Nitrogen Tripod Ligand/Oxygen Tripod Ligand Indium(III) Complexes: The First Structurally Characterized Trofimenko−Kläui Complex $[\eta^5\text{-}(C_5H_5)Co\{P(OCH_3)_2(O)\}_3InHB(pz)_3][InCl_4]$ (pz = pyrazol-1-yl)

Wolfgang Kläui,*[a] Wilfried Peters,[a] Norbert Liedtke,[a] Swiatoslaw Trofimenko,[b] Arnold L. Rheingold,[b] and Roger D. Sommer[b]

Keywords: Hard and soft acids and bases concept (HSAB) / Symbiosis and antisymbiosis / Indium / (Cyclopentadienyl)tris(diorganylphosphito-*P*)cobaltate(1−) / Hydrotris(pyrazol-1-yl)borate / Mixed-ligand complexes

Indium(III) complexes $[L_RInTp^*]X$ {L_R = (cyclopentadienyl)-tris[diorganylphosphi(ni)to-*P*]cobaltate(1−) $[\eta^5\text{-}(C_5H_5)Co\{PR_2(O)\}_3]^-$, R = OCH_3, CH_2CH_3; Tp* = hydrotris(3,5-dimethylpyrazol-1-yl)borate} have been prepared from $[Tp^*InCl_2(NCCH_3)]$ and AgL_{OMe} or TlL_{Et}. Alternatively, equilibration of a 1:1 mixture of the homoleptic complexes $[In(L_{OMe})_2][PF_6]$ and $[In(Tp)_2][PF_6]$ in aqueous methanol slowly yielded the heteroleptic indium(III) complex $[L_{OMe}InTp][PF_6]$. An X-ray crystal structure determination revealed a *fac*-N_3O_3 coordination sphere for the $[L_{OMe}InTp][InCl_4]$ complex. These indium compounds represent the first structurally characterized complexes where the tripodal oxygen ligand L_R and the tripodal nitrogen ligand Tp are coordinated to the same metal center. Indium(III) is classified as a class a, i.e. a hard metal ion, but it evidently prefers an antisymbiotic arrangement of ligands.

Introduction

Jørgensen defined chemical symbiosis as the fact that hard bases (electronegative donor atoms) attached to a given central atom make it a harder Lewis acid by retaining their valence electrons thus maintaining a high positive charge on the central atom.[1] Soft bases (donor atoms of low electronegativity) attached to the same central atom give up their valence electrons thereby reducing its positive charge and making it a softer Lewis acid. Pearson, on the other hand, pointed out that class b metal ions very often behave in an antisymbiotic manner. Thus, soft bases attached to an already soft Lewis acid decrease its affinity towards another soft base.[2] Antisymbiosis can be explained on the basis of the *trans* effect or *trans* influence and is most pronounced in square planar $4d^8$ and $5d^8$ complexes. Symbiosis seems to be the preferred behaviour of class a, i.e. hard metal ions.

The tridentate oxygen and nitrogen ligands **1** and **2** (see Figure 1), that we introduced some time ago,[3,4] are both facially coordinating monoanionic six-electron ligands. The tripodal nitrogen ligands, abbreviated herein as Tp, exhibit coordination chemistry resembling that of cyclopentadienyl or pentamethylcyclopentadienyl ligands. On the other hand, tripodal oxygen ligands, abbreviated herein as L_R, are very hard and weak ligands. Indeed, they are weaker than water and nearly as hard as fluoride. Both form 2:1 complexes with a wide variety of main group and transition metal ions M^{2+} and M^{3+}. All our attempts to synthesize hard-soft mixed-ligand 2:1 complexes starting from metal salts MX_2 and alkali metal salts of **1** and **2** have been unsuccessful. We obtained only mixtures of the homoleptic complexes and the question that arises is whether this was a consequence of strict symbiosis? In the following, we describe the synthesis and characterization of octahedral mixed-ligand indium(III) complexes, i.e. indium(III) complexes with an InN_3O_3 coordination polyhedron.

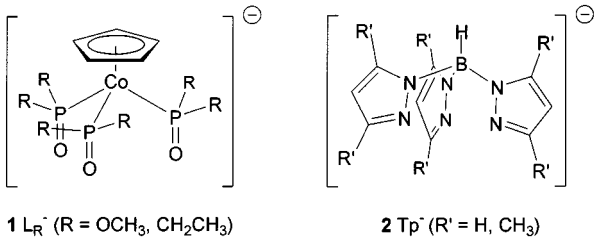

Figure 1. Structures of Kläui's and Trofimenko's ligands **1** and **2**

Results and Discussion

Preparative Results

Reactions of the silver and thallium salts of the oxygen ligands, e.g. AgL_{OMe} (**1a**) and TlL_{Et} (**1b**), with the indium complex $[Tp^*InCl_2(NCCH_3)]$ (**6**)[5] lead to compounds $[L_{OMe}InTp^*][AgCl_2]$ (**3d**) and $[L_{Et}InTp^*]Cl$ (**3c**) (see Figure 2).

The reactions of the silver and thallium salts are fast and go to completion. The corresponding alkali metal salts re-

[a] Institut für Anorganische Chemie und Strukturchemie I der Heinrich-Heine-Universität,
Universitätsstraße 1, 40225 Düsseldorf, Germany
Fax: (internat.) + 49-(0)211/811-2287
E-mail: klaeui@uni-duesseldorf.de
[b] Department of Chemistry and Biochemistry, University of Delaware,
Newark, Delaware 19716, USA

 © WILEY-VCH Verlag GmbH, 69451 Weinheim, 2001 1434−1948/01/0303−0693 $ 17.50+.50/0

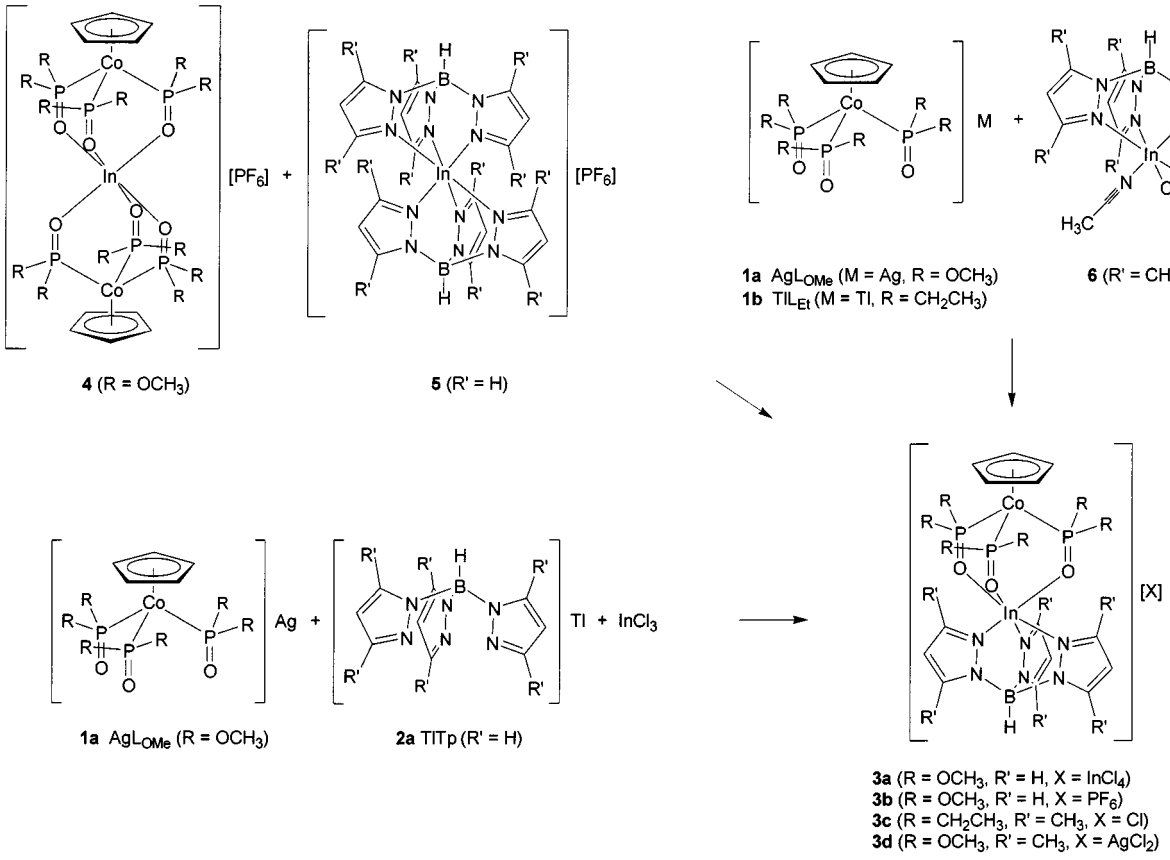

Figure 2. Synthesis and schematic structures of the indium(III) complexes

act more sluggishly and the need to separate the remaining starting compounds makes purification of the complexes **3** more difficult.

We had no evidence as to whether the successful preparation of the heteroleptic indium complexes $[L_{OMe}InTp^*]^+$ and $[L_{Et}InTp^*]^+$ was kinetically or thermodynamically controlled. Therefore, we performed a second experiment in which indium chloride was treated with AgL_{OMe} (**1a**) and TlTp (**2a**) in a mixture of dichloromethane, acetone, and methanol. $[L_{OMe}InTp][InCl_4]$ (**3a**) was isolated in almost quantitative yield. We could not detect any of the homoleptic complexes $[In(L_{OMe})_2]^+$ or $[In(Tp)_2]^+$. Finally, we tried to equilibrate an equimolar mixture of the homoleptic compounds $[In(L_{OMe})_2][PF_6]$ (**4**) and $[In(Tp)_2][PF_6]$ (**5**) in methanol/water. At room temperature, we found there to be very little or no ligand exchange. After refluxing the solution for 2 d, we were able to recover the heteroleptic compound $[L_{OMe}InTp][PF_6]$ (**3b**) together with some of the unchanged homoleptic complexes **4** and **5**. However, the solubilities of **3b**, **4**, and **5** are rather similar and we have not been able to separate the compounds. Identification of **3b**, **4**, and **5** was nevertheless possible on the basis of their ^1H and ^{31}P NMR spectra. Complete equilibration could not be attained by prolonged heating. The Tp ligand is slowly hydrolyzed under these conditions.

Complexes **3** were obtained as bright-yellow crystals, and were found to be stable in moist air and soluble in acetone, nitromethane, and dichloromethane, moderately soluble in chloroform, diethyl ether, and methanol/water mixtures, and insoluble in hydrocarbons.

MS Data, IR Spectra, and Conductivity Measurements

The mass spectra of complexes **3** were measured by the fast atom bombardment (FAB^+) ionization technique using a nitrobenzyl alcohol matrix. The molecular ion peaks $[L_RInTp]^+$ and $[L_RInTp^*]^+$ were the base peaks of the spectra and could easily be recognized from the characteristic isotope pattern. The only other strong peaks were those corresponding to the fragment $[L_RIn + H]^+$, generated by loss of the Tp or Tp* ligand from the molecular ion.

The IR spectra of complexes **3a**−**3d** were found to be dominated by the characteristic absorptions of the ligands **1**[6] and **2**.[4] Conductivity measurements[7] of 10^{-3} M solutions of **3a** and **3d** in nitromethane indicated that these compounds behave as 1:1 electrolytes in solution.

1D and 2D NMR Spectra

The ^1H NMR spectra of **3a**−**3d** feature only a few peaks that can easily be assigned to either ligand **1** or ligand **2**. In complexes **3a** and **3b**, the pyrazol-1-yl protons give rise to an AMX spin system and the ^1H NMR spectra reveal local C_{3v} symmetry of the ligands. In the ^1H NMR spectra of **3c** and **3d**, the protons of the methyl groups in the 3- and 5-positions of the pyrazol-1-yl rings appear as singlets, as do the 4-H protons (ratio 3:3:1), again indicating local C_{3v}

Table 1. Chemical shifts (δ) of the free ligands and of the heteroleptic complexes **3c** and **3d**; pz = pyrazol-1-yl, L_R^- = (cyclopentadienyl)tris-[diorganylphosphi(ni)to-*P*]cobaltate(1−)

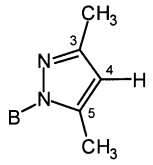

Compound	^{1}H NMR							^{31}P{1H} NMR
	3-CH_3-pz (Tp^{*-})	4-H-pz (Tp^{*-})	5-CH_3-pz (Tp^{*-})	C_5H_5 (L_R^-)	OCH_3 (L_{OMe}^-)	CH_2CH_3 (L_{Et}^-)	CH_2CH_3 (L_{Et}^-)	P (L_R^-)
NaL_{OMe} [a]	–	–	–	5.06	3.61			110.0
TlL_{Et} (**1b**)[a]	–	–	–	4.88	–	1.22	2.10 2.30	108.5
KTp*[b]	2.05[c]	5.58	2.21[c]	–	–	–	–	–
$[L_{OMe}InTp^*][AgCl_2]$ (**3d**)[a]	2.46	5.88	2.40	5.46	3.84	–	–	117.8
$[L_{Et}InTp^*]Cl$ (**3c**)[a]	2.36	5.81	2.35	5.47	–	1.31	2.5	119.7

[a] [D_1]Chloroform. – [b] [D_6]Acetone. – [c] The 3- and 5-positions of the pyrazol-1-yl rings were not distinguished.

symmetry of the ligands. The two upfield resonances due to the methyl groups cannot be unequivocally assigned to the 3- and 5-positions solely on the basis of the 1D ^{1}H NMR spectrum.[8]

In the ^{31}P{^{1}H} NMR spectra, the phosphito and phosphinito groups of the tripodal oxygen ligand give rise to a singlet resonance at δ ≈ 110, which is broadened by quadrupolar relaxation (^{59}Co, I = 7/2). Coordination of the ligand to indium(III) decreases the electronic shielding and δ^{31}P is consequently shifted to lower field by about 10 ppm to δ ≈ 120 (see Table 1).

The ^{1}H NMR spectrum of ligand **1a** features a four-line pattern ("*virtual* quadruplet") due to the methoxy groups of L_{OMe}^- (OCH_3, $[A[X_3]_2]_3$ spin system, $^3J_{H\text{-}P}$ = 11.1 Hz). These resonances are shifted to lower field in **3d** as compared to those in **1** (see Table 1). The ^{1}H NMR spectrum of the ligand L_{Et}^- (**1b**) features unresolved multiplet patterns due to the methyl groups (CH_2CH_3, $[A[X_3YZ]_2]_3$ spin system) and the methylene groups (CH_2CH_3, $[A[X_3YZ]_2]_3$ spin system), which are shifted to lower field in **3c**. Coordination to indium(III) also shifts the signals due to the pyrazol-1-yl ring protons and methyl groups to lower field (see Table 1).

All the NMR-spectroscopic data of compounds **3** are in agreement with their formulation as mixed-ligand complexes $[L_RInTp]^+$ and $[L_RInTp^*]^+$ in solution. However, the chemical shift differences between the mixed-ligand complexes and the homoleptic complexes are rather small and are not always sufficient to discern e.g. $[L_{Et}InTp^*]^+$ from an equimolar mixture of $[In(L_{Et})_2]^+$ and $[In(Tp^*)_2]^+$. We have recently found[9] that the coordination of an oxygen ligand and a nitrogen ligand to the same indium ion can be proven by 2D ^{1}H NOESY NMR spectroscopy. In this way, one can identify $[L_RInTp]^+$ and $[L_RInTp^*]^+$ and exclude fast ligand exchange between homoleptic and heteroleptic complexes.[9]

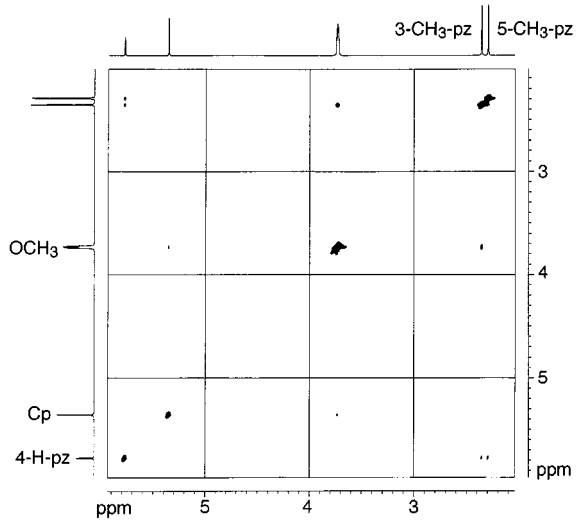

Figure 3. 2D ^{1}H NOESY NMR spectrum of **3d** ([D_6]acetone); a strong cross-peak is observed between the methoxy groups of the oxygen ligand and *only one* (!) of the pyrazol-1-yl ring methyl groups of the nitrogen ligand

Table 2. 2D ^{1}H NOESY NMR correlations in the heteroleptic complex $[L_{OMe}InTp^*][AgCl_2]$ (**3d**); pz = pyrazol-1-yl, L_{OMe}^- = (cyclopentadienyl)tris(dimethylphosphito-*P*)cobaltate(1−)

NOE correlation	
of H-	with H-
OCH_3 (L_{OMe}^-)	C_5H_5 (L_{OMe}^-), 3-CH_3-pz
C_5H_5 (L_{OMe}^-)	OCH_3 (L_{OMe}^-)
4-H-pz	3-CH_3-pz, 5-CH_3-pz
3-CH_3-pz	4-H-pz, OCH_3 (L_{OMe}^-)
5-CH_3-pz	4-H-pz

Such NOESY NMR spectra (see Figure 3, Table 2) show correlation signals between the cyclopentadienyl ligand and the methoxy groups of the oxygen ligand, as well as interac-

tions between the pyrazol-1-yl 4-H ring proton and the 3-CH_3-pz and 5-CH_3-pz methyl groups. Additionally, a strong cross-peak is observed between the methoxy groups of the oxygen ligand and only *one* of the pyrazol-1-yl ring methyl groups of the nitrogen ligand, a result that can only be obtained if both ligands are coordinated to the same metal ion, thus confirming the spatial proximity of the two ligands as depicted in Figure 2. This cross-peak also leaves no ambiguity concerning the assignment of 3-CH_3 and 5-CH_3 of the pyrazol-1-yl rings.

We expected the mixed-ligand complexes identified in solution to also exist in the solid state. A single-crystal X-ray analysis of complex **3a** confirmed this hypothesis (see Figure 4).

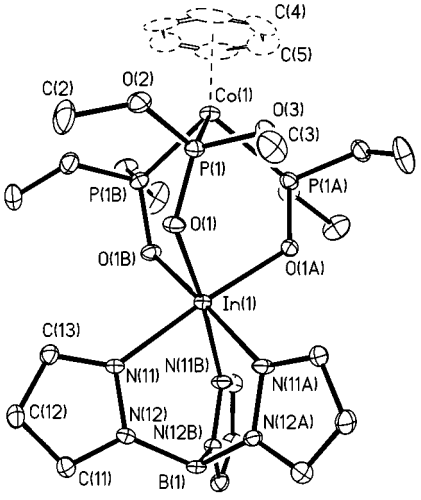

Figure 4. Thermal ellipsoid plot (at a 30% probability level) for the cation of **3a**; the disordered cyclopentadienyl ring is represented by the six atoms above Co(1); hydrogen atoms and the $[InCl_4]^-$ ion are omitted for the sake of clarity

Crystal Structure of $[L_{OMe}InTp][InCl_4]$ (3a)

A thermal ellipsoid plot of **3a** is shown in Figure 4; for crystal data see Table 3. Both ions in the lattice are positioned along a threefold axis. The Cp ring of the ligand is perpendicular to the crystallographic threefold axis. As a result, threefold disorder is imposed upon the five-membered ring. For the Cp system, two unique positions of the C atoms were found in the asymmetric unit. The occupancy for each position was set at 0.83325 so that C(4) and C(5) represent one-third of the cyclopentadienyl ring. The distance from Co(1) to the centroid of the calculated ring was found to be 1.69 Å. The hydrogen atoms on C(4) and C(5) were ignored.

Conclusions

The results of this study have shown that the hard class a metal ion indium(III) can behave in an antisymbiotic manner. The different steric properties of the Tp and Tp* ligands do not influence the course of the reaction.

As far as we are aware, there have been no detailed investigations of the preferences for symbiosis or antisymbiosis of hard metal ions. Hegetschweiler[10] has looked at the coordination chemistry of 1,3,5-triamino-1,3,5-trideoxy-*cis*-inositol (taci) towards the Group 13 metal ions Al^{3+}, Ga^{3+}, and Tl^{3+}. It was found that taci can act as a tridentate ligand in four different binding modes (O_3, O_2N, ON_2, and N_3). X-ray crystal structure determinations revealed AlO_6, GaN_3O_3, and TlN_6 coordination spheres for the respective $[M(taci)_2]^{3+}$ complexes. These results fit nicely with our finding of an InN_3O_3 coordination sphere for the $[L_RInTp]^+$ and $[L_RInTp^*]^+$ complexes.

Table 3. Crystal data and structure refinement for **3a**

Empirical formula	$C_{20}H_{33}BCl_4CoIn_2N_6O_9P_3$
Formula mass	1035.61
Temperature	173(2) K
Wavelength	0.71073 Å
Crystal system	cubic
Space group	$P2(1)3$
Unit cell dimensions	a = 15.6051(2) Å
b = 15.6051(2) Å	
c = 15.6051(2) Å	
Volume	3800.14(8) Å^3
Z	4
Density (calculated)	1.810 Mg/m^3
Absorption coefficient	2.092 mm^{-1}
F(000)	2040
Crystal size	0.30 × 0.25 × 0.20 mm
θ range for data collection	2.26 to 28.36°
Index ranges	$-20 \le h \le 18$
	$-19 \le k \le 20$
	$-20 \le l \le 20$
Reflections collected	17289
Independent reflections	3077 [R(int) = 0.0427]
Completeness to θ = 28.36°	97.7%
Absorption correction	empirical from SADABS
Max. and min. transmission	0.6797 and 0.5725
Refinement method	full-matrix least squares on F^2
Data/restraints/parameters	3077/0/142
Goodness-of-fit on F^2	1.681
Final R indices [$I > 2\sigma(I)$]	R_1 = 0.0309, wR_2 = 0.0601
R indices (all data)	R_1 = 0.0348, wR_2 = 0.0613
Absolute structure parameter	0.05(2)
Largest diff. peak and hole	0.328 and −0.519 e Å^{-3}

Although the synthesis of $[L_RMTp]$ (M = Pb, Sn; R = OCH_2CH_3) has been reported in the literature,[11] the complexes were not characterized by X-ray analysis. We tried to synthesize $[L_{OEt}PbTp]$ (**9**) according to the published procedure (Figure 5). At 328 K, the 1D ^{1}H NMR spectrum of the product displayed two sets of signals like those reported in the literature,[11] which could readily be assigned to the two ligands with local C_{3v} symmetry. At 223 K, a doubling of the number of signals was observed. These well-separated signals were indicative of the presence of three species, which we assign as the heteroleptic complex $[L_{OEt}PbTp]$ (**9**) and the homoleptic complexes $[(L_{OEt})_2Pb]$ (**10**) and $[Tp_2Pb]$ (**11**). This hypothesis was supported by the relevant intensity ratios. The existence of **9** was corroborated by a 2D ^{1}H NOESY NMR spectrum (223 K), which showed a cross-peak between the OCH_2CH_3 groups of the oxygen ligand and only one of the pyrazol-1-yl ring protons of the nitrogen ligand. A 2D ^{1}H EXSY NMR spectrum (223 K) featured interchange signals between the pyrazol-1-yl ring protons in the 3- and 5-positions as well as between both Cp signals of the oxygen ligand, thus revealing an equilibrium

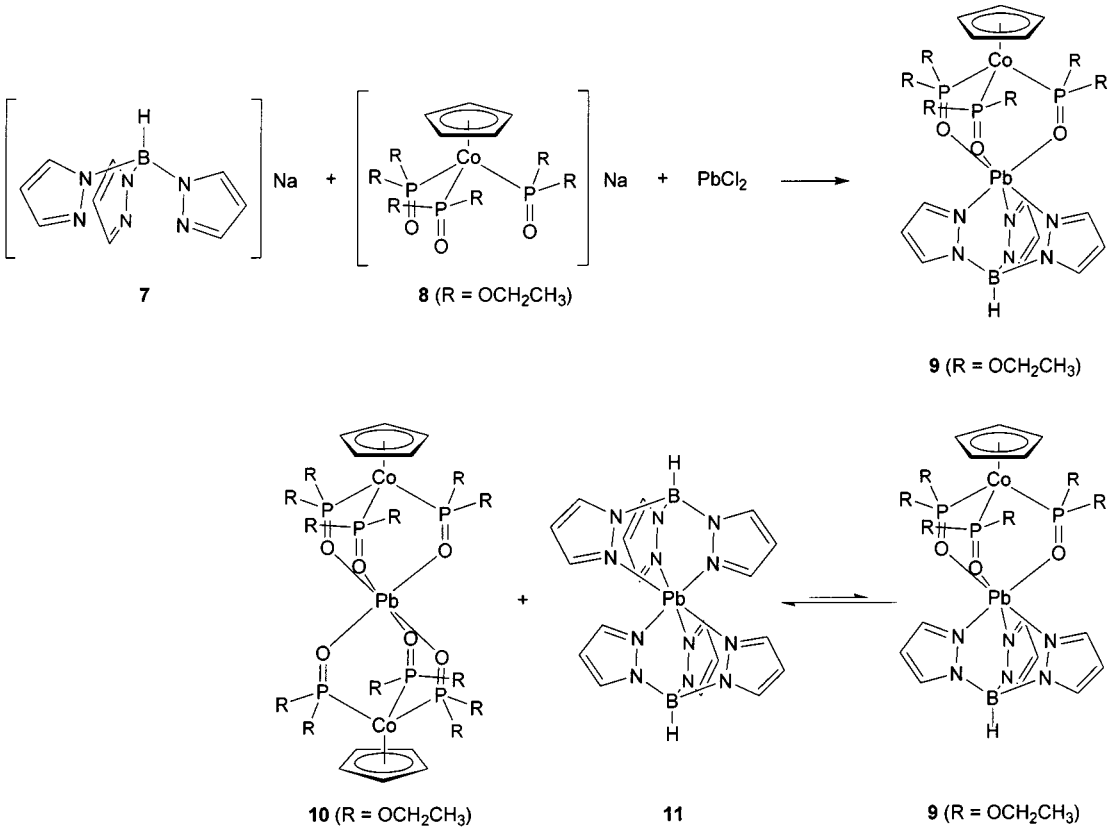

Figure 5. Equilibrium between the homoleptic and heteroleptic lead(II) complexes

Table 4. ^{207}Pb chemical shifts (δ) of the homoleptic and heteroleptic lead(II) complexes; Tp = tris(pyrazol-1-yl)borate, L_{OEt} = (cyclopentadienyl)tris(diethylphosphito-*P*)cobaltate; lead chemical shifts are highly dependent on temperature and concentration (0.05 M solution in $CDCl_3$)

Compound		^{207}Pb NMR ($\nu_{1/2}$/Hz)		
		Literature values	303 K	223 K
1:1 mixture of **10** and **11**		–	–	−2037, −1614 (120), −1309 (96)
"[TpPbL$_{OEt}$]"	(**9**)	−1613 (110)	–	−2032 (362), −1615 (193), −1311 (169)
[(L$_{OEt}$)$_2$Pb]	(**10**)	−2034 (320)	−2056 (55) sept., $^2J_{PbP}$ = 72 Hz	−2005 (335)
[(Tp)$_2$Pb]	(**11**)	−895 (600)	−1244 (72)	−1312 (99)

between **9**, **10**, and **11** in solution. At ambient temperatures, this equilibrium is fast on the proton NMR time scale.

The ^{31}P{^{1}H} NMR spectrum featured two well-separated signals at 223 K, which could be assigned to **9** and **10**. The ^{207}Pb NMR spectrum showed the resonances of the homoleptic complexes **10** and **11**, as well as a third signal that could most probably be assigned to **9** (see Table 4).

A solution of a mixture of the homoleptic complexes **10** and **11** in a 1:1 molar ratio exhibits exactly the same spectroscopic properties and gives an identical elemental analysis as reported for **9** in the literature. The very similar physical properties of these complexes as well as the fast equilibrium between **9**, **10**, and **11** in solution most probably account for the fact that neither Reger[11] nor ourselves have been able to isolate **9** as a pure compound.

It seems impossible to make general predictions as to whether a class a, i.e. a hard metal ion, will prefer a symbiotic or an antisymbiotic ligand arrangement. A more systematic investigation should give better insight into the relationship between HSAB properties and symbiotic and antisymbiotic behaviour.

Experimental Section

General Procedures: Standard inert-atmosphere techniques were used for syntheses and sample manipulations. The solvents were dried by standard methods, distilled under nitrogen, and stored over 4 Å molecular sieves prior to use. Acetone p.a. and nitromethane p.a. (E. Merck, Darmstadt) were used as obtained and stored over 4 Å molecular sieves. – ^{1}H, 2D ^{1}H NOESY, 2D ^{1}H EXSY,

$^{31}P\{^1H\}$, and ^{207}Pb NMR spectra were recorded with a Bruker Analytische Meßtechnik DRX 500 NMR spectrometer from 0.05 M solutions. The ^1H NMR spectra were calibrated against the residual proton signals of the solvents as internal references ([D_6]acetone: δ_H = 2.08; [D_1]chloroform: δ_H = 7.24), while the $^{31}P\{^1H\}$ NMR spectra were referenced to external 85% H_3PO_4. Chemical shifts are accurate to within ±0.01 ppm for δ^1H, ±0.1 ppm for $\delta^{31}P$, and ±1 ppm for $\delta^{207}Pb$. For acquisition of the ^{207}Pb NMR spectra, the following parameters were typically used: sweep width 10^5 Hz, 4 k data points, 90° pulse. ^{207}Pb chemical shifts are reported downfield from tetramethyllead using 1 M aq. $Pb(NO_3)_2$ ($\delta^{207}Pb$ = −2961) as an external standard. The phase-sensitive NOESY spectra[12] were obtained with 512 t_1 increments and 2048 data points in t_2; 16 free induction decays were collected for each value of t_1. After zero-filling and multiplying both dimensions with a q sine function, the data were Fourier-transformed into a 1024 × 1024 matrix. The mixing time used was 0.9 s. − Infrared spectra were recorded with a Bruker Analytische Meßtechnik IFS 66 FT-IR spectrometer. − FAB^+ mass spectra were recorded with a Finnigan MAT 8200 mass spectrometer. − Elemental analyses were provided by the Institut für Pharmazeutische Chemie at the Heinrich-Heine-Universität Düsseldorf and the Mikroanalytisches Labor Pascher, Remagen. − Conductivity measurements were performed using a Schott CG 851 conductometer. − The sodium salt of **1**[13] and compounds **1a**,[9] **1b**,[14] **3a**,[9] **3b**,[9] **4**,[9] **5**,[9] **6**,[5] **7**,[4] **8**,[15] **10**,[16] and **11**[4] were prepared according to published procedures. The thallium salt **2a** was prepared from KTp and Tl_2CO_3 according to procedures for analogous TlTp compounds.[17] All other compounds were purchased from commercial sources.

Crystal Structure Determination of 3a: Diffraction data were collected with a Siemens P4 diffractometer equipped with a CCD area detector. Crystal data are presented in Table 3. The cubic unit cell was determined using reflections collected from three series of 15 frames in distinct regions of space. Final unit-cell refinement was performed by a least-squares fitting of 6886 reflections. The systematic absences were consistent with the space groups $P2_13$ and $P4_232$; Laue group symmetry supported the former choice. The E statistics for the data, with a value of 0.687, also supported this choice. The structure was solved by direct methods and the remaining atoms were located by difference Fourier synthesis. The reported absolute stereochemistry was confirmed by refinement of the Flack parameter [0.05(2)]. Non-hydrogen atoms were refined anisotropically. Hydrogen atoms were placed in calculated positions and treated as isotropic contributions with thermal parameters defined as 1.2 or 1.5 times that of the parent atom. All software and sources of scattering factors are contained in the SHELXTL program library (version 5.10, G. Sheldrick, Bruker-AXS, Madison, WI).

Crystallographic data (excluding structure factors) for the structure reported in this paper have been deposited with the Cambridge Crystallographic Data Centre as supplementary publication no. CCDC-151641. Copies of the data can be obtained free of charge on application to CCDC, 12 Union Road, Cambridge CB2 1EZ, UK [Fax: (internat.) + 44-1223/336-033; E-mail: deposit@ccdc.cam.ac.uk].

Preparations

{(Cyclopentadienyl)tris(dimethylphosphito-*P*)cobalt-*O*,*O*′,*O*′′}-{hydrotris(3,5-dimethylpyrazol-1-yl)borato-*N*,*N*′,*N*′′}indium Dichloroargentate [L_{OMe}InTp*][$AgCl_2$] (3d): A colourless solution of **6** (0.44 g, 0.92 mmol) in dichloromethane (20 mL) was treated with **1a** (0.52 g, 0.92 mmol) and the resulting mixture was stirred at room temperature. After a few minutes, the solution turned cloudy and the precipitation of a white solid was observed. The reaction mixture was stirred overnight, then filtered through Celite, and the filtrate was concentrated in vacuo. The resulting yellow residue was redissolved in the minimum volume of dichloromethane and this solution was treated with an excess of *n*-hexane. A pale-yellow oily residue precipitated immediately, which solidified on ultrasound treatment. The yellow solid was repeatedly washed with small amounts of *n*-hexane and dried in vacuo. Slow diffusion of diethyl ether into a dichloromethane solution yielded yellow crystals. Yield: 0.86 g (94%). − ^1H NMR (298 K, [D_1]chloroform): δ = 2.40 (s, 9 H, 5-CH_3-pz), 2.46 (s, 9 H, 3-CH_3-pz), 3.84 (virt. q, [A[X_3]$_2$]$_3$ $^3J_{H-P}$ = 11.1 Hz, 18 H, OCH_3 L_{OMe}), 5.46 (s, 5 H, C_5H_5 L_{OMe}), 5.88 (s, 3 H, 4-H-pz). − $^{31}P\{^1H\}$ NMR (298 K, [D_1]chloroform): δ = 117.8 {s, [*A*[X_3]$_2$]$_3$, *P*(O)OCH_3}. − IR (KBr): $\tilde{\nu}$ = 2559 cm^{-1} (m) ν(B−H), 1103 (vs), 1071 (vs) ν(P=O), 647 (m), 587 (s) δ(P=O). − $C_{26}H_{45}AgBCl_2CoInN_6O_9P_3$ (1041.94): calcd. C 29.97, H 4.35, N 8.07, Ag 10.35, In 11.02; found C 30.07, H 4.36, N 8.05, Ag 10.2, In 11.0. − FAB^+ MS; *m*/*z* (%): 863 [M − Cl]$^+$ (100), 567 [L_{OMe}In + H]$^+$ (43). − Conductivity (10^{-3} M solution of **3d** in nitromethane): Λ = 73 μS.

{(Cyclopentadienyl)tris(diethylphosphinito-*P*)cobalt-*O*,*O*′,*O*′′}-{hydrotris(3,5-dimethylpyrazol-1-yl)borato-*N*,*N*′,*N*′′}indium Chloride [L_{Et}InTp*]Cl (3c): According to the procedure described above for **3d**, complex **3c** was obtained as a yellow powder from **6** (0.70 g, 1.46 mmol) and **1b** (0.94 g, 1.46 mmol). Yield: 1.26 g (97%). − ^1H NMR (298 K, [D_1]chloroform): δ = 1.31 {m, [A[X_3YZ]$_2$]$_3$, 18 H, P(O)CH_2CH_3 L_{Et}}, 2.35 (s, 9 H, 5-CH_3-pz), 2.36 (s, 9 H, 3-CH_3-pz), 2.5 {m, [A[X_3YZ]$_2$]$_3$, 12 H, P(O)CH_2CH_3 L_{Et}}, 5.47 (d, 5 H, $^3J_{H-P}$ = 0.4 Hz, C_5H_5 L_{Et}), 5.81 (s, 3 H, 4-H-pz). − $^{31}P\{^1H\}$ NMR (298 K, [D_1]chloroform): δ = 119.7 {s, [*A*[X_3YZ]$_2$]$_3$, *P*(O)OCH_3}. − IR (KBr): $\tilde{\nu}$ = 2555 cm^{-1} (m) ν(B−H), 1070 (vs) ν(P=O), 648 (m), 538 (vs) δ(P=O). − $C_{32}H_{57}BClCoInN_6O_3P_3$ (886.01): calcd. C 43.34, H 6.48, N 9.48; found C 41.85, H 6.55, N 9.11. − FAB^+ MS; *m*/*z* (%): 851 [M − Cl]$^+$ (100), 555 [L_{Et}In + H]$^+$ (48).

Acknowledgments

This work was supported by the Fonds der Chemischen Industrie. We thank K. Hegetschweiler for helpful discussions. N. L. wishes to thank B. Tommes for assistance with the preparative work.

[1] C. K. Jørgensen, *Inorg. Chem.* **1964**, *3*, 1201.
[2] R. G. Pearson, *Inorg. Chem.* **1973**, *12*, 712.
[3] W. Kläui, *Angew. Chem.* **1990**, *102*, 661; *Angew. Chem. Int. Ed. Engl.* **1990**, *29*, 627.
[4] S. Trofimenko, *Scorpionates: The Coordination Chemistry of Polypyrazolylborate Ligands*, Imperial College London, **1999**, and references therein.
[5] A. H. Cowley, C. J. Carrano, R. L. Geertz, R. A. Jones, C. M. Nunn, *Angew. Chem.* **1988**, *100*, 306; *Angew. Chem. Int. Ed. Engl.* **1988**, *27*, 277.
[6] W. Kläui, K. Dehnicke, *Chem. Ber.* **1978**, *111*, 451.
[7] W. J. Geary, *Coord. Chem. Rev.* **1971**, *7*, 81.
[8] C. Lopez, R. M. Claramunt, D. Sanz, C. Foces Foces, F. H. Cano, R. Faure, E. Cayon, J. Elguero, *Inorg. Chim. Acta* **1990**, *176*, 195.
[9] W. Kläui, N. Liedtke, W. Peters, *Magn. Res. Chem.* **1999**, *37*, 867.
[10] K. Hegetschweiler, M. Ghisetta, T. F. Fässler, R. Nesper, H. W. Schmalle, G. Rihs, *Inorg. Chem.* **1993**, *32*, 2032.
[11] D. L. Reger, Y. Ding, A. L. Rheingold, R. L. Ostrander, *Inorg. Chem.* **1994**, *33*, 4226.
[12] J. Jeener, P. Bachmann, R. R. Ernst, *J. Chem. Phys.* **1979**, *71*, 4546.
[13] W. Kläui, B. Lenders, B. Hessner, K. Evertz, *Organometallics* **1988**, *7*, 1357.

[14] W. Kläui, A. Kremer-Aach, N. Liedtke, unpublished results.
[15] W. Kläui, *Z. Naturforsch., B* **1979**, *34*, 1403.
[16] E. M. Holt, W. Kläui, J. J. Zuckerman, *J. Organomet. Chem.* **1987**, *335*, 29.
[17] S. Trofimenko, J. C. Calabrese, P. J. Domaille, J. S. Thompson, *Inorg. Chem.* **1989**, *28*, 1091.

Received July 19, 2000
[I00285]

The Heterotrimetallic Complex [Ni(acacen)KLa(pta)$_4$]: Structural and Thermochemical Studies

Natalia Kuzmina,[a] Mikhail Ryazanov,[a] Irina Malkerova,[b] Andrei Alikhanyan,[b] and Alain N. Gleizes*[c]

Keywords: Potassium / Lanthanum / Nickel / Mass spectrometry / Thermochemistry

The heterotrimetallic species [Ni(acacen)KLa(pta)$_4$] [H_2acacen and Hpta being *N,N′*-ethylenebis(acetylacetonimine) and 1,1,1-trifluoro-5,5-dimethyl-2,4-hexanedione, respectively] was obtained by interaction of Ni(acacen) with KLa(pta)$_4$ in chloroform. From the X-ray, single crystal structure determination, the potassium cation acts as a bridge between the complex anion [La(pta)$_4$]$^-$ and the neutral complex Ni(acacen). Sublimation, thermal behaviour, pressure, and composition of the vapour phase have been investigated for both [Ni(acacen)KLa(pta)$_4$] and the parent complexes Ni(acacen) and KLa(pta)$_4$, by means of thermal analysis and mass spectrometry using a Knudsen cell. The heterotrimetallic molecule was not found in the saturated vapour. Two processes take place upon heating: [Ni(acacen)KLa(pta)$_4$]$_{(s)}$ → [KLa(pta)$_4$]$_{(s)}$ + Ni(acacen)$_{(g)}$ and [KLa(pta)$_4$]$_{(s)}$ → [KLa(pta)$_4$]$_{(g)}$. The standard free energy of formation for [Ni(acacen)KLa(pta)$_4$] have been estimated ($\Delta G_f^0{}_{380K}$ = −6.1±2 kJ/mol). [Ni(acacen)KLa(pta)$_4$] can be sublimed completely at low pressure because both parent complexes KLa(pta)$_4$ and Ni(acacen) are volatile.

Introduction

Volatile heterometallic complexes are interesting as prospective single-source precursors for the growth of heterometallic thin-film materials by chemical vapour deposition from metal-organic precursor molecules (MOCVD).[1] The coordination chemist′s problem is then to combine at the least two metal elements, into a congruently vaporizing metal-organic complex. Generally, the metal elements do not belong to the same chemical family, and they present different metal complex chemistries and thermochemistries. Various synthetic strategies can be applied.[1] In order to prepare volatile complexes incorporating a *d* and an *f* or an *s* element, we have developed a strategy based on the use of *d* metal complexes as neutral ligands to coordinatively saturate an *f* or an *s* element cation in one of its β-diketonates.[2−5]

We present here results about an unusual heterotrimetallic complex, which results from interaction between the heterobimetallic complex KLa(pta)$_4$ and Ni(acacen).

[a] Moscow State University, Department of Inorganic Chemistry, Leninskie Gory, 119899 Moscow, Russia
E-mail: kuzmina@inorg.chem.msu.ru
[b] Kurnakov Institute of General and Inorganic Chemistry RAS, 31 Leninskii Prosp., 117233, Moscow, Russia
E-mail: alikhanyan@ionchran.rinet.ru
[c] Ecole Nationale Supérieure de Chimie de Toulouse, INPT, CIRIMAT-UMR 5085,
118 route de Narbonne, 31077 Toulouse cedex 4, France
E-mail: agleizes@ensct.fr

Results and Discussion

Synthesis and Crystal Structure of [Ni(acacen)KLa(pta)$_4$]

The heterotrimetallic complex [Ni(acacen)KLa(pta)$_4$] was obtained as a single-phased, red-brown, crystalline product by simple interaction of Ni(acacen) with KLa(pta)$_4$ in chloroform. It crystallises in the triclinic system, with a space group of $P\bar{1}$, and unit-cell volume 2769 Å^3. The unit-cell comprises two centrosymmetrically related asymmetric units.

The asymmetric unit is made of one of each constituent: a complex anion [La(pta)$_4$]$^-$, a cation K$^+$, and a neutral complex Ni(acacen) (Figure 1). The potassium acts as a link

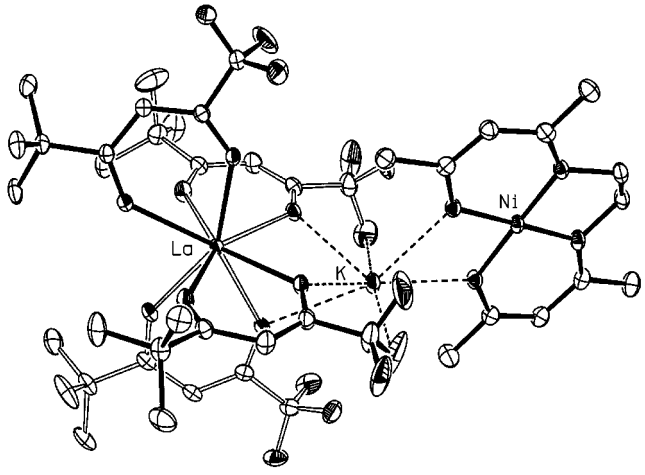

Figure 1. The heterotrimetallic entity [Ni(acacen)KLa(pta)$_4$]; ellipsoids are at their 30% probability level; ellipsoids with octant shading are for non-carbon atoms

 © WILEY-VCH Verlag GmbH, 69451 Weinheim, 2001 1434−1948/01/0303−0701 $ 17.50+.50/0

Table 1. Selected distances [Å] and angles [deg] in [Ni(acacen)KLa(pta)$_4$]

Around K		Around La		Around Ni	
K−O(2)	2.661(3)	La−O(1b)	2.421(2)	Ni−O(1)	1.857(2)
K−O(1a)	2.677(3)	La−O(2d)	2.439(2)	Ni−O(2)	1.859(3)
K−O(1c)	2.731(3)	La−O(2a)	2.470(3)	Ni−N(1)	1.853(3)
K−O(1)	2.742(3)	La−O(2b)	2.490(3)	Ni−N(2)	1.858(3)
K−F(1c)	2.843(5)	La−O(2c)	2.494(3)	O(1)−Ni−O(2)	84.01(11)
K−O(1d)	2.914(3)	La−O(1a)	2.521(3)	O(1)−Ni−N(1)	94.73(13)
K−F(1a)	2.949(4)	La−O(1c)	2.532(3)	O(2)−Ni−N(2)	94.16(13)
		La−O(1d)	2.532(2)	N(1)−Ni−N(2)	87.21(14)
K···La	3.9421(11)				
K···Ni	3.7780(11)			Ni···Ni[a]	4.8000(14)
				Ni···Ni[b]	6.5691(15)
				N(1)−C(11)−C(12)−N(2)	-35.9(4)

[a] Code of symmetry operations: 1 − x, − y, 1 − z. − [b] −x, −y, 1 − z.

between the two metal complexes, being in contact with the two oxygen atoms of Ni(acacen), and three oxygen and two fluorine atoms of [La(pta)$_4$]$^-$. Selected bond lengths and angles are presented in Table 1.

Around La (Figure 2), the four triangles LaO(1a)O(2a), LaO(1b)O(2b), LaO(1c)O(2c), and LaO(1d)O(2d) are almost perpendicular to each other, making angles ranging from 85.5(1)° to 89.6(1)° with each other. Dihedral angles about O(1i)O(2i) between these planes and respective mean planes of atoms O(1i), O(2i), C(1i), C(2i), C(3i), C(4i), C(5i) are 12.4(1)° and 12.9(1)° for ligands *b* and *d*, and 4.0(2)° and 4.2(2)° for ligands *a* and *c*, respectively. The coordination polyhedron around La is close to a bicapped trigonal prism, with O(1a)O(2a)O(1b) and O(1d)O(2d)O(2c) as the triangular faces, O(2b) and O(1c) at the capping vertices.

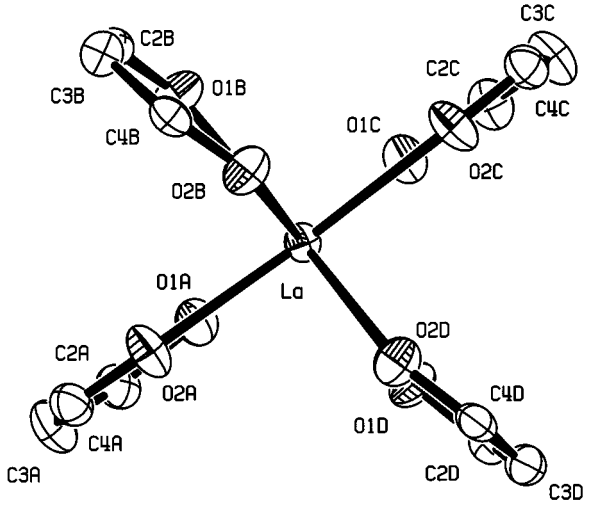

Figure 2. A view of the La(pta)$_4^-$ entity; for the sake of clarity, *tert*-butyl and trifluoromethyl groups have been omitted

Cerium(IV) in Ce(pta)$_4$ and cerium(III) in (NH$_4$)Ce(pta)$_4$ have been recently reported to have a square antiprism coordination geometry.[6] Distortion from expected square antiprism in the present compound is likely to result from the cation K$^+$, which tightly binds two *pta* oxygen atoms: K−O(1a) = 2.677(3) Å and K−O(1c) = 2.731(3) Å. Potassium next neighbouring atoms are the *acacen* oxygen atoms O(1) and O(2) at 2.742(3) Å and 2.661(3) Å, respectively, the *pta* oxygen O(1d) at 2.914(3) Å, and the fluorine atoms F(1c), F(1a), F(2d), and F(2a) at 2.843(4) Å, 2.949(4) Å, 3.295(3) Å, and 3.358(4) Å, respectively.

In Ni(acacen) (Figure 3−5), slight deviations from planarity are evident, besides the torsion angle N(1)C(11)C(12)N(2) of −35.9(4)°. The N_2O_2 environment of the nickel atom is slightly tetrahedrally distorted, with atom to mean plane distances of ±0.04 Å. The planes defined by atoms Ni, O(1), and N(1) on one hand and Ni, O(2), and N(2) on the other hand make an angle of 3.5(3)°. In both ketoimine moieties, planar OC_3 and NC_3 parts make an angle of circa 5° with each other. The Ni(acacen) entities are related by inversion. They partially overlap, giving rise to stacks parallel to the *a* axis with distances between mean planes alternatively equal to 3.66 Å for inversion through (1/2, 0, 1/2), and to 3.85 Å for inversion through (0, 0, 1/2). Figure 3 and Figure 4 show that the overlap is more extended for entities separated by 3.66 Å than by 3.85 Å. Intra-stack Ni···Ni distances are 4.800(1) Å and 6.569(1) Å, alternatively (Figure 5).

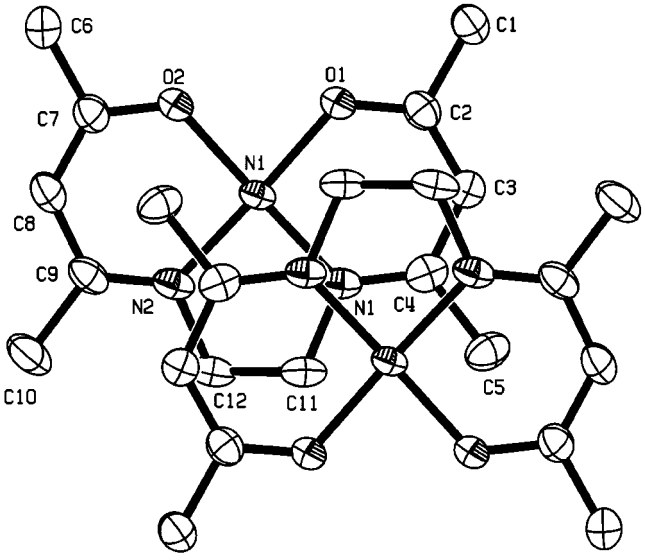

Figure 3. Overlap scheme of centrosymmetrically related Ni(acacen) entities in [Ni(acacen)KLa(pta)$_4$] through inversion at (1/2, 0, 1/2)

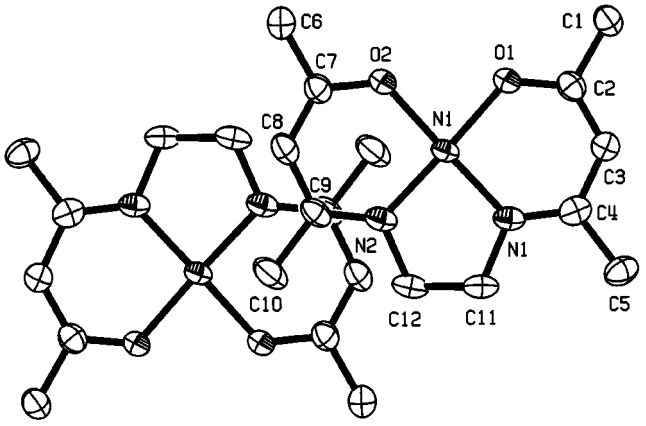

Figure 4. Overlap scheme of centrosymmetrically related Ni(acacen) entities in [Ni(acacen)KLa(pta)$_4$] through inversion at (0, 0, 1/2)

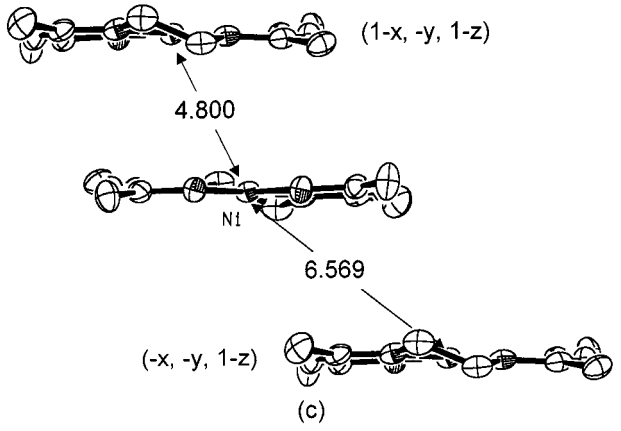

Figure 5. Overlap schemes of centrosymmetrically related Ni(acacen) entities in [Ni(acacen)KLa(pta)$_4$], a side view of the stacking repeat unit

Table 2. Tentative inventory of van der Waals contacts in [Ni(acacen)KLa(pta)$_4$]

F···CH$_3$		CH$_3$···CH$_3$	
F(2a)···C(52d)[a]	3.243(6)	C(51a)···C(52b)[b]	4.007(7)
F(2a)···C(10)[c]	3.324(5)	C(52a)···C(51b)[d]	3.950(7)
F(2b)···C(51d)[a]	3.380(5)	C(53a)···C(53a)[e]	3.427(12)
		C(53b)···C(53d)[b]	3.922(7)
F···CH$_2$		C(52d)···C(1)[f]	3.876(7)
F(2c)···C(11)[g]	3.222(5)		
F(2c)···C(12)[g]	3.215(5)	CH$_3$···CH	
F(1d)···C(11)[f]	3.255(5)	C(3b)···C(52a)[h]	3.535(7)
		C(3d)···C(51c)[d]	3.757(6)
F···CH		C(52d)···C(3)[f]	3.976(7)
F(1d)···C(8)[i]	3.419(5)		

[a] Code of symmetry operations: $x, y-1, z$. – [b] $-x, 1-y, -z$; – [c] $-x, -y, 1-z$. – [d] $x-1, y, z$; – [e] $-x, -y, -z$; – [f] $x, 1+y, z$; – [g] $1-x, -y, 1-z$. – [h] $1+x, y, z$. – [i] $-x, 1-y, 1-z$.

Table 2 shows the results of a screening of van der Waals contacts. They consist of contacts between F atoms and $-CH_3$, $-CH_2$, or $-CH$ groups, and between $-CH_3$ and $-CH_3$ or $-CH$ groups. There are no van der Waals contacts between F atoms.

For Ni(acacen) entities separated by 3.66 Å, the distances from one entity to the centrosymmetrically related one [N(1)···N(1) = 3.66 Å and N(2)···C(4) = 3.70 Å] suggest interactions between π-electrons of partial double bonds N(1)–C(4) and N(2)–C(9). In the same way, a strong interaction between the methyl group about C(5) and electrons delocalized on bonds between atoms O(2), C(7), C(8), C(9), and N(2) of the centrosymmetrically related *acacen* ligand is suggested by the fact that C(5) is at 3.7–3.8 Å from these atoms and at 3.441(4) Å from the mean plane of the ligand. The methylene group about C(11) is possibly involved in the same kind of interaction to a lesser extent: C(11) is at 3.6–3.7 Å from atoms O(1) and N(1) of the related entity and 3.412(5) Å from mean plane of the corresponding *acacen*. For entities separated by 3.85 Å, the methyl group about C(10) for each entity is at 3.630(6) Å from the mean plane of atoms O(2), C(7), C(8), C(9), and N(2) of the related entity.

Thermal Analyses and Vacuum Sublimation

The results of thermal analyses for [Ni(acacen)KLa(pta)$_4$] have been correlated with those for parent complexes KLa(pta)$_4$ and Ni(acacen).

The thermogravimetric analysis curves for KLa(pta)$_4$ and Ni(acacen) are shown in Figure 6, a and 6, b respectively. A single-stepped, quasi total (>98%) weight loss occurs at 165–230 °C and 205–285 °C, respectively for KLa(pta)$_4$ and Ni(acacen). This corresponds predominantly to sublimation. The thermogravimetric curve for [Ni(acacen)KLa(pta)$_4$] (Figure 6, c) shows two stages of weight loss. The major weight loss (70%) occurs in the temperature range 180–330 °C, which corresponds to sublimation. The second, smoother stage (weight loss of about 20%) occurs in the range 330–500 °C. This may correspond to partial thermal decomposition of the complex. The nonvolatile residue amounted to 6% of the initial weight, confirming that sublimation is mainly responsible for the weight loss.

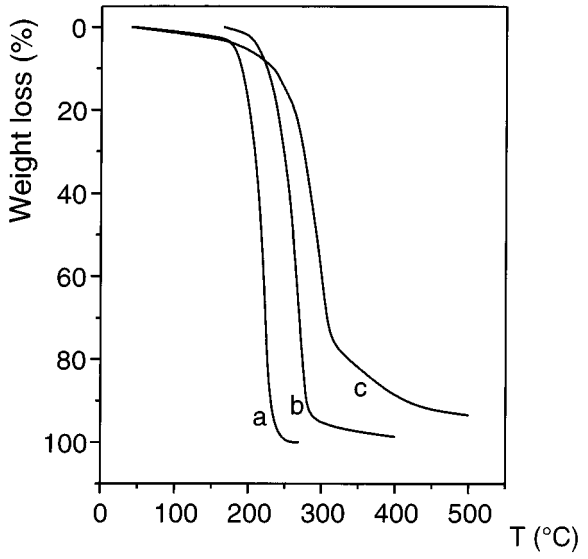

Figure 6. Thermal gravimetric analyses under vacuum (0.01 Torr) for a) KLa(pta)$_4$, b) Ni(acacen), c) [Ni(acacen)KLa(pta)$_4$]

[Ni(acacen)KLa(pta)$_4$] was submitted to isothermal vacuum sublimation (0.01 Torr). The sample was totally sub-

limed at 200 °C, yielding a single, homogeneous sublimate at the cold end of the reactor tube. Results of elemental analyses for the sublimate were the same as for the starting [Ni(acacen)KLa(pta)$_4$]. However, this experiment did not show whether sublimation occurred with or without dissociation. In order to determine whether [KLa(pta)$_4$Ni(acacen)] exists in the vapour phase, or dissociates into gaseous KLa(pta)$_4$ and Ni(acacen), which would recombine at the cold part of the reactor, mass-spectrometry experiments were carried out for [Ni(acacen)KLa(pta)$_4$] and the component complexes KLa(pta)$_4$ and Ni(acacen).

Mass Spectrometry of [Ni(acacen)], [KLa(pta)$_4$] and [Ni(acacen)KLa(pta)$_4$]

[KLa(pta)$_4$]

The mass spectra of [KLa(pta)$_4$] were recorded in the temperature range 394−420 K (Table 3). The major species were lanthanum-containing [La(pta)$_3$]$^+$, [La(pta)(OCCF$_3$CH$_2$)]$^+$ and [La(pta)$_4$]$^+$. However, the heterobimetallic molecular ion [KLa(pta)$_4$]$^+$ was observed over the temperature range, thus indicating that no decomposition of [KLa(pta)$_4$] into K(pta) and La(pta)$_3$ occurs upon sublimation. At 418 K, the vapour pressure of [KLa(pta)$_4$] is equal to $4.2\cdot10^{-2}$ Pa. Congruent sublimation has been reported for other ionic bimetallic complexes of lanthanide fluorinated β-diketonates. The compound [NaCe(pta)$_4$] sublimes without decomposition according to published mass spectrometry data.[6] A similar spectrum was obtained for Cs[Y(hafa)$_4$], which was the first volatile heterobimetallic complex investigated by mass spectrometry.[7] The tendency to form lanthanum-fluorine containing species is supported by our data too (Table 3). The formation of such species upon fragmentation is likely to result from migration of fluorine atoms from the ligands to the metal centre, a process favoured by the hard-acid character of lanthanides.[8]

[Ni(acacen)]

[Ni(acacen)] sublimes congruently in the temperature range 349−412 K. At 393 K, the vapour pressure of [Ni(acacen)] is equal to $1.4\cdot10^{-1}$ Pa. The standard enthalpy of sublimation for [Ni(acacen)] was found to be 127.7 ± 0.3 kJ/mol from mass spectrometry data (Table 4), in good agreement with the value of 129.1±0.9 kJ/mol, measured by effusion in the range 402−450 K.[9] [Ni(acacen)] is more volatile than the related nickel Schiff-base complex, Ni(salen), which sublimes in the range 459−545 K.[2] The difference in volatility is likely to result from stronger π interactions between the phenyl groups in solid Ni(salen)[10] with respect to Ni(acacen), which does not contain such groups. [Ni(acacen)] has a volatility that compares with those of nickel acetylacetonate[11] and nickel acetylacetoniminate.[12]

[Ni(acacen)KLa(pta)$_4$]

Mass spectra were recorded at 390 K and 419 K. They show ions containing either Ni, or La, or La and K (Table 3), thus indicating that the heterotrimetallic molecule is not present in the saturated vapour. Relative intensities of La-containing species tend to increase on increasing temperature. It may be inferred that two processes take place upon heating are, accroding to Equation (1) and Equation (2):

$$[Ni(acacen)KLa(pta)_4]_{(s)} \rightarrow [KLa(pta)_4]_{(s)} + Ni(acacen)_{(g)} \quad (1)$$

$$[KLa(pta)_4]_{(s)} \rightarrow [KLa(pta)_4]_{(g)} \quad (2)$$

The temperature dependence of ion current intensities was measured for Ni-containing species in the temperature range 350−419 K. The vapour pressure of Ni(acacen) over

Table 3. Intensities of main ion currents (relative units) in mass spectra of [KLa(pta)$_4$], Ni(acacen) and [Ni(acacen)KLa(pta)$_4$) (U = 60 eV)

[KLa(pta)$_4$] (415 K)		[Ni(acacen)] (407 K)		[Ni(acacen)KLa(pta)$_4$)] (390 K)		[Ni(acacen)KLa(pta)$_4$)] (419 K)	
[KLa(pta)$_4$]$^+$	0.12	[Ni(acacen)]$^+$	1.00	[Ni(acacen)]$^+$	1.00	[Ni(acacen)]$^+$	1.00
[La(pta)$_4$]$^+$	0.64	[NiOC(CH$_3$)CH$_2$C(CH$_3$)NC]$^+$	0.69	[NiOC(CH$_3$)CH$_2$C(CH$_3$)NC]$^+$	0.66	[NiOC(CH$_3$)CH$_2$C(CH$_3$)NC]$^+$	0.26
[La(pta)$_3$]$^+$	1.00	[NiOC(CH$_3$)CH$_2$NC]$^+$	0.10	[KLa(pta)$_4$]$^+$	0.02	[KLa(pta)$_4$]$^+$	0.05
[LaF(pta)$_2$(OCCF$_3$)]$^+$	0.10	[CH$_3$C(O)CH$_2$CN]$^+$	0.08	[KLa(pta)$_3$]$^+$	0.01	[KLa(pta)$_3$]$^+$	0.01
[La(pta)$_2$]$^+$	0.01			[La(pta)$_4$]$^+$	0.01	[La(pta)$_4$]$^+$	0.02
[La(pta)(OCCF$_3$CH$_2$]$^+$	0.93			[La(pta)$_3$]$^+$	0.02	[La(pta)$_3$]$^+$	0.48
[LaOF(pta)]$^+$	0.32			[La(pta)$_2$OC(CH$_3$)$_3$CHCO]$^+$	0.04	[La(pta)$_2$OC(CH$_3$)$_3$CHCO]$^+$	0.05
				[La(pta)$_2$OCF$_3$CHCO]$^+$	0.02	[La(pta)$_2$OCF$_3$CHCO]$^+$	0.64
				[La(pta)$_2$]$^+$	0.04	[La(pta)$_2$]$^+$	0.01
				[La(pta)OCCF$_3$CH$_2$]$^+$	0.05	[LaOCC(CH$_3$)$_3$]$^+$	0.01
				[LaOCC(CH$_3$)]$^+_3$	0.04		

Table 4. Temperature dependence of saturated vapour pressures of Ni(acacen) and [Ni(acacen)KLa(pta)$_4$)]

Complex	A[a]	B[a]	T range [K]	$\Delta_s H^0_T$ [kJ/mol]
Ni(acacen)	6667 ± 155	16.11 ± 0.08	349−412	128 ± 3
[Ni(acacen)KLa(pta)$_4$)]	7633 ± 160	17.74 ± 0.11	350−419	146 ± 10

[a] A and B are coefficients of the equation $\log P_{Pa} = -A/T + B$.

[Ni(acacen)KLa(pta)$_4$] (Table 4) is lower (2.1 10^{-2} Pa at 393 K) than over solid Ni(acacen), due to formation of the heterotrimetallic complex. From measured saturated vapour pressures of Ni(acacen) over [Ni(acacen)KLa(pta)$_4$] and over Ni(acacen), the activity of Ni(acacen) at 380 K was found to be $a_{[Ni(acacen)]} = 0.15$. The standard free energy of formation of [Ni(acacen)KLa(pta)$_4$] according to Equation (3) was found to be $\Delta G_f^0{}_{380K} = -6.1 \pm 2$ kJ/mol.

$$[KLa(pta)_4]_{(s)} + Ni(acacen)_{(s)} \rightarrow [Ni(acacen)KLa(pta)_4]_{(s)} \quad (3)$$

Conclusion

The complex [Ni(acacen)KLa(pta)$_4$] is an interesting example of a heterometallic compound in which a cation, namely K^+, acts as a bridge between two metal complexes. In coordination chemistry, examples of heterometallic compounds with bridging ligands abound, and usually, polydentate ligands act as bridges between two metal centres. One further possibility is to have a neutral metal complex acting as a ligand towards the coordinatively unsaturated metal centre of a second complex, as is the case for instance for the series of complexes of formulae [M(SB)Ln(β-dik)$_3$] (M = Cu, Ni, SB = Schiff base such as *saloph*, *salen*, *acacen*, β-dik = *thd*, *pta*, *hfa*, *fod*) that we are investigating.[2,3] In the case of [Ni(acacen)KLa(pta)$_4$], both complex entities [Ni(acacen)] and [La(pta)$_4^-$] are coordinatively saturated, but oxygen donor atoms from ligands *pta* and *acacen* may form additional bridging bonds. It is worth pointing out that some of the fluorine atoms of the β-diketone participate to this bridge, so that the question arises of the existence of such complexes with nonfluorinated β-diketones about the lanthanide cation.

According to thermodynamic data, the energy of interaction between Ni(acacen) and KLa(pta)$_4$] is rather weak. Upon heating, the complex [Ni(acacen)KLa(pta)$_4$] dissociates into its parent complexes Ni(acacen) and KLa(pta)$_4$, and sublimation may be complete thanks to the volatility of both components.

Experimental Section

Preparation and Characterization of the Complex [Ni(acacen)KLa(pta)$_4$]: The starting materials H_2(acacen), Ni(acacen), were obtained according to literature methods.[13] The preparation of KLa(pta)$_4$, was adapted from that of NaCe(thd)$_4$.[6] − Elemental analyses (C, H, N) were carried out by the Microanalytical Service of the Moscow State University. − IR spectra were recorded on a Perkin−Elmer 1750 FTIR spectrophotometer for KBr disks in the 4000−300 cm^{-1} region.

[Ni(acacen)KLa(pta)$_4$] was obtained as follows: A solution of Ni(acacen) (112 mg, 0.4 mmol) in 50 mL of chloroform was slowly added to a solution of [KLa(pta)$_4$] (383 mg 0.4 mmol) in chloroform. The red solution was then heated under reflux for 2 h. Slow evaporation of the resulting solution afforded dark red crystals (445 mg, yield 90%). − $C_{44}H_{58}F_{12}KLaN_2NiO_{10}$ (1239): calcd. C 42.61, H 4.68, N 2.26; found C 42.52, H 4.80, N 2.29. − IR: $\tilde{\nu}$ = 2980, 1635, 1540, 1520, 1480, 1425, 1380, 1360, 1285, 1240, 1160, 1120, 975, 950, 915, 840, 800, 760, 700, 650, 545, 485 cm^{-1}.

X-ray Structure Study: Crystal data: formula $C_{44}H_{58}F_{12}KLaN_2NiO_{10}$, mol. weight = 1239.6 amu, monoclinic, $P\bar{1}$, a = 9.984(2), b = 12.455(2), c = 23.064(4) Å, α = 101.68(2)°, β = 98.96(2)°, γ = 91.58(2)°, Z = 2, d = 1.487 g.cm^{-3}, μ = 1.27 mm^{-1}. − Data collection: Stoe Imaging Plate Diffraction System (IPDS), Oxford Cryosystems cooler device, monochromated Mo-K_α radiation, T = 140 K, crystal size 0.75×0.17×0.10 mm, crystal-to-detector distance 80 mm, 208 exposures (2 minutes/exposure), $0 < \varphi < 249.6°$, φ oscillation 1.2°, $1.45 < \theta_{max} < 24.20°$, coverage of the unique set 93%. Measured reflections 21835, observed (expected) unique reflections 8234 (8852). Crystal decay monitored by measuring 200 reflections per image, only statistical fluctuations observed. Intensities corrected for Lorentz and polarisation effects, not for absorption (average cylindrical μr = 0.1). − Structural analysis and refinement: analysis by Patterson and Fourier map techniques, refinement by full-matrix, least-squares techniques, using the SHELX-93 program.[14] All H atoms introduced at calculated positions using a riding model. Anisotropic displacement parameters for non-H atoms: 640 parameters for 8234 reflections. R = 0.034 [7208 $F_o > 4\sigma(F_o)$] and 0.040 for all data, R_w = 0.087, GooF = 1.06 e.

Thermal Analyses: Thermogravimetric and differential thermal analyses under vacuum (0.01 Torr) were carried out on a Sinku-Riko TGD-7000 thermal analyzer, at a heating rate of 10°/min. Isothermal dynamic sublimation experiments were run with samples (100 mg) placed in glass test tubes for periods of 30 min at 200 °C and a pressure of 0.01 Torr. Weight loss was equal to 100%. The sublimate was collected in cold part of reactor and analysed. − $C_{44}H_{58}F_{12}KLaN_2NiO_{10}$ (1239.6) : calcd. C 42.61, H 4.68, N 2.26; found C 42.76, H 4.76, N 1.81.

Mass Spectrometry and Study of the Vapour Phase: The mass spectra of Ni(acacen), KLa(pta)$_4$ and [Ni(acacen)KLa(pta)$_4$] were recorded on a MS 1301 spectrometer having a 50−1500 amu mass range, and using 60 eV ionising electrons. The complexes were vapourised from a Knudsen effusion cell. The ratio of surface of evaporation to surface of the effusion hole was about 600. The cell temperature was measured with a Pt/Pt(Rh) thermocouple (±0.1 K). The experiments were carried out in ranges 349−412 K for Ni(acacen), 394−420 K for KLa(pta)$_4$ and 350−420 K for [Ni(acacen)KLa(pta)$_4$]. The main ion peaks in mass spectra of Ni(acacen), KLa(pta)$_4$ and [Ni(acacen)KLa(pta)$_4$] are given in Table 3.

Vapour pressures *versus* temperature were determined by means of isothermal vapourisation experiments and use of the Herz−Knudsen equation. Enthalpies of sublimation were calculated from the temperature dependencies of ion current intensities by using Clausius−Clapeyron equation and a least-squares method.

Crystallographic data (excluding the structure factor tables) for the structure reported in this paper have been deposited with the Cambridge Crystallographic Data Centre as supplementary publication CCDC-147101. Copies of the data can be obtained free of charge on application to CCDC, 12 Union Road, Cambridge CB2 1EZ, UK [Fax: (internat.) + 44(1223)336−033; E-mail: deposit@ccdc.cam.ac.uk].

Acknowledgments

Financial support from the Russian Foundation for Basic Research (RFBR, grant 99−03−32800) and INTAS (contract # 95−118) is

acknowledged. Gratitude is expressed to Mr. B. Donadieu (Laboratoire de Chimie de Coordination du CNRS, Toulouse) for helpful assistance in using a Stoe Image Plate Diffraction System.

[1] A. N. Gleizes, *Chem. Vap. Deposition* **2000**, *6*, 155−173.
[2] A. Gleizes, M. Julve, N. Kuzmina, A. Alikhanyan, F. Lloret, I. Malkerova, J. L. Sanz, F. Senocq, *Eur. J. Inorg. Chem.* **1998**, 1169−1174.
[3] A. N. Gleizes, F. Senocq, M. Julve, J. L. Sanz, N. Kuzmina, S. Troyanov, I. Malkerova, A. Alikhanyan, M. Ryazanov, A. Rogachev, E. Dedlovskaya, *J. Phys. IV France* **1999**, *9*, 943−951.
[4] A. S. Alikhanyan, I. P. Malkerova, N. P. Kuzmina., A. Gleizes, M. Julve, J. L. Sanz-Lloret, I. L. Eremenko, *Russian J. Inorg. Chem.* **1999**, *44*, 973−976 (russ.).
[5] N. P. Kuzmina, A. Yu. Rogachev, F. M. Spiridonov, E. M. Dedlovskaya, V. A. Kezko, A. Gleizes, G. Battiston, *Russ. J. Inorg. Chem.* **2000**, *45*, 1468−1475.
[6] M. Becht, K.-H. Dahmen, V. Gramlich, A. Marteletti, *Inorg. Chim. Acta* **1996**, *248*, 27−33.
[7] S. J. Lippard, *J. Am. Chem. Soc.* **1966**, *88*, 4300−4301.
[8] S. M. Schildcrout, *Inorg. Chem.* **1985**, *24*, 760−765.
[9] M. A. V. Ribeiro da Silva, M. D. M. C. Ribeiro da Silva, M. J. S. Monte, J. M. Gonçalves, E. M. R. Fernandes, *J. Chem. Soc., Dalton Trans.* **1997**, 1257−1262.
[10] A. G. Manfredotti, C. Guastini, *Acta Crystallogr.* **1982**, *C38*, 863−867.
[11] P. M. Burkinshaw, C. T. Mortimer, *Coord. Chem. Rev.* **1983**, *48*, 101−155.
[12] R. G. Charles, *Thermochim. Acta* **1980**, *38*, 315−327.
[13] P. J. McCarthy, R. Horey, *J. Am. Chem. Soc.* **1955**, *77*, 5820−5823.
[14] G. M. Sheldrick, *SHELX-97*, University of Göttingen, Germany.

Received July 26, 2000
[I00298]

On the Commonality of Speciation of Inorganic Solutes in Superacids, Strong Bases, Molten Salts, and Water

Thomas A. O'Donnell[a]

Keywords: Inorganic solute speciation / Superacids / Molten salts / Unusual oxidation states / Disproportionation

When dealing with inorganic solutes in protic solvents such as superacids, ammonia, and water, and especially in the case of molten salts, the authors of most textbooks and specialised reviews treat solution processes in each solvent or class of solvent separately, and rarely, if ever, draw the separate sections together to indicate the commonality of the solution processes from a generalised acid-base viewpoint. Initially in this review three chemically-simple solution media, H_2O, anhydrous HF, and molten chloroaluminates, are used to illustrate the generality of the behaviour of Cr^{III} in the three solvents. In neutral media "$Cr(OH)_3$", CrF_3, and $CrCl_3$ are sparingly soluble, whereas in basic media the solvo-anions $Cr(OH)_4^-$, CrF_6^{3-}, and $CrCl_6^{3-}$ are the dominant species. In acidic media Cr^{3+} cations, solvated to a greater or less extent, are formed. In highly acidic media, transition metal cations in very low oxidation states can be generated, e.g. Ti^{2+}, U^{3+}, and Sm^{2+}, as well as homopolyatomic cations, such as I_2^+, Se_8^{2+}, Te_6^{4+}, N_5^+, and Hg_3^{2+}. Each of these cations would disproportionate in aqueous solutions and, indeed, they do so on addition of sufficient base, even in HF or chloroaluminates. Under oxidising conditions solvo-anions in high oxidation states, e.g. CrO_4^{2-}, AgF_4^- and NiF_6^{2-}, are stable in basic media. Solute speciation in sulfur acids and ammonia is dealt with briefly because most investigation of homopolyatomic cations and anions has been carried out in these solvents. The overall aim of this review is to demonstrate the generality of inorganic solute speciation in all ionising solvents. It is proposed here that the primary determinant of speciation in all media is the level of acidity or basicity of the solvent rather than its chemical composition or its temperature domain.

1. Introduction

Dissolution processes in ionising media for simple ionic solids, such as the halides, nitrates, sulfates, and other oxoanions of the elements of Groups I and II of the Periodic Table are relatively straightforward, yielding solvated cations and anions in aqueous and nonaqueous media unless the ions, usually the anions, undergo solvolysis. The vast majority of inorganic compounds, particularly those of the transition elements, do not follow this simple pattern. So the nature of solute-solvent interaction for these compounds assumes great importance in considering their solution processes.

[a] Department of Chemical Engineering,
The University of Melbourne,
Parkville Victoria 3010, Australia

All too frequently, in the presentation of the solution chemistry of inorganic compounds in a range of ionising media, textbooks, and even specialised monographs and book series deal in separate sections or chapters with ionisation, dissolution, and solvolysis processes in solvents such as water, basic solvents such as ammonia and amides, and in acidic media such as sulfuric acid, fluorosulfuric acid, and hydrogen fluoride. This is especially the case in the presentation of chemistry in molten salts which, being nonprotic and frequently in elevated temperature domains, are perceived as being very different from protic or even nonprotic solvents which are liquid at or near ambient temperature.

The six-volume series[1] which gives the most extensive coverage of chemistry in nonaqueous solvents is structured in this way. Furthermore, in most earlier presentations, solvents such as H_2SO_4 and liquid NH_3 have been referred to as being "acidic" or "basic" (relative to H_2O). It is im-

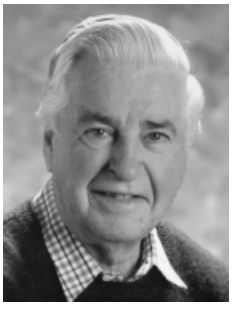

Tom O'Donnell was born at Ballarat, Australia, in 1923 and is a graduate of the University of Melbourne – Ph.D. (1954) and D.Sc. (1971). He was a member of the academic staff of the Melbourne School of Chemistry from 1949 to 1988 when he retired as Professor of Inorganic Chemistry. He spent a sabbatical year at Cambridge in 1955 with Professor H. J. Emeléus in order to commence research in inorganic fluorine chemistry. His earliest work was on systematisation of the chemical reactivity of the higher fluorides of d- and f-transition elements. Later he studied acid-base reactions and solute speciation in anhydrous HF and extended this to similar studies in other superacids. On retirement he joined the Melbourne Department of Chemical Engineering where he has worked collaboratively on fluoride-based chemistry directed towards development of novel commercial processes.

MICROREVIEWS: This feature introduces the readers to the authors' research through a concise overview of the selected topic. Reference to important work from others in the field is included.

 © WILEY-VCH Verlag GmbH, D-69451 Weinheim, 2001 1434–1948/01/0101–0021 $ 17.50+.50/0

portant to stress that, *as separate solvent systems*, 100% H_2SO_4 and anhydrous NH_3 are neutral media, each of which can be made more acidic by addition of appropriate Bronsted or Lewis acids (e.g. SO_3 or NH_4^+) or more basic by addition of suitable bases, such as HSO_4^- or NH_2^-.

Very rarely are the separate sections either presented or drawn together to indicate the commonality of the solution processes from a generalised acid-base viewpoint. This review sets out to demonstrate this commonality. Much of the material is drawn from a recent book[2] which was written, in part, to draw the attention of specialised researchers interested in chemistry in highly acidic media to these generalisations. The book also serves as a reference in the presentation and discussion of some superacid solution work carried out at the University of Melbourne which is not yet in readily available journals, as well as in the re-interpretation of some earlier published work from other groups. The present review extends the generalisation concept to include basic solvents such as ammonia and to describe recently reported chemistry in superacids, e.g. synthesis of the homopolyatomic cation N_5^+ and generation of AgF_4^- and NiF_6^{2-}, fluoro-anions of transition elements in very high oxidation states.

In the first two major sections of this review, solution speciation will be compared for three solvents only, namely water, anhydrous HF, and molten chloroaluminates. In most presentations of nonaqueous chemistry, water serves as the primary reference solvent. A vast amount of physical and inorganic chemistry has been studied in aqueous solution and a wide range of solvated cationic and anionic species has been characterised spectroscopically. These three solvent media have been chosen because comparison of spectra recorded in each of these media has allowed reliable postulations to be made about the extent of solvation of transition metal cations in these media. Additionally, HF and chloroaluminates were selected as the nonaqueous media because they have special properties concerned with their stability and self-ionisation, to be discussed below.

To those not familiar with solution chemistry in anhydrous HF, this solvent may seem to be an unlikely choice for a model solvent system, given its reactivity towards the usual materials of construction of scientific apparatus; but, with the availability of spectroscopic and electrochemical equipment constructed from fluorocarbons such as Teflon and KelF, synthetic sapphire and platinum, manipulation of and physico-chemical investigation of HF solutions in closed systems is now reasonably straightforward.

There are two main reasons why anhydrous HF is the superacid of choice for generation of highly-reducing stable monatomic transition metal cations in very low oxidation states, such as Ti^{2+} and Sm^{2+}, which reduce H_2O, and of highly oxidising transition metal solvo-anions with the metals in very high oxidation states, such as NiF_6^{2-} and AgF_4^- which oxidise water:

(i) it has a very large useable potential range of 4 to 4.5 volt between anodic and cathodic generation of F_2 and H_2. This compares with a range of about 2 volt, depending on pH, for H_2O.

(ii) it has the widest range of acidity-basicity of any of the superacids. HF exhibits this large acidity-basicity range because it undergoes a simple self-ionisation to about the same extent as H_2O, as discussed below.

Intrinsically, HF is so acidic that no compound is known to act as a Bronsted acid towards it. In the equations below, the self-ionisation equilibria [Equation (1)] are shown schematically as being shifted by the addition of the weak Lewis acid BF_3 [Equation (2)] and the strong Lewis acid SbF_5 [Equation (3)], to give the most acidic protic solutions yet generated:

$$3\,HF \rightleftharpoons H_2F^+ + HF_2^- \quad (1)$$

$$2\,HF + BF_3 \rightleftharpoons H_2F^+ + BF_4^- \quad (2)$$

$$2\,HF + SbF_5 \rightleftharpoons H_2F^+ + SbF_6^- \quad (3)$$

By simple addition of a soluble fluoride, e.g. NaF, HF can be made more basic than any other superacid.

Levels of acidity and basicity in different superacidic media can be compared reliably using values of the Hammett Acidity Function, H_o. These were measured by Gillespie and co-workers for HSO_3F[3] and HF[4] solutions. Table 1 shows that, whereas pure HSO_3F and pure HF have identical value for H_o, additions of only 0.4 m base (F^-) and 0.4 m acid (SbF_5) to HF cause much greater changes in acidity and basicity than additions of 0.4 m base (SO_3F^-) and 0.4 m acid [$SbF_2(SO_3F)_3$] to HSO_3F. This is a reflection of the magnitudes of the autoprotolysis constants for the two superacids, as cited in Table 1.

The very high levels of acidity, or more specifically, the very low levels of basicity in HF containing Lewis acids are such that stable unusual cationic species such as Ti^{2+} and Sm^{2+} (Section 2.2.2) and I_2^+ and the recently characterised N_5^+ (Section 2.2.3) can be generated in HF. Enhanced basicity allows generation of stable anions such as NiF_6^{2-} and AgF_4^- (Section 2.3.2).

The small value of the autoprotolysis constant for HF means that large increases in basicity of HF will occur as very small amounts of base added. A practical consequence is that "neat" HF, as obtained by repeated distillation, will contain sufficient of the most likely impurity, H_2O which acts as a strong Bronsted base, that such a liquid will have a value for H_o much less than that of −15.1 determined for pure HF. Gillespie and Liang[4] showed experimentally that addition to HF of as little as 0.1 mol% of water reduced the observed H_o to −10.66. Extrapolation of their plot of H_o vs. concentration of H_2O in HF suggests strongly that even minute concentrations of water and other impurities that can be protonated will produce a medium with values of H_o for "neat" HF of around −11, an observation that has been made experimentally.

The first transition metal cations generated in HF solutions acidified with the weak Lewis acid BF_3 were Ni^{2+}, Co^{2+}, Pr^{3+}, and Nd^{3+} [5] – all cations in "normal" oxidation states. These cations were characterised by comparison of their HF spectra with previously reported aqueous spec-

Table 1. Dependence of acidity/basicity levels of superacids on the magnitude of autoprotolysis constants

Superacid	Autoprotolysis constant [mol^2 kg^{-2}]	Values of Hammett Acidity Function, H_o		
		Lewis base added (0.4 m)	Pure acid	Lewis acid added (0.4 m)
HF	3×10^{-13}	−9.63	−15.1	−20.64
HSO_3F	3.8×10^{-8}	−13.24	−15.1	−17.71

tra and were so similar that the same level of solvation was postulated for the cations in both solvents.[5]

The term "normal" oxidation state is used here where an ion in that oxidation state is stable in aqueous solution. The terms "unusually low" or "unusually high" are used for ions which would be unstable in aqueous solution, e.g. Ti^{2+} or NiF_6^{2-}.

Another rich source of spectra available for comparative purposes with those for cations in HF was the work of Gruen and colleagues who recorded spectra of a range of dipositive transition metal cations in molten $AlCl_3$,[6] which is the pure acid of the chloroaluminate system, and in chloroaluminates at elevated temperatures.[7] Later workers carried out voltammetric investigations[8] in chloroaluminates which are liquid at room temperature and these also provided insights into the interpretation of ionic spectra in HF and other solvents.

Frequently ionisation in molten salt media is extremely complex, showing a multiplicity of interdependent ionic equilibria. This is particularly the case for melts of metallurgical or geological interest. Chloroaluminate melts are mixtures of $AlCl_3$ and an ionic chloride such as NaCl or, in the case of media which are liquid at or near ambient temperature, a salt such as *N*-butylpyridinium chloride ($BuPy^+Cl^-$). These exhibit relatively simple *solvent* speciation and so can be viewed as model systems for molten salt investigations. More importantly in the present context, they provide a nonprotic medium in which acidity and basicity can be controlled accurately. A 1:1 mixture of $AlCl_3$, the acid of the system, and NaCl (or BuPyCl) provides the neutral medium $Na^+AlCl_4^-$ (or $BuPy^+AlCl_4^-$), Cl^- being the base of the chloroaluminate solvent system. So any excess of NaCl over $AlCl_3$ constitutes a basic medium and, conversely, excess of $AlCl_3$ provides an acidic medium, as indicated in Figure 1. Consequently acid-base dependent *solute* speciation can be studied under controlled conditions and, as with HF, unusual ionic species which are unstable in H_2O can be generated, presenting a potentially rich area for new synthetic work.

High temperature chloroaluminates have a large useable potential range − from cathodic deposition of Al to anodic release of Cl_2. Room temperature chloroaluminates have a more restricted range because of oxidation or reduction of the organic cation.

2. Acid-base Dependence of Speciation of Transition Metals in H_2O, HF and Chloroaluminates

Figure 2 gives a brief summary of solution behaviour in the ionising media H_2O, HF, and chloroaluminates and provides the basis for a discussion of the general nature of the dependence of solute speciation on acidity or basicity of the medium. The solution behaviour of chromium(III), which is characteristic of many transition metals, is discussed first to illustrate typical solute speciation in each solvent in the absence of applied reduction or oxidation. Superimposed on this framework are several of the currently known species that can be generated when oxidants or reductants are added to the basic or acidic medium in each case.

2.1 Neutral Media

There is general acceptance of the insolubility of the so-called hydroxides of the transition metals in neutral water. The precipitates obtained when an aqueous solution is neutralised are not the simple hydroxides [idealised as $Cr(OH)_3$ in Figure 2] but are complex mixtures of metal centres with which are associated H_2O, OH^-, and even O^{2-} as bridging or terminal ligands. The key characteristic is that these aggregates carry no overall charge and so polymerise to form sparingly soluble nonstoichiometric compounds.

CrF_3 is typical of the neutral binary fluorides of First Row Transition Elements in "normal" oxidation states, each of which, along with some Main Group fluorides such as AlF_3, has very low solubility in anhydrous HF.

A survey of a large body of published work shows that neutral binary chlorides show similar behaviour in chloroaluminates. $CoCl_2$, $NiCl_2$, $FeCl_2$, $NpCl_3$, $NpCl_4$, and lanthanide trichlorides have all been reported as precipitating from neutral chloroaluminates. A specific reference is found in the work of Osteryoung and colleagues.[8] Cyclic voltammo-

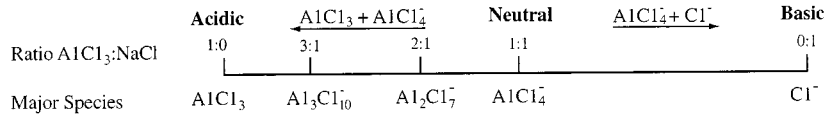

Figure 1. Acid-base dependence of solvent speciation in chloroaluminates (from *Superacids and Acidic Melts as Inorganic Chemical Reaction Media*, VCH, New York, **1993**)

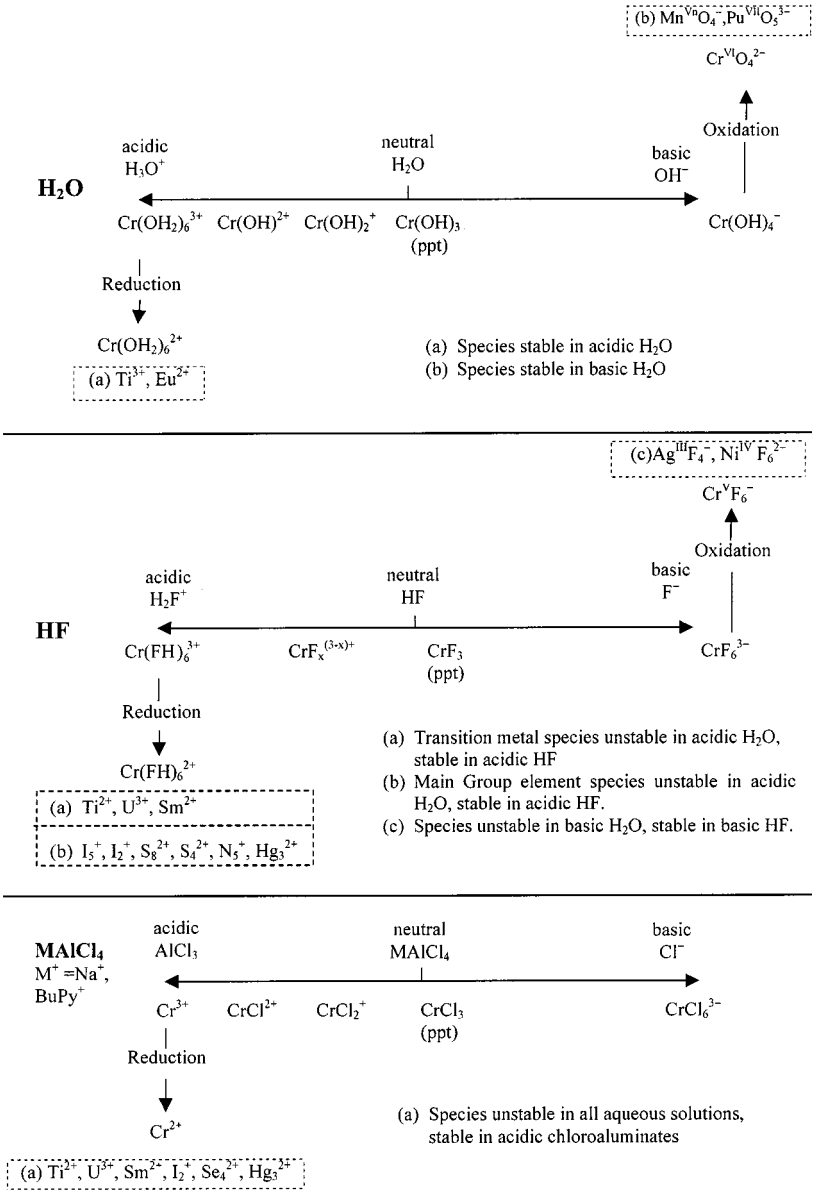

Figure 2. Generalised scheme for dependence of solute speciation on acidity and basicity in ionising solvents

grams were recorded in $AlCl_3-BuPyCl$ for the $Fe^{III}-Fe^{II}$ system from a basic medium ($AlCl_3/Cl^-$, 0.75:1) to acidic ($AlCl_3/Cl^-$, 2:1). This work will be discussed in greater detail in the section below; but in the present context, it is relevant to quote this report which shows that precipitation of $FeCl_2$ occurs near neutrality, commencing near a melt ratio of $AlCl_3/Cl^-$, 0.99:1 with redissolution occurring in the 1.1:1 acidic melt.

2.2 Acidified Media

2.2.1 Cations in "Normal" Oxidation States

First Row transition elements and metallic Main Group elements occur as aquo-cations, e.g. $Cr(OH_2)_6^{3+}$, $Fe(OH_2)_6^{3+}$ $Al(OH_2)_6^{3+}$, etc., in strongly acid, noncomplexing aqueous solution (e.g. in aqueous $HClO_4$). As indicated in Figure 2, hydroxo-complexation occurs progressively as the solution approaches neutrality, together with more complex species such as $Cr_2(OH)_2^{4+}$, $Cr_3(OH)_4^{5+}$, etc., the ratio of charge to metal decreasing as neutrality is approached. In addition to hydroxo-complexation, there is the possibility of a vast range of complexed cations, depending on the availability in the acidic aqueous solutions of other potential ligands. As the simplest of examples, species such as $[Cr(H_2O)_5Cl]^{2+}$ and $[Cr(H_2O)_4Cl_2]^+$ can be formed if the solution contains Cl^-.

As stated above, binary fluorides of transition metals are sparingly soluble in "neat" HF. The equilibrium [Equation (4)]

$$MF_n + (n + m)\,HF \rightleftharpoons M(HF)_m^{n+} + nHF_2^- \quad (4)$$

lies overwhelmingly to the left. The weak Lewis acid BF_3 and the strong Lewis acid SbF_5 react as in Equation (5) and Equation (6),

$$BF_3 + HF_2^- \rightleftharpoons BF_4^- + HF \quad (5)$$

$$SbF_5 + HF_2^- \rightleftharpoons SbF_6^- + HF \quad (6)$$

displacing the equilibrium in Equation (4) to markedly increase the concentration of solvated M^{n+} cations. The weak acid BF_3 produces solutions in HF of dispositive *d*-transition metal cations. The strong acid SbF_5 was required to dissolve *d*-transition metal trifluorides.

CrF_3 dissolves in HF−SbF_5 to give the lowest of the spectra in Figure 3.[9]

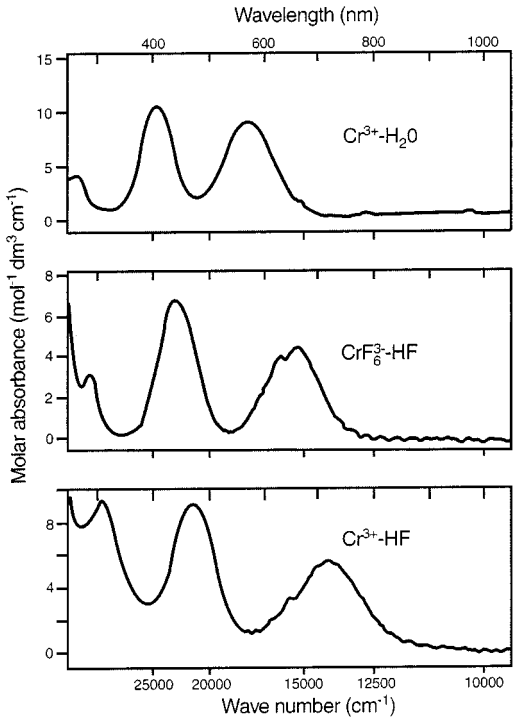

Figure 3. UV/Visible spectra of chromium(III) as $Cr(OH_2)_6^{3+}$ in H_2O, CrF_6^{3-} in HF, and $Cr(FH)_6^{3+}$ in HF (from *Superacids and Acidic Melts as Inorganic Chemical Reaction Media*, VCH, New York, **1993**)

Evidence for the existence of the six-coordinate cation $Cr(FH)_6^{3+}$ is provided by a comparison of the HF−SbF_5 spectrum with the known spectrum for $Cr(OH_2)_6^{3+}$ and with the experimentally observed spectra, which are virtually identical, for CrF_6^{3-} dissolved in both H_2O and HF. CoF_2 dissolved in HF−BF_3[5] gives a broad, shouldered peak very similar to that for $Co(H_2O)_6^{2+}$ in water and to that in Figure 4(b), indicating octahedral coordination, i.e. $Co(FH)_6^{2+}$, rather than tetrahedral coordination which would give a more intense and complex spectrum like that in Figure 4(a).

In the Melbourne research program, cations in acidified anhydrous HF were shown to have the same solvent coordination as in H_2O for Cr^{3+}, Co^{2+}, Ni^{2+}, Fe^{2+}, Cu^{2+}, Pr^{3+}, Nd^{3+}, and many others. Some degree of spectral band broadening with reduction in acidity was ascribed to formation of fluorocations in solutions nearer to neutrality. There was no spectroscopic evidence for coordination to the cations in HF solution of solvo-anions of the Lewis acids, eg. BF_4^-, SbF_6^-, etc.

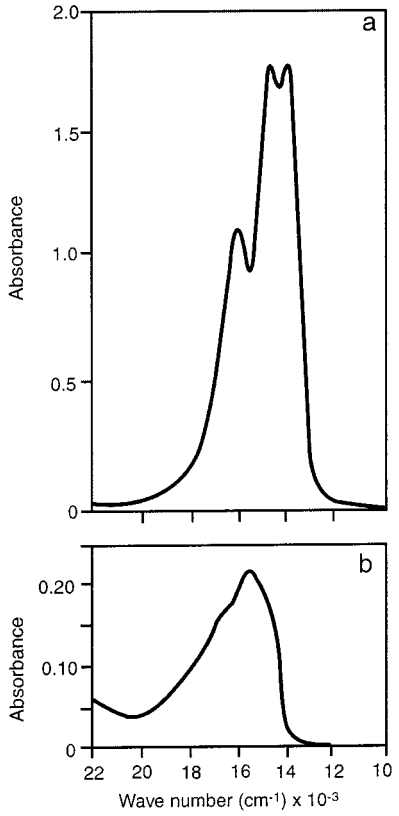

Figure 4. UV/Vis spectra of cobalt(II) (a) as $CoCl_4^{2-}$ in basic chloride melt and (b) as Co^{2+} in acidic chloroaluminate melt (from *Superacids and Acidic Melts as Inorganic Chemical Reaction Media*, VCH, New York, **1993**)

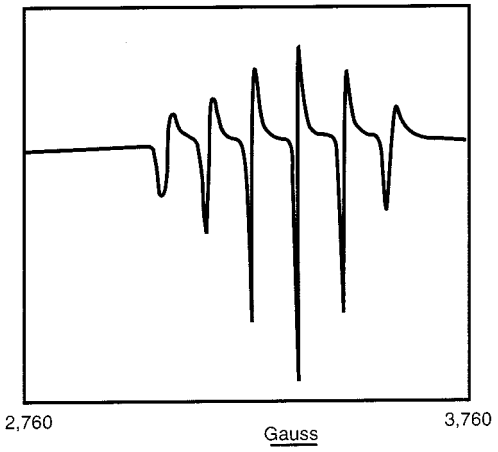

Figure 5. ESR spectrum of manganese(II) in AsF_5/HF (from *Superacids and Acidic Melts as Inorganic Chemical Reaction Media*, VCH, New York, **1993**)

The ESR spectrum of a solution of MnF_2 in HF−AsF_5 (Figure 5)[9] provided excellent evidence for existence of the cation $Mn(FH)_6^{2+}$. The ESR spectrum of the HF solution is very similar to that for $Mn(OH_2)_6^{2+}$ in H_2O, showing the characteristic six lines due to the interaction of the unpaired electrons with the nuclear spin of 5/2 on the manganese.

Øye and Gruen[6] recorded spectra of the dichlorides of the *3d* transition elements from Ti to Cu in $AlCl_3$, the pure acid of the chloroaluminate system, at 227°C. Their evidence points to cation formation in all cases. Their Co^{II} spectrum was the broad band of Figure 4(b), similar to that for $Co(OH_2)_6^{2+}$, whereas in earlier work in a basic chloride melt (the eutectic LiCl−KCl) Gruen and McBeth[7] had observed the spectrum in Figure 4(a), which is virtually identical to that for $CoCl_4^{2-}$ in an aqueous solution containing excess Cl^-.

Few researchers studying solutions of compounds of transition elements in chloroaluminates have been prepared to postulate directly the existence of solvated cations, as such, in acidic media whereas there is general agreement that the species in basic media are chloro-anions, as will be presented below.

Osteryoung's voltammetric investigation of the $Fe^{III}-Fe^{II}$ system in $AlCl_3$−BuPyCl[8] provides spectacular evidence for change in speciation as acidity and basicity of the medium are varied. Using potentiometry, they demonstrated the existence of $FeCl_4^-$ and $FeCl_4^{2-}$ in basic solution and they showed, as in Figure 6, that as the medium was made acidic the redox potential for $Fe^{III}-Fe^{II}$ changed by about 1.8 volt. Obviously there is a drastic change in solute speciation and it has been proposed[2a] that, on acidification, the electroactive species change from being anionic to being cationic.

In cyclic voltammetry, a value of 62 mV for ΔE_p, the difference between the cathodic and the anodic peak potentials, is observed for a system that is perfectly electrochemically reversible; but this value increases with decrease in reversibility. Reference to Figure 6 shows that, not only is there a vast and rapid change in peak positions in passing through neutrality, but electrochemical reversibility decreases as indicated by increase in values of ΔE_p.

A major criterion for electrochemical reversibility is that the stereochemistries of reduced and oxidised species are identical, as in basic melts. The present author has postulated[2a] that this would also be the case if, in strongly acidic chloroaluminate media, the electroactive species were the cations, Fe^{3+} and Fe^{2+}, each weakly but identically solvated. Some proposed intermediate equilibria, which are pCl dependent, are shown in Figure 6 and are based on the fact that Fe^{III} is known to form complexes with Cl^- and other ligands more strongly than does Fe^{II}, i.e. in weakly acidic medium $FeCl_2^+$ and $FeCl^+$ could be the dominant chloro complexes of Fe^{III} and Fe^{II}. Such nonidentical coordination geometry would contribute to nonreversibility leading to

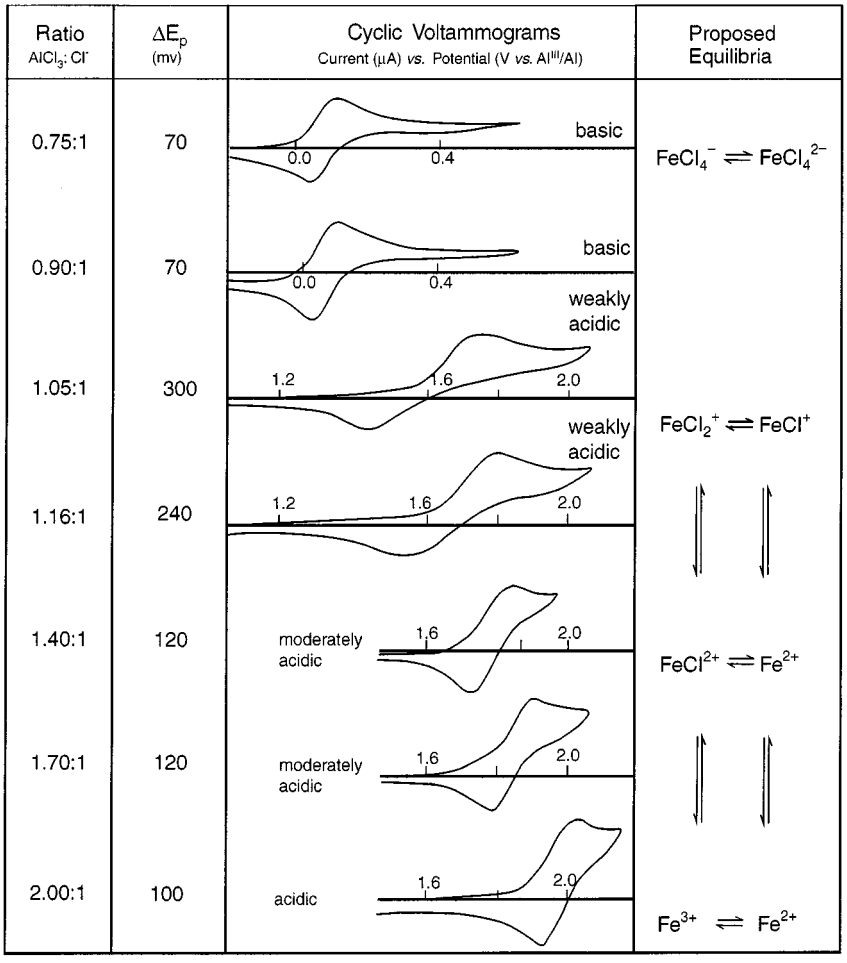

Figure 6. Cyclic voltammograms for $Fe^{III}-Fe^{II}$ in chloroaluminates of varying acidity and basicity (from *Superacids and Acidic Melts as Inorganic Chemical Reaction Media*, VCH, New York, **1993**)

greater values of ΔE_p. The present author has discussed the re-interpretation of this work and other evidence for simple cation formation in chloroaluminates in more detail elsewhere.[2b]

2.2.2 Transition Metal Cations in Unusually Low Oxidation States

Earlier, those cationic oxidation states which are stable in water were classified as "normal". There are certain low oxidation states which can be generated in aqueous solution only under strongly acidic conditions. It is possible to produce stable aqueous solutions of Cr^{2+} by reduction of Cr^{III} under acidic conditions in the absence of air. Similarly a few other low oxidation state cations can be generated in acidic aqueous solution, e.g., V^{2+}, Eu^{2+}, and Ti^{3+}. Ions such as Ti^{2+}, Yb^{2+}, Sm^{2+}, and Zr^{3+}, which can be generated in nonaqueous media, would reduce water, even when strongly acidified.

After being generated electrolytically or by chemical reduction in H_2O, U^{III} is known to be oxidised over relatively short time periods to U^{IV}, reducing H_2O. In 1976, O'Donnell treated metallic U with HF saturated with the weak nonoxidising Lewis acid BF_3 and generated lilac-coloured solutions containing U^{3+} which were stable indefinitely.[10] The acidified HF was reduced to H_2. Spectrum (b) in Figure 7 is that for U^{3+} in HF−BF_3 and can be compared with Spectrum 7(a) which was recorded while U was maintained in oxidation state III in acidic aqueous solution, using continuous electrolysis.[11]

Subsequently, treatment of metallic Ti with strongly acidic HF−SbF_5 yielded a solution containing Ti^{2+} [12]

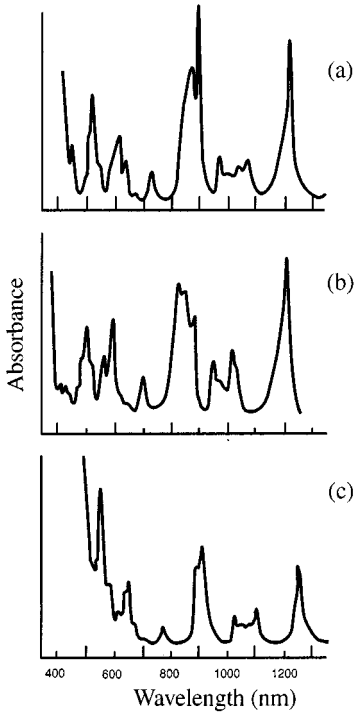

Figure 7. Spectra of uranium(III) in (a) 1 M $DClO_4$ (b) BF_3/HF, and (c) $AlCl_3$/BuPyCl, 2:1 (from *Superacids and Acidic Melts as Inorganic Chemical Reaction Media*, VCH, New York **1993**)

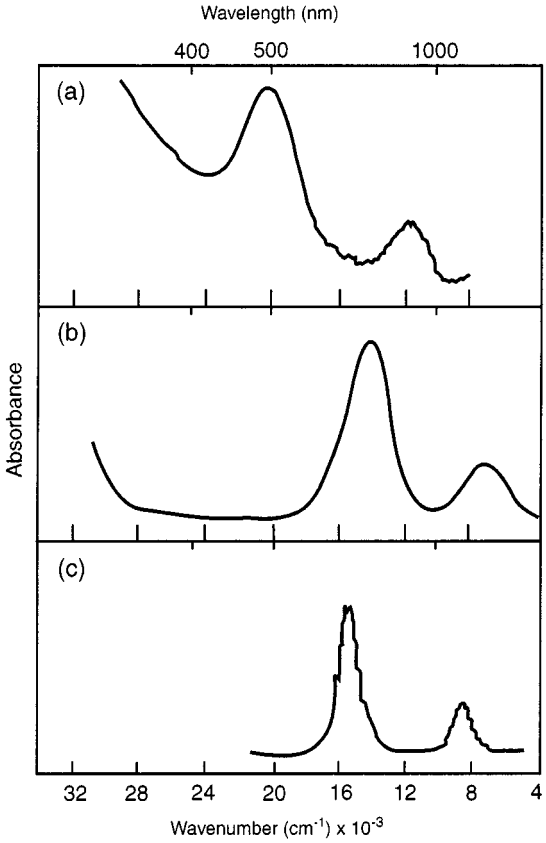

Figure 8. Spectra of titanium(II) in (a) SbF_5/HF, (b) molten $AlCl_3$ (c) crystalline NaCl at 10 K (doped at 1% level) (from *Superacids and Acidic Melts as Inorganic Chemical Reaction Media*, VCH, New York **1993**)

characterised initially by comparison of the HF spectrum (Figure 8a) with that previously reported[6] for that of $TiCl_2$ in molten $AlCl_3$ (Figure 8b), which has been interpreted[2c] as being the spectrum for weakly solvated Ti^{2+}.

Six-coordination in $Ti(HF)_6^{2+}$ was supported by similarity of the HF spectrum to that for $TiCl_2$ doped at 1% level into a host crystal of NaCl in which the coordination number is six (Figure 8c).[13] Not unexpectedly solvated V^{2+} and Cr^{2+}, generated in similar fashion, were observed in acidified HF.[12] The lanthanide metals Eu, Yb, and Sm reacted with neat anhydrous HF to give Eu^{2+}, Yb^{2+}, and Sm^{2+} and H_2.[14]

Belgian researchers[15] conducted potentiometric and spectroscopic studies of U^{III} and U^{IV} in the low temperature (40°C) melt BuPyCl−$AlCl_3$. The similarity of their spectrum (Figure 7c) in the acidic melt ($AlCl_3$/BuPyCl, 2:1) to the spectra for U^{3+} in H_2O and in HF (Figure 7a and 7b) strongly suggest the existence of cationic U^{III} in this melt. The spectrum for U^{III} in basic chloride melts,[16] where the absorbing species is postulated to be an anionic chloro-complex of U^{III}, is very different from that in the acidic melt, showing a broad very intense absorption in the region 400−700 nm and no sign of the sharp peak above 1200 nm observed in the acidic melt spectrum.

As indicated above, the spectrum (Figure 8b) recorded by Øye and Gruen[6] for a solution of $TiCl_2$ in the pure acid, $AlCl_3$, indicates the presence of Ti^{2+}.

Gilbert and co-workers[17] conducted electrochemical and spectroscopic studies for lanthanide(III)−lanthanide(II) systems in 40°C melts ranging from acidic ($AlCl_3$/BuPyCl, >60:<40), through weakly acidic ($AlCl_3$, 60 to 50.1 mol%) to neutral and basic. Over this acidity-basicity range, values of $E_{1/2}$ for the $Ln^{III}-Ln^{II}$ systems shifted to more cathodic potentials. They postulated formation of anionic chloro-complexes in basic media and they reported low solubilities of lanthanide dichlorides and trichlorides near neutrality. They proposed cationic species such as Sm^{3+} and Sm^{2+} in acidic melts, with $SmCl^{2+}$ nearer to neutrality and anionic species such as $SmCl_6^{3-}$ in basic media.

It will be demonstrated in Section 2.2.4 that addition of the base F^- to acidified HF or of the base Cl^- to acidic chloroaluminates containing cations such as U^{3+} and Ti^{2+} causes disproportionation of the cations to form the metal and a higher oxidation state fluoride or chloride in each case. Stability of these low oxidation state cations in these acidic media demonstrates the low basicity of these media, i.e. there is not sufficient of the base F^- or Cl^- to cause instability of the cations.

2.2.3 Homopolyatomic Cations of Non-metallic Elements

The pioneering work on generation of homopolyatomic cations such as I_2^+, I_3^+, Br_3^+, S_4^{2+}, Se_8^{2+}, and Te_6^{4+} *in solution* was initiated by Gillespie and the bulk of the experimental work was carried out by his co-workers who prepared them in oleums and in HSO_3F and characterised them spectroscopically. Their existence and stability in sulfur acids will be discussed in Section 3.1.1. These cations cannot exist even in acidified aqueous solution because the medium is too basic. They would disproportionate on contact with water, as will be discussed in Section 2.2.4.

A relatively small amount of work has been done on generation and stability of homopolyatomic cations in HF and in chloroaluminates − the two solvent systems other than H_2O being discussed in the major part of this review. Gillespie and Passmore[18] reported isolation of solid $S_8^{2+}(AsF_6^-)_2$ from addition of sulfur to an AsF_5-HF solution [Equation (7)]:

$$S_8 + 3\,AsF_5 \xrightarrow{HF} S_8^{2+} + 2\,AsF_6^- + AsF_3 \quad (7)$$

AsF_5 acts as oxidant, Lewis acid, and source of AsF_6^- to provide both a superacidic reaction medium and a counter-ion of sufficiently weak basicity to prevent disproportionation of the cation. *Electrophilic cations which are stable in strongly acidic solutions require very weakly nucleophilic counter-ions to be stabilised in the solid state.*

Using Gillespie's spectral data to identify iodine cations in HF solutions, Besida and O'Donnell[19] determined the acidity thresholds at which polyiodine cations were formed in HF solutions. They treated excess of iodine with controlled amounts of elemental F_2 in HF solutions ranging from basic to strongly acidic. In separate solutions, decreasing concentrations of NaF were used to reduce the basicity of the medium and known concentrations of the Lewis acids of increasing strength, NbF_5, TaF_5, and SbF_5, were used to increase the acidity in controlled fashion. They demonstrated that the only species detected in basic solutions were I_2 and IF_5, shown in Section 2.2.4 to be the final disproportionation products for polyiodine cations in basic media. I_5^+, the iodine cation with the smallest charge-to-atom ratio, was not formed until a threshold H_o value of −10.95 was reached, the value for neutral HF being −15.1, as stated earlier. I_5^+ and I_3^+ were in co-existence until an H_o value of about −15. Then, I_3^+ and I_2^+ co-existed, with I_2^+ becoming the dominant species. I_2^+ was the only species detectable for H_o values more negative than −16.20. These reactions were shown to be reversible in the manner shown in Section 2.2.4, i.e. cations of high charge-to-atom ratio disproportionate on addition of base.

Recently, Christe and colleagues[20] have reported a spectacular example of a stable homopolyatomic cation in N_5^+, the third known all-nitrogen entity after N_2 itself and N_3^-. The potentially unstable cation — its enthalpy of formation has been calculated as being about 1470 kJ mol^{-1} — was generated in superacidic medium at low temperature and isolated as a solid compound with the weakly basic anion AsF_6^-. They treated $N_2F^+AsF_6^-$, formed by direct reaction of *cis*-N_2F_2 and AsF_5, with HN_3 in anhydrous HF at −78°C and isolated the solid product $N_5^+AsF_6^-$, which is marginally stable at ambient temperature but stable indefinitely at −78°C. There is indirect chemical evidence that the acidity of the HF reaction medium may have been enhanced by availability of some free AsF_5 formed during the reaction.

While several nonmetal homopolyatomic cations have been reported in chloroaluminates, very little definitive work has been reported on relating the stability of these cations to acidity-basicity levels in molten chloroaluminates. Initially I_5^+ and I_3^+ were synthesised by reacting fused stoichiometric amounts of I_2, ICl, and $AlCl_3$ to form I_5AlCl_4 and I_3AlCl_4 i.e. under neutral conditions, Cl^- reacting with $AlCl_3$ to form the neutral $AlCl_4^-$.[21] Increased acidity was required to stabilise I_2^+ in the melt 63 mol% $AlCl_3$/37 mol% NaCl.[22]

2.2.4 Base-induced Disproportionation of Cations

It has been seen that generation of stable solutions of monatomic cations of transition metals in unusually low oxidation states and of homopolyatomic nonmetal cations is possible in highly acidic media, i.e. in media of very low basicity. Addition of an appropriate base to such solutions renders the cations unstable due to disproportionation.

The necessity for an acidic medium for these cation is indicated by the observation that gradual addition of a basic solution of NaF to a solution of U^{3+} in HF/BF_3[2d] led to the formation of metallic U and solid UF_4 according to the Equation (8):

$$4\,U^{3+} + 12\,F^- \rightarrow U + 3\,UF_4 \quad (8)$$

A more complex disproportionation was observed when F^- was added to a solution of Ti^{2+} in $HF-SbF_5$ where the formation of metallic Ti was accompanied by formation of fluorides of Ti in oxidation states III and IV.[2e]

Homopolyatomic nonmetal cations are susceptible to step-wise disproportionation reactions on gradual addition of base to solutions of the cations in superacids. Quantitative investigation[19] has shown that with increasing basicity, the cation I_2^+ in $HF-SbF_5$ disproportionates firstly to I_3^+ and IF_5, Equation (9), then to I_5^+ and IF_5, Equation (10), and finally to I_2 and IF_5, Equation (11):

$$14\ I_2^+ + 5\ F^- \rightleftharpoons 9\ I_3^+ + IF_5 \quad (9)$$

$$12\ I_3^+ + 5\ F^- \rightleftharpoons 7\ I_5^+ + IF_5 \quad (10)$$

$$5\ I_5^+ + 5\ F^- \rightleftharpoons 12\ I_2 + IF_5 \quad (11)$$

These lead to the overall reaction, Equation (12):

$$10\ I_2^+ + 10\ F^- \rightleftharpoons 9\ I_2 + 2\ IF_5 \quad (12)$$

(IF_3 was shown spectroscopically to be a minor component of the products of disproportionation of polyiodine cations in HF solutions).

Small increases in available base cause disproportionation of I_2^+ to I_3^+ and I_5^+. When available F^- is comparable with or somewhat greater than the concentration of I_2^+, total disproportionation occurs to elemental I_2 and an essentially covalent compound of iodine in a higher oxidation state than in the parent cation. These reactions were shown to be reversible. When the disproportionation products I_2 and IF_5 were added to HF solutions of varying acidity, mutual oxidation and reduction, i.e., conproportionation, yielded the products I_5^+, I_3^+, and I_2^+ as the acidity was increased even when each reactant was in ten-fold excess. It is apparent that, *unless a very powerful oxidant or reductant is present*, the level of acidity of the medium is the principal determinant of cationic speciation, regardless of whether oxidant or reductant is in excess i.e. regardless of reaction stoichiometry.

This pattern of stabilization of cations in unusual oxidation states in media of low basicity and their disproportionation on addition of base, which has now been well established quantitatively for iodine cations, appears to be quite general for homopolyatomic cations and for cations of transition metals in low oxidation states. It applies, regardless of the nature of the cations or of the media, to all the cations listed in Section 3.1.1. Even though many of the experimental observations are fragmentary, reports on synthesis and stability of cations in superacids other than HF and in chloroaluminates are all consistent with the scheme outlined above.

It is interesting to note that Hg_2^{2+}, the only homopolyatomic cation which has been shown to be stable in aqueous solution, disproportionates to metallic Hg and a Hg^{II} compound on addition of base. Furthermore the less stable Hg_3^{2+}, prepared in both chloroaluminate and in HSO_3F, disproportionates to Hg and a compound of Hg^{II} on contact with water.[23]

There is indirect but highly plausible evidence for disproportionation of U^{III} in nearly-neutral chloroaluminates in the work of Morrey and colleagues,[24,25] who prepared UCl_3 in situ in a series of sealed tubes by heating small amounts of U with very much larger comparable volumes of metallic Al and of chloroaluminate melts which ranged from acidic ($AlCl_3$/KCl, 2:1) through neutral (1:1) to basic (0.4:1). After prolonged heating, followed by quenching, each of the immiscible layers, metallic Al and chloroaluminates, was analysed for U. The uranium content of the metallic Al phase was very low when the chloroaluminate phase was strongly acidic or strongly basic but very much higher when the salt layer was nearly neutral. They reported different spectra for the U^{III} species in acidic and in basic melts. The present author has reinterpreted[2f] their work by postulating that U^{III} is present as stable cationic and anionic species in acidic and in basic melts but that near neutrality, U^{III} disproportionates to U^0 and U^{IV} in similar fashion as in Equation 8. Metallic U dissolves preferentially in the Al^0 phase and U^{IV}, present as a chlorouranate(IV) in the melt layer, is reduced to U^{III} by Al providing a cyclic disproportionation reaction leading to continually increasing concentrations of U^0 in the Al^0 layer.

Sørlie and Øye[26] dissolved $TiCl_2$ in $AlCl_3$ and reproduced the earlier spectrum (Figure 8b) recorded by Øye and Gruen.[6] They then recorded spectra for $TiCl_2$ dissolved in chloroaluminates of increasing basicity by progressive addition of KCl until the molar ratio was KCl/$AlCl_3$, 51:49. As neutrality was approached a large new band, possibly for $TiCl^+$, was observed with the original two bands characteristic of Ti^{2+} still present. In the basic melt (51:49) the spectrum changed dramatically to that observed by them for $TiCl_3$ in a basic melt. They reported that metallic Ti deposited on the walls of the spectroscopic cell in this slightly basic melt. Their observations are consistent with an idealised disproportionation reaction, Equation (13):

$$3\ Ti^{2+} + 12\ Cl^- \rightarrow Ti + 2\ TiCl_6^{3-} \quad (13)$$

2.2.5 Anions in Acidified Media

While several cations in unusually low oxidation states can be generated in highly acidic aqueous media, there does not appear to be anything particularly unusual about anion speciation in these media. A wide range of simple, familiar anions, e.g. halides, oxo-anions, carboxylates etc. can exist in acidified aqueous solutions as stable species, free or protonated to molecular species.

A much more limited range of anions can exist in the extremely acidic solvent HF. These are F^- itself, anions formed by Lewis acid-base interaction in HF e.g. BF_4^-, SbF_6^- and anions of superacids of comparable strength with HF, e.g. SO_3F^-. Other anions are fully protonated or solvolysed. Cl^- is protonated to HCl which is expelled from solution because of its insolubility and volatility. Carboxylates are doubly protonated to cationic species. Most oxo-anions undergo solvolysis, e.g. NO_3^- gives NO_2^+ and SO_4^{2-} forms SO_3F^-. The nonavailability of those simple anions which act as strong ligands in aqueous solution, e.g. Cl^-, means that metal cations undergo simple solvation in HF with no further complexation of the type exemplified for chlorochromium (III) cations in Section 2.2.1.

Little information is available on possible anionic species in chloroaluminates other than those derived from the me-

dium or from solutes which are usually added as anhydrous chlorides. So the only anions reported in acidic media are Cl^- and those derived from the Lewis acid, namely $AlCl_4^-$, $Al_2Cl_7^-$ etc.

2.3 Base-enhanced Media

This section deals with H_2O, HF, and chloroaluminates to which the conjugate base of the solvent has been added. The anhydrous NH_3 solvent system, where the *neutral* medium is more basic than H_2O, will be discussed in section 3.2.

2.3.1 Anions in Normal Oxidation States

To an extent even greater than in acidic aqueous media, basic aqueous solutions can support a wide range of simple anions such as halides, oxo-anions, carboxylates, etc. In basic H_2O, solvo-anions of transition metals in normal oxidation states whose hydroxides are amphoteric can form e.g. $Cr(OH)_4^-$, $Zn(OH)_4^{2-}$, $Al(OH)_4^-$ etc.

The situation in basic HF is not very different from that in acidic HF. Most simple anions are protonated or solvolysed. In addition to F^-, the stable anions are those derived from interaction between F^- and a Lewis acid. Very weak Lewis acids will form fluoro-anions in basic HF more extensively than in acidic HF e.g. MoF_6^-, TiF_6^{2-} etc.

A similar situation exists in chloroaluminates. Cl^- interacts with binary chlorides to produce chlorometallate anions[7] with the metal in the same oxidation state as in the parent chloride, e.g., $CrCl_3$, $CoCl_2$, $NiCl_2$, $ZnCl_2$, etc. form $CrCl_6^{3-}$, $CoCl_4^{2-}$, $NiCl_4^{2-}$, $ZnCl_4^{2-}$, etc.

2.3.2 Solvo-anions of Metals in High Oxidation States

Reference to Figure 2 shows that, to the extent that information is available, a general property of solvents made strongly basic is the ability to allow preparation of stable anions based on metals in high oxidation states coordinated by ligands derived from the solvent. Thus, oxidation of chromate(III), $Cr(OH)_4^-$, in basic water yields chromate(VI), CrO_4^{2-}, Examples of other oxo-anions prepared by oxidation in strongly basic aqueous solution are MnO_4^- and PuO_5^{3-}, for which the metals are in oxidation state VII, the latter being very unusual for Pu.

The spectra in Figure 3 show that chromium(III) is soluble in basic HF as CrF_6^{3-}. Fluorochromate(V), CrF_6^- (see Figure 2) has been shown to be stable in basic anhydrous HF.[27] Solid CrF_5, prepared by fluorination of CrF_3, was added to an HF solution containing $NF_4^+HF_2^-$ – i.e. a basic solution – to yield $NF_4^+CrF_6^-$, a very powerful oxidant.

There have been several reported preparations of fluoronickelate(IV), NiF_6^{2-}, which is stable in HF. Stein and coworkers electrolysed strongly basic HF (0.5 to 1.5 M in KF) using a nickel anode and generated red NiF_6^{2-}, in solution.[28]

Žemva and colleagues used the very powerful oxidant KrF_2 to react with AgF_2 and NiF_2 in HF in the presence of XeF_6 at −60°C and produced the solids $[XeF_5^+Ag^{III}F_4^-]$[29] and $[(Xe_2F_{11}^+)_2Ni^{IV}F_6^{2-}]$.[30] XeF_6 ionises extensively in HF to form XeF_5^+ and F^-, providing both the basic HF solution necessary for the formation of the high oxidation state anions in solution and the counterions XeF_5^+ and $Xe_2F_{11}^+$ for isolation of the solid products.

More recently Bartlett has reported quantitative oxidation of NiF_2 and AgF_2 to $[Ni^{IV}F_6^{2-}]$[31] and $[Ag^{III}F_4^-]$[32] at room temperature using ultra violet – or sunlight – irradiated F_2 in very strongly basic HF (KF/HF ≈ 1:4). The anions were isolated as the stable solids K_2NiF_6 and $KAgF_4$.

There does not appear to have been any work done on generation in basic chloroaluminates of chloro-anions of metals in very high oxidation states. This would appear to be a potentially fruitful synthetic route to new chlorides and chloro-anions, particularly as the very reliable voltammetric procedures developed for investigations in room temperature chloroaluminates could be used to indicate attainability of high oxidation states.

3. Other Ionising Media

In order to demonstrate in some depth the general nature of the dependence of formation and stability of cationic and of anionic species on acidity and basicity of the medium, the content of this article, to date, has been limited to speciation in H_2O, HF, and chloroaluminates, media for which a reasonably broad range of experimental information is available.

There is good reason to believe that the generalities propounded for these three solvents hold good for all ionising acid-base media. Two other types of media will now be considered briefly, the anhydrous sulfur acids (oleums and fluorosulfuric acid) and strongly basic media, particularly anhydrous ammonia. The principal reasons for adding these are that homopolyatomic cations, which were discussed briefly for HF and chloroaluminates, were first identified systematically in sulfur acids. Further, it is a corollary of the fact that homopolyatomic cations are stable in highly acidic media that homopolyatomic anions, e.g., the Zintl ions, are generated in strongly basic media such as NH_3. To the extent that information is available, it can be shown that transition metal ionisation in these solvents follows the same trends as in the three solvents discussed to date.

3.1 Sulfur Acids

3.1.1 Homopolyatomic Non-metal Cations

Earlier, in Sections 2.2.3 and 2.2.4 there was an account of a quantitative Melbourne study of the dependence of stability of iodine cations on acidity and basicity levels in HF.[19] This is the only such study in HF that has been reported. However, virtually all of the pioneering work on generation in solution of cations of iodine, bromine, sulfur,

selenium, and tellurium had emanated earlier from Gillespie's group at McMaster University, Ontario. He and Passmore published an early review of that work which is relatively short and very readable.[33] More recently Passmore and colleagues have reviewed the field exhaustively.[34]

From nearly 200 years ago there had been reports of highly coloured solutions of I_2, S_8, Se_8, and Te in oleums (H_2SO_4 containing excess SO_3). Formation of oxo-cations or oxo-anions was proposed to account for these colours. Gillespie showed conclusively that the coloured species in oleums and in HSO_3F were the homopolyatomic cations I_2^+, I_4^{2+}, I_3^+, I_5^+, Br_3^+, Te_6^{4+}, Te_4^{2+}, Se_4^{2+}, Se_8^{2+}, Se_{10}^{2+}, S_4^{2+}, S_8^{2+}, and S_{19}^{2+}.

The basis for Gillespie's very elegant methodology in this area is illustrated below in the generation of Se_8^{2+} and Se_4^{2+}. He used the powerful oxidant peroxydisulfuryldifluoride ($S_2O_6F_2$) in appropriately varying stoichiometric amounts in the solvent HSO_3F to oxidise the elements, in this case Se. $S_2O_6F_2$, on reduction, yields two SO_3F^- anions. SO_3F^- is the base of the solvent and has a greatly enhanced ionic mobility in the solvent and so can be monitored conductometrically. After reaction, he and his coworkers determined the number of ionic particles in solution by cryoscopy and the number of SO_3F^- ions by an original specialised conductance method. For the oxidation of Se_8 by $S_2O_6F_2$ in the stoichiometric ratio 1:1 in HSO_3F, they demonstrated cryoscopically that there were three particles per mol of Se_8, two of which were shown to be SO_3F^- ions by conductance measurements, indicating that the third particle was doubly positively charged, Equation (14):

$$Se_8 + S_2O_6F_2 \rightarrow Se_8^{2+} + 2\,SO_3F^- \quad (14)$$

If 1:2 stoichiometry were to be used, six particles would be observed, four of which would be SO_3F^- ions, so that Se_4^{2+} would be the reaction product, Equation (15):

$$Se_8 + 2\,S_2O_6F_2 \rightarrow 2\,Se_4^{2+} + 4\,SO_3F^- \quad (15)$$

In the oleum experiments, SO_3 acted both as the Lewis acid and as a less specific oxidant.

The McMaster group recorded UV/Visible spectra to characterise each of the cations in oleums or HSO_3F and in many cases isolated solid products containing the cations, necessarily associated with weakly basic anions, and determined their structures by X-ray diffraction techniques.

On addition of base, SO_3F^- or HSO_4^-, all of these cations disproportionate to a cation of lower charge-to-atom ratio and a covalent compound in a higher oxidation state, in similar fashion to the disproportionation of iodine cations as discussed in Section 2.2.4. Ultimately, on addition of sufficient base, they disproportionate to the element and a covalent compound.

Table 2 shows two general trends for the dependence of the stability of polyatomic cations of S, Se and Te on the level of acidity of the medium. The media are all based on 100% H_2SO_4, made either acidic with SO_3 or, in one case, weakly basic with HSO_4^-. Values of H_o listed in Table 2 are taken from the work of Gillespie, Robinson, and Peel[35] and are based on the experimental conditions, such as addition of SO_3 or of HSO_4^- to H_2SO_4, cited in the reports of the preparation of each of the cations. Consideration of the threshold acidities for stabilisation of the sulfur cations shows that the higher the ratio of charge-to-atom, the higher is the required acidity, i.e., the lower the basicity of the medium. Less base is required to cause disproportionation of S_4^{2+} than for S_8^{2+} and S_{19}^{2+} in turn. For the cations of the same structure and charge S_4^{2+}, Se_4^{2+}, and Te_4^{2+}, the smaller the atomic number of the element the higher is the acidity required for stabilisation, i.e., the lower the basicity of the medium. There is greater attenuation of charge over Te_4^{2+} than for Se_4^{2+} and S_4^{2+}, in turn, i.e., Te_4^{2+} is the least electrophilic of the three cations and can exist with a greater availability of base without disproportionating. *These stability trends for chalcogen cations hold for all homopolyatomic cations of metals and nonmetals in other acidic solvents*, but less comprehensive data are available to allow similar quantitative comparisons for these other solvents.

3.1.2 Transition Metal Cations

Little work has been reported in the open literature on generation of cations or solvo-anions of transition metals in the sulfur acids. In Melbourne work the spectra of solvated Co^{2+}, Ni^{2+}, and Cr^{3+} were recorded after adding appropriate Lewis acids to oleums, HSO_3F, and CF_3SO_3H.[2g] $Co(HSO_4)_2$ was shown to be sparing soluble in 100% H_2SO_4. Addition of SO_3 caused marked increase in the Co^{II} concentration and the spectrum was that for six-coordinate Co^{II} (Figure 4b). Electrolysis was conducted in a three-compartment cell with Co^{II} in 20% $SO_3-H_2SO_4$ in the central compartment. Spectrometric analysis showed that Co^{II} moved quantitatively to the cathode compartment, with no detectable Co^{II} in the anode compartment, indicating the existence of solvated Co^{2+} in the oleum solution.

For most of these Melbourne studies,[2g] Co^{II} was chosen as a model solute because of the major differences in spectra for four-coordinate and six-coordinate Co^{II} (Figure 4a and 4b). $Co(SO_3F)_2$ and $Co(CF_3SO_3)_2$ were both found to be sparingly soluble in "neat" HSO_3F and CF_3SO_3H but dissolved when the Lewis acids SbF_5 and $B(OSO_2CF_3)_3$ were added to the two superacids. In each case spectra were very similar to that in Figure 4b indicating, as with $Co(H_2O)_6^{2+}$ and $Co(HF)_6^{2+}$, six-coordinate solvated cation formation in each case. Table 3 shows the similarity of the spectra in H_2O, the four superacids and $AlCl_3$. For spectra of all the *d*-transition metal cations studied, small shifts of peak positions relative to aqueous solutions were observed for all the superacids with larger shifts in chloroaluminates.

Table 2. Dependence of charge on chalcogen cations on acidity of the medium

Cation	S_4^{2+}	S_8^{2+}	S_{19}^{2+}
Medium	>40% $SO_3-H_2SO_4$	>15% $SO_3-H_2SO_4$	>5% $SO_3-H_2SO_4$
Hammett Function	−14.1	−13.2	−12.7
Cation	S_4^{2+}	Se_4^{2+}	Te_4^{2+}
Medium	>40% $SO_3-H_2SO_4$	100% H_2SO_4	$HSO_4^- - H_2SO_4$
Hammett Function	−14.1	−11.9	−11

Table 3. Peak positions for cobalt (II) in acidified water, superacids, and in acidic melts; sh = shoulder

Solvent	H_2O	HF	HSO_3F
Peak positions [nm]	458 sh 510	471 sh 532	477 sh 545
Solvent	CF_3SO_3H	$SO_3-H_2SO_4$	$AlCl_3$
Peak positions [nm]	482 sh 555	483 sh 540	590 sh 633

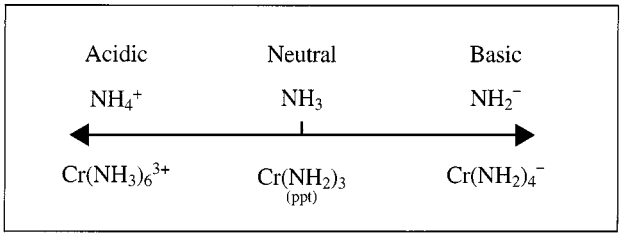

Figure 9. Dependence of Cr^{III} speciation in liquid NH_3 on acidity and basicity of the medium

3.2 Strongly Basic Media

3.2.1 Homopolyatomic Anions

The converse of stabilisation of homopolyatomic cations containing elements of fractional positive charge in strongly acidic (i.e. weakly basic) media is the formation of homopolyatomic anions containing elements of fractional negative charge in media which in the "neat" state are much more basic than H_2O.

Historically, this class of anion dates back to the work of Zintl in Germany about 1930. He reduced PbI_2, dissolved in NH_3, with strongly basic solutions of Na in NH_3 to produce the ions Pb_7^{4-} and Pb_9^{4-} in solution. Zintl also generated Sn_9^{4-} and a range of anions A_n^{3-} (for A = As, Sb, Bi and n = 3, 5, 7) as well as dinegative polyatomic anions of Se and Te. Some four decades later ethylenediamine, more basic than NH_3 and, unlike NH_3, a liquid at room temperature, was used as a medium to produce many more polyatomic anions. This field has been reviewed by Corbett.[36]

Much work has been done on isolation of solid products containing the polyatomic anions for structure determination; but that lies outside the scope of this very brief survey of these anions *in solution*. However very little systematic work has been done on deliberate variation of the acidity or basicity of NH_3 by adding NH_4^+ or NH_2^- to study anion stability. There are some incidental observations[2h] that suggest strongly that these anions are more stable when the base NH_2^- is added and that they decompose on addition of the acid NH_4^+ − the opposite of the behaviour of polyatomic cations in acidic media, as expected.

3.2.2 Solute Speciation of Transition Metals

Figure 2 was used to indicate the generality of solute speciation in H_2O, superacids and molten salts i.e. solvated cations exist in acidified medium, sparingly soluble "binary" uncharged polymeric compounds in neutral medium and solvo-anions in the medium to which excess base has been added. A survey of solute speciation[37] shows that a similar situation holds in liquid NH_3, as indicated in Figure 9.

$CrCl_3$ dissolves in "neat" NH_3 to give $Cr(NH_3)_6^{3+}$ as well as $Cr(NH_3)_5Cl^{2+}$ (c.f. $Cr(H_2O)_5Cl^{2+}$ in water).[37] At first sight, it might seem surprising that solvated cations, rather than polymeric amides, are formed in "neat" NH_3 which undergoes the self-ionisation, Equation (16):

$$2\,NH_3 \rightleftharpoons NH_4^+ + NH_2^- \qquad (16)$$

The self-ionisation constant, K_i, for this equilibrium is extremely small, being about 10^{-33} mol^2L^{-2} at −50 C.[37] The dependence of the acidity − basicity range in a protic solvent on its autoprotolysis constant was discussed in Section 1, where it was shown that minute traces of H_2O, acting as a Bronsted base in HF, could reduce the H_o value for HF by as much as four units. The most likely impurity in NH_3 is reported as being H_2O[37] which acts as a Bronsted acid to produce NH_4^+ and OH^-, the latter being an "innocent" ion in NH_3 in the acid-base sense. Because of the very small autoprotolysis constant for NH_3, traces of H_2O will greatly increase the acidity of the medium, favouring formation of cationic species.

Solute speciation in NH_3 parallels that in other solvents.[37] Thus addition of NH_2^- to $Cr(NH_3)_6^{3+}$ in NH_3 gives insoluble, polymeric chromium amide, $[Cr(NH_2)_3]_n$, which is amphoteric and forms soluble $Cr(NH_2)_4^-$ on further addition of NH_2^-. VCl_3 dissolves in "neat" NH_3 to form $V(NH_3)_6^{3+}$ as well as $[V(NH_3)_5NH_2]^{2+}$ which is the counterpart of $[V(H_2O)_5OH]^{2+}$ in water. Addition of NH_2^- gives $[V(NH_2)_3]_n$ and then $V(NH_2)_4^-$. The divalent metals Mn^{II}, Fe^{II}, Co^{II}, Ni^{II}, Cu^{II}, and Zn^{II} all form $M(NH_3)_6^{2+}$ in solution and give the amides $[M(NH_2)_2]_n$ on addition of NH_2^-.

Transition metals in higher "normal" oxidation states undergo more complex solvolysis[37] giving species like $TiCl(NH_2)_3$. Deprotonation of NH_3 to NH_2^- can proceed further to formation of imide, NH^{2-}, and nitride, N^{3-}, and many anionic species for metals in relatively high oxidation states are reported to be more complex through coordination of these latter two species, as in $[TiNH_2(NH)_2]^-$ and $[Zr(NH_3)_2(N)_2]^{2-}$. These are somewhat akin to Ti and Zr species containing OH^- and O^{2-} ligands in aqueous solution and in solids derived from aqueous solutions.

3.2.3 Anions of Transition Metals in Unusually Low Oxidation States

Unlike the situation in superacids where solvo-anions can be generated which contain transition metals in unusually high oxidation states (Section 2.3.2), anions based on transition metals in unusually low oxidation states have been generated in NH_3. Reduction by metallic K in NH_3 at −33°C of the entities $[Ni(CN)_4]^{2-}$, $[Pt(NH_3)_4]^{2+}$, $Mn_2(CO)_{10}$, and $Fe(CO)_5$ led to formation of $[Ni(CN)_4]^{4-}$, $Pt(NH_3)_4$, $[Mn(CO)_5]^-$, and $[Fe(CO_4]^{2-}$ with the metals in formal oxidation states Ni^0, Pt^0, Mn^{-1}, and Fe^{-II}.

Conclusion

In Figure 2 and Figure 9, chromium(III) has been used to show that there is a common pattern of acid-base dependent solute speciation in the solvents H_2O, HF, NH_3, and chloroaluminates. Uncharged binary polymeric precipitates form in neutral medium.

Moderate increase in acidity leads to formation of cations, solvated to greater or less degree, particularly when considering transition elements of the First Row of the Periodic Classification. (Transition elements of the Second and Third Rows normally occur in high oxidation states and rarely occur as discrete monatomic cations in aqueous solutions. For example Mo and W normally exist in aqueous solution as molybdates and tungstates which, in some instances, are polymeric).

Elements other than chromium have been used to demonstrate that provision of a *highly acidic* medium can allow generation and stabilisation of cations of metals in unusually low oxidation state or, except for H_2O, homopolyatomic cations of metallic and nonmetallic elements. More specifically, a highly acidic medium is one of very low basicity − sufficiently low to prevent disproportionation of the cations. Superacidic conditions happen to be a convenient way of providing media of very low basicity. H_2O is too basic to allow existence of the homopolyatomic cations or of many of the low-oxidation-state transition metal cations generated in superacids.

When the uncharged precipitate is amphoteric, moderate increase in basicity of the medium will lead to formation of solvo-anions − complexes of the metal and the base of each solvent, e.g. $Cr(OH)_4^-$, CrF_6^{3-}, and $CrCl_6^{3-}$. It appears that many more binary chlorides are amphoteric in molten chloride media than is the case for precipitates in H_2O, HF, and most solvents. When each of the media is made *very strongly basic*, generation of very high oxidation states is possible for chromium and other metals in the solvo-anions.

For most solvent systems there is less information available on solute speciation across a wide range of acidity and basicity than is the case for the three solvents presented in Figure 2. Sulfur acids and ammonia have been included to show that the available information on solute speciation is consistent with the patterns outlined in this review. Thus the solvated cation $Cr(NH_3)_6^{3+}$, the neutral polymer $[Cr(NH_2)_3]_n$ and the solvo-anion $Cr(NH_2)_4^-$ are generated in acidic, neutral and basic NH_3. Further, inclusion of these two solvent systems indicates that some converse relationships exist between highly acidic and highly basic media. Thus homopolyatomic cations are stable in superacidic media while homopolyatomic anions are stable in NH_3 and ethylenediamine. Solvo-anions of transition metals in very high oxidation states can be generated in superacidic media, such as HF, while anions of transition metals in very low oxidation states are formed in basic media such as NH_3.

The only class of molten salt system presented here has been the chloroaluminates because of the ease of adjusting the acidity or basicity of the medium and because of the relative simplicity of ionic speciation in the molten salt itself. By comparison, molten silicates for example, where the acid of the system is SiO_2, the base is O^{2-} and the species in a neutral silicate is SiO_4^{4-}, are extremely complex. However it is to be expected that extremely complex silicate systems, like geological magma or metallurgical slags, would lend themselves to similar investigation and interpretation of solute species.

There are good reasons to believe that the systematisation demonstrated in this review for a limited number of solvents holds generally for acid-base interaction of inorganic solutes with all ionising solvents. What emerges from this overview is that, as a generalisation, the levels of acidity or basicity of solvent systems, rather than their chemical composition or temperature domain, are the principal determinants of charge and oxidation state of ionic species in solution.

[1] *The Chemistry of Non-aqueous Solvents*, (Ed.: J. J. Lagowski), Vols I-VB, Academic Press, New York, **1966−1978**.
[2] T. A. O'Donnell, *Superacids and Acidic Melts as Inorganic Chemical Reaction Media*, VCH, New York, **1993**. − [2a]pp. 143−145. − [2b]pp. 139−145, 156−158. − [2c]pp. 167−173. − [2d]pp. 177−178. − [2e]p. 166. − [2f]pp. 183−184. − [2g]pp. 136−139. − [2h]pp. 191−193.
[3] R. J. Gillespie, T. E. Peel, *J. Am. Chem. Soc.* **1973**, *95*, 5173.
[4] R. J. Gillespie, J. Liang, *J. Am. Chem. Soc.* **1988**, *110*, 6053.
[5] C. G. Barraclough, R. W. Cockman, T. A. O'Donnell, *Inorg. Chem.* **1977**, *16*, 673.
[6] H. A. Øye, D. M. Gruen, *Inorg. Chem.* **1964**, *3*, 836.
[7] D. M. Gruen, R. L. McBeth, *Pure Appl. Chem.* **1963**, *6*, 23.
[8] C. Nanjundiah, K. Shimizu, R. A. Osteryoung, *J. Electrochem. Soc.* **1982**, *129*, 2474.
[9] C. G. Barraclough, R. W. Cockman, T. A. O'Donnell, M. J. Snare, *Inorg. Chem.* **1988**, *27*, 4504.
[10] M. Baluka, N. Edelstein, T. A. O'Donnell, *Inorg. Chem.* **1981**, *20*, 3279.
[11] D. Cohen, W. T. Carnell, *J. Phys. Chem.* **1960**, *64*, 1933.
[12] C. G. Barraclough, R. W. Cockman, T. A. O'Donnell, W. S. J. Schofield, *Inorg. Chem.* **1982**, *21*, 2519.

[13] D. H. Brown, A. Hunter, W. E. Smith, *J. Chem. Soc., Dalton Trans.* **1979**, 79.
[14] C. G. Barraclough, R. W. Cockman, T. A. O'Donnell, *Inorg. Chem.* **1991**, *30*, 340.
[15] R. De Waele, L. Heerman, W. D'Olieslager, *J. Less-Common Metals* **1986**, *122*, 319.
[16] D. M. Gruen, R. L. McBeth, *J. Inorg. Nucl. Chem.* **1959**, *9*, 290.
[17] J. P. Schoebrechts, B. P. Gilbert, G. Duyckaerts, *J. Electroanal. Chem.* **1983**, *145,* 127.
[18] R. J. Gillespie, J. Passmore, *J. Chem. Soc., Chem. Commun.* **1969**, 1333.
[19] J. Besida, T. A. O'Donnell, *Inorg. Chem.* **1989**, *28*, 1669.
[20] K. O. Christe, W. W. Wilson, J. A. Sheehy, J. A. Boatz, *Angew. Chem. Int. Ed.* **1999**, *38*, 2004.
[21] D. J. Merryman, J. D. Corbett, P. A. Edwards, *Inorg. Chem.* **1975**, *14*, 428.
[22] K. Tanemoto, G. Mamantov, R. Marassi, G. M. Begun, *J. Inorg. Nucl. Chem.* **1981**, *43*, 1779.
[23] B. D. Cutforth, C. G. Davies, P. A. W. Dean, R. J. Gillespie, P. R. Ireland, P. K. Ummat, *Inorg. Chem.* **1973**, *12*, 1343.
[24] R. H. Moore, J. R. Morrey, E. E. Voiland, *J. Phys. Chem.* **1963**, *67*, 744.
[25] J. R. Morrey, R. H. Moore, *J. Phys. Chem.* **1963**, *67*, 748.
[26] M. Sørlie, H. A. Øye, *Inorg. Chem.* **1981**, *20*, 1384.
[27] R. Bougon, W. W. Wilson, K. O. Christe, *Inorg. Chem.* **1985**, *24*, 2286.
[28] L. Stein, J. M. Neil, G. R. Alms, *Inorg. Chem.* **1969**, *8*, 2472.
[29] K. Lutar, A. Jesih, B. Žemva, *Rev. Chim. Miner.* **1986**, *23*, 565.
[30] A. Jesih, K. Lutar, I. Leban, B. Žemva, *Inorg. Chem.* **1989**, *28*, 2911.
[31] J. M. Whalen, G. M. Lucier, L. Chacón, N. Bartlett, *J. Fluor. Chem.* **1998**, *88*, 107.
[32] G. M. Lucier, J. M. Whalen, N. Bartlett, *J. Fluor. Chem.* **1998**, *89*, 101.
[33] R. J. Gillespie, J. Passmore, *Acc. Chem. Res.* **1971**, *4*, 413.
[34] N. Burford, J. Passmore, J. C. P. Sanders, in *From Atoms to Polymers − Isoelectronic Analogues* (Eds.: J. F. Liebman, A. Greenberg), VCH Publishers Inc., **1989**, pp. 53−108.
[35] R. J. Gillespie, T. E. Peel, E. A. Robinson, *J. Am. Chem. Soc.* **1971**, *93*, 5083.
[36] J. D. Corbett, *Chem. Rev.* **1985**, *85*, 363.
[37] J. J. Lagowski, G. M. Moczygemba, in *The Chemistry of Nonaqueous Solvents* (Ed.: J. J. Lagowski), Vol 2, **1967**, Academic Press, pp. 319−371.

Received March 27, 2000
[I00119]

The Reductive and Oxidative Half-Reactions and the Role of Copper Ions in Plant and Mammalian Copper−Amine Oxidases

Alessandra Padiglia,[a] Rosaria Medda,[a] Andrea Bellelli,[b] Enzo Agostinelli,[c] Laura Morpurgo,[c] Bruno Mondovi',[c] Alessandro Finazzi Agrò,[d] and Giovanni Floris[a][‡]

Keywords: Oxidases / Mammalian amine oxidase / Copper / Cofactors / 6-Hydroxydopa

In this review, the nature and characteristics of the prosthetic group, the intermediates in the catalytic mechanism, and the role of the copper in plant copper–amine oxidases from pea and lentil seedlings are compared with the corresponding features of mammalian amine oxidase from bovine serum. All these enzymes contain the same organic cofactor derived from the modification of a protected tyrosyl residue. Considering the catalytic mechanism, plant amine oxidase may be referred to as a "protein radical enzyme", operating through a free radical located on the cofactor. This is in contrast to bovine serum amine oxidase, which forms the free-radical intermediate only to a minor extent in the course of the catalytic cycle. A scheme for the catalytic mechanism is proposed in order to account for this difference.

I. Introduction

Copper-containing amine oxidases [amine−oxygen oxidoreductase (deaminating) (copper/TPQ-containing); EC 1.4.3.6] are homodimers, in which each subunit (MW 70−90 KDa) contains one tightly bound Cu^{II} ion and one 6-hydroxydopa quinone (TPQ) moiety as prosthetic groups. These enzymes catalyze the oxidative deamination of primary amines by transferring two electrons from the amines to molecular oxygen. The catalytic mechanism can be divided into two half-reactions, namely enzyme reduction by the substrate [Equation (1)] followed by enzyme re-oxidation by molecular oxygen [Equation (2)].

$$E_{ox} + R-CH_2-NH_3^+ \rightarrow E_{red}-NH_2 + R-CHO \quad (1)$$

$$E_{red}-NH_2 + O_2 \rightarrow E_{ox} + NH_3 + H_2O_2 \quad (2)$$

Amine oxidases are ubiquitous enzymes, occurring in microorganisms (fungi and bacteria),[1] plants,[2] and mammals.[3] In the plant kingdom, the presence of amine oxidases was first demonstrated in 1949.[4] Since then, plant amine oxidases from various species of several families have been purified to homogeneity and characterized,[2] the best known and studied being those from seedlings of the pulses lentil[2] (*Lens esculenta*) and pea[5] (*Pisum sativum*) and that from *Euphorbia characias* (a shrub) latex.[6] Mammalian amine oxidases have also been actively investigated for over 40 years, well-studied examples being those from pig kidney,[7−9] human placenta,[10,11] bovine serum,[12−15] pig plasma,[16] and equine plasma.[17] The nature of the covalently bound cofactor and the number of active sites, as well as the role of copper and the reaction mechanism have been also investigated over many years.

Abbreviations used: Cu−AO: copper−amine oxidase; BSAO: bovine serum amine oxidase; LSAO: lentil seedling amine oxidase; PSAO: pea seedling amine oxidase; TPQ: 6-hydroxydopa (2,4,5-trihydroxyphenylethylamine) quinone.

II. The Organic Cofactor and Copper

The presence of an organic cofactor in copper−amine oxidases has been sought for almost 60 years and its nature has been the subject of much debate.[18] Prior to 1984, the most likely candidate was considered to be a covalently bound pyridoxal 5-phosphate[19] (Figure 1, A), but this hypothesis could never be proved. During the 1970s, a new dissociable cofactor was identified in bacterial glucose dehydrogenase and methanol dehydrogenase, which was eventually demonstrated to be pyrrole quinoline quinone by X-ray diffraction analysis[20] (Figure 1, B). This led to the suggestion that pyrrole quinoline quinone might be the active site cofactor of a range of eukaryotic proteins, including copper amine oxidases from bovine serum,[21,22] pig kidney,[23] and pea seedlings.[24] Finally, in 1990, Klinman and co-workers[25] demonstrated that 6-hydroxydopa quinone (TPQ, Figure 1, C), derived from the oxidation of an in

[a] Department of Sciences Applied to Biosystems, University of Cagliari,
09100 Cagliari, Italy
[b] CNR Center of Molecular Biology University of Rome "La Sapienza",
00100 Rome, Italy
[c] Department of Biochemical Sciences "A. Rossi Fanelli", University of Rome "La Sapienza",
00100 Rome, Italy
[d] Department of Experimental Medicine, University of Rome "Tor Vergata",
00100 Rome, Italy
[‡] Correspondence address: Dipartimento di Scienze Applicate ai Biosistemi Università di Cagliari,
Città Universitaria, 09042 Monserrato (CA), Italy
Fax: (internat.) + 39-070/675-4523
E-mail: florisg@unica.it

 © WILEY-VCH Verlag GmbH, D-69451 Weinheim, 2001 1434−1948/01/0101−0035 $ 17.50+.50/0

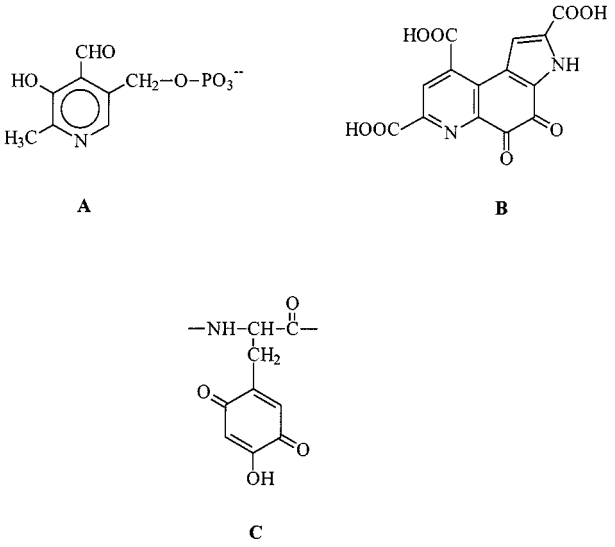

Figure 1. Structural formulae of some cofactors: **A**: pyridoxal 5-phosphate; **B**: pyrrole quinoline quinone; **C**: 6-hydroxydopa quinone

trinsic tyrosine in the amino acid sequence in a post-translational event, is in fact the redox cofactor of eukaryotic amine oxidases.[26] A sequence Asn−TPQ−Asp/Glu was identified in these enzymes,[27] and the cDNA-derived amino acid sequence of *Lens esculenta* (EMB Data Bank accession number X64201),[28] *Hansenula polymorpha*,[26] bovine serum (EMBL Data Bank accession number Q29437),[29] *Pisum sativum* (GB Data Bank accession number L39931),[30] *Cicer arietinum* (EMB Data Bank accession number AJ009825),[31] and *Euphorbia characias* (GB Data Bank accession number AF171698)[6] amine oxidases revealed that a tyrosine codon corresponds to the TPQ cofactor in the mature protein.

Besides TPQ, amine oxidases also contain copper in a 1:1 stoichiometric ratio with the organic cofactor. The crystal structure of PSAO[5] shows that the copper atom is coordinated by three histidine side chains and two water molecules (Figure 2), with the shortest distance between TPQ and the copper atom being ca. 6 Å. Extended X-ray absorption fine-structure (EXAFS) analysis has been used to define the

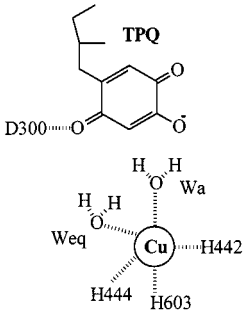

Figure 2. Structural arrangement of the copper center and the organic cofactor in the active site of pea amine oxidase; the copper ion is coordinated by three protected His residues (H442, H603, and H444) and two water molecules (Wa = axial water; We = equatorial water);[5] D300 has been identified as a base required in the active site for the catalytic mechanism

Alessandra Padiglia, PhD in Comparative Biochemistry of Ecosystems; specialized in Toxicology. Currently she is researcher of Biochemistry and Molecular Biology, Faculty of Science, University of Cagliari (Italy). She is working on purification and characterization of enzymatic proteins, and on plant genes.

Rosaria Medda, Researcher of Biochemistry, Faculty of Medicine, University of Cagliari (Italy). She is working on purification and characterization of enzymatic proteins, and on metabolism of diamines and polyamines.

Andrea Bellelli, Researcher at the "Centro di Biologia Molecolare", Consiglio Nazionale delle Ricerche (CNR), Rome, Italy. His main research interests are oxygen-carrying proteins and enzymes with oxidase activity.

Enzo Agostinelli, Associate Professor of Applied Biochemistry, Faculty of Pharmacy, University of Rome "La Sapienza" (Italy). He improved his knowledge on intracellular microinjection and electroporation techniques in U.S.A. He is studying the nature and functionality of the catalytic site of amine oxidase from bovine serum.

Laura Morpurgo, Researcher at the "Centro di Biologia Molecolare", Consiglio Nazionale delle Ricerche (CNR), Rome, Italy. She improved her knowledge at the Inorganic Chemistry Laboratory of Oxford (UK) and at the Laboratory of Chromatography of Rome (Italy). Her researche is concerned with metal complexes and with structure−function relationships in copper-containing proteins.

Bruno Mondovi', PhD in Biochemistry and PhD in Applied Biochememistry. Currently he is Full Professor of Applied Biochememistry, Faculty of Pharmacy, University of Rome "La Sapienza" (Italy). He is working on structure and function of copper proteins and on biochemical mechanisms of heat sensitivity of cancer cells.

Alessandro Finazzi Agrò, Full Professor of Enzymology, Faculty of Medicine, University of Rome "Tor Vergata" (Italy) and currently Rector of the same University. Since 35 years he is studying copper proteins and copper enzymes with respect to their biochemical, physiological and pathological roles.

Giovanni Floris, Associate Professor of Biochemistry and Molecular Biology, Faculty of Science, University of Cagliari (Italy). He is working on purification and characterization of enzymatic proteins, particularly on plant amine oxidases.

MICROREVIEWS: This feature introduces the readers to the authors' research through a concise overview of the selected topic. Reference to important work from others in the field is included.

structure of the copper site in both the oxidized and dithionite-reduced states of some amine oxidases.[32]

III. The Number of Actives Sites

Since all the amine oxidases described so far are homodimers, a problem arose concerning the number of active sites present in the molecule. This problem has mainly been tackled by titrating the enzyme with irreversible inhibitors. The conflicting results obtained on titrating amine oxidases with carbonyl reagents have been rationalized for LSAO and PSAO.[33,34] The titration of highly purified samples extrapolates to 1 mol of inhibitor per enzyme subunit, indicating the presence of two active quinones moieties per protein dimer. A similar result was reported for the titration of highly purified samples of BSAO with phenylhydrazine,[35] but Morpurgo et al.[14] subsequently found that only one enzyme subunit actually reacts with this inhibitor. A somewhat higher value, 1.1−1.3 mol/dimer, was obtained with other reagents, e.g. semicarbazide and 2-hydrazinopyridine.[36,37] In these cases, the reaction of one mol of inhibitor/dimer was faster than the subsequent reaction, which led to the generation of a spectroscopically different adduct.

IV. Optical and EPR Spectroscopy

In addition to the protein absorbance maximum at ca. 280 nm, oxidized Cu−AOs show an absorption band in the visible region associated with their distinctive pink color. The visible spectra of TPQ cofactor models show maxima at 480−484 nm,[38,39] consistent with theoretical calculations. Indeed, the maximum absorbance observed for most mammalian Cu−AOs is very close to 480 nm. In the plant enzymes, this band is red-shifted to 498 nm, probably because of specific interactions with amino acid residues in the active site. Removal of copper from the amino oxidases from both LSAO[40] and *Euphorbia* latex[6] under non-reducing conditions shifts the band to 480 nm. Reconstitution of the metal-depleted protein with cobalt does not restore the native spectrum of LSAO and the absorption maximum remains at 480 nm.[41] In the case of BSAO, the visible band maximum is unaffected by metal depletion and Co^{2+} substitution.[42] The extinction coefficients for some Cu−AOs are listed in Table 1.

Table 1. Extinction coefficients ($mM^{-1}\ cm^{-1}$) of the amine oxidases from pea and lentil seedlings and from bovine serum at pH = 7; wavelengths are given in italics

Enzyme	Oxidized form	Reduced form
PSAO	4.9 (*498*), 300 (*278*)[34]	–
LSAO	4.5 (*498*), 245 (*278*)[33]	7.1 (*464*) 4.6 (*434*)[47]
BSAO	3.8 (*480*), 310 (*280*)[74]	–

The copper ion in Cu−AOs is EPR-detectable and its spectrum falls in the category of so-called type-2 Cu EPR spectra.[43] Native LSAO exhibits a typical type-2 copper spectrum in a tetragonal field, characterized by $g_{\|} = 2.32$ and $A_{\perp} = 153$ G, and by the absence of superhyperfine structure.[44] The same applies to BSAO, for which the EPR parameters are $g_{\|} = 2.30$ and $A_{\perp} = 155$ G.[45]

V. The Reaction Mechanism

A. The Reductive Half-Reaction

A plausible kinetic scheme for the catalytic mechanism of Cu−AOs is presented in Scheme 1. It might be somewhat redundant since plant and mammalian enzymes behave differently and some of them may fail to populate all the intermediates, at least under the usual experimental conditions, as detailed below.

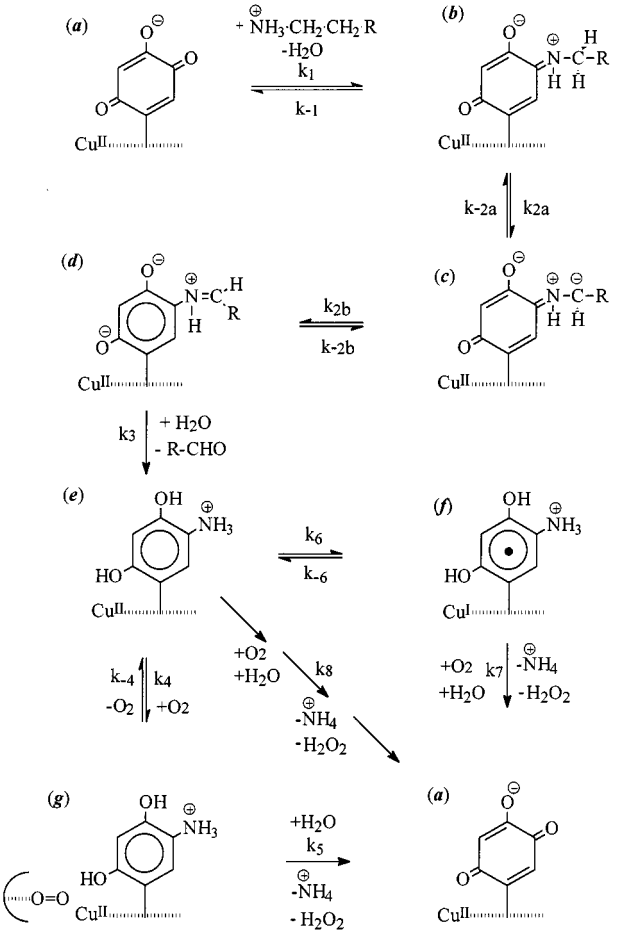

Scheme 1. Catalytic mechanism of Cu−AOs: (***a***) resting oxidized enzyme; (***b***) Cu^{II}−quinone ketimine, the substrate Schiff base; (***c***) Cu^{II}−carbanion species; (***d***) Cu^{II}−quinolaldimine, the product Schiff base; (***e***) Cu^{II}−aminoresorcinol; (***f***) Cu^{I}−semiquinolamine radical; (***g***) Cu^{II}−aminoresorcinol−oxygen complex

Step 1: Cu^{II}−Quinone Ketimine

The amine substrate binds to the carbonyl function of TPQ in the resting oxidized enzyme [Cu^{II}−TPQ (***a***)] to form a substrate Schiff base [Cu^{II}−quinone ketimine (***b***)]. In the case of BSAO, Hartmann and co-workers[46] demon-

strated that the quinone and quinone ketimine oxidized forms of the enzyme, both of which absorb at 480 nm, are spectroscopically distinguishable since only ***b*** shows a shoulder at 340 nm. In order to maximize the population of the quinone ketimine species in the catalytic cycle of LSAO, Floris and co-workers used different substrates. With γ-aminobutanoic acid as the substrate,[47] a marked delay (4 min) was observed before bleaching of the enzyme, indicative of the formation of the quinone ketimine intermediate. The authors were unable to distinguish the "pink" spectrum of the latter from that of the quinone species.

Step 2: Cu^{II}−Carbanion Species

The oxidation of the amine substrate involves base-catalyzed abstraction of a proton from C1 with the formation of a Cu^{II}−carbanion species (***c***). The formation of the carbanion species was demonstrated in the case of BSAO using *para*-substituted benzylamines.[48] The carbanion species generated in the case of LSAO was later trapped with the electrophilic reagent tetranitromethane.[49] The active site base was identified as Asp300 in PSAO.[5] It is worth noting that the stereospecificity of proton abstraction in the reaction with *Escherichia coli* AO, coupled with the mutagenesis data, shows beyond any doubt that Asp383 is the catalytic base.[50] The protected Asp381 seems to play a similar role in BSAO.[37]

Step 3: Cu^{II}−Quinolaldimine

Transformation of the Cu^{II}−carbanion (***c***) into the product Schiff base, the Cu^{II}−quinolaldimine (***d***), is associated with the bleaching of the 498 nm absorption band. This intermediate is the most elusive species involved in the reaction mechanism of AOs. The tautomeric form of the quinolaldimine (a quino-imine) was identified in both LSAO[40] and BSAO[46] using the poor substrate *p*-(dimethylamino)benzylamine.

Step 4: Cu^{II}−Aminoresorcinol

Oxidation of the bound substrate (followed by hydrolysis) releases the aldehydic product, leaving the Cu^{II}−aminoresorcinol derivative (***e***) bearing a bound ammonia molecule. This species is still colorless. Hartmann and co-workers[46] demonstrated a complex time evolution of the "colorless" component in BSAO, attributed to the transformation of quinolaldimine into aminoresorcinol, although they were unable to assign a defined difference spectrum to this reaction. That the aldehyde is released after hydrolysis of the imine, leaving the amino group bound to the cofactor, has been demonstrated in both mammalian and plant AOs.[6,35,40]

In conclusion, comparison of the spectroscopic changes described above with Scheme 1 clearly shows that the chemistry of TPQ implies the involvement of more than three different species. Indeed, the "pink" oxidized Cu^{II}−TPQ derivatives and the "colorless" reduced forms have at least been demonstrated to represent "families" of derivatives rather than pure chemical species. The species ***a***, ***b***, and ***c*** in Scheme 1 are believed to be pink, albeit with slightly different spectra,[50] whereas species ***d*** and ***e*** are colorless.

B. The Oxidative Half-Reaction

In contrast to the detailed studies on the reductive half-reaction [Equation (1)], little is known about the oxidative half-reaction in plant enzymes [Equation (2)]. This reaction has, however, been well characterized in the case of BSAO.[51,52]

Cu^{I}−Semiquinolamine Radical

Hill and Mann[19] reported that solutions of PSAO turned from pink to yellow when an appropriate substrate was added under anaerobic conditions. The absorption band of the oxidized enzyme, with a maximum at about 500 nm, disappeared immediately and was replaced by three bands centered at 465, 435, and 350 nm. The authors concluded that the yellow product was the enzyme−substrate complex. Years after this observation, the yellow intermediate was proposed to be a free radical on the basis of its EPR spectrum, which shows a well-resolved hyperfine structure due to coupling with the various protons of an aromatic ring. The presence of copper ions has been shown to be essential for the observation of the free-radical EPR signal.[53] Since the identification of TPQ as the cofactor of several amine oxidases,[25] unequivocal evidence has been obtained for the generation of a Cu^{I}−semiquinone by substrate reduction under anaerobic conditions in plant amine oxidases.[40,54]

When a good substrate such as putrescine is added to LSAO, the broad absorption band at 498 nm disappears instantaneously, indicative of rapid conversion of the TPQ cofactor to a colorless species, the Cu^{II}−aminoresorcinol (***e***), which is predominant in the steady state. If the amine concentration is high enough to fully consume the available oxygen, the solution turns yellow owing to the emergence of new absorption bands centered at 434 and 464 nm.[40,47,54] These are indicative of the formation of Cu^{I}−semiquinolamine free radical species (***f***), in which the substrate-derived nitrogen is covalently bound to the aromatic ring system.[55−57] The extinction coefficients of substrate-reduced LSAO at pH = 7 and 298 K are reported in Table 1. It may be estimated from EPR measurements that under these experimental conditions the population of the radical species lies in the range 40−50%, the remaining fraction of the enzyme being in the form of Cu^{II}−aminoresorcinol. The yellow radical species ***f*** is in a sense "pure", since it does not share its spectrum with other species. However, it occurs in an equilibrium mixture with species ***e***.[54,58] It proved possible to stabilize the Cu^{I}−aminoresorcinol by treating the radical with dithionite, thus allowing the spectrum of the pure colorless species to be recorded.[47] The addition of substrate to LSAO under anaerobic conditions at room temperature led to a marked decrease in the EPR signal attributed to Cu^{II}, while a new signal appeared at $g \approx 2$, at a field modulation amplitude lower than 1 G. This signal intensified with time, reached a

maximum after 5 min of incubation, and thereafter was found to be stable in the frozen sample or in anaerobic liquid solutions. Admission of air led to a gradual disappearance of this signal. These features are indicative of a free radical. In the case of the pea enzyme, Dooley et al.[54] showed that ca. 40% of the Cu^{II} is reduced to Cu^{I} after the addition of substrate to the native enzyme under anaerobiotic conditions, indicating that the Cu^{I}−semiquinolamine and the Cu^{II}−aminoresorcinol are in equilibrium. The interconversion rate constants of these two species were estimated by *T*-jump methods to be $k_{+6} = k_{-6} = 2{\cdot}10^4\ s^{-1}$ [58] (Table 2), taking advantage of the large equilibrium ΔH. Indeed, the Cu^{I}−semiquinolamine EPR signal, monitored as a function of temperature, could not be detected below about 258 K, but was observed to increase on going from 283 to 298 K, the highest temperature investigated.[58][59]

Table 2. Rate constants for the individual steps described in Scheme 1; all data for BSAO are due to Bellelli et al.,[52] whereas those for LSAO are due to Bellelli et al.[65] and Medda et al.,[47] except the values for k_6/k_{-6} for LSAO, which are due to Turowski;[58] the value of k_7 for LSAO has been calculated assuming that the maximum population attained by the radical species is 50%[47]

BSAO Species

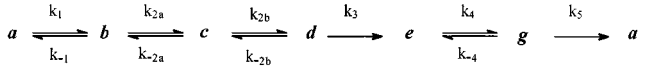

LSAO Species

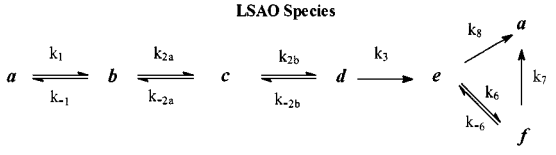

	BSAO	LSAO
k_1 [$M^{-1}s^{-1}$]	$9{\cdot}10^4$	$4{\cdot}10^5$
k_{-1} [s^{-1}]	250	3
$k_{2\ (a\ and\ b)}$ [s^{-1}]	1.2	≥ 200
$k_{-2\ (a\ and\ b)}$ [s^{-1}]	0.01	negligible
k_3 [s^{-1}]	3.3	100
k_4 [$M^{-1}s^{-1}$]	$3.6{\cdot}10^5$	−
k_{-4} [s^{-1}]	33	−
k_5 [s^{-1}]	20	−
k_6 [s^{-1}]	−	$2{\cdot}10^4$
k_{-6} [s^{-1}]	−	$2{\cdot}10^4$
k_7 [$M^{-1}s^{-1}$]	−	$6{\cdot}10^7$
k_8 [$M^{-1}s^{-1}$]	−	$5{\cdot}10^5$

The intensities of the absorbances at 464 and 434 nm of reduced LSAO observed at pH = 7 were found to decrease at both acidic and alkaline pH values, and faded completely at extreme pH values (pH < 5 or > 10).[47] The titration data were fitted to an equilibrium between Cu^{I}−semiquinolamine and the bleached Cu^{II}−aminoresorcinol controlled by two independent ionizable groups with $pK_1 = 5.7$ and $pK_2 = 7.9$: Cu^{I}−semiquinolamine (pH = 7) ⟷ Cu^{II}−aminoresorcinol (pH= 5 or 10)

The shape and position, but not the relative intensities, of the absorption bands were found to be independent of the substrate used.[40,47][60]

Mechanism of Proton-Coupled Electron-Transfer to Dioxygen

In an extensive study of the re-oxidation of bovine serum Cu−amine oxidase (one of those enzymes that do not populate the Cu^{I}−semiquinolamine radical), Su and Klinman[51] reported a detailed analysis of the chemical and kinetic mechanisms of dioxygen conversion into hydrogen peroxide not requiring the conversion of Cu^{II} to Cu^{I}. A hydrophobic niche in the vicinity of the oxygen atom at the C2 position of the reduced cofactor has been identified as the putative dioxygen binding site in the X-ray structure of the active form of the eukaryotic yeast *Hansenula polymorpha*.[61] Reaction of dioxygen with the semiquinolamine does not lead to superoxide release, but two proton-transfer steps are probably coupled to the release of bound H_2O_2 after the formation of a metal-bound hydroperoxide.[62] Since in mammalian amine oxidases the radical species is not present to any significant extent (ca. 1%),[15] it is reasonable to assume that both forms of the reduced enzyme (***e*** and ***f***) can react with O_2 to release H_2O_2 and ammonia, thereby regenerating the Cu^{II}−quinone species.[47] This is also supported by kinetic evidence. It is worthy of note that at least in some Cu−AOs a labile complex with O_2 is formed before oxidation takes place.[51] The reaction of Cu^{II}−aminoresorcinol with oxygen should not be considered as surprising, since the model compound (2,4,5-trihydroxybenzyl)hydantoin is rapidly oxidized by atmospheric O_2 to TPQ−hydantoin.[25] A similar reaction has also been proposed for BSAO.[38]

Stopped-Flow Experiments

Since some of the TPQ derivatives encountered in the catalytic cycle are short-lived and elusive, transient spectroscopy (i.e. stopped-flow methodology) has been exploited in an effort to characterize the spectra and reactivities of as many intermediates as possible. In a typical stopped-flow experiment, the three spectroscopic components, i.e. pink, colorless, and yellow are easily resolved, at least in those Cu−AOs that populate the radical species. The spectroscopic information obtainable is, however, insufficient to resolve all the intermediates, given that some of them have very similar spectra, and a three- or four-step scheme is usually sufficient to describe the time courses recorded. For this review, we carried out an extensive re-evaluation of our data on BSAO and LSAO using the same kinetic scheme, in order to simplify the comparison.

When oxidized LSAO is mixed with putrescine, the bleaching of the 498-nm band is a second-order process, but does not reach completion as the steady-state mixture contains significant amounts of the quinone and aminoresorcinol derivatives. The precise amounts of the latter depend on the chemical nature and concentration of the substrate. This result is in contrast to that obtained for BSAO, for which bleaching is minimal and the steady-state mixture contains mostly the quinone and quinone ketimine derivatives. The following step, i.e. the conversion of ketimine into aldimine, is fast with LSAO and slow with BSAO, consistent with the

isotopic effect observed using dideuterated benzylamine.[63][64] Release of the aldehyde product is usually fast in plant Cu−AOs, at least when physiological substrates are used, and slow in BSAO. This step yields the aminoresorcinol derivative of TPQ, a reduced and bleached species that reacts slowly with oxygen. In the case of BSAO, a labile oxygen complex forms[51] (Scheme 1, ***g***), making the re-oxidation non-second-order,[52] while with LSAO the same complex decays immediately to the oxidized enzyme and the time courses recorded conform to second-order kinetics.

In plant Cu−AOs at a neutral pH value, the aminoresorcinol rapidly equilibrates with the semiquinolamine radical, which attains a population of 40−50%.[54,58] The reactivity of the radical towards dioxygen is 20- to 100-fold higher than that of aminoresorcinol, thus the apparent rate constant for re-oxidation is close to half of that of the radical species[65] (Table 2). Because of the high efficiency of the oxidation reaction, the value of K_m for dioxygen is low in most or all Cu−AOs, irrespective of the complexity of the reaction mechanism. From the rate constants reported in Table 2, a complete and consistent kinetic characterization of the catalytic cycle can be put forward, even though the accuracy of the parameters is low (with SDs between 20 and 50%) due to the redundancy of the kinetic mechanism. In our opinion, such a complete description, even if approximate, is desirable since it allows comparison with the steady-state parameters and hence guarantees a much higher degree of confidence than the determination of the rate constants for single steps.

Under the same experimental conditions as used for LSAO, BSAO does not show the 460−350-nm spectrum typical of the radical species,[46,52] while a radical giving a low-intensity signal 1−2% of the intensity of the copper signal is detected in the room-temperature EPR spectrum.[51,54] According to Dooley,[54] the low concentration does not preclude a catalytic relevance of this radical, while Su and Klinman[51] proposed that the predominant Cu^{II}−aminoresorcinol is the species that reacts with O_2 forming a Cu^{II}−peroxide intermediate. The latter hypothesis is consistent with much experimental data that show Co^{II}-substituted BSAO to be catalytically competent and thus suggest a metal structural function[42,66,69] and/or a Lewis acid role.[45] The nature of the radical in BSAO has recently been questioned, as it also forms when the enzyme is largely inactivated by reaction with hydrogen peroxide.[70]

The Role of Copper

As mentioned above, besides TPQ, amine oxidases also contain copper ions in a 1:1 stoichiometric ratio with the organic cofactor. Since TPQ undergoes reversible redox chemistry even in the absence of copper,[71,72] the function of the metal center in the catalytic mechanism is controversial. Crucial questions are the role of copper ions in the catalytic mechanism and their valence state during the catalytic cycle. Partial answers are now available for each of these questions. In plant enzymes, copper ions have been shown to be involved in the re-oxidation of the substrate-reduced enzyme in the presence of oxygen. It has been unequivocally demonstrated that copper ion reduction occurs in PSAO and LSAO,[40,47,54][58] and that this is coupled to the appearance of a characteristic radical species of the reduced TPQ (the Cu^{I}−semiquinolamine). Through a detailed analysis of fully Cu-depleted, half and fully Cu-reconstituted, and Co-, Ni-, and Zn-substituted lentil amine oxidase, Floris and co-workers[41] have shown that copper ions are also essential for the faster catalytic rate of plant enzymes as compared with mammalian amine oxidases.

The effects of copper ion removal and Co^{II} substitution have been studied in detail with BSAO. In the Cu-depleted protein, the rate of TPQ reduction by benzylamine was found to decrease by a factor of about 10^3 without a substantial change in the enzyme−substrate affinity, the rate of binding to hydrazine inhibitors decreased substantially, and the re-oxidation process was no longer observed.[42] Co^{II} substitution partly restored the catalytic activity (up to 10−40%), decreased K_m to an extent depending on the amino substrate, restored the reactivity towards hydrazine inhibitors to almost the native level,[69] and led to an almost 50-fold increase in the oxygen K_m.[73] Thus, the Co^{II} derivative represents a distinct enzyme from the native one, with quite different kinetic parameters. This implies that the metal center has no redox role in BSAO,[42,74,75] but it may have a structural role and may act as a Lewis acid by modulating the pK_a value of the water molecule through which it is bonded to TPQ−O_2.[37]

Concluding Remarks

Amine oxidases are extensively studied enzymes owing to their ubiquitous distribution in living systems, even though their role has not yet been unambiguously established. The kinetic mechanism of these copper−carbonyl enzymes has only recently been elucidated, following the discovery of the long-sought organic cofactor. Both, copper ions and TPQ, are essential for the enzyme function. However, while the redox cycling of TPQ has been well documented in every enzyme tested, a change in the valence of the copper ions is found only in plant enzymes, which are much more active than their animal homologues. The reduction of copper ions is accompanied by the appearance of a very characteristic radical species, although this has not been proven to be an essential step in the enzymatic mechanism. Nonetheless, plant amine oxidases are nowadays rightly considered as belonging to the group of so-called radical enzymes. A full understanding of their mode of action will require further experiments involving site-directed mutagenesis, while that of their physiological role might be advantageously applied in the construction of "knock-out" organisms lacking the amine oxidase gene.

Acknowledgments

This study was supported in part by funds from the MURST (60%), from the C.N.R. Target Project on Biotechnology, and from contract nos. 97.03975.CT04, 97.04376.CT14, and 98.0115.CT14.

[1] R. A. Cooper, P. F. Knowles, D. E. Brown, M. A. McGuirl, D. M. Dooley, *Biochem. J.* **1992**, *288*, 337−340.

[2] R. Medda, A. Padiglia, G. Floris, *Phytochemistry* **1995**, *39*, 1−9.

[3] W. McIntire, C. Hartmann, in: *Principles and Applications of Quinoproteins* (Ed.: V. L. Davidson), Marcel Dekker, Inc., New York, **1992**, chapter VI.

[4] E. Werle, E. Pechmann, *Justus Liebigs Ann. Chem*. **1949**, *562*, 44−60.

[5] V. Kumar, D. M. Dooley, H. C. Freeman, J. M. Guss, I. Harvey, M. A. McGuirl, M. C. J. Wilce, V. Zubak, *Structure* **1996**, *4*, 943−955.

[6] A. Padiglia, R. Medda, A. Lorrai, B. Murgia, J. Z. Pedersen, A. Finazzi Agrò, G. Floris, *Plant Physiol.* **1998**, *117*, 5193−5198.

[7] B. Mondovì, G. Rotilio, M. T. Costa, A. Finazzi Agrò, E. Chiancone, R. E. Hansen, H. Beinert, *J. Biol. Chem.* **1967**, *242*, 1160−1167.

[8] A. Rinaldi, P. Vecchini, G. Floris, *Prep. Biochem*. **1982**, *12*, 11−28.

[9] V. Steinebach, B. W. Groen, S. S. Wijmenga, W. M. A. Niessen, J. A. Jongejan, J. A. Duine, *Anal. Biochem.* **1995**, *230*, 159−166.

[10] M. J. Crabbe, W. G. Bardsley, *Biochem. J.* **1974**, *139*, 183−189.

[11] F. Morel, A. Surla, P. V. Vignais, *Biochem. Biophys. Res. Comm.* **1992**, *187*, 178−186.

[12] C. W. Tabor, H. Tabor, S. M. Rosenthal, *J. Biol. Chem.* **1954**, *8*, 645−661.

[13] H. Yamada, K. T. Yasunobu, *J. Biol. Chem.* **1962**, *237*, 1511−1516.

[14] L. Morpurgo, E. Agostinelli, B. Mondovì, L. Avigliano, R. Silvestri, G. Stefanich, M. Artico, *Biochemistry* **1992**, *31*, 2615−2621.

[15] J. P. Klinman, D. Mu, *Annu. Rev. Biochem*. **1994**, *63*, 299−344.

[16] K. D. S. Yadav, P. F. Knowles, *Eur. J. Biochem.* **1981**, *114*, 139−144.

[17] S. R. Carter, M. A. McGuirl, D. E. Brown, D. M. Dooley, *J. Inorg. Biochem.* **1994**, *56*, 127−141.

[18] E. A. Zeller, *Adv. Enzymol. Relat. Subj. Biochem*. **1942**, *2*, 93−112.

[19] J. M. Hill, P. J. G. Mann, *Biochem. J.* **1964**, *91*, 171−182.

[20] S. A. Salisbury, H. S. Forrest, W. B. T. Cruse, O. Kennard, *Nature (London)* **1979**, *280*, 843−844.

[21] C. L. Lobenstein-Verbeek, J. A. Jongejan, J. A. Duine, *FEBS Lett*. **1984**, *170*, 305−309.

[22] M. Ameyama, M. Hayasashi, K. Matsuchita, E. Shinagawa, O. Adachi, *Agric. Biol. Chem*. **1984**, *48*, 561−565.

[23] R. A. van der Meer, J. A. Jongejan, J. Frank, J. A. Duine, *FEBS Lett.* **1986**, *6*, 111−114.

[24] Z. Glatz, J. Kovàr, L. Macholàn, P. Pec, *Biochem. J.* **1987**, *242*, 603−606.

[25] S. M. Janes, D. Mu, D. Wemmer, A. J. Smith, S. Kaur, D. Maltby, A. L. Burlingame, J. P. Klinman, *Science* **1990**, *248*, 981−987.

[26] D. Mu, S. M. Janes, A. J. Smith, D. E. Brown, D. M. Dooley, J. P. Klinman, *J. Biol. Chem.* **1992**, *267*, 7979−7982.

[27] S. M. Janes, M. M. Palcic, C. H. Scaman, A. J. Smith, D. E. Brown, D. M. Dooley, M. Mure, J. P. Klinman, *Biochemistry* **1992**, *31*, 12147−12154.

[28] A. Rossi, M. Petruzzelli, A. Finazzi Agrò, *FEBS Lett.* **1992**, *301*, 253−257.

[29] D. Mu, K. F. Medzihradszky, G. W. Adams, P. Mayer, W. M. Hines, A. L. Burlingame, A. J. Smith, D. Cai, J. P. Klinman, *J. Biol. Chem*. **1994**, *269*, 9926−9932.

[30] A. J. Tipping, M. J. McPherson, *J. Biol. Chem.* **1995**, *270*, 16939−16946.

[31] G. Rea, M. Laurenzi, E. Tranquilli, R. D'Ovidio, R. Federico, R. Angelini, *FEBS Lett*. **1998**, *437*, 177−182.

[32] D. M. Dooley, R. A. Scott, P. F. Knowles, C. M. Colangelo, M. A. McGuirl, D. Brown, *J. Am. Chem. Soc.* **1998**, *120*, 2599−2605.

[33] A. Padiglia, R. Medda, G. Floris, *Biochem. Int.* **1992**, *28*, 1097−1107.

[34] M. M. McGuirl, C. D. McCahon, K. A. McKeown, D. M. Dooley, *Plant Physiol.* **1994**, *106*, 1205−1211.

[35] S. M. Janes, J. P. Klinman, *Biochemistry* **1991**, *30*, 4599−4605.

[36] D. De Biase, E. Agostinelli, G. De Matteis, B. Mondovì, L. Morpurgo, *Eur. J. Biochem.* **1996**, *237*, 93−99.

[37] G. De Matteis, E. Agostinelli, B. Mondovì, L. Morpurgo, *J. Biol. Inorg. Chem.* **1999**, *4*, 348−353.

[38] M. Mure, J. P. Klinman, *J. Am. Chem. Soc*. **1993**, *115*, 7117−7127.

[39] M. Bossa, G. O. Morpurgo, L. Morpurgo, *Biochemistry* **1994**, *33*, 4425−4431.

[40] R. Medda, A. Padiglia, J. Z. Pedersen, G. Rotilio, A. Finazzi Agrò, G. Floris, *Biochemistry* **1995**, *34*, 16375−16381.

[41] A. Padiglia, R. Medda, J. Z. Pedersen, A. Finazzi Agrò, A. Lorrai, B. Murgia, G. Floris, *J. Biol. Inorg. Chem.* **1999**, *4*, 608−613.

[42] E. Agostinelli, G. De Matteis, A. Sinibaldi, B. Mondovì, L. Morpurgo, *Biochem. J.* **1997**, *324*, 497−501.

[43] B. G. Malmström, L.-E. Andreasson, B. Reinhammar, in: *The Enzymes* (Ed.: P. D. Boyer), Academic Press, New York, NY, **1975**.

[44] G. Rotilio, in: *Structure and Function of Amine Oxidase* (Ed.: B. Mondovì), CRC Press Inc., Boca Raton, Florida, **1985**.

[45] L. Morpurgo, E. Agostinelli, O. Befani, B. Mondovì, *Biochem. J.* **1987**, *248*, 865−870.

[46] C. Hartmann, P. Brzovic, J. P. Klinman, *Biochemistry* **1993**, *32*, 2234−2241.

[47] R. Medda, A. Padiglia, A. Bellelli, P. Sarti, S. Santanchè, A. Finazzi Agrò, G. Floris, *Biochem. J.* **1998**, *332*, 431−437.

[48] C. Hartmann, J. P. Klinman, *Biochemistry* **1991**, *30*, 4605−4611.

[49] R. Medda, A. Padiglia, J. Z. Pedersen, G. Floris, *Biochem. Biophys. Res. Commun*. **1993**, *196*, 1349−1355.

[50] C. M. Wilmot, J. M. Murray, G. Alton, M. R. Parson, M. A. Convery, V. Blakeley, A. S. Corner, M. M. Palcic, P. F. Knowles, M. J. McPherson, S. E. V. Phillips, *Biochemistry* **1997**, *36*, 1608−1620.

[51] Q. Su, J. P. Klinman, *Biochemistry* **1998**, *37*, 12513−12525.

[52] A. Bellelli, L. Morpurgo, B. Mondovì, E. Agostinelli, *Eur. J. Biochem.* **2000**, *267*, 3264−3269.

[53] A. Finazzi Agrò, A. Rinaldi, G. Floris, G. Rotilio, *FEBS Lett.* **1984**, *176*, 378−380.

[54] D. M. Dooley, M. A. McGuirl, D. E. Brown, P. N. Turowski, W. S. McIntire, P. F. Knowles, *Nature* **1991**, *349*, 262−264.

[55] J. Z. Pedersen, S. El-Sherbini, A. Finazzi Agrò, G. Rotilio, *Biochemistry* **1992**, *31*, 8−12.

[56] J. McCracken, J. Peisach, C. E. Cote, M. A. McGuirl, D. M. Dooley, *J. Am. Chem. Soc*. **1992**, *114*, 3715−3720.

[57] D. M. Dooley, D. E. Brown, A. W. Clague, J. N. Kemsley, C. D. McCahon, M. A. McGuirl, P. N. Turowski, W. S. McIntire, J. A. Farrar, A. J. Thomson, in: *Bioinorg. Chem. of Copper* (Eds.: K. D. Karlin, Z. Tyeklár) Chapman & Hall, Inc., New York, NY, **1993**.

[58] P. N. Turowski, M. A. McGuirl, D. M. Dooley, *J. Biol. Chem.* **1993**, *268*, 17680−17682.

[59] P. Moenne-Loccoz, N. Nakamura, V. Steinebach, J. A. Duine, M. Mure, J. P. Klinman, J. Sanders-Loehr, *Biochemistry* **1995**, *34*, 7020−7026.

[60] R. Medda, A. Padiglia, J. Z. Pedersen, A. Lorrai, G. Floris, *Biochem. Mol. Biol. Int*. **1997**, *40*, 629−637.

[61] R. Li, J. P. Klinman, F. S. Mathews, *Structure* **1998**, *6*, 293−307.

[62] J. P. Klinman, *Chem. Rev.* **1996**, *96*, 2541−2561.

[63] B. Olsson, J. Olsson, G. Pettersson, *Eur. J. Biochem*. **1976**, *71*, 375−382.

[64] M. Palcic, J. P. Klinman, *Biochemistry* **1983**, *22*, 5957−5966.

[65] A. Bellelli, A. Finazzi Agrò, G. Floris, M. Brunori, *J. Biol. Chem.* **1991**, *266*, 654−657.

[66] L. Morpurgo, E. Agostinelli, J. Muccigrosso, F. Martini, B. Mondovì, L. Avigliano, *Biochem. J.* **1989**, *260*, 19−25.

[67] L. Morpurgo, E. Agostinelli, B. Mondovì, B. L. Avigliano, *Biol. Met.* **1990**, *3*, 114−117.

[68] E. Agostinelli, L. Morpurgo, C. Wang, A. Giartosio, B. Mondovì, *Eur. J. Biochem*. **1994**, *222*, 727−732.

[69] E. Agostinelli, G. De Matteis, B. Mondovì, L. Morpurgo, *Bi-*

ochem. J. **1998**, *330*, 383−387.
[70] P. Pietrangeli, S. Nocera, P. Fattibene, X. T. Wang, B. Mondovì, L. Morpurgo, *Biochem. Biophys. Res. Commun.* **2000**, *267*, 174−178.
[71] M. Mure, J. P. Klinman, *J. Am. Chem. Soc*. **1995**, *117*, 8698−8706.
[72] M. Mure, J. P. Klinman, *J. Am. Chem. Soc*. **1995**, *117*, 8707−8718.
[73] G. De Matteis, Ph.D. Dissertation, Faculty of Sciences, University of Rome "La Sapienza", **1999**.
[74] S. Suzuky, T. Sakurai, A. Nakahara, T. Manabe, T. Okuyama, *Biochemistry* **1983**, *22*, 1630−1635.
[75] S. Suzuky, T. Sakurai, A. Nakahara, T. Manabe, T. Okuyama, *Biochemistry* **1986**, *25*, 338−341.

Received March 29, 2000
[I00120]

Modelling the Hydrodenitrogenation of Aromatic N-Heterocycles in the Homogeneous Phase

Claudio Bianchini,*[a] Andrea Meli,[a] and Francesco Vizza[a]

Keywords: Hydrodenitrogenation / Homogeneous catalysis / Nitrogen heterocycles / C−N Bond cleavage

Recent legislation directed at reducing nitrogen levels in fossil fuels has led to numerous studies of the hydrodenitrogenation (HDN) process, whereby nitrogen is removed from organic compounds in petroleum feedstocks. In this review a comprehensive study of the coordination, activation, hydrogenation, hydrogenolysis and denitrogenation of N-heterocycles assisted by transition metal complexes in either fluid solution or single-site systems, is reported. Furthermore, similarities to the reactions occurring in the HDN process over commercial heterogeneous catalysts are also discussed.

Introduction

Under the business pull and environmental push, increasing research efforts are being made to design more efficient catalysts for the hydrodenitrogenation (HDN) of fossil fuels. To this purpose, studies applying molecular complexes have provided valuable mechanistic information on the adsorption modes of aromatic N-heterocycles as well as their hydrogenation and hydrogenolysis reactions. All relevant HDN modelling studies are reviewed in this paper that also provides a brief overview of the heterogeneous HDN mechanisms.

Petroleum and other fossil fuel feedstocks are contaminated by variable amounts of organic compounds containing sulfur, nitrogen and oxygen and, to a much lesser extent, by inorganic compounds, mainly in the form of metalloporphyrins. The presence of all these substances considerably damages the refining processes employed to upgrade feedstocks to product fuels, and ultimately lowers the quality of the latter. Indeed, besides poisoning the catalysts for the cracking and reforming reactions, hydrocarbons containing heteroatoms generate, upon combustion, dangerous polluting agents such as sulfur and nitrogen oxides (SO_x, NO_x).

[a] Istituto per lo Studio della Stereochimica ed Energetica dei Composti di Coordinazione, ISSECC − CNR,
Via J. Nardi 39, I-50132 Firenze, Italy
Fax: (internat.) +39-055/245-8366
E-mail: bianchin@fi.cnr.it

Claudio Bianchini (left) was born in Florence, Italy, in 1949 and received his ''Laurea'' in Chemistry from the University of Florence in 1973. Upon graduation, he joined the Chemistry Department as a bourse-holder (1974−1975). He then moved to the Research Center of the pharmaceutical industry A. Menarini in Florence (1976−1977) as research officer. In 1977, he was offered a position at ISSECC-CNR, Florence, by Prof. L. Sacconi. Currently Director of ISSECC, his research interests include homogeneous and heterogeneous catalysis (HDS, HDN, polymerisation and copolymerisation of olefins), asymmetric catalysis and organometallic reactions. He has authored about 300 papers and patents.

Andrea Meli (center) was born in Florence, Italy, in 1948 and received his ''Laurea'' in Chemistry from the University of Florence in 1974. In 1976, he joined ISSECC-CNR where he is presently first-class researcher and responsible of the catalysis department. His current research interests are in the field of homogeneous and heterogeneous catalysis (HDS, HDN, polymerisation and copolymerisation of olefins) and high-pressure NMR spectroscopy. He has authored about 170 papers and patents.

Francesco Vizza (right) was born in Cirò, Italy, in 1957 and received his ''Laurea'' in Biology from the University of Florence in 1982. In 1986, he joined ISSECC-CNR where he is presently researcher and responsible of a catalysis laboratory. His current research interests are in the field of homogeneous and heterogeneous catalysis (HDS, HDN, polymerisation and copolymerisation of olefins), metal complexes in therapy and diagnostics, high-pressure NMR spectroscopy. He has authored about 85 papers and patents.

MICROREVIEWS: This feature introduces the readers to the authors' research through a concise overview of the selected topic. Reference to important work from others in the field is included.

 © WILEY-VCH Verlag GmbH, D-69451 Weinheim, 2001 1434−1948/01/0101−0043 $ 17.50+.50/0

The discovery of heavy oil reservoirs world-wide and the growing use of coal and oil shale for the production of fuels are pushing the petrochemical industry to invest an increasing amount of human and financial resources in the research and development of more efficient catalysts for removing heteroatoms from fossil fuels. This purification is currently carried out under hydrotreating conditions in the presence of heterogeneous catalysts and, depending on the element to be removed, involves four main chemical processes: hydrodesulfurisation (HDS), hydrodenitrogenation (HDN), hydrodeoxygenation (HDO) and hydrodemetalation (HDM) [Equations (1) to (4)].[1]

$$C_aH_bS + c\ H_2 \rightarrow H_2S + C_aH_d$$
Hydrodesulfurisation (HDS) (1)

$$C_aH_bN + c\ H_2 \rightarrow NH_3 + C_aH_d$$
Hydrodenitrogenation (HDN) (2)

$$C_aH_bO + c\ H_2 \rightarrow H_2O + C_aH_d$$
Hydrodeoxygenation (HDO) (3)

$$ML + a\ H_2 + b\ H_2S \rightarrow MS_b + LH_c$$
Hydrodemetalation (HDM) (4)

Of the four heterogeneous reactions outlined above, HDS has received, and is still receiving, the greatest attention for two principal reasons. Sulfur, contained in thiols, sulfides, disulfides and thiophenic molecules, is actually the most abundant heteroatom in fossil fuels and is also the element with the highest environmental impact. Furthermore, sulfur compounds are largely responsible for the poisoning of the hydrotreating catalysts. The importance of sulfur removal from crude oil feedstocks has therefore directed most of the R&D investments toward the HDS reaction, and in particular toward the design of more efficient heterogeneous catalysts. In parallel to studies under both actual and model reactor conditions, a considerable contribution to a better understanding of the HDS mechanism has been provided by homogeneous studies involving soluble metal complexes.[3−6] It is a common belief that many recent progresses in the field of heterogeneous HDS catalysis have been made with the contribution of the mechanistic information provided by the homogeneous studies.

Related to environmental push and business pull, increasing attention is now being paid to the HDN reaction. Indeed, the degradation of nitrogen compounds to ammonia and hydrocarbons consumes more hydrogen than any other hydrotreating reaction, and therefore any improvement in the efficiency of HDN catalysis would cause an immediate business advantage. From the environmental perspectives, nitrogen oxides and sulfur oxides contribute almost equally to the ravaging phenomenon known as "acid rain". Further, nitrogen oxides contribute to enhance the "greenhouse" effect and are certainly at the forefront in the undesired production of ground-level ozone that damages lung tissue, reduces lung function and sensitises the lungs to other irritants.[1,2]

Although nitrogen is largely produced in the combustion of air/hydrocarbon mixtures, the removal of nitrogen from feedstocks is of enormous importance and constitutes a major technological challenge for the 21st Century.

Nitrogen in petroleum and coal is contained in various organic compounds, which include five- and six-membered heterocycles, aliphatic and aromatic amines and nitriles. Some representative nitrogen compounds in fossil fuels are shown in Figure 1 (polyalkyl substitution is largely diffuse among cyclic compounds).

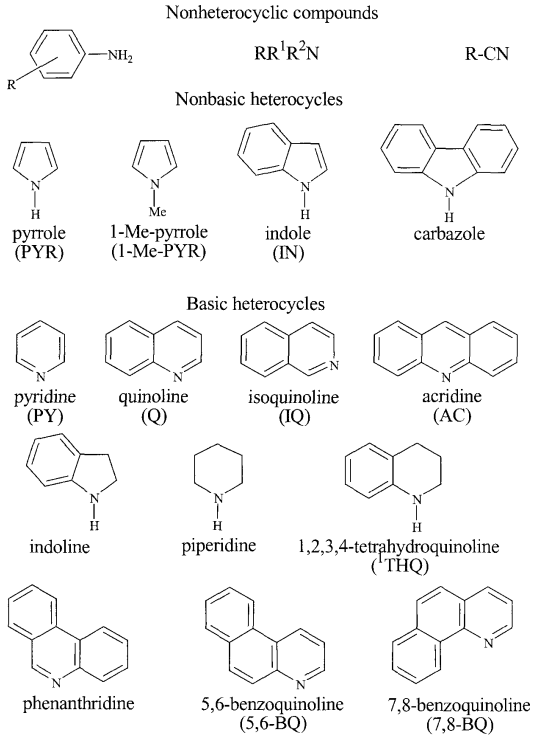

Figure 1. Some representative nitrogen compounds in fossil fuels

Amines and nitriles are less abundant and their degradation is efficiently performed under hydrotreating conditions applying commercial catalysts. The HDN of the aromatic heterocycles, generally pyrroles, indoles, quinolines and pyridines, is much more difficult to accomplish, even more than the HDS of fused-ring thiophenes. Moreover, HDN of the aromatic N-heterocycles requires a greater amount of H_2 than HDS of thiophenes, as the latter does not necessarily involve the saturation of the heterocyclic ring prior to hydrogenolysis.[1,7]

Although the intimate mechanism of metal-catalysed HDN is still far from being understood completely, a relatively rough mechanistic picture of this reaction is now available based on the combined efforts of heterogeneous and homogeneous studies. The former have provided data on product distribution, kinetics and selectivity, whereas the latter have contributed to the elucidation of the binding of the nitrogen substrates to metal centres and the mechanisms of fundamental steps such as the hydrogen-transfer from metal to coordinated substrate and the C-N bond scission.

Unlike HDS, no review article on homogeneous modelling studies of HDN has recently appeared, and therefore a complete overview of the interactions between single metal sites and N-heterocycles, alone or in combination with H_2, is missing in the relevant literature. Aimed at filling this gap, we have written this short review which takes into account

all recent results regarding the activation of N-heterocycles by soluble metal complexes, and also tries to provide some clues which will enable a comparison between heterogeneous and homogeneous HDN-related reactions.

The Heterogeneous HDN Reaction

General Information

In actual refinery reactors, HDN occurs simultaneously with all the other hydrotreating processes that include HDS, HDO, HDM, hydrodearomatisation (HDA), and hydrocracking. The reaction parameters are generally optimised for the HDS reaction, and therefore the experimental conditions and the catalysts employed are not the optimal ones for HDN, as the degradation of nitrogen compounds requires longer reaction times, as well as higher temperature and H_2 pressures than that of thiophenes.[1,7]

The HDN reaction is commonly performed at high temperatures (350−500 °C) and hydrogen pressures (200 bar), over heterogeneous catalysts composed of a γ-alumina support covered by metal sulfides. Mo or W are essential "components" but increased catalytic activity is achieved with the use of variable amounts of late transition metals such as Co, Ni, Ru, Rh, Ir, and Pt, which are called "promoters". Commercial catalysts are prepared by coimpregnation of γ-alumina with aqueous solutions of both a metal component salt (e.g. a Mo salt like $[NH_4][Mo_7O_{24}]$) and a promoter salt [e.g. a Co salt like $Co(NO_3)_3$], followed by reductive sulfidation with sulfur-containing compounds like H_2S, thiophene or CS_2. The Co and Mo exist primarily as Co_9S_8 and MoS_2.[8] The presence of H_2S during the reaction is believed to favour HDN, as it avoids the formation of metal oxides, which are much less active than metal sulfides. An active role of H_2S in the C−N bond scission step has also been demonstrated (vide infra).[9] The most efficacious HDN catalysts are based on Mo and Ni, probably because these catalysts exhibit the best performance in HDA.

In spite of significant progress in the field of surface characterisation (MES, EXAFS, FTIR, XAS, EPR spectroscopy, etc.), it has been concluded that the activity of the catalysts is related to sites located somewhere along the edges of small MoS_2 or Co(Ni)−Mo−S nanoclusters.[1a,10] In particular, the role of the promoters is still a matter of debate. According to a commonly accepted interpretation of HDS catalysed by "Co(Ni)−Mo(W)−S" phases,[1a,10,11] the active centres for the activation of the thiophenic molecules are the promoter atoms located at the edge plane of a MoS_2 single slab, whereas H_2 activation takes place on MoS_2 (or WS_2). The key role of the promoters in the activation of thiophenes has been confirmed by various homogeneous studies[3−6] that also agree with the conclusion that the desulfurisation requires the cooperation of more than one metal centre (component-promoter or promoter-promoter), and the multipoint coordination of the first C−S bond scission product (e.g. thiolate groups).[5a,12−14] A similar mechanistic picture may be proposed for HDN, e.g. the sulfur vacancies associated with Mo^{II} cations located at the edges of the MoS_2 crystallites are the sites where the hydrogenation of the N-heterocycles takes place, while the hydrogenolysis reactions would occur on acidic Mo−SH groups formed by interaction of M=S units with protons derived from the dissociation of H_2S over the catalyst surface.[1a]

It has been experimentally proven that aromatic nitrogen molecules undergo HDN via preliminary hydrogenation of the heterocyclic ring, followed by C−N bond scission (hydrogenolysis). The hydrogenation of the heterocyclic ring is necessary to reduce the high energy required to cleave the carbon−nitrogen bond that, in a typical N-heterocycle, is close to that of a C=N double bond.[7a]

Since the hydrogenation of the heterocycle to a saturated amine occurs prior to C−N bond cleavage, the position of the hydrogenation equilibrium actually controls the removal of the nitrogen atom, particularly when the hydrogenolysis rate is much slower than the hydrogenation rate. Unfavoured hydrogenation equilibria would result in a low concentration of saturated amine with the consequent decrease of the overall HDN rate. Accordingly, high pressures of H_2 are required for efficient HDN. The equilibrium constants for the hydrogenation of typical substrates such as quinoline (Q) and pyrrole (PYR) decrease with increasing temperatures as the ring reductions are exothermic. However, the hydrogenolysis and overall HDN equilibria are favourable, even at temperatures as high as 500 °C. Although the hydrogenation equilibria are unfavourable, the effect of higher hydrogen partial pressures, such as those used in industrial hydroprocessing, is to force the equilibria considerably toward the hydroprocessing products.[7a] Besides disfavouring the hydrogenation/hydrogenolysis equilibria, a low H_2 pressure may also lead to the undesired production of polycondensed N-heterocycles *via* catalytic dehydrogenation.[15] Indeed, kinetic modelling of the HDN process indicates that dehydrogenation of partially hydrogenated substrates such as tetrahydroquinoline (THQ) can be competitive with C−N bond cleavage, even in the presence of H_2.[7]

Adsorption Modes of N-Heterocycles over Heterogeneous Catalysts

In spite of many research efforts over the last twenty years and the progress made in developing surface spectroscopic techniques, very little is known about the detailed structure of the edges of the MoS_2 crystallites or Co(Ni)−Mo−S nanoclusters, as well as the nature of the active sites. This lack of information has strongly limited our knowledge of the interactions between N-heterocycles and the catalyst sites. As a result many hypotheses, often contradictory to each other, have been forwarded, but no precise conclusion has been reached.

A common belief is that basic heterocycles, such as Q, interact with the metal sites over the catalyst surface by two principal modes: *end-on* through the nitrogen atom and *side-on* through either ring (Figure 2). It is also agreed that in the absence of steric congestion provided by α-substituents, Q preferentially uses the nitrogen atom for interaction with the catalyst. In contrast, *side-on* coordination is fa-

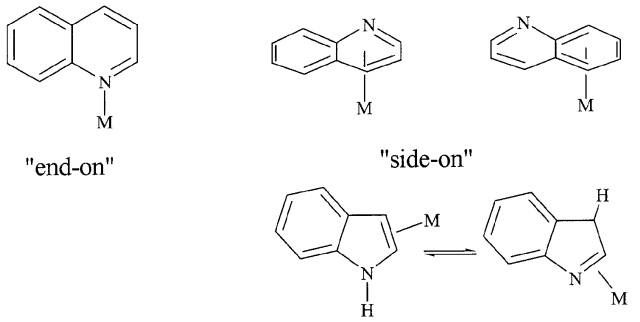

Figure 2. Postulated interactions of Q with the metal sites over the catalyst surface

voured for non-basic rings such as PYR and its higher homologues in which the nitrogen lone pair is not available for coordination.

In order to exemplify the level of uncertainty regarding the adsorption modes of N-heterocycles over the catalyst surface, Figure 3 shows the bonding modes of Q and THQ that have been proposed for HDN-active Ni^{2+} supported on SiO_2-Al_2O_3.[16]

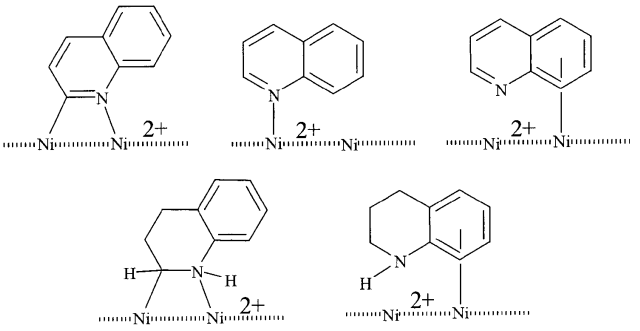

Figure 3. Proposed adsorption modes of Q and THQ over Ni^{2+} supported on SiO_2-Al_2O_3

HDN vs. Other Hydrotreating Processes

The nitrogen-containing compounds are more easily adsorbed over the catalyst surface than most of the heteroatom and aromatic compounds in fossil fuels. The adsorption of nitrogen compounds is so efficient that an almost continuous film may cover the catalyst surface. However, not all molecules undergo HDN due to the many possible unfavourable orientations. The strong tendency of nitrogen compounds for adsorption apparently disfavours adsorption of other substrates and ultimately inhibits other hydrotreating reactions, which, in some circumstances, may even favour HDN. Indeed, it has been found that the H_2S produced by HDS, although competing with the nitrogen compounds for adsorption (thus reducing the hydrogenation rate), promotes the hydrogenolysis step (vide infra).[9] Similarly, the H_2O formed in the HDO of many phenols and other O-heterocycles seems to enhance the overall HDN rate.[9a,17]

Principal Reaction Pathways and Mechanisms Proposed for Heterogeneous HDN

The principal reaction pathways proposed for the heterogeneous HDN of the model substrate Q[1,7,18] are shown in Scheme 1. A sequence of similar steps has also been suggested to occur for the HDN of PYR.

The most efficient and selective HDN of Q would proceed via the reaction sequence **a→b→c**, which does not involve the hydrogenation of the carbocyclic ring. The **a→b→c** sequence consumes less hydrogen than any other path, and also yields high quality product fuels as the residual aromaticity in the denitrogenated products increases the octane rating. However, most of Q undergoes HDN via the alternative sequence **a→d→e→f** that involves the hydrogenation of both rings and therefore consumes twice the amount of H_2, yielding propylcyclohexane. In neutral or basic media, the hydrogenation of the heterocyclic ring is faster than that of the carbocycle, i.e. the hydrogenation of Q to 1,2,3,4-tetrahydroquinoline (^{1}THQ) is faster than that of Q to 5,6,7,8-tetrahydroquinoline (^{5}THQ). In turn, the hydrogenation of ^{5}THQ to decahydroquinoline (DHQ) is faster than that of ^{1}THQ. This observation has been associated to the high π-electron density of the heterocyclic ring. It has been proposed that the hydrogenolysis of ^{1}THQ to *o*-propylaniline is slower than its hydrogenation to DHQ, because the adsorption of ^{1}THQ over the catalyst surface is hampered by its resonance form containing a double bond between the nitrogen atom and the proximal carbocyclic carbon atom.

Using the analogy of metal-catalysed hydrogenation of aromatics, it is proposed that the hydrogenation of N-heterocycles to saturated cyclic amines involves the formation of metal π-adducts, followed by a reductive π→s shift once the two consecutive hydrogen transfers have occurred from vicinal S−H groups. The mechanism is analogous to that reported by Kwart for the HDS of thiophene.[19] It has also been proposed that the metal centre activates the aromatic ring, behaving as an electrophile that delocalises the ring electron density.[7b]

The hydrogenolysis of the C−N bonds in N-heterocycles is much more difficult to accomplish than the hydrogenation of the rings as well as the hydrogenolysis of C−S bonds. Indeed, homogeneous C−N scissions in N-heterocycles are very rare and exclusively stoichiometric in nature,[3c][3d] whereas several C−S bond insertions occurring in solution catalysts have been reported.[3−6] There is little doubt that the higher bond energy of C−N bonds as compared with C−S bonds (by 3−9 kcal mol^{-1}) contributes in making the catalysts less efficient for HDN than for HDS, under comparable experimental conditions.[7]

From a mechanistic viewpoint, the C−N bond cleavage has been suggested to occur through either a Hofmann-type elimination (HE) or a nucleophilic substitution (SN), both reactions being promoted by a base (Scheme 2).[20]

In this mechanistic picture, the first C−N bond cleavage in ^{1}THQ would require the cooperation of a protic acid whose conjugate base B^- may participate in either HE or SN mechanisms (Scheme 3). Many species present on the catalyst surface under hydrotreating conditions may act either as bases or nucleophiles: sulfydryl groups (SH^-) generated by the heterolytic splitting of H_2S, hydride ions (H^-), hydroxyl ions (OH^-) or even neutral molecules such as H_2S,

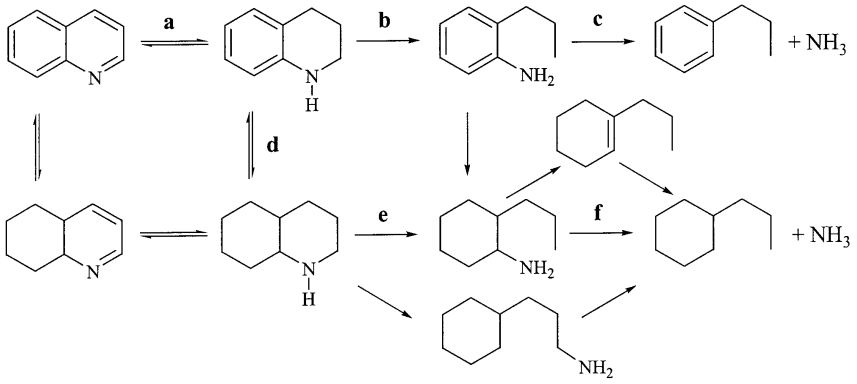

Scheme 1

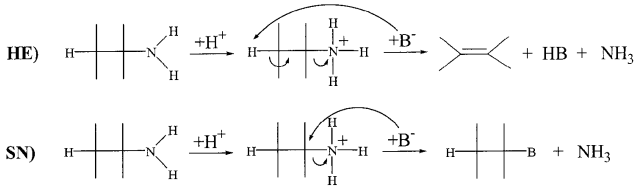

Scheme 2

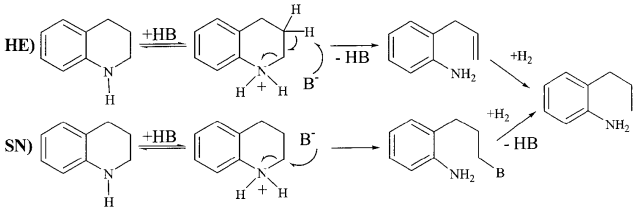

Scheme 3

H_2O, NH_3 or amines. In this mechanistic picture, the increase in the rate of hydrogenolysis by addition of H_2S, has been explained in terms of the enhanced production of H^+ and SH^- groups on the catalyst surface upon heterolytic splitting of H_2S.[7]

The second C−N bond cleavage to give NH_3 and *n*-propylcyclohexane completes the HDN process of Q consuming an overall amount of seven H_2 molecules per nitrogen atom. Furthermore, this step may occur through either HE or SN mechanisms.

It is worth noting that the saturation of the heterocyclic C_α atom is necessary to cleave the C−N bond *via* an SN mechanism, while both the C_α and C_β carbon atoms must have sp^3 hybridisation to allow for a C-N bond cleavage to occur *via* a HE mechanism. In the case of Q, this means that the hydrogenation of both rings is necessary to cleave the C−N bond *via* either mechanism, which is consistent with the formation of *n*-propylcyclohexane as the main HDN product (Scheme 4).

The interaction of the surface metal atoms with saturated N-heterocycles has been the object of model studies by Laine and co-workers.[7c,21] It has been suggested that the C−N scission in saturated heterocycles may not require acidic sites, but rather metal centres. Two possible pathways have been proposed for the HDN of piperidine which differ from each other with respect to the nature of the interme-

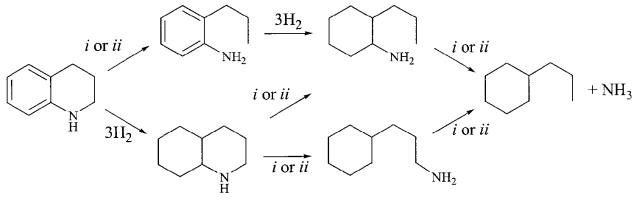

i = **HE** (+H^+, +B^-, -HB) + H_2
ii = **SN** (+H^+, +B^-) + (H_2, -HB)

Scheme 4

diate formed, either a metal alkyl species (**a**) or a metal alkylidene species (**b**) (Scheme 5). In either case, the first step has been suggested to involve the oxidative addition of the C−H bond adjacent to the nitrogen atom to give a metal(hydride) species. The subsequent migration of the hydride from the metal to either the C_α atom or the N atom of an η^2-piperidinyl ligand determines the nature of the intermediate that is ultimately hydrogenated to a primary amine.

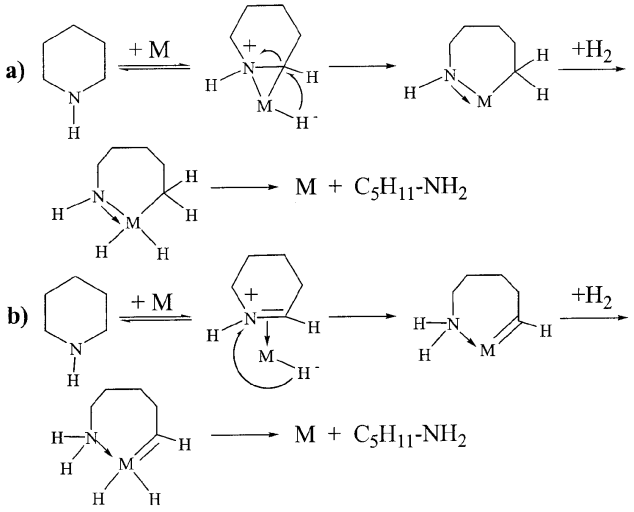

Scheme 5

Model studies on the HDN of piperidine have also contributed to rationalise the beneficial effect of H_2S and H_2O on the rate of C−N hydrogenolysis. Nucleophilic attack by either molecule at the C_α atom would form sulfur-con-

taining intermediates that undergo hydrolytic C−N bond cleavage faster than in the absence of H_2S or H_2O.[7,9,17]

Similar mechanisms have also been proposed to account for the increased rate of C−N hydrogenolysis observed in the presence of other nucleophiles such as NH_3. However, under actual reactor conditions, the addition of NH_3 inhibits HDN, because NH_3 prevails over all the other nitrogen compounds for the interaction with the surface coordination vacancies.[7]

Homogeneous Modelling Studies

Homogeneous modelling studies involving soluble transition metal complexes represents one of the most fruitful approaches in providing mechanistic information on the elementary steps involved in the hydrotreating of fossil fuels. HDN model studies in solution are not as numerous and detailed as those involving HDS. Nonetheless, much of our current understanding of HDN is based on structural and reactivity information obtained in the homogeneous phase, in particular on four relevant issues: modes of bonding between N-heterocycles and metal centres, reactivity of coordinated N-heterocycles, elementary steps of metal-catalysed hydrogenation of N-heterocycles, insertion of metal centres into C−N bonds. A common strategy in HDN modelling is to react mononuclear or polynuclear metal complexes, containing either coordination vacancies or weakly bound ligands, with N-heterocycles.

Common model substrates are PYR, indole (IN), pyridine (PY), and Q together with their alkyl-substituted derivatives and/or their partially or completely hydrogenated products. These model substrates may be divided in two main categories according to the donor properties of the nitrogen atom. In compounds like PYR (pK_a = 0.4) and IN (pK_a = −3.6), the nitrogen lone pair is delocalised over the five-membered ring and is not available for interaction with electrophiles. In contrast, the nitrogen atom in PY (pK_a = 5.2) or Q (pK_a = 4.9) is a good nucleophile susceptible to attack by various electrophilic metal fragments. The different character of the nitrogen atom in the two types of substrates and the presence of aromatic carbocyclic rings is believed to remarkably influence their interaction with the heterogeneous catalyst surface and, consequently, the mechanisms for reduction. The homogeneous studies have indeed proved that both the basicity of the nitrogen atom and the presence of carbocyclic rings determine the binding mode of N-heterocycles to single metal sites, and ultimately control the further reactivity of the M−N heterocycle ensemble.

Binding Modes of N-Heterocycles in Transition Metal Complexes

A) Complexes with Pyrrole and Pyrrolyl Ligands

All known bonding modes of PYR and pyrrolyl ions, or their alkylated analogues, in mononuclear complexes are illustrated in Figure 4.

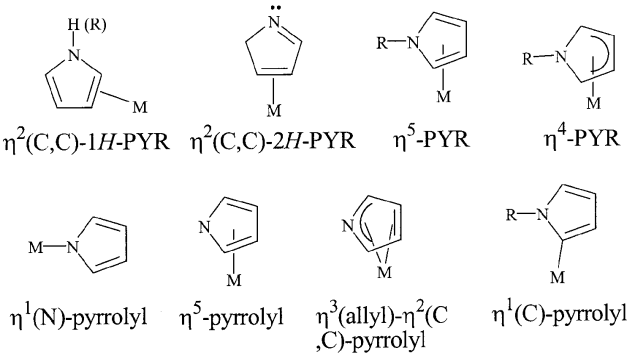

Figure 4. Known bonding modes of PYR and pyrrolyl ions in mononuclear complexes

No complex containing an η^1(N)-PYR ligand has ever been reported, even in the 3*H*-pyrrolidine structure which has been authenticated for IN (vide infra). The most numerous complexes are the η^5-PYR ones,[22] but some examples containing η^2(C,C)-PYR ligands have also been characterised.[23] The η^4 mode has been observed in one complex only.[24]

Metal complexes containing pyrrolyl ligands are ubiquitous in the periodic table, and common coordination modes are the η^1(N) and η^5 modes.[22a,25−27] However, depending on the nature of the supporting metal fragment, each bonding mode may be viewed as involving two distinct electronic forms.[27e]

The pyrrolyl group may be generated in situ by metal-assisted N−H activation of PYR,[26] or provided as a metal salt after N−H deprotonation with a base.[27] In the first case, a high-energy low-valent metal fragment is required to lower the energy barrier for N−H insertion, while $NC_4H_4^-M^+$ reagents (M = Na, K) are commonly reacted with electrophilic metal fragments. C−H bond activation to give η^1(C) pyrrolyl(hydride) metal complexes has also been described.[26c]

The interaction with polynuclear complexes to give an adduct containing intact PYR has never been reported. Either N−H and/or C−H bond activation is commonly observed, yielding bridging pyrrolyl ligands (Figure 5).[27a,27e,28,29]

Selective C−H bond cleavage of N-methylpyrrole is promoted by the dimer $[Cp^*IrH_3]_2$ ($Cp^* = C_5Me_5$), which, under comparable experimental conditions, is able to cleave both thiophene and 2-methylthiophene[28] (Scheme 6). This different reactivity is consistent with a higher energy barrier for C−N insertion than for C−S insertion, as is observed in heterogeneous HDN/HDS.

N−H activation, followed by two dehydrogenation steps has been found to transform pyrrolidine into an imidoyl ligand (Scheme 7).[30]

A particular type of pyrrolyl ligand is that found in the Mo dimer $[(Cp'Mo)_2(S_2CH_2)(\mu\text{-}S)(\mu\text{-}S\text{-pyrrolyl})]^+$, obtained by Rakowski DuBois upon nucleophilic attack by the electron-rich PYR molecule at the disulfide bond in $[(Cp'Mo)(\mu\text{-}S)_2(S_2CH_2)]_2^{2+}$ ($Cp' = C_5H_5$, C_5H_4Me) (Scheme 8).[31] A mechanism has been proposed which in-

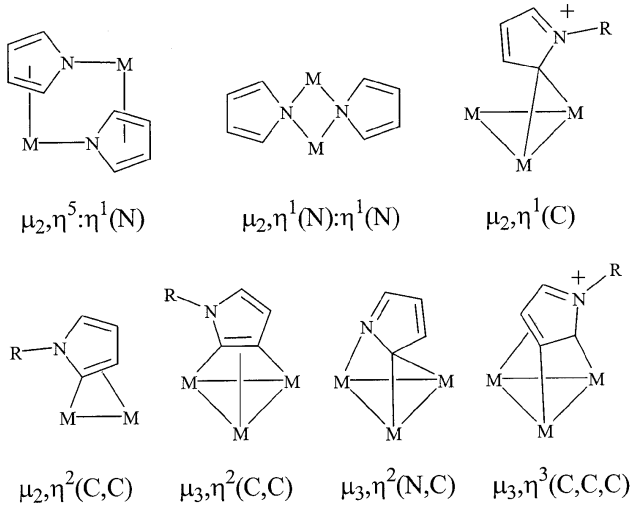

Figure 5. Bonding modes of pyrrolyl ligands in polynuclear complexes

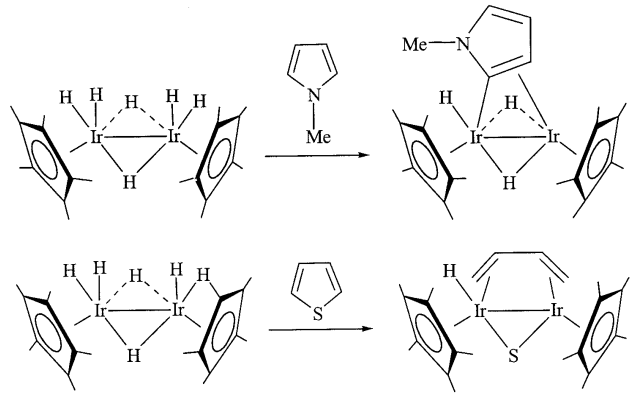

Scheme 6

volves heterolytic scission of the S-S bond by the nucleophilic ring, followed by loss of a proton from the heterocycle to give a 1:1 mixture of μ-pyrrolylthiolate and μ-SH dimers. Alkyl-substituted pyrroles such as 1-Me-PYR or 1,2,5-Me_3-PYR behave similarly, but the regiochemistry of electrophilic addition may vary depending on the position of the substituent.

The ability of the pyrrole ring to attack S-S bonds is not diminished, neither when a metal is bound to the nitrogen atom as in Scheme 9 for $[ReCl_2(PMe_2Ph)_3(\eta^1(N)\text{-pyrrolyl})]$, nor when the nitrogen and a β-carbon atom are engaged in bonding to a metal and to a sulfur atom (Scheme 10). The selectivity for substitution at the β-position has been attributed to the steric bulk of pyrrole N-substituent.[31]

The formation of the unusual (η^1(C)-pyrrolyl)-SMo_2, Re-(μ,η^1(N):η^1(C)-pyrrolyl)-SMo_2 and Re-(μ,η^1(N):η^1(C):η^1(C)-pyrroldiyl)-$(SMo_2)_2$ groupings represents quite interesting models of the potential interaction of electron-rich N-heterocycles with a sulfided metal surface. Indeed, the presence of disulfide moieties over HDS/HDN catalysts has been demonstrated. Moreover, previous studies of thiophene adsorption over MoS_2 catalysts have hypothesised a S−S interaction between the surface sulfur and the substrate.[1,7]

B) Complexes with Indole, Indolyl, Indoline, and Indolinyl Ligands

Indole (IN) differs from PYR by a condensed arene ring. This makes a great difference in the interaction with metal centres and produces a larger variety of possible coordination modes (Figure 6). Indeed, the presence of the carbocyclic ring allows IN to bind a metal centre using the arene ring, leading to the important η^6 mode.[32] Examples of η^1(N)-IN complexes have also been reported that may be better described as η^1(N)-3H-indolenine species.[33−35]

The indolyl anion coordinates mononuclear fragments using the nitrogen (η^1(N) mode),[26a][26e,35] the heterocyclic ring (η^5 mode),[32d,36] or the carbocyclic ring (η^6 mode).[32b]

An interesting case of base-assisted η^6-IN → η^5-indolyl shift[32d] is illustrated in Scheme 11, while an acid-promoted η^1(N)-indolyl → η^1(N)-indolenine conversion[35] is shown in Scheme 12. Treating indolenine complexes with hydride produces η^1(N)-indolinyl derivatives.[32a][35b]

Electron-rich metal fragments can react with 2-substituted IN, yielding either kinetic C−H or thermodynamic N−H insertion products.[26d]

Like PYR,[31] 1-Me-IN has been found to react with the μ-S_2 tetramer $[(Cp'Mo\mu\text{-}S)_2(S_2CH_2)]_2^{2+}$ to give the elec-

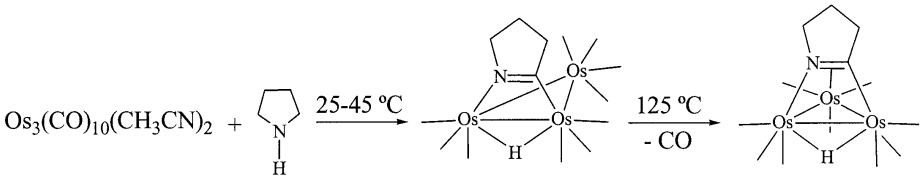

Scheme 7

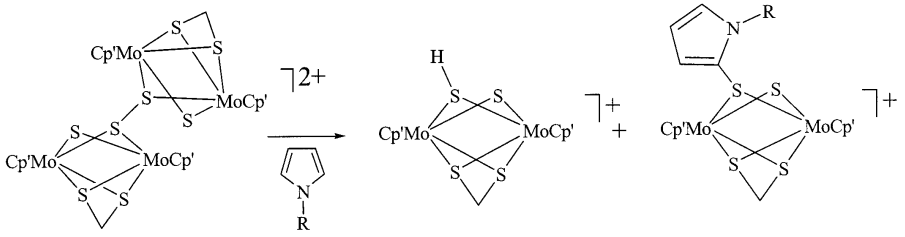

Scheme 8

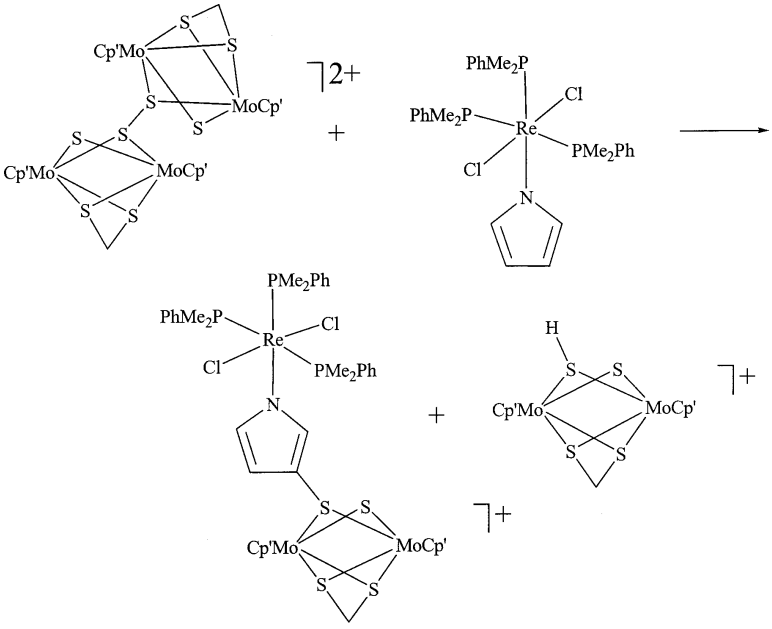

Scheme 9

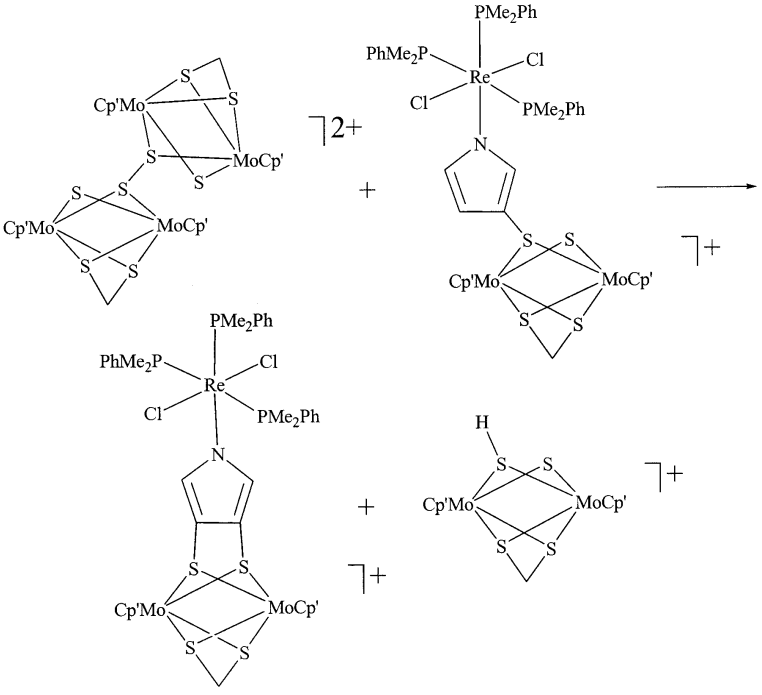

Scheme 10

trophilic substitution product (Scheme 13). The reaction is mechanistically similar to that with PYR.

The coordination chemistry of indoline, obtained by selective hydrogenation of the heterocyclic ring of IN, has also been investigated.[32a] η^6 and η^1(N) Coordination modes, as well as their interconversion, have been reported.[31,35b,37] Of particular relevance are the studies carried out by Rakowski DuBois on the coordination, acid/base properties and activation of indoline by (*p*-cymene)Ru^{II} fragments.[32a,37] The complex [(*p*-cymene)Ru(η^1-indoline)$(CH_3CN)_2$)]$(OTf)_2$ converts to [(*p*-cymene)Ru(η^6-indoline)]$(OTf)_2$ upon gentle heating in CH_2Cl_2 and can be deprotonated to give the corresponding (η^1-indolinyl) complex[37] (Scheme 14). The reactivity of the latter compound is described in a following section.

The presence of the carbocyclic ring widens the range of possible bonding modes of IN to metal clusters.[34,38] As shown in Figure 7, IN, indolyl, indoline or indolinyl ligands may use both nitrogen and carbon atoms from either ring to bind metal centres.[34,38]

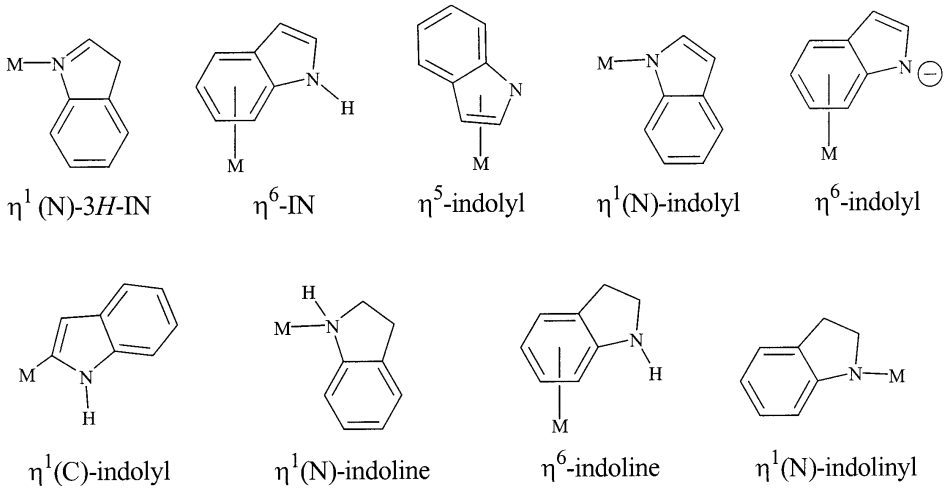

Figure 6. Known bonding modes of IN derivatives in mononuclear complexes

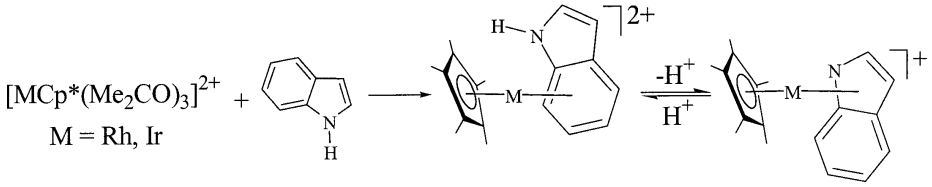

Scheme 11

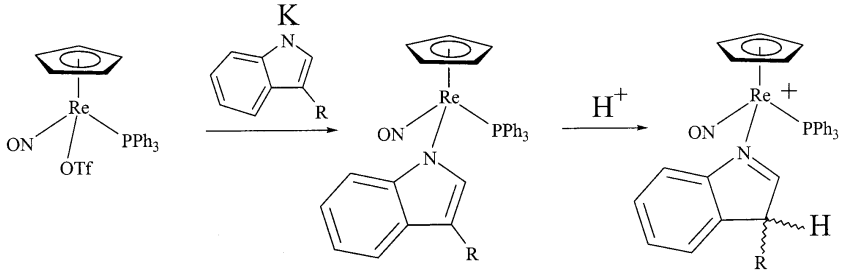

Scheme 12

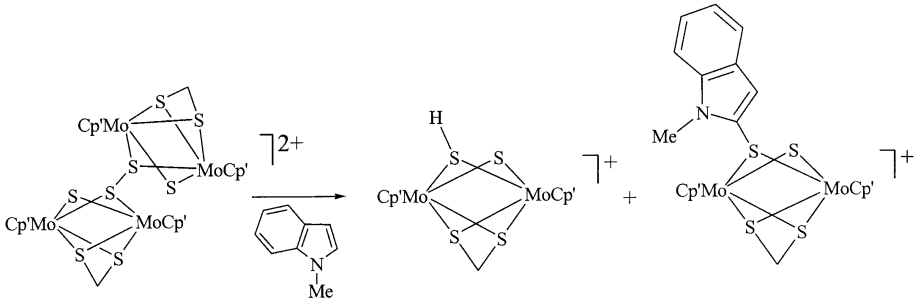

Scheme 13

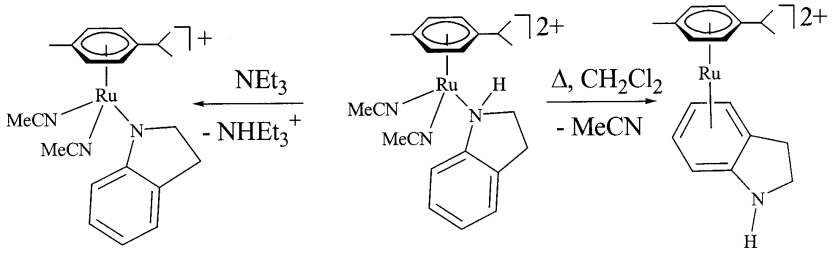

Scheme 14

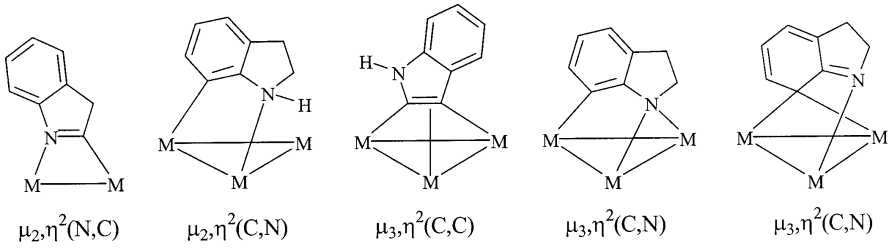

Figure 7. Bonding modes of IN to metal clusters

C) Complexes with Carbazole

The coordination chemistry of carbazole has scarcely been investigated. Only N−H bond activation to give η^1(N)-carbazoyl products has been reported.[26c,39] Interestingly, the reaction of [Cp*Rh(PMe_3)(H)(Ph)] with carbazole[26c] yields a C−H insertion kinetic product that thermally converts to a thermodynamic N-H insertion product (Figure 8).

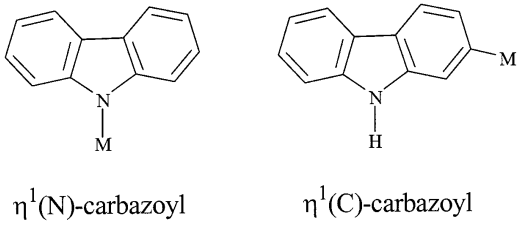

Figure 8. Known modes of carbazoyl coordination

D) Complexes with Pyridine, Quinoline, and Derivatives

The known bonding modes of PY and its alkyl-substituted derivatives to single metal sites are illustrated in Figure 9.

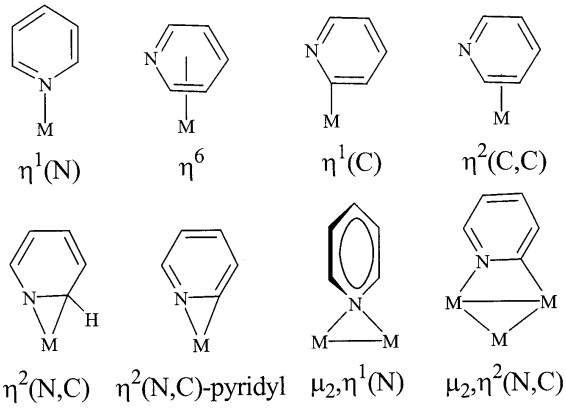

Figure 9. Known bonding modes of pyridine derviatives to single metal sites

The most common coordination for PY is through the nitrogen atom, which uses its lone pair for interaction with Lewis acceptors.[40,41] Unlike thiophene,[3−6] the nitrogen atom in η^1(N)-PY complexes is retained in the ring plane.[42] Formally, monohapto-PY complexes are also the η^1(C) ones obtained from C−H bond activation by electron-rich metal fragments.[43]

Another quite common coordination mode of PY is the η^6 mode, whose formation does not necessarily require the presence of alkyl substituents in the 2,6 positions of the ring to hinder the η^1(N) mode.[41,44]

Many homogeneous studies of PY coordination have centred on the η^1(N) and η^6 modes, and the factors controlling their interconversion and/or prevalence.[41] With the use of the isostructural and isolelectronic Ru^{II} and Rh^{III} complexes [Cp(or Cp*)M(CH_3CN)$_3$]$^{n+}$, Fish and co-workers have found that, in the absence of steric constraints, the η^1(N) mode prevails over the η^6 mode, particularly with the more electrophilic Rh^{III} centre.[41c] For example, [Cp*Rh(CH_3CN)$_3$]$^{2+}$ reacts with 2-methylpyridine and 2,6-dimethylpyridine yielding compounds of the formula [Cp*Rh(η^1(N)-PY)(CH_3CN)$_2$]$^{2+}$, while the sterically encumbered 2,4,6-trimethylpyridine[41c] forms the η^6 adduct [Cp*Rh(η^6-PY)]$^{2+}$. An interesting reactivity path is displayed by [CpRu(CH_3CN)$_3$]$^+$, in which the Ru^{II} centre is more electron-rich than Rh^{III} in the analogous complex. The greater propensity of Ru^{II} to stabilise the η^6 mode *via* π-backbonding from a filled metal orbital to a π* orbital of PY, has allowed Fish to follow the η^1(N)→η^6 interconversion of 2-methylpyridine and 2,4-dimethylpyridine illustrated in Scheme 15. The initially formed η^1(N) complex slowly loses MeCN and converts to the thermodynamic η^6-PY product. This rearrangement has been proposed to involve an η^4-PY intermediate.[41a,41d]

With unsubstituted PY, the stable adduct [CpRu(η^1(N)-PY)$_3$]$^+$ is obtained.[41d] However, when Cp* is employed to make the Ru centre more electron-rich, the complex [Cp*Ru(η^1(N)-PY)$_3$]$^+$ is a kinetic product that thermally converts to the corresponding η^6 derivative (Scheme 16).[41b]

The only example of PY acting as a bridge between two metal centres through the nitrogen atom has been found in Mo_2O_2[S_2P(O*i*Pr)$_2$]$_2$(μ-*O*)(μ-S)[μ,η^1(N)-PY] (Scheme 17).This compound is of particular relevance to HDN because of the presence of two Mo atoms in a sulfur-rich environment. In this Mo dimer, the PY ring is almost coplanar with the bridging O and S atoms, while the Mo-N distances are longer than regular Mo-N distances.[45]

Another rare binding mode of a pyridine substrate is the η^2(C,C) mode which has been described by Taube and coworkers for 2,6-dimethylpyridine (lutidine) (Scheme 18).[46] This interesting coordination mode is exclusively stabilised by the electron-rich [Os(NH_3)$_5$]$^{2+}$ fragment, and rearranges to the η^1(N) mode a one-electron oxidation. The η^2(C,C)→η^1(N) rearrangement of lutidine raises much interest as it relates the bonding mode of the N-heterocycle with the metal oxidation state. Indeed, the active metal

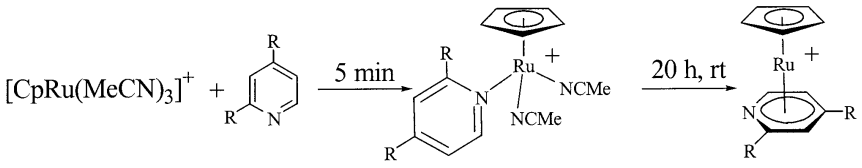

Scheme 15

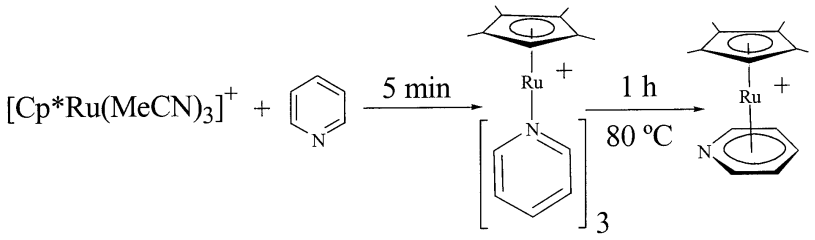

Scheme 16

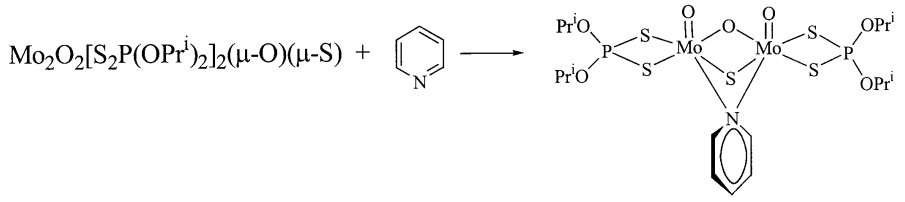

Scheme 17

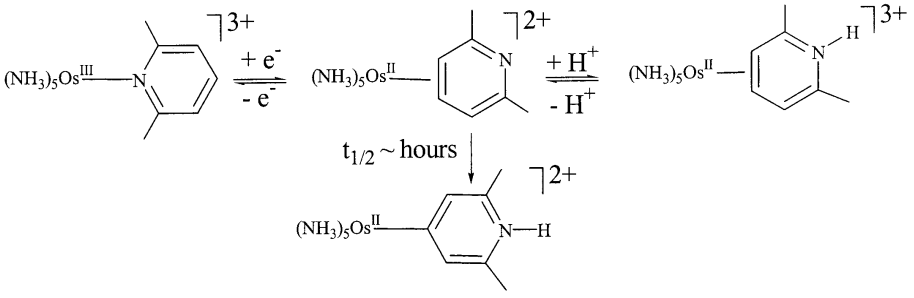

Scheme 18

centres of heterogeneous HDS/HDN catalysts may have different oxidation states due to electron-transfer processes involving both surface and bulk metal atoms.[1]

Interestingly, the η^2(C,C) mode of lutidine rearranges with time to give an Os^{II} lutidinium ylide. In contrast, the η^2(C,C) mode is maintained when $[Os(NH_3)_5(\eta^2$-lutidine$)]^{2+}$ is protonated to give a lutidinium derivative.

All the bonding modes that have been described so far represent valid models for the adsorption of PY over the catalyst surface. None of them, however, has been found to be a precursor to C−N bond scission. In contrast, the η^2(N,C) mode effectively activates the PY ring toward C−N scission. These C−N insertions will be commented on in a separate section, while the known η^2(N,C) metal complexes are reviewed below.

The first η^2(N,C)-PY complex, $[(silox)_3Ta(\eta^2$(N,C)-$NC_5H_5)]$, was prepared by Wolczanski in 1988 through the simple procedure illustrated in Scheme 19 (silox = tBu_3SiO^-).[47] The structure of $[(silox)_3Ta(\eta^2$(N,C)-$NC_5H_4R)]$ is consistent with a Ta^V metallaaziridine where the aromaticity of PY has been interrupted by strong Ta(dπ)→PY(π*) back-bonding.[47b]

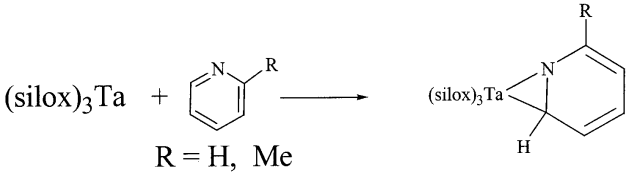

Scheme 19

Reaction of $[(silox)_3Ta(\eta^2$(N,C)-$NC_5H_5)]$ with 2-picoline and lutidine give similar η^2(N,C) products whose formation have been proposed to occur by nucleophilic attack of the starting Ta^{III} compound at the LUMO of the N-heterocycle

(predominantly C=N π*). A detailed in situ NMR spectroscopic study with the sterically congested lutidine shows that C−H bond activation may compete kinetically with η^2(N,C) coordination (Scheme 20).

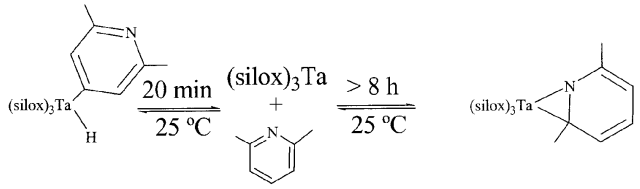

Scheme 20

Similar starting materials such as $(silox)_3M$ (M = Sc, Ti, V) react with PY in a conventional manner leading to η^1(N) derivatives.[47b] The absence of four electron repulsion problems in the Sc, Ti and V derivatives has been invoked to account for the selective formation of η^1(N) adducts.

Reduction of $[(silox)_3NbCl_2]$ with Na/Hg in PY affords a kinetic η^2(N,C)-PY product which thermally undergoes C−N insertion (vide infra).[47a]

Another Ta compound containing a η^2(N,C) pyridine ligand is $[(DIPP)_2ClTa(\eta^2(N,C)\text{-}2,4,6\text{-}NC_5H_2tBu_3)]$ (DIPP = $2,6\text{-}OC_6H_3iPr_2$) obtained by Wigley and co-workers by nitrile insertion into a tantallacyclopentadiene complex.[48]

Besides precursors to C−N bond scission, transients with η^2(N,C) pyridine ligands have been proposed to be critical to C_α−H activation leading to complexes containing a dihapto $NC_5H_4^-$ ligand.[49] The first of such compounds with unsubstituted PY, $Cp^*Lu(\eta^2(N,C)\text{-}NC_5H_4)$, was reported by Watson.[49b] A few years later, Bercaw reported the synthesis of $[Cp^*Sc(\eta^2(N,C)\text{-}NC_5H_4),]$[49a] while Ti derivatives with 2-substituted pyridines have been described by Teuben.[49c] A common synthetic procedure to these η^2(N,C)-pyridyl compounds involves the reaction of the substrate with alkyl or hydride complexes as shown in Scheme 21 for the Sc derivative. An in situ NMR spectroscopic study with the precursor Cp*ScMe has suggested the formation of the intermediate, the η^1(N)-PY adduct, prior to C−H insertion.[49a]

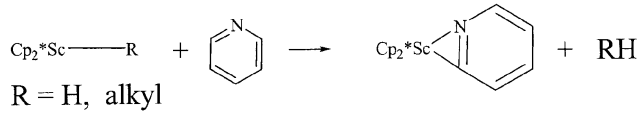

Scheme 21

PY uses the N atom and the C_α atom for coordination in the triosmium cluster $[Os_3(\mu\text{-}H)\ (\mu\text{-}NC_5H_4)(CO)_{10}]$, but two distinct metal centres are involved (Figure 9).[50]

The coordination chemistry of Q does not differ significantly from that of PY, except for the interactions with polynuclear metal complexes. In this case, the presence of the carbocyclic ring allows a larger variety of bonding modes.

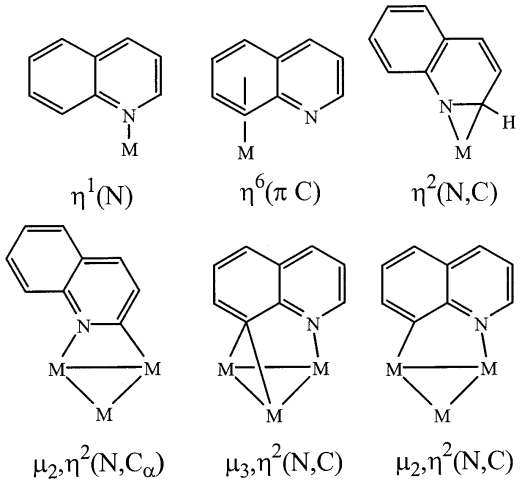

Figure 10. Known modes of Q coordination in transition metal complexes

Figure 10 summarises all the known coordination modes of Q in both mononuclear and polynuclear metal complexes.

Like PY, the most common coordination mode of Q in mononuclear complexes is the η^1(N),[40,41] which may be in equilibrium with the $\eta^6(\pi C)$.[41,44] No example of η^6coordination involving the heterocyclic ring (πN) has ever been reported.

An $\eta^1(N)\rightarrow\eta^6(\pi C)$ rearrangement analogous to that already described for PY is illustrated in Scheme 22.[41a][41d] The complex $[CpRu(CH_3CN)_3]^+$ reacts with Q yielding a kinetic η^1(N) product that converts to the thermodynamic $\eta^6(\pi C)$ derivative by decoordination of acetonitrile.

Substitution of Cp* for Cp increases the π back-bonding capability of the Ru centre, and the $\eta^6(\pi C)$ complex is formed in a straightforward manner with no evidence of the η^1(N) adduct.[41d]

The η^1(N)-Q mode may also be a precursor to the η^2(N,C) mode, as shown in Scheme 23, for the conversion of $[(DIPP)_3Ta\{\eta^1(N)\text{-}Q\}Cl_2]$ to $[(DIPP)_3Ta\{\eta^2(N,C)\text{-}Q\}]$ (DIPP = $2,6\text{-}OC_6H_3iPr_2$). This reaction requires an increase of the electron density at the metal centre to allow for an efficient $M(d\pi)\rightarrow Q(\pi^*)$ back-bonding interaction.[51]

The multipoint activation of Q and alkyl-substituted quinolines has been studied with the clusters $Ru_3(CO)_{12}$ [52] and $Os_3(CO)_{10}(CH_3CN)_2$.[21a,53] The main bonding modes are summarised in Figure 10, while the reactivity of the resulting products will be reviewed in the next section. In all cases, N-coordination is accompanied by C-H insertion by an adjacent metal centre.

Tetrahydroquinoline (THQ) has been the subject of many studies aimed at investigating the dehydrogenation of partially reduced N-heterocycles over heterogeneous catalysts. $Ru_3(CO)_{12}$ reacts with THQ to give a bis-Q complex with a $\mu_2,\eta^2(N,C_\alpha)$ coordination mode (Scheme 24).[52] Dehydrogenation of THQ to Q has also been found to occur by reaction with either $[Os_3(CO)_{10}(CH_3CN)_2]$[53] or $Os_3(CO)_{12}$.[21a]

In conclusion, PY and Q exclusively use the nitrogen atom for coordination when the metal centre is electrophilic

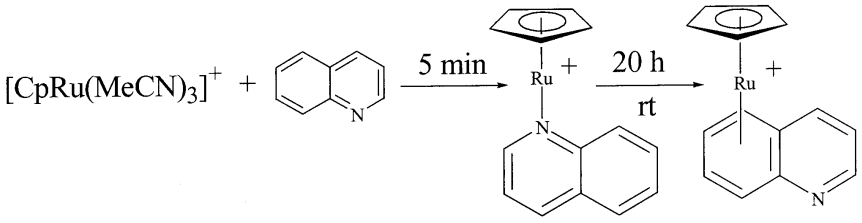

Scheme 22

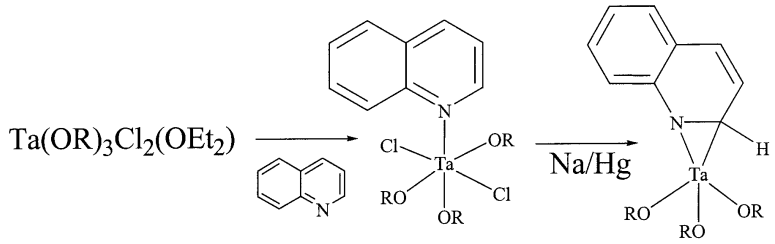

Scheme 23

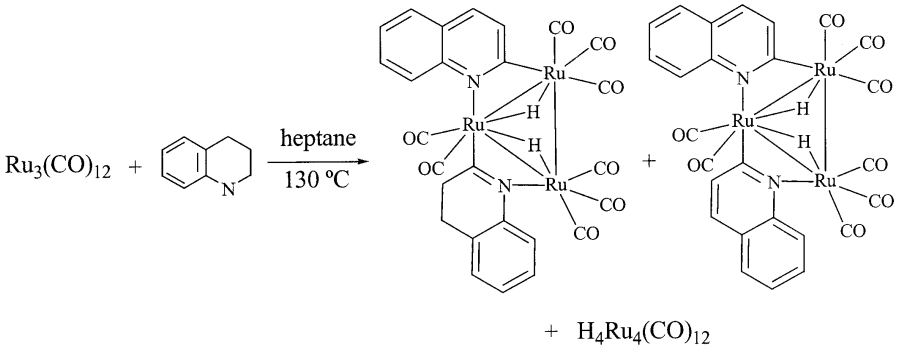

Scheme 24

in nature and only one free site is available. When three coordination vacancies are available and the metal centre has filled dπ orbitals for πback bonding, the preferred bonding mode is the η^6, either πN or πC depending on the substrate. When two free sites are available, the electronic nature of the metal centre dictates whether the substrate binds the metal using two carbon atoms or the nitrogen and the C_α atom. Electron-rich systems based on late-transition metals prefer the olefinic η^2(C,C) mode, while electrophilic early-transition metal systems stabilise the η^2(N,C) mode. As will be shown in the next section, the binding mode of the N-heterocycle ultimately controls the reactivity of the activated substrate.

E) Complexes with Other Basic Polyaromatic N-Heterocycles

Isoquinoline, 5,6-benzoquinoline, 7,8-benzoquinoline, acridine, and phenanthridine have been found to bind single metal centres in either a η^1(N) or a η^6(πC) fashion.[41c,44a,53a]

Like PY and Q, the triosmium cluster $[Os_3(CO)_{10}(CH_3CN)_2]$ reacts with polyaromatic N-heterocycles, such as 5,6-benzoquinoline and phenanthridine, yielding μ_3,η^2(N,C,C) complexes (Scheme 25).[53] Phenanthridine also forms a μ_2,η^2(N,C_α) complex similar to that with Q.

Reactivity of Coordinated N-Heterocycles

Upon coordination, the chemical reactivity of N-heterocycles is generally enhanced as compared with the free molecules. However, no general rule can be given. Indeed, besides the nature of the metal fragment, the reactivity of coordinated N-heterocycles depends on the substrate, the degree and regioselectivity of ring substitution, and the bonding mode. The reactivity studies reported in this section are just a selection of those that are representative of the possible chemical processes occurring during HDN. The catalytic hydrogenation reactions of N-heterocycles will be reviewed separately.

A) Pyrrole and Derivatives

In contrast to free PYR, which protonates at the α-position preferentially and under forcing conditions ($pK_a = -1$), η^2(C,C)-pyrrole in $[Os(NH_3)_5(2,3\text{-}\eta^2\text{-}2,5\text{-dimethylpyrrole})]^{2+}$, undergoes selective protonation by mild acids at the β-carbon away from the metal to produce a 3*H*-pyrrolium species (Scheme 26).[23a] In the presence of a weak base,

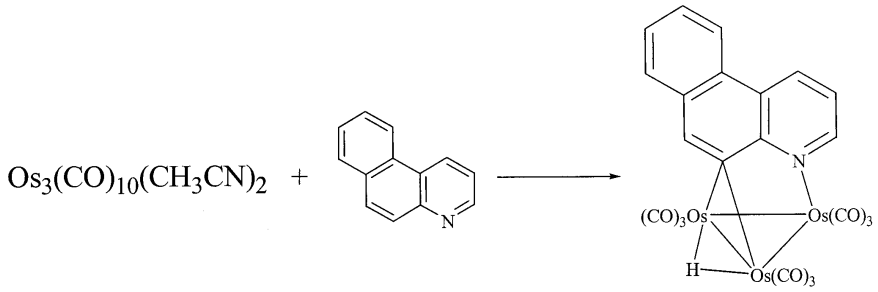

Scheme 25

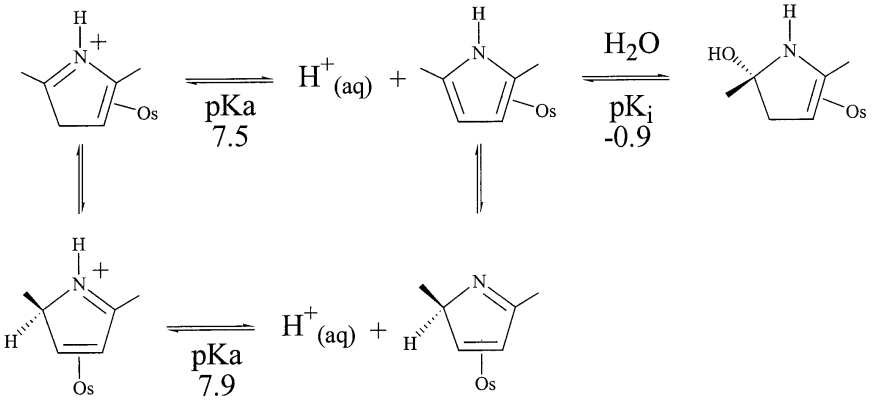

Scheme 26

the 3H-pyrrolium complex is converted into the 2H-pyrrolium tautomer that can be deprotonated at the nitrogen to give a neutral 2H-PYR ligand bonded to Os through the C_3-C_4 double bond. Nucleophilic addition of OH^-, from H_2O, to the enamine-like C=C bond in the starting η^2(C,C)-pyrrole complex has also been observed.

The η^5-pyrrolyl complexes [(*p*-cymene)M(NC_4Me_4)]OTf (M = Ru, Os) are readily converted into the corresponding η^5-PYR by selective alkylation at the nitrogen atom (Scheme 27).[22a] Interestingly, the η^5-PYR ligand in [(*p*-cymene)M($MeNC_4Me_4$)]($OTf)_2$ undergoes regio- and stereoselective hydride addition to an α-carbon atom to give a η^4-$MeNC_4Me_4H$ derivative. This compound reacts with protic acids, leading to further PYR reduction and dissociation from the metal as an iminium salt.

In a complex redox chemical process, the dimer [$(tmeda)_2$-Nb_2Cl_5Li(tmeda)] reacts with the 2,5-dimethylpyrrole lithium salt 2,5-$Me_2C_4H_2NLi$ to give a mixture of two products that have been confirmed by single-crystal X-ray analyses (Scheme 28) (tmeda = *N*,*N*,*N*′,*N*′-tetramethylethylendiamine).[27a]

The neutral product contains Nb^{III} and Nb^{IV} ions in different coordination geometries. The Nb^{IV} centre is coordinated by a terminal hydride ligand and by two η^5-pyrrolyl rings one of which is also η^1(N)-bonded to the Nb^{III} centre. The coordination of the latter metal is completed by another η^1(N)-pyrrolyl ligand, a bidentate tmeda molecule and a bridging CH_2 group that comes from the fragmentation of tmeda (N-Me cleavage, followed by C-H insertion). The anionic product [{(2,5-$Me_2C_4H_2N)_2Nb$}{(η^5-2,5-$Me_2C_4H_2N$)(2,5-$Me_2C_4H_2N$)Nb}(μ-N)(μ,η^1:η^1:η^4-1,4-$Me_2C_4H_2$)] is much more interesting as it contains a denitrogenated pyrrole ring. The anion, isolated as the $[(tmeda)_2Nb_2Cl_5Li(tmeda)]^+$ salt, contains two Nb^{IV}

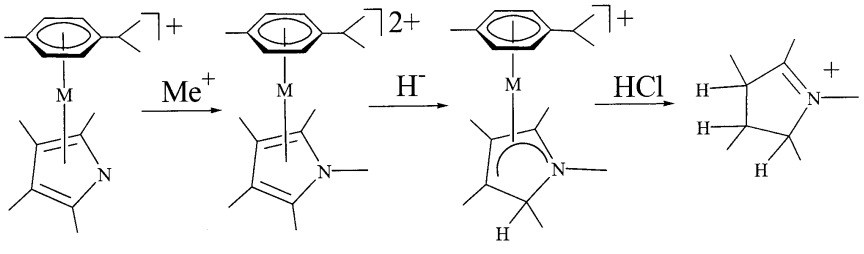

Scheme 27

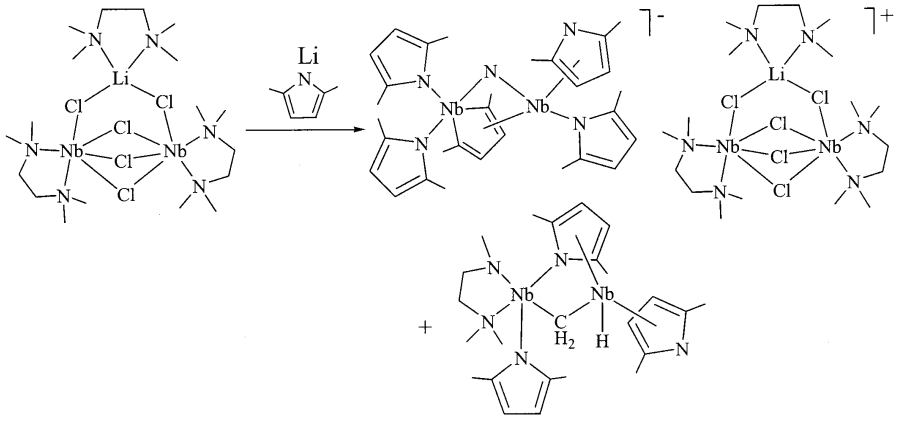

Scheme 28

centres connected by a nitride ligand and by a dienediyl group. Three η^1(N) and one η^5 pyrrolyl rings complete the coordination spheres.

The overall reaction (Scheme 28) thus corresponds to the simultaneous cleavages of C-N bonds in both the pyrrole ring and the saturated amine. The formation of the anionic product has been suggested to involve the cooperative attack of the two Nb^{II} centres on one pyrrolyl anion. The four electrons necessary to form the nitride and the dienediyl group are obtained from the five electrons provided by the oxidation of the four Nb^{II} centres during the formation of the anion and cation.

B) Indole and Derivatives

Besides undergoing deprotonation of the nitrogen atom to give η^5-indolyl complexes (Scheme 11), η^6-IN complexes are activated toward nucleophilic substitution at the carbocyclic ring,[32c,54] as well as reduction of the heterocyclic ring.[32a] Although the latter process has been found to involve a heterogeneous catalyst, 5% Rh/C, it is important to have demonstrated that η^6 coordination through the carbocyclic ring promotes the hydrogenation of the heterocyclic portion of the molecule to give an η^6-indoline complex (Scheme 29). Activation by carbanions towards nucleophilic addition has also been shown for η^6-indoline.[32a]

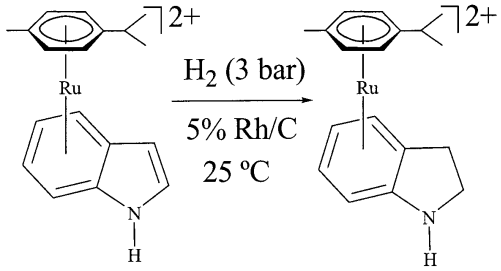

Scheme 29

A common reaction path of η^1(N)-indolyl complexes is their transformation into η^1(N)-indolenine derivatives upon selective protonation of the β-carbon atom (Scheme 12).[35]

The much lower propensity of N-heterocycles as compared with S- and O-heterocycles to undergo C-heteroatom insertion by metal fragments is shown by the reactions of $[Mn(CO)_3(\eta^6\text{-IN})]$, $[Mn(CO)_3(\eta^6\text{-BT})]$ (BT = benzothiophene) and $[Mn(CO)_3(\eta^6\text{-BF})]$ (BF = benzofuran) with $Pt(PPh_3)_3$ (Scheme 30).[55−57] Under comparable conditions, Pt inserts into the C_2-S[55] and C_2-O[56] bond of BT or BF, respectively, while the remote activation[55] of the IN heterocyclic[57] ring by $Mn(CO)_3$ exclusively results in N-H insertion with the formation of the heteronuclear trimer $[(CO)_3Mn(\mu^2,\eta^6,\eta^1(N)\text{-}C_8H_6N)]_2[Pt(PPh_3)_2]$.

Unlike mononuclear species, polynuclear metal complexes containing bridging ligands derived from N−H or C−H activation of N-heterocycles (see Figure 5 and 7) generally behave as thermodynamic sinks and do not react further with H_2, nucleophiles or electrophiles even under harsh experimental conditions.

Dehydrogenation of indoline to indole by thermolysis of metal clusters containing C-H inserted indoline has been observed,[37] while indoline has been employed as a hydrogen source for the transfer hydrogenation of olefins in the presence of $[RhCl(PPh_3)_3]$.[57] A possible pathway for indoline dehydrogenation is shown in Scheme 31.

C) Pyridine, Quinoline and Derivatives

For PY the η^1(N) mode represents the simplest way of approaching a metal centre possessing a free coordination site. In the η^1-mode however, no activation of the heterocycle takes place. In order to increase the chemical reactivity of PY, a metal centre must have at least two free sites for coordination.

In the dihapto mode through two carbon atoms,[46] as in $[Os(NH_3)_5(\eta^2\text{-lutidine})]^{2+}$, the pyridine ring can be protonated intermolecularly at nitrogen, or even intramolecularly deprotonated at carbon as shown in Scheme 18. Although interesting, the transformations illustrated in Scheme 24 are by far less exciting than those observed when PY is activated by a metal centre through the η^2(N,C) mode: in this case, the HDN-crucial C−N bond cleavage may indeed occur. The first evidence for metal C−N insertion was reported by Wigley in 1992, who reacted the metallaaziridine complex $[(DIPP)_2ClTa(\eta^2(N,C)\text{-}2,4,6\text{-}NC_5H_2tBu_3)]$ with $LiHBEt_3$ in THF at low temperatures obtaining the C−N insertion product $[(DIPP)_2Ta\{=NCtBu=CHCtBu=CHCHtBu\}]$ (Scheme 32).[51d]

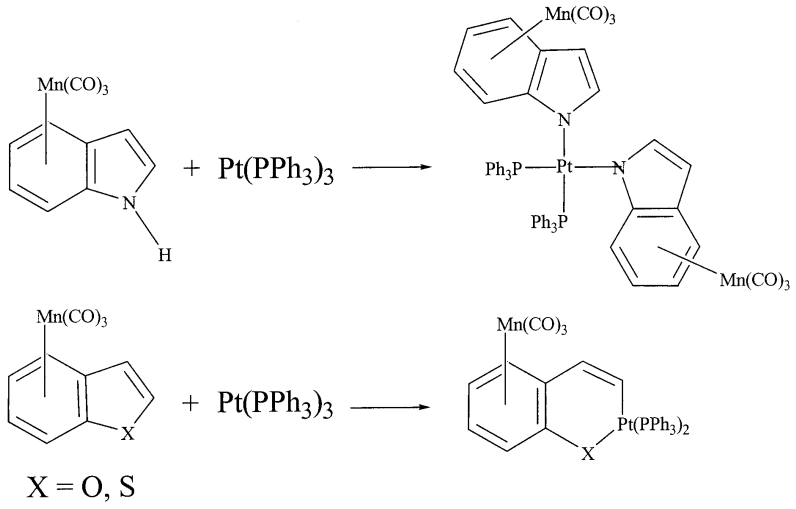

Scheme 30

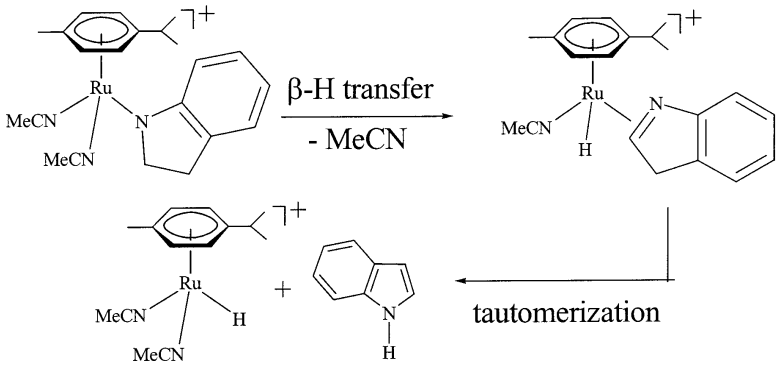

Scheme 31

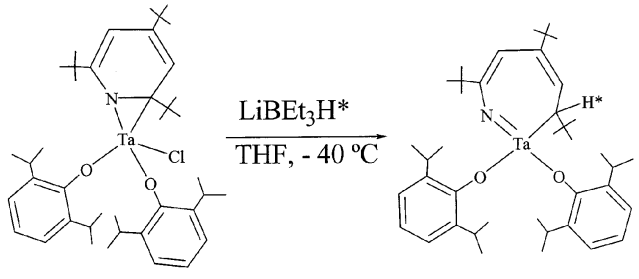

Scheme 32

Experiments with carbon nucleophiles (RMgCl, MeLi) in place of $LiHBEt_3$, have provided valuable information to discriminate between the two possible pathways (*exo*-attack vs. *endo*-attack) to PY C−N scission (Scheme 33).[51b,51c] It has been established that the reaction occurs *via* an intramolecular *endo*-attack of the hydride that migrates to the PY Cα atom as a σ-nucleophile.

A major conclusion of Wigley's study is that bonding of PY in the η^2(N,C) fashion allows the Cα atom (a formal sp^2 carbon) to attain sp^3 hybridisation, and thereby renders this carbon atom susceptible to nucleophilic attack. However, the presence of the *t*Bu groups in $[(DIPP)_2ClTa\{\eta^2(N,C)\text{-}2,4,6\text{-}NC_5H_2tBu_3\}]$ is of mandatory importance for the occurrence of the nucleophile-promoted C-N bond cleavage. Indeed, neither the related Ta complex $[(silox)_3Ta\{\eta^2(N,C)\text{-}NC_5H_5\}]$[51a] nor the Q derivative $[(DIPP)_2Ta\{\eta^2(N,C)\text{-}Q\}]$[51a] undergoes C−N insertion upon nucleophilic addition. Nonetheless, Wigley's compound represents an excellent model to gain an insight into some relevant issues of HDN, e.g. it supports the hypothesis which states that the cobalt-promoter effect in the $MoS_2/\gamma\text{-}Al_2O_3$ catalyst is that where the electron density increases on the surface metal atoms *via* electron transfer.[1] Moreover, the fact that the C−N scission step occurs with the

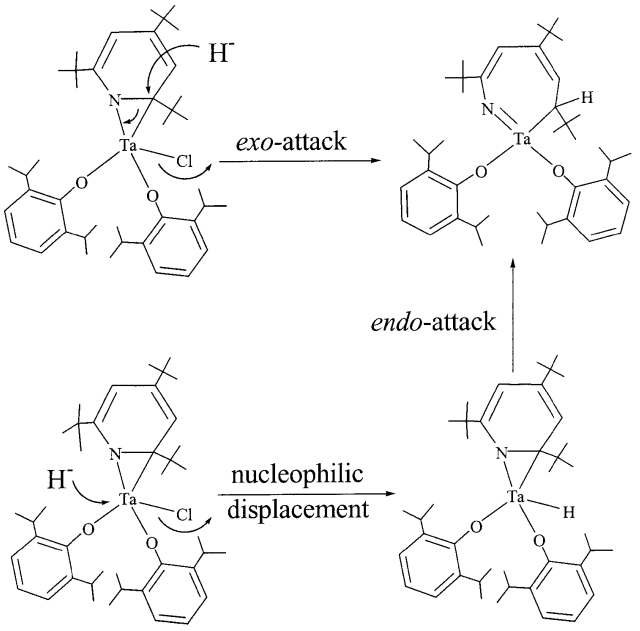

Scheme 33

formation of an imido moiety (M=NR) is consistent with the ultimate elimination of ammonia by hydrogenolysis of the C−N inserted product.

An intriguing case of metal-assisted ring-opening of PY has been reported by Wolczanski using the low-valent $(silox)_3Nb$ fragment that binds PY in the η^2(N,C) mode (Scheme 34).[47a] Unlike $[(DIPP)_2ClTa\{\eta^2(N,C)$-2,4,6-$NC_5H_2tBu_3\}]$, $[(silox)_3Nb\{\eta^2(N,C)$-$NC_5H_5\}]$ undergoes C−N insertion by thermolysis in benzene at 70 °C only. The reaction gives 0.5 equiv. of PY and 0.5 equiv of $[(silox)_3Nb{=}CHCH{=}CHCH{=}CHN{=}Nb(silox)_3]$ as a thermodynamic mixture of *cis,cis*-, *trans,cis*-, *trans,trans*- and *cis,trans*-isomers.

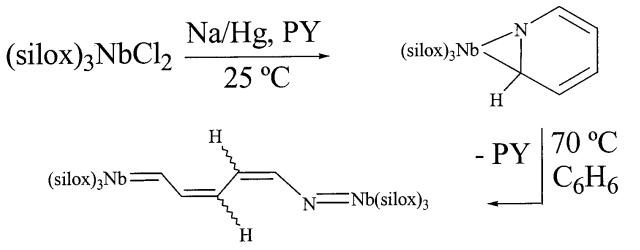

Scheme 34

Hydrogenation and Hydrogenolysis of N-heterocycles Catalysed by Transition Metal Complexes

Under actual HDN conditions, the hydrogenation of N-heterocycles is much more facile than the subsequent C−N hydrogenolysis.[7] This trend is observed also when soluble metal complexes are used as models for heterogeneous HDN catalysts. Indeed, while several examples of hydrogenation of N-heterocycles to the corresponding cyclic amines (partially or fully saturated) have been reported, only one case of hydrogenolysis promoted by a homogeneous catalyst has been described so far. Moreover, the real nature of this hydrogenolysis process is still rather doubtful.

A) Hydrogenolysis of Pyridine

Under water-gas shift (wgs) conditions and in the presence of $Rh_6(CO)_{16}$, PY has been found to undergo both hydrogenation to piperidine and hydrogenolysis to various bis(piperidinyl)alkanes (Scheme 35).[58] The formation of the latter compounds has been proposed to involve extrusion of NH_3 from the intermediate 1,4-dihydropyridine to give glutaraldehyde, which in turn reacts with piperidine and hydrogen to form the bis(piperidinyl) products. The absence of both particulate metal in the reactor and reactivity when the rhodium metal was substituted for $Rh_6(CO)_{16}$ confirmed the homogeneous nature of the process. However, the lack of further studies supporting the homogeneity of this HDN reaction, the harsh experimental conditions (150 °C, 800 psi CO), and the proven capability of heterogeneous catalysts to promote the conversion of PY illustrated in Scheme 35,[59] have contributed in raising doubts on the homogeneous nature of the overall process.

B) Hydrogenation of Pyridine, Quinoline, Indole and Derivatives

The first example of selective hydrogenation of PY to piperidine was reported in 1970 by Jardine and McQuillin.[60] The reaction was carried out in DMF at 1 bar H_2 in the presence of $Rh(PY)_3Cl_3/NaBH_4$. The same catalyst system was found to be effective for the reduction of Q to THQ (see below). In either case, no kinetic or mechanistic information was provided. In contrast, an in-depth study[61] is available for the hydrogenation of 2-methylpyridine to 2-methylpiperidine catalysed by $[Cp^*Rh(MeCN)_3]^{2+}$. Deuterium labelling experiments, competitive studies and reactions with isolated intermediates allowed Fish and co-workers to address many relevant issues regarding the hydrogenation of pyridines in the presence of this Rh^{III} precursor (Scheme 36a).[41,61]

On the basis of the deuteration pattern observed when D_2 was substituted for H_2, it was concluded that the reductions of the C=N and C=C bonds are reversible. The reversibility of H_2 addition to the C=N bond was suggested to be promoted by the allylic nature of the reduction product, i.e. $NH{-}CH_2{-}C{=}C$, which is highly activated toward rearomatisation of the N-ring by dehydrogenation. Another remarkable observation made by Fish was that six-membered mononuclear N-heterocycles such as PY and derivatives are much less prone to undergo hydrogenation than bi- and trinuclear N-ring compounds (e.g. quinolines, benzoquinolines, acridines) due to their higher resonance stabilisation energy. This finding led Fish to conclude that the initial C=N bond hydrogenation which actually disrupts the aromaticity of the molecule, is the most critical hydrogenation step in the overall reduction process. The reduction of 1,2,5,6-tetrahydropyridine (THPY) with D_2 in the presence of $[Cp^*Rh(MeCN)_3]^{2+}$ (exclusive deuterium incorporation in the C_3 and C_4 carbon atoms, Scheme 36b) and the independent synthesis of $[Cp^*Rh(\eta^1(N)$-THPY$(MeCN)_2]^{2+}$

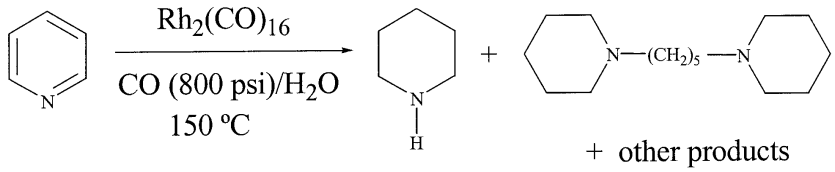

Scheme 35

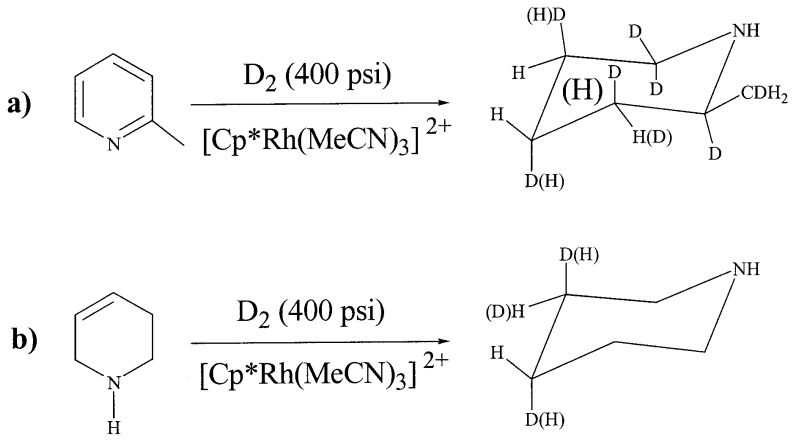

Scheme 36

provided two additional pieces of HDN-relevant information: i) η^1(N)-THPY complexes are not intermediate to piperidine production; ii) partially hydrogenated N-heterocycles are easily dehydrogenated to their aromatic precursors, thus confirming that C-N bond cleavage for cyclic amines is not thermodynamically favoured over rearomatisation.[61]

Laine's idea to use late transition metal carbonyls, capable of promoting the wgs reaction, for the hydrogenation of PY, prompted other researchers to follow this route. In all cases, however, polyaromatic heterocycles such as Q, 5,6-benzoquinoline (5,6-BQ), 7,8-benzoquinoline (7,8-BQ), acridine (AC) and derivatives, were employed as model substrates. In no case was the HDN of the N-heterocycle observed.

Under either wgs or synthesis-gas (sg) conditions, Fish employed a variety of metal carbonyls or phosphane-modified metal carbonyls for the reduction of polyaromatic heterocycles.[62] Selective hydrogenation of the heterocyclic ring was achieved with $Fe(CO)_5$, $Mn_2(CO)_8(PBu_3)_2$ and $Co_2(CO)_6(PBu_3)_2$. Under wgs conditions, $RuCl_2(CO)_2(PPh_3)_2$ and $H_4Ru_4(CO)_{12}$ proved to be inactive due to competitive coordination of CO, while efficient regioselective hydrogenation of the substrate was achieved using H_2 gas. In all cases, however, high temperatures (180−200 °C) were needed and very low turnovers [mol substrate (mol catalyst^{-1})] were obtained.[62] The reactivity of $Fe(CO)_5$ toward selective reduction of the heterocyclic ring under wgs conditions was also reported by Kaesz and co-workers for Q, isoquinoline (IQ) and AC.[63] Improved catalytic efficiency (up to 87 turnovers) was obtained adding both a base and a phase-transfer agent. Finally, various substituted quinolines and isoquinolines were selectively hydrogenated in the heterocyclic ring with $Rh_6(CO)_{16}$ under wgs conditions.[64] However, unlike PY,[58] no HDN product was formed. It was also reported that 4-methyl-Q was selectively converted into 4-methyl-THQ under wgs conditions, whereas 4-methyl-5,6,7,8-THQ was exclusively obtained using H_2 gas.[64]

It was possible to apply mild reaction conditions only with more complex ligand systems than CO, and hence study the mechanism and kinetics of hydrogenation of polyaromatic N-heterocycles.

The first detailed mechanistic studies of homogeneous hydrogenation of polyaromatic substrates have been reported by Fish and co-workers who employed the Rh^I and Ru^{II} precatalyts $[(PPh_3)_3RhCl]$[65] and $[(PPh_3)_3RuHCl]$[66] under mild experimental conditions (85 °C, 310 psi H_2, benzene). The Rh complex was actually shown to convert into $(PPh_3)_3Rh(H)_2Cl$ by treatment with H_2. As a general trend, the relative hydrogenation rates decreased in the order phenanthridine > AC > Q > 5,6-BQ > 7,8-BQ, which reflects the influence of both steric and electronic effects. All substrates were regioselectively hydrogenated at the heteroaromatic ring; only AC was converted into a mixture of 9,10-dihydroacridine and 1,2,3,4-tetrahydroacridine. The hydrogenation of Q was found to be inhibited by the presence of pyridines and THQ in the reaction mixture, due to competing coordination to the metal centre; all the other substrates had no appreciable effect on the rate of Q hydrogenation. In the case of the Rh catalyst, Q reduction was promoted in the presence of IN, PYR, carbazole and even of sulfur-heterocycles such as thiophene, benzothiophene and dibenzothiophene.

The substitution of D_2 for H_2 in the reduction of Q, catalysed by either $(PPh_3)_3RhCl$ or $(PPh_3)_3RuHCl$, provided the following pieces of information: i) the hydrogenation of the C=N bond is reversible; ii) the C_3-C_4 double bond is irre-

versibly hydrogenated in a stereoselective cis manner; iii) the C_8-H bond in the carbocyclic ring is activated (most likely by cyclometalation). Based on deuterium labelling experiments and of reactions with isolated compounds, Fish proposed a sound mechanism for the hydrogenation of Q with $[(PPh_3)_3Rh(H)_2Cl]$ or $[(PPh_3)_3RuHCl]$, which however, did not distinguish between intra- and intermolecular reduction of the C_3-C_4 double bond. This mechanism is not shown here for the simple reason that, some years later, the same author reported a similar and more complete mechanistic picture using $[Cp^*Rh(MeCN)_3]^{2+}$ as the catalyst precursor (vide infra).

The catalytic performances of $[(PPh_3)_3RuCl_2]$, $[(PPh_3)_3RhCl]$, $[(PPh_3)_3RuHCl(CO)]$, $[(PPh_3)_3OsHCl(CO)]$, $[Rh(cod)(PPh_3)_2]^+$ and $[Ir(cod)(PPh_3)_2]^+$ (cod = 1,5-cyclooctadiene) in the selective hydrogenation of Q to THQ have been investigated by Sánchez-Delgado and Gonzáles (150 °C, 30 bar H_2, toluene).[67] The Rh complex was by far the most active [initial rate ca. 200 mol Q (mol cat)$^{-1}$ h^{-1}], while the Os complex was the least efficient [initial rate ca. 5 mol Q (mol cat)$^{-1}$ h^{-1}]. The latter observation is consistent with the kinetic sluggishness of third-row metals. Some chemical factors affecting the activity of the Ru complex $[(PPh_3)_3RuHCl(CO)]$ were investigated in detail. Coordinating solvents such as MeCN or MeOH, or added ligands such as CO quenched the catalysis. The addition of acid or base gave adverse effects, the base acting as an inhibitor; water did not apparently affect the catalytic rate.

A study relating the rate of hydrogenation of Q to THQ with the nature of the metal centre has recently been reported by López-Linares and co-workers.[68] Several catalyst systems were prepared by adding either Tp or Tp* [Tp = tris(pyrazolyl)borate; Tp* = tris(3,5-dimethylpyrazolyl)borate] to toluene solutions of $[Rh(cod)Cl_2]_2$, $[Ir(cod)Cl_2]_2$, $[Ir(coe)Cl_2]_2$ (coe = cyclooctene) and $RuCl_2(MeCN)_4$. Preformed $TpIr(C_2H_4)_2$ was also tested. Rhodium formed the most active catalysts. As a general trend, the activity was found to increase with the ease of formation of Tp or Tp* complexes, while the presence of ligands capable of competing with Q for coordination decreased the hydrogenation rate, e.g. coe and ethylene which can undergo competitive metal insertion into sp^2 C−H bonds.

Deuterium gas experiments, monitored by both NMR spectroscopic and GC/MS analysis, and in situ high-pressure NMR spectroscopic reactions were very helpful to draw out the mechanism reported in Scheme 37 for the hydrogenation of Q to THQ catalysed by the Rh^{III} complex $[Cp^*Rh(MeCN)_3]^{2+}$ (40 °C, 500 psi H_2, CH_2Cl_2).[61] The regioselectivity and degree of deuterium incorporation are shown in the scheme just to help the reader in following the authors' conclusions.

Salient features of the postulated mechanism are: i) η^1(N) bonding of Q to Rh with the loss of complexed MeCN, followed by the formation of a hydride; ii) reversible 1,2-N=C bond hydrogenation, most likely by a η^2(N,C) coordination as later shown by Wolczanski[47] and Wigley;[48] iii) migration of Cp*Rh from nitrogen to the C_3-C_4 double bond; iv) reversible C_3-C_4 double bond reduction; v) Cp*Rh complexation to the carbocyclic ring, followed by C_6-H and C_8-H bond activation; vi) $\eta^6(\pi C)$ coordination of THQ, followed by ligand exchange with Q to continue the catalytic cycle. In this mechanistic picture, the Rh centre goes through the catalytic process with the unusual III→V→III oxidation/reduction cycle. Some intermediate complexes[41e] in the catalytic cycle were isolated and characterised, i.e. $[Cp^*Rh(\eta^1(N)\text{-}Q)(MeCN)_2]^{2+}$ and $[Cp^*Rh(\eta^6(\pi C)\text{-}THQ)]^{2+}$. The critical role of η^1(N) coordination for selective nitrogen ring reduction was also demonstrated by the much higher catalytic activity of $[Cp^*Rh(MeCN)_3]^{2+}$ vs. the Ru analogue $[Cp^*Ru(MeCN)_3]^+$, which indeed forms a more stable $\eta^6(\pi N)$ complex.[41]

The mechanism illustrated in Scheme 37 also accounts for the $[Cp^*Rh(MeCN)_3]^{2+}$-assisted regioselective hydrogenation of pyridines, benzoquinolines, AC as well as indoles and benzothiophene.[61] The observation that the relative hydrogenation rates decreased in the order AC > Q > 5,6-BQ > 2-Me-Q > 2-Me-PY was attributed to both electronic and steric effects. In particular, the rate decreased with increasing basicity and steric hindrance at the nitrogen atom. A different case is represented by 7,8-BQ that showed the highest relative rate and, in competitive reactions, was found to remarkably enhance the rate of hydrogenation of Q and other substrates as well. It was proposed that the enhanced rate is due to a hydrogen transfer mechanism, which is consistent with the role of nitrogen compounds as hydrogen-donor solvents in coal liquefaction.[61]

The deuteration pattern of THQ found by Fish is rather similar to that reported by Laine for the hydrogenation of Q with the clusters $H_2Os_3(CO)_{10}$ and $Os_3(CO)_{12}$, as well as real sulfided Co-Mo/γ-Al_2O_3 heterogeneous catalysts.[21a][69] Some differences in the deuteration pattern, in particular the presence of more deuterium in the 4-position and less in the 2-position, have been interpreted in terms of the occurrence of oxidative addition of the Os cluster to C-H bonds in Q and 1,4-hydrogenation as well (Scheme 38).

By combination of kinetic and chemical methods, and using $[Rh(cod)(PPh_3)_2]PF_6$ as the catalyst precursor, Sánchez-Delgado and co-workers have provided a further insight into the mechanism of the regioselective hydrogenation of Q to THQ.[70] The experimental rate law was $r_i = k_{cat}[Rh][H_2]^2$ with $k_{cat} = 50 \pm 6$ M^{-2} s^{-1} at 370 K and the following thermodynamic parameters were obtained: $\Delta H = 9 \pm 1$ kcal mol^{-1}, $\Delta S = -27.0 \pm 0.3$ eu. The isolation of $[Rh(cod)(Q)_2]PF_6$ at the end of the catalysis (370 K, ≤1 bar H_2, toluene), and the observation that the rate of hydrogenation of the partially reduced substrate dihydroquinoline (DHQ) was comparable with that of Q, allowed Sánchez-Delgado to propose the mechanism illustrated in Scheme 39.

The catalytic cycle starts with the displacement of PPh_3 by Q in the Rh^I precursor to give the bis-Q compound $[Rh(cod)(Q)_2]^+$, which then reacts with H_2 to give the Rh^{III} dihydride $[Rh(cod)(H)_2(Q)_2]^+$. After the C=N bond has been rapidly and reversibly reduced by two consecutive hydride transfers, a η^2(C,C)-DHQ complex is formed which

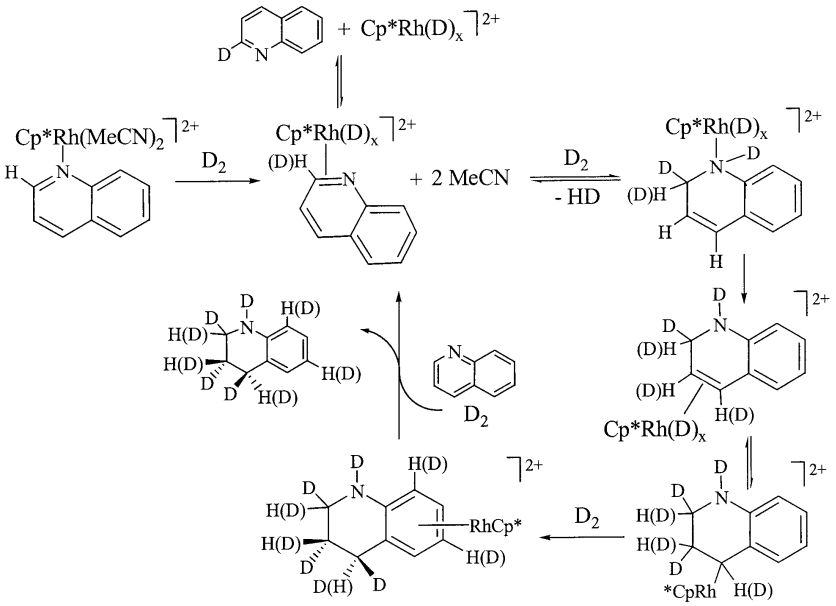

Scheme 37

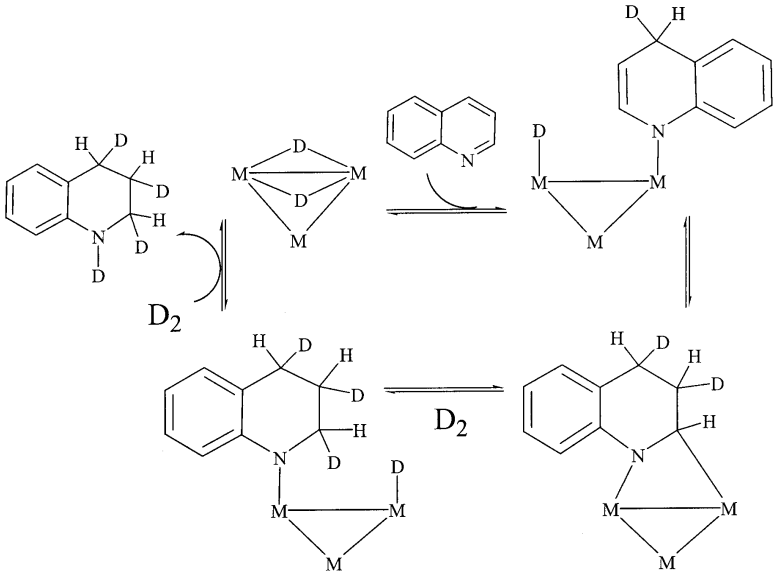

Scheme 38

slowly reacts with H_2 to give THQ. The irreversible displacement of THQ from rhodium by Q regenerates the bis-Q complex to continue the catalysis. According to the kinetic studies, the overall process that converts DHQ to THQ constitutes the rate-limiting step. Besides accounting for the kinetic results, the mechanism proposed by Sánchez-Delgado comprises steps that are commonly encountered in rhodium-catalysed olefin hydrogenation mechanisms where, unlike the Fish mechanism, the rhodium metal goes through the catalysis with the usual III→I→III reduction/oxidation cycle.

Kinetic studies for Q reduction to THQ have also been reported by Rosales and co-workers for the Ru^{II} complex $[RuH(CO)(MeCN)(PPh_3)_2]BF_4$.[71] At low hydrogen pressure, the experimental rate law $r_i = k_{cat}\,[Ru_0][H_2]^2$ (k_{cat} = 28.5 $M^{-2}\,s^{-1}$ at 398 K) was quite similar to that found by Sánchez-Delgado. In contrast, at high H_2 pressure, a first-order dependence of the reaction rate with respect to the hydrogen concentration was observed. The proposed mechanism involves a rapid and reversible partial hydrogenation of bonded Q, followed by a rate-determining second hydrogenation of DHQ.

A zero-order dependence on the substrate concentration is not a general kinetic rule for the homogeneous hydrogenation of Q to THQ. A much more complex kinetic law was actually found for the reaction catalysed by the Rh^{I} complex [(triphos)Rh(DMAD)]PF_6 (triphos = $CH_3C(CH_2PPh_2)_3$; DMAD = dimethyl acetylenedicarboxylate).[72] Monitoring the formation of THQ with time by GC at a fixed temperature of 60 °C showed that the rate is

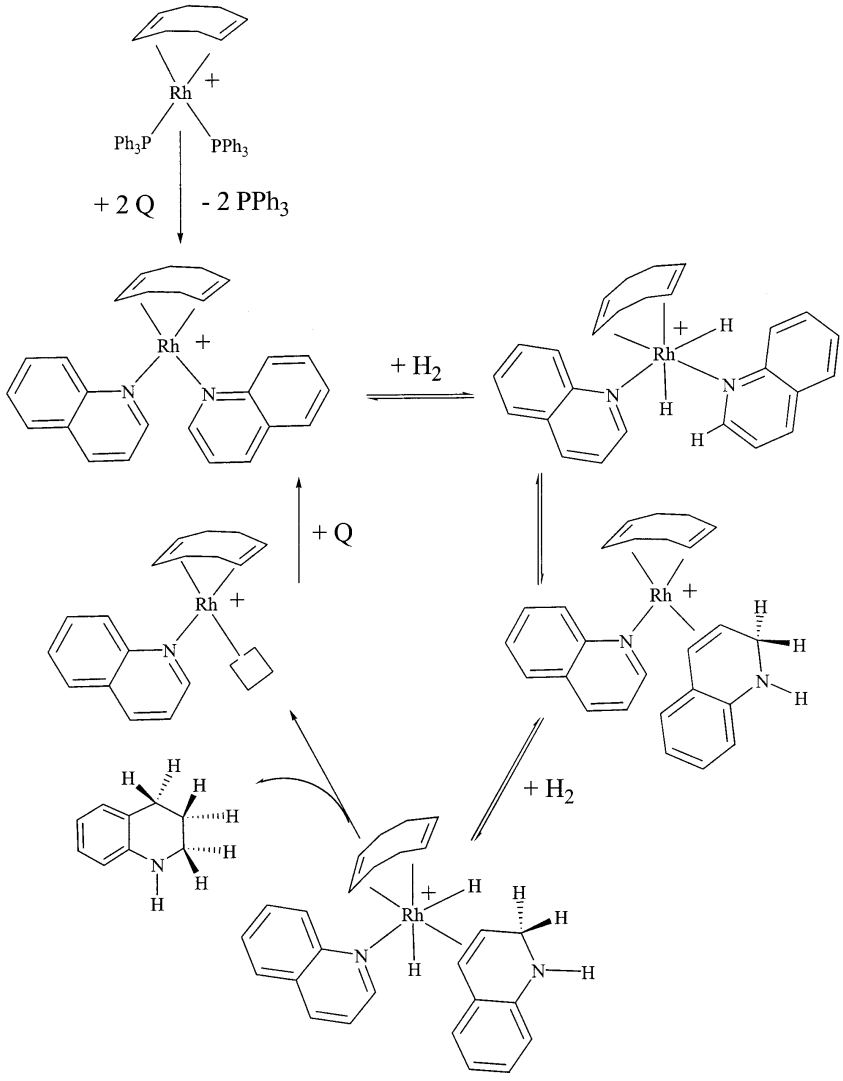

Scheme 39

first-order with respect to both H_2 (from 4 to 30 bar) and catalyst concentration (from 36 to 110 mM). In contrast, an inverse dependence of the hydrogenation rate with respect to Q concentration was found. The empirical rate law $r = k''\,[Rh][H_2][Q]^2$, where $k'' = k\,(a + b[Q] + c[Q]^2)^{-1}$, was proposed to account for the inhibiting effect of Q concentration and the experimental observation that the rate tends to be second-order for very low Q concentrations (< 30 mM) and zero-order for very high Q concentrations (> 70 mM). Depending on the concentration of Q, the experimental rate law thus simplifies to $r = k/c\,[Rh][H_2]$, to $r = k/a\,[Rh][H_2][Q]^2$ or to $r = k\,(b + c[Q])^{-1}[Rh][H_2][Q]$. On the basis of the kinetic study, deuterium labelling and high-pressure NMR spectroscopic experiments under catalytic conditions, as well as the identification of catalytically relevant intermediates, a mechanism was proposed which essentially differs from that reported by Sánchez-Delgado for the rate-limiting step, i.e. the reversible reduction of the C=N bond instead of that of the $C_3{=}C_4$ bond (irreversible) (Scheme 40). The overall hydrogenation of the C=N bond, which actually disrupts the aromaticity of Q, was proposed as rate-determining step also in light of the independent reduction of isolated 2,3-dihydroquinoline that, under comparable experimental conditions, was reduced faster than Q. Also, the lack of deuterium incorporation into the carbocyclic ring of both THQ and Q ruled out η^6-Q or η^6-THQ complexes.

The Rh catalyst generated from [(triphos)Rh(DMAD)]PF_6 underwent deactivation with time, due to the formation of catalytically inactive Rh^I monohydrido complexes by heterolytic splitting of H_2 promoted by the basic environment of the reaction.[73] The addition of an excess of strong protic acid such as triflic acid, CF_3SO_3H, to the catalytic mixture was sufficient to overcome this drawback and induce a remarkable rate enhancement: at 40 °C and 30 bar H_2, the tof [mol substrate (mol cat)$^{-1}$ h^{-1}] increased from 40 to 95 by addition of a 20-fold excess of acid.[72] The acid was shown to convert inactive Rh^I into active

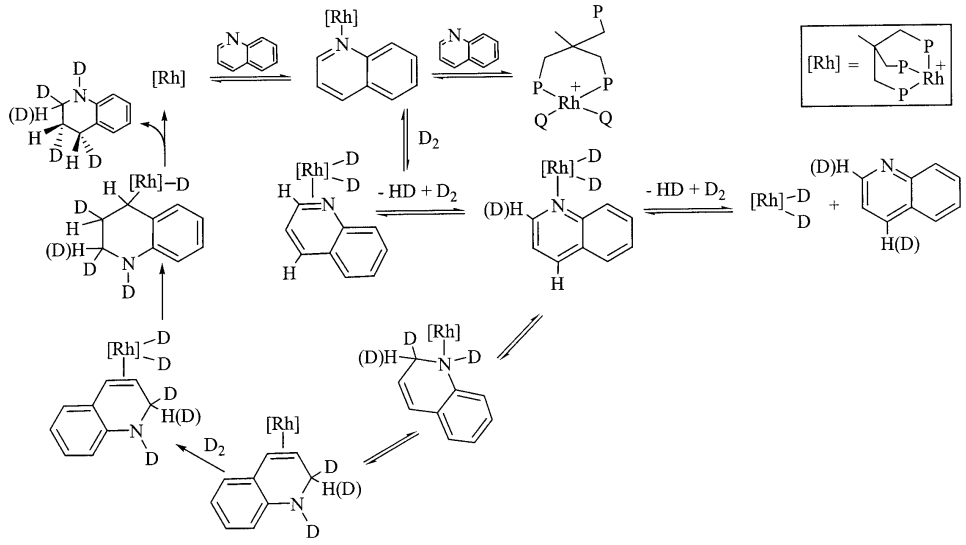

Scheme 40

Rh^{III}. Based on this finding, the addition of strong protic acids was also found to be of mandatory importance for generating a catalytically active system from [(triphos)Ru(-MeCN)$_3$](O$_3$SCF$_3$)$_2$ which, under neutral conditions, is almost inactive for Q reduction. Indeed, treatment of the ruthenium compound with H_2 produces ammonia which preferentially coordinates, over Q, to the metal centre. Moreover, in the basic environment of the reaction, the presence of moisture[73a,74] was found to give the catalytically inactive dimer [(triphos)Ru(μ-OH)$_3$Ru(triphos)]$^+$. The protic acid inhibits the formation of both NH_3 adducts and the (μ-OH)$_3$ dimer, thus allowing the hydrogenation of Q to THQ to proceed smoothly with a tof of 65.[72]

The catalyst precursor [RuH(CO)(MeCN)$_2$(PPh$_3$)$_2$]BF$_4$ was also employed to catalyse the hydrogenation of various polyaromatic N-heterocycles under relatively mild conditions (125 °C, 4 bar H_2, xylene or toluene).[75] The reactivity order AC > Q >> 5,6-BQ > 7,8-BQ > IN > IQ was in line with previous trends and reflects steric and electronic effects. In particular, the greater propensity to reduction of AC as compared with Q was attributed to the higher resonance stabilisation energy of this latter, while the almost negligible reduction of IQ was accounted for by the higher basicity of the N atom in this substrate. A kinetic study was carried out for the reduction of AC to 9,10-dihydroacridine. Unlike Q, the experimental rate law was $r = k_{cat}$ [Ru][H_2] and the postulated mechanism involves, as the determining step, the hydrogenation of coordinated AC in [RuH(CO)(η^1(N)-AC)(MeCN)(PPh$_3$)$_2$]$^+$, yielding 9,10-dihydroacridine and the coordinatively unsaturated complex [RuH(CO)(MeCN)(PPh$_3$)$_2$]$^+$.

In homogeneous phase, IN is much more difficult to reduce than Q as shown by the limited number of known catalysts {e.g. (PPh$_3$)$_3$RuHCl[66] and [RuH(CO)(-MeCN)(PPh$_3$)$_2$]BF$_4$ [75]}, as well as their very scarce activity (tof's ≤1). Indeed, the η^1(N) coordination, which is critical for selective nitrogen ring reduction in Q, is virtually unknown for IN which prefers to bind to metal centres using the carbocyclic ring (vide infra). In the latter coordination mode, the C=N bond is not activated and too many sites at the metal centre are occupied so that the oxidative addition of H_2 is very difficult to accomplish. Consistently, the hydrogenation of IN is generally inhibited when the reaction mixture contains basic substrates such as Q, THQ, and PY. To the best of our knowledge, the only catalyst that is able to regioselectively hydrogenate IN to indoline with an acceptable tof is [(triphos)Rh(DMAD)]PF$_6$, on the condition that a protic acid is added to the catalytic mixture.[3a–3d,7] By using equivalent amounts of triflic acid and IN tof's as high as 100 were obtained already at 60 °C and 30 bar H_2. It was experimentally shown that indoline was actually formed by reduction of the protonated form of IN, the 3H-indolium cation which possesses a localised C=N bond.[72]

Aqueous-Biphase Hydrogenation of N-Heterocycles

The remarkable progress recently achieved in the field of water-soluble catalysts and the actual possibility of applying aqueous-biphase catalysis to large volume reactions[76] have encouraged the petrochemical industry to look at aqueous-catalysis as an alternative method for removing sulfur and nitrogen impurities from distillates. Recent publications[73c,77–79] and patents[80] show that the hydrogenation and hydrogenolysis of aromatic heterocycles in biphasic media is indeed technically feasible.

The selective hydrogenation of N-heterocycles has been achieved by researchers at PDVSA-INTEVEP with the use of water-soluble Ru^{II} catalysts stabilised by either triphenylphosphane trisulfonate (TPPTS) or triphenylphosphane monosulfonate (TPPMS) ligands.[77,80] As a general procedure, the catalysts were prepared in situ from RuCl$_3$·3H$_2$O and excess phosphane in water, and the resulting solution was added to a hydrocarbon solution containing various model N-heterocycles such as Q, AC, and IQ. The biphasic reactions were performed under relatively drastic experimental conditions (130–170 °C, 70–110 bar H_2) and gave

the selective reduction of the heterocyclic ring. It was generally observed that nitrogen compounds did not inhibit the hydrogenation of added thiophenic substrates. In fact, in some cases a promoting effect was observed. The beneficial effect of the N-compounds on the rate of hydrogenation of thiophenes has been attributed to the catalyst protection by amines, which are better nucleophiles than thioethers. As a matter of fact, the major ruthenium product isolated from the aqueous phase after hydrogenation of a BT/Q mixture with $RuCl_3 \cdot 3H_2O/TPPMS_{(excess)}$ in water/decalin was $RuHCl(TPPMS)_2(THQ)_2$ (**A** in Figure 11).

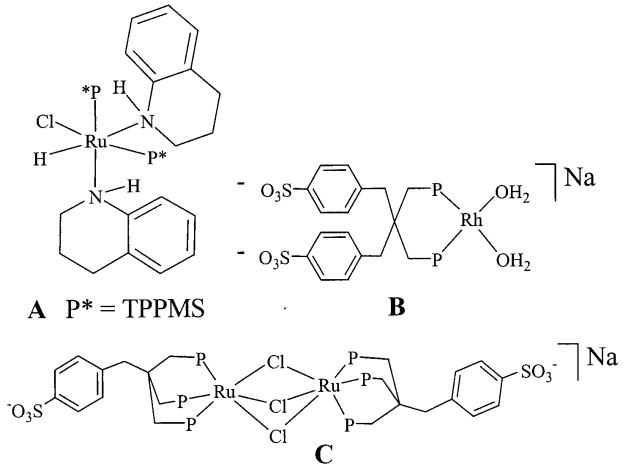

Figure 11. Water-soluble ruthenium complexes

The regioselective reduction of Q to THQ in water/hydrocarbon has been achieved also with bidentate and tridentate water-soluble ligands. In particular, the diphosphane $(NaO_3S(C_6H_4)CH_2)_2C(CH_2PPh_2)_2$ ($Na_2DPPPDS$) was found to form quite active systems in combination with rhodium and ruthenium.[5a,78] The Rh^I complex $[(DPPPDS)Rh(H_2O)_2]Na$ (**B** in Figure 11) was actually isolated and employed in water/*n*-octane to hydrogenate 1:1 mixtures of Q and BT at high temperatures (160 °C). Only the N-heterocycle was efficiently reduced (tof = 50), BT hydrogenation to 2,3-dihydrobenzothiophene (DHBT) being only marginal (tof = 2). A similar selectivity was found for the catalytic system $RuCl_3 \cdot H_2O/2Na_2DPPPDS$, prepared in situ. In contrast, the individual hydrogenation rates for Q and BT have been reported to be similar (tof = 30 at 140 °C, 30 bar H_2, water/*n*-heptane) and independent of the presence of either substrate when the dimeric complex $Na[\{(sulphos)Ru\}_2(\mu\text{-}Cl)_3]$ (**C** in Figure 11) was employed as precatalyst[79] [sulphos = tridentate ligand $^-O_3S(C_6H_4)CH_2C(CH_2PPh_2)_3$]. No attempt was made to determine whether the dimeric structure of the precursor was maintained during the catalysis. However, since the mononuclear complex $[(sulphos)Ru(MeCN)_3]^+$ has been found to catalyse the hydrogenation of BT to DHBT in water/decalin at a very similar rate,[79b] it is likely that disruption of the dimeric structure of C occurs under catalytic conditions. Under biphasic conditions, also the zwitterionic Rh^I complex (sulphos)Rh(cod) has been tested as a catalyst precursor for the hydrogenation of heterocycles. Although a modest catalyst for the hydrogenation of BT to DHBT, it is very efficient for the hydrogenation of Q to THQ (tof = 20 at 160 °C, 30 bar H_2, water/*n*-heptane).[79b]

Hydrogenation of N-Heterocycles by Supported Molecular Catalysts

In order to gain an insight into the reactivity of isolated metal surface sites under hydrotreating conditions, molecular catalysts of proven effectiveness for the hydrogenation of heteroaromatic rings have been heterogenised following different procedures.

The first of such approaches was reported by Fish in 1985. The molecular catalyst of choice was $Rh(PPh_3)_3Cl$, that the same author had shown to be active for the regioselective reduction of various polynuclear heteroaromatics.[81] The molecular precursor was tethered to 2% crosslinked phosphinated polystyrene-divinylbenzene and the resulting heterogeneous catalyst (**A** in Figure 12) was employed to hydrogenate Q, AC, 5,6-BQ and 7,8-BQ in benzene solution (85 °C, 310 psi H_2). The order of activity was identical to that in the homogeneous phase,[65] AC>Q>5,6-BQ>7,8-BQ, but the initial rates of the heterogeneous hydrogenations were from 10 to 20 times faster. This remarkable increased rate was essentially attributed to steric requirements surroundings the active metal centre in the tethered com-

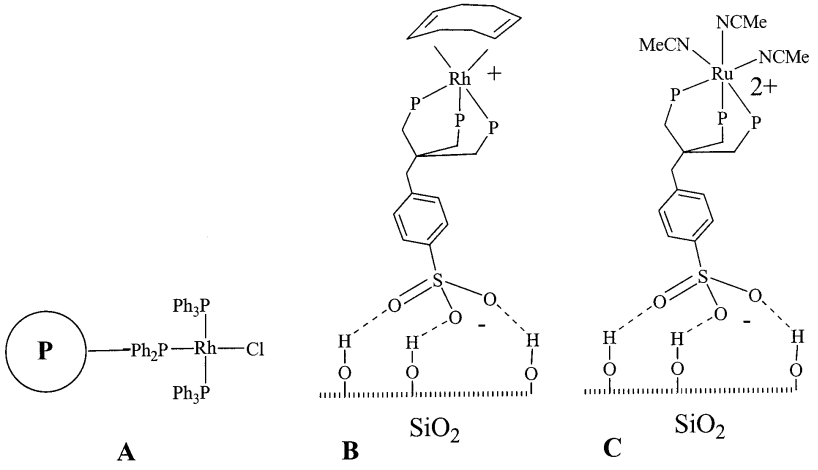

Figure 12. Supported molecular catalysts

plex, which apparently would favour the coordination of the N-heterocycles by disfavouring that of PPh_3. The regioselectivity of hydrogenation was even higher than that in the homogeneous phase as no formation of 1,2,3,4-tetrahydroacridine was observed. The deuteration pattern of the heteroaromatic ring after a catalytic reaction with D_2 was identical to that observed in the homogeneous phase, except for the lack of deuterium incorporation at position 8 of the carbocyclic ring. The supported catalyst was also employed to hydrogenate N-heterocycles in model coal liquid containing pyrene, tetralin, *p*-cresol, 2-methylpyridine and methylnaphthahalene. An increased rate was observed which was attributed to the ability of some constituents, especially *p*-cresol, to stabilise unsaturated rhodium species formed in the course of the catalysis.

The silica-supported hydrogen-bonded (SHB) rhodium complexes (sulphos)Rh(cod)/SiO_2 and [(sulphos)Ru(-MeCN)$_3$](SO$_3$CF$_3$)/SiO_2 (**B** and **C** in Figure 12), successfully employed to hydrogenate olefins in heterogeneous phase,[82][83] have been found to hydrogenate Q in *n*-octane (100 °C, 30 bar H_2) yielding selectively THQ with tof's as high as 100.[84] In line with the behaviour of the $Rh(PPh_3)_3Cl$/P-$Rh(PPh_2)_2Cl$ system,[81] both (sulphos)Rh(cod)/SiO_2 and [(sulphos)Ru(MeCN)$_3$](SO$_3$CF$_3$)/SiO_2 have been found to be more efficient catalysts than the homogeneous and aqueous-biphasic counterparts with triphos or sulphos ligands. The enhanced rate observed for the heterogeneous reactions has been attributed to the fact that, unlike in fluid solution systems, the heterogenised complexes do not undergo dimerisation to give catalytically inactive species.

Conclusions

The results described in this report define transition metal complexes as viable models for mimicking many steps occurring in heterogeneous HDN and allow the following conclusions to be drawn.

The η^1(N) and η^2(N,C) coordination modes of N-heterocycles are crucial for their hydrogenation and hydrogenolysis, respectively. In particular, it is evident that the regioselective hydrogenation of the heteroaromatic rings is effectively accomplished by late transition metals (promoters) in high oxidation states. Also, an acidic environment is generally found to promote efficient hydrogenation pathways. C−N bond cleavage is a difficult task that is best accomplished when the substrate uses the η^2(N,C) mode for binding an early transition metal in relatively low oxidation state. In all the cases reported, however, the C−N insertion step requires the transfer of a hydride ligand from the metal centre to the C−N carbon atom, which is consistent with a hydrolytic C−N insertion. The ultimate denitrogenation step apparently requires the cooperation of two metal centres as is commonly found for the homogeneous desulfurisation of thiophenes.[3−6,12] Accordingly, it does not seem likely that a single metal site can coordinate a N-heterocycle, insert into a C−N bond and finally remove the nitrogen atom.

Given the complexity of the HDN process and the many alternative or concomitant mechanisms that may be in operation even on the surface of the same catalyst, the homogeneous modelling studies must be considered with extreme caution. Most of the spectator ligands in solution reactions are actually not representative of the pool of ligands available to industrial hydrotreating catalysts. The model N-heterocycles generally employed (Q, PYR, IN) represent a fraction of nitrogen compounds in fossil fuels, and the environment of the reactions is extremely different. Nonetheless, we have shown here that many reactions involving transition metal complexes and N-heterocycles show sound analogies with related reactions occurring over the surface of heterogeneous catalysts. These analogies and the relative mechanistic information continue to give HDN modelling a great boost.

Acknowledgments

The Ministero dell'Ambiente of Italy is gratefully acknowledged for financial support (contract PR1/C).

[1] [1a]H. Topsøe, B. S. Clausen, F. E. Massoth, *Hydrotreating Catalysis*, Springer-Verlag, Berlin Heidelberg, **1996**. − [1b]J. Scherzer, A. J. Gruia, *Hydrocracking Science and Technology*, Marcel Dekker, New York, **1996**. − [1c]C. N. Satterfield, *Heterogeneous Catalysis in Industrial Practice*, McGraw-Hill, New York, **1991**.

[2] M. L. Occelli, R. Chianelli, *Hydrotreating Technology for Pollution Control*, Marcel Dekker, New York, **1996**.

[3] [3a]R. J. Angelici, in *Transition Metal Sulphides − Chemistry and Catalysis* (Eds: T. Weber, R. Prins, R. A. van Santen), Kluwer, Dordrecht, **1998**, 89−127. − [3b]R. J. Angelici, *Polyhedron* **1997**, 16, 3073−3088. − [3c]R. J. Angelici, *Bull. Soc. Chim. Belg.* **1995**, *104*, 265−282. − [3d]R. J. Angelici, in *Encyclopedia of Inorganic Chemistry* (Ed.: R. B. King), John Wiley, New York, **1994**, Vol. 3, 1433−1443. − [3e]R. J. Angelici, *Coord. Chem. Rev.* **1990**, *105*, 61−76. − [3f]R. J. Angelici, *Acc. Chem. Res.* **1988**, ***21***, 387−394.

[4] T. B. Rauchfuss, *Prog. Inorg. Chem.* **1991**, *39*, 259−329.

[5] [5a]C. Bianchini, A. Meli, in *Transition Metal Sulphides − Chemistry and Catalysis* (Eds.: T. Weber, R. Prins, R. A. van Santen), Kluwer, Dordrecht, **1998**, 129−154. − [5b]C. Bianchini, A. Meli, *Acc. Chem. Res.* **1998**, *31*, 109. − [5c]C. Bianchini, A. Meli in *Aqueous-Phase Organometallic Catalysis − Concepts and Applications* (Eds.: B. Cornils, W. A. Herrmann), VCH, Weinheim, **1998**, 477−485. − [5d]C. Bianchini, A. Meli, in *Applied Homogeneous Catalysis with Organometallic Compounds* (Eds.: B. Cornils, W. A. Herrmann), VCH, Weinheim, **1996**, Vol. 2, 969−979. − [5e]C. Bianchini, A. Meli, *J. Chem. Soc., Dalton Trans.* **1996**, 801−814.

[6] R. A. Sánchez-Delgado, *J. Mol. Catal.***1994,** *86*, 287−307.

[7] [7a]M. J. Girgis, B. C. Gates, *Ind. Eng. Chem. Res.* **1991**, *30*, 2031−2058. − [7b]T. C. Ho, *Catal. Rev. − Sci. Eng*. **1988**, *30*, 117−160. − [7c]R. M. Laine, *Catal. Rev. − Sci. Eng*. **1983**, *25*, 459−474. − [7d]J. R. Katzer, R. Sivasubramanian, *Catal. Rev. − Sci. Eng*. **1979**, *20*, 155−208. − [7e]B. C. Gates, J. R. Katzer, G. C. A Schuit, *Chemistry of Catalytic Processes*, McGraw-Hill, New York, **1979**, Cap. 6.

[8] [8a]P. Grange, *Catal. Rev. − Sci. Eng*. **1980**, *21*, 135−143. − [8b]G. Hagenbach, Ph. Courty, B. Delmon, *J. Catal.* **1973**, *31*, 264−268. − [8c]D. Pirotte, J. M. Zabala, P. Grange, B. Delmon, *Bull. Soc. Chim. Belg.* **1981**, *90*, 1239−1245.

[9] [9a]C. N. Satterfield, C. M. Smith, M. Ingalis, *Ind. Eng. Chem. Process Des. Dev.* **1985**, *24*, 1000−1004. − [9b]S. H. Yang, C. N. Satterfield, *Ind. Eng. Chem. Process Des. Dev.* **1984**, *23*, 20−28. − [9c]S. H. Yang, C. N. Satterfield, *J. Catal*. **1983**, *81*, 168−173. − [9d]C. N. Satterfield, S. Gültekin, *Ind. Eng. Chem. Process Des. Dev.* **1981**, *20*, 62−68. − [9e]C. N. Satterfield, D. L. Carter, *Ind. Eng. Chem. Process Des. Dev.* **1981**, *20*, 538−540.

[10] [10a] S. Harris, R. R. Chianelli, *J. Catal*. **1986**, *98*, 17−25. −

[10b] H. Topsøe, R. Candia, N.-Y. Topsøe, B. S. Clausen, *Bull. Soc. Chim. Belg.* **1984**, *93*, 783−790. − [10c] H. Topsøe, B. S. Clausen, *Catal. Rev. − Sci. Eng*. **1984**, *26*, 395−401.
[11] A. N. Startsev, *Catal. Rev. − Sci. Eng*. **1995**, *37*, 353−423.
[12] [12a] C. Bianchini, M. V. Jiménez, A. Meli, S. Moneti, V. Patinec, F. Vizza, *Organometallics* **1997**, *16*, 5696−5705. − [12b] C. Bianchini, M. V. Jiménez, C. Mealli, A. Meli, S. Moneti, V. Patinec, F. Vizza, *Angew. Chem. Int. Ed. Engl.* **1996**, *35*, 1706−1708.
[13] [13a] D. A. Vicic, W. D. Jones, *Organometallics* **1997**, *16*, 1912−1919. − [13b] W. D. Jones, R. M. Chin, *J. Am. Chem. Soc.* **1994**, *116*, 198−203.
[14] [14a] M. D. Curtis, S. H. Druker, *J. Am. Chem. Soc*. **1997**, *119*, 1027−1036. − [14b] U. Riaz, O. J. Curnow, M. D. Curtis, *J. Am. Chem. Soc.* **1994**, *116*, 4357−4363.
[15] L. Y. Chiang, J. W. Swirczewski, R. Kastrup, C. S. Hsu, R. B. Upasani, *J. Am. Chem. Soc.* **1991**, *113*, 6574−6584.
[16] R. H. Fish, J. N. Michaels, R. S. Moore, H. Heinemann, *J. Catal.* **1990**, *123*, 74−85.
[17] [17a] C. N. Satterfield, S. H. Yang, *J. Catal*. **1983**, *81*, 335−346. − [17b] C. N. Satterfield, C. M. Smith, *Ind. Eng. Chem. Process Des. Dev.* **1986**, *25*, 942−949.
[18] R. Prins, M. Jian, M. Flechsenhar, *Polyhedron* **1997**, 16, 3235−3246.
[19] [19a] H. Kwart, J. Katzer, J. Horgan, *J. Phys. Chem.* **1982**, *86*, 2641−2648. − [19b] H. Kwart, G. C. A. Schuit, B. C. Gates, *J. Catal*. **1980**, *61*, 128−134.
[20] N. Nelson, R. B. Levy *J. Catal*. **1979**, *58*, 485−488.
[21] [21a] Eisenstadt, C. M. Giandomenico, M. F. Frederick, R. M. Laine, *Organometallics* **1985**, *4*, 2033−2039. − [21b] R. M. Laine, *J. Mol. Catal.* **1983**, *21*, 119−132.
[22] [22a] F. Kvietok, V. Allured, V. Carperos, M. Rakowski DuBois, *Organometallics* **1994**, *13*, 60−68. − [22b] N. Kuhn, *Bull. Soc. Chem. Belg*. **1990**, *99*, 707−712.
[23] [23a] W. H. Myers, J. I. Koontz, W. D. Harman, *J. Am. Chem. Soc.***1992**, *114*, 5684−5692. − [23b] W. H. Myers, M. Sabat, W. D. Harman, *J. Am. Chem. Soc.***1991**, *113*, 6682−6683. − [23c] R. Cordone, W. D. Harman, H. Taube *J. Am. Chem. Soc.***1989**, *111*, 5969−5970.
[24] D. S. Glueck, F. J. Hollander, R. G. Bergman, *J. Am. Chem. Soc.***1989**, *111*, 2719−2721.
[25] M. Rakowski DuBois, *Coord. Chem. Rev.* **1998**, *174*, 191−205.
[26] [26a] T. Morikita, M. Hirano, A. Sasaki, S. Komiya, *Inorg. Chim. Acta* **1999**, *291*, 341−354. − [26b] M. S. Driver, J. F. Hartwig, *Organometallics* **1997**, *16*, 5706−5715. − [26c] W. D. Jones, L. Dong, A. W. Myers, *Organometallics* **1995**, *14*, 855−861. − [26d] G. C. Hsu, W. P. Kosar, W. D. Jones, *Organometallics* **1994**, *13*, 385−396. − [26e] F. T. Ladipo, J. S. Merola, *Inorg. Chem.* **1990**, *29*, 4172−4173.
[27] [27a] M. Tayebani, S. Gambarotta, G. P. A. Yap, *Angew. Chem. Int. Ed.* **1998**, *37*, 3002−3005. − [27b] M. Rakowski DuBois, K. G. Parker, C. Ohman, B. C. Noll, *Organometallics* **1997**, *16*, 2325−2334. − [27c] W. J. Kelly, W. E. Parthun, *Organometallics* **1992**, *11*, 4348−4350. − [27d] K. J. Chase, R. F. Bryan, M. K. Woode, R. N. Grimes, *Organometallics* **1991**, *10*, 2631−2642. − [27e] N. Kuhn, G. Henkel, J. Kreutzberg, *Angew. Chem. Int. Ed. Engl.* **1990**, *29*, 1143−1144. − [27f] E. Carmona, J. M. Marin, P. Palma, M. Paneque, M. Poveda, *Inorg. Chem.* **1989**, *28*, 1895−1900. − [27g] A. Efraty, N. Jubran, A. Doldman, *Inorg. Chem.* **1982**, *21*, 868−873. − [27h] M. D. Fayer, C. B. Harris, *Inorg. Chem.* **1969**, *8*, 2792−2796.
[28] D. A. Vicic, W. D. Jones, *Organometallics* **1999**, *18*, 134−138.
[29] [29a] A. J. Arce, R. Machado, Y. De Sanctis, M. V. Capparelli, R. Atencio, J. Manzur, A. J. Deeming, *Organometallics* **1997**, *16*, 1735−1742. − [29b] A. J. Arce, J. Manzur, M. Marquez, Y. De Sanctis, A. J. Deeming, *J. Organomet. Chem.* **1991**, *412*, 177−193. − [29c] A. J. Deeming, A. J. Arce, Y. De Sanctis, M. W. Day, K. I. Hardcastle, *Organometallics* **1989**, *8*, 1408−1413.
[30] [30a] M. Day, D. Espitia, K. I. Hardcastle, S. E. Kabir, E. Rosenberg, *Organometallics* **1991**, *10*, 3550−3553.[30b] E. Rosenberg, S. E. Kabir, K. I. Hardcastle, M. Day, E. Wolf, *Organometallics* **1990**, *9*, 2214−2217.
[31] M. Rakowski DuBois, L. D. Vasquez, R. F. Ciancianelli, B. C. Noll, *Organometallics* **2000**, *in press.*
[32] [32a] S. Chen, L. Vasquez, B. C. Noll, M. Rakowski DuBois, *Organometallics* **1997**, *16*, 1757−1764. − [32b] S. Chen, V. Carperos, B. C. Noll, R. J. Swope, M. Rakowski DuBois, *Organometallics* **1995**, *14*, 1221−1231. − [32c] R. M. Moriarty, U. S. Gill, Y. Y. Ku, *J. Organomet. Chem*. **1988**, *350*, 157−190. − [32d] C. White, S. J. Thompson, P. M. Maitlis, *J. Chem. Soc., Dalton Trans.* **1977**, 1654−1661.
[33] O. Yamauchi, M. Takani, K. Toyoda, H. Masuda, *Inorg. Chem.* **1990**, *29*, 1856−1860.
[34] [34a] K. I. Hardcastle, H. Minassian, A. J. Arce, Y. De Sanctis, A. J. Deeming, *J. Organomet. Chem.* **1989**, *368*, 119−130. − [34b] R. Robson, *Inorg. Chim. Acta* **1982**, *57*, 71−77.
[35] [35a] S. Chen, B. C. Noll, L. Peslherbe, M. Rakowski DuBois, *Organometallics* **1997**, *16*, 1089−1092. − [35b] T. J. Johnson, A. M. Aris, J. A. Gladysz, *Organometallics* **1994**, *13*, 3182−3193.
[36] J. A. D. Jeffreys, C. Metters, *J. Chem. Soc., Dalton Trans.* **1977**, 1624−1627.
[37] L. Vasquez, B. C. Noll, M. Rakowski DuBois, *Organometallics* **1998**, *17*, 976−981.
[38] S. E. Kabir, D. S. Kolwaite, E. Rosenberg, L. G. Scott, T. McPhillips, R. Duque, M. Day, K. I. Hardcastle, *Organometallics* **1996**, *15*, 1979−1988.
[39] J. J. Garcia, A. L. Casado, A. Iretskii, H. Adams, P. M. Maitlis, *J. Organomet. Chem.* **1998**, *558*, 189−192.
[40] J. Reedijk, in *Comprehensive Coordination Chemistry* (Eds.: G. Wilkinson, R. D. Gillard, J. McCleverty), Pergamon Press, Oxford, **1987**, Vol. 2.
[41] [41a] R. H. Fish, H-S. Kim, R. H. Fong, *Organometallics* **1991**, *10*, 770−777. − [41b] R. H. Fish, R. H. Fong, A. Than, E. Baralt, *Organometallics* **1991**, *10*, 1209−1212. − [41c] R. H. Fish, E. Baralt, H-S. Kim, *Organometallics* **1991**, *10*, 1965−1971. − [41d] R. H. Fish, H-S. Kim, R. H. Fong, *Organometallics* **1989**, *8*, 1375−1377. − [41e] R. H. Fish, H-S. Kim, J. E. Babin, R. D. Adams, *Organometallics* **1988**, *7*, 2250−2252.
[42] B. Chaudret, F. A. Jalón, M. Pérez-Manrique, F. Lahoz, F. J. Plou, R. Sánchez-Delgado, *New J. Chem*. **1990**, *14*, 331−338.
[43] H. E. Selnau, J. S. Merola, *Organometallics* **1993**, *12*, 1583−1591.
[44] [44a] B. Chaudret, F. A. Jalón, *J. Chem. Soc., Chem. Commun*. **1988**, 711−713. − [44b] E. J. Wucherer, E. L. Muetterties, *Organometallics* **1987**, *6*, 1691−1695. − [44c] R. H. Morris, J. M. Ressner, *J. Chem. Soc., Chem. Commun.* **1983**, 909−910.
[45] [45a] M. G. B. Drew, P. J. Baricelli, P. C. H. Mitchell, A. R. Read, *J. Chem. Soc., Dalton Trans.* **1983**, 649−655. − [45b] M. G. B. Drew, P. C. H. Mitchell, A. R. Read, *J. Chem. Soc., Chem. Commun*. **1982**, 238−239.
[46] [46a] R. Cordone, D. W. Harman, T. Taube, *J. Am. Chem. Soc.* **1989**, *111*, 2896−2900. − [46b] R. Cordone, T. Taube, *J. Am. Chem. Soc* **1987**, *109*, 8101−8102.
[47] [47a] T. S. Kleckley, J. L. Bennett, P. T. Wolczanski, E. B. Lobkowsky, *J. Am. Chem. Soc.* **1997**, *119*, 247−248. − [47b] K. J. Covert, D. R. Neithamer, M. C. Zonnevylle, R. E. LaPointe, C. Schaller, P. T. Wolczanski, *Inorg. Chem*. **1991**, *30*, 2494−2508. − [47c] D. R. Neithamer, L. Parkanyi, J. F. Mitchell, P. T. Wolczanski, *J. Am. Chem. Soc*. **1988**, *110*, 4421−4423.
[48] [48a] D. P. Smith, J. R. Strickler, S. D. Gray, M. A. Bruck, R. S. Holmes, D. E. Wigley, *Organometallics.* **1992**, *11*, 1275−1288. − [48b] J. R. Strickler, M. A. Bruck, D. E. Wigley. *J. Am. Chem. Soc*. **1990**, *112*, 2814−2816.
[49] [49a] M. E. Thompson, S. M. Baxter, A. R. Bulls, B. J. Burger, M. C. Nolan, B. D. Santarsiero, W. P. Schaefer, J. E. Bercaw, *J. Am. Chem. Soc.* **1987**, *109*, 203−219. − [49b] P. L. Watson, *J. Chem. Soc., Chem. Commun.* **1983**, 276−277. − [49c] E. Klei, J. H. Teuben, *J. Organomet. Chem.* **1981**, *214*, 53−59.
[50] A. J. Deeming, M. J. Stchedroff, C. Whitaker, A. J. Arce, Y. De Sanctis, J. W. Steed, *J. Chem. Soc., Dalton Trans.* **1999**, 3289−3294.
[51] [51a] K. J. Weller, P. A. Fox, S. D. Gray, D. E. Wigley, *Polyhedron* **1997**, *16*, 3139−3163. − [51b] K. J. Weller, S. D. Gray, P. Briggs, D. E. Wigley, *Organometallics* **1995**, *14*, 5588−5597. − [51c] S. D. Gray, K. J. Weller, M. A. Bruck, P. Briggs, D. E. Wigley, *J. Am. Chem. Soc.* **1995**, *117*, 10678−10693. − [51d] S. D. Gray, D. P. Smith, M. A. Bruck, P. Briggs, D. E. Wigley, *J. Am. Chem. Soc.* **1992**, *114*, 5462−5463.
[52] R. H. Fish, T.-J. Kim, J. L. Stewart, J. H. Bushweller, R. K. Rosen, J. W. Dupon, *Organometallics* **1986**, *5*, 2193−2198.
[53] [53a] R. Smith, E. Rosenberg, *Organometallics* **1999**, *18*, 3519−3527. − [53b] E. Arcia, D. S. Kolwaite, E. Rosenberg, K. Hardcastle, J. Ciurash, R. Duque, R. Gobetto, L. Milone, D.

Osella, M. Botta, W. Dastrù, A. Viale, I. Fiedler, *Organometallics* **1998**, *17*, 415−426.
[54] L. S. Hegedus, *Angew. Chem. Int. Ed. Engl.* **1988**, *27*, 1113−1126.
[55] [55a] C. A. Dullaghan, G. B. Carpenter, D. A. Sweigart, D. S. Choi, S. S. Lee, Y. K. Chung, *Organometallics* **1997**, *16*, 5688−5695. − [55b] C. A. Dullaghan, X. Zhang, D. Walther, G. B. Carpenter, D. A. Sweigart, *Organometallics* **1997**, *16*, 5604−5606. − [55c] S. Sun, C. A. Dullaghan, D. A. Sweigart, *J. Chem. Soc., Dalton Trans.* **1996**, 4493−4507.
[56] X. Zhang, E. J. Watson, C. A. Dullaghan, S. M. Gorun, D. A. Sweigart, *Angew. Chem. Int. Ed.* **1999**, *38*, 2206−2208.
[57] D. A. Sweigart, private communication.
[58] R. M. Laine, D. W. Thomas, L. W. Cary, *J. Org. Chem.* **1979**, *44*, 4964−4966.
[59] K. Kindler, D. Mathies, *Chem. Abstr.* **1960**, *54*, 19731b.
[60] I. Jardine, F. J. McQuillin, *J. Chem. Soc. D* **1970**, 626.
[61] Baralt, E., Smith, S. J., Hurwitz, J., Horváth, I. T. e Fish, R. H. *J. Am. Chem. Soc.* **1992**, *114,* 5187−5196.
[62] R. H. Fish, A. Thormodsen, G. A. D. Cremer, *J. Am. Chem. Soc.* **1982**, *104*, 5234−5237.
[63] T. J. Lynch, M. Banah, H. D. Kaesz, C. D. Porter, *J. Org. Chem*. **1984**, *49*, 1266−1270.
[64] S. I. Murahashi, Y. Imada, H. Hirai, *Tetrahedron Lett*. **1987**, *28*, 77−80.
[65] R. H. Fish, J. L. Tan, A. Thormodsen, *J. Org. Chem*. **1984**, 49, 4500−4505.
[66] R. H. Fish, J. L. Tan, A. Thormodsen, *Organometallics* **1985**, *4*, 1743−1747.
[67] R. A. Sánchez-Delgado, E. Gonzalez, *Polyhedron* **1989**, *8* 1431−1436.
[68] Y. Alvarado, M. Busolo, F. López-Linares, *J. Mol. Cat. A* **1999**, *142*, 163−167.
[69] R. M. Laine, *New J. Chem*. **1987**, *11*, 543−547.
[70] R. A. Sánchez-Delgado, D. Rondón, A. Andriollo, V. Herrera, G. Martin, B Chaudret, *Organometallics* **1993**, *12*, 4291−4296.
[71] M. Rosales, Y. Alvarado, M. Boves, R. Rubio, H. Soscun, R. Sánchez-Delgado, *Trans. Met. Chem*. **1995**, *20*, 246−251.
[72] M. Macchi, Ph. D. Dissertation, Università di Trieste (Italy), **1999**.
[73] [73a] C. Bianchini, A. Meli, S. Moneti, F. Vizza, *Organometallics* **1998**, *17*, 2636−2645. − [73b] C. Bianchini, J. A. Casares, A. Meli, V. Sernau, F. Vizza, R. A. Sánchez-Delgado, *Polyhedron* **1997**, *16*, 3099−3114. − [73c] C. Bianchini, A. Meli, V. Patinec, V. Sernau, F. Vizza, *J. Am. Chem. Soc*. **1997**, *119*, 4945−4954.
[74] C. Bianchini, A. Meli, S. Moneti, W. Oberhauser, F. Vizza, V. Herrera, A. Fuentes, R. A. Sánchez-Delgado, *J. Am. Chem. Soc*. **1999**, *121*, 7071−7080.
[75] M. Rosales, J. Navarro, L. Sanchez, A. Gonzales, Y. Alvarado, R. Rubio, C. De la Cruz, T. Rajmankina, *Trans. Met. Chem*. **1996**, *21*, 11−15.
[76] [76a] B. Cornils, W. A. Herrmann, *Aqueous-Phase Organometallic Catalysis − Concepts and Applications*, VCH, Weinheim, **1998**. − [76b] B. Cornils, W. A. Herrmann, in *Applied Homogeneous Catalysis with Organometallic Compounds* (Eds.: B. Cornils, W. A. Herrmann), VCH, Weinheim, **1996**, Vol. 2, 575−601.
[77] D. E. Páez, A. Andriollo, F. López-Linares, R. E. Galiasso, J. A. Revete, R. A. Sánchez-Delgado, A. Fuentes, *Am. Chem. Soc. Div. Fuel Chem. Symp. Prepr.*, **1998**, *43*, 563−567.
[78] [78a] CNR (C. Bianchini, A. Meli, F. Vizza), **1999**, PCT/EP97/06493. − [78b] CNR (C. Bianchini, A. Meli, F. Vizza), **1996**, IT FI96A000272.
[79] [79a] I. Rojas, F. López-Linares, N. Valencia, C. Bianchini, *J. Mol. Cat. A* **1999**, *144*, 1−6. − [79b] C. Bianchini, M. Macchi, A. Meli, W. Oberhauser, F. Vizza, manuscript in preparation. − [79c] C. Bianchini, P. Frediani, V Sernau, *Organometallics* **1995**, *14*, 5458−5460.
[80] [80a] INTEVEP S. A. (D. E. Páez, A. Andriollo, R. A. Sánchez-Delgado, N. Valencia, R. E. Galiasso, F. López-Linares), **1999**, US 5.958.223. − [80b] INTEVEP S. A. (D. E. Páez, A. Andriollo, R. A. Sánchez-Delgado, N. Valencia, F. López-Linares, R. E. Galiasso), **1998**, US 5.753.584.
[81] R. H. Fish, A. D. Thormodsen, H. Heinemann, *J. Mol. Cat*. **1985**, *31*, 191−198.
[82] C. Bianchini, D. G. Burnaby, J. Evans, P. Frediani, A. Meli, W. Oberhauser, R. Psaro, L. Sordelli, F. Vizza, *J. Am. Chem. Soc*. **1999**, *121*, 5961−5969.
[83] C. Bianchini, V. Dal Santo, A. Meli, W. Oberhauser, R. Psaro, F. Vizza, *Organometallics* **2000**, *19*, 2433−2444.
[84] C. Bianchini, A. Meli, W. Oberhauser, F. Vizza, manuscript in preparation.

Received April 28, 2000
[I00171]

A Novel Dimanganese(II) Complex with Two Chloride Bridges − A Two-Electron Oxidation System

Isabel Romero,[a] Marie-Noëlle Collomb,*[a] Alain Deronzier,*[a] Antoni Llobet,[b] Emmanuel Perret,[c] Jacques Pécaut,[c] Laurent Le Pape,[c] and Jean-Marc Latour*[c]

Keywords: Manganese / N ligands / Biomimetic synthesis / Structure elucidation / Electrochemistry

A new kind of binuclear μ-chloro complex of manganese with two bpea ligands [bpea = *N*,*N*-bis(2-pyridyl methyl) ethylamine] has been synthesized and structurally characterized. A thorough electrochemical study shows that this complex exhibits a two-electron reversible oxidation leading to the stable dimanganese(III) complex.

Introduction

One-electron transfers are ubiquitous in chemistry as well as in biology.[1] However, activation of diatomic substrates such as dioxygen and dinitrogen requires multielectron transfers, which are often performed by metal clusters at enzyme active sites.[2] Moreover, in specific instances, multielectron transfers can be crucial because one-electron transfers may lead to deleterious effects. This is the case for catalases, the enzymes which carry out the disproportionation of hydrogen peroxide into water and molecular oxygen.

Most of these enzymes are hemoproteins, but a few bacterial catalases are known to possess a dinuclear manganese center at their active site.[3] It is generally believed that the Mn pair shuttles between the two oxidation states $Mn^{II}-Mn^{II}$ and $Mn^{III}-Mn^{III}$ during the catalytic cycle,[3a] thereby avoiding one-electron transfers which would produce hydroxyl radicals. The $Mn^{II}-Mn^{III}$ mixed-valent state is never observed under the normal conditions where the catalase reaction occurs. The structure and mechanism of action of this active center remains poorly defined, and in order to gain insight into the structure and the disproportionation mechanism, many efforts have been devoted in the past decade to designing simple model molecules.[4] Many of these model systems contain two Mn^{II} ions bridged by ligands like carboxylate,[5] phenoxide,[6] alkoxide[7] or, more rarely, by chloride.[8] These compounds can undergo the two following distinct one-electron exchanges [Equation (1) and (2)]:

$$Mn^{II}Mn^{II} \underset{\longleftarrow}{\xrightarrow{(E_{1/2})_1}} Mn^{II}Mn^{III} + e^- \quad (1)$$

$$Mn^{II}Mn^{III} \underset{\longleftarrow}{\xrightarrow{(E_{1/2})_2}} Mn^{III}Mn^{III} + e^- \quad (2)$$

with formation of a mixed-valence $Mn^{II}-Mn^{III}$ species[5] whose stability is expressed by the disproportionation constant (K_d), determined from the separation of the redox potentials of the two one-electron steps. The stability of the mixed-valent state depends on the degree of electronic coupling of the two metal ions[9] and, for uncoupled metal ions, a direct two-electron redox transition at a single electrochemical potential is expected. It has been stressed recently that for dimanganese(II) species to achieve a high efficiency of catalase-like activity, formation of the mixed-valence $Mn^{II}-Mn^{III}$ state must be disfavored.[3b] In this context, it is somewhat surprising that the electrochemical behavior of dimanganese $Mn^{II}-Mn^{II}$ complexes has been only scarcely examined in detail. Indeed, only for three of these systems a direct two-electron redox transition has been proposed.[5c,8b,10] We report here the synthesis, crystal structure and magnetic properties of a new di-Mn^{II} complex with a bis-μ-chloro unit $Mn_2(\mu\text{-}Cl)_2(bpea)_2Cl_2$ **(1)** [bpea = *N*,*N*-bis(2-pyridylmethyl)ethylamine]. A thorough electrochemical study reveals that **1** exhibits a clean , two-electron reversible oxidation system leading to the stable di-Mn^{III} complex.

Results

Solid State Structure

When $MnCl_2$ dissolved in water was allowed to react with an ethanolic solution of the bpea ligand at ambient temperature, the colorless solution turned yellow and **1** could be crystallized by slow evaporation of the solution. The structure of this binuclear complex was determined by an X-ray crystallographic study (Figure 1).

[a] Laboratoire d'Electrochimie Organique et de Photochimie Rédox, UMR CNRS 5630, Université Joseph Fourier Grenoble 1,
B. P. 53, 38041 Grenoble cedex 9, France
[b] Departament de Quimica, Universitat de Girona, Campus de Montilivi, E-17071 Girona, Spain
[c] DRFMC-Laboratoire de Chimie Inorganique et Biologique, UMR CEA−CNRS-UJF 5046, CEA-Grenoble, 38054 Grenoble Cedex, France

 © WILEY-VCH Verlag GmbH, D-69451 Weinheim, 2001 1434−1948/01/0101−0069 $ 17.50+.50/0

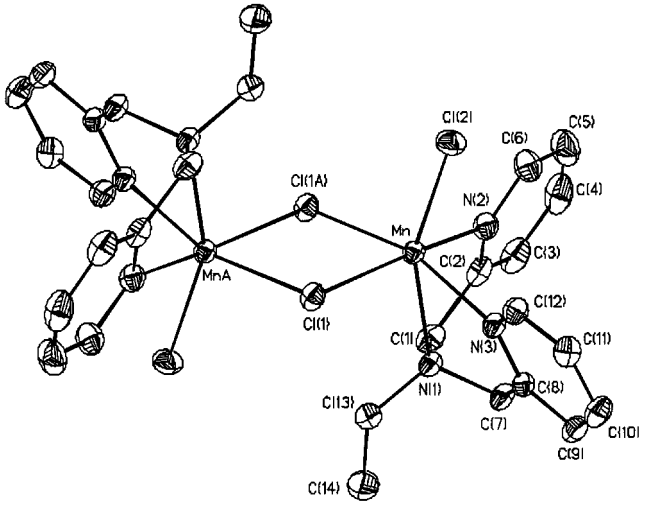

Figure 1. Molecular structure of **1**; selected bond lengths (Å) and angles (°): Mn−Mn#1 3.786, Mn−Cl(1) 2.5374(9), Mn−Cl(2) 2.4249(8), Mn−N(1) 2.4246(16), Mn−N(2) 2.2811(17), Mn−N(3) 2.2657(16), Mn−Cl(1) 2.5683(7); Mn(1)−Cl(1)−Mn#1 95.72(2), Cl(2)−Mn−Cl(1) 98.17(2), N(1)−Mn−Cl(1) 99.65(4), N(2)−Mn−Cl(1) 165.63(4), N(3)−Mn−Cl(1) 88.96(4), N(1)−Mn−Cl(2) 156.43(4), N(2)−Mn−Cl(2) 94.18(5), N(3)−Mn−Cl(2) 92.77(5), N(2)−Mn−N(1) 70.68(5), N(3)−Mn−N(1) 72.30(6), N(3)−Mn−N(2) 97.78(5), Cl(1)−Mn−Cl(1)#1 84.28(2), Cl(2)−Mn−Cl(1)#1 103.73(3), N(1)−Mn−Cl(1)#1 93.32(4), N(2)−Mn−Cl(1)#1 85.69(4), N(2)−Mn−Cl(1)#1 162.88(4)

Each Mn atom is bound by three nitrogen atoms from a facially coordinated bpea ligand, and three chloride ions, in an octahedrally distorted fashion. The two manganese atoms are bridged by a pair of chloride ions leading to an Mn_2Cl_2 diamond core. The two manganese atoms are equivalent since the complex has a rotational C_2 symmetry axis passing through the center of this core. Owing to the presence of the symmetry axis the Mn_2Cl_2 core is strictly planar and the Mn−Mn bond length is 3.786 Å. The two Mn−Cl bridging bond lengths are slightly different [2.5374(8) and 2.5683(7) Å] and longer than the terminal Mn−Cl bond lengths (2.4249 Å). All these structural features are similar to those of other structurally characterized $Mn^{II}Mn^{II}$ di-μ-chloro complexes.[10]

Magnetic and Spectroscopic Properties

The temperature dependence of the product of the molar susceptibility and temperature (χT) at 0.5, 1, 2.5 and 5 T is shown for **1** in Figure 2. In the range from 300 to 100 K, χT is constant at ca. 8.5 $cm^3 \cdot K \cdot mol^{-1}$, which is close to the value expected for two independent spins $S = 5/2$ (8.75 $cm^3 \cdot K \cdot mol^{-1}$). At lower temperatures, χT increases to reach a maximum whose value and temperature depends on the applied magnetic field (11.5 $cm^3 \cdot K \cdot mol^{-1}$ at 4 K for 0.5 T, 10.6 $cm^3 \cdot K \cdot mol^{-1}$ at 6 K for 1 T, 9.9 $cm^3 \cdot K \cdot mol^{-1}$ at 14 K for 2.5 T and 9.0 $cm^3 \cdot K \cdot mol^{-1}$ at 60 K for 5 T). This behavior is typical of a metal pair experiencing a ferromagnetic interaction. In those cases where the exchange interaction and the zero-field splittings are of comparable magnitudes, full diagonalization of the matrix is required to treat all field- and temperature-dependent data. Preliminary fit-

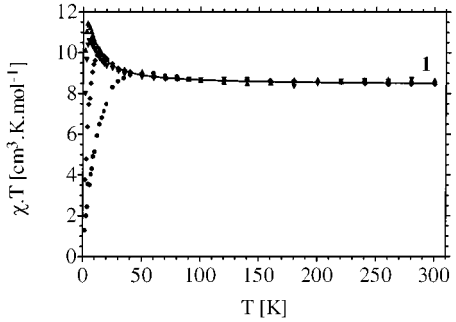

Figure 2. Temperature dependence of the product of the molar magnetic susceptibility and temperature for a microcrystalline sample of **1** (7.91×10^{-5} mol except at 2.5 T, 6.60×10^{-5} mol) at 0.5 (▲), 1 (▼), 2.5 (◆) and 5 T (•); solid line is the best least-square fit to the magnetic data

tings of the susceptibility data (Figure 2) with an expression based on a Heisenberg Hamiltonian ($J = -2J\ S_1S_2$), as described in the Experimental Section, were performed in the temperature range where the D effects are negligible. This led to an estimate of the magnetic exchange interaction of $J = 0.34$ (3) cm^{-1}.

The solution EPR spectra have been recorded in dichloromethane (Figure 3) and in acetonitrile to investigate the nuclearity of the complex, either in the absence or presence of the electrolyte $[(nBu)_4N]ClO_4$ in order to duplicate the electrochemical conditions. The two spectra are essentially identical, which points to the absence of chemical change induced by the electrolyte. They exhibit features extending from 50 to more than 800 mT as is normal for dimanganese(II) species.[12] Nevertheless, owing to the fact that some distorted mononuclear manganese(II) compounds possess similar transitions,[13] the dinuclearity of the complexes in solution cannot be taken for granted on the basis of these spectra. We were definitely able to prove this, however, through the observation of intense EPR transitions in the parallel mode, a property expected only for integer spins[14] and which rules out that the active species is mononuclear. The EPR spectra in acetonitrile are quite similar, except for a minor amount of mononuclear decomposition products. Therefore the EPR study undoubtedly shows that **1** exists as a dinuclear entity in solution as well as in the solid state. The very small modification of the

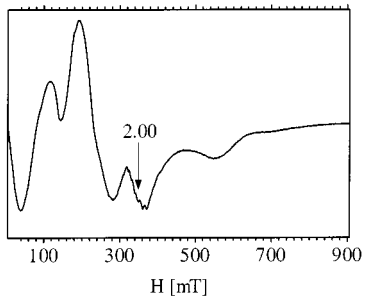

Figure 3. X-band EPR spectrum of **1** at a concentration of 1 mM in dichloromethane at 4.2 K; instrumental parameters: microwave frequency (9.6545 GHz), microwave power (0.2 mW), modulation amplitude (10 G), modulation frequency (100 kHz), sweep time 168 s; the six hyperfine lines centered at $g \approx 2.02$ are attributed to a minor mononuclear Mn(II) impurity

whole spectrum shape with temperature in the range 3.8−50 K is in agreement with the small exchange-coupling obtained from magnetization measurements.

The dinuclearity of the complex in solution is shown again by an electrospray mass spectral study. Indeed, the compound appears as a complex pattern at m/z = 669−677 which corresponds to $([(bpea)ClMn(\mu\text{-}Cl)_2Mn(bpea)]^+$. A theoretical mass analysis of the isotopic pattern confirms the presence of three chlorine atoms.

Electrochemical Properties

The cyclic voltammogram (CV) of **1** (1×10^{-3} M) in CH_3CN containing 0.1 M $[(nBu)_4N]ClO_4$ under Ar is shown in Figure 4. The CV exhibits a two-electron reversible oxidation wave corresponding to the $Mn^{II}Mn^{II}/Mn^{III}Mn^{III}$ redox system ($E_{1/2}$ = 0.63 V; ΔE_p = 80 mV, scan rate = 100 mVs^{-1}). A two-electron oxidation second wave only poorly reversible is also seen at $E_{1/2}$ = 1.41 V. The two-electron transfer nature of the waves is based on the intensity of the peaks compared to that of a one-electron transfer, and on coulometric experiments (v.i.). The first two-electron process [Equation (3)] can be decomposed in the two, reversible one-electron exchanges depicted in Equations (1) and (2) and the standard potentials $(E_{1/2})_1$ and $(E_{1/2})_2$ of each electron transfer can be calculated from the ΔE_p of the overall process.[15] The values of $(E_{1/2})_1$ and $(E_{1/2})_2$ are 0.60 and 0.66 V, respectively, giving $K_d = 1.2 \times 10^{-1}$. These data indicate that the two one-electron transfers occur at similar potentials and that the mixed-valence species $Mn^{II}Mn^{III}$ is only poorly stable.

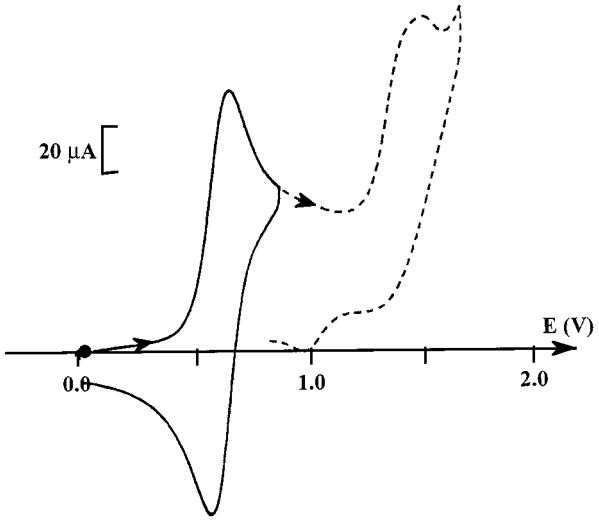

Figure 4. CV in CH_3CN + 0.1 M $[(nBu)_4N]ClO_4$ of a 1 mM solution of **1** at a platinum electrode (5 mm diameter); scan rate: 100 mV s^{-1}

$$Mn^{II}Mn^{II} \rightleftharpoons Mn^{III}Mn^{III} + 2e^- \qquad (3)$$

The $Mn^{III}Mn^{III}$ species could be prepared by an exhaustive electrolysis carried out at E_{appl} = 0.8V in CH_3CN. The initial yellow solution turned green-brown [λ_{max}= 416 (shoulder) and 534 nm]. The formation of a $Mn^{III}Mn^{III}$ species is clearly demonstrated by voltamperometry experiments conducted at a Pt rotating disk electrode. After electrolysis, the anodic initial wave at $E_{1/2}$ = 0.63 V is retained as a cathodic one. However, the yield of $Mn^{III}Mn^{III}$ species is only 85% as judged by a comparison of the height of the wave recorded before and after electrolysis. A slight excess of coulometry is observed (2.3 electrons per complex). EPR spectroscopy showed that the oxidized solution is EPR silent except for a small contribution from a mononuclear Mn(II) decomposition product. It should be noted, however, that besides the $Mn^{III}Mn^{III}$ complex, a species exhibiting a quasi reversible oxidation wave at $E_{1/2}$ = 0.98 V is generated in a 15% yield, as determined by the rotating disk experiment. No attempt has been made to identify this new species.

Discussion

Electrochemical and spectroscopic studies have revealed that **1** exhibits reversible two-electron exchanges between dimanganese(II) and dimanganese(III) states. The latter state can be oxidized further in a two-electron process, but this transfer is less reversible. A two-electron oxidation of dimanganese(II) centers has been proposed recently for two complexes with aliphatic bridges.[5c][8b] This behavior is interpreted as arising from the independency of the two metal sites in agreement with an insulating effect of the aliphatic chain. In this respect, it is worth noting that the ΔE_p of the overall process has been observed to decrease (from 128 to ca 75 mV) in dimanganese complexes of binucleating amine ligands when the length of the aliphatic chain distance increases from 2 to 3−4 methylene groups, and therefore the Mn−Mn distance from 6.3 to 8.3 Å.[8b] Such a two-electron transfer was proposed also for a (μ-alkoxo)(μ-acetato) compound[10] where the carboxylate was supposed to play a similar insulating role.[3b] Indeed the two sites must be electronically uncoupled in order not to bring any stabilization of the mixed-valent state. It therefore appears that in **1** the bridging chlorides, while structurally linking the two manganese ions, are actually isolating them electronically from one another. A comparison with the above-mentioned complexes reveals that in **1**, although ΔE_p is small (80 mV), the Mn−Mn distance is short 3.8 Å, which points to a strong effect of the chloride bridges. This electronic uncoupling is reflected in the very weak magnetic coupling of the two Mn ions.

Experimental Section

General: All syntheses and electrochemical experiments were performed under an argon atmosphere. Electrochemical equipment and procedures have been described previously.[16] Potentials are referred to an Ag | 10 mM Ag^+ reference electrode in CH_3CN + 0.1 M electrolyte. The potentials referenced to that system can be converted into SCE by adding 300 mV. The bpea ligand was prepared following a literature method.[11]

$Mn_2(\mu\text{-}Cl)_2(bpea)_2Cl_2$ (1): To an aqueous solution (4 mL) of $MnCl_2$ (0.110 g, 0.88 mmol) was added an ethanol solution (4 mL) of bpea ligand (0.200 g, 0.88 mmol) with stirring. The resulting pale yellow solution was stirred for one hour, then filtered three times to remove any impurity and evaporated to dryness at room temperature. The white microcrystalline powder formed was redissolved in acetonitrile and colorless crystals were obtained by slow evaporation of this solution at room temperature. The crystals of **1** (0.125 mg, yield 40%) were collected by filtration, washed with diethyl ether and dried in air.

IR (KBr): $\tilde{\nu}$ = 1600 (s), 1571 (m), 1475 (m), 1464 (w), 1432 (s), 1384 (m), 1361 (m), 1342 (w), 1303 (m), 1290 (m), 1268 (w), 1248 (w), 1211 (w), 1173 (w), 1150 (s), 1119 (m), 1099 (m), 1069 (w), 1044 (s), 1015 (s), 995 (m), 985 (w), 964 (w), 935 (w), 896 (w), 852 (w), 821 (m), 767 (s), 736 (w), 722 (w), 638 (m), 514 (w), 504 (w), 470 (w), 415 (m) cm^{-1}. – $C_{28}H_{34}Cl_4Mn_2N_6$ (706.29): calcd. C 47.59, H 4.81, N 11.89; found C 47.29, H 4.79, N 11.72.

X-ray Crystal Structure Analysis of 1: $C_{28}H_{34}Cl_4Mn_2N_6$, M = 706.29; monoclinic, space group $P2_1/c$, a = 10.1085(19), b = 16.399(7), c = 10.089(3) Å, α = 90, β = 109.771(17), γ = 90, V = 1573.9(9) $Å^3$, T = 298(2) K, Z = 2, F (000) = 724, D_c = 1.490 $g{\cdot}cm^{-3}$, μ = 1.171 mm^{-1}. The data sets for the single-crystal X-ray studies were collected with Mo-K_α radiation on a Bruker SMART diffractometer. All calculations were performed on a Silicon Graphics system, using the SHELXTL program.[17] The structure was solved by direct methods and refined by full-matrix least-squares on F_2.

Crystallographic data (excluding structure factors) for the structure(s) included in this paper have been deposited with the Cambridge Crystallographic Data Centre as supplementary publication no. CCDC-146219. Copies of the data can be obtained free of charge on application to CCDC, 12 Union Road, Cambridge CB2 1EZ, UK [Fax: (internat.) + 44-1223/336-033; Email: deposit@ccdc.cam.ac.uk].

Magnetic measurements were performed using a Quantum Design MPMS SQUID magnetometer operating at 0.5–5 T over the temperature range 2–300 K. The powdered samples were contained in a kel-F bucket which was calibrated independently at the same fields and temperatures. The raw data were corrected for the sample holder contribution, and the molar susceptibility corresponds to the resulting magnetization per mol and per magnetic field unit. The subtracted diamagnetic contribution of **1** was evaluated at -429×10^{-6} $cm^3{\cdot}mol^{-1}$. The fitting procedure was effected in the range 12, 25, 60, 120–300 K at 0.5, 1, 2.5 and 5T, respectively. The fitting function, based on an Heisenberg Hamiltonian $-2J\ S_1{\cdot}S_2$, was c [(1 – α) 2Mn(II,II) + 8.75 α] + 2TIP. T, with c to take into account uncertainties concerning the exact composition of the powder; 2α, the proportion of mononuclear Mn(II) seen by EPR; 2Mn(II,II), the Van Vleck formula for such a complex including parameters g and J, and TIP the Temperature Independent Paramagnetism and/or a ferromagnetic contribution. G was fixed to 2. The fit gave J = +0.34 (3) cm^{-1}, c = 0.96 (1), α = 0 (fixed) and TIP = 0 (fixed).

Low temperature EPR spectra were recorded on an X-band Bruker EMX spectrometer equipped with an Oxford Instruments ESR-900 continuous-flow helium cryostat and an ER-4116 OM Bruker cavity. Magnetic field values were measured with an EMX-035M NMR gaussmeter.

Infrared spectra were recorded with a Perkin–Elmer Spectrum GX FTIR Spectrometer as KBR pellets.

[1] S. Skourtis, D. N. Beratan, in *Electron Transfer in Chemistry* (Ed.: V. Balzani), Vol. 1, Wiley-VCH, in press.
[2] R. E. Sharp, S. K. Chapman, *Biochim. Biophys. Acta* **1999**, *1432*, 143–158.
[3] [3a]J. E. Penner-Hahn, in *Manganese Redox Enzymes* (Ed.: V. L. Pecoraro), VCH Publishers, New York, **1992**, pp 29–45. – [3b]G. C. Dismukes, *Chem. Rev.* **1996**, *96*, 2909–2926.
[4] V. L. Pecoraro, M. J. Baldwin, A. Gelasco, *Chem. Rev.* **1994**, *94*, 807–826.
[5] [5a] M. Devereux, M. Mc Cann, M. T. Carey, M. Curran, G. Ferguson, C. Cardin, M. Guvery, F. Quillet, *J. Chem. Soc., Dalton Trans.* **1995**, 771–776. – [5b] T. Tanase, S. J. Lippard, *Inorg. Chem.* **1995**, *34*, 4682–4690. – [5c] D. F. Xiang, X. S. Tan, W. T. Tang, F. Xue, T. C. W. Mak, *Polyhedron* **1998**, *17*, 1375–1380.
[6] [6a] H. Okawa, H. Sakiyama, *Pure Appl. Chem.* **1995**, *67*, 273–280. – [6b] T. Nagata, J. Mizukami, *J. Chem. Soc., Dalton Trans.* **1995**, 2825–2830.
[7] P. J. Pessiki, G. C. Dismukes, *J. Am. Chem. Soc.* **1994**, *116*, 898–903.
[8] [8a] B. C. Unni Nar, J. E. Sheats, R. Ponteciello, D. Van Engen, V. Petrouleas, G. C. Dismukes, *Inorg. Chem.* **1989**, *28*, 1582–1587. – [8b] S. J. Brudenell, L. Spiccia, A. M. Bond, G. D. Fallon, D. C. R. Hockless, G. Lazarev, P. J. Mahon, E. R. T. Tiekink, *Inorg. Chem.* **2000**, *39*, 881–892.
[9] P. J. Pessiki, S. V. Khangulov, D. M. Ho, G. C. Dismukes, *J. Am. Chem. Soc.* **1994**, *116*, 891–897.
[10] [10a] E. Sinn, *J. Chem. Soc., Dalton Trans.* **1975**, 162–165. – [10b] F. H. Köhler, N. Hebendanz, U. Thewalt, B. Kanellakopulos, R. Klenze, *Angew. Chem. Int. Ed. Engl.* **1984**, *23*, 721–723. – [10c] A. Garoufis, S. Kasselouri, S. Boyatzis, C. P. Raptopoulou, *Polyhedron* **1999**, *18*, 1615–1620.
[11] S. Pal, M. K. Chan, W. H. Armstrong, *J. Am. Chem. Soc.* **1992**, *114*, 6398–6406.
[12] S. V. Khangulov, P. J. Pessiki, V. V. Barynin, D. E. Ash, G. C. Dismukes, *Biochemistry* **1995**, *34*, 2015–2025.
[13] A. Bencini, D. Gatteschi, in *Transition Metal Chemistry* (Eds.: G. A. Mason and B. N. Figgis), Vol. 8, Chap. 1, M. Dekker, New York, **1982**.
[14] A. Abragam, B. Bleaney, *Electron Paramagnetic Resonance of Transition Ions*, Clarendon Press, Oxford, **1970**.
[15] D. Richardson, H. Taube, *Inorg. Chem.* **1981**, *20*, 1278–1285.
[16] M. N. Collomb Dunand Sauthier, A. Deronzier, I. Romero, *J. Electroanal. Chem.* **1997**, *436*, 219–225.
[17] G. M. Sheldrick, SHELXTL version 5.1. *An Integrated System for Solving, Refining and Displaying Crystal Structures from Diffraction Data*, Siemens Analytical X-ray Instruments, Madison, WI, **1990**.

Received July 3, 2000
[I00260]

Activation of C−H Bonds in Five-Membered Heterocycles by a Half-Sandwich Yttrium Alkyl Complex

Stefan Arndt,[a] Thomas P. Spaniol,[a] and Jun Okuda*[a]

Keywords: Yttrium / Chelates / C−H activation / Lewis acids / Heterocycles

The highly labile half-sandwich alkyl complex [Y(η^5:η^1-$C_5Me_4SiMe_2NCMe_3$)(CH_2SiMe_3)(THF)] smoothly undergoes σ-bond metathesis with furan and thiophene in pentane to give tetramethylsilane and the sparingly soluble complexes [Y(η^5:η^1-$C_5Me_4SiMe_2NCMe_3$)(μ-2-C_4H_3X)]$_2$ (X = O, S). They dissolve in THF to give the THF adducts [Y(η^5:η^1-$C_5Me_4SiMe_2NCMe_3$)(2-C_4H_3X)(THF)$_n$]. Pyrrole reacts with [Y(η^5:η^1-$C_5Me_4SiMe_2NCMe_3$)(CH_2SiMe_3)(THF)] to give the Lewis base-free pyrrolide [Y(η^5:η^1-$C_5Me_4SiMe_2NCMe_3$)(NC_4H_4)]$_n$.

Introduction

Since the first report by Watson on intermolecular C−H bond activation involving lanthanocene alkyl complexes,[1] systematic studies by Bercaw et al. have established the σ-bond metathesis to be a general reaction type whenever metal complexes with an $f^x d^0$-electron configuration undergo C−H bond activation reactions.[2] In particular, the decamethyllanthanocenes [Ln(η^5-C_5Me_5)$_2$X]$_2$ (X = H, alkyl) were shown to undergo a variety of reactions with aromatic compounds[3] including furan and thiophene.[3e] The latter reaction recently allowed the development of an elegant method to synthesize 2-thienyl-functionalized polyethylenes by combining C−H bond activation with ethylene insertion chemistry.[4] While exploring the polymerization activity of lanthanide alkyls and hydrides supported by the sterically more accessible linked amido-cyclopentadienyl ligands [Ln(η^5:η^1-$C_5Me_4SiMe_2NCMe_3$)X],[5a,5b] we have noticed the absence of C−H bond activation processes, e.g. involving aromatic solvents or THF. We wish to report here that the highly labile yttrium alkyl [Y(η^5:η^1-$C_5Me_4SiMe_2NCMe_3$)(CH_2SiMe_3)(THF)] undergoes a C−H bond activation reaction with furan and thiophene.

Results and Discussion

When the labile half-sandwich alkyl complex [Y(η^5:η^1-$C_5Me_4SiMe_2NCMe_3$)(CH_2SiMe_3)(THF)] (**1**), most conveniently prepared in situ from $YCl_3(THF)_{3.5}$ and $LiCH_2SiMe_3$, followed by reaction with $(C_5Me_4H)SiMe_2NHCMe_3$,[5] is treated with an excess of furan or thiophene in pentane at ambient temperature, tetramethylsilane and sparingly soluble precipitates of the presumably dimeric complexes [Y(η^5:η^1-$C_5Me_4SiMe_2NCMe_3$)(μ-2-C_4H_3X)]$_2$ (X = O, **2**; S, **3**) are formed in good yield (Scheme 1). Elemental analysis indicates the absence of THF in these complexes. In analogy to the crystallographically characterized 2-thienyl permethylyttrocene complex [Y(η^5-C_5Me_5)$_2$(μ-2-C_4H_3S)]$_2$, recently reported by Hessen et al.,[4] the crystal structure determination of **2**[6] reveals a dimeric structure. The two "metallocene-like" Y(η^5:η^1-$C_5Me_4SiMe_2NCMe_3$) fragments are connected by two bridging 2-furyl ligands. The $C_5Me_4SiMe_2NCMe_3$ ligands are arranged in a transoidal fashion. Due to severe disorder of the 2-furyl bridges, details of the structure determination will be published in due course. Both complexes dissolve in THF to give the corresponding monomeric THF complexes that can be fully characterized by ^{1}H and ^{13}C NMR spectroscopy. Most diagnostically, the yttrium-bound 2-carbon atoms in **2** and **3** give rise to doublets at δ = 204 and 176, with $^1J_{YC}$ = 59 and 55 Hz, respectively. The NMR spectra at room temperature in [D_8]THF indicate the presence of a mirror plane. Upon cooling a solution of **2** below −60 °C, the enantiotopic $SiMe_2$ and C_5Me_4 resonances decoalesce, indicating the slowing down of the THF dissociation process. The aromatic resonances do not change significantly suggesting free

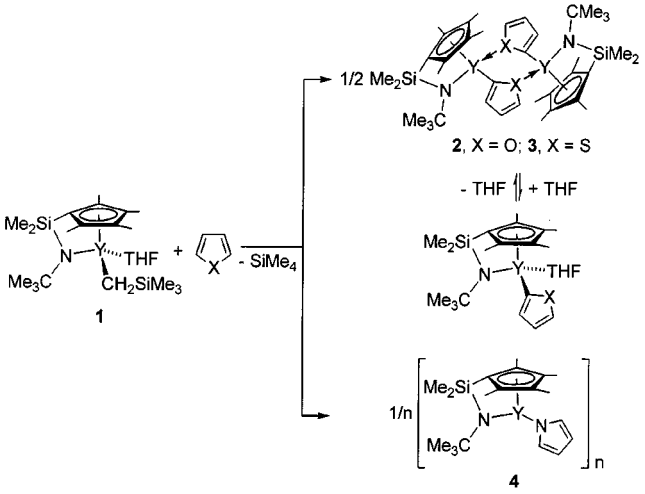

Scheme 1

[a] Institut für Anorganische Chemie und Analytische Chemie, Johannes Gutenberg-Universität Mainz
Duesbergweg 10−14, 55099 Mainz, Germany
E-mail: okuda@mail.uni-mainz.de

 © WILEY-VCH Verlag GmbH, D-69451 Weinheim, 2001 1434−1948/01/0101−0073 $ 17.50+.50/0

rotation about the yttrium-2-carbon bond without a strong yttrium-heteroatom coordination.

A pseudo first-order rate law was found for the reaction of [Y(η^5:η^1-$C_5Me_4SiMe_2NCMe_3$)(CH_2SiMe_3)(THF)] (**1**) with a 32-fold excess of thiophene in [D_8]THF to give **2** (Figure 1). The activation parameters $\Delta H^{\ddagger} = 68 \pm 1$ kJ mol^{-1} and $\Delta S^{\ddagger} = -85 \pm 3$ J K^{-1} mol^{-1} were calculated from the temperature dependence of the rate constants (Figure 2). The negative entropy is in accordance with an associative process. A well-defined arrangement of the reactants in the transition state can be inferred. Although the THF in **1** was previously shown to be labile,[5b] examples for stable five-coordinate complexes of the type [Y(η^5:η^1-$C_5Me_4SiMe_2NCMe_3$)(X)($L)_2$] (X = one-, L = two-electron ligand) were recently reported.[5b,5c]

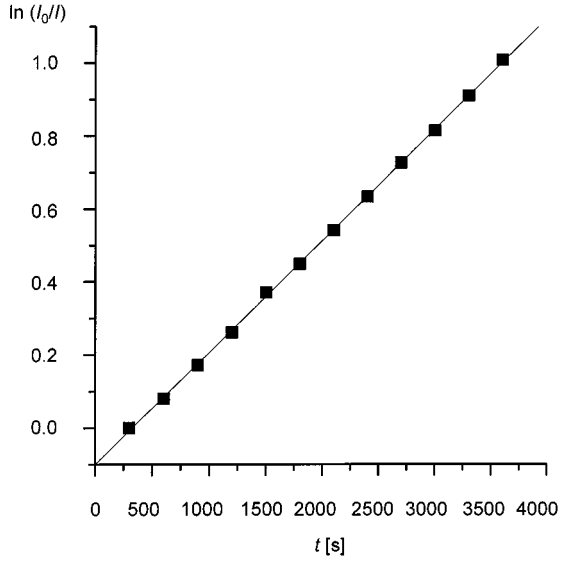

Figure 1. Reaction of [Y(η^5:η^1-$C_5Me_4SiMe_2NCMe_3$)(CH_2-$SiMe_3$)(THF)] (**1**) with thiophene in [D_8]THF: plot of ln(I_0/I) vs. t at 25 °C

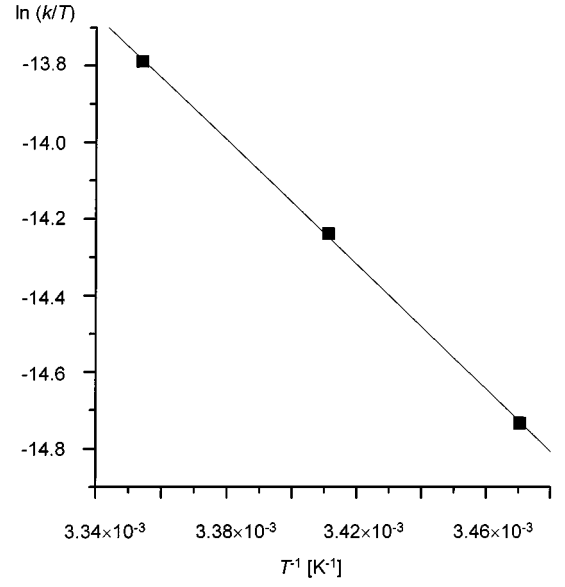

Figure 2. Reaction of [Y(η^5:η^1-$C_5Me_4SiMe_2NCMe_3$)(CH_2-$SiMe_3$)(THF)] (**1**) with thiophene in [D_8]THF: Eyring plot

In contrast to furan and thiophene, pyrrole reacts with the alkyl **1** in pentane in a stoichiometric ratio under protolysis to give the pyrrolide [Y(η^5:η^1-$C_5Me_4SiMe_2$-$NCMe_3$)(NC_4H_4)] (**4**) in good yield. This compound is sparingly soluble, even in THF, but dissolving in [D_5]pyridine allowed the recording of NMR spectra, presumably as the pyridine adduct [Y(η^5:η^1-$C_5Me_4SiMe_2NCMe_3$)-(NC_4H_4)([D_5]pyridine)$_n$]. The low solubility suggests a dimeric structure for **4**, although the related amido complexes of the type [Ln(η^5:η^1-$C_5Me_4SiMe_2NCMe_3$){$N(SiMe_3)_2$}] (Ln = Y, Nd, Sm, Lu) are all monomeric.[7] The crystallographically characterized monomeric lutetocene pyrrolide [Lu(η^5-$C_5H_5)_2$($NC_4H_2Me_2$-2,5)(THF)] (Ln = Y, Lu) was also reported to be insoluble.[8] The room temperature NMR spectroscopic data of the pyridine adduct of **4** [Y(η^5:η^1-$C_5Me_4SiMe_2NCMe_3$)(NC_4H_4)([D_5]pyridine)$_n$] are in agreement with the presence of a mirror plane, indicating a solution structure in which the pyridine ligand is rapidly exchanging its site at the chiral metal center.

In summary we have shown that the labile alkyl [Y(η^5:η^1-$C_5Me_4SiMe_2NCMe_3$)(CH_2SiMe_3)(THF)] smoothly undergoes σ-bond metathesis not only with dihydrogen[5a] and phenylsilane,[5b] but also with furan and thiophene to give metalated products. Further extension of this C−H bond activation chemistry is underway.

Experimental Section

General: All experiments were performed under argon by using standard Schlenk or glove-box techniques. Solvents were purified, dried and distilled under argon. − ^{1}H, ^{13}C, and ^{29}Si NMR: Bruker DRX 400; all spectra at 25 °C; ^{1}H: 400 MHz, ^{13}C: 101 MHz, ^{29}Si: 79.5 MHz. − Elemental analyses: Microanalytical laboratory of this department.

[Y(η^5:η^1-$C_5Me_4SiMe_2NCMe_3$)(μ-2-C_4H_3O)]$_2$ (2) and [Y(η^5:η^1-$C_5Me_4SiMe_2NCMe_3$)(2-C_4H_3O)([D_8]THF)$_n$]: A solution of furan (750 μL, 10.0 mmol) in hexane (3 mL) was layered on neat hexane (4.5 mL) which was already layered on top of [Y(η^5:η^1-C_5Me_4Si-Me_2NCMe_3)(CH_2SiMe_3)(THF)] (**1**) (300 mg, 0.6 mmol) dissolved in toluene (3 mL). Colorless crystals (163 mg, 66%) formed upon standing over a period of 6 days at 5 °C. − ^{1}H NMR ([D_8]THF): δ = 0.39 [s, 6 H, $Si(CH_3)_2$], 1.26 [s, 9 H, $C(CH_3)_3$], 2.01, 2.02 [s, 2 × 3 H, $C_5(CH_3)_4$], 6.04 (m, 1 H, C_4H_3O-3), 6.22 (d, $^3J_{HH}$ = 2.9 Hz, 1 H, C_4H_3O-4), 7.46 (m, 1 H, C_4H_3O-5). − ^{1}H NMR ([D_8]THF, −100 °C): δ = 0.33, 0.36 [s, 2 × 3 H, $Si(CH_3)_2$], 1.26 [s, 9 H, $C(CH_3)_3$], 1.71, 1.84, 1.95, 2.01 [s, 4 × 3 H, $C_5(CH_3)_4$], 6.01 (br, 1 H, C_4H_3O-3), 6.17 (br, 1 H, C_4H_3O-4), 7.49 (m, 1 H, C_4H_3O-5). − ^{13}C{^{1}H} NMR ([D_8]THF): δ = 5.8 [$Si(CH_3)_2$], 8.6, 11.9 [$C_5(CH_3)_4$], 32.3 [$C(CH_3)_3$], 51.7 [s, $C(CH_3)_3$], 104.0 [$C_5(CH_3)_4$ at Si], 104.6, 116.4 (s, C_4H_3O), 118.7, 123.8 [$C_5(CH_3)_4$], 139.8 (s, C_4H_3O). 204.4 (d, $^1J_{YC}$ = 59 Hz, C_4H_3O-2). − ^{29}Si{^{1}H} NMR ([D_8]THF): δ = 28.8 (d, $^2J_{SiY}$ = 2 Hz). − $C_{38}H_{60}N_2O_2Si_2Y_2$ (810.9): calcd. C 56.29, H 7.46, N 3.45; found C 55.07, H 7.37, N 3.58.

[Y(η^5:η^1-$C_5Me_4SiMe_2NCMe_3$)(μ-2-C_4H_3S)]$_2$ (3) and [Y(η^5:η^1-$C_5Me_4SiMe_2NCMe_3$)(2-C_4H_3S)([D_8]THF)$_n$]: A suspension of anhydrous YCl_3 (586 mg, 3.0 mmol) in THF (20 mL) was heated to 60 °C for 30 min. The solvent was then removed in vacuo and the residue taken up in pentane (24 mL). At −78 °C a solution of $LiCH_2SiMe_3$ (860 mg, 9.1 mmol) in pentane (24 mL) was added.

After stirring for 2 h at 0 °C the reaction mixture was filtered and the filtrate treated with neat $(C_5Me_4H)SiMe_2NHCMe_3$ (715 mg, 2.8 mmol). After stirring for 2 h at 0 °C and filtration, the filtrate containing the alkyl $[Y(\eta^5{:}\eta^1\text{-}C_5Me_4SiMe_2NCMe_3)(CH_2SiMe_3)(THF)]$ was treated with thiophene (3.9 mL, 48.0 mmol) and stirred for 1.5 h at room temperature. The supernatant was decanted off from the colorless precipitate which was washed with pentane (2 × 10 mL) to give colorless microcrystals (711 mg, 56%) − ^{1}H NMR ([D$_8$]THF): δ = 0.43 [s, 6 H, Si(CH$_3$)$_2$], 1.32 [s, 9 H, C(CH$_3$)$_3$], 1.98, 2.05 [s, 2 × 6 H, C$_5$(CH$_3$)$_4$], 6.97 (dd, $^3J_{HH}$ = 2.9 Hz and 4.4 Hz, 1 H, C$_4$H$_3$S-3), 7.09 (d, $^3J_{HH}$ = 2.9 Hz, 1 H, C$_4$H$_3$S-4), 7.31 (d, $^3J_{HH}$ = 4.4 Hz, 1 H, C$_4$H$_3$S-5). − ^{13}C{^{1}H} NMR ([D$_8$]THF): δ = 5.9 [Si(CH$_3$)$_2$], 8.9, 11.8 [C$_5$(*C*H$_3$)$_4$], 32.5 [C(*C*H$_3$)$_3$], 52.1 [*C*(CH$_3$)$_3$], 104.1 [*C*$_5$(CH$_3$)$_4$ attached to Si], 119.3, 123.6 [*C*$_5$(CH$_3$)$_4$], 124.2, 124.3, 131.4 (C$_4$H$_3$S), 176.7 (d, $^1J_{YC}$ = 55 Hz, C$_4$H$_3$S-2). − ^{29}Si{^{1}H} NMR ([D$_8$]THF): δ = 23.5. − $C_{38}H_{60}N_2S_2Si_2Y_2$ (843.0): calcd. C 54.14, H 7.17, N 3.32, S 7.61; found C 54.61, H 7.18, N 3.32, S 7.64.

Kinetics: Compound **1** (20 mg, 40 μmol) was dissolved in a mixture of [D$_8$]THF (400 μL) and thiophene (100 μL, 1260 μmol) and ^{1}H NMR spectra (2 scans) were recorded every 5 min. over a period of 1 h at 15, 20 and 25 °C. The rate constants were obtained by a plot of $\ln(I_0/I)$ vs. t. Integrals of the β-CH$_2$ groups of THF were used as internal standard for calibrating the integrals I of the YCH$_2$ group; $I_0 = I(t = 0\text{ s})$. $k(T = 288\text{ K}) = (1.15 \pm 0.04) \times 10^{-4}\text{ s}^{-1}$, $k(T = 293\text{ K}) = (1.92 \pm 0.02) \times 10^{-4}\text{ s}^{-1}$, $k(T = 298\text{ K}) = (3.06 \pm 0.02) \times 10^{-4}\text{ s}^{-1}$. The kinetic isotope effect using [D$_4$]thiophene at 298 K was $k_H/k_D = 6.4$.

$[Y(\eta^5{:}\eta^1\text{-}C_5Me_4SiMe_2NCMe_3)(NC_4H_4)]_n$ (4) and $[Y(\eta^5{:}\eta^1\text{-}C_5Me_4SiMe_2NCMe_3)(NC_4H_4)([D_5]pyridine)_m]_n$: A suspension of **1** (200 mg, 0.4 mmol) in hexane (3 mL) was treated with neat pyrrole (28 μL, 0.4 mmol) at 25 °C and the reaction mixture stirred at 0 °C for 2 h. Colorless microcrystals (107 mg, 65%) were obtained by filtration. − ^{1}H NMR ([D$_5$]pyridine): δ = 0.81 [s, 6 H, Si(CH$_3$)$_2$], 1.42 [s, 9 H, C(CH$_3$)$_3$], 1.74, 2.07 [s, 2 × 6 H, C$_5$(CH$_3$)$_4$], 6.69, 7.09 (br s, 2 × 2 H, NC$_4$H$_4$). − ^{13}C{^{1}H} NMR ([D$_5$]pyridine): δ = 9.0 [Si(*C*H$_3$)$_2$], 11.3, 15.0 [C$_5$(*C*H$_3$)$_4$], 34.8 [C(*C*H$_3$)$_3$], 54.7 [*C*(CH$_3$)$_3$], 107.2 [*C*$_5$(CH$_3$)$_4$ attached to Si], 108.6, 124.7 (s, NC$_4$H$_4$), 127.2 [*C*$_5$(CH$_3$)$_4$]; one signal for the C$_5$(CH$_3$)$_4$ carbon is obscured by solvent signals. − ^{29}Si{^{1}H} NMR ([D$_5$]pyridine): δ = 28.1 (d, $^2J_{SiY}$ = 2 Hz). − $C_{19}H_{31}N_2SiY$ (404.5): calcd. C 56.42, H 7.73, N 6.93; found C 56.51, H 7.62, N 7.25.

Acknowledgments

Generous financial support by the Fonds der Chemischen Industrie and the Deutsche Forschungsgemeinschaft is gratefully acknowledged.

[1] [1a] P. L. Watson, *J. Am. Chem. Soc.* **1982**, *104*, 337−339. − [1b] P. L. Watson, *J. Am. Chem. Soc.* **1983**, *105*, 6491−6495. − [1c] P. L. Watson, G. W. Parshall, *Acc. Chem. Res.* **1985**, *18*, 51−56.

[2] M. E. Thompson, S. M. Baxter, A. R. Bulls, B. J. Burger, M. C. Nolan, B. D. Santarsiero, W. P. Schaefer, J. E. Bercaw, *J. Am. Chem. Soc.* **1987**, *109*, 203−219.

[3] [3a] P. L. Watson, *J. Chem. Soc., Chem. Commun.* **1983**, 276−277. − [3b] W. J. Evans, T. A. Ulibarri, J. W. Ziller, *Organometallics* **1991**, *10*, 134−142. − [3c] K. H. den Haan, Y. Wielstra, J. H. Teuben, *Organometallics* **1987**, *6*, 2053−2060. − [3d] M. Booij, A. Meetsma, J. H. Teuben, *Organometallics* **1991**, *10*, 3246−3252. − [3e] B. J. Deelman, M. Booij, A. Meetsma, J. H. Teuben, H. Kooijman, A. L. Spek, *Organometallics* **1995**, *14*, 2306−2317. − [3f] N. S. Radu, S. L. Buchwald, B. Scott, C. J. Burns, *Organometallics* **1996**, *15*, 3913−3915.

[4] [4a] S. N. Ringelberg, A. Meetsma, B. Hessen, J. H. Teuben, *J. Am. Chem. Soc.* **1999**, *121*, 6082−6083. − [4b] B. Hessen, S. N. Ringelberg, G.-J. Meppelder, J. H. Teuben, *Polym. Prepr. (Am. Chem. Soc., Div. Polym. Chem.)* **2000**, *41(1)*, 397−398.

[5] [5a] K. C. Hultzsch, T. P. Spaniol, J. Okuda, *Angew. Chem.* **1999**, *111*, 163−165; *Angew. Chem. Int. Ed.* **1999**, *38*, 227−230. − [5b] K. C. Hultzsch, P. Voth, K. Beckerle, T. P. Spaniol, J. Okuda, *Organometallics* **2000**, *19*, 228−243. − [5c] S. Arndt, P. Voth, T. P. Spaniol, J. Okuda, *Organometallics* in press.

[6] Yellow crystal, 0.37 × 0.44 × 0.90 mm, $C_{38}H_{60}N_2O_2Si_2Y_2$, T = 293(2) K, a = 14.89(1), b = 23.845(2), c = 11.5086(9) Å, V = 4086.1(6) Å^3, orthorhombic space group *Cmca* (No. 66), Z = 4, $D_{calcd.}$ = 1.318 g cm^{-3}.

[7] [7a] Y. Mu, W. E. Piers, M.-A. MacDonald, M. J. Zaworotko, *Can. J. Chem.* **1995**, *73*, 2233−2238. − [7b] S. Tian, V. M. Arrendondo, C. L. Stern, T. J. Marks, *Organometallics* **1999**, *18*, 2568−2570.

[8] H. Schumann, P. R. Lee, A. Dietrich, *Chem. Ber.* **1990**, *123*, 1331−1334.

Received August 9, 2000
[I00310]

Mechanistic Comparison of the Nickel(0)-Catalyzed Homo-Oligomerization and Co-Oligomerization of Alkynes and Nitriles[‡]

John J. Eisch,*[a] Xin Ma,[a] Kyoung I. Han,[a] John N. Gitua,[a] and Carl Krüger[b]

Dedicated on the occasion of his 75th birthday to Professor Günther Wilke, an outstanding pioneer in transition metal catalyzed organic synthesis

Keywords: Organometallics / Metallacycles / Oligomerizations / Alkynes / Nitriles / Nickel

A comparative mechanistic study of the nickel(0)-catalyzed homo-oligomerization and co-oligomerization of alkynes and of nitriles has been undertaken, with diphenylacetylene and benzonitrile, towards an array of nickel(0) reagents, such as finely divided nickel, $(COD)_2Ni$, (Bpy)(COD)Ni, $(Et_3P)_4Ni$, (Bpy)(PhC≡CPh)Ni and $(COD)_2Ni$–$MeAlCl_2$ combinations in donor (THF) and nondonor (PhMe or neat substrate) solvents. Special attention has been given to the detailed molecular structures of the initial 1:1 adducts, (Bpy)(PhC≡CPh)Ni, $(Ph_3P)_3$(PhC≡CPh)Ni and $[(Ph_3P)(PhC{\equiv}N)Ni]_4$ by a consideration of XRD and IR data. Data from the single crystal XRD analysis of (Bpy)(PhC≡CPh)Ni, reported here for the first time, are shown to be in excellent accord with the presence of a 2,3-diphenylnickelacyclopropene ring for the (PhC≡CPh)Ni moiety with almost coplanar chelating coordination of the bipyridyl ligand, rather than with the presence of simple "side-on" coordination of the alkyne with the metal center. A parallel analysis of XRD and IR data for the two benzonitrile-nickel(0) complexes, which were drawn from previous publications, has concluded that the nickel in $(Ph_3P)_3$(PhC≡N)Ni is coordinated in an "end-on" fashion and the nickel centers in $[(Ph_3P)(PhC{\equiv}N)Ni]_4$ are coordinated as bridges between nitrile units in both an "end-on" and "side-on" manner. The stereochemistry of the acid hydrolysis of the nickelacyclopropene complex to (*E*)- or (Z)-alkene was shown to depend on the structure of the cleaving acid; parallel hydrolysis of nitrile-nickel complexes has shown that "end-on" complexes regenerate the nitrile, while "side-on" complexes lead to the aldehyde. In homo-oligomerization of diphenylacetylene or other alkyne the clean cyclotrimerization to the benzene derivative was shown to proceed by way of a nickelacyclopentadiene intermediate, as was evident by chemical trapping. The homo-oligomerization of benzonitrile by nickel(0) was found not to lead to 2,4,6-triphenyl-1,3,5-triazine, as claimed in the literature, but rather solely to benzyl phenyl ketone, the dimeric hydrolysis product. The attempted co-oligomerization of diphenylacetylene and benzonitrile with ordinary nickel(0) complexes led only to the homocyclotrimer of the alkyne. Only when the alkyne was prebonded to the nickel, as in (Bpy)(PhC≡N)Ni, could significant amounts of a codimerization product with the nitrile be observed. The origin of the triazine, claimed in a previous report to form from benzonitrile and Raney nickel, has been traced to the presence of adventitious moisture and air. Other unexpected products formed from nickel(0) complexes and benzonitrile have been shown to arise from oxidative addition reactions of nickel(0) with various σ C–E bonds.

Introduction

The nickel-catalyzed selective cyclooligomerizations of alkynes by Walter Reppe's group in the 1940s[1] and the analogous cyclooligomerizations of 1,3-alkadienes by Günther Wilke and co-workers[2] in the succeeding two decades were seminal discoveries in ushering in the current era of transition metal-mediated organic synthesis.[3] Wilke's studies in particular, with their focus on detecting and trapping reactive intermediates and on probing the steric and electronic effects of metal ligands on reactivity, have provided researchers in this flourishing field with a stellar paradigm for steering and optimizing such metal-catalyzed organic reactions.

Reppe's empirical findings that acetylene is principally cyclotrimerized into benzene by nickel(0) catalysts, such as $(Ph_3P)_2(CO)_2Ni$, but is largely cyclotetramerized into the unstable cyclooctatetraene by such nickel(II) salts as $Ni(CN)_2$ [1a,4] or by nickel(0) complexes having labile ligands $[(COD)_2Ni]$[5] have long piqued the curiosity of many chemists. Subsequent detailed mechanistic studies of these oligomerizations have adduced cogent and persuasive evidence that reactive nickelacyclopropene (**1**) and nickelacyclopentadiene (**2**) rings are pivotal intermediates in both cyclooligomerizations and that trimerization to **3** or tetramerization to **4** hinges on whether **2** reacts with a third alkyne (path a) or undergoes autodimerization (path b) (Scheme 1).[2c,6–13]

[‡] Organic Chemistry of Subvalent Transition Metal Complexes, 20. – Part 19: J. J. Eisch, J. R. Alila, *Organometallics*, **2000**, *19*, 1211.

[a] Department of Chemistry, The State University of New York at Binghamton,
Binghamton, New York 13902–6016, U.S.A.
[b] Max-Planck-Institut für Kohlenforschung,
45470 Mülheim (Ruhr), Germany

 © WILEY-VCH Verlag GmbH, D-69451 Weinheim, 2001 1434–1948/01/0101–0077 $ 17.50+.50/0

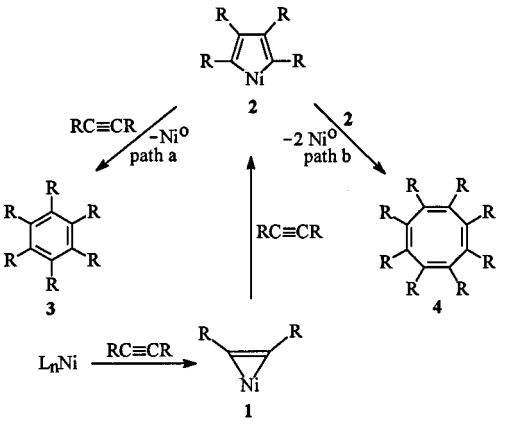

Scheme 1

The varying prevalence of path a or path b has been suggested to depend upon the ligands L_n on nickel and the substituents R on the acetylene monomer.[12]

In light of the intricate mechanistic features involved in such oligomerizations, we were curious to learn to what extent organic nitriles or azaacetylenes, R−C≡N, might undergo similar homo-cyclooligomerization or co-cyclotrimerization with alkynes by nickel metal catalysis. Two brief publications offered encouragement: benzonitrile (**5**) was reported to cyclotrimerize to 2,4,6-triphenyl-1,3,5-triazine (**6**) [Equation (1)] when heated at reflux with $Fe(CO)_5$ or $Fe_2(CO)_9$ [14] or when allowed to reflux with Raney nickel for many hours.[15] However, attempts by other workers to reproduce the formation of triazine **6** over carefully dried and deoxygenated Raney nickel or even on pure nickel surfaces were unsuccessful.[16] No reports of the nickel-catalyzed co-cyclotrimerization of alkynes and nitriles have been found, even though such oligomerizations by cobalt catalysis are common and have received much attention.[17] In the present report we establish that benzonitrile can be co-dimerized with an alkyne but only by intermediacy of an alkyne-nickel(0) complex. Furthermore, benzonitrile can indeed be oligomerized by nickel(0) complexes but in an entirely different manner not involving the formation of triazine **6**. The structural and electronic reasons for these divergent oligomerization pathways followed by alkynes and by nitriles under nickel(0)-mediation will be elucidated in light of the actual and probable organonickel intermediates.

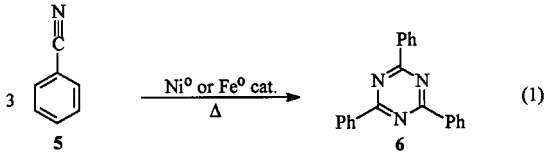

(1)

Results and Discussion

Structures of Initial 1:1 Complexes of Nickel(0) with Alkynes or with Nitriles

Such cyclotrimerizations of alkynes have as their common starting intermediate 1:1 adducts with nickel(0) that have been isolated, where appropriate ligands are present, and characterized by spectroscopic and single crystal X-ray structural analyses. Here we present such characterization of 2,2-bipyridyl(η^2-diphenylacetylene)nickel (**7**), where an essentially planar interaction of both the bipyridyl group and the C≡C bond with the nickel center is evident (Figure 1). The average Ni−C (acetylenic) separation of 1.86 ± 0.01 Å is comparable with *sigma* Ni−C bonds involving sp^2-hybridized carbon centers, such as the Ni−C bond of 1.89 ± 0.01 Å in structure **8**.[18] Moreover, the supposed acetylenic C−C separation of 1.30 ± 0.005 Å is more congruent with the presence of a C=C rather than a C≡C bond in **7**[19] (Table 1). Finally, complex **7** displays a sharp absorption at 1770 cm^{-1} in its infrared spectrum, shifted by 330 cm^{-1} to lower frequencies than the C≡C stretch of unsymmetrically substituted acetylenes such as phenylacetylene. An absorption of 1770 cm^{-1} in complex **7** is in much closer agreement with a C=C bond stretching vibration,

Professor Günther Wilke was born in Heidelberg, Germany, on February 23, 1925, where he was to obtain both the Abitur at the Humanistisches Gymnasium and the doctorate degree in 1951 at the Universität Heidelberg upon completion of structural studies on lignin under the direction of Professor Karl Freudenberg. Shortly thereafter, he joined Karl Ziegler's research group as scientific assistant at the Max-Planck-Institut für Kohlenforschung in Mülheim (Ruhr) and participated in bringing Ziegler's recent discoveries in organoaluminum chemistry and low-pressure ethylene polymerization to economic fruition. Since his curiosity was strongly aroused by the seminal discovery of the Nickel Effect by Ziegler and Holzkamp, he launched his independent research program in 1956 with the systematic investigation of the effect of nickel and other transition metals on reactions of main-group organometallics. Over the next 40 years he pursued the exciting and unforeseen ramifications of such research, which have led to the novel template syntheses of medium-sized carbocycles, the regioselective oligomerizations of alkenes and alkadienes as well as the asymmetric syntheses of carbon skeletons. Interwoven with such discoveries have been many pioneering mechanistic studies that have elucidated the governing roles of the transition metal and its ligands in these novel carbon-carbon bond coupling processes. During the period of 1969-1993 as successor to Karl Ziegler, he directed the MPI during a flourishing period of expansion of its research activities and facilities. In over 220 publications and numerous patents he disseminated the classic research results of his many doctoral students and published with Peter Jolly the authoritative, two-volume treatment of "The Organic Chemistry of Nickel" (1974, Academic Press). Among many honors for his scientific discoveries may be cited the Ruhr-Preis für Kunst und Wissenschaften and both the Emil Fischer Medaille and the Karl-Ziegler-Preis of the Gesellschaft Deutscher Chemiker. His outstanding enthusiasm and skill in the art of laboratory experimentation finds a fitting parallel in his keen interest in and a notable private collection of contemporary art. As a young scientist it was this senior author's pleasure and honor to work closely with Günther Wilke, the master experimentalist, during a yearlong postdoctoral fellowship in Professor Ziegler's institute in 1956.

which in unconjugated disubstituted *cis*-alkenes absorb near 1670 cm^{-1}. Accordingly, a nickelacyclopropene or nickelirene structure seems to be a more important resonance structure contributor (**7a**) with a nickel(II) oxidation state than does resonance structure **7b** where the nickel center is viewed as in a Ni(0) oxidation state and as only accepting electron density from its ligand donors, diphenylacetylene and 2,2-bipyridyl. As will be evident, the nickelirene structure **7a** also proves to be the more useful molecular model for understanding the courses of chemical reactions undergone by **7** with various electrophilic or unsaturated organic reagents.

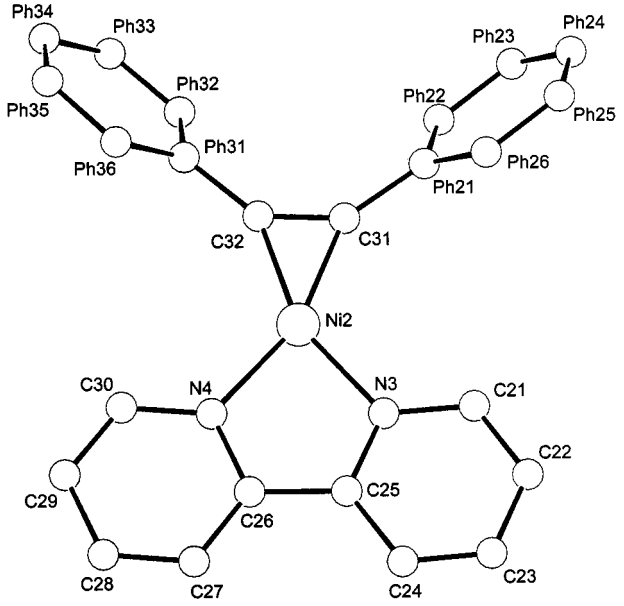

Figure 1. Structure and atom numeration of one of the independent molecules of 2,2-bipyridyl (η^2-diphenylacetylene)nickel found in the asymmetric unit cell of **7**

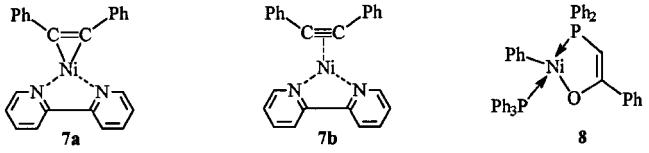

A number of spectroscopic and single crystal X-ray structural analyses of 1:1 adducts of benzonitrile with nickel(0) complexes have been published. The two XRD studies are most valuable in establishing that the nickel(0) center can coordinate with the nitrile group in both an "end-on" (**9a**) and a "side-on" (**9b**) manner.

As was established in the structure of (benzonitrile)tris(triphenylphosphane)nickel(0) (**10**), "end-on" coordination of Ni° was evident (Ni−N bond length of 1.89 ± 0.011 Å and Ni−N−C bond angle of 173 ± 7°).[20] Similarly, the

Table 1. Selected bond lengths and angles of 2,2′-bipyridyl(η^2-diphenylacetylene)nickel **(7)**

Bond lengths [Å][a]	Min. value	Max. value	Av. value
$C_{11}-C_{12}$	1.296	1.306	1.301
$C_{31}-C_{32}$	1.289	1.299	1.294
Ni_1-C_{11}	1.854	1.860	1.857
Ni_2-C_{31}	1.843	1.849	1.846
Ni_1-C_{12}	1.866	1.872	1.869
Ni_1-C_{32}	1.856	1.862	1.859
$C_{11}-Ph_1$	1.445	1.455	1.450
$C_{31}-Ph_{21}$	1.458	1.468	1.463
$C_{12}-Ph_{11}$	1.446	1.456	1.451
$C_{32}-Ph_{31}$	1.450	1.460	1.455
Bond angles [°]			
$C_{11}-Ni_1-C_{12}$	40.8	41.0	40.9
$C_{31}-Ni_2-C_{32}$	40.8	41.0	40.9
$Ni_1-C_{11}-C_{12}$	69.9	70.3	70.1
$Ni_2-C_{31}-C_{32}$	69.9	70.3	70.1
$Ni_1-C_{12}-C_{11}$	68.9	69.3	69.1
$Ni_2-C_{32}-C_{31}$	68.8	69.2	69.0

[a] The pairwise grouping of bond lengths and bond angles in the Table are the measured values for the two independent molecules of **7** found in the asymmetric cell. The first value in each pair is for the molecular and the atom numeration shown in Figure 1. The second value in each pair is that of the second molecule not shown in any figure. However, the atom numeration in the second molecule has the following atom correspondence to molecule one/ C_{11} = C_{31}; C_{12} = C_{32}; Ni_1 = Ni_2; Ph_1 = Ph_{21}; Ph_{11} = Ph_{31}.

structure of the clathrate compound, tetrakis[(benzonitrile)(triphenylphosphane)nickel(0)] (**11**),[21] incorporating various hydrocarbon solvent molecules, actually has the Ni^0 centers simultaneously coordinated to adjacent benzonitrile units in an "end-on" and a "side-on" manner (**11,** schematically drawn). Since complexes **10** and **11** are in equilibrium with each other, one can conclude that "end-on" coordination of the nickel center is the stronger primary binding mode with the nitrile group and that "side-on" bonding is only ancillary to it. The "end-on" Ni−N bond length of 1.90 Å is similar to that in **7** but the Ni−N−C bond angle at 167° deviates more from linearity. The "side-on" Ni−C bond length at 1.85 Å is comparable to Ni−C bonds with sp^3-hybridized carbons (vide supra).

Infrared spectral data on complexes **10** and **11** provide a useful insight into such "end-on" and "side-on" coordination. The nitrile stretch in uncomplexed benzonitrile at 2230 cm^{-1} is lowered to 2150 cm^{-1} by "end-on" coordination as in **10**.

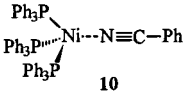

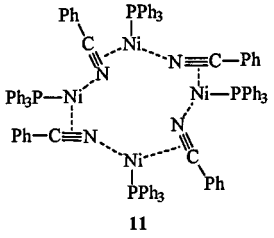

On the other hand, complex **11** displays a strong band at 1850 cm^{-1}. Again, such a stretching frequency lies much closer to a C=N stretch (1470−1690 cm^{-1}) than to a C≡N

stretch (2100−2200 cm^{-1}). Thus, it again appears that for such "side-on" coordination, the resonance contribution of a nickel(II) system, namely, azanickelacyclopropene (**12a**) would seem to be more important than that of a nickel(0) *pi*-complex (**12b**).

As confirmation of the importance of structure **12a** is the observed C−N bond length of 1.26 Å, considerably longer than the C≡N bond (1.16 Å) and very comparable with those of C=N linkages (1.26−1.30 Å).[21]

These infrared data from nickel(0)-benzonitrile complexes of known structure can now conversely be used to evaluate the type of bonding in unknown structures. Thus the complex, (benzonitrile) (2,2-bipyridyl)nickel(0) (**13**), which has a sharp absorption at 2105 cm^{-1} must have "end-on" coordination.[22] This is undoubtedly the complex formed initially when (2,2-bipyridyl)(1,5-cyclooctadiene) nickel(0) interacts with benzonitrile (vide infra).

Bipyridyl---Ni---N≡C—Ph
13

Protonolysis of the Initial 1:1 Complexes of Nickel(0) with Alkynes or with Nitriles

The stereochemical course of the protonolysis of 2,3-diphenylnickelirene·2,2-bipyridyl (**7a**) depends strikingly upon the solvent and the specific nature of the proton source. When **7a** was treated with 85% H_3PO_4 in THF or with glacial HOAc, almost quantitative yields of only *cis*-stilbene (**14**) were obtained. On the other hand, when the protonolysis was conducted with 6N aqueous HCl, a pale red precipitate of PhCH=CPh(NiCl·Bpy) (**15**) was formed almost immediately in 90% yield. The remaining 10% of the starting material had been converted into a 9:1 mixture of *cis*- and *trans*-stilbenes. The stereochemistry of the stilbenyl C−Ni bond in intermediate **15** was established by treating **15** first with HOAc and determining that only *trans*-stilbene (**16**) was produced. Then in a separate experiment **15** was treated with DOAc with the result that *trans*-stilbene-d_1 (**16a**) was formed. Since HOAc did not cause isomerization of the stilbenyl group in the protonolysis of **7a**, it is reasonable that it would not cause isomerization in the protonolysis of intermediate **15**. Therefore, isomerization of the stilbenyl group must have occurred during the formation of **15** from **7a** under the action of HCl. That only one proton is added in the formation of **15** from **7a** was verified by treating **7a** with DCl. The deuteriated **15a** formed was treated in separate experiments with either HOAc or DOAc. Both experiments generated only *trans*-stilbenes but the former experiment gave the d_1-isotope (**16a**) while the latter only the $d_{1,2}$-isotope (**16b**). These interrelated reactions are depicted in Scheme 2.

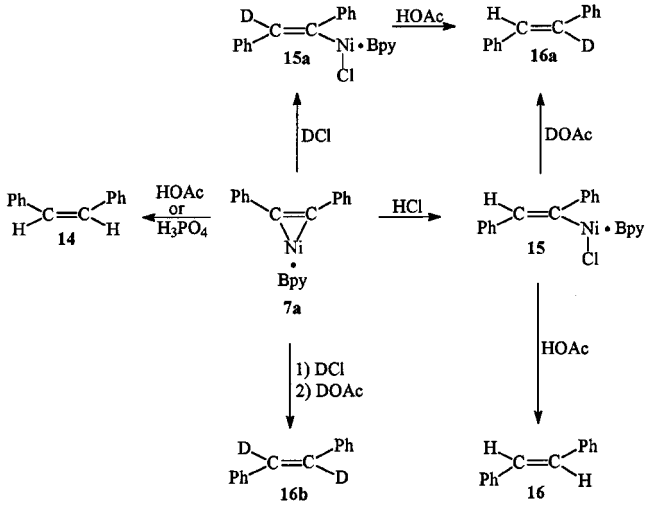

Scheme 2

A congruent explanation for the retention of configuration on the protonolysis of the first C−Ni bond in **7a** by acetic acid or by phosphoric acid may lie in the ability of these acids to deliver a proton via a six-membered coordinated transition state (**17**). By contrast, the ionic transition state **18**, formed by HCl in water, can easily isomerize by ring-opening, to form the sterically most stable ion (**19**) [Equation (2)]:

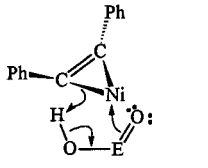

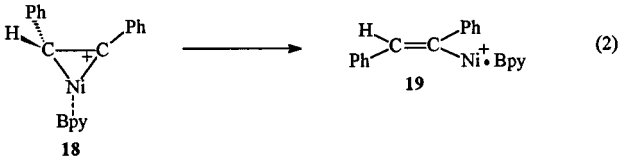

Up to the present work, little has been known about the course of protonolysis of "end-on" or "side-on" nickel-nitrile complexes. It has been reported that complex **13**, which can now be assigned an "end-on" structure, regenerates benzonitrile essentially quantitatively after being treated with a weak acid like acetylacetone. Even dilute HNO_3 produces only recovered benzonitrile.[22] Given the known resistance of nitriles to reduction or to hydrolysis, this result may not be surprising. In the present work it is therefore noteworthy to report that the treatment of benzonitrile in THF with nickel complexes, such as $(COD)_2Ni$, (Bpy)(COD)Ni or $(Et_3P)_4Ni$ and hydrolytic workup produces benzaldehyde in yields of 5−15%. We conclude that such benzaldehyde must have arisen from the hydrolysis of a "side-on"-coordinated nickel complex like **12a**, which can

be considered as having much azanickelacyclopropene character (vide supra). The intermediate benzaldehyde imine (**20**) should hydrolyze easily to benzaldehyde (**21**) [Equation (3)].

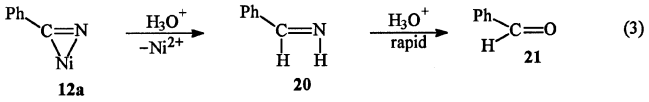

Oligomerization Reactions of Alkynes and Nitriles by Nickel(0) Complexes

Oligomerizations with (2,2′-Bipyridyl)(diphenylacetylene)-nickel(0) (7a)

Complex **7a** catalyzes the cyclotrimerization of diphenylacetylene (**22**) to hexaphenylbenzene (**23**) in refluxing toluene but at a significantly slower rate than with $(COD)_2Ni$ as catalyst, which effects comparable conversions to **23** in refluxing THF in half the time (Scheme 3).

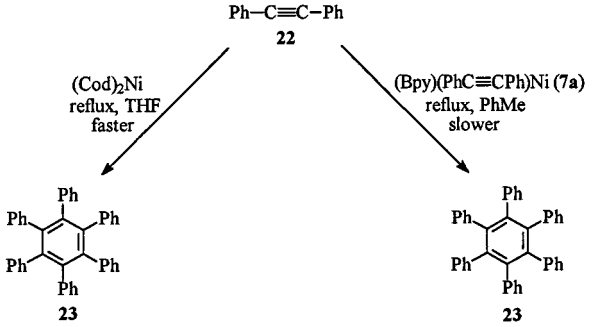

Scheme 3

The cyclotrimerization of dimethyl acetylenedicarboxylate (**24**) catalyzed by **7a** to hexamethyloxycarbonylbenzene (**25**) occurs in refluxing benzene faster than that of **22** in refluxing toluene. When the cyclotrimerization of **24** with **7a** was carried out at 25 °C in THF, up to 20% of the product was the mixed cyclotrimer, 1,2,3,4-tetramethyloxycarbonyl-5,6-diphenylbenzene (**26**) (Scheme 4). This finding supports the conclusion that at lower temperatures some of complex **7a** is stable and undergoes insertions of **24**, ultimately leading via **27** to **26.** At higher temperatures especially, **7a** decomposes with the transfer of Bpy·Ni to **24** with the formation of **28**, which leads to the formation of **25** (Scheme 5). These findings support the previously proposed

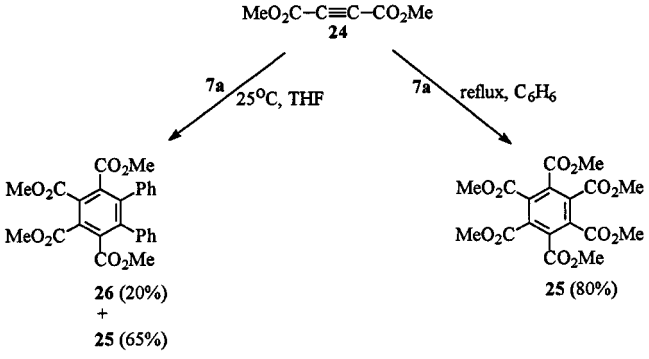

Scheme 4

hypothesis that nickelirenes, such as **7a** and **28**, are discrete and crucial intermediates in the cyclooligomerization of alkynes by nickel(0) complexes.[11−13]

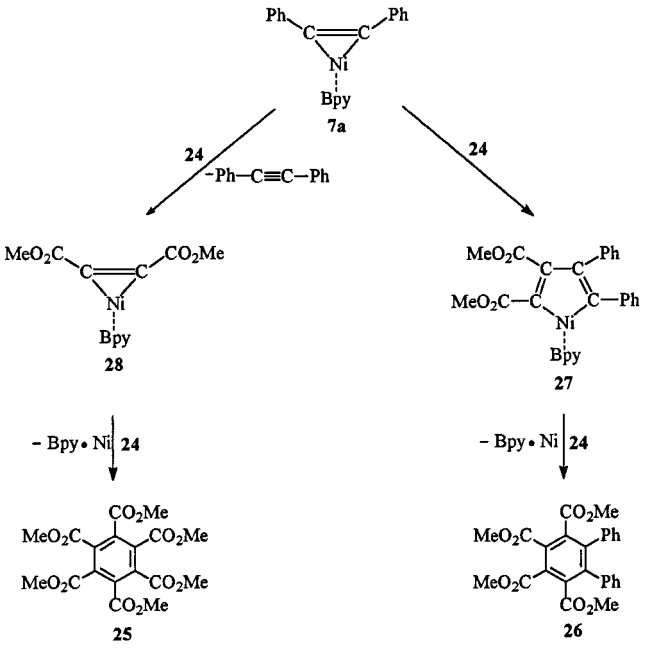

Scheme 5

Attempted Co-oligomerizations of Diphenylacetylene (22) and Benzonitrile (5) by Nickel(0) Complexes

The interaction of a 2:1 mixture of **22** and **5** with one equivalent of $(COD)_2Ni$ in refluxing THF led to a 65% yield of hexaphenylbenzene (**23**) and 3% of *cis*-stilbene (**14**) but no discernible oligomer involving incorporation of benzonitrile, such as pentaphenylpyridine. This result implies that benzonitrile cannot compete with diphenylacetylene in the crucial insertion step with the nickelirene intermediate **29** (L = COD) (Scheme 6 depicting the competitively faster formation of **31** and hence **23** from **7a** and the much slower formation of **30**, which would lead to pentaphenylpyridine). The validity of this inference was substantiated by subjecting the more stable and less reactive nickel complex **7a** to the action of benzonitrile alone in THF at 25°C, without any competing alkyne. Indeed, hydrolytic workup gave up to 40% of the *cis*- and *trans*-isomeric 1,2,3-triphenylpropen-1-ones (**32**), convincing evidence that azanickelole **30** had formed from **7a** by insertion of benzonitrile (Scheme 7).

Attempted Homo-Oligomerizations of Benzonitrile (5) by Nickel(0) Complexes

Many careful and systematic variations have been attempted to reproduce the reported cyclotrimerization of **5** over Raney nickel in refluxing benzonitrile with the formation of 2,4,6-triphenyl-1,3,5-triazine (**6**) [Equation (1)].[15] To avoid possible contaminants present in the typical samples of Raney nickel, such as aluminum metal and NaOH, as well as moisture and dihydrogen, the attempted

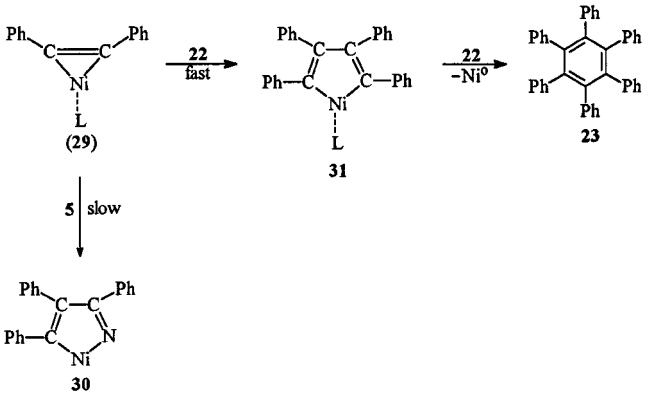

Scheme 6.

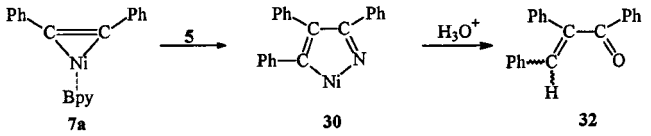

Scheme 7

oligomerizations were also carried out with pure nickel metal powders, prepared under argon by the alkylative reduction of nickel salts with *n*-butyllithium in THF at −78°C. In the complete absence of traces of oxygen and of moisture, such nickel metal led to little or no **6** even after 2 days at 190 °C. Only when moist air was admitted during reflux did noticeable amounts of **6** form (5−10% of **5**) and other unusual reaction products appear (vide infra). We are forced to agree with the conclusion of Oehme and Pracejus[16] that a pure nickel metal surface is incapable of catalyzing the cyclotrimerization of benzonitrile under the conditions reported by Heldt.[15]

Since our previous experience with the coupling and cleavage reactions of nickel(0) complexes has shown that such reactions are especially favored in donor solvents at or below 25 °C, we then undertook a study of the reaction of benzonitrile with nickel(0) complexes in THF. As reported above, protonolysis of such reaction mixtures gave benzaldehyde (**21**), most likely stemming from the protonolysis of a "side-on" complex [Equation (3), **12a**]. But an additional, most surprising hydrolysis product was also isolated, namely benzyl phenyl ketone (**33**). No trace of any other dimeric or trimeric product, such as benzil (**34**) or triazine **6** was detected. The yields of benzaldehyde and benzyl phenyl ketone obtained with different ratios of $(COD)_2Ni$ and nitrile are noteworthy: with a 1:2 $(COD)_2Ni$:**5** ratio, the yields of **21** and **33** were 13% and 15%, with 70% of nitrile **5** remaining. When a reverse ratio of 2:1 $(COD)_2Ni$:**5** was employed, all of the benzonitrile was consumed and again only **33** and **21** were found in the reaction products, this time in a ratio of 96:4.

These results show that the formation of ketone **33** is fostered by the stoichiometric action of more than one nickel atom per nitrile. Clearly, when a 1:2 $(COD)_2Ni$:**5** ratio is employed, $(COD)_2Ni$ is the limiting reagent and hence only about one-third of the benzonitrile can react. In explaining the origin of ketone **33**, we suggest that the coupling of the nitrile carbons must occur in an unusual manner, certainly not involving a straightforward reductive dimerization as depicted in Equation 4.[23] Were such an ordinary reductive coupling to have occurred, an intermediate diazanickelole (**35**) would have formed and would undoubtedly have hydrolyzed to benzil (**34**), a product noteworthy by its absence in this reaction.

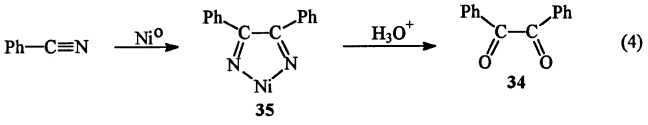

To account for the formation of ketone **33**, therefore, we propose a cyclodimerization of two "end-on"-coordinated nickel(0) complexes of benzonitrile (**36**) by agency of nickel(0) to form a (3,4,-diphenyl-1,2-diazacyclobutadiene)nickel(0) complex of type **37**. Protonolytic decomposition of **37** would reasonably be expected to lead via **38**−**40** to ketone **33** (Scheme 8). Currently, our efforts are directed toward isolating a suitably ligated derivative of **37** for confirmatory XRD and protonolysis studies. There is ample precedent for the stable complexation of the cyclobutadiene ring with nickel(0), typified by (η^4-tetraphenylcyclobutadiene)bis(triethylphosphane)nickel(0), whose structure has been confirmed by an XRD study.[11] Also, the mode of protonolytic cleavage of this latter structure partly resembles that of **35**: glacial acetic acid leads to the formation of (*E,E*)-1,2,3,4-tetraphenyl-1,3-butadiene.

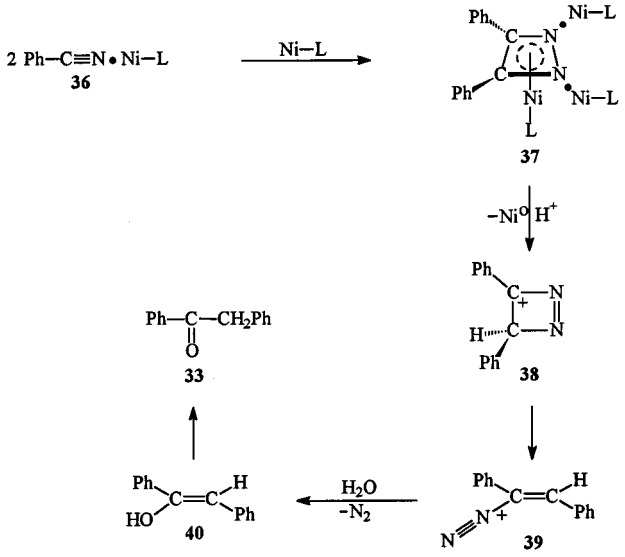

Scheme 8

Although such complexations between benzonitrile and nickel(0) are relatively stable at 25°C, they are easily disrupted at higher temperatures. For example, conducting the reaction of (Bpy)(COD)Ni with benzonitrile in THF at 25°C gives, upon hydrolysis, 20% of ketone **33**, whereas the same reaction conducted in refluxing THF gives no trace of **33**. Even at room temperature, such reactions can lead to decyanation of the nitrile, especially those nitriles with

electron-withdrawing substituents, as shown in Equation (5). With electron-donating substituents, oxidative addition of C−CN bonds to nickel(0) occurs more slowly [Equation (6)].

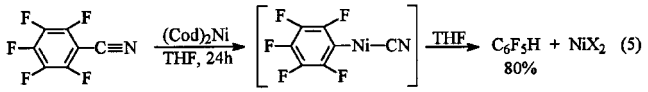

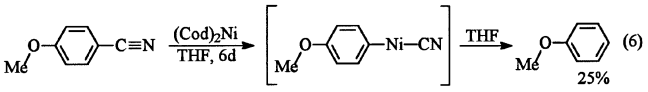

The usual aryl aldehyde and substituted benzyl phenyl ketone were also detected upon hydrolysis of the latter reaction mixture.

During our attempts to reproduce the cyclotrimerization of benzonitrile reported by Heldt[15] as occurring on nickel metal in refluxing **5**, we did observe significant decyanation, as was evident by low recovery of **5** (<50%) and by the detection of cyanide ion in the hydrolysis products with the "Prussian Blue" test.

Significant, Unexpected Reactions Occurring between Benzonitrile and Nickel(0) Complexes

Formation of Benzamide (41) and 2,4,6-Triphenyl-1,3,5-triazine (6)

From the present study and the previous work of Oehme and Pracejus[16] it is clear that under a completely inert atmosphere and anhydrous conditions neither a clean nickel surface nor a nickel(0) complex reacts with pure benzonitrile at temperatures up to 200 °C to produce any triazine **6**. However, in the presence of adventitious moist air such nickel(0) complexes convert the nitrile to benzamide (**41**) even at 25 °C. Nickel(II) salts, in turn, have been shown to convert benzamide into the triazine **6** at elevated temperatures.[16] The so-called catalytic hydration of nitriles to amides, reported over 40 years ago, involves heating aqueous suspensions of amides with nickel metal catalysts of the Raney or Urushibara type under an air atmosphere.[24] In the light of our present findings, we can now propose a rational reaction mechanism involving the formation of a "side-on" complex on the nickel surface (**42,** with **5**), its air-oxidation to **43** and the hydrolysis via enaminate **44** to the amide **41** (Scheme 9). In keeping with the intermediacy of **42**, significant reduction of the nitrile to the amine or even reductive cleavage to ammonia has been observed.

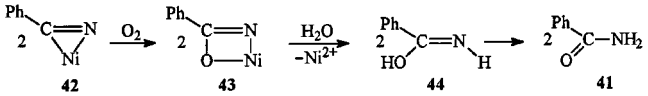

Scheme 9

Ethylation of Benzonitrile (5) in the Presence of Tetrakis(triethylphosphane)nickel(0) (45)

As with other nickel(0) complexes, the triethylphosphane complex **45** reacted with benzonitrile to produce small amounts of benzaldehyde (5%) and benzyl phenyl ketone (10%) upon hydrolysis. But, surprisingly, ethyl phenyl ketone (**46**) was also formed in 60% yield. Since the only discernible source of the ethyl group is the Et_3P ligand, we are led to suggest that the Ni(0) center, in the presence of benzonitrile (**9a**) undergoes an oxidative addition into the ethyl-phosphorus bond of a Et_3P unit (Scheme 10). Decomposition of **47** in either a heterolytic or a homolytic fashion would yield **48**, whose hydrolysis would provide ketone **46**. Although an unusual reaction for phosphane complexes themselves at 25 °C, the following C−P bond cleavage reaction has been observed in refluxing hexane [Equation (7)].[25] Clearly an oxidative addition to the Ni(0) center must be involved. Pending further study, it remains unclear as to whether such reactions are promoted by light or radical sources.

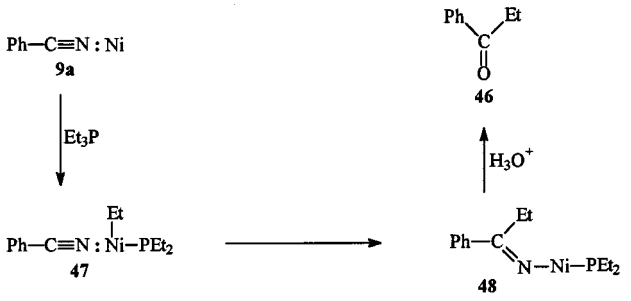

Scheme 10

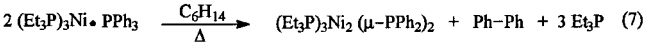

Isobutylation of Benzonitrile (5) by Triisobutylaluminum (49) in the Presence of Bis(1,5-cyclooctadiene)nickel(0) (50)

Nitriles react with diisobutylaluminum hydride at 20−25 °C to give aldehydes upon hydrolysis but they do not react with triisobutylaluminum at such temperatures. Only when nitriles are heated with Bu_3Al does reaction occur but then hydroalumination, rather than carbalumination, is the observed outcome, leading again to aldehydes or primary amines.[26] Therefore, the extraordinary reaction of benzonitrile with 1:1 mixture of Bu_3Al and $(COD)_2Ni$ to yield isobutyl phenyl ketone (**51**) in 42% yield deserves particular attention. Such a yield results from reactions of 1:1:1 mixtures of the reactants conducted in toluene either over seven days at 25 °C or 24 hours at reflux. Traces of benzyl phenyl ketone (**33**) and benzophenone (1−5%) were also detected.

To account for the formation of ketone **51**, an oxidative addition of the Ni(0) center of **9a** into the isobutyl-aluminum bond is reasonable, similar to that depicted in Scheme 10 to form **52** which decomposes in an analogous fashion to **53**, whose hydrolysis would yield **51** (Scheme 11). That the yield of **51** levels off under 50% may be a consequence of strong Lewis base (**53**) complexing with half of

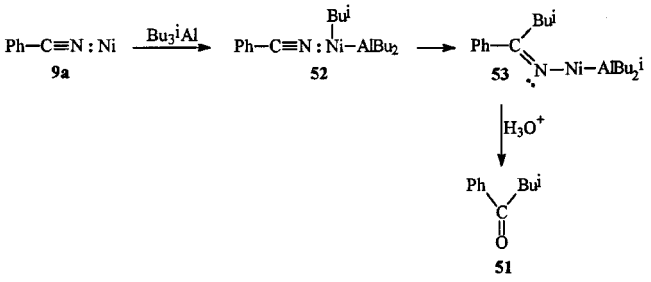

Scheme 11

the available Bu_3Al and preventing it from reacting with **9a**. As to the mechanism of reaction, there is evidence from the reaction of diphenylacetylene with 1:1 combinations of iBu_3Al and $(COD)_2Ni$ that both photochemical- and radical-promoted processes may be operative.[27]

The small but significant yield of benzophenone is noteworthy: the above-mentioned oxidative addition of Ni(0) into aryl-cyano bonds [Equations (5) and (6)] is undoubtedly the cause. At 25 °C the resulting phenylnickel cyanide (**54**) would be sufficiently stable to add to the nitrile **5** to form adduct **55**, whose hydrolysis would lead to benzophenone (Scheme 12):

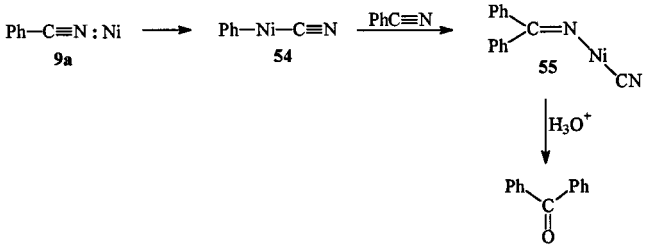

Scheme 12

Conclusions

These parallel studies of the homo-oligomerization and co-oligomerization of alkynes and nitriles show how pivotal the initial 1:1 adduct of nickel(0) and the triple-bonded substrate is on the course of such oligomerizations. With alkynes the reactive "side-on" complex can best be viewed as a nickelacyclopropene or nickelirene both in terms of its molecular structural properties and its chemical reactions. The 1:1 nickel(0) complex with nitriles can be "end-on" as well as "side-on" (azanickelacyclopropene) with evidence existing that "end-on" complexation is the more stable mode and the more important precursor to the homo-oligomerization, nickelodecyanation and several unusual addition reactions of nitriles. In the co-oligomerization of alkynes and nitriles the greater stability of the "side-on" complex of nickel(0) with the alkyne monomer over the corresponding "side-on" complex of nickel(0) with nitriles results in essentially exclusive homocyclotrimerization of the alkyne. Only in the absence of free alkyne can the nickelacyclopropene apparently be intercepted by the nitrile leading to a co-dimer with the alkyne. In the homo-oligomerization of nitriles the 1:1 "end-on" complexation with nickel(0) appears to lead to an unusual stoichiometric dimerization apparently in the form of an $\eta^4-1,2$-diazacyclobutadiene-nickel(0) precursor complexed in a "corner-on" fashion with two nickel(0) units.

Experimental Section

Instrumentation, Analysis and Starting Reagents: All reactions were carried out under a positive pressure of anhydrous, oxygen-free argon. All solvents employed with organometallic compounds were dried and distilled from a sodium metal-benzophenone ketyl mixture prior to use.[28] The IR spectra were recorded with a Perkin−Elmer instrument, model 457 and samples were measured either as mineral oil mulls or as KBr films. The NMR spectra (^1H and ^{13}C) were recorded with a Bruker spectrometer, model EM-360 and tetramethylsilane (TMS) was used as the internal standard. The chemical shifts reported are expressed in the δ-scale and in parts per million (ppm) from the reference TMS signal. The GC/MS measurements and analyses were performed with a Hewlett-Packard GC 5890/Hewlett-Packard 5970 Mass-Selective-Detector instrument. The gas chromatographic analyses were carried out with a Hewlett-Packard instrument, model 5880, provided with a 6 ft OV-101 packed column or with a Hewlett-Packard instrument, model 5890, having a 30 m SE-30 capillary column, respectively. Melting points were determined on a Thomas-Hoover Unimelt capillary melting point apparatus and are uncorrected. The $(COD)_2Ni$ was prepared according to a procedure adapted from those of Semmelhack[29] and of Schunn.[30] The yield of product has been improved to 95% by purifying the starting materials with extreme care.

The $(Et_3P)_4Ni$ was prepared according to the method of Cundy[31] and the (Bpy)(COD)Ni by the procedure of Dinjus et al.[32] The complex, (Bpy)(Ph−C≡C−Ph)Ni (**7**), was prepared according to the following modified procedure, which is based upon the method of Eisch and Piotrowski.[33]

A suspension of $(COD)_2Ni$ (2.91 g, 10.6 mmol) in 40 mL THF was treated with 2,2′-bipyridyl (1.70 g, 10.7 mmol) in 10 mL THF at 25 °C and the reaction mixture stirred for 1 h. After the solvent was removed under reduced pressure, the viscous dark purple residue was dried under vacuum overnight. Then 50 mL of THF was introduced to dissolve this black-purple solid and diphenylacetylene (1.89 g, 10.6 mmol) in 20 mL of THF was then added dropwise. The reaction mixture was then stirred at 25 °C for 15 h, after which time THF was removed under reduced pressure and the black viscous residue dried under vacuum for 16 h in order to remove the cyclooctadiene. Then 50 mL of THF was used to extract the residue and the mixture filtered. The filtrate was concentrated to about 20 mL and pentane was then introduced in small portions. After the first precipitation was observed, another 15 mL of pentane was added. The mixture was allowed to stand at 25 °C for 2 h to complete the crystallization. The black crystalline solid was then filtered off and was washed with small portions of pentane three times and then dried under vacuum for 4 h. The yield of the product was 3.00 g (72%). Such crystals were employed for X-ray crystallographic structure determination. − IR (mineral oil): $\tilde{\nu}$ = 710(s), 730(s), 755(s), 765(m), 775(m), 850(w), 1025(s), 1490(m), 1570(w), 1590(s), 1740(br, w), 1770(m).

General Procedures: All steps in the preparation, transfer, and main reactions of the metal salts and organometallic reagents studied here were conducted under an atmosphere of anhydrous and oxygen-free argon. All solvents and apparatus were likewise freed of

traces of dissolved or adsorbed moisture and oxygen by published procedures and then maintained under argon. Methods and techniques for working under anhydrous and anaerobic conditions have been described previously.[28] In the hydrolysis procedure employed for the workup of all nickel(0) reaction mixtures, it proved essential that the aqueous HCl be thoroughly free of oxygen and that both freeze-thaw cycles in vacuum and readmission of argon be conducted to that end. Because of the small-scale runs the presence of oxygen during hydrolysis greatly reduced the amounts of benzaldehyde and benzyl phenyl ketone isolated.

Protonolysis of (Bpy)(Ph−C≡C−Ph)Ni (7): A solution of **7** (1.00 g, 2.55 mmol) in 20 mL of THF under argon was treated with 10 mL of degassed 85% H_3PO_4 at 25 °C for 4 h to form an off-white precipitate and a blue solution. Hydrolytic workup gave an organic extract containing only *cis*-stilbene (**14**) (0.73g, 95%), as determined by IR, ^1H and ^{13}C NMR spectroscopy.

A similar solution of **7** was treated with degassed 6 N aqueous HCl with prompt formation of a pale red-colored precipitate, which corresponded to a 90% yield of PhCH=CPh(NiCl·Bpy) (**15**) based upon a Ni analysis of 14.0% (calcd. 13.63%), as well as a positive test for Cl anion upon sodium fusion, and IR spectroscopy: $\tilde{\nu}$ = 700(s), 740(s), 790(s), 910(m), 1040(m), 1080(m), 1500 (m, occurring in C=C−M groupings), 1540 (vw), 1580(w), 1600(m). The filtrate was shown by GC/MS analysis to contain *cis*- and *trans*-stilbenes (**14** and **16**) in a 9:1 ratio.

Treatment of the pale red solid **15** with glacial acetic acid in THF gave, upon hydrolytic workup, a quantitative yield of only *trans*-stilbene.

Finally, a 1.00-g sample of **7** in THF was treated with degassed 6 N DCl in D_2O to give the deuteriated pale red solid, PhCD=CPh(NiCl·Bpy) (**15a**). In separate reactions then, **15a** was treated either with HOAc in THF or with DOAc in THF. In the former reaction, only *trans*-stilbene-d_1, $C_6H_5CD{=}CHC_6H_5$ (**16a**), was formed. In the latter reaction, only *trans*-stilbene-$d_{1,2}$, $C_6H_5CD{=}CDC_6H_5$ (**16b**), was found.

Cyclotrimerization of Diphenylacetylene (22) by (Bpy)(Ph−C≡C−Ph)Ni (7): A sample of **7** (395 mg, 1.0 mmol) and diphenylacetylene (1.00 g, 5.6 mmol) was heated in refluxing toluene for 2 days. During this time a white precipitate formed in the dark red solution. After hydrolytic workup the solid was filtered off and shown to be hexaphenylbenzene (**23**) (0.75g, 75%). − IR (mineral oil): $\tilde{\nu}$ = 700(m), 735(w), 790(w), 1380(m), 1465(s). − m.p. >400°C. The organic layer contained mainly unchanged **22** and traces of stilbenes **14** and **16**.

Cyclotrimerization of Dimethyl Acetylenedicarboxylate (24) by (Bpy)(Ph−C≡C−Ph)Ni(0): A sample of **7** (5.5 mmol, 2.17 g) and **24** (15 mmol, 2.13 g) was heated in refluxing benzene for 36 h. Usual hydrolytic workup provided an 80% yield (1.70 g) of hexamethyloxycarbonylbenzene (**25**) , m.p. 186−188°C (from THF/H_2O), identified by MS and ^1H NMR spectroscopic data. Traces of stilbenes, but no hexamethylbenzene, were observed.

Co-cyclotrimerization of Dimethyl Acetylenedicarboxylate (24) and Diphenylacetylene Derived from (Bpy)(Ph−C≡C−Ph)Ni (7): A sample of **7** (5.9 mmol, 2.33g) and **24** (13 mmol 1.85g) dissolved in 30 mL of THF was stirred for 18 h at 25 °C. After hydrolytic workup and column chromatographic separation of the organic products on silica gel (40−60 mesh) with ethyl ether/hexane as the eluting solvent, the following products were obtained and identified by MS and ^1H NMR spectroscopic data: hexamethyloxycarbonylbenzene (65%) (**25**); 1,2,3,4-tetramethyloxycarbonyl-5,6-diphenylbenzene (**26**) (20%), m.p. 221−222°C. − ^1H NMR ($CDCl_3$): δ = 3.42 (s, 6 H), 7.03 (s, 5 H). − IR (mineral oil): $\tilde{\nu}$ = 710(s), 1000(m), 1100(s), 1210(m), 1460(s). − dimethyl fumarate (10%). − m.p. 102−103°C. − ^1H NMR ($CDCl_3$): δ = 3.78 (s, 6 H), 6.80 (s, 2 H); and *trans*-stilbene (5%).

Attempted Co-oligomerization of Diphenylacetylene (22) and Benzonitrile (5) in the Presence of $(COD)_2Ni$: To a solution of $(COD)_2Ni$ (62.0 mg, 0.226 mmol) in 5 mL THF was added a mixture of benzonitrile (232 mg, 2.26 mmol) and diphenylacetylene (805 mg, 4.52 mmol) in 10 mL of THF. The reaction mixture was then stirred at 25 °C for 24 h. A 2-mL sample of the reaction mixture was hydrolyzed with 4 mL of 3N HCl. The organic layer was then neutralized with sodium bicarbonate and dried over magnesium sulfate. The solvent was removed under reduced pressure and the product mixture was analyzed by GC. Diphenylacetylene (conversion of 5%), benzonitrile (conversion of less than 1%) and *cis*-stilbene (yield of 3%) were identified by the co-injection of authentic samples.

The rest of the reaction mixture was heated at reflux for 24 h. After one hour of reflux a white solid separated and the color of the solution turned brown. When the reaction mixture was cooled to 25 °C, the crystalline solid was filtered off from the solution and washed twice with small amounts of THF. The organic layer was hydrolyzed with 20 mL of 3 N aqueous HCl and neutralized with aqueous $NaHCO_3$. The organic layer was dried over $MgSO_4$ and the solvent was removed under reduced pressure. Analysis by GC showed the presence of diphenylacetylene (**22**) (33%), benzonitrile (**5**) (85%) and *cis*-stilbene (3%) (**14**). The white solid, 512 mg (65%), was confirmed to be hexaphenylbenzene (**23**) by the following spectral characterization: ^1H NMR ($CDCl_3$, TMS): δ = 6.84 (m). − ^{13}C NMR ($CDCl_3$): δ = 125.13, 126.54, 131.36, 140.28 and 140.60 (m). − IR (KBr): $\tilde{\nu}$ = 559(vs), 690(vs), 728(vs), 780(vs), 1028(s), 1072(s), 1406(vs), 1448(vs), 1500(vs), 1607(vs), 3040(vs), 3070(s), 3090 (m) cm^{-1}. − MS (70eV): *m/z* = 534 [M^+]. A mass spectral search for the parent ion of pentaphenylpyridine, 548, was negative.

Reaction of (Bpy)(PhC≡CPh)Ni (7) with Benzonitrile (5): A solution of (Bpy)(PhC≡CPh)Ni (228 mg, 0.580 mmol) in 10 mL THF was cooled to −78 °C, after which pure benzonitrile (107 mg, 0.598 mmol) was added dropwise. The reaction mixture was warmed to 25 °C and stirred at this temperature for 2 days. The reaction mixture was then heated at reflux for 6 h and then quenched with 20 mL of 2N aqueous HCl. The organic layer was neutralized with aqueous $NaHCO_3$ and dried over anhydrous $MgSO_4$. According to GC/MS analysis and co-injection with authentic samples (provided by American Peptid Corp., Sunnyvale, CA), the *cis*- and *trans*-1,2,3-triphenylpropen-1-ones (**32**) were found to be the main products. Total yield of the *cis*- and *trans*-isomers was 40%. *cis*-Stilbene (**14**) (53%) was also one of the main products. Minor products (≈2%) were 1,2,3,4-tetraphenyl-1,3-butadiene isomers and *trans*-stilbene. Spectral characterization of the products by GC-MS analysis follows: *cis*- and *trans*-1,2,3-triphenylpropen-1-ones: $C_{21}H_{16}O$: *m/z* = 284 $[M]^{\cdot+}$, 179 $[C_{14}H_{11}]^{\cdot+}$, 105 $[C_7H_5O]^{\cdot+}$, 77 $[C_6H_5]^{\cdot+}$, isomeric butadiene derivatives of MF, $C_{28}H_{22}$: *m/z* = 358 $[M]^{\cdot+}$, 267 $[C_{21}H_{15}]^{\cdot+}$, 179 $[C_{14}H_{11}]^{\cdot+}$, 178 $[C_{14}H_{10}]^+$. − IR spectrum (thin film): C=O absorption of 1,2,3-triphenylpropen-1-one at 1652 cm^{-1}.

Similar reactions were carried out in toluene both at 25 °C and under reflux. The workup procedures were identical with that of the reaction carried out in THF. For the reaction in toluene at 25 °C for 8 days, the *cis*- and *trans*-stilbenes **14** and **16** were the main

products with a *cis*- to *trans* ratio of 1.3:1.0 and the total yield in stilbenes of 68%. Also 31% of diphenylacetylene was recovered from the nickel complex. The reaction carried out in toluene under reflux for 8 h gave only 10% of *cis*-stilbene with 85% of the diphenylacetylene recovered. Traces (<2%) of hexaphenylbenzene were found but neither the 1,2,3,-triphenylpropen-1-ones nor the 1,2,3,4-tetraphenyl-1,3-butadienes were detected.

Oligomerization of Benzonitrile (5) Mediated by Various Nickel(0) Complexes

By $(COD)_2Ni$: To a solution of $(COD)_2Ni$ (289 mg, 1.05 mmol) in 10 mL THF was added benzonitrile (0.215 mL, 216 mg, 2.10 mmol) dropwise at 25 °C and the reaction mixture then stirred for 7 days. The color of the solution changed immediately from yellow to red and then slowly to dark-brown. Samples withdrawn at reaction times of 24 h, 48 h and 7 days were hydrolyzed with 3 N aqueous HCl, neutralized with aqueous $NaHCO_3$ and finally dried over anhydrous $MgSO_4$. The resulting product mixtures were analyzed by GC and GC-MS. After 7 days at 25 °C the main products were identified as benzaldehyde (**21**) (13%) and benzyl phenyl ketone (**33**) (15%) with the conversion of benzonitrile at about 30%. When small amounts of dry air were slowly admitted to the reaction mixture, variable amounts of benzamide were detected in the hydrolysis products. Characterization of benzyl phenyl ketone by GC:MS: $C_{14}H_{12}O$: m/z = 196 $[M]^{\cdot+}$, 105 $[C_7H_5]^{\cdot+}$, 91 $[C_7C_7]^{\cdot+}$, 77 $[C_6H_5]^{\cdot+}$.

A similar reaction run to the foregoing was conducted, except that a 2:1 ratio of $(COD)_2Ni$:**5** was allowed to react in THF for 24 h. Hydrolytic workup showed that an 80% material recovery was obtained with the complete consumption of benzonitrile and the formation of a 96:4 molar ratio of **33:21**.

The reaction of benzonitrile with $(COD)_2Ni$ was also conducted in neat benzonitrile. Thus, freshly distilled and degassed benzonitrile (3 mL, 29.4 mmol) was added to $(COD)_2Ni$ (245 mg, 0.892 mmol) at 0 °C whereupon the reaction mixture changed immediately from yellow to bright red. After 10 min at 0 °C 15 mL of 3N hydrochloric acid was added. The usual workup procedure showed that 10% of benzaldehyde but less than 5% of benzyl phenyl ketone was formed. The same reaction carried out at 25 °C over 24 h yielded no **33** and only 10% of benzaldehyde.

By $(COD)_2Ni$ and iBu$_3$Al: The dropwise addition of iBu$_3$Al (0.25 mL, 1.00 mmol) to a solution of $(COD)_2Ni$ (275 mg, 1.00 mmol) in 10 mL of toluene turned the initially yellow solution brown. Subsequent introduction of benzonitrile (0.10 mL, 1.00 mmol) caused the gradual development of a red color. The resulting mixture was stirred for 7 days, hydrolyzed and after the usual workup analyzed by GC-MS procedures. A 42% yield (68 mg) of isobutyl phenyl ketone (**49**) was obtained: MS (70 eV): m/z = 162 $[M]^{\cdot+}$, 120 $[C_8H_8O]^{\cdot+}$, 105 $[C_6H_5CO]^{\cdot+}$, 77 $[C_6H_5]^{\cdot+}$. − IR (Film): $\tilde{\nu}$ = 1680 cm^{-1}. Benzyl phenyl ketone (5%) and benzophenone (1%) were also identified.

By $(Et_3P)_4Ni$: To a solution of the phosphane complex (458 mg, 0.914 mmol) in 15 mL of THF was added benzonitrile (0.186 mL, 188 mg, 1.83 mmol) of. The color of the solution changed from red-purple to green immediately. The reaction mixture was stirred at 25 °C for 7 days. Usual hydrolytic workup and a GC/MS analysis of the organic products showed that ethyl phenyl ketone (**44**) was the main product (60%, 130 mg) and **21** (5%) and **33** (10%) were minor products.

44: MS: m/z = 134 $[M]^{\cdot+}$, 105 $[PhCO]^{\cdot+}$, 77 $[C_6H_5]^{+}$. − IR (film): $\tilde{\nu}$ = 1684 cm^{-1}.

By (Bpy)(COD)Ni: To the freshly made complex **7** (0.82 mmol) were added 15 mL of THF and benzonitrile (0.166 mL, 168 mg, 1.63 mmol). The reaction mixture was stirred at 25 °C for 7 days with no apparent color change of the dark solution. The reaction was quenched with 20 mL of 2 N aqueous HCl and then neutralized with aqueous $NaHCO_3$. The GC analysis of the dried organic layer showed that benzyl phenyl ketone **33** had formed in 20% yield, but benzaldehyde was found in only 5% yield. The conversion of benzonitrile was 30%.

The same reaction carried out at reflux for 24 h, but only benzaldehyde was obtained in a yield less than 5%; no deoxybenzoin was detected.

By $Ni(acac)_2$/Et_3Al: To a mixture of $Ni(acac)_2$ (203 mg, 0.791 mmol) and benzonitrile (0.161 mL, 163 mg, 1.58 mmol) in 15 mL of toluene was added slowly triethylaluminum (0.216 mL, 180 mg, 1.58 mmol). The color of the solution turned immediately from green to dark brown. After the reaction mixture had been stirred at 25 °C for 24 h, hydrolytic workup and analysis showed that **33** was formed in 15% yield.

By $(COD)_2Ni/MeAlCl_2$: a) Adding Benzonitrile to the Mixture of $(COD)_2Ni$-$MeAlCl_2$ in Toluene: One milliliter of a 1 M hexane solution of $MeAlCl_2$ was added dropwise to a solution of $(COD)_2Ni$ (276 mg, 1.00 mmol) in 10 mL of toluene. The formation of a nickel mirror and a black precipitate were immediately formed. To this mixture was added benzonitrile (0.10 mL, 1 mmol) and the reaction mixture stirred at 25 °C for 24 h. The usual workup procedure and subsequent GC analysis showed that no reaction between benzonitrile and the nickel complex had occurred. Of interest is that about 90% of the 1,5-cyclooctadiene had been isomerized to its 1,3-isomer.

b) Adding $(COD)_2Ni$ to the Mixture of Benzonitrile and $MeAlCl_2$ in Toluene: A solution of $(COD)_2Ni$ (291 mg, 1.06 mmol) in 8 mL of toluene was added to a mixture of benzonitrile (0.11 mL, 1.06 mmol) and 1.06 mL of a 1 M hexane solution of $MeAlCl_2$ in 7 mL toluene and the reaction mixture then stirred for 24 h at 25 °C. After hydrolysis and GC analysis benzyl phenyl ketone (**33**) was found in 20% yield but no trace of benzaldehyde was detected.

By comparison, a similar reaction run in which the $MeAlCl_2$ was added to a mixture of $(COD)_2Ni$ and benzonitrile in toluene led to the formation of no organic products.

Oligomerization of Substituted Benzonitriles by $(COD)_2Ni$

Pentafluorobenzonitrile: A reddish solution of $(COD)_2Ni$ (1.27 mmol) and 2.54 mmol of the nitrile in 10 mL of THF was stirred at 25 °C for 24 h, during which time it turned pale yellow. Usual hydrolytic workup permitted the recovery of only 20% of the nitrile and yielded only pentafluorobenzene and no other organic products. It is assumed that any nickel(0) complex with the nitrile underwent decyanation with the loss of the C_6F_5 group (vide infra).

4-Methoxybenzonitrile: A red solution of $(COD)_2Ni$ (1.00 mmol) and 2.0 mmol of the nitrile in 10 mL of THF was stirred at 25 °C for 24 h, during which time it turned dark brown. Usual hydrolytic workup and GC-MS and NMR analysis showed the presence of 75% of the nitrile, 15% of 4-methoxybenzyl 4-methoxyphenyl ketone and 10% of 4-methoxybenzaldehyde with only a trace of anisole (material balance of 90%).

In an identical reaction extended over 6 days, the material balance fell to 60% and anisole was now a significant product (25%).

Reaction of Nickel Metal with Benzonitrile at Reflux: To a solution of $Ni(acac)_2$ (2.56 g 10.0 mmol) in 30 mL of THF was added *n*-

butyllithium (12.5 mL, 20.0 mmol, 1.6 M in hexane) at −78 °C, and the resulting mixture was allowed to come to 25 °C over 2 hours. The black suspension was then evaporated to dryness under reduced pressure. Under argon dry benzonitrile (degassed under Ar and freshly distilled from P_2O_5, 13 mL, 0.13 mol) was added and the reaction mixture was heated at reflux (190−195 °C) for 40 hours. The resulting dark gray suspension was evaporated to dryness under vacuum and the solid residue was then slurried with toluene and hydrolyzed with 3 N aqueous HCl. Concentration of the dried toluene extract led to the deposition of 2,4,6-triphenyltriazine (**6**) (50 mg, 0.5%): ^{1}H NMR ($CDCl_3$): δ = 7.61−7.58 (m, 9 H), 8.80−8.77 (d of d, 6 H). − ^{13}C NMR ($CDCl_3$): δ = 128.64, 128.99, 132.49, 136.31, 171.71). Evaporation of the toluene filtrate left a residue of 45% of recovered benzonitrile.

The reaction of nickel metal with refluxing benzonitrile was repeated six times, with the nickel metal being generated initially from either $NiBr_2$ or $Ni(acac)_2$ and two equivalents of *n*-butyllithium in THF, as described above. In each case, only traces of **6**, or none at all, were detected in the benzonitrile residue.

The low recovery of benzonitrile in certain runs (<50%) was an indication of decomposition of **5** by catalytic decyanation.[34] Verification of this side reaction was obtained by cooling the unhydrolyzed reaction mixture and filtering off the yellow brown precipitate. This solid was freed of organic matter by extraction with toluene to leave a residue of nickel metal and $Ni(CN)_2$. The presence of $Ni(CN)_2$ was established by a "Prussian Blue" test. The addition of aqueous ammonium hydroxide dissolved the $Ni(CN)_2$, leaving the Ni metal residue. To this ammoniacal extract were added, successively, aqueous $FeSO_4$ and then aqueous $FeCl_3$, whereupon a deep blue precipitate formed.

Reaction of Nickel Metal with Benzonitrile at Reflux (Presence of Oxygen and Moisture): In conducting the foregoing reaction it was observed in certain runs that the initially dark gray nickel suspensions turned to a yellow-green color. This color change was shown to be caused by adventitious entry of moist air into the reaction vessel. In such runs, 2,4,6-triphenyl-1,3,5-triazine and other reaction products were found upon hydrolysis. Thus a reaction run as the foregoing with $Ni(acac)_2$ as the source of Ni metal gave a yellow-brown suspension after 50 h at 195 °C under an argon atmosphere. The toluene extract was concentrated to 25 mL and then was allowed to stand at −10 °C for several days to allow crystallization. After the supernatant liquid was removed with a cannula the cluster of deposited red crystals, which proved unsuitable for XRD analysis, was quenched with degassed 6 N HCl. After Et_2O extraction the organic layer was neutralized with sodium bicarbonate, dried over anhydrous magnesium sulfate and evaporated under reduced pressure. The major organic product proved to be 1,3-diphenyl-1,3-propanedione (30 mg, 5%). − ^{1}H NMR ($CDCl_3$) δ = 4.63 (s, 2 H, diketone tautomer), 6.86 (s, 1 H, enolate vinyl hydrogen), 7.57−7.47 (m, 6 H), 8.11 (d, 4 H), 16.85 (s, 1 H, enolate OH). − ^{13}C NMR ($CDCl_3$): δ = 93.17, 127.17, 128.68, 132.47, 135.61, 185.78. − MS (Positive Ion Electrospray): *m*/*z* = 225 $[MH]^+$, 105.

After the usual hydrolytic workup of the supernatant liquid the organic residue obtained was purified by flash chromatography [silica gel, gradient elution with hexanes, hexanes/dichloromethane (4:1), and hexanes/ethyl acetate (3:1)] to give 2,4,6-triphenyl,1,3,5-triazine (**6**, 2%, based on starting **5**) and 4,5,6-triphenylpyrimidine (0.3%), for which latter product the following spectral data were obtained: ^{1}H NMR ($CDCl_3$): δ = 7.60−7.52 (m, 9 H), 8.03 (s, 1 H), 8.31−8.29 (d of d, 4 H), 8.74−8.72 (d of d, 2 H). − ^{13}C NMR ($CDCl_3$): δ = 110.31, 127.31, 128.45, 128.50, 128.92, 130.62, 130.76, 137.63, 164.82. − DEPT (CH only): δ = 110.30, 127.29, 128.44, 128.49, 128.92, 130.63, 130.76. − CIMS: 309 $[MH]^+$, 205, 102).

The product mixture from the last chromatographic fraction was concentrated and the residue was analyzed by ^{1}H and ^{13}C NMR spectroscopy. Small amounts of hexaphenylbenzene and benzamide (<1%) were observed. The origin of these products can be reasonably ascribed to the benzamide formed from benzonitrile by adventitious moist air[35] and detailed consideration of their generation will be the subject of future publications.

X-ray Crystallographic Study of 2,2′-Bipyridyl(η^2-diphenylacetylene)nickel (7): Crystal Mounting and Data Collection: A black crystal of **7**, 0.58 × 0.58 × 0.14 mm in size, was mounted with a perfluorinated polyether oil on the tip of a glass fiber on the goniometer head and cooled immediately by an argon current to −173 °C. Intensity data were collected with an Enraf−Nonius CAD4 diffractometer by a coupled ω-2θ scan technique with speeds varying from 1.0 to 10.0°/min depending on the standard deviation to intensity ratio of a preliminary 10°/min scan. The radiation employed was Mo-K_α with a graphite monochromator. The crystals of molecular weight 393.1 g mol^{-1} have two independent molecules per unit cell and have a calculated density of 1.35 Mg m^{-3}; they belong to the monoclinic crystal system and the space group of $P2_1/c$, No. 14. The two independent molecules in the asymmetric unit cell of **7** have the same atom separations within the margin of experimental error. They differ only with respect to their torsion angles. Both Ni centers are absolutely planar (sum of angles equals 360°. All other geometrical data correspond to expected values.

The absorption corrections were made by the ψ-scan method. Observed reflections were defined as those reflections with $I \geq 2\sigma(I)$. Only these were used in the solution and refinement of the structure (*F* refinement). For refinement based on F^2 all reflections were used. Refinement was done by least-squares; the quantity minimized was $\Sigma w(|Y_o| - |Y_c|)^2$, with $Y = F$ or F^2. Computations were done using VAX, Sun4, and Silicon Graphics computers. In addition to several locally written programs, the following software was used: S. L. Lawton, R. A. Jacobson, TRACER (cell reduction), United States Energy Commission, Report IS-1141, Iowa State University, USA, **1965**. P. Coppens, L. Leiserowitz, D. Rabinovich, DATAP (data reduction), *Acta Crystalogr.* **1965**, *18*, 1035. G. M. Sheldrick, SHELXS-86 (crystal structure determination), *Crystallographic Computing 3* (Eds: G. M. Sheldrick, C. Krüger, R. Goddard), Clarendon Press, Oxford, **1985**, dp. 185. G. M. Sheldrick, *SHELXL-93* (least-squares refinement), University of Göttingen, **1993**. E. Egert, G. M. Sheldrick, *PATSEE* (structure solution), *Acta Crystallogr.* **1985**, A41, 262. P. Main, S. J. Fiske, S. E. Hull, L. Lessinger, G. Germain, J.-P. Declercq, M. M. Woolfson, *MULTAN80* (structure solution), University of York, England and Louvain, Belgium, **1980**. W. R. Busing, K. O. Martin, H. A. Levy, *GFMLX a highly modified version of ORFLS* (full-matrix least-squares refinement), Report ORNL-TM-305, Oak Ridge National Laboratory, Tennessee, USA, **1962**; H. D. Flack, (enantiomorph-polarity estimation), *Acta Crystallogr.* **1983**, *A39*, 876. P. Roberts, G. M. Sheldrick, *XANADU* (calculation of best planes, torsion angles and idealized hydrogen atom positions), University of Cambridge, England, **1976**. R. E. Davis, D. R. Harris, *DAESD* (calculation of distances and angles), Roswell Park Mem. Inst., USA, **1970**. V. Schomaker, K. N. Trueblood, *RIGID* (rigid-body analysis) *Acta Crystallogr.* **1968**, B24, 63. C. K. Johnson, *ORTEP* (thermal ellipsoid plot program), Report ORNL-5138, Oak Ridge National Lab., Tennessee, USA, **1976**. E. Keller, *SCHAKAL* (molecular drawing), *Chem. Unserer Zeit* **1986**, *20*, 178. B. W. van der Waal, *FSYN* (slant

plane Fourier syntheses), Technical University of Enschede, Netherlands, **1975.** *SYBYL* (molecular calculations), Tripos Associates, Inc., St. Louis. *INSIGHT*/*DISCOVER*, Biosym Technologies, San Diego, USA.

Crystallographic data (excluding structure factors) for the structure reported in this paper have been deposited with the Cambridge Crystallographic Data Centre as supplementary publication no. CCDC-144795. Copies of the data can be obtained free of charge on application to CCDC, 12 Union Road, Cambridge CB2 1EZ, UK (Fax: (internat.) + 44-1223/336-033; E-mail: deposit@ccdc.cam.ac.uk].

Acknowledgments

The foregoing research was initiated under a grant from the U. S. National Science Foundation, fostered with support of the U. S. Department of Energy, and brought to a successful conclusion with financial aid to the principal investigator through an Alexander von Humboldt Senior Scientist Award. Valuable orienting experiments and technical assistance have been provided by Drs. Mona Singh and Yun Qian.

[1] Leading literature citations: [1a] W. Reppe, O. Schlichting, K. Klager, T. Toepel, *Justus Liebigs Ann. Chem.* **1948**, *560*, 1. – [1b] W. Reppe, O. Schlichting, H. Meister, *Justus Liebigs Ann. Chem.* **1948**, *560*, 93. – [1c] W. Reppe, W. Schweckendiek, *Justus Liebigs Ann. Chem.* **1948**, *560*, 104.

[2] Comprehensive reviews of such oligomerizations: [2a] B. Bogdanovic, B. Henc, A. Lösler, B. Meister, H. Pauling, G. Wilke, *Angew. Chem.* **1974**, *85*, 39. – [2b] G. Wilke, *J. Organomet. Chem.* **1980**, *200*, 349. – [2c] J. J. Eisch, S. R. Sexsmith, *Res. Chem. Intermed.* **1990**, *13*, 149.

[3] *Comprehensive Organometallic Chemistry II*, Vol. 12 (Eds.: E. W. Abel, F. G. A. Stone, G. Wilkinson), Pergamon Press, Oxford, **1995**.

[4] Overviews: [4a] J. W. Copenhaver, M. H. Bigelow, *Acetylene and Carbon Monoxide Chemistry*, Reinhold, New York, **1960**. – [4b] G. N. Schrauzer, *Adv. Organomet. Chem.***1964**, *2*, 1.

[5] The actual catalyst for the cyclotetramerization of acetylene is thought to be "naked" nickel(0) in all cases ("naked" meaning, in G. Wilke's view, that the ligands available to nickel, such as COD, are easily displaced by the alkyne.) The induction period observed for the oligomerization with nickel(II) salts is thought to entail the necessary reduction of nickel(II) to nickel(0), the actual catalyst. If nickel(0) is added at the start, there is no induction period and the oligomerization starts promptly (Professor Günther Wilke, observations and views communicated personally to J. J. E., **1985**). In addition, cf. G. Wilke, *Pure Appl. Chem.* **1978**, *50*, 677.

[6] J. J. Eisch, J. E. Galle, *J. Organomet. Chem.* **1975**, *96*, C23.

[7] J. J. Eisch, G. A. Damesevitz, *J. Organomet. Chem.* **1975**, *96*, C19.

[8] J. J. Eisch, A. A. Aradi, K. I. Han, *Tetrahedron Lett*. **1983**, *24*, 2073.

[9] J. J. Eisch, A. M. Piotrowski, K. I. Han, C. Krüger, Y. H. Tsay, *Organometallics* **1985**, *4*, 225.

[10] J. J. Eisch, *Pure & Applied Chem*. **1984**, *56*, 35.

[11] J. J. Eisch, A. M. Piotrowski, A. A. Aradi, C. Krüger, M. J. Romano, *Z. Naturforsch.* **1985**, *40b*, 624.

[12] J. J. Eisch, J. E. Galle, A. A. Aradi, M. P. Boleslawski, *J. Organomet. Chem.* **1987**, *312*, 399.

[13] J. J. Eisch, A. A. Aradi, M. A. Lucarelli, Y. Qian, Tetrahedron Symposium-in-*Print* **1998**, *54*, 1169.

[14] S. F. A. Kettle, L. E. Orgel, *Proc. Chem. Soc.* **1959**, 307.

[15] W. Z. Heldt, *J. Organomet. Chem.* **1966**, *6*, 292.

[16] G. Oehme, H. Pracejus, *Z. Chem.* **1969**, *9*, 140.

[17] Leading references: [17a]H. Yamazaki, Y. Wakatsuki, *Tetrahedron Lett.* **1973**, 3383. – [17b] Y. Wakatsuki, H. Yamazaki, *Synthesis* **1976**, 26. – [17c] H. Bönnemann, R. Brinkmann, H. Schlenkluhn, *Synthesis* **1974**, 575.

[18] W. Keim, F. H. Kowaldt, R. Goddard, C. Krüger, *Angew. Chem.* **1978**, *90*, 493.

[19] The reported C=C separation in cyclopropene is 1.304 ± 0.003 Å: L. V. Vilkov, V. S. Mastryukov, N. I. Sadova, *Determination of the Geometrical Structure of Free Molecules*, Mir Publishers, Moscow, **1983**, p. 122.

[20] I. W. Bassi, C. Benedicenti, M. Calcaterra, G. Rucci, *J. Organomet. Chem.* **1976**, *117*, 285.

[21] I. W. Bassi, C. Benedicenti, M. Calcaterra, R. Intrito, G. Rucci, C. Santini, *J. Organomet. Chem.* **1978**, *144*, 225.

[22] M. Uchino and S. Ikeda, *J. Organomet.Chem.***1971**, *33*, C41.

[23] J. J. Eisch, Y. Qian, M. Singh, *J. Organomet. Chem.* **1996**, *512*, 207: 9-Fluorenone reacts with Ni(0) complexes to yield, upon hydrolysis, a 25% yield of the dimeric pinacol, 9,9-dihydroxy-9,9′-bifluorenol.

[24] [24a] K. I. Watanabe, *Bull. Chem. Soc. Japan* **1959**, *32*, 1290. – [24b] K. I. Watanabe, *Bull. Chem. Soc. Japan* **1964**, *37*, 1325. – [24c] K. I. Watanabe, K. Saki, *Bull. Chem. Soc. Japan* **1966**, *39*, 8.

[25] D. R. Fahey, J. E. Mahan, *J. Am. Chem. Soc.* **1976**, *98*, 4499.

[26] H. Lehmkuhl, K. Ziegler, H. G. Gellert in *Methoden der Organischen Chemie*, E. Müller, ed., Thieme Verlag, Stuttgart, vol. XIII/4, 1970, pp. 239–241.

[27] J. J. Eisch, X. Ma, M. Singh, G. Wilke, *J. Organomet. Chem.* **1997**, *527*, 301. This communication was put into print without the Elsevier Publishers sending the galley proofs to the senior author for his approval as they had promised. As a result, the published communication contains many errors in typography and layout. Since Elsevier has declined to publish this version as a corrigendum, the senior author (JJE) has been forced to prepare a completely corrected and emended version of this communication. Interested researchers can receive a copy of this corrected version by writing to the senior author.

[28] J. J. Eisch, *Organometallic Syntheses*, Vol. 2, Academic Press, New York, **1981**.

[29] M. F. Semmelhack, *Organic Reactions*, Vol. 19, Wiley, New York **1972**, p. 178.

[30] R. A. Schunn, *Inorganic Syntheses*, Vol. 15, Wiley, New York, **1974**, p. 5.

[31] C. S. Cundy, *J. Organomet. Chem.* **1974**, *69*, 305.

[32] E. Dinjus, I. Gorski, E. Uhlig, H. Walther, *Z. Anorg. Allg. Chem.* **1976,** *75*, 422.

[33] J. J. Eisch, A. M. Piotrowski, unpublished studies.

[34] For leading references to reductive cyanation by main-group and transition metal reagents, cf. J. March, *Advanced Organic Chemistry*, 4th ed., Wiley, New York, **1992**, p. 634.

[35] Precedents for the transformations of benzamide into the products observed in this reaction have been observed: 1) into triazine **6**: ref. [16]; 2) into diphenylacetylene (**22**) by subvalent titanium reagents: R. Dams, M. Malinowski, H. J. Geise, Recl. Trav. Chim. Pays-*Bas* **1982**, *101*, 112; 3) the co-oligomerization of benzonitrile, diphenylacetylene and possibly $Ni(CN)_2$ into 4,5,6-triphenylpyrimidine: Scheme 7, the present work; 4) the cyclotrimerization of **22** into hexaphenylbenzene (**23**) by nickel(0): ref.[11] and the present work; and 5) the possible coupling of two molecules of benzonitrile and $Ni(CN)_2$ by nickel(0) to form precursors to 1,3-diphenyl-1,3-propanedione coupling related to that in Scheme 8, the present work.

Received March 29, 2000
[I00121]

Reductive Activation of Tripod Cobalt Compounds: Oxidative Addition of H−H, P−H, and Sn−H Functions

Ute Winterhalter,[a] Laszlo Zsolnai,[a] Peter Kircher,[a] Katja Heinze,[a] and Gottfried Huttner*[a]

Dedicated to Prof. Dr. Peter Paetzold on the occasion of his 65th birthday

Keywords: Tripodal ligands / Cobalt / Reductive activation / Oxidative addition / Tin hydrides / Diphosphene

Treatment of the *tripod* compounds *tripod*$CoCl_2$ (**1**), and *tripod*CoCl (**2**), [*tripod* = $CH_3C(CH_2PPh_2)_3$] in THF solution under argon atmosphere with strong reducing agents such as KC_8 leads to the generation of reactive species. While the dinitrogen compound *tripod*$Co(N_2)$Co*tripod* (**3**), which is formed under N_2 atmosphere, is rather unreactive, the species formed under argon atmosphere undergo selective reactions with compounds containing P–H or Sn–H functions. With $PhPH_2$ as the reagent, the diphosphene compound *tripod*Co(η^2-PhP=PPh) (**8**), is formed in a yield (44%) similar to that achieved in the preparation of **8** from **2** and PhPHNa (60%). With Ph_3SnH as the reagent, *tripod*$CoSnPh_3$ (**9**), is obtained (yield 61%), while reaction with Bu_3SnH produces *tripod*$Co(H)_2SnBu_3$ (**10a**, 50%). The Co^I species **9** undergoes oxidative addition of dihydrogen to produce the Co^{III} compound *tripod*$Co(H)_2SnPh_3$ (**10b**), which is an analogue of **10a**. The properties of these new compounds are characterized by the usual analytical techniques, including NMR spectroscopy, cyclic voltammetry, and X-ray analysis.

Introduction

The chemistry of [*tripod*Co] templates − *tripod* = $CH_3C(CH_2PPh_2)_3$ − is well developed for the Co^{II} [1] and Co^{III} [2] oxidation states, while low-valent derivatives are still rare. On the other hand, it is well-known that templates L_3Co (L = PMe_3)[3] also possess a rich chemistry with Co in lower oxidation states. A possible entry into the chemistry of low-valent [*tripod*Co] compounds is the reduction of easily accessible [*tripod*Co^{II}] compounds such as *tripod*$CoCl_2$ (**1**) (Scheme 1),[4] by electropositive metals. Using zinc powder as the reductant,[5] the Co^I compound *tripod*CoCl (**2**), is produced,[4,6] which in itself allows access to the chemistry of [*tripod*Co^I] derivatives.[5] Reduction of **1** with Na/Hg has been found to produce *tripod*$Co(N_2)$Co*tripod* (**3**).[7]

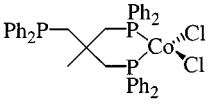

1

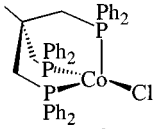

2

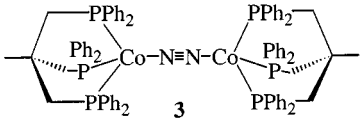

3

Scheme 1

The Co^0 compound **3** has already been tested with regard to its propensity to act as a precursor for other low-valent [*tripod*Co] species.[8] It was found, however, to be rather unreactive, while the solutions from which it is obtained are reactive due to the presence of some undefined by-products.[8] Although the reactions of such solutions with CO_2 or CS_2 furnished only the oxidized products incorporating η^2-CO_3 and η^2-S_2CO ligands,[8] their observed reactivity indicates that reduction of the metal in **1** produces highly reactive species.

In this paper, we report on the results obtained upon reduction of **1** in THF solution by KC_8 or activated Mg (Scheme 2). While *tripod*$Co(N_2)$Co*tripod* (**3**), is obtained as one of the products when this reduction is carried out under dinitrogen, reduction under argon atmosphere produces highly reactive species that undergo oxidative addition with P−H and Sn−H functions, thereby leading to derivatives such as *tripod*$Co(P_2Ph_2)$ (**8**), and *tripod*$Co(H)_2(SnR_3)$ (**10**).

Results and Discussion

Reductions of 1 and 2: Products and By-Products

Products

Reduction of a THF solution of **1** with various reductants was monitored by UV/Vis/NIR spectrophotometry,

[a] Anorganisch-Chemisches Institut der Universität Heidelberg, Im Neuenheimer Feld 270, 69120 Heidelberg, Germany
Fax: (internat.) + 49-(0)6221/545707

 © WILEY-VCH Verlag GmbH, D-69451 Weinheim, 2001 1434−1948/01/0101−0089 $ 17.50+.50/0

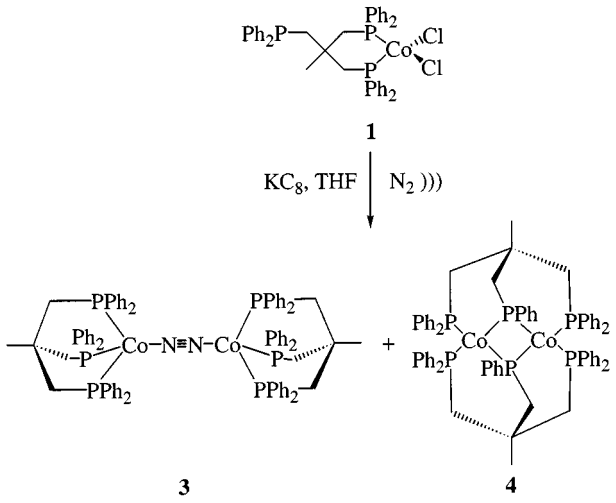

Scheme 2

this being the only simple tool suitable for analysing these highly sensitive and strongly paramagnetic solutions. Reduction with KC_8 as well as with Na/Hg under N_2 was found to produce solutions showing a strong band at around 1130 nm and a weaker absorption at around 680 nm (Figure 1b; Table 1). The relative intensities of these two bands was found to vary to some extent in different experiments, while no conditions could be found under which one of these two bands was absent. Reduction of **1** under an N_2 atmosphere with activated Mg led to spectra of type a (Figure 1a) with just one prominent band at 1130 nm. The same type of spectrum was obtained when **2** was reduced with KC_8 under N_2. Reduction of **1** or **2** under argon atmosphere with KC_8 produced solutions that characteristically showed spectra of type c (Figure 1c). The same type of spectrum was observed when **1** was reduced with Na/Hg under Ar. If the spectrum contained any signature of *tripod*-Co(N_2)Co*tripod*, **3**, this should be the band at around 1130 nm (Figure 1a). For comparison purposes, **3** was prepared by reacting **2** with KC_8 under N_2. On layering the THF solution obtained by this procedure with petroleum ether (boiling range 40−60 °C), crystals of **3** were produced. These crystals were analysed by measuring the lattice constants [a = 1794(3) pm, b = 1531.1(9) pm, c = 1279(1) pm, α = 90°, β = 94.16(6)°, γ = 90°], which were found to be identical to those reported for **3** in the literature.[7] The UV/Vis/NIR spectrum of a solution of this authentic crystalline sample of **3** in THF was recorded. The band at around 1130 nm (Figure 1a) was found to coincide with the intrinsic absorption of **3** [λ_{max} (ε) = 405 (8000), 718 (550), 1134 nm (4700) $M^{-1}cm^{-1}$]. This result, together with the result obtained by comparing the UV/Vis/NIR spectra in Figure 1 (a, b: N_2 atmosphere; c: Ar atmosphere), indicates that the compound giving rise to the band at 1130 nm, which is only present when the experiment is performed under N_2, is the dinitrogen compound **3** itself. The compound giving rise to the band at 680 nm (Figure 1, b and c) is not identified as such. Again, on the basis of the UV/Vis/NIR spectra, it cannot be the Co^I species *tripod*CoCl that shows a completely different spectrum[4] [λ_{max} (ε) = 530 (120, sh), 826 (150), 1131 (430), 1224 (450) $M^{-1}cm^{-1}$].

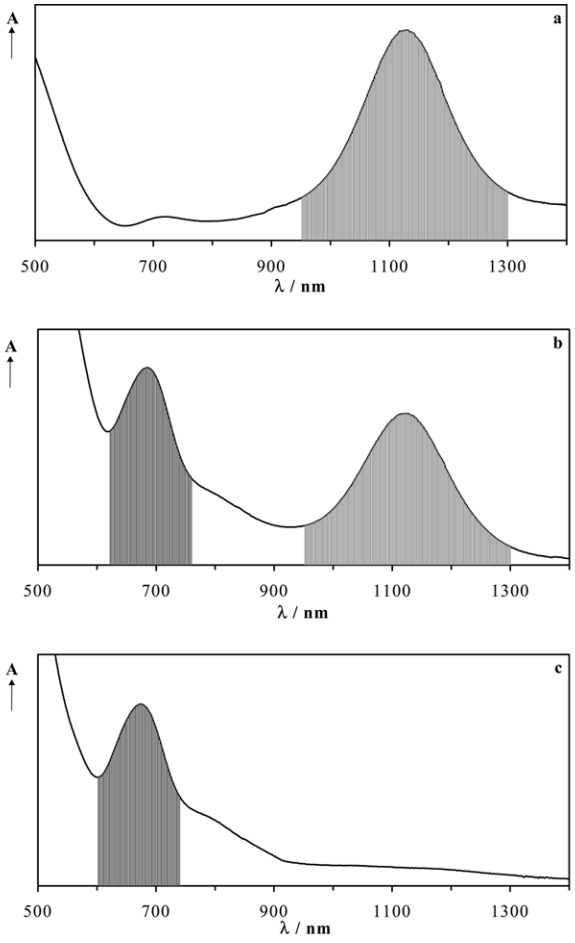

Figure 1. Electronic spectra of solutions obtained by reducing THF solutions of **1** or **2** under N_2 or Ar.
a: Spectrum of **3**, N_2 atmosphere. − **b**: Spectrum observed after reducing **1** or **2** under an N_2 atmosphere; for experimental conditions, see Table 1. − **c**: As **b**, but with Ar atmosphere instead of N_2; for experimental conditions, see Table 1

Table 1. Starting compounds, reductants, and inert gases used to produce compounds with the spectral signature shown in Figure 1

Comp.	Reductant	Atmosphere	Spectrum
1	Mg	N_2	a
2	KC_8	N_2	a
1	KC_8	N_2	b
1	Na/Hg	N_2	b
1	KC_8	Ar	c
2	KC_8	Ar	c
1	Na/Hg	Ar	c

By-Products

The nature of the compound giving rise to the absorption at 680 nm is not known. It is, however, known that this species is the reactive one since **3** (band at 1130 nm, Figure 1a and 1b) is unreactive with respect to the reactions reported in this paper. Only solutions showing the absorption at 680 nm have been found to undergo reactions with

the reagents used. Among the products generated upon reduction of **1**, the dicobalt species $[CH_3C(CH_2PPh_2)_2CH_2PPh]_2Co_2$ (**4**), is occasionally obtained in low yields in the form of a crystalline material.

The constitution of **4** shows that it is only a minor by-product that cannot be responsible for the generation of the compounds obtained upon reactions of solutions showing the band at 680 nm with various substrates (see later). Thus, **4** has been dephenylated at the *tripod* ligand, whereas all the products described herein contain an intact ligand. The FAB mass spectrum of crystalline **4** shows peaks at m/z = 1212 [M^+] and 606 [M^{2+}]. The structure of **4** has been determined by X-ray analysis (Figure 2, Table 2 and 8).

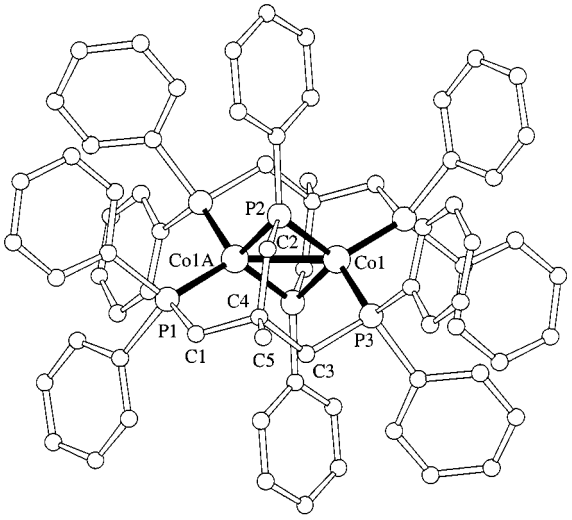

Figure 2. Structure of **4**, which has crystallographic inversion symmetry; atoms related to atom *i* by this symmetry are labelled as atom *i*A throughout

Table 2. Selected bond lengths [pm], bond angles [°], and torsion angles [°] in **4**

	4
Co1−P1A[a]	215.23(7)
Co1−P2	215.17(8)
Co1−P3	213.69(7)
Co1−P2A	216.07(7)
Co1−Co1A	233.41(6)
P1−C1	189.0(3)
P2−C2	184.7(3)
P3−C3	185.7(3)
$P-C_{Ph}$	183.3(3)−184.9(3)
$C_{CH_2}-C4$	155.0(4)−156.6(4)
P1A−Co1−P2	126.94(3)
P1A−Co1−P2A	95.11(3)
P1A−Co1−P3	113.24(3)
P2−Co1−P2A	114.46(2)
P2−Co1−P3	92.45(3)
P2A−Co1−P3	116.40(3)
P1A−Co1−Co1A	129.53(3)
P2A−Co1−Co1A	57.04(2)
P2−Co1−Co1A	57.42(2)
P3−Co1−Co1A	116.82(3)
Co1−P2−Co1A	65.54(2)
P2−Co1−P3−C3	56.1
Co1−P3−C3−C4	−65.7
P3−C3−C4−C2	5.2
C3−C4−C2−P2	50.4
C4−C2−P2−Co1	−42.5
C2−P2−Co1−P3	−13.3
P2−Co1A−P1−C1	−44.6
Co1A−P1−C1−C4	16.3
P1−C1−C4−C2	48.7
C1−C4−C2−P2	−75.8
C4−C2−P2−Co1A	32.3
C2−P2−Co1A−P1	23.7

[a] Atom labels refer to Figure 2. The molecular structure shows centrosymmetric symmetry. In Figure 2, the atom related to atom *i* by this symmetry is labelled as atom *i*A.

The formation of **4** from **1** may possibly be rationalized by considering that in THF solutions of **1** the *tripod* ligand is present in a bidentate binding mode with only two of its donor groups coordinated to the metal and the third one remaining as a dangling arm.[4] Since it has been shown that reductive dephenylation[9] of *tripod* ligands may occur in complexes as well as in the free ligand, it is tempting to assume that in the case of **1** the noncoordinated PPh_2 group is preferentially dephenylated. This assumption might explain the formation of the phosphido group of the ligand $[CH_3C(CH_2PPh_2)_2CH_2PPh]^-$ in **4**.

The molecules of **4** are centrosymmetric, containing a dicobalt unit at the centre. This unit is bridged by two CH_2PPh^- phosphido groups in a μ_2 manner. Each of these phosphido groups is part of one $[CH_3C(CH_2PPh_2)_2CH_2PPh]^-$ tripodal entity, with the two CH_2PPh_2 groups of each of these ligands coordinating to a Co centre (Figure 2). Each Co centre is thus coordinated by four P atoms in a coordination polyhedron that is best described as distorted tetrahedral, with the corresponding P−Co−P angles in the range 92.5−126.9° (Table 2). The binding mode of the $[CH_3C(CH_2PPh_2)_2CH_2PPh]^-$ ligand in **4** is similar to that observed for the $[CH_3C(CH_2PPh_2)_2CH_2S]^-$ ligand in $\{[CH_3C(CH_2PPh_2)_2CH_2S]_2Ni_2\}^{2+}$,[10] where the thiolate function acts as a μ_2 bridging group. In this dinickel compound, the coordination geometry about the Ni centres is idealized square planar, in contrast to the idealized tetrahedral surroundings of the Co centres in **4**. As a consequence, there is some strain in the chelate scaffolding of **4**. The six-membered chelate rings formed by the phosphido phosphorus, one phosphane donor, and the three-carbon chain at each of the two Co centres (Figure 2) have rather irregular twist conformations (torsion angles in Table 2). The most marked twists are seen along the sequences P2−Co1−P3−C3 (56.1°) and C3−C4−C2−P2 (50.4°). These torsion angles are of similar size and equal sign as characteristic for a twist conformation. The corresponding torsion angles P2−Co1A−P1−C1 (−44.6°) and C1−C4−C2−P2 (−75.8°) in the chelate cycle about Co1A are also similar in size and equal in sign as befits a twist conformation.

In terms of its bonding, **4** is an analogue of $(PMe_3)_4(\mu_2\text{-}PMe_2)_2Co_2$,[3c] in which the phosphane and phosphido groups act as isolated ligands as opposed to being covalently linked in **4**. The basic geometries of these two compounds are correspondingly similar. Both compounds show a planar $[Co_2(\mu_2\text{-}P_2)]$ cyclic arrangement with short transannular Co−Co distances of just 236 pm in the PMe_3 derivative and 233 pm in **4**. The short Co−Co distance in the

former has been interpreted in terms of the formation of a Co−Co double bond, in agreement with the diamagnetism of this compound as inferred from its NMR spectra. No NMR spectra of **4** could be recorded since, once crystallized, the compound proved to be insoluble in both apolar (toluene) and polar (CH_2Cl_2, DMA, THF) solvents. Although the diamagnetism of **4** has not been proved experimentally, the close similarity of the basic structural arrangements in $(PMe_3)_4(\mu_2\text{-}PMe_2)_2Co_2$ and **4** can be taken to indicate similar bonding.

A selective synthesis of **4** might be envisaged as being possible through the reaction of $[CH_3C(CH_2PPh_2)_2CH_2PPh]^-$ with Co salts under reductive conditions. For this purpose, the *tripod* ligand $CH_3C(CH_2PPh_2)_2CH_2PHPh$ (**6**), was synthesized from the easily accessible precursor $CH_3C(CH_2PPh_2)_2CH_2Cl$, **5** (Scheme 3).[10]

5 **6**

Scheme 3

Thus, a solution of **5** in DMSO was treated with a solution of PhPHK, prepared from KO*t*Bu and $PhPH_2$, in the same solvent, to furnish the *tripod* ligand **6**. After chromatographic workup, **6** was obtained as a viscous, colourless oil in 82% yield.

When a THF solution of **6** was treated with $CoCl_2$, a green solution was obtained, which, by analogy with the reaction of *tripod* with $CoCl_2$, could be expected to contain η^2-**6**·$CoCl_2$.

Addition of KC_8 to such a solution resulted in a brown slurry, from which minor amounts ($\leq$ 5%) of **4** could be isolated by crystallization. That **4** had indeed been formed was confirmed by the mass spectrum of the material produced, which was identical to those obtained from crystalline samples of **4** prepared starting from *tripod* (see above), as well as by comparison of the unit cell dimensions determined for crystals of the relevant samples.

The formation of **4** from *tripod*$CoCl_2$ under the strongly reducing conditions used to generate the dinitrogen compound **3** under an atmosphere of dinitrogen (Figure 1a) or a reactive species (Figure 1c) under argon is evidently a minor side reaction since all the other products described in this paper, as obtained from such strongly reducing solutions, are found to contain the intact $CH_3C(CH_2PPh_2)_3$ ligand showing no signs of dephenylation.

Reactivity of the Solutions Obtained from 1 or 2 by Reduction in THF under Argon

The THF solutions obtained by reducing *tripod*$CoCl_2$ (**1**), or *tripod*CoCl (**2**), with strong reducing agents such as KC_8 or Na/Hg under argon atmosphere all showed the same type of UV/Vis/NIR spectrum (Figure 1c). Irrespective of the coordination compound (**1** or **2**) or reductant (KC_8, Na/Hg) from which they are obtained (Table 1), these solutions are henceforth referred to as "solution **A**". Once formed, solution **A** does not react with N_2. The spectral signature remains unchanged when the argon atmosphere is replaced by N_2. Condidering their method of preparation, it is probable that these solutions contain [*tripod*Co] species with Co in a low oxidation state. With this in mind, it seemed appropriate to test their reactivity with regard to oxidative addition reactions. A series of substrates containing N−H, P−H, or Sn−H bonds as constituents potentially able to undergo oxidative addition was therefore tested.

N−H Functions

With $H_2N-NHPh$ as the substrate, initial oxidative addition might well be followed by a dehydrogenation reaction leading to compounds containing PhN_2H as the ligand.[11b] Since [*tripod*Co] compounds containing hydrazido ligands in a η^2 coordination mode are well-characterized species,[11] it was hoped that formation of any such products would be recognized by comparison with the authentic compounds. When solution **A** was treated with $H_2N-NHPh$, a colour change from red-brown to red was observed. Evaporation of the solvent left an oily residue, which solidified after repeated treatment with petroleum ether (boiling range 40−60 °C). FAB mass spectrometric analysis showed that this solid contained $[tripodCo(H)_3Cotripod]^+$ [*m*/*z* = 1369 (M^+)] and presumably also *tripod*Co(η^2-PhNNH) [*m*/*z* = 789 (M^+)]. The latter compound has previously been prepared from $[tripodCo(\eta^2\text{-}PhNNH_2)]^+$ by deprotonation[11b] All attempts to isolate it in a pure state from the above reaction were unsuccessful.

Besides N−H bond addition, the oxidative addition of hydrazine might also involve oxidative cleavage of the N−N bond. In order to obtain a model for the type of compound that might ensue from such an N−N bond scission, the diamido derivative $[tripodCo(\mu\text{-}NH_2)_2Cotripod](BPh_4)_2$ (**7**), was prepared from *tripod*$CoCl_2$, **1**, and $NaNH_2$ (Scheme 4).

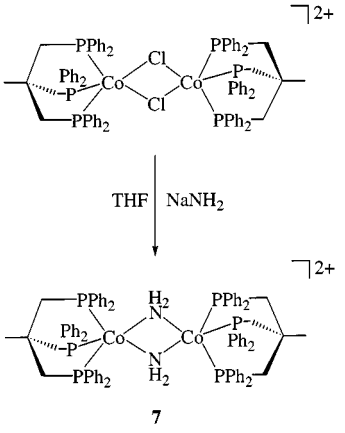

7

Scheme 4

The BPh_4^- salt of **7** was obtained as a microcrystalline brown powder and was completely characterized by all the appropriate analytical techniques (Table 6 and 7, see exp.

Section), including by single-crystal X-ray analysis (Figure 3).

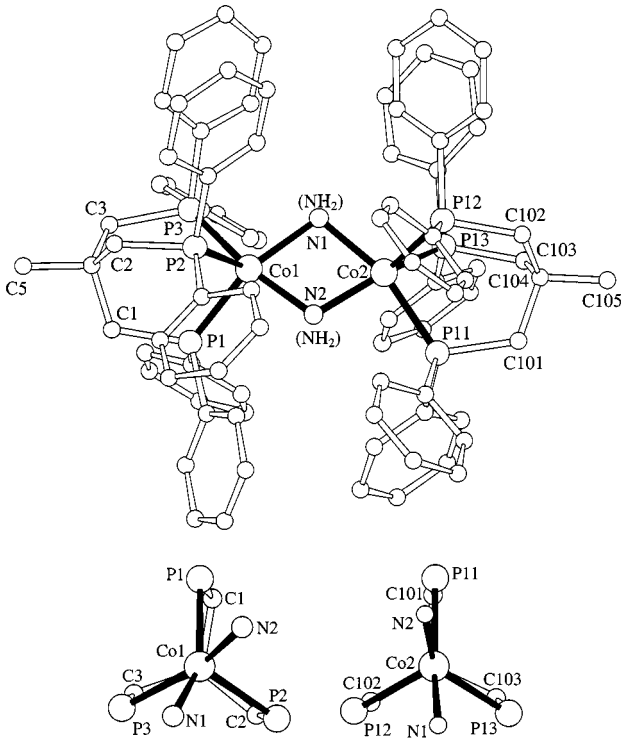

Figure 3. Structure of **7**: Bridging by the NH_2 groups is asymmetric (not shown); the individual positions of the bridging NH_2 groups could be refined using the split-atom technique; the bottom part of the figure shows the coordination polyhedra in a projection onto the relevant P_3 planes; the environment around Co1 (left-hand side) is idealized square pyramidal, while the coordination of Co2 is better described as idealized trigonal bipyramidal (right-hand side). Due to disorder problems, individual geometrical parameters are not accurate and hence are not explicitly given in this paper. Crystallographic data are nevertheless available (see exp. Section, X-ray Crystallographic Study).

Elucidation of the molecular structure of **7** is hampered by partial disorder of the bridging ligands. Its crystal structure is isotypical with that of [*tripod*Co(μ-OH)$_2$Co*tripod*](BPh$_4$)$_2$,[12] where the same type of disorder phenomena, with a minimum of two split positions for each OH group, has been found.[12] Although, in spite of this disorder, the constitution and overall geometry of **7** are clearly apparent, the individual distances and angles are subject to large errors. The Co−Co distance in **7** amounts to 308 pm, while that in its hydroxy analogue is 306 pm.[12] The Co−P distances range from 220 to 231 pm in **7**; in its OH analogue they lie in the range 223−229 pm.[12] The Co−N distances in **7** were determined as 197 pm and 189 pm, while the Co−O distances in the analogue measure 195 pm and 184 pm. It is clear from these figures that X-ray analysis cannot differentiate between the presence of μ-OH or μ-NH_2 bridges. The presence of μ-NH_2 bridges in **7** could, however, be proved by IR spectroscopy (CsI). The μ-OH groups in [*tripod*Co(μ-OH)$_2$Co*tripod*]$^{2+}$ give rise to an infrared absorption at 3260 cm^{-1}.[12] **7** shows no absorption in this region, but has absorptions at 3350 (m), 3313 (w), 3248 (m), 3197 (w), 3158 (w), and 3120 (w) cm^{-1} in the range characteristic for N−H vibrations. **7** crystallizes in the space group *P*1 with one molecule per unit cell such that no crystallographic symmetry restriction is imposed on it. The observed structure has no apparent symmetry higher than C_1 and hence four N−H vibrations are to be expected. The fact that six N−H vibrations are observed is in agreement with the observation that the individual NH_2 groups occupy different positions with respect to the [*tripod*Co Co*tripod*] entity, since the apparent disorder could be resolved by the split-atom technique. The coordination geometries about the Co centres are close to square pyramidal in one part of the molecule (Co1) and close to trigonal bipyramidal in the other part (Co2) (Figure 3, bottom). From these structural data, it appears that **7** may exist in different isomeric forms, a hypothesis that is supported by the fact that a total of six N−H bands are observed. The ESR data of the paramagnetic compound **7** [μ_{eff} (295 K) = 2.1 μ_B per molecule] are also in agreement with this hypothesis. Dichloromethane solutions of **7** show two signals at 298 K {g_1 = 2.11 [A_1 = 24 G]; g_2 = 2.09 [A_2 = 28 G]}. At least two different d^7 Co^{II} centres are therefore present in **7**. ESR spectra obtained in a CH_2Cl_2/THF glass at 100 K are not sufficiently resolved to determine the number of isomers present. An average *g* value of 2.11 and hyperfine coupling modulations corresponding to coupling constants of 34 G and 29 G are observed.

Having established the properties of **7**, the possibility of similar compounds having been formed in the reaction of solution **A** with $H_2N-NHPh$ can be ruled out. Reaction of solution **A** with NH_3 neither produced any species similar to **7**, nor could any secondary product resulting from this reaction be identified.

P−H Functions

In view of the well-documented capacity of [*tripod*Co] templates to generate[13] and bind ligands containing P−P bonds, $PhPH_2$ was tested as a substrate potentially able to undergo oxidative addition with the species present in solution **A**. While the initial product of this reaction could not be observed, the dehydrogenation product *tripod*Co(P_2Ph_2) (**8,** Scheme 5) was obtained in 44% yield. The reaction of solution **A** with $PhPH_2$ was accompanied by a gradual colour change from red-brown to red. Evaporation of the solvent left a red powder, from which analytically pure **8** was isolated by chromatography.

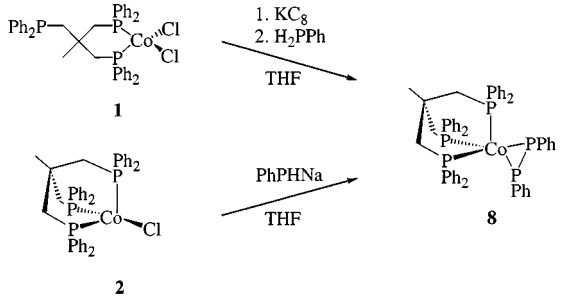

Scheme 5

Single crystals of **8** were obtained by layering a concentrated solution in acetone first with ethanol and then with

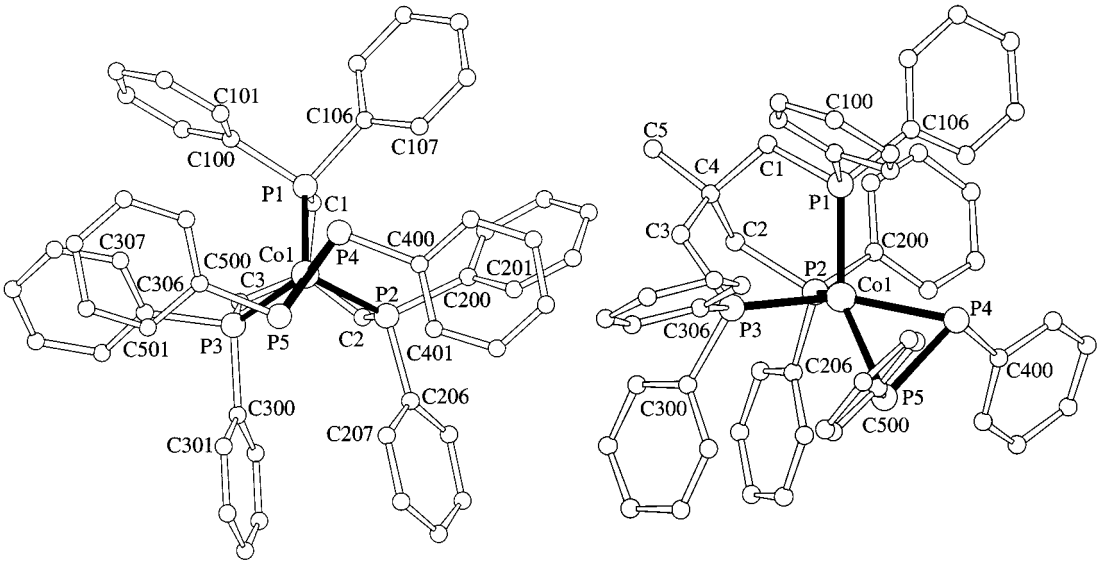

Figure 4. Structure of the diphosphene derivative **8**: Left-hand side: projection onto the plane formed by the three *tripod* phosphorus donor atoms; the torsion angles in Table 3 involving Hz_i refer to this projection; right-hand side: general view

petroleum ether (boiling range 40−60 °C). Its structure is shown in Figure 4 and the salient distances and angles are presented in Table 3. Crystallographic details are given in Table 8. The coordination geometry about cobalt may be viewed as idealized tetrahedral if the centre of the P−P bond is seen as occupying one corner of this idealized tetrahedron (Figure 4). In another view, an idealized square-pyramidal coordination geometry is apparent, with the two phosphorus centres of the diphosphene ligand, P4 and P5, and the two phosphorus donors of the *tripod* ligand, P1 and P3, forming the base and P2 the apex (Figure 4). Considering the distances between the phosphorus centres of the *tripod* ligand and the cobalt atom, this latter view appears to be more realistic since the apical bond Co1−P2 (225 pm) is significantly longer than the equatorial ones Co1−P1 (219 pm), Co1−P3 (219 pm) (see Table 3). The Co−P bonds involving the phosphorus centres of the diphosphene ligand are distinctly longer (234 pm, Table 3) than those to the *tripod* ligand. The distance P4−P5 (212.8 pm, Table 3) is characteristic of a side-on-coordinated P−P double bond. It is longer than the uncoordinated P−P double bond in free diphosphenes.[14−17] The diphosphene ligand in **8** shows a *trans* configuration (Figure 4). The bonds to the phenyl groups point slightly outwards, away from the Co atom. The torsion angle C400−P4−P5−C500 is 149°. This torsion is symmetrical with respect to the Co1−P4−P5 coordination plane, with the two torsion angles Co1−P4−P5−C500 (−103.3°) and Co1−P5−P4−C400 (−108.0°) being almost equal (Figure 4).

An independent synthesis of **8** was achieved by the reaction of *tripod*CoCl, **2**, with PhPHNa, which furnished the compound in 60% yield [a somewhat higher yield (70%) was obtained when *tripod*$CoCl_2$, **1**, was used as the starting compound]. The straightforward formation of **8** by reaction of PhPHNa with **1** or **2** is in contrast to the reaction of MesPHLi or IsPHLi (Mes = 2,4,6-trimethylphenyl, Is = 2,4,6-triisopropylphenyl) with these starting compounds.

Table 3. Selected bond lengths [pm], bond angles [°], and torsion angles [°] in **8**

	8
Co1−P1	219.31(9)
Co1−P2	225.01(9)
Co1−P3	219.37(8)
Co1−P4	233.60(9)
Co1−P5	234.07(9)
P4−P5	212.8(1)
P4−C400	184.1(3)
P5−C500	184.8(3)
P1−Co1−P2	90.61(3)
P1−Co1−P3	94.36(3)
P1−Co1−P4	100.86(3)
P1−Co1−P5	144.19(3)
P2−Co1−P3	90.95(3)
P2−Co1−P4	113.40(3)
P2−Co1−P5	121.45(3)
P3−Co1−P4	150.84(3)
P3−Co1−P5	100.08(3)
P4−Co1−P5	54.13(3)
Co1−P4−P5	63.05(3)
Co1−P4−C400	111.74(9)
P5−P4−C400	102.9(1)
Co1−P5−P4	62.82(3)
Co1−P5−C500	107.77(9)
P4−P5−C500	103.36(9)
Co1−P1−C1−C4	11.2
Co1−P2−C2−C4	18.2
Co1−P3−C3−C4	22.5
C400−P4−P5−C500	148.6
Co1−P4−P5−C500	−103.3
Co1−P5−P4−C400	−108.0
Hz1−P1−C100−C101[a]	15.0
Hz1−P1−C106−C107	51.7
Hz2−P2−C200−C201	32.6
Hz2−P2−C206−C207	32.7
Hz3−P3−C300−C301	15.4
Hz3−P3−C306−C307	57.4

[a] The torsion angles involving Hz at the bottom of the table are defined as follows: P−Hz designates a vector that is vertical with respect to the plane formed by the three *tripod* phosphorus donor atoms and points towards the observer when, in a projection onto this plane, the vector Co−C4 points away from the observer, such that C4 lies below this plane. [1c]

With these reactants, inseparable mixtures were obtained. Mass spectra gave no indication of the formation of products analogous to **8**. It thus appears that the bulky organic substituents (Mes, Is) impede the formation of the corresponding R_2P_2 ligands. Analysis of the product mixtures obtained from these bulky phosphanes is complicated by the fact that the compounds are paramagnetic, thus preventing the use of many analytical methods. This is a problem pertaining to many of the reactions described in this paper. The only reliable means of assessment is single-crystal X-ray analysis, which, however, requires suitable single crystals, which are not always easy to obtain.

Sn−H Functions

Next we analysed the reactivity of Sn−H functions in the given context. The reason for selecting stannanes as substrates was due to the fact that phosphane Co templates are known to form stable Co−Sn bonds.[3a] When solutions **A** were treated with Ph_3SnH, a slight colour change from red-brown to red was observed over a period of 12 hours. By chromatographic workup, the compound *tripod*$CoSnPh_3$ (**9**, Scheme 6), was isolated from the reaction mixture in yields of around 60%. **9** could also be obtained through the reaction of **2** with Ph_3SnLi. As an analogue of **9**, $(PMe_3)_3$-$CoSnPh_3$ [3a] has previously been prepared by Klein et al. by means of a salt metathesis reaction starting from $(PMe_3)_3CoCl$. The 16-electron d^8 compound **9** is paramagnetic, as expected for tetrahedral coordination. Its magnetic moment amounts to 3.2 μ_B, indicating the presence of two unpaired electrons. The UV/Vis/NIR spectrum of **9** (Table 7) exhibits features characteristic for compounds of the type *tripod*CoX[6] with one band at 950 nm (ε = 95) and a broad maximum at 1470 nm (ε = 170). In comparison with the spectrum of *tripod*CoCl {530 nm [ε = 120, sh], 826 nm [ε = 150], 1131 nm [ε = 430], 1224 nm [ε = 450]},[4] where the two long-wavelength bands are resolved into two individual maxima, the long-wavelength band of **9** must correspond to the envelope of two unresolved absorptions. The reaction of **2** with Ph_3SnLi could be monitored by UV/Vis/NIR spectroscopy. It was found that with the protocol described in the Experimental Section, the reaction is quantitative. Single crystals of **9** were obtained by layering THF solutions with petroleum ether (boiling range 40−60 °C).

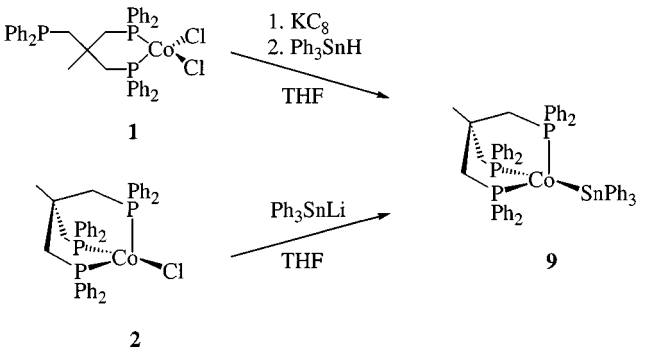

Scheme 6

X-ray analysis confirmed the idealized tetrahedral coordination of the Co centre in **9** (Figure 5). The mutual arrangement of the three phenyl groups of the $SnPh_3$ ligand and the six phenyl groups of the *tripod* ligand appears to impose steric problems. One of the phenyl groups of the *tripod* ligand (C100−C105 at P1) and one of the phenyl groups of the $SnPh_3$ unit (C400−C405) show disorder with respect to their rotational positions about their P−C_{ipso} and Sn−C_{ipso} axes, respectively. The positions shown for these groups in Figure 5 correspond to the orientation that is adopted by 70% of the molecules within the crystal.

The fact that this disorder is seen for both of these rings to approximately the same extent (relative occupancies of 70:30) indicates that the rotational motions of the phenyl groups are strongly coupled. It would appear that this steric interference is mirrored in the position of the tin centre. For an undisturbed molecule of the type *tripod*CoX, the ligand

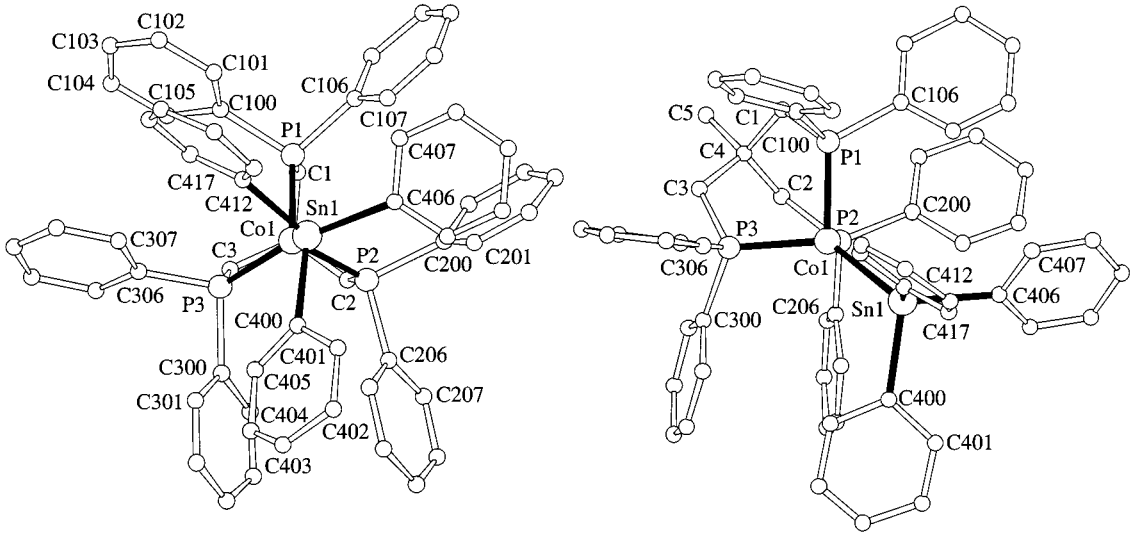

Figure 5. Structure of **9**: In the solid state the phenyl rings C100−C105 and C400−C405 are found to be disordered over two rotational positions in a 7:3 ratio; the major conformer is shown here; the left-hand figure corresponds to a projection of the structure onto the plane formed by the three *tripod* phosphorus donor atoms; the right-hand figure gives a general view of the compound

atom X would be expected to be located on the idealized trigonal axis of the P_3Co entity. This is indeed found for compounds such as *tripod*CoX (X = Cl,[4] Br,[6] NO[18]). In **9**, the tin centre shows a significant deviation from this coaxial position (Figure 5, left-hand side). The Co−P distances [219.6(3)−220.9(4) pm] are marginally shorter than those in *tripod*CoCl, **2** [224.2(3) pm][4] or $(PMe_3)_3CoSnPh_3$ [222(1) pm].[3a] The Co−Sn distance of 258.5(2) pm (Table 4) closely resembles that found in $(PMe_3)_3CoSnPh_3$ [259.0(2) pm].[3a]

In contrast to the reaction of Ph_3SnH with solution **A** [obtained by reduction of *tripod*$CoCl_2$ (**1**), with KC_8], which gives *tripod*$CoSnPh_3$, **9**, Bu_3SnH produces the dihydride compound *tripod*$Co(H)_2SnBu_3$, **10a** (Scheme 7).

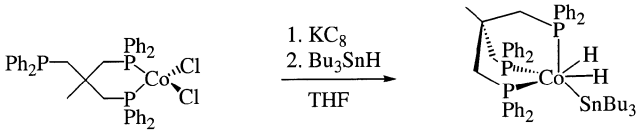

1 **10a**

Scheme 7

Table 4. Selected bond lengths [pm], bond angles [°], and torsion angles [°] in **9**, **10b**, and **11**

	9	**10b**[a]	**11**[b]
Co1−P1	220.9(4)	214.8(1)	220.9(1)
Co1−P2	219.6(3)	217.5(1)	218.7(1)
Co1−P3	220.6(3)	216.9(1)	217.7(1)
Co1−Sn1	258.5(2)	249.39(7)	256.14(7)
Co1−X	−	137(4)	171.0(4)
Co1−Y	−	135(4)	−
C6−O6	−	−	117.8(4)
Sn1−X	−	236	−
Sn1−Y	−	225	−
Sn1−C400	220(1)	219.5(4)	219.3(4)
Sn1−C406	220(1)	218.4(4)	217.7(4)
Sn1−C412	221(1)	217.8(5)	219.5(4)
P1−Co1−P2	91.0(1)	96.23(4)	97.55(4)
P1−Co1−P3	94.4(1)	93.06(5)	90.51(4)
P2−Co1−P3	92.4(1)	92.12(4)	90.66(4)
P1−Co1−Sn1	120.7(1)	139.75(4)	102.81(3)
P2−Co1−Sn1	118.07(9)	110.63(3)	95.77(3)
P3−Co1−Sn1	130.7(1)	114.50(4)	164.26(3)
P1−Co1−X	−	86(2)	133.3(1)
P2−Co1−X	−	178(2)	129.2(1)
P3−Co1−X	−	87(2)	89.1(1)
P1−Co1−Y	−	88(2)	−
P2−Co1−Y	−	88(2)	−
P3−Co1−Y	−	178(2)	−
X−Co1−Sn1	−	68(2)	75.7(1)
Y−Co1−Sn1	−	64(2)	−
X−Co1−Y	−	92(2)	−
C400−Sn1−Co1	114.1(2)	121.5(1)	111.4(1)
C406−Sn1−Co1	120.0(3)	121.2(1)	128.0(1)
C412−Sn1−Co1	119.0(3)	110.3(1)	113.8(1)
C400−Sn1−C406	101.5(4)	104.7(2)	102.3(2)
C400−Sn1−C412	100.2(4)	95.2(2)	97.3(1)
C406−Sn1−C412	98.6(4)	98.4(1)	99.3(1)
Co1−P1−C1−C4	7.4	22.2	23.0
Co1−P2−C2−C4	14.4	11.1	10.6
Co1−P3−C3−C4	14.2	16.2	18.6
Hz1−P1−C100−C101[c]	29.2	11.7	12.3
Hz1−P1−C106−C107	23.7	55.7	−14.9
Hz2−P2−C200−C201	15.0	22.3	47.9
Hz2−P2−C206−C207	26.2	36.9	29.1
Hz3−P3−C300−C301	26.9	32.2	24.3
Hz3−P3−C306−C307	29.8	26.2	35.5
Co1−Sn1−C400−C_{ortho}[d]	135.6	−97.5	−95.7
Co1−Sn1−C406−C_{ortho}[d]	90.7	−101.0	−142.9
Co1−Sn1−C412−C_{ortho}[d]	−170.7	178.9	−150.2

[a] **10b** with X = H1, Y = H2. − [b] **11** with X = C6−O6. − [c] The torsion angles involving Hz at the bottom of the table are defined as follows: P−Hz designates a vector that is vertical with respect to the plane formed by the three *tripod* phosphorus donor atoms and points towards the observer when, in a projection onto this plane, the vector Co−C4 points away from the observer, such that C4 lies below this plane [1c] (see Figures 5−7). − [d] C_{ortho} refers to the C atom that points towards the observer when viewed along the Sn−Co axis.

10a was obtained in the form of a yellow-brown crystalline material in about 50% yield after chromatographic separation. In accordance with its formal Co^{III} oxidation state, it is a diamagnetic compound. Its ^1H NMR spectrum shows well-resolved signals in the appropriate integral ratios for all the organic groups (Table 5). The signal due to the Co-bonded hydrogens is observed at $\delta = -13.4$ with a relative intensity corresponding to two protons. This signal shows satellites induced by ^{119}Sn coupling with a coupling constant of 170 Hz, which is clearly too small for covalent Sn−H bonding (*cf.* Ph_3SnH: $^1J_{^{119}SnH} = 1900$ Hz), but rather indicates a secondary interaction of the metal-bonded hydrogen atoms with the tin nucleus.

For compounds involving this type of agostic interaction, coupling constants in the range 150−330 Hz[19] have been found to be characteristic. $^2J_{PH}$ coupling is not resolved at 200 MHz, the only effect of ^{31}P decoupling being a marginal reduction in the line width. The presence of Co−H bonds in **10a** is also indicated by infrared absorptions at 1948 and 1909 cm^{-1} (Table 7), the intensities of which are similar to those of the C−H vibrations at around 3000 cm^{-1}. This high relative intensity rules out the possible interpretation that these two bands might originate from a harmonic or combination vibration. The energy of the vibrations corresponds to energies reported for Co−H vibrations in other hydride compounds.[20] The appearance of two $\tilde{\nu}$(Co−H) absorptions corresponds to the symmetric and antisymmetric vibrations. The $^{31}P\{^1H\}$ NMR spectrum of **10a** shows a broad resonance at $\delta = 46$ (line width 380 Hz). The appearance of this signal does not change significantly on cooling to 193 K, the only effect being a reduction of the line width (105 Hz). Observations of this nature have occasionally been made with [*tripod*Co^{III}] derivatives in the past.[2e] From this observation, it is evident that − over the temperature range studied − the relative orientation of the *tripod* ligand with respect to the coligands is dynamic. The ^{119}Sn NMR spectrum of **10a** shows one signal at $\delta = 17.8$ (Table 5), in the typical range for metal−bonded SnR_3 groups.[19b]

Cyclic voltammograms show − rather unexpectedly at first glance − that **10a** is reversibly oxidized at $E_{1/2} = -390$ mV. Since the formal oxidation state of the cobalt in compound **10a** is +III, oxidation of the metal would imply the formation of Co^{IV}, which is highly improbable given the nature of the ligands present. A possible explanation for this finding is the hypothesis that oxidation of **10a** leads to oxidative coupling of its hydride ligands to produce a η^2-coordinated dihydrogen ligand (Scheme 8).

Table 5. NMR spectroscopic data for compounds **10a**, **10b**, **11**

	^{1}H NMR	^{13}C{^{1}H} NMR	^{31}P{^{1}H} NMR	^{119}Sn NMR
10a[a]	−13.4 (s, $^1J_{^{119}SnH}$ = 170 Hz, 2 H, Co−*H*), 0.8 (m, 6 H, Bu-C*H*$_2$), 0.9 (m, 9 H, Bu-C*H*$_3$), 1.3−1.4 (m, 6 H, Bu-C*H*$_2$), 1.5−1.6 (m, 6 H, Bu-C*H*$_2$, 3 H *tripod*-C*H*$_3$), 2.3 (br. s, 6 H, C*H*$_2$P), 7.0−7.3 (m, 30 H, aromatic *H*)	14.2 (s, Bu-*C*H$_3$), 16.4 (s, Bu-*C*H$_2$), 28.8 (s, Bu-*C*H$_2$), 31.3 (s, Bu-*C*H$_2$), 36.4 (m, *C*H$_2$P), 37.9 (m, *tripod*-*C*H$_3$), 127.6−141.9 (aromatic *C*)	46.0 (m)	17.8 (m)
10b	−13.2 (s, $^1J_{^{119}SnH}$ = 220 Hz, 2 H, Co−*H*), 1.6 (s, 3 H *tripod*-C*H*$_3$), 2.3 (br. s, 6 H, C*H*$_2$P), 6.8−7.7 (m, 45 H, aromatic *H*)	36.1 (m, *C*H$_2$P), 37.8 (m, *tripod*-*C*H$_3$), 125.4−152.7 (aromatic *C*)	44.3 (m), 47.1 (m),[b] 43.8 (m)[b]	
11[a]	1.6 (s, 3 H *tripod*-C*H*$_3$), 2.4 (br. s, 6 H, C*H*$_2$P), 6.8−7.3 (m, 45 H, aromatic *H*)	36.4 (s, C_q), 37.1 (m, *C*H$_2$P), 38.1 (m, *tripod*-*C*H$_3$), 126.6−149.6 (aromatic *C*)	28.7 (br. s)	−31.4 (br. s)

[a] The data for **10a** were collected on a Bruker Avance DRX 300 instrument at 300.130 MHz (^{1}H), 121.495 MHz (^{31}P{^{1}H}), 75.468 MHz (^{13}C{^{1}H}); ^{13}C{^{1}H} NMR spectroscopic data for **11** were measured on a Bruker Avance DRX 500 spectrometer at 125.758 MHz; all the other data refer to measurements on a Bruker Avance DPX 200 instrument. − [b] T = 178 K.

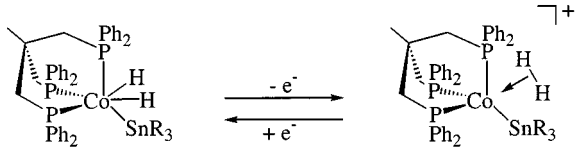

10a, b **B**

a: R = Bu
b: R = Ph

Scheme 8

In the 17-electron species **B** obtained after oxidation, cobalt is in its conventional +II oxidation state. Attempts to isolate **B** after oxidation of **10a** with ferrocenium salts have not yet been successful.

The fact that the 16-electron Co^{I} compound **9** and the 18-electron Co^{III} compound **10a** are both stable suggests that **9** should react with Lewis bases to form 18-electron Co^{I} compounds *tripod*CoSnPh$_3$L′.[21] This expectation is borne out by the reaction of **9** with carbon monoxide, which leads to the carbonyl derivative *tripod*Co(CO)SnPh$_3$ (**11**, Scheme 9).

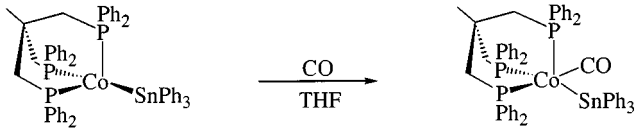

9 **11**

Scheme 9

Solutions of **9** change their colour from red to orange-yellow after a few minutes of exposure to carbon monoxide. From such a solution, **11** was isolated in 70% yield as a microcrystalline orange powder. Crystals were obtained by vapour diffusion of diethyl ether into a dichloromethane solution (Figure 6, Table 4 and 8)

The coordination of the cobalt centre in **11** is intermediate between trigonal bipyramidal and square pyramidal, as is often observed for compounds of the type *tripod*CoLL′. Angles and distances fall within their normal ranges (Table 4).

Analytical data (Table 6 and 7) and the NMR spectra (Table 5) of **11** are in full agreement with its constitution. The ^{119}Sn resonance is observed at δ = −31.4. Only one ^{31}P signal is observed, in agreement with the usual dynamic behaviour of five-coordinate compounds. No change in the appearance of the ^{31}P{^{1}H} NMR signal in the temperature range 293−193 K is observed. In the IR spectrum, the carbonyl group gives rise to a strong absorption at ν(CO) = 1853 cm^{-1} (Table 7). The cyclic voltammogram shows that the Co^{I} species **11** is reversibly oxidized at $E_{1/2}$ = −140 mV, indicating the relative stability of the cationic Co^{II} species [*tripod*Co(CO)SnPh$_3$]$^+$.

The carbonyl addition reaction of **9** is analogous to the reaction of (PMe$_3$)$_3$CoSnPh$_3$ with CO.[3a] In contrast to the (PMe$_3$)$_3$Co template, for which prolonged exposure of (PMe$_3$)$_3$Co(CO)SnPh$_3$ to CO leads to substitution of PMe$_3$ by CO, producing (PMe$_3$)$_2$Co(CO)$_2$SnPh$_3$, the *tripod* metal template of **11** remains unaffected. Solutions of **11** may be kept under CO for hours without any noticeable decomposition.

Comparing **9** with **10a**, the most plausible "oxidant" should be the dihydrogen. When a THF solution of **9** was stirred under 1 bar of H$_2$, the red colour of **9** was replaced by the yellow colour of **10b** within six hours (Scheme 10).

After chromatography, **10b** was isolated as a yellow microcrystalline powder. The ^{1}H NMR resonance of the hydride groups is observed at δ = −13.2, and ^{119}Sn satellites ($^1J_{^{119}SnH}$ = 220 Hz) indicate agostic HSn interactions.[19] In the IR spectrum, bands corresponding to the Co−H vibrations[20] are found at 1903 and 1888 cm^{-1} (Table 7). The intensities of these bands are again comparable to that of the strongest band in the ν̃(C−H) vibration region. The

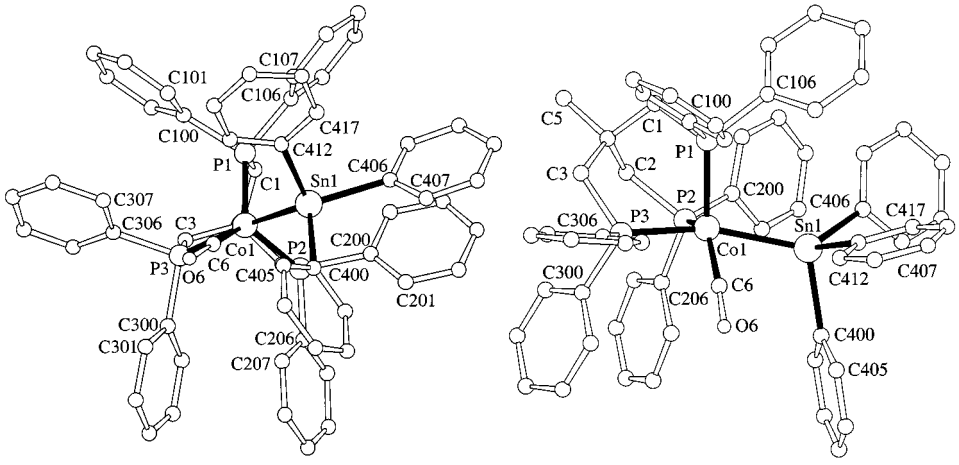

Figure 6. Structure of **11**: The left-hand side shows a projection onto the plane defined by the three *tripod* phosphorus donor atoms, the dummy vectors P_i-Hz_i in Table 4 refer to this view; the right-hand figure shows a general view of **11**

Table 6. Analytical data for compounds **7** to **11**

No.	Formula (M)	MS *m/z* (%) [Frag.]	$C_{calcd.}$ C_{found}	$H_{calcd.}$ H_{found}	$X_{calcd.}$ X_{found}	M.p. (°C)
7	$C_{130}H_{122}N_2P_6B_2Co_2\cdot 3CH_2Cl_2$	FAB: 1398 (1) [M^+], 1382 (6) [$M^+ - NH_4$],	69.68	5.63	1.22[a]	155
	2292.54	1322 (5) [$M^+ - Ph$], 698, (22) [M^{2+}], 683 (100) [*tripod*Co^+]	70.01	5.78	0.73[a]	(dec.)
8	$C_{53}H_{49}P_5Co$	EI: 899 (100) [M^+], 683 (87) [*tripod*Co^+]	70.75	5.49	17.21[b]	210
	899.77		70.59	5.49	17.04[b]	(dec.)
9[c]	$C_{59}H_{54}P_3CoSn$	–	68.56	5.27	8.99[b]	230
	1033.64		67.92	5.26	8.21[b]	
10a[c]	$C_{53}H_{68}P_3CoSn$	FAB: 931 (27) [$M^+ - Bu + O$]	65.25	7.03	9.52[b]	197
	975.69		64.89	7.01	8.19[b]	
10b[c]	$C_{59}H_{56}P_3CoSn$	FAB: 1034 (8) [$M^+ - 2$ H], 683 (27) [*tripod*Co^+]	–	–	–	171
	1035.64		–	–	–	(dec.)
11	$C_{60}H_{54}CoSnO$	FAB: 1062 (7) [M^+], 711 (8) [*tripod*Co(CO)$^+$], 683 (55)	67.88	5.13	8.75[b]	241
	1061.69	[*tripod*Co^+], 673 (100) [*tripod*O_3^+]	67.66	5.35	8.46[b]	(dec.)

[a] X = N. – [b] X = P. – [c] Compounds **9** and **10** are very air-sensitive. Due to this sensitivity, no microanalytical data could be determined for **10b** with the equipment available.

Table 7. Analytical data for compounds **7** to **11**

No.	CV Potential[a]	UV/Vis/NIR λ_{max} [nm] (ε) [$M^{-1}cm^{-1}$]	IR: $\tilde{\nu}$ [cm^{-1}]	μ_{eff} (μ_B) 295 K
7	E_p^C = −730mV (reverse scan: 40 mV); E_p^A = 970 mV (reverse scan: 270 mV)	344 (4120), 444 (725), 789 (420), 1175 (br, 140)[b]	N−H: 3350 (m), 3313 (w), 3248 (m), 3197 (w), 3158 (w), 3120 (w) [c]	2.1
8	$E_{1/2}$ = −65 mV (qrev. ox., ΔE = 100 mV), E_p^C = −610 mV (reverse scan: − 50 mV); E_p^A = 740 mV; ΔE_{Fc} = 190 mV	511 (sh, 1750), 681 (260), 1134 (br, 220)[d]	–	2.1
9	E_p^R = −30 mV (qrev. ox.,:ΔE = 125 mV); E_p^A = 170 mV, E_p^R = 355 mV; E_p^A = 1050 mV; E_p^C = −1270 mV; ΔE_{Fc} = 135 mV	485 (180), 593 (sh, 60), 949 (95), 1470 (br, 170)[d]	–	3.2
10a	$E_{1/2}$ = −390 mV (rev. ox.), ΔE = 145 mV; E_p^A = 860 mV, E_p^C = −1970 mV, ΔE_{Fc} = 140 mV	364 (sh, 870)[b]	Co−H: 1948 (m), 1909 (sh) [c]	–
	$E_{1/2}$ = −140 mV (rev. ox.), ΔE = 175 mV; E_p^A = 815 mV (reverse scan: 490 mV); ΔE_{Fc} = 135 mV	–	Co−H: 1903 (m), 1888 (m) [e]	–
11	$E_{1/2}$ = −140 mV (rev. ox.), ΔE = 105 mV; E_p^A = 1350 mV; ΔE_{Fc} = 135 mV	296 (19000), 344 (sh, 12000)[b]	CO: 1853 (vs) [c]	–

[a] All measurements were performed in CH_2Cl_2 solutions at scan speeds of 200 mVs^{-1}. – [b] Solvent: CH_2Cl_2. – [c] CsI. – [d] Solvent: THF. – [e] KBr.

$^{31}P\{^1H\}$ NMR spectrum of **10b** shows one signal at 298 K, which, in terms of its line width and shift, corresponds to that observed for **10a**. On cooling solutions of **10b** in CD_2Cl_2, the signal increases in intensity and starts to split into two components with an approximate ratio of 2:1 at 193 K. At 178 K, the lowest attainable temperature due to

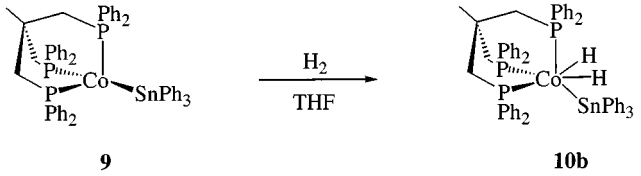

9 **10b**

Scheme 10

solubility problems, the individual absorptions are not yet separated and the signals are still broad (line width = 170 Hz).[2e] The signal with a relative intensity of one is seen at $\delta = 47$, that corresponding to a relative intensity of two at $\delta = 44$. Resolution of the individual resonances of the phosphorus nuclei of coordinated *tripod* ligands has occasionally been observed and has also been quantitatively analysed in terms of the rotation of the *tripod*Co template relative to the co-ligands.[5] The splitting of the $^{31}P\{^1H\}$ NMR signal of **10b** into two components with relative intensities of 2:1 indicates that the rigid conformation observed at low temperatures should have approximate C_S symmetry. Like **10a**, the Co^{III} compound **10b** was found to be reversibly oxidized. Oxidation occurs at $E_{1/2} = -140$ mV and, by the same arguments as discussed for **10a**, it is assumed that the oxidation process is not metal-centred but transforms the hydride ligands into a coordinated dihydrogen ligand leading to a compound of type **B** (Scheme 8).

The structure of **10b** has been elucidated by single-crystal X-ray analysis (Figure 7, Table 4 and 8).

Crystals of **10b** were obtained of exposing THF solutions of **10b** to a vapour phase of petroleum ether (boiling range 40−60 °C) for several days. The conformation adopted by **10b** in the solid state (Figure 7) is close to mirror symmetric with respect to the bonds radiating from the cobalt and tin centres (Figure 7, left-hand side). The rotational positions of the phenyl rings at P2 and P3 are also close to being mirror symmetric, within a range of about 30° (see torsion angles in Table 4). The rotational positions of the phenyl groups at the $SnPh_3$ ligand also conform to this idealized mirror symmetry, with the phenyl group C412−C417 lying in the mirror plane and the two remaining phenyl groups lying in positions mirror symmetric to each other [the torsion angles $Co-Sn-C_x-C_{ortho}$ refer to the *ortho* carbons C401, C407, and C417, as shown in Figure 7. This selection follows the convention of measuring the rotational positions of aryl groups with respect to the *ortho* carbon atom that is closest to the observer with respect to the projection shown in Figure 7 (left-hand side). With the selection of torsion angles thus made, a mirror symmetric arrangement of the phenyl groups of C400, C406 is indicated by torsion angles of equal size and equal sign, as is indeed found (−97.5° and −101.0°, Table 4)].

The approximate mirror symmetry exhibited by **10b** in the solid state must correspond to a globally optimal conformation since $^{31}P\{^1H\}$ NMR spectroscopy (see above) shows that the low-temperature conformation of **10b** is in fact mirror symmetric.

The positions of the hydride ligands have been inferred from electron density maps and refined by least-squares methods. The Co−H distances are around 136 pm, with an H−Co−H angle of around 90° (Table 4). The distances of these hydride ligands from the tin centre are around 230 pm (Table 4), making them definitely too long for a conventional Sn−H bond. Their interaction with the tin nucleus is nevertheless apparent from the Sn−H coupling constant of 220 Hz (Table 5). In spite of the fact that the cobalt centre is six-coordinate in **10b**, its coordination geometry is not octahedral (Figure 7, right-hand side). While all the Co-centred angles involving a phosphorus and a hydrogen ligand are close to 90° (or 180°, respectively; see Table 4), the angles involving the tin centre deviate from the ideal octahedral values by 20−30° throughout (Table 4). With **10b** being a Co^{III} derivative, the expected coordination polyhedron would be an octahedron. Considering the wealth of information available concerning the structures of six-coordinate Co^{III} compounds, **10b** represents a rare

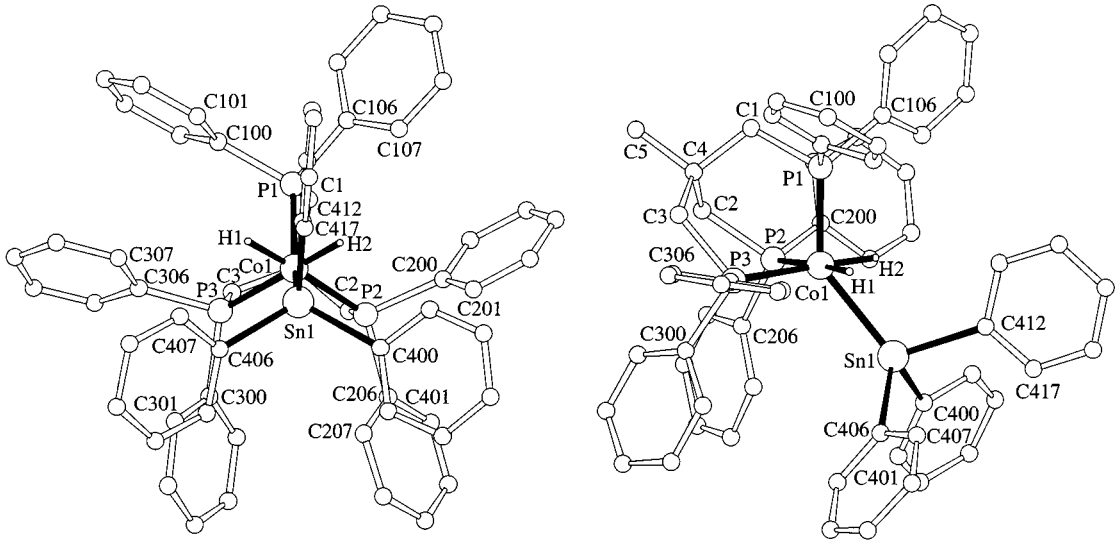

Figure 7. Structure of **10b**: The left-hand side diagram shows a projection of the structure onto the plane defined by the three *tripod* phosphorus donor atoms; the dummy vectors P_i-Hz_i in Table 4 refer to this view; the right-hand figure shows a general view of **10b**

Table 8. Crystal data for **4**, **7**, **8**, **9**, **10b**, and **11**

Compound	**4**	**7**	**8**	**9**	**10b**	**11**
Formula	$C_{70}H_{68}P_6Co_2\cdot 2.25\ CH_2Cl_2$	$C_{130}H_{122}P_6Co_2N_2B_2\cdot 1.5\ (CH_3)_2CO$	$C_{53}H_{49}P_5Co\cdot 0.75\ (CH_3)_2CO$	$C_{59}H_{54}P_3CoSn$	$C_{59}H_{56}P_3CoSn$	$C_{60}H_{54}P_3OCoSn\cdot 1.3\ CH_2Cl_2$
Molecular mass [g]	1404.01	2037.7	943.26	1033.64	1035.57	1171.97
Crystal size [mm]	0.2 × 0.25 × 0.25	0.3 × 0.2 × 0.2	0.2 × 0.2 × 0.15	0.2 × 0.2 × 0.1	0.15 × 0.2 × 0.2	0.05 × 0.2 × 0.3
Crystal system	triclinic	triclinic	monoclinic	monoclinic	orthorhombic	orthorhombic
Space group (No.)	$P\bar{1}$ (2)	$P1$ (1)	$P2_1/n$ (14)	$P2_1/n$ (14)	$Pna2_1$ (33)	$P2_12_12_1$ (19)
a [pm]	1110.80(2)	1389.1(3)	1347.5(3)	1402.7(3)	1919.0(4)	1359.8(3)
b [pm]	1149.30(2)	1561.7(3)	959.5(2)	1876.1(3)	1354.7(3)	1635.6(3)
c [pm]	1368.50(3)	1683.8(3)	3636.5(7)	1894.7(3)	1904.9(4)	2488.3(5)
α [°]	68.55(1)	114.77(1)	90	90	90	90
β [°]	86.73(1)	91.70(2)	96.98(3)	91.21(1)	90	90
γ [°]	81.14(1)	111.54(2)	90	90	90	90
V [10^6 pm^3]	1606.65(6)	3011(1)	4667(2)	4985(2)	4952(2)	5534(2)
Z	1	1	4	4	4	4
$d_{x.}$ [g cm^{-3}]	1.451	1.164	1.343	1.370	1.389	1.407
T [K]	200		200	200	200	200
No. of rflns. for cell param.	–	30	–	28	–	–
Scan range	4.9 ≤ 2Θ ≤ 56°	4.9 ≤ 2Θ ≤ 50°	3.1 ≤ 2Θ ≤ 52°	4.2 ≤ 2Θ ≤ 48°	3.7 ≤ 2Θ ≤ 56°	3.4 ≤ 2Θ ≤ 55°
Method	ω scan, Δω = 0.5°	ω scan, Δω = 0.6°	ω scan, Δω = 1.0°	ω scan, Δω = 0.6°	ω scan, Δω = 1.0°	ω scan, Δω = 1.0°
Scan speed	–	dω/dt = 10°min^{-1}	–	dω/dt = 10°min^{-1}	–	–
s frame^{-1}	20	–	5	–	2	3
No. rflns. measured	45008	10459	61896	8183	46221	49871
No. unique rflns.	6722	10459	9180	7829	11869	12711
No. rflns. observed	5786	7047	6488	4972	8885	10754
Observation criterion	$I \geq 2\sigma$	$I \geq 2\sigma$	$I \geq 2\sigma$	$I \geq 2\sigma$	$I \geq 2\sigma$	$I \geq 2\sigma$
No. param. refined	387	811	575	504	590	671
Resid. el. density [10^{-6} e pm^{-3}]	0.41	1.37	0.75	1.07	0.68	1.27
R_1/R_W [%] (refinement on F^2)	4.4/12.6	9.0/26.6	4.4/9.9	8.1/19.7	4.1/8.5	3.8/9.9

example of a significant deviation from the prototype octahedral coordination. Figure 7 (right-hand side) suggests that steric factors alone cannot be responsible for this observation. It thus appears that the agostic interactions between the cobalt-bonded hydrogens and the cobalt−tin bond might be the driving force for the observed distortion.

Conclusion

Solutions obtained by reduction of *tripod*$CoCl_2$ (**1**) or *tripod*CoCl (**2**) with electropositive metals in THF are highly reactive. Upon reaction with $PhPH_2$, they produce the diphosphene derivative *tripod*Co(η^2-PhP=PPh) (**8**). With R_3SnH they form *tripod*$CoSnR_3$ (**9**) or *tripod*$Co(H)_2SnR_3$ (**10**). The paramagnetic Co^I species *tripod*$CoSnPh_3$ undergoes oxidative addition of H_2 to produce *tripod*$Co(H)_2SnPh_3$ (**10b**). The Co^{III} compound **10b** is unique in so far as it has a very distorted octahedral geometry that allows for agostic H−Sn interactions and in that it undergoes reversible one-electron oxidation, which is assumed to be ligand-centred, producing the Co^{II} species [*tripod*Co(η^2-H_2)$SnPh_3$]$^+$.

Experimental Section

General Remarks: Unless otherwise noted, all manipulations were carried out under argon using standard Schlenk techniques. All solvents were dried by standard methods and distilled under argon or dinitrogen.[22] For ultrasonic activation of reaction mixtures, a "Bender & Hobein, Laboson 200" ultrasonic bath was used. The solvents CD_2Cl_2 and $CDCl_3$ used for NMR spectroscopic measurements were degassed by three successive "freeze-pump-thaw" cycles and dried with 4 Å molecular sieves. − NMR: Bruker Avance DPX 200 at 200.120 MHz (^{1}H), 50.323 MHz (^{13}C{^{1}H}), 81.015 MHz (^{31}P), and 74.631 MHz (^{119}Sn); T = 303 K unless stated otherwise; chemical shifts (δ) in ppm with respect to (residual protons in) CD_2Cl_2 (^{1}H: δ = 5.32; ^{13}C: δ = 53.80) and $CDCl_3$ (^{1}H: δ = 7.27; ^{13}C: δ = 77.00) as internal standards; ^{31}P chemical shifts (δ) in ppm with respect to 85% H_3PO_4 (^{31}P: δ = 0) as external standard. − IR: Bruker IFS-66; CsI or KBr discs or Nujol mulls. − EPR: Bruker ESP 300E (X-band, external standard diphenylpicrylhydrazyl). All measurements were made at 293 K and 100 K in a standard cavity ER 4102St. − Magnetic measurements: Faraday balance, Bruker B-E 15 C8 electromagnet, Bruker B-H 15 field controller, Sartorius M 25 D-S vacuum microbalance; calibration with $K_3[Fe(CN)_6]$. All measurements were carried out at 293 K. − UV/Vis/NIR: Perkin−Elmer Lambda 19. − Fast-atom bombardment (FAB) MS: Finnigan MAT 8230, xenon, matrix: 4-nitrobenzyl alcohol; electron impact (EI) MS: 70 eV. − Elemental analyses: Microanalytical Laboratory of the Organisch-Chemisches Institut, Universität Heidelberg. With the techniques used, problems arise with highly air- and temperature-sensitive compounds such as **9**, **10a**, and **10b** during the preparation of the test samples. The customary degree of accuracy is therefore not always attainable with these materials. The wet chemical analysis of phosphorus contents is occasionally disturbed by the presence of tin in the same sample. The corresponding analytical data will therefore also have higher margins of error. − Melting points: Gallenkamp MFB-595 010 apparatus; uncorrected values. − Cyclic voltammetry: Metrohm "Universal Meß- und Titriergefäß", Metrohm RDE 628 GC electrode, platinum electrode, SCE electrode, Princeton Applied Re-

search potentiostat model 273; samples 10^{-3} M in 0.1 M nBu_4NPF_6/CH_2Cl_2. Reactions described as reversible show a square-root dependence of current vs. scan speed in the range 50 to 1000 mVs^{-1}. All potentials are quoted relative to the saturated calomel electrode.

Materials: 1,1,1-Tris[(diphenylphosphanyl)methyl]ethane, *triphos*,[23] was prepared according to the literature procedure. All other materials were obtained from commercial sources and were used as received. Silica gel (Kieselgel z.A. 0.06−0.20 mm, J. T. Baker Chemicals B. V.) used for chromatography and kieselgur (Erg. B.6, Riedel de Haen AG) were degassed at 1 mbar for 24 h and saturated with argon.

General Procedure for the Synthesis of Solution A: A solution of **1**[4] (377 mg, 0.50 mmol) in THF (20 mL) was added to KC_8 (1.25 mmol), prepared by heating potassium (50 mg, 1.25 mmol) with graphite (120 mg, 10 mmol), and the suspension was sonicated until the colour changed to orange-brown. The reaction mixture was then filtered through kieselgur.

Synthesis of *tripod*Co(N_2)Co*tripod* (3): The following manipulations were carried out under a dry N_2 atmosphere:

Method a: A suspension of **2**[5] (359 mg, 0.50 mmol) in THF (20 mL) was added to KC_8 (1.50 mmol) and the mixture was sonicated until the colour turned to dark red. The supernatant reaction mixture was then removed from the insoluble material by means of a syringe. On layering this solution with petroleum ether (boiling range 40−60 °C), red crystals were obtained.

Method b: A solution of **1**[4] (377 mg, 0.50 mmol) in THF (20 mL) was added to activated Mg (2 g) (for activation: Mg filings were vigorously stirred in vacuo at 250 °C for 1 h) and the mixture was stirred until a dark-red colour developed. The supernatant reaction mixture was then removed from the unchanged Mg by means of a syringe. On layering this solution with petroleum ether (boiling range 40−60 °C), red crystals were obtained. − UV/Vis/NIR (THF): λ_{max} (ε) = 405 (8000), 718 (550), 1134 nm (4700 M^{-1} cm^{-1}). − Crystallographic data: see text.

Synthesis of [1,1-Bis(diphenylphosphanomethyl)-1-(phenylphosphanomethyl)]ethane (6): A solution of KO*t*Bu (689 mg, 6.14 mmol) and $PhPH_2$ (675 mg, 6.14 mmol) in DMSO (40 mL) was slowly added to a solution of 1-chloro-2-bis(diphenylphosphanylmethyl)propane (**5**)[10] (1.95 g, 4.10 mmol) in DMSO (30 mL). The reaction mixture was stirred for 4 h at 100 °C. The solvent was then removed in vacuo and the residue was purified by column chromatography on silica gel, eluting with petroleum ether (boiling range 40−60 °C)/diethyl ether, 9:1; R_f = 0.47. Yield: 1.84 g (3.35 mmol, 82%) as a colourless, viscous substance. − $C_{35}H_{35}P_3$ (548.58): calcd. C 76.63, H 6.43, P 16.94; found C 76.73, H 6.70, P 16.54. − ^{1}H NMR ($CDCl_3$): δ = 1.2 (br. s, 3 H, CH_3), 2.3 (br. s, 2 H, CH_2PHPh), 2.6 (br. s, 4 H, C$H_2$$PPh_2$), 4.0 (br. s, $^1J_{PH}$ = 204 Hz, 1 H, P*H*Ph), 6.9−7.9 (m, 25 H, arom. H). − ^{31}P NMR ($CDCl_3$): δ = −71.4 (d, $^1J_{PH}$ = 204 Hz, 1 P, PHPh), −26.8 (s, 2 P, PPh_2). − ^{13}C{^{1}H} NMR ($CDCl_3$): δ = 29.3 (m, CH_3), 37.3−38.3 (m, *C*H_2PHPh, Cq), 43.1 (m, *C*$H_2$$PPh_2$), 128.0−140.6 (arom. C). − MS (EI); *m*/*z* (%): 547 (17) [M^+ − H], 471 (100) [M^+ − Ph], 363 (19) [M^+ − PPh_2]. − IR (Nujol): $\tilde{\nu}$(P−H) = 2282 (vs) cm^{-1}.

Synthesis of [*tripod*Co(NH_2)$_2$Co*tripod*](BPh_4)$_2$ (7): To a solution of **1**[4] (754 mg, 1.00 mmol) in THF (40 mL) (blue solution) were added $NaBPh_4$ (342 mg, 1.00 mmol) (solution turned red) and $NaNH_2$ (78 mg, 2.00 mmol). After the colour of the mixture had turned brown, the solvent was removed in vacuo. The residue was redissolved in CH_2Cl_2, this solution was filtered through 5 cm kieselgur, and the solvent was removed to leave 682 mg (0.67 mmol, 67%) of a brown powder. Recrystallization from acetone/diethyl ether yielded orange crystals suitable for X-ray structure analysis (see exp. Section, X-ray Crystallographic Study). − EPR (CH_2Cl_2, 295 K): g_1 = 2.11 (A_1 = 24 G); g_2 = 2.09 (A_2 = 28 G). − EPR (THF/CH_2Cl_2, 100 K): g_{av} = 2.11 (A = 34, 29 G). − For additional analytical data, see Table 6 and 7.

Synthesis of *tripod*Co(P_2Ph_2) (8). − Method a: At −60 °C, a solution of **1**[4] (566 mg, 0.75 mmol) in THF (30 mL) was added to a solution of PhPHLi [24b] (1.65 mmol), prepared by adding *n*BuLi (0.66 mL, 2.5 M in hexane) to a solution of $PhPH_2$ (182 mg, 0.18 mL, 1.65 mmol) in THF (20 mL). The colour changed from blue to red and the mixture was stirred for 30 min. at room temperature. The solvent was then removed in vacuo, and the residue was suspended in petroleum ether (boiling range 40−60 °C) and flash chromatographed on silica gel. After elution with 200 mL of petroleum ether (boiling range 40−60 °C), the product was eluted with diethyl ether as a red band, removal of the solvent from which gave 485 mg (0.54 mmol, 72%) of a microcrystalline powder. Red crystals, suitable for X-ray structure analysis, were obtained by layering a saturated acetone solution with ethanol and petroleum ether (boiling range 40−60 °C).

Method b: To solution **A**, prepared from **1**[4] (0.50 mmol) and KC_8 (1.25 mmol) (see above), was added $PhPH_2$ (170 mg, 0.17 mL, 1.54 mmol). After stirring for 2 h, the colour had changed to red and the solvent was removed in vacuo. The residue was taken up in petroleum ether (boiling range 40−60 °C). Chromatographic workup as described above gave 198 mg (0.22 mmol, 44%) of **8**.

Method c: A modification of Method a, starting from **1**[4] (566 mg, 0.75 mmol) and PhPHNa [24a] (1.65 mmol) [prepared by adding Na (38 mg, 1.65 mmol) to a solution of $PhPH_2$ (182 mg, 0.18 mL, 1.65 mmol) in THF (20 mL) and sonicating until the Na had dissolved] gave 472 mg (0.53 mmol, 70%) of compound **8**.

Method d: In a further modification of Method a, **8** was prepared starting from **2**[5] (359 mg, 0.50 mmol) suspended in THF (25 mL) and a solution of PhPHLi [24b] or PhPHNa[24a] (1.10 mmol) in THF (20 mL). Yield: 270 mg (0.30 mmol, 60%). − For analytical data, see Table 6 and 7.

Synthesis of *tripod*CoSnPh_3 (9). − Method a: A suspension of **2**[5] (359 mg, 0.50 mmol) in THF (15 mL) was added to a THF solution of Ph_3SnLi[25] (0.90 mmol), prepared by adding *n*BuLi (0.36 mL, 2.5 M in toluene) to a solution of Ph_3SnH (315 mg, 0.90 mmol) in THF (15 mL). The initially brown suspension turned red and the reaction mixture was stirred overnight. After removal of the solvent, the residue was suspended in petroleum ether (boiling range 40−60 °C) and flash chromatographed on silica gel. After elution with 200 mL of petroleum ether (boiling range 40−60 °C), the product was eluted with diethyl ether as a red band, removal of the solvent from which gave 340 mg (0.33 mmol, 66%) of a red microcrystalline powder. Red crystals, suitable for X-ray structural analysis, were obtained by layering a saturated THF solution with petroleum ether (boiling range 40−60 °C).

Method b: Compound **9** was prepared by adding Ph_3SnH (895 mg, 2.55 mmol) to solution **A**, prepared from **1**[4] (0.85 mmol) and KC_8 (2.13 mmol) (see above), and stirring overnight. Chromatographic workup (as described above) yielded 540 mg (0.52 mmol, 61%) of **9**. − For analytical data, see Table 6 and 7.

Synthesis of *tripod*Co($H)_2SnBu_3$ (10a): To solution **A**, prepared from **1**[4] (0.85 mmol) and KC_8 (2.13 mmol) (see above), was added

Bu_3SnH (745 mg, 0.68 mL, 2.56 mmol). After stirring overnight, the solvent was removed in vacuo. The residue was suspended in petroleum ether (boiling range 40−60 °C). Chromatographic workup (as described for compound **9**) gave 410 mg (0.42 mmol, 50%) of a yellow-brown microcrystalline solid. Recrystallization from acetone at −20 °C afforded 210 mg (0.22 mmol, 25%) as yellow crystals. − For analytical data, see Table 6 and 7.

Synthesis of *tripod*Co(H)$_2$SnPh$_3$ (10b): A solution of **9** (620 mg, 0.60 mmol) in THF (30 mL) was saturated with H_2 at 1 bar and stirred for 6 h. The red colour of the reaction mixture turned yellow. After removal of the solvent, the residue was suspended in petroleum ether (boiling range 40−60 °C). Chromatographic workup (as described for compound **9**) gave upon removal of the solvent 420 mg (0.41 mmol, 68%) of a yellow microcrystalline powder. A concentrated THF solution was distributed between several test tubes (Ø = 1 cm), which were placed in a Schlenk tube (250 mL). Petroleum ether (boiling range 40−60 °C) was introduced into the Schlenk tube, vapour diffusion of which into the THF solutions yielded yellow single crystals suitable for X-ray structure analysis. − For analytical data, see Table 6 and 7.

Synthesis of *tripod*Co(CO)SnPh$_3$ (11): CO was bubbled through a solution of **9** (620 mg, 0.60 mmol) in THF (30 mL) for 10 min. The red colour of the solution turned orange. The solvent was then removed in vacuo, the residue was suspended in petroleum ether (boiling range 40−60 °C), and chromatographed on kieselgur. After elution with 200 mL of petroleum ether (boiling range 40−60 °C), the orange product was eluted with toluene. Removal of the solvent in vacuo from the appropriate fraction gave 445 mg (0.42 mmol, 70%) of **11** as an orange microcrystalline solid. A concentrated dichloromethane solution was distributed between several test tubes (Ø = 1 cm), which were placed in a Schlenk tube (250 mL). Diethyl ether was introduced into the Schlenk tube, vapour diffusion of which into the CH_2Cl_2 solutions yielded orange single crystals suitable for X-ray structure analysis. − For analytical data, see Table 6 and 7.

X-ray Crystallographic Study: Measurements were made on a Siemens P4 four-circle diffractometer (**7**, **9**) or on a Nonius-Kappa CCD diffractometer (**4**, **8**, **10b**, **11**) using graphite-monochromated Mo-K_α radiation throughout. For the measurements on the Siemens P4 four-circle diffractometer, the intensities of three check reflections (measured every 100 reflections) remained constant throughout the data collection, thus indicating crystal and electronic stability. The data collected on the Siemens P4 diffractometer were corrected in the usual manner, including by an experimental absorption correction. The data collected on the Nonius Kappa CCD device were processed using the standard Nonius software.[26] All calculations were performed using the SHELXT-PLUS software package. Structures were solved by direct methods with the SHELXS-97 program and refined with the SHELXL-97 program.[27,28] Graphical handling of the structural data during solution and refinement was performed with XPMA.[29] Structural representations were generated using Winray 32.[30] Atomic coordinates and anisotropic thermal parameters of nonhydrogen atoms were refined by full-matrix least-squares calculations. The data relating to the structure determinations are compiled in Table 8. Compound **7**: The nitrogens of the amido groups are disordered over two positions with s.o.f.s of 0.75 and 0.25. The acetone solvent molecules were found to be distributed over four sites with s.o.f.s of 0.5, 0.4, 0.35, and 0.25. The disordered atoms were refined isotropically. Due to these disorder problems, the refinement converged only to $R_1 = 9.0\%$ and $R_2 = 26.6\%$, hence discussion of the bond lengths and angles is omitted. Compound **9**: One phenyl ring (C100−C105) was found to be disordered over two orthogonal orientations with s.o.f.s of 0.7 and 0.3. These atoms were refined isotropically. One phenyl ring of the $SnPh_3$ ligand (C400−C405) was found to be disordered over two rotational positions with s.o.f.s of 0.6 and 0.4. The angle between the orientations is 40°. Compound **10b**: The crystal of **10b** examined was found to be a racemic twin, the Flack *x* parameter being 0.267. The metal-bonded hydrogens H1 and H2 were located in the difference map and refined isotropically.

Crystallographic data (excluding structure factors) for the structures reported in this paper have been deposited with the Cambridge Crystallographic Data Centre as supplementary publication nos. CCDC-143127 (**4**), CCDC-143131 (**7**), CCDC-143130 (**8**), CCDC-143129 (**9**), CCDC-143126 (**10b**), and CCDC-143128 (**11**). Copies of the data can be obtained free of charge on application to the CCDC, 12 Union Road, Cambridge CB2 1EZ, U.K. [Fax: (internat.) +44 (0)1223/336033; E-mail: deposit@ccdc.cam.ac.uk].

Acknowledgments

We are grateful to the German Science Foundation (DFG), SFB 247, the VW Foundation (Stiftung Volkswagenwerk), and the Fonds der Chemischen Industrie for financial support. The technical support of T. Jannack (mass spectrometry), D. Günauer (cyclic voltammetry), and the Microanalytical Laboratory of the Institute of Organic Chemistry is gratefully acknowledged.

[1] For cobalt(II), see for instance: [1a]L. Sacconi, F. Mani, *Trans. Met. Chem*. **1982**, *8*, 179−252. − [1b]V. Sernau, G. Huttner, M. Fritz, B. Janssen, M. Büchner, C. Emmerich, O. Walter, L. Zsolnai, D. Günauer, T. Seitz, *Z. Naturforsch*. **1995**, *50b*, 1638−1652. − [1c]S. Beyreuther, J. Hunger, G. Huttner, S. Mann, L. Zsolnai, *Chem. Ber*. **1996**, *129*, 745−757.

[2] For cobalt(III), see for instance: [2a]R. B. King, L. W. Houk, K. H. Panell, *Inorg. Chem*. **1969**, *8*, 1042−1048. − [2b]C. Bianchini, D. Masi, C. Mealli, A. Meli, G. Martini, F. Laschi, P. Zanello, *Inorg. Chem.* **1987**, *26*, 3683−3693. − [2c]S. Vogel, G. Huttner, L. Zsolnai, *Z. Naturforsch*. **1993**, *48b*, 641−652. − [2d]C. A. Ghilardi, F. Laschi, S. Midollini, A. Orlandini, G. Scapacci, P. Zanello, *J. Chem. Soc., Dalton Trans.* **1995**, 531−540. − [2e]K. Heinze, G. Huttner, L. Zsolnai, A. Jacobi, P. Schober, *Chem. Eur. J.* **1997**, *3*, 732−743.

[3] See for instance: [3a]H.-F. Klein, K. Ellrich, D. Neugebauer, O. Orama, K. Krüger, *Z. Naturforsch.* **1983**, *38b*, 303−310. − [3b]D. A. Buckingham, C. R. Clark, *Comprehensive Coordination Chemistry*, Pergamon Press, **1987**, *Vol. 4*, 635−900. − [3c]H.-F. Klein, M. Gaß, U. Zucha, B. Eisenmann, *Z. Naturforsch*. **1988**, *43b*, 927−932. − [3d]H.-F. Klein, X. Li, H. Sun, A. Brand, M. Lemke, U. Flörke, H.-J. Haupt, *Inorg. Chim. Acta* **2000**, *298 (1)*, 70−75.

[4] K. Heinze, G. Huttner, L. Zsolnai, P. Schober, *Inorg. Chem*. **1997**, *36*, 5457−5469.

[5] R. Rupp, A. Frick, G. Huttner, P. Rutsch, U. Winterhalter, A. Barth, P. Kircher, L. Zsolnai, *Eur. J. Inorg. Chem.* **2000**, *3*, 523−536.

[6] L. Sacconi, S. Midollini, *J. Chem. Soc., Dalton Trans.* **1972**, 1213−1216.

[7] F. Cecconi, C. A. Ghilardi, S. Midollini, S. Moneti, A. Orlandini, M. Bacci, *J. Chem. Soc., Chem. Commun*. **1985**, 731−733.

[8] F. Cecconi, C. A. Ghilardi, S. Midollini, S. Moneti, A. Orlandini, *J. Organomet. Chem*. **1987**, *323*, C5−C9.

[9] [9a]O. Walter, T. Klein, G. Huttner, L. Zsolnai, *J. Organomet. Chem*. **1993**, *458*, 63−81. − [9b]M. Büchner, G. Huttner, U. Winterhalter, A. Frick, *Chem. Ber./Recueil* **1997**, *130*, 1379−1392. − [9c]O. Walter, M. Büchner, G. Huttner, *J. Organomet. Chem*. **1997**, *529*, 103−106.

[10] G. Rheinhard, R. Soltek, G. Huttner, A. Barth, O. Walter, L. Zsolnai, *Chem. Ber*. **1996**, *129*, 97−108.

[11] [11a] S. Vogel, A. Barth, G. Huttner, Th. Klein, L. Zsolnai, R. Kremer, *Angew. Chem*. **1991**, *103*, 325−327; *Angew. Chem. Int. Ed. Engl*. **1991**, *30*, 303−304. − [11b] V. Körner, G. Huttner, S.

Vogel, A. Barth, L. Zsolnai, *Chem. Ber./Recueil* **1997**, *130*, 489−492.
[12] C. Mealli, S. Midollini, L. Sacconi, *Inorg. Chem*. **1975**, *14*, 2513−2521.
[13] See for instance: [13a] M. Di Vaira, C. A. Ghilardi, S. Midollini, L. Sacconi, *J. Am. Chem. Soc*. **1978**, *100*, 2550−2551. – [13b] M. Di Vaira, L. Sacconi, *Angew. Chem*. **1982**, *94*, 338−351, *Angew. Chem. Int. Ed. Engl*. **1982**, *21*, 330. – [13c] M. Di Vaira, L. Sacconi, P. Stoppioni, *J. Organomet. Chem*. **1983**, *250*, 183−195. – [13d] A. Barth, G. Huttner, M. Fritz, L. Zsolnai, *Angew. Chem*. **1990**, *102*, 956−958, *Angew. Chem. Int. Ed. Engl.* **1990**, *29*, 929.
[14] M. Yoshifuji, I. Shima, N. Inamoto, K. Hirotsu, T. Higuchi, *J. Am. Chem. Soc*. **1981**, *103*, 4587−4589. For more recent examples, see refs.[15,16]
[15] L. Weber, *Chem. Rev.* **1992**, *92*, 1839−1906.
[16] CSD: F. H. Allen, J. E. Davis, J. J. Galloy, O. Johnson, O. Kennard, C. F. Macrae, E. M. Mitchell, G. F. Mitchell, J. M. Smith, D. Watson, *J. Chem. Inf. Comput. Sci*. **1991**, *31*, 187−204.
[17] For an early example concerning the bond lengths of η^2-side-on-coordinated *versus* free P−P double bonds, see ref.[15] – [17a] J. Borm, L. Zsolnai, G. Huttner, *Angew. Chem.* **1983**, *95*, 1018; *Angew. Chem. Int. Ed. Engl.* **1983**, *22*, 977.
[18] [18a] P. Dapporto, S. Midollini, A. Orlandini, L. Sacconi, *Inorg. Chem*. **1976**, *15*, 2768−2774. – [18b] S. Vogel, G. Huttner, L. Zsolnai, C. Emmerich, *Z. Naturforsch*. **1993**, *48b*, 353−363.
[19] [19a] U. Schubert, S. Gilbert, S. Mock, *Chem. Ber*. **1992**, *125*, 835−837. – [19b] S. Gilbert, M. Knorr, S. Mock, U. Schubert, *J. Organomet. Chem*. **1994**, *480*, 241−254.
[20] A. Sacco, R. Ugo, *J. Chem. Soc.* **1964**, *3*, 3274−3277.
[21] D. L. DuBois, D. W. Meek, *Inorg. Chem*. **1976**, *15*, 3076−3083.
[22] Organikum, Deutscher Verlag der Wissenschaften, Berlin, **1990**.
[23] A. Muth, Diplomarbeit, University of Heidelberg, **1989**.
[24] [24a] R. Batchelor, T. Birchall, *J. Am. Chem. Soc*. **1982**, *104*, 674−679. – [24b] Z. Hou, T. L. Breen, D. W. Stephan, *Organometallics* **1993**, *12*, 3158−3167.
[25] A. G. Davies, *Organotin Chemistry*, VCH, Weinheim, **1997**, *Chapter 17*, 253.
[26] DENZO−SMN, Data processing software, Nonius **1998**; http://www.nonius.com
[27] [27a] G. M. Sheldrick, *SHELXS-97, Program for Crystal Structure Solution*, University of Göttingen, **1997**; http://shelx.uni-ac.gwdg.de/shelx/index.html – [27b] G. M. Sheldrick, *SHELXL-97, Program for Crystal Structure Refinement*, University of Göttingen, **1997**; http://shelx.uni-ac.gwdg.de/shelx/index.html
[28] *International Tables for X-ray Crystallography*, Vol. 4, Kynoch Press, Birmingham, U.K., **1974**.
[29] L. Zsolnai, G. Huttner, *XPMA*; http://www.rzuser.uni-heidelberg.de/~v54/xpm.html, Universität Heidelberg, **1994**.
[30] R. Soltek, *Winray 32*; http://www.rzuser.uni-heidelberg.de/~v54/xpm.html, Universität Heidelberg, **2000**.

Received April 17, 2000
[I00148]

Synthesis and X-ray Structure of Metalated Rhodium(II) Catalysts with a Chiral Phospholane

Francisco Estevan,[a] Peter Krueger,[b] Pascual Lahuerta,*[a] Eduardo Moreno,[a] Julia Pérez-Prieto,*[c] Mercedes Sanaú,[a] and Helmut Werner*[b]

Dedicated to Professor R. Uson on the occasion of his 75th birthday

Keywords: Carbocycles / Chirality / Diazo compounds / P ligands / Rhodium

The reaction of $Rh_2(O_2CR)_4$ (R = CH_3, CF_3) with the chiral phosphane (2*S*,5*S*)-2,5-dimethyl-1-phenylphospholane (PC* H), results in the formation of two diastereoisomers of $Rh_2(O_2CCR)_2(PC^*)_2$, with (*P*) and (*M*) configuration. These can easily be isolated by chromatographic methods to obtain enantiomerically pure Rh^{II} compounds. Preliminary catalytic studies have shown that they induce moderate asymmetry in the cyclization of 5-aryl-1-diazo-2-pentanones and 1-diazo-5-hexen-2-one. X-ray analysis of the (*M*) diastereoisomer with formula $Rh_2(O_2CCCH_3)_2(PC^*)_2$ is reported. The crystallographic parameters are as follows: space group $P2_12_12$ (orthorhombic) with *a* = 12.1347(11) Å, *b* = 14.5870(13) Å, *c* = 9.8171(9) Å.

Introduction

After the first report that the reaction of rhodium acetate and triphenylphosphane readily forms the bis(cyclometalated) compound $Rh_2(O_2CCH_3)_2[(C_6H_4)PPh_2]_2$,[1] it has been confirmed that this reaction can be extended to other rhodium carboxylates and to other arylphosphanes,[2−4] yielding the homologous metalated compounds $Rh_2(O_2CR)_2(PC)_2$, (PC = metalated phosphane; R = CH_3, CF_3; Scheme 1). Kinetic studies confirmed that the cyclometalation reaction was catalysed by protic acids.[5]

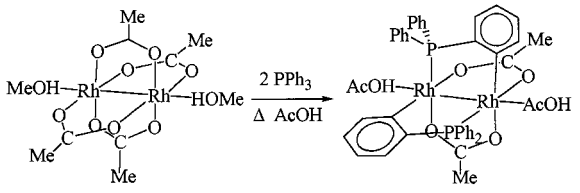

Scheme 1. *ortho*-Metalation reactions in binuclear dirhodium compounds

Different transition-metal compounds have been used as catalysts in the transformation of α-diazocarbonyl compounds, but the compounds of rhodium(II) have shown general utility.[6] We have reported that the bis(cyclometalated) complexes $Rh_2(O_2CR)_2(PC)_2$, exhibit excellent chemoselectivity in the catalytic intramolecular C−H insertion reactions of α-diazo compounds, where this reaction is competing with aromatic substitution.[7] In these compounds, the presence of two different ligands, the metalated phosphane and the carboxylate, allowed for a modulation of the electronic and steric properties of the catalyst which influence the activity and selectivity of the catalytic reactions.

Many efforts have been devoted to obtain chiral rhodium(II) complexes suitable for asymmetric induction in carbene transfer reactions. In this context, great success has been achieved by using rhodium(II) compounds having four chiral carboxylates[8] or amidate groups[9] as bridging ligands. As the bis(cyclometalated) complexes $Rh_2(O_2CR)_2(PC)_2$ with head-to-tail arrangement are inherently chiral, we have recently reported the isolation of the pure enantiomers [see (*P*) and (*M*) notation in Scheme 2]

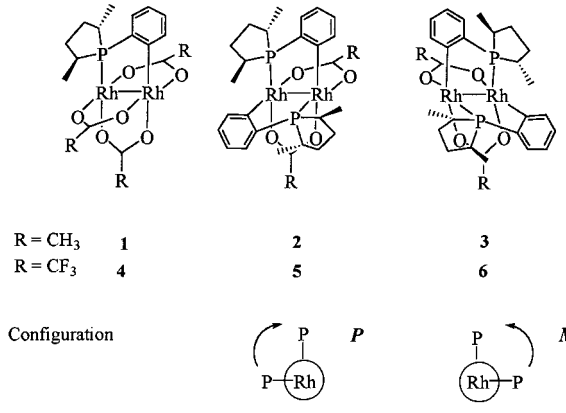

Scheme 2. Structures of compounds $Rh_2(O_2CCR)_3(PC^*)$ and $Rh_2(O_2CCR)_2(PC^*)_2$ [(*P*) and (*M*) isomers]

[a] Dep. de Química Inorgánica, Facultad de Químicas, Universidad de Valencia,
Dr. Moliner 50, 46100 Burjassot-Valencia, Spain
Fax: (internat.) + 34-96/386-4322
E-mail: pascual.lahuerta@uv.es
[b] Institut für Anorganische Chemie, Universität Würzburg,
Am Hubland, 97074 Würzburg, Germany
[c] Dep. de Química Orgánica, Facultad de Farmacia, Universidad de Valencia,
Av. Vicent A. Estelles, s/n, 46100 Burjassot-Valencia, Spain
Fax: (internat.) + 34-96/386-4939,
E-mail: julia.perez@uv.es

 © WILEY-VCH Verlag GmbH, D-69451 Weinheim, 2001 1434−1948/01/0101−105 $ 17.50+.50/0

resulting from the metalation of PPh_3.[10] These enantiomers induced identical enantiomeric control, but with opposite *ee* values (36% *ee*; 70% yield), in the C−H insertion reaction of 1-diazo-5-phenyl-2-pentanone.

An alternative and previously unused approach to the preparation of chiral bis(cyclometalated) rhodium(II) compounds, is by the reaction of rhodium(II) carboxylates with a chiral $PhPR_2$* phosphane. Owing to the inherent chirality of $Rh_2(O_2CR)_2(PC)_2$ dimers,[10] this process would result in the formation of two diastereoisomers, which could be isolated to perform catalytic assays. Furthermore, since bis(cyclometalated) compounds having basic phosphanes have proved to be reactive and selective in carbene transfer reactions,[7] our primary objective was the generation of new, enantiomerically pure, cyclometalated rhodium(II) derivatives with chiral, electron-rich phospholanes[5] as ligands.

We describe in this paper the synthesis of several cyclometalated rhodium(II) compounds resulting from the reaction of rhodium acetate or rhodium trifluoroacetate and (2*S*,5*S*)-2,5-dimethyl-1-phenylphospholane (PC*H). The crystal structure of one of the isolated diastereoisomers of formula $Rh_2(O_2CCH_3)_2(PC^*)_2 \cdot 2\,CH_3CO_2H$ is also reported. Their utility in asymmetric induction has been studied in C−H insertion and cyclopropanation reactions of model diazo ketones. The observed enantioselectivities, though moderate, compare favourably with those obtained for other types of chiral rhodium(II) complexes[11,12] and reveal the great potential of these compounds in asymmetric catalysis.

Results and Discussion

Rhodium(II) acetate and (2*S*,5*S*)-2,5-dimethyl-1-phenylphospholane (molar ratio 1:2.2) were heated at reflux in a mixture of toluene and acetic acid (3:1). The reaction was considerably slow and did not go to completion even after 33 h. From this reaction mixture, three new compounds were isolated by column chromatography: the monometalated compound $Rh_2(O_2CCH_3)_3(PC^*)$ (**1**) (43%) and the two diastereoisomers $Rh_2(O_2CCH_3)_2(PC^*)_2$ [(*P*) isomer] (**2**) (23%) and $Rh_2(O_2CCH_3)_2(PC^*)_2$ [(*M*) isomer] (**3**) (13%).

These compounds exchange the carboxylate groups upon treatment with trifluoroacetic acid, to form the corresponding trifluoroacetate derivatives $Rh_2(O_2CCF_3)_3(PC^*)$ (**4**), $Rh_2(O_2CCF_3)_2(PC^*)_2$ [(*P*) isomer] (**5**), and $Rh_2(O_2CCF_3)_2(PC^*)_2$ [(*M*) isomer] (**6**) (Scheme 2).

The reaction of rhodium(II) trifluoroacetate and the phospholane was considerably faster and, after 16 h at room temperature in CH_2Cl_2 solution, the two bismetalated compounds **5** (32%) and **6** (14%) were formed. Under these conditions, the monometalated compound **4** was not detected in solution.

Crystal Structure of 3

A schematic drawing of the structure of compound **3** together with selected bond lengths and angles, is presented in Figure 1. In the dinuclear complex **3**, the two rhodium atoms are bridged by two acetate groups and by two phospholane molecules metalated at the phenyl ring; two oxygen atoms of two acetic acid molecules occupying the axial positions, complete the slightly distorted octahedral coordination (bond angles in the range 83.00−93.90 Å) around the metal centres. As observed in all the related compounds, each of these acetic acid molecules undergoes an O···H−O interaction with one oxygen atom of each bridging acetate group. The value of the Rh−Rh bond length 2.5036(6) Å falls within the range reported for dirhodium compounds of comparable structure.[13]

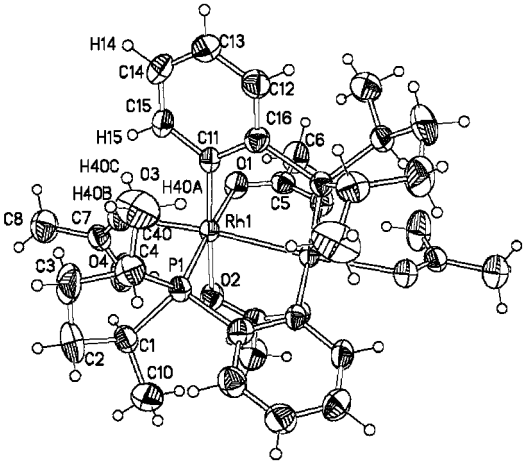

Figure 1. ORTEP diagram of the complex (*M*)-**3**·$(HO_2CCH_3)_2$; selected bond lengths [A] and angles [°]: Rh1−Rh1A 2.5036(6), Rh1−C16 1.992(4), Rh1−O2 2.196(2), Rh1−O3 2.370(3), Rh1−O1 2.139(2), Rh1−P1 2.2187(10); C16−Rh1−O1 89.45(12), O1−Rh1−O2 83.00(10), O1−Rh1−P1 175.15(8), C16−Rh1−O3 94.59(12), C16−Rh1−O2 172.43(12), P1−Rh1−O3 93.90(7)

The crystal structure determination confirmed that compound **3** has the (*M*) configuration. Consequently, compound **6** will have the same configuration while compounds **2** and **5** must have the (*P*) configuration (Scheme 2). An interesting feature in compound **3** is that the methyl group attached to C1 of the phospholane ring is oriented toward the metalated phenyl ring of the same phosphane ligand (intra-ligand interaction), while the methyl group attached to C4 points towards the metalated phenyl ring of the other phosphane (inter-ligand interaction). A simple molecular model built for compound **2** (or **5**) shows that for the (*P*) configuration only the intra-ligand interaction can be generated as is shown in Scheme 3.

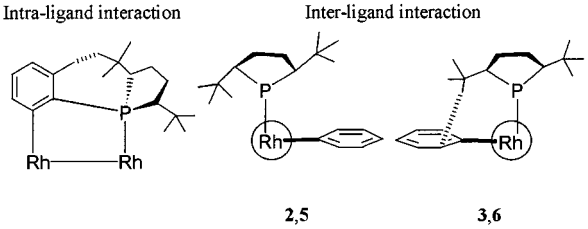

Scheme 3. Model of inter- and intra-ligand interactions in compounds **2**, **3**, **5**, **6**

Spectroscopic Data

All the new compounds were characterised by ^1H, ^{13}C, and ^{31}P NMR spectroscopy. The ^{31}P NMR spectrum of

compound **1**, with only one metalated phosphane ligand, displays a characteristic doublet of doublets due to the coupling to both rhodium nuclei ($\delta = 35.9$; $^1J_{RhP} = 152$ Hz, $^2J_{RhP} = 3$ Hz). In contrast, the bis(cyclometalated) compounds show a multiplet corresponding to the AA′ part of an AA′XX′ system at lower chemical shift values ($\delta = 27.4$ and 28.3). As expected, the three acetate groups of compound **1** are magnetically different and this is reflected in the ^{1}H and ^{13}C NMR spectroscopic data.

The molecules of compound **3** have a crystallographic C_2 symmetry axis. This symmetry is apparently retained in solution as the four methyl groups of the phospholane ligands are equivalent in the ^{1}H NMR spectrum in a pairwise manner. These two signals are of equal intensity and integrate as 6 H each. They appear as doublets of doublets, showing coupling to one proton and to the phosphorus atom. The other three bis(cyclometalated) compounds show a similar pattern of signals for the phospholane ligands. The difference in chemical shift values for the methyl groups of the phospholane ligands is relatively small ($\delta \approx 0.6$) for compounds **2** and **5** but it is larger for complexes **3** and **6** ($\delta \approx 1.2$). This can be attributed to the different environments of the methyl groups in the (*P*) and (*M*) configurations and also to the possible H···H interactions (Scheme 3).

A careful NMR spectroscopy study carried out for compounds **5** and **6** confirmed that the supposed H···H interactions (see above) also occur in solution. The ^{1}H NMR spectrum of **6** displays three multiplet signals in the aromatic region which, based on COSY experiments, were assigned as following: $\delta = 6.85$ (H^{12}), 6.95 (H^{13} and H^{14}), and 7.56 (H^{15}). The signals at $\delta = 0.28$ and 0.93 were assigned to the methyl groups of the phospholane and appeared as very characteristic doublets of doublets owing to the coupling to the phosphorus atom and to the H^1 and H^4 protons whose signals appeared as multiplets at $\delta = 2.86$ and 2.33 , respectively. The assignment of these signals was made with an NOE experiment.

Irradiation of the methyl resonance at $\delta = 0.93$ led to an enhancement of the signal at $\delta = 2.86$, assigned to H^1, and also of the signal at $\delta = 6.85$ (Scheme 4). This is in agreement with an intra-ligand interaction between H^{12} and the protons of the methyl group attached to C^1. Irradiation of the methyl signal at $\delta = 0.28$ resulted in an enhancement of the intensity of the signal at $\delta = 2.33$, assigned to H^4, and also of the signals at $\delta = 6.95$ and 7.56. This result supports the interaction between the protons of the methyl group attached to C^4 and two aromatic protons, H^{15} and probably H^{14}.

Different results were obtained when this experiment was performed with isomer **5**. The ^{1}H NMR spectrum of **5** displays four signals in the aromatic region which, based on COSY experiments, were assigned as follows: $\delta = 6.74$ (H^{12}), 6.86 (H^{13}), 6.98 (H^{14}), 7.57 (H^{15}). We use the same labelling scheme as in compound **6** to identify the hydrogen atoms in compound **5**. The signals at $\delta = 0.04$ and 1.26 were assigned to the methyl groups of the phospholane and appeared again doublets of doublets. The protons H^1 and H^4 gave rise to a broad signal at $\delta = 2.37$.

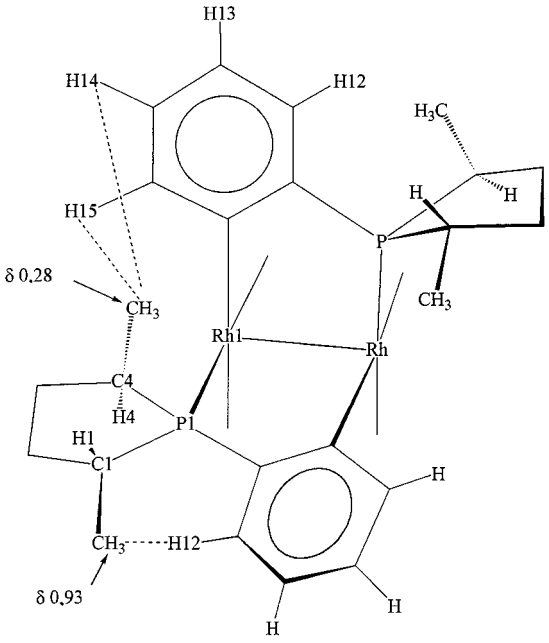

Scheme 4. NOE experiment for compound **6**

In an NOE experiment (Scheme 5), irradiation of the methyl signal at $\delta = 0.04$ led to an enhancement of the intensity of the signal at $\delta = 2.37$, due to an interaction with H^1, and to that of the signal at $\delta = 6.74$. This result is indicative of an interaction between the protons of the methyl group attached to C^1 and the aromatic proton H^{12}. Irradiation of the methyl resonance at $\delta = 1.26$ gave only an enhancement of the signal at $\delta = 2.37$, due to an interaction with H^4, but not of any other signal in the aromatic region. These results support the *P*-configuration of compound **5**.

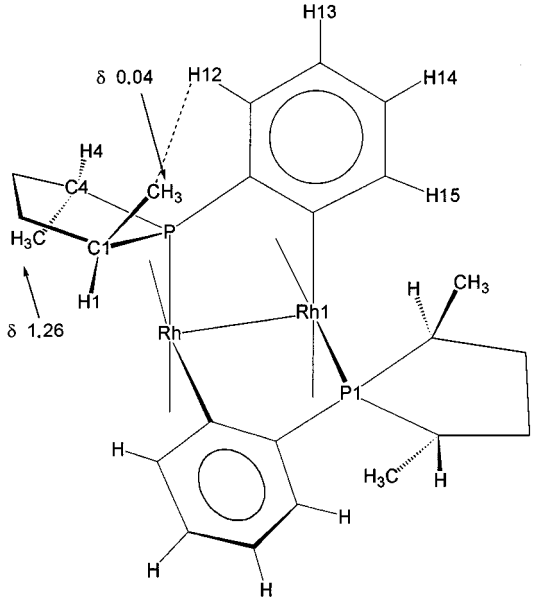

Scheme 5. NOE experiment for compound **5**

Exploratory Catalytic Studies

1-Diazo-2-alkanones were prepared from the corresponding acid by reaction with ethyl chloroformate, followed by treatment with freshly prepared diazomethane.

Catalytic reactions were performed by the addition of the rhodium(II) complex (1 mol-%) to an anhydrous dichloromethane solution containing the diazo compound; the reaction mixture was heated at reflux for 1 h. After cooling, the solution was filtered through a short plug of silica gel to remove the catalyst, and the solvent was evaporated under reduced pressure. The residue was analysed by ^1H and ^{13}C NMR spectroscopy.

We mainly studied the ability of the diastereoisomers (*P*)-**5** and (*M*)-**6** to induce a C−H insertion reaction of diazo compounds **7** (Scheme 6). Complex (*M*)-**6** catalysed the cyclisation of **7** with high yield but only a small variation in enantiomeric control was observed by the introduction of electron-withdrawing or electron-donating groups on the benzene ring of the organic substrate (Scheme 6). It is worth mentioning that although the enantiomeric control offered by these rhodium(II) compounds was modest, complexes containing chiral carboxamidates catalyse intramolecular aliphatic C−H insertion of 1-diazo-2-alkanones with practically no asymmetric induction.[11] Surprisingly, in the case of (*P*)-**5**, the diazo compounds **7** were recovered unchanged after several hours of heating in the presence of the rhodium catalyst.

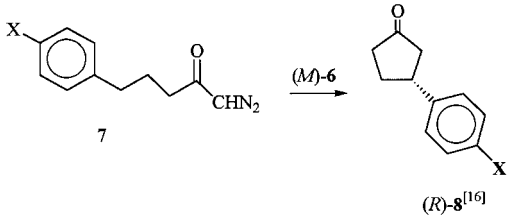

7 (*R*)-**8**[16]

	Yield (%)	% ee[15]
X = H	85	39
X = Cl	93	33
X = OCH_3	80	37

Scheme 6. C−H insertion of 1-diazo-5-aryl-2-pentanones

Both diastereoisomers (*M*)-**6** and (*P*)-**5** were able to transform the 1-diazo ketone **9** in high yield, but the sense and extent of the enantiotopic selection were different (Scheme 7). It is interesting to note that low enantiomeric control has been achieved in the intramolecular cyclopropanation of this type of diazo compound catalysed by chiral rhodium(II) carboxamides.[14] In particular, the cyclisation of the diazo ketone **9** using those catalysts have only provided levels of enantiomeric control in the 3−23% *ee* range.[12]

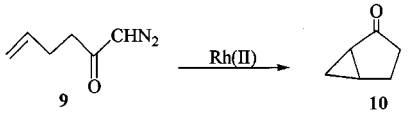

9 10

	Yield (%)	% ee[15]	
(*P*)-**5**	84	52	(1*S*,5*R*)[17]
(*M*)-**6**	90	22	(1*R*,5*S*)
Rh_2(carboxamidates)$_4$[12]	50-94	3-23	

Scheme 7. Cyclopropanation of 1-diazo-5-hexen-2-one

Conclusion

In summary, we explored the synthesis of chiral bis(cyclometalated) rhodium(II) compounds based on the use of a chiral phosphane. The reaction of dirhodium carboxylates with (2*S*,5*S*)-2,5-dimethyl-1-phenylphospholane led to two types of dimers with different environments around the Rh centre. Diastereoisomers were easily isolated by chromatographic methods. Preliminary catalytic studies showed their different efficiencies in inducing asymmetry in the cyclisation of model 1-diazo carbonyl compounds. The level of enantiomeric control, although moderate, is promising since other rhodium(II) catalysts have shown less selectivity in the transformation of this type of diazo compound. The availability of other chiral 2,5-disubstituted phospholanes[18] can allow further studies to determine the influence of the electronic and steric effects of the phosphane ligand on the reactivity and selectivity of these new chiral rhodium(II) catalysts.

Experimental Section

All reactions were carried out under argon, using standard Schlenk techniques. $Rh_2(O_2CCF_3)_4$ was prepared by literature procedures.[19] Other starting materials (besides the phospholane) were commercially available and used as received. Solvents were degassed and used without further purification. − NMR spectra were recorded with Bruker AC-200 and Varian Unity-300 spectrometers. Chemical shifts (δ values) are given relative to TMS (^1H, ^{13}C), and to 85% H_3PO_4 aqueous solution (^{31}P). Coupling constants (*J*) are given in Hertz.

Preparation of (2*S*,5*S*)-2,5-Dimethyl-1-phenylphospholane: This ligand was prepared according to literature procedures.[18]

Synthesis of Acetate Complexes 1−3: $Rh_2(O_2CCH_3)_4$ (206 mg, 0.433 mmol) and (2*S*,5*S*)-2,5-dimethyl-1-phenylphospholane (183 mg, 0.952 mmol) were heated at reflux in a mixture of toluene/acetic acid (6 mL, 3:1) for 33 h. After cooling, the solvent was evaporated under reduced pressure and the resulting violet solid was dissolved in CH_2Cl_2.The solution was purified by chromatography on silica gel. Elution with CH_2Cl_2/ether/acetone (50:10:1) separated a dark blue band from a green band. The blue band was collected and the solvent was evaporated. Crystallisation of the residue from acetone/hexane gave $Rh_2(O_2CCH_3)_3$(PC) (**1**) as a dark blue solid. Yield 115 mg (43%). − ^1H NMR ($CDCl_3$): δ = 0.63 (dd, J_{PH} = 13.8, J_{HH} = 6.8, 3 H, CH_3 ring), 1.03 (dd, J_{PH} = 15.6, J_{HH} = 6.9, 3 H, CH_3 ring), 1.71 (s, 3 H, CH_3 *cis*), 1.78 (s, 3 H, CH_3 *cis*), 2.11 (s, 3 H, CH_3 *trans*), 1.20−2.90 (m, 6 H, CH_2, CH ring), 6.60−9.00 (m, 4 H, C_6H_4). − $^{31}P\{^1H\}$ NMR ($CDCl_3$): δ = 35.9 (dd, $^1J_{RhP}$ = 152, $^2J_{RhP}$ = 3). − The green band was redissolved in CH_2Cl_2.The solution was chromatographed on silica gel. Elution with CH_2Cl_2/acetone (5:1) led to a separation into two green bands. The green solutions were concentrated to dryness and dissolved in acetone. Addition of hexane precipitated green solids, which were dried in vacuum.

Fraction 1: Compound **2** [(*P*) isomer], 75 mg (23%). − ^1H NMR ($CDCl_3$): δ = 0.04 (dd, J_{PH} = 14.3, J_{HH} = 7.0, 6 H, CH_3 ring), 1.21 (dd, J_{PH} = 15.5, J_{HH} = 7.0, 6 H, CH_3 ring), 1.40−3.00 (m, 12 H, CH_2, CH ring), 2.15−2.25 (s, 6 H, CH_3COO) 6.70−7.52 (m, 8 H, C_6H_4). − $^{31}P\{^1H\}$ NMR ($CDCl_3$): δ = 27.9 (AA′XX′ system).

Fraction 2: Compound **3** [(*M*) isomer], 41 mg (13%). – ^{1}H NMR ($CDCl_3$): δ = 0.33 (dd, J_{PH} = 15.1, J_{HH} = 7.1, 6 H, CH_3 ring), 0.97 (dd, J_{PH} = 13.6, J_{HH} = 6.9, 6 H, CH_3 ring), 1.40−3.00 (m, 12 H, CH_2, CH ring), 2.07−2.2 (s, 6 H, CH_3CO_2) 6.80−7.00 (m, 6 H, C_6H_4), 7.58 (dd J = 5.2, J = 2.7 2 H, C_6H_4). – $^{31}P\{^1H\}$ NMR ($CDCl_3$): δ = 27.4 (AA′XX′ system).

Synthesis of Trifluoroacetate Derivative 4: $Rh_2(O_2CCH_3)_3(PC)$ (**1**) (58 mg, 0.1 mmol) was dissolved in CH_2Cl_2 and after trifluoroacetic acid (0.77 mL, 10 mmol) was added, the solution was stirred for 2 h. The solvent was removed under vacuum and the crude solid was dissolved in CH_2Cl_2 (1 mL).The solution was purified by chromatography on silica gel. Elution with CH_2Cl_2 gave a blue band from which a blue solid was obtained after evaporation of the solvent. – ^{1}H NMR ($CDCl_3$): δ = 0.60 (dd, J_{PH} = 15.8, J_{HH} = 6.6, 3 H, CH_3 ring), 1.22 (dd, J_{PH} = 16.6, J_{HH} = 6.9, 3 H, CH_3 ring), 0.94−2.80 (m, 6 H, CH_2, CH ring), 6.98−8.53 (m, 4 H, C_6H_4). – $^{31}P\{^1H\}$ NMR ($CDCl_3$): δ = 36.3 (dd, $^1J_{RhP}$ = 141, $^2J_{RhP}$ = 4).

Synthesis of Trifluoroacetate Derivatives 5 and 6: $Rh_2(O_2CCF_3)_4$ (100 mg, 0.21 mmol) and (2*S*,5*S*)-2,5-dimethyl-1-phenylphospholane (188 mg, 0.46 mmol) were stirred in CH_2Cl_2 (6 mL) for 16 h. The solvent was evaporated under reduced pressure and the resulting violet solid was worked up as described for the acetate derivatives **2** and **3**.

Compound 5 [(*P*) Isomer]: 116 mg (32%). – ^{1}H NMR ($CDCl_3$): δ = 0.04 (dd, J_{PH} = 15.5, J_{HH} = 7.0, 6 H, CH_3 ring), 1.26 (dd, J_{PH} = 16.0, J_{HH} = 6.2, 6 H, CH_3 ring), 0.80−2.50 (m, 12 H, CH_2, CH ring), 6.74 (t, J = 7.7, 2 H, C_6H_4), 6.86 (t, J = 7.4, 2 H, C_6H_4), 6.98 (t, J = 7.5, 2 H, C_6H_4), 7.58 (dd J = 7.9, J = 3.6, 2 H, C_6H_4). – $^{31}P\{^1H\}$ NMR ($CDCl_3$): δ = 29.1 (AA′XX′ system).

Compound 6 [(*M*] Isomer]: 48 mg (14%). – $[\alpha]_D$ = +423 (c = 0.04, $CHCl_3$). – ^{1}H NMR ($CDCl_3$): δ = 0.28 (dd, J_{PH} = 15.4, J_{HH} = 7.2, 6 H, CH_3 ring), 0.93 (dd, J_{PH} = 15.5, J_{HH} = 8.5, 6 H, CH_3 ring), 1.4−3.00 (m, 12 H, CH_2, CH ring), 6.85 (m, 2 H, aromatic H), 6.95 (m, 4 H, aromatic H), 7.56 (m, 2 H, aromatic H). – $^{31}P\{^1H\}$ NMR ($CDCl_3$): δ = 27.4 (AA′XX′ system).

Crystallographic Data Collection and Refinement of the Structure: A Siemens SMART CCD diffractometer was used for data collection on crystals of the compound. Unit-cell dimensions were determined by a least fit of 50 reflections, ($2.07° < \theta < 23.32°$) The crystal structure determination was done by direct methods, using SHELXTL V 5.05;[20] the refinement on F^2 was done using all reflections. The positions of all non-hydrogen atoms were deduced from difference Fourier maps and were refined anisotropically. Hydrogen atoms were placed in their geometrically generated positions and were refined riding on the carbon atom to which they are attached. Green single crystals were grown in CH_2Cl_2/hexane. $C_{32}H_{46}O_8P_2Rh_2$: crystal size 0.3 × 0.25 × 0.3 mm, M = 826.45, orthorhombic, space group $P2_12_12$ with a = 12.1347(11), b = 14.5870(13), c = 9.8171(9) Å, V = 1737.7(3) Å^3 and Z = 2 ($\rho_{calcd.}$ = 1.579 g cm^{-3}), μ (Mo-K_α) = 1.088 mm^{-1}. 3932 reflections measured, 2174 unique (R_{int} = 0.0212), which were used in all calculations. Data/parameters 2174:205. The final R value was 0.0187 ($wR2$ = 0.042). Crystallographic data (excluding structure factors) for the structure reported in this paper have been deposited with the Cambridge Crystallographic Data Centre as supplementary publication no. CCDC-142404. Copies of the data can be obtained free of charge on application to CCDC, 12 Union Road, Cambridge CB2 1 EZ, UK [Fax: (internat.) + 44-1223/336-033; E-mail: deposit@ccdc.cam.ac.uk].

Acknowledgments

We thank the Dirección General de Investigación Científica y Técnica (DGICYT) (Project PB94−0988) and the EC (Project TMR Network ERBFMRXCT 60091).

[1] A. R. Chakravarty, F. A. Cotton, D. A. Tocher, J. H. Tocher, *Organometallics* **1985**, *4*, 8.
[2] [2a] F. Barceló, F. A. Cotton, P. Lahuerta, R. Llusar, M. Sanaú, W. Schwotzer, M. A. Ubeda, *Organometallics* **1986**, *5*, 808. – [2b] F. Barceló, F. A. Cotton, P. Lahuerta, M. Sanaú, W. Schwotzer, M. A. Ubeda, *Organometallics* **1987**, *6*, 1105. – [2c] F. A. Cotton, P. Lahuerta, J. Payá, F. Barceló, M. A. Ubeda, *Inorg. Chem.* **1988**, *27*, 1010. – [2d] P. Lahuerta, J. Payá, X. Solans, M. A. Ubeda, *Inorg. Chem.* **1992**, *31*, 385. – [2e] P. Lahuerta, E. Peris, M. A. Ubeda, S. García-Granda, M. R. Díaz, *J. Organomet. Chem.* **1993**, *455*, C10. – [2f] F. Estevan, G. Gonzalez, P. Lahuerta, M. Martinez, E. Peris, R. van Eldik, *J. Chem. Soc., Dalton Trans.* **1996**, 1045.
[3] [3a] E. C. Morrison, D. A. Tocher, *J. Organomet. Chem.***1991**, *408*, 105. – [3b] E. C. Morrison, D. A. Tocher, *Inorg. Chim. Acta* **1989**, *157*, 139.
[4] M. V. Borrachero, F. Estevan, S. García-Granda, P. Lahuerta, J. Latorre, E. Peris, M. Sanaú, *J. Chem. Soc., Chem. Commun.* **1993**, *24*, 1864.
[5] [5a] G. González, P. Lahuerta, M. Martinez, E. Peris, M. Sanaú, *J. Chem. Soc., Dalton Trans* **1994**, 545. – [5b] G. González, M. Martinez, F. Estevan, A. García-Bernabé, P. Lahuerta, E. Peris, M. A. Ubeda, R. Diaz, S. García-Granda, B. Tejerina, *New J. Chem.* **1996**, *20*, 83.
[6] M. P. Doyle, M. A. McKervey, *Chem. Commun.* **1997**, 983.
[7] [7a] F. Estevan, P. Lahuerta, J. Pérez-Prieto, S. E. Stiriba, M. A. Ubeda, *Synlett* **1995**, *11*, 1121. – [7b] F. Estevan, P. Lahuerta, J. Pérez-Prieto, M. Sanaú, S. E. Stiriba, M. A. Ubeda, *Organometallics* **1997**, *16*, 880.
[8] [8a] S. Hashimoto, N. Watanabe, S. Ikegami, *Tetrahedron Lett.* **1990**, *31*, 5173. – [8b] M. Anada, S. Hashimoto, *Tetrahedron Lett.* **1998**, *39*, 79.
[9] [9a] M. P. Doyle, W. R. Winchester, J. A. A. Hoorn, V. Lynch, S. H. Simonsen, R. Ghosh, *J. Am. Chem. Soc.* **1993**, *115*, 9968. – [9b] M. P. Doyle, Q-L. Zhov, A. B. Dyatkin, D. A. Ruppar, *Tetrahedron Lett.* **1995**, *36*, 7579.
[10] D. F. Taber, S. C. Malcolm, K. Bieger, P. Lahuerta, M. Sanaú, S. E. Stiriba, J. Pérez-Prieto, M. A. Monge, *J. Am. Chem. Soc.* **1999**, *121*, 860.
[11] P. Müller, P. Polleaux, *Helv. Chim. Acta* **1994**, *77*, 645.
[12] M. P. Doyle, M. Y. Eismont, Q. L. Zhou, *Russ. Chem. Bull.* **1997**, *46*, 955.
[13] F. A. Cotton, R. A. Walton, *Multiple Bonds Between Metal Atoms*; Clarendon Press, Oxford, **1993**.
[14] M. P. Doyle, D. C. Forbes, *Chem. Rev.* **1998**, *98*, 911.
[15] The *ee* values were based on GC analysis with a 2,3-di-*O*-acetyl 6-*O*-*tert*-butyldimethylsilyl beta CDX column.
[16] The absolute configuration of **8** was determined by correlation of the sign of the rotation of polarized light with that of the known enantiomer: L. A. Paquette, J. P. Gilday, C. S. Ra, *J. Am. Chem. Soc.* **1987**, *109*, 6858.
[17] The absolute configuration of **10** was determined by correlation of the sign of the rotation of polarized light with that of the known enantiomer: [17a]D. A. Lighter, D. E. Jackman, *Tetrahedron Lett.* **1975**, 3051. –[17b] E. A. March, K. A. Nelson, *Tetrahedron* **1987**, *43*, 679.
[18] [18a] M. J. Burk, J. E. Feaster, R. L. Harlow, *Tetrahedron: Asymmetry* **1991**, *2*, 569. – [18b] M. J. Burk, J. E. Feaster, R. L. Harlow, *J. Am. Chem. Soc.* **1990**, *115*, 10125−10138. – [18c] M. J. Burk, J. E. Feaster, R. L. Harlow, *Organometallics* **1990**, *9*, 2653.
[19] S. A. Johnson, H. R. Hunt, H. M. Neumann, *Inorg. Chem.* **1963**, *2*, 960.
[20] *SHELXTL V 5.05*, AXS Siemens, **1996**.

Received April 20, 2000
[I00157]

Disc-Like Chiral Palladium and Platinum Complexes: Synthesis and Mesomorphic Properties

Belkiz Bilgin Eran,*[a] Dirk Singer,[b] and Klaus Praefcke[c]

Dedicated to Professor Dr. R. Miethchen on the occasion of his 60th birthday

Keywords: Liquid crystals / Metallomesogens / Charge-transfer complexes / Palladium organyls / Platinum organyls

ortho-Palladated and -platinated benzalimines are a widely studied novel type of liquid-crystals. These sheet-shaped materials contain two or even four metal atoms and carry eight and twelve flexible side-chains, respectively. Here we present the preparation and mesomorphic properties of dinuclear chiral homologues of such sheet-like compounds. On their own, the chiral members of the dinuclear cyclopalladated series exhibit no liquid-crystalline properties, but show mesophase inductions (Col_h-phase) in mixtures with an electron-acceptor, e.g., 2,4,7-trinitrofluorenone (**TNF**). A diplatinated chiral analogue, however, monotropically exhibits the cholesteric nematic discotic (N_D^*) type of mesophase. Mixtures of this platinum nematogen with **TNF** also show the induction of a columnar mesophase (Col_h) due to charge-transfer interactions.

Introduction

Cyclometallated complexes containing platinum group metals are of considerable academic and commercial interest and have grown to be a significant subject in current liquid-crystal research.[1,2] Within this field *ortho*-palladated metal organyls − organometallic compounds with metal-carbon bonds − originally attracted interest because of their promising combinations of properties attributed to transition-metal complexes and to the self-organization in liquid-crystalline phases.[1,2] Most cyclopalladated mesogens found so far are calamitic in nature, and they are either rod-shaped in the case of mononuclear complexes or can be viewed as twin-mesogens made up by two rod-shaped moieties fused by means of bridging groups. Consequently, usually typical nematic and/or smectic phases consistent with their rod-like structures are observed.

However, by changing the number and position of the peripheral alkyl chains of such *ortho*-metallated mesogens more sheet-like or ellipsoid shapes can be obtained, leading to the formation of the nematic discotic (N_D) type of mesophase.[2,3] We have studied structure-property relations for such sheet-like *ortho*-metallated complexes by varying both their core section (bridging ligands and the metal atom) as well as their aliphatic periphery.[3−7]

Chiral mesophases formed by chiral mesogens are of special interest with respect to their electro-optical properties and possible applications resulting from these properties. The number of sheet- or disc-like chiral mesogens in general and particularly of those exhibiting the cholesteric-nematic discotic (N_D^*) type of mesophase found so far is quite limited.[8,9] Here, we report the synthesis and liquid-crystalline properties of the first chiral members of flat, sheet-like dinuclear palladium and platinum organyls.

Result and Discussion

Chirality can be introduced into sheet-like dinuclear palladium or platinum organometallic compounds of the type

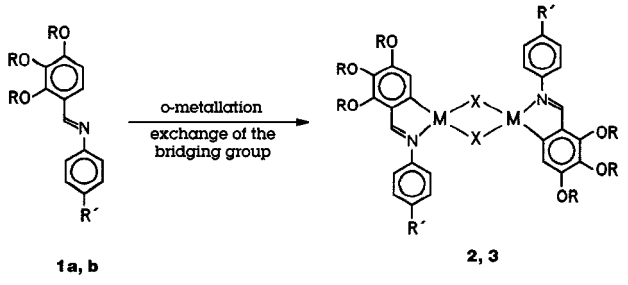

1a, 2: R = C_6H_{13}, R´ = O

1b, 3: R = C_6H_{13}, R´ = O

2: M = Pd, **a**: X = Cl; **b**: X = Br; **c**: X = SCN; **3**: M = Pt, X = Cl

Scheme 1

[a] Department of Chemistry, Yildiz Teknik Üniversitesi
80270 Istanbul, Turkey
Fax: (internat.) +90-212/2245013
E-mail: bilgin@yildiz.edu.tr
[b] Department of Chemistry, Howard University
Washington, DC 20059, USA
Fax: (internat.) +1-202/8065442
E-mail: dsinger@polymer.chem.howard.edu
[c] Technische Universität Berlin, J4
10623 Berlin, Germany
Fax: (internat.) +49-(0)30/31424298
E-mail: kp@chem.tu-berlin.de

 © WILEY-VCH Verlag GmbH, D-69451 Weinheim, 2001 1434−1948/01/0101−0111 $ 17.50+.50/0

studied here (see Scheme 1) through their peripheral aliphatic chains, either in the aniline- or in the benzaldehyde-derived[10] parts of the ligands.

Dinuclear palladium organyls in general can be obtained from imines, for example **1a** in Scheme 1, by *ortho*-palladation of the ligands with palladium acetate in glacial acetic acid. Exchange of the acetato-bridges with hydrochloric acid leads to chloro-bridged dinuclear palladium complexes (**2a**) from which the bromo- and thiocyanato-bridged homologues **2b** and **c** are accessible by simple exchange reactions with KBr and KSCN, respectively. The dinuclear chloro-bridged platinum complexe **3** (cf. Scheme 1) on the other hand, was obtained by direct *ortho*-platination of the respective imine ligand **1b** with (di-μ-chloro-bis(η^3-2-methylallylplatinum).

The chiral ligands **1a** and **b** were synthesized from 4-nitrophenol, by the usual etherification with the corresponding alkyl tosylates. These tosylates[9] are easily prepared from the hydrogenation product of (*S*)-β-*citronellol* and from (*S*)-*2-methylbutyl alcohol*, respectively, and the citronellol derivative is given as an example in Scheme 2. Reduction of the 4-nitrophenol ethers with Fe/HCl followed by acid-catalyzed condensation with 2,3,4-tri(hexyloxy)-benzaldehyde[11] gave the new chiral imines **1a** and **b**.

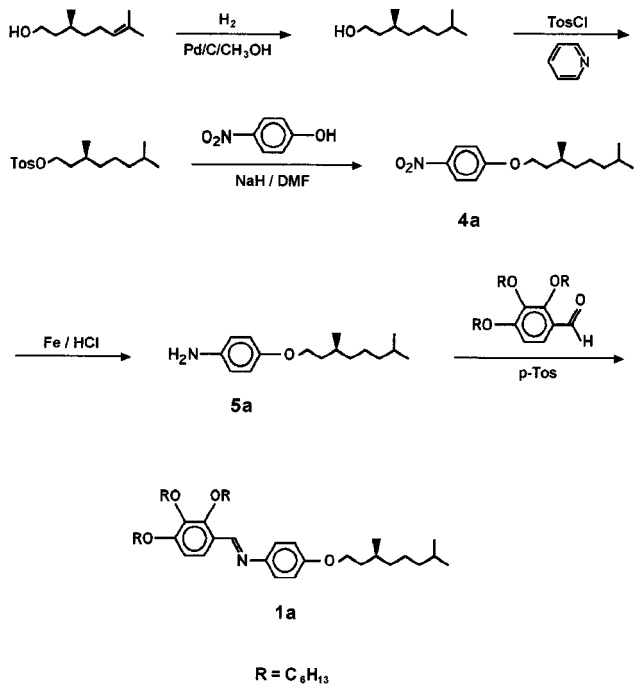

Scheme 2

The new ligands **1a** and **b** as well as their metal complexes **2a**−**c** and **3** were characterized by ^{1}H and ^{13}C NMR spectroscopy and gave correct elemental analysis (see Experimental Section). Furthermore, ^{1}H and ^{13}C NMR spectroscopic data for the dipalladium organyls **2a**−**c** and the diplatinum organyl **3** are very similar to those of non-chiral analogs with planar structures and antiparallel orientations of their ligands, as shown by X-ray analysis.[6]

No mesophase formation could be observed for the chloro-, bromo- and thiocyanato-bridged chiral dinuclear palladium organometallic compounds **2a**, **b** or **c**, respectively, in contrast to their achiral analogs,[4] which all exhibit the nematic-discotic ($\mathbf{N_D}$) type of mesophase monotropically. These palladium and platinum organometallic compounds with eight peripheral chains all show a tendency for significant supercooling and slow crystallization. However, when using hot-stage polarizing microscopy even with cooling rates as high as 100 K/min, no formation of a mesophase could be observed by cooling **2a**−**c** from their isotropic phases.

The new diplatinum organyl **3**, on the other hand, carrying two short chiral side-chains exhibits a monotropic cholesteric nematic-discotic mesophase (N_D^*).

The thermal transition data of these four new chiral metallocyclic compounds are summarized in Table 1.

Table 1. Phase transition temperatures *T* (°C) and enthalpies (kJ mol^{-1}) of **2a**−**c** and **3**:
Cr: crystalline, N_D*: cholesteric nematic discotic and Iso: isotropic

Organometallic compound	M	X	Cr	*T*[a]	N_D^*	Iso
2a	Pd	Cl	•	65.3 (38.6)	–	•
2b	Pd	Br	•	67.2 (58.4)	–	•
2c	Pd	SCN	•	98.7 (53.8)	–	•
3	Pt	Cl	•	90.1 (39.1)	{• 72.2 (0.3) }	•

[a] Mettler TA 3000/DSC-30 S with TA 72.5 software. Heating rates 5 K min^{-1} for the melting process, the entalpies are given in parentheses. To prevent crystallization the clearing process of **3** was measured with 10 K min^{-1}.

The properties of the sheet-like[3−7] and calamitic[12] dinuclear palladium and platinum organyls found so far allow for the conclusion that the number and kind of side-chains play a determining role in the formation of the liquid-crystalline phase. The type of metal (Pd or Pt), on the other hand, has only very little or no influence on the type and stability of the mesophase formed. In general, for sheet-like members a more or less coplanar arrangement of the ligands is a further requirement for the formation of nematic discotic phases. A comparison of the phase transition data of the chiral dinuclear palladium organyls **2a**−**c** with their achiral analogs[4] shows that the two bulkier and chiral 3,7-dimethyloctyloxy chains in **2a**−**c** led to lower melting temperatures and prevented the formation of a mesophase, at least in the observable temperature range. We attribute this to the steric hindrance to a nematic packing due to the methyl groups and not to an effect of the chirality per se.

It should be emphasized here that the two chiral lateral chains in the ligands of the dinuclear platinum organyl **3** differ from those present in the series of di-palladium complexes **2**. In the diplatino mesogen **3**, the chiral center is nearer to the molecular core and, most probably more important, these two chains are significantly shorter and lack the terminal branching. Therefore, a very fluid cholesteric nematic discotic (N_D^*) mesophase with "strain" or fingerprint texture and strong thermal fluctuations is observed on cooling **3** from the isotropic melt. The phase transition from

the N_D^* phase to the isotropic liquid is very sharp; the clearing enthalpy of 0.3 kJ/mol is within the range of 0.1−0.4 kJ/mol, common for nematic discotic mesophases.[4,6,11,13]

Nematic discotic phases are usually observed in systems composed of flat, sheet-like molecules lacking significant intermolecular interactions perpendicular to their molecular plane. For such systems, even minor changes in the packing of the peripheral aliphatic chains can favor or prevent the self-organization in a mesophase.

In systems composed of electron-rich flat molecules, strong attractive interactions between these molecules can often be introduced by charge-transfer interactions with a suitable electron-acceptor, for example 2,4,7-trinitrofluorenone (**TNF**). In these systems, the mixed interactions perpendicular to the molecular planes are significantly stronger than those between molecules of the same kind, leading to the formation of columnar mesophases with an alternating stacking of electron-donor and -acceptor molecules.[13−15]

The new chiral sheet-like dinuclear palladium organometallic compounds **2a**−**c**, not liquid-crystalline in their pure state, all formed charge-transfer complexes with 2,4,7-trinitrofluorenone (**TNF**) as indicated by a change of color to brown-red. As expected, an induced mesophase was formed in mixtures of the chiral sheet-like dinuclear chloro- and bromo-bridged compounds **2a** and **b**, respectively. In contact preparations with **TNF**, each showed the formation of induced hexagonal columnar (Col_h) mesophases, a behavior already observed for their achiral dipalladium and diplatinum analogs.[4,6,13] On cooling from the isotropic phase, droplets with linear defects as well as star-shaped domains with homeotropic orientation and hexagonal symmetry were formed, developing into a mosaic texture similar to that observed for the Col_h phase of **TNF** complexes of the achiral dinuclear palladium and platinum analogs.[4,6,13]

Contact mixtures of the thiocyanato-bridged derivative **2c** with **TNF**, on the other hand, show the stabilization of the nematic cholesteric phase in the contact zone, as was observed for its achiral thiocyanato-bridged palladium and platinum analogs.[4,6,13] So far, dinuclear palladium and platinum organyls with eight peripheral chains and a thiocyanato- and (in one case) a iodo-bridge are the only examples[13] showing the stabilization of the nematic discotic type of mesophase by charge-transfer interactions with a strong electron acceptor, for example **TNF**, rather then the induction of a nematic columnar one.[15−17]

The maximum clearing temperatures of the charge-transfer complexes of the dipalladium organometallic compounds **2a**−**c** and the diplatinum mesogen **3** with **TNF** in contact preparations are summarized in Table 2, as determined by polarizing microscopy.

It is interesting to note that in contact mixtures of the palladium organyl **2c** and **TNF,** on cooling from the isotropic phase, textures typical for cholesteric nematic phases are only formed in regions with low **TNF** concentrations; in the areas of higher **TNF** contents, Schlieren textures characteristic of achiral nematic phases are observed.

Table 2. Thermomesomorphic properties of charge-transfer complexes generated by mixing the chiral dinuclear palladium organyls **2a**−**c** and platinum organyl **3**, respectively, with 2,4,7-trinitrofluorenone (**TNF**). The maxima of the clearing temperatures are put in parentheses; Col_h: hexagonal columnar, N: nematic

TNF complex of	M	X	mesophase[a]
2a	Pd	Cl	Col_h (145 °C)
2b	Pd	Br	Col_h (86 °C)
2c	Pd	SCN	N* and N (79 °C)
3	Pt	Cl	Col_h (189 °C)

[a] Results based on contact preparations. The phase transition temperatures have been determined by hot stage polarizing microscopy (heating rate 5 K min^{-1}).

As expected, an induced mesophase is also formed in mixtures of the chiral sheet-like dinuclear platinum organometallic compound **3** with **TNF**. Contact preparations of **3** with **TNF** exhibit a highly viscous induced mesophase up to 189 °C. On cooling from the isotropic liquid, droplets with linear defects as well as star-shaped domains with homeotropic orientation and hexagonal symmetry are formed, developing into a mosaic texture similar to that observed for the Col_h phases of **TNF** complexes of dinuclear palladium and platinum analogs.[4,6,13]

Conclusion

The series of dinuclear palladium organometallic compounds **2a**−**c** with two chiral peripheral chains each are not liquid-crystalline, most probably because of the space requirements of these citronellol-derived side-chains. The shorter chiral (*S*)-2-methylbutyloxy chains present in the diplatinum complex **3**, on the other hand, allow for the formation of a monotropic cholesteric nematic discotic mesophase. All of the dipalladium organyls **2a**−**c** and the diplatinum complex **3** form charge-transfer complexes with strong electron acceptors such as 2,4,7-trinitrofluorenone (**TNF**). These charge-transfer complexes exhibit enantiotropic columnar hexagonal (Col_h) induced mesophases or in the case of the thiocyanato-bridged di-palladium complex **2c**, a stabilized cholesteric nematic discotic phase. Dinuclear chiral *ortho*-metallated compounds of the type studied here seem to be incapable of forming enantiotropic cholesteric nematic mesophases, similar to their achiral analogs, which also only form monotropic nematic-discotic phases. However, the charge-transfer induced hexagonal columnar mesophases of mixtures of **TNF** with **2a**, **b** and **3** and the stabilized cholesteric nematic phase in the binary system **TNF/2c** make these dinuclear metal organometallic compounds suitable for studying the relationship between molecular chirality and mesophase chirality in the nematic as well as in higher-ordered hexagonal columnar phases. Besides charge-transfer complexes with achiral electron-acceptors such as **TNF**, those with the enantiomers of 2-(2,4,5,7-tetranitrofluorenyliden aminooxy propionic acid (**TAPA**) should allow for a detailed study of the influence of molecular chirality on mesophase properties.

Experimental Section

The characterizations of the compounds **1**−**5** presented here are based on correct elemental analyses (Perkin−Elmer Series II CHNS/O Analyzer 2400) and on various spectroscopic data, e.g., ^{1}H, ^{13}C NMR (Bruker WH-400 or AM-270 spectrometers, respectively, $CDCl_3$ solutions), IR (Beckmann 9, CCl_4 solutions) and MS (Varian MAT 711). Only structurally relevant resonances are given below.

Phase transition data were determined by differential scanning calorimetry (Mettler TA 3000/DSC-30 S with TA 72.5 software) and by polarizing microscopy (Leitz Laborlux 12 Pol with a hotstage Mettler FP 82 with heating rates of 5 or 10 K min^{-1} in both methods. To obtain cooling rates of up to 100 K/min a Linkam hotstage THMS 600 system with a TMS 91/C 9196 controller combination was employed).

Synthesis of the 4-Nitrophenol Ethers 4a and b: A solution of 4-nitrophenol (13.91 g, 100 mmol) {**4b**: (8.35 g, 60 mmol)} in dry DMF (80 mL) {**4b**: 50 mL} was added dropwise at ambient temperature under argon and with stirring to a suspension of sodium hydride (60 wt.% suspension in paraffin oil, 4.40 g, 110 mmol) {**4b**: (2.64 g, 66 mmol)} in dry DMF (30 mL) {**4b**: 20 ml}. After stirring this mixture for 2h at room temperature, a solution of (*S*)-3,7-dimethyloctyl tosylate[9] (31.25 g, 100 mmol, prepared by hydrogenation of commercially available citronellol followed by routine tosylation, Scheme 2) in dry DMF (50 mL) or (*S*)-2-methylbutyl tosylate[9] (14.54 g, 60 mmol) in dry DMF (30 mL), respectively, was added. The reaction mixtures were stirred at 80 °C for 12 h or 4 h, respectively, and, after cooling, poured into ice water. After extraction with diethyl ether and usual workup procedures, the crude products were purified by flash-column chromatography on silica gel with petroleum ether/ethyl acetate mixtures (20:1 and 10:1) as eluents.

(*S*)-4-(3,7-Dimethyloctyloxy)nitrobenzene (4a): Yield: 24.30 g (87%) yellow oil. − ^{1}H NMR: δ = 8.18, 6.93 (2d, $J \approx 9$ Hz each; 2 arom. H), 4.14−4.03 (m; OCH_2). − ^{13}C NMR: δ =164.19, 141.27 (2s, 2 arom. C), 125.85, 114.36 (2d, 2 arom. CH each), 67.21 (t, OCH_2). − GC/MS; *m*/*z* (%): 279 (6) [M$^+$], 140 (7) [$C_{10}H_{20}$], 57 (100). − $C_{16}H_{25}NO_3$ (279.4): MS (HR); *m*/*z*: 279.1834 [M$^+$]; calcd.: 279.1834.

(*S*)-4-(2-Methylbutyloxy)nitrobenzene[18] **(4b):** Yield: 10.53 g (84%) yellow oil. − ^{1}H NMR: δ = 8.19, 6.94 (2d, $J \approx 9$ Hz each; 2 arom. H), 3.91, 3.83 (2 dd, $J \approx 6.5$ Hz and 9 Hz, respectively, OCH_2). − ^{13}C NMR: δ =164.37, 141.26 (2s, 2 arom. C), 125.85, 114.36 (2d, 2 arom. CH each), 73.58 (t, OCH_2). − GC/MS; *m*/*z* (%): 209 (12) [M$^+$], 139 (28) [M$^+$ − C_5H_{10}], 70 (100) [C_5H_{10}]. − $C_{11}H_{15}NO_3$ (209.2): MS (HR); *m*/*z*: 209.1052 [M$^+$]; calcd. 209.1052.

Synthesis of the Chiral Aniline Compounds 5a and b: A mixture of (*S*)-4-(3,7-dimethyloctyloxy)nitrobenzene (**4a**, 5.59 g, 20 mmol) or (*S*)-4-(2-methylbutyloxy)nitrobenzene (**4b**, 4.18 g, 20 mmol),[18] respectively, with a suspension of iron powder (6.14 g, 110 mmol) in ethanol/water (50 mL:10 mL) and HCl (20%, 0.6 mL) was heated at reflux for 4 h or 2 h. After the addition of $NaHCO_3$ powder (1.93 g, 23 mmol) to the boiling reaction mixture, the mixture was heated at reflux for 1 h and filtered hot. The crude products were extracted from the residues with hot ethanol and, after removal of the solvent, purified by flash column chromatography on silica gel using petroleum ether/ethyl acetate (5:1) as eluent.

(*S*)-4-(3,7-Dimethyloctyloxy)aniline (5a): Yield: 3.90 g (78%) orange oil. − ^{1}H NMR: δ = 6.75, 6.64 (2d, $J \approx 9$ Hz each; 2 arom. H), 3.96−3.86 (m, OCH_2), 3.41 (s, broad, NH_2). − ^{13}C NMR: δ = 152.25, 139.76 (2s, 2 arom. C), 116.34, 115.58 (2d, 2 arom. CH each), 66.92 (t, OCH_2). − GC/MS; *m*/*z* (%): 249 (2.7) [M$^+$], 109 (100) [M$^+$ − $C_{10}H_{20}$]. − IR (CCl_4): $\tilde{\nu}$ = 3460 and 3383 cm^{-1} (NH_2). − $C_{16}H_{27}NO$ (249.4): MS (HR); *m*/*z*: 249.2093 [M$^+$]; calcd.: 249.2093.

(*S*)-4-(2-Methylbutyloxy)aniline[18] **(5b):** Yield: 3.10 g (86%) yellow oil. − ^{1}H NMR: δ = 6.75, 6.64 (2d, $J \approx 9$ Hz each; 2 arom. H), 3.75, 3.65 (2 dd; $J \approx 6.5$ Hz and 9 Hz, respectively, OCH_2), 3.41 (s, broad, NH_2). − ^{13}C NMR: δ =152.46, 139.69 (2s, 2 arom. C), 116.32, 115.58 (2d, 2 arom. CH each), 73.58 (t, OCH_2). − GC/MS; *m*/*z* (%): 179 (13) [M$^+$], 109 (100) [M$^+$ − C_5H_{10}]. − IR (CCl_4): $\tilde{\nu}$ = 3460 and 3383 cm^{-1} (NH_2). − $C_{11}H_{17}NO$ (179.3): MS (HR); *m*/*z*: 179.1310 [M$^+$]; calcd.: 179.1310.

Synthesis of the Imine Ligands 1a and b: The imines **1a** and **b** were prepared in the usual way[4] by a *p*-toluenesulfonic acid (40 mg) catalyzed condensation of 2,3,4-tri(hexyloxy)benzaldehyde[11] (4.07 g, 10 mmol) with **5a** (3.74 g, 15 mmol) or with **5b** (2.69 g, 15 mmol) in toluene (50 mL) and purified by column chromatography on basic aluminum oxide using petroleum ether/ethyl acetate (20:1 to 5:1) as eluent.

(*S*)-*N*-[4-(3,7-Dimethyloctyloxy)phenyl]-2,3,4-tris(hexyloxy)-benzalimine (1a): Yield: 5.79 g (91%) orange oil. − ^{1}H NMR: δ = 8.77 (s, HC=N), 7.83, 6.73 (2 d, $J \approx 9$ Hz each; 2 arom. H of the benzyliden rings), 7.19, 6.91 (2 d, $J \approx 9$ Hz each; 4 arom. H of the N-substituted phenyl rings), 4.10 (t, $J \approx 6.5$ Hz; OCH_2), 4.06−3.94 (m, 3 OCH_2). − ^{13}C NMR: δ =157.46, 156.09, 154.03, 145.64, 141.29, 123.24 (6 s, 6 arom. C), 154.44 (d, HC=N), 122.11, 122.07, 114.92, 108.59 (4 d; 1, 2, 2 and 1 arom. CH), 74.84, 73.67, 68.76, 66.58 (4 t, 4 OCH_2). − MS; *m*/*z* (%): 637 (12) [M$^+$], 496 (2) [M$^+$ − $C_{10}H_{21}$], 389 (100) [M$^+$ − $C_{16}H_{26}NO$]. − $C_{41}H_{67}NO_4$ (637.9): MS (HR); *m*/*z*: 637.5070 [M$^+$]; calcd.: 637.5070.

(*S*)-*N*-[4-(2-Methylbutyloxy)phenyl]-2,3,4-tris(hexyloxy)benzalimine (1b): Yield: 4.80 g (85%) orange oil. − ^{1}H NMR: δ = 8.77 (s, HC=N), 7.84, 6.74 (2 d, $J \approx 9$ Hz each; 2 arom. H of the benzyliden rings), 7.19, 6.92 (2 d, $J \approx 9$ Hz each; 4 arom. H of the N-substituted phenyl rings), 4.11 (t, $J \approx 6.5$ Hz; OCH_2), 4.07−3.92 (m, 2 OCH_2), 3.84, 3.75 (2 dd, $J \approx 6.5$ Hz and 9 Hz, respectively; OCH_2 of the chiral alkyl chain). − ^{13}C NMR: δ =157.67, 156.09, 154.03, 145.62, 141.29, 123.25 (6 s, 6 arom. C), 154.43 (d, HC=N), 122.09, 122.07, 114.93, 108.59 (4 d; 1, 2, 2 and 1 arom. CH), 74.85, 73.68, 73.16, 68.76 (4 t, 4 OCH_2). − MS; *m*/*z* (%): 567 (6.5) [M$^+$], 496 (6.2) [M$^+$ − C_5H_{11}], 389 (100) [M$^+$ − $C_{11}H_{16}NO$]. − $C_{36}H_{57}NO_4$ (567.8): MS (HR); *m*/*z*: 567.4288 [M$^+$]; calcd.: 567.4288.

Synthesis of the Dinuclear Chloro-Bridged Palladium Organyl 2a: The palladium organometallic compound **2a** was prepared in two steps from the chiral imine ligand **1a** first by reacting 1**a** (5 mmol) with palladium acetate $Pd_3(OAc)_6$ (5 mmol) in glacial acetic acid followed by treatment of the red intermediate product (2 mmol) with a mixture of 2-propanolic hydrochloric acid (0.1 N) according to a description regarding the achiral analogs published elsewhere.[4,5] The desired palladium organometallic compound **2a** was purified by several recrystallizations from ethanol/acetone.

Di-μ-chlorobis[3,4,5-tris(hexyloxy)-2-{[[(*S*)-4-(3,7-dimethyloctyloxy)phenyl]imino]-methyl}phenyl-*C*,*N*]dipalladium(II) (2a): Yield: 2.30 g (74%) yellow crystals. − ^{1}H NMR: δ = 7.99 (s, 2 HC=N), 7.31−7.19, 6.88−6.79 (2 m, broad; 8 arom. H of the N-substituted phenyl rings), 6.57 (s, broad; 2 arom. H of the Pd-substituted phenyl rings), 4.11, 3.85 (2 t, $J \approx 6.5$ Hz each; 2 OCH_2

each), 4.03−3.92 (m, 4 OCH_2). − ^{13}C NMR: δ =170.16 (d, 2 HC=N), 158.63, 155.15, 152.01, 148.87, 140.92, 137.90, 131.68 (7 s, 14 arom. C), 124.00, 114.58, 111.33 (3 d; 4, 4 and 2 arom. CH), 74.64, 73.68, 68.98, 66.53 (4 t, 8 OCH_2). − $C_{82}H_{132}Cl_2N_2O_8Pd_2$ (1557.7): calcd. C 63.23, H 8.54, N 1.80; found C 62.94, H 8.59, N 2.12.

Synthesis of the Bromo- and Thiocyanato-Bridged Palladium Organyls 2b and c: The bromo- and thiocyanato-bridged palladium organometallic compounds **2b** and **2c** were prepared from the analogous chloro-bridged compound **2a** by simple exchange reactions with potassium bromide and potassium thiocyanate, respectively, in dichloromethane/acetone under argon at room temperature. The crude products were purified by recrystallization from methanol/acetone.

Di-μ-bromobis[3,4,5-tris(hexyloxy)-2-{[[(*S*)-4-(3,7-dimethyloctyloxy)phenyl]imino]-methyl}phenyl-*C*,*N*]dipalladium(II)(2b): The halogen-exchange reaction (Cl → Br) was carried out by stirring **2a** (0.31 g, 0.2 mmol) and KBr (0.71 g, 6 mmol) in a mixture of CH_2Cl_2 (60 mL) with acetone (30 mL) for 5 d. Yield: 280 mg (85%) yellow crystals. − ^1H NMR: δ = 8.03 (s, 2 HC=N), 7.28−7.21, 6.89−6.82 (2 d, broad; 8 arom. H of the *N*-substituted phenyl rings), 6.76 (s, broad; 2 arom. H of the Pd-substituted phenyl rings), 4.10, 3.85 (2 t, $J \approx 6.5$ Hz each; 2 OCH_2 each), 4.04−3.93 (m, 4 OCH_2). − ^{13}C NMR: δ =170.76 (d, 2 HC=N), 158.20, 155.35, 151.95, 150.80, 143.10, 137.55, 132.36 (7 s, 14 arom. C), 124.56, 114.61, 114.09 (3 d; 4, 2 and 4 arom. CH), 74.62, 73.60, 68.72, 66.52 (4 t, 8 OCH_2). − $C_{82}H_{132}Br_2N_2O_8Pd_2$ (1646.6): calcd. C 59.81, H 8.08, N 1.70; found C 59.16, H 8.13, N 1.82.

Bis[μ-(thiocyanato-*N*:*S*)]bis[3,4,5-tris(hexyloxy)-2-{[[(*S*)-4-(3,7-dimethyloctyloxy)phenyl]imino]methyl}phenyl-*C*,*N*]dipalladium(II) (2c):The halogen-exchange reaction (Cl → SCN) was carried out by stirring **2a** (0.31 g, 0.2 mmol) and KSCN (0.58 g, 6 mmol) in a mixture of CH_2Cl_2 (60 mL) with acetone (30 mL) for 5 d. Yield: 290 mg (90%) yellow green crystals. − ^1H NMR: δ = 8.12 (s, 2 HC=N), 7.26, 6.91 (2 d, $J \approx 9$ Hz each; 8 arom. H of the N-substituted phenyl rings), 6.18 (s, 2 arom. H of the Pd-substituted phenyl rings), 4.11, 3.85 (2 t, $J \approx 6.5$ Hz each; 2 OCH_2 each), 4.07−3.97 (m, 4 OCH_2). − ^{13}C NMR: δ =170.25 (d, 2 HC=N), 158.37, 155.56, 152.63, 149.69, 143.38, 137.81, 133.60, 126.02 (8 s, 14 arom. C and 2 SCN), 123.95, 114.30, 114.85 (3 d; 4, 4 and 2 arom. CH), 74.64, 73.61, 68.71, 66.65 (4 t, 8 OCH_2). − IR (CCl_4): $\tilde{\nu}$ = 2151 cm^{-1} (SCN). − $C_{84}H_{132}N_4O_8S_2Pd_2$ (1603.0): calcd. C 62.94, H 8.30, N 3.49; found C 62.75, H 8.48, N 3.47.

Synthesis of the Dinuclear Platinum Organyl 3: A solution of the chiral imine **1b** (1.16 g, 2.05 mmol) in dichloromethane (20 mL) was added under Ar to a suspension of di-μ-chloro-bis(η^3-2-methylallylplatinum)[19] (0.57 g, 1.0 mmol) in dry methanol (15 mL). After stirring the reaction mixture at room temperature for 25 d, an orange precipitate was filtered off. The chiral platinum organometallic compound **3** was purified by several crystallizations from methanol/acetone.

Based on the ^1H NMR spectroscopic data for **3** we assume this chiral platinum organometallic compound to be a mixture of two isomers, at least in solution, as reported in a previous paper for the achiral diplatinum analogue.[6] This is probably due to the different orientations of the two ligands i.e., parallel or antiparallel to each other.

Di-μ-chlorobis[3,4,5-tris(hexyloxy)-2-{[[(*S*)-4-(2-methylbutyloxy)phenyl]imino]-methyl}phenyl-*C*,*N*]diplatin(II) (3): Yield: 635 mg (40%) orange crystals. − ^1H NMR: δ = 8.12, 8.09 (2 s, ratio 1 (*anti*):0.2 (*syn*); HC=N), 7.30, 6.88 as well as 7.20, 6.80 (2 × 2 d, $J \approx 8.5$ Hz each; arom. H of the *N*-substituted phenyl rings), 6.64, 6.46 (2 s, ratio 0.2 (*syn*):1 (*anti*); arom. H of the Pt-substituted phenyl rings), 4.12, 3.98 (2 t, $J \approx 6.5$ Hz each; 2 OCH_2 each), 3.90−3.68 (m, 4 OCH_2). − ^{13}C NMR: δ =172.12 (d, 2 HC=N), 158.77, 157.15, 152.76, 142.19, 136.69, 134.75, 131.09 (7 s, 14 arom. C), 124.77, 114.23, 110.27 (3 d; 4, 4 and 2 arom. CH), 74.52, 73.45, 73.15, 68.64 (4 t, 8 OCH_2). − $C_{72}H_{112}Cl_2N_2O_8Pt_2$ (1594.8): calcd. C 54.23, H 7.08, N 1.76; found C 54.05, H 6.89, N 1.62.

Acknowledgments

B. Bilgin Eran wishes to thank the Yildiz Teknik Üniversitesi Research Fond and Devlet Planlama Teskilati (DPT) (State Planning Organization Turkey) for supplying a polarizing microscope. K. Praefcke is grateful to the Deutsche Forschungsgemeinschaft, Bonn (Sonderforschungsbereich Sfb 335 "Anisotrope Fluide", project C 3), the Fonds der Chemischen Industrie, Frankfurt/Main, the Gesellschaft von Freunden der Technischen Universität Berlin, and to the Technische Universität Berlin, Germany, for financial support of their liquid-crystal work.

[1] A.-M. Giroud-Godquin, P. M. Maitlis, *Angew. Chem. Int. Ed. Engl.* **1991**, *30*, 375−402; P. Espinet, M. A. Esteruelas, L. A. Oro, J. L. Serrano, E. Sola, *Coord. Chem. Rev.* **1992**, *117*, 215−274; D. W. Bruce, in: D. W. Bruce, D. O′Hare (Eds.), *Inorganic Materials*, John Wiley & Sons, Chichester, New York, Brisbane, Toronto, Singapore, **1992**, chapter 8; D. W. Bruce, *J. Chem. Soc., Dalton Trans.* **1993**, 2983−2989; A. P. Polishchuk, T. V. Timofeeva, *Russ. Chem. Rev*s. **1993**, *62*, 291−321; S. A. Hudson, P. M. Maitlis, *Chem. Rev.* **1993**, *93*, 861−885; L. Oriol, J. L. Serrano, *Adv. Mater.* **1995**, *7*, 348−369.

[2] J. L. Serrano, ed., *Metallomesogens, Synthesis, Properties, and Applications*, VCH, Weinheim, New York, Basel, Cambridge, Tokyo, **1996**.

[3] K. Praefcke, J. D. Holbrey, N. Usol′tseva, *Mol. Cryst. Liq. Cryst.* **1996**, *288*, 189−200; K. Praefcke, J. D. Holbrey, N. Usol′tseva, D. Blunk, *Mol. Cryst. Liq. Cryst.* **1997**, *292*, 123−139.

[4] K. Praefcke, D. Singer, B. Gündogan, *Mol. Cryst. Liq. Cryst.* **1992**, *223*, 181−195.

[5] B. Gündogan, K. Praefcke, *Chem. Ber.* **1993**, *126*, 1253−1255; K. Praefcke, D. Singer, B. Gündogan, K. Gutbier, M. Langner, *Ber. Bunsenges. Phys. Chem.* **1994**, *98,* 118−122; N. Usol′tseva, K. Praefcke, D. Singer, B. Gündogan, *Liq. Cryst.* **1994**, *16*, 601−616; N. Usol′tseva, G. Hauck, H. D. Koswig, K. Praefcke, B. Heinrich, *Liq. Cryst.* **1996**, *20*, 731−739; B. Heinrich, K. Praefcke, D. Guillon, *J. Mater. Chem.* **1997**, *7*, 1363−1372.

[6] K. Praefcke, B. Bilgin, J. Pickardt, M. Borowski, *Chem. Ber.* **1994**, *127*, 1543−1545; B. Bilgin, *Ph. D. Dissertation*, Faculty 5 / Chemistry, Technische Universität Berlin, Germany **1996**.

[7] K. Praefcke, B. Bilgin, N. Usol′tseva, B. Heinrich, D. Guillon, *J. Mater. Chem.* **1995**, *5*, 2257−2264; K. Praefcke, B. Bilgin, J. Pickardt, M. Borowski, *J. Organomet. Chem.* **1999**, *592*, 155−161.

[8] J. Malthete, C. Destrade, H. T. Nguyen, J. Jaques, *Mol. Cryst. Liq. Cryst.* **1981**, *64*, 233−238; C. Destrade, H. T. Nguyen, J. Malthete, J. Jaques, *Phys. Lett.* **1980**, *79A*, 189−192; B. Kohne, K. Praefcke, *Chimia* ***1987,*** 41, 196−198; D. Krüerke, H.-S. Kitzerow, G. Heppke, V. Vill, *Ber. Bunsenges. Phys. Chem.* **1993**, *97*, 1371−1375.

[9] M. Langner, K. Praefcke, D. Krüerke, G. Heppke, *J. Mater. Chem.* **1995**, *5*, 693−699.

[10] Regarding this latter type of ligands: K. Praefcke, M. Fehlinger, B. Bilgin Eran, unpubl. results.

[11] K. Praefcke, B. Kohne, B. Gündogan, D. Singer, D. Demus, S. Diele, G. Pelzl, U. Bakowsky, *Mol. Cryst. Liq. Cryst.* **1991**, *198*, 393−405.

[12] J. Barbera, P. Espinet, E. Lalinde, M. Marcos, J. L. Serrano, *Liq. Cryst.* **1987**, *2*, 833−842; M. Marcos, M. B. Ros, J. L. Serrano, *Liq. Cryst.* **1988**, *3*, 1129−1136; M. A. Ciriano, P.

Espinet, E. Lalinde, M. B. Ros, J. L. Serrano, *J. Molec. Struct.* **1989**, *196*, 327−341; M. B. Ros, N. Ruiz, J. L. Serrano, P. Espinet, *Liq. Cryst.* **1991**, *9*, 77−86; M. J. Baena, J. Barbera, P. Espinet, A. Ezcurra, M. B. Ros, J. L. Serrano, *J. Am. Chem. Soc.* **1994**, *116,* 1899−1906.

[13] D. Singer, A. Liebmann, K. Praefcke, J. H. Wendorff, *Liq. Cryst.* **1993**, *14*, 785−794; K. Praefcke, D. Singer, *Mol. Mat.* **1994**, *3*, 265−270; K. Praefcke, J. D. Holbrey, *J. Inclusion Phen., Molec. Recogn. Chem.* **1996**, *24*, 19−41.

[14] S. Zamir, D. Singer, N. Spielberg, E. J. Wachtel, H. Zimmermann, R. Poupko, Z. Luz, *Liq. Cryst*. **1996**, *21*, 39−50.

[15] K. Praefcke, D. Singer in *Handbook of Liquid Crystals*, **1998**, *2B*, chapter XVI, p. 945−967 (Eds.: D. Demus, J. Goodby, G. W. Gray, H.-J. Spiess, V. Vill), Wiley-VCH, Weinheim, New York, Chichester, Brisbane, Singapore, Toronto and references cited therein.

[16] K. Praefcke, D. Singer, B. Kohne, M. Ebert, A. Liebmann, J. H. Wendorff, *Liq. Cryst.* **1991**, *10*, 147−159.

[17] H. Bengs, O. Karthaus, H. Ringsdorf, C. Baehr, M. Ebert, J. H. Wendorff, *Liq. Cryst.* **1991**, *10*, 161−168.

[18] H. Ringsdorf, C. Urban, W. Knoll, M. Sawodny, *Makromol. Chem.* **1992**, *193*, 1235−1247.

[19] D. J. Mabbott, B. E. Mann, P. M. Maitlis, *J. Chem. Soc., Dalton Trans.* **1977**, 294−299.

Received April 25, 2000
[I00160]

Vanadium(III) and -(IV) Complexes with *O,N*-Chelating Aminophenolate Ligands: Synthesis, Characterization and Activity in Ethene/Propene Copolymerization

Henk Hagen,[a] Jaap Boersma,[a] Martin Lutz,[b] Anthony L. Spek,[b] and Gerard van Koten*[a]

Keywords: Vanadium / Phenolates / Catalysis / Polymerizations / Alkenes

Monoanionic, potentially bi- or terdentate aminophenolates, ($[OC_6H_3(CH_2NMe_2)$-2-R-4$)]^-$, R = H (**a**), Me (**b**), *t*Bu (**c**), Cl (**d**), N=NPh (**e**), MeO (**f**) and $[OC_6H_2(CH_2NMe_2)_2$-2,6-Me-4$]^-$ (**g**)), have been used in the synthesis of well-defined vanadium-based catalysts for the polymerization of α-olefins. The reaction of $[Cp_2V]$ with the parent phenol of **g** resulted in oxidation of the vanadium(II) nucleus to obtain the vanadium(III) (tris)phenolate $[V(OC_6H_2(CH_2NMe_2)_2$-2,6-Me-4$)_3]$ (**1**). Vanadium(III) aminophenolates could not be obtained by reaction of $[VCl_3(THF)_3]$ with the sodium phenolates because of incorporation of NaCl. However, use of the corresponding silyl ether $Me_3SiOC_6H_3(CH_2NMe_2)$-2-Me-4 (**2**) resulted in the formation of the chlorovanadium (bis)phenolate $[VCl(OC_6H_3(CH_2NMe_2)$-2-Me-4$)_2]$ (**3**). Attempts to oxidize **3** to the corresponding dichlorovanadium(IV) (bis)phenolate were not successful. No reaction was observed with CuCl, AgCl and $PbCl_2$. A dark blue compound **4** was obtained with $CuCl_2$, which was tentatively assigned as a V^{III}/Cu^{II} dinuclear species. Treatment of the vanadium(IV) oxo (bis)phenolates **5a**–**5f** with $SOCl_2$ in benzene at room temperature or in toluene at reflux temperature resulted in the formation of dark blue compounds **6a**–**6f**, whose stoichiometries indicated excess chloride. Only when **5a** and **5d** were reacted with $SOCl_2$ at −70 °C could the desired dichlorovanadium (bis)phenolates $[VCl_2(OC_6H_4(CH_2NMe_2)-2)_2]$ (**7a**) and $[VCl_2(OC_6H_3(CH_2NMe_2)$-2-Cl-4$)_2]$ (**7d**) be obtained. X-ray crystal structure determination of **1** and **3** showed that both compounds have a trigonal bipyramidal geometry with two aminophenolate ligands bound in a bidentate η^2-*O,N* fashion to the vanadium center in similar ways. The compounds **1**, **3**, **6** and **7** were tested for ethene/propene copolymerization.

Introduction

Although the activity of vanadium-based catalysts is often inferior to that of other systems, their use has several advantages, such as (1) the preparation of high molecular weight polymers with narrow molecular weight distributions, (2) the preparation of ethene/α-olefin copolymers with high α-olefin incorporation, and (3) the preparation of syndiotactic polypropene.[1] One of the reasons for the reduced activity of vanadium-based catalysts is their deactivation during the polymerization process due to the reduction of catalytically active vanadium species to less active or even inactive low-valent species. One way to overcome this problem would be the stabilization of the higher oxidation states of the vanadium center by ancillary ligands. To this end, we recently set out to study the use of mono-anionic, potentially bidentate aminophenolate ligands (see Figure 1). These ligands have been chosen since vanadium systems with oxygen-containing ligands are known to give polymers with narrow molecular weight distributions,[2] while the nitrogen donor atom can help in stabilizing the high oxidation state of the vanadium center by V−N coordination. In addition to the latter effect, an *ortho*-amino functionality itself represents a substituent with considerable bulk, which can prevent bimolecular deactivation pathways of the vanadium catalyst.[1,3] Finally, the electronic properties of the vanadium center can be considerably influenced by varying the *meta* and *para* substituents on the phenolate ring, as we have recently shown for vanadium(IV) oxo (bis)phenolate complexes.[4] It turns out that these ligands cannot be employed in vanadium(V) chemistry, since the *ortho*-amino function causes reduction of the vanadium(V) center to vanadium(IV).[5] Therefore, in our further studies we have focused on employing these *ortho*-aminophenolate ligands in systems with the vanadium center in the formal 3^+ or 4^+ oxidation state.

a R = H **d** R = Cl **g**

b R = Me **e** R = N=NPh

c R = *t*Bu **f** R = MeO

Figure 1. Selected *ortho*-aminophenolate ligands

[a] Debye Institute, Department of Metal-Mediated Synthesis, Utrecht University,
Padualaan 8, 3584 CH Utrecht, The Netherlands
E-mail: g.vankoten@chem.uu.nl
[b] Bijvoet Center for Biomolecular Research, Crystal and Structural Chemistry, Utrecht University,
Padualaan 8, 3584 CH Utrecht, The Netherlands
E-mail: a.l.spek@chem.uu.nl

 © WILEY-VCH Verlag GmbH, D-69451 Weinheim, 2001 1434−1948/01/0101−0117 $ 17.50+.50/0

Results and Discussion

In the course of our attempts to synthesize vanadium(II) phenolates, we have treated $[Cp_2V]$ with the bis(amino)-phenol $HOC_6H_2(CH_2NMe_2)_2$–2,6-Me-4 (see Scheme 1). Instead of the expected vanadium(II) (bis)phenolate, this reaction gave a bright orange compound, which was identified by X-ray crystallography (vide infra) as the vanadium(III) (tris)phenolate $[V(OC_6H_2(CH_2NMe_2)_2\text{-}2,6\text{-}Me\text{-}4)_3]$ (**1**). The formal 3^+ oxidation state of vanadium in **1** was confirmed by its magnetic susceptibility ($\mu_{eff} = 2.52\ \mu_b$), which is characteristic of a d^2 high-spin complex.[6] Oxidation of low-valent vanadium(II) to vanadium(III) by phenols with the concomitant formation of molecular hydrogen is not uncommon. The formation of vanadium(III) species can be avoided only when phenols with larger *ortho*-substituents like *i*Pr, *t*Bu or Ph are used.[7] This oxidation is not restricted to phenols themselves, but also occurs when sodium phenolates are used. In the latter case, however, a disproportionation reaction occurs with the formation of the vanadium(III) phenolate and metallic vanadium.[8]

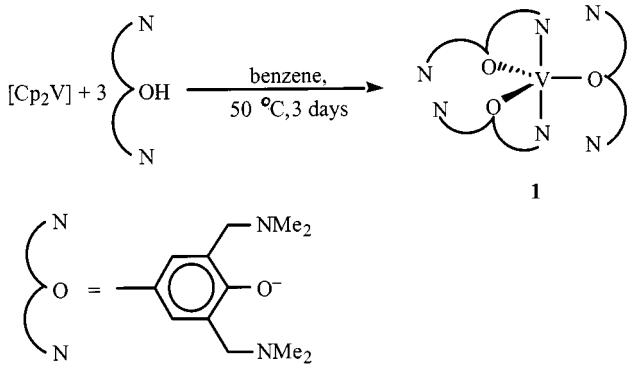

Scheme 1. Synthesis of the vanadium(III) (tris)phenolate **1**

In our further studies $[VCl_3(THF)_3]$ was used as the starting material for the synthesis of vanadium(III) aminophenolate complexes. It must be noted that a salt metathesis reaction with the corresponding sodium phenolate gave non-reproducible results. Depending on the temperature and the solvent used, none or only part of the expected amount of NaCl precipitated from the reaction mixture, indicating the formation of hetero di- or tri-nuclear complexes. The exact nature of these complexes was not determined but examples of such compounds are known in lanthanide chemistry.[9] In this kind of complex the aminophenolate ligands form bridges between different metal atoms via the oxygen atoms while the amino nitrogen atoms coordinate to either the metal or sodium. To overcome the problem of NaCl incorporation the corresponding silyl ether, $Me_3Si\text{-}OC_6H_3(CH_2NMe_2)$-2-Me-4 (**2**), was used. Treatment of $[VCl_3(THF)_3]$ with two equivalents of the silyl ether **2** in refluxing THF (see Scheme 2) resulted in the formation of the chlorovanadium (bis)phenolate $[VCl(OC_6H_3(CH_2NMe_2)\text{-}2\text{-}Me\text{-}4)_2]$ (**3**), which was isolated as a moderately air-sensitive, crystalline orange solid.

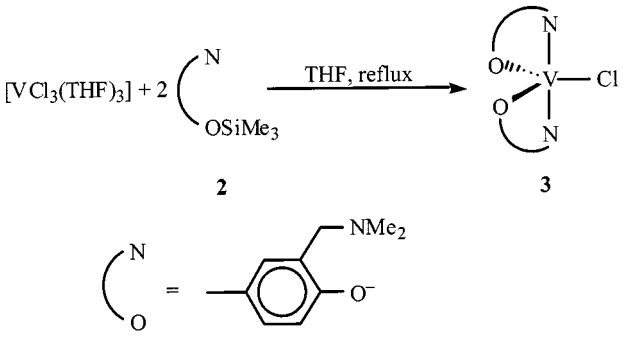

Scheme 2. Synthesis of the chlorovanadium (bis)phenolate **3**

Synthesis of Vanadium(IV) Phenolates

Rather than using VCl_4, which is an inconvenient starting material because of its volatility and oxidative nature, we attempted to use the chlorovanadium (bis)phenolate **3** as starting material for the synthesis of the corresponding dichlorovanadium(IV) (bis)phenolate. Attempts to oxidize **3** with CuCl, AgCl or $PbCl_2$ were in vain, as no reaction was observed. However, when $CuCl_2$ was used a dark blue complex (**4**) was almost immediately formed (Scheme 3). Although the exact nature of **4** remains unclear, elemental analysis indicated the isolation of a complex with a $V(OR)_2CuCl_3{\cdot}CH_2Cl_2$ stoichiometry (OR = $OC_6H_3(CH_2NMe_2)$-2-Me-4). Complex **4** is insoluble in alkanes, aromatic solvents like benzene and toluene, and Et_2O. It is poorly soluble in chloroform and reasonably soluble in CH_2Cl_2 and THF. The severe line-broadening in the ^1H NMR spectrum of **4** in CD_2Cl_2 indicates that it is a paramagnetic species.

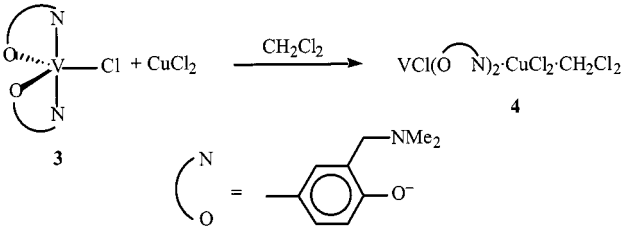

Scheme 3. Synthesis of the dinuclear vanadium/copper compound **4**

For a complex with the observed V:Cu:anion stoichiometry, three combinations of V/Cu oxidation states are conceivable, viz. V^{III}/Cu^{II}, V^{IV}/Cu^{I} or V^{V}/Cu^{0}. In view of the V^{IV}/V^{V} oxidation potential, the V^{V}/Cu^{0} combination is not likely. Oxidation of the vanadium nucleus in **4** by $CuCl_2$ to vanadium(IV) would result in the formation of a complex with a paramagnetic, EPR active vanadium center and a diamagnetic copper(I) center. EPR analysis of a 2 mM solution of **4** in CH_2Cl_2 showed the characteristic octet of a vanadium(IV) compound. Since the signal was very weak, it is most likely caused by an impurity. This would mean that the vanadium nucleus has not been oxidized in the re-

action with $CuCl_2$ and we believe that **4** is best described as a V^{III}/Cu^{II} dinuclear species.

In view of these results, another route to dichlorovanadium(IV) (bis)phenolate complexes was studied, i.e. the reaction of vanadyl complexes, $[VO(OR)_2]$ (**5a**−**5f**),[4] with thionyl chloride. In this reaction the $[V{=}O]^{2+}$ unit is transformed into a $[VCl_2]^{2+}$ unit with the liberation of SO_2.[10] Treatment of compounds **5** with excess $SOCl_2$ in benzene at room temperature or in toluene at reflux temperature gave dark blue/green compounds (**6a**−**6f**), which are insoluble in alkanes, aromatics like benzene and toluene, and Et_2O. They are slightly to very soluble in THF, CH_2Cl_2 and MeCN.

None of the elemental analyses of compounds **6**[11] agreed with the formula $VCl_2(OR)_2$, but they all had stoichiometries containing various amounts of excess chlorine. The amount of additional chlorine appears to be independent of both reaction time and reaction temperature. Also the presence of approximately half an equivalent of sulfur is remarkable. Attempts to grow crystals suitable for a crystal structure determination failed and so far this has hampered the identification of these complexes.

When exactly one equivalent of thionyl chloride was added to **5a** at −70 °C the desired dichlorovanadium (bis)-phenolate, $[VCl_2(OC_6H_4(CH_2NMe_2)\text{-}2)_2]$ (**7a**) was obtained in a 76% yield (see Scheme 4). During this reaction a toluene-insoluble solid with a Cl:V ratio greater than two was also formed, as is also the case when the reaction is carried out at room temperature (vide supra).[12] Treatment of the vanadyl (bis)phenolates **5c** and **5d** with thionyl chloride at −70 °C resulted in the formation of the desired dichloro compound $[VCl_2(OC_6H_3(CH_2NMe_2)\text{-}2\text{-}Cl\text{-}4)_2]$ (**7d**) in the case of **5d**, whereas for **5c** a compound (**7c**) with a Cl:V ratio of 3.5 was found.[13] Compounds **7a**, **7c** and **7d** are dark blue, insoluble in alkanes, sparingly soluble in aromatics like benzene and toluene, but very soluble in polar solvents like CH_2Cl_2, THF and MeCN.

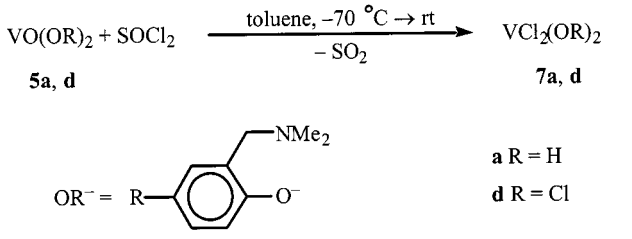

Scheme 4. Synthesis of the vanadium dichloro (bis)phenolates **7a** and **7d**

The difference in reactivity between compounds **5** and a large number of vanadyl Schiff base complexes, $[VOL_2]$, is remarkable. The latter all give the corresponding dichlorovanadium complexes in high yields.[14] The only difference between the present $[VO(OR)_2]$ complexes and the Schiff base containing $[VOL_2]$ complexes is the presence of an sp^3 amine nitrogen in the former vs. an sp^2 imine nitrogen atom in the latter. Unfortunately, the mechanism of the reaction of $[VOL_2]$ with thionyl chloride is not known. If, however, a vanadium(V) species is formed in a side reaction, then this could be an explanation for the different results in the reactions of compounds **5**. It is known that vanadium(V) compounds can be reduced by trialkylamines. Moreover, when the vanadium(V) species contains a halogen, this amine will be recovered as the trialkylammonium halide.[15] The source of the proton in this reaction is not known. Recently we reported that the use of *ortho*-aminophenolates in vanadium(V) chemistry gave rise to the formation of vanadium(IV) compounds.[5] Consequently, the formation of a vanadium(V) chloride in the reaction of **5** with $SOCl_2$ would immediately result in the reduction of the vanadium(V) nucleus to yield a vanadium(IV) vanadate species and a quaternary ammonium substituent (see Scheme 5). As two amine functionalities are present in the molecule, the reaction sequence can occur twice. The results we obtained in the synthesis of compounds **7** led us to believe that indeed a change in oxidation state is responsible for this behavior. The oxidation potential of the *t*Bu-substituted vanadyl complex is lower than those of the H- and Cl-substituted complexes (ΔE_{ox} = 60 and 130 mV, respectively).[4] A complex with a lower oxidation potential would easily lead to the formation of an unstable vanadium(V) complex, and from there to a vanadium(IV) complex with ammonium substituents and excess chlorine. The reason that this behavior is not observed for the Schiff base complexes could be twofold. Firstly, the side-reaction involving the oxidation to vanadium(V) does not occur because of their higher oxidation potentials. Secondly, the side reaction is an equilibrium. If the oxidation to vanadium(V) would occur, no chlorovanadate species would be formed as the vanadium(V) center is not reduced by an imine function. Instead it may react to return to the starting vanadium(IV) compound and subsequently react with $SOCl_2$ to form the dichlorovanadium compound.

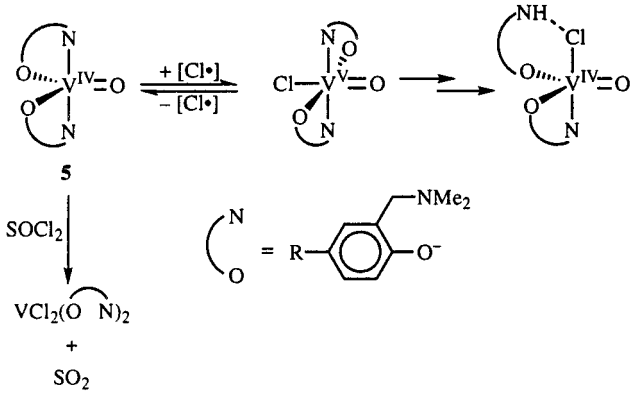

Scheme 5. Postulated reaction mechanism for the formation of an ammonium vanadate(IV) species

IR analysis corroborated the suggestion that **6** are ammonium chlorovanadate complexes. Comparison of the IR spectrum of **6b**[16] with the one of the ammonium chlorovanadate complex $[VOCl_2(OC_6H_2(CH_2NMe_2)\text{-}2\text{-}Me\text{-}4\text{-}(CH_2NHMe_2)\text{-}6)]$,[4] revealed that the 2900−2800 cm^{-1} regions (i.e., the region in which the complex resonance pattern for the intramolecular hydrogen bond is found) are very similar.

Solid-State Structures of 1 and 3

The ^{1}H NMR spectra of the vanadium(III) complexes display broad peaks with no substructure due to the paramagnetism of these d^2 compounds. This means little or no structural information can be obtained with NMR. The high-spin state of these compounds makes them also inaccessible to conventional X-band EPR analysis.[17] Consequently, in order to get information about the structure, a single crystal X-ray structure determination is of great importance. Crystallization of **1** from hexane gave single crystals suitable for X-ray crystal structure analysis. The molecular structure of **1** is depicted in Figure 2. Selected bond lengths and angles are given in Table 1. The geometry around the vanadium center is a distorted trigonal bipyramid (21% on the Berry pseudorotation path between D_{3h} and C_{4v} [18]). The three oxygen atoms are in the equatorial plane (Σ(O−V−O) = 359.82°) while the two coordinating nitrogen atoms are in the apical positions (N1−V−N3 = 171.74(8)°); i.e., two bis(amino)phenolate ligands are bonded in a bidentate η^2-*O*,*N* fashion to the vanadium center in a similar way. The third phenolate ligand is bonded in an η^1-*O* monodentate fashion. The V-O and O-C bond lengths and the V-O-C bond angles fall within the range reported for vanadium(III) phenolates (1.818-1.927 Å, 1.315-1.378 Å and 132.2-158.3°, respectively).[19] The V−O−C angle of the monodentate bonded ligand is considerably larger than those in the chelate rings. This allows more π-bonding to the vanadium center, which is reflected in a slight shortening of the V−O bond.

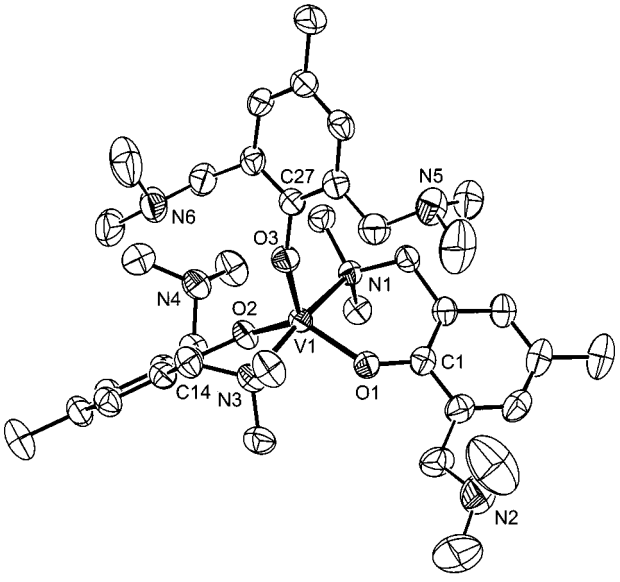

Figure 2. Displacement ellipsoid plot of **1**, drawn at 50% probability; hydrogen atoms are omitted for clarity; only one conformation of the disordered aminobenzyl groups is shown

Crystallization of **3** from toluene gave single crystals suitable for an X-ray crystal structure determination. The molecular structure is depicted in Figure 3 and pertinent bond lengths and bond angles are given in Table 2. The geometry around the vanadium center is trigonal bipyramidal as in **1**. It has crystallographic C_2 symmetry with the symmetry axis along the V−Cl bond. The equatorial plane is formed by the two oxygen atoms of the phenolate ligands and the chlorine atom. The apical positions are occupied by the coordinating nitrogen atoms (N1−V−N1′ = 175.65(18)°). The V−Cl bond length (2.2923(16) Å) lies in the range reported for vanadium(III) chlorides (2.277−2.418 Å).[20a,20c] The bond lengths and bond angles involving the bidentate η^2-*O*,*N* bonded ligand are comparable to those in **1**. Compound **3** cocrystallizes with one equivalent of toluene.

Table 1. Selected bond lengths and bond angles for **1**

Bond lengths (Å)			
V1−O1	1.876(2)	V1−N3	2.189(2)
V1−O2	1.866(2)	O1−C1	1.350(3)
V1−O3	1.853(2)	O2−C14	1.350(3)
V1−N1	2.195(2)	O3−C27	1.345(3)
Bond angles (deg)			
O1−V1−O2	126.31(8)	V1−O3−C27	148.1(2)
O1−V1−O3	116.83(8)	N1−V1−N3	171.74(8)
O2−V1−O3	116.68(8)	O1−V1−N1	88.61(7)
V1−O1−C1	133.48(18)	O2−V1−N3	88.56(8)
V1−O2−C14	134.2(2)		

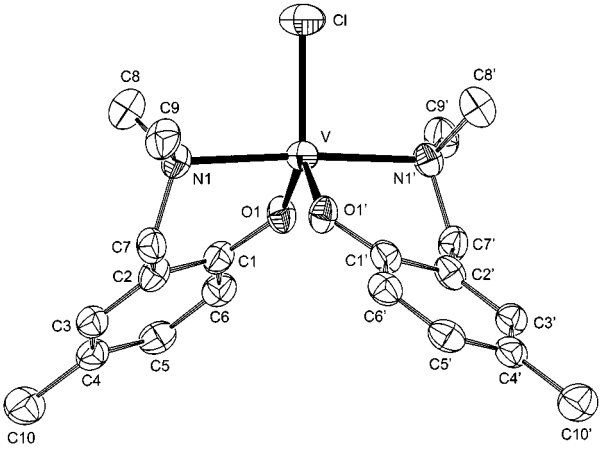

Figure 3. Displacement ellipsoid plot of **3**, drawn at 50% probability; hydrogen atoms are omitted for clarity; symmetry operation ′: $-x$, y, $0.5-z$

Table 2. Selected bond lengths and bond angles for **3**

Bond lengths (Å)			
V − Cl	2.2923(16)	V−O1	1.854(3)
V − N1	2.187(3)	O1−C1	1.345(4)
Bond angles (deg)			
Cl − V − O1	122.38(8)	O1−V−N1	88.71(11)
Cl − V − O1′	122.38(8)	N1−V−N1′	175.65(18)
O1 − V − O1′	115.23(16)	V−O1−C1	133.4(2)

Polymerization Tests

The vanadium(III) and -(IV) compounds obtained in this work were tested for ethene/propene copolymerization. The

polymerization tests were carried out in pentamethylheptane (PMH) at 30° C for a period of 10 minutes. The ethene/propene pressure was 8 bar and the ethene/propene molar ratio was kept constant at 1:2. $Et_{1.5}AlCl_{1.5}$ was used as cocatalyst. The reaction vessel was loaded with 500 mL of PMH, 20 equivalents of cocatalyst and the monomers. The catalysts (± 25 μmol), dissolved or suspended in toluene, were injected into the reaction vessel without premixing of the cocatalyst. The results of these preliminary tests are listed in Table 3.

Table 3. Ethene/propene copolymerization results with vanadium aminophenolate complexes

Complex [a]	Yield (g)	Activity[b]	C_3 (mass%)	η[c] (dL/g)	Mw[d]
1	0.9	27	n.d.	n.d.	–
3	5.3	159	37.5	5.86	6.7
6a	0.7	21	n.d.	n.d.	–
6c	2.6	78	38.2	8.15	10.5
6e	4.6	138	39.1	7.29	9.0
6f	0.7	21	n.d.	n.d.	–
7c	7.4	222	32.3	4.95	5.0
7d	6.3	189	29.5	5.95	6.3

[a] Polymerization conditions: 25 μmol [V], 20 equiv. $Et_{1.5}AlCl_{1.5}$, 500 mL PMH, 30 °C, 8 bar ethene/propene ratio 1:2, 10 min. reaction time. – [b] Activity in kg/mol[V]·h·bar. – [c] Intrinsic viscosity measured in decalin at 135 °C. – [d] Molecular weight in g/mol $\times 10^{-5}$.

The activities found vary over one order of magnitude, with the activities of complexes **6** significantly lower than those of **7**. The reason for these lower activities is probably the poor solubility of the former complexes, as only **6e** is slightly soluble in toluene whereas **6a**, **6c** and **6f** are completely insoluble in toluene. The activity of **1** is low in comparison with **3**. The reason for this difference is probably the rate of formation of the catalytically active species. The steric bulk of the pendant amino substituents probably hinders the approach of an aluminium species, which is necessary for ligand exchange with subsequent formation of a vanadium alkyl compound.

IR analysis of the polymers shows that the incorporation of propene varied between approximately 30 and 40%. The molecular weights of the polymers were calculated based on their intrinsic viscosities (in decalin at 135°). The molecular weights varied between 5.0×10^5 and 10.5×10^5 g/mol. When these results are compared to those reported by Gambarotta and co-workers for tetravalent $(R_2N)_2VCl_2$ (R = *i*Pr, Cy) complexes[21] some differences can be noted. The activities are of the same order of magnitude (430 and 165 kg EP/mol[V]·h·bar, respectively). The molecular weight (Mw = 2293000 for R = *i*Pr) is much higher, but the propene incorporation is slightly lower (27%). Unfortunately, it is difficult, if not impossible, to make a fair comparison with the results reported in the literature. Often the conditions are different or details of the polymerization reactions are not mentioned.

Experimental Section

General: All reactions were performed in an atmosphere of dry, oxygen-free dinitrogen using standard Schlenk techniques. Solvents were carefully dried and distilled prior to use. $[Cp_2V]$,[22] $[VCl_3(THF)_3]$,[23] the phenols **b** and **g**,[24] and the vanadium oxo (bis)phenolates **5a**–**5f** were prepared according to literature procedures. $SOCl_2$ was distilled from quinoline. Et_3N was distilled from CaH_2. All other chemicals were obtained from commercial sources and used as received. Elemental analyses were performed by H. Kolbe, Mikroanalytisches Laboratorium, Mülheim, Germany. ^1H NMR spectra were recorded on a Bruker AC300 spectrometer or a Varian Unity Inova 300 spectrometer. EPR spectra were recorded on a Bruker ESP 300 spectrometer.

Synthesis of $[V(OC_6H_2(CH_2NMe_2)_2$–2,6-Me-4$)_3]$ (1): A mixture of $[Cp_2V]$ (0.44 g, 2.42 mmol) and $HOC_6H_2(CH_2NMe_2)_2$–2,6-Me-4 (1.96 g, 8.82 mmol) in benzene (40 mL) was stirred for 50 hours at 70 °C during which time the color slowly changed from purple to green. After removal of the solvent in vacuo a green oil was obtained. Leaving the oil to stand yielded two crops of a red solid (1.04 g; 60%). Recrystallization from hexane at 4 °C gave bright orange crystals. Mp: 129 °C. – $C_{39}H_{63}N_6O_3V$: calcd. C 65.52, H 8.88, N 11.76; found C 65.33, H 8.89, N 11.80. – IR (KBr, cm^{-1}): 2998(m), 2972(s), 2941(s), 2903(s), 2851(s), 2828(s), 2909(s), 2758(s), 2728(m), 2714(m), 1780(w), 1609(w), 1576(w), 1468(s), 1362(m), 1300(s), 1283(s), 1256(s), 1172(m), 1146(m), 1042(m), 1005(m), 984(m), 872(s), 845(s), 826(s), 638(m), 600(m), 557(m). – Magnetic susceptibility: $\mu_{eff} = 2.52\mu_b$.

Synthesis of $Me_3SiOC_6H_3(CH_2NMe_2)$-2-Me-4 (2): A solution of $HOC_6H_4(CH_2NMe_2)$-2-Me-4 (**b**) (11.41 g, 68.63 mmol) in Et_2O (25 mL) was added dropwise to a stirred solution of Me_3SiCl (11.3 mL, 89.3 mmol) and Et_3N (12.4 mL, 89.3 mmol) in Et_2O (300 mL). A white precipitate was immediately formed and the resulting mixture was stirred for 16 hours. The precipitate was subsequently removed by filtration. The filtrate was concentrated in vacuo to give a yellowish oil. This oil was flash-distilled to give **2** as a colorless oil (13.13 g; 80%). – ^1H NMR (300 MHz, $CDCl_3$): δ = 0.27 (s, 9 H, $SiMe_3$), 2.25 (s, 6 H, NMe_2), 2.28 (s, 3 H, Me), 3.37 (s, 2 H, CH_2), 6.69 (d, 1 H, $^3J_{H,H}$ = 8 Hz, Ar-H^6), 6.92 (dd, 1 H, $^3J_{H,H}$ = 8 Hz, $^4J_{H,H}$ = 2 Hz, Ar–H^5), 7.13 (d, 1 H, $^4J_{H,H}$ = 2 Hz, Ar–H^3).

Synthesis of $[VCl(OC_6H_3(CH_2NMe_2)$-2-Me-4$)_2]$ (3): A solution of $Me_3SiOC_6H_3(CH_2NMe_2)$-2-Me-4 (**2**) (4.44 g, 18.70 mmol) in THF (20 mL) was added dropwise to a stirred suspension of $[VCl_3(THF)_3]$ (3.52 g, 9.42 mmol) in THF (50 mL). A dark red solution was immediately obtained, which was then heated at reflux for one hour. After removal of the solvent in vacuo the residue was extracted with toluene (80 mL) and the resulting solution was left to stand for several days, yielding bright orange crystals (0.74 g; 16%). Cooling the supernatant solution to −20 °C gave a second crop (0.98 g; 21%). M.p.: 122 °C. – $C_{20}H_{28}N_2O_2VCl{\cdot}C_7H_8$: calcd. C 63.97, H 7.16, N 5.53; found C, 63.29, H 6.83, N 5.50.

Synthesis of $[VCl(OC_6H_3(CH_2NMe_2)$-2-Me-4$)_2CuCl_2]$ (4): $CuCl_2$ (0.39 g, 2.90 mmol) was added as solid to a stirred solution of $[VCl(OC_6H_3(CH_2NMe_2)$-2-Me-4$)_2{\cdot}C_7H_8]$ (**3**) (0.9 g, 1.7 mmol) in CH_2Cl_2 (50 mL). The color changed to dark blue within a few minutes. The mixture was stirred for two days after which it was filtered. The volume of the solution was reduced to 30 mL in vacuo. The solution was layered with Et_2O (30 mL) and left to stand for three days. A dark blue oil was formed which upon drying in vacuo yielded a dark blue solid (0.94 g; 87%). – $C_{21}H_{30}N_2O_2VCuCl_3{\cdot}CH_2Cl_2$: calcd. C 39.77, H 4.77, N 4.42; Cl, 27.95; found C, 39.73, H 5.38, N 4.39; Cl, 27.60.

Synthesis of $[VCl_2(OC_6H_4(CH_2NMe_2)-2)_2]$ (7a): $SOCl_2$ (1.5 mL, 2.1 M in toluene, 3.2 mmol) was added to a stirred suspension of

$[VO(OC_6H_4(CH_2NMe_2)\text{-}2)_2]$ (**5a**) (1.14 g, 3.10 mmol) in toluene (40 mL) at −70 °C. The solution was allowed to slowly warm to room temperature, during which it turned dark green and a dark colored precipitate was formed. After stirring for an additional 16 hours the solution was separated from the precipitate by centrifugation/decantation and the residue was extracted twice with toluene (40/20 mL). The volume of the combined toluene fractions was reduced to 15 mL in vacuo after which pentane (40 mL) was added. The solvent was removed by centrifugation/decantation and the residue was washed with pentane (2 × 25 mL). Compound **7a** was obtained as a dark blue powder after drying in vacuo (0.99 g, 76). − $C_{18}H_{24}N_2O_2VCl_2$: calcd. C 51.20, H 5.73, N 6.63; V, 12.06; Cl, 16.79; found C, 50.99, H 5.75, N 6.49; V, 11.83; Cl, 16.65. − EPR (toluene): A_{iso} = 84.1 Gauss; g_{iso} = 1.955.

Synthesis of $[VCl_2(OC_6H_3(CH_2NMe_2)\text{-}2\text{-}Cl\text{-}4)_2]$ (7d): Compound **7d** was prepared in a similar way to **7a** starting from $[VO(OC_6H_3(CH_2NMe_2)\text{-}2\text{-}Cl\text{-}4)_2]$ (**5d**) (0.53 g, 1.22 mmol) and $SOCl_2$ (0.6 mL, 2.1 M in toluene, 1.2 mmol) and was obtained as a dark blue powder (0.32 g, 54). − $C_{18}H_{22}N_2O_2VCl_4$: calcd. C 44.02, H 4.52, N 5.70; Cl, 28.87; found C, 43.88, H 4.50, N 5.67; Cl, 28.84. − EPR (toluene): A_{iso} = 84.00; g_{iso} = 1.953.

X-ray Crystallographic Structure Determination and Refinements. Orange crystals of **1** suitable for X-ray diffraction were grown by cooling a saturated hexane solution to 4 °C while orange crystals of **3**·C_7H_8 were grown from toluene at room temperature. X-ray intensities were measured on an Enraf−Nonius CAD4T diffractometer with rotating anode and graphite monochromator (Mo−$K\alpha$, λ = 0.71073 Å).

Crystal structure of **1**: Yellow block, 0.25 × 0.25 × 0.25 mm^3. The structure was solved with direct methods (SHELXS86[25]) and refined with the program SHELXL93[26] against F^2 for all reflections up to a resolution of $(\sin\theta/\lambda)_{max}$ = 0.65 Å^{-1}. An absorption correction was not considered necessary. Non-hydrogen atoms were refined freely with anisotropic displacement parameters; hydrogen atoms were refined as rigid groups. Three of the uncoordinated aminobenzyl groups were refined with disorder models.

Crystal structure of **3**: Yellow plate, 0.38 × 0.30 × 0.05 mm^3. The structure was solved with Patterson methods (DIRDIF97[27]) and refined with the program SHELXL97[28] against F^2 of all reflections up to a resolution of $(\sin\theta/\lambda)_{max}$ = 0.59 Å^{-1}. An absorption correction based on Psi-scans was applied (0.87−0.97 transmission). Non-hydrogen atoms were refined freely with anisotropic displacement parameters; hydrogen atoms were refined as rigid groups. The crystal structure contains large voids (670 Å^3) filled with disordered toluene molecules. Their contribution to the structure factors was secured by back-Fourier transformation (program PLATON,[29] CALC SQUEEZE, 196 e/unit cell)

Both structures were checked for higher symmetry with the program PLATON.[29] Crystal data and details of the data collection are shown in Table 4. Geometrical calculations and illustrations were performed with PLATON.[29]

Crystallographic data (excluding structure factors) for the structures reported in this paper have been deposited with the Cambridge Crystallographic Data Centre as supplementary publications no. CCDC-139534 (**1**) and -139535 (**3**). Copies of the data can be obtained free of charge on application to CCDC, 12 Union Road, Cambridge CB2 1EZ, UK [Fax: (internat.) + 44-1223/336-033; E-mail: deposit@ccdc.cam.ac.uk].

Table 4. Crystallographic data for **1** and **3**.

	1	**3**
Empirical formula	$C_{39}H_{63}N_6O_3V$	$C_{20}H_{28}N_2O_2VCl\cdot C_7H_8$
Formula weight	714.91	506.995
Crystal system	Triclinic	Orthorhombic
Space group	$P\bar{1}$ (No. 2)	*Pbcn* (No. 60)
a, Å	9.2793(7)	11.712(2)
b, Å	13.9788(10)	16.4182(16)
c, Å	17.4615(12)	13.5356(16)
α, deg	110.474(5)	90
β, deg	99.989(6)	90
γ, deg	96.252(6)	90
V, Å^3	2054.1(3)	2602.8(6)
Z	2	4
D_{calc}, g cm^{-3}	1.156	1.294
μ (Mo $K\alpha$), mm^{-1}	0.28	0.496
F(000)	772	1072
T, K	225	150
θ range	1.28−27.46	2.14−25.00
hkl range	−11 → 12, −16 → 18, −22 →15	−13 → 1, −19 → 19, −16 → 0
Measured reflections	12616	4488
Unique reflections	9388	2289
Observed refl. [$I > 2\sigma(I)$]	6519	1300
Parameters/restraints	510/0	119/0
Final $R1$[a]	0.061	0.0563
Final $wR2$[b]	0.165	0.1339
Goodness of fit	1.019	0.96
Residual electron density	−0.34 → 0.73	−0.18 → 0.43

[a] $R1 = \Sigma||F_c| - |F_c||/\Sigma|F_c|$ based on observed reflections. − [b] $wR2 = [\Sigma[w(F_o^2 - F_c^2)^2]/\Sigma[w(F_o^2)^2]]^{1/2}$ based on all reflections.

Acknowledgments

This work was carried out in connection with NIOK, The Netherlands Institute for Catalysis Research, and was supported by the Department of Economic Affairs of The Netherlands. Crystallographic studies were supported in part (M.L., A.L.S.) by the Council for the Chemical Sciences of the Netherlands Organization for Scientific Research (CW-NWO). Polymerization tests and polymer analysis were carried out at the DSM Research B.V., Sittard, the Netherlands. EPR analyses were carried out at the Department of Atomic and Interface Physics, Utrecht University, The Netherlands by Dr. E. E. van Faassen. IR and Raman analyses of **6b** were carried out at the Department of Analytical Molecular Spectroscopy, Utrecht University, The Netherlands by Dr. B. T. G. Lutz.

[1] V. J. Murphy, H. Turner, *Organometallics* **1997**, *16*, 2495, and references therein.
[2] F. J. Karol, S.-C. Kao, *New J. Chem.* **1994**, *18*, 97.
[3] [3a] F. Preuss, H. Becker, J. Kaub, W. S. Sheldrick, *Z. Naturforsch., Teil B* **1988**, *43*, 1195. − [3b] J.-K. F. Buijink, A. Meetsma, J. H. Teuben, H. Kooijman, A. L. Spek, *J. Organomet. Chem.* **1995**, *497*, 161.
[4] H. Hagen, A. Barbon, E. E. van Faassen, B. T. G. Lutz, A. L. Spek, G. van Koten, *Inorg. Chem.* **1999**, *38*, 4079.
[5] H. Hagen, C. Bezemer, J. Boersma, H. Kooijman, M. Lutz, A. L. Spek, G. van Koten, *Inorg. Chem.* **2000**, *39*, 3970.
[6] The spin-only value for a $S = 2$ system is 2.83 μ_b. However for $3d^2$ complexes the departure from the spin-only value can be large due to a contribution of the orbital angular momentum. D. F. Shriver, P. W. Atkins, C. H. Langford, *Inorganic Chemistry*; Oxford University Press: Oxford, 1990; p. 214.
[7] [7a] R. K. Minhas, J. J. H. Edema, S. Gambarotta, A. Meetsma, *J. Am. Chem. Soc.* **1993**, *115*, 6710. − [7b] M. J. Scott, W. Christian, A. Wilisch, W. H. Armstrong, *J. Am. Chem. Soc.* **1990**, *112*, 2429.
[8] S. Gambarotta, F. van Bolhuis, M. Y. Chiang, *Inorg. Chem.* **1987**, *26*, 4301.

[9] M. P. Hogerheide, J. T. B. H. Jastrzebski, J. Boersma, W. J. J. Smeets, A. L. Spek, G. van Koten, *Inorg. Chem.* **1994**, *33*, 4431.
[10] M. Pasquali, A. Torres-Filho, C. Floriani, *J. Chem. Soc., Chem. Commun.* **1975**, 534.
[11] **6a**: Anal. found C 42.58, H 4.84, N 4.63, Cl 26.12, V 8.60, S 2.30. Based on nitrogen analysis 4.63 ≈ 2 N: MW = 605; stoichiometry: 21.4 C; 29.0 H; 4.5 Cl; 1.0 V; 0.4 S. Based on residual mass: 4.1 O. **6c**: Anal. found C 46.05, H 5.81, N 3.80; Cl, 26.97. Based on nitrogen analysis 3.80 ≈ 2 N: MW = 737; stoichiometry: 28.3 C; 42.5 H; 5.6 Cl. **6d**: Anal. found C 38.03, H 3.86, N 4.43, Cl 34.29. Based on nitrogen analysis 4.43 ≈ 2 N: MW = 632; stoichiometry: 20.0 C; 24.2 H; 6.1 Cl. **6e**: Anal. found C 56.34, H 4.83, N 12.33; Cl, 13.51. Based on nitrogen analysis 12.33 ≈ 6 N: MW = 682; stoichiometry: 32.0 C; 32.6 H; 2.6 Cl. **6f**: Anal. found C 43.98, H 5.02, N 4.17; Cl, 23.49; V, 8.43, S 3.51. Based on nitrogen analysis 4.17 ≈ 2 N: MW = 672; stoichiometry: 24.6 C; 33.7 H; 4.5 Cl; 1.1 V; 0.7 S. Based on residual mass: 4.8 O.
[12] The residue in the case of **7a** contained three equivalents of chlorine. Anal. found C 47.44, H 5.38, N 5.90, Cl 22.35. Based on nitrogen analysis 5.90 ≈ 2 N: MW = 475; stoichiometry: 18.8 C; 25.3 H; 3.0 Cl.
[13] **7c**: Anal. found C 53.85, H 7.01, N 4.67; Cl, 20.59. Based on nitrogen analysis 4.67 ≈ 2 N: MW = 600; stoichiometry: 26.9 C; 41.7 H; 3.5 Cl.
[14] [14a] M. Pasquali, F. Marchetti, C. Floriani, *Inorg. Chem.* **1979**, *18*, 2401. – [14b] A. Jezierski, J. B. Raynor, *J. Chem. Soc., Dalton Trans.* **1981**, 1. – [14c] V. Vergopoulos, S. Jantzen, N. Julien, E. Rose, *Z. Naturforsch., Teil B* **1994**, *49*, 1127. – [14d] H. Schmidt, M. Bashispoor, D. Rehder, *J. Chem. Soc., Dalton Trans.* **1996**, 3865.
[15] K. L. Baker, D. A. Edwards, G. W. A. Fowles, R. G. Williams, *J. Inorg. Nucl. Chem.* **1967**, *29*, 1881.
[16] IR (Poflu mull, cm^{-1}): 3000, 2953, 2917, 2855, 2715, 1594, 1483, 1254, 1225, 1150, 1100, 975, 926, 905, 861, 832, 709, 686, 661. – Raman (MeCN, cm^{-1}): 1604, 1485, 1277, 1142, 1117, 929, 860, 755, 563, 547, 378.
[17] To study paramagnetic d^2 complexes high-field EPR has to be used: P. L. W. Tregenna-Pigott, H. Weihe, J. Bendix, A.-L. Barra, H.-U. Güdel, *Inorg. Chem.* **1999**, *38*, 5928 and references therein.
[18] R. R. Holmes, *Progress in Inorg. Chem.* **1984**, *32*, 119, and references therein.
[19] [19a] R. A. Henderson, D. L. Hughes, Z. Janas, R. L. Richards, P. Sobota, S. Szafert, *J. Organomet. Chem.* **1998**, *554*, 195. – [19b] C. Floriani, M. Mazzanti, A. Chiesi-Villa, Guastine, C. *Angew. Chem. Int. Ed. Engl.* **1988**, *27*, 576. – [19c] P. G. Cozzi, C. Floriani, A. Chiesi-Villa, C. Rizzoli, *Inorg. Chem.* **1995**, *34*, 2921. – [19d] W. C. A. Wilisch, M. J. Scott, W. H. Armstrong, *Inorg. Chem.* **1988**, *27*, 4335.
[20] [20a] A. T. Vlahos, T. A. Kabanos, C. P. Raptopoulos, A. Terzis, *Chem. Commun.* **1997**, 269. – [20b] M. B. O′Donoghue, W. M. Davis, R. R. Schrock, W. M. Reiff, *Inorg. Chem.* **1999**, *38*, 243. – [20c] C. M. Grant, B. J. Stamper, M. J. Knapp, K. Folting, J. C. Huffman, D. N. Hendrickson, G. Christou, *J. Chem. Soc., Dalton Trans.* **1999**, 3399. – [20d] P. B. Hitchcock, D. L. Hughes, G. J. Leigh, J. R. Sanders, J. S. de Souza, *Chem. Commun.* **1996**, 1985.
[21] N. Desmangles, S. Gambarotta, C. Bensimon, S. Davis, H. Zahalka, *J. Organomet. Chem* **1998**, *562*, 53.
[22] F. H. Köhler, W. Prössdorf, *Z. Naturforsch., Teil B* **1977**, *32*, 1026.
[23] E. Kurras, *Naturwissenschaften* **1959**, *5*, 171.
[24] *Methoden der Organischen Chemie*, 4th ed., J. Houben, T. Weyl, Eds., Georg Thieme Verlag: Stuttgart, Germany, **1957**, Vol. 11/1; p. 756.
[25] G. M. Sheldrick, *SHELXS-86 Program for crystal structure solution*; University of Göttingen, Germany, **1986**.
[26] G. M. Sheldrick, *SHELXL-93 Program for crystal structure refinement*; University of Göttingen, Germany, **1993**.
[27] P. T. Beurkens, G. Admiraal, G. Beurskens, W. P. Bosman, S. García-Granda, R. O. Gould, J. M. M. Smits, C. Smykalla, *The DIRDIF97 program system, Technical report of the Crystallographic Laboratory*; University of Nijmegen, The Netherlands, 1997
[28] G. M. Sheldrick, *SHELXL-97 Program for crystal structure refinement*; University of Göttingen, Germany, **1997**.
[29] A. L. Spek, *PLATON A multipurpose crystallographic tool*; Utrecht University, The Netherlands, **1998**.

Received February 11, 2000
[I00046]

Bis(*ortho*)-Chelated Bis(phosphanyl)aryl Ruthenium(II) Complexes Containing an η^1-*P*-Monodentate or μ-Bridging η^1-*P*,η^1-*P*′ Bonded R−PCHP Arene Ligand, 1-R-3,5-$(CH_2PPh_2)_2C_6H_3$ [R = H, Br, or, Si(*n*-$CH_2CH_2C_8F_{17})_3$] — Cyclometalation Reaction Intermediates and Potential Catalysts for Use in Fluorinated Biphasic Systems

Paulo Dani,[a] Bodo Richter,[a] Gerard P. M. van Klink,[a] and Gerard van Koten*[a]

Keywords: Ruthenium / Monoanionic terdentate *P,C,P*′-bisphospanylaryl / Cyclometalation / P ligands / Fluorine

Mono- and binuclear ruthenium(II) complexes containing ligands derived from the *meta*-bis(phosphanyl)arene ligand 1-R-3,5-$(CH_2PPh_2)_2C_6H_3$ [R–PCHP: R = H (**5**), Br (**3**), or Si(*n*-$CH_2CH_2C_8F_{17})_3$ (**4**)] have been synthesized and fully characterized. On reaction of equimolar amounts of the ruthenium starting material (e.g. $[RuCl_2(PPh_3)_3]$) and the *meta*-bis(phosphanyl)arene, complexes of the type $[RuCl\{C_6H_2(CH_2PPh_2)_2$-2,6-R-4$\}(PPh_3)]$ are invariably isolated, which contain only one $[C_6H_3(CH_2PPh_2)_2$-2,6$]^-$ monoanionic ligand η^3-*P,C,P*′-bonded to Ru. Monitoring of this reaction by ^1H and ^{31}P NMR has shown it to proceed via intermediate species having an apparently η^3-*P,C,P*′-bonded PCP ligand and a second *meta*-bis(phosphanyl)arene ligand that is either η^1-P-bonded or μ-η^1-P,η^1-P′-bridging between two [RuCl(PCP)] units. The synthesis of the first PCP "pincer"-type ligand with a polyfluorinated "pony tail" is detailed, viz. compound **4** as well as the corresponding ruthenium complex [RuCl{(*n*-C_8F_{17}-$CH_2CH_2)_3$Si–PCP}], **7**. The latter compound is soluble in fluorinated solvents and hence represents the first ruthenium "pincer" complex that may find use in fluorinated biphasic systems.

Introduction

Bis(phosphanes) exhibit a rich coordination chemistry upon interaction with a wide range of metal centers. As shown in Figure 1, various mono- and multimetallic complexes can be formed. Complexes with *cis*-η^2-*P,P*′-coordinated ligands are by far the most common as compared with the so-called "dangling" η^1-*P* (monodentate) coordination motif.[1] The coordination mode can be greatly affected by the length of the chain linking the two donor groups and by the type of substituents present either in the organic backbone or at the donor atoms.[2] The use of bis(phosphane) ligands capable of forming *trans*-spanning complexes (often with a carbon chain containing five or more atoms) is likely to lead to the observation of a different binding mode. This involves not only the coordination of the two P-donors, but also that of a formal carbanion localized at a central position in the backbone. This is clearly a result of C−H bond activation (i.e. orthometalation).[3] Thus, true organometallic species can be generated from bis(phosphane) ligands through appropriate choice of the linking backbone. This is exemplified by the "pincer" ligands of the general formula shown in Figure 1 (the monoanionic η^3-*P,C,P*′-coordinating PCP ligand) and Figure 2.

Such properties of *trans*-spanning ligands are particularly evident in the coordination behavior of bis(phosphane) ligands of the type R−PCHP (Figure 2), in which a rigid *m*-xylylenediyl organic fragment links the two P donor groups.[3a,4]

Reaction of these R−PCHP ligands with transition metal complexes frequently results in the formation of metalated complexes containing a formal monoanionic (i.e. η^3-*P,C,P*′)-coordinated R−PCP ligand. Only a few cases are known where the ligand is bonded as a neutral (noncyclometalated) R−PCHP species. Examples of this type of bonding are observed in just a few square-planar d^8 metal complexes,[5−7] tetrahedral silver compounds,[8] and the octahedral ruthenium species **1**[9] and **2**[10] (Figure 3).

In the present paper, the coordination and cyclometalation properties of the R−PCHP ligands 1-Br-3,5-$(CH_2PPh_2)_2C_6H_3$ (**3**), 1-(*n*-$C_8F_{17}CH_2CH_2)_3$Si-3,5-$(CH_2PPh_2)_2C_6H_3$ (**4**), and 3,5-$(CH_2PPh_2)_2C_6H_4$ (**5**) (R = H, see Figure 2) are reported in more detail. The formation of species with *P*-coordinated neutral R−PCHP ligands and their involvement in the generation of cyclometalated compounds with monoanionic η^3-*P,C,P*′-coordinated R−PCP ligands has been observed.

Results and Discussion

Ruthenium Complexes of R−PCP Ligands

The fluorine-rich ligand (*n*-$C_8F_{17}CH_2CH_2)_3$Si−PCHP (**4**) (Scheme 1) was obtained in excellent yield (94%) by dir-

[a] Department of Metal-Mediated Synthesis, Debye Institute, Utrecht University,
Padualaan 8, 3584 CH Utrecht, The Netherlands
Fax: (internat.) +31-30/252-3615
E-mail: g.vankoten@chem.uu.nl

 © WILEY-VCH Verlag GmbH, D-69451 Weinheim, 2001 1434−1948/01/0101−0125 $ 17.50+.50/0

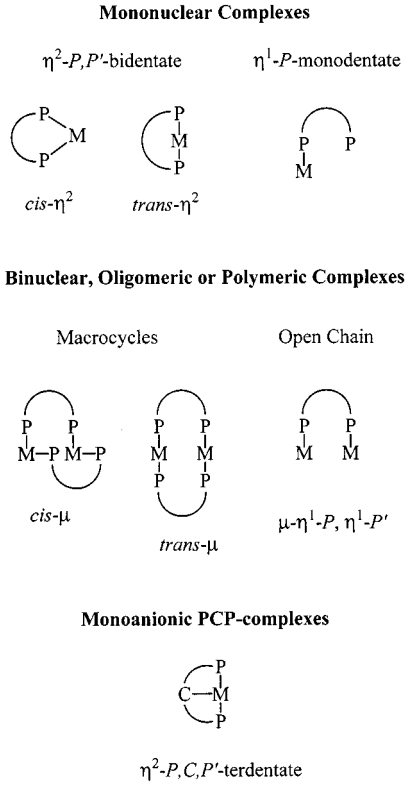

Figure 1. Possible coordination modes of bis(phosphane) ligands and of a monoanionic η^3-*P,C,P′*-coordinated PCP ligand derived from C−H activation

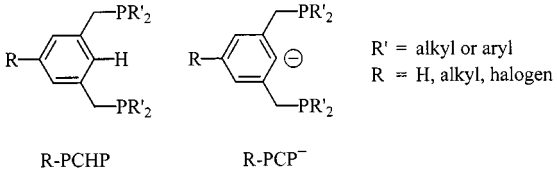

Figure 2. R−PCHP-type ligands and their respective monoanionic R−PCP derivatives

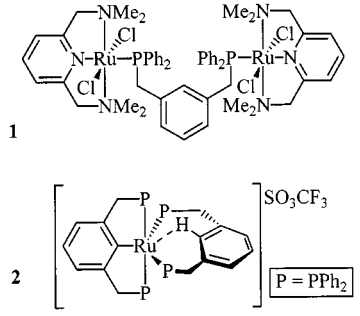

Figure 3. Octahedral ruthenium species with a neutral PCHP ligand

ect lithium/halogen exchange of the 5-bromo *meta*-bis(phosphane) ligand **3** with two equiv. of *t*BuLi followed by quenching of the resulting 5-lithio derivative with $(n\text{-}CH_2CH_2C_8F_{17})_3SiBr$. Reactions of **3** and **4** with one equiv. of $[RuCl_2(PPh_3)_3]$ in refluxing 1,2-dichloroethane (Scheme 1) resulted in the formation of the 16-electron, neutral ruthenium(II) compounds [RuCl{$C_6H_2(CH_2PPh_2)_2$-2,6-R-4}(PPh_3)] [R = Br, **6**; $(n\text{-}C_8F_{17}CH_2CH_2)_3Si$, **7**], containing a monoanionic η^3-*P,C,P′*-bonded R−PCP ligand, in about 70% yield in each case.

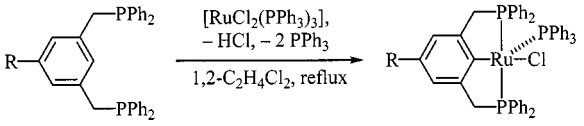

3, R = Br
4, R = Si(n-$CH_2CH_2C_8F_{17}$)$_3$
5, R = H

6 (72%)
7 (71%)
8 (90%)[12-14]

Scheme 1. Synthesis of [RuCl(R−PCP)(PPh_3)] complexes

In the $^{31}P\{^1H\}$ NMR spectrum of **6**, the phosphorus resonance attributable to the cyclometalated Br−PCP ligand appears as a doublet at $\delta = 36.74$ while the phosphorus nucleus of the PPh_3 moiety resonates as a triplet at $\delta = 80.62$ ($^2J_{PP} = 32$ Hz). A coupling constant of this magnitude is characteristic of a *cis* arrangement of the PPh_3 unit in relation to the two magnetically equivalent PCP phosphorus nuclei.[11] The ^1H NMR spectrum of **6** shows a set of two multiplets attributable to the diastereotopic benzylic protons, indicating the absence of a plane of symmetry containing the benzylic carbon atoms, but showing the presence of an apparent plane of symmetry bisecting the Ru−Cl−P(PPh_3)−C_{ipso} atoms. This leads to enantiotopic *ortho*-CH_2PPh_2 substituents. Similar ^1H and ^{31}P NMR spectra have been observed for the fluorinated-tail complex **7**. In addition to the respective resonances observed for **6**, the ^1H NMR spectrum of **7** shows two multiplets in the ranges $\delta = 0.90-1.10$ and $1.95-2.25$, each set of signals integrating for six protons, clearly attributable to the methylene protons present in the fluorinated chain.

All the spectroscopic features suggest that **6** and **7** are structural analogues of the reported parent complex [RuCl(H−PCP)(PPh_3)] (**8**, cf. **6** with R = H).[12−14] Thus, these new complexes have a distorted square-pyramidal geometry in solution, with a PPh_3 ligand in the apical position and a basal plane formed by the monoanionic η^3-*P,C,P′*-coordinated R−PCP ligand and the Cl ligand.

Ruthenium Complexes Containing One Neutral R−PCHP Ligand

The method outlined in Scheme 1 was one of our initial synthetic protocols that we applied to the synthesis of [RuCl(R−PCP)(PPh_3)] [R = H (**8**), Ph][12] complexes. This method has proven to be of general use. However, some drawbacks have been encountered for R groups containing sensitive functionalities (e.g., when R = $SiMe_3$, desilylation can occur).[10,15] Other chlorinated solvents can be used as the reaction medium, such as CH_2Cl_2 or *o*-dichlorobenzene. However, 1,2-dichloroethane has been shown to be the best choice in terms of reaction times (typically 1−2 h), yields, and ease of work-up of the resulting products. When the reactions are carried out in refluxing CH_2Cl_2, the lower temperature leads to an appreciable decrease in the rate of the reaction such that the final complex is obtained only after three days. On the other hand, this retardation has allowed us the opportunity to gain insight into the various

stages of the reaction leading to the formation of species such as **6** and **8**.

On monitoring the 1:1 molar reaction of **3** with $[RuCl_2(PPh_3)_3]$ in refluxing CH_2Cl_2 by ^{31}P NMR spectroscopy, the signal attributable to **3** ($\delta = -9.07$) is seen to disappear within 5 min. At the same time, a broad and intense singlet at $\delta \approx -4.5$ is observed, which is characteristic of free PPh_3, together with intense but very broad signals between $\delta = 30$ and 90. This suggests the occurrence of intra- and/or intermolecular exchange processes involving displacement of PPh_3 ligand(s) of $[RuCl_2(PPh_3)_3]$ by the more basic benzylic ligand **3**. This results in the formation of a complex mixture of oligomeric species. Within 1−2 h, the broad signals gradually fade in intensity with the concomitant appearance of a set of two doublets located at $\delta =$ 40.05 and 40.30 (the latter is normally very weak), a triplet at $\delta = 83.75$ ($J_{PP} = 30$ Hz), and a singlet at $\delta = -10.06$. At this stage, it is already possible to observe very weak patterns due to the final compound **6** (doublet and triplet resonances at $\delta = 36.74$ and 80.62, respectively). Obviously, as the reaction progresses the signals due to **6** become stronger at the expense of the other signals present. It should be noted that similar behavior was observed when ligand **5** was used in such an experiment.

The magnitude and multiplicity of J_{PP} gives an excellent indication of the mutual arrangement of the phosphanes[11] around the metal center and allows the assignment of structural features of the intermediate species formed en route to the final product (e.g. **6**). The coupling constant data pointed to the presence of Ru complexes containing an η^2-*P,P′*-bonded ligand as exemplified, for instance, by structures **A** and **B** (Figure 4). Such complexes have often been postulated as precursors in cyclometalations of bis(phosphane) donor ligands. However, the chemical shifts are typical for a bis(*ortho*)-metalated η^3-*P,C,P′*-bonded PCP ligand containing a third phosphorus nucleus in an apical position *trans* to a vacant site.[10−13,16] For instance, in the ^{31}P NMR spectrum of the cationic Ru^{II} complex **2**, the only known complex containing both an η^2-*P,P′* PCHP and an η^3-*P,C,P′*-coordinated PCP ligand attached to the same metal center, the ^{31}P resonance of the P nuclei of the bidentate bonded *meta*-bis(phosphane) PCHP ligand is seen at around $\delta = 18-20$, while the nuclei of the η^3-*P,C,P′*-coordinated PCP ligand give rise to a broad signal (room temp.) centered at $\delta = 40$.[17] Therefore, the initially formed species consists of the μ-η^1-*P*,η^1-*P′* (cf. **C**) or the η^1-*P*-coordinated species **D** (Figure 4). The latter compounds already contain a bis(*ortho*)-metalated η^3-*P,C,P′* R−PCP ligand but differ from the final complex **6** in that the apical position is occupied by a second R−PCHP ligand instead of PPh_3. In this way, the singlet at $\delta = -10.06$ can be assigned to the dangling PPh_2 group of **D** and the doublet at $\delta = 40.30$ to the phosphorus of the bis(*ortho*)-metalated ligand. On this basis, the signal at $\delta = 83.75$ should therefore be comprised of two superimposed triplets.

In accordance with this hypothesis, compounds **9** and **10** were detected when $[RuCl_2(PPh_3)_3]$ was reacted with excess Br−PCHP (2 to 3 equiv. of Br−PCHP were used instead of 1, cf. step *a* in Scheme 2), and when **6** was directly reacted with one equiv. of Br−PCHP (step *b* in Scheme 2). Furthermore, the addition of further $[RuCl_2(PPh_3)_3]$ to a mixture of complexes **9** and **10** (CH_2Cl_2) followed by refluxing overnight (step *c* in Scheme 2) afforded **6** in 53% isolated yield.

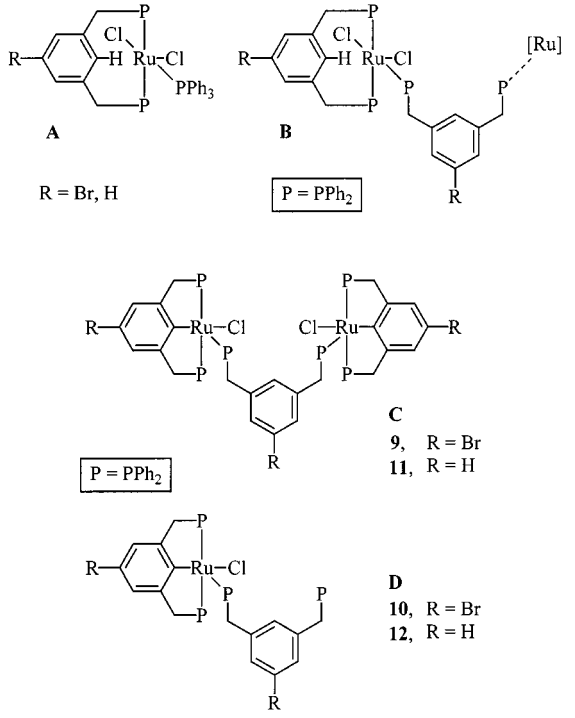

Figure 4. Postulated and observed intermediates in cyclometallation of bis(phosphane) donor ligands

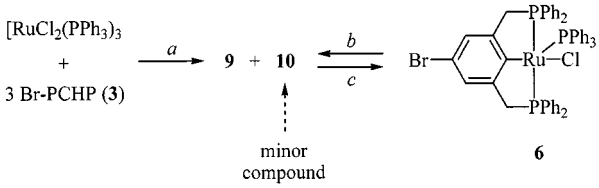

Scheme 2. Conditions: (a) CH_2Cl_2, reflux for 3 days; (b) 1 equiv. of Br−PCHP, CH_2Cl_2, 1 h at room temp.; (c) 1 equiv. of $[RuCl_2(PPh_3)_3]$, CH_2Cl_2, overnight reflux

From the ^1H and ^{13}C NMR spectra of a mixture of **9** and **10** (the latter present to an extent of 11%), most of the features of **9** and some of the features of **10** could be established. Thus, the presence of a bis(*ortho*)-metalated Br−PCP ligand is clearly apparent from the ^{13}C NMR spectrum, where $Ru-C_{ipso}$ of **9** appears at $\delta = 173.85$ as a characteristic doublet ($^2J_{CP} = 16$ Hz).[14] The diastereotopic benzylic protons of the cyclometalated ligand give rise to signals at $\delta = 2.67$ and 3.63 in the ^1H NMR spectrum, each with integrals corresponding to four protons. On the other hand, all of the benzylic protons of the bridging Br−PCHP ligand appear as a single doublet at $\delta = 3.10$ ($^2J_{HP} = 9$ Hz). The aromatic protons of the xylylene group of the Br−PCHP ligand give rise to two singlets at considerably higher field, at $\delta = 4.82$ and 5.47, respectively, with relative integrals of 1:2. These features further confirm the idealized square-pyramidal structure of this compound and emphas-

ize the symmetric disposition of the bridging ligand, where the diastereotopic benzylic protons are magnetically equivalent. In the case of **10**, two of the benzylic protons of the bis(*ortho*)-metalated ligand and all the benzylic protons of the η^1-*P*-bonded Br−PCHP ligand are coincidentally located in the same spectral region (δ = 3.30−3.80), while the two remaining benzylic protons appear as a multiplet at δ = 2.83. The xylylene protons of the Br−PCHP ligand are nonequivalent and appear as singlets at δ = 5.68, 5.82, and 5.90. It should be mentioned that transition metal complexes containing a neutral η^1-*P* monodentate R−PCHP ligand have not previously been reported. To the best of our knowledge, this coordination mode has only been observed in Ag compounds of the H−PCHP ligand (P = PPh_2).[25]

The **C**- and **D**-type species were also observed in similar reactions involving **5** (i.e. complexes **11** and **12**). However, in the case of the H−PCHP ligand, the concentration of species **12** was too low to allow its characterization by ^1H and ^{13}C NMR spectroscopy.

Further evidence for the absence of PPh_3 in complexes such as **C** was obtained from the reaction of $RuCl_3 \cdot 3H_2O$ with an excess of H−PCHP in methanol (Scheme 3). Spectroscopically pure complex **11** was isolated as a green solid in low yield (14%). Similar spectroscopic features to those of **9** were observed, with the exception of the multiplicity of the xylylene protons of the bridging H−PCHP ligand. In **11**, they appear as a singlet (δ = 5.42), a doublet (δ = 5.69, $^3J_{HH}$ = 8 Hz), and a triplet (δ = 5.99, $^3J_{HH}$ = 8 Hz).

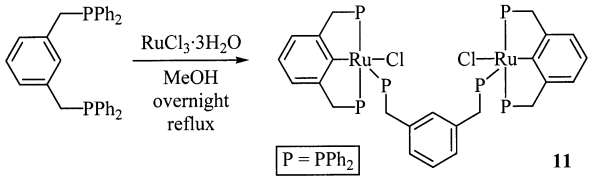

Scheme 3. Formation of **11** using $RuCl_3 \cdot 3\,H_2O$ as starting material

The fluorinated arylruthenium(II) "pincer" complex **7** is the first example of a ruthenium compound containing three fluorinated C_{10} tails ("pony tails") connected to the *para*-position of the PCP ligand through a silicon branching point. A very interesting feature of **7**, which has 43.2 wt% of fluorine, is its solubility in fluorocarbon solvents. Initially, **7** was synthesized to facilitate the separation of the arylruthenium(II) compound from the free PPh_3 present in the crude reaction mixture. Thus, the mixture could be separated by dissolving **7** in FC-72 (perfluorohexanes), a solvent in which PPh_3 is insoluble. This property also gives a clear indication of the presence of an $(n\text{-}C_8F_{17}CH_2CH_2)_3Si$ group in the complex molecule for species such as **6** and **8**, which would otherwise be completely insoluble in FC-72. Our intention for **7** and analogous fluorinated organometallic compounds is to explore their chemistry in fluorinated biphasic catalysis.[18] In this context, we have already prepared the NCN complex **13** (Figure 5) containing 35.8 wt% of fluorine, and have used it as a model complex for the selective addition of CCl_4 to methyl methacrylate (Kharasch addition) under both standard and fluorinated biphasic conditions.[19,20]

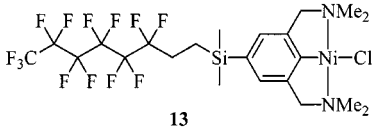

Figure 5. Fluorinated arylruthenium(II) pincer **13** used for the Kharasch addition reaction under biphasic conditions

It is interesting to note that in the syntheses of **6** and **7**, the Br−C and Si−C bonds remain unaffected by the applied synthetic protocol. This is in sharp contrast to the Si−aryl bond cleavage observed using the ligand Me_3Si−PCHP under similar conditions.[13,15] Such a process (i.e. desilylation) is thought to be promoted by HCl formed in the ruthenation reaction[13,15] and to follow an electrophilic aromatic substitution mechanism.[21] Therefore, the presence of electron-withdrawing groups on the aromatic ring can be expected to disfavor such reactivity. Indeed, it is observed that the electron density at the Si atom, as measured by ^{29}Si NMR spectroscopy, is significantly lower in $(n\text{-}C_8F_{17}CH_2CH_2)_3Si$−aryl compounds than in their Me_3Si−aryl analogues.[22]

Oxidative addition of low-valent (coordinatively unsaturated) ruthenium complexes to C−halide bonds is a well-documented process.[23] However, in the synthesis of **6** no species originating from this type of reactivity were detected and the retention of the C−Br bond in the product was clearly established by ^{13}C NMR spectroscopy and elemental analysis. This bond was also unaffected during an attempt to form a bimetallic complex through the coupling of two molecules of **6**. This was performed in combination with a nickel-containing catalyst. The starting complex **6** was recovered quantitatively at the end of the procedure.

The observations made thus far suggest that the displacement of the η^1-*P* or μ-η^1-*P*,η^1-*P*′ bonded R−PCHP ligand from species such as **C** and **D** is probably the rate-limiting step of this reaction, rather than the C−H activation that occurs during the cyclometalation step. In the early stages of the reaction of $[RuCl_2(PPh_3)_3]$ with R−PCHP, the latter readily displaces the PPh_3 ligands coordinated at the ruthenium center, forming a mixture of species, most likely oligomeric in nature (Scheme 4). The extent to which this process occurs is likely to be dictated by the chelate-coordinative properties of the R−PCHP ligand relative to those of PPh_3. A fast and, under the applied reaction conditions, irreversible cyclometalation reaction proceeds, this being the origin of species of types **C** and **D**. As in this reaction the molar ratio of $[RuCl_2(PPh_3)_3]$ to R−PCHP is 1:1, the formation of complexes such as **C** and **D** implies the existence of Ru centers depleted of such ligands. The excess free PPh_3 present slowly displaces coordinated R−PCHP ligands, which are then trapped by the metal centers lacking a cyclometalated R−PCP ligand. Therefore, one of the roles of complexes such as **9**, **10**, **11**, and **12** in the formation of [RuCl(R−PCP)(PPh_3)] complexes would appear to be to serve as reservoirs of R−PCHP ligands. Naturally, the R−PCHP released from species **C** and **D** can also react

with the final complex [RuCl(R−PCP)(PPh_3)], replacing the PPh_3 and reforming **C** and **D**. However, this does not lead to any progress in the overall process in the direction of formation of complexes [RuCl(R−PCP)(PPh_3)].

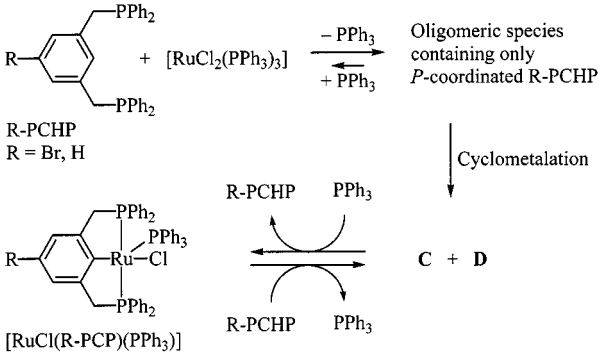

Scheme 4. Formation of [RuCl(R−PCP)(PPh_3)] complexes by reacting [$RuCl_2(PPh_3)_3$] with R−PCHP ligands

Conclusions

In this paper, we have focussed on the reaction of the [$RuCl_2(PPh_3)_3$] starting material with R−PCHP ligands having PPh_2 groups connected through a rigid *m*-xylylenediyl organic fragment. When equimolar amounts of [$RuCl_2(PPh_3)_3$] and the R−PCHP ligands were mixed, a chemo- and regioselective reaction was observed involving one of the C−H bonds of the *m*-xylylenediyl fragment, thereby leading to the exclusive formation of complexes of the type [RuCl(R−PCP)(PPh_3)]. Analysis carried out in the course of the reaction has shown the intermediacy of monomeric and dimeric Ru complexes containing an η^3-*P,C,P′* R−PCP ligand and an η^1-*P* R−PCHP ligand bonded to the same metal center. The displacement of the R−PCHP ligand apparently constitutes the rate-determining step in this reaction, and hence C−H bond activation does not greatly affect the overall rate. In this sense, the observed intermediates operate as reservoirs, slowly releasing R−PCHP fragments during the course of the reaction.

In the R−PCHP-type ligand, the R group, located in the *meta*-position in relation to the two CH_2PPh_2 fragments, offers an additional potentially reactive site to the metal center or to species present in the reaction mixture under the employed conditions. However, no interactions involving this part of the ligand molecule were observed.

Finally, complex **7** represents the first example of an Ru compound bearing three fluorinated tails connected to the *para*-position of a PCP ligand. An interesting solubility in a fluorinated solvent (FC-72) has been shown, which is a prerequisite for future investigations concerning the use of **7** as a catalyst or catalyst precursor in biphasic systems.

Experimental Section

General Remarks: All experiments were performed under a dry nitrogen atmosphere using standard Schlenk techniques. Benzene, alkanes, and Et_2O were dried with sodium using benzophenone as indicator. Dichloromethane was dried with CaH_2. 1,2-Dichloroethane and FC-72 were degassed using the freeze-pump-thaw technique. − ^1H, ^{13}C, ^{19}Si, and ^{31}P NMR spectra were recorded at 25 °C on a Bruker AC200 or on a Varian Unity INOVA 300 NMR spectrometer. Chemical shifts are given in ppm relative to $(CH_3)_4Si$ (^1H, ^{13}C, and ^{19}Si NMR spectra) or a capillary containing 85% H_3PO_4 (^{31}P NMR spectra). − 5-Bromo-*m*-xylene was purchased from Aldrich Chem. Co. and was used without further purification. [$RuCl_2(PPh_3)_3$],[24] **5**,[25] **8**,[12] 1-Br-3,5-$(CH_2Br)_2C_6H_3$,[26] and $BrSi(n\text{-}CH_2CH_2C_8F_{17})_3$ [27] were prepared according to literature procedures. Attempted homocouplings using a nickel catalyst were performed following a procedure described previously.[28]

Synthesis of 1-Br-3,5-$(CH_2PPh_2)_2C_6H_3$ (3): A three-necked 500 mL round-bottomed flask containing an ammonia condenser and a magnetic stirring bar was connected to a nitrogen line and then immersed in an acetone/dry-ice bath. After about 250 mL of ammonia had been condensed, sodium (1.38 g, 60 mmol) was added in small chunks. After 30 min, solid PPh_3 (7.87 g, 30 mmol) was added to the intensely blue-colored solution, causing a color change to pale-yellow. After a further 40 min, dry ammonium bromide (2.94 g, 30 mmol) was slowly added, followed after another 15 min by solid 1-Br-3,5-$(CH_2Br)_2C_6H_3$ (5.14 g, 15 mmol) in a single portion. The acetone/dry-ice bath was then removed. After evaporation of the ammonia (4 h), the residual material was extracted with degassed water (2 × 100 mL) and diethyl ether (4 × 100 mL). The combined organic extracts were dried with $MgSO_4$. After filtration, the volatiles were removed in vacuo from the filtrate to leave a white solid. Recrystallization from MeOH was sometimes necessary to purify the compound. Yield: 60−70%. − $C_{32}H_{27}BrP_2$ (553.5): calcd. C 69.45, H 4.92; found C 69.41, H 4.88. − M.p. 95−97 °C. − ^1H NMR (200 MHz, $CDCl_3$): δ = 3.26 (s, 4 H, CH_2), 6.75 (s, 1 H, CH-4), 6.91 (s, 2 H, CH-2,6), 7.20−7.45 (m, 20 H, aromatic). − $^{13}C\{^1H\}$ NMR (75 MHz, $CDCl_3$): δ = 35.9 (d, $^1J_{CP}$ = 17 Hz, CH_2), 122.2 (s, CBr), 128.7 (d, $^3J_{CP}$ = 7 Hz, *m*-Ph), 129.1 (s, *p*-Ph), 129.4 (t, $^3J_{CP}$ = 7 Hz, CH-4), 130.1 (d, $^3J_{CP}$ = 9 Hz, CH-2,6), 133.1 (d, $^2J_{CP}$ = 19 Hz, *o*-Ph), 138.1 (d, $^1J_{CP}$ = 15 Hz, C_{quat} of Ph), 139.8 (d, $^2J_{CP}$ = 9 Hz, C-3,5). − $^{31}P\{^1H\}$ NMR (81 MHz, $CDCl_3$): δ = −9.07 (s).

Synthesis of 1-Si(n-$CH_2CH_2C_8F_{17})_3$-3,5-$(CH_2PPh_2)_2C_6H_3$ (4): To a solution of **3** (1.11 g, 2 mmol) in diethyl ether (50 mL) at −80 °C was added 2 equiv. of a hexane solution of *t*BuLi. After 40 min., a solution of $BrSi(n\text{-}CH_2CH_2C_8F_{17})_3$ (2.90 g, 2 mmol) in diethyl ether (80 mL) was transferred into the organolithium solution at −80 °C by means of a cannula. After 1 h, the system was slowly allowed to warm to room temperature (overnight). A $^{31}P\{^1H\}$ NMR spectrum recorded thereafter indicated quantitative conversion. Compound **4** was separated from the LiBr by repeated extractions with pentane. Yield: 3.46 g (1.9 mmol, 94%). − $C_{62}H_{39}F_{51}P_2Si$ (1842.9): calcd. C 40.41, H 2.13, F 52.58, P 3.36, Si 1.52; found C 40.54, H 2.23, F 52.46, P 3.28, Si 1.55. − ^1H NMR (300 MHz, $CDCl_3$): δ = 0.85−0.97 (m, 6 H, CH_2−Si), 1.80−2.10 (m, 6 H, CH_2−CF_2), 3.45 (s, 4 H, CH_2−P), 6.65 (m, 2 H, CH-2,6), 7.25 (s, 1 H, CH-4), 7.30−7.55 (m, 20 H, P−Ph). − $^{13}C\{^1H\}$ NMR (75 MHz, $CDCl_3$): δ = 1.5 (s, CH_2−Si), 25.8 (t, $^2J_{CF}$ = 24 Hz, CH_2−CF_2), 36.2 (vt, CH_2−P), 100.0−126.0 (m, all C−F), 128.7 (d, $^3J_{CP}$ = 6.72 Hz, *m*-Ph), 129.2 (s, *p*-Ph), 131.1 (s, Si−C_{quat}), 132.4 (m, CH-4), 133.4 (d, $^2J_{CP}$ = 18 Hz, *o*-Ph), 138.2 (m, C_{quat}−CH_2PPh_2), 138.4 (d, $^1J_{CP}$ = 15 Hz, C_{quat} of P−Ph); CH-2,6 was not found. − $^{31}P\{^1H\}$ NMR (81 MHz, C_6D_6): δ = −8.66 (s). − $^{29}Si\{^1H\}$ NMR (60 MHz, $CDCl_3$): δ = 0.49 (s).

Synthesis of [RuCl{4-Br-2,6-$(CH_2PPh_2)_2C_6H_2$}(PPh_3)] (6). − Method A: A solution of 1-Br-3,5-$(CH_2PPh_2)_2C_6H_3$ (0.58 g,

1.1 mmol) in 1,2-dichloroethane (10 mL) was added dropwise to a hot solution of $[RuCl_2(PPh_3)_3]$ (1.05 g, 1.1 mmol) in 40 mL of the same solvent. After refluxing for 2 h, the volatiles were removed under reduced pressure and the remaining solid was washed sequentially with hexane (2 × 5 mL), a 1:1 mixture of hexane/diethyl ether (1 × 5 mL), and diethyl ether (2 × 5 mL). Yield: 0.72 g (72%).

Method B: Complex **9** (0.0681 g, containing 11% of **10**) and $[RuCl_2(PPh_3)_3]$ (0.0316 g, 0.033 mmol) were dissolved in CH_2Cl_2 (10 mL) and the solution was refluxed overnight. The volatiles were then removed under reduced pressure and the remaining solid was washed sequentially with hexane (2 × 5 mL), a 1:1 mixture of hexane/diethyl ether (1 × 5 mL), and diethyl ether (2 × 5 mL). Yield: 0.0500 g (50%).

6: M.p. > 200 °C. − $C_{50}H_{41}BrClP_3Ru$ (951.2): calcd. C 63.13, H 4.34, P 9.77, Cl 3.73, Br 8.40, Ru 10.63; found C 63.08, H 4.26, P 9.65, Cl 3.79, Br 8.28, Ru 10.78. − ^{1}H NMR (300 MHz, CD_2Cl_2): δ = 2.37 (br. d, $^2J_{HH}$ = 16 Hz, 2 H, CH_2), 3.45 (dvt, $^2J_{HH}$ = 16 Hz, $^2J_{HP}$ = 6 Hz, 2 H, CH_2), 6.86 (m, 6 H, *m*-PPh_3), 6.95 (m, 4 H, *m*-PPh_2), 7.08 (m, 6 H, *o*-PPh_3), 7.11 (m, 4 H, *o*-PPh_2), 7.12−7.15 (m, 5 H, *p*-PPh_2 and *p*-PPh_3), 7.13 (2 H, CH-3,5), 7.39 (m, 4 H, *m*-PPh_2), 7.44 (m, 2 H, *p*-PPh_2), 7.85 (m, 4 H, *o*-PPh_2). − ^{13}C{^{1}H} NMR (75.5 MHz, CD_2Cl_2): δ = 39.1 (vt, $^{vt}J_{CP}$ = 15 Hz, CH_2), 116.0 (s, C−Br), 125.7 (vt, $^{vt}J_{CP}$ = 9 Hz, C-3,5), 127.4 (d, $^3J_{CP}$ = 10 Hz, *m*-PPh_3), 128.4 (vt, $^{vt}J_{CP}$ = 4 Hz, *m*-PPh_2), 128.8 (vt, $^{vt}J_{CP}$ = 4 Hz, *m*-PPh_2), 129.45−129.50 (two s, *p*-PPh_3 and *p*-PPh_2), 130.3 (s, *p*-PPh_2), 132.7 (vt, $^{vt}J_{CP}$ = 5 Hz, *o*-PPh_2), 133.1 (vt, $^{vt}J_{CP}$ = 5 Hz, *o*-PPh_2), 134.0 (m, C_{quat}−PPh_2), 134.4 (d, $^2J_{CP}$ = 10 Hz, *o*-PPh_3), 135.5 (vt, $^{vt}J_{CP}$ = 17 Hz, C_{quat}−PPh_2), 136.4 (d, $^1J_{CP}$ = 52 Hz, C_{quat}−PPh_3), 153.0 (vt, $^{vt}J_{CP}$ = 9 Hz, C-2,6), 172.8 (d, $^2J_{CP}$ = 17 Hz, Ru−C_{ipso}). − ^{31}P{^{1}H} NMR (121 MHz, CD_2Cl_2): δ = 36.74 (d, 2 P, Br−PCP), 80.62 (t, $^2J_{PP}$ = 32 Hz, 1 P, PPh_3).

Synthesis of [RuCl{$C_6H_2(CH_2PPh_2)_2$-2,6-Si(*n*-$CH_2CH_2C_8F_{17})_3$-4}-(PPh_3)] (7): $[RuCl_2(PPh_3)_3]$ (0.16 g, 0.17 mmol) and *meta*-bis(phosphane) **4** (0.31 g, 0.17 mmol) were dissolved in 1,2-dichlorobenzene and the solution was refluxed for 2 h. The volatiles were then removed under reduced pressure and the green-colored solid residue was extracted with FC-72 (5 × 2 mL). The insoluble material (free PPh_3) was separated from the green solution by filtration through Celite mounted in a disposable pipette. This extraction−filtration operation was performed twice in order to obtain the final product **7** free from PPh_3. Yield: 0.27 g (0.12 mmol, 71%). − FAB-MS showed a fragmentation peak at *m*/*z* = 2205.71 [M^+ − Cl] and also peaks characteristic of the loss of C_nF_m fragments. − ^{1}H NMR (300 MHz, CD_2Cl_2): δ = 0.90−1.10 (m, 6 H, CH_2−Si), 1.95−2.25 (m, 6 H, CF_2−CH_2), 2.73 (br. d, $^2J_{HH}$ = 16 Hz, 2 H, CH_2−P), 3.44 (m, 2 H, CH_2−P), 6.20−7.90 (m, aromatic), 8.08 (br. s, 4 H, *o*-PPh_2). − ^{13}C NMR (50 MHz, $CDCl_3$): δ = 1.5 (s, CH_2−Si), 26.0 (t, $^3J_{CF}$ = 24 Hz, *C*H_2−CF_2), 38.9 (t, $^1J_{CP}$ = 15 Hz, CH_2−P), 100.0−124.0 (m, CF_n), 121.8 (s), 127.1 (d, $^4J_{CP}$ = 11 Hz, *m*-PPh_3), 128.06 (vt, *m*-PPh_2), 128.59 (m, *m*-PPh_2), 129.0−129.5 (m, *p*-PPh_3 and *p*-PPh_2), 130.1 (s, *p*-PPh_2), 132.5 (vt, *o*-PPh_2), 134.1 (d, $^3J_{CP}$ = 8 Hz, *o*-PPh_3), 135.6 (m, C_{quat}), 136.7 (s, C_{quat}), 151.9 (vt, C_{quat}); resonances of Ru−C_{ipso} and C_{quat}−PPh_2 were too weak to be located). − ^{31}P{^{1}H} NMR (81 MHz, C_6D_6): δ = 36.11 (d, 2 P, PPh_2), 82.26 (t, $^2J_{PP}$ = 32 Hz, 1 P, PPh_3).

Synthesis of [{RuCl[$C_6H_2(CH_2PPh_2)_2$-2,6-Br-4]}$_2${μ-η^1-*P*,η^1-*P*′-[$C_6H_3(CH_2PPh_2)_2$-3′,5′-Br-1′]}] (9) and (10). − Method A: A solution of $[RuCl_2(PPh_3)_3]$ (0.96 g, 1.0 mmol) and **3** (1.11 g, 2.0 mmol) in CH_2Cl_2 (30 mL) was refluxed for 3 days. The volatiles were then removed under reduced pressure and the residual dark-green material was washed with hexane (8 × 10 mL) and Et_2O (2 × 4 mL). After drying in vacuo, 0.95 g of a light-green solid was obtained, which was found to consist of **9** (89%) and **10** (11%).

Method B: Addition of ligand **3** (0.0200 g, 0.0360 mmol) to a solution of **6** (0.0688 g, 0.0720 mmol) in CH_2Cl_2 (10 mL) and stirring for 1 h at room temp. led to a mixture of complexes **9** and **10** in a 2:1 ratio. However, starting materials were still present, despite the use of excess ligand, which thwarted the isolation of **9** and **10** from the reactants after the standard work-up (see above) with hexane and Et_2O.

[{RuCl[$C_6H_2(CH_2PPh_2)_2$-2,6-Br-4]}$_2${μ-η^1-*P*,η^1-*P*′-[$C_6H_3(CH_2PPh_2)_2$-3′,5′-Br-1′]}] (9): ^{1}H NMR (300 MHz, $CDCl_3$): δ = 2.67 (br. d, $^2J_{HH}$ = 16 Hz, 4 H, CH_2 of Br−PCP), 3.10 (d, $^2J_{HP}$ = 9 Hz, 4 H, CH_2 of Br−PCHP), 3.63 (dm, $^2J_{HH}$ = 16 Hz, 4 H, CH_2 of Br−PCP), 4.82 (s, 1 H, CH-4′), 5.47 (s, 2 H, CH-2′,3′), 6.30−7.90 (m, aromatic), 8.00−8.20 (m, 8 H, *o*-PPh_2). − ^{13}C{^{1}H} NMR (75.5 MHz, CD_3Cl): δ = 39.6 (m, all CH_2), 115.3 (s, C−Br of Br−PCP), 119.9 (s, C−Br of Br−PCHP), 125.0 (m, aromatic CH), 126.8 (m, aromatic CH), 128.3 (m, aromatic CH), 128.6 (m, aromatic CH), 129.1 (s, aromatic CH), 129.8 (s, aromatic CH), 130.3 (m, aromatic CH), 131.1 (m), 131.7 (m, aromatic CH), 132.8 (d, J_{CP} = 9 Hz, aromatic CH), 133.0 (m), 134.2 (m, C_{quat}), 136.2 (d, J_{CP} = 12 Hz, C_{quat}), 151.3 (vt, $^{vt}J_{CP}$ = 9 Hz, C-2,6 of Br−PCP), 173.9 (br. d, $^2J_{CP}$ = 16 Hz, Ru−C_{ipso}). − ^{31}P{^{1}H} NMR (81 MHz, CD_3Cl): δ = 40.05 (d, 4 P, Br−PCP), 83.75 (t, $^2J_{PP}$ = 31 Hz, 2 P, Br−PCHP).

[RuCl{$C_6H_2(CH_2PPh_2)_2$-2,6-Br-4}{η^1-*P*-[$C_6H_3(CH_2PPh_2)_2$-3′,5′-Br-1′]}] (10): Due to the low concentration of this compound, as well as to overlap with the stronger signals of the bridging complex, only a few of its ^{1}H NMR resonances could be assigned. For the same reasons, the carbon resonances were to weak too be detected. − ^{1}H NMR (300 MHz, $CDCl_3$): δ = 2.83 (m, 2 H, CH_2 of the non-coordinated CH_2PPh_2 group), 3.30−3.80 (m, 6 H, CH_2 of the coordinated CH_2PPh_2 groups), 5.68 (s, 1 H, CH-2′ or 4′ or 6′), 5.82 (s, 1 H, CH-2′ or 4′ or 6′), 5.90 (s, 1 H, CH-2′ or 4′ or 6′). − ^{31}P{^{1}H} NMR (81 MHz, CD_3Cl): δ = −10.06 (s, 1 P, non-coordinated PPh_2), 40.3 (d, 2 P, Br−PCP), 83.8 (t, 1 P, coordinated PPh_2 of Br−PCHP , $^2J_{PP}$ = 31 Hz).

Synthesis of [{RuCl[$C_6H_3(CH_2PPh_2)_2$-2,6]}$_2${μ-η^1-*P*,η^1-*P*′-[C_6H_4-$(CH_2PPh_2)_2$-1′,3′]}] (11): A solution of $RuCl_3{\cdot}3H_2O$ (0.18 g, 0.70 mmol) in methanol (10 mL) was refluxed for 1 h. Compound **5** (0.50 g, 1.05 mmol) was then added as a solid and reflux was continued overnight. After removal of the volatiles under reduced pressure, pure **11** could be extracted from the green-colored solid residue with benzene. Yield: 0.0700 g (14%). − ^{1}H NMR (300 MHz, C_6D_6): δ = 2.81 (br. d, $^2J_{HH}$ = 16 Hz, 4 H, CH_2 of H−PCP), 3.42 (d, $^2J_{HP}$ = 9 Hz, 4 H, CH_2 of H−PCHP), 3.62 (dvt, $^2J_{HH}$ = 16 Hz, 4 H, CH_2 of H−PCP), 5.42 (s, 1 H, CH-2′), 5.69 (d, $^3J_{HH}$ = 8 Hz, 2 H, CH-2′,4′), 5.99 (t, $^3J_{HH}$ = 8 Hz, 1 H, CH-3′), 6.60−6.85 (m, 22 H, aromatic), 6.90−7.25 (m, 26 H, aromatic), 7.35−7.45 (m, 10 H, aromatic), 8.10−8.20 (m, 8 H, *o*-Ph); not all resonances were detected due to overlapping with C_6D_6 carbon signal. − ^{13}C{^{1}H} NMR (75.5 MHz, C_6D_6): δ = 40.6 (m, all CH_2), 121.6 (s, CH aromatic), 122.9 (t, J_{CP} = 9 Hz), 126.6 (s), 126.9 (d, J_{CP} = 10 Hz), 130.8−131.3 (m), 132.4 (vt, $^{vt}J_{CP}$ = 5 Hz), 133.5−133.9 (m), 135.2−136.1 (m), 151.1 (vt, $^{vt}J_{CP}$ = 9 Hz, C_{quat}, C-2,6), 175.3−175.9 (m, Ru−C_{ipso}). − ^{31}P{^{1}H} NMR (81 MHz, C_6D_6): δ = 40.90 (d, 4 P, H−PCP), 85.22 (t, $^2J_{PP}$ = 32 Hz, 2 P, H−PCHP).

Acknowledgments

This work was financially supported by the Conselho Nacional de Desenvolvimento Científico e Tecnológico (CNPq), Brazil, and the Council for Chemical Sciences of the Netherlands Organization for Scientific Research (CW-NWO). Dr. R. A. Gossage (Department of Chemistry, Acadia University, Wolfville, Nova Scotia, Canada) is kindly thanked for discussions and corrections of the manuscript.

[1] For compounds having dangling phosphorus groups, see: [1a]R. J. Mawby, D. Morris, E. M. Thorsteinson, F. Basolo, *Inorg. Chem.* **1966**, *5*, 27−33. − [1b] Q.-B. Bao, S. J. Landon, A. L. Rheingold, T. M. Haller, T. B. Brill, *Inorg. Chem.* **1985**, *24*, 900−908. − [1c] B. L. Shaw, M. J. Smith, G. N. Stretton, *J. Chem. Soc., Dalton Trans.* **1988**, 725−727. − [1d] P. McQuade, N. P. Rath, L. Bartow, *Inorg. Chem.* **1999**, *38*, 5468−5670 and references therein.

[2] For reviews, see: [2a] B. L. Shaw, *Adv. Chem. Ser.* **1982**, *196*, 101−115. − [2b] W. Levason, C. A. McAuliffe, *Adv. Inorg. Chem. Radiochem.* **1972**, *14*, 173−253. − [2c] D. M. A. Minahan, W. E. Hill, C. A. McAuliffe, *Coord. Chem. Rev.* **1984**, *55*, 31−54. − [2d] J. C. Bailar, *J. Chem. Educ.* **1981**, *58*, 674−681.

[3] [3a] C. J. Moulton, B. L. Shaw, *J. Chem. Soc., Dalton Trans.* **1976**, 1020−1024. − [3b] M. A. Bennett, R. N. Johnson, I. B. Tomkins, *J. Organomet. Chem.* **1977**, *128*, 73−84. − [3c] P. W. Clark, *J. Organomet. Chem.* **1977**, *137*, 235−255.

[4] [4a] H. Rimml, L. M. Venanzi, *J. Organomet. Chem.* **1983**, *259*, C6−C7. − [4b] F. Gorla, L. M. Venanzi, A. Albinati, *Organometallics* **1994**, *13*, 43−54.

[5] R. J. Cross, A. R. Kennedy, K. W. Muir, *J. Organomet. Chem.* **1995**, *478*, 227−233.

[6] A. Vigalok, O. Uzan, L. J. W. Shimon, Y. Ben-David, J. M. L. Martin, D. Milstein, *J. Am. Chem. Soc.* **1998**, *120*, 12539−12544.

[7] In the absence of other interactions, the square-planar complexes containing μ-η^1-*P*,η^1-*P*′-PCEP ligands (E = H or alkyl group) are expected to be symmetrical with equivalent phosphorus nuclei. This is observed for the platinum complexes reported in refs. [5] and [6]. However, we recently isolated a dimeric platinum complex containing two μ-η^1-*P*,η^1-*P*′-H−PCHP ligands, in which the phosphorus atoms are nonequivalent as a result of additional non-bonding interactions. M. Albrecht, P. Dani, M. Lutz, A. L. Spek, G. van Koten, *J. Am. Chem. Soc.*, in press.

[8] F. Caruso, M. Camalli, H. Rimml, L. M. Venanzi, *Inorg. Chem.* **1995**, *34*, 673−679.

[9] I. del Río, R. A. Gossage, M. Lutz, A. L. Spek, G. van Koten, *J. Organomet. Chem.* **1999**, *583*, 69−79.

[10] P. Dani, T. Karlen, R. A. Gossage, W. J. J. Smeets, A. L. Spek, G. van Koten, *J. Am. Chem. Soc.* **1997**, *119*, 11317−11318.

[11] [11a] D. J. Cole-Hamilton, G. Wilkinson, *J. Chem. Soc., Dalton Trans.* **1977**, 797−804. − [11b] D. J. Cole-Hamilton, G. Wilkinson, *Nouv. J. Chim.* **1977**, *1*, 141−155.

[12] T. Karlen, P. Dani, D. M. Grove, P. Steenwinkel, G. van Koten, *Organometallics* **1996**, *15*, 5687−5694.

[13] G. Jia, H. M. Lee, H. P. Xia, I. D. Williams, *Organometallics* **1996**, *15*, 5453−5455.

[14] P. Dani, G. P. M. van Klink, G. van Koten, *Eur. J. Inorg. Chem.* **2000**, 1465−1470.

[15] P. Dani, M. Albrecht, G. P. M. van Klink, G. van Koten, *Organometallics*, in press.

[16] M. E. van der Boom, H.-B. Kraatz, L. Hassner, Y. Ben-David, D. Milstein, *Organometallics* **1999**, *18*, 3873−3884.

[17] P. Dani, M. A. M. Toorneman, G. P. M. van Klink, W. J. J. Smeets, A. L. Spek, G. van Koten, *Organometallics*, in press.

[18] E. de Wolf, G. van Koten, B.-J. Deelman, *Chem. Soc. Rev.* **1999**, *28*, 37−41.

[19] H. Kleijn, J. T. B. H. Jastrzebski, R. A. Gossage, H. Kooijman, A. L. Spek, G. van Koten, *Tetrahedron* **1998**, *54*, 1145−1152.

[20] We have also synthesized a PPh_3 derivative containing a fluorine-rich substituent at the para-position of each phenyl ring. The corresponding Wilkinson-type catalyst has been produced and tested in an olefin hydrogenation reaction, giving successful results in terms of both activity and ease of separation by extraction with fluorinated solvents. B. Richter, B.-J. Deelman, G. van Koten, *J. Mol. Cat. A: Chem.* **1999**, *145*, 317−321.

[21] [21a] C. Eaborn, *J. Chem. Soc. B* **1969**, 21−24. − [21b] C. Eaborn, *J. Organomet. Chem.* **1975**, *100*, 43−57. − [21c] B. Bennetau, J. Dunogues, *Synlett* **1993**, 171−176.

[22] B. Richter, E. de Wolf, B.-J. Deelman, G. van Koten, *J. Org. Chem.* **2000**, *65*, 3885−3893.

[23] T. Naota, H. Takaya, S.-I. Murahashi, *Chem. Rev.* **1998**, *98*, 2599−2660.

[24] P. S. Hallman, T. A. Stephenson, G. Wilkinson, *Inorg. Synth.* **1970**, *12*, 237−240.

[25] F. Caruso, M. Camalli, H. Rimml, L. M. Venanzi, *Inorg. Chem.* **1995**, *34*, 673−679.

[26] W. Ried, H. Bodem, *Chem. Ber.* **1956**, *89*, 2328−2331.

[27] [27a] A. Studer, D. P. Curran, *Tetrahedron* **1997**, *53*, 6681−6696. − [27b] A. Studer, P. Jeger, P. Wipf, D. P. Curran, *J. Org. Chem.* **1997**, *62*, 2917−2924.

[28] I. Colon, D. R. Kelsey, *J. Org. Chem.* **1986**, *51*, 2627−2637.

Received May 12, 2000
[I00172]

Steric Factors Affecting the Brønsted Acidity of Aluminosilsesquioxanes

Maria D. Skowronska-Ptasinska,[a] Robbert Duchateau,*[a] Rutger A. van Santen,[a] and Glenn P. A. Yap[b]

Keywords: Aluminosilicates / Silsesquioxanes / Aluminum / Silicon / Zeolite analogues

By reacting $AlMe_3$ with two equivalents of (*c*-$C_5H_9)_7Si_7O_9(OH)_2OSiR_3$, the corresponding Brønsted acidic aluminosilsesquioxanes [(*c*-$C_5H_9)_7Si_7O_{11}(OSiR_3)$]Al[(*c*-$C_5H_9)_7Si_7O_{10}(OH)OSiR_3$] [$SiR_3$ = $SiMe_3$ (**1a**), $SiMePh_2$ (**1b**)] are obtained. These complexes readily react with triethylamine to yield the corresponding ammonium salts {[(*c*-$C_5H_9)_7Si_7O_{11}(OSiR_3)]_2Al$}$^-${$HNEt_3$}$^+$ (**2a**,**b**). Hydrogen bonding between the acidic SiO(H)→Al proton and the pendant silyl ether function is effectively reduced by increasing the steric bulk of the silyl ether substituents, resulting in a higher acidity for **1b** compared to that of **1a**. With the silsesquioxane ligand (*c*-$C_5H_9)_8Si_8O_{11}(OH)_2$, which lacks pendant silyl ether functions, the acidic proton cannot satisfactorily be stabilized and this renders the putative Brønsted acid [(*c*-$C_5H_9)_8Si_8O_{13}$]Al[(*c*-$C_5H_9)_8Si_8O_{12}(OH)$] unstable. In the absence of proton acceptors, the disproportionation product [(*c*-$C_5H_9)_8Si_8O_{13}]_3Al_2$ (**3**) is formed instead of the Brønsted acid. However, in the presence of triethylamine, the initially formed Brønsted acid readily transfers its proton to the amine, affording the ammonium salt {[(*c*-$C_5H_9)_8Si_8O_{13}]_2Al$}$^-${$HNEt_3$}$^+$ (**4**).

Introduction

Acidic aluminum sites in zeolites, clays, and aluminosilicates play an important role in acid-catalyzed reactions.[1] In recent years, several soluble aluminum complexes based on incompletely condensed silsesquioxanes have been prepared and successfully employed as homogeneous models for aluminosilicates and zeolites.[2−5] This paper concerns the further development of molecular cluster analogues of zeolitic acidic sites, which are either inherently useful as catalysts or serve as model systems facilitating detailed mechanistic analysis. Recently, we reported the synthesis and characterization of the aluminosilsesquioxane {[(*c*-$C_5H_9)_7Si_7O_{11}(OSiMe_3)$]Al[(*c*-$C_5H_9)_7Si_7O_{10}(OH)OSiMe_3$]} (**1a**),[4] the first homogeneous model of a hydrogen-bonded Brønsted acidic aluminosilicate site as found, for example, in zeolite HY.[1] The strong intramolecular hydrogen bond between the acidic SiO(*H*)→Al proton and the pendant silyl ether oxygen (Si*O*$SiMe_3$) was found to dramatically lower the Brønsted acidity of this complex. In an effort to produce more acidic aluminosilsesquioxanes, we have now synthesized aluminosilsesquioxane complexes with diminished intramolecular hydrogen bonding.

Results and Discussion

To reduce hydrogen bonding as observed in **1a**,[4] the silsesquioxane (*c*-$C_5H_9)_7Si_7O_9(OH)_2OSiMePh_2$ with a considerably more bulky silyl ether substituent was synthesized.[6] Brønsted acids of the type {[(*c*-$C_5H_9)_7Si_7O_{11}(OSiR_3)$]Al[(*c*-$C_5H_9)_7Si_7O_{10}(OH)OSiR_3$]} [$SiR_3$ = $SiMe_3$ (**1a**); $SiMePh_2$ (**1b**)] may readily be prepared by treatment of silsesquioxane solutions with $AlMe_3$ in toluene, although the reaction rate strongly depends on the silyl ether substituent (Scheme 1). Whereas for SiR_3 = $SiMe_3$ the reaction reaches completion within minutes at 0 °C, when R is the more bulky $MePh_2$ group, significant retardation is seen and heating to reflux (1 h) is required in order to obtain the Brønsted acid {[(*c*-$C_5H_9)_7Si_7O_{11}(OSiMePh_2)$]Al[(*c*-$C_5H_9)_7Si_7O_{10}(OH)OSiMePh_2$]} (**1b**) in reasonable yield. In the presence of triethylamine, the Brønsted acids (**1a**,**b**) are selectively transformed into the corresponding ammonium salts {[(*c*-$C_5H_9)_7Si_7O_{11}(OSiR_3)]_2Al$}$^-${$HNEt_3$}$^+$ [SiR_3 = $SiMe_3$ (**2a**),[4] $SiMePh_2$ (**2b**); Scheme 1].

In the ^{1}H NMR spectrum of **1a**, the OH resonance is seen at δ = 8.50, characteristic of a hydrogen-bonded acidic hydroxyl group.[7] In contrast, the OH resonance of **1b** is significantly shifted to higher field, appearing at δ = 4.90. This high-field shift may conceivably be the result of either reduced hydrogen bonding or of decreased acidity of the hydroxyl group.[4,7] The observed higher frequency of the O−H stretching vibration of **1b** (3366 cm^{-1}) compared to that of **1a** (3150 cm^{-1}) is in line with decreased hydrogen bonding. Hence, it can be concluded that increasing the steric bulk of the pendant silyl ether function does indeed reduce hydrogen bonding and should render **1b** more acidic than **1a**.

To determine the relative acidities of **1a** and **1b**, the ammonium salt {[(*c*-$C_5H_9)_7Si_7O_{11}(OSiMe_3)]_2Al$}$^-${$HNEt_3$}$^+$ (**2a**) was treated with an equimolar amount of the Brønsted acid {[(*c*-$C_5H_9)_7Si_7O_{11}(OSiMePh_2)$]Al[(*c*-$C_5H_9)_7Si_7O_{10}(OH)OSiMePh_2$]} (**1b**). As was assumed on the basis of the

[a] Dutch Polymer Institute/Schuit Institute of Catalysis, Eindhoven University of Technology,
P. O. Box 513, 5600 MB Eindhoven, The Netherlands
Fax: (internat.) +31-40/2455054
E-mail: R.Duchateau@tue.nl
[b] University of Ottawa,
Ottawa, Ontario, K1N 6N5, Canada

 © WILEY-VCH Verlag GmbH, D-69451 Weinheim, 2001 1434−1948/01/0101−0133 $ 17.50+.50/0

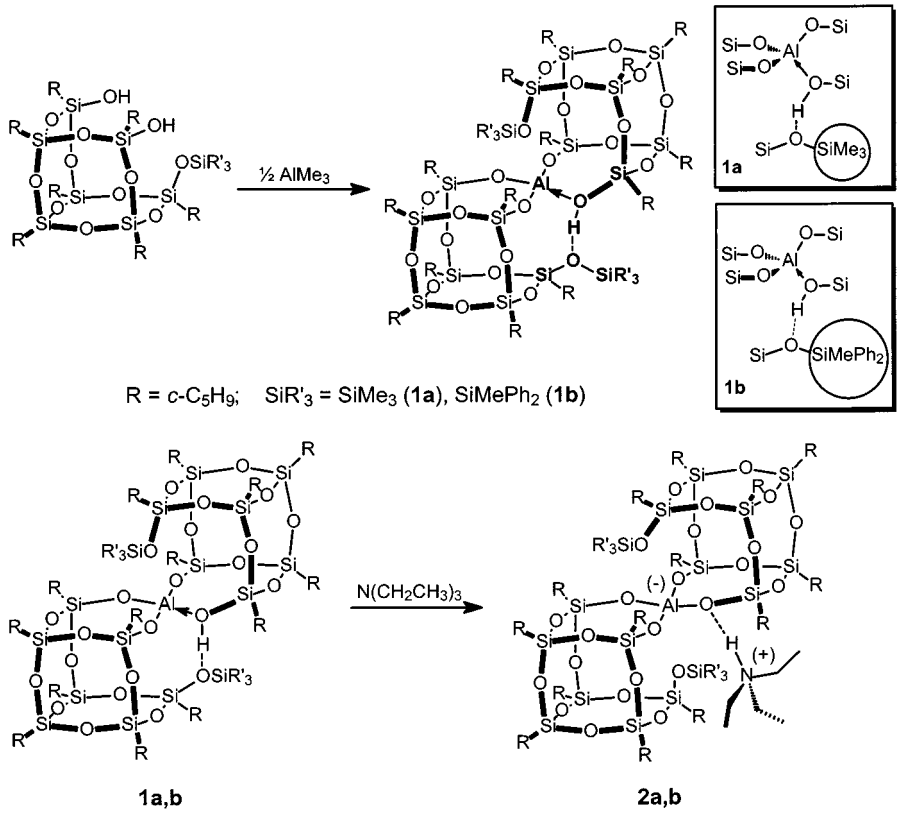

Scheme 1

NMR and IR spectroscopic data, the equilibrium (^{1}H NMR) that was set up revealed that **1b** is indeed a stronger acid than **1a** ($\Delta pK_{a(\mathbf{1a}-\mathbf{1b})} = 1.1$).

The NMR spectra of the ammonium salts **2a**,**b** are significantly simplified compared to those of the corresponding asymmetric Brønsted acids **1a**,**b** and are consistent with a C_2 symmetric structure.[4] With shifts ranging from δ =

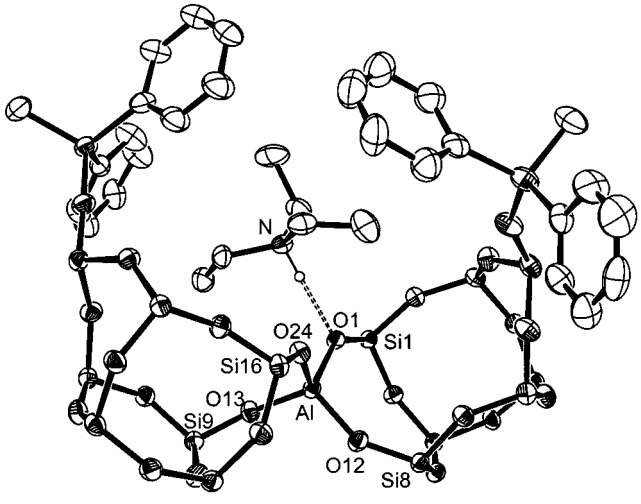

Figure 1. Molecular structure of **2b**; cyclopentyl substituents are omitted for the sake of clarity; thermal ellipsoids are scaled to enclose 30% of the electron density; selected bond lengths [A]: Al−O1 1.764(4), Al−O12 1.721(4), Al−O13 1.731(4), Al−O24 1.743(4), Si1−O1 1.604(4), Si8−O12 1.586(4), Si9−O13 1.586(4), Si16−O24 1.587(4), N−O1 2.885(6); angles [deg]: O1−Al−O12 112.4(2), O13−Al−O24 109.0(2), O1−Al−O24 104.1(2), O12−Al−O13 111.8(2)

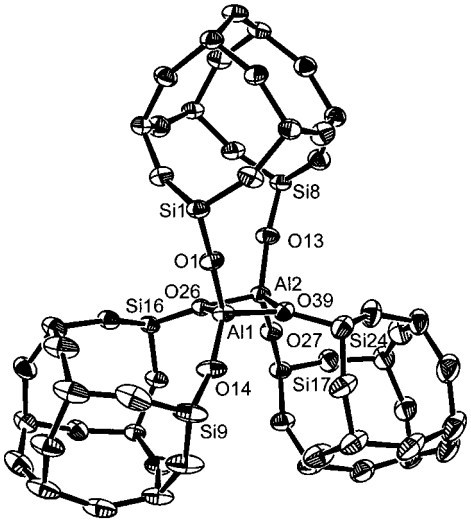

Figure 2. Perspective ORTEP plot of **3**; cyclopentyl substituents are omitted for the sake of clarity; thermal ellipsoids are scaled to enclose 30% of the electron density; selected bond lengths [Å]: Al1−O1 1.684(7), Al2−O13 1.674(7), Al1−O14 1.676(7), Al2−O27 1.665(7), Al1−O26 1.833(6), Al2−O26 1.835, Al1−O39 1.826(7), Al2−O39 1.837(7), O1−Si1 1.568(7), O13−Si8 1.584(7), O14−Si9 1.576(7), O27−Si17 1.602(7), O26−Si16 1.649(6), O39−Si24 1.653(7); angles [deg]: O1−Al1−O14, 117.4(4), O1−Al1−O26 111.3(3), O1−Al1−O39 112.1(3), O14−Al1−O26 115.2(3), O14−Al1−O39 112.4(4), O26−Al1−O39 83.7(3), O13−Al2−O27 118.7(4), O13−Al2−O26 111.3(3), O13−Al2−O39 110.6(3), O27−Al2−O26 110.8(3), O27−Al2−O39 116.6(3), O26−Al2−O39 83.4(3), Al1−O26−Al2 95.5(3), Al1−O39−Al2 95.6(3), Si1−O1−Al1 176.4(5), Si8−O13−Al2 173.2(5), Si9−O14−Al1 162.8(5), Si17−O27−Al2 173.7(5), Si16−O26−Al1 129.1(4), Si16−O26−Al2 133.1(4), Si24−O39−Al1 136.8(4), Si24−O39−Al2 126.9(4)

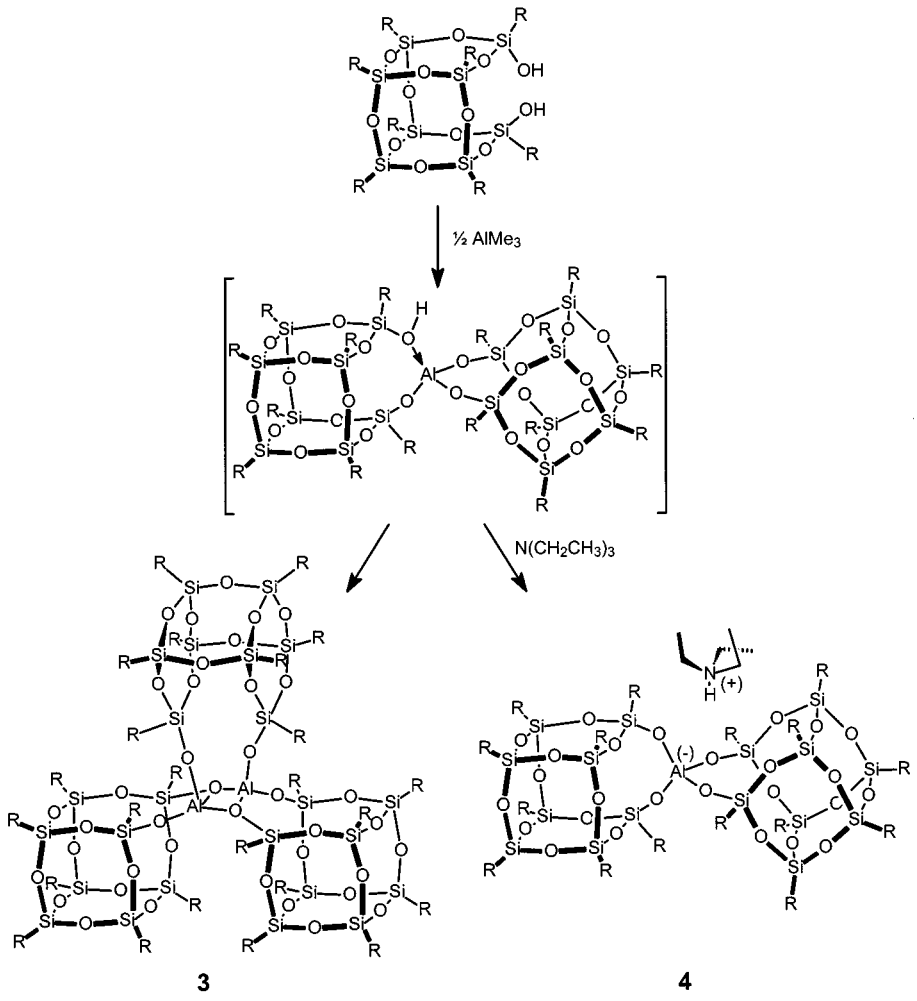

Scheme 2

9.69−9.27, the Et_3NH resonances for **2a**,**b** are virtually identical. It is interesting to note that for **2b** the $HNEt_3$ methylene protons appear as a doublet of multiplets ($^3J_{HH}$ = 68 Hz), whereas for **2a** only a single multiplet is observed. This effect may possibly be attributed to a difference in hydrogen bonding between the ammonium proton and the Al−O−Si oxygen in **2a**,**b**. The X-ray structure of **2a** reveals that the ammonium ion is hydrogen bonded to the aluminosilsesquioxane fragment.[4] In contrast, the molecular structure of the slightly more bulky cyclohexyl analogue of **2a** consists of a nonbonded ion pair.[3] Although still hydrogen bonded, due to its larger steric bulk the ammonium cation in **2b** (Figure 1) is coordinated significantly less effectively than in **2a**. Therefore, the $^3J_{HH}$ coupling, and thus the N−H bond strength, can be expected to increase on going from **2a** to **2b**, as is indeed observed.

The above results support the proposition that hydrogen bonding between the SiO(*H*)→Al proton and the silyl ether function is effectively reduced by increasing the steric bulk of the pendant silyl ether function, which, in turn, results in increased acidity of the complex. If instead a silsesquioxane ligand lacking such a silyl ether function is used, such hydrogen bonding will be prevented, which may result in an even stronger Brønsted acid. To test this hypothesis, we studied the silsesquioxane $(c\text{-}C_5H_9)_8Si_8O_{11}(OH)_2$, which is accessible by a similar route as its cyclohexyl-substituted analogue, as recently reported by Feher et al.[8] Treatment of toluene solutions of $(c\text{-}C_5H_9)_8Si_8O_{11}(OH)_2$ with half an equivalent of $AlMe_3$ led to a rapid reaction. The only aluminosilsesquioxane compound recovered after crystallization was the bimetallic $[(c\text{-}C_5H_9)_8Si_8O_{13}]_3Al_2$ (**3**), and not the expected Brønsted acid, $[(c\text{-}C_5H_9)_8Si_8O_{13}]Al[(c\text{-}C_5H_9)_8Si_8O_{12}(OH)]$ (Scheme 2). However, when the reaction of $(c\text{-}C_5H_9)_8Si_8O_{11}(OH)_2$ with $AlMe_3$ was carried out in the presence of NEt_3, the ammonium salt $\{[(c\text{-}C_5H_9)_8Si_8O_{13}]_2Al\}^-\{HNEt_3\}^+$ (**4**) was formed (Scheme 2). The fact that in the presence of an amine the ammonium salt **4** is obtained suggests that, in the absence of a proton acceptor, the proton of the initially formed Brønsted acid is highly reactive. Consequently, the unstable Brønsted acid disproportionates into the thermodynamically more stable complex **3**.

Figure 2 shows the molecular structure of **3**. The tetrahedral aluminum centers are connected by two bridging μ-OSi groups and by one silsesquioxane ligand, which is bonded in an η^1-fashion to each aluminum atom. The average η^1-O_{Si}−Al bond length of 1.675(7) Å compares well with those in $[(Ph_3SiO)_2Al(O\mathit{t}Bu)]_2$ [av. η^1-O_{Si}−Al = 1.690(3)

Å][9a] and $[(Ph_2Si)_2O_3]_4Al_4(OH)_4{\cdot}4OEt_2$ [av. η^1-O_{Si}−Al = 1.698(3) Å][9a] and is significantly shorter than, for example, that in the Lewis base adduct $[(c\text{-}C_6H_{11})_7Si_7O_{12}]AlO{=}PPh_3$ [av. η^1-O_{Si}−Al = 1.717(4) Å][2] or those in the anionic $\{[(c\text{-}C_5H_9)_7Si_7O_{11}(OSiR'_3)]_2Al\}^-\{HNEt_3\}^+$ {av. η^1-O_{Si}−Al: 1.741(5) Å [SiR'_3 = $SiMe_3$ (**2a**)],[4] 1.740(4) [SiR'_3 = $SiMePh_2$ (**2b**)]}. With an average distance of 1.833(7) Å, the (μ-O_{Si})−Al bonds are normal for bridging (μ-RO)−Al bonds.[9] The Si−O bond lengths [av. 1.605(7) Å] are similar to those found in the silsesquioxane compounds ($c\text{-}C_6H_{11})_8Si_8O_{13}[N(H)Ph]_2$ [1.609(2)−1.630(2) Å] and ($c\text{-}C_6H_{11})_8Si_8O_{13}S$ [1.610(2)−1.693(2) Å].[10]

Concluding Remarks

In summary, the strength of the intramolecular hydrogen bond found in **1a−b** may be effectively tuned by altering the steric bulk of the silyl ether substituent. Increased steric bulk leads to less effective hydrogen bonding, which, in turn, renders the complex more acidic. However, when the acidic proton is not satisfactorily stabilized (as, for example, by hydrogen bonding), then the Brønsted acid becomes unstable and is liable to undergo further reactions.

Experimental Section

General Remarks: All manipulations were performed under an argon atmosphere using glove box (Braun MB-150 GI) and Schlenk techniques. Solvents were distilled from Na (toluene), K (THF), or Na/K alloy (hexanes, [D_6]benzene) and stored under argon. Triethylamine and [D_1]chloroform were dried over 4 Å molecular sieves. − IR spectra were recorded on a Nicolet Avatar 360 spectrophotometer equipped with an ATR (golden gate) device. − NMR spectra were recorded on a Varian Mercury 400 MHz (^{1}H, 400 MHz; ^{13}C, 100 MHz) or a Varian Inova 500 MHz (^{29}Si, 99 MHz) spectrometer at 25 °C. Chemical shifts are reported in ppm and are referenced to residual solvent resonances (^{1}H, ^{13}C) or an external standard (^{29}Si, TMS, δ = 0). − $(c\text{-}C_5H_9)_7Si_7O_9(OH)_3$[2] and $(c\text{-}C_5H_9)_7Si_7O_9(OSiMePh_2)(OH)_2$[11] were prepared according to literature procedures. $(c\text{-}C_5H_9)_8Si_8O_{12}$ was prepared by the Pt-catalyzed hydrosilylation of $(c\text{-}C_5H_9)_7Si_8O_{12}H$ in refluxing cyclopentene. $(c\text{-}C_5H_9)_8Si_8O_{11}(OH)_2$ was prepared by treating $(c\text{-}C_5H_9)_8Si_8O_{12}$ with CF_3SO_3H as described by Feher et al.[8]

$[(c\text{-}C_5H_9)_7Si_7O_{11}(OSiMePh_2)]Al[(c\text{-}C_5H_9)_7Si_7O_{10}(OH)(OSiMePh_2)]$ (1b): To a solution of $(c\text{-}C_5H_9)_7Si_7O_9(OH)_2OSiMe_2Ph$ (3.22 g, 3.00 mmol) in toluene (25 mL) was added $AlMe_3$ (0.75 mL, 2.0 M solution in *n*-heptane, 1.5 mmol) at 0 °C. After stirring for 1 h at room temperature, the mixture was refluxed for a further 1 h. The volatiles were then evaporated and the product was recrystallized from hexane (7 mL) at room temperature, yielding **1b** (2.33 g, 1.07 mmol, 72%) as colorless crystals. − ^{1}H NMR ([D_6]benzene): δ = 0.88 (m, 6 H, $SiCH_3$), 1.17 (m, 14 H, $CH{-}C_5H_9$), 1.65 (m, 112 H, $CH_2{-}C_5H_9$), 4.90 (s, 1 H, OH), 7.30 (m, 6 H, Ph), 7.85 (m, 4 H, Ph). − ^{13}C{^{1}H} NMR ([D_6]benzene): δ = 0.03 (s, $SiCH_3$), 22.67, 22.87, 22.90, 23.62, 24.93 (s, $CH{-}C_5H_9$), 27.27, 27.36, 27.43, 27.52, 27.98, 28.09, 28.50 (s, $CH_2{-}C_5H_9$), 128.07, 130.26, 134.57 (Ph). − ^{29}Si{^{1}H} NMR ([D_6]benzene): δ = −67.48, −66.91, −64.66, −64.29, −63.53 [s, $(\equiv O)_3SiC_5H_9$], −9.89 (s, $SiMePh_2$) (1:1:1:2:2:1 ratio). − $C_{96}H_{153}AlO_{24}Si_{16}$ (2167.61): calcd. C 53.19, H 7.11; found C 53.03, H 7.24.

$\{[(c\text{-}C_5H_9)_7Si_7O_{11}(OSiMePh_2)]_2Al\}^-\{Et_3NH\}^+$ (2b): At 0 °C, $AlMe_3$ (0.5 mL, 2.0 M solution in *n*-heptane, 1.0 mmol) was added to a stirred solution of $(c\text{-}C_5H_9)_7Si_7O_9(OH)_2OSiMePh_2$ (2.15 g, 2.01 mmol) and NEt_3 (0.3 mL, 2.2 mmol) in toluene (30 mL). After stirring at room temperature for 1 h, the volatiles were evaporated. The crude product was recrystallized from hexane (15 mL) at 0 °C, yielding **2b** (1.20 g, 0.53 mmol, 53%) as colorless crystals. − ^{1}H NMR ([D_6]benzene): δ = 0.73 (s, 6 H, $SiCH_3$), 0.89 [m, 9 H, $HN(CH_2CH_3)_3$], 1.23 (m, 14 H, $CH{-}C_5H_9$), 1.65 (m, 112 H, $CH_2{-}C_5H_9$), 2.63 [dm, ^3J(H,H) = 68 Hz, 6 H, $HN(CH_2CH_3)_3$], 7.23 (m, 12 H, Ph), 7.70 (m, 8 H, Ph), 9.29 (s, 1 H, $HNEt_3$). − ^{13}C{^{1}H} NMR ([D_6]benzene): δ = 0.21 (s, $SiCH_3$), 8.84 (s, NCH_2CH_3), 23.05, 23.31, 24.31, 24.50, 24.63, 25.51, 25.91 (s, $CH{-}C_5H_9$, 1:1:1:1:1:1:1 ratio), 27.05, 27.13, 27.25, 27.33, 27.46, 27.62, 28.06, 28.12, 28.30, 28.57, 28.67, 28.93 (s, $CH_2{-}C_5H_9$), 45.59 (s, NCH_2CH_3), 127.99, 128.04, 129.87, 134.43, 134.50, 137.57, 137.86, (s, Ph). − ^{29}Si{^{1}H} NMR ([D_6]benzene): δ = −67.03, −66.46, −64.48, −64.23, −64.14, −63.61 [s, $(\equiv O)_3SiC_5H_9$], −11.79 (s, $SiMePh_2$) (1:1:1:2:1:1:1 ratio). − $C_{102}H_{168}AlNO_{24}Si_{16}$ (2268.81): calcd. C 54.00, H 7.46; found C 53.63, H 7.52.

$[(c\text{-}C_5H_9)_8Si_8O_{13}]_3Al_2$ (3): At 0 °C, $AlMe_3$ (0.5 mL, 2.0 M in *n*-heptane, 1.0 mmol) was added to a stirred solution of $(c\text{-}C_5H_9)_8Si_8O_{11}(OH)_2$ (1.98 g, 2.00 mmol) in toluene (10 mL). After stirring overnight at room temperature, the volatiles were removed in vacuo and the remaining white solid was crystallized from hexane (5 mL) to yield **3** (1.00 g, 0.33 mmol, 66%) as colorless crystals. − ^{1}H NMR ([D_6]benzene): δ = 1.23 (m, 8 H, $CH{-}C_5H_9$), 1.75 (br. m, 64 H, $CH_2{-}C_5H_9$). − ^{13}C{^{1}H} NMR ([D_6]benzene): δ = 22.62, 22.69, 22.93, 23.20, 23.78, 24.44, 25.52 (s, $CH{-}C_5H_9$), 27.39, 27.45, 27.64, 27.76, 28.01, 28.58 ($CH_2{-}C_5H_9$). − ^{29}Si{^{1}H} NMR ([D_6]benzene): δ = −69.89, −69.51, −68.85, −68.40, −68.23, −67.56, −67.40, −65.78, −64.98, −60.56. − $C_{120}H_{216}Al_2O_{39}Si_{24}$ (3011.04): calcd. C 47.87, H 7.23; found C 47.93, H 7.29.

$\{[(c\text{-}C_5H_9)_8Si_8O_{13}]_2Al\}^-\{Et_3NH\}^+$ (4): The procedure used was similar to that described for **2b**, starting from $(c\text{-}C_5H_9)_8Si_8O_{11}(OH)_2$ (0.64 g, 0.65 mmol). The crude product was recrystallized from hexane (6 mL) at 0 °C, yielding **4** (0.42 g, 0.20 mmol, 61%) as colorless crystals. − ^{1}H NMR ([D_6]benzene): δ = 0.92 [m, 9 H, $N(CH_2CH_3)_3$], 1.06 (m, 4 H, $CH{-}C_5H_9$), 1.21 (m, 12 H, $CH{-}C_5H_9$), 1.80 (m, 128 H, $CH_2{-}C_5H_9$), 2.78 [m, 6 H, $N(CH_2CH_3)_3$], 9.94 (s, 1 H, $HNEt_3$). − ^{13}C{^{1}H} NMR ([D_6]benzene): δ = 8.26 [s, $N(CH_2CH_3)_3$], 22.89, 23.87, 26.42 (s, $CH{-}C_5H_9$, 2:4:2 ratio), 27.44, 27.52, 27.58, 27.61, 27.84, 28.67, 28.43, 28.72 (s, $CH_2{-}C_5H_9$), 45.02 [s, $N(CH_2CH_3)_3$]. − ^{29}Si{^{1}H} NMR ([D_6]benzene): δ = −68.66, −67.39, −65.17 (s, 2:1:1 ratio). − $C_{86}H_{160}AlNO_{26}Si_{16}$ (2100.56): calcd. C 49.17, H 7.68; found C 49.75, H 7.84.

X-ray Crystal Structure Analyses of 2b and 3: Single crystals of **2b** and **3** suitable for X-ray structure analysis were grown from saturated hexane solutions. Data were collected on a Bruker AX SMART 1 K CCD diffractometer using Mo-K_α radiation (λ = 0.71073 Å).

For **2b**: $C_{102}H_{168}AlNO_{24}Si_{16}{\cdot}(C_6H_{14})$ (M_r: 2345.59): T = 203(2) K, 0.2 × 0.1 × 0.1 mm, monoclinic, $P2_1/n$, a = 24.947(2) Å, b = 19.032(2) Å, c = 28.629(3) Å, β = 111.718(2)°, V = 12628(2) Å^3, Z = 4, $\rho_{calcd.}$ = 1.234 gcm^{-3}, μ(Mo-K_α) = 2.32 cm^{-1}. A total of 81069 reflections were collected, of which 13217 were considered unique. The structure was solved by direct methods using SHELXS-97[12] and subsequent difference Fourier maps. A final refinement on F^2 converged at R_1 = 0.0595, wR_2 = 0.1662.

For **3**: $C_{120}H_{216}Al_2O_{39}Si_{24}$ (M_r: 3011.05): T = 236(2) K, 0.1 × 0.1 × 0.02 mm, triclinic $P1$(bar), a = 19.047(4) Å, b = 19.355(4) Å, c = 24.662(6) Å, α = 105.540(4)°, β = 91.650(5)°, γ = 103.428(5)°, V = 8480(3) Å^3, Z = 2, $\rho_{calcd.}$ = 1.179 gcm^{-3}, μ(Mo-K_α) = 2.52 cm^{-1}. A total of 66657 reflections were collected, of which 15296 were considered unique. The structure was solved by direct methods using SHELXS-97[12] and subsequent difference Fourier maps. A final refinement on F^2 converged at R_1 = 0.0831, wR_2 = 0.2347.

Crystallographic data (excluding structure factors) for the structures reported in this paper have been deposited with the Cambridge Crystallographic Data Centre as supplementary publication nos. CCDC-143922 (**26**) and -143923 (**3**). Copies of the data can be obtained free of charge on application to the CCDC, 12 Union Road, Cambridge CB2 1EZ, U.K. [Fax (internat.): +44-1223/336-033; E-mail: deposit@ccdc.cam.ac.uk].

Acknowledgments

This work was financed by the Dutch Polymer Institute and the Schuit Institute of Catalysis, who are gratefully acknowledged.

[1] [1a] P. A. Jacobs, *Carbonigenic Activity of Zeolites*, Elsevier, Amsterdam, **1977**. – [1b] I. E. Maxwell, W. H. J. Stork, in *Introduction to Zeolite Science and Practice* (Eds.: H. van Bekkum, E. M. Flanigen, J. C. Jansen), Elsevier Science Publishers B.V., **1991**. – [1c] J. E. Naber, K. P. de Jong, W. H. J. Stork, H. P. C. E. Kuipers, M. F. M. Post, in *Zeolites and Related Microporous Materials: State of the Art 1994* (Eds.: J. Weitkamp, H. G. Karge, H. Pfeifer, W. Hölderich), Elsevier Science B.V., **1994**.

[2] [2a] F. J. Feher, T. A. Budzichowski, K. J. Weller, *J. Am. Chem. Soc.* **1989**, *111*, 7288. – [2b] F. J. Feher, K. J. Weller, *Organometallics* **1990**, *9*, 2638. – [2c] F. J. Feher, K. J. Weller, J. W. Ziller, *J. Am. Chem. Soc.* **1992**, *114*, 9686.

[3] F. T. Edelmann, Y. K. Gun′ko, S. Giessmann, F. Olbrich, *Inorg. Chem.* **1999**, *38*, 210.

[4] R. Duchateau, R. J. Harmsen, H. C. L. Abbenhuis, R. A. van Santen, A. Meetsma, S. K.-H. Thiele, M. Kranenburg, *Chem. Eur. J.* **1999**, *5*, 3130.

[5] H. C. L. Abbenhuis, H. W. G. van Herwijnen, R. A. van Santen, *Chem. Commun.* **1996**, 1941.

[6] Silsesquioxanes with even more bulky silyl ether substituents [e.g. $OSiPh_3$ and $OSi(SiMe_3)_3$] could not be synthesized.

[7] H. Koller, G. Engelhardt, R. A. van Santen, *Topics in Catalysis* **1999**, *9*, 163.

[8] F. J. Feher, D. Soulivong, A. G. Eklund, *Chem. Commun.* **1998**, 399.

[9] [9a] M. Veith, M. Jarczyk, V. Huch, *Angew. Chem.* **1997**, *109*, 140; *Angew. Chem. Int. Ed. Engl.* **1997**, *36*, 117. – [9b] M. Veith, M. Jarczyk, V. Huch, *Angew. Chem.* **1998**, *110*, 105; *Angew. Chem. Int. Ed. Engl.* **1998**, *37*, 105.

[10] F. J. Feher, D. Soulivong, F. Nguyen, J. W. Ziller, *Angew. Chem.* **1998**, *110*, 2808; *Angew. Chem. Int. Ed. Engl.* **1998**, *37*, 2663.

[11] H. C. L. Abbenhuis, A. D. Burrows, H. Kooijman, M. Lutz, M. T. Palmer, R. A. van Santen, A. L. Spek, *Chem. Commun.* **1998**, 2627.

[12] [12a] G. M. Sheldrick, *Acta Cryst.* **1990**, *A46*, 467. – [12b] G. M. Sheldrick, *SHELX-97: Program for the Solution and Refinement of Crystal Structures*, University of Göttingen, Germany, **1997**.

Received May 5, 2000
[I00182]

(Pyrazolylborato)zinc−Aldehyde Complexes

Rainer Walz,[a] Michael Ruf,[a] and Heinrich Vahrenkamp*[a]

Keywords: Zinc / Aldehydes / Phenoxide complexes / Structural chemistry / Pyrazolylborate complexes

The zinc hydroxide complex $Tp^{Cum,Me}Zn–OH$ [**1**, $Tp^{Cum,Me}$ = tris(3-cumenyl-5-methylpyrazolyl)borate] reacts with trichloroacetaldehyde and pentafluorobenzaldehyde to form the complexes $Tp^{Cum,Me}Zn–O(CHOH)R$, containing the aldehyde ligands as the deprotonated aldehyde hydrates. **1** and 2-formylphenol, 2,6-diformylphenol and 2-formylthiophenol undergo condensation with the formation of the corresponding phenolate and thiophenolate complexes, in which one formyl group of each is coordinated to the zinc center as part of a six-membered chelate ring. The aldehyde–hydrate and aldehyde–phenolate bonding modes, which were confirmed by three structure determinations, represent two new kinds of aldehyde attachment to transition metal centers.

Introduction

Aldehyde functions belong to the standard functions of preparative organic chemistry, and metal salts are frequently used to increase their reactivity by Lewis acid activation.[1,2] For mechanistic considerations and for improving the knowledge about their basic coordination chemistry, it is therefore worthwhile to gain information on the bonding interactions between metal ions and the aldehyde CO functions. Due to the fact that aldehydes are very poor donor ligands, the number of isolated and structurally characterized aldehyde complexes is limited. Prior to our own work, only nine structures of such complexes with monodentate *O*-coordinated aldehyde ligands have been reported.[3]

Zinc salts, specifically zinc chloride, are among the most common activators for the reactivity of organic carbonyl functions. This holds for preparative organic chemistry,[1,2] as well as for enzymatic reactions: Two prominent representatives of the alcohol dehydrogenase class of enzymes, horse liver alcohol dehydrogenase (LADH, converting alcohols to aldehydes)[5,6] and yeast alcohol dehydrogenase (YADH, converting aldehydes to alcohols),[7,8] are zinc enzymes. All this provides ample motivation to study the coordination chemistry of zinc with alcohol and aldehyde ligands and to find out about the zinc-mediated reactivity of the corresponding substrates.

As we began our work in the preparative and structural chemistry of zinc−aldehyde complexes, only a small handful of these complexes had been described and only three structures reported.[3,9] We contributed several dozen compounds, including structural models for the alcohol dehydrogenases, and determined their structures.[4,9−12] Our findings underlined the general statement that monodentate aldehydes are very weak donors, and can be attached to zinc ions only in the absence of nitrogen or even weak oxygen donors, and that the combination with nitrogen donors is possible only when the aldehyde function forms a favorable chelate ligand together with them. Thus, one important bonding type, i.e. the monodentate attachment of an aldehyde molecule to a zinc ion in a "natural" environment, that is one with N and O or S donors, is still unknown.

We had experienced that encapsulating tris(pyrazolyl)borate (Tp) ligands are good mimics for a protein-like environment for zinc ions, thus allowing for the synthesis of structural models and mechanistic investigations of enzyme-like situations.[13] Moreover, the counterparts of the aldehydes in LADH or YADH reactivity, the alcohols, had already been attached to zinc ions together with the Tp ligands.[14−18] We therefore hoped that in a suitable TpZn environment, aldehydes might be induced to bind to the zinc center with their C=O functions. In order to ensure maximum protection of the substrates, we chose $Tp^{Cum,Me}$ as the Tp ligand with the most spacious substituents, and we used $Tp^{Cum,Me}Zn−OH$ (**1**),[19] bearing OH as a good leaving group,[13,20] as the reagent for the aldehyde substrates.

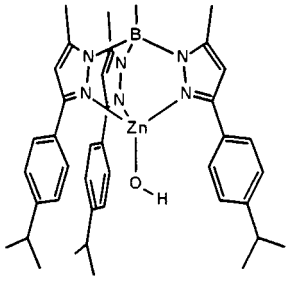

$Tp^{Cum,Me}Zn$-OH (1)

Results and Discussion

Complexes of Hydrated Aldehydes

Treatment of **1** with simple aliphatic or aromatic aldehydes in nonprotic solvents did not produce any noticeable

[a] Institut für Anorganische und Analytische Chemie der Universität Freiburg,
Albertstrasse 21, 79104 Freiburg, Germany
Fax: (internat.) + 49-(0)761/203-6001
E-mail: vahrenka@uni-freiburg.de

 © WILEY-VCH Verlag GmbH, D-69451 Weinheim, 2001 1434−1948/01/0101−0139 $ 17.50+.50/0

effects in the ^{1}H NMR spectra, and the reagents remained unchanged after removal of the solvent. However, aldehydes with electronegative substituents did react with **1**. Trichloroacetaldehyde and pentafluorobenzaldehyde were converted into complexes **2** and **3**. This conversion is accompanied by a shift of the ν(OH) band in the IR spectra to 3532 (**2**) and 3597 (**3**) cm^{-1}, and a shift of the OH resonance in the NMR spectra to δ = 4.10 (in $CDCl_3$) in both cases.

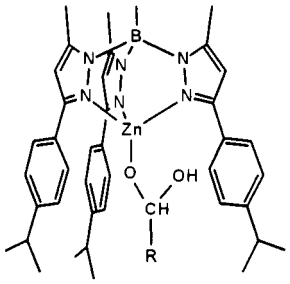

2: R = CCl_3 **3**: R = C_6F_5

Compounds **2** and **3** are α-hydroxyalkoxide complexes, i.e. they can be derived from the hydrated aldehydes. This could be verified for **2** by the synthesis from **1** and trichloroacetaldehyde hydrate (chloral hydrate). These hydrates, just like the aliphatic alcohols with electronegative substituents,[17] are sufficiently acidic to react with **1** by condensation. The direct formation of **2** and **3** under anhydrous conditions, however, is not a condensation reaction. It results from a nucleophilic attack of the Zn−OH function at the aldehyde carbon atom, followed by a concerted process of Zn−O(aldehyde) bond formation and Zn−O(OH) bond breaking. We have elucidated a trajectory for this type of reactions of TpZn−OH complexes by kinetic, structural and theoretical investigations.[20,21] In specific cases it corresponds to the initial stage of aldehyde hydration which is catalyzed as an abiotic process by zinc enzymes like carbonic anhydrase,[22] and which has been modeled for the catalytic hydration of acetaldehyde with zinc complexes of macrocyclic ligands.[23,24,25] The encapsulation provided by the Tp ligand and the uncharged nature of **2** and **3** renders these complexes stable and inert enough to be isolable as images of catalytic intermediates. This has been observed many times before for such images in the form of TpZn−X complexes.[13]

The structure determination of **2** (Figure 1) identifies the complex as belonging to the basic class of TpZn−OX complexes with monodentate OX ligands. There is little distortion of the threefold symmetry of the TpZn unit [O−Zn−N 120.9-124.6(1)°, N−Zn−N 91.1-96.9(1)°, Zn−O roughly on the threefold symmetry axis], and the Zn····O(OH) distance of 3.37 Å is outside the bonding range. The Zn−O bond length is as short as those in other TpZn−OR and TpZn−OH complexes,[14,17,18,19] and the bending angle Zn−O−C is at the lower end of its range.[17,18]

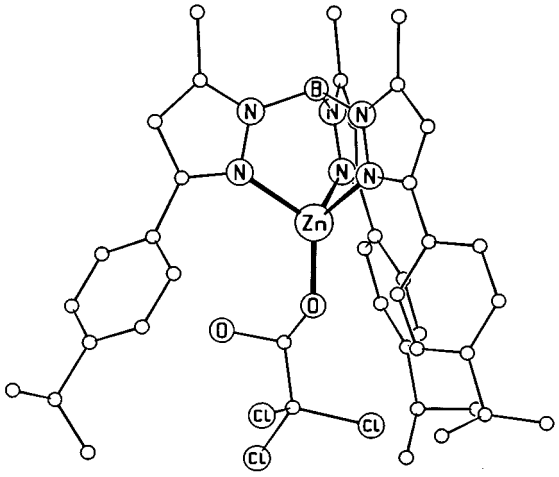

Figure 1. Molecular structure of complex **2**; selected bond lengths [Å] and angles [°]: Zn−O 1.865(2), Zn−N 2.063(3), 2.036(3), 2.040(3), C−O(Zn) 1.364(5), C−O(OH) 1.395(5), Zn−O−C 125.5(2)

In terms of a mechanistic discussion the structure of **2** corresponds to the completion of the first step of catalytic aldehyde hydration, i.e. the complete breaking of the old Zn−O bond and the complete formation of the new Zn−O bond. There are no other α-hydroxyalkoxide complexes of zinc available for comparison, but the situation resembles that in zinc carboxylate complexes. The structures of the latter[26] display a smooth transition from symmetrically bidentate to purely monodentate coordination of the carboxylate ligand, thereby outlining a simple trajectory for the reaction discussed here, namely the hydration of an aldehyde. Thus, there is good evidence that this reaction proceeds by the four-center mechanism which also applies to all other hydrolytic reactions of the TpZn−OH complexes.[20] This mechanism might be verified here by ^{17}O labeling studies. However, this would be doomed to be futile, as Parkin[27] showed that the lability and mobility of these systems lead to rapid ^{17}O scrambling over all possible positions.

Complexes of 2-Formylphenols

We had observed previously[17] that TpZn−phenolates, unlike simple TpZn−alkoxides, are easy to isolate and are stable against hydrolysis. In the course of these studies we had found IR-spectroscopic evidence for chelating aldehyde coordination in the TpZn complex of $HOAr^2$. Subsequent studies[20] then showed that, other than what was originally thought, five-coordinate zinc ions in TpZn complexes are not uncommon and CO coordination to zinc ions as part of five- or six-membered chelate rings is possible in TpZn complexes of e.g. hydroxamates, β-hydroxy ketonates or β-diketonates.[15,28] We therefore extended our investigations of the TpZn−phenolate complexes to those of phenolates with carbonyl-containing functional groups in the β-positions. We found evidence for aldehyde coordination with the formyl-substituted phenols $HOAr^1$ and $HOAr^2$, as well as with the thiophenol $HSAr^1$. The 2-hydroxymethylphenol

($HOAr^3$) was included in this investigation for comparative purposes.

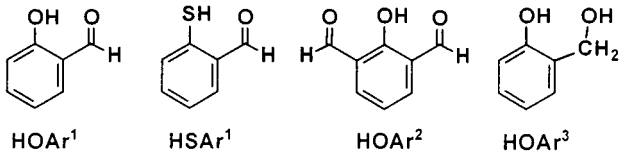

$HOAr^1$ $HSAr^1$ $HOAr^2$ $HOAr^3$

We have already described the preparation of complexes **6** and **7**, derived from $HOAr^2$ and $HOAr^3$.[17] The new complexes **4** and **5** were formed in reasonable yields from **1** and the corresponding phenol in dichloromethane. Two significant pieces of evidence point to the zinc−aldehyde coordination in **4**−**6**, firstly a shift of −15 to −20 cm^{-1} for the aldehyde bands in the IR spectra of **4** (1655 cm^{-1}), **5** (1651 cm^{-1}) and **6** (1648 cm^{-1}) in comparison with those of the free aldehydes; and secondly a shift of more than −2 ppm for the aldehyde proton in the NMR spectra (see Experimental Section). In comparison, the ^1H NMR resonances of the OCH_2 groups of the ligand $HOAr^3$ appear virtually unchanged in its complex **7**.

$Tp^{Cum,Me}Zn\text{-}OAr^1$ **4** $Tp^{Cum,Me}Zn\text{-}SAr^1$ **5**

$Tp^{Cum,Me}Zn\text{-}OAr^2$ **6** $Tp^{Cum,Me}Zn\text{-}OAr^3$ **7**

The structures of complexes **4**, **6** and **7** were determined, see Figure 2 and 3 and Table 1. Complex **7** can be compared with **2** or the other phenolate and alkoxide complexes[17,18] having a symmetrical coordination of the Tp ligand, a roughly trigonal symmetry of the TpZn−O unit, a rather short Zn−O bond, and a distinctly noncoordinating CH_2OH unit. Complexes **4** and **6**, on the other hand, are quite similar, having one aldehyde function attached as a fifth donor to the zinc center, and containing the aldehyde−phenolate ligand as part of a six-membered chelate ring.

The coordination geometry of the zinc center in **4** and **6** is very close to trigonal bipyramidal, as seen by the nearly linear O2−Zn−N1 arrangement. In agreement with this, the Zn−N bond lengths differ significantly and the Zn−O1 line is bent away from the Zn−B line defining a trigonal axis of the Tp ligand. The Zn−O2 bond is 0.27 (**4**) and 0.19 (**6**) Å longer than the Zn−O1 bond. This is because of two reasons, the Zn−O(aldehyde) interaction is weaker than the Zn−O(phenolate) interaction, and Zn−O2 defines the axial direction of the trigonal bipyramid. The O1−C bond lengths are typical for zinc phenolates,[17,29] the O2−C bond lengths are characteristically short and almost unchanged in comparison with those in free aldehydes.[10−12]

There is a considerable variation in the Zn−O(aldehyde) bond lengths, mostly due to changes in coordination numbers and geometries around the zinc center.[4,10−12] Five-coordinated zinc complexes of pyridine-2-carbaldehydes[11] have the closest geometrical relation to **4** and **6**; but their Zn−O distances vary extensively. It can be stated, however, that for complexes in which nitrogen donors compete with aldehyde ligands, **4** and **6** are among those that have the

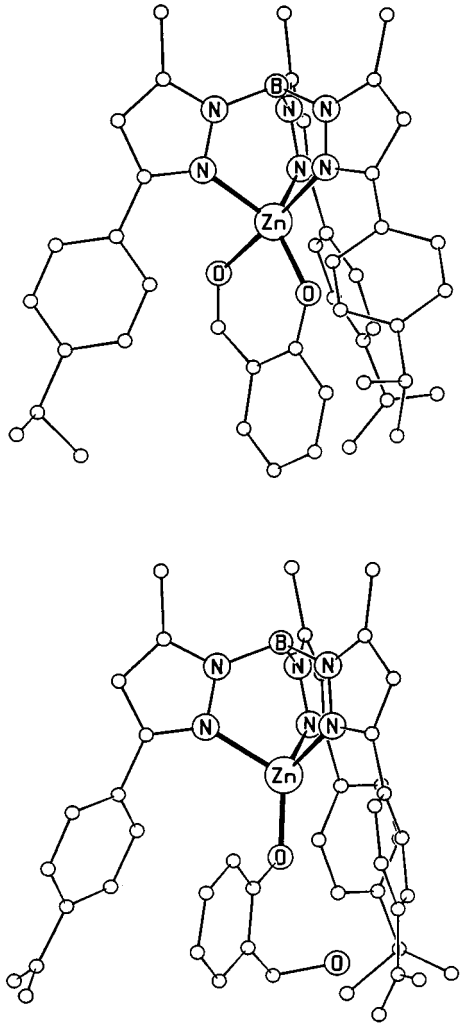

Figure 2. Comparison of the structures of **4** (top) and **7** (bottom)

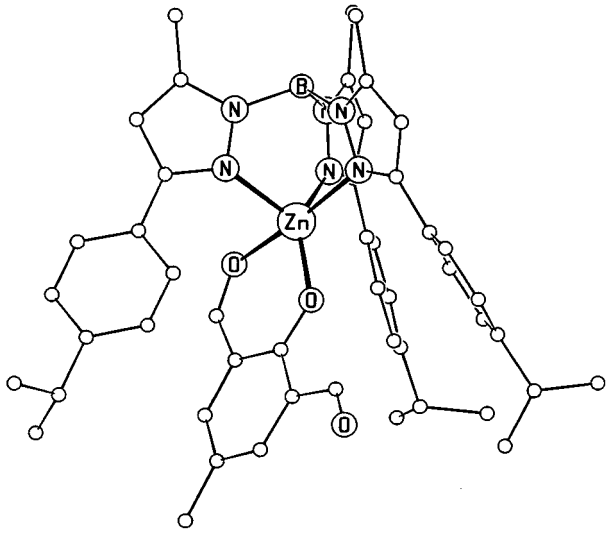

Figure 3. Molecular structure of **6**

Table 1. Structural comparison of **4**, **6** and **7** [Å, °]

	4	**6**	**7**
Zn−N1	2.213(2)	2.159(3)	2.011(3)
Zn−N2	2.038(2)	2.059(3)	2.044(3)
Zn−N3	2.046(2)	2.046(3)	2.053(3)
Zn−O1	1.904(2)	1.921(2)	1.859(2)
Zn−O2	2.173(2)	2.210(3)	4.473(2)
O1−C	1.302(3)	1.305(4)	1.346(4)
O2−C	1.230(3)	1.225(5)	1.437(7)
O1−Zn−N1	93.4(1)	100.7(1)	124.1(1)
O1−Zn−N2	136.3(1)	136.2(1)	125.6(1)
O1−Zn−N3	128.1(1)	123.2(1)	119.8(1)
O1−Zn−O2	87.9(1)	86.7(1)	−
O2−Zn−N1	177.5(1)	171.9(1)	−
Zn−O1−C	132.2(2)	131.9(2)	123.1(2)
Zn−O2−C	123.8(2)	124.0(3)	−

shortest, i.e. strongest, Zn−O(aldehyde) interactions. In this respect **4** and **6** resemble the TpZn−β-diketonate complexes[17,28] which also have six-membered chelate rings and short Zn−O bonds. Apparently, in a TpZn(X)(Y) environment the six-membered chelate ring is a more strain-free alternative for the attachment of X and Y to the zinc ion than the common five-membered chelate ring. This has helped to create stable Zn−O(aldehyde) ligation inside the TpZn pocket, which yields the significant information that zinc−aldehyde interactions can be strong enough to overcome the reluctance of the encapsulated TpZn−X complexes to increase the coordination number of the zinc ion from four to five.

Conclusions

This work has provided two new bonding modes of aldehydes to zinc ions, the attachment as anions of the aldehyde hydrates and the attachment as part of bidentate O,O donors forming six-membered chelate rings. Unlike in the previous examples, the aldehydes under these conditions can form stable zinc complexes even in the presence of several good nitrogen donors. It is likely that the protection offered by the encapsulating pyrazolylborate ligands and the uncharged molecular nature of the complexes have helped to make them accessible.

The structures of the aldehyde complexes yield two pieces of information in terms of catalytic or enzymatic aldehyde interconversions. Firstly, they support a consistent mechanistic picture of the nucleophilic attack at carbonyl functions, exemplified here by aldehyde hydration. Secondly, they visualize the increase of the coordination number of the zinc ion from four to five, even when the weakly coordinating aldehydes are the fifth ligands. For the processes during the action of the LADH or YADH enzymes, this means that a coligand, cosubstrate or reagent may be present at the zinc ion during the catalytic turnover.

Experimental Section

The general working and measuring conditions were as in ref. [30] Reagents, except for **1**,[19] $HSAr^1$ [31] and $HOAr^2$,[32] were obtained commercially.

Complex 2: A solution of **1** (500 mg, 0.72 mmol) in 30 mL of dichloromethane and 40 mL of acetonitrile was treated with freshly distilled trichloroacetaldehyde (531 mg, 528 μL, 3.60 mmol) and stirred for 20 h. After concentrating to 30 mL in vacuo, the solution was left standing at −4 °C for several weeks. 341 mg (49%) of **2** was precipitated as colorless crystals, m.p. 178 °C, which were washed with a few mL of petroleum ether. − $C_{41}H_{48}BCl_3N_6O_2Zn{\cdot}2CH_3CN{\cdot}2H_2O$ (839.4 + 82.1 + 36.0): calcd. C 56.44, H 6.10, N 11.70; found C 56.47, H 5.68, N 10.44. − ^{1}H NMR ($CDCl_3$): δ = 1.18 (d, *J* = 6.9 Hz, 18 H, *i*Pr), 1.55 (s, 4 H, H_2O), 1.98 (s, 6 H, CH_3CN), 2.45 [s, 9 H, Me(pz)], 2.83 (sept, *J* = 6.9 Hz, 3 H, *i*Pr), 4.00 [s, 1 H, CH (aldehyde)], 6.11 [s, 3 H, H (pz)], 7.22 (d, *J* = 8.2 Hz, 6 H, Ph), 7.55 (d, *J* = 8.2 Hz, 6 H, Ph).

Complex 3: 1 (200 mg, 0.29 mmol) and C_6F_5CHO (569 mg, 2.90 mmol) in 40 mL of dichloromethane were stirred for 20 h. The solvent was removed in vacuo and the residue washed with a few mL of acetonitrile. Recrystallization from acetonitrile/dichloromethane (3:1) yielded 86 mg (33%) of **3** as colorless crystals, m.p. 225 °C. − $C_{46}H_{48}BF_5N_6O_2Zn$ (888.1): calcd. C 62.21, H 5.45, N 9.46; found C 61.15, H 5.90, N 10.15. − ^{1}H NMR ($CDCl_3$): δ = 1.23 (d, *J* = 6.9 Hz, 18 H, *i*Pr), 2.53 [s, 9 H, Me (pz)], 2.91 (sept, *J* = 6.9 Hz, 3 H, *i*Pr), 4.09 [s, 1 H, CH (aldehyde)], 6.19 [s, 3 H, H (pz)], 7.29 (d, *J* = 8.2 Hz, 6 H, Ph), 7.64 (d, *J* = 8.2 Hz, 6 H, Ph).

Complex 4: 1 (200 mg, 0.29 mmol) and $HOAr^1$ (35 mg, 0.31 μL, 0.29 mmol) in 30 mL of dichloromethane were stirred for 4 h. The solvent was removed in vacuo and the residue dissolved in 20 mL of acetone. Slow concentration over several weeks yielded 179 mg (53%) of **4** as yellow crystals, m.p. 181 °C. − $C_{46}H_{51}BN_6O_2Zn$ (796.2): calcd. C 69.40, H 6.46, N 10.56; found C 68.37, H 6.40, N 10.46. − ^{1}H NMR ($CDCl_3$): δ = 1.16 (d, *J* = 6.9 Hz, 18 H, *i*Pr), 2.58 [s, 9 H, Me (pz)], 2.78 (sept, *J* = 6.9 Hz, 3 H, *i*Pr), 6.21 [s, 3 H, H(pz)], 6.41 (t, *J* = 7.8 Hz, 1 H, OPh), 6.65 (d, *J* = 7.8 Hz, 1 H, OPh), 7.09 (d, *J* = 8.2 Hz, 6 H, Ph), 7.22 (m, 2 H, OPh), 7.54 (d, *J* = 8.2 Hz, 6 H, Ph), 7.87 [s, 1 H, CH (aldehyde)].

Complex 5: 1 (200 mg, 0.29 mmol) and $HSAr^1$ (46 mg, 0.89 mmol) in 40 mL of dichloromethane were stirred for 4 h. The solvent was removed in vacuo and the residue dissolved in 30 mL of methanol/dichloromethane (4:1). Slow concentration over several weeks yielded 121 mg (49%) of **5** as yellow crystals, m.p. 217 °C. − $C_{46}H_{51}BN_6OSZn$ (812.2): calcd. C 68.02, H 6.33, N 10.35; found C 66.73, H 6.65, N 9.25. − ^{1}H NMR ($CDCl_3$): δ = 1.21 (d, *J* = 6.9 Hz, 18 H, *i*Pr), 2.51 [s, 9 H, Me(pz)], 2.81 (sept, *J* = 6.9 Hz, 3 H, *i*Pr), 6.19 [s, 3 H, H (pz)], 7.09 (d, *J* = 8.2 Hz, 6 H, Ph), 7.22 (m, 3 H, SPh), 7.49 (d, *J* = 8.2 Hz, 6 H, Ph), 7.64 (d, *J* = 8.4 Hz, 1 H, SPh), 7.95 [s, 1 H, CH (aldehyde)].

Structure Determinations:[33] The crystals were obtained directly from the reaction solutions and used without drying in vacuo. They were immersed in fluorinated polyether oil and immediately placed in the nitrogen stream of the diffractometer's cooling system. Diffraction data were recorded at ca. −100 °C using the ω/2θ technique with a Nonius CAD4 diffractometer fitted with a molybdenum tube (K_α, λ = 0.7107 Å) and a graphite monochromator and treated without absorption corrections. The structures were solved with direct methods and refined anisotropically with the SHELX program suite.[34] Hydrogen atoms were included with fixed distances and isotropic temperature factors 1.5 times those of their attached atoms. Parameters were refined against F^2. The *R* values are defined as $R_1 = \Sigma|F_o - F_c|/\Sigma F_o$ and $wR_2 = \{\Sigma[w(F_o^2 - F_c^2)^2]\Sigma[w(F_o^2)^2]\}^{1/2}$. Drawings were produced with SCHAKAL.[34] Table 2 lists the crystallographic data.

Table 2. Crystallographic details

	2	**4**	**6**	**7**
Empirical formula	$C_{45}H_{58}BCl_3N_8O_4Zn$	$C_{46}H_{51}BN_6O_2Zn$	$C_{49}H_{55}BCl_2NO_3Zn$	$C_{46}H_{53}BN_6O_2Zn$
Molecular mass	957.5	796.2	923.1	798.2
Crystal size [mm]	0.5 × 0.4 × 0.3	0.6 × 0.5 × 0.4	0.4 × 0.4 × 0.3	0.5 × 0.4 × 0.3
Space group	$P\bar{1}$	$P\bar{1}$	$P2_1/c$	$P\bar{1}$
Z	2	2	4	2
a [Å]	12.270(2)	10.603(7)	12.233(1)	12.530(3)
b [Å]	14.140(3)	11.048(7)	23.234(5)	13.139(3)
c [Å]	16.730(3)	18.419(2)	17.270(3)	14.132(3)
α [°]	73.14(3)	95.760(6)	90	86.85(3)
β [°]	75.20(3)	99.770(6)	108.01(1)	68.29(3)
γ [°]	67.16(3)	91.650(5)	90	89.32(3)
V [Å^3]	2526.2(8)	2113.3(3)	4668.1(1)	2158.2(8)
d(calcd.) [gcm^{-3}]	1.65	1.25	1.31	1.23
μ(Mo-K_α) [mm^{-1}]	1.02	0.63	0.69	0.61
hkl range	h: −15 to 14 k: −17 to 17 l: −20 to 20	h: −13 to 13 k: −13 to 0 l: −22 to 22	h: 0 to 16 k: 0 to 32 l: −23 to 22	h: −15 to 14 k: −16 to 16 l: −17 to 0
Measured reflections	18708	8723	12903	8842
Independent reflections	9096	8271	12903	8479
Observed refl. [$I > 2\sigma(I)$]	6805	5743	8466	6132
Parameters	559	505	559	505
Refined reflections	9096	8271	12903	8479
R_1(obs.refl.)	0.059	0.042	0.075	0.054
wR_2(all refl.)	0.167	0.123	0.238	0.181
Residual electron density [e/Å^3]	+ 0.9 −0.5	+ 0.4 −0.3	+ 1.2 −1.1	+ 0.6 −0.3

Acknowledgments

This work was supported by the Deutsche Forschungsgemeinschaft and by the Fonds der Chemischen Industrie. We thank Drs. W. Deck and M. Tesmer for help during the crystallographic work.

[1] *Comprehensive Organic Synthesis* (Eds.: B. M. Trost, I. Fleming, S. L. Schreiber), Pergamon Press, Oxford, **1991**.
[2] *Comprehensive Organic Functional Group Transformations* (Eds.: A. R. Katritzky, O. Meth-Cohn, C. W. Rees), Pergamon Press, Oxford, **1995**.
[3] For a compilation of references, see ref.[4]
[4] B. Müller, H. Vahrenkamp, *Eur. J. Inorg. Chem.* **1999**, 117−127.
[5] H. Eklund, B. Nordström, E. Zeppezauer, G. Söderlund, I. Ohlsson, T. Boiwe, B. O. Söderberg, O. Tapia, C. I. Brändén, A. Akeson, *J. Mol. Biol.* **1976**, *102*, 27−59.
[6] S. Ramaswamy, H. Eklund, B. V. Plapp, *Biochemistry* **1994**, *33*, 5230−5237.
[7] F. M. Dickinson, *Eur. J. Biochem.* **1974**, *41*, 31−36.
[8] A. J. Ganzhorn, B. V. Plapp, *J. Biol. Chem.* **1988**, *263*, 5446−5454.
[9] B. Müller, H. Vahrenkamp, *Angew. Chem.* **1994**, *106*, 2164−2165; *Angew. Chem. Int. Ed. Engl.* **1994**, *33*, 2089−2090.
[10] B. Müller, H. Vahrenkamp, *Eur. J. Inorg. Chem.* **1999**, 129−135.
[11] B. Müller, H. Vahrenkamp, *Eur. J. Inorg. Chem.* **1999**, 137−144.
[12] B. Müller, A. Schneider, M. Tesmer, H. Vahrenkamp, *Inorg. Chem.* **1999**, *38*, 1900−1907.
[13] H. Vahrenkamp, *Acc. Chem. Res.* **1999**, *32*, 589−596.
[14] R. Alsfasser, M. Ruf, S. Trofimenko, H. Vahrenkamp, *Chem. Ber.* **1993**, *126*, 703−710.
[15] M. Ruf, K. Weis, I. Brasack, H. Vahrenkamp, *Inorg. Chim. Acta* **1996**, *250*, 271−281.
[16] M. Ruf, F. A. Schell, R. Walz, H. Vahrenkamp, *Chem. Ber.* **1997**, *130*, 101−104.
[17] R. Walz, K. Weis, M. Ruf, H. Vahrenkamp, *Chem. Ber.* **1997**, *130*, 975−980.
[18] C. Bergquist, G. Parkin, *Inorg. Chem.* **1999**, *38*, 422−423.
[19] M. Ruf, H. Vahrenkamp, *Inorg. Chem.* **1996**, *35*, 6571−6578.
[20] M. Rombach, C. Maurer, K. Weis, E. Keller, H. Vahrenkamp, *Chem. Eur. J.* **1999**, *5*, 1013−1027.
[21] M. Bräuer, E. Anders, S. Sinnecker, W. Koch, M. Rombach, H. Brombacher, H. Vahrenkamp, *J. Chem. Soc., Chem. Commun.* **2000**, 647−648.
[22] Y. Pocker, J. E. Meany, *Biochemistry* **1965**, *4*, 2535−2541.
[23] P. J. Wooley, *J. Chem. Soc., Perkin Trans. 2* **1977**, 318−324.
[24] R. H. Prince, P. J. Wooley, *J. Chem. Soc., Dalton Trans.* **1972**, 1548−1554.
[25] E. Kimura, T. Shiota, T. Koike, M. Shiro, M. Kodama, *J. Am. Chem. Soc.* **1990**, *112*, 5805−5811.
[26] For a compilation of references, see ref.[20]
[27] A. Looney, R. Han, K. McNeill, G. Parkin, *J. Am. Chem. Soc.* **1993**, *115*, 4690−4697.
[28] A. Kremer-Aach, W. Kläui, R. Bell, A. Strerath, H. Wunderlich, D. Mootz, *Inorg. Chem.* **1997**, *36*, 1552−1563.
[29] C. O. Rodriguez de Barbarin, N. A. Bailey, D. E. Fenton, Q. Y. He, *Inorg. Chim. Acta* **1994**, *219*, 205−208.
[30] M. Förster, R. Burth, A. K. Powell, T. Eiche, H. Vahrenkamp, *Chem. Ber.* **1993**, *126*, 2643−2648.
[31] F. Mayer, *Liebigs Ann. Chem.* **1931**, *488*, 259−296.
[32] F. Ullmann, K. Brittner, *Chem. Ber.* **1909**, *42*, 2539−2548.
[33] Crystallographic data for the structure reported in this paper have been deposited with the Cambridge Crystallographic Data Centre as supplementary publication no. CCDC-144035 (**2**), -144036 (**4**), -144037 (**6**) and -144038 (**7**). Copies of the data can be obtained free of charge on applicaton to CCDC, 12 Union Road, Cambridge CB2 1EZ, UK [Fax: (internat.) + 44-1223/336-033; E-mail: deposit@ccdc.cam.ac.uk]
[34] G. M. Sheldrick, *SHELXS-86* and *SHELXL-93*, Programs for Crystal Structure Determination, Universität Göttingen, **1986** and **1993**.
[35] E. Keller, Program *SCHAKAL for Windows*, Universität Freiburg, **1999**.

Received May 12, 2000
[I00191]

Structural Studies and Solution Dynamics of Complexes of Magnesium with the *N,N*-Dimethylaminomethylferrocenyl Ligand

Naka Seidel,[a] Klaus Jacob,*[a] Axel K. Fischer,[b] Claus Pietzsch,[c] Pierro Zanello,[d] and Marco Fontani[d]

Keywords: Chelates / Chirality / Cyclic voltammetry / Magnesium / Moessbauer spectroscopy

The reaction of {*C,N*-[Fe(η^5-C_5H_5)(η^5-C_5H_3(CH_2NMe_2)-2)]}Li, (FcN)Li, with magnesium bromide affords the magnesate complex $Li_2Mg(FcN)_2Br_2(OEt_2)_2$ **(1)**. Extraction of **1** with diethyl ether yields $(FcN)_2Mg(OEt_2)$ **(2).** The reaction of (FcN)Li with magnesium halides and THF directly affords $(FcN)_2Mg(THF)$ **(3)**. In solution, these compounds appear as a mixture of diastereomers, whereas in the solid state they each crystallize as a single *rac*-diastereomer. The ratio of *rac*-*meso*-diastereomers in solution is solvent- and temperature-dependent, consistent with an intermolecular exchange between the diastereomers. An intramolecular dynamic phenomenon involving dissociation and recoordination of Mg–N bonds was also observed.

Introduction

In the last decade the dimethylaminomethylferrocenyl unit (FcN) has become an extremely versatile ligand for the synthesis of stable organometallic complexes containing metals from the entire periodic table. On the one hand the geometric properties of the ligand give rise to effective steric shielding and stabilization upon coordination to a metal, and, on the other hand, the ligand is flexible enough to adapt various coordination modes.[1] The most abundant coordination mode is (*C,N*)-bidentate, with the α-carbon atom from the substituted Cp-ring and the amine nitrogen as donors to the same metal (Figure 1), such as found in the following compounds: $(FcN)_2TlCl$,[2] $(FcN)SiCl_3$,[3] $(FcN)_2Pt$,[4] (FcN)PtCl(DMSO),[5] $(FcN)_2VCl$,[6] and $CpTi(FcN)Cl_2$.[6] The X-ray diffraction analyses of $Cp_2M(FcN)_2$ (M = Ti, Zr, Hf),[7] $Cp_2Ti(FcN)Cl$[6] and $(FcN)_2Yb(\mu\text{-}Cl)_2Li(THF)_2$ [8] revealed a monodentate *C*-bonded FcN. The FcN ligand can also act as a carbon bridging ligand, as found in $Li[Cp_2Y(FcN)_2]$,[9] $[(FcN)Cu]_4$ [10] and $[(FcN)Ag]_4$.[11] Another μ-(*C,N*)-bridging mode is found in $[(FcN)HgCl]_2$ [12] and $[(FcN)Au]_2$.[4] Some compounds show more than one coordination mode around the same metal, as, for instance, in the thallium compound $(FcN)_3Tl$,[13] with two bidentate and one monodentate FcN ligands. In solution, this compound appears to be dynamic, but this aspect was not well investigated. Recently, we investigated the dynamic behavior of the lead compound $(FcN)_2Pb$.[14] A rapid dissociation of one of the Pb−N bonds and recoordination occurs in solution, whereas in the solid state both FcN ligands are (*C,N*)-bidentate bonded.

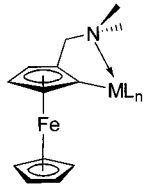

Figure 1. FcN as a bidentate ligand

The FcN ligand is chiral.[15] Therefore, when two or more FcN ligands are coordinated in one molecule this could give rise to the formation of diastereomers. Moreover, the chirality can be used as a "marker" to study intermolecular exchange processes, that could not have been observed otherwise. For instance, in the case of $(FcN)_2SiCl_2$ only the *meso*-form was found, whereas for $(FcN)_2SiMe_2$ both *rac*- and *meso*-diastereomers were formed, which could subsequently be separated by crystallization.[16] The silicon diastereomers obviously do not exchange. In contrast, for the first time, an intermolecular exchange between the diastereomers was demonstrated for $(FcN)_2Pb$.

Organomagnesium compounds, and in particular Grignard reagents, play an important role in organic synthesis. In order to explain the outcome and selectivity of alkylations with these compounds, it is of utmost importance to understand their structures in solution as well as in the solid state.[17,18] With this in mind, it was decided to use the FcN ligand for a thorough study of the structure and dynamics of this highly useful class of reagents.

[a] Institut für Anorganische Chemie der Martin-Luther-Universität Halle-Wittenberg,
Geusaer Straße 88, 06217 Merseburg, Germany
[b] Chemisches Institut der Otto-von-Guericke-Universität Magdeburg,
Universitätsplatz 2, 39106 Magdeburg, Germany
[c] Institut für Angewandte Physik, Technische Universität Bergakademie Freiberg,
Bernhard von Cotta Straße 4, 09596 Freiberg, Germany
[d] Dipartimento di Chimica dell'Università di Siena,
Pian dei Mantellini 44, I-53100 Siena, Italy

 © WILEY-VCH Verlag GmbH, 69451 Weinheim, 2001 1434−1948/01/0101−0145 $ 17.50+.50/0

Results and Discussion

The reaction of magnesium bromide with two equivalents of (FcN)Li,[19] in diethyl ether at room temperature, furnishes deep-red crystals of $[Li_2Mg(FcN)_2Br_2(OEt_2)_2]$ **(1)**, in 80% yield (Scheme 1). The same product is formed when the starting compounds are mixed in a ratio of 1:1; half of the $MgBr_2$ is left unchanged. Compound **1** may be considered as a trapped intermediate during the formation of the diorganomagnesium compounds $(FcN)_2Mg$ discussed below. It is interesting to note that in these and other reactions with (FcN)Li and MgX_2 no Grignard compounds (FcN)MgX are formed.[20]

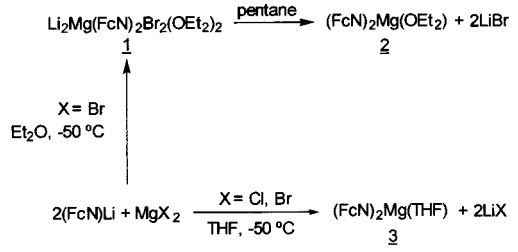

Scheme 1

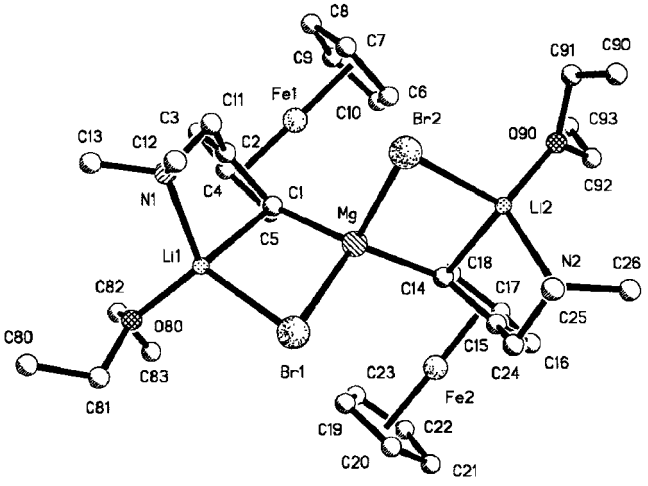

Figure 2. The molecular structure of **1**

Compound **1** crystallizes solely as a *rac*-diastereomer. The results of the X-ray diffraction analysis show that **1** is a magnesate compound where $Li(OEt_2)$ moieties are linked to the "$MgBr_2$" unit by *C*-bridging FcN groups. The molecular structure of **1** is shown in Figure 2 and the most important molecular dimensions are summarized in Table 1. The central magnesium atom shows a distorted tetrahedral coordination geometry with angles ranging from 98.06(4)°(Br1−Mg−Br2) to 119.8(2)° (C14−Mg−C1). The magnesium-bromide bond distances correspond approximately with the sum of the ionic radii of Br^- and Mg^{2+} [sum of ionic radii 263 pm,[21] Mg−Br1 = 260.08(13), Mg−Br2 = 260.52(13) pm]. The bromide-lithium bonds are somewhat shorter than the sum of the ionic radii [Br1−Li1 250.8(7), Br2−Li2 249.3(7) pm; sum of ionic radii 255 pm].[21] The lithium atoms are also four coordinate with angles ranging from 92.2(3)° (N1−Li1−C1) to 117.8(4)° (O80−Li1−C1) for Li1 and from 95.2(3)° (N2−Li2−C14) to 118.9(4)° (O90−Li2−N2) for Li2. The nitrogen atoms show an appreciable deviation from a tetrahedral geometry. The angles range from 97.1(3)° (C24−N2−Li2) to 118.2(3)° (C25−N2−Li2). The sum of the angles around the oxygens of the coordinating diethyl ether molecules is 359.5(5) [O80], and 359.0(4) pm [O90]. The best planes of the spiro system (Li1−C1−Mg−Br1, Li2−C14−Mg−Br1) are almost rectangular (82.6°).

Extraction of compound **1** with boiling pentane affords $[(FcN)_2Mg(OEt_2)]$ **(2)** in quantitative yield in the form of orange crystals (Scheme 1). The X-ray diffraction analysis of **2** (vide infra) reveals that the compound exists in the solid state as a *rac*-diastereomer.

Reaction of magnesium chloride with two equivalents of (FcN)Li and a small excess of tetrahydrofuran in ether furnishes orange crystals of $[(FcN)_2Mg(THF)]$ **(3)**, in 80% yield (see Scheme 1). The X-ray diffraction analysis shows that **3** also crystallizes as a *rac*-diastereomer. The alternative method of preparing **3** is from the reaction of magnesium

Table 1. Selected molecular dimensions in complex **1**; bond lengths [Å], angles [°] (ESDs are in parentheses)

Mg−C1	2.169(4)	Fe1−C(1m)[a]	1.653
Mg−C14	2.167(4)	Fe1−C(2m)	1.658
Li1−C1	2.390(8)	Fe2−C(3m)	1.642
Li2−C14	2.311(8)	Fe2−C(4m)	1.652
Mg−Li1	3.029(7)	Li1−N1	2.074(8)
Mg−Li2	2.994(7)	Li2−N2	2.065(7)
Mg−Br1	2.6008(13)	Li1−Br1	2.508(7)
Mg−Br2	2.6052(13)	Li2−Br2	2.493(7)
C1−Mg−C14	119.8(2)	Li1−O80	1.894(8)
Br1−Mg−Br2	98.06(4)	Li2−O90	1.911(7)
N1−Li1−C1	92.2(3)	N2−Li2−C14	95.2(3)
N1−Li1−Br1	113.2(3)	N2−Li2−Br2	109.5(39
O80−Li1−C1	117.8(4)	O90−Li2−C14	112.6(3)
O80−Li1−Br1	115.5(3)	O90−Li2−Br2	115.7(3)
Li1−N1−C(11−13)	99.8(3) to 117.5(4)	Li2−N2−C(24−26)	97.1(3) to 118.2(3)
Br1−Mg−C1−Li1	7.9(2)	Br2−Mg−C1−Li1	-92.3(2)
Br1−Mg−C14−Li2	104.9(2)	Br2−Mg−C14−Li2	1.2(2)

[a] The suffix 'm' denotes the centroid of a Cp ring.

bromide with two equivalents of (FcN)Li in a mixture of tetrahydrofuran and toluene.

The crystal structures of **2** and **3** are very similar, and therefore they will be discussed together, with parameters for compound **3** given in square brackets. Compound **2** crystallizes in the space group $P2_12_12_1$, and compound **3** in the space group $P2_1/n$. The X-ray structures of **2** and **3**, with their atomic numbering schemes, are shown in Figure 3 and 4. Bond distances and angles are given in Table 2. The crystal structures of both compounds are built up from discrete monomers. The magnesium atom is five-coordinate with two (*C,N*)-chelate-bonded FcN ligands and one *O*-bonded ether molecule in **2** (tetrahydrofuran in **3**). The coordination geometry shows a 59% [63%] distortion from a trigonal bipyramid towards a square pyramid along the Berry pseudorotation coordinate.[22] The distortion is defined by bending of the C1−Mg−C14 angle around the N1−Mg−N2 axis. The small bite angle of the FcN ligands (C−Mg−N ca 79°) causes distortions around the α-carbon atoms and nitrogen atoms. For instance, although the C−N−C angles have ideal values, the Mg−N1−C11 and Mg−N2−C24 angles {99.85(1) [100.90(3)] and 97.89(2)° [102.46(3)°], respectively} are smaller than the other Mg−N−C angles. Similarly, the C2−C1−Mg and C15−C14−Mg angles {110.1(1)° [110.8(2)°] and 110.0(2)° [111.1(2)°], respectively} are smaller than C5−C1−Mg and C18−C14−Mg angles {144.4(2) [144.2(2)] and 145.0(2)° [145.2(2)°], respectively}. The sum of the angles around the oxygen atom is 359.9(2)° [359.9(2)°], indicating an almost perfect trigonal geometry. The puckering in the tetrahydrofuran molecule in **3** is described as an envelope with C29 sticking out of the plane defined by the other four atoms in the ring.

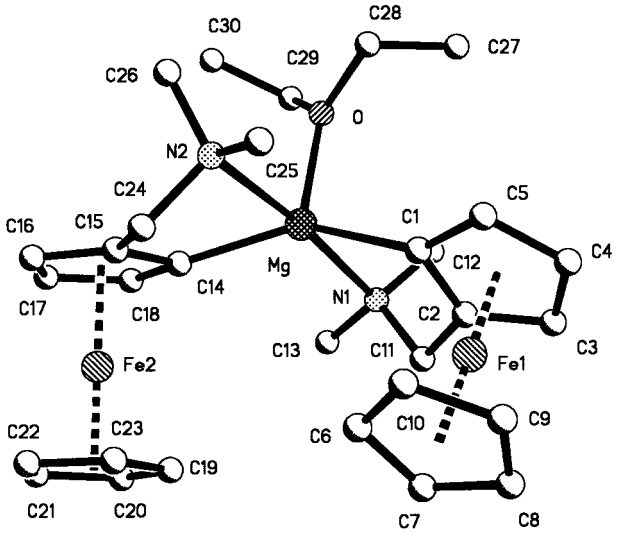

Figure 3. The molecular structure of **2**

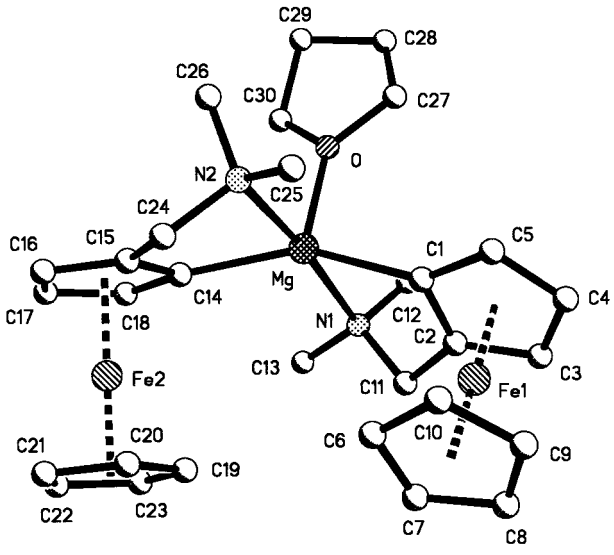

Figure 4. The molecular structure of **3**

The ^1H and ^{13}C NMR spectroscopic data in $[D_8]$THF at 21 °C of all three compounds are virtually identical and correspond to the solvated $(FcN)_2Mg$ species. The solution data show the presence of two diastereomers in a ratio of 3:1. In order to distinguish both diastereomers in solution, it occurred to us that **2**, as a chiral compound, crystallizes

Table 2. Selected molecular dimensions in complexes **2** and **3**; bond lengths [Å], angles [°] (ESDs are in parentheses)

	2	**3**		**2**	**3**
Mg−C1	2.150(2)	2.151(2)			
Mg−C14	2.152(2)	2.160(2)	Fe1−C(1m)[a]	1.652	1.648
Mg−N1	2.412(2)	2.421(2)	Fe1−C(2m)	1.658	1.657
Mg−N2	2.465(2)	2.419(2)	Fe2−C(3m)	1.652	1.656
Mg−O	2.084(2)	2.077(2)	Fe2−C(4m)	1.661	1.660
C1−Mg−C14	147.68(8)	150.59(9)	Mg−N1−C11	95.75(11)	100.80(13)
N1−Mg−N2	172.73(7)	172.34(7)	Mg−N2−C24	97.79(12)	102.36(13)
C1−Mg−O	105.35(7)	102.40(8)	C2−C1−Mg	110.14(13)	110.8(2)
C14−Mg−O	106.96(7)	107.01(8)	C15−C14−Mg	110.0(2)	111.1(2)
N1−Mg−O	94.37(6)	92.02(7)	C5−C1−Mg	144.4(2)	144.4(2)
N2−Mg−O	92.89(7)	95.63(7)	C18−C14−Mg	145.0(2)	145.2(2)
C1−Mg−N1	78.89(7)	78.07(8)	C14−Mg−N2	78.69(7)	78.00(8)
C11−N1	1.493(3)	1.488(3)	N1−C12	1.471(3)	1.474(3)
C24−N2	1.489(3)	1.484(3)	N1−C13	1.476(3)	1.467(3)
C11−N1−C(av.)	109.2(2)	109.2(2)	N2−C25	1.474(3)	1.475(3)
C24−N2−C(av.)	109.5(2)	109.4(2)	N2−C26	1.468(3)	1.474(3)

[a] The suffix 'm' denotes the centroid of a Cp ring.

in the asymmetrical space group $P2_12_12_1$. Therefore in a single crystal, compound **2** exists as either the (*R*,*R*)- or (*S*,*S*)-diastereomer, which should prevent the conversion into the *meso*-diastereomer in solution, and therefore result in only one set of signals in the NMR spectra. The ^{1}H NMR spectrum of one single crystal indeed revealed signals of only one compound. By comparison, it was deduced that these signals belong to the major diastereomer, indicating that the *rac*-diastereomer is prevalent in solution at room temperature.

The NMR spectroscopic data at room temperature show only one set of signals for both FcN groups in each diastereomer, indicating intramolecular exchange (Table 3). Below −20 °C in [D$_8$]THF the signals of the methyl groups of the *rac* diastereomer start to broaden; those of the *meso*-(FcN)$_2$Mg broaden at −40 °C. At −60 °C there are two signals for the methyl groups of *rac*-(FcN)$_2$Mg at δ = 2.25 and 2.95. This diastereomer has C_2-symmetry along the Mg−O axis and therefore both FcN ligands are equivalent and only two signals for the methyl groups are expected. In contrast, due to lack of symmetry, *meso*-(FcN)$_2$Mg should exhibit four signals for the methyl groups. At −90 °C we observed two broad signals at δ = 2.10 and 2.65, and it is likely that the signals of the *meso*-diastereomer have not reached decoalescence completely. The temperature-dependent NMR spectroscopic data could be explained by a rapid dissociation and recoordination of the Mg−N bonds.

The ratio of diastereomers measured in different solvents ([D$_8$]THF, [D$_8$]toluene, C$_6$D$_6$) is temperature dependent (at room temp. 2.8, 2.5, and 2, respectively). This suggests an intermolecular exchange between diastereomers. The proportion of the *rac*-diastereomer is higher at lower temperatures. This observation is reminiscent to those of the plumbylene compound (FcN)$_2$Pb, with the difference that, for the latter compound, the *meso*-diastereomer is prevalent. The equilibrium constant K (*rac*/*meso*) gradually changes from 2.8 at +25 °C to 12.0 at −90 °C in [D$_8$]THF. Plotting ln$K$ against 1/T (Van't Hoff plot) gives a straight line from which the thermodynamic parameters ΔH = −5.92 kJ mol^{-1} K^{-1} and ΔS = −12.1 J mol^{-1} K^{-1} were obtained (r = 0.9819).

The mechanistic pathway for the observed intermolecular exchange most likely involves electron-deficient three-center two-electron interactions (see Scheme 2). It invokes a simultaneous migration of two σ-bonded FcN groups through an intermediate with carbon-bridged FcN groups. Although this mechanism is very similar to that proposed for (FcN)$_2$Pb, it is fundamentally different. In the lead compound, exchange of FcN ligand probably proceeds via a preliminary Pb−Pb interaction, whereas for the magnesium compound such an interaction is highly unlikely.

The redox behavior of complex **3** has been examined by electrochemical techniques. At any rate, the appearance of a primary, single-stepped two-electron oxidation points out that the two ferrocene units do not communicate electronically each other.

Figure 5 shows the anodic cyclic voltammetric profile exhibited by complex **3** in dichloromethane solution.

The single-stepped two-electron oxidation at $E^{\circ\prime}$ = +0.41 V (accompanied with a yellow-to-blue color change) has features of chemical reversibility (at 0.05 Vs^{-1}: i_{pc}/i_{pa} = 0.9; ΔE_p = 70 mV, blue-to-yellow change). The blue color is typical of the formation of the ferrocenium cation.

The oxidation potential may be compared with that of FcNH ($E^{\circ\prime}$ = +0.38 V). After exhaustive two-electron oxidation-reduction it displays a reversible anodic process at

Table 3. ^{1}H NMR spectroscopic data for **2** in [D$_8$]THF

[a]		NMe_2	CH_2N	CpFe	C_5H_3
21 °C	*rac*-	2.55 (s, 12 H)	3.03 (d, 2 H, J = 14) 3.59 (d, 2 H, J = 14)	4.06 (s, 10 H)	3.84 (s, 2 H) 4.00 (s, 2 H) 4.13 (s, 2 H)
	meso-	2.42 (s, 12 H)	2.86 (d, 2 H, J = 13) 3.83 (d, 2 H, J = 13)	4.11 (s, 10 H)	3.88 (s, 2 H) 3.98 (s, 2 H)[b]
−90 °C	*rac*-	2.25 (s, 6 H) 2.95 (s, 6 H)	3.11 (d, 2 H, J = 14) 3.50 (d, 2 H, J = 14)	4.13 (s, 10 H)	4.11 (s)[b] 4.16 (s, 2 H)
	meso-	2.10 (s, br, 6 H) 2.65 (s, br, 6 H)	2.49 (d, 2 H, J = 13)[b]	4.16 (s, 10 H)	3.92 (s, 2 H) 4.07 (s, br, 4 H)[b]

[a] The ^{1}H NMR spectroscopic data of **1** and **3** are virtually identical. − [b] Not all signals were observed, due to the overlap with other signals.

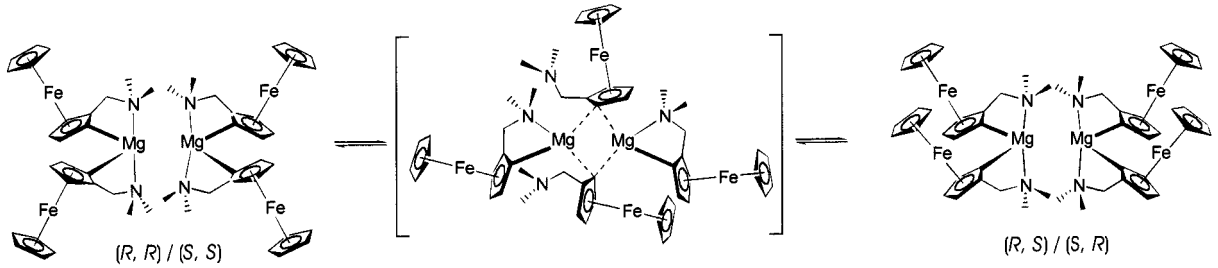

Scheme 2

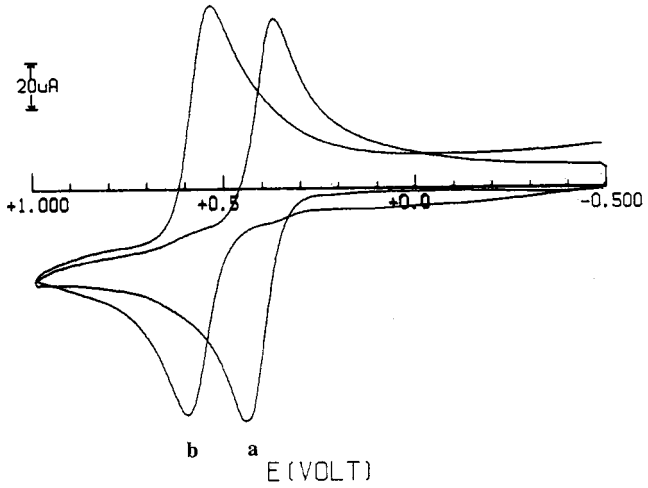

Figure 5. Cyclic voltammograms recorded on a platinum electrode in CH_2Cl_2 solution containing **1** (1.8×10^{-3} mol dm^{-3}) and $[NBu_4][PF_6]$ (0.2 mol dm^{-3}) before (a) and after (b) a cycle of exhaustive oxidation and reduction

$E^{\circ\prime}$ = +0.57 V (at 0.05 Vs^{-1}: ΔE_p = 76 mV), indicating decomposition of the compound (Figure 5b).

The Mössbauer parameters of **1** and **3** are shown in Table 4. The isomer shifts do not differ significantly from those of (FcN)Li,[23] titanium or vanadium compounds.[6]

Table 4. Mössbauer parameters for compounds **1** and **3** (78 K, referenced against α-iron foil)

Compound[a]	δ[b] [mm s^{-1}]	q.s.[c] [mm s^{-1}]	Γ[d] [mm s^{-1}]
1	0.520(2)	2.367(4)	0.324(7)
2	0.485(7)	2.33(2)	0.36(2)

[a] Numbers in parentheses correspond to the experimental error in the last significant figures. – [b] Isomer shift. – [c] Quadrupole splitting. – [d] Half-width at half height.

The data in Table 4 show lower values of *q.s.* for measured compounds relative to the *q.s.* in ferrocene [2.40(3) mm s^{-1}].[23] Such a decrease in *q.s.* is associated with electron-withdrawing substituents on the ferrocenyl moieties, and may be due to the binding of the Mg units to the FcN ligand. Nevertheless, this change is very small, indicating that the Fe^{II} orbitals are not very sensitive to ring substituents.

Conclusions

The diorganomagnesium compounds **1**–**3** are highly dynamic in solution. Although all three compounds only crystallize as (*C,N*)-bonded *rac*-diastereomers, a mixture of *meso*- and *rac*-diastereomers forms in solution. The *rac*/*meso*-ratio is solvent- and temperature-dependent, and consistent with an intermolecular exchange between diastereomers. An intramolecular dynamic process of dissociation and recoordination of Mg–N bonds is responsible for the equivalency of both FcN groups in solution.

Experimental Section

General Remarks: All experiments were carried out using standard Schlenk techniques under purified argon atmosphere. Solvents were distilled from sodium benzophenone ketyl prior to use. The commercial products *n*-butyllithium (1.6 M solution in hexane), magnesium chloride, magnesium bromide and dimethylaminomethylferrocenylferrocene were used without further purification. The known starting material (FcN)Li was prepared according to the literature.[19] – ^{1}H and ^{13}C NMR spectra were recorded on a Varian Unity 500 spectrometer. – Materials and apparatus for electrochemistry have been described elsewhere.[24] All potential values are referred to the Saturated Calomel Electrode (SCE). Under the present experimental conditions {dichloromethane solution containing $[NBu_4][PF_6]$ (0.2 mol dm^{-3})} the one-electron oxidation of ferrocene occurs at $E^{\circ\prime}$ = + 0.38 V. – Mössbauer data were recorded at 78 K on a Wissel spectrometer with a ^{57}Co source in a rhodium matrix, 1.8 GBq.

Synthesis of $[Li_2Mg(FcN)_2Br_2(OEt_2)_2]$ (1): (FcN)Li (5.00 g, 20.1 mmol) was added to a suspension of $MgBr_2$ (1.84 g, 10.0 mmol) in diethyl ether (150 mL) at −50 °C with vigorous stirring. After 1 h the reaction mixture was allowed to warm to room temperature whilst stirring, affording a clear orange-colored solution. The volume of the solution was reduced to the point of crystallization after one day and stored at 7 °C to give product **1** as orange air- and moisture-sensitive crystals. Yield: 6.64 g, 80%. – $C_{34}H_{52}Br_2Fe_2Li_2MgN_2O_2$ (830.49): calcd. C 49.17, H 6.31, N 3.37, Br 19.24; found C 49.21, H 6.35, N 3.32, Br 19.31. – ^{1}H NMR ([D$_8$]THF, room temp.; *meso*-diastereomer in square brackets): δ = 2.57 (s, 12 H, NMe_2) [2.42 (s, 12 H, NMe_2)], 3.03 (d, $^1J_{C,H}$ = 14 Hz, 2 H, CH_2N) [2.85 (d, $^1J_{C,H}$ = 13 Hz, 2 H, CH_2N], 3.60 (d, $^1J_{C,H}$ = 14 Hz, 2 H, CH_2N) [3.83 (d, $^1J_{C,H}$ = 13 Hz, 2 H, CH_2N], 4.06 (s, 10 H, C_5H_5) [4.11 (s, 10 H, C_5H_5)], 3.83 (s, 2 H, C_5H_3) [3.88 (s, 2 H, C_5H_3)], 3.99 (s, 2 H, C_5H_3) [3.97 (s, 4 H, C_5H_3)], 4.12 (s, 2 H, C_5H_3).

Synthesis of $[(FcN)_2Mg(OEt_2)]$ (2): Crystals of **1** were filtered off, and exhaustively extracted with pentane. The pentane solution was stored in a freezer at −30 °C to give product **2** as deep-reddish air- and moisture-sensitive crystals. Yield: 5.31 g, 80%. – $C_{30}H_{42}Fe_2MgN_2O$ (582.67): calcd. C 61.84, H 7.26, N 4.81; found C 61.92, H 7.32, N 4.75. – ^{13}C{^{1}H} NMR ([D$_8$]THF, room temp.; *meso*-diastereomer in square brackets): δ = 47.1 [46.7] (NMe_2), 63.0 [63.4] ($-CH_2N$), 76.5 [77.2] ($C_5H_3-CH_2NMe_2$), 95.4 [95.0] (C_5H_3-Mg).

Synthesis of $[(FcN)_2Mg(THF)$ (3)]: (FcN)Li (2.90 g, 11.6 mmol) was added to a suspension of $MgBr_2$ (1.07 g, 5.8 mmol) in 150 mL of toluene and 5 mL tetrahydrofuran at −78 °C with constant stirring. The orange-colored reaction mixture was stirred for 24 h. Workup as for **2**. Deep-reddish crystals of **3** were obtained after cooling the pentane solution to −30 °C. Yield: 2.93 g, 85%. – $C_{30}H_{40}Fe_2MgN_2O$ (580.65): calcd. C 62.05, H 6.94, N 4.83; found C 61.98, H 6.89, N 4.90. – ^{1}H NMR ([D$_8$]THF, room temp.; *meso*-diastereomer in square brackets): δ = 2.55 (s, 12 H, NMe_2) [2.42 (s, 12 H, NMe_2)], 3.03 (d, $^1J_{C,H}$ = 14 Hz, 2 H, CH_2N) [2.86 (d, $^1J_{C,H}$ = 13 Hz, 2 H, CH_2N)], 3.59 (d, $^1J_{C,H}$ = 13 Hz, 2 H, CH_2N) [3.83 (d, $^1J_{C,H}$ = 13 Hz, 2 H, CH_2N)], 4.06 (s, 10 H, C_5H_5) [4.11 (s, 10 H, C_5H_5)], 3.84 (s, 2 H, C_5H_3) [3.88 (s, 2 H, C_5H_3)], 4.00 (s, 2 H, C_5H_3) [3.98 (s, 4 H, C_5H_3)], 4.13 (s, 2 H, C_5H_3).

X-ray Structure Analyses of 1, 2 and 3: Crystal and numerical data of the structure determinations are given in Table 5. Crystals were covered with inert oil and mounted on a glass fiber, and then trans-

Table 5. Crystallographic data for **1**, **2** and **3**

	1	**2**	**3**
Empirical formula	$C_{34}H_{52}Br_2Fe_2Li_2MgN_2O_2$	$C_{30}H_{42}Fe_2MgN_2O$	$C_{30}H_{40}Fe_2MgN_2O$
Molecular mass	830.49	582.67	580.65
Crystal dimensions [mm]	0.80 × 0.50 × 0.40	0.55 × 0.50 × 0.16	0.40 × 0.24 × 0.12
Crystal system	monoclinic	orthorhombic	monoclinic
Space group	*C2/c*	$P2_12_12_1$	$P2_1/n$
a [Å]	34.3791(5)	10.4576(4)	12.2948(2)
b [Å]	11.2325(2)	11.3446(4)	10.59530(10)
c [Å]	22.3681(4)	24.1390(7)	21.8177(2)
α [°]	90	90	90
β [°]	115.8970(10)	90	97.7310(10)
γ [°]	90	90	90
V [Å^3]	7770.3(2)	2863.8(2)	2816.29(6)
Z	8	4	4
$d_{calcd.}$ [g cm^{-3}]	1.420	1.351	1.369
T [K]	173(2)	173(2)	163(2)
μ [mm^{-1}]	2.850	1.060	1.078
θ_{max} [°]	28.3	28.3	28.2
No. rflns.	25637	19229	18512
No. unique rflns.	9545	6994	6925
No. rflns. observed	6132	6183	5173
Structure determination	Direct methods	Direct methods	Direct methods
Refinement	on F^2 in SHELXL	on F^2 in SHELXL	on F^2 in SHELXL
No. parameters refined	414	332	329
$R_1[I > 2\sigma(I)]$	0.0529	0.0587	0.0395
wR_2 (all data)	0.1282	0.0627	0.0846
Goodness-of-fit (on F^2)	1.017	1.084	1.046

ferred to the diffractometer in a stream of a cold gas (Bruker AXS Smart CCD System with LT-2 low-temperature adapter). Monochromatic Mo-K_α radiation (λ = 71.073 pm) was used. Data were corrected for Lorentz and polarization effects. Absorption correction (multi-scan method SADABS) was employed. The structures were solved by direct methods using the SHELXS program and refined by full-matrix least-squares against F^2 with SHELXL-97.[25] All non-hydrogen atoms were refined with anisotropic thermal parameters. All hydrogen atoms were found in the difference Fourier map and refined isotropically.

Crystallographic data (excluding structure factors) for the reported structures have been deposited with the Cambridge Crystallographic Data Centre as supplementary publication no. CCDC-113801 (**1**), -113802 (**2**), -113803 (**3**). Copies of data can be obtained free of charge on application to CCDC, 12 Union Road, Cambridge CB2 1EZ, UK [Fax: (internat.) +44-1223/336-093; E-mail: deposit@ccdc.cam.ac.uk].

Acknowledgments

N. S. thanks Dr. Adolphus A. H. van der Zeijden for fruitful discussions. K. J. thanks the Deutsche Forschungsgemeinschaft DFG for financial support, N. S. thanks the DFG program "Graduierten-Kolleg: Synthese und Reaktionsverhalten von Organometallverbindungen und Metallkomplexen" for a fellowship, P. Z. thanks University of Siena for financial support (ex-quota 60%).

[1] F. T. Edelmann, K. Jacob, *J. Prakt. Chem.* **1998**, *340*, 393−407.
[2] K. Jacob, J. Scholz, K. Merzweiler, C. Pietzsch, *J. Organomet. Chem*. **1997**, *527*, 109−115.
[3] W. Palitzsch, C. Pietzsch, K. Jacob, F. T. Edelmann, T. Gelbrich, V. Lorenz, M. Puttnat, G. Roewer, *J. Organomet. Chem*. **1998**, *554*, 139−146.
[4] K. Jacob, F. Voigt, K. Merzweiler, C. Pietzsch, *J. Organomet. Chem*. **1997**, *545−546*, 421−433.
[5] P. Ramani R. Ranatunge-Bandarage, B. H. Robinson, J. Simpson, *Organometallics* **1994**, *13*, 500−510.
[6] P. B. Hitchcock, D. L. Hughes, G. J. Leigh, J. R. Sanders, J. S. de Souza, *J. Chem. Soc., Dalton Trans.* **1999**, 1161−1174.
[7] K.-H. Thiele, C. Krüger, R. Boese, G. Schmid, T. Bartik, G. Pályi, *Z. Anorg. Allg. Chem*. **1990**, *590*, 55−64.
[8] H. Gornitzka, A. Steiner, D. Stalke, U. Kilimann, F. T. Edelmann, K. Jacob, K.-H. Thiele, *J. Organomet. Chem*. **1992**, *439*, C6−C10.
[9] K. Jacob, M. Schäfer, A. Steiner, G. M. Sheldrick, F. T. Edelmann, *J. Organomet. Chem*. **1995**, *487*, C18−C20.
[10] A. Nesmeyanov, Yu. T. Struchkov, N. N. Sedova, V. G. Andrianov, Yu. V. Volgin, V. A. Sazonova, *J. Organomet. Chem*. **1977**, *137*, 217−221.
[11] A. Nesmeyanov, N. N. Sedova, Yu. T. Struchkov, V. G. Andrianov, E. N. Stakheeva, V. A. Sazonova, *J. Organomet. Chem*. **1978**, *153*, 115−122.
[12] L. G. Kuz'mina, Yu. T. Struchkov, D. A. Lemenovskii, I. F. Urasovskii, I. E. Nifanev, L. G. Perevalova, *Koord. Khim*. **1983**, *9*, 1212−1219.
[13] K. Jacob, J. Scholz, C. Pietzsch, F. T. Edelmann, *J. Organomet. Chem*. **1995**, *501*, 71−77.
[14] N. Seidel, K. Jacob, A. A. H. van der Zeijden, H. Menge, K. Merzweiler, C. Wagner, *Organometallics* **2000**, *19*, 1438−1441.
[15] K. Schlögl , M. Fried, *Monatsh. Chem*. **1964**, *95*, 558−575.
[16] W. Palitzsch, C. Pietzsch, M. Puttnat, K. Jacob, K. Merzweiler, P. Zanello, A. Cinquantini, M. Fontani, G. Roewer, *J. Organomet. Chem*. **1999**, *587*, 9−17.
[17] V. C. R. Grignard, *Hebd. Seances Acad. Sci*. **1900**, *130*,1322.
[18] P. R. Markies, O. S. Akkerman, F. Bickelhaupt, W. J. J. Smeets, A. L. Spek, *Adv. Organomet. Chem.* **1991**, *32*, 147−226.
[19] M. D. Rausch, G. A. Moser, C. F. Maede, *J. Organomet. Chem*. **1973**, *51*, 1−12.
[20] The Grignard compound (FcN)MgBr can be obtained by reaction of $(FcN)_2Mg$ and $MgBr_2$ in ether. (FcN)MgBr was preliminary characterized by ^1H and ^{13}C NMR spectroscopy. In the Schlenk-type equilibrium the Grignard compound is obviously favored. N. Seidel, K. Jacob, *Unpublished results.*
[21] *CRC Handbook of Chemistry and Physics*, 78th Edition, CRC Press, Boca Raton, New York **1997**, Section 12−14.
[22] R. R. Holmes, *Prog. Inorg. Chem*. **1984**, *32*, 119−236.
[23] K. Jacob, W. Palitzsch, *Z. Anorg. Allg. Chem*. **1994**, *620*, 1489−1493.

[24] A. Togni, M. Hobi, G. Rihs, G. Rist, A. Albinati, P. Zanello, D. Zech, H. Keller, *Organometallics* **1994**, *13*, 1224−1234.
[25] G. M. Sheldrick, SHELXS, *Program for Crystal Structure Determination*, University of Göttingen, Germany, **1986**; SHELXL-97, *Program for Crystal Structure Refinement*, University of Göttingen, Germany, **1997**.

Received May 23, 2000
[I00201]

The First Spacer-Bridged Tetraorganodistannoxanes with a Mixed Double Ladder Structure[‡]

Michael Mehring,[a] Ingo Paulus,[a] Bernhard Zobel,[a] Markus Schürmann,[a] Klaus Jurkschat,*[a] Andrew Duthie,[b] and Dainis Dakternieks*[b]

Keywords: Tin / Distannoxanes / Oxo complexes / Electrospray mass spectrometry

The reaction of $Me_3SiCH_2Cl_2Sn(CH_2)_3SnCl_2Ph$ (**6**) with $(tBu_2SnO)_3$ gave a statistical mixture of the corresponding tetraorganodistannoxanes whereas the reaction of the spacer-bridged ditin tetrachlorides $RCl_2Sn(CH_2)_4SnCl_2R$ (**3**, R = Me_3CCH_2; **4**, R = Me_2CHCH_2; **10**, R = Me_3SiCH_2) with the polymeric spacer-bridged ditin oxides $[R(O)Sn(CH_2)_4Sn(O)R]_n$ (**7**, R = Me_2CHCH_2; **8**, R = Me_3CCH_2; **11**, R = Me_3SiCH_2) provided the mixed double ladder compounds $\{[R(Cl)Sn(CH_2)_4Sn(Cl)R][R'(Cl)Sn(CH_2)_4Sn(Cl)R']O_2\}_2$ (**9**, R = Me_3CCH_2, R′ = Me_2CHCH_2; **12**, R = Me_3CCH_2, R′ = Me_3SiCH_2) in almost quantitative yield. In solution, **9** and **12** are in equilibrium with their corresponding dimers, as was evidenced by ^{119}Sn NMR spectroscopy, molecular mass determination, and electrospray mass spectrometry. The molecular structures of **9** and **12** were established by single crystal X-ray diffraction.

Introduction

Currently, there is much interest in dimeric tetraorganodistannoxanes $[R_2(X)SnOSn(X)R_2]_2$ (X = halogen, OH, $R'CO_2$, NCS; R, R′ = alkyl, aryl)[1−5] since these compounds are reported to be efficient homogeneous catalysts in various organic reactions such as transesterification under virtually neutral conditions,[6] highly selective acylation of alcohols,[7] urethane formation,[8] and alkyl carbonate synthesis.[9] X-ray crystallography has illustrated the dimeric nature of a large number of tetraorganodistannoxanes and NMR spectroscopic studies show that this structural arrangement is retained in solution.[1−5] However, only a few examples of monomeric species for both solution and in the solid state have been reported.[2,4,10−13]

In contrast to the symmetrically substituted tetraorganodistannoxanes, unsymmetrically substituted ones, such as $[Bu_2(X)SnOSn(Y)Bu_2]_2$ (X = O_2CMe, Cl, OPh, OMe; Y = Cl, OPh, OMe),[2,4] $[tBu_2(Cl)SnOSn(Cl)R_2]_2$ (R = Me, Et, *i*Pr, *n*Bu),[14] $[tBu_2(OH)SnOSn(Cl)R_2]_2$ (R = *n*Bu, cyclohexyl),[14,15] $[Ph_2(Cl)SnOSn(OH)Ph_2]_2{\cdot}2(CH_3)_2CO$[16] and $Et_2BrSnOSnBrPr_2$[17] have attracted less attention and only four of these compounds have been characterized by X-ray crystallography.[14−16]

For some time we have been interested in the synthesis, structure, and catalytic activity of the spacer-bridged tetraorganodistannoxanes $\{[R(X)Sn-Z-Sn(X)R]O\}_n$ [X = Cl, F, OH, OAc; R = alkyl; Z = $(CH_2)_3$, $(CH_2)_4$, $CH_2SiMe_2CH_2$, $CH_2SiMe_2CCSiMe_2CH_2$].[18−21] In the solid state, these compounds exhibit either a dimeric (*n* = 2) or a double ladder structure (*n* = 4). Furthermore, the first triple ladder $\{[R(Cl)Sn(CH_2)_3Sn(Cl)(CH_2)_3Sn(Cl)R]O_{1.5}\}_4$ (R = Me_3SiCH_2) was reported, in which three $Sn_4Cl_4O_2$ layers are connected through trimethylene bridges.[22] The most convenient synthetic methodologies for the preparation of compounds of the type $\{[R(Cl)Sn-Z-Sn(Cl)R]O\}_n$ (*n* = 2, 4) are (i) the reaction of a spacer-bridged ditin tetrachloride $RCl_2Sn-Z-SnCl_2R$ with $(tBu_2SnO)_3$ as the oxygen transfer reagent and (ii) the reaction of a spacer-bridged ditin tetrachloride with the corresponding spacer-bridged polymeric ditin oxide $[R(O)Sn-Z-Sn(O)R]_n$.

In solution, most of the spacer-bridged distannoxanes retain their solid-state structure, but in the cases of Z = $(CH_2)_4$ and X = Cl, OAc, and Z = $(CH_2)_3$ and X = OAc, equilibria between dimers and tetramers have been observed. These kinetically labile species show higher catalytic activity in acylation reactions than the kinetically more inert double ladder compounds.[18]

Here we report our attempts to prepare mixed tetraorganodistannoxanes and present the X-ray single crystal structure analyses of $\{[R(Cl)Sn(CH_2)_4Sn(Cl)R][R'(Cl)Sn(CH_2)_4Sn(Cl)R']O_2\}_2$ (**9**, R = Me_3CCH_2, R′ = Me_2CHCH_2; **12**, R = Me_3CCH_2, R′ = Me_3SiCH_2), the first mixed double ladders containing two different organic groups R and R′.

Results and Discussion

The unsymmetrically substituted ditin precursor $Me_3SiCH_2Cl_2Sn(CH_2)_3SnCl_2Ph$ (**6**) was prepared by reac-

[‡] This work contains parts of the Diploma thesis of M. Mehring, Dortmund University, 1995, and of the planned Ph. D. thesis of I. Paulus.

[a] Lehrstuhl für Anorganische Chemie II der Universität Dortmund,
44221 Dortmund, Germany,
Fax: (internat.) + 49-(0)231/755-5048,
E-mail: kjur@platon.chemie.uni-dortmund.de
[b] Centre for Chiral and Molecular Technologies,
Deakin University,
Geelong, Victoria 3217, Australia

 © WILEY-VCH Verlag GmbH, 69451 Weinheim, 2001 1434−1948/01/0101−0153 $ 17.50+.50/0

tion of Ph_3SnNa (**1**) with $Cl(CH_2)_3SnPh_2CH_2SiMe_3$[22] (**2**) to give $Me_3SiCH_2Ph_2Sn(CH_2)_3SnPh_3$ (**5**) which was converted into its tetrachloro-substituted derivative **6** by reaction with $HgCl_2$ (Scheme 1).

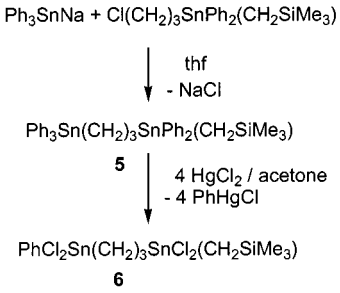

Scheme 1. Synthesis of the unsymmetrically substituted trimethylene-bridged ditin compound **6**

The reaction of compound **6** with one-third molar equivalent $(tBu_2SnO)_3$ gave a complex reaction mixture. The ^{119}Sn NMR spectrum of this mixture displayed 23 signals in the range of $\delta = -90$ to -210, in addition to the resonance at $\delta = 55$ (assigned to tBu_2SnCl_2). This is close to the 24 signals expected for a statistical distribution of 5 possible isomers with a double ladder arrangement (Scheme 2). It is most likely that the missing signal is superimposed with one of the 23 signals. Attempts to isolate a single isomer failed.

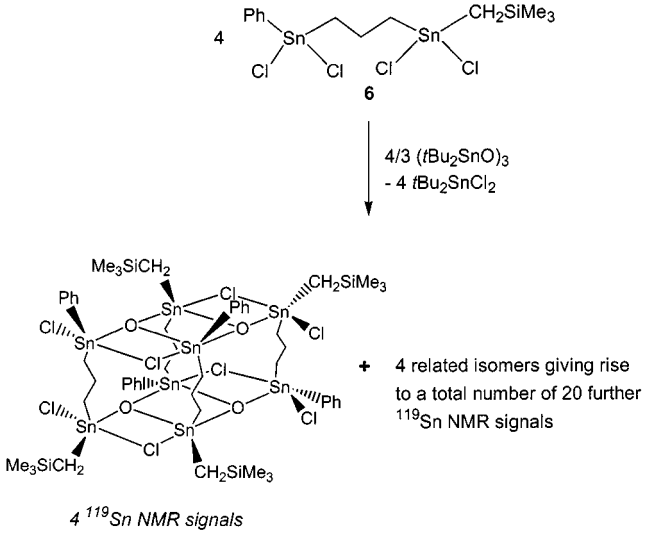

Scheme 2. Reaction of compound **6** with $(tBu_2SnO)_3$ giving a statistical mixture of double ladder isomers

However, the reaction of the spacer-bridged ditin tetrachloride $RCl_2Sn(CH_2)_4SnCl_2R$ (**3**, R = Me_3CCH_2) with the spacer-bridged ditin oxide $[R(O)Sn(CH_2)_4Sn(O)R]_n$ (**7**, R = Me_2CHCH_2), as well as the reaction of $RCl_2Sn(CH_2)_4SnCl_2R$ (**4**, R = Me_2CHCH_2) with $[R(O)Sn(CH_2)_4Sn(O)R]_n$ (**8**, R = Me_3CCH_2) in toluene resulted in the almost quantitative formation of the mixed double ladder compound $\{[R(Cl)Sn(CH_2)_4Sn(Cl)R][R'(Cl)Sn(CH_2)_4Sn(Cl)R']O_2\}_2$ (**9**, R = Me_3CCH_2, R′ = Me_2CHCH_2) (Scheme 3). Analogously, the reactions of $RCl_2Sn(CH_2)_4SnCl_2R$ (**10**, R = Me_3SiCH_2) with $[R(O)Sn(CH_2)_4Sn(O)R]_n$ (**8**, R = Me_3CCH_2), and $RCl_2Sn(CH_2)_4SnCl_2R$ (**3**, R = Me_3CCH_2) with $[R(O)Sn(CH_2)_4Sn(O)R]_n$ (**11**, R = Me_3SiCH_2), gave $\{[R(Cl)Sn(CH_2)_4Sn(Cl)R][R'(Cl)Sn(CH_2)_4Sn(Cl)R']O_2\}_2$ (**12**, R = Me_3CCH_2, R′ = Me_3SiCH_2) in almost quantitative yield. The mixed double ladder compounds **9** and **12** were also formed by mixing equimolar amounts of the symmetrically substituted double ladders $\{[R(Cl)Sn(CH_2)_4Sn(Cl)R]O\}_4$, **14** (R = Me_3CCH_2) and **15** (R = Me_2CHCH_2), and **13** (R = Me_3SiCH_2) and **14** (R = Me_3CCH_2), respectively, as was shown by ^{119}Sn NMR experiments in $CHCl_3/CDCl_3$ (Scheme 3). After 2 h of heating at reflux, a complex mixture of different double ladders was observed, whereas after 3 d of heating at reflux, the conversion of the starting double ladders into the mixed ones **9** and **12**, was complete. In contrast to the tetramethylene-bridged double ladders reported here the trimethylene-bridged double ladders $\{[R(Cl)Sn(CH_2)_3Sn(Cl)R]O\}_4$ are kinetically inert and do not show the formation of mixed double ladders.[23]

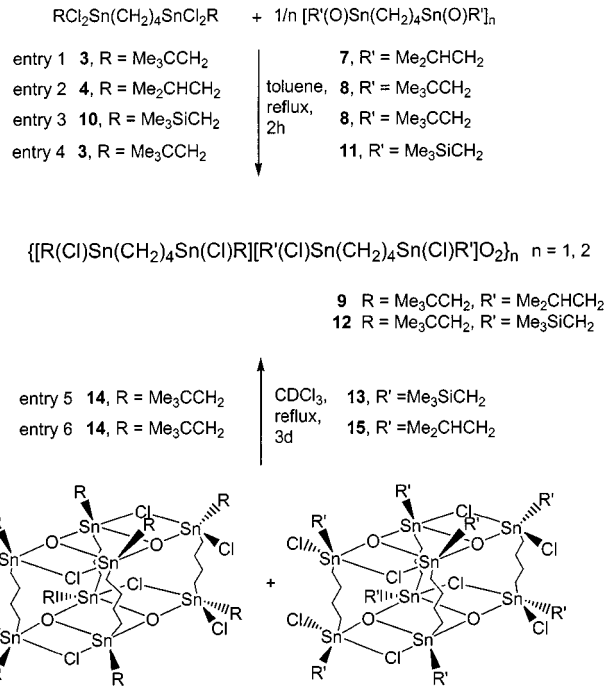

Scheme 3. Syntheses of the mixed tetramethylene-bridged tetraorganodistannoxanes **9** and **12**

The molecular structure of compounds **9** and **12** are shown in Figure 1 and Figure 2, respectively. Crystallographic data are given in Table 3 and selected geometrical parameters are listed in Table 1. The compounds **9** and **12** form centrosymmetric tetramers in which two $Sn_4Cl_4O_2$ units are linked through four tetramethylene bridges giving a double ladder arrangement. The $Sn_4Cl_4O_2$ layer is almost planar with the greatest deviation from the plane for Cl(2) [0.232(2) Å] in **9** and Cl(3) [0.360(2) Å] in **12**. Each tin atom has a distorted trigonal-bipyramidal geometry. For the exocyclic tin atoms, two carbon atoms and one oxygen atom occupy the equatorial positions and two chlorine atoms the axial positions, while for the endocyclic tin atoms the equat-

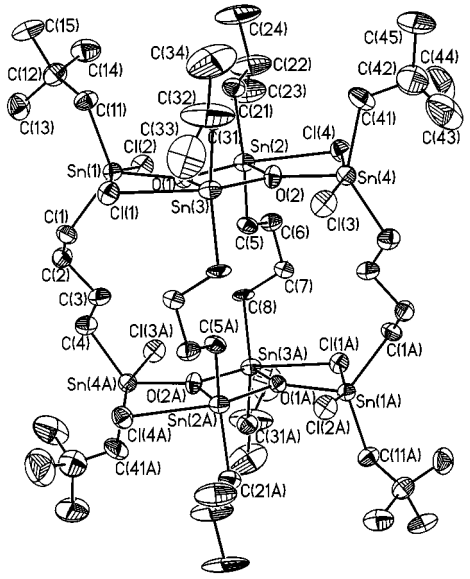

Figure 1. General view (SHELXTL-Plus) of **9** showing 30% probability displacement ellipsoids and the atom numbering scheme (symmetry transformations used to generate equivalent atoms: $a = -x + 1, -y, -z - 1$)

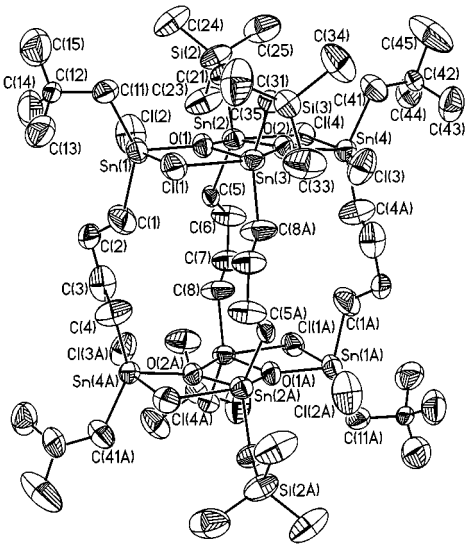

Figure 2. General view (SHELXTL-Plus) of **12** showing 30% probability displacement ellipsoids and the atom numbering scheme (symmetry transformations used to generate equivalent atoms: $a = -x + 1, -y, -z - 1$)

orial positions are occupied by two carbon atoms and one oxygen atom and the axial positions by one oxygen atom and one chlorine atom. In both structures the neopentyl groups Me_3CCH_2 are attached to the exocyclic tin atoms, and the isobutyl groups Me_2CHCH_2 (in **9**) and the trimethylsilylmethyl groups Me_3SiCH_2 (in **12**) are bound to the endocyclic ones. The bond lengths and bond angles (Table 1) correspond to those of previously described ladder[14] and double ladder structures.[18,19] The Sn−O bond lengths for the exocyclic tin atoms, Sn(1)−O(1) and Sn(4)−O(2), are 2.021(5) and 2.017(5) Å, respectively, for **9**, and 2.017(3) and 2.009(3) Å, respectively, for **12**. In the four-membered Sn_2O_2 ring the Sn−O bonds are somewhat

Table 1. Selected bond lengths [Å] and angles [°] for **9** and **12**

	9	**12**		**9**	**12**
Sn(1)−O(1)	2.021(5)	2.017(3)	Sn(3)−O(1)	2.065(5)	2.052(3)
Sn(1)−Cl(1)	2.809(2)	2.751(2)	Sn(3)−O(2)	2.134(5)	2.140(3)
Sn(1)−Cl(2)	2.434(2)	2.478(2)	Sn(3)−Cl(1)	2.686(2)	2.752(2)
Sn(2)−O(1)	2.125(5)	2.127(3)	Sn(3)−Cl(3)	3.326(3)	3.272(2)
Sn(2)−O(2)	2.051(5)	2.058(3)	Sn(4)−O(2)	2.017(5)	2.009(3)
Sn(2)−Cl(2)	3.320(2)	3.248(2)	Sn(4)−Cl(3)	2.488(2)	2.474(2)
Sn(2)−Cl(4)	2.760(2)	2.724(2)	Sn(4)−Cl(4)	2.733(2)	2.760(2)
O(1)−Sn(1)−C(1)	120.5(3)	106.2(2)	C(31)−Sn(3)−C(8)	144.4(3)	144.5(3)
O(1)−Sn(1)−C(11)	109.6(3)	114.8(2)	O(1)−Sn(3)−Cl(1)	77.3(1)	76.0(1)
C(1)−Sn(1)−C(11)	123.5(3)	136.7(3)	C(31)−Sn(3)−Cl(1)	89.5(3)	88.1(2)
O(1)−Sn(1)−Cl(2)	86.3(2)	85.5(1)	O(2)−Sn(3)−Cl(1)	151.1(1)	150.4(1)
C(11)−Sn(1)−Cl(2)	107.3(3)	96.5(2)	C(8)−Sn(3)−Cl(1)	93.7(2)	92.2(2)
C(1)−Sn(1)−Cl(2)	100.6(2)	99.9(3)	O(2)−Sn(3)−C(8)	97.4(3)	96.0(2)
O(1)−Sn(1)−Cl(1)	75.0(2)	76.5(1)	O(2)−Sn(4)−C(41)	104.3(3)	110.3(2)
C(11)−Sn(1)−Cl(1)	85.4(2)	90.9(2)	O(2)−Sn(4)−C(4)	118.4(3)	109.7(3)
C(1)−Sn(1)−Cl(1)	84.0(2)	85.6(3)	C(41)−Sn(4)−C(4)	136.3(4)	137.9(3)
Cl(2)−Sn(1)−Cl(1)	160.3(1)	162.0(1)	O(2)−Sn(4)−Cl(3)	86.6(2)	85.0(1)
O(2)−Sn(2)−C(5)	107.1(3)	114.9(4)	C(41)−Sn(4)−Cl(3)	95.7(3)	96.4(2)
O(2)−Sn(2)−C(21)	109.6(3)	109.1(2)	C(4)−Sn(4)−Cl(3)	95.3(2)	99.7(3)
C(5)−Sn(2)−C(21)	142.1(3)	135.5(5)	O(2)−Sn(4)−Cl(4)	76.9(2)	76.4(1)
O(2)−Sn(2)−O(1)	74.6(2)	74.6(1)	C(41)−Sn(4)−Cl(4)	90.2(3)	91.0(2)
C(5)−Sn(2)−O(1)	99.5(3)	98.0(5)	C(4)−Sn(4)−Cl(4)	91.1(2)	85.9(3)
C(21)−Sn(2)−O(1)	98.8(3)	99.6(2)	Cl(3)−Sn(4)−Cl(4)	163.4(1)	161.3(1)
O(2)−Sn(2)−Cl(4)	75.7(2)	76.5(1)	Sn(1)−Cl(1)−Sn(3)	82.5(1)	82.0(1)
C(5)−Sn(2)−Cl(4)	89.5(2)	95.2(4)	Sn(2)−Cl(4)−Sn(4)	82.2(1)	82.2(1)
C(21)−Sn(2)−Cl(4)	90.7(3)	88.6(2)	Sn(1)−O(1)−Sn(3)	125.0(2)	125.0(1)
O(1)−Sn(2)−Cl(4)	150.3(1)	151.1(1)	Sn(1)−O(1)−Sn(2)	128.4(2)	128.2(2)
O(1)−Sn(3)−C(31)	109.9(3)	109.6(2)	Sn(3)−O(1)−Sn(2)	105.5(2)	105.6(2)
O(1)−Sn(3)−O(2)	74.1(2)	74.5(1)	Sn(4)−O(2)−Sn(2)	125.2(3)	124.7(2)
C(31)−Sn(3)−O(2)	96.6(3)	101.1(2)	Sn(4)−O(2)−Sn(3)	129.0(3)	129.8(2)
O(1)−Sn(3)−C(8)	105.4(3)	104.9(3)	Sn(2)−O(2)−Sn(3)	105.7(2)	104.9(2)

lengthened, with the longest bonds found for Sn(2)−O(1) [2.125(5) Å] and Sn(3)−O(2) [2.134(5) Å] (**9**), and for Sn(2)−O(1) [2.127(3) Å] and Sn(3)−O(2) [2.140(3) Å] (**12**). Two of the chlorine atoms of each monolayer form Sn−Cl−Sn bridges [Sn(1)−Cl(1)−Sn(3) 82.5(1)° (**9**), 82.0(1)° (**12**), Sn(2)−Cl(4)−Sn(4) 82.2(1)° (**9**), 82.2(1)° (**12**)], with Sn(1)−Cl(1), Sn(3)−Cl(1), Sn(4)−Cl(4) and Sn(2)−Cl(4) bond lengths of 2.809(2), 2.686(2), 2.733(2), and 2.760(2) Å (**9**), respectively, and 2.751(2), 2.752(2), 2.760(2), and 2.724(2) Å (**12**), respectively. The chlorine atoms Cl(2) and Cl(4) can be regarded as non-bridging, although the Sn(2)−Cl(2) [3.320(2) Å (**9**), 3.248 (2) Å (**12**)] and Sn(3)−Cl(3) [3.326(3) Å (**9**), 3.272 (2) Å (**12**)] distances are shorter than the sum of the van der Waals radii of tin and chlorine (3.97 Å).[24] The Sn(1)−Cl(2) and Sn(4)−Cl(3) bond lengths are 2.434(2) and 2.488(2) Å (**9**), respectively, and 2.478(2) and 2.474(2) Å (**12**), respectively, which are slightly longer than the Sn−Cl single bond length of 2.39 Å.[22]

An equilibrium between tetrameric double ladder structures ($n = 4$) and dimers ($n = 2$) has been previously reported for $CHCl_3$ solutions of the tetramethylene-bridged tetraorganodistannoxanes $\{[R(Cl)Sn(CH_2)_4Sn(Cl)R]O\}_n$ (**13**, R = Me_3SiCH_2; **14**, R = Me_3CCH_2; **15**, Me_2CHCH_2), which showed degrees of association with $n = 3.9$, 2.3, and 2.5, respectively.[18] The molecular mass determination of **9** in $CHCl_3$ showed $M = 1639$ g mol^{-1} ($c = 20$ mg mL^{-1}), which is indicative of the existence in solution of an equilibrium between double ladder structures (**9a−c**) (calcd. for **9a−c**: $M = 2035$ g mol^{-1}) and the dimer **9d** (calcd. for **9d**: $M = 1018$ g mol^{-1}) (Scheme 4). Compound **12** has a molecular mass $M = 1191$ g mol^{-1} ($c = 20$ mg mL^{-1}) in $CHCl_3$, showing that the dimer **12d** (calcd. for **12d**: $M = 1077$ g mol^{-1}) dominates at this concentration (Scheme 4). The molecular mass of **12** increases at higher concentration ($M = 1689$ g mol^{-1}, $c = 145$ mg mL^{-1}), showing that the equilibrium is shifted towards formation of double ladders **12a−c** (calcd. for **12a−c**: $M = 2155$ g mol^{-1}) (Scheme 5).

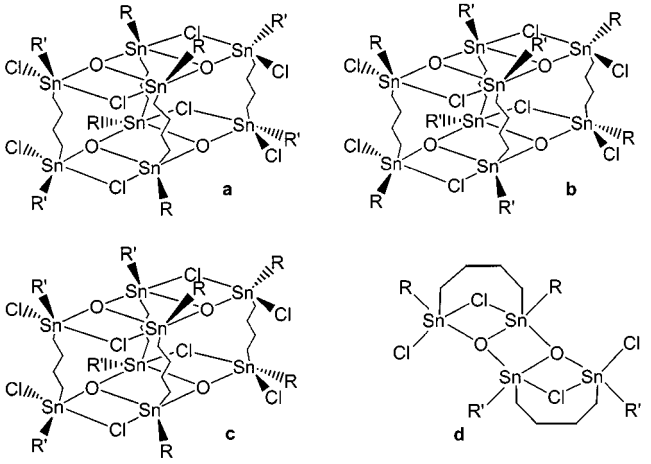

Scheme 4

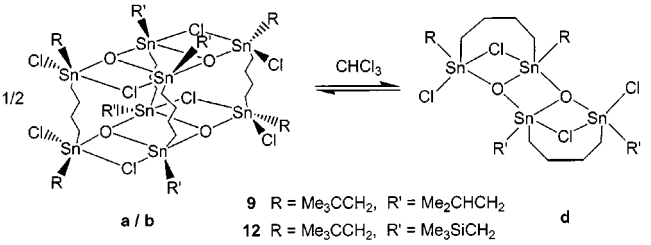

Scheme 5. Dimer-tetramer equilibrium in solutions of **9** (R = Me_3CCH_2, R′ = Me_2CHCH_2) and **12** (R = Me_3CCH_2, R′ = Me_3SiCH_2)

The ^{119}Sn NMR spectroscopic data in $CDCl_3$ of the mixed double ladders **9** and **12**, and of the related simple double ladders **13−15** are given in Table 2. A solution of crystalline **9** in toluene shows two pairs of signals of equal integral ratio at δ = −85.2 (26%)/−148.5 (27%) and at δ = −86.4 (15%)/−147.9 (15%) which are assigned with caution to **9a** and **9b**. The resonances at δ = −78.7 (5%),−150.2 (5%), and −85.4 (4%),−152.7 (3%) are assigned with caution to one of the two possible isomers of the dimer **9d**, but we were not able to discriminate the *cis* and the *trans* isomer. In principal, these signals could also be assigned to the tetramer **9c** (Scheme 4), for which four signals of equal integral ratio are expected. However, the molecular mass determination of a solution of **9** in $CHCl_3$ is indicative of an equilibrium between tetramers and dimers, and thus we assign the four signals to the dimer **9d** rather than to the tetramer **9c**. In $CDCl_3$ solution, **9** displays two signals of equal integral ratio at δ = −83.0 (36%) and δ = −145.2 (35%) which are assigned to **9a** and/or **9b,** and three signals for the dimer **9d** [δ = −78.2 (7%), −84.2 (7%), −144.4 (14%)]. The missing signal is likely to be superimposed with the signal at δ = −144.4. Furthermore, one signal of minor intensity was observed at δ = −146.9 (1%).

Table 2. ^{119}Sn NMR spectroscopic data in $CDCl_3$ for compounds of the type $\{[R(Cl)Sn(CH_2)_4Sn(Cl)R][R'(Cl)Sn(CH_2)_4Sn(Cl)R']O_2\}_2$; chemical shifts are given in δ values and coupling constants [$^2J(^{119}Sn-O-^{119/117}Sn)$] in Hz

		Sn_{exo}		Sn_{endo}	
9	R = Me_3CCH_2	−78.2 [74]	7%	−144.4 [66]	14%
	R′ = Me_2CHCH_2	−84.2 [57]	7%		
		−83.0 [61]	36%	−145.2 [70]	35%
				−146.9	1%
12	R = Me_3CCH_2	−68.5	5%	−144.9	5%
	R′ = Me_3SiCH_2	−83.8	5%		
		−70.6	1%	−143.2	2%
		−85.6	1%		
		−84.5 [64]	27%	−140.7 [64]	33%
		−87.0 [60]	11%	−139.5 [62]	10%
13	R = R′ = Me_3SiCH_2	−66.7	50%	−137.3	50%
14	R = R′ = Me_3CCH_2	−83.1	25%	−146.8	25%
		−85.4	25%	−147.3	25%
15	R = R′ = Me_2CHCH_2	−78.7 [62]	8%	−143.1 [70]	8%
		−79.1 [66]	42%	−144.8 [61]	42%

The ^{119}Sn NMR spectrum of **12** in toluene shows two pairs of signals of equal integral ratio at δ = −83.8 (23%)/−145.5 (23%) and at δ = −86.9 (11%)/−144.3 (12%), which are assigned with caution to the tetramers **12a** and **12b**

(Scheme 4). Furthermore, two sets of four signals are observed at δ = −68.8 (5%), −83.3 (5%), −146.2 (5%), and −149.4 (5%) and at δ = −71.3 (2%), −85.4 (3%), −143.0 (3%), and −147.9 (3%), which are assigned to the *cis* and *trans* isomer of **12d** (Scheme 4). The ^{119}Sn NMR spectroscopic experiments of **12** in $CDCl_3$ at concentrations of c = 145 mg mL^{-1} and c = 290 mg mL^{-1} gave similar results: The tetramers **12a** and **12b** are characterized by two sets of signals at −84.5 (27%)/−140.7 (33%) and at δ = −87.0 (11%)/−139.5 (10%). It is most likely that the signal at δ = −140.7 is superimposed with two resonances of the corresponding dimer. This assumption is supported by the observation of only six additional resonances at δ = −68.5 (5%), −70.6 (1%), −83.8 (5%), −85.6 (1%), −143.2 (2%), and −144.9 (5%) for the *cis* and the *trans* isomer of the dimer **12d** instead of the expected eight signals.

On the basis of the ^{119}Sn NMR spectroscopic experiments in $CDCl_3$ at c = 145 mg mL^{-1} the dimer/tetramer ratio of **12** was estimated to be approximately 1:1, which is in accordance with the molecular mass determination at the same concentration. It is worth noting that signals of the symmetrically substituted double ladders **13**−**15** are not detected in the ^{119}Sn NMR spectra of analytically pure **9** or **12**.

The structure of the double ladders can formally be divided into a spacer-bridged organostannoxane core to which two spacer-bridged ditin tetrachlorides $RCl_2Sn(CH_2)_4SnCl_2R$ are coordinated. The addition of $RCl_2Sn(CH_2)_4SnCl_2R$ (**10**, R = Me_3SiCH_2) to a solution of **12** in a 1:1 molar ratio gave a partial exchange (Scheme 6). The ^{119}Sn NMR spectrum in $CDCl_3$ shows the signals of the starting materials $RCl_2Sn(CH_2)_4SnCl_2R$ (**10**, R = Me_3SiCH_2) and **12**, a resonance at δ = −113.0 assigned to $RCl_2Sn(CH_2)_4SnCl_2R$ (**3**, R = Me_3CCH_2), two resonances at δ = −67.7 and −138.4 assigned to the simple double ladder **13**, and additional resonances at δ = −85.7, −100 ($W_{1/2}$ = 600 Hz), and −147 ($W_{1/2}$ = 600 Hz), for which no assignment is made.

In the case of the trimethylene-bridged double ladder $\{[R(Cl)Sn(CH_2)_3Sn(Cl)R]O\}_4$ (R = Me_3SiCH_2), no exchange was observed upon addition of a trimethylene-bridged ditin tetrachloride $RCl_2Sn(CH_2)_3SnCl_2R$ (R = Me_3CCH_2), which hints at the higher kinetic stability of the former compound compared with the tetramethylene-bridged double ladders.

The electrospray mass spectra of **9** and **12**, in acetonitrile/dichloromethane solution (9:1), show cluster patterns that are consistent with the species formed by ionization of dimers as well as of tetrameric double ladder compounds. The negative ion ESMS spectrum of **9** shows a cluster pattern which is centered at m/z = 2040 and which is assigned to the major species [**9a**−**c** + Cl]$^-$ (calcd. m/z = 2071), [**9a**−**c** + OH]$^-$ (calcd. m/z = 2051), and [**9a**−**c** − Cl + 2 OH]$^-$ (calcd. m/z = 2033). Compound **12** shows a similar cluster pattern centered at m/z = 2170 which is indicative of the species [**12a**−**c** + Cl]$^-$ (calcd. m/z = 2191), [**12a**−**c** + OH]$^-$ (calcd. m/z = 2173), and [**12a**−**c** − Cl + 2 OH]$^-$ (calcd. m/z = 2153). Species corresponding to the symmetrically substituted double ladders $\{[R(Cl)Sn(CH_2)_4Sn(Cl)R]O\}_4$ (**13**, R = Me_3SiCH_2; **14**, R = Me_3CCH_2; **15**, R = Me_2CHCH_2) were not observed, which, in accordance with the NMR spectroscopic experiments discussed above, shows that there is no equilibrium between mixed double ladders and symmetrically substituted double ladders. In the ESMS spectrum of **9** and **12**, additional cluster patterns are observed which are centered at m/z = 1032 and m/z = 1105, respectively. These patterns are assigned to doubly charged species such as [**9a**−**c** + 2 OH]$^{2-}$ (calcd. m/z = 1034) and [**9a**−**c** − Cl + 3 OH]$^{2-}$ (calcd. m/z = 1025) and [**12a**−**c** + 2 OH]$^{2-}$ (calcd. m/z = 1095) and [**12a**−**c** + 2 Cl]$^{2-}$ (calcd. m/z = 1113), rather than to the corresponding anions of the dimers **9d** and **12d**. Nevertheless, we cannot exclude that the cluster patterns of the latter are superimposed by the patterns of the doubly charged species. There are also cluster patterns of low intensity at m/z = 531 and m/z = 558 (**9**), and m/z = 558 and m/z = 590 (**12**), which are consistent with the anions **A**−**C** (Scheme 7). The formation of **A**−**C** can be explained by the dissociation of the dimers **9d**/**12d** and the complexation of a chloride.

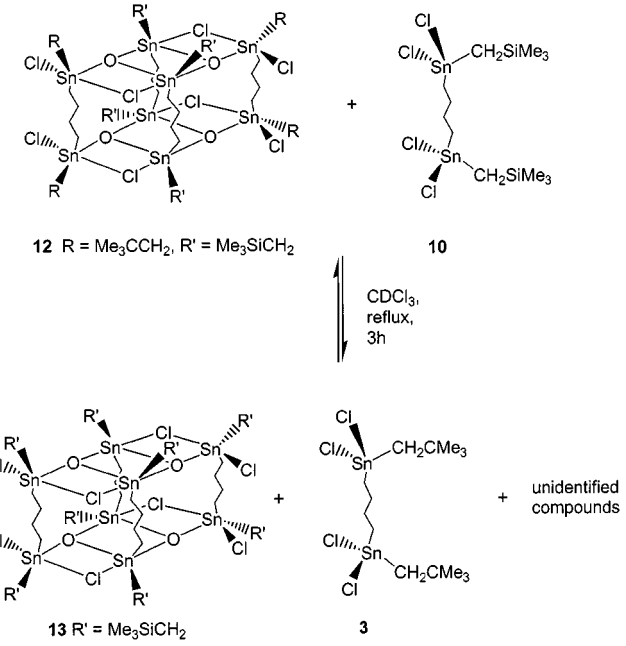

Scheme 6. Reaction of the mixed tetramethylene-bridged tetraorganodistannoxane **12** with the tetramethylene-bridged ditin tetrachloride **10**

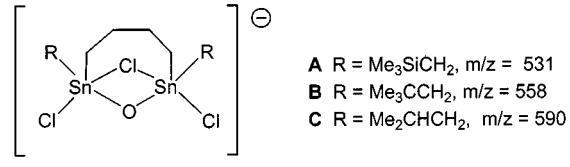

Scheme 7

In the ESMS spectra of both **9** and **12**, patterns of high intensity were observed, which are assigned to the complexes [$RCl_2Sn(CH_2)_4SnCl_2R$ + Cl]$^-$ (**9**, R = Me_3CCH_2

with m/z = 613, Me_2CHCH_2 with m/z = 585; **12**, R = Me_3CCH_2 with m/z = 613, Me_3SiCH_2 with m/z = 645). This observation is in agreement with the NMR spectroscopic experiment showing partial exchange of the tetrachloride fragment $RCl_2Sn(CH_2)_4SnCl_2R$ (**3**, R = Me_3CCH_2) in **12** upon addition of $RCl_2Sn(CH_2)_4SnCl_2R$ (**10**, R = Me_3SiCH_2) to a $CHCl_3$ solution of **12** (Scheme 6).

Conclusion

The synthesis of a mixed double ladder starting from the unsymmetrically substituted $(Me_3SiCH_2)Cl_2Sn(CH_2)_3SnCl_2Ph$ (**6**) failed. However, two convenient synthetic methods for the preparation of the first mixed double ladders $\{[R(Cl)Sn(CH_2)_4Sn(Cl)R][R'(Cl)Sn(CH_2)_4Sn(Cl)R']O_2\}_2$ (**9**, R = Me_3CCH_2, R′ = Me_2CHCH_2; **12**, R = Me_3CCH_2, R′ = Me_3SiCH_2) and their characterization by X-ray crystallography are given. In contrast to the previously reported trimethylene-bridged double ladders, the tetramethylene-bridged species are kinetically labile in solution and mixed double ladders are formed by scrambling reactions between the related simple double ladders. Furthermore, the mixed tetramethylene-bridged species seem to be thermodynamically more stable than the related simple species, since no simple double ladders were detected after the quantitative formation of the mixed double ladder compounds. Nevertheless, the partial substitution of fragments such as $RCl_2Sn(CH_2)_4SnCl_2R$ in the mixed double ladders is possible. These observations give an explanation for the fact that tetramethylene-bridged organostannoxanes are more efficient catalysts in transesterification reactions than the trimethylene-bridged analogues.[18] This work is a further step toward the fine tuned catalyst design of spacer-bridged distannoxanes.

Experimental Section

General Remarks: All solvents were dried and purified by standard procedures. − Bruker DPX-300 and DRX-400 spectrometers were used to obtain ^1H and ^{119}Sn NMR spectra. ^1H and ^{119}Sn chemical shifts δ are given in ppm and were referenced against Me_4Si and Me_4Sn, respectively. No integration of the signals in the ^1H NMR spectra is given as a result of their partial superimposition. − Molecular mass determinations were performed with a Knaur osmometer in $CHCl_3$ at 59 °C. − The organotin chlorides $RCl_2Sn(CH_2)_4SnCl_2R$ (**3**, R = Me_3CCH_2; **4**, R = Me_2CHCH_2; **10**, R = Me_3SiCH_2) and oxides $[R(O)Sn(CH_2)_4Sn(O)_2R]_n$ (**8**, R = Me_3CCH_2; **7**, R = Me_2CHCH_2; **11**, R = Me_3SiCH_2) were prepared according to literature procedures.[18] − Electrospray mass spectra were obtained with a Platform II single quadrupole mass spectrometer (Micromass, Altrincham, UK) using an acetonitrile/dichloromethane (9:1) mobile phase. Acetonitrile/dichloromethane solutions (0.1 mM) of the compounds were injected directly into the spectrometer using a Rheodyne injector equipped with a 100 μL loop. A Harvard 22 syringe pump delivered the solutions to the vaporization nozzle of the electrospray ion source at a flow rate of 10 μL min^{-1}. Nitrogen was used as both a drying gas and for nebulization with flow rates of approximately 200 mL min^{-1} and 20 mL min^{-1}, respectively. Pressure in the mass analyzer region was usually about $4\cdot10^{-5}$ mbar. Typically, 50 signal-averaged spectra were collected.

Synthesis of $(Me_3SiCH_2)Cl_2Sn(CH_2)_3SnCl_2Ph$ (6): To a solution of hexaphenyldistannane (2.00 g, 2.86 mmol) and naphthalene (100 mg, 1.28 mmol) in THF (30 mL), sodium (0.14 g, 6.09 mmol) was added in small portions. After stirring the resulting solution for 18 h, a solution of (3-chloropropyl)diphenyl(trimethylsilylmethyl)tin (**2**) (1.25 g, 2.86 mmol) in THF (10 mL) was added dropwise at −50 °C. The resulting suspension was stirred for 48 h during which time it was warmed up. The resulting solid material was filtered. After evaporation of the solvent, the resulting crude oily product was dissolved in hot hexane (5 mL) and the solid material was filtered. The solvent was removed in vacuo, giving 2.99 g 1-[diphenyl(trimethylsilylmethyl)stannyl]-3-(triphenylstannyl)-propane (**5**) as a yellow oil {^{119}Sn NMR ($CHCl_3/CDCl_3$, 111.92 MHz): δ = −63.5 [$^4J(^{119}Sn-^{117/119}Sn)$ = 56 Hz], −103.9 [$^4J(^{119}Sn-^{117/119}Sn)$ = 54 Hz]}. The intermediate product **5** was dissolved in acetone (20 mL) and a solution of $HgCl_2$ (4.32 g, 15.88 mmol) in acetone (20 mL) was added dropwise at 0 °C. The suspension was stirred overnight and filtered. The solvent was removed in vacuo giving an oily residue, which was suspended in diethyl ether (50 mL). Again, it was filtered and the solvent was evaporated. The resulting solid residue was extracted with hexane (40 mL) in a Soxhlet apparatus for 72 h, giving 1.77 g (53%) of **6** as a beige solid with a m.p. of 74−75 °C. − ^1H NMR (400.13 MHz, $CDCl_3$): δ = 0.17 (s, 9 H, $SiMe_3$), 0.88 [s, 2 H, $SiCH_2$, $^2J(^{119}Sn-^1H)$ = 93 Hz], 1.83 (t, 2 H, $SnCH_2$), 2.07 (t, 2 H, $SnCH_2$), 2.39 (quint, 2 H, CH_2), 7.48−7.63 (m, 5 H, H_{Ph}). − ^{13}C NMR ($CDCl_3$, 100.63 MHz): δ = 1.0 ($SiMe_3$), 11.9 [$^1J(^{13}C-^{119}Sn)$ = 226 Hz, CH_2Si], 20.9 (CH_2), 27.6 [$^1J(^{13}C-^{119}Sn)$ = 369 Hz, CH_2Sn], 29.2 [$^1J(^{13}C-^{119}Sn)$ = 331 Hz, CH_2Sn], 129.6 [$^3J(^{13}C-^{119}Sn)$ = 60 Hz, C_m], 131.7 [$^4J(^{13}C-^{119}Sn)$ = 27 Hz, C_p], 134.6 [$^2J(^{13}C-^{119}Sn)$ = 48 Hz, C_o], 138.6 [$^1J(^{13}C-^{119}Sn)$ = 598 Hz, C_i]. − ^{119}Sn NMR (111.92 MHz, $CHCl_3/CDCl_3$): δ = 38.2 [$^4J(^{119}Sn-^{117/119}Sn)$ = 158 Hz], 130.0 [$^4J(^{119}Sn-^{117/119}Sn)$ = 159 Hz]. − $C_{13}H_{22}Cl_4SiSn_2$ (585.7): calcd. C 26.66, H 3.79; found C 26.30, H 3.80.

Reaction of $(Me_3SiCH_2)Cl_2Sn(CH_2)_3SnCl_2Ph$ (6) with $(tBu_2SnO)_3$ (NMR Spectroscopic Experiment): $(tBu_2SnO)_3$ (140 mg, 0.56 mmol) was added to a solution of $(Me_3SiCH_2)Cl_2Sn(CH_2)_3SnCl_2Ph$ (**6**) (330 mg, 0.56 mmol) in CH_2Cl_2 (3 mL). The resulting solution was heated at reflux for 5 min. The solvent was evaporated, the residue washed with pentane (5 mL) and dissolved in CH_2Cl_2 (2.5 mL). A ^{119}Sn NMR spectrum of this solution was measured. − ^{119}Sn NMR (111.91 MHz, $CH_2Cl_2/D_2O_{capillary}$) δ = −53.7 ($tBu_2SnCl_2$), −84.5 [$^2J(^{119}Sn-^{117/119}Sn)$ = 73 Hz], −86.4 [$^2J(^{119}Sn-^{117/119}Sn)$ = 75 Hz], −90.8 [$^2J(^{119}Sn-^{117/119}Sn)$ = 73 Hz], −92.2 [$^2J(^{119}Sn-^{117/119}Sn)$ = 72 Hz], −94.2, −96.2 [$^2J(^{119}Sn-^{117/119}Sn)$ = 60 Hz], −100.2 [$^2J(^{119}Sn-^{117/119}Sn)$ = 62 Hz], −132.1 [$^2J(^{119}Sn-^{117/119}Sn)$ = 71 Hz], −132.3, −132.5 [$^2J(^{119}Sn-^{117/119}Sn)$ = 72 Hz], −134.5 [$^2J(^{119}Sn-^{117/119}Sn)$ = 68 Hz], −137.6 [$^2J(^{119}Sn-^{117/119}Sn)$ = 63 Hz], −164.1, −165.4, −166.2, −168.5 [$^2J(^{119}Sn-^{117/119}Sn)$ = 78 Hz], −170.5, −209.5, −209.7, −210.9 [$^2J(^{119}Sn-^{117/119}Sn)$ = 83 Hz], −212.2 [$^2J(^{119}Sn-^{117/119}Sn)$ = 88 Hz], −214.0 [$^2J(^{119}Sn-^{117/119}Sn)$ = 73 Hz], −214.9 [$^2J(^{119}Sn-^{117/119}Sn)$ = 82 Hz].

[Synthesis of $\{[R(Cl)Sn(CH_2)_4Sn(Cl)R]_2[R'(Cl)Sn(CH_2)_4Sn(Cl)R']_2O_2\}_2$ (9, R = Me_3CCH_2, R′ = Me_2CHCH_2). − Method A:

$[R(O)Sn(CH_2)_4Sn(O)R]_n$ (R = Me_2CHCH_2) (100 mg, 0.23 mmol) was added to a solution of $RCl_2Sn(CH_2)_4SnCl_2R$ (R = Me_3CCH_2) (131 mg, 0.23 mmol) in toluene (25 mL) at room temperature. The resulting suspension was stirred at room temperature for 1 h and heated at reflux for 2 h until the solution became clear. Crystallization from toluene at room temperature yielded 218 mg (94%) of **9** as colorless crystals with m.p. 214−216 °C. − **Method B:** $[R(O)Sn(CH_2)_4Sn(O)_2R]_n$ (R = Me_3CCH_2) (100 mg, 0.21 mmol) was added to a solution of $RCl_2Sn(CH_2)_4SnCl_2R$ (R = Me_2CHCH_2) (117 mg, 0.21 mmol) in toluene (25 mL) at room temperature. The resulting suspension was stirred at room temperature for 1 h and heated at reflux for 2 h until the solution became clear. Crystallization from toluene at room temperature yielded 203 mg (94%) of **9** as colorless crystals with m.p. 214−216 °C. − **Method C (in situ Preparation, NMR Spectroscopic Experiment):** $\{[R(Cl)Sn(CH_2)_4Sn(Cl)R]O\}_4$ (**15**, R = Me_2CHCH_2) (53 mg, 0.24 mmol) was added to a solution of $\{[R(Cl)Sn(CH_2)_4Sn(Cl)R]O\}_4$ (**14**, R = Me_3CCH_2) (50 mg, 0.24 mmol) in $CDCl_3$ (2 mL), and the resulting solution was heated at reflux for 3 d. A ^{119}Sn NMR spectrum of this solution was recorded after t = 4 d. − ^{119}Sn NMR (149.21 MHz, $CDCl_3$) δ = −78.2 [$^2J(^{119}Sn-^{117/119}Sn)$ = 74 Hz, 7%], −83.0 [$^2J(^{119}Sn-^{117/119}Sn)$ = 61 Hz, 36%], −84.2 [$^2J(^{119}Sn-^{117/119}Sn)$ = 57 Hz, 7%], −144.4 [$^2J(^{119}Sn-^{117/119}Sn)$ = 66 Hz, 14%], −145.2 [$^2J(^{119}Sn-^{117/119}Sn)$ = 70 Hz, 35%], −146.9 (1%). − ^{119}Sn NMR (111.92 MHz, toluene/D_2O cap.): δ = −78.7 [$^2J(^{119}Sn-^{117/119}Sn)$ = 67 Hz, 5%], −85.2 [$^2J(^{119}Sn-^{117/119}Sn)$ = 65 Hz, 26%], −85.4 (4%), −86.4 [$^2J(^{119}Sn-^{117/119}Sn)$ = 65 Hz, 15%], −147.9 [$^2J(^{119}Sn-^{117/119}Sn)$ = 66 Hz, 15%], −148.5 [$^2J(^{119}Sn-^{117/119}Sn)$ = 67 Hz, 27%], −150.2 (5%), −152.7 (3%). − ^{1}H NMR (400.13 MHz, C_6D_6): δ = 1.04 (d, Me_2CH), 1.16 (s, Me_3C), 1.17 (s, Me_3C), 1.23 (d, Me_2CH), 1.24 (d, Me_2CH), 1.40 (s, Me_3C), 1.90−2.42 (complex pattern, CH_2), 2.47 (m, Me_2CH), 2.76 (m, Me_2CH). − Molecular mass determination ($CHCl_3$, 20 mg mL^{-1}): 1639 g mol^{-1}. − $C_{52}H_{112}Cl_8O_4Sn_8$ (2035.0): calcd. C 30.69, H 5.55; found calcd. C 30.61, H 5.58%.

Synthesis of $\{[R(Cl)Sn(CH_2)_4Sn(Cl)R]_2[R'(Cl)Sn(CH_2)_4Sn(Cl)R']_2O_2\}_2$ (12, R = Me_3CCH_2, R′ = Me_3SiCH_2). − Method A: In a similar manner to compound **9** the distannoxane **12** was prepared from $RCl_2Sn(CH_2)_4SnCl_2R$ (R = Me_3CCH_2) (347 mg, 0.60 mmol) and $[R(O)Sn(CH_2)_4Sn(O)R]_n$ (R = Me_3SiCH_2) (300 mg, 0.60 mmol), and obtained as a colorless solid (0.62 g, 96%) with m.p. 197−198 °C. − **Method B:** Analogously the reaction of $RCl_2Sn(CH_2)_4SnCl_2R$ (R = Me_3SiCH_2) (456 mg, 0.75 mmol) and $[R(O)Sn(CH_2)_4Sn(O)R]_n$ (R = Me_3CCH_2) (350 mg, 0.75 mmol) gave **12** as a colorless solid (0.79 g, 98%). − **Method C (NMR Spectroscopic Experiment):** $\{[R(Cl)Sn(CH_2)_4Sn(Cl)R]O\}_4$ (**13**, R = Me_3SiCH_2) (53 mg, 0.24 mmol) was added to a solution of $\{[R(Cl)Sn(CH_2)_4Sn(Cl)R]O\}_4$ (**14**, R = Me_3CCH_2) (50 mg, 0.24 mmol) in $CDCl_3$ (2 mL), and the resulting solution was heated at reflux for 3 d. ^{119}Sn NMR spectra of this solution were recorded after t = 1 h, 1 d, and 3 d. − ^{119}Sn NMR (149.21 MHz, $CDCl_3$): δ = −68.5 (5%), −70.6 (1%), −83.8 (5%), −84.5 (27%), −85.6 (1%), −87.0 (11%), −139.5 (10%), −140.7 (33%), −143.2 (2%), −144.9 (5%). − ^{119}Sn NMR (111.92 MHz, toluene, D_2O cap.): δ = −68.8 (5%), −71.3 (2%), −83.3 [$^2J(^{119}Sn-^{117/119}Sn)$ = 67 Hz, 5%], −83.8 [$^2J(^{119}Sn-^{117/119}Sn)$ = 66 Hz, 23%], −85.4(3%), −86.9 [$^2J(^{119}Sn-^{117/119}Sn)$ = 66 Hz, 11%], −143.0 (3%), −144.3 [$^2J(^{119}Sn-^{117/119}Sn)$ = 66 Hz, 12%], −145.5 [$^2J(^{119}Sn-^{117/119}Sn)$ = 67 Hz, 23%], −146.2 [$^2J(^{119}Sn-^{117/119}Sn)$ = 67 Hz, 5%], −147.9 (3%), −149.4 [$^2J(^{119}Sn-^{117/119}Sn)$ = 67 Hz, 5%]. − ^{1}H NMR (400.13 MHz, [D_8]toluene): δ = 0.21 (s, Me_3Si), 0.22 (s, Me_3Si), 0.41 (s, Me_3Si), 1.08 (s, Me_3C), 1.11 (s, CH_2Si), 1.15 (s, Me_3C), 1.19 (s, CH_2Si), 1.34 (s, Me_3C), 1.36 (s, CH_2Si), 1.85−2.21 (complex pattern, CH_2). − Molecular mass determination ($CHCl_3$, 20 mg mL^{-1}): 1191 g mol^{-1}, ($CHCl_3$, 145 mg mL^{-1}): 1689 g mol^{-1}. −

Table 3. Crystallographic data for **9** and **12**

	9	**12**
Empirical formula	$C_{52}H_{112}Cl_8O_4Sn_8$	$C_{52}H_{120}Cl_8O_4Si_4Sn_8{\cdot}C_6H_6$
Formula mass	2034.54	2233.07
Crystal system	triclinic	triclinic
Crystal size [mm]	0.20 × 0.20 × 0.20	0.30 × 0.25 × 0.20
Space group	$P\bar{1}$	$P\bar{1}$
a [Å]	10.996(1)	12.746(1)
b [Å]	12.247(1)	13.529(1)
c [Å]	16.807(1)	16.117(1)
α [°]	69.019(1)	79.424(1)
β [°]	87.145(1)	69.207(1)
γ [°]	65.013(1)	62.388(1)
V [Å^3]	1901.7(3)	2301.7(3)
Z	1	1
$\rho_{calcd.}$ [Mg/m^3]	1.777	1.611
μ [mm^{-1}]	2.898	2.451
F(000)	992	1098
θ range [°]	2.98 to 25.68	3.16 to 25.37
Index ranges	$-13 \le h \le 13$ $-12 \le k \le 14$ $-20 \le l \le 20$	$-12 \le h \le 12$ $-13 \le k \le 16$ $-18 \le l \le 19$
No. of reflns. collected	18520	26367
Completeness to θ_{max}	85.3	92.3
no. of independent reflns./R_{int}	6156/0.0580	7805/0.0260
no. of reflns. observed with [$I > 2\sigma(I)$]	2780	3885
no. of refined param.	335	406
GooF (F^2)	0.822	0.939
$R1$ (F) [$I > 2\ \sigma(I)$]	0.0431	0.0371
$wR2$ ($F2$) (all data)	0.1312	0.1021
$(\Delta/\sigma)_{max}$	< 0.001	< 0.001
Largest diff peak/hole [e/Å^3]	0.714/−0.776	0.539/−0.484

$C_{52}H_{120}Cl_8O_4Si_4Sn_8$ (2155.4): calcd. C 28.98, H 5.61; found calcd. C 29.35, H 5.45.

Reaction of $\{[R(Cl)Sn(CH_2)_4Sn(Cl)R]_2[R'(Cl)Sn(CH_2)_4Sn(Cl)R']_2O_2\}_2$ (12, R = Me_3CCH_2, R' = Me_3SiCH_2) with $RCl_2Sn(CH_2)_4SnCl_2R$ (3, R = Me_3CCH_2) (NMR Spectroscopic Experiment): Compound **3** (72 mg, 0.34 mmol) was added to a solution of **12** (72 mg, 0.34 mmol) in $CDCl_3$ (2 mL). The resulting solution was heated at reflux for 3 h and a ^{119}Sn NMR spectrum was recorded. − ^{119}Sn NMR (149.21 MHz, $CDCl_3$): δ = −131.4, −113.0, −66.7, −67.5, −69.7, −82.9, − 83.5, −84.7, −85.3, −86.1, −100 ($W_{1/2}$ = 600 Hz), −137.4, −138.5, −139.6, −142.4, −144.8, −147 ($W_{1/2}$ = 600).

Addition of $RCl_2Sn(CH_2)_3SnCl_2R$ (R = Me_3CCH_2) to a Solution of $\{[R(Cl)Sn(CH_2)_3Sn(Cl)R]O\}_4$ (R = Me_3SiCH_2) (NMR Spectroscopic Experiment): $RCl_2Sn(CH_2)_3SnCl_2R$ (R = Me_3CCH_2) (56 mg, 0.10 mmol) was added to a solution of the double ladder (216 mg, 0.10 mmol) in CH_2Cl_2 (3 mL). The resulting solution was heated at reflux for 2 h and a ^{119}Sn NMR spectrum (149.21 MHz, CH_2Cl_2/D_2O cap.) was recorded which showed the signals of the starting materials at δ = −96.1 [$^2J(^{119}Sn-^{117/119}Sn)$ = 67 Hz], −132.9 [$^2J(^{119}Sn-^{117/119}Sn)$ = 69 Hz] and δ = 107.9 [$RCl_2Sn(CH_2)_3SnCl_2R$, R = Me_3CCH_2].

Crystallography: Intensity data for the colorless crystals grown from benzene were collected with a Nonius KappaCCD diffractometer with graphite-monochromated Mo-K_α (0.71069 Å) radiation at 291 K. The data collection covered almost the whole sphere of reciprocal space with 360 frames by ω-rotation (Δ/ω = 1°) at two times 10 s (**9**) and 20 s (**12**) per frame. The crystal-to-detector distance was 2.7 cm (**9**) and 3.0 cm with a detector-θ-offset of 5° (**2**). Crystal decay was monitored by repeating the initial frames at the end of data collection. On analysis of the duplicate reflections, there was no indication for any decay. The data were not corrected for absorption effects. The structure was solved by direct methods SHELXS97[25] (Sheldrick, **1990**) and successive difference Fourier syntheses. Refinement applied full-matrix least-squares methods SHELXL97[26] (Sheldrick, **1997**). − The H atoms were placed in geometrically calculated positions using a riding model ($C-H_{prim.}$ 0.96 Å, $C-H_{sec.}$ 0.97 Å; H_{aryl} C−H 0.93), and for **9** refined with a common isotropic temperature factor [U_{iso} 0.148(7) Å^2] and for **12** with isotropic temperature factors constrained to be 1.5 times those of the carrier atom. − Disordered tetramethylene, *tert*-butyl (**12**), and isobutyl (**9**) groups were found with occupancies of 0.3333 [C(43′), C(44′)], 0.5 [C(3), C(5), C(3′), C(5′)], and 0.6666 [C(43), C(44)] in **12** and of 0.15 [C(32′)] and 0.85 [C(32)] in **9**. − Atomic scattering factors for neutral atoms and real and imaginary dispersion terms were taken from International Tables for X-ray Crystallography.[27] The figures were created by SHELXTL[28] (Sheldrick, **1991**). Crystallographic data are given in Table 3 and selected bond lengths and angles in Table 1. Crystallographic data for the structures reported in this paper have been deposited with the Cambridge Crystallographic Data Centre as supplementary publications nos. CCDC-144264 (**9**) and CCDC-144265 (**12**). Copies of the data can be obtained free of charge on application to CCDC, 12 Union Road, Cambridge CB21EZ, UK [Fax: (internat.) + 44-1223/336-033; E-mail: deposit@ccdc.cam.ac.uk].

Acknowledgments

We thank the Deutsche Forschungsgemeinschaft, the Fonds der Chemischen Industrie and the Australian Research Council (ARC) for financial support.

[1] R. Okawara, M. Wada, *J. Organomet. Chem.* **1963**, *1*, 81−88.
[2] D. C. Gross, *Inorg. Chem.* **1989**, *28*, 2355−2359.
[3] A. G. Davies, *Organotin Chemistry*, VCH, Weinheim, **1997**.
[4] O. Primel, M.-F. Llauro, R. Pétiaud, A. Michel, *J. Organomet. Chem.* **1998**, *558*, 19−33.
[5] F. Ribot, C. Sanchez, A. Meddour, M. Gielen, E. R. T. Tiekink, M. Biesemans, R. Willem, *J. Organomet. Chem.* **1998**, *552*, 177−186.
[6] J. Otera, N. Dan-oh, H. Nozaki, *J. Org. Chem.* **1991**, *56*, 5307−5311.
[7] A. Orita, A. Mitsutome, J. Otera, *J. Org. Chem.* **1998**, *63*, 2420−2421.
[8] R. P. Houghton, A. W. Mulvaney, *J. Organomet. Chem.* **1996**, *517*, 107−113.
[9] E. N. Suciu, B. Kuhlmann, G. A. Knudsen, R. C. Michaelson, *J. Organomet. Chem.* **1998**, *556*, 41−54.
[10] Y. Meada, R. Okawara, *J. Organomet. Chem.* **1967**, *10*, 247−256.
[11] T. Yano, K. Nakashima, J. Otera, R. Okawara, *Organometallics* **1985**, *4*, 1501−1503.
[12] S. P. Narula, S. K. Bharadwaj, H. K. Sharma, G. Mairesse, P. Barbier, G. Nowogrocki, *J. Chem. Soc., Dalton Trans.* **1988**, 1719−1723.
[13] S. Brooker, F. T. Edelmann, D. Stalke, *Acta Crystallogr.* **1991**, *C47*, 2527−2529.
[14] D. Dakternieks, K. Jurkschat, S. van Dreumel, E. R. T. Tiekink, *Inorg. Chem.* **1997**, *36*, 2023−2029.
[15] U. Baumeister, D. Dakternieks, K. Jurkschat, M. Schürmann, *Main Group Met. Chem.,* manuscript submitted.
[16] J. F. Vollano, R. O. Day, R. R. Holmes, *Organometallics* **1984**, *3*, 745−750.
[17] T. Harada, *Rep. Sci. Res. Inst., Tokyo* **1948**, *24*, 177−181.
[18] M. Mehring, M. Schürmann, I. Paulus, D. Horn, K. Jurkschat, A. Orita, J. Otera, D. Dakternieks, A. Duthie, *J. Organomet. Chem.* **1999**, *574*, 176−192.
[19] D. Dakternieks, K. Jurkschat, D. Schollmeyer, H. Wu, *Organometallics* **1994**, *13*, 4121−4123.
[20] M. Schulte, M. Schürmann, D. Dakternieks, K. Jurkschat, *Chem. Commun.* **1999**, 1291−1292.
[21] B. Zobel, M. Schürmann, K. Jurkschat, D. Dakternieks, A. Duthie, *Organometallics* **1998**, *17*, 4096−4104.
[22] M. Mehring, M. Schürmann, H. Reuter, D. Dakternieks, K. Jurkschat, *Angew. Chem.* **1997**, *109*, 1150−1152; *Angew. Chem. Int. Ed. Engl.* **1997**, *36*, 1112−1114.
[23] M. Mehring, diploma thesis **1996**, University of Dortmund, Germany.
[24] P. G. Harrison, *Compounds of tin: general trends* (Ed.: P. J. Smith,); Blackie Academic & Professional, London, **1998**, vol. 1, pp. 10−61.
[25] G. M. Sheldrick, *Acta Crystallogr.* **1990**, *A46*, 467−473.
[26] G. M. Sheldrick, University of Göttingen, Germany, **1997**.
[27] *International Tables for Crystallography*, Dordrecht: Kluwer Academic Publishers, **1992**, vol. C.
[28] G. M. Sheldrick, *SHELXTL V5.1* Software Reference Manual, Bruker AXS, Inc., Madison, Wisconsin, USA, **1997**.

Received May 26, 2000
[I00217]

A General Synthetic Pathway to Lewis Base-Stabilized, Monomeric Group 13/15 Compounds

Florian Thomas,[a] Stephan Schulz,*[a] and Martin Nieger[a]

Keywords: Semiconductors / Heterocycles / Donor-acceptor systems / Cage compounds / Aluminum / Gallium

Reactions of an equimolar amount of 4-(dimethylamino)pyridine (dmap) with several Al–E heterocycles $[R_2AlE(SiMe_3)_2]_x$ (E = P, As; R = Me, x = 3; R = Et, x = 2) and Ga–Sb heterocycles $[R_2GaSb(SiMe_3)_2]_x$ (R = Me, x = 3; R = Et, x = 2) in hexane offers a general pathway for the formation of monomeric, Lewis base-stabilized compounds of the type dmap–$(R_2)ME(SiMe_3)_2$ (M = Al, R = Me, E = P **1**, As **2**; R = Et, E = As **3**; M = Ga, E = Sb, R = Me **4**, Et **5**). Compounds **1**, **2**, **3** and **5** have been characterized by single-crystal X-ray diffraction.

Introduction

Over the last two decades, the synthesis of monomeric group 13/15 compounds of the type $R_2MER'_2$ has received growing interest owing to their fascinating bonding properties.[1] In addition, compounds of the type $[R_2MER'_2]_x$, which may serve as so-called single-source precursors for the preparation of the corresponding semiconducting binary materials, are still in the focus of very intense studies. These compounds are usually obtained in the form of heterocycles (x = 2, 3), heterocubanes (x = 4) or more highly associated cages (x > 4), both in solution and in the solid state, as a result of the tendency of the triele atom to utilize its vacant p-valence orbital by increasing its coordination number from 3 to 4. Monomeric group 13/15 compounds $R_2MER'_2$ are only formed with sterically extremely bulky ligands on both M and E, which inhibit the formation of oligomers and lead to the formation of kinetically stabilized monomers.[2] Recently, we demonstrated a synthetic route for the formation of electronically stabilized monomeric compounds. Monomeric, Lewis base-stabilized organoaluminum stibides[3] and bismuthides[4] of the type dmap−$(R_2)AlE(SiMe_3)_2$ (E = Sb, Bi) were obtained by ring-cleavage reactions of the corresponding heterocycles $[R_2AlER'_2]_x$ with 4-(dimethylamino)pyridine (dmap). The triele atom is coordinatively and electronically saturated by interaction with the strong base, while the *lone pair* of the pentele atom is still active for coordination chemistry. Prior to our studies, only a few examples of structurally characterized, Lewis base-stabilized amino-, phosphanyl-, and arsanylalane monomers had been reported. $Me_3N-Al(H_2)NR_2$ and $Me_3N-Al(H_2)As(SiMe_3)_2$ were synthesized by the reaction of $H_3Al-NMe_3$ with sterically bulky secondary amines[5] and $As(SiMe_3)_3$,[6] respectively. Reactions of $H_2AlCl-NMe_3$ with $LiEMes_2$ (E = P, As; Mes = 2,4,6-$Me_3C_6H_2$) led to the formation of $Me_3N-Al(H_2)EMes_2$.[7] Unfortunately, no general pathway for the synthesis of this specific class of compounds has been developed so far. The reactions are limited to Me_3N-stabilized AlH_3 or H_2AlCl as starting compounds. However, the desired monomeric compounds are of particular interest because they may serve as general building blocks for the synthesis of bimetallic complexes of the type dmap−$(R_2)ME(R'_2)-M'L_n$ (M = triele; E = pentele; M′ = transition metal),[8] where the pentele atom bridges a "soft" transition metal and a "hard" main-group metal fragment.[9] Complexes of this type can be considered as transition metal derivatives of an amphoteric main group element ligand.[10] Up to now, $Me_3N-(Me_3SiCH_2)_2-AlP(Ph)_2-Cr(CO)_5$ is the only structurally characterized compound of this type, which was prepared in a very special reaction by Beachley et al.[10a,11] However, this specific reaction pathway couldn't be successfully expanded to the synthesis of other comparable bimetallic complexes.

In this paper we wish to present our extended studies on ring-cleavage reactions of Al−E heterocycles containing the lighter homologues of group 15, P and As, as well as on Ga−Sb heterocycles, demonstrating the general and convenient purpose of this particular reaction type for the synthesis of the desired class of compounds.

Results

The reaction of equimolar amounts of 4-(dimethylamino)-pyridine (dmap) with several Al−E heterocycles $[R_2AlE(SiMe_3)_2]_2$ (E = P, As; R = Me, Et) in hexane resulted in the formation of the corresponding Lewis base-stabilized monomers **1**−**3** in almost quantitative yield (Scheme 1). Monomers prepared in this way are extremely sensitive to-

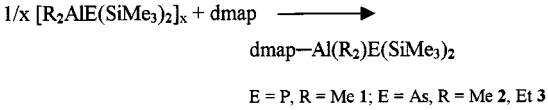

Scheme 1. Synthesis of monomeric, Lewis base-stabilized phosphanyl- and arsanylalanes

[a] Institut für Anorganische Chemie der Universität Bonn, Gerhard-Domagk-Straße 1, D-53121 Bonn, Germany
Fax: (internat.) +49-228/73-5327
E-mail: sschulz@uni-bonn.de

 © WILEY-VCH Verlag GmbH, 69451 Weinheim, 2001 1434−1948/01/0101−0161 $ 17.50+.50/0

wards air and moisture, particularly in solution. At −30 °C, compounds **1**−**3** were obtained as crystalline, light yellow solids.

The ^{1}H and ^{13}C NMR spectra of **1**−**3** show resonances due to the organic ligands bound to the metal centers and the expected resonances of dmap. Integration of the signals due to the organic ligands and dmap indicated a 1:1 stoichiometry of dmap:$R_2AlE(SiMe_3)_2$ (E = P, As; R = Me, Et). The proton resonances of the organic ligands bound to the metal centers appear further downfield (MeAl, EtAl, and Me_3Si resonances) than those of the starting heterocycles, while those of the dmap molecule are shifted upfield. These findings are in agreement with results observed for similar borane adducts,[12] and correspond to a partial rearrangement of the charge distribution within the aromatic ring as shown in Scheme 2.

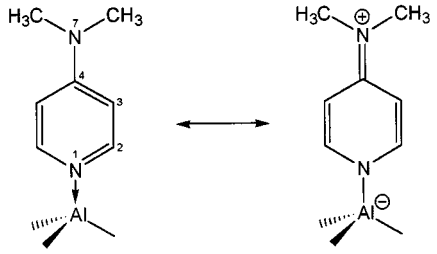

Scheme 2

Single-crystal X-ray analyses of **1** (Figure 1), **2** (Figure 2), and **3** (Figure 3) clearly show the presence of monomeric $R_2AlE(SiMe_3)_2$ molecules, to which one dmap molecule is coordinated. Compounds **2** and **3** crystallize in the triclinic space group $P\bar{1}$ (no. 2), while **1** crystallizes in the monoclinic space group $P2_1/c$ (no. 14). Both **1** and **2** crystallize with two independent molecules in the asymmetric unit.

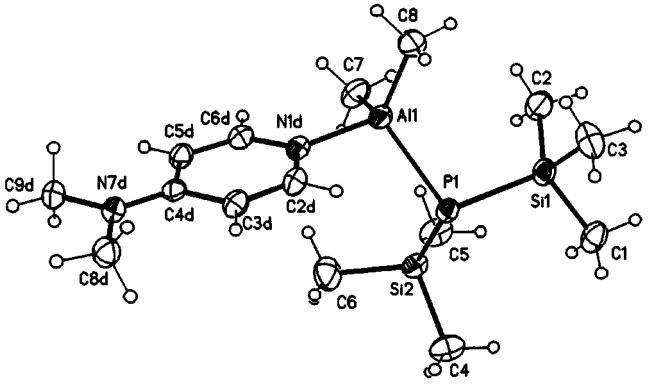

Figure 1. ORTEP diagram (50% probability ellipsoids) showing the solid-state structure and atom-numbering scheme for **1**; for clarity, only one independent molecule of the asymmetric unit is presented; selected bond lengths [pm] and angles [°]: Al1−N1d 198.4(2), Al1−P1 237.9(1), Al1−C7 197.7(2), Al1−C8 197.7(2), P1−Si1 223.6(1), P1−Si2 223.7(1); C7−Al1−C8 115.3(1), Si1−P1−Si2 104.8(1), N1d−Al1−P1 101.0(1), Si1−P1−Al1 102.5(1), Si2−P1−Al1 101.8(1)

As found in the corresponding monomers of the higher homologues dmap−$Al(R_2)E(SiMe_3)_2$ (R = Me, Et, E = Sb, Bi),[3,4] the substituents bonded to Al and the particular pentele atom adopt a staggered conformation relative to one another. The average Al−C bond lengths (**1**: 197.7, 197.5; **2**: 196.9, 196.6; **3**: 197.7 pm) and C−Al−C bond angles [**1**: 115.3(1), 114.6(1)°; **2**: 114.7(2), 115.7(2)°; **3**: 115.3(2)°] are within the expected ranges, while the E−Si bond lengths (**1**: 223.7, 222.9; **2**: 233.8, 233.9; **3**: 233.8 pm) are at the lower end of typical E−Si bond lengths.[13] They are only slightly shorter than in the starting compounds {average E−Si distances found in $[Me_2AlP(SiMe_3)_2]_2$: 225.9

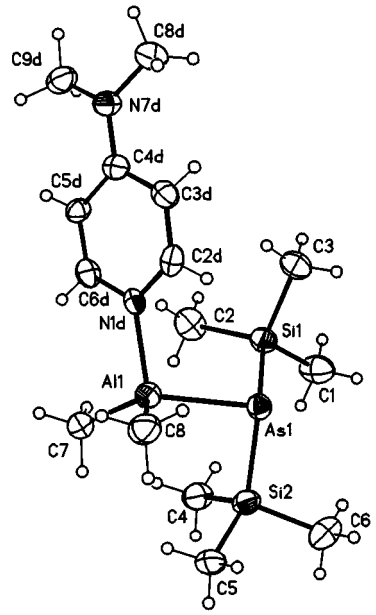

Figure 2. ORTEP diagram (50% probability ellipsoids) showing the solid-state structure and atom-numbering scheme for **2**; for clarity, only one molecule of the asymmetric unit is presented; selected bond lengths [pm] and angles [°]: Al1−N1d 197.5(4), Al1−As1 247.2(2), Al1−C7 196.5(4), Al1−C8 197.3(4), As1−Si1 233.7(2), As1−Si2 233.8(2); C7−Al1−C8 114.7(2), Si1−As1−Si2 101.1(1), N1d−Al1−As1 104.5(2), Si1−As1−Al1 105.0(1), Si2−As1−Al1 98.0(1)

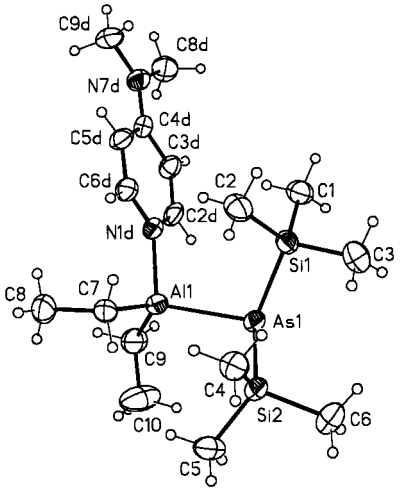

Figure 3. ORTEP diagram (50% probability ellipsoids) showing the solid-state structure and atom-numbering scheme for **3**; selected bond lengths [pm] and angles [°]: Al1−N1d 198.8(3), Al1−As1 247.3(1), Al1−C7 196.5(4), Al1−C9 198.9(3), As1−Si1 233.4(1), As1−Si2 234.1(1); C7−Al1−C9 115.3(2), Si1−As1−Si2 101.3(1), N1d−Al1−As1 105.0(1), Si1−As1−Al1 103.5(1), Si2−As1−Al1 101.8(1)

pm; $[Me_2AlAs(SiMe_3)_2]_2$: 234.5 pm; $[Et_2AlAs(SiMe_3)_2]_2$: 234.9 pm}.

The Al−N bond lengths [**1**: 198.4(2), 197.7(2); **2**: 197.5(4), 198.9(4); **3**: 198.8(3) pm] are almost the same as those observed in the corresponding monomeric compounds of the heavier group 15 elements dmap−(R_2)AlE$(SiMe_3)_2$ (R = Me, Et, E = Sb, Bi), indicating the strong donor capacity of dmap. In addition, the almost equal Al−N distances demonstrate that the particular pentele atom does not have a significant electronic influence on the Lewis acidity of the Al fragment. Typical Al−N distances of adducts with tricoordinated N centers are comparable [e.g. 2-methylpyridine−$AlCl_3$: 194.2(2) pm, stronger Lewis acid],[14] while adducts with tetracoordinated N centers show significantly longer Al−N distances [e.g. $Me_3Al-NMe_3$: 210(1) pm; $H_3Al-NMe_3$: 206.3(8) pm (gas phase); Me_3Al-NH_3: 200.4(5) pm (powder diffraction); H_3Al-tmp (tmp = 2,2,6,6-tetramethylpiperidine): 204(1) pm].[15] However, compounds containing stronger Lewis acids [e.g. $Cl_3Al-NMe_3$: 196(1) pm (single-crystal analysis)[16]; 194.5(35) pm (electron diffraction)[17]] show comparable Al−N distances. Compared to analogous Lewis base-stabilized monomers of the type $Me_3N\rightarrow Al(R_2)ER'_2$, the dmap adducts show the shortest Al−N distances [Al−N (in pm): $Me_3N\rightarrow Al(H_2)N(tmp)_2$ 205.8(2);[5a] $Me_3N\rightarrow Al(H)(Cl)N(SiMe_3)_2$ 201.6(5);[5b] $Me_3N\rightarrow Al(H_2)As(SiMe_3)_2$ 199.8(7);[6] $Me_3N\rightarrow Al(H_2)PMes_2$ 200.9(8)[7]].

The Al−P [237.9(1), 237.4(1) pm **(1)**] and Al−As bond lengths [247.2(2), 247.0(2) **(2)**, 247.3(1) pm **(3)**] are also relatively short. Comparable Al−P distances in phosphanylalanes were found in the monomeric compounds $Trip_2AlP(Ada)(SiPh_3)$ [234.2(2) pm][18] (Trip = 2,4,6-iPr$_3$C$_6$H$_2$) and Tmp_2AlPPh_2 [237.7(1) pm],[2a] while the Lewis base-stabilized monomer $Me_3N\rightarrow Al(H_2)PMes_2$ shows a slightly longer distance [240.9(3) pm].[7] The Al−As distances in **2** and **3** [247.2(2), 247.0(2); 247.3(1) pm] are almost the same as those in monomeric $Tmp_2AlAsPh_2$ [248.5(2) pm][2a] but slightly longer than those in $Me_3N\rightarrow Al(H_2)As(SiMe_3)_2$ [243.8(2) pm][6] and $Me_3N-Al(H)AsSi(iPr)_3]_2$.[19] The shortest Al−As distances were found in the borazine analogue [Mes*AlAsPh]$_3$·Et$_2$O (Mes* = 2,4,6-tBu$_3$C$_6$H$_2$), which, however, only has tricoordinated Al centers.[20] The comparable Lewis base-stabilized monomer $Me_3N-Al(H_2)As(SiMe_3)_2$ is sterically less hindered than **2** and **3** and contains a slightly stronger Lewis acidic Al center due to the weaker +I effect of the H- relative to the Me-substituents. The Al−P and Al−As distances agree very well with the sum of the covalent radii of the corresponding central atoms (Al−P: 235 pm; Al−As: 246 pm).[21] Interestingly, the starting heterocycles show significantly longer Al−E distances. The average Al−E distances found in $[Me_2AlP(SiMe_3)_2]_2$ (245.7 pm), $[Me_2AlAs(SiMe_3)_2]_2$ (253.6 pm) and $[Et_2AlAs(SiMe_3)_2]_2$ (253.5 pm) are elongated by 8 (Al−P) and 6 pm (Al−As), respectively. In contrast, the Al−E distances of the corresponding monomeric stibides [dmap−(Me_2)AlSb$(SiMe_3)_2$: 269.1(1) pm; dmap−(Et_2)AlSb$(SiMe_3)_2$: 267.9(1) pm][3] and bismuthide [dmap−(Me_2)AlBi$(SiMe_3)_2$: 275.5(2) pm][4] are on average less shortened (Al−Sb: 3−5 pm; Al−Bi: 2 pm) compared to those of the starting heterocycles {$[Me_2AlSb(SiMe_3)_2]_3$: 271.9 pm;[22] $[Et_2AlSb(SiMe_3)_2]_2$: 273.5 pm;[23] $[Me_2AlBi(SiMe_3)_2]_3$: 277.4 pm[24]}. Obviously, intramolecular steric repulsion between the ligands is less intense within the heterocycles of the heavier homologues of group 15 owing to the increasing atomic radii of the penteles from P to Bi.

Besides the structural similarity of **1**, **2**, **3**, and the higher homologues dmap−(R_2)AlE$(SiMe_3)_2$ (R = Me, Et, E = Sb, Bi)[3,4] in almost every structural feature, the compounds show one remarkable difference: The Si−E−Si and Si−E−Al bond angles decrease significantly with increasing atomic number of the group 15 element. While the Si−P−Si angles in **1** are 104.8(1) and 102.9(1)°, the corresponding Si−As−Si angles in **2** [101.1(1) and 101.9(1)°] and **3** [101.3(1)°] are smaller. The corresponding stibides dmap−Al(R_2)Sb$(SiMe_3)_2$ [R = Me 97.6(2)°; Et 99.1(1)°] and bismuthides dmap−Al(R_2)Bi$(SiMe_3)_2$ [R = Me 95.7(1)°; Et 97.4(1)°] again show significantly reduced angles. These findings are in agreement with the well-known tendency within group 15 trihydrides H_3E, which show constantly decreasing H−E−H angles from 106.8° (NH_3)[25] to 91.3° (SbH_3),[26] as well as in triphenyl [C−E−C angles decrease from 102.8° (PPh_3), 100.1° ($AsPh_3$), 97.8° ($SbPh_3$) to 93.9° ($BiPh_3$)][27] and trimethyl derivatives Me_3E [C−E−C angles decrease from 110.6° (NMe_3)[28] to 94.2° ($SbMe_3$)].[29] Only $BiMe_3$ shows a slightly bigger C−Bi−C angle of 96.7°.[30] The smaller bond angles of the stibides and bismuthides relative to the amides result both from the decreased steric repulsion between the $SiMe_3$ groups owing to the increased E−Si bond length and from the increased s-character of the *lone pair* and the increased p-character of the bonding electron pairs due to relativistic effects and the lanthanide-contraction (inert-pair effect).[31]

In an attempt to prove the generality of the described reaction pathway for the synthesis of group 13/15 monomers, we also investigated reactions of Ga−Sb heterocycles $[R_2GaSb(SiMe_3)_2]_x$ (R = Me, x = 3; R = Et, x = 2) with dmap. Again, the monomeric compounds dmap−Ga(R_2)Sb$(SiMe_3)_2$ (R = Me **4**, Et **5**, Scheme 3) were obtained in almost quantitative yield. However, they are more temperature labile than the Al derivatives and start to decompose significantly at room temperature both in solution and in the solid state. Therefore, the reaction has to be performed between −10 and 0 °C and the resulting monomers have to be stored at −30 °C.

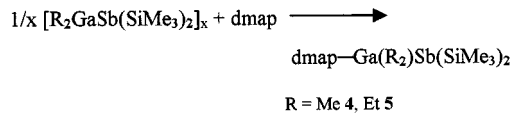

Scheme 3. Synthesis of monomeric, Lewis base-stabilized stibinogallanes

Single crystals of **5** were obtained from a solution in hexane at −30 °C. Compound **5** crystallizes in the triclinic space group $P\bar{1}$ (no. 2). **5** (Figure 4) is isostructural to the corresponding Al derivative dmap−Al(Et_2)Sb$(SiMe_3)_2$[3] and shows comparable Ga−C (199.4 pm) and Sb−Si distances

(255.0 pm) as well as C−Ga−C [117.2(2) °] and Si−Sb−Si bond angles [99.3(1) °].

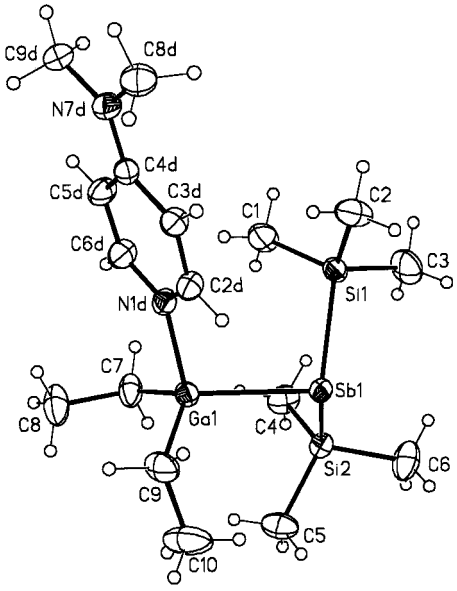

Figure 4. ORTEP diagram (50% probability ellipsoids) showing the solid-state structure and atom-numbering scheme for **5**; selected bond lengths [pm] and angles [°]: Ga1−N1d 206.6(2), Ga1−Sb1 264.8(1), Ga1−C7 198.5(2), Ga1−C9 200.3(2), Sb1−Si1 254.8(1), Sb1−Si2 255.3(1); C7−Ga1−C9 117.2(2), Si1−Sb1−Si2 99.3(1), N1d−Ga1−Sb1 103.6(1), Si1−Sb1−Ga1 100.6(1), Si2−Sb1−Ga1 99.3(1)

In contrast, the Ga−N distance is much longer [206.6(2) pm], demonstrating the reduced Lewis acidity of the Et_2Ga- relative to the Et_2Al-fragment, but almost the same as in 2-(methyl)pyridine−$Ga(Me_2)Cl$ [206.6(3) pm].[32] However, 4-(methyl)pyridine−$Ga(Mes_2)SeMes$, which also contains a tricoordinated N base, shows a slightly longer Ga−N distance [209.5(3) pm],[33] while in the methylene-bridged compound $Me_3N{-}Ga(CH_2CMe_2)CH_2P(Ph_2){-}Cr(CO)_5$, which contains a tetracoordinated N center, the Ga−N distance is significantly increased [223.5(3) pm].[10c] Very recently, Gladfelter et al. described the synthesis of several quinuclidine-stabilized amido- and azidogallanes by the reaction of quinuclidine-stabilized dichlorogallane quin−$Ga(H)Cl_2$ with Li amides and azides. The X-ray structures of four compounds showed dative Ga−N distances between 206 and 210 pm,[34] which are comparable to that found in $Me_3N{-}GaH_3$ [208.1(4) pm].[35] The Ga−Sb distance of 264.8(1) pm found in **5** is the shortest Ga−Sb bond length ever observed. It is also shorter than the Al−Sb distances found in the Lewis base-stabilized Al−Sb monomers (267−270 pm).[3] An analogous tendency was observed for the Al−Sb and Ga−Sb heterocycles {e.g. $[Me_2MSb(SiMe_3)_2]_3$: 270.2(1)−273.8(1) pm (M = Al),[22] 267.7(1)−271.4(1) pm (M = Ga)[36]; $[Et_2MSb(SiMe_3)_2]_2$: 272.3(1), 272.9(1) pm (M = Al),[23] 271.8(1), 272.9(1) pm (M = Ga)[37]}. Although the covalent radii of Al and Ga are almost the same (Al 125 pm; Ga 126 pm), the Ga−Sb heterocycles tend to have slightly shorter inter-metallic bond lengths than the Al−Sb compounds.

Conclusions

Four- and six-membered group 13/15 heterocycles can be cleaved by reaction with the strong Lewis base 4-(dimethylamino)pyridine (dmap). Previous reports on Al−Sb and Al−Bi heterocycles are extended in these studies to the corresponding Al−P and Al−As heterocycles as well as to Ga−Sb compounds. In all cases, Lewis base stabilized monomers of the type dmap−$M(R_2)E(SiMe_3)_2$ were formed in almost quantitative yield. This convenient reaction type seems to be a general, useful synthetic pathway for the synthesis of the desired class of compounds, allowing access to a wide variety of monomeric group 13/15 compounds. The coordination chemistry of the resulting monomers is currently under investigation.

Experimental Section

General Considerations: All manipulations were performed in a glovebox under a Ar-atmosphere or by standard Schlenk techniques. $[Me_2GaSb(SiMe_3)_2]_3$ [36] and $[Et_2GaSb(SiMe_3)_2]_2$ [37] were prepared by literature methods. Although the synthesis of $[Me_2AlP(SiMe_3)_2]_2$,[38] $[Me_2AlAs(SiMe_3)_2]_2$,[39] and $[Et_2AlAs(SiMe_3)_2]_2$ [40] is described in the literature, these compounds were prepared by the dehydrosilylation reaction between the corresponding alane R_2AlH and $E(SiMe_3)_3$ according to a procedure described previously.[22,23] − ^1H and $^{13}C\{^1H\}$ spectra were recorded using a Bruker AMX 300 spectrometer, using C_6D_5H as internal reference (δ^1H = 7.154; $\delta^{13}C$ = 128.0). − Elemental analyses were performed at the Mikroanalytisches Laboratorium der Universität Bonn.

General Preparation of dmap −Al(R$_2$)E(SiMe$_3$)$_2$: 4-(Dimethylamino)pyridine (2.00 mmol) was added to a solution of the respective Al−E heterocycle (1.00 mmol) in hexane and the resulting suspension was heated at reflux for 30 min. The resulting clear, slightly yellow solution was stored at −30 °C. After 10 h, compounds **1**−**3** were obtained as colorless or light yellow solids.

dmap −Al(Me$_2$)P(SiMe$_3$)$_2$ (1): Yield 0.66 g (1.85 mmol, 93%). − ^1H NMR (300 MHz, C_6D_6, 25 °C): δ = 0.02 (d, $^3J_{P-H}$ = 1.6 Hz, 6 H, AlMe), 0.56 (d, $^3J_{P-H}$ = 3.9 Hz, 18 H, $SiMe_3$), 2.00 (s, 6 H, NMe_2), 5.71 [d, $^3J_{H-H}$ = 6.4 Hz, 2 H, C(3)-H], 8.26 [dd, $^{3,4}J_{H-H}$ = 5.6 / 1.5 Hz (AA′XX′), 2 H, C(2)-H]. − $^{13}C\{^1H\}$ NMR (50 MHz, C_6D_6, 25 °C): δ = −4.4 [AlMe (d, $^2J_{C-P}$ = 12.5 Hz)], 6.1 [$SiMe_3$ (d, $^2J_{C-P}$ = 10.4 Hz)], 38.6 (NMe_2), 106.9 [C(3)-H], 148.0 [C(2)-H], 155.3 [C(4)]. − $C_{15}H_{34}AlN_2PSi_2$ (356.57): calcd. C 50.50, H 9.64; found C 50.71, H 9.88.

dmap −Al(Me$_2$)As(SiMe$_3$)$_2$ (2): Yield 0.75 g (1.88 mmol, 94%). − ^1H NMR (300 MHz, C_6D_6, 25 °C): δ = 0.03 (s, 6 H, AlMe), 0.61 (s, 18 H, $SiMe_3$), 1.92 (s, 6 H, NMe_2), 5.58 (d, $^3J_{H-H}$ = 6.6 Hz, 2 H, C(3)-H), 8.18 (dd, $^{3,4}J_{H-H}$ = 5.8 / 1.5 Hz, 2 H, C(2)-H). − $^{13}C\{^1H\}$ NMR (50 MHz, C_6D_6, 25 °C): δ = −4.1 (AlMe), 6.3 ($SiMe_3$), 38.6 (NMe_2), 106.8 [C(3)-H], 147.3 [C(2)-H], 155.5 [C(4)]. − $C_{15}H_{34}AlAsN_2Si_2$ (400.52): calcd. C 45.14, H 8.60; found C 45.28, H 8.71.

dmap −Al(Et$_2$)As(SiMe$_3$)$_2$ (3): Yield 0.74 g (1.72 mmol, 86%). − ^1H NMR (300 MHz, C_6D_6, 25 °C): δ = 0.60 (s, 18 H, $SiMe_3$), 0.86 (q, $^3J_{H-H}$ = 8.1 Hz, 4 H, Et-CH_2), 1.51 (t, $^3J_{H-H}$ = 8.1 Hz, 6 H, Et-CH_3), 1.91 (s, 6 H, NMe_2), 5.58 [d, $^3J_{H-H}$ = 7.3 Hz, 2 H, C(3)-H], 8.20 [dd, $^{3,4}J_{H-H}$ = 5.9 / 1.4 Hz, 2 H, C(2)-H]. − $^{13}C\{^1H\}$

Table 1. Crystallographic data and measurements for dmap−Al(Me_2)P($SiMe_3$)$_2$ (**1**), dmap−Al(Me_2)As($SiMe_3$)$_2$ (**2**), dmap−Al(Et_2)As($SiMe_3$)$_2$ (**3**), and dmap−Ga(Et_2)Sb($SiMe_3$)$_2$ (**5**)

	1	**2**	**3**	**5**
Empirical formula	$C_{15}H_{34}AlN_2PSi_2$	$C_{15}H_{34}AlAsN_2Si_2$	$C_{17}H_{38}AlAsN_2Si_2$	$C_{17}H_{38}GaN_2SbSi_2$
M [g mol^{-1}]	356.57	400.52	428.57	518.14
Crystal system	monoclinic	triclinic	triclinic	triclinic
Space group	$P2_1/c$ (No. 14)	$P\bar{1}$ (No. 2)	$P\bar{1}$ (No. 2)	$P\bar{1}$ (No. 2)
a [Å]	14.3849(3)	9.4486(6)	9.4839(6)	9.5773(3)
b [Å]	13.1337(3)	16.1715(13)	9.9883(8)	10.3393(4)
c [Å]	24.2830(6)	16.4331(14)	14.0512(11)	14.1058(5)
α [deg]		69.504(4)	78.462(4)	77.594(2)
β [deg]	102.011(2)	73.748)4)	77.301(5)	76.594(2)
γ [deg]		87.298(4)	70.398(4)	69.676(2)
V [Å^3]	4487.28(18)	2254.4(3)	1211.63(16)	1260.26(8)
Z	8	4	2	2
Radiation (wavelength, Å)	Mo-K_α (0.71073)	Mo-K_α (0.71073)	Mo-K_α (0.71073)	Mo-K_α (0.71073)
μ [mm^{-1}]	0.266	1.650	1.540	2.237
temp. [K]	123(2)	123(2)	123(2)	123(2)
D_{calcd} [g cm^{-3}]	1.056	1.180	1.175	1.365
Crystal dim. [mm]	0.35 × 0.30 × 0.15	0.20 × 0.10 × 0.05	0.30 × 0.25 × 0.05	0.35 × 0.15 × 0.10
$2\theta_{max}$ [deg]	56.6	50.0	50.0	56.6
No. of rflns. rec.	46610	31736	15304	21830
No. of nonequiv. rflns. rec.	10622	7916	4252	5999
R_{merg}	0.047	0.132	0.083	0.062
No. of parameters refined	383	383	210	210
$R1$[a]; $wR2$[b]	0.032, 0.092	0.051, 0.082	0.042, 0.095	0.027, 0.067
Goodness of fit[c]	1.034	0.868	0.964	1.040
Final max, min Δρ [e Å^{-3}]	0.288, −0.252	0.434, −0.602	0.754, −0.508	0.661, −1.511

[a] $R1 = \Sigma(||F_o| - |F_c||)/\Sigma|F_o|$ [for $I > 2\sigma(I)$]. − [b] $wR2 = \{\Sigma[w(F_o^2 - F_c^2)^2]/\Sigma[w(F_o^2)^2]\}^{1/2}$. − [c] Goodness of fit = $\{\Sigma[w(|F_o^2| - |F_c^2|)^2]/(N_{observns} - N_{params})\}^{1/2}$.

NMR (50 MHz, C_6D_6, 25 °C): δ = 4.3 (Et-CH_2), 6.1 ($SiMe_3$), 10.6 (Et-CH_3), 38.1 (NMe_2), 106.4 [C(3)-H], 147.0 [C(2)-H], 155.1 [C(4)]. − $C_{17}H_{38}AlAsN_2Si_2$ (428.57): calcd. C 47.63, H 8.91; found C 47.46, H 8.67.

General Preparation of dmap −Ga(R_2)Sb($SiMe_3$)$_2$: 4-(Dimethylamino)pyridine (2.00 mmol) was added to a solution of the respective Ga−Sb heterocycle (1.00 mmol of the dimer, 0.67 mmol of the trimer) in hexane at −10 °C. The resulting suspension was stirred at this temperature for 1 h, slowly warmed to 0 °C over 2 h, filtered, and stored at −30 °C. After 10 h, compounds **4** and **5** were obtained as colorless or light yellow solids, which are thermolabile. They decompose significantly in solution at 25 °C within 30 min. ^{13}C NMR spectra could therefore not be obtained.

dmap −Ga(Me_2)Sb($SiMe_3$)$_2$ (4): Yield 0.66 g (1.34 mmol, 67%). − ^1H NMR (300 MHz, C_6D_6, 25 °C): δ = 0.39 (s, 4.4 H, $GaMe_2$), 0.65 (s, 14 H, $SiMe_3$), 2.05 (s, 6 H, NMe_2), 5.69 [d, $^3J_{H-H}$ = 6.9 Hz, 2 H, C(3)-H], 8.10 [d, $^3J_{H-H}$ = 5.7 Hz, 2 H, C(2)-H]. − $C_{15}H_{34}GaN_2SbSi_2$ (489.45): calcd. C 36.73, H 6.95; found C 35.81, H 6.78.

dmap −Ga(Et_2)Sb($SiMe_3$)$_2$ (5): Yield 0.67 g (1.29 mmol, 60%). − ^1H NMR (300 MHz, C_6D_6, 25 °C): δ = 0.67 (s, 18 H, $SiMe_3$), 1.03 (q, $^3J_{H-H}$ = 7.9 Hz, 4 H, Et-CH_2), 1.52 (t, $^3J_{H-H}$ = 8.0 Hz, 6 H, Et-CH_3), 1.99 (s, 6 H, NMe_2), 5.67 [d, $^3J_{H-H}$ = 5.7 Hz, 2 H, C(3)-H], 8.13 [d, $^3J_{H-H}$ = 6.0 Hz, 2 H, C(2)-H]. − $C_{17}H_{38}GaN_2SbSi_2$ (518.14): calcd. C 39.43, H 7.41; found C 39.11, H 7.02.

X-ray Structure Solution and Refinement: Crystallographic data of **1**, **2**, **3**, and **5** are summarized in Table 1. Figure 1−4 show the ORTEP diagrams of the solid-state structures of **1**, **2**, **3**, and **5**. Data were collected on a Nonius Kappa-CCD diffractometer. The structures of **1**, **2**, **3**, and **5** were solved by Patterson methods (SHELXS-97)[41] and refined by full-matrix least-squares on F^2 (SHELXL-97).[42] All non-hydrogen atoms were refined anisotropically and hydrogen atoms by a riding model. Empirical absorption corrections were applied (**2**, **3**, and **5**). The crystallographic data of **1**, **2**, **3**, and **5** (excluding structure factors) have been deposited with the Cambridge Crystallographic Data Centre as supplementary publication no. CCDC-144769 (**1**), CCDC-144768 (**2**), CCDC-144767 (**3**), and CCDC-144770 (**5**). Copies of the data can be obtained free of charge on application to CCDC, 12 Union Road, Cambridge, CB21EZ [Fax: (Internat.) +44-1223/336-033; E-mail: deposit@ccdc.cam-ak.uk].

Acknowledgments

S. Schulz would like to thank the Deutsche Forschungsgemeinschaft DFG and F. Thomas the Theodor-Laymann-Stiftung der Universität Bonn for Fellowship awards. Financial support was given by the DFG, the Fonds der Chemischen Industrie, the Bundesministerium für Bildung, Wissenschaft, Forschung und Technologie (BMBF) and Prof. E. Niecke, Universität Bonn.

[1] P. P. Power, *Chem. Rev.* **1999**, *99*, 3463−3503.
[2] [2a] K. Knabel, I. Krossing, H. Nöth, H. Schwenk.-Kirchner, M. Schmidt-Amelunxen, T. Seifert, *Eur. J. Inorg. Chem.* **1998**, 1095−1114. − [2b] W.-P. Leung, C. M. Y. Chan, B.-M. Wu, T. C. W. Mak, *Organometallics* **1996**, *15*, 5179−5184. − [2c] J. Prust, P. Müller, C. Rennekamp, H. W. Roesky, I. Uson, *J. Chem. Soc., Dalton. Trans.* **1999**, 2265−2266. − [2d] P. J. Brothers, P. P. Power, *Adv. Organomet. Chem.* **1996**, *39*, 1−69. − [2e] R. J. Wehmschulte, K. Ruhlandt-Senge, P. P. Power, *Inorg. Chem.* **1994**, *33*, 3205−3207. − [2f] E. K. Byrne, L. Parkanyi, K. H. Theopold, *Science* **1988**, *241*, 332−334.
[3] S. Schulz, M. Nieger, *Organometallics* **2000**, *19*, 2640−2642.
[4] S. Schulz, F. Thomas, M. Nieger, *Organometallics* in the press.
[5] [5a] J. L. Atwood, G. A. Koutsantonis, F.-C. Lee, C. L. Raston, *J. Chem. Soc., Chem. Commun.* **1994**, 91−92. − [5b] M. G. Gardiner, G. A. Koutsantonis, S. M. Lawrence, F.-C. Lee, C. L. Raston, *Chem. Ber.* **1996**, *129*, 545−549. − [5c] J. F. Janik, E. N. Duesler, R. T. Paine, *J. Organomet. Chem.* **1997**, *539*, 19−25.
[6] J. F. Janik, R. L. Wells, P. S. White, *Inorg. Chem.* **1998**, *37*, 3561−3566.

[7] D. A. Atwood, L. Contreras, A. H. Cowley, R. A. Jones, M. A. Mardones, *Organometallics* **1993**, *12*, 17−18.
[8] F. Thomas, S. Schulz, M. Nieger, manuscript in preparation.
[9] Terminology "weak" and "hard" are used in the context of the HSAB principle. − [9a] R. G. Pearson, *J. Am. Chem. Soc.* **1988**, *110*, 7684−7690. − [9b] W. B. Jensen, *Chem. Rev.* **1978**, *78*, 1−22.
[10] [10a] C. Tessier-Youngs, C. Bueno, O. T. Beachley, Jr., M. R. Churchill, *Inorg. Chem.* **1983**, *22*, 1054−1059. − [10b] C. Tessier-Youngs, W. J. Youngs, O. T. Beachley, Jr., M. R. Churchill, *Organometallics* **1983**, *2*, 1128−1138. − [10c] O. T. Beachley, Jr., M. A. Banks, J. P. Kopasz, R. D. Rogers, *Organometallics* **1996**, *15*, 5170−5174.
[11] Nöth et al. described the synthesis of the comparable borylphosphanylchromium complex $(Me_2N)_2BP(Ph)_2-Cr(CO)_5$, but no X-ray structure was reported. H. Nöth, S. N. Sze, *Z. Naturforsch.* **1978**, *33b*, 1313−1317.
[12] G. M. J. Lesley, A. Woodward, N. J. Taylor, T. B. Marder, *Chem. Mater.* **1998**, *10*, 1355.
[13] Typically, P−Si bond lengths range from 223 to 230 pm and As−Si distances from 233 to 235 pm.
[14] L. M. Engelhardt, P. C. Junk, C. L. Raston, B. W. Skelton, A. H. White, *J. Chem. Soc., Dalton Trans.* **1996**, 3297−3301.
[15] See for example: [15a]J. Müller, U. Ruschewitz, O. Indris, H. Hartwig, W. Stahl, *J. Am. Chem. Soc.* **1999**, *121*, 4647−4652. − [15b] J. L. Atwood, G. A. Koutsantonis, F.-C. Lee, C. L. Raston, *J. Chem. Soc., Chem. Commun.* **1994**, 91−92. − [15c] A. Haaland, *Angew. Chem.* **1989**, *101*, 1017−1032; *Angew. Chem. Int. Ed. Engl.* **1989**, *28*, 992−1007. − [15d]A. Haaland, in *Coordination Chemistry of Aluminum* (Ed. G. H. Robinson), VCH Verlagsgesellschaft, Weinheim **1993**.
[16] D. F. Grant, R. C. G. Killean, J. L. Lawrence, *Acta Crystallogr. Sect. B* **1969**, *25*, 377−378.
[17] A. Almenningen, A. Haaland, T. Haugen, D. P. Novak, *Acta Chem. Scand.* **1973**, *27*, 1821−1823.
[18] R. J. Wehmschulte, K. Ruhlandt-Senge, P. P. Power, *Inorg. Chem.* **1994**, *33*, 3205−3207.
[19] M. Driess, S. Kunz, K. Merz, H. Pritzkow, *Chem. Eur. J.* **1998**, *4*, 1628−1632.
[20] R. J. Wehmschulte, P. P. Power, *J. Am. Chem. Soc.* **1996**, *118*, 791−797.
[21] A. F. Hollemann, E. Wiberg, *Lehrbuch der Anorganischen Chemie*, 101. Auflage, Walter de Gruyter, Berlin, **1995**, p. 1838−1840.
[22] S. Schulz, M. Nieger, *Organometallics* **1999**, *18*, 315−319.
[23] S. Schulz, M. Nieger, *Organometallics* **1998**, *17*, 3398−3400.
[24] S. Schulz, M. Nieger, *Angew. Chem.* **1999**, *111*, 1020; *Angew. Chem. Int. Ed.* **1999**, *38*, 967.
[25] A. F. Hollemann, E. Wiberg, *Lehrbuch der Anorganischen Chemie*, 101. Auflage, Walter de Gruyter, Berlin, **1995**.
[26] A. W. Jache, G. S. Blevins, W. Gordy, *Phys. Rev.* **1955**, *97*, 680−698.
[27] [27a] N. J. Holmes, *J. Organomet. Chem.* **1997**, *545*, 111−115. − [27b] M. J. Aroney, *J. Chem. Soc., Dalton Trans.* **1994**, 2827−2834.
[28] B. Beagley, T. G. Hewitt, *Trans. Faraday Soc.* **1968**, *64*, 2561−2563.
[29] B. Beagley, A. R. Medwid, *J. Mol. Struc.* **1977**, *38*, 229−230.
[30] B. Beagley, K. T. McAloon, *J. Mol. Struc.* **1973**, *17*, 429−430.
[31] For a detailed discussion see for example: W. Kutzelnigg, *Angew. Chem.* **1984**, *96*, 262−286; *Angew. Chem. Int. Ed. Engl.* **1984**, *23*, 272−296.
[32] Y. Koide, J. A. Francis, S. G. Bott, A. R. Barron, *Polyhedron* **1998**, *17*, 983−991.
[33] H. Rahbarnoohi, R. L. Wells, L. M. Liable-Sands, G. P. A. Yap, A. L. Rheingold, *Organometallics* **1997**, *16*, 3959−3964.
[34] B. Luo, V. C. Young, Jr., W. L. Gladfelter, *Inorg. Chem.* **2000**, *39*, 1705−1709.
[35] P. T. Brain, H. E. Brown, A. J. Downs, T. M. Greene, E. Johnson, S. Parsons, D. W. H. Rankin, B. A. Smart, C. Y. Tang, *J. Chem. Soc., Dalton Trans.* **1998**, 3685−3691
[36] S. Schulz, M. Nieger, *J. Organomet. Chem.* **1998**, *570*, 275−278.
[37] E. E. Foos, R. J. Jouet, R. L. Wells, A. L. Rheingold, L. M. Liable-Sands, *J. Organomet. Chem.* **1999**, *582*, 45−52.
[38] [38a] L. K. Krannich, C. L. Watkins, S. J. Schauer, *Organometallics* **1995**, *14*, 3094−3097. − [38b] L. K. Krannich, C. L. Watkins, S. J. Schauer, C. H. Lake, *Organometallics* **1996**, *15*, 3980−3984. − [38c] F. Hey-Hawkins, M. F. Lappert, J. L. Atwood, S. G. Bott, *J. Chem. Soc., Dalton Trans.* **1991**, 939−948.
[39] R. L. Wells, A. T. McPhail, T. M. Speer, *Eur. J. Solid State Inorg. Chem.* **1992**, *29*, 63−79.
[40] R. L. Wells, A. T. McPhail, T. M. Speer, *Organometallics* **1992**, *11*, 960−963.
[41] G. M. Sheldrick, SHELXS-97, Program for Structure Solution: *Acta Crystallogr. Sect. A* **1990**, *46*, 467.
[42] G. M. Sheldrick, *SHELXL-97*, Program for Crystal Structure Refinement, Universität Göttingen, **1997**.

Received June 28, 2000
[I00255]

Isolation and Structural Characterization of New Indium(III) Aqua Complexes: *trans*-$[InCl_2(H_2O)_4]^+$ and *trans*-$[InCl_4(H_2O)_2]^-$ as Supramolecular Adducts with Cucurbituril and Related Studies

Denis G. Samsonenko,[a] Maxim N. Sokolov,[a] Alexander V. Virovets,[a] Natalya V. Pervukhina,[a] and Vladimir P. Fedin*[a]

Keywords: Indium / Aluminum / Solid-state structures / Supramolecular chemistry / Aqua complexes / Cucurbituril

Aqua and aqua-chloride complexes of Al^{III} and In^{III} have been isolated from aqueous solutions and structurally characterized by X-ray analysis as supramolecular adducts with cucurbituril. Using this approach, *trans*-$[InCl_2(H_2O)_4]^+$ and *trans*-$[InCl_4(H_2O)_2]^-$ species were detected and isolated for the first time as parts of supramolecular assemblies of $[InCl_2(H_2O)_4]_3Cl_3\cdot(C_{36}H_{36}N_{24}O_{12})\cdot4H_2O$ (**1**) and $(H_3O)_3[InCl_4(H_2O)_2]_3\cdot2(C_{36}H_{36}N_{24}O_{12})\cdot17H_2O$ (**2**). The hexaaqua indium(III) cation is present in $[In(H_2O)_6](NO_3)_3\cdot(C_{36}H_{36}N_{24}O_{12})\cdot9H_2O$ (**3**), and its geometry has been established by X-ray crystallography for the first time. The preparation and crystal structure of an Al^{III} hexaaqua ion – cucurbituril adduct $[Al(H_2O)_6]Cl_3\cdot(C_{36}H_{36}N_{24}O_{12})\cdot18H_2O$ (**4**) is also reported. A comparison of In^{III} with its analogs in Group 13 shows closer similarity between In^{III} and Tl^{III} in the chloroaqua complexes than between In and its lighter congeners.

Introduction

Knowledge about coordination chemistry of Group 13 metals (Al − Tl) has rapidly expanded in the last decade.[1,2] This development involves both the introduction of new ligands and more careful examining of "old" and "simple" compounds. Still, detailed information of the nature of the species that are present even in simple systems is often lacking. Thus, from solutions of In^{III} in aqueous HCl, only $[InCl_6]^{3-}$ [2] and $[InCl_5(H_2O)]^{2-}$ [3] could be isolated so far. No other ionic species with higher H_2O/Cl ratios have been identified, except for a serendipitous preparation of a thiotrithiazyl salt, $[S_4N_3]^+[cis\text{-}InCl_4(H_2O)_2]^-$.[4] The *fac*-isomer of $[InCl_3(H_2O)_3]$ is also known. It is formed as a side-product from the reaction of $InCl_3$ with *n*-butyl acetate in hexane.[5a] The same *fac*-$[InCl_3(H_2O)_3]$ moieties also exist in $[InCl_3(H_2O)_3]\cdot$18-crown-6[5b] and in $[InCl_3(H_2O)_3]\cdot$3dioxane.[5c] Curiously enough, $InCl_3\cdot4H_2O$ contains five-coordinate $[InCl_3(H_2O)_2]$ units enmeshed in a network of hydrogen bonding with solvated water molecules.[6]

Recently we became interested in the isolation and structural characterization of often elusive aqua-complexes and mixed-ligand species containing coordinated aqua ligands by employing a supramolecular approach − crystallization with cucurbituril (*Cuc*).[7] Cucurbituril is a macrocyclic cavitand with two identical carbonyl-fringed portals.[8] It can coordinate alkali metal ions such as Na^+, K^+, Rb^+, Cs^+, Ca^{2+} directly, acting as a ligand.[9] It also forms strong hydrogen bonds of the N−H···O type with aliphatic and aromatic amines [10] and we expected even stronger hydrogen bonding with coordinated water molecules of aqua complexes which would enable their crystallization. This expectation has been validated and we wish to report the structures of $[InCl_2(H_2O)_4]_3Cl_3\cdot(C_{36}H_{36}N_{24}O_{12})\cdot4H_2O$ (**1**), $(H_3O)_3[InCl_4(H_2O)_2]_3\cdot2(C_{36}H_{36}N_{24}O_{12})\cdot17H_2O$ (**2**), and $[In(H_2O)_6](NO_3)_3\cdot(C_{36}H_{36}N_{24}O_{12})\cdot9H_2O$ (**3**) as well as of an Al complex, $[Al(H_2O)_6]Cl_3\cdot(C_{36}H_{36}N_{24}O_{12})\cdot18H_2O$ (**4**).

Results and Discussion

The synthesis of the supramolecular adducts **1**−**4** is straightforward. Cucurbituril is not soluble in water, but moderately soluble in 3 M HCl, in neutral KNO_3 solution as well as in solutions of other alkaline metals (due to the metal coordination to the C=O groups of *Cuc*). We also found that *Cuc* is soluble in aqueous solutions of In^{III} and Al^{III} salts, and in this case that the hydrogen bonding between the coordinated waters and the carbonyls of *Cuc* is operative, instead of the expected direct coordination as X-ray analyses show. The products are separated as colorless single crystals suitable for X-ray studies. They lose their water of crystallization very easily, so that **3** and **4** become opaque and lose their crystallinity in air within a few minutes. This fact explains the unsatisfactory agreement between the analytically deduced formula of **3** as the heptahydrate and the stoichiometry found by X-ray analysis (nonahydrate).

The structure of the *trans*-$[InCl_2(H_2O)_4]^+$ cation and the crystal packing in **1** are shown in Figure 1 and Figure 2. This is the first crystal structure in which *Cuc* molecules occupy a crystallographic position with the highest possible symmetry, D_{6h} (6/*mmm*). They form one-layered hexagonal packing with channels running along the *c* axis. There are outer-sphere Cl^- anions [Cl(3)] disordered over 12 positions around the centers of *Cuc* molecules, the Cl···Cl distances being 0.83 − 2.21 Å. The cation lies in the positions with

[a] Institute of Inorganic Chemistry, Russian Academy of Sciences, pr. Lavrentjeva 3, Novosibirsk 630090, Russia
E-mail: cluster@che.nsk.su

 © WILEY-VCH Verlag GmbH, 69451 Weinheim, 2001 1434−1948/01/0101−0167 $ 17.50+.50/0

D_{2h} (*mmm*) site symmetry and is also disordered over two orientations around the Cl−In−Cl (*c*) axis. Solvent water molecules [O(1w)] and another counterion Cl^- [Cl(2)] form columns along the $\bar{6}$ axis, Cl···O distances being 3.19 Å. Our attempts to resolve the disorder by assuming a space group with lower symmetry were unsuccessful. Selected bond lengths and angles are given in Table 1.

In the crystal structure of **2**, there are two different isomers, *cis* and *trans*, of the $[InCl_4(H_2O)_2]^-$ anion (Figure 3). The In−Cl and In−OH_2 bond lengths are similar in both isomers. The *cis* anion forms a hydrogen bond with and

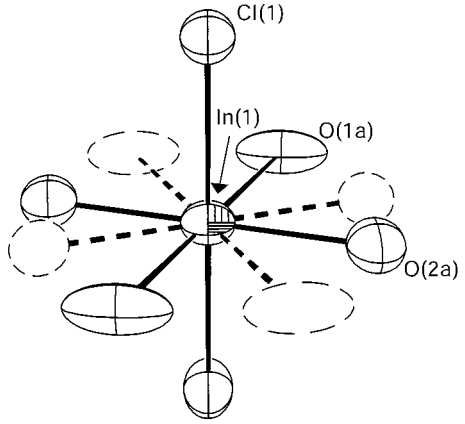

Figure 1. *trans*-$[In(H_2O)_4Cl_2]^+$ cation in **1** (50% probability ellipsoids). The second orientation is shown by dashed lines

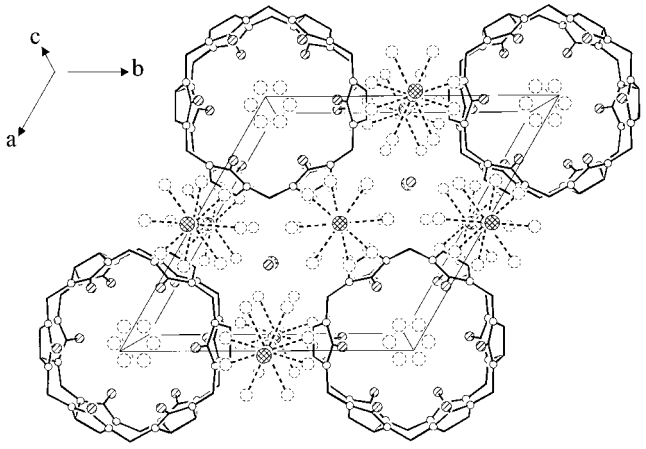

Figure 2. Crystal packing in **1**. Disordered atoms are shown by dashed lines

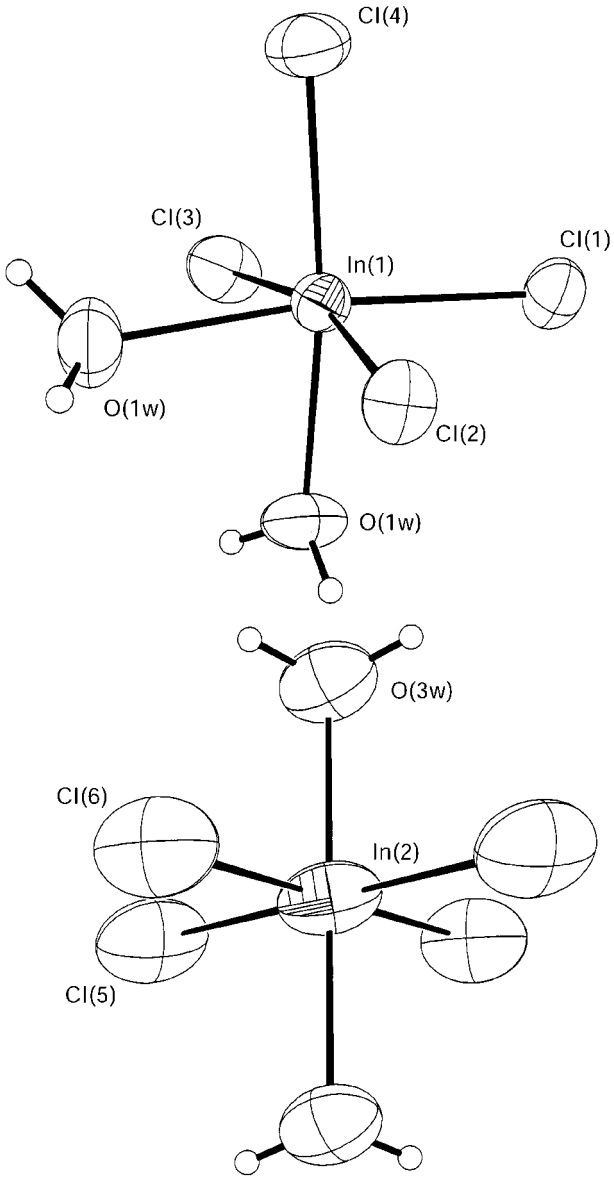

Figure 3. *cis*- (top) and *trans*-$[In(H_2O)_2Cl_4]^-$ (bottom) anion in **2** (50% probability ellipsoids)

O···O distance of 2.64 Å between the coordinated water and an oxygen atom of the *Cuc* molecule. All *Cuc* molecules also contain disordered water in the center of the "barrel".

Table 1. Main bond lengths [Å] and valence angles [°] in **1** (symmetry transformations used to generate equivalent atoms: #1 − *x*,−*y* + 1,−*z*; #2 − *x*,−*x* + *y*, *z*; #3 − *x*,−*x* + *y*,−*z* − 1; #4 − *x* + *y*, *y*, *z*)

In(1)−Cl(1)	2.423(5)	C(11)−N(11)	1.353(8)
In(1)−O(1a)	2.363(16)	N(11)−C(111)	1.454(7)
In(1)−O(2a)	2.118(18)	N(11)−C(11b)	1.448(9)
C(11)−O(11)	1.234(12)		
Cl(1)−In(1)−Cl(1)#1	180	O(11)−C(11)−N(11)	124.9(4)
O(1a)−In(1)−Cl(1)	90	N(11)#2−C(11)−N(11)	110.2(8)
O(1a)−In(1)−Cl(1)#1	90	C(11)−N(11)−C(111)	111.1(7)
O(1a)#1−In(1)−O(1a)	180	C(11)−N(11)−C(11b)	124.4(6)
O(2a)−In(1)−O(1a)#1	97.4(7)	C(11b)−N(11)−C(111)	123.4(7)
O(2a)−In(1)−O(1a)	82.6(7)	N(11)−C(111)−C(111)#3	103.7(5)
O(2a)−In(1)−O(2a)#1	180	N(11)−C(11b)−N(11)#4	112.2(7)

In the crystal, the *Cuc* molecules form parquet-like packing with anions between them (Figure 4). There are a lot of intermolecular hydrogen bonds between coordinated, solvent water, and the *Cuc* molecules. Our attempts to locate H_3O^+ cations were unsuccessful. Selected bond lengths and angles are given in Table 2.

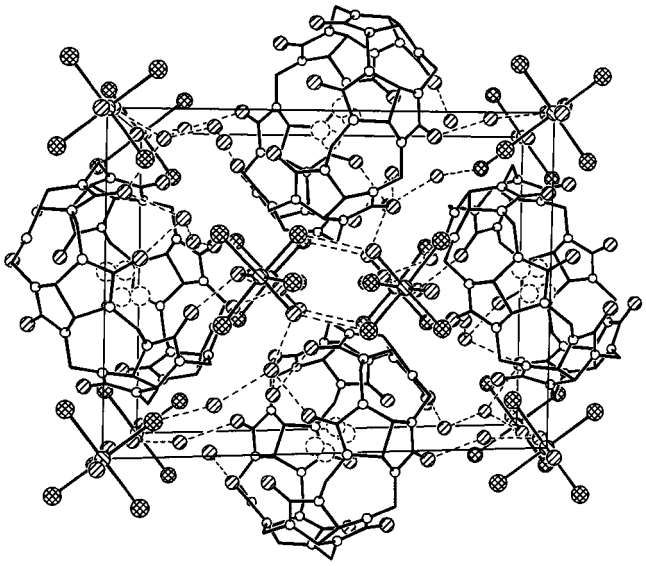

Figure 4. Crystal packing in **2**, view along the *a* axes. Hydrogen bonds are shown as dashed lines

Table 2. Main bond lengths [Å] and valence angles [°] in **2** (symmetry transformations used to generate equivalent atoms: #1 $-x,-y,-z+2$)

In(1)−Cl(1)	2.4637(13)	In(1)−O(2w)	2.252(4)
In(1)−Cl(2)	2.4626(13)	In(2)−O(3w)	2.237(5)
In(1)−Cl(3)	2.4778(14)	In(2)−Cl(5)	2.455(2)
In(1)−Cl(4)	2.4472(14)	In(2)−Cl(6)	2.470(2)
In(1)−O(1w)	2.222(4)		
Cl(1)−In(1)−Cl(3)	93.38(5)	O(1w)−In(1)−O(2w)	82.21(19)
Cl(2)−In(1)−Cl(1)	94.50(4)	O(2w)−In(1)−Cl(1)	172.19(14)
Cl(2)−In(1)−Cl(3)	165.90(5)	O(2w)−In(1)−Cl(2)	85.66(13)
Cl(4)−In(1)−Cl(1)	96.35(5)	O(2w)−In(1)−Cl(3)	84.95(14)
Cl(4)−In(1)−Cl(2)	96.00(5)	O(2w)−In(1)−Cl(4)	91.39(14)
Cl(4)−In(1)−Cl(3)	94.73(6)	O(3w)#1−In(2)−O(3w)	180
O(1w)−In(1)−Cl(1)	90.00(13)	O(3w)−In(2)−Cl(5)	91.68(17)
O(1w)−In(1)−Cl(2)	86.49(11)	O(3w)−In(2)−Cl(5)#1	88.32(17)
O(1w)−In(1)−Cl(3)	81.83(11)	O(3w)−In(2)−Cl(6)	89.16(16)
O(1w)−In(1)−Cl(4)	172.96(13)	O(3w)−In(2)−Cl(6)#1	90.84(16)

The crystal structure of **3** gives the first example of a structurally characterized $[In(H_2O)_6]^{3+}$ cation (Figure 5). The $In-OH_2$ distances are shorter than those found in the $[InCl_4(H_2O)_2]^-$ anion in **2**. Cucurbituril molecules are associated with indium aqua-cations by hydrogen bonds between portal oxygen atoms and water molecules, the O···O distances being 2.637 − 2.835 Å. In the crystal packing, these aggregates form parquet-like layers (Figure 6) connected by hydrogen bonds to solvent water molecules. Selected bond lengths and angles are given in Table 3.

The crystal of compound **4** contains $[Al(H_2O)_6]^{3+}$ cations, Cl^- anions, water and *Cuc* molecules associated by hydrogen bonds. One of the cations is disordered over two

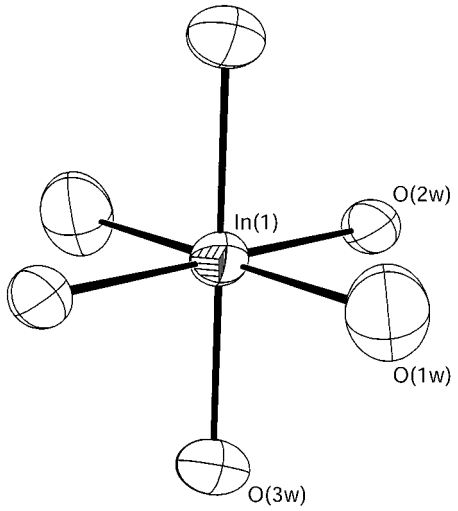

Figure 5. Crystallographically independent $[In(H_2O)_6]^{3+}$ cation in **3** (50% probability ellipsoids)

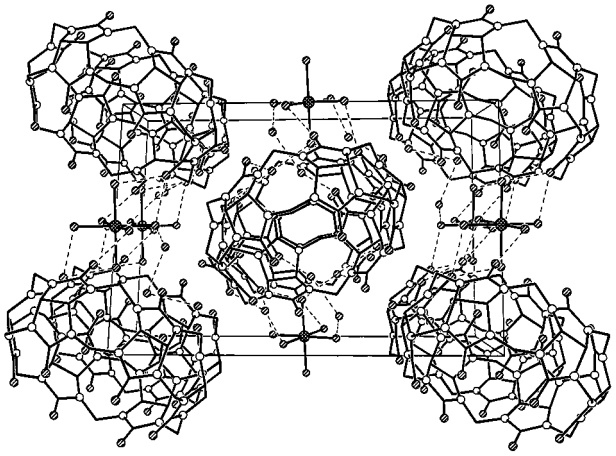

Figure 6. Crystal packing in **3**, view along the *a* axis. Hydrogen bonds are shown as dashed lines.

Table 3. Main bond lengths [Å] and valence angles [°] in **3** (symmetry transformations used to generate equivalent atoms: #1 $-x-2,-y+2,-z+3$; #2 $-x,-y+1,-z+2$)

In(1)−O(1w)	2.152(8)	In(2)−O(4w)	2.149(7)
In(1)−O(2w)	2.139(6)	In(2)−O(5w)	2.141(6)
In(1)−O(3w)	2.142(7)	In(2)−O(6w)	2.136(8)
O(1w)−In(1)−O(1w)#1	180	O(4w)−In(2)−O(4w)#2	180
O(2w)−In(1)−O(1w)	88.4(3)	O(5w)−In(2)−O(4w)	87.9(3)
O(2w)−In(1)−O(1w)#1	91.6(3)	O(5w)−In(2)−O(4w)#2	92.1(3)
O(2w)#1−In(1)−O(2w)	180	O(5w)−In(2)−O(5w)#2	180
O(2w)−In(1)−O(3w)	89.7(3)	O(6w)−In(2)−O(4w)	89.5(3)
O(2w)−In(1)−O(3w)#1	90.3(3)	O(6w)−In(2)−O(4w)#2	90.5(3)
O(3w)−In(1)−O(1w)	89.3(3)	O(6w)−In(2)−O(5w)	88.2(3)
O(3w)−In(1)−O(1w)#1	90.7(3)	O(6w)−In(2)−O(5w)#2	91.8(3)
O(3w)−In(1)−O(3w)#1	180	O(6w)−In(2)−O(6w)#2	180

orientations with relative weights 0.793(6)/0.207(6) (Figure 7). Crystal packing (Figure 8) is based on the *pseudo*-body-centered motif of *Cuc* molecules with aluminum aqua-cations between them. Each *Cuc* molecule contains water molecule disordered over six positions around its

center. Selected bond lengths and angles are given in Table 4.

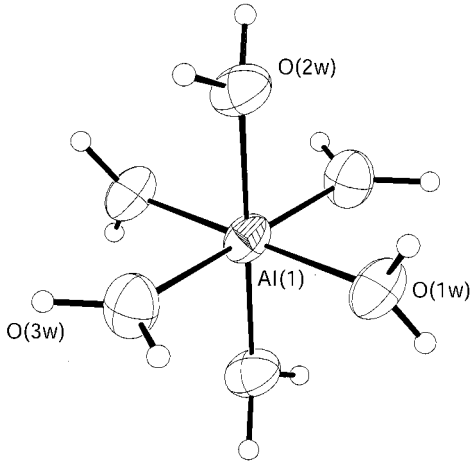

Figure 7. Crystallographically independent $[Al(H_2O)_6]^{3+}$ cations in **4** (50% probability ellipsoids)

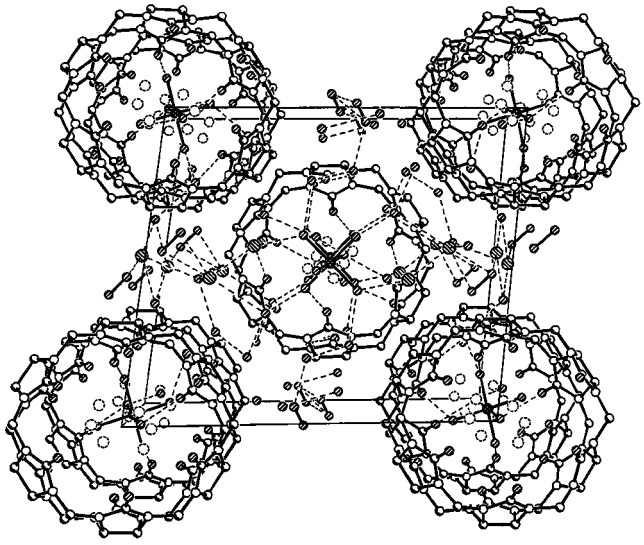

Figure 8. Crystal packing in **4**, view along the *a* axis. Hydrogen bonds are shown as dashed lines

The observed In−O distances in the hexaaqua indium cation of **3** are in good agreement with the value obtained from the X-ray study of aqueous solutions of In^{III} perchlorate, 2.16 Å.[11a] The same cation is present in the crystals of In alums, $M^{I}In(SO_4)_2{\cdot}12H_2O$, though here quantitative structural data are lacking.[11b] In^{III} nitrate forms hydrates with 3, 4 or 5 water molecules, but to the best of our knowledge there is no direct structural information for any of these hydrates. Both the stoichiometry and the spectroscopic evidence of NO_3^- coordination exclude the presence of $[In(H_2O)_6]^{3+}$ in these compounds.[11c] In^{III} also coordinates nitrate in solutions,[11c] where the species $[In(H_2O)_5(\eta^1\text{-}NO_3)]^{2+}$ has been postulated, but in our case all three nitrates are in the outer sphere. The *trans*-$[InCl_2(H_2O)_4]^+$ cation found in **1** has its counterpart in Tl chemistry − *trans*-$[TlX_2(H_2O)_4]^+$ (X = Cl, Br, CN).[12] The analogy with Tl extends further still, because for both metals, crystals of the tetrahydrates $MCl_3{\cdot}4H_2O$ contain trigonal bipyramidal $MCl_3(H_2O)_2$ molecules.[6,13] But for the tetrahalo complexes this analogy does not hold, with Tl^{III} giving only tetrahedral species $TlCl_4^-$,[12] whereas for In^{III} both *cis*- and *trans*-$[InCl_4(H_2O)_2]^-$ have been isolated, although $InCl_4^-$ [14] is also known. Of the lighter Group 13 metals, no evidence exists for Al of any mixed $[AlX_{6-n}(H_2O)_n]^{n-3}$ (X = Cl, Br, I) species both in the solid state and in solution, whereas for Ga there is ample evidence for them.[15] However, only $[GaX_4]^-$ salts with large organic cations could be isolated from aqueous solutions of Ga^{III} halides.[1] Thus, the $[InCl_4(H_2O)_2]^-$ species so far have no analogs among the other Group 13 metals.

Experimental Section

General: The salts, $AlCl_3{\cdot}6H_2O$ and "$In(NO_3)_3{\cdot}4.5H_2O$" were of commercial quality and used without further purification. Cucur-

Table 4. Main bond lengths [Å] and valence angles [°] in **4**.

Al(1)−O(1w)	1.869(3)	Al(2)−O(6w)	1.868(4)
Al(1)−O(2w)	1.880(3)	Al(2)−O(41w)	1.864(14)
Al(1)−O(3w)	1.876(3)	Al(2)−O(51w)	1.870(13)
Al(2)−O(4w)	1.877(4)	Al(2)−O(61w)	1.855(13)
Al(2)−O(5w)	1.880(4)		
O(1w)−Al(1)−O(1w)#1[a]	180	O(6w)−Al(2)−O(4w)#2	90.45(19)
O(1w)−Al(1)−O(2w)#1	90.69(13)	O(6w)−Al(2)−O(4w)	89.55(19)
O(1w)−Al(1)−O(2w)	89.31(13)	O(6w)−Al(2)−O(5w)	90.7(2)
O(1w)#1−Al(1)−O(2w)	90.69(13)	O(6w)−Al(2)−O(5w)#2	89.3(2)
O(1w)−Al(1)−O(3w)	89.12(13)	O(6w)−Al(2)−O(6w)#2	180
O(1w)#1−Al(1)−O(3w)	90.88(13)	O(41w)−Al(2)−O(41w)#2	180
O(2w)#1−Al(1)−O(2w)	180	O(51w)−Al(2)−O(41w)	90.4(7)
O(3w)−Al(1)−O(2w)#1	90.82(13)	O(51w)−Al(2)−O(41w)#2	89.6(7)
O(3w)−Al(1)−O(2w)	89.18(13)	O(51w)−Al(2)−O(51w)#2	180
O(3w)−Al(1)−O(3w)#1	180	O(61w)−Al(2)−O(41w)	89.8(6)
O(4w)#2−Al(2)−O(4w)	180	O(61w)−Al(2)−O(41w)#2	90.2(6)
O(4w)#2−Al(2)−O(5w)	89.0(2)	O(61w)−Al(2)−O(51w)	90.5(6)
O(4w)−Al(2)−O(5w)	91.0(2)	O(61w)#2−Al(2)−O(61w)	180
O(5w)−Al(2)−O(5w)#2	180		

[a] Symmetry transformations used to generate equivalent atoms: #1 $-x,-y+1,-z+1$; #2 $-x-1,-y,-z+2$.

Table 5. Crystal data and structure refinement for **1**−**4**

Compound	**1**	**2**	**3**	**4**
Formula	$C_{36}H_{68}Cl_9In_3N_{24}O_{28}$	$C_{72}H_{127}Cl_{12}In_3N_{48}O_{50}$	$C_{36}H_{66}InN_{27}O_{36}$	$C_{36}H_{84}AlCl_3N_{24}O_{36}$
Crystal system	hexagonal	triclinic	triclinic	triclinic
Space group	*P6/mmm*	$P\bar{1}$	$P\bar{1}$	$P\bar{1}$
Unit cell dimensions	a = 14.407(1)	a = 12.7408(6)	a = 13.036(2)	a = 12.843(1)
[Å, °]	c = 10.331(1)	b = 13.7375(7)	b = 13.525(2)	b = 15.730(1)
		c = 18.216(1)	c = 19.520(3)	c = 17.745(1)
		α = 90.627(5)	α = 89.58(1)	α = 81.801(5)
		β = 101.568(4)	β = 84.93(1)	β = 83.575(6)
		γ = 92.194(4)	γ = 70.89(1)	γ = 74.255(6)
Volume [Å^3]	1857.0(3)	3120.7(3)	3238.4(9)	3405.0(4)
Z	1	1	2	2
D (calcd.) [Mg/m^3]	1.742	1.721	1.608	1.524
Crystal size [mm]	0.40 × 0.36 × 0.28	0.68 × 0.28 × 0.24	0.40 × 0.35 × 0.14	0.35 × 0.30 × 0.24
μ(Mo-K_α) [mm^{-1}]	1.337	0.913	0.481	0.257
Absorption correction	Integration	Integration	2 ψ-scans	5 ψ-scans
Reflns. collected	2320	11430	10036	12432
Unique reflns.	689	11049	9592	11863
R[int]	0.0215	0.0134	0.0302	0.0169
Observed reflns.	675	9551	6561	8643
Final R indices [$F \geq 4\sigma(F)$] [a]	$R1$ = 0.0750,	$R1$ = 0.0595,	$R1$ = 0.0833,	$R1$ = 0.0810,
	$wR2$ = 0.3212	$wR2$ = 0.1773	$wR2$ = 0.2522	$wR2$ = 0.2355
R indices (all data)	$R1$ = 0.0755,	$R1$ = 0.0672,	$R1$ = 0.1044,	$R1$ = 0.1050,
wR2 = 0.3217	$wR2$ = 0.1867	$wR2$ = 0.2650	$wR2$ = 0.2631	
GooF on F^2	3.155	1.079	1.022	1.023

[a] Definitions: $R1 = \Sigma\# \mid |F_o| - |F_c| \mid / \Sigma\# |F_o|$, $wR2 = \{\Sigma\# [\, w(F_o^2 - F_c^2)^2 \,] / \Sigma\# [\, w(F_o^2)^2 \,]\}^{1/2}$, GoF = $\{\Sigma\# [\, w(F_o^2 - F_c^2)^2 \,]/(n-p)\}^{1/2}$.

bituril hydrate (water content corresponds approximately to that of the hexahydrate) was from Merck. *p*-Toluenesulfonic acid was purchases from Aldrich Chemical Company, Inc. Elemental analysis was performed by the analytical service of the Institute of Organic Chemistry SB RAS (Novosibirsk). The nitrate in **3** was determined by ion-exchange chromatography.

X-ray Structure Determination: The diffraction measurements for compounds **1**−**4** were performed at room temperature (293 K) with Bruker P4 (**1**, **4**) and Enraf−Nonius CAD4 (**2**, **3**) four-cycle diffractometers using graphite-monochromated Mo-K_α radiation (λ = 0.71073 Å). The crystals of **3** and **4** were sealed onto quartz capillaries with traces of mother liquor to avoid decomposition by dehydration. The unit cell was determined from setting angles of 24 reflections in the $9 \leq \theta \leq 15°$ range. Data were collected using standard techniques (θ/2θ scans with variable speed) up to $2\theta_{max} = 50°$. Structures were solved by direct methods using SHELXS97[16] (**1**, **4**) and SIR97[17] (**2**, **3**) programs. The hydrogen atoms of cucurbituril molecules were refined in rigid-body approximation. Some hydrogen atoms of water molecules were found in difference electron-density maps and refined by applying geometrical constraints. In the structure **3**, one of the NO_3^- ions appears to be disordered over several positions and therefore our attempts to locate it were unsuccessful. Nevertheless, the chemical analysis data for **3** are in good agreement with the proposed formula.

Crystallographic data for the structures reported in this paper have been deposited with the Cambridge Crystallographic Data Center as supplementary publication no. CCDC-144322 (**1**), -144323 (**2**), -144324 (**3**), -144325 (**4**). Copies of the data can be obtained free of charge on application to the CCDC, 12 Union Road, Cambridge CB2 1EZ, U.K. [Fax: (internat.) +44 (0)1223/336033; E-mail: deposit@ccdc.cam.ac.uk].

$[InCl_2(H_2O)_4]_3Cl_3\cdot(C_{36}H_{36}N_{24}O_{12})\cdot 4H_2O$ (1): $In(NO_3)_3\cdot 4.5H_2O$ (0.70 g, 1.8 mmol) was dissolved in a solution of cucurbituril (5 mL, 20 mM) in HCl (3 M) and kept at room temperature in an open beaker. Colorless hexagonal prisms of **1** separated after one week. Yield − 0.025 g (13%). − $C_{36}H_{68}N_{24}O_{28}Cl_9In_3$: calcd. C 22.19, H 3.52, N 17.25, Cl 16.37; found C 20.18, H 3.80, N 16.16, Cl 16.32.

$(H_3O)_3[InCl_4(H_2O)_2]_3\cdot 2(C_{36}H_{36}N_{24}O_{12})\cdot 17H_2O$ (2): In an aqueous solution of KNO_3 (1 M) and Hpts (0.01 M) was dissolved cucurbituril to a concentration 6.7 mM of cucurbituril. The white lamellar crystals were separated after standing for one day and a fraction of them (0.22 g) were dissolved in HCl (16 mL, 3 M). $In(NO_3)_3\cdot 4.5H_2O$ (60 mg, 0.15 mmol) was dissolved in the solution (5 mL). Colorless prismatic crystals of **2** separated after one week. Yield − 0.015 g (7%). − $C_{72}H_{127}Cl_{12}In_3N_{48}O_{50}$: calcd. C 26.73, H 3.96, N 20.78, Cl 13.15; found C 26.18, H 3.67, N 20.41, Cl 12.15.

$[In(H_2O)_6](NO_3)_3\cdot(C_{36}H_{36}N_{24}O_{12})\cdot 9H_2O$ (3): In a solution of $In(NO_3)_3\cdot 4.5H_2O$ (3.94 g, 10.13 mmol) in water (10 mL), cucurbituril (0.10 g, 0.085 mmol) was dissolved after heating for 15 min on a hot plate. The solution was filtered and left in an open beaker for 1 day. Large colorless crystals of **3** separated, which, however, lost two water molecules. Yield − 0.081 g (19%). − $C_{36}H_{62}N_{27}O_{34}In$: calcd. C 28.23, H 4.08, N 24.69, NO_3^- 11.86, In 7.50; found C 28.00, H 4.07, N 24.85, NO_3^- 12.88, In 8.09.

$[Al(H_2O)_6]Cl_3\cdot(C_{36}H_{36}N_{24}O_{12})\cdot 18H_2O$ (4): In a solution of $AlCl_3\cdot 6H_2O$ (0.12 g, 0.5 mmol) in water (10 mL), cucurbituril (30 mg, 0.026 mmol) was dissolved after heating for 15 min on a hot plate. The solution was filtered and left in an open beaker for 4 days. Large colorless crystals of **4** separated, which, however, rapidly lost their water (1−2 minutes) and disintegrated when they were taken out of the mother liquor.

Acknowledgments

We are grateful to the Russian Foundation for Basic Research for supporting this work. We thank Dr. B. S. Smolyakov and Mrs. S. N. Filimonova for nitrate determination.

[1] A. J. Downs (Ed.), *Chemistry of Aluminium, Gallium, Indium and Thallium*, Blackie Academic and Professional, Glasgow, **1993**.

[2] [2a] H.-U. Schlimper, M. L. Ziegler, *Z. Naturforsch*. **1972**, *27b*, 377. – [2b] A. T. Pilyukova, V. V. Pokrovski, A. V. Samodelov, *Zh. Neorg. Khim*. **1965**, *10*, 1748. – [2c] J.-P. Wignacourt, G. Novogrocki, G. Mairesse, P. Barbier, *Rev. in Inorg. Chem*. **1980**, *2*, 207. – [2d] C. Reber, H. U. Guedel, G. Meyer, F. Schleid, C. A. Paul, *Inorg. Chem*. **1989**, *28*, 3249.

[3] [3a] H. P. Klieg, E. Kummer, L. A. Alexander, *J. Am. Chem. Soc*. **1948**, *70*, 3064. – [3b] J. P. Wignacourt, G. Mairesse, P. Barbier, *Cryst. Struct. Comm*. **1976**, *5*, 293. – [3c] O. Knop, T. S. Cameron, D. Adhiekesavalu, B. R. Vincent, J. A. Jenkins, *Can. J. Chem*. **1987**, *65*, 1527. – [3d] X. Solons, M. C. Moron, F. Palacio, *Acta Crystallogr*. **1988**, *C44*, 965.

[4] M. L. Ziegler, H. U. Schlimper, B. Nuber, J. Weiss, G. Ertl, *Z. Anorg. Allg. Chem*. **1975**, *415*, 193.

[5] [5a] D. R. Aris, W. Errington, G. R. Willey, *Acta Crystallogr*. **1999**, *C55*, 1746. – [5b] N. R. Streltsova, M. G. Ivanov, S. D. Vashchenko, V. K. Belskii, I. I. Kalinichenko, *Koord. Khim*. **1991**, *17*, 646. – [5c] S. H. Whitlow, E. J. Gabe, *Acta Crystallogr*. **1975**, *B31*, 2534.

[6] J. P. Wignacourt, G. Mairesse, P. Barbier, *Can. J. Chem*. **1982**, *60*, 1747.

[7] [7a] M. N. Sokolov, A. V. Virovets, D. N. Dybtsev, O. A. Gerasko, V. P. Fedin, R. Hernandez-Molina, W. Clegg, A. G. Sykes, *Angew. Chem*. **2000**, *112*, 1725; *Angew. Chem. Int. Ed.* **2000**, *39*, 1659. – [7b] V. P. Fedin, A. V. Virovets, M. N. Sokolov, D. N. Dybtsev, O. A. Gerasko, W. Clegg, *Inorg. Chem*. **2000**, in press.

[8] [8a] R. Behrend, E. Meyer, F. Rusche, *Liebigs Ann. Chem*. **1905**, *339*, 1. – [8b] W. A. Freeman, W. L. Mock, N. −Y. Shih, *J. Am. Chem. Soc*. **1981**, *103*, 7367.

[9] [9a] Y. −M. Jeon, J. Kim, D. Whang, K. Kim, *J. Am. Chem. Soc*. **1996**, *118*, 9790. – [9b] D. Whang, J. Heo, J.H. Park, K. Kim, *Angew. Chem. Int. Ed.* **1998**, *37*, 78. – [9c] J. Heo, S.-Y. Kim, D. Whang, K. Kim, *Angew. Chem. Int. Ed.* **1999**, *38*, 641. – [9d] J. Heo, J. Kim, D. Whang, K. Kim, *Inorg. Chim. Acta* **2000**, *297*, 307. – [9e] W. A. Freeman, *Acta Cryst*. **1984**, *B40*, 382.

[10] W. L. Mock, in: *Comprehensive Supramolecular Chemistry* **1996**, *Vol. 2*, 477.

[11] [11a] Y. Marcus, *Chem. Rev*. **1988**, *88*, 1475. – [11b] S. P. Best, J. K. Beattie, R. S. Armstrong, *J. Chem.Soc., Dalton Trans*. **1984**, 2611. – [11c] G. V. Kozhevnikova, G. Keresztury, *Inorg. Chim. Acta* **1985**, *98*, 59.

[12] J. Blixt, J. Glaser, J. Mink, I. Persson, P. Persson, M. Sandström, *J. Am. Chem. Soc.* **1995**, *117*, 5089.

[13] J. Glaser, *Acta Chem. Scand., Ser. A* **1979**, *33*, 789.

[14] T. Staffel, G. Meyer, *Z. Anorg. Allg. Chem.* **1990**, *585*, 38.

[15] [15a] M. J. Taylor, *Polyhedron* **1990**, *9*, 207. – [15b] D. G. Tuck, *Pure Appl. Chem*. **1983**, *55*, 1477. – [15c] I. Bányai, J. Glaser, *J. Am. Chem. Soc.* **1989**, *111*, 3186. – [15d] I. Bányai, J. Glaser, *J. Am. Chem. Soc*. **1990**, *112*, 4703.

[16] G. M. Sheldrick, *SHELX-97 Release 97−2*, Göttingen University, Germany, **1998.**

[17] A. Altomare, M. C. Burla, M. Camalli, G. L. Cascarano, C. Giacovazzo, A. Guagliardi, A. G. G. Moliterni, G. Polidori, R. Spagna, *J. Appl. Cryst*. **1999**, *32*, 115.

Received May 16, 2000
[I00202]

Synthesis and Structures of Aminoalkoxyalanes

Heinrich Nöth,*[a] Andreas Schlegel,[a] Bakthan Singaram,[b] Jörg Knizek,[a][+] Peter Mayer,[a][+] and Thomas Seifert[a][+]

Dedicated to Professor Hubert Schmidbaur on the occasion of his 65th birthday

Keywords: Aluminum / Amino alcohols / Hydrido complexes / NMR spectroscopy

Reactions of various amino alcohols with $AlH_3{\cdot}NMe_3$ in hydrocarbons or ethers yielded the corresponding aminoalkoxyalanes $R_2N(X)_nOAlH_2$ **1**–**4** which are dimeric in the solid state. The structures of **1**–**4** show a characteristic Al_2O_2 ring system with pentacoordinated Al atoms. Pentacoordination is also observed in bis(–)-*R*-ephedrinoalane **(5)** which is, however, monomeric. Reduction of acetophenone with (–)-*R*-ephedrinoalane **(3)** proceeded without any noticeable stereoselectivity. Temperature-dependent ^{27}Al NMR studies suggest that the well-defined structures found in the solid state are not retained in solution.

Introduction

Although $LiAlH_4$ and $NaBH_4$ are amongst the most widely used hydride reducing reagents,[1] their stereoselectivity is negligible.[2] Therefore, modifications of these hydrides by suitable substituents to achieve adequate stereo- and enantioselectivity have been investigated. Amongst these reagents is lithium binaphtholato-*tert*-butoxy hydrido aluminate, Noyori′s reagent, which shows very high enantioselectivity.[3] The factors which control the reaction mechanism, and consequently the stereoselectivity, are not yet fully understood. The main reason for this lies in the lack of knowledge concerning the composition of the active reducing species in solution. Recently, we have shown that the stability of alkoxyaluminum hydrides and alkali metal organyloxohydridoaluminates in solution depends on the nature of the substituents at the Al centers.[4] In principle, it should be possible to turn AlH_3 into a reagent with high stereo- and possibly enantioselectivity, for instance by introducing chiral substituents.[5] In this paper we describe new aminoalkoxoalanes, some of them with chiral centers, as well as some temperature-dependent ^{27}Al NMR studies, which provide information about their nature in solution.

Synthesis

The synthesis of aminoalkoxo alanes was performed by allowing the amino alcohols R*OH to react with $AlH_3{\cdot}NMe_3$ [see Equation (1) and (2)] particularly those leading to alanes of type R^*OAlH_2, because their hydride content is higher than that of the alanes $(R^*O)_2AlH$.

$$R^*OH + AlH_3{\cdot}NMe_3 \rightarrow R^*OAlH_2 + NMe_3 + H_2 \quad (1)$$

$$2R^*OH + AlH_3{\cdot}NMe_3 \rightarrow (R^*O)_2AlH + NMe_3 + 2\,H_2 \quad (2)$$

$$2\,R^*OAlH_2 \rightarrow (R^*O)_2AlH + AlH_3 \quad (3)$$

The reactions were performed in tetrahydrofuran or toluene with *N*,*N*-dimethylaminoethanol, *N*,*N*-dimethylaminopropanol, (−)-(*S*)-1-methylpyrrolidine-2-methanol, (*N*-methyl-L-prolinol) or (−)-*N*-methylephedrine. Common to all these amino alcohols is the tertiary amino group. Reactions in a 1:1 ratio led to the alane derivatives **1**−**4**, while the 2:1 reaction of the ephedrine with $AlH_3{\cdot}NMe_3$ yielded the bis(aminoalkoxo)alane **5**.

Compounds **1**−**4** proved to be dimeric in the solid state. Because no compounds of type $R^*OAlH_2{\cdot}NMe_3$ [R*O = $R_2N(CH_2)_nO$] were obtained, it is evident that the amino group of the amino alcohol has displaced the Me_3N ligand from the Al center. Taking this into account, several different structural units may result, as depicted by Formulae **A**−**G**.

Although the dimeric nature of these compounds is ascertained in the solid state to be of type **B**, it cannot be excluded that the compounds may adopt other structures in solution.

Reduction of acetophenone with the ephedrinoalane **3** resulted in practically no stereospecific induction; these experiments will therefore not be described.

Spectroscopic Properties

^{27}Al NMR spectroscopy should allow us to distinguish between **A** and **C**, with tetracoordinated Al centers, and types **B**, **D**, and **F**, with pentacoordinate Al atoms. A structure of type **G** should result in two ^{27}Al resonances with a quintet for the AlH_4 anion in the proton-coupled spectrum. For a structure of type **E**, a single broad resonance is be expected (exchange signal). The resonances for structures

[a] Department of Chemistry, University of Munich, Butenandtstraße 5−13, House D, 81377 München, Germany
Fax: (internat.) +49-89/2180-7455
E-mail: H.Noeth@lrz.uni-muenchen.de
[b] Department of Chemistry, University of California, Santa Cruz, California, USA
[+] X-ray structure analysis.

 © WILEY-VCH Verlag GmbH, 69451 Weinheim, 2001 1434−1948/01/0101−0173 $ 17.50+.50/0

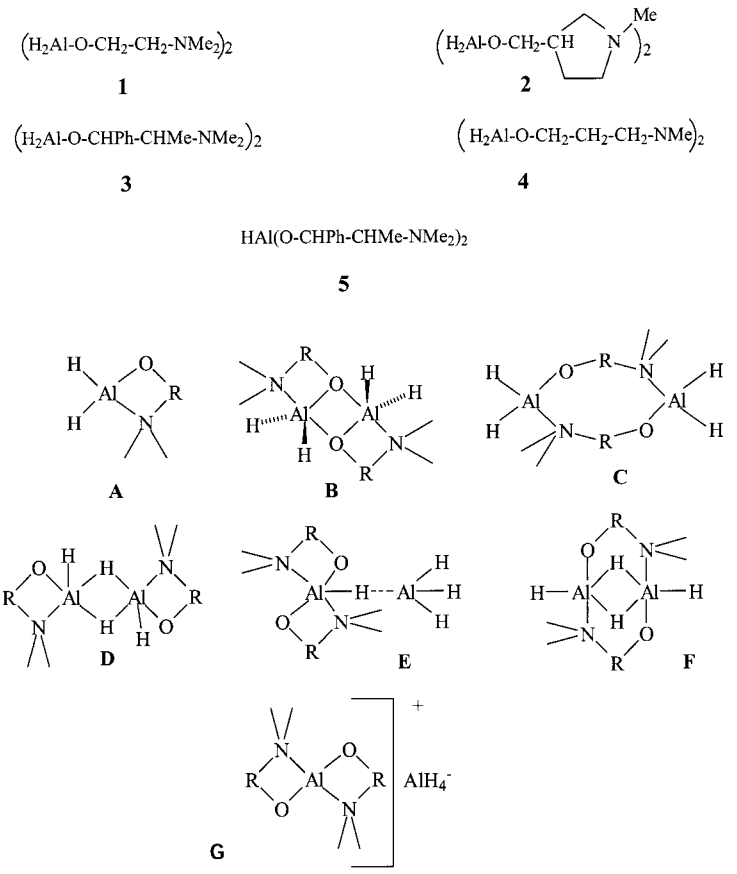

with pentacoordinate Al centers should appear further upfield, indicating electronically better shielded atoms. Table 1 lists the ^{27}Al NMR shifts and IR spectroscopic data for the Al−H stretching vibrations.

Table 1. ^{27}Al chemical shifts of compounds **1**−**5** (main signal) in [D$_8$]toluene at 27 °C (δ in ppm, half-height width $h_{1/2}$ in Hz) and νAlH (in cm^{-1}) in the IR spectra

	δ^{27}Al	$h_{1/2}$	νAlH$_2$/AlH
1	91	1090	1755, 1716
2	91	1880	1767, 1730
3	96	4260	1811, 1776
4	92	1970	1749, 1715
5	83	3690	1777

With the exception of compound **5**, all ^{27}Al resonances lie in the narrow range of 91−96 ppm. All signals are quite broad, and it was not possible to resolve ^{27}Al,^{1}H-coupling. This is in agreement with the rather high asymmetry about the Al center which allows for rapid relaxation. The δ^{27}Al values are by themselves not necessarily a convincing argument for tetra- or pentacoordination because the observed chemical shifts are on the border of tetra- and pentacoordination.[6] However, by comparing these data with those of (ROAlH$_2$)$_2$ (R = alkyl, δ^{27}Al = 115−130),[4,7] featuring tetracoordination for Al, then the δ^{27}Al values for compounds **1**−**5** support pentacoordination in toluene solution (*vide infra*). This is particularly evident for compound **5** with δ^{27}Al = 83. The most striking difference between alkoxyalanes with small alkyl groups and the aminoalkoxyalanes is that, in solution, the latter are not subject to ligand exchange, which would lead to AlH$_3$ and bis(aminoalkoxy)alanes, as shown in Equation (3).

Although the dimeric nature of compounds **1**−**4** were ascertained by X-ray structure analysis, there are alternatives as depicted by formulae **D**−**F**.

A structure of type **E**, which might even become ionic as shown in **G**, can be excluded immediately because only a single ^{27}Al NMR signal is observed in toluene solution and none for AlH$_4^-$. This also excludes structures with two chemically and spectroscopically different Al centers. Isomers **D** and **F** should be discernible from structure **B** by IR spectroscopy: the absorptions for terminal AlH groups and for tetracoordinated Al atoms are expected in the range of 1800−1900 cm^{-1}, and for the bridging AlH$_2$Al groups at about 1650 cm^{-1}.[4,7,8] The presence of two IR absorptions in the range from 1703−1777 cm^{-1} can be assigned to antisymmetric and symmetric AlH$_2$ vibrations for pentacoordinated Al centers, and this rules out the presence of structures **D** and **F** in solution.

However, the temperature-dependent ^{27}Al NMR spectra of compound **1** in toluene reveal that the situation in toluene is more complex (see Figure 1). Firstly, the spectra show the presence of hexacoordinated species which seem to gain in concentration at low temperature. On warming the solution, the dominant signal at δ ≈ 60 (−70 °C) moves to δ ≈ 90 at higher temperature, indicating a rapid equilibrium between penta- and tetracoordinated species. However, with

increasing temperature the signal not only becomes sharper, as expected, but rather at 20 °C the δ = 91 signal represents a contribution of >90% by a pentacoordinated Al species. We assume that this signal represents a situation of a rapid equilibrium [see Equation (4)] between various molecules having penta- and tetracoordinated centers. $^{1}J(^{27}Al,^{1}H)$ could not be observed at any temperature owing to the considerable line widths (1090−4250 Hz). Similar ^{27}Al NMR spectra were observed for compounds **2**−**4**. Therefore, there is no single species present in solution, and this should be reflected in the reactions of these compounds. Equation (4) describes the state of these molecules in solution.

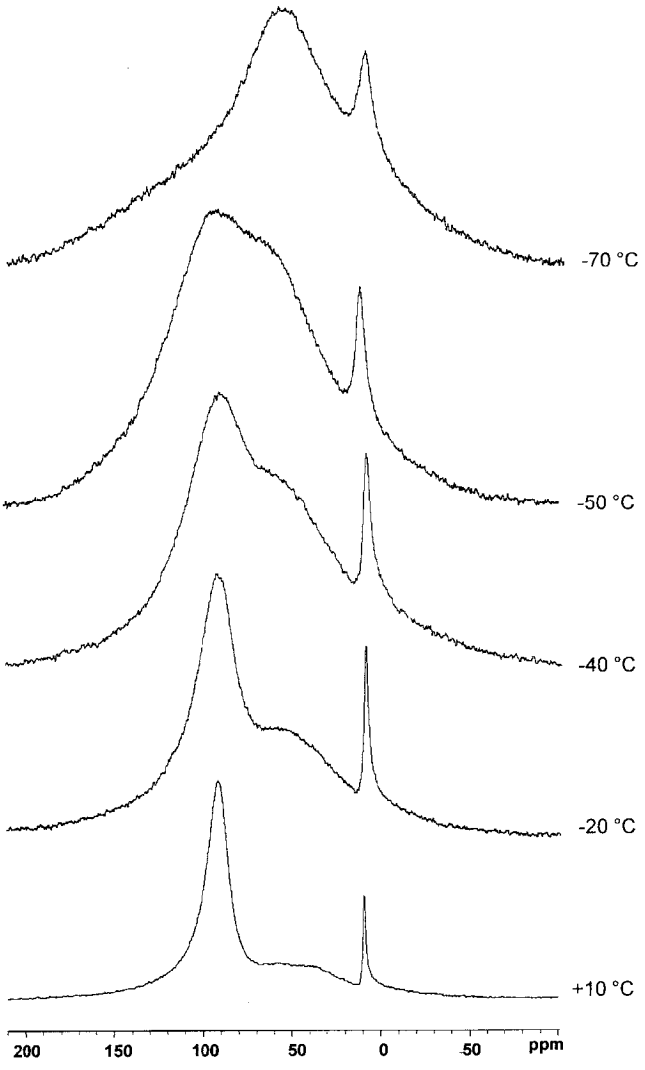

Figure 1. Temperature-dependent ^{27}Al NMR spectra of compound **1** in deuterated toluene

Evidence for the stability of the dimeric entities of compounds **1**−**4** comes from mass spectra. In all cases, the $[M_2 - 2\ H]^+$ ion has been detected, demonstrating that the compounds are volatile, but not as monomeric units; rather, they also retain their dimeric state of aggregation in the gas phase. Compound **5**, however, is monomeric in the gas phase in agreement with its structure in the crystal.

Molecular Structures

Compounds **1**−**5** were obtained as single crystals, and their structures were determined by X-ray methods. Figure 2−6 represent the molecular structures. The general features of these structures are: i) all compounds are dimeric in the solid state, except **5**, even though they all have pentacoordinated Al atoms, and ii) the presence of a central, planar, or almost planar, Al_2O_2 four-membered ring. Compounds **1**, **2**, and **3** contain aminoalkoxy groups forming a five-membered ring with the Al atom. This geometry induces a considerable distortion about the Al centers from a trigonal bipyramidal arrangement. As expected, the Al−O bond in the "trigonal plane" is shorter than the Al−O bond in the axial position. Except for compound **1**, where the sum of the bond angles for this plane is only 349.2°, almost perfect "planes" are present in compounds **2**−**5** (359 ± 1°).

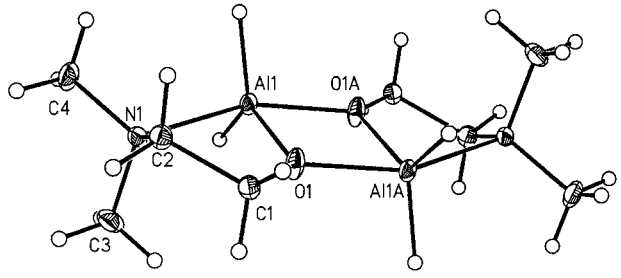

Figure 2. Molecular structure of dimeric *N*,*N*-dimethylaminoethoxyalane **(1)**; thermal ellipsoids are drawn on a 25% probability scale; selected bond lengths (in Å): Al1−O1 1.850(2), Al1−O1A 1.903(2), Al1−N1 2.133(2), Al1−H1 1.50(2), Al1−H2 1.54(3).; selected bond angles (in °): O1−Al−O1A 75.61(8), Al1−O1−C1 122.6(1), Al1A−O1−C1 132.4(1), Al1−O1−Al1A 104.39(8), N1−Al1−O1 79.71(7), N1−Al1−O1A 154.50(7), H1−Al1−H2 120(1), H1−Al−O1 125.4(9), H2−Al1−O1 114(1), N1−Al1−H1 92.9(9), N1−Al−H2 94(1)

The axis N1−Al1−O1A in the centrosymmetric molecule **1** is bent towards the equatorial Al1−O1 bond (see Figure 2), and the deviations from the 90° angles (axial to equatorial) result from ring strain both of the Al_2O_2 four-membered ring [O1−Al1−O1A 75.61(8)°] as well as of the five-membered Al−O−C−C−N ring [distorted envelope configuration with N1−Al1−O1 = 79.71(7)°].

In contrast to **1**, which crystallizes in the centrosymmetric monoclinic space group $P2_1/n$, compounds **2** and **3**

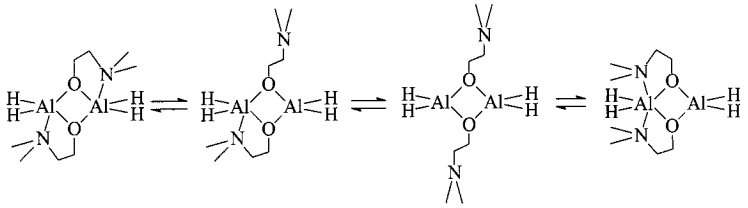

(4)

crystallize in the acentric monoclinic space group $P2_1$, as expected for the presence of chiral aminoalkoxy ligands. There are two independent molecules of **2** in the unit cell, both having the same configuration but a different conformation (see Figure 3). The sum of bond angles for the atoms around the "trigonal plane" is 360°, and the H−Al−H bond angle is close to 120°. The Al−N coordination generates a new chiral center at the nitrogen atom, the absolute stereoconfiguration being of the *S*-type. The two "terminal" pyrrolidine rings are oriented towards the same side with respect to the Al_2O_2 ring, resulting in a "boat conformation", and the two molecules reveal an (*S,R*) and an (*R,R*) configuration. The CH_2O moiety of the prolinato group forms a shorter Al−O distance within the five-membered $AlNC_2O$ ring than to the Al atom of the next H_2Al-OR' unit [1.833(2) vs. 1.919(2) Å].

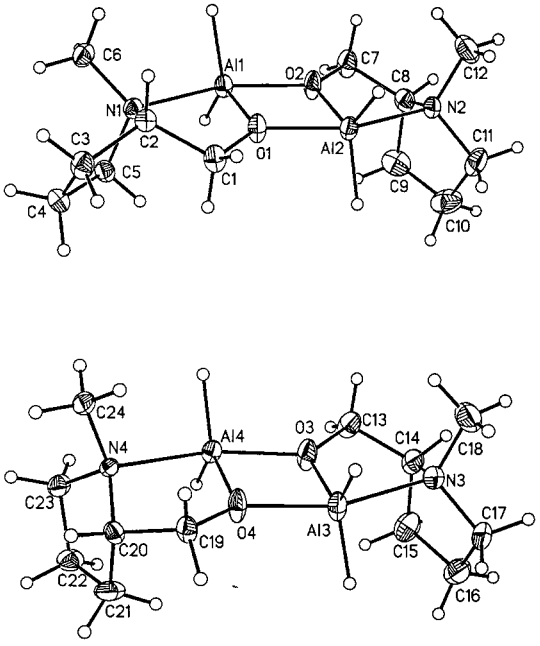

Figure 3. Molecular structure of dimeric *N*-methyl-L-prolinatoalane **(2)**; thermal ellipsoids represent a 25% probability; selected bond lengths (in Å): Al1−O1 1.833(2), Al1−O2 1.919(2), Al1−N1 2.141(2), Al2−O1 1.901(2), Al1−H1 1.51(3), Al1−H2 1.59(3), Al2−H3 1.51(3), Al2−H4 1.55(3); selected bond angles (in °): O1−Al1−O2 74.73(9), N1−Al1−O1 80.73(9), N1−Al1−O2 155.46(9), H1−Al1−H2 118(2), H1−Al1−O1 122(1), H2−Al1−O1 120(1), N1−Al1−H1 92(1), N1−Al1−H2 94(1), Al1−O1−Al2 105.4(1), Al1−O1−C1 122.0(2), Al2−O1−C1 132.5(2), O2−Al2−O1 75.20(9), O2−Al2−N2 80.33(9), O1−Al2−N2 155.5(1)

In compound **3** (Figure 4), we observe a slightly nonplanar Al_2O_2 ring [sum of bond angles = 354.98(8)°]. The geometry around the two Al atoms indicates a strongly distorted trigonal bipyramid, the axial N−Al−O bonds being 153.28(8)° and 150.57(8)°, respectively. However, there is a perfect "trigonal plane" as shown by the sum of the bond angles (360°). But we find the same sum of bond angles for atoms H1B, O1 and N2 around atom Al1. This indicates that the geometry at the Al atoms can also be considered as a distorted "tetragonal pyramid". This involves atoms H1A, O1, O2 and N2 as the base and H1B as the top of the pyramid. It is, of course, evident that the absolute stereoconfiguration at atoms C3 and C14, as well as at C2 and C13 (*R* or *S*), has not changed, as demonstrated by the analogous arrangement of the phenyl groups with respect to the Al_2O_2 ring.

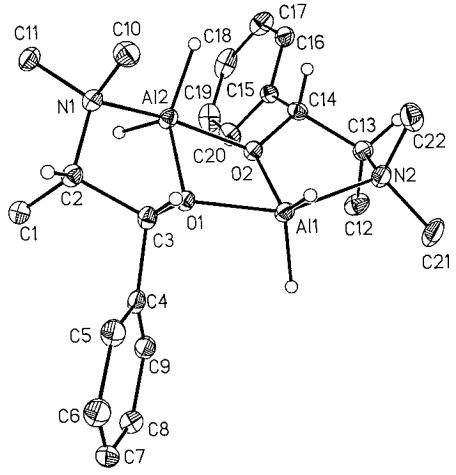

Figure 4. Molecular structure of dimeric (−)-*N*-methylephedrinatoalane **(3)**; thermal ellipsoids are depicted on a 25% probability scale; selected bond lengths (in Å): Al1−O1 1.940(2), Al1−O2 1.848(2), Al1−N2 2.145(2), Al2−O1 1.870(2), Al2−O2 1.920(2), Al2−N1 2.140(2), Al1−H1A 1.59(3), Al1−H1B 1.54(2); selected bond angles (in °): O1−Al1−O2 75.88(7), O1−Al1−N2 153.23(8), N2−Al1−O2 80.92(8), H1A−Al1−H1B 119(1), H1A−Al1−O2 127.1(9), H1B−Al1−O2 114.2(9), O1−Al1−H1A 92.7(9), O1−Al1−H1B 105.5(9), N2−Al1−H1A 90.7(9), N2−Al1−H1B 97(1), O1−Al2−O2 75.85(7), O1−Al2−N1 80.61(8), Al2−O1−C3 121.1(1), Al2−N1−C2 105.7(1)

Compound **4**, a derivative of *N*,*N*-dimethylaminopropanol, differs from the other dimeric aminoalkoxyalanes as the trigonal bipyramid is less distorted owing to the formation of a six-membered $AlOC_3N$ ring, which exerts less ring strain (Figure 5). Consequently, the axial N−Al−O bond is now 164.43(6)°, approximately 10° wider than in compounds **1**−**3**. Like compound **1**, compound **4** is also centrosymmetric. Nevertheless, due to the different Al−O bond lengths and the sharp bond angles O1−Al1−O1A [77.96(5)°] and Al1−O1−Al1A [102.04(6)°], the H−Al−O bond angles are quite different [128.6 and 113.1(7)°]. The six-membered rings are present in a chair conformation.

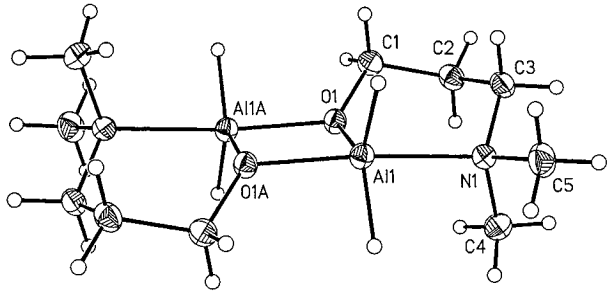

Figure 5. Molecular structure of dimeric (dimethylamino)propanolatoalane **(4)**; thermal ellipsoids depict a 25% probability; selected bond lengths (in Å): Al1−O1 1.834(1), Al1−O1A 1.930(1), Al1−N1 2.127(1), Al1−H1 1.53(2), Al1−H2 1.55(1); selected bond angles (in °): O1−Al1−O1A 77.96(5), Al1−O1−Al1A 102.04(5), Al1−O1−C1 125.8(1), Al1A−O1−C1 125.8(1), H1−Al1−H2 118(1), H1−Al1−O1 128.6(7), H2−Al1−O1 113.1(7), N1−Al1−O1A 164.43(6), N1−Al1−H1 87.3(6), N1−Al1−H2 91.7(7)

In contrast to the mono(aminoalkoxy)alane compound **5**, the bis(ephedrino)alane is monomeric but also features a pentacoordinated Al center (Figure 6). The molecule shows a twofold axis lying in the Al−H vector. While the axial positions of the slightly distorted pentagonal bipyramid are occupied by the nitrogen atoms [N−Al−N(0A) 174.3°] the trigonal plane is formed by the hydride hydrogen atom and two oxygen atoms, all bond angles for this plane being 120°. The Al−O bond lengths are shorter (1.760 Å) than in compounds **1**−**4**, while the Al−N bond lengths are almost the same as in the other compounds reported here.

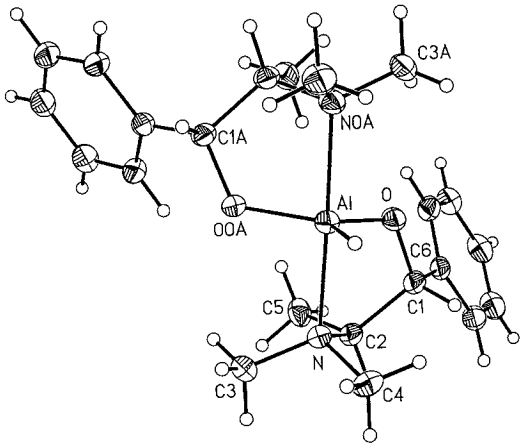

Figure 6. ORTEP plot of the molecular structure of bis(ephedrino)alane **(5)**; thermal ellipsoids represent a 25% probability; aromatic and methyl hydrogen atoms are omitted for clarity; selected bond lengths (in Å): Al−O 1.7603(2), Al−N 2.138(2), Al−H 1.83(2), O−C1 1.398(2), N−C3 1.478(3), N−C4 1.478(3); selected bond angles (in °): O−Al−O(0A) 119.9(1), O−Al−N 92.54(7), O−Al−N(0A) 84.61(7), O−Al−N 174.3(1), O−Al−H 120.0(1)N−Al−H 92.9(1). C1−O−Al 119.4(1), C3−N−C4 107.4(2), C2−N−Al 103.0(1)

Discussion

Amino alcohols react smoothly in a 1:1 molar ratio with $AlH_3{\cdot}NMe_3$, providing aminoalkoxyalanes $R_2N(CH_2)_nOAlH_2$ quantitatively. During the reaction, not only is H_2 formed but also the Me_3N coordinated to AlH_3 is displaced by the amino group of the amino alcohol, a displacement that is most likely entropy-driven owing to the formation of five- or six-membered rings in which the amino group coordinates to the Al center. It is typical for compounds **1**−**4** that the Al atoms are pentacoordinated, two monomeric $R_2N(CH_2)_nOAlH_2$ units form dimers by Al−O coordination which leads to a central Al_2O_4 four-membered ring with two significantly different Al−O bond lengths. The O−Al−O bond angles are rather acute (about 75°) while the Al−O−Al bond angles are quite wide (about 105°), with the oxygen atoms residing in a planar Al_2C environment. Similar structures have been found for aminoalkoxy-diorganylalanes $[R_2N(CH_2)_nOAlR_2']_2$-gallanes and $[R_2N(CH_2)_nOGaR_2]$.[9] These classes of compounds are also dimeric. However, they may become monomeric by increasing the size of the ligand. Thus, the Me_2Al and the Me_2Ga derivatives of the darvon alcohol [(+)-(2*S*,3*R*)-4-dimethylamino-1,2-diphenyl-2-butanol] are monomeric in the solid state.[10] Interestingly, reactions of R_2AlCl (R = Me, Et) with amino alcohols not only gives access to dimeric aminoalkoxy alkyl chloroalanes $[R^*OAl(R)Cl]_2$ but, in the case of Me_2AlCl and (*S*)-α,α-diphenyl-2-pyrrolidinyl methanol, an ionic complex $\{MeAl(R^*O)_2AlMe]^+[MeAlCl_3]^-$ is formed.[12] Although compounds **1**−**5** are the first structurally characterized aminoalkoxyalanes, one gallium homologue has been reported previously: *N*,*N*′′-dimethylaminoethoxydihydridogallane.[11] The bond lengths in the gallium compound are slightly longer than in the comparable aluminium compounds, and this holds also for the alane and gallane (E = Al, Ga) pairs of $[t\text{BuOEH}_2]_2$.[7b] Table 2 shows a comparison of the structural parameters of the dimeric compounds **1**−**4** with similar aminoalkoxydiorganylalanes.

First of all, it can be noted that the $Al-O_{ax}$ bond lengths are approximately up to 0.09 Å longer than the $Al-O_{eq}$ bonds. In general, the Al−O and particularly the Al−N bond lengths of the diorganylamine derivatives are longer than those of the alane derivatives, while the $N-Al-O_{ax}$ bond angles do not vary by more than 3.5°. Furthermore, a comparison of the only two closely related pairs of alane and gallane derivatives is also included in Table 2.

Bond lengths are generally somewhat longer for the gallium compounds,[6b] while the bond angles are almost identical.[7b] Although pentacoordination at Al is the structural feature for all aminoalkoxydihydridoalanes described here,

Table 2. Comparison of bond lengths (in Å) and bond angles (in °) in structurally related dimeric aminoalkoxyalanes and dimeric alkoxydialkylalanes; (−)MEP = (−)-*N*-methylephedrine, (−)NMP = *N*-methyl-L-proline

	d(Al−N)	*d*(Al-$_{ax}$)	*d*(Al-$_{eq}$)	N−Al−O	ref.
$[Me_2NCH_2CH_2OAlH_2]_2$, **1**	2.133(3)	1.903(2)	1.850(2)	154.50(7)	-
$[Me_2NCH_2CHMeOAlMe_2]_2$	2.246(2)	1.927(1)	1.852(1)	151.0(1)	[8]
$[2\text{-}C_5H_4NCH_2OAl\textit{i}Bu]_2$	2.130(5)	1.935(5)	1.853(5)	151.7(2)	[12]
$[(-)MEP-AlH_2]_2$, **3**	2.143(2)	1.940(2)	1.848(2)	153.23(8)	-
$[(-)MEP-AlMe_2]_2$	2.193(8)	1.946(7)	1.864(6)	151.6(3)	[11]
$[(-)NMP-AlH_2]_2$, **2**	2.141(2)	1.919(2)	1.833(2)	155.4(9)	-
$[Me_2N(CH_2)_3O-AlH_2]_2$, **4**	2.127(1)	1.930(1)	1.834(1)	164.43(6)	-
	d(Al−H) or *d*(Ga−H)		*d*(Al−O) or *d*(Ga−O)		ref.
$[Me_2NCH_2CH_2OAlH_2]_2$, **1**	1.50(2), 1.54(2)		1.850(2), 1.903(2)		-
$[Me_2NCH_2CH_2O-GaH_2]_2$	1.50(7), 1.73(5)		1.911(3), 2.053(3)		[10]
$[Me_3CO-AlH_2]_2$	1.55(4), 1.55(5)		1.810(3), 1.815(3)		[6b]
$[Me_3CO-GaH_2]_2$	1.61(10), 1.69(12)		1.908(9), 1.902(9)		[6b]

the situation in solution is different. At ambient temperature, the ^{27}Al NMR spectra demonstrate the dominating presence of a dimer. However, a temperature-dependent series of ^{27}Al NMR as well as ^{1}H and ^{13}C NMR spectra clearly show that the room-temperature spectrum represents an averaged dynamic situation. The line width is also indicative of this assumption. Furthermore, at low temperature a significant amount of hexacoordinated Al centers is present besides the pentacoordinated Al and possibly the tetracoordinated species. Therefore, a comparatively complex situation exists in solution. A more detailed study will be needed to evaluate the kinetics and energetics of the species involved in the equilibrium (4). Taking these equilibria into account, the practical absence of any stereoselective reduction of acetophenone with prolinolatodihydridoalane or (+)-*N*-methylephedrinodihydridoalane can be understood.

Experimental Section

All manipulations were carried out using Schlenk techniques under an N_2 atmosphere, using flame-dried glassware. $AlH_3{\cdot}NMe_3$ was prepared from $[Me_3NH]Cl$ and $LiAlH_4$.[15] The amino alcohols are commercially available and were used as supplied. NMR: Jeol GSX 270 and Jeol EX 400:TMS C_6D_6, $AlCl_3$ in H_2O, LiCl in D_2O as standards. Routine spectra were recorded at 24.5 °C. − IR: Nicolet FT, range 4000−400 cm^{-1}. − X-ray: Siemens P4 diffractometer, Mo-K_α-radiation, graphite monochromator, CCD area detector. − C,H,N analysis was performed with an automated analyzer. Al was determined by TEDA titration.

Dimeric *N,N*-Dimethylaminoethoxyalane (1): $AlH_3{\cdot}NMe_3$ (0.71 g, 7.9 mmol) was dissolved in toluene (25 mL). At −25 °C a solution of $Me_2NCH_2CH_2OH$ (0.71 g, 8 mmol) in toluene (10 mL) was added slowly with stirring. After the gas evolution had ceased, the solution was reduced in vacuo to about half of its volume. The crystals that separated at −20 °C were isolated. Toluene was then removed partially from the filtrate. Compound **1** (810 mg, 86.9%) was isolated; m.p. 184−186 °C (dec.). − ^{1}H NMR (C_6D_6): δ = 1.95 (s, 12 H, N*Me*$_2$), 1.96 [t,^{3}J(H,H) = 5.6 Hz, 4 H, NC*H*$_2$], 3.57 [t,^{3}J(H,H) = 5.6 Hz, 4 H, OC*H*$_2$], ca. 4 (broad, 4 H, Al*H*$_2$). − ^{13}C NMR (C_6D_6): δ = 44.3 (N*Me*$_2$), 55.4 (N*C*H$_2$), 58.4 (O*C*H$_2$). − ^{27}Al NMR (C_6D_6): δ = 91 ($h_{1/2}$ = 1090 Hz), 94 ($h_{1/2}$ = 900 Hz). − IR (Nujol, Hostaflon): ṽ: 3000 vs, 2978 vs, 2921 vs, 2885 vs, 2841 vs, 2808 sh, m, 2800 sh, m, 2794 m, 1755 vs/1719 vs [νAlH$_2$], 1496 m, 1459 vs, 1438 s, 1429 s, 1403 m, 1378 m, 1354 m, 1277 vs, 1254 vs, 1185 vs, 1089 vs, 1073 vs, 955 vs, 908 vs, 825 vs, 779 vs, 748 vs, 718 vs, 684 m, 556 vs, 550 vs cm^{-1}. − MS (70 eV): *m*/*z* = 233 [(**1**)$_2$ − H]$^+$, 203 [(**1**)$_2$ − 2 Me − H]$^+$. − $C_8H_{24}Al_2O_2N_2$ (234.3): calcd. C 41.02, H 10.33, Al 23.04, N 11.96; found C 40.58, H 9.85, Al 23.11, N 11.34.

Dimeric *N*-Methylprolinatoalane (2): To a stirred solution of $AlH_3{\cdot}NMe_3$ (0.84 g, 9.5 mmol) in toluene (10 mL) was added dropwise a solution of *N*-methylprolinol [(*S*)-2-hydroxymethyl-1-methylpyroline, 1.06 g, 9.5 mmol] in toluene (10 mL). After gas evolution had ceased, stirring was continued for one hour. Repeated crystallisations at −78 °C gave colorless needles (2.45 g, 90.4%), m.p. 134−151 °C (dec.). − ^{1}H NMR (C_6D_6): δ = 1.18−1.27 (m, 1 H), 1.34−1.42 (m, 1 H), 1.78−1.94 (m, 3 H), 1.99−2.03 (m, 1 H), 2.04 (s, 3, NC*H*$_3$), 3.18−3.24 (m, 1 H), 3.51 [dd, *J*(H,H) = 2.1 Hz, 11 Hz, 1 H], 3.63 [dd, *J*(H,H) = 4.7 Hz, 11 Hz, 1 H). − ^{13}C NMR: δ = 21.3 (*C*H$_2$), 27.6 (*C*H$_2$), 43.7 (N*C*H$_3$), 56.1 (N*C*H$_2$), 57.9 (N*C*H), 67.6 (O*C*H$_2$). − ^{27}Al NMR: δ = 91 ($h_{1/2}$ = 1880 Hz). − IR (Nujol, Hostaflon): ṽ: 2971 vs, 2939 vs, 2907 s, 2873 vs, 2813 w, 1767 vs/1730 vs, [νAlH$_2$], 1486 w, 1477 w, 1460 s, 1451 w, 1422 m, 1381 m, 1365 m, 1351 m, 1340 m, 1319 m, 1298 m, 1281 m, 1253 m, 1241 m, 1215 m, 1193 m, 1141 s, 1097 vs, 1060 s, 1043 s, 1029 vs, 996 vs, 920 vs, 897 m, 886 m, 831 vs, 810 vs, 773 vs, 737 vs,br, 633 vs, 577 vs, 560 vs, 537 vs cm^{-1}. − MS (70 eV): *m*/*z* = 286 [M$^+$], 285 [M$^+$ − H], 284 [M$^+$ − 2 H], 269 [M$^+$ − 2 H − CH$_3$], 256 [M$^+$ − 2 CH$_3$], 255 [M$^+$ − H − 2 CH$_3$]. − $C_{12}H_{28}Al_2N_2O_2$ (286.32): calcd. C 50.34, H 9.86, Al 9.42, N 9.78; found C 49.29, H 9.99, Al 9.15, N 9.35.

Dimeric (−)-Ephedrinoalane (3)$_2$: As described for **2**, $AlH_3{\cdot}NMe_3$ (1.73 g, 19.4 mmol) in toluene (17.1 mL) was treated with (−)-(1*R*,2*S*)-2-dimethylamino-1-phenyl-propanol (2.68 g, 15.0 mmol) dissolved in toluene (27.3 mL). Crystallisation at −20 °C yielded **3** (2.75 g, 88.8%) as colorless crystals, m.p. 166 °C (dec.), softening at ≈139 °C. − ^{1}H NMR (C_6D_6): δ = 0.69 [d, ^{3}J(H,H) = 7.2 Hz, 6 H, 3-*H*], 1.89 (s, 6 H, NC*H*$_3$), 2.15 (s, 6 H, NC*H*$_3$), 2.47 [dq, ^{3}J(H,H) = 5.4 Hz, 2 H, 2-*H*], 4.1 (s, br., 4 H, Al*H*$_2$), 5.41 [d, ^{3}J(H,H) = 5.4 Hz, 2 H, 1-*H*], 7.06 [dd, ^{3}J(H,H) = 7.5 Hz, 2 H, *p*-*H*(Ar)], 7.22 [dd, ^{3}J(H,H) = 7.5 Hz, 4 H, *m*-*H*(Ar)], 7.55 [d,^{3}J(H,H) = 7.5 Hz, 4 H, *o*-*H*(Ar)]. − ^{13}C NMR (C_6D_6): δ = 10.5 (*C*H$_3$), 40.6 (N*C*H$_3$), 46.2 (N*C*H$_3$), 65.5 (N*C*H), 72.9 (O*C*H), 127.3, 127.7, 127.9 (*C*−Ar), 140.9 [*i*-*C*(Ar)]. − ^{27}Al NMR (C_6D_6): δ = 96 ($h_{1/2}$ = 4260 Hz) − IR (Nujol, Hostaflon): ṽ: 3082 m, 3060 m, 3024 s, 3007 s, 2989 vs, 2925 s, 2901 vs, 2890 vs, 2869 vs, 2847 s, 2798 m, 1811 vs/1776 vs/1703 vs, br.(ν AlH$_2$), 1604 m, 1492 m, 1463 vs, 1449 vs, 1432 vs, 1406 vs, 1386 vs, 1364 m, 1349 m, 1302 m, 1243 m, 1217 m, 1196 m, 1177 m, 1129 m, 1109 vs, 1101 vs, 1070 vs, 1010 vs, 961 vs, 899 vs, 865 vs, 850 vs,sh, 824 s, 789 vs, 758 vs, 742 vs, 726 vs,sh, 716 vs, 703 vs, 661 vs, 591 vs, 574 vs; (toluene): ṽ = 1805 vs,sh, 1784 vs,br, 1748 vs,br cm^{-1}. − $C_{22}H_{36}Al_2N_2O_2$ (414.49): calcd. C 63.75, H 8.75, Al 13.02, N 6.76; found C 63.01, H 8.62, Al 12.85, N 6.40.

Dimeric *N,N*-Dimethylaminopropanolatoalane (4)$_2$: To $AlH_3{\cdot}NMe_3$ (0.84 g, 9.5 mmol) in toluene (10 mL) was added a solution of $Me_2N(CH_2)_3OH$ (0.97 g, 9.45 mmol) in toluene (10 mL) at −10 °C, while stirring. Stirring was continued for 30 minutes after gas evolution had ceased. Crystallisation at −20 °C gave **4** (1.09 g, 87.9%) as colorless prisms, melting in the range of 118−133 °C. − ^{1}H NMR (C_6D_6): δ = 1.19 [tt, ^{3}J(H,H) = 5.5 Hz, 4 H, 2-*H*], 2.00 (s, 12 H, N*Me*$_2$), 2.15 [t, ^{3}J(H,H) = 5.5 Hz, 4 H, NC*H*$_2$], 3.90 [t, ^{3}J(H,H) = 5.5 Hz, 4 H, OC*H*$_2$]. − ^{13}C NMR (C_6D_6): δ = 26.3 (C2), 45.6 (N*Me*$_2$), 59.4 (N*C*H$_2$), 64.0 (O*C*H$_2$). − ^{27}Al NMR (C_6D_6): δ = 92 ($h_{1/2}$ = 1970 Hz) − IR (Nujol, Hostaflon): ṽ = 3009 s, 3004 s, 2993 s, 2960 vs, 2926 vs, 2904 vs, 2876 vs, 2866 vs, 2840 s, 2806 m, 1749 vs/1715 vs (νAlH$_2$), 1475 vs, 1455 s, 1429 vs, 1398 w, 1385 w, 1377 w, 1356 w, 1301 m, 1269 s, 1252 m, 1234 s, 1184 s, 1170 s, 1098 vs, 1087 vs, 1049 vs, 1016 vs, 967 s, 900 vs, 862 vs, 772 vs, 748 vs, 721 vs, 598 vs, 558 vs, 545 vs cm^{-1}. − $C_{10}H_{28}O_2N_2Al_2$ (262.30): calcd. C 45.79, H 10.76, Al 20.57, N 10.68; found C 44.95, H 10.99, Al 20.43, N 10.09.

Bis(ephedrino)alane (5): To a stirred solution of $AlH_3{\cdot}NMe_3$ (0.49 g, 5.5 mmol) in diethyl ether (10 mL) was added a solution of (−)-(1*R*,2*S*)-2-dimethylamino-1-phenylpropanol (1.97 g, 11.0 mmol) in tetrahydrofuran (10 mL). After addition, stirring was continued for 1 hour. All volatile material was then removed from the solution in vacuo. Crystallisation of the solid residue at −20 °C from toluene/hexane (2:1, 15 mL) gave clear crystals (1.78 g, 84%), m.p. 86 °C, softening ≈70 °C. − ^{1}H NMR (C_6D_6): δ = 0.97 [d,^{3}J(H,H) = 7.2 Hz, 6 H, 3-*H*], 2.30 (s, 6 H, NC*H*$_3$), 2.38 (s, 6 H, NC*H*$_3$), 2.31−2.36 [m,^{3}J(H,H) ≈ 5 Hz, 2 H, 2-*H*], 5.34 [d,

Table 3. Crystallographic data and data referring to data collection and structure solution of compounds **1**–**5**

Compound	1	**2**	**3**	**4**	**5**
Empirical formula	$C_8H_{24}Al_2N_2O_2$	$C_{12}H_{28}Al_2N_2O_2$	$C_{22}H_{36}Al_2N_2O_2$	$C_{10}H_{28}Al_2N_2O_2$	$C_{29}H_{41}AlN_2O_2$
Formula mass	234.25	286.32	414.49	262.30	476.62
Cryst. size [mm]	0.3×0.3×0.35	0.22 ×0.25 ×0.35	0.20 ×0.20 ×0.30	0.30 ×0.35 ×0.40	0.35×0.3×0.27
Crystal system	monoclinic	monoclinic	monoclinic	monoclinic	hexagonal
Spące group	*P*2(1)/*n*	*P*2(1)	*P*2(1)	*P*2(1)/*c*	*P*3(1)21
a [Å]	6.073(3)	6.7904(1)	8.343(3)	6.8829(3)	12.2199(9)
b [Å]	10.645(4)	14.2260(2)	12.223(3)	10.6099(5)	12.2199(9)
c [Å]	10.721(4)	17.2732(3)	11.789(3)	11.1632(4)	15.865(1)
α [°]	90	90	90	90	90
β [°]	95.25(2)	93.632(1)	91.48(1)	102.477(1)	90
γ [°]	90	90	90	90	120
V [Å^3]	690.2(5)	1665.24(4)	1201.7(6)	795.96(6)	2051.7(3)
Z	2	4	2	2	3
ρ(calcd.), [Mg/m^3]	1.127	1.142	1.145	1.094	1.157
μ [mm^{-1}]	0.194	0.172	0.139	0.175	0.101
F(000)	256	624	448	288	774
Index range	$-1 \le h \le 7$ $-13 \le k \le 12$ $-12 \le l \le 7$	$-8 \le h \le 8$ $-18 \le k \le 18$ $-20 \le l \le 20$	$-9 \le h \le 9$ $-13 \le k \le 13$ $-13 \le l \le 13$	$-8 \le h \le 8$ $-3 \le k \le 13$ $-15 \le l \le 9$	$-14 < h < 14$ $-13 < k < 14$ $-19 < l < 19$
2 θ [°]	53.86	58.62	49.42	58.72	51.52
Temp. [K]	173(2)	193(2)	193	183(2)	200
Refl. collected	1420	9644	5920	4462	15 703
Refl. unique	1004	6368	3826	1452	2618
Refl. observed (4σ)	976	5513	3202	1295	1904
R (int.)	0.1326	0.0196	0.0239	0.0142	0.0591
No. variables	75	361	275	83	161
Weighting scheme[a] *x*/*y*	0.0906/0.1991	0.03020/0.61670	0.04300/0.000	0.0567/0.1557	0.06520/0.000
GOOF	1.122	1.074	1.014	1.094	0.923
Final *R* (4σ)	0.0526	0.0419	0.0379	0.0316	0.0409
Final *wR*2	0.1444	0.0850	0.0775	0.0949	0.1029
Larg. res. peak [e/Å^3]	0.416	0.168	0.141	0.159	0.280

[a] $w^{-1} = \sigma^2F_o^2 + (xP)^2 + yP$; $P = (F_o^2 + 2F_c^2)/3$

^3J(H,H) = 4 Hz, 2 H, 1-*H*], {7.10–7.18 (m), 7.30 [dd, ^3J(H,H) = 7.8 Hz], 7.44 [d, ^3J(H,H) = 7.8 Hz], 20 H}. – ^{13}C NMR (C_6D_6): δ = 11.15 (*C*H$_3$), 43.5 (N*C*H$_3$), 46.5 (N*C*H$_3$), 68.2 (N*C*H), 73.0 (O*C*H), 126.2, 126.3, 128.2 (*C*–Ar), 146.5 [*i*-*C*(Ar)]. – ^{27}Al NMR (C_6D_6): δ = 83 ($h_{1/2}$ = 3690 Hz); in diethyl ether: 81 ($h_{1/2}$ = 2370 Hz). – IR (Nujol, Hostaflon): $\tilde{\nu}$ = 3081 m, 3066 m, 3023 s, 3000 vs, 2993 vs, 2980 vs, 2925 vs, 2908 vs, 2879 vs, 2865 vs, 2845 vs, 2823 vs, 2797 vs, 1777 vs,br, ν AlH$_2$, 1601 m, 1491 vs, 1461 vs, 1453 vs, 1447 vs, 1434 vs, 1406 m, 1386 vs, 1347 s, 1300 m, 1289 m, 1243 m, 1216 vs, 1196 m, 1167 m, 1127 vs, 1102 s, 1087 m, 1066 vs, 1017 vs, 955 vs, 921 m, 893 vs, 864 s, 855 s,sh, 826 m, 790 vs, 762 vs, 742 vs, 734 s, 710 vs, 690 vs, 675 s, 626 s, 608 vs cm^{-1}. – MS (70 eV): *m*/*z* = 384, 383 [M$^+$ – 2 H], 312, 311 [M$^+$ – $CH_3CHN(CH_3)_2$ – 2 H]. – $C_{22}H_{34}AlN_2O_2$ (385.51): calcd. C 68.54, H 8.89, N 7.27, Al 6.99; found C 67.80, H 9.25, N 6.55, Al 6.54.

X-ray Structure Determinations: Single crystals were transferred from the toluene suspensions onto precooled polyfluoroether oil (–30 °C) and the selected specimen was mounted on the tip of a glass fiber. This was transferred to the goniometer head which was cooled by a stream of N_2 gas to 193 K (LT2 device). After optically aligning the crystal, five different sets in χ of 15 frames each were collected (Δ = 0.3°), and the data were used to calculate the cell dimensions (SMART program).[16] Data collection was performed by using the hemisphere mode of the SMART program. Data for a total of 1290 frames were collected at two different χ-settings with Δ = 0.3°. The data was reduced with the program SAINT[17] and an empirical adsorption correction was applied (SADABS). The structures were solved (SHELXTL)[18] by direct methods and the non-hydrogen atoms were refined anisotropically. The positions of the H atoms bonded to Al were taken from the difference Fourier map; all others were either taken from the Fourier map or placed in calculated positions and included in the final refinement cycles. Compound **5** crystallized as **5**·0.5C_7H_8. The toluene molecule is disordered. Refinement was performed with SOF = 0.5 for two orientations. No hydrogen atoms were included for the toluene molecules. Relevant data referring to crystallography, data collection and refinement are summarized in Table 3.

Crystallographic data (excluding structure factors) for the structures reported in this paper have been deposited with the Cambridge Data Centre as supplementary publication no. CCDC-148492–148496 (**1**–**5**). Copies of the data can be obtained free of charge on application to CCDC, 12 Union Road, Cambridge C32.1 EZ, UK [Fax: (internat.) +44-1223/336-033. E-mail: deposit@ccdc.cam.ac.uk].

Acknowledgments

We thank the Fonds der Chemischen Industrie and particularly Chemetall GmbH for support of this study. Furthermore, we would like to acknowledge the cooperation of Dipl.-Chem. K. Knabel, Dr. Martina Vosteen and Dr. R. Waldhör for recording the NMR spectra, and Mrs. D. Ewald for measuring the mass spectra.

[1] [1a] A. Hajos, *Komplexe Hydride*, VEB Deutscher Verlag der Wissenschaften, Berlin, **1966**. – [1b] H. Nöth, E. Wiberg. *Fortschr. Chem. Forsch.* **1967**, *8*, 321–436. – [1c] H. C. Brown, S. Krishnamurthy, *Tetrahedron* **1979**, *35*, 567–607. – [1d] J. Seyden-Penne, *Reductions by the Alumino- and Borohydrides in Organic Synthesis*, VCH Publishers, Weinheim, New York, **1991**.

[2] E. C. Ashby, J. R. Boone, *J. Org. Chem.* **1976**, *41*, 2890–2903, and ref. [1d].

[3] R. Noyori, *Pure Appl. Chem.* **1981**, *53*, 2315–2322; R. Noyori,

I. Tomino, Y.Tanimoto, M. Nishizawa, *J. Am. Chem. Soc.* **1984**, *106*, 6709−6716, *J. Am. Chem. Soc.* **1984**, *106*, 6716−6725.
[4] [4a] H. Nöth, A. Schlegel, J. Knizek, H. Schwenk, *Angew. Chem.* **1997**, *109*, 2754−2758; *Angew. Chem. Int. Ed. Engl.* **1997**, *36*, 2640−2643. − [4b] H. Nöth, A. Schegel, J. Knizek, W. Ponikwar, T. Seifert, *Chem. Eur. J.* **1998**, *4*, 2191−2203.
[5] J. P. Vigneron, I. Jacquet, *Tetrahedron* **1976**, *32*, 939−944.
[6] [6a] R. Benn, A. Rufinska, H. Lehmkuhl, E. Janssen, C. Krüger, *Angew. Chem. Int. Ed. Engl.* **1983**, *22*, 808−809. − [6b] R. Benn, E. Janssen, H. Lehmkuhl, A. Rufinska, *J. Organomet. Chem.* **1987**, *333*, 155−168.
[7] [7a] H. Nöth, H. Suchy, *Z. Anorg. Allg. Chem.* **1968**,*358,* 44−66. − [7b] M. Veith, S. Faber, H. Wolfanger, V. Huch, *Chem. Ber.* **1996**, *129*, 381−384.
[8] J. Weidlein, U. Müller, K. Dehnicke, *Schwingungsfrequenzen* vol. I, Thieme Publ. Stuttgart, **1981**; A. P. Kurbakova, L. A. Leites, V. V. Gavrilinko, Yu. N. Karaksin, L. I. Zakharkin, *Spectrochim. Acta* **1975**, *31 A*, 281−286.
[9] K.-H. Thiele, E. Hecht, T. Gelbrich, U. Dümichen, *J. Organomet. Chem.* **1997**, *540*, 89−94 and refs. cited therein; E. Hecht, T. Gelbrich, W. Wernik, R. Weimann, K.-H. Thiele, J. Sieler, H. Schumann, *Z. Anorg. Allg. Chem.* **1998**, *624*, 1061−1066; T. Gelbrich, E. Hecht, K.-H. Thiele, J. Sieler, *J. Organomet. Chem.* **2000**, *595*, 21−30.
[10] R. Kumar, M. L. Sierra, J. P. Oliver, *Organometallics* **1994**, *13*, 4285−4293.
[11] S. J. Rettig, A. Storr, J. Trotter, *Can. J. Chem.* **1975**, *53*, 58−66.
[12] M. L. Sierra, V. S. J. de Mel, J. P. Oliver, *Organometallics* **1989**, *8*, 2486−2488.
[13] M. R. P. van Vliet, P. Buysingh, G. van Koten, K. Vrieze, B. Kojic-Prodic. A. L. Spek *Organometallics* **1985**, *4*, 1701−1707.
[14] E. Hecht, T. Gelbrich, K.-H. Thiele, J. Sieler, *Z. Anorg. Allg. Chem.* **2000**, *626*, 180−186.
[15] J. K. Ruff, *Inorg. Synth.* **1967**, *9*, 30−37.
[16] Siemens Analytical Instruments, SMART, Version 4.1.
[17] Siemens Analytical Instruments, SAINT. Version 4.1.
[18] G. W. Sheldrick, University of Göttingen, **1993**.

Received March 27, 2000
[I00118]

Alkylthiolatoalanes and Alkylthiolatohydridoaluminates

Jörg Knizek,[a] Heinrich Nöth,*[a] and Andreas Schlegel[a]

Dedicated to Prof. Dr. Drs. h. c. Rolf Huisgen on the occasion of his 80th birthday

Keywords: Aluminum / Lithium / S ligands / Hydrides / Structure elucidation

Reactions of thiols RSH (R = Et, *i*Pr, *t*Bu) with $AlH_3{\cdot}NMe_3$ lead to $RSAlH_2{\cdot}NMe_3$ or $(RS)_2AlH{\cdot}NMe_3$ compounds, depending on the stoichiometry. Similarly, the 1:1 reaction of $LiAlH_4$ with RSH (R = Et, *i*Pr) in ether produces $LiAlH_3SR$, however, in the case of $NaAlH_4$ and *i*PrSH in THF, ligand exchange of $NaAlH_3(SR)$ to $NaAlH_4$, $NaAlH_2(SR)_2$ and $NaAlH(SR)_3$ occurs. A byproduct of the formation of $LiAlH(StBu)_3$ (**6**), in ether is $[(Et_2O)LiAlH(StBu)_3{\cdot}LiStBu]_2$ (**7**). Reaction of a 1:1 mixture of $LiAlH_4$ with $AlH_3{\cdot}NMe_3$ and HS*t*Bu (1:1:5) leads to $LiAlH(StBu)_3{\cdot}AlH(StBu)_2NMe_3$ (**8**). Compounds **5**, **7** and **8** were characterized by X-ray structure determinations. All molecules contain tetracoordinated Al centers.

Introduction

Aluminum compounds containing aluminum−sulfur bonds are comparatively less well studied than the thermodynamically more stable compounds with Al−O bonds.[1] Therefore, most of them are hydrolytically unstable in spite of the fact that alkanethiols are more acidic than alcohols, even if sulfur is less electronegative than oxygen. This can be readily rationalized by the theory of the HSAB principle. In consonance with this well-known principle is the observation that in dimethylaluminum complexes of thiophene a C-bridging is preferred over an Al−S interaction.[2] However, Al−S bridging in thioalanes is a well-known feature.[3] For instance, Me_2AlSMe is dimeric both in the solution and gas phase, and dimerization occurs via Al−S bonds.[4] However, this compound forms a chain structure in the solid phase.[4] If bulky R groups are introduced as in $Al(SAr)_3$, $RAl(SR)_2$ and $R_2Al(SR)$ (R = *t*Bu, Ar = 2,4,6-$tBu_3C_6H_2$), monomeric arylthioalanes with three-coordinated Al atoms are kinetically stabilized.[5] Not surprisingly, this demonstrates the tendency of oligomerization. So far only a few studies have been concerned with the reaction of thiols with aluminum hydride.[6] For instance, thiomorpholine reacts with $AlH_3{\cdot}NMe_3$ to produce dimeric $H_2Al[\mu\text{-}N(CH_2)_4S]$, a nitrogen-bridged dimeric substituted alane;[6a] this unit, in the solid state, forms a two-dimensional network via Al−S interactions generating pentacoordinated Al centers.

The reaction of $LiAlH_4$ with $(Et_2HN{-}CH_2{-}CH_2{-}SH)Cl$ yields $AlH(SCH_2CH_2NEt_2)_2$ irrespective of a 1:1 or 1:2 stoichiometry. It is assumed that $H_2AlSCH_2CH_2NEt_2$ is formed in a first stage followed by ligand exchange to give AlH_3 and $AlH(SCH_2CH_2NEt_2)_2$.[6a] Moreover, a number of other thiolatoalanes, H_2AlSR, have been reported.[6b,6c] Alkylthiolatoalanes smell even worse than the thiols, a long-standing experience of the senior author,[7] and this may be a reason why these compounds have not been very attractive for a closer investigation. The purpose of the study reported here was to compare the formation and structures of some thiolatoalanes and thiolatohydridoaluminates with those of organyloxoalanes and alkali metal organyloxohydridoaluminates.[8,9]

Synthesis

Two routes have been employed to prepare alkylthiolatoalanes as depicted in Equation (1) to (3).

$$AlH_3{\cdot}NMe_3 + RSH \longrightarrow RSAlH_2{\cdot}NMe_3 + H_2 \quad (1)$$

R	Et	*i*Pr	*t*Bu
	1	2	3

$$AlH_3 + tBuSH \longrightarrow \underset{\mathbf{4}}{tBuSAlH_2} + H_2 \quad (2)$$

$$AlH_3{\cdot}NMe_3 + 2\,tBuSH \longrightarrow \underset{\mathbf{5}}{(tBuS)_2AlH{\cdot}NMe_3} + 2\,H_2 \quad (3)$$

Compound **1,** a liquid, fumed in contact with air, solidified at − 20 °C and decomposed on distillation under vacuum. This also holds for the liquid compounds **2** and **3**. Complexed trimethylamine was not released under vacuum; in contrast to alkoxyalane−trimethylamines (particularly with alkyl = Me, Et, *n*Pr)[8,10] which are prone to ligand exchange to give polymeric and insoluble products of various compositions. The alkylthiolatoalanes showed no tendency of this behavior. Solvent-free $tBuSAlH_2$ resulted according to Equation (2). However, the ^{27}Al NMR spectrum of the solution in ether suggests that the compound is present as $tBuSAlH_2{\cdot}OEt_2$. It looses the coordinated ether in vacuo readily, and the ether-free compound is a moisture-sensitive white powder.

[a] Department of Chemistry, University of Munich
Butenandtstraße 5−13, 81377 München, Germany

 © WILEY-VCH Verlag GmbH, 69451 Weinheim, 2001 1434−1948/01/0101−0181 $ 17.50+.50/0

When $LiAlH_4$ was allowed to react with thiols, the amount of H_2 liberated depended on the stoichiometry involved [Equation (4)].

$$MAlH_4 + n\,RSH \longrightarrow MAlH_{4-n}(SR)_n + nH_2 \quad (4)$$
$$M = Li, Na;\ R = Et, i\text{Pr}, t\text{Bu}$$

$$2\,NaAlH_2(S\text{-}i\text{Pr})_2 \leftrightarrow NaAlH_3(S\text{-}i\text{Pr}) + NaAlH(S\text{-}i\text{Pr})_3 \quad (5)$$

$$2\,NaAlH_3(S\text{-}i\text{Pr}) \rightarrow NaAlH_4 + NaAlH_2(S\text{-}i\text{Pr})_2 \quad (6)$$

1:1 reactions of $LiAlH_4$ with EtSH or *i*PrSH in ether gave a solution which shows only a single ^{27}Al NMR signal at $\delta = 115$; this demonstrates not only the formation of $LiAlH_3(SR)$ but also proves its stability against ligand exchange. For the analogous organyloxyhydridoaluminates this kind of ligand exchange is typical,[9−11] and all members of the series $LiAlH_{4-n}(OR)_n$ can be detected in solution. However, when *i*PrSH was allowed to react with $NaAlH_4$ in THF in a 1:1 ratio the ^{27}Al NMR spectrum reveals the presence of at least three species [$NaAlH_4$, $NaAlH_2(S\textit{i}Pr)_2$ and $NaAlH(S\textit{i}Pr)_3$] in solution, as shown in Equation (5).

Treatment of $LiAlH_4$ in ether with *t*BuSH in a 1:3 ratio yielded compound **6** which was isolated as $Et_2O{\cdot}LiAlH(S\textit{t}Bu)_3$. However, in addition to this main product small amounts of crystals separated from the solution, and an X-ray structure analysis proved them to be $(Et_2O){\cdot}LiAlH(S\textit{t}Bu)_3{\cdot}LiS\textit{t}Bu$ (**7·Et$_2$O**). Most likely this compound was formed in a reaction sequence described by Equation (7) to (9).

$$LiAlH_4 + 3\,{}^t\text{BuSH} \longrightarrow \underset{\mathbf{6}}{LiAlH(S^t\text{Bu})_3} + 3\,H_2 \quad (7)$$

$$LiAlH(S^t\text{Bu})_3 + Et_2O \rightarrow HAl(S^t\text{Bu})_2{\cdot}OEt_2 + LiS^t\text{Bu} \quad (8)$$

$$LiAlH(S^t\text{Bu})_3 + LiS^t\text{Bu} \rightarrow \underset{\mathbf{7}}{LiAlH(S\text{-}^t\text{Bu})_3\,LiS^t\text{Bu}} \quad (9)$$

Obviously, $LiAlH(S\textit{t}Bu)_3$ behaves as a Lewis acid and adds $LiS\textit{t}Bu$ through its *t*BuS groups. In order to test whether $LiAlH(S\textit{t}Bu)_3$ would add an alane as a Lewis base, we employed $(t\text{BuS})_2AlH{\cdot}NMe_3$. As shown in Equation (10) a 1:1 mixture of $LiAlH_4$ and $AlH_3{\cdot}NMe_3$ reacted smoothly with *t*BuSH to produce the compound $LiAlH(S\textit{t}Bu)_3{\cdot}AlH(S\textit{t}Bu)_2{\cdot}NMe_3$ (**8**). However, the alane acted as a ligand only for the Li center with the formation of Li−S bonds, and no NMe_3 displacement from $(t\text{BuS})_2AlH{\cdot}NMe_3$ occurred.

$$LiAlH_4 + AlH_3{\cdot}NMe_3 + 5\,HS^t\text{Bu} \rightarrow \underset{\mathbf{8}}{LiAlH(S^t\text{Bu})_3{\cdot}\,AlH(S^t\text{Bu})_2{\cdot}\,NMe_3} + 5\,H_2 \quad (10)$$

NMR-Spectroscopic Data

As already indicated, only a single ^{27}Al NMR signal can be observed for the alkylthiolatoalanes **1**−**5**. Table 1 lists the relevant data.

Compounds **1**−**3** are tetracoordinated at the Al atom as shown by the low-field resonances. The signals are not very broad, nevertheless no Al−H coupling can be observed. Compound **4**, in ether solution, shows a better shielded Al center than compounds **1**−**3**. However, in benzene solution the Al nucleus of the ether-free compound **4** exhibits no change in shielding, but an enormous increase in the line width. This is an indication of the association of monomeric molecules in solution, probably through hydrogen bonds [Equation (11)]. If **4** were present in solution with pentacoordinated Al centers, the signal would then appear at an even higher field ($\delta \approx 110-120$). The ^{27}Al NMR spectrum of **4** in benzene solution also shows a low-intensity signal at $\delta = 9$ which points to the presence of a hexacoordinated species.

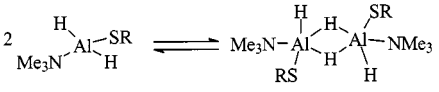

(11)

In contrast to alkoxyalanes, the shielding of the ^{27}Al nucleus is only marginally influenced by the number of RS substituents (compare **3** with **5**). However, this is not the case for the alkylthiolatohydridoaluminates; here, $\delta(^{27}Al)$ changes in the same manner as for the $AlH_{4-n}(OR)_n^-$ species.[9,11c] A higher degree of RS substitution leads to a successive deshielding of the ^{27}Al nucleus. The solution for the 1:1 reaction of $NaAlH_4$ with *i*PrSH shows three ^{27}Al NMR

Table 1. ^{27}Al NMR spectroscopic data of alkylthiolatoalanes and alkylthiolatohydridoaluminates (δ in ppm, $h_{1/2}$ in Hz)

	1	**2**	**3**	**4**	**5**	**6**	**7**
$\delta^{27}Al$	152	151	147	132	147	136	147
$h_{1/2}$	1053	1126	1103	1510	924	4390	1000
Solvent	C_6D_6	C_6D_6	C_6D_6	Et_2O	C_6D_6	C_6D_6	C_6D_6
δ (^7Li)	−	−	−	−	−	0.26	0.70
Solvent						Ether	C_6D_6
	$LiAlH_3SEt$	$LiAlH_3S\textit{i}Pr$	$LiAlH_2(S\textit{i}Pr)_2$	$LiAlH(S\textit{t}Bu)_3$			
$\delta^{27}Al$	115	115	128	131, 133			
Solvent	Ether	Ether	Ether	THF, Ether			

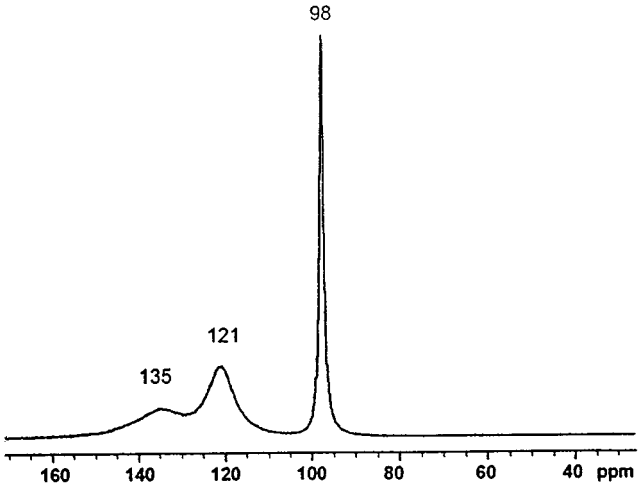

Figure 1. ^{27}Al NMR spectrum of a solution of "$NaAlH_2(SiPr)_2$" in THF to show the presence of various species; signals at δ = 98, 121 and 135 are assigned to $NaAlH_4$, $NaAlH_2(SiPr)_2$ and $NaAlH(SiPr)_3$

signals (see Figure 1). The sharp signal stems from $NaAlH_4$, the signal at δ = 135 is due to $NaAlH(SiPr)_3$ and the signal at δ = 121 due to $NaAlH_2(SiPr)_2$ (exchange). $NaAl(SiPr)_4$ is not present as this would give rise to a sharp and easily detectable signal.

IR Data

Table 2 contains a list of Al−H stretching bands. Compounds **2** and **3** exhibit a strong band in the narrow region 1805−1808 cm^{-1}, and compound **5** a strong and sharp band at 1840 cm^{-1}. Therefore, two electronegative RS groups strengthen the Al−H bond. This is in agreement with the series of compounds $AlH_{3-n}X_n{\cdot}OEt_2$ (X = Cl, Br).[12] Compound **4** shows a band for a terminal Al−H stretching vibration at 1846 cm^{-1}. In addition, there is a strong broad band ranging from 1750 to 1570 cm^{-1}, which is due to an Al−H−Al bridging mode. A band at 1699 cm^{-1} is observed for compound **2** (solid in Nujol mull) which also proves the presence of bridging hydrides. Consequently, this compound does not seem to be present as monomeric $iPrSAlH_2{\cdot}NMe_3$, but it is associated through Al−H−Al bridges. This is because the IR data exclude the presence of an Al−(SR)−Al bridge. The Al−H(terminal) stretching vibrations for the hydridoaluminates are found in the 1850-cm^{-1} region, which are associated with tetracoordinated Al centers.

Table 2. Al−H strechting bands (in cm^{-1}) for compounds **2**−**6** and **8**; for further data see Experimental Section

	2	**3**	**4**	**5**	**6**	**8**
νAlH_2	1808	1805	1846	1840	1829	1858, 1782
νAl−H−Al	1699	–	1750−1570	–	–	–

Molecular Structures

The structural features deduced from IR- and NMR-spectroscopic data of compounds **1**−**5** are ascertained by the determination of the molecular structure of **5** by X-ray structure analysis. This compound crystallizes in space group $P2_1/c$. The Al center is surrounded by two S atoms, one N and one H atom in a distorted tetrahedral array (see Figure 2).

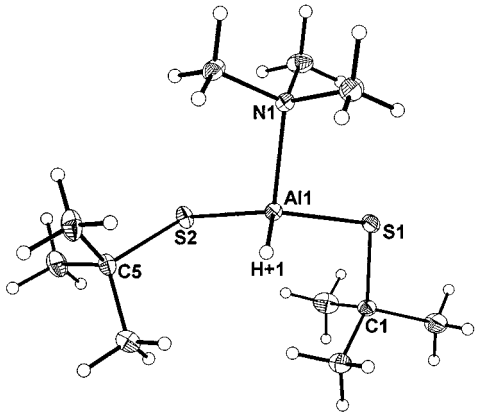

Figure 2. ORTEP plot of the molecular structure of the crystal of $HAl(StBu)_2{\cdot}NMe_3$ (**5**); thermal ellipsoids are shown on a 25% probability scale; selected bond lengths [Å] and angles [°] (esd values in parentheses): Al1−S1 2.2496(5), Al1−S2 2.2296(5), Al1−N1 2.020(1), Al1−H1 1.50(2), S1−C1 1.861(1), S2−C5 1.863(1); N1−Al1−S1 98.46(3), N1−Al1−S2 106.19(4), S1−Al1−C2 112.00(2), H1−Al1−N1 102.9(6), H1−Al1−S1 118.1(6), H1−Al1−S2 116.2(6), Al1−S1−C1 106.44(4), Al1−S2−C5 108.20(5), C10−N1−C9 109.2(1), C10−N1−C11 108.5(1), C9−N1−C11 107.6(1), C10−N1−Al1 112.70(8), C11−N1−Al1 110.09(8), C9−N1−Al1 108.6(9)

The Al−S bond lengths (average 2.240 Å) are shorter than the Al−S dative bond in $[tBuAl(\mu\text{-}OC_6H_4\text{-}2\text{-}SMe)]_2$ [2.778(1) Å].[13] The latter is comparable with the Al−S bond lengths in $AlH(SCH_2CH_2NEt_2)_2$ (average 2.725 Å)[14] with its pentacoordinated Al center. Thus, the difference in bond lengths between the tetracoordinated Al center in **5** and the pentacoordinated Al atom in $AlH(SCH_2CH_2NEt_2)_2$ is ca. 0.49 Å. It is also significantly longer than in the tricoordinated Al compound $Al(SC_6H_2tBu_3)_3$ [2.185(8) Å].[15] Al−S−C bond angles are wider than the H−S−C bond angles in thiols (96−101°).[16]

Crystals obtained from the 1:3 reaction of $LiAlH_4$ with *t*BuSH were suspected to be $LiAlH(StBu)_3$ but proved to be the ether adduct of dimeric $LiAlH(StBu)_3{\cdot}LiStBu$ (**7**) by X-ray structure analysis. The molecular structure as found for the solid state is represented in Figure 3.

The centrosymmetric dimer features a planar central Li_2S_2 ring with open S−Li−S bond angles [103.9(3)°] and rather sharp Li−S−Li angles [76.1(3)°]. Each lithium atom is tetracoordinated, atom Li1 is surrounded by three sulfur atoms and one oxygen atom, while atom Li2 coordinates to four sulfur atoms. It should be noted that the Li−S bonds to the tetracoordinated S4 atom (average 2.429 Å) are slightly shorter than the Li−S bonds to the tricoordinated

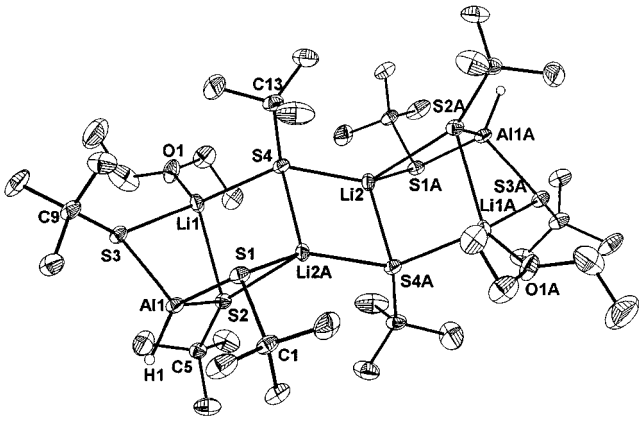

Figure 3. Molecular structure of the crystal of **7·OEt$_2$**; thermal ellipsoids are depicted on a 25% probability level; hydrogen atoms bonded to C atoms are not shown for clarity; selected atom distances [Å] and bond angles [°] (esd values in parentheses): Al1−H1 1.39(1), Al1−S1 2.259(2), Al1−S2 2.263(2), Al1−S3 2.242(2), Al1−S1 3.250(8), Li1−O1 1.889(9), Li1−S2 2.548(9), Li1−S3 2.563(9), Li1−S4 2.427(9), Li1−Li2A 3.39(1), Li2−Li2A 2.98(2), Li2A−S4 2.404(8), Li2−S1A 2.494(8), Li2−S4A 2.431(8), Li2−S2A 2.803(9), Li2A−S1 2.494(8), Li2A−S2 2.803(9), S1−C1 1.854(5), S2−C5 1.858(5), S3−C9 1.848(5), S4−C13 1.838(5); H1−Al1−S1 112(2), H1−Al1−S2 116(4), H1−Al1−S3 117(4), S1−Al1−S2 102.83(8), S1−Al1−S3 110.16(8), S2−Al1−S3 96.80(7), S1−Li2a−S4 137.6(3), S1−Li2A−S2 89.4(3), O1−Li1−S4 1o8.9(4), O1−Li1−S2 127.5(4), Al1−S1−Li2A 90.2(2), Al1−S2−Li2A 82.7(2), Al1−S2−Li1 84.8(2), Al1−S3−Li1 84.8(2), LI1−S4−Li2 139.1(3), Li1−S4−Li2A 88.4(3), Li2−S4−Li2A 76.1(3)

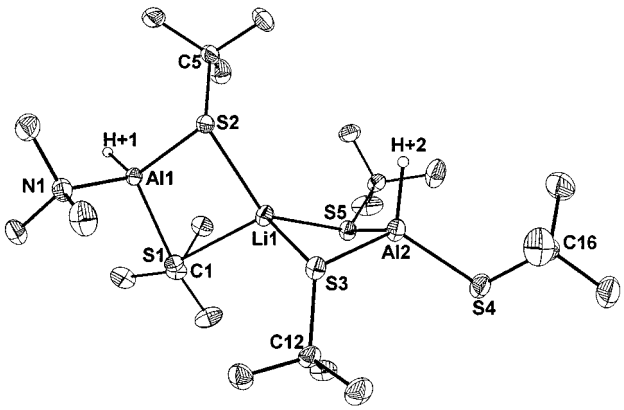

Figure 4. ORTEP presentation of the molecular structure of the crystal of **8**; thermal ellipsoids are drawn on a 25% probability level; H atoms bonded to carbon atoms are omitted for clarity; selected atom distances [Å] and bond angles [°] (esd values in parentheses): Al1−H1 1.48(4), Al1−N1 1.979(3), Al1−S1 2.246(1), Al1−S2 2.243(1), Al2−H2 1.58(4), Al2−S3 2.281(2), Al2−S4 2.237(2), Al2−S5 2.293(2), Li1−S1 2.489(6), Li1−S2 2.551(6), Li1−S3 2.491(6), Li1−S5 2.445(6), S1−C1 1.865(4), S2−C5 1.866(4), S3−C12 1.866(4), S4−C16 1.865(4), S5−C20 1.858(4); N1−Al1−S1 103−7(1), N1−Al1−S2 106.2(1), S1−Al1−S2 103−67(5). Al1−S−Li1 83.5(2), Al1−S2−Li1 82.2(2), S1−Li1−S2 88.8(2), S3−Li1−S5 88.5(2), S1−Li1−S3 109.8(2), S2−Li1−S5 136.5(3), S2−Li1−S3 108.7(2), DS1−Li1−S5 112.9(2), Li1−S5−C20 127.2(2)

S atoms. Atom Li1 binds to only two sulfur atoms of the $HAl(StBu)_3^-$ unit, and these bonds are the longest ones (2.548, 2.563 Å) while the bond Li1−S4 adopts an intermediate position (2.494 Å). The shortest Al−S bond is Al1−S2 [2.263(2) Å], atom S2 being tetracoordinated. It features a very large Li2A−S2−C5 bond angle of 155.1(2)°. All S−Al−S bond angles are rather sharp (96−103°), and, consequently, the H−Al−S bond angles are wide (112−117°). This asymmetry for a tetracoordinated Al atom with respect to a tetrahedral array is also present at the Li atoms.

A much simpler molecular structure is observed for compound **8**, $LiAlH(StBu)_3{\cdot}AlH(StBu)_2{\cdot}NMe_3$, as shown in Figure 4. One can readily note that it is an addition product of $HAl(StBu)_2{\cdot}NMe_3$ and $LiAlH(StBu)_3$. The metal ions are tetracoordinated and the skeleton of the molecule can be described as a spirocycle with the Li atom at the spiro center. This Li atom coordinates to four sulfur atoms with Li−S bond lengths ranging from 2.489(6) to 2.511(6) Å. There are two pairs of sharp S−Li−S bond angles (88°) and two wide ones (136°). The coordination geometry around both Al atoms is a strongly distorted tetrahedral geometry. The distortion is greater for Al1 than for Al2. At Al2, the S−Al−S bond angles are all different, the smallest one is S3−Al2−S5 with only 97.66(5)°, probably due to the coordination of these S atoms to Li1. In contrast, the angle S3−Al2−S4 is rather wide, 117.49(6)°, while the angle S5−Al2−S4 [109.19(6)°] is almost a perfect tetrahedral angle.

Discussion

Although the present study on the interaction of thiols with alane·trimethylamine, $LiAlH_4$ and $NaAlH_4$ is not as complete as analogous studies with alcohols,[8−11] some generalizations can be deduced. As expected, when the thiols, which are more acidic than alcohols, react, the amount of hydrogen evolved and the formation of the products are determined by the stochiometry involved. While AlH_3 in ether reacts with alcohols (ROH) having small R groups (R = Me, Et, Pr), to produce not very well defined products of composition $AlH_{3-n}(OR)_n$, only single-type species $AlH_2(SR){\cdot}NMe_3$ and $AlH_2(SR){\cdot}NMe_3$, which are stable against ligand exchange at ambient temperatures, are formed in the reaction of alane trimethylamine with thiols. Compound $AlH_2SEt{\cdot}NMe_3$ associates in the solid state through hydride bridges, and the IR spectra clearly show that there are no Al−S−Al bridging bonds. In contrast, compounds $ROAlH_2$ are characterized by Al−O−Al bridges.[17] This difference can readily be explained by the HASB theory. The softer base H^- is preferred as a bridging ligand over sulfur, and the IR spectra of the compounds $RSAlH_2{\cdot}NMe_3$ indeed show the presence of Al−H−Al bridges,[18] while in the case of alkoxyalanes the Al−O bonds are thermodynamically favored. No bands attributable to Al−H−Al vibrations are present for $(tBuS)_2AlH{\cdot}NMe_3$ (**5**) in agreement with its molecular structure.

Reactions of $MAlH_4$ with RSH have concentrated on the $LiAlH_4$/*t*BuSH and $NaAlH_4$/*i*PrSH systems, particularly on the former. For the first system, the product expected by

the stoichiometry of the reaction has been found to be $LiAlH(StBu)_3$ (**6**). However, in addition, a small amount of the dimeric compound $LiAlH(StBu)_2{\cdot}LiStBu$ (**7**) is also formed, demonstrating that $LiHAl(StBu)_3$, whose structure is still unknown, may act as a Lewis base through its RS groups. This has been verified by the addition of the alane $(tBuS)_2AlH{\cdot}NMe_3$ to $LiHAl{\cdot}(StBu)_3$ in compound **8**. This is a feature that needs further investigation; a similar behavior is, as yet, unknown in alkoxyaluminate chemistry. However, an investigation of Noyori's reagent[19,20] revealed many unexpected aspects showing that even hexacoordinated aluminates are readily formed.[21] We will report on these results shortly.

It is expected that the Al−S bond length would increase with increasing coordination number, and this can be demonstrated for the compounds investigated. All Al atoms of compounds **5**, **7** and **8** are tetracoordinated while the S atoms have coordination numbers 2, 3 and 4, respectively. Average Al−S bonds are as follows: $Al^{(4)}-S^{(2)}$ = 2.239 Å, $Al^{(4)}-S^{(3)}$ = 2.244 Å, and $Al^{(4)}-S^{(4)}$ = 2.457 Å. In addition, the average Al−S bond length $Al^{(6)}-S^{(2)}$ has been found to be 2.399 Å.[22] (Coordination numbers are set here in superscript). Therefore, we observe an increase in the Al−S bond lengths as the coordination number of sulfur increases. The $Al^{(4)}-S^{(2)}$ bond length is shorter than the $Al^{(6)}-S^{(2)}$ bond lengths by 0.016 Å. This trend was to be expected. Li−S bond lengths give no clear separation between $Li^{(4)}-S^{(3)}$ and $Li^{(4)}-S^{(4)}$, the former span the range from 2.489 to 2.566 Å, the latter from 2.457 to 2.548 Å. These data are in agreement with known structures of lithium thiolates,[23] the shortest being 2.39 Å found in $(Et_2O)_2Li(trip-S)_2In(S-trip)_2$ (trip = 2,4,6-triisopropylphenyl).

Experimental Section

All experiments were performed under anhydrous conditions and dinitrogen using Schlenk techniques. $LiAlH_4$ was supplied by Chemetall GmbH and $AlH_3{\cdot}NMe_3$ prepared form $LiAlH_4$ and $[Me_3NH]Cl$.[24] The thiols used were obtained commercially. − NMR: Jeol GSX 270 and EX 400; standards: $AlCl_3$ in H_2O (1 M), C_6D_6, $SiMe_3$. − IR: Nicolet 20 FT spectrometer (4000−400 cm^{-1}) as Nujol/Hostaflon mulls. − X-ray: Siemens P4 diffractometer with CCD area detector and LT2 low-temperature device. − Elemental analysis: C, H, N in the microanalytical laboratory of the institute; Al complexometrically. Partial hydrolysis was noted in weighing small samples for elemental analysis. This may be the reason for several significant deviations between calculated and found values.

Alkylthiolatoalanes and Lithium(alkylthiolato)hydridoaluminates. − General Procedure: The hydrides ($AlH_3{\cdot}NMe_3$, AlH_3 in ether, $LiAlH_4$ or $NaAlH_4$) were dissolved or suspended in toluene, ether or THF. While stirring, a solution of the thiol in the respective solvent was added (1:1, 1:2 ratio), and stirring was continued until gas evolution had ceased. No elemental analysis was performed when ^{27}Al NMR spectra proved that only a single compound was present.

Ethylthiolatoalane·Trimethylamine (1): Prepared from $AlH_3{\cdot}NMe_3$ (0.68 g, 7.63 mmol) in toluene (5 mL), and EtSH (0.47 g, 7.63 mmol) in toluene (4 mL). Addition at −4 °C, 2 h stirring at ambient temperature. An oil remained after stripping off all volatiles in vacuo. This oil solidified on standing to a waxy mass. − ^{27}Al NMR (70 MHz, C_6D_6): δ = 152 ($h_{1/2}$ = 1053 Hz). − ^1H NMR (270 MHz, C_6D_6): δ = 1.33 [t, ^3J(H,H) = 7.5 Hz, 3 H, CH_3CH_2S-], 2.00 (s, 9 H, NCH_3), 2.67 [q, ^3J(H,H) = 7.5 Hz, 2 H, CH_3CH_2S-], 4.0 (br, 2 H, AlH_2). − ^{13}C NMR (68 Hz, C_6D_6): δ = 20.9 (CH_3CH_2S-), 21.5 (br., CH_3CH_2S-), 46.9 (NCH_3).

Isopropylthiolatoalane·Trimethylamine (2): Prepared from $AlH_3{\cdot}NMe_3$ (560 mg, 6.28 mmol) in toluene (10 mL) and *i*PrSH (480 mg, 6.28 mmol) in toluene (5 mL) at 0 °C, 2 h stirring at ambient temperature. All volatiles were removed in vacuo. Yield: 950 mg (92.7%). − ^{27}Al NMR (104 MHz, C_6D_6): δ = 151 ($h_{1/2}$ = 1126 Hz). − ^1H NMR (400 MHz, C_6D_6): δ = 1.43 [d, ^3J(H,H) = 6.6 Hz, 6 H, CH_3(*i*Pr)], 1.97 (s, 9 H, NCH_3), 3.25 [qq, ^3J(H,H) = 6.6 Hz, 1 H, CH(*i*Pr)], 4.08 (br., AlH_2). − ^{13}C NMR (100 MHz, C_6D_6): δ = 29.7 [CH_3(*i*Pr)], 47.0 (NCH_3), 32.6 [br., CH(*i*Pr)]. − IR (CsBr): $\tilde{\nu}$ = 2975 (vs), 2953 (vs), 2916 (vs), 2857 (vs), 1808 (vs, νAlH_2), 1699 (m, br., νAlH_{br}), 1480 (vs), 1463 (vs), 1447 (vs), 1406 (m), 1379 (m), 1363 (s), 1244 (s), 1152 (s), 1102 (m), 1050 (m), 1015 (m), 994 (vs), 887 (m), 816 (s), 792 (vs), 746 (vs), 702 (vs), 650 (vs, br), 626 (vs), 552 (s), 501 (s) cm^{-1}.

***tert*-Butylthiolatoalane·Trimethylamine (3):** Prepared from $AlH_3{\cdot}NMe_3$ (1.18 g, 13.2 mmol) in toluene (10 mL) and Me_3CSH (1.19 g, 13.2 mmol) in toluene (10 mL) at −15 °C. The resulting solution was stirred for 1 h at 20 °C. After removal of all volatiles, 2.20 g (92.8%) of an oily liquid remained, m.p. 10−15 °C. − ^{27}Al NMR (70 MHz, C_6D_6): δ = 147 ($h_{1/2}$ = 1103 Hz). − ^1H NMR (270 MHz, C_6D_6): δ = 1.97 [s, 9 H, CH_3(*t*Bu)], 1.59 (s, 9 H, NCH_3). − ^{13}C NMR (68 MHz, C_6D_6): δ = 37.1 [CH_3(*t*Bu)], 42.4 [br., C_q(tBu)], 47.3 (NCH_3). − IR (CsBr): $\tilde{\nu}$ = 2972 (vs), 2957 (vs), 2937 (vs), 2921 (vs), 2894 (s), 2862 (s), 1805 (vs,νAlH_2), 1480 (vs), 1462 (vs), 1361 (vs), 1244 (m), 1164 (m), 1156 (m), 1103 (w), 995 (vs), 818 (m), 792 (m, sh), 754 (vs), 732 (s), 705 (vs), 659 (s, br.), 625 (s), 583 (m), 521 (m), 501 (m), 464 (m) cm^{-1}.

***tert*-Butylthiolatoalane (4):** $LiAlH_4$ (25.42 mmol) in Et_2O (20 mL) was converted into AlH_3 by reaction with $AlCl_3$ (1.17 g, 8.47 mmol), dissolved in ether (20 mL), followed by addition of Me_3CSH (3.06 g, 32.9 mmol) in ether (10 mL). After 2 h, the insoluble material was separated and ether removed from the filtrate in vacuo. An oil remained that proved to contain Et_2O by NMR spectroscopy. It was treated several times with small amounts of pentane and the residue was then kept in vacuo for several hours. This produced a white powder. Yield: 4.00 g (66.6%). −^{27}Al NMR (70 MHz, Et_2O): δ = 132 ($h_{1/2}$ = 1510 Hz), (C_6D_6): δ = 132 ($h_{1/2}$ = 6632 Hz), 9 ($h_{1/2}$ = 3061 Hz). − ^1H NMR (270 MHz, C_6D_6): δ = 1.58 [s, 9 H, CH_3(*t*Bu)], ca. 4.5 (br., AlH_2). − ^{13}C NMR (68 MHz, C_6D_6): δ = 14.7 (CH_3), 47.8 [C_q(*t*Bu)]. − IR (Nujol, Hostaflon): $\tilde{\nu}$ = 2962 (vs), 2937 (vs), 2925 (vs), 2900 (vs), 2862 (vs), 1846 (vs, br.)/ca.1750−1570 (s, br.) (νAlH_n), 1472 (vs), 1460 (vs), 1395 (s), 1369 (s, sh), 1364 (s), 1159 (m), 810 (vs, br.), 744 (vs, br), 688 (vs, br), 666−600 (vs, br), 576 (s, br) cm^{-1}. − $C_4H_{11}AlS$ (118.17): calcd. C 40.66, H 9.38; found C 37.62, H 8.50.

Bis(*tert*-butylthiolato)alane·Trimethylamine (5): Prepared from $AlH_3{\cdot}NMe_3$ (920 mg, 10.3 mmol) in toluene (15 mL) and Me_3CSH (1.86 g, 20.7 mmol) in toluene (8 mL) at −15 °C. The resulting solution was stirred for 1 h followed by reduction of the volume of the solution by ca. 50%. From this solution crystals separated at −20 °C. Yield: 2.41 g (93.4%), m.p. 62 °C. − ^{27}Al NMR (70 MHz, C_6D_6): δ = 147 ($h_{1/2}$ = 924 Hz). − ^1H NMR (270 MHz, C_6D_6): δ = 1.71 [s, 18 H, CH_3(*t*Bu)], 1.94 (s, 9 H, NCH_3). − ^{13}C NMR

(68 MHz, C_6D_6): δ = 37.1 [CH_3(tBu)], 47.3 (NCH_3). − IR (Nujol, Hostaflon): $\tilde{\nu}$ = 2975 (vs), 2957 (vs), 2938 (vs), 2900 (vs), 2733 (vs), 1840 (vs, νAlH_2), 1482 (vs), 1471 (s), 1458 (s), 1444 (m), 1423 (m), 1406 (s), 1390 (m), 1360 (s), 1245 (s), 1241 (s), 1212 (s), 1166 (vs), 1150 (vs), 1110 (s), 1105 (s), 1024 (m), 997 (vs), 988 (vs), 819 (vs), 657 (vs), 628 (vs), 580 (vs), 528 (vs), 493 (vs), 460 (s) cm^{-1}. − $C_{10}H_{25}AlNS_2$ (250.42): calcd. C 47.96, H 10.06, Al 10.78, N 5.59; found C 46.33, H 8.61, Al 10.45, N 5.31.

Lithium Tris(*tert*-butylthiolato)hydridoaluminate (6) and Its 1:1 Adduct with Lithium *tert*-Butylthiolate (7): A solution of Me_3CSH (4.81 g, 53.3 mmol) in ether (20 mL) was allowed to react with $LiAlH_4$ (17.76 mmol) in ether (20 mL). A slightly turbid solution formed. On keeping the clear solution at 0 °C for several days, a small amount of crystals of (**7**)$_2$ formed. This was confirmed by X-ray structure analysis. From the filtrate all volatile materials were removed in vacuo, and the residue washed several times with small amounts of pentane. On keeping the solid material under vacuum (10^{-3} Torr) all the ether could be removed from **6**. Yield: 4.75 g (71%), m.p. 136 °C (dec.). − ^{27}Al NMR (70 MHz, C_6D_6): δ = 136 ($h_{1/2}$ = 4392 Hz); (Et_2O): δ = 133 ($h_{1/2}$ = 1782 Hz); (THF): δ = 131 ($h_{1/2}$ = 1535 Hz). − ^{7}Li NMR (105 MHz, Et_2O): δ = 0.26 ($h_{1/2}$ = 64.9 Hz). − ^{1}H NMR (270 MHz, C_6D_6): δ = 1.10 [t, br., ^3J(H,H) = 7.0 Hz, 6 H, $CH_3(Et_2O)$], 1.70 [s, 27 H, CH_3(*t*Bu)], 3.33 [dd, br., ^3J(H,H) = 7.0 Hz, 4 H, $CH_2(Et_2O)$]. − ^{13}C NMR (68 MHz, C_6D_6): δ = 15.1 [$CH_3(Et_2O)$], 36.2 [CH_3(*t*Bu)], 45.1 (C_q), 65.7 [$CH_2(Et_2O)$]. − IR (Nujol, Hostaflon): $\tilde{\nu}$ = 2973 (vs), 2959 (vs), 2938 (vs), 2921 (vs), 2894 (vs), 2859 (vs), 1829 (vs, νAlH_2), 1472 (s), 1458 (s), 1389 (m), 1362 (vs), 1216 (m), 1187 (m), 1167 (vs), 1153 (vs), 1106 (m), 1097 (s), 1069 (s), 1027 (m), 839 (w), 820 (s), 657 (vs), 613 (vs), 578 (vs) cm^{-1}. − $C_{12}H_{38}AlLiS_3$ (302.47): calcd. C 47.65, H 9.33, Al 8.92; found C 47.16, H 9.30, Al 8.55.

Lithium Pentakis(*tert*-butylthiolato)dihydridodialuminate·Trimethylamine (8): A solution of $LiAlH_4$ (8.08 mmol) in ether (5 mL) was added to a solution of AlH_3·NMe_3 (720 mg, 8.08 mmol) in toluene (10 mL), followed by dropwise addition of Me_3CSH (3.64 g, 40.4 mmol), dissolved in toluene (5 mL), at −20 °C. Stirring was continued for 1 h, and ether removed at 10 Torr from the solution. On cooling to −20 °C needles of **8** separated. From the filtrate all volatiles were removed in vacuo giving **8**, m.p. 147−150 °C (dec.). − ^{27}Al NMR (104 MHz, C_6D_6): δ = 147 ($h_{1/2}$ = 998 Hz). − ^{7}Li NMR (105 MHz, C_6D_6): δ = 0.70 ($h_{1/2}$ = 11.0 Hz). − ^{1}H NMR (270 MHz, C_6D_6): δ = 1.72 [s, br., CH_3(*t*Bu)], 1.73 [s, br., CH_3(*t*Bu)], 1.92 (s, NCH_3). − ^{13}C NMR (68 MHz, C_6D_6): δ = 36.4 [br., CH_3(*t*Bu)], 37.1 [CH_3(*t*Bu)], 43.2 (C_q), 47.3 (NCH_3). − IR (Nujol, Hostaflon): $\tilde{\nu}$ = 2969 (vs), 2957 (vs), 2938 (vs), 2929 (vs), 2894 (vs), 2859 (vs), 1858 (vs)/1782 (vs, νAlH_2), 1481 (s), 1472 (s), 1459 (s), 1446 (w), 1406 (m), 1360 (vs), 1309 (m, br.), 1244 (s, br.), 1236 (vs), 1212 (m), 1166 (vs), 1152 (vs), 1111 (m), 1105 (m), 997 (m), 986 (vs), 815 (s), 653 (vs), 628 (s), 578 (m) cm^{-1}. − $C_{23}H_{56}Al_2S_5LiN$ (567.94): calcd. C 48.64, H 9.94, Al 9.50, N 2.47; found C 46.86, H 9.22, Al 9.13, N 1.86.

Crystal Structure Determinations: Single crystals of compounds **5**, **7**, and **8** were covered with perfluoroether oil, the selected crystal mounted on the tip of a glass fiber and placed on a goniometer head. The goniometer head was then fitted on the support of a Siemens P4 diffractometer equipped with a low-temperature device LTP2 and a CCD area detector. Graphite-monochromated Mo-K_α radiation was used for measurements. Preliminary unit-cell determinations were performed with the reflection data of a total of 75 frames taken in five different orientations of 15 frames each by changing φ by 0.3° increments. Data collection was performed with the program HEMISHERE and 5 s/frame exposure time with two

Table 3. Crystal data and data of collection parameters and results of refinement

Compound	**5**	**7**	**8**
Empirical formula	$C_{11}H_{28}AlNS_2$	$C_{20}H_{47}AlLi_2OS_4$	$C_{23}H_{56}Al_2LiNS_5$
Molecular mass	265.44	472.68	567.89
Crystal size [mm]	0.20 × 0.30 × 0.40	0.3 × 0.5 × 0.5	0.10 × 0.10 × 0.40
Crystal system	monoclinic	monoclinic	monoclinic
Space group	$P2_1/c$	$P2_1/n$	$P2_1/n$
a [Å]	15.1505(1)	15.385(7)	11.646(3)
b [Å]	9.6977(2)	10.709(6)	18.351(3)
c [Å]	11.8115(2)	18.75(1)	17.118(3)
β [°]	110.323(1)	107.542(8)	102.176(8)
V [Å^3]	1627.37(4)	2944.9(27)	3576.1(13)
Z	4	4	4
ρ(calcd.) [Mg/m^3]	1.083	1.066	1.055
μ [mm^{-1}]	0.358	0.360	0.385
F(000)	584	1032	1240
Index range	$-18 \le h \le 18$, $-11 \le k \le 12$, $-14 \le l \le 15$	$-18 \le h \le 16$, $-13 \le k \le 13$, $-24 \le l \le 24$	$-13 \le h \le 13$, $-21 \le k \le 21$, $-19 \le l \le 19$
2θ [°]	57.92	58.42	49.42
T [K]	183(2)	183(2)	193(2)
Refl. collected	8968	16503	16658
Refl. unique	3197	5722	5713
Refl. observed (4σ)	2742	2856	4558
R (int.)	0.0164	0.0864	0.0319
No. variables	149	276	347
Weighting scheme[a] *x*/*y*	0.03910/0.3364	0.0590/7.8456	0.0575/5.6772
GOOF	1.044	1.168	1.060
Final *R*(4σ)	0.0268	0.0537	0.0564
Final *wR*2	0.0685	0.1341	0.1346
Largest residual peak [e/Å^3]	0.265	0.619	1.621

[a] $w^{-1} = \sigma^2F_o^2 + (xP)^2 + yP$; $P = (F_o^2 + 2F_c^2)/3$.

different χ settings. Data of a total of 1290 frames were collected and reduced using the program SAINT including absorption correction with the program SADABS. The structures were solved by direct methods (SHELXPLUS).[25] All non-hydrogen atoms were refined anisotropically, H atom positions at Al were taken from the difference Fourier data, and the H atom positions on C were calculated. These were included in the final refinement with a riding model, while the AlH hydrogen atoms were freely refined with fixed isotropic *U* values in the final cycles of refinement. All refinements proceeded normally. Relevant data are summarized in Table 3. Crystallographic data (excluding structure factors) for the structures reported in this paper have been deposited with the Cambridge Crystallographic Data Centre as supplementary publication no. CCDC-143572 (**5**), -143573 (**7**·OEt_2), -143574 (**8**). Copies of the data can be obtained free of charge on application to CCDC, 12 Union Road, Cambridge CB2 1EZ, UK [Fax: (internat.) + 44-1223/336-033; E-mail: deposit@ccdc.cam.ac.uk].

Acknowledgments

We thank Fonds der Chemischen Industrie and Chemetall GmbH for their generous support for this study, Mrs. E. Kiesewetter for measuring the IR spectra and Mrs. D. Kaeser for performing the elemental analyses of the rather smelly substances.

[1] *Chemistry of Aluminium, Gallium, Indium and Thallium* (Ed.: A. J. Downs), Blackie Academic Professional, London, Glasgow, New York, Tokyo, Melbourne, Madras, **1993**, chapter 8.
[2] H. Rahbarnoohi, R. Kumar, M. J. Heeg, J. P. Oliver, *Organometallics* **1994**, *13,* 3300−3308.
[3] D. J. Brauer, G. D. Stucky, J. Am. Chem. *Soc.* **1969**, *91*, 5462−5466.
[4] A. Haaland, O. Stokkeland, J. Weidlein, *J. Organomet. Chem.* **1975**, *94*, 353−360.
[5] R. J. Wehmschulte, K. Ruthlandt-Senge, P. P. Power, *Inorg. Chem.* **1995**, *34*, 2593−2599.
[6] [6a] C. Jones, F. C. Lee, G. A. Koutsantonis, M. G. Gardiner, C. L. Raston, J. Chem. Soc. *Chem. Commun.* **1996**, 829−833. − [6b] W. Marconi, A. Mazzei, F. Bonati, M. de Malde, *Z. Naturforsch, Part B* **1963**, *18,* 3−5. − [6c]A. Mazzei, F. Bonati, W. Marconi, G. Manana, G. Castelfranchi, Ital. Patent 68730; *Chem. Abstr.* **1967**, *66*, P2724.
[7] H. Nöth, Dissertation, University of Munich, **1954**.
[8] A. Schlegel, H. Nöth, H. Schwenk-Kirchner, *Angew. Chem.* **1997**, *109*, 2754−2758.; *Angew. Chem. Int. Ed. Engl.* **1997**, *36*, 2640−2645.
[9] A. Schlegel, J. Knizek, I. Krossing, H. Nöth, W. Ponikwar, *Chem. Eur. J.* **1998**, *4*, 2191−2203.
[10] A. Schlegel, Dissertation, University of Munich, **1999.**
[11] [11a] H. C. Brown, C. J. Shoaf, J. Am. Chem. *Soc.* **1964**, *86*, 1079−1085. − [11b] N. Ya. Turova, M. I. Karporskaya, A. V. Novoselova, *J. Gen. Chem. USSR* **1966**, *47*, 1231−1237. − [11c] L. I. Zakharkin, D. N. Maslin, V. V. Gavrilova, *J. Gen. Chem. USSR* **1966**, *36*, 2000−2006. − [11d] J. Fusek, F. Hanousek, F. Haruda, Coll. Czech. *Chem. Commun.* **1976**, *41*, 187−192.
[12] J. Weidlein, U. Müller, K. Dehnicke, *Schwingungsfrequenzen*, G. Thieme Verlag, Stuttgart, New York, **1981.**
[13] D. G. Henndershot, M. Barber, R. Kumar, J. P. Oliver, *Organometallics* **1991**, *10*, 3302−3309.
[14] C. Jones, F. C. Lee, G. A. Koutsantonis, M. G. Gardiner, C. L. Raston, *J. Chem. Soc. Dalton Trans.* **1996**, 829−233.
[15] K. Ruthland-Senge, P. P. Power, *Inorg. Chem.* **1991**, *30*, 2633−2637.
[16] *Interatomic Distances*, Special Publ. No. 18, Royal Soc. Chem., London, **1968**.
[17] M. Veith, S. Faber, H. Wolfanger, V. Huch, *Chem. Ber.* **1996**, *129*, 381−384.
[18] J. L. Atwood, F. R. Bennet, F. M. Elms, C. Jones, C. L. Raston, K. D. Robinson, *J. Am. Chem. Soc.* **1991**, *113*, 8183−8185.
[19] R. Noyori, I. Tomino, M. Yamada, M. Nishizawa, *J. Am. Chem. Soc.* **1984**, *106,* 6709−6716.
[20] R. Noyori, *Pure Appl. Chem.* **1981**, *53*, 2315−2322.
[21] Max Suter, Diploma Thesis, University of Munich, **1999**; A. Schlegel, PhD Thesis, University of Munich, **1999**. See also ref.[10]
[22] H. Nöth, P. Konrad, *Chem. Ber.* **1983**, *116*, 3552−3558
[23] *Lithium Chemistry* (Eds.: A.-M. Sapse, P. v. Rague-Schleyer), J. Wiley Interscience, New York, Chichester, Brisbane, Toronto, Singapore, **1995**., chapter 8.
[24] J. K. Ruff, *Inorg. Synth.* **1967**, *9*, 30−37.
[25] *SHELXPLUS*, *SAINT*, *SMART*, *SADABS*, Siemens Analytical Instrumentation, Madison, **1995**, Version 4.1.

Received May 29, 2000
[I00163]

Metal Assembly of Cyclodextrin Recognition Sites

Johanna M. Haider[a][+] and Zoe Pikramenou*[a][+]

Keywords: Cyclodextrins / Supramolecular chemistry / Receptors / Coordination chemistry / Molecular devices

Cyclodextrin recognition sites are assembled in macromolecular structures by using metal assembly principles. Methylated cyclodextrins are functionalised with bidentate bipyridine and tridentate terpyridine units to give versatile receptor ligands, β-CD–mbpy and β-CD–ttp, respectively, for metal complexation. Tris-cyclodextrin complexes are prepared by reaction of the β-CD–mbpy receptor with iron(II) and by reaction of β-CD–ttp with europium(III). The latter leads to a luminescent complex with three recognition sites around the luminescent metal core. Bis-cyclodextrin complexes are prepared by addition of iron(II) to β-CD–ttp. The characterisation of the compounds and their luminescent properties are reported.

Introduction

Receptors for small molecule recognition are popular building blocks in supramolecular design.[1] Artificial receptors have been developed from either multiple covalent bond synthesis or self-assembly principles for applications that range from biomedical research to the sensor field.[2] The design of optical molecular sensors based on recognition events has attracted much interest for the technological development of molecular devices.[3] Photoactive metal centres have been appended to calixarene[4] or cyclodextrin[5] receptor molecules for sensing ion or molecule recognition events. We are interested in employing cyclodextrins as rigid receptors that bind photoactive guests leading to the spatial organisation of energy or electron donor-acceptor arrays based on transition metals. Cyclodextrins are particularly attractive natural host molecules, water soluble, with a hydrophobic well-defined cavity.[6] Formation of transition metal arrays for photoinduced processes have been previously developed by using covalent bond bridges[7] or hydrogen-bond interfaces[8] to bring the metal centres together in one array. The importance of the cyclodextrin approach is that light-induced processes can be observed between two photoactive units held together by *non-covalent* interactions in aqueous solutions.[9]

The design of cyclodextrin-based organised arrays requires functionalisation of the cyclodextrin glucose units which can be achieved by modifying and using synthetic routes established in carbohydrate chemistry.[10] Metal centres have been attached to both discrete sugar units[11] and functionalised cyclodextrins,[12] primarily for developing models for enzymatic catalysis or sensors. In order to increase the number of guest interaction sites in cyclodextrin recognition systems the design of molecules with more than one cyclodextrin binding sites is attractive. Previous methods to link more than one cyclodextrin have employed covalent bond multi-step synthesis using bridges such as bipyridines,[13] porphyrins,[14] or organoselenium moieties.[15] Such bridged bis-cyclodextrin compounds have shown interesting catalytic properties for ditopic recognition of substrates.[13a] In this paper the assembly of cyclodextrins using coordination principles to yield complexes with multiple cyclodextrin recognition sites around a central metal core is reported. Our approach, using metal centres to assemble receptors, provides metal-directed spatial control of the receptors so that directional intramolecular energy or electron transfer processes between the central metal core and the guest species included in the receptor sites can take place when the metal core is photoactive. Metal centres have been previously employed to bring hydrogen-bonded recognition sites together.[16]

We wish to report the assembly of two or three functionalised cyclodextrins around a metal centre depending on the coordination preference of the metal core; octahedral metal centres and nine-coordinate lanthanide ions are used to spatially organise cyclodextrins functionalised with bidentate (β-CD−mbpy) and tridentate units (β-CD−ttp). Metal coordination properties allow the assembly of three cyclodextrins, which has not previously been investigated via covalent bond synthesis.

Results and Discussion

Synthesis

To incorporate a bidentate site on the cyclodextrin rim a new monosubstituted cyclodextrin 2,2′-bipyridine derivative was synthesised by attaching a monohydroxy permethylated cyclodextrin to the 4-position of a 2,2′-bipyridine to give β-CD−mbpy. Bipyridine functionalised cyclodextrins have been previously prepared either by William-

[a] Current address: School of Chemistry, University of Birmingham,
Edgbaston, Birmingham B15 2TT, UK
Fax: (internat.) +44-121/414-4403
E-mail: Z.Pikramenou@bham.ac.uk
[+] Previous address: Department of Chemistry, University of Edinburgh,
Kings Buildings, Edinburgh, EH9 3JJ, UK

 © WILEY-VCH Verlag GmbH, 69451 Weinheim, 2001 1434−1948/01/0101−0189 $ 17.50+.50/0

son ether synthesis at the 5,5′- or 6-positions of the bipyridine,[12c] thioether formation at 5,5′-disubstituted bipyridines[13a] or via "phosphinimine" type reactions of 5-methylamino bipyridines.[17] We employed the Williamson ether synthesis as a convenient route to attach the 4-position of a 4,4′-dimethyl 2,2′-bipyridine onto the cyclodextrin. We chose the 4-position both to avoid steric crowding around the metal (a problem with the 6-substituents) and to ensure good electronic coupling for communication of a redox active guest with the metal in photoinduced intramolecular processes. The functionalised cyclodextrin was prepared from the monohydroxy permethylated β-cyclodextrin[18] and 4-bromomethyl, 4′methyl-2,2′-bipyridine. The latter was prepared by modification of a procedure of monosilylation of the dimethyl 2,2′-bipyridine[19] followed by bromination with BrF_2CCF_2Br (Scheme 1).

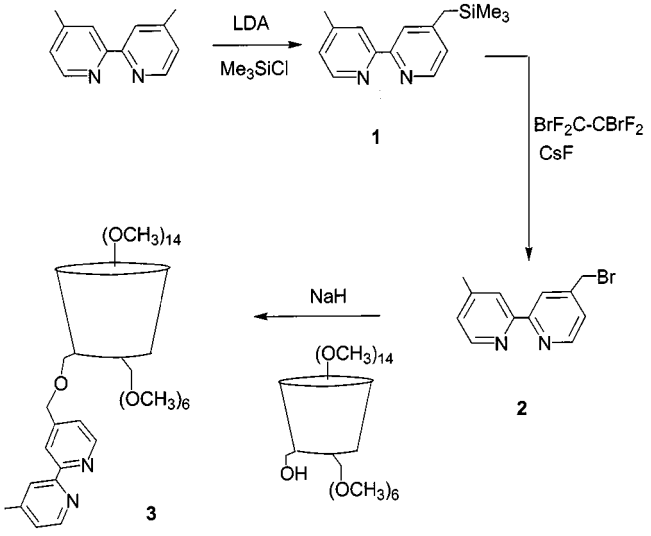

Scheme 1

The 4-substituted bipyridine was shown to be more reactive towards the ether formation under similar conditions than the analogous 6- and 5- substituted bipyridines. The β-CD−mbpy is an attractive ligand due to its versatile solubility in both halogenated solvents and water which is important not only in the handling and purification of the compound but also in the metal complex formation.

Simple addition of Fe^{II} to a methanolic solution of β-CD−mbpy results in a deep red colour which is attributed to a complex with three cyclodextrins around the iron centre, $[Fe(\beta\text{-CD}-\text{mbpy})_3]^{2+}$ (Scheme 2). Solubility of the complex is enhanced by the presence of the methylated cyclodextrins and chromatographic methods have been more effective for isolation of the complex rather than recrystallization used in the analogous $[Fe(mbpy)_3][PF_6]_2$ complex.

Three cyclodextrins can potentially be assembled around a metal by using a tridentate binding site (such as a tolylterpyridine unit) attached on the cyclodextrin (β-CD−ttp) and a nine coordinate lanthanide, such as europium, (Scheme 3). We have previously reported such a functionalised cyclodextrin β-CD−ttp.[9] Europium(III) ions do not possess strong ligand field preference, adopting high coordination numbers in solution and they are known to form a tris-complex with 2,2′:6,′2′′ terpyridine. Upon addition of three equivalents of β-CD−ttp in an ethanolic solution of europium chloride the tris-cyclodextrin complex, $[Eu(\beta\text{-CD}-\text{ttp})_3]^{3+}$, is formed.[20]

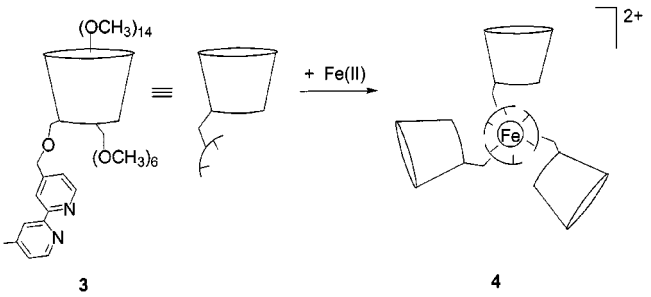

Scheme 2

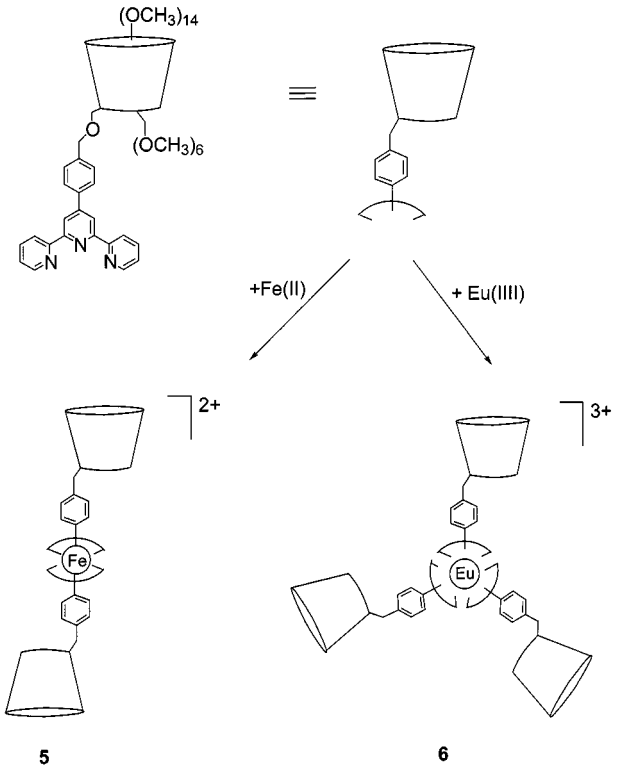

Scheme 3

When a metal with octahedral geometry is employed with the tridentate functionalised cyclodextrin two cyclodextrins are assembled around the metal; when Fe^{II} is reacted with β-CD−ttp a strong purple coloured complex of $[Fe(\beta\text{-CD}-\text{ttp})_2]^{2+}$ is formed.

Characterisation

NMR, UV/Vis spectroscopy together with mass spectrometric analysis were employed to confirm the identification of the compounds. Electrospray mass spectrometry has proven to be an important technique in the identification of self-assembled polymetallic systems.[21] In our case it has been successfully applied in cyclodextrin systems. In Table 1 the electrospray mass spectrometry data of the complexes

Table 1. Electrospray mass spectrometry data of metallo-cyclodextrins

Metal Complex	*m/z*, corresponding fragment
$[Fe(\beta\text{-CD}-mbpy)_3][PF_6]_2$	2422, $\{M-2\ [PF_6]\}^{2+}$
	1717, $\{M-2\ [PF_6]-1\ CD_f\}^{2+}$[a]
	1010, $\{M-2\ [PF_6]-2\ CD_f\}^{2+}$
$[Eu(\beta\text{-CD}-ttp)_3][PF_6]_3$	1788, $\{M-3\ [PF_6]\}^{3+}$
	1347, $\{M-3\ [PF_6]+Na\}^{4+}$
	1765, $\{M-2\ [PF_6]\}^{2+}$
	1184, $\{M-2\ [PF_6]+Na\}^{3+}$
$[Fe(\beta\text{-CD}-ttp)_2][PF_6]_2$	894, $\{M-2\ [PF_6]+2\ Na\}^{4+}$

[a] CD_f = [6-monohydroxy permethylated β-cyclodextrin−H].

The H_{Glu}-6,6′ pair of the substituted glucose of the cyclodextrin also becomes diastereotopic, one proton is shifted to δ = 4.06 and shows a cross peak in the 2D TOCSY with the other one at δ = 3.71. Distinct from the cyclodextrin proton manifold are the six primary methoxy groups at δ = 3.34, 3.32, 3.31, 3.30, 3.28, 3.27 and the H_{Glu}-2 glucose protons at δ = 3.18−3.12. Full assignment of the cyclodextrin protons also agrees with previously detailed studies of permethylated cyclodextrins.[22]

The $[Fe(\beta\text{-CD}-mbpy)_3][PF_6]_2$ complex is diamagnetic which indicates that the cyclodextrin substitution does not induce any steric hindrance, which is known to be responsible for spin crossover phenomena in iron complexes.[23] In

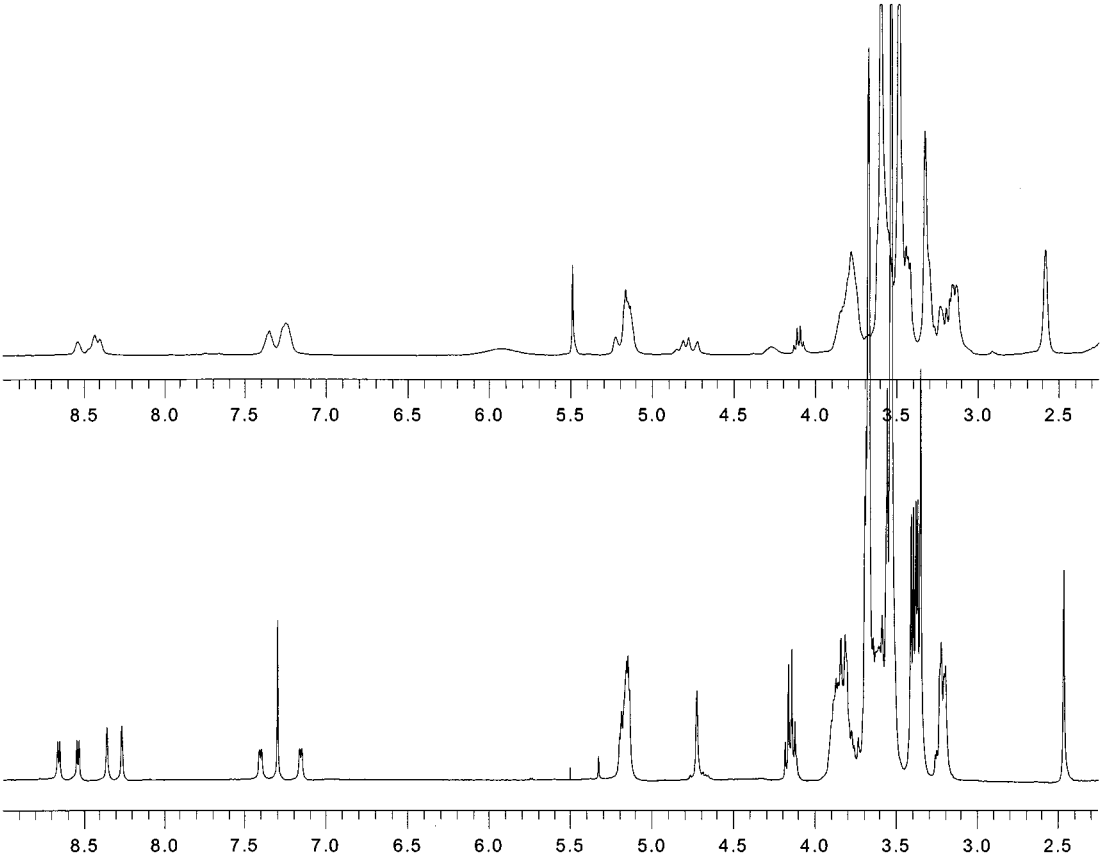

Figure 1. The 360 MHz ^1H NMR spectra of β-CD−mbpy (bottom) in $CDCl_3$ and $[Fe(\beta\text{-CD}-mbpy)_3][PF_6]_2$ (top) in CD_3CN

are presented. The data confirm the formulation of the bis- and tris-cyclodextrin complexes.

In the ^1H NMR spectrum of the β-CD−mbpy ligand, shown in Figure 1, the characteristic anomeric protons of the glucose units are non-equivalent due to the mono-substitution; five of them overlap (multiplet at δ = 5.4) while two separate doublets appear at δ = 5.12 and 5.10 (J = 4 Hz).

Substitution of the bipyridine unit is confirmed by the shift of the methylene group from δ = 4.43 in the bromide derivative to δ = 4.66 in β-CD−mbpy. The splitting of the signal as an AB pattern due to the diastereotopic protons upon attachment to the chiral cyclodextrin also confirms this. The rest of the aromatic protons appear as six signals. the ^1H NMR spectrum of the complex (Figure 1), the complexation with the β-CD−mbpy is confirmed by the shift, of the H-6,6′ protons of the bipyridine, to lower frequencies. The aromatic proton peaks are broader than are usually observed which may be due to the presence of the two *fac* and *mer* isomers[24] or to a very small impurity of iron(III)[25] which is difficult to exclude due to the high solubility of the complex. The complex UV/Vis absorption spectrum shows the characteristic MLCT absorption at 530 nm which agrees with the model compound which is a tris-bipyridine iron(II) complex without the cyclodextrin receptor.

The purple bis-cyclodextrin iron complex $[Fe(\beta\text{-CD}-ttp)_2][PF_6]_2$ was characterised by 600 MHz ^1H NMR

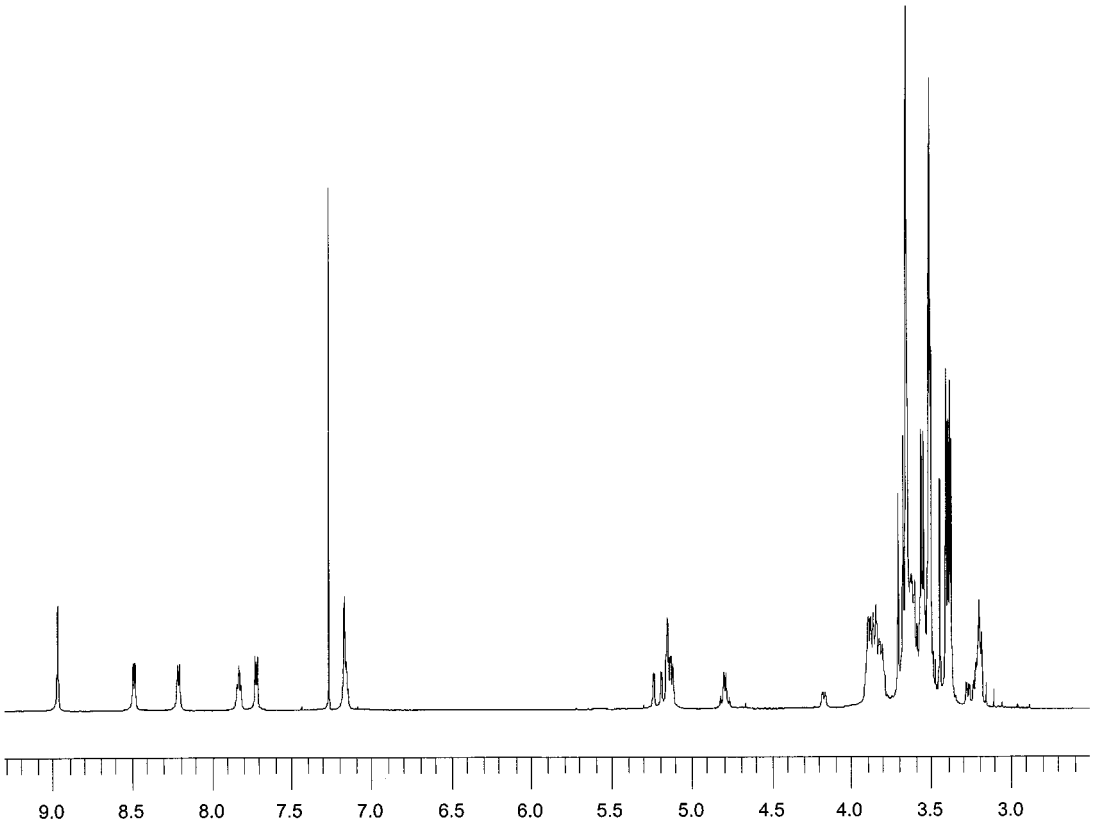

Figure 2. The 600 MHz ^{1}H NMR spectrum of $[Fe(\beta\text{-CD}-ttp)_2][PF_6]_2$ in $CDCl_3$

spectroscopy (Figure 2). The H-6 protons of the terpyridine unit show a 1.55 ppm shift at lower frequencies with respect of the chemical shift in the ligand spectrum attributed to metal coordination.[26] The methylene protons on the benzyl ring are diastereotopic appearing as a doublet of doublets at $\delta = 4.75$ where the methylene diastereotopic protons of the substituted glucose ring appear at $\delta = 4.15$ and 3.80, the latter is obscured by the rest of the cyclodextrin protons ($\delta = 3.15-3.90$). This was assigned from the ^{1}H-^{1}H COSY contour plot. Acetonitrile solutions of the iron complex display a typical MLCT absorption band at 569 nm. No luminescence was detected upon excitation to the MLCT band for either the bipyridine or the terpyridine cyclodextrin complexes. This is not surprising since both iron(II) bipyridine and terpyridine complexes bear low lying metal-centred states that provide radiationless pathways for luminescence quenching.[27]

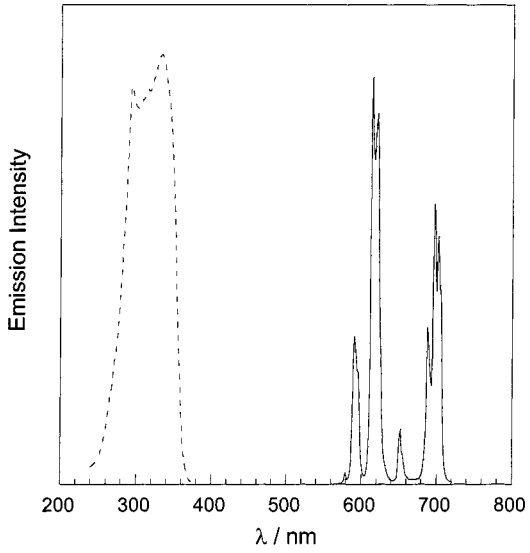

Figure 3. Emission ($\lambda_{exc} = 330$ nm, solid line) and excitation ($\lambda_{em} = 616$ nm, dashed curve) spectra of $[Eu(\beta\text{-CD}-ttp)_3]^{3+}$ in acetonitrile corrected for PMT and lamp response, respectively

Luminescence Spectroscopy

The europium complex was characterised by electrospray mass spectrometry and NMR spectroscopy. In the ^{1}H NMR spectrum of the perchlorate salt of the complex, the observed chemical shifts of the terpyridine protons are consistent with previously reported studies of europium terpyridine complexes.[28] The complex is stable in most organic solvents but dissociates in the presence of water as expected for lanthanide terpyridine complexes.[28] The europium ion was selected as a luminescent probe with well explored photophysical properties. Acetonitrile solutions of the complex exhibit strong red luminescence, characteristic of the europium ion upon excitation at the ligand band (Figure 3). The excitation spectrum upon monitoring the 616 nm europium emission shows a band centred at 320 nm corresponding to the ligand π-π^* transition which is in agreement with the absorption spectrum of the complex. The tolyl-terpyri-

dine units act as light-harvesting centres for collecting the energy and transferring it to the lanthanide centre.

Conclusions

Metal assembly of polypyridine functionalised cyclodextrins leads to the formation of complexes with two or three cyclodextrin receptor sites around the metal core. The employment of methylated cyclodextrins leads to versatile soluble ligands for metal complex formation. The metallo-receptors developed in this study can take part in photoactive processes occurring in more than one direction in space through the metal core and the guests. We are currently studying the ruthenium(II) analogues of these receptors because of their attractive photophysical properties for inducing energy or electron transfer processes.

Experimental Section

General Procedures and Materials: All starting materials were purchased from Aldrich unless otherwise indicated. β-Cyclodextrin (Acros) was recrystallized from water and dried under vacuum at 80 °C for 8 hours. $RuCl_3 \cdot xH_2O$ was provided from Johnson & Matthey as a loan. Solvents used in synthetic procedures were analytical grade apart from the ones used in size exclusion chromatography and spectroscopic studies where HPLC grade solvents were used. THF was freshly distilled from sodium under nitrogen. All ligand synthetic procedures were carried out under a nitrogen atmosphere. Thin layer chromatography (TLC) analyses were performed on either Merck silica gel 60 glass plates or Merck alumina gel 60 glass plates as indicated. Biobeads SX3 was used as a stationary phase for size exclusion chromatography. Cyclodextrins were detected by an oxidising solution consisting of anisaldehyde/acetic acid/methanol/sulfuric acid in a 2:45:430:22 ratio followed by heating at around 100 °C.

NMR spectra were recorded on Bruker DRX 360 and Varian Inova 600 spectrometers. The protons on the glucose units were indicated as H_{Glu} in the assignments. Fast atom bombardment mass spectrometry was performed on a Kratos MS-50 spectrometer and electrospray on a Quattro instrument at the EPSRC Mass Spectrometry Service Centre in Swansea.

Absorption spectra were recorded on a Perkin−Elmer Lambda 16 UV/Vis spectrometer. Emission and excitation spectra were recorded on a Photon Technology International QM-1 steady state spectrometer described elsewhere.[29]

4′-Methyl-{4-(trimethylsilyl)methyl}-2,2′-bipyridine (1): To a solution of LDA (Fluka, 1.05 g, 9.78 mmol) in freshly distilled THF (20 mL) a solution of 4,4′-dimethyl-2,2′-bipyridine (1.50 g, 8.15 mmol) in the same solvent (50 mL) was added dropwise at −78 °C. The dark brown mixture was kept stirring at that temperature for an hour. Trimethylsilyl chloride (1.06 g, 9.78 mmol) was added under vigorous stirring and after 20 s the reaction was quenched with absolute EtOH (10 mL), where upon the solution turned green. The cold reaction mixture was poured into an aqueous saturated $NaHCO_3$ solution and was left to reach room temperature. The mixture was extracted by dichloromethane (3 × 40 mL) and the combined organic phases were dried over anhydrous Na_2SO_4. After filtration and evaporation of the solvent TLC analysis of the mixture showed the presence of mono- and bis- silyl-substituted products (silica gel deactivated with NH_3, R_f = 0.68 and 0.86, respectively). Pure product was obtained after column chromatography (silica gel deactivated by addition of 10% triethylamine to the eluent system: EtOAc/cyclohexane 3:7) (yield: 1.5 g, 72%).

^{1}H NMR (360 MHz, $CDCl_3$): δ = 8.51 (d, J = 4.98 Hz, 1 H, H-6), 8.45 (d, J = 5.26 Hz, 1 H, H-6′), 8.21 (s, 1 H, H-3′), 8.04 (s,1 H, H-3), 7.09 (dd, J = 4.97 Hz, J = 1 Hz, 1 H, H-5′), 6.93 (dd, J = 5.01 Hz, J = 1 Hz, 1 H, H-5), 2.41 (s, 3 H, 4′-methyl), 2.19 (s, 2 H, 4-methylene), 0.02 (s, 9 H, CH_3-Si).

4-Bromomethyl-4′-methyl-2,2′-bipyridine (2): Caesium fluoride (0.475 g, 3.125 mmol) and $BrF_2C-CBrF_2$ (0.813 g, 3.125 mmol) were added to a solution of **(1)** (0.4 g, 1.56 mmol) in dry DMF (5 mL). The reaction was followed by TLC (deactivated silica, EtOAc/hexane 1:4) (R_f(product) = 0.43). The reaction reached completion after 4−5 h and the mixture was then poured into water (10 mL) and extracted by EtOAc (3 × 50 mL). The combined organic phases were washed with brine, dried over Na_2SO_4, filtered and the solvent evaporated. The brown oil was purified by column chromatography (deactivated silica ethyl acetate/cyclohexane 1:4) to give a slightly yellow oil (yield: 0.3 g, 73%).

^{1}H NMR (360 MHz, $CDCl_3$): δ = 8.60 (d, J = 4.99 Hz, 1 H, H-6), 8.49 (d, J = 4.96 Hz, 1 H, H-6′), 8.37 (s, 1 H, H-3), 8.19 (s, 1 H, H-3′), 7.29 (dd, J = 4.95 Hz, J = 1 Hz, 1 H, H-5), 7.11 (dd, J = 5.03 Hz, J = 1 Hz, 1 H, H-5′), 4.43 (s, 2 H, 4- methylene), 2.39 (s, 3 H, 4′-methyl).

6-Mono[4-methyl(4′-methyl-2,2′-bipyridyl)]-permethylated β-cyclodextrin (β-CD−mbpy) (3): 6-Monohydroxy permethylated β-cyclodextrin (0.8 g, 0.565 mmol) was dissolved in freshly distilled THF (15 mL). NaH (100 mg, 60% suspension in oil, 2.6 mmol) was added and a white precipitate was formed. A solution of (**2**) (208 mg, 0.789 mmol) in THF (5 mL) was added. The mixture was left to reflux for 12 h, quenched with brine (5 mL) and the solvent was evaporated. The residue was treated with brine (10 mL) and extracted with dichloromethane (3 × 40 mL). The combined organic phases were dried over Na_2SO_4, filtered and the solvent was evaporated. The compound was purified through column chromatography (Biobeads SX3, acetone). Yield 0.3 g, 33%.

^{1}H NMR (600 MHz, $CDCl_3$): δ = 8.58 (d, J = 5 Hz, 1 H, H-6), 8.46 (d, J = 5 Hz, 1 H, H-6′), 8.28 (s, 1 H, H-3), 8.19 (s, 1 H, H-3′), 7.33 (dd, J = 5 Hz, J = 1 Hz, 1 H, H-5), 7.09 (dd, J = 5 Hz, J = 1 Hz, 1 H, H-5′), 5.12 −5.07 (H_{Glu}-1, 7 H), 4.66 (dd, J = 13.5 Hz, J = 19.0 Hz, 2 H, CH_2 on C-4-bpy), 4.06 (dd, J = 6.8 Hz, J = 3.85 Hz, 1 H, H_{Glu}-6), 3.83−3.12 (m, H_{Glu}-2,3,4,5,6, $-OCH_{3Glu}$), 2.39 (s, 3 H, -CH_3 on C-4′).

[Fe(β-CD−mbpy)$_3$][PF$_6$]$_2$ (4): A solution of $[NH_4]_2Fe(SO_4)_2 \cdot 6H_2O$ (12 mg, 0.03 mmol) in water (1 mL) was added to a solution of (**3**) (150 mg, 0.09 mmol) in MeOH (2 mL). The mixture immediately turned dark purple and was left stirring for 30 min. The mixture was treated with a methanolic solution of NH_4PF_6, following extraction with dichloromethane (3 × 20 mL) and column chromatography (Biobeads SX3, acetone) the complex was obtained in 45% yield (70 mg).

^{1}H NMR (360 MHz, $CDCl_3$): δ = 8.55, 8.42 (2 H, H-3,-3′), 7.35, 7.25 (4 H, H-5,-5′, H-6,-6′), 5.25 −5.10 (7 H, H_{Glu}-1), 4.80 (2 H, CH_2 on C-4-bpy), 4.25 (1 H, H_{Glu}-6), 3.9−3.1 (m, H_{Glu}-2,3,4,5,6, $-OCH_{3Glu}$), 2.6 (3 H, $-CH_3$ on C-4′). − UV/Vis (MeOH) (ε/$M^{-1}cm^{-1}$): λ = 520 nm (9770), 351 (9700), 297 (83400), 289 (88100). − ESI MS (CH_3CN): m/z = 2422{M − 2[PF_6]}$^{2+}$.

$[Fe(\beta\text{-CD}-ttp)_2][PF_6]_2$ (5): To a solution of β-CD−ttp (50 mg, 0.029 mmol) in methanol (1 mL) a solution of $(NH_4)_2Fe(SO_4)_2$ in the same solvent (5.6 mg, 0.014 mmol) was added. The complex formed immediately giving a strong purple coloured solution. The mixture was heated for a few minutes to 50 °C, cooled to room temperature and a solution of ammonium hexafluorophosphate (4.8 mg, 0.028 mmol) in methanol (1 mL) was added. There was no precipitation due to the high solubility of the methylated cyclodextrin and the complex was isolated following extraction by dichloromethane (74 mg, yield: 73%).

^{1}H NMR (600 MHz, $CDCl_3$): δ = 8.98 (s, 4 H, H-3′), 8.48 (d, *J* = 7.9 Hz, 4 H, H-3), 8.19 (d, *J* = 7.7 Hz, 4 H, H_o), 7.80 (dd, *J* = 6.4, 6.8 Hz, 4 H, H-4), 7.71 (d, *J* = 7.7 Hz, 4 H, H_m), 7.19- 7.15 (m, 4 H, H-5,6), 5.24−5.10 (m, 7 H, H_{Glu}-1), 4.78 (dd, *J* = 7.6 Hz, 4 H, $-CH_2$-benzyl), 4.18 (dd, *J* = 10.7 Hz, *J* = 2.9 Hz, 2 H, H_{Glu}-6), 4.0−3.0 (m, H_{Glu}-2,3,4,5,6 $-OCH_{3Glu}$). − FAB-MS (nitrobenzyl alcohol matrix): *m*/*z* = 3674 $\{M - [PF_6]\}^+$, 3530 $\{M - 2[PF_6]\}^+$. − UV/Vis (MeOH) (ε/ $M^{-1}cm^{-1}$): λ = 568 nm (13800), 313 (37500) 286 (46000).

$[Eu(\beta\text{-CD}-ttp)_3][PF_6]_3$ (6): 6-Monotolylterpyridine permethylated β-cyclodextrin, β-CD−ttp (100 mg, 57 mmol) was dissolved in absolute EtOH (2 mL) and a hot solution of $Eu(NO_3)_3{\cdot}5H_2O$ (8.56 mg, 19 mmol) in the same solvent (1 mL) was added. The mixture was refluxed for 3 hours, the volume was reduced and NH_4PF_6 in EtOH (1 mL) was added. As no precipitate was formed, the mixture was extracted in dichloromethane (2 mL) following evaporation of the solvent. It was filtered through a Millipore column to remove the excess of NH_4PF_6, to yield 85 mg of the complex after solvent evaporation (yield 79%).

ESI-MS (MeOH/EtOH): *m*/*z* = 1788 $\{M - 3[PF_6]\}^{3+}$. − ^{1}H NMR (300 MHz, CD_3CN): δ = 16.14 (H-6), 7.18 ($H_{o/m}$), 6.95 (H-4), 6.6 ($H_{o/m}$), 6.3 (H-5), 5.1 (H_{Glu}-1), 4.6 ($-CH_2$-benzyl), 4.0−3.0 (rest of cyclodextrin protons), 2.5−2.4 (H3, 3′). − UV/Vis (CH_2Cl_2): λ = 280, 330 nm.

Acknowledgments

We are grateful to EPSRC for financial support to J. M. H. (GR/L91788), Drs. N. Spencer, C. M. Hewage and M. Chavarot for obtaining the NMR spectra and Dr. A. M. W. Cargill Thompson for helpful discussions. We also wish to thank Johnson & Matthey for a loan of ruthenium trichloride.

[1] F. Vögtle, *Comprehensive Supramolecular Chemistry*; Volume 2, (Exec. Eds. J. L. Atwood, J. E. D. Davies, D. D. MacNicol, F. Vögtle), Elsevier Science, Oxford, **1996**.

[2] [2a] S. H. Gellman, Special Issue on Molecular Recognition, *Chem. Rev.* **1997**, *97*, issue 5. − [2b] D. Gutsche, *Calixarenes, Monographs in Supramolecular Chemistry* (Series Editor: J. F. Stoddart), The Royal Society of Chemistry, Cambridge, **1991**. − [2c] F. Diedrich, *Cyclophanes*, *Monographs in Supramolecular Chemistry*, (Series Editor: J. F. Stoddart), The Royal Society of Chemistry, Cambridge, **1991**.

[3] [3a] A. P. de Silva, H. Q. N. Gunaratne, T. Gunnlaugsson, A. J. M. Huxley, C. P. McCoy, J. T. Rademacher, T. E. Rice, *Chem. Rev.* **1997**, *97*, 1515. − [3b] W. K. Hartmann, M. Montellaro, Z. Pikramenou, D. G. Nocera, in *Chemosensors of Ion and Molecule Recognition* (Ed. J.-P. Desvergne and A. W. Czarnik), NATO ASI Series C, 492, Kluwer Academic Publishers, **1997**, 159. − [3c] T. Mizuno, T. Fukumatsu, M. Takeuchi, S Shinkai, *J. Chem. Soc., Perkin Trans. 1* **2000**, 407.

[4] P. D. Beer, Z. Chen, A. J. Goulden, A. Grieve, D. Hesek, F. Szemes, T. Wear, *J. Chem. Soc., Chem. Commun.* **1994**, 1269.

[5] [5a] M. A. Mortellaro, D. G. Nocera, *J. Am. Chem. Soc*. **1996**, *118*, 7414. − [5b] Z. Pikramenou, J.-a Yu, R. B. Lessard, A. Ponce, P. A. Wong, D. G. Nocera, *Coord. Chem. Rev.* **1994,** *132,* 181.

[6] M. V. Rekharsky, Y. Inoue, *Chem. Rev.* **1998**, *98*, 1875.

[7] [7a] E. C. Constable, P. Harverson, C. E. Housecroft, *J. Chem. Soc., Dalton Trans.* **1999**, 3693. − [7b] L. De Cola, P. Belser, *Coord. Chem. Rev.* **1998,** *177*, 301. − [7c] R. Ziessel, M. Hissler, A. El-Ghayoury, A. Harriman, *Coord. Chem. Rev.* **1998,** *180*, 1251. − [7d] F. Barigelletti, L. Flamigni, J.-P. Collin, J.-P. Sauvage, *Chem. Commun.* **1997**, 333.

[8] [8a] T. H. Ghaddar, E. W. Castner, S. S. Isied, *J. Am. Chem. Soc*. **2000**, *122,* 1233. − [8b] M. D. Ward, C. M. White, F. Barigelletti, N. Armaroli, G. Calogero, L. Flamigni, *Coord. Chem. Rev.* **1998,** *171*, 481. − [8c] D. J. Hurley, Y. Tor, *J. Am. Chem. Soc*. **1998**, *120,* 2194. − [8d] E. C. Constable, R. A. Fallahpour, *J. Chem. Soc., Dalton Trans.* **1996**, 2389.

[9] [9a] S. Weidner, Z. Pikramenou, *Chem. Commun.* **1998**, 1473. − [9b] J. M. Haider, M. Chavarot, L. De Cola, Z. Pikramenou, to be submitted.

[10] A. R. Khan, P. Forgo, K. J. Stine, V. T. D'Souza, *Chem. Rev.* **1998**, *98*, 1977**.**

[11] E. C. Constable, S. Mundwiler, *Polyhedron* **1999**, *18***,** 2433.

[12] [12a] E. Rizzarelli, G. Vecchio, *Coord. Chem. Rev.* **1999**, *188*, 343. − [12b] R. Breslow, S. D. Dong, *Chem. Rev.* **1998**, *98*, 1997. − [12c] R. Deschenaux, M. M. Harding, T. Ruch, *J. Chem. Soc., Perkin Trans 2* **1993**, 1251.

[13] [13a] B. Zhang, R. Breslow, *J. Am. Chem. Soc*. **1997**, *119*, 1676. − [13b] R. Deschenaux, A. Greppi, T. Ruch, H.-P. Kriemler, F. Raschdorf, R. Ziessel, *Tetrahedron Lett*. **1994**, *35*, 2165.

[14] [14a] W.-H. Chen, J.-M. Yan, Y. Tagashira, M. Yamaguchi, K. Fujita, *Tetrahedron Lett.* **1999**, *40*, 891. − [14b] R. Breslow, X. Zhang, R. Xu, M. Maletic, R. Merger, *J. Am. Chem. Soc*. **1996**, *118*, 11678. − [14c] Y. Kuroda, M. Ito, T. Sera, H. Ogoshi, *J. Am. Chem. Soc*. **1993**, *115*, 7003.

[15] Y. Liu, C. C. You, Y. Chen, T. Wada, Y. Inoue, *J. Org. Chem*. **1999**, *64*, 7781.

[16] B. Linton, A. D. Hamilton, *Chem. Rev.* **1997**, *97*, 1669.

[17] F. Charbonier, T. Humbert, A. Marsura, *Tetrahedron Lett*. **1999**, *40*, 4047.

[18] Z. Chen, J. S. Bradshaw, M. L. Lee, *Tetrahedron Lett*. **1992**, *33*, 1177.

[19] [19a] S. A. Savage, A. P. Smith, C. L. Fraser, *J. Org. Chem.* **1998**, *63*, 10048. − [19b] U. S. Schubert, C. Eschenbaumer, G. Hochwimmer, *Tetrahedron Lett*. **1998**, *39,* 8643.

[20] [20a] Lanthanide terpyridine complexes have been previously prepared: D. A. Durham, G. H. Frost, F. A. Hart, *J. Inorg. Nucl. Chem.* **1969**, *31*, 833. − [20b] G. H. Frost, F. A. Hart, C. Heath, M. B. Hursthouse, *J. Chem. Soc., Chem. Commun.* **1969**, 1421. − [20c] M. G. Drew, P. B. Iveson, M. J. Hudson, J. O. Liljenzin, L. Spjuth, P. Y. Cordier, A. Enarsson, C. Hill, C. Madic, *J. Chem. Soc., Dalton Trans.* **2000**, 821.

[21] [21a] F. M. Romero, R. Ziessel, A. Dupont-Gervais, A. Van Dorsselaer, *Chem. Commun*. **1996**, 551. − [21b] G. Hopfgartner, F. Vilbois, C. Piguet, *Rapid Communications in Mass Spectrometry* **1999**, *13*, 302.

[22] [22a] J. R. Johnson, N. Shankland, I. H. Sadler, *Tetrahedron* **1985**, *41*, 3147. − [22b] C. M. Spencer, J. F. Stoddart, R. Zarzycki, *J. Chem. Soc., Perkin Trans.2* **1987**,1323.

[23] D. Onggo, J. M. Hook, A. D. Rae, H. A. Goodwin, *Inorg. Chim. Acta* **1990**, *173*, 19.

[24] T. J. Rutherford, D. A. Reitsma, F. R. Keene, *J. Chem. Soc., Dalton Trans.* **1994**, 3659.

[25] E. Sinn, *Inorg. Chim. Acta* **1969**, *3*, 11.

[26] E. C. Constable, A. M. W. Cargill Thompson, D. A. Tocher, M. A. Daniels, *New J. Chem*. **1992**, *16*, 855.

[27] E. Amouyal, M. Mouallem-Bahout, G. Calzaferri, *J. Phys. Chem.* **1991** *95*, 7641.

[28] [28a] R. D. Chapman, R. T. Loda, J. P. Riehl, R. W. Schwartz, *Inorg. Chem*. **1984**, *23,* 1652. − [28b] C. Mallet, R. P. Thummel, C. Hery, *Inorg. Chim. Acta* **1993**, *210,* 223.

[29] N. W. Alcock, P. R. Barker, J. M. Haider, M. J. Hannon, C. L. Painting, Z. Pikramenou, E. A. Plummer, K. Rissanen, P. Saarenketo, *J. Chem. Soc., Dalton Trans.* **2000,** 1447.

Received March 30, 2000
[I00123]

An Unusual Oxidation of 1,5-Dimethyl-2,4-bis(dialkylamino)-1,5-diaza-2,4-diphosphinan-6-one with Hexafluoroacetone

Igor V. Shevchenko,*[a] Rostislav N. Mikolenko,[a] Alexander N. Chernega,[b] Eduard B. Rusanov,[b] and Hansjoerg Grützmacher[c]

Dedicated to Professor Michael Lattman on the occasion of his 50th birthday

Keywords: Methylenediphosphane / Hexafluoroacetone / Carbodiphosphorane / Ylides / Wittig reaction / Oxidations

The oxidation of heterocycles **5a,b**, or **9** containing a methylenediphosphane unit, with hexafluoroacetone does not lead to the expected dioxaphospholane heterocycles, but yields unstable carbodiphosphoranes **6a,b** or ylide **10** respectively, which then react easily with HFA to give the stable intermediate products **7a,b** or **11** of the Wittig reaction.

Introduction

It is well-known that the oxidation of phosphanes with hexafluoroacetone (HFA) usually leads to the formation of 1,3- or 1,4-dioxaphospholane heterocycles.[1–4] Recently, however, we showed that this is not the only possible pathway for this reaction and that the presence of a methylene group in an α-position to the phosphorus atom may direct the reaction in an unusual way.[5,6] For example, bis[bis(dialkylamino)phosphinyl]methanes **1a,b** easily react with only two equivalents of HFA quantitatively, giving carbodiphosphoranes **2a,b** (Scheme 1).

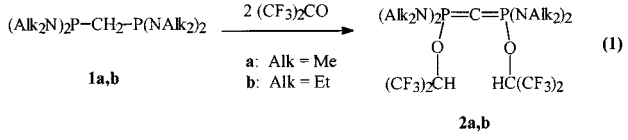

Scheme 1

Results and Discussion

In order to demonstrate the scope of this unusual reaction, we decided to employ other diphosphanes containing the structural fragment P–CH_2–P. It was interesting, for example, to investigate the reaction of HFA with compounds in which this fragment was a part of a heterocyclic system. As a model system we chose 1,5-dimethyl-2,4-bis(dialkylamino)-1,5-diaza-2,4-diphosphinan-6-one **5a,b**.[7]

The reactivity of **5a,b** in the reaction with HFA did not differ much from that of **1a,b**. The reaction proceeded smoothly at room temperature when gaseous HFA was slowly bubbled through a solution of **5a** or **5b** in dichloromethane at 20 °C. However, only small quantities of the expected cyclic carbodiphosphoranes **6a,b** could be detected in the reaction mixture by NMR spectroscopy. Unlike carbodiphosphoranes **2a,b**, compounds **6a,b** underwent addition of one more equivalent of HFA to give the heterocycles **7a,b**, which were the main product in this reaction (Scheme 2). The rate of addition of HFA to carbodiphosphoranes **6a,b** evidently exceeded the rate of their own formation; with HFA as limiting reagent, the content of **6a,b** did not grow and the starting material **5a,b** remained in the reaction mixture.

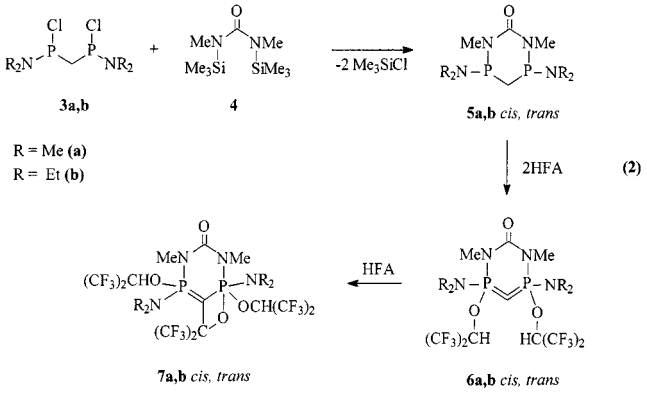

Scheme 2

These results are consistent with the only known example of the addition of HFA to hexaphenylcarbodiphosphorane.[8] Here, the same type of [1,2]oxaphosphetane was obtained by a cyclic addition. However the reaction required excess HFA and heating to 50 °C.

[a] Institute of Bioorganic Chemistry,
Murmanskaya Street 1, 02094 Kiev, Ukraine
Fax: (internat.) + 38-044/573-2552
E-mail: ishev@bpci.kiev.ua; ishev@bioorg.kiev.ua
[b] Institute of Organic Chemistry,
Murmanskaya Street 5, 02094 Kiev, Ukraine
Fax: (internat.) + 38-044/573-2643
E-mail: iochkiev@ukrpack.net
[c] Laboratorium für Anorganische Chemie, ETH-Zentrum,
Universitätstraße 6, CH-8092 Zürich
Fax: (internat.) + 41-1/632-1090
E-mail: gruetz@inorg.chem.ethz.ch

 © WILEY-VCH Verlag GmbH, 69451 Weinheim, 2001 1434–1948/01/0101–0195 $ 17.50+.50/0

Starting heterocycles **5a,b** were obtained in high yield by the addition of silylated urea **4** to methylene-bis(diethylaminochlorophosphanes) **3a,b** and were used in the reaction with HFA without purification. They existed as *cis*- and *trans*-isomers, depending on the position of the substituents at the phosphorus atoms with respect to the cycle. The *cis*-isomer of **5** is kinetically more stable and its formation is favored. The *trans*-isomer **5-*trans*** is thermodynamically more stable and the *cis*/*trans* ratio after reaching equilibrium between the isomers is 1:9. The rate of transformation of **5-*cis*** into **5-*trans*** depends on the solvent used in the reaction.[7] This gave us the possibility to use varying *cis*/*trans* ratios from 1:1 to 1:9 when **5a,b** was reacted with HFA.

The products of this reaction, compounds **7a,b**, also formed *cis*- and *trans*-isomers. However, unlike the starting heterocycles **5a,b**, they exist independently of each other and do not show any tendency to interconvert one into the other. That is why the observed ratio between the isomers of product **7** reflects the isomer distribution of the starting compound **5** before reaction with HFA.

When compounds **5a,b** were prepared in diethyl ether, the initial ratio between the isomers was 1:1 and after reaction with HFA the products **7a,b** were obtained with the same ratio of isomers. Each isomer displays two characteristic doublets in the ^{31}P NMR spectrum. Compounds **7a,b** are stable crystalline products and were isolated as a mixture of *cis*- and *trans*-isomers. The ratio of the isolated material corresponded to the one seen in solution and since both have equal solubility, they could not be separated. Attempts to separate them by liquid chromatography led to their substantial decomposition on the surface of silica gel, even though compounds **7a,b** do not react with water in the absence of silica gel.

When **5a,b** were prepared in dichloromethane, the *cis*/*trans* equilibrium ratio (1:9) was rapidly reached. The addition of HFA to this isomeric mixture gave the same distribution of isomers in the reaction products **7a,b**. The predominant content of **7a,b-*trans*** allowed for their isolation as pure crystalline substances. The structures of **7a,b-*trans*** are consistent with their NMR spectra. For example, the ^{31}P NMR spectrum of **7a** shows two doublets at −42 ppm and 33 ppm, which are characteristic of the ylide and spirophosphorane phosphorus atoms respectively. The ^{1}H and ^{13}C NMR spectra showed the non-equivalence of dialkylamino groups. All CF_3 groups of **7a,b-*trans*** are nonequivalent and give rise to six independent multiplets in the ^{19}F NMR spectra. Two of them do not show FH coupling, as they belong to the CF_3 groups connected to the four-membered ring.

The structure of compound **7b-*trans*** was confirmed by a single-crystal X-ray diffraction study. The general view of the molecule is shown in Figure 1. It should be noted that heterocycles of this type have not been studied by structural methods yet.[9]

The central 6-membered ring P(1)P(2)N(1)N(2)C(1)C(2) in this compound is almost planar: deviations from the least-square plane do not exceed 0.070 Å. The 4-membered heterocycle P(2)O(3)C(1)C(12) is planar within 0.026 Å.

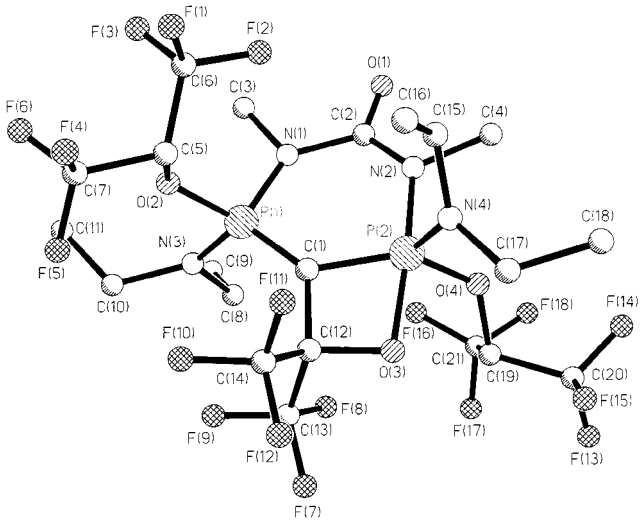

Figure 1. Perspective view and labelling scheme for the molecule **7b-*trans*** (H atoms are omitted for clarity). Selected bond lengths [Å] and angles [°]: P(1)−N(1) 1.634(3), P(1)−C(1) 1.668(4), P(2)−C(1) 1.738(4), P(2)−N(2) 1.773(3), P(2)−O(3) 1.779(3), O(3)−C(12) 1.407(4), N(1)−C(2) 1.421(5), N(2)−C(2) 1.352(5), C(1)−C(12) 1.507(5); N(1)−P(1)−C(1) 105.8(2), C(1)−P(2)−N(2) 98.3(2), C(12)−O(3)−P(2) 94.9(2), C(2)−N(1)−P(1) 129.3(3), C(2)−N(2)−P(2) 132.3(3), C(12)−C(1)−P(2) 93.1(2), P(1)−C(1)−P(2) 132.2(2), N(2)−C(2)−N(1) 121.1(3), O(3)−C(12)−C(1) 95.9(3)

The dihedral angle between the planes of the 6- and 4-membered cycles is 11.63°. All nitrogen atoms have a trigonal coordination sphere (corresponding sums of bond angles lie within a narrow range: 358.6−360.0°). Atom P(1) has significantly distorted tetrahedral coordination whereas atom P(2) has a trigonal bipyramidal coordination, with atoms O(3) and N(2) being in axial and atoms C(1), N(4), O(4) in equatorial positions.

Together with **7a,b**, small quantities of the cyclic carbodiphosphoranes **6a,b** were detected in the reaction mixture (about 5−10% based on ^{31}P NMR spectrum). These compounds also exist as *cis*- and *trans*-isomers. Each of them displays a singlet in the range of 40−44 ppm. This value is consistent with the chemical shifts of acyclic carbodiphosphoranes **2a,b**. As a strong base, **6a,b** can react with ammonium hydrochlorides to give salts **8a,b**. Since chlorophosphanes **3a,b** were frequently contaminated with small amounts of dialkylammonium chloride, salts **8a,b** were found in the reaction mixture with a yield of about 3−4%. When the reaction was carried out in THF, **8b** crystallized from the reaction mixture as a colorless crystalline product. *A priori*, this compound should also give rise to two isomers. However, only one isomer of **8b** was formed, as is evident from the ^{31}P NMR spectrum where only one singlet

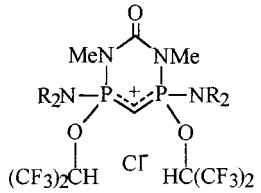

8a,b

at 44.05 ppm is observed. The X-ray analysis of a single crystal revealed that this is the *cis*-isomer (Figure 2). The hexafluoroisopropoxide groups form two chelating units, which embrace the chlorine anion forming the thermodynamically stable structure. The chlorine atom is kept by the two hydrogen bonds which is only possible for the *cis*- but not for the *trans*-isomer (Cl···C(5) 3.323(9), Cl···C(12) 3.377(9) Å).

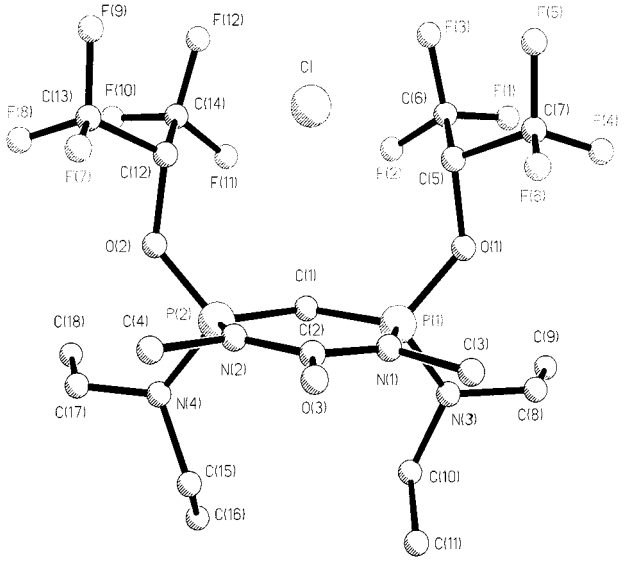

Figure 2. Perspective view and labelling scheme for the molecule **8b-*cis*** (H atoms are omitted for clarity). Selected bond lengths [Å] and angles [°]: P(1)−N(1) 1.654(10), P(1)−C(1) 1.671(11), P(2)−C(1) 1.662(11), P(2)−N(2) 1.661(10), N(1)−C(2) 1.39(2), N(2)−C(2) 1.364(14); N(1)−P(1)−C(1) 107.4(5), C(1)−P(2)−N(2) 106.3(5), C(2)−N(1)−P(1) 129.5(9), C(2)−N(2)−P(2) 130.9(9), P(1)−C(1)−P(2) 125.5(7), N(2)−C(2)−N(1) 119.5(13)

As in compound **7b-*trans***, the central 6-membered ring P(1)P(2)N(1)N(2)C(1)C(2) of **8b-*cis*** is almost planar: deviations do not exceed 0.060 Å. Atoms P(1) and P(2) have significantly distorted tetrahedral coordination. These data differ from the results of X-ray analyses, which we obtained earlier for the *cis*- and *trans*-isomers of the sulfur-derivative of heterocycle **5b**. These isomers showed noticeably distorted ring conformations, while the distortions at the phosphorus atoms were less pronounced than in **7b**-*trans* and **8b**-*cis*.[10] Owing to the $n_{N(1,2)}-\pi_{C=O}$ conjugation, the N(1)−C(2) and N(2)−C(2) bonds of **8b-*cis*** and **7b-*trans*** are noticeably shorter than the standard value of 1.45 Å for the $N(sp^2)-C(sp^2)$ single bond.[11] Comparison of the geometrical parameters of **8b-*cis*** and **7b-*trans*** with the corresponding values in related systems[10,12−14] shows delocalization of electron density over the N(1)−P(1)−C(1)−P(2)−N(2) bond system for the former molecules. It is noteworthy that unlike compound **7b-*trans***, in which the P(1)=C(1) double bond is localized as is indicated by the rather different bond lengths [P(1)−C(1) 1.668(4), P(2)−C(1) 1.738(4) Å], charge delocalization over the P(1)−C(1)−P(2) system [P(1)−C(1) 1.671(11), P(2)−C(1) 1.662(11) Å] is observed in **8b-*cis***.

For the further studies of the reactions of $P-CH_2-P$-containing heterocycles with HFA we used compound **9**. Its structure is rather close to that of **5a,b**, but instead of dialkylamino groups the two phosphorus atoms are bridged by one more urea unit. The reaction of compound **9** with HFA is slower and after 48 h in a sealed tube, a polymeric product of uncertain structure (82%) and compound **11** (18%) were obtained (Scheme 3). Since compound **11** is poorly soluble in dichloromethane, which was used as a solvent, it crystallized directly from the reaction mixture as colorless crystals.

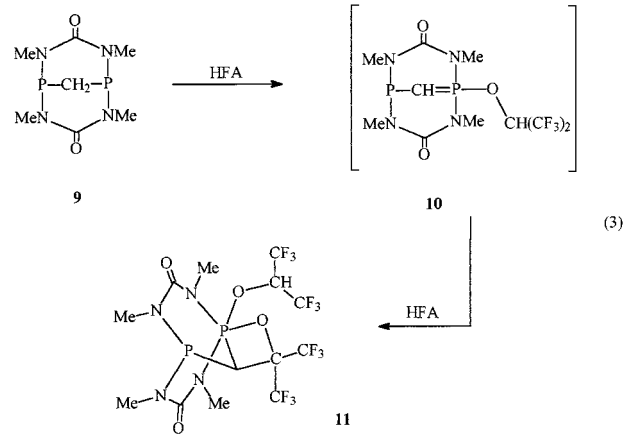

Scheme 3

Unlike **5**, the phosphorus atoms of compound **9** are less nucleophilic, as they are bonded to two amide nitrogen atoms. That is why the reaction of **9** with HFA involves only one of the two phosphorus atoms. Although we could not detect it, we assumed that in this case the first reaction product, the ylide intermediate **10**, undergoes two simultaneous processes: polymerization and addition of HFA across the P=C bond to give **11**.

The structure of **11** was determined by NMR spectroscopic and analytical data. The ^1H NMR spectrum shows the non-equivalence of the all four methyl groups, the characteristic multiplet of the $(CF_3)_2CH$ unit at 5.48 ppm and doublet of doublets of the P−CH−P proton at 4.82 ppm. All CF_3 groups are also non-equivalent and display separate multiplets in the ^{19}F NMR spectrum. The interesting feature of this compound is that the two CF_3 groups at the four-membered cycle show a through-space coupling with the tricoordinated phosphorus atom. This phosphorus atom appears as a multiplet at 61 ppm in the ^{31}P NMR spectrum, whereas the other phosphorus atom gives rise to a doublet at −43 ppm.

Thus, the reaction of the $P-CH_2-P$ containing heterocycles **5** and **9** with hexafluoroacetone did not lead to the formation of the expected 1,3,2- or 1,4,2-dioxaphospholane heterocycles with a pentacoordinated phosphorus atom, but yielded derivatives of cyclic carbodiphosphoranes with tetracoordinated ylide phosphorus atoms.

Experimental Section

All operations were performed under nitrogen in a dry box. The solvents were dried by the usual procedures. The NMR spectra were recorded on JEOL FX-90Q and Varian 300 MHz spectro-

meters. The ^{1}H and ^{13}C NMR chemical shifts were referenced to tetramethylsilane (TMS). The ^{31}P NMR chemical shifts were measured using 85% aqueous orthophosphoric acid as an external standard. As usual, high frequency shifts were given positive signs. The digital resolutions were 0.25 Hz, 0.5 Hz and 1.25 Hz for ^{1}H-, ^{13}C- and ^{31}P NMR spectra respectively.

Synthesis of Compounds 3a,b: Compounds **3a,b** can be obtained with a 35−40% yield (after distillation) from methylene-bis(dichlorophosphane)[17] and dialkylamine. Use of silylated dialkylamine increases the yield to 50%. It is more convenient, however, to prepare fully substituted tetra(dialkylamino)methylenediphosphane **1a,b**, which can be isolated by distillation in 75−80% yield, and mix it subsequently with one equivalent of starting methylene-bis(dichlorophosphane) without solvent.

Synthesis of Compound 7a-*trans*: *N,N′*-Dimethyl-*N,N′*-bis(trimethylsilyl)urea[18] **4** (154 mg, 0.663 mmol) was added to a solution of methylene-bis(dimethylaminochlorophosphane) **3a** (150 mg, 0.638 mmol) in dichloromethane (1.5 mL), and the mixture was stirred at room temperature for 15 min. The reaction mixture was then placed in a 5-mm NMR tube and gaseous HFA (40 mL, 1.79 mmol) was slowly bubbled through it at room temperature using a syringe with a thin needle. The solvent was removed in vacuo 10 min after the addition of HFA and the residue was extracted with hexane (2 × 5 mL). The hexane solution was concentrated in vacuo to a volume of 5 mL and then cooled to −15 °C. In 48 h colorless crystals of **7a-*trans*** were separated and dried in vacuo. Yield 120 mg (25%), m.p. 101−102 °C. − ^{1}H NMR (89.56 MHz, $CDCl_3$): δ = 2.59 (d, $^{3}J_{PH}$ = 13.2 Hz, 6 H, N(CH_3)$_2$), 2.75 (d, $^{3}J_{PH}$ = 15.1 Hz, 6 H, N(CH_3)$_2$), 2.78 (d, $^{3}J_{PH}$ = 16.8 Hz, 3 H, NCH_3), 2.86 (d, $^{3}J_{PH}$ = 10.0 Hz, 3 H, NCH_3), 5.18 (m, 1 H, CHCF$_3$), 5.42 (m, 1 H, CHCF$_3$). − ^{13}C NMR (22.5 MHz, $CDCl_3$): δ = 28.6 (s, 1 C, NCH$_3$), 35.7 (s, 1 C, NCH$_3$), 36.8 (s, 2 C, N(CH$_3$)$_2$), 37.6 (d, $^{2}J_{PC}$ = 8.5 Hz, 2 C, N(CH$_3$)$_2$), 67.0−75.5 (m, 3 C, CH(CF$_3$)$_2$), 120.4 (q, $^{1}J_{FC}$ = 282.8 Hz, 2 C, CF$_3$), 121.3 (q, $^{1}J_{FC}$ = 279.2 Hz, 2C, CF$_3$), 123.5 (q, $^{1}J_{FC}$ = 289.0 Hz, 2C, CF$_3$), 153.8 (dd, $^{2}J_{PC}$ = 10.9 Hz, $^{2}J_{PC}$ = 11.2 Hz, C=O). − ^{19}F NMR (282.2 MHz, $CDCl_3$): δ = −72.99 (m, CF$_3$), −73.47 (m, CF$_3$), −74.08 (m, CF$_3$), −74.62 (m, CF$_3$), −76.17 (m, CF$_3$), −77.27 (m, CF$_3$). − ^{31}P NMR (36.2 MHz, $CDCl_3$): δ = −42.0 (d, $^{2}J_{PP}$ = 75.6 Hz), 33.1 (d, $^{2}J_{PP}$ = 75.6 Hz). − $C_{17}H_{20}F_{18}N_4O_4P_2$ (748.29): calcd. C 27.29, H 2.69; found C 27.18, H 2.82.

Synthesis of Compound 7b-*trans*: *N,N′*-Dimethyl-*N,N′*-bis(trimethylsilyl)urea[18] **4** (128 mg, 0.550 mmol) was added to a solution of methylene-bis(dimethylaminochlorophosphane) **3b** (150 mg, 0.515 mmol) in dichloromethane (2 mL), and the mixture was stirred at room temperature for 45 min. The solvent was then removed in vacuo and the remaining oil was allowed to stay at 25 °C for 30 min in order for the *cis*- and *trans*-isomers of **3b** to reach equilibrium. Subsequently, the oil was dissolved in CH_2Cl_2 (1 mL), the solution was placed in a 5-mm NMR tube and gaseous HFA (32 mL, 1.44 mmol) was slowly bubbled through the solution using a syringe equipped with a thin needle. The solvent was removed in vacuo 10 min after the addition of HFA, and the residue was extracted with hexane (2 × 3 mL). The hexane solution was concentrated in vacuo to a volume of 1 mL and then cooled to −15 °C. The colorless crystals of **7b-*trans*** formed over 24 h were separated and dried in vacuo. Yield 116 mg (29%), m.p. 120−121 °C. − ^{1}H NMR (89.56 MHz, $CDCl_3$): δ = 1.04 (t, $^{3}J_{HH}$ = 7.1 Hz, 6 H, NCH$_2$CH_3), 1.17 (t, $^{3}J_{HH}$ = 7.1 Hz, 6 H, NCH$_2$CH_3), 2.84 (d, $^{3}J_{PH}$ = 7.3 Hz, 3 H, NCH_3), 2.91 (d, $^{3}J_{PH}$ = 10.3 Hz, 3 H, NCH_3), 3.09 (m, 8 H, NCH_2CH$_3$), 5.11 (m, 1 H, CHCF$_3$), 5.35 (m, 1 H, CHCF$_3$). − ^{13}C NMR (22.5 MHz, $CDCl_3$): δ = 11.97 (s, 1 C, NCH$_2$CH_3), 12.14 (s, 1 C, NCH$_2$CH_3), 14.0 (s, 2 C, NCH$_2$CH_3), 30.0 (s, 1 C, NCH$_3$), 36.1 (s, 1 C, NCH$_3$), 37.7 (d, $^{2}J_{PC}$ = 8.6 Hz, 2 C, NCH$_2$CH$_3$), 42.3 (s, 2 C, NCH$_2$CH$_3$), 65.0−76.2 (m, 3 C, CH(CF$_3$)$_2$), 120.5 (q, $^{1}J_{FC}$ = 286.5 Hz, 2 C, CF$_3$), 121.5 (q, $^{1}J_{FC}$ = 284.1 Hz, 2C, CF$_3$), 123.5 (q, $^{1}J_{FC}$ = 286.4 Hz, 2C, CF$_3$), 153.8 (dd, $^{2}J_{PC}$ = 10.9 Hz, $^{2}J_{PC}$ = 11.1 Hz, 1 C, C=O). − ^{19}F NMR (282.2 MHz, $CDCl_3$): δ = −72.29 (m, 3 F, CF_3), −72.86 (m, 3 F, CF_3), −74.10 (m, 3F, CF_3), −74.17 (m, 3 F, CF_3), −74.39 (m, 3 F, CF_3), −75.51 (m, 3 F, CF_3). − ^{31}P NMR (36.2 MHz, $CDCl_3$): δ = −38.2 (d, $^{2}J_{PP}$ = 74.2 Hz), 36.0 (d, $^{2}J_{PP}$ = 74.2 Hz). − $C_{21}H_{28}F_{18}N_4O_4P_2$ (804.40): calcd. C 31.36, H 3.51; found C 31.69, H 3.58.

Synthesis of Compound 8b-*cis*: *N,N′*-Dimethyl-*N,N′*-bis(trimethylsilyl)urea[18] **4** (134 mg, 0.578 mmol) was added to a solution of methylene-bis(dimethylaminochlorophosphane) **3b** (160 mg, 0.550 mmol) in THF (4 mL), and the mixture was stirred at room temperature for 15 min. The solvent and all volatiles were then removed in vacuo (0.05 Torr) for 15 min, and the remaining oil was dissolved again in THF (4 mL). The solution was then placed in a 10-mm NMR tube and gaseous HFA (17 mL, 0.755 mmol) was slowly bubbled through the solution using a syringe equipped with a thin needle. The reaction mixture was allowed to stay at −15 °C. Colorless crystals of **8b-*cis*** formed over 24 h were separated and dried in vacuo. Yield 13 mg (3.6%). − ^{1}H NMR (89.56 MHz, $CDCl_3$): δ = 1.22 (t, $^{3}J_{HH}$ = 7.1 Hz, 12 H, NCH$_2$CH_3), 3.04 (d, $^{3}J_{PH}$ = 6.2 Hz, 6 H, NCH_3), 3.25 (m, 8 H, NCH_2CH$_3$, 1 H, PCHP), 7.46 (m, 2 H, CHCF$_3$). − ^{19}F NMR (84.26 MHz, $CDCl_3$): δ = −72.98 (d, $^{3}J_{FH}$ = 41.0 Hz, 12 F, CF_3). − ^{31}P NMR (36.2 MHz, $CDCl_3$): δ = 44.0 (s, 2 P).

Synthesis of Compound 11: Gaseous hexafluoroacetone (20.5 ml; 0.914 mmol) was condensed into a solution of bicyclic compound **9** (113 mg; 0.456 mmol) in dichloromethane (1 mL) in a glass tube. The tube was sealed and kept at room temperature for 3 d. The colorless crystalline product formed in the reaction mixture was then filtered off, washed with dichloromethane (0.3 mL) and dried in vacuo (0.05 mm). Yield 49 mg (18.5%), m.p. 120−121 °C. − ^{1}H NMR ($CDCl_3$): δ = 2.93 (d, $^{3}J_{HP}$ = 9.4 Hz, 3 H, NCH_3), 2.99 (d, $^{3}J_{HP}$ = 10.2 Hz, 3 H, NCH_3), 3.14 (d, $^{3}J_{HP}$ = 9.4 Hz, 3 H, NCH_3), 3.18 (d, $^{3}J_{HP}$ = 12.6 Hz, 3 H, NCH_3), 4.82 (dd, $^{2}J_{HP}$ = 6.1 Hz, $^{2}J_{HP}$ = 26.1 Hz, 1 H, P−CH−P), 5.48 (d of hept., $^{3}J_{HP}$ = 14.9 Hz, $^{3}J_{HF}$ = 5.6 Hz, 1 H, HC(CF$_3$)$_2$). − ^{19}F NMR (84.26 MHz, $CDCl_3$): δ = −77.93 (m, CF$_3$), −74.11 (m, CF$_3$), −73.18 (m, CF$_3$), −70.98 (m, CF$_3$). − ^{31}P NMR ($CDCl_3$): δ = −43.3 (d, $^{2}J_{PP}$ = 65.0 Hz, 1 P), 61.3 (m, $^{2}J_{PP}$ = 65.0 Hz, 1 P). − $C_{13}H_{14}F_{12}N_4O_4P_2$ (580.21): calcd. C 26.91, H 2.43; found C 27.07, H 2.54.

X-ray Crystal Structure Determination of Compounds 7b-*trans* and 8b-*cis*: Crystal data, data collection and processing parameters are given in Table 1. All crystallographic measurements were performed at 20 °C on a CAD-4-Enraf−Nonius diffractometer using graphite-monochromated Mo-K_α radiation (λ = 0.71069 Å) and ω-2θ scan mode (the ratio of the scanning rates ω/2θ = 1.2). Unit-cell parameters were calculated from the setting angles of 22 strong, high-angle carefully centered reflections with $13 > \theta > 12°$ for **7b-*trans*** and $11 > \theta > 10°$ for **8b-*cis***. Three reflections were chosen as intensity standards and were measured every 3600 s of X-ray exposure time, and three orientation control reflections were measured every 147 reflection. Correction for crystal decay (ca. 13% for **7b-*trans*** and 8% for **8b-*cis***) was applied during the processing of data sets. All data were corrected for Lorentz and polarization effects but not for absorption. Both structures were solved by direct methods.[15] Non-hydrogen atoms were refined against F by the full-matrix least-squares technique[16] in the anisotropic approxi-

Table 1. Crystal data and structure refinement parameters of compounds **7b-*trans***, **8b-*cis***

	7b-*trans*	**8b-*cis***
Empirical formula	$C_{21}H_{28}F_{18}N_4O_4P_2$	$C_{18}H_{29}ClF_{12}N_4OP_2$
a [Å]	10.452(2)	13.314(5)
b [Å]	11.732(1)	12.896(4)
c [Å]	14.908(3)	17.613(6)
α [°]	68.00(1)	90
β [°]	78.81(1)	105.48(3)
γ [°]	73.79(1)	90
V [Å^3]	1619	2914
Z	2	4
d [g × cm^{-3}]	1.65	1.54
Crystal system	Triclinic	Monoclinic
Space group	P-1 (N2)	$P2_1/c$ (N14)
μ [mm^{-1}]	0.27	0.34
F(000)	812	1376
Crystal size [mm]	0.27 × 0.40 × 0.50	0.03 × 0.15 × 0.15
Index ranges	$0 < h < 10$	$0 < h < 14$
	$-11 < k < 12$	$0 < k < 13$
	$-15 < l < 15$	$-19 < l < 18$
θ_{max} [°]	22	22.7
No. of reflections:		
Collected	4220	4314
Independent	3953	3894
in refinement ($I > 0$)	3069	3037
with $I > 2\sigma(I)$	2789	1418
R(int)	0.015	0.043
No. of refined parameters	442	281
Final R factors ($I > 2\sigma(I)$):		
R_1 (F)	0.042	0.098
R_w (F^2)	0.112	0.178
GOF	1.044	1.005
Weighting coefficients:		
A	0.065	0.082
B	1.238	0
Largest peak/hole [e cm^{-3}]	0.21/−0.24	0.28/−0.29

mation. All hydrogen atoms in **7b-*trans*** were located in the difference Fourier maps. For **8b-*cis*** all hydrogen atoms were placed in calculated positions. In both structures, the hydrogen atoms were included in the final refinement riding their supporting carbon atoms. The weighting scheme $\omega^{-1} = \sigma^2(F_o^2) + (AP)^2 + BP$, with $P = (F_o^2 + 2F_c^2)/3$ was used. − Crystallographic data (excluding structure factors) for the structures reported in this paper have been deposited with the Cambridge Crystallographic Data Centre as supplementary publication no. CCDC-141691 (**7b-*trans***) and CCDC-141692 (**8b-*cis***). Copies of the data can be obtained free of charge on application to CCDC, 12 Union Road, Cambridge CB2 1EZ, UK (Fax: (internat.) +44−1223/336−033; E-mail: deposit@ccdc.cam.ac.uk).

Acknowledgments

We thank the Swiss National Science Foundation for financial support. We are indebted to Mr. T. Kaschner for his cooperation.

[1] M. Witt, K. S. Dathathreyan, H. W. Roesky, Inorganic Chemistry of Hexafluoroacetone, *Adv. Inorg. Chem. Radiochem.,* **1986**, *30*, 223−312.
[2] R. Burgada, R. Setton, "Preparation, Properties and Reactions of Phosphoranes", in: *The Chemistry of Organophosphorus Compounds*, ed. F. R. Hartley, in *The Chemistry of Functional Groups*, Series ed. S. Patai, Wiley, Chichester, New York, Brisbane, Toronto, Singapore, 1994, vol. 3; chapter 3, pp. 185−272.
[3] F. U. Seifert, G.-V. Röschenthaler, *J. Fluorine Chem.,* **1995**, *70*, 171−174.
[4] I. Neda, C. Melnicky, A. Vollbrecht, A. Fischer, P. G. Jones, R. Schmutzler, *Z. Anorg. Allg. Chem.* **1996**, *622*, 1047−1059.
[5] I. V. Shevchenko, *Chem Commun.* **1998**, 1203−1204.
[6] I. Shevchenko, R. Mikolenko, S. Loss, H. Grützmacher, *Eur. J. Inorg. Chem.* **1999**, 1665−1671.
[7] I. V. Shevchenko, M. V. Furmanova, V. P. Kukhar, R. Schmutzler, *Z. Naturforsch. B* **1992**, *47*, 258−262.
[8] G. H. Birum, C. N. Matthews, *J. Org. Chem.* **1967**, *32*, 3554−3559.
[9] Cambridge Crystallography Data Base, Release Spring **1999**.
[10] I. V. Shevchenko, A. Fischer, P. G. Jones, R. Schmutzler, *Chem. Ber.* **1994**, *127*, 1247−1250.
[11] M. Burke-Laing, M. Laing, *Acta Crystallogr. (B).* **1976**, *32*, 3216−3224.
[12] I. V. Shevchenko, P. G. Jones, A. Fischer, R. Schmutzler, *Heteroatom Chem.* **1992**, *3*, 177−180.
[13] R. E. Marsh, *Acta Crystallogr. (B)* **1997**, *53*, 317.
[14] E. Fluck, F. Rosche, G. Heckmann, F. Weller, *Heteroatom Chem.* **1995**, *6*, 355−363.
[15] G. M. Scheldrick, SHELXS-86. Program for the Solution of Crystal Structures, University of Goettingen, Göttingen, Germany, **1986**.
[16] G. M. Scheldrick, SHELXS-93. Program for the Refinement of Crystal Structures, University of Göttingen, Goettingen, Germany, **1993**.
[17] Z. S. Novikova, A. A. Prishchenko, I. F. Lutsenko, *Zh. Obshch. Khim.* **1977**, *47*, 775−781.
[18] J. F. Klebe, J. B. Bush, Jr., J. E. Lyones, *J. Am. Chem. Soc.* **1964**, *86*, 4400.

Received April 3, 2000
[I00130]

Diastereoselective Homochiral Self-Assembly Between Anions and Cation in Solution

Olivier Maury,*[a] Jérôme Lacour,[b] and Hubert Le Bozec*[a]

Keywords: Chiral recognition / NMR spectroscopy / Ruthenium / Self-assembly / Supramolecular chemistry

Diastereoselective homochiral self-assembly occurs in solution by mixing the propeller-like racemic tris(DEAS-bpy) ruthenium(II) cation **B** [DEAS-bpy = 4,4′-bis(diethylaminostyryl)-[2,2′]-bipyridine)] and the racemic TRISPHAT anion **A** [TRISPHAT = tris(tetrachlorobenzenediolato)phosphate(V)]. This phenomenon is clearly shown by ^{1}H NMR spectroscopic studies which reveal: (i) the existence of a rapid equilibrium between their homochiral and heterochiral associations, (ii) at room temperature, the preferential formation of the homochiral ion pairs with a ratio homochiral/heterochiral = 72:28, and (iii) at 243 K, the almost pure homochiral associations ($\mathbf{B}^{\Lambda}$,$\mathbf{A}^{\Lambda}{}_2$) and ($\mathbf{B}^{\Delta}$,$\mathbf{A}^{\Delta}{}_2$).

Introduction

Propeller-like molecules are potential candidates for diastereoselective self-assembly, where chiral supramolecules are spontaneously formed from a mixture of racemic components. Such types of chiral recognition have generally been observed in the solid state.[1] The recognition driving force is mainly due to the formation of intermolecular hydrogen bonds, the helicity of both compounds ensuring the spatial compatibility of the H-donor and acceptor groups.[2] Moreover, a few examples of self-assembly have also been observed for propeller-like H-bond-free molecules: spontaneous homochiral segregation occurred during the formation of columnar liquid crystals[3] or during gel crystallization,[4] the homochiral association of the propellers ensuring the optimal packing. Chiral recognition phenomena have also been observed among guest tris(diimine) metal complexes when intercalated into host mineral clays.[5]

D_3-symmetric propeller-like molecules are particularly interesting as a new class of octupolar chromophores for nonlinear optics (NLO).[6] Coordination chemistry is a powerful tool to design such compounds,[7] and recently we[8] and others[9] have reported the large molecular hyperpolarisability of octahedral ruthenium(II) complexes [Ru(bpy′)$_3$][PF$_6$]$_2$, where bpy′ is a functionalized 2,2′-bipyridine. With the aim of increasing the NLO activity of such systems, we became interested in the association of Ru^{II} cationic octupoles with counter anions also having a D_3 propeller-like topology. We sought to use the propeller-like tris(tetrachlorobenzenediolato)phosphate(V) anion [TRISPHAT] **A** (Figure 1) which was recently described as a chiral shift agent,[10] a chiral inducer onto Fe^{II} complexes[11] and for its ion-pair chromatographic-resolution properties.[12]

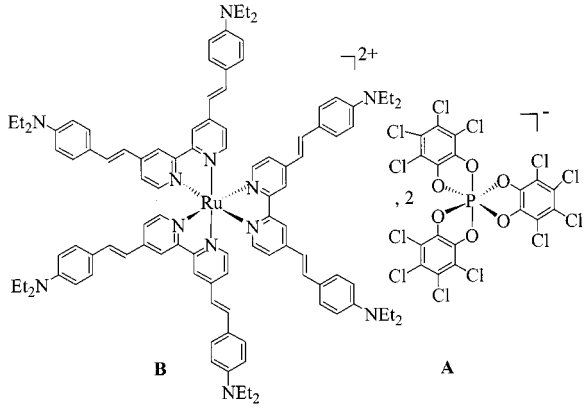

Figure 1. TRISPHAT anion **A** (Δ) and [Ru(DEAS-bpy)$_3$]$^{2+}$ cation **B** (Δ) (DEAS-bpy = 4,4′-bis(diethylaminostyryl)-[2,2′]-bipyridine)

In this article, we wish to describe the synthesis and ^{1}H NMR spectroscopic studies of the association between a racemic D_3-symmetric ruthenium tris(DEAS-bpy) dication {where DEAS-bpy represents 4,4′-bis(diethylaminostyryl)-[2,2′]-bipyridine} and the racemic TRISPHAT anion which reveals a remarkable diastereoselective, homochiral self-assembly phenomenon in solution.

Results and Discussion

The tris(bipyridyl) ruthenium complex (**B**,[PF$_6$]$_2$) is classically prepared by reacting [RuCl$_2$(DMSO)$_4$] with DEAS-bpy (three equivalents) in refluxing DMF, followed by an anionic exchange with NaPF$_6$. The TRISPHAT salt (**B**,**A**$_2$) is obtained either from the chloride or the hexafluorophosphate salts by anion metathesis with [HNBu$_3$][TRISPHAT] (Scheme 1). This new complex is much more soluble than the corresponding PF$_6$ salt in chlorinated solvents allowing its purification by using silica-gel column chromatography with dichloromethane as eluent. The spectroscopic and

[a] Organométallique et Catalyse: Chimie et Electrochimie Moléculaire, UMR 6509 CNRS − Université de Rennes 1, Campus de Beaulieu, 35042 Rennes cedex, France
Fax: (internat.) +33-299/28 69 39
E-mail: lebozec@univ-rennes1.fr
[b] Département de Chimie Organique, quai Ernest Ansermet 30, CH-1211 Genève 4, Switzerland

 © WILEY-VCH Verlag GmbH, 69451 Weinheim, 2001 1434−1948/01/0101−0201 $ 17.50+.50/0

analytical data are given in the Experimental Section. The aromatic parts of the ^{1}H NMR spectra of (**B**,[PF_6]$_2$) and (**B**,**A**$_2$) are displayed in Figure 2. For the TRISPHAT salt, a strong deshielding of the H_6 proton is observed ($\Delta\delta$ = +0.5 ppm) while the bipyridyl protons H_3 and H_5, as well as the protons of the styryl substituents (H_7-H_{11}), are displaced to higher field when compared to those of the corresponding hexafluorophosphate salt. A similar, but weaker, effect can be observed in the corresponding ^{13}C NMR spectra (see Experimental Section), with the C_6 carbons being shifted downfield ($\Delta\delta$ = +1.0 ppm).

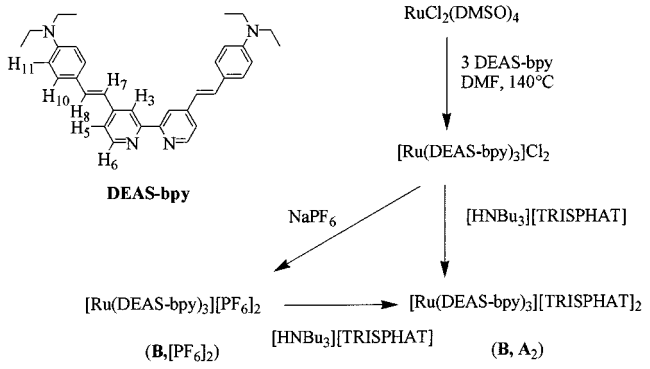

Scheme 1. Synthesis of (**B**,**A**$_2$) and indexation of DEAS-bpy

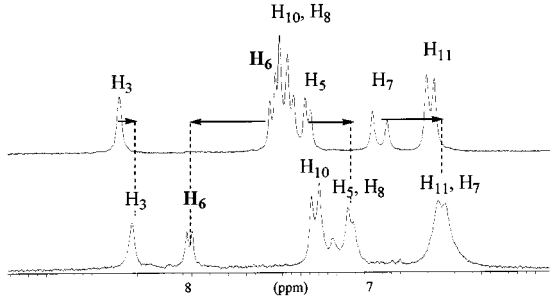

Figure 2. Effect of the counter-anion on the aromatic region of the ^{1}H NMR spectra of (**B**,[PF_6]$_2$) (up) and (**B**,**A**$_2$)

It is worth noting that the TRISPHAT anion **A** and the Ru^{II} complex **B** exist as two configurationally stable Λ and Δ enantiomers.[13] Their association should afford a mixture of diastereoisomeric complexes consisting of two couples of enantiomeric homochiral (**B**$^{\Lambda}$,**A**$^{\Lambda}_2$), (**B**$^{\Delta}$,**A**$^{\Delta}_2$) and heterochiral (**B**$^{\Lambda}$,**A**$^{\Delta}_2$), (**B**$^{\Delta}$,**A**$^{\Lambda}_2$) derivatives. Surprisingly, the ^{1}H NMR spectrum of the racemic mixture (CD_2Cl_2, 293 K) shows only one set of signals for the bipyridyl ligands (Figure 2) suggesting either a dynamic phenomenon or the selective formation of one diastereoisomer. Lowering the temperature to 243 K results in a slight shift and broadening of the signals, but no splitting of the ^{1}H NMR signals is observed (Figure 3). On the other hand, a direct observation of diastereoisomers by NMR spectroscopy should be possible through exchange between *rac* (**B**,[PF_6]$_2$) and the partially resolved chiral cinchonidinium−Δ TRISPHAT salt **A**$^{\Delta}$ ([α]$_D$ = −320, *de* = 86%).[14] The ^{1}H NMR spectrum of this mixture (298 K), shows two sets of signals for the bipyridyl ligands, corresponding to the expected mixture of homochiral and heterochiral diastereoisomers (Figure 4a).[15] The H_6 and $H_{6'}$ protons give signals of equal intensity at δ = 8.17 and 7.54, values which are notably different from that observed for the racemic mixture (unique signal, δ = 7.98, Figure 4f or Figure 2). At this stage no direct explanation could be given; since the TRISPHAT enantiomeric excess seems to have a large influence on the NMR spectra, two other experiments were carried out.

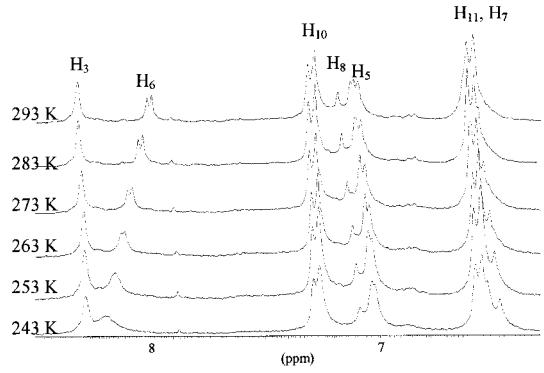

Figure 3. Variable temperature ^{1}H NMR spectra of *rac* (**B**,**A**$_2$) complexes (CD_2Cl_2, 300 MHz)

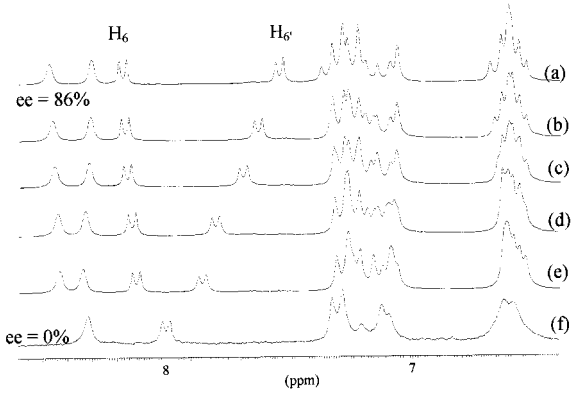

Figure 4. Aromatic part of the ^{1}H NMR spectra (CD_2Cl_2, 200 MHz, 293 K)of (**B**,**A**$_2$) (**A**$^{\Delta}$, *ee* = 86%) (a); *rac* (**B**,**A**$_2$) (f); during the addition of *rac* ([$HNBu_3$],**A**) to the solution of (**B**,**A**$_2$) (**A**$^{\Delta}$, *ee* = 86%) (b-e)

In order to decrease the TRISPHAT enantiomeric excess, *rac* (**B**,**A**$_2$) was incrementally added to the solution obtained with partially resolved TRISPHAT, containing mainly the (**B**$^{\Delta}$,**A**$^{\Delta}_2$) and (**B**$^{\Lambda}$,**A**$^{\Delta}_2$) diastereoisomers (Figure 4a). The convergence of the H_6 and $H_{6'}$ proton NMR probes is observed whereas their relative intensities remain equal, clearly indicating that these two signals are due to Δ−[Ru(DEAS-bpy)$_3$]$^{2+}$ and Λ−[Ru(DEAS-bpy)$_3$]$^{2+}$ propellers in a TRISPHAT-oriented medium. The dependence of the H_6 and $H_{6'}$ chemical shifts on TRISPHAT's *ee* is due to rapid equilibria involving the homochiral and heterochiral associations. For the two rapid equilibria, the position of the H_6 and $H_{6'}$ coalescence signals δ_{obs} is given by the equation: $\delta_{obs} = x\delta_{HOMO} + (1 - x)\delta_{HETERO}$ [Equation (a)] where x represents the relative amount of the homochiral species and δ_{HOMO} and δ_{HETERO} the chemical shift of the pure diastereoisomers. This equation allows the de-

termination of the relative amount of both homochiral and heterochiral diastereoisomers.

Finally, in order to quantify the role of the TRISPHAT enantiomeric excess, small amounts of *rac* ([$HNBu_3$],**A**) were successively added to a solution of (**B**,$\mathbf{A_2}$) ($\mathbf{A^{\Delta}}$, *ee* = 86%, Figure 4a). The evolution of the ^1H NMR spectra (Figure 4b−e) also shows that, for both family of protons, the intensity is retained, whereas their chemical shifts converge. For each **B** enantiomer, the positions of H_6 and $H_{6'}$ traduce the homochiral/heterochiral composition of the equilibria in Equations (1) and (2), respectively (vide supra).

$$(\mathbf{B^{\Delta}},\mathbf{A^{\Delta}_2}) + 2\,[HNBu_3][\mathbf{A^{\Lambda}}] \rightleftharpoons (\mathbf{B^{\Delta}},\mathbf{A^{\Lambda}_2}) + 2\,[HNBu_3][\mathbf{A^{\Delta}}] \quad (1)$$

$$(\mathbf{B^{\Lambda}},\mathbf{A^{\Delta}_2}) + 2\,[HNBu_3][\mathbf{A^{\Lambda}}] \rightleftharpoons (\mathbf{B^{\Lambda}},\mathbf{A^{\Lambda}_2}) + 2\,[HNBu_3][\mathbf{A^{\Delta}}] \quad (2)$$

As shown in Scheme 2, the chemical shifts of H_6 and $H_{6'}$ vary linearly with the TRISPHAT enantiomeric excess. The validity of Equation (a) is enforced by the fact that the straight lines intercept the Y-axis at the same point (δ = 8.07) corresponding to the racemic mixture *rac* (**B**,$\mathbf{A_2}$), experimentally recorded at δ = 7.98 (Figure 4f). Of particular interest, the slopes of the straight lines are very different, showing a different evolution of the two equilibria in Equations (1) and (2) during the addition of *rac* **A** (and especially the isomer $\mathbf{A^{\Lambda}}$). Both equilibria are displaced to the right but the shift of the equilibrium in Equation (2) is about five times[16] more pronounced than that of the equilibrium in Equation (1), clearly showing that, under these experimental conditions,[17] the homochiral association is spontaneously preferred to the heterochiral one.

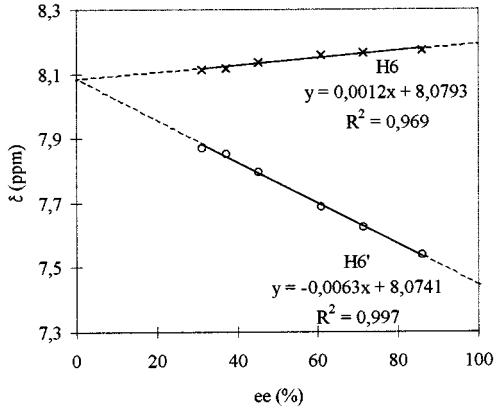

Scheme 2. H_6 and $H_{6'}$ chemical shift vs. TRISPHAT's *ee*

Extrapolation of the straight lines to *ee* = 100% allows the determination of the theoretical chemical shift for the pure homochiral (H_6, δ_{HOMO} = 8.19) and heterochiral ($H_{6'}$, δ_{HETERO} = 7.44) isomers. Thus, according to equation (a), the unique $H_6/H_{6'}$ signal of the racemic mixture (**B**,$\mathbf{A_2}$) at δ = 7.98 allows the determination of x = 0.72. This traduces for each $[Ru(DEAS\text{-}bpy)_3]^{2+}$ enantiomer, the rapid equilibrium between the 72% homochiral [($\mathbf{B^{\Lambda}}$,$\mathbf{A^{\Lambda}_2}$) or ($\mathbf{B^{\Delta}}$,$\mathbf{A^{\Delta}_2}$)] and 28% heterochiral [($\mathbf{B^{\Lambda}}$,$\mathbf{A^{\Delta}_2}$) and ($\mathbf{B^{\Delta}}$,$\mathbf{A^{\Lambda}_2}$)] diastereoisomers. In other words, the homochiral isomer is 0.56 kcal·mol^{-1} more stable than the heterochiral one at 298 K in CH_2Cl_2.

This result can also be used to explain the variable-temperature ^1H NMR experiment of *rac* (**B**,$\mathbf{A_2}$) in CD_2Cl_2 (Figure 3), where the ratio of homochiral/heterochiral diastereoisomers linearly increases with the lowering of the temperature leading toward the formation of the thermodynamically favored homochiral form.

Conclusion

As previously noticed, tris(bipyridyl) metal complexes (M = Fe, Ru) have already been associated with the TRISPHAT anion but only in its enantiopure form,[10−12] the same association with racemic TRISPHAT giving rise to insoluble salts.[11] In contrast, the use of functionalized DEAS-bpy, which leads to an enhanced solubility of the corresponding ruthenium salt, allows the study of the association with racemic TRISPHAT. The enantiopure TRISPHAT anion is known to form a diastereoselective, homochiral ion-pair with the labile tris(4,4′-dimethyl-[2,2′]-bipyridine) iron(II) dication.[11] In the present work, we show that the same homochiral association occurs between racemic TRISPHAT and the nonlabile propeller-like ruthenium complex. Moreover, this recognition is temperature dependant, leading to the almost pure homochiral associations ($\mathbf{B^{\Lambda}}$,$\mathbf{A^{\Lambda}_2}$) or ($\mathbf{B^{\Delta}}$,$\mathbf{A^{\Delta}_2}$) at 243 K. Such diastereoselective self-assembly has already been observed by Swager et al. for neutral, propeller-like metal complexes during the formation of columnar liquid crystals, the homochiral segregation being driven by the optimization of the packing.[3] In this paper, the self-assembly occurs in solution between charged propeller-like compounds. The driving force is thought to be the minimization of the electrostatic interactions, the anion/cation distance being shorter in the homochiral association (Figure 5).

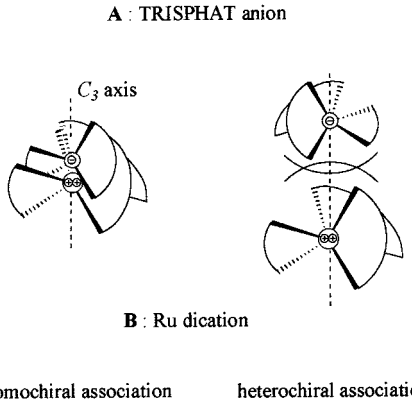

Figure 5. Schematic representation of both homochiral and heterochiral interactions

Finally, the assembly of octupolar anions and cations opens the way towards the design of supramolecular materials for nonlinear optics. Studies are now in progress to examine the NLO activity of such multi-octupolar compounds.

Experimental Section

General: All reactions were routinely performed under argon using Schlenk techniques. − NMR spectra (^{1}H, ^{13}C, ^{31}P) were recorded on a BRUKER DPX 200 (operating at 200.12 MHz for ^{1}H, 50.32 MHz for ^{13}C and 81.91 MHz for ^{31}P) or on a BRUKER AC 300 (operating at 300.13 MHz for ^{1}H) spectrometers. NMR spectroscopic data are listed in parts per million (ppm) and are reported relative to 85% H_3PO_4 (^{31}P) or to tetramethylsilane (^{1}H, ^{13}C), residual solvent peaks being used as internal standard (CD_2Cl_2: ^{1}H: δ = 5.25; ^{13}C: δ = 53.45). Complete attribution of the ^{1}H and ^{13}C spectra required 2D experiments [COSY, H−C correlation (hmqc and hmbc sequences)]. − UV/Vis spectra were recorded on a BIO-TEK/KONTRON UVIKON 941 spectrophotometer in dichloromethane solution. − High resolution mass spectrometry measurements (FAB) were performed by the Centre Regional de Mesures Physiques de l'Ouest (Rennes, France) and elemental analysis by the Service Central d'Analyse du CNRS (Solaize, France). Solvents are simply distilled prior to use. $[RuCl_2(DMSO)_4]$[18] and the ligand 4,4′-bis(diethylaminostyryl)-[2,2′]-bipyridine[19] were prepared using published methods. The complex (**B**,$[PF_6]_2$) has already been published[9] but its NMR spectroscopic data are completed for comparison.

Characterization of (B,$[PF_6]_2$): ^{1}H NMR (CD_2Cl_2, 298 K): δ = 8.32 (br. s, 6 H, H_3), 7.5 (d, ^1J = 6 Hz, 6 H, H_6), 7.44 (d, ^1J = 8 Hz, 12 H, H_{10}), 7.35 (d, ^1J = 16 Hz, 6 H, H_8), 7.31 (d, ^1J = 6 Hz, 6 H, H_5), 6.89 (d, ^1J = 16 Hz, 6 H, H_7), 6.6 (d, J = 8 Hz, 12H, H_{11}), 3.3 (br. m, 24 H, H_{12}), 1.1 (t, ^1J = 6.5 Hz, 36H, H_{13}). − ^{13}C NMR (CD_2Cl_2, 298 K): δ = 157.0 (C_2), 150.0 (C_6), 149.1 (C_{12}), 147.6 (C_4), 137.2 (C_8), 129.5 (C_{10}), 122.8 (C_5), 122.3 (C_9), 120.1 (C_3), 117.6 (C_7), 111.6 (C_{11}), 44.6 (C_{13}), 12.4 (C_{14}). − ^{31}P NMR (CD_2Cl_2, 298 K): δ = −144 (hept, J = 712 Hz). − UV/Vis (CH_2Cl_2): λ_{max} = 520 (150000), 446 nm (142000). − HRMS-FAB ($C_{102}H_{114}F_6N_{12}PRu$, {[B][$PF_6$]}$^+$): calcd. 1753.8004; found1753.7971.

Preparation of (B,[TRISPHAT]$_2$): $[RuCl_2(DMSO)_4]$ (250 mg, 51.6 mmol, 1 equiv.) and 4,4′-bis(diethyl-aminostyryl)-2,2′-bipyridine (777 mg, 1.55 mmol, 3 equiv.) were dissolved in dimethylformamide (10 mL). The dark red solution was stirred overnight in refluxing DMF. After cooling to room temperature, [$HNBu_3$][TRISPHAT] (986 mg, 1.03 10^{-3} mol, 2 equiv.) was added. After stirring for 30 min. at room temperature, a dark red solid was precipitated out by addition of water (100 mL). The complex was filtered off and purified by column chromatography (silica gel, CH_2Cl_2). The solvent was removed under vacuum to afford a dark red microcrystalline powder (1.22 g, 67% yield). − ^{1}H NMR (CD_2Cl_2, 298 K): δ = 8.29 (br. s, 6 H, H_3), 7.98 (d, ^1J = 6 Hz, 6 H, H_6), 7.3 (d, ^1J = 8 Hz, 12 H, H_{10}), 7.1 (d, ^1J = 16 Hz, 6 H, H_8), 7.09 (d, ^1J = 6 Hz, 6 H, H_5), 6.62 (d, ^1J = 16 Hz, 6 H, H_7), 6.6 (d, ^1J = 8 Hz, 12 H, H_{11}), 3.3 (br. m, 24 H, H_{12}), 1.1 (t, ^1J = 6.5 Hz, 36 H, H_{13}). − ^{13}C NMR (CD_2Cl_2, 298 K): δ = 156.9 (C_2), 151.0 (C_6), 149.0 (C_{12}), 147.0 (C_4), 136.3 (C_8), 129.4 (C_{10}), 122.5 (C_5), 122.2 (C_9), 119.9 (C_3), 117.3 (C_7), 111.4 (C_{11}), 44.5 (C_{13}), 12.4 (C_{14}), 141.6 (d, J = 6 Hz, TRISPHAT), 122.66 (TRISPHAT), 114.0 (d, J = 20 Hz, TRISPHAT). − ^{31}P NMR (CD_2Cl_2, 298 K): δ = −80.5 (s). − UV/Vis (CH_2Cl_2): λ_{max} = 520 (146000), 447 nm (143000). − HRMS-FA) ($C_{120}H_{114}Cl_{12}N_{12}O_6PRu$, {**B**,[TRISPHAT]}$^+$): calcd. 2377.3995; found 2377.3927. − $C_{138}H_{114}Cl_{24}N_{12}O_{12}P_2Ru$: calcd. C 52.68, H 3.65, N 5.34; found C 51.97, H 3.64, N 5.15.

Reaction Between (B,A_2) (A^A, *ee* = 86%) and *rac* ([$HNBu_3$],[A]): In an NMR tube, (**B**,A_2) (A^A, *ee* = 86%) (40 mg, 1.3 × 10^{-5} mol) was dissolved in CD_2Cl_2 (1 mL). *Rac* ([$HNBu_3$],[**A**]) was added in small fractions directly weighed in the NMR tube. After each addition an NMR spectrum was recorded. The experiment was conducted until a precipitate appeared. The resulting NMR spectra are shown in Figure 4.

Acknowledgments

The authors thank Dr. A. Bondon for fruitful discussions.

[1] J. M. Lehn, *Supramolecular Chemistry: Concepts and Perspectives. 1st ed.* VCH. Weinheim, **1995**, Chapter 9.
[2] R. Kuroda, *Inorg. Chem.* **1991**, *30*, 4954−4959 and references cited therein.
[3] S. T. Trzaska, H. F. Hsu, T. M. Swager, *J. Am. Chem. Soc.* **1999**, *121*, 4518−4519. Such a resolution phenomenon has already been observed with disc-shape molecules, see: A. R. A. Palmans, J. A. J. M. Vekemans, E. E. Havinga, E. W. Meijer, *Angew. Chem. Int. Ed. Engl.* **1997**, *36*, 2649−2651.
[4] R. Andrés, M. Gruselle, B. Malézieux, M. Verdager, J. Vaissermann, *Inorg. Chem*. **1999**, *38*, 4637−4646.
[5] [5a] J. Breu, N. Raj, C. R. A. Catlow, *J. Chem. Soc., Dalton Trans.* **1999**, 835−845.[5b] J. Breu, C. R. A. Catlow, *Inorg. Chem*. **1995**, *34*, 4504−4510.[5c] H. Sato, A. Yamagishi, S. Kato, *J. Am. Chem. Soc*. **1992**, *114*, 10933−10940.
[6] [6a] I. Ledoux, J. Zyss, *Chem. Rev.* **1994**, *94*, 77−105.[6b] O. Riant, G. Bluet, S. Brasselet, N. Druze, I. Ledoux, F. Lefloch, A. Skiebniewsky, J. Zyss, *Mol. Cryst. Liq. Cryst.* **1998**, *322*, 35−42.
[7] H. Le Bozec, T. Renouard, *Eur. J. Inorg. Chem.* **2000**, 229−239.
[8] C. Dhenaut, I. Ledoux, I. D. W. Samuel, J. Zyss, M. Bourgault, H. Le Bozec, *Nature* **1995**, *374*, 339−342.
[9] F. W. Vance, J. T. Hupp, *J. Am. Chem. Soc.* **1999**, *121*, 4047−4053.
[10] [10a] J. Lacour, C. Ginglinger, F. Favarger, S. Torche-Haldimann, *Chem. Commun.* **1997**, 2285−2286.[10b] C. Ginglinger, D. Jeannerat, J. Lacour, S. Jugé, J. Uziel, *Tetrahedron Lett*. **1998**, *39*, 7495−7498.
[11] J. Lacour, J. J. Jodry, C. Ginglinger, S. Torche-Haldimann, *Angew. Chem. Int. Ed.* **1998**, *37*, 2379−2380.
[12] J. Lacour, S. Torche-Haldimann, J. J. Jodry, C. Ginglinger, F. Favarger, *Chem. Commun.* **1998**, 1733−1734.
[13] In the case of $[Ru(bpy)_3]^{2+}$ complex see: W. W. Brant, F. P. Dwyer, E. C. Gyarfas, *Chem. Rev.* **1954**, *54*, 959. In the case of the TRISPHAT anion, no racemisation is observed below 60 °C.
[14] [14a] J. Lacour, C. Ginglinger, C. Grivet, G. Bernardinelli, *Angew. Chem. Int. Ed.* **1997**, *36*, 608−610.[14b] J. Lacour, C. Ginglinger, F. Faverger, *Tetrahedron Lett.* **1998**, *39*, 4825−4828.
[15] The chiral shift-reagent ability of the TRISPHAT anion is confirmed by the downfield shift of the H_6 proton which is more pronounced for the homochiral association (H_6) than for the heterochiral ($H_{6'}$) one. Since H_6 and $H_{6'}$ are the most sensitive protons in term of chemical shift, they are used as NMR probes for this study.
[16] In Scheme 2, the ratio of the slope is equal to 5.25.
[17] All the experiments were carried out in dichloromethane. The influence of the solvent polarity was not studied.
[18] I. P. Evans, A. Spencer, G. Wilkinson, *J. Chem. Soc., Dalton Trans.* **1973**, 204−209.
[19] A. Juris, S. Campagna, I. Bidd, J.-M. Lehn, R. Ziessel, *Inorg. Chem.* **1988**, *27*, 4007−4011.

Received April 4, 2000
[I00134]

Copper Complexes as Functional Models for Dopamine β-Hydroxylase – Mechanistic Study of Oxygen Atom Transfer from Cu/O Species to Benzylic C−H Bonds[‡]

Ingrid Blain,[a] Michel Giorgi,[a] Innocenzo De Riggi,[b] and Marius Réglier*[a]

Keywords: Copper / Enzymes / Radicals / RPY2 ligand / Oxygen atom transfer / O-O activation

The mechanism of the oxygen atom transfer reaction mediated by copper-oxygen species has been studied through a substrate-binding ligand approach. Oxidations of copper 5-X-IndPY2 type complexes in which an electron donating (X = OMe) or withdrawing group (X = CN) substitutes the aromatic nucleus in position 5, lead to compounds **2b,c** and **3b,c** resulting from benzylic hydroxylations. With these complexes, where one of the benzylic positions is influenced by a *para* substituent (leading to **2b,c**) while the other suffers influence from the *meta* group (leading to **3b,c**), we observe that the ratio **2**:**3** > 1 is in favor of a certain electrophilicity of the copper/oxygen species responsible for the hydroxylations. While a concerted mechanism cannot be excluded, the results are in favor of a two-step mechanism involving radical species.

Introduction

The mechanism of O_2 activation by copper-containing mono-oxygenases such as dopamine β-hydroxylase (DBH; benzylic hydroxylation of dopamine into noradrenaline) is of current interest.[1] Given that this enzymatic process involves the formation of highly reactive Cu/O radical species, which are responsible for hydrogen atom abstraction from the substrate, the Cu/O_2 chemistry has been the subject of recent investigations and considerable progress in the understanding of structural and spectroscopic aspects was made through biomimetic studies using copper complexes as active site models.[2,3] Recently, using the substrate-binding ligand approach,[4] Itoh and co-workers have described the first benzylic hydroxylation at the β-position of a tertiary amino group similarly to that of DBH.[5] This approach involved the study of copper complexes derived from RPY2-type ligands, in which a phenethylamine "substrate" is covalently bound to the tertiary amino group of the ligand, favoring conditions for an intramolecular oxygen atom transfer. An important feature of Itoh's hydroxylation is that not only does it occur during the reaction of the [PhenPY2]Cu^{I} complex with O_2 (condition I) but also under conditions close to the enzymatic reaction where the [PhenPY2]Cu^{II} complex is reduced first by benzoin before the reaction with O_2 (condition II). A detailed study of intermediates formed under condition I showed that upon reaction with O_2 the first step is the formation of the side-on $[L_2Cu_2(\mu\text{-}\eta^2\text{:}\eta^2\text{-}O_2)]^{2+}$ species.[6] A detailed kinetic study including solvent, *p*-substituent and the kinetic deuterium isotope effects suggested the rate-determining step of the benzylic hydroxylation of the ligand to be the O−O bond homolysis of the μ-η^2:η^2-peroxodicopper(II) intermediate to give a bis(μ-oxo)dicopper species $[Cu_2^{III}(\mu\text{-}O)_2]^{2+}$ (Scheme 1: **A** → **B**).[7]

In order to get more information on the Oxygen Atom Transfer to the Ligand (OATL) involved in these reactions (Scheme 1: **B** → **C**), we studied the reaction of copper complexes derived from a RPY2 ligand in which a 2-aminoindane "substrate" is used.[8] Due to a five-membered ring structure fused to an aromatic nucleus, 2-aminoindane is a very promising substrate for studying the stereochemistry of the transfer of an oxygen atom. Indeed, 2-aminoindane possesses two benzylic stereogenic centers, each bearing two hydrogen atoms and the stereochemistry of aminoindanols obtained after hydroxylation (*cis* vs. *trans*) can be regarded as an indicator for the stereoselectivity of the oxygen atom transfer.[9] On the other hand, the two equivalent benzylic positions in 2-aminoindane can be differentiated by benzylic mono substitution with a deuterium atom (Scheme 2: **1a**). In this way, the process involving an insertion into a C−H bond competes with a process involving an insertion into a C−D bond. The ratio of compounds **2**:**3** (Scheme 2) resulting from these two processes is related to the deuterium kinetic isotope effect (DKIE) of the reaction.

[‡] Aminoindanes in Oxygen Transfer Reactions, 3. − Part 2: ref.[8]; part 1: ref.[9]

[a] Chimie, Biologie et Radicaux Libres, UMR-CNRS 6517, Universités d'Aix-Marseille 1 et 3, Faculté des Sciences et Techniques de Saint Jérôme, case 432, av. Escadrille Normandie-Niemen, 13397 Marseille Cedex 20, France
Fax: (internat.) +33-4/9198-3208
E-mail: marius.reglier@lbs.u-3mrs.fr
[b] Synthèse, Catalyse et Chiralité, UMR-CNRS 6516, Université d'Aix-Marseille 3, Faculté des Sciences et Techniques de Saint Jérôme, ENSSPICAM, av. Escadrille Normandie-Niemen, 13397 Marseille Cedex 20, France

 © WILEY-VCH Verlag GmbH, 69451 Weinheim, 2001 1434−1948/01/0101−0205 $ 17.50+.50/0

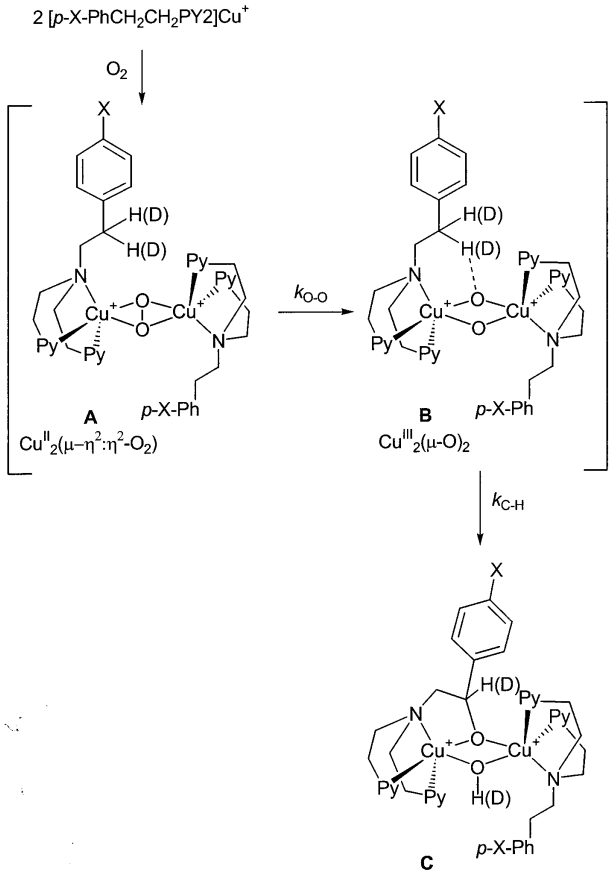

Scheme 1. Substrate-binding ligand approach

With copper complexes derived from ligand **1a** (Table 1, runs 1−2), we demonstrated that the oxygen atom transfer occurs with retention of configuration and we determined a DKIE of 11 and 7.6 for conditions I and II, respectively. In order to study the substituent effect on the oxygen atom transfer reaction and using the same strategy, we describe now the elaboration of new ligands **1b,c** in which an electron donating (OMe) or withdrawing group (CN) substitutes the aromatic nucleus in position 5. With these ligands, where one of the benzylic positions is influenced by a *para* substituent while the other suffers influence from the *meta* group, the oxygen atom transfer should be influenced by various electronic factors and the ratio of compounds **2**:**3** resulting from this transformation should give information on the k_{para}/k_{meta} ratio as well as the mechanism of the OATL process.

Results and Discussion

The ligands 5-X-IndPY2 **(1b,c)** and 7-X-TetralPY2 **(1d,e)** were synthesized by Michael addition of the corresponding primary amines to freshly distilled 2-vinyl pyridine in a methanol/acetic acid mixture. The copper(I) complexes [5-X-IndPY2]$CuPF_6$ and [7-X-TetralPY2]$CuPF_6$ were prepared by reaction of $[CH_3CN]_4CuPF_6$ and the corresponding ligands in dichloromethane. The corresponding copper(II) complexes [5-X-IndPY2]$Cu(CF_3SO_3)_2$ and [7-X-TetralPY2]$Cu(CF_3SO_3)_2$ were obtained in nearly quantitative yields by complexation of the ligands with $Cu(CF_3SO_3)_2$ in methanol. Recrystallization from dichloromethane using the diethyl ether vapor diffusion technique afforded blue crystals of [7-OMe-TetralPY2]$Cu(CF_3SO_3)_2$ which were suitable for X-ray diffraction analysis (Table 2, Figure 1).

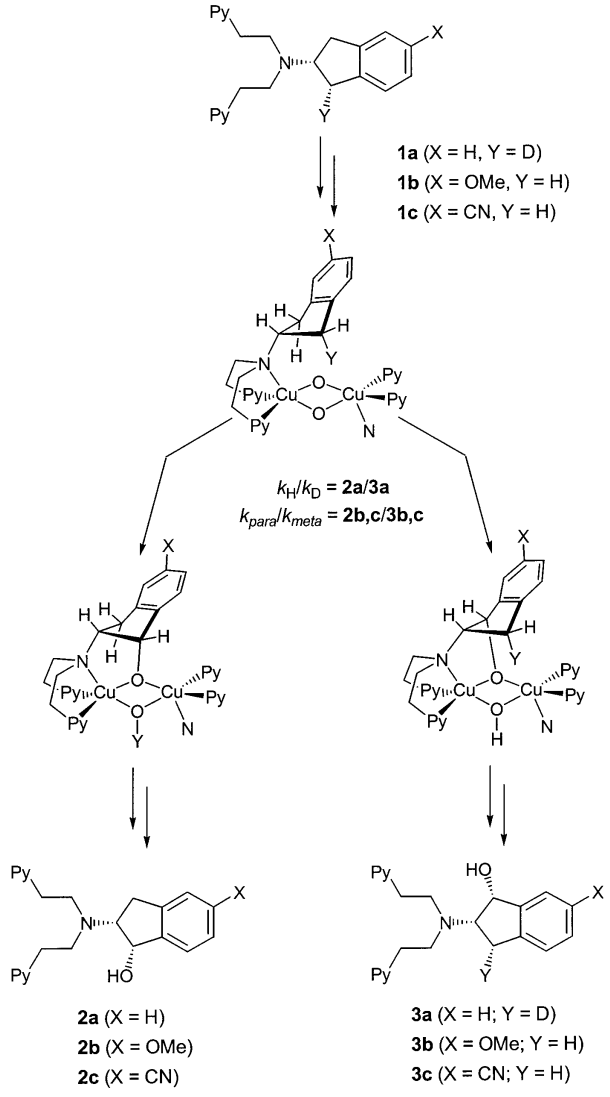

Scheme 2. 2-Aminoindane in substrate-binding ligand approach

The oxidation of copper complexes derived from 5-X-IndPY2 ligands **1b,c** was performed in dichloromethane under conditions I and II. After demetallation of the resulting copper(II) complexes with 35% aqueous ammonia the oxidation products were analyzed by NMR spectroscopy. Under condition I, the oxidation led to a 1:1 mixture of the recovered ligands **1b,c** and the two hydroxylated ligands **2b,c** and **3b,c** (Table 1, runs 3 and 5). Under condition II, these two compounds **2b,c** and **3b,c** were also obtained but in quantitative yields (Table 1, runs 4 and 6). Because it was impossible to separate them by chromatography, their structure and the ratios were determined by NMR spectroscopic analysis of the mixture. To achieve this, the first task was the complete assignment of all protons and carbons by

Table 1. Oxidation of copper complexes derived from ligands 5-X-IndPY2 (**1b,c**) and 7-X-TetralPY2 (**1d,e**)

Runs	Ligands	Conditions[a]	Product distributions	**2:3**
1	*cis*-d-IndPY2 (**1a**)	I	**1a** (51%) + **2a** (45%) +**3a** (4%)	11.0
2		II	**2a** (88%) +**3a** (12%)	7.6
3	5-MeO-IndPY2 (**1b**)	I	**1b** (57%) + **2b** (33%) + **3b** (10%)	3.3
4		II	**2b** (81%) + **3b** (19%)	4.3
5	5-CN-IndPY2 (**1c**)	I	**1c** (58%) + **2c** (25%) + **3c** (17%)	1.5
6		II	**2c** (70%) + **3c** (30%)	2.3
7	TetralPY2 (**1d**)	I	**1d** (75%) + **3d** (25%)	–
8		II	**3d** (100%)	–
9	7-MeO-TetralPY2 (**1e**)	I	**1e** (75%) + **3e** (25%)	–
10		II	**3e** (100%)	–

[a] Condition I: 2 mM solution of copper(I) complex in dichloromethane placed under dioxygen atmosphere for one day. Condition II: 1.6 mM solution of copper(II) complex in dichloromethane reduced by benzoin (2 equiv.) in the presence of NEt_3 (2 equiv.) for two hours under argon, then placed under dioxygen atmosphere for one day.

Table 2. Crystallographic data for [7-MeO-TetralPY2]Cu$(CF_3SO_3)_2$

Crystal data	
Formula	$C_{27}H_{29}CuF_6N_3O_7S_2$
M_r	749.21
Crystal system	Monoclinic
Space group	$P2_1/c$
a [Å]	9.93(3)
b [Å]	12.80(4)
c [Å]	27.59(3)
β [°]	90.162(2)
V [Å^3]	3508(2)
$D_{calcd.}$ [g cm^{-3}]	1.42
Z	4
F(000) [e]	1532
μ (Mo-K_α) [cm^{-1}]	8.1
T [K]	298
Scan mode	ω/2θ
Scan width [°]	2.7 + 0.4 tanθ
$2\theta_{max}$ [°]	48.04
Measured refl.	6880
Unique refl.	6151
Refl. used for ref.	2212
Absorption correction	none
Ref. parameters	331
H atoms	included not refined
R[a]	0.088
R_w	0.163
w	unit
$(shift/e.s.d.)_{max}$	1.04
Goodness of fit	5.198
$\Delta\rho_{fin}$(max/min) [eÅ^{-3}]	0.84/-0.69

[a] We could not obtain a very good R value during the structure refinement because the diffracted intensities (high mosaicity and anisotropic shape of the samples) and the resolution (few intensities could be measured until 2θ = 48°) were low. As the absorption corrections did not give better results, we did not use them in the last refinement cycles.

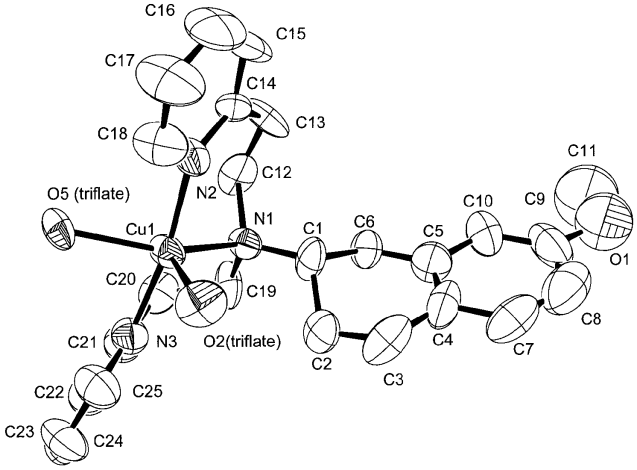

Figure 1. ORTEP representation of [7-MeO-TetralPY2]-Cu$(CF_3SO_3)_2$ at the 30% probability level; selected bond lengths in Å: Cu1−O2 2.23(2), Cu1−O5 2.15(5), Cu1−N1 2.08(3), Cu1−N2 2.05(2), Cu1−N3 1.98(2); selected bond angles in °: O2−Cu1−O5 97.6(12), O2−Cu1−N1 113.6(8), O2−Cu1−N2 85.3(8), O2−Cu1−N3 94.8(10), O5−Cu1−N1 148.7(13), O5−Cu1−N2 85.7(13), O5−Cu1−N3 85.0(13), N1−Cu1−N2 94.4(7), N1−Cu1−N3 94.2(9), N2−Cu1−N3 170.6(8)

homo- and heteronuclear correlation experiments (COSY gradient, HMQC and HMBC). Then two dimensional NOESY sequences revealing several interesting Nuclear Overhauser Effects (NOE) allowed us to attribute the fine structure of compounds **2b,c** and **3b,c** (Scheme 3). First of all, an NOE between protons H_1 and H_2 allowed the assignment of the *cis* stereochemistry of the 1,2-amino alcohol. In order to attribute the structure of the major compound, we first localized on the ^{1}H NMR spectra protons in the *ortho* position of the X substituent (numbered H_4 for **2b,c** and H_7 for **3b,c**). In both cases these protons show an NOE with the two benzylic protons H_3 for the major isomers, while the minor isomers show an NOE with proton H_1. These results indicate unambiguously that the major isomers correspond to the *para*-hydroxy compounds **2b,c**, and the minor isomer to the *meta*-hydroxy compounds **3b,c**. Integration of protons corresponding to **2b,c** and **3b,c** gave the *para*/*meta* ratios reported in Table 1.

In compounds **1b,c**, whatever the nature of the substituent (OMe vs. CN) and under reaction conditions I or II, hydroxylation preferentially occurs in the *para* position. The effects are more important for the electron donating OMe group (**2b**/**3b** = 3.3 and 4.3) than for the electron-withdrawing CN (**2c**/**3c** = 1.5 and 2.3). This is in favor of a certain electrophilicity of the copper/oxygen species responsible for the hydroxylations. In one of our previous studies, the higher DKIE observed under condition I compared to that of condition II (11 vs. 7.6) was rationalized as the occurrence of two different copper-oxygen intermediates.[10] Though being low, the differences observed in the **2**:**3** ratios confirm once again this former interpretation. Under condition I, the occurrence of a bis(μ-oxo)dicopper

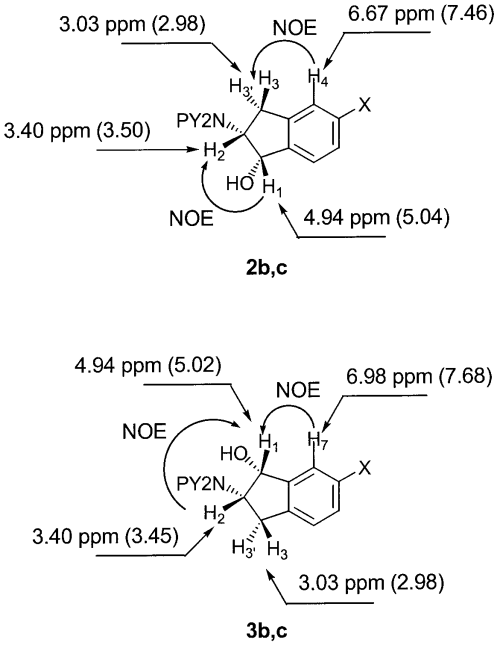

Scheme 3. Some Nuclear Overhauser Effects observed with compounds **2b,c** and **3b,c**. Chemical shifts are reported for X = MeO and in parenthesis for X = CN

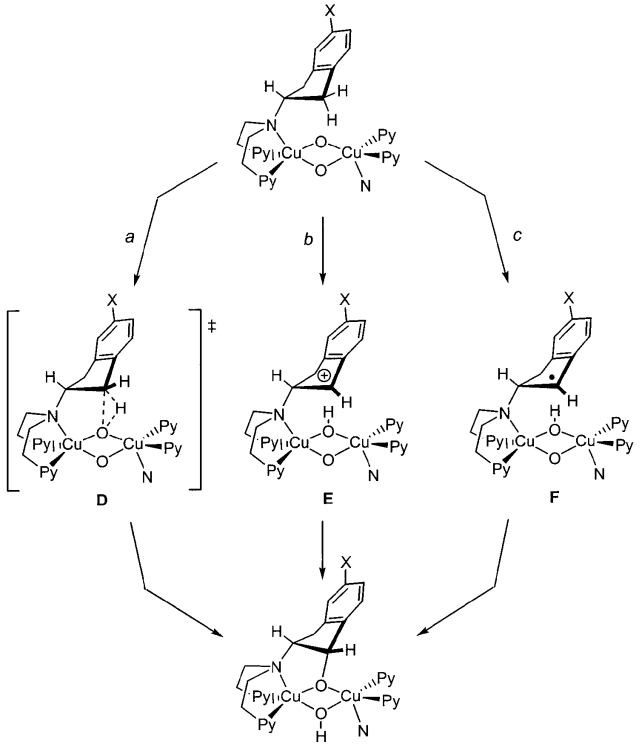

Scheme 4. Possible mechanisms for the oxygen atom transfer

species $[Cu_2^{III}(\mu\text{-}O)_2]^{2+}$ is now well accepted as the principal active species in oxygen atom transfer. But in the presence of benzoin (condition II), the structure of the active copper/oxygen species is less clear and several structures can be proposed. Among them, species involving the mixed valence $[Cu^{II}Cu^{III}(\mu\text{-}O)_2]^{2+}$ intermediates or the oxygen radical species $[Cu^{II}-O^{\bullet}]^{+}$ ($\equiv [Cu^{III}-O^{-}]^{+}$) are very attractive.[10] Possible pathways consistent with these structures and an intramolecular oxygen atom insertion into the benzylic C−H bond are presented in Scheme 4. The high **2**:**3** ratios observed with 5-OMe-IndPY2 ligand (Table 1, runs 3 and 4) could be in favor of a hydride abstraction (Scheme 4, pathway *b*) and a carbocation intermediate **E**. Although these values indicate transition-state stabilization by an electron donating group, they are small compared with values normally observed in reactions involving benzylic carbocation intermediates. Moreover, with the 5-CN-IndPY2 ligand, we would expect a more marked effect in favor of the *meta* product **3c**. Indeed, according to the Hammet equation $\log(k/k_0) = \sigma\rho$,[11] values of $\log(k_{para}/k_{meta})$ can be estimated by the expression $\rho(\sigma_p-\sigma_m)$. Considering that for reactions involving benzylic carbocation intermediates, the ρ value is less than −2, we would expect a k_{para}/k_{meta} ratio of 6 and 0.6 for MeO and CN groups, respectively.[12] These results, which seem to be unfavorable to the intermediacy of **E**, could be in favor of a concerted mechanism (Scheme 4: pathway *a*) where a positive minimal charge development in the transition state may be envisaged. However, initial radical formation (Scheme 4: pathway *c*) by a hydrogen atom abstraction by the Cu−O core seems to be more reasonable, since Mayer has recently shown that metal-oxo complexes can oxidize hydrocarbons by a hydrogen-atom abstraction mechanism which is attributed to their thermodynamic affinity for a hydrogen atom ($\equiv H^+ + e^-$).[13] This proposal is all the more reasonable as similar values of the k_{para}/k_{meta} ratio are often seen in radical-generating systems. Indeed, for benzylic H abstraction of *p*- or *m*-substituted toluenes by *t*BuOO$^{\bullet}$ (*t*BuO$^{\bullet}$) radical the ratios k_{para}/k_{meta} were found to be 3.14[14] and 1.3[14] (1.0[15]) for OMe and CN groups, respectively.[16]

All of our results and those described in the literature, concern hydroxylation occurring in the β position of a tertiary amino group of the ligand. In order to study the factors that govern the oxygen atom transfer, we decided to examine the hydroxylation of ligands derived from 2-aminotetralin compounds. Like 2-aminoindane, 2-aminotetralin possesses two benzylic carbons but one is in the β position while the second is in the γ position with respect to the amino group. Moreover, the γ position can be activated by a OMe substituent in position 7 of the aromatic ring and it would be interesting to know whether this activation would be enough for directing the hydroxylation towards this benzylic position. Under both oxidation conditions, hydroxylation takes place at the β benzylic carbon even when an OMe substituent is present in position 7 of the aromatic ring (Table 1, runs 7−10). This is evident from the ^{1}H NMR spectrum, which shows a doublet at δ = 4.65 (**3d**) and 4.60 (**3e**) with coupling constants ^3J = 3.4 Hz characteristic for a *cis* stereochemistry.[17] Our results demonstrate that the six-membered transition state is more favorable than the seven-membered one even when an OMe

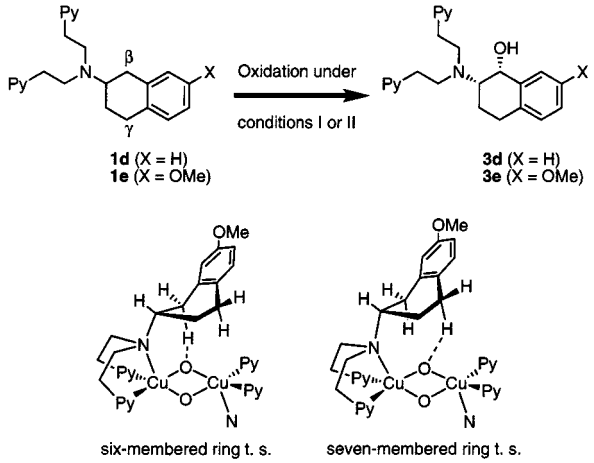

Scheme 5. 7-X-TetralPY2 ligands **1d,e** in oxygen atom transfer reaction

substituent activates the γ benzylic position (Scheme 5). It might be hazardous to consider the Cu−O core as an oxygen centered radical, however, we can see here a similarity to Barton's reaction where an intramolecular δ C−H bond activation by an alkoxy radical takes place.[18]

Conclusion

Several examples of OATL are described in the literature demonstrating that the substrate binding ligand approach gives valuable information about the active species involved in the copper−dioxygen activation. However, two problems remain. The first one concerns the mechanism of the oxygen atom transfer. The question is to determine whether the oxygen atom transfer occurs in a concerted pathway or in a two step process involving radical intermediates. For the moment, it is difficult to answer this fundamental question. More experiments are needed, notably using a radical clock fixed on the tertiary amino group of the ligand. The second problem concerns the catalytic aspect of the oxygen atom transfer. Few examples of oxygen atom transfer from a copper center to an exogenous substrate are known.[19,20] To achieve this, the substrate association in the copper coordination sphere still remains to be solved.[21] We think this will be an exciting challenge for the organic chemist.

Experimental Section

General: Solvents were freshly distilled under Ar (MeOH/Mg, Et_2O/Na-benzophenone ketyl, CH_3CN/CaH_2 and CH_2Cl_2/P_2O_5). Deoxygenation of solvents and solutions was carried out by 3 vacuum/purge cycles. Preparations and handling of air sensitive compounds were carried out using standard Schlenk techniques. Commercial starting materials were used without further purification, except for 2-vinylpyridine, which was distilled prior to use. 2-Amino-5-methoxyindane was prepared in two steps from 5-methoxy-1-indanone by a procedure described in the literature.[22] 2-Amino-5-cyanoindane was prepared in six steps from 5-bromo-1-indanone.[23] 2-Aminotetralin and 2-amino-7-methoxytetralin were obtained by reductive amination of the corresponding 2-tetralones.[24] NMR spectra were recorded at 25 °C on Bruker AC-200 or AMX-400 spectrometers. Chemical shifts are reported in ppm as δ values downfield from an internal standard of TMS. Homo- and heteronuclear correlations were obtained by COSY gradient, HMQC and HMBC techniques with a 5 mm reverse probehead using a *z* field gradient. 2D-NOESY experiments were performed with a 5 mm $^1H/^{13}C$ DUAL probehead.

Ligands 1b−e: To absolute MeOH were added 2-vinylpyridine, primary amine and acetic acid. After refluxing for several days, MeOH was evaporated and 15% NaOH was added. The product was extracted with CH_2Cl_2 and the organic layer dried over Na_2SO_4. Evaporation of CH_2Cl_2 under reduced pressure (18 Torr) left the crude product. Flash chromatography (SiO_2, CH_2Cl_2/MeOH 95:5) afforded the pure ligands (Table 3).

1b: ^1H NMR (200 MHz, $CDCl_3$): δ = 2.65−2.85 (m, 2 H), 2.90−3.10 (m, 10 H), 3.65−3.80 (m, 1 H), 3.75 (s, 3 H), 6.60−6.75 (m, 2 H), 7.00−7.20 (m, 5 H), 7.55 (td, *J* = 7.5 and 1.7 Hz, 2 H), 8.50 (ddd, *J* = 4.8, 1.7 and 1 Hz, 2 H). − ^{13}C NMR (50.3 MHz, $CDCl_3$): δ = 36.1 (CH_2-ind), 36.2 (2 CH_2), 37.3 (CH_2-ind), 51.5 (2 CH_2), 55.4 (CH_3O), 63.6 (CHN), 110.0 (CH-aryl), 112.2 (CH-aryl), 121.1 (2 CH-pyr), 123.4 (2 CH-pyr), 125.0 (CH-aryl), 133.8 (C-aryl), 136.2 (2 CH-pyr), 143.2 (C-aryl), 149.3 (2 CH-pyr), 158.7 (C-aryl), 160.7 (2 C-pyr).

1c: ^1H NMR (200 MHz, $CDCl_3$): δ = 2.70−3.10 (m, 12 H), 3.75 (m, 1 H), 7.20 (d, *J* = 8.2 Hz, 1 H), 7.30−7.40 (m, 6 H), 7.55 (td, *J* = 7.5 and 1.7 Hz, 2 H), 8.50 (ddd, *J* = 5.5, 1.7 and 1 Hz, 2 H). − ^{13}C NMR (50.3 MHz, $CDCl_3$): δ = 35.8 (2 CH_2), 36.4 (CH_2-ind), 40.0 (CH_2-ind), 51.2 (2 CH_2), 62.7 (CHN), 109.9 (C-aryl), 119.4 (CN), 121.2 (2 CH-pyr), 123.4 (2 CH-pyr), 125.2 (CH-aryl), 127.9 (CH-aryl), 130.5 (CH-aryl), 136.3 (2 CH-pyr), 143.0 (C-aryl), 147.6 (C-aryl), 149.2 (2 CH-pyr), 160.2 (2 C-pyr).

1d: ^1H NMR (200 MHz, $CDCl_3$): δ = 1.50−1.70 (m, 1H), 2.00−1.85 (m, 1H), 2.95−3.05 (m, 13 H), 6.96−7.10 (m, 8H), 7.54 (td, *J* = 7.5 and 1.7 Hz, 2 H), 8.51 (ddd, *J* = 4, 1.7 and 1 Hz, 2 H). − ^{13}C NMR (50.3 MHz, $CDCl_3$): δ = 25.0 (CH_2-tetral), 29.7 (CH_2-tetral), 32.3 (CH_2-tetral), 38.0 (2 CH_2), 50.9 (2 CH_2), 56.9 (CHN), 121.1 (2 CH-pyr), 123.6 (2 CH-pyr), 125.5 (CH-aryl), 125.6 (CH-aryl), 128.5 (CH-aryl), 129.4 (CH-aryl), 136.1 (2 CH-pyr), 136.3 (2 C-aryl), 149.1 (2 CH-pyr), 160.7 (2 C-pyr).

1e: ^1H NMR (200 MHz $CDCl_3$): δ = 1.55 (qd, *J* = 11.7 and 6.5 Hz, 1 H), 1.85−2.00 (m, 1 H), 2.65−2.76 (m, 4 H), 2.90−3.07 (m, 9 H), 3.72 (s, CH_3O), 6.53 (d, *J* = 2.7 Hz, 1 H), 6.62 (dd, *J* = 8.2 and 2.7 Hz, 1 H), 6.92 (d, *J* = 8.2 Hz, 1 H), 7.03−7.12 (m, 4 H), 7.52 (td, *J* = 7.6 and 1.7 Hz, 2 H), 8.48 (ddd, *J* = 5.8, 1.7 and 1 Hz, 2 H). − ^{13}C NMR (50.3 MHz, $CDCl_3$): δ = 26.0 (CH_2-tetral), 28.9 (CH_2-tetral), 32.5 (CH_2-tetral), 38.0 (2 CH_2), 50.9 (2 CH_2), 55.2 (CH_3O), 57.0 (CHN), 112.0 (CH-aryl), 113.9 (CH-aryl), 121.1 (2 CH-pyr), 123.6 (2 CH-pyr), 128.4 (C-aryl), 129.4 (CH-aryl), 136.1 (2 CH-pyr), 137.4 (C-aryl), 149.2 (2 CH-pyr), 157.4 (C-aryl), 160.6 (2 C-pyr).

Copper(II) Complexes: To a solution of $Cu(CF_3SO_3)_2$ in MeOH was added dropwise a solution of the ligand in MeOH. This mixture was then stirred for 30 min. MeOH was evaporated in vacuo and Et_2O was added. The precipitate was filtered off, washed with Et_2O and dried in vacuo to give the copper(II) complexes as blue solids (Table 4).

General Procedure for the Oxidation of Copper(I) Complexes by O_2 (Condition I): To a solution of $[CH_3CN]_4CuPF_6$ (100 μmol) in degassed CH_2Cl_2 (50 mL) was added dropwise a solution of ligand **1b−e** (100 μmol) in CH_2Cl_2 (50 mL). The mixture was allowed to stir under Ar for 1 h, and then exposed to O_2 atmosphere for 24

Table 3. Preparation of ligands **1b−e**

Ligands	**1b**	**1c**	**1d**	**1e**
Primary amines	2-amino-5-MeO-indane 540 mg (3.3 mmol)	2-amino-5-CN-indane 126 mg (0.8 mmol)	2-aminotetralin 438 mg (3 mmol)	2-amino-7-MeO-tetralin 332 mg (1.9 mmol)
Vinylpyridine	3.5 mL (33 mmol)	1.7 mL (15.7 mmol)	6.5 mL (60 mmol)	4.1 mL (38 mmL)
MeOH	8 mL	2 mL	16 mL	8 mL
AcOH	0.75 mL	0.36 mL	1.37 mL	4.1 mL
Yields	374 mg (1 mmol, 30%).	156 mg (0.42 mmol, 53%)	226 mg (0.63 mmol, 21%)	220 mg (0.57 mmol, 30%)

Table 4. Preparation of copper(II) complexes [RPY2]Cu(CF_3SO_3)$_2$

Copper(II) complexes	[5-MeOIndPY2] Cu(CF_3SO_3)$_2$	[5-CNIndPY2] Cu(CF_3SO_3)$_2$	[TetralPY2] Cu(CF_3SO_3)$_2$	[7-MeOTetralPY2] Cu(CF_3SO_3)$_2$
Ligands	**1b** (400 mg, 1 mmol)	**1c** (370 mg, 1 mmol)	**1d** (360 mg, 1 mmol)	**1e** (390 mg, 1 mmol)
Cu(CF_3SO_3)$_2$	350 mg (0.97 mmol)	350 mg (0.97 mmol)	350 mg (0.97 mmol)	350 mg (0.97 mmol)
MeOH	15 mL	15 mL	15 mL	15 mL
Yields	700 mg (952 µmol, 95%)	680 mg (931 µmol, 93%)	690 mg (959 µmol, 96%)	710 mg (947 µmol, 95%)
Analysis	$C_{26}H_{27}N_3CuS_2O_7F_6$ (735.17) calcd. C 42.48, H 3.70, N 5.72 found C 42.58, H, 3.62, N 5.81	$C_{26}H_{24}N_4CuS_2O_6F_6$ (730.16) calcd. C 42.77, H 3.31, N 7.67 found C 42.82, H 3.35, N 7.72	$C_{26}H_{27}N_3CuS_2O_6F_6$ (719.17) calcd. C 43.42, H 3.78, N 5.84 found C 43.38, H 3.72, N 5.93	$C_{27}H_{29}N_3CuS_2O_7F_6$ (749.20) calcd. C 43.29, H 3.90, N 5.61 found C 43.38, H 3.72, N 5.55

h. Then, CH_2Cl_2 was evaporated in vacuo and Et_2O was added and the precipitate obtained was centrifuged, washed with Et_2O and dried in vacuo to give a mixture of copper(II) complexes. This mixture was dissolved in CH_2Cl_2 (20 mL), washed with 35% NH_4OH (5 mL), brine (3 × 5 mL) and dried over Na_2SO_4. Evaporation of CH_2Cl_2 under reduced pressure (18 Torr) gave the crude product. Flash chromatography (SiO_2, CH_2Cl_2/MeOH 90:10) afforded the recovered ligands **1b−e** and a mixture of compounds **2b,c** and **3b,c** (**3d,e**).

General Procedure for the Oxidation of Copper(II) Complexes by O_2 in the Presence of Benzoin (Condition II): To a solution of copper(II) complex (100 µmol) in degassed CH_2Cl_2 (6 mL) were added benzoin (200 µmol) and NEt_3 (200 µmol). This mixture was stirred under Ar for 2 h and then exposed to O_2 atmosphere for 24 h. CH_2Cl_2 was evaporated in vacuo and Et_2O was added. The precipitate obtained was centrifuged, washed with Et_2O and dried in vacuo to give a mixture of copper(II) complexes. This mixture was dissolved in CH_2Cl_2 (20 mL), washed with 35% NH_4OH (5 mL), brine (3 × 5 mL) and dried over Na_2SO_4. Evaporation of CH_2Cl_2 under reduced pressure (18 Torr) gave the crude product. Flash chromatography (SiO_2, CH_2Cl_2/MeOH 90:10) afforded compounds **2b,c** and **3b,c** (**3d,e**).

2b: ^{1}H NMR (400 MHz, $CDCl_3$): δ = 2.95 (dd, *J* = 15 and 7 Hz, 1 H), 2.98−3.09 (m, 5 H), 3.10−3.25 (m, 4 H), 3.40 (m, 1 H), 3.75 (s, CH_3O), 4.94 (d, *J* = 5 Hz, 1 H), 6.71−6.75 (m, 2 H), 7.08 (ddd, *J* = 7, 5 and 1 Hz, 2 H), 7.12 (d, *J* = 8 Hz, 2 H), 7.33 (d, *J* = 9 Hz, 1 H), 7.55 (td, *J* = 8 and 2 Hz, 2 H), 8.50 (bd, *J* = 5 Hz, 2 H). − ^{13}C NMR (100.6 MHz, $CDCl_3$): δ = 34.3 (CH_2-Ind), 34.4 (2 CH_2), 49.9 (2 CH_2), 55.4 (CH_3O), 67.0 (CHN), 72.7 (CHOH), 110.3 (CH-aryl), 112.9 (CH-aryl), 121.5 (2 CH-pyr), 123.7 (2 CH-pyr), 126.5 (CH-aryl), 135.6 (C-aryl), 136.6 (2 CH-pyr), 143.4 (C-aryl), 149.4 (2 CH-pyr), 160.0 (2 C-pyr), 160.5 (C-aryl).

2c: ^{1}H NMR (400 MHz, $CDCl_3$): δ = 2.95−3.00 (m, 5 H), 3.02 (m, 1 H), 3.08−3.20 (m, 4 H), 3.50 (m, 1 H), 5.04 (d, *J* = 5.4 Hz, 1 H), 7.05−7.10 (m, 4 H), 7.45−7.50 (m, 3 H), 7.53 (td, *J* = 8 and 2 Hz, 2 H), 8.46 (dd, *J* = 5 and 1.6 Hz, 2 H). − ^{13}C NMR (100.6 MHz, $CDCl_3$): δ = 34.4 (CH_2-Ind), 34.5 (2 CH_2), 49.6 (2 CH_2), 66.3 (CHN), 73.4 (CHOH), 119.2 (CN), 123.6 (2 CH-pyr), 112.1 (C-aryl), 121.4 (2 CH-pyr), 126.1 (CH-aryl), 128.4 (CH-aryl), 131.2 (CH-aryl), 136.5 (2 CH-pyr), 142.8 (C-aryl), 148.7 (C-aryl), 149.1 (2 CH-pyr), 159.6 (2 C-pyr).

3b: ^{1}H NMR (400 MHz, $CDCl_3$): δ = 2.95 (dd, *J* = 15 and 7 Hz, 1 H), 2.98−3.09 (m, 5 H), 3.10−3.25 (m, 4 H), 3.40 (m, 1 H), 3.76 (s, CH_3O), 4.94 (d, *J* = 5 Hz, 1 H), 6.88 (dd, *J* = 8 and 2 Hz, 1 H), 6.98 (d, *J* = 2 Hz, 1 H), 7.20−7.00 (m, 1 H), 7.08 (ddd, *J* = 7, 5 and 1 Hz, 2 H), 7.12 (d, *J* = 8 Hz, 2 H), 7.55 (td, *J* = 8 and 2 Hz, 2 H), 8.50 (bd, *J* = 5 Hz, 2 H). − ^{13}C NMR (100.6 MHz, $CDCl_3$): δ = 33.1 (CH_2-Ind), 34.4 (2 CH_2), 49.9 (2 CH_2), 55.5 (CH_3O), 66.9 (CHN), 73.7 (CHOH), 110.3 (CH-aryl), 115.5 (CH-aryl), 121.5 (2 CH-pyr), 123.7 (2 CH-pyr), 125.6 (CH-aryl), 135.6 (C-aryl), 136.6 (2 CH-pyr), 143.4 (CH-aryl), 149.4 (2 CH-pyr), 159.2 (C-aryl), 160.0 (2 C-pyr).

3c: ^{1}H NMR (400 MHz, $CDCl_3$): δ = 2.95−3.00 (m, 5 H), 3.02 (m, 1 H), 3.08−3.20 (m, 4 H), 3.45 (m, 1 H), 5.02 (d, *J* = 5.8 Hz, 1 H), 7.05−7.10 (m, 4 H), 7.28 (d, *J* = 8 Hz, 1H), 7.45−7.50 (m, 1 H), 7.53 (td, *J* = 8 and 2 Hz, 2 H), 7.68 (d, *J* = 1 Hz, 1 H), 8.46 (dd, *J* = 5 and 1.6 Hz, 2 H). − ^{13}C NMR (100.6 MHz, $CDCl_3$): δ = 34.0 (CH_2-Ind), 34.5 (2 CH_2), 49.6 (2 CH_2), 66.4 (CHN), 73.2 (CHOH), 110.6 (CH-aryl), 119.2 (CN), 121.4 (2 CH-pyr), 123.6 (2 CH-pyr), 125.6 (CH-aryl), 129.1 (CH-aryl), 132.6 (CH-aryl), 136.5 (2 CH-pyr), 144.8 (C-aryl), 147.4 (C-aryl), 149.1 (2 CH-pyr), 159.6 (2 C-pyr).

3d: ^{1}H NMR (200 MHz, $CDCl_3$): δ = 2.00 (m, 1 H), 2.62−3.10 (m, 10 H), 3.10−3.30 (m, 1 H), 4.65 (d, *J* = 3.4 Hz, 1 H), 6.98−7.10 (m, 5 H), 7.10−7.20 (m, 2 H), 7.35 (m, 1 H), 7.50 (td, *J* = 7.5 and 2 Hz, 2 H), 8.48 (dd, *J* = 5 and 1 Hz, 2 H). − ^{13}C NMR (50.3 MHz, $CDCl_3$): δ = 19.9 (CH_2-tetral), 29.5 (CH_2-tetral), 35.8 (2 CH_2), 49.7 (2 CH_2), 61.6 (CHN), 68.34 (CHOH), 121.2 (2 CH-pyr), 123.6 (2 CH-pyr), 126.0 (CH-aryl), 127.6 (CH-aryl), 128.2 (CH-aryl), 130.6 (CH-aryl), 136.3 (2 CH-pyr), 137.4 (2 C-aryl), 149.0 (2 CH-pyr), 160.0 (2 C-pyr).

3e: ^{1}H NMR (200 MHz, $CDCl_3$): δ = 1.95 (m, 2 H), 2.60−3.30 (m, 11 H), 3.80 (s, CH_3O), 4.60 (d, *J* = 3.4 Hz, 1 H), 6.75 (dd, *J* = 8.6 and 2.8 Hz, 1 H), 6.90 (d, *J* = 2.8 Hz, 1 H), 7.10−6.95 (m, 5 H), 7.50 (td, *J* = 7.5 and 2 Hz, 2 H), 8.50 (dd, *J* = 5, 2 and 1 Hz, 2 H). − ^{13}C NMR (50.3 MHz, $CDCl_3$): δ = 20.2 (CH_2-tetral), 28.7 (CH_2-tetral), 35.9 (2 CH_2), 49.8 (2 CH_2), 55.4 (CH_3O), 61.6 (CHN), 68.5 (CHN), 114.2 (C-aryl), 114.8 (CH-aryl), 121.2 (2 CH-pyr), 123.6 (2 CH-pyr), 128.5 (C-aryl), 129.2 (C-aryl), 136.3 (2 CH-pyr), 138.5 (C-aryl), 149.1 (2 CH-pyr), 157.9 (C-aryl), 160.2 (2 C-pyr).

X-ray Structure Analysis: Crystal data for [7-OMe-TetralPY2]-$Cu(CF_3SO_3)_2$ together with details of the X-ray diffraction experiment, are reported in Table 4.

Crystallographic data for the structure reported in this paper has been deposited at the Cambridge Crystallographic Data Center as supplementary publication no. CCDC-137161. Copies of the data can be obtained free of charge on application to CCDC, 12 Union Road, Cambridge CB2 1EZ, UK [Fax: (internat.) +44-1223/336-033, E-mail: deposit@chemcrys.cam.ac.uk].

Acknowledgments

This research was supported by the *CNRS* and the *French Ministry of Universities*. The authors are grateful to Dr. A. Heumann for a number of enlightening discussions.

[1] J. P. Klinman, *Chem. Rev.* **1996**, *96*, 2541−2561; W. Kaim, J. Rall, *Angew. Chem.* **1996**, *108*, 47−64; *Angew. Chem. Int. Ed. Engl.* **1996**, *35*, 43−60.

[2] K. D. Karlin, S. Kaderli, A. D. Zuberbühler, *Acc. Chem. Res.* **1997**, *30*, 139−147.

[3] N. Kitajima, Y. Moro-Oka, *Chem. Rev.* **1994**, *94*, 737−757.

[4] M. Réglier, E. Amadéi, E. H. Alilou, F. Eydoux, M. Pierrot, B. Waegell, *Bioinorganic Chemistry of Copper* (Eds.: K. D. Karlin, Z. Tiecklar), Chapman and Hall, **1993**, 348−362.

[5] S. Itoh, T. Kondo, M. Komatsu, Y. Ohshiro, C. Li, N. Kanehisa, Y. Kai, S. Fukuzumi, *J. Am. Chem. Soc.* **1995**, *117*, 4714−4715.

[6] References for $L_2Cu_2(\mu\text{-}\eta^2\text{:}\eta^2\text{-}O_2)^{2+}$ species with L = RPY2: I. Sanyal, M. Mahroof-Tahir, S. Nasir, P. Ghosh, B. I. Cohen, Y. Gultneh, R. Cruse, A. Farooq, K. D. Karlin, S. Liu, J. Zubieta, *Inorg. Chem.* **1992**, *31*, 4322−4332; ref.; $HB(3,5\text{-}i\text{Pr}_2\text{pz})_3$, N. Kitajima, K. Fujisawa, Y. Moro-Oka, K. Toriumi, *J. Am. Chem. Soc.* **1989**, *111*, 8975−8976; $P(2,4\text{-}i\text{Pr}_2\text{im})_3$: T. N. Sorrel, W. E. Allen, P. S. White, *Inorg. Chem.* **1995**, *34*, 952−960; $i\text{Pr}_3$-tacn: S. Mahapatra, J. A. Halfen, E. C. Wilkinson, L. Que Jr., W. B. Tolman, *J. Am. Chem. Soc.* **1994**, *116*, 9785−9786.

[7] S. Itoh, H. Nakao, L. M. Berreau, T. Kondo, M. Komatsu, S. Fukuzumi, *J. Am. Chem. Soc.* **1998**, *120*, 2890−2899.

[8] I. Blain, P. Bruno, M. Giorgi, E. Lojou, D. Lexa, M. Réglier, *Eur. J. Inorg. Chem.* **1998**, 1297−1304.

[9] A. A. Mitrochkine, F. Eydoux, G. Gil, M. Réglier, *Eur. J. Org. Chem.* **1998,** 1171−1176.

[10] I. Blain, M. Giorgi, I. De Riggi, M. Réglier, *Eur. J. Inorg. Chem.* **2000**, 393−398.

[11] C. D. Johnson, *The Hammett Equation*; Cambridge University Press: Cambridge, U. K. **1973**.

[12] For the MeO group, $\sigma_p = -0.27$ and $\sigma_m = 0.12$ and for the CN group $\sigma_p = 0.66$ and $\sigma_m = 0.56$: C. Hansch, A. Leo, R. W. Taft, *Chem. Rev.* **1991**, *91*, 165−195.

[13] K. Wang, J. M. Mayer, *J. Am. Chem. Soc.* **1997**, *119*, 1470−1471; J. M. Mayer, *Acc. Chem. Res.* **1998**, *31*, 441−450.

[14] J. A. Howard, J. H. B. Chenier, *J. Am. Chem. Soc.***1973**, *95*, 3054−3055.

[15] H. Sakurai, A. Hosomi, *J. Am. Chem. Soc.* **1967**, *89*, 458−460.

[16] Recently, a recent report confirmed the electropilicity of copper−oxygen core: S. Itoh, M. Taki, H. Nakao, P. L. Holland, W. B. Tolman, L. Que, Jr., S. Fukuzumi, *Angew. Chem. Int. Ed.* **2000**, *39*, 398−400.

[17] D. W. Patrick, L. K. Truesdale, S. A. Biller, K. B. Sharpless, *J. Org. Chem.* **1978**, *43*, 2628−2638.

[18] D. H. R. Barton, *Pure Appl. Chem.* **1968**, *16*, 1. R. H. Hesse, *Adv. Free Radical Chem.* **1969**, *3*, 83.

[19] H. V. Obias, Y. Lin, N. N. Murthy, E. Pidcock, E. I. Solomon, M. Ralle, N. J. Blackburn, Y.-M. Neuhold, A. D. Zuberbühler, K. D. Karlin, *J. Am. Chem. Soc.* **1998**, *120*, 12960−12961.

[20] M. A. Lockwood, T. J. Blubaugh. M. Coler, S. Lovell, J. M. Mayer, *Angew. Chem. Int. Ed.* **1999**, *38*, 225−227.

[21] R. J. M. Klein Gebbink, C. F. Martens, P. J. A. Kenis, R. J. Jansen, H.-F. Nolting, V. A. Solé, M. C. Feiters, K. D. Karlin, R. J. M. Nolte *Inorg. Chem.* **1999**, *38*, 5755−5768.

[22] I. Blain, Ph. D. Dissertation, Univ. of Aix-Marseille III, **1998**.

[23] J. G. Cannon, J. A. Perez, R. K. Bhatnagar, J. P. Long, F. M. Sharabi, *J. Med. Chem*. **1982**, *25*, 1442−1446.

[24] J. A. Howard, J. H. B. Chenier, *J. Am. Chem. Soc.* **1973**, *95*, 3054.

Received April 12, 2000
[I00143]

Organometallic Polymers with the Backbone Consisting of Ferrocene and Bimetallic Tetracarboxylates

Wen-Mei Xue,[a] Fritz E. Kühn,*[a] Eberhardt Herdtweck,[a] and Quanchang Li[a]

Keywords: Ferrocene / Molybdenum / Multiple bonds / Oligomers / Rhodium

The tetranuclear compounds $Mo_2(O_2CCF_3)_4(FPA)_2$ (**1**), $Rh_2(O_2CCH_3)_4(FPA)_2$ (**2**), and $Rh_2(O_2CCF_3)_4(FPA)_2$ (**3**) (FPA = ferrocenyl-4-pyridylacetylene) have been synthesized by the reaction of bimetallic tetraacetates with FPA in a 1:2 stoichiometry. They have been investigated as models of oligomeric and polymeric complexes of analogous composition. UV/Vis absorption spectroscopy and cyclic voltammetry indicate that $Rh_2(O_2CCF_3)_4$ possesses the strongest inductive effect of the three bimetallic tetracarboxylates examined in this study. Complex **1** was additionally characterized by single crystal X-ray analysis, revealing a Mo–Mo distance of 214.22(3) pm, which is elongated in comparison to $Mo_2(O_2CCF_3)_4$ [209.0(4) pm], and a Mo–N distance of 250.4(2) pm. Oligomers with backbones consisting of 1,1′-bis(4-pyridylethynyl)ferrocene (BPEF) and bimetallic tetracarboxylates, $[M_2(O_2CR)_4(BPEF)]_n$ (M = Mo, R = CF_3, **4**; M = Rh, R = CH_3, **5**; M = Rh, R = CF_3, **6**), have been prepared by treating the bimetallic tetracarboxylates with BPEF in a 1:1 molar ratio. The terminal groups and the number of repeating units have been estimated by elemental analyses. The oligomeric complexes **5** and **6** are insoluble in all common solvents. Complex **4** dissolves in strongly coordinating donor solvents due to replacement of the BPEF ligands by solvent molecules.

Introduction

Polymers and oligomers containing metal-metal bonds in the backbone may display novel conductive, optical, and magnetic properties.[1] A number of bimetallic carboxylates[1f,2a] have been linked by bidentate axial ligands, resulting in one-dimensional polymeric species. Pyrazine has been used to link $Cr_2(O_2CCH_3)_4$,[2b] $Mo_2(O_2CCH_3)_4$,[3a] $Cu_2(O_2CCH_3)_4$,[3b] and $Ru_2\{O_2C(CH_2)_6CH_3\}_4$.[3c] $Mo_2(O_2CCF_3)_4$ units have been linked by 9,10-anthraquinone, 2,6-dimethyl-1,4-benzoquinone, 1,4-naphthoquinone,[3d] and 2,5-dimethyl-*N*,*N*′-dicyanoquinone diimine (2,5-DM-DCNQI).[3e] $Mo_2(O_2CCH_3)_4$ units have been bridged by 4,4′-bipyridine,[3a] 1,2-bis(dimethylphosphanyl)ethane (dmpe) and tetramethylethylenediamine (tmed).[3f] $Rh_2(O_2CC_2H_5)_4$ units have been linked by phenazine and durenediamine ligands, respectively.[2c] Phenazine has also been employed to connect cationic $Ru_2(O_2CC_2H_5)_4^+$ complexes to afford polymers.[2d] However, to the best of our knowledge, examples of oligomers and polymers based on bimetallic monomers with organometallic spacing groups are not yet known in the literature.[1f] This paper describes the first representatives of bimetallic oligomers bridged by π-conjugated ferrocene derivatives. $Mo_2(O_2CCF_3)_4$ is feasible as a building block because, in principle, the quadruple bond allows a delocalization of electrons along the oligomer chain. Dirhodium tetracarboxylates $Rh_2(O_2CCH_3)_4$ and $Rh_2(O_2CCF_3)_4$ are also employed, taking advantage of their air- and moisture-stability. The replacement of CH_3 by CF_3 is recommended for increasing the solubility and the metal-axial ligand interaction in the oligomer.

Ferrocene-containing complexes are currently receiving much attention due to their increasing role in the rapidly growing area of materials science. They have been of use as charge-transfer complexes and polymers,[4] molecular sensors,[5] and in nonlinear optics.[6] The favorable electrochemical properties of ferrocene make this molecule a particularly promising candidate for incorporation into polymer chains. It is quite obvious that ferrocene polymers are more likely to display exceptional properties when the different metal centers are intimately coupled through suitable unsaturated bridging units.[7] We therefore explore an oligomer system containing both ferrocene and metal-metal bonds in the backbone. Introduction of bimetallic complexes into the ferrocene-based oligomers combines the advantages of both the ferrocene and the metal-metal bonds. Additionally, it allows the use of a wider diversity of metals (Mo, Rh, Re, Cu, Cr, W, Pt, Ru, etc.) and equatorial ligands which may be helpful in fine-tuning the oligomer properties.

Results and Discussion

Tetranuclear Complexes

Preparation and Characterization

In order to better understand the electronic and electrochemical properties of oligomeric complexes of analogous composition, complexes **1**–**3** were synthesized as models by the reaction of dirhodium- or dimolybdenum-tetracarboxylate with the monodentate FPA ligand in a 1:2 molar ratio as shown in Equation (1).

[a] Anorganisch-Chemisches Institut der Technischen Universität München,
Lichtenbergstraße 4, 85747 Garching bei München, Germany
Fax: (internat.) +49-89/289-13473
E-mail: fritz.kuehn@ch.tum.de

 © WILEY-VCH Verlag GmbH, 69451 Weinheim, 2001 1434–1948/01/0101–0213 $ 17.50+.50/0

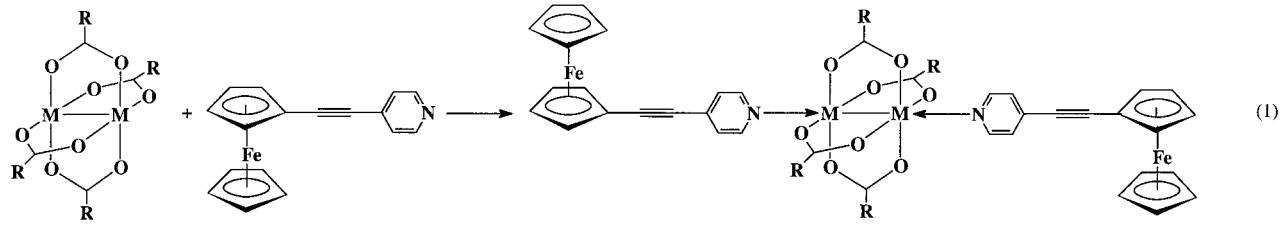

FPA

	M	R
1	Mo	CF_3
2	Rh	CH_3
3	Rh	CF_3

(1)

The dimolybdenum compound **1** decomposes when exposed to air within a couple of hours in the solid state and within 10 minutes in solution. The dirhodium complexes **2** and **3** are air stable. Compounds **1** and **3** are soluble in most polar organic solvents, e.g. CH_2Cl_2, $CHCl_3$, MeCN, THF, etc., but **2** is only soluble in CH_2Cl_2 and $CHCl_3$, due to the commonly lower solubility of acetyl complexes in comparison to trifluoroacetyl compounds.[2a]

The IR active C≡C stretching vibration gives rise to bands at 2207, 2205, and 2206 cm^{-1} respectively for compounds **1**–**3**. This vibration is slightly lower in energy in all cases than in the free FPA ligand (2210 cm^{-1}). The pyridyl ring stretching vibration appears at 1601, 1603, and 1604 cm^{-1}, the corresponding signal of FPA at 1594 cm^{-1}.

The pyridyl protons of **2** [$\delta(H_\alpha)$ = 9.11, $\delta(H_\beta)$ = 7.72] show their resonances at lower field than the free ligand FPA (δ = 8.53 and 7.32, respectively). In contrast, up-field shifts of the α-ring pyridyl protons are observed in compounds **1** (δ = 8.03) and **3** (δ = 8.27), possibly due to the strong electron-withdrawing effect of the trifluoroacetyl ligands, which diminish backbonding effects from the bimetallic cores. The ferrocene proton resonances are comparable for compounds **1**–**3** and the free ligand. The proton NMR signal of the CH_3CO_2 group is shifted downfield in CD_2Cl_2 from δ = 1.76 [axial ligand free $Rh_2(O_2CCH_3)_4$] to δ = 1.88 in the case of complex **2**, demonstrating that electron density must be shifted back to the ferrocenyl unit in the latter molecule. The ^{13}C NMR spectroscopic data of the CH_3 moiety shows the same trend [δ = 23.5 in the starting material $Rh_2(O_2CCH_3)_4$ and δ = 30.1 in the axially ligated product compound].

Attempts to prepare mixed-valence complexes by chemical oxidation have not yet been successful. Treatment of $Rh_2(O_2CCH_3)_4(FPA)_2$ with I_2 in dichloromethane at room temperature resulted in no reaction, while the same treatment carried out on $Mo(O_2CCF_3)_4(FPA)_2$ led to immediate decomposition.

Structural Investigation

The molecular structure of compound **1** together with selected interatomic distances, angles and torsion angles are shown in Figure 1. The neutral complex crystallizes in the space group *P*1(bar) (No. 2). Quadruply bonded dimolybdenum complexes with four bridging $(O_2CCF_3)^-$ ligands usually exhibit a crystallographic center of inversion in the solid state, as does compound **1**. The two pyridyl ligands coordinate to the molybdenum atoms in the axial positions and are slightly bent [Mo_a–Mo–N 165.85(5)°]. Compound **1** and all other 11 crystallographically characterized compounds with a $[Mo_2(\mu\text{-}O_2CCF_3)_4]$ building block exhibit a very similar core geometry.[8] As expected the $[Mo_2(\mu\text{-}O_2CCF_3)_4]$ unit has a nearly idealized D_{4h} symmetry. The observed Mo–Mo bond length of 214.22(3) pm in **1** is found at the upper end of the known range for Mo–Mo quadruple bonds. The elongation of the Mo–Mo bond in comparison to the starting material {$[Mo_2(\mu\text{-}O_2CCF_3)_4]$, *d*(MoMo) = 209.0(4) pm} is clearly due to the electron donor capability of the axial ligands. Donation of additional electron density to a quadruple bond leads to a weakening of the Mo–Mo interaction, caused by the involvement of antibonding orbitals. The Mo–O distances do not vary significantly. The Mo-pyridyl bond is comparatively long [Mo–N 250.4(2) pm], indicating relatively weak molybdenum–nitrogen interactions. However, the Mo–N distance is shorter than expected from the sum of the van der Waals radii (Mo–N: 382 pm) but longer than the sum of the covalent radii (Mo–N: 215 pm).[8] The NMR and IR data described above are in good agreement with all these observations.

Electronic Absorption Spectra

Any perturbation of the electronic structure of the ferrocenes should lead to a bathochromic shift of the respective UV/Vis transitions. Figure 2 presents a comparison of the UV/Vis spectra of complex **2** and FPA. A peak at 365 nm (13600 M^{-1} cm^{-1}) and a broad band around 451 nm (3040 M^{-1} cm^{-1}) in **2** are assigned to d-d transitions in the ferrocene unit.[9] FPA shows similar absorptions at 352 nm (2320 M^{-1} cm^{-1}) and 449 nm (760 M^{-1} cm^{-1}) but significantly lower extinction coefficients. The higher energy d-d transition bands in the spectra of complexes **1** and **3** are probably shoulders of π-π* absorptions. As shown in Table 1, the lower energy absorptions appear around 451 nm (2340 M^{-1} cm^{-1}) and 466 nm (6310 M^{-1} cm^{-1}) in the derivatives **1** and **3**. In addition to the d-d transitions, the spectra show a strong peak assigned to a π-π* transition at about 310 nm: FPA, 304 nm (12800 M^{-1} cm^{-1}); **1**, 305 (37499); **2**, 308 (32800); **3**, 316 (47500). The shift to longer wavelength absorptions in the case of derivatives **1**–**3** compared to unco-

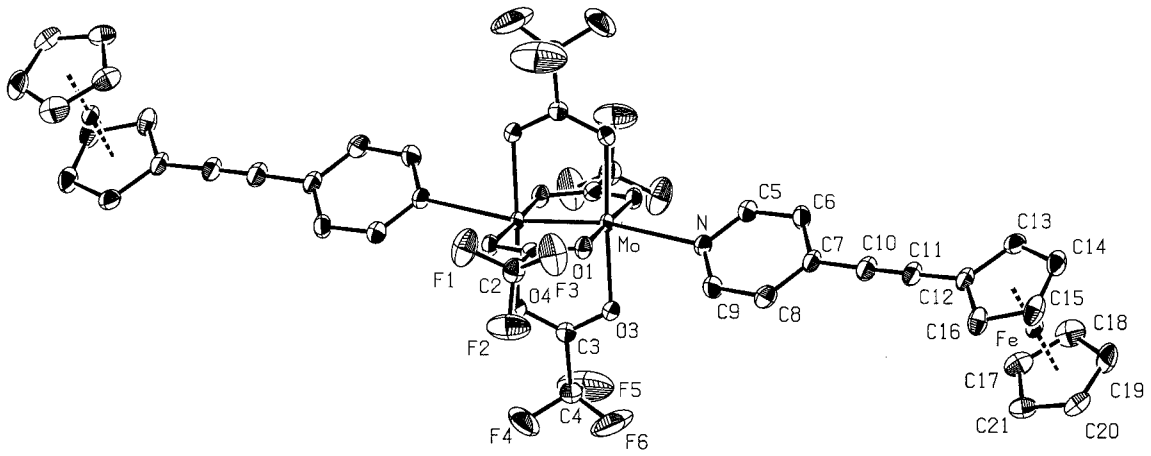

Figure 1. ORTEP drawing of the molecular structure of **1** in the solid state; thermal ellipsoids are at the 50% probability level; hydrogens omitted for clarity; selected bond lengths [pm], angles and torsion angles [°]: Mo−Mo_a 214.22(3), Mo−O1 214.45(19), Mo−O3 213.6(2), Mo_a−O2 211.22(19), Mo_a−O4 211.6(2), Mo−N 250.4(2), C10−C11 120.0(4); O1−Mo−$O2_a$ 177.25(7), O3−Mo−$O4_a$ 177.26(7), O1−Mo−O3 91.23(7), O1−Mo−$O4_a$ 88.19(7), $O4_a$−Mo−$O2_a$ 91.58(7), $O2_a$−Mo−O3 88.87(7), Mo_a−Mo−N 165.85(5); O1−Mo−Mo_a−O2 −0.09(7), O3−Mo−Mo_a−O4 −0.61(7); translation of symmetry code to equivalent positions: $a = 1 - x, 2 - y, -z$

ordinated FPA is probably due to the inductive effects of the dimetallic moieties. The degree of deviation of the bathochromic shifts of both d-d and π-π* transitions of complex **3** vs. FPA are bigger than in the case of compound **2**, due to the strong electron-withdrawing effect of the trifluoroacetyl groups. Complexes **1** and **3** bear the same carboxylato ligand, but the shifts of both d-d and π-π* bands in **3** vs. FPA are more pronounced than in derivative **1**. This reflects the fact that the Lewis acidity of $Rh_2(O_2CCF_3)_4$ is higher than that of $Mo_2(O_2CCF_3)_4$.

Electrochemical Properties

As depicted in Figure 3, the cyclic voltammogram of complex **2** in CH_2Cl_2 exhibits two subsequently reversible anodic couples. The first oxidation with $E_{1/2} = 0.18$ V is assigned to the oxidation of the two ferrocene units, whereas the second with $E_{1/2} = 0.52$ V is due to the oxidation process $[Rh_2]^{5+/4+}$. The coordination of dirhodium(II) by FPA results in a pronounced cathodic shift of $[Rh_2]^{5+/4+}$ from the parent $Rh_2(O_2CCH_3)_4$ (0.90 V), probably due to the strong electron-donating ability of FPA. The weak anodic shift of $Fe^{3+/2+}$ in complex **2** compared to FPA (0.12 V) is probably caused by the inductive effect of the acetate ligands in $Rh_2(O_2CCH_3)_4$. This effect compensates at least partially the electron deficiency of the Rh centers. As presented in Table 1, the $Fe^{3+/2+}$ oxidation potentials of **1** and **3** are also anodically shifted to 0.17 V and 0.27 V respectively from the parent FPA. Moreover, the shift of compound **3** vs. free FPA is more remarkable than the one in **1** and **2**, reflecting the negative inductive effect of the trifluoroacetate ligands of $Rh_2(O_2CCF_3)$. This result is consistent with the results obtained from electron absorption spectroscopy (see above).

FPA gives a half-peak width $W_{1/2}$ of 237 mV, whereas complex **1** displays a $W_{1/2}$ of 297 mV. Although the $Fe^{3+/2+}$ oxidation peak width of **1** is 60 mV broader than that of

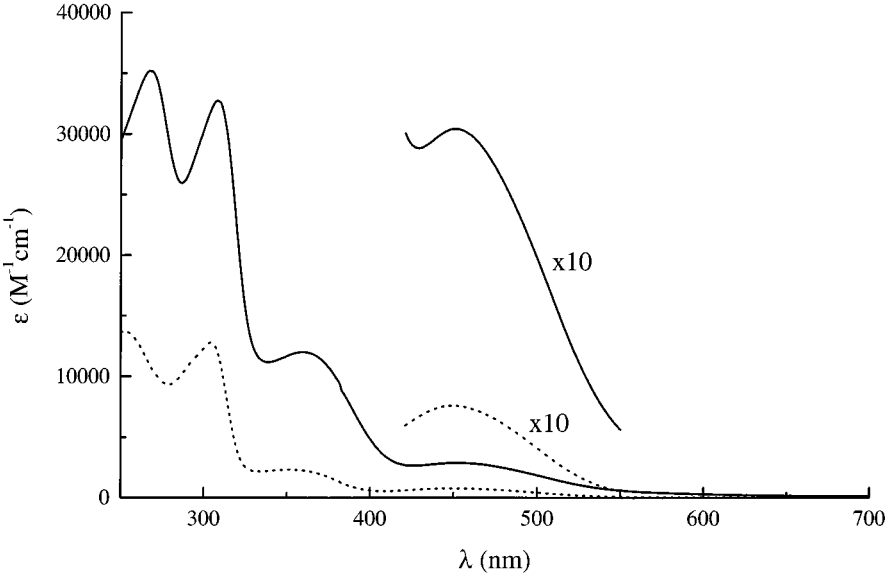

Figure 2. UV/Vis absorption spectra of $Rh_2(O_2CCH_3)_4(FPA)_2$ (**2**, solid line) and FPA (dotted line) in CH_2Cl_2 at room temperature

Table 1. Ferrocene oxidation potentials and electronic absorptions of the complexes and ligands at room temperature

Material	E (ΔE_p)/$Fe^{3+/2+}$ [a]	λ_{max},[b] nm (ε, 10^3 м$^{-1}$ cm^{-1})
$Mo_2(O_2CCF_3)_4(FPA)_2$ **1**	0.17 (80)	305 (37.4), 451 (2.34)
$Rh_2(O_2CCH_3)_4(FPA)_2$ **2**	0.18 (61)	267 (35.2), 308 (32.8), 365 (13.6), 451 (3.04)
$Rh_2(O_2CCF_3)_4(FPA)_2$ **3**	0.27 (62)	260 (6.39), 316 (9.46), 466 (6.31)
$[Mo_2(O_2CCF_3)_4(BPEF)]_n$ **4**	0.41 (61)[c][d] −0.20 (ir)[e]	304 (16.6), 439 (1.19)[c][f]
FPA	0.12 (72)	304 (12.8), 352 (2.32), 449 (0.76)
BPEF	0.43 (ir)[c] −0.22 (ir)[e]	308 (16.9), 350 (3.55), 458 (0.87)[c] 311 (19.6), 350 (4.16), 457 (1.04)

[a] Performed in deoxygenated CH_2Cl_2 solutions except otherwise stated. Potentials in volts vs. ferrocene (0.00 V with ΔE_p = 95 mV in CH_2Cl_2 and 66 mV in CH_3CN). Scan rate is 50 mV/s except otherwise stated. $\Delta E_p = E_{pa} - E_{pc}$ (mV). − [b] Measured in CH_2Cl_2 solutions except otherwise stated. − [c] Measured in CH_3CN. − [d] Scan rate is 200 mV/s. − [e] Measured in THF. − [f] Molarity is based on the repeating unit.

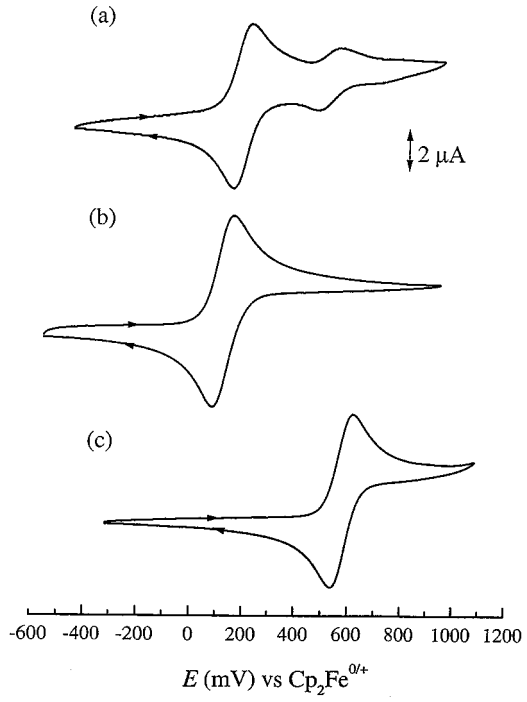

Figure 3. Cyclic voltammograms of (a) $Rh_2(O_2CCH_3)_4(FPA)_2$ (**2**), (b) FPA and (c) $Rh_2(O_2CCH_3)_4$ at the same scan rate of 50 mV/s in CH_2Cl_2 with 0.1 м TBAH at room temperature

FPA, both DPV and SQW measurements reveal a single process. A single $Fe^{3+/2+}$ oxidation wave as narrow as that of FPA is observed for both compounds **2** and **3**. The apparent lack of interaction between the ferrocene units in the tetranuclear complexes might be due to the less favorable energetic positions of the available orbitals in the complexes, the relatively weak Mo-axial ligand interactions and the presence of the rather long conjugating units between the ferrocene fragments.

Thermogravimetry

The complexes **1**−**3** and their precursor complexes $Mo_2(O_2CCF_3)_4$, $Rh_2(O_2CCF_3)_4$, $Rh_2(O_2CCH_3)_4$, and FPA have been examined by thermogravimetry (TG). While the bimetallic starting materials sublime with onset temperatures of 226 °C [$Mo_2(O_2CCF_3)_4$], 278 °C [$Rh_2(O_2CCH_3)_4$], and 312 °C [$Rh_2(O_2CCF_3)_4$], FPA starts to decompose at 229 °C, the tetrameric product complexes **1** and **2** are more stable than both their precursor complexes, with decomposition onset temperatures of 247 °C and 296 °C. However, compound **3** decomposes with a lower onset temperature (275 °C) than its bimetallic precursor $Rh_2(O_2CCF_3)_4$. The product complexes **1**−**3** are therefore in general significantly more stable than the least stable starting material, two of them are even more thermally stable than both precursors. This clearly proves the formation of product compounds of significant stability.

Oligomeric and Polymeric Complexes

Preparation and Characterization

The one-dimensional organometallic oligomer $[Mo_2(O_2CCF_3)_4(BPEF)]_n$ (**4**) with alternating ferrocene units and dimolybdenum quadruple bonds in the π-conjugated chain is obtained by the reaction of $Mo_2(O_2CCF_3)_4$ with one equivalent of BPEF [BPEF = 1,1′-bis(4-pyridylethynyl-)ferrocene] as shown in Equation 2. The orange solid is readily soluble in THF, moderately soluble in CH_3CN, and insoluble in all other common organic solvents. The solid state IR spectrum exhibits the characteristic C≡C stretching vibration at 2211 cm^{-1} and the C−F stretching vibration at 1193 cm^{-1}. These bands are nearly identical in energy to those in free BPEF [ν(C≡C) = 2208 cm^{-1}] and $Mo_2(O_2CCF_3)_4$ [ν(C−F) = 1192 cm^{-1}]. The strong band at 1592 cm^{-1} attributed to the pyridyl ring shifts to 1603 cm^{-1} after ligation.

Elemental analyses are consistent with an oligomer or polymer having the stoichiometry $Mo_2(O_2CCF_3)_4$/BPEF = 1:1. The ^1H NMR spectroscopic data of δ($H_α$-pyridyl) (δ = 8.42) and δ($H_β$-pyridyl) (δ = 7.21) in **4** ([D_8]THF) are nearly identical with those of BPEF (δ = 8.46 and 7.19, respectively), and it is impossible to estimate the number of repeating units n in **4** from the ^1H NMR spectroscopic data. Besides the pyridyl protons, the ferrocene protons (δ($H_α$-C_5H_4) = 4.61, δ($H_β$-C_5H_4) = 4.42) also display a similar chemical shift compared to those of free BPEF (δ = 4.57 and 4.37, respectively). The major difference is that the pyridyl protons in **4** show broad signals at room temperature. They become broader and shift to lower field [δ($H_α$) = 8.78, δ($H_β$) = 7.31] at +55 °C, but split to a doublet with peaks

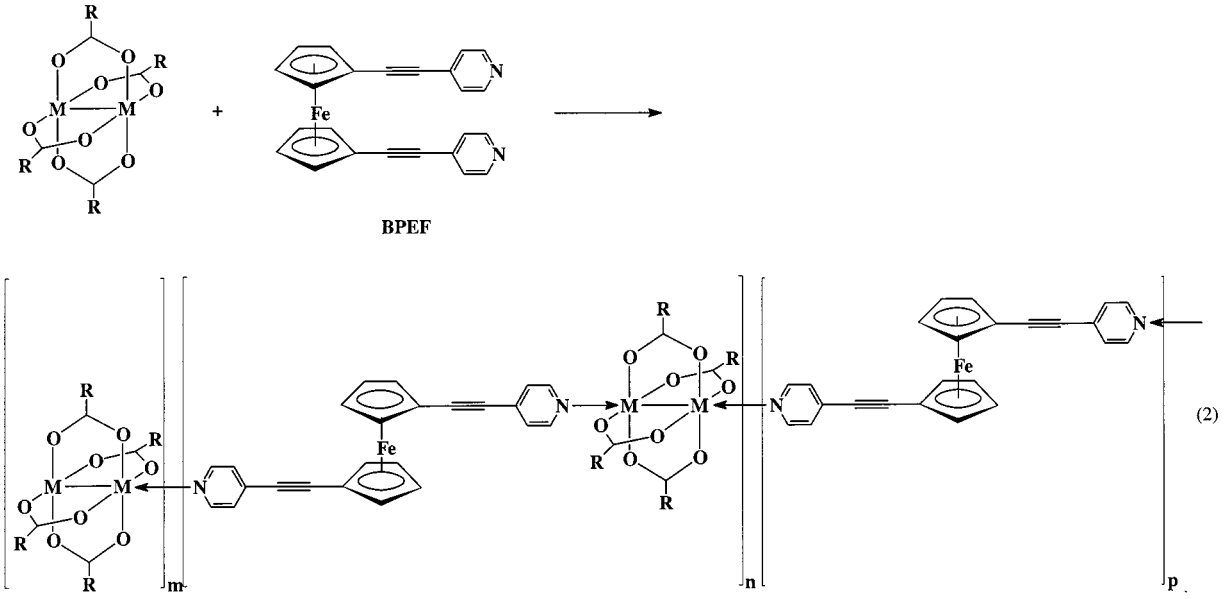

	M	R	m	n	p
4	Mo	CF_3	0	unknown	0
5	Rh	CH_3	1	ca. 3	0
6	Rh	CF_3	0	9-14	1

at δ = 8.38 and 7.20, respectively, at −80 °C. This behavior is probably due to a temperature-dependent fluxionality in the system. At lower temperatures the whole structure is more rigid. Increasing the temperature leads to significant thermal movements, causing a broadening of the signals. Free BPEF does not show temperature dependence in its NMR spectrum. The ^{13}C NMR chemical shift of the R−CO_2 carbon atom in complex **4** (δ = 166.7, [D_8]THF) is not significantly different from that in $Mo_2(O_2CCF_3)_4$ (δ = 167.0). Therefore it is assumed that the oligomer chain of complex **4** may be broken due to the combined effects of weak metal-axial ligand interactions and the relatively strong coordinating ability of the solvent THF which is present in high excess. It is known that the strong σ component found in Mo−Mo quadruple bonds ($\sigma^2\pi^4\delta^2$) prevents stronger binding of any low-lying orbitals at the axial positions.[2a] A huge excess of the coordinating solvent THF is therefore very likely to break the oligomer chain. It was reported that the dissolution of $[Ru_2(O_2C(CH_2)_6CH_3)_4(pyrazine)]_n$ in coordinating solvents such as THF and MeOH also resulted in breaking of the polymer chain.[3c] We have reported the preparation of $[Mo_2(\mu\text{-}O_2CCH_3)_2(\mu\text{-}dppma)_2(NC_5H_4\text{-}R)_2]^{2+}$ recently. A mixture of nitrile and pyridine ligated complexes is obtained if the reaction is conducted in acetonitrile instead of dichloromethane.[11] Chemical ionization mass spectrometry (CI-MS) measurements of oligomer **4** also indicate that the metal-axial ligand interaction is weak, showing two major peaks corresponding to $BPEF^+$ and $[Mo_2(O_2CCF_3)_4]^+$ but no parent oligomer ion.

At an onset temperature of ca. 273 °C the oligomer **4** breaks down, producing sublimed $Mo_2(O_2CCF_3)_4$ units. Further heating results in gradual decomposition of the residue and gives a residual weight of 30% at 800 °C under He atmosphere as shown by TGA analysis (Figure 4). It is to be noted, however, that the onset of sublimation for the starting material $[Mo_2(O_2CCH_3)_4]$ is more than 45 °C below the onset of the first decomposition step of compound **4** (226 °C). Derivative **4** is also significantly more stable than the analogous tetrameric complex **1** (see above). This not only proves that complex **4** is not merely a mixture of starting materials, but also explains why all the $[Mo_2(O_2CCH_3)_4]$ incorporated in derivative **4** does not sublime when the oligomeric structure breaks down. The temperature is already significantly above the sublimation temperature of the dimolybdenum precursor so that only part of it is still able to sublime; the remaining residue decomposes gradually.

In the solid state, compound **4** is stable in air for a couple of hours, but in solution it decomposes within 10 min when exposed to air. In order to obtain air stable organometallic oligomers of this type, $Rh_2(O_2CCH_3)_4$ and $Rh_2(O_2CCF_3)_4$ were employed to yield oligomers **5** and **6** as shown in Equation (2). It is additionally anticipated that $Rh_2(O_2CCF_3)_4$ leads to stronger metal-axial ligand interactions because it is a stronger Lewis acid than $Rh_2(O_2CCH_3)_4$. Accordingly, neither compound **5** nor complex **6** are soluble in any common solvents. THF and acetonitrile are unable to break the axial interactions between the dirhodium core and the BPEF ligands, in contrast to the case of compound **4**.

The IR spectra of **5** and **6** exhibit characteristic C≡C stretching vibrations at 2208 and 2210 cm^{-1}, respectively. Derivative **6** additionally shows the C−F stretching vibration at 1194 cm^{-1}. These data are comparable with those of free BPEF [ν(C≡C) = 2208 cm^{-1}] and free $Rh_2(O_2CCF_3)_4$ [ν(C−F) = 1190 cm^{-1}].

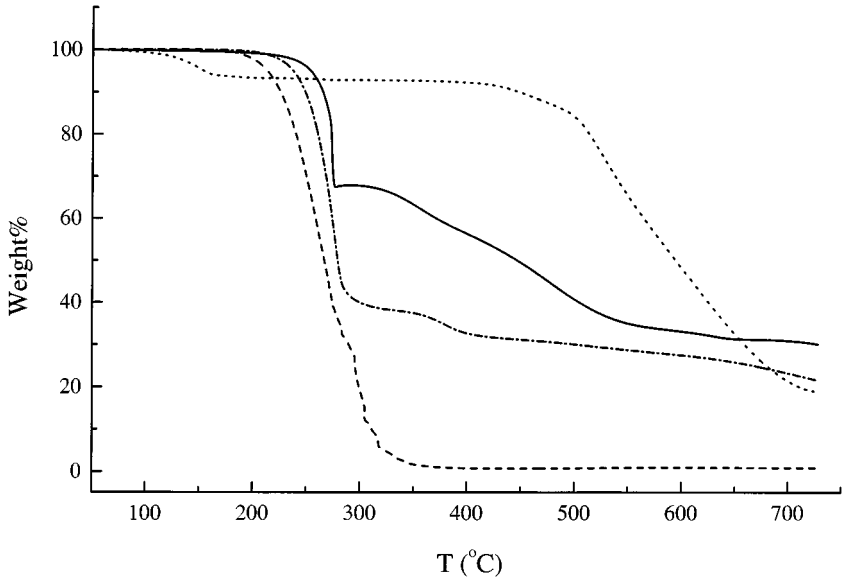

Figure 4. Plot of percent weight loss versus temperature for the thermal decomposition of $[Mo_2(O_2CCF_3)_4(BPEF)]_n$ (**4**, solid line), $Mo_2(O_2CCF_3)_4$ (dashed line), BPEF (dotted line), and $Mo_2(O_2CCF_3)_4(FPA)_2$ (**1**) (dashed-dotted line)

The poor solubility of complexes **5** and **6** prevents successful measurements of NMR spectra and the determination of the molecular mass in solution. However, the elemental analyses provide a rough way of estimating the number of repeating units and the terminal groups of the oligomers. The analytical results for complex **5** suggest the terminal groups are $Rh_2(O_2CCH_3)_4$ because the carbon content is much lower than that assumed for a stoichiometry $Rh_2(O_2CCH_3)_4$/BPEF = 1:1. The calculated elemental percentages are compared to the experimental data in Table 2. The percentages of H, N, and Fe are not sensitive enough to the extension of the oligomer chain, but those of C and Rh are quite informative. Taking the absolute error of the C analyses as 0.3%, and of the Rh analyses of 1%, the oligomer **5** has the composition of $[Rh_2(O_2CCH_3)_4]_{n+1}(BPEF)_n$ (n is around 3, most likely a mixture of oligomers with different lengths) and the average molecular mass is 2933. In the same manner, the composition of oligomer **6** is assumed to be $[Rh_2(O_2CCF_3)_4]_n(BPEF)_{n+1}$ (n = 9−14), the terminal groups are BPEF, and the molecular mass is in the range of 9803 to 15034 (Table 2). Considering the well-defined onset of sublimation for the complexes **4**−**6** (see below) it is unlikely that these derivatives still contain a significant amount of the starting materials (which can be removed easily by washing − see Experimental Section). Therefore the results obtained from elemental analysis should at least give a reliable estimation of the size of the oligomers.

The TGA profiles of complexes **5** and **6** are in principle similar to that of compound **4**. Oligomer **5** is thermally stable under a He atmosphere until the temperature reaches ca. 300 °C. Then the polymer structure breaks down and $Rh_2(O_2CCH_3)_4$ starts to sublime. Again, the longer chain of compound **5** is somewhat more stable than the tetranuclear model compound **2** (see above). Further heating results in gradual decomposition of the residue and gives a residual weight of 53% at 730 ° C. $Rh_2(O_2CCH_3)_4$ without any axial ligands has a sublimation onset temperature of about 20 °C (278 °C) below that of the oligomer **5**. Compound **6** is thermally stable under He below 320 °C. The residual weight is 28% at 730 °C. Despite the fact that the tetranuclear complex **3** is less stable than $Rh_2(O_2CCF_3)_4$, its oligomeric analogue **6** is more stable than this precursor (decomposition onset at 312 °C, see above). These data are additional proof of the significant interactions in the bimetallic complexes with the axial BPEF ligands.

Electrochemical Properties

The insolubility of oligomers **5** and **6** prevents investigation of their electrochemical properties in solution, but the properties of complex **4** were investigated by cyclic voltammetry. The usual solvent for the oxidation of ferrocene is dichloromethane due to its inertness towards ferrocenium-type ions. However, we employed acetonitrile and tetrahydrofuran for the measurements because complex **4** is much more soluble in these solvents. It is to be noted, however, that the data obtained are probably not representative of the oligomeric compound **4** but only of fragments of it and therefore have to be regarded with great caution. Dissolved complex **4** displays an irreversible $Fe^{3+/2+}$ oxidation at −0.20 V in THF, which is comparable to the parent BPEF (−0.22 V). The $Fe^{3+/2+}$ oxidation wave of BPEF (0.43 V) is still irreversible in MeCN. However, when the scan rate reaches 200 mV/s, a reversible curve with $E_{1/2}$ = 0.41 V is observed for compound **4** dissolved in acetonitrile. The fact that the oxidation potential for the dissolved derivative **4** is very close to that of free starting material supports the view of a breakdown of the oligomeric structure in solution.

Electronic Absorption Spectra

BPEF shows d-d transitions at 350 nm (3550 M^{-1} cm^{-1}) and 458 nm (870 M^{-1} cm^{-1}), as well as π-π* transition at 308 nm (16900 M^{-1} cm^{-1}) in CH_3CN. It is anticipated that

Table 2. Estimation of the terminal groups and the number of repeated units of oligomers **5** and **6** by elemental analyses

$[Rh_2(O_2CCH_3)_4]_{n+1}(BPEF)_n$ (n is ca. 3) **5** Ratio[a]	Formula	fw	C%	H%	N%	F%	Fe%	Rh%
Found			42.74	3.54	2.94	–	6.03	27.6
3:2	$C_{72}H_{68}Fe_2N_4O_{24}Rh_6$	2102.47	41.13	3.26	2.66	–	5.31	29.38
4:3	$C_{104}H_{96}Fe_3N_6O_{32}Rh_8$	2932.71	42.59	3.30	2.87	–	5.71	28.08
5:4	$C_{136}H_{124}Fe_4N_8O_{40}Rh_{10}$	3762.95	43.41	3.32	2.98	–	5.94	27.36
1:1	$(C_{32}H_{28}FeN_2O_8Rh_2)_n$	n×830.24	46.29	3.40	3.37	–	6.73	24.79

$[Rh_2(O_2CCF_3)_4]_n(BPEF)_{n+1}$ (n = 9–14) **6**

Ratio[b]	Formula	fw	C%	H%	N%	F%	Fe%	Rh%
Found			38.00	1.66	2.85	20.52	5.35	19.4
8:9	$C_{280}H_{144}F_{96}Fe_9N_{18}O_{64}Rh_{16}$	8757.26	38.40	1.66	2.88	20.83	5.74	18.80
9:10	$C_{312}H_{160}F_{108}Fe_{10}N_{20}O_{72}Rh_{18}$	9803.39	38.23	1.65	2.86	20.93	5.70	18.89
10:11	$C_{344}H_{176}F_{120}Fe_{11}N_{22}O_{80}Rh_{20}$	10846.24	38.06	1.64	2.84	21.02	5.67	18.98
11:12	$C_{376}H_{192}F_{132}Fe_{12}N_{24}O_{88}Rh_{22}$	11892.06	37.94	1.63	2.83	21.09	5.64	19.04
12:13	$C_{408}H_{208}F_{144}Fe_{13}N_{26}O_{96}Rh_{24}$	12937.88	37.88	1.62	2.81	21.15	5.62	19.09
13:14	$C_{440}H_{224}F_{156}Fe_{14}N_{28}O_{104}Rh_{26}$	13987.90	37.76	1.61	2.80	21.19	5.60	19.13
14:15	$C_{472}H_{240}F_{168}Fe_{15}N_{30}O_{112}Rh_{28}$	15034.02	37.71	1.61	2.80	21.23	5.57	19.17
15:16	$C_{504}H_{256}F_{180}Fe_{16}N_{32}O_{120}Rh_{30}$	16080.15	37.71	1.60	2.79	21.17	5.56	19.20
1:1	$(C_{32}H_{16}F_{12}FeN_2O_8Rh_2)_n$	n×1046.13	36.74	1.54	2.68	21.79	5.34	19.67

[a] Stoichiometry $Rh_2(O_2CCH_3)_4$:BPEF. – [b] Stoichiometry $Rh_2(O_2CCF_3)_4$:BPEF.

these absorption bands move to longer wavelengths and exhibit stronger extinction coefficients when BPEF forms an oligomer with $Mo_2(O_2CCF_3)_4$ in complex **4** for the same reasons as in the tetranuclear model complex **1**. However, the UV/Vis spectrum of dissolved complex **4** in CH_3CN does not show these features. The d-d and π-π* transitions of the dissolved derivative **4** are comparable to BPEF both in energy and in intensity, except that the d-d absorption around 350 nm appears as a shoulder of the π-π* absorption band of dissolved **4**. This behavior again supports the view that destruction of the oligomeric structure of **4** by the donor solvents occurs.

Conclusions

A new type of organometallic oligomer with the backbone consisting of bimetallic tetracarboxylates and a π-conjugated ferrocene derivative is easily generated by mixing the precursor compounds in solution at room temperature. The terminal groups and the number of repeating units are estimated by elemental analysis. The poor solubility of $[Rh_2(O_2CCH_3)_4]_{n+1}(BPEF)_n$ ($n \approx 3$) (**5**) and $[Rh_2(O_2CCF_3)_4]_n(BPEF)_{n+1}$ (n = 9–14) (**6**) prevents investigation of their electronic and electrochemical properties. The properties of dissolved $[Mo_2(O_2CCF_3)_4(BPEF)]_n$ (**4**) in MeCN and THF solutions are not related to the behavior of the real oligomer due to coordination competition between BPEF and the donor solvents. TGA studies prove the strength of the metal-axial interactions in the oligomeric complexes **4**–**6**. The electronic and electrochemical investigations of the tetranuclear model compounds indicate that the ferrocene units are electronically noncommunicating. Further research in this field will include modification of the tetracarboxylate ligands, bimetallic centers and ferrocene bridges in order to enhance the solubility of the oligomers and increase the electronic coupling within the oligomeric chains. Work in this direction is currently under way in our laboratory.

Experimental Section

General: All preparations and manipulations were carried out under an oxygen- and water-free argon atmosphere using standard Schlenk techniques. Solvents were dried by standard procedures, distilled, and stored under argon over 4-Å molecular sieves. $Mo_2(O_2CCF_3)_4$,[2e] $Rh_2(O_2CCH_3)_4$,[11] and $Rh_2(O_2CCF_3)_4$[12] were prepared according to the literature methods. – Elemental analyses were performed at the Mikroanalytisches Labor of the TU München in Garching. – ^1H and ^{13}C NMR were recorded by a Jeol JNM GX-400 spectrometer. – IR spectra were obtained on a Perkin–Elmer FT-IR spectrometer using KBr pellets as IR matrix. – Electronic absorption spectra were recorded using a Perkin–Elmer Lambda 2 UV/Vis spectrometer. – Cyclic voltammograms were recorded with a computer-controlled Model 173 Potentiostat/galvanostat (EG&G Princeton Applied Research) in argon-saturated and dry solutions with tetrabutylammonium hexafluorophosphate (TBAH, 0.1 M) as supporting electrolyte. The working electrode was platinum and the reference electrode silver wire. Potentials are quoted vs. the ferrocene/ferrocenium couple as internal standard. – TGA was performed using a Perkin–Elmer TGA 7 Thermogravimetric Analyzer with a heating rate of 15 °C/min.

Ferrocenyl-4-pyridylacetylene (FPA): Synthesized from ferrocenylacetylene[13] and 4-bromopyridine hydrochloride using a modified literature procedure.[14] Decomposes at 154 °C. – $C_{17}H_{13}FeN$ (287.14): calcd. C 71.11, H 4.56, N 4.88; found C 71.25, H 4.47, N 4.59. – Positive FAB-MS: m/z = 288 $[FPA + H^+]^+$. – Selected IR (KBr): $\tilde{\nu}$ = 2210 s (C≡C), 1636 m, 1594 vs, 1536 m, 1455 m, 1411 m, 1103 m, 1040 m, 1023 m, 1004 m, 987 m, 927 m, 817 vs, 538 m, 499 s, 483 s cm^{-1}. – ^1H NMR (CD_2Cl_2, room temp.): δ = 4.25 (s, 5 H, C_5H_5), 4.31 (t, 2 H, H_β-C_5H_4), 4.54 (t, 2 H, H_α-C_5H_4), 7.32 (d, 2 H, H_β-C_5H_4N), 8.53 (d, 2 H, H_α-C_5H_4N). – ^{13}C NMR

(CD_2Cl_2, room temp.): δ = 69.9, 70.4, 72.1 (C_5H_5 & C_5H_4), 83.6 (C_5H_4CC), 94.3 (CCC_5H_4N), 125.5 (C_β-C_5H_4N), 132.3 (C_γ-C_5H_4N), 150.1 (C_α-C_5H_4N).

1,1′-Bis(4-pyridylethynyl)ferrocene (BPEF): Synthesized by a modified literature procedure for 1,1′-bis(phenylethynyl)ferrocene.[10] A mixture of 1,1′-diiodoferrocene[15] (1.0 g, 2.3 mmol), 4-ethynylpyridine[16] (0.60 g, 5.8 mmol), $Pd(PPh_3)_4$ (0.10 g, 0.090 mmol), CuI (0.018 g, 0.090 mmol), and (iPr)$_2$NH (40 mL) was heated at reflux for 24 h. The solvent was removed under vacuum, and the residue extracted with H_2O/CH_2Cl_2. The organic layer was washed with H_2O, dried with $MgSO_4$, and chromatographed on a SiO_2 (70−220 mesh) column. Successive elution with CH_2Cl_2 and CH_2Cl_2/THF (1:1) led to the development of three bands. The third band in reddish-orange color afforded 0.70 g (89%) of the product. Decomposes at 155 °C. − $C_{24}H_{16}FeN_2$ (387.85): calcd. C 74.26, H 4.13, N 7.22; found C 73.98, H 4.37, N 7.01. − positive FAB-MS: *m/z*: 389 [BPEF + H^+]$^+$. − selected IR (KBr): $\tilde{\nu}$ = 2208 s (C≡C), 1633 m, 1592 vs, 1536 m, 1405 m, 1261 s, 1097 s, 1030 s, 997 m, 932 m, 817 vs, 801 vs, 540 m, 498 s cm^{-1}. − ^{1}H NMR ($CDCl_3$, room temp.): δ = 4.37 (t, 4 H, H_β-C_5H_4), 4.57 (t, 4 H, H_α-C_5H_4), 7.19 (d, 4 H, H_β-C_5H_4N), 8.46 (d, 4 H, H_α-C_5H_4N). − ^{13}C NMR ($CDCl_3$, room temp.): δ = 68.0, 71.4, 73.4 (C_5H_4), 84.5 (C_5H_4CC), 92.4 (CCC_5H_4N), 125.2 (C_β-C_5H_4N), 131.8 (C_γ-C_5H_4N), 149.6 (C_α-C_5H_4N).

$Mo_2(O_2CCF_3)_4(FPA)_2$ (1): A CH_2Cl_2 solution (25 mL) containing $Mo_2(O_2CCF_3)_4$ (0.10 g, 0.16 mmol) and FPA (0.10 g, 0.35 mmol) was stirred at room temperature for 2 h. The solvent was removed under oil pump vacuum and the residue was washed with *n*-hexane. Yield: 0.16 g, 82%. Slow evaporation of the diethyl ether solution of **1** gave crystals suitable for single crystal X-ray analysis. − $C_{42}H_{26}F_{12}Fe_2Mo_2N_2O_8$ (1218.23): calcd. C 41.41, H 2.15, N 2.30; found C 41.16, H 2.24, N 2.19. − Selected IR (KBr): $\tilde{\nu}$ = 2207 s (C≡C), 1601 vs, 1421 m, 1220 vs, 1193 vs. (C−F), 1170 vs, 1155 vs, 1004 s, 925 m, 856 m, 816 s, 779 m, 730 s, 596 m, 538 m, 499 m cm^{-1}. − ^{1}H NMR (CD_2Cl_2, room temp.): δ = 4.23 (s, 10 H, C_5H_5), 4.33 (t, 4 H, H_β-C_5H_4), 4.53 (t, 4 H, H_α-C_5H_4), 7.24 (d, 4 H, H_β-C_5H_4N), 8.03 (d, 4 H, H_α-C_5H_4N). − ^{13}C NMR (CD_2Cl_2, room temp.): δ = 70.2, 70.5, 72.3 (C_5H_5 & C_5H_4), 83.2 (C_5H_4CC), 126.0 (C_β-C_5H_4N), 149.2 (C_α-C_5H_4N), 166.6 (CO_2).

$Rh_2(O_2CCH_3)_4(FPA)_2$ (2): A solution of FPA (0.14 g, 0.50 mmol) in THF (10 mL) was added to a THF solution (30 mL) of $Rh_2(O_2CCH_3)_4$ (0.10 g, 0.23 mmol). The orange precipitate was collected and washed with Et_2O after being stirred at room temperature for 2 h. Yield: 0.18 g, 78%. − $C_{42}H_{38}Fe_2N_2O_8Rh_2$ (1016.28): calcd. C 49.64, H 3.77, N 2.76; found C 49.51, H 3.79, N 2.46. − Selected IR (KBr): $\tilde{\nu}$ = 2205 vs (C≡C), 1593 vs, 1450 m, 1429 vs, 1344 m, 1217 m, 1171 m, 1107 m, 1061 m, 1012 m, 925 m, 826 s, 694 s, 628 m, 600 m, 541 m, 500 s, 483 m, 446 m cm^{-1}. − ^{1}H NMR (CD_2Cl_2, room temp.): δ = 1.88 (s, 12 H, CH_3), 4.31 (s, 10 H, C_5H_5), 4.38 (t, 4 H, H_β-C_5H_4), 4.63 (t, 4 H, H_α-C_5H_4), 7.72 (d, 4 H, H_β-C_5H_4N), 9.11 (s, br, 4 H, H_α-C_5H_4N). − ^{13}C NMR (CD_2Cl_2, room temp.): δ = 30.1 (CH_3), 70.2, 70.6, 72.4 (C_5H_5 & C_5H_4), 126.9 (C_β-C_5H_4N), 150.6 (C_α-C_5H_4N), 191.4 (CO_2).

$Rh_2(O_2CCF_3)_4(FPA)_2$ (3): A solution of FPA (0.096 g, 0.33 mmol) in Et_2O (20 mL) was added to a solution of $Rh_2(O_2CCF_3)_4$ (0.10 g, 0.15 mmol) in Et_2O (10 mL). The orange precipitate was collected and washed with Et_2O after being stirred at room temperature for 2 h. Yield: 0.090 g, 49%. − $C_{42}H_{26}F_{12}Fe_2N_2O_8Rh_2$ (1232.16): calcd. C 40.94, H 2.13, N 2.27; found C 40.50, H 1.98, N 2.16. − selected IR (KBr): $\tilde{\nu}$ = 2206 vs (C≡C), 1662 vs, 1604 vs, 1456 m, 1424 m, 1223 vs, 1193 vs (C−F), 1172 vs, 1016 m, 925 m, 858 m, 818 s, 786 m, 738 s, 603 m, 540 m, 501 m cm^{-1}. − ^{1}H NMR ([D$_8$]THF, room temp.): δ = 4.26 (s, 10 H, C_5H_5), 4.39 (s, 4 H, H_β-C_5H_4), 4.61 (s, 4 H, H_α-C_5H_4), 7.46 (d, 4 H, H_β-C_5H_4N), 8.27 (d, 4 H, H_α-C_5H_4N). − ^{13}C NMR ([D$_8$]THF, room temp.): δ = 70.1, 72.8 (C_5H_5 & C_5H_4), 83.5 (C_5H_4CC), 99.6 (CCC_5H_4N), 113.3 (CF_3), 126.6 (C_β-C_5H_4N), 135.6 (C_γ-C_5H_4N), 152.3 (C_α-C_5H_4N), 175.7 (CO_2).

$[Mo_2(O_2CCF_3)_4(BPEF)]_n$ (4): A CH_2Cl_2 solution (10 mL) of BPEF (0.050 g, 0.13 mmol) was added to a CH_2Cl_2 solution (10 mL) of $Mo_2(O_2CCF_3)_4$ (0.071 g, 0.11 mmol), immediately giving an orange precipitate. After being stirred at room temperature for 2 h, the precipitate was collected and washed with Et_2O. Yield: 0.095 g (84%). − $(C_{32}H_{16}F_{12}FeN_2Mo_2O_8)_n$ ($n \times$ 1032.2): calcd. C 37.24, H 1.56, F 22.09, Fe 5.41, Mo 18.90, N 2.71; found C 37.56, H 1.50, F 23.51, Fe 3.88, Mo 19.24, N 2.67. − Selected IR (KBr): $\tilde{\nu}$ = 2211 m (C≡C), 1633 m, 1603 vs, 1424 m, 1222 vs, 1193 vs (C−F), 1159 vs, 1002 m, 856 m, 824 m, 780 m, 731 vs, 595 s, 502 m cm^{-1}. − ^{1}H NMR ([D$_8$]THF, room temp.): δ = 4.42 (s, 4 H, H_β-C_5H_4), 4.61 (s, 4 H, H_α-C_5H_4), 7.21 (s, 4 H, H_β-C_5H_4N), 8.42 (s, br, 4 H, H_α-C_5H_4N). − ^{13}C NMR ([D$_8$]THF, room temp.): δ = 72.3, 74.2 (C_5H_4), 85.2 (C_5H_4CC), 93.0 (CCC_5H_4N), 114.6 (CF_3), 126.0 (C_β-C_5H_4N), 132.5 (C_γ-C_5H_4N), 150.6 (C_α-C_5H_4N), 166.7 (CO_2).

$[Rh_2(O_2CCH_3)_4]_{n+1}(BPEF)_n$ ($n \approx$ 3) (5): A THF solution (15 mL) of $Rh_2(O_2CCH_3)_4$ (0.057 g, 0.13 mmol) was added to a THF solution (5 mL) of BPEF (0.050 g, 0.13 mmol). The orange precipitate was collected and washed with THF after being stirred at room temperature for 2 h. Yield: 0.10 g, 93%. − $C_{104}H_{96}Fe_3N_6O_{32}Rh_8$ (2932.71): calcd. C 42.59, H 3.30, Fe 5.71, N 2.87, Rh 28.07; found C 42.74, H 3.54, Fe 6.03, N 2.94, Rh 27.6. − selected IR (KBr): $\tilde{\nu}$ = 2208 m (C≡C), 1592 vs, 1500 m, 1429 vs, 1346 m, 1216 m, 1046 m, 1027 m, 1010 m, 827 m, 696 s, 628 m, 555 m, 478 m cm^{-1}.

$[Rh_2(O_2CCF_3)_4]_n(BPEF)_{n+1}$ (n = 9−14) (6): A CH_2Cl_2 solution (10 mL) of $Rh_2(O_2CCF_3)_4$ (0.039 g, 0.059 mmol) was quickly added to a CH_2Cl_2 solution (10 mL) of BPEF (0.023 g, 0.059 mmol). The reddish-orange precipitate was collected after 1 h and washed with Et_2O. Yield: 0.055 g, 86%. − For calculated analytical data refer to Table 2; found C 38.00, H 1.66, F 20.52, Fe 5.35, N 2.85, Rh 19.4. − Selected IR (KBr): $\tilde{\nu}$ = 2210 m (C≡C), 1666 vs, 1606 s, 1426 m, 1222 vs, 1194 vs (C−F), 1169 vs, 1016 m, 858 m, 828 m, 786 m, 738 s, 540 m, 503 m cm^{-1}.

X-ray Crystallography: Crystal data and details of the structure determination are presented in Table 3. A clear red-brown plate (0.25 × 0.15 × 0.05 mm) was employed for the analysis. Preliminary examination and data collection were carried out on a Kappa CCD area detecting diffraction system (NONIUS; MACH^3) equipped with a rotating anode and graphite monochromated Mo-K_α radiation (NONIUS; FR 591). The unit cell parameters were obtained by full-matrix least-squares refinements of 31046 reflections. Data collection were performed at 153 K (exposure time: 60 s per frame; 9 sets, and Ω-scans, Δ/ΔΩ: 1°; *d*x: 40.0 mm). A total number of 19385 reflections were collected. Raw data were corrected for Lorentz and polarization effects, corrected for absorption and decay effects and scaled with the program DENZO-SMN. After merging (R_{int} = 0.0184) a sum of 4089 independent reflections remained and were used for all calculations. All "heavy atoms" of the asymmetric unit were refined anisotropically. All hydrogen atoms were located in the difference Fourier map and refined with individual isotropic temperature parameters. Full-matrix least-squares refinements were carried out by minimizing $\Sigma w(F_o^2 - F_c^2)^2$ with SHELX-97 weighting scheme and stopped at shift/err < 0.001. Neutral atom scattering factors for all atoms and anomalous dispersion

corrections for the non-hydrogen atoms were taken from *International Tables for Crystallography.* All calculations were performed on a DEC 3000 AXP workstation and an Intel Pentium II PC, with the STRUX system, including the programs PLATON, SIR92, and SHELX-97.[17]

Table 3. Selected crystallographic data for $[Mo_2(O_2CCF_3)_4(FPA)_2]$ (**1**)

Empirical formula	$C_{42}H_{26}F_{12}Fe_2Mo_2N_2O_8$
fw	1218.23
Crystal system	triclinic
Space group	$P\bar{1}$
a [pm]	1034.29(2)
b [pm]	1040.16(3)
c [pm]	1175.90(3)
α [deg]	100.876(1)
β [deg]	115.989(1)
γ [deg]	95.447(1)
V [10^6 pm^3]	1093.88(5)
Z	1
$\rho_{calcd.}$ [g cm^{-3}]	1.849
F_{000}	600
μ [mm^{-1}]	1.316
Θ range [deg]	2.04 to 25.58
Data collcd (*h,k,l*)	±12, ±12, ±14
No. of reflections collected	19385
No. of independent reflections (all data)	4089
No. of observed reflections [$I_o > 2\sigma(I_o)$]	3796
No. of parameters refined	359
$R1$[a] [$I_o > 2\sigma(I_o)$/all data]	0.0265/0.0291
$wR2$[b]	0.0662
GOF[c]	1.034
Weights *a*/*b*[d]	0.0241/1.4782
$\Delta\rho_{max/min}$ [e Å^{-3}]	1.07/−0.54

[a] $R1 = \Sigma(||F_o| - |F_c||)/\Sigma|F_o|$. – [b] $wR2 = [\Sigma w (F_o^2 - F_c^2)^2/\Sigma w (F_o^2)^2]^{1/2}$. – [c] $GOF = [\Sigma w (F_o^2 - F_c^2)^2/(NO - NV)]^{1/2}$. – [d] $w = 1/[\sigma^2(F_o^2) + (a*P)^2 + b*P]$ with P: [max (0 or F_o^2) + $2F_c^2$]

Crystallographic data (excluding structure factors) for the structures reported in this paper have been deposited with the Cambridge Crystallographic Data Centre as supplementary publication no. CCDC-150833 (**1**). Copies of the data can be obtained free of charge on application to CCDC, 12 Union Road, Cambridge CB2 1EZ, UK [Fax: (internat.) +44-1223/336-033; E-mail: deposit@ccdc.cam.ac.uk].

Acknowledgments

W.-M. X. thanks the Alexander von Humboldt Foundation for a postdoctoral research associate fellowship. Professor W. A. Herrmann is acknowledged for continuous support of our work. Professor D. Wabner and Mr. T. Görlach are acknowledged for helpful discussions concerning cyclovoltammetry and DPV measurement.

[1] [1a] *Inorganic materials* (Eds.: D. W. Bruce, D. O'Hare), Wiley, **1992**. – [1b] *Extended Linear Chain Compounds*, *Vol. 1–3*, (Ed.: J. S. Miller), Plenum, New York, **1982**. – [1c] L. Oriol, J. L. Serrano, *Adv. Mater.* **1995**, *7*, 348. – [1d] N. G. Connelly, W. E. Geiger, *Adv. Organomet. Chem.* **1984**, *23*, 1. – [1e] N. G. Connelly, W. E. Geiger, *Adv. Organomet. Chem.* **1985**, *24*, 87. – [1f] M. H. Chisholm, *Acc. Chem. Res.* **2000**, *33*, 53 and references cited therein.

[2] [2a] *Multiple Bonds Between Metal Atoms* (Eds.: F. A. Cotton, R. A. Walton), 2nd edition, Oxford University Press, London, **1993**. – [2b] F. A. Cotton, T. R. Felthouse, *Inorg. Chem.* **1980**, *19*, 328. – [2c] F. A. Cotton, T. R. Felthouse, *Inorg. Chem.* **1981**, *20*, 600. – [2d] F. A. Cotton, Y. Kim, T. Ren, *Inorg. Chem.* **1992**, *31*, 2723. – [2e] F. A. Cotton, J. G. Norman, *J. Coord. Chem.* **1971**, *1*, 161.

[3] [3a] M. Handa, K. Kasamatsu, K. Kasuge, M. Mikuriya, T. Fujii, *Chem. Lett.* **1990**, 1753. – [3b] B. Morison, R. C. Hughes, Z. G. Soos, *Acta Crystallogr.* **1975**, *B31*, 762. – [3c] J. L. Wesemann, M. H. Chrisholm, *Inorg. Chem.* **1997**, *36*, 3258. – [3d] M. Handa, H. Matsumoto, D. Yashioka, R. Nukada, M. Mikuriya, I. Hiromitsu, K. Kasuge, *Bull. Chem. Soc. Jpn.* **1998**, *71*, 1811. – [3e] X. Ouyang, C. Campana, K. R. Dunbar, *Inorg. Chem.* **1996**, *35*, 7188. – [3f] M. C. Kerby, B. W. Eichhorn, J. A. Creighton, K. P. C. Vollhardt, *Inorg. Chem.* **1990**, *29*, 1319.

[4] [4a] A. Togni, M. Hobi, G. Rihs, G. Rist, A. Albinati, P. Zanello, D. Zech, H. Keller, *Organometallics* **1994**, *13*, 1224. – [4b] R. Rulkens, A. J. Lough, I. Manners, S. R. Lovelace, C. Grant, W. E. Geiger, *J. Am. Chem. Soc.* **1996**, *118*, 12683. – [4c] F. F. Debiani, T. Gmeinwieser, E. Herdtweck, F. Jäkle, F. Laschi, M. Wagner, P. Zanello, *Organometallics* **1997**, *16*, 4776. – [4d] F. F. Debiani, F. Jäkle, M. Spiegler, M. Wagner, P. Zanello, *Inorg. Chem.* **1997**, *36*, 2103. – [4e] M. Fontani, F. Peters, W. Scherer, W. Wachter, M. Wagner, P. Zanello, *Eur. J. Inorg. Chem.* **1998**, 1453. – [4f] M. Grosche, E. Herdtweck, F. Peters, M. Wagner, *Organometallics* **1999**, *18*, 4669.

[5] [5a] R. W. Wagner, P. A. Brown, T. E. Johnson, J. S. Lindsey, *J. Chem. Soc., Chem. Commun.* **1991**, 1463. – [5b] E. C. Constable, *Angew. Chem. Int. Ed. Engl.* **1991**, *30*, 407.

[6] See, for example: – [6a] K. L. Kott, D. A. Higgins, R. J. McMahon, R. M. Corn, *J. Am. Chem. Soc.* **1993**, *115*, 5342. – [6b] Z. Yuan, N. J. Taylor, Y. Sun, T. B. Marder, I. D. Williams, L.-T. Cheng, *J. Organomet. Chem.* **1993**, *449*, 27. – [6c] Z. Yuan, G. Stringer, I. R. Jobe, D. Kreller, K. Scott, L. Koch, N. J. Taylor, T. B. Marder, *J. Organomet. Chem.* **1993**, *452*, 115. – [6d] Benito, J. Cano, R. Martinez-Manez, J. Paya, J. Soto, M. Julve, F. Loret, M. D. Marcos, E. Sinn, *J. Chem. Soc., Dalton Trans.* **1993**, 1999.

[7] P. Nguyen, P. Gómez-Elipe, I. Manners, *Chem. Rev.* **1999**, *99*, 1515, and references therein.

[8] 3d Search and Research Using the Cambridge Structural Database; F. H. Allen, O. Kennard, *Chemical Design Automation News* **1993**, *8*, 1 and 31–37. The refcodes are as follows: BEYFIU, BURTEN, BURTIR (2x), MOTFAC, REPPUX, TFACMO, TIZWUU, TUFVIZ, VOZCIW, WEJZIU.

[9] T. H. Barr, W. E. Watts, *J. Organomet. Chem.* **1968**, *15*, 177.

[10] [10a] W.-M. Xue, F. E. Kühn, G. Zhang, E. Herdtweck, *J. Organomet. Chem.* **2000**, *596*, 177. – [10b] W.-M. Xue, F. E. Kühn, G. Zhang, E. Herdtweck, G. Raudaschl-Sieber, *J. Chem. Soc., Dalton Trans.* **1999**, 4103.

[11] G. A. Rempel, P. Legzdius, H. Smith, G. Wilkinson, *Inorg. Synth.* **1972**, *13*, 90.

[12] J. Kitchens, J. L. Bear, *Thermochimica Acta* **1970**, *1*, 537.

[13] M. Rosenblum, N. Brawn, J. Papenmeier, M. Applebaum, *J. Organomet. Chem.* **1966**, *6*, 173.

[14] J. T. Lin, J. J. Wu, C.-S. Li, Y. S. Wen, K.-J. Lin, *Organometallics* **1996**, *15*, 5028.

[15] R. F. Kovar, M. D. Rausch, H. Rosenberg, *Organomet. Chem. Synth.* **1970/1971**, *1*, 173.

[16] L. D. Ciana, A. Haim, *J. Heterocyclic Chem.* **1984**, *21*, 607.

[17] Data collection and data reduction: [17a] B. V. Nonius, NONIUS MACH3 *Operating System Version 5.1*, Delft, The Netherlands, **1994**. – [17b] Z. Otwinowski, W. Minor, *Methods in Enzymology* **1997**, *276*, 307. – [17c] *Tables for Crystallography*, Vol. C, Tables 6.1.1.4 (pp. 500–502), 4.2.6.8 (pp. 219–222), and 4.2.4.2 (pp. 193–199), Ed. A. J. C. Wilson, Kluwer Academic Publishers, Dordrecht, The Netherlands, **1992**. – [17d] G. Artus, W. Scherer, T. Priermeier, E. Herdtweck, *STRUX-V, A Program System to Handle X-ray Data*, TU München, Germany, **1997**. Structure solution: [17e] SIR92: A. Altomare, G. Cascarano, C. Giacovazzo, A. Guagliardi, M. C. Burla, G. Polidori, M. Camalli, , *J. Appl. Cryst.* **1994**, *27*, 435. Structure refinement: [17f] G. M. Sheldrick, *SHELXL-97*, University of Göttingen, Göttingen, Germany, **1998**. Graphics: [17g] A. L. Spek, *PLATON, A Multipurpose Crystallographic Tool*, Utrecht University, Utrecht, The Netherlands, **1999**.

Received April 17, 2000
[I00153]

Theoretical Studies of $[Os_3(CO)_{10}(\alpha\text{-Diimine})]$: Structures, Frontier Orbitals and Bonding

Maria José Calhorda,*[a,b] Elke Hunstock,[a] Luís F. Veiros,[c] and František Hartl[d]

Keywords: Osmium / Cluster compounds / DFT calculations / Charge transfer / Molecular orbitals / Diimines

DFT calculations were performed on $Os_3(CO)_{10}$(α-diimine) clusters, for α-diimine = DAB (1,4-diaza-1,3-butadiene), PYCA (σ-*N*,σ-*N*′-pyridine-2-carbaldehyde-imine), and BIPY (2,2′-bipyridine). Geometry optimizations were performed for several models of the possible isomers under different conditions. Axial isomers were always found to be the most stable, in agreement with the available X-ray determined structures. A full optimization of the geometry was required in order to improve the quality of the results, but the distances tended to be longer than the experimental ones. In spite of these shortcomings, the nature of the frontier orbitals, showing the increasing localization of the cluster LUMO in the α-diimine ligand as this is expanded (45, 65, 76% for DAB, PYCA, and BIPY, respectively), was consistent with the increasing MLCT character of the HOMO–LUMO transition along the series. Extended Hückel calculations were able to reproduce these trends qualitatively.

Introduction

There is a significant number of theoretical studies dealing with binary carbonyl transition metal clusters. The $M_3(CO)_{12}$ triad (M = Fe, Ru, Os) has been the object of a very important fraction of such studies, the relevant issue being that the iron derivative exhibits C_{2v} symmetry and has two bridging carbonyls over one edge, while both the ruthenium and the osmium clusters only possess terminal carbonyls. Several levels of theory have been used, starting from semiempirical extended Hückel (EH) and INDO calculations, up to HF and MP2 calculations, and more recently DFT methods.[1] Semiempirical methods can be applied to all clusters, independently of their size and symmetry, and this is their main advantage. On the other hand, more sophisticated methods can give a better answer to specific problems and become more reliable when trying to predict structures of molecules. From our previous experience, it is known that DFT methods are very adequate for dealing with first-row transition-metal clusters, while MP2 becomes the best choice for third-row derivatives. On the other hand, MP2 takes considerable time and requires extensive computer capabilities when studying large systems.[2]

Theoretical studies of mixed clusters containing other ligands besides carbonyls are less common, although they involve much chemistry.[3] The influence of the nature of the ligands on carbonyl bridge formation has been studied and it was found that coordination of π-donors can increase the tendency to form carbonyl bridges in clusters of second-row transition metals, such as ruthenium or rhodium, when they are absent in the binary carbonyl parent cluster.[4] Some publications address the triosmium clusters in detail. Morokuma and co-workers studied the bonding in $Os_3(CO)_9(C_6H_6)$ using single-point MP2 energy calculations on HF-optimized structures, and EH for orbital analysis.[5] Some of us qualitatively analyzed the bonding of *ortho*-metallated α-diimines to $HOs_3(CO)_9$.[6a]

In this work, DFT calculations[7] performed under different conditions and on models of three $Os_3(CO)_{10}$(α-diimine) clusters are described, and the reliability of extended Hückel[8] calculations on these systems is discussed. This study was prompted by the rich photochemistry[9] and intriguing electrochemistry[6] exhibited by these clusters. Di- and trinuclear transition-metal carbonyls with the α-diimine ligand have been found to undergo a photochemical metal−metal bond homolysis from a low-lying σπ* excited state, in which σ represents the metal−metal bonding orbital and π* represents the lowest unoccupied orbital of the α-diimine. This excited state is either directly optically available or can be occupied by surface crossing from the metal-to-α-diimine (MLCT) states.[10] Experimental results indicate that a similar situation also applies to the $Os_3(CO)_{10}$(α-diimine) clusters which produce diradicals in non-coordinating or weakly coordinating solvents upon irradiation with visible light.[9] This knowledge can be used to check the accuracy of our model compounds, as will be discussed later.

[a] ITQB, Quinta do Marquês, EAN, Apart. 127, 2781-901 Oeiras, Portugal
[b] Departamento de Química e Bioquímica, Faculdade de Ciências, Universidade de Lisboa, 1749−016 Lisboa, Portugal
[c] Centro de Química Estrutural, IST, Av. Rovisco Pais, 1049-001 Lisboa, Portugal
[d] Universiteit van Amsterdam, Institute of Molecular Chemistry, Nieuwe Achtergracht 166, 1018 WV Amsterdam, The Netherlands

 © WILEY-VCH Verlag GmbH, 69451 Weinheim, 2001 1434−1948/01/0101−0223 $ 17.50+.50/0

Results and Discussion

Molecular Structures

Three model α-diimine ligands were considered in this work, namely DAB (1,4-diaza-1,3-butadiene), PYCA (σ-*N*,σ-*N*′-pyridine-2-carbaldehyde-imine), and BIPY (2,2′-bipyridine), as depicted in Scheme 1. They differ by the progressive replacement of the imine C=N bonds by pyridine rings.

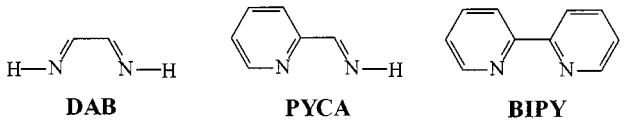

Scheme 1

The $Os_3(CO)_{10}$(DAB) cluster (**1**) was the first to be studied (see Experimental Section for details) and the availability of the X-ray structure of the related $Os_3(CO)_{10}$(*i*Pr-DAB)[11] provided a good starting point for the calculations. In principle, two alternative structures are possible for this cluster with the α-diimine σ-*N*,σ-*N*′-chelated to a single osmium atom, namely the axial and the equatorial one, as depicted in Scheme 2, left and right.

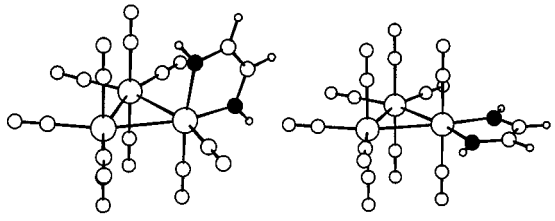

Scheme 2

The axial isomer (left) has no symmetry (C_1), while the equatorial isomer has two mirror planes and a twofold rotation axis. The first model was very similar to what can be seen in Scheme 2, since the terminal carbonyl groups were forced to lie on the Os3 plane or to be perpendicular to it. The other variables were optimized. The axial isomer (**1aL**) was found by DFT calculations to be more stable by 0.83 eV. A relatively large basis set (see basis set L in Experimental Section) was used for these two initial calculations. A reduced basis set (see Experimental Section) was used afterwards (**1a**) because the size of the other ligands (PYCA and BIPY) prevented the use of the larger one. Obviously, the same conditions must be used in order to compare results for the three α-diimine ligands. Extended Hückel calculations[8] led to a similar result, namely that the axial isomer was more stable by 0.75 eV.

The features of the rigid models **1aL** and **1a** significantly deviated from those of the available crystal structure of $Os_3(CO)_{10}$(*i*Pr-DAB). Besides the distances, to which we shall come back, the angles were totally different. Therefore, the model for the more stable axial isomer was improved, making it more flexible by allowing all the torsion angles to vary (**1b**). The calculated DFT energy dropped by 0.71 eV. A single-point calculation was also performed using the coordinates of the experimental structure (**1c**). The energies cannot be compared, as there are two isopropyl substituents on the DAB nitrogen atoms. However the nature of the frontier orbitals should be similar if the model is reliable, and calculated and experimental bond lengths can therefore be compared. The geometry of the axial isomer, with C_1 symmetry, was also optimized using *Gaussian 94*[12] (**1d**; HF; see Experimental for details). A general idea of the structural differences between the five calculations of the axial isomer can be inferred from the drawings in Scheme 3, showing the rigid model (**1a**), the more flexible model (**1b**), the experimental structure on the top right (**1c**), the rigid model (basis set L; **1aL**), and the flexible model (Gaussian; **1d**).

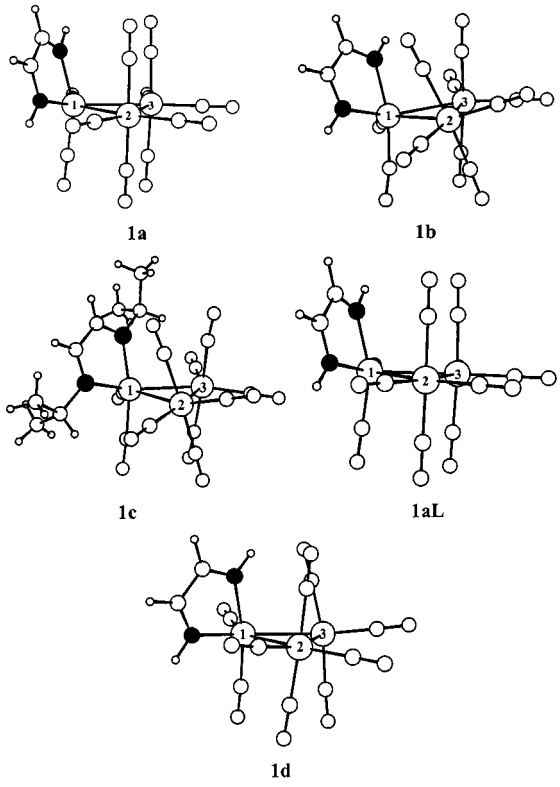

Scheme 3

The most relevant distances (Os−Os and Os−N) are listed in Table 1, and while the main features of the observed structure are reproduced in the calculations, the distances tend to be too long when DFT methods are used (**1a, 1b**). Although only the HF approach could be used owing to the size of the cluster, the distances (**1d**) are in

Table 1. Selected distances (pm) in several models and calculation levels of $Os_3(CO)_{10}$(DAB) (**1a, 1aL, 1b, 1d**) and in $Os_3(CO)_{10}$(*i*Pr-DAB) (**1c**)

Bond/Model	**1a**	**1aL**	**1b**	**1c** (exp.)	**1d**[a]
Os1−Os2	305.0	303.2	297.9	287.7	292.3
Os1−Os3	301.6	301.3	300.6	288.0	292.5
Os2−Os3	303.7	304.6	299.9	286.7	296.9
Os1−N1	212.0	210.9	213.7	211.4	215.5
Os1−N2	212.0	210.9	209.3	206.6	207.3

[a] HF calculations.

better agreement with the experimental ones (**1c**), especially with respect to the Os−Os bonds.

The first two columns in Table 1 demonstrate the effect of the basis set. The larger one (**1aL**) leads to shorter distances, but exceeded our computing capabilities when we moved to the larger α-diimine ligands. A comparison of the values in columns **1a** and **1b** shows, however, that the effect of using a better model is more important. Indeed, the full geometry optimization is more effective in reducing bond lengths than increasing the basis set. For instance, Os1−Os2 drops from 305.0 pm in **1a** to 303.2 in **1aL** with the better basis set, but to 297.9 pm in **1b**, with a better model and a small basis set, getting closer to the experimental value of 287.7 pm (**1c**).When the same model is used and one compares DFT and HF, it can be seen that this last method leads to shorter Os−Os bond lengths. The computation time is increased, though, and one of the Os−N bonds is even longer. The size and lack of symmetry of compound **1** precluded an MP2 calculation, although recent calculations on the more symmetric $Os_3(CO)_{12}$ showed MP2 to reproduce distances better.[2]

Another interesting aspect of the experimental structure, also reproduced by the full optimization procedure, concerns the torsion angles around the carbonyl groups. Although a list of their values is of limited value, it can be noted that some of them move away from the perpendicular to the Os3 plane by up to 25°, as clearly seen in Scheme 3. The HF structure (**1d**) has bond lengths in good agreement with the experimental structure (**1c**), but the torsion angles are very different, and the carbonyls bend in the wrong direction, revealing the limitations of this approach. The overall picture provided by the DFT-optimized structure is more realistic, despite the long bond lengths.

The introduction of the first pyridine ring changes DAB into PYCA (Scheme 1). As the ligand is asymmetric, there are more possible isomers for the model compound $Os_3(CO)_{10}$(PYCA) (**2**), as the two axial isomers (**2a1, 2a2**) shown in Scheme 4 (top and center) are not equivalent. The equatorial isomer (**2a3**) is the more symmetric one, with a mirror plane (C_s).

There is no X-ray structure available for compound **2** or a related one. DFT calculations with the standard basis set, keeping the carbonyls perpendicular to or on the Os_3 plane, were performed for the three isomers. The most stable is the axial isomer **2a1**. The other axial isomer **2a2** has a higher energy (0.18 eV), while the equatorial **2a3**, with an energy 0.31 eV higher than **2a1**, is the least stable. For this $Os_3(CO)_{10}$(PYCA) cluster, EH calculations showed the axial species **2a2** to be the most stable, followed by **2a3** (0.28 eV) and **2a1** (2.23 eV). This result can be traced to steric repulsion between the pyridine ring of the ligand and the carbonyls perpendicular to the Os_3 plane, as no geometry optimization was made. The DFT calculations, allowing for these repulsions to be relieved during the geometry-optimization process, led to a more likely order of stability, with **2a1** being the most stable isomer.[13] Also, since the carbonyl groups are much stronger π-acceptors than the α-diimines, *cis*-$Os_3(CO)_2$ geometries (as in the axial isomers) are more stable than structures with carbonyls in *trans* positions (the equatorial isomer) competing for π back donation from the same metal orbitals.

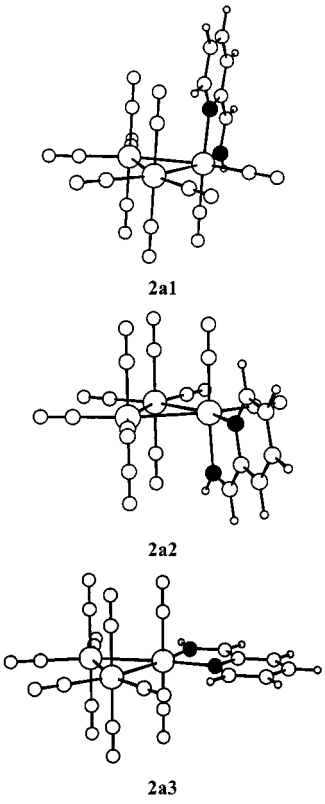

Scheme 4

A full optimization of the axial isomer (**2b**), taking all the degrees of freedom into account, resulted in a more stable cluster (0.94 eV), as expected from the study of the DAB derivatives. A complete geometry optimization using Gaussian94 HF, was also performed (**2d**). The representation of the geometries clarify the changes in the carbonyl positions which take place as the model improves (Scheme 5). The relevant distances are given in Table 2.

These distances can be compared with those of $Os_3(CO)_{10}$(*i*Pr-DAB) given in Table 1. The conclusions are similar to those drawn above, namely that DFT methods give too long distances. The HF calculation leads to shorter Os−Os bonds, but on the other hand one of the Os−N bonds is the largest. Interestingly, for this system, the carbonyls occupy the same positions as in the DFT-optimized structures and in $Os_3(CO)_{10}$(*i*Pr-DAB), in opposition to what was found for the model DAB cluster.

The third cluster studied was $Os_3(CO)_{10}$(BIPY) (**3**). There are two isomers, an axial and an equatorial one, similar to those in Scheme 2. A complete optimization of both isomers was performed using DFT calculations, and the axial isomer was found to be more stable by 0.52 eV. The drawings of the optimized structures of the (**3b1**) axial and equatorial (**3b2**) isomers and the X-ray structure of $Os_3(CO)_{10}$(BIPY) (**3c**)[14] are represented in Scheme 6. Both the calculated Os−Os and Os−N distances are too long compared with the observed ones (Table 3).

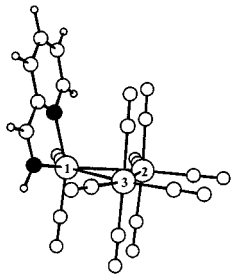

2a1

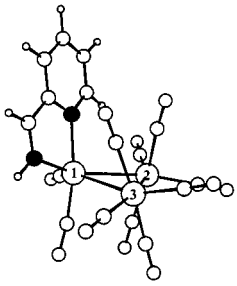

2b

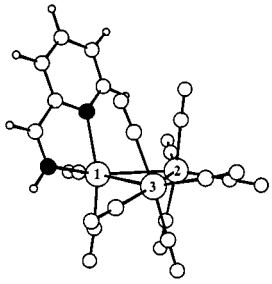

2d

Scheme 5

Table 2. Selected distances (pm) in several models and calculation levels of $Os_3(CO)_{10}$(PYCA) (**2a1, 2b, 2d**)

Bond/Model	**2a1**	**2b**	**2d**[a]
Os1−Os2	308.6	293.7	289.6
Os1−Os3	300.6	304.1	296.6
Os2−Os3	300.2	297.2	297.1
Os1−N1	217.3	222.5	226.3
Os1−N2	217.3	211.9	211.7

[a] HF calculations.

Since the geometry of the two isomers of $Os_3(CO)_{10}$(BIPY) was fully optimized, they can be compared more reliably. From the two drawings in Scheme 6, it can be seen that the carbonyls do not need to distort so much away from directions perpendicular to the Os3 plane in the case of the equatorial isomer. This reflects a smaller number of steric repulsive interactions in the axial isomer of the cluster. This steric constraints are reflected in the EH relative energies of the two isomers (idealized geometries with carbonyls perpendicular or in the plane of Os_3): the axial isomer is less stable by 2.07 eV. If the carbonyls are allowed to bend back, away from the α-diimine ligand, the energy immediately starts to drop. It is worth noting that in the DAB cluster, where steric repulsions are negligible, the axial

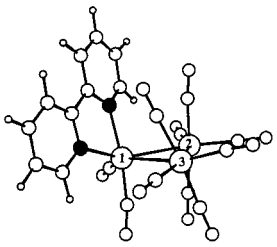

3b1

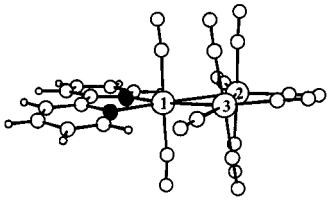

3b2

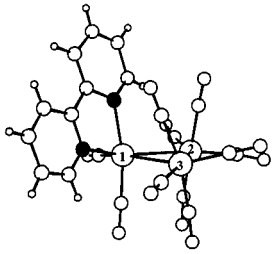

3c

Scheme 6

Table 3. Selected distances (pm) in the axial (**3b1**) and equatorial (**3b2**) isomers of $Os_3(CO)_{10}$(BIPY) and in the experimental structure (**3c**).

Bond/Model	**3b1**	**3b2**	**3c**
Os1−Os2	292.2	301.9	284.1
Os1−Os3	309.5	301.1	290.1
Os2−Os3	297.7	303.8	288.4
Os1−N1	219.8	219.4	217.9
Os1−N2	220.3	220.3	209.0

isomer was found to be the most stable by EH calculations. The introduction of the pyridine rings reverses this pattern and demands further optimization of the geometry (as done in the DFT calculations).

The Os−Os distances are the same in $Os_3(CO)_{10}$(BIPY) and in $Os_3(CO)_{10}$(*i*Pr-DAB) within experimental error, so that any of them can be used to check the calculations on $Os_3(CO)_{10}$(PYCA).

A Qualitative View of the Bonding

The three α-diimine ligands DAB, PYCA, and BIPY have an increasingly large π-system. The bonding of DAB to the cluster is achieved by σ-donation from the two equivalent nitrogen lone-pair orbitals, as the symmetric and antisymmetric combinations, to empty cluster orbitals localized in Os1. There is also a back-donation component from the cluster to the second π* (DAB), LUMO. The set of π orbitals of DAB is very similar to that of 1,3-butadiene, taking into account the different electronegativities of carbon

and nitrogen. The interaction between DAB and $Os_3(CO)_{10}$ is depicted on the right hand side of Figure 1 (EH calculations). The corresponding interaction with PYCA is shown on the left hand side.

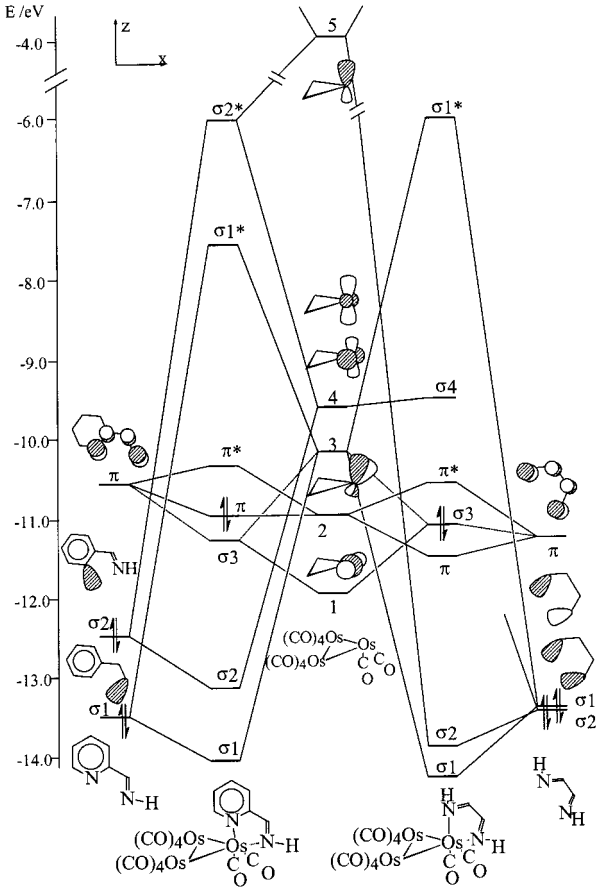

Figure 1. Molecular orbital diagram between the cluster fragment $Os_3(CO)_{10}$ (center) and DAB (right) or PYCA (left), showing the most relevant interactions

The presence of the pyridine ring lifts the degeneracy between the two nitrogen lone pairs. The π* (PYCA) LUMO, the acceptor orbital, is largely localized on the same atoms as in DAB, but lies at higher energy owing to the larger number of nodes (not shown). As a consequence, the LUMO of the triosmium clusters, which is the antibonding combination arising from this back-donation component involving π* (PYCA), is expected to possess different a character in the two clusters. In $Os_3(CO)_{10}$DAB, the energy match is better, the interaction stronger, the covalent character more pronounced, and the levels are delocalized between the carbonyl−osmium fragment and the DAB ligand. For $Os_3(CO)_{10}$PYCA, the energy match is not as good, and the cluster LUMO is much more located on the π* (PYCA) orbital (closer in energy) than on the cluster core. The trend is qualitatively the same as one moves to BIPY. The corresponding π* (BIPY) LUMO lies at a higher energy than that of PYCA, and the cluster LUMO becomes even more localized on the BIPY ligand. We come back to these features in the next section.

The Frontier Orbitals (DFT) and the MLCT Transition

As was discussed above, the agreement between experimental and calculated structures using DFT methods improves when the model is improved and a full optimization is performed. The other feature associated with the different models which changes significantly is the composition of the frontier orbitals. This is of great importance because one of the aims of the present study is to understand and compare the character of the lowest-energy electronic transition in the three investigated clusters, and a reliable way of determining that orbital composition is essential.

The results for the $Os_3(CO)_{10}$(DAB) models compared with those of the experimental structure are given in Table 4.

Table 4. Composition of the frontier orbitals (%) of two models of $Os_3(CO)_{10}$(DAB) (**1a, b**) and of $Os_3(CO)_{10}$(*i*Pr-DAB) (**1c**)

	1a			**1b**				**1c**		
m.o.	Os1	Os2,3	DAB	Os1	Os2,3	DAB	m.o.	Os1	Os2,3	DAB
75a	23	10	26	20	15	16	93a	18	12	13
74a[a]	11	24	21	11	17	45	92a[a]	8	12	53
73a[b]	20	12	39	15	17	39	91a[b]	15	19	33
72a	57	7	16	14	44	3	90a	21	26	14
71a	20	41	5	32	21	9	89a	12	41	2
70a	40	21	12	48	19	9	88a	57	10	13

[a] LUMO. − [b]HOMO.

There is a striking difference in the composition of the LUMO, as one moves from the more primitive (**1a**), to the better model (**1b**), and to the real structure (**1c**). The LUMO becomes much more localized on the DAB ligand, going from only 21%, to 45%, and 53%, the last two numbers being comparable. The HOMO is not as sensitive to the type of model.

Table 5. Composition of the frontier orbitals (%) of two models of $Os_3(CO)_{10}$(PYCA) (**2a1, 2b**)

	2a1			**2b**		
m.o.	Os1	Os2,3	PYCA	Os1	Os2,3	PYCA
84a	22	12	24	23	18	11
83a[a]	8	19	40	7	11	65
82a[b]	22	15	34	18	21	28
81a	10	59	10	21	34	4
80a	27	33	6	23	33	7
79a	33	30	8	49	21	7

[a] LUMO. − [b] HOMO.

Table 6. Composition of the frontier orbitals (%) of the model and the observed structure of $Os_3(CO)_{10}$(BIPY) (**3b1, c**)

	3b1			**3c**		
m.o.	Os1	Os2,3	BIPY	Os1	Os2,3	BIPY
93a	18	17	30	1	1	96
92a[a]	5	7	76	3	3	87
91a[b]	20	24	19	21	23	13
90a	25	29	5	19	29	9
89a	23	34	7	11	40	7
88a	51	20	4	56	15	6

[a] LUMO. − [b] HOMO.

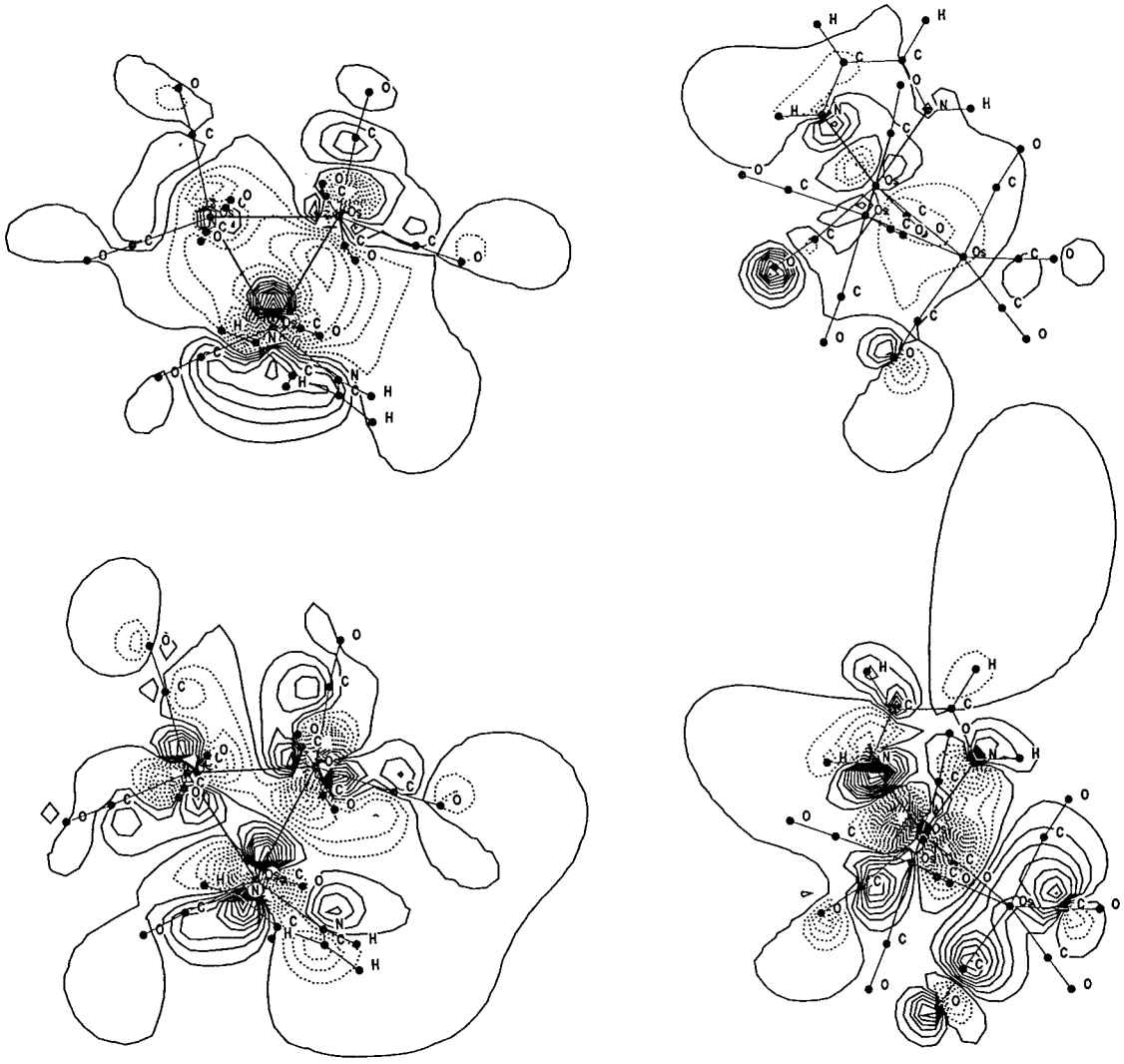

Figure 2. Wavefunction contour plots of the HOMO (top) and LUMO (bottom) of $Os_3(CO)_{10}$(DAB) (**1b**), in the Os_3 plane (left) and in the N−Os−N plane (right)

The same behavior has been found for the $Os_3(CO)_{10}$-(PYCA) cluster (Table 5).

It can be seen that the LUMO has only a contribution of 40% of the ligand in the primitive model, which increases to 65% in **2b**. Conversely, the ligand contribution to the HOMO drops. There is no structure of the cluster, so these values cannot be checked. For $Os_3(CO)_{10}$(BIPY) (Table 6) only the best model (**3b1**) was calculated (full optimization) and there is an experimental structure (**3c**).

There is a good agreement between the composition of the orbitals of the model and of the observed structure, suggesting that our model, in spite of its limitations with regard to the reproduction of bond lengths, describes accurately the nature of the frontier orbitals.

The character of the frontier orbitals can be seen in a better way in the two-dimensional wavefunction plots of Figure 2. In two-dimensional plots, a convenient plane to plot the wavefunction contours must be chosen. In the $Os_3(CO)_{10}$(α-diimine) clusters, the relevant planes are those defined by N−Os−N and by Os_3. We show in Figure 2 both the HOMO and the LUMO for $Os_3(CO)_{10}$(DAB) (**1b**), as two-dimensional plots in the Os_3 plane (left) and in the N−Os−N plane (right).

The same representation is given for $Os_3(CO)_{10}$(BIPY) (**3b1**), in order to compare the character of the orbitals (Figure 3).

The relative energies of the molecular orbitals are also important for the analysis of the electronic transitions. They also depend on the model used to describe the cluster, as can be seen from the selection given in Table 7, for models of $Os_3(CO)_{10}$(DAB) (**1a, 1b**) and $Os_3(CO)_{10}$(*i*Pr-DAB) (**1c**). The HOMO−LUMO gap is 1.76 eV for $Os_3(CO)_{10}$(*i*Pr-DAB) (**1a**), close to the value obtained for the flexible model **1b** (1.66 eV), but much larger than the result obtained with the rigid model **1a** (1.46 eV).

Finally, in Table 8 we give the relative energies of the frontier orbitals for the flexible models of the axial isomers of the three clusters (**1b, 2b, 3b1**) and $Os_3(CO)_{10}$(BIPY). The HOMO−LUMO gap varies with the α-diimine ligand, going from 1.66 eV for the DAB cluster, to 1.50 eV for the

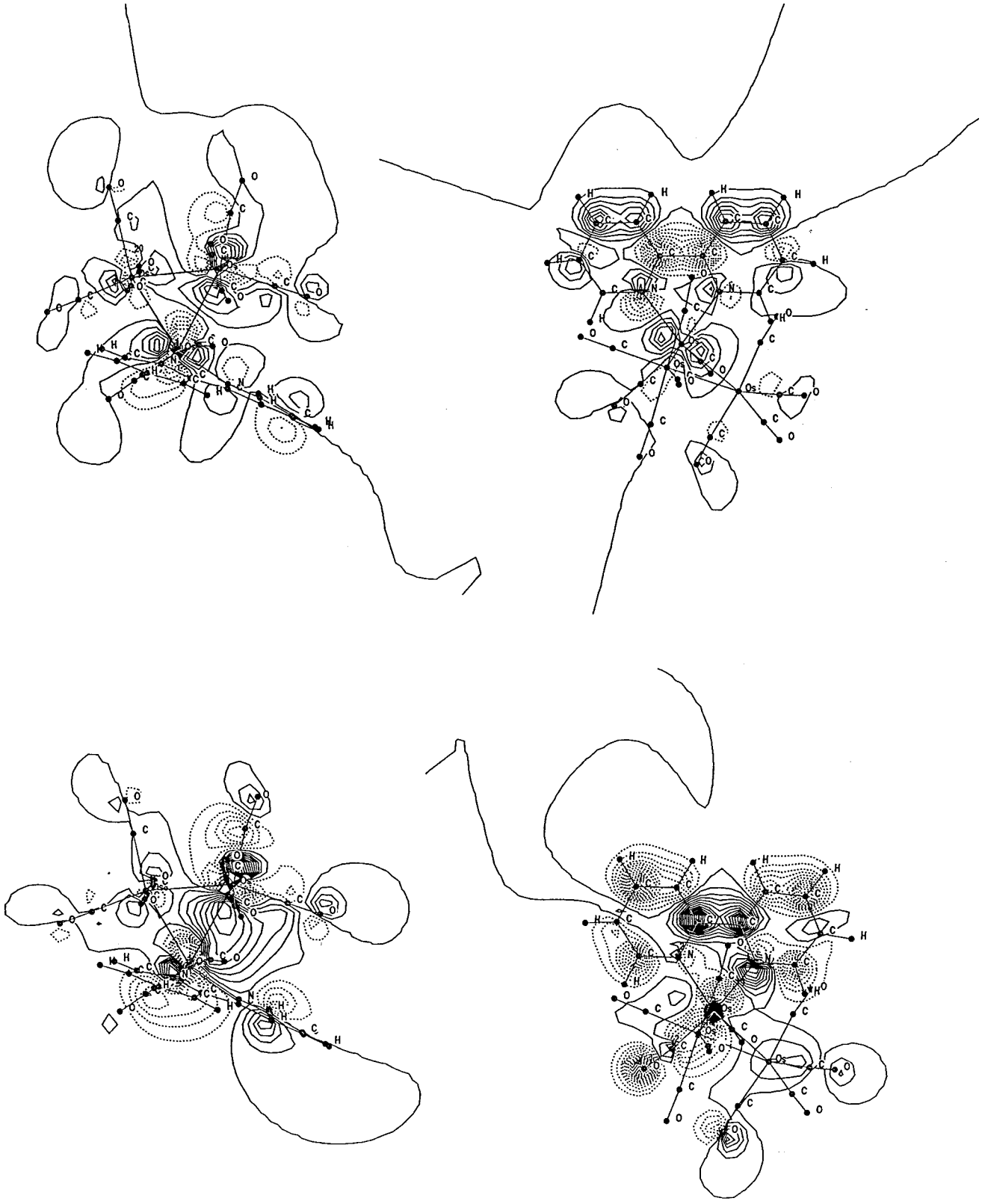

Figure 3. Wavefunction contour plots of the HOMO (top) and LUMO (bottom) of $Os_3(CO)_{10}$(BIPY) (**3b1**), in the Os_3 plane (left) and in the N−Os−N plane (right)

PYCA cluster, and 1.41 eV for the BIPY cluster. It becomes smaller as the HOMO becomes more localized in the metals and the LUMO in the diimine.

Final Remarks

As discussed above, the LUMO becomes progressively more localized on the α-diimine ligand as one moves from

Table 7. Energies of the frontier orbitals (eV) of models of $Os_3(CO)_{10}$(DAB) (**1a, 1b**) and $Os_3(CO)_{10}$(*i*Pr-DAB) (**1c**)

	1a	**1b**		**1c**
m.o.			m.o.	
75a	−3.28	−3.24	93a	−2.72
74a[a]	−3.76	−3.99	92a[a]	−3.51
73a[b]	−5.22	−5.65	91a[b]	−5.27
72a	−5.70	−6.01	90a	−5.65
71a	−6.03	−6.07	89a	−5.70
70a	−6.33	−6.43	88a	−6.12

[a] LUMO. – [b] HOMO.

Table 8. Energies of the frontier orbitals (eV) of models of $Os_3(CO)_{10}$(α-diimine) (**1b, 2b, 3b1**) and $Os_3(CO)_{10}$(BIPY) (3**c**)

	1b	**2b**		**3b1**	**3c**
m.o.		m.o.		m.o.	
75a	−3.24	84a	−3.17	93a	−3.15	−3.06
74a[a]	−3.99	83a[a]	−3.89	92a[a]	−3.72	−3.74
73a[b]	−5.65	82a[b]	−5.39	91a[b]	−5.13	−5.16
72a	−6.01	81a	−5.83	90a	−5.66	−5.51
71a	−6.07	80a	−5.89	89a	−5.80	−5.55
70a	−6.43	79a	−6.39	88a	−6.26	−6.23

[a] LUMO. – [b] HOMO.

DAB, to PYCA, to BIPY in $Os_3(CO)_{10}$(α-diimine) (45, 65, 76% from **1b, 2b, 3b1**, respectively) and the HOMO on the metal-carbonyl core (32, 39, 44%), indicating that the cluster core-to-ligand charge-transfer character of the HOMO−LUMO transition increases along the series. This trend agrees well with the previously published resonance Raman spectra of the clusters $Os_3(CO)_{10}$(α-diimine) (α-diimine = *i*Pr-DAB, *i*Pr-PYCA, BIPY).[9a][9b] The spectra document that in the case of the *i*Pr-DAB-derivative, the HOMO−LUMO transition possesses a pronounced metal−ligand bonding-to-antibonding rather than charge-transfer character, in agreement with its negligible solvatochromism.[15] For the *i*Pr-PYCA and BIPY-derivatives, the resonance Raman spectra and negative solvatochromism[9b] manifest a significant charge transfer character of this first electronic transition. This difference is also reflected in the limited tendency of the clusters $Os_3(CO)_{10}$(R-DAB) (R = alkyl) to produce charge-separated zwitterions from the diradical intermediates photogenerated upon the HOMO−LUMO excitation, in sharp contrast to the photochemistry of the R-PYCA and, in particular, BIPY-derivatives.[9a] Such conversion demands localization of the excited electron mainly in the π* orbital of the α-diimine ligand, which is not the case in the strongly π-delocalized Os−DAB metallacycle (see Table 4, model **1b**).

The extended Hückel method does not give a good result for predicting relative energies of isomers, in the absence of a geometry optimization, but leads to a good description of the nature of the frontier orbitals, reflecting the progressive contribution of the α-diimine ligand to the LUMO and of the three osmium atoms to the HOMO in the $Os_3(CO)_{10}$(α-diimine) clusters.

Experimental Section

All Density Functional Theory calculations were performed using the Amsterdam Density Functional program package (ADF).[17,18] The Local Spin Density (LSD) exchange correlation potential was used with the Local Density Approximation of the correlation energy (Vosko−Wilk-Nusair).[19] Gradient-corrected geometry optimizations were performed using Becke's[20] exchange and Perdew's[21] correlation functionals, and included relativistic effects, treated by a quasi-relativistic method where Darwin and mass-velocity terms are incorporated.[23]

The inner shells of Os (1s−5p) were frozen, for both the large (L) and reduced basis sets. A triple-ζ STO basis set was used for the valence part of Os (5d−6s), additionally augmented by one diffuse 6p function. For C and N, the 2s and 2p valence shells were described by a triple-ζ STO basis, augmented by one 3d polarization function. For O and H a double-ζ STO basis was used. In the large (L) case, the 2s and 2p shells of C, O and N and the 1s shell of H are triply split and augmented by two polarization functions (3d+4f for C, O, N; 2p+3d for H).

The Hartree−Fock (HF) geometry optimizations were performed using Gaussian94.[12] For Os, the inner shells (1s−4f) were replaced by relativistic effective core potentials of Hay and Wadt,[24] thus including the outermost core orbitals into the SCF procedure. These orbitals were fully contracted while the valence shells were described by a double-ζ STO basis completed by two additional diffuse 6p functions.[25] For the ligand atoms C, O, N and H, standard basis sets (6−31G) were used. The geometry optimizations were performed without any symmetry constraints, except for the equatorial isomers (C_s symmetry).

The extended Hückel method with modified H_{ij} values was used.[26] The basis set for the metal atoms consisted of *n*s, *n*p and (*n-1*)d orbitals. The s and p orbitals were described by single Slater-type wavefunctions, and the d orbitals were taken as contracted linear combinations of two Slater-type wavefunctions. The parameters used for Os were (H_{ii}/eV, ζ): 6s −8.17, 2.452; 6p −4.81, 2.429; 5d −11.84, 5.571, 2.416 (ζ_2), 0.6372 (C_1), 0.5598 (C_2). Standard parameters were used for other atoms. The calculations were performed on model clusters with idealized structures based on the real structures quoted throughout the text. The results were compared with the real structures, when available, producing qualitatively similar results. The bond lengths (Å) were as follows: Os−Os 2.90, Os−C(CO) 1.95, Os−N 2.15, Os−C 2.15, C−O 1.15, C−N 1.40, C−C 1.40, C−H 1.08, N−H 1.08.

Acknowledgments

M. J. C. and E. H. gratefully acknowledge funding from the TMR Network "Metal Clusters in Catalysis and Organic Synthesis". This work is also part of a European collaboration COST Action D14, project D14/0001/99.

[1] [1a] B. E. R. Schilling, R. Hoffmann, *J. Am. Chem. Soc.* **1979**, *101*, 3456. – [1b] J. Li, K. Jug, *Inorg. Chim. Acta.* **1992**, *196*, 89. – [1c] E. J. Baerends, A. Rosa, *New J. Chem.* **1991**, *15*, 815. – [1d] D. G. J. Evans, *J. Chem. Soc., Chem. Commun.* **1983**, 675. – [1e] B. Delley, M. C. Manning, D. E. Ellis, J. Berkowitz, W. C. Trogler, *Inorg. Chem.* **1982**, *21*, 2247. – [1f] J. W. Lauher, *J. Am. Chem. Soc.* **1986**, *108*, 1521. – [1g] D. Braga, A. Roger, B. F. G. Johnson, *Inorg. Chim. Acta* **1990**, *174*, 185. – [1h] A. Sironi, *Inorg. Chem.* **1992**, *31*, 299. – [1i] P. T. Chesky, M. B. Hall, *Inorg. Chem.* **1983**, *22*, 2998. – [1j] R. D. Barreto, T. P. Fehlner, L.-Y. Hsu, S. G. Shore, *Inorg. Chem.* **1986**, *25*, 3572.

– [1k] M. A. Gallop, M. P. Gomez-Sal, C. E. Housecroft, B. F. G. Johnson, J. Lewis, S. M. Owen, P. R. Raithby, A. H. Wright, *J. Am. Chem. Soc.* **1992**, *114*, 2502. – [1l] J.-F. Halet, J.-Y. Saillard, R. Lissillour, M. J. McGlinchey, G. Jaouen, *Inorg. Chem.* **1985**, *24*, 218. – [1m] G. L. Griewe, M. B. Hall, *Inorg. Chem.* **1988**, *27*, 2250. – [1n] F. A. Cotton, X. Feng, *Inorg. Chem.* **1991**, *30*, 3666. – [1o] R. L. DeKock, K. S. Wong, T. P. Fehlner, *Inorg. Chem.* **1982**, *21*, 3203. – [1p] C. Mealli, *J. Am. Chem. Soc*. **1985**, *107*, 2245. – [1q] A. R. Pinhas, T. A. Albright, P. Hofmann, R. Hoffmann, *Helv. Chim. Acta* **1980**, *63*, 29.

[2] E. Hunstock, C. Mealli, M. J. Calhorda, J. Reinhold, *Inorg. Chem.* **1999**, *38*, 5053.

[3] [3a] *The Chemistry of Metal Cluster Complexes* (Eds.: D. F. Shriver, H. D. Kaesz, R. D. Adams), VCH, Cambridge, **1990**. – [3b] *Catalysis by Di- and Polynuclear Metal Cluster Complexes* (Eds.: R. D. Adams, F. A. Cotton), Wiley-VCH, Canada, **1998**.

[4] [4a] D. Braga, F. Grepioni, M. J. Calhorda, L. F. Veiros, *Organometallics* **1995**, *14*, 1992. – [4b] D. Braga, F. Grepioni, M. J. Calhorda, H. Wadepohl, S. Gebert, L. F. Veiros, *Organometallics* **1995**, *14*, 5350.

[5] J.-F. Riehl, N. Koga, K. Morokuma, *Organometallics* **1993**, *12*, 4788.

[6] [6a] J. Nijhoff, F. Hartl, J. W. M. van Outersterp, D. J. Stufkens, M. J. Calhorda, L. F. Veiros, *J. Organomet. Chem.***1999**, *573*, 121. – [6b] F. Hartl, J. W. M. van Outersterp, D. J. Stufkens, manuscript in preparation.

[7] R. G. Parr, W. Young, *Density Functional Theory of Atoms and Molecules,* Oxford University Press, New York, **1989**.

[8] [8a] R. Hoffmann, *J. Chem. Phys.* **1963**, *39*, 1397. – [8b] R. Hoffmann, W. N. Lipscomb, *J. Chem. Phys.* **1962**, *36*, 2179.

[9] [9a] J. Nijhoff, M. J. Bakker, F. Hartl, D. J. Stufkens, W.-F. Fu, R. van Eldik, *Inorg. Chem.* **1998**, *37*, 661. – [9b] J. W. M. van Outersterp, Garriga, M. T. Oostenbrink, H. A. Nieuwenhuis, D. J. Stufkens, F. Hartl, *Inorg. Chem.* **1995**, *34*, 6312. – [9c] J. Nijhoff, M. J. Bakker, F. Hartl, D. J. Stufkens, *J. Organomet. Chem.* **1999**, *572*, 271. – [9d] J. Nijhoff, F. Hartl, D. J. Stufkens, *Organometallics* **1999**, *18*, 4380.

[10] [10a] D. J. Stufkens, M. P. Aarnts, J. Nijhoff, B. D. Rossenaar, A. Vlček Jr., *Coord. Chem. Rev.* **1998**, *171*, 93. – [10b] D. J. Stufkens, A. Vlček Jr., *Coord. Chem. Rev.* **1998**, *177*, 127.

[11] R. Zoet, T. B. H. Jastrzebski, G. van Koten, T. Mahabiersing, K. Vrieze, D. Heijdenrijk, C. H. Stam, *Organometallics* **1988**, *7*, 2108.

[12] M. J. Frisch, G. W. Trucks, H. B. Schlegel, P. M. W. Gill, B. G. Johnson, M. A. Robb, J. R. Cheeseman, T. A. Keith, G. A. Petersson, J. A. Montgomery, K. Raghavachari, M. A. Al-Daham, V. G. Zakrzewski, J. V. Ortiz, J. B. Foresman, J. Cioslowski, B. B. Stefanov, A. Nanayakkara, M. Challacombe, C. Y. Peng, P. A. Ayala, W. Chen, M. W. Wong, J. L. Andres, E. S. Replogle, R. Gomperts, R. L. Martin, D. J. Fox, J. S. Binkley, D. J. Defrees, J. Baker, J. P. Stewart, M. Head-Gordon, C. Gonzalez, J. A. Pople, *Gaussian 94*, Gaussian Inc., Pittsburgh, PA, **1994**.

[13] R. Zoet, G. van Koten, K. Vrieze, A. J. M. Duisenberg, A. L. Spek, *Inorg. Chim. Acta*, **1988**, *148*, 71.

[14] N. E. Leadbeter, J. Lewis, P. R. Raithby, G. N. Ward, *J. Chem. Soc., Dalton Trans.* **1997**, 2511.

[15] For $Os_3(CO)_{10}$(*i*Pr-DAB) the lowest-energy absorption band is found at λ_{max} = 522 nm in toluene, THF, acetone, acetonitrile and pyridine. Bakker, M. J., Undergraduate scientific report, University of Amsterdam, 1996.

[16] M. P. Aarnts, M. P. Wilms, K. Peelen, J. Fraanje, K. Goubitz, F. Hartl, D. J. Stufkens, E. J. Baerends, A. Vlček, *Inorg. Chem.* **1996**, *35*, 5468.

[17] *Amsterdam Density Functional (ADF) program*, release 2.01 Vrije Universiteit: Amsterdan, The Netherlands, **1995**.

[18] [18a] E. J. Baerends, D. Ellis, P. Ros, *Chem. Phys.* **1973**, *2*, 41. – [18b] E. J. Baerends, P. Ros, *Int. J. Quantum Chem.* **1978**, *S12*, 169. – [18c] P. M. Boerrigter, G. te Velde, E. J. Baerends, *Int. J. Quantum Chem.* **1988**, *33*, 87. – [18d] G. te Velde, E. J. Baerends, *J. Comp. Phys.* **1992**, *99*, 84.

[19] S. H. Vosko, L. Wilk, M. Nusair, *Can. J. Phys.* **1980**, *58*, 1200.

[20] [20a] A. D. Becke, *J. Chem. Phys.* **1987**, *88*, 1053. – [20b] A. D. Becke, *Phys. Rev.* **1988**, *A38*, 3098.

[21] [21a] J. P. Perdew, *Phys. Rev.* **1986**, *B33*, 8822. – [21b] J. P. Perdew, *Phys. Rev.* **1986**, *B34*, 7406.

[22] [22a] L. Versluis, T. Ziegler, *J. Chem. Phys.* **1988**, *88*, 322. – [22b] L. Fan, T. Ziegler, *J. Chem. Phys.* **1991**, *95*, 7401.

[23] [23a] T. Ziegler, V. Tschinke, E. J. Baerends, J. G. Snijders, W. Ravenek, J. Phys. *Chem.* **1989**, *93*, 3050. – [23b] J. G. Snijders, E. J. Baerends, *Mol. Phys.* **1978**, *36*, 1789. – [23c] J. G. Snijders, E. J. Baerends, P. Ros, *Mol. Phys.* **1979**, *38*, 1909.

[24] P. J. Hay, W. R. Wadt, *Technical Report*, Los Alamos National Laboratory, **1990.**

[25] P. J. Hay, W. R. Wadt, *J. Chem. Phys.* **1985**, *82*, 299.

[26] J. H. Ammeter, H.-J. Bürgi, J. C. Thibeault, R. Hoffmann, *J. Am. Chem. Soc.* **1978**, *100*, 3686.

Received April 17, 2000
[I00155]

Chromium and Tungsten Carbene Complexes of Thieno[3,2-*b*]thiophene

Marilé Landman,[a] Helmar Görls,[b] and Simon Lotz*[c]

Keywords: Carbene complexes / Dinuclear complexes / Chromium / Tungsten / Sulfur heterocycles

Dinuclear carbene complexes with 3,6-dimethylthieno[3,2-*b*]thienylene (T′T′) and thieno[3,2-*b*]thienylene (TT) spacers were prepared using the classical Fischer method. Their reactivity in solution towards oxygen, as well as their structural features were investigated. Chromium and tungsten carbene complexes were synthesized via dilithiation of the thienothiophene, followed by the addition of the appropriate metal carbonyl complex and subsequent alkylation with triethyloxonium tetrafluoroborate. Monocarbene [M{C(OEt)T′T′H}$(CO)_5$], (M = Cr, **1**; W, **4**), biscarbene [$(CO)_5$M{C(OEt)T′T′C(OEt)}M$(CO)_5$], (M = Cr, **2**; W, **5**), and the products [M{C(OEt)T′T′C(O)OEt} $(CO)_5$], (M = Cr, **3**; W, **6**), where a metal moiety of **2** and **5** has been replaced by an ester functionality, were isolated. The reaction product afforded in the reaction of $Cr(CO)_6$ with lithiated thieno[3,2-*b*]thiophene, [Cr{C(OEt)TTC(O)Bu}$(CO)_5$], **7**, did not resemble any of the products isolated in the similar reaction of $Cr(CO)_6$ with lithiated 3,6-dimethylthieno[3,2-*b*]thiophene.

Introduction

The current interest in thiophenes as molecules with potential electro-optical properties for use as molecular devices[1] was recently extended to include thieno[3,2-*b*]thiophenes.[2] Research in this area has unfortunately been impeded by the lack of convenient synthetic methods. Since the discovery of the first stable transition metal carbene complex by Fischer and Maasböl in 1964,[3] research in this field has been extensive with wide application possibilities. Several mononuclear, as well as dinuclear[4] biscarbene complexes with various spacers have been prepared. The first biscarbene complex containing two different metal moieties, contains a 2,2′-bithienylene (T−T) spacer and was published in 1995,[5] however, the synthetic method was unsatisfactory. In this paper the syntheses of carbene complexes containing thieno[3,2-*b*]thiophene and 3,6-dimethylthieno[3,2-*b*]thiophene as bridging units in dinuclear biscarbene complexes are reported. This work represents an extension of previously published dinuclear biscarbene complexes with thienylene (T) spacers, [$(CO)_2$ L_3M{C(OEt)TC(OEt)}M$L_3(CO)_2$], (M = Cr, L = CO; M = W, L = CO; M = Mn, L = Cp, MeCp).[6]

In an attempt to enhance the electron density and transmission properties of thieno[3,2-*b*]thiophene for potential application in non-linear optics, the synthesis of 2-arylthieno[3,2-*b*]thiophene was planned.[7] Various synthetic routes were proposed for this synthesis and intermediates containing metal fragments as substituents such as 2-tributylstannylthieno[3,2-*b*]thiophene, (thieno[3,2-*b*]thiophen-2-yl)boronic acid, and 2-thieno[3,2-*b*]thienylzinc chloride were prepared from lithio precursors. A number of α-substituted thienothiophene compounds have been synthesized in a similar manner via the monolithiated derivative e.g. selenium and tellurium compounds.[8] Several silyl compounds[9] were synthesized via the use of 2,5-disubstituted thieno[3,2-*b*]thiophenes, prepared by dilithiation of thieno[3,2-*b*]thiophene and followed by the subsequent reaction with electrophiles.

Results and Discussion

Examples of compounds containing thienothiophenes as bridging spacers are limited in the literature and mostly confined to main group metal compounds. The synthesis of thieno[3,2-*b*]thiophene was based on the work of Goldfarb and co-workers,[10] but several of the reaction steps were revised to obtain higher yields.[11,12,13] Since no practical short-step synthesis for thieno[3,2-*b*]thiophene, or substituted derivatives thereof, was available in the literature, the utilization of thienothiophenes in coordination chemistry with transition metals has been neglected. However, in 1994, Choi and co-workers[14] reported a one-pot synthesis of 3,6-dimethylthieno[3,2-*b*]thiophene, which promoted investigation of the properties of these molecules in coordination chemistry. This synthesis was based on the discovery made by Teste and Lozac'h[15] that the reaction of 2,5-dimethyl-3-hexyne-2,5-diol with elemental sulfur afforded 3,6-dimethylthieno[3,2-*b*]thiophene, although the yield was low. Choi re-examined this reaction and varied the reaction conditions until 3,6-dimethylthieno[3,2-*b*]thiophene was obtained in a reasonable yield.

[a] Department of Chemistry, University of South Africa,
P.O. Box 392, South Africa, 0003
Fax: (internat.) +27−12/4298549
E-mail: landmm@alpha.unisa.ac.za
[b] Friedrich-Schiller-Universität, Institut für Anorganische und Analytische Chemie,
Lessingstrasse 8, 07743, Jena, Germany
Fax: (internat.) +49−3641/948121
E-mail: goerls@xa.nlwl.uni-jena.de
[c] Department of Chemistry, University of Pretoria,
Pretoria, South Africa, 0002
Fax: (internat.) +27−12/3625297
E-mail: slotz@postino.up.ac.za

 © WILEY-VCH Verlag GmbH, 69451 Weinheim, 2001 1434−1948/01/0101−0233 $ 17.50+.50/0

The novel carbene complexes **2** and **5** were synthesized using the classical Fischer method. The dimetallation of thieno[3,2-*b*]thiophene and 3,6-dimethylthieno[3,2-*b*]thiophene was based on the method described by Bugge.[13] The reactions were carried out in hexane and TMEDA was introduced together with butyllithium to form 2,7-dilithio species at elevated temperatures. Formation of biscarbene complexes followed after addition of the metal hexacarbonyl and subsequent quenching with the alkylating agent $Et_3O{\cdot}BF_4$. The synthetic procedure for the preparation of these complexes is outlined in Scheme 1.

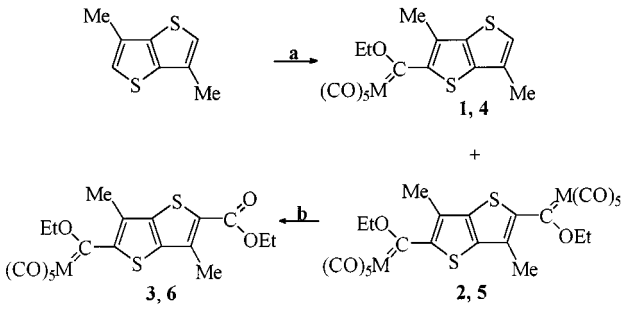

M = Cr, **1-3**
M = W, **4-6**

Scheme 1. Synthesis of the novel carbene complexes **1**−**6**; reagents: (a) 2 equiv. *n*BuLi, $M(CO)_6$, $Et_3O{\cdot}BF_4$; (b) O_2

Carbene complexes of chromium, complexes **1** and **2**, were crystallized from hexane/dichloromethane (1:1) solutions to affording red-orange needles for the monocarbene complex and purple-black crystals for the biscarbene complex. X-ray diffraction studies confirmed the structures of these compounds. Similar products, complexes **3** and **4**, were obtained for tungsten and characterized spectroscopically. Complexes **3** and **6** are suggested to have formed in solution by oxidation of the air-sensitive biscarbene complexes, involving trace amounts of oxygen.[6]

Complex **7** was isolated from the reaction between $Cr(CO)_6$ and thieno[3,2-*b*]thiophene and did not resemble any of the products obtained from the similar reaction with 3,6-dimethylthieno[3,2-*b*]thiophene. Although the synthetic procedure followed was identical, only complex **7** was isolated instead of the expected monocarbene and biscarbene complexes. The yield of **7** was low and implies the formation of other unstable compounds. The structural elucidation of this complex was based on the data collected with the use of NMR spectroscopy, infrared data, and mass spectrometry.

A possible reaction route to **7** is attributed to the enhanced acidity exhibited by the protons of the unsubstituted thienothiophene. Hence, the suggested formation of product **7**, as is illustrated in Scheme 2, can be explained by reaction of a deprotonated thienothiophene monocarbene complex and a metal butyl carbene to give a dinuclear ylide intermediate. Elimination of an ethoxy group follows and after subsequent oxidation of the more reactive metal butyl carbene end of the biscarbene, the final product, complex **7**, is afforded. TMEDA acts as a base and deprotonates the ring at the 7-position of the monocarbene complex, while its conjugated acid assists in the removal of the ethoxy group from the ylide.

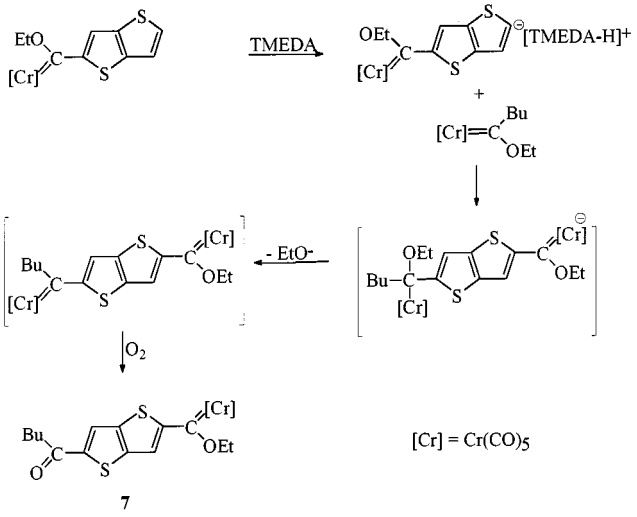

Scheme 2. Suggested formation of complex **7**

The complexes were fully characterized and their NMR spectra recorded in deuterated chloroform. The monocarbene complexes, **1** and **4**, display a quadruplet signal for the H7 proton due to coupling with the methyl group on C6. This methyl signal is observed as a doublet and a coupling constant of ca. 1 Hz is determined for this four-bond coupling. It is interesting to note the significant difference in chemical shift values of the methylene resonance of the carbene ethoxy substituent on the spectra of the three tungsten complexes compared with the same signal on the spectra of the chromium complexes. The chemical shift is observed significantly more upfield for the tungsten complexes than for the chromium complexes, denoting that these resonance values are fairly characteristic for a specific metal and unaffected by the substituent on the 7-position of the 3,6-dimethylthieno[3,2-*b*]thiophene unit. Also characteristic is the position of the methylene resonances of the ester groups at $\delta \approx 4.35$ for both complexes **3** and **6**, which shows that the influence of the different metals is not transferred through the ligand to the other side of the thienothiophene rings. This was also observed for the corresponding thiophene complexes.[6] On the proton, as well as on the carbon NMR spectra of complexes **3** and **6** evidence for the further decomposition of these products to the 2,7-bis(ethyl ester) of 3,6-dimethylthieno[3,2-*b*]thiophene is observed and signifies the reactivity in solution towards oxygen of not only the biscarbene but also of the resulting monocarbene-ester complexes over prolonged periods of time.

Carbene carbon chemical shifts are found at characteristic values for the different metals on the ^{13}C NMR spectra. The values fall within the range of $\delta = 317-319$ for the chromium complexes, while these resonances are observed at $\delta = 292-297$ on the tungsten spectra. This same sequence is noted for the position of the $M(CO)_5$ peaks on the different spectra. The difference in chemical shift value ($\Delta\delta$) of the carbonyl resonances is approximately 10 ppm,

with tungsten upfield from chromium. The methylene carbons of the carbene ethoxy group of the different metal spectra reveal the opposite trend, with the resonances of the chromium complexes observed upfield from those of the tungsten complexes.

The lower wavenumbers observed on the infrared spectra of the monocarbene complexes **1** and **4** compared with those of the biscarbene complexes, and the decomposition products, indicate stronger metal-carbonyl back bonding and thus a decrease in C−O bond order. This implies weaker metal to carbene carbon π-bonding. Alternatively, the substituents on the carbene carbon may play a greater role in stabilizing the electrophilic carbene carbon. The values reported for the monocarbene complexes of chromium and tungsten containing a phenyl substituent, $[Cr(CO)_5C(OEt)Ph]$[16] and $[W(CO)_5C(OMe)Ph]$,[17] are even higher than for the thiophene complexes, implying that the phenyl unit is a poorer donor of electron density relative to the thienyl or, consequently, the thienothienyl substituent.

From the structures of complexes **1** and **2**, as shown in Figure 1 and Figure 2, it is noted that the heteroaromatic spacer, the carbene carbon and the metal atom are all coplanar for both structures. The metal fragment is orientated towards the sulfur atom and away from the methyl substituent on the ring in complex **1**. For complex **2**, the two $Cr(CO)_5$ metal fragments are found on opposite sides of the spacer ligand, positioned towards the sulfur atom and away from the methyl substituent on the ring. This is in contrast with the structure of the biscarbene complex of chromium pentacarbonyl, constituting a thienylene.[6] In this complex, the metal fragments are found on the same side of the thiophene ring and on the side opposite to the sulfur atom in the ring. However, for the biscarbene complex of chromium pentacarbonyl with biphenylene as the bridging ligand, the metal moieties are again on opposite sides of the axis connecting the two carbene carbon atoms.[4b] The Cr metal is approximately octahedrally arranged, with two of the *cis*-carbonyl ligands bending away from the carbene carbon. This is indicated by the bond angles of 94.5(1)° for both the C(12)−Cr(1)−C(1) and C(12A)−Cr(1)−C(1) angles in **1** and 93.1(1)° for both the angles C(7)−Cr−C(1) and C(9)−Cr(1)−C(1) in **2**. On considering the positions of the ethyl group of the ethoxy substituent relative to the metal fragment in the solid state, the (*Z*)-isomer of this complex along the carbene−O bond is observed. This is in accordance with the observation in the literature that the (*Z*)-isomer is by far the most popular arrangement in the crystal structures of ethoxy- or methoxy-substituted carbene complexes of octahedrally coordinated metals.[18] Suggested delocalization in the ring system is promoted by the observed bond lengths, which are all very similar and correspond to distances between characteristic $C(sp^2)$ single bonds and $C(sp^2)$ double bonds.[19] In contrast to the observation made for complex **1** where only the one thiophene unit is affected, delocalization in complex **2** occurs throughout the whole heteroarene system, aided by the influence of the second metal fragment, which is absent in complex **1**.

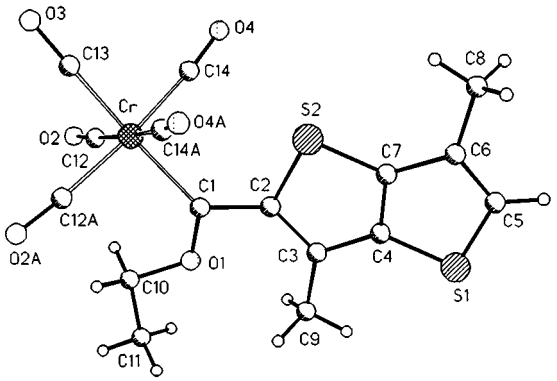

Figure 1. Molecular structure of complex **1**; selected bond lengths [Å] and angles [°]: Cr1−C1 2.081 (4), S1−C5 1.722(4), S1−C2 1.751(4), S2−C7 1.721(5), S2−C4 1.729(4), C1−C2 1.469(6), C2−C3 1.413(6), C3−C4 1.411(6), C4−C5 1.377(6), C5−C6 1.341(7), C6−C7 1.431(6), O1−C1−C2 104.9(3), O1−C1−Cr1 128.6(3), C2−C1−Cr1 126.5(3)

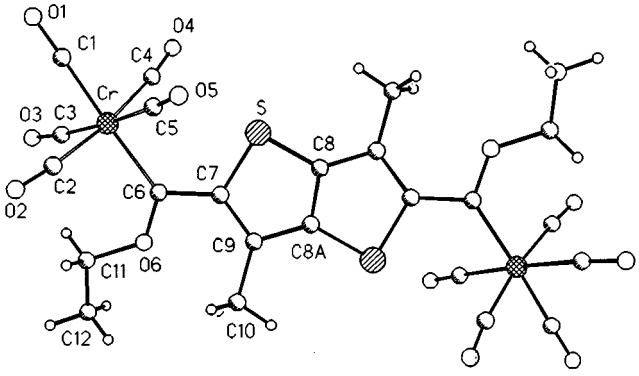

Figure 2. Molecular structure of complex **2**; selected bond lengths [Å] and angles [°]: Cr−C1 2.068(3), S−C4A 1.721(2), S−C2 1.745(3), C1−C2 1.473(4), C2−C3 1.393(4), C3−C4 1.415(4), C4A−C4 1.378(5), O6−C1−C2 105.0(2), O6−C1−Cr 129.2(2), C2−C1−Cr 125.7(2)

Conclusion

Transition metal biscarbene complexes with conjugated spacers are still limited in the literature. In this paper, we have reported the syntheses of biscarbene complexes with thienothiophene spacers, comprising two fused thiophene units. On comparing the relative stabilities in solution of these novel complexes with those of biscarbene complexes of thiophene, as described in the literature,[6] it was found that by increasing the number of thiophene units in the spacer, the stability of the complexes improves. However, formal stability studies were not conducted but the rate of decomposition of the individual complexes in solution was taken as a criterion. Biscarbene complexes convert into monocarbene-ester products within minutes after being dissolved in acetone or THF.

Experimental Section

General Remarks: All NMR spectra were recorded in deuterated chloroform, unless stated otherwise, using TMS as an internal

standard on a Bruker ARX-300 spectrometer. − Infrared spectra were recorded on a BOMEM FT-IR spectrophotometer using dichloromethane as solvent unless otherwise specified. − Mass spectra were recorded at ca. 70 eV on a Finnigan Mat 8200 instrument, using the electron impact method.

All reactions were performed in an inert atmosphere of either nitrogen or argon by using standard Schlenk techniques and vacuum-line methods. Solvents were dried and distilled under nitrogen prior to use. − Column chromatography was carried out under nitrogen using either silica gel (particle size 0.063−0.200 nm) or neutral aluminium oxide as resin. − Most chemicals were used directly without prior purification. The following compounds were prepared using known literature methods: 3,6-dimethylthieno[3,2-*b*]thiophene,[14] 2,3,5-tribromothiophene,[11] 3-bromothiophene,[12] ethyl (3-thienylthio)acetate,[10] ethyl (2-formyl-3-thienylthio)acetate,[13] thieno[3,2-*b*]thiophene carboxylic acid, thieno[3,2-*b*]thiophene[12], and triethyloxonium tetrafluoroborate.[20]

Revised Synthesis of Thieno[3,2-*b*]thiophene: Synthesis of 2,3,5-tribromothiophene was effected according to the method described by Brandsma and Verkruijsse,[11] and involved the reaction of bromine (180.00 mL; 3.50 mol) and thiophene (80.00 mL, 1.00 mol) in a 48% aqueous HBr/diethyl ether solution (400 mL/100 mL) at elevated temperatures (75°C). The target product (97%) and HBr were formed. Reduction of 2,3,5-tribromothiophene (321.00 g, 1.00 mol) to obtain 3-bromothiophene (55%),[12] was performed using zinc dust (196.00 g, 3.00 mol) in 175 mL of acetic acid. Reaction of 3-bromothiophene (90.50 g, 0.55 mol) with elemental sulfur (17.60 g, 0.55 mol), followed by the addition of ethyl bromoacetate (61.4 mL, 0.55 mol), afforded ethyl (3-thienothio)acetate (73%). On reacting this acetate-substituted thiophene (26.60 g, 0.13 mol) with phosphorus oxychloride (30.00 g, 0.19 mol) in *N*,*N*-dimethylformamide (14.00 g, 0.19 mol) afforded ethyl(2-formyl-3-thienothio)acetate (85%) in a Vilsmeier formylation reaction.[13] Cyclization and the subsequent decarboxylation of this compound yielded thieno[3,2-*b*]thiophene.[10]

Chromium Carbene Complexes 1, 2, and 3: 3,6-Dimethylthieno[3,2-*b*]thiophene (0.67 g, 4.00 mmol) was dissolved in 50 mL of hexane. TMEDA (1.20 mL, 8.00 mmol) and *n*-butyl lithium (5.5 mL, 8.8 mmol) were added at room temperature. The mixture was refluxed for 45 minutes and then cooled to 0 °C. After the addition of 50 mL of THF, $Cr(CO)_6$ (1.76 g, 8.00 mmol) was added and the suspension stirred for an hour. The color of the reaction changed to dark brown. After completion of the reaction, the solvent was removed in vacuo. The residue was dissolved in 20 mL of dichloromethane. Triethyloxonium tetrafluoroborate (1.50 g, 8.10 mmol) was dissolved in 20 mL of dichloromethane and this was added to the cooled reaction mixture (−20 °C). An immediate color change to a purple solution was observed. Stirring was maintained for a further hour while the temperature was allowed to reach room temperature. The mixture was then filtered, the solvent removed, and the remainder purified on a silica gel column. Three products were isolated, starting with pure hexane as eluent and gradually increasing the polarity of the solvent by adding dichloromethane. The first was the orange monocarbene complex **1**. The second purple complex was the biscarbene complex **2**, while the third red-orange compound was characterized as **3**. This complex was isolated using a hexane/dichloromethane mixture (1:1) as eluent.

1: Yield 0.55 g (33%), m.p.173−177 °C. − $C_{16}H_{12}CrO_6S_2$ (416.4): calcd. C 46.15, H 2.91; found C 46.36, H 3.05. − IR (ν_{CO}; CH_2Cl_2) = 2055 (m), 1979 (w), 1938 (vs) cm^{-1}. − ^1H NMR ($CDCl_3$, 300.135 MHz): δ = 7.18 (q, ^4J = 1.2 Hz, 1 H, H^7), 5.19 (q, ^3J = 7.0 Hz, 2 H, OCH_2CH_3), 2.47 (s, 3 H, Me^3), 2.41 (d, ^4J = 1.2, 3 H, Me^6), 1.71 (t, ^3J = 7.0, 3 H, OCH_2CH_3). − ^{13}C NMR ($CDCl_3$, 75.1 MHz): δ = 318.7 (carbene carbon), 222.8, 216.8 (CO), 150.1 (C^2), 144.7 (C^4), 142.6 (C^5), 130.8 (C^3), 129.5 (C^6), 128.2 (C^7), 76.4 (OCH_2CH_3), 18.6 (Me^3), 15.6 (OCH_2CH_3), 14.7 (Me^6). − MS (EI); *m*/*z*: 416 [M^+], 388 [M^+ − CO], 360 [M^+ − 2 CO], 332 [M^+ − 3 CO], 304 [M^+ − 4 CO], 276 [M^+ − 5 CO].

2: Yield 1.25 g (47%), $C_{24}H_{16}O_{12}S_2Cr_2$ (664.5): calcd. C 43.38, H 2.43; found C 43.61, H 2.62. − IR (ν_{CO}; CH_2Cl_2) = 2053 (m), 1986 (w), 1941 (vs) cm^{-1}. − ^1H NMR ($CDCl_3$, 300.135 MHz): δ = 5.19 (q, ^3J = 7.1 Hz, 4 H, OCH_2CH_3), 2.47 (s, 6 H, Me^3), 1.74 (t, ^3J = 7.1 Hz, 6 H, OCH_2CH_3). − ^{13}C NMR ($CDCl_3$, 75.1 MHz): δ = 223.6, 216.3 (CO), 167.7 (C^2), 149.8 (C^4), 131.9 (C^3), 76.6 (OCH_2CH_3), 17.6 (Me^3), 15.5 (OCH_2CH_3). − MS (EI); *m*/*z*: 636 [M^+ − CO], 552 [M^+ − 4 CO], 524 [M^+ − 5 CO].

3: Yield 0.23 g (12%), $C_{19}H_{16}O_8S_2Cr$ (488.5): calcd. C 46.72, H 3.31; found C 46.86, H 3.45. − IR (ν_{CO}; CH_2Cl_2) = 2057 (m), 1984 (w), 1940 (vs) cm^{-1}. − ^1H NMR ($CDCl_3$, 300.135 MHz): δ = 5.20 (q, ^3J = 6.9 Hz, 2 H, OCH_2CH_3−M), 4.35 (q, ^3J = 7.2 Hz, 2 H, OCH_2CH_3−O), 2.70 (s, 3 H, Me^3), 2.43 (s, 3 H, Me^6), 1.72 (t, ^3J = 6.9 Hz, 3 H, OCH_2CH_3−M), 1.38 (t, ^3J = 7.2 Hz, 3 H, OCH_2CH_3−O). − ^{13}C NMR ($CDCl_3$, 75.1 MHz): δ = 317.9 (carbene carbon), 223.3, 216.7 (CO), 163.6 (C^2), 163.1 (C^7), 142.7 (C^4), 142.0 (C^5), 130.6 (C^3), 129.7 (C^6), 76.4 (OCH_2CH_3−M), 61.4 (OCH_2CH_3−O), 17.7 (Me^3), 15.6 (OCH_2CH_3−M), 15.0 (Me^6), 14.4 (OCH_2CH_3−O). − MS (EI); *m*/*z*: 488 [M^+], 460 [M^+ − CO], 432 [M^+ − 2 CO], 404 [M^+ − 3 CO], 376 [M^+ − 4 CO], 348 [M^+ − 5 CO].

Tungsten Carbene Complexes 4, 5, and 6: 3,6-Dimethylthieno[3,2-*b*]thiophene (0.34 g, 2.00 mmol) was dissolved in 30 mL of hexane. TMEDA (0.60 mL, 4.00 mmol) and *n*-butyl lithium (2.80 mL, 4.40 mmol) were added to this solution at room temperature. The same procedure was followed as for the chromium analog with the addition of $W(CO)_6$ (1.40 g, 4.00 mmol). For alkylation triethyloxonium tetrafluoroborate (0.74 g, 4.00 mmol) was used. On purification using column chromatography, three bands separated. The eluent used involved hexane/dichloromethane mixtures of various compositions. While the first product was isolated using pure hexane as eluent, a 1:1 mixture was used to isolate the third product. The first monocarbene complex **4** was isolated as an orange solid. The second purple complex was characterized as the biscarbene complex **5**, while the third red-orange band was identified as **6**.

4: Yield 0.45 g (41%), m.p.187−189 °C. − $C_{16}H_{12}O_6S_2W$ (548.3): calcd. C 35.05, H 2.21; found C 35.23, H 2.40. − IR (ν_{CO}; CH_2Cl_2) = 2063 (m), 1989 (w), 1933 (vs) cm^{-1}. − ^1H NMR ($CDCl_3$, 300.135 MHz): δ = 7.22 (q, ^4J = 1.1 Hz, 1 H, H^7), 5.02 (q, ^3J = 7.1 Hz, 2 H, OCH_2CH_3), 2.48 (s, 3 H, Me^3), 2.41 (d, ^4J = 1.1 Hz, 3 H, Me^6), 1.69 (t, ^3J = 7.1 Hz, 3 H, OCH_2CH_3). − ^{13}C NMR ($CDCl_3$, 75.1 MHz): δ = 292.6 (carbene carbon), 201.9, 197.8 (CO), 150.2 (C^2), 144.1 (C^4), 144.1 (C^5), 132.1 (C^3), 131.0 (C^6), 128.8 (C^7), 79.0 (OCH_2CH_3), 18.9 (Me^3), 15.4 (OCH_2CH_3), 14.6 (Me^6). − MS (EI); *m*/*z*: 548 [M^+], 520 [M^+ − CO], 492 [M^+ − 2 CO], 464 [M^+ − 3 CO], 436 [M^+ − 4 CO], 408 [M^+ − 5 CO].

5: Yield 0.67 g (36%), $C_{24}H_{16}O_{12}S_2W_2$ (928.3): calcd. C 31.05, H 1.74; found C 31.14, H 1.82. − IR (ν_{CO}; CH_2Cl_2) = 2062 (m), 1983 (w), 1938 (vs) cm^{-1}. − ^1H NMR ($CDCl_3$, 300.135 MHz): δ = 5.04 (q, ^3J = 7.1 Hz, 4 H, OCH_2CH_3), 2.48 (s, 6 H, Me^3), 1.72 (t, ^3J = 7.1 Hz, 6 H, OCH_2CH_3). − ^{13}C NMR ($CDCl_3$, 75.1 MHz): δ = 202.2, 197.3 (CO), 164.9 (C^2), 149.3 (C^4), 123.5 (C^3), 79.6 (OCH_2CH_3), 18.4 (Me^3), 15.3 (OCH_2CH_3). − MS (EI); *m*/*z*: 932

[M^+], 903 [M^+ − CO], 874 [M^+ − 2 CO], 818 [M^+ − 4 CO], 788 [M^+ − 5 CO].

6: Yield 0.11 g (9%), $C_{19}H_{16}O_8S_2W$ (620.3): calcd. C 36.79, H 2.61; found C 37.01, H 2.82. − IR (ν_{CO}; CH_2Cl_2) = 2065 (m), 1985 (w), 1936 (vs) cm^{-1}. − ^1H NMR ($CDCl_3$, 300.135 MHz): δ = 5.03 (q, ^3J = 7.2 Hz, 2 H, OCH_2CH$_3$−M), 4.36 (q, ^3J = 7.2 Hz, 2 H, OCH_2CH$_3$−O), 2.70 (s, 3 H, Me^3), 2.44 (s, 3 H, Me^6), 1.70 (t, ^3J = 7.2 Hz, 3 H, OCH$_2$$CH_3$−M), 1.39 (t, ^3J = 7.2 Hz, 3 H, OCH$_2$$CH_3$−O). − ^{13}C NMR ($CDCl_3$, 75.1 MHz): δ = 296.3 (carbene carbon), 202.3, 197.8 (CO), 162.8 (C^2), 159.3 (C^7), 144.7 (C^4), 141.3 (C^5), 130.0 (C^3), 129.7 (C^6), 79.5 (OCH_2CH$_3$−M), 61.5 (OCH_2CH$_3$−O), 18.4 (Me^3), 15.2 (OCH$_2$$CH_3$−M), 14.8 (Me^6), 14.2 (OCH$_2$$CH_3$−O). − MS (EI); *m*/*z*: 620 [M^+], 592 [M^+ − CO], 564 [M^+ − 2 CO], 536 [M^+ − 3 CO], 508 [M^+ − 4 CO], 480 [M^+ − 5 CO].

Chromium Carbene Complex 7: Thieno[3,2-*b*]thiophene (0.56 g, 4.00 mmol) was dissolved in 30 mL of hexane. THF (100 mL) was added together with TMEDA (1.20 mL, 8.00 mmol) and *n*-butyllithium (5.50 mL, 8.80 mmol). The mixture was refluxed for 45 minutes and cooled to 0 °C, after which 100 mL of THF was added. $Cr(CO)_6$ (1.70 g, 8.00 mmol) was introduced and the mixture was stirred for an hour at room temperature. The solvent was evaporated and triethyloxonium tetrafluoroborate (1.50 g, 8.00 mmol), dissolved in 30 mL of dichloromethane, was added at −30 °C. The mixture was stirred for 15 minutes in the cold and for a further 45 minutes at room temperature, after which it was filtered and the solvent evaporated. The residue was column chromatographed with a hexane/dichloromethane (1:1) solution to yield the purple-pink product **7**.

7: Yield 0.79 g (42%), $C_{19}H_{16}O_7S_2Cr$ (472.5): calcd. C 48.30, H 3.42; found C 48.51, H 3.59. − IR (ν_{CO}; CH_2Cl_2) = 2058 (m), 1978 (w), 1943 (vs) cm^{-1}. − ^1H NMR ($CDCl_3$, 300.135 MHz): δ = 8.33 (s, 1 H, H^3), 7.82 (s, 1 H, H^6), 5.21 (q, ^3J = 7.0 Hz, 2 H, OCH_2CH$_3$−M), 2.93 [t, ^3J = 7.5 Hz, 2 H, C(O)CH_2CH$_2$CH$_2$CH$_3$], 1.74 [t, ^3J = 7.5 Hz, 2 H, C(O)CH$_2$$CH_2CH_2CH_3$], 1.69 (t, ^3J = 7.0 Hz, 3 H, OCH$_2$$CH_3$−M), 1.42 [t, ^3J = 7.5 Hz, 2 H, C(O)CH$_2$CH$_2$$CH_2CH_3$], 0.95 [t, *J* = 7.5 Hz, 3 H, C(O)CH$_2$CH$_2$CH$_2$$CH_3$]. − ^{13}C NMR ($CDCl_3$, 75.1 MHz): δ = 317.0 (carbene carbon), 223.5, 217.5 (CO), 194.5 (C=O), 164.0 (C^2), 155.1 (C^7), 146.8, 139.4, 134.4 (C^3, C^4, C^5, C^6, C^{10}, C^{11}), 75.7 (OCH_2CH$_3$−M), 43.0 [C(O)CH_2CH$_2$CH$_2$CH$_3$], 25.5 [C(O)CH$_2$$CH_2CH_2CH_3$], 22.8 [C(O)CH$_2CH_2$$CH_2CH_3$], 15.1 (OCH$_2$$CH_3$−M), 13.9 [C(O)CH$_2CH_2CH_2$$CH_3$]. − MS (EI); *m*/*z*: 472 [M^+], 444 [M^+ − CO], 416 [M^+ − 2 CO], 388 [M^+ − 3 CO], 360 [M^+ − 4 CO], 332 [M^+ − 5 CO].

X-ray Crystallographic Study: The intensity data for the compounds were collected at −90 °C on a Nonius−Kappa CCD diffractometer, using graphite-monochromated Mo-K_α radiation. Data were corrected for Lorentz and polarization effects, but not for absorption.[21,22] The structures were solved by direct methods (SHELXS)[23] and refined by full-matrix least squares techniques against F_o^2 (SHELXL-97)[24]. The hydrogen atoms of the structures were included at calculated positions with fixed thermal parameters. All non-hydrogen atoms were refined anisotropically. XP (SIEMENS Analytical X-ray Instruments, Inc.) was used for structure representations. One molecule of chromium hexacarbonyl co-crystallized with two molecules of the monocarbene complex **1**. Other experimental details are given in Table 1. Crystallographic data (excluding structure factors) for the structures reported in this paper have been deposited with the Cambridge Crystallographic Data Centre as supplementary material publication nos. CCDC-142023 (**1**) and CCDC-142024 (**2**). Copies of the data can be obtained free of charge on application to CCDC, 12 Union Road, Cambridge CB21EZ, UK [Fax: (internat.) +44 1223/336-033; E-mail: deposite@ccdc.cam.ac.uk].

Acknowledgments

We wish to thank Mr E. Palmer for the NMR measurements and the University of Pretoria and the Foundation for Research and Development, Pretoria, for financial assistance.

Table 1. Crystallographic data and data related to data acquisition and refinement for compounds **1** and **2**

	1		**2**	
Empirical formula	$CrC_{16}H_{12}O_6S_2 \cdot 0.5\ Cr(CO)_6$		$C_{24}H_{16}Cr_2O_{12}S_2$	
Formula mass	526.41		664.49	
Temperature	183(2) K		183(2) K	
Wavelength	0.71073 Å		0.71073 Å	
Crystal system	monoclinic		triclinic	
Space group	*C*2/m		*P*−1	
Unit cell dimensions	*a* = 30.4690(9) Å	α = 90°	*a* = 6.4052(5) Å	α = 71.172(5)°
	b = 7.5136(4) Å	β = 90.930(2)°	*b* = 8.8481(7) Å	β = 82.010(5)°
	c = 9.5477(4) Å	γ = 90°	*c* = 13.0304(6) Å	γ = 83.681(3)°
Volume	2185.5(2) Å^3		690.51(8) Å^3	
Z	4		1	
Density (calculated)	1.600 Mg/m^3		1.598 Mg/m^3	
Absorption coefficient	0.998 mm^{-1}		0.999 mm^{-1}	
F(000)	1064		336	
Crystal size	0.35 × 0.30 × 0.25 mm		0.30 × 0.30 × 0.10 mm	
Theta range for data collection	2.79 to 23.23°		3.22 to 23.31°	
Index ranges	$-33 \le h \le 33$, $-8 \le k \le 0$, $-10 \le l \le 10$		$0 \le h \le 7$, $-9 \le k \le 9$, $-13 \le l \le 14$	
Reflections collected	2961		3832	
Independent reflections	1620 [*R*(int) = 0.0233]		1857 [*R*(int) = 0.027]	
Refinement method	Full-matrix least-squares on F^2		Full-matrix least-squares on F^2	
Data/restraints/parameters	1587/0/175		1824/0/181	
Goodness-of-fit on F^2	0.947		1.047	
Final R indices [$I>2\sigma(I)$]	*R*1 = 0.0356, *wR*2 = 0.1120		*R*1 = 0.0356, *wR*2 = 0.1039	
R indices (all data)	*R*1 = 0.0437, *wR*2 = 0.1377		*R*1 = 0.0386, *wR*2 = 0.1154	
Largest diff. peak and hole	0.350 and −0.356 e·Å^{-3}		0.247 and −0.379 e·Å^{-3}	

[1] J. M. Tour, *Chem. Rev.* **1996**, *96*, 37.
[2] J. Nakayama, H. Dong, K. Sawada, A. Ishii, S. Kumakura, *Tetrahedron* **1996**, *52*, 471.
[3] E. O. Fischer and A. Maasböl, *Angew. Chem.* **1964**, *76*, 645; *Angew. Chem. Int. Ed. Engl.* **1964**, *3*, 580.
[4] [4a] E. O. Fischer, W. Röll, N. H. T. Huy, K. Ackermann, *Chem. Ber.* **1982**, *115*, 2951. – [4b] N. H. T. Huy, P. LeFloch, F. Robert, Y. Jeannin, *J. Organomet. Chem.* **1987**, *327*, 211. – [4c] C. Hartbaum, G. Roth, H. Fischer, *Eur. J. Inorg. Chem.* **1998**, 191. – [4d] D. W. Macomber, M-H. Hung, P. Madhukar, M. Liang, R. D. Rogers, *Organometallics* **1991**, *10*, 737.
[5] S. Maiorana, A. Papagni, E. Licandro, A. Persoons, K. Clay, S. Houbrechts, W. Porzio, *Gazz. Chim. Ital.* **1995**, *125*, 377.
[6] Y. M. Terblans, H. M. Roos, S. Lotz, *J. Organomet. Chem.* **1998**, *566*, 133.
[7] D. Prim, G. Kirsch, *J. Chem. Soc., Perkin Trans. 1* **1994**, 2603.
[8] M. Blenkle, P. Boldt, C. Bräuchle, W. Grahn, I. Ledoux, H. Nerenz, S. Stadler, J. Wichern, J. Zyss, *J. Chem. Soc., Perkin Trans. 2* **1996**, 1377.
[9] L. S. Fuller, B. Iddon, K. A. Smith, *J. Chem. Soc., Perkin Trans. 1* **1997**, 3465.
[10] Y. A. L. Goldfarb, V. P. Litvinov, S. Ozolin, *Izv. Akad. Nauk. SSSR, Ser. Khim.* **1965**, 510.
[11] L. Brandsma, H. D. Verkruijsse, *Synth. Commun.* **1988**, *18*, 1763.
[12] S. Gronowitz, T. Raznikiewicz, *Org. Synth. Coll.* **1973**, *5*, 149.
[13] A. Bugge, *Acta Chem. Scand.* **1968**, *22*, 63.
[14] K. S. Choi, K. Sawada, H. Dong, M. Hoshino, J. Nakayama, *Heterocycles* **1994**, *38*, 143.
[15] J. Teste, N. Lozac'h, *Bull. Soc. Chim. Fr.* **1955**, 422.
[16] M. Y. Darensbourg, D. J. Darensbourg, *Inorg. Chem.* **1970**, *9*, 32.
[17] E. O. Fischer, A. Maasböl, *Chem. Ber.* **1967**, *100*, 2445.
[18] [18a] O. S. Mills, A. D. Redhouse, *J. Chem. Soc. A* **1968**, 642. – [18b] G. Huttner, B. Krieg, *Chem. Ber.* **1972**, *105*, 67. – [18c] U. Schubert, *Organometallics* **1982**, *1*, 1085.
[19] F. H. Allen, O. Kennard, D. G. Watson, L. Brammer, A. G. Orpen, R. Taylor, *J. Chem. Soc., Perkin Trans 2* **1987**, S1.
[20] H. Meerwein, *Org. Synth.* **1966**, *46*, 113.
[21] *COLLECT*, Data Collection Software; Nonius B. V., Netherlands, **1998**.
[22] Z. Otwinowski, W. Minor, *Processing of X-ray Diffraction Data Collected in Oscillation Mode* in: *Methods in Enzymology, Vol.276, Macromolecular Crystallography, Part A* (Eds.: C. W. Carter, R. M. Sweet), pp. 307–326, Academic Press, **1997**.
[23] G. M. Sheldrick, *Acta Crystallogr. Sect. A* **1990**, *46*, 467–473.
[24] G. M. Sheldrick, *SHELXL-97* (Release 97-2), University of Göttingen, Germany, **1997**.

Received April 25, 2000
[I00164]

Redox Characteristics and Anion Association Behaviour of Stereoisomeric Forms of Mono- and Oligonuclear Metal Complexes Using High Pressure Electrochemistry

Brett D. Yeomans,[a] Laurence S. Kelso,[a] Peter A. Tregloan,[b] and F. Richard Keene*[a]

Keywords: Anion association / Stereochemistry / High-pressure electrochemistry / Mixed-valence / Ruthenium polypyridyl

The effect of the presence of the anions PF_6^-, BF_4^-, ClO_4^-, and tosylate$^-$ on the potentials of the $Ru^{III/II}$ redox processes in a series of mono-, di-, and trinuclear complexes involving polypyridyl ligands are reported. The anions gives rise to a cathodic shift in the respective redox potentials in the sequence $PF_6^- < BF_4^- \approx ClO_4^- <$ tos$^-$, with the magnitude of the shifts being largest for the tri-nuclear and smallest for the mononuclear species. In one dinuclear complex, a variation of anion was also observed to affect the difference in potentials between the [6+/5+] and [5+/4+] couples. These effects are consistent with known specific association of the anions with metal complexes of this type. In the presence of PF_6^-, high-pressure electrochemical studies revealed the molar volume changes for successive redox couples in di- and trinuclear complexes were almost invariant ($\Delta V_{complex}$ = 24 ± 2 cm^3 mol^{-1}) and consistent with the value for mononuclear species. This constancy is interpreted in terms of isolated $Ru^{III/II}$ processes in all complexes and implies that the electrostrictive effects on solvent are limited to a very short range.

Introduction

We have recently established that the stereochemical relationship of the components in mono- and oligonuclear species influences intramolecular electron and energy transfer processes between them. These studies have included the variation in lifetimes of the charge-separated excited states in the four geometric isomers of the chromophore-quencher complex $[Ru(Me_2bpy)(bpy\text{-}A)(bpy\text{-}D)]^{4+}$ {Me_2bpy = 4,4′-dimethyl-2,2′-bipyridine; bpy-A = bpy-MV^{2+} = (4′-methyl-2,2′-bipyridin-4-yl)methyl-1′-methyl-4,4′-bipyrinediium cation (MV^{2+} is an acceptor quencher); bpy-D = bpy-PTZ = 4′-methyl-2′,2-bipyridin-4-yl)methyl]phenothiazine (PTZ is a donor quencher)},[1,2] the variation in redox characteristics of the diastereoisomers of the two dimetallic systems $[\{Ru(pp)_2\}_2(\mu\text{-azo})]^{4+}$ {azo = azobis(2-pyridine),

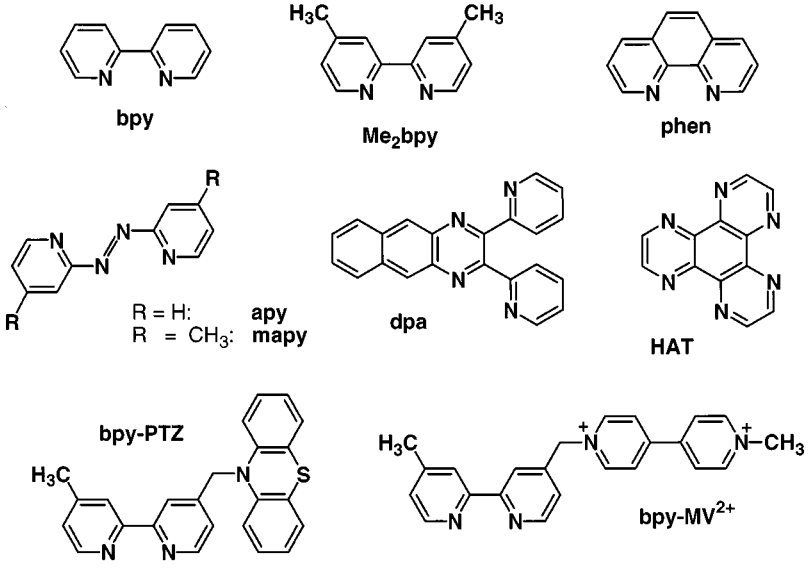

apy, or azobis(4-methyl-2-pyridine), mapy; pp = 2,2′-bipyridine (bpy) or Me_2bpy} and $[\{Ru(bpy)_2\}_2(\mu\text{-dpa})]^{4+}$ {dpa = 2,3-bis(2-pyridyl)-1,4-diaazaanthracene},[3,4] and the variation of excited state lifetimes for the diastereoisomers of the dinuclear $[\{Ru(pp)_2\}_2(\mu\text{-HAT})]^{4+}$ and trinuclear

[a] School of Biomedical and Molecular Sciences, James Cook University, Townsville, Queensland 4811, Australia
Fax: (internat.) + 61-7/4781-4600
E-Mail: Richard.Keene@jcu.edu.au
[b] School of Chemistry, University of Melbourne, Parkville, Victoria 3052, Australia
Supporting information for this article is available on the WWW under http://www.wiley-vch.de/home/eurjic or from the author.

 © WILEY-VCH Verlag GmbH, 69451 Weinheim, 2001 1434−1948/01/0101−0239 $ 17.50+.50/0

$[\{Ru(pp)_2\}_3(\mu\text{-HAT})]^{6+}$ complexes involving the bridging ligand HAT {pp = bpy or phen (1,10-phenanthroline); HAT = 1,4,5,8,9,12-hexaazatriphenylene}.[5]

At this stage, because of the limited number of examples available, the factors which give rise to dependence of such physical characteristics on the stereochemistry are not yet clear.

As part of our stereochemical studies, we have also established a general cation-exchange chromatographic procedure which allows the separation of stereoisomers of mono- and oligonuclear complexes.[3−10] The mechanism of the separation involves differential association of the anion of the eluent with the stereoisomers of the substrate cation, and NMR titration studies reveal the association has π-stacking and hydrophobic components.[4,7,8] More detailed studies of complex−anion (and probably complex−solvent) interactions will complete our understanding of the more intimate mechanistic details of the factors which contribute to the discrimination.

Recent reports have shown that electrochemical techniques such as cyclic voltammetry and differential pulse voltammetry performed at high pressure may be used to measure redox reaction volume changes (ΔV_{cell}) for electrochemical cells involving reactions of transition metal complexes.[11] Further, the experimental ΔV_{cell} can be resolved into reference electrode and working electrode contributions and the latter in turn broken into electrostrictive and intrinsic components, so that the technique can provide otherwise inaccessible information on the solvational and structural changes which accompany metal complex reduction processes − in both aqueous and non-aqueous solutions.

For systems such as those listed above, the technique therefore had immediate appeal in probing the nature of differences in the redox characteristics of stereoisomeric forms of the same complex, and in investigating the differences in anion/solvent interactions between similar structures. The present paper reports the first such investigations.

Results and Discussion

Syntheses

Synthesis and Separation. The synthesis of $[\{Ru(bpy)_2\}_2(\mu\text{-dpa})](PF_6)_4$ was achieved by heating a 2:1 mixture of $[Ru(bpy)_2Cl_2]$ and the dpa ligand in methanol/water for 24 h. An alternative procedure involved heating an ethylene glycol solution of the reactants in a microwave oven: however, this method produced a lower yield of the dinuclear complex, with an increase in the production of mononuclear $[Ru(bpy)_2(dpa)]^{2+}$.

The dinuclear species $[\{Ru(bpy)_2\}_2(\mu\text{-dpa})]^{4+}$ exists in two diastereoisomeric forms, one *racemic* (consisting of the ΔΔ/ΛΛ enantiomeric pairs) and the other *meso* (ΔΛ). The diastereoisomers were separated by cation-exchange chromatography: the *rac* diastereoisomer appeared to be less stable than the *meso*, and underwent slow decomposition in the solid form.

For diastereoisomer characterisation, the resolution of one of the diastereoisomers unequivocally establishes its identity as *rac*. We have developed chromatographic methods for separation of enantiomers by ion-exchange chromatography, using chiral eluents.[5,7,12] Cation-exchange chromatography of the two separated diastereoisomers of $[\{Ru(bpy)_2\}_2(\mu\text{-dpa})]^{4+}$ (isolated from Bands 1 and 2 of the their chromatographic separation) using an aqueous solution of sodium (−)-*O*,*O*′-dibenzoyl-L-tartrate as the eluent showed that the product from Band 2 separated further into two bands (designated 2A and 2B), therefore unambiguously identifying it as the *rac* form. The isolated cations from this resolution had equal and opposite CD spectra (Figure 1).

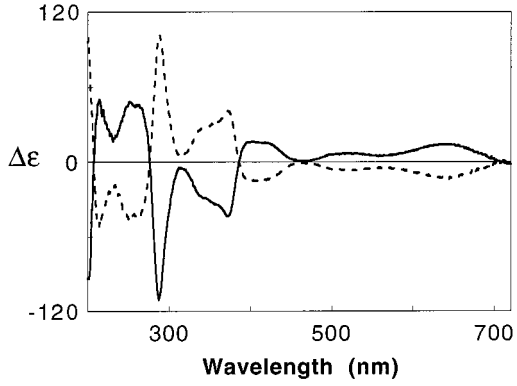

Figure 1. CD spectra (CH_3CN solution) of the ΔΔ (- - - - -) and ΛΛ (——) enantiomers of *rac*-$[\{Ru(bpy)_2\}_2(\mu\text{-dpa})](PF_6)_4$

On the basis of Exciton Theory and by comparison with previous resolutions of similar species,[5] Band 2A was assigned as ΔΔ and Band 2B as ΛΛ.

Electrochemistry

Redox potentials were determined by cyclic and differential pulse voltammetry in CH_3CN solution containing 0.1 M supporting electrolyte. The anion of the electrolyte was observed to affect the redox potentials associated with the $Ru^{III/II}$ couples in mono-, di-, and trinuclear complexes, and the separation between the formally [5+/4+] and [6+/5+] processes in dinuclear systems.

The $[FeCp_2]^{+/0}$ couple was employed as the reference in these studies, and this couple itself is known to be solvent and electrolyte dependent.[13,14] Consequently, the $[FeCp^*_2]^{+/0}$ redox couple (Cp* = pentamethylcyclopentadienyl anion), which is less susceptible to anion and solvent interactions,[14] was also used as a reference; however, we found little difference for $[FeCp_2]^{+/0}$ vs. $[FeCp^*_2]^{+/0}$ in the range of electrolytes employed {$E_{1/2}$ values of $[FeCp_2]^{+/0}$ vs. $[FeCp^*_2]^{+/0}$ in acetonitrile/0.1 M $[(n\text{-}C_4H_9)_4N]X$ solution were 520 mV (X = BF_4^-), 512 mV (PF_6^-), 510 mV (ClO_4^-), and 507 mV (tos^-; tosylate ion}. On this basis, the reasonable assumption is made that the data reported reflect only the changes in potential associated with working electrode half-cell of the particular complex involved.

Table 1. Electrolyte-anion dependence of redox potentials of complexes vs. $[FeCp_2]^{+/0}$ in CH_3CN/0.1 M $[(n\text{-}C_4H_9)_4N]X$

	Anion X^-	$E_{1/2}$ (mV) [3+/2+]	$E_{1/2(1)}$ (mV) [5+/4+]	$E_{1/2(2)}$ (mV) [6+/5+]	$\Delta E_{1/2}$ (mV)
$[Ru(bpy)_3]^{n+}$	PF_6^-	904			
	tos^-	852			
$[Ru(Me_4bpy)_3]^{n+}$	PF_6^-	652			
	tos^-	612			
$[Ru(phen)_3]^{n+}$	PF_6^-	892			
	tos^-	860			
$[Ru(phen)_2(HAT)]^{n+}$	PF_6^-	1172			
	BF_4^-	1140			
	ClO_4^-	1184			
	tos^-	1072			
$\Delta\Lambda$(*meso*)-$[\{Ru(phen)_2\}_2(\mu\text{-HAT})]^{n+}$	PF_6^-		1160	1384	224
	BF_4^-		1160	1356	196
	ClO_4^-		1106	1310	204
	tos^-		972	1054	86
$\Delta\Lambda$(*meso*)-$[\{Ru(bpy)_2\}_2(\mu\text{-dpa})]^{n+}$	PF_6^-		1069	1262	193
	BF_4^-		1008	1200	192
	ClO_4^-		1025	1200	175
	tos^-		962	1082	120
$\Delta\Delta/\Lambda\Lambda$(*rac*)-$[\{Ru(bpy)_2\}_2(\mu\text{-dpa})]^{n+}$	PF_6^-		1088	1263	175
	BF_4^-		1048	1203	155
	ClO_4^-		1049	1202	153
	tos^-		990	1094	104

The dependencies of redox potentials of complexes studied in this work on the anion of the electrolyte are listed in Table 1. There is a cathodic shift of potentials in solutions containing certain electrolyte anions, with tos^- having the greatest effect. The induced shifts are less for $Ru^{III/II}$ couples in monouclear complexes (50 mV for complexes containing only bpy and phen ligands and their derivatives; 100 mV for mononuclear complexes containing the ligand HAT) than those) in dinuclear systems for the formally [5+/4+] (100−200 mV) and [6+/5+] processes (150−300 mV.

For the mononuclear complex couples $[Ru(bpy)_3]^{3+/2+}$, $[Ru(Me_4bpy)_3]^{3+/2+}$, and $[Ru(phen)_3]^{3+/2+}$, a cathodic shift in the redox potential was observed in the order $PF_6^- < BF_4^- < ClO_4^- < tos^-$, with the same trend being observed for $[Ru(phen)_2(HAT)]^{3+/2+}$ but of larger magnitude. Ion-pairing between the cationic complex and electrolyte anion would be expected to result in a cathodic shift in the redox potential due to the lesser net charge of the ion-pair,[13,14] so the shift of potentials to less positive values in solutions with different electrolyte anions can be correlated with differential ion-pairing;[4,8] i.e. the tos^- anion interacts with the complex to a greater extent than does PF_6^-. The effect observed for $[Ru(phen)_2(HAT)]^{3+/2+}$ suggests an even greater interaction.

For dinuclear complexes, the electrochemistry of $[\{Ru(Me_2bpy)_2\}_2(\mu\text{-mapy})]^{4+}$,[3] $[Ru(phen)_2(HAT)]^{2+}$, $[\{Ru(phen)_2\}_2(\mu\text{-HAT})]^{4+}$, and $[\{Ru(phen)_2\}_3(HAT)]^{6+}$ [5] have been reported elsewhere. In the present study, in CH_3CN/0.1 M $[(n\text{-}C_4H_9)_4N]PF_6$ solution the diastereoisomers of $[\{Ru(bpy)_2\}_2(\mu\text{-dpa})]^{4+}$ each exhibited two reversible one-electron oxidations corresponding to successive oxidation of the metal centres, and multiple reversible ligand-based reductions. However, the *meso* and *rac* forms differed (Figure 2); in the *meso* complex the first oxidation ($E_{1/2(1)}$) occurred at a less positive potential than the *rac* form, resulting in a greater separation of the two oxidations ($\Delta E_{1/2}$). The separation between such oxidations in a dinuclear species is used as an indication of the degree of M−M interaction.[15]

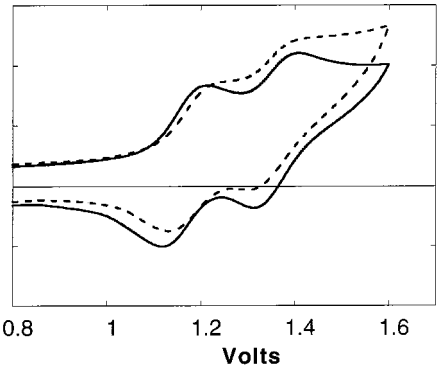

Figure 2. Cyclic voltammograms (CH_3CN/0.1 M $[(n\text{-}C_4H_9)_4N]PF_6$ solution) of the *meso*- (——) and *rac*- (- - - - -) diastereoisomers of $[\{Ru(bpy)_2\}_2(\mu\text{-dpa})]^{n+}$ {[5+/4+] and [6+/5+] couples only}

In dinuclear systems, the anions also affect this separation between [5+/4+] $\{E_{1/2(1)}\}$ and [6+/5+] $\{E_{1/2(2)}\}$ redox couples. For example, $\Delta E_{1/2}$ for $\Delta\Lambda$-$[\{Ru(bpy)_2\}_2(\mu\text{-dpa})]^{4+}$ ranged from 193 mV $\{[(n\text{-}C_4H_9)_4N]PF_6\}$ to 120 mV $\{[(n\text{-}C_4H_9)_4N]tos\}$, with $\Delta E_{1/2}$ decreasing in the order $PF_6^- > BF_4^- > ClO_4^- > tos^-$. Even more dramatic effects were observed for $[\{Ru(phen)_2\}_2(\mu\text{-HAT})]^{4+}$ (Table 1). The effects were always in the order that the separation for $PF_6^- > BF_4^- > tos^-$: the effect of ClO_4^- was more variable, but generally comparable with that of BF_4^-. In all cases, the absolute potentials of both couples shifted, and the greater negative shift of the [6+/5+] couple leads to the decrease in separation. Changing the electrolyte cation {e.g.

$[(C_2H_5)_4N]ClO_4$ cf. $[(n\text{-}C_4H_9)_4N]ClO_4$} made no difference to the voltammetry.

For dinuclear species, ion-pairing offers one possible explanation for the remarkable observations of the dependence of $\Delta E_{1/2}$ on the identity of the anion in the electrolytes. For these dinuclear complexes, on purely electrostatic grounds ion-pairing would be stronger for the [6+]/[5+] couple (cf. [5+]/[4+]) because of the larger charges involved, resulting in $E_{1/2(2)}$ ([6+]/[5+]) shifting more cathodically than $E_{1/2(1)}$.

An alternative rationalization of the effect is more speculative. Recent work has shown specific interactions between a variety of aliphatic and aromatic anions with ruthenium(II) complexes containing polypyridyl ligands,[8] and in the case of dinuclear species, specific interactions have been identified in the region between the metal centres. The presence of the anion(s) in that region might result in an increased metal−metal separation, with the resultant decrease in metal−metal interaction manifested in a smaller separation between the two metal-based oxidations ($\Delta E_{1/2}$), as observed for tos^- (for which the association would be strongest) with $[\{Ru(bpy)_2\}(\mu\text{-dpa})]^{4+}$ and $[\{Ru(phen)_2\}_2(\mu\text{-HAT})]^{4+}$.

Spectroelectrochemistry

Detailed spectroelectrochemical studies of the dinuclear complexes bridged by apy and mapy have previously been reported.[3] Similar studies were undertaken in the present work for the complexes $[\{Ru(phen)_2\}_2(\mu\text{-HAT})]^{4+}$, $[\{Ru(phen)_2\}_3(\mu\text{-HAT})]^{6+}$, and $[\{Ru(bpy)_2\}_2(\mu\text{-dpa})]^{4+}$, and the absorption data for the resulting electrogenerated species are collated and presented as Supporting Information (Table S1). All three compounds showed clear isosbestic points for the first oxidation process, and reversibility was demonstrated by coincidence of the various isosbestic points during the reverse reduction step, which led to ultimate recovery of the starting compound.

For the dinuclear complexes the first oxidation was a one-electron process, producing the mixed-valence species $[(pp)_2Ru^{III}(\mu\text{-L})Ru^{II}(pp)_2]^{5+}$ (pp = bpy or phen) which possess intense intervalence charge transfer or metal-to-metal charge transfer (MMCT) bands in the near infrared (NIR) region of the spectrum. The formation of such a band in a spectroelectrochemical experiment is shown for the oxidation of *meso*-$[\{Ru(phen)_2\}_2(\mu\text{-HAT})]^{4+}$ in Figure 3. Additionally, the overlayed spectra of $[\{Ru(bpy)_2\}_2(\mu\text{-dpa})]^{4+}$ and its electrogenerated [5+] and [6+] analogues are shown in Figure 4. The first oxidation of both these dinuclear complexes was accompanied by a 50% decrease in the intensity of their respective MLCT absorptions (at 15600 cm^{-1} and 18200 cm^{-1}, respectively). This is consistent with the notional conversion of one of the d^6 metal centres in each dimer to a d^5 entity. The band attributed to the $d\pi(Ru^{II})\rightarrow\pi^*$(bridge) MLCT absorption collapsed completely following removal of a second electron.

An analysis of the NIR absorbances using Hush theory[16,17] reveals a large discrepancy between calculated and experimentally derived values of $\Delta\nu_{1/2}$ (Table 2). While a strong solvent dependency may account for this (our measurements were primarily carried out in CH_3CN solution), the non-applicability of the theory suggests a large degree of delocalisation and thus strongly interacting (Robin and Day "Class III") behaviour.[18−20] This is further supported by the unsymmetrical (non-gaussian) appearence of the bands and the apparent fine structure within the NIR region absorbances. No differences in band energy, intensity or shape were observed between the diastereoisomeric pairs of the dinuclear species investigated.

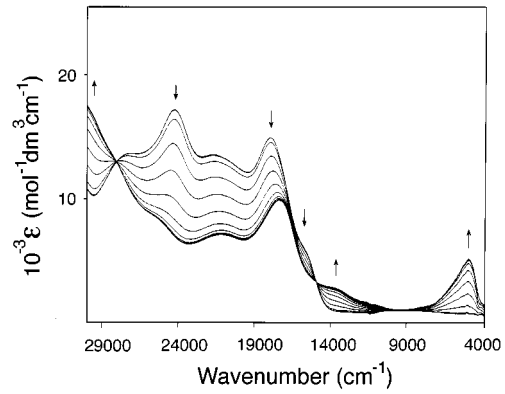

Figure 3. Spectroelectrochemical study of one-electron oxidation of *meso*-$[\{Ru(phen)_2\}_2(\mu\text{-HAT})]^{4+}$ (CH_3CN/0.1 M $[(n\text{-}C_4H_9)_4N]ClO_4$ solution)

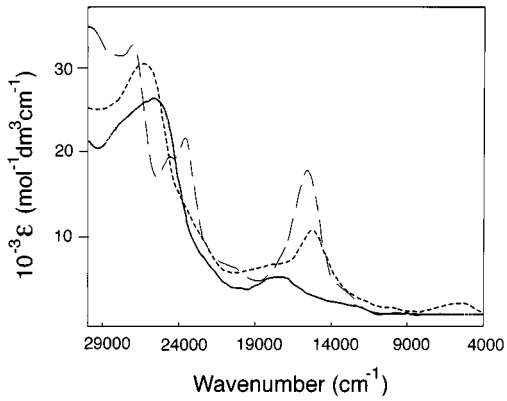

Figure 4. UV/Visible spectra of $[\{Ru(bpy)_2\}_2(\mu\text{-dpa})]^{4+}$ (− − − −) and the electrogenerated 5+ (- - - - -) and 6+ (——) analogues (CH_3CN/0.1 M $[(n\text{-}C_4H_9)_4N]ClO_4$ solution)

Table 2. MMCT band analysis of mixed-valence dinuclear species in CH_3CN solution at −32 °C

Dinuclear Complex	$\tilde{\nu}_{max}$ [cm^{-1}]	$\Delta\tilde{\nu}_{1/2}$ (calcd.) [cm^{-1}]	$\Delta\tilde{\nu}_{1/2}$ (exp.) [cm^{-1}]
$[\{Ru(bpy)_2\}_2(\mu\text{-dpa})]^{5+}$	5600	3600	2800
$[\{Ru(bpy)_2\}_2(\mu\text{-mapy})]^{5+}$ [3]	6900	3990	1600
$[\{Ru(phen)_2\}_2(\mu\text{-HAT})]^{5+}$	5200	3470	1700
$[\{Ru(*phen*)_2\}_2(\mu\text{-HAT})]^{5+}$	8200	4350	1900

For the dinuclear complexes, some problems were encountered when attempts were made to fully oxidize both metal centres to the trivalent state. A spectrum of $[\{Ru(bpy)_2\}_2(\mu\text{-dpa})]^{6+}$ was obtained at −32 °C, however the compound was only metastable when held at a high anodic potential for extended periods of time. A gradual

reduction in the absorption intensity was observed across the entire spectral region and following regeneration the original [4+] cation also exhibited a reduced intensity.

We were unable to observe the $[\{Ru(phen)_2\}_2(\mu\text{-HAT})]^{6+}$ cation. Subjecting the [5+] species to high anodic potentials over a 3 h period led to a new unidentified [6+] compound in which one or more of the phenanthroline ligands appeared to have undergone oxidation. The product species is characterised by an intense absorption at 11300 cm^{-1} which can tentatively be assigned as a $\sigma(\text{ligand})\rightarrow d^5(Ru^{III})$ (LMCT) transition. The oxidation of phenanthroline to 1,10-phenanthroline-5,6-dione while coordinated to a ruthenium or cobalt(III) centre is a well-documented phenomenon: the reaction is known to proceed readily (and at much lower potentials) relative to the oxidation of an uncoordinated ligand.[21,22] This oxidative conversion was completely irreversible, however the new species was itself very stable and displayed its own completely reversible spectroelectrochemistry. Upon reduction to the 5+ state, this new complex exhibited a unique MMCT band which predictably collapsed upon further reduction to a [4+] species (Figure 5). Repeated oxidations and reductions via bulk electrolysis gave reproducible isosbestic points and uniform absorption intensities.

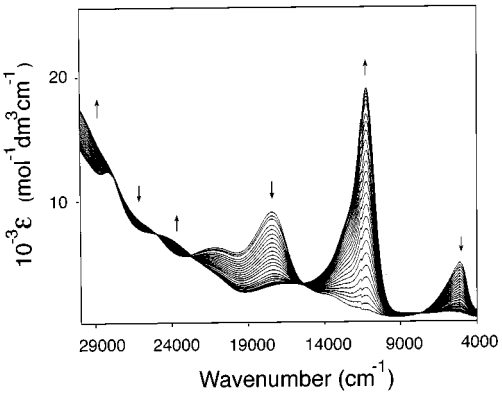

Figure 5. Spectroelectrochemical trace of the reduction of $[\{Ru(*phen*)_2\}_2(\mu\text{-HAT})]^{5+}$ (CH_3CN/0.1 M $[(n\text{-}C_4H_9)_4N]ClO_4$ solution)

Reduction of the dinuclear complexes bridged by dpa or HAT led to rapid decomposition of the original [4+] species. Re-oxidation of the dpa species produced a compound whose visible spectrum was very similar to that of $[Ru(bpy)_2(dpa)]^{2+}$. This is consistent with a previous spectroelectrochemical investigation of $[\{Ru(bpy)_2\}_2(\mu\text{-dpp})]^{4+}$ where it was determined that mononuclear $[Ru(bpy)_2(dpp)]^{2+}$ was produced via de-chelation of dinuclear starting material subjected to large cathodic potentials.[18]

The spectroelectrochemistry of the $[\{Ru(phen)_2\}_3(\mu\text{-HAT})]^{6+}$ trinuclear complex presented none of the problems associated with the dinuclear species. Two successive oxidations {[6+]→[7+] and [7+]→[8+]} and two reversible reductions {[6+]→[5+] and [5+]→[4+]} were easily achieved. The starting compound was also regenerated without any appreciable degradation. No NIR absorption bands were observed for the potentially mixed-valent [5+] or [6+] species. The absence of a MMCT transition implies that electron density is totally delocalised across the entire molecule and hence removal of an electron from the system only results in a small change in the effective charge on all three metal centres. This is borne out by the relatively small differences between the visible absorption spectra following each successive redox event.

High-Pressure Electrochemistry

High-pressure voltammetry techniques enable the measurement of molar volume changes of electron-transfer reactions.[11] The standard molar volume change ($\Delta V°_{cell}$) for a redox reaction is given by $\Delta V°_{cell} = (d\Delta G°/dP)$, or $\Delta V°_{cell} = -nF(dE°/dP)$, where n is the number of electrons transferred and F is the Faraday constant. The cell reaction volume (ΔV_{cell}) of a redox couple can therefore be determined by measuring the pressure dependence of $E_{1/2}$ for the redox couple. ΔV_{cell} is the sum of the two half-cell components, $\Delta V_{complex}$ and ΔV_{ref}, arising from the molar volume changes of the reference and working electrodes, respectively. The same reference {Ag/Ag^+ (0.01 M in CH_3CN)} was employed for all experiments; ΔV_{ref} for this system has been determined to be -20.7 cm^3 mol^{-1}.[11] Using this value for ΔV_{ref}, molar volumes changes for the reduction processes of the complexes, $\Delta V_{complex}$, were then calculated and are listed with the measured ΔV_{cell} values in Table 3.

The $\Delta V_{complex}$ will be made up of two components, ΔV_{elec} and ΔV_{intr}: the former is an electrostrictive contribution arising from interaction of solvent molecules and counterions with the ionic charge of the complex, and the latter is an intrinsic contribution arising from bond length and structural changes within the molecule. For the ruthenium complexes containing polypyridyl ligand studied here, minimal structural changes occur within the $Ru^{III/II}$ redox process,[23] so that the major component of $\Delta V_{complex}$ will be ΔV_{elec}, reflecting the interaction of solvent and electrolyte with the complex cation.

While there is little influence of the anion on the value of $\Delta V_{complex}$ for the mononuclear species $[Ru(phen)_2(HAT)]^{3+/2+}$ {$\Delta V_{complex} = 22.2$ cm^3 mol^{-1} in $[(n\text{-}C_4H_9)_4N]PF_6$ and 20.0 cm^3 mol^{-1} in $[(C_2H_5)_4N]ClO_4$}, in all other complexes studied there appears to be a significant effect, which is noticably more positive (by 7−12 cm^3 mol^{-1}) in PF_6^- than in ClO_4^- media. This effect is presumably related to the specific interactions/association of some anions: it is consistent with a greater release of solvent in the presence of the less strongly associated anion PF_6^- because the effective complex charge is higher, and $\Delta V_{complex}$ is proportional to Δz^2 (see below). The discrimination of the anions in dinuclear complexes indicates that the region between the metal centres is additionally important.[8]

For all species except the monomer, shifts in $E_{1/2}$ at 1 bar indicate that ClO_4^- associates more strongly than PF_6^-, and the differences in ΔV values seem to parallel the differences (or lack thereof) in $E_{1/2}$ measured in the respective media. However, leaving aside the data for the $[Ru(phen)_2(HAT)]^{3+/2+}$ couple in perchlorate media, the values of $\Delta V_{complex}$ are remarkably constant across charge

Table 3. ΔV_{cell} and corresponding molar volume changes ($\Delta V_{complex}$) for reduction of mono-, di-, and trinuclear complexes in CH_3CN/0.1 M $[(n\text{-}C_4H_9)_4N]X$ ($X = PF_6^-$, ClO_4^-) solution

Redox Couple	Δz^2	0.1 M $[(n\text{-}C_4H_9)_4N]PF_6$ ΔV_{cell} cm^3mol^{-1}	$\Delta V_{complex}$[a] cm^3mol^{-1}	0.1 M $[(C_2H_5)_4N]ClO_4$ ΔV_{cell} cm^3mol^{-1}	$\Delta V_{complex}$ [a] cm^3mol^{-1}
$[Ru(phen)_2(HAT)]^{3+/2+}$	5	+1.5	+22.2	−0.7	+20.0
ΔΔ/ΛΛ-$[\{Ru(phen)_2\}_2(\mu\text{-HAT})]^{6+/5+}$	11	+0.7	+21.4	−8.6	+12.1
ΔΔ/ΛΛ-$[\{Ru(phen)_2\}_2(\mu\text{-HAT})]^{5+/4+}$	9	+4.7	+25.4	−7.6	+13.1
ΔΛ-$[\{Ru(phen)_2\}_2(\mu\text{-HAT})]^{6+/5+}$	11	+1.1	+21.8	−6.1	+14.6
ΔΛ-$[\{Ru(phen)_2\}_2(\mu\text{-HAT})]^{5+/4+}$	9	+1.7	+22.4	−5.5	+15.2
ΔΔΔ/ΛΛΛ-$[\{Ru(phen)_2\}_3(\mu\text{-HAT})]^{8+/7+}$	15	+2.4	+23.1		
ΔΔΔ/ΛΛΛ-$[\{Ru(phen)_2\}_3(\mu\text{-HAT})]^{7+/6+}$	13	+4.2	+24.9		
ΔΔ/ΛΛ-$[\{Ru(bpy)_2\}_2(\mu\text{-dpa})]^{6+/5+}$	11	+2.9	+23.6	−4.5	+16.2
ΔΔ/ΛΛ-$[\{Ru(bpy)_2\}_2(\mu\text{-dpa})]^{5+/4+}$	9	+4.4	+25.1	−2.4	+18.3
ΔΛ-$[\{Ru(bpy)_2\}_2(\mu\text{-dpa})]^{6+/5+}$	11	+4.6	+25.3	−4.6	+16.1
ΔΛ-$[\{Ru(bpy)_2\}_2(\mu\text{-dpa})]^{5+/4+}$	9	+5.2	+25.9	−2.2	+18.5
ΔΔ/ΛΛ-$[\{Ru(Me_2bpy)_2\}_2(\mu\text{-mapy})]^{5+/4+}$	9	+2.9	+23.6		
ΔΛ-$[\{Ru(Me_2bpy)_2\}_2(\mu\text{-mapy})]^{5+/4+}$	9	+3.4	+24.1		

[a] $\Delta V_{complex} = \Delta V_{cell} - \Delta V_{ref}$ ($\Delta V_{ref} = -20.7\ cm^3\ mol^{-1}$); ref.[11]

changes and across complexes within each charge change group ($\Delta V_{complex} = 24 \pm 2\ cm^3\ mol^{-1}$). Furthermore, there does not appear to be any significant difference in $\Delta V_{complex}$ between the diastereoisomers within the $[\{Ru(bpy)_2\}_2(\mu\text{-dpa})]^{n+}$ and $[\{Ru(phen)_2\}_2(\mu\text{-HAT})]^{n+}$ species: the values of $\Delta V_{complex}$ for the *meso* isomers of both dinuclear complexes are generally within $2\ cm^3\ mol^{-1}$ of the *rac* form, which is not significantly greater than experimental error.

This is a surprising result. Previous studies have discussed the correlation between electrostrictive changes ΔV_{elec} and $\Delta z^2/r$ $\{\Delta z^2 = (z_{ox})^2 - (z_{red})^2$; r = radius of species$\}$.[24] Calculated van der Waal's volumes for the mono-, di-, and trinuclear complexes $\{[Ru(phen)_2(HAT)]^{n+}$, $[\{Ru(phen)_2\}_2(\mu\text{-HAT})]^{n+}$, and $[\{Ru(phen)_2\}_2(\mu\text{-HAT})]^{n+}\}$ were 518, 847, and 1177 Å^3, respectively: even allowing for the approximation incurred because of the non-spherical nature of the di- and trinuclear species, the constancy of $\Delta V_{complex}$ cannot be accounted for by this simple $\Delta z^2/r$ relationship.

A rationalization for the effect may be found in ion association, which is known to occur between the cationic mono-, di-, and trinuclear complexes used in this study and a variety of anions.[8] Indeed, NMR titration studies of the interaction of a number of mononuclear (2+) and dinuclear (4+) complexes with strongly associating anions were interpreted to indicate a 2:1 and 4:1 ratio of anions/cation, respectively.[8] Accordingly, the "effective charge" would be expected to be less than the formal charge in these species. Furthermore, if in di- and trinuclear species there were differences in the extent of association between the oxidized and reduced forms, then their effective charges would also be less than the formal charges, and actually closer to the charges applying to the mononuclear situation. Thus for each redox couple in the systems studied, the measured values of $\Delta V_{complex}$ could be similar. This situation is represented by the Equation (1).

$$[M^{n+} \ldots pX^-]^{(n-p)+} + e^- \rightarrow [M^{(n-1)+} \ldots (p-q)X^-]^{(n-p-1+q)+} + qX^- \quad (1)$$

However, consideration of the Nernst equation would a require a linear relationship between $E_{1/2}$ and $\ln[X^-]$ with a slope of $-0.059q$ (q is the number of anions released from association on a one-electron reduction of the substrate).[25] Our studies of the dependence of $E_{1/2}$ on the concentration of the anion indicated that there was no significant release of associated anions on reduction within any nuclearity regime.

Another rationale has its basis within the nature of the redox changes. Regardless of the nuclearity, each redox process involves a change at one ruthenium centre from oxidation state III to II. The observed consistency of $\Delta V_{complex}$ values may indicate that the effects on solvent are localised around individual ruthenium centres. In other words, the system behaves as a sequence of localised 3+/2+ charge changes and that in all cases Δz^2 is effectively 5, regardless of the overall charge. The consistent value of ca. $20-26\ cm^3\ mol^{-1}$ is in agreement with the [3+/2+] couples measured both in this work, and in other independent observations of [3+/2+] reductions: e.g. $\Delta V_{complex} = 22.2\ cm^3\ mol^{-1}$ (acetonitrile/0.1 M $[(C_2H_5)_4]ClO_4$) for $[Fe(phen)_3]^{3+/2+}$.[11] The interpretation that all centres are acting as independent $Ru^{III/II}$ couples appears to be in conflict with the communication between the metal centres in the di- and trinuclear species, as evidenced by our observation of MMCT bands in such complexes (discussed above). However, in 1,4-pyrazine-bridged dinuclear ruthenium complexes, in which there is also strong communication between the metal centres, reaction entropies ($\Delta S°$) for successive redox changes are independent of the oxidation state of the second Ru centre, and correspond to the $\Delta S°$ values for the corresponding mononuclear moieties. This was interpreted to demonstrate that the entropy change upon reduction of the Ru was caused by short-range effects not reaching further than two solvent molecules.[26] It is not unreasonable to conclude that the constancy of the values of $\Delta V_{complex}$ across successive redox changes and across complexes within each charge

group observed in the present work reflects isolated events where the solvent effect is limited to a short range.

Experimental Section

Physical Measurements: Electronic spectra were recorded using a Cary 5E UV/Vis/NIR spectrophotometer. NMR spectra were recorded on Bruker AM300 or Varian Mercury 300 MHz spectrometers. Electrochemical measurements at atmospheric pressure were performed in an argon-filled drybox using a Bioanalytical Systems (BAS) 100A electrochemical analyzer. Cyclic voltammetry in acetonitrile employed a platinum disk (1 mm diameter) working electrode, platinum wire counter electrode and Ag/Ag^+ (0.01 M) reference electrode. Solutions contained 0.1 M $[(n\text{-}C_4H_9)_4N]PF_6$ or $[(C_2H_5)_4N]ClO_4$ as electrolyte. Typically, scan rates were 100−200 mV s^{-1}. Ferrocene ($[FeCp_2]$ was added as an internal standard after each experiment (oxidation at +0.095 V vs. Ag/Ag^+). For differential pulse voltammetry (DPV) measurements the conditions used were scan rate 4 mV/s, pulse amplitude 50 mV, pulse width 60 msec and pulse period 1 s. Spectra of oxidized and reduced species were obtained at 240 K by electrogeneration within a cryostatted optical semi-thin-layer electrochemical (OSTLE) cell, utilizing a Perkin−Elmer Lambda 9 UV/Vis/NIR spectrophotometer, as described previously.[27] High resolution mass spectra were obtained at the Australian Institute of Marine Science (Townsville) on a Bruker BioApex 47e ICR Mass Spectrometer with an electrospray source, using solutions ca. 2 μg/mL in acetonitrile.

The high pressure electrochemical cell is a development of our earlier design[24,28] and has a sample volume of ca. 1 mL, uses a 1 mm Pt disk working electrode, 2 mm Pt disk counter electrode and a Ag/Ag^+ (0.01 M in 0.1 M supporting electrolyte) reference electrode separated from the working solution by a Vycor™ frit mounted in a flexible Teflon™ sleeve.[11] The high-pressure electrochemical experiments were performed in acetonitrile solution containing 0.1 M $[(n\text{-}C_4H_9)_4N]PF_6$ or $[(C_2H_5)_4N]ClO_4$ as supporting electrolyte: samples were prepared in air, then purged with N_2 before closing the cell and mounting it in the high pressure bomb, thermostatted at 298 K. Cyclic voltammetry and differential pulse experiments were carried out using a MacLab potentiostat and data acquisition system with E-Chem software (AD Instruments). Data were recorded at intervals of about 500 psi (34 bar) up to the maximum pressure, allowing the cell to thermally equilibrate for about 20 mins between measurements, and then at intermediate pressures as the pressure was lowered, to check the integrity of measurements over the period of the measurements, typically 4 h.

Materials: Ammonium hexafluorophosphate (Aldrich), potassium hexafluorophosphate (Aldrich), 2,3-diaminonaphthalene (Fluka), sodium toluene-4-sulfonate (sodium tosylate; Aldrich), tetra-*n*-butylammonium hexafluorophosphate {$[(n\text{-}C_4H_9)_4N]PF_6$; Aldrich}, tetra-*n*-butylammonium perchlorate {$[(n\text{-}C_4H_9)_4N]ClO_4$; Fluka}, tetra-*n*-butylammonium tosylate {$[(n\text{-}C_4H_9)_4N]$tos; Fluka}, tetraethylammonium perchlorate {$[(C_2H_5)_4N]PF_6$; Kodak Eastman}, and decamethylferrocene (Aldrich) were used as supplied. SP Sephadex C-25 (Pharmacia) was used for chromatographic separation of ruthenium complexes.[4] HPLC grade acetonitrile (BDH) was used for electrochemical measurements; all other solvents were of reagent grade and used without purification. The ruthenium complexes $[Ru(bpy)_2Cl_2]\cdot 2\,H_2O$,[29] $[Ru(pp)_3](PF_6)_2$ {pp = bpy, phen, or Me_4bpy (4,4′,5,5′-tetramethyl-2,2′-bipyridine)},[12] $[Ru(phen)_2(HAT)](PF_6)_2$,[5] $[\{Ru(phen)_2\}_2(\mu\text{-HAT})](PF_6)_4$,[5] $[\{Ru(phen)_2\}_3(\mu\text{-HAT})](PF_6)_6$,[5] and $[\{Ru(bpy)_2\}_2(\mu\text{-mapy})](PF_6)_4$ and $[\{Ru(Me_2bpy)_2\}_2(\mu\text{-mapy})](PF_6)_4$[3] were prepared and purified by literature methods.

2,3-Bis(2-pyridyl)-1,4-diazaanthracene (dpa): Preparation by a modified procedure of Goodwin and Lions[30] for 2,3-bis(2-pyridyl)quinoxaline. 2,3-Diaminonaphthalene (1.0 g, 6.3 mmol) and 2,2′-pyridil (= di-2-pyridylglyoxal; 1.34 g, 6.3 mmol) were refluxed in ethanol (20 cm^3) for 0.5 h. The volume of the reaction mixture was reduced to half via rotary evaporation. The yellow crystalline solid was collected by filtration and recrystallised from ethanol. Yield: 1.53 g (77%); m.p. 184−185 °C. ^{13}C NMR ($CDCl_3$): δ = 123.0, 124.0, 126.9, 127.8, 128.6, 134.2, 136.6, 137.6, 148.3, 153.0, 157.5.

$[\{Ru(bpy)_2\}_2(\mu\text{-dpa})](PF_6)_4$. − Method A: 2,3-Bis(2-pyridyl)-1,4-diazaanthracene (dpa; 31.7 mg, 0.095 mmol) was dissolved in nitrogen-purged 50% aqueous methanol (20 cm^3). $[Ru(bpy)_2Cl_2]\cdot 2\,H_2O$ (105 mg; 0.202 mmol) was added and the mixture heated at reflux for 24 h. Methanol was removed via rotary evaporation and the crude product precipated from the aqueous solution by addition of a saturated solution of KPF_6. A dark green solid was isolated by vacuum filtration and washed sparingly with water. Purification was achieved by cation-exchange chromatography (SP-Sephadex C-25; eluent 0.5 M NaCl). A claret band of mononuclear material eluted first, followed by the desired dark green product, which was isolated as the PF_6^- salt. Yield: 117 mg (71%). ESMS (accurate mass): observed *m/z* 1597.1009 (most abundant isotope peak within cluster); $[C_{62}H_{46}N_{12}Ru_2](PF_6)_3^+$ requires 1597.1005.

Method B: A mixture of $[Ru(bpy)_2Cl_2]\cdot 2\,H_2O$ (170 mg, 0.33 mmol) and dpa (50 mg; 0.15 mmol) in ethylene glycol (3 cm^3) was heated in a modified microwave oven[31] (Sharp model R-2V55; 600 W, 2450 MHz) on medium-high power for 5 min. The green solution was poured into distilled water (50 cm^3) and a saturated solution of KPF_6 added dropwise yielding a dark green solid, which was collected and washed with distilled water. Purification of the crude product was achieved as above. Yield: 85 mg (33%).

Column Conditions for Separation/Resolution of $[\{Ru(bpy)_2\}_2(\mu\text{-dpa})](PF_6)_4$: Separation of the diastereoisomers and resolution of the enantiomers of the *rac* form were achieved by cation exhange chromatography on SP Sephadex C-25 support using 0.25 M sodium toluene-4-sulfonate and 0.075 M sodium (−)-*O*,*O*′-dibenzoyl-L-tartrate as eluents, respectively.[7] The diastereoisomers separated after passing through an effective column length (ECL) of 150 cm (the *meso* band eluting first). Resolution to give the two enantiomers (ΔΔ and ΛΛ) of the *rac* form was achieved over an ECL of 80 cm. All products were precipitated as the PF_6^- salts by addition of a saturated solution of KPF_6 to each green band after elution. Diastereoisomeric ratio (*rac*/*meso*): 44:56. Enantiomeric ratio (ΔΔ/ΛΛ): 49:51.

Acknowledgments

This work was supported by the Australian Research Council, James Cook University and the University of Melbourne. The authors would like the thank Dr. Graham Heath (Australian National University) for use of the OSTLE facilities, Dr Len Barbour (University of Alabama) for the van der Waal's volume calculations, and Professors Royce Murray (University of North Carolina, Chapel Hill, USA) and Joseph Hupp (Northwestern University, Evanston, USA) for valuable discussions.

[1] T. J. Rutherford, F. R. Keene, *Inorg. Chem.* **1997**, *36*, 2872−2878.

[2] J. A. Treadway, P. Chen, T. J. Rutherford, F. R. Keene, T. J. Meyer, *J. Phys. Chem. A* **1997**, *101*, 6824−6826.
[3] L. S. Kelso, D. A. Reitsma, F. R. Keene, *Inorg. Chem.* **1996**, *35*, 5144−5153.
[4] F. R. Keene, *Chem. Soc. Rev.* **1998**, *27*, 185−193.
[5] T. J. Rutherford, O. Van Gijte, A. Kirsch-De Mesmaeker, F. R. Keene, *Inorg. Chem.* **1997**, *36*, 4465−4474.
[6] D. A. Reitsma, F. R. Keene, *J. Chem. Soc., Dalton Trans.* **1993**, 2859−2860.
[7] N. C. Fletcher, P. C. Junk, D. A. Reitsma, F. R. Keene, *J. Chem. Soc., Dalton Trans.* **1998**, 133−138.
[8] N. C. Fletcher, F. R. Keene, *J. Chem. Soc., Dalton Trans.* **1999**, 683−689.
[9] F. R. Keene, *Coord. Chem. Rev.* **1997**, *166*, 122−159.
[10] T. J. Rutherford, F. R. Keene, *Inorg. Chem.* **1997**, *36*, 3580−3581.
[11] T. W. Swaddle, P. A. Tregloan, *Coord. Chem. Rev* **1999**, *187*, 255−289.
[12] T. J. Rutherford, P. A. Pellegrini, J. Aldrich-Wright, P. C. Junk, F. R. Keene, *Eur. J. Inorg. Chem.* **1998**, 1677−1688.
[13] J. T. Hupp, *Inorg. Chem.* **1990**, *29*, 5010−5012.
[14] J. Ruiz, D. Astruc, *C.R. Acad. Sci. Paris* **1998**, 21−27.
[15] D. E. Richardson, H. Taube, *Inorg. Chem.* **1981**, *20*, 1278−1285.
[16] N. S. Hush, *Progr. Inorg. Chem.* **1967**, *8*, 391−444.
[17] G. C. Allen, N. S. Hush, *Progr. Inorg. Chem.* **1967**, *8*, 357−389.
[18] K. Kalyanasundaram, M. K. Nazeeruddin, *Inorg. Chim. Acta* **1994**, *226*, 213−230.
[19] R. J. Crutchley, *Adv. Inorg. Chem.* **1994**, *41*, 273−325.
[20] C. E. B. Evans, G. P. A. Yap, R. J. Crutchley, *Inorg. Chem.* **1998**, *37*, 6161−6167.
[21] N. C. Thomas, K. Pringle, G. B. Deacon, *J. Chem. Educ.* **1989**, *66*, 516−517.
[22] R. D. Gillard, R. E. E. Hill, R. Maskill, *J. Chem. Soc. (A)* **1970**, 707−710.
[23] A. Juris, S. Barigelletti, S. Campagna, V. Balzani, P. Belser, A. von Zelewsky, *Coord. Chem. Rev.* **1988**, *84*, 85−277.
[24] J. I. Sachinidis, R. D. Shalders, P. A. Tregloan, *Inorg. Chem.* **1994**, *33*, 6180−6168.
[25] A. J. Bard, L. R. Faulkner, *Electrochemical Methods*, John Wiley, New York, **1980**.
[26] H. L. Blonk, A. M. Roelofsen, T. Frelink, M. J. Anders, J. E. J. Schmitz, J. G. M. van der Linden, J. J. Steggerda, *J. Phys. Chem.* **1992**, *96*, 6004−6012.
[27] C. M. Duff, G. A. Heath, *Inorg. Chem.* **1991**, *30*, 2528−2535.
[28] J. Sachinidis, R. D. Shalders, P. A. Tregloan, *J. Electroanal. Chem.* **1992**, *327*, 219- 234.
[29] T. Togano, N. Nagao, M. Tsuchida, H. Kumakura, K. Hisamatsu, F. S. Howell, M. Mukaida, *Inorg. Chim. Acta* **1992**, *195*, 221−225.
[30] H. A. Goodwin, F. Lions, *J. Am. Chem. Soc.* **1959**, *81*, 6415−6422.
[31] D. M. P. Mingos, D. R. D. Baghurst, *Chem. Soc. Rev.* **1991**, *20*, 1−47.

Received April 26, 2000
[I00165]

Formation of Metallamacrocycles from Palladium(II), Platinum(II) and Copper(I) Complexes and the Ditopic Ligands [{*p*-(Ph_2PO)C_6H_4}$_2$$CMe_2$], [{2-$Ph_2PO$-3,5-($Me_3C$)$_2$$C_6H_2$}$_2$S], [{*p*-[($C_{10}H_6O$)$_2$PO]$C_6H_4$}$_2$$CMe_2$]

Carmela Grazia Arena,[a] Dario Drommi,[a] Felice Faraone,*[a] Claudia Graiff,[b] and Antonio Tiripicchio[b]

Keywords: Macrocycles / Metallacycles / Palladium / Platinum / Copper

The new ligands bis(phosphinito) [{2-Ph_2PO-3,5-(Me_3C)$_2$$C_6H_2$}$_2$S] (**4**) and chiral bis(phosphite) [{*p*-[($C_{10}H_6O$)$_2$PO]C_6H_4}$_2$$CMe_2$] (**5**) were synthesised and their reactions with palladium(II), platinum(II), copper(I) substrates were studied. The ligand **3** [{*p*-(Ph_2PO)C_6H_4}$_2$$CMe_2$], previously reported by us, was also used in the same reactions. Ligands **3** and **5** formed 28-membered metallamacrocycles while ligand **4** afforded the analogous compound only in the reaction with the copper(I) substrate. In the reaction of **3** with [Pd(PhCN)$_2$Cl$_2$] the metallamacrocycle [PdCl$_2$(μ-**3**)]$_2$ (**6**) or the oligomer [Pd$_2$Cl$_4$(μ-**3**)]$_n$ (**7**) were formed, depending on the molar ratio used. The reaction of **3** with [Pd(η^3-C_3H_5)Cl]$_2$ afforded compound {[Pd(η^3-C_3H_5)Cl]$_2$(μ-**3**)} (**8**). The allylpalladium macrocycle [Pd(η^3-C_3H_5)(μ-**3**)]$_2$[OTf]$_2$ (**9**) was obtained by treating a solution of **8** in THF with $AgCF_3SO_3$. The reactions of ligand **3** with [Pt(COD)I$_2$] or [Cu(NCCH$_3$)$_4$]BF$_4$ led to the formation of metallamacrocycles [PtI$_2$(μ-**3**)]$_2$ (**10**) and [Cu$_2$(μ-**3**)$_2$][BF$_4$]$_2$·2CH$_3$CN (**11**), respectively. The structure of **10** was also elucidated by X-ray analysis. Reactions of **4** with palladium(II) and platinum(II) complexes afforded a mixture of two very different compounds in almost an equimolar ratio. An X-ray analysis established that one is a mononuclear compound, formed by modification of the ligand **4**, containing a P,S-chelate, namely {PdCl$_2${[2-Ph_2PO-3,5(Me_3C)$_2$$C_6H_2$][3,5-($Me_3C$)$_2$$C_6H_2$OH]S}] (**12**). The reaction between [Cu(NCCH$_3$)$_4$]BF$_4$ and **4** afforded the ionic metallamacrocycle [Cu(μ-**4**)][BF$_4$]$_2$·2CH$_3$CN (**14**). In compound **10**, the size of the central cavity formed by the bridging ligand **3** was determined.

Introduction

In the last twenty years a number of studies have indicated that hydrogen bond formation is not the unique mode through which the supramolecular self-assembly of molecules can occur and coordination bond formation was found to be a very useful tool to promote supramolecular self-assembly processes.[1a,2] In fact the preferred coordination numbers, the geometry of transition metal complexes and the shape of the bi- and polydentate ligands drives a spontaneous supramolecular self-assembly process to give metallamacrocycles with trigonal, square-planar, and tetrahedral coordinated metal ions.[2] In this context, a renewed interest in metallamacrocycles has recently been observed. Additionally, they can potentially act as host molecules in the generation of supramolecular architectures.[3] Several bi- or polydentate rigid aromatic nitrogen ligands have been used in reactions with transition metal complexes, generally in a square-planar configuration, to induce metallamacrocyclic structure formation.[1,4] Recently,[5] "flexible" non-chelating proligands HE-EH [HE-EH = 1,4-($HOCH_2$)$_2$$C_6H_4$, 1,3-($HOCH_2$)$_2$$C_6H_4$, (4-$HOC_6H_4$)$_2$$CH_2$] have been used in the reaction with [Mo(NO)(tp*)I$_2$]$_2$ {tp* = HB(3,5-$Me_2C_3HN_2$)$_3$} in the presence of NEt_3, to afford the dinuclear metallacyclophanes [Mo(NO)(tp*)(E-E)]$_2$ as the major product. In these reactions, kinetic control in the formation of the dinuclear metallamacrocycles was observed.

Lately,[6] we have synthesized the large valence angle bis(*p*-phosphinito) ligands [*p*-(Ph_2PO)C_6H_4]$_2$X (X = O, **1**; S, **2**; CMe_2, **3**), designed to induce a bridging coordination in transition metal complexes. The reactions of **1**−**3** with [Ru(*p*-cymene)Cl$_2$]$_2$, [Rh(C_5Me_5)Cl$_2$]$_2$, [Rh(C_5H_5)(CO)$_2$]$_2$ gave dinuclear complexes in which the two metal centres are bridged by only one phosphinito ligand.[6]

In this paper we report the synthesis of the new ligands bis(phosphinito) [{2-Ph_2PO-3,5-(Me_3C)$_2$$C_6H_2$}$_2$S] (**4**) and chiral bis(phosphite) [{*p*-[($C_{10}H_6O$)$_2$PO]C_6H_4}$_2$$CMe_2$] (**5**), and the reactions of **3**, **4** and **5** with palladium(II), platinum(II), and copper(I) substrates. The crystal structures of the dichloromethane solvates of the macrocyclic dinuclear complex [Pt{[*p*-(Ph_2PO)C_6H_4]$_2$$CMe_2$}I$_2$]$_2$ (**10**) and of [PdCl$_2${[2-Ph_2PO-3,5-(CMe_3)$_2$$C_6H_2$][3,5-($CMe_3$)$_2$-$C_6H_2$OH]S}] (**12**) are also reported.

Results and Discussion

Synthesis of Ligands 4 and 5

In order to synthesise a bis(phosphinito) ligand with a bigger steric requirement than ligands **1**−**3**, we prepared

[a] Dipartimento di Chimica Inorganica, Chimica Analitica e Chimica Fisica-Università di Messina,
Salita Sperone 31, Vill. S. Agata, 98166 Messina, Italy
[b] Dipartimento di Chimica Generale ed Inorganica, Chimica Analitica, Chimica Fisica, Università di Parma, Centro di Studio per la Strutturistica Diffrattometrica del CNR,
Parco Area delle Scienze 17A, 43100 Parma, Italy

 © WILEY-VCH Verlag GmbH, 69451 Weinheim, 2001 1434−1948/01/0101−0247 $ 17.50+.50/0

ligand **4** which has sulfur as the bridging atom, two phosphinito groups at the 2-position, and four *tert*-butyl groups as substituents in the aromatic moieties.

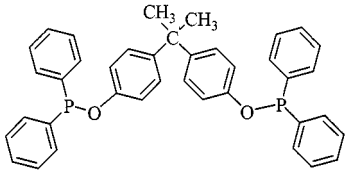

3

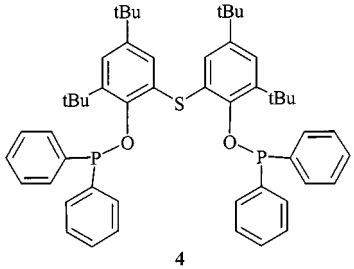

4

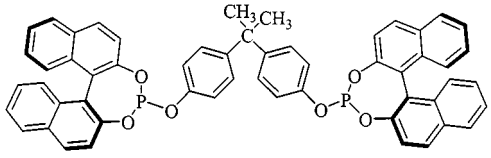

5

Ligand **4** was synthesised by treating 4,4′,6,6′-di-*tert*-butyl-2,2′-thiobisphenol[7] with PPh_2Cl and an excess of NEt_3 in toluene at room temperature. Several recrystallisations from hexane gave the pure product **4** as a white moderately air-stable powder, which was analysed by $^{31}P\{^1H\}$, ^1H NMR spectroscopy and GCMAS. In the $^{31}P\{^1H\}$ NMR spectrum ($CDCl_3$ solution), a singlet appears at $\delta = 117.1$ and in the ^1H NMR two singlets at $\delta = 1.26$ and 1.31 due to *tert*-butyl groups as well as signals due to aromatic groups are seen. In the mass spectrum, a molecular peak at 810 was observed.

Ligand **5** has the same backbone as **3**, but it is chiral owing to the presence of two chiral configurationally resolved binaphthol groups. It was prepared by lithiation of 2,2-bis(4-hydroxyphenyl)propane in THF and subsequent addition of the lithium derivative to a solution of (*S*)-(1,1′-binaphthalene-2,2′-dioxy)chlorophosphane[8] in the same solvent at room temperature. The pure product was isolated as a white, air-sensitive powder and characterised by NMR spectroscopy. The $^{31}P\{^1H\}$ NMR spectrum (C_6D_6 solution), shows a singlet at $\delta = 144.79$ while the ^1H NMR exhibits a signal at $\delta = 1.47$ due to the CH_3 groups as well as two doublets at $\delta = 6.96$ and 7.0 ($J = 3$ Hz) due to the *p*-substituted phenyl groups. Multiplets in the range $\delta = 7.45-7.64$ due to the binaphthyl protons are also observed.

Ligands **3**−**5** were designed to induce a bridging coordination to transition metal centres. Structural determination of dinuclear Ru^{II} complexes containing ligand **3** proved that the P−P distance is longer than 9 Å[6] and therefore a *cis* or *trans* chelating bonding mode for ligands **3** and **5** is not expected.

Reactions of Ligands 3−5 with Palladium(II), Platinum(II) and Copper(I) Complexes

The reaction of **3** with $[Pd(PhCN)_2Cl_2]$ in a 1:1 molar ratio in toluene produced a yellow precipitate which was analysed as metallamacrocycle $[PdCl_2(\mu\text{-}\mathbf{3})]_2$ (**6**).

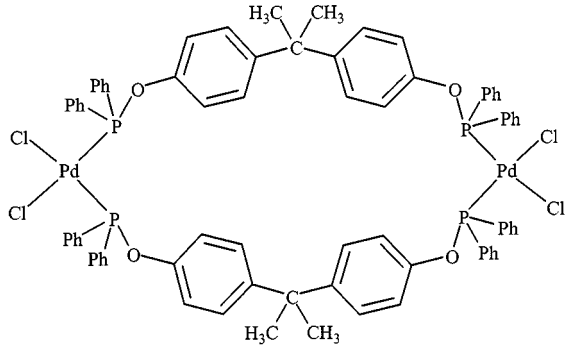

6

It is air-stable, soluble in chlorinated solvents and proved to be non-conducting in acetone solution. In agreement with the proposed structure, the $^{31}P\{^1H\}$ NMR spectrum ($CDCl_3$), shows a singlet at $\delta = 109.0$ while the ^1H NMR spectrum features a singlet at $\delta = 1.46$ due to the $C(CH_3)_2$ group together with the characteristic resonances of phenyl rings.

When a solution of **3** in toluene was added to a solution of $[Pd(PhCN)_2Cl_2]$ in the same solvent in a 1:2 molar ratio, an orange-brown precipitate quickly formed which was insoluble in common organic solvents and analysed as $[Pd_2Cl_4(\mathbf{3})]$ (**7**). Compound **7** dissolves moderately only in coordinating solvents such as CH_3CN and DMF.

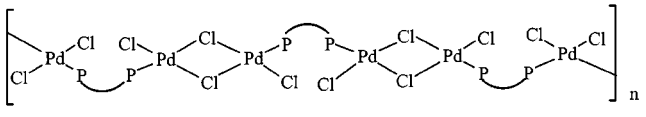

7

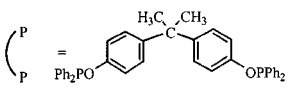

The $^{31}P\{^1H\}$ NMR spectrum of **7** in CD_3CN shows a resonance at $\delta = 106.3$ as a sharp singlet which is consistent with a symmetric geometry. The ^1H NMR spectrum shows a singlet at $\delta = 1.37$ due to the isopropyl group, together with the signals of the aromatic rings in the correct integration ratio. Although it was not possible to obtain useful information from the mass spectrum because of the wide fragmentation of the compound **7**, on the basis of NMR spectroscopic data and the observed chemical properties, we

deduced that **7** was an oligomer, $[Pd_2Cl_4(\mu\text{-}\mathbf{3})]_n$, in which the chloride and the phosphinito ligands alternately coordinate as bridges to palladium(II) centres. In coordinating solvents such as CH_3CN and DMF, a break of the chloro bridge probably occurs but the oligomeric structure is maintained. Furthermore, the ^1H NMR spectra of **7** (CD_3CN solution) shows features which indicate that scrambling processes take place. The proposed structure of **7** is in agreement with the trend of the palladium(II) to give bi- and polynuclear chloro-bridged compounds.[9] Reaction of $[Pd(\eta^3\text{-}C_3H_5)Cl]_2$ with **3** in a 1:1 molar ratio afforded the expected dinuclear compound $\{[Pd(\eta^3\text{-}C_3H_5)Cl]_2(\mu\text{-}\mathbf{3})\}$ (**8**) in which the two metal atoms are bridged by only one phosphinito ligand.

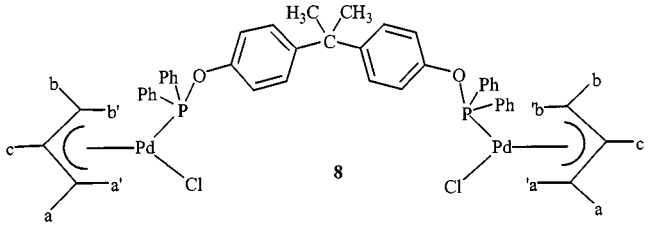

8

This is corroborated by the $^{31}P\{^1H\}$ NMR spectrum ($CDCl_3$ solution), which shows a sharp singlet at δ = 123.29, indicating a plane of symmetry in the molecule. In the ^1H NMR spectrum, the singlet at δ = 1.55 was assigned to the isopropyl group. A ^1H NOESY experiment made the assignment of each allylic proton signal possible: two broad multiplets at δ = 2.20 (^3J = 12 Hz, $H_{b'}$) and at δ = 3.13 (J = 6 Hz, H_b), two doublets of doublets at δ = 3.57 (^3J = 11 Hz, J_{PH} = 15 Hz, Ha′) and at δ = 4.67 (J_{PH} = 7 Hz, H_a), one multiplet at δ = 5.22 (H_c). Phase-sensitive 2D-^1H NOESY spectrum shows NOE peaks between H_c and its vicinal H_a and H_b protons. The analysis of the NMR spectroscopic data led us to conclude that a dynamic process, fast on the NMR time scale, was taking place and that it involved all the allylic protons in the molecule. This process is due to two concurrent $\eta^3-\eta^1-\eta^3$ rearrangements of the allylic fragment.[10]

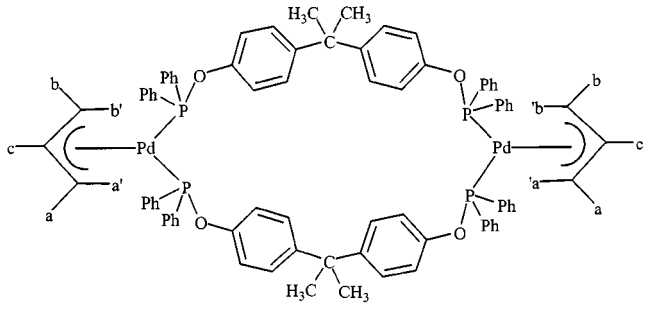

9

In order to prepare an allylpalladium macrocycle, a solution of $\{Pd(\eta^3\text{-}C_3H_5)Cl]_2(\mu\text{-}\mathbf{3})\}$ (**8**) in THF was initially treated with $AgCF_3SO_3$ in a 1:2 molar ratio, and after filtration of the AgCl precipitate, was further treated with 1 equivalent of **3**. The white dinuclear allylpalladium macrocycle $[Pd(\eta^3\text{-}C_3H_5)(\mu\text{-}\mathbf{3})]_2[OTf]_2$ (**9**) was obtained in good yield and was characterised by microanalysis, NMR spectroscopy and conductivity measurements.

The presence of a broad signal at δ = 120.6 in the $^{31}P\{^1H\}$ NMR spectrum ($CDCl_3$), revealed a complex fluxional process in the complex. This was further supported by the broadness of the signals observed in the ^1H NMR spectra recorded over a wide range of temperatures.

Reaction of $[Pt(COD)I_2]$ with ligand **3** in an equimolar ratio proceed in a similar way to that with $[Pd(PhCN)_2Cl_2]$. Addition of ligand **3** to a toluene solution of $[Pt(COD)I_2]$ led to the formation of metallamacrocycle $[PtI_2(\mu\text{-}\mathbf{3})]_2$ (**10**) as a yellow precipitate which was characterized by NMR spectroscopy and X-ray analysis. As expected, the $^{31}P\{^1H\}$ NMR spectrum ($CDCl_3$) displays a peak at δ = 81.81, together with satellites due to $^{195}Pt-P$ coupling (J_{PtP} = 3968 Hz), and the ^1H NMR spectrum features all ligand signals in the correct integration ratio.

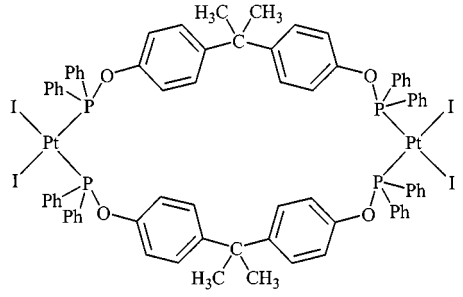

10

Crystal Structure of $[PtI_2(\mu\text{-}3)]_2\cdot 2CH_2Cl_2$ ($\mathbf{10}\cdot 2CH_2Cl_2$)

A view of the structure of complex **10** is shown in Figure 1, together with the numbering system. Selected bond lengths and angles are given in Table 1. The metallamacrocycle has an imposed crystallographic C_2 symmetry.

The coordination at Pt is square-planar and involves two P atoms mutually in *cis* position and two I atoms. The two Pt−I [2.6523(11) and 2.6562(9) Å] and Pt−P [both 2.259(2) Å] bond lengths are equal. The most interesting feature is the 28-membered metallacycle; the conformation of the ring is shown in Figure 2. The central cavity seems to be too small to bind even small guest molecules. Critical cross-ring interatomic distances are C23···C23′ (3.983 Å), C23−C24′ and C23′−C24 (4.078 Å). The apex indicates an atom related by the twofold axis. The Pt−Pt′ and C7−C7′ separations are 13.071 and 8.974 Å, respectively. Furthermore, two phenyl groups at P2 point to the same side of the ring, facing one another, the shortest contacts involving C31···C31′ (3.690 Å), C31−C32′ and C31′−C32 (3.983 Å). It is worth noting that the O2 atom is involved in an intermolecular hydrogen bond with the Cl2 atom [O2···Cl2 = 3.048(5), Cl2···H2 = 2.32(5) Å; 02−H2−Cl2 = 157(5)°].

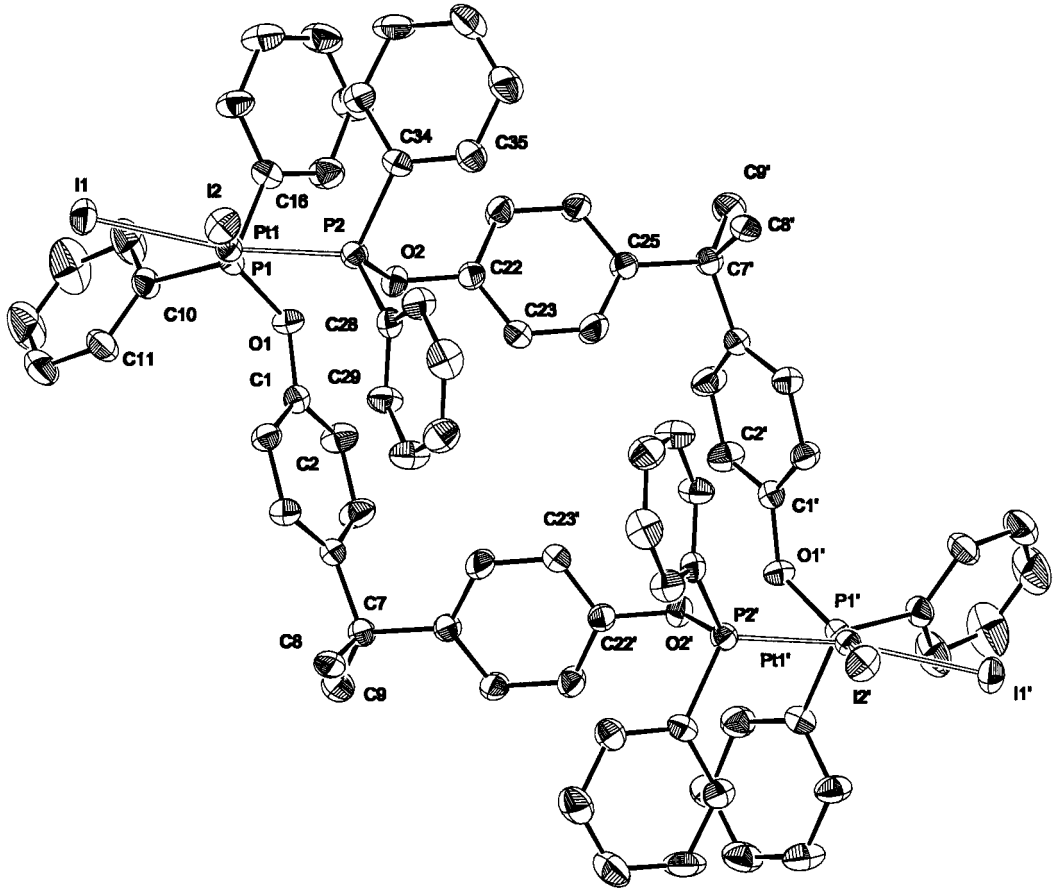

Figure 1. ORTEP view of the structure of the complex **10** together with the numbering scheme; the ellipsoids for the atoms are drawn at the 30% probability level

The reaction between $[Cu(NCCH_3)_4]BF_4$ and ligand **3** in a 1:1 molar ratio in dichloromethane solution, afforded the metallamacrocycle $[Cu_2(\mu\text{-}\mathbf{3})_2][BF_4]_2{\cdot}2CH_3CN$ (**11**) as a white solid. Conductivity measurements in methanol solution proved that compound **11** is a 2:1 electrolyte. The $^{31}P\{^1H\}$ NMR spectrum displays a singlet at $\delta = 99.06$, while the ^1H NMR spectrum ($CDCl_3$ solution) in addition to the expected signals, also shows a singlet at $\delta = 1.55$ due to the CH_3CN molecule of crystallisation. The coordination of acetonitrile to the metal centre can be excluded, since the observed chemical shift is the same as that of the free CH_3CN.

Reactions of **4** with Pd^{II} and Pt^{II} complexes gave different results from those reported for ligands **3**. Addition of one equivalent of **4** to a solution of $[Pd(PhCN)_2Cl_2]$ in toluene afforded a mixture of two very different compounds, **12** and **13**, in a 42:58 ratio, each giving rise to a singlet at $\delta = 135.66$ and 78.79, respectively, in the $^{31}P\{^1H\}$ NMR spectrum ($CDCl_3$).

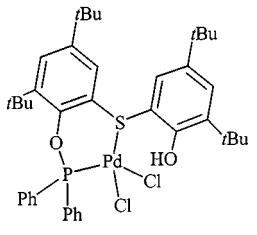

12

Fractional crystallisation from CH_2Cl_2/hexane allowed us to separate the two compounds. Thus, **12** was obtained as yellow crystals which exhibit only a signal at $\delta = 135.66$ in the $^{31}P\{^1H\}$ NMR in $CDCl_3$. An X-ray analysis carried out on these crystals established that it has formula $[PdCl_2\{[2\text{-}Ph_2PO\text{-}3,5\text{-}(CMe_3)_2C_6H_2][3,5\text{-}(CMe_3)_2\text{-}C_6H_2OH]S\}]$.

Crystal Structure of $[PdCl_2\{[2\text{-}Ph_2PO\text{-}3,5\text{-}(CMe_3)_2C_6H_2]\text{-}[3,5\text{-}(CMe_3)_2\text{-}C_6H_2OH]S\}]{\cdot}2CH_2Cl_2$ (**12**·2CH_2Cl_2)

A view of the structure of complex **12** is shown in Figure 3 together with the numbering system. Selected bond lengths and angles are given in Table 2. The coordination at Pd is square-planar and involves two Cl atoms and the P1 and S1 from the chelating ligand, obtained by fragmentation of **4**. The six-membered chelating ligand is in a boat conformation with the two near-planar S1PdP101 and 01C13C18S1 moieties forming a dihedral angle of 41.1(1)°. The Pd−P1 and Pd−S1 bond lengths are 2.1985(15) and 2.2770(13) Å, respectively. The Pd−Cl1 and Pd−Cl2 bond lengths, 2.3149(14) and 2.3769(15) Å respectively, are rather different; the bond *trans* to the P atom is longer.

In light of the structure determined for **12**, we may consider two hypotheses based on this result. One could explain the hydrolysis of one P−O bond in the pure ligand as being due to the presence of water in the solvent. However, this can be excluded since the reaction was repeated several

Table 1. Selected bond lengths [Å] and angles [°] for **10·2CH$_2$Cl$_2$** (symmetry transformations used to generate equivalent atoms: ′ $-x + 1, y, -z + 1/2$)

Bond lengths	
Pt(1)−P(2)	2.259(2)
Pt(1)−P(1)	2.259(2)
Pt(1)−I(1)	2.6523(11)
Pt(1)−I(2)	2.6562(9)
P(1)−O(1)	1.625(5)
P(2)−O(2)	1.632(5)
O(1)−C(1)	1.399(8)
O(2)−C(22)	1.400(8)
C(1)−C(2)	1.365(10)
C(1)−C(6)	1.380(10)
C(2)−C(3)	1.380(11)
C(3)−C(4)	1.384(11)
C(4)−C(5)	1.396(10)
C(4)−C(7)	1.533(10)
C(5)−C(6)	1.372(10)
C(7)−C(25)′	1.541(10)
C(22)−C(27)	1.367(10)
C(22)−C(23)	1.372(10)
C(23)−C(24)	1.385(11)
C(24)−C(25)	1.384(11)
C(25)−C(26)	1.379(10)
C(25)−C(7)′	1.541(10)
C(26)−C(27)	1.398(10)
Bond angles	
P(2)−Pt(1)−P(1)	96.86(7)
P(2)−Pt(1)−I(1)	168.82(5)
P(1)−Pt(1)−I(1)	89.90(5)
P(2)−Pt(1)−I(2)	84.73(5)
P(1)−Pt(1)−I(2)	176.53(5)
I(1)−Pt(1)−I(2)	88.07(2)
C(25)′−C(7)−C(4)	108.1(6)
O(1)−P(1)−Pt(1)	120.0(2)
O(2)−P(2)−Pt(1)	109.11(19)
C(1)−O(1)−P(1)	128.5(4)
C(22)−O(2)−P(2)	123.8(4)
C(2)−C(1)−O(1)	114.7(6)

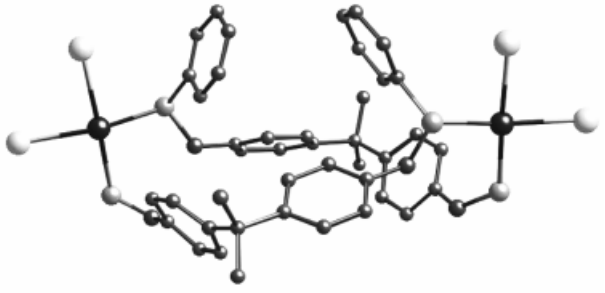

Figure 2. View of the 28-membered metallacycle of **10**; six phenyl groups (two at P1 and P1′ and one at P2 and P2′) are omitted for clarity

times under rigorously anhydrous conditions and the same result was obtained. Furthermore, the reaction between the Cu complex and the same sample of ligand **4** used in the reaction with [Pd(PhCN)$_2$Cl$_2$] in toluene, gave a product (see below) which does not arise from P−O bond hydrolysis in ligand **4**. Another possibility is that a very complicated reaction takes place which could involve sulfur coordination to the palladium centre. In this case, a lengthening and breaking of one P−O bond can occur by a probable, but not experimentally proven, contribution of the solvent. Undoubtedly, the characterization of **13** is fundamental to the understanding of this reaction. Unfortunately, several attempts to obtain suitable crystals for X-ray analysis of **13** failed so far. However, other studies have to be conducted to give insight into this reaction.

Reaction of [Pt(COD)I$_2$] with 1 equivalent of ligand **4** produced a mixture of compounds, as could be inferred by the presence of several peaks in the $^{31}P\{^1H\}$ NMR spectrum. It is also likely that a product similar to **12** can be formed in this reaction. Differently from palladium, reaction between [Cu(NCCH$_3$)$_4$]BF$_4$ and ligand **4** in a 1:1 molar ratio in toluene afforded the white ionic metallamacrocycle [Cu(μ-**4**)][BF$_4$]$_2$·2CH$_3$CN (**14**), which was soluble in chlorinated solvents, acetone and methanol. Compound **14** was found to be a 1:2 electrolyte in methanol solution.

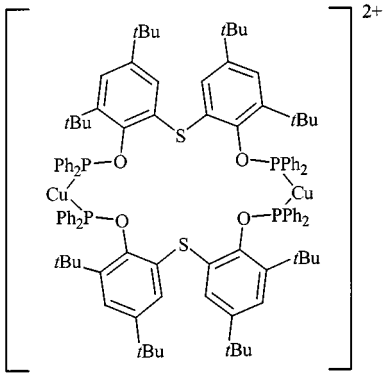

14

Complex **14** presents elemental analysis and NMR spectroscopic data fully consistent with the proposed structure. Indeed, only two sharp singlets are present for *tert*-butyl groups in the ^1H NMR spectrum, consistent with the proposed symmetric structure. Furthermore, a sharp singlet at $\delta = 108.81$ is present in the $^{31}P\{^1H\}$ NMR spectrum.

On the basis of the similar structural features of ligands **3** and **5**, we expect a similar behaviour in the reactions between **5** and Pd, Pt and Cu complexes. Only in the case of the reaction with the Cu complex, was it not possible synthesise a product in pure form. A rapid degradation of the initially formed macrocycle probably occurs in solution.

The reaction of [Pd(PhCN)$_2$Cl$_2$] with ligand **5** in toluene and in a 1:1 molar ratio, led to the formation of an orange-brown precipitate, which shows a singlet at $\delta = 107.68$ together with two signals of very low intensity at $\delta = 86.6$ and 85.7 in the $^{31}P\{^1H\}$ NMR spectrum ($CDCl_3$). However, several recrystallisations from toluene/hexane made it possible to obtain the pure chiral metallamacrocycle [Pd(μ-**5**)Cl$_2$]$_2$ (**15**).

Its $^{31}P\{^1H\}$ NMR spectrum ($CDCl_3$) features only the signal at $\delta = 107.68$, while all expected signals in the correct integration ratio are present in the ^1H NMR spectrum. By adding ligand **5** to a solution of [Pt(COD)I$_2$] in toluene, the metallamacrocycle [Pt(μ-**5**)I$_2$]$_2$ (**16**) precipitated as a yellow solid. The resulting compound was not in a pure form, but

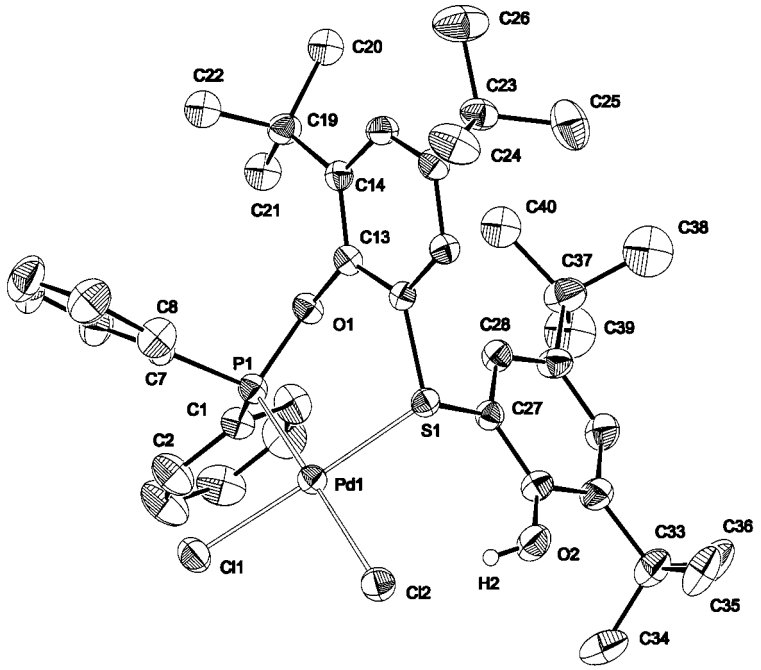

Figure 3. ORTEP view of the structure of the complex **12** together with the numbering scheme; the ellipsoids for the atoms are drawn at the 30% probability level

Table 2. Selected bond lengths [Å] and angles [°] for **12·2CH$_2$Cl$_2$**

Bond lengths	
Pd(1)−P(1)	2.1985(15)
Pd(1)−S(1)	2.2770(13)
Pd(1)−Cl(1)	2.3149(14)
Pd(1)−Cl(2)	2.3769(15)
S(1)−C(18)	1.784(5)
S(1)−C(27)	1.796(5)
P(1)−O(1)	1.633(3)
O(1)−C(13)	1.385(6)
O(2)−C(32)	1.343(7)
C(13)−C(18)	1.400(6)
Bond angles	
P(1)−Pd(1)−S(1)	93.41(6)
P(1)−Pd(1)−Cl(1)	87.13(6)
S(1−Pd(1)−Cl(1)	176.52(5)
P(1)−Pd(1)−Cl(2)	175.24(5)
S(1)−Pd(1)−Cl(2)	87.72(6)
Cl(1)−Pd(1)−Cl(2)	92.01(6)
C(18)−S(1)−C(27)	103.1(2)
C(18)−S(1)−Pd(1)	110.87(15)
C(27)−S(1)−Pd(1)	110.57(17)
O(1)−P(1)−Pd(1)	114.31(13)
C(13)−O(1)−P(1)	125.8(3)
C(18)−C(13)−O(1)	119.9(4)
C(13)−C(18)−S(1)	124.4(4)

repeated recrystallisations from toluene/hexane allowed us to obtain the pure compound **16**. It was characterised by elemental analyses, $^{31}P\{^1H\}$ and ^1H NMR spectroscopy. In the $^{31}P\{^1H\}$ NMR spectrum, a singlet at δ = 84.06 (J_{PtP} 5543) is present.

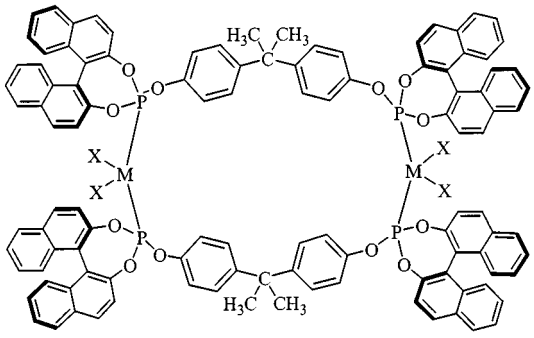

M = Pd, X = Cl, **15** M = Pt, X = I, **16**

Conclusion

A new class of dinuclear metallamacrocycles [M(μ-**L**)X$_2$]$_2$ [M = Pd^{II}, Pt^{II}, Cu^{I}] characterised by a 28-membered ring was obtained using the ditopic ligands **3** and **5**. In the case of **4**, only the Cu^{I}-based dinuclear macrocycle was formed with this ligand. Different results were achieved with Pd^{II} and Pt^{II} complexes on account of sulfur being involving in the course of the reaction. The lack of formation of cyclic tri- and tetranuclear species in the reaction of **3** with Pd^{II}, Pt^{II} and Cu^{I} substrates is a consequence both of the geometry of ligand **3** and of thermodynamic factors owing to the very strong metal−phosphorus bond. Another consequence of the ligand geometry is that when ligand **3** was used in the reaction with [Ru(η^6-*p*-cymene)Cl$_2$]$_2$, only the dinuclear complex {[Ru(η^6-*p*-cymene)Cl$_2$]$_2$[μ-(*p*-Ph$_2$POC$_6$H$_4$)$_2$C(Me)$_2$]} was obtained[6] and attempts to ob-

tain bi- and tetranuclear metallamacrocycles were unsuccessful. The formation of the dinuclear metallamacrocycles $[M(\mu\text{-}L)X_2]_2$ (M = Pd^{II}, Pt^{II}, Cu^{I}, L = **3**, **5**) was promoted by the presence of *cis*-coordinated labile ligands in the starting complexes. Thus, the reaction of $[M(PPh_3)_4]$ (M = Pt, Pd) with dihalobenzophenone afforded the dinuclear complex $\{[MX(PPh_3)_2]_2[(\mu\text{-}(C_6H_4)_2CO]\}$ (M = Pt, X = I, M = Pd, X = Br, I) and failed to give $\{[MX_2(PPh_3)]_2[(\mu\text{-}(C_6H_4)_2CO]_2\}$.[11]

A very interesting aspect connected with the formation of metallamacrocycles is the introduction of chirality by suitable self-assembly building blocks. At least five different ways of rationally designed chiral supramolecular species have been indicated.[12] Stang successfully used an appropriate metal complex bearing (*R*)-(+)-BINAP as the chiral ancillary ligand for the synthesis of chiral palladium(II) and platinum(II) supramolecular square-planar species.[12] The use of the ditopic chiral ligand **5** made the synthesis of chiral palladium(II)- and platinum(II)-based macrocycles possible.

From this work we conclude that chiral dinuclear square-planar metallamacrocycles can be obtained by spontaneous self-assembly of building units of palladium(II) and platinum(II) complexes containing labile ligands and the chiral bidentate ligand **5**. This methodology can be extensively used owing to the great number of chiral ligands, with different geometric properties, which should prove to be bi- and tridentate functional building blocks for the synthesis of chiral supramolecular squares. Up to now, the use of chiral dinuclear square-planar metallamacrocycles as organometallic reagents is an unexplored topic.

The ability for molecular recognition of these new metallamacrocycles depends on the size of the cavity formed. On the basis of the X-ray crystal structure of the complex **10·2CH$_2$Cl$_2$** the cavity determined by meaningful cross-ring interatomic distances seems to be too small to bind guest molecules. We are actually trying to synthesize different types of bis(phosphinito) ligands with the aim of obtaining metallamacrocycles that can act as host molecules in the formation of supramolecular species.

Experimental Section

All syntheses were performed under argon or nitrogen using standard Schlenk-tube techniques. Freshly distilled, dry, and oxygen-free solvents were used throughout. [D_6]Benzene (99.5+%) and [D_3]chloroform (99.8+%) were used as received from Aldrich Chemical Co. All other reagents were of the highest purity grade commercially available and were used without further purification. Redox Analytical Laboratories, Milan, performed microanalyses. ^{1}H, ^{31}P and ^{13}C NMR spectra were obtained with a Bruker AMX R-300 spectrometer equipped with a broad-band probe operating at 300.13, 121.49 and 75.46 MHz, respectively [δ (ppm) relative to Me_4Si, *J* (Hz)]. $^{31}P\{^1H\}$ spectra were run using an aqueous H_3PO_4 sample (85%) as external reference (δ = 0). Standard pulse sequences were employed for ^{1}H-2D-NOESY. Mixing times of 0.8 s were used for the phase-sensitive NOESY experiments. $[Cu(NCCH_3)_4]BF_4$[13], $[\{p\text{-}(Ph_2PO)C_6H_4\}_2CMe_2]$,[6] and 4,4′,6,6′-di-*tert*-butyl-2,2′-thiobisphenol[7] were prepared by standard methods. IR spectra of KBr pellets were recorded with a Perkin−Elmer FT-IR 1720 spectrometer. GLC analyses were performed with a Carlo Erba HRGC 5160 series Mega instrument using a 25-m Mega OV1 column.

[{2-Ph$_2$PO-3,5-(CMe$_3$)$_2$C$_6$H$_2$}$_2$S] (4): The synthetic procedure was essentially the same as previous described for **1**, using a solution of PPh_2Cl (1.98 g, 9.00 mmol) and a solution of 4,4′,6,6′-di-*tert*-butyl-2,2′-thiobisphenol (2.00 g, 4.50 mmol) and NEt_3 (1.45 g, 14.3 mmol) in toluene (40 mL each). The reaction mixture was warmed to room temperature and then kept under continuous stirring for 72 h. The ligand **4** was obtained as a white solid by filtration of the resulting mixture and crystallisation from toluene/hexane (1:3, v/v). Yield 87% (3.17 g, 3.90 mmol). − $C_{52}H_{60}O_2P_2S$ (811.0): calcd. C 77.01, H 7.46, S 3.95; found C 76.97, H 7.49, S 3.91. − ^{1}H NMR ($CDCl_3$): δ = 1.26 [s, 18 H, $C(CH_3)_3$], 1.31 [s, 18 H, $C(CH_3)_3$], 7−7.12 (m, 12 H, CH), 7.28 (d, ^3J = 2.5 Hz, 2 H, CH), 7.39 (d, ^3J = 2.5 Hz, 2 H, CH), 7.61−7.67(m, 8 H, CH). − $^{31}P\{^1H\}$ NMR ($CDCl_3$): δ = 117.21 (s).

[{*p*-[(C$_{10}$H$_6$O)$_2$PO]C$_6$H$_4$}$_2$CMe$_2$] (5): *n*BuLi solution in hexanes (1.6 M, 1.09 mL, 0.112 g, 1.75 mmol) was added dropwise to a solution of 2,2-bis(4-hydroxyphenyl)propane (0.200 g, 0.876 mmol) in THF (20 mL) at −78 °C. The white mixture was added to a solution of (*S*)-(1,1′-binaphthalene-2,2′-dioxy)chlorophosphane in THF (3 mL) at 0 °C. The resulting pale yellow solution was allowed to reach room temperature and stirred for ca. 2 h. The solution was then dried under vacuum and extracted with toluene (3 × 5 mL). Decreasing the solution volume followed by the addition of hexane led to the formation of a white solid. The pure ligand **3** was isolated, washed with small volumes of hexane and finally dried under vacuum with a yield of 70% (0.525 g, 0.613 mmol). − $C_{55}H_{38}O_6P_2$ (856.8): calcd. C 77.10, H 4.47; found C 77.3, H 4.49. − ^{1}H NMR (C_6D_6): δ = 1.47 [s, 6 H, $C(CH_3)_2$], 6.96−7.65 (m, 24 H, CH). − $^{31}P\{^1H\}$ NMR (C_6D_6): δ = 144.79 (s).

[PdCl$_2$(μ-3)]$_2$ (6): Ligand **3** (0.165 g, 0.260 mmol), dissolved in toluene (5 mL), was treated with a solution of $[Pd(PhCN)_2Cl_2]$ (0.100 g, 0.260 mmol) in toluene (30 mL). A yellow solid precipitated immediately and was separated from the mother solution after ca. 1 h, washed with toluene (3 × 1 mL), diethyl ether (1 × 1 mL) and then dried under vacuum. Yield 82% (0.166 g, 0.107 mmol). − $C_{78}H_{68}Cl_4O_4P_4Pd_2$ (1548): calcd. C 60.52, H 4.43; Cl, 9.16; found C 60.16, H 4.34; Cl, 8.93. − ^{1}H NMR ($CDCl_3$): δ = 1.46 [s, 6 H, $C(CH_3)_2$], 6.45 (d, ^3J = 8.4 Hz, 4 H, CH), 6.70 (d, ^3J = 8.7 Hz, 4 H, CH), 7.28−7.46 (m, 12 H, CH), 7.66−7.69 (m, 8 H, CH). − $^{31}P\{^1H\}$ NMR ($CDCl_3$): δ = 109.03 (s).

[Pd$_2$Cl$_4$(μ-3)]$_n$ (7): The orange compound **7** was prepared from $[Pd(PhCN)_2Cl_2]$ (0.080 g, 0.208 mmol) and **3** (0.062 g, 0.104 mmol) as described above for compound **6**. Yield 75% (0.074 g, 0.078 mmol). − $C_{39}H_{34}Cl_4O_2P_2Pd_2$ (951.3): C. 49,24; H. 3,60; Cl. 14,91; found C. 49,20; H. 3,63; Cl. 14,87. − ^{1}H NMR (CD_3CN): δ = 1.37 [s, 6 H, $C(CH_3)_2$], 6.25 (d, ^3J = 8.7 Hz, 4 H, CH), 6.52 (d, ^3J = 8.9 Hz, 4 H, CH), 6.86−7.69 (m, 20 H, CH). − $^{31}P\{^1H\}$ NMR (CD_3CN): δ = 106.32 (s).

{[Pd(η^3-C$_3$H$_5$)Cl]$_2$(μ-3)} (8): To a solution of $[Pd(\eta^3\text{-}C_3H_5)Cl]_2$ (0.05 g, 0.137 mmol) in dichloromethane (10 mL) was added ligand **3** (0.082 g, 0.137 mmol). The resulting yellow solution was stirred for 1 h and then reduced to 3 mL in vacuo. Addition of hexane (10 mL) led to the formation of a yellow precipitate. Yield 72% (0.048 g, 0.050 mmol). − $C_{45}H_{44}Cl_2O_2P_2Pd_2$(962.5): calcd. C 56.15, H 4.61; Cl, 7.37; found C 56.25, H 4.53; Cl, 6.99. − ^{1}H NMR ($CDCl_3$): δ = 1.55 [s, 6 H, $C(CH_3)_2$], 2.20 [d (br.), ^3J = 12 Hz, 2

H, $H_{b'}$], 3.13 [d (br.), ^3J = 6 Hz, 2 H, H_b], 3.57 [dd (br.), ^3J = 11 Hz, J_{HP} 15 Hz, 2 H, $H_{a'}$], 4,67 [dd (br.), J_{HP} 7 Hz, 2 H, H_a], 5.22 [m (br.), 2 H, H_c], 6.99 (d, ^3J = 5 Hz, 4 H, H_e), 7.01 (d, ^3J = 5 Hz, 4 H, H_d), 7.43−7.45 (m, 12 H, $H_{m,p}$), 7.85−7.93 (m, 8 H, H_o). − $^{31}P\{^1H\}$ NMR ($CDCl_3$): δ = 123.29 (s).

[Pd(η³-C_3H_5)(μ-3)]$_2$[OTf]$_2$ (9): The bridge complex **8** (0.077 g, 0.080 mmol) was dissolved in dichloromethane (10 mL) and $AgCF_3SO_3$ (0.041 g, 0.16 mmol) was added with continuous stirring. After 5 min, ligand **3** (0.048 g, 0.080 mmol), dissolved in THF (2 mL), was added to the suspension and the mixture stirred for a further 1 h. The mixture was filtered through Celite, and the solution was concentrated to a small volume; addition of hexane and vigorous shaking led to the formation of **9** as a white solid. Yield 65% (0.093 g, 0.050 mmol). − $C_{86}H_{78}F_6O_{10}P_4S_2Pd_2$ (1786): calcd. C 57.82, H 4.40, S 3.59; found C 57.3, H 4.20, S 3.74. − ^1H NMR ($CDCl_3$): δ = 1.53 [s, 12 H, $C(CH_3)_2$], 3.33 [s (br.), 2H, $H_{b'}$], 3.48 [s (br.), 2 H, H_b], 3.87 [s (br.), 2 H, $H_{a'}$], 3.95 [s (br.), 2 H, H_a], 5.32 [m (br.), 2 H, H_c], 6,48 [d (br.), ^3J = 8 Hz, 8 H, H_e], 7,02 [d (br.), ^3J = 10 Hz, 4 H, H_d], 7,41−7.46 [m (br.), $H_{m,p}$, 24 H], 7,83−7.86 [m (br.), 16 H, H_o]. − $^{31}P\{^1H\}$ NMR ($CDCl_3$): δ = 120,6 [s (br.)].

[PtI_2(μ-3)]$_2$ (10): The dinuclear complex was prepared by reaction of ligand **3** (0.089 mg, 0.143 mmol) with a solution of [Pt(COD)I_2] (0.080 g, 0.143 mmol) in toluene (30 mL). A yellow precipitate was immediately obtained. The reaction mixture was stirred for 1 h and then the solvent was removed. The precipitate was washed with toluene (3 × 1 mL) and finally dried in vacuo. Yield 78% (0.117 g, 0.056 mmol). − $C_{78}H_{68}I_4O_4P_4Pt_2$ (2091): calcd. C 44.8, H 3.28, I 24.28; found C 45.15, H 3.39, I 24.60. − ^1H NMR ($CDCl_3$): δ = 1.51 [s, 6 H, $C(CH_3)_2$], 6.35 (d, ^3J = 8.4 Hz, 4 H, CH), 6.72 (d, ^3J = 8.3 Hz, 4 H, CH), 7.16−7.41 (m, 12 H, CH), 7.63−7.70 (m, 8H, CH). − $^{31}P\{^1H\}$ ($CDCl_3$): δ = 81.81 (s, J_{PtP} = 3968 Hz).

[Cu(μ-3)]$_2$[BF_4]$_2$·2CH_3CN (11): A dichloromethane solution containing ligand **3** (0.095 g, 0.159 mmol) was added dropwise to a solution of [Cu(CH_3CN)$_4$]BF_4 (0.050 g, 0.159 mmol) in CH_2Cl_2 (10 mL). The colourless solution was kept under continuous stirring for ca. 1 h, filtered through Celite and concentrated under vacuum until a volume of 1 mL was achieved. Further addition of hexane (10 mL) led to the formation of a white solid which was isolated, washed several times with hexane and dried. Yield 87% (0.109 g, 0.069 mmol). − $C_{82}H_{74}B_2Cu_2F_8N_2O_4P_4$ (1576): calcd. C 62.49, H 4.73, N 1.78; found C 62.29, H 4.93, N 1.59. − ^1H NMR ($CDCl_3$): δ = 1.49 [s, 6 H, $C(CH_3)_2$], 1.98 (s, 6 H, CH_3), 6.7 (d, ^3J = 8.4 Hz, 4 H, CH), 6.93 (d, ^3J = 8.3 Hz, 4 H, CH), 7.35−7.43 (m, 20 H, CH). − $^{31}P\{^1H\}$ NMR ($CDCl_3$): δ = 99.06 (s). − Λ [ohm^{-1} cm^2 mol^{-1}] (5 10^{-4} − 10^{-3} M CH_3OH) = 182.

[$PdCl_2$\{[2-Ph_2PO-3,5-$(MeC)_2C_6H_2$][3,5-$(Me_3Cl_2C_6H_2OH]S$\}] (12): A solution of [Pd($PhCN$)$_2$$Cl_2$] (0.050 g, 0.130 mmol) in toluene (10 mL) was treated with a toluene solution of ligand **4** (0.105 g, 0.130 mmol). The yellow solution was stirred for ca. 30 min and then reduced to a small volume (1 mL). By crystallization from a toluene/hexane mixture, a yellow solid was obtained. Yield 78% (0.081 g, 0.101 mmol). − $C_{40}H_{51}Cl_2O_2PSPd$ (804.2): calcd. C 59.74, H 6.39, Cl 8.82, S 3.99; found C 59.37, H 6.31, Cl 8.26, S 4.23. − ^1H NMR ($CDCl_3$): δ = 0.99 [s, 9 H, $C(CH_3)_3$], 1.03 [s, 9 H, $C(CH_3)_3$], 1.30 [s, 9 H, $C(CH_3)_3$], 1.31 [s, 9 H, $C(CH_3)_3$], 6.34 (d, ^3J = 2.1 Hz, 1 H, CH_{Ar}), 7.21−7.71 (m, 14 H, CH). − $^{31}P\{^1H\}$ ($CDCl_3$): δ = 135.66 (s).

[Cu(μ-4)]$_2$[BF_4]$_2$·CH_3CN (14): The white compound **13** was prepared from [Cu(CH_3CN)$_4$]BF_4 (0.080 g, 0.254 mmol) and the ligand **4** (0.206 g, 0.254 mmol) as described above for the compound **11**. Yield 89% (0.222 g, 0.113 mmol). − $C_{106}H_{123}B_2Cu_2F_8NO_4P_4S_2$ (1963): calcd. C 64.83, H 6.31, N 0.71, S 3.26; found C 64.48, H 6.42, N 0.80, S 2.95. − ^1H NMR ($CDCl_3$): δ = 0.87 [s, 18 H, $C(CH_3)_3$], 1.24 [s, 18 H, $C(CH_3)_3$], 2.26 (s, 3 H, CH_3), 7.01−7.40 (m, 24 H, CH). − $^{31}P\{^1H\}$ NMR ($CDCl_3$): δ = 108.81 (s). − Λ [ohm^{-1} cm^2 mol^{-1}] (5 10^{-4} − 10^{-3} M CH_3OH) = 183.

[$PdCl_2$(μ-5)]$_2$ (15): Ligand **5** (0.110 g, 0.128 mmol), dissolved in toluene (5 mL), was added dropwise with continuous stirring to a solution of [Pd($PhCN$)$_2$$Cl_2$] (0.05 g, 0.128 mmol) in toluene (10 mL). A yellow-orange solid began to precipitate. After 2 h, the solid was isolated from the reaction mixture, washed with toluene (3 × 1 mL), and dried under vacuum. Yield 73% (0.097 g, 0.046 mmol). − $C_{110}H_{76}Cl_4O_{12}P_4Pd_2$ (2068): calcd. C 63.88, H 3.70, Cl 6.86; found C 63.56, H 4.04, Cl 6.93. − ^1H NMR ($CDCl_3$): δ = 1.27 [s, 6 H, $C(CH_3)_2$], 6.25 (d, ^3J = 6.6 Hz, CH, 4 H), 5.5 (d, ^3J = 6.6 Hz, 4 H, CH), 7.27−7.65 (m, 12 H, CH), 7.89−8.01 (m, 8 H, CH). − $^{31}P\{^1H\}$ NMR ($CDCl_3$): δ = 107.68 (s).

[PtI_2(μ-5)]$_2$ (16): The yellow bridge species was synthesized by the reaction of a solution of [Pt(COD)I_2] (0.050 g, 0.089 mmol) in toluene (10 mL) with a toluene solution of ligand **5** (0.076 mg, 0.089 mmol), using the same procedure for the synthesis of **16**. Yield 78% (0.116 g, 0.045 mmol). − $C_{110}H_{76}I_4O_{12}P_4Pt_2$ (2611): calcd. C 50.59, H 2.93, I 19.44; found C 50.28, H 2.59, I 19,60. − ^1H NMR ($CDCl_3$): δ = 1.27 [s, 6 H, $C(CH_3)_2$], 6.36 (d, ^3J = 8.8 Hz, 4 H, CH), 6.63 (d, ^3J = 8.3 Hz, 4 H, CH), 7.16−7.88 (m, 20 H, CH). − $^{31}P\{^1H\}$ NMR ($CDCl_3$): δ = 84.06 (s, J_{PtP} 5543 Hz).

X-ray Structure Determination of 10·2CH_2Cl_2 and 12·2CH_2Cl_2: The crystals of both complexes were obtained by crystallization from dichloromethane solutions and molecules of solvent were found in them. The intensity data of both complexes were collected at room temperature with a Siemens AED (**10·2CH_2Cl_2**) and with an Enraf−Nonius CAD 4 (**12·2CH_2Cl_2**) single-crystal diffractometer using graphite-monochromated Mo-K_α (**10·2CH_2Cl_2**) and Cu-K_α (**12·2CH_2Cl_2**) radiation and the θ/2θ scan technique. Crystallographic and experimental details for both structures are summarized in Table 3. A correction for absorption was made for both complexes [maximum and minimum value for the transmission coefficient was 1.000 and 0.487 (**10·2CH_2Cl_2**), 1.000 and 0.697 (**12·2CH_2Cl_2**).[14] The structures were solved by Patterson and Fourier methods and refined by full-matrix least-squares procedures (based on F_o^2) with anisotropic thermal parameters in the last cycles of refinement for all the non-hydrogen atoms, except for the carbon and chlorine atoms of the solvent molecules (**10·2CH_2Cl_2**) and except for the carbon atoms of the two isobutyl groups which were found disordered in two positions with an occupancy factor of 0.5 (**12·2CH_2Cl_2**). In both structures, the hydrogen atoms were introduced into the geometrically calculated positions and refined riding on the corresponding parent atoms. In the final cycles of refinement a weighting scheme $w = 1/[\sigma^2F_o^2 + (0.0533\ P)^2]$ (**10·2CH_2Cl_2**) and $w = 1/[\sigma^2F_o^2 + (0.1271\ P)^2]$ (**12·2CH_2Cl_2**) where $P = (F_o^2 + 2\ F_c^2)/3$ was used. All calculations were carried out with the DIGITAL AlphaStation 255 computers of the "Centro di Studio per la Strutturistica Diffrattometrica" del CNR, Parma, using the SHELX-97 systems of crystallographic computer programs.[15] The supplementary material for the structures includes the lists of atomic coordinates for the non-H atoms, of calculated coordinates for the hydrogen atoms, of anisotropic thermal parameters and complete lists of bond lengths and angles. The details of the crystal structure investigations have been deposited in the Cambridge Crystallographic Data Centre as supplementary publications no. CCDC-143608 (**10·2CH_2Cl_2**) and -143609 (**12·2CH_2Cl_2**). Copies of the data can be obtained free of charge on application to CCDC,

Table 3. Crystal data and structure refinement for **10·2CH$_2$Cl$_2$** and **12·2CH$_2$Cl$_2$**; $R1 = \Sigma|F_o - F_c|/|\Sigma(F_o)$ $wR2 = \{\Sigma[w(F_o^2 - F_c^2)^2]/\Sigma[w(F_o^2)^2]\}^{1/2}$

	10·2CH$_2$Cl$_2$	**12·2CH$_2$Cl$_2$**
Empirical formula	$C_{78}H_{68}I_4O_4P_4Pt_2 \cdot 2CH_2Cl_2$	$C_{40}H_{51}Cl_2PPdS \cdot 2CH_2Cl_2$
Formula mass	2260.84	973.99
Temperature	293(2) K	293(2) K
Wavelength	0.71144 Å	1.54184 Å
Crystal system	monoclinic	monoclinic
Space group	*C*2/*c*	$P2_1/n$
Unit cell dimensions	$a = 31.436(5)$Å	$a = 14.740(4)$Å
	$b = 16.563(4)$Å	$b = 19.851(5)$Å
	$c = 15.894(4)$Å	$c = 16.272(4)$Å
	$\beta = 101.28(6)°$	$\beta = 93.17(6)°$
Volume	8116(3) Å^3	4754(2) Å^3
Z	4	4
Density (calcd.)	1.850 Mg/m^3	1.361 Mg/m^3
Absorption coefficient	52.23 cm^{-1}	72.28 cm^{-1}
F(000)	4320	2008
Crystal size	0.32 × 0.25 × 0.21 mm	0.12 × 0.22 × 0.22 mm
θ range [°]	3.08−27.10	3.52−70.02
Index ranges	$-40 \le h \le 39, -6 \le k \le 21, -19 \le l \le 20$	$-17 \le h \le 17, 0 \le k \le 24, 0 \le l \le 19$
Reflections collected	11581	9313
Independent reflections	8909 [*R*(int) = 0.1353]	8995 [*R*(int) = 0.0554]
Obs. refl [$I > 2\sigma(I)$]	4772	6097
Data/restr./param.	8909/6/448	8995/0/482
Goodness-of-fit on F^2	0.838	0.981
Final *R* indices [$I > 2\sigma(I)$]	*R1* = 0.0421, *wR2* = 0.0905	*R1* = 0.0589, *wR2* = 0.1704
R indices (all data)	*R1* = 0.0959, *wR2* = 0.1035	*R1* = 0.0831, *wR2* = 0.1883

12 Union Road, Cambridge CB2 1EZ, UK [Fax: (internat.) + 44-1223/336-033, E-mail: deposit@ccdc.cam.ac.uk].

Acknowledgments

We thank MURST for financial support.

[1] [1a] S. Leininger, B. Olenyuk, P. J. Stang, *Chem. Rev.* **2000**, *100*, 853. − [1b] P. J. Stang, Chem. *Eur. J.* **1998**, *4*, 19. − [1c] P. N. W. Baxter, *Metal Ion Directed Assembly of Complex Molecular Architectures and nanostructures* in *Comphrensive Supramolecular Chemistry*, vol. 9 (Series Ed.: J-M. Lehn; Volume Eds.: J. P. Sauvage, M. W. Hosseini), Pergamon, Oxford, **1996**, chapter 5, p. 165. − [1d] G. X. Liu, R. Puddephatt, *Organometallics* **1996**, *15*, 5257. − [1e] S. Achar, J. J. Vittal, R. Puddephatt, *Organometallics* **1996**, *15*, 43.

[2] [2a] J. A Whiteford, C. V. Lu, P. J. Stang, *J. Am. Chem. Soc.* **1997**, *119*, 2524. − [2b] P. J. Stang, D. H. Cao, S. Saito, A. A. M. Arif, *J. Am. Chem. Soc.* **1994**, *117*, 6273. − [2c] P. J. Stang, D. H. Cao, *J. Am. Chem. Soc.* **1994**, *116*, 4981.

[3] C. J. Jones, *Chem. Soc. Rev.* **1998**, *27,* 289.

[4] [4a] P. J. Stang, B. Olenyuk, *Acc. Chem. Res.* **1997**, *30*, 502. − [4b] F. Makoto, K. Ogura, *Bull. Chem. Soc. Jpn.* **1996**, *69*, 1471.

[5] F. S. McQuillan, H. Chen, T. A. Hamor, C. J. Jones, H. A. Jones, P. Sidebotham, *Inorg. Chem*. **1999**, *38*, 1555.

[6] C. G. Arena, D. Drago, M. Panzalorto, G. Bruno, F. Faraone, *Inorg. Chim. Acta* **1999**, *292*, 84.

[7] S. D. Pastor, J. D Spivack, L. P Steinhuebel, *J. Heterocycl. Chem.* **1984**, *21*, 1285.

[8] G. Franciò, C. G. Arena, F. Faraone, C. Graiff, M. Lanfranchi, A. Tiripicchio, *Eur. J. Inorg. Chem.* **1999**, 1219.

[9] F. R. Hartley, *The Chemistry of Platinum and Palladium*, Applied Science Publishers Ltd., Ripple Road, Barking, Essex, England, **1973**.

[10] P. S. Pregosin, R. Salzmann, *Coord. Chem. Rev.* **1996**, *155*, 35

[11] J. Manna, C. J. Kuchl, J. A. Whiteford, P. J. Stang, *Organometallics* **1997**, *16*, 1897.

[12] M. Fuss, H. U. Siehl, B. Olenyuk, P. J. Stang, *Organometallics* **1999**, *18*, 758.

[13] G.J. Kubas, *Inorg. Synth*. **1979**, *19*, 90.

[14] N. Walker, D. Stuart, *Acta Crystallogr., Sect. A* **1983**, *39* 158. − F. Ugozzoli, *Comput. Chem.* **1987**, *11*, 109.

[15] G. M. Sheldrick, *SHELX-97, Program for the Solution and the refinement of Crystal Structures*, Universität Göttingen, Germany, **1997**.

Received April 28, 2000
[I00167]

Enthalpies of Sublimation of $M(\eta^5\text{-}C_5H_5)_2Cl_2$ (M = Ti, Zr, Hf, V, Nb, W) Complexes

Hermínio P. Diogo,[a] Manuel E. Minas da Piedade,*[a] Jorge M. Gonçalves,[b] Manuel J. S. Monte,[b] and Manuel A. V. Ribeiro da Silva[b]

Keywords: Transition metals / Metallocenes / Knudsen effusion / Thermochemistry

The standard molar enthalpies of sublimation of $M(\eta^5\text{-}C_5H_5)Cl_2$ (M = Ti, V, Zr, Nb, Hf, and W) compounds, at 298.15 K, were determined by the Knudsen effusion method to be: 124.4±2.9 kJmol^{-1} (M = Ti), 108.5±4.6 kJmol^{-1} (M = Zr), 110.2±2.9 kJmol^{-1} (M = Hf), 140.1±7.4 kJmol^{-1} (M = V), 127.4±4.4 kJmol^{-1} (M = Nb), and 120.7±8.6 kJmol^{-1} (M = W). The results obtained show a tendency to linearly decrease with increasing metal atomic radius.

Introduction

The study of bent metallocenes has generated a wealth of fundamental chemistry and some major commercial applications (e.g. new Ziegler-Natta catalysts for the production of polyethylene and polypropylene).[1] These studies have also raised an increasing number of questions about the energetics of reactivity and bonding in these complexes as one tries to rationalise the observed reactions and molecular structures.[2]

The enthalpies of sublimation of $M(\eta^5\text{-}C_5H_5)_2Cl_2$ (M = Ti, Zr, Hf, V, Nb, Ta, Mo, W) complexes are of considerable importance in the study of the energetics of transition metal-ligand bonds. Bis(cyclopentadienyl) compounds, $M(\eta^5\text{-}C_5H_5)_2L_n$ (M = Ti, Zr, Hf, V, Nb, Ta, Mo, W; L = H, halogen, CO, alkyl, alkene, aryl, alkoxide, thiolate, phosphane, etc.; n = 1−3), have been extensively used as models for investigating the general trends of M−L bond dissociation enthalpies in group 4−6 transition metals.[3−9] Absolute M−L bond dissociation enthalpies in these complexes can, in principle, be obtained by calculating the enthalpy of reaction (1) from the gas phase enthalpies of formation of $M(\eta^5\text{-}C_5H_5)_2L_n$, $M(\eta^5\text{-}C_5H_5)_2$, and L:

$$M(\eta^5\text{-}C_5H_5)_2L_n\,(g) \rightarrow M(\eta^5\text{-}C_5H_5)_2\,(g) + nL\,(g) \quad (1)$$

$$DH^o(M-L) = \Delta_fH^o[M(\eta^5\text{-}C_5H_5)_2, g]/n + \Delta_fH^o(L, g) - \Delta_fH^o[M(\eta^5\text{-}C_5H_5)_2L_n, g]/n \quad (2)$$

where $DH^o(M-L)$ denotes a bond dissociation enthalpy for n = 1 and a mean bond dissociation enthalpy for n = 2 or 3.

[a] Centro de Química Estrutural, Complexo Interdisciplinar, Instituto Superior Técnico,
1049-001 Lisboa, Portugal
Fax: (internat.) + 351-21/8464455/57
E-mail: pcmemp@alfa.ist.utl.pt
[b] Centro de Investigação em Química, Departamento de Química, Faculdade de Ciências, Universidade do Porto,
Rua do Campo Alegre, 687, 4169-007 Porto, Portugal
Fax: (internat.) + 351-22/6082822
E-mail: risilva@fc.up.pt

Unfortunately, although many $\Delta_fH^o[M(\eta^5\text{-}C_5H_5)_2L_n, g]$ and $\Delta_fH^o(L, g)$ values are available,[3−9] the enthalpies of formation of the $M(\eta^5\text{-}C_5H_5)_2$ fragments are not known. In order to overcome this problem, all $DH^o(M-L)$ values reported up to now for $M(\eta^5\text{-}C_5H_5)_2L_n$ compounds have been anchored in the mean M−Cl bond dissociation enthalpies of the corresponding dichlorides. This has been done by considering reaction (3) and Equation 4:

$$M(\eta^5\text{-}C_5H_5)_2L_n\,(g) + 2\,Cl\,(g) \rightarrow M(\eta^5\text{-}C_5H_5)_2Cl_2\,(g) + nL\,(g) \quad (3)$$

$$DH^o(M-L) = 2\,DH^o(M-Cl)/n + \Delta_fH^o[M(\eta^5\text{-}C_5H_5)_2Cl_2, g]/n + \Delta_fH^o(L_n, g) - \Delta_fH^o[M(\eta^5\text{-}C_5H_5)_2L_n, g]/n - 2\Delta_fH^o(Cl, g)/n \quad (4)$$

The calculation of $DH^o(M-L)$ from Equation 4 requires knowledge of the values of $DH^o(M-Cl)$ and $\Delta_fH^o[M(\eta^5\text{-}C_5H_5)_2Cl_2, g]$. The M−Cl bond dissociation enthalpies in $M(\eta^5\text{-}C_5H_5)Cl_2$ have been estimated from the corresponding values in the homoleptic molecules MCl_x.[3−5,8] The enthalpies of formation of $M(\eta^5\text{-}C_5H_5)_2Cl_2$ in the gaseous state can be derived from Equation 5.

$$\Delta_fH^o[M(\eta^5\text{-}C_5H_5)_2Cl_2, g] = \Delta_fH^o[M(\eta^5\text{-}C_5H_5)_2Cl_2, cr] + \Delta_{sub}H^o[M(\eta^5\text{-}C_5H_5)_2Cl_2] \quad (5)$$

The enthalpies of sublimation of $M(\eta^5\text{-}C_5H_5)_2Cl_2$ are therefore needed to calculate $DH^o(M-L)$ from Equation 4.

The $\Delta_{sub}H^o[M(\eta^5\text{-}C_5H_5)_2Cl_2]$ values are also interesting since they are directly related to the intermolecular forces that dictate the solid state structures of the $M(\eta^5\text{-}C_5H_5)_2Cl_2$ compounds. They can therefore be useful in the development of methods for predicting crystal structures or enthalpies of sublimation of organometallic compounds based on atom-atom potential calculations.[10] The ability to predict crystal structures has of course a major impact in areas of great current chemical research activity, such as crystal engineering,[11] while the enthalpy of sublimation and vapour pressures of organometallic compounds are important in, for example, the design of chemical vapour deposition (CVD) processes.[12]

 © WILEY-VCH Verlag GmbH, 69451 Weinheim, 2001 1434−1948/01/0101−0257 $ 17.50+.50/0

Only the enthalpies of sublimation of $Ti(\eta^5\text{-}C_5H_5)_2Cl_2$, $Zr(\eta^5\text{-}C_5H_5)_2Cl_2$, and $Hf(\eta^5\text{-}C_5H_5)_2Cl_2$ have been measured up to now,[8,9,13,14] and some discrepancies exist in cases where more than one independent result has been reported. The importance of $\Delta_{sub}H^o[M(\eta^5\text{-}C_5H_5)_2Cl_2]$ for the research topics mentioned above led us to undertake their systematic determination for group 4−6 transition metals.

Results and Discussion

The enthalpies of sublimation of the $M(\eta^5\text{-}C_5H_5)_2Cl_2$, compounds were derived from vapour pressure versus temperature measurements, using three different Knudsen effusion apparatuses.[15−18] For M = Ti, Zr, Hf, V, and W, the vapour pressures, p (Table 1), were determined as a function of the temperature, T, from the mass of sample, m, lost by the cell during the time t, according to:[19]

$$p = \frac{m}{AtK_C}\sqrt{\frac{2\pi RT}{M}} \quad (6)$$

where M is the molar mass of the effusing vapour, A is the area of the effusion hole, R is the gas constant, and K_C is the Clausing factor given by Equation 7.[19]

$$K_C = \frac{8r}{3l + 8r} \quad (7)$$

In Equation 7, l and r represent the thickness and the radius of the effusion hole, respectively. The vapour pressure data in Table 1 were fitted to the Clausius−Clapeyron Equation 8.[20]

$$\ln p = -\frac{a}{T} + b \quad (8)$$

and the enthalpies of sublimation of the dichloride complexes at the mean temperature, T_m, of the experiments were obtained as $\Delta_{sub}H^o(T_m) = aR$, where R is the gas constant. The values of $\Delta_{sub}H^o(T_m)$, and of the constants a and b in Equation 8 are indicated in Table 2. The uncertainties quoted correspond to σt_s, where σ is the standard error and t_s the Student's factor for a 95% confidence level.[21] Plots of Equation 8 for $Ti(\eta^5\text{-}C_5H_5)_2Cl_2$, $Zr(\eta^5\text{-}C_5H_5)_2Cl_2$, $Hf(\eta^5\text{-}C_5H_5)_2Cl_2$, $V(\eta^5\text{-}C_5H_5)_2Cl_2$, and $W(\eta^5\text{-}C_5H_5)_2Cl_2$ are shown in Figure 1. The lines for the titanium, zirconium and hafnium complexes are based on the values of the corresponding a and b constants for the global results in Table 2.

In the case of $Nb(\eta^5\text{-}C_5H_5)_2Cl_2$, the mass of compound effusing from the Knudsen cell was monitored with a quartz crystal resonator detector.[17,18] If a thin film of any substance is deposited on the surface of a quartz crystal resonator, a shift Δf, of the main resonance frequency, f, is observed, which is a function of the mass of the coating, m.[22] Under the conditions of our experiment, the rate of change of the resonance frequency of the quartz crystal, v, with the time, t, is proportional to the rate of effusion of the compound from the cell, m/t:[17,18]

$$v = \frac{\Delta f}{t} = C_f\frac{m}{t} \quad (9)$$

where C_f is a proportionality constant. Equations 6 and 9 lead to:

$$p = \frac{v}{C_f AK_C}\sqrt{\frac{2\pi RT}{M}} \quad (10)$$

and, therefore, according to Equations 8 and 10, a plot of $\ln(vT^{1/2})$ against $1/T$ should give a straight line:

$$\ln(vT^{1/2}) = -\frac{a}{T} + b' \quad (11)$$

of slope $a = \Delta_{sub}H^o(T_m)/R$, and ordinate b. By fitting Equation 11 to the v and T data given in Table 1 for $Nb(\eta^5\text{-}C_5H_5)_2Cl_2$ it was possible to derive the values of a, b', and

Table 1. Vapour pressures of $M(\eta^5\text{-}C_5H_5)_2Cl_2$ compounds

$Ti(\eta^5\text{-}C_5H_5)_2Cl_2$ [a]			$Zr(\eta^5\text{-}C_5H_5)_2Cl_2$				$Hf(\eta^5\text{-}C_5H_5)_2Cl_2$			$V(\eta^5\text{-}C_5H_5)_2Cl_2$		$Nb(\eta^5\text{-}C_5H_5)_2Cl_2$		$W(\eta^5\text{-}C_5H_5)_2Cl_2$	
T/K	p/Pa hole 1	p/Pa hole 3	T/K	p/Pa hole 1	p/Pa hole 2	p/Pa hole 3	T/K	p/Pa hole 1	p/Pa hole 3	T/K	p/Pa hole 4	T/K	10^2v/s^{-2} hole 5	T/K	p/Pa hole 4
399.30	0.1141	0.1089	377.74	0.2261	0.2077	0.2062	366.21	0.1408	0.1327	459.8	0.1374	388.6	0.32964	466.5	0.0302
400.82	0.1377	0.1297	379.19		0.2565	0.2519	369.19	0.1825	0.1736	462.2	0.1664	390.1	0.38306	470.7	0.0408
402.34	0.1453	0.1524	380.85	0.3081	0.2947	0.2900	372.20	0.2395	0.2384	465.1	0.2045	391.7	0.44764	472.2	0.0442
405.25	0.1873	0.1918	382.10	0.3096	0.3142	0.2996	375.10	0.3180	0.3032	468.3	0.2426	393.2	0.50993	473.1	0.0448
407.30	0.2286	0.2265	383.62	0.3765	0.3565	0.3565	378.20	0.4240	0.4053	470.0	0.2829	394.7	0.57993	477.8	0.0604
409.75	0.2900	0.2877	385.35	0.4370	0.3869	0.3873	381.17	0.5232	0.5105	471.9	0.3306	396.2	0.71288	478.3	0.0660
412.35	0.3680	0.3573	386.84	0.4982	0.4616	0.4846	384.25	0.7234	0.7047	477.1	0.4859	397.7	0.76842	482.9	0.0808
414.55	0.4219	0.4157	388.08	0.5087	0.5433	0.5154	387.18	0.9023	0.8920	477.5	0.4916	399.1	0.88632	485.3	0.0933
417.42	0.5412	0.5173	389.57	0.6387	0.5849	0.5895						400.7	1.00661		
420.40	0.6959	0.6784	391.16		0.6499	0.6902						402.3	1.21577		
422.32	0.8054	0.7817	392.65	0.8133	0.7635	0.7339						403.6	1.28136		
424.05	0.9222	0.9178										405.0	1.53338		

[a] Hole dimensions: (1) A = 0.596 mm^2, r = 0.436 mm, l = 0.049 mm; (2) A = 0.754 mm^2, r = 0.490 mm, l = 0.049 mm; (3) A = 0.862 mm^2, r = 0.524 mm, l = 0.049 mm; (4) A = 0.440 mm^2, r = 0.374 mm, l = 0.0209 mm.

Table 2. Values of the constants in Equations 8 and 11 and enthalpies of sublimation of the $M(\eta^5\text{-}C_5H_5)_2Cl_2$ compounds at the average temperature of the experiments (T_m)

M	Hole no.	T_m/K	a	b[a] or b[b]	$\Delta_{sub}H^o(T_m)$/kJmol^{-1}
Ti	1	411.68	14307±334	33.66±0.82	
	3	411.68	14244±281	33.49±0.69	
	Global results	411.68	14275±211	33.58±0.52	118.7±1.8
Zr	1	385.20	12633±1116	31.95±2.88	
	2	385.20	12343±821	31.15±2.13	
	3	385.20	12591±805	31.79±2.08	
	Global results	385.20	12511±517	31.60±1.33	104.0±4.3
Hf	1	376.70	12669±360	32.62±0.95	
	3	376.70	12892±333	33.18±0.88	
	Global results	376.70	12781±287	32.90±0.77	106.3±2.4
V	4	468.7	15824±795	32.42±1.69	131.6±6.6
Nb	5	396.8	14729±470	35.17±1.18	122.5±3.9
W	4	475.9	13464±935	25.38±1.96	111.9±7.8

[a] See Equation 8, for M = Ti, Zr, Hf, V, W. – [b] See Equation 11, for M = Nb.

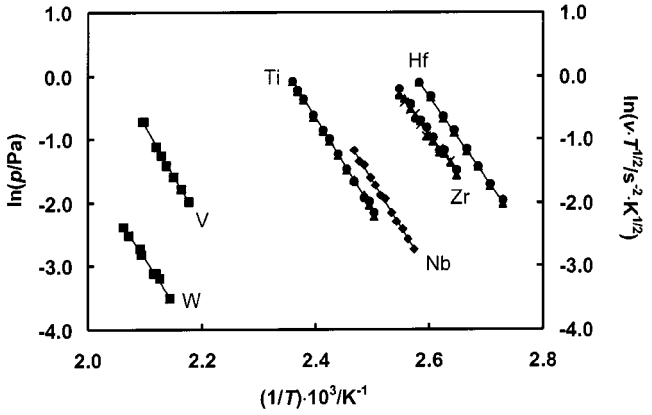

Figure 1. Plots of the Clausius–Clapeyron equation for the $M(\eta^5\text{-}C_5H_5)_2Cl_2$ (M = Ti, Zr, Hf, V, W) compounds and of $\ln(vT^{1/2})$ versus $1/T$ for $Nb(\eta^5\text{-}C_5H_5)_2Cl_2$ (see text). (•) – hole 1, (×) – hole 2, (▲) – hole 3, (■) – hole 4, (◆) – hole 5

$\Delta_{sub}H^o(T_m)$ indicated in Table 2. The uncertainties quoted were calculated as described above for the other complexes. A representation of $\ln(vT^{1/2})$ versus $1/T$ for $Nb(\eta^5\text{-}C_5H_5)_2Cl_2$, based on the a and b constants in Table 2, is also shown in Figure 1.

The enthalpies of sublimation of the $M(\eta^5\text{-}C_5H_5)_2Cl_2$ compounds, at 298.15 K, were derived from:

$$\Delta_{sub}H^o(298.15\ K) = \Delta_{sub}H^o(T_m) + \Delta_{sub}C_p^o(298.15 - T_m) \quad (12)$$

by using the $\Delta_{sub}H^o(T_m)$ data in Table 2 and an estimated value $\Delta_{sub}C_p^o = -(50\pm20)$ JK^{-1}mol^{-1}.[23] The results obtained are shown in Table 3.

As mentioned in the Introduction, only the enthalpies of sublimation of $Ti(\eta^5\text{-}C_5H_5)_2Cl_2$,[8,9,13,14] $Zr(\eta^5\text{-}C_5H_5)_2Cl_2$,[8,9,13,14] and $Hf(\eta^5\text{-}C_5H_5)_2Cl_2$[8,9,13] had been previously measured. Correction of the reported values from their reference temperatures to 298.15 K, using Equation 12 and $\Delta_{sub}C_p^o = -(50\pm20)$ JK^{-}·^{1}mol^{-1}, led to the results in Table 3. Note, however, that the information needed to recalculate the corresponding uncertainties using the Student's factor is lacking in the literature. The errors in the published data included in Table 3 may, therefore, be underestimated relative to those quoted for our values.

Table 3 shows that the standard molar enthalpies of sublimation of $Ti(\eta^5\text{-}C_5H_5)_2Cl_2$, $Zr(\eta^5\text{-}C_5H_5)_2Cl_2$, and $Hf(\eta^5\text{-}C_5H_5)_2Cl_2$ proposed in this paper agree, within the experimental error, with those obtained by Balducci et al.[13] and by Rabinovich et al.,[8,9] using effusion methods. Our value for $\Delta_{sub}H^o[Zr(\eta^5\text{-}C_5H_5)_2Cl_2]$ is also in good agreement with a mass spectrometric result published by Kiser et al.[14] A large discrepancy exists, however, between the $\Delta_{sub}H^o[Ti(\eta^5\text{-}C_5H_5)_2Cl_2]$ value reported by Kiser et al.[14] and those obtained by us and other authors. The enthalpy of sublimation of $\Delta_{sub}H^o[W(\eta^5\text{-}C_5H_5)_2Cl_2]$ in Table 3 is also ca. 16 kJmol^{-1} higher than an estimate of 104.6±4.2 kJmol^{-1} reported by Tel'noi et al.[8]

Finally, it is interesting to note that a linear least squares analysis of a representation of the $\Delta_{sub}H^o[M(\eta^5\text{-}C_5H_5)_2Cl_2]$ (M = Ti, Zr, Hf, V, Nb, W) values reported in this paper versus the atomic radii of the metals, r_M,[24] (Table 3), leads to (Figure 2):

$$\Delta_{sub}H^o[M(\eta^5\text{-}C_5H_5)_2Cl_2]/kJmol^{-1} = -0.972(r_M/pm) + 263.3 \quad (13)$$

with a regression coefficient of 0.9. Equation 13 reproduces the experimental $\Delta_{sub}H^o[M(\eta^5\text{-}C_5H_5)_2Cl_2]$ values with a maximum error of 10 kJmol^{-1}, and predicts that $\Delta_{sub}H^o[Ta(\eta^5\text{-}C_5H_5)_2Cl_2] = 124\pm10$ kJmol^{-1}, and $\Delta_{sub}H^o[Mo(\eta^5\text{-}C_5H_5)_2Cl_2] = 131\pm10$ kJmol^{-1}. Attempts to measure the enthalpies of sublimation of $Ta(\eta^5\text{-}C_5H_5)_2Cl_2$, and $Mo(\eta^5\text{-}C_5H_5)_2Cl_2$ in the Lisbon laboratory failed due to decomposition of the samples before a measurable mass loss from the Knudsen cell could be obtained.

Conclusion

The enthalpies of sublimation of the $M(\eta^5\text{-}C_5H_5)_2Cl_2$ compounds reported in this paper (*i*) decrease from the first to the second transition series, (*ii*) remain almost constant from the second to the third transition series, and (*iii*) decrease across a transition series. This trend shows a remarkably good linear correlation with the atomic radii of the metals. The significance of this correlation to the nature of the intermolecular potentials in these molecules needs to

Table 3. Enthalpies of sublimation of the $M(\eta^5\text{-}C_5H_5)_2Cl_2$ compounds, at 298.15 K, in $kJmol^{-1}$,[a] and atomic radii of the metals (r_M) in pm[b]

Group 4	Group 5	Group 6
M = Ti (r_M = 144.8) 124.4±2.9 (this work) 102±13[c] 120.2±3.7[d] 118.9±3.5[e]	**M = V** (r_M = 132.1) 140.1±7.4 (this work)	
M = Zr (r_M = 160) 108.5±4.6 (this work) 103±13[c] 105.6±3.1[d] 106.7±3.1[e]	**M = Nb** (r_M = 142.9) 127.4±4.4 (this work)	**M = Mo** (r_M = 136.2) (131±10)
M = Hf (r_M = 156.4) 110.2±2.9 (this work) 107.3±2.4[c] 106.4±2.8[d]	**M = Ta** (r_M = 143) (124±10)	**M = W** (r_M = 137) 120.7±8.6 (this work)

[a] Values in parentheses were estimated from Equation 13. – [b] Ref.[24]. – [c] Ref.[14]. – [d] Ref.[8,9]. – [e] Ref.[13].

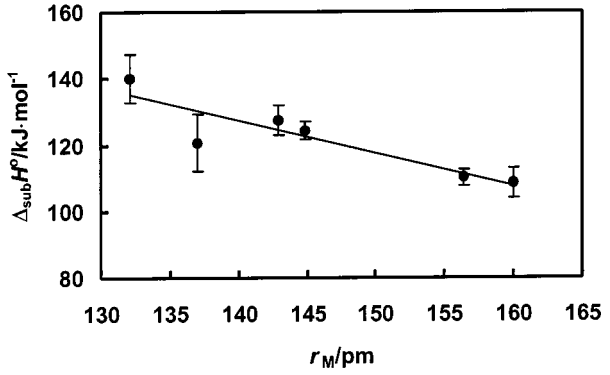

Figure 2. Enthalpies of sublimation of the $M(\eta^5\text{-}C_5H_5)_2Cl_2$ compounds, at 298.15 K, versus the atomic radii, r_M of the metals

be investigated. The obtained $\Delta_{sub}H°[M(\eta^5\text{-}C_5H_5)_2Cl_2]$ data will also enable an improvement in the reliability of bond dissociation enthalpies derived for bis(cyclopentadienyl) compounds, which are one of the most important model systems used to study the systematics of bonding energetics in transition metal compounds.

Experimental Section

General: All syntheses were carried out under argon atmosphere, by standard Schlenk techniques. Solvents were dried as recommended by Perrin et al.[25] and distilled and stored under argon atmosphere. The $W(\eta^5\text{-}C_5H_5)_2H_2$ used in the preparation of $W(\eta^5\text{-}C_5H_5)_2Cl_2$ was synthesised as described by Green and Knowles[26] and purified by sublimation at 353 K and 0.13 Pa.

C, H, N elemental analysis were performed with a Carlo Erba 1106 elemental analyser. Infrared spectra were obtained with a Perkin–Elmer 683 spectrophotometer calibrated with polystyrene film. Band intensities are referred to as following: vs, very strong; s, strong; m, medium; w, weak.

Materials: $Ti(\eta^5\text{-}C_5H_5)_2Cl_2$ was prepared as recommended by Samuel[27] and purified by sublimation at 333 K and 0.13 Pa. – $C_{10}H_{10}Cl_2Ti$: calcd. C 48.24, H 4.05; found C 48.20, H 4.03. – IR (KBr, cm^{-1}): 3120 m, 1445 s, 1375 w, 1028 m, 1015 s, 874 m, 820 vs.

$Zr(\eta^5\text{-}C_5H_5)_2Cl_2$ was synthesised as described in the literature[27–29] and purified by sublimation at 363 K and 1.3 Pa. – $C_{10}H_{10}Cl_2Zr$: calcd. C 41.09, H 3.45; found C 41.03, H 3.47. – IR (KBr, cm^{-1}): 3100 m, 1865 w, 1760 w, 1660–1640 w, 1435 s, 1360 m, 1115 m, 1065 w, 1020–1015 vs, 935–920 w, 860–840 vs, 815 vs.

$Hf(\eta^5\text{-}C_5H_5)_2Cl_2$ (Aldrich, 98%) was purified by sublimation at 390 K and 0.13 Pa. – $C_{10}H_{10}Cl_2Hf$: calcd. C 31.64, H 2.65; found C 31.59, H 2.62. – IR (KBr, cm^{-1}): 3115 m, 1440 s, 1367 w, 1023 s, 1013 s, 855–840s, 814 vs.

$V(\eta^5\text{-}C_5H_5)_2Cl_2$ (Aldrich, 95%) was purified by sublimation at 463 K and 0.13 Pa. – $C_{10}H_{10}Cl_2V$: calcd. C 47.65, H 4.00; found C 47.59, H 3.94. – IR (KBr, cm^{-1}): 3100 m, 1450 m, 1370 w, 1015–1025 w, 1013 s, 890 w, 830 vs.

$Nb(\eta^5\text{-}C_5H_5)_2Cl_2$ was synthesised as described in the literature[30] and purified by sublimation at 363 K and 1.3 Pa. – $C_{10}H_{10}Cl_2Nb$: calcd. C 40.85, H 3.43; found C 40.60, H 3.68. – IR (KBr, cm^{-1}): 3100 m, 1435 m, 1360 w, 1260 w, 1120 w, 1070 w, 1020 s, 870 m, 820 vs.

The method of preparing $W(\eta^5\text{-}C_5H_5)_2Cl_2$ [31] was adapted from that given by Cooper and Green.[32] Dropwise addition of chloroform to a solution of $W(\eta^5\text{-}C_5H_5)_2H_2$ in toluene, under argon atmosphere, at room temperature, gave green crystals of $W(\eta^5\text{-}C_5H_5)_2Cl_2$. These were washed with diethyl ether and dried at room temperature in a filter funnel connected to a water aspirator pump. The product obtained was washed with dichloromethane in a Soxhlet apparatus for 24 h, until colourless extracts were observed, and dried under vacuum (318 K, 1.3 Pa). – $C_{10}H_{10}Cl_2W$: calcd. C 31.20, H 2.62; found C 31.40, H 2.60. – IR (KBr, cm^{-1}): 3110 m, 1430 m, 1360 w, 1265 vw, 1110 vw, 1010 m, 875 m, 835 s, 800 m, 585 w.

Apparatus: The Knudsen effusion apparatus used in the Porto laboratory to measure the vapour pressures of the complexes $Ti(\eta^5\text{-}C_5H_5)_2Cl_2$, $Zr(\eta^5\text{-}C_5H_5)_2Cl_2$, and $Hf(\eta^5\text{-}C_5H_5)_2Cl_2$ has been reported.[15] This apparatus enables the simultaneous operation of three Knudsen cells. In the present work, the effusion holes had a thickness of 0.049 mm, and the areas were 0.596 mm^2 (hole 1), 0.754 mm^2 (hole 2), and 0.862 mm^2 (hole 3). The cells were immersed in a silicone oil bath whose temperature was controlled to within ±0.001 K using a Tronac PTC 40 thermostat. The temperature of the sample was assumed to be identical to the temperature

of the bath, which was measured to ±0.01 K with an Amarell calibrated mercury thermometer. In a typical experiment, each cell was charged with ca. 300 mg of sample and the observed mass loss was determined to $\pm 10^{-5}$ g with a Mettler H54 balance. The duration of the runs varied from 3 h to 6 h and the corresponding mass losses from the cell varied between 10 mg and 30 mg.

In the Lisbon laboratory, the vapour pressures of V(η^5-$C_5H_5)_2Cl_2$ and W(η^5-$C_5H_5)_2Cl_2$ were measured with the Knudsen effusion setup previously described.[16] The temperature range of the apparatus was, however, extended up to ca. 650 K by replacement of the water bath with a Termolab tubular furnace surrounding the brass block containing the effusion cell. The temperature of the furnace was controlled to ±0.1 K by a Eurotherm 902P thermostatic unit and a K type thermocouple placed in contact with the inner wall of the furnace. The equilibrium temperature inside the cell was assumed to be identical to the temperature of the brass block. This temperature was measured with a Tecnisis 100 Ω platinum resistance thermometer embedded in the block and connected in a four wire configuration to a Keithley 2000 multimeter. The average of all temperature readings acquired during a constant 10 s interval was stored in the buffer memory of the multimeter. The mean value of the total number of readings accumulated by the multimeter during a run was taken as the corresponding sample temperature. The bronze cell used in the experiments[16a][16b] had an effusion hole with an area of 0.440 mm^2, and a thickness of 0.0209 mm. In a typical run, the cell was charged with ca. 250 mg of sample and the observed mass loss was determined to $\pm 10^{-5}$ g with a Sartorius 2474 balance. The duration of the experiments varied between ca. 21 h and 23 h for V(η^5-$C_5H_5)_2Cl_2$, and 18 h and 25 h for W(η^5-$C_5H_5)_2Cl_2$. The corresponding sample mass losses from the cell were in the ranges ca. 15 mg − 56 mg and 4 mg − 13 mg, respectively.

The compound Nb(η^5-$C_5H_5)_2Cl_2$ was studied using an improved version[18] of the Knudsen effusion apparatus with a quartz crystal microbalance detector, described by Burkinshaw and Mortimer.[17] The cylindrical Knudsen cell with an external diameter of 13 mm, an internal diameter of 6 mm, and a depth of 8 mm, was made of steel. The cell was closed by screwing on a steel lid containing a central effusion hole. The hole has the shape of diverging conical orifice with the smaller section (0.8 mm diameter) facing the interior of the cell. The complete cell was screwed into an electrically heated cylindrical steel block, inside the vacuum chamber of an Edwards 306 vacuum coating unit, equipped with a Edwards FTM3 film thickness monitor incorporating a water cooled quartz crystal resonator (6 MHz). The temperature of the block was controlled to ±0.1 K by an Eurotherm 815 unit. The temperature of the sample was measured by a Labfacility P100/0620 platinum resistance thermometer screwed to the bottom of the effusion cell. The vapour effusing from the Knudsen cell condensed on the quartz crystal resonator which was positioned above the effusion hole. The changes in the oscillation frequency of the crystal were monitored as a function of time by a Philips Frequency Counter PM. The pressure inside the vacuum chamber was maintained at ca. $6 \cdot 10^{-5}$ Pa by an Edwards system consisting of an E2M12 rotary pump and a E04 diffusion pump with a liquid nitrogen trap. In the study of Nb(η^5-$C_5H_5)_2Cl_2$ the cell was initially charged with ca. 200 mg of compound, and the temperature of the furnace was raised until the rate of sublimation corresponded to a rate of frequency change, *v*, greater than ca. 10 Hz min^{-1}. When equilibrium was established the frequency counter readings were acquired as a function of time for 45−60 min. The experiment was repeated at successively higher temperatures separated by ca. 2 K.

Acknowledgments

This work was supported by the PRAXIS XXI and SAPIENS programmes (Projects PRAXIS/PCEX/QUI/62/96 and SAPIENS/35406/99). We also thank Ana L. F. Pires for assistance in the measurements of the vapour pressures of Ti(η^5-$C_5H_5)_2Cl_2$ and Zr(η^5-$C_5H_5)_2Cl_2$, and Dr. Jay Labinger (Beckman Institute, California Institute of Technology) for providing the Ta(η^5-$C_5H_5)_2Cl_2$ sample used in attempts to measure its enthalpy of sublimation.

[1] For leading references see: [1a]*Comprehensive Organometallic Chemistry* (Eds.: G. Wilkinson, F. G. A. Stone, E. W. Abel), Pergamon, Oxford, **1982**. − [1b]*Comprehensive Organometallic Chemistry II* (Eds.: E. W. Abel, F. G. A. Stone, G. Wilkinson), Pergamon, Oxford, **1995**. − [1c]*Metallocenes: Synthesis, Reactivity, Applications* (Eds.: A. Togni, R. L. Alterman), Wiley-VCH, Weinheim, **1998**.

[2] For leading references see: [2a]*Metal-Ligand Bonding Energetics in Organotransition Metal Compounds* (Ed.: T. J. Marks), Polyhedron Symposium-in-Print, *7*, **1988**. − [2b]*Bonding Energetics in Organometallic Compounds* (Ed.: T. J. Marks), ACS Symposium Series 428, American Chemical Society, Washington, **1990**. − [2c]*Energetics of Organometallic Species* (Ed.: J. A. Martinho Simões), NATO ASI Ser., Ser. C, Vol. 367, Kluwer, Dordrecht, **1992**. − [2d]S. P. Nolan, in *Encyclopedia of Inorganic Chemistry* (Ed.: R. B. King), John Wiley, Chichester, **1994**, Vol. 1, 307−318. − [2e]P. B. Dias, M. E. Minas da Piedade, J. A. Martinho Simões, *Coord. Chem. Rev.* **1994**, *135/136*, 737−807.

[3] G. Pilcher, H. A. Skinner in *The Chemistry of the Metal-Carbon Bond* (Eds.: F. R. Hartley, S. Patay), John Wiley, New York, **1982**, Chapter 2.

[4] A. R. Dias, J. A. Martinho Simões, *Polyhedron* **1988**, *16/17*, 1531−1544.

[5] J. A. Martinho Simões, J. L. Beauchamp, *Chem. Rev.* **1990**, *90*, 629−688.

[6] H. P. Diogo, J. A. Simoni, M. E. Minas da Piedade, A. R. Dias, J. A. Martinho Simões, *J. Am. Chem. Soc.* **1993**, *115*, 2764−2774.

[7] J. A. Martinho Simões, *Organometallic Thermochemistry Data* in NIST Chemistry WebBook, NIST Standard Reference Database Number 69 (Eds.: W. G. Mallard, P. J. Linstrom), National Institute of Standards and Technology, Gaithersburg, February 2000, (http://webbook.nist.gov/chemistry).

[8] V. I. Tel'noi, I. B. Rabinovich, *Russ. Chem. Rev.* **1977**, *46,* 689−705.

[9] I. B. Rabinovich, V. P. Nistratov, V. I. Tel'noi, M. S. Sheiman, *Thermochemical and Thermodynamic Properties of Organometallic Compounds*, Begell House, New York, **1999**.

[10] See, for example, [10a] A. J. Pertsin, A. I. Kitaigorodsky, *The Atom-Atom Potential Method. Applications to Organic Molecular Solids*, Springer Verlag, Berlin, **1987**. − [10b] *Theoretical Aspects and Computer Modelling of the Molecular Solid State*, (Ed.: A. Gavezzotti), John Wiley, Chichester, **1997**.

[11] *Crystal Engineering: From Molecules and Crystals to Materials* (Eds.: D. Braga, F. Grepioni, A. G. Orpen) NATO Science Series C, Vol. 538, Kluwer, Dordrecht, **1999**.

[12] See, for example, [12a] *The Chemistry of Metal CVD*, (Ed. T. T. Kodas, M. J. Hampden-Smith), John Wiley, New York, **1994**. − [12b] H. D. Kaesz, A. Zinn, L. Brandt, in *Encyclopedia of Inorganic Chemistry* (Ed.: R. B. King), John Wiley, Chichester, **1994**, Vol. 4, 2205−2219. − [12c] H. O. Pierson, *Handbook of Chemical Vapour Deposition (CVD)*, 2nd Ed., Noyes Publications, New Jersey, **1999**.

[13] G. Balducci, G. Bardi, G. de Maria, R. Gigli, *VII All-Union Calorimetry Conference*, Moscow, Russia, **1977**, 33−34.

[14] R. W. Kiser, J. G. Dillard, D. L. Dugger, *Adv. Chem. Ser.* **1968**, *72*, 153−180.

[15] M. A. V. Ribeiro da Silva, M. J. S. Monte, *Thermochim. Acta* **1990**, *171*, 169−183.

[16] [16a]J. C. G. Calado, A. R. Dias, M. E. Minas da Piedade, J. A. Martinho Simões, *Rev. Port. Quim.* **1980**, *22*, 53−62. − [16b] H. P. Diogo, M. E. Minas da Piedade, A. C. Fernandes, J. A. Martinho Simões, M. A. V. Ribeiro da Silva, M. J. S. Monte, *Thermochim. Acta* **1993**, *228*, 15−22. − [16c] R. C. Santos, *Tese de Doutoramento*, Instituto Superior Técnico, Lisboa, Portugal, **2000**.

[17] P. M. Burkinshaw, C. T. Mortimer, *J. Chem. Soc., Dalton Trans.* **1984**, 75−77.
[18] J. M. Gonçalves, *Tese de Doutoramento*, Universidade do Porto, Porto, Portugal, **1996**.
[19] See for example, [19a] S. Dushman, *Scientific Foundations of Vacuum Technique*, Wiley, New York, **1949**. − [19b] E. D. Cater, *The Effusion Method at Age 69: Current State of the Art*, in Proceedings of the 10th Materials Research Symposium on Characterization of High Temperature Vapors and Gases, Vol. I, (Ed.: J. Hastie) National Bureau of Standards Special Publication 561/1, Washington, **1979**, 3−36.
[20] See for example, J. D. Cox, G. Pilcher, *Thermochemistry of Organic and Organometallic Compounds*, Academic Press, London, **1970**.
[21] G. A. Korn, T. M. Korn, *Mathematical Handbook for Scientists and Engineers*, McGraw-Hill, New York, **1968**.
[22] G. Z. Sauerbrey, *Z. Phys.* **1959**, *155*, 206−222.
[23] J. B. Pedley, University of Sussex, personal communication as cited in reference 13. The error of ±20 $JK^{-1}mol^{-1}$ was assumed in the present paper.
[24] J. Emsley, *The Elements*, 2nd ed. (revised), Clarendon Press, Oxford, **1992**
[25] D. D. Perrin, W. L. F. Armarego, D. R. Perrin, *Purification of Laboratory Chemicals*, 2nd Ed., Pergamon, Oxford, **1980**.
[26] M. L. H. Green, P. J. Knowles, *J. Chem. Soc., Perkin Trans. 1* **1973**, 989−991.
[27] E. Samuel, *Bull. Soc. Chim. Fr.* **1966**, *11*, 3548−3564.
[28] E. Samuel, R. Setton, *C. R. Hebd. Seances Acad. Sci.* **1962**, *254*, 308−309.
[29] H. P. Diogo, *Tese de Doutoramento*, Instituto Superior Técnico, Lisboa, Portugal, **1993**.
[30] L. E. Manzer, *Inorg. Chem.* **1977**, *16*, 525−528.
[31] M. E. Minas da Piedade, *Tese de Doutoramento*, Instituto Superior Técnico, Lisboa, Portugal, **1988**.
[32] R. L. Cooper, M. L. H. Green, *J. Chem. Soc. (A)* **1967**, 1155−1160.

Received May 8, 2000
[I00187]

Further Investigation into the Platinum-Activated Addition of Diphenylsulfimide to Acetonitrile; the X-ray Crystal Structure of $[PPh_4][PtCl_2(Ph_2SNC(Me)NH)]_2Cl$

Paul F. Kelly*[a] and Alexandra M. Z. Slawin[b]

Keywords: Sulfur / Nitrogen / Platinum / Sulfimides / Nitriles

Reaction of Ph_2SNH (**1**) with $[PtCl_2(MeCN)_2]$ (1:1 ratio) in MeCN at 50 °C results in the formation of $[PtCl_2\{Ph_2SNC(Me)NH\}]$ (**3**); without heating $[Pt(Ph_2SNH)\{Ph_2SNC(Me)NH\}Cl]Cl$ (**2**) is the primary product. Attempts to grow X-ray quality crystals of **3** have not succeeded; it does, however, form a crystalline 2:1 adduct with $[PPh_4]Cl$ (**3a**), the structure of which confirms the presence of the bidentate $Ph_2SNC(Me)NH$ ligand hydrogen-bonded to the chloride anion. Reaction of **3** with three equivalents of **1** and two of $Tl[PF_6]$ results in the formation of $[Pt(Ph_2SNH)_2\{Ph_2SNC(Me)NH\}_2][PF_6]_2$ (**4**), the first example of a complex containing the $[Ph_2SNC(Me)N(H)]$ unit acting as a monodentate ligand, bound through the nitrogen atom.

Introduction

As part of our continuing interest in the coordination chemistry of sulfur−nitrogen species[1] we have recently reported on the reactivity of *S*,*S*′-diphenylsulfimide, Ph_2SNH (**1**), towards a number of metal centres, including copper (resulting in *trans*-$[CuCl_2(Ph_2SNH_2)]$ which, uniquely for a neutral Cu^{II} species exhibits square-planar and pseudo-tetrahedral allogons),[2] cobalt,[3] and platinum.[4] During investigations into reactions involving the latter metal we discovered that the reaction of two equivalents of **1** with $PtCl_2(MeCN)_2$ resulted in the formation of $[Pt(Ph_2SNH)\{Ph_2SNC(Me)NH\}Cl]Cl$ (**2**) rather than the expected simple substitution product. In effect one of the incoming sulfimide units had added to a metal-bound acetonitrile − an addition that does not take place in the absence of the metal centre (or indeed in the presence of a metal other than platinum, at least amongst those we have investigated so far). The resulting nitrile/sulfimide ligand binds in a bidentate fashion through a nitrogen and a sulfur atom; indeed, one of the most interesting aspects of this reaction was the fact that **2** constitutes the first example of a sulfimide unit binding to a metal centre through a sulfur atom. Here we present the results of further investigations into this reaction.

Results and Discussion

Upon first isolating **2** from the 2:1 reaction of **1** with $PtCl_2(MeCN)_2$ we made preliminary, tentative assumptions about the reaction mechanism. Given that nucleophilic attack upon coordinated nitriles is well known[5] we anticipated that this would be the first stage, with the resulting *N*-bound monodenate ligand then chelating by removal of the other nitrile (and S−Pt bond formation). Then the second sulfimide would displace a chloride to give the final product. In order to go some way to confirming this suggestion we have now analysed the analogous equimolar reaction, which should, on the basis of the latter mechanism, generate $[PtCl_2\{Ph_2SNC(Me)NH\}]$ (**3**). The latter does indeed form, though not in as straightforward a manner as we had anticipated. Within a short time of complete addition of the reagents a crystalline material starts to form; rather than being **3**, however, IR spectroscopy indicates that this material is in fact **2**. If, however, the crude mixture at this stage is heated to ca. 50 °C for two hours any solids present redissolve and the colour of the solution gradually changes from pale yellow to a bright lemon colour. After precipitation of a small amount of impurity with Et_2O, the main reaction product can be retrieved by evaporation of the solvent and trituration of the oily residue with cold ether. Although, unfortunately, we have yet to grow crystals suitable for single crystal diffraction, the resulting bright yellow material may be formulated as **3** by a combination of IR, NMR, and microanalysis.

Further confirmation of its nature comes when crystallisation is attempted in the presence of $[PPh_4]Cl$. We initially performed this in the hope that the chloride would break the Pt−S bond thus giving a monodentate $[Ph_2SNC(Me)NH]$ ligand. In fact this does not happen (though, as we will see, we can achieve this in other ways); rather, the chloride binds through hydrogen bonds to two units of **3** to give the adduct **3a** (Figure 1).

Within the Pt−S−N−C−N metallacycle of **3a** there appears to be minimal difference in geometry between the two independent units and indeed between them and the previously reported values for **2**. While the planes of the two metallacycles are inclined at an angle of 53° to each other,

[a] Department of Chemistry, Loughborough University, Loughborough, Leicester, LE11 3TU, UK
[b] Department of Chemistry, University of St.Andrews, St. Andrews, Fife, KY16 9ST, UK

 © WILEY-VCH Verlag GmbH, 69451 Weinheim, 2001 1434−1948/01/0101−0263 $ 17.50+.50/0

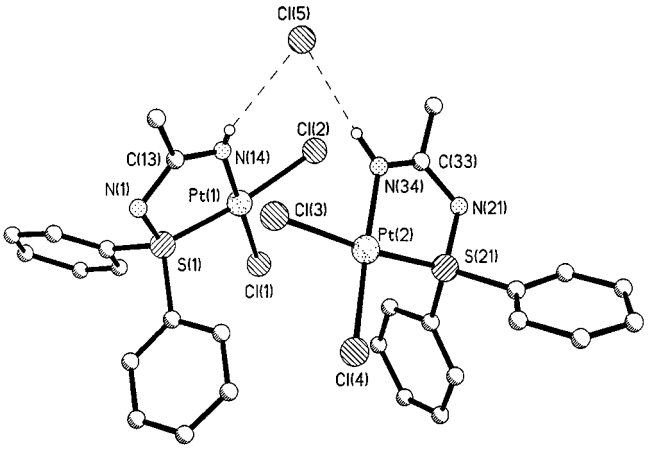

Figure 1. The X-ray crystal structure of **3a** (omitting the $[PPh_4]^+$ cation)

the average H···Cl interaction distance is 2.33 Å, and the average N−H−Cl angle 160°. The resulting structure is interesting for a number of reasons. Firstly it confirms the tendency of the N−H bonds of coordinated sulfimide units to get involved in significant hydrogen bonding interactions. In the case of previously noted examples, the formation of such bonds was undoubtedly aided by the fact that they were part of cation−anion interactions;[3,6] here this is obviously not the case, though the significant interactions are present nonetheless.

In addition, of course, it confirms the basic structure of **3**; further confirmation, and of the original mechanism we put forward, comes when **3** is treated with **1**. Within a few minutes of addition in MeCN crystals of **2** (confirmed by IR) begin to form. We can thus be confident that the kind of mechanism shown in Scheme 1 applies to the system as a whole. As **1** is slowly added to the system during the 1:1 reaction **3** starts to form; once formed it then acts as a competitor to the $PtCl_2(MeCN)_2$. Unreacted **1** can thus either undergo nitrile addition to give more **3** or substitution on the **3** that has been formed in order to give **2**. The latter appears to be preferred, meaning that by the end of addition of **1** the mixture consists of **2** and, presumably, unchanged $PtCl_2(MeCN)_2$. This mixture can, however, be driven through to **3** by heating, suggesting that the unchanged sulfimide ligand in **2** is actually quite labile.

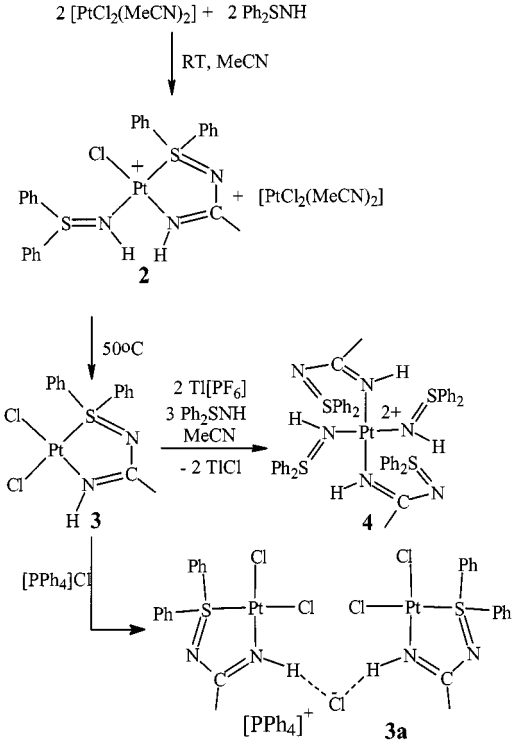

Scheme 1. Summary of the reactions to form **2**, **3**, **3a**, and **4**

An important feature of **3** is its obvious potential as a reagent with which to probe the properties of the bidentate ligand − in particular its lability. A significant result in this area is obtained when **3** (formed in situ) is treated with $Tl[PF_6]$ and three equivalents of **1**. The thallium salt displaces chloride from **3** with, presumably, MeCN taking up the vacant site. This intermediate then reacts with three equivalents of **1** to produce a new species, **4**, which may be isolated in crude form by centrifugation of the mixture (in order to separate the bulk of the finely divided TlCl generated in the reaction) followed by filtration and removal of the solvent. Trituration of the oily product with Et_2O yields an off-white solid from which crystalline material may be grown by slow diffusion of Et_2O into a solution in MeCN.

We can formulate **4** as $[Pt(Ph_2SNH)_2\{Ph_2SNC(Me)NH\}_2][PF_6]_2$ by a combination of microanalysis, IR, NMR. X-ray crystallography also backs this up, though we do not formally present the results here as the structure suffers from poor quality [unit cell: triclinic, space group $P\bar{1}$; a = 10.4943(2), b = 11.0252(3), c = 14.1772(4) Å; α = 107.45(1), β = 100.295(1), γ = 110.441(1)°]. Its does, however, confirm that the Pt centre now exhibits two unchanged sulfimide ligands and two sulfimide/nitrile addition ligands both bound in monodentate fashion as shown in Scheme 1. As for the mechanism of formation of **4**, we can reasonably assume that the initial reaction of $Tl[PF_6]$ with **3** replaces at least one of the halides with MeCN which can then react with **1**, possibly giving $[Pt(Ph_2SNC(Me)NH)_2]$ as an intermediate. Additional molecules of **1** then substitute into this by breaking Pt−S bonds.

In conclusion, the isolation of **3** in good yield will allow us to probe the substitution properties of this new class of chelating ligand. The isolation of **4** is important insofar as it indicates that the new ligands formed in the platinum-assisted sulfimide/nitrile reactions are not constrained to chelation and thus may ultimately prove to be labile. The displacement and isolation of such addition products as free species would provide us with interesting new (and undoubtedly reactive) systems that cannot be generated by direct sulfimide/nitrile reactions. It would also raise the intriguing possibility of adjusting the reaction system to allow the platinum to act catalytically. Work towards this end is currently underway.

Experimental Section

All reactions were carried out under dry nitrogen; MeCN was dried and distilled from calcium hydride, diethyl ether from sodium. −

IR spectra were run with a Perkin−Elmer PE2000 spectrometer; NMR with a Bruker AC250 spectrometer; microanalysis was performed by Loughborough's Departmental service. − Ph_2SNH (**1**) was prepared by our previously reported variation upon the literature route.[6]

3: A solution of $[PtCl_2(MeCN)_2]$ (61 mg, 0.18 mmol) in MeCN (10 mL) was treated with a solution of **1** (36 mg, 0.18 mmol) in the same solvent (10 mL) added over a period of 1 min, with stirring. The resulting mixture was then heated to 50 °C and stirred at this temperature for 2 h during which time the solution colour changed from pale yellow to a bright lemon. At this point the volume of the solvent was reduced to ca. 5 mL in vacuo and Et_2O (50 mL) added with stirring. This resulted in the formation of a small amount of a flocculant white precipitate which was filtered off and the solution reduced to dryness in vacuo then triturated with Et_2O to give a bright yellow product. Yield 60 mg, 67%. − IR (key bands, i.e. non-phenyl): $\tilde{\nu}$ = 3296 cm^{-1} (ms, νN−H), 1529 (s, νC−N), 808 (m, νN−S), 356 (mw, νPt−Cl), 331 (m, νPt−Cl). − ^1H NMR ($CDCl_3$): δ = 8.13 (m, 4 H, phenyl), 7.65 (m, 6 H, phenyl), 2.43 (s, 3 H, CH_3). − $C_{14}H_{14}Cl_2N_2PtS$ (508.3): calcd. C 33.1, H 2.8, N 5.5; found C 32.9, H 2.8, N 5.7. − Crystallisation by slow diffusion of Et_2O into a CH_2Cl_2 solution to which $[PPh_4]Cl$ had been added resulted in well-formed yellow crystals of the adduct $[PPh_4][PtCl_2(Ph_2SNC(Me)NH)]_2Cl$ (**3a**).

4: A crude solution of **3** in MeCN was generated as above from $[PtCl_2(MeCN)_2]$ (43 mg, 0.12 mmol) and **1** (25 mg, 0.12 mmol) (with heating for2 h followed by cooling to room temperature) and treated with $Tl[PF_6]$ (86 mg, 0.25 mmol). This resulted in the immediate production of a finely divided white solid within a pale brown/red solution; the mixture thus formed was stirred for 1 min then solid **1** (73 mg, 0.36 mmol) added. After stirring for 1 h at 60 °C, the mixture was cooled to room temperature and stirred overnight. At this stage it was centrifuged to separate out the bulk of the very finely divided solid present and then filtered through Celite, the solvent volume reduced to a few mL and Et_2O (50 mL) added with stirring. The resulting brown/orange oil was triturated with Et_2O to give the crude product as an off-white solid. Yield 116 mg. Microanalysis reveals this material to be contaminated with variable amounts of a CHN-free impurity, presumably TlCl, which proves surprisingly difficult to remove; the IR spectrum is, however, identical to that of pure crystalline material generated by slow diffusion of Et_2O into an MeCN solution. Yield of the crystalline material is typically half that of the crude material; however, we believe that the bulk of this shortfall reflects decomposition in solution over the time taken for crystallisation (the solution darkens appreciably over a period of days, even in an inert atmosphere) rather than there being a high impurity level in the crude material. − IR (key bands, i.e. non-phenyl): 3366 cm^{-1} (ms), 3320 (m) (both ν N−H), 1542 (s,ν C−N), 918 (m, ν N−S), 842 (vs, br., ν P−F). − ^1H NMR (CD_3CN): δ = 7.74 (m, 2 H, phenyl), 7.62 (m, 4 H, phenyl), 7.36 (m, 14 H, phenyl), 2.41 (s, 3 H, CH_3). − $C_{52}H_{50}F_{12}N_6P_2PtS_4$ (1372.3): C 45.5, H 3.7, N 6.1; found C 45.3, H 3.9, N 6.2.

Crystal Data for 3a: $C_{52}H_{48}Cl_5N_4PPt_2S_2$, M = 1391; triclinic, space group $P\bar{1}$; a = 11.96(1), b = 22.83(1), c = 10.703(6) Å, α = 92.00(5), β = 111.51(6) γ = 77.48(6)°; V = 2651(3) $Å^3$, Z = 2, calculated density: 1.743 gcm^{-3}. Yellow prism, dimensions 0.3 × 0.1 × 0.08 mm, μ (Mo-K_α) = 56.50 cm^{-1}, λ = 0.71069 Å, F(000) = 1352. − Data were collected (using a Rigaku AFC7S diffractometer with graphite-monochromated Mo-K_α radiation) by the ω-2θ scan technique to a maximum 2θ value of 50.0°. Of 9820 measured reflections 9333 were unique. An empirical absorption correction was applied resulting in transmission factors ranging from 0.66 to 1.00. − Structure analysis and refinement: The structure was solved by direct methods and refined by full-matrix least squares against F. Non-hydrogen atoms were refined anisotropically; hydrogen atoms were included but not refined. Refinement against F led to R = 0.042 [$R = \Sigma(|F_o| - |F_c|)/\Sigma|F_o|$], Rw = 0.045. The maximum/minimum residual electron densities in the final ΔF map were 1.33 and −1.96 $e^-/Å^3$; calculations were performed using the teXsan crystallographic software package of Molecular Structure Corporation.[7] Crystallographic data (excluding structure factors) for the structure reported in this paper have been deposited with the Cambridge Crystallographic Data Centre as supplementary publication no. CCDC-143676. Copies of the data can be obtained free of charge on application to CCDC, 12 Union Road, Cambridge CB2 1EZ, UK [Fax: (internat.) + 44-1223/336-033; E-mail: deposit@ccdc.cam.ac.uk].

Acknowledgments

The authors acknowledge Johnson Matthey for loans of precious metals.

[1] P. F. Kelly, A. M. Z. Slawin, A. Soriano-Rama, *J. Chem. Soc., Dalton Trans.* **1996**, 53−59 and references therein.
[2] P. F. Kelly, A. M. Z. Slawin, K. W. Waring, *J. Chem. Soc., Dalton Trans.* **1997**, 2853−2854.
[3] P. F. Kelly, A. M. Z. Slawin, K. W. Waring, *Inorg. Chem. Commun.* **1998**, *1*, 249−250
[4] P. F. Kelly, A. M. Z. Slawin, *Chem. Commun.* **1999**, 1081−1082.
[5] R. A. Michelin, M. Mozzon, R. Bertani, *Coord. Chem. Rev.* **1996**, *147*, 299−338.
[6] P. F. Kelly, S.-M. Man, A. M. Z. Slawin, K. W. Waring, *Polyhedron* **1999**, *18*, 3173−3179.
[7] *teXsan: Crystal Structure Analysis Package*, Molecular Structure Corporation, Texas, USA, **1985**, **1992**.

Received May 15, 2000
[I00194]

New Alkyl−Cobalt(III) Complexes with Tridentate Amino−Oxime Ligands: Synthesis, Structure, and Reactivity

Renata Dreos,[a] Alessandro Felluga,[a] Giorgio Nardin,[a] Lucio Randaccio,*[a] Patrizia Siega,[a] and Giovanni Tauzher*[a]

Keywords: Cobalt / Tridentate ligands / Alkylations / Vitamins / N ligands

The oxidative addition of alkyl halides to the Co^{I} species generated by the reduction of $[Co^{III}(LNHpy)(HLNHpy)](ClO_4)_2$ (**1**), where HLNHpy is the tridentate 2-(2-pyridylethyl)amino-3-butanone oxime ligand and LNHpy is its conjugate base, led to the formation of a new class of organocobalt complexes of general formula $[RCo^{III}(LNHpy)(HLNHpy)](ClO_4)$ [R = Me (**2a**), Et (**2b**), CH_2CF_3 (**2c**), *n*Bu (**2d**), and CH_2Cl (**2e**)]. All the complexes were characterised by ^1H and ^{13}C NMR spectroscopy. The X-ray structures of **2a**, **2b** and **2c** provide evidence for a pseudo-octahedral configuration, where HLNHpy and LNHpy act as bi- and tridentate ligands, respectively. The axial geometry in **2a** is closer to that found in methylcobalamin than that reported for other models, suggesting steric and electronic *cis* influences of the equatorial ligands close to those of the corrin nucleus. The solution properties and the reactivity show strong analogies with those of the previously known Vitamin B_{12} models.

Introduction

Previous studies on classical models for coenzyme B_{12}, such as alkylcobaloximes $LCo(DH)_2R$ (Scheme 1a, DH = monoanion of dimethylglyoxime, R = alkyl, L = neutral Lewis base), have been aimed at elucidating the factors that affect the properties of the Co−C bond. Experimental evidence shows that steric and electronic factors are both important in this context.[1] The recent structural results on B_{12} enzymes have shown that in some of the enzyme-bound B_{12} coenzymes, the benzimidazole residue is replaced in the coordination to Co by the imidazole moiety of a histidine of the protein chain.[2] This finding has renewed interest in the nature of the Co−L bond in simple models.[3,4,5] The early hypothesis[1] that the Co−L distance is influenced by the orientation of the planar L ligand, measured by the torsional angle φ around that bond, has been confirmed.[6−8] In orientation A (Scheme 2), when φ is close to 0, the Co−L distance is found to be shorter by about 0.03 Å than in orientation B (Scheme 2), corresponding to φ close to 90°. Typically, orientation A is found in cobaloximes, whereas orientation B is found in iminocobaloxime analogues (Scheme 1b). However, in the lariat-type complexes[8] (Scheme 1c), derived from iminocobaloximes, the values of φ and of the Co−py distance are similar to those in the cobaloxime analogues. In fact, in the lariat-type complexes, although derived from iminocobaloximes, orientation A is imposed by the conformational rigidity of the pentadentate ligand.

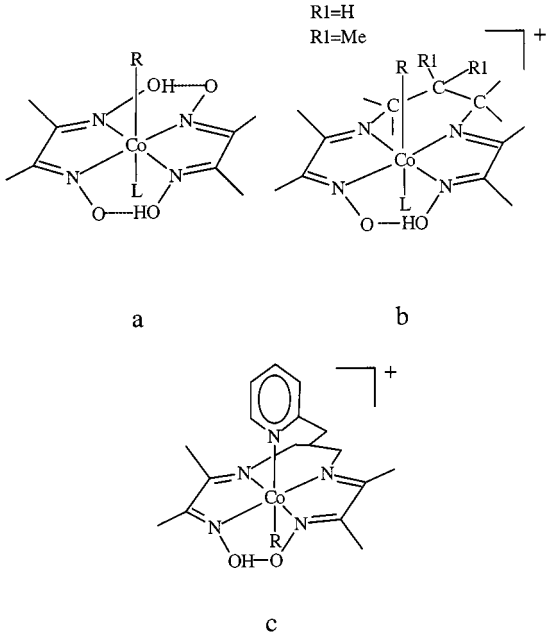

Scheme 1

Less definitive indications about the influence of the L orientation on the Co−C bond in the ground state has been found so far. In fact, structural (Co−R distance) and spectroscopic (ν_{Co-Me}) evidences have suggested that orientation B may correspond to a weaker Co−C bond than in orientation A.[7] On the other hand, FT-Raman studies did not detect any change in the Co−C force constants even in base-on and base-off cobalamins.[9] Furthermore, recent studies[10] on the interaction of adenosylcobinamides with hindered bases, (1,2-Me_2Im, 2-Mepy and 2,6-Me_2py) have provided evidence for a dominant effect of the axial base on the transition state of the Co−C bond-cleavage process.

[a] Dipartimento di Scienze Chimiche, Università degli Studi di Trieste
Via L. Giorgieri 2, 34127 Trieste, Italy
Fax: (internat.) + 39-040/676-3903
E-mail: randaccio@univ.trieste.it

 © WILEY-VCH Verlag GmbH, 69451 Weinheim, 2001 1434−1948/01/0101−0267 $ 17.50+.50/0

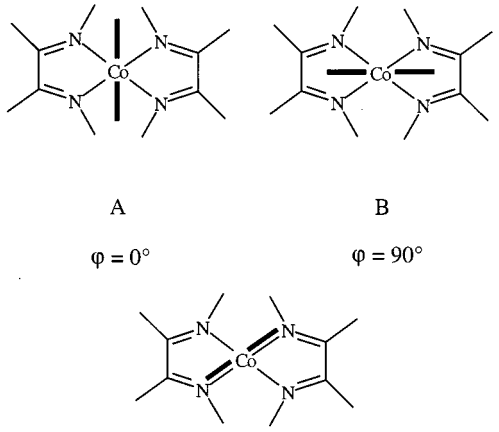

Scheme 2

In order to obtain further insight into the above points, we have synthesised a new class of organocobalt derivatives $[RCo(LNHpy)(HLNHpy)]ClO_4$, (**2**) (HLNHpy = 2-(2-pyridylethyl)amino-3-butanone oxime) derived from $[Co(LNHpy)(HLNHpy)](ClO_4)_2$ (**1**),[11] (Scheme 3). The geometry of **2** is reminiscent of the lariat-type complexes,[8] which combine the corrin-like features of the iminocobaloximes with an appended axial base. However, they differ from the latter by having a more crowded equatorial moiety, owing to the side substituents at the amino C−N fragments. Therefore, complexes **2** could potentially mimic the interactions between axial and equatorial moieties in cobalamins better than previous models.

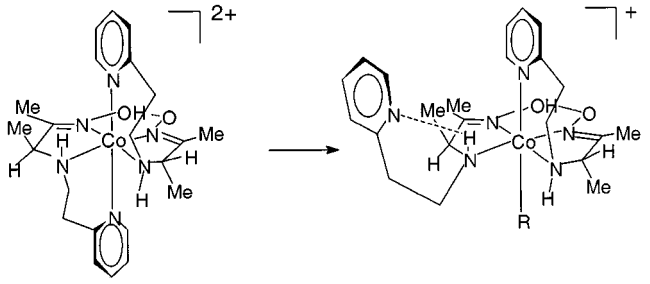

1 **2**

Scheme 3

The synthesis and NMR characterisation of a series of complexes of type **2** [R= Me (**2a**), Et (**2b**), CH_2CF_3 (**2c**), *n*Bu (**2d**), CH_2Cl (**2e**)], the crystal structure of **2a**, **2b**, **2c** as well as the reactivity of the Me derivative are reported and their ability to model the B_{12} system is discussed.

Results

Synthesis

The organometallic complexes of type **2** were obtained according to Equation (1).

$$[Co^{III}(LNHpy)(HLNHpy)]^{2+} \xrightarrow{NaBH_4, PdCl_2} [Co^{I}(LNHpy)(HLNHpy)]$$
$$[Co^{I}(LNHpy)(HLNHpy)] \xrightarrow{RX} [R\text{-}Co^{III}(LNHpy)(HLNHpy)]^{+} + X^{-} \quad (1)$$

The process involves the oxidative addition of the appropriate alkyl halide to the nucleophilic Co^I species, which may be generated in situ by the reduction of **1** with $NaBH_4$/$PdCl_2$. Similar synthetic routes have been extensively exploited to obtain cobalt complexes containing highly unsaturated equatorial ligands. Generally, the Co^I species are obtained from Co^{III} by the use of $NaBH_4$.[12] We observed[11] that although the reduction of **1** with $NaBH_4$ does not proceed beyond the formation of a Co^{II} species, the complete reduction to Co^I could be achieved by the addition of a catalytic amount of $PdCl_2$ to the reaction mixture. The formation of Co^I is recognisable by its nucleophilic reactivity toward alkyl halides, but the dark brown solutions are extremely sensitive to oxygen and this prevented further characterisation. It is noteworthy that the Co^{II} complex obtained by reduction with $NaBH_4$ is unreactive toward alkyl iodides (see Discussion). Several attempts to synthesise organometallic derivatives with bulky alkyl groups such as iC_3F_7, iC_3H_7, and adamantyl were carried out, but the Co^I species failed to react with the corresponding alkyl halide. Even after several hours, Co^I was unchanged and its presence could be verified by the addition of CH_3I to the reaction mixture, which rapidly led to the formation of the methyl derivative.

Reactivity of the Methyl Derivative 2a

Like alkylcobalamins[13] and synthetic alkylcobalt(III) chelates,[14] complex **2a** is light-sensitive. The photolysis of an aqueous solution of the complex in the presence of oxygen produced formaldehyde and complex **1**. This result may be rationalised by the assumption that the initial step is the homolysis of the Co−C bond, which produces a Co^{II} species and methyl radicals. In the presence of oxygen they are oxidised, giving **1** and formaldehyde, which are the expected products of aerobic photolysis.[13]

The methyl-transfer reaction occurs from complex **2a** to $Co^{II}(DH)_2(H_2O)_2$. The reaction was carried out in the dark under nitrogen. After exposure to air, complex **1** and $CH_3Co^{III}(DH)_2H_2O$ were isolated and identified [Equation (2)].

$$[CH_3Co^{III}(LNHpy)(HLNHpy)]^{+} + [Co^{II}(DH)_2] \longrightarrow$$
$$[Co^{II}(LNHpy)(HLNHpy)]^{+} + [CH_3Co^{III}(DH)_2H_2O] \quad (2)$$
$$[Co^{II}(LNHpy)(HLNHpy)]^{+} \xrightarrow{O_2} [Co^{III}(LNHpy)(HLNHpy)]^{2+}$$

Since the process occurs in the absence of light, it can be formulated as a direct transfer of the methyl radical to the acceptor. The Co^{II} species arising from the dealkylation gives **1** after oxidation in the air. The complex **2a** also

methylates Vitamin B_{12r} under the experimental conditions described above [Equation (3)].

$$[CH_3Co^{III}(LNHpy)(HLNHpy)]^+ + \text{Vit. } B_{12r} \longrightarrow CH_3B_{12} + [Co^{II}(LNHpy)(HLNHpy)]^+ \quad (3)$$

The exchange reaction of the chelate moiety of **2a** has been successfully carried out in one case: A methanolic solution of **2a**, dimethylglyoxime, and pyridine (allowed to stand overnight) produced $CH_3Co^{III}(DH)_2py$ as a product. It seems likely that the reaction proceeds by the stepwise replacement of the two amino oxime ligands by dimethylglyoxime.

X-ray Structures

The ORTEP[15] drawings of **2a**−**2c** are given in Figure 1, crystal data in Table 1. For **2a**, only the ORTEP drawing of one of the two crystallographically nonequivalent molecules (A) is shown. Complexes **2** can formally be described as being derived from parent compound **1**, by substitution of one axial pyridyl moiety with the R group. Complex **1** can

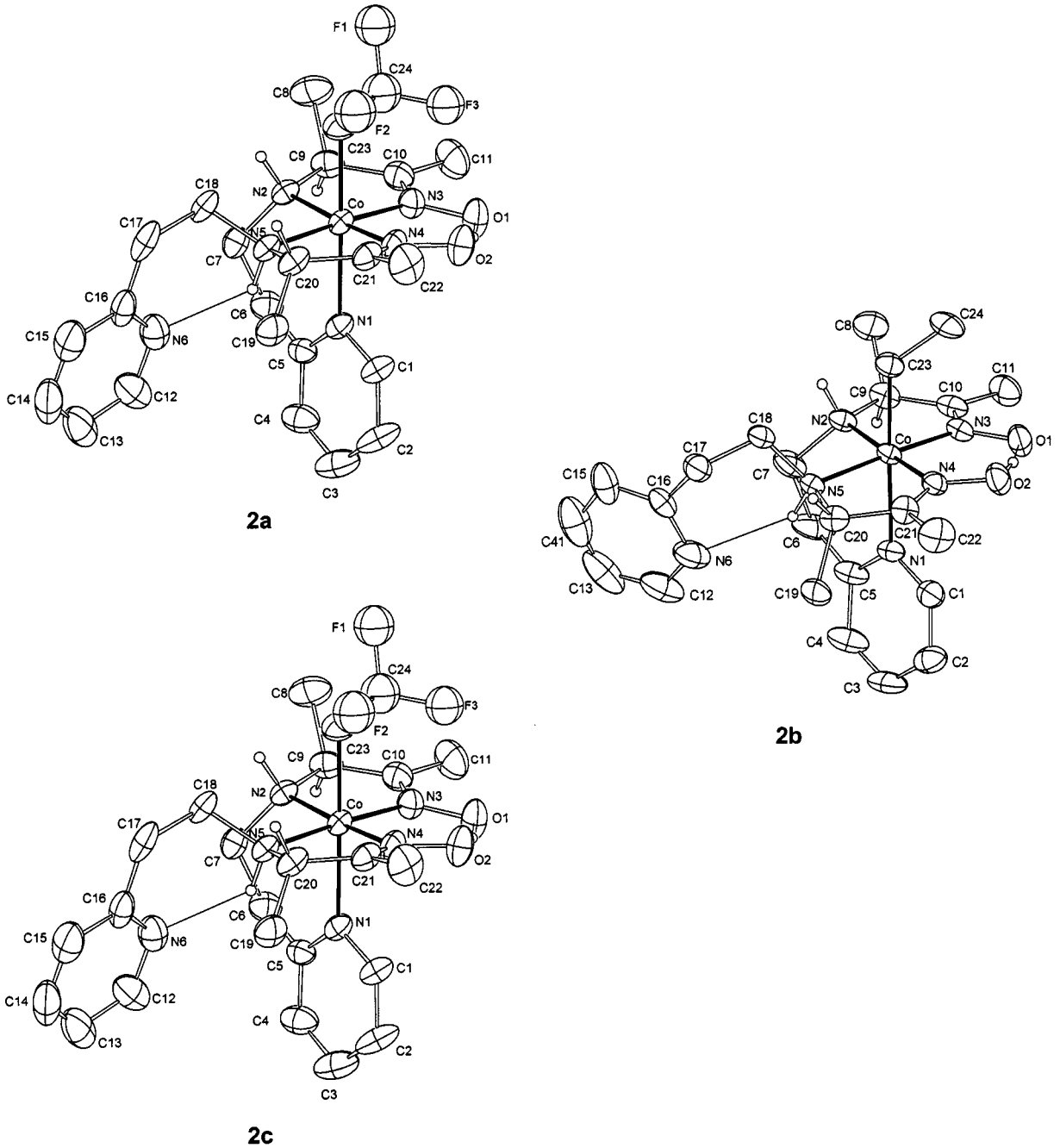

Figure 1. ORTEP diagram with the numbering scheme for the non-hydrogen atoms of one of the two crystallographic independent molecules of **2a**, **2b**, and **2c**

therefore, to a good approximation, be considered as a structural reference for complexes **2** (Scheme 3). The pendant pyridyl group in complexes **2** is anchored through N6 to the N5 amino atom by a short intramolecular hydrogen bond in the range of 2.861(8)−3.020(8) Å (Table 2). The two oximic O atoms of LNHpy and HLNHpy are hydrogen-bonded, with O···O distances ranging from 2.401(7) to 2.432(7) Å (Table 2). The average of the values is shorter by about 0.07 Å than that of 2.487(2) Å, obtained by averaging 140 values found in cobaloximes.[1b] Analysis of the N−O bonds in the three complexes and of the Fourier difference maps did not allow for location of the H oxime bridge, which was assumed to be bonded to O2 (see below), so that LNHpy acts as a tridentate and HLNHpy as a bidentate ligand.

The coordination around N1 is such that the two Co−N1−C angles differ by up to about 10°, the largest value being on the side of the 2-ethylene chain (Table 2). Such an asymmetric coordination of the axial N donor is typical of lopsided ligands, such as Me_3Bzm,[1] and of lariat-type complexes of Scheme 1c.[8]

The axial distances, together with the torsion angle around the Co−N1 bond, φ, are given in Table 3. The Co−N1 distances reflect the notable *trans* influence of the alkyl group in complexes **2**, relative to that of the pyridyl group in **1**. The Co−C bond length in complexes **2** appears to increase with the bulk and to decrease with the electron-withdrawing ability of R, in agreement with previous findings in cobaloximes.[19]

Table 1. Crystal data and structure refinement for complexes **2a**, **2b** and **2c**

Compound	**2a**	**2b**	**2c**
Empirical formula	$C_{24.50}H_{39}ClCoN_6O_{6.50}$	$C_{24}H_{38.50}ClCoN_6O_{6.25}$	$C_{24.50}H_{36}Cl_2CoF_3N_6O_6$
Formula weight	616.00	605.49	697.42
Temperature [K]	293(2)	293(2)	293(2)
Wavelength [Å]	0.71073	0.71073	0.71073
Crystal system, space group	monoclinic, $P2_1/n$	monoclinic, $P2_1/n$	monoclinic, $C2/c$
a [Å]	22.581(2)	16.868(4)	16.090(2)
b [Å]	11.907(2)	9.6950(10)	15.165(3)
c [Å]	22.788(3)	17.218(4)	25.837(4)
β [°]	106.370(8)	91.38(2)	105.220(10)
V [Å^3]	5878.7(14)	2814.9(10)	6083(2)
Z, calcd. density [Mg/m^3]	8, 1.392	4, 1.429	8, 1.523
Absorption coefficient [mm^{-1}]	0.724	0.754	0.807
F(000)	2592	1274	2888
Crystal size [mm]	0.3 × 0.6 × 0.9	0.2 × 0.3 × 0.7	0.2 × 0.3 × 0.6
Range for data collect. [°]	2.05 to 27.97	5.01 to 26.02	5.02 to 26.02
Reflections collected/unique	7955/7554 [R(int) = 0.0232]	5675/5494 [R(int) = 0.0287]	6238/5951 [R(int) = 0.0402]
Data/restraints/parameters	7554/0/675	5494/0/347	5951/9/354
Goodness-of-fit on F^2	1.037	0.984	1.037
Final R indices [$I > 2\sigma(I)$]	$R1$ = 0.0724, $wR2$ = 0.2483	$R1$ = 0.0747, $wR2$ = 0.2044	$R1$ = 0.0877, $wR2$ = 0.2315
R indices (all data)	$R1$ = 0.0724, $wR2$ = 0.2483	$R1$ = 0.1413, $wR2$ = 0.2712	$R1$ = 0.1681, $wR2$ = 0.2760
Largest diff. peak and hole [e.Å^{-3}]	0.903 and −0.930	0.721 and −0.804	0.934 and −0.826

The bending angle, α, between the two equatorial five-membered rings and the displacement, d, of Co out of the four N equatorial donor plane are given in Table 3. The displacement occurs towards the axial pyridyl group in A and B molecules of **2a** and towards R in **2b** and **2c**, and reflects the difference in bulk between R and the *trans*-pyridyl group.[16] In all the complexes, the pyridyl ligand is tilted out of the axial direction and the tilt can be measured by the dihedral angle, γ, between the mean planes of the pyridyl ligand and of the four equatorial N donors. The values of γ in **1** and **2**, (Table 3), are close to those observed in py (82.3°) and 1,5,6-trimethylbenzimidazole (Me_3Bzm) (81.0°) iminocobaloximes with methyl substituents on the propylene bridge (Scheme 1b, R1 = Me).[17]

Equatorial coordination distances and angles in complexes **2** are given in Table 2 together with those of **1**. In complexes **2**, the Co−N4 distances are slightly shorter than those of Co−N3. This supports the previous assignment of the oxime bridge H atom.[18]

NMR Characterisation

The characterisation in solution was performed by ^{1}H and ^{13}C NMR spectroscopy in [D_6]DMSO. The (LNHpy)(HLNHpy) moiety gives rise to strikingly similar ^{1}H NMR spectra for all five complexes. The spectrum of **2c** is described as an example. The CH_3 protons give rise to two doublets at δ_H = 0.66 and 1.32 (CH_3CH) and two singlets at δ_H = 1.78 and 2.05 ($CH_3C{=}N$), each signal integrating for three protons. Ethylenic CH_2 protons generate four partially overlapped multiplets in the range δ_H = 2.88−3.44, the total integration corresponding to eight protons. The signals for the CH protons at δ_H = 3.75 and 3.82 appear as broad multiplets, and those for the NH protons at δ_H = 4.75 and 5.47 as a broad doublet and a broad singlet, respectively; each of these signals integrates for one proton. On addition of D_2O to the DMSO solution, the NH signals did not disappear, indicating a slow exchange on the NMR time scale. In $CDCl_3$ solution, the NH doub-

Table 2. Selected bond lengths [Å] and angles [°] for **1** and **2**

	2a(A)	**2a**(B)	**2b**	**2c**	**1**(A)	**1**(B)
Co−N1	2.134(5)	2.185(5)	2.168(5)	2.160(6)	2.033(4)	2.045(5)
Co−N2	1.996(5)	1.983(5)	1.964(5)	1.991(5)	1.991(5)	1.988(5)
Co−N3	1.888(6)	1.900(6)	1.893(5)	1.903(6)	1.912(5)	1.914(5)
Co−N4	1.888(5)	1.893(5)	1.879(5)	1.887(6)	1.911(5)	1.902(4)
Co−N5	2.018(5)	2.005(5)	2.035(5)	2.021(6)	1.980(5)	1.961(5)
Co−N6	−	−	−	−	2.017(5)	1.983(5)
Co−C23	1.960(7)	1.983(7)	2.015(6)	1.998(8)	−	−
N1−Co−N2	92.2(2)	93.2(2)	90.3(2)	91.8(2)	94.0(2)	94.4(2)
N1−Co−N3	89.2(2)	88.0(2)	89.1(2)	89.2(2)	85.5(2)	83.2(2)
N1−Co−N4	92.1(2)	90.3(2)	91.1(2)	91.6(2)	92.7(2)	91.2(2)
N1−Co−N5	88.7(2)	90.2(2)	87.7(2)	87.6(2)	90.3(2)	90.6(2)
N1−Co−C23	177.3(3)	175.3(3)	177.9(2)	178.7(3)	−	−
N1−Co−N6	−	−	−	−	176.4(2)	174.2(2)
N2−Co−N3	81.9(2)	82.3(2)	81.6(2)	82.2(3)	82.0(2)	81.2(2)
N2−Co−N4	175.6(2)	176.5(2)	178.2(2)	176.6(3)	173.1(2)	174.3(2)
N2−Co−N5	98.4(2)	97.8(2)	98.5(2)	98.7(2)	99.1(2)	97.7(2)
N2−Co−C23	90.4(3)	90.6(3)	91.8(2)	86.9(3)	−	−
N2−Co−N6	−	−	−	−	89.1(2)	89.9(2)
N3−Co−N4	97.5(3)	97.7(2)	97.4(2)	97.7(3)	96.9(2)	97.7(2)
N3−Co−N5	177.9(3)	178.3(2)	176.8(2)	176.7(2)	175.7(2)	173.8(2)
N3−Co−C23	90.5(3)	89.8(3)	90.9(2)	90.7(4)	−	−
N3−Co−N6	−	−	−	−	93.2(2)	93.6(2)
N4−Co−N5	82.4(2)	82.3(2)	82.6(2)	82.0(3)	82.6(2)	83.1(2)
N4−Co−C23	85.3(3)	85.9(3)	86.8(2)	89.7(3)	−	−
N4−Co−N6	−	−	−	−	84.2(2)	84.4(2)
N5−Co−C23	91.6(3)	91.9(3)	92.4(2)	92.6(3)	−	−
N5−Co−N6	−	−	−	−	91.0(2)	92.6(2)
Co−N1−C1	116.9(4)	118.6(4)	117.0(4)	116.6(5)	117.2(3)	116.7(3)
Co−N1−C5	126.4(5)	125.0(4)	125.6(5)	126.1(5)	126.0(4)	124.8(3)
Co−N6−C12	−	−	−	−	116.3(3)	116.2(4)
Co−N6−C16	−	−	−	−	126.9(3)	126.1(3)
O1·····O2	2.402(7)	2.401(7)	2.432(7)	2.408(8)	2.388(7)	2.421(6)
N5·····N6	2.861(8)	2.968(8)	3.020(8)	2.894(8)	−	−

let (belonging to the bidentate ligand) shifts downfield to δ_H = 5.74, whereas the NH singlet shifts upfield to δ_H = 4.60; the different behaviour could be due to the formation of an intramolecular hydrogen bond between the proton of the NH doublet and the nitrogen atom of the noncoordinated pyridine, as found in the solid state. Aromatic protons generate two series of partially overlapped signals, of correct multiplicity and intensity, in the δ_H range 8.41−7.30. The oxime proton resonates at δ_H = 19.6. This value, very close to that found in the lariat-type complexes[8] and shifted remarkably downfield with respect to that of cobaloximes[20] and imino cobaloximes,[21] suggests a strong hydrogen bond.

The main difficulty in the assignment of ^{1}H and ^{13}C NMR spectra of the (LNHpy)(HLNHpy) moiety lied in distinguishing between the resonances of the tridentate and of the bidentate ligands. An almost complete assignment of ^{1}H and ^{13} C signals was performed for **2c** using homonuclear and heteronuclear shift correlation 2D NMR (H,H- and H,C-COSY), HMBC and DIFNOE spectroscopy. Shift assignments for the other alkyl complexes were made according to those of **2c** (Table 4 and 5).

The protons bonded to the α-carbon atom of the axial alkyl groups show a remarkable downfield shift with respect to those of the corresponding cobaloximes (+1.07 ppm for Me, +1.25 ppm for Et, and +1.14 ppm for CH_2CF_3)[20] although a direct comparison is not thoroughly meaningful, because the spectra of the latter were recorded in $CDCl_3$ and the solvent significantly influences the chemical shift of the Cα protons in complexes **2**. The effect is much weaker for protons that are more distant from the metal centre. For R = Et and *n*Bu, the CH_2 resonances in the ^{1}H NMR spectrum are partially buried; for R = CH_2CF_3, the CH_2 protons give rise to a quadruplet owing to coupling with fluorine ($^3J_{HF}$ = 15 Hz). It is noteworthy that in the CH_2Cl derivative, these protons generate an AB spectrum ($^2J_{HH}$ = 5 Hz) owing to the coupling between diastereotopic geminal protons.

Discussion

Complexes **2** are structurally similar to lariat-type complexes, but with some additional features. In fact, the equatorial moiety is more crowded with respect to the latter model, because of the side substituents on the amino C−N, pointing above and below the equatorial plane. Furthermore, the values of φ, found in complexes **1** and **2**, make them "representatives" of the orientation C of Scheme 2, as compared with cobaloximes and lariat complexes, which exhibit orientation A, and iminocobaloximes, which exhibit orientation B. However, the relative flexibility of the ethylene chain bearing the coordinated pyridyl group allows for a rotation, even if limited, of the axial py residue around the Co−N1 bond. This rotation is somewhat less restricted than in lariat-type complexes.[8] In fact, there is clear evid-

Table 3. Axial distance (Å) in some B_{12} models, as well as φ (°), γ (°), and α (°) values; data are from ref.[1], unless otherwise stated

(LNHpy)(HLNHpy)[a] Compound	**1**	**1**	**2c**	**2a**	**2a**	**2b**
R	Py(A)[a]	py(B)[a]	CH_2CF_3[b]	Me(A)[b]	Me(B)[b]	Et[b]
Co−N1/Å	2.033(4)	2.045(5)	2.160(6)	2.134(5)	2.185(5)	2.168(5)
Co−N6/Å	2.017(5)	1.983(5)	−	−	−	−
φ/°	48	44	44	38	48	36
φ′/°	30	28	−	−	−	−
Co−C/Å	−	−	1.998(8)	1.960(7)	1.983(7)	2.015(6)
d/Å	0.022	−0.004	0.002	0.018	0.015	−0.016
α/°	17	13	16	9	14	8
γ/°	81	75	84	82	82	80
γ′/°	86	89	−	−	−	−
$pyCo(DH)_2R$						
R	Cl[b]	CH_2CF_3[c]	Me[c]	Et[c]		
Co−Nax/Å	1.956	2.041(4)	2.068(3)	2.081(3)		
φ/°	6	0	1	0		
Co−R/Å	−	2.010(3)	1.998(5)	2.035(5)		
d/Å	0	0.01	0.05	0.05		
α/°	2	1	3	9.1		
γ/°	89	90	89	90		
$Me_3Bzm[(DO)(DOH)pn]R$[d]						
R	Cl[c]	CH_2CF_3	Me	Et		
Co−N_{ax}/Å	1.993(6)	2.060(3)	2.100(3)	2.105(3)		
φ/°	86	80	115	119		
Co−R/Å	−	2.026(4)	2.011(3)	2.041(4)		
d/Å	0.06	0.06	0.09	0.10		
α/°	13	16.6	13.8	16.7		
γ/°	89	84	88	89		
(C1py)h[e]						
R	Cl	Me(A)	Me(B)			
Co−N_{ax}/Å	1.959(4)	2.06(1)	2.07(1)			
φ/°	0	0	0			
Co−R/Å	2.237(2)	2.05(2)	1.99(2)			
d/Å	0.02	0.02	0.04			
α/°	1.6	−1.8	−4.4			
γ/°	90	90	90			

[a] This work, excluding **1** from ref.[11] − [b] S. Geremia, R. Dreos, L. Randaccio, G. Tauzher, L. Antolini, *Inorg. Chim. Acta* **1994**, *216*, 125. − [c] L = py. − [d] ref.[4] − [e] ref.[8]

Table 4. ^1H NMR chemical shifts of $[RCo(LNHpy)(HLNHpy)]ClO_4$ complexes in $[D_6]DMSO$

R	*ortho*	*meta*[a]		*para*	NH	CH	CH_2-CH_2	CH_3 [b]		O··H··O	axial R
nC_4H_9[c]	8.41 (d)	7.69 (d)	7.54 (t)	8.03 (t)	4.74(bs)	3.60 (bm)	3.32−2.76	1.73 (s)	1.34 (d)	19.40 (s)	CH_3 0.94 (t)
	8.18 (d)	7.31 (d)	7.25 (t)	7.76 (t)	4.50 (bd)	3.73 (bm)	(bm, 8 H)	2.00 (s)	0.84 (d)		CH_2 1.09 (m), 1.44(m), 2.77(m)
C_2H_5 [c]	8.41 (d)	7.69 (d)	7.54 (t)	8.03 (t)	4.70 (bs)	3.58 (bm)	3.31−2.74	1.73 (s)	1.35 (d)	19.41 (s)	CH_3 0.46 (t)
	8.19 (d)	7.31 (d)	7.25 (t)	7.75 (t)	4.44 (bd)	3.72 (bm)	(bm, 8 H)	2.00 (s)	0.84 (d)		CH_2 2.99(q)
CH_3 [c]	8.42 (d)	7.72 (d)	7.55 (t)	8.04 (t)	4.87 (bs)	3.57 (bm)	3.32−2.73	1.72 (s)	1.33 (d)	19.41 (s)	1.89 (s)
	8.29 (d)	7.33 (d)	7.27 (t)	7.77 (t)	4.44 (bd)	3.67 (bm)	(bm, 8 H)	1.99 (s)	0.77 (d)		
CH_2Cl[c]	8.45 (d)	7.75 (d)	7.55 (t)	8.05 (t)	5.08(bs)	3.71 (bm)	3.40−2.84	1.77 (s)	1.39 (d)	19.36 (s)	5.02
	8.34 (d)	7.34 (d)	7.28 (t)	7.78 (t)	4.65 (bd)	3.78 (bm)	(bm, 8 H)	2.04 (s)	0.72 (d)		4.98 ($^2J_{H-H}$ = 5 Hz)
CH_2CF_3 [c]	8.41 (d)	7.76 (d)	7.55 (t)	8.05 (t)	5.47 (bs)	3.75 (bm)	3.44−2.88	1.78 (s)	1.32 (d)	19.60 (s)	2.55 (q)
	8.36 (d)	7.35 (d)	7.30 (t)	7.80 (t)	4.75 (bd)	3.82 (bm)	(bm, 8 H)	2.05 (s)	0.66 (d)		

[a] The first column is for *meta* protons bonded to C4 and C15, the second column for protons bonded to C2 and C13. − [b] The first column is for methyl groups adjacent to C=N, the second column for methyl groups adjacent to CH. − [c] Data in the upper line refer to the tridentate ligand, data in the lower line refer to the bidentate ligand.

ence that the orientation of the py moiety also appreciably influences the length of the Co−N1 bond, so that the expected trend in the *trans* influence with R is modified (see below). Thus, for the same ligand *trans* to N1 (and N6 in **1**) larger φ values correspond to longer Co−N1 distances. In fact, the values of φ and of the Co−N1 distance in mole-

Table 5. ^{13}C NMR chemical shifts of [RCo(LNHpy)(HLNHpy]ClO_4 complexes in [D_6]DMSO

R	C10 C21	C5 C16	C1 C12	C4 C13	C2 C15	C3 C14	C9 C20	C6 C17	C7 C18[a]	C8 C19	C11 C22	axial R group
nC_4H_9[b]	156.75	159.57	150.57	126.55	123.26	138.60	60.94	30.21	45.89	17.17	12.74	CH_3 13.79
	160.54	159.02	148.01	123.77	121.94	137.13	61.50	32.22	49.64	18.87	14.13	CH_2 22.76, 24.30, 33.55
C_2H_5 [b]	156.68	159.53	150.61	126.53	123.24	138.58	60.89	30.21	45.82	17.13	12.73	CH_3 17.06
	160.54	159.00	148.03	123.71	121.92	137.08	61.55	32.25	49.62	18.81	14.12	CH_2 18.05
CH_3 [b]	156.82	159.13	150.78	126.78	123.30	138.74	60.35	30.14	45.06	17.74	12.74	
	169.50	159.06	148.12	123.73	121.96	137.12	61.58	32.21	50.74	18.53	13.89	
CH_2Cl [b]	157.45	160.32	151.30	127.08	123.46	139.05	59.86	30.30	44.54	16.79	13.15	43.08
	160.76	158.96	148.14	123.77	122.07	137.22	61.45	32.02	50.25	18.38	14.32	
CH_2CF_3 [b]	158.63	160.01	151.10	127.31	123.56	139.13	59.09	30.00	43.61	16.25	13.42	CF_3 133 (q)
	161.52	159.06	148.21	123.80	122.14	137.33	61.40	31.92	50.57	18.52	14.55	

[a] Resonances not assigned separately. − [b] Data in the upper line refer to the tridentate ligand, data in the lower line refer to the bidentate ligand.

cule A are smaller than those in molecule B of **2a**. Analogously, the Co−N1 bond is longer than the Co−N6 bond and φ is larger than φ′ in both molecules A and B of **1** (Table 3). This suggests that the φ values of 36° in **2b** and of 44° in **2c** should correspond to a short- and a long-type Co−N1 bond, respectively. Therefore, it appears that the Co−N(py) distance *trans* to the same donor reaches the largest value when φ approaches 50°, which corresponds to orientation C in Scheme 2. That this conformation is the most strained, is also suggested by the increase in the bending α angle when φ approaches 50°, as shown in Figure 2, where the α/φ plot is reported for complexes **1** and **2**.

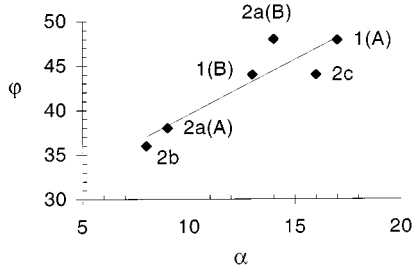

Figure 2. Dependence of the torsion angle φ around the Co−N1 bond on the bending angle α between the two equivalent five-membered rings in complexes **1** and **2**; A and B refer to the two independent molecules of **1** and **2a**

Taking these observations into account, it is of interest to compare the geometry of the axial fragment in complexes **2** with that in the analogous alkylcobaloximes and other related B_{12} models. In the latter series, the Co−N(ax) distance increases with an increase in the σ-donating ability of R, for L ligands with very similar φ values. Thus, in cobaloximes and iminocobaloximes, for which φ ≈ 0 and 90°, respectively, the order of increasing Co−py distances is Cl << CH_2CF_3 < Me < Et. Furthermore, for a given R, the Co−py bond is lengthened, when φ ≈ 90° (in complexes of Scheme 1, b) with respect to that observed when φ ≈ 0° (in complexes of Scheme 1, a and c), irrespective of the type of equatorial moiety. For complexes **2**, the apparently anomalous trends in Co−N(ax) distances with R as well as the differences between the A and B molecules of **2a** (and in the same molecule of **1**) can easily be interpreted if both contributions are considered. In fact, the distance Co−N1 of 2.134(5) Å (R = Me, φ = 38°) in molecule A of **2a**, is shorter than in **2b** [2.168(5) Å] (R = Et, φ = 36°), as is the case with the other B_{12} models. Analogously, the distance of 2.185(5) Å (R = Me φ = 48°) in molecule B of **2a** is longer than in **2c** [2.160(6) Å] (R = CH_2CF_3, φ = 44°). The influence of the torsion angle on the Co−N1 distance can be evaluated in **1**, where the two axial Co−N1 distances (φ ≈ 45°) are longer that those of Co−N6 (φ ≈ 30°). Therefore, the Co−N1 distance is the result of a compromise between the energies involved in the torsion around N1 and in the Co−N1 stretching. These structural features are in agreement with recent molecular mechanics calculations for $LCo(DH)_2Me$ (L is a planar N donor ligand) based on a new approach which also takes the contribution of the electronic *trans* influence into account.[5] These calculations have furnished profiles of the strain energy against the φ angle, which is characterised by a large maximum centred at φ = 90° and a minimum at φ = 0°, the difference in height ranging from 8 to 40 kJ/mol and increasing with the L bulk.[5] In addition, the large maximum at approximately φ = 90° has a fine structure, consisting of two nearly equal maxima at about 55° and 145°, separated by a relative minimum at φ = 90°. This suggested that orientation C (Scheme 2) is energetically even less favoured than orientation B. The corresponding plot of calculated Co−N(ax) distances against φ shows a profile very similar to that of the strain energy with a Co−N bond lengthening at φ = 50° which increases from 0.03 to 0.06 Å depending on the bulk of L. The Co−R distances follow the same trend in all the series of Table 3, reflecting the effects of the bulk and the σ-donating ability of R.[19]

Recent accurate Co−Me and Co−N axial distances of 1.979(4) and 2.162(4) Å, respectively, have been reported in MeCbl.[22] Hence, one of the most interesting structural features of model **2** is that the geometry of the axial N−Co−Me fragment is much closer to that of MeCbl (where the axial N ligand is a benzimidazole residue) than any other previously proposed B_{12} model, as shown by a comparison of the axial distances in several B_{12} models and MeCbl (Table 6).

The present complexes also show many solution properties characteristic of cobalamins and of their synthetic models. Significant parallels include the observation of the

Table 6. Comparison of the axial distances [Å] in MeCbl and in methyl derivatives of several B_{12} models

	Co−Me	Co−Nax
MeCbl	1.979(4)	2.162(4)
2a	1.960(7), 1.983(7)	2.134(5), 2.185(5)
MeCo[(DH)(DOH)pn]py	2.003(3)	2.106(3)
MeCo[(DH)(DOH)pn] Me_3Bzm	2.011(3)	2.100(3)
MeCo(C1py)	1.99(2), 2.05(2)	2.07(1)
MeCo$(DH)_2$py	1.998(5)	2.068(3)
MeCo$(DH)_2Me_3$Bzm	1.989(2)	2.060(2)

Co^{III}/Co^{II} and Co^{II}/Co^{I} redox series, the reactions of the Co^{I} species with alkylating agents to give organocobalt derivatives, the photochemically induced Co−C cleavage and the alkyl-transfer reactions to radical acceptors. On the other hand, there are some distinctive aspects in the chemical behaviour of these novel models which deserve attention. One is the appreciable influence of the steric factors, which is clearly indicated by the anomalous trend in the *trans* influence (see structural results) and by the fact that it is apparently impossible to prepare derivatives with bulky alkyl groups, such as isopropyl, adamantyl and perfluoroisopropyl, which have been reported for previously known models.[1,23] The observed methyl transfer from **2a** to $Co^{II}(DH)_2$ and Vitamin B_{12r} may also be interpreted in terms of steric factors that lower the stability of Co−C bond in these amino−oximato complexes.

The electronic factors appear to be less important in determining the stability of the Co−C bond. In this regard, it should be noted that both alkylcobalamines and their simple models, contain highly unsaturated ligands that allow for an extensive electronic delocalisation over the equatorial plane, while the alkyl−cobalt complexes **2** contain only two unconjugated C=N bonds in their chelating system. It follows that a high extent of unsaturation of the equatorial ligand is not a necessary prerequisite for the formation of stable alkyl−cobalt complexes. This result is not unexpected; at least in a few cases, the synthesis of alkyl−cobalt compounds containing completely saturated polyamine (N4) macrocycles has been successfully achieved.[24−26] On the contrary, electronic factors play a relevant role in stabilising the lowest oxidation state of the metal ion. Thus, both the higher lability of the Co^{I} derivative of the complex (**1**) and the more drastic conditions required for its formation, relative to the formation of the corresponding cobal(I)oximes, may be ascribed to the lower extent of unsaturation present in the equatorial ligand. In at least one case it was unequivocally proved that the Co^{II}/Co^{I} reduction is responsive to the extent of unsaturation present in the ligand; a greater unsaturation causes an anodic shift in the half-wave potentials.[27] This trend justifies, at least qualitatively, the experimental observations reported above.

The last point to stress is the inability of the Co^{II} species derived from **1** to react with alkyl halides to give the corresponding alkyl−cobalt species by means of a free radical process. This behaviour is somewhat unexpected because both photochemical and alkyl-transfer processes involve homolytic cleavage of the Co−C bond, thereby providing clear evidence for the tendency of these complexes to react through radical processes. In addition, the majority of the Co^{II} forms of the Vitamin B_{12} models and Vitamin B_{12r} itself have been found to be reactive toward alkyl halides. On the basis of kinetic studies[28] the following stepwise free-radical mechanism [Equation (4)] has been proposed for these series of compounds:

$$LCo^{II} + RX \longrightarrow LCo^{III}X + R \quad \text{(slow)}$$

$$LCo^{II} + R \longrightarrow LCo^{III}R \quad \text{(fast)} \qquad (4)$$

$$2LCo^{II} + RX \longrightarrow LCo^{III}X + LCo^{III}R$$

Likewise, the lack in reactivity of the Co^{II} form of **1** can be attributed to its inability to abstract the halogen from the alkyl halide in the slow step rather than to its low tendency to trap free alkyl radicals.

Conclusions

Tridentate amino−oxime ligands are effective in stabilising the Co^{III}−C bond, as the analogous tridentate imino−oxime ligands.[29,30] The methyl derivative undergoes photolytic homolysis and is a better methyl donor than methylcobaloxime. These organometallic complexes can therefore be considered as suitable models for the B_{12} system (alkylcobalamin), such as the well-known alkylcobaloximes and other related models.[1] A distinctive feature of this new model is the appreciable influence of steric factors on their chemical behaviour. This is clearly indicated by the anomalous trend in the *trans* influence and by the fact that it is apparently impossible to prepare derivatives with bulky alkyl groups, such as *i*Pr, adamantyl and perfluoroisopropyl, which, on the contrary, have been reported for previously known models. In this respect, they more closely parallel the alkylcobalamin chemistry. Furthermore, the axial distances in the methyl derivative, very close to those recently reported for methylcobalamin, make them a better B_{12} structural model than any other previously reported.[22] Structural evidence is given that this behaviour can be related to the crowded equatorial moiety, which interacts with

the axial ligands more strongly than in cobaloximes. A recent comparison[22] of the structural, spectroscopic and electrochemical properties of alkylcobalamins with those of alkylcobaloximes suggests that the corrin ligand makes more electronic charge available on Co than on the $(DH)_2$ ligand (electronic *cis* influence), and that the longer Co−N axial distances in cobalamins are also due to ring electronic influence. Both the longer Co−N1 bonds and the increased difficulty in the Co^{III}/Co^{I} reduction, relative to alkylcobaloximes, suggests a higher charge density on Co in complexes **2**. The present models are possibly also electronically closer to cobalamins. These compounds therefore seem to offer a better opportunity to study the influence of steric factors on the formation and cleavage of the Co−C bond, than that provided by previous B_{12} models. Finally, the easy substitution of the chelating ligand, which occurs without cleavage of the Co−Me bond, suggests the possibility of preparing new series of otherwise inaccessible organometallic compounds.

Experimental Section

Vitamin B_{12a} and methylcobalamin were purchased from Aldrich. $CH_3Co(DH)_2H_2O$, $CH_3Co(DH)_2py$, and $Co(DH)_2(H_2O)_2$ were prepared by previously reported methods.[12] All other reagents and chemicals were commercial products and were used without further purification. − ^1H and ^{13}C NMR spectra were recorded with a Jeol EX-400 (^1H at 400 MHz and ^{13}C at 100.4 MHz) from [D_6]DMSO solutions with TMS as internal standard. Two-dimensional homonuclear and heteronuclear correlated spectra (H,H and H,C COSY) were obtained using the instrument's automatic programme. The HMBC spectrum of $[CF_3CH_2Co(LNHpy)(HLNHpy)]ClO_4$ in [D_6]DMSO was obtained as a 2048 × 256 data matrix with 64 scans (preceded by 4 dummy scans) per t_1 value and a PDBS (pulse delay between scans) of 1.00 s. An 8.7 μs 90° PW (pulse width) of ^{13}C was used. Values of Δ_1 (the delay between the first 90° proton pulse and the first 90° ^{13}C pulse) and Δ_2 (the delay between the first and the second 90° ^{13}C pulse) were 3.6 and 62.5 ms, respectively.

Syntheses: The same synthetic procedure was followed for all the $[RCo(LNHpy)(HLNHpy)]ClO_4$ complexes (R = Me, Et, *n*Bu, CH_2Cl, CH_2CF_3). − ***CAUTION:*** *Although no problems were encountered in the present study, perchlorate salts are potentially explosive and should only be handled in small quantities!* − The reactions were performed at room temperature, under an inert atmosphere and in the dark. In a typical experiment, a solution of NaOH (0.20 g, 5.00 mmol) in water (2 mL) was added to a suspension of complex **1** (1.00 g, 1.49 mmol) in methanol (150 mL). The resulting clear solution was treated with $NaBH_4$ (0.12 g, 4.70 mmol), dissolved in a minimum volume of water, followed by three drops of $PdCl_2$ solution, prepared by the addition of conc. HCl to a suspension of $PdCl_2$ (1.00 g) in water (20 mL) until complete dissolution had occurred. When the solution assumed a dark brown colour (after 15 min), a solution of the appropriate alkyl iodide (7.45 mmol, i.e. 5 equiv. with respect to the complex) in methanol (10 mL) was added. After about 30 min, the dark brown solution turned to bright orange. At this point, the flow of N_2 was suspended and the methanol was removed in a rotary evaporator at 40 °C. The aqueous suspension was extracted with CH_2Cl_2 (2 × 50 mL) and the residual water removed from the organic phase by treatment with anhydrous Na_2SO_4. After filtration, the solution was concentrated to 10 mL, passed through a chromatographic column of Al_2O_3 and eluted with CH_2Cl_2. A solution of the pure product was obtained (50 mL). The by-products, which were most strongly bound, could eventually be eluted with methanol. Diisopropyl ether was then added until the solution became turbid, and the suspension was allowed to stand overnight. Crystals of the desired product were recovered by filtration and air-dried. In order to obtain crystals suitable for X-ray analysis or for a better purification, the products were treated as follows.

$[CH_3Co(LNHpy)(HLNHpy)]ClO_4·0.5CH_3COCH_3$ (2a): Some drops of water were added to a saturated solution of the complex in acetone, followed by diisopropyl ether, until the solution became turbid. After standing in the dark in a stoppered vessel for 2 d, orange crystals were collected by filtration and air-dried. Yield: 0.31 g (34%). − $C_{24.5}H_{39}ClCoN_6O_{6.5}$ (616.0): calcd. C 47.8, H 6.4, N 13.6; found C 47.9, H 6.4, N 13.6.

$[C_2H_5Co(LNHpy)(HLNHpy)]ClO_4$ (2b): Recrystallised as above; red crystals were obtained. Yield: 0.28 g (31%). − $C_{24}H_{38}ClCoN_6O_6$ (610.0): calcd. C 47.9, H 6.4, N 14.0; found C 48.0, H 6.3, N 13.7.

$[CF_3CH_2Co(LNHpy)(HLNHpy)]ClO_4·0.5CH_2Cl_2$ (2c): Recrystallised by the diffusion of diisopropyl ether stratified over a saturated solution of the complex in dichloromethane. Yellow crystals were collected by filtration and air-dried. Yield: 0.37 g (36%). − $C_{24.5}H_{36}Cl_2CoF_3N_6O_6$ (697.4): calcd. C 42.2, H 5.2, N 12.1; found C 42.5, H 5.2, N 12.2.

[*n*-C_4H_9Co[(LNHpy)(HLNHpy)]ClO_4 (2d): Recrystallised as above; red crystals were obtained. Yield: 0.25 g (27%). − $C_{26}H_{42}ClCoN_6O_6$ (629.1): calcd. C 49.6, H 6.75, N 13.4; found C 49.4, H 6.7, N 12.8.

$[ClCH_2Co(LNHpy)(HLNHpy)]ClO_4$(2e): Recrystallised as above; yellow crystals were obtained. Yield: 0.42 g (45%). − $C_{23}H_{35}Cl_2CoN_6O_6$ (621.4): calcd. C 44.5, H 5.7, N 13.5; found C 44.4, H 5.7, N 13.3.

Substitution of the Chelating System by Dimethylglyoxime: Dimethylglyoxime (0.114 g, 0.98 mmol) and pyridine (0.5 mL) were added to a solution of complex **2a** (0.300 g, 0.49 mmol) in methanol (20 mL). The solution was allowed to stand for 5 h at room temperature in the dark. Water (5 mL) was then added to the solution. After evaporation of the methanol, orange crystals of $CH_3Co(DH)_2py$ were collected by filtration (0.154 g, 82%) and identified by ^1H NMR ($CDCl_3$): δ_H = 0.82 (3 H, CH_3−Co), 2.13 (12 H, CH_3−C), 7.33, 7.73, 8.62 (5 H, C_5H_5N). Following the same procedure, but with exclusion of pyridine, no reaction was observed and the starting complex was recovered. After recrystallisation, the complex was identified by elemental analysis. − $C_{24.5}H_{39}ClCoN_6O_{6.5}$ (616.0): calcd. C 47.8, H 6.4, N 13.6; found C47.6, H 6.3, N 13.3.

Transmethylation Reaction on $Co(DH)_2(H_2O)_2$: A solution of complex **2a** (0.100 g, 0.17 mmol) in methanol (20 mL) was treated with $Co^{II}(DH)_2(H_2O)_2$ (0.055 g, 0.17 mmol, 1 equiv.) under N_2, in the dark at room temperature. After 5 h, the solution was allowed to stand in air, water (5 mL) was added and the methanol was removed in a rotary evaporator. The aqueous residue was extracted with CH_2Cl_2. By evaporation of the solvent, the complex **1** was obtained and identified by ^1H NMR spectroscopy. The aqueous phase, concentrated in air with exclusion of light, gave red crystals of $CH_3(DH)_2H_2O$ identified by ^1H NMR (CD_3OD): δ_H = 0.67 (3 H, CH_3−Co), 2.24 (12 H, CH_3−C).

Transmethylation of Complex 2a on Vitamin B_{12r}: The reaction was carried out under nitrogen, in the dark and at room temperature. A solution of Vitamin B_{12a} (0.050 g) in water (25 mL) was reduced to Vitamin B_{12r} as described in the literature.[14] A solution of the complex **2a** (0.100 g) in methanol (25 mL) was then added and the reaction mixture was allowed to stand overnight. After the evaporation of methanol and the addition of acetone (30 mL), a red microcrystalline precipitate formed slowly. The product (0.030 g, 70%) was collected by filtration, air-dried, and identified as methylcobalamin by comparison of its UV/Vis and ^{1}H NMR spectra in D_2O with those of an authentic sample.

Photolysis of Complex 2a: A solution of $[CH_3Co(LNHpy)(HLNHpy)]ClO_4$ (0.100 g, 0.17 mmol) in water (50 mL) was exposed to sunlight for 1 h. It was then concentrated in air after the addition of a few drops of a saturated solution of $NaClO_4$. Red crystals of complex **1** were collected by filtration and identified by ^{1}H NMR spectroscopy. A solution of **2** (2 mg) in water (1 mL) was photolysed; the formaldehyde present in the filtrate was detected by the chromotropic acid test.[31]

Structure Determination: Single crystals, suitable for X-ray data collection of **2**, were grown as already reported in syntheses. Single-crystal X-ray data were collected at room temperature with a CAD4 Enraf−Nonius diffractometer using graphite-monochromated Mo-K_α radiation (λ= 0.71073 Å). Cell parameters were determined from 25 carefully selected reflections. Data were corrected for Lorentz polarisation effects and for absorption by the ψ-scan technique. Detailed crystallographic data are presented in Table 1. − The structures were solved by Patterson methods followed by Fourier syntheses and refined by full-matrix least-squares cycles. All the calculations were carried out with SHELXS (solution of structures) and SHELXL (refinement of structures) programs.[32] The hydrogen atoms were set in calculated positions and allowed to ride on the atoms to which they are linked. One water molecule at 0.25 occupancy and one acetone molecule at 0.5 occupancy were located in the unit cell of **2b** and **2c**, respectively. Other refinement conditions are given in Table 1. Crystallographic data (excluding structure factors) reported in this paper have been deposited at the Cambridge Crystallographic Data Centre and allocated the deposition numbers CCDC-145122 (**2a**), -145123 (**2b**), and -145124 (**2c**). Copies of the data can be obtained free of charge on application to CCDC, 12 Union Road, Cambridge CB2 1IZ, UK [Fax: (internat.) + 44-1223/336-033; E-mail: deposit@ccdc.cam.ac.uk].

Acknowledgments

We thank the Ministero della Ricerca Scientifica e Tecnologica (Roma) (PRIN 9803184222) and the Consiglio Nazionale delle Ricerche (CNR) for financial support.

[1] [1a] N. Bresciani Pahor, M. Forcolin, L. G. Marzilli, L. Randaccio, M. F. Summers, P. J. Toscano, *Coord. Chem. Rev.* **1985**, *63*, 1−125. − [1b] L. Randaccio, N. Bresciani Pahor, E. Zangrando, L. G. Marzilli, *Chem. Soc. Rev.* **1989**, *18*, 225−250. − [1c] L. Randaccio, *Comments Inorg. Chem.* **1999**, 21, 327−376.

[2] [2a] F. Mancia, N. H. Keep, A. Nakagawa, P. F. Leadlay, S. McSweeney, B. Rasmussen, P. Boske, O. Diat, P. R. Evans, *Structure* **1996**, *4*, 339−350. − [2b] C. L. Drennan, S. Huang, J. T. Drummond, R. G. Mattews, M. L. Ludwig, *Science* **1994**, *226*, 1669−1670. − [2c] R. Reitzer, K. Gauber, C. Jogl, U. G. Wagner, H. Bothe, W. Buckel, C. Kratky, *Biochemistry* **1999**, *38*, 891−902. − [2d] N. Shibata, J. Mesuda, T. Tobimatsu, T. Toraya, K. Suto, Y. Morimoto, N. Yasuoca, *Structure* **1999**, *7*, 997−1007.

[3] J. M. Sirovatka, R. G. Finke, *J. Am. Chem. Soc.* **1997**, *119*, 3057−3067.

[4] [4a] S. M. Polson, R. Cini, C. Pifferi, L. G. Marzilli, *Inorg. Chem.* **1997**, *36*, 314−322. − [4b] S. J. Moore, A. Kutikov, R. J. Lachicotte, L. G. Marzilli, *Inorg. Chem.* **1999**, *38*, 768−776.

[5] S. Geremia, M. Calligaris, L. Randaccio, *Eur. J. Inorg. Chem.* **1999**, 981−992.

[6] R. Cini, S. J. Moore, L. G. Marzilli, *Inorg. Chem.* **1998**, *37*, 6890−6897.

[7] S. Hirota, S. M. Polson, J. M. Puskett, Jr., S. J. Moore, M. B. Mitchell, L. G. Marzilli, *Inorg. Chem.* **1996**, *35*, 5646−5653.

[8] [8a] A. Gerli, M. Sabat, L. G. Marzilli, *J. Am. Chem. Soc.* **1992**, *114*, 6711−6718. − [8b] L. G. Marzilli, A. Gerli, A. M. Calafat, *Inorg. Chem.* **1992**, *31*, 4617−4627.

[9] [9a] S. Dang, R. Padmakumar, N. Maiti, R. Banerjee, T. G. Spiro, *J. Am. Chem. Soc.* **1998**, *120*, 9947−9948 and references therein. − [9b] J. M. Puckett, Jr., M. B. Mitchell, S. Hirota, L. G. Marzilli, *Inorg. Chem.* **1996**, *35*, 4656−4662 and references therein.

[10] J. M. Sirovatka, R. G. Finke, *Inorg. Chem.* **1999**, *38*, 1697−1707.

[11] L. Catalano, R. Dreos, G. Nardin, L. Randaccio, G. Tauzher, S. Vuano, *J. Chem. Soc., Dalton Trans* **1996**, 4269−4274.

[12] B. D. Gupta, S. Roy, *Inorg.Chim.Acta* **1988**, *146*, 209−221.

[13] H. P. C. Hogenkamp, *Biochemistry* **1966**, *5*, 417−422.

[14] G. N. Schrauzer, J. W. Sibert, R. J. Windgassen, *J. Am. Chem. Soc.* **1968**, *20*, 6681−6688.

[15] C. K. Johnson, ORTEP; Report ORNL-5138; Oak Ridge National Laboratory: Oak Ridge, TN, **1976**.

[16] S. Geremia, L. Randaccio, E. Zangrando, L. Antolini, *J. Organomet. Chem.* **1992**, *425*, 131−139.

[17] P. G. Yohannes, N. Bresciani Pahor, L. Randaccio, E. Zangrando, L. G. Marzilli, *Inorg. Chem.* **1988**, *27*, 4738−4744.

[18] L. Randaccio, S. Geremia, R. Dreos-Garlatti, G. Tauzher, F. Asaro, G. Pellizer, *Inorg. Chim. Acta* **1992**, *194*, 1−8.

[19] L. Randaccio, S. Geremia, E. Zangrando, C. Ebert, *Inorg. Chem.* **1994**, *33*, 4641−4650.

[20] H. A. O. Hill and K. G. Morallee, *J. Chem.Soc. A* **1969**, 554−559.

[21] W. O. Parker, Jr., E. Zangrando, N. Bresciani Pahor, L. Randaccio, L. Marzilli, *Inorg. Chem.* **1986**, *19*, 3491−3497.

[22] L. Randaccio, M. Furlan, S. Geremia, M. Slouf, I. Srenova, D. Toffoli, *Inorg. Chem.*, in press.

[23] P. J. Toscano, H. Brand, S. Liu, J. Zubieta, *Inorg. Chem.* **1990**, *29*, 2101− 2105.

[24] T. S. Roche, J. F. Endicott, *Inorg. Chem.* **1974**, *13*, 1575−1580.

[25] T. S. Roche, J. F. Endicott, *J. Am. Chem. Soc.* **1972**, *94*, 8622−8623.

[26] A. Bakac, J. H. Espenson, *Inorg. Chem.* **1987**, *26*, 4353−4355.

[27] A. M. Tait, F. V. Lovecchio, D. H. Busch, *Inorg. Chem.* **1977**, *16*, 2206− 2212.

[28] J. Halpern, *Ann. N. Y. Acad.Sci.* **1974**, *239*, 2−21.

[29] R. Dreos, G. Tauzher, D. H. Trendafilova, G. Nardin, L. Randaccio, *Inorg. Chem.* **1996**, *35*, 2715−2716.

[30] R. Dreos, E. Herlinger, G. Tauzher, S. Vuano, G. Nardin, L. Randaccio, *Organometallics* **1998**, *17*, 2366−2369.

[31] C. E. Bricker, W. A. Vail, *Anal. Chem.* **1950**, *22*, 720−722.

[32] [32a] *SHELXS-86, Program for Structure Solution*: G. M. Sheldrick, *Acta Crystallogr., Sect. A* **1990**, *46*, 467. − [32b] G. M. Sheldrick, *SHELXL-93, Program for Structure Refinement*; Universität Göttingen, Göttingen, Germany, **1993**.

Received June 15, 2000
[I00238]

Quinone Oxygen-Coordinated Palladium(II) Complexes with Anthraquinone Ligands Bearing *N*-Heterocyclic Coordination Sites

Toshiyuki Moriuchi,[a] Takuo Watanabe,[a] Isao Ikeda,[a] Akiya Ogawa,[b] and Toshikazu Hirao*[a]

Keywords: Coordination modes / Quinones / Crystal engineering / Palladium / Redox chemistry

The coordination properties of anthraquinone ligands bearing *N*-heterocyclic coordination sites to divalent palladium, and structural characterization of the quinone oxygen-coordinated palladium(II) complexes are described. The intramolecular NH···O (quinone) hydrogen bond [N(1)···O(2), 2.617 Å] was observed in the crystal structure of 1-chloro-8-[2-(2-pyridyl)ethylamino]-9,10-anthraquinone (**1a**). The anthraquinone moieties of **1a** are oriented in a face-to-face manner to form π-stacks in the crystal, with an interplanar distance of ca. 3.5 Å between the neighboring anthraquinone moieties. Complexation of **1a** with $Pd(OAc)_2$ afforded the palladium(II) complex **2a**. The quinone oxygen, which is bent out of the anthraquinone plane, is coordinated to the palladium(II) center, which is substituted by the amino nitrogen in a position *trans* to the pyridyl nitrogen in the crystal structure **2a**. 1-(2-Phenylethylamino)-8-[2-(2-pyridyl)ethylamino]-9,10-anthraquinone (**1b**) was also found to form the 1:1 quinone oxygen-coordinated palladium(II) complex **2b**. The single-crystal X-ray structure determination of **2b** shows the existence of two independent molecules in the asymmetric unit. These two molecules are present in a good mirror image relationship, indicating conformational enantiomers. Furthermore, they are overlapped in a face-to-face manner to form the π-stack dimer, which arranges in a herringbone motif with the virtues of offset stacking and edge-to-face contacts in the crystal packing. Starting from 1,5-bis[2-(2-pyridyl)ethylamino]-9,10-anthraquinone (**1c**) bearing two *N*-heterocyclic coordination sites, the conjugated palladium(II) homobimetallic complex **2c** was obtained. Two palladium atoms are bridged by the quinone moiety to afford a redox-active conjugated homobimetallic complex system. The crystal structure of **2c** reveals that two palladium atoms are disposed on opposite faces of the anthraquinone plane, accompanied by the bend of the quinone oxygens out of the anthraquinone plane. The anthraquinone moieties of **2c** are arranged in an edge-to-face orientation in the crystal packing. In the palladium(II) complexes **2b**–**c**, the d,π-conjugated system is interconnected through a π-π interaction between the π-conjugated systems. The cyclic voltammograms of these quinone oxygen-coordinated palladium(II) complexes **2a**–**c** show two redox couples based on the quinone moiety, which are positively shifted relative to the free quinone ligands.

Introduction

Efficient redox processes of transition metal complexes are one of the key factors in developing versatile systems for new materials and catalytic redox reactions. Since ligand coordination greatly contributes to redox processes, ligand design is often crucial for the construction of an efficient redox system. From this point of view, the redox-active quinone ligands, which are present in three redox forms (the reduced hydroquinone dianions, the partially reduced semiquinone radical anions, and the oxidized neutral quinones) are considered to permit an efficient redox system. A variety of transition metal complexes with *o*-quinones or their reduced forms have been prepared and studied extensively.[1] For *p*-quinone ligands, Bäckvall has demonstrated the involvement of the π-coordination of *p*-quinone to a Pd^0 center in the Pd-catalyzed oxidation of olefins and conjugated dienes.[2] The redox properties of the Pd^0 complexes with π-bound *p*-quinone ligands have also been investigated.[3] However, the *p*-quinone complexes, in which a quinone oxygen coordinates to a high valent transition metal, have not been investigated extensively,[4] despite the elucidation of their coordination and redox properties in catalysis. In our previous papers,[5] the π-conjugated molecule, *N,N′*-bis(4′-dimethylaminophenyl)-1,4-benzoquinone diimine, was introduced to the palladium(II) complex bearing the *N*-heterocyclic tridentate podand ligand, affording a redox-active π-conjugated palladium(II) homobimetallic complex, in which the redox properties of the quinone diimine moiety are modulated by complexation. These results prompted us to investigate the redox properties of the transition metal complexes with *p*-quinones and to characterize the complexes structurally. Another interesting feature depends on the π-π interactions between the anthraquinone aromatic rings in the crystal packing.[6] This interaction could induce architecturally controlled self-assembly, leading to molecular aggregates in the solid state. The π-π interaction between the π-conjugated moieties of the conjugated complexes is considered to be one of the most convenient approaches for the assembly of the conjugated complexes. In this context, we herein report the coordination properties of anthraquinone ligands bearing *N*-heterocyclic coordination sites to

[a] Department of Applied Chemistry, Faculty of Engineering, Osaka University, Yamada-oka, Suita, Osaka 565−0871, Japan
E-mail: hirao@ap.chem.eng.osaka-u.ac.jp
[b] Department of Chemistry, Faculty of Science, Nara Women's University, Kitauoyanishi-machi, Nara 630−8506, Japan

 © WILEY-VCH Verlag GmbH, 69451 Weinheim, 2001 1434−1948/01/0101−0277 $ 17.50+.50/0

divalent palladium, and the structural characterization of the quinone oxygen-coordinated palladium(II) complexes.

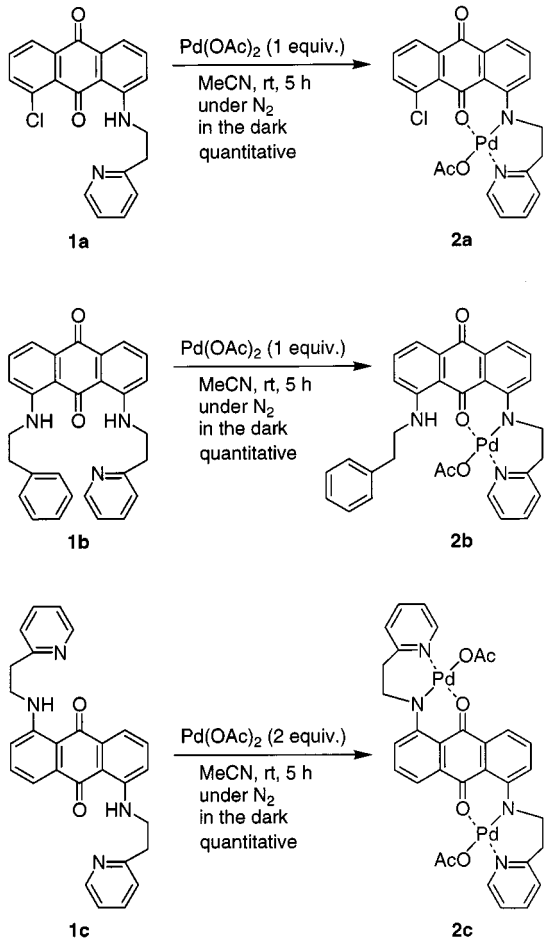

Scheme 1

Results and Discussion

The anthraquinone ligands **1a–c** were prepared from the corresponding chloroanthraquinones and 2-(2-aminoethyl)-pyridine (Scheme 1). These anthraquinone ligands were fully characterized by spectroscopic techniques and elemental analysis. The FT-IR spectra of the anthraquinone ligands **1a–c** show hydrogen-bonded NH and C=O stretching bands (**1a**: 3286 and 1635 cm^{-1}, **1b**: 3263 and 1620 cm^{-1}, **1c**: 3255 and 1620 cm^{-1}, Table 1). The crystal structure of **1a** supports the presence of an intramolecular hydrogen bond between NH and C=O (quinone) [N(1)···O(2), 2.617 Å; H···O(2), 1.88 Å, Figure 1 and Table 2], indicating a slightly longer carbonyl bond [O(2)–C(13), 1.224 Å] than the non-hydrogen bonded carbonyl bond [O(1)–C(6), 1.216 Å]. Selected bond lengths and bond angles are listed in Table 3. It is notable that the anthraquinone moieties of **1a** are oriented in a face-to-face

Table 1. Selected spectroscopic data

	FT-IR		$E_{1/2}$ (V) [a]	
	ν_{N-H} (cm^{-1})	$\nu_{C=O}$ (cm^{-1})	q/sq	sq/hq
1a	3286	1658, 1635	-1.44	-1.94
2a	——	1651, 1620	-1.32	-1.73
1b	3263	1658, 1620	-1.56	-1.98
2b	3332	1643, 1620	-1.40	-1.81
1c	3255	1620	-1.57	-1.87
2c	——	1620	-1.31	-1.61

[a] V vs. Fc/Fc^+.

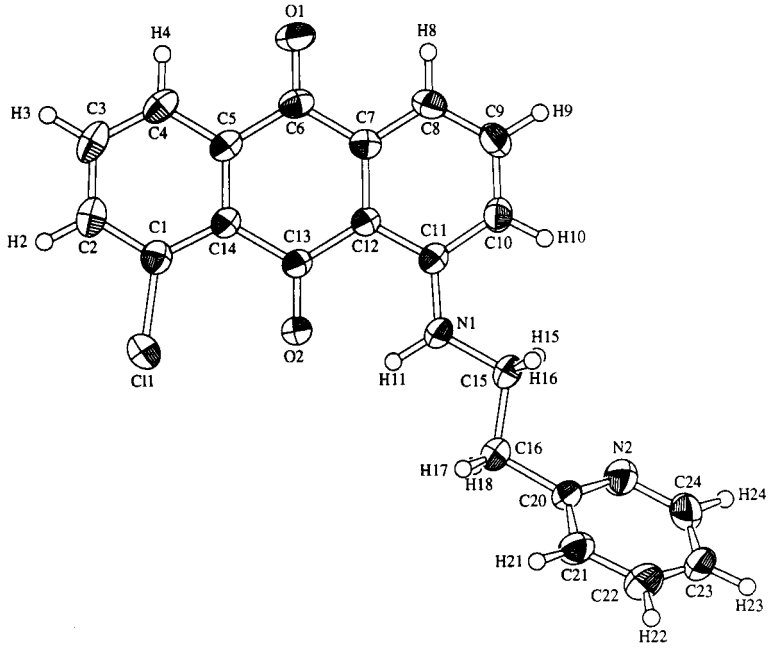

Figure 1. Molecular structure of **1a** (40% probability ellipsoids)

manner with an interplanar distance of ca. 3.5 Å between the neighboring anthraquinone moieties, which form π-stacks in the crystal as shown in Figure 2. The arrangement of π-stacks represents an offset π-stacked geometry which places one carbonyl oxygen atom directly above the carbonyl carbon atom of the neighboring molecule.

Complexation of **1a** with $Pd(OAc)_2$ in acetonitrile afforded the 1:1 palladium(II) complex **2a** (Scheme 1). The formation of **2a** was followed by spectrophotometric titration. Thus, the absorption around 647 nm due to **2a** appeared and increased until the ratio of [**1a**]/[$Pd(OAc)_2$] was 1:1, with concomitant disappearance of the absorption of

Table 2. Crystallographic data for **1a**, **2a**, **2b**, and **2c**

	1a	**2a**	**2b**	**2c**
Empirical formula	$C_{21}H_{15}N_2O_2Cl$	$C_{23}H_{17}N_2O_4ClPd \cdot H_2O$	$C_{31}H_{27}N_3O_4Pd$	$C_{32}H_{28}N_4O_6Pd_2 \cdot CH_3CN$
Formula weight	362.81	545.27	611.97	818.45
Crystal system	monoclinic	monoclinic	triclinic	triclinic
Space group	$P2_1/n$ (No. 14)	$P2_1/c$ (No. 14)	$P\bar{1}$ (No. 2)	$P\bar{1}$ (No. 2)
a [Å]	7.054(3)	10.212(9)	16.822(4)	16.895(3)
b [Å]	10.605(3)	8.004(4)	14.750(3)	16.932(4)
c [Å]	22.582(2)	26.005(3)	11.021(3)	14.441(4)
α [°]			89.99(2)	112.54(2)
β [°]	94.02(2)	93.91(2)	108.77(2)	111.65(2)
γ [°]			90.00(2)	62.44(2)
V [Å^3]	1685.0(7)	2120(1)	2588(1)	3288(1)
Z	4	4	4	4
D_{calcd} [g cm^{-3}]	1.430	1.708	1.570	1.653
μ(Mo Kα) [cm^{-1}]	2.45	10.41	7.61	11.47
T [°C]	23	23	23	23
λ(Mo Kα) [Å]	0.71069	0.71069	0.71069	0.71069
R [a]	0.062	0.042	0.059	0.058
R_w [b]	0.101	0.031	0.063	0.069

[a] $R = \Sigma||F_o| - |F_c||/\Sigma|F_o|$. – [b] $R_w = [\Sigma w(|F_o| - |F_c|)^2/\Sigma wF_o^2]^{1/2}$.

Table 3. Selected bond lengths [Å] and bond angles [°] for **1a**, **2a**, and **2b**

	1a	**2a**	**2b** [a]	
Bond lengths				
Pd–O(2)	----	1.970(3)	1.985(7)	1.987(7)
Pd–O(3)	----	2.031(3)	2.058(8)	2.056(8)
Pd–N(1)	----	1.974(3)	1.994(8)	1.985(8)
Pd–N(2)	----	2.010(4)	2.026(9)	2.015(9)
O(1)-C(6)	1.216(7)	1.217(6)	1.24(1)	1.23(1)
O(2)-C(13)	1.224(6)	1.266(5)	1.28(1)	1.28(1)
N(1)-C(11)	1.365(7)	1.327(5)	1.32(1)	1.34(1)
C(10)-C(11)	1.421(8)	1.447(6)	1.40(1)	1.42(1)
C(11)-C(12)	1.424(7)	1.457(6)	1.45(1)	1.42(1)
C(12)-C(13)	1.474(8)	1.414(6)	1.44(1)	1.42(1)
C(13)-C(14)	1.508(7)	1.502(6)	1.48(1)	1.49(1)
Bond angles				
O(2)–Pd–O(3)	----	85.5(1)	91.1(3)	91.0(3)
O(2)–Pd–N(1)	----	90.8(1)	88.4(3)	88.4(3)
O(3)–Pd–N(2)	----	89.3(2)	85.8(4)	86.1(4)
N(1)–Pd–N(2)	----	94.4(2)	94.5(3)	94.4(4)
O(2)–Pd–N(2)	----	172.5(2)	175.6(3)	175.8(3)
O(3)–Pd–N(1)	----	176.3(1)	175.7(4)	176.0(4)
C(13)-O(2)-Pd	----	127.6(3)	129.4(7)	128.4(7)
C(11)-N(1)-Pd	----	124.1(3)	124.7(7)	124.1(7)
O(2)-C(13)-C(14)	119.6(5)	113.7(4)	115.0(10)	113.4(10)
O(2)-C(13)-C(12)	121.5(5)	125.2(4)	122.7(9)	123.9(10)
C(11)-C(12)-C(13)	120.5(5)	122.4(4)	123.2(9)	123.1(10)
C(12)-C(11)-N(1)	122.2(5)	124.9(4)	124.2(9)	124.6(10)
C(10)-C(11)-N(1)	120.0(5)	119.7(4)	119.6(10)	119.0(10)
C(11)-N(1)-C(15)	123.1(5)	117.4(4)	116.6(9)	116.9(9)

[a] Two independent molecules exist in the asymmetric unit.

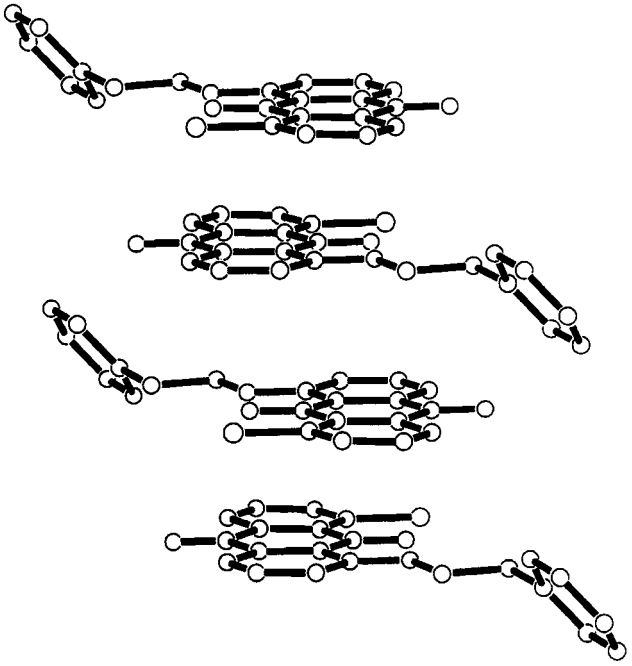

Figure 2. Crystal packing diagram of **1a** showing extended π-stacking

1a around 505 nm (Figure 3). This result supports the formation of the 1:1 complex **2a**. The structure of the isolated complex **2a** was elucidated by ^{1}H NMR spectroscopy. The absence of an amine proton in the ^{1}H NMR spectrum indicates the displacement of the acetate ligands of $Pd(OAc)_2$ by the amino nitrogen of **1a**. The down-field shift

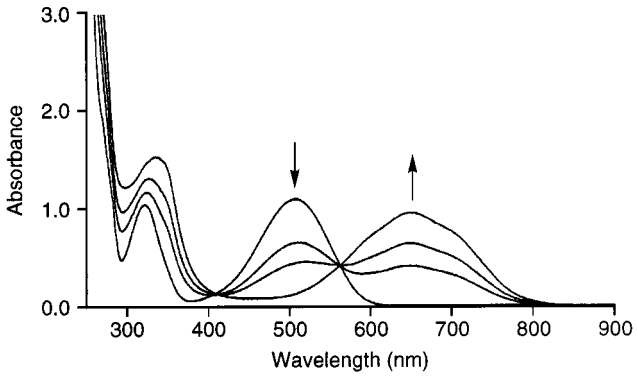

Figure 3. UV/Vis spectra on successive treatment of **1a** (1.0×10^{-4} M) with $Pd(OAc)_2$ (0, 0.4, 0.6, 1.0×10^{-4} M) in MeCN under argon

of the pyridyl protons implies the coordination of the pyridyl nitrogen to palladium.

Further structural information for **2a** was obtained by an X-ray crystal structure determination (Figure 4 and Table 2). The quinone oxygen and pyridyl nitrogen atoms coordinate to palladium in a *trans* fashion. The coordinated quinone carbonyl bond [O(2)−C(13), 1.266 Å] is longer than the uncoordinated one [O(1)−C(6), 1.217 Å], which is consistent with the observation of two kinds of C=O stretching bands (1651 and 1620 cm^{-1}) in the FT-IR spectrum of **2a**. The bond lengths of both N(1)−C(11) and C(12)−C(13) are shortened upon complexation [**1a**: N(1)−C(11), 1.365 Å; C(12)−C(13), 1.474 Å; **2a**: N(1)−C(11), 1.327 Å; C(12)−C(13), 1.414 Å]. The O(2)−C(13)−C(12) and C(12)−C(11)−N(1) angles increase slightly to accommodate the palladium atom [**1a**: O(2)−C(13)−C(12), 121.5°; C(12)−C(11)−N(1), 122.2°; **2a**: O(2)−C(13)−C(12), 125.2°; C(12)−C(11)−N(1), 124.9°]. Additionally, the palladium center deviates considerably from the anthraquinone plane. The coordination

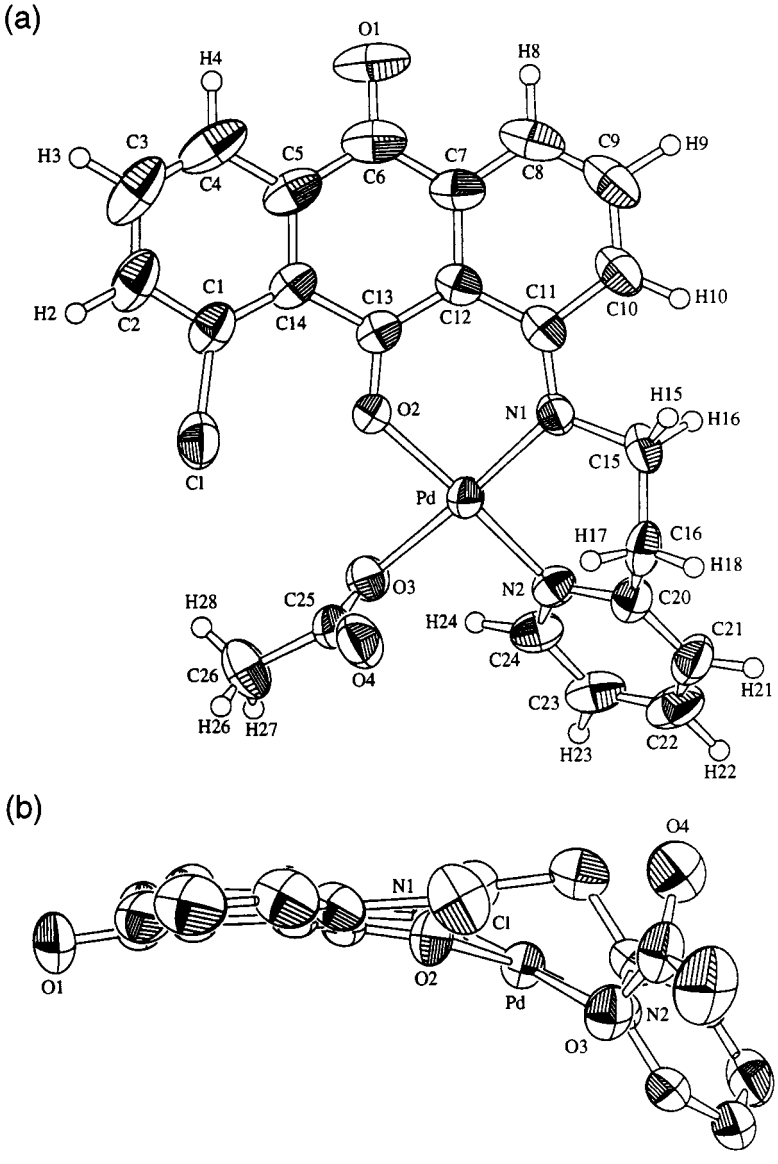

Figure 4. (a) Top view and (b) side view of the molecular structure of **2a** (40% probability ellipsoids. Hydrogen atoms are omitted for clarity)

geometry is almost square planar with the palladium-bonded amino nitrogen in a position *trans* to the acetoxy group. Another interesting feature lies in the nonplanar anthraquinone skeleton of **2a**, which is in sharp contrast to the planar one of **1a**. The two phenyl rings in the anthraquinone moiety form a V shape intersecting at C(6) and C(13) with a dihedral angle of 15.2°, where O(1) and O(2) are bent slightly out of the anthraquinone plane, as shown in Figure 4b. The π-stacks observed for **1a** are not observed in the crystal packing of **2a**, possibly due to the nonplanar anthraquinone skeleton (Figure 5).

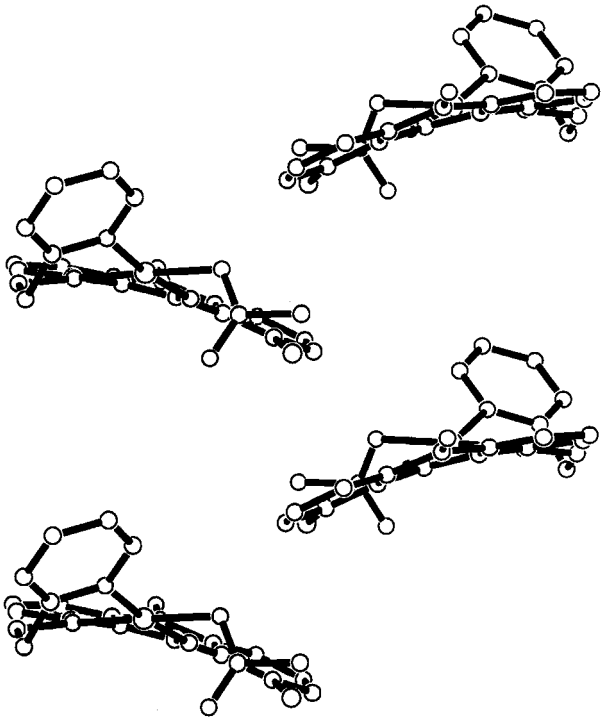

Figure 5. Crystal packing diagram obtained for **2a**

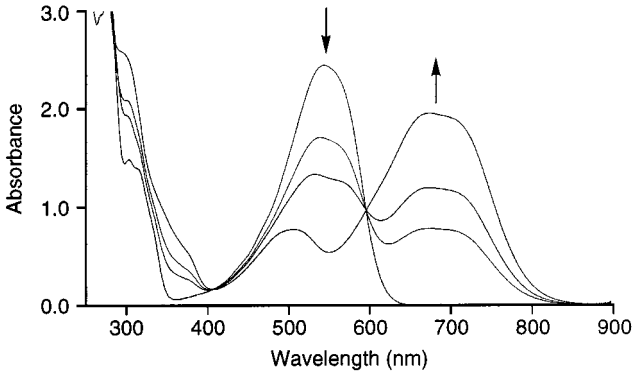

Figure 6. UV/Vis spectra on successive treatment of **1b** (1.0×10^{-4} M) with $Pd(OAc)_2$ (0, 0.4, 0.6, 1.0×10^{-4} M) in MeCN under argon

On the basis of these observations, the complexation behavior and molecular arrangement of the unsymmetrical anthraquinone ligand **1b** was studied to gain insight into the effect of the pendant group at the 8-position. Treatment of **1b** with $Pd(OAc)_2$ in acetonitrile afforded the 1:1 complex **2b** (Scheme 1). A similar spectral change was observed to support the formation of the palladium(II) complex **2b**, which exhibited a broad band around 675 nm (Figure 6). In the ^{1}H NMR spectrum of the isolated complex **2b**, the down-field shift of the pyridyl protons, and no shift of the phenylethyl group indicate that the nitrogen of the phenylethylamino group does not coordinate.

The crystal structure of **2b** is also characterized by a quinone oxygen-coordinated square planar geometry, in which the palladium atom is deviated from the anthraquinone plane, as observed in **2a** (Figure 7 and Table 2). As **2b** crystallized in the space group $P\bar{1}$ with $Z = 4$, two independent molecules exist in the asymmetric unit. Noteworthy, they are present in a good mirror image relationship as depicted in Figure 8. However, the barrier of interconversion of these

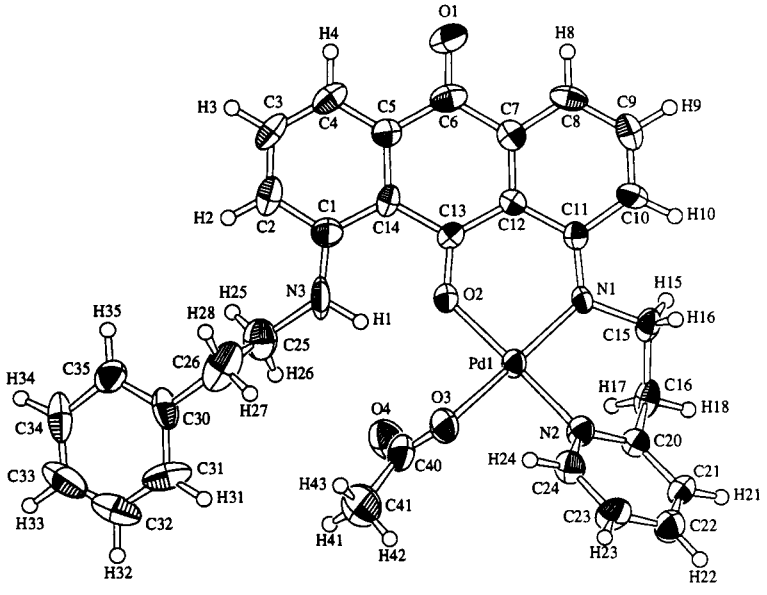

Figure 7. Molecular structure of **2b** (40% probability ellipsoids)

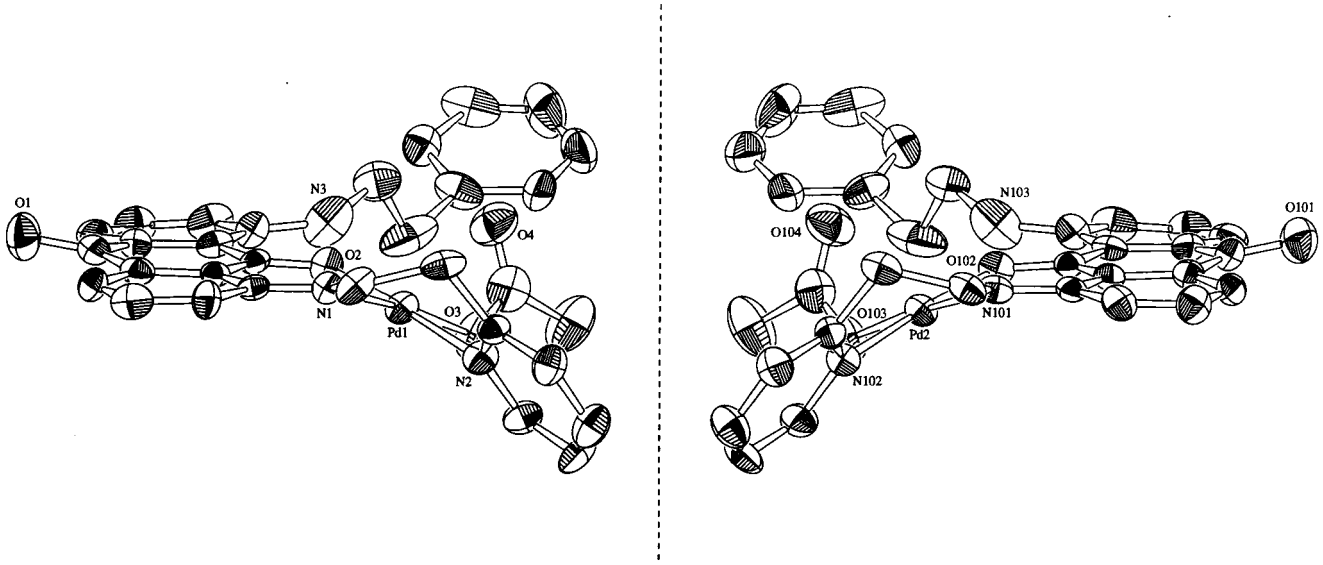

Figure 8. Conformational enantiomers of **2b** (40% probability ellipsoids); the enantiomorphs are related by the mirror plane

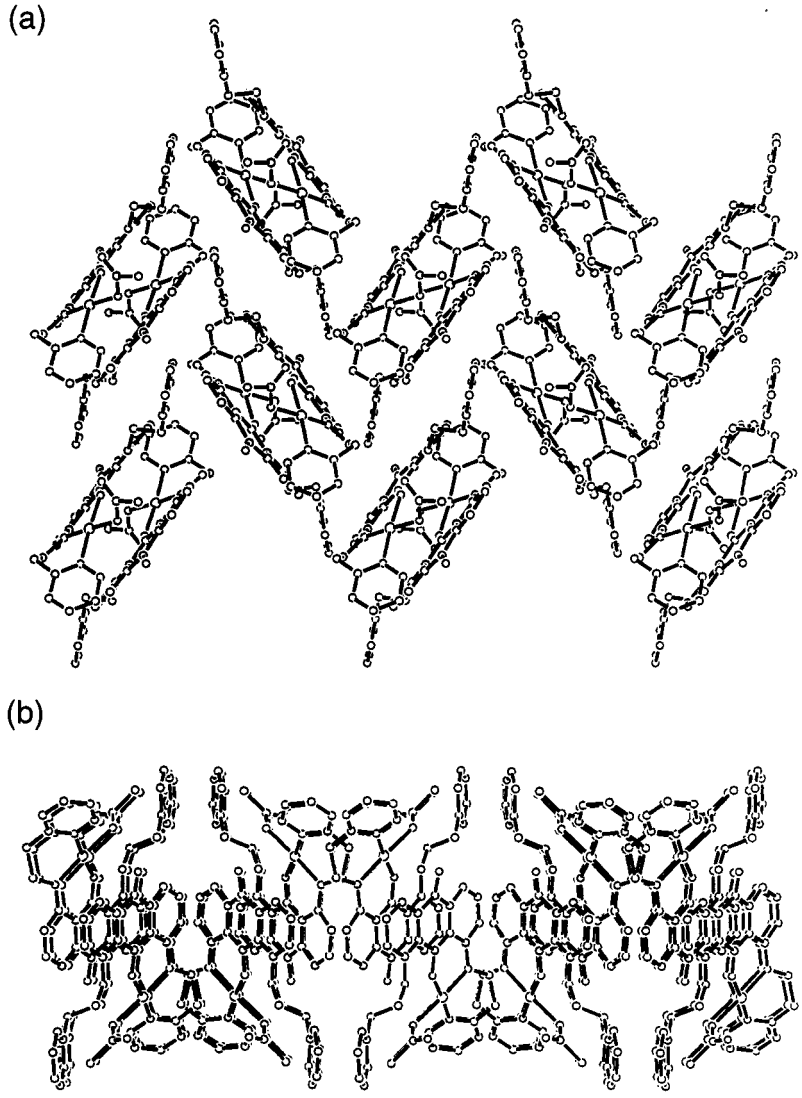

Figure 9. (a) Top view and (b) side view of the herringbone packing of the π-stack dimer in the crystal packing of **2b**

conformational enantiomers is low in solution. In the crystal packing (Figure 9), these enantiomers are present in a face-to-face manner with an interplanar distance of ca. 3.5 Å between the anthraquinone moieties, which form a π-

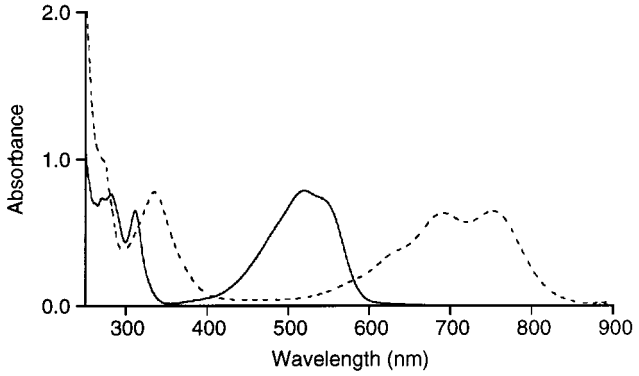

Figure 10. UV/Vis spectra of **1c** (−) (5.0×10^{-5} M) and **2c** (− −) (5.0×10^{-5} M) in CH_2Cl_2 under argon

stacked dimer that arranges in a herringbone motif with the virtues of offset stacking and edge-to-face contacts. Additionally, intramolecular hydrogen bonding between NH and C=O (quinone) [N(3)···O(2), 2.60 Å; H···O(2), 1.8 Å; N(103)···O(102), 2.60 Å; H···O(102), 1.8 Å] remains upon complexation.

Terminal bimetallic complexes with π-conjugated bridging spacers have recently received much attention as functional materials.[7] From this point of view, the construction of a conjugated bimetallic complex system with the 1,5-disubstituted anthraquinone ligand **1c** was examined. Treatment of **1c** with two equivalents of $Pd(OAc)_2$ in acetonitrile led to the formation of the conjugated palladium(II) homobimetallic complex **2c** as shown in Scheme 1. Only one kind of proton signal in ^1H NMR spectrum and only one C=O stretching

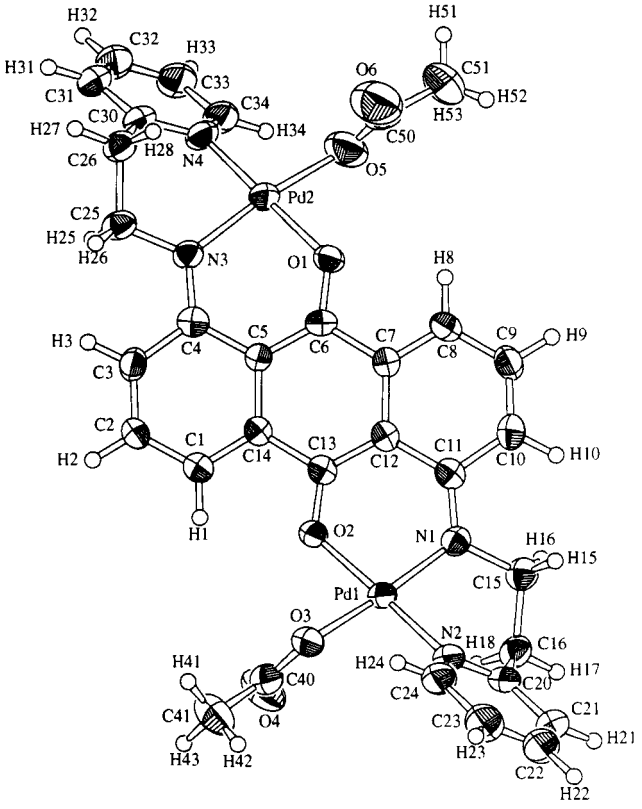

Figure 11. Molecular structure of **2c** (40% probability ellipsoids)

Table 4. Selected bond lengths [Å] and bond angles [°] for **2c**[a]

Bond lengths					
Pd(1)–O(2)	1.967(7)	1.962(7)	Pd(2)–O(1)	1.977(8)	1.960(8)
Pd(1)–O(3)	2.027(8)	2.039(8)	Pd(2)–O(5)	2.07(1)	2.034(8)
Pd(1)–N(1)	1.982(9)	1.974(9)	Pd(2)–N(3)	1.954(9)	1.969(9)
Pd(1)–N(2)	1.995(10)	2.02(1)	Pd(2)–N(4)	2.009(10)	2.010(9)
O(2)-C(13)	1.27(1)	1.27(1)	O(1)-C(6)	1.26(1)	1.26(1)
N(1)-C(11)	1.33(1)	1.33(1)	N(3)-C(4)	1.34(1)	1.36(1)
C(10)-C(11)	1.44(1)	1.43(1)	C(3)-C(4)	1.43(2)	1.43(1)
C(11)-C(12)	1.46(1)	1.45(1)	C(4)-C(5)	1.46(1)	1.45(1)
C(12)-C(13)	1.40(1)	1.42(1)	C(5)-C(6)	1.40(1)	1.39(1)
C(13)-C(14)	1.49(1)	1.48(1)	C(6)-C(7)	1.50(1)	1.48(1)
Bond angles					
O(2)–Pd(1)–O(3)	88.8(3)	85.4(3)	O(1)–Pd(2)–O(5)	88.2(4)	85.7(3)
O(2)–Pd(1)–N(1)	90.2(3)	91.4(3)	O(1)–Pd(2)–N(3)	90.0(3)	90.7(3)
O(3)–Pd(1)–N(2)	87.7(4)	90.2(4)	O(5)–Pd(2)–N(4)	88.5(4)	89.6(4)
N(1)–Pd(1)–N(2)	93.0(4)	93.0(4)	N(3)–Pd(2)–N(4)	92.5(4)	94.2(4)
O(2)–Pd(1)–N(2)	175.8(4)	173.8(4)	O(1)–Pd(2)–N(4)	174.9(4)	172.1(4)
O(3)–Pd(1)–N(1)	172.8(3)	176.8(3)	O(5)–Pd(2)–N(3)	168.9(4)	175.9(4)
C(13)-O(2)-Pd(1)	124.4(7)	128.7(7)	C(6)-O(1)-Pd(2)	124.1(7)	127.9(7)
C(11)-N(1)-Pd(1)	121.6(7)	124.4(7)	C(4)-N(3)-Pd(2)	123.8(8)	124.8(7)
O(2)-C(13)-C(14)	113.6(9)	115.1(9)	O(1)-C(6)-C(7)	114.3(9)	113.1(9)
O(2)-C(13)-C(12)	125.9(10)	124.3(10)	O(1)-C(6)-C(5)	125(1)	125.5(9)
C(11)-C(12)-C(13)	122.3(9)	123.3(9)	C(4)-C(5)-C(6)	123.1(9)	123.6(10)
C(12)-C(11)-N(1)	124.3(10)	125.1(10)	C(5)-C(4)-N(3)	123.1(10)	123.6(9)
C(10)-C(11)-N(1)	120(1)	119.9(9)	C(3)-C(4)-N(3)	120(1)	120.5(10)
C(11)-N(1)-C(15)	119.2(10)	117.1(9)	C(4)-N(3)-C(25)	116.6(9)	116.3(9)

[a] Two independent molecules exist in the asymmetric unit.

band (1620 cm^{-1}) in the FT-IR spectrum were detected, indicating the symmetrical coordination of two quinone oxygens to each palladium. Two low-energy bands with maxima around 753 and 691 nm were observed in the UV/Vis spectrum (Figure 10). The structure of **2c** was confirmed by an X-ray crystal structure determination (Figure 11 and Table 2). In the asymmetric unit, there are two independent molecules with almost the same conformation since **2c** crystallized in the space group $P\bar{1}$ with $Z = 4$. Selected bond lengths and bond angles are summarized in Table 4. Both quinone oxygens participate in the coordination to each palladium. The coordination geometry around both palladium centers is almost the same. Two palladium atoms are disposed on opposite faces of the anthraquinone plane, accompanied by the

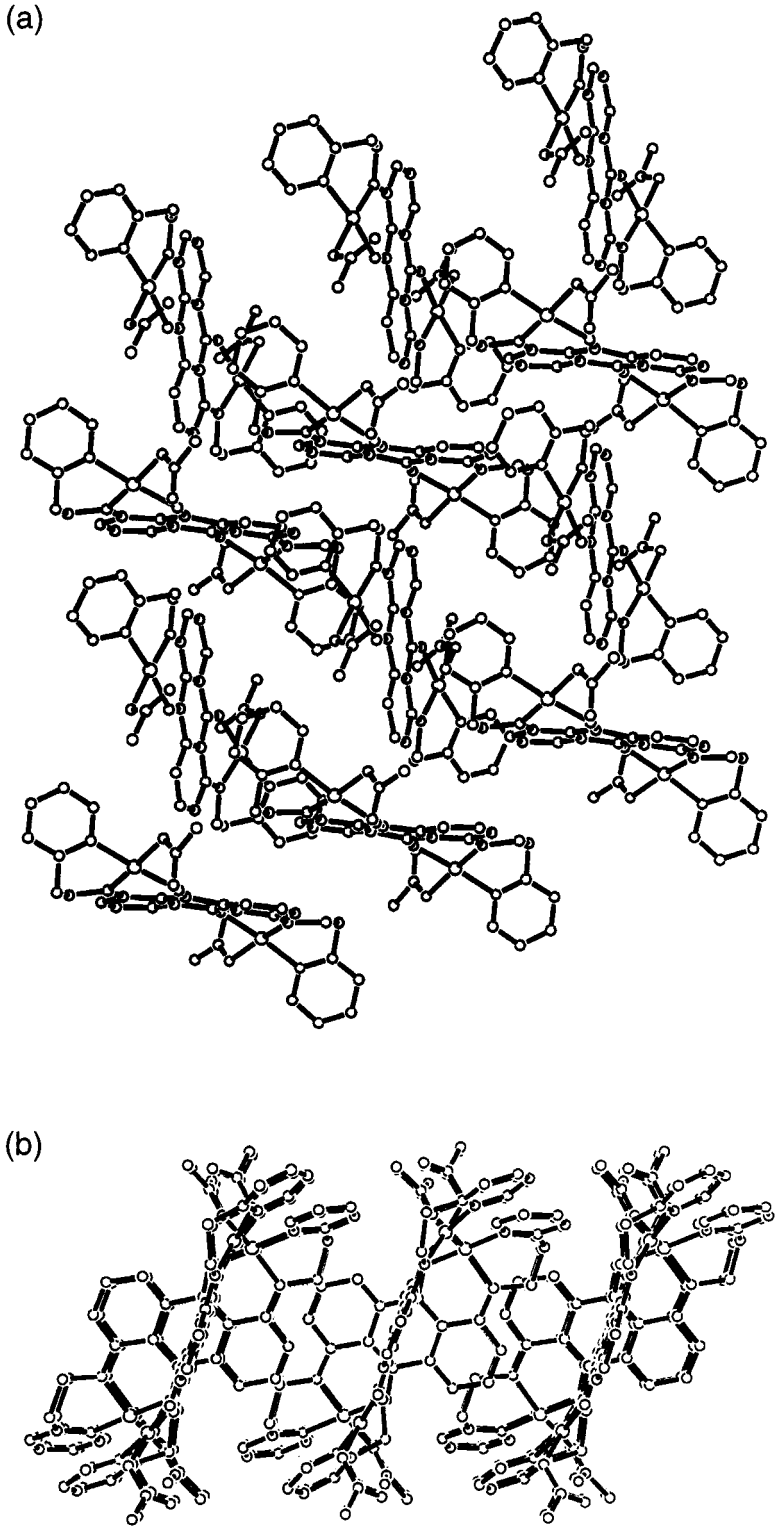

Figure 12. (a) Top view and (b) side view of the crystal packing diagram of **2c** showing edge-to-face π-π interactions

bend of quinone oxygens which lie out of the anthraquinone plane. Two palladium atoms are bridged by the quinone moiety to afford a redox-active conjugated homobimetallic complex. Two independent molecules are interconnected by an edge-to-face interaction between the anthraquinone rings in the crystal packing, as shown in Figure 12.

The redox properties of **1** and **2** were investigated by cyclic voltammetry in CH_2Cl_2. Electrochemical interest in the palladium(II) complexes in this study lies in the redox properties of the anthraquinone ligands because the complexation contributes to the electronic state. The redox potentials as listed in Table 1 are given vs. the standard Fc/Fc^+ redox couple. The quinone oxygen-coordinated palladium(II) complex **2a** shows two redox couples ($E_{1/2}$ = −1.73 V and −1.32 V vs. Fc/Fc^+) assignable to stepwise one-electron reductions of the anthraquinone moiety to give the corresponding reduced species. These redox couples are positively shifted relative to the free anthraquinone ligand **1a** ($E_{1/2}$ = −1.94 V and −1.44 V vs. Fc/Fc^+) as illustrated in Figure 13. As expected, the palladium(II) homobimetallic complex **2c** exhibits a more anodic shift due to the binding of two divalent palladium. Compared with the uncomplexed one, the complexed quinone is considered to be stabilized as an electron sink.

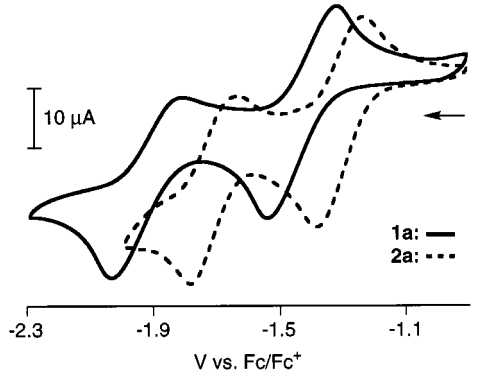

Figure 13. Cyclic voltammograms of **1a** (1.0×10^{-3} M) and **2a** (1.0×10^{-3} M) in CH_2Cl_2 (0.1 M nBu_4NClO_4) at a glassy carbon working electrode with scan rate = 100 mV/s under Ar

Conclusion

The anthraquinone ligands **1** bearing *N*-heterocyclic coordination sites have been shown to form the quinone oxygen-coordinated palladium(II) complexes. The X-ray crystal structure determination of the palladium(II) complex **2** indicates the coordination of the quinone oxygen to palladium. The conjugated palladium(II) homobimetallic complex **2c** was obtained in the case of the anthraquinone ligand bearing two *N*-heterocyclic coordination sites. The results reported in this paper reveal the aggregation properties of anthraquinone derivatives in a solid state. The anthraquinone ring plays an important role in the arrangement through the π-π interactions in the crystal packing. The quinone oxygen-coordinated palladium(II) complexes **2** exhibit two redox couples based on the quinone moiety, suggesting that the complexed quinones can be considered to be stabilized as an electron sink. In the palladium(II) complexes **2b−c**, the d,π-conjugated system is revealed to interconnect through π-π interactions between the π-conjugated systems. The controlled assembly of the redox-active conjugated complexes is envisaged to permit potential applications as functioning components of molecular devices.

Experimental Section

General Methods: All reagents and solvents were purchased from commercial sources and were further purified by standard methods, if necessary. Melting points were determined on a Yanagimoto Micromelting Point apparatus and were uncorrected. Infrared spectra were obtained with a Perkin−Elmer model 1605 FT-IR. ^1H NMR spectra were recorded on a Bruker AM-600 (600 MHz) or a JEOL JNM-GSX-400 (400 MHz) spectrometer with tetramethylsilane as an internal standard. Mass spectra were run on a JEOL JMS-DX303HF mass spectrometer. Electronic spectra were obtained using a Hitachi U-3000 spectrophotometer.

Synthesis of 1-Chloro-8-[2-(2-pyridyl)ethylamino]-9,10-anthraquinone (1a): A mixture of 1,8-dichloroanthraquinone (0.554 g, 2.0 mmol), 2-(2-aminoethyl)pyridine (1.22 g, 10.0 mmol), 4-dimethylaminopyridine (0.020 g, 0.16 mmol), and triethylamine (2.05 g, 20 mmol) in toluene (30 mL) was stirred under argon at reflux temperature for 7 days. After evaporation of the toluene in vacuo, the resulting mixture was dissolved in chloroform, washed with saturated $NaHCO_3$ aqueous solution and brine, and dried over $MgSO_4$. The anthraquinone ligand **1a** (reddish brown needles) was isolated in 68% yield by silica-gel column chromatography and purified by recrystallization from chloroform/hexane. − M.p. 168−170 °C (uncorrected). − R_f = 0.45 (ethyl acetate). − IR (KBr): $\tilde{\nu}$ = 3286 (NH), 1658 (C=O), 1635 (C=O) cm^{-1}. − ^1H NMR (400 MHz, CD_3CN): δ = 3.19 (t, J = 6.8 Hz, 2 H), 3.79 (q, J = 6.8 Hz, 2 H), 7.20 (ddd, J = 7.8, 4.9, 1.1 Hz, 1 H), 7.28 (dd, J = 8.7, 1.1 Hz, 1 H), 7.31 (ddd, J = 7.8, 1.1, 0.9 Hz, 1 H), 7.46 (dd, J = 7.4, 1.1 Hz, 1 H), 7.59 (dd, J = 8.7, 7.4 Hz, 1 H), 7.66 (dd, J = 8.0, 7.7 Hz, 1 H), 7.68 (td, J = 7.8, 1.9 Hz, 1 H), 7.82 (dd, J = 8.0, 1.4 Hz, 1 H), 8.18 (dd, J = 7.7, 1.4 Hz, 1 H), 8.56 (ddd, J = 4.9, 1.9, 0.9 Hz, 1 H), 9.60 (br, 1 H). − MS (EI): m/z = 362 [M^+]. − $C_{21}H_{15}N_2ClO_2$ (362.81): calcd. C 69.52, H 4.17, N 7.72, Cl 9.77; found C 69.26, H 4.09, N 7.64, Cl 9.86.

Synthesis of 1-(2-Phenylethylamino)-8-[2-(2-pyridyl)ethylamino]-9,10-anthraquinone (1b): A mixture of **1a** (0.36 g, 1.0 mmol), 2-phenylethylamine (0.30 g, 2.5 mmol), 4-dimethylaminopyridine (0.010 g, 0.10 mmol), and tripropylamine (1.43 g, 10 mmol) in xylene (20 mL) was stirred under argon at reflux temperature for 7 days. After evaporation of the xylene in vacuo, the resulting mixture was dissolved in chloroform, washed with saturated $NaHCO_3$ aqueous solution and brine, and dried over $MgSO_4$. The anthraquinone ligand **1b** (purple needles) was isolated in 53% yield by silica-gel column chromatography and purified by recrystallization from chloroform/hexane. − M.p. 183−184 °C (uncorrected). − R_f = 0.44 (ethyl acetate/chloroform 1:1 v/v). − IR (KBr): $\tilde{\nu}$ = 3263 (NH), 1658 (C=O), 1620 (C=O) cm^{-1}. − ^1H NMR (600 MHz, $CDCl_3$): δ = 3.08 (t, J = 7.4 Hz, 2 H), 3.24 (t, J = 7.1 Hz, 2 H), 3.59 (q, J = 7.4 Hz, 2 H), 3.77 (q, J = 7.1 Hz, 2 H), 7.04 (d, J = 8.5 Hz, 1 H), 7.10 (d, J = 8.5 Hz, 1 H), 7.18 (dd, J = 7.6, 4.7 Hz, 1 H), 7.26−7.29 (m, 2 H), 7.31−7.37 (m, 4 H), 7.48 (dd, J = 8.5, 7.6 Hz, 2 H), 7.55 (d, J = 7.6 Hz, 2 H), 7.62 (td, J = 7.6, 1.7 Hz, 1 H), 8.62 (dd, J = 4.7, 1.7 Hz, 1 H), 9.69 (br, 1 H), 9.73 (br, 1 H).

− MS (EI): m/z = 447 [M^+]. − $C_{29}H_{25}N_3O_2 \cdot 0.25H_2O$ (452.04): calcd. C 77.06, H 5.69, N 9.30; found C 77.04, H 5.57, N 9.29.

Synthesis of 1,5-Bis[2-(2-pyridyl)ethylamino]-9,10-anthraquinone (1c): A mixture of 1,5-dichloroanthraquinone (1.39 g, 5.0 mmol), 2-(2-aminoethyl)pyridine (3.05 g, 25 mmol), 4-dimethylaminopyridine (0.050 g, 0.40 mmol), and tripropylamine (7.16 g, 50 mmol) in toluene (70 mL) was stirred under argon at reflux temperature for 7 days. After evaporation of the toluene in vacuo, the resulting mixture was dissolved in chloroform, washed with saturated $NaHCO_3$ aqueous solution and brine, and dried over $MgSO_4$. The anthraquinone ligand **1c** (red brown needles) was isolated in 12% yield by silica-gel column chromatography and purified by recrystallization from chloroform/hexane. − M.p. 169−170 °C (uncorrected). − R_f = 0.30 (ethyl acetate). − IR (KBr): $\tilde{\nu}$ = 3255 (NH), 1620 (C=O) cm^{-1}. − ^1H NMR (400 MHz, CD_3CN): δ = 3.17 (t, J = 6.9 Hz, 4 H), 3.76 (q, J = 6.9 Hz, 4 H), 7.15 (dd, J = 8.5, 1.0 Hz, 2 H), 7.21 (ddd, J = 7.7, 4.9, 1.0 Hz, 2 H), 7.32 (ddd, J = 7.7, 1.0, 0.8 Hz, 2 H), 7.45 (dd, J = 7.5, 1.0 Hz, 2 H), 7.55 (dd, J = 8.5, 7.5 Hz, 2 H), 7.69 (td, J = 7.7, 1.9 Hz, 2 H), 8.54 (ddd, J = 4.9, 1.9, 0.8 Hz, 2 H), 9.70 (br, 2 H). − MS (EI): m/z = 448 (M^+). − $C_{28}H_{24}N_4O_2 \cdot 0.5H_2O$ (457.53): calcd. C 73.51, H 5.51, N 12.25; found C 73.29, H 5.33, N 12.15.

General Procedure for the Preparation of the Palladium(II) Complex 2: To anthraquinone ligand **1** (0.20 mmol) in acetonitrile (40 mL) was added an acetonitrile solution (10 mL) of $Pd(OAc)_2$ (44.9 mg, 0.20 mmol) under argon. For the preparation of **2c**, two equiv. of $Pd(OAc)_2$ were used. Stirring at room temperature for 5 h in the dark afforded a blue solution. After evaporation of the solvent in vacuo, the palladium(II) complex **2** was quantitatively isolated by recrystallization from acetonitrile.

2a: M.p. 235−236 °C (decomp.). − IR (KBr): $\tilde{\nu}$ = 1651 (C=O), 1620 (C=O) cm^{-1}. − ^1H NMR (400 MHz, CD_3CN): δ = 1.85 (s, 3 H), 3.26−3.30 (m, 2 H), 3.55−3.58 (m, 2 H), 7.27 (dd, J = 8.8, 1.8 Hz, 1 H), 7.30−7.36 (m, 3 H), 7.53 (d, J = 7.7 Hz, 1 H), 7.63 (dd, J = 8.0, 7.8 Hz, 1 H), 7.79 (dd, J = 8.0, 1.4 Hz, 1 H), 7.93 (td, J = 7.7, 1.6 Hz, 1 H), 8.14 (dd, J = 7.8, 1.4 Hz, 1 H), 8.49 (dd, J = 5.8, 1.6 Hz, 1 H). − MS (FAB): m/z = 469 [M − OAc + 1]$^+$. − $C_{23}H_{17}ClN_2O_4Pd \cdot H_2O$ (545.29): calcd. C 50.66, H 3.51, N 5.14, Cl 6.50; found C 50.74, H 3.51, N 5.38, Cl 6.55.

2b: M.p. 244−245 °C (decomp.). − IR (KBr): $\tilde{\nu}$ = 1643 (C=O), 1620 (C=O) cm^{-1}. − ^1H NMR (400 MHz, CD_2Cl_2): δ = 1.87 (s, 3 H), 2.94−2.98 (m, 2 H), 3.14−3.16 (m, 2 H), 3.51−3.56 (m, 4 H), 7.03−7.06 (m, 1 H), 7.08 (dd, J = 9.1, 1.1 Hz, 1 H), 7.20−7.31 (m, 7 H), 7.32 (dd, J = 6.9, 1.1 Hz, 1 H), 7.41 (ddd, J = 7.6, 1.4, 0.8 Hz, 1 H), 7.43−7.45 (m, 2 H), 7.83 (td, J = 7.6, 1.5 Hz, 1 H), 8.58 (ddd, J = 5.9, 1.5, 0.8 Hz, 1 H), 8.73 (br, 1 H). − MS (FAB) m/z = 553 [M − OAc + 1]$^+$. − $C_{31}H_{27}N_3O_4Pd \cdot 0.5H_2O$ (621.0): calcd. C 59.96, H 4.54, N 6.77; found C 60.07, H 4.49, N 7.07.

2c: M.p. 245−246 °C (decomp.). − IR (KBr): $\tilde{\nu}$ = 1620 (C=O) cm^{-1}. − ^1H NMR (600 MHz, CD_2Cl_2): δ = 1.86 (s, 6 H), 3.11−3.13 (m, 4 H), 3.43−3.46 (m, 4 H), 6.91 (d, J = 9.2 Hz, 2 H), 7.12 (dd, J = 9.2, 7.0 Hz, 2 H), 7.14 (ddd, J = 7.6, 5.6, 1.2 Hz, 2 H), 7.25 (d, J = 7.0 Hz, 2 H), 7.29 (dd, J = 7.6, 1.2 Hz, 2 H), 7.72 (td, J = 7.6, 1.4 Hz, 2 H), 8.47 (dd, J = 5.6, 1.4 Hz, 2 H). − MS (FAB): m/z = 660 [M − 2 OAc + 1]$^+$. − $C_{32}H_{28}N_4O_6Pd_2 \cdot CH_3CN$ (818.49): calcd. C 49.89, H 3.82, N 8.56; found C 49.25, H 3.61, N 8.95.

Electrochemical Experiments: The cyclic voltammetry measurements were performed on a BAS CV-50 W voltammetry analyzer in deaerated CH_2Cl_2, containing 0.1 M nBu_4NClO_4 as a supporting electrolyte, at 298 K, with a three-electrode system consisting of a highly polished glassy carbon working electrode (BAS), a platinum auxiliary electrode (BAS), and an Ag/AgCl (0.01 M) reference electrode (BAS), at 100 mV/s scan rate. Potentials are given vs. Fc/Fc^+ as an internal standard.

X-ray Crystal Structure Determination: All measurements for **1a**, **2a**, **2b**, and **2c** were made on a Rigaku AFC5R diffractometer with graphite monochromated Mo-K_α radiation and a rotating anode generator. The structures of **1a**, **2a**, and **2b** were solved by direct methods and expanded using Fourier techniques. The structure of **2c** was solved by heavy-atom Patterson methods and expanded using Fourier techniques. The non-hydrogen atoms were refined anisotropically. The H atoms involved in hydrogen bonding were located in electron density maps. The remainder of the H atoms were placed in idealized positions and allowed to ride with the C atoms to which each is bonded. Crystallographic details are given in Table 2. Crystallographic data (excluding structure factors) for the structures reported in this paper have been deposited with the Cambridge Crystallographic Data Centre as supplementary publication no. CCDC-146561 for **1a**, -146562 for **2a**, -146563 for **2b**, and -146564 for **2c**. Copies of the data can be obtained free of charge on application to CCDC, 12 Union Road, Cambridge CB2 1EZ, UK [Fax: (internat.) +44-1223/336-033; E-mail: deposit@ccdc.cam.ac.uk].

Acknowledgments

This work was financially supported in part by a Grant-in-Aid for Scientific Research on Priority Areas from the Ministry of Education, Science, and Culture, Japan. Thanks are also due to the Analytical Center, Faculty of Engineering, Osaka University for the use of their facilities.

[1] [1a] C. G. Pierpont, H. H. Downs, T. G. Rukavina, *J. Am. Chem. Soc.* **1974**, *96*, 5573. − [1b] R. M. Buchanan, S. L. Kessel, H. H. Downs, C. G. Pierpont, D. N. Hendrickson, *J. Am. Chem. Soc.* **1978**, *100*, 7894. − [1c] S. R. Sofen, D. C. Ware, S. R. Cooper, K. N. Raymond, *Inorg. Chem.* **1979**, *18*, 234. − [1d] C. G. Pierpont, R. M. Buchanan, *Coord. Chem. Rev.* **1981**, *38*, 45. − [1e] M. E. Cass, D. L. Greene, R. M. Buchanan, C. G. Pierpont, *J. Am. Chem. Soc.* **1983**, *105*, 2680. − [1f] M. W. Lynch, D. N. Hendrickson, B. J. Fitzgerald, C. G. Pierpont, *J. Am. Chem. Soc.* **1984**, *106*, 2041. − [1g] M. Haga, E. S. Dodsworth, A. B. P. Lever, *Inorg. Chem.* **1986**, *25*, 447. − [1h] H. Masui, A. B. P. Lever, P. R. Auburn, *Inorg. Chem.* **1991**, *30*, 2402. − [1i] D. M. Adams, A. Dei, A. L. Rheingold, D. N. Hendrickson, *Angew. Chem. Int. Ed. Engl.* **1993**, *32*, 880. − [1j] L. F. Joulié, E. Schatz, M. D. Ward, F. Weber, L. J. Yellowlees, *J. Chem. Soc., Dalton Trans.* **1994**, 799. − [1k] C. G. Pierpont, C. W. Lange, *Prog. Inorg. Chem.* **1994**, *41*, 331. − [1l] A. M. Barthram, R. L. Cleary, R. Kowallick, M. D. Ward, *Chem. Commun.* **1998**, 2695.

[2] [2a] J. E. Bäckvall, S. E. Byström, R. E. Nordberg, *J. Org. Chem.* **1984**, *49*, 4619. − [2b] J. E. Bäckvall, A. Gogoll, *Tetrahedron Lett.* **1988**, *29*, 2243. − [2c] J. E. Bäckvall, R. B. Hopkins, H. Grennberg, M. M. Mader, A. K. Awasthi, *J. Am. Chem. Soc.* **1990**, *112*, 5160. − [2d] A. Thorarensen, A. Palmgren, K. Itami, J. E. Bäckvall, *Tetrahedron Lett.* **1997**, *38*, 8541. − [2e] K. Bergstad, H. Grennberg, J. E. Bäckvall, *Organometallics* **1998**, *17*, 45.

[3] [3a] M. Hiramatsu, H. Nakano, T. Fujinami, S. Sakai, *J. Organomet. Chem.* **1982**, *236*, 131. − [3b] M. Hiramatsu, K. Shiozaki, T. Fujinami, S. Sakai, *J. Organomet. Chem.* **1983**, *246*, 203. − [3c] R. A. Klein, C. J. Elsevier, F. Hartl, *Organometallics* **1997**, *16*, 1284.

[4] [4a] S. S. Massoud, R. B. Jordan, *Inorg. Chem.* **1991**, *30*, 4851. − [4b] A. DelMedico, P. R. Auburn, E. S. Dodsworth, A. B. P. Lever, W. J. Pietro, *Inorg. Chem.* **1994**, *33*, 1583.

[5] T. Moriuchi, S. Bandoh, M. Miyaishi, T. Hirao, *Eur. J. Inorg. Chem.* in press.

[6] [6a] C. J. da Cunha, S. S. Fielder, D. V. Stynes, H. Masui, P. R. Auburn, A. B. P. Lever, *Inorg. Chim. Acta* **1996**, *242*, 293. – [6b] K. Ochiai, Y. Mazaki, S. Nishikiori, K. Kobayashi, S. Hayashi, *J. Chem. Soc., Perkin Trans. 2* **1996**, 1139. – [6c] B. S. Joshi, T. Rho, P. L. Rinaldi, W. Liu, T. A. Wagler, M. G. Newton, D. Lee, S. W. Pelletier, *J. Chem. Crystallogr.* **1997**, *27*, 553.

[7] [7a] M. Haga, T. Ano, K. Kano, S. Yamabe, *Inorg. Chem.* **1991**, *30*, 3843. – [7b] J.-P. Sauvage, J.-P. Collin, J.-C. Chambron, S. Guillerez, C. Coudret, V. Balzani, F. Barigelletti, L. De Cola, L. Flamigni, *Chem. Rev.* **1994**, *94*, 993. – [7c] W. Weng, T. Bartik, J. A. Gladysz, *Angew. Chem. Int. Ed. Engl.* **1994**, *33*, 2199. – [7d] M. D. Ward, *Chem. Soc. Rev.* **1995**, 121. – [7e] N. Le Narvor, L. Toupet, C. Lapinte, *J. Am. Chem. Soc.* **1995**, *117*, 7129. – [7f] A. Harriman, R. Ziessel, *Chem. Commun.* **1996**, 1707. – [7g] O. Lavastre, J. Plass, P. Bachmann, S. Guesmi, C. Moinet, P. H. Dixneuf, *Organometallics* **1997**, *16*, 184. – [7h] N. D. Jones, M. O. Wolf, D. M. Giaquinta, *Organometallics* **1997**, *16*, 1352. – [7i] M. M. Richter, A. J. Bard, W. Kim, R. H. Scmehl, *Anal. Chem.* **1998**, *70*, 310. – [7j] J. A. McCleverty, M. D. Ward, *Acc. Chem. Res.* **1998**, *31*, 842. – [7k] M. Hissler, A. El-ghayoury, A. Harriman, R. Ziessel, *Angew. Chem. Int. Ed.* **1998**, *37*, 1717. – [7l] T. Bartik, W. Weng, J. A. Ramsden, S. Szafert, S. B. Falloon, A. M. Arif, J. A. Gladysz, *J. Am. Chem. Soc.* **1998**, *120*, 11071. – [7m] E. C. Constable, C. E. Housecroft, E. R. Schofield, S. Encinas, N. Armaroli, F. Barigelletti, L. Flamigni, E. Figgemeier, J. G. Vos, *Chem. Commun.* **1999**, 869.

Received July 3, 2000
[I00264]

Rhodium(I) Complexes with $OPPy_2Ph$ and $OPPy_3$ (Py = 2-Pyridyl), and Their Behavior in Hydrogenation Reactions

Juan A. Casares,[a] Pablo Espinet,*[a] José M. Martín-Alvarez,[a] Gustavo Espino,[b] Mercedes Pérez-Manrique,[b] and Florencia Vattier[b]

Dedicated to Professor Angel Alberola on the occasion of his 70th birthday

Keywords: Alkenes / Hydrogenations / N ligands / Phosphanes / Rhodium

The reaction of $[Rh_2(\mu\text{-}Cl)_2(COD)_2]$ (COD = 1,5-cyclooctadiene) or $[Rh_2(\mu\text{-}Cl)_2(TFB)_2]$ (TFB = tetrafluorobenzobicyclo[2.2.2]octatriene) with the N-donor chelating ligand $OPPy_2Ph$ (Py = 2-pyridyl) in the presence of $TlBF_4$ affords cationic complexes $[Rh(diene)(OPPy_2Ph)](BF_4)$ (**1**, diene: COD; **2**, diene: TFB). Compounds **1** or **2** react with CO to give $[Rh(CO)_2(OPPy_2Ph)](BF_4)$ (**4**), which is also obtained by treatment of $[Rh_2(\mu\text{-}Cl)_2(CO)_4]$ with $OPPy_2Ph$ and $TlBF_4$. In a similar way, the complexes $[Rh(diene)(OPPy_3)](BF_4)$ (**5**, diene: COD; **6**, diene: TFB) are obtained when using $OPPy_3$; they react with CO to give $[Rh_2(\mu\text{-}CO)_3(OPPy_3)_2](BF_4)_2$ (**9**). The behavior of the complexes in solution is reported. The complexes with $OPPy_3$, **5** and **6**, show equivalence of the three Py groups in their NMR spectra. Complex **5** is square-planar in the solid state, and in solution, and the uncoordinated and coordinated Py groups undergo fast exchange in solution. Complex **6** is pentacoordinated in the solid state and in solution, and its Py groups exchange their coordination sites in a fast topomerization process. The single-crystal X-ray structures of **5** and **6** have been solved. The behavior of **1** and **5** as catalysts in hydrogenation reactions of cyclohexene, acetone, and cyclohexanone is also reported.

Introduction

Recent years have seen a renascence of interest in the study of multidentate nitrogen-donor ligands and their use in homogeneous catalysis.[1] N-donor ligands have some advantages over P-donors: mainly their higher stability towards oxidation, allowing a longer life for the catalysts. Because of this, cationic complexes of rhodium(I) with diolefins and N-donor ligands have been studied in catalyzed reduction processes of unsaturated organic compounds,[2] and the scope of these reactions has successfully been extended to the synthesis of chiral products, with fairly good enantiomeric excess.[1,3] Amongst the N-donor ligands, the most widely used are anionic substituted pyrazolylborates, because they can stabilize both rhodium(I) and rhodium(III) complexes, and it is possible to modulate the steric hindrance around the metal by properly choosing the substituents on the Pz rings.[4] The most important electronic variation that can be introduced onto ligands is a change in overall charge, and neutral tris-chelate ligands have indeed been tested in parallel with anionic pyrazolates $[HB(^RPz)_3]^-$. Good results have been obtained with substituted 1,4,7-triazacyclononane,[5] while other neutral *fac*-terdentate ligands, such as trispyrazolylmethane or trispyridylmethane have been less intensely studied in comparison.[6] Terdentate planar ligands such as *terpy* cannot be compared with the previous ones because of their very different geometrical restrictions and electronic properties.[7]

We have shown previously that, in Pd chemistry, $OPPy_2Ph$ (Py = 2-pyridyl) coordinates through the N atoms, in such a way that the two pyridyl rings are disposed obliquely respective to the coordination plane of the metal, giving rise to a six-membered ring in a "boat" conformation, with the Ph group lying above the metal.[8] $OPPy_3$ behaves similarly, but the third Py group can pentacoordinate the metal (as happens in some fluxional process intermediates), enabling $OPPy_3$ to act either as a bidentate or as a tridentate ligand. Pentacoordination might be more accessible for Rh than for in Pd. We report here the synthesis of complexes of rhodium(I) with these ligands and diolefins (COD = 1,5 cyclooctadiene and TFB = tetrafluorobenzobicyclo[2.2.2]octatriene) or carbon monoxide, as well as the behavior of the cationic diolefin complexes in catalytic hydrogenation of ketones and olefins.

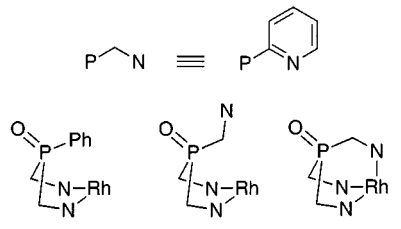

[a] Departamento de Química Inorgánica, Facultad de Ciencias, Universidad de Valladolid,
Prado de la Magdalena s.n., 47005 Valladolid, Spain
E-mail: espinet@qi.uva.es
[b] Departamento de Química, Facultad de Ciencias, Universidad de Burgos,
Pza. Misael Bañuelos, 09002 Burgos, Spain

 © WILEY-VCH Verlag GmbH, 69451 Weinheim, 2001 1434−1948/01/0101−0289 $ 17.50+.50/0

Results and Discussion

a) Complexes with $OPPy_2Ph$

The complexes $[Rh(COD)(OPPy_2Ph)](BF_4)$ (**1**) and $[Rh(TFB)(OPPy_2Ph)](BF_4)$ (**2**) were prepared as yellow, crystalline solids by treatment of $OPPy_2Ph$ with the corresponding $[Rh_2(\mu\text{-}Cl)_2(diene)_2]$ in the presence of $TlBF_4$. Their IR spectra in the solid state show the expected ν(P=O) band at wavelengths similar to those of the free ligands, which rules out coordination of the oxygen in the complexes .

Compounds **1** and **2** can adopt two conformations: with either the oxygen (**A**) or the aromatic free ring (**B**) towards the metal. In any case, the coordination plane of the metal is not a symmetry plane (Scheme 1). Their ^1H NMR spectra in $CDCl_3$ show signals for only one conformer in each case: six nonequivalent nuclei for the 1,5-COD ligand in **1**; and two aliphatic and two olefinic signals for **2**. In order to determine which conformer is present in solution, a NOESY spectrum of **1** was recorded. As shown in Figure 1, both olefinic protons give NOEs with the pyridine H-6, while one of them gives a clear NOE cross peak with the phenyl group. This supports conformer **B**, with the phenyl ring towards the metal; in line with the situation found for Pd[8] and analogous tris(pyrazolyl)borate complexes of rhodium(I).[4k−4m]

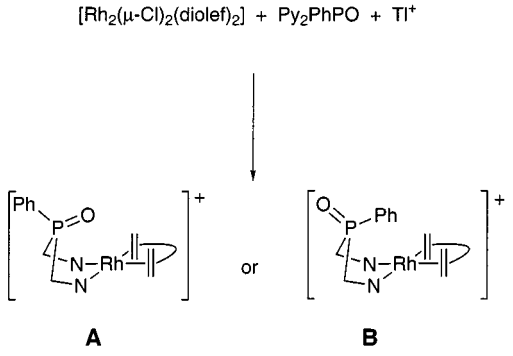

Scheme 1. Diolefin: COD (**1**); TFB (**2**)

In deuterated acetone, however, complexes **1** and **2** are fluxional and exhibit exchange between the upper and lower halves of the COD or TFB, respectively. Both feature olefinic protons in coalescence at room temperature, while at −60 °C these have split into two well defined signals. For **2**, this exchange is also observable in the ^{19}F NMR spectrum, which changes from an ABCD spin system pattern at −40 °C to an AA′BB′ one at room temperature (Figure 2). The ^{31}P NMR spectra are not affected by the exchange, showing only one doublet for each compound in all the temperature range studied. This suggests that the fluxionality observed in the ^1H and ^{19}F spectra is not associated with any conformational change in the coordinated ligand $OPPy_2Ph$. On the contrary, the solvent-dependence of the process strongly points to a pentacoordinated intermediate in which either the Py groups, the double bonds, or both, exchange their coordination sites. These fluxional processes are common in $[Rh(diene)(L-L)]^+$ complexes, and it has been shown that the exchange rate in noncoordinating solvents is increased by the presence of traces of Cl^- anions, or by adventitious acetone.[7,9,10]

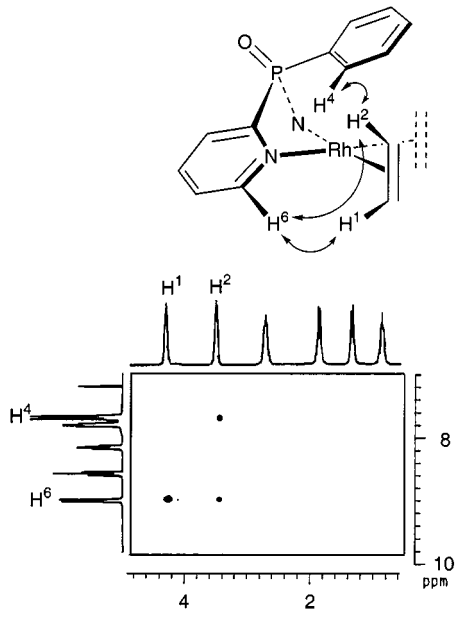

Figure 1. NOESY spectrum of **1** in $CDCl_3$ at 273 K

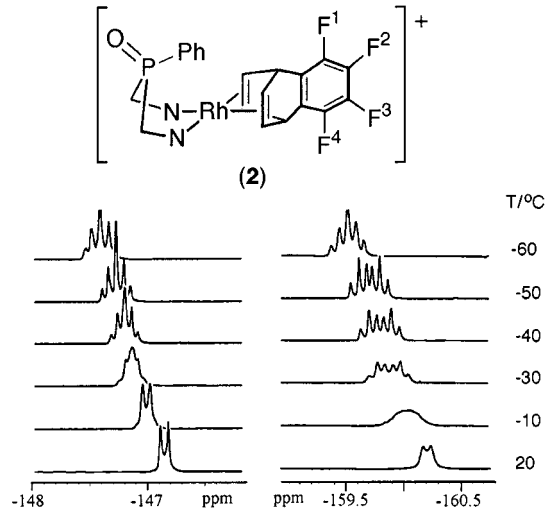

Figure 2. ^{19}F NMR spectra of **2** in $[D_6]$acetone at different temperatures. F^1 and F^4 (ca. −147) become equivalent at room temperature, due to diolefin rotation. The same is observed for F^2 and F^3 (ca. −160)

By bubbling CO through a dichloromethane solution of **1**, it is easy to obtain a dicarbonyl complex $[Rh(CO)_2(OPPy_2Ph)]BF_4$ (**3a**), which shows ν(CO) at 2104 and 2047 cm^{-1} [(Equation (1)].

$$[Rh(COD)(OPPy_2Ph)] + CO \rightarrow [Rh(CO)_2(OPPy_2Ph)]BF_4 + COD \quad (1)$$

Attempts at isolating neutral carbonyl complexes with $OPPy_2Ph$ were unsuccessful. The reaction of $[Rh_2(\mu\text{-}Cl)_2(CO)_4]$ with $OPPy_2Ph$ (1:1) was monitored in deuterated chloroform by NMR techniques. The ^{31}P and ^1H

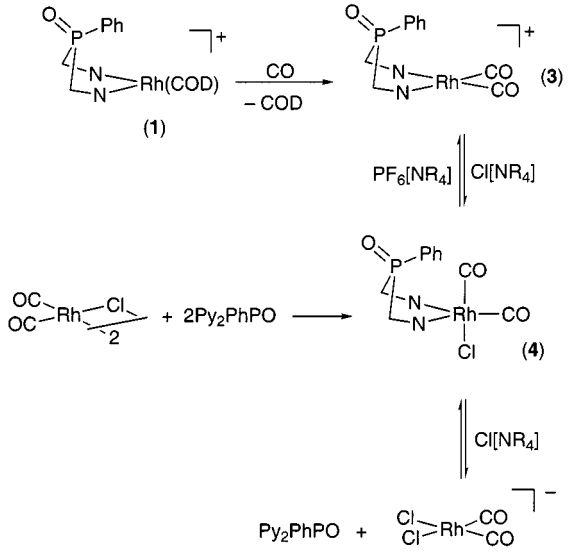

Scheme 2

NMR spectra at room temperature show a mixture of the cation in complex **3** (9%, presumably with Cl^- as the counter-anion), the desired chlorocarbonyl compound $[RhCl(CO)_2(OPPy_2Ph)]$ **4** (70%) and free ligand $OPPy_2Ph$ (21%) (Scheme 2). In agreement with the NMR results, the Infrared spectrum of a comparable solution in CH_2Cl_2 at room temperature shows six carbonyl bands, corresponding to a mixture of the three *cis* dicarbonyl complexes in equilibrium: two from the cationic compound **3**, two from the neutral chlorodicarbonyl complex **4** (at 2035 and 2095 cm^{-1}), and two corresponding to the anion $[Rh(Cl)_2(CO)_2]^-$ (at 2071 and 1995 cm^{-1}).[11] At −60 °C, there is a small change in the ratio of products, but no new signals appear. The addition of an excess of $[Et_3BzN]Cl$ to the solution shifts the equilibrium completely, displacing the $OPPy_2Ph$ ligand, and only $[Rh(Cl)_2(CO)_2]^-$ is observed in the IR spectrum. In contrast, the addition of a large amount of $[Bu_4N][PF_6]$ shifts the equilibrium toward **3**, and the other two complexes disappear.

The donor ability of the $OPPy_2Ph$-N,N ligand can be evaluated from the stretching bands of the carbonyl groups in the IR spectra of the complexes. For all of these, the ν(CO) values are shifted to higher frequency, not only relative to the analogous complexes with bipyridine, but also relative to the complexes with monodentate pyridine or other nonplanar chelating ligands like bispyrazolylmethane or bidentate imidazolyl ligands like $(mim)_2CH_2$ (mim = *N*-methylimidazol-2-yl).[12] Since the geometry of the ligand does not permit a good π interaction with the metal, this has to be attributed more to a poorer donor ability in the $OPPy_2Ph$-N,N ligand than to a higher π acceptor character. This is reinforced by the electron-withdrawing ability of the P=O group, compared to geometrically similar ligands such $(Py)_2S$.[12c] The overall effect is that $OPPy_2Ph$-N,N behaves as a rather labile N-donor ligand, which can easily be removed from the rhodium (I) complexes.

b) Complexes with $OPPy_3$

Diolefin Complexes

The diolefin complexes $[Rh(COD)(OPPy_3)](BF_4)$ (**5**) and $[Rh(TFB)(OPPy_3)](BF_4)$ (**6**) were prepared as yellow, crystalline solids by treatment of $OPPy_3$ with the corresponding $[Rh_2(\mu\text{-}Cl)_2(diene)_2]$ in the presence of $TlBF_4$ (Scheme 3). In these compounds, the $OPPy_3$ ligand can act either in bidentate or in tridentate fashion, giving tetracoordinated or pentacoordinated complexes, respectively. For ligands containing pyridyl groups, the values of $\nu(CN)_{Py}$ indicate whether they are coordinated or not:[9,13] the uncoordinated Py groups exhibit this band at 1574 cm^{-1}, but it moves to higher frequency when coordinated. The IR spectrum of **5** in the solid state shows two bands at 1587 and 1572 cm^{-1}, one of coordinated and one of free Py; thus the compound seems to be square-planar with only two coordinated Py groups. In contrast, the IR spectra of **6** in the solid state shows just one $\nu(CN)_{Py}$ absorption at 1586 cm^{-1}; hence the three Py groups are coordinated and the compound is pentacoordinated in the solid state. In agreement with this interpretation, the ν(P=O) bands in **5** (1206 cm^{-1}) appear at almost the same value as in the free ligand, while the coordination of the third Py group shifts this stretching band to 1230 cm^{-1} in **6**. This shift has previously been observed in other complexes in which the $OPPy_3$ ligand coordinates in a tridentate mode,[14] and is related to the decrease in the CPC angle around the phosphorus, which is accompanied by an increase in the P=O strength, as also observed, for instance, in strained cyclic ketones.[15−17]

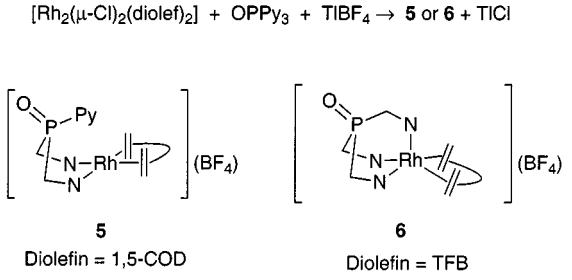

Scheme 3. Diolefin: COD (**5**); TFB (**6**)

In order to evaluate these structural hypotheses and other structural features, the structures of **5** and **6** were deter-

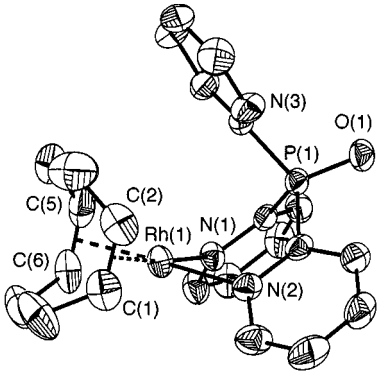

Figure 3. ORTEP plot of $[Rh(COD)(OPPy_3)](BF_4)$·acetone (**5**·Me_2CO)

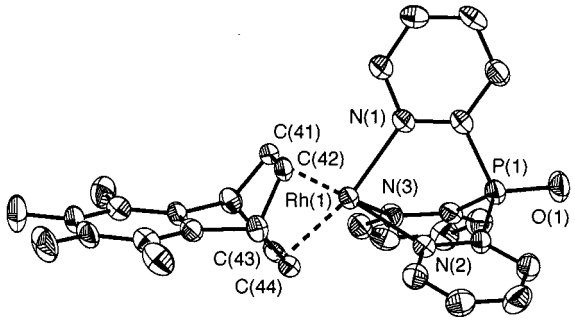

Figure 4. ORTEP plot of $[Rh(TFB)(OPPy_3)](BF_4)\cdot C_{2.5}O$ (**6**·$C_{2.5}O$)

Table 1. Selected bond lengths [pm] and angles [°] in $[Rh(COD)(OPPy_3)](BF4)\cdot Me_2CO$ (**5**·Me_2CO) and $[Rh(TFB)(OPPy_3)](BF_4)\cdot C_{2.5}O$ (**6**·$C_{2.5}O$)

5·Me_2CO		**6**·$C_{2.5}O$	
Bond lengths [Å]			
Rh(1)−N(1)	2.125(4)	Rh(1)−N(1)	2.126(6)
Rh(1)−N(2)	2.112(5)	Rh(1)−N(2)	2.279(5)
Rh(1)−C(1)	2.158(6)	Rh(1)−N(3)	2.269(5)
Rh(1)−C(2)	2.143(6)	Rh(1)−C(41)	2.061(6)
Rh(1)−C(5)	2.157(7)	Rh(1)−C(42)	2.068(6)
Rh(1)−C(6)	2.138(7)	Rh(1)−C(43)	2.169(7)
C(1)−C(2)	1.391(10)	Rh(1)−C(44)	2.155(7)
C(5)−C(6)	1.359(10)	C(41)−C(42)	1.436(9)
		C(43)−C(44)	1.366(10)
Bond angles [deg]			
N(2)−Rh(1)−N(1)	87.51(18)	C(41)−Rh(1)−N(1)	97.0(2)
N(2)−Rh(1)−C(6)	160.2(3)	C(42)−Rh(1)−N(1)	97.8(2)
N(1)−Rh(1)−C(6)	95.2(2)	N(1)−Rh(1)−C(44)	159.0(2)
N(2)−Rh(1)−C(2)	93.0(3)	N(1)−Rh(1)−C(43)	156.8(2)
N(1)−Rh(1)−C(2)	155.6(3)	C(41)−Rh(1)−N(3)	115.4(2)
N(2)−Rh(1)−C(5)	162.9(3)	C(42)−Rh(1)−N(3)	156.0(2)
N(1)−Rh(1)−C(5)	91.5(2)	N(1)−Rh(1)−N(3)	86.1(2)
N(2)−Rh(1)−C(1)	92.4(2)	C(44)−Rh(1)−N(3)	114.4(2)
N(1)−Rh(1)−C(1)	166.7(3)	C(43)−Rh(1)−N(3)	88.8(2)
		C(41)−Rh(1)−N(2)	154.4(2)
		C(42)−Rh(1)−N(2)	113.7(2)
		N(1)−Rh(1)−N(2)	86.4(2)
		C(44)−Rh(1)−N(2)	89.1(2)
		C(43)−Rh(1)−N(2)	116.3(2)
		N(3)−Rh(1)−N(2)	90.2(2)

mined by X-ray diffraction methods, and their corresponding ORTEP diagrams are shown in Figure 3 and Figure 4, respectively. Selected bond lengths and angles for both structures are listed in Table 1.

Molecular Structure of [Rh(COD)(OPPy$_3$)](BF$_4$)·Acetone (5·Acetone)

The rhodium atom has an essentially square-planar geometry. Its deviation from the plane defined by N1, N2, and the midpoints of the olefinic bonds is 0.038 Å. The neutral ligand is acting as an *N,N*-chelate, as expected, and the six-membered chelate ring shows a boat conformation. The Rh−N bond lengths (2.125 and 2.112 Å) are within the normal range for pyridine ligands bonded to Rh^I. The distance from the third nitrogen atom to the rhodium (3.975 Å) is clearly out of the bonding interaction range (sum of the van der Waals radii: 3.15 Å). The coordinated pyridyl rings are inclined relative to the coordination plane, making angles of 126.3° and 122.8°. The conformer found is the one that places the uncoordinated pyridyl ring above the coordination plane: similar to conformer **B** in Scheme 1. This structure should render the olefinic moieties above and below the coordination plane nonequivalent in the NMR.

Molecular Structure of [Rh(TFB)(OPPy$_3$)](BF$_4$)·xAcetone (6·xAcetone)

Its geometry can be described as distorted trigonal bipyramidal, with one of the nitrogen atoms (N1) and the midpoints of one olefinic bond (M2) in axial positions (angle N1−Rh1−M2 = 167.51°). The equatorial plane is defined by the other two nitrogen atoms (N2 and N3) and M1 (the midpoint between carbon atoms C41 and C42), with the rhodium atom lying 0.039 Å above this plane. From the rhodium, the distance to the axial nitrogen is shorter than those to the equatorial nitrogen atoms (2.126 vs. 2.279 and 2.269 Å), as found in other *tbp* structures.[18] The olefinic bond in the equatorial plane is longer than the one in the axial position, as a consequence of stronger π backbonding in the equatorial position. This effect also explains the shorter distances from rhodium to the carbon atoms in the equatorial double bond than to those in the axial double bond. Other interatomic distances in the TFB ligand are similar to the values obtained in other rhodium-TFB complexes. [19]

The hapticity of the $OPPy_3$ ligand (κ^2 or κ^3) depends on the diene coordinated to the rhodium. This dependence has been reported and studied for poly(pyrazolyl)borato complexes.[4i−4n] It has been proposed that dienes with a larger bite angle, such as COD, favor a κ^2 structure, while dienes with a smaller bite angle favor the κ^3 coordination mode. In complex **6**, the bite angle of the TFB ligand is 69.71°, resulting in a pentacoordinated structure with the three pyridyl rings bonded to the rhodium.

Behavior in Solution of Diolefin Complexes with OPPy$_3$

In spite of this solid state structural difference for **5** and **6**, in solution they behave more similarly. Their ^1H NMR spectra both show only one signal for all the olefinic protons, and the three Py rings are equivalent, while $J^{103}_{Rh-}{}^{31}_{P}$ is maintained even at high temperature (50 °C). The ^{19}F NMR spectrum of **6** corresponds to an AA′BB′ spin system, even at −60 °C. These data reveal the existence of fast intramolecular fluxional processes for both complexes; however, these are not the same in each case. In fact, their IR spectra in Cl_2CH_2 solution and in the solid state are almost identical. Hence, **5** remains square-planar [$\nu(CN)_{Py}$ at 1574 and 1589 cm^{-1}], with the free and the coordinated Py groups exchanging rapidly in solution. On the other hand, **6** remains pentacoordinated in solution [$\nu(CN)_{Py}$ at 1590 and 1586 cm^{-1}], and the observed equivalence of the Py groups and the fluorine nuclei is due to the fast exchange of coordination sites in the pentacoordinated complex.

Carbonyl Complexes

The carbonylation of **5** in dichloromethane gives a mixture of *cis*-dicarbonyls [ν(CO) at 2105 and 2049 cm^{-1}, and

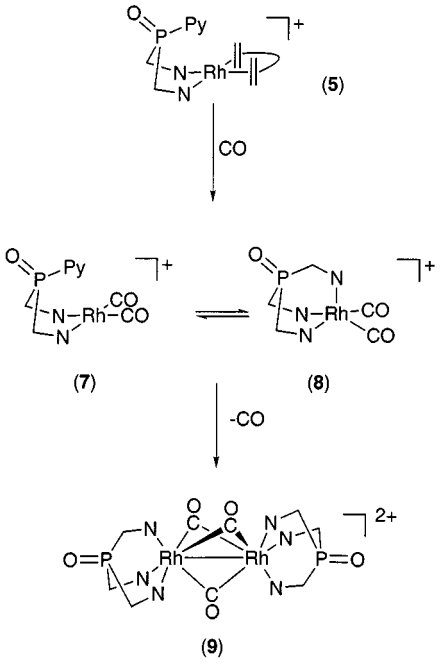

Scheme 4

at 2085 and 2021 cm^{-1}], corresponding to the formation of square-planar (**7**) and pentacoordinated (**8**) complexes (Scheme 4). This process is followed by the precipitation of an insoluble product with only one ν(CO) absorption at 1836 cm^{-1}, elemental analysis of which agrees with the formulation $[Rh_2(\mu\text{-}CO)_3(OPPy_3)_2](BF_4)_2$ (**9**). Analogous products are obtained when using triazacyclononane,[5a] $HCPz_3$,[6b] $MeGaPz_3$,[6c] or $[HBPz_3]^-$ [4k] as ligands. By removing the solvent and washing the resulting oil with n-hexane, it is possible to obtain a mixture of **7**, **8**, and **9a**, but if the oil is then redissolved in tetrahydrofuran and refluxed for 30 min, all the monomeric dicarbonyls are transformed into **9a**.

The carbonylation process was monitored by ^1H and ^{31}P NMR spectroscopy. A solution of **5** was prepared under nitrogen and cooled in an ice bath at 0 °C. After bubbling CO through for 10 min, the solution was placed in the NMR probe, previously thermostated at 0 °C. The spectrum showed that all the starting compound **5** had reacted, giving free cyclooctadiene, only one group of pyridyl signals in the ^1H NMR, and one doublet at 13.2 ($^3J_{Rh\text{-}P}$ = 7.12 Hz) in the ^{31}P NMR. The spectrum did not change on cooling to −60 °C, showing that the exchange between the square-planar and pentacoordinated isomers is very fast. After warming the sample to 0 °C, nitrogen was bubbled through the solution until **9** started to precipitate; the spectra recorded at this point showed a decrease in intensity of the aromatic signals assigned to (**7** + **8**) relative to the signals of the residual 1,5-COD, reflecting the insolubility of **9a**. After the NMR experiment, the solution was left at room temp. for one hour, and a yellow-green solid was formed. The solution was filtered and the solid was characterized as **9a** by its IR spectrum. A GC of the solution showed that 1,5-cyclooctadiene was the only organic product of the reaction.

The reaction of $OPPy_3$ with $[Rh_2(\mu\text{-}Cl)_2(CO)_4]$ in dichloromethane proceeds with CO evolution, to give $[Rh_2(\mu\text{-}CO)_3(OPPy_3)_2][RhCl_2(CO)_2]_2$ (**9b**) as a dark red, insoluble compound [ν(CO) = 2066, 1989, and 1834 cm^{-1}]. Attempts at obtaining a neutral chlorocarbonyl complex were unsuccessful.

c) Catalytic Experiments

The hydrogenation of cyclohexene, acetone, and cyclohexanone, using the cationic complexes **1** and **5** as catalysts, was examined. Significant hydrogenation rates were only observed above 50 °C. An almost linear increase of the rate of hydrogenation with pressure was found. Hydrogenation of a 1:1 mixture of cyclohexene and cyclohexanone showed a clear preference for the hydrogenation of cyclohexene. Representative catalytic experiments are summarized in Table 2.

Table 2. Results of the catalysis experiments

Complex	Time[a] [min]	Cyclohexanone	Acetone	Cyclohexene[b]
1[c]	30	4.6	2.1	27 (30)
1[c]	60	18	7.5	55 (57)
1[c]	120	43	18	78 (80)
5[c]	30	12	6.0	47 (40)
5[c]	60	20	10	67 (61)
5[c]	120	48	20	78 (64)
1[d]	30	3.1		30
1[d]	60	13		54
1[d]	120	29		72
5[d]	30	8.5		11
5[d]	60	19		47
5[d]	120	36		56

[a] Reaction conditions: Catalyst 0.014 mmol; Substrate 28 mmol; solvent: 18 mL of a solution of NaOH 0.04 mol dm^{-3} in methanol; $P(H_2)$ 10 bar; T: 80 °C. – [b] The data in parentheses have been obtained using pure methanol as solvent, without base. – [c] The substrate was only cyclohexanone, only acetone or only cyclohexene in each case. – [d] The substrate was a mixture of cyclohexanone (1.4 mmol) and cyclohexene (1.4 mmol).

The behavior of the two catalysts is very similar. The conversion rates obtained with **5** are slightly higher than with **1**, while the selectivity follows the opposite trend. In the light of the very different chemical behavior found for the complexes with $OPPy_3$ and $OPPy_2Ph$, a greater difference had been expected for the catalytic experiments. The similarity in catalytic behavior suggests that probably, thanks to the poor donor ability of the ligands under catalytic conditions (low concentration of complex, large excess of substrates, and high pressure of hydrogen), there is decoordination of the nitrogen ligand to give the active compound, the complexes with $OPPy_3$ and $OPPy_2Ph$ being the resting state for the catalyst. This hypothesis is further supported by the observation that addition of an excess of ligand to the solution (complex: ligand ratio = 1:1) leads to a nearly 50% decrease in catalytic activity.

Conclusion

The $OPPy_3$ and $OPPy_2Ph$ ligands are nitrogen-based ligands containing sp^2-hybridized nitrogen donors. Com-

pared with geometrically analogous anionic pyrazolylborates, both similarities and differences are found. They are very similar in coordination and dynamic behavior. However, 2-pyridylphosphane oxides are weaker ligands than pyrazolylborates. Because of this they are unable to withstand working conditions currently used in catalytic reactions.

Experimental Section

General Remarks: All manipulations were conducted with rigorous exclusion of air. Solvents were dried by known procedures and distilled under nitrogen prior to use. − ^{1}H NMR (300.16 MHz), ^{19}F NMR (282.4 MHz), and ^{31}P NMR (121.4 MHz) spectra were recorded on a Bruker ARX 300 instrument equipped with a VT-100 variable-temperature probe. Chemical shifts are reported from tetramethylsilane (^{1} H), CCl_3F (^{19}F), or H_3PO_4 (85%) (^{31}P), with positive shifts downfield, and at ambient probe temperature unless otherwise stated. NOESY experiments were carried out with a standard program, operating in phase-sensitive mode, with a 5% random variation in the evolution time, to avoid COSY cross-peaks, and with a mixing time equal to T_1 of the olefinic signals as measured by inversion recovery. − Combustion CHN analyses were made on a Perkin−Elmer 2400 CHN microanalyzer. − Infrared spectra were recorded on a Perkin−Elmer 843 (range 4000−200 cm^{-1}) with Nujol mulls between polyethylene sheets, or in dichloromethane solution between NaCl plates. − The catalytic reactions were monitored by GLC on a Hewlett−Packard II 5890, using an HP-FFAP column and with mesitylene as internal standard. The precursors $[Rh_2(\mu\text{-}Cl)_2(1,5\text{-}COD)_2]$,[20] $[Rh_2(\mu\text{-}Cl)_2(TFB)_2]$,[21] $[Rh_2(\mu\text{-}Cl)_2(CO)_4]$ and the ligands $OPPy_2Ph$ and $OPPy_3$ were prepared by published methods.[22]

$[Rh(OPPy_2Ph)(COD)]BF_4$ (1): A suspension of $[Rh_2(\mu\text{-}Cl)_2(COD)_2]$ (200 mg, 0.41 mmol) in acetone (20 mL) was treated with $TlBF_4$ (236 mg, 0.81 mmol) and $OPPy_2Ph$ (238 mg, 0.85 mmol). After 30 min stirring at room temperature, the TlCl was filtered off and the yellow solution was concentrated to dryness in vacuum. The yellow residue was recrystallized from dichloromethane-diethyl ether, washed with diethyl ether and vacuum dried. Yield 409 mg (87%). − $C_{24}H_{25}BF_4N_2OPRh$ (578.16): calcd. C 49.86, H 4.36, N 4.82; found C 49.68, H 4.16, N 4.57. − ^{1}H NMR ($CDCl_3$): δ = 8.93 (m, 2 H), 8.56 (m, 2 H), 8.11 (m, 2 H), 7.82 (m, 3 H), 7.63 (m, 4 H), 4.14 (m, 2 H), 3.44 (m, 2 H), 2.64 (m, 2 H), 1.82 (m, 2 H), 1.22 (m, 2 H), 0.85 (m, 2 H). − ^{31}P NMR: δ = 18.7 (d, $^3J_{Rh\text{-}P}$ = 7.56 Hz). − IR (Nujol mull): $\nu(CN)_{Py}$ 1587 cm^{-1}; ν(P=O) 1203 cm^{-1}.

$[Rh(TFB)(OPPy_2Ph)]BF_4$ (2): A suspension of $[Rh_2(\mu\text{-}Cl)_2(TFB)_2]$ (100 mg, 0.14 mmol) in acetone (15 mL) was treated with $TlBF_4$ (80 mg, 0.28 mmol) and $OPPy_2Ph$ (77 mg, 0.28 mmol). After 30 min stirring at room temperature, the TlCl was filtered off and the yellow solution was concentrated to dryness in vacuum. The yellow residue was recrystallized from dichloromethane-diethyl ether, washed with diethyl ether and vacuum dried. Yield 139 mg (73%). − $C_{28}H_{19}BF_8N_2OPRh$ (696.2): calcd. C 48.31, H 2.75, N 4.02; found C 48.71, H 2.90, N 4.03. . − ^{1}H NMR ([D$_6$]acetone): δ = 9.04 (m, 2 H), 8.36 (m, 2 H), 8.14 (m, 2 H), 3.94 (m, 4 H), 1.65 (m, 4 H), 1.83 (m, 4 H). − ^{31}P NMR: δ = 18.6 (d, $^3J_{Rh\text{-}P}$ = 6.8 Hz). − ^{19}F NMR: δ = −147.15 (m, 2 F), −150.1 (4 F, BF_4^-), −160.20 (m, 2 F). − IR (Nujol mull): $\nu(CN)_{Py}$ 1589 cm^{-1}; ν(P=O) 1214 cm^{-1}.

$[Rh(CO)_2(OPPy_2Ph)]BF_4$ (3a): Carbon monoxide was bubbled through a solution of **1** (130 mg 0.225 mmol) in dichloromethane (20 mL) for 2 h. The resulting pale yellow solution was concentrated to 5 mL and diethyl ether was added. The yellow solid formed was filtered off, washed with diethyl ether and vacuum dried. Yield 80 mg (67%). − $C_{18}H_{13}BF_4N_2O_3PRh$ (525.9): calcd. C 41.09, H 2.47, N 5.34; found C 41.22, H 2.53, N 5.22. − ^{31}P NMR: δ = 19.6 (d, $^3J_{Rh\text{-}P}$ = 9.6 Hz). − ^{1}H NMR ($CDCl_3$): δ = 9.23 (m, Py), 8.58 (m), 8.22 (m), 7.82 (m), 7.64 (m, Ph). − IR (Nujol mull): ν(CO) 2092, 2035 cm^{-1}; $\nu(CN)_{Py}$ 1594 cm^{-1}; ν(P=O) 1212 cm^{-1}.

Reaction of $[Rh_2(\mu\text{-}Cl)_2(CO)_2]$ with $OPPy_2Ph$: $Rh_2(\mu\text{-}Cl)_2(CO)_4$ (220 mg, 0.55 mmol) and $OPPy_2Ph$ (320 mg, 1.1 mmol) were dissolved in 20 mL of dichloromethane. The solution was split into three aliquots; one was used as reference, another was used to study by IR the effect of adding $[Et_3BzN]Cl$, and the third was used to study by IR the reactivity with $[Bu_4N][PF_6]$.

$[Rh(CO)_2(OPPy_2Ph)][RhCl_2(CO)_2]$ (3b): $Rh_2(\mu\text{-}Cl)_2(CO)_4$ (110 mg, 0.27 mmol) and $OPPy_2Ph$ (80 mg, 0.27 mmol) were dissolved in 10 mL of dichloromethane. The solution was filtered and 5 mL of ethanol were added. After concentration to 5 mL, **3b** crystallized as yellow plates. Yield 135 mg (73%). − $C_{20}H_{13}Cl_2N_2O_5PRh_2$ (669.00): calcd. C 35.70, H 1.93, N 4.16; found C 35.91, H 2.00, N 4.11. − ^{31}P NMR ([D$_6$]acetone): δ = 19.97 (d, $^3J_{Rh\text{-}P}$ = 7.4 Hz). − ^{1}H NMR ([D$_6$]acetone): δ = 9.49 (m, Py), 8.68 (m), 8.56 (m), 8.01 (m), 7.86 (m, Ph), 7.78 (m), 7.51 (m). − IR: ν(CO) 2098, 2065, 2038, 1991 cm^{-1}; $\nu(CN)_{Py}$ 1590 cm^{-1}; ν(PO) 1213 cm^{-1}.

$[Rh(COD)(OPPy_3)]BF_4$ (5): The procedure was as described for **1**, but $OPPy_3$ (237 mg, 0.85 mmol) was added instead of $OPPy_2Ph$. Yield 790 mg (84%). − $C_{23}H_{24}BF_4N_3OPRh$ (579.2): calcd. C 47.70, H 4.18, N 7.26; found C 47.55, H 4.15, N 7.12. − ^{31}P NMR: δ = 14.7 (d, $^3J_{Rh\text{-}P}$ = 5.56 Hz). − ^{1}H NMR: δ = 9.00 (m, Py), 8.33 (m), 8.13 (m); 3.91, 1.65 and 1.86 (br. signals, COD). − IR (Nujol mull): $\nu(CN)_{Py}$ 1587 and 1572 cm^{-1}, ν(P=O) 1206 cm^{-1}. Single crystals of $5{\cdot}Me_2CO$ suitable for X-ray diffraction were formed by slow diffusion of a solution of the complex in acetone-ethanol (2:1) and *n*-hexane at room temperature.

$[Rh(TFB)(OPPy_3)]BF_4$ (6): The procedure was as described for **2**, but $OPPy_3$ (77 mg, 0.14 mmol) was used instead of $OPPy_2Ph$. Yield 135 mg (70%). − $C_{27}H_{18}BF_8N_3OPRh$ (697.1): calcd. C 46.52, H 2.60, N 6.03, found C 46.58, H 2.73, N 5.98. − ^{31}P NMR ([D$_6$]acetone): δ = 3.0 (d, $^3J_{Rh\text{-}P}$ = 6.8 Hz). − ^{19}F NMR: δ = −147.2 (m, 2 F), −150.3 (4 F, BF_4^-), −160.5 (m, 2 F). − ^{1}H NMR: δ = 9.64 (m, Py), 8.65 (m), 8.43 (m) and 7.96 (m), 6.13 (m, TFB) and 3.94 (m). − IR (Nujol mull): ν_{Py}(CN) 1586 cm^{-1}, νP=O 1230 cm^{-1}. Single crystals of $\mathbf{6}{\cdot}x Me_2CO$ suitable for X-ray diffraction were formed by slow diffusion of a solution of the complex in acetone-ethanol (2:1) into *n*-hexane at room temperature.

$[Rh_2(\mu\text{-}CO)_3(OPPy_3)_2](BF_4)_2$ (9a): Carbon monoxide was bubbled through a solution of **2** (150 mg 0.235 mmol) in dichloromethane (20 mL) for 2 h. The solvent was evaporated and the residue was dissolved in THF (10 mL) and refluxed for 30 min. The insoluble green solid formed was filtered off, washed with diethyl ether and vacuum dried. Yield 72 mg (60%). − $C_{33}H_{24}B_2F_8N_6O_5P_2Rh_2$ (1026.0): calcd. C 38.63, H 2.34, N 8.22; found C 38.70, H 2.41, N 8.17. − IR (Nujol mull): ν(CO) 1836 cm^{-1}; $\nu(CN)_{Py}$ 1593 cm^{-1}; ν(PO) 1236 cm^{-1}.

$[Rh_2(\mu\text{-}CO)_3(OPPy_3)_2][RhCl_2(CO)_2]_2$ (9b): $[Rh_2(\mu\text{-}Cl)_2(CO)_4]$ (100 mg, 0.25 mmol) and Py_3PO (155 mg, 0.55 mmol) were dissolved in 10 mL of dichloromethane; the solution was stirred until the CO evolution ceased (two hours). The insoluble dark red solid

Table 3. Crystal data and structure refinement for **5**·Me_2CO and **6**·$C_{2.5}O$

	5·Me_2CO	**6**·$C_{2.5}O$
	Crystal Data	
Empirical formula	$C_{26}H_{30}BF_4N_3O_2PRh$	$C_{29.5}H_{18}BF_8N_3O_2PRh$
Formula weight	637.22	743.16
Crystal system	Monoclinic	Monoclinic
Space group	$P2_1/n$	$C2/c$
a [Å]	8.572(2)	29.868(6)
b [Å]	16.374(5)	10.775(2)
c [Å]	19.790(5)	18.064(3)
β [deg]	99.192(5)	99.960(4)
V [Å^3]	2741.9(13)	5725.8(18)
Z	4	8
$D_{calcd.}$ [g cm^{-3}]	1.544	1.724
Absorption coefficient [mm^{-1}]	0.737	0.740
F(000)	1296	2952
Crystal size [mm]	0.04 × 0.10 × 0.11	0.03 × 0.11 × 0.11
	Data Collection	
Temperature [K]	303(2)	293(2)
Theta range for data collection	1.62 to 21.98°	2.01 to 23.31°
Wavelength [Å]	0.71073 (Mo-K_α)	0.71073 (Mo-K_α)
Index ranges	$-9 \le h \le 8$, $0 \le k \le 17$, $0 \le l \le 20$	$-33 \le h \le 32$, $0 \le k \le 11$, $0 \le l \le 20$
Reflections collected	10834	13388
Independent reflections	3336 (R_{int} = 0.0550)	4128 (R_{int} = 0.0487)
Observed reflections [$I > 2\sigma(I)$]	2196	2880
	Refinement	
Data/restraints/parameters	3336/0/345	4128/0/411
Goodness-of-fit on F^2	0.901	1.006
Final R indices [$I > 2\sigma(I)$]	R_1 = 0.0419, wR_2 = 0.0953	R_1 = 0.0506, wR_2 = 0.1388
R indices (all data)	R_1 = 0.0722, wR_2 = 0.1037	R_1 = 0.0773, wR_2 = 0.1583
Largest diff. peak and hole [e Å^{-3}]	0.571 and −0.364	2.483 and −0.505

formed, $[Rh_2(\mu\text{-}CO)_3(OPPy_3)_2][RhCl_2(CO)_2]_2$ was filtered, washed with dichloromethane and vacuum dried. Yield 145 mg (80%). − $C_{37}H_{24}Cl_4N_6O_9P_2Rh_4$ (1312.2): calcd. C 33.90, H 1.85, N 6.40; found C 33.91, H 1.80, N 6.42.

X-ray Crystallography: Suitable single crystals were mounted on glass fibers, and diffraction measurements were made using a Bruker SMART CCD area-detector diffractometer with Mo-K_α radiation (λ = 0.71073 Å).[23] Intensities were integrated from several series of exposures, each exposure covering 0.3° in ω, the total data set being a hemisphere.[24] Absorption corrections were applied, based on multiple and symmetry-equivalent measurements.[25] The structure was solved by Patterson synthesis or direct methods and refined by least-squares on weighted F^2 values for all reflections (see Table 3).[26] All nonhydrogen atoms were assigned anisotropic displacement parameters and refined without positional constraints. Hydrogen atoms were taken into account at calculated positions and their positional parameters were refined. Refinement proceeded smoothly to give R_1 = 0.0419 for **5**·acetone and R_1 = 0.0621 for **6**, based on the reflections with $I > 2\sigma(I)$. Further refinement for **6**, including a molecule of acetone with one carbon in a special position led to a final R_1 value of 0.0505 for **6**·$C_{2.5}O$. Hydrogen atoms of the acetone in **6**·$C_{2.5}O$ were not included in the calculations. Complex neutral-atom scattering factors were used.[27] Crystallographic data (excluding structure factors) for the structures **5**·acetone and **6**·$C_{2.5}O$ reported in this paper have been deposited with the Cambridge Crystallographic Data Centre as Supplementary Publication numbers CCDC-144233 (**5**·Me_2CO) and CCDC-144234 (**6**·$C_{2.5}O$). Copies of the data can be obtained free of charge on application to the CCDC, 12 Union Road, Cambridge CB2 1EZ, U.K. [Fax: (internat.) +44-1223/336-033; E-mail: deposit@ccdc.cam.ac.uk].

Catalytic Experiments. − Hydrogenation with Molecular Hydrogen: In each experiment, 0.014 mmol of the rhodium complex and 28 mmol of the substrate were dissolved in 18 mL of a 0.04 M solution of sodium hydroxide in methanol. After stirring for some minutes in order to dissolve the complex completely, the solution was transferred to a previously deaerated high pressure reactor containing a magnetic bar for stirring the solution; the reactor was then filled with the desired pressure of hydrogen and connected to a thermostated oil bath. The course of the reaction was followed by taking a sample of the solution at different times and refilling the reactor to the previous pressure. The solutions were analyzed by GC. The homogeneity of the catalysis was tested by adding a large excess of mercury to the reaction vessel (Hg:catalyst = 100:1).

Acknowledgments

Financial support by the Dirección General de Enseñanza Superior (Project No. PB96−0363) and the Junta de Castilla y León (Project No. VA18/97) are gratefully acknowledged.

[1] A. Togni, L. M.Venanzi, *Angew. Chem. Int. Ed. Engl.* **1994**, *33*, 497−526, and references therein.
[2] [2a] B. R. James, *Homogeneous Hydrogenation,* Wiley Interscience, New York, **1973**. − [2b] R. S. Dickson *Homogeneous Catalysis with Compounds of Rhodium and Iridium*, D. Reidel, Dordrecht, **1985**. − [2c] P. J. Collman, L. S. Hegedus, R. G. Norton, R. G. Finke, *Principles and Applications of Organotransition Metal Chemistry*, M. Walley, **1987**, Chap. 10.
[3] [3a] H. Takaya, O. Tetsuo, T. R. Noyori, Chap. 1 in *Catalytic*

Asymmetric Synthesis (Ed.: I. Ojima), VCH, New York, **1993**. – [3b] G. Zassinovich, G. Mestroni, S. Cladiali, *Chem. Rev.* **1992**, *92*, 1051–1069.

[4] [4a] S. Trofimenko, *Chem. Rev.* **1993**, *93*, 943–980. – [4b] N. Kitajima, W. B. Tolman, *Prog. Inorg. Chem.* **1995**, *43*, 419–531; for recent examples see: [4c] A. F. Hill, A. J. P. White, D. J. Williams, J. D. E. T. Wilton-ely, *Organometallics* **1998**, *17*, 3152–3154. – [4d] S. Ikeda, Y. Maruyama, F. Ozawa, *Organometallics* **1998**, *17*, 3770–3774. – [4e] T. O. Northcutt, R. J. Lachicotte, W. D. Jones, *Organometallics* **1998**, *17*, 5148–5152. – [4f] D. D. Wick, T. O. Northcutt, R. J. Lachicotte, W. D. Jones, *Organometallics* **1998**, *17*, 4484–4492. – [4g] W. J. Oldman, D. M. Heinekey, *Organometallics* **1997**, *16*, 467–470. – [4h] H. Katayama, K. Yamamura, Y. Miyaki, F. Ozawa, *Organometallics* **1997**, *16*, 4497–4500. – [4i] M. Akita, K. Ohta, Y. Takahasi, S. Hikichi, Y. Moro-Oka, *Organometallics* **1997**, *16*, 4121–4128. – [4j] N. G. Connelly, D. J. H. Emslie, B. Metz, A. G. Orpen, M. J. J. C. S. Quayle, *Chem. Commun.* **1996**, 2289–2290. – [4k] D. Sanz, M. D. Santa-María, R. M. Claramunt, M. Cano, J. V. Heras, J. A. Campo, F. A. Ruíz, E. Pinilla, A. Monge, *J. Organomet. Chem.* **1996**, *526*, 341–350. – [4l] U. E. Bucher, A. Currao, R. Nesper, H. Rüeger, L. M. Venanzi, E. Younger, *Inorg. Chem.* **1995**, *34,* 66–74. – [4m] M. Cocivera, T. J. Desmond, G. Ferguson, B. Kaitner, F. J. Lalor, D. J. O′Sullivan, *Organometallics* **1982**, *1*, 1125–1132. – [4n] M. Cocivera, G. Ferguson, B. Kaitner, F. J. Lalor, D. J. O′Sullivan, M. Parvez, B. Ruhl, *Organometallics* **1982**, *1*, 1132–1139.

[5] [5a] B. de Bruin, J. J. Donners, R. de Gelder, J. M. Smits, A. W. Gal, *Eur. J. Inorg. Chem.* **1998**, 401–406. – [5b] H. Zhen, C. Wang, Y. Hu, T. C. Flood, *Organometallics* **1998**, *17*, 5397–5405. – [5c] B. de Bruin, M. J. Boerakker, J. J. Donners, B. E. Christiaans, P. P. Schlebos, R. de Gelder, J. M. Smits, A. L. Spek, A. W. Gal, *Angew. Chem. Int. Ed. Engl.* **1997**, *36*, 19, 2064–2067. – [5d] R. Zhou, C. Wang, Y. Hu, T. C. Flood, *Organometallics* **1997**, *16*, 434–441. – [5e] L. Wang, J. R. Sowa, C. Wang, R. S. Lu, P. G. R. Gassman, T. C. Flood, *Organometallics* **1996**, *15*, 4240–4246. – [5f] L. Wang, C. Wang, R. Bau, T. C. Flood, *Organometallics* **1996**, *15*, 491–498. – [5g] P. Chaudhuri, K. Wieghardt, Prog. *Inorg. Chem.* **1987**, *35*, 329–436. – [5h] J. M. Johnson, J. E. Bulkowski, A. L. Rheingold, B. C. Gates, *Inorg. Chem*. **1987**, *26*, 2644.

[6] [6a] M. A. Esteruelas, L. A. Oro, M. C. Apreda, C. Foces-Foces, F. H. Cano, R. M. Claramunt, C. López, J. Elguero, M. Begtrup, *J. Organomet. Chem.* **1988**, *344*, 93–108. – [6b] M. A. Esteruelas, L. A. Oro, R. M. Claramunt, C. López, J. L. Lavandera, J. Elguero, *J. Organomet. Chem.* **1989**, *366*, 245–255. – [6c] B. N. Lonie, S. J. Rettig, A. Storr, J. Trotter, *Can. J. Chem.* **1984**, *62*, 633.

[7] [7a] H. F. Haarman, F. R. Bregman, J.-M. Ernsting, N. Veldman, A. Spek, K. Vrieze, *Organometallics* **1997**, *16*, 54–67. – [7b] H. F. Haarman, J.-M. Ernsting, M. Kranenburg, H. Kooijman, N. Veldman, A. L. Spek, P. W. N. M. van Leeuwen, K. Vrieze, *Organometallics* **1997**, *16*, 887–900.

[8] J. A. Casares, P. Espinet, J. M. Martínez de Ilarduya, Y. S. Lin, *Organometallics* **1997**, *16*, 770–779.

[9] M. A. Alonso, J. A. Casares, P. Espinet, K. Soulantica, J. Charmant, A. G. Orpen, *Inorg. Chem*. **2000**, *39*, 705–711.

[10] [10a] H. I. Heitner, S. J. Lippard, *Inorg. Chem.* **1972**, *11*, 1447–1453. – [10b] K. Vrieze, P. W. N. M. van Leeuwen, *Prog. Inorg. Chem.* **1971**, *14*, 1–63. – [10c] H. I. Heitner, S. J. Lippard, *J. Am. Chem. Soc.* **1970**, *92*, 3486.

[11] R. P. Huges, Chap 35, pg 282 in "*Comprehensive Organometallic Chemistry*", (Eds.: G. Wilkinson, F. G. Stone, E. W. Abel), Pergamon Press, **1982**.

[12] [12a] R. Usón, L. A. Oro, C. Claver, M. A. Garralda, *J. Organomet. Chem.* **1976**, *105*, 365–374. – [12b] L. A. Oro, M. Esteban, R. M. Claramunt, J. Elguero, C. Foces-Foces, F. H. Cano, *J. Organomet. Chem.* **1984**, *276*, 79–87. – [12c] G. Tresoldí, P. Piraino, E. Rotondo, E. Faraone, *J. Chem. Soc., Dalton Trans.* **1991**, 425–430. – [12d] S. Elgafi, L. D. Field, B. A. Messerle, P. T. Turner, T. W. Hambley, *J. Organomet. Chem.* **1999**, *588*, 69–77.

[13] [13a] M. P. Anderson, A. L. Casalnuovo, B. J. Johnson, B. N. Mattson, A. M. Mueting, L. H. Pignolet, *Inorg. Chem.* **1988**, *27*, 1649–1658. – [13b] H.-H. Wang, A. L. Casalnuovo, B. J. Johnson, A. M. Mueting, L. H. Pignolet, *Inorg. Chem.* **1988**, *27*, 325–331. – [13c] L. Costella, A. Del Zotto, A. Mezzetti, E. Zangrando, P. Rigo, *J. Chem. Soc., Dalton Trans.* **1993**, 3001–3008. – [13d] A. Del Zotto, A. Mezzetti, P. Rigo, *J. Chem. Soc., Dalton Trans.* **1994**, 2257–2264. – [13e] A. Del Zotto, G. Nardin, P. Rigo, *J. Chem. Soc., Dalton Trans.* **1995**, 3343–3351.

[14] J. A. Casares, P. Espinet, R. Hernando, G. Iturbe, F. Villafañe, *Inorg. Chem.* **1997**, *36*, 44–49.

[15] W. Kemp, *Organic Spectroscopy*, MacMillan Press, Bath, **1978**.

[16] An alternative explanation is based on the "Gutmann Rules" (see ref.[17]).The coordination of the Py groups to the rhodium center implies a shift of electron density from oxygen to phosphorus, reinforcing the bonding between them.

[17] J. E. Huheey, *Inorganic Chemistry. Principles of Structure and Reactivity*, 3rd ed., Harper & Collins, **1983**, 309–312.

[18] A compilation of rhodium-nitrogen distances in square-planar and pentacoordinated complexes can be found in ref.[7a]

[19] [19a] M. A. Esteruelas, F. J. Lahoz, M. Oliván, E. Oñate, L. A. Oro, *Organometallics* **1994**, *13*, 3315–3323. – [19b] F. J. Lahoz, A. Tiripicchio, M. Tiripicchio-Carmellini, L. A. Oro, M. T. Pinillos, *J. Chem. Soc., Dalton Trans.* **1985**, 1487.

[20] G. Giordano, R. H. Crabtree, *Inorg. Synthesis* **1990**, *28*, 88.

[21] D. M. Roe, A. G. Massey, *J. Organomet. Chem.***1971**, *28*, 273.

[22] [22a] G. Newcome, D. C. Hagen, *J. Org. Chem.* **1978**, *43*, 947–949. – [22b] J. A. MacCleverty, G. Wilkinson, *Inorg. Synthesis* **1990**, *28*, 84.

[23] SMART V5.051 diffractometer control software, Bruker Analytical X-ray Instruments Inc., Madison, WI, **1998**.

[24] SAINT V6.02 integration software, Bruker Analytical X-ray Instruments Inc., Madison, WI, **1999**.

[25] G. M. Sheldrick, *SADABS: A program for absorption correction with the Siemens SMART system;* University of Göttingen, Germany, **1996**.

[26] *SHELXTL program system version 5.1;* Bruker Analytical X-ray Instruments Inc., Madison, WI, **1998**.

[27] International Tables for Crystallography, Kluwer, Dordrecht, **1992**, vol. C.

Received December 1, 1999
[I99430]

The First Example of a True "Turnbull's Blue" Family Compound with Trapped Iron Oxidation States

Vitaly V. Pavlishchuk,*[a] Iryna A. Koval,[a] Eugeny Goreshnik,[b] Anthony W. Addison,*[c] Gerard A. van Albada,[d] and Jan Reedijk[d]

Keywords: Prussian blue / Magnetic susceptibility / Valence trapping / Iron / Macrocycles

The first compound of a true Turnbull's Blue family [i.e. an iron(II) hexacyanoferrate(III)] complex with valence-trapped states of iron – $[Fe([9]ane\text{-}S_3)_2]_3[Fe(CN)_6]_2\cdot 2H_2O$ (Ukrainian Red, UR) was synthesized. It crystallizes in the trigonal space group P3, a = 12.038(8) Å, b = 12.038(8) Å, c = 14.342(7) Å, α = 90.00°, β = 90.00°, γ = 120.00°. The unit cell of UR consists of separate $[Fe([9]ane\text{-}S_3)_2]^{2+}$ cations, $[Fe(CN)_6]^{3-}$ anions and 5.3 molecules of water. Encapsulation of the Fe^{II} in the homoleptic thioether environment plays the dual role of stabilizing Fe^{II} and protecting the central metal ion from direct bridging with hexacyanoferrate(III) anions. The absence of such interactions and trapping of iron oxidation states in the cations and anions was demonstrated by X-ray diffraction and magnetic susceptometry. Magnetic measurements are consistent with diamagnetic Fe^{II} inside the macrocyclic moieties and S = 1/2 for Fe^{III} in the hexacyanoferrate(III) anions.

Introduction

Until the 1960's Turnbull's Blue was believed to be iron(II) hexacyanoferrate(III), $Fe_3[Fe(CN)_6]_2$. This saga began 300 years ago when Berlin and Diesbach prepared Prussian Blue, also called Berlin Blue. The Prussian Blue synthesis heralded not only the discovery of a new family of cyanides, but initiated a whole field of coordination chemistry. Prussian Blue was ascribed as being the iron(III) hexacyanoferrate(II), $Fe_4[Fe(CN)_6]_3$, in contrast to the similarly intense blue pigment Turnbull's Blue. Recently[1–3] all these various iron cyanides have been consolidated into a single family of Prussian Blues (PB's). In this paper we use this name solely in reference to iron-containing cyanoferrates. Only since the 1960s have the identities of Prussian ($Fe_4[Fe(CN)_6]_3$) and Turnbull's Blues ("$Fe_3[Fe(CN)_6]_2$") been elucidated by magnetochemistry and Mössbauer spectroscopy.[2,4–10] These methods, as well as subsequent X-ray examination[11] revealed that Prussian Blue and Turnbull's Blue are both iron(III) hexacyanoferrates(II), containing high spin Fe^{3+} cations and $[Fe(CN)_6]^{4-}$ with low-spin Fe^{II}, linked by cyanide bridges. Thus, a real "Turnbull's Blue" simultaneously containing Fe^{II} and $[Fe(CN)_6]^{3-}$ has never been reported. Detailed examination of PB's molecular and electronic structures suggest a significant exchange interaction between ions, and valence delocalization[1,10,12,13] along the Fe–C≡N–Fe bonds. All PB′s have been assigned as Robin and Day Class II mixed-valence systems.[14] In such systems partial valence delocalization occurs, and two oxidation states are still distinguishable by physical methods. Until now, only polymeric PB's with magnetic interaction or valence delocalization between iron atoms have been described in the literature.[1,10,12,13,16–18] The detection of high-temperature ferromagnetic ordering in a number of PB-family complexes containing different metal ions connected by CN^- bridges has stimulated the design and study of new magnetic materials based on these compounds.[1,15–21] The recent discovery of photoinduced magnetization in a cobalt-containing PB analog may be of practical interest for the development of photochemically tunable molecular magnets.[22] From this point of view, the synthesis of true Turnbull's Blue complexes with trapped oxidation states is still a challenge and is of significant fundamental interest. Blocking of such iron-iron interactions may be achieved by shielding the iron cations with homoleptic macrocyclic ligands, generating around them a coordinatively saturated environment which precludes any bridging by anions. Comparison of the magnetic and electronic properties of complexes containing cyano bridges with those that do not can reveal the details of the roles of such bridging groups in superexchange interactions between the metal centers. In this paper we report the synthesis and properties of the first

[a] L. V. Pisarzhevskii Institute of Physical Chemistry of the National Academy of Sciences of the Ukraine,
252039, Kiev, prosp. Nauki, 31, The Ukraine
Fax:(internat.) +380 44 265 6216
E-mail: pavlisvv@phyche.freenet.kiev.ua
[b] Department of Chemistry, I. Franko Lviv State University,
290005, Lviv, The Ukraine
[c] Department of Chemistry, Drexel University,
Philadelphia, PA 19104, USA
Fax: (internat.) +1-215/895-1265
E-mail: addisona@drexel.edu
[d] Leiden Institute of Chemistry, Gorlaeus Laboratories, Leiden University,
P. O. Box 9502, 2300 RA Leiden, The Netherlands
Fax: (internat.) +31 71 527 4451
E-mail: reedijk@chem.leidenuniv.nl

 © WILEY-VCH Verlag GmbH, 69451 Weinheim, 2001 1434–1948/01/0101–0297 $ 17.50+.50/0

example of a true Turnbull's Blue (i.e. iron(II) hexacyanoferrate(III)) complex with valence-trapped states of iron − $[Fe([9]ane\text{-}S_3)_2]_3[Fe(CN)_6]_2\cdot 2H_2O$, which we refer to as Ukrainian Red (UR).

Results and Discussion

Synthesis

The reaction of $[Fe([9]ane\text{-}S_3)_2](ClO_4)_2$ with $K_3[Fe(CN)_6]$ in aqueous solution in molar ratio 3:2 results in precipitation of shiny ruby colored crystals of product, while the color of the solution changes to dull yellow. If the reaction mixture is allowed to stand for several days an additional amount of product forms, along with a minor amount of classic PB colloid. The analytical data agree with the formula $[Fe([9]ane\text{-}S_3)_2]_3[Fe(CN)_6]_2\cdot 2H_2O$ for the bulk product, while an X-ray diffraction study proves the constitution of a single crystal to be $[Fe([9]ane\text{-}S_3)_2]_3[Fe(CN)_6]_2\cdot 5.3H_2O$ (vide infra). Ukrainian Red shows no sign of redox exchange between its cations and anions during crystallization, so in contrast to classical PB's, the Fe^{III} ions in UR remain as hexacyanoferrate(III) anions, and the Fe^{II} ions are muffled by two trithiamacrocyclic ligands. Its composition thus matches formally the *virtual* classic Turnbull's Blue composition ($Fe_3[Fe(CN)_6]_2$), but with iron(II) in macrocyclic moieties. The hexathiamacrocyclic environment around Fe lends significant relative stabilization to the Fe^{2+} oxidation state[23] and because of the consequently high $E_{1/2}$ value[23] for the $[Fe([9]ane\text{-}S_3)_2]^{3+/2+}$ couple, the hexacyanoferrate(III) ions cannot oxidize $[Fe([9]ane\text{-}S_3)_2]^{2+}$ to $[Fe([9]ane\text{-}S_3)_2]^{3+}$. In addition, the macrocyclic shielding in UR prevents the formation of cyanide bridges between Fe^{II} and Fe^{III} and thus is also crucial for preventing electron delocalization between these two iron atoms in different oxidation states. $[Fe([9]ane\text{-}S_3)_2]_3[Fe(CN)_6]_2\cdot 2H_2O$ is insoluble in most common solvents. In order to confirm the integrity of the iron centers during the reaction and the absence of interactions between them in the complex salt, we investigated the crystal and molecular structure of UR as well as its IR and optical spectra and magnetochemical behavior.

Table 1. Crystal data for Ukrainian Red

Empirical formula	$C_{48}H_{76}Fe_5N_{12}O_2S_{18}$
Formula mass	1709.6
Crystal System	trigonal
Space group	*P*3
Dimensions	0.22 × 0.12 × 0.10
a (Å)[a]	12.038(8)
b (Å)	12.038(8)
c (Å)	14.342(7)
α	90.00
β	90.00
γ	120.00
V (Å^3)	1800(3)
Z	1
$\rho_{calcd.}$ (g cm^{-3})	1.632(3)
μ(Mo-K_α, cm^{-1})	15.61
R_{int}	0.039
$wR(F^2)$	0.037

[a] The standard deviations are reported in parentheses.

Molecular Structure and Physical Properties of Ukrainian Red

Crystallographic parameters for $[Fe([9]ane\text{-}S_3)_2]_3[Fe(CN)_6]_2\cdot 2H_2O$ are given in Table 1. Selected bond lengths and angles are summarized in Table 2. A perspective view appears in Figure 1.

Table 2. Selected bond lengths (Å) and bond angles (°) in Ukrainian Red

Bond lengths			
Fe(1)−S(1)	2.23(1)	Fe(1)−S(1a)	2.23(1)
Fe(1)−S(1b)	2.23(1)	Fe(1)−S(6)	2.27(1)
Fe(1)−S(6a)	2.27(1)	Fe(1)−S(6b)	2.27(1)
Fe(2)−S(2)	2.24(1)	Fe(2)−S(2a)	2.24(1)
Fe(2)−S(2b)	2.24(1)	Fe(2)−S(5)	2.27(1)
Fe(2)−S(5a)	2.28(1)	Fe(2)−S(5b)	2.27(11)
Fe(3)−S(3)	2.23(1)	Fe(3)−S(3a)	2.23(1)
Fe(3)−S(3b)	2.23(1)	Fe(3)−S(4)	2.25(1)
Fe(3)−S(4a)	2.25(1)	Fe(3)−S(4b)	2.25(1)
Fe(4)−C(10)	1.91(2)	Fe(4)−C(10a)	1.91(2)
Fe(4)−C(10b)	1.91(2)	Fe(4)−C(15)	1.95(1)
Fe(4)−C(15a)	1.95(2)	Fe(4)−C(15b)	1.95(1)
Fe(5)−C(1)	1.95(2)	Fe(5)−C(1a)	1.95(2)
Fe(5)−C(1b)	1.95(2)	Fe(5)−C(11)	1.94(2)
Fe(5)−C(11a)	1.94(2)	Fe(5)−C(11b)	1.94(2)
C(1)−N(3)	1.16(2)	C(10)−N(2)	1.14(2)
C(15)−N(1)	1.15(2)	C(11)−N(4)	1.12(3)
Angles[a]			
S(1)−Fe(1)−S(6)	90.8(4)	S(1)−Fe(1)−S(6a)	179.6(5)
S(1)−Fe(1)−S(6b)	90.3(4)	S(1a)−Fe(1)−S(1b)	89.6(4)
S(1a)−Fe(1)−S(6)	90.3(4)	S(1a)−Fe(1)−S(6a)	90.8(4)
S(1a)−Fe(1)−S(6b)	179.6(5)	S(1b)−Fe(1)−S(6)	179.6(5)
S(1b)−Fe(1)−S(6a)	90.3(4)	S(1b)−Fe(1)−S(6b)	90.8(4)
S(1)−Fe(1)−S(1a)	89.6(4)	S(1)−Fe(1)−S(1b)	89.6(4)
S(6)−Fe(1)−S(6a)	89.3(4)	S(6)−Fe(1)−S(6b)	89.3(4)
S(6a)−Fe(1)−S(6b)	89.3(4)	S(2)−Fe(2)−S(2a)	90.7(3)
S(2)−Fe(2)−S(2b)	90.7(3)	S(2)−Fe(2)−S(5)	93.8(3)
S(2)−Fe(2)−S(5a)	175.1(4)	S(2)−Fe(2)−S(5b)	87.4(3)
S(2a)−Fe(2)−S(2b)	90.7(3)	S(2a)−Fe(2)−S(5)	87.4(3)
S(2a)−Fe(2)−S(5a)	93.8(3)	S(2a)−Fe(2)−S(5b)	175.1(4)
S(2b)−Fe(2)−S(5)	175.1(4)	S(2b)−Fe(2)−S(5a)	87.4(3)
C(10)−Fe(4)−C(10a)	94.7(8)	C(10)−Fe(4)−C(10b)	94.7(8)
C(10)−Fe(4)−C(15)	94.3(7)	C(10)−Fe(4)−C(15a)	81.9(7)
C(10)−Fe(4)−C(15b)	170.6(8)	C(10a)−Fe(4)−C(10b)	94.7(8)
C(10a)−Fe(4)−C(15)	170.6(8)	C(10a)−Fe(4)−C(15a)	94.3(7)
C(10a)−Fe(4)−C(15b)	81.9(7)	C(10b)−Fe(4)−C(15)	81.9(7)
C(10b)−Fe(4)−C(15a)	170.6(8)	C(10b)−Fe(4)−C(15b)	94.3(7)
C(15)−Fe(4)−C(15a)	89.6(6)	C(15)−Fe(4)−C(15b)	89.6(6)
C(15a)−Fe(4)−C(15b)	89.6(6)	C(1)−Fe(5)−C(1a)	92.7(8)
C(1)−Fe(5)−C(1b)	92.7(8)	C(1)−Fe(5)−C(11)	91.2(8)
C(1)−Fe(5)−C(11a)	89.0(8)	C(1)−Fe(5)−C(11b)	175.6(9)
C(1a)−Fe(5)−C(11a)	91.2(8)	C(1b)−Fe(5)−C(11a)	175.6(9)
C(1b)−Fe(5)−C(11b)	91.2(8)	C(11)−Fe(5)−C(11b)	87.0(9)
C(11)−Fe(5)−C(11b)	87.0(8)	C(1a)−Fe(5)−C(11b)	87.0(9)

[a] Standard deviations in parentheses.

The unit cell of UR consists of separate $[Fe([9]ane\text{-}S_3)_2]^{2+}$cations, $[Fe(CN)_6]^{3-}$ anions and 5.3 molecules of water (Figure 2). The macrocyclic cations are arranged in UR in such a way that the macrocyclic ligands form an unusual linear tube, along whose central axis the iron(II) ions are situated (Figure 3). Two nonequivalent $[Fe(CN)_6]^{3-}$ anions balance the positive charge of the cations, while water molecules occur in the unit cell in two

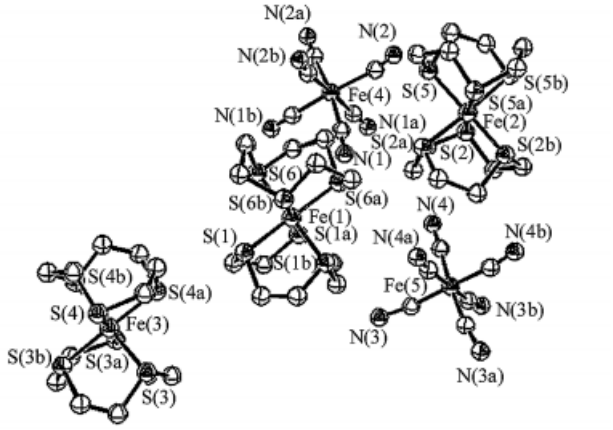

Figure 1. Molecular structure of Ukrainian Red. For clarity of presentation, water molecules and hydrogen atoms are not shown

independent positions with occupancies 1 and 0.77 (the multiplicity of each position is 3, thus $3+3 \times 0.77$ gives 5.3 water molecules in unit cell). The cations and anions are not connected by CN^- bridges, as is evident from Figure 1. There is no evidence for the existence of hydrogen bonding inside the unit cell.

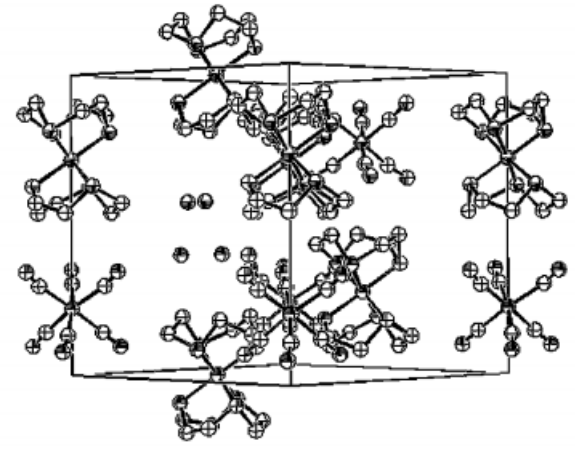

Figure 2. Unit cell content of Ukrainian Red

Similarities between the lattice building blocks in UR and in the starting reagents might be anticipated. Indeed, comparison of the Fe−C bond lengths in UR with those in $K_3[Fe(CN)_6]$[25] shows no significant differences. In the potassium salt, all the Fe−C distances are approximately equal (1.93−1.95 Å), whereas in UR these values vary within slightly larger limits (1.91 and 1.95 Å). These differences between the Fe−C distances are not significant relative to their standard deviations (Table 2) and thus may reveal that the equivalence of the Fe−C bonds is inherited by UR. In the potassium salt, the cyanide ligand $C\equiv N^-$ bond lengths are practically constant (1.14−1.16 Å).[24] In UR, they are also within these limits and the mean $[Fe(CN)_6]^{3-}$ radius (the distance between Fe and N) in UR is close to that in $K_3[Fe(CN)_6]$.[25] Previously, a dynamic Jahn−Teller effect in $K_3[Fe(CN)_6]$ was detected by magnetic circular dichroism[26] and Mössbauer spectroscopy,[27] while a static Jahn−Teller distortion was demonstrated for $[Fe([9]ane\text{-}S_3)_2](PF_6)_3$ by Mössbauer spectroscopy.[28] The bond lengths in UR offer no clear evidence in favor of a Jahn−Teller distortion in $[Fe(CN)_6]^{3-}$. Nonetheless, deviations of the C−Fe−C angles from 90° (Table 2) along with nonlinearity of the Fe−C≡N units in UR (Figure 1, Table 2) leave room for speculation about the existence of a Jahn−Teller distortion in this compound.

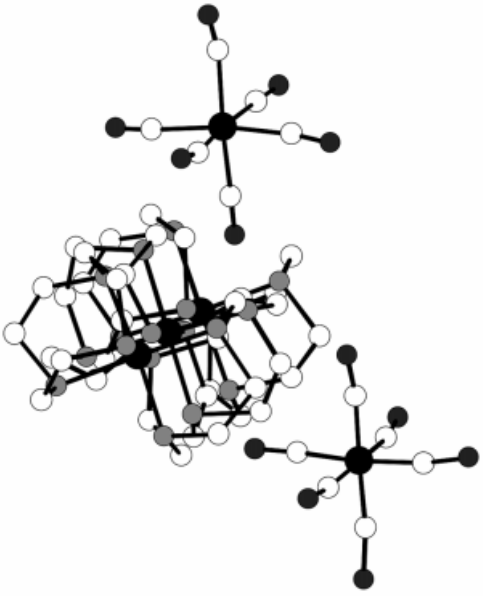

Figure 3. A perspective view of UR

The structural parameters for two of the three $[Fe([9]ane\text{-}S_3)_2]^{2+}$ cations in the UR unit cell (Table 2) also differ slightly from those described earlier in the literature.[23] The angles around Fe(1) of the central macrocycle (Table 2) coincide with those found in $[Fe([9]ane\text{-}S_3)_2](ClO_4)_2$. However, the corresponding angles in the two terminal macrocyclic cations are different (Table 2).[23] The Fe−S distances in UR vary between 2.23 and 2.27 Å, while in the parent $[Fe([9]ane\text{-}S_3)_2](ClO_4)_2$ these values are within 0.01 Å of 2.25 Å.[23] The terminal $[Fe([9]ane\text{-}S_3)_2]^{2+}$ in UR show slightly distorted octahedra as shown by some bond angle deviations from 90° (Table 2). These minor distortions in the cation structure in UR can be attributed to the influence of lattice packing in this compound.

The IR spectrum of UR contains a sharp band at 2100 cm^{-1} with a weaker satellite at 2113 cm^{-1} and a broad shoulder at lower frequency. These absorptions are attributed to the $\nu_{C\equiv N}$ mode of the nonbridging cyanide groups. The splitting of this mode and its broadening at lower frequencies may be attributed to the presence of the different types of cyanide anions in UR.

The reflectance spectrum of UR (Figure 4) shows two strong absorptions at 23,641 and 18,587 cm^{-1}, which originate from the individual ions. The band at 18,587 cm^{-1} is attributed to the $A_{1g} \rightarrow T_{1g}$ d-d transition in the octahedral low-spin d^6 $[Fe([9]ane\text{-}S_3)_2]^{2+}$ cations, as observed in $[Fe([9]ane\text{-}S_3)_2](ClO_4)_2$.[23] The second $A_{1g} \rightarrow T_{2g}$ d-d transition normally observed in $[Fe([9]ane\text{-}S_3)_2]^{2+}$ at 25,316 cm^{-1} is obscured in UR by the broad charge transfer band,

π t_{2u} (CN^-) $\rightarrow$ t_{2g} (Fe^{III}). The band at 23,641 cm^{-1} in UR also arises from hexacyanoferrate(III) and is attributed to σ t_{1u} (CN^-) $\rightarrow$ t_{2g} (Fe^{III}) charge transfer.[29] In contrast to PB, and as expected for this structure, there is no sign of an intervalence charge transfer band in UR in the region 6,600−30,300 cm^{-1}. Unfortunately, the insolubility of UR in common solvents prevents measurements of its optical spectrum in solution.

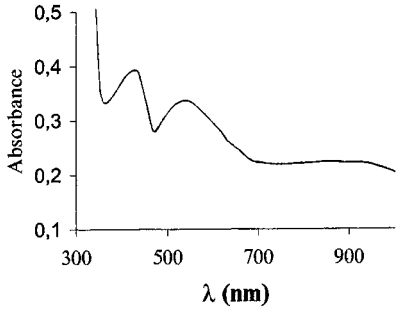

Figure 4. Electronic spectrum of UR in $BaSO_4$ matrices

The magnetochemical results for UR are consistent with the structural and spectral data. The temperature dependence of χT for UR was fitted in agreement with a $^2T_{2g}$ $[Fe(CN)_6]^{3-}$ ground state split under the influence of spin-orbit coupling in the magnetic field model[30,31] (Figure 5):

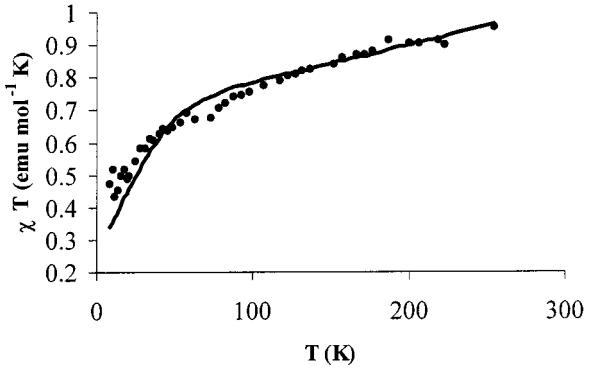

Figure 5. Variable-temperature magnetic data for UR. The solid line was calculated from Equation 1 with $\lambda = -72 \pm 6$ cm^{-1}, $\kappa = 0.75 \pm 0.03$, $TIP = 0.0015 \pm 0.0001$ emu; experimental data. ($R = [\Sigma(\chi_{obs} - \chi_{calc})^2/\Sigma\chi^2_{obs}]^{1/2}$) = 0.029

$$\chi_M = \frac{N\beta^2}{3kT}\left[\frac{3x(1+k)^2 - 8(2+k)^2 + \{30x(1-k)^2 + 8(2+k)^2\}e^{3x/2}}{9x\{1+2e^{3x/2}\}}\right] + TIP$$

κ is the orbital reduction factor, and $x = \kappa\lambda/3$ while the other symbols have their usual meanings. The additional term for temperature independent paramagnetism was introduced in order to reflect coupling between the singlet ground state and nonthermally populated excited states for the low-spin Fe^{2+} cations in the macrocyclic moieties.[31]

The susceptibility data for UR fit well to the above model under the assumption that significant magnetic exchange interactions between ions in the salt are absent. κ-Values for $[Fe(CN)_6]^{3-}$ in previous work[32−37] were also derived without consideration of magnetic exchange at even very low temperatures in $K_3[Fe(CN)_6]$.[38] The calculated κ = 0.75 for the $[Fe(CN)_6]^{3-}$ ion in UR reflects considerable covalency in this anion. The literature values for κ vary between 0.56 and 0.90; however, our value is close to that reported by Figgis.[37] The substantial reduction of λ (ref. between −250[37] and −400[35] cm^{-1}) also might be considered as evidence for the existence of a Jahn−Teller effect[34,35] in the hexacyanoferrate ions in UR. The separation of the $[Fe(CN)_6]^{3-}$ anions from each other is too great (9.5 Å) for significant magnetic exchange between iron(III) atoms.

Conclusion

Summarizing the results of this study, we would like to emphasize that almost three centuries have passed before a compound having a composition consistent with the original Turnbull's Blue formulation was synthesized. Success was achieved mainly due to the chosen synthetic strategy of encapsulating the Fe^{II} inside the homoleptic thioether environment. Such coordination plays the dual role of stabilizing Fe^{II} and protecting the central metal ion from direct bridging with hexacyanoferrate(III) anions. The absence of such interactions and trapping of iron oxidation states in the cations and anions was demonstrated by X-ray diffraction and magnetic susceptibility. In contrast to the classical PB's, assigned as Class II mixed valence systems,[14] UR is a Robin and Day Class I compound which shows no sign of valence delocalization in its spectroscopic and magnetic properties. This study also confirms the significant role of CN^- bridges in the magnetic interactions normally found in PB complexes. Shielding by the macrocyclic ligands prevents magnetic interactions between metal centers, so that UR shows no magnetic exchange between iron atoms. Further work is underway, involving coordinatively unsaturated $[M[9]ane-S_3]^{n+}$ building blocks and hexacyanoferrate/chromate(III) as potential sources of ferromagnetic materials.

Experimental Section

General Remarks: All reactants and solvents were of reagent grade and used as purchased; $[Fe([9]aneS_3)_2](ClO_4)_2$ was prepared according to the procedure reported by Wieghardt and co-workers.[23]

Physical Measurements: Infrared spectra were measured on a Carl Zeiss-Jena Specord M 75IR spectrometer using KBr pellets. Electronic spectra were recorded by the diffuse reflectance technique using $BaSO_4$ matrices on a Carl Zeiss-Jena Specord M-40 spectrophotometer. The magnetochemical behavior of the complex in the 5−278 K temperature range was studied using a fully automated Manics DSM-8 susceptometer. Data were corrected for diamagnetic contributions, estimated from the Pascal constants.[30]

$[Fe([9]aneS_3)_2]_3[Fe(CN)_6]_2 \cdot 2H_2O$ (Ukrainian Red): An aqueous solution of $K_3[Fe(CN)_6]$ (0.088 g, 0.27 mmol) was slowly added to an aqueous solution of $[Fe([9]ane-S_3)_2](ClO_4)_2$ (0.246 g, 0.40 mmol).

After half an hour, dark ruby colored prisms formed, which were filtered off, washed with water and ethanol and dried in air. Yield: 0.20 g, 63%. Elemental analysis; calcd. for $C_{48}H_{76}Fe_5N_{12}O_2S_{18}$: calcd. C 33.7, H, 4.48, N, 9.83, S, 33.8, Fe, 16.3; found calcd. C 33.6, H, 4.41, N, 9.89, S, 33.6, Fe, 16.0%. IR (cm^{-1}, KBr disc): 3386 (ν_{O-H}), 2113, 2101 ($\nu_{C\equiv N}$). Optical spectrum (solid state) : $\tilde{\nu}_{max}$, cm^{-1}: 23,641, 18,587.

X-ray Crystallographic Study: For X-ray diffraction, the selected crystal was mounted in a glass capillary, set on the goniometer head and carefully centered. X-ray intensity data were measured on an automated four-circle Dartch diffractometer with graphite-monochromated Mo-K_α radiation in the θ-2θ scan mode. Rotation and Weissenberg photographs gave preliminary parameters for the trigonal unit cell and Laue class 3 was defined. Any systematic absences were found and space group $P3$ was assigned to the unit cell. The cell parameters were least-squares refined using 24 reflections in the range: $25° \leq 2\theta \leq 30°$. The structure was solved using the CSD program package[20]. Iron and sulfur atoms were found by direct methods, the positions of other non-hydrogen atoms being derived from Fourier synthesis. All H atoms were found by difference Fourier synthesis, and their positional and overall thermal parameters were refined isotropically. Crystallographic data for Ukrainian Red are presented in Table 1. Crystallographic data (excluding structure factors) for the structure reported in this paper have been deposited with the Cambridge Crystallographic Data Centre as supplementary publication no. CCDC-138604. Copies of the data can be obtained free of charge on application to CCDC, 12 Union Road, Cambridge CB2 1EZ, UK [Fax: (internat.) + 44(1223)336−033; E-mail: deposit@ccdc.cam.ac.uk].

Acknowledgments

The authors wish to thank M. Prushan for helpful discussion and Drexel University for support.

[1] K. R. Dunbar, R. A. Heintz, *Prog. Inorg. Chem*. **1997**, *45*, 283−391.
[2] R. E. Wilde, S. N. Ghosh, B. J. Marshall, *Inorg. Chem*. **1970**, *9*, 2512−2516.
[3] H. Holtzman, *Ind. Eng. Chem*. **1945**, *37*, 855−859.
[4] A. Ito, M. Suenaga, K. Ono, *J. Chem. Phys.* **1968**, *48*, 3597−3599.
[5] L. M. Epstein, *J. Chem. Phys.* **1962**, *36*, 2731−2737.
[6] E. Fluck, W. Kerler, W. Neuwirth, *Angew. Chem. Int. Ed. Engl.* **1963**, *2*, 277−287.
[7] J. F. Duncan, P. W. R. Wigley, *J. Chem. Soc*, **1963**, 1120−1125.
[8] K. Maer, Jr., M. L. Beasley, R. L. Collins, W. O. Milligan, *J. Am. Chem. Soc*. **1998**, *90*, 3201−3208.
[9] K. Chandra, D. Raj, S. P. Puri, *J. Chem. Phys.* **1967**, *46*, 1466−1468.
[10] B. Mayoh, P. Day, *J. Chem. Soc., Dalton Trans.* **1976**, 1483−1486.
[11] H. J. Buser, D. Schwarzenbach, W. Petter, A. Ludi, *Inorg. Chem*. **1977**, *16*, 2704−2710.
[12] H. Vahrenkamp, A. Geiss, G. N. Richardson, *J. Chem. Soc., Dalton Trans.* **1997**, 3643−3651.
[13] B. Mayoh, P. Day, *J. Chem. Soc., Dalton Trans.* **1976**, 1483−1486.
[14] M. B. Robin, P.Day, *Adv. Inorg. Radiochem.* **1967**, *10*, 248−422.
[15] M. Ketterle, J. Fiedler, W. Kaim, *Chem. Commun.* **1998**, 1701−1702.
[16] E. Dujardin, S. Ferlay, X. Phan, C. Desplanches, C. Cartier dit Moulin, P. Sainctavit, F. Baudelet, E. Dartyge, P. Veillet, M. Verdaguer, *J. Am. Chem. Soc*. **1998**, *120*, 11347−11352.
[17] T. Mallah, S. Thiébaut, M. Verdaguer, P. Veillet, *Science*, **1993**, *262*, 1554−1556.
[18] V. Gadet, T. Mallah, I. Castro, P. Veillet, M. Verdaguer, *J. Am. Chem. Soc*. **1992**, *114,* 9213−9214.
[19] Ø. Hatlevik, W. E. Buschmann, J. Zhang, J. L. Manson, J. S. Miller, *Adv. Mater.* **1999,** *11,* 914−918.
[20] M. Ohba, N. Usuki, N. Fukita, H. 'kawa, *Angew. Chem. Int. Ed.* **1999,** *38,* 1795−1798.
[21] M. Verdaguer, *Science*, **1996**, *272*, 698−699.
[22] O. Sato, T. Iyoda, A. Fujishima, K. Hashimoto, *Science*, **1996**, *272*, 704−705.
[23] K. Wieghardt, H.-J. Küppers, J. Weiss, *Inorg. Chem.* **1985**, *24*, 3067−3071
[24] L. G. Akselrud, P. Y. Zavalii, Yu. N. Grin, V. K. Pecharsky, B. Baumgartner, E. Wolfel, *Materials Science Forum* **1993**, *133−136*, 335−340.
[25] B. N. Figgis, B. W. Skelton, A. H. White, *Aust. J. Chem*. **1978**, *31*, 1195−1199.
[26] H. Kobayashi, M. Shimiu, Y. Kaizu, *Bull. Chem. Soc. Jpn*. **1970**, *43*, 2321−2325.
[27] P. Gütlich, R. Link, A. X. Trautwein, in Mössbauer Spectroscopy in Transition Metal Chemistry, Springer-Verlag, Heidelberg, **1978**.
[28] H.-J. Küppers, K. Wieghardt, B. Nuber, J. Weiss, E. Bill, A. X. Trautwein, *Inorg. Chem.* **1987**, *26*, 3762−69.
[29] A. B. P. Lever. "Inorganic Electronic Spectroscopy", 2nd ed.; Elsevier: Amsterdam, **1984**, 258−262.
[30] E. A. Bourdeaux, L. N. Mulay. "Theory and application of Molecular Paramagnetism", Wiley-Interscience, New York, **1976**, 509 PP.
[31] O. Kahn, "Molecular Magnetism", VCH, New York, **1993**, 380 PP.
[32] F. R. McKim, W. P. Wolf, *Proc. Phys. Soc. B*, **1956**, *69*, 1231−1236.
[33] B. Bleaney, M. C. M. O'Brien, *Proc. Phys. Soc. B*, **1956**, *69*, 1216−1230.
[34] B. N. Figgis, *Trans. Faraday. Soc*., **1961**, *57*, 198−203.
[35] B. N. Figgis, *Trans. Faraday. Soc*., **1961**, *57*, 204−209.
[36] J. Baker, B. N. Figgis, *J. Chem. Soc., Dalton Trans.* **1975**, 598−602.
[37] J. Baker, B. N. Figgis. *Aust. J. Chem.* **1982**, *35*, 265−275.
[38] B. N. Figgis, J. Lewis. *Prog. Inorg. Chem*. **1964**, *6*, 237−240.

Received January 28, 2000
[I00029]

Intramolecular Dynamics of Asymmetric Lanthanide(III) Porphyrin Sandwich Complexes in Solution

Sergey P. Babailov,*[a] Athanassios G. Coutsolelos,[b] Alexander Dikiy,[c] and Georgios A. Spyroulias[d]

Keywords: NMR spectroscopy / Lanthanides / Phenyl ring rotation / Metalloporphyrins

Temperature dependencies of the ^{1}H NMR spectra of asymmetric double-decker complexes of DyH(oep)(tpp) (**I**) and LuH(oep)(tpp) (**II**), where tpp is tetraphenylporphyrin and oep is octaethylporphyrin, have been analyzed. The kinetic and thermodynamic parameters for intramolecular phenyl ring rotations have been determined. The rotation in (**I**) is characterized by k(298 K) = 11.4 s^{-1}, $\Delta H^{\ddagger}$ = 48.0±6.0 kJ mol^{-1}, while in (**II**) the derived parameters are found to be k(298 K) = 14.0 s^{-1}, $\Delta H^{\ddagger}$ = 65.5±7.1 kJ mol^{-1}. The possible reasons for the different characteristics of these complexes are discussed. The structural parameters calculated for **I** and YbH(oep)(tpp) (**III**), indicate close similarities between the complexes. Nevertheless, it appears that the principal values of the molar paramagnetic susceptibility tensor (χ_i) differ significantly in these complexes.

Introduction

A number of physico-chemical studies on sandwich-complexes containing lanthanide metal(III) or metal(IV) ions and porphyrin ligands have been reported in the literature. These studies have been carried out using techniques such as UV/Vis, CD[1a−1g], low-temperature NIR spectroscopy[2c,2d], NMR,[1a−1c,2b−2e,3b−3d] resonance Raman (RR),[4c,4d,5a−5d] and electron spin resonance[1c,3c,4d] spectroscopies, as well as electrochemistry,[1d,2,3a] photophysics,[4a,4b] and X-ray crystal structure studies[1b,1c,2d,6]. Presently, the thermodynamic, structural, and electronic properties of these complexes are well known, both in solution and in the solid state. Recently, a new phenomenon, involving intramolecular rotation of the decker rings about each other in symmetrical sandwich complexes has been discovered and studied using CD and NMR spectroscopies.[1f,1g] The investigation of the dynamic properties of double-decker complexes represents an interesting area in metalloporphyrin chemistry and attracts the interest of researchers.

[a] Institute of Inorganic Chemistry SB RAS,
pr. Lavrentyev 3, 630090, Novosibirsk, Russia
[b] Chemistry Department, University of Crete,
P. O. Box 1470, 714 09-Heraklion, Crete, Greece
Fax: (internat.) +30 81/393 601
E-mail: coutsole@chemistry.uch.gr
[c] Institute of Agricultural Chemistry, University of Bologna,
Viale Berti Pichat 10, 40127, Bologna, Italy
Fax: (internat.) +39 051/20 99 792
E-mail: alex@flash.iaca.unibo.it
[d] CERM - Universita′ di Firenze Dipertimento di Chimica,
Polo Scientifico,
Via Luigi Sacconi 6, 50019 Sesto Fiorentino (FI), Italy
Fax: (internat.) +39 055/42 09 253
E-mail: georgios@alpha.cerm.unifi.it
Supporting information for this article is available on the WWW under http://www.wiley-vch.de/home/eurjic or from the author.

Although intramolecular dynamic processes involving motions, like phenyl ring rotation, in lanthanide porphyrin sandwich complexes were partially investigated, this motion was not sufficiently elucidated and described. The phenyl rings rotation-rate has been determined for the symmetric YbH(tpp)$_2$ complex at room temperature by the analysis of NOESY cross-peaks intensities.[3e] However, the activation parameters of the phenyl ring rotation were not measured. In this report we use the dynamic NMR approach[7a−7d] to obtain the phenyl rings rotation rate and the activation enthalpy for this process in solution on the asymmetric double-decker complexes DyH(oep)(tpp) (**I**) and LuH(oep)(tpp) (**II**).[3d,3e] The schematic representation of the complexes structure is illustrated in Figure 1. In addition, the results obtained by using pseudo-contact shifts and lanthanide-induced enhancements of longitudinal relaxation rates experienced by some protons of paramagnetic DyH(oep)(tpp) and YbH(oep)(tpp) (**III**) reveal that the structures of the complexes are very similar, with only a slight decrease in distances between the planes of porphyrin ligands upon increase in the atomic number of the lanthanide ions. This result has been interpreted as being due to so-called lanthanide contraction.

Results and Discussion

We have already reported the complete ^{1}H NMR signal assignment of complexes **I-III**.[3d,3e] The signal assignment was based on 1D NOE technique as well as on 2D NOESY, ROESY, TOCSY, and COSY experiments.

The intramolecular phenyl ring rotation rate for complex **II** was determined from the measurements of the temperature dependence of its ^{1}H NMR spectrum. ^{1}H NMR spectra of complex **II** at different temperatures are shown in Figure 2. ^{1}H NMR signals corresponding to *endo-ortho*,

 © WILEY-VCH Verlag GmbH, 69451 Weinheim, 2001 1434−1948/01/0101−0303 $ 17.50+.50/0

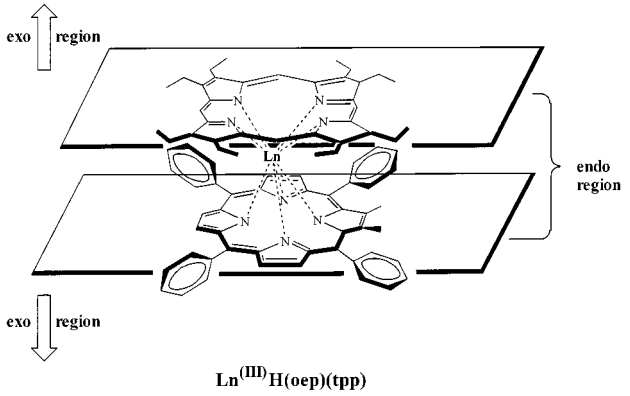

Figure 1. Schematic representation of the asymmetric LnH(oep)(tpp) complexes

exo-ortho, *endo-meta*, *exo-meta* protons are broadened with an increase in temperature, which is consistent with pairwise exchange between the sites: (*endo-ortho*) ⇄ (*exo-ortho*), and (*endo-meta*) ⇄ (*exo-meta*) (see Table 1). The first-order rate constant, k, for the intramolecular exchange processes was determined by comparison of calculated and observed temperature dependent linewidths of (*endo-ortho*), (*exo-ortho*), (*endo-meta*), and (*exo-meta*) ^{1}H NMR signals, according to a procedure reported for the uncoupled two-site exchange case.[7a,7e] Activation parameters were determined using the Eyring Kinetic Equation (1) from weighted least squares {$\ln[k(T)/T]$ versus $1/T$}[7a,7b,7e] where R is the gas constant, k_B is the Boltzmann constant and h is the Planck constant.

$$\ln[k(T)/T] = -\Delta H^{\ddagger}/RT + \Delta S^{\ddagger}/R + \ln(k_B/h) \quad (1)$$

The activation enthalpy of the phenyl rings rotation for **II** was found to be $\Delta H^{\ddagger} = 65.5 \pm 7.1$ kJ mol^{-1} with k(298 K) = 14.0 s^{-1}. We have also calculated the free energy of activation $\Delta G^{\ddagger} = 67.7 \pm 7.1$ kJ mol^{-1} at 95° C in order to compare it with data previously reported. The value obtained for the phenyl ring-flip activation free en-

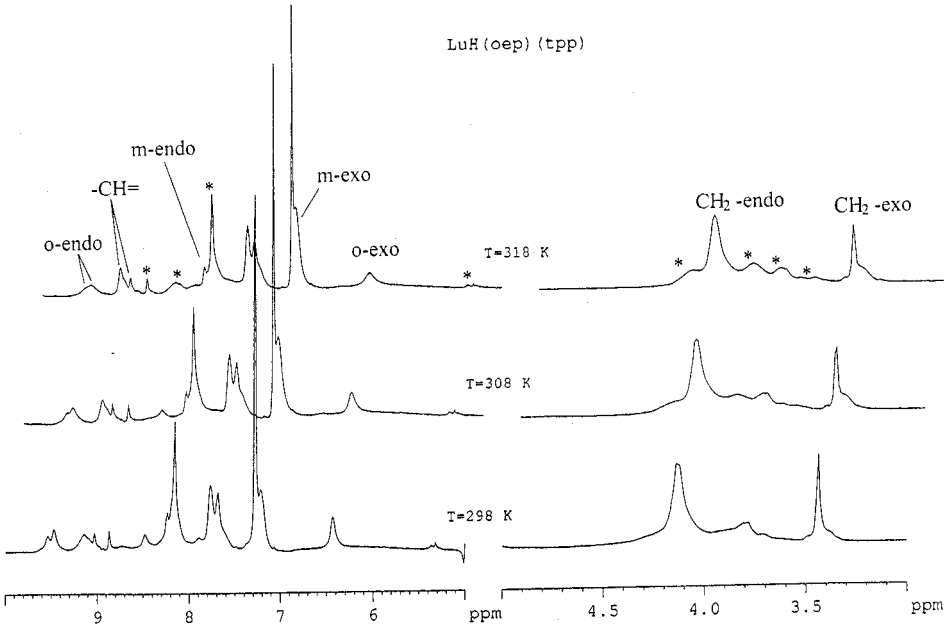

Figure 2. 500-MHz ^{1}H NMR spectra of LuH(oep)(tpp) (complex **II**) in $CDCl_3$ solution at various temperatures

Table 1. ^{1}H NMR observed chemical shifts (δ), hyperfine shifts (Δδ), longitudinal relaxation times (T_1) and calculated structural parameters of the LnH(oep)(tpp) complexes in $CDCl_3$ at 298 K

	Yb (**III**)[3e]				Dy (**I**)[3e]				Lu (**II**)[3d]
assignment	Δδ, ppm	Δδ/B(Yb)[a]	T_1,[b] ms	r/r(CH$_3$)[c]	Δδ, ppm	Δδ/B(Dy)[a]	T_1,[b] ms	r/r(CH$_3$)[c]	δ,[d] ppm
meso	30.4	0.78	8.0	0.76	−21.7	0.12	1.5	0.75	9.1
endo-CH$_2$	25.4	0.65	13.9	0.84	−6.6	0.037	7.2	0.96	4.1
exo-CH$_2$	17.4	0.44	18.7	0.88	−8.2	0.045	7.5	0.97	3.7
endo-ortho	1.3	0.033	21.7	0.90	−59.3	0.33	4.0	0.87	9.4
exo-ortho	3.7	0.094	34.0	0.97	16.2	−0.09	3.4	0.85	6.4
para	0.8	0.02	251.3	1.36	−9.6	0.05	52.6	1.34	7.6
endo-meta	−1.3	0.033	150.7	1.25	−21.9	0.02	31.9	1.23	8.1
exo-meta	−1.1	−0.028	157.6	1.26	−3.4	0.019	30.1	1.22	7.2
CH$_3$	2.4	0.06	40.2	1.0	−3.8	0.02	9.3	1.0	1.3
pyrrolic	−28.0	−0.71	9.3	0.78	−69.5	0.38	2.4	0.80	8.1

[a] B(Yb) = 39.2 and B(Dy) = −181.0, Bleaney's constants. − [b] Measured at 500 MHz. − [c] r − effective distance between the lanthanide cation and the resonated proton. − [d] Chemical shifts relative to TMS.

ergy in **II** is in good agreement with that found for the Ru(CO)(*i*Pr tpp) complex ($\Delta G^{\ddagger}$ = 77.8 kJ mol^{-1} at 95° C).[7e]

In order to compare the thermodynamic parameters of the phenyl ring flipping in LnH(oep)(tpp) complexes across the lanthanide series, including the activation enthalpy in the Lu complex, which is the last member of the series, the analogous parameters were determined for the Dy^{III} complex (**I**). The temperature dependence of ^{1}H NMR spectra of **I** within the temperature range 288 K to 306 K (data not shown) was investigated. No significant temperature dependent changes of the ^{1}H NMR linewidth were observed in addition to the Curie−Weiss dependence of the hyperfine shifts.[7b] This phenomenon can be explained by considering that the exchange rates between the sites (*endo-ortho*) ⇄ (*exo-ortho*), and (*endo-meta*) ⇄ (*exo-meta*) are smaller with respect to broadening of these signals due to lanthanide-induced enhancements of the relaxation rates (Table 1).

In order to determine the phenyl ring rotation rate constants for **I**, the temperature dependence of the 1D NOE spectra was investigated. The temperature variation of 1D NOE spectra of **I** is shown in Figure 3. The 1D NOE spectra were obtained by saturating *endo-ortho* and *endo-meta* signals. Upon saturation of *endo-ortho* and *endo-meta* signals, strong negative connectivities with signals *exo-ortho* and *exo-meta,* respectively, are observed. A temperature decrease results in a decrease of intensities of these negative peaks. This is consistent with the observed negative peaks being due to saturation transfer. We used these experimental data to evaluate the rate constants for the rotation of the phenyl rings. The time dependence of the longitudinal magnetization in an observed site at a transfer of saturated spins from the irradiated site is well known.[7a] During the irradiation the absorption intensity in the observed site [$v(t)$] falls off exponentially to a new steady state level [$v(\infty)$] due to transfer of saturated spins from the irradiated site. The rate of attainment of the new steady state, as well as its intensity, is determined by T_1 and the pre-exchange lifetime ($1/k$) of the observed site. Therefore, the rate constants were obtained using the following ratio [Equation (2)][7a] where $v(0)$ is the absorption intensity in the observed site without irradiation of another site.

$$k = [v(0) - v(\infty))/(v(\infty)\ T_1] \quad (2)$$

The measured intensities of the saturation transfer spectra (Figure 3) allowed us to determine the phenyl ring-flip rate constant [k(298 K) = 11.4 s^{-1}] and the activation enthalpy for this process ($\Delta H^{\ddagger}$ = 48.0±6.0 kJ mol^{-1}).

An increase of the activation enthalpy along the series of lanthanide oep-tpp sandwich complexes reflects a larger steric barrier. Therefore, the differences in activation enthalpy of complexes **II** with respect to **I** may be related to a slight decrease of the porphyrin inter-plane distance. This is consistent with the ionic radius decrease along the series of lanthanide metals, known as *"lanthanide contraction"*.

In order to access this possibility, we have analyzed the available NMR and structural data on these complexes using Equation (3). It was assumed that the dipolar term dominates in the lanthanide-induced enhancements of spin-lattice relaxation rates on the ligand nuclei for **I** and **III**. The comparison of the calculated values of the structural parameter [$r(i)/r(CH_3)$], where r is distance between the lanthanide cation and the resonated proton,[10a−10c] (Table 1) for **I** and **III** reveals that the corresponding values in both complexes are rather similar although not identical.

$$r(i)/r(CH_3) = [T_1(i)/T_1(CH_3)]^{1/6} \quad (3)$$

The observed small differences between two complexes can be due either to an error in determination of $T_1(i)$ values or to minor structural differences.

A theoretical ratio has been previously reported for the variation of the pseudo-contact shifts in a series of isostructural Ln complexes.[11a,11b] In order to compare the hyperfine shifts of **I** with corresponding values of **II** (Table 1),

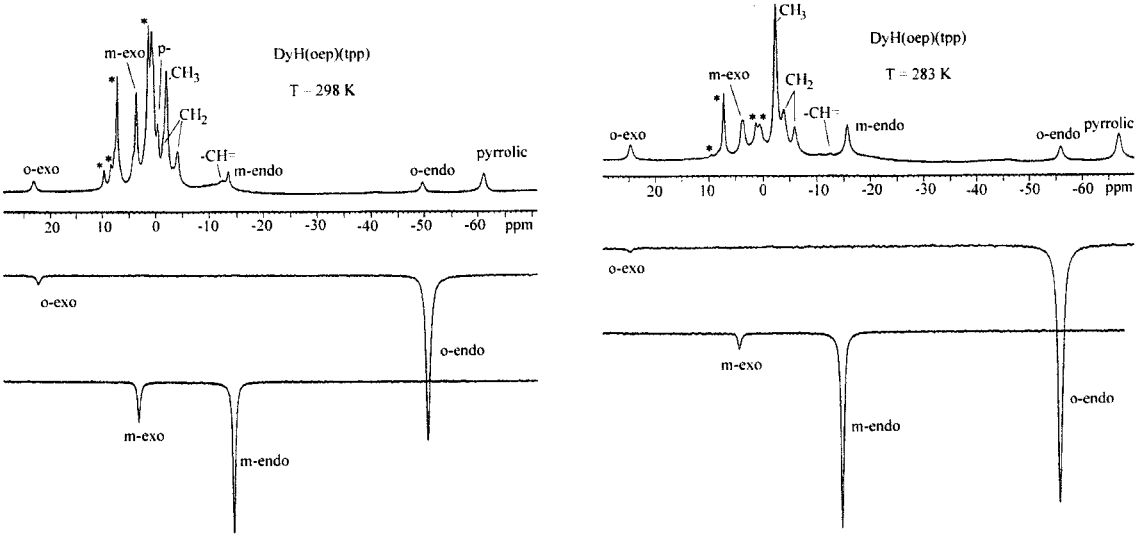

Figure 3. 500-MHz ^{1}H NMR 1D NOE difference spectra of DyH(oep)(tpp) (complex **I**) in $CDCl_3$ solution at various temperatures; assignment of diastereotopic phenyl proton peaks is reported; the asterisks indicate solvent or/and impurities

the parameters $\Delta\delta/B(\mathrm{Ln})$, where $\Delta\delta$ is the hyperfine shift and $B(\mathrm{Ln})$ is the Bleaney's constant,[11a,11b] were calculated. The analysis of Table 1 indicates that there is no correlation between the corresponding values of these parameters for complexes **I** and **III**. This means that the principal values (χ_i) of the molar paramagnetic susceptibility tensor change drastically from **I** to **III**, while only minor structural differences between these complexes occur. This behavior can be rationalized as due both to the effect of lanthanide contraction and to the macrocyclic nature (as basicity, planarity, etc.) of the ligand. These results are in rather good agreement with the study of complexes of macrocyclic polyether 18-crown-6 with paramagnetic lanthanide cations.[11b] The values of $(\chi_z - \chi_{av})/B(\mathrm{Ln})$ parameter are found to change monotonically three times with increase in the atomic number of Ln for Ln = Ce, Nd, and Pr with minor changes in the effective angle H−(18-crown-6)−Ln with C_2 axis of symmetry of the complexes. Therefore, the significant variation of molar paramagnetic susceptibility between complexes **I** and **III** are proposed to be related to a slight decrease of the distance between the planes of porphyrin ligands. This distance decreasing is relative to the increase in the number of lanthanide *f* electrons, which consequently results to lanthanide ionic radius contraction.

Experimental Section

Complexes **I**−**III** were synthesized according to the methods previously described.[1e,3d] Samples for NMR spectroscopy were prepared by dissolving **I**−**III** in deuterated chloroform. NMR spectra were recorded using MSL 200 and DRX 500 Bruker spectrometers operating at 200.13 and 500.13 MHz Larmor frequencies, respectively. Recycle delays and irradiation times ranged from 50 to 350 ms and from 20 to 200 ms, respectively. The spectra were calibrated by assigning the residual chloroform signal at 298 K to a shift from TMS of $\delta = 7.23$. 1D NOE spectra were recorded in difference mode using acquisition schemes previously described.[8a,8b] The chemical shift values of the diamagnetic LuH(oep)(tpp) complex[3d,3e] were used to calculate the hyperfine shifts for paramagnetic complexes **I** and **III**.

Longitudinal relaxation times were measured using a nonselective inversion recovery pulse sequence.[9a] The T_1 values were obtained from a two-parameter fit of the data to an exponential recovery function. In all cases the magnetization recovery was found to be exponential within the accuracy of the experiment, as expected for fast relaxing nuclei with little cross relaxation and favorable chemical exchange conditions.[9b]

Solution temperature was controlled using a Bruker B-VT 1000 temperature controller. Fourier-transformed spectra were subjected to complete line shape analysis[7a,7b,7d] on a Pentium-166 computer to obtain rate data for complexes **II**.

Supporting Information Available (see also footnote on the first page of this article): Temperature variations of $\ln(k)$ for DyH(oep)(tpp) in deuterated chloroform (Figure S1). Temperature variations of $\ln(k)$ for LuH(oep)(tpp) in deuterated chloroform (Figure S2).

Acknowledgments

We wish to acknowledge the RFFI for support (grant No. 00−03−33011a). We are grateful to Professors Ivano Bertini and Claudio Luchinat (University of Florence) for their insightful comments on the manuscript.

[1] [1a] J. W. Buchler, H. G. Kapellmann, M. Knoff, K.-L. Lay, S. Pfeifer, *Z. Naturforsch* **1983**, *38B*, 1339−1345. − [1b] J. W. Buchler, A. De Cian, J. Fischer, M. Kihn-Botulinski, H. Paulus, R. Weiss, *J. Am. Chem. Soc.* **1986**, *108*, 3652−3659. − [1c] J. W. Buchler, A. De Cian, J. Fischer, M. Kihn-Botulinski, R. Weiss, *Inorg. Chem.* **1988**, *27*, 339−345. − [1d] J. W. Buchler, B. Scharbert, *J. Am. Chem. Soc.* **1988**, *110*, 4272−4276. − [1e] G. A. Spyroulias, C. Raptopoulou, D. de Montauzon, A. Mari, R. Poilblanc, A. Terzis, A. G Coutsolelos, *Inorg. Chem.* **1999**, *38*, 1683−1696. − [1f] M. Takeuchi, T. Imada, S. Shinkai, *Angew. Chem. Int. Ed.* **1998**, *37*, 2096−2099. − [1g] K. Tashiro, T. Fujiwara, K. Konishi, T. Aida, *Chem. Commun.* **1998**, 1121−1122.

[2] [2a] J. W. Buchler, K. Elsässer, M. Kihn-Botulinski, B. Scharbert, *Angew. Chem. Int. Ed. Engl.* **1986**, *25*, 286−287. − [2b] J. W. Buchler, P. Hammerschmitt, I. Kaufeld, J. Löffler, *Chem. Ber.* **1991**, 2151−2159. − [2c] J. W. Buchler, M. Kihn-Botulinski, B. Scharbert, *Z. Naturforsch* **1988**, *43B*, 1371−1380. − [2d] J. W. Buchler, A. De Cian, J. Fischer, P. Hammerschmitt, J. Löffler, B. Scharbert, R. Weiss, *Chem. Ber.* **1989**, *122*, 2219−2228. − [2e] J. W. Buchler, M. Kihn-Botulinski, J. Löffler, M. Wicholas, *Inorg. Chem.* **1989**, *28*, 3770−3772.

[3] [3a] J. W. Buchler, J. Löffler, *Z. Naturforsch.* **1990**, *45B*, 531−542. − [3b] E. M. Davoras, G. A. Spyroulias, E. Mikros, A. G. Coutsolelos, *Inorg. Chem.* **1994**, *33*, 3430−3434. − [3c] J. W. Buchler, M. Kihn-Botulinski, J. Löffler, B. Scharbert, *New, J. Chem.* **1992**, *16*, 545−553. − [3d] G. A. Spyroulias, A. G. Coutsolelos, *Inorg. Chem.* **1996**, *35*, 1382−1385. − [3e] I. Bertini, A. Coutsolelos, A. Dikiy, C. Luchinat, G. A. Spyroulias, A. Troganis, *Inorg. Chem.* **1996**, *35*, 6308−6315.

[4] [4a] X. Yan, D. Holten, *J. Phys. Chem.* **1988**, *92*, 409−414. − [4b] O. Bilsel, J. Rodriguez, D. Holten, *J. Phys. Chem.* **1990**, *94*, 3508−3512. − [4c] J. K. Duchowski, D. F. Bocian, *J. Am. Chem. Soc.* **1990**, *112*, 3312−3318. − [4d] R. J. Donohoe, J. K. Duchowski, D. F. Bocian, *J. Am. Chem. Soc.* **1988**, *110*, 6119−6124.

[5] [5a] J. K. Duchowski, D. F. Bocian, *J. Am. Chem. Soc.* **1990**, *112*, 8807−8811. − [5b] J. K. Duchowski, D. F. Bocian, *Inorg. Chem.* **1990**, *29*, 4158−4160. − [5c] J.-H. Perng, J. K. Duchowski, D. F. Bocian, *J. Phys. Chem.* **1990**, *94*, 6684−6691. − [5d] J.-H. Perng, J. K. Duchowski, D. F. Bocian, *J. Phys. Chem.* **1991**, *95*, 1319.

[6] G. A. Spyroulias, A. G. Coutsolelos, C. Raptopoulou, A. Terzis, *Inorg. Chem.* **1995**, *34*, 2476−2479.

[7] [7a] J. Sandstrom, *Dynamic NMR Spectroscopy*, Academic Press: London, **1982**. − [7b] S. P. Babailov, Yu. G. Krieger, *J. Struct. Chem.* **1998**, *39*, 580. − [7c] S. Forsen, R. A. Hoffman, *J. Chem. Phys.* **1963**, *39*, 2892. − [7d] S. F. Lincoln, *Prog. React. Kinet.* **1977**, *9*, 1−91. − [7e] S. S. Eaton, G. R. Eaton, R. H. Holm, *J. Organomet. Chem.* **1972**, *39*, 179−195.

[8] [8a] L. Banci, I. Bertini, C. Luchinat, M. Piccioli, A. Scozzafava, P. Turano, *Inorg. Chem.* **1989**, *28*, 4650−4656. − [8b] L. B. Dugad, G. N. La Mar, L. Banci, I. Bertini, *Biochemistry* **1990**, *29*, 2263−2271.

[9] [9a] R. L. Vold, J. S. Waugh, M. P. Klein, D. E. Phelps, *J. Chem. Phys.* **1968**, *48*, 3831−3832. − [9b] G. N. La Mar, J. S. de Ropp, in: *Biological Magnetic Resonance* (Eds.: L. J. Berliner, J. Reuben); Plenum Press: New York, **1993**; *12*, 1−78.

[10] [10a] G. C. Levy, U. E. Edlung, C. Holloway, *J. Magn. Res.* **1976**, *24*, 375−387. − [10b] C. A. M. Vijverberg, J. A. Peters, A. P. G. Kieboom, et al., *Tetrahedron* **1986**, *42*, 1567. − [10c] T. J. Swift, in: *NMR of Paramagnetic Molecules* (Eds.: G. N. La Mar); Academic Press: New York, **1973**.

[11] [11a] B. Bleaney, *J. Magn. Res.* **1972**, *25*, 91. − [11b] S. P. Babailov, Yu. G. Krieger, *J. Struct. Chem.* **1990**, *31*, 65.

Received June 16, 2000
[I00239]

Boron-Bridged Group-4 *ansa*-Metallocene Complexes

Pamela J. Shapiro[a]

Keywords: Group-4 elements / Metallocenes / Boron bridge / Lewis acids / Alkene polymerization

Boron-bridged group-4 *ansa*-metallocene complexes are newcomers to the field of metallocene-mediated olefin polymerization catalysis. Because of the Lewis acidity of the boron bridge, it is more reactive than the more common carbon and silicon bridges. It is also more vulnerable to cleavage from the ligand framework by nucleophilic agents. A primary goal of our work is to involve the boron bridge more actively in the reaction chemistry of the metallocene while keeping the bridge intact.

Introduction

Metallocenophanes and *ansa*-Metallocenes

The earliest examples of interannular-bridged metallocenes are ferrocene derivatives and are called ferrocenophanes in association with the nomenclature system for bridged, aromatic, organic compounds.[1−3] The first examples of interannular-bridged metallocene complexes of the group-4 transition metals were synthesized by Katz and by Bernal;[4,5] however, Brintzinger is responsible for popularizing these systems and for popularizing the term "*ansa*-metallocene".[6] The latin prefix *ansa* (for bent handle, attached at both ends) was also borrowed from the organic nomenclature for bridged aromatic compounds. The term *ansa*-metallocene has generally been applied to bridged, bent-metallocene complexes of main-group metals,[7−10] the early transition metals (groups 3−7)[11−22] and the lanthanide metals,[23−27] whereas the term metallocenophane continues to be used for the bridged sandwich compounds of iron and ruthenium.[28−30]

Group-4 *ansa*-metallocene complexes are currently favored for the stereocontrol that they afford in Ziegler−Natta-type olefin polymerization catalysis.[31−33] These complexes are also popular as catalysts for various asymmetric organic transformations.[34] Although a number of different bridging groups have been introduced, carbon and silicon moieties are most common and have served a primarily structural role, that of fixing the cyclopentadienyl, indenyl, or fluorenyl rings of the metallocene in a specific orientation with respect to the active site. The bridge has also been designed to direct the stereochemistry of ring addition during metallocene formation;[11] however, to date, there has been little *chemical* participation of the *ansa* moiety in the reactions occurring at the transition metal center.[25]

This chemical participation has been one of the goals of our research. To this effect we have incorporated an electrophilic borylidene moiety in the *ansa* position of the metallocene. One of our objectives is the activation of the transition metal center by the boron bridge in a manner currently accomplished by external Lewis acid coactivators. The potential to couple geometry changes at the boron bridge with chemistry occurring at the transition metal center is another attractive feature of this new class of *ansa*-metallocenes.

Although related to the boron-bridged systems described herein, group-4 metallocenes with dangling boryl groups will not be covered in this review article. Participation of the dangling boryl group in the chemistry of the transition metal has been demonstrated by Piers and co-workers.[35] Bochmann and co-workers have modeled intramolecular activation of ligands on the metal center by boron.[36] Their examples indicate that the ability of the Lewis-acidic boryl

[a] Department of Chemistry, University of Idaho
Moscow, ID 83844-2343, USA
Fax: (internat.) + 1-208/885-6173
E-mail: shapiro@uidaho.edu

The author was born in Boston, Massachusetts (USA) in 1962. Her interest in transition metal mediated catalysis was inspired by her undergraduate research experience in the laboratories of Professor K. B. Sharpless while she was earning her Bachelor of Science degree at MIT. She received her training in synthetic and mechanistic organometallic chemistry as a Ph.D. student in the research group of Professor J. E. Bercaw at Caltech in Pasadena, CA. After a postdoctoral year at DuPont's Experimental Station in Wilmington, DE, in 1991 she joined the chemistry faculty at the University of Idaho where she is currently Associate Professor of Inorganic Chemistry.

MICROREVIEWS: This feature introduces the readers to the authors' research through a concise overview of the selected topic. Reference to important work from others in the field is included.

 © WILEY-VCH Verlag GmbH, 69451 Weinheim, 2001 1434−1948/01/0202−0321 $ 17.50+.50/0

group to activate the metal complexes intramoleculary by σ-ligand abstraction is very sensitive to the proximity of the boryl group to the ligands. In this respect, dangling the boryl group over the active site of the metal center is more effective than including it within the interannular bridge of the metallocene. Nevertheless, *inter*molecular activation of the metal center of another complex by the boron bridge is still possible and does occur. Additional examples of group-4 metallocene complexes with dangling boryl groups are found in ref.[37−40,41b]

Syntheses of Boron-Bridged *ansa*-Metallocenes

Manners and co-workers reported the first example of a [1]borylidene-bridged metallocene, which was prepared by treating 1,1′-dilithioferrocene with an aminodichloroborane.[30] Unfortunately, a similar approach for introducing a boron atom between the cyclopentadienyl rings of metallocene complexes of the more reactive group-4 metals is not possible since further metallation of the cyclopentadienyl ring is unlikely in the presence of the electrophilic group-4 metal center. Instead, the boron-bridged dicyclopentadienyl ligand framework must be assembled prior to its attachment to the group-4 metal center.

In 1979, Jutzi and Seufert reported a method for the synthesis of cyclopentadienylboranes involving the reaction of haloboranes with cyclopentadienyltrimethylsilanes and -trimethylstannanes.[41a] The presence of an additional trimethylsilyl substituent on the cyclopentadienyl ring allows the further attachment of a titanium trichloride fragment by reaction with $TiCl_4$.[41b] The avoidance of salt-metathesis reactions in these synthetic steps is attractive due to the vulnerability of the boron−cyclopentadienyl linkage to cleavage by strong nucleophiles.[42] In 1995, Reetz and co-workers reported using this chemistry to form boron-substituted zirconocenes.[37] We have also employed this chemistry for the synthesis of the boron-bridged titanium homobimetallic complex **II** and the *ansa*-zirconocene complex **III** shown in Scheme 1.[43]

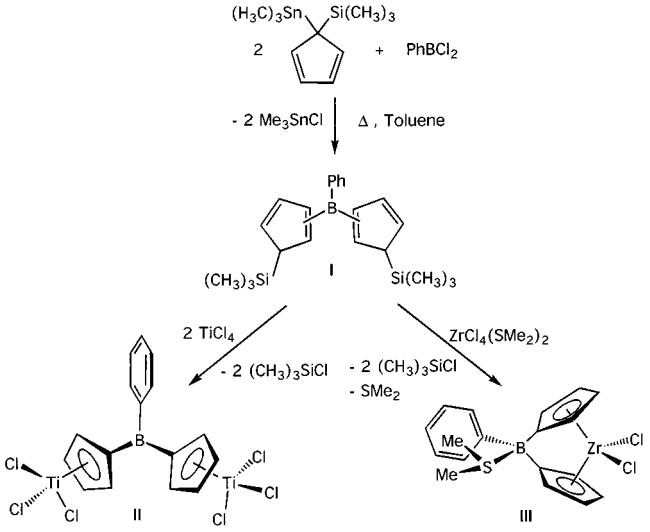

Scheme 1. Syntheses of boron-bridged titanium homobimetallic complex **II** and *ansa*-zirconocene complex **III**

The more labile trimethylstannyl substituents on the cyclopentadienyl rings are required for the ring borylation step. Formation of an *ansa*-metallocene was not expected from the reaction of ligand **I** with $TiCl_4$ since it has been shown that the attachment of only *one* cyclopentadienyl ligand to the titanium center is possible by this dehalodesilation route.[44] On the other hand, although zirconium tetrachloride has been shown to readily metallate two trimethylsilylcyclopentadiene rings by this route, it is completely unreactive toward ligand **I**, as are $[ZrCl_4(THF)_2]$ and $[ZrCl_4(THT)_2]$ (THT = tetrahydrothiophene). Fortunately, $[ZrCl_4(SMe_2)_2]$ does react with **I** to form the *ansa*-metallocene **III**, in which one of the dimethyl sulfide ligands is retained as an adduct on the phenylborylidene bridge. The attachment of an electropositive boron atom to the ring system apparently deactivates the silyl substituents toward electrophilic substitution by Zr^{IV} such that only a non-oligomeric, weakly solvated source of $ZrCl_4$ is suitable. Even when **I** is treated with two equivalents of $[ZrCl_4(SMe_2)_2]$, the *ansa*-metallocene is formed preferentially. We have used this same reaction to generate various other boryl-cyclopentadienylzirconium complexes, including $[\{Ph_2(SMe_2)B(C_5H_4)\}ZrCl_3]$ and $[\{(C_6F_5)_2(SMe_2)B(C_5H_4)\}ZrCl_3]$,[45] in which the boryl group is pendant to but not bridging between the cyclopentadienyl rings.

We believe that the dimethyl sulfide assists in the formation of the *ansa* complex since its coordination to the boron rehybridizes the single-atom bridge from an sp^2 to an sp^3 geometry which can better accommodate the bent-metallocene structure. As we were preparing to publish our findings, we discovered a report on the synthesis of the base-free version of **III** by Rufanov and co-workers.[46] These authors employed bis(trimethylstannyl)cyclopentadiene as the precursor to their boron-bridged ligand, forming the stannylated analog of **I**, which was treated directly with $ZrCl_4$. A mononuclear, *ansa*-metallocene structure was proposed for the base-free species, although an X-ray crystal structure was not obtained, and the molecular weight of the complex was not determined. The validity of this assignment is still in question, and we have not yet successfully prepared the base-free *ansa*-metallocene either by the Rufanov method or by complete removal the dimethyl sulfide adduct from **III**.

Lewis Aciditiy of Phenylborylidene Bridge

Efforts to abstract the Lewis base adduct from **III** with a stronger Lewis acid have been, so far, unsuccessful. Surprisingly, when either **III** or the related *tert*-butyl isocyanide complex are combined with an equimolar amount of $B(C_6F_5)_3$ in CD_2Cl_2, only partial abstraction of the Lewis base adduct (30−37%) by $B(C_6F_5)_3$ from the phenylborylidene bridge is observed by ^1H and ^{19}F NMR spectroscopy at 273 K.[47] We expected the boron atom of the phenylborylidene bridge to have an electrophilicity more comparable to that of BPh_3 based on its substitution. Indeed, ν(CN) for the *tert*-butyl isocyanide analog of **III**, $[\{(Ph)(tBuNC)B(\eta^5\text{-}C_5H_4)_2\}ZrCl_2]$, is identical to that of $Ph_3B(CN-tBu)$ (2272 cm^{-1})[48] and substantially lower than that of

$(C_6F_5)_3B(CN-tBu)$ (2310 cm^{-1}).[49] Thus, we surmise that the greater affinity of **III** for its Lewis base adducts arises from the relief of the internal strain which would exist in the sp^2-hybridized boron bridge.

The reactivity of the borylidene bridge in **III** also reveals a Lewis acidity more comparable to that of $B(C_6F_5)_3$ than BPh_3, since **III** is able to accomplish methide abstraction in a manner similar to that of $B(C_6F_5)_3$. For example, reaction of **III** with Cp^*_2AlMe ($Cp^* = C_5Me_5$) affords the pentamethylaluminocenium cation $[Cp^*_2Al]^+$ with $[(Ph)(Me)B(\eta^5\text{-}C_5H_4)_2ZrCl_2]^-$ as the counteranion [Equation (1)]. $B(C_6F_5)_3$, but not BPh_3, reacts in a similar manner with Cp^*_2AlMe.[47]

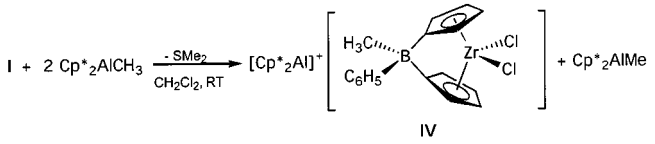

IV

The formation of **IV** is important as it indicates the possibility of stabilizing a borate-bridged *ansa*-zirconocene complex as a zwitterion (Figure 1).

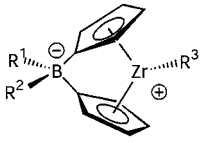

Figure 1. Hypothetical borate-bridged *ansa*-zirconocene zwitterion

It is clear, however, that the countercation plays a role in the stability of the borate bridge. The stability of **IV**, with its permethylaluminocenium countercation, suggests that a sterically hindered, non-intrusive countercation is desirable. This is further supported by the synthesis of a variety of stable borate-bridged *ansa*-zirconocene salts by treating **III** with $[Bu_4N]X$ (X = Cl, Br, I, BF_4, BH_4) and $[(Ph_3P)_2N]Cl$.[45] The borylidene bridge in **III**, like $B(C_6F_5)_3$, also abstracts a methyl anion from Cp_2ZrMe_2, as indicated by ^1H and ^{11}B NMR spectra of the reaction. We are currently trying to isolate and fully characterize the product of this reaction.

Alkylation of Boron-Bridged *ansa*-Zirconocene Complexes

Alkylation of the transition metal center is an essential step in forming an active catalyst center for olefin polymerization and other applications in catalysis. The vulnerability of the electrophilic boron bridge to nucleophilic attack and subsequent cleavage from the cyclopentadienyl ring is probably responsible for our unsuccessful efforts to alkylate complex **III** using conventional organometallic alkylating reagents such as alkyllithium, Grignard, alkylzinc, and alkylaluminum reagents. Such cleavage of the boryl group from the cyclopentadienyl ligand has been encountered in other cases.[43,49]

Dynamic behavior observed in the variable-temperature ^1H NMR spectra of **III** revealed that the dimethyl sulfide adduct is only weakly coordinated to the boron. It is readily replaced by more tightly coordinating ligands, such as PMe_3, to form $[\{Ph(PMe_3)B(\eta^5\text{-}C_5H_4)_2\}ZrCl_2]$ (**V**) which, unlike **III**, is non-labile on the NMR time scale [Equation (2)].[43]

III V

This substitution protects the boron sufficiently to allow alkylation of the zirconium center by alkyllithium and Grignard reagents to form complexes of the type $[\{Ph(PMe_3)B(\eta^5\text{-}C_5H_4)_2\}ZrR_2]$ (R = CH_2SiMe_3, $CH_2C_6H_5$), which can be activated with either $B(C_6F_5)_3$ or $[PhMeNH]^+[B(C_6F_5)_4]^-$ toward ethylene and propene polymerization.[45] A related phenylborylidene-bridged bis(indenyl)zirconium dichloride complex was recently reported by Reetz and co-workers.[50] The trimethylphosphane adduct of this complex, upon activation with MAO (MAO = methylalumoxane), was found to be a better catalyst for the polymerization of propene than the diethyl ether adduct, presumably due to stronger complexation of the boron by PMe_3. Similarly, complex **V**, with its tightly coordinating PMe_3, is activated by MAO toward olefin polymerization. Complex **III**, however, with its weakly coordinating SMe_2, is completely inactive under the same reaction conditions. Complex **IV** and other borate-bridged complexes such as $[NEt_4]^+[\{Ph(Cl)B(\eta^5\text{-}C_5H_4)_2\}ZrCl_2]^-$ and $[(Ph_3P)_2N]^+[\{Ph(Cl)B(\eta^5\text{-}C_5H_4)_2\}ZrCl_2]^-$ are also activated by MAO toward olefin polymerization, although their activities in the polymerization of ethylene were found to be lower than that of **V**.[47]

Other Boron-Bridged Group-4 Metallocene Complexes

The phenyl group on the borylidene bridge may be replaced with other substituents for the purpose of fine-tuning the electrophilicity of the boron. By using BBr_3 instead of $PhBCl_2$ in the ligand synthesis shown in Scheme 1, we are able to prepare ligand **VI**, in which the bromine is readily replaced by other moieties, such as the pentafluorophenyl group in ligand **VII**. These ligands were used to prepare complexes **VIII** and **IX** (Scheme 2). A variable-temperature ^1H NMR study shows that, in contrast to complex **III**, the dimethyl sulfide adduct in complex **IX** is non-labile on the NMR time scale.[45]

An X-ray crystal structure of complex **IX** confirmed its formulation but the structure is highly disordered with an unidentified solvent molecule. A preliminary ORTEP drawing of the molecule is shown in Figure 2.[51]

Introduction of an amido group onto the boron bridge allows the isolation of base-free group-4 *ansa*-metallocenes complexes, examples of which have been reported by Braunschweig and by Ashe (Figure 3).[52,53] π-Electron donation from the nitrogen to the boron is evident in the X-ray crystal structures of these complexes and is presumably responsible for the greater stability of the base-free boron

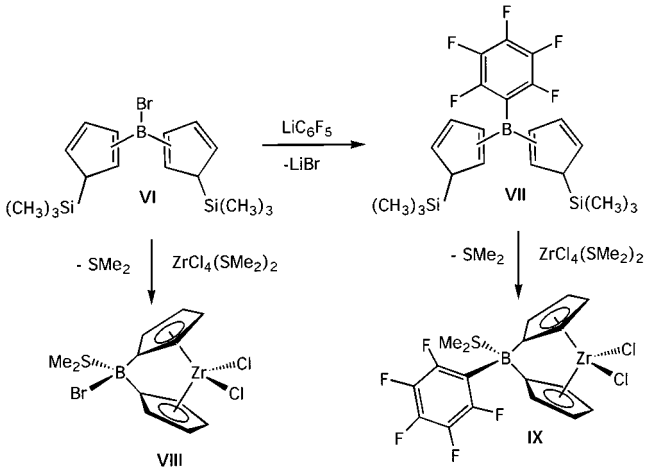

Scheme 2. Variations on the substitution of the boron bridge

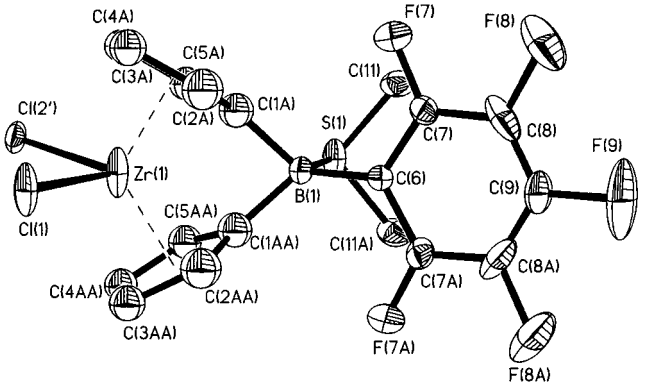

Figure 2. Preliminatry ORTEP drawing of the molecular structure of **IX**; thermal ellipsoids are drawn at 30% probability

bridges. Complex **XI**, upon activation with MAO, exhibits polymerization activities in the range exhibited by Me_2Si-bridged zirconocenes.

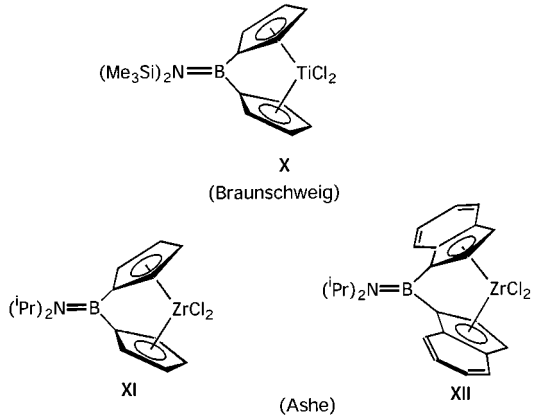

Figure 3. Amidoborylidene-bridged *ansa*-metallocene complexes of Ti^{IV} and Zr^{IV}

As mentioned above, Reetz and co-workers have recently reported the synthesis of a bis(indenyl)zirconium dichloride complex with different Lewis bases coordinated to the phenylborylidene bridge (**XIII**, Figure 4).[50] Reaction of the dianionic indenyl ligand with $ZrCl_4$ affords a 1:1 mixture of *rac*- and *meso*-metallocene isomers, from which the *rac* isomer can be selectively crystallized in 12% yield. The PMe_3 adduct of this system exhibits high propene polymerization activity as well as high selectivity for an isotactic polymer. Base-free, methylborylidene- and tris(trimethylsilyl)borylidene-bridged analogs of C_2-symmetric bis(indenyl)zirconium complexes were reported separately by Rufanov and co-workers, although no X-ray crystallographic data confirming the structures are available.[54]

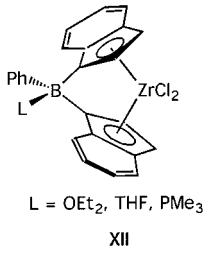

Figure 4. Phenylborylidene-bridged *rac*-bis(indenyl)zirconium complex prepared by Reetz and co-workers

A new paradigm for the synthesis of interannularly bridged metallocenes involving the formation of a donor/acceptor linkage between a Lewis-acidic boryl substituent on one ring of the metallocene and a Lewis-basic substituent on the opposite ring was introduced by Starzewski and co-workers (**XIV**, Figure 5).[55] This self-assembly approach to bridge formation affords enormous synthetic control and versatility in the design of the *ansa*-metallocene complexes since the electronic and steric properties of the donor and acceptor components are easily varied and the final stereochemistry of the metallocene, i.e. the relative orienation of asymmetrically substituted cyclopentadienyl rings or indenyl rings, is more easily controlled.

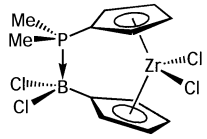

Figure 5. Donor/acceptor *ansa*-zirconocene complex introduced by Starzewski and co-workers

Structural Features of Boron-Bridged *ansa*-Zirconocene and -Titanocene Complexes

Table 1 lists selected geometric features of crystallographically characterized boron-, silicon-, and 1-, 2-, and 3-carbon-bridged metallocenes. The bite angle ε of the bridge, the dihedral angle α between the ring planes, and the angle γ formed by the metal center and the ring centroids are defined in Figure 6.

The narrowing of γ and the widening of α relative to the two-carbon- and three-carbon-bridged complexes reflects the distortion of the *ansa*-metallocenes from a "normal" geometry. The degree of distortion caused by a boron bridge is much larger than that of a silicon bridge but not quite as large as the distortion in a carbon-bridged *ansa*-metallocene.

Large changes in the size of the bridge bite angle ε produce relatively small changes in γ and α. For instance, despite a difference of over 5° in the bridge bite angles for the

Table 1. Selected angles [°] for various C-, Si-, and B-bridged *ansa*-metallocene complexes

Complex	X	Bridge angle ε	Ring-ring dihedral α	Ct–M–Ct γ	Ref.
	–$(CH_2)_3$–	—	53.3	130.2	65
	–$(CH_2)_2$–	—	53	128	6
	Me_2Si	89.5(1)	51.2	128.7(1)	65
	H_2C	97	63, 68	121, 122	6
	$(Me_3Si)_2NB$	98.3(6)	61.8	124.4	53
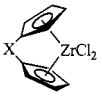	–$(CH_2)_3$–	—	50.2	129	65
	Me_2Si	93.2(2)	56.8	125.4(3)	65
	Me_2C	99.8	71.4	116.6	66
	$Ph(SMe_2)B$	101.1(2)	65.9	121.3(2)	44
	$Ph(PMe_3)B$	100.1(3)	68.5	121.1(6)	44
	$Ph(Me)B^{\ominus}$	97.2	65.2	120.5	48
	$Ph(Cl)B^{\ominus}$	99.4	65.9	120.9	48
	$(iPr)_2NB$	103.9(3)	65.5	119.6	54
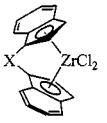	–$(CH_2)_2$–[a]	—	60.4	125.3	67
	Me_2C	100.3(3)	70.8	118.3	68
	Me_2Si	94.57(6)	61.94	119.04	62
	(THF)PhB	101.5(2)	67.2	122.3(8)	51
	$Ph(PMe_3)B$	99.4(2)	66.7	121.5(7)	51
	$(iPr)_2NB$	104.9	66.8	121.6	54

[a] This complex contains tetrahydroindenyl ligands.

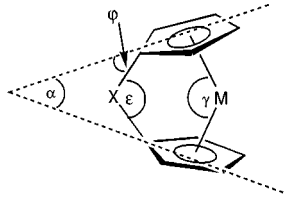

Figure 6. Illustration of *ansa*-metallocene angles listed in Table 1

final two entries of Table 1, the magnitudes of γ and α for the two complexes are nearly identical. This is due to a compensating distortion, represented by angle φ, in which the bridging atom bends away from the plane of the cyclopentadienyl or indenyl rings. The bending distortion of the bridge for the final complex (φ =18° and 20°) is greater than that of the preceding complex (φ =16° and 16.5°).

The bite angles of the base-free amidoborylidene-bridged species, complexes **II**, **XI**, and **XII**, are quite narrow for sp^2-hybridized boron atoms (cf. the 127° bridge angle for the bimetallic titanium complex **II** shown in Scheme 1[39]), illustrating the considerable strain experienced by an sp^2-hybridized boron atom in the *ansa* position.

Increasing the reaction space about the transition metal center by reducing the size of the bridge has been found to improve metallocene catalyst activity in some instances[56–58] and diminish it in others.[59][60] The effect of ring tilt on the olefin polymerization activity of metallocene catalysts is somewhat unpredictable because it depends on the type of rings comprising the ligand framework as well as on their substitution.[61–63] For example, [$Me_2Si(Ind)_2ZrCl_2$] generates a better catalyst for propene polymerization than [$Me_2C(Ind)_2ZrCl_2$] upon activation with MAO;[61] however, the reverse is true when the indenyl rings are substituted with *tert*-butyl groups at the 3-position.[63]

We have already noted from the data in Table 1 that the boron-bridged metallocenes are more distorted from a relaxed metallocene geometry than the silicon-bridged complexes but less distorted than the carbon-bridged complexes. Polymerization studies to date have shown that, with suitable protection of the boron, the activity and isospecificity of the boron-bridged complexes can be comparable to that of silicon-bridged analogs.[50,53] Furthermore, the potential to tune the electronic properties of the boron bridge, and consequently the transition metal center,[64] expands the range of ligand modification opportunities available for controlling the activity and selectivity of the metallocene catalyst.

Summary

The viability of boron-bridged goup-4 *ansa*-metallocene complexes as olefin polymerization catalysts that are competitive with the more common carbon- and silicon-bridged systems has been demonstrated. Although the boron bridge tends to be more vulnerable to nucleophilic attack and subsequent cleavage from the metallocene rings, tightly coordinating Lewis bases can protect it from this type of degradation. Furthermore, anionic borate bridges remain intact when accompanied by a suitable countercation.

Base-free, boron-bridged species have been prepared by introducing substituents that can donate additional π-electrons to the empty p orbital on the boron. In the absence of such stabilization, the sp^2-hybridized boron bridge behaves as a strong Lewis acid because of the internal strain it experiences in the *ansa* position, strain which can be somewhat relieved by rehybridization of the boron to sp^3 through the coordination of a Lewis base. This property, together with the ability of the boron to coordinate a wide variety Lewis bases, expands the potential functionality of the *ansa* bridge well beyond the structural role that it normally plays.

Acknowledgments

I thank my talented co-workers listed in the references for their contributions to this chemistry, and I am grateful to the National Science Foundation and the University of Idaho for their support. I am also grateful to Dr. Brendan Twamley (University of Idaho) for calculating many of the angles in Table 1 from the original crystal structure data and for proof-reading this manuscript.

[1] T. H. Barr, W. E. Watts, *Tetrahedron* **1968**, *24*, 3219–3235.
[2] T. H. Barr, W. E. Watts, *Tetrahedron* **1968**, *24*, 6111–6118.
[3] H. L. Lentzner, W. E. Watts, *Chem. Commun.* **1970**, 26–27.
[4] T. J. Katz, N. Acton, *Tetrahedron Lett.* **1970**, *28*, 2497–2499.

[5] B. R. Davis, I. Bernal, *J. Organomet. Chem.* **1971**, *30*, 75−87.
[6] J. A. Smith, J. v. Seyerl, G. Huttner, H.-H. Brintzinger, *J. Organomet. Chem.* **1979**, *173*, 175−185.
[7] R. Littger, N. Metzler, H. Nöth, M. Wagner, *Chem. Ber.* **1994**, *127*, 1901−1908.
[8] M. Rieckhoff, U. Pieper, D. Stalke, F. T. Edelmann, *Angew. Chem. Int. Ed. Engl.* **1993**, *32*, 1079−1081.
[9] K. M. Kane, P. J. Shapiro, R. Cubbon, A. Vij, A. L. Rheingold, *Organometallics* **1997**, *16*, 4567−4571.
[10] P. J. Shapiro, K. M. Kane, A. Vij, D. Stelck, G. J. Matare, R. L. Hubbard, B. Caron, *Organometallics* **1999**, *18*, 3468−3473.
[11] J. P. Mitchell, S. Hajela, S. K. Brookhart, K. I. Hardcastle, L. M. Henling, J. E. Bercaw, *J. Am. Chem. Soc.* **1996**, *118*, 1045−1053.
[12] S. L. J. Conway, L. H. Doerrer, J. C. Green, M. L. H. Green, A. Scottow, A. H. H. Stephens, *J. Chem. Soc., Dalton Trans.* **2000**, 329−333.
[13] S. L. J. Conway, L. H. Doerrer, M. L. H. Green, *Organometallics* **2000**, *19*, 630−637.
[14] A. Chernega, J. Cook, M. L. H. Green, L. Labella, S. J. Simpson, J. Souter, A. H. H. Stephens, *J. Chem. Soc., Dalton Trans.* **1997**, 3225−3243.
[15] D. Churchill, J. H. Shin, T. Hascall, J. M. Hahn, B. M. Bridgewater, G. Parkin, *Organometallics* **1999**, *18*, 2403−2406.
[16] D. M. Heinekey, C. E. Radzewich, *Organometallics* **1999**, *18*, 3070−3074.
[17] F. Schaper, M. Rentzsch, M. H. Prosenc, U. Rief, K. Schmidt, H.-H. Brintzinger, *J. Organomet. Chem.* **1997**, *534*, 67−69.
[18] H. Schwemlein, H. H. Brintzinger, *J. Organomet. Chem.* **1983**, *254*, 69−73.
[19] G. Dorer, J. Diebold, O. Weyand, H. H. Brintzinger, *J. Organomet. Chem.* **1992**, *427*, 245−255.
[20] D. T. Mallin, M. D. Rausch, Y.-G. Lin, S. Dong, J. C. W. Chien, *J. Am. Chem. Soc.* **1990**, *112*, 2030−2131.
[21] M. L. H. Green, N. Isihara, *J. Chem. Soc., Dalton Trans.* **1994**, 657−665.
[22] U. Dietrich, M. Hackmann, B. Rieger, M. Klinga, M. Leskelä, *J. Am. Chem. Soc.* **1999**, 4348−4355.
[23] C. Qian, Z. Gang, G. Lijun, *J. Organomet. Chem.* **1996**, *525*, 23−30.
[24] F. T. Edelmann, M. Rieckhoff, I. Haiduc, I. Silaghi-Dumitrescu, *J. Organomet. Chem.* **1993**, *447*, 203−208.
[25] P. W. Roesky, C. L. Stern, T. J. Marks, *Organometallics* **1997**, *16*, 4705−4711.
[26] H. Schumann, F. Erbstein, J. Demtschuk, R. Weimann, *Z. Anorg. Allg. Chem.* **1999**, *625*, 1457−1465.
[27] J. Eppinger, M. Spiegler, W. Hieringer, W. Herrman, R. Anwander, *J. Am. Chem. Soc.* **2000**, *122*, 3080−3096.
[28] M. Heberhold, *Angew. Chem. Int. Ed. Engl.* **1995**, *34*, 1837−1839.
[29] J. K. Pudelski, D. P. Gates, R. Rulkens, A. J. Lough, I. Manners, *Angew. Chem. Int. Ed. Engl.* **1995**, *34*, 1506−1508.
[30] H. Braunschweig, R. Dirk, M. Müller, P. Nguyen, R. Resendes, D. P. Gates, I. Manners, *Angew. Chem. Int. Ed. Engl.* **1997**, *36*, 2338−2340.
[31] H. H. Brintzinger, D. Fischer, R. Mülhaupt, B. Rieger, R. M. Waymouth, *Angew. Chem. Int. Ed. Engl.* **1995**, *34*, 1143−1170.
[32] *Metalorganic Catalysts for Synthesis and Polymerization* (Ed.: W. Kaminsky), Springer, Berlin, **1999**.
[33] *Ziegler Catalysts: recent scientific innovations and technological improvements* (Eds.: G. Fink, R. Mulhaupt, H. H. Brintzinger), Springer-Verlag, Berlin, **1995**.
[34] A. H. Hoveyda, J. P. Morken, *Angw. Chem. Int. Ed. Engl.* **1996**, *35*, 1262−1284.
[35] Y. Sun, R. E. v. H. Spence, W. E. Piers, M. Parvez, G. P. A. Yap, *J. Am. Chem. Soc.* **1997**, *119*, 5132−5143.
[36] S. J. Lancaster, S. Al-Benna, M. Thornton-Pett, M. Bochmann, *Organometallics* **2000**, *19*, 1599−1608.
[37] M. T. Reetz, H. Brümmer, M. Kessler, J. Kuhnigk, *Chimia* **1995**, *49*, 501−503.
[38] M. Bochmann, S. J. Lancaster, O. B. Robinson, *J. Chem. Soc., Chem. Commun.* **1995**, 2081−2082.
[39] S. A. Larkin, J. T. Golden, P. J. Shapiro, G. P. A. Yap, D. M. J. Foo, A. L. Rheingold, *Organometallics* **1996**, *15*, 2393−2398.
[40] J. Ruwwe, G. Erker, R. Fröhlich, *Angew. Chem. Int. Ed. Engl.* **1996**, *35*, 80−82.
[41] [41a] P. Jutzi, A. Seufert, *J. Organomet. Chem.* **1979**, *169*, 327−355. − [41b] P. Jutzi, A. Seufert, *J. Organomet. Chem.* **1979**, *169*, 373−380.
[42] H. Grundke, P. I. Paetzold, *Chem. Ber.* **1971**, *104*, 1136−1146.
[43] D. S. Stelck, P. J. Shapiro, N. Basickes, *Organometallics* **1997**, *16*, 4546−4550.
[44] C. H. Winter, X.-X. Zhou, D. A. Dobbs, M. J. Heeg, *Organometallics* **1991**, *10*, 210−214.
[45] D. S. Stelck, P. J. Shapiro, unpublished results.
[46] K. A. Rufanov, V. V. Kotov, N. B. Kazennova, D. A. Lemenovskii, E. V. Avtomonov, J. Lorberth, *J. Organomet. Chem.* **1996**, *525*, 287−289.
[47] C. T. Burns, D. S. Stelck, P. J. Shapiro, A. Vij, K. Kunz, G. Kehr, T. Concolino, A. L. Rheingold, *Organometallics* **1999**, *18*, 5432−5434.
[48] H. Jacobsen, H. Berke, S. Döring, G. Kehr, G. Erker, R. Frölich, O. Meyer, *Organometallics* **1999**, *18*, 1724−1735.
[49] F. A. Shafiq, K. A. Abboud, D. E. Richardson, J. M. Boncella, *Organometallics* **1998**, *17*, 982−985.
[50] M. T. Reetz, M. Willuhn, C. Psiorz, R. Goddard, *Chem. Commun.* **1999**, 1105−1106.
[51] Preliminary crystal data for **IX** at 193(2) K with Mo-K_α (λ = 0.71073 Å) radiation: $C_{18}H_{16}Cl_2F_5SZr$; M = 532.30; monoclinic, space group $P2_1/m$; a = 10.1562(4), b = 13.2711(2), c = 10.5087(4) Å, β = 118.071(2)°; V = 1249.79(7) Å^3; Z = 2; $\rho_{calcd.}$ = 1.414 Mg/m^3; μ = 0.74 mm^{-1}, φ range 2.20−28.35°; GOF on F_o^2 = 1.528 for 3057 unique reflections and 145 parameters, $R1$ = 0.1649, $wR2$ = 0.4549. The Cp rings are disordered over 2 sites and one Cl atom is disordered across the mirror plane. There is an unidentified solvent molecule present. This compound is currently being recrystallized for further structural studies.
[52] H. Braunschweig, C. von Koblinski, R. Wang, *Eur. J. Inorg. Chem.* **1999**, 69−73.
[53] A. J. Ashe, X. Fang, J. W. Kampf, *Organometallics* **1999**, *18*, 2288−2290.
[54] K. Rufanov, E. Avtomonov, N. Kazennova, V. Kotov, A. Khvorost, D. Lemenovskii, J. Lorberth, *J. Organomet. Chem.* **1997**, *536−537*, 361−373.
[55] K. Aleksander, O. Starzewski, W. M. Kelly, A. Stumpf, D. Freitag, *Angew. Chem. Int. Ed.* **1999**, *38*, 2439−2442.
[56] W. E Piers, P. J. Shapiro, J. E. Bercaw, *Synlett* **1990**, 2, 74−84.
[57] G. Jeske, L. E. Schock, P. N. Swepston, H. Schumann, T. J. Marks, *J. Am. Chem. Soc.* **1985**, *107*, 8091−8103.
[58] Y. Obora, O. Tetsuo, C. L. Stern, T. J. Marks, *J. Am. Chem. Soc.* **1997**, *119*, 3745−3755.
[59] G. Jeske, H. Lauke, H. Mauermann, H. Schumann, T. J. Marks, *J. Am. Chem. Soc.* **1985**, *107*, 8111−8118.
[60] M. R. Gagné, C. L. Stern, T. J. Marks, *J. Am. Chem. Soc.* **1992**, *114*, 275−294.
[61] [61a] W. A. Herrmann, J. Rohrmann, E. Herdtweck, W. Spaleck, A. Winter, *Angew. Chem. Int. Ed. Engl.* **1989**, *28*, 1511−1512. − [61b] W. Spaleck, M. Antberg, V. Dolle, R. Klein, J. Rohrmann, A. Winter, *New J. Chem.* **1990**, *14*, 499−503. − [61c] W. Spaleck, M. Antberg, M. Aulbach, B. Bachmann, V. Dolle, S. Haftka, F. Küber, J. Rohrmann, A. Winter, in ref.[33], pp. 83−97.
[62] J. A. Ewen, M. J. Elder, in ref.[33], pp. 99−109.
[63] [63a] L. Resconi, F. Piemontesi, I. Camurati, O. Sudmeijer, I. E. Nifant′ev, P. V. Ivchenko, L. G. Kuz′mina, *J. Am. Chem. Soc.* **1998**, *120*, 2308−2321. [63b] L. Resconi, L. Cavallo, A. Fait, F. Piemontesi, *Chem. Rev.* **2000**, *100*, 1253−1345.
[64] G. C. Bazan, W. D. Cotter, Z. J. A. Komon, R. A. Lee, R. J. Lachicotte, *J. Am. Chem. Soc.* **2000**, *122*, 1371−1380.
[65] C. S. Bajgur, W. R. Tikkanen, J. L. Petersen, *Inorg. Chem.* **1985**, *24*, 2539−2546.
[66] R. M. Shaltout, J. Y. Corey, N. P. Rath, *J. Organomet. Chem.* **1995**, *503*, 205−212.
[67] F. R. W. P. Wild, M. Wasiucionek, F. Huttner, H. H. Brintzinger, *J. Organomet. Chem.* **1985**, *288*, 63−67.
[68] A. Z. Voskoboynikov, A. U. Agarkov, E. A. Chernyshev, I. P. Beletskaya, A. V. Churakov, L. G. Kuz′mina, *J. Organomet. Chem.* **1997**, *530*, 75−82.

Received May 3, 2000
[I00177]

The Effect of Internal Hydroxy Groups in Chiral Diphosphane Rhodium(I) Catalysts on the Asymmetric Hydrogenation of Functionalized Olefins

Armin Börner[a]

Keywords: Asymmetric synthesis / Cooperative effects / Hydrogenation / Phosphanes / Rhodium

The unique effects of internal hydroxy groups in chiral rhodium(I) diphosphane catalysts on the asymmetric hydrogenation of functionalized olefins are summarized. In the first part, effects caused by the additional functional group on the rate and enantioselectivity of the catalytic reaction with Rh^I-diphosphane complexes are shown. For comparison, the results obtained with relevant parent catalysts or complexes bearing alkoxy groups are also considered. Subsequently, mechanistic studies which may explain the rate-reducing as well as the *ee*-enhancing effect of hydroxy groups are discussed in detail. Furthermore, the subtle competitive interplay between the hemilabile behaviour of hydroxy groups and their ability to establish hydrogen bonding within the framework of the ligand or between the ligand and the substrate is shown. Proof is given that conformationally flexible ligands bearing hydroxy groups can respond to varying electronic features of the catalytic centre and the substrate. Finally, the beneficial effect of hydroxy groups on the fine-tuning of diphosphane catalysts of low performance is demonstrated for some examples. This modification resulted in catalysts which afforded the chiral hydrogenation product in up to 99% *ee*.

Introduction

The effective control of stereoselective transformations is at the centre of modern organic chemistry research.[1] In stereodifferentiating catalysis employing transition metal complexes, two principal interactions between the catalyst and the prochiral substrate can be identified and these interactions enable chiral recognition: stereodiscriminating bond formation and diastereoselective repulsive interactions. These factors lead to diastereomeric intermediates with different thermodynamic stabilities and consequently in different concentration ratios. The diastereomeric intermediates in turn react to form the enantiomeric products. Owing to the energy differences of the intermediates, the rates are more or less different. For most catalytic reactions, the thermodynamic stabilities of the intermediates as well as the rate constants of the pre-equilibrium and the rate-determining steps are not available and cannot be predicted by theoretic methods. Consequently, the design of asymmetric catalysts is mainly based on trial and error.

To optimize chiral catalysts of low performance, several approaches have been envisaged. The most common way is to increase the bulkiness of selected parts of the ligand or to ensure rigid or restrained conformations of the catalyst.[2,3] Achiwa[4] and RajanBabu[5] showed that in some cases electronic effects can be advantageously employed for the fine-tuning of chiral catalysts. Most of these approaches consider the chiral catalyst as being static and focus on the construction of conformationally fixed molecules and do not take the varying steric and electronic features of catalytic intermediates or different substrates into consideration.[6]

[a] Institut für Organische Katalyseforschung an der Universität Rostock e.V.
Buchbinderstraße 5/6, 18055 Rostock, Germany
Fax: (internat.) +49-381/466-9324
E-mail: armin.boerner@ifok.uni-rostock.de

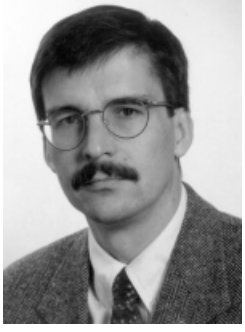

Armin Börner received his Ph.D. in 1984 from the University of Rostock (Germany) with Prof. H. Kristen, working in the field of carbohydrate chemistry. He moved to the Department of Complex Catalysis of the Academy of Sciences of the former GDR, at that time led by Prof. H. Pracejus. After some research stays in the pharmaceutical industry and abroad (1981, Debrecen, Hungary; 1987, Hyderabad, India), he joined the group of Prof. H. B. Kagan at the Laboratoire Synthèse Asymétrique at Orsay (France) in 1991 for a postdoctoral position. In 1992 he joined the "Asymmetric Catalysis" group at the Max-Planck-Gesellschaft (leader Prof. R. Selke), where he finished his habilitation in 1994. In 1993/94 he was a guest lecturer at the University of Würzburg. Currently, he is working as head of department at the Institut für Organische Katalyseforschung (IfOK). In 2000 he was appointed a C3-professor for "Asymmetric Catalysis" at the university of Rostock. His main research is focused on basic research in asymmetric catalysis with transition metals and its application in industry.

MICROREVIEWS: This feature introduces the readers to the authors' research through a concise overview of the selected topic. Reference to important work from others in the field is included.

 © WILEY-VCH Verlag GmbH, 69451 Weinheim, 2001 1434–1948/01/0202–0327 $ 17.50+.50/0

In 1992 Sawamura and Ito addressed the question of the benefit of secondary interactions in asymmetric metal catalysis.[7] Since that time, we and several other groups have elaborated the synthesis and application of chiral ligands containing additional functional groups. The aim was to control the conformational fluxionality within diastereomeric catalyst−substrate assemblies by electrostatic interactions,[8] π,π-interactions,[9] charge-transfer interactions,[10] hydrogen bonding,[11] Lewis acid/base interactions[12] or by inclusion in crown ethers.[13]

In particular, we were interested in investigating the influence of hydroxy groups in the backbone of conventional chiral diphosphane Rh^I-catalysts on the asymmetric hydrogenation. This reaction is of pivotal importance from an academic point of view[14] as well as for practical applications.[15] In the beginning of the research, we focused our attention on the synthesis of chiral hydroxy phosphanes and developed main strategies for their preparation. This work has recently been reviewed.[16] In this paper we will concentrate on the effects caused by hydroxy groups in diphosphane metal catalyst on the asymmetric hydrogenation. Simultaneously, reasons for these peculiar effects will be discussed. It should be noted that the effect of other "active" functional groups like amino or carboxylate groups are also worth being elaborated on, but are not considered here in detail.[7] Other typical features of phosphane ligands bearing hydroxy groups, such as the improvement of the solubility of the catalyst in water,[17] transformations into other functional groups[18] or the construction of heterobimetallic catalysts[12d,12e] have been discussed elsewhere.

In order to illustrate the distinct behaviour of the hydroxy group in the hydrogenation catalysts, comparison with closely related catalysts acting under the same conditions is necessary. From this point of view, valuable information can be derived particularly by comparison with analogous catalysts bearing alkoxy groups. The beneficial effect of alkoxy functionalities, especially that of the OMe group in asymmetric hydrogenation, has been more thoroughly investigated and employed in the past.[19] Principally, the OMe and the OH groups have some common features in catalysis, e.g. both can act as hemilabile ligands[20] and show a "windshield wiper effect" if properly placed,[21] but only the latter is able to serve as a hydrogen-bond donor. In this review, similarities between both are analyzed, but evidence will be also provided to show that the structural differences can have a significant influence on the course of the rhodium-catalyzed asymmetric hydrogenation.

Effects and Preliminary Results

As far back as 1982, Knowles et al. briefly noted that by substitution of the methoxy groups in the industrially applied DiPAMP[22] ligand (**1-OMe)** by OH groups (**1-OH**), a hydrogenation catalyst was obtained which exhibited good enantioselectivity but rather poor reactivity.[23] This sporadic observation indicated for the first time that the hydroxy group may be used for enantiocontrol. Furthermore, a relationship between the additional functional group and the lowered rate of the asymmetric hydrogenation was found.

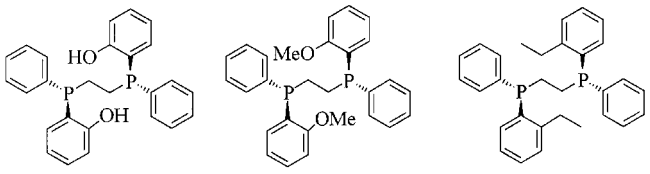

1-OH **1-OMe (DiPAMP)** **1-Et**

In the same year, Amma and Stille reported the synthesis of (*R*)-1,2-bis(diphenylphosphanyl)propan-3-ol (**2-OH**).[24]

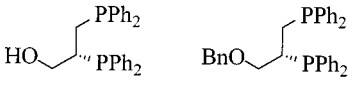

2-OH **2-OBn**

Attempts to utilize this ligand in the asymmetric hydrogenation of (*Z*)-*N*-acetylamino acrylic and (*Z*)-*N*-acetylamino cinnamic acid (AH), which are commonly used as standard substrates,[25] failed owing to the poor activity of the relevant Rh^I complex. Interestingly, by benzylation of the OH group (ligand **2-OBn**) an active catalyst was obtained.

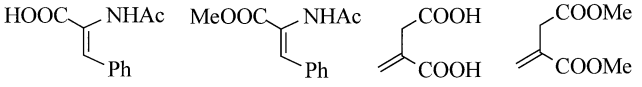

AH **AMe** **ItH_2** **$ItMe_2$**

We explored the same catalytic reaction with the homologous ligand **3-OH**.[26] The corresponding Rh-catalyst hydrogenated AH and its methyl ester (AMe) very slowly. This negative effect could be overcome by protection of the OH-group as the benzyl ether (**3-OBn**).

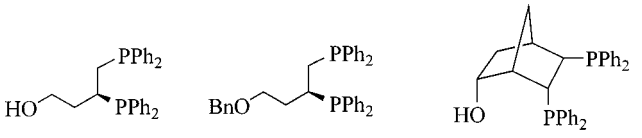

3-OH **3-OBn** **4 (HO-NorPHOS)**

At this time we concluded that an attractive interaction between the OH group and other parts of the catalyst−substrate complexes could be responsible for the observed decelerating effect. It is worth mentioning that the hydrogenations described above were performed in a large excess of methanol. In general, with parent catalysts no rate-reducing effects were observed in this solvent. That means that the effect of the hydroxy group could unambiguously be attributed to intramolecular and not to intermolecular interactions. In a ligand based on a rigid carbon skeleton such as **4**, this interaction should be disturbed. Indeed, **HO-NorpHOS** gave a hydrogenation catalyst with an activity similar to Brunner's **NorPHOS**, in spite of the fact that

the former was also based on the 4-hydroxy-1,2-bis(diphenylphosphanyl)butane moiety like **3-OH**.[27]

In the meantime, other groups also reported interesting catalytic effects observed after functionalization of phosphane catalysts. Thus, Dahlenburg and Kurth found that by incorporation of hydroxy groups, bis-trialkylphosphanes such as **5-H** may get profit in the Rh^I-catalyzed asymmetric hydrogenation of AH.[28] **5-OH** showed a 12% higher enantioselectivity than was observed with the parent ligand.

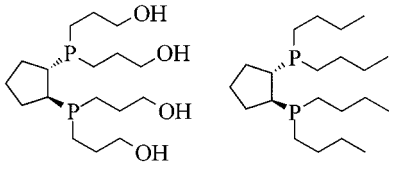

5-OH **5-H**

All the 1,2-diphosphanes described above form five-membered chelates with rhodium(I). Owing to the low conformational flexibility of this chelate size, attractive interactions of the additional functional group may be hindered or even overridden by steric effects. For example, Imamoto et al. found similarly high *ee*'s by application of a rhodium(I) complex with the DiPAMP analogous ligand **1-Et**.[29] Based on this result, they advocated the idea that the effect of the methoxy group in the DiPAMP−Rh-catalyst is based preferentially on steric reasons. A change of the reaction rate owing to the nonpolar ethyl group was not reported. Prompted by this result, we next turned our attention to the synthesis and application of conformationally flexible seven-membered chelates of the DIOP type like **6-OH** and **7-OH**.[30]

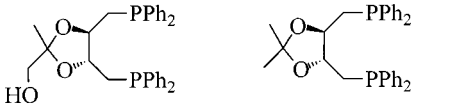

6-OH **6-H (DIOP)**

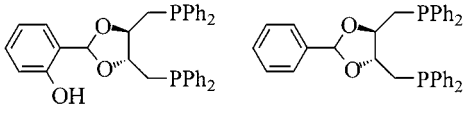

7-OH **7-H**

Surprisingly, under reduced H_2 pressure, Rh^I catalysts based upon these hydroxy phosphanes reduced the standard substrates more slowly than their parent catalysts derived from **DIOP** and **7-H**.[31] These results gave evidence that a remote OH group may also influence the rate and thus the mechanism of the asymmetric reaction. In several instances, improved enantioselectivities were also noted owing to the effect of the hydroxy group, but this correlation was not generally valid for all pairs of ligands tested. Interestingly, the X-ray structural analysis of the precatalyst [Rh(**6-OH**)(COD)]BF_4 gave no evidence that the OH group interfered with the rhodium centre. In contrast the hydroxy group was found to be situated far away from the metal. This fact indicated that the decisive interaction of the functional group with the catalytic centre is of low energy and may first come into play during the catalytic cycle or at least after coordination of the prochiral substrate.

Recently, Kagan et al. noted a striking enhancement of the enantioselectivity from 45% *ee* to more than 85% *ee* in the hydrogenation of AH, when the isopropylidene-protected bis-ferrocene ligand **8-Isoprop** was replaced by the corresponding diols **8-OH**.[32] It is noteworthy, that the increase in the *ee* found with these OH substituted nine-membered chelates was almost independent of the configurations at the 2,3-positions (**8(a-c)-OH**).

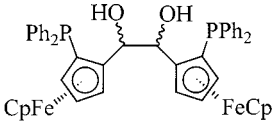

8a-OH (1*R*,2*R*)
8b-OH (1*S*,2*S*)
8c-OH (1*R*,2*S*)

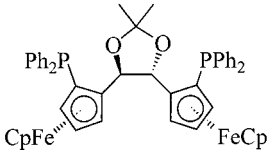

8-Isoprop

Mechanistic Studies

To better elaborate the dual effect of the OH group, we required a suitable model catalyst. As discussed above, conformers of 1,2-diphosphane chelates might be too rigid to permit a clear differentiation between attractive interactions within the catalyst−substrate assembly and sterically driven effects due to the 5-membered ring. Furthermore, because of the conformational rigidity, low hydrogenation rates are generally characteristic for these hydrogenation catalysts. Therefore, decelerating effects caused by additional functional groups may entirely block the catalytic reaction (vide supra). Conformationally flexible seven-membered chelates and therefore more active catalysts based on 1,4-bis(diphenylphosphanyl)butane ligands bearing one or two hydroxy groups in the carbon chain seemed to be much better suited. In addition, since other stabilizing groups are not present in these model complexes, catalytic effects can clearly be traced to the effect of the oxygen functionalities.

In a first study, we compared the Rh^I complexes of (*S*)-1,4-bis(diphenylphosphanyl)butan-2-ol (**9-OH**) and its methyl ether (**9-OMe**) in the asymmetric hydrogenation of AH, itaconic acid (ItH_2) and their corresponding methyl esters (AMe, $ItMe_2$).[33] The results are listed in Table 1. For comparison, results obtained with the Rh-complex of 1,4-bis(diphenylphosphanyl)butane (DPPB) are also included, representing a seven-membered chelate ring without any additional coordinating groups.[34a]

Table 1. Hydrogenations with [Rh(ligand)(COD)]BF_4

Ligand[a]	AH t [min][b]	*ee* [%]	AMe t [min][b]	*ee* [%]	ItH_2 t [min][b]	*ee* [%]	$ItMe_2$ t [min][b]	*ee* [%]
DPPB	<2	–	<2	–	<2	–	<2	–
9-OMe	6	4.6 (*S*)	13	5.3 (*S*)	1.5	8.3 (*R*)	15	2.6 (*R*)
9-OH	15	41.7 (*S*)	35	25.6 (*S*)	2.5	45.2 (*R*)	20	24.8 (*R*)
11-OMe	150[c]	0.6 (*S*)	420[d]	23.7 (*R*)[d]	6.0[c]	22.4 (*S*)	80[d]	7.6 (*S*)[d]
11-OH	420[c]	36.3 (*R*)	1920[d]	32.2 (*R*)[d]	15.0[c]	56.8 (*S*)	–[e]	–
13-OH	<2	–	<2	–	<2	–	<2	–

[a] Molar ratio catalyst/substrate = 1:100, 1 bar H_2 in methanol, room temp.; substrates: **AH**, **AMe**, **ItH_2**, **$ItMe_2$**. – [b] Corresponds to the time when 100% consumption of hydrogen was observed. – [c] In the original publication (ref.[34a]) times for 50% consumption of hydrogen were given. – [d] D. Heller, A. Börner, unpublished results. – [e] Hydrogenation proceeded only under elevated pressure.

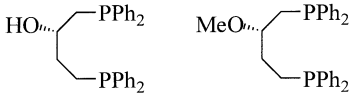

9-OH **9-OMe**

The latter is the most active catalyst in this series. It is remarkable that in comparison to the unfunctionalized catalyst, the incorporation of the methoxy as well as the hydroxy group diminished the rate of the reaction. This comparison nicely illustrates that the decelerating effect is not only restricted to the hydroxy but also to the methoxy group bearing catalysts.[35] In our opinion, this effect of the OMe group has been underestimated in the past.[36]

It is clear that the hydroxy group bearing catalyst gave generally superior enantioselectivities. In some cases, improvement of the selectivity by more than 35% *ee* was achieved relative to the catalyst based on **9-OMe**. In particular, the hydrogenation of substrate acids profits from this effect. Simultaneously with the enhancement of the enantioselectivity, a serious decrease in the activity was observed. In general, no change in the sense of the induced chirality was observed when **9-OH** was used instead of **9-OMe**. Interestingly, X-ray structural analysis and $^{31}P\{^1H\}$ NMR spectroscopic studies of the relevant precatalysts gave no evidence of a close proximity of the oxygen functional groups to the metal centre. This result again implicated that the decisive interaction takes place more in certain catalytic species rather than in the precatalyst.

Of relevance to this discussion are results by Huttner et al. with cationic Rh^I complexes based on chiral 1,3-bis(diarylphosphanyl)propan-2-ol (**10-OH**).[37] In the hydrogenation of standard substrates, no reduced rate was found relative to the corresponding OMe substituted catalyst (**10-OMe**). The OH group bearing catalyst was even more active than its OMe counterpart. No significant difference in the stereodiscriminating abilities of both ligands was observed. NMR spectroscopic investigations of the precatalysts in solution revealed that among different twist and chair conformations present in a dynamic equilibrium, no species was found with the oxygen group coordinated at the rhodium centre. Apparently, the absence of catalytic effects in this system commonly attributed to the OH group can be described as being a result of the high stability of the relevant conformations of the six-membered chelate which does not allow the OH group to play an active role in the chirality transfer.

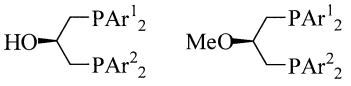

10-OH **10-OMe**

In order to enhance the tendency of the hydroxy group to approach the catalytic centre, we incorporated in the butane chain of **9-OH** a second hydroxy group in a *threo* position in order to create **11-OH**.[34] For comparison, the corresponding dimethoxy ligand (**11-OMe**) was synthesized in a similar way.

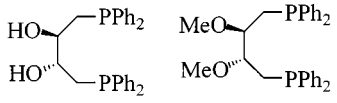

11-OH **11-OMe**

Rh^I complexes of these ligands were proofed for the asymmetric hydrogenation of standard substrates in methanol.[34a] Results are also shown in Table 1. In comparison to catalysts with only one oxygen group (**9-OMe**, **9-OH**) the incorporation of the second oxygen group further diminished the rate. As was also found with single oxygen-substituted ligands, exchange of the methoxy by hydroxy groups resulted in a significant increase in selectivity by up to 35% *ee*.

The X-ray structural analyses of the precatalysts based on **9-OH** and **9-OMe** showed some agreements but also striking differences. Neither structure was C_2 symmetric as the structures of the ligands imply. In the former, the phosphorus atoms are bonded to the rhodium with different interatomic distances (2.283 Å and 2.377 Å). Furthermore, one of the enantiotopic hydroxy groups interacts with the metal (2.396 Å) to a degree never before observed in related methoxyphosphane complexes derived from DiPAMP[38] or Nagel's PyrPHOS.[39] Owing to this interaction the seven-membered chelate is forced to adopt a boat conformation (see Scheme 1, **A**). As anticipated, one important driving force for the formation of the five-membered O–Rh–P

cycle is the pseudo-equatorial arrangement of the hydroxy group in the fused six-membered ring which is fixed in a distorted chair conformation.

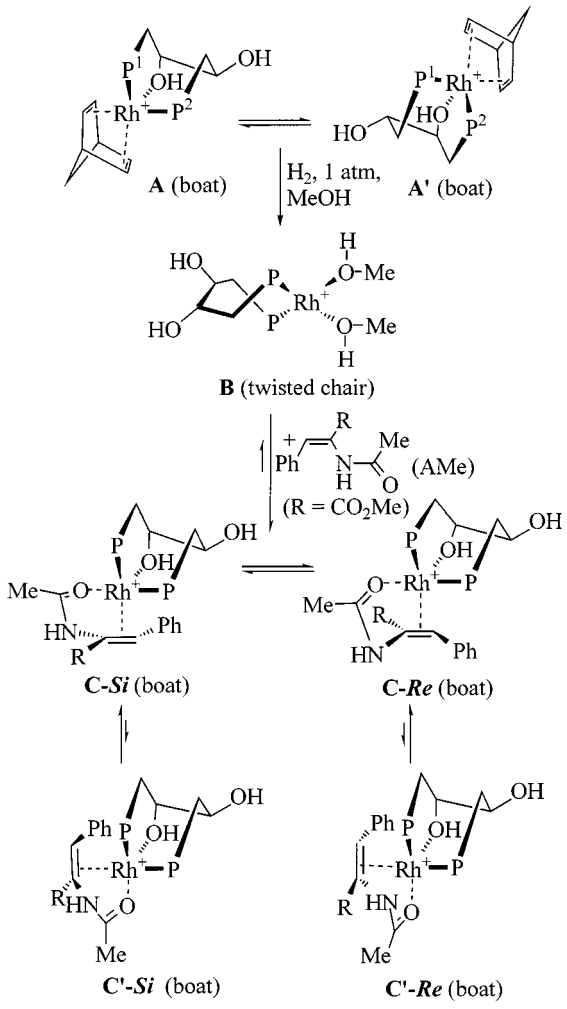

Scheme 1. The counter-ligand-dependent O−Rh-interactions at different stages of the asymmetric hydrogenation of AMe (*P*−Ph groups are omitted)

For the structure of [Rh(COD)(**11-OMe**)]BF_4, different features were noted. Both phosphorus atoms are thus bonded at approximately equal distances to the metal. The most important difference in comparison to the hydroxy complex is the distance between rhodium and the oxygen of the neighbouring ether group (3.282 Å). This is a difference of more than 0.9 Å.

The occurrence of the five-membered O−Rh−P chelate should be also confirmed in solution. To have a model compound for this investigation, *cis*-3-diphenylphosphanyl-4-hydroxytetrahydrofuran[40] was synthesized and its cationic Rh^I complex **12** was spectroscopically characterized in solution.[41] Particularly valuable for this discussion was the observation in the $^{31}P\{^1H\}$ NMR spectrum of the downfield shift of the phosphorus signal at δ = 40.1 owing to the formation of the five-membered chelate.[42]

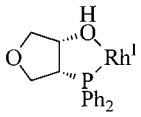

12

With this result in hand, we analyzed the $^{31}P\{^1H\}$ NMR spectra of the precatalyst [Rh(NBD)(**11-OH**)]BF_4 in CD_3OD, since CH_3OH was the solvent of the hydrogenation. (Figure 1a). The complex was characterized at ambient temperature by a doublet at δ = 18.1 which showed a coalescence at 243 K when the temperature was lowered. The spectrum at 189 K displayed two sets of well-separated double doublets at δ = 44.0 (J_{Rh-P} = 141.5 Hz, J_{P-P} = 41.4 Hz) and δ = −2.7 (J_{Rh-P} = 129.1 Hz, J_{P-P} = 41.4 Hz) produced by two nonequivalent phosphorus atoms. Keeping the typical downfield resonance of the five-membered hydroxy phosphane rhodium chelate **12** in mind, the resonance at δ = 44.0 could be unambiguously assigned to this ring size. The coordination of the oxygen causes the seven-membered ring to adopt the boat conformation **A** (Scheme 1) as concluded from the X-ray structural analysis. The typical change of the band shapes with decreasing temperature gave clear evidence that the doublet observed at room temperature was characteristic of a rapid exchange of the phosphane signals. This interchange of upfield with downfield and downfield with upfield phosphorus resonances caused by the alternate coordination of the two hydroxy groups was not distinguishable on the NMR time scale at ambient temperatures. Due to the C_2-symmetry of the ligand boat structures **A** and **A′** are identical.

The methoxy complex [Rh(COD)(**11-OMe**)]BF_4 showed a different behaviour with decreasing temperature (Figure 1b). The coalescence temperature was 35 K lower than in the hydroxy complex. Even at 177 K the doublets of doublets were less separated. Additionally, at δ = 17.2 a doublet was observed which corresponds in shift and coupling to that of the cationic Rh(DPPB)-complex. The signal could therefore clearly be assigned to a C_2-symmetric complex and proved that at low temperatures this complex also existed in a conformation where the oxygen atoms did not interact with the metal (Scheme 2, twisted chair-conformation **B**). Owing to these measurements, considerable differences in the populations of the conformers **A** and **B** of the hydroxy and methoxy complexes were concluded. This difference was explained by repulsive interactions between the oxygen group and the phenyl rings of the phosphanyl moiety. Increasing size of the oxygen substituent prevented the ligand from binding in the η^3-coordination mode. Further proof for this assumption came from the comparison with the corresponding bis-*O*-Ph_3Si-substituted complex. No Rh−O interaction was found owing to the bulky silyl groups.

The precatalyst in turn was converted into the catalytically active species by hydrogenation of the stabilizing diolefin (Scheme 1).[34b] The $^{31}P\{^1H\}$ NMR spectrum of the bis-methanol complex **B** at room temperature showed a doublet at δ = 47.5. In comparison to the bis-olefin com-

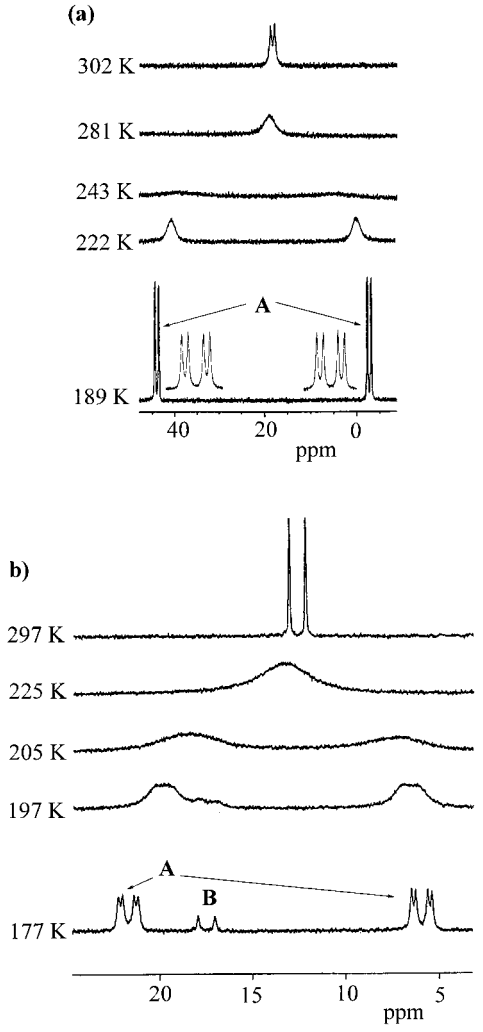

Figure 1. $^{31}P\{^1H\}$ NMR spectra of the complexes [Rh(NBD)(**11-OH**)]BF_4 (a) and [Rh(COD)(**11-OMe**)]BF_4 (b) in CD_3OD at different temperatures; the relevant equilibrium of the conformers is depicted in Scheme 1 (top) and Scheme 2, respectively

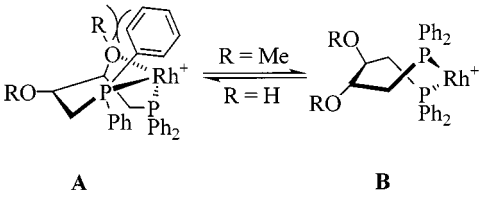

Scheme 2. Influence of the size of the *O*-substituent on the equilibrium of metal-coordinated and uncoordinated conformers

plex, the downfield shift was caused by the strong π-donor, but weak π-acceptor properties of the *O*-coordinated solvent.[43] However, no dynamic phenomenon was observed at all accessible temperatures. This was a clear indication that in contrast to the precatalyst in the catalytically active species, the interaction of the hydroxy groups with the metal was fully suspended. The complex existed exclusively in the relaxed C_2-symmetric twisted chair conformation **B**. This behaviour was rationalized by the decrease in the Lewis-acidity of rhodium(I) caused by the coordination of methanol, hence the interaction of the metal with the OH group (Lewis-base) is disfavoured.

This finding clearly illustrated that in the precatalyst not only steric interactions assisted by the second hydroxy group forces the hydroxy group to approach the metal, but also attractive interactions come into play. This result was additionally confirmed by a combined ^{103}Rh NMR density-functional study.[44] It was calculated that the "pure electronic" effect of the coordinated OH group causes an upfield shift of more than 150 ppm in the ^{103}Rh NMR spectrum relative to the resonance of the same conformation of the non-functionalized complex.

By addition of a non-symmetric prochiral substrate such as AMe, catalyst−substrate complexes were formed from the solvent complex (Scheme 1, **C**).[34b] In contrast to corresponding complexes of related 1,4-diphosphanes like DPPB, the solvent−complex was fully consumed by the substrate. This result agrees well with the small Michaelis constant measured in the hydrogenation of AMe with [Rh(**11-OH**)$(MeOH)_2$]BF_4. The peculiar pattern of the spectrum was rationalized by the assumption of a tripodal coordination of the hydroxy phosphane ligand. In principle, because of the stereofacial coordination of prochiral AMe to rhodium, the alternate coordination of both hemilabile OH ligands should produce a spectrum characterising four diastereomeric substrate complexes (**C-*Si***, **C-*Re***, **C′-*Si***, **C′-*Re***). But the only complexes found were those where the phosphane *trans* to the carbonyl oxygen was involved in the six-membered O−P−Rh chelate (**C-*Si***, **C−R*e***). Up to now there is no rationale for this preference.

In general, these results showed that electronically different counter-ligands can significantly influence the "arm-off arm-on"-mechanism between the hydroxy group and the metal and consequently the conformation of the chiral catalyst. Furthermore, these results provided evidence that the coordination of the OH group takes place stereoselectively in catalyst−substrate complexes with electronically non-symmetric substrates.

Basically, the tripodal coordination mode of the ligand and the bidentate coordination of the prochiral dehydroamino acid produces 18-electron Rh^I complexes. For the subsequent oxidative addition of hydrogen, which is considered as the rate-determining step in the asymmetric hydrogenation,[45] prior decomplexation of the hemilabile ligand is necessary (Scheme 3, **A** → **B** → **D**). Obviously, this feature is responsible for the lowering of the hydrogenation rate observed in the presence of hemilabile OH and OMe ligands. In other words, the concentration of the inactive 18-electron complexes and the rate of decomplexation determines the rate of the hydrogenation.

Unexpected proof for this assumption derived from the hydrogenation in a non-polar solvent.[34b] In contrast to the reaction in methanol in CH_2Cl_2 the hydrogenation proceeded approximately fivefold faster without affecting the enantioselectivity. The temperature-dependent $^{31}P\{^1H\}$ NMR spectra of the precatalyst in $CD_2Cl_2/CHCl_2F$ strikingly differed from those observed in CD_3OD. Thus at low temperature, a C_2-symmetric complex featuring no Rh−O interactions was preferentially found. The corresponding complex with tripodal coordination of the chiral ligand was

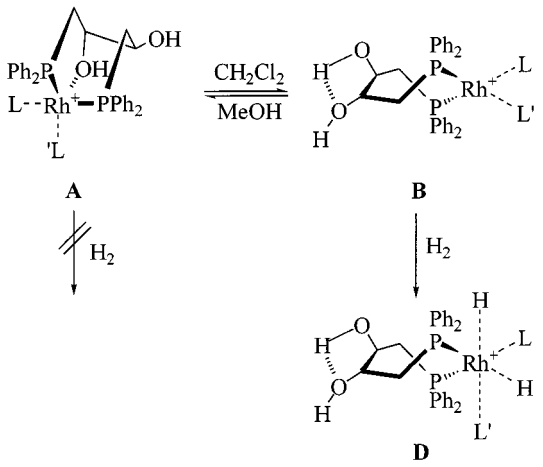

Scheme 3. HO/Rh- and HO/HO-interactions of **11-OH** complexes and their influence on the reactivity towards H_2 (L,L′ = diolefin, MeOH, bidentate substrate)

observed only in a small quantity. In the IR spectrum in solution the formation of intramolecular hydrogen bonding between the OH groups was observed (**B**, Scheme 3). Evidently, in a nonpolar solvent this strong intramolecular hydrogen bonding is more favoured than the (weak) interaction of one of the hydroxy groups with rhodium (**A**). When the Rh−O interaction is suspended, the hydrogenation can operate unhindered. In methanol the intramolecular hydrogen bonding is cleaved and the Rh−O interaction dominates. The complex is converted into an inactive state. Macroscopically, the decrease in the concentration of the active catalyst−substrate complex is expressed in the deceleration of the hydrogenation.

In the model system discussed above, the formation of the η^3-coordinated species was assisted by the *threo* arrangement of the hydroxy groups, which in the chelate cycle caused the pseudo-equatorial orientation of the uncoordinated OH group. We therefore anticipated that by changing the geometry of the *threo* 2,3-diol moiety to *erythro*, the Rh−O interaction should be disfavoured. Simultaneously, the tendency for the formation of the intramolecular hydrogen bonding should be improved.[46] In order to give evidence for this hypothesis, the required (achiral) (2*R*,3*S*)-1,4-bis(diphenylphosphanyl)butane-2,3-diol (**13-OH**) was synthesized.[47]

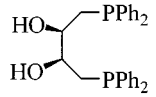

13-OH

IR solid state spectra and $^{31}P\{^1H\}$ NMR of [Rh(**13-OH**)(COD)]BF_4 in CD_3OD revealed also for this precatalyst an intramolecular interaction between the OH group and the Rh centre. However, the small difference in the chemical shift of $\delta = 21.9$ is in remarkable contrast to the value observed for the relevant *threo*-complex ($\Delta\nu = 46.7$ ppm), but corresponds to the difference found with [Rh(**11-OMe**)(COD)]BF_4 ($\Delta\nu = 16.1$ ppm). As discussed above for the latter, a higher dominance of the bidentate coordination mode in methanol was concluded. Obviously, in addition to η^3-coordinated species, the *erythro*-complex also showed considerable amounts of η^2-coordinated conformations at ambient temperature. Interestingly, in the $^{31}P\{^1H\}$ NMR spectra of relevant catalyst−substrate complexes, no significant differences between catalyst−substrate complexes of **11-OH** and **13-OH** at low temperature could be found, which is in contrast to observations made with precatalysts.

Results of hydrogenation experiments with (achiral) [Rh(**13-OH**)(COD)]BF_4 are also given in Table 1. Inspection of all the values clearly shows that hydrogenations with this complex were superior. The hydrogenation times measured with this catalyst were even shorter than with the catalyst bearing only a single hydroxy group (**9-OH**). Its activity was similar to that of the Rh(DPPB) catalyst. This result showed that the typical decelerating effect of the OH group can be fully suspended by a second OH group.

It should be reminded that an accelerating effect on the hydrogenation of dehydroamino acid derivatives has been already achieved with the **11-OH** catalyst when the reaction was carried out in a non-polar solvent. The change from methanol to CH_2Cl_2 facilitated the formation of an intramolecular hydrogen bond and shifted the equilibrium from η^3- to η^2-coordination.

Recently, it could be shown that this hydrogen bonding between the *threo* OH groups was easily disrupted by the addition of triphenylphosphane oxide owing to the favoured intermolecular hydrogen bonding between P=O and one of the OH groups.[47] The other hydroxy group coordinated to the rhodium. This cleavage reaction could be also initiated when the P=O fragment was incorporated in an appropriate prochiral substrate like 3-dimethylphosphono-butenoate (DP), a phosphonate analogue of dimethyl itaconate (Scheme 4). $^{31}P\{^1H\}$ NMR spectroscopic studies in deuterated methanol showed that in a mixture of [Rh(**11-OMe**)$(MeOH)_2$]BF_4 and a fivefold excess of the prochiral substrate, the bis-solvent complex (**B**) was exclusively present. The observation of this complex gave proof of the low stability of the diastereomeric catalyst−substrate complexes.

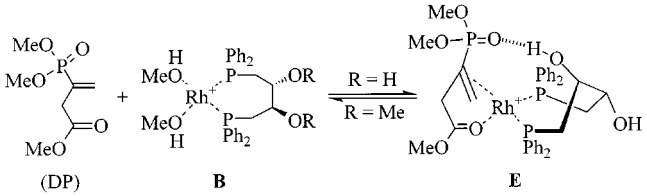

Scheme 4. Shift of the equilibrium between solvent complex and catalyst−substrate complex in dependence on the substituent R in CD_3OD as solvent

In contrast, by addition of DP to [Rh(**11-OH**)$(MeOH)_2$]$^+$ predominantly the resonances of a catalyst−substrate complex (**E**) were observed, revealing its high thermodynamic stability. The typical shift of the signals indicated that, surprisingly, no interaction between one of the OH groups and the metal centre took place. It was assumed that the Rh−O interaction is suspended owing to

an intramolecular hydrogen bonding between the OH group and the P=O functionality.

Results of the asymmetric hydrogenation are listed in Table 2. As can be clearly seen, with [Rh(**11-OMe**)(COD)]BF_4 very poor conversion occurred. The hydrogenation product was obtained in 24% *ee*. In striking contrast, the rhodium complex based on **11-OH** reduced the prochiral substrate much faster, to give the saturated product with 83% *ee*. This is an increase of approximately 60%.

Table 2. Asymmetric hydrogenation of (*E*)-methyl 3-dimethoxyphosphorylbut-2-enoate (DP) with [Rh(COD)(Ligand)]BF_4

Ligand[a]	Solvent	*t*/2[min][b]	*ee*[%]
11-OMe	methanol	>1000	24 (*S*)
11-OH	methanol	220	83 (*S*)
11-OH	CH_2Cl_2	no conversion	–

[a] For conditions of the hydrogenation compare Table 1. – [b] Time required for 50% consumption of hydrogen.

It is remarkable that by application of [Rh(**11-OH**)(COD)]BF_4 in dichloromethane as solvent, no conversion was observed. As discussed above, it can be concluded that an intramolecular hydrogen bonding between one of the OH groups and the P=O group of the substrate is established in both solvents. While in MeOH the remaining OH group is engaged by the solvent affording a 16-electron species and therefore allowing the oxidative addition of hydrogen to proceed, in dichloromethane this OH group couples to the rhodium centre. The η^3-coordinated complexes produced are catalytically inactive and therefore hinder the hydrogenation. This assumption also explains the dramatic reversal of the hydrogenation activity by changing from AMe which is a poor hydrogen-bond acceptor to the strong hydrogen-bond acceptor DP in MeOH and dichloromethane, respectively. With the former substrate, the catalytically inactive η^3-complexes are dominant in MeOH, whereas in case of the latter, η^3-complexes dominate in dichloromethane.

The previously reviewed studies illustrate the high mobility of the internal hydroxy groups in appropriate metal complexes and their decisive role in the establishment of pre-equilibria between catalyst and catalyst–substrate complexes. In some cases, relationships between structure and catalytic properties could be deduced. Simultaneously, gradual (size) and fundamental (H-bonding) differences in the behaviour of OH and OMe groups became obvious. Clearly, the characterization of precatalysts or individual stable catalyst–substrate complexes alone does not allow for a reliable conclusion on macroscopically observed overall rates and enantioselectivities. The rate constants of the pre-equilibrium steps and of the rate-determining steps are required in order to determine the special role of the catalytically unreactive η^3-coordinated catalyst–substrate complexes on the enantioselectivity. Unfortunately, up to now the complete set of data under hydrogenation conditions has not been accessible owing to the great complexity of relevant model systems. Several features remain speculative. For example, this holds for the stabilization of hydrido alkyl rhodium complexes by the OH group beyond the oxidative addition of H_2, as was found by Brown et al. in relevant DiPAMP substrate complexes.[48] Furthermore, the question of the effect of potential attractive interactions between the proton of the functional group and metal-bonded hydride[49] has up to now not been addressed at all.

In summary, results observed with tailored model catalysts and model substrates clearly illustrates that the negative effect on the rate, frequently observed with Rh^I hydrogenation catalysts bearing hydroxy phosphanes as ligands, can be entirely overcome by the co-operative effect of an appropriately placed second hydroxy group or a strong hydrogen-bond accepting group such as P=O incorporated in the substrate. As a result we can take full advantage of the positive effect on the enantioselectivity. It has to be verified that the superior enantioselectivities in the asymmetric hydrogenation of standard substrates such as AH and ItH_2 as outlined above can also be explained by a (weak) intramolecular hydrogen bonding between the hydroxy groups of the ligand and the carboxylic group of the substrate during the catalytic cycle.

First Applications in Highly Enantioselective Asymmetric Hydrogenations

As seen above, the incorporation of hydroxy groups can dramatically improve the stereodiscriminating properties of

Table 3. Asymmetric hydrogenation with cationic Rh^I complexes based on RoPHOS-ligands

Ligand[a]	Substrate	*ee* [%]
14-OBn[b]	AH	93.6 (*S*)
14-OMe[b]	AH	97.0 (*S*)
14-OH[c]	AH	>99.0 (*S*)
14-OBn[b]	AMe	96.0 (*S*)
14-OMe[b]	AMe	98.3 (*S*)
14-OH[c]	AMe	>99.0 (*S*)

[a] 1–3 bar H_2 in methanol at room temp.; catalyst:substrate = 1:100. – [b] [Rh(Ligand)COD)]BF_4 was used. – [c] Precatalyst was prepared by mixing [Rh(COD)$_2$]PF_6 with **10-OH**.

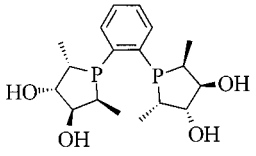

14-OH

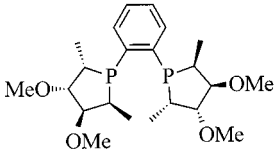

14-OMe

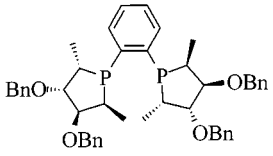

14-OBn

(RoPHOS)

chiral hydrogenation catalysts. Recently, we[50] and later, the groups of Zhang[51] and RajanBabu[52] found access to a new class of functionalized DuPHOS ligands derived from D-mannitol called RoPHOS (**14**). As shown in Table 3, benzyloxy,[50b] methoxy[53] and hydroxy groups[51] at the 3- and 4-positions of the phospholane moiety have a different effect on the enantioselectivity. Thus, with the OH bearing ligand **14-OH**, more than 99% *ee* could be achieved in the hydrogenation of AH and AMe. Although the increase is small, a significant gain in the enantioselectivity was achieved.

More dramatic effects were recently reported by Brown et al. in the hydrogenation of methyl *N*-acyl cinnamates with BPE-RoPHOS hybrid ligands.[54] The most striking results are listed in Table 4. Thus, by utilization of the ligand **15-H**, a hybrid of the well-known and individually efficient ligands BPE and DiPAMP, poor enantioselectivity was achieved. Incorporation of remote methoxy groups (**15-OMe**) in the phospholane increased the *ee*. The highest enhancement was obtained because of the assistance of the hydroxy groups (ligand **15-OH**). In some cases, in comparison to the parent ligand **15-H**, a difference of up to 90% resulted owing to the remote hydroxy groups.

Table 4. Asymmetric hydrogenation with cationic Rh^I complexes based on BPE/RoPHOS−DiPAMP hybrid ligands

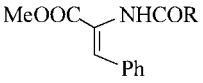

Ligand[a]	R (Substrate)	*ee* [%]
15-H	Me	38 (*S*)
15-OMe	Me	85 (*S*)
15-OH	Me	92 (*S*)
15-H	*tert*-Bu	5 (*R*)
15-OMe	*tert*-Bu	67 (*S*)
15-OH	*tert*-Bu	88 (*S*)
15-H	Ph	–
15-OMe	Ph	77 (*S*)
15-OH	Ph	90 (*S*)

[a] 1.3 bar H_2 in methanol; catalyst:substrate = 1:100; the precatalyst was prepared by mixing $[Rh(COD)_2]PF_6$ with BH_3-ligand adducts in the presence of HBF_4−OMe_2.

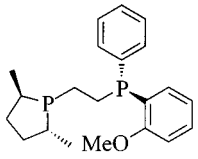

15-H
(BPE-DiPAMP hybrid)

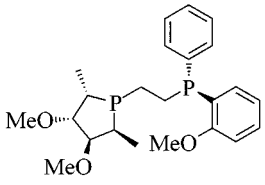

15-OMe

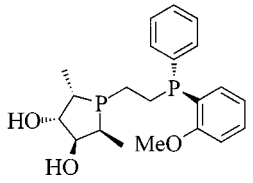

15-OH

(RoPHOS-DiPAMP hybrids)

Concluding Remarks

Results summarised herein show the great academic challenge, but also the high potential associated with the use of internal hydroxy groups in chiral rhodium diphosphane catalysts for tuning the reactivity and the enantioselectivity of asymmetric hydrogenations. The crucial issue lies in the large number and variety of competing binding sites in relevant polyfunctionalized catalyst−substrate complexes. These features are related to the action of enzymes. Modelling of individual interactions, studies of equilibria and evaluation of their effect on the rate and the enantioselectivity are therefore of great importance for the proper placement of additional functional groups within the catalyst. The effective control of such secondary interactions opens new perspectives for the enantiodiscrimination of prochiral substrates and gives access to a new generation of biomimetic catalysts.

There are an increasing number of reports in the literature indicating that hydroxy groups in phosphorus ligands may also influence other metal-catalyzed transformations, such as hydroformylations,[55] transfer hydrogenations[56]or Baylis−Hillman reactions.[51b] In some of these reports, the reduced rate of the catalytic reaction was problematic. The progress achieved over the last years in asymmetric hydrogenation with Rh^I hydroxy phosphane catalysts is an encouraging sign that the decelerating effect of the hydroxy group can also be overcome in these reactions by the employment of suitable substrates and/or appropriate reaction conditions.

Acknowledgments

The author is grateful for the financial support provided by the Max-Planck-Gesellschaft, BASF AG (Ludwigshafen), Bmbf (Förderkennzeichen 03C0304A), NATO and the Fonds der Chemischen Industrie. I wish to thank all co-workers and colleagues involved in this research project over the last years. In particular I deeply appreciate the collaboration of Dr. J. Holz, Dr. R. Kadyrov, PD Dr. D. Heller, Dr. W. Baumann, Dr. S. Borns, Dr. A. Kless, Dr. M. Quirmbach (IfOK Rostock), Dr. R. Stürmer (BASF), and PD Dr. M. Bühl (MPI Mülheim). I thank Prof. Dr. em. R. Selke for kind support of this work. It is a pleasure for me to acknowledge the skilled technical assistance by Mrs. G. Voß and Mrs. C. Pribbenow.

[1] [1a] *Asymmetric Synthesis* (Ed.: J. D. Morrison), Academic Press, Orlando, **1985**, vol. 1−5. – [1b] *Catalytic Asymmetric Synthesis* (Ed.: I. Ojima), VCH, New York, **1993**. – [1c] R. Noyori, *Asymmetric Catalysis in Organic Synthesis* Wiley, New York, **1994**. – [1d] *Comprehensive Asymmetric Catalysis* (Eds.: E. N. Jacobsen, A. Pfaltz, H. Yamamoto), Springer, Heidelberg, **1999**, vol. I−III.

[2] J. M. Brown, P. L. Evans, *Tetrahedron* **1988**, *44*, 4905−4916; V. A. Pavlow, E. Klabunovskii, Yu. T. Struchkov, A. A. Voloboev,

A. I. Yanovski, *J. Mol. Catal.* **1988**, *44*, 217−243; H. Brunner, A. Winter, J. Breu, *J. Organomet. Chem.* **1998**, *553*, 285−306; P. Dierkes, P. W. N. M. van Leeuwen, *J. Chem. Soc., Dalton Trans.* **1999**, 1519−1529.

[3] The principle of double stereodifferentiation is also a powerful tool for the improvement of the enantioselectivity, but without relevance for the discussion herein: S. Masamune, W. Choy, J. S. Petersen, L. R. Sita, *Angew. Chem.* **1985**, *97*, 1−31; *Angew. Chem. Int. Ed. Engl.* **1985**, *24*, 1−31.

[4] K. Inoguchi, S. Sakuraba, K. Achiwa, *Synlett* **1992**, 169−178.

[5] T. V. RajanBabu, A. L. Casalnuovo, *J. Am. Chem. Soc.* **1992**, *114*, 6265−6266; T. V. RajanBabu, T. A. Ayers, G. A. Halliday, K. K. You, J. C. Calabrese, *J. Org. Chem.* **1997**, *62,* 6012−6028; T. V. RajanBabu, B. Radetich, K. K. You, T. A. Ayers, A. L Casalnuovo, J. C. Calabrese, *J. Org. Chem.* **1999**, *64*, 3429−3447.

[6] N. M. Brunkan, P. S. White, M. R. Gagné, *Angew. Chem.* **1998**, *110*, 1615−1618; *Angew. Chem. Int. Ed.* **1998**, *37*, 1579−1582.

[7] M. Sawamura, Y. Ito, *Chem. Rev.* **1992**, *92*, 857−871.

[8] I. Yamada, K. Fukui, Y. Aoki, S. Ikeda, M. Yamaguchi, T. Yamagishi, *J. Organomet. Chem.* **1997**, *539*, 115−120; I. Yamada, M. Ohkuouchi, M. Yamaguchi, T. Yamagishi, *J. Chem. Soc., Perkin Trans. 1* **1997**, 1869−1873.

[9] G. B. Jones, B. J. Chapman, *Synthesis* **1995**, 475−497 and references cited therein.

[10] H. Brunner, R. Störiko, F. Rominger, *Eur. J. Inorg. Chem.* **1998**, 771−781.

[11] T. Hayashi, K. Kanehira, T. Hagihara, M. Kumada, *J. Org. Chem.* **1988**, *53*, 113−120.

[12] [12a] A. Börner, J. Ward, K. Kortus, H. B. Kagan, *Tetrahedron: Asymmetry* **1993**, *4*, 2219−2228. − [12b] L. B. Fields, E. N. Jacobsen, *Tetrahedron: Asymmetry* **1993**, *4*, 2229−2240. − [12c] B. F. M. Kimmich, C. R. Landis, D. R. Powell, *Organometallics* **1996**, *15*, 4141−4146. − [12d] A. Kless, C. Lefeber, A. Spannenberg, R. Kempe, W. Baumann, J. Holz, A. Börner, *Tetrahedron* **1996**, *52*, 14599−14606. − [12e] M. Quirmbach, A. Kless, J. Holz, V. Tararov, A. Börner, *Tetrahedron: Asymmetry* **1999**, *10*, 1803−1811.

[13] C. R. Landis, R. A. Sawyer, E. Somsook, *Organometallics* **2000**, *19*, 994−1002; D. K. MacFarland, C. R. Landis, *Organometallics* **1996**, *15*, 483−485; M. Sawamura, Y. Nakayama, W.-M. Tang, Y. Ito, *J. Org. Chem.* **1996**, *61*, 9090−9096.

[14] P. A. Chaloner, M. Esteruelas, F. Joó, L. A. Oro, *Homogeneous Hydrogenation*, Kluwer, 1994; J. Halpern, in ref.[1a], Vol. 5, 41−69; M. Nógrády, *Stereoselective Synthesis*, VCH, Weinheim, **1995**, 45−65; J.-P. Genêt, in *Advanced Asymmetric Synthesis* (Ed.: G. R. Stephenson), Chapman & Hall, London, **1996**, 146−180; J. M. Brown, in ref.[1d], 121−182.

[15] H. Takaya, T. Ohta, R. Noyori, in ref.[1b], 1−39 and in ref.[1c], 1−94; H. B. Kagan, *C. R. Acad. Sci. Paris Serie IIb*, **1996**, *322*, 131−143; R. A. Sheldon, *Chirotechnology*, Marcel Dekker, New York, **1993**, 271−303; A. Börner, J. Holz, in *Transition Metals for Organic Synthesis* (Eds.: M. Beller, C. Bolm), Wiley-VCH, **1998**, vol. 2, 3−13.

[16] J. Holz, M. Quirmbach, A. Börner, *Synthesis* **1997**, 983−1006; J. Holz, M. Quirmbach, L. Götze, A. Börner, *Rec. Res. Develop. Org. Chem.* **1998***, 2*, 685−711.

[17] D. J. Brauer, P. Machnitzki, T. Nickel, O. Stelzer, *Eur. J. Inorg. Chem.* **2000**, 65−73. J; Holz, D. Heller, R. Stürmer, A. Börner, *Tetrahedron Lett.* **1999**, *40*, 7059−7062; R. Selke, J. Holz, A. Riepe, A. Börner, *Chem. Eur. J.* **1998**, *4*, 769−771.

[18] See, e.g. S. Trinkhaus, R. Kadyrov, R. Selke, J. Holz, L. Götze, A. Börner, *J. Mol. Catal. A: Chemical* **1999**, *144*, 15−26; A. Kless, J. Holz, D. Heller, R. Kadyrov, R. Selke, C. Fischer, A. Börner, *Tetrahedron: Asymmetry* **1996**, *7*, 33−36.

[19] See e.g. [19a] N. W. Alcock, J. M. Brown, J. C. Jeffery, *J. Chem. Soc., Chem. Commun.* **1974**, 829−830. − [19b] C. R. Johnson, T. Imamoto, *J. Org. Chem.* **1987**, *52*, 2170−2174. − [19c] K. Burgess, M. J. Ohlmeyer, K. H. Whitmire, *Organometallics* **1992**, *11*, 3588−3600. − [19d] U. Nagel, T. Krink, *Angew. Chem.* **1993**, *105*, 1099−1101; *Angew. Chem. Int. Ed. Engl.* **1993**, *32*, 1052−1054. − [19e] A. M. Allgeier, E. T. Singewald, C. A. Mirkin, C. L. Stern, *Organometallics* **1994**, *13*, 2928−2930.

[20] J. C. Jeffrey, T. B. Rauchfuss, *Inorg. Chem.* **1979**, *18*, 2658−2666; J. J. Schneider, *Nachr. Chem.* **2000**, *48*, 614−620.

[21] A. Bader, E. Lindner, *Coord. Chem. Rev.* **1991**, *108*, 27−110.

[22] W. S. Knowles, *Acc. Chem. Res.* **1983**, *16*, 106−112.

[23] W. S. Knowles, W. C. Christopfel, K. E. Koenig, C. F. Hobbs, in *Catalytic Aspects of Metal Phosphane Complexes* (Eds. E. C. Aleya, D. W. Meek), American Chemical Society, Washington, **1982**, p. 325, 330.

[24] J. Amma, J. K. Stille, *J. Org. Chem.* **1982**, *47*, 468−473.

[25] U. Nagel, J. Albrecht, *Top. Catal.* **1998**, *5*, 3−23.

[26] A. Börner, J. Ward, W. Ruth, J. Holz, A. Kless, D. Heller, H. B. Kagan, *Tetrahedron* **1994**, *50*, 10419−10430.

[27] J. Ward, A. Börner, H. B. Kagan, *Tetrahedron: Asymmetry* **1992**, *3*, 849−852.

[28] L. Dahlenburg, V. Kurth, *J. Organomet. Chem.* **1999**, *585*, 315−325.

[29] T. Imamoto, H. Tsuruta, Y. Wada, H. Masuda, K. Yamaguchi, *Tetrahedron Lett.* **1995**, *36*, 8271−8274.

[30] A. Börner, J. Holz, A. Kless, D. Heller, U. Berens, *Tetrahedron Lett.* **1994**, *33*, 6071−6074; J. Holz, A. Börner, A. Kless, S. Borns, S. Trinkhaus, R. Selke, D. Heller, *Tetrahedron: Asymmetry* **1995**, *6*, 1973−1988.

[31] D. Heller, J. Holz, S. Borns, A. Spannenberg, R. Kempe, U. Schmidt, A. Börner, *Tetrahedron: Asymmetry* **1997**, *8*, 213−222.

[32] O. Riant, O. Samuel, T. Flessner, S. Taudien, H. B. Kagan, *J. Org. Chem.* **1997**, *62*, 6733−6745.

[33] A. Börner, A. Kless, R. Kempe, D. Heller, J. Holz, W. Baumann, *Chem. Ber.* **1995**, *128*, 767−773.

[34] [34a] S. Borns, R. Kadyrov, D. Heller, W. Baumann, A. Spannenberg, R. Kempe, J. Holz, A. Börner, *Eur. J. Inorg. Chem.* **1998**, 1291−1295.− [34b] S. Borns, R. Kadyrov, D. Heller, W. Baumann, J. Holz, A. Börner, *Tetrahedron: Asymmetry* **1999**, *10*, 1425−1431.

[35] Frequently, the decelerating effect of the alkoxy group may be suspended owing to the engagement of the ligating oxygen atom in a conformationally rigid heterocycle in the backbone of the ligand. A prominent example is DIOP (H. B. Kagan, T.-P. Dang, *J. Am. Chem. Soc.* **1972**, *94*, 6429−6433). Relevant rhodium catalysts exhibit extremely high hydrogenation activities for the substrates considered herein.

[36] Ref.[19c], footnote 49; ref.[19d]; Reduced hydrogenation activities were also reported for some diphosphanes catalysts bearing amino groups: K. Achiwa. Y. Ohga, Y. Iitaka, *Chem. Lett.* **1979**, 865−868; Y. Ohga, Y. Iitaka, K. Achiwa, *Chem. Lett.* **1980**, 861−864; K. Achiwa, P. A. Chaloner, D. Parker, *J. Organomet. Chem.* **1981**, *218*, 249−260; W. Hu, C.-C. Chen, G. Xue, A. S. C. Chan, *Tetrahedron: Asymmetry* **1998**, *9*, 4183−4192 and references therein. In some cases the decelerating effect of the amino group could be overcome by *N*-acylation.

[37] J. Karas, G. Huttner, K. Heinze, P. Rutsch, L. Zsolnai, *Eur. J. Inorg. Chem.* **1999**, 405−420.

[38] B. McCulloch, J. Halpern, M. R. Thompson, C. R. Landis, *Organometallics* **1990**, *9*, 1392−1395.

[39] U. Nagel, T. Krink, *Chem. Ber.* **1993**, *126*, 1091−1100. *Chem. Ber.* **1993**, *126*, 309−316.

[40] A. Börner, J. Holz, J. Ward, H. B. Kagan, *J. Org. Chem.* **1993**, *58*, 6814−6817.

[41] A. Börner, A. Kless, J. Holz, W. Baumann, A. Tillack, R. Kadyrov, *J. Organomet. Chem.* **1995**, *490,* 213−219.

[42] The shift to longer wavelengths in the IR spectrum of complex **12** in $CDCl_3$ indicated the increase of the acidity of the hydroxy group owing to coordination.

[43] J. M. Brown, P. A. Chaloner, A. G. Kent, B. A. Murrer, P. N. Nicholson, D. Parker, P. J. Sidebottom, *J. Organomet. Chem.* **1981**, *216*, 263−276.

[44] M. Bühl, W. Baumann, R. Kadyrov, A. Börner, *Helv. Chim. Acta* **1999**, *82*, 811−820.

[45] A. S. C. Chan, J. J. Pluth, J. Halpern, *J. Am. Chem. Soc.* **1980**, *102*, 5952−5954.

[46] It is interesting to note that Rh−N interactions in 1,2-dipyridyl-substituted 1,2-bis(diphenylphosphanyl)ethane metal complexes are also dependent on the relative stereochemistry of both pyridyl groups. While the interaction has been found with the *erythro* ligand, no Rh−N contact occurred in case of the *threo* ligand. J. L. Bookham, D. M. Smithies, M. T. Pett, *J. Chem. Soc., Dalton Trans.* **2000**, 975−980; J. L. Bookham, D. M. Smithies, *J. Organomet. Chem.* **1999**, *577*, 305−315.

[47] J. Holz, R. Kadyrov, S. Borns, D. Heller, A. Börner, *J. Organomet. Chem.* **2000**, *603*, 61−68.

[48] J. A. Ramsden, T. D. W. Claridge, J. M. Brown, *J. Chem. Soc., Chem. Commun.* **1995**, 2469−2471.
[49] For recent publications, see: D.-H. Lee, H. J. Kwon, B. P. Patel, L. M. Liable-Sands, A. L. Rheingold, R. H. Crabtree, *Organometallics* **1999**, *18*, 1615−1621; R. H. Crabtree, O. Eisenstein, G. Sini, E. Peris, *J. Organomet. Chem.* **1998**, *567*, 7−11; J. A. Ayllón, C. Gervaux, S. Sabo-Etienne, B. Chaudret, *Organometallics* **1997**, *16*, 2000−2002.
[50] [50a] R. Stürmer, A. Börner, J. Holz, G. Voß, DE 19725796, **1998**. − [50b] Holz, M. Quirmbach, U. Schmidt, D. Heller, R. Stürmer, A. Börner, *J. Org. Chem.* **1998**, *63*, 8031−8034.
[51] [51a] W. Li, Z. Zhang, D. Xiao, X. Zhang, *Tetrahedron Lett.* **1999**, *40*, 6701−6704. − [51b] W. Li, Z. Zhang, D. Xiao, X. Zhang, *J. Org. Chem.* **2000**, *65*, 3489−3496.
[52] Y.-Y. Yan, T. V. RajanBabu, *Org. Lett.* **2000**, *2*, 199−202; Y.-Y. Yan, T. V. RajanBabu, *J. Org. Chem.* **2000**, *65*, 900−906.
[53] J. Holz, D. Heller, R. Stürmer, A. Börner, unpublished results.
[54] D. Carmichael, H. Doucet, J. M. Brown, *Chem. Commun.* **1999**, 261−262.
[55] R. Kadyrov, J. Heinicke, M. K. Kindermann, D. Heller, C. Fischer, R. Selke, A. K. Fischer, P. G. Jones, *Chem. Ber.* **1997**, *130*, 1663−1670; I. D. Kostas, C. G. Screttas, *J. Organomet. Chem.* **1999**, *585*, 1−6; D. Selent, D. Röttger, K.-D. Wiese, A. Börner, *Angew. Chem.* **2000**, *112*, 1694−1696; *Angew. Chem. Int. Ed.* **2000**, *39*, 1639−1641.
[56] A. M. d'A. Rocha Gonsalves, J. C. Bayón, M. M. Pereira, M. E. S. Serra, J. P. R. Pereira, *J. Organomet. Chem.* **1998**, *553*, 199−204; M. Quirmbach, J. Holz, V. I. Tararov, A. Börner, *Tetrahedron* **2000**, *56*, 775−780.

Received May 17, 2000
[I00200]

Second-Order Optical Nonlinearities in Coordination Chemistry: The Case of Bis(salicylaldiminato)metal Schiff Base Complexes

Pascal G. Lacroix[a]

In memory of my greatly respected mentor Professor Olivier Kahn

Keywords: Nonlinear optics / Metal complexes / Schiff bases / Molecular devices

Since the mid-1980s, there has been a growth of interest in the search and development of molecular second-order nonlinear optical (NLO) materials that possess various device applications. Beside the most traditional donor-acceptor ("push-pull") organic chromophores (e.g. the stilbene family), chemists have increasingly extended their field of investigations to newer generations of organic molecules of greater complexity. In recent years, coordination complexes through their unique characteristics such as various redox and magnetic properties, in addition to their great diversity of geometries, have introduced a new dimension to the area. This review attempts to summarize the NLO capabilities of bis(salicylaldiminato)metal Schiff base complexes: (*i*) chromophores with enhanced hyperpolarizabilities (β) can be obtained by virtue of the coordinated metal center; (*ii*) the use of chiral substituents allows the engineering of the chromophores into various non-centrosymmetric environments and efficiencies of about 10 times that of urea in second-harmonic generation; (*iii*) the general trend observed for the high temperature stability in this family of chromophores, while combined with the large β×μ products, makes these systems interesting candidates for their incorporation into poled polymers with high glass transition temperatures (*Tg*); (*iv*) the possibility for β modulation induced by magnetic transition is also seen with respect to the concept of molecular switching.

1. Introduction

Materials which exhibit highly nonlinear optical (NLO) responses are currently of great scientific and technological interest.[1] While inorganic solids such as $LiNbO_3$ and KH_2PO_4 have traditionally attracted the widest attention,[2] it is now recognized that molecular-based materials possess many superior NLO characteristics: ultrafast response times, lower dielectric constants, better processability as thin-film devices, and enhanced non-resonant NLO responses relative to the traditional inorganic solids.[3] When a molecule is subjected to laser light [i.e. very high intensity electric field (*E*)], the polarization of the molecule is expressed by Equation (1).[4]

$$\mu(E) = \mu_0 + \alpha E + \beta E^2 + \ldots \quad (1)$$

In this expression, μ_0 is the permanent dipole moment, α the linear polarizability, and β the quadratic hyperpolarizability (origin of the NLO response). According to the widely used two-level model,[5] β can be described in terms of a ground and first excited state, having a charge-transfer character, and is related to the energy of the optical transition (ΔE), its oscillator strength (*f*), and the difference between the ground and excited state dipole moments ($\Delta\mu$) through Equation 2).

$$\beta = \frac{3e^2\hbar f \Delta\mu}{2m(\Delta E)^3} \times \frac{(\Delta E)^4}{\left((\Delta E)^2 - (2\hbar\omega)^2\right)\left((\Delta E)^2 - (\hbar\omega)^2\right)} \quad (2)$$

[a] Laboratoire de Chimie de Coordination, CNRS, 205 route de Narbonne,
31077 Toulouse Cedex, France
Fax: (internat.) + 33-5/61553003
E. mail: pascal@lcc-toulouse.fr

The author was born in Dole, France. He received his PhD under the supervision of Prof. Olivier Kahn, at the university of Orsay (France) in 1989. He entered the field of nonlinear optics as a postdoctoral fellow, with Prof. Tobin J. Marks, at Northwestern University (Evanston, USA) from 1989 to 1991. He then returned to Orsay, where he pursued in the field of hybrid magnetic-NLO materials designed by intercalation chemistry. He moved to the Laboratoire de Chimie de Coordination (Toulouse, France) in 1994. His current research interest concerns multi-property materials with nonlinear optical, magnetic, and conducting properties.

MICROREVIEWS: This feature introduces the readers to the authors' research through a concise overview of the selected topic. Reference to important work from others in the field is included.

 © WILEY-VCH Verlag GmbH, 69451 Weinheim, 2001 1434−1948/01/0202−0339 $ 17.50+.50/0

The largest β values are obtained when the molecules contain π-electronic systems with charge asymmetry arising from contributions from the substituents-induced asymmetry. This situation is optimized with "push-pull" molecules, in which the magnitude of β can be correlated with the electron-donating and -accepting strength of the substituent,[6] but can also be enhanced by increasing the path of conjugation between the substituents.[7] The most traditional experimental determination of β is the Electric-Field-Induced-Second-Harmonic (EFISH) method,[8] which requires the molecules to be aligned by a strong electric field by means of their static dipole moments (μ). Therefore, the EFISH signal is proportional to β×μ. Measurements of β can also be carried out with the Hyper-Raleigh Scattering (HRS) method,[9] which does not require electric fields, and therefore is suitable for nonpolar and ionic chromophores.

The polarization of a macroscopic material is again given by an expression analogous to Equation (1), where the macroscopic polarization (P) is expressed by Equation (3).

$$P = \chi^{(1)}E + \chi^{(2)}E^2 + \ldots \quad (3)$$

$\chi^{(2)}$ is the quadratic susceptibility and is related to the underlying β. An important point to note is that for $\chi^{(2)}$ to be non-zero, the material needs to be non-centrosymmetric. This can be explained by the fact that $P(-E) = -P(E)$ in a centrosymmetric material. Therefore, $\chi^{(2)}(-E)(-E) = -(\chi^{(2)}E^2)$, and $\chi^{(2)} = 0$. Consequently, the search for materials with efficient quadratic nonlinearities has to be conducted in two steps which include: (*i*) the designing of molecular structures with a large β value, and (*ii*) the engineering of the chromophores into non-centrosymmetric environments.

Several examples of chromophores are shown in Table 1. They all have been successfully embodied into non-centrosymmetric environments in the solid state following various methodologies. The oldest strategy in crystal engineering for $\chi^{(2)}$ NLO materials is chirality, which ensures the crystallization of a pure enantiomer in a non-centrosymmetric space group. Methyl 2-[(2,4-dinitrophenyl)amino]propanoate (MAP, **1**) was the first $\chi^{(2)}$ NLO material studied in depth, which exploited this strategy.[10] Among several alternative attempts, we have previously reported on the intercalation of cationic chromophores such as 4′-dimethylamino-1-methylstilbazolium (DAMS, **2**) into lamellar matrices as a possible route towards highly efficient $\chi^{(2)}$ NLO materials.[11] However, the method which has been widely adopted since the late 1980s requires poling the chromophores at high temperatures in polymers with high glass transition temperatures (*Tg*).[12] Disperse Red One (DR1, **3**) is an example of an organic chromophore which has widely been investigated in poled polymers for fifteen years.[13] High *Tg* NLO polymers have recently been reviewed.[14]

The macroscopic NLO properties are usually measured by Second-Harmonic Generation (SHG), and the results are expressed as the d_{33} tensor component of $\chi^{(2)}$ in poled polymer materials,[14] or as the SHG efficiency versus that of urea in the Kurtz−Perry powder test[15] for microcrystalline solids. However, it has to be emphasized that this test, which has a modest reliability, is not sufficient to fully understand the origin and extent of the NLO response.

Table 1. Examples of chromophores for which non-centrosymmetric solid-state environments have been obtained by crystal growth (**1**), intercalation into layered host matrices (**2**) or as functionalized poled polymers (**3**)

Compounds	[ref.]
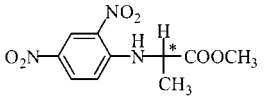 **1**	[10]
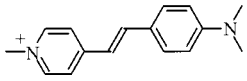 **2**	[11]
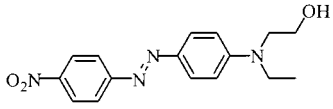 **3**	[13]

2. Organometallic and Inorganic Chromophores

2.1. "Push-pull" Organometallic Chromophores

Besides organic molecules, which up to now have been the most widely investigated systems, organometallic structures should be intriguing candidates as second-order NLO chromophores by virtue of their low-energy electronic charge-transfer excitations. The report in 1987 that *cis*-1-ferrocenyl-2-(4-nitrophenyl)ethylene[16] exhibited an SHG efficiency 62 times that of urea has motivated many organometallic chemists to enter the field. As a result, a number of reports of organotransition metal systems with NLO properties have appeared in the literature.[17] Nevertheless, in the late 1980s, despite many synthetic efforts, the measured NLO responses of organometallic chromophores were almost invariably lower than those of π-organic chromophores of comparable molecular dimensions. Understanding the reasons for such modest NLO responses became possible when the Zerner Intermediate Neglect of Differential Overlap (ZINDO) method in conjunction with the Sum Over States (SOS) formalism made the NLO response−electronic structure relationships available.[18] It was pointed out that many organometallics possess pseudo-centrosymmetric electronic environments and, therefore, lack the extreme electronic asymmetry required for large second-order NLO responses.[19] This tendency is illustrated

in Table 2 where the calculated hyperpolarizabilities of organometallics are compared with a stilbene analogue.[18]

Table 2. Comparison of calculated molecular hyperpolarizabilities for organometallic chromophores and a prototypical organic structures (ref.[18])

Compound	β ($\times 10^{-30}$ cm^5 esu^{-1})
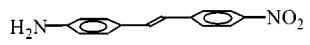 **4**	65.9
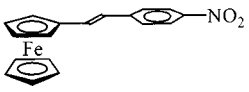 **5**	30.8
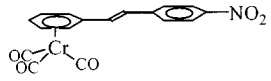 **6**	23.5

Our interest in the field of coordination complexes based NLO chromophores started at this point, by examination of $(CO)_5W-L$ (where L represents an extended π-organic system).[20] The reason for this choice is related to the topological similarity to the conventional push-pull organic chromophores which could offer attracting alternatives to the aforementioned η^5-ferrocenyl complexes and (η^6-arene)chromium structures. Our study pointed out the versatility of the pyridine$-W(CO)_5$ based chromophores (Table 3) in which $-W(CO)_5$ usually acts as a donor,[21] in compounds **7**−**9**, and by contrast with the withdrawing effect of the pyridine$-W(CO)_5$ moiety evidenced in **10**. The molecular orbital analysis indicates that the carbonylmetal fragment acts as σ-acceptor, forcing the adjacent pyridine ring to become the molecular LUMO. As a consequence, the seemingly innocent pyridine becomes a strong acceptor.[20] Since the early 1990s, the interest in using a metal center for converting a pyridine into a strong acceptor for NLO purposes has grown with respect to the concept of octupolar chromophores,[22] which are non-centrosymmetric and nonpolar molecules (e.g. point groups T_d, and D_{3d}). NLO (pyridine)metal complexes, including intriguing new octupolar architectures, have recently been reviewed by Le Bozec.[23]

2.2. A New Approach in the Search of Inorganic NLO Candidates

Until the early 1990s, the main strategy in the design of metal-organic NLO chromophores was to simply mimic organic molecules by using metal centers instead of organic donors[16,17a,17b]. The ferrocene derivative **5** is probably the best example that illustrates this methodology. However, the fact that the NLO response of such chromophores was almost invariably lower than that of π-organics gave rise to the idea that copying organic NLO structures by means of organometallic substituents might not have been the best guideline towards coordination compounds with enhanced optical nonlinearities. This idea becomes more relevant in the case of inorganic complexes, where the d-electrons are more strongly held by the metal atom than in the case of organometallic compounds. This difference can raise difficulties in the designing of classical push-pull chromophores, within the framework of a two-level model built up in the realm of organic chemistry with extended π-conjugated electronic structures.

Table 3. Comparison of experimental (EFISH) molecular hyperpolarizabilities for a series of $(CO)_5W-$pyridine derivatives and for stilbazole-based chromophores at 1.907 μm (**7**−**9**) and 1.064 μm (**10**−**11**)

Compounds	β ($\times 10^{-30}$ cm^5 esu^{-1})	[ref.]
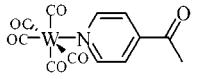 **7**	-9.3	[17a]
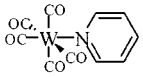 **8**	-4.4	[17a]
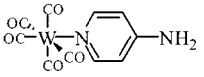 **9**	-2.1	[17a]
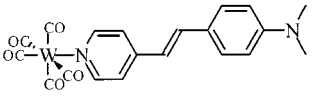 **10**	61	[20]
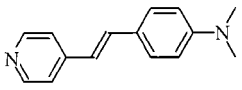 **11**	28	[20]

Our interest in inorganic chromophores started in 1990 by a short theoretical investigation of (pentammine)ruthenium derivatives. A lot of work had been devoted to mixed-valence Ru^{II}/Ru^{III} complexes[24] since the initial report on the mixed-valence $[Ru(NH_3)_5]_2pz^{5+}$ (**12**, Figure 1) by Creutz and Taube.[25] In this compound an electron is almost fully delocalized with $(Ru^{II})^{1/2}/(Ru^{III})^{1/2}$ centers (class III in the Robin−Day classification of mixed-valence systems[26]). Consequently, the $(NH_3)_5Ru^{II}$ fragment can formally be seen as a very strong electron donor. However, although ruthenium-based complexes have exhibited sizeable NLO responses as push-pull chromophores in some cases (e.g. $\beta = 70 \times 10^{-30}$ cm^3 esu^{-1} for compound **13**[27]), the

largest NLO responses were reported in compounds in which the pyridine−Ru^{II} fragments act as electron acceptors and not donors (e.g. $\beta = 2200 \times 10^{-30}$ cm^3 esu^{-1} for the octupolar systems **14**[28]). This versatility prompted us to greatly modify our approach to inorganic chromophores in the early 1990s. It became increasingly clear that the traditional donor/acceptor chemical guidelines would probably no longer be fully sufficient in finding the best candidates in chromophore design.

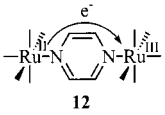

12

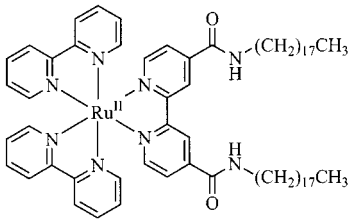

13

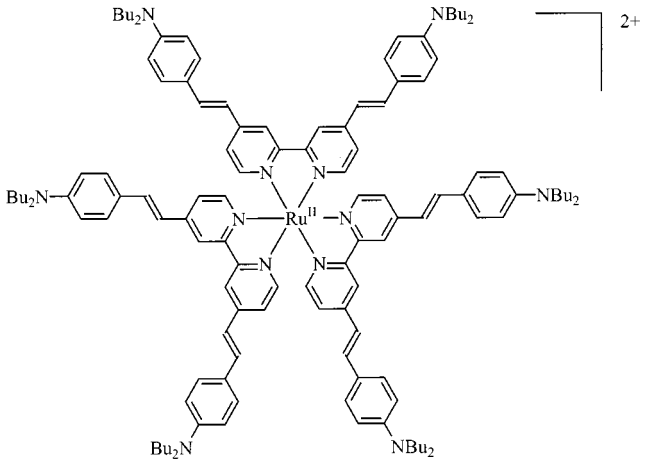

14

Figure 1. Ruthenium-based charge-transfers in mixed valence complexes **12** and NLO chromophores **13**, and **14**; the five NH_3 of $Ru(NH_3)_5$ are omitted for clarity in **12**

To avoid tedious synthetic programs, with the outcome of uncertain NLO properties, theoretical quantum procedures have been very helpful in the last decade.[18] We became convinced that the search for new families of inorganic chromophores should require preliminary calculations conducted on idealized molecular structures for selecting new inorganic candidates with sizeable nonlinearities. The criteria for the selection is as follows: $\beta_{complex} > \beta_{ligand}$, the comparison between experimental and calculated data being the test to prove the relevance of the quantum description of the properties. Our methodology is summarized in Scheme 1. Besides the gain in synthesis time, this approach is an attempt to fully understand what orbitals are actually involved in the NLO response, and finally to provide chemical guidelines for designing molecules with enhanced capabilities. In conclusion to this section, it is worth noting the tetrahedral cobalt(II) complex with two 1-(*p*-dimethylaminophenylhydrazono)-2-(*p*-nitrophenylimino)ethane ligands reported in 1992 by Simon et al.[29] Although the complex did not follow the traditional push-pull structures, the authors provided evidence for enhanced nonlinearities after metal complexation. The reasons for such behavior are probably related to a better conjugation within the donor−acceptor chromophore by virtue of the metal center. This example also illustrates the fact that pure chemical intuition may no longer be fully appropriate in predicting the extent of the NLO response, and emphasizes the need for efficient screening methods for selecting inorganic NLO materials. This approach has been successfully used in the design of bis(salicylaldiminato)metal Schiff base complexes with NLO capabilities.

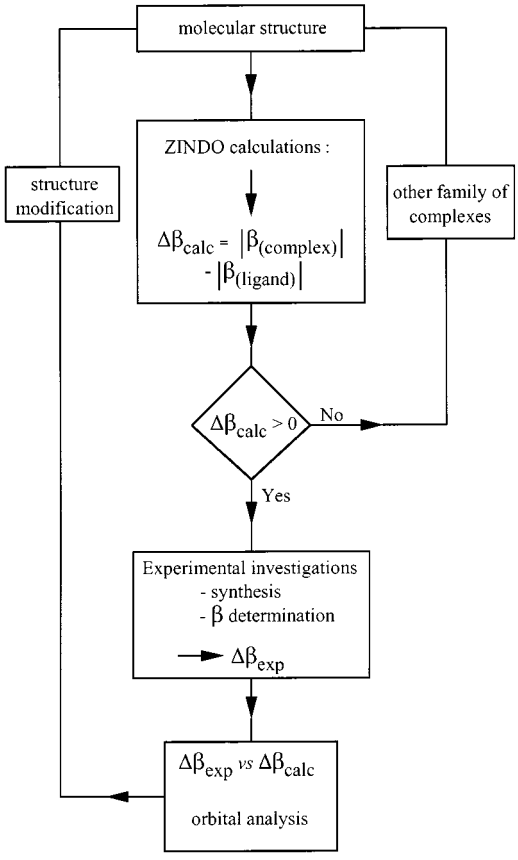

Scheme 1

3. Bis(salicylaldiminato)metal Schiff Base Complexes

3.1. Complexes with NLO Responses Larger than that of the Related Ligands

The first report of an NLO metal complex of the tetradentate salen [*N*,*N*′-bis(salicyleneaminato)ethylene] ligand

was that of Thompson et al. in 1991.[30] The authors observed second-harmonic generation in M^{III}-(salen)Py−$NHCH_2X$ derivatives. However, in these systems, the metal−salen core was probably not directly involved in the charge-transfer process responsible for the NLO response, but was rather used to enhance the NLO response of an apical substituted pyridine ligand, in a way similar to that observed in **10** or **14**. The report by Di Bella et al.[31] on various Ni(salen) (**15**, Table 4) derivatives with experimental sizeable NLO responses opened interesting perspectives for metal complexes. In contrast with the widely investigated push-pull organic chromophores, such complexes offer a large variety of structures that allows to locate the metal atom in a more strategic position at the center of the charge-transfer system, making better use of the metal d-orbital hybridization schemes in an organic environment. Importantly, it was proven by a ZINDO theoretical analysis that the NLO response of Ni(salen) complexes is dominated by the HOMO → LUMO transition, in which the nickel atom acts as a donor. This result indicates that this family of derivatives can offer suitable candidates for the strategy introduced in the preceding section.

The best result, which successfully applied this methodology was obtained in the investigation of the NLO properties of ligand **16**, compared with that of the corresponding nickel(II) complex **17** (Table 4).[32] It was shown that the complex exhibits an enlarged NLO response relative to that of the free ligand, with experimental β values of 109 and 235×10^{-30} cm^5 esu^{-1} for **16** and **17**, respectively. In this family, a slight red shift of about 15 nm upon metal complexation provides a modest β enhancement. Moreover, the intrinsic role of the metal center can be understood from a comparative analysis of the calculated data for **16** and **17**. In contrast to the two-level description of the NLO properties of push-pull organic chromophores, the data indicate that two transitions (1→2 and 1→3) are involved in the NLO response for both ligand and metal complex. The differences in electronic populations between the ground state and the two excited states are shown in Figure 2 for **16** and **17**. The picture clearly reveals the enhancement of the intramolecular charge transfer, once the metal atom has been introduced in the molecular structure. This suggests that the metal center, which acts as a donor, favors the conjugation of the chromophore, and hence allows a larger charge transfer in the excited states. One may expect various NLO responses by simply changing the nature of the metal center in this family of inorganic chromophores, a situation that would provide a possibility for optimizing β, once a suitable ligand has been selected. This has been achieved for the Zn^{II} derivative, with a β value of 400×10^{-30} cm^5 esu^{-1}, roughly twice that of the Ni^{II} complex. However, the orbital origin of this difference was not clarified, because of the different geometries between Zn^{II} and Ni^{II} complexes. The search for bis(salicylaldiminato)metal Schiff base complexes with NLO capabilities has been further optimized with the design of compound **18**.[33] However, the β enhancement upon complexation is modest and the metal center itself behaves as a weak donor, in contrast to the situation encountered in **17**, and depicted in Figure 2.

Besides the large β value, it has to be emphasized here that this family of derivatives exhibits excellent thermal stabilities (e.g. 360, 400, and 300 °C for **15**, **17**, and **18**, respectively). It is now generally believed that molecular second-order NLO materials will enter the marketplace, depending on the ability of the chromophores to be poled in

Table 4. Experimental (EFISH) NLO responses of various bis(salicylaldiminato)metal Schiff base complexes (ref.[31,32])

Compounds		β ($\times10^{-30}$ cm^5 esu) 1.34 μm	1.9 μm	Compounds		β ($\times10^{-30}$ cm^5 esu) 1.34 μm	1.9 μm
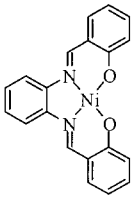	**15**	-20.5		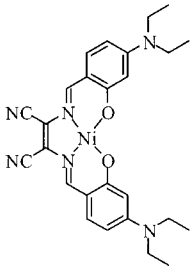	**17**	235	800 ($\beta\times\mu$)
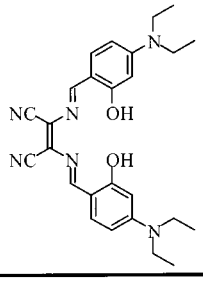	**16**	109		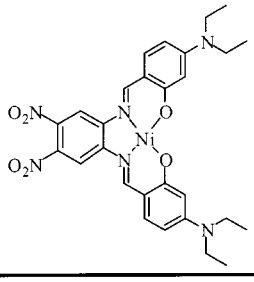	**18**		1530 ($\beta\times\mu$)

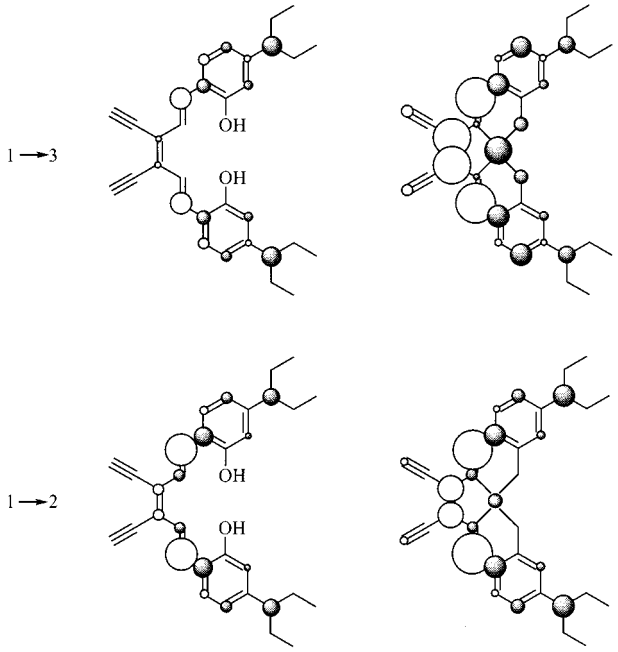

Figure 2. Difference in electronic populations between the ground state and the two excited states for **16** (left) and **17** (right); the black (white) contributions indicate a decrease (increase) in electron density in the charge-transfer process

polymers with very high glass transition temperatures.[12a] The rationale is that if *Tg* is far above the device's operating temperature, the alignment will not decay significantly over the life-time of the device. For stable and efficient poling, it has been realized that polymers with *Tg* higher than 250 °C have to be used and consequently, a good thermal stability has become an important prerequisite for $\chi^{(2)}$ NLO materials. This is undoubtedly one of the major characteristics of metal−salen derivatives. An important point to note is that the poling process requires the use of external electric fields. Therefore although β is the origin of the NLO effect, $\beta\times\mu$ is the molecular figure of merit for poled polymer films. The NLO response of **18** ($\beta\times\mu = 1530\times10^{-48}$ cm^5 D esu^{-1} at 1.907 μm, which corresponds to a static $\beta_0\times\mu = 968\times10^{-48}$ cm^5 D esu^{-1} at zero frequency) can be compared with that of the best organic candidates of similar molecular size.[3a] Although μ enhancement rather than β enhancement is mostly responsible for the large $\beta\times\mu$ value, this large NLO response definitely establishes the potential of these derivatives in the poled polymer approach.

Several metal−salen-based polymers have already been reported,[34] one of them using NLO monomers (polymer **19**, Figure 3).[35] On the other hand, the compounds were found to be rather insoluble, and no NLO effects have been reported. The crystal structure of a chain made of Mn^{III}(salen)(4-pyridylglycinate) blocks (**20**) has also been reported.[36] The structure reveals head-to-tail alignment of adjacent dipoles, but adjacent polymer chains are antiparallel, so no NLO effects are observed. To the best of our knowledge, the only report of NLO properties for an amorphous polymer containing metal Schiff base complexes has been that of poled polyhydroxystyrene doped with chromophore **18** (5% w/w). It exhibits a d_{33} value of 0.65 pm V^{-1} at 1.907 μm, and retains 85% of its NLO response after one week.[33] Although this value is a sizable NLO response for host-guest systems, larger d_{33} values (ca. 10 pm V^{-1}) would require functionalized polymers with chromophores covalently bonded. This has not been achieved yet.

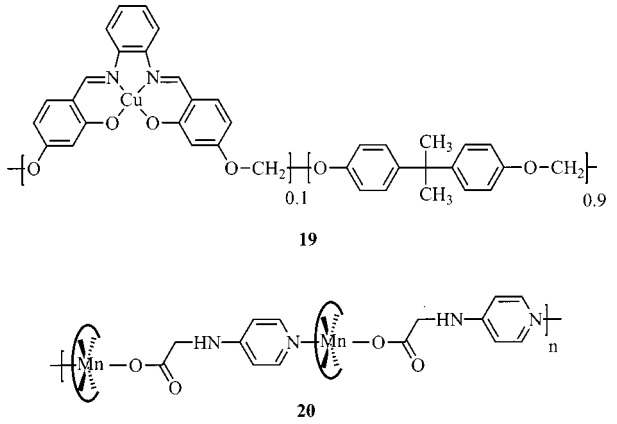

Figure 3. Chains containing bis(salicylaldiminato)metal Schiff base, with NLO capabilities; the ellipse represents a salen ligand in **20**

3.2. Chiral Complexes Efficient in Second-Harmonic Generation

In 1996, Chiang reported on an Fe^{III} derivative **21** (Figure 4), which was found to crystallize in the non-centrosymmetric $P6_5$ space group, with a powder efficiency twice that of urea.[37] The origin of the quadratic NLO response was attributed to both the pyridine−Fe π-system and the salen ligand, the first component most likely being dominant. In contrast to **21**, the Cambridge data base reveals that most of the crystal structures of bis(salicylaldiminato)metal complexes reported to date exhibit centrosymmetric space groups. In particular, bis(salicylaldiminato)nickel(II) complexes all possess centrosymmetric crystal structures, except those made with a chiral diamine (pure enantiomer). This observation strongly supports the idea that derivatives such as **15**−**18** will most likely exhibit vanishing NLO properties due to crystal centrosymmetry.

As is well known, chirality provides the chemist with a means of guaranteeing that crystallization of a pure enantiomer will occur in a non-centrosymmetric space group. In order to promote SHG efficiencies in the solid state, careful examination of Figure 2 provides interesting chemical

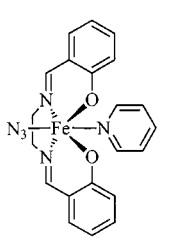

Figure 4. Fe^{III} complex exhibiting two charge-transfer transitions in the salen ligand and in the pyridine−Fe^{III} π-system

guidelines. It appears that the "C=N−C" linkage plays an important role as the withdrawing counterpart of the chromophore, in terms of charge transfer, whereas the contribution of the nitrile substituent is weak. Thus, complexes such as **22**−**24** (Table 5) are preferred in which the "C=N−C" linkage is present, with the addition of two asymmetric carbon atoms to force the crystallization into a non-centrosymmetric space group for the pure (1*R*−2*R* or 1*S*−2*S*) enantiomers. Complex **22** is the first bis(salicylaldiminato)-based metal complex on which this methodology was successfully applied for NLO purposes.[38] However, an unexpectedly low SHG efficiency, < 0.25 times that of urea was observed, arising from a pseudo-centrosymmetric crystal structure.

Table 5. SHG powder efficiencies (vs. urea) of chiral bis(salicylaldiminato)metal Schiff base complexes at 1.907 μm

Compounds		Efficiencies	[ref.]
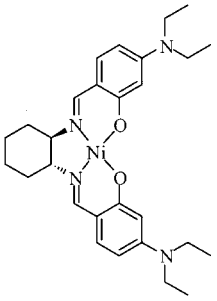	**22**	< 0.25	[38]
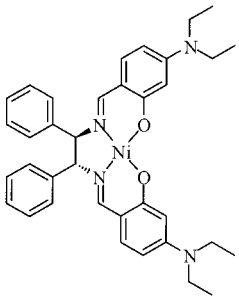	**23**	13	[39]
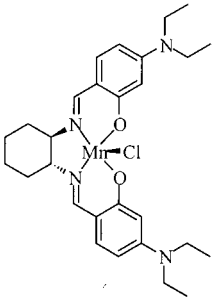	**24**	8	[38]

This strategy was further optimized in complex **23**, which crystallizes in the non-centrosymmetric $P2_1$ space group, and to date exhibits the highest SHG efficiency (13 × that of urea) in this class of materials.[39] The structure−NLO property relationships established by Zyss lead to the *d* component of $\chi^{(2)}$ given in Equation (4) where θ is defined as the angle between β and the 2_1 two-fold axis of the crystal, and *N*, the concentration of chromophores per volume unit.[40]

$$d_{ZXX} = N\beta\cos\theta\sin^2\theta \quad (4)$$

θ is equal to 57.8° for **23** and corresponds to an angular factor of 0.381. This value must be compared with the $2/\sqrt{3} = 0.385$ theoretical value which maximizes the angular factor for the most favorable crystal structure.[40] Consequently, the molecular orientation of **23** is optimized in the solid, and an efficiency 13 times that of urea is probably close to the upper limit for bis(salicylaldiminato)nickel(II) Schiff base complexes based on this π-electronic structure.

The deleterious effect of pseudo-centrosymmetry on the bulk SHG efficiency of molecules such as **22** can tentatively be related to the fact that the chiral substituent lies near the mean plane of the chromophore. Therefore, two isomers made from (1*R*,2*R*)-cyclohexanediyl or (1*S*,2*S*)-cyclohexanediyl, placed on top of each other almost coincide. Indeed, a calculation indicates that an average distance between the carbon atoms of the cyclohexanediyl and the NiO_2N_2 plane of **22** is to 0.31 Å. In other words, the molecule is "weakly chiral" in the sense of the quantification of chirality developed by Mislow.[41] By contrast, the out-of-plane displacement of the chiral substituents is large in **23**, in which the centroids of the phenyl substituents are located about 3.2 Å apart from the NiO_2N_2 plane. This difference can account for an enhanced "degree of chirality" for **23** relative to that of **22**.

To encourage out-of-plane displacements, alternative chromophores were envisioned such as **24**. Beside an SHG efficiency 8 times that of urea, **24** exhibits a different optical spectrum with a red shift, strongly indicative of reduced transition energy [Δ*E* in Equation (2)], and hence an enhanced β value.[38] It is worth mentioning that **24** brings about NLO chromophores with additional magnetic ($S = 2$) capabilities. The possibilities for interplay between magnetic and NLO behaviors will be discussed in the next section.

3.3. A Possibility for NLO Switching in Metal Schiff Base Complexes

Coordination complexes offer a large variety of magnetic properties by virtue of the coordination metal center,[42] that could bring about NLO chromophores with unique characteristics as multi-property building blocks. However, the possibility for direct interplay between both properties remains a challenging question. Di Bella et al. have shown that, on passing from close-shell Ni^{II}(salophen) to open-shell Cu^{II} or Co^{II} analogues **25** (Figure 5), experimental β values could increase from −20 to −50, and −170 $\times 10^{-30}$ cm^5 esu^{-1}, respectively.[43] This effect has been ascribed to the different natures of the electronic excited states. By contrast, we have investigated the paramagnetic complex **26**, which is the Cu^{II} analogue of **17**.[32] EFISH measurements revealed a β value of 200×10^{-30} cm^5 esu^{-1}, which is comparable with the 235×10^{-30} cm^5 esu^{-1} value measured for **17** within the range of uncertainty of the EFISH method.

However, various recent investigations have pointed out the possibility of β enhancement in organic radicals.[44,45] Such observations open interesting perspectives towards a possible interplay between magnetic and NLO behaviors.

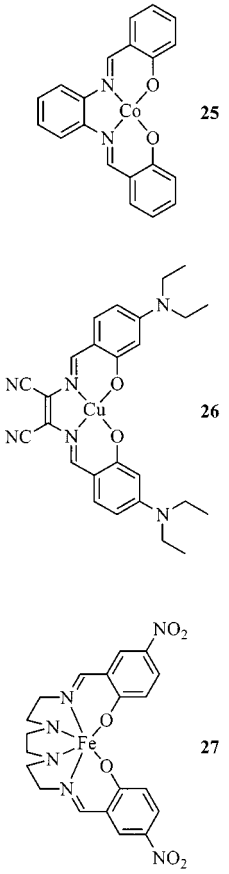

Figure 5. Paramagnetic bis(salicylaldiminato)metal Schiff base complexes with NLO capabilities

The possibility of bulk NLO modulation occurring upon ferromagnetic phase transition in a material containing NLO chromophores can be theoretically envisioned. It has long been known that a rotation of the axis of linearly polarized light occurs on passage through a magnetized material. This is commonly called the Faraday rotation.[46] This effect, which modifies the angle between *E* (the electric field component of the light) and β, should therefore modulate the NLO behavior of the solid. Nevertheless, the β value of the chromophores would not be affected by such a magnetic transition. By contrast, in bis(salicylaldiminato) Schiff base complexes, the spin carrier is the NLO chromophore itself. Therefore, one might wonder if this unique characteristic could encourage a relationship between both properties at the molecular level.

The first evidence for β modulation occurring upon magnetic phase transition has recently been reported in compound **27** (Figure 5).[47] Compound **27** is an iron(II) derivative, which reveals metal-to-ligand charge-transfer capabilities. The frontier orbitals of **27** are shown in Figure 6. By virtue of the two nitro substituents, the compound exhibits the push-pull character required for a sizable β value. At high temperatures, the two chromophores present in the crystal unit cell are equivalent (spin state, $S = 2$), and therefore possess the same β. Interestingly, the compound undergoes a spin transition ($S = 2 \rightarrow S = 0$) in two steps upon cooling down. A phase at intermediate temperature (around 150 K) has been observed in which one half of the chromophores are $S = 0$, and one half are $S = 2$.[48] This unique characteristic allows us to calculate the hyperpolarizability for both spin states in nearly identical solid-state environments. It is found that an enhancement of the static hyperpolarizability (β_0) of about 25% (36.9 to 45.9 $\times 10^{-30}$ cm^5 esu^{-1}) occurs on passing from $S = 0$ to $S = 2$. The main origin of this effect is likely to be related to geometry modifications occurring in the coordination sphere of the metal center.

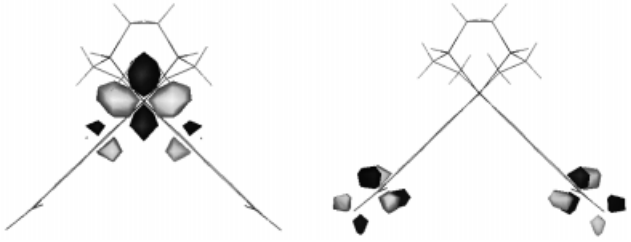

Figure 6. HOMO (left) and LUMO (right) for **27**

In these last few years, the intriguing concept of molecular switches has attracted great interest from a variety of perspectives.[49,50] These molecular NLO materials have recently been reviewed.[51] The switch is usually achieved by isomerization or redox/proton transfer. For example, Coe et al. have reported on an efficient redox switching in ruthenium(II) complexes.[52] By contrast, **27** is the first example of a new class of molecules in which a β switch could be envisioned from a magnetic phenomenon. However, in order to be fully convincing, a switch should be attached to an "on and off" behavior, which has not yet been observed.

4. Concluding Remarks

Until the late 1980s the push-pull one-dimensional electronic model has been the basis of almost every NLO chromophore such as the typical benchmark *p*-nitroaniline molecule. We have reported on various examples of ferrocene-, $W(CO)_5$-, or $Ru(NH_3)_5$-based organometallic and inorganic molecules for which an unexpectedly low NLO response has suggested, in the early 1990s, that the design of chromophores could be reconsidered aside from the traditional push-pull framework in coordination chemistry. Owing to the ability of computational models to provide efficient screening methods of selection, a new family of bis(salicylaldiminato) Schiff base complexes has finally emerged. It is worth noting that, in most reports on these materials, a large part of the work was invariably devoted to theoretical investigations of the properties.

Various Schiff-base complexes have now been reported to exhibit significant β enhancement upon metal complexation. For instance, Espinet et al. have recently ob-

tained Pd^{II} and Pt^{II} complexes in which β_0 enhancements as high as 80% of those of the corresponding ligands were measured.[53] In the present paper, we have presented a class of bis(salicylaldiminato) Schiff base complexes, which appear to be thermally robust NLO materials possessing large $\beta\times\mu$ products. Therefore, they provide interesting candidates for incorporation into high *Tg* polymer matrices. The next challenging goal for this research program would be to be able to covalently link the best of the bis(salicylaldiminato) Schiff base complexes (e.g. **17** and **18**) into polymers, such as polyimides. Beside the poled polymers approach, versatile synthetic methodologies allow for the design of chiral derivatives, with solid-state SHG efficiencies or paramagnetic multifunctional building blocks, in which the properties are expected to be related in some way to the concept of molecular switches. As the NLO field matures, it can be anticipated that materials with switchable NLO responses will find various novel applications.

Acknowledgments

The experimental work reported from our group was performed by F. Averseng, G. Lenoble, I. Malfant, C. Lepetit, and J. C. Daran. NLO measurements were performed by K. Nakatani (ENS Cachan), and early ZINDO calculations by S. Di Bella (University of Catania). The author is grateful to all of them.

[1] [1a] Y. R. Shen, *The Principles of Nonlinear Optics*, Wiley, New York, **1984**. – [1b] N. P. Prasad, D. J. Williams, *Introduction to Nonlinear Optical Effects in Molecules and Polymers*, Wiley, New York, **1991**. – [1c] J. Zyss, *Molecular Nonlinear* Optics, Academic Press, New York, **1994**. – [1d] H. S. Nalwa, S. Miyata, *Nonlinear Optics of Organic Molecules and Polymers*, CRC Press, New York, **1997**.

[2] S. K. Kurtz, in: *Nonlinear Optical Materials – Laser Handbook*, vol. 1 (Ed. F. T. Arecchi, E. O. Schultz-DuBois), North-Holland, Amsterdam, **1972**, p. 923.

[3] For recent reviews see: [3a] L. R. Dalton, A. W. Harper, R. Ghosn, W. H. Steier, M. Ziari, H. Fetterman, Y. Shi, R. V. Mustacich, A. K. Y. Jen, K. J. Shea, *Chem. Mater.* **1995**, *7*, 1060. – [3b] R. G. Benning, *J. Mater. Chem.* **1995**, *5*, 365. – [3c] T. Verbiest, S. Houbrechts, M. Kauranen, K. Clays, A. Persoons, *J. Mater. Chem.* **1997**, *7*, 2175.

[4] J. L. Oudar, D. S. Chemla, *J. Chem. Phys.* **1977**, *66*, 2664.

[5] J. L. Oudar, *J. Chem. Phys.* **1977**, 67, 446.

[6] D. J. Williams, *Angew. Chem. Int. Ed. Engl.* **1984**, *23*, 690.

[7] For example: [7a] M. Blanchard-Desce, V. Alain, P. V. Bedworth, S. R. Marder, A. Fort, C. Runser, M. Barzoukas, S. Lebus, R. Wortmann, *Chem. Eur. J.* **1997**, *3*, 1091. – [7b] M. Blanchard-Desce, J.-M. Lehn, M. Barzoukas, C. Runser, A. Fort, G. Puccetti, I. Ledoux, J. Zyss, *Nonlinear Opt.* **1995**, *10*, 23. – [7c] M. Blancherd-Desce, J.-M. Lehn, M. Barzoukas, I. Ledoux, J. Zyss, *Chem. Phys.* **1994**, *181*, 281.

[8] B. F. Levine, C. G. Betha, *J. Chem. Phys.* **1975**, *63*, 2666.

[9] [9a] K. Clays, A. Persoons, *Phys. Rev. Lett.* **1991**, *66*, 2980. – [9b] K. Clays, A. Persoons, *Rev. Sci. Instrum.* **1992**, *63*, 3285.

[10] J. Oudar, R. Hierle, *J. Appl. Phys.* **1977**, *48*, 2669.

[11] P. G. Lacroix, R. Clément, K. Nakatani, J. Zyss, I. Ledoux, *Science* **1994**, *263*, 658.

[12] [12a] R. Dagani, in: *Chem. Eng. News* **1996**, March 4, p. 22. – [12b] M. Eich, G. C. Bjorklund, D. Y. Yoon, *Polym. Adv. Technol.* **1990**, *1*, 189.

[13] Among recent examples for the NLO use of DR1, see: [13a] D. H. Choi, J. H. Park, T. H. Rhee, N. Kim, S.-D. Lee, *Chem. Mater.* **1998**, *10*, 705. – [13b] N. Tirelli, U. W. Suter, A. Altomare, R. Solaro, F. Ciardelli, S. Follonier, C. Bosshard, P. Günter, *Macromolecules* **1998**, *31*, 2152. – [13c] H. Jiang, A. K. Kakkar, *Macromolecules* **1998**, *31*, 2501.

[14] H. S. Nalwa, T. Watanabe, S. Miyata, in ref.[1d], chapter 4.

[15] [15a] S. K. Kurtz, T. T. Perry, *J. Appl. Phys.* **1968**, *39*, 3798. – [15b] J. P. Dougherty, S. K. Kurtz, *J. Appl. Crystallogr.* **1976**, *9*, 145.

[16] M. L. H. Green, S. R. Marder, M. E. Thompson, J. A. Bandy, D. Bloor, P. V. Kolinsky, R. J. Jones, *Nature* **1987**, *330*, 360.

[17] Among reviews of NLO organometallics see: [17a] L. T. Cheng, W. Tam, G. R. Meredith, S. R. Marder, *Mol. Cryst. Liq. Cryst.* **1990**, *189*, 137. – [17b] S. R. Marder, in: *Inorganic Materials* (Ed.: D. W. Bruce, D. O'Hare), John Wiley & Sons: New York, **1992**, pp 115. – [17c] N. J. Long, *Angew. Chem. Int. Ed. Engl.* **1995**, *34*, 21. – [17d] I. R. Whittall, A. M. McDonagh, M. G. Humphrey, M. Samoc, *Adv. Organomet. Chem.* **1998**, *42*, 291.

[18] D. R. Kanis, M. A. Ratner, T. J. Marks, *Chem. Rev.* **1994**, *94*, 195.

[19] D. R. Kanis, M. A. Ratner, T. J. Marks, *J. Am. Chem. Soc.* **1992**, *114*, 10338.

[20] D. R. Kanis, P. G. Lacroix, M. A. Ratner, T. J. Marks, *J. Am. Chem. Soc.* **1994**, *116*, 10089.

[21] M. S. Wrighton, H. B. Abrahamson, D. L. Morse, *J. Am. Chem. Soc.* **1976**, *98*, 4105.

[22] [22a] J. Zyss, *J. Chem. Phys.* **1993**, *98*, 6583. – [22b] J. Zyss, I. Ledoux, *Chem. Rev.* **1994**, *94*, 77.

[23] H. Lebozec, T. Renouard, *Eur. J. Inorg. Chem.* **2000**, 229.

[24] Among several reviews, see for example: [24a] H. Taube, *Angew. Chem. Int. Ed. Engl.* **1984**, *23*, 329. – [24b] C. Creutz, *Prog. Inorg. Chem.* **1983**, *30*, 1.

[25] C. Creutz, H. Taube, *J. Am. Chem. Soc.* **1969**, *91*, 3988.

[26] M. B. Robin, P. Day, *Adv. Inorg. Chem. Radiochem.* **1967**, *10*, 247.

[27] H. Sakaguch, H. Nakamura, T. Nagamura, T. Ogawa, T. Matsuo, *Chem. Lett.* **1989**, 1715.

[28] C. Dhenaut, I. Ledoux, I. D. F. Samuel, J. Zyss, M. Bourgault, H. Le Bozec, *Nature* **1995**, *374*, 339.

[29] T. Thami, P. Bassoul, M. A. Petit, J. Simon, A. Fort, M. Barzoukas, A. Villaeys, *J. Am. Chem. Soc.* **1992**, *114*, 915.

[30] W. Chiang, M. E. Thompson, D. VanEngen, J. W. Perry, *Spec. Publ. R. Soc. Chem.* **1991**, *91*, 210.

[31] S. Di Bella, I. Fragala, I. Ledoux, M. A. Diaz-Garcia, P. G. Lacroix, T. J. Marks, *Chem. Mater.* **1994**, *6*, 881.

[32] P. G. Lacroix, S. Di Bella, I. Ledoux, *Chem. Mater.* **1996**, *8*, 541.

[33] F. Averseng, P. G. Lacroix, I. Malfant, G. Lenoble, P. Cassoux, K. Nakatani, I. Maltey-Fanton, J. A. Delaire, A. Aukauloo, *Chem. Mater.* **1999**, *11*, 995.

[34] See for example: [34a] D. Wöhrle, P. Buttner, *Polym. Bull. (Berlin)* **1985**, *13*, 57. – [34b] R. P. Kingsborough, T. M. Swager, *Adv. Mater.* **1998**, *10*, 1003.

[35] D. Vitalini, P. Mineo, S. Di Bella, I. Fragalà, P. Maravigna, E. Scamporrino, *Macromolecules* **1996**, *29*, 4478.

[36] W. Chiang, D. M. Ho, D. Vanengen, M. E. Thompson, *Inorg. Chem.* **1993**, *32*, 2886.

[37] W. Chiang, D. Vanengen, M. E. Thompson, *Polyhedron* **1996**, *15*, 2369.

[38] G. Lenoble, P. G. Lacroix, J.-C. Daran, S. Di Bella, K. Nakatani, *Inorg. Chem.* **1998**, *37*, 2158.

[39] F. Averseng, P. G. Lacroix, I. Malfant, F. Dahan, K. Nakatani, *J. Mater. Chem.* **2000**, *10*, 1013.

[40] J. Zyss, J. L. Oudar, *Phys. Rev.* **1982**, *A26*, 2028.

[41] A. B. Buda, T. Auf der Heyde, K. Mislow, *Angew. Chem. Int. Ed. Engl.* **1992**, *31*, 989.

[42] O. Kahn, *Molecular Magnetism*, VCH, Weinheim, **1993**.

[43] S. Di Bella, I. Fragalà, I. Ledoux, T. J. Marks, *J. Am. Chem. Soc.* **1995**, *117*, 9481.

[44] S. Di Bella, I. Fragalà, T. J. Marks, M. A. Ratner, *J. Am. Chem. Soc.* **1996**, *118*, 12747.

[45] I. Malfant, N. Cordente, P. G. Lacroix, C. Lepetit, *Chem. Mater.* **1998**, *10*, 4079.

[46] J. F. Dillon, *J. Appl. Phys.* **1968**, *39*, 922.

[47] F. Averseng, C. Lepetit, P. G. Lacroix, J. P. Tuchagues, *Chem. Mater.*, in press.

[48] D. Boinnard, A. Bousseksou, A. Dworkin, J. M. Savariault, F. Varret, J. P. Tuchagues, *Inorg. Chem.* **1994**, *33*, 271.

[49] J. M. Lehn, *Supramolecular Chemistry – Concepts and Perspectives*, VCH, Weinheim, **1995**.

[50] M. D. Ward, *Chem. Soc. Rev.* **1995**, *24*, 121.

[51] B. J. Coe, *Chem. Eur. J.* **1999**, *5*, 2464.
[52] B. J. Coe, S. Houbrechts, I. Asselberghs, A. Persoons, *Ang. Chem. Int. Ed.* **1999**, *38*, 366.
[53] J. Buey, S. Coco, L. Díez, P. Espinet, J. M. Martín-Alvarez, J. A. Miguel, S. García-Granda, A. Tesouro, I. Ledoux, J. Zyss, *Organometallics* **1998**, *17*, 1750.

Received May 22, 2000
[I00209]

Dynamic Behaviour, Solution and Crystal Structure of an Allylmolybdenum/Oxo/Hydroxo Heterocubane

Cornelia Borgmann,[a] Christian Limberg,*[a] Sven Cunskis,[a] and Peter Kircher[a]

Dedicated to Prof. Dr. Günter Helmchen on the occasion of his 60th birthday

Keywords: Allyl complexes / Cubanes / Molybdenum / NMR spectroscopy / Rearrangements

The synthesis of a highly unsymmetrical, chiral oxometallocubane anion $[\{(\pi\text{-}C_3H_5)Mo(CO)_2\}_4(\mu_3\text{-}OH)_3(\mu_3\text{-}O)]^-$ built up from organometallic moieties and oxo ligands is described. Its structure was investigated not only in the solid state (X-ray diffraction analysis) but also in solution applying modern sophisticated NMR techniques. It was thereby possible to identify a trigonal twist rearrangement as the process responsible for the fluxional behaviour of this compound in solution: the (π-allyl)Mo moieties are highly mobile, rotating on the "oxo surface" even at –65 °C. This complex can be regarded as a suitable model for (π-allyl)Mo units incorporated into molybdenum oxide surfaces.

Introduction

Organotransition metal oxide complexes are noteworthy in representing a link between solid, more or less ionic metal oxides and low-valent molecular organometallic systems. Despite their potential model character with respect to oxidation intermediates[1,2] — for instance in processes where organic substrates are converted catalytically on metal oxide surfaces — there are as yet surprisingly few known representatives with organic ligands other than Cp.[1–4] One example of heterogeneous catalysis, where organometallic oxo moieties might play a significant role, entails the oxidation of propene at bismuthmolybdates by O_2 to yield acrolein:[5,6] the rate determining step is proposed to lead to surface intermediates with π-allyl Mo units embedded in an oxidic environment, and this stimulates research with the aim of preparing molecular complexes being modelled on this situation.

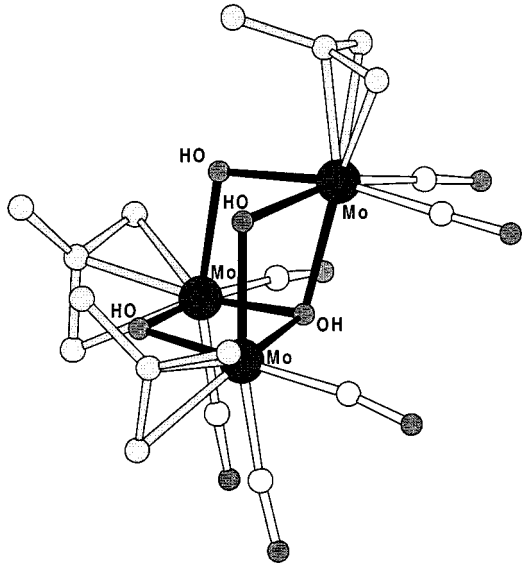

Figure 1. Molecular structure of **1**;[7] hydrogen atoms are omitted for clarity

Results and Discussion

In a recent study[7] we were able to prepare a complex anion $[\{(C_4H_7)Mo(CO)_2\}_3(\mu\text{-}OH)_3(\mu_3\text{-}OH)]^-$ **(1)** with (π-methallyl)Mo units in a *hydroxide* ligand sphere by treatment of $[Mo(\pi\text{-methallyl})(CO)_2(NCCH_3)_2(THF)]O_3SCF_3$ **(2)** with KOH/18-crown-6. Methallyl ligands were chosen instead of allyl ligands as they often facilitate the interpretation of NMR spectra and, additionally, provide a kinetic stabilisation for labile compounds. However, looking at the crystal structure of **1** (Figure 1), it occurred to us that the methyl substituents at the allyl groups also have an influence on the product formation: the structure can be considered as being derived from a neutral cubane-like arrangement, where one corner, a $[(\pi\text{-}C_4H_7)Mo(CO)_2]^+$ unit, is missing because the methyl groups occupy the corresponding space. This suggested analogous experiments with the allyl-derivative of **2**, **2′**.[7] Reacting this compound with KOH/18-crown-6 (Scheme 1) provided, after appropriate

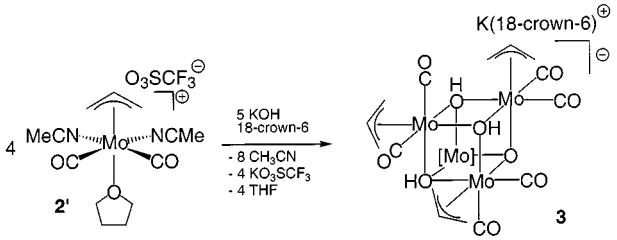

Scheme 1

[a] Universität Heidelberg, Anorganisch-Chemisches Institut, Im Neuenheimer Feld 270, 69120 Heidelberg, Germany
Fax: (internat.) + 49-6221/545-707
E-mail: Limberg@sun0.urz.uni-heidelberg.de

 © WILEY-VCH Verlag GmbH, 69451 Weinheim, 2001 1434–1948/01/0202–0349 $ 17.50+.50/0

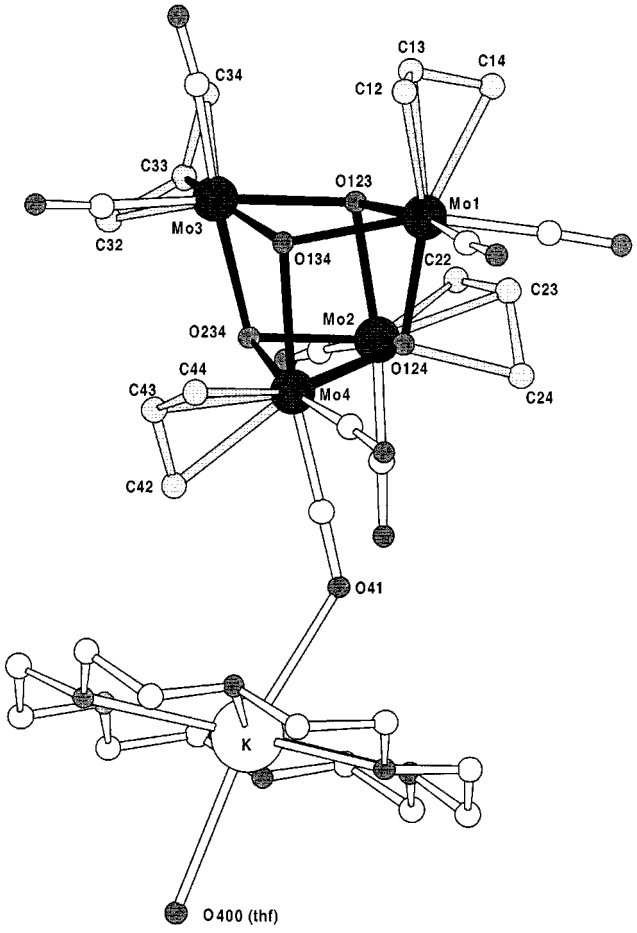

Figure 2. Molecular structure of one of the two independent, enantiomeric molecules of **3** found in the unit cell; all hydrogen atoms (and the additional 7.5 THF molecules within the cell) are omitted for clarity; selected bond lengths and angles (in Å and °): Mo(3)−O(234/123) 2.237(7)/2.261(7), Mo(1)−O(123/134) 2.327(6)/2.253(7), Mo(2)−O(123) 2.261(7), Mo(4)−O(134/234) 2.306(8)/2.259(7), Mo(3)−O(134) 2.143(8), Mo(2)−O(234) 2.195(7), Mo(2)−O(124) 2.118(7), Mo(1/4)−O(124) 2.050(7)/2.093(7), Mo(1)−C(12/13/14) 2.389(10)/2.237(11)/2.314(11), K(1)−O(41) 2.738(9), K(1)−O(400) 2.954(13); Mo(4)−O(124)−Mo(1) 108.9(3), Mo(4)−O(124)−Mo(2) 105.0(3), Mo(1)−O(124)−Mo(2) 108.8(3), Mo(3)−O(134)−Mo(4) 106.6(3), Mo(3)−O(134)−Mo(1) 106.9(3), Mo(1)−O(134)−Mo(4) 95.3(3)

work up, compound **3** as red crystals, one of which was analysed by X-ray diffraction (Figure 2).

The Solid-State Structure of 3

Indeed, the sterically less demanding allyl ligands allow a fourth $[(\pi\text{-}C_3H_5)Mo(CO)_2]^+$ unit to complete the cubane-like geometry. This, however, further polarises the OH ligands thereby enhancing their acidity. Accordingly, after the formation of the neutral product $[\{(\pi\text{-}C_3H_5)Mo(CO)_2\}_4(\mu_3\text{-}OH)_4]$ one proton is abstracted by excess [(18-crown-6)K]OH leading to **3** which possesses a highly unsymmetrical (chiral) anion $[\{(\pi\text{-}C_3H_5)Mo(CO)_2\}_4(\mu_3\text{-}OH)_3(\mu_3\text{-}O)]^-$. Two of these anions can be found within the unit cell, each of them being connected through a carbonyl oxygen atom [(O(41) in Figure 2] to a K^+ cation coordinated by a crown ether and a THF molecule [O(400)]. The two resulting ion pairs **3** in the cell are enantiomers. None of the hydroxylic protons could be located in the structure analysis, so it is not immediately obvious which of the O atoms corresponds to the oxo ligand. However, this can be inferred from a comparison of the Mo−O bond lengths within **3**. Most of them can be assigned to one of two relatively narrow distance ranges i.e. **I:** Mo(3)−O(234/123) 2.237(7)/2.261(7), Mo(1)−O(123/134) 2.327(6)/2.253(7), Mo(2)−O(123) 2.261(7), Mo(4)−O(134/234) 2.306(8)/2.259(7) Å; **II:** Mo(3)−O(134) 2.143(8), Mo(2)−O(234) 2.195(7) Å. The group **I** bonds all have CO ligands bound *trans* to them, while group **II** bonds are located *trans* to allyl ligands and are somewhat shorter as the *trans* influence of the allyl group is weaker than that of CO. Only the bonds of O(124) do not fit into these groups: Mo(2)−O(124) [2.118(7) Å] with a CO ligand in the *trans* position clearly lies out of the region defined by the group **I** bonds, which are considerably longer. Furthermore, Mo(4)−O(124) and Mo(1)−O(124) (*trans* to allyl) are, at 2.050(7) and 2.093(7) Å, significantly shorter than the group **II** bonds. It is therefore reasonable to assign O(124) to the O^{2-} ligand within the complex.[8]

Compound **3** can thus be considered as a suitable, *soluble* model for (π-allyl)Mo units incorporated in molybdenum oxide surfaces, and a detailed NMR spectroscopic analysis of its dynamics promised to provide valuable information. The determination of the solution structure of **3** formed the basis for such an investigation.

The Solution Structure of 3

When dissolved in [D_8]THF, compound **3** shows, at room temp. (apart from the signals due to the crown ether), only three broad signals corresponding to averaged resonances of all H_{syn}, H_{anti}, and H_{meso} protons, i.e. **3** is highly fluxional in solution. No OH signals can be seen. On cooling of the sample, the spectrum dramatically changes in a continuous fashion until a stationary situation is reached at −65 °C. At this point a geometry of the anionic framework corresponding to the one in the crystal structure is frozen out on the ^{1}H NMR time scale, as shown by HSQC, HMBC,

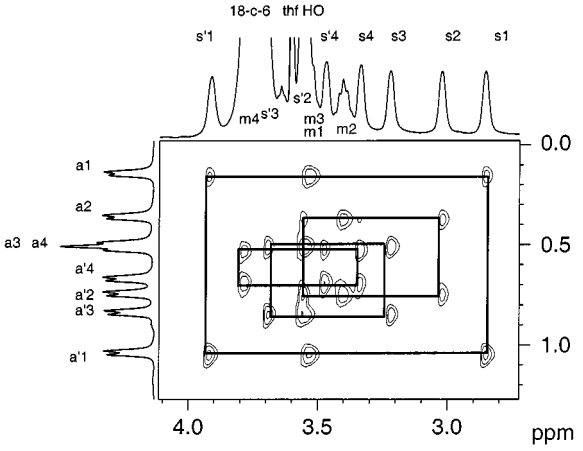

Figure 3. TOCSY NMR spectrum of **3** (500 MHz, [D_8]THF, −65 °C)

Table 1. ^{1}H and ^{13}C NMR shifts of the nuclei belonging to the four different allyl groups in **3** (500 MHz, [D$_8$]THF, −65 °C)

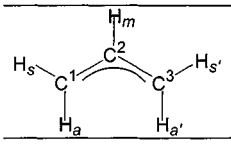

	^{13}C			^{1}H				
Allyl group	C^1	C^2	C^3	H$_a$	H$_{a'}$	H$_m$	H$_s$	H$_{s'}$
1	49.8	64.7	77.7	0.14	1.04	3.54	2.85	3.91
2	53.3	60.5	81.0	0.36	0.74	3.39	3.02	3.55
3	55.0	59.3	79.1	0.50	0.84	3.55	3.22	3.64
4	53.5	58.3	79.4	0.52	0.67	3.78	3.34	3.47

TOCSY and NOESY NMR experiments: Each proton belonging to the anion of **3** now shows an individual signal (see Figure 3, where the absorptions of all the allylic protons and their correlations in the TOCSY spectrum are shown), and applying the above-mentioned methods it was possible to assign[9] all of them to a certain position in one of four allyl groups, as indicated in Table 1. The structure frozen out at that temperature thus has to belong to the C_1 point group. Furthermore, the signals of the OH protons can now be observed: A resonance at $\delta = -1.1$ with an integral of one proton should be assigned[10] to the HO(123) ligand, and a second one appearing at $\delta = 4.4$ must belong to HO(134).[12] Moreover, the NOESY spectrum reveals that the signal of HO(234) is hidden by the overlapping resonances of H$_{s'}$ belonging to allyl group 2, H$_m$ of allyl group 3 and H$_m$ of allyl group 1. All other features can also be interpreted in terms of the structure shown in Figure 2, but assignments other than the ones mentioned would be less unambiguous.

Dynamics of 3

Considering **3** as a model, and having identified the solution structure of its anion as being equivalent to the one in the solid state structure, the most important remaining question concerns the type of dynamic process responsible for the changes of the spectrum observed on annealing of the sample. Recently, we have been able to show[13] that in [(π-allyl)(CO)$_2$Mo(OR)$_3$] complex metal fragments the allyl ligands themselves are comparatively rigid (i.e. they are not involved in π-σ-π rearrangements or other processes involving Mo−C bond breaking), but that the (allyl)Mo(CO)$_2$ moiety is capable of "rotating" on the trigonal sphere formed by the three alkoxide ligands by a trigonal twist rearrangement[14−16] (see Figure 4). This process, which has been proved only for a few examples in the literature,[13−17] is also important in the case of **3**: in the NOESY spectrum, where the time scale is different from that of a "normal" ^{1}H NMR spectrum due to the long mixing times, exchange cross peaks with characteristic phases can be found between the signals within each of the proton groups (*syn*, *anti*, *meso*, OH), indicating that even at −65 °C there is a motion by which, for instance, not only the *anti* protons belonging to *one* allyl group but also those belonging to *different* allyl ligands become equivalent. This finding can only be understood if trigonal twist arrangements are operative. If, for instance, the (allyl)Mo(2)(CO)$_2$ unit of **3** as shown in Figure 2 is rotated (viewing this unit as shown in Figure 4) anticlockwise by 120° on the O(123/124/234) surface, the enantiomer of the structure shown in Figure 2 is obtained, which of course has identical NMR properties, but the ligands on Mo(4) now correspond to those of Mo(1) (and vice versa), while H$_2$C(22) has turned into H$_2$C(24). This causes typical exchange peaks in the NOESY spectrum, for instance, between the two H$_a$ signals, the two H$_s$ signals, the two H$_{a'}$ signals etc. belonging to C(22) and C(24). On further annealing this process becomes faster until the protons of the allyl groups on Mo(4) and Mo(1) [as well as those of C(22) and C(24)] become indistinguishable also on the time scale of the ^{1}H NMR spectrum showing coalescence. Similar effects occur when two or even three (allyl)Mo units rotate simultaneously, so that the dramatic changes of the spectra with temperature are understandable (the case becomes even more complicated if allowance for shifts of the hydroxylic protons is made at higher temperatures, which is not unreasonable).

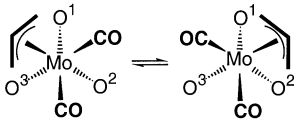

Figure 4. Trigonal twist rearrangement of a (π-allyl)Mo moiety on an oxo surface

In conclusion a novel organometallic oxomolydocubane **3** has been synthesised in a controlled fashion and analysed structurally. There is only one other compound known with a soft π-allyl and a hard oxo ligand being connected to one and the same Mo centre: [{(C$_4$H$_7$)Mo(CO)$_2$(bipy)}$_2$(μ-MoO$_4$-κ*O*,κ*O*′)], which is insoluble in all common solvents.[18] For **3**, however, it could be unequivocally proved that on dissolution not only does its constitution remain intact but the chiral structure it adopts in the crystal is thermodynamically favoured also in solution. Even at −65 °C the (π-allyl)Mo moieties are mobile, rotating an the "oxo surface". From the latter finding, conclusions can also be drawn concerning the dynamics of molybdenum oxide-supported (π-allyl)Mo fragments, as, for instance, those poten-

tially formed as intermediates during the oxidation of propene with bismuthmolybdates.

Experimental Section

Synthesis of 3: A solution of AgO_3SCF_3 (0.51 g, 2.0 mmol) in 8 mL THF was added to a solution of **2′**[7] (0.62 g, 2.0 mmol) with a cannula. Immediately, AgCl precipitated as a greyish solid. The filtrate was added to a suspension of KOH (0.18 g, 3.0 mmol) and 18-crown-6 (0.79 g. 3.0 mmol) in 10 mL THF. After stirring for 3 h the precipitated white K(18-crown-6)O_3SCF_3 was filtered off from the red-orange solution, which was subsequently layered with 100 mL of light petroleum. Storing at −20 °C for 6 days yielded 0.41 g (0.3 mmol) of analytically pure, crystalline **3·3.75THF** corresponding to a yield of 55%. ^{1}H and ^{13}C NMR (500 MHz, [D$_8$]THF): see Table 1. − IR (KBr): $\tilde{\nu}$ = 1915 (br, s)/1821 (br, s) [ν(CO)], 3606 (m)/3563 (m) [ν(OH)] cm^{-1}. − $C_{39}H_{61}KMo_4O_{19.75}$ (1267.78) [**3·1.75 THF**; 2 molecules of THF per molecule of **3** are lost on drying]: calcd. C 36.95, H 4.85; found C 36.59, H 5.11.

X-ray Crystallography

3·3.75THF: $C_{32}H_{47}KMo_4O_{18}\cdot C_{15}H_{30}O_{3.75}$, M_r = 14.12, monoclinic, space group *Cc*, Z = 4, a = 13.756(3), b = 28.077(6), c = 33.650(7) Å, β = 101.72(3), V = 12725.00 Å^3, 3.4 < 2θ < 52.0°, ω-scan, T = 200 K, δ_{cald} = 1.547 g cm^{-3}, measured 31925, independent 24490, and observed reflections 20526 with $I > 2\sigma(I)$, Lp correction, 1472 refined parameters with R = 0.070, residual electron density (max./min.): 1.244/−0.911 eÅ^{-3}; Mo-K_α radiation, λ = 0.71073 Å, was used and the structures were solved by direct methods (program: SHELXS-97) and refined versus F^2 (program: SHELXL-97) with anisotropic temperature factors for all non-hydrogen atoms, apart from C(22) and some of the atoms belonging to the THF molecules, which could only be refined isotropically.

Crystallographic data (excluding structure factors) for the structure(s) included in this paper have been deposited with the Cambridge Crystallographic Data Centre as supplementary publication no. CCDC-146570. Copies of the data can be obtained free of charge on application to CCDC, 12 Union Road, Cambridge CB2 1EZ, UK [Fax: (internat.) + 44-1223/336-033; Email: deposit@ccdc.cam.ac.uk].

Acknowledgments

We are grateful to the *Deutsche Forschungsgemeinschaft* and the *Fonds der Chemischen Industrie* for financial support in the form of a Heisenberg-Stipendium (C. L.) and funding.

[1] See, for instance: O. I. Guzyr, J. Prust, H. W. Roesky, C. Lehmann, M. Teichert, F. Cimpoesu, *Organometallics* **2000**, *19*, 1549 and references cited.
[2] J. Sundermeyer, *Angew. Chem.* **1993**, *105*, 1195; *Angew. Chem. Int. Ed. Engl.* **1993**, *32*, 1144 and references cited.
[3] W. A. Herrmann, *Angew. Chem.* **1988**, *100*, 1269; *Angew. Chem. Int. Ed. Engl.* **1988**, *27*, 1297 and references cited.
[4] F. Bottomley, L. Sutin, *Adv. Organomet. Chem.* **1988**, *28*, 339 and references cited.
[5] R. K. Grasselli, J. D. Burrington, *Ind. Engl. Chem. Prod. Res. Dev.* **1984**, *23*, 394.
[6] J. Belgacem, J. Kress, J. A. Osborn, *J. Mol. Cat.* **1994**, *86*, 267.
[7] C. Borgmann, C. Limberg, E. Kaifer, H. Pritzkow, L. Zsolnai, *J. Organomet. Chem.* **1999**, *580*, 214.
[8] Repeated crystallisations of **3** applying various techniques and solvent mixtures yielded crystals differing in their space groups and the numbers of THF molecules within the unit cells; the structure of the anion, however, always remained identical to the one depicted in Figure 2 (within the frames given by the errors). In one case the protons at the O(134) and O(234) atoms could even be located.
[9] The signals of the *syn* and *anti* protons connected to a certain terminal C atom were identified by means of HSQC and HMBC NMR spectra, while the two terminal CH_2 groups belonging to one and the same allyl group (i.e. $C^1H_aH_s$ and $C^3H_{a'}H_{s'}$ connected through C^2H_m, compare the designations in Table 1) were correlated by TOCSY NMR spectra (Figure 3).
[10] NMR studies concerning the anion **1**[7] and other carbonyl(hydroxo)molybdenum complexes[11] showed that μ_x-OH resonances are increasingly shifted to higher field, the more CO ligands can be found *trans* to the *x* Mo−OH bonds, and HO(123) bears the maximum of three CO ligands in *trans* position to it.
[11] J. T. Lin, S. K. Yeh, G. H. Lee, Y. Wang, *J. Organomet. Chem.* **1989**, *361*, 89.
[12] In a NOESY NMR spectrum this signal shows intense cross peaks to only two of the eight *anti* protons ($H_{a'}$ of the allyl groups designated as 2 and 4 in Table 1), and it is therefore reasonable to assign it to HO(134) as, unlike HO(234), it is exactly in such a situation where it is close only to the *anti* protons at C(44) and C(12).
[13] C. Borgmann, C. Limberg, L. Zsolnai, K. Heinze, *Z. Naturforsch.* **1999**, *54b*, 473.
[14] J. W. Faller, D. A. Haitko, R. D. Adams, D. F. Chodosh, *J. Am. Chem Soc.* **1977**, *99*, 1654.
[15] J. W. Faller, D. A. Haitko, R. D. Adams, D. F. Chodosh, *J. Am. Chem Soc.* **1979**, *101*, 865.
[16] R. A. Brown, S. Endud, J. Friend, J. M. Hill, M. W. Whiteley, *J. Organomet. Chem.* **1988**, *339*, 283.
[17] See also: P. Espinet, R. Hernado, G. Iturbe, F. Villafane, A. G. Orpen, I. Pascual, *Eur. J. Inorg. Chem.* **2000**, 1031 and references cited.
[18] C. Borgmann, C. Limberg, L. Zsolnai, *Chem. Commun.* **1998**, 2729.

Received August 11, 2000
[I00312]

Self-Assembly of Nickel(II) Complexes of New Bis-Bidentate Schiff Base Ligands[‡]

Laura Carbonaro,[a] Mauro Isola,*[a] Vincenzo Liuzzo,[a] Fabio Marchetti,[b] Federica Balzano,[c] Christian Silvio Pomelli,[a] and Andrea Raffaelli[c]

Keywords: Nickel / Schiff bases / Self assembly / N ligands / Supramolecular chemistry

Nickel(II) complexes derived from three new bis-bidentate Schiff bases, H_2L^{1-3}, having two *N*-*n*-propyl-salicylaldiminate units linked by an O–$(CH_2)_n$–O spacer (n = 4, 8, 12, respectively) at the 3-position of the salicyl moieties, are described. The pyridine adduct of the complex with the shorter spacer forms a cyclic trinuclear structure, $[Ni_3(L^1)_3(py)_6]$ (**2**), in the solid state, where each Ni^{II} ion is octahedrally coordinated by two N,O-bidentate arms of two different ligands and two pyridine nitrogens. The base with n = 8 leads to the double-helical dinuclear complex, $[Ni_2(L^2)_2]$·THF (**3**), which is the first example of a structurally characterised helicate based on a square-planar N_2O_2 coordination geometry. In $CHCl_3$ solution, **3** undergoes a disassembly process which results in an equilibrium mixture where the mononuclear species is largely predominant.

In recent years there has been increasing interest in the dinuclear and polynuclear coordination complexes of relatively simple ligands which exhibit, in solution and/or in the solid state, unusual, in some cases unexpected, structural complexity.[1] Helicates,[2] grids,[3] boxes and rings[4] are examples of supramolecular structures generated by the complexation of multidentate ligands with metal ions.

Interesting studies have been devoted to the development of synthetic procedures in order to prepare new multidentate ligands exhibiting the potential ability to give bridged polynuclear species. In particular, a number of attractive ligands with bidentate, chelating binding sites with flexible spacers between them have recently been reported.[5]

Here we describe a general procedure for the facile preparation of new tetradentate Schiff base ligands containing two N,O-bidentate chelating moieties linked through flexible polymethylene dioxo spacers, and their coordination behaviour with nickel(II).

The ligands H_2L^1, H_2L^2 and H_2L^3 were prepared in good yields (ca. 50%) by reaction of the dianion of 2,3-dihydroxybenzaldehyde with the appropriate alkyl α,ω-dibromide in dimethyl sulfoxide,[6] followed by the treatment of the resulting dialdehydes with *n*-propylamine. Reaction of the ligands with $Ni(OAc)_2·4H_2O$ in a 1:1 molar ratio in ethanol afforded the complexes **1a–c** as light-green solids (Scheme 1).

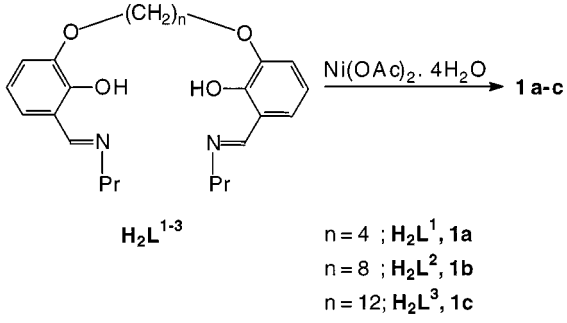

Scheme 1

Elemental analyses suggest the formation of 1:1 complexes for all three systems; however, **1a** exhibits quite different properties from those of both **1b** and **1c**. While the latter complexes have relatively low melting points (190–192 °C and 120–122 °C, respectively) and are moderately (Et_2O, dioxane) or very soluble (chloroform, THF, toluene) in organic solvents, **1a** has a melting point >320 °C and is insoluble in most common organic solvents, suggesting a higher structural complexity. However, **1a** is soluble in pyridine (py), and on addition of Et_2O to the pyridine solution the crystalline green solid **2**, analysing as **1a·2py**, precipitates; this material is paramagnetic, while **1a** is diamagnetic, similar to **1b** and **1c**. These data suggest that nickel(II) adopts a square-planar (SP) coordination geometry in **1a–c** and a nonplanar geometry in the pyridine adduct **2**, at least in the solid state.

[‡] This work is part of the thesis of V. L. in partial fulfillment for the requirements of the degree of Philosophy Doctor of Chemical Sciences.

[a] Dipartimento di Chimica e Chimica Industriale, Università di Pisa, Via Risorgimento 35, I-56126 Pisa, Italy
Fax: (internat.) +39-50/918-210
E-mail: misola@dcci.unipi.it
[b] Dipartimento di Ingegneria Chimica, dei Materiali, delle Materie Prime e Metallurgia, Università degli Studi di Roma "La Sapienza", Via del Castro Laurenziano 7, I-00161 Roma, Italy
[c] Centro di Studio del CNR per le Macromolecole Stereordinate ed Otticamente Attive, Via Risorgimento 35, I-56126 Pisa, Italy

 © WILEY-VCH Verlag GmbH, 69451 Weinheim, 2001 1434–1948/01/0202–0353 $ 17.50+.50/0

Electrospray ionization mass spectroscopy (ESI-MS) of acetonitrile solutions of **1b**, **1c** and **2** indicates the presence of Ni^{II}/ligand 1:1 complexes, but higher mass peaks, corresponding to 2:2 aggregates or species resulting from their fragmentation, suggest the existence in solution of dinuclear complexes, in substantial amounts for **2**, and in small amounts for **1b** and **1c**. The spectrum of **2** also shows a very weak peak corresponding to a trinuclear species.

The ^{1}H NMR spectrum of **2** in $CDCl_3$ shows broad signals whose chemical shift depends on the concentration (mainly for the imine and aromatic protons and for the *ortho* protons of the complexed pyridine) suggesting the presence of an equilibrium involving Ni^{II} ions in a nonplanar environment. Single crystals of **2** were grown from pyridine/diethyl ether and studied by X-ray diffraction. The complex is the cyclic trimer $[Ni_3(L^1)_3(py)_6]$ shown in Figure 1. Each nickel(II) ion is octahedrally coordinated by two pairs of O,N coordination sites of two different ligands and two pyridine nitrogens. The molecule posses a pseudo threefold axis (C_3), that in the Figure points out of the page. As the ligands turn around as a helix fragment, the molecule is chiral, but forms racemic crystals because helices of opposite chirality regularly alternate in the centrosymmetric $P2_1/c$ space group.

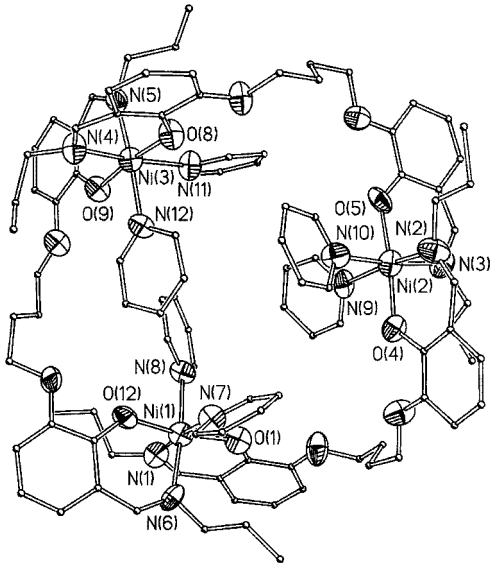

Figure 1. Crystal structure of **$[Ni_3(L^1)_3(py)_6]$** (**2**); Ni, O and N atoms are represented by 30% probability thermal ellipsoids; C atoms are represented by small spheres and H atoms are omitted for clarity; relevant bond lengths (Å) and angles (°): Ni(1)−O(1) 2.007(12), Ni(1)−O(12) 2.02(1), Ni(1)−N(1) 2.11(1), Ni(1)−N(6) 2.11(1), Ni(1)−N(8) 2.15(1), Ni(1)−N(7) 2.16(1), Ni(2)−O(4) 2.00 (1), Ni(2)−O(5) 2.02(1), Ni(2)−N(2) 2.12(1), Ni(2)−N(3) 2.14(2), Ni(2)−N(9) 2.16(1), Ni(2)−N(10) 2.22(1), Ni(3)−O(9) 1.988(9), Ni(3)−O(8) 2.013(9), Ni(3)−N(4) 2.10(1), Ni(3)−N(5) 2.11(1), Ni(3)−N(12) 2.17(1), Ni(3)−N(11) 2.20(1); O(1)−Ni(1)−O(12) 169.6(4), O(1)−Ni(1)−N(1) 89.4(5), O(12)−Ni(1)−N(1) 97.7(5), O(1)−Ni(1)−N(6) 98.5(5), O(12)−Ni(1)−N(6) 89.5(4), N(1)−Ni(1)−N(6) 86.9(5), O(1)−Ni(1)−N(8) 86.3(5), O(12)−Ni(1)−N (8) 86.2(5), N(1)−Ni(1)−N(8) 89.5(5), N(6)−Ni(1)−N(8) 174.0(5), O(1)−Ni(1)−N(7) 86.8(4), O(12)−Ni(1)−N(7) 86.8(5), N(1)−Ni(1)−N(7) 173.3(5), N(6)−Ni(1)−N(7) 88.2(5), N(8)−Ni(1)−N(7) 95.7(5), O(4)−Ni(2)−O(5) 173.9(4), O(4)−Ni(2)−N(2) 89.0(5), O(5)−Ni(2)−N(2) 96.4(5), O(4)−Ni(2)−N(3) 94.4(5), O(5)−Ni(2)−N(3) 88.0(5), N(2)−Ni(2)−N(3) 93.9(6), O(4)−Ni(2)−N(9) 83.2(5), O(5)−Ni(2)−N(9) 91.1(5), N(2)−Ni(2)−N(9) 170.1(5), N(3)−Ni(2)−N(9) 92.8(5), O(4)−Ni(2)−N(10) 90.4(5), O(5)−Ni(2)−N(10) 87.5(5), N(2)−Ni(2)−N(10) 83.4(6), N(3)−Ni(2)−N(10) 174.5(6), N(9)−Ni(2)−N(10) 90.4(5), O(9)−Ni(3)−O(8) 173.0(4), O(9)−Ni(3)−N(4) 95.3(5), O(8)−Ni(3)−N(4) 89.4(5), O(9)−Ni(3)−N(5) 88.4(5), O(8)−Ni(3)−N(5) 96.9(5), N(4)−Ni(3)−N(5) 88.3(5), O(9)−Ni(3)−N(12) 84.1(4), O(8)−Ni(3)−N(12) 90.5(5), N(4)−Ni(3)−N(12) 93.3(5), N(5)−Ni(3)−N(12) 172.5(5), O(9)−Ni(3)−N(11) 90.2(5), O(8)−Ni(3)−N(11) 85.3(4), N(4)−Ni(3)−N(11) 174.2(5), N(5)−Ni(3)−N(11) 89.9(5), N(12)−Ni(3)−N(11) 89.2(5)

Single crystals of the complex **$[Ni_2(L^2)_2]\cdot$THF** (**3**) were obtained by slow evaporation of a solution of **1b** in THF/Et_2O. X-ray diffraction analysis shows that dinuclear molecules (Figure 2) result from the coordination of two $(L^2)^{2-}$ ligands to two nickel centres. Each metal atom is linked in a *trans*-square-planar (*trans*-SP) geometry by two N,O-coordination sites of different ligands. The nickel atoms and chelating groups lie approximately on parallel planes (max. deviations 0.31 and 0.22 Å, respectively) spaced by 3.46 Å. The planes are bonded by two octyl chains which are twisted forming a double helix. On going from Ni(1) to Ni(2) the chains twist by a quarter of a turn. The whole molecule possesses a *pseudo* D_2 symmetry, one of the two-fold axes passing through the nickel atoms.

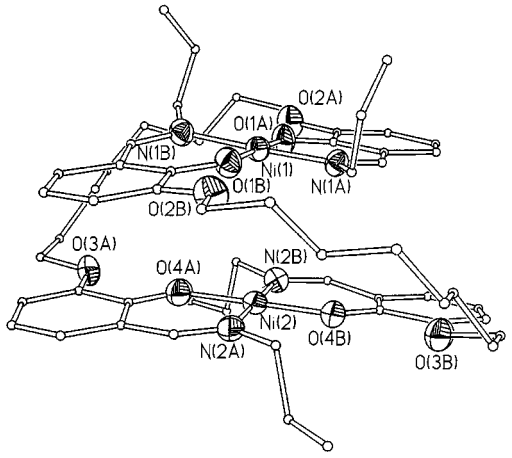

Figure 2. Perspective view of the molecular structure of **$[Ni_2(L^2)_2]\cdot$THF** (**3**); Ni, O and N atoms are represented by 30% probability thermal ellipsoids; C atoms are represented by small spheres, and H atoms and clathrated THF are omitted for clarity; only the most populated positions of the disordered propyl groups are shown; relevant bond lengths (Å) and angles (°): Ni(1)−O(1A) 1.844(8), Ni(1)−O(1B) 1.852(8), Ni(1)−N(1A) 1.908(8), Ni(1)−N(1B) 1.925(9), Ni(2)−O(4A) 1.858(7), Ni(2)−O(4B) 1.859(7), Ni(2)−N(2B) 1.892(11), Ni(2)−N(2A) 1.909(10); O(1A)−Ni(1)−O(1B) 177.4(49), O(1A)−Ni(1)−N(1A) 92.9(4), O(1B)−Ni(1)−N(1A) 87.9(4), O(1A)−Ni(1)−N(1B) 86.4(4), O(1B)−Ni(1)−N(1B) 92.9(4), N(1A)−Ni(1)−N(1B) 178.0(4), O(4A)−Ni(2)−O(4B) 179.6(4), O(4A)−Ni(2)−N(2B) 86.6(4), O(4B)−Ni(2)−N(2B) 93.4(4), O(4A)−Ni(2)−N(2A) 92.8(4), O(4B)−Ni(2)−N(2A) 87.2(4), N(2B)−Ni(2)−N(2A) 179.4(4)

The square-planar geometry found for **3** is rather unusual[7] for double-stranded helical complexes, but not surprising in this case. In fact it is known[8] that in bis(*N*-alkylsalicylaldiminato)nickel(II) complexes, in the absence of space-demanding alkyl substituents, the nickel atom exhibits planar geometry.

The ^{1}H NMR spectra of a $CDCl_3$ solution of microcrystalline **1b** and **1c** show a major set (>90%) of resonances and some signals of very low intensity. The major reson-

ances, corresponding to a largely predominant species, and the minor set of signals can be assigned, according to the ESI-MS data, to the mononuclear and dinuclear complexes, respectively. The mononuclear complexes have been characterized by ROESY analysis (see Experimental Section). As far as the set of minor resonances is concerned, it can be unambiguously assigned, at least in the case of **1b**, to the dinuclear species interconverting with the mononuclear complex in solution. In fact, the ^{1}H NMR spectra of a $CDCl_3$ solution of **3** recorded at different times after dissolution of the solid sample shows a decrease of the intensity of the signals corresponding to the dinuclear species and a concomitant increase of the intensity of the resonances due to the mononuclear complex (Figure 3a and Figure 3b). When equilibrium is reached (>29 h), the spectrum is identical to that of the mononuclear complex **1b** (Figure 3b and Figure 3c).

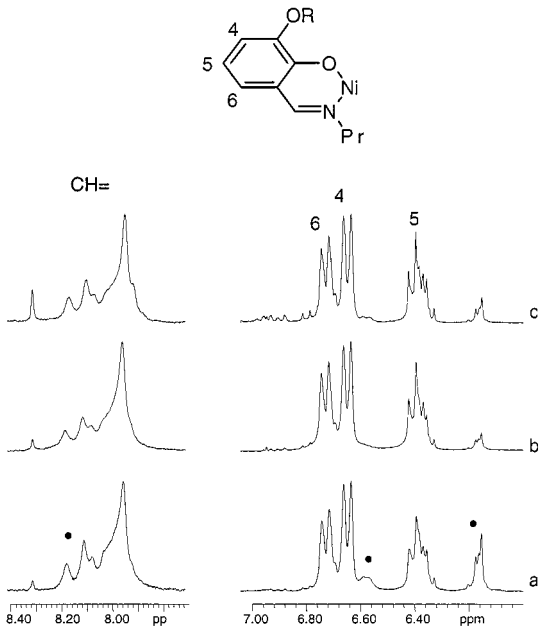

Figure 3. ^{1}H NMR (300 MHz, $CDCl_3$, 25 °C) spectral regions corresponding to aromatic and imine protons of: (a) the dinuclear complex **3** after 10 min, (b) the dinuclear complex **3** after 29 h and (c) complex **1b**; a filled circle denotes resonances corresponding to the dinuclear species

The existence of an interconversion equilibrium between dinuclear and mononuclear species is also demonstrated by a ^{1}H NMR saturation transfer experiment. In fact, the selective irradiation of the resonance at $\delta = 6.16$, corresponding to the dinuclear species, produces saturation transfer at $\delta = 6.38$, corresponding to the resonance of the H_5 proton of the mononuclear species (Figure 4).

Thus, while in the solid state the ligand $(\mathbf{L^2})^{2-}$ is able to coordinate each chelating arm to a different metal centre to give a bridged dinuclear species, in solution it prefers to act as a tetradentate chelate to a single Ni^{II} ion, presumably in a *cis*-SP geometry; in fact, a space filling representation[9] of **1b** indicates that the spacer appears not to be long enough to make accessible to Ni^{II} ion the sterically preferred *trans*-SP coordination geometry. Moreover, molecular mechanics calculations[9] suggest that the system consisting of two mononuclear units of **1b** with the Ni^{II} ion adopting a *cis*-SP coordination geometry is more stable (ca. 4 kcal/mol in vacuo, ca. 9 kcal/mol in THF solution) than the calculated minimum-energy dinuclear structure, whose distances and angles are in good agreement with those found by X-ray analysis. These results indicate that the octamethylene bridging unit supplies the ligand $(\mathbf{L^2})^{2-}$ with optimal geometric requirements to easily wrap about the Ni^{II} ions to produce both mono- and dinuclear complexes with a small energetic difference, and that the solvation energy and crystal packing forces must play a fundamental role in the stabilisation of either species.

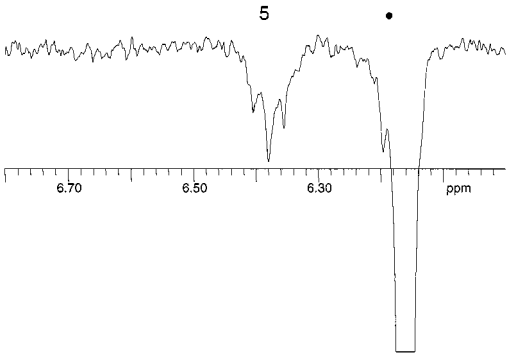

Figure 4. Saturation transfer difference spectrum (300 MHz, $CDCl_3$, 25 °C) of equilibrium mixture **3/1b** corresponding to the irradiation of the resonance at $\delta = 6.16$

Finally, it can be envisaged that structural modifications of the spacer (length and flexibility) and of the steric hindrance of the substituents on the imine nitrogen atoms, combined with the stereoelectronic preference of the metal ion, could easily modulate the coordination geometry of this new class of bis-bidentate ligands, in order to favour the self-assembly process of high-nuclearity species. Work along these lines is in progress.

Experimental Section

IR spectra were collected on a Perkin−Elmer Paragon 500 FTIR spectrophotometer and electronic absorption spectra with a Perkin−Elmer Lambda 9 spectrophotometer in chloroform; λ_{max} in nm and ε in $M^{-1}\,cm^{-1}$. ESI mass spectra were recorded on a PE Sciex API III plus triple quadrupole mass spectrometer equipped with an Atmospheric Pressure Ionization source and an articulated Ionspray interface. The sample was dissolved in chloroform (1 mg/mL) and diluted 1:100 with acetonitrile. Experimental conditions included: IS voltage, 5.5 kV; OR voltage, 90 V.

NMR measurements were performed on a Varian VXR-300 spectrometer in $CDCl_3$ as solvent; the temperature was controlled by the Varian control unit (±0.1 °C). ^{1}H NMR chemical shifts are referenced to TMS as external standard. The 2D NMR spectra were obtained by using standard sequences. The phase-sensitive ROESY spectra were acquired with a spectral width of 3000 Hz in 2 K data points using 8 scans for each of the 256 t_1 increments, with a mixing time ranging from 200−600 ms. A Gaussian function was applied for processing in both dimensions.

In the saturation transfer experiments, selective irradiation was applied for up to 2 s immediately prior to the observation pulse (with a 1-ms interval to allow for electronic recovery), and a total pulse interval of 3 s was used. The spectra were acquired in an interleaved fashion, first by saturating the resonance of interest and then by applying the decoupler significantly off-resonance. The difference spectra were obtained by subtracting the transformed off-resonance spectrum from the on-resonance spectrum.

Preparation of the Dialdehydes: To a solution of 2,3-dihydroxybenzaldehyde (6.5 g, 47 mmol) in anhydrous DMSO (100 mL) was added NaH (2.5 g, 104 mmol) under nitrogen. After stirring for 1 h at room temperature, 23 mmol of the appropriate dibromide was added and the resulting solution was allowed to stir for 24 h. The reaction mixture was poured into water (300 mL) and washed with chloroform. The aqueous layer was subsequently acidified with 6 M HCl and extracted with chloroform (3 × 50 mL). The combined chloroform extracts were dried over anhydrous Na_2SO_4, filtered, concentrated under reduced pressure, and methanol (20 mL) added. A colourless solid was obtained, which was filtered off and dried. Yields: from 60% to 65%.

1,4-Bis(3-formyl-2-hydroxy)phenoxybutane: m.p. 153−155 °C. − IR (Nujol): $\tilde{\nu}$ = 1646 cm^{-1} (C=O). − ^1H NMR ($CDCl_3$): δ = 11.07 (s, 2 H, OH), 9.93 (s, 2 H, CHO), 7.18−6.96 (m, 6 H, C_6H_3), 4.18 (t, 4 H, CH_2O), 2.11 [t, 4 H, $(CH_2)_2$]. − $C_{18}H_{18}O_6$ (330.33): calcd. C 65.45, H 5.49; found C 65.19, H 5.63.

1,8-Bis(3-formyl-2-hydroxy)phenoxyoctane: m.p. 116−119 °C. − IR (Nujol): $\tilde{\nu}$ = 1646 cm^{-1} (C=O). − ^1H NMR ($CDCl_3$): δ = 11.02 (s, 2 H, OH), 9.91 (s, 2 H, CHO), 7.18−6.96 (m, 6 H, C_6H_3), 4.04 (t, 4 H, CH_2O), 1.89−1.42 [m, 12 H, $(CH_2)_6$]. − $C_{22}H_{26}O_6$ (386.44): calcd. C 68.38, H 6.78; found C 68.89, H 7.10.

1,12-Bis(3-formyl-2-hydroxy)phenoxydodecane: m.p. 92 °C. − IR (Nujol): $\tilde{\nu}$ = 1646 cm^{-1} (C=O). − ^1H NMR ($CDCl_3$): δ = 11.03 (s, 2 H, OH), 9.94 (s, 2 H, CHO), 6.96−7.18 (m, 6 H, C_6H_3), 4.07 (t, 4 H, CH_2O), 1.89−1.31 [m, 20 H, $(CH_2)_{10}$]. − $C_{26}H_{34}O_6$ (442.55): calcd. C 70.56, H 7.74; found C 70.32, H 7.53.

Preparation of the Ligands H_2L^{1-3} and Their Ni^{II} Complexes: The Schiff bases were synthesised following standard procedures. A mixture of dialdehyde (2.2 mmol) and *n*-propylamine (12 mmol) in ethanol (20 mL) was heated to reflux for 2 h. After cooling, a yellow solid precipitated out on addition of water. Recrystallisation from $CHCl_3$/hexane afforded yellow crystalline material. Yields: 80−90%.

H_2L^1: m.p. 108−110 °C. − IR (Nujol): $\tilde{\nu}$ = 1628 cm^{-1} (C=N). − ^1H NMR ($CDCl_3$): δ = 14.19 (s, 2 H, OH), 8.33 (s, 2 H, CH=N), 6.99−6.74 (m, 6 H, C_6H_3), 4.16 (t, 4 H, CH_2O), 3.58 (t, 4 H, CH_2N), 2.16 [t, 4 H, $(CH_2)_2$], 1.74 (m, 4 H, CH_2), 1.01 (t, 6 H, CH_3). − $C_{24}H_{32}N_2O_4$ (412.52): calcd. C 69.88, H 7.82, N 6.79; found C 69.74, H 7.94, N 6.67. − UV/Vis: λ_{max} (10^{-3} ε) = 243 (sh) (17), 262 (23), 305 (sh) (4.1), 330 (5.4), 425 (0.92).

H_2L^2: m.p. 84−86 °C. − IR (Nujol): $\tilde{\nu}$ = 1627 cm^{-1} (C=N). − ^1H NMR ($CDCl_3$): δ = 14.22 (s, 2 H, OH), 8.33 (s, 2 H, CH=N), 6.95−6.74 (m, 6 H, C_6H_3), 4.04 (t, 4 H, CH_2O), 3.57 (t, 4 H, CH_2N), 1.92−1.44 (m, 16 H, CH_2), 1.00 (t, 6 H, CH_3). − $C_{28}H_{40}N_2O_4$ (468.63): calcd. C 71.76, H 8.60, N 5.98; found C 71.24, H 8.88, N 5.60. − UV/Vis: λ_{max} (10^{-3} ε) = 243 (sh) (18), 262 (25), 305 (sh) (4.6), 330 (5.8), 425 (1.0).

H_2L^3: m.p. 73−75 °C. − IR (Nujol): $\tilde{\nu}$ = 1629 cm^{-1} (C=N). − ^1H NMR ($CDCl_3$): δ = 14.19 (s, 2 H, OH), 8.32 (s, 2 H, CH=N), 6.95−6.74 (m, 6 H, C_6H_3), 4.04 (t, 4 H, CH_2O), 3.58 (t, 4 H, CH_2N), 1.95−1.31 (m, 24 H, CH_2), 1.00 (t, 6 H, CH_3). − $C_{32}H_{48}N_2O_4$ (524.74): calcd. C 73.25, H 9.22, N 5.34; found C 72.92, H 9.22, N 5.03. − UV/Vis: λ_{max} (10^{-3} ε) = 243 (sh) (19), 262 (26), 305 (sh) (4.8), 330 (6.0), 425 (1.0).

The reaction of H_2L^{1-3} with Ni^{II} acetate tetrahydrate in a 1:1 molar ratio in ethanol at room temperature gave light green solids. A solution of H_2L^{1-3} (2 mmol) in EtOH (20 mL) was added dropwise to a solution of $Ni(CH_3COO)_2{\cdot}4H_2O$ (2 mmol) in EtOH (20 mL). After stirring at room temperature for 2 h, green microcrystalline **1a**,**1b** and **1c,** respectively**,** were collected by filtration, washed with diethyl ether and dried in vacuo. Yields: 90%. The adduct **2** was obtained by addition of Et_2O to a pyridine solution of **1a.**

$[Ni_x(L^1)_x]$ (1a): m.p. >320 °C. − IR (Nujol): $\tilde{\nu}$ = 1612 cm^{-1} (C=N). − $C_{24}H_{30}N_2NiO_4$ (469.20): calcd. C 61.44, H 6.44, N 5.97; found C 61.57, H 6.70, N 5.42.

$[Ni_3(L^1)_3(py)_6]$ (2): m.p. 120−125 °C (dec.). − IR (Nujol): $\tilde{\nu}$ = 1617 cm^{-1} (C=N). − ESI-MS: *m*/*z* (%) = 413 (100) $[H_2L^1 + H]^+$, 469 (90) $[NiL^1 + H]^+$, 881 (50) $[Ni(L^1)_2 + 3H]^+$, 938 (traces) $[(NiL^1)_2 + H]^+$, 1426 (traces) $[(NiL^1)_3 + Na]^+$. − ^1H NMR ($CDCl_3$): δ = 9.16 (4 H, Py), 7.73 (2 H, Py), 7.45 (4 H, Py), 6.85 (2 H, Ph), 6.69 (2 H, Ph), 6.32 (2 H, Ph), 4.43 (2 H, CH=N), 3.87 (4 H, CH_2), 1.87 (8 H, CH_2), 1.60 (4 H, CH_2), 0.99 (6 H, CH_3). − $C_{102}H_{120}N_{12}Ni_3O_{12}$ (1872.2): calcd. C 65.09, H 6.43, N 8.93; found C 64.25, H 5.86, N 8.69 − UV/Vis: λ_{max} (10^{-3} ε) = 251 (141), 268 (156), 335 (26.7), 420 (12.6), 625 (0.26).

$[NiL^2]$ (1b): m.p. 190−192 °C ($CHCl_3$/hexanes). − IR (Nujol): $\tilde{\nu}$ = 1611 cm^{-1} (C=N). − ESI-MS: *m*/*z* (%) = 469 (25) $[H_2L^2 + H]^+$, 525 (100) $[NiL^2 + H]^+$, 1051 (traces) $[(NiL^2)_2 + H]^+$. − ^1H NMR ($CDCl_3$): δ = 7.96 (s, 2 H, CH=N), 6.71 (dd, 2 H, H_6), 6.63 (dd, 2 H, H_4), 6.38 (dd, 2 H, H_5), 3.82 (t, 4 H, CH_2O), 3.53 (t, 4 H, CH_2N), 1.95 (m, 4 H, CH_2CH_2N), 1.74 (m, 4 H, CH_2CH_2O), 1.42 (m, 4 H, $CH_2CH_2CH_2O$), 1.35 (m, 4 H, $CH_2CH_2CH_2CH_2O$), 1.00 (t, 6 H, CH_3). − $C_{28}H_{38}N_2NiO_4$ (525.31): calcd. C 64.02, H 7.29, N 5.33; found C 64.28, H 7.49, N 5.32. − UV/Vis: λ_{max} (10^{-3} ε) = 251 (43), 268 (51), 335 (8.9), 420 (4.2), 625 (0.12).

$[Ni_2(L^2)_2]{\cdot}THF$ (3): m.p. 134−135 °C (THF/Et_2O). − IR (Nujol): $\tilde{\nu}$ = 1611 cm^{-1} (C=N). − ESI-MS identical to that of **1b**. − ^1H NMR, see text. − $C_{56}H_{76}N_4Ni_2O_8{\cdot}C_4H_8O$ (1122.7): calcd. C 64.19, H 7.54, N 4.99; found C 64.45, H 7.87, N 4.73. − UV/Vis: λ_{max} and ε (calculated taking into account the concentration of the NiN_2O_2 unit) are identical to those of **1b**.

$[NiL^3]$ (1c): m.p. 120−122 °C ($CHCl_3$/hexanes). − IR (Nujol): $\tilde{\nu}$ = 1611 cm^{-1} (C=N). − ESI-MS: *m*/*z* (%) = 525 (100) $[H_2L^3 + H]^+$, 581 (95) $[NiL^3 + H]^+$, 1106 (traces) $[Ni(L^3)_2 + 3H]^+$, 1161 (traces) $[(NiL^3)_2 + H]^+$. − ^1H NMR ($CDCl_3$): δ = 7.59 (s, 2 H, CH=N), 6.71 (dd, 2 H, H_6), 6.62 (dd, 2 H, H_4), 6.38 (dd, 2 H, H_5), 3.81 (t, 4 H, CH_2O), 3.51 (t, 4 H, CH_2N), 1.96 (m, 4 H, CH_2CH_2N), 1.73 (m, 4 H, CH_2CH_2O), 1.41 (m, 4 H, $CH_2CH_2CH_2O$), 1.40−1.20 (m, 12 H, CH_2), 1.00 (t, 6 H, CH_3). − $C_{32}H_{46}N_2NiO_4$ (581.41): calcd. C 66.11, H 7.97, N 4.82; found C 66.16, H 8.25, N 4.66. − UV/Vis: λ_{max} (10^{-3} ε) = 251 (45), 268 (54), 335 (8.4), 420 (4.0), 625 (0.09).

X-ray Crystallographic Study: X-ray diffraction measurements were carried out with a Siemens P4 diffractometer equipped with graphite-monochromated Mo-K_α radiation (λ = 0.71073 Å). Compound **2**, green square-section needle-like crystals, in part hollow as square tubes, $C_{102}H_{120}N_{12}Ni_3O_{12}$; M = 1882.23; T = 293(2) K, monoclinic, space group $P2_1/c$ (No. 14); a = 9.078(4), b = 34.150(14), c = 32.815(9) Å, U = 10173(7) $Å^3$; Z = 4; μ = 0.613 mm^{-1}; crystal size (mm) 0.92 × 0.23 × 0.22. 12353 reflections collected, 9455 independent, R_{int} = 0.1514. The structure was solved by the automatic direct methods of the SIR97 programme.[10] The structure was refined by full-matrix least-squares methods with the SHELX97 program.[11] Owing to the relatively high internal R value, calculated on the equivalent reflections, anisotropic thermal factors were used only for Ni, N and O atoms. The hydrogen atoms were introduced in calculated positions and allowed to ride on the connected heavy atoms. Final reliability factors for 652 parameters,

refined with no restraints: R_1 = 0.1158 calculated for 4893 reflections with $I > 2\sigma(I)$, wR_2 = 0.2201 for all 9455 reflections in the refinement; *GOF* = 1.187.

Compound **3**, deep olive green prismatic crystals, $C_{60}H_{88}N_4Ni_2O_9$; M = 1126.76; T = 293(2) K, Orthorhombic, space group $Pna2_1$ (No. 33); a = 14.813(2), b = 21.540(2), c = 18.277(2) Å, U = 5831.7(11) Å^3; Z = 4; μ = 0.703 mm^{-1}; crystal size (mm) 0.58 × 0.38 × 0.19. 4911 reflections collected, 4245 independent, R_{int} = 0.0282. The structure was solved by standard automatic direct methods and refined by least-squares methods. Abnormally high values of thermal factors and inconsistent geometry revealed a conformational disorder in two of the terminal propyl groups and in the clathrated THF. The two propyl groups were refined as distributed in two different conformations with a constrained geometry, while the THF molecule was refined with a fixed conformation taken from a well-refined structure in the literature.[11] At the end of the refinement, residual peaks and holes of 0.403 and −0.339 e·Å^{-3} were present around the disordered solvent molecule of the difference Fourier map. The solution and constrained refinement were done by means of the SHELX97 programme.[12] Final reliability factors for 632 parameters, refined with five restraints: R_1 = 0.0583 calculated for 3020 reflections with $I > 2\sigma(I)$, wR_2 = 0.0904 for all 4245 reflections in the refinement; *GOF* = 1.023.

Crystallographic data (excluding structure factors) for the structures reported in this paper have been deposited with the Cambridge Crystallographic Data Centre as supplementary publication no. CCDC-147138 (**2**) and -147139 (**3**). Copies of the data can be obtained free of charge on application to CCDC, 12 Union Road, Cambridge CB2 1EZ, UK [Fax: (internat.) + 44-1223/336-033; E-mail: deposit@ccdc.cam.ac.uk].

Acknowledgments

We thank Professor F. Calderazzo for helpful discussions. Financial support from Ministero dell'Università e della Ricerca Scientifica (MURST) and Consiglio Nazionale delle Ricerche (CNR) is acknowledged.

[1] J.-M. Lehn, *Supramolecolar Chemistry, Concepts and Perspectives*, VCH, Weinheim, **1995**; F. Vögtle, *Supramolecular Chemistry*, John Wiley & Sons, Chichester, **1991**.

[2] Reviews and very recent references: C. Piguet, G. Bernardinelli, G. Hopfgartner, *Chem. Rev.* **1997**, 97, 2005−2062; E. C. Constable, *Prog. Inorg. Chem.* **1994**, 42, 67−138; P. J. Stang, *Chem. Eur. J.* **1998**, 4, 19−27; A. von Zelewsky, O. Mamula, *J. Chem. Soc., Dalton Trans.* **2000**, 219−231; G. Baum, E. C. Constable, D. Fenske, C. E. Housecroft, T. Kulke, *Chem. Eur. J.* **1999**, 5, 1862−1873; G. Baum, E. C. Constable, D. Fenske, C. E. Housecroft, T. Kulke, M. Neuburger, M. Zehnder, *J. Chem. Soc., Dalton Trans.* **2000**, 945−959; M. J. Hannon, S. Bunce, A. J. Clarke, N. W. Alcock, *Angew. Chem. Int. Ed.* **1999**, 38, 1277−1278; M.-H. Shu, W.-Y. Sun, C.-Y. Duan, Y.-J. Fu, W.-J. Zhang, W.-X. Tang, *J. Chem. Soc., Dalton Trans.* **1999**, 729−734; N. K Solanki, A. E. H. Wheatley, S. Radojevic, M. McPartlin, M. A. Halcrow, *J. Chem. Soc., Dalton Trans.* **1999**, 521−523; M. Greenwald, D. Wessely, E. Katz, I. Willner, Y. Cohen, *J. Org. Chem.* **2000**, 65, 1050−1058; Y. Zhang, L. Jianmin, M. Nishiura, H. Hou, W. Deng, T. Imamoto, *J. Chem. Soc., Dalton Trans.* **2000**, 293−297; R. L. Paul, S. M. Couchman, J. C. Jeffery, J. A. McCleverty, Z. R. Reeves, M. D. Ward, *J. Chem. Soc., Dalton Trans.* **2000**, 845−851.

[3] J. Rojo, J.-M. Lehn, G. Baum, D. Fenske, O. Waldmann, P. Müller, *Eur. J. Inorg. Chem.* **1999**, 517−522; J. Rojo, F. Romero-Salguero, J.-M. Lehn, G. Baum, D. Fenske, *Eur. J. Inorg. Chem.* **1999**, 1421−1428; A. M. Garcia, F. J. Romero-Salguero, D. M. Bassani, J.-M. Lehn, G. Baum, D. Fenske, *Chem. Eur. J.* **1999**, 5, 1803−1808.

[4] N. Matsumoto, Y. Motoda, T. Matsuo, T. Nakashima, N. Re, F. Dahan. J.-P. Tuchagues, *Inorg. Chem.* **1999**, 38, 1165−1173; K. Yamanari, I. Fukuda, Y. Kushi, A. Fuyuhiro, N. Kubota, T. Fukuo, R. Arakawa, *Inorg. Chem.* **1998**, 37, 5611−5618; M. J. Hannon, C. L. Painting, W. Errington, *Chem. Commun.* **1997**, 307−308; C. M. Hartshorn, P. Steel, *Chem. Commun.* **1997**, 541−542; P. L. Jones, K. J. Byrom, J. C. Jeffery, J. A. McCleverty, M. D. Ward, *Chem. Commun.* **1997**, 1361−1362; G. R. Newkome, T. J. Cho, C. N. Moorefield, G. R. Baker. R. Cush, P. S. Russo, *Angew. Chem. Int. Ed.* **1999**, 38, 3717−3721; A. Neels, H. Stoeckli-Evans, *Inorg. Chem.* **1999**, 38, 6164−6170; B.-L. Fei, W.-Y. Sun, K.-B. Yu, W.-X. Tang, *J. Chem. Soc., Dalton Trans.* **2000**, 805−811; X.-H. Bu, H. Morishita, K. Tanaka, K. Biradha, S. Furusho, M. Shiiionoya, *Chem. Commun.* **2000**, 971−972.

[5] N. Yoshida, H. Oshio, T. Ito, *J. Chem. Soc., Perkin Trans. 2* **1999**, 975−983 and references therein; N. Yoshida, K. Ichikawa, M. Shiro, *J. Chem. Soc., Perkin Trans. 2* **2000**, 17−26 and references therein; B. J. McNelis, L. C. Nathan, C. J. Clark, *J. Chem. Soc., Dalton Trans.* **1999**, 1831−1834; K. L. V. Mann, J. C. Jeffery, J. A. McCleverty, M. D. Ward, *J. Chem. Soc., Dalton Trans.* **1998**, 3029−3035 and references therein; A. G. J. Ligtenbarg, E. K. van den Beuken, A. Meetsma, N. Veldman, W. J. J. Smeets, A. L. Spek, B. L. Feringa, *J. Chem. Soc., Dalton Trans.* **1998**, 263−270; C. Provent, P. Chautemps, G. Gellon, J.-L. Pierre, *Bull. Soc. Chim. Fr.* **1997**, 134, 487−493.

[6] V. Kessar, Y. P. Gupta, T. Mohammed, K. Sawal, *J. Chem. Soc., Chem. Commun.* **1983**, 400−401.

[7] Recently, D. Datta and co-workers have described the preparation of a dinuclear diamagnetic Ni^{II}−N4 complex, for which molecular mechanics calculations suggest the existence of a minimum-energy double-stranded helical structure (M. Zimmer, D. A. Tocher, G. K. Patra, J. P. Naskar, D. Datta, *Indian J. Chem.* **1999**, 38A, 1087−1091).

[8] R. Knoch, H. Elias, H. Paulus, *Inorg. Chem.* **1995**, 34, 4032−4040.

[9] All calculations were performed with GAUSSIAN (GAUSSIAN 99, Revision A.10, Gaussian Inc., Pittsburg PA, 1998) using the UFF force field and the PCM model of solvation (J. Tomasi, M. Persico, *Chem. Rev.* **1994**, 94, 2027−2094).

[10] A. Altomare, M. C. Burla, M. Camalli, G. L. Cascarano, C. Giacovazzo, A. Guagliardi, A. G. G. Molitemi, G. Polidori, R. Spagna, *J. Appl. Crys.* **1999**, 32, 115−119.

[11] A. Klauck, K. Seppelt, *Angew. Chem. Int. Ed. Engl*, **1994**, *33*, 93.

[12] G. M. Sheldrick, SHELXL97, A FORTRAN program for the solution and refinement of X-ray structures, University of Göttingen, **1997**.

Received July 24, 2000
[I00288]

$(C_7H_{13}N_2)_3Al$ – The First Tris(diketiminato)metal Complex[‡]

Norbert Kuhn,*[a] Stefan Fuchs,[a] and Manfred Steimann[a]

Dedicated to Professor Max Schmidt on the occasion of his 75th birthday

Keywords: Aluminum / Chelates / N ligands / Vinamidines / Coordination chemistry

The stable tris(diketiminato)metal complex $(C_7H_{13}N_2)_3Al$ (**4**) is obtained from $Me_3N{\cdot}AlH_3$ and the vinamidine $C_7H_{14}N_2$ (**1**). The X-ray structure analysis of the complex **4** reveals a distorted octahedral coordination of the nitrogen atoms at the aluminum centre.

Introduction

(β-Diketiminato)metal complexes of main group[1–12] and transition[13–18] elements, including compounds of the types $VinMX_2$, $VinMX_3$ and Vin_2M (Vin = η^2-diketiminato), have drawn increasing interest in the past years. In contrast to their ketiminato and diketonato analogues, complexes of the type Vin_3M are unknown, as yet. In the course of our investigations on vinamidine[19,20] aluminum chelates[1,2,21,22] we have tried to fill this gap, and present now the first tris(diketiminato)metal complex.

Results and Discussion

The title compound **4** is obtained from the vinamidine **1**[23] and $Me_3N{\cdot}AlH_3$ as colourless crystals in moderate yield, the isolable alane **2**[21] being the intermediate (Scheme 1). The compound is also formed by reacting the cationic complex **3**[22] (X = Cl, Br) with alkali metal vinamidinates, as confirmed by NMR spectroscopy.

The X-ray structure analysis of **4** (Figure 1) reveals a distorted octahedral coordination geometry at the metal centre. Owing to the increased coordination number, the geometry of the VinAl fragments exhibits a significant difference to that found for **2** and **3** (X = BPh_4) due to a lengthening of the Al–N bonds and a decrease in the N–Al–N bond angles [Al–N 2.002(18) to 2.0626(17) Å, N–Al–N 86.19(7) to 91.39(7) °]. There is no indication of steric overcrowding, for example by distortion of the near planar ring fragments or by unusual lengthening of bonds.

The NMR spectroscopic data of **4** are in the expected range (see Exp. Sect.). The ^{27}Al NMR signal (δ = 15.5) is shifted to high field in relation to **2**[21] and **3**;[22] this is caused by the increase of the coordination number at the metal centre.[24,25] Although it is present as its molecular ion in the mass spectrum (EI), we have not succeeded in subliming this compound without decomposition. As expected, compound **4** is less sensitive towards nucleophilic attack (e.g. towards hydrolysis) than **3**, apparently due to its lower charge density.

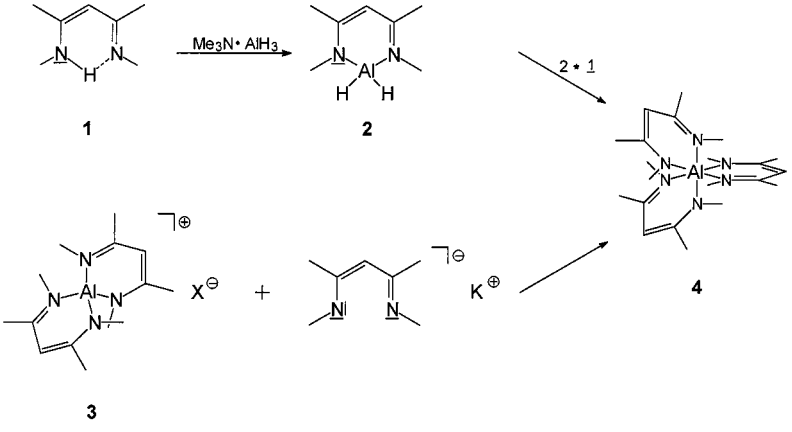

Scheme 1

There are only a moderate number of examples involving a sixfold nitrogen coordination at Al. Apparently, these

[‡] Vinamidines, 9. – Part 8: Ref.[22]

[a] Institut für Anorganische Chemie der Universität Tübingen, Auf der Morgenstelle 18, 72076 Tübingen, Germany
Fax: (internat.) +49-7071/295-306
E-mail: kuhn@uni-tuebingen.de

 © WILEY-VCH Verlag GmbH, 69451 Weinheim, 2001 1434–1948/01/0202–0359 $ 17.50+.50/0

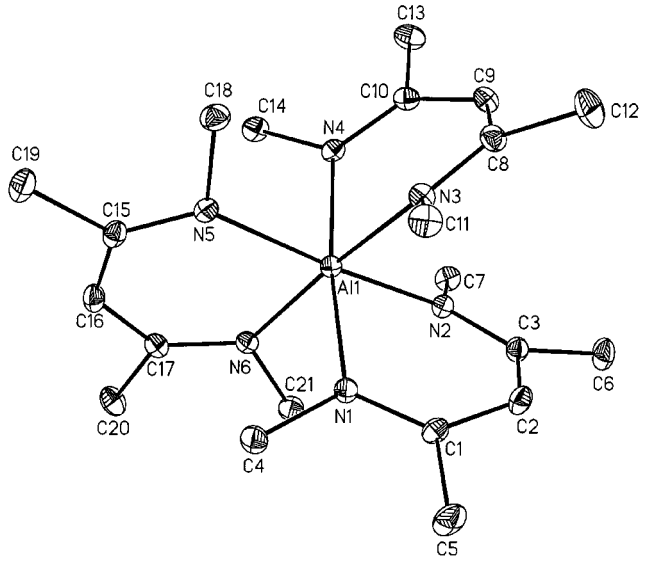

Figure 1. View of $C_{21}H_{39}AlN_6$ (**4**) in the crystal lattice; selected bond lengths (Å) and angles (°): Al(1)−N(1) 2.0011(18), Al(1)−N(2) 2.0275(18), Al(1)−N(3) 2.0232(17), Al(1)−N(4) 2.0002(18), Al(1)−N(5) 2.0552(18), Al(1)−N(6) 2.0626(17), N(1)−C(1) 1.328(3), C(1)−C(2) 1.400(3), C(2)−C(3) 1.404(3), C(3)−N(2) 1.319(3), N(3)−C(8) 1.327(3), C(8)−C(9) 1.402(3), C(9)−C(10) 1.402(3), C(10)−N(4) 1.327(3), N(5)−C(15) 1.326(3), C(15)−C(16) 1.398(3), C(16)−C(17) 1.399(3), C(17)−N(6) 1.330(2); N(1)−Al(1)−N(2) 87.82(7), N(3)−Al(1)−N(4) 87.39(7), N(5)−Al(1)−N(6) 88.84(7), N(1)−Al(1)−N(4) 173.18(7), N(2)−Al(1)−N(5) 173.79(7), N(3)−Al(1)−N(6) 173.73(7), Al(1)−N(1)−C(1) 123.14(13), N(1)−C(1)−C(2) 122.62(18), C(1)−C(2)−C(3) 125.59(18), C(2)−C(3)−N(2) 123.03(17), C(3)−N(2)−Al(1) 122.24(13), Al(1)−N(3)−C(8) 121.60(13), N(3)−C(8)−C(9) 122.81(18), C(8)−C(9)−C(10) 125.36(18), C(9)−C(10)−N(4) 122.66(18), C(10)−N(4)−Al(1) 123.12(13), Al(1)−N(5)−C(15) 127.64(14), N(5)−C(15)−C(16) 124.20(18), C(15)−C(16)−C(17) 127.77(18), C(16)−C(17)−N(6) 124.03(18), C(17)−N(6)−Al(1) 127.44(14)

compounds are stabilised by the low steric demand of the ligands (see, for example, $[Al(NH_3)_6]^{3+}$,[26] $[Al(MeCN)_6]^{3+}$,[27,28] $[Al(N_3)_3py_3]$[29]) and by chelate effects as observed for pyrazolylborato,[30] amidinato[31] and triazenido[32−34] complexes. In addition, some cage compounds are known.[35−38]

In summary, the surprising absence of Vin_3M complexes from the literature in the case of the *N*-methylated ligand may be a consequence of synthetic reasons rather than low stability. In fact, we have not been able to prepare **4** starting from aluminum halides and vinamidines or their alkali metal derivatives, as yet. We are continuing our efforts to find a general route, especially to transition metal Vin_3M complexes, which are of interest as chiral counterparts of the well-known diketonato complexes $(acac)_3M$.[39]

Experimental Section

General Remarks: All synthetic experiments were routinely carried out in purified solvents under argon. *N*-methyl-4-(methylimino)-2-penten-2-amine (**1**)[23] and $Me_3N{\cdot}AlH_3$ [40] were prepared according to published procedures. NMR: Bruker AC 250; MS: Finnigan MAT 311A; X-ray: Siemens P4.

Preparation of Tris{η²-*N*-methyl-4-(methylimino)-2-penten-2-aminato}alane (4): A solution of $Me_3N{\cdot}AlH_3$ (0.18 g, 2.0 mmol) in toluene (10 mL) was added slowly to a solution of **1** (0.76 g, 6.0 mmol) in toluene (20 mL). After stirring for 24 h, the solvent was removed in vacuo and the residue dissolved again in 20 mL toluene. The filtered solution was evaporated to dryness and the remaining solid recrystallised from toluene/pentane to give **4** (0.32 g, 40%) as colourless crystals. − ^{1}H NMR ([D$_6$]benzene): δ = 1.81 (s, 18 H, 4,6-Me), 2.79 (s, 18 H, 1,3-Me), 4.63 (s, 3 H, 5-H). − ^{13}C NMR ([D$_6$]benzene): δ = 22.6 (4,6-Me), 37.1 (1,3-Me), 95.1 (C5), 166.4 (C4,6). − ^{27}Al NMR ([D$_6$]benzene, $[Al(H_2O)_6]^{3+}$ ext.): δ = 15.5. − MS (EI, 70 eV, Vin = $C_7H_{13}N_2$): *m*/*z* (%) = 401 (5) [M^+ − H], 277 (20) [M^+ − Vin], 126 (70) [Vin^+], 111 (78) [Vin^+ − Me], 96 (100) [Vin^+ − 2Me] and further fragments. − $C_{21}H_{39}AlN_6$ (402.56): calcd. C 62.66, H 9.76 N 20.88; found C 62.27, H 10.04, N 20.49.

X-ray Crystallographic Study: $C_{21}H_{39}AlN_6$, triclinic, M = 402.56 g cm^{-3}, space group = $P\bar{1}$ (No. 2), T = 293 K, Mo-K_α, a = 8.687(2), b = 8.904(3), c = 17.004(2) Å, α = 87.314(19), β = 78.230(17), γ = 63.99(2) °, Z = 2, D = 1.157 g cm^{-3}, μ = 0.106 mm^{-1}, crystal size 0.25 × 0.25 × 0.35 mm^3, θ range for data collection 2.45 to 27.50°, 8048 reflections collected, 5227 independent reflections [R(int) = 0.0363], direct methods, no adsorption correction; final R indices [$I > 2\sigma(I)$]: $R1(wR2)$ = 0.0496 (0.1268); R indices (all data): $R1(wR2)$ = 0.0748 (0.1488); GooF = 1.911. Hydrogen atoms calculated, not refined. − Crystallographic data (excluding structure factors) for the structure reported in this paper have been deposited with the Cambridge Crystallographic Data Centre as supplementary publication no. CCDC-151144. Copies of the data can be obtained free of charge on application to CCDC, 12 Union Road, Cambridge CB2 1EZ, UK [Fax: (internat.) +44-1223/336-033; E-mail: deposit@ccdc.cam.ac.uk].

Acknowledgments

This work was generously supported by the Deutsche Forschungsgemeinschaft and the Fonds der Chemischen Industrie. We acknowledge Professor R. Boese (Essen) for helpful discussions.

[1] N. Kuhn, A. Kuhn, M. Speis, D. Bläser, R. Boese, *Chem. Ber.* **1990**, *123*, 1301.
[2] N. Kuhn, J. Fahl, S. Fuchs, M. Steimann, G. Henkel, *Z. Anorg. Allg. Chem.* **1999**, *625*, 2108.
[3] N. Kuhn, M. Speis, *Inorg. Chim. Acta* **1988**, *145*, 5.
[4] N. Kuhn, A. Kuhn, R. Boese, N. Augart, *J. Chem. Soc., Chem. Commun.* **1989**, 975.
[5] N. Kuhn, A. Kuhn, J. Lewandowski, M. Speis, *Chem. Ber.* **1991**, *124*, 997.
[6] B. Quian, D. L. Ward, M. R. Smith, III, *Organometallics* **1998**, *17*, 3070.
[7] C. E. Radzewich, M. P. Coles, R. F. Jordan, *J. Am. Chem. Soc.* **1998**, *120*, 9384.
[8] C. E. Radzewich, I. A. Guzei, R. F. Jordan, *J. Am. Chem. Soc.* **1999**, *121*, 8673.
[9] F. Cosledan, P. B. Hitchcock, M. F. Lappert, *Chem. Commun.* **1999**, 705.
[10] M. R. Kopp, B. Neumüller, *Z. Anorg. Allg. Chem.* **1999**, *625*, 739.
[11] C. Cui, H. W. Roesky, H. Hao, H.-G. Schmidt, M. Noltemeyer, *Angew. Chem. Int. Ed.* **2000**, *39*, 1815.
[12] P. J. Bailey, C. M. E. Dick, S. Fabre, S. Parsons, *J. Chem. Soc., Dalton Trans.* **2000**, 1655.
[13] J. E. Parks, R. H. Holm, *Inorg. Chem.* **1968**, *7*, 1408.
[14] R. Knorr, A. Weiß, *J. Chem. Soc., Chem. Commun.* **1977**, 173.
[15] R. Uhrhammer, D. G. Black, T. G. Gardner, J. D. Olsen, R. F. Jordan, *J. Am. Chem. Soc.* **1993**, *115*, 8493.

[16] P. B. Hitchcock, M. F. Lappert, D.-S. Liu, *J. Chem. Soc., Chem. Commun.* **1994**, 2637.
[17] L. Kakaliou, W. J. Scanlon, IV, B. Quian, S. W. Baek, M. R. Smith, III, D. H. Morty, *Inorg. Chem.* **1999**, *38*, 5964.
[18] R. Vollmerhaus, M. Rahim, R. Tomaszewski, S. Xin, N. J. Taylor, S. Collins, *Organometallics* **2000**, *19*, 2161.
[19] D. Lloyd, H. McNab, *Angew. Chem. Int. Ed. Engl.* **1976**, *15*, 459.
[20] D. Lloyd, H. McNab, *Advances in Heterocyclic Chemistry* **1993**, *56*, 1.
[21] N. Kuhn, S. Fuchs, M. Steimann, *Z. Anorg. Allg. Chem.* **2000**, *626*, 1387.
[22] N. Kuhn, S. Fuchs, C. Maichle-Mößmer, E. Niquet, *Z. Anorg. Allg. Chem.* **2000**, *626*, 2248.
[23] S. G. McGeachin, *Can. J. Chem.* **1968**, *46*, 1903.
[24] R. Benn, A. Rufinska, H. Lehmkuhl, E. Janssen, C. Krüger, *Angew. Chem. Int. Ed. Engl.* **1983**, *22*, 779.
[25] J. W. Akitt, *Progress in NMR Spectroscopy* **1989**, *21*, 1.
[26] D. Peters, J. Bock, H. Jacobs, *J. Less Common Met.* **1989**, *154*, 243.
[27] E. Babian-Kibala, Hong Chen, F. A. Cotton, L. M. Daniels, L. R. Falvello, G. Schmid, Z. Yao, *Inorg. Chim. Acta* **1996**, *250*, 359.
[28] F. Favier, J. L. Pascal, C. Belin, M. Tillard-Carbonnel, *Acta Crystallogr.* **1997**, *53C*, 1234.
[29] R. A. Fischer, A. Miehr, H. Sussek, H. Pritzkow, E. Herdtweck, J. Müller, O. Ambacher, T. Metzger, *Chem. Commun.* **1996**, 2685.
[30] D. J. Darensbourg, E. L. Maynard, M. W. Holtcamp, K. K. Klausmeyer, J. H. Reibenspies, *Inorg. Chem.* **1996**, *35*, 2682.
[31] L. M. Engelhardt, M. G. Gardiner, C. Jones, P. C. Junk, C. L. Raston, A. H. White, *J. Chem. Soc., Dalton Trans.* **1996**, 3053.
[32] J. T. Leman, A. R. Barron, J. W. Ziller, R. M. Kren, *Polyhedron* **1989**, *8*, 1909.
[33] J. T. Leman, J. Braddock-Wilking, A. J. Coolong, A. R. Barron, *Inorg. Chem.* **1993**, *32*, 4324.
[34] J. Braddock-Wilking, J. T. Leman, C. T. Farrar, S. C. Larsen, D. J. Singel, A. R. Barron, *J. Am. Chem. Soc.* **1995**, *117*, 1736.
[35] J. F. Janik, E. N. Duesler, R. T. Paine, *Inorg. Chem.* **1988**, *27*, 4335.
[36] F. Moise, W. T. Pennington, G. H. Robinson, *J. Coord. Chem.* **1991**, *24*, 93.
[37] Z. Jiang, L. V. Interrante, D. Kwon, F. S. Tham, R. Kullnig, *Inorg. Chem.* **1992**, *31*, 4815.
[38] M.-D. Li, C.-C. Chang, S.-T. Liu, G.-H. Lee, Y. Wang, S.-M. Peng, *Organometallics* **1994**, *13*, 1504.
[39] R. C. Mehrotra, R. Bohra, D. P. Gaur, *Metal β-Diketonates and Allied Derivatives*, Academic Press, London, **1978**.
[40] R. A. Kovar, J. O. Callaway, *Inorg. Synth.* **1977**, *17*, 36.

Received September 20, 2000
[I00354]

Versatility of the Nature of the Magnetic Gadolinium(III)−Vanadium(IV) Interaction − Structure and Magnetic Properties of Two Heterobinuclear [Gd, V(O)] Complexes

Jean-Pierre Costes,*[a] Françoise Dahan,[a] Bruno Donnadieu,[a] Javier Garcia-Tojal,[a] and Jean-Pierre Laurent[a]

Keywords: Schiff bases / Vanadium / Lanthanides / Magnetic properties

It has been known for a long time that the magnetic exchange interaction between copper and gadolinium ions is always ferromagnetic. Very recently, three exceptions to this general trend were revealed. They involve complexes associating a gadolinium(III) ion with a copper(II) ion or with radicals of the nitroxide or semiquinone types. We want to show that this trend is more general than expected, for such a behavior can also be observed in heterobinuclear vanadyl-gadolinium complexes.

Introduction

The interest given to magnetic interactions between rare earth ions and other types of spin carriers has been focused mainly on gadolinium(III) derivatives containing free radicals[1−4] or copper(II)[5−11] complexes. Very few examples involving nickel(II), cobalt(II), iron(III) and vanadium(IV)[12] ions have been reported. In all these species the interaction between gadolinium(III) and the other paramagnetic center was found to be ferromagnetic. Recently three exceptions to this general trend were revealed; they involve radicals of the nitroxide and semiquinone types[13,14] and a copper(II) complex.[15] Preliminary studies show that an antiferromagnetic behavior is also observed in new trinuclear(Gd, Cu_2) complexes. In search of original examples of antiferromagnetic coupling we have considered the systems consisting of the gadolinium(III) and vanadium(IV) ions and several ligands H_2L^i derived from 2-hydroxy-3-methoxybenzaldehyde.

Results and Discussion

In two instances we succeeded in obtaining well-defined, crystalline complexes by very slow and careful addition of the suitable mononuclear precursors $L^iV(O)$ to $Gd(NO_3)_3{\cdot}6H_2O$, in acetone.[16] Chemical analysis data lead to the following formulae: $[L^1V(O)Gd(H_2O)(NO_3)_3]{\cdot}H_2O$ (**1**) and $[L^2V(O)\{(CH_3)_2CO\}Gd(NO_3)_3]$ (**2**) [H_2L^1 and H_2L^2 stand for *N*,*N*′bis(3-methoxysalicylidene)-1,2-diamino-2-methylpropane and *N*,*N*′-bis(3-methoxysalicylidene)-1,3-diamino-2,2′-dimethyl-propane, respectively].

The heterobinuclear nature of **1** and **2** is supported by the molecular structures[17] shown in Figure 1 and 2. In each compound the metallic ions are doubly bridged by two phenolato oxygen atoms [O(1) and O(2)] of the ligand L^i. The most pertinent difference between the two complexes concerns the GdO_2V bridging core, which is almost planar in **1** with a dihedral angle α between the [O(1)−Gd−O(2)] and [O(1)−V−O(2)] planes of 3.5(7)°, while in compound **2** the value is 20.7(l)°. The related Gd···V separations are equal to 3.5191(5) and 3.5043(4) Å in **1** and **2**, respectively. In both compounds, gadolinium(III) is decacoordinated, although in **2** the coordination sphere comprises four oxygens from L^2 and six from three chelating NO_3, while in **1** one chelating NO_3 is replaced by one monodentate (NO_3) and a water molecule. This water molecule is involved in a hydrogen bonding network through an uncoordinated H_2O and a bound NO_3. Nevertheless, the intermolecular Gd···Gd distance is large [7.7512(2) Å] and slightly shorter than in **2** [8.3816(4) Å], where hydrogen bonds are absent. The vanadium(IV) ion is pentacoordinated in **1** and hexacoordinated in **2** due to the presence of an additional acetone molecule which is loosely bound in an axial position. The vanadium-oxo bond has the same length in both complexes, while the basal bonds are slightly shorter in **1** than in **2**. The metal ions are displaced from the mean basal planes by 0.6183(5) and 0.3418(4) Å in **1** and **2**, respectively. All the intermolecular metal contacts are large (≥7.47 Å) with the exception of a V···V separation of 5.7665(7) Å in **2**. The analogous value in **1** is 7.475(l) Å. However, the lack of bridging pathway between the two V^{IV} ions militates against the possibility of a discernible interaction. Finally, the magnetic data for both complexes may be analyzed on the basis of isolated binuclear species.

From our previous work,[12a] compound **1** has a ferromagnetic ($S_T = 4$) ground state with a coupling constant J of 1.5 cm^{-1}. As for **2**, the profile of the $\chi_M T$ vs. T curve (Figure 3) differs significantly from that of **1** and suggests an antiferromagnetic ($S_T = 3$) ground state. In the 2−300 K

[a] Laboratoire de Chimie de Coordination du CNRS, UPR 8241, liée par conventions à l'Université Paul Sabatier et à l'Institut National Polytechnique de Toulouse,
205 route de Narbonne, 31077 Toulouse Cedex, France
Fax: (internat.) + 33-5/61553003
E-mail: costes@lcc-toulouse.fr

 © WILEY-VCH Verlag GmbH, 69451 Weinheim, 2001 1434−1948/01/0202−0363 $ 17.50+.50/0

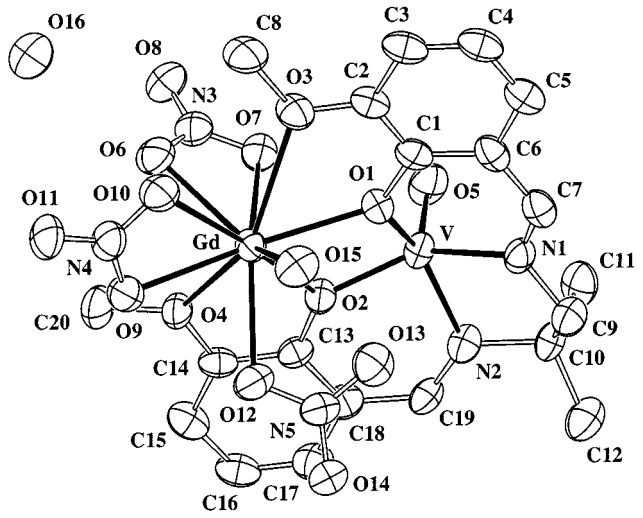

Figure 1. Zortep drawing of **1** with thermal ellipsoids at the 50% probability level; hydrogen atoms are omitted; selected bond lengths [Å] and angles [°]: V−O(l) 1.942(2), V−O(2) 1.937(2), V−O(5) 1.588(3), Gd−O(1) 2.376(2), Gd−O(2) 2.424(2), O(l)−V−O(2) 80.82(9), O(l)−Gd−O(2) 63.19(7), Gd−O(1)−V 108.76(9), Gd−O(2)−V 107.08(9), V···Gd 3.5191(5)

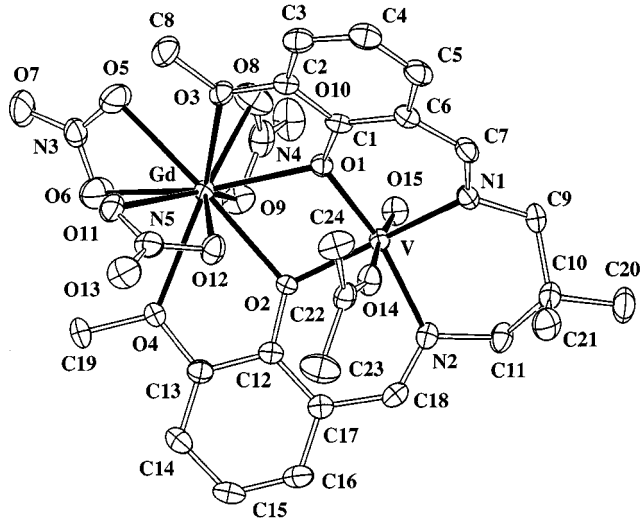

Figure 2. Zortep drawing of **2** with thermal ellipsoids at the 50% probability level; hydrogen atoms are omitted; selected bond lengths [Å] and angles [°]: V−O(l) 1.988(2), V−O(2) 1.986(1), V−O(15) 1.588(2), Gd−O(l) 2.405(2), Gd−O(2) 2.414(2), O(1)−V−O(2) 80.25(6), O(1)−Gd−O(2) 64.20(5), Gd−O(l)−V 105.42(6), Gd−O(2)−V 105.14(6), V···Gd 3.5043(4)

range, fitting the experimental data to the expression[18] derived from the Hamiltonian $H = -JS_{Gd}\cdot S_V$ yields $J = -2.6$ cm^{-1}, $g_{Gd} = 2.0$ and $g_V = 2.1$, the agreement factor R $[(\chi_M T_{calcd.} - \chi_M T_{obs})^2/(\chi_M T_{obs})^2]$ being equal to 3.8×10^{-5}. There is no sign of secondary effects (intermolecular coupling, zero field splitting, ...). The nature of the ground state is definitely substantiated by field-dependent magnetization measurements. Up to 5×10^4 G, the data comply with the values calculated from the Brillouin function for an $S_T = 3$, $g = 2.1$ spin system.

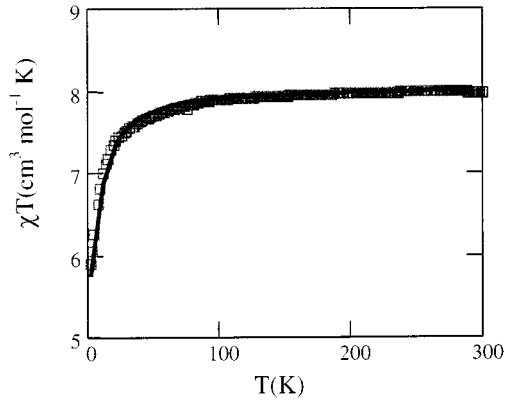

Figure 3. Plot of $\chi_M T$ vs. T for **2** (1000 G); the solid line represents the best data fit

Finally, the present work shows that the magnetic changeability which has so far been observed for (Gd, radical)[13,14] and (Gd, Cu)[15] complexes is also a property of the [Gd, V(O)] compounds. In the two series of bimetallic complexes, a lengthening of the diimino chain of the ligand (from N−C−C−N to N−C−C−C−N) is responsible for a spin-state reversal (from $S = 4$ to $S = 3$). Concurrently there is a significant increase in the bending of the bridging core. The present data reinforce the suggestion[13−15] that the nature and magnitude of the (Gd, M) [M = organic radical, copper(II), vanadium(IV)] interactions result from a sensitive balance between two opposite contributions. The available interaction models[7,18−21] stress the importance of charge transfer (CT) excited states in stabilizing selectively either a low-spin or a high-spin state. The former case corresponds to a CT between two singly occupied orbitals (from $3d_{Cu}$ or $3d_{VO}$ to $4f_{Gd}$) while the second originates from a CT from a singly occupied orbital ($3d_{Cu}$ or $3d_{VO}$) to an empty orbital ($6s_{Gd}$ or more probably $5d_{Gd}$) . These CT-based mechanisms do not seemingly conflict with the observation that the spin states of the binuclear complexes are little affected by the symmetry change of the magnetic orbitals of the second spin carrier (d_{xy} vs. $d_{x^2-y^2}$ type) but are significantly dependent on the planarity of the bridging network.

Experimental Section

Starting materials were purchased from Acros and Aldrich (*o*-vanillin, 1,3-diamino-2,2′-dimethylpropane, 1,2-diamino-2-methylpropane, vanadyl sulfate and gadolinium nitrate hexahydrate), and used without further purification. The compounds were synthesized as follows.

Vanadyl Complexes: The monomeric vanadyl entities were prepared by addition of an aqueous solution of vanadyl sulfate (10 mmol, 1.63 g) to a mixture of *o*-vanillin (20 mmol, 3.04 g) and the corresponding diamine (10 mmol; 0.88 and 1.02 g, for **1** and **2** respectively) in boiling methanol. The precipitates were filtered off, washed with methanol and diethyl ether, and dried under vacuum.

$L^1VO(H_2O)$: Moss green powder, yield 52%. − $C_{20}H_{24}N_2O_6V$ (439.36): calcd. C 54.7, H 5.5, N 6.4; found C 54.5, H 5.3, N 6.0.

− Selected IR bands: $\tilde{\nu}$ = 3481, 2930, 1617, 1552, 1470, 1443, 1401, 1297, 1248, 1225, 1083, 975, 855, 748, 734 cm^{-1}.

$L^2VO(H_2O)$: Light green powder, yield 58%. − $C_{21}H_{26}N_2O_6V$ (453.39): calcd. C 55.6, H 5.8, N 6.2; found C 55.5, H 5.9, N 6.1. − Selected IR bands: $\tilde{\nu}$ = 3435, 2954, 1652, 1618, 1555, 1471, 1453, 1432, 1412, 1392, 1326, 1297, 1248, 1224, 1086, 1066, 958, 859, 733 cm^{-1}.

Vanadyl-Gadolinium Complexes. The vanadyl precursors (1 mmol) were dissolved in acetone and equimolar amounts of the corresponding lanthanide nitrates (1 mmol) were added. Stirring for 90 minutes at room temperature [$L^1VO(H_2O)$ precursor] or stirring and boiling for 40 minutes [$L^2VO(H_2O)$ precursor] yielded green precipitates that were filtered off, washed with acetone and diethyl ether, and dried under vacuum. Dark green crystals of the gadolinium derivatives suitable for X-ray studies were obtained by slow diffusion in a cell device. In the case of **2**, solutions of both gadolinium nitrate and the corresponding precursor in acetone were allowed to react for 10 days at room temperature. Compound **1** required a dichloromethane/acetone (5:2) solution in the compartment occupied by the vanadyl monomer, and the diffusion was carried out at 255 K during nine days.

$[L^1VOGd(NO_3)_3(H_2O)](H_2O)$ (1): Green precipitate, yield 69%. − $C_{20}H_{26}GdN_5O_{16}V$ (800.63): calcd. C 30.0, H 3.3, N 8.8; found C 30.1, H 3.0, N 8.8. − Selected IR bands: $\tilde{\nu}$ = 3470, 2977, 1615, 1560, 1521, 1462, 1437, 1400, 1384, 1306, 1281, 1249, 1226, 1078, 1005, 859, 746 cm^{-1}.

$[L^2VO(C_3H_6O)Gd(NO_3)_3]$ 2. Green precipitate, yield 56%. − $C_{24}H_{30}GdN_5O_{15}V$ (836.71): calcd. C 34.4, H 3.6, N 8.4; found C 34.5, H 3.3, N 8.3. − Selected IR bands: $\tilde{\nu}$ = 3391, 2962, 1703, 1630, 1609, 1567, 1521, 1489, 1473, 1435, 1311, 1283, 1245, 1230, 1064, 995, 857, 741, 735 cm^{-1}.

Acknowledgments

J. G.-T. thanks the University of Burgos and the City Hall of Burgos for his Postdoctoral Fellowship. J.-P. C., F. D., B.D., and J.-P. L. thank the Centre National Scientifique (CNRS), France, for financial support.

[1] C. Benelli, A. Caneschi, D. Gatteschi, J. Laugier, P. Rey, *Angew. Chem. Int. Ed. Engl.* **1987**, *26*, 913−915.
[2] [2a] C. Benelli, A. Caneschi, D. Gatteschi, L. Pardi, P. Rey, D. P. Shum, R. L. Carlin, *Inorg. Chem.* **1989**, *28*, 272−275. − [2b] C. Benelli, A. Caneschi, D. Gatteschi, L.Pardi, P. Rey, *Inorg. Chem.* **1990**, *29*, 4223−4228.
[3] C. Benelli, A. Caneschi, D. Gatteschi, L. Pardi, *Inorg. Chem.* **1992**, *31*, 741−746.
[4] J. P. Sutter, M. L. Kahn, S. Golhen, L. Ouahab, O. Kahn, *Chem. Eur. J.* **1998**, *4*, 571−576.
[5] A. Bencini, C. Benelli, A. Caneschi, R. L. Carlin, A. Dei, D. Gatteschi, *J. Am. Chem. Soc.* **1985**, *107*, 8128−8136.
[6] C. Benelli, A. Caneschi, D. Gatteschi, O. Guillou, L. Pardi, *Inorg. Chem.* **1990**, *29*, 1750−1755.
[7] M. Andruh, I. Ramade, E. Codjovi, O. Guillou, O. Kahn, J. C. Trombe, *J. Am. Chem. Soc.* **1993**, *115*, 1822−1829.
[8] C. Benelli, A. J. Blake, P. E. Y. Milne, J. M. Rawson, R. E. P. Winpenny, *Chem. Eur. J.* **1995**, *1*, 614−618.
[9] J. P. Costes, F. Dahan, A. Dupuis, J. P. Laurent, *Inorg. Chem.* **1996**, *35*, 2400−2402.
[10] I. Ramade, O. Kahn, Y. Jeannin, R. Robert, *Inorg. Chem.* **1997**, *36*, 930−936.
[11] J. P. Costes, F. Dahan, A. Dupuis, *Inorg. Chem.* **2000**, *39*, 165−168 and references cited therein.
[12] [12a] J. P. Costes, A. Dupuis, J. P. Laurent, *J. Chem. Soc., Dalton Trans.* **1998**, 735−736. − [12b] J. P. Costes, A. Dupuis, J. P. Laurent, *Eur. J. Inorg. Chem.* **1998**, 1543−1546 and references cited therein.
[13] C. Lescop, D. Luneau, E. Belorisky, P. Fries, M. Guillot, P. Rey, *Inorg. Chem.* **1999**, *38*, 5472−5473.
[14] A. Caneschi, A. Dei, D. Gatteschi, L. Sorace, K. Vostrikova, *Angew. Chem. Int. Ed.* **2000**, *39*, 246−248.
[15] J. P. Costes, F. Dahan, A. Dupuis, J. P. Laurent, *Inorg. Chem.* **2000**, *39*, 169−173.
[16] Crystals were obtained at 255 K for **1** and 295 K for **2**. In the case of **1**, we were unable to collect the data at a temperature lower than 255 K without destroying the crystal.
[17] Crystal structures analysis: The data were collected on a STOE IPDS diffractometer with Mo-K_α radiation. The structures were solved using direct methods (SHELXS-97) and refined on F^2 (SHELXL-97). A numerical absorption correction was used for **1**.
1: $C_{20}H_{26}GdN_5O_{16}V$, M_r = 800.65, monoclinic, space group $P2_1/n$, a = 16.234(2), b = 10.4958(7), c = 16.467(2) Å, β = 90.99(1)°, V = 2805.4(5) Å^3, Z = 4, $\rho_{calcd.}$ = 1.896 Mg·m^{-3}, $F(000)$ = 1584, λ = 0.71073 Å, μ(Mo-K_α) = 2.761 mm^{-1}, T = 255 K, crystal size 0.25 × 0.15 × 0.10 mm^3. Of the 24339 reflections collected ($3.3 < 2\theta < 52.1°$), 5448 were independent; max./min. residual electron density 0.703/−1.159 e/Å^3, $R1$ = 0.0294 [$I > 2\sigma(I)$], $wR2$ = 0.0603 (all data).
2: $C_{24}H_{30}GdN_5O_{15}V$, M_r = 836.72, monoclinic, space group $P2_1/c$, a = 9.992(1), b = 17.556(2), c = 18.293(2) Å, β = 105.68(1)°, V = 3089.4(6) Å^3, Z = 4, $\rho_{calcd.}$ = 1.799 Mg·m^{-3}, $F(000)$ = 1664, λ = 0.71073 Å, μ(Mo-K_α) = 2.509 mm^{-1}, T = 160 K, crystal size 0.50 × 0.25 × 0.13 mm^3. Of the 18864 reflections collected ($2.9 < 2\theta < 48.4°$), 4523 were independent; max./min. residual electron density 0.832/−0.338 e/ Å^3, $R1$ = 0.0198 [$I > 2\sigma(I)$], $wR2$ = 0. 0438 (all data).
Crystallographic data (excluding structure factors) for the structures reported in this paper have been deposited with the Cambridge Crystallographic Data Centre as supplementary publication no. CCDC-146861 **(1)** and -146862 **(2)**. Copies of the data can be obtained free of charge on application to CCDC, 12 Union Road, Cambridge CB2 IEZ, UK [Fax: (internat.) +44-1223/336-033; E-mail: deposit@ccdc.cam.ac.uk].
[18] P. U. Anderson, in *Magnetism* (Eds.: G. T. Rado, H. Suhl), Academic Press,New York, **1963**; Vol.1, Chapter 2.
[19] J. B. Goodenough, in *Magnetism and the Chemical Bond*, Interscience, New York, **1963**.
[20] R. Hotzelmann, K. Wieghardt, U. Flörke, H. J. Haupt, D. C. Weatherburn, J. Bonvoisin, G. Blondin, J. J.Girerd, *J. Am. Chem. Soc.* **1992**, *114*, 1681−1696.
[21] H.Weihe, H.U. Güdel, H. Toflund, *Inorg. Chem.* **2000**, *39*, 1351−1362 and references cited therein.

Received October 16, 2000
[I00391]

$Fe_9O_3(OC_2H_5)_{21}\cdot C_2H_5OH$ – A New Structure Type of an Uncharged Iron(III) Oxide–Alkoxide Cluster

Michael Veith,*[a] Frank Grätz,[a] and Volker Huch[a]

Keywords: Iron / Oxo compounds / Alkoxides / Cluster compounds / Magnetic properties

A new nona iron(III) oxide-alkoxide cluster has been prepared by the treatment of $FeCl_3$ with three equivalents of sodium ethoxide. The molecule is the first example of a neutral iron(III) alkoxide cluster based on OEt ligands and shows a paramagnetic moment of 13.4(1) μ_B at 293 K in the solid state.

Introduction

Iron(III) oxides, alkoxides and hydroxides show a great structural diversity, the most remarkable feature being the formation of charged and uncharged clusters by formal condensation.[1] The iron atoms in such compounds are often linked by oxygen atoms. The remaining ligands on the iron atoms may be hydroxide,[2–5] carboxylate,[4–7] alkoxide,[6,8,9] multipodal amino-organic,[10] or amino hydroxyorganic[2] groups, to mention just a few possibilities. The structural building blocks of such iron oxide clusters are often FeO_6 octahedra (less frequently FeO_5 bipyramids or square pyramids) linked by oxygen atoms, which show twofold to sixfold coordination. The new cluster $Fe_9O_3(OEt)_{21}\cdot EtOH$ described here is the first example of such an aggregate containing, apart from bridging oxygens, only the alkoxide group OEt as ligand.

Results and Discussion

In our attempt to synthesise the alkoxide[11–13] $Fe(OC_2H_5)_3$[14] by reaction of iron(III) chloride with sodium ethoxide following established routes, we noticed that a solid brown compound could be isolated in about 60% yield. The X-ray crystal structure analysis of this molecular compound revealed a new structure type within iron(III) alkoxide clusters (see Figure 1). It also showed that the compound is made up of three oxygen atoms, nine iron(III) atoms, twenty-one alkoxide ligands and an alcohol molecule coordinated to one of the Fe centres. The molecular formulation $Fe_9O_3(OC_2H_5)_{21}\cdot C_2H_5OH$ **(1)** has been confirmed by elemental analysis. The oxygen atoms in the cluster presumably come from the residual water in C_2H_5OH.[15] The molecule has the lowest point symmetry C_1 which is due to asymmetric adduct formation of a neutral ethanol molecule.

Leaving this extra ligand apart an almost *mm*2 (C_{2v}) symmetry can be attributed to the rest of the molecule (neglecting the orientations of the ethyl groups). A pseudo-twofold axis runs through the iron atom Fe(1) and the central oxygen atom O(6) which connects three metal atoms in a trigonal planar coordination sphere. The other two oxygen atoms are in the centres of very distorted Fe_4 tetrahedra, the distortion being due to an important elongation of one of the edges [Fe(2)···Fe(4) and Fe(3)···Fe(5)]. These elongated edges are the only ones which are not bridged by μ_2-OC_2H_5. While most of the iron atoms have one terminal OC_2H_5 ligand, Fe(1), Fe(2) and Fe(3) are completely integrated in the oxygen bridge network, and Fe(6) has an additional C_2H_5OH neutral ligand. At Fe(1) there are four μ_2-OC_2H_5 terminal bridges, while at Fe(2) and Fe(3) there are three. Fe(4), Fe(5) and Fe(6) are almost octahedrally coordinated by oxygen atoms, while all other iron atoms are in distorted trigonal bipyramidal oxygen coordination spheres. The largest deviation from trigonal bipyramidal geometry is found for Fe(1), which is better described as square pyramidal with respect to the nearest oxygen atoms. Altogether there are six terminal OC_2H_5 ligands, fifteen bridging μ_2-OC_2H_5 groups and an additional neutral C_2H_5OH ligand. There is a neat dependence of Fe–O distances and coordination numbers on the atoms involved in the bond as well as on the site of the coordination polyhedron (axial versus equatorial): Fe–λ^4O = 201.1(7) pm, Fe–λ^3O = 191.1(1)

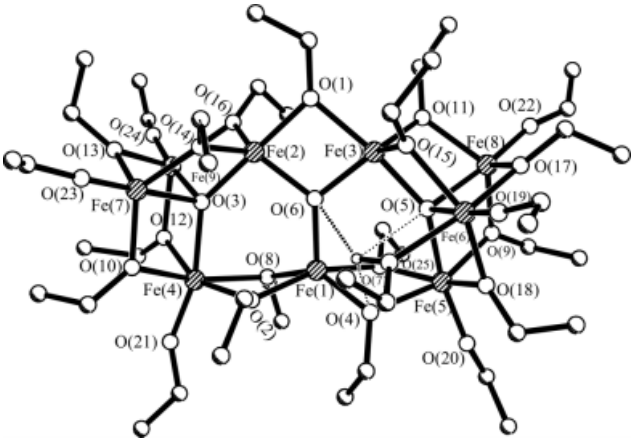

Figure 1. X-ray crystal structure of the iron(III)oxide–alkoxide $Fe_9O_3(OC_2H_5)_{21}\cdot C_2H_5OH$

[a] Institut für Anorganische Chemie, Universität d. Saarlandes
Postfach 151150, D-66701 Saarbrücken, Germany
Fax: (internat.) +49-681/302-3995
E-mail: veith@rz.uni-sb.de

 © WILEY-VCH Verlag GmbH, 69451 Weinheim, 2001 1434–1948/01/0202–0367 $ 17.50+.50/0

pm and Fe−OC_2H_5 (μ_2) = 200.9(0) pm; Fe−OC_2H_5 (terminal) = 178.7(3) pm (mean values). As anticipated, the neutral alcohol ligand at Fe(6) has the longest Fe−O bond [219.0(5) pm]. Interestingly, all μ_2-OC_2H_5 bridges are found at the equatorial sites of the trigonal bipyramidally coordinated iron atoms. The proton of the alcohol ligand can be located and serves as a bridging atom (hydrogen bond) between O(25) and O(4), O(5) and O(6).

The magnetic moment[16−19] of $Fe_9O_3(OC_2H_5)_{21}\cdot C_2H_5OH$ in the solid state is μ_{eff} = 13.4(1) B.M. at 293 K.[20]

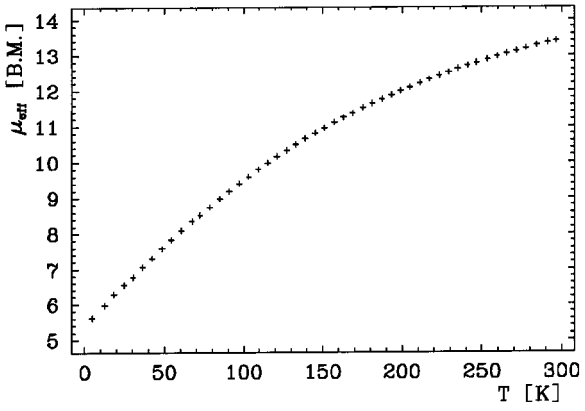

Figure 2. Plot of the magnetic moment (μ_{eff} [B.M.]) of solid **1** versus temperature [K] (see ref.[20])

From the steady shortening of the magnetic moment of crystalline cluster **1** with decreasing temperature (Figure 2) an antiferromagnetic exchange interaction within the molecule can be deduced.[20]

The values found have to be compared to a calculated value for one independent high spin Fe^{3+} ion of μ_{eff} = 5.92 B.M. The crystals seem to be ferrimagnetic, and this is currently being investigated further.[21] Interestingly, the cluster **1** when dissolved in benzene shows a tendency to dissociate. Cryoscopic measurements in the same solvent give a molecular weight of about 510 g/mol. This corresponds to a fragmentation into several species from the original cluster (molecular weight, 1543.0 g/mol) and is more than the simple release of the neutral ethanol ligand. As a solid residue from the benzene solution of cluster **1** we have isolated a compound which analysed as "$Fe_5O(OC_2H_5)_{13}$". We are currently investigating the structural and physical consequences of this decomposition which is driven by simple change of the solvent. Further studies on this system are underway.[21]

Experimental Section

$Fe_9O_3(OC_2H_5)_{21}\cdot C_2H_5OH$ (1): The solvent C_2H_5OH was distilled from sodium and kept over molecular sieves. Under a dry nitrogen atmosphere anhydrous $FeCl_3$ (4.428 g, 27.3 mmol) was added to a solution of sodium ethoxide [formed in situ from sodium (1.886 g, 82.0 mmol) and C_2H_5OH (20 mL)] in ethanol. The mixture was stirred under reflux for 100 h. After removing the solvent under reduced pressure the residue was distilled at 200 °C/0.01 Torr; the product crystallizes on cooling as a brown solid. Yield 2.735 g (60%). − $C_{44}H_{111}Fe_9O_{25}$: calcd. C 34.3, H 7.3, Fe 32.6; found C 34.2, H 7.3, Fe 32.1. − M..p.: 90 °C.

X-ray Crystallography

A crystal suitable for X-ray crystallography was isolated from an ethanol solution of **1**. Stoe IPDS diffractometer, Mo-K_α radiation (λ = 71.073 pm), 293 K, crystal size 0.2 × 0.18 × 0.12 mm, triclinic, space group $P\bar{1}$ with a = 1247.4(2) pm, b = 1746.2(3) pm, c = 1814.1(4) pm, α = 68.02(3)°, β = 84.58(3)°, γ = 88.45(3)°, V = 3647.7(12) × 10^6 pm^3, Z = 2, ρ = 1.405 Mg·m^{-3}, μ = 1.798 mm^{-1}, 2.07° ≤ θ ≤ 24.08°, −14 ≤ h ≤ 13, −19 ≤ k ≤ 20, −20 ≤ l ≤ 20, 23099 measured reflections, 10729 independent, $R1$ = 0.0627, $wR2$ = 0.1553, GOF = 0.928, no restraints, 483 parameters, remaining electron density max. 0.717 × 10^{-6} min. −0.652 × 10^{-6} e·pm^{-3}.

The structure described in this paper was solved with the heavy-atom method and refined towards F^2 for all observed reflections (solution and refinement with SHELXS-97 and SHELXL-97, hydrogen atoms were calculated in an ideal tetrahedral geometry and optimised).

Crystallographic data for the structure reported in this paper have been deposited with the Cambridge Crystallographic Data Centre as supplementary publication CCDC-149596. Copies of the data can be obtained free of charge on application to CCDC, 12 Union Road, Cambridge CB2 IEZ, UK [Fax: (internat.) + 44-1223/336-033; E-mail: deposit@ccdc.cam.ac.uk].

[1] K. S. Hagen, *Angew. Chem. Int. Ed. Engl.* **1992**, *31*, 1010.
[2] S. L. Heath, A. K. Powell, *Angew. Chem. Int. Ed. Engl.* **1992**, *31*, 191.
[3] C. J. Harding, R. K. Henderson, A. K. Powell, *Angew. Chem. Int. Ed. Engl.* **1993**, *32*, 570.
[4] S. M. Gorun, S. J. Lippard, *Nature* **1986**, *319*, 666.
[5] S. M. Gorun, G. C. Papaefthymiou, R. B. Frankel, S. J. Lippard, *J. Am. Chem. Soc.* **1987**, *109*, 3337.
[6] K. L. Taft, S. J. Lippard, *J. Am. Chem. Soc.* **1990**, *112*, 9629.
[7] I. Shweky, L. E. Pence, G. C. Papaefthymiou, R. Sessoli, J. W. Yun, A. Bino, S. J. Lippard, *J. Am. Chem. Soc.* **1997**, *119*, 1037.
[8] A. Caneschi, A. Cornia, S. J. Lippard, *Angew. Chem. Int. Ed. Engl.* **1995**, *34*, 467.
[9] K. Hegetschweiler, H. W. Schmalle, H. M. Streit, V. Gramlich, H. U. Hund, I. Erni, *Inorg. Chem.* **1992**, *31*, 1299.
[10] V. S. Nair, K. S. Hagen, *Inorg. Chem.* **1992**, *31*, 4048.
[11] R. C. Mehrotra, J. of Non-*Crystalline Solids* **1988**, *100*, 1.
[12] K. G. Caulton, L. G. Hubert-Pfalzgraf, *Chem. Rev.* **1990**, 969.
[13] M. Veith, S. Mathur, V. Huch, *Inorg. Chem.* **1996**, *35*, 7295.
[14] D. C. Bradley, R. K. Multani, W. Wardlaw, *J. Chem. Soc.* **1958**, 126.
[15] A. Caneschi, A. Cornia, A. C. Fabretti, D. Gatteschi, *Angew. Chem. Int. Ed. Engl.* **1995**, *34*, 2716.
[16] R. W. Adams, E. Bishop, R. L. Martin, G. Winter, *Aust. J. Chem.* **1966**, *19*, 207.
[17] K. Hegetschweiler, A. Corina, D. Gatteschi, L. Hausherr-Primo, V. Gramlich, *Inorg. Chem.* **1996**, *35*, 4414.
[18] A. Caneschi, A. Cornia, S. J. Lippard, G. C. Papaefthymiou, R. Sessoli, *Inorg. Chim. Acta* **1996**, *243*, 295.
[19] K. L. Taft, G. C. Papaefthymiou, S. J. Lippard, *Inorg. Chem.* **1994**, *33*, 1510.
[20] We thank Dr. J. Ensling (Universität Mainz) for the magnetic measurements and for discussion of the results.
[21] P. Gütlich, J. Ensling, M. Veith, F. Grätz, V. Huch, to be published.

Received July 12, 2000
[I00274]

Ruthenium(III) Coordination to the Exocyclic Nitrogen of 9-Methyladenine and Stabilisation of the Rare Imine Tautomer by Intramolecular Hydrogen Bonding

Aldrik H. Velders,[a] Bart van der Geest,[a] Huub Kooijman,[b] Anthony L. Spek,[b] Jaap G. Haasnoot,[a] and Jan Reedijk*[a]

Keywords: Ruthenium / Bioinorganic chemistry / N ligands / Crystal structure / Hydrogen bonds

The X-ray structure of *trans*-[$RuCl_3(dmtp)_2$(9-MeAde)] shows that this compound is the first crystallographic example of a ruthenium(III) complex with an adenine derivative coordinated as a monodentate ligand through the exocyclic *N*6 nitrogen; two intramolecular hydrogen bonds stabilise the coordination of the adenine, which is present as a neutral ligand in the rare tautomeric imine form with a unique short C6–N6 distance of 1.293(3) Å.

Introduction

In the search for new antitumour-active metal compounds, several chlororuthenium complexes have proven to be promising candidates for clinical studies.[1] In particular, complexes of the type *trans*-$[RuCl_4(L)_2]^-$, with L a heterocyclic ligand like imidazole or indazole, have shown good activity against platinum-resistant tumours.[2,3] The hydrolysis properties[4] of these complexes, and their binding to biologically available ligands present in proteins[5] and nucleic acids,[6] appear to be important factors in the study of a structure-activity relationship. The anionic tetrachlororuthenium(III) complexes are to be considered as prodrugs that hydrolyse rapidly in vivo to form relatively stable neutral *trans*-$[RuCl_3(H_2O)(L)_2]$ complexes.[7] By using the bicyclic nitrogen heterocycle 5,7-dimethyl[1,2,4]triazolo[1,5-*a*]pyrimidine, dmtp, we have directly synthesised the first hydrolysis product of such antitumour complexes, *trans*-$[RuCl_3(H_2O)(dmtp)_2]\cdot H_2O$, in which intramolecular hydrogen-bonding interactions of the two dmtp ligands stabilise the coordinated water molecule.[8] This monoaquabis(dmtp)ruthenium(III) complex appears to be a very useful compound for the investigation of the binding properties of this type of ruthenium(III) antitumour complex with biological molecules, such as the heterocyclic nitrogen ligands present in nucleic acids (purines and pyrimidines). In this paper the synthesis and characterisation of the reaction product of *trans*-$[RuCl_3(H_2O)(dmtp)_2]\cdot H_2O$ with the DNA model base 9-methyladenine, 9-MeAde (Figure 1), *trans*-$[RuCl_3(dmtp)_2$(9-MeAde)] (**1**) is presented. The adenine is present in the rare imine tautomer and coordinates to the ruthenium through the exocyclic N6 nitrogen.

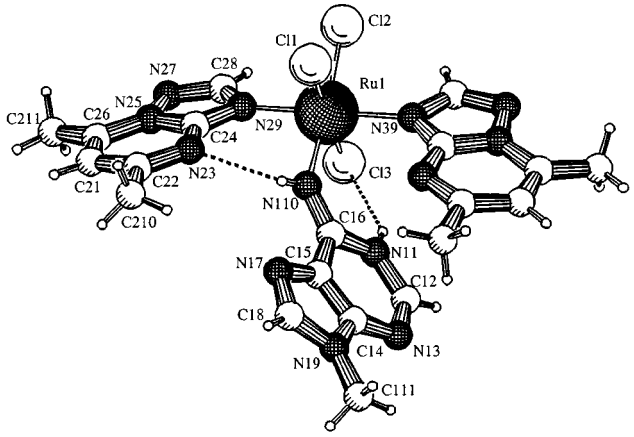

Figure 1. Molecular structure of **1**; intramolecular hydrogen bonding is indicated with dotted lines; the co-crystallised solvent molecule is omitted for clarity; selected metal-ligand bond lengths (Å) and angles (°): Ru(1)−Cl(1) 2.3329(8), Ru(1)−Cl(2) 2.3852(8), Ru(1)−Cl(3), 2.3772(8), Ru(1)−N(29) 2.083(2), Ru(1)−N(39) 2.090(2), Ru(1)−N(110) 2.035(2); Cl(1)−Ru(1)−Cl(3) 178.64(3), N(29)−Ru(1)−N(39) 178.00(8), Cl(2)−Ru(1)−N(110) 175.82(7); donor···acceptor (D···A) distances (Å) and donor−hydrogen···acceptor (D−H···A) angles (°) of the intramolecular hydrogen bonds: N(11)−H···Cl(3) 3.22(9) and 144(3); N(11)−H···N(23) 2.936(3) and 140(3).

Coordination of metal ions to the exocyclic N6 of adenine is difficult, but can occur after deprotonation of the amine.[9] Crystallographic evidence for coordination to the exocyclic nitrogen of deprotonated adenine derivatives has been observed with molybdenum complexes,[10] in a dinuclear platinum complex,[11] and in trinuclear rhodium[12] and ruthenium(II) arene complexes.[13] Crystallographic reports of exocyclic coordination of adenine derivatives in the imine form are even less well-known and have been reported only for a mercury compound,[14] a dimolybdenum complex,[15] and a platinum adduct.[16,17] In DNA, adenine is mainly present in the amine form (Scheme 1) with the N6 and N1 nitrogens acting as hydrogen donor and acceptor atoms, respectively, involved in base pairing with thymine. The imine form of adenine can result in nucleobase mispairing and therefore it is of great biological importance to get a de-

[a] Leiden Institute of Chemistry, Gorlaeus Laboratories, Leiden University,
P. O. Box 9502, 2300 RA Leiden, The Netherlands
Fax: (internat.) +31-71/527-4671
E-mail: reedijk@chem.leidenuniv.nl
[b] Bijvoet Center for Biomolecular Research, Crystal and Structural Chemistry, Utrecht University,
Padualaan 8, 3584 CH, Utrecht, The Netherlands

 © WILEY-VCH Verlag GmbH, 69451 Weinheim, 2001 1434−1948/01/0202−0369 $ 17.50+.50/0

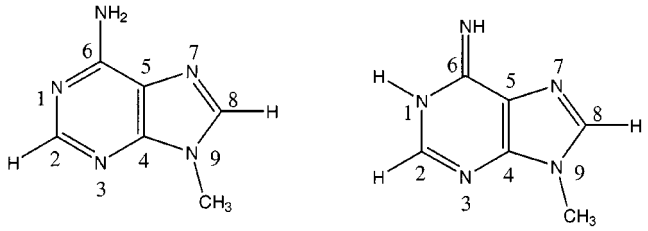

Scheme 1. Tautomeric structures of 9-MeAde: the amine form (left) and the imine form (right)

tailed understanding of the factors influencing the formation and properties of such metal complexes.[18−20]

The crystal structure of *trans*-[$RuCl_3(dmtp)_2$(9-MeAde)] (Figure 1) shows a neutral six-coordinated ruthenium(III) complex with three chloride ions in a *mer* configuration, the two dmtp ligands are coordinated through the triazole N9 nitrogens in a mutual *trans* head-to-head orientation. The Ru−N(9) and Ru−Cl bond distances and angles are comparable to those found in related complexes, such as, for example,[8] *trans*-[$RuCl_3(H_2O)(dmtp)_2$]·H_2O and[21] *trans*-[$RuCl_3(H_2O)(admtp)_2$]·H_2O which also display a quasi-octahedral stereochemistry with two *trans*-located triazolopyrimidine ligands. The 9-MeAde is coordinated to the ruthenium through the exocyclic N6 atom, completing the coordination sphere. In the difference density map a hydrogen atom is clearly visible at the N1 site, indicating that the 9-MeAde is neutral and present in the imine form. Also, the short C6−N6 distance of 1.293(3) Å is typical for the imine form of adenine. The average C−N distance for amine groups coordinated to transition metals is 1.39 Å (596 entries in the Cambridge Structural Database, version April 1999).

The N3 site of triazolopyrimidine ligands is known to form intramolecular hydrogen bonds easily with other coordinated ligands like water molecules or amines.[8,21,22] Also, in **1** the N3 atom of one of the two dmtp ligands is involved in an intramolecular hydrogen bond, in this case with the imine proton of the 9-MeAde. The tautomeric imine form of 9-MeAde in **1** is furthermore stabilised by an intramolecular hydrogen bond between the proton on the endocyclic nitrogen N1 and one of the *cis*-coordinated chloride ions. Both hydrogen bonds constrain the 9-MeAde to orient in a *syn* orientation with respect to the N(1) site.

The crystal structure of [$Ru(NH_3)_5$(1-$MeCyt^-$)]$(PF_6)_2$, where 1-$MeCyt^-$ stands for the anion of the pyrimidine 1-methylcytosine,[23] was the first crystallographic report of a DNA base coordinating through the exocyclic nitrogen to a ruthenium(III) complex. More recently, a trinuclear ruthenium-arene complex[13] has been reported in which a deprotonated adenine coordinates contemporaneously through the N1, N7 and N6 nitrogens. The present 9-MeAde complex **1** is the first crystallographic evidence of a purine coordinated to a ruthenium ion though its exocyclic amine as a monodentate ligand in the rare tautomeric imine form. The Ru−N(110) bond length of 2.035(2) Å is significantly shorter than the Ru−N(29) and Ru−N(39) distances [2.083(2) and 2.090(2) Å, respectively] and suggests a considerable π-bonding between the ruthenium and the 9-MeAde ligand.

Ruthenium complexes are known to coordinate preferentially to the N7 nitrogens of oxopurines;[24−27] the N7 is, however, not necessarily the most likely binding site of aminopurines. In fact, in the late seventies it was suggested on the basis of DNA binding studies with single- and double-stranded DNA that ruthenium(III) ammine complexes do not preferentially bind to the N7 of adenine, but possibly coordinate to adenine through the exocyclic nitrogen N6.[28] The absorption spectrum of **1** in the near-UV and visible part of the electromagnetic spectrum shows two main absorption bands at 360 and 500 nm, which have also been observed in several ruthenium(III) ammine complexes with adenine-like ligands.[29,30] The present study unambiguously confirms these absorptions to be characteristic for a ruthenium(III) ion coordinated to the exocyclic, imine group of a nucleobase.

In the solid-state structure of **1**, the two dmtp ligands are not equivalent, but it is likely that in solution all three heterocyclic ligands are to some extent flexible and can rotate around their Ru−N axes. This, in fact, can be concluded from the ^1H NMR spectroscopic data of **1**, in which the two dmtp ligands are indistinguishable. The ^1H NMR spectrum of **1** (Figure 2) shows largely shifted and broadened resonances which is caused by the presence of the paramagnetic ruthenium(III) centre. On the basis of the relative intensities of the peaks, and by comparison with related complexes, the dmtp[8,21,31] and adenine[32,33] proton resonances have been assigned. The dipolar contribution to the isotropic shifts in a ruthenium(III) adenine-κ^{N6} complex are relatively small and the shifts of the H2 and H8 protons can be attributed mainly to the contact contributions;[33] the large shifts of the 9-MeAde ring protons are therefore consistent with a strong π-overlap.

In conclusion, the structure of complex **1** indicates that the use of the triazolopyrimidine dmtp offers the possibility to stabilise, isolate and study the interaction of potential ruthenium antitumour complexes with biological targets like the DNA bases. The intramolecular hydrogen bonds between the dmtp and the 9-MeAde in **1** are not likely to be a prerequisite for N6 coordination, but do play an important role in facilitating the isolation and characterisation of this mode of coordination. The hydrogen-bond interac-

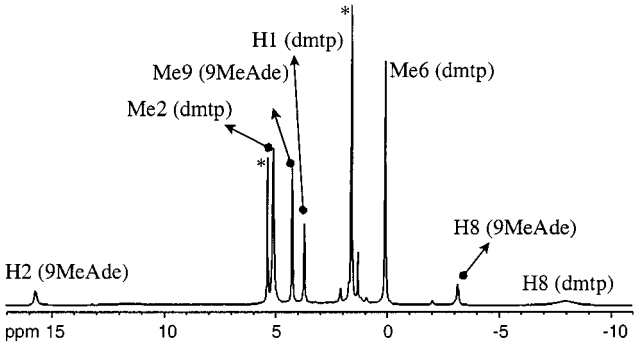

Figure 2. ^1H NMR spectrum of **1** in CD_2Cl_2; the proton numbering is as given in Figure 1; the asterisks indicate residual solvent signals

tion of the N1(H) with a coordinated chloride, on the other hand, is likely to be of influence on the coordination to the adenine N6, also in other (antitumour-active) chlororuthenium complexes. Such a stabilisation of the imine form through (hydrogen) bonding with the N(1) and N(6) of the adenine would inhibit the formation of a normal base pair with thymine; instead, mispairing with guanine or adenine bases might be favoured which eventually can lead to mutations.[18,34,35] The interaction of *trans*-$[RuCl_3(H_2O)(dmtp)_2]\cdot H_2O$ with other nucleobases, as well as the subsequent reactions of the formed adducts, are current subjects of investigation.

Experimental Section

General Remarks: NMR: Data were obtained at 300.13 MHz on a Bruker DPX 300 MHz spectrometer (for CD_2Cl_2 as solvent, δ_H = 5.33 at 295 K). The ^1H NMR signals of **1** could be identified as the paramagnetically shifted and broadened signals with relatively fast relaxation times (on the order of milliseconds). The magnetic moment of **1** was determined on a Johnson Matthey Alfa Product Magnetic Susceptability Balance MK I. Elemental analyses were performed by the Microanalytical Laboratory, University College, Dublin (Ireland). UV/Vis spectra were obtained on a Perkin−Elmer Lambda 900 spectrophotometer. The ligand 5,7-dimethyl[1,2,4]triazolo[1,5-*a*]pyrimidine (dmtp) and *trans*-$[RuCl_3(H_2O)(dmtp)_2]\cdot H_2O$ were prepared as described previously.[8] 9-Methyladenine was prepared by methylation of adenine with methyl iodide.[36]

***trans*-[$RuCl_3$(9-MeAde-*N*6)$(dmtp)_2$] (1):** A mixture of *trans*-$[RuCl_3(H_2O)(dmtp)_2]\cdot H_2O$ (0.10 g, 0.2 mmol) and 9-MeAde (0.10 g, 0.7 mmol) was heated in 20 mL ethanol (98%) at 75 °C, without stirring. After 15 minutes, the colour of the initially yellowish suspension turned to dark red and after 30 minutes a red microcrystalline powder precipitated, which was isolated by filtration and washed with ethanol and diethyl ether. Yield, 60 mg (50%). The compound was dissolved in a dichloromethane/ethanol mixture (3:1) and red crystals were obtained by diethyl ether diffusion into this solution. The crystals obtained in this way were not stable in air for long periods of time, most likely because of evaporation of co-crystallised solvent molecules; the X-ray data analyses were done on crystals freshly taken out of the mother liquor. $C_{20}H_{23}Cl_3N_{13}$ (652): calcd. C 36.8, H 3.58, Cl 16.3, N 27.9; found C 35.5, H 3.52, Cl 16.5, N 26.4. − The effective magnetic moment, μ_{eff}, of the complex was determined to be 1.9 Bohr magneton at 20 °C, which is in the range of that expected for a single-electron system like a low-spin ruthenium(III) ion.[37] $-^1H$ NMR ([CD_2Cl_2, at 25 °C): δ = −8.0 [2 H, H8 (dmtp)], −3.1 [1 H, H8 (9-MeAde)], 0.1 [6 H, Me6 (dmtp)], 3.7 [2 H, H1 (dmtp)], 4.2 [3 H, Me9 (9-MeAde)], 5.1 [6 H, Me2 (dmtp)], 15.7 [1 H, H2 (9-MeAde)]. − UV/Vis (CH_2Cl_2): λ = 362 nm (ε = $7.12\cdot10^3$ м$^{-1}$ cm^{-1}), 500 (ε = $2.48\cdot10^3$ м$^{-1}$ cm^{-1}).

X-ray Crystallographic Study: $C_{20}H_{23}Cl_3N_{13}Ru\cdot1/2CH_2Cl_2$, M_r = 695.39, red, plate-shaped crystal (0.02 × 0.20 × 0.40 mm), triclinic, space group *P*1(bar) with *a* = 9.7336(12), *b* = 11.2417(15), *c* = 13.924(2) Å, α = 80.922(7), β = 74.505(8) and γ = 75.410(8)°, *V* = 1414.2(3) Å^3, *Z* = 2, D_x = 1.633 g cm^{-3}, μ(Mo-K_α) = 0.96 mm^{-1}. All data, where relevant, are given with disordered solvent contribution. 15167 Reflections were measured (6389 independent, R_{int} = 0.0461, 1.6° < θ < 27.5°, T = 150 K, Mo-K_α radiation, graphite monochromator, λ = 0.71073 Å) on a Nonius KappaCCD diffractometer with rotating anode; no absorption correction was applied. The structure was solved by automated direct methods (SHELXS-86,[38]). Full-matrix least-squares refinement of 345 parameters on F^2 (SHELXL-97,[38]) resulted in a final *R*1 value of 0.0356 (*wR*2 = 0.0789, GoF = 1.021). H atoms were introduced at calculated positions and included riding on their carrier atoms except for the N−H hydrogens which were located on a difference Fourier map and whose positions were refined. A cavity (1/2,1/2,1/2) with a volume of 206 Å^3 per unit cell was filled with disordered solvent (most likely dichloromethane); the associated electron density was taken into account with the PLATON/SQUEEZE procedure.[39] A total of 42 e per unit cell was found (consistent with the presence of one CH_2Cl_2 molecule) and corrected for. Final residual density was in the range −0.81 to 0.50 e Å^{-3}.

Crystallographic data (excluding structure factors) for the structure(s) reported in this paper have been deposited with the Cambridge Crystallographic Data Centre as supplementary publication no. CCDC-149915. Copies of the data can be obtained free of charge on application to CCDC, 12 Union Road, Cambridge CB2 1EZ, UK [Fax: (internat.) +44-1223/336-033; E-mail: deposit@ccdc.cam.ac.uk].

Acknowledgments

The authors thank Johnson & Matthey (UK) for their generous loan of $RuCl_3\cdot3H_2O$. This research is sponsored by the Council of Chemical Sciences of the Netherlands Organisation for Scientific Research (NWO), and also support by COST Action D8/0017/97 (Metals in medicine) is kindly acknowledged.

[1] M. J. Clarke, F. Zhu, D. R. Frasca, *Chem. Rev.* **1999**, *99*, 2511.
[2] B. K. Keppler, M. Henn, U. M. Juhl, M. R. Berger, R. Niebl, F. E. Wagner, *Progr. in Clin. Biochem.* **1989**, *10*, 41−69.
[3] B. K. Keppler, *New J. Chem.* **1990**, *14*, 389−403.
[4] O. M. N. Dhubhghaill, W. R. Hagen, B. K. Keppler, K. G. Lipponer, P. J. Sadler, J. Chem. Soc., *Dalton Trans.* **1994**, 3305−3310.
[5] F. Kratz, M. Hartmann, B. K. Keppler, L. Messori, *J. Biol. Chem.* **1994**, *269*, 2581−2588.
[6] M. Hartmann, T. J. Einhauser, B. K. Keppler, *Chem. Commun.* **1996**, 1741−1742.
[7] K.-G. Lipponer, E. Vogel, B. K. Keppler, *Metal-Based Drugs* **1996**, *3*, 243−259.
[8] A. H. Velders, L. Pazderski, F. Ugozzoli, M. Biagini-Cingi, A. M. Manotti-Lanfredi, J. G. Haasnoot, J. Reedijk, *Inorg. Chim. Acta* **1998**, *273*, 259−265.
[9] B. Lippert, *Progr. in Inorg. Chem.* **1989**, *37*, 1−97.
[10] L. Y. Kuo, M. G. Kanatzidis, M. Sabat, A. L. Tipton, T. J. Marks, *J. Am. Chem. Soc.* **1991**, *113*, 9027−9045.
[11] G. Trovo′, G. Bandoli, M. Nicolini, B. Longato, *Inorg. Chim. Acta* **1993**, *211*, 95−99.
[12] D. P. Smith, E. Baralt, B. Morales, M. M. Olmstead, M. F. Maestre, R. H. Fish, *J. Am. Chem. Soc.* **1992**, *114*, 10647−10649.
[13] S. Korn, W. S. Sheldrick, *J. Chem. Soc., Dalton Trans.* **1997**, 2191−2199.
[14] F. Zamora, M. Kunsman, M. Sabat, B. Lippert, *Inorg. Chem.* **1997**, *36*, 1583−1587.
[15] E. F. Day, C. A. Crawford, K. Folting, K. R. Dunbar, G. Christou, *J. Am. Chem. Soc.* **1994**, *116*, 9339−9340.
[16] J. Arpalahti, K. D. Klika, *Eur. J. Inorg. Chem.* **1999**, 1199−1201.
[17] J. Viljanen, K. D. Klika, R. Sillanpaa, J. Arpalahti, *Inorg. Chem.* **1999**, *38*, 4924−4925.
[18] B. Lippert, H. Schoellhorn, U. Thewalt, *Inorg. Chim. Acta* **1992**, *198−200*, 723−732.

[19] J. Sponer, J. E. Sponer, L. Gorb, J. Leszczynski, B. Lippert, *J. Phys. Chem. (A)* **1999**, *103*, 11406−11413.
[20] J. V. Burda, J. Sponer, J. Leszczynski, *J. Biol. Inorg. Chem.* **2000**, *5*, 178−188.
[21] A. H. Velders, F. Ugozzoli, M. Biagini-Cingi, A. M. Manotti-Lanfredi, J. G. Haasnoot, J. Reedijk, *Eur. J. Inorg. Chem.* **1999**, 213−215.
[22] J. M. Salas, M. A. Romero, M. P. Sanchez, M. Quiros, *Coord. Chem. Rev.* **1999**, *195*, 1119−1142.
[23] B. J. Graves, D. J. Hodgson, *J. Am. Chem. Soc.* **1979**, *101*, 5608−5612.
[24] V. M. RodriguezBailey, K. J. LaChanceGalang, P. E. Doan, M. J. Clarke, *Inorg. Chem.* **1997**, *36*, 1873−1883.
[25] K. J. LaChanceGalang, M. Zhao, M. J. Clarke, *Inorg. Chem.* **1996**, *35*, 6021−6026.
[26] M. J. Clarke, H. Taube, *J. Am. Chem. Soc.* **1974**, *96*, 5413−5419.
[27] M. E. Kastner, K. F. Coffey, M. J. Clarke, S. E. Edmonds, K. Eriks, *J. Am. Chem. Soc.* **1981**, *103*, 5747−5752.
[28] M. J. Clarke, M. Buchbinder, A. Kelman, *Inorg. Chim. Acta* **1978**, *27*, L87−L88.
[29] M. J. Clarke, *J. Am. Chem. Soc.* **1978**, *100*, 5068−5075.
[30] M. J. Clarke, *Inorg. Chem.* **1980**, *19*, 1103−1104.
[31] A. H. Velders, *Ph. D. thesis*, Leiden University, **2000**.
[32] M. J. Clarke, *Prog. Clin. Biochem. Med.* **1989**, *10*, 25−39.
[33] V. M. RodriguezBailey, M. J. Clarke, *Inorg. Chem.* **1997**, *36*, 1611−1618.
[34] O. Kennard, W. N. Hunter, *Angew. Chem. Int. Ed. Engl.* **1991**, *30*, 1254−1277.
[35] M. D. Topal, J. R. Fresco, *Nature* **1976**, *263*, 285−289.
[36] E. G. Talman, W. Bruning, J. Reedijk, A. L. Spek, N. Veldman, *Inorg. Chem.* **1997**, *36*, 854−861.
[37] E. A. Seddon, K. R. Seddon, *The Chemistry of Ruthenium*, Elsevier, Amsterdam, The Netherlands **1984**.
[38] G. M. Sheldrick, SHELXL-97 Program for crystal structure determination. University of Göttingen, Germany, **1997**.
[39] A. L. Spek, PLATON A multi-purpose crystallographic tool. Utrecht University, The Netherlands, 2000. Internet: http://www.cryst.chem.uu.nl/platon/.

Received July 31, 2000
[I00302]

Synthesis and Reactivity of Monoborylacetylene Derivatives

Yiqun Gu,[a] Hans Pritzkow,[a] and Walter Siebert*[a]

Dedicated to Prof. Ulrich Müller on the occasion of his 60th birthday

Keywords: Alkynes / Boranes / Boron / Hydroboration / Phenols

The catechol-substituted monoborylacetylenes **1a**–**d** are obtained from the reaction of bis(diisopropylamino)borylacetylene with catechol derivatives and 2,2′-biphenol. The catalytic trimerization of **1a**–**d** with $[(\eta^5\text{-}C_5H_5)Co(CO)_2]$ yields isomeric mixtures of the triborylbenzene derivatives **2a,2a′**, **2b,2b′**, and **2c,2c′**. The reaction of **2a,2a′** with mesitylllithium provides the hexamesityl-substituted 1,3,5-triborylbenzene **2e**. Hydroboration of **1a** with catecholborane affords a mixture of 1,1-bis(1,3,2-benzodioxaborol-2-yl)ethene (**3a**) and *trans*-1,2-bis(1,3,2-benzodioxaborol-2-yl)ethene (**4a**). Hydroboration of **1a** and **3a** with one or two mol of $HBCl_2$ and subsequent substitution of the chlorine atoms of the product with catechol leads in each case to the 1,1,1-trisborylmethane derivative **5a** in 83 and 78% yield, respectively, which forms the tris(THF) adduct **5a**$(thf)_3$. Treatment of **5a** with *t*BuLi yields 1,1,1-tris[di(*tert*-butyl)boryl]ethane **6a**. $[Co_2(CO)_8]$ reacts with **1a** to give 3-(1,3,2-benzodioxaborol-2-yl)-1,2-bis(tricarbonylcobalta)tetrahedrane **(9a)**. The new compounds have been characterized by NMR spectroscopy and mass spectrometry as well as by X-ray structure analyses for **1a**, **3a**, **5a**, **5a**$(thf)_3$, and **9a**.

Introduction

Alkynylboranes are interesting synthons for a variety of compounds. Köster et al.[1] prepared monoborylacetylenes by reacting amine-stabilized dialkylchloroboranes with metal acetylides. The addition of diethyl ether-trifluoroborane to the formed adducts leads to donor-free borylacetylenes. Thermally stable monoborylacetylenes[2,3] are obtained with electron-donating groups such as dialkylamino or alkoxy, which reduce the Lewis acidity at the boron center. Dialkoxyborylacetylenes[4,5] may be formed from the corresponding aminoacetylenes. In the reaction of metal acetylides with dialkoxyhaloboranes the halogen atom as well as the alkoxy substituents are replaced. In contrast, the reaction of diaminohaloboranes with metal acetylides leads to the expected compounds in good yields. Here we report on the synthesis and properties of the catechol-substituted monoborylacetylene derivatives **1a−c**.

Results and Discussion

Synthesis and Properties of Monoborylacetylenes (1)

For the preparation of catechol-substituted monoborylacetylenes bis(diisopropylamino)borylacetylene[6] is reacted in THF with two equivalents of HCl and one equivalent of catechol or biphenol, leading to the monoborylacetylenes **1a−d** in 46 to 68% yield (Scheme 1). The colorless solids may be sublimed in vacuo (**1a−c**) or recrystallized (**1d**); the melting points of the products are between 45 °C (**1c**) and 115 °C (**1d**). Compounds **1a−c** are soluble in common organic solvents whereas **1d** dissolves only in toluene and THF and forms a stable THF adduct.

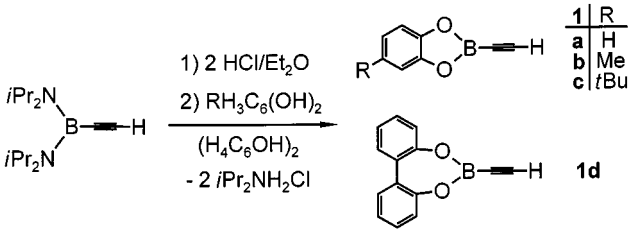

Scheme 1

The ^1H NMR spectra of **1a−d** exhibit a singlet for the acetylenic proton between δ = 2.77 (**1a**) and 2.37 (**1d**). In the ^{13}C NMR spectra the signals of the α carbon atoms (bound to boron) were not observed; the signals for the β carbon atoms (δ = 94−86) are shifted to lower field relative to alkylacetylenes (δ = 70−80),[7] which may indicate an interaction of the empty orbital at boron with the π system of the triple bond. Also, the oxygen atoms in **1a−c** may compete for the empty orbital at boron. In **1d** the boron atom is in bonding contact with the oxygen atom of one THF molecule. The ^{11}B NMR signal for **1d** is shifted to higher field (δ = 15.9) relative to the values for **1a** (δ = 24.1), **1b**, and **1c** (both δ = 24.3). The X-ray structure analysis of **1a** (Figure 1) reveals an almost linear B−C−C−H moiety. The boron atom is trigonal coordinated, and the heterocycle is almost planar. Compound **1a** has approximately C_{2v} symmetry, the C≡C distance [1.195(3) Å] is slightly widened relative to other R−C≡C−R compounds[8] (1.183 Å) and the B−C bond [1.520(4) Å] is short

[a] Anorganisch-Chemisches Institut der Universität Heidelberg, Im Neuenheimer Feld 270, 69120 Heidelberg, Germany
Fax: (internat.) + 49-6221/545-609

 © WILEY-VCH Verlag GmbH, 69451 Weinheim, 2001 1434−1948/01/0202−0373 $ 17.50+.50/0

for a B−C single bond. This is in agreement with structural data for oxygen-substituted diborylacetylenes.[6,9]

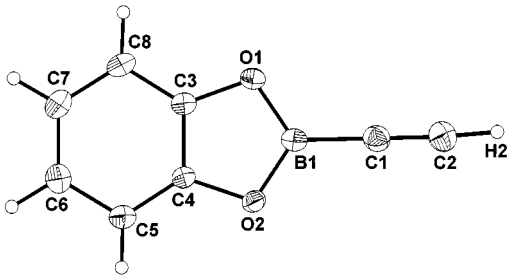

Figure 1. Molecular structure of **1a** in the crystal; selected bond length [Å] and angles [°]: B1−O1 1.387(3), B1−O2 1.372(3), B1−C1 1.520(4), C1−C2 1.195(3), C2−H2 1.00(3); O1−B1−O2 112.3(2), O1−B1−C1 123.2(2), O2−B1−C1 124.4(2), B1−C1−C2 178.7(2), C1−C2−H2 176(1)

Trimerization of 1 to Triborylbenzene Derivatives (2)

Only a few triborylbenzene derivatives are known;[10,11] these have been prepared in low yields by Grignard reactions. The synthesis of substituted arenes by cobalt-catalyzed trimerization of alkynes is well established and has led to a broad application in organic synthesis.[12] Very recently we obtained hexaborylbenzene derivatives by cyclotrimerization of diborylacetylenes in the presence of catalytic amounts of (η^5-cyclopentadienyl)dicarbonylcobalt.[13,14] Analogously, in refluxing toluene the monoborylacetylenes **1a−c** form isomeric mixtures of the triborylbenzene derivatives **2a,2a′**, **2b,2b′**, and **2c,2c′** in good yields (>50%; Scheme 2). The 1,3,5- and 1,2,4-isomers could not be separated.

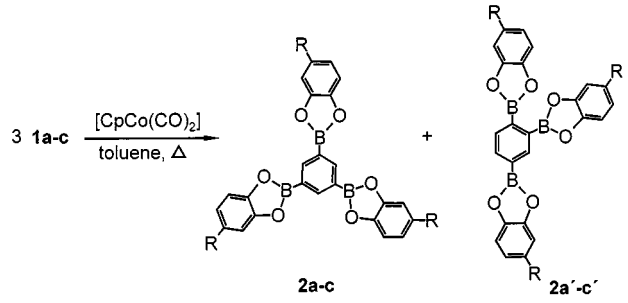

Scheme 2

The mixtures of **2a−c,2a′−c′** are light brown, air-stable solids. The product **2a,2a′** is not soluble in most organic solvents; it partially dissolves in methanol, however, with slow decomposition and formation of catBOMe ($\delta^{11}B$ = 18). In contrast, **2b,2b′** and **2c,2c′** easily dissolve in THF and CH_2Cl_2.

The ^{11}B NMR spectra exhibit broad signals at δ = 30.1 for **2a,2a′** (in [D_4]MeOH), δ = 29.6 for **2b,2b′**, and δ = 33.9 for **2c,2c′** (in CD_2Cl_2). In the ^1H NMR spectrum of **2a,2a′** several signals appear in the arene region. The pattern for *ortho* substitution of the catechol group is found between δ = 6.60 and 6.76. A multiplet between δ = 8.1 and 7.5 is assigned to the central rings of **2a,a′**. In the ^{13}C NMR spectrum, three signals at δ = 146.2, 120.9, and 116.3 are found for the carbon atoms of the catechol groups. A signal at δ = 131.6 is assigned to the hydrogen-substituted carbon atoms of the central aromatic ring of the symmetrical isomer **2a**. Resonances at δ = 141.6, 137.9, and 134.7 are due to the central aromatic carbon atoms (CH) of the unsymmetrical derivative **2a′**. The ^1H NMR spectra of **2b,2b′** and **2c,2c′** indicate that the unsymmetrical derivatives are the main products. In the aromatic region, these compounds exhibit multiplets for the substituted catechol groups at δ = 6.44−6.66 for **2b,2b′** (in [D_4]MeOH) and δ = 7.17−7.43 for **2c,2c′** (in CD_2Cl_2). A second multiplet at δ = 7.50−7.77 in the spectrum of **2b,b′** is generated by the three unsymmetrical protons of the central arene ring. The corresponding signals for **2c′** can be fully assigned: the two adjacent protons give rise to two doublets of doublets at δ = 8.31 ($^3J_{HH}$ = 7.5 Hz, $^4J_{HH}$ = 1.3 Hz) and δ = 8.14 ($^3J_{HH}$ = 7.5 Hz, $^5J_{HH}$ = 0.8 Hz), the resonance for the remaining proton appears as a pseudo triplet at δ = 8.74 (averaged $J_{HH} \approx 1$ Hz). In addition, the nine methyl groups of the three *tert*-butyl substituents of **2c′** result in two signals at δ = 1.37 and 1.35, integrating for nine and eighteen protons respectively, which belong to the groups in the 2- and 1,4-positions. The ^{13}C NMR spectra also indicate the predominant formation of the unsymmetrical structures **2b′** and **2c′**. In the aromatic region of the ^{13}C NMR spectra of **2c,2c′** 19 of the expected 21 signals for the nonboron-bound carbon atoms can be distinguished. A signal for the central C(H) carbon atoms in the symmetrical structure is not found, which means either that **2c** is not present or that its concentration is very low. In the spectra of the products **2a,2a′** and **2b,2b′**, however, the presence of small amounts of the isomers **2a** and **2b** is clearly seen. Beside the aromatic ^{13}C resonances for **2a′/2b′**, signals at δ = 131.6 and 130.7 are assigned to the central C(H) atoms in **2a** and **2b**, respectively.

The reaction of **2a,2a′** with mesityllithium provides the hexamesityl-substituted triborylbenzene derivative **2e** in 49% yield (Scheme 3). Its spectroscopic data and the X-ray structure analysis confirm that the symmetric isomer 1,3,5-tris(dimesitylboryl)benzene (**2e**) has been formed. This compound was first prepared in 2% yield from 1,3,5-tribromobenzene Grignard reagent and fluorodimesitylborane.[11]

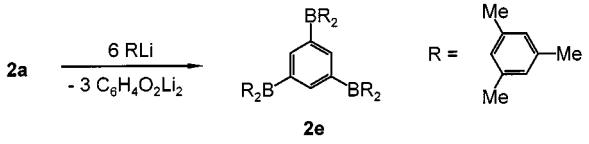

Scheme 3

Hydroboration of 1a to Yield 1,1-Bis(1,3,2-benzodioxaborol-2-yl)ethene (3a), *trans*-1,2-Bis(1,3,2-benzodioxa-borol-2-yl)ethene (4a), and 1,1,1-Tris(1,3,2-benzodioxaborol-2-yl)ethane (5a)

Alkynes and alkenes are hydroborated regioselectively by 1,3,2-benzodioxaborole (catecholborane).[15] The reaction of the monoborylacetylene **1a** with catecholborane at 80 °C leads to a mixture of 1,1-bis(1,3,2-benzodioxa-borol-2-yl)ethene (**3a**) and a small amount of *trans*-1,2-bis(1,3,2-benzo-

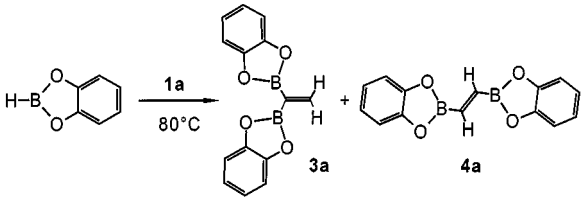

Scheme 4

dioxaborol-2-yl)ethene (**4a**) in 86% yield (Scheme 4).[16] The *cis*-addition of catecholborane proceeds regioselectively favoring the formation of the 1,1-isomer **3a**. Only a minor amount of the 1,2-isomer **4a** is obtained. Related 1,2-derivatives with a *cis*-arrangement have been reported by Marder and Norman,[17] and isomeric 1,1-diborylethene derivatives have been synthesized by Matteson.[18] Colorless **3a** melts at 105 °C with decomposition, it is soluble in toluene, benzene, and THF.

In the NMR spectra only signals for **3a** were found, indicating that the amount of the 1,2-derivative **4a** is rather small. However, its formation was unambiguously proven by X-ray structure analysis (see below). The ^{1}H NMR spectrum of **3a** exhibits a multiplet signal between δ = 6.60−6.93 for the aromatic protons and for the alkene hydrogen atoms. In the ^{13}C NMR spectrum one finds three signals at δ = 148.8, 123.1, and 112.9 for the aromatic carbon atoms. One sharp signal for the CH_2 carbon atom of the ethene unit at δ = 154.9 proves the presence of the 1,1-isomer, its chemical shift is similar to that of comparable compounds.[19,20] In the ^{11}B NMR spectrum one signal appears at δ = 32.2.

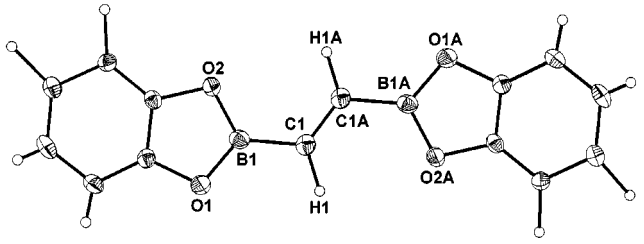

Figure 2. Molecular structure of **4a** in the crystal; selected bond lengths [Å] and angles [°]: C1−C1a 1.348(10), C1−B1 1.554(8), B1−O1 1.386(7), B1−O2 1.386(7), C1−H1 1.12(5); C1a−C1−B1 122.3(6), C1−B1−O1 125.8(5), C1−B1−O2 122.8(5), O1−B1−O2 111.4(5)

In the solid state the molecule **4a** (Figure 2) has a crystallographic inversion center at the midpoint of the C=C double bond and is almost planar (max. dev. 0.04 Å) resulting in C_{2h} symmetry. Both the B and C atoms of the ethene unit are planar coordinated. The heterocycles are almost planar and they are in a coplanar arrangement (dihedral angle: 0°). The length of the C1−C1a bond [1.348(10) Å] is that of a double bond and the B−C bonds [1.554(8) Å] are a bit shorter than single bonds.

As indicated above, the hydroboration of **1a** with catecholborane stops after the first *cis*-addition. However, **3a** reacts with $HBCl_2$,[21,22] and subsequent substitution of the Cl atoms by catechol leads to 1,1,1-triborylethane **(5a)** in

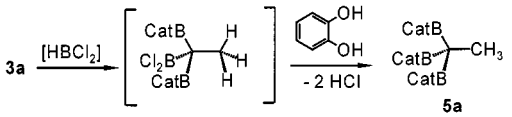

Scheme 5

78% yield (Scheme 5). It is a colorless solid, which is soluble in toluene, THF, and dichloromethane. The spectroscopic data of **5a** are discussed below.

The hydroboration of **1a** with $[HBCl_2]$ and subsequent substitution of the chlorine atoms by catechol groups leads to 1,1,1-triborylethane **(5a)** in 83% yield (Scheme 6). The solid is recrystallized from THF to yield the THF adduct **5a**$(thf)_3$; in toluene it loses THF and forms crystalline **5a**. Both compounds have been studied by X-ray structure analyses (see below). The related compound $[(MeO)_2B]_3CCH_3$ has been reported previously.[18]

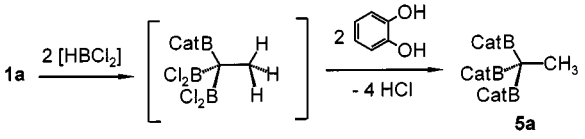

Scheme 6

The ^{1}H NMR spectrum of **5a** indicates a C_3 symmetry with three boryl substituents bonded to one carbon atom. The *ortho* substitution pattern for the aromatic region is observed between δ = 6.67−6.97, and a singlet appears at δ = 2.04 for the methyl group. The ^{13}C NMR spectroscopic data confirm the assignments from the ^{1}H NMR spectrum. The ^{11}B NMR spectrum shows one broad signal at δ = 35.

The X-ray diffraction study reveals that **5a**$(thf)_3$ has approximately C_{3v} symmetry (Figure 3 and 4). The heterocycles are almost planar. The boron-bound carbon atom is almost tetrahedral, and the C1−C2 bond is 1.556(5) Å. All B−C and B−O bond lengths in **5a**$(thf)_3$ are normal. The distances from the boron to the oxygen atoms of the THF molecules (2.72−2.91 Å) are relatively short. This, and the geometrical arrangement of the THF molecules, suggests a very weak interaction between these atoms. A similar arrangement was found in 1,1,2,2-tetrakis(1,3,2-benzodioxaborol-2-yl)ethane·2THF.[9] The THF-free solid-state structure of **5a** is almost identical to that of **5a**$(thf)_3$. No significant changes in bond lengths and angles are observed, which means that the influence of the THF molecules in **5a**$(thf)_3$ on its structural parameters is negligible.

1,1,1-Tris[di(*tert*-butyl)boryl]ethane (6a)

Treatment of **5a** with *t*BuLi results in the formation of 1,1,1-tris[di(*tert*-butyl)boryl]ethane (**6a**) in 12% yield (Scheme 7). Compound **6a** is a colorless, thermally stable liquid, which does not form any *closo*-C_2B_3 carborane by elimination of trisorganoboranes. In the mass spectrum of **6a** the molecular ion M^+ is absent; however, M^+ patterns for the C_2B_3 carborane derivative **7a** (m/z = 258) and for the C_2B_4 carborane derivative **8a** [m/z = 325, $(M - H)^+$] appear. These carboranes are most likely formed in the mass spectrometer. The ^{11}B NMR spectrum does not show

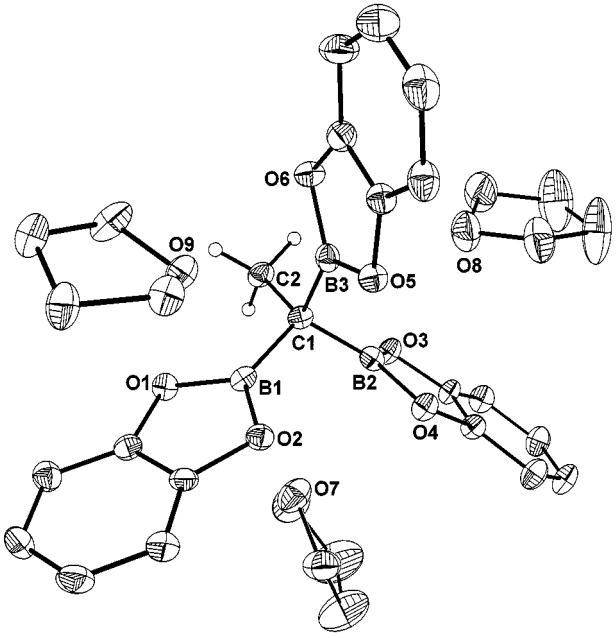

Figure 3. Molecular structure of **5a(thf)$_3$** in the crystal; selected bond lengths [Å] and angles [°]: C1−C2 1.556(5), C1−B1 1.544(6), C1−B2 1.564(6), C1−B3 1.569(6), B1−O1 1.407(5), B1−O2 1.395(5), B2−O3 1.397(5), B2−O4 1.385(5), B3−O5 1.387(6), B3−O6 1.395(6); B1−C1−C2 110.8(3), B1−C1−B2 110.2(3), B1−C1−B3 105.9(3), B2−C1−B3 108.5(3), C2−C1−B2 110.5(3), C2−C1−B3 110.9(3). Selected bond lengths [Å] and angles [°] for **5a**: C−C 1.556 [1.554−1.557(3)], C−B 1.568 [1.560−1.581(3)], B−O 1.385 [1.380−1.398(3)], B−C−C 110.4−113.1(2), B−C−B 103.3−113.1(2)

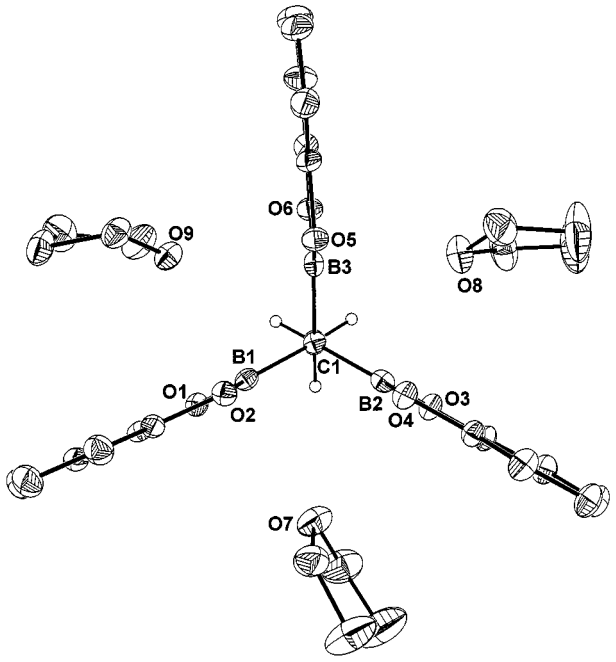

Figure 4. Molecular structure of **5a(thf)$_3$** as viewed along the C1−C2 vector

any signal for the carboranes, it contains only the signal for **6a** at δ = 83.4. The ^{1}H NMR spectrum exhibits two singlets at δ = 1.92 and 1.11 in the ratio 1:18, the ^{13}C NMR spectrum shows two signals at δ = 14.1 and 30.3, the carbon atoms adjacent to boron are not detected.

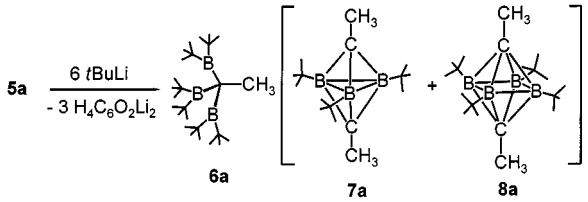

Scheme 7

3-(1,3,2-Benzodioxaborol-2-yl)-1,2-bis(tricarbonylcobalta)-tetrahedrane (9a)

Dicobaltahexacarbonyl-η^2-alkyne complexes are obtained by reacting alkynes with $Co_2(CO)_8$.[23] Analogously, the monoborylacetylene **1a** reacts with [$Co_2(CO)_8$] in hexane with elimination of CO to give complex **9a** (Scheme 8).

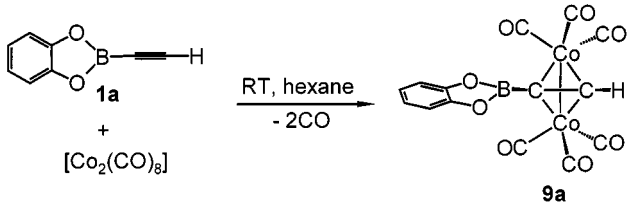

Scheme 8

Chromatographic workup of the dark brown solution and crystallization from toluene gives dark crystals of **9a** in 42 % yield. It is soluble in hexane, toluene, THF, or CH_2Cl_2, although it decomposes when exposed to light or heat. In the ^{1}H NMR spectrum the aromatic protons appear as an *ortho* pattern between δ = 6.70−6.94, the aliphatic proton gives a singlet at δ = 5.83 and is thus shifted downfield by more than 3 ppm relative to **1a** (δ = 2.77). This has been explained in related compounds by the electronegativity of the Co_2C_2 unit and the anisotropy effect of the C≡O groups. In the ^{13}C NMR spectrum three signals appear at δ = 149.0, 123.2, and 112.8 for the aromatic carbon atoms. The signal for CO at δ = 200 is broadened by intramolecular CO exchange. A broad signal at δ = 71 is found for the boron-bonded carbon, whereas the signal for the other carbon atoms appears at δ = 81.9. The ^{11}B NMR signal at δ = 32.6 is shifted downfield by 8 ppm with respect to that of **1a** (δ = 24.1).

The X-ray diffraction study confirms the structure of **9a** as that of a tetrahedrane (Figure 5). The almost linear B−C−C−H moiety in **1a** has been altered by the complexation, the angles are decreased to 151.0(2)° (B1−C2−C1) and 141(1)° (C2−C1−H1). The atoms C1−C2−Co1−Co2 form a distorted tetrahedrane, the dihedral angle O1−B1−C2−C1 is 11.9°. The Co−Co bond length of 2.48 Å is comparable with other data,[24] the distance between the carbon atoms of the tetrahedrane [1.334(3) Å] is 0.14 Å longer than the C−C bond in **1a**, and is of the same magnitude as a double bond.[24b,24c]

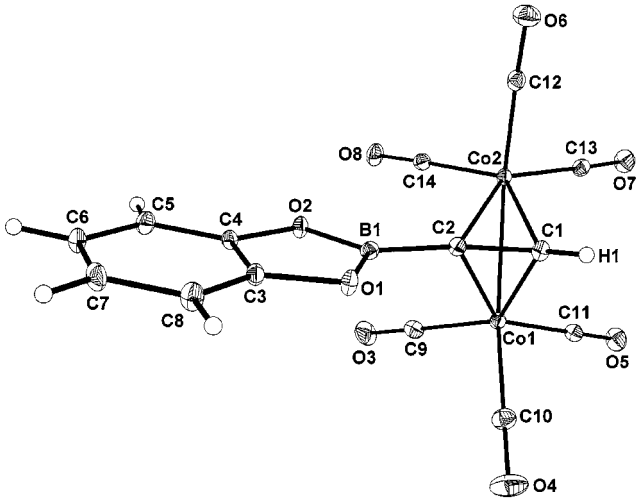

Figure 5. Molecular structure of **9a** in the crystal; selected bond lengths [A] and angles [°]: C1−C2 1.334(3), C1−Co1 1.956(2), C1−Co2 1.957(2), C2−Co1 1.991(2), C2−Co2 1.976(2), Co1−Co2 2.480(1), C2−B1 1.528(3); H1−C1−C2 141(1), C1−C2−B1 151.0(2), Co1−C1−Co2 78.67(7), Co1−C2−Co2 77.41(7), C1−C2−Co1 68.9(1), C1−C2−Co2 69.4(1), C2−C1−Co1 71.7(1), C2−C1−Co2 70.9(1), C1−Co1−C2 39.51(8), C1−Co2−C2 39.66(8), C1−Co1−Co2 50.68(6), C2−Co1−Co2 51.03(5)

Experimental Section

General: All reactions were carried out under a purified nitrogen atmosphere. The solvents were dried according to published procedures. − NMR: Bruker AC 200 or DRX 200 and Jeol FX-90 Q (^{11}B, external standard, $BF_3{\cdot}OEt_2$; ^{1}H, ^{13}C, standards were the signals of the residual protons in the deuterated solvents, calculated relative to TMS). − MS: Finnigan MAT 8230, ZAB-2F VG-Micromass and Jeol MS station JMS 700. − The following compounds were prepared according to literature procedures: bis(diisopropylamino)borylacetylene,[6] catecholborane.[15] * Boron carbide formation often reduces the found values.

1,3,2-Benzodioxaborol-2-yl-acetylene (1a), 1,3,2-(5-Methylbenzo)-dioxaborol-2-yl-acetylene (1b), 1,3,2-(5-*tert*-Butyl-benzo)dioxaborol-2-yl-acetylene (1c), and 2-Ethinyldibenzo[d.f]-1,3,2-dioxaborepine·THF (1d·thf): To a stirred solution of bis(diisopropylamino)borylacetylene (3.307 g, 14.0 mmol) in 50 mL of THF at −78 °C was added $HCl{\cdot}OEt_2$ (3.12 M; 10 mL, 31.2 mmol) within 30 min. Stirring was continued for 30 min., and NH_2iPr_2Cl formed as a white solid. Then, 14.0 mmol of the corresponding aromatic diol (**1a:** 1.540 g of catechol; **1b:** 1.744 g of 4-methylcatechol; **1c:** 2.330 g of 4-*tert*-butylcatechol; **1d:** 2.644 g of 2,2′-biphenol) dissolved in 10 mL of THF was added and the reaction mixture was allowed to warm overnight to room temperature. After filtration of the solid the solution was reduced almost to dryness. The products **1a**, **1b**, and **1c** were sublimed, **1d** was crystallized from THF.

1a: 1.227 g (61%), m.p. 53 °C. − ^{1}H NMR (200 MHz, $CDCl_3$): δ = 2.77 (s, 1 H, C≡CH), 7.24−7.14 (m, 4 H, C_6H_4). − ^{13}C NMR (50 MHz, $CDCl_3$): δ = 93.7 (br., C≡*C*H), 113.7, 124.3, 148.5 (C_6H_4), B*C* not observed. − ^{11}B NMR (64 MHz, $CDCl_3$): δ = 24.1. − EI-MS: *m*/*z* (%) = 144 (100) [M^+]. − HR-EIMS: *m*/*z* = 144.0382 [M^+], calcd. for $^{12}C_8{}^1H_5{}^{11}B^{16}O_2$: 144.0383 (Δ = 0.1 mmu).

1b: 1.009 g (46%), m.p. 48 °C. − ^{1}H NMR (200 MHz, $CDCl_3$): δ = 2.36 (s, 3 H, CH_3), 2.75 (s, 1 H, C≡CH), 7.12−6.88 (m, 3 H, C_6H_3). − ^{13}C NMR (50 MHz, $CDCl_3$): δ = 21.3 (CH_3), 93 (br., C≡*C*H), 112.0, 113.3, 123.8, 133.4, 145.4, 147.6 (C_6H_3), B*C* not observed. − ^{11}B NMR (64 MHz, $CDCl_3$): δ = 24.3. − EI-MS: *m*/*z* (%) = 158 (100) [M^+]. − $C_9H_7BO_2$ (158.0): calcd. C 68.43, H 4.47; found C 67.24, H 4.64.

1c: 1.915 g (68%), m.p. 45 °C. − ^{1}H NMR (200 MHz, $CDCl_3$): δ = 1.31 (s, 9 H, CH_3), 2.75 (s, 1 H, C≡CH), 7.28−7.14 (m, 3 H, C_6H_3). − ^{13}C NMR (50 MHz, $CDCl_3$): δ = 31.7 (CH_3), 34.9 [*C*(CH_3)$_3$], 93 (br., C≡*C*H), 110.0, 111.7, 120.1, 144.3, 145.2, 147.4 (C_{ar}), B*C* not observed. − ^{11}B NMR (64 MHz, $CDCl_3$): δ = 24.3. − EI-MS: *m*/*z* (%) = 200 (24.6) [M^+], 185 (100) [$M^+ - CH_3$]. − $C_{12}H_{13}BO_2$ (200.0): calcd. C 72.05, H 6.55; found C 71.38, H 6.51.

1d·THF: 2.715 g (66%), m.p. 115 °C (dec.). − ^{1}H NMR (200 MHz, $CDCl_3$): δ = 1.94 (quint, 4 H, THF), 2.37 (s, 1 H, C≡CH), 4.00 (t, 4 H, THF), 7.45−7.02 (m, 8 H, H_{ar}). − ^{13}C NMR (50 MHz, $CDCl_3$): δ = 25.3 (THF), 69.5, 86 (br., C≡*C*H), 121.3, 124.1, 128.7, 129.2, 129.7, 153.1 (C_{ar}), B*C* not observed. − ^{11}B NMR (64 MHz, $CDCl_3$): δ = 15.9. − EI-MS: *m*/*z* (%) = 220 (100) [M^+]. − HR-EIMS: *m*/*z* = 220.0698 [M^+], calcd. for $^{12}C_{14}{}^1H_9{}^{11}B^{16}O_2$: 220.0696 (Δ = 0.2 mmu).

Tris(1,3,2-benzodioxaborol-2-yl)benzene Isomers (2a,2a′), Tris[1,3,2-(5-methylbenzo)dioxaborol-2-yl]benzene Isomers (2b,2b′), and Tris[1,3,2-(5-*tert*-butylbenzo)dioxaborol-2-yl]benzene Isomers (2c,2c′): Monoborylacetylene (**1a:** 0.865 g; **1b:** 0.956 g; **1c:** 1.209 g; 6.0 mmol) and (η^5-cyclopentadienyl)dicarbonylcobalt (0.055 g, 0.3 mmol, 5 mol-%) were heated in 15 mL of toluene for 24 h under reflux. The solid was separated and washed several times with small amounts of solvent (**2a,2a′:** THF and CH_2Cl_2; **2b,2b′:** toluene and CH_2Cl_2; **2c,2c′:** hexane) and dried in vacuum.

2a,2a′: 1.345 g (52%), m.p. 237 °C. − ^{1}H NMR (200 MHz, [D$_4$]MeOH): δ = 6.76−6.60 (m, 12 H, C_6H_4), 8.10−7.50 (m, 3 H, C_6H_3). − ^{13}C NMR (50 MHz, [D$_4$]MeOH): δ = 116.3, 120.9 (C_6H_4), 131.6 (C_6H_3, central, symm.), 134.7, 137.9, 141.7 (C_6H_3, central, unsymm.), 146.2 (C_6H_4). − ^{11}B NMR (64 MHz, [D$_4$]MeOH): δ = 30.1. − EI-MS: *m*/*z* (%) = 432 (100) [M^+]. − HR-EIMS: *m*/*z* = 432.1183 [M^+], calcd. for $^{12}C_{24}{}^1H_{15}{}^{11}B_3{}^{16}O_6$: 432.1148 (Δ = 3.6 mmu). − $C_{24}H_{15}B_3O_6$ (431.8): calcd. C 66.76, H 3.50; found C 65.28*, H 3.72.

2b,2b′: 1.550 g (55%), m.p. 220 °C. − ^{1}H NMR (200 MHz, [D$_4$]MeOH): δ = 2.18 (s, 9 H, CH_3), 6.66−6.44 (m, 9 H, C_6H_3, terminal), 7.64−7.50, 7.77 (each br., 3 H, C_6H_3, central). − ^{13}C NMR (50 MHz, [D$_4$]MeOH): δ = 21.0 (CH_3), 116.5, 117.4, 121.4 (C_6H_3, terminal), 130.7 (C_6H_3, central, symm.), 132.1 (C_6H_3, central, unsymm.), 134.5 (C_6H_3, terminal), 137.9, 141.1 (C_6H_3, central, unsymm.), 144.1, 146.3 (C_6H_3, terminal). − ^{11}B NMR (64 MHz, [D$_4$]MeOH): δ = 29.6. − EI-MS: *m*/*z* (%) = 474 (100) [M^+]. − HR-EIMS: *m*/*z* = 474.1643 [M^+], calcd. for $^{12}C_{27}{}^1H_{21}{}^{11}B_3{}^{16}O_6$: 474.1617 (Δ = 2.6 mmu). − $C_{27}H_{21}B_3O_6$ (473.9): calcd. C 68.43, H 4.47; found C 67.39, H 4.71.

2c′: 1.858 g (52%), m.p. 190 °C. − ^{1}H NMR (200 MHz, CD_2Cl_2): δ = 1.35 (s, 18 H, CH_3), 1.37 (s, 9 H, CH_3), 7.43−7.17 (m, 9 H, C_6H_3, terminal), 8.14 (dd, 3 H, $^3J_{HH}$ = 7.5 Hz, $^5J_{HH}$ = 0.8 Hz), 8.31 (dd, 3 H, $^3J_{HH}$ = 7.5 Hz, $^4J_{HH}$ = 1.3 Hz, H adj.), 8.74 (pseudo triplet, 3 H, averaged $J_{HH} \approx$ 1 Hz). − ^{13}C NMR (50 MHz, CD_2Cl_2): δ = 31.9 (CH_3), 35.2 [*C*(CH_3)$_3$], 110.32, 110.36, 110.40, 111.87, 111.93, 111.95 [C(H) catechol, adj. to C(O)] 120.06, 120.13, 120.21 [C(H) catechol, adj. to C(CH_3)$_3$], 146.58, 146.62 [*C*(CH_3)$_3$], 147.25, 147.33, 147.42, 148.80, 148.84 [C(O)], BC not observed. − ^{11}B NMR (64 MHz, CD_2Cl_2): δ = 33.9. − EI-MS: *m*/*z* (%) = 600 (90) [M^+], 585 (100) [$M^+ - CH_3$]. − HR-EIMS: *m*/*z* = 600.2994

[M^+], calcd. for $^{12}C_{36}{}^{1}H_{39}{}^{11}B_3{}^{16}O_6$: 600.3026 (Δ = 3.2 mmu). − $C_{36}H_{39}B_3O_6$ (600.1): calcd. C 72.05, H 6.55; found C 70.44*, H 6.53.

1,3,5-Tris(dimesitylboryl)benzene (2e): To a suspension of **2a,2a′** (0.210 g, 0.44 mmol) in toluene (30 mL) was added a solution of MesLi·OEt_2 (1.191 g) in Et_2O (10 mL) at −20 °C. The mixture was then heated for 3 h under reflux. After removal of the solvents the reaction mixture was worked-up by column chromatography (SiO_2/THF). Recrystallization from toluene yielded 0.330 g of **2e** (49%), m.p. 235 °C. − ^{1}H NMR (200 MHz, $CDCl_3$): δ = 1.88 (s, 36 H, *o*-CH_3), 2.23 (s, 18 H, *p*-CH_3), 6.70 (s, 12 H, C_6H_2), 7.50 (s, 3 H, C_6H_3). − ^{13}C NMR (50 MHz, $CDCl_3$): δ = 21.2 (CH_3), 23.4, 128.0, 138.4, 140.5 (C_6H_2), 145.1 (C_6H_3), B*C* not observed. − ^{11}B NMR (29 MHz, [D_8]toluene): δ = 88. − EI-MS: *m*/*z* (%) = 822 (2) [M^+ − H], 703 (6) [M^+ − Mes − H], 574 (12) [M^+ − $BMes_2$], 324 (54) [M^+ − 2$BMes_2$ − H], 249 (91) [$BMes_2$]$^+$, 120 (100) [MesH]$^+$, 105 (75) [$MesH^+$ − Me].

Bis(1,3,2-benzodioxaborol-2-yl)ethenes (3a and **4a):** A solution of **1a** (0.800 g, 5.6 mmol) and CatBH·THF (1.067 g, 5.6 mmol) in 20 mL of THF was heated at 80 °C under reflux for 4 h. Then the solvent was partially removed in vacuum and a white solid (1.267 g, 86%, m.p. 105 °C dec.) separated. It contained **3a** and a small amount of **4a**, which was not detected by NMR spectroscopy but obtained by crystallization from toluene.
3a: ^{1}H NMR (200 MHz, C_6D_6): δ = 6.93−6.60 (m, 8 H, C_6H_4), 6.99 (s, 2 H, BCH). − ^{13}C NMR (50 MHz, C_6D_6): δ = 112.8, 123.0, 148.8 (C_6H_4), 154.9 (CH_2). − ^{11}B NMR (64 MHz, C_6D_6): δ = 32.2. − EI-MS: *m*/*z* (%) = 264 (30) [M^+]. − $C_{14}H_{10}B_2O_4$ (263.8): calcd. C 63.73, H 3.82; found C 63.18, H 4.13.

1,1,1-Tris(1,3,2-benzodioxaborol-2-yl)ethane (5a): Procedure A: To a solution of **1a** (1.941 g, 13.5 mmol) in 50 mL of pentane was added BCl_3 (6 mL, 69.1 mmol) at −20 °C. Then triethylsilane (4.00 g, 34.4 mmol) in 10 mL of pentane was added very slowly at −20 °C. After 2 h of stirring at room temperature the solution was cooled to −20 °C and catechol (3.053 g, 27.7 mmol) in 10 mL of THF was added within 40 min. After 18 h of stirring at room temperature the solid was isolated by filtration, washed several times with hexane and dried in vacuum. Recrystallization from toluene yielded **5a** (4.282 g, 83%).
Procedure B: To a suspension of **3a** (1.543 g, 5.8 mmol) in 30 mL of pentane was added BCl_3 (2 mL, 23.0 mmol) at −20 °C. Then, triethylsilane (0.900 g, 7.7 mmol) in 20 mL of pentane was very slowly added. After 2 h of stirring at room temperature the solution was cooled to −20 °C and catechol (0.644 g, 5.8 mmol) in 5 mL of THF was added within 30 min. The reaction mixture was stirred for 18 h at −20 °C. Thereafter the solid was separated, washed several times with hexane, and dried in vacuum. Recrystallization from toluene yielded **5a** (1.731 g, 78%), m.p. 155 °C (dec.) − ^{1}H NMR (200 MHz, C_6D_6): δ = 2.04 (s, 3 H, CH_3), 6.97−6.67 (m, 12 H, C_6H_4). − ^{13}C NMR (50 MHz, C_6D_6): δ = 12.2 (CH_3), 112.8, 122.9, 149.0 (C_6H_4). − ^{11}B NMR (64 MHz, C_6D_6): δ = 35.4. − EI-MS: *m*/*z* (%) = 384 (100) [M^+]. − HR-EIMS: *m*/*z* = 384.1169 [M^+], calcd. for $^{12}C_{20}{}^{1}H_{15}{}^{11}B_3{}^{16}O_6$: 384.1147 (Δ = 2.1 mmu). − $C_{20}H_{15}B_3O_6$ (383.8): calcd. C 62.59, H 3.94; found C 61.01*, H 4.27.

1,1,1-Tris[di(*tert*-butyl)boryl]ethane (6a): A suspension of **5a** (1.00 g, 2.6 mmol) in 70 mL of hexane was reacted at −70 °C with 9 mL of *t*BuLi. After stirring at −20 °C the mixture was heated for 5 h under reflux. Separation of the solid resulted in a yellow solution, which was slowly concentrated under reduced pressure (50 Torr). The yellow, oily residue was distilled at 80 °C/0.4 Torr to yield **6a** (0.122 g, 12%). − ^{1}H NMR (200 MHz, $CDCl_3$): δ = 1.11 [s, 54 H, $C(CH_3)_3$], 1.92 (s, 3 H, CH_3). − ^{13}C NMR (50 MHz, $CDCl_3$): δ = 14.1 (CH_3), 30.3 [$C(CH_3)_3$], B*C* not observed. − ^{11}B NMR (29 MHz, $CDCl_3$): δ = 83.4. − EI-MS: *m*/*z* (%) = 325 (0.8) [M^+(**8a**) − H], 258 (1.2) [M^+(**7a**)], 243 (1.9) [M^+(**7a**) − Me], 41 (100).

3-(1,3,2-Benzodioxaborol-2-yl-1,2-bis(tricarbonylcobalta)tetrahedrane (9a): To a solution of $Co_2(CO)_8$ (2.034 g, 5.9 mmol) in 30 mL of hexane at −20 °C was slowly added **1a** (0.856 g,

Table 1. Data for the crystal structure analyses

	1a	**4a**	**5a(thf)$_3$**	**5a**	**9a**
Empirical formula	$C_8H_5BO_2$	$C_{14}H_{10}B_2O_4$	$C_{20}H_{15}B_3O_6{\cdot}3C_4H_8O$	$C_{20}H_{15}B_3O_6$	$Co_2C_{14}H_5BO_8$
Formula weight	143.93	263.84	600.06	383.50	429.85
Crystal system	tetragonal	monoclinic	monoclinic	orthorhombic	triclinic
Space group	$I4_1/a$	$P2_1/n$	$P2_1/n$	*Pbca*	$P\bar{1}$
Unit cell *a* [Å]	16.96(3)	5.870(3)	11.883(9)	11.996(2)	6.7766(1)
b [Å]	16.96(3)	6.002(3)	11.959(10)	30.683(4)	7.6633(1)
c [Å]	10.43(2)	17.693(9)	22.725(16)	39.120(5)	15.5942(3)
α [°]	90	90	90	90	100.385(1)
β [°]	90	96.95(4)	91.09(6)	90	94.252(1)
γ [°]	90	90	90	90	102.229(1)
Volume [Å^3]	2999(9)	618.8(5)	3229(4)	14399(3)	773.15(2)
Z	16	2	4	32	2
Density [g/cm^3]	1.275	1.416	1.234	1.416	1.846
μ [mm^{-1}]	0.089	0.100	0.087	0.101	2.186
F(000)	1184	272	1272	3168	424
Crystal size [mm]	0.80 × 0.50 × 0.20	0.35 × 0.35 × 0.30	0.90 × 0.60 × 0.35	0.38 × 0.21 × 0.13	0.46 × 0.17 × 0.03
θ-range[°]	24.94	23.96	22.50	26.36	28.28
Index ranges (*h*, *k*, *l*)	0/20, 0/20, 0/12	−6/6, 0/6, 0/20	−12/11, 0/12, 0/24	0/14, 0/38, 0/48	−9/8, −10/9, 0/20
No. of reflections	1325	876	4183	14670	3750
observed [$I > 2\sigma_I$]	949	590	2307	9532	3087
Parameters	120	111	403	1285	246
*R*1 [$I > 2\sigma_I$]	0.0384	0.0598	0.0588	0.0444	0.0279
*wR*2	0.0917	0.2013	0.1544	0.1162	0.0697
T (K)	203(2)	203(2)	203(2)	173(2)	173(2)
Max. residual electron density [e/Å^3]	0.13/−0.15	0.30/−0.33	0.22/−0.19	0.29/−0.25	0.67/−0.36

5.9 mmol) in 20 mL of hexane. After stirring for 3 days at 20 °C the solvent was removed and the reaction mixture separated by column chromatography (florisil): with n-hexane red-brown $Co_2(CO)_8$, and with toluene brown **9a** was eluted (1.082 g, 42%), m.p. 125 °C (dec.). – ^{1}H NMR (200 MHz, C_6D_6): δ = 5.83 (s, 1 H, CH), 6.94–6.70 (m, 4 H, H_{ar}),. – ^{13}C NMR (50 MHz, C_6D_6): δ = 71 (br., CB), 81.9 (CH), 112.8, 123.2, 149.0 (C_{ar}), 200 (br., CO). – ^{11}B NMR (64 MHz, C_6D_6): δ = 32.6. – EI-MS: *m/z* (%) = 430 (12) [M^+], 402 (39) [M^+ – CO], 374 (6) [M^+ – 2CO], 346 (16) [M^+ – 3CO], 318 (36) [M^+ – 4CO], 290 (91) [M^+ – 5CO], 262 (46) [M^+ – 6CO], 118 (100) [Bcat – H]$^+$. – HR-EIMS: *m/z* = 429.8763 [M^+], calcd. for $^{12}C_{14}{}^1H_5{}^{11}B^{16}O_8{}^{59}Co_2$: 429.8741 (Δ = 2.2 mmu).

X-ray Crystal Structure Analyses of 1a, 4a, 5a, 5a(thf)$_3$ and 9a: Table 1 contains details of the structures. The intensities for **1a**, **4a**, and **5a(thf)$_3$** were measured with a four-circle diffractometer, and for **9a** and **5a** with a CCD area detector (Mo-K_α radiation, λ = 0.71073 Å, graphite monochromator, ω-scans). The structures were solved by direct methods (SHELXS-86)[25] and refined by least-square methods based on F^2 with all measured reflections (SHELXL-97)[26]. For **1a**, **4a**, **5a** and **9a** the hydrogen atoms were located by difference Fourier synthesis and refined isotropically; for **5a(thf)$_3$** the hydrogen atoms were inserted in calculated positions. Crystallographic data (excluding structure factors) for the structures reported in this paper have been deposited with the Cambridge Crystallographic Data Centre as supplementary publication nos. CCDC-148514 (**1a**), -148515 (**4a**), -148516 [**5a(thf)$_3$**], -150265 (**5a**), and -148517 (**9a**). Copies of the data can be obtained free of charge on application to CCDC, 12 Union Road, Cambridge CB2 1EZ, UK [Fax: (internat.) +44-1223/336-033; E-mail: deposit@ccdc.cam.ac.uk].

Acknowledgments

Support of this work by the Deutsche Forschungsgemeinschaft (SFB 247), the Fonds der Chemischen Industrie, and the BASF AG is gratefully acknowledged. We thank Dr. Peter Greiwe for helpful discussions.

[1] R. Köster, H. J. Horstschäfer, P. Binger, *Liebigs Ann. Chem.* **1968**, *717*, 1.
[2] J. Soulié, P. Cadiot, *Bull. Soc. Chim. Fr.* **1966**, 3846.
[3] B. Wrackmeyer, H. Nöth, *Z. Naturforsch.* **1974**, *29b*, 564.
[4] For exchange of amino for oxygen substituents, see: R. J. Brotherton, A. L. McCloskey, J. L. Boone, H. M. Manasevit, *J. Am. Chem. Soc.* **1960**, *82*, 6245.
[5] C. Blanchard, E. Framery, M. Vaultier, *Synthesis* **1996**, 46.
[6] H. Schulz, G. Gabbert, H. Pritzkow, W. Siebert, *Chem. Ber.* **1993**, *126*, 1593.
[7] M. Hesse, H. Meier, B. Zeeh, *Spektroskopische Methoden in der Organischen Chemie*, 4. Aufl., Thieme Verlag, Stuttgart, **1991.**
[8] F. H. Allen, O. Kennard, D. G. Watson, L. Brammer, A. G. Orpen, R. Taylor, *J. Chem. Soc., Perkin Trans.* **1987**, *2*, 1.
[9] M. Bluhm, A. Maderna, H. Pritzkow, S. Bethke, R. Gleiter, W. Siebert, *Eur. J. Inorg. Chem.* **1999**, 1693.
[10] D. R. Stern, R. M. Washburn, U. S. Pat. 3092652, C. A. 11556, **1963**.
[11] K. Okada, T. Sugawa, M. Oda, *J. Chem. Soc., Chem. Commun.* **1992**, 74.
[12] K. P. C. Vollhard, *Angew. Chem.* **1984**, *96*, 525; *Angew. Chem. Int. Ed. Engl.* **1984**, *23*, 539.
[13] A. Maderna, H. Pritzkow, W. Siebert, *Angew. Chem.* **1996**, *108*, 1664; *Angew. Chem. Int. Ed. Engl.* **1996**, *35*, 1501.
[14] C. Ester, A. Maderna, H. Pritzkow, W. Siebert, *Eur. J. Inorg. Chem.* **2000**, 1177.
[15] G. W. Kabalka, *Org. Prep. Proced. Int.* **1977**, *9*, 133.
[16] Y. Gu, Dissertation, University of Heidelberg, **1999**.
[17] T. B. Marder, N. C. Norman, *Topics in Catalysis* **1998**, *5*, 63.
[18] D. S. Matteson, *Synthesis* **1975**, 147.
[19] F. Lhermitte, B. Carboni, *Synlett* **1996**, 377.
[20] M. Hildenbrand, H. Pritzkow, U. Zenneck, W. Siebert, *Angew. Chem.* **1984**, *96*, 371; *Angew. Chem. Int. Ed. Engl.* **1984**, *23*, 371.
[21] H. C. Brown, N. Ravindran, *J. Am. Chem. Soc.* **1973**, *95*, 2396.
[22] R. Soundararajan, D. S. Matteson, *J. Org. Chem.* **1990**, *55*, 2274; T. Deforth, H. Pritzkow, W. Siebert, *Angew. Chem.* **1995**, *107*, 748; *Angew. Chem. Int. Ed. Engl.* **1995**, *34*, 681.
[23] [23a] P. Galow, A. Sebald, B. Wrackmeyer, *J. Organomet. Chem.* **1983**, *259*, 253. – [23b] R. S. Dickson, P. J. Fraser, *Adv. Organomet. Chem.* **1974**, *12*, 323. – [23c] H. Greenfield, H. W. Sternberg, R. A. Friedel, J. H. Wotiz, R. Markby, I. Wender, *J. Am. Chem. Soc.* **1956**, *78*, 120. – [23d] U. Kruerke, W. Hübel, *Chem. Ber.* **1961**, *94*, 2829.
[24] [24a] C. Elschenbroich, A. Salzer, *Organometallchemie*, Verlag Teubner, Stuttgart, **1993**. – [24b] W. G. Sly, *J. Am. Chem. Soc.* **1959**, *81*, 18. – [24c] F. A. Cotton, J. D. Jamerson, B. R. Stults, *J. Am. Chem. Soc.* **1976**, *98*, 1774.
[25] G. M. Sheldrick, *SHELXS86*, University of Göttingen, **1986**.
[26] G. M. Sheldrick, *SHELXL97*, University of Göttingen, **1997**.

Received May 10, 2000
[I00189]

Syntheses and Reactivity of Exocyclic Unsaturated Heterodiborolanes and Their Diborylhexadiene Precursors − Formation of 2-Aza-4,5-dicarba-*nido*-hexaboranes(6)

Peter Greiwe,[a] Volker Beez,[a] Hans Pritzkow,[a] and Walter Siebert*[a]

Dedicated to Prof. Dr. Herbert Schumann on the occasion of his 65th birthday

Keywords: Heterocarboranes / Heterocycles / Hydroborations / Heteroboranes / Boron

The aryl-substituted 3,4-diboryl-2,4-hexadienes **4c–e** are generated when 3,4-bis(dimethoxyboryl)-2,5-dimethyl-2,4-hexadiene (**4a**) and 3,4-bis(dichloroboryl)-2,5-dimethyl-2,4-hexadiene (**4b**) react with two equivalents of xylyllithium or duryllithium. Cyclization reactions of **4b** with heptamethyldisilazane and of **4c** with $MeN(SiMe_3)_2$, $S(SiMe_3)_2$, and $O(SiMe_3)_2$ lead to the corresponding 2,5-diaryl-3,4-diisopropylidene-1-hetero-2,5-diborolanes **5a,b**, **6**, and **7** in excellent yields. 1-Aza-2,5-di-*tert*-butyl-3,4-diisopropylidene-1-methyl-2,5-diborolane (**5c**) is obtained from the reaction of **5a** with two equivalents of *tert*-butyllithium. When the azadichlorodiborolane **5a** is reacted with $Li[BH_4]$ or $Li[DurBH_3]$ the Cl atoms are replaced by hydrogen or duryl and the liberated BH_3 hydroborates the isopropylidene groups to form the 2-aza-4,5-dicarba-4,5-diisopropyl-2-methyl-*nido*-hexaboranes **10a,b**. The new compounds are characterized by MS and ^1H, ^{11}B and ^{13}C NMR spectroscopy. X-ray structure analyses of **4c** and **4e** show that the two halves of the hexadienes are rotated by 80 to 90°. The solid state structures of the three duryl-substituted heterodiborolanes **5b**, **6**, and **7** reveal twist conformations of the C_2B_2X rings.

Introduction

A number of larger azacarboranes with 10−12 vertices are known,[1] but, to the best of our knowledge, examples of smaller clusters with C,B,N framework atoms have not been published. Recently, we reported the hydroboration of appropriate heterocycles to produce carborane[2a] and heterocarborane[2b] compounds. In particular a combined substitution/hydroboration reaction of the thiadiborolane **1** with $Li[RBH_3]$ produces the 4,5-dicarba-2-thia-*nido*-hexaborane(5) derivatives **2a−d** and the thiadicarbanonaborane(8) **3**.[2b]

Analogously, it should be possible to synthesize other heterocarboranes as well. We describe here corresponding reactions of the 1-aza-1-methyl-2,5-diborolane **5a** to give derivatives of the new class of 2-aza-4,5-dicarba-*nido*-hexaboranes(6) (**10**). In addition, the syntheses of some boron-alkyl-substituted 1-aza-, 1-thia-, and 1-oxa-2,5-diborolanes are reported. They are potential precursors for heterodicarba-*nido*-hexaboranes.

Results and Discussion

3,4-Diboryl-2,4-hexadienes

Attempts to replace the chlorine atoms in **1** by alkyl groups using organometallic reagents were not successful, as cleavage of B−S bonds occurred. However, as will be demonstrated, such chlorine substitution is possible in the case of the azadiborolane **5a**. Because of this limitation, a generally applicable approach to substituted heterodiborolanes was developed. The key compounds are 3,4-bis(monoorganoboryl)-substituted 2,4-hexadienes of type **4**, which can be transformed into heterodiborolanes.

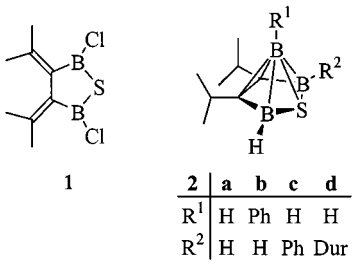

1

2	**a**	**b**	**c**	**d**
R^1	H	Ph	H	H
R^2	H	H	Ph	Dur

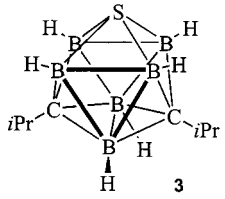

3

In the bis(dimethoxy)- and bis(dichloroboryl)hexadienes **4a,b**, each of the boryl groups may be monosubstituted when bulky xylyllithium or duryllithium are used, to give the compounds **4c−e**. Whereas **4d** is isolated in 70% yield by distillation, the yield of the crystalline duryl compound **4e** was considerably less (13%). The chlorine derivative **4c** was obtained by recrystallization from hexane in 40% yield. When the sterically less demanding *tert*-butyllithium was reacted with **4a,b**, mixtures of alkylated species with different substitution patterns were obtained (Scheme 1).

The derivatives **4d,e** are not suitable for cyclization reactions because the methoxy groups are unreactive toward trimethylsilyl reagents. Also, attempts to exchange OMe for Cl in **4d** using an excess of BCl_3 or PCl_5 did not lead to

[a] Anorganisch-Chemisches Institut der Universität Heidelberg, Im Neuenheimer Feld 270, 69120 Heidelberg, Germany
Fax: (internat.) +49-(0)6221/54-5609
E-mail: ci5@ix.urz.uni-heidelberg.de

 © WILEY-VCH Verlag GmbH, 69451 Weinheim, 2001 1434−1948/01/0202−0381 $ 17.50+.50/0

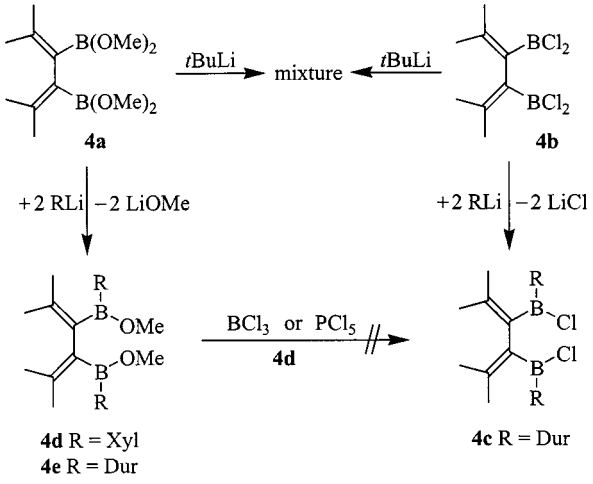

Scheme 1

the desired chlorine compound. Either **4d** did not react or decomposition occurred.

Heterodiborolanes

Cyclization reactions of 1,2-bis(dichloroboryl)- or 1,2-bis[chloro(organo)boryl]arenes, -alkenes, and -alkanes with reagents carrying trimethylsilyl as leaving groups have been successfully employed in the syntheses of various five and six-membered heterocycles.[3] Accordingly, compound **4b** reacts with one equivalent of $MeN(SiMe_3)_2$ to give the azadiborolane **5a** in 90% yield as a pale-yellow, air-sensitive liquid. In spite of the bulky duryl groups, compound **4c** yields the corresponding azadiborolane **5b** almost quantitatively when allowed to react with equimolar amounts of $MeN(SiMe_3)_2$. The formation of the duryl-substituted thia- and oxadiborolanes **6** and **7**, on the other hand, requires an excess of $O(SiMe_3)_2$ or $S(SiMe_3)_2$, the absence of solvent, and higher temperatures (120 °C). Under these conditions, **6** and **7** are obtained in very good yields (Scheme 2).

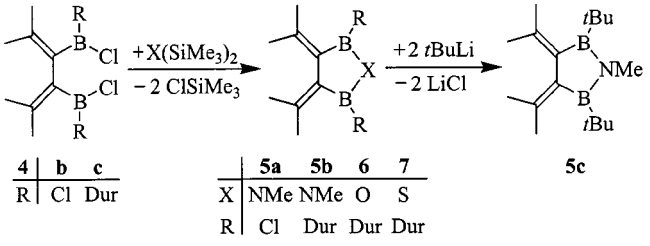

4	b	c
R	Cl	Dur

	5a	5b	6	7
X	NMe	NMe	O	S
R	Cl	Dur	Dur	Dur

Scheme 2

As shown above, monosubstitution of the boryl groups in the hexadienes **4a,b** can only be carried out when bulky substituents are used thus blocking a second substitution. A possible way to introduce smaller groups is the replacement of Cl in chloro-heterodiborolanes by alkyl groups; however, this was not successful for **1**. Only the azadiborolane **5a** is readily derivatized by this method. When treated with two equivalents of *tert*-butyllithium, compound **5a** generates the alkylated azadiborolane **5c** as a colorless, thermally labile liquid in 63% yield.

Azadicarba-*nido*-hexaboranes(6)

The only product of the reaction of **5a** with $Li[DurBH_3]$ is the 2-aza-4,5-dicarba-3-duryl-4,5-diisopropyl-2-methyl-*nido*-hexaborane (**10a**) carrying a duryl group in an equatorial position. This result is in agreement with the analogous reaction of the sulfur compound **1** with $Li[DurBH_3]$, whereas the reaction of **1** with $Li[PhBH_3]$ gives two isomers.[2b] This different behavior has been explained[2b] by a different reactivity of the lithium borates. In the first case, a duryl group would initially be transferred to the five-membered ring, which is then hydroborated by BH_3 to form the thiacarborane **2d**. In the second case, $Li[PhBH_3]$ would substitute the chlorine atoms by either hydrogen *or* a phenyl group and a mixture of two compounds (**2b,c**) is obtained. Such reasoning is not necessary if one assumes that the aryl group is always transferred first to give intermediates of type **5e,f** (if the starting material is **5a**) or the corresponding thia derivative (if the starting material is **1**), followed by hydroboration of the double bonds. This leads to a bicyclic organoborane of type **9** (and its thia analog) in which the boryl groups can easily change places by a rearrangement process prior to formation of the cluster structure (Scheme 3). Thus the finding of a mixture of two products (**2b,c**) having the phenyl group in either the apex *or* equatorial position and of only one product with an equatorial duryl substituent (**2d**, **10a**) can be explained by steric reasons. A duryl group in the apex position is strongly disfavored because the *ortho*-methyl groups would come very close to the isopropyl groups and the equatorial boron atoms.[4] For a phenyl group there is no such steric restriction, and both positions are possible.

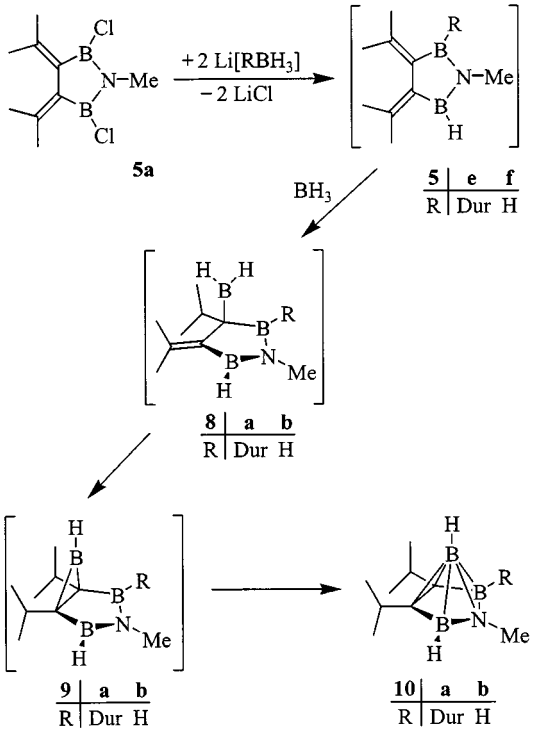

5	e	f
R	Dur	H

8	a	b
R	Dur	H

9	a	b
R	Dur	H

10	a	b
R	Dur	H

Scheme 3

When **5a** is allowed to react with $Li[BH_4]$, a complex mixture of BH-substituted products is formed (Scheme 3). Three of them can be separated by GC/MS analysis. The compound with the shortest retention time is easily identified as the 2-aza-4,5-dicarba-4,5-diisopropyl-2-methyl-*nido*-hexaborane(6) (**10b**) by MS. The molecular peak is found at $m/z = 175$ and its *nido* structure is inferred from the ^{11}B NMR spectroscopic data. The two other compounds with longer retention times show MS peaks at $m/z = 189$ and 349, respectively. The first peak may be assigned to a product which is formed by hydroboration of **5f** with two equivalents of BH_3; the isotopic distribution pattern supports the presence of an additional BH_3 relative to **10b**. The isotopic pattern of the compound with $m/z = 349$ is in agreement with a molecular formula of $(i\text{PrC})_4(BH)_6(NMe)_2$ suggesting "dimerization" of the azacarborane **10b** or its precursors **8b** or **9b**. Since several structural isomers are possible, a geometry is not proposed at this point.

Spectroscopic and Structural Characterization

Both, the ^1H and ^{13}C NMR spectra of the diborylhexadienes **4c–e** exhibit two signals for the isopropylidene methyl groups. For the aryl ring C atoms in **4d** not adjacent to boron, three resonances are found consistent with freely rotating xylyl groups. The *ortho*-methyl groups of the aryl substituents in **4d,e** produce a strongly broadened signal which shows that ring rotation is somewhat restricted. The NMR spectra of the chlorine derivative **4c** show four singlets for the duryl-methyl protons, and all six aromatic carbon atoms can be distinguished, implying a fully restricted rotation about the B–C bond at ambient temperature. Surprisingly, only one slightly broadened signal for the methyl carbon atoms of the duryl groups is found.

The ^{11}B NMR shifts of the aza- and oxadiborolanes **5b** and **6** are almost identical ($\delta = 55$ and 54, respectively) and the *tert*-butyl derivative **5c** gives a signal at $\delta = 58$, whereas the value for the thiadiborolane **7** is $\delta = 72$. Although the ^1H and ^{13}C NMR spectroscopic data suggest that the duryl groups can rotate freely in **5b** and **6**, the data for **7** are consistent with a restricted rotation, which might be explained by the larger B–S distances compared to B–N and B–O, and the accompanying geometrical changes (see below).

The composition of **10a** follows from the ^1H and ^{11}B NMR and the mass spectra. Although **10a** could not be separated fully from by-products, most of the ^1H NMR signals were assigned. Four doublets are observed for the isopropyl groups and four singlets for the duryl substituents, as expected for the *nido* structure shown in Scheme 3. This is supported by the ^{11}B NMR spectroscopic data showing one doublet at $\delta = -41.5$ ($^1J_{BH} = 202$ Hz) for the apex BH, a second doublet at $\delta = 13.5$ ($^1J_{BH} = 130$ Hz, equatorial BH), and a singlet at $\delta = 23.1$ (equatorial B-duryl). Among the signals of the product mixture obtained from the reaction of **5a** with $Li[BH_4]$, the ^{11}B NMR spectroscopic data of **10b** can be identified when compared to those of **10a**. The equatorial boron atoms give a doublet at $\delta = 13.6$ ($^1J_{BH} = 155$ Hz) and for the apical boron a signal at $\delta = -45.2$ ($^1J_{BH} = 202$ Hz) is found. These data are very similar to those measured for the closely related thiacarborane **1d**, and calculated values[2b] and are in line with the proposed *nido*-6-⟨V⟩ clusters with a pentagonal aperture derived from a pentagonal bipyramid by removal of one apical vertex. This geometry was found for the solid state structure of **1d**. Both azacarboranes show NMR signals for one five-connected boron atom in the high-field region having large B–H coupling constants which are typical of apical bonding situations.[5] At lower field resonances for two three-connected boron atoms are found exhibiting coupling constants in the normal range for equatorial bonding.[5] The alternative *nido*-6-⟨IV⟩ structure established for $N_2B_4H_6$ derivatives which represents a fragment of a pentagonal bipyramid with a missing vertex at the base[6] can thus be excluded. Such a geometry has two kinds of four-connected boron atoms and would give rise to NMR signals in the region between the values found for **10a,b**.

Single crystal X-ray diffraction studies showed that the unit cell of the crystals of **4e** contained two independent molecules with crystallographic C_2 symmetry. The solid state structures of **4c** (Figure 1) and **4e** exhibit, as expected, similar features. The $Me_2C{=}C{-}B(OMe)/Cl$ units are

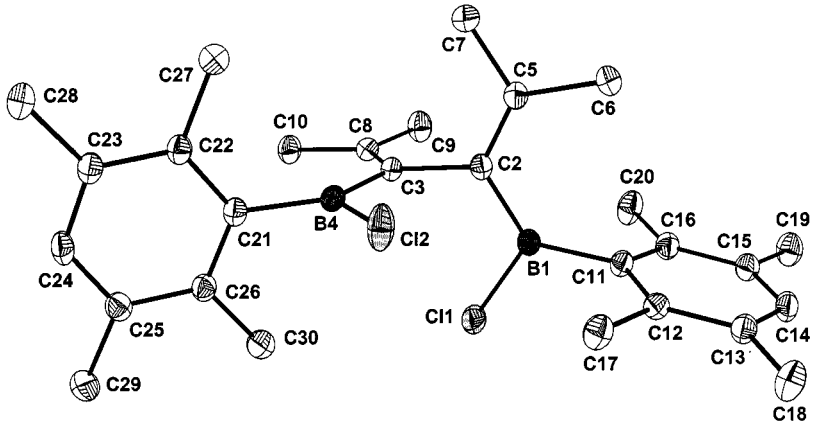

Figure 1. Molecular structure of **4c**; selected bond lengths [Å] (corresponding data for **4e** in square brackets): C3–C8 1.355(3) [1.328(8)], C2–C5 1.360(3) [1.355(8)], C2–C3 1.529(3) [1.520(10), 1.510(11)], C3–B4 1.540(4) [1.574(9)], C2–B1 1.541(4) [1.560(10)], B4–Cl2 1.799(3) [B–O 1.374(8)] B1–Cl1 1.802(3) [B–O 1.377(8)], B4–C21 1.582(4) [1.589(9)], B1–C11 1.581(4) [1.590(8)]

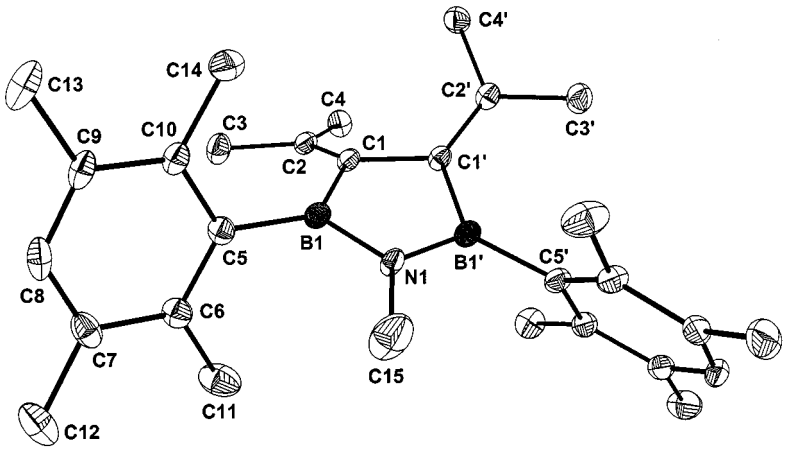

Figure 2. Molecular structure of **5b**; selected bond lengths [Å] and angles [°]: C1−C1′ 1.501(6), C1−C2 1.353(4), C1−B1 1.567(5), B1−C5 1.575(5), B1−N1 1.425(4), N1−C15 1.462(7); C2−C1−C1′−C2′ 51.0

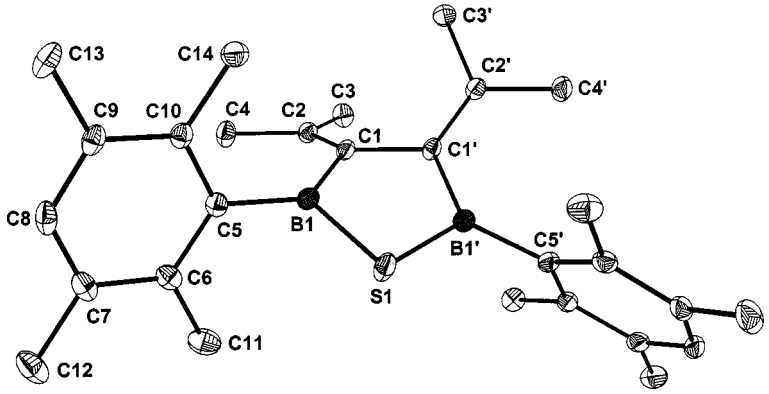

Figure 3. Molecular structure of **7**; selected bond lengths [Å] and angles [°] (corresponding data for **6** in square brackets): C1−C1′ 1.508(3) [1.500(4)], C1−C2 1.359(2) [1.358(3)], C1−B1 1.552(2) [1.571(3)], B1−C5 1.572(2) [1.570(5)], B1−S1 1.824(2) [B1−O1 1.400(2)]; C2−C1−C1′−C2′ 53.8 [50.2]

planar and the two halves of the molecules are rotated by 90° (**4c**) and by 78 and 82° in the two independent molecules of **4e**. This difference is most probably due to crystal packing effects. The duryl groups are positioned almost perpendicular to the $Me_2C{=}C{-}B(OMe)/Cl$ plane (85/89° in **4c** and 88/87° in **4e**).

The molecular structures of **5b** (Figure 2), **6** and **7** (Figure 3) exhibit C_2 symmetry, the axis bisects the C1−C1′ bond and runs through the heteroatom. The five-membered rings are twisted about the C1−C1′ bond by 17.9° (**5b**), 16.0° (**6**) and 22.3° (**7**), respectively (B1−C1−C1′−B1′ torsion angles). Because of the steric bulk, the two neighboring isopropylidene groups are twisted about the double bonds by 18.5° (**5b**), 19.0° (**6**), and 18.1° (**7**) as determined from the [C1′−C1−B1]/[C4−C3−C2] interplanar angles. The duryl groups adopt angles of 67° (**5b**), 66° (**6**), and 69° (**7**) with the corresponding C1−B1−X planes.

Conclusion

In this paper we report a route to transform the azaorganoborane heterocycle **5a** into the 2-aza-4,5-dicarba-*nido*-hexaboranes **10a,b**. The synthetic strategy involves a substitution/hydroboration reaction of **5a** with $Li[RBH_3]$ (R = H, Dur) to give the hydrido-1-aza-2,5-diborolanes **5e,f** which are hydroborated by the freed BH_3. Presumably, the final products **10a,b** are formed via the intermediates **8a,b** and **9a,b**. This reaction sequence allows the formation of other heterodicarbahexaboranes.

Experimental Section

All reactions and manipulations were performed in dry glassware under argon or nitrogen using standard Schlenk techniques. Solvents were distilled from appropriate drying agents under inert gas before use. − $Et_2O{\cdot}BF_3$ was used as the external standard for ^{11}B NMR. As internal references for ^1H and ^{13}C NMR spectra the signals of the deuterated solvents were used and calculated for TMS. NMR: Bruker AC 200 and Bruker DRX 200. − MS: Varian MAT CH7 and GCMS HP 5971. − The following starting materials were prepared by literature methods: lithium durylborate,[7] xylyllithium,[8] duryllithium.[8] Hexamethyldisilathiane, hexamethyldisiloxane, and heptamethyldisilazane were commercially obtained.

3,4-Bis[(chloro)durylboryl]-2,5-dimethyl-2,4-hexadiene (4c): A sample of duryllithium ($DurLi{\cdot}OEt_2$; 5.14 g, 24.8 mmol), obtained from DurBr and LiBu, was suspended in 150 mL of hexane, cooled to 0 °C, and **4b** (3.35 g, 12.4 mmol), dissolved in 20 mL of hexane, was added. The mixture was refluxed for 2.5 h and the precipitate

filtered off and washed twice with 20 mL of hexane. The filtrates were concentrated and cooled to −30 °C. Colorless **4c** (2.31 g, 5 mmol, 40%) precipitated from the solution. − ^{1}H NMR (C_6D_6, 200 MHz): δ = 1.77, 1.82 (2 s, 2 × 6 H, $(CH_3)_2C$), 2.09, 2.10 (2 s, 2 × 6 H, *m*-aryl-CH_3), 2.24, 2.42 (2 s, 2 × 6 H, *o*-aryl-CH_3), 6.88 (s, 2 H, aryl). − ^{11}B NMR (C_6D_6, 64 MHz): δ = 61. − ^{13}C NMR (C_6D_6, 50 MHz): δ = 19.4 (aryl-CH_3), 26.7, 23.7 [2 × C(*C*H_3)$_2$], 131.5, 131.8, 132.5, 133.8, 134.2 (5 × C_{aryl}), 145, 147 [both br, B*C*C$(CH_3)_2$ and BC_{aryl}], 164.1 [*C*$(CH_3)_2$]. − EI-MS: *m*/*z* (%) = 467 [M^+], (19), 432 [M^+ − Cl] (100), 413 (71), 332 [M^+ − Dur] (23).

3,4-Bis[(2,6-dimethylphenyl)methoxyboryl]-2,5-dimethyl-2,4-hexadiene (4d) and 3,4-bis[(duryl)methoxyboryl]-2,5-dimethyl-2,4-hexadiene (4e): The same procedure as described for **4c** was used. Instead of recrystallization the solvent was stripped off and the remaining viscous product was distilled under high vacuum. Yields: 790 mg (2 mmol, 70%) of **4d** and 100 mg (0.2 mmol, 13%) of **4e**. Compound **4e** crystallizes at room temp. after a few hours, whereas **4d** becomes a glass-like solid

4d: ^{1}H NMR ($CDCl_3$, 200 MHz): δ = 1.65, 1.69 [2 s, 2 × 6 H, C$(CH_3)_2$], 2.15 (s, broad, 12 H, aryl-CH_3), 3.38 (O−CH_3), 6.91 (d, $^3J_{HH}$ = 7.5 Hz, 4 H, aryl), 7.08 (t, $^3J_{HH}$ = 7.5 Hz, 2 H, aryl). − ^{11}B NMR ($CDCl_3$, 64 MHz): δ = 47. − ^{13}C NMR ($CDCl_3$, 50 MHz): δ = 21.3 (aryl-CH_3), 22.4, 24.0 [C(*C*H_3)$_2$], 53.5 (O−CH_3), 126.1, 127.1, 137.9 (3 × C_{aryl}), 141, 143 [both br, B*C*C$(CH_3)_2$ and BC_{aryl}], 147.3 [*C*$(CH_3)_2$]. − EI-MS: *m*/*z* (%) = 402 (22) [M^+], 298 (8) [M^+ − xylyl], 224 (66) [M^+ − (BXylOMe) − OMe], 209 (58) [M^+ − (BXylOMe) − OMe − Me], 147 (100) [XylBOMe$^+$].

4e: ^{1}H NMR (C_6D_6, 200 MHz): δ = 1.84, 1.86 [2 s, 2 × 6 H, $(CH_3)_2$C], 2.17 (s, 12 H, *m*-aryl-CH_3), 2.22 (s, br, 12 H, *o*-aryl-CH_3), 3.32 (s, 6 H, O−CH_3), 6.90 (s, 2 H, duryl). − ^{11}B NMR (C_6D_6, 64 MHz): δ = 49. − ^{13}C NMR ($CDCl_3$, 50 MHz): δ = 18.3, 19.6 (aryl-CH_3), 22.7, 24.4 [2 × C(*C*H_3)$_2$], 53.4 (O−CH_3), 131.1, 133.3, 133.7 (3 × C_{aryl}), 147.6 [*C*$(CH_3)_2$]. − EI-MS: *m*/*z* (%) = 458 (12) [M^+], 325 (9) [M^+ − duryl], 309 (4), 252 (37) [M^+ − DurB$(OMe)_2$], 237 (31), 175 (100) [DurBOMe$^+$].

1-Aza-2,5-dichloro-3,4-diisopropylidene-1-methyl-2,5-diborolane (5a): Heptamethyldisilazane (1.52 g, 8.69 mmol) was added at room temp. to a solution of **4b** (2.36 g, 8.69 mmol) in 50 mL of hexane. The mixture was refluxed for 4 h, the solvent evaporated and the residue distilled at 58 °C/8 × 10^{-3} mbar to give 1.80 g (7.8 mmol, 90%) of colorless, air-sensitive **5a**. − ^{1}H NMR (C_6D_6, 200 MHz): δ = 1.71, 2.15 [2 s, 2 × 6 H, $(CH_3)_2$C, *exo* and *endo*], 2.89 (s, 3 H, N−CH_3). − ^{11}B NMR (C_6D_6, 64 MHz): δ = 44. − ^{13}C NMR (C_6D_6, 50 MHz): δ = 23.1, 26.4 [2 × C(*C*H_3)$_2$, *exo* and *endo*], 29.7 (N−CH_3), 137 [br, B*C*−C$(CH_3)_2$], 146.0 [*C*$(CH_3)_2$]. − EI-MS: *m*/*z* (%) = 229 (51) [M^+], 214 (100) [M^+ − CH_3], 200 (7) [M^+ − C_2H_5], 122 (25) [M^+ − C_8H_{11}].

1-Aza-2,5-diduryl-3,4-diisopropylidene-1-methyl-2,5-diborolane (5b): Heptamethyldisilazane (325 mg, 1.85 mmol) was added to a solution of **4c** (650 mg, 1.4 mmol) in 25 mL of hexane. The mixture was stirred for 15 h, filtered and the solvent removed in vacuo. According to the ^{1}H NMR spectrum the reaction was almost quantitative. Recrystallization from hexane at −80 °C gave 425 mg (1 mmol, 70%) of colorless **5b**. − ^{1}H NMR (C_6D_6, 200 MHz): δ = 1.81, 1.84 [2 s, 2 × 6 H, $(CH_3)_2$C], 2.16, 2.26 [2 s, 2×12 H, aryl-CH_3], 2.56 (N−CH_3), 6.94 (s, 2 H, duryl). − ^{11}B NMR (C_6D_6, 64 MHz): δ = 55. − ^{13}C NMR (C_6D_6, 50 MHz): δ = 19.0, 19.6 (aryl-CH_3), 25.9, 23.2 [C(*C*H_3)$_2$], 31.6 (N−CH_3), 131.3, 133.5 (2 × C_{aryl}), 142.5 (C_{aryl}H), 143, 144 [both br, B*C*C$(CH_3)_2$ and BC_{Aryl}]. − EI-MS: *m*/*z* (%) = 425 (100) [M^+], 382 (17) [M^+ − C$(CH_3)_2$], 356 (12), 291 (17) [M^+ − Dur].

1-Aza-2,5-di-*tert*-butyl-3,4-diisopropylidene-1-methyl-2,5-diborolane (5c): *tert*-Butyllithium (24 mmol, 1.7 M in pentane) was added to a solution of **5a** (2.74 g, 12 mmol) in hexane at −50 °C. The mixture was stirred for 15 h at room temp., the liquid separated from the precipitate and the solvent removed in vacuo. The remaining oil was distilled at 10^{-2} mbar and a bath temperature of 50−90 °C yielding 2.06 g (7.5 mmol, 63%) of **5c**. Part of the product decomposed under these conditions to a dark brown solid. − ^{1}H NMR ($CDCl_3$, 200 MHz): δ =1.19 (s, 18 H, *t*Bu), 1.66, 1.82 [2 s, 2×6 H, $(CH_3)_2$C], 2.88 (s, 3 H, N−CH_3). − ^{11}B NMR (C_6D_6, 64 MHz): δ = 58. − ^{13}C NMR (C_6D_6, 50 MHz): δ = 21.4 [*C*$(CH_3)_2$], 22.9, 26.9 [2 × C(*C*H_3)$_2$], 28.6 [C(*C*H_3)$_3$], 32.9 (N−CH_3), 126.0 [*C*$(CH_3)_2$], 150 [br, B*C*C$(CH_3)_2$]. − EI-MS: *m*/*z* (%) = 273 (28) [M^+], 216 (24) [M^+ − *t*Bu], 174 (10) [M^+ − C$(CH_3)_2$], 160 (16), 41 (100) [$C_3H_5^+$].

2,5-Diduryl-3,4-diisopropylidene-1-oxa-2,5-diborolane (6): A sample of **4c** (400 mg) was refluxed for six hours in 10 mL of hexamethyldisiloxane. After removal of all volatile components, pure **6** remained as a colorless solid. − ^{1}H NMR (C_6D_6, 200 MHz): δ = 1.69, 1.86 [2 s, 2×6 H, $(CH_3)_2$C], 2.12, 2.33 (2 s, 2×12 H, aryl-CH_3), 6.94 (s, 2 H, duryl). − ^{11}B NMR (C_6D_6, 64 MHz): δ = 54. − ^{13}C NMR (C_6D_6, 50 MHz): δ = 19.5, 19.3 (2 × aryl-CH_3), 23.5, 25.6 [2 × C(*C*H_3)$_2$], 132.1, 133.5, 134.5 (C_{aryl}H), 147.5 [*C*$(CH_3)_2$]. − m.p. 190 °C (dec.). − EI-MS: *m*/*z* (%) = 412 (100) [M^+], 278 (25) [M^+ − Dur], 252 (38) [M^+ − DurBO].

2,5-Diduryl-3,4-diisopropylidene-1-thia-2,5-diborolane (7): A sample of **4c** (800 mg, 1.71 mmol) was heated for 4 h to 120 °C in 5 mL of hexamethyldisilathiane. The yellow solution was cooled to room temp. which caused the product to precipitate. The colorless solid **7** (610 mg, 1.4 mmol, 83%) was separated and washed with cold hexane. − ^{1}H NMR ($CDCl_3$, 200 MHz): δ = 1.77, 1.82 [2 s, 2 × 6 H, $(CH_3)_2$C], 2.07 (s, 6 H, aryl-CH_3), 2.21 (s, 18 H, aryl-CH_3), 6.92 (s, 2 H, duryl). − ^{11}B NMR ($CDCl_3$, 64 MHz): δ = 72. − ^{13}C NMR ($CDCl_3$, 50 MHz): δ = 18.9, 19.3 (2 × *m*-aryl-CH_3), 19.5, 19.8 (2 × *o*-aryl-CH_3), 22.8, 25.4 [2 × C(*C*H_3)$_2$], 131.2, 132.3, 132.5, 133.1, 133.5 (5 × C_{aryl}), 145 [br, B*C*−C$(CH_3)_2$ or BC_{aryl}], 145.5 [*C*$(CH_3)_2$], 148 [br, B*C*−*C*$(CH_3)_2$ or BC_{aryl}]. − EI-MS: *m*/*z* (%) = 428 (100) [M^+], 294 (20) [M^+ − Dur], 253 (69) [M^+ − C$(CH_3)_2$ − Dur].

2-Aza-4,5-dicarba-3-duryl-4,5-diisopropyl-2-methyl-*nido*-hexaborane(6) (10a): Lithium durylborate (990 mg, 6.2 mmol) was suspended in 60 mL of hexane. Compound **5a** (720 mg, 3.1 mmol) was added at room temp. and the mixture was stirred for 48 h. The solution was separated from the precipitate, the solvent evaporated and the residue distilled at 90−100 °C/8 × 10^{-3} mbar to yield 142 mg of a colorless oil consisting mostly of **10a**. − ^{1}H NMR ($CDCl_3$, 200 MHz): δ = 0.95, 0.99, 1.17, 1.20 [4 d, 4×3 H, CH(C*H*$_3$)$_2$, $^3J_{HH}$ = 8 Hz], 2.16, 2.19 (2 s, 2 × 3 H, *m*-methyl), 2.21, 2.23 (2 s, 2 × 3 H, *o*-methyl), 2.62 (s, 3 H, *N*-methyl), 6.88 (s, 1 H, *p*-aryl-CH). − ^{11}B NMR (C_6D_6, 64 MHz): δ = 23.1 (s, B-duryl), 13.5 (d, B_{eq}H, $^1J_{BH}$ = 130 Hz), −41.5 (d, B_{apical}H, $^1J_{BH}$ = 202 Hz). − EI-MS: *m*/*z* (%) = 295 (20) [M^+ − B], 280 (3) [M^+ − B − CH_3], 252 (10) [M^+ − B − C_3H_7], 43 (100) [$C_3H_7^+$], 41 [$C_3H_5^+$].

2-Aza-4,5-dicarba-4,5-diisopropyl-2-methyl-*nido*-hexaborane(6) (10b): Li[BH_4] (155 mg, 5.75 mmol) was suspended in 50 mL of hexane and **5a** (660 mg, 2.88 mmol) was added at room temp. After 5 h of stirring at 40 °C, the solvent was removed at 1 mbar and the remaining colorless oil condensed into a dry-ice cooled trap. − ^{11}B NMR (C_6D_6, 64 MHz): δ = −45.2 (d, B_{apical}, $^1J_{BH}$ = 202 Hz), 13.6 (d, B_{eq}, $^1J_{BH}$ = 155 Hz). − EI-MS: *m*/*z* (%) = 175 (22) [M^+], 160 (10) [M^+ − Me], 146 (11) [M^+ − NMe], 132 (45) [M^+ − *i*Pr], 41 (100) [$C_3H_5^+$].

Table 1. Crystal data and structure refinement for **4c**, **4e**, **5b** **6** and **7**

	4c	**4e**	**5b**	**6**	**7**
Empirical formula	$C_{28}H_{38}B_2Cl_2$	$C_{30}H_{44}B_2O_2$	$C_{29}H_{41}B_2N$	$C_{28}H_{38}B_2O$	$C_{28}H_{40}B_2O_{0.09}S_{0.91}$
Formula weight	467.10	458.27	425.25	412.20	428.87
Crystal system	monoclinic	orthorhombic	monoclinic	monoclinic	monoclinic
Space group	$P2_1/c$	$P2na$	$C2/c$	$C2/c$	$C2/c$
a [Å]	10.867(5)	8.852(4)	23.547(12)	23.555(15)	24.3272(16)
b [Å]	11.993(6)	13.814(7)	9.351(7)	9.139(5)	8.7071(6)
c [Å]	21.416(11)	23.761(11)	14.866(9)	15.018(9)	15.4201(10)
α [°]	90	90	90	90	90
β [°]	95.90(3)	90	126.83(3)	127.87(3)	128.412(1)
γ [°]	90	90	90	90	90
V [Å^3]	2776(2)	2906(2)	2620(3)	2552(3)	2559.3(3)
Z	4	4	4	4	4
Calcd. density [g/cm^3]	1.118	1.048	1.078	1.073	1.113
Absorp. coeff. [mm^{-1}]	0.247	0.062	0.060	0.061	0.133
F(000)	1000	1000	928	896	933
Crystal size [mm]	0.65 × 0.50 × 0.35	0.60 × 0.30 × 0.25	0.55 × 0.45 × 0.06	0.65 × 0.40 × 0.35	0.18 × 0.24 × 0.34
Θ_{max} [°]	26.00	23.00	25.00	25.00	28.30
Index ranges	−13/13, 0/14, 0/26	0/8, 0/15, 0/26	−17/25, −11/0, −17/17	−17/28, −10/0, −17/17	−31/25, 0/11, 0/20
No. of reflections					
Unique	5460	2037	1989	2240	3092
Observed [$I > 2\sigma(I)$]	5460	2802	1989	2240	8705
Transmission	0.999−0.875	0.998−0.914		0.999−0.964	0.928−0.763
Parameters	304	322	157	218	222
Final R indices					
$R1$ [$I > 2\sigma(I)$]	0.0527	0.0503	0.0595	0.0441	0.0441
$wR2$	0.1304	0.1055	0.1486	0.1102	0.1102
Res. electron dens.[e/Å^3]	+0.225 / −0.286	+0.171 / −0.185	+0.188 / −0.335	+0.175 / −0.128	+0.332 / −0.532

Crystal Structure Determinations: Crystal data and details of the structure determinations are presented in Table 1. Data collection for **4c**, **4e**, **5b**, and **6**: Siemens Stoe AED2 diffractometer (Mo-K_α radiation, ω-scans) at −70 °C; for **7**: Bruker AXS Smart 1000 area detector (Mo-K_α, ω-scans) at −100 °C. The structures were solved by direct methods (SHELXS 86)[9] and refined by least-squares based on F^2 with all measured reflections (SHELXL 97)[9] using anisotropic temperature factors for non-hydrogen atoms. Hydrogen atoms were located and refined isotropically (**6**, **7**) or inserted in calculated positions (**4c**, **4e**, **5b**). The structure refinement of **7** revealed that sulfur was partially replaced by oxygen (ca. 9%).

Crystallographic data (excluding structure factors) for the structures reported in this paper have been deposited with the Cambridge Crystallographic Data Centre as supplementary publication nos. CCDC-146539 (**4c**), -146540 (**4e**), -146541 (**5b**), -146542 (**6**), and -146543 (**7**). Copies of the data can be obtained free of charge on application to CCDC, 12 Union Road, Cambridge CB2 1EZ, UK [Fax: (internat.) +44-1223/336-033; E-mail: deposit@ccdc.cam.ac.uk].

Acknowledgments

Support of this work by the Deutsche Forschungsgemeinschaft (Schwerpunktprogramm Polyeder), the Fonds der Chemischen Industrie and the BASF AG is gratefully acknowledged.

[1] V. A. Brattsev, S. P. Knyazev, G. N. Danilova, V. I. Stanko, *Zh. Obshch. Khim.* **1975**, *45*, 1393−94; Engl. Ed. p. 1364; A. E. Wille, K. Su, P. J. Carroll, L. G. Sneddon, *J. Am. Chem. Soc.* **1996**, *118*, 6407−6421; J. Plesek, B. Stibr, D. Hnyk, T. Jelinek, S. Hermanek, J. D. Kennedy, M. Hofmann, P. v. R. Schleyer, *Inorg. Chem.* **1998**, *37*, 3902−3909.

[2] [2a] W. Siebert, R. Hettrich, H. Pritzkow, *Angew. Chem.* **1994**, *106*, 215−217; *Angew. Chem. Int. Ed. Engl.* **1994**, *33*, 203−204. − [2b] V. Beez, P. Greiwe, H. Pritzkow, M. Hofmann, P. v. R. Schleyer, W. Siebert, *Eur. J. Inorg. Chem.* **1998**, 1775−1779.

[3] P. Frankhauser, M. Drieß, H. Pritzkow, W. Siebert, *Chem. Ber.* **1994**, *127*, 329−331; W. Siebert, H. Schmidt, R. Full, *Z. Naturforsch.* **1980**, *35b*, 873−81; W. Haubold, A. Gemmler, *Chem. Ber.* **1980**, *113*, 3352−56; W. Haubold, U. Kraatz, *Chem. Ber.* **1979**, *112*, 1083.

[4] As simple modeling of such a carborane shows the only possible orientation for an apical duryl group is parallel to the basal B−B and C−C vectors. Even in this position the *ortho*-methyl groups are very close to the isopropyl substituents and the equatorial boron atoms, but these steric interactions do not seem to be severe enough that one would completely exclude the possibility of a duryl group in the apical position. There are only two feasible ways from which such a carborane could originate: by an exchange of two boryl groups in **9a** or by a hydroboration with 1,2-diduryldiborane(6). Both reactions would involve intermediates with even shorter duryl−isopropyl contacts, too short for nonbonding interactions. Thus a carborane with a duryl group in an apical position should be stable but in the above discussed cases duryl−isopropyl interactions make the bicyclic intermediates energetically inaccessible so that a carborane cannot form this way.

[5] J. Kroner, B. Wrackmeyer, *J. Chem. Soc., Faraday Trans. 2* **1976**, *72*, 2283.

[6] P. Paetzold, B. Redenz-Stormanns, R. Boese, *Chem. Ber.* **1991**, *124*, 2435−2441; R. Boese, B. Kröckert, P. Paetzold, *Chem. Ber.* **1987**, *120*, 1913−1915.

[7] A. Berndt, *Angew. Chem.* **1993**, *105*, 1034; *Angew. Chem. Int. Ed. Engl.* **1993**, *32*, 985.

[8] E. Wehman, J. T. B. H. Jastrzebski, J.-M. Ernsting, D. M. Grove, G. v. Koten, *J. Organomet. Chem.* **1988**, *353*, 133−143; instead of the aryl iodide the bromide was used.

[9] G. M. Sheldrick, SHELXS-86, SHELXL97, University of Göttingen.

Received July 5, 2000
[I00267]

Reactions of Diboratetrahalides(4) with Boriranylideneboranes − Formation, Reactivity, and Structures of Cyclic Tetraborylmethanes and Isomeric Diborylmethyleneborane Derivatives

Andreas Ziegler,[a] Hans Pritzkow,[a] and Walter Siebert*[a]

Dedicated to Prof. Dr. Günter Helmchen on the occasion of his 60th birthday

Keywords: Boranes / Diboration / Hyperconjugation / Cyclizations

Reaction of the boriranylideneboranes **1a**,**b**,**c** with tetrahalogenodiboranes(4) leads to two types of products. In the case of **1a** the cyclic tetraborylmethane derivatives **2a**,**a′** are formed in high yield, whereas **1b**,**c** yield the isomeric linear diborylmethyleneboranes **3b**,**c**. Compound **2a** reacts with diethylamine, (dimethylamino)trimethylsilane, and lithium pyrrolidinide to give the 1,3-diboretanes **4a**,**b**,**c**. The composition of the products was determined from spectroscopic data and X-ray structure analyses of **2a**, **3c**, **4a**, and **4c**.

Introduction

In 1969 the first synthesis of tetraborylmethane derivatives was reported. Stone et al.[1] obtained the tetrakis(dichloroboryl)methane (**A**), which was characterized by mass spectrometry, in a co-condensation reaction of carbon and borontrichloride. At the same time, Matteson et al. synthesized the oxygen-substituted derivatives **B** and **C**.[2−5] These compounds are widely used in organic synthesis.

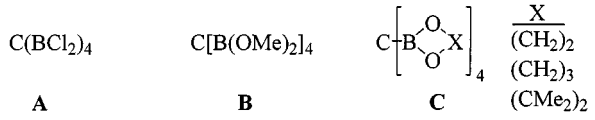

A **B** **C**

Tetraborylmethane [$C(BH_2)_4$] has been the subject of theoretical studies. Schleyer et al. calculated the energy differences between the tetrahedral and the planar structure of methane derivatives.[6] It was found that electropositive substituents like lithium or boron should stabilize the planar tetracoordinate configuration by reducing the energy difference of 630 kJ/mol between tetrahedral and planar methane. For nonclassical (planar) methane, boron and lithium should act as σ-donor and π-acceptor substituents. The formation of a three-center, two-electron bond means that all substituents must lie in the same plane. Recently, the X-ray structure analysis of $C[B(OMe)_2]_4$ revealed, as expected, that it has the classical tetrahedral structure.[7]

We present here reactions of the nonclassical boriranylideneboranes **1a**,**b**,**c**, first prepared by Berndt et al. in the early 1980s,[8,9] with tetrahalogenodiboranes(4). In the case of the *tert*-butyl-substituted compound **1a**, the addition of B_2X_4 (X = Cl, Br) leads to **2a**,**a′**, which are the first tetraborylmethane derivatives with two different substituents at the central carbon atom (Scheme 1). In contrast, **1b**,**c** and B_2Cl_4 form the linear products **3b**,**c** in good yields. To our surprise the reactivity of **2a**,**a′** is rather weak. Substitutions to form definite products occur with amines to give **4a**,**b**,**c**.

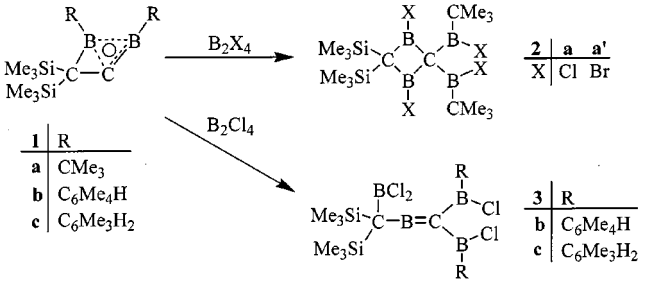

Scheme 1

Results and Discussion

Synthesis and Reactivity

The tetraborylmethanes **2a** and **2a′** are formed in excellent yields upon addition of B_2X_4 (X = Cl, Br) to a solution of **1a** in hexane at low temperature. The spectroscopic data of **2a**,**a′** are similar; **2a** is a colorless, low melting, crystalline solid, which shows only one ^{11}B NMR signal at δ = 69 for all boron atoms. In the ^1H NMR spectrum the expected signals for $SiMe_3$ and CMe_3 are observed. The ^{13}C NMR spectrum of **2a** exhibits the resonances of the methyl groups of the trimethylsilyl and *tert*-butyl substituents at δ = 3.7 and 29.6, respectively. The quaternary carbon atoms of CMe_3 and Si_2CB_2 give broad signals at δ = 31 and 58, respectively. A low-field temperature-dependent signal at δ = 79 is detected for the central carbon atom of CB_4.

Compound **2a′** is less stable than **2a**. Decomposition of freshly prepared, colorless **2a′** is visible by the increase of a

[a] Anorganisch-Chemisches Institut der Universität Heidelberg, Im Neuenheimer Feld 276, 69120 Heidelberg, Germany
Fax: (internat.) +49-6221/545-609
E-mail: ci5@ix.urz.uni-heidelberg.de

 © WILEY-VCH Verlag GmbH, 69451 Weinheim, 2001 1434−1948/01/0202−0387 $ 17.50+.50/0

brown color. The CI mass spectra of **2a′** exhibits the molecular ion peak [M^+] at $m/z = 648$ with an intensity of 2%.

The reaction of B_2Cl_4 with the aryl-substituted compounds **1b**,**c** yields slightly yellow crystals of **3b**,**c** with a molecular mass of 622 and 594, respectively. The ^{11}B NMR spectra show, for both compounds, one broad signal, which splits at higher temperature into two peaks with a 1:1 intensity. The signal at lower field belongs to the two equivalent boron atoms, the second signal is formed by superposition of signals for the remaining boron centers. The expected signals appear in the ^1H and the ^{13}C NMR spectra of **3b**,**c**, the signals for CB_3 are broad and located at $\delta = 95$ and 96, respectively.

In an attempt to substitute the four chlorine atoms at boron by amino substituents, compound **4a** was synthesized by treating **2a** with an excess of diethylamine in hexane (Scheme 2). This type of compound is already known in the literature and was first prepared by Berndt et al.[10,11] It is obtained as a colorless solid in good yield. During the reaction, one of the carbon−boron bonds is cleaved with protonation of the carbon atom by the amine. The ^{11}B NMR spectrum of **4a** shows only one signal at $\delta = 45$ for all three boron atoms. For the methylene protons of the diethylamine groups of the ring, an ABX_3 system appears due to the prochiral carbon ring atom. The resonance for the proton at HCB_3 is located at $\delta = 0.37$, as indicated by a two-dimensional ^1H, ^{13}C NMR study. The remaining signals of **4a** are in the expected areas. In the ^{13}C NMR spectrum the CB_3 signal is located at $\delta = 28$.

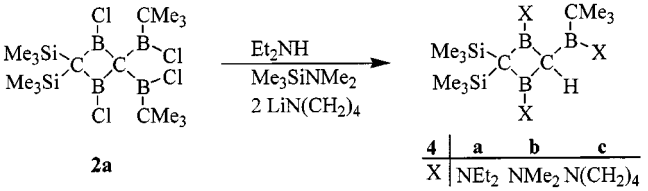

Scheme 2

In another attempt to synthesize a tetraborylmethane derivative with four amino groups, compound **2a** was treated with four equivalents of (dimethylamino)trimethylsilane. The only product isolated in this reaction is **4b**, an analog of **4a**. The origin of the hydrogen in **4b** is not known, although it might come from the *tert*-butyl group of the cleaved boryl group. However, the expected cleavage product, a (dimethylamino)boracyclopropane, was not detected. Compound **4b** was characterized by ^1H, ^{13}C and ^{11}B NMR spectroscopy. A CI mass spectrum of **4b** shows the molecular ion peak [$M^+ + 1$] at $m/z = 394$ as the base peak.

To obtain further information on the reactivity of **2a**, attempts were made to substitute only two of the four chlorine atoms at boron by amino substituents. When **2a** is treated with two equivalents of lithium pyrrolidinide, the formation of **4c** is observed. Its composition was determined by NMR and MS spectroscopy and an X-ray structure analysis.

Crystal Structures

Single crystals of **2a** were grown from a hexane solution at −20 °C. Figure 1 shows a molecule of **2a**. The torsion angle C1−B1−B2−C2 is very small (4.5°) so that the four-membered ring is almost planar. The bond lengths C1−B1 and C1−B2 are 1.555 and 1.547 Å, which are shortened in comparison to C2−B1 and C2−B2 (1.605 and 1.606 Å). The bond lengths C1−Si1 and C1−Si2 (1.912 and 1.914 Å) are longer than the corresponding distances in **4a** and **4c**. We explain these data by C−Si hyperconjugation of the ring boron atoms with the C1−Si1 and C1−Si2 bonds in **2a**. Tetracoordinate C2 is not a planar carbon center, it has a normal tetrahedral environment of four boron atoms.

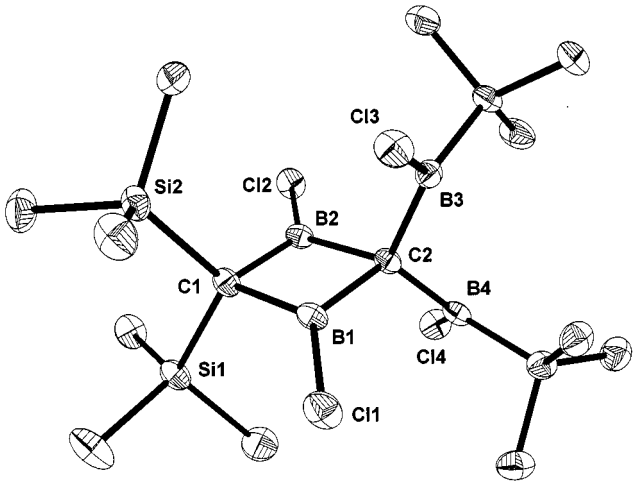

Figure 1. Structure of **2a** in the crystal; selected bond lengths [Å] and angles [°]: B1−C1 1.555(3), B1−C2 1.605(3), B2−C1 1.547(3), B2−C2 1.606(3), C2−B3 1.575(2), C2−B4 1.573(3), C1−Si1 1.912(2), C1−Si2 1.914(2); B1−C1−B2 80.4(1), B1−C2−B2 77.2(1), C1−B1−C2 101.0(1), C1−B2−C2 101.2(1), B3−C2−B4 113.4(1), torsion angle C1−B1−B2−C2 4.5(2)

Crystals of the compounds **3b**,**c** suitable for X-ray structure analyses were obtained from hexane at −20 °C. Both structures are disordered in the crystal. Only the structure of **3c** (Figure 2) will be discussed here because of its better crystallographic data. The most prominent feature is the linear C1−B1=C2 unit. The short B1−C2 bond length of 1.416 Å is in the range of a C=B double bond, the bond length C1−B1 (1.472 Å) is in between that of a single and a double bond. The C1−B3 bond is, at 1.732 Å, very long. Most surprising is the small B1−C1−B3 angle of 101.0°, which is a large deviation from the normal tetrahedral angle. The observed lengthening of the C1−B3 bond length in connection with the decreased bond angle and the short C1−B1 bond is explained by hyperconjugation of the C1−B3 sigma bond with the empty orbital at B1.[8]

Crystals of **4a** were obtained from hexane, whereas **4c** formed crystals in a solution of toluene. Only the structure of **4a** is discussed here. Selected bond lengths and angles of both molecules are listed in the legend of Figure 3. The four-membered ring of **4a** is slightly folded (8.7°). The B−N distances (1.397−1.414 Å) are in the range of those in other aminoboranes. The angles in the ring are very similar to those of **2a**.

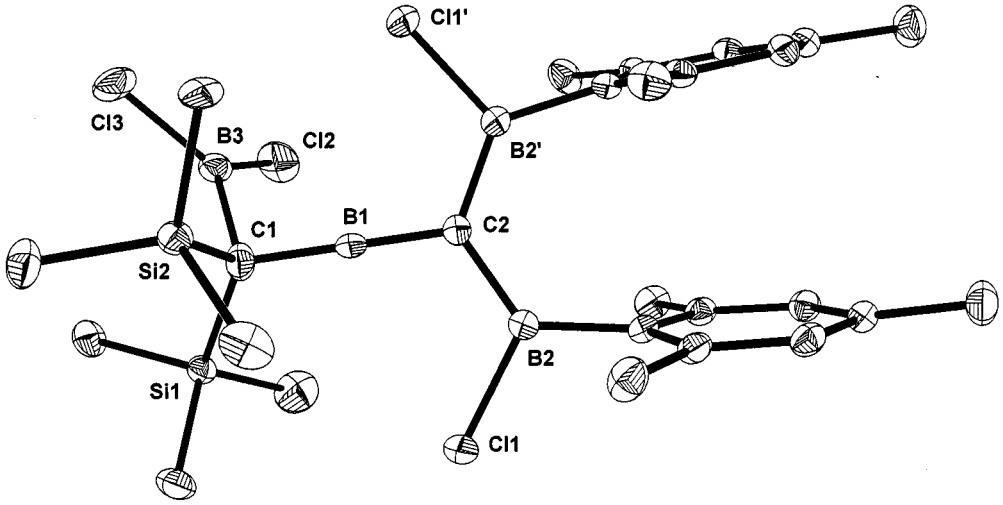

Figure 2. Structure of **3c** in the crystal; selected bond lengths [Å] and angles [°]: B1−C2 1.416(4), B1−C1 1.472(4), B2−C2 1.523(2), B3−C1 1.732(4), C1−Si1 1.878(1), C1−Si2 1.905(1); B1−C2−B2 117.5(1), B1−C1−B3 101.0(1), B1−C1−Si1 105.6(1), B1−C1−Si2 117.4(1), C2−B1−C1 180.00

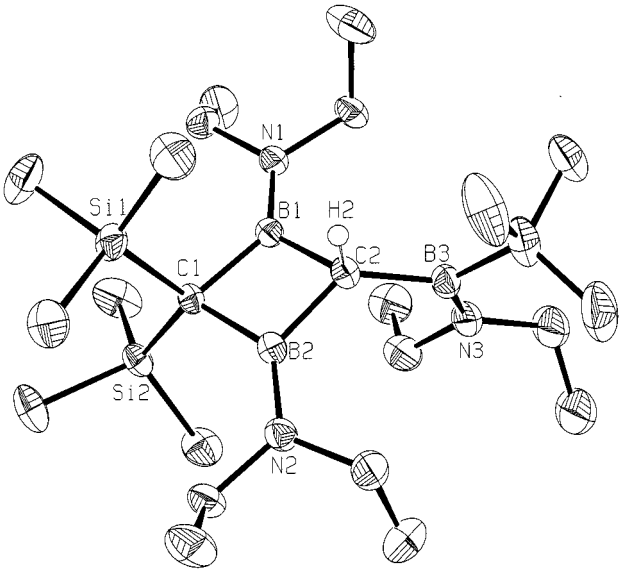

Figure 3. Structure of **4a** in the crystal; selected bond lengths [Å] and angles [°]: B1−C1 1.622(2), B1−C2 1.600(2), B2−C1 1.621(2), B2−C2 1.599(2), C2−B3 1.581(2), C1−Si1 1.881(1), C1−Si2 1.882(1), B1−N1 1.400(2), B2−N2 1.397(2), B3−N3 1.414(2);B1−C1−B2 79.5(1), B1−C2−B2 80.8(1), C1−B1−C2 99.2(1), C1−B2−C2 99.3(1), B2−C2−B3 129.6(1), B1−C2−B3 129.8(1), torsion angle C1−B1−B2−C2 8.7(2). − Selected bond lengths [Å] and angles [°] for **4c**: B1−C1 1.622(3), B1−C2 1.593(3), B2−C1 1.614(3), B2−C2 1.597(3), C2−B3 1.568(3), C1−Si1 1.879(2), C1−Si2 1.875(2), B1−N1 1.387(3), B2−N2 1.389(3), B3−N3 1.405(3); B1−C1−B2 78.1(2), B1−C2−B2 79.4(2), C1−B1−C2 99.2(2), C1−B2−C2 99.4(2), B2−C2−B3 129.7(2), B1−C2−B3 129.7(2), torsion angle C1−B1−B2−C2 14.8(2)

Conclusion

Reaction of the boriranylideneboranes **1a**,**b**,**c** with tetrahalogenodiboranes(4) leads to the cyclic tetraborylmethane derivatives **2a**,**a′** or to the isomeric diborylmethyleneboranes **3b**,**c**. The substitution of the chlorine atoms of **2a** by amino groups yields the triamino derivatives **4a**,**b**,**c**, with unexpected cleavage of one of the exocyclic C−B bonds.

Experimental Section

General: Reactions were carried out under dry argon or nitrogen, using standard Schlenk techniques. Solvents were dried, distilled, and saturated with nitrogen. Glassware was dried with a heat-gun under high vacuum. − ^{1}H and ^{13}C NMR: Bruker DRX 200 spectrometer and Bruker AC 500, ^{11}B NMR: Bruker DRX 200 spectrometer, NMR references are $(CH_3)_4Si$ and $BF_3{\cdot}Et_2O$. − Mass spectra were obtained with a ZAB-2F VH Micromass CTD spectrometer and high resolution mass spectra with a Joel MS Station JMS-700 spectrometer. − Melting points (uncorrected) were measured with a Büchi apparatus using capillaries which were filled under argon or nitrogen, and sealed.

4,4-Bis(*tert*-butylchloroboryl)-1,3-dichloro-2,2-bis(trimethylsilyl)-1,3-diboretane (2a): B_2Cl_4 (0.74 g, 4.50 mmol) was condensed into a solution of **1a** (1.33 g, 4.34 mmol) in 10 mL of hexane at −85 °C. The mixture was allowed to warm to room temperature. The solvent and all volatile components were removed under vacuum, and the colorless solid obtained was crystallized from hexane at −20 °C. Yield: 1.88 g (92%), m.p.: 78−81 °C. − ^{1}H NMR (200 MHz, $CDCl_3$): δ = 0.22 [s, 18 H, $Si(CH_3)_3$], 1.07 [s, 18 H, $C(CH_3)_3$]. − ^{11}B NMR (64 MHz, $CDCl_3$): δ = 69. − ^{13}C NMR (125 MHz, $CDCl_3$, 223 K): δ = 3.7 [q, $Si(CH_3)_3$], 29.6 [q, $C(CH_3)_3$], 31 [br. s, $C(CH_3)_3$], 58 (br. s, CB_2), 79 (br. s, CB_4). − CI-MS: *m*/*z* (%) = 470 (6) [M^+], 455 (13) [$M^+ - CH_3$], 433 (100) [M^+ − Cl]. − HR-MS (CI): *m*/*z* = 433.1790 [M^+ − Cl]; calcd. $^{12}C_{16}{}^1H_{36}{}^{35}Cl_3{}^{29}Si_2{}^{11}B_4$: 433.1794 (Δ*mm*: 0.4).

1,3-Dibromo-4,4-bis(bromo-*tert*-butylboryl)-2,2-bis(trimethylsilyl)-1,3-diboretane (2a′): B_2Br_4 (0.16 g, 0.31 mmol) was condensed into a solution of **1a** (0.10 g, 0.31 mmol) in 10 mL of hexane at −85 °C. The mixture was allowed to warm to room temperature. The solvent and all volatile components were removed under vacuum, and a colorless solid was obtained. Yield: 0.16 g (82%). − ^{1}H NMR (200 MHz, $CDCl_3$): δ = 0.32 [s, 18 H, $Si(CH_3)_3$], 1.21 [s, 18 H, $C(CH_3)_3$]. − ^{11}B NMR (64 MHz, $CDCl_3$): δ = 70. − ^{13}C NMR (125 MHz, C_6D_6): δ = 3.2 [q, $Si(CH_3)_3$], 29.4 [q, $C(CH_3)_3$], 32 [br. s, $C(CH_3)_3$], 61 (br. s, CB_2), 86 (br. s, CB_4). − CI-MS: *m*/*z* (%) = 648 (2) [M^+], 633 (3) [$M^+ - CH_3$], 567 (100) [M^+ − Br].

[Bis(trimethylsilyl)(dichloroboryl)methyl]-1,1-bis(chlorodurylboryl)-methyleneborane (3b): B_2Cl_4 (1.11 g, 6.80 mmol) was condensed

into a solution of **1b** (3.36 g, 6.80 mmol) in 45 mL of hexane at −85 °C. The mixture was allowed to warm to room temperature. The product was filtered and the colorless solid obtained was crystallized from hexane at −80 °C. Yield: 2.27 g (50%), m.p.: 189−191 °C (dec.). − ^{1}H NMR (200 MHz, $CDCl_3$): δ = 0.65 [s, 18 H, $Si(CH_3)_3$], 1.91 (s, 12 H, *o*- and *m*-CH_3), 1.94 (s, 12 H, *o*- and *m*-CH_3), 6.54 (s, 2 H, *p*-H). − ^{11}B NMR (96 MHz, $CDCl_3$): δ = 54, 62 (1:1). − ^{13}C NMR (50 MHz, $CDCl_3$): δ = 2.7 [q, $Si(CH_3)_3$], 18.9 (q, *o*- or *m*-CH_3), 19.5 (q, *o*- or *m*-CH_3), 130.8 (d, *p*-C), 131.4 (s, *o*- or *m*-C), 132.2 (s, *o*- or *m*-C), 142 (br. s, *i*-C). − ^{13}C NMR(125 MHz, CD_2Cl_2, 183 K, additional signals): δ = 44 (br. s, CB_2), 95 (br. s, CB_3). − EI-MS: *m*/*z* (%) = 622 (44) [M^+], 512 (76) [$M^+ - Me_3SiCl$]. − HR-MS (EI): *m*/*z* = 620.2135 [M^+]; calcd. $^{12}C_{28}{}^1H_{44}{}^{35}Cl_4{}^{29}Si_2{}^{11}B_4$: 620.2162 (Δ*mm*: 2.7).

[Bis(trimethylsilyl)(dichloroboryl)methyl]-1,1-bis(chloromesitylboryl)methyleneborane (3c): B_2Cl_4 (1.22 g, 7.47 mmol) was condensed into a solution of **1c** (2.07 g,4.81 mmol) in 45 mL of hexane at −85 °C. The mixture was allowed to warm to room temperature, and then kept for 15 h at −20 °C to yield yellow crystals of **3c**. Yield: 0.94 g (33%), m.p.: 146−148 °C (dec.). − ^{1}H NMR (200 MHz, $CDCl_3$): δ = 0.61 [s, 18 H, $Si(CH_3)_3$], 2.03 (s, 12 H, *o*-CH_3), 2.11 (s, 6 H, *p*-CH_3), 6.35 (s, 4 H, *m*-H). − ^{11}B NMR (64 MHz, $CDCl_3$, 298 K): δ = 60. − ^{11}B NMR (64 MHz, toluene, 333 K): δ = 57, 65. − ^{13}C NMR (125 MHz, $CDCl_3$, 223 K): δ = 3.2 [q, $Si(CH_3)_3$], 22.0 (q, *p*-CH_3), 23.2 (q, *o*-CH_3), 45 (br. s, CB_2), 96 (br. s, CB_3), 126.8 (d, *m*-C), 136.5 (s, *o*-C), 137.5 (s, *p*-C), 140 (s, *i*-C). − CI-MS: *m*/*z* (%) = 594 (20) [M^+], 558 (60) [M^+ − Cl]. − HR-MS (EI): *m*/*z* = 592.1803 [M^+]; calcd. $^{12}C_{26}{}^1H_{40}{}^{35}Cl_4{}^{29}Si_2{}^{11}B_4$: 592.1811 (Δ*mm*: 0.8).

4-(*tert*-Butyldiethylaminoboryl)-1,3-bis(diethylamino)-2,2-bis(trimethylsilyl)-1,3-diboretane (4a): Compound **2a** (0.10 g, 0.21 mmol) was dissolved in 8 mL of hexane and diethylamine (0.12 g, 1.70 mmol) was added at −30 °C. The mixture was allowed to warm to room temperature and then was refluxed for three days. After filtration, part of the solvent was removed under vacuum, and the solution was cooled to −80 °C to give colorless crystals, m.p.: 230−233 °C. Yield: 0.04 g (42%). − ^{1}H NMR (500 MHz, $CDCl_3$): δ = 0.03 [s, 9 H, $Si(CH_3)_3$], 0.10 [s, 9 H, $Si(CH_3)_3$], 0.37 (s, 1 H, B_3CH), 0.89 (t, 3 H, NCH_2CH_3), 0.97 (t, 9 H, NCH_2CH_3), 0.98 [s, 9 H, $C(CH_3)_3$], 1.04 (t, 6 H, NCH_2CH_3), 2.71 (q, 2 H, NCH_2CH_3), 2.95 (dq, 2 H, NCH_2CH_3), 3.05−3.25 (m, 4 H, NCH_2CH_3), 2.22 (q, 2 H, NCH_2CH_3), 3.34 (dq, 2 H, NCH_2CH_3). − ^{11}B NMR (64 MHz, $CDCl_3$): δ = 45. − ^{13}C NMR (125 MHz, $CDCl_3$, 223 K): δ = 3.2 [q, $Si(CH_3)_3$], 4.9 [q, $Si(CH_3)_3$], 13.2 (q, NCH_2CH_3), 14.2 (q, NCH_2CH_3), 14.3 (q, NCH_2CH_3), 18 (br. s, CB_2), 22 [br. s, $C(CH_3)_3$], 28 (br. s, CB_3), 31.2 [q, $C(CH_3)_3$], 39.3 (t, NCH_2CH_3), 40.9 (t, NCH_2CH_3), 41.0 (t, NCH_2CH_3), 44.5 (t, NCH_2CH_3). − CI-MS: *m*/*z* (%) = 477 (5) [M^+], 420 (100) [$M^+ - C(CH_3)_3$]. − HR-MS (EI): *m*/*z* = 477.4482 [M^+]; calcd. $^{12}C_{24}{}^1H_{58}{}^{11}B_3{}^{14}N_3{}^{29}Si_2$: 477.4449 (Δ*mm*: 3.3).

4-(*tert*-Butyldimethylaminoboryl)-1,3-bis(dimethylamino)-2,2-bis(trimethylsilyl)-1,3-diboretane (4b): Compound **2a** (0.22 g, 0.47 mmol) was dissolved in 10 mL of toluene and (dimethylamino)trimethylsilane (0.22 g, 1.87 mmol) was added at −25 °C. The mixture was allowed to warm to room temperature and was then refluxed for two days. The solvent and volatile compounds were removed under vacuum to yield an orange solid. The crude product was sublimed to give 0.06 g (32%) of **4b**. − ^{1}H NMR (200 MHz, $CDCl_3$): δ = 0.02 [s, 9 H, $Si(CH_3)_3$], 0.06 [s, 9 H, $Si(CH_3)_3$], 0.30 (s, 1 H, B_3CH), 0.97 [s, 9 H, $C(CH_3)_3$], 2.41 (s, 3 H, NCH_3), 2.64 (s, 6 H, NCH_3), 2.77 (s, 6 H, NCH_3), 2.80 (s, 3 H, NCH_3). − ^{11}B NMR (64 MHz, $CDCl_3$): δ = 45. − ^{13}C NMR (50 MHz, $CDCl_3$): δ = 3.1 [q, $Si(CH_3)_3$], 4.7 [q, $Si(CH_3)_3$], 21 (br. s, CB_2), 23 [br. s, $C(CH_3)_3$], 28 (br. s, CB_3), 31.2 [q, $C(CH_3)_3$], 40.4 (q, NCH_3), 40.5 (q, NCH_3), 41.7 (q, NCH_3), 44.5 (q, NCH_3). − CI-MS: *m*/*z* (%) = 394 (100) [$M^+ + 1$]. − HR-MS (EI): *m*/*z* = 336.2820 [$M^+ - C(CH_3)_3$]; calcd. $^{12}C_{14}{}^1H_{37}{}^{11}B_3{}^{14}N_3{}^{29}Si_2$: 336.2835 (Δ*mm*: 1.5).

4-(*tert*-Butylpyrrolidylboryl)-1,3-dipyrrolidyl-2,2-bis(trimethylsilyl)-1,3-diboretane (4c): A suspension of lithium pyrrolidinide (0.09 g, 1.20 mmol) in 20mL of hexane was added dropwise to a solution

Table 1. Crystal data and structure refinement for **2a**, **3c**, **4a**, and **4c**

	2a	**3c**	**4a**	**4c**
Empirical formula	$C_{16}H_{36}B_4Cl_4Si_2$	$C_{26}H_{40}B_4Cl_4Si_2$	$C_{24}H_{58}B_3N_3Si_2$	$C_{24}H_{52}B_3N_3Si_2$
Formula weight	469.67	593.80	477.34	471.30
Crystal system	monoclinic	monoclinic	monoclinic	monoclinic
Space group	$P2_1/n$	$C2/c$	$P2_1/n$	$P2_1/c$
Unit cell				
a [Å]	13.926(7)	15.7018(10)	12.1986(6)	21.0269(4)
b [Å]	11.899(6)	14.7365(9)	16.0124(8)	17.5429(3)
c [Å]	16.961(8)	15.2120(10)	16.9864(8)	17.0373(4)
β [°]	112.75(2)	112.175(1)	107.725(1)	108.693(1)
V [Å^3]	2592(2)	3259.5(4)	3160.4(3)	5953.1(2)
Z	4	4	4	8
Calcd. density [g/cm^3]	1.204	1.210	1.003	1.052
Absorp. coeff. [mm^{-1}]	0.550	0.452	0.128	0.135
F(000)	992	1248	1064	2080
Crystal size [mm]	0.65 × 0.60 × 0.50	0.51 × 0.27 × 0.23	0.54 × 0.38 × 0.29	0.46 × 0.38 × 0.20
Θ_{max} [°]	25.0	28.3	28.3	25.7
Index ranges	−16/15, 0/14, 0/20	−20/18, 0/19, 0/20	−16/15, 0/21, 0/22	−25/24, 0/21, 0/20
No. of reflections				
Unique	4563	3960	7622	11316
Observed [$I > 2\sigma(I)$]	3982	2957	5819	8689
Transmission	0.954−1.000	0.739−0.894	0.788−0.894	0.761−0.894
Parameters	250	226	522	602
Final *R* indices				
*R*1 [$I > 2\sigma(I)$]	0.0296	0.0444	0.0407	0.0566
*wR*2	0.0801	0.1329	0.1147	0.1680
Largest diff. peak/hole [e/Å^3]	+0.30 / −0.21	+0.66 / −0.36	+0.41 / −0.15	+0.57 / −0.53

of **2a** (0.28 g, 0.60 mmol) in 10 mL of hexane at −55 °C. The mixture was allowed to warm to room temperature and then was refluxed overnight. The solvent and volatile compounds were removed under vacuum, and the crude orange product was crystallized from toluene to give orange **4c**. Yield: 0.14 g (48%). − ^{1}H NMR (200 MHz, C_6D_6): δ = 0.28 [s, 9 H, $Si(CH_3)_3$], 0.34 [s, 9 H, $Si(CH_3)_3$], 1.24 [s, 9 H, $C(CH_3)_3$], 1.52 (m, 12 H, NCH_2CH_2), 2.76−3.52 (m, 12 H, NCH_2), signal for B_3CH was not observed. − ^{11}B NMR (64 MHz, C_6D_6): δ = 44. − ^{13}C NMR (50 MHz, C_6D_6): δ = 3.7 [q, $Si(CH_3)_3$], 5.0 [q, $Si(CH_3)_3$], 24.1 (t, NCH_2CH_2), 25.7 (t, NCH_2CH_2), 27.0 (t, NCH_2CH_2), 28.9 (t, NCH_2CH_2), 31.0 [q, $C(CH_3)_3$], 44.3 (t, NCH_2), 48.8 (t, NCH_2), 50.0 (t, NCH_2), 52.3 (t, NCH_2), CB signals were not observed. − EI-MS: *m/z* (%) = 471 (1) [M^+], 414 (100) [$M^+ - C(CH_3)_3$]. − HR-MS (EI): *m/z* = 471.4000 [M^+]; calcd. $^{12}C_{24}{}^1H_{52}{}^{11}B_3{}^{14}N_3{}^{29}Si_2$: 471.3979 (Δ*mm*: 2.1).

X-ray Structure Determinations of 2a, 3c, 4a, and 4c: Crystal data and details of the structure determinations are listed in Table 1. Intensity data for **3c**, **4a**, and **4c** were collected at 173 K with a Bruker AXS Smart 1000 and for **2a** at 210 K with a Siemens Stoe AED2 diffractometer (Mo-K_α radiation, λ = 0.7107 Å, graphite monochromator, ω-scan). The structures were solved by direct methods and refined by least-squares methods based on F^2 with all measured reflections (SHELXTL NT5.1).[12] All non-hydrogen atoms were refined anisotropically. One of the two independent molecules in **4c** is disordered.

Crystallographic data (excluding structure factors) for the structures reported in this paper have been deposited with the Cambridge Crystallographic Data Centre as supplementary publication nos. CCDC-147172 (**2a**), CCDC-147173 (**3c**), CCDC-147174 (**4a**), CCDC-147175 (**4c**). Copies of the data can be obtained free of charge upon application to CCDC, 12 Union Road, Cambridge CB2 1EZ, UK [Fax: (internat.) + 44-1223/336-033; E-mail: deposit@ccdc.cam.ac.uk].

Acknowledgments

This work was supported by the Deutsche Forschungsgemeinschaft (SFB 247 and SSP Polyeder) and the Fonds der Chemischen Industrie.

[1] J. E. Dobson, P. M. Tucker, F. G. A. Stone, R. Schaeffer, *J. Chem. Soc. (A)* **1969**, 1882.
[2] R. B. Castle, D. S. Matteson, *J. Organomet. Chem.* **1969**, *20*, 19−28.
[3] D. S. Matteson, *Synthesis* **1975**, 147.
[4] D. S. Matteson, R. J. Wilcsek, *J. Organomet. Chem.* **1973**, *57*, 231.
[5] D. S. Matteson, R. A. Davis, L. A. Hagelee, *J. Organomet. Chem.* **1974**, *69*, 45.
[6] J. B. Collins, J. D. Dill, E. D. Jemmis, Y. Apeloig, P. v. R. Schleyer, R. Seeger, J. A. Pople, *J. Am. Chem. Soc.* **1976**, *98*, 5419.
[7] A. Bethäuser, H. Pritzkow, W. Siebert, unpublished results.
[8] A. Berndt, *Angew. Chem.* **1993**, *105*, 1034−1058; *Angew. Chem. Int. Ed. Engl.* **1993**, *32*, 985 and references cited therein.
[9] C. Wieczorek, J. Allwohn, G. Schmidt-Lukasch, R. Hunold, W. Massa, A. Berndt, *Angew. Chem.* **1990**, *102*, 435; *Angew. Chem Int. Ed. Engl.* **1990**, *29*, 398 and references cited therein.
[10] A. Hoefner, B. Ziegler, R. Hunold, W. Massa, A. Berndt, *Angew. Chem.* **1991**, *103*, 580; *Angew. Chem Int. Ed. Engl.* **1991**, *30*, 594.
[11] R. Hunold, M. Allwohn, J. Stadler, W. Massa, P. v. R. Schleyer, A. Berndt, *Angew. Chem.* **1989**, *101*, 759−761; *Angew. Chem Int. Ed. Engl.* **1989**, *28*, 781.
[12] G. M. Sheldrick, SHELXTL NT5.1, Bruker AXS, Madison, Wisconsin **1999**.

Received August 17, 2000
[I00320]

Molecular "Floppyness" and the Lewis Acidity of Silanes: A Density Functional Theory Study

Holger Fleischer[a]

This paper is dedicated to Prof. Dr. Karl Hensen on the occasion of his 65th birthday

Keywords: Coordination chemistry / Density functional calculations / Lewis acids / Silanes

A comprehensive set of Lewis acid-base adducts of silanes was investigated by means of the density functional theory geometry optimization [B3LYP/6–31G(d)], and thermochemical calculations, [B3LYP/6–311+G(2d,p)//B3LYP/6–31G(d)]. Complex formation was found to weaken Si–Cl and Si–Br bonds more than Si–F or Si–H bonds. Comparable distances between Si and a Lewis base L (L = NH_3, OH_2, F^-) are shorter in hexa- than in pentacoordinated complexes. The molecular structures of the pentacoordinated Si complexes allowed for a mapping of an S_N2 reaction pathway by correlating the lengths of the Si–X and Si–L bonds. Complex formation was found to be exothermic for most of the coordination compounds, and the analysis of the natural atomic charges revealed a high ionic character of the dative bonds. Formation of the anionic complexes and of $SiH_2X_2(py)_2$ is most exothermic with X = Cl or Br and otherwise most exothermic with X = F. Only small enthalpy differences were found between the *trans* and *cis* configurations of $SiF_4(py)_2$. The standard free enthalpy of complex formation is negative only for complexes between halosilanes and F^-, i.e. all other silane Lewis base adducts are thermodynamically unstable under standard conditions with respect to dissociation. It is inferred that the existence of some of the silicon complexes in the solid state or in solution is caused by stabilizing intermolecular forces, and silanes are classified as very weak Lewis acids. The thermochemistry of complex formation was analyzed in terms of molecular "floppyness" of the silanes and the energy of interaction between the deformed silane and the Lewis base. The enhanced complex stability of $SiCl_4(py)_2$ compared to $SiH_4(py)_2$ and of $GeF_4(NH_3)$, $[GeF_5]^-$ and $[GeF_6]^{2-}$ compared to the analogues silane adducts does not result from a stronger Lewis acid base interaction but from an increased "floppyness" of $SiCl_4$ and GeF_4 compared to SiH_4 and SiF_4, respectively.

Introduction

While many compounds of group 13 elements act as Lewis acids due to their electron deficiency, the driving force for the formation of hypervalent silanes must be different. Many adducts of silanes with Lewis bases have been characterized,[1] and hypervalent compounds have long since been the subject of many experimental[2] and theoretical[3] investigations; some are even of pharmaceutical interest.[4] Several review articles have been published in this field.[5] Hence, since Si atoms can participate in donor acceptor interactions, the corresponding silanes were said to be Lewis acids.

But does the Lewis acidity of, for example, $SiCl_4$ follow from the existence of $SiCl_4(py)_2$ *in the solid state*? And why does $SiCl_4(py)_2$ exist and $SiH_4(py)_2$ does not?[1f] Most complexes between silanes and typical Lewis bases are hitherto found only in the solid state or in polar solvents, some exist at very low temperatures only with matrix isolation,[6] and $SiF_4(NH_3)$ is the only example of a silane adduct known to the author, that has been detected in the gas phase, but at very low temperatures.[7]

Thus two questions arise: first, how does the Lewis acidity of silanes depend on their molecular properties, and second, is the existence of adducts between silanes and Lewis bases at room temperature at all enabled by intermolecular forces, in contrast to group 13 Lewis acids like BX_3, AlX_3 and GaX_3 (X = H, alkyl, halogen) whose adducts with Lewis bases are known to exist in the gas phase under normal conditions (see e.g. reference 8)? $SiH_2Cl_2(py)_2$ was recently calculated to be thermodynamically unstable under normal conditions with respect to dissociation into SiH_2Cl_2 and pyridine.[9] It is thus of interest to look at the thermodynamic stability of a more comprehensive set of silicon complexes, including different coordination numbers, donor atoms and substitution patterns of the silicon atom. Some of the molecules investigated exist in the solid state, i.e. $SiH_3Cl(OMe_2)$,[10] $SiH_2Cl_2(py)_2$,[1f,9] $SiH_2Br_2(py)_2$,[1f] $SiF_4(py)_2$,[11] $SiCl_4(py)_2$,[12] $SiF_4(NH_3)_2$,[13], $SiF_4(NH_3)$,[6] SiF_5^-,[14] and SiF_6^{2-},[15] the others are model compounds, i.e. $SiH_3X(NH_3)$, $SiX_4(NH_3)$ and $SiH_3X(OH_2)$, $SiH_2F_2(py)_2$, $SiH_4(py)_2$, $[SiH_3XF]^-$, $[SiH_4F]^-$, $[SiCl_4F]^-$, $[SiH_4F_2]^{2-}$ and $[SiCl_4F_2]^{2-}$ (X = F, Cl, Br for complexes of SiH_3X and SiH_2X_2 and X = H, F, Cl for complexes of SiX_4, py = pyridine).[16,18] To investigate the matter of "genuine" Lewis acidity of silanes, no molecules such as silatranes or 1-sila-8-dimethylaminonaphthalene, whose potential donor and acceptor sites are forced into close proximity, and where an interaction is favored by molecular steric strains, were considered. Furthermore, no chelating or macrocyclic

[a] Institut für Anorganische Chemie und Analytische Chemie, Johannes Gutenberg Universität Mainz, Duesberg Weg 10–14, 55099 Mainz, Germany
Email: fleische@mail.uni-mainz.de

 © WILEY-VCH Verlag GmbH, 69451 Weinheim, 2001 1434–1948/01/0202–0393 $ 17.50+.50/0

Lewis bases were included in the study to avoid their stabilizing effect on complexes.

Geometry optimizations for molecules as large as $SiCl_4(py)_2$ (27 atoms, 166 electrons), with a full-electron Hartree-Fock (HF) method using a reasonable basis set [e.g. 6−31G(d)], followed by CI (configuration interaction) or MP*n* (n-th order Møller Plesset perturbation) calculations to account for electron correlation exceeded the limits of the available computational resources. Hence a DFT (density functional theory) approach[19,20] was chosen which includes dynamic electron correlation effects without requiring as many computational resources as the above quoted methods do. In the present paper, the results of DFT geometry optimizations and thermochemical calculations on coordination compounds of different silanes will be presented, and molecular factors influencing the Lewis acidity of and dative bonds[21,22] to silanes will be discussed

Results and Discussion

Molecular Structures

Selected structural parameters are given in Table 1 to 3 (See Figure 1 for a graphical overview of the complexes).

Table 1. Selected structural parameters from optimized geometries of SiH_3X and their Lewis acid base adducts

	r_e(Si−X)	x[a]	r_e(Si−H)	r_e(Si−L)	l[a]	a(XSiH)
SiH_3F (C_{3v})	161.3	1.000	148.5			109.2
$SiH_3F(NH_3)$ (C_{3v})	163.2	1.012	148.4	256.4	1.328	104.3
$SiH_3F(NMe_3)$ (C_3)	163.5	1.014	148.6	248.5	1.288	103.0
$SiH_3F(OH_2)$ (C_s)	162.3	1.006	148.3[b]	276.0	1.445	108.4[b]
$[SiH_3F_2]^-$ (D_{3h})	172.0	1.066	152.7	172.0	0.910	90.0
SiH_3Cl (C_{3v})	207.9	1.000	148.2			108.6
$SiH_3Cl(NH_3)$ (C_{3v})	213.6	1.027	147.9	250.8	1.299	102.2
$SiH_3Cl(OH_2)$ (C_s)	210.5	1.013	147.8[b]	273.4	1.431	105.5[b]
$SiH_3Cl(OMe_2)$ (C_s)	210.5	1.013	147.8[b]	271.7	1.423	105.5[b]
$SiH_3Cl(OMe_2)$[c]	214.2	-		227.2		99.4[b]
$[SiH_3ClF]^-$ (C_{3v})	261.4	1.257	148.8	167.6	0.887	81.6
SiH_3Br (C_{3v})	222.9	1.000	148.2			108.8
$SiH_3Br(NH_3)$ (C_{3v})	228.6	1.026	147.9	250.7	1.299	102.3
$SiH_3Br(OH_2)$ (C_s)	225.3	1.011	147.9[b]	273.6	1.432	105.7[b]
$[SiH_3BrF]^-$ (C_{3v})	276.0	1.238	148.6	167.4	0.886	81.4

[a] See text for definition of x and l. − [b] Averaged value over symmetrically nonequivalent Si−H bonds and X−Si−H angles. − [c] Single crystal X-ray diffraction structure from Reference 10. Atomic distances represent an r_α instead of an r_e structure.

Table 3. Selected structural parameters from optimized geometries of SiX_4, GeF_4, and their Lewis acid base adducts

	r_e(Si−X)	x[a]	r_e(Si−L)	l[a]	a(X[a]SiX[e])[33]
SiH_4 (T_d)	148.6	1.000			
$SiH_4(py)_2$ (D_{2h})	156.0	1.050	203.6	1.055	
$[SiH_4F_2]^{2-}$ (D_{4h})	164.4	1.106	176.8	0.935	
$SiH_4(NH_3)$ (C_{3v})	148.4/149.7[b]	1.007	302.6	1.568	106.8
$[SiH_4F]^-$ (C_{3v})	152.9/161.3[b]	1.085	171.7	0.908	88.2
SiF_4 (T_d)	157.9	1.000			
$SiF_4(py)_2$ (D_{2h})	167.0	1.058	198.3	1.027	
$SiF_4(NH_3)_2$ (C_{2h})	166.9	1.057	197.4	1.023	
$[SiF_6]^{2-}$ (O_h)	172.0	1.089	172.0	0.910	
$SiF_4(NH_3)$ (C_{3v})	160.8/161.2[b]	1.021	214.4	1.111	98.1
$SiF_4(NMe_3)$ (C_3)	161.3/161.7[b]	1.024	217.0	1.124	96.8
$[SiF_5]^-$ (D_{3h})	164.2/167.3[b]	1.060	167.3	0.885	90.0
GeF_4	171.0	1.000			
$[GeF_6]^{2-}$	182.2	1.065	182.2	0.944	
$GeF_4(NH_3)$	174.0/173.3[b]	1.013	215.9	1.096	96.9
$[GeF_5]^-$	175.9/177.8[b]	1.040	177.8	0.921	90.0
$SiCl_4$ (T_d)	204.7	1.000			
$SiCl_4(py)_2$ (C_{2h})	221.6	1.083	204.6	1.060	
$[SiCl_4F_2]^{2-}$ (D_{4h})	232.7	1.137	164.5	0.870	
$SiCl_4(NH_3)$ (C_{3v})	210.3/211.7[b]	1.034	216.6	1.122	97.2
$[SiCl_4F]^-$ (C_{3v})	215.2/224.4[b]	1.096	164.5	0.870	90.0

[a] See text for definition of x and l. x is not given for equatorial Si−X bonds in SiX_4(L). − [b] The first of the two values refers to the equatorial, the second to the apical Si−X bond.

The molecular geometry of the complexes may give an indication of the strength of the Lewis acid/base interaction in terms of atomic distances and distortion of silane and Lewis base from their ground state geometries. According to Pauling,[34] the bond length is an indication of the bond strength, i.e. the shorter Si−L bond (L = O for OH_2, OMe_2; L = N for NH_3, NMe_3 and py; L = F for F^-) should be the stronger one.[35] As different X and L are to be compared with each other, relative lengths are used instead of r_e(Si−X) and r_e(Si−L). Accordingly, r_e(Si−X) is divided by r_e(Si−X) of the parent silane to give the relative length $x = r_e(Si-X)/r_e(Si-X)_{silane}$ and r_e(Si−L) is divided by the sum of the covalent radii of Si and L to give the relative length $l = r_e(Si-L)/[r_{cov}(Si) + r_{cov}(L)]$. (Covalent radii are taken from reference 36 and are 122, 118, 75, 73 and 71 pm for Ge, Si, N, O and F, respectively). In the complex anions, in $SiH_3X(L)$ and in $SiH_2X_2(py)_2$, r_e(Si−L) decreases for a given complex with X in the order H > F > Cl > Br, and, for a given L, the relative lengths of the Si−X bond, x, increases in the same order, the only excep-

Table 2. Selected structural parameters from optimized geometries of SiH_2X_2 and their Lewis acid base adducts

	r_e(Si−X)	x[a]	r_e(Si−H)	r_e(Si−N)	l[a]	τ(CNSiX)[b]
SiH_2F_2 (C_{2v})	160.1	1.000	147.9			
$SiH_2F_2(py)_2$ (D_{2h})	171.1	1.069	150.4	208.5	1.080	0.0
SiH_2Cl_2 (C_{2v})[c]	206.5	1.000	147.6			
$SiH_2Cl_2(py)_2$ (C_{2h})[c]	229.1	1.109	148.3	203.9	1.056	60.5
SiH_2Br_2 (C_{2v})	221.8	1.000	147.6			
$SiH_2Br_2(py)_2$ (C_{2h})	242.7	1.094	148.0	202.4	1.049	66.1

[a] See text for definition of x and l. − [b] Parameter represents the torsion between one N−C bond of pyridine and one Si−X bond. − [c] Values from reference 9.

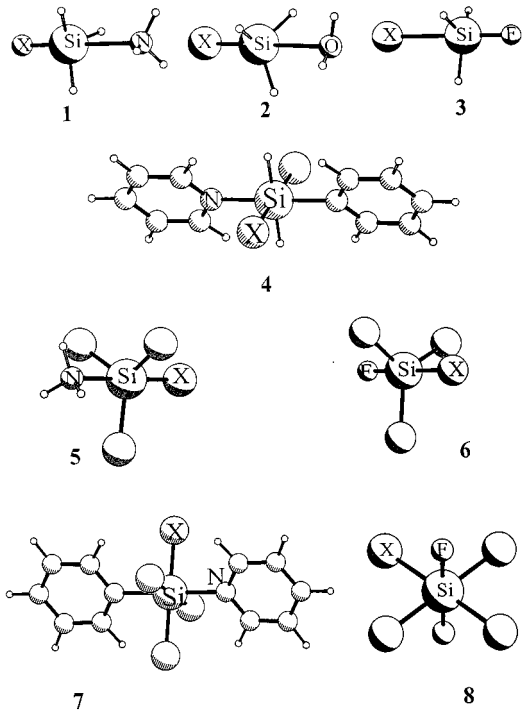

Figure 1. Molecular graphics of the hypervalent compounds investigated (only those systems are shown, in which X is varied) $SiH_3X(NH_3)$ **1**, $SiH_3X(OH_2)$ **2**, $[SiH_3XF]^-$ **3**, $SiH_2X_2(py)_2$ **4** (X = F, Cl, Br); $SiX_4(NH_3)$ **5**, $[SiX_4F]^-$ **6**, $SiX_4(py)_2$ **7**, $[SiX_4F_2]^{2-}$ **8** (X = H, F, Cl)

tions being $[SiH_4F]^-$ and $[SiH_3F_2]^-$. For the other complexes, $SiX_4(NH_3)$ and $SiX_4(py)_2$, Si−N is shortest with X = F.

The relative length *x* increases with L in the order L = O < N << F^- and the relative length *l* decreases in the same order. Thus, *l* and *x* suppose F^- to be the strongest of all Lewis bases studied in the present work.

Considering the electrically neutral amine-silane complexes, r_e(Si−N) is smaller in the hexacoordinated compounds $SiX_4(py)_2$, $SiH_2X_2(py)_2$ and $SiF_4(NH_3)_2$ than in the pentacoordinated $SiX_4(NH_3)$, $SiH_3X(NH_3)$, $SiH_3F(NMe_3)$ and $SiF_4(NMe_3)$, and smaller in $SiX_4(NH_3)$ and $SiF_4(NMe_3)$ than in $SiH_3X(NH_3)$ and $SiH_3F(NMe_3)$. The difference in r_e(Si−N) between $SiF_4(py)_2$ and $SiF_4(NH_3)_2$, and between $SiF_4(NMe_3)$ and $SiF_4(NH_3)$, is marginal, while r_e(Si−N) is shorter in $SiH_3F(NMe_3)$ than in $SiH_3F(NH_3)$. These results suppose that the Si−N distance is mainly determined by electronic and not by steric factors. The nature of the Si−L bond in $SiH_3X(L)$ and $SiX_4(L)$ was analyzed in terms of second order perturbation in a natural orbital basis (see Table 4). It is not the absolute values of these energies that are of interest, but, for comparable complexes, their relative orders. In complexes $SiH_3X(L)$, the interaction of the lone pair of L with the anti-bonding orbital of the apical Si−X bond, n(L)−σ*(Si−X), was found to play the major role, a result that rationalizes the considerable lengthening of the Si−X bond due to interaction of L with Si. Compared to n(L)−σ*(Si−X), the interaction between the lone pair of L and the anti-bonding orbitals of the equatorial Si−H bonds, n(L)−σ*(Si−H), is rather small. In $SiX_4(L)$, the apical Si−X bond is only slightly longer than the equatorial ones, and in $GeF_4(NH_3)$, $r_e(Ge-F^a)$ is even smaller than $r_e(Ge-F^e)$, a relation well reflected by the NBO interaction energies (see Table 4).

Structure Correlation

Interpreting the pentacoordinated complexes in terms of structure correlation[37] as "snapshots" of an S_N2 reaction path, with the nucleophile and the nucleofuge occupying the apical positions of a trigonal bipyramid, a smaller *l* requires a bigger *x* and vice versa. As can be seen from Figure 2a, the pentacoordinated complexes give a reasonably good correlation between *x* and *l*, in contrast to the hexacoordinated ones (see Figure 2b). The deformations of SiH_3X and SiX_4, as measured by the difference of *a*(HSiX) and

Table 4. Second order perturbation energies for the interaction of Lewis base L and SiH_3X, SiH_2X_2, SiX_4 and GeF_4 in an NBO basis[a]

	n(L)-σ*(Si−X)	n(L)-σ*(Si−Y)[b]		n(L)-σ*(E−X)[c]	n(L)-σ*(Ei−Y)[b,c]
$SiH_3F(OH_2)$	24.0	4.5[d] (3)	$SiH_4(NH_3)$	17.8	3.8 (3)
$SiH_3Cl(OH_2)$	28.8	5.9[d] (3)	$SiF_4(NH_3)$	51.2	46.6 (3)
$SiH_3Br(OH_2)$	31.0	6.2[d] (3)	$SiCl_4(NH_3)$	53.3	53.3 (3)
$SiH_3F(NH_3)$	44.7	9.5 (3)	$[SiH_4F]^-$	88.2	47.9 (3)
$SiH_3Cl(NH_3)$	56.1	12.8 (3)	$[SiF_5]^-$	72.0	65.8 (3)
$SiH_3Br(NH_3)$	59.8	13.1 (3)	$[SiCl_4F]^-$	51.9	47.4 (3)
$[SiH_3F_2]^-$	79.2	47.0 (3)	$GeF_4(NH_3)$	74.8	106.6 (3)
$[SiH_3ClF]^-$	131.3	36.7 (3)	$[GeF_5]^-$	79.0	127.1 (3)
$[SiH_3BrF]^-$	137.9	35.5 (3)			
	n(L)-3p_z(Si)[e]	n(X)-3p_z(Si)[e]		n(L)-3p_z(Si)[e]	n(X)-3p_z(Si)[e]
$SiH_2F_2(py)_2$	313.5 (2)	57.1 (2)	$SiH_4(py)_2$	387.3 (2)	–
$SiH_2Cl_2(py)_2$	378.8 (2)	40.5 (2)	$SiF_4(py)_2$	331.4 (2)[f]	57.6 (4)
$SiH_2Br_2(py)_2$	402.8 (2)	42.1 (2)	$SiCl_4(py)_2$	367.8 (2)	50.6 (4)

[a] Energies are given in kJ mol^{-1}. Values in parentheses represent the multiplicity of the given type of second order interaction in the actual complex. – [b] Y = H for complexes of SiH_3X, and Y = X^e for complexes of SiX_4. – [c] E = Si for SiX_4, E = Ge for GeF_4 – [d] Average value from three n(O)-σ*(Si−H) interactions. – [e] *z* axis of cartesian system is defined by the two L atoms, i.e. of all three 3p orbitals of Si, 3p_z can best overlap with the lone pairs of L. – [f] In $SiF_4(py)_2$, an additional n(N)−3s(Si) interaction of 299.4 kJ mol^{-1} is present.

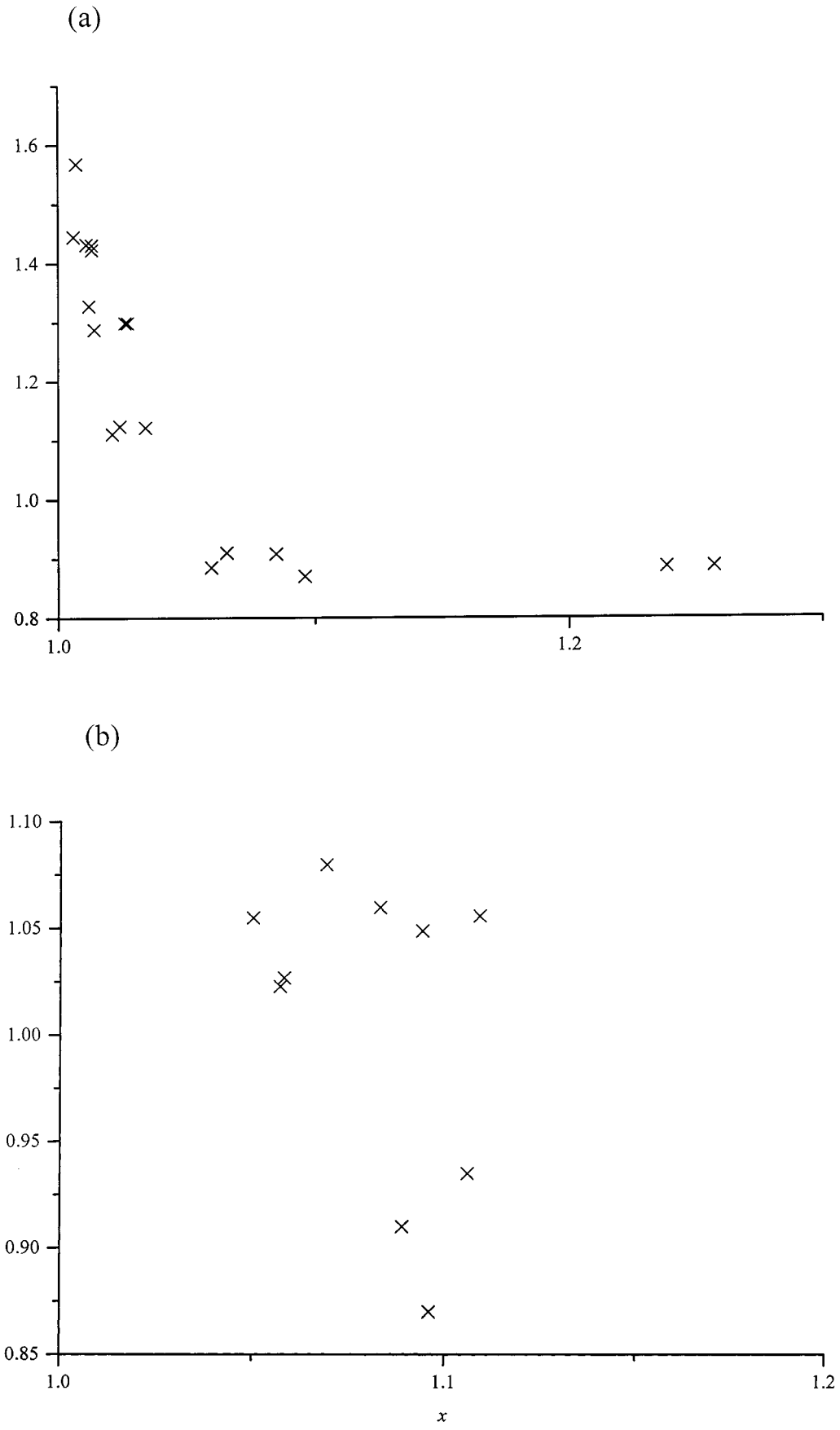

Figure 2. Correlation between the relative length of the Si−X bond, *x*, and the relative lengths of the Si−L bond, *l*, for (a) pentacoordinated (b) hexacoordinated Si complexes; for details see text

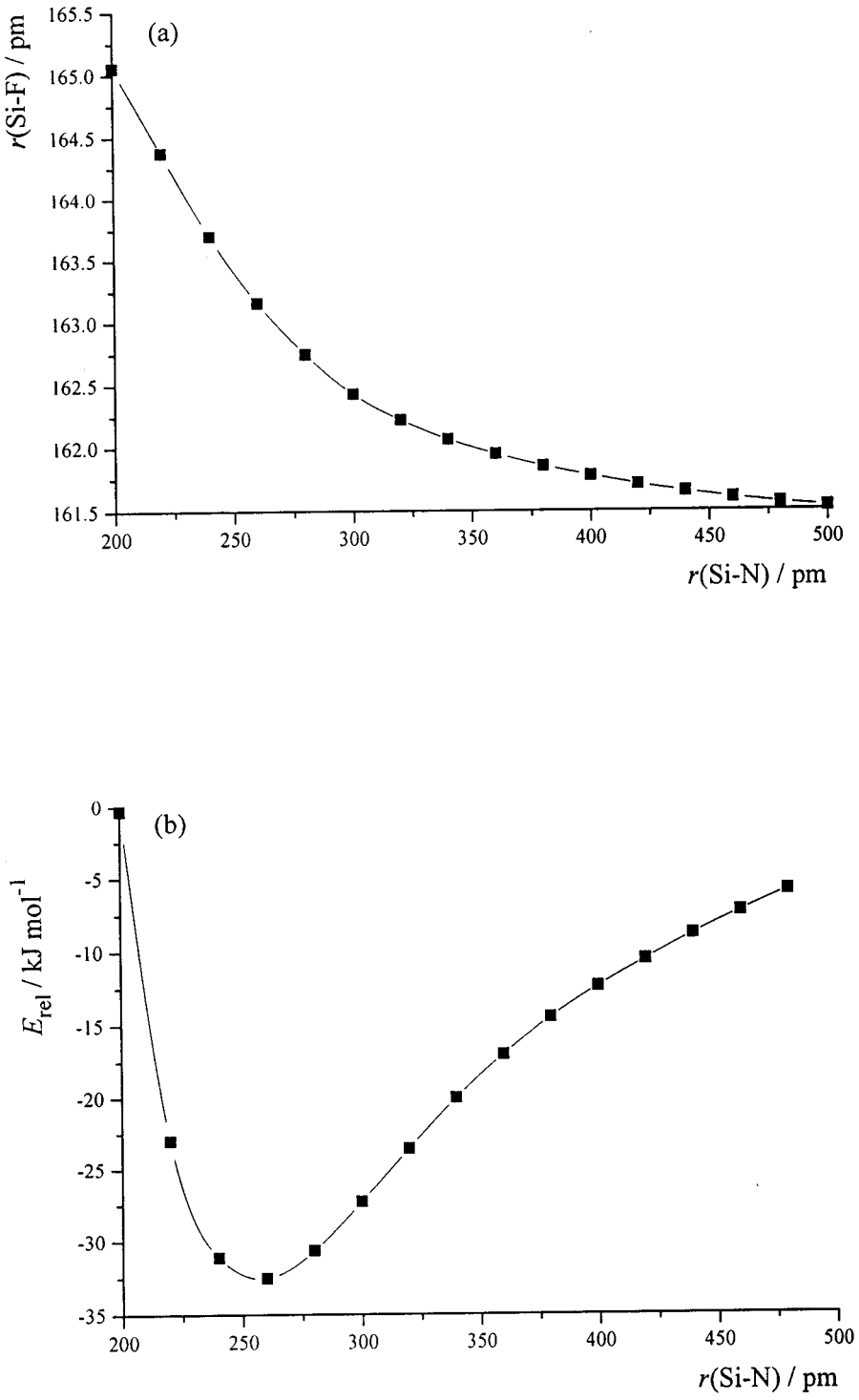

Figure 3. (a) Correlation between r(Si−N) and r(Si−F) in $SiH_3F(NH_3)$; (b) Relaxed potential energy scan (B3LYP/6−31G(d)) for r(Si−N) of $SiH_3F(NH_3)$; $E_{rel} = 0$ represents complete dissociation

$a(X^aSiX^e)$ between the complex and the silane, corroborate the structure correlation, as the approaching nucleophile L pushes the H and X^e atoms away towards X^a and narrows a(HSiX) and $a(X^aSiX^e)$. For $SiH_3F(NH_3)$, a relaxed potential energy scan was performed by changing r(Si−N) in a stepwise manner and optimization of the remaining parameters. The potential energy as a function of r(Si−N) (b) and a correlation of r(Si−N) with r(Si−F) (a) are given in Figure 3. The latter shows a typical pattern for a correlation with mutual weakening of the bonds as it occurs in an S_N2 mechanism, analogous to Figure 2a.

Comparison to Solid State Structures

$SiH_3Cl(OMe)_2$ presents a striking example of a dative bond to Si that is shorter in the solid state than in the isolated molecule (see Table 1). This difference is attributed to

stabilizing intermolecular contacts in the solid state.[10] The shorter Si−O bond in the solid state corresponds to a longer Si−Cl bond, an example for structure correlation within different "phases". The considerable shift of the Si−O distance by changes in the molecular environment implies that the curvature of the potential energy surface, $\partial^2 V/\partial r_e(Si-O)^2$, at its minimum is small, i.e. the bond is weak. This weakness applies also for the Si−N bond in $SiH_3F(NH_3)$ (see Figure 3). r(Si−N) can be varied around the equilibrium distance over a range of 75 pm without increasing the energy by more than 5 kJ mol^{-1}.

Thermochemistry of Complex Formation: Structural "Stiffness" vs. Energy of Interaction

Since the energy, enthalpy and free enthalpy of complex formation are state functions, their values do not depend on the way in which the complex is formed. It is useful to divide the complex formation from silane (S) and Lewis base (L) into two steps. First, the molecules of the silane and the Lewis base are deformed from their ground state geometries, S(GS) and L(GS), to their complex geometry, S(CG) and L(CG), the energy required being ΔE_{def}(S) [Equation (1a)] and ΔE_{def}(L) [Equation (1b)].

$$S(GS) \rightarrow S(CG) \quad (1a)$$

$$L(GS) \rightarrow L(CG) \quad (1b)$$

In all complexes, ΔE_{def}(L) proved to be only a small fraction of ΔE_{def}(S), and only ΔE_{def}(S) is further considered.

The deformed silane and Lewis base then interact and form the complex [Equation (2)].

$$S(CG) + n\ L(CG) \rightarrow SL_n \quad (2)$$

The energy of the process shown in Equation (2), V, represents the strength of interaction. Since the energy required for Equation (1a) may even vary for the same silane and the same coordination number, a study of ΔE_{def}(S) from the ground state geometry to a well defined distorted geometry was performed. For hexacoordinated complexes of SiH_2X_2 and SiX_4, the silane molecules were "flattened", i.e. the geometry optimization was performed with the symmetry restricted to D_{2h} for SiH_2X_2 and D_{4h} for SiX_4. To account for the pentacoordinated complexes of SiH_3X and SiX_4, the molecules were optimized with a trigonal pyramidal structure, which means that the HSiX angles in SiH_3X and the XSiX angles in SiX_4 between the unique X atom and the other X atoms were fixed to 90°. This symmetry is designated as "C_{3v}(tp)". The energy necessary for these kinds of deformations is a measure of the "floppyness" of the silane to adopt the geometry in a given complex. Values for ΔE_{def}(S) are given in Table 7.

The standard enthalpy of complex formation, ΔH_c^{298}, and the standard free enthalpy of complex formation, ΔG_c^{298}, obtained in the present study exhibit partially very small absolute values (see Table 5a and 5b), hence counterpoise calculations are essential to correct them for the basis set superposition error (bsse).[31,32,38] Counterpoise-corrected

Table 5. (a) Enthalpies of complex formation, ΔH_c^{298}; (b) free enthalpies of complex formation, ΔG_c^{298}; (c) basis set superposition errors for the thermochemistry of complex formation; for details see text

(a)[a]

Silane	SiH_3X (CN_{Si} = 5)			SiX_4 (CN_{Si} = 5)		SiX_4 (CN_{Si} = 6)		SiH_2X_2 (CN_{Si} = 6)
Lewis base	NH_3	H_2O	F^-	NH_3	F^-	py	F^-	py
X = H				3.2	−143.2	123.1	200.1	
F	−13.2	−5.5	−214.7	−23.4	−296.0	−57.1	−89.1	2.4
Cl	−10.1	−3.9	−269.4	13.8	−306.3	3.8	−257.4	−15.9
Br	−10.4	−3.7	−294.3					−26.1

(b)[b]

Silane	SiH_3X (CN_{Si} = 5)			SiX_4 (CN_{Si} = 5)		SiX_4 (CN_{Si} = 6)		SiH_2X_2 (CN_{Si} = 6)
Lewis base	NH_3	H_2O	F^-	NH_3	F^-	py	F^-	py
X = H				27.4	−112.4	215.1	269.6	
F	23.4	22.7	−178.7	16.7	−260.9	38.3	−12.2	100.9
Cl	27.0	24.1	−237.8	60.3	−275.5	107.5	−188.8	80.4
Br	26.8	23.7	−262.6					71.8

(c)

Silane	SiH_3X (CN_{Si} = 5)			SiX_4 (CN_{Si} = 5)		SiX_4 (CN_{Si} = 6)		SiH_2X_2 (CN_{Si} = 6)
Lewis base	NH_3	H_2O	F^-	NH_3	F^-	py	F^-	py
X = H				1.6	8.3	3.2	17.2	
F	3.2	2.2	9.6	7.0	11.7	19.2	26.7	19.0
Cl	3.1	2.1	10.1	6.2	15.4	17.1	31.7	16.2
Br	3.1	2.1	9.0					15.0

[a] $SiH_3F(NMe_3)$: −16.4, $SiH_3Cl(OMe_2)$: −5.4, $SiF_4(NMe_3)$: −23.5, $SiF_4(NH_3)_2$: −62.3, $GeF_4(NH_3)$: −65.0, $[GeF_5]^-$: −347.3, $[GeF_6]^{2-}$: −191.7. − [b] $SiH_3F(NMe_3)$: 27.5, $SiH_3Cl(OMe_2)$: 25.9, $SiF_4(NMe_3)$: 25.8, $SiF_4(NH_3)_2$: 15.3, $GeF_4(NH_3)$: −26.1, $[GeF_5]^-$: −312.0, $[GeF_6]^{2-}$: −115.3.

Table 6. (a) Energies of deformation for the silanes from the ground state geometry to the geometry in the complexes ΔE_{def}(S) in kJ mol^{-1}; (b) counterpoise corrected energies of interaction, V^{cc}, for the silanes (CG) with the specified Lewis bases in kJ mol^{-1}; for details see text

(a)[a]

Silane	SiH_3X (CN_{Si} = 5)			SiX_4 (CN_{Si} = 5)		SiX_4 (CN_{Si} = 6)		SiH_2X_2 (CN_{Si} = 6)
Lewis base	NH_3	H_2O	F^-	NH_3	F^-	py	F^-	py
X = H				2.1	113.9	375.4	402.7	
F	4.2	0.2	105.1	75.2	219.9	285.6	333.0	218.7
Cl	10.2	2.0	197.9	78.0	196.5	285.1	368.7	229.1
Br	8.3	1.2	172.2					208.3

(b)[b]

Silane	SiH_3X (CN_{Si} = 5)			SiX_4 (CN_{Si} = 5)		SiX_4 (CN_{Si} = 6)		SiH_2X_2 (CN_{Si} = 6)
Lewis base	NH_3	H_2O	F^-	NH_3	F^-	py	F^-	py
X = H				−3.3	−247.0	−264.6	−178.2	
F	−21.8	−9.3	−310.3	−101.1	−505.8	−342.0	−397.8	−225.7
Cl	−25.5	−9.9	−460.5	−68.2	−490.0	−283.7	−599.4	−257.8
Br	−23.8	−8.7	−461.3					−249.6

[a] $GeF_4(NH_3)$: 64.9, $[GeF_5]^-$: 155.0, $[GeF_6]^{2-}$: 220.9. − [b] $GeF_4(NH_3)$: −132.0, $[GeF_5]^-$: −490.6, $[GeF_6]^{2-}$: −390.5.

Table 7. Energies of deformation, ΔE_{def}(silane) (kJ mol^{-1}) for structurally distorted silanes and GeF_4; for details see text

	ΔE_{def}		ΔE_{def}
SiH_3F (C_{3v} tp)	95.3	SiH_2F_2 (D_{2h})	207.5
SiH_3Cl (C_{3v} tp)	84.7	SiH_2Cl_2 (D_{2h})	206.3
SiH_3Br (C_{3v} tp)	78.5	SiH_2Br_2 (D_{2h})	197.4
SiH_4 [C_{3v}(tp)]	88.1	SiH_4 (D_{4h})	373.7
SiF_4 [C_{3v}(tp)]	199.2	SiF_4 (D_{4h})	261.1
GeF_4 [C_{3v}(tp)]	147.2	GeF_4 (D_{4h})	182.6
$SiCl_4$ [C_{3v}(tp)]	169.6	$SiCl_4$ (D_{4h})	252.8

values are indicated by the superscript "cc". Differences in ΔH_c^{298} between different complexes can subsequently be analyzed in terms of ΔE_{def}(S) vs. V^{cc}.

Lewis Bases with N or O Donor Atoms

The formation of $SiH_3X(L)$ from SiH_3X and L is more exothermic for L = NH_3 than for L = OH_2, a result that is in accordance with the n(L)−σ*(Si−X) energies already presented (vide infra), and reflects the enhanced Lewis basicity of NH_3 compared to H_2O. ΔH_c^{298} of $SiH_3X(L)$ is more negative for X = F than for X = Cl or X = Br, and Table 6 reveals that this is due to the small ΔE_{def}, despite V^{cc} being smaller for $SiH_3F(L)$ than for $SiH_3Cl(L)$ or $SiH_3Br(L)$.

With $SiX_4(NH_3)$ on the other side, complex formation is exothermic only for X = F and even more endothermic for X = Cl than for X = H, and the differences in ΔH_c^{298} between different X groups are much bigger than for $SiH_3X(NH_3)$. Both, ΔE_{def} and V^{cc}, are very small for SiH_4, in accordance with the long Si−N bond in $SiH_4(NH_3)$ (see Table 3). The reduced stability of $SiCl_4(NH_3)$ relative to $SiF_4(NH_3)$ can be attributed entirely to the stronger interaction between SiF_4 and NH_3 (see Table 6), with ΔE_{def} being about equal for the two complexes. As with $SiF_4(NH_3)$/$SiCl_4(NH_3)$, the increased stability of $SiF_4(py)_2$ relative to $SiCl_4(py)_2$ is due to the difference in V^{cc} and not in ΔE_{def}. It is striking that one of the "classical" silicon complexes, $SiCl_4(py)_2$,[1b] exhibits a positive ΔH_c^{298}, in contrast to the formation of *solid* $SiCl_4(py)_2$ from $SiCl_4$ and pyridine, which is distinctly exothermic. Formation of $SiH_4(py)_2$ is even less favored, but this is caused by $\Delta E_{def}(SiH_4)$ being bigger than $\Delta E_{def}(SiCl_4)$, while V^{cc} of $SiH_4(D_{4h})$ and $SiCl_4(D_{4h})$ with pyridine are nearly equal. This means that the different Lewis acidities of SiH_4 and $SiCl_4$ are not caused by different electron-withdrawing forces of the ligands, but are due to different ΔE_{def}.

The variable differences in ΔH_c^{298} for penta- and hexacoordinated complexes of SiH_4 on one hand and of SiF_4/$SiCl_4$ on the other have their cause in different trends of $\Delta E_{def}[SiX_4,C_{3v}(tp)]$ and $\Delta E_{def}[SiX_4(D_{4h})]$ and in the different degrees of deformation of SiX_4 in $SiX_4(L)$. ΔE_{def} $[SiH_4,C_{3v}(tp)]$ is about 100 kJ mol^{-1} smaller and $\Delta E_{def}[SiH_4(D_{4h})]$ about 100 kJ mol^{-1} bigger than the respective values for SiF_4 and $SiCl_4$.

Only recently, and also by means of DFT calculations, Gillespie and co-workers related the weaker Lewis acidity of BF_3 relative to BCl_3 to the higher energy that is necessary to achieve a pyramidalization of the former.[8] The authors take the greater strength of the B−F bond relative to the B−Cl bond, and ligand close-packing effects as the causes for this effect and favor them over the "classical" explanation in terms of an n(X)−p_π(B) interaction. In the present work, a second order perturbation analysis of $SiX_4(D_{4h})$ in an NBO basis reveals substantial stabilization for X = F and Cl (440 and 436 kJ mol^{-1} for each molecule, respectively) through an n(X)−3p_π(Si) interaction. In $SiF_4(py)_2$, and $SiCl_4(py)_2$, this kind of interaction is reduced to 232 and 204 kJ mol^{-1}, respectively, but is still considerably high. Due to the absence of lone pairs, this interaction cannot operate with X = H. The significantly lower $\Delta E_{def}(D_{4h})$ for SiF_4 and $SiCl_4$ compared to SiH_4 cannot be due to bond

strengths, as the Si−H bond is weaker than the Si−F and Si−Cl bonds, nor due to a stronger repulsion between X atoms, as H atoms are smaller and less charged than F atoms. Instead, the above mentioned $n(X)-3p_{\pi}(Si)$ interaction (see Table 4), which stabilizes the deformed states of SiF_4 and $SiCl_4$, is seen to be responsible for the results outlined in Table 7.

Comparing $SiH_2X_2(py)_2$ and $SiX_4(py)_2$, ΔH_c^{298} of $SiF_4(py)_2$ is much more negative than ΔH_c^{298} of $SiH_2F_2(py)_2$, whereas ΔH_c^{298} of $SiCl_4(py)_2$ is slightly positive and ΔH_c^{298} of $SiH_2Cl_2(py)_2$ is negative (see Table 5a). Similar relations are found for $SiH_3X(NH_3)/SiX_4(NH_3)$ (X = F, Cl), where the formation of $SiF_4(NH_3)$ and $SiH_3Cl(NH_3)$, is much more exothermic than that of $SiH_3F(NH_3)$ and $SiCl_4(NH_3)$. Hence, SiH_2Cl_2 and SiF_4 are more Lewis acidic than SiH_2F_2 and $SiCl_4$, and SiH_3Cl and SiF_4, more acidic than $SiCl_4$ and SiH_3F. For the pyridine complexes, this order is due to $\Delta E_{def}(SiH_2X_2)$ being smaller than $\Delta E_{def}(SiX_4)$ and V^{cc} of $SiH_2Cl_2(py)_2$ bigger than that of $SiH_2F_2(py)_2$.

Considering the N and O donor complexes, V^{cc} is bigger in the hexacoordinated than in the pentacoordinated ones, which reflects the different $r_e(Si-L)$, i.e. short Si−L bonds correspond to strong interactions and vice versa. These differences can be explained in terms of second order NBO interactions (see Table 4). In the pentacoordinated complexes, the Si−L bonds result mainly from $n(L)-\sigma^*(Si-X)$ interactions, while in hexacoordinated complexes, $n(L)-3p_z(Si)$ interactions dominate. Due to a smaller difference in the NBO energies and a bigger overlap integral of n(L) and $3p_z(Si)$, compared to n(L) and $\sigma^*(Si-X)$, the second order $n(L)-3p_z(Si)$ energy is considerably bigger than the $n(L)-\sigma^*(Si-X)$ energy.

In terms of ΔG_c^{298} (see Table 5b), none of the neutral Lewis bases NH_3, NMe_3, py, OH_2 and OMe_2 forms complexes with silanes that are thermodynamically stable under normal conditions. This is in accordance with results on some SiF_4-amine adducts which are completely dissociated in the gas phase under normal conditions.[39]

Figure 3b shows the results of a relaxed potential energy scan for $SiH_3F(NH_3)$ in which the potential energy is given as a function of $r(Si-N)$. The curve represents a typical Morse-type potential. No barrier of activation occurs that could kinetically stabilize any thermodynamically labile complex towards dissociation or would prevent complex formation. The existence or nonexistence of this type of complex thus depends on thermodynamic factors only, with the solid state or polar environments providing additional stabilization.

A comparison of $SiF_4(NH_3)$ with $GeF_4(NH_3)$ reveals a higher thermodynamic stability of the latter (see Table 5). Approximately the same values of ΔE_{def} allow for a more enhanced distortion of GeF_4 (see Table 3), which, in turn, gives a stronger interaction with NH_3, as can be seen from V^{cc}.

F^- as Lewis Base

While NH_3, OH_2, their methyl derivatives and pyridine cannot substitute a halide or hydride from an Si center without charge separation, substitution reactions of silanes with F^- according to Equations (3a)−(3c) do not generate electric charges.

$$SiH_3X + F^- \rightarrow SiH_3F + X^- \quad (3a)$$

$$SiX_4 + F^- \rightarrow SiX_3F + X^- \quad (3b)$$

$$SiX_4 + 2\,F^- \rightarrow SiX_2F_2 + 2\,X^- \quad (3c)$$

For X = F, these reactions proceed in a thermochemically neutral manner, they are exothermic for X = Cl, Br and endothermic for X = H, in accordance with results of Gronert et al.[40]

The absolute value of ΔH_c^{298} as a function of the Lewis bases in complexes $SiH_3X(L)$, $SiX_4(L)$ and $SiX_4(L)_2$ is much bigger for $L = F^-$ than for the neutral ligands (see Table 5). The heavier the atom X is, the more exothermic becomes the complex formation with $L = F^-$, $[SiH_4F_2]^{2-}$ being the only complex exhibiting positive ΔH_c^{298} and ΔG_c^{298}. All other F^- complexes are thermodynamically stable with respect to dissociation into silane and F^-.

Gutsev calculated $[SiF_6]^{2-}$ to be unstable towards dissociation into $[SiF_5]^-$ and F^-, and to exhibit a metastable octahedral geometry with respect to ionization ($[SiF_6]^{2-} \rightarrow [SiF_6]^- + e^-$, see also reference 18).[41] The thermodynamic instability of $[SiF_6]^{2-}$ is confirmed in the present study, with $\Delta H^{298} = -206.9$ and $\Delta G^{298} = -248.7$ kJ mol^{-1} for the reaction $[SiF_6]^{2-} \rightarrow [SiF_5]^- + F^-$ [B3LYP/6−311+(2d,p)//B3LYP/6−31G(d)]. Furthermore, formation of SiF_6^{2-} is not much more exothermic than that of $SiF_4(py)_2$ or $SiF_4(NH_3)_2$. The existence of SiF_6^{2-}must thus be due to intermolecular stabilization, either in the solid state or in solution.

As with $GeF_4(NH_3)$, $[GeF_5]^-$ and $[GeF_6]^{2-}$ are thermodynamically more stable than their silicon analogues. In contrast to $SiF_4(NH_3)$ and $GeF_4(NH_3)$, the degree of deformation of SiF_4 and GeF_4 in $[EF_5]^-$ and $[EF_6]^{2-}$ (E = Si, Ge) is the same. It is hence striking, that V^{cc} for $[EF_5]^-$ and $[EF_6]^{2-}$ is even more negative for E = Si, and the overall increased thermodynamic stability of $[GeF_5]^-$ and $[GeF_6]^{2-}$ results from significantly smaller values of $\Delta E_{def}(GeF_4)$ compared to $\Delta E_{def}(SiF_4)$ (see Table 6 and 7).

Table 8. ΔH^{298} for reactions according to Equations 3a−c

X =	H	Cl	Br
reaction 3a		−195.9	−241.1
3b	93.8	−212.9	
3c	162.0	−426.8	

The more negative ΔH^{298} (see Table 8) for a given reaction, the more negative is the corresponding ΔH_c^{298} (see Table 5). Notably, ΔH_c^{298} is always more negative than the corresponding ΔH^{298}, i.e. in contrast to anions with pentacoordinated carbon atoms, which represent transition states in S_N2 reactions, silanes form complexes, that are thermodynamically stable toward decomposition either into SiH_3X/SiX_4 and F^- or $SiH_3F/SiFX_3$ and X^-. With the anionic complexes, Haaland's distinction between covalent

and dative bonds (see reference 22) comes to its limits. For example, the two Si−F bonds in $[SiH_3F_2]^-$ (D_{3h}) are equivalent by symmetry and the criterion of least-energy bond cleavage defines the Si−F bond that is broken first as dative, since dissociation would favorably be heterolytic, giving SiH_3F and F^-. The other one is subsequently defined as covalent, since least-energy cleavage will give SiH_3 and F instead of SiH_3^+ and F^-. Distinction between a covalent and a dative Si−F bond would thus be arbitrary. Taking $[SiH_3ClF]^-$, the first bond to be broken is either Si−F or Si−Cl, which would be defined as dative, giving either SiH_3Cl and F^- or SiH_3F and Cl^-, and leaving the other as covalent. This is an arbitrary distinction as well, but here between two nonequivalent bonds and this cannot be justified. It is suggested for such cases to extend Haaland's definition, and to define the dative bond as that whose heterolytic cleavage costs less energy, which in the present case is the Si−Cl bond. Thus, in contrast to the complexes with N/O donors, where the Si−L bond formed is the dative bond, in complexes with F^- as Lewis base, Si−Cl and Si−Br bonds become dative, as can be seen from ΔH^{298} in Table 8, which represent the enthalpy differences of the heterolytic bond cleavage [see Equations (3a)−(3c)]. It is this qualitative difference between F^- and N/O donors which is seen as the cause of the different trends of Lewis acidity outlined above.

Natural Atomic Charges

Atomic charges should indicate the ionic character of bonds in hypervalent Si compounds and its dependence on X and L. Natural atomic charges[28,29] are directly related to the eigenvalues of the density matrix expressed in terms of natural atomic orbitals and are thus more reliable than Mulliken atomic charges.[28]

The highest values for q_{Si} are always with X = F (see Table 9). q_{Si} varies little with L, if X = F and *decreases* in this case on coordination in all cases except $[SiH_3F_2]^-$. For X ≠ F, q_{Si} *increases* on coordination in most cases, and is most positive in the complex anions. An increase of charge of the central atom on coordination was previously found for $SiH_2Cl_2(py)_2$, $[SiH_4F]^-$ and $[SiH_5]^-$, but also for $[GeH_5]^-$ and $[SnH_5]^-$.[9,40] A similar relationship holds for q_X. It varies little for X = F, for which it is most negative (except for $[SiH_3XF]^-$) and it is more negative in the hypervalent than in the tetravalent silanes. Comparing $[SiX_4F]^-$ to $[SiX_4F_2]^{2-}$ and $SiF_4(NH_3)$ to $SiF_4(NH_3)_2$, q_X is more

Table 9. Natural atomic charges (a) of the Si atom, (b) of X and (c) of L (L = N for NH_3, NMe_3, py; L = O for H_2O, Me_2O; L = F for F^-).

(a)[a]

X =	H	F	Cl	X =	F	Cl	Br
SiX_4 (T_d)	0.63	2.46	1.38	SiH_2X_2 (C_{2v})	1.77	1.11	0.93
SiX_4 (D_{4h})	1.21	2.43	1.35	SiH_2X_2 (D_{2h})	1.74	1.17	0.99
SiX_4 [C_{3v}(tp)]	0.50	2.42	1.37	$SiH_2X_2(py)_2$	1.67	1.21	1.10
$SiX_4(NH_3)$	0.65	2.45	1.41	SiH_3X (C_{3v})	1.29	0.92	0.82
$[SiX_4F]^-$	0.90	2.40	1.61	SiH_3X [C_{3v}(tp)]	1.19	0.87	0.78
$SiX_4(py)_2$	0.85	2.44	1.47	$SiH_3X(NH_3)$	1.26	0.92	0.83
$[SiX_4F_2]^{2-}$	1.20	2.37	1.84	$SiH_3X(OH_2)$	1.27	0.92	0.92
				$[SiH_3XF]^-$	1.35	1.16	1.13

(b)[b]

X =	H	F	Cl		F	Cl	Br
SiX_4 (T_d)	−0.16	−0.62	−0.34	SiH_2X_2 (C_{2v})	−0.62	−0.38	−0.30
SiX_4 (D_{4h})	−0.30	−0.61	−0.34	SiH_2X_2 (D_{2h})	−0.63	−0.43	−0.34
SiX_4 [C_{3v}(tp)][c]	−0.13	−0.61	−0.34	$SiH_2X_2(py)_2$	−0.70	−0.57	−0.52
$SiX_4(NH_3)$[c]	−0.17	−0.64	−0.40	SiH_3X (C_{3v})	−0.61	−0.40	−0.32
$[SiX_4F]^-$ [c]	−0.30	−0.68	−0.49	SiH_3X [C_{3v}(tp)]	−0.66	−0.48	−0.42
$SiX_4(py)_2$	−0.29	−0.68	−0.47	$SiH_3X(NH_3)$	−0.64	−0.470	−0.41
$[SiX_4F_2]^{2-}$	−0.43	−0.73	−0.62	$SiH_3X(OH_2)$	−0.63	−0.43	−0.37
				$[SiH_3XF]^-$	−0.72	−0.79	−0.77

(c)[d]

X =	H	F	Cl		F	Cl	Br
$SiX_4(NH_3)$	−1.11	−1.15	−1.13	$SiH_2X_2(py)_2$	−0.53	−0.54	−0.54
$[SiX_4F]^-$	−0.71	−0.69	−0.67	$SiH_3X(NH_3)$	−1.12	−1.12	−1.11
$SiX_4(py)_2$	−0.50	−0.57	−0.58	$SiH_3X(OH_2)$	−0.94	−0.93	−0.93
$[SiX_4F_2]^{2-}$	−0.74	−0.73	−0.68	$[SiH_3XF]^-$	−0.72	−0.68	−0.68

[a] $SiF_4(NH_3)_2$: 2.40, $SiF_4(NMe_3)$: 2.47; $SiH_3F(NMe)_3$: 1.27; $SiH_3Cl(OMe)_2$: 0.92. − [b] $SiF_4(NH_3)_2$: −0.69; $SiF_4(NMe_3)$: −0.64; $SiH_3F(NMe)_3$: −0.64; $SiH_3Cl(OMe)_2$: −0.43. − [c] Abundance weighted average of apical and equatorial q_X. − [d] $SiF_4(NH_3)_2$: −1.13; $SiF_4(NMe_3)$: −0.59; $SiH_3F(NMe)_3$: −0.53; $SiH_3Cl(OMe)_2$: −0.58. $q_N(NH_3) = -1.11$, $q_N(NMe_3) = -0.49$, $q_N(py) = -0.45$, $q_O(H_2O) = -0.93$, $q_O(Me_2O) = -0.56$, $q_F(F^-) = -1.00$.

negative in the hexacoordinated complexes. In $SiX_4[C_{3v}(tp)]$, $SiX_4(NH_3)$ and $[SiX_4F]^-$, q_X is more negative for the apical than for the equatorial X. It is interesting to note that the reduced negative charge on the donor atom in NMe_3 compared to NH_3 (and as well in OMe_2 compared to OH_2) has little influence on q_{Si}.

For SiH_3X, SiH_2X_2 and their complexes, $q_{H(Si)}$ (not given in Table 9) becomes more negative in the order X = Br < Cl < F.

The increase in the charge difference between Si and X on complex formation in most cases gives a hint of a pronounced ionic nature of the interaction between Si and L, increasing in the order X = H < Br < Cl < F and, consequently, $SiH_3X < SiH_2X_2 < SiX_4$. In the course of the complex formation, electron density is shifted from and to the periphery of the molecule, i.e. X becomes more negatively and the H atoms of the ligands more positively charged. This shift will certainly favor intermolecular coulombic and charge-dipole interactions and hence gives a reasonable explanation for the stabilization of the otherwise unstable silane-amine complexes in polar solutions and in the solid state.

Alternative Complex Configurations: *cis* vs. *trans*

It has already been established [3d,22,42,43] that in pentacoordinated Si complexes with a trigonal bipyramidal configuration, the most stable structure has the Lewis base, i.e. the dative bond, in an apical rather than an equatorial position [*cf.* $SiF_4(NMe_3)$ vs. PF_4NMe_2 in ref.[22]]. In the present paper, $SiF_4(py)_2$ was chosen to investigate the case of *cis* (C_2) vs. *trans* (D_{2h}) configuration in distorted octahedral complexes. All known XRD structures of hexacoordinated Si complexes of the SiA_4B_2 type that are not configurationally strained, i.e. that do not contain chelating Lewis bases or the Si atom as a member of a ring system, exhibit a *trans*- rather than a *cis* configuration.[9,11–13,44,45]

Since the Si–N bond is longer in the *cis*- than in the *trans* complex, and, regarding the *cis* complex, the Si–F bonds *trans* to the Si–N bonds are shorter than the two Si–F bonds in mutual *trans* position (see Figure 4), the *trans*-effect of F is obviously stronger than that of N. The bond angles around the Si atom in *cis*-$SiF_4(py)_2$ are: *a*(F^bSiF^b) 101.5, *a*(F^aSiF^a) 161.7, *a*(F^aSiF^b) 95.3 and 96.3, *a*(NSiN) 84.5, *a*($NSiF^a$) 82.9 and 83.5, *a*($NSiF^b$) 87.0 and 171.5° ("a" denotes the two F atoms *trans* to each other, "b" denotes the other two). In spite of the huge differences in their molecular structures, ΔH_c^{298} is surprisingly very similar for the two configurations, with a difference of only 7.6 kJ mol^{-1} in favor of the *trans* complex. The much stronger interaction due to a shorter contact distance between py and SiF_4(CG) in the *trans* complex is nearly entirely compensated by the energy of deformation, which is much bigger for the *trans* complex (285.6 kJ mol^{-1}) than for the *cis* complex (216.6 kJ mol^{-1}). Since the energy difference between the *cis* and *trans* configurations is rather small, the domination of the *trans* configuration in all SiA_2B_4 complexes in the solid state is assumed to be mainly a crystal packing effect.

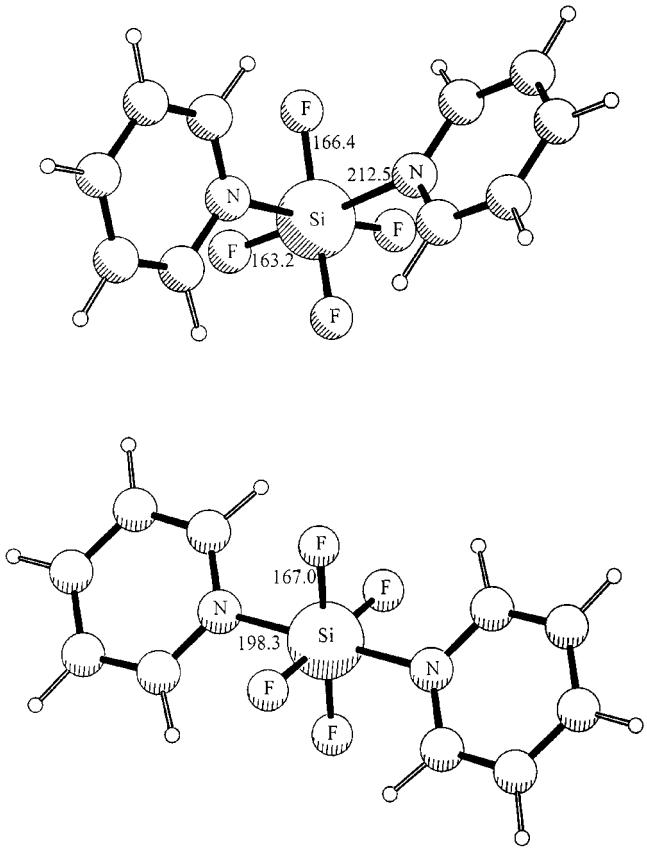

Figure 4. Molecular graphics of *cis*- (above) and *trans*-$SiF_4(py)_2$ with selected interatomic distances

Comparison of the B3LYP/6–311+G(2d,p)//B3LYP/6–31G(d) Approach to More Sophisticated Models and Experimental Results

$SiF_4(NH_3)$ is the only silane adduct with a known gas-phase structure, and it was taken as a probe for the reliability of the B3LYP/6–31G(d) geometry optimizations for the present subject.[46] Since the N and F atoms exhibit large negative charges according to NBO analyses (see Table 9), the geometry of $SiF_4(NH_3)$ was optimized with the B3LYP/6–311+G(2d,p) model to reveal the influence of diffuse functions on the molecular structure. Additionally, an MP2/6–311+G(2d,p) geometry optimization was performed to compare the MP2 and the B3LYP level. Furthermore, with $SiH_3F(NH_3)$, another comparison of the B3LYP and the MP2 model was performed.

The data in Table 10a demonstrate that *r*(Si–F) and *a*(F^aSiF^e) agree very well between all theoretical models and the experiment. The Si–N bond is too long with all model chemistries, MP2/6–311+G(2d,p) giving the closest value. A good agreement between DFT- and MP2-optimized covalent bond lengths and angles is also achieved for $SiH_3F(NH_3)$.

The dative bond is far more sensitive to the chosen method of geometry optimization and the basis set than the covalent bonds are. Complex formation is estimated to be more exothermic with the MP2 method of electron correla-

Table 10. Selected parameters (a) from the experimental and theoretically optimized molecular structure of $SiF_4(NH_3)$; (b) from theoretically optimized molecular structure of $SiH_3F(NH_3)$

(a)

	B3LYP(I)[a]	B3LYP(II)[b]	MP2(I)[c]	MP2(II)[d]	exp[e]
r(Si−F^a)	161.2	160.9	160.9	161.2	161.2
r(Si−F^e)	160.8	160.5	160.3	160.8	160.8
r(Si−N)	214.4	213.0	210.8	214.4	209.0
a(F^{e}SiF^a)	98.1	97.7	97.7	97.7	97.7
ΔE_{form}	−33.1	−32.5	−41.3	−43.9	

(b)

	B3LYP(I)[a]	B3LYP(II)[b]	MP2(II)[d]
r(Si−F)	163.2	163.7	163.5
r(Si−H)	148.4	147.3	146.5
r(Si−N)	256.4	267.0	261.5
a(HSiF)	104.3	103.9	103.7
ΔE_{form}	−21.1	−21.4	−27.6

[a] B3LYP(I): B3LYP/6−311+G(2d,p)//B3LYP/6−31G(d). − [b] B3LYP(II): B3LYP/6−311+G(2d,p). − [c] MP2: MP2/6−311+G(2d,p). − [d] MP2/D95G(p,d) from ref.[47] − [e] Structure from ref.[7]

tion than with B3LYP, while diffuse functions have a minor influence.

Conclusion

The aim of the present work was to give a comprehensive study of the Lewis acidity of silanes and to have a closer look at its molecular origins. The method of partitioning the energy of complex formation into a deformation energy, ΔE_{def}, and an interaction energy, V, together with an analysis of the nature of the dative bond in terms of natural bond orbitals and natural atomic charges proved to be very useful for this purpose. Silanes were shown to be weak Lewis acids towards neutral N and O donor Lewis bases. The energy gained by interaction with these donor atoms is, in many cases, not much bigger, and in quite a few cases even smaller, than the energy necessary to change the geometry of the silane from the ground state to that in the complex, leading to comparably small values of ΔH_c^{298}. Since the formation of the complex reduces the number of molecules, ΔS_c^{298} of the system is negative. This fact leads to a positive value of ΔG_c^{298} for all complexes with N and O donor atoms. Only complexes of silanes with the very strong Lewis base F^- exhibit a negative standard free enthalpy of formation. A comparison of SiF_4 and GeF_4 shows that the latter is a stronger Lewis acid than SiF_4, but not due to a stronger interaction with Lewis bases, but due to a more floppy ground-state geometry, resulting in smaller ΔE_{def}. The DFT calculations in the present paper rationalize why complexes between silanes and N/O donating Lewis bases were never observed in the gas phase under standard conditions. The atomic charges, the changes in bond lengths during complex formation and, compared to N and O donors, the significantly more exothermic reactions of halosilanes with F^- suggest that the interaction between Si and the donor atoms exhibit an highly ionic character, increasing from SiH_3X to SiH_2X_2 to SiX_4 and from X = Br to Cl to F. Silanes are classified as very weak Lewis acids due to the "stiffness" of their molecular structure and only with very strong Lewis bases or stabilized by intermolecular forces in solution of the solid state, Lewis base adducts of silanes can exist at room temperature.

Experimental Section

Theoretical Methods

All calculations were performed on various servers of the Zentrum für Datenverarbeitung, Universität Mainz, using the GAUSSIAN94 software package.[23] The geometries of all molecules were fully optimized under the respective symmetry constraints using a 6−31G(d) basis set and density functional theory (DFT)[19] employing a combination of local, gradient-corrected, and exact exchange functionals according to the prescription of Becke[24] and the gradient-corrected correlation functional of Lee, Yang and Parr[25] [B3LYP/6−31G(d)] (for basis set terminology see e.g. reference 26). All stationary points were characterized by calculation of analytic force constants. With the same model chemistry, natural atomic charges were calculated and second order perturbation energies in a natural orbital basis were calculated.[27−29] Taking the B3LYP/6−31G(d) optimized geometries, single-point energies were calculated at the B3LYP level using Pople's 6−311+G(2d,p) basis set.[30] H^{298} and G^{298} were obtained from B3LYP/6−311+G(2d,p)//B3LYP/6−31G(d) energies and unscaled B3LYP/6−31G(d) thermal corrections. Using the B3LYP/6−31G(d) optimized geometries of the complexes, B3LYP/6−311+G(2d,p) counterpoise calculations were performed to correct the energy of interaction between Si and the donor atoms for the basis set superposition error (bsse).[31,32]

All thermochemical quantities (i.e. ΔE, ΔH, ΔG and V) are given in kJ mol^{-1}, all atomic distances in pm, all bond and torsional angles in degree and all charges in fractions of the elemental charge (1.609×10^{-19} C).

Acknowledgments

The author thanks the Fonds der Chemischen Industrie for a grant and the Zentrum für Datenverarbeitung, Johannes Gutenberg Universität Mainz, for providing the computational resources.

[1] [1a] W. R. Trost, *Nature* **1952**, *169*, 289−290. − [1b] U. Wannagat, Z. Schwarz, H. Voss, *Z. Anorg. Allg. Chem.* **1954**, *277*, 73−88. − [1c] B. J. Aylett, *J. Inorg. Nucl. Chem.* **1958**, *5*, 292−295. − [1d] E. Schnell, *Monatsh. Chem.* **1962**, *93*, 1136−1144. − [1e] I. R. Beattie, *Quart. Rev. Chem. Soc.* **1963**, *17*, 382−405. − [1f] H. J. Campbell-Ferguson, E. A. V. Ebsworth, *J. Chem. Soc. A*, **1966**, 1508−1514; **1967**, 705−712. − [1g] U. Wannagat, K. Hensen, F. Vielberg, *Monatsh. Chem.* **1968**, *99*, 431−437.

[2] [2a] B. J. Helmer, R. West, R. J. P. Corriu, M. Poirier, G. Royo, A. de Saxce, *J. Organomet. Chem.* **1983**, *251*, 295−298. − [2b] A. R. Bassindale, T. Stout, *J. Chem. Soc., Chem. Commun.* **1984**, 1387−1389. − [2c] D. G. Anderson, A. J. Blake, S. Cradock, E. A. V. Ebsworth, D. W. H. Rankin, H. E. Robertson, A. J. Welch, *J. Chem. Soc., Dalton Trans.* **1986**, 91−95. − [2d] D. Kummer, S. C. Chaudhry, T. Debaerdemaeker, U. Thewalt,

Chem. Ber. **1990**, *123*, 945−951. − [2e] K. M; Kane, F. M. Lemke, J. L. Petersen, *Inorg. Chem.* **1995**, *34*, 4085−4091. − [2f] K. Hensen, F. Gebhardt, M. Bolte, *Z. Anorg. Allg. Chem.* **1997**, *623*, 633−636. − [2g] N. W. Mitzel, A. J. Blake, D. W. H. Rankin, *J. Am. Chem. Soc.* **1997**, *119*, 4143−4148. − [2h] P. Boudjouk, S. D. Kloos, B-K. Kim, M. Page, D. Thweatt, *J. Chem. Soc., Dalton Trans.* **1998**, 877−879. − [2i] H. H. Karsch, P. A. Schlüter, M. Reisky, *Eur. J. Inorg. Chem.* **1998**, 442−426.

[3] [3a] A. Greenberg, C. Plant, C. A. Venanzi, *THEOCHEM*, **1991**, *80*, 291−301. − [3b] M. S. Gordon, M. T. Carroll, J. H. Jensen, L. P. Davis, L. W. Burggraf, R. M. Guidry, *Organometallics* **1991**, *10*, 2657−2660. − [3c] G. I. Csonka, P. Hencsei, *J. Comput. Chem.* **1994**, *15*, 385−394. − [3d] J. M. Anglada, C. Bo, J. M. Bofill, R. Crehuet, J. M. Poblet *Organometallics* **1999**, *18*, 5584−5593.

[4] R. Tacke, D. Reichel, M., Kropfgans, P. G. Jones, E. Mutschler, J. Gross, X. Hou, M. Waeldbrock, G. Lambrecht, *Organometallics* **1995**, *14*, 251−262.

[5] [5a] S. N. Tandura, M. G. Voronkov, M. V. Alekseev, *Top. Curr. Chem.* **1986**, *131*, 99−156. − [5b] R. R. Holmes, *Chem. Rev.* **1990**, *90*, 17−31. − [5c] C. Chuit, R. J .P. Corriu, C. Reye, J. C. Young, *Chem. Rev.* **1993**, *93*, 1371−1448.

[6] T. J. Lorenz, B. S. Ault, *Inorg. Chem.* **1982**, *21*, 1758−1761.

[7] R. S. Ruoff, T. Emilsson, A. I. Jaman, T. C. Germann, H. S. Gutowsky, *J. Chem. Phys.* **1992**, *96*, 3441−3446.

[8] B. D. Rowsell, R. J. Gillespie, G. L. Heard, *Inorg. Chem.* **1999**, *38*, 4659−4662.

[9] K. Hensen, T. Stumpf, M. Bolte, C. Näther, H. Fleischer, *J. Am. Chem. Soc.* **1998**, *120*, 10402−10408.

[10] A. J. Blake, S. Cradock, E. A. V. Ebsworth, K. C. Franklin, *Angew. Chem.* **1990**, *102*, 87−89; *Angew. Chem. Int. Ed. Engl.* **1990**, *29*, 76−78.

[11] V. A. Bain, R. C. G. Killean, M. Webster, *Acta Cryst.* **1969**, *B25*, 156−159.

[12] O. Bechstein, B. Ziemer, D. Hass, S. I. Trojanov, V. B. Rybakov, G. N. Maso, *Z. Anorg. Allg. Chem.* **1990**, *582*, 211−216.

[13] C. Plitzko, G. Meyer, *Z. Anorg. Allg. Chem.* **1996**, *622*, 1646−1650.

[14] F. Olbrich, R. J. Lagow, *Z. Anorg. Allg. Chem.* **1995**, *621*, 1929−1932.

[15] W. C. Hamilton, *Acta Cryst.* **1962**, *15*, 353−360.

[16] Due to the presence of protic hydrogen atoms, $SiH_3X(NH_3)$, $SiH_3X(OH_2)$ (X = Cl, Br) and $SiCl_4(NH_3)$ are thermodynamically unstable with respect to the formation of di-/oligosilazanes and NH_4X (L = NH_3), or disiloxanes and HX (L = H_2O).[17] Since this reaction channel does not interfer with the subject studied, these compounds can still serve as models for dative Si−N and Si−O interactions.

[17] R. Fessenden, J. Fessenden *Chem. Rev.* **1961**, *61*, 361−388.

[18] Only a few isolated dianionic species were calculated to be stable towards a single electron oxidation according to $A^{2-} \rightarrow A^- + e^-$ (personal correspondence, Dr. Thomas Sommerfeld, University of Perugia, Italy.) and it is suspected that none of the dianions investigated herein are members of this set. This aspect was anyhow not subject of the present study.

[19] R. G. Parr, W. Yang, *Density-Functional Theory of Atoms and Molecules*, Oxford University Press, **1989**.

[20] T. Ziegler, *Chem. Rev.* **1991**, *91*, 651−667.

[21] In the present study, covalent and dative bonds are distinguished according to the definition of Haaland.[22] A chemical bond between two atoms is called covalent, if the lowest energy channel of dissociation leads to a homolytic cleavage, and dative if it is cleaved heterolytically.

[22] A. Haaland, *Angew. Chem.* **1989**, *101*, 1017−1032; *Angew. Chem. Int. Ed. Engl.* **1989**, *28*, 992−1007.

[23] GAUSSIAN 94, Revision E.2, M. J. Frisch, G. W. Trucks, H. B. Schlegel, P. M. W. Gill, B. G. Johnson, M. A. Robb, J. R. Cheeseman, T. Keith, G. A. Petersson, J. A. Montgomery, K. Raghavachari, M. A. Al-Laham, V. G. Zakrzewski, J. V. Ortiz, J. B. Foresman, J. Cioslowski, B. B. Stefanov, A. Nanayakkara, M. Challacombe, C. Y. Peng, P. Y. Ayala, W. Chen, M. W. Wong, J. L. Andres, E. S. Replogle, R. Gomperts, R. L. Martin, D. J. Fox, J. S. Binkley, D. J. Defrees, J. Baker, J. P. Stewart, M. Head-Gordon, C. Gonzalez, J. A. Pople, Gaussian, Inc., Pittsburgh PA, **1995**.

[24] A. D. Becke, *J. Chem. Phys.* **1993**, *98*, 5648−5652.

[25] C. Lee, W. Yang, R. G. Parr, *Phys. Rev.* **1988**, *B37*, 785−789.

[26] W. J. Hehre, L. Radom, P. v. R. Schleyer, J. A. Pople, Ab initio *Molecular Orbital Theory*; Wiley, New York, **1986**.

[27] The term "model chemistry" refers to a distinct method of calculation combined with a distinct basis set e. g. B3LYP/6−311+G(2d,p), see also reference 26.

[28] A. E. Reed, R. B. Weinstock, F. Weinhold, *J. Chem. Phys.* **1985**, 83, 735−746.

[29] A. E. Reed, L. A. Curtiss, F. Weinhold, *Chem. Rev.* **1988**, *88*, 899−926.

[30] R. Krishnan, J. S. Binkley, R. Seeger, J. A. Pople, *J. Chem. Phys.* **1980**, *72*, 650−654.

[31] S. F. Boys, F. Bernardi, *Mol. Phys.* **1970**, *19*, 553−566.

[32] D. W. Schwenke, D. G. Truhlar, *J. Chem. Phys.* **1985**, *82*, 2418−2426.

[33] The indices "a" and "e" refer to apical and equatorial positions in a trigonal pyramidal or a trigonal bipyramidal structure.

[34] L. Pauling, *The Nature of the Chemical Bond and the Structure of Molecules and Crystals*, 3rd ed., Cornell University Press, **1960**.

[35] Recent ab initio investigations on complexes with dative Al→W interactions revealed bigger dissociation energies for adducts with longer bonds. See R. A. Fischer, M. M. Schulte, J. Weiss, L. Zsolnai, A. Jacobi, G. Huttner, G. Frenking, C. Boehme, S. F. Vyboishchikov, *J. Am .Chem. Soc.* **1998**, *120*, 1237−1248.

[36] *Tables of Interatomic Distances and Configurations in Molecules and Ions*, Ed. L. Sutton, Spec. Publ. No 11 and 18, The Chemical Society, London **1958** and **1965**.

[37] H. B. Bürgi, *Perspectives in Coordination Chemistry* (Eds.: A. F. Williams, C. Floriani, A. E. Merbach), p. 1−29, Helvetica Chimica Acta, Basel, **1992**.

[38] In this respect, recently published energy calculations for coordinative Si−N interactions which were not corrected for the bsse are to be taken with care. See: H. Bock, Z. Havlas, V. Krenzel, *Angew. Chem.* **1998**, *110*, 3305−3307; *Angew. Chem. Int. Ed.* **1998**, *37*, 3163−3166.

[39] C. J. Porritt, *Chem. Ind. (London)* **1979**, 215.

[40] S. Gronert, R. Glaser, A. Streitwieser, *J. Am. Chem. Soc.* **1989**, *111*, 3111−3117.

[41] G. L. Gutsev, *Chem. Phys. Lett.* **1991**, *184*, 305−309.

[42] C. J. Marsden, *Inorg. Chem.* **1983**, *22*, 3177−3178.

[43] J. A. Deiters, R. R. Holmes, *J. Am. Chem. Soc.* **1987**, *109*, 1686−1692.

[44] H. Fleischer, K. Hensen, T. Stumpf, *Chem. Ber.* **1996**, *129*, 765−771.

[45] M. Kettner, Ph.D. Thesis, University of Frankfurt/Main, **1999**.

[46] From the experiment, an r_g structure was obtained, while ab initio and DFT geometry optimizations lead to r_e structures. Since the experiment was performed at a temperature of 3 K, r_e and r_g should not differ too much for bond lengths, with $r_g > r_e$.

[47] A. R. Rossi, J. M. Jasinski, *Chem. Phys. Lett.* **1990**, *169*, 399−404.

Received May 12, 2000
[I00193]

Open-Chain Polyamine Ligands Bearing an Anthracene Unit − Chemosensors for Logic Operations at the Molecular Level

Sérgio Alves,[a] Fernando Pina,*[a] M. Teresa Albelda,[b] Enrique García-España,*[b] Conxa Soriano,[c] and Santiago V. Luis*[d]

Keywords: Polyamines / Nickel / Copper / Zinc / Cadmium / Sensors / Logic gates

In this work the absorption and the fluorescence emission properties as well as the protonation sequence of three open chain polyamine ligands of different dimensions bearing an anthracene unit were studied. The protonation and stability constants with Ni^{2+}, Cu^{2+}, Zn^{2+}, and Cd^{2+} have been determined in 0.15 mol·dm^{-3} NaCl at 298.1 ± 0.1 K. The values of both protonation and stability constants follow the expected trends according to the number of nitrogen donors, sequence of chelate rings and hydrophilic–hydrophobic balance. Chelation enhancement of the fluorescence emission (CHEF) was observed for some complexes of these ligands with Zn^{2+} and Cd^{2+}. In contrast the analog complexes containing $Cu^{2+}$and Ni^{2+} exhibit a chelation enhancement of the quenching (CHEQ) except for the complexes with the largest chain where some protonated metal complexes are emissive. These systems are explored from the point of view of chemosensors for logic operations at the molecular level.

Introduction

The tendency towards miniaturization has been a constant objective in many scientific applications, in particular those related to the construction of electronic components. The smaller size is associated with better performance and greater speed.[1,2] However, miniaturization based on top-down approaches, like lithographic techniques, seems to have reached its lower limits.[3,4] One possible alternative to overcome this drawback is the use of the bottom up approach. In this strategy molecules are viewed as elementary components performing a single act, and an assembly of molecular components as a device capable of executing a given function.[4,5]

Molecular analogs of electronic devices are important research tools. There is also a possibility of their future application in a chemical computer.[4−8] In order to mimic semiconductor logic gates, switches based on systems operating in liquid solutions (liquid logic) have been described.[8−13] De Silva and co-workers reported several examples of these systems constituted by a receptor and a fluorophore separated by a spacer.[8,10−13] The input signal (1,0) is obtained through the binding of metal ions or protons to the receptor, while the output signal (0,1) is generally detected by the presence of light emission. In a different approach, based on a pseudo rotaxane, the groups of Balzani and Stoddart were able to describe a conceptual XOR logic gate.[14]

In recent years our groups have been involved in the synthesis and photochemical characterization of chemosensors containing an aromatic hydrocarbon unit and bearing a polyamine receptor unit.[15−19] These molecules are capable of sensing not only cations,[15−18] but also anions.[19] In the case of H^+, Zn^{2+}, and Cd^{2+} we observed an enhancement of the fluorescence emission upon chelation (CHEF), while a quenching effect (CHEQ) can be detected for chelation of ATP, Cu^{2+}, and Ni^{2+}.[8,18,19]

In this work we explore the potential of a series of compounds containing one anthracene moiety, linked to a polyamine chain by an anthrylic carbon atom and their metal complexes. The purpose of this is for mimicking the electronic logic gates.

The systems reported here show a high versatility, because depending on pH, different logic gates, based on metal ion coordination (exhibiting CHEQ and CHEF effects), can be designed.

Results and Discussion

Protonation and Stability Constants

The protonation constants of **L3** and **L4** (Scheme 1) and the stability constants for their interaction with the metal ions Ni^{2+}, Cu^{2+}, Zn^{2+}, and Cd^{2+} are shown in Tables 1, 2,

[a] Departamento de Química, Centro de Química Fina e Biotecnologia, Universidade Nova de Lisboa,
Quinta da Torre, 2825 Monte de Caparica, Portugal
E-mail fjp@dq.fct.unl.pt
[b] Departament de Química Inorgànica, Facultat de Química, Universitat de València,
c/Dr. Moliner 50, 46100 Burjassot (València), Spain
E-mail: enrique.garcia-es@uv.es
[c] Departament de Química Orgànica, Facultat de Farmàcia, Universitat de València,
Avda. Vicent Andrés Estellés s/n, 46100 Burjassot (València)
[d] Departament de Química Inorgànica i Orgànica, Universitat Jaume I,
c/Borriol s/n, 12080 Castellón, Spain
E-mail: luiss@mail.uji.es

 © WILEY-VCH Verlag GmbH, 69451 Weinheim, 2001 1434−1948/01/0202−0405 $ 17.50+.50/0

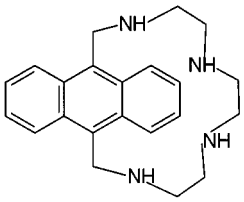

L1

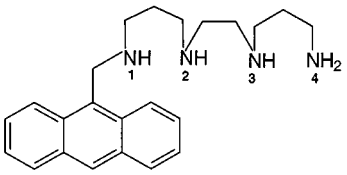

L2

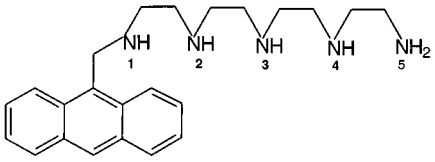

L3

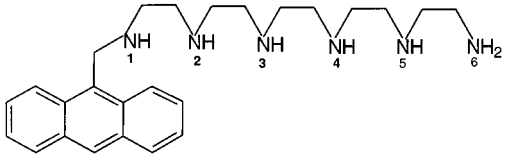

L4

Scheme 1

Table 1. Logarithms of the protonation constants for the receptors **L3** and **L4** determined in NaCl 0.15 mol·dm^{-3} at 298.1 ± 0.1 K

Reaction	L3	L4	L2
H+L ⇌ HL[a]	10.27(4)[b]	10.05(1)	10.28
H+ HL ⇌ H_2L	9.16(5)	9.18(1)	9.21
H+ H_2L ⇌ H_3L	7.83(8)	8.42(1)	7.65
H+ H_3L ⇌ H_4L	4.96(1)	6.69(1)	5.59
H+ H_4L ⇌ H_5L	2.9(1)	4.22(2)	–
H+ H_5L ⇌ H_6L	–	2.33(3)	–
logβ[c]	35.1	40.9	32.7

[a] Charges omitted by clarity. – [b] Values in parentheses are standard deviations in the last significant figure. – [c] log $\beta = \Sigma \log K_{HjL}$.

and 3 respectively. All constants were determined in 0.15 mol·dm^{-3} NaCl at 298.1 ± 0.1 K.

The trend of the protonation constants (Table 1) can be largely interpreted in terms of minimization of coulombic repulsion between same sign charges.[20] **L3** presents three large constants [log K_1 − log K_3 = 2.4 or $\Delta(\log K_1/K_3)$ = 2.4] and two much lower constants for the fourth and fifth protonation steps [$\Delta(\log K_3/K_4)$ = 2.87, $\Delta(\log K_4/K_5)$ = 2.06]. **L4** displays even higher constants than **L3** in its first three protonation steps [$\Delta(\log K_1/K_3)$ = 1.63] an intermediate value for the fourth protonation step [$\Delta(\log K_3/K_4)$ = 1.75] and a group of two lower constants for the fifth and sixth protonation steps [$\Delta(\log K_5/K_6)$ = 1.9]. The first three protons binding the free polyamine **L3** can bind non-adjacent nitrogen atoms and therefore electrostatic repulsion will not be very large at this stage. The fourth protonation has to occur, however, adjacent to two already protonated nitrogen atoms yielding an important basicity decrease.

For **L4**, the situation is slightly different. The first three protons can bind the receptor through distant enough nitrogen atoms to yield even higher constants than **L3** (see Figure 1). The fourth protonation, however, will have to take place close to only one protonated centre yielding a smaller basicity reduction than that observed for the fourth step of **L3**.

Another point of interest is to compare these protonation constants with those reported in the literature for the polyamines, 1,4,7,10,13-pentaazatridecane (tetren, **L5**) and 1,4,7,10,13,16-hexaazahexadecane (penten, **L6**). The larger hydrophilicity of **L5** and **L6** is denoted in their higher protonation constants. This fact can be ascribed to the greater stabilisation by hydrogen bonding of **L5** and **L6,** containing primary nitrogen atoms at both ends, to the solvent water molecules.

The stability constants of the metal complexes of **L3** and **L4**, presented in Table 2 and Table 3, fulfil some of the general aspects of the coordination chemistry of polyamine ligands. Firstly, the Cu^{2+} complexes of both ligands are the ones displaying the largest stabilities; the stability trend observed $Cu^{2+} > Ni^{2+} > Zn^{2+}$ follows the expected tendency

Table 2. Stability constants for the interaction of **L3** with Cu^{2+}, Zn^{2+}, and Cd^{2+} determined in NaCl 0.15 mol·dm^{-3} at 298.1 ± 0.1 K

Reaction	Ni^{2+}	Cu^{2+}	Zn^{2+}	Cd^{2+}
M + L ⇌ ML[a]	13.2(1)	18.15(7)[b]	11.73(1)	8.36(2)
ML + H ⇌ MHL	8.2	7.57	8.28	9.98
M + LH ⇌ MHL	11.1	15.37	9.74	8.07
MHL + H ⇌ MH_2L	5.1	4.61	5.4	5.48
MH_2L + H ⇌ MH_3L	–	3.48	–	–
ML + OH ⇌ ML(OH)	3.3	3.66	5.38	–
M + L + H_2O ⇌ ML(OH) + H^+	2.7(1)	8.1(1)	3.88(8)	–

[a] Charges omitted by clarity. – [b] Values in parentheses are standard deviations in the last significant figure.

Table 3. Stability constants for the interaction of **L4** with Ni^{2+}, Cu^{2+}, Zn^{2+}, and Cd^{2+} determined in NaCl 0.15 mol·dm^{-3} at 298.1 ± 0.1 K

Reaction	Ni^{2+}	Cu^{2+}	Zn^{2+}	Cd^{2+}
M + L ⇌ ML[a]	15.2(1)[b]	18.45(5)	12.84(5)	10.07(5)
ML + H ⇌ MHL	7.31	9.31	8.21	9.82
M + LH ⇌ MHL	12.5	17.71	11.0	9.85
MHL + H ⇌ MH_2L	6.12	5.03	6.22	6.62
MH_2L + H ⇌ MH_3L	–	3.58	–	–
ML + OH ⇌ ML(OH)	–	–	4.9	–
M + L + H_2O ⇌ ML(OH) + H^+	–	–	4.01(4)	–

[a] Charges omitted by clarity. – [b] Values in parentheses are standard deviations in the last significant figure.

according to the general Irving−Williams order of stability for octahedral complexes. The stability of the Cd^{2+} complexes is, for the two ligands, slightly lower than that found for the Zn^{2+} complexes. It is interesting to note that, particularly for Cu^{2+}, the stability constants of the different complexes do not increase much from **L3** to **L4**. Although deriving coordination numbers from values of the free energy terms alone can often be misleading, comparison of the values of the stability constants with those presented by analogous complexes can provide useful information with respect to this. The stability of the $[CuL]^{2+}$ complexes of **L3** and **L4** (see Table 2 and Table 3) is clearly lower than those presented by the $[CuL]^{2+}$ complexes of **L5**, log K_{CuL} = 22.8, and **L6**, log K_{CuL} = 22.40(5),[21] and even slightly lower than that presented by the open-chain tetraamine 1,4,7,10-tetraazadecane, log K_{CuL} = 20.05. Therefore, all of this data, together with the presence of different protonated complex species seem to suggest that four nitrogen atoms are involved in the coordination sphere of the Cu^{2+} complexes of both polyamines. This point is further supported by comparison with the tetraamine **L2**, that also contains an anthracene fragment. The complex $[Cu\mathbf{L2}]^{2+}$ whose crystal structure denoted a 4-coordination of the Cu^{2+} by the nitrogen donors of the ligand,[18] presents a slightly higher stability than $[Cu\mathbf{L3}]^{2+}$ and $[Cu\mathbf{L4}]^{2+}$, again suggesting the same number of co-ordinated nitrogens. The higher stability of $[Cu\mathbf{L2}]^{2+}$ (log K_{CuL2} = 19.45) with respect to $[Cu\mathbf{L3}]^{2+}$ and $[Cu\mathbf{L4}]^{2+}$ can be ascribed to the better bite produced by an alternated sequence of five and six-membered chelate rings. For the other metal ions studied, Ni^{2+}, Zn^{2+}, and Cd^{2+}, similar comparisons with related polyamines also suggest four as the most likely number of nitrogen donors involved in the first co-ordination sphere of the metals (log K_{NiL2} = 11.61, log K_{ZnL2} = 8.62, log K_{CdL2} = 8.20, ref.[18]).

Electronic Absorption and Fluorescence Emission Studies

For all systems the molar fraction distribution of the different species in solution was calculated with the constants determined by potentiometry, and used to fit the absorption and the fluorescence emission titration curves.

Protonation Effects

The electronic absorption spectra of the free ligands reported in Scheme 1 do not change significantly with pH, in contrast with the fluorescence emission intensities which are dramatically dependent on the protonation state of the compounds (see Figure 1). In previous work carried out with the smaller ligands **L1** and **L2**, we reported that their fully protonated forms exhibit the highest emission intensity.[18] According to the NMR spectroscopic data, the first and second deprotonation steps occur on the two central

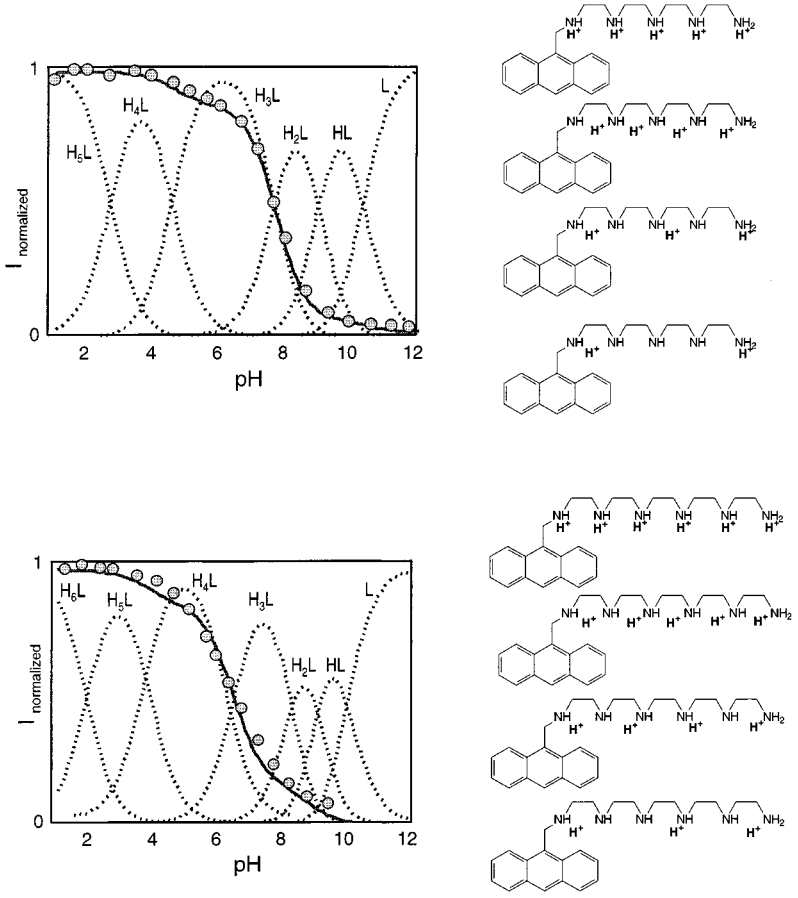

Figure 1. Fluorescence emission titration curves and molar fraction distributions of the ligands in the absence of metal ions; **L3**: λ_{exc} = 387 nm, λ_{em} = 420 nm; **L4**: λ_{exc} = 378 nm, λ_{em} = 418 nm

nitrogens of the chain. However, while the first deprotonation has only a small effect in the intensity of the fluorescence emission, the second one gives rise to its complete disappearance. The quenching effect can be accounted for by the thermodynamically favourable intramolecular photo-induced electron transfer from the lone pairs of the amine to the excited anthracene unit. This process is prevented by the protonation of the nitrogens, because protonation increases the oxidation potential by amounts of the order of 2 eV, changing the process from exergonic to endergonic. In the case of the macrocycle **L1** and its open-chain analog compound **L2**, the existence of one proton shared by the two central nitrogen atoms seems to be sufficient to prevent the quenching process. For this reason the complete quenching effect is only observed when both central nitrogens 2 and 3 are not protonated.

This pattern is repeated in the case of the compounds **L3** and **L4**.

A large quenching effect is observed only for the forms in which nitrogens 2 and 3 are completely deprotonated. It is worthwhile noting that deprotonations occurring on nitrogen atoms located at large distances from the anthracene ($n \geq 4$) do not produce significant quenching effects. This result can be explained by the well-known decrease of the electron transfer efficiency with the distance. According to CPK models the most suited nitrogen atoms for such a transfer seem to be those located at positions 2 and 3.

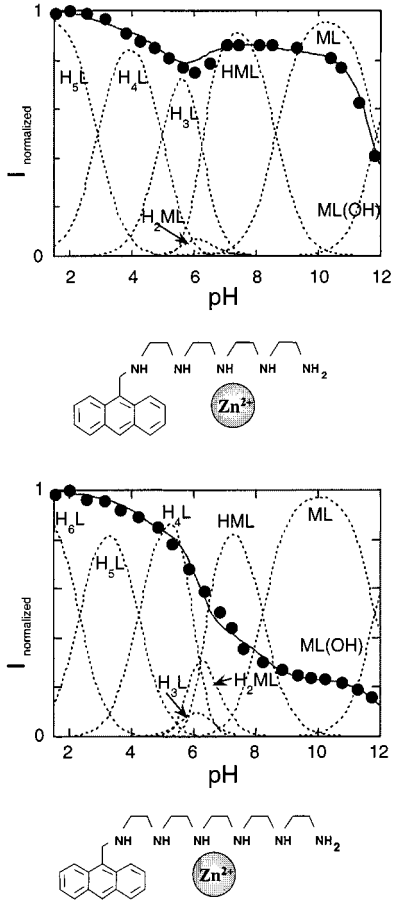

Figure 2. Fluorescence emission titration curves and molar fraction distributions of the ligands in the presence of Zn^{2+}; **L3**: λ_{exc} = 388 nm, λ_{em} = 420 nm; **L4**: λ_{exc} = 379 nm, λ_{em} = 418 nm

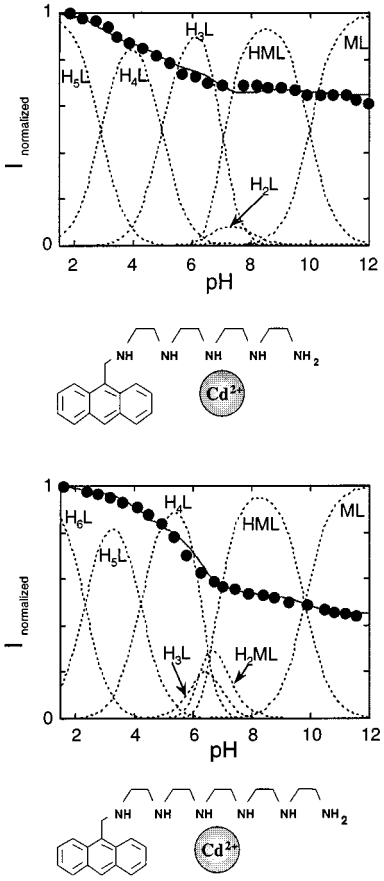

Figure 3. Fluorescence emission titration curves and molar fraction distributions of the ligands in the presence of Cd^{2+}; **L3**: λ_{exc} = 380 nm, λ_{em} = 419 nm; **L4**: λ_{exc} = 382 nm, λ_{em} = 418 nm

Chelation Enhancement of the Fluorescence Emission (CHEF)

It is well documented that metal cations like Zn^{2+} and Cd^{2+}, can give rise to complexes exhibiting fluorescence emission.[18,22,23] Figure 2 and Figure 3 show the fluorescence emission titration curves of the compounds **L3** and **L4**, in the presence of equimolar quantities of Zn^{2+} and Cd^{2+}, respectively. As reported in previous work, the zinc complexes of ligands containing a polyamine chain linked to an aromatic hydrocarbon unit are generally emissive except for the hydroxo species.[17,18] In principle, any positively charged substrate capable of binding to the nitrogen lone pairs could prevent the electron transfer. However, the interaction with metal cations can also give rise to other non-emissive excited states (charge transfer) or promote the quenching by energy transfer involving the metal. This is not the case for Zn^{2+} and Cd^{2+}, because these metal cations posses a d^{10} electronic configuration and, thus no charge transfer process (except metal-ligand CT when low energy empty ligand orbitals are available) or energy transfer is expected to occur. Therefore, for ligands **L2**−**L4** coordination of Zn^{2+} and Cd^{2+} produce a chelation enhancement of the fluorescence emission (CHEF effect).

On this basis, the species $[ZnL4]^{2+}$ showing a lower emission intensity than its analogous $[ZnL2]^{2+}$ [18] and $[ZnL3]^{2+}$ is an exception. This behaviour can be explained by the fact that Zn^{2+} is coordinated by only four nitrogen atoms. In the case of the species $[ZnL4]^{2+}$ there would be two non-coordinated deprotonated nitrogens (one more than in **L3**), and probably one of these nitrogens can get closer to the anthracene. Attempts to obtain suitable crystals of these complexes for X-ray diffraction in order to support our interpretation have unfortunately been unsuccessful.

In general, there is an important difference between Zn^{2+} and Cd^{2+} complexes in the basic pH region, because Cd^{2+}, differently from Zn^{2+}, does not easily form the non-emissive hydroxo complexes. This fact permits the existence of strong emissions, for example at pH = 12, which can be explored for practical purposes, vide infra. Finally, the species $[CdL4]^{2+}$ is also less emissive than its analogs $[CdL3]^{2+}$ and $[CdL2]^{2+}$, probably by the same reason pointed out for the Zn^{2+} complexes.

Chelation Enhancement of the Quenching (CHEQ)

Contrarily to Zn^{2+} and Cd^{2+}, many other metal cations are able to quench the emission when forming the corresponding complexes giving rise to the appearance of CHEQ effects. Cu^{2+} and Ni^{2+} are representative examples (see Figure 4 and Figure 5, respectively). This quenching effect can be explained by the existence of deactivation channels involving the metal orbitals. Energy transfer for both metal ions as well as electron transfer in the case of Cu^{2+}, have been claimed as possible mechanisms of deactivation.

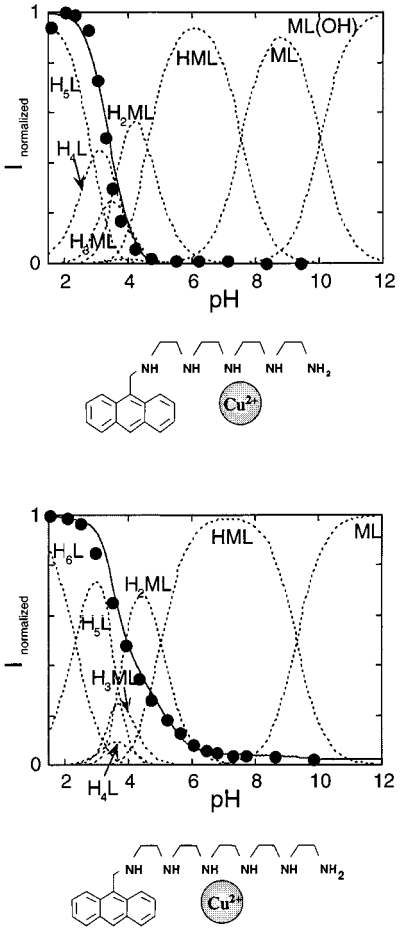

Figure 4. Fluorescence emission titration curves and molar fraction distributions of the ligands in the presence of Cu^{2+}; **L3**: λ_{exc} = 391 nm, λ_{em} = 418 nm; **L4**: λ_{exc} = 379 nm, λ_{em} = 418 nm

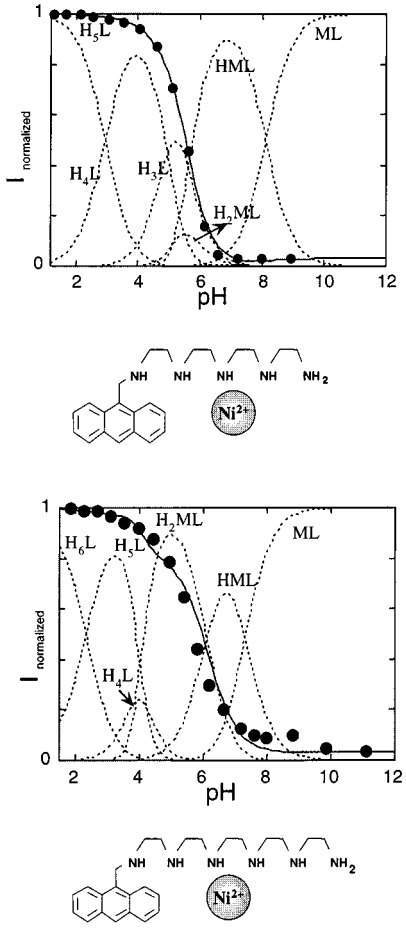

Figure 5. Fluorescence emission titration curves and molar fraction distributions of the ligands in the presence of Ni^{2+}; **L3**: λ_{exc} = 378 nm, λ_{em} = 418 nm; **L4**: λ_{exc} = 379 nm, λ_{em} = 418 nm

In Figure 4, the fluorescence emission titration curves of the ligands in the presence of Cu^{2+} are shown. As in the previous examples the dimension of the chain affects the emissive properties of the complexes. Comparing the Cu^{2+} complexes of these ligands, the most interesting feature is the existence of a slightly emissive $[CuH_2L4]^{4+}$ species, and a relatively strong emissive species, $[CuH_3L4]^{5+}$. In this case, we can expect that the metal ion to be coordinated by nitrogens 4, 5 and 6, is far enough away from the anthracene so as to decrease the metal-chromophore interaction.

Inspection of Figure 5, shows that while the $[NiL]^{2+}$ complexes are not emissive, strong emissions can be detected for some of the protonated complexes. Once more the most intense emission is observed for the ligand possessing the largest chain, $[NiH_2L4]^{4+}$. This behaviour can be explained as follows: i) by increasing the length of the chain, metal adducts containing protonated nitrogens are allowed to be formed ii) in these species the metal is more

distant from the fluorophore making their interactions difficult.

Logic Gates

In Figure 6 we represent the fluorescence emission titration curves of the complexes formed between **L3** and equimolar quantities of the metal cations Zn^{2+}, Cd^{2+},Cu^{2+}, and Ni^{2+}. This figure constitutes the basis for the following discussion.

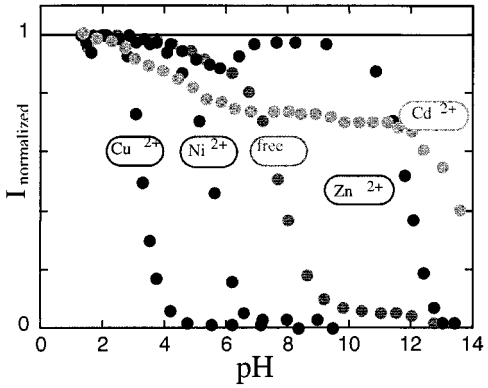

Figure 6. Comparison of the fluorescence emission of **L3** at 420 nm for the various metal ions; excitation wavelengths: Free − 387 nm; Zn^{2+} − 388 nm; Cd^{2+} − 380 nm; Cu^{2+} − 391 nm; Ni^{2+} − 378 nm

As reported previously by other authors[8,14] switching systems based on external impulses can be designed. In the present system we consider the impulses as the addition of a metal (symbol 1), or non addition, (symbol 0). Fluorescence emission intensity was used as an output signal as follows: i) if the emission reaches more than 60% of the maximum emission intensity of the free ligand at the considered wavelength the output is considered (1); ii) if the emission lies below 10% of the maximum emission intensity, the output is considered (0). It should be noted that this treatment is similar to the one used in electronics: for example in the case of the TTL family of logic gates the 1 level is considered approximately between 2 and 5 V, and the 0 level is between 0 and 0.8 V.[24]

Logic Gates Based on a CHEQ-CHEQ Pair

The first example concerns the use of a pair of metal ions both giving rise to CHEQ effects (Scheme 2).

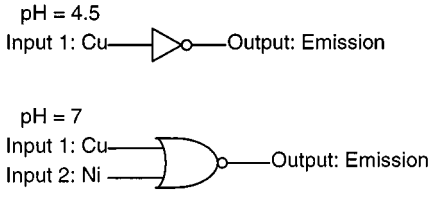

Cu^{2+}	Ni^{2+}	pH = 4.5	pH = 7
0	0	1	1
0	1	1	0
1	0	0	0
1	1	0	0
		NOT Cu^{2+}	NOR

Scheme 2

At pH = 1 the ligand is completely protonated and thus the system behaves independently of the metals giving in all case an output of 1. In terms of the electrical circuit analogy it means that the current flows in all circumstances and the output is 1 (third column in the table of Scheme 2). At pH = 4.5 (fourth column in the table), the situation is different. When neither Cu^{2+} nor Ni^{2+} are added to the solution of **L3** (inputs 0 in first and second column), the emission from the free ligand is observed, and the output is 1 (see Figure 6). Exclusive addition of Ni^{2+} at this pH value (input 0 for Cu^{2+}, input 1 for Ni^{2+}) gives rise to an emissive situation (output 1), while exclusive addition of Cu^{2+} leads to a quenching effect (output 0). When both metals are added (inputs 1 for Cu^{2+} and Ni^{2+}) it can be noted that the binding constant of Cu^{2+} is much higher than that of Ni^{2+}, resulting in a quenching effect (output 0). In terms of the logic table it can be considered as **NOT Cu^{2+}** since this column shows a positive answer (output 1) only when Cu^{2+} is absent. At pH = 7.0, both metal ions give rise to a quenching effect and the result is a **NOR** logic gate. The addition of any metal ion separately or both simultaneously gives an output of 0. Finally at pH = 10.0 the emission is quenched by electron transfer even in the absence of metal ions (output 0 in all cases). This means that no current can flow through the electrical circuit.

Logic Gates Based on a CHEF-CHEF Pair

When Zn^{2+} and Cd^{2+}, both exhibiting CHEF effects are used, a different set of logical gates is obtained, Scheme 3. At pH < 7 the situation is similar to that observed for $Ni^{2+}$and Cu^{2+} at pH = 1 and the output is always 1. At pH = 10.0, however, both metals compete for binding to the chemosensor and the two adducts show fluorescence emission, a situation that leads to an **OR** logic gate. At pH = 12.7 the response of the system is equal to the input of Cd^{2+}, because the association constant of $[CdL]^{2+}$ is much higher than the non emissive $[ZnL(OH)]^{+}$.

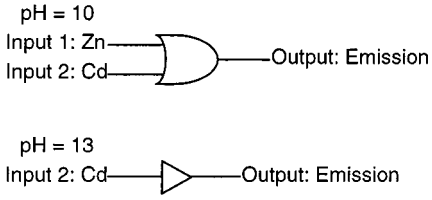

Zn^{2+}	Cd^{2+}	pH = 10	pH = 13
0	0	0	0
0	1	1	1
1	0	1	0
1	1	1	1
		OR	Cd^{2+}

Scheme 3

Logic Gates Based on a CHEF-CHEQ Pair

Another possibility is to combine metal ions that show CHEF and CHEQ effects (Scheme 4). In the case of Zn^{2+} and Cu^{2+}, the logic gates at pH = 1.0 (output 1 in all cases) and 5.0 (**NOT Cu^{2+}**) are similar to those described for Cu^{2+} and Ni^{2+} at pH = 1.0 and 4.5, respectively. However, in the

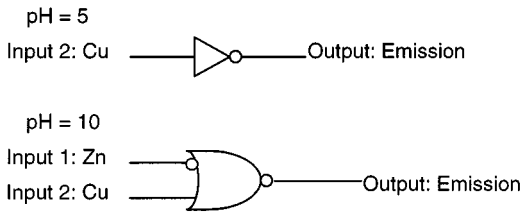

Zn^{2+}	Cu^{2+}	pH = 5	pH = 10
0	0	1	0
0	1	0	0
1	0	1	1
1	1	0	0
		NOT Cu^{2+}	NOT($Zn^{2+} \Rightarrow Cu^{2+}$)

Scheme 4

case of the logic gate at pH = 10, the complexes with Cu^{2+} are stronger than those of Zn^{2+} leading to a set of outputs which are equivalent to a negation of the implication $\mathbf{Zn^{2+} \Rightarrow Cu^{2+}}$. In this case an output 1 is obtained only when Zn^{2+} is present but Cu^{2+} is absent.

Experimental Section

Materials: Synthesis of receptors **L1**−**L2** has been accomplished as described in ref.[18]

***N*¹-(2-Aminoethyl)-N²[2-{[2-(anthrylmethyl)aminoethyl]amino}-ethyl]ethane-1,2-diamine:** Compound L3 was synthesised by an alternative procedure consisting of the reaction of a five-fold excess of the free amine tetraethylenepentaamine (3.76 g 20 mmol) with anthracene-9-carbaldehyde (0.82 g 4 mmol) to give the imine. To the solution in ethanol (75 mL) sodium borohydride (0.33 g 8.6 mmol) was added and the mixture was stirred at room temperature for 24 hours. The ethanol was removed at reduced pressure. The resulting residue was treated with water and the functionalised amine was extracted with dichloromethane (3 × 30 mL). The organic phase was washed with water and dried with anhydrous sodium sulfate and the solvent evaporated to yield the free amine, which was dissolved in ethanol and precipitated as a hydrochloride salt. (Yield 62%; 1.4 g). mp: 219−222 °C. − ^{1}H NMR (D_2O): δ_H = 3.15−3.32 (m, 14 H); 3.51 (t, 2 H), 5.19 (s, 2 H); 7.45 (t, 2 H); 7.56 (t, 2 H); 8.00 (d, 2 H); 8.12 (d, 2 H); 8.55 (s, 1 H). − ^{13}C NMR (D_2O): δ_C = 35.6, 43.7, 44.0, 44.7, 122.8, 125.9, 128.2, 129.8, 130.7, 131.2. − $C_{23}N_5H_{38}Cl_5$ (561.85): calcd. C 49.17, N 12.47, H 6.82; found C, 49.3, N, 12.6, H, 7.0.

***N*¹-[2-{(2-Aminoethyl)amino}ethyl]-*N*²-[{2-[{2-(anthrylmethyl)-amino}ethyl]amino}ethyl]ethane-1,2-diamine:** Compound **L4** was prepared as **L3**, by reaction of penthaethylenehexaamine and anthracene-9-carbaldehyde. (Yield 63%; 1.61 g) m.p. 189−192 °C. − ^{1}H NMR (D_2O) δ_H = 3.34−3.44 (m, 20 H); 4.94 (s, 2 H); 7.42 (t, 2 H); 7.53 (t, 2 H); 7.86 (d, 2 H); 7.97 (d, 2 H); 8.29 (s, 1 H). − ^{13}C NMR (D_2O): δ_C = 35.5, 43.5, 43.6, 44.8, 119.7, 122.5, 125.6, 127.9, 129.5, 130.2, 130.7. − $C_{25}N_6H_{44}Cl_6$ (641.38): calcd. C 46.7, N 13.09, H 6.9; found C, 47.1, N, 13.3, H, 7.2.

NaCl used as a background electrolyte, was a Merck suprapur product. CO_2-free NaOH and HCl solutions were prepared following the procedure reported in ref.[20]

Spectrophotometric and Spectrofluorimetric Titrations: Absorption spectra were recorded on a Perkin−Elmer Lambda 6 spectrophotometer and fluorescence emission on a SPEX F111 Fluorolog spectrofluorimeter. HCl and NaOH were used to adjust the pH values that were measured on a Metrohm 713 pH meter. Linearity of the fluorescence emission was checked in the concentration range 10^{-5} mol·dm^{-3} to 10^{-6} mol·dm^{-3}. The absorbance of the excitation wavelength was maintained lower than ca. 0.15. When excitation was carried out at wavelengths different from the isosbestic points, a correction for the absorbed light was performed.

Emf Measurements: The potentiometric titrations were carried out at 298.1 ± 0.1 K in NaCl 0.15 mol·dm^{-3}. The experimental procedure (burette, potentiometer, cell, stirrer, microcomputer, etc.) have been fully described elsewhere.[25] The acquisition of the emf data was performed with the computer program PASAT.[26] The reference electrode was an Ag/AgCl electrode in saturated KCl solution. The glass electrode was calibrated as an hydrogen-ion concentration probe by titration of previously standardized amounts of HCl with CO_2-free NaOH solutions and the equivalent point was determined by the Gran's method,[27] which gives the standard potential, $E°'$, and the ionic product of water [pK_w = 13.73(1)]. The concentrations of the different metal ions employed were determined gravimetrically by standard methods. NaCl was used as the supporting electrolyte instead of the more usual $NaClO_4$, due to the slightly higher solubility of the receptors in this medium.

The computer program HYPERQUAD,[28] was used to calculate the protonation and stability constants. The titration curves for each system (ca. 100 experimental points corresponding to at least three measurements, pH range investigated 2−10, concentration of metals and L ranging from $1{\cdot}10^{-3}$ to $5{\cdot}10^{-3}$ mol·dm^{-3}) were treated either as a single set or as separate curves without significant variations in the values of the stability constants. Finally, the data sets were merged together to give the final stability constants. Moreover, in the case of Ni^{2+}, measurements were made both in formation and in dissociation (from acid to alkaline pH and vice versa) to check the reversibility of the reactions.

NMR Measurements: The ^{1}H and ^{13}C NMR spectra were recorded on Varian UNITY 300 and UNITY 400 spectrometers, operating at 299.95 and 399.95 MHz for ^{1}H and at 75.43 and 100.58 MHz for ^{13}C. The spectra were obtained at room temperature in D_2O or $CDCl_3$ solutions. For the ^{13}C NMR spectra dioxane was used as a reference standard (δ = 67.4) and the solvent signal for the ^{1}H spectra. The probe temperature was regulated with a variable temperature accessory. Adjustments to the desired pH were made using drops of DCl or NaOD solutions The pH was calculated from the measured pD values using the correlation, pH = pD − 0.4.[29]

Acknowledgments

This work was supported by DGICYT PB-97-0796 and PRAXIS/P/QUI/10074/1998 and a Ph. D. Grant (S. A.). One of us (M. T. A.) wants to thank the Conselleria d' Educació i Ciència for a Ph. D. Grant.

[1] L. F. Lindoy, *Nature* **1993**, *364*, 17−18.
[2] P. Ball, L. Garwin, *Nature* **1993**, *355*, 761−766.
[3] A. L. Robinson, *Science (Washington D.C.)* **1984**, *223*, 267−268.
[4] K. E. Drexler, *Nanosystems: Molecular Machinery, Manufacturing and Computation*; Wiley, New York, **1992**.
[5] J.-M. Lehn, *Supramolecular Chemistry*; VCH,: Weinheim, **1995**.
[6] V. Balzani, F. Scandola, *Supramolecular Photochemistry*, Horwood: Chichester, **1991**; chapter 12.
[7] J. Millman, A. Grabel *Microelectronics*; McGraw-Hill: New York, **1998**; chapter 6.
[8] A. P. de Silva, C. P. McCoy, *Chem. Ind.* **1994**, 992−996.

[9] V. Balzani, A. Credi, F. Scandola, *Chim. Ind. (Rome)* **1997**, *79*, 751−759.
[10] A. P. de Silva, H. Q. N. Gunaratne, C. P. McCoy, *Nature* **1993**, *364*, 42−44.
[11] R. A. Bissel, A. P. de Silva, H. Q. N. Gunaratne, P. L. M. Lynch, G. E. M. Maguire, C. P. McCoy, K. R. A. S. Sandanayake, *Top. Curr. Chem.* **1993**, *168*, 223−264.
[12] A. P. de Silva, I. M. Dixon, H. Q. N. Gunaratne, T. Gunnlaugsson, Pamela R. S. Maxwell, T. E. Rice, *J. Am. Chem. Soc.* **1999**, *121*, 1393−1394.
[13] A. P. de Silva, N. D. McClenaghan, *J. Am. Chem. Soc.* **2000**, *122*, 3965−3966.
[14] A. Credi, V. Balzani, S. J. Langford, J. F. Stoddart, *J. Am. Chem. Soc.* **1997**, *119*, 2679−2681.
[15] M. A. Bernardo, A. J. Parola, F. Pina, E. Garcia-España, V. Marcelino, S. V. Luís, J. F. Miravet, *J. Chem. Soc., Dalton Trans* **1995**, 993−997.
[16] M. A. Bernardo, J. A. Guerrero, E. Garcia-España, S. V. Luis, J. M. Llinares, F. Pina, J. A. Ramirez, C. Soriano, *J. Chem. Soc., Perkin Trans. 2* **1996**, 2335−2342.
[17] M. A. Bernardo, E. García-España, J. Latorre, S. V. Luis, J. M. Llinares, F. Pina, J. A. Ramírez, C. Soriano, *Inorg. Chem.* **1998**, *37*, 3935−3942.
[18] M. A. Bernardo, F. Pina, B. Escuder, E. García-España, M. L. Godino-Salido, J. Latorre, S. V. Luis, J. A. Ramírez, C. Soriano, *J. Chem. Soc., Dalton Trans.* **1999**, 915−921.
[19] M. T. Albelda, M. A. Bernardo, E. Garcia-España, M. L. Godino-Salido, S. V. Luis, M. J. Melo, F. Pina, C. Soriano, *J. Chem. Soc., Perkin Trans 2* **1999**, 2545−2549.
[20] A. Bencini, A. Bianchi, E. García-España, M. Micheloni, J. A. Ramírez, *Coordination Chemistry Reviews* **1999**, *188*, 97−156.
[21] E. Martell, R. M. Smith, R. J. Motekaitis; *NIST Critically Selected Stability Constants of Metal Complexes Database*, NIST Standard Reference Database, version 4, **1997**.
[22] A. W. Czarnik, *Acc. Chem. Res.* **1994**, *27*, 302−307.
[23] A. W. Czarnik, *Fluorescent Chemosensors for Ion and Molecule Recognition*, American Chemical Society, Washington DC, **1992**.
[24] H. Taub, *Digital circuits and microprocessors*, McGraw-Hill, **1982**.
[25] E. García-España, M.-J. Ballester, F. Lloret, J.-M. Moratal, J. Faus, A. Bianchi, *J. Chem. Soc., Dalton Trans.* **1988**, 101−104.
[26] M. Fontanelli, M. Micheloni, *Proceedings of the I Spanish−Italian Congress on Thermodynamics of Metal Complexes*, Diputación de Castellón, Castellón, Spain, **1990**.
[27] G. Gran, *Analyst (London)* **1952**, *77*, 881; F. J. Rossotti, H. Rossotti, *J. Chem. Educ.* **1965**, *42*, 375−378.
[28] A. Sabatini, A. Vacca, A. Gans, P. Gans, *Talanta* **1996**, *43*, 1739−1753.
[29] A. K. Convington, M. Paabo, R. A. Robinson, R. G. Bates, *Anal. Chem.* **1968**, *40*, 700−706.

Received May 18, 2000
[I00204]

Heteroleptic Rare Earth Double-Decker Complexes with Porphyrinato and 2,3-Naphthalocyaninato Ligands − Preparation, Spectroscopic Characterization, and Electrochemical Studies

Jianzhuang Jiang,*[a] Wei Liu,[a,b] Ka-Lok Cheng,[b] Ka-Wo Poon,[b] and Dennis K. P. Ng*[b]

Keywords: Lanthanides / Actinides / Porphyrins / Phthalocyanines / Sandwich complexes

A series of RE(Nc)(TBPP) (**1**–**12**) complexes [RE = La, Pr, Nd, Sm, Eu, Gd, Tb, Dy, Y, Ho, Er, Tm; Nc = 2,3-naphthalocyaninate; TBPP = *meso*-tetrakis(4-*tert*-butylphenyl)porphyrinate] and Eu[Nc(*t*Bu)$_4$](TClPP) [Nc(*t*Bu)$_4$ = tetra(*tert*-butyl)-2,3-naphthalocyaninate; TClPP = *meso*-tetrakis(4-chlorophenyl)-porphyrinate] (**13**) have been prepared by a one-pot procedure which involves the treatment of RE(acac)$_3$·*n*H$_2$O (acac = acetylacetonate) with the corresponding metal-free porphyrins and naphthalonitriles in the presence of 1,8-diazabicyclo[5.4.0]undec-7-ene (DBU) in *n*-octanol. These novel double-deckers have been spectroscopically characterized. A one-electron reduction and three one-electron oxidations have been revealed by electrochemical methods. The potentials of all these processes depend linearly on the ionic radii of the central metal ions, giving a relatively large potential difference (0.50–0.57 V) between the first oxidation and the first reduction processes.

Introduction

Tetrapyrrole derivatives such as porphyrins and phthalocyanines are able to form sandwich complexes with a range of metal ions including rare earths, actinides, group 4 transition metals, and some main group elements (e.g. Bi, In, Sn).[1] The resulting double- and triple-decker complexes possess intriguing and unique electronic and optical properties which render them useful in materials science. Bis(phthalocyaninato) rare earth complexes RE(Pc)$_2$,[2] for example, can be used in electrochromic devices,[3] field-effect transistors,[4] gas and herbicide sensors,[5] and optically addressed spatial light modulators.[6] While the chemistry and properties of both homoleptic and heteroleptic complexes with these two types of ligands have been extensively studied, little is known about the naphthalocyanine analogues which contain a more delocalized π system. It is expected that sandwich complexes containing these larger macrocyclic ligands should have distinct properties compared with the Pc counterparts owing to the narrower energy gap between the highest occupied and the lowest unoccupied molecular orbitals (HOMO and LUMO).[7,8]

A number of naphthalocyanine-containing double-[8,9] and triple-decker[8b,10] complexes have been reported, but virtually all of them are confined to lutetium complexes. Sandwich-type Nc[2] complexes of other metals have only appeared very recently.[11] It has been well documented that the electronic properties of these sandwich complexes depend on the ring-to-ring separation, which can be altered by the size of the metal center.[12] Studies of a whole series of analogous complexes with different metal centers are therefore of special importance.

We have recently developed an efficient synthetic pathway for heteroleptic sandwich complexes which involves a cyclic tetramerization of dicyanobenzenes using RE(ring)(acac) [RE = Eu, Y; ring = Pc, Por] as the template.[2,13] This method has been utilized to prepare the first hetereoleptic Nc and Por complexes Eu(Nc)(TPyP) and Eu[Nc(SC$_{12}$H$_{25}$)$_8$](TPyP).[2,14] We report herein an extension of this work which involves a simplified one-pot procedure leading to a series of (naphthalocyaninato)(porphyrinato) rare earth double-decker complexes. The spectroscopic and electrochemical properties of these novel sandwich compounds are also described herein.

Results and Discussion

The preparation of the mixed double-deckers RE(Nc)(TBPP) (RE = La, Pr, Nd, Sm, Eu, Gd, Tb, Dy, Y, Ho, Er, Tm) (**1**−**12**) was mainly based on our previously described procedure,[2,13,14] but the prior generation of the half-sandwich complexes RE(TBPP)(acac) was found to be not necessary. Thus a one-pot procedure involving the metal-free porphyrin H$_2$(TBPP), RE(acac)$_3$·*n*H$_2$O, naphthalonitrile, and DBU in *n*-octanol could also lead to the desired products (Scheme 1). Similar to the RE(Por)$_2$ [Por = TPP or OEP][2,12b,15] and RE[Nc(*t*Bu)$_4$]$_2$ series,[2,11b] the yield of these mixed sandwiches decreases gradually with the size of the central metal ion (Table 1), showing that, for all these double-deckers, complexes with a smaller metal center are more difficult to obtain, probably due to

[a] Department of Chemistry, Shandong University, Jinan 250100, China
Fax: (internat.) +86-(0)531/856-5211
E-mail: jzjiang@sdunetnms.sdu.edu.cn
[b] Department of Chemistry, The Chinese University of Hong Kong, Shatin, N. T., Hong Kong, China
Fax: (internat.) +852/2603−5057
E-mail: dkpn@cuhk.edu.hk

 © WILEY-VCH Verlag GmbH, 69451 Weinheim, 2001 1434−1948/01/0202−0413 $ 17.50+.50/0

an increase in steric compression of the two macrocyclic ligands. The europium analogue Eu[Nc(*t*Bu)$_4$](TClPP) (**13**) was prepared similarly using the metal-free porphyrin H$_2$(TClPP)[2] and 6-*tert*-butylnaphthalonitrile.

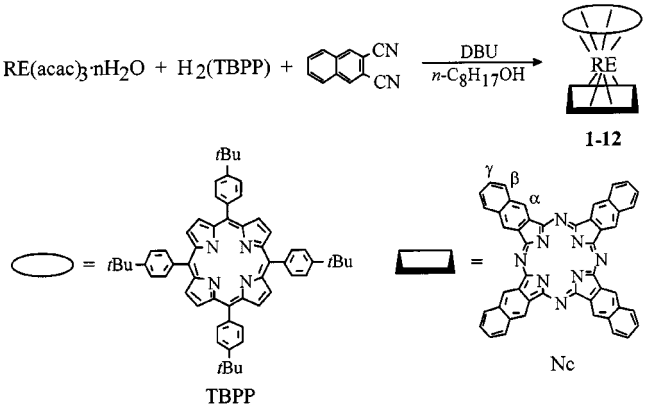

Scheme 1. Synthesis of heteroleptic rare earth double-deckers

All these double-deckers, after being purified by column chromatography and recrystallization, were essentially pure as shown by thin-layer chromatography. However, satisfactory analytical data could not be obtained. This might be due to the presence of traces of impurities which could not be completely removed by conventional purification methods.[16] The compounds, however, were unambiguously characterized with a range of spectroscopic methods. The matrix-assisted laser desorption/ionization time-of-flight (MALDI-TOF) mass spectra of all these compounds showed prominent signals attributed to the molecular ions, of which the isotopic patterns were in good agreement with the respective simulated spectra (Table 1).

Figure 1 shows the absorption spectrum of Pr(Nc)(TBPP) (**2**), which is representative for the spectra of this series of compounds. The spectral features resembled those of the Pc counterparts RE^{III}(Pc)(Por)[12c,13b,13c,17] and the previously reported Nc complexes Eu(Nc)(TPyP) and Eu[Nc(SC$_{12}$H$_{25}$)$_8$](TPyP),[14] and thus could be assigned in a similar manner. As shown in Table 1, the Nc B band (323−329 nm) and the TBPP B band (414−424 nm) are rather insensitive to the metal center. By analogy with the Pc analogues RE^{III}(Pc)(Por), the weak absorption at 479−482 nm and the near-IR band at 1025−1146 nm may arise from a hole localized on the Nc ring. The latter signal shifts gradually to the red as the size of the tervalent metal center decreases from La to Tm, which was also seen for the Pc counterparts.[12c] This observation suggests that this near-IR absorption should not be due to an intramolecular ring-to-ring charge-transfer transition as proposed previously.[14,18] For such a transition, a reverse trend should be observed because the π-π interactions between the rings will become stronger when the ring-to-ring separation decreases along the series.[12b,12c,19] This charge-transfer transition band, however, could not be detected for these complexes up to 2400 nm and the reason remains unclear at this stage. Another remarkable feature for these Nc double-deckers is the relatively intense Q bands at 549−583 and 612−635 nm, which are almost invisible in the Pc analogues.[12c,13b,13c,17] Both of these signals experience a hypsochromic shift when the size of the metal center decreases.

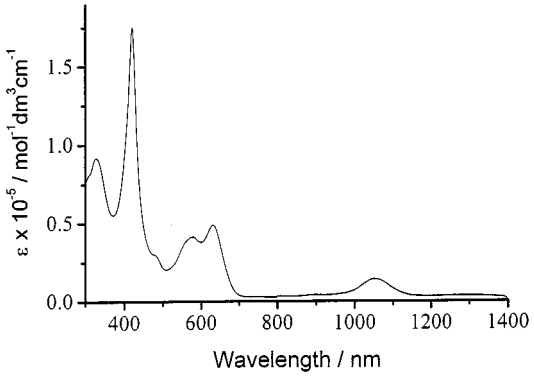

Figure 1. Electronic absorption spectrum of Pr(Nc)(TBPP) (**2**) in CHCl$_3$

The presence of Nc π radical anion (Nc$^{\bullet-}$) in these single-hole complexes was also corroborated by the strong IR marker band at 1319−1325 cm^{-1} (Table 1),[11b,11c] which is also a diagnostic band for the Pc π radical anion (Pc$^{\bullet-}$).[20] Due to the presence of this unpaired electron, these complexes, like other single-hole analogues, are usually NMR

Table 1. Reaction yields and spectral data for the double-deckers **1**−**13**

Compound	Yield (%)	Mass (*m*/*z*)[a]	*v* (Nc$^{\bullet-}$) (cm^{-1})	λ_{max} (nm) (log ε)[b]					
La(Nc)(TBPP) (**1**)	73	1690	1319	323 (4.95)	424 (5.19)	482 (4.40)	583 (4.57)	635 (4.67)	1025 (4.10)
Pr(Nc)(TBPP) (**2**)	76	1692	1319	329 (4.96)	421 (5.24)	480 (4.47)	579 (4.62)	630 (4.69)	1053 (4.16)
Nd(Nc)(TBPP) (**3**)	71	1694	1320	327 (4.94)	419 (5.27)	481 (4.46)	574 (4.59)	628 (4.65)	1064 (4.10)
Sm(Nc)(TBPP) (**4**)	70	1703	1320	325 (4.94)	419 (5.21)	481 (4.47)	563 (4.59)	622 (4.63)	1084 (4.10)
Eu(Nc)(TBPP) (**5**)	67	1703	1322	326 (4.91)	417 (5.08)	480 (4.45)	561 (4.58)	621 (4.60)	1096 (4.09)
Gd(Nc)(TBPP) (**6**)	63	1707	1322	327 (5.00)	417 (5.17)	481 (4.54)	558 (4.67)	620 (4.69)	1104 (4.17)
Tb(Nc)(TBPP) (**7**)	50	1708	1323	323 (4.98)	417 (5.13)	489 (4.52)	555 (4.64)	617 (4.66)	1120 (4.14)
Dy(Nc)(TBPP) (**8**)	42	1713	1323	327 (4.92)	417 (5.12)	480 (4.46)	555 (4.69)	616 (4.58)	1131 (4.08)
Y(Nc)(TBPP) (**9**)	43	1639	1323	326 (4.91)	419 (5.11)	479 (4.45)	552 (4.58)	614 (4.57)	1131 (4.09)
Ho(Nc)(TBPP) (**10**)	38	1715	1324	327 (4.84)	416 (5.17)	480 (4.38)	553 (4.52)	615 (4.50)	1132 (4.00)
Er(Nc)(TBPP) (**11**)	32	1718	1323	327 (4.90)	414 (5.03)	481 (4.44)	550 (4.56)	613 (4.55)	1139 (4.06)
Tm(Nc)(TBPP) (**12**)	29	1719	1325	328 (4.89)	415 (5.01)	482 (4.44)	549 (4.58)	612 (4.55)	1146 (4.10)
Eu[Nc(*t*Bu)$_4$](TClPP) (**13**)	66	1841	1327	334 (4.97)	419 (5.20)	479 (4.52)	555 (4.52)	642 (4.67)	1072 (4.24)

[a] Mass corresponding to the most abundant isotopic peak of the molecular ion. − [b] Recorded in CHCl$_3$.

Table 2. ^{1}H NMR spectroscopic data for the reduced form of selected double-deckers in $CDCl_3$/[D_6]DMSO (1:1)

Compound	NMR spectroscopic data[a]
La(Nc)(TBPP) (**1**)[b]	8.91 (s, 8 H, H_α), 7.97 (dd, J = 3.0, 6.0 Hz, 8 H, H_β), 7.44 (s, 8 H, H_{pyr}), 7.26 (br s overlapping with the residue $CHCl_3$ peak, H_γ), 6.47 (br s, 4 H, C_6H_4), 6.17 (br s, 4 H, C_6H_4), 5.95 (br s, 4 H, C_6H_4), 5.54 (br s, 4 H, C_6H_4), 0.68 (s, 36 H, *t*Bu)
Nd(Nc)(TBPP) (**3**)[b]	8.02 (br s, 12 H, H_α and C_6H_4), 7.73 (dd, J = 3.0, 6.0 Hz, 8 H, H_β), 7.62 (s, 8 H, H_{pyr}), 7.43 (dd, J = 3.0, 6.0 Hz, 8 H, H_γ), 7.25 (br s, 4 H, C_6H_4), 6.82 (br s, 4 H, C_6H_4), 4.59 (br s, 4 H, C_6H_4), 0.79 (s, 36 H, *t*Bu)
Sm(Nc)(TBPP) (**4**)[c]	8.98 (s, 8 H, H_α), 8.27 (dd, J = 3.3, 5.7 Hz, 8 H, H_β), 7.47 (dd, J = 3.3, 5.7 Hz, 8 H, H_γ), 7.26 (s, 8 H, H_{pyr}), 6.88 (br s, 4 H, C_6H_4), 6.68 (br s, 4 H, C_6H_4), 5.75 (br s, 4 H, C_6H_4), 5.22 (br s, 4 H, C_6H_4), 1.10 (s, 36 H, *t*Bu)
Eu(Nc)(TBPP) (**5**)[c]	10.95 (s, 8 H, H_α), 10.34 (br s, 4 H, C_6H_4), 9.36 (dd, J = 3.3, 6.0 Hz, 8 H, H_β), 8.31 (dd, J = 3.3, 6.0 Hz, 8 H, H_γ), 7.50 (br s, 4 H, C_6H_4), 7.28 (br s, 12 H, H_{pyr} and C_6H_4), 6.30 (br s, 4 H, C_6H_4), 1.78 (s, 36 H, *t*Bu)
Eu[Nc(*t*Bu)$_4$](TClPP) (**13**)[c]	10.79−11.17 (m, 8 H, H_α), 10.19 (br s, 4 H, C_6H_4), 9.29−9.37 (m, 8 H, H_β), 8.45−8.49 (m, 4 H, H_γ), 7.34 (br s, 4 H, C_6H_4), 7.20−7.24 (br s, 12 H, H_{pyr} and C_6H_4), 6.04 (br s, 4 H, C_6H_4), 2.10 (s, 36 H, *t*Bu)

[a] Given as: chemical shift (δ) (multiplicity, relative intensity and assignment) where s = singlet, br s = broad signal, d = doublet, m = multiplet. − [b] Recorded in the presence of $NaBH_4$. − [c] Recorded in the presence of hydrazine hydrate.

silent. We employed the strategy developed by L'Her[8a,21] using hydrazine hydrate or $NaBH_4$ as the reducing agent to generate the monoanionic $[RE^{III}(ring\text{-}1)(ring\text{-}2)]^-$ or protonated $RE^{III}H(ring\text{-}1)(ring\text{-}2)$ species, in which both the macrocycles become diamagnetic. We were able to obtain satisfactory ^{1}H NMR spectroscopic data for the reduced form of the La, Nd, Sm, and Eu double-deckers (Table 2). The spectra for the Pr, Dy, and Tm analogues, however, were hard to interpret which could be related to the different magnetic properties of the metal ions. It is worth noting that NMR spectroscopic data for such sandwich-type complexes having a paramagnetic metal center are rare indeed.[1]

Figure 2 shows the ^{1}H NMR spectra of the two Eu^{III} double-deckers **5** and **13** in the presence of hydrazine hydrate. It can be seen that the Nc α protons of the reduced form of **5** resonate as a singlet at δ = 10.95 because of the symmetrical Nc ring. The corresponding signal for **13** appears as a multiplet at δ = 10.79−11.17 due to the presence of a mixture of constitutional isomers and the non-equivalence of these α protons. The assignment for the Nc β and γ protons' signals (at ca. δ = 9.3 and 8.4, respectively) for these two compounds is supported by the smaller integration observed for the latter for **13**. Similar to other sandwiches containing a TPP ligand or its derivatives,[1b,17b,22] four distinct broad signals appear for the *ortho* and *meta* aryl protons in both cases, suggesting that there is a restricted rotation about the C(*meso*)−C(aryl) bonds.

The electrochemical behavior of all the double-deckers **1**−**13** in CH_2Cl_2 was investigated by cyclic voltammetry (CV) and differential pulse voltammetry (DPV). The voltammograms generally displayed four quasi-reversible couples assignable to the first three one-electron oxidations and the first one-electron reduction of the sandwich compounds (Table 3); all of them are ligand-based processes. Figure 3 shows the cyclic voltammogram of Sm(Nc)(TBPP) (**4**), which is typical. The second one-electron reduction process, which was commonly seen in related double-deckers, could not be revealed for these complexes under the present conditions due to a solvent breakdown. As shown in Figure 4, the potentials of all these processes are linearly dependent on the ionic radius of the metal center,

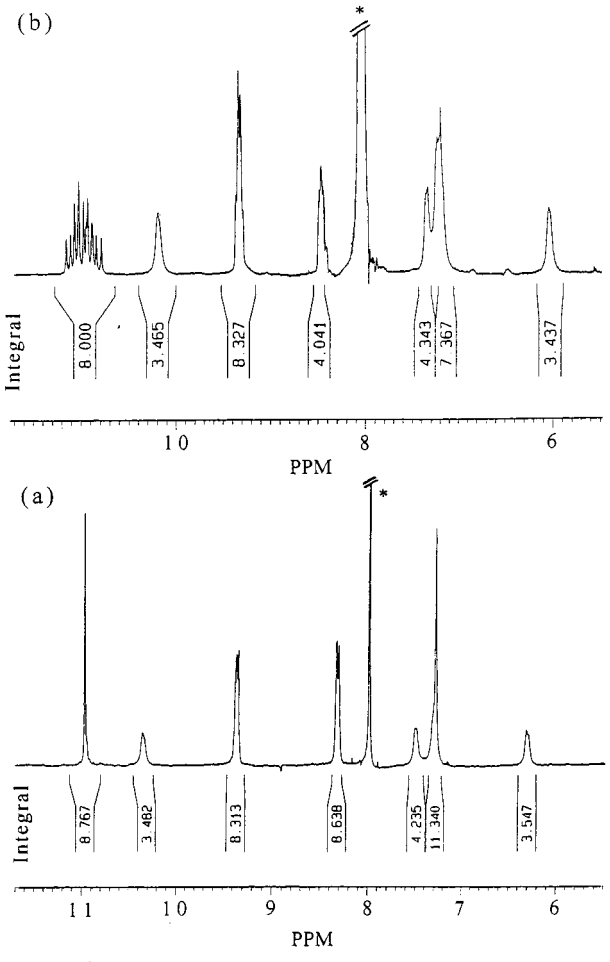

Figure 2. ^{1}H NMR spectra of (a) Eu(Nc)(TBPP) (**5**) and (b) Eu[Nc(*t*Bu)$_4$](TClPP) (**13**) in the presence of a small amount of hydrazine hydrate in $CDCl_3$/[D_6]DMSO (1:1); * indicates the signal for hydrazine hydrate

with a positive gradient for the first oxidation and the first reduction processes and a negative gradient for the second and third oxidation processes. The linear correlation observed between these potentials and the ionic radii of the central metals indicates that π-π interactions are probably present in these heteroleptic double-deckers. The potential difference between the first oxidation and the first reduction

Table 3. Electrochemical data for the double-deckers **1**−**13**

Compound[a]	$E_{1/2}$ (oxd.3)	$E_{1/2}$ (oxd.2)	$E_{1/2}$ (oxd.1)	$E_{1/2}$ (red.1)
La(Nc)(TBPP) (**1**)	1.32	1.02	0.55	0.05
Pr(Nc)(TBPP) (**2**)	1.35	1.04	0.54	0.02
Nd(Nc)(TBPP) (**3**)	1.38	1.05	0.54	0.04
Sm(Nc)(TBPP) (**4**)	1.40	1.08	0.52	0.00
Eu(Nc)(TBPP) (**5**)	1.38[b]	1.04	0.46	-0.06
Gd(Nc)(TBPP) (**6**)	1.41	1.08	0.49	-0.04
Tb(Nc)(TBPP) (**7**)	1.41[b]	1.11	0.48	-0.07
Dy(Nc)(TBPP) (**8**)	1.44	1.09	0.47	-0.06
Y(Nc)(TBPP) (**9**)	1.45	1.09	0.44	-0.07
Ho(Nc)(TBPP) (**10**)	1.45	1.10	0.45	-0.07
Er(Nc)(TBPP) (**11**)		1.12	0.44	-0.10
Tm(Nc)(TBPP) (**12**)	1.47	1.11	0.42	-0.10
Eu[Nc(*t*Bu)$_4$](TClPP) (**13**)	1.43[b]	1.16	0.53	-0.04

[a] Recorded with [Bu$_4$N][PF$_6$] as electrolyte in CH_2Cl_2 (0.1 M) at ambient temperature. Potentials were obtained by cyclic voltammetry with a scan rate of 100 mV s^{-1}, and are expressed as half-wave potentials ($E_{1/2}$) in volts relative to SCE unless otherwise stated. − [b] By differential pulse voltammetry.

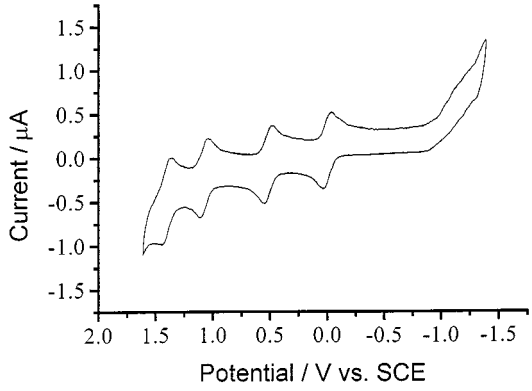

Figure 3. Cyclic voltammogram of Sm(Nc)(TBPP) (**4**) in CH_2Cl_2 containing 0.1 M [Bu$_4$N][PF$_6$] at a scan rate of 100 mV s^{-1}

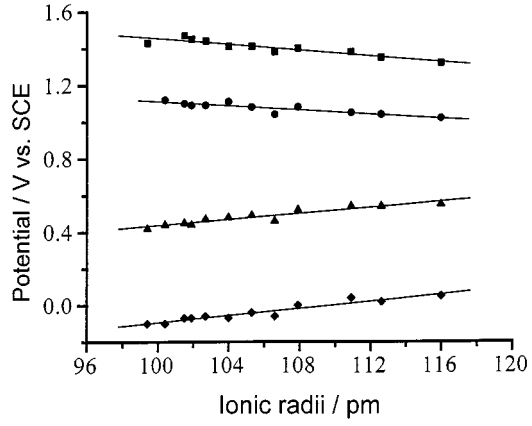

Figure 4. Redox potentials of RE(Nc)(TBPP) (**1**−**12**) as a function of the ionic radii of the RE^{III} ions;[28] ◆ = first reduction, ▲ = first oxidation, ● = second oxidation, ■ = third oxidation

is rather insensitive to the metal center with a value ranging from 0.50 to 0.57 V. These values, which can reflect the HOMO−LUMO gap of the complexes, are slightly larger than those of the Pc counterparts RE^{III}(Pc)(TPP) (0.45−0.48 V)[12c] and are significantly larger than those of the bis(naphthalocyaninato) analogues (0.29−0.37 V).[8,11b,11c]

In summary, we have prepared a series of rare heteroleptic rare-earth double-decker complexes containing porphyrinato and 2,3-naphthalocyaninato ligands by a simple one-pot procedure. It is envisaged that this methodology can be extended readily to other heteroleptic sandwich systems. Having a more delocalized macrocyclic ligand, these complexes have been found to exhibit distinct spectroscopic and electrochemical properties compared with those of the Pc counterparts.

Experimental Section

n-Octanol was distilled from sodium. The electrolyte [Bu$_4$N][PF$_6$] was recrystallized twice from tetrahydrofuran prior to use. All other reagents and solvents were of reagent grade and used as received. Naphthalonitrile,[23] 6-*tert*-butylnaphthalonitrile,[23] H$_2$(TBPP),[24] H$_2$(TClPP),[24] and RE(acac)$_3$·*n*H$_2$O[25] were prepared by previously described methods. − UV/Vis: Hitachi U-3300. − Near-IR: Hitachi U-3100. − IR: Perkin−Elmer 1600. − MALDI-TOF-MS: Bruker BIFLEX III, α-cyano-4-hydroxycinnamic acid as matrix. − Electrochemical measurements were carried out with a BAS CV-50 W voltammetric analyzer. The cell comprised inlets for a platinum-sphere working electrode, a silver-wire counter electrode and an Ag/AgNO$_3$ (0.1 M in MeCN) reference electrode which was connected to the solution by a Luggin capillary whose tip was placed close to the working electrode.[26] Typically, a 0.1 M solution of [Bu$_4$N][PF$_6$] in CH_2Cl_2 containing the sample was purged with nitrogen for 20 min, then the voltammograms were recorded at ambient temp. Potentials were referenced to the Ag/Ag$^+$ couple in MeCN, which was taken as +0.31 V vs. the saturated calomel electrode (SCE) as determined for this system previously using ferrocene as an internal standard.[27]

General Procedure for the Preparation of RE(Nc)(TBPP) (1−12) and Eu[Nc(*t*Bu)$_4$](TClPP) (13): A mixture of RE(acac)$_3$·*n*H$_2$O (0.10 mmol), H$_2$(TBPP) or H$_2$(TClPP) (0.05 mmol), naphthalonitrile or 6-*tert*-butylnaphthalonitrile (0.40 mmol), and DBU (50 mg, 0.33 mmol) in *n*-octanol (4 mL) was refluxed overnight (>18 h) under nitrogen to give a dark green solution. The volatiles were then removed under reduced pressure and the residue was chromatographed on a silica gel column with CH_2Cl_2/hexane (1:2) as eluent to remove the unchanged metal-free porphyrin as the first fraction. The column was further eluted with $CHCl_3$ to give a greenish blue band containing the desired double-decker. The crude product was further purified by the same chromatographic procedure followed

by recrystallization from a mixture of $CHCl_3$ and MeOH to give a dark blue powder. The yields together with the characterizing data for these complexes are given collectively in Table 1.

Acknowledgments

Financial support from the Natural Science Foundation of China (Grant No. 29701002), the State Educational Ministry of China, the Natural Science Foundation of Shandong Province, the Science Committee of Shandong Province, Shandong University, State Key Laboratory of Rare Earths at the Peking University, the Hong Kong Research Grants Council, and The Chinese University of Hong Kong is gratefully acknowledged.

[1] [1a] D. K. P. Ng, J. Jiang, *Chem. Soc. Rev.* **1997**, *26*, 433−442. − [1b] J. W. Buchler, D. K. P. Ng, in *The Porphyrin Handbook* (Eds.: K. M. Kadish, K. M. Smith, R. Guilard), Academic Press, San Diego, **2000**, vol. 3, chapter 20. − [1c] J. Jiang, K. Kasuga, D. P. Arnold, in *Handbook of Advanced Electronic and Photonic Materials* (Ed.: H. S. Nalwa), Academic Press, San Diego, **2000**, in press.

[2] Abbreviations used for tetrapyrrole derivatives: Nc = 2,3-naphthalocyaninate, Nc(tBu)$_4$ = tetra(*tert*-butyl)-2,3-naphthalocyaninate, Nc($SC_{12}H_{25}$)$_8$ = 3,4,12,13,21,22,30,31-octakis(dodecylthio)-2,3-naphthalocyaninate, OEP = octaethylporphyrinate, Pc = phthalocyaninate, Por = general porphyrinate, TBPP = *meso*-tetrakis(4-*tert*-butylphenyl)porphyrinate, TClPP = *meso*-tetrakis(4-chlorophenyl)porphyrinate, TPP = *meso*-tetraphenylporphyrinate, TPyP = *meso*-tetra(4-pyridyl)-porphyrinate.

[3] [3a] M. M. Nicholson, in *Phthalocyanines: Properties and Applications* (Eds.: C. C. Leznoff, A. B. P. Lever), VCH, New York, **1993**, vol. 3, pp. 71−117. − [3b] T. Komatsu, K. Ohta, T. Fujimoto, I. Yamamoto, *J. Mater. Chem.* **1994**, *4*, 533−536. − [3c] R. Jones, A. Krier, K. Davidson, *Thin Solid Films* **1997**, *298*, 228−236.

[4] [4a] M. Madru, G. Guillaud, M. Al Sadoun, M. Maitrot, C. Clarisse, M. Le Contellec, J.-J. André, J. Simon, *Chem. Phys. Lett.* **1987**, *142*, 103−105. − [4b] R. Madru, G. Guillaud, M. Al Sadoun, M. Maitrot, J.-J. André, J. Simon, R. Even, *Chem. Phys. Lett.* **1988**, *145*, 343−346. − [4c] C. Clarisse, M. T. Riou, M. Gauneau, M. Le Contellec, *Electron. Lett.* **1988**, *24*, 674−675. − [4d] G. Guillaud, M. Al Sadoun, M. Maitrot, J. Simon, M. Bouvet, *Chem. Phys. Lett.* **1990**, *167*, 503−506.

[5] [5a] J. Souto, M. L. Rodríguez, J. A. Desaja, R. Aroca, *Int. J. Electronics* **1994**, *76*, 763−769. − [5b] P. Bassoul, T. Toupance, J. Simon, *Sensors Actuators B* **1995**, *26−27*, 150−152. − [5c] K. R. Rickwood, D. R. Lovett, B. Lukas, J. Silver, *J. Mater. Chem.* **1995**, *5*, 725−729. − [5d] B. Liang, C. Yuan, Y. Wei, Y. Zhang, D. Jiang, S. Zhang, A. Lu, *Synth. Met.* **1997**, *88*, 219−223. − [5e] J. Alvarez, J. Souto, M. L. Rodríguez-Méndez, J. A. de Saja, *Sensors Actuators B* **1998**, *48*, 339−343.

[6] M. Guéna, Z. Y. Wu, M. L'Her, A. Pondaven, C. Cadiou, *Appl. Phys. Lett.* **1998**, *72*, 765−767.

[7] E. Ortí, R. Crespo, M. C. Piqueras, F. Tomás, *J. Mater. Chem.* **1996**, *6*, 1751−1761.

[8] [8a] F. Guyon, A. Pondaven, P. Guenot, M. L'Her, *Inorg. Chem.* **1994**, *33*, 4787−4793. − [8b] F. Guyon, A. Pondaven, J.-M. Kerbaol, M. L'Her, *Inorg. Chem.* **1998**, *37*, 569−576.

[9] [9a] M. Bouvet, J. Simon, *Chem. Phys. Lett.* **1990**, *172*, 299−302. − [9b] N. Ishikawa, O. Ohno, Y. Kaizu, *Chem. Phys. Lett.* **1991**, *180*, 51−56. − [9c] N. Ishikawa, O. Ohno, Y. Kaizu, *J. Phys. Chem.* **1993**, *97*, 1004−1010. − [9d] M. Bouvet, P. Bassoul, J. Simon, *Mol. Cryst. Liq. Cryst.* **1994**, *252*, 31−38. − [9e] M. Passard, J. P. Blanc, C. Maleysson, *Thin Solid Films* **1995**, *271*, 8−14. − [9f] M. Passard, A. Pauly, J. P. Germain, C. Maleysson, *Synth. Met.* **1996**, *80*, 25−28.

[10] F. Guyon, A. Pondaven, M. L'Her, *J. Chem. Soc., Chem. Commun.* **1994**, 1125−1126.

[11] [11a] J. Jiang, D. P. Arnold, H. Yu, *Polyhedron* **1999**, *18*, 2129−2139. − [11b] J. Jiang, W. Liu, K.-W. Poon, D. Du, D. P. Arnold, D. K. P. Ng, *Eur. J. Inorg. Chem.* **2000**, 205−209. − [11c] T. Nyokong, F. Furuya, N. Kobayashi, D. Du, W. Liu, J. Jiang, *Inorg. Chem.* **2000**, *39*, 128−135. − [11d] J. Jiang, L. Rintoul, D. P. Arnold, *Polyhedron* **2000**, *19*, 1381−1394.

[12] [12a] J. W. Buchler, B. Scharbert, *J. Am. Chem. Soc.* **1988**, *110*, 4272−4276. − [12b] J. W. Buchler, P. Hammerschmitt, I. Kaufeld, J. Löffler, *Chem. Ber.* **1991**, *124*, 2151−2159. − [12c] D. Chabach, M. Tahiri, A. De Cian, J. Fischer, R. Weiss, M. El Malouli Bibout, *J. Am. Chem. Soc.* **1995**, *117*, 8548−8556.

[13] [13a] J. Jiang, W. Liu, W.-F. Law, J. Lin, D. K. P. Ng, *Inorg. Chim. Acta* **1998**, *268*, 141−144. − [13b] J. Jiang, M. T. M. Choi, W.-F. Law, J. Chen, D. K. P. Ng, *Polyhedron* **1998**, *17*, 3903−3908. − [13c] J. Jiang, J. Xie, M. T. M. Choi, Y. Yan, S. Sun, D. K. P. Ng, *J. Porphyrins Phthalocyanines* **1999**, *3*, 322−328.

[14] J. Jiang, D. Du, M. T. M. Choi, J. Xie, D. K. P. Ng, *Chem. Lett.* **1999**, 261−262.

[15] J. W. Buchler, J. Hüttermann, J. Löffler, *Bull. Chem. Soc. Jpn.* **1988**, *61*, 71−77.

[16] Satisfactory analytical data could be obtained for Eu[Nc(tBu)$_4$]$_2$ and Eu[Nc($SC_{12}H_{25}$)$_8$]$_2$, which had been purified by gel-permeation chromatography repeatedly using Bio-beads SX-1 (Bio-rad) followed by recrystallization (see ref.[11c]).

[17] [17a] T.-H. Tran-Thi, T. A. Mattioli, D. Chabach, A. De Cian, R. Weiss, *J. Phys. Chem.* **1994**, *98*, 8279−8288. − [17b] J. Jiang, T. C. W. Mak, D. K. P. Ng, *Chem. Ber.* **1996**, *129*, 933−936.

[18] There is now substantial evidence that the hole in this class of complexes is delocalized over both macrocycles at least to a certain extent. On this basis, this characteristic near-IR band should be more correctly assigned to an electronic transition from a bonding orbital constructed from the HOMO of each ring to a half-occupied antibonding orbital (see ref.[1b]).

[19] [19a] J. W. Buchler, K. Elsässer, M. Kihn-Botulinski, B. Scharbert, S. Tansil, *ACS Symp. Ser.* **1986**, *321*, 94−104. − [19b] G. Ostendorp, H. Homborg, *Z. Anorg. Allg. Chem.* **1996**, *622*, 1222−1230.

[20] K. M. Kadish, G. Moninot, Y. Hu, D. Dubois, A. Ibnlfassi, J.-M. Barbe, R. Guilard, *J. Am. Chem. Soc.* **1993**, *115*, 8153−8166.

[21] [21a] A. Pondaven, Y. Cozien, M. L'Her, *New J. Chem.* **1992**, *16*, 711−718. − [21b] C. Cadiou, A. Pondaven, M. L'Her, P. Jéhan, P. Guenot, *J. Org. Chem.* **1999**, *64*, 9046−9050.

[22] [22a] J. Jiang, R. L. C. Lau, T. W. D. Chan, T. C. W. Mak, D. K. P. Ng, *Inorg. Chim. Acta* **1997**, *255*, 59−64. − [22b] J. Jiang, W. Liu, W.-F. Law, D. K. P. Ng, *Inorg. Chim. Acta* **1998**, *268*, 49−53.

[23] E. I. Kovshev, V. A. Puchnova, E. A. Luk'yanets, *Zh. Org. Khim.* **1971**, *7*, 369−371.

[24] G. H. Barnett, M. F. Hudson, K. M. Smith, *J. Chem. Soc., Perkin Trans. 1* **1975**, 1401−1403.

[25] J. G. Stites, C. N. McCarty, L. L. Quill, *J. Am. Chem. Soc.* **1948**, *70*, 3142−3143.

[26] D. T. Sawyer, A. Sobkowiak, J. L. Roberts, Jr., *Electrochemistry for Chemists*, 2nd ed., Wiley, New York, **1995**, chapter 6.

[27] Y.-L. Wong, J.-F. Ma, W.-F. Law, Y. Yan, W.-T. Wong, Z.-Y. Zhang, T. C. W. Mak, D. K. P. Ng, *Eur. J. Inorg. Chem.* **1999**, 313−321.

[28] R. D. Shannon, *Acta Cryst.* **1976**, *A32*, 751−767. The radii of the metal ions at the coordination number 8 were taken.

Received May 30, 2000
[I00219]

Olefins Coordinated at a Highly Electrophilic Site − Dicationic Palladium(II) Complexes and Their Equilibrium Reactions with Nucleophiles

Christine Hahn,[a] Pasquale Morvillo,[a] and Aldo Vitagliano*[a]

Dedicated to Professor Paolo Corradini on the occasion of his 70th birthday

Keywords: Palladium / Alkene complexes / Nucleophilic additions / Tridentate ligands / Aminations

Dicationic olefin palladium(II) complexes [Pd(PNP)(olefin)]$(BF_4)_2$ [olefin = ethylene, propene, styrene, (*Z*)-2-butene, (*E*)-2-butene, norbornene; PNP = 2,6-bis(diphenylphosphanylmethyl)pyridine] have been prepared and characterized by ^1H, ^{13}C, and ^{31}P NMR spectroscopy. The coordinated double bond in these complexes is strongly electrophilic, and easily adds a variety of nucleophiles NuH (H_2O, MeOH, aliphatic and aromatic amines). This reaction competes with olefin displacement in a rapidly reversible equilibrium process, as a result of which the addition products can also be obtained starting from the substituted compounds [Pd(PNP)(NuH)]$(BF_4)_2$ and the appropriate olefin. Equilibrium constants for the addition and substitution reactions have been determined in a number of cases. Proton abstraction from [Pd(PNP)(CHRCHR′NuH)]$^{2+}$ by $NaHCO_3$ quantitatively drives the equilibrium to β-functionalized alkyl complexes of the general formula [Pd(PNP)(CHRCHR′Nu)](BF_4), which are unusually stable to β-H elimination.

Introduction

(Olefin)palladium(II) complexes are important intermediates in organic syntheses and catalytic processes,[1] where the addition of nucleophiles to the C=C double bond is the crucial step. This offers numerous possibilities for the functionalization of simple olefins.[2] Among these, the hydroamination process, which was first investigated in the early 1970s, has recently attracted renewed attention.[3] The electrophilic character of the coordinated olefin is enhanced by an increase in the positive charge on the metal center,[4] as also shown by the ability of cationic Pd^{II} complexes to promote olefin polymerization[5] and copolymerization[6] reactions. Accordingly, very high reactivity would, in principle, be expected for complexes where the metal center bears a net (+2) charge, thus making such species appealing targets for investigation. On the other hand, a net (+2) charge would also enhance the electrophilic character and hardness of the metal center, and in such species the soft olefinic ligand can be expected to be readily displaceable, even by weak ligands and/or nucleophiles. Consequently, dicationic alkene complexes are expected to be accessible only within a rather narrow range of conditions and their reactivity is not readily predictable in advance. In line with the above considerations, no dicationic Pd^{II} complex of a simple monoolefin had been described in the literature[7] until we reported[8] the synthesis and characterization of two compounds of the formula [Pd(PNP)(CH_2=CHR)]$(BF_4)_2$ [PNP = 2,6-bis(diphenylphosphanylmethyl)-pyridine;[9] R = H, Ph], together with their reactions with secondary aliphatic amines. A number of questions arose from the above study, e.g. concerning the range of accessible (+2) charged complexes, their reactivity with nucleophiles weaker than aliphatic amines, and the nature (kinetic or thermodynamic) and extent of the competition between nucleophilic addition and displacement. In the present paper, we address these issues, presenting some quantitative evidence for the high electrophilicity of the olefin and for the interplay between addition and substitution reactions in these species. We also report the generation of a rare class of non-chelating β-functionalized (alkyl)Pd^{II} derivatives that are thermally stable and do not undergo β-H elimination.[10−13]

Results and Discussion

Synthesis and Characterization of [Pd(PNP)(olefin)]$^{2+}$ Complexes

The dicationic (olefin)palladium(II) complexes [Pd(PNP)(olefin)]$(BF_4)_2$ [olefin: CH_2=CH_2 (**1**), CH_2=CHMe (**2**), CH_2=CHPh (**3**), (*Z*)-MeCH=CHMe (**4**), (*E*)-

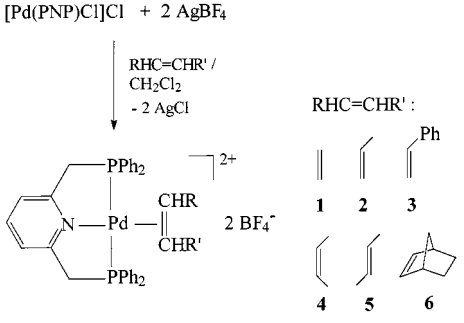

(1)

[a] Dipartimento di Chimica, Università di Napoli "Federico II", Via Mezzocannone 4, 80134 Napoli, Italy
Fax: (internat.) + 39-081/674199
E-mail: alvitagl@unina.it

 © WILEY-VCH Verlag GmbH, 69451 Weinheim, 2001 1434−1948/01/0202−0419 $ 17.50+.50/0

MeCH=CHMe (**5**), norbornene (**6**)] were prepared by reaction of the chloro complex [Pd(PNP)Cl]Cl[14] with two equivalents of silver tetrafluoroborate in the presence of an excess of the olefin according to Equation (1). The preparation of complexes **1** and **3** by the same procedure has been described previously.[8] In an alternative synthetic route, the norbornene complex **6** could be prepared by displacement of ethylene with an excess of norbornene [Equation (2)] and was obtained in high yield in an analytically pure state.

$$\underset{\mathbf{1}}{[Pd(PNP)(CH_2{=}CH_2)](BF_4)_2} \xrightarrow[-\ CH_2{=}CH_2]{\text{norbornene/ } CH_2Cl_2} \underset{\mathbf{6}}{[Pd(PNP)(\text{norbornene})](BF_4)_2} \quad (2)$$

The complexes **2** and **4**−**6** were characterized by ^{31}P, ^{1}H, and ^{13}C NMR spectroscopy. They were found to be moderately stable in dichloromethane and nitromethane solution at room temperature and may be stored for months under a dry atmosphere. They slowly decompose in moist air, as was also observed for the ethylene and styrene complexes **1** and **3**.[8] The ^{1}H and ^{31}P NMR spectra of the complexes (see Experimental Section) indicate an averaged C_2 symmetry for the propene complex **2** and an averaged C_{2v} symmetry for the complexes **4** and **6** and hence a fast rotation of the olefin about the Pd−double bond axis in each case. The spectrum of the propene complex **2** does not show substantial changes on cooling down to 203 K, indicating that at this temperature olefin rotation is still fast on the NMR time scale. The pattern observed for the propene complex **2** also indicates that at room temperature the exchange (dissociation−reassociation) of the olefin is slow on the NMR time scale. This was confirmed for all the complexes examined by the appearance of well-separated signals for the protons of free and coordinated olefin when a small amount of free olefin was added to each sample.

The ^{13}C chemical shifts of the olefinic carbon atoms in the complexes **1**−**6** are listed in Table 1, together with the corresponding coordination-induced shifts Δδ. A rather uniform albeit modest upfield shift is observed: The average Δδ is −15 ppm for the methine carbon atoms (except in the case of norbornene) and −33 ppm for the methylene carbon atoms, confirming previous observations for complexes **1** and **3**.[8] As pointed out previously,[8] the small values of Δδ are consistent with the high positive charge present on the central ion (as compared with the isoelectronic Rh^{I} complexes[15]) and with a consequent presumably low contribution of π-back-donation to the metal−olefin bond.[16]

Table 1. ^{13}C NMR chemical shifts of the coordinated olefins in **1**−**6** ($\Delta\delta = \delta_{coord} - \delta_{free}$)

Olefin	δ(=CH_2)	Δδ(=CH_2)	δ(=CH)	Δδ(=CH)
$CH_2{=}CH_2$ [8]	88.0	−35.3		
MeCH=CH_2	86.4	−29.6	118.1	−16.5
PhCH=CH_2 [8]	77.2	−34.8	120.2	−15.3
(*Z*)-MeCH=CHMe			110.9	−14.4
(*E*)-MeCH=CHMe			107.8	−17.6
Norbornene			105.2	−30.5

Olefin Displacement

As mentioned in the previous section, in complexes **1**−**6** at room temperature the olefin exchange is slow on the NMR time scale, which seems to be a rather unusual feature for coordinatively unsaturated Pd^{II} complexes.[17] However, the exchange is fast on the laboratory time scale, as shown by an experiment in which free ethylene was added to an NMR sample of the propene complex **2** at room temperature. The ^{1}H NMR spectrum of the mixture, recorded within 3 min of mixing, showed the presence of both species **1** and **2**, the relative abundances of which remained unchanged with time, indicating a rapid equilibration of the olefin complexes. The equilibrium constant for the exchange [Equation (3)] of ethylene for propene was estimated as $K = 1.4$ by integration of the NMR signals of the four species involved. Similar experiments were performed on complexes **3**−**5**, allowing estimation of the respective equilibrium constants [Equation (3)].

$$\underset{\mathbf{2\text{-}5}}{[Pd(PNP)(\text{olefin})](BF_4)_2} + CH_2{=}CH_2 \quad \Big\Vert K\,(CD_2Cl_2) \quad (3)$$

olefin	*K*
propene	1.4
E-2-butene	3
Z-2-butene	6
styrene	26

$$\underset{\mathbf{1}}{[Pd(PNP)(CH_2{=}CH_2)](BF_4)_2} + \text{olefin}$$

The relative stabilities of the olefin complexes seem to be determined essentially by steric factors. It is worth noting that (*E*)-2-butene gives a more stable complex than (*Z*)-2-butene, in contrast to the sequence typically found for (2-butene)metal complexes.[16,18] This most likely arises from the C_2 symmetry of the "pocket" created by the PNP ligand, which is better suited for hosting the (*E*)- as compared to the (*Z*)-olefin. The substantially lower stability of the styrene complex **3** can be ascribed to a steric interaction between the phenyl groups, which was revealed by its X-ray structure.[8]

As anticipated in the introduction, the olefin in complexes **1**−**6** is easily displaced, even by ligands that are usually weakly coordinative towards d^8 ions. Dissolution in acetone led to loss of the olefin from all of the complexes, while saturation of dichloromethane solutions of **1**, **2**, or **3** with water followed by evaporation of the solvent furnished the aqua complex **7** [Equation (4)]. The displacement of ethylene by acetonitrile, giving complex **8**, proved to be even more favorable. In the latter two cases, the equilibrium constants for the exchange [Equation (4)] were determined by

^{1}H NMR measurements in CD_2Cl_2/CD_3NO_2 (4:1) and were found to be $K = 5{\cdot}10^{-2}$ and $K = 9{\cdot}10^{2}$ for **7** and **8**, respectively.

$$[Pd(PNP)(CH_2{=}CH_2)](BF_4)_2 + L \quad \mathbf{1}$$

L	K (CD_2Cl_2/CD_3NO_2)
H_2O	$5 \cdot 10^{-2}$
CH_3CN	$9 \cdot 10^{2}$

$$[Pd(PNP)(L)](BF_4)_2 + CH_2{=}CH_2 \qquad (4)$$

L = H_2O **7**; CH_3CN **8**

Reactions with Nucleophiles

Complexes **1**−**6** were treated with a number of nucleophiles, including water, methanol, and aliphatic and aromatic amines. In many cases, the reaction mixtures were directly analyzed by ^{1}H NMR, which revealed details that would have remained undetected in normal preparative experiments and hence provided a quantitative estimation of the factors controlling the behaviour of the system.

Reactions with H_2O

As mentioned above, treatment of the ethylene complex **1** with an excess of H_2O resulted in the displacement of the olefin with production of the aqua complex $[Pd(PNP)(H_2O)](BF_4)_2$ (**7**) [Equation (4)], which was isolated and characterized by ^{1}H NMR. However, when the reaction was performed in an NMR tube using an excess of ethylene and a drop of water (resulting in a biphasic mixture), signals appeared in the spectrum indicative of a partial conversion of **1** to addition products (see below). These addition products were almost undetectable in the absence of an excess of heterogeneous water. This qualitatively indicated the occurrence of an overall equilibrium, in which the nucleophilic attack on the coordinated olefin was followed by proton transfer to the water phase (see Scheme 1). Indeed, when the reaction was performed in the presence of solid $NaHCO_3$ (ca. 2 equiv.), the equilibrium was seen to be quantitatively shifted towards the addition products, which could be isolated as a solid mixture and were assigned the mono- and dialkylated structures **9** and **10** (Scheme 1). In the ^{1}H NMR spectrum of the mixture, two sets of signals are seen for the $[PdCH_2CH_2O]$ moiety at $\delta = 2.02$ and 3.44 for **9** and at $\delta = 1.79$ and 2.79 for **10**. Integration of these signals reveals a ratio of ca. 1:3. Correspondingly, two different signals are observed for the PCH_2 group of the coordinated PNP ligand, at $\delta = 4.38$ and $\delta = 4.44$, respectively, in the same 1:3 ratio. Reductive degradation of the product mixture with $NaBH_4$ in $[D_8]$THF gave a solution in which the ^{1}H NMR signals of ethanol and diethyl ether were found in the same 1:3 ratio as observed for **9** and **10** (corresponding to a molar ratio of 1:1.5), thus independently confirming the above assignments.

Both the substitution reaction and the nucleophilic attack were found to be readily reversible. Indeed, addition of 5 equiv. of concentrated HBF_4 to a sample of the alkyl derivatives **9** and **10** in the presence of free ethylene resulted in the formation of **1**. Also, treatment of the aqua complex

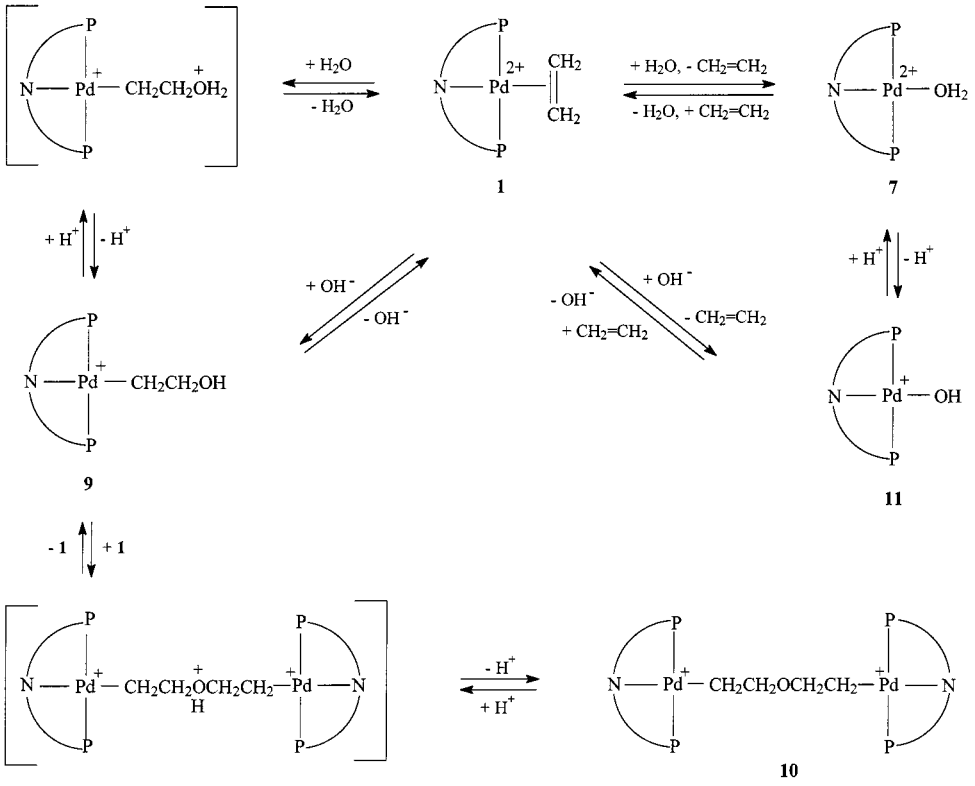

Scheme 1

7 with $NaHCO_3$ in dichloromethane saturated with ethylene likewise produced the same mixture of alkyl derivatives **9** and **10**. The formation of **10** was also performed in a stepwise manner, i.e. by first abstracting a proton from the coordinated water in **7** with an excess of $NaHCO_3$, giving the hydroxo complex $[Pd(PNP)(OH)]BF_4$ (**11**), and then treating the isolated complex **11** with ethylene. The latter reaction was monitored by ^1H NMR, which revealed the initial formation of the monoalkylated species **9** followed by partial conversion to **10**.

A similar set of equilibria were revealed in the case of the propene complex **2**. The major observed addition product (80% based on Pd) was the mononuclear primary alkyl derivative **12**, corresponding to a Markovnikov addition. Two pertinent differences from the ethylene case were qualitatively apparent. Firstly, the addition products were barely detectable in the absence of added $NaHCO_3$, indicating that the addition reaction is appreciably less favored than in the case of ethylene. Secondly, the binuclear species **13** was only produced as a minor product (20% based on Pd), probably reflecting the steric repulsion between two secondary carbon atoms linked to the same oxygen atom.

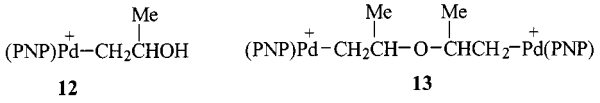

12 **13**

Reactions with MeOH

Dissolution of the ethylene complex **1** in CD_3OD produced a strongly acidic solution, the ^1H NMR spectrum of which revealed the presence of the addition product $[D_3]$**14**, a substitution product $[D_3]$**15**, and free ethylene in a molar ratio of 1:1:1. In the case of the propene complex **2**, the addition product $[D_3]$**16** was formed to a lesser extent (corresponding ratio 1:4:4), while for the styrene complex **3**, only the substitution product $[D_3]$**15** and free styrene were detectable in solution. Small amounts of the addition products were also detectable in the case of the 2-butene complexes **4** and **5**. Addition of an excess of free olefin to the solutions of **1** and **2** led to an increase in the relative amounts of the corresponding addition products **14** and **16**, respectively. These results indicate that in methanol solution two fast equilibrium reactions are operative [Equation (5) and Equation (6)].

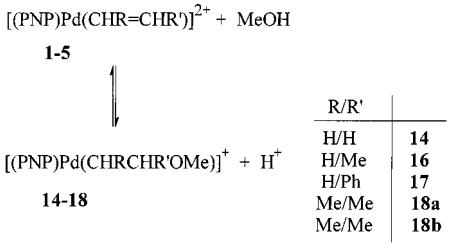

R/R'	
H/H	**14**
H/Me	**16**
H/Ph	**17**
Me/Me	**18a**
Me/Me	**18b**

(5)

The equilibrium constants for the overall reaction [Equation (7)] were estimated for ethylene, propene, and the two

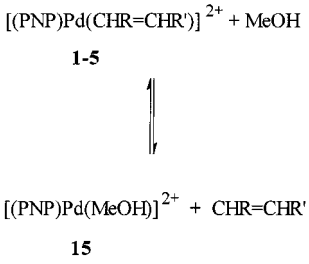

(6)

2-butenes, giving a relative measure of the stabilities of the (β-methoxyalkyl)palladium species compared with the respective free olefins.

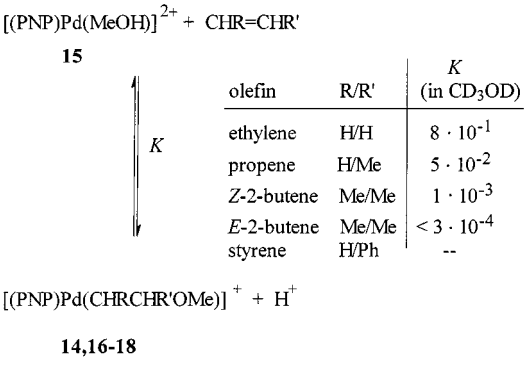

olefin	R/R'	K (in CD_3OD)
ethylene	H/H	$8 \cdot 10^{-1}$
propene	H/Me	$5 \cdot 10^{-2}$
Z-2-butene	Me/Me	$1 \cdot 10^{-3}$
E-2-butene	Me/Me	$< 3 \cdot 10^{-4}$
styrene	H/Ph	--

(7)

In the case of the ethylene complex **1**, the equilibrium represented by Equation (7) also results in a site exchange of the α- and β-protons of the alkyl chain. This exchange was actually revealed at room temperature by a ^1H NMR saturation transfer experiment, in which irradiation of either of the CH_2 groups caused a partial transfer of magnetization to the other CH_2 unit as well as to the free $CH_2=CH_2$ molecules, indicating that the overall exchange [Equation (7)] takes place at a rate comparable to the relaxation rates ($1-10\ s^{-1}$).

In line with our expectations, when the complexes **1**–**5** were treated with 2 equiv. of $NaHCO_3$ in methanol in the presence of an excess of free olefin, the equilibrium represented by Equation (7) was driven to completion leading to quantitative formation of the corresponding β-methoxyalkyl complexes **14** and **16**–**18**, which could be isolated. In the case of the ethylene complex **1**, the nucleophilic attack was also performed in a CH_2Cl_2 solution using 4 equiv. of MeOH, which led to the same result. High regioselectivity was achieved in the reactions of the propene and styrene complexes **2** and **3**, which gave **16** and **17**, respectively, in better than 97% abundances.[19] The structures of **16** and **17** were independently confirmed by reductive cleavage of the complexes with $NaBH_4$ in CD_3OD, which gave $CH_3CH(Me)OMe$ and $CH_3CH(Ph)OMe$, respectively. Addition of methanol to the (*Z*)- and (*E*)-2-butene complexes **4** and **5** furnished the diastereomers **18a** and **18b**, respectively, which could be distinguished by virtue of the slight but significant differences in their ^1H NMR spectra (see Experimental Section). The structures of **18a** and **18b** were

assigned assuming *trans* attack on the respective olefin complexes **4** and **5**. Although at present we are unable to provide any *direct* evidence for this assumption,[20] the alternative possibility of a *cis* addition (i.e. a true migratory insertion) seems unlikely in the light of previous knowledge on the stereochemistry of nucleophilic addition.[21] However, *circumstantial* evidence regarding this matter comes from the fact that although cationic (alkyl)(olefin) complexes of palladium(II) with bidentate ligands undergo rather fast insertion,[5] the isolated methyl derivative $[Pd(PNP)(CH_3)]BF_4$ is totally unreactive towards ethylene.[22]

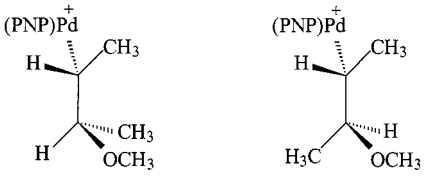

18a **18b**

The obtained β-methoxyalkyl complexes are quite stable as solids and in solution, both when the σ-bonded carbon atom is primary (as in **14**, **16**, and **17**) and when it is secondary (as in **18a**,**b**). No interconversion between the two diastereomers **18a** and **18b** was observed in dichloromethane solution over a period of one week.

In spite of the commonly encountered high reactivity of norbornene, no addition product of methanol could be obtained from complex **6**, possibly because of steric instability of the σ-alkyl derivative that would be produced by the nucleophilic attack, or (as suggested by a referee) because of inertness of *exo*-η^2-norbornene towards *trans* addition.

In an attempt to cleave the Pd−C σ-bond protolytically, the β-methoxyalkyl complexes were treated with gaseous HCl in CD_2Cl_2 solution, allowing direct monitoring of the reaction by NMR. However, this led to an immediate reversion of the nucleophilic addition through heterolytic fragmentation. The respective olefin was liberated, along with MeOH and $[Pd(PNP)Cl]BF_4$.

$$\underset{\textbf{14, 16-18}}{[(PNP)Pd(CHRCHR'OMe)]BF_4} \xrightarrow{\substack{HCl\ (g)/\\ CD_2Cl_2}} [Pd(PNP)Cl]BF_4 + CHR{=}CHR' + MeOH \qquad (8)$$

For the complexes **18a** and **18b**, the reversion of the addition led almost exclusively to the formation of (*Z*)- and (*E*)-2-butene, respectively, which provides evidence for the microscopic reversibility of this reaction.

Reactions with Amines

The reactions of the secondary alkylamines piperidine and dimethylamine with the ethylene and styrene complexes **1** and **3** were recently reported from a purely preparative point of view.[8] We have now investigated the process in more detail and have extended the studies to less basic aromatic amines. After adding an excess of ethylene to a solution (0.007 mol L^{-1}) of the isolated dimethylamine complex **19**,[8] an equilibrium was attained within about 1 h at 283 K. The final solution contained the addition product **20**−H^+ together with very small but measurable amounts of the starting complex **19**. The ratio **20**−H^+/**19** was found to be proportional to the concentration of free ethylene, confirming the existence of the equilibrium and allowing estimation of the equilibrium constant for the formal "insertion"[23] reaction represented by Equation (9) ($K = 3 \cdot 10^4$ L mol^{-1}).

$$\underset{\textbf{19}}{[(PNP)Pd(Me_2NH)]^{2+}} + CH_2{=}CHR \quad \Big\Vert K_{ins}(CD_2Cl_2)$$

olefin	K_{ins} [L mol^{-1}]
ethylene	$3 \cdot 10^4$
propene	10^2

$$[(PNP)Pd(CH_2CHRNHMe_2)]^{2+} \qquad (9)$$

R = H, **20**-H^+,
R = Me, **21**-H^+

Similar experiments were performed using propene and styrene as the olefins. In the case of propene, the addition product **21**−H^+ was formed in an equilibrium reaction, the estimated constant for which was $K = 10^2$ L mol^{-1}. In the case of styrene, no addition product could be detected. However, when the reaction was performed starting from the styrene complex **3** and an excess (4 equiv.) of Me_2NH was added, the primary alkyl derivative **22** was formed immediately and completely isomerized within 1 h to the secondary (anti-Markovnikov) alkyl derivative **23** (Scheme 2). The same reaction with excess Me_2NH was also performed with the propene complex **2**, resulting in a mixture of **21** (82%) and the anti-Markovnikov product **24** (18%). The regiochemical assignments of the products **21**−**24** were confirmed by in situ reduction with sodium borohydride and ^1H NMR identification of the resulting amines. The higher stability of the secondary (anti-Markovnikov) alkyl derivative **23** compared to **22** is in contrast to the common trend shown by alkylmetal complexes (primary > secondary >> tertiary), but seems to reflect a common outcome in amination reactions of styrene.[3a]

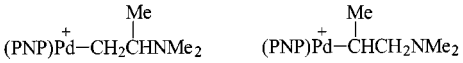

21 **24**

Experiments similar to those described above were performed using aniline as a nucleophile. Starting from a solution (0.015 mol L^{-1}) of the isolated aniline complex **25** containing 0.1 mol L^{-1} of free ethylene, an equilibrium distribution of 10:1 between the starting complex and the addition product **26**−H^+ was attained within a few minutes. The estimated equilibrium constant for the formal "insertion"[23] reaction [Equation (10)] is $K = 1$ L mol^{-1}. Upon addition of $NaHCO_3$ (2 equiv.), the equilibrium was quantitatively driven towards the addition product **26**, which was

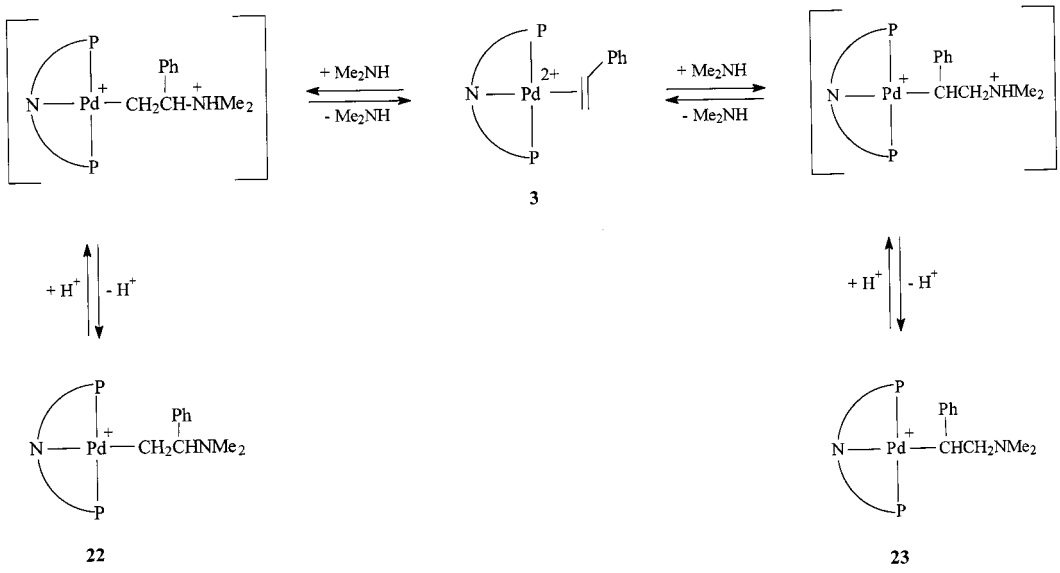

Scheme 2

formed together with small amounts of the dialkylated product **27**.[24]

$$[(PNP)Pd(PhNH_2)]^{2+} + CH_2{=}CH_2 \quad (\mathbf{25})$$

$$\Big\Vert \; K_{ins} = 1\ L\ mol^{-1}\ (CD_2Cl_2/CD_3NO_2) \qquad (10)$$

$$[(PNP)Pd(CH_2CH_2NH_2Ph)]^{2+} \quad (\mathbf{26}\text{-}H^+)$$

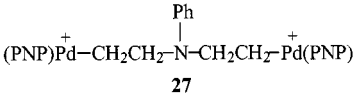

27

In the above experiments, the equilibrium concentration of the ethylene complex **1** was below the limit of detection, hence the equilibrium constants for the substitution and addition reactions could not be directly evaluated. In order to estimate their individual values, the equilibrium constants of two auxiliary substitution reactions [Equation (11) and Equation (12)] were determined by ^{1}H NMR.

$$[(PNP)Pd(PhNH_2)]^{2+} + MeCN \quad (\mathbf{25})$$

$$\Big\Vert \; K = 4 \cdot 10^{-3}\ (CD_2Cl_2/CD_3NO_2) \qquad (11)$$

$$[(PNP)Pd(MeCN)]^{2+} + PhNH_2 \quad (\mathbf{8})$$

By combining these values with that for the ethylene displacement by acetonitrile [$K = 9{\cdot}10^2$, see Equation (4)], the equilibrium constants for the substitution (K_{sub}) and addition (K_{add}) reactions with aniline and dimethylamine were estimated. The values are reported in Table 2, together with the corresponding values for the propene complex **2**.

$$[(PNP)Pd(Me_2NH)]^{2+} + PhNH_2 \quad (\mathbf{19})$$

$$\Big\Vert \; K = 4 \cdot 10^{-4} \qquad (12)$$

$$[(PNP)Pd(PhNH_2)]^{2+} + Me_2NH \quad (\mathbf{25})$$

Table 2. Approximate values of the equilibrium constants for the addition (K_{add}), substitution (K_{sub}), and "insertion" (see ref.[23]) ($K_{ins} = K_{add}/K_{sub}$) reactions of **1** and **2** with amines

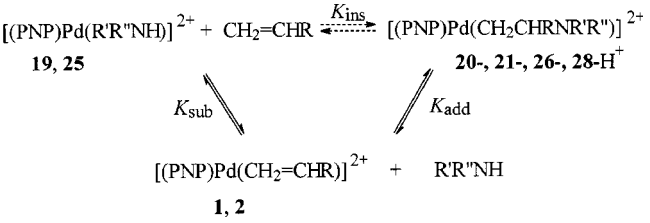

((Scan 19)) Amine	Me_2NH			$PhNH_2$		
Olefin	K_{ins} [L·mol^{-1}]	K_{add} [L·mol^{-1}]	K_{sub}	K_{ins} [L·mol^{-1}]	K_{add} [L·mol^{-1}]	K_{sub}
$CH_2{=}CH_2$	$3{\cdot}10^4$	10^{13}	$6{\cdot}10^8$	1	$2{\cdot}10^5$	$2{\cdot}10^5$
$CH_2{=}CHMe$	$1{\cdot}10^2$	10^{11}	$1{\cdot}10^9$	$5{\cdot}10^{-2}$	$1.5{\cdot}10^4$	$3{\cdot}10^5$

The K_{add} values given in Table 2 show that nucleophilic attack on the coordinated olefin is a quite favorable process in the dicationic complex, even when the nucleophile is a poorly basic aromatic amine. Moreover, the acidic β-ammonioalkyl derivative generated in the reaction can be further converted into the more stable β-aminoalkyl species through proton abstraction by an auxiliary base. When the basicity of the amine decreases, the nucleophilic attack is less favored, but at the same time the β-ammonioalkyl derivative is more acidic, and a successive proton abstraction becomes more favored. Therefore, the overall reaction in the presence of an auxiliary base is expected to be driven to a similar extent towards the (β-aminoalkyl)palladium derivative. In view of these considerations, we treated complexes **1** and **2** with primary aromatic amines of varying basicity (ranging from 4-methoxyaniline, pK_a = 5.3 to 2-chloroaniline, pK_a = 2.6) and $NaHCO_3$ (2 equiv.) in the presence of an excess of the respective gaseous olefins. The (β-aminoethyl)Pd^{II} compounds **26** and **28−34** were indeed obtained in good yields (Scheme 3) as cream-colored solids and were characterized by ^1H NMR.

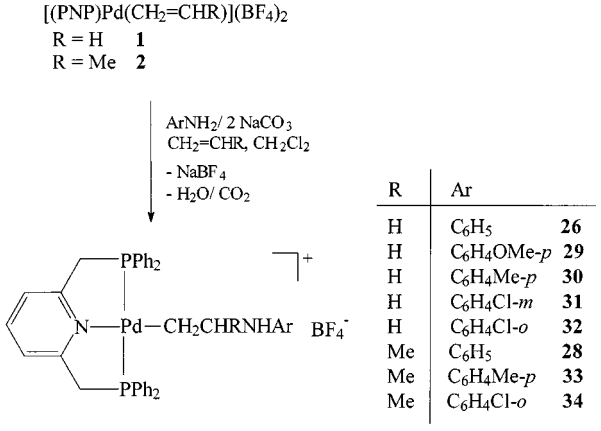

R	Ar	
H	C_6H_5	**26**
H	C_6H_4OMe-*p*	**29**
H	C_6H_4Me-*p*	**30**
H	C_6H_4Cl-*m*	**31**
H	C_6H_4Cl-*o*	**32**
Me	C_6H_5	**28**
Me	C_6H_4Me-*p*	**33**
Me	C_6H_4Cl-*o*	**34**

Scheme 3

The structures of the propene derivatives **28**, **33**, and **34** were assigned essentially as in the case of the water and methanol adducts, and indicated selective attack at the secondary carbon atom (Markovnikov addition). As in the case of the corresponding β-methoxyalkyl species **14** and **16−18**, the complexes **26** and **28−34** can be stored indefinitely as solids and are also stable in solution; no evidence for β-H elimination was observed after a week in dichloromethane. This stability towards β-H elimination is quite exceptional in (alkyl)Pd species that are not stabilized by four- or five-membered ring formation.[11] It most likely arises from the impossibility of the putative hydride ligand to access either of the *cis* positions, both of them being firmly bound by the two phosphane "arms" of the PNP ligand. It is noteworthy in this respect that the only β-functionalized open-chain alkyl Pd^{II} derivatives hitherto isolated are *trans*-$[Pd(PMe_3)_2(CH_2CH_2Y)Br]$ (Y = CO_2Me, CN).[13]

Conclusions

The use of the tridentate "pincer" ligand PNP has allowed the unprecedented isolation of stable dicationic (olefin)Pd^{II} complexes, and the subject of nucleophilic addition to Pd^{II}-coordinated olefins has been re-examined using these dicationic complexes as substrates. The σ-alkyl derivatives resulting from the nucleophilic attack are remarkably stable towards β-H elimination, as a consequence of the unavailability of the adjacent coordination sites. Since side-reactions arising from β-H elimination do not take place, for the first time approximate equilibrium data could be obtained for the nucleophilic addition and for the competitive substitution reaction. The results indicate that in a dicationic Pd^{II} complex the olefin is highly activated towards nucleophilic addition (much more so than in neutral species[25]), both kinetically and thermodynamically. It is relevant to note in this respect that in monocationic complexes containing a ligand isoelectronic and isostructural with PNP (i.e. PCP), no nucleophilic attack on a coordinated olefin is observed.[26] The coordinated double bond actually acts as a strong electrophile, as indicated by its ability to capture a lone pair from methanol and to successively protonate a base as weak as methanol itself. Viewed from another perspective, the σ-alkyl derivatives resulting from the nucleophilic attack are strongly stabilized by the residual positive charge on the metal ion, and it appears that the C−Pd σ-bond is *more* stabilized by the positive charge than the Pd−N bond of a coordinated amine. Thus, the formal "insertion"[23] of the olefin into the Pd−N bond is thermodynamically favored (Table 2), while it was found to be *disfavored* in the case of neutral species.[27] This finding could be relevant for the development of synthetically useful hydroaminations, because olefin displacement, which is considered to be a serious obstacle to achieving such processes,[3a] might become a minor concern or even be of no consequence in the case of dicationic species.

Experimental Section

General: All reactions were carried out under dry nitrogen. CH_2Cl_2 was refluxed with CaH_2, MeOH with $Mg/Mg(OMe)_2$, and diethyl ether with Na/benzophenone. The solvents were distilled prior to use. CD_2Cl_2, CD_3NO_3, and $CDCl_3$ were dried with 4-Å molecular sieves. $AgBF_4$ was obtained from ABCR and was used without further purification. The aromatic amines RNH_2 were obtained from Aldrich and were distilled prior to use. − NMR spectra were recorded with Varian Gemini 200, Bruker AC-200, Bruker AC-250, and Bruker WH-400 instruments. ^1H NMR shifts were referenced to the resonances of the residual protons in the solvents and the ^{13}C NMR shifts to the solvent resonances (δ = 53.8, CD_2Cl_2; δ = 62.8, CD_3NO_2). For the ^{31}P NMR spectra, H_3PO_4 (85%) was used as an external standard.

Syntheses: The complexes [Pd(PNP)Cl]Cl,[14] $[Pd(PNP)(CH_2=CHR)](BF_4)_2$ [R = H (**1**), Ph (**3**)], and $[Pd(PNP)(L)](BF_4)_2$ [L = MeCN (**8**), Me_2NH (**19**), pyridine (**35**)][8] were prepared according to previously described procedures.

[Pd(PNP)(olefin)](BF$_4$)$_2$ (2, 4−6). − General Procedure: A mixture of [Pd(PNP)Cl]Cl (200 mg, 0.306 mmol) and $AgBF_4$ (121 mg, 0.620 mmol) in CH_2Cl_2 (10 mL) was saturated with the appropriate gaseous olefin (in the case of norbornene 10 equiv. of the olefin was added). After stirring the mixture for 10 min, the precipitate was filtered off. In the case of 2-butenes and norbornene, the precipitate (containing the product) was washed with nitromethane (1 mL, free from any nitrile!). The product was precipitated from the solution by the dropwise addition of diethyl ether. The solid was collected by filtration, washed with diethyl ether, and dried in vacuo.

2: Yield 191 mg (0.243 mmol, 78%); ivory-colored solid; m.p. 181 °C (dec.). − $C_{34}H_{33}B_2F_8NP_2Pd$ (797.62): calcd. C 51.20, H 4.17, N 1.76; found C 50.91, H 4.21, N 1.69. − ^{1}H NMR (200 MHz, CD_2Cl_2): δ = 1.51 (d, J_{HH} = 6.2 Hz, 3 H, CH_3), 4.56 (d pseudo t, J_{HH} = 17.2 Hz, N_{HP} = 5.4 Hz, 2 H, PCH_aH$_b$), 4.66 (d, J_{HH} = 14.8 Hz, 1 H, =CH_2), 4.70 (d, J_{HH} = 7.8 Hz, 1 H, =CH_2), 5.21 (d pseudo t, J_{HH} = 17.2 Hz, N_{HP} = 5.0 Hz, 2 H, PCH$_a$$H_b$), 6.00 (br, 1 H, =CH), 7.59−8.02 (m, 23 H, Ph, py). − ^{13}C NMR (50 MHz, CD_2Cl_2): δ = 21.5 (s, CH_3), 44.9 (pseudo t, N_{CP} = 12.8 Hz, PCH_2), 86.3 (s, =CH_2), 118.1 (s, =CH), 124.5 (pseudo t, N_{CP} = 25.5 Hz, Ph$_i$), 124.5 (br, py-3,5), 125.5 (pseudo t, N_{CP} = 27.3 Hz, Ph$_{i'}$), 131.2−131.3 (br, Ph$_m$), 133.8 (pseudo t, N_{CP} = 5.7 Hz, Ph$_o$), 134.9 (s, Ph$_p$), 135.1 (pseudo t, N_{CP} = 7.7 Hz, Ph$_{o'}$), 144.1 (s, py-4), 161.1 (br, py-2,6). − ^{31}P NMR (CH_2Cl_2, 81 MHz): δ = 46.9 (s).

4: Yield 196 mg (0.242 mmol, 79%); pale-yellow solid; m.p. 205 °C (dec.). − $C_{35}H_{35}B_2F_8NP_2Pd$ (811.64): calcd. C 51.79, H 4.35, N 1.73; found C 51.56, H 4.20, N 1.63. − ^{1}H NMR (200 MHz, CD_2Cl_2): δ = 1.69 (br. d, J_{HH} = 3.6 Hz, 6 H, CH_3), 4.83 (pseudo t, N_{HP} = 5.2 Hz, 4 H, CH_2), 5.97 (br. q, 2 H, =CH), 7.50 (d, J_{HH} = 7.8 Hz, 2 H, py-3,5), 7.71 (m, 12 H, Ph), 7.83−8.03 (m, 9 H, py, Ph). − ^{13}C NMR (50 MHz, CD_2Cl_2): δ = 17.5 (s, CH_3), 44.2 (pseudo t, N_{CP} = 14.8 Hz, PCH_2), 110.8 (s, =CH), 124.8 (br, py-3,5), 131.2 (pseudo t, N_{CP} = 5.6 Hz, Ph$_m$), 134.7 (s, Ph$_p$), 134.9 (pseudo t, N_{CP} = 7.5 Hz, Ph$_o$), 144.2 (s, py-4), 160.4 (br, py-2,6). − ^{31}P NMR (CH_2Cl_2, 81 MHz): δ = 45.3 (s).

5: Yield 211 mg (0.260 mmol, 85%); pale-yellow solid. − $C_{35}H_{35}B_2F_8NP_2Pd$ (811.64): calcd. C 51.79, H 4.35, N 1.73; found C 51.50, H 4.16, N 1.60. − ^{1}H NMR (400 MHz, CD_2Cl_2): δ = 1.47 (br. d, J_{HH} = 3.6 Hz, 6 H, CH_3), 4.76 (d pseudo t, N_{HP} = 5.6 Hz, J_{HH} = 17.4 Hz, 2 H, PCH_aH$_b$), 5.14 (d pseudo t, N_{HP} = 4.6 Hz, J_{HH} = 17.4 Hz, 2 H, PCH$_a$$H_b$), 5.86 (br. m, 2 H, =CH), 7.67−8.00 (m, 22 H, Ph, py), 8.11 (t, J_{HH} = 8.0 Hz, 1 H, py-4). − ^{13}C NMR (100 MHz, CD_2Cl_2): δ = 19.1 (s, CH_3), 43.7 (pseudo t, N_{CP} = 14.1 Hz, PCH_2), 107.8 (s, =CH), 124.6 (pseudo t, N_{CP} = 5.3 Hz, py-3,5), 124.7 (pseudo t, N_{CP} = 27.1 Hz, Ph$_i$), 125.5 (pseudo t, N_{CP} = 26.1 Hz, Ph$_{i'}$), 130.5 (br, Ph$_m$), 133.1 (pseudo t, N_{CP} = 5.3 Hz, Ph$_o$), 134.3 (s, Ph$_p$), 134.3 (Ph$_{o'}$), 134.4 (s, Ph$_{p'}$), 144.2 (s, py-4), 160.3 (br, py-2,6). − ^{31}P NMR (CH_2Cl_2, 81 MHz): δ = 45.5 (s).

6. − Method A: According to the general procedure: yield 235 mg (0.251 mmol, 82%), ivory-colored solid. − **Method B:** To a solution of **1** (150 mg, 0.191 mmol) in CH_2Cl_2 (5 mL) was added ca. 10 equiv. of norbornene (2 mmol). After stirring the mixture for 1 h, the product was precipitated by the dropwise addition of diethyl ether. The solid was filtered off, washed three times with diethyl ether, and dried in vacuo. Yield 175 mg (0.187 mmol, 98%). − $C_{38}H_{37}B_2F_8NP_2Pd{\cdot}CH_2Cl_2$ (934.63): calcd. C 50.12, H 4.21, N 1.50; found C 49.80, H 4.03, N 1.39. − ^{1}H NMR (200 MHz, CD_2Cl_2): δ = 0.77 (m, 1 H, norbornene), 1.34 (m, 1 H, norbornene), 1.55 (br, 4 H, norbornene), 1.94 (br, norbornene), 4.92 (t, J_{HP} = 4.2 Hz, 2 H, =CH, norbornene), 4.95 (pseudo t, N_{HP} = 5.0 Hz, 4 H, PCH_2), 7.57 (d, J_{HH} = 7.4 Hz, 2 H, py-3,5), 7.69−7.73 (m, 12 H, Ph), 7.86−7.98 (m, 9 H, Ph, py). − ^{13}C NMR (50 MHz, CD_3NO_2): δ = 23.6 (s, norbornene), 43.9 (s, norbornene), 46.0 (pseudo t, N_{CP} = 14.6 Hz), 54.5 (s, norbornene), 105.2 (s, =CH, norbornene), 124.6 (pseudo t, N_{CP} = 5.6 Hz, py-3,5), 125.4 (pseudo t, N_{CP} = 27.3 Hz, Ph$_i$), 130.7 (pseudo t, N_{CP} = 5.6 Hz, Ph$_m$), 134.1 (pseudo t, N_{CP} = 7.4 Hz, Ph$_o$), 134.7 (s, Ph$_p$), 144.2 (s, py-4), 159.9 (s, py-2,6). − ^{31}P NMR (81 MHz, CH_2Cl_2): δ = 50.4 (s).

[Pd(PNP)(H$_2$O)](BF$_4$)$_2$ (7): To a solution of **1** (100 mg, 0.127 mmol) in CH_2Cl_2 (6 mL) was added ca. 50 equiv. of H_2O (100 μL). After stirring for a few minutes, a yellow crystalline solid precipitated, which was collected by filtration, washed several times with diethyl ether, and dried in vacuo. Yield 90%. − ^{1}H NMR (200 MHz, CD_2Cl_2): δ = 3.0 (v br, H_2O), 4.45 (br, 4 H, PCH_2), 7.54−8.05 (m, 23 H, Ph, py).

Reactions of 1 and 2 with H$_2$O: To a solution of **1** or **2** (100 mg) in CH_2Cl_2 (6 mL), saturated with ethylene or propene, respectively, 2 equiv. of $NaHCO_3$ and 50 equiv. of H_2O were added. The mixture was then stirred for 3 h, the solid was filtered off, and the solvent was removed under reduced pressure. A solid was obtained, which was recrystallized from CH_2Cl_2/diethyl ether.

9/10: Yield 87 mg (97% based on Pd); pale-yellow solid. − ^{1}H NMR (200 MHz, $CDCl_3$): **9**: δ = 2.02 (m, 2 H, $PdCH_2$), 3.44 (m, 2 H, CH_2), 4.44 (pseudo t, N_{HP} = 4.6 Hz, 4 H, PCH_2), 7.35−7.73 (m, 23 H, Ph, py). − **10**: δ = 1.79 (m, 2 H, $PdCH_2$), 2.78 (m, 2 H, CH_2), 4.38 (pseudo t, N_{HP} = 4.6 Hz, 4 H, PCH_2), 7.35−7.73 (m, 23 H, Ph, py). − ^{31}P NMR (81 MHz, CH_2Cl_2): **9/10**: δ = 24.1 (s).

12/13: Yield 82 mg (92% based on Pd); orange-yellow solid. − ^{1}H NMR (200 MHz, $CDCl_3$): **12**: δ = 0.81 (d, J_{HH} = 6.0 Hz, 3 H, CH_3), 2.01 (m, 2 H, $PdCH_2$), 3.66 (m, 1 H, CH), 4.44 (pseudo t, N_{HP} = 4.6 Hz, 4 H, PCH_2), 7.15−7.75 (m, 23 H, Ph, py). − **13**: δ = 1.17 (d, J_{HH} = 4 Hz, 3 H, CH_3), 2.01 (m, 2 H, $PdCH_2$), 3.65 (m, 1 H, CH), 4.44 (pseudo t, N_{HP} = 4.6 Hz, 4 H, PCH_2), 7.15−7.75 (m, 23 H, Ph, py). − ^{31}P NMR (81 MHz, CH_2Cl_2): **12/13**: δ = 22.3 (s), 23.7 (s).

Reductive Degradation with NaBH$_4$: To a suspension of 20 mg of the appropriate product mixture (**9/10** or **12/13**) in [D$_8$]THF (0.7 mL), cooled in an ice-bath, was added excess $NaBH_4$. After stirring for 1 h at room temperature, the dark-brown solution was filtered and the filtrate was analyzed by ^{1}H NMR spectroscopy.

[Pd(PNP)(OH)]BF$_4$ (11): A mixture of **7** (100 mg, 0.129 mmol) and 2 equiv. of $NaHCO_3$ in CH_2Cl_2 (5 mL) was stirred for 1.5 h. The mixture was then filtered and the product was precipitated from the filtrate by the dropwise addition of diethyl ether. The orange-yellow solid was collected by filtration, washed with diethyl ether, and dried in vacuo. Yield 85 mg (124 mmol, 96%). − ^{1}H NMR (200 MHz, CD_2Cl_2): δ = 4.21 (pseudo t, N_{HP} = 4.4 Hz, 4 H, PCH_2), 7.15−7.75 (m, 23 H, Ph, py). − ^{31}P NMR (81 MHz, CH_2Cl_2): δ = 22.3 (s).

Reactions of [Pd(PNP)(CHRCHR′)](BF$_4$)$_2$ (1−5) with MeOH. − General Procedure: To a solution of **1−5** (100 mg) in MeOH (2 mL) cooled to 0 °C were added an excess of the appropriate olefin and 2 equiv. of $NaHCO_3$. The mixture was stirred for 3 h, the precipitate was filtered off, and the solvent was removed under reduced pressure. A beige solid was obtained in each case, which was recrystallized from CH_2Cl_2/diethyl ether.

[Pd(PNP)(CH$_2$CH$_2$OMe)]BF$_4$ (14): Yield 85%. − $C_{34}H_{34}BF_4NOP_2Pd$ (727.82): calcd. C 56.11, H 4.71, N 1.93; found

C 55.73, H 4.73, N 1.82. – ^{1}H NMR (200 MHz, CD_2Cl_2): δ = 2.00 (m, 2 H, $PdCH_2$), 2.85 (s, 3 H, OCH_3), 3.10 (m, 2 H, CH_2), 4.43 (pseudo t, N_{HP} = 4.6 Hz, 4 H, PCH_2), 7.48–7.94 (m, 23 H, Ph, py). – ^{31}P NMR (81 MHz, CH_2Cl_2): δ = 24.4 (s).

[Pd(PNP){$CH_2CH(Me)OMe$}]BF_4 (16): Yield 86%. – $C_{35}H_{36}BF_4NOP_2Pd \cdot CH_2Cl_2$ (826.73): calcd. C 52.30, H 4.63, N 1.69; found C 51.26, H 4.46, N 1.62. – ^{1}H NMR (400 MHz, CD_2Cl_2): δ = 0.68 (d, J_{HH} = 5.9 Hz, 3 H, CH_3), 1.67 (m, 1 H, $PdCH_2$), 2.20 (m, 1 H, $PdCH_2$), 2.74 (s, 3 H, OCH_3), 3.05 (m, 1 H, CH), 4.28–4.40 (m, 4 H, PCH_2), 7.50–7.68 (m, 22 H, Ph, py), 7.91 (t, J_{HH} = 7.8 Hz, 1 H, py-4).

[Pd(PNP){$CH_2CH(Ph)OMe$}]BF_4 (17): Yield 80%. – ^{1}H NMR (200 MHz, CD_2Cl_2): δ = 2.00 (m, 1 H, PCH_2), 2.19 (m, 1 H, $PdCH_2$), 2.65 (s, 3 H, OCH_3), 3.78 (m, 1 H, CH), 4.41 (m, PCH_2), 6.84 (m, 2 H, CPh), 7.12 (m, 3 H, CPh), 7.49–7.95 (m, 23 H, PPh, py). – ^{31}P NMR (81 MHz, CH_2Cl_2): δ = 24.7 (s).

[Pd(PNP){CH(Me)CH(Me)OMe}]BF_4 [18a, obtained from (*Z*)-2-butene]: Yield 83%. – ^{1}H NMR (200 MHz, CD_2Cl_2): δ = 0.82 (d, J_{HH} = 5.6 Hz, 3 H, CH_3), 0.92 (m, 3 H, CH_3), 2.74 (m, 2 H, CH–CH), 2.92 (s, 3 H, OCH_3), 4.31 (pseudo t, N_{HP} = 4.2 Hz, 4 H, PCH_2), 7.44–7.95 (m, 23 H, Ph, py). – ^{31}P NMR (81 MHz, CH_2Cl_2): δ = 21.8 (s).

[Pd(PNP){CH(Me)CH(Me)OMe}]BF_4 [18b, obtained from (*E*)-2-butene]: Yield 81%. – ^{1}H NMR (200 MHz, CD_2Cl_2): δ = 0.93 (d, J_{HH} = 5.4 Hz, 3 H, CH_3), 1.04 (m, 3 H, CH_3), 2.72 (s, 3 H, OCH_3), 2.74 (m, 2 H, CH–CH), 4.35 (m, 4 H, PCH_2), 7.45–7.93 (m, 23 H, Ph, py).

Reductive Degradation of 16 and 17 with $NaBH_4$: To a solution of 20 mg of compound **16** or **17** in CD_3OD (0.7 mL), cooled in an ice-bath, was added excess $NaBH_4$. After stirring for 1 h at room temperature, the dark-brown solution was filtered and the filtrate was analyzed by ^{1}H NMR spectroscopy. – ^{1}H NMR: $CH_3CH(Me)OCD_3$: δ = 1.14 (d, J_{HH} = 6.2 Hz, 6 H, CH_3), 3.50 (sept, J_{HH} = 6.2 Hz, 1 H, CH).; $CH_3CH(Ph)OCD_3$: δ = 1.41 (d, J_{HH} = 6.1 Hz, 3 H, CH_3), 4.34 (q, J_{HH} = 6.1 Hz, 1 H, CH), 7.28 (m, 5 H, Ph).

Treatment of 14, 16–18a,b with HCl: Gaseous HCl was bubbled through solutions of **14**, **16–18a,b** in CD_2Cl_2, which led to a color change from orange to yellow. The ^{1}H NMR spectra of these solutions were found to feature signals attributable to both the free olefin and $[Pd(PNP)Cl]^+$.

[Pd(PNP)(MeOH)]$(BF_4)_2$ (15): Compound **1** (100 mg) was dissolved in MeOH (5 mL) and the solvent was removed under reduced pressure. This procedure was repeated twice more. Finally, the yellow solid was washed with diethyl ether and dried in vacuo. Yield 95%. – ^{1}H NMR (200 MHz, CD_2Cl_2): δ = 3.17 (br, 1 H, OH), 3.38 (s, 3 H, CH_3), 4.49 (pseudo t, N_{HP} = 4.6 Hz, 4 H, PCH_2), 7.48–8.01 (m, 23 H, Ph, py).

Reactions of 19 with Ethylene and Propene: Solutions of **19** (3 mg) in CD_2Cl_2 (0.6 mL) were saturated with ethylene and propene, respectively.

[(PNP)$PdCH_2CH_2NHMe_2$]$^{2+}$ (20–H^+): NMR: δ = 1.82 (m, 2 H, $PdCH_2$), 2.28 (s, 6 H, NMe_2), 2.79 (m, 2 H, NCH_2), 4.52 (pseudo t, N_{HP} = 5.0 Hz, 4 H, PCH_2), 7.48–8.02 (m, 23 H, Ph, py).

[(PNP)$PdCH_2CH(Me)NHMe_2$]$^{2+}$ (21–H^+): NMR: δ = 0.82 (d, J_{HH} = 6.2 Hz, 3 H, CH_3), 1.79 (m, 1 H, $PdCH_2$), 1.92 (m, 1 H, $PdCH_2$), 2.15 (s, 3 H, NCH_3), 2.22 (s, 3 H, NCH_3), 2.89 (m, 1 H, CH), 4.56 (pseudo t, N_{HP} = 4.6 Hz, 4 H, PCH_2), 7.55–8.02 (m, 23 H, Ph, py).

Reaction of 3 with Me_2NH: Two NMR tubes were prepared, each containing a solution of **3** (8 mg) in CD_2Cl_2 (0.6 mL) with 4 equiv. of gaseous Me_2NH. A ^{1}H NMR spectrum was recorded immediately after the addition of the amine.

[(PNP)$PdCH_2CH(Ph)NMe_2$]$^+$ (22): NMR: δ = 1.68 [s, 6 H, $N(CH_3)_2$], 2.28 (m, 1 H, $PdCH_2$), 2.48 (m, 1 H, $PdCH_2$), 3.44 (m, 1 H, CH), 4.37 (pseudo t, 4 H, N_{HP} = 4.4 Hz, PCH_2), 6.55 (d, 2 H, J_{HH} = 8.2 Hz, Ph), 7.06 (m, 3 H, Ph), 7.53–7.98 (m, 23 H, PPh, py). – For the reductive degradation, an excess of $NaBH_4$ (dissolved in a drop of CD_3OD) was added instantly to one of the two solutions. After 20 min, its ^{1}H NMR spectrum was recorded again, which now featured signals due to $CH_3CH(Ph)NMe_2$. – The second sample was again analyzed by ^{1}H NMR after 1 h.

[(PNP)$PdCH(Ph)CH_2NMe_2$]$^+$ (23): NMR: δ = 1.89 [s, 6 H, $N(CH_3)_2$], 2.48 (m, 1 H, NCH_2), 2.68 (m, 1 H, PdCH), 3.98 (m, 1 H, NCH_2), 4.26 (d pseudo t, N_{HP} = 4.6 Hz, J_{HH} = 17 Hz, 2 H, PCH_aH_b), 4.40 (d pseudo t, N_{HP} = 4.4 Hz, J_{HH} = 17 Hz, 2 H, PCH_aH_b), 6.41 (d, J_{HH} = 7 Hz, 2 H, Ph), 6.87 (m, 3 H, Ph), 7.50–7.92 (m, 23 H, PPh, py). – After treatment of the solution with $NaBH_4$ (CD_3OD) as described above, the signals of $PhCH_2CH_2NMe_2$ were detectable.

Reaction of 2 with 4 Equiv. of Me_2NH: The reaction was carried out in an NMR tube in a similar manner as described for the reaction of **3** with Me_2NH.

[(PNP)$PdCH_2CH(Me)NMe_2$]$^+$ (21): ^{1}H NMR (200 MHz, CD_2Cl_2): δ = 0.70 (d, J_{HH} = 6.2 Hz, 3 H, CH_3), 1.85 (m, 1 H, $PdCH_2$), 1.97 (s, 6 H, NCH_3), 2.05 (m, 1 H, $PdCH_2$), 2.62 (m, 1 H, CH), 4.48 (pseudo t, N_{HP} = 4.6 Hz, 4 H, PCH_2), 7.57–7.98 (m, 23 H, Ph, py).

[(PNP)$PdCH(Me)CH_2NMe_2$]$^+$ (24): ^{1}H NMR (200 MHz, CD_2Cl_2): δ = 1.02 (d pseudo t, J_{HH} = 7.0 Hz, N_{HP} = 3 Hz, 3 H, CH_3), 1.84 (s, 6 H, NCH_3), 4.36 (pseudo t, N_{HP} = 4.4 Hz, 4 H, PCH_2), 7.55–8.02 (m, 23 H, Ph, py). The remaining signals for CH and CH_2 are overlapped with the signals due to **21**.

[Pd(PNP)($PhNH_2$)]$(BF_4)_2$ (25): To a solution of **1** (100 mg) in CH_2Cl_2 (3 mL) was added aniline (0.5 mL). After stirring for a few minutes, an ivory-colored solid crystallized, which was collected by filtration, washed three times with diethyl ether, and dried in vacuo. Yield 85%. – $C_{37}H_{34}B_2F_8N_2P_2Pd \cdot 0.75CH_2Cl_2$ (912.27): calcd. C 49.70, H 3.92, N 3.07; found C 49.79, H 3.91, N 3.14. – ^{1}H NMR (200 MHz, CD_2Cl_2): δ = 4.59 (pseudo t, N_{HP} = 4.8 Hz, 4 H, PCH_2), 5.70 (br, 2 H, NH_2), 6.67 (d, J_{HH} = 7.6 Hz, 2 H, NPh), 6.89 (m, 3 H, NPh), 7.55–7.80 (m, 22 H, Ph, py), 7.88 (t, J_{HH} = 7.6 Hz, 1 H, py-4).

Reactions of 25 with Ethylene and Propene: A solution of **24** (8 mg) in CD_2Cl_2/CD_3NO_2 (6:1) (0.6 mL) was saturated with either ethylene or propene. Since the signals of the addition products appear in the spectra at relatively low intensity and are partly overlapped by the signals of **25**, the full set of signals could not be detected.

[(PNP)$PdCH_2CH_2NH_2Ph$]$^{2+}$ (25–H^+): NMR: δ = 2.12 (m, 1 H, $PdCH_2$), 3.28 (m, 1 H, NCH_2), 4.47 (pseudo t, N_{HP} = 4.8 Hz, 4 H, PCH_2).

[(PNP)$PdCH_2CH(Me)NH_2Ph$]$^{2+}$ (26–H^+): NMR: δ = 0.92 (d, J_{HH} = 6.0 Hz, 3 H, CH_3).

Preparation of [Pd(PNP)($CH_2CHRNHAr$)]$(BF_4)_2$ (26, 28–34) – General Procedure: A solution of **1** or **2** (100 mg) in CH_2Cl_2 (2 mL) was cooled to 0 °C and saturated with the appropriate olefin; 2

equiv. of $NaHCO_3$ and 4 equiv. of $ArNH_2$ were then added. After stirring the mixture for 3 h, the precipitate was filtered off and the filtrate was concentrated to dryness under reduced pressure. A beige solid was obtained, which was recrystallized from CH_2Cl_2/diethyl ether.

[Pd(PNP)(CH_2CH_2NHPh)]BF_4 (26): Yield 87%. – $C_{39}H_{37}BF_4N_2P_2Pd{\cdot}0.5CH_2Cl_2$ (831.31): calcd. C 57.07, H 4.60, N 3.37; found C 56.72, H 4.58, N 3.26. – ^{1}H NMR (200 MHz, CD_2Cl_2): δ = 2.09 (m, 2 H, $PdCH_2$), 2.93 (br, 2 H, CH_2N), 3.41 (br, 1 H, NHPh), 4.43 (pseudo t, N_{HP} = 4.6 Hz, 4 H, PCH_2), 5.98 (d, J_{HH} = 7.6 Hz, 2 H, NPh_o), 6.54 (t, J_{HH} = 7.4 Hz, 1 H, NPh_p), 6.92 (t, J_{HH} = 7.4 Hz, 2 H, NPh_m), 7.53–7.88 (m, 22 H, Ph, py), 7.94 (t, J_{HH} = 7.2 Hz, 1 H, py-4). – ^{31}P NMR (81 MHz, CH_2Cl_2): δ = 23.8 (s).

[Pd(PNP)($CH_2CH_2NHC_6H_4OMe$-*p*)]BF_4 (29): Yield 80%. – ^{1}H NMR (200 MHz, $CDCl_3$): δ = 2.05 (m, 2 H, $PdCH_2$), 2.86 (br, 2 H, NCH_2), 3.07 (br, 1 H, NH), 3.68 (s, 3 H, CH_3) 4.45 (pseudo t, N_{HP} = 4.8 Hz, 4 H, PCH_2), 5.95 (d, J_{HH} = 9.2 Hz, 2 H, NC_6H_4), 6.54 (d, J_{HH} = 9.2 Hz, 2 H, NC_6H_4), 7.50–7.82 (m, 23 H, Ph, py). – ^{31}P NMR (81 MHz, CH_2Cl_2): δ = 23.6 (s).

[Pd(PNP)($CH_2CH_2NHC_6H_4Me$-*p*)]BF_4 (30): Yield 84%. – ^{1}H NMR (200 MHz, $CDCl_3$): δ = 2.05 (m, 2 H, $PdCH_2$), 2.15 (s, 3 H, CH_3), 2.89 (br, 2 H, NCH_2), 3.19 (br, 1 H, NH), 4.44 (pseudo t, N_{HP} = 4.6 Hz, 4 H, PCH_2), 5.80 (d, J_{HH} = 8.2 Hz, 2 H, NC_6H_4), 6.73 (d, J_{HH} = 8.2 Hz, 2 H, NC_6H_4), 7.49–7.74 (m, 23 H, Ph, py). – ^{31}P NMR (81 MHz, CH_2Cl_2): δ = 23.6 (s).

[Pd(PNP)($CH_2CH_2NHC_6H_4Cl$-*m*)]BF_4 (31): Yield 81%. – ^{1}H NMR (200 MHz, $CDCl_3$): δ = 2.03 (m, 2 H, $PdCH_2$), 2.79 (br, 2 H, CH_2N), 3.50 (br, 1 H, NH), 4.45 (pseudo t, N_{HP} = 4.2 Hz, 4 H, PCH_2), 5.88 (m, 2 H, NC_6H_4Cl), 6.48 (d, J_{HH} = 8.2 Hz, 1 H, NC_6H_4Cl), 6.81 (t, J_{HH} = 8.4 Hz, 1 H, NC_6H_4Cl), 7.52–7.72 (m, 23 H, Ph, py). – ^{31}P NMR (81 MHz, CH_2Cl_2): δ = 23.6 (s).

[Pd(PNP)($CH_2CH_2NHC_6H_4Cl$-*o*)]BF_4 (32): Yield 81%. – $C_{39}H_{36}BF_4N_2P_2Pd \cdot 1.5\,CH_2Cl_2$ (950.68): calcd. C 51.11, H 4.13, N 2.94; found C 50.76, H 4.01, N 2.86. – ^{1}H NMR (200 MHz, $CDCl_3$): δ = 2.09 (m, 2 H, $PdCH_2$), 2.94 (br, 2 H, CH_2N), 4.03 (br t, J_{HH} = 5.0 Hz, 1 H, NH), 4.46 (pseudo t, N_{HP} = 4.8 Hz, 4 H, PCH_2), 5.78 (d, J_{HH} = 8.0 Hz, 1 H, NC_6H_4Cl), 6.48 (d, J_{HH} = 7.8 Hz, 1 H, NC_6H_4Cl), 6.78 (t, J_{HH} = 8.0 Hz, 1 H, NC_6H_4Cl), 7.11 (d, J_{HH} = 7.8 Hz, 1 H, NC_6H_4Cl), 7.46–7.83 (m, 23 H, Ph, py).

[Pd(PNP){$CH_2CH(Me)NHPh$}]BF_4 (28): Yield 83%. – ^{1}H NMR (250 MHz, CD_2Cl_2): δ = 0.84 (d, J_{HH} = 6.3 Hz, 3 H, CH_3), 1.94 (m, 1 H, CH_2), 2.20 (m, 1 H, CH_2), 3.12 (d, J_{HH} = 9.1 Hz, 1 H, NH), 3.27 (m, 1 H, CH), 4.39 (pseudo t, N_{HP} = 4.7 Hz, 4 H, PCH_2), 5.87 (d, J_{HH} = 7.8 Hz, 2 H, NPh), 6.53 (t, J_{HH} = 7.5 Hz, 1 H, NPh), 6.87 (t, J_{HH} = 7.8 Hz, 2 H, NPh), 7.48–7.75 (m, 22 H, PPh, py-3,5), 7.95 (t, 1 H, py-4).

[Pd(PNP){$CH_2CH(Me)NHC_6H_4Me$-*p*}]BF_4 (33): Yield 86%. – ^{1}H NMR (200 MHz, CD_2Cl_3): δ = 0.83 (d, J_{HH} = 7.0 Hz, 3 H, CH_3), 1.92 (m, 1 H, CH_2), 2.15 (s, 3 H, CH_3) 2.20 (m, 1 H, CH_2), 2.96 (d, J_{HH} = 9.0 Hz, 1 H, NH), 3.24 (m, 1 H, CH), 4.38 (pseudo-t, N_{HP} = 4.5 Hz, 4 H, PCH_2), 5.82 (d, J_{HH} = 7.1 Hz, 2 H, NC_6H_4), 6.71 (d, J_{HH} = 7.1 Hz, 2 H, NC_6H_4), 7.50–7.95 (m, 23 H, PPh, py).

[Pd(PNP)($CH_2CH(Me)NHC_6H_4Cl$-*o*)]BF_4 (34): Yield 81%. – ^{1}H NMR (200 MHz, $CDCl_3$): δ = 0.85 (d, J_{HH} = 6.2 Hz, 3 H, CH_3), 1.89 (m, 1 H, CH_2), 2.21 (m, 1 H, CH_2), 3.27 (m, 1 H, CH), 3.93 (d, J_{HH} = 9.0 Hz, 1 H, NH), 4.46 (pseudo t, N_{HP} = 4.6 Hz, 4 H, PCH_2), 5.74 (d, J_{HH} = 7.4 Hz, 1 H, NC_6H_4Cl), 6.46 (t, J_{HH} = 7.0 Hz, 1 H, NC_6H_4Cl), 6.73 (t, J_{HH} = 7.8 Hz, 1 H, NC_6H_4Cl), 7.09 (d, J_{HH} = 8 Hz, 1 H, NC_6H_4Cl), 7.44–7.85 (m, 23 H, PPh, py).

Reaction of 26 with 1: To a solution of **26** (7 mg) in CD_2Cl_2 (0.6 mL) saturated with ethylene, **1** (8 mg) was added, which led to a color change to reddish. An excess of $NaHCO_3$ was added and the mixture was stirred overnight, after which it had become yellow.

27: ^{1}H NMR (200 MHz): δ = 1.74 (m, 4 H, $PdCH_2$), 2.78 (t br, J = 7.8 Hz, 4 H, CH_2N), 4.35 (pseudo-t, N_{HP} = 4.8 Hz, 8 H, PCH_2), 5.73 (d, J_{HH} = 8.0 Hz, 2 H, NPh_o), 6.33 (t, J_{HH} = 7.2 Hz, 1 H, NPh_p), 6.62 (t, J_{HH} = 7.2 Hz, 1 H, NPh_m), 7.41–7.96 (m, 46 H, Ph, py).

Equilibrium Constant Determinations: The equilibrium constants for the exchange and addition reactions were determined by ^{1}H NMR analysis of equilibrium mixtures at 298 K (methanol addition reactions) or 283 K (all other cases) in CD_2Cl_2 or CD_2Cl_2/CD_3NO_2 (4:1) solution (c = 7–15 mM). With one exception (addition of Me_2NH to propene complex **2**), the reported values are the average result of three measurements run at different olefin or ligand concentrations. Very unbalanced exchange equilibria [e.g. Equation (11)] were handled by treating a solution of the most stable complex with a large excess of the exchanging ligand. The amine addition equilibria (olefin "insertion"[23]) were handled by treating a solution of the pure [Pd(PNP)(amine)]$(BF_4)_2$ complex (**19** or **25**) with an excess of the olefin. In this approach, the amount of free amine in the solution was made negligible and hence the simultaneous occurrence of proton-transfer equilibria to the free base could also be neglected. For the ligand-exchange reactions solutions (0.015 M) of **2**–**5** [Equation (3)], **1** [Equation (4), L = H_2O], and **25** [Equation (11)] were prepared and treated with an excess of the appropriate substituting ligand. In the case of the ethylene/MeCN exchange [Equation (4)], a solution of **8** was treated with a large excess of ethylene. The equilibrium constant for the $PhNH_2/Me_2NH$ exchange [Equation (12)] could not be determined directly because of an overlapping of all the relevant signals of the four species. Therefore, the constants of two further auxiliary equilibria were measured, involving the exchanges pyridine/Me_2NH (K = 1 in CD_2Cl_2) and $PhNH_2$/pyridine ($K = 4{\cdot}10^{-4}$ in CD_2Cl_2/CD_3NO_2).

Acknowledgments

We thank the Deutsche Akademie der Naturforscher Leopoldina (BMBF-LPD 9801-4) (C. H.) and the MURST (PRIN 9803243241) for financial support. We also thank the CIMCF, Università di Napoli "Federico II" for providing access to NMR facilities. We are grateful to Prof. D. Steinborn for helpful discussions.

[1] [1a] R. F. Heck, *Palladium Reagents in Organic Synthesis*, Academic Press, New York, **1985**. – [1b] J. Tsuji, *Palladium Reagents and Catalysts: Innovation in Organic Synthesis*, Wiley, Chichester, **1995**.

[2] [2a] B. Åkermark, J.-E. Bäckvall, K. Zetterberg, *Acta Chem. Scand.* **1982**, *B36*, 577–585. – [2b] J.-E. Bäckvall, E. E. Björkman, *J. Org. Chem.* **1980**, *45*, 2893–2898. – [2c] J.-E. Bäckvall, S. Byström, *J. Org. Chem.* **1982**, *47*, 1126–1128. – [2d] N. Oshima, Y. Hamatani, H. Fukui, H. Suzuki, Y. Moro-Oka, *J. Organomet. Chem.* **1986**, *303*, C21–C24. – [2e] K. F. McDaniel, in: *Comprehensive Organometallic Chemistry II* (Eds.: E. W. Abel, A. Stone, G. Wilkinson), Pergamon Press, London, **1995**, vol. 12, pp. 601–622. – [2f] J. P. Collman, L. S. Hegedus, J. R. Norton, R. G. Finke, *Principles and Application of Organotransition Metal Chemistry*, University Science Books, Mill Valley, CA, **1987**, pp. 410–415.

[3] [3a] T. E. Müller, M. Beller, *Chem. Rev.* **1998**, *98*, 675−703. − [3b] R. Taube, in: *Applied Homogeneous Catalysis with Organometallic Compounds* (Eds.: B. Cornils, W. A. Herrmann), VCH, Weinheim, **1996**, vol. 1, pp. 507−520. − [3c] H. M. Senn, P. E. Blöchl, A. Togni, *J. Am. Chem. Soc.* **2000**, *122*, 4098−4107.

[4] [4a] G. Annibale, L. Maresca, G. Natile, A. Tiripicchio, M. Tiripicchio Camellini, *J. Chem. Soc., Dalton Trans.* **1982**, 1587−1591. − [4b] S. Sasaki, K. Maruta, K. Ohkubo, *Inorg. Chem.* **1987**, *26*, 2499−2505.

[5] [5a] L. K. Johnson, S. Mecking, M. Brookhart, *J. Am. Chem. Soc.* **1996**, *118*, 267−268. − [5b] L. K. Johnson, C. M. Killian, M. Brookhart, *J. Am. Chem. Soc.* **1995**, *117*, 6414.

[6] [6a] E. Drent, P. H. M. Budzelaar, *Chem. Rev.* **1996**, *96*, 663−681. − [6b] E. Drent, W. W. Jager, *Polym. Mater. Sci. Eng.* **1997**, *76*, 100−104.

[7] Dicationic Pd^{II} complexes of the chelating olefin 1,5-cyclooctadiene have been reported: [7a] R. Roulet, R. Vouillamoz, *Helv. Chim. Acta* **1974**, *57*, 2139−2140. − [7b] E. Rotondo, G. Tresoldi, F. Faraone, R. Pietropaolo, *Inorg. Chem.* **1976**, *15*, 2102−2107.

[8] C. Hahn, A. Vitagliano, F. Giordano, R. Taube, *Organometallics* **1998**, *17*, 2060−2066.

[9] W. V. Dahlhoff, S. M. Nelson, *J. Chem. Soc. A* **1971**, 2184−2190.

[10] While alkylpalladium species stabilized by chelation are well known,[11] β-functionalized open-chain (alkyl)Pd^{II} derivatives are limited to coordinatively saturated species[12] and to the recently isolated $[Pd(PMe_3)_2(CH_2CH_2Y)Br]$ (Y = CO_2Me, CN).[13]

[11] A. J. Canty, in: *Comprehensive Organometallic Chemistry II* (Eds.: E. W. Abel, A. Stone, G. Wilkinson), Pergamon Press, London, **1995**, vol. 9, pp. 225−290.

[12] [12a] H. Kurosawa, N. Asada, *Tetrahedron Lett.* **1979**, *3*, 255−256. − [12b] T. Majima, H. Kurosawa, *J. Chem. Soc., Chem. Commun.* **1977**, 610−611.

[13] Y. Kayaki, I. Shimizu, A. Yamamoto, *Chem. Lett.* **1995**, 1089−1090.

[14] G. Vasapollo, C. F. Nobile, A. Sacco, *J. Organomet. Chem.* **1985**, *296*, 435−441.

[15] C. Hahn, J. Sieler, R. Taube, *Chem. Ber.* **1997**, *130*, 939−945.

[16] H. Kurosawa, T. Majima, N. Asada, *J. Am. Chem. Soc.* **1980**, *102*, 6996−7003.

[17] [17a]E. Ban, R. P. Hughes, J. Powell, *J. Organomet. Chem.* **1974**, *69*, 455−472.[17b] W. Partenheimer, B. Durham, *J. Am. Chem. Soc.* **1974**, *96*, 3800−3805.

[18] [18a] M. Herberhold, in: *Metal π-Complexes*, Elsevier Science Publ. Co., Amsterdam, London, New York, **1974**, vol. 2, part II, p. 126. − [18b] M. E. Cucciolito, V. De Felice, A. Panunzi, A. Vitagliano, *Organometallics* **1989**, *8*, 1180−1187.

[19] The ^1H NMR spectrum of **16** shows three multiplets (1 H each) at δ = 3.05, 2.20, and 1.67, and a doublet (3 H) at δ = 0.68, which can be assigned to the $-CH_2CH(Me)-$ fragment, the most downfield signal being attributable to a −CH−O fragment. In a homodecoupling experiment, irradiation of the signal at δ = 3.05 led to decoupling of the methyl doublet at δ = 0.68, thus unambiguously assigning the former to the C*H*Me proton and thereby pointing to a structure corresponding to a Markovnikov addition (**16**). In the ^1H NMR spectrum of **17**, two multiplets at δ = 2.00 and 2.19 are seen for the $Pd-CH_2$ moiety, while a multiplet at δ = 3.78 (1 H) can be assigned to the C*H*Ph fragment to which the methoxy group is bound.

[20] The best way of establishing the stereochemistry of the addition would be an X-ray structure determination of either **18a** or **18b**, but as yet we have been unable to obtain suitable crystals of the complexes. The methine H−H coupling constants (7.1 and 9.1 Hz, respectively, in CD_3OD) could also be useful for this purpose, but only in conjunction with a detailed theoretical study aimed at establishing the conformational distribution of the species. To be reliable, such a QM/MM investigation should take in account the interactions with the solvent and the counterion, which is beyond the scope of the present paper and might be worthy of a separate study.

[21] [21a] J. E. Bäckvall, B. Åkermark, S. O. Ljunggren, *J. Am. Chem. Soc.* **1979**, *101*, 2411−2416. − [21b] J. A. Davies, in: *Comprehensive Organometallic Chemistry II* (Eds.: E. W. Abel, A. Stone, G. Wilkinson), Pergamon Press, London, **1995**, vol. 9, p. 312.

[22] C. Hahn, A. Vitagliano, unpublished results.

[23] The term "insertion" refers only to the formal outcome of the reaction and does not have any mechanistic implication. It is likely that the actual mechanism involves a (bimolecular) substitution of the amine ligand followed by external *trans* nucleophilic attack on the coordinated olefin.

[24] To confirm the assigned structure, the dinuclear complex **27** was independently prepared by the reaction of **1** with **26** in the presence of 2 equivs. of $NaHCO_3$; see Experimental Section.

[25] B. Åkermark, J. E. Bäckvall, L. S. Hegedus, K. Zetterberg, K. Siirala-Hansèn, K. Sjöberg, *J. Organomet. Chem.* **1974**, *72*, 127−138.

[26] H. B. Kraatz, D. Milnstein, *J. Organomet. Chem.* **1995**, *488*, 223−232.

[27] In the reactions of amines with *trans*-[(amine)(olefin)$PdCl_2$] complexes, the olefin displacement was found to irreversibly preclude nucleophilic addition.[25]

Received June 23, 2000
[I00251]

Imine Versus Amine Donors in Iron-Based Ethylene Polymerisation Catalysts

George J. P. Britovsek,[a] Vernon C. Gibson,*[a] Sergio Mastroianni,[a] Daniel C. H. Oakes,[a] Carl Redshaw,[a] Gregory A. Solan,[a] Andrew J. P. White,[a] and David J. Williams[a]

Keywords: Alkenes / Polymerizations / Iron / N ligands

The synthesis and characterisation of iron(II) dichloro complexes containing neutral tridentate nitrogen ligands of the type 2-arylaminoalkyl-6-aryliminoalkylpyridine [2-ArNHCR(Me)-6-ArN=CR]C_5H_3N (R = H, Ar = 2,6-*i*$Pr_2C_6H_3$ or 2,4,6-$Me_3C_6H_2$; R = Me, Ar = 2,6-*i*$Pr_2C_6H_3$)] and 2,6-bis(arylaminomethyl)pyridine [2,6-$(ArNHCH_2)_2$]C_5H_3N (Ar = 2,6-*i*$Pr_2C_6H_3$) are described and their activity in ethylene polymerisation is compared with their 2,6-bis(aryliminoalkyl)pyridine analogues.

Introduction

Transition metal-catalyzed olefin polymerisation is currently a subject of intense academic and industrial interest. The need for greater control over the products of olefin polymerisation, combined with advances in the understanding of homogeneous polymerisation systems, have resulted in the development of highly active single-site olefin polymerisation catalysts such as Group 4 metallocenes and the ''constrained geometry'' catalysts'.[1−5] The development of non-metallocene early transition metal catalysts, and in particular the discovery of highly active late transition metal based systems, have signposted the way forward for further developments in catalytic olefin polymerisation.[6,7] The discovery by Brookhart and co-workers in 1995 of highly active nickel and palladium olefin polymerisation catalysts containing the α-diimine ligand frame[8] has been followed by extensive studies on variations of the α-diimine ligand.[9−11] In addition, many other non-diimine neutral bidentate ligands have been screened for olefin polymerisation activity, a large number by in situ methods.[7,12] However, to date, no other donor combinations have matched the high activities obtained with α-diimine ligands, suggesting a special feature of these systems that has yet to be fully understood.

A second family of highly active late transition metal polymerisation catalysts based on 2,6-bis(imino)pyridine complexes of iron and cobalt, was reported independently by ourselves,[13] Bennett and Brookhart in 1998.[14] The effects of ligand changes, especially at the aryl (Ar) and imino carbon (R) substituents, on the activity and product selectivity of these bis(imino)pyridine iron and cobalt catalysts (**I**) have been studied in detail,[15−17] as well as the polymerisation of propene[18−20] and applications in reactor blending.[21,22] Only a few variations on the core bis(imino)-pyridine skeleton have been reported; for example, a neutral tridentate bis(oxazolinyl)pyridine ligand[23] and monoanionic tridentate bis(imino)pyrollide,[24] bis(amino)phenyl and bis(phosphanyl)amide ligands.[25] These variations have resulted in very low catalyst activities. With a view to obtaining a greater understanding of structure-activity relationships in the [N,N,N]Fe catalyst system, we have targeted alternative tridentate [N,N,N] chelate ligands. A relatively straightforward modification to the ligand frame is to replace one, or both, of the imine groups by amine donors, examples being 2-aminoalkyl-6-iminoalkylpyridine complexes of type **II** and the 2,6-bis(aminoalkyl)pyridine species of type **III** (see Figure 1). The synthesis and characterisation of complexes of type **II** and **III** are described and their ethylene polymerisation activity is discussed and compared to the parent bis(imino)pyridine system **I**.

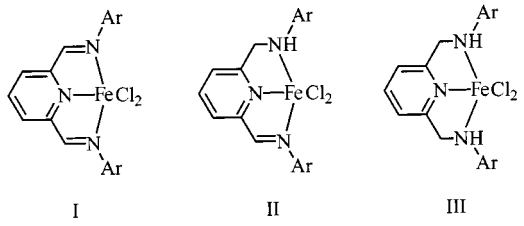

Figure 1. Pyridyldiimine (**I**), pyridylimineamine (**II**) and pyridyldiamine (**III**) iron complexes

Results and Discussion

Synthesis of ligands and complexes

A convenient method of preparing 2-aminoalkyl-6-iminoalkylpyridines is by exploiting attack by nucleophilic reagents at the imine carbon atoms.[26] We have recently shown that $AlMe_3$ reacts with bis(imino)pyridines to give products of the type {[2-ArNCR(Me)-6-ArN=CR]-C_5H_3N}$AlMe_2$ (**1a−c**, Scheme 1) in which only one of the imino functionalities is attacked to generate an amide donor.[27] Hydrolysis of these complexes, followed by extraction with pentane and workup, affords ligands **2a−c** as pale yellow crystalline solids.

[a] Department of Chemistry, Imperial College, South Kensington, London SW7 2AY, U.K.
E-mail: V.Gibson@ic.ac.uk

 © WILEY-VCH Verlag GmbH, 69451 Weinheim, 2001 1434−1948/01/0202−0431 $ 17.50+.50/0

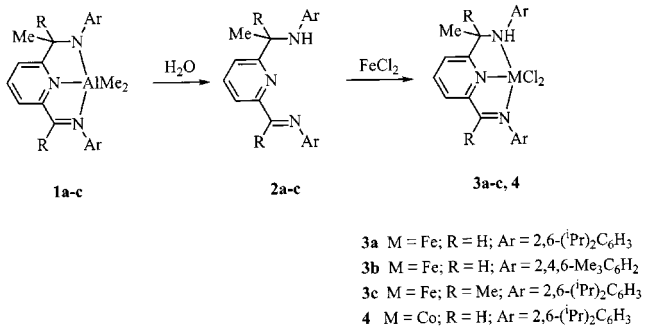

Scheme 1

The ^{1}H NMR spectra of **2a**−**c** confirm the presence of the amine protons as broad resonances in the range δ = 4.3−4.5, and the infrared spectra show N−H stretches in the region 3355−3365 cm^{-1}. A single crystal X-ray structure of **2a** shows the molecule to possess a *transoid* relationship between the imine and amine groups (Figure 2), a geometry that is different to the *cisoid* conformation in the metal complexes (see **3a**, Figure 3). There is only a small (ca. 7°) out-of-plane rotation of the C=N double bond relative to the pyridyl ring, whereas the 2,6-diisopropylphenyl ring system is oriented essentially orthogonally (ca. 87°). The *transoid* conformation observed here for the pyridyl imine unit is typical for such species in the solid state,[18,28,29] i.e. there has to be an approximate 180° rotation about the C(2)−C(9) bond for chelation of the pyridyl and imino nitrogen atoms to a metal centre. In contrast to the in-plane conformation of the conjugated imine group, there is a marked deviation of the saturated "amine arm" from co-planarity with the pyridyl ring, the N(1)−C(6)−C(7)−N(7) torsion angle being 65°. Centrosymmetrically related pairs of molecules pack such that the edge of ring **A** of one molecule is directed into the face of ring **B** of another; the centroid···centroid distance is 4.94 Å, and is consistent with an aromatic···aromatic edge-to-face interaction.

Treatment of **2a**−**c** with $FeCl_2$ in *n*BuOH at elevated temperature gives complexes **3a**−**c** as pale blue solids. Analogous to the bis(imino)pyridine systems, these complexes are

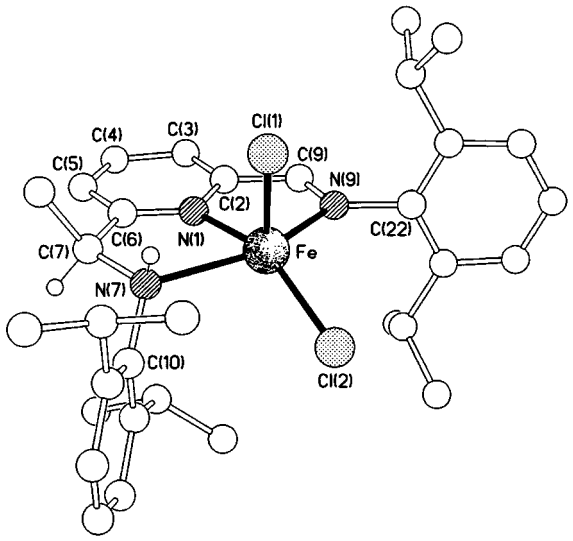

Figure 3. The molecular structure of **3a**; selected bond lengths (Å) and angles (°): Fe−N(1) 2.115(7), Fe−N(7) 2.310(8), Fe−N(9) 2.217(8), Fe−Cl(1) 2.311(3), Fe−Cl(2) 2.243(2), C(7)−N(7) 1.489(12), C(9)−N(9) 1.281(12); N(1)−Fe−N(9) 75.4(3), N(1)−Fe−Cl(2) 148.0(2), N(9)−Fe−Cl(2) 102.9(2), N(1)−Fe−N(7) 73.5(3), N(9)−Fe−N(7) 148.5(3), Cl(2)−Fe−N(7) 101.2(2), N(1)−Fe−Cl(1) 102.8(2), N(9)−Fe−Cl(1) 102.3(2), Cl(2)−Fe−Cl(1) 108.6(1), N(7)−Fe−Cl(1) 88.8(2)

paramagnetic, with μ_{eff} typically between 5.4 and 5.6 BM, indicating four unpaired electrons; they were further characterized by IR, MS and microanalysis. The IR spectra of **3a**−**c** show ν(N−H) stretches at ca. 3300 cm^{-1}. Crystals of **3a** suitable for a single crystal structure determination were grown from a concentrated acetonitrile solution. The X-ray analysis of **3a** shows[30] (Figure 3) that the partially saturated ligand (**2a**) complexes to the iron(II) centre in a similar way to its unsaturated analogue,[13,14] the N(7)−C(7)−py−C(9)−N(9) component being co-planar to within 0.07 Å, with the iron atom lying 0.07 Å out of this plane. The five-membered chelate ring containing the amino nitrogen atom N(7) is also almost planar, the torsional twist about the C(6)−C(7) bond being only ca. 6°. The geometry at iron is distorted square pyramidal with *cis* angles in the range 73.5(3) to 108.6(1)°, the iron atom lying 0.43

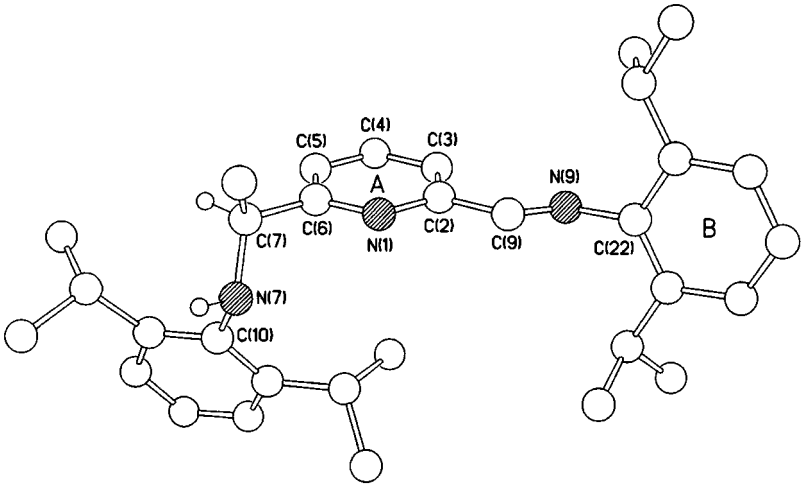

Figure 2. The molecular structure of **2a**; selected bond lengths (Å): C(7)−N(7) 1.473(8), C(9)−N(9) 1.255(8)

Å out of the basal plane in the direction of the apical atom Cl(1). The most noticeable feature in the pattern of bonding is the weak nature of the Fe−N(7) linkage [2.310(8) Å] — a distance equal to that to the apical chlorine centre Cl(1) [2.311(3) Å] — and a consequent shortening of the Fe−N(9) bond to 2.217(8) Å {*cf.* 2.238(4) and 2.250(4) Å in the related bis(imino)pyridine iron dichloride species[13−15]}. The Fe−N(1) bond length is, as expected, shorter at 2.115(7) Å, as is the distance to the basal chlorine [2.243(2) Å]. Both of the 2,6-diisopropylphenyl substituents are oriented approximately orthogonally to the basal coordination plane, the ca. 81° twist about the N(9)−C(22) bond facilitating characteristic C−H···N(pπ) interactions[31] between the isopropyl methine hydrogen atoms and the imine nitrogen [N(9)]; the H···N distances are 2.41 and 2.44 Å. The amine nature (i.e. sp^3 hybridisation) of the N(7) nitrogen precludes any such interaction here, and results in a distinct folding of the C(10) aryl substituent out of the N(7)−C(7)−py−C(9)−N(9) plane — the C(22) phenyl carbon atom is virtually coplanar with this plane (deviation ca. 0.03 Å) whilst C(10) lies 1.06 Å below it, such that the N−Ar bond is inclined by ca. 42° to this plane. This deviation will strongly affect the steric influence of the ligand on the remaining metal coordination sites. Finally, there are no dominant intermolecular interactions of note, although there is evidence for a weak C−H···Cl hydrogen bond between the imine C−H group [C(9)] in one molecule and the apical chorine [Cl(1)] in another; the C···Cl and H···Cl distances are 3.34 and 2.57 Å, respectively, with a C−H···Cl angle of 137°.

2,6-Bis(2,6-diisopropylphenylaminomethyl)pyridine **(5)** (see Scheme 2) was readily prepared according to a procedure by McConville and co-workers, from the reaction of 2,6-bis(bromomethyl)pyridine with LiNHAr (Ar = 2,6-diisopropylphenyl).[32] However, this potentially tridentate chelate does not react with anhydrous $FeCl_2$ in *n*BuOH, nor in THF; there is no colour change on mixing and warming to 80 °C, and after workup, only starting materials are recovered. In case this outcome may have been a consequence of the modified disposition of the large aryl groups imposed by the sp^3-hybridised nitrogen centres, we also attempted a similar reaction between 2,6-bis(diphenylaminomethyl)pyridine and $FeCl_2$ but again complexation did not occur. An alternative method, recently described by Calderazzo et al.,[33] was investigated by refluxing a mixture of pyridyldiamine ligand **5** and $FeCl_2$·thf in toluene overnight. This route leads to the desired complex **6** in high yield as blue/green crystals (Scheme 2). The compound is air stable and readily soluble in polar solvents such as dichloromethane or THF, but decomposes in acetone. Satisfactory microanalysis, IR and magnetic data (μ_{eff} = 5.08 BM) as well as X-ray crystallographic analysis confirm the structure of **6** to be the expected five-coordinate [N,N,N]$FeCl_2$ complex.

Depending upon the method of crystallization, two different crystalline forms are produced, one monoclinic (**6a**, Figure 4), obtained from a hot saturated toluene solution and the other orthorhombic (**6b**, Figure 5), grown from cold (−30 °C) toluene. In the monoclinic form, the ligand is tridentate, binding to the iron centre through the pyridyl and the two amine nitrogen atoms in a fashion analogous to that seen in the imine/amine complex **3a**. The geometry at iron is still distorted square pyramidal, but with the iron atom lying 0.61 Å out of the basal plane; the *cis* angles are in the range 74.2(1) to 115.6(1)°. The two five-membered chelate rings are nonplanar, there being torsional twists of ca. 26 and 18° about the C(2)−C(7) and C(6)−C(8) bonds, respectively. Interestingly, these twists are in opposite senses, thus producing δ and λ conformations, respectively, for the two rings, whereas the configurations at the two amino centres are the same. As expected, the Fe−N(1) distance [2.118(4) Å] is significantly shorter than that to the two amine nitrogens, which are the same at 2.313(4) and 2.328(4) Å for N(7) and N(8), respectively, values essentially the same as that to the amino nitrogen in **3a**. Similarly, the Fe−Cl(axial) distance [2.313(2) Å] is longer than its basal counterpart [2.269(2) Å]. In common with **3a**, the two 2,6-diisopropylphenyl ring systems are oriented approximately orthogonally to the basal coordination plane. Although both the amine nitrogen atoms N(7) and N(8) are pyramidal, as a consequence of the different folds of the five-membered chelate rings only one of the 2,6-diisopropylphenyl rings is folded out of the basal coordination plane, the other having its N(7)−C(9) linkage virtually in plane. This results in an overall geometry very similar to that seen in the imine-amine structure **3a**. The only intermolecular packing interaction of note is a weak π-π stacking of pairs of C(21) containing 2,6-diisopropylphenyl rings of adjacent molecules; the mean interplanar separation is 3.85 Å.

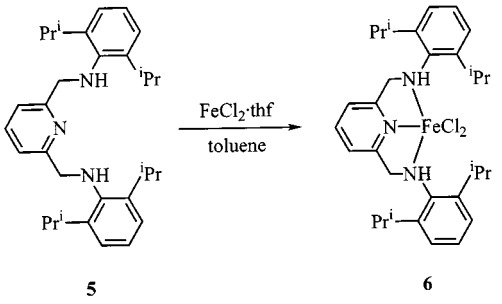

5 **6**

Scheme 2

The orthorhombic form of the complex **(6b)** has crystallographic C_2 symmetry about an axis passing along the Fe···N(1)···C(4) vector. The conformations of the two five-membered chelate rings are both λ relative to the *S* configurations at the amino centres (Figure 5); the torsional twists about the C(2)−C(5) bonds are ca. 17°. Accompanying this difference in the conformational/configurational relationship (*cf.* that in **6a**) is a change from a square pyramidal to a trigonal bipyramidal coordination geometry for the iron with N(1), Cl and ClA forming the equatorial plane. The angles subtended at iron by these three atoms are all, within statistical significance, 120°; the axial bonds [Fe−N(5)] subtend an angle of 153.8(2)°. The Fe−N(1) and Fe−N(5) bond lengths [2.095(5) and 2.322(4) Å, respectively] do not differ significantly from those in **6a**. In contrast to the asymmetric Fe−Cl bond lengths in **3a** and **6a**, here they are

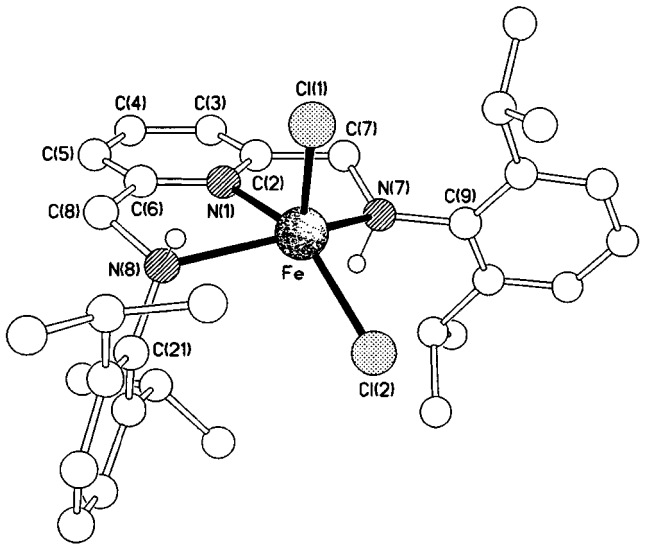

Figure 4. The molecular structure of the monoclinic form of **6** (**6a**) showing also the square pyramidal geometry at iron; selected bond lengths (Å) and angles (°): Fe−N(1) 2.118(4), Fe−N(7) 2.313(4), Fe−N(8) 2.328(4), Fe−Cl(1) 2.313(2), Fe−Cl(2) 2.269(2), C(7)−N(7) 1.445(6), C(8)−N(8) 1.507(6); N(1)−Fe−Cl(2) 142.87(12), N(1)−Fe−N(7) 74.16(14), Cl(2)−Fe−N(7) 91.09(12), N(1)−Fe−Cl(1) 103.32(12), Cl(2)−Fe−Cl(1) 113.75(7), N(7)−Fe−Cl(1) 115.61(14), N(1)−Fe−N(8) 76.48(14), Cl(2)−Fe−N(8) 101.42(11), N(7)−Fe−N(8) 145.2(2), Cl(1)−Fe−N(8) 88.94(12)

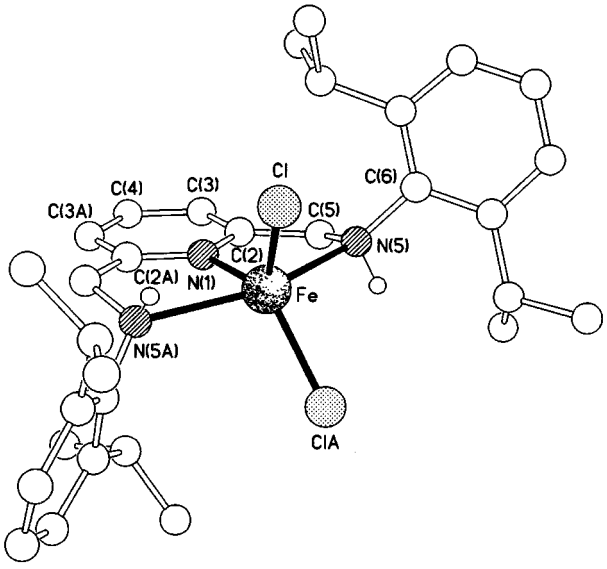

Figure 5. The molecular structure of the orthorhombic form of **6** (**6b**) showing also the trigonal bipyramidal geometry at iron; selected bond lengths (Å) and angles (°): Fe−N(1) 2.095(5), Fe−N(5) 2.322(4), Fe−Cl 2.277(2), C(5)−N(5) 1.479(6); N(1)−Fe−Cl 120.03(5), N(1)−Fe−ClA 120.03(5), Cl−Fe−ClA 119.94(9), N(1)−Fe−N(5A) 76.91(10), Cl−Fe−N(5A) 90.80(12), ClA−Fe−N(5A) 102.29(12), N(1)−Fe−N(5) 76.91(10), Cl−Fe−N(5) 102.29(12), ClA−Fe−N(5) 90.80(12), N(5A)−Fe−N(5) 153.8(2)

symmetric at 2.277(2) Å, there being no axial/basal distinction. The essentially orthogonal relationship between the 2,6-diisopropylphenyl ring systems and the N_3Fe coordination plane is retained, but in contrast to **6a**, because of the C_2 symmetry and the pyramidalisation at the amine nitrogens, one of the 2,6-diisopropylphenyl is directed "up" and the other "down". There are no intermolecular packing interactions of consequence.

For bis(imino)pyridine iron complexes we have shown previously that, depending on the aryl substituents of the ligand (e.g. 2,6-diisopropylphenyl versus mesityl), either square based pyramidal or trigonal bipyramidal geometries are observed in the solid state.[15] Here we see that, in the case of complex **6**, different geometries (**6a** and **6b**) are obtained depending on the method of crystallisation. These results suggest a small energy difference between the two geometries, indicating stereochemical nonrigidity of $[N,N,N]FeCl_2$ complexes, a behaviour that is not uncommon for five-coordinate complexes.[34]

Ethylene Polymerisation Results

The results of ethylene polymerization tests at 1 bar and 10 bar with precatalysts **3a−c**, **4** and **6** with methylaluminoxane (MAO) as activator are collected in Table 1. For comparison, the polymerisation results of the previously reported pyridyldiimine iron precatalysts **7** and **8** are also included (Figure 6). Two sets of polymerisation tests are shown in Table 1. Tests at 1 bar were carried out in a Schlenk flask at room temperature, with no scavenger and toluene as the solvent. High pressure tests (10 bar) were performed in a 1 litre autoclave at 35 °C, with triisobutylaluminium as a scavenger and isobutane as the solvent.

The results collected in Table 1 show that all of the new pyridylimine amine (**3a−c**) and pyridyldiamine (**6**) iron complexes are active ethylene polymerisation catalysts under these conditions. However, it is also apparent that the activities of these new precatalysts are dramatically reduced relative to the pyridyldiimine catalysts **7** and **8** (run 10 and 11). The highest activities of 90−110 g/mmol·h·bar are obtained with complex **3c**, which is derived from the pyridyldiketimine ligand (as in complex **8**). The precatalysts **3a** and **3b**, derived from aldimine precursors, generally show lower activities, around 20 g/mmol·h·bar. This difference in activity parallels the trends observed for aldimine (**7**) versus ketimine (**8**) precatalysts based on pyridyldiimine ligands (runs 10 and 11).[15] The very low activity observed for the pyridylimine amine cobalt precursor **4** (run 7) compared to the iron analogue **3a** (run 1) is equally not surprising, bearing in mind that, in general, for pyridyldiimine systems, cobalt precatalysts are an order of magnitude less active than their iron counterparts. Substitution of both imine donors for amine donors as in precatalyst **6** leads to a further decrease in activity, typically to around 10 g/mmol·h·bar. A similar behaviour of diimine versus diamine donors is observed in nickel ethylene polymerisation systems, where the saturated bis(2,6-diisopropylphenyl)ethylene diamine ligand showed only very low activity relative to the α-diimine analogue.[12]

Previously we have shown for pyridyldiimine iron polymerisation catalyst **8**, that the rate of propagation is first order in ethylene, resulting in a linear increase of the yield of polyethylene with pressure.[15] Although we have not carried out a systematic study of the effect of pressure on these new pyridylimine amine systems, the results in Table 1 show

Table 1. Results of ethylene polymerization runs using precatalysts **3a−c**, **4**, **6−8**

Run	Precatalyst (μmol)	Activator (mmol/equiv.)	T (C)	P (bar)	Yield (g)	Activity (g mmol^{-1} h^{-1} bar^{-1})	M_n	M_w	M_w/M_n
1[a]	**3a** (20)	MAO (8/400)	25	1	0.4	20			
2[b]	**3a** (25)	MAO (10/400)	35	10	5.2	21	30000	210000	7.1
3[a]	**3b** (20)	MAO (8/400)	25	1	0.4	18			
4[b]	**3b** (27)	MAO (10/400)	35	10	3.7	14	21000	177000	8.4
5[a]	**3c** (20)	MAO (8/400)	25	1	2.1	90			
6[b]	**3c** (25)	MAO (10/400)	35	10	27.8	110	161000	896000	5.5
7[a]	**4** (20)	MAO (8/400)	25	1	0.06	3			
8[a]	**6** (20)	MAO (8/400)	25	1	0.21	11			
9[b]	**6** (25)	MAO (10/400)	35	10	0.70	3	3000	63000	21.1
10[c]	**7** (6)	MAO (1.2/200)	35	10	18.2	305	3400	132000	38.9
11[c]	**8** (0.5)	MAO (0.5/1000)	50	10	26.9	5340	64000	611000	9.5

[a] Schlenk-test conditions: Toluene solvent (40 mL), reaction time 1 hour. − [b] High pressure reactor conditions: Isobutane solvent (0.5 L), reaction time 1 hour, Al*i*Bu$_3$ scavenger (2 mL of a 1 M solution). − [c] Results for precatalysts **7** and **8** taken from ref.[15]

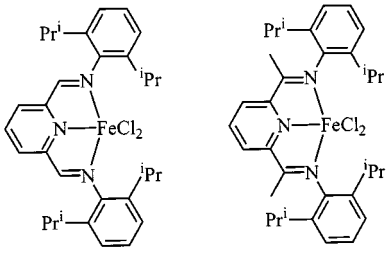

7 **8**

Figure 6. 2,6-Bis(imino)pyridine iron precatalysts **7** and **8**

the difference between 1 bar and 10 bar tests. With a tenfold increase in pressure (similar amount of catalyst in each case) an approximate tenfold increase in polymer yield is observed, suggesting that for these systems the rate of propagation is also first order in ethylene.

Molecular weight data have only been obtained for the pyridyl imine amine systems which showed moderate activity (Table 1). The M_w value for the polyethylene obtained with the ketimine-derived imine amine catalyst **3c** is comparable to the parent pyridyl diimine catalyst **8**. The aldimine-derived analogue **3a** gives a lower value for M_n and M_w than for **3c**, but follows the same trend as seen for pyridyl diimine systems (cf. Runs 2 and 6 versus 10 and 11), including a negligible difference between 2,6-diisopropyl and mesityl substituents (**3a** versus **3b**, runs 2 and 4).

In conclusion, we have synthesized and characterized a series of complexes containing neutral tridentate [N,N,N] ligands. The 2-aminoalkyl-6-iminoalkyl-pyridine iron complexes of type **II** (Figure 1) show moderate activity in ethylene polymerisation, whereas a 2,6-bis(alkylamino)pyridyl iron complex of type **III** shows only low activity. Interestingly, although the activities are significantly lower than the related pyridyldiimine catalysts, similar trends upon ligand variation, both in activity as well as in polymer properties, are observed. A possible reason for the lower activity relative to bis(imino)pyridine systems is the weakness of the amino-iron interaction, which may lead to dissociation of the amine arm in these catalysts. However, the lack of conjugation through the ligand backbone may also be significant, as may the orientation of the amino aryl substituent in hindering access of monomer to the active site or growth of the polymer chain.

Experimental Section

General: All manipulations were carried out under an atmosphere of nitrogen using standard Schlenk and cannula techniques or in a conventional nitrogen-filled glove-box. Solvents were refluxed over an appropriate drying agent, and distilled and degassed prior to use. Elemental analyses were performed by the microanalytical services of the Department of Chemistry at Imperial College, Medac Ltd. or SACS at the University of North London. NMR spectra were recorded on a Bruker spectrometer at 250 MHz (^{1}H), and 62.9 MHz (^{13}C) at 293 K; chemical shifts are referenced to the residual protio impurity of the deuterated solvent; coupling constants are quoted in Hz. Mass spectra were obtained using either Fast Atom Bombardment (FAB), Electron Impact (EI) or Chemical Ionization (CI). Magnetic susceptibility studies were performed using an Evans balance or the Evans NMR method (solvent CD_2Cl_2; reference: cyclohexane).

Materials: The ligands 2,6-bis[(2,6-diisopropylphenylimino)methyl-]pyridine,[15] and 2,6-bis[(2,6-diisopropylphenylamino)methyl]pyridine (**5**),[32] as well as pyridinedicarboxaldehyde,[35] $FeCl_2$·thf[33] and the aluminium complexes **1a−c**[27] were prepared according to established procedures while 2,6-diacetylpyridine, MAO (10% solution in toluene) and all anilines were purchased from Aldrich Chemical Co. All other chemicals were obtained commercially and used as received unless stated otherwise.

Synthesis of Ligands and Complexes

6-[(2,6-Diisopropylphenylamino)-1-ethyl]-2-[(2,6-diisopropylphenylimino)methyl]pyridine (2a): Pentane (40 mL) was added to [C_5NH_3{CH=N(2,6-*i*Pr$_2$-C$_6$H$_3$)}{CHMeN(2,6-*i*Pr$_2$-C$_6$H$_3$)}]AlMe$_2$ (**1a**; 5.79 g, 11.0 mmol) followed by slow addition of an equal volume of water. After stirring for a further 3 h the pentane was stripped off. The aqueous phase was then extracted into chloroform (3 × 30 mL), filtered, dried over $MgSO_4$ and taken to dryness to give analytically pure [C_5NH_3{CH=N(2,6-*i*Pr$_2$-C$_6$H$_3$)}-{CHMeNH(2,6-*i*Pr$_2$-C$_6$H$_3$)}] (**2a**; 4.14 g, 80%). − ^{1}H NMR ($CDCl_3$, 293 K): δ = 8.38 (s, 1 H, N=CH), 8.17 [d, ^3J(HH) = 7.7, 1 H, Py-H$_m$], 7.73 [app. t, ^3J(HH) = 7.7, 1 H, Py-H$_p$], 7.3−7.0 (m, 7 H, Ar-H, Py-H$_m$), 4.48 [d, ^3J(HH) = 10.4, 1 H, N-H], 4.3−4.4 (m, 1 H, N−CHMe), 3.31 [sept, ^3J(HH) = 6.8, 2 H, CHMe$_2$], 3.02 [sept, ^3J(HH) = 6.8, 2 H, CHMe$_2$], 1.49 [d, ^3J(HH) = 6.6, 3 H,

N−CHMe], 1.3−1.2 (m, 18 H, $CHMe_2$), 1.09 (d, 6 H, $CHMe_2$). − CI MS: m/z = 470 [$(M + H)^+$]. − IR (Nujol mull): $\tilde{\nu}$ = 3356 cm^{-1} [ν(N−H)]. − $C_{32}H_{43}N_3$ (469.71): calcd. C 81.88, H 9.17, N 8.96; found C 82.21, H 9.30, N 8.71.

Crystal Data for 2a: $C_{32}H_{43}N_3$, M = 469.7, monoclinic, space group $P2_1/c$ (no. 14), a = 16.208(2), b = 10.364(1), c = 17.664(3) Å, β = 100.67(1)°, V = 2916.1(6) $Å^3$, Z = 4, D_c = 1.070 g cm^{-3}, μ(Cu-K_α) = 4.70 cm^{-1}, F(000) = 1024, T = 293 K; clear plates, 0.23 × 0.07 × 0.02 mm, Siemens P4/RA diffractometer, ω-scans, 4065 independent reflections. The structure was solved by direct methods and the non-hydrogen atoms were refined anisotropically using full-matrix least-squares based on F^2 to give R_1 = 0.096, wR_2 = 0.191 for 1619 independent observed reflections [$|F_o| > 4\sigma(|F_o|)$, $2\theta \leq 116°$] and 317 parameters.
Crystallographic data (excluding structure factors) for this structure have been deposited with the Cambridge Crystallographic Data Centre as supplementary publication no. CCDC-149266. Copies of the data can be obtained free of charge on application to CCDC, 12 Union Road, Cambridge CB2 1EZ, UK [Fax: (internat.) + 44-1223/336-033; Email: deposit@ccdc.cam.ac.uk].

6-[(2,4,6-Trimethylphenylamino)-1-ethyl]-2-[(2,4,6-trimethylphenylimino)methyl]pyridine (2b): Prepared in the same way as described for compound **2a**, from Al complex **1b**. Yield 75%. − ^{1}H NMR ($CDCl_3$, 293 K): δ = 8.28 (s, 1 H, N=CH), 8.07 [d, ^3J(HH) = 7.8, 1 H, Py-H_m], 7.64 [app. t, ^3J(HH) = 7.8, 1 H, Py-H_p], 7.14 (d, 1 H, Py-H_m), 6.84 (s, 2 H, Ar-H), 6.70 (s, 2 H, Ar-H), 4.43 [br, q, ^3J(HH) = 6.5, 1 H, N−CHMe], 4.31 (s, br, 1 H, N−H), 2.23 (s, 3 H, Ar-Me_p), 2.18 (s, 6 H, Ar-Me_o), 2.13 (s, 3 H, Ar-Me_p), 2.07 (s, 6 H, Ar-Me_o), 1.36 (d, 3 H, NCHMe). − CI MS: m/z = 385 [$(M + H)^+$]. − IR (Nujol mull): $\tilde{\nu}$ = 3359 cm^{-1} [ν(N−H)]. − $C_{26}H_{31}N_3$ (385.55): calcd. C 81.04, H 8.05, N 10.91; found C 81.44, H 8.39, N 10.79.

6-[2-(2,6-Diisopropylphenylamino)-2-isopropyl]-2-[(2,6-diisopropylphenylimino)ethyl]pyridine (2c): Prepared in the same way as described for compound **2a**, from Al complex **1c**. Yield 71%. − ^{1}H NMR ($CDCl_3$, 293 K): δ = 8.25 [d, ^3J(HH) = 7.7, 1 H, Py−H_m], 7.79 (app. t, ^3J(HH) = 7.7, 1 H, Py-H_p), 7.59 (d, 1 H, Py-H_m), 7.2−7.0 (m, 6 H, Ar-H), 4.47 (s, br, 1 H, N−H), 3.31 [sept, ^3J(HH) = 6.7, 2 H, $CHMe_2$], 2.77 [sept, ^3J(HH) = 6.7, 2 H, $CHMe_2$], 2.24 (s, 3 H, N=CMe), 1.51 (s, 6 H, N−CMe_2), 1.17 (d, 12 H, $CHMe_2$), 1.07 (d, 12 H, $CHMe_2$). − EI MS: m/z = 497 [M^+]. − IR (Nujol mull): $\tilde{\nu}$ = 3362 cm^{-1} [ν(N−H)]. − $C_{34}H_{47}N_3$ (497.77): calcd. C 82.09, H 9.46, N 8.45; found C 82.39, H 9.71, N 8.30.

{6-[(2,6-Diisopropylphenylamino)-1-ethyl]-2-[(2,6-diisopropylphenylimino)methyl]pyridine}iron(II) Dichloride (3a): $FeCl_2$ (0.20 g, 1.57 mmol) was dissolved in hot *n*-butyl alcohol (10 mL) at 80 °C. A suspension of **2a** (0.72 g, 1.62 mmol) in *n*-butyl alcohol was added dropwise at 80 °C. The reaction mixture turned blue. After stirring at 80 °C for 15 minutes the reaction was allowed to cool to room temperature. The reaction volume was then reduced to a few millilitres and diethyl ether added to precipitate [C_5NH_3{CH=N(2,6-iPr_2-C_6H_3)}{CHMeNH(2,6-iPr_2-C_6H_3)}]$FeCl_2$ (**3a**; 0.76 g, 83%) as a blue powder, which was subsequently washed three times with diethyl ether (10 mL). − μ_{eff} (Evans Balance): 5.6 BM. − IR (Nujol): $\tilde{\nu}$ = 3303 cm^{-1} [ν(N−H)]. − FAB MS: m/z = 596 [M^+], 560 [M^+ − Cl]. − $C_{32}H_{43}N_3FeCl_2$ (596.46): calcd. C 64.43, H 7.21, N 7.05; found C 64.70, H 7.19, N 6.99.

Crystal Data for 3a: $C_{32}H_{43}Cl_2N_3Fe$, M = 596.4, orthorhombic, space group $P2_12_12_1$ (no. 19), a = 13.433(2), b = 13.449(3), c = 18.624(3) Å, V = 3365(1) $Å^3$, Z = 4, D_c = 1.177 g cm^{-3}, μ(Mo-K_α) = 6.30 cm^{-1}, F(000) = 1264, T = 293 K; deep red blocks, 0.57 × 0.40 × 0.23 mm, Siemens P4/PC diffractometer, ω-scans, 3302 independent reflections. The structure was solved by direct methods and the non-hydrogen atoms were refined anisotropically using full-matrix least-squares based on F^2 to give R_1 = 0.065, wR_2 = 0.113 for 1968 independent observed absorption corrected reflections [$|F_o| > 4\sigma(|F_o|)$, $2\theta \leq 50°$] and 347 parameters. The absolute chirality of **3a** (which undergoes spontaneous resolution upon crystallisation) was determined by an R-factor test [R_1^+ = 0.0648, R_1^- = 0.0666].
Crystallographic data (excluding structure factors) for this structure have been deposited with the Cambridge Crystallographic Data Centre as supplementary publication no. CCDC-149267. Copies of the data can be obtained free of charge on application to CCDC, 12 Union Road, Cambridge CB2 1EZ, UK [Fax: (internat.) + 44-1223/336-033; Email: deposit@ccdc.cam.ac.uk].

{6-[(2,4,6-Trimethylphenylamino)-1-ethyl]-2-[(2,4,6-trimethylphenylimino)methyl]pyridine}iron(II) Dichloride (3b): Complex **3b** was prepared by an analogous route to that outlined for complex **3a** from $FeCl_2$ (0.15 g, 1.18 mmol) and ligand **2b** (0.44 g, 1.18 mmol). Yield: 0.46 g, 80%. − μ_{eff} (Evans Balance): 5.4 BM. − IR (Nujol): $\tilde{\nu}$ = 3307 cm^{-1} [ν(N−H)]. − FAB MS: m/z = 511 [M^+], 476 [M^+ − Cl]. − $C_{26}H_{31}Cl_2N_3Fe$ (512.30): calcd. C 60.94, H 6.05, N 8.20; found C 60.11, H 6.12, N 7.98.

{6-[2-(2,6-Diisopropylphenylamino)-2-isopropyl]-2-[(2,6-diisopropylphenylimino)ethyl]pyridine}iron(II) Dichloride (3c): Complex **3c** was prepared by an analogous route to that outlined for **3a** from $FeCl_2$ (0.15 g, 1.18 mmol) and **2c** (0.59 g, 1.18 mmol). Yield: 0.46 g, 62%. − μ_{eff} (Evans Balance): 5.6 BM. − IR (Nujol): $\tilde{\nu}$ = 3301 cm^{-1} [ν(N−H)]. − FAB MS: m/z = 623 [M^+], 588 [M^+ − Cl]. − $C_{34}H_{47}Cl_2N_3Fe$ (624.52): calcd. C 65.38, H 7.53, N 6.73; found C 65.31, H 7.89, N 7.31.

{6-[(2,6-Diisopropylphenylamino)-1-ethyl]-2-[(2,6-diisopropylphenylimino)methyl]pyridine}cobalt(II) Dichloride (4): Complex **4**[30] was prepared by an analogous route to that outlined for **3a** from $CoCl_2$ (0.15 g, 1.15 mmol) and **2a** (0.54 g, 1.15 mmol). Yield: 0.48 g, 70%. − μ_{eff}(Evans Balance): 4.6 BM. − IR (Nujol mull): $\tilde{\nu}$ = 3304 cm^{-1} [ν(N−H)]. − FAB MS: m/z = 599 [M^+], 563 [M^+ − Cl], 528 [M^+ −2Cl].

[2,6-Bis(2,6-diisopropylphenylaminomethyl)pyridine]iron(II) Dichloride (6): A suspension of the pyridyldiamine ligand **5** (0.45 g; 1.0 mmol) and $FeCl_2$·thf (1 equiv.) in toluene (50 mL) was refluxed overnight. Upon cooling to room temperature, the product precipitated as blue/green crystals (**6a**), which were washed with toluene and pentane and dried in vacuo. Another batch of crystals were grown from a saturated toluene solution at −30 °C (**6b**). Yield: 0.51 g (87%). − μ_{eff} (Evans NMR method): 5.08 BM. − $C_{31}H_{43}N_3FeCl_2$·0.5thf (620.51): calcd. C 63.88, H 7.63, N 6.77; found C 64.07, H 7.77, N 6.52.

Crystal Data for 6a (monoclinic form): $C_{31}H_{43}N_3Cl_2Fe$·0.5C_7H_8, M = 630.5, monoclinic, space group $P2_1/n$ (no. 14), a = 9.789(2), b = 14.750(4), c = 24.757(3) Å, β = 95.79(1)°, V = 3556(1) $Å^3$, Z = 4, D_c = 1.178 g cm^{-3}, μ(Mo-K_α) = 6.00 cm^{-1}, F(000) = 1340, T = 293 K; blue/straw dichroic needles, 0.77 × 0.17 × 0.17 mm, Siemens P4/PC diffractometer, ω-scans, 6268 independent reflections. The structure was solved by the heavy atom method and all the major occupancy non-hydrogen atoms were refined anisotropically using full-matrix least-squares based on F^2 to give R_1 = 0.066, wR_2 = 0.137 for 3276 independent observed reflections [$|F_o| > 4\sigma(|F_o|)$, $2\theta \leq 50°$] and 438 parameters.

Crystallographic data (excluding structure factors) for this structure have been deposited with the Cambridge Crystallographic Data Centre as supplementary publication no. CCDC-149268. Copies of the data can be obtained free of charge on application to CCDC, 12 Union Road, Cambridge CB2 1EZ, UK [Fax: (internat.) + 44-1223/336-033; Email: deposit@ccdc.cam.ac.uk].

Crystal Data for 6b (orthorhombic form): $C_{31}H_{43}N_3Cl_2Fe{\cdot}3C_7H_8$, M = 860.8, orthorhombic, space group *Pccn* (no. 56), a = 25.815(2), b = 10.106(1), c = 18.516(1) Å, V = 4830.6(5) Å^3, Z = 4 (the complex has crystallographic C_2 symmetry), D_c = 1.184 g cm^{-3}, μ(Cu-K_α) = 37.9 cm^{-1}, F(000) = 1840, T = 183 K; pale yellow plates, 0.53 × 0.47 × 0.07 mm, Siemens P4/RA diffractometer, ω-scans, 3564 independent reflections. The structure was solved by direct methods and all the major occupancy non-hydrogen atoms were refined anisotropically using full-matrix least-squares based on F^2 to give R_1 = 0.068, wR_2 = 0.168 for 2253 independent observed absorption corrected reflections [$|F_o| > 4\sigma(|F_o|)$, $2\theta \leq 124°$] and 288 parameters.
Crystallographic data (excluding structure factors) for this structure have been deposited with the Cambridge Crystallographic Data Centre as supplementary publication no. CCDC-149269. Copies of the data can be obtained free of charge on application to CCDC, 12 Union Road, Cambridge CB2 1EZ, UK [Fax: (internat.) + 44-1223/336-033; Email: deposit@ccdc.cam.ac.uk].

General Polymerization Procedures: (a) *High Pressure Tests*: A 1 litre stainless steel reactor was baked out under a nitrogen flow for at least 1 h at >85 °C and subsequently cooled to the temperature of polymerization. Isobutane (0.5 L) and trialkylaluminum (triisobutylaluminum) were introduced into the reactor and stirred at the reaction temperature for at least 1 hour. Ethylene was introduced by over-pressure and the difference between the total pressure and the initial pressure (isobutane and nitrogen: ca. 10 bar) is the pressure quoted in Table 1. The catalyst solution in toluene was then injected under nitrogen. The reactor pressure was maintained constant throughout the polymerization run by computer controlled addition of ethylene. The polymerization time was 60 minutes. Runs were terminated by venting off volatiles and the reactor contents were isolated, washed with aqueous HCl, methanol and dried in a vacuum oven at 50 °C.

(b) *Schlenk-line 1 bar ethylene Tests*: The precatalyst was dissolved in toluene (40 mL) and MAO (10 wt% in toluene) added to produce an orange solution. The Schlenk tube was placed in a water bath, purged with ethylene and the contents magnetically stirred and maintained under ethylene (1 bar) for the duration of the polymerization (60 minutes). The polymerization was terminated by the addition of aqueous hydrogen chloride. The solid PE was recovered by filtration, washed with methanol (50 mL) and dried (vacuum oven at 50 °C).

Acknowledgments

bp Chemicals Ltd and the Engineering and Physical Sciences Research Council are thanked for financial support. Drs J. Boyle and G. Audley are thanked for NMR and GPC measurements, respectively.

[1] H. H. Brintzinger, D. Fischer, R. Mülhaupt, B. Rieger, R. M. Waymouth, *Angew. Chem. Int. Ed. Engl.* **1995**, *34*, 1143−1170.
[2] W. Kaminsky, *J. Chem. Soc., Dalton Trans.* **1998**, 1413−1418.
[3] H. G. Alt, A. Köppl, *Chem. Rev.* **2000**, *100*, 1205−1222.
[4] M. Bochmann, *J. Chem. Soc., Dalton Trans.* **1996**, 255−270.
[5] A. L. McKnight, R. M. Waymouth, *Chem. Rev.* **1998**, *98*, 2587−2598.
[6] G. J. P. Britovsek, V. C. Gibson, D. F. Wass, *Angew. Chem. Int. Ed.* **1999**, *38*, 428−447.
[7] S. D. Ittel, L. K. Johnson, M. Brookhart, *Chem. Rev.* **2000**, *100*, 1169−1203.
[8] L. K. Johnson, C. M. Killian, M. Brookhart, *J. Am. Chem. Soc.* **1995**, *117*, 6414−6415.
[9] T. Schleis, J. Heinemann, T. P. Spaniol, R. Mülhaupt, J. Okuda, *Inorg. Chem. Commun.* **1998**, *1*, 431−434.
[10] T. Schleis, T. P. Spaniol, J. Okuda, J. Heinemann, R. Mülhaupt, *J. Organomet. Chem.* **1998**, *569*, 159−167.
[11] P. B. MacKenzie, L. S. Moody, C. M. Killian, J. A. Ponasik, Jr., J. P. McDevitt, (Eastman Chemical Company), WO 98/40374, **1998**.
[12] L. K. Johnson, J. Feldman, K. A. Kreutzer, S. J. McLain, M. A. Bennett, E. B. Coughlin, D. S. Donald, L. T. Jennings Nelson, A. Parthasarathy, X. Shen, W. Tam, Y. Wang, (DuPont), WO 97/02298, **1997** [*Chem. Abstr.* **1997**, *126*, 199931].
[13] G. J. P. Britovsek, V. C. Gibson, B. S. Kimberley, P. J. Maddox, S. J. McTavish, G. A. Solan, A. J. P. White, D. J. Williams, *Chem. Commun.* **1998**, 849−850.
[14] B. L. Small, M. Brookhart, A. M. A. Bennett, *J. Am. Chem. Soc.* **1998**, *120*, 4049−4050.
[15] G. J. P. Britovsek, M. Bruce, V. C. Gibson, B. S. Kimberley, P. J. Maddox, S. Mastroianni, S. J. McTavish, C. Redshaw, G. A. Solan, S. Strömberg, A. J. P. White, D. J. Williams, *J. Am. Chem. Soc.* **1999**, *121*, 8728−8740.
[16] B. L. Small, M. Brookhart, *J. Am. Chem. Soc.* **1998**, *120*, 7143−7144.
[17] G. J. P. Britovsek, S. Mastroianni, G. A. Solan, S. P. D. Baugh, C. Redshaw, V. C. Gibson, A. J. P. White, D. J. Williams, M. R. J. Elsegood, *Chem. Eur. J.* **2000**, *6*, 2221−2231.
[18] B. L. Small, M. Brookhart, *Macromolecules* **1999**, *32*, 2120−2130.
[19] M. S. Brookhart, B. L. Small, (DuPont/UNC), WO 98/30612, **1998** [*Chem. Abstr.* **1998**, *129*, 149375r].
[20] C. Pellecchia, M. Mazzeo, D. Pappalardo, *Macromol. Rapid Commun.* **1998**, *19*, 651−655.
[21] S. Mecking, *Macromol. Rapid Commun.* **1999**, *20*, 139−143.
[22] S. Mecking, (Targor GmbH), WO 98/38228, **1998**.
[23] K. Nomura, W. Sidokmai, Y. Imanishi, *Bull. Chem. Soc. Jpn.* **2000**, *73*, 599−605.
[24] D. M. Dawson, D. A. Walker, M. Thornton-Pett, M. Bochmann, *J. Chem. Soc., Dalton Trans.* **2000**, 459−466.
[25] P. T. Matsunaga, (Exxon Chemical Patents Inc.), WO 99/57159, **1999**.
[26] G. van Koten, J. T. B. H. Jastrzebski, K. Vrieze, *J. Organomet. Chem.* **1983**, *250*, 49−61.
[27] M. D. Bruce, V. C. Gibson, C. Redshaw, G. A. Solan, A. J. P. White, D. J. Williams, *Chem. Commun.* **1998**, 2523−2524.
[28] P. R. Meehan, E. C. Alyea, G. Ferguson, *Acta Cryst.* **1997**, *C53*, 888−890.
[29] A. L. Vance, N. W. Alcock, J. A. Heppert, D. H. Busch, *Inorg. Chem.* **1998**, *37*, 6912−6920.
[30] The cobalt analogue **4** of **3a**, is isomorphous: orthorhombic, space group $P2_12_12_1$ (no. 19), a = 13.426(2), b = 13.441(4), c = 18.455(8) Å, V = 3330(2) Å^3.
[31] P. N. Jagg, P. F. Kelly, H. S. Rzepa, D. J. Williams, J. D. Woollins, W. Wylie, *J. Chem. Soc., Chem. Commun.* **1991**, 942−944.
[32] F. Guérin, D. H. McConville, J. J. Vittal, *Organometallics* **1996**, *15*, 5586−5590.
[33] F. Calderazzo, U. Englert, G. Pampaloni, E. Vanni, *C. R. Acad. Sci. Paris, Série II c* **1999**, *2*, 311−319.
[34] E. L. Muetterties, *Acc. Chem. Res.* **1970**, *3*, 266−273.
[35] N. W. Alcock, R. G. Kingston, P. Moore, C. Pierpoint, *J. Chem. Soc., Dalton Trans.* **1984**, 1937−1943.

Received July 13, 2000
[I00275]

Inductive Effects in Ruthenium-Modified Amino Acids

Bernd Geißer,[a] Thomas Skrivanek,[b] Ute Zimmermann,[b] Derk J. Stufkens,[c] and Ralf Alsfasser*[a]

Keywords: Bioinorganic chemistry / Amino acids / Luminescence / Ruthenium

Emission spectroscopy has been used to probe and quantify electronic interactions mediated by alkyl side chains in a homologous series of amino acids. The ω-amine functions of diaminopropionic acid (DAPA), diaminobutyric acid (DABA), ornithine, and lysine were covalently labeled with a luminescent $[Ru(bipy)_3]^{2+}$ fragment. Protonation of the α-amine function results in a significant dependence of nonradiative excited-state decay rates on the number of methylene groups, *n*, in the respective side chain. Two analogous series of compounds in which the α-amino acid moiety was replaced by $R–NH_2$ or $R–NMe_3^+$ have been studied for comparison. It was found that the emission energies of the chromophore and the pK_A values of the remote amine functional groups in our complexes are both affected by inductive effects which can be described by a Hammett–Taft type relationship. We were able to show that the induction decays with $1/n$, where n = the number of methylene groups separating the chromophore from the amine and ammonium functions. A qualitative description of the phenomenon is given in terms of acid base theory.

Introduction

Peptides and peptide analogues are among the most versatile components for the biomimetic development of new compounds and materials. Examples include pharmaceuticals,[1] enzyme mimetics,[2–4] building blocks for combinatorial catalyst screenings,[5–7] light-harvesting peptides[8,9] and model compounds for electron-transfer proteins.[10–13] The unsurpassed adaptability of peptide scaffolds is achieved by a surprisingly simple building-block design. It remains a fascinating practical and intellectual challenge for chemists to study and understand the subtle interactions between individual amino acid functions which as a whole determine the function of the assembly.

The basic starting point for investigations of electronic interactions between side-chain functional groups and their microenvironment is amino acids and small peptides. Absorption[14,15] and resonance Raman spectra[16] and the characterization of photodegradation products[17] provide evidence for charge transfer processes involving the amide backbone and aromatic side chains. These processes can be modulated by inductive effects imposed by additional functional groups. An *N*-terminal ammonium ion has been shown to induce higher rates of photoinduced electron transfer reactions in phenylalanine containing peptides.[18]

A related effect is also responsible for the unusual photophysical properties of the ruthenium-substituted amino acids **1a–4a** shown in Figure 1. We have recently shown[19] that the ruthenium-based emission is quenched by protonation of the remote amino acid NH_2 group. Nonradiative decay rates increase as the number of methylene groups, *n*, decreases. Questions concerning the origin of this be-

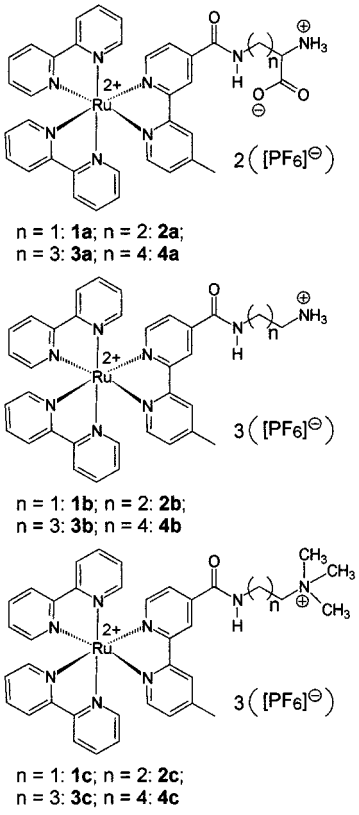

Figure 1. Structures of all compounds investigated in this work

[a] Institute of Inorganic Chemistry, University of Erlangen, Egerlandstraße 1, 91058 Erlangen, Germany
Fax: (internat.) + 49–9131/852–7387
E-mail: Alsfasser@chemie.uni-erlangen.de
[b] Institute of Physical Chemistry, University of Erlangen, Egerlandstraße 3, 91058 Erlangen, Germany
[c] Institute of Molecular Chemistry, University of Amsterdam, Nieuwe Achtergracht 166, 1018 WV Amsterdam, The Netherlands

 © WILEY-VCH Verlag GmbH, 69451 Weinheim, 2001 1434–1948/01/0202–0439 $ 17.50+.50/0

havior have prompted us to study the amine and tetraalkylammonium derivatives **1b−4b** and **1c−4c**, respectively (Figure 1). Our results now enable us to propose a model which explains our observations.

The inductive effect of an ammonium functional group is interpreted in terms of acid-base interactions as defined by the ECT concept developed by Drago et al.[20,21] A semiquantitative analysis is possible by the introduction of a distance dependent Hammett−Taft σ-parameter.[22,23] This conceptual framework may contribute to a better understanding of inductive effects and serve as a starting point for more detailed quantitative analyses of electronic interactions in peptides and proteins.

Results

Synthesis and Characterization

The amine derivatives **1b−4b** were prepared analogously to the amino acids **1a−4a** starting from the succinimide ester $[Ru(bipy)_2(m\text{-OSu})](PF_6)_2$ [9] and the respective mono-*t*Boc protected diamine. Reaction of **1b−4b** with an excess of methyl iodide afforded the trimethylammonium complexes **1c−4c**. All compounds were purified by ion-exchange column chromatography and isolated as hexafluorophosphate salts. The products were characterized and their purity checked by ^{1}H NMR spectroscopy, FAB-MS, and C,H,N-elemental analysis.

NMR Titrations

Ground state pK_A values of the amine groups in **1b−4b** were determined by the same method as described recently for the amino acid complexes **1a−4a**.[19] The respective α-CH resonances were plotted as a function of pH (D_2O) and the curves were fit to a two-state acid base equilibrium.[24,25] Table 1 summarizes the pK_A values determined for the amine functions of our complexes together with some literature data.

Table 1. pK_A(NH_2/NH_3^+) values of **1a−4a**[19] and **1b−4b** as determined by NMR- (pK_A) and luminescence spectroscopy (pK_A*), respectively

Compound	pK_A	pK_A*
1a	8.59 ± 0.02	8.82 ± 0.05
2a	9.33 ± 0.02	9.37 ± 0.09
3a	9.64 ± 0.02	10.21 ± 0.19
4a	9.80 ± 0.03	10.10 ± 0.51
1b	9.21 ± 0.01	9.27 ± 0.04
2b	10.23 ± 0.03	10.18 ± 0.07
3b	10.75 ± 0.01	10.80 ± 0.16
4b	11.22 ± 0.02	10.37 ± 0.37
DAPA[26]	6.68	
DABA[26]	8.19	
Orn[26]	8.78	
Lys[26]	9.12	
Ethylenediamine[27]	10.71/7.56	
Propylenediamine[27]	10.94/9.03	
Butylenediamine[27]	11.15/9.71	
Asn[26]	8.72	
Gln[26]	9.01	

The pK_A values of the respective amine functions in **1a−4a** and **1b−4b** are strongly affected by the presence of the ruthenium chromophore. The α-NH_3^+ groups of our ruthenium-substituted amino acids are considerably less acidic than those of the respective parent compounds diaminopropionic acid (DAPA), diaminobutyric acid (DABA), ornithine, and lysine.[26] Similarly, the pK_A values of the ammonium groups in **1b−4b** are higher than those reported for the second protonation of the respective diamine.[27] It is interesting to note that the pK_A values obtained for **1a** and **2a** compare well with those reported for the two ω-amido-α-amino acids asparagine and glutamine. This suggests that the amino acid groups are more strongly affected by the amide function than by the ruthenium complex fragment.

Absorption and Resonance Raman Spectra

The UV/Visible spectra of the twelve complexes **1(a-c)−4(a-c)** are indistinguishable within experimental error and are typical for polypyridyl ruthenium complexes. No significant spectral changes are observable at pH values ranging from 0 to 14. A characteristic broad band at 457 nm with a shoulder at 430 nm is assigned to the MLCT transitions involving the unsubstituted and amide-substituted bipyridine ligands.

Resonance Raman spectra for **1a** were collected in order to evaluate further the contributions of the different bipyridine ligands to the absorption bands. Excitation wavelengths (λ_{exc}) of 433, 457.9, and 488 nm, respectively, were used which cover the MLCT band of the complex. Measurements at three different pH values (1, 7, and 12) show that the spectra do not vary significantly with pH.

The strongest bands are summarized in Table 2. They are found above 1000 cm^{-1} and belong to stretching vibrations of the ligands. No vibration of the amino acid moiety is resonance enhanced. The relative signal intensities significantly depend on the excitation wavelength. A comparison with $[Ru(bipy)_3]^{2+}$ shows that bands at 1608, 1563, 1320, and 1176 cm^{-1} can be assigned to vibrations involving the unsubstituted bipyridine rings in **1a**. They are strongest at λ_{exc} = 433 nm indicating that the shoulder at the high-energy end of the MLCT band is due to a Ru → bipy charge transfer. Transitions involving the amide-substituted ligand occur at lower energy, which is evident from the Raman bands at 1622, 1547, 1277, and 1214 cm^{-1} which increase as λ_{exc} is raised to 488 nm. Finally, the strongest Raman band is located at 1491 cm^{-1} and reveals a shoulder at its low-energy end (ca. 1483 cm^{-1}) when λ_{exc} = 488 nm.

Table 2. Selected resonance Raman bands ($\tilde{\nu}$, cm^{-1}) assignable to the unsubstituted (bipy) and amino acid substituted (bipy−AA) bipyridine ligands of **1a**

Ligand	1. Set	2. Set	3. Set	4. Set	5. Set
bipy	1608	1563	1491	1320	1176
bipy−AA	1622	1547	1483 (sh)	1277	1214

Table 3. Cyclic voltammetry data for **1a−4a**, **1b−4b**, and **1c−4c**

Compd.	$Ru^{II/III}$ obsd. $E_{1/2}$, V (ΔEp, mV)	Ligand reductions obsd. $E_{1/2}$, V (ΔEp, mV)		
1a	1.33 (80)	−1.30 (70)	−1.49 (70)	−1.72 (70)
2a	1.33 (90)	−1.31 (70)	−1.54 (60)	−1.73 (80)
3a	1.32 (100)	−1.30 (60)	−1.54 (50)	−1.75 (90)
4a	1.32 (90)	−1.31 (60)	−1.51 (130)	−1.72 (110)
1b	1.33 (90)	−1.27 (70)	−1.47 (70)	−1.71 (110)
2b	1.33 (90)	−1.22 (80)	−1.46 (90)	−1.70 (90)
3b	1.32 (80)	−1.22 (80)	−1.46 (70)	−1.70 (80)
4b	1.32 (90)	−1.23 (70)	−1.46 (80)	−1.70 (80)
1c	1.31 (100)	−1.33 (80)	−1.54 (80)	−1.83 (110)
2c	1.32 (90)	−1.34 (80)	−1.54 (80)	−1.83 (110)
3c	1.32 (90)	−1.34 (80)	−1.54 (80)	−1.77 (100)
4c	1.32 (90)	−1.34 (80)	−1.53 (90)	−1.73 (90)

Our data compare well with time-resolved resonance Raman studies reported by Meyer et al[28] for the lysine derivative **4a** in acetonitrile. The assignment of the low-energy transitions to charge-transfer processes involving the amide-substituted pyridine ring is consistent with a lower reduction potential of this ligand. It is important for the arguments presented in the following discussion that the MLCT transition involving the amino acid ligand bpy-DAPA is largely obscured by transitions to the unsubstituted bipyridines. This prevents an accurate determination of λ_{max} for the Ru → bpy-DAPA transition.

Cyclic Voltammetry

The cyclic voltammogram of each complex in acetonitrile is characterized by four reversible waves. Table 3 summarizes these data. Oxidation of the respective ruthenium(II) center is observed at a potential of ca. +1.32 V (vs. Ag/AgCl). The first ligand reduction occurs at a potential of ca. −1.3 V. Consistent with literature data of related complexes,[29] and our resonance Raman studies, we assign this wave to the reduction to the amide-substituted pyridine ring.

Whereas the oxidation waves are clearly independent of the bipyridine substituents, small differences are observed for the ligand reduction potentials. The amine complexes **1b−4b** appear to be more easily reducible than their amino acid and tetraalkylammonium analogues **1a,c-4a,c**. However, considering the broad waves which are typical for the class of complexes investigated this difference may not be significant.

Emission Spectra

The emission spectra of **1a−4a** and **1b−4b** are strongly pH dependent. In Figure 2, the uncorrected maximum emission intensities are plotted as a function of pH. Two protonation steps are clearly separated in each case. The inflection point at ca. pH 0.5 is assigned to protonation of the amide link.[19] The second inflection is due to protonation/deprotonation of the respective amine functions. The magnitude of the observed change in luminescence intensity depends on the number of methylene spacers separating the amide link from the α-C atom. The spectra of the amino acids and the ethylenediamine derivatives show very similar pH dependences except for a significant difference in the observed pK_A values. All luminescence titration curves yield pK_A values for the amine groups which are very similar to those obtained by NMR spectroscopy, suggesting similar acid-base properties of the ground and excited states. The results obtained from emission spectroscopy are also summarized in Table 1.

Lifetime measurements performed for all complexes at pH 0, 4.8, and 12 confirm our findings from steady state measurements. We have repeated and reproduced all lifetime experiments reported earlier[19] in order to assure that all data were obtained under the same conditions. These results are presented in Table 4. Amide protonation at low pH values results in large nonradiative decay rates (τ = ca. 60 ns) for all compounds. In the pH range between the two inflections shown in Figure 2, lifetimes increase with the number of methylene spacers, *n*. The values obtained for **1a** (τ = 345 ns) and **1b** (τ = 355 ns) at pH 4.8 compare well. At pH 12 we find very similar values of ca. 420 ns for all four amino acids. In the case of the amine derivatives **1b−4b** this number is slightly smaller (396 ns). We think that this difference is significant and may be due to medium effects associated with the high base concentration. As will be shown in the Discussion section, high pH values also

Table 4. pH-Dependent luminescence lifetimes τ (ns) of **1a−4a**, **1b−4b**, and **1c−4c**

Compd.	pH 0	pH 4.8	pH 12
1a	64 ± 1	345 ± 8	427 ± 2
2a	77 ± 1	389 ± 5	427 ± 2
3a	61 ± 1	428 ± 7	420 ± 3
4a	59 ± 1	430 ± 1	413 ± 1
1b	53 ± 1	355 ± 1	396 ± 3
2b	54 ± 1	389 ± 2	402 ± 2
3b	50 ± 1	404 ± 2	405 ± 2
4b	50 ± 1	407 ± 1	404 ± 2
1c	61 ± 1	352 ± 4	345 ± 3
2c	53 ± 2	399 ± 3	393 ± 1
3c	52 ± 1	423 ± 2	412 ± 1
4c	50 ± 1	422 ± 1	412 ± 2

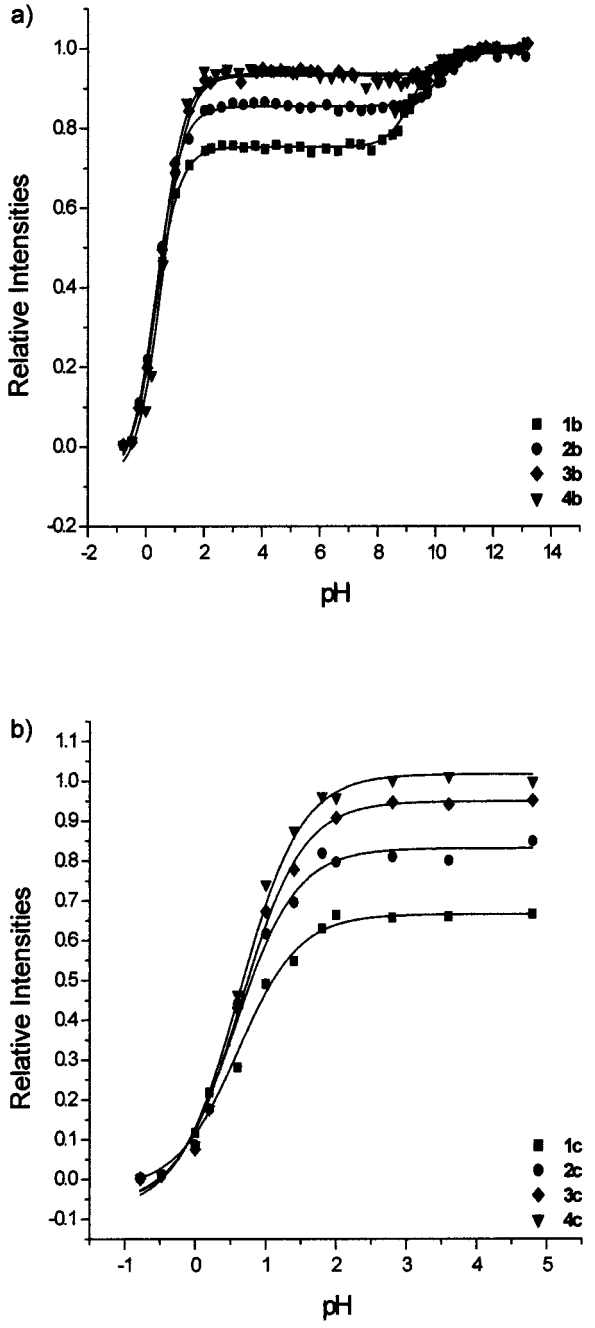

Figure 2. Luminescence intensities of (a) **1b−4b** and (b) **1c−4c** as a function of pH; intensities of **1b−4b** are relative to the values of the respective compound at pH 12, intensities of **1c−4c** are relative to the value of **4c** at pH 4.8

affect the lifetimes of the trimethylammonium complexes **1c−4c**.

The trimethylammonium complexes **1c−4c** were prepared in order to evaluate possible contributions of NH bonds to nonradiative decay processes.[30] The compounds exhibit lifetimes of 352 ns (**1c**), 399 ns (**2c**), 423 ns (**3c**), and 422 ns (**4 c**) at pH 4.8. These numbers also compare well with the data obtained for our series of amino acids, indicating that NH bonds are not involved in energy dissipation pathways. Slightly smaller values are observed at pH 12, indicating a small contribution of the basic medium to excited-state decay processes. In summary, our results demonstrate that a zwitterionic amino acid function, an ammonium ion, and a tetraalkylammonium ion have the same effects on the excited state properties of a $[Ru(bipy)_3]^{2+}$ chromophore.

Discussion

Our data demonstrate that the luminescence properties of the $[Ru(bipy)_3]^{2+}$ chromophores in **1(a-c)−4(a-c)** are affected by protonation of the amide link at very low pH, as well as by the presence of NR_4^+ functions in (i) the zwitterionic amino acid groups of **1a−4a**, (ii) the ammonium ions in **1b−4b**, and (iii) the trimethylalkylammonium groups in **1c−4c**. Two conclusions can be drawn from a comparison of the three series of compounds investigated: (i) the reduced lifetimes of the compounds with short alkyl spacers originate from the intramolecular presence of an NR_4^+ function and do not require a zwitterionic amino acid structure, and (ii) a direct participation of NH units in energy dissipation pathways is ruled out since the $RNMe_3^+$ compounds **1c−4c** do not differ significantly from the RNH_3^+ derivatives **1a,b−4a,b**. The latter conclusion is particularly important since hydrogen bonding to the solvent[31] and high energy NH vibrations are known to significantly effect nonradiative decay rates in other systems.[30]

It is evident from the emission spectra shown in Figure 3 that decreasing intensities are associated with a small but significant band-shift to lower energies. This observation suggests that the energy gap between the excited state and the ground state is affected. A contribution to the nonradiative decay rate constants according to the energy gap law is therefore evident. However, the differences between the emission maxima are very small making a quantitative analysis difficult. Figure 4 contains a plot of ln*k* versus emission energies which includes literature data reported for $[Ru(bipy)_3]^{2+}$.[32] The comparison in Figure 4b clearly shows that, in fact, the very small shift in energies observed for our compounds is sufficient to account for the observed differences in nonradiative decay rates. It should be noted that $[Ru(bipy)_3]^{2+}$ cannot be included without caution since linear energy-gap relationships are only expected within a series of closely related complexes. In addition, it has been reported that solvent effects in hydroxylic solutions may result in significant deviations from a simple linear energy-gap dependence.[33,34] As is shown in Figure 4b the linear fit obtained for our complexes alone is slightly steeper than that obtained if $[Ru(bipy)_3]^{2+}$ is included. However, we think the data show that the structure and pH-dependent nonradiative decay rates of our complexes can conveniently be explained in terms of the energy-gap law. This is important since we do not have any evidence for other well-known effects such as the participation of low lying d-d excited states,[35] solvent reorganization,[36] or different geometric displacements in the excited state.[37,38] These phenomena should manifest themselves in ligand loss or emission band shapes.

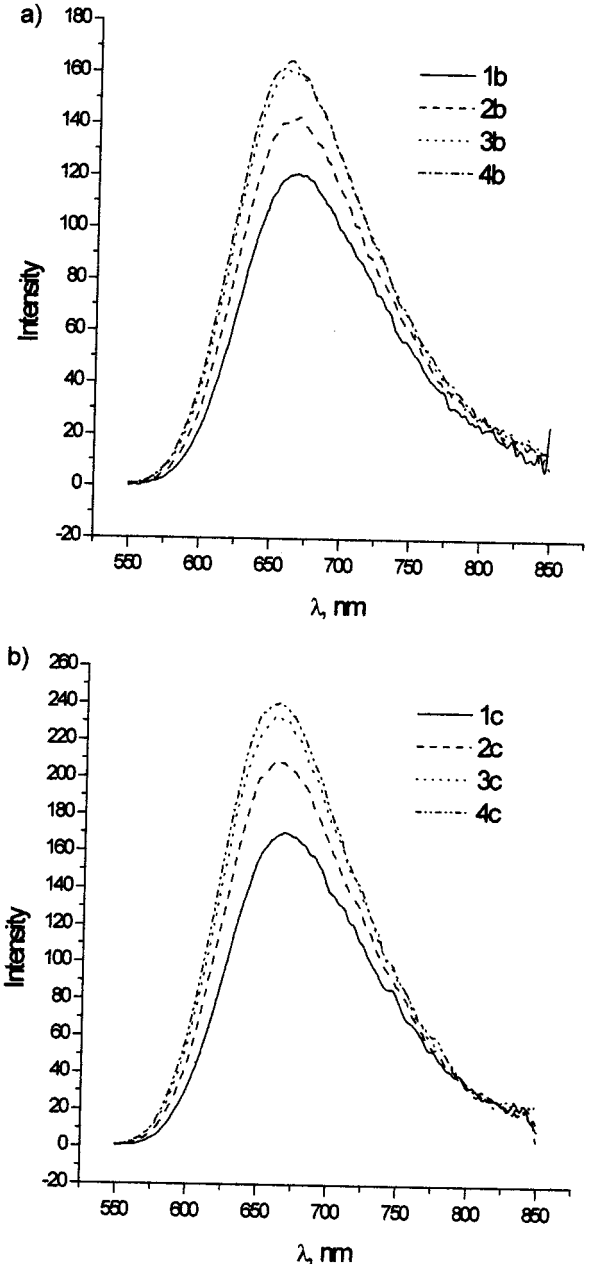

Figure 3. Corrected luminescence spectra measured at pH 4.8: a) **1b−4b**, b) **1c−4c**

The origin of the decreasing emission energies is most likely an inductive effect caused by the ammonium groups in our complexes. An electronic interaction between the ruthenium chromophore and the remote amine functions is evident from the ground state pK_A values given in Table 1. The NH_3^+ groups in **1a−4a** and **1b−4b** become more acidic as the number of methylene groups decreases. Similarly, the electron affinity of the ruthenium chromophore must increase in the presence of an ammonium group. This results in a lower HOMO−LUMO energy gap and explains our observations. A similar effect has been described by Seidel et al., who reported the influence of *N*-terminal ammonium groups on photoinduced electron transfer rates in tyrosine peptides.[18]

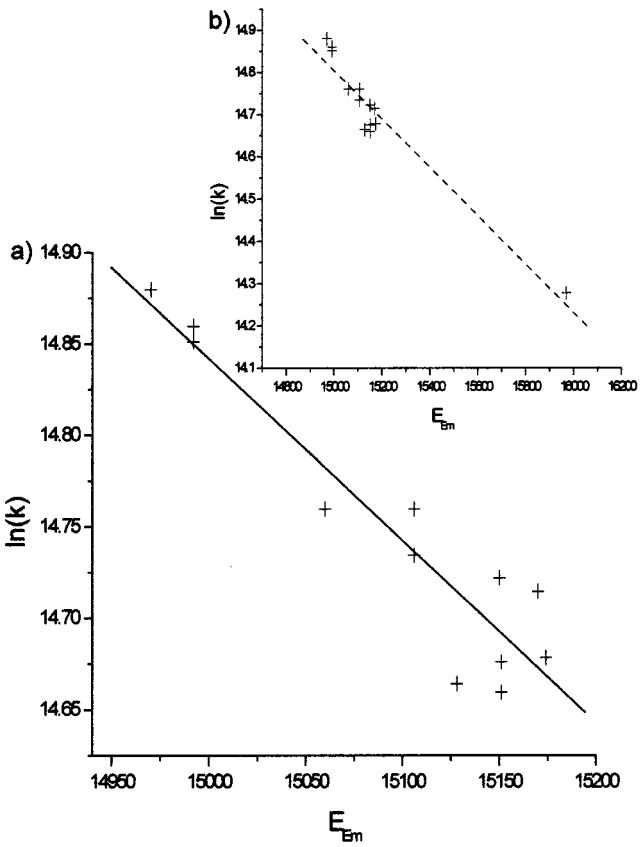

Figure 4. (a) Plot of ln k vs. E_{em} (pH = 4.8) for all compounds reported in this work; (b) comparison with the literature value reported for $[Ru(bipy)_3]^{2+}$ (see ref. [49])

Further support for an explanation which only involves an energy gap law relationship comes from the behavior of our complexes at low pH values. We have shown in a previous article[19] that protonation of the amide oxygen atom in **1a−4a** is associated with a large red shift of the emission energies. Resonance structures of the excited state can be drawn with the negative charge localized at the amide functional group and it is evident that protonation of this group will result in a lower reduction potential of the substituted bipyridine ligand.

We suggest that a qualitative description of the observed phenomena can be given in terms of acid-base interactions between the Lewis acid NR_4^+ and the Lewis basic amide link. Drago et al.[20,21] have developed the ECT-concept which splits acid-base interactions into three contributions. The first one, $C_{acid}C_{Base}$, describes covalent interactions and is irrelevant here since acid and base are separated by an alkyl chain in our complexes. The second one, $E_{Acid}E_{Base}$, originates in electrostatic interactions and may be the most important in determining the pK_A(NH_2/NH_3^+) values in **1b−4b**. The third contribution, $R_{Acid}T_{Base}$, (R: Receptance, T: Transmission) refers to an exchange of electron density between the acid and the base. The ECT parameters are closely related to the physical parameters electron affinity (EA), ionization energy (IE), and electronegativity as defined by the Jaffé scale.[39−41] Consideration of the electron transfer interaction $R_{Acid}T_{Base}$ may explain why a zwitter-

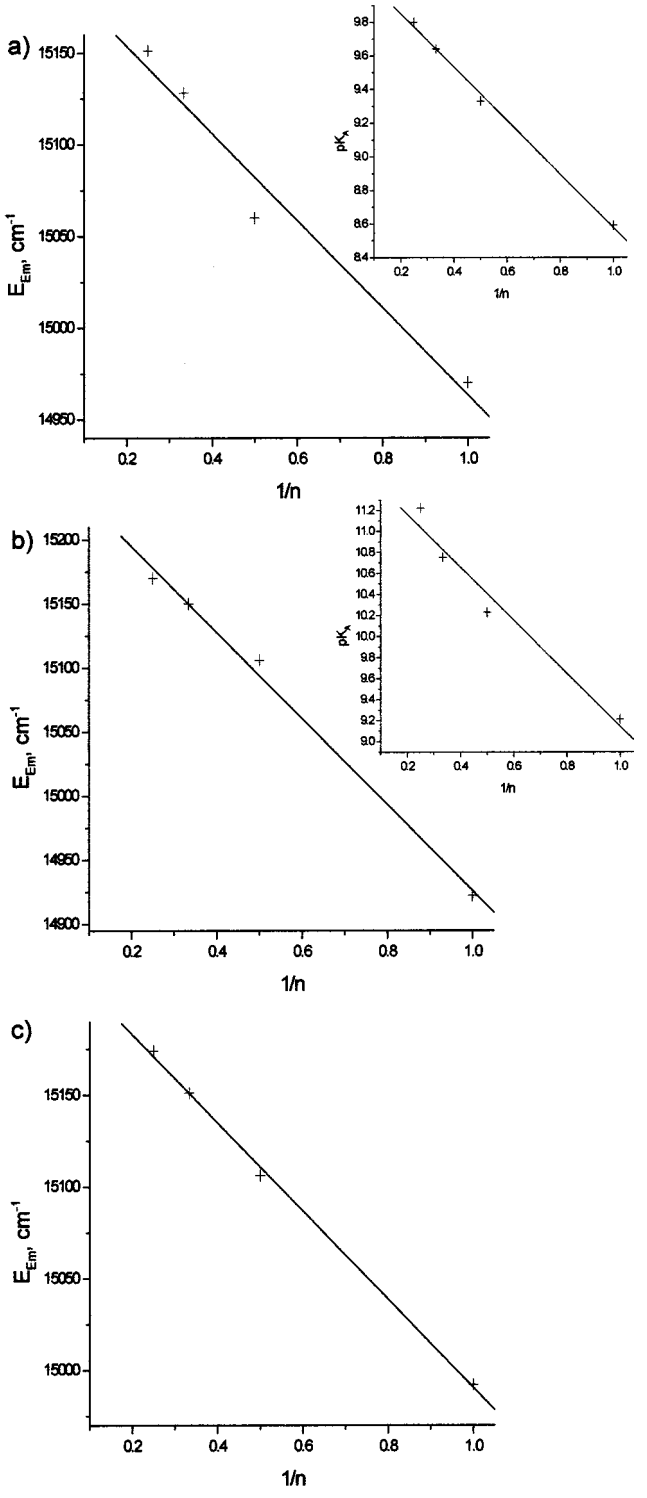

Figure 5. Plots of pK_A values (NH_2/NH_3^+) and emission energies (pH 4.8), respectively, vs. 1/*n*: (a) **1a−4a**, (b) **1b−4b**; (c) plot of the emission energies of **1c−4c** at pH 4.8 vs. 1/*n*

ionic amino acid (0 charge) and an ammonium function (+1 charge) can have the same effect on the LUMO energy of a conjugated chromophore.

The significant changes in pK_A(NH_2/NH_3^+) values observed for our amino acid (**1a−4a**) and amine (**1b−4b**) complexes indicate that inductive effects have to be relevant not only in the excited states, but also in the ground states of the molecules. It must therefore be explained why the decreased HOMO−LUMO gap is not manifest in changes of the absorption spectra and reduction potentials. The differences in emission energies, ΔE_{em}, are on the order of 2 kJ/mol between the two extremes within each series (**1a/4a**, **1b/4b**, **1c/4c**). This would correspond to an estimated change in redox potentials of ca. 20 mV, a value which is not significant within the experimental error of our cyclic voltammograms. As has been discussed above, the same is true for the absorption spectra of our complexes, which are largely obscured by overlapping MLCT bands. The resonance Raman spectra show that the MLCT transition to the substituted bipy ligand is covered by the Ru → bipy transition, which is more intense due to the presence of two unsubstituted bipyridine ligands. This makes a determination of the absorption energy corresponding to the Ru → substituted bipy transition impossible. It is evident that effects which are readily observable by emission spectroscopy cannot be determined by either absorption spectroscopy or cyclic voltammetry.

Inductive effects are usually described semi-quantitatively by linear free-energy relationships such as the Hammett[22] and Taft[23] equations. In a correlation analysis, rate constants or physical properties such as chemical shifts or IR frequencies[42] are plotted as a function of a parameter, σ, which is a measure of the magnitude of the electron-donating or -withdrawing effect imposed by a functional group. In our study the functional groups do not vary and the inductive effect is only a function of the number of methylene groups separating the chromophore from the ammonium function. As is shown in Figure 5, both pK_A values and emission energies give reasonably good straight lines when they are plotted against 1/*n*, where *n* is the number of methylene spacers as defined by Figure 1. Consequently, ln*k* also shows a linear dependence on 1/*n* and pK_A, respectively. This is shown in Figure 6. Thus, 1/*n* describes the decrease of σ with increasing alkyl chains separating a Lewis acid from a Lewis base. This relationship holds for zwitterionic amino acids as well as for ammonium ions and should therefore be a measure of similar effects in a large variety of different compounds including peptides and proteins.

Though four data points are a small basis for a quantitative correlation all the series behave similarly, thus supporting our interpretation. An interesting aspect is revealed by the ln*k* vs. 1/*n* plots obtained for the trimethylammonium complexes **1c−4c** at pH 4.8 and pH 12. The two lines are parallel with slightly higher nonradiative decay rates observed at high base concentration. This observation can be assigned to a medium effect which is comparable to the small ionic-strength contributions observed for nonradiative decay rates of the $[Ru(bipy)_3]^{2+}$ excited state.[43]

A few problems should finally be noted. Due to their inherent flexibility, alkyl chains prevent a quantitative analysis of distance effects between two functional groups. The number of bonds or the number of methylene groups, *n*, has to be used instead. In addition, the amide link applied in our study may result in the formation of *syn* and *anti*

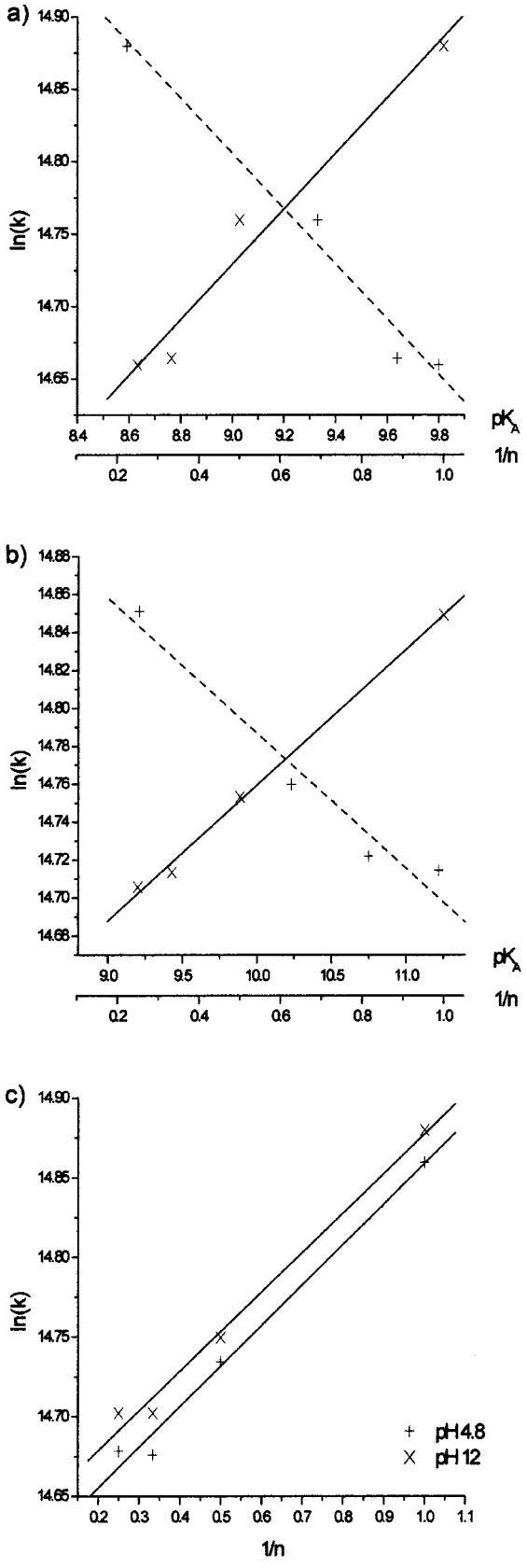

Figure 6. Plots of ln k vs. 1/n (solid lines, x) and pK_A values (dashed lines, +), respectively: (a) **1a−4a**, (b) **1b−4b**; (c) Plot of ln k vs. 1/n for **1c−4c** at pH 4.8 and pH 12, respectively

isomers which is a known complication in the quantitative analysis of photoinduced electron-transfer reactions involving amide-bridged donor-acceptor dyads.[44] Furthermore, alkyl bridges are known to effect electrostatic interactions since they modify the microscopic dielectric constant between the two relevant functional groups.[45] As a consequence, our empirical correlations are not suitable for a quantitative evaluation of different contributions such as the magnitude of electrostatic ($E_{Acid}E_{Base}$) or electron transfer ($R_{Acid}T_{Base}$) interactions. Detailed theoretical studies will be required to tackle these problems. However, with our proposed model we provide a starting point for such investigations.

Conclusions

Our studies concerning the photophysical properties of chromophore-substituted amino acids have lead us to propose a model for the interpretation of inductive effects in amino acids and peptides. Two observations are particularly important:
(1) The pK_A value of a remote functional group and the HOMO−LUMO gap of a chromophore are linearly related. This may be relevant for the interpretation of pH titration curves particularly in small molecular assemblies were meaningful assignments of pK_A values can be made.
(2) 1/n can be used to describe the decay of the electronic Hammett−Taft parameter, σ, when an increasing alkyl bridge separates two functional groups. Our data show that σ/n is significant in **1a** but very small in the lysine derivative **4a**. This may help to define the limiting case for "through-bond" interactions mediated by amino acid side chains in small peptide assemblies[13,28,29,46] and proteins.[47]

Experimental Section

Materials: $[Ru(bipy)_2Cl_2]$[48], $[Ru(bipy)_2(m\text{-OH})](PF_6)_2$ [9] and $[Ru(bipy)_2(m\text{-OSu})](PF_6)_2$ (m = 4-carbonyl-4′-methyl-2,2′-bipyridine, m-OSu = 4-carboxysuccinimidoester-4′-methyl-2,2′-bipyridine) were prepared according to the method reported by Erickson et al.[9] $RuCl_3$ was a donation from Degussa. Reagent grade solvents were obtained from Roth, NMR solvents from Aldrich and all other chemicals from Fluka. Water for preparations was demineralized. All reactions were carried out under argon.

Spectra were recorded with the following instruments: UV/Vis: Shimadzu UV-2101PC. − IR (KBr pellets): Mattson Polaris FT IR. − ^{1}H NMR: Bruker Avance DPX 300. All chemical shifts are referenced to residual solvent signals as internal standards previously referenced to TMS, with high-frequency shifts recorded as positive. Pyridine resonances are labelled "b" for the bipy, and "m" for the substituted bipy ligands, respectively. − Elemental analysis: Carlo Erba EA 1106. − FAB: Micromass ZabSpec mass spectrometer.

$[Ru(bipy)_2\{m\text{-}CONH(CH_2)_nNH_3^+\}](PF_6)_3$ (n = 2: 1b, 3: 2b, 4: 3b, 5: 4b). − General Procedure: $[Ru(bipy)_2(m\text{-OH})](PF_6)_2$ and HOSu (1.1 equiv.) were dissolved in acetonitrile (5 mL) and the solution was cooled to 0 °C. Dicyclohexylcarbodiimide (DCC, 2.5 equiv.) was added and the red suspension was stirred at 0 °C for 5 h. The

precipitated urea was filtered off and washed several times with small amounts of acetonitrile. The *N*-Boc-monoprotected diamine (1.2 equiv.) was added to the filtrate and the reaction mixture was stirred for 1.5 h at 41 °C. After removal of all the acetonitrile by rotary evaporation, the residue was suspended in a mixture of dioxane (20 mL) and 4 N HCl (6 mL) and stirred for 1 h at 0 °C. All solvent was removed by rotary evaporation and the residue dried under vacuum. The obtained solid was dissolved in water (100 mL), neutralized with 2 M NaOH and purified by ion exchange chromatography (Sephadex CM-50) with an NaCl gradient in aqueous phosphate buffer (0.6 mM, pH = 7.2). A first band was obtained at 10 mM NaCl which contained traces of $[Ru(bipy)_2(m\text{-}OH)]^{2+}$. The product was eluted with 80 mM NaCl. Rotary evaporation to dryness afforded an orange solid which was suspended in a minimum volume of methanol. The suspension was filtered to remove insoluble salts, all methanol stripped by rotary evaporation and the resulting red solid dried in vacuo.

The crude products were dissolved in water (20 mL), precipitated with a 1.5-fold excess of NH_4PF_6 in water (1 mL) and stirred for 1 h at room temp. HPF_6 (60%, 1.5 equiv.) was added to yield the compounds in their fully protonated form. After 10 min. the brown-orange precipitate was isolated by filtration, washed with cold 0.1 M HPF_6 (3 × 5 mL) and dried in a vacuum desiccator over silica gel.

1b: Yield: 890 mg (74%). − ^{1}H NMR (300 MHz, CD_3OD): δ = 2.58 (s, 3 H, m4′-CH_3), 3.22 (t, 2 H, $CH_2CH_2NH_3^+$), 3.73 (t, 2 H, $CH_2CH_2NH_3^+$), 7.34 (d, 1 H, m5′), 7.47 (m, 4 H, b5), 7.62 (d, 1 H, m5), 7.79 (m, 5 H, 4 × b6, m6′), 7.94 (d, 1 H, m6), 8.09 (m, 4 H, b4), 8.64 (m, 5 H, 4 ×b3, m3′), 8.95 (s, 1 H, m3). − IR (KBr pellets, cm^{-1}): $\tilde{\nu}$ = 3080 (m), 2926 (m), 1657 (m), 1543 (m), 1466 (m), 1449 (m), 1311 (m), 842 (vs, PF_6^-), 765 (s), 559 (s). − UV/Vis (H_2O): λ_{max} (lg ε, M^{-1} cm^{-1}) = 456 (4.24), 288 (4.95), 245 nm (4.44). − FAB$^+$ (*m*-NBA): *m*/*z* = 961 [$M^+ - PF_6^-$], 815 [$M^+ - 2\ PF_6^-$]. − $C_{34}H_{33}F_{18}N_8OP_3Ru{\cdot}H_2O$ (1105.6 + 18): calcd. C 36.34, H 3.14, N 9.97; found C 36.44, H 3.10, N 9.66.

2b: Yield: 951 mg (78%). − ^{1}H NMR (300 MHz, CD_3OD): δ = 1.96 (q, 2 H, $CH_2CH_2CH_2NH_3^+$), 2.59 (s, 3 H, m4′-CH_3), 3.04 [t, 2 H, $(CH_2)_2CH_2NH_3^+$], 3.55 [t, 2 H, $CH_2(CH_2)_2NH_3^+$], 7.34 (d, 1 H, m5′), 7.47 (m, 4 H, b5), 7.61 (d, 1 H, m5), 7.80 (m, 5 H, 4 × b6, m6′), 7.91 (d, 1 H, m6), 8.09 (m, 4 H, b4), 8.64 (m, 5 H, 4 ×b3, m3′), 8.96 (s, 1 H, m3). − IR (KBr pellets, cm^{-1}): $\tilde{\nu}$ = 3114 (m), 3083 (m), 2934 (m), 1630 (m), 1544 (m), 1465 (m), 1447 (m), 1261 (m), 1163 (m), 845 (vs, PF_6^-), 766 (s), 559 (s). − UV/Vis (H_2O): λ_{max} (lg ε, M^{-1} cm^{-1}) = 456 (4.24), 288 (4.95), 245 nm (4.45). − FAB$^+$ (*m*-NBA): *m*/*z* = 975 [$M^+ - PF_6^-$], 830 [$M^+ - 2\ PF_6^-$]. − $C_{35}H_{35}F_{18}N_8OP_3Ru{\cdot}H_2O$ (1119.7 + 18): calcd. C 36.95, H 3.28, N 9.85; found C 36.64, H 3.34, N 9.36.

3b: Yield: 890 mg (72%). − ^{1}H NMR (300 MHz, CD_3OD): δ = 1.74 (m, 4 H, -$CH_2CH_2CH_2CH_2NH_3^+$), 2.59 (s, 3 H, m4′-CH_3), 2.98 [m, 2 H, $(CH_2)_3CH_2NH_3^+$], 3.49 [m, 2 H, $CH_2(CH_2)_3NH_3^+$], 7.34 (d, 1 H, m5′), 7.47 (m, 4 H, b5), 7.61 (d, 1 H, m5), 7.78 (m, 5 H, 4 × b6, m6′), 7.91 (d, 1 H, m6), 8.10 (m, 4 H, b4), 8.65 (m, 5 H, 4 ×b3, m3′), 8.96 (s, 1 H, m3). − IR (KBr pellets, cm^{-1}): $\tilde{\nu}$ = 3117 (m), 3083 (m), 2939 (m), 1652 (m), 1543 (m), 1466 (m), 1448 (m), 1239 (m), 1163 (m), 843 (vs, PF_6^-), 765 (s), 559 (s). − UV/Vis (H_2O): λ_{max} (lg ε, M^{-1} cm^{-1}) = 456 (4.22), 287 (4.94), 246 nm (4.44). − FAB$^+$ (*m*-NBA): *m*/*z* = 989 [$M^+ - PF_6^-$], 843 [$M^+ - 2\ PF_6^-$]. − $C_{36}H_{37}F_{18}N_8OP_3Ru{\cdot}3H_2O$ (1133.7 + 54): calcd. C 36.40, H 3.64, N 9.43; found C 35.93, H 3.29, N 9.66.

4b: Yield: 750 mg (75%). − ^{1}H NMR (300 MHz, CD_3OD): δ = 1.47 [m, 2 H, $(CH_2)_3CH_2CH_2NH_3^+$], 1.69 [m, 4 H, $CH_2CH_2CH_2(CH_2)_2NH_3^+$], 2.58 (s, 3 H, m4′-$CH_3$), 2.95 [t, 2 H, $(CH_2)_4CH_2NH_3^+$], 3.46 [t, 2 H, $CH_2(CH_2)_4NH_3^+$], 7.33 (d, 1 H, m5′), 7.46 (m, 4 H, b5), 7.61 (d, 1 H, m5), 7.79 (m, 5 H, 4 × b6, m6′), 7.91 (d, 1 H, m6), 8.09 (m, 4 H, b4), 8.64 (m, 5 H, 4 ×b3, m3′), 8.95 (s, 1 H, m3). − IR (KBr pellets, cm^{-1}): $\tilde{\nu}$ = 3078 (m), 2933 (m), 1652 (m), 1544 (m), 1465 (m), 1444 (m), 1240 (m), 1139 (m), 844 (vs, PF_6^-), 764 (s), 559 (s). − UV/Vis (H_2O): λ_{max} (lg ε, M^{-1} cm^{-1}) = 455 (4.24), 286 (4.95), 246 nm (4.44). − FAB$^+$ (*m*-NBA): *m*/*z* = 1003 [$M^+ - PF_6^-$], 858 [$M^+ - 2\ PF_6^-$]. − $C_{37}H_{39}F_{18}N_8OP_3Ru{\cdot}2H_2O$ (1147.7 + 36): calcd. C 37.54, H 3.66, N 9.47; found C 37.23, H 3.78, N 9.34.

[Ru(bipy)$_2${*m*-CONH(CH$_2$)$_n$N(CH$_3$)$_3^+$}](PF$_6$)$_3$ (*n* = 2: 1c, 3: 2c, 4: 3c, 5: 4c). − General Procedure: $[Ru(bipy)_2\{m\text{-}CONH(CH_2)_n\text{-}NH_3^+\}](PF_6)_3$ (**1b−4b**; 0.27 mmol), sodium carbonate (5.1 mmol, 540 mg) and sodium iodide (0.14 mmol, 20 mg) were suspended in acetonitrile (20 mL). After 10 min., methyl iodide (0.98 mmol, 61 μL) was added and the red suspension was stirred in the dark for 2 days. Insoluble salts were filtered off, all solvent stripped by rotary evaporation and the resulting red solid dried overnight under vacuum. The complexes were purified by ion-exchange chromatography and isolated as described above for the diamine compounds, except that no HPF_6 was used and the products were washed with cold 10 mM aqueous NH_4PF_6 (3 × 5 mL).

1c: Yield: 228 mg (72%). − ^{1}H NMR (300 MHz, CD_3OD): δ = 2.58 (s, 3 H, m4′-CH_3), 3.21 (s, 9 H, $N(CH_3)_3^+$), 3.61 [t, 2 H, $CH_2CH_2N(CH_3)_3^+$], 3.90 [t, 2 H, $CH_2CH_2N(CH_3)_3^+$], 7.34 (d, 1 H, m5′), 7.46 (m, 4 H, b5), 7.61 (d, 1 H, m5), 7.78 (m, 5 H, 4 × b6, m6′), 7.92 (d, 1 H, m6), 8.09 (m, 4 H, b4), 8.58 (s, 1 H, m3′), 8.65 (d, 4 H, 4 ×b3), 8.92 (s, 1 H, m3). − IR (KBr pellets, cm^{-1}): $\tilde{\nu}$ = 3118 (m), 3087 (m), 1674 (s), 1541 (m), 1470 (m), 1448 (m), 1309 (m), 841 (vs, PF_6^-), 765 (s), 558 (s). − UV/Vis (H_2O): λ_{max} (lg ε, M^{-1} cm^{-1}) = 457 (4.23), 288 (4.95), 245 nm (4.45). − FAB$^+$ (*m*-NBA): *m*/*z* = 1003 [$M^+ - PF_6^-$], 858 [$M^+ - 2\ PF_6^-$]. − $C_{37}H_{39}F_{18}N_8OP_3Ru{\cdot}H_2O$ (1147.7 + 18): calcd. C 38.1, H 3.55, N 9.61; found C 38.35, H 3.49, N 9.54.

2c: Yield: 223 mg (72%). − ^{1}H NMR (300 MHz, CD_3OD): δ = 2.14 [q, 2 H, $CH_2CH_2CH_2N(CH_3)_3^+$], 2.59 (s, 3 H, m4′-CH_3), 3.16 [s, 9 H, $N(CH_3)_3^+$], 3.44 [m, 2 H, $(CH_2)_2CH_2N(CH_3)_3^+$], 3.58 [t, 2 H, $CH_2(CH_2)_2N(CH_3)_3^+$], 7.33 (d, 1 H, m5′), 7.48 (m, 4 H, b5), 7.61 (d, 1 H, m5), 7.77 (m, 4 H, 4 × b6), 7.88 (d, 1 H, m6′), 8.09 (m, 4 H, b4), 8.58 (s, 1 H, m3′), 8.65 (m, 4 H, 4 × b3), 8.95 (s, 1 H, m3). − IR (KBr pellets, cm^{-1}): $\tilde{\nu}$ = 3118 (m), 3088 (m), 2966 (m), 1671 (s), 1541 (m), 1468 (m), 1448 (m), 1309 (m), 840 (vs, PF_6^-), 765 (s), 558 (s). − UV/Vis (H_2O): λ_{max} (ε, M^{-1} cm^{-1}) = 456 (17000), 289 (90000), 244 nm (28500). − FAB$^+$ (*m*-NBA): *m*/*z* = 1162 [M^+], 1017 [$M^+ - PF_6^-$], 871 [$M^+ - 2\ PF_6^-$]. − $C_{38}H_{41}F_{18}N_8OP_3Ru{\cdot}H_2O$ (1161.8 + 18): calcd. C 38.69, H 3.67, N 9.50; found C 38.52, H 3.65, N 9.18.

3c: Yield: 224 mg (70%). − ^{1}H NMR (300 MHz, CD_3OD): δ = 1.71 [q, 2 H, $(CH_2)_2CH_2CH_2N(CH_3)_3^+$], 1.89 [q, 2 H, $CH_2CH_2(CH_2)_2N(CH_3)_3^+$], 2.58 (s, 3 H, m4′-$CH_3$), 3.10 [s, 9 H, $N(CH_3)_3^+$], 3.34 [t, 2 H, $(CH_2)_3CH_2N(CH_3)_3^+$], 3.54 [t, 2 H, $CH_2(CH_2)_3N(CH_3)_3^+$], 7.34 (d, 1 H, m5′), 7.47 (m, 4 H, b5), 7.61 (d, 1 H, m5), 7.79 (m, 4 H, 4 × b6), 7.87 (m, 2 H, m6′, m6), 8.09 (m, 4 H, b4), 8.59 (s, 1 H, m3′), 8.66 (m, 4 H, 4 × b3), 8.94 (s, 1 H, m3). − IR (KBr pellets, cm^{-1}): $\tilde{\nu}$ = 3086 (m), 1736 (m), 1665 (s), 1542 (m), 1468 (m), 1448 (m), 1310 (m), 841 (vs, PF_6^-), 765 (s), 558 (s). − UV/Vis (H_2O): λ_{max} (lg ε, M^{-1} cm^{-1}) = 456 (4.25), 287 (4.95), 245 nm (4.45). − FAB$^+$ (*m*-NBA): *m*/*z* = 1031 [$M^+ - PF_6^-$], 886 [$M^+ - 2\ PF_6^-$]. − $C_{39}H_{43}F_{18}N_8OP_3Ru{\cdot}H_2O$ (1175.8 + 18): calcd. C 39.24, H 3.80, N 9.39; found C 38.91, H 3.75, N 9.00.

4c: Yield: 234 mg (71%). − ^{1}H NMR (300 MHz, CD_3OD): δ = 1.45 [m, 2 H, $(CH_2)_3CH_2CH_2N(CH_3)_3^+$], 1.75 [m, 4 H, $CH_2CH_2CH_2(CH_2)_2N(CH_3)_3^+$], 2.58 (s, 3 H, m4′-$CH_3$), 3.08 [s, 9 H, $N(CH_3)_3^+$], 3.29 [t, 2 H, $(CH_2)_4CH_2N(CH_3)_3^+$], 3.48 [t, 2 H, $CH_2(CH_2)_4N(CH_3)_3^+$], 7.30 (d, 1 H, m5′), 7.46 (m, 4 H, b5), 7.55 (d, 1 H, m5), 7.75 (m, 4 H, 4 × b6), 7.83 (m, 2 H, m6′, m6), 8.07 (m, 4 H, b4), 8.53 (s, 1 H, m3′), 8.59 (d, 4 H, 4 × b3), 8.88 (s, 1 H, m3). − IR (KBr pellets, cm^{-1}): $\tilde{\nu}$ = 3085 (m), 1734 (m), 1667 (s), 1541 (m), 1468 (m), 1448 (m), 1310 (m), 842 (vs, PF_6^-), 765 (s), 558 (s). − UV/Vis (H_2O): λ_{max} (lg ε, M^{-1} cm^{-1}) = 456 (4.27), 288 (4.95), 245 nm (4.44). − FAB$^+$ (*m*-NBA): *m*/*z* = 1045 [M^+ − PF_6^-], 900 [M^+ − 2 PF_6^-]. − $C_{40}H_{45}F_{18}N_8OP_3Ru{\cdot}H_2O$ (1189.8 + 18): calcd. C 39.78, H 3.92, N 9.28; found C 39.86, H 4.30, N 9.06.

Methods: Steady state luminescence spectra were recorded in deoxygenated demineralized water with a Perkin−Elmer LS 50B spectrofluorimeter equipped with a red-sensitive Hamamatsu R928 photomultiplier tube. 10 μM solutions of the complexes at different pH values were used and the emission spectra were corrected for imperfections of the instrument.

The emission and NMR titration curves for $[Ru(bipy)_2\{m\text{-}CONH(CH_2)_nNH_3^+\}](PF_6)_3$ **1b−4b** were obtained as described previously.[19]

Emission lifetimes were measured following excitation of the sample with a laser pulse at 450 nm as delivered by a Nd-YAG laser (B.M. Industries, 5021 DNS/DPS 10, λ = 1064 nm, harmonic generation of 532, 355 and 266 nm, respectively, laser pulse with $\tau_L \approx 6$ ns, beam diameter $d = 7$ mm and maximal repetition rate $f = 10$ Hz, laser pulse energy E_L at the location of the sample ≈ 1 mJ) coupled with an optical parametrical oscillator (OPO, B.M. Industries, OP 901) for generation of the excitation wavelength. Time-resolved detection of the luminescence of the sample after laser excitation was done with a photomultiplier tube in combination with a monochromator (λ_{em} = 630 nm, time resolution 250 ns and 20 ns). The signal of the photomultiplier was read out by a digital storage oscilloscope (DSO, Gould 4072) and transferred to a personal computer for processing, storage and output. All measurements were made with samples previously deoxygenated by purging with nitrogen. The complex concentration was 10 μM in all cases.

Cyclic voltammetry was performed with a PAR potentiostat 263 using a three-electrode cell with glassy carbon working, Ag/AgCl reference and Pt counter electrodes. Deoxygenated acetonitrile solutions of the complexes containing $TBABF_4$ (10^{-1} M) as supporting electrolyte were used. $E_{1/2}$ values were calculated from half the difference between E_P values for the anodic and cathodic waves from cyclic voltammograms. The ferrocene-ferrocenium couple was observed at 0.45 V (ΔE_P = 88 mV) in acetonitrile under the measurement conditions.

[1] F. Osterkamp, B. Ziemer, U. Koert, M. Wiesner, P. Raddatz, S. L. Goodman, *Chem. Eur. J.* **2000**, *6*, 666−683.
[2] B. Imperiali, R. S. Roy, *J. Am. Chem. Soc.* **1994**, *116*, 12083−12084.
[3] B. Imperiali, R. S. Roy, *Tetrahedron Lett.* **1996**, *37*, 2129−2132.
[4] T. Carell, J. Butenandt, *Angew. Chem.* **1997**, *109*, 1590−1593; *Angew. Chem. Int. Ed. Engl.* **1997**, *36*, 1461−1464.
[5] B. M. Cole, K. D. Shimizu, C. A. Krueger, J. P. A. Harrity, M. L. Snapper, A. H. Hoveyda, *Angew. Chem.* **1996**, *108*, 1776−1779; *Angew. Chem. Int. Ed. Engl.* **1996**, *35*, 1668−1671.
[6] B. Jandeleit, D. J. Schaefer, T. S. Powers, H. W. Turner, W. H. Weinberg, *Angew. Chem.* **1999**, *111*, 2648−2689; *Angew. Chem. Int. Ed.* **1999**, *38*, 2495−2532.
[7] K. D. Shimizu, B. M. Cole, C. A. Krueger, K. W. Kuntz, M. L. Snapper, A. H. Hoveyda, *Angew. Chem.* **1997**, *109*, 1782−1785; *Angew. Chem. Int. Ed. Engl.* **1997**, *36*, 1703−1707.
[8] D. G. McCafferty, B. M. Bishop, C. G. Wall, S. G. Hughes, S. L. Mecklenburg, T. J. Meyer, B. W. Erickson, *Tetrahedron* **1995**, *51*, 1093−1106.
[9] B. M. Peek, G. T. Ross, S. W. Edwards, G. J. Meyer, T. J. Meyer, B. W. Erickson, *Int. J. Pept. Protein Res.* **1991**, *38*, 114−123.
[10] M. R. DeFelippis, M. Faraggi, M. H. Klapper, *J. Am. Chem. Soc.* **1990**, *112*, 5640−5642.
[11] M. Faraggi, M. R. DeFelippis, M. H. Klapper, *J. Am. Chem. Soc.* **1989**, *111*, 5141−5145.
[12] E. Galoppini, M. A. Fox, *J. Am. Chem. Soc.* **1996**, *118*, 2299−2300.
[13] S. S. Isied, M. Y. Ogawa, J. F. Wishart, *Chem. Rev.* **1992**, *92*, 381−394.
[14] X. G. Chen, P. Li, J. S. W. Holtz, Z. Chi, V. Pajcini, S. A. Asher, L. A. Kelly, *J. Am. Chem. Soc.* **1996**, *118*, 9705−9715.
[15] V. Pajcini, X. G. Chen, R. W. Bormett, S. J. Geib, P. Li, S. A. Asher, E. G. Lidiak, *J. Am. Chem. Soc.* **1996**, *118*, 9716−9726.
[16] Y. Wang, R. Purrello, S. Georgiou, T. G. Spiro, *J. Am. Chem. Soc.* **1991**, *113*, 6368−6377.
[17] R. R. Hill, J. D. Coyle, D. Birch, E. Dawe, G. E. Jeffs, D. Randall, I. Stec, T. M. Stevenson, *J. Am. Chem. Soc.* **1991**, *113*, 1805−1817.
[18] C. Seidel, A. Orth, K.-O. Greulich, *Photochem. Photobiol.* **1993**, *58*, 178−184.
[19] B. Geißer, A. Ponce, R. Alsfasser, *Inorg. Chem.* **1999**, *38*, 2030−2037.
[20] R. S. Drago, D. C. Ferris, N. Wong, *J. Am. Chem. Soc.* **1990**, *112*, 8953−8961.
[21] R. S. Drago, N. Wong, D. C. Ferris, *J. Am. Chem. Soc.* **1991**, *113*, 1970−1977.
[22] L. P. Hammett, *Chem. Rev.* **1936**, *17*, 125−136.
[23] R. W. Taft, Jr., *Separation of Polar, Steric and Resonance Effects in Reactivity* (Ed.: M. S. Newman), Wiley, New York, **1956**, pp 556ff.
[24] A. M. Josceanu, P. Moore, S. C. Rawle, P. Sheldon, S. M. Smith, *Inorg. Chim. Acta* **1995**, *240*, 159−168.
[25] K. H. Scheller, V. Scheller-Krattiger, R. B. Martin, *J. Am. Chem. Soc.* **1981**, *103*, 6833−6839.
[26] T. Kiss, *Complexes of Amino Acids* (Ed.: K. Burger), Ellis Horwood, New York, **1990**, pp 56−134.
[27] R. C. Weast, *CRC Handbook of Chemistry and Physics* 51st ed., The Chemical Rubber Co., Cleveland, **1970**.
[28] S. L. Mecklenburg, B. M. Peek, J. R. Schoonover, D. G. McCafferty, C. G. Wall, B. W. Erickson, T. J. Meyer, *J. Am. Chem. Soc.* **1993**, *115*, 5479−5495.
[29] S. L. Mecklenburg, D. G. McCafferty, J. R. Schoonover, B. M. Peek, B. W. Erickson, T. J. Meyer, *Inorg. Chem.* **1994**, *33*, 2974−2983.
[30] T. R. Thomas, R. J. Watts, G. A. Crosby, *J. Chem. Phys.* **1973**, *59*, 2123−2131.
[31] H. Sun, M. Z. Hoffman, *J. Phys. Chem.* **1993**, *97*, 11956−11959.
[32] J. van Houten, R. J. Watts, *J. Am. Chem. Soc.* **1976**, *98*, 4853−4858.
[33] J. V. Caspar, B. P. Sullivan, E. M. Kober, T. J. Meyer, *Chem. Phys. Lett.* **1982**, *91*, 91−95.
[34] J. V. Caspar, T. J. Meyer, *J. Am. Chem. Soc.* **1983**, *105*, 5583−5590.
[35] B. Durham, J. V. Caspar, J. K. Nagle, T. J. Meyer, *J. Am. Chem. Soc.* **1982**, *104*, 4803−4810.
[36] Z. Murtaza, D. K. Graff, A. P. Zipp, L. A. Worl, W. E. Jones, W. D. Bates, T. J. Meyer, *J. Phys. Chem.* **1994**, *98*, 10504−10513.
[37] G. F. Strouse, J. R. Schoonover, R. Duesing, S. Boyde, W. E. Jones, Jr., T. J. Meyer, *Inorg. Chem.* **1995**, *34*, 473−487.
[38] J. A. Treadway, B. Loeb, R. Lopez, P. A. Anderson, F. R. Keene, T. J. Meyer, *Inorg. Chem.* **1996**, *35*, 2242−2246.
[39] J. Hinze, H. H. Jaffé, *J. Am. Chem. Soc.* **1962**, *84*, 540−546.
[40] J. Hinze, H. H. Jaffé, *J. Phys. Chem.* **1963**, *67*, 1501−1506.
[41] J. Hinze, M. A. Whitehead, H. H. Jaffé, *J. Am. Chem. Soc.* **1963**, *85*, 148−154.
[42] P. Zuman, R. Patel, *Techniques in Organic Reaction Kinetics*, Wiley, New York, **1984**.

[43] G. L. Gaines, *J. Phys. Chem.* **1979**, *83*, 3088−3091.
[44] F. D. Lewis, J. M. Wagner-Brennan, J. M. Denari, *J. Phys. Chem. A* **1998**, *102*, 519−525.
[45] J. G. Kirkwood, F. H. Westheimer, *J. Chem. Phys.* **1938**, *6*, 506−512.
[46] S. L. Mecklenburg, B. M. Peek, B. W. Erickson, T. J. Meyer, *J. Am. Chem. Soc.* **1991**, *113*, 8540−8542.
[47] H. B. Gray, J. R. Winkler, *Annu. Rev. Biochem.* **1996**, *65*, 537−561.
[48] B. P. Sullivan, D. J. Salmon, T. J. Meyer, *Inorg. Chem.* **1978**, *17*, 3334−3341.
[49] J. van Houten, R. J. Watts, *Inorg. Chem.* **1978**, *17*, 3381−3385.
Received July 14, 2000
[I00276]

Construction of Various Supramolecules by π−π Interactions: Self-Assembly of Nickel(II) Macrocyclic Complexes Containing Pyridine Pendant Arms with Bidentate Ligands

Kil Sik Min[a] and Myunghyun Paik Suh*[a]

Keywords: Macrocyclic ligands / Nickel / Self-assembly / π−π interactions / Supramolecular chemistry

The supramolecular compounds, $[Ni(C_{20}H_{32}N_8)(en)](ClO_4)_2 \cdot 2\,H_2O$ (**1**), $[Ni(C_{20}H_{32}N_8)(isonicotinate)_2]$ (**2**), and $[Ni(C_{20}H_{32}N_8)(BQDC)] \cdot 3\,H_2O$ (**3**), have been constructed by the self-assembly of a nickel(II) macrocyclic complex containing pyridyl pendant rings, $[Ni(C_{20}H_{32}N_8)](ClO_4)_2 \cdot 2\,H_2O$, with ethylenediamine (hereafter noted en), isonicotinic acid, and potassium 2,2′-biquinoline-4,4′-dicarboxylate, ($K_2BQDC \cdot 3\,H_2O$), respectively, in $MeCN/H_2O$. The X-ray crystal structure of **1** indicates that one en coordinates a nickel(II) macrocyclic complex to form a folded macrocyclic complex, which ends up with a stacking dimer via C–H···π and offset face-to-face π–π interactions between the pyridine pendant groups. The X-ray crystal structure of **2** indicates that two isonicotinate ions coordinate a nickel(II) macrocyclic complex at the axial positions and the pyridine groups of the coordinated isonicotinates are involved in offset face-to-face π–π interactions, which gives rise to a 1D chain. The 1D chains are linked together via the offset face-to-face π–π interactions between the pyridine groups of the macrocycle to generate a 2D network. The X-ray crystal structure of **3** indicates that each $BQDC^{2-}$ ion coordinates two nickel(II) macrocyclic complexes and each nickel(II) macrocyclic unit binds two $BQDC^{2-}$ ions at the axial positions to form a 1D chain. The 1D chains experience the intramolecular hydrogen bonding as well as the interchain offset face-to-face π–π interactions between the pyridyl pendant rings of the macrocycle and the $BQDC^{2-}$ ions, which gives rise to a 2D sheet. Between the 2D sheets herringbone π–π interactions exist, which results in a 3D framework.

Introduction

Self-assembly of organic molecules and metal-ion building blocks may yield a new generation of multidimensional supramolecular networks. In the assembly of the supramolecules, hydrogen bonding,[1] π−π stacking interaction,[2] and C−H···π interaction[3], besides the metal−ligand coordination, are utilized to induce intermolecular interactions.[4] In particular, supramolecules built by noncovalent interactions between aromatic rings are of great importance because of the potential applications for molecular recognition,[5] catalysis,[6] stabilizing protein structure,[7] and molecular devices.[8] To become a new class of solid materials, the supramolecules should be insoluble and the frameworks should be maintained, even after the removal of the guest molecules or restored upon reintroduction of the guest molecules. For this purpose, extensive intermolecular interactions, hopefully multidimensional ones, should exist in the solid. In particular, the control of dimensionality of the supramolecules is a challenging subject in the self-assembly since the ancillary ligation by solvent or anion may result in low dimensionality.

To obtain insoluble supramolecules which are constructed by the extensive π−π stacking interactions as well as the metal−ligand coordination, we have employed in the self-assembly the nickel(II) macrocyclic complex containing pyridine pendants (**A**) as a metal building block and the bidentate ligands such as en, isonicotinate, and 2,2′-biquinoline-4,4′-dicarboxylate ($BQDC^{2-}$) as the organic building blocks (Figure 1). We have obtained a dimer $[Ni(C_{20}H_{32}N_8)(en)](ClO_4)_2 \cdot 2\,H_2O$ (**1**), a 2D sheet $[Ni(C_{20}H_{32}N_8)(isonicotinate)_2]$ (**2**), and a 3D network $[Ni(C_{20}H_{32}N_8)(BQDC)] \cdot 3\,H_2O$ (**3**), respectively, from the self-assembly. Here, we report X-ray crystal structures and properties of these supramolecules.

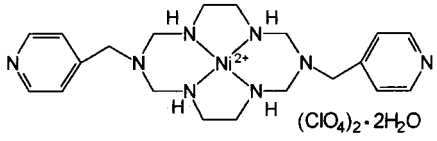

A: $[Ni(L)](ClO_4)_2 \cdot 2H_2O$

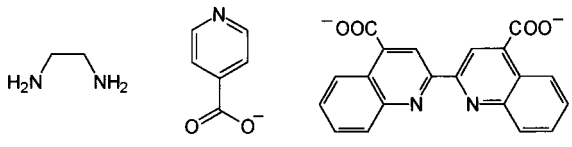

en **isonicotinate** **$BQDC^{2-}$**

Figure 1. Building blocks employed in the self-assembly of **1**−**3**

[a] School of Chemistry and Center for Molecular Catalysis, Seoul National University, Seoul 151-742, Republic of Korea
Fax: (internat.) + 82-2/886-8516
E-mail: mpsuh@plaza.snu.ac.kr

Supporting information for this article is available on the WWW under http://www.wiley-vch.de/home/eurjic or from the author.

 © WILEY-VCH Verlag GmbH, 69451 Weinheim, 2001 1434−1948/01/0202−0449 $ 17.50+.50/0

Results and Discussion

Properties and X-ray Crystal Structure of $[Ni(C_{20}H_{32}N_8)(en)](ClO_4)_2 \cdot 2\,H_2O$ (1)

Compound **1** was prepared in $MeCN/H_2O$ by the self-assembly of nickel(II) macrocyclic complex **A** with en. It is soluble in DMF, DMSO, and $MeNO_2$/MeOH. The infrared spectrum (Nujol mull) shows $\nu_{C=N}$ of pyridine pendant rings at 1605 cm^{-1}, ν_{NH} of the primary amines of en at 3335 and 3270 cm^{-1}, and ν_{NH} of the secondary amines of macrocycle at 3182 cm^{-1}. The value of molar conductance (Λ_M) measured in DMSO is 70 $\Omega^{-1}cm^2mol^{-1}$, which corresponds to a 1:2 electrolyte.[9] The electronic absorption spectrum shows a d−d transition band at 532 nm (ε = 9), which corresponds to the characteristic chromophore of a nickel(II) ion coordinated with an N_4 macrocycle and an N_2 bidentate ligand.[10]

An ORTEP drawing of **1** is shown in Figure 2a and the selected bond lengths and angles are listed in Table 1. The nickel(II) ion displays distorted octahedral coordination geometry by coordination with the four secondary amine nitrogen atoms of the macrocycle in a folded conformation and the two nitrogen atoms of en in the *cis* positions. The average Ni−N bond length is 2.136(1) Å, which is longer than that for octahedral nickel(II) complex coordinated with N_4O_2 donors.[11] In the structure, one pyridine pendant group of the macrocyclic complex experiences C−H···π interaction[3] as well as offset face-to-face π−π interaction[2,12] with a pyridine pendant group belonging to a neighboring macrocyclic complex, which leads to a stacked dimer (Figure 2b). For the C−H···π interaction, the distance between the centroid of the pyridine pendant ring and the nearest carbon atom of the pendant group is 3.579 Å (H11A···centroid 2.699 Å, C11−H11A···centroid 159.4°).[13] For the π−π stacking interaction, the interplanar separation of the aromatic rings is 3.63−3.65 Å (centroid···centroid 4.741 Å) and the dihedral angle between the ring planes is 0.0°. The lattice water molecules form hydrogen bonds with the nitrogen atoms of the pyridine pendant groups: O9···N9 2.875(5) Å, O10···N10 2.789(5) Å. In addition, the oxygen atoms of the perchlorate anion form hydrogen bonds with a secondary amine of the macrocycle [O8···N4($-x$ + 1, $-y$ + 1, $-z$ + 1) 3.172(5) Å, O8−H4−N4 171.2°] and the primary amines of en [O3···N7($-x$, $-y$ + 1, $-z$) 3.155(6) Å, O3−H7A−N7 162.1°; O1···N8(x, y − 1, z) 3.202(6) Å, O1−H8B−N8 170.2°].

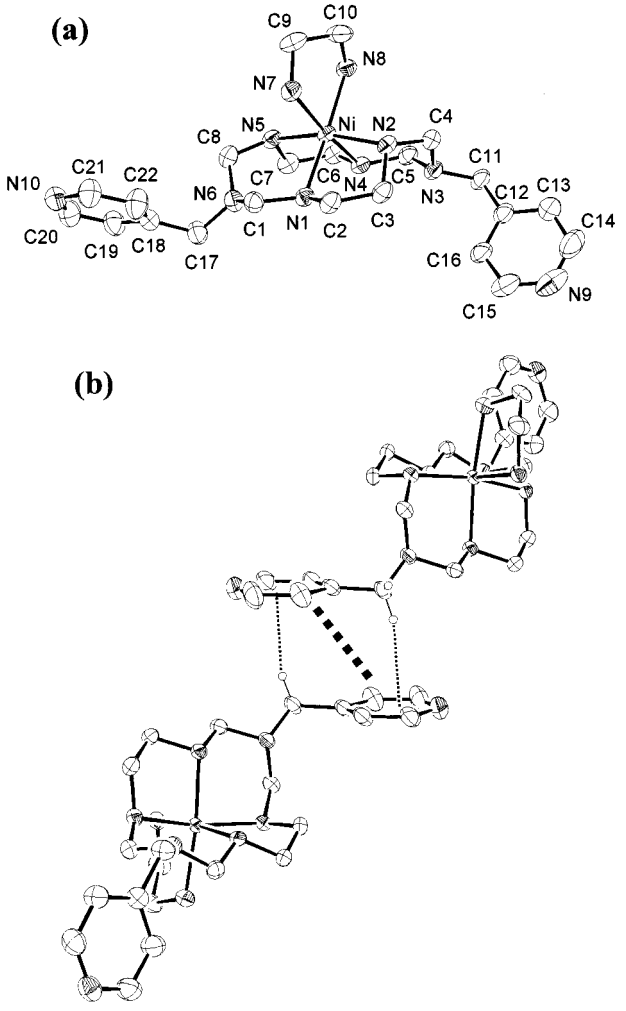

Figure 2. (a) ORTEP drawing of **1** with atomic numbering scheme; the atoms are represented by 40% probable thermal ellipsoids; (b) perspective view of **1**, showing a dimer; the C−H···π interactions are indicated as •••; the offset face-to-face π−π interaction between pyridine groups leading to a dimer is indicated as ■■■

Table 1. Selected bond lengths [Å] and angles [°] for **1**−**3**

$[Ni(C_{20}H_{32}N_8)(en)](ClO_4)_2 \cdot 2\,H_2O$ (**1**)			
Ni−N1	2.124(3)	Ni−N5	2.138(3)
Ni−N2	2.151(3)	Ni−N7	2.140(3)
Ni−N4	2.115(3)	Ni−N8	2.146(3)
N1−Ni−N2	82.21(10)	N2−Ni−N8	95.91(12)
N1−Ni−N4	94.44(11)	N4−Ni−N5	82.64(11)
N1−Ni−N5	88.63(11)	N4−Ni−N7	171.88(12)
N1−Ni−N7	93.47(12)	N4−Ni−N8	91.98(11)
N1−Ni−N8	173.26(11)	N5−Ni−N7	95.73(13)
N2−Ni−N4	88.79(11)	N5−Ni−N8	94.22(13)
N2−Ni−N5	166.95(11)	N7−Ni−N8	80.18(12)
N2−Ni−N7	94.10(13)		
$[Ni(C_{20}H_{32}N_8)(isonicotinate)_2]$ (**2**)			
Ni−N1	2.062(5)	O1−C11	1.247(8)
Ni−N2	2.021(6)	O2−C11	1.255(8)
Ni−O1	2.135(4)	N3−C1[a]	1.421(9)
N1−Ni−N2	86.8(2)	O1−C11−O2	127.7(5)
N1−Ni−O1	91.94(16)	O1−C11−C12	116.4(7)
N2−Ni−O1	92.60(17)	O2−C11−C12	115.9(6)
$[Ni(C_{20}H_{32}N_8)(BQDC)] \cdot 3\,H_2O$ (**3**)			
Ni−N1	2.048(5)	O1−C11	1.238(7)
Ni−N2	2.080(5)	O2−C11	1.251(7)
Ni−O1	2.110(4)	C14−C14[b]	1.410(12)
N1−Ni−N2	84.91(18)	O1−C11−O2	125.1(7)
N1−Ni−O1	93.50(18)	O1−C11−C12	114.6(6)
N2−Ni−O1	91.6(2)	O2−C11−C12	120.2(6)

[a] Marked atoms are generated by symmetry operations: $-x$, $-y$, $-z$. − [b] $-x$ − 1, $-y$, $-z$.

Properties and X-ray Crystal Structure of [Ni($C_{20}H_{32}N_8$)(isonicotinate)$_2$] (2)

Compound **2** was prepared in MeCN/H_2O by the self-assembly of nickel(II) macrocyclic complex **A** with isonicotinate. It is insoluble in any solvents. The infrared spectrum (Nujol mull) shows $\nu_{C=N}$ of pyridine pendant groups at 1596 cm^{-1}, $\nu_{C=O}$ of the carboxylate groups coordinating the macrocyclic complex at 1547 cm^{-1}, and ν_{NH} of the secondary amines of macrocycle at 3213 and 3140 cm^{-1}. Two split secondary amine peaks of the nickel(II) complex indicate that the compound has two kinds of secondary amines, which is attributed to the hydrogen bonding interactions of the two secondary amines of the macrocycle as revealed by the X-ray crystal structure. The diffuse reflectance spectrum shows maximum absorption at 510 nm, which corresponds to the characteristic chromophore for the nickel(II) ion coordinated with N_4O_2 donors.[10]

An ORTEP drawing of **2** is shown in Figure 3a and the selected bond lengths and angles are listed in Table 1. The coordination geometry around the nickel(II) ion is a tetragonally distorted octahedron in which the nickel(II) ion is coordinated with the four secondary amine nitrogen atoms of the macrocycle in the square-planar fashion and two oxygen atoms from two isonicotinate ions at the axial sites. The average Ni−N and Ni−O bond lengths are 2.053(2) and 2.130(3) Å, respectively. All pyridine groups of the isonicotinate ions coordinating nickel(II) ions are involved in offset face-to-face π−π interactions by themselves (centroid···centroid 3.673 Å),[12] which leads to a supramolecular 1D polymer propagating along the *c* axis (Figure 3b). The interplanar separation and the offset angle between the ring planes of isonicotinate ions are 3.46−3.47 Å and 11.2°, respectively. Within a 1D chain, the free carbonyl oxygen atom of the coordinated carboxylate ion forms an intramolecular hydrogen bond with the secondary amine of the macrocycle [O2···N2 2.883(6) Å, O2−H2−N2 155.6°]. Therefore, two C−O bond lengths of the carboxylate group are not significantly different although one is coordinated [1.247(8) Å] and the other is uncoordinated [1.255(8) Å] to the nickel(II) ion. The 1D polymers are linked together via offset face-to-face π−π interactions between the pyridine rings of the macrocycle, which leads to a 2D network extending along the [1$\bar{1}$0] plane (Figure 3c). The pyridine rings are positioned completely parallel to each other with the dihedral angle of 0.0°. The intercentroid distance and the offset angle between the ring planes are 4.847 Å and 47.6°, respectively.

Properties and X-ray Crystal Structure of [Ni($C_{20}H_{32}N_8$)(BQDC)] · 3 H_2O (3)

Compound **3** was prepared in MeCN/H_2O by the self-assembly of nickel(II) macrocyclic complex **A** with 2,2′-biquinoline-4,4′-dicarboxylate ($BQDC^{2-}$). It is stable and does not loose guest water molecules upon exposure to the atmosphere. The compound is insoluble in any solvents. The infrared spectrum (Nujol mull) of **3** shows ν_{NH} of the secondary amines of macrocycle at 3276 and 3181 cm^{-1}, $\nu_{C=N}$ of pyridine pendant groups at 1600 cm^{-1}, and $\nu_{C=O}$ of the carboxylate groups of $BQDC^{2-}$ at 1579 cm^{-1}. Two split secondary amine peaks of the nickel(II) complex indicate that the macrocycle has two kinds of secondary amines due to the hydrogen bonding interactions, which is revealed by the X-ray crystal structure. The diffuse reflectance spectrum shows maximum absorption at 502 nm, which corresponds to the characteristic chromophore for the nickel(II) ion coordinated with N_4O_2 donors.[10] The TGA trace of **3** (Figure S1, Supporting Information) shows a weight loss of 5.65% at 80 °C, corresponding to the loss of three guest water molecules per unit formula. No chemical decomposition was observed up to 250 °C.

An ORTEP drawing of **3** is shown in Figure 4a and the selected bond lengths and angles are listed in Table 1. Each nickel(II) ion of macrocyclic complex **A** is coordinated by two carboxylate oxygen atoms of $BQDC^{2-}$ ion at the axial positions as well as the N_4 macrocycle to display a distorted octahedral coordination geometry. Since each $BQDC^{2-}$ ion binds two metal ions in an *exo*-bidentate mode, **3** becomes a linear coordination polymer (Figure 4b). The average Ni−N and Ni−O bond lengths are 2.064(3) and 2.110(3) Å, respectively. The aromatic ring of $BQDC^{2-}$ ion is tilted [dihedral angle = 67.5(2)°] with respect to the square coordination plane of the macrocycle. The $BQDC^{2-}$ bridging ligand is not planar since the dihedral angle between the carboxylate group and the aromatic ring of $BQDC^{2-}$ ion is 30.6(3)°. The dihedral angle between the carboxylate plane and the macrocyclic coordination plane involving nickel atom is 87.4(6)°. Within a 1D chain, intramolecular hydrogen bonding interactions exist between the uncoordinated oxygen atoms of carboxylate and the secondary amines of the macrocycle to form stable six-membered rings [O2···N1 2.915(7) Å, O2−H1−N1 150.7°]. Compound **3** has two kinds of 1D chains. The linear chains are linked by the offset face-to-face π−π interactions[12] between the aromatic groups of the $BQDC^{2-}$ ions belonging to a chain, and the pyridine pendant groups of the macrocycle belonging to the adjacent linear chains, which leads to a 2D network extending along the (002) plane (Figure 4c). The interplanar separation and the dihedral angle between the aromatic ring of $BQDC^{2-}$ ion and the pyridine pendant group of macrocyclic complex are 3.32−3.55 Å and 5.87°, respectively. Between the layers, there exist the herringbone π−π interactions between the $BQDC^{2-}$ ion and the pyridine pendant ring of macrocycle, which gives rise to a 3D network (Figure 4d). The distance between the centroids is 5.237 Å, and the dihedral angle between the pendant pyridine group and the aromatic ring of $BQDC^{2-}$ ion is 75.1(1)°. The separation between the layers is 10.697 Å. The shortest Ni···Ni distance within a linear chain is 13.451(5) Å and that between the linear chains is 12.968(4) Å. The lattice water molecules are located in the cavities created by the packed chains. The void volume of cavities per unit cell is 648 Å^3 (15.4%) as estimated by PLATON.[14] In addition, the lattice water molecules form hydrogen bonds with the uncoor-

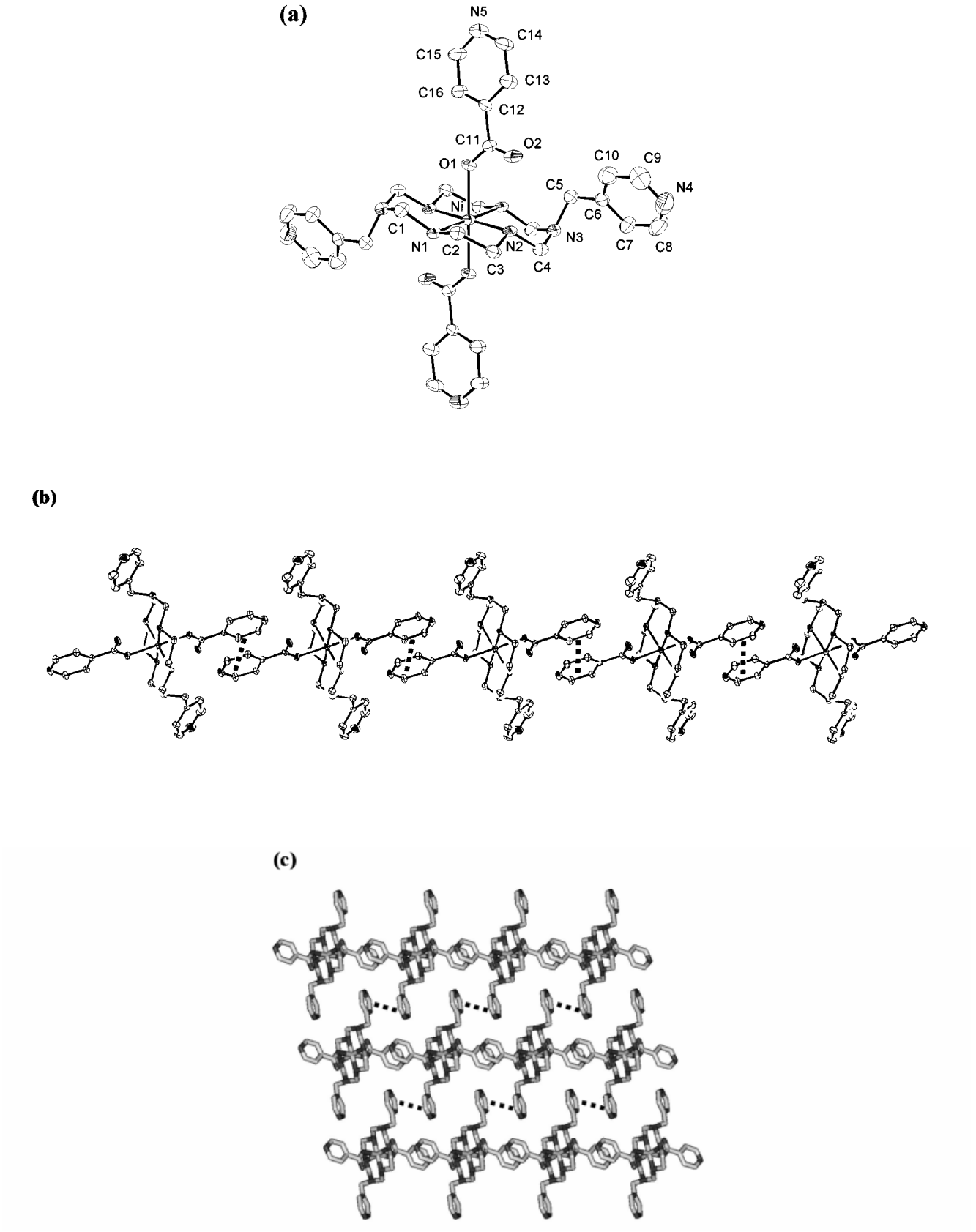

Figure 3. (a) ORTEP drawing of **2** with atomic numbering scheme; the atoms are represented by 40% probable thermal ellipsoids; (b) perspective view of **2** showing a 1D chain; the offset face-to-face π−π interactions between the coordinated isonicotinate ions are indicated as ■■■; (c) extended 2D structure of **2**; the interchain offset face-to-face π−π interactions are indicated as ■■■

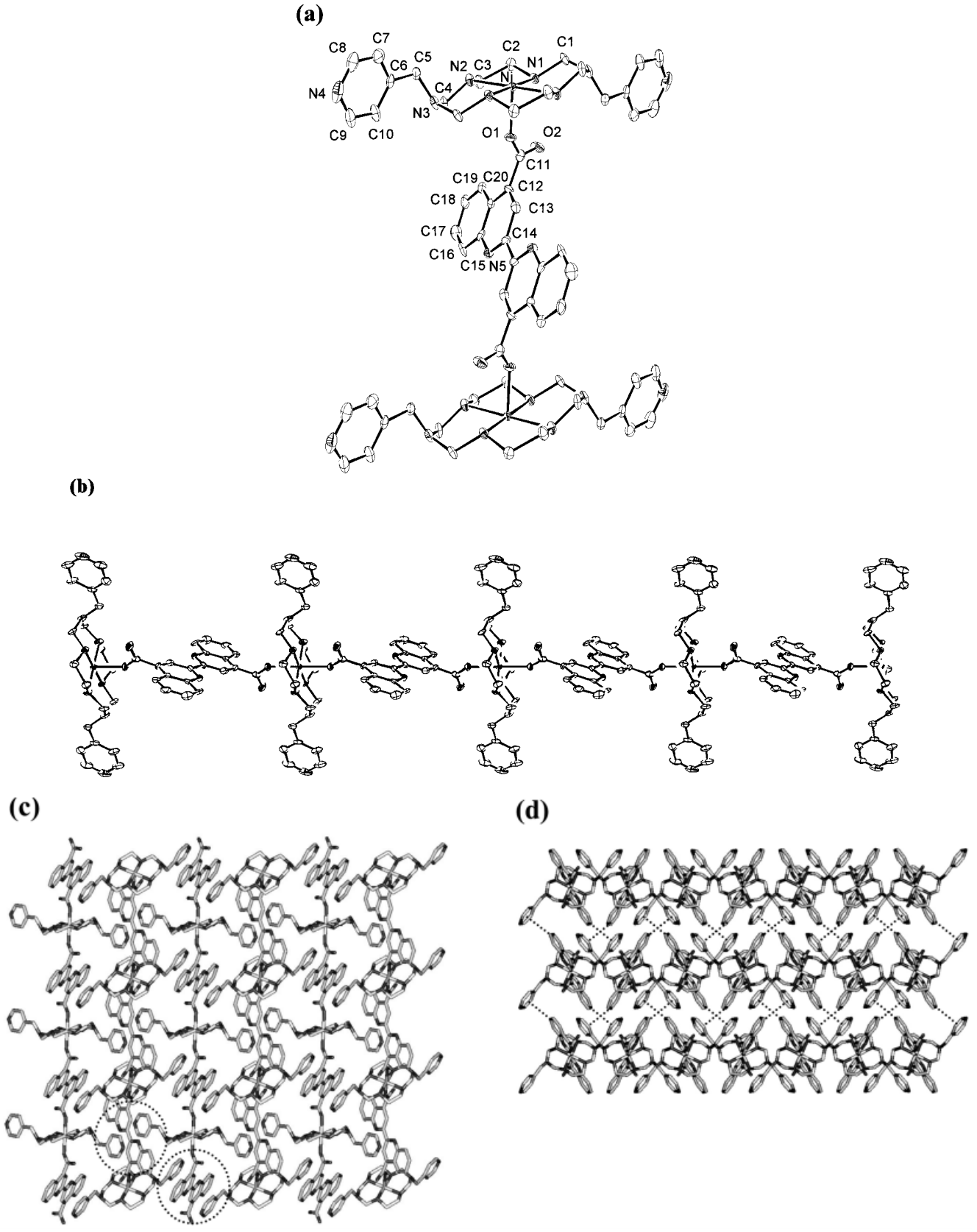

Figure 4. (a) ORTEP drawing of **3** with atomic numbering scheme; the atoms are represented by 20% probable thermal ellipsoids; (b) perspective view of **3** showing a 1D chain; (c) extended 2D structure of **3**; the interchain offset face-to-face π−π interactions are indicated as dotted circles; (d) side view of the packed structure of **3** showing the herringbone π−π interactions between the 2D layers, which are indicated as ●●●

dinated carboxylate oxygen atom [O2···O3($-1 + x$, y, z) = 2.757(8) Å], with the pyridine nitrogen atom of the macrocycle [O3···N4($1 + x$, $-0.5 - y$, $0.5 + z$) = 3.041(11) Å], and with the other lattice water molecule (O3···O4 = 2.754(7) Å).

Conclusion

We have constructed several supramolecules having structures of dimer, 2D sheet, and 3D framework by the self-assembly of a nickel(II) macrocyclic complex containing pyridyl pendant rings (**A**) with organic bidentate ligands such as en, isonicotinate, and 2,2′-biquinoline-4,4′-dicarboxylate, respectively. The supramolecules are assembled by the π−π stacking interactions involving aromatic rings of the organic ligand and the pyridine pendant groups attached to the macrocyclic ligand.

Experimental Section

General: All chemicals and solvents used in the synthesis were of reagent grade and used without further purification. − Infrared spectra were recorded with a Perkin−Elmer 2000 FT-IR spectrophotometer. − Elemental analyses were performed by the analytical laboratory of Seoul National University. − UV/Vis diffuse reflectance spectra were recorded with a Cary 300 Bio UV/Vis spectrophotometer. − Thermogravimetric analysis (TGA) and differential scanning calorimetry (DSC) were performed at a scan rate of 5 °C/min using a DuPont TGA 2050 TA instrument and a DuPont DSC 2100 TA instrument, respectively.

Safety Note: *Although we have experienced no problem with the compounds reported in this work, perchlorate salts of metal complexes with organic ligands are often explosive and should be handled with great caution!*

$[Ni(C_{20}H_{32}N_8)](ClO_4)_2 \cdot 2\,H_2O$ (A):[15] To a stirred methanol solution (75 mL) of $Ni(OAc)_2 \cdot 4\,H_2O$ (12.4 g, 0.05 mol), were slowly added ethylenediamine (6.8 mL, 0.10 mol), paraformaldehyde (6.0 g, 0.20 mol), and 4-(aminomethyl)pyridine (10.8 g, 0.10 mol). The mixture was heated at reflux for 24 h. The solution was filtered while hot and the filtrate was concentrated to ca. 1/5 of the original volume. $HClO_4$ (60%, 20 mL) was added to the yellow-brown solution and the solution was allowed to stand in a refrigerator until yellow crystals of $[Ni(L + 2\,H)](ClO_4)_4 \cdot 2\,H_2O$ formed, these were filtered off, washed with methanol, and dried in air. Yield: 35%. To an MeCN suspension (40 mL) of $[Ni(L + 2\,H)](ClO_4)_4 \cdot 2\,H_2O$ (2.5 g), was added an excess amount of triethylamine (2 mL). The complex went into the solution and yellow crystals of $[Ni(L)](ClO_4)_2 \cdot 2\,H_2O$ (**A**) formed in a few minutes. The crystals were filtered off, washed with water, and dried in air. − FT IR (Nujol mull, cm^{-1}): $\tilde{\nu}$ = 3590 (s, br.), 3195 (s), 1650 (m), 1605 (s), 1565 (m), 1100 (s), 625 (s). − UV/Vis ($MeNO_2$): λ_{max} [nm] (ε [M^{-1} cm^{-1}]) = 450 (68). − $C_{20}H_{36}Cl_2N_8NiO_{10}$ (678.2): calcd. C 35.42, H 5.35, N 16.52; found C 35.24, H 4.93, N 16.59.

$[Ni(C_{20}H_{32}N_8)(en)](ClO_4)_2 \cdot 2\,H_2O$ (1): To an MeCN/H_2O (v/v; 1:1, 20 mL) solution of **A** (0.50 g, 0.74 mmol), was added dropwise an MeCN solution (5 mL) of ethylenediamine (0.044 g, 0.74 mmol) at room temperature. The color of the solution turned from yellow to purple. The solution was allowed to stand at room temperature. The purple crystals formed, which were filtered off, washed with MeOH, and dried in air. Yield: 83%. − FT IR (Nujol mull, cm^{-1}): $\tilde{\nu}$ = 3650 (s), 3335 (s), 3270 (s), 3182 (s), 1605 (s), 1565 (s), 1100 (s). − UV/Vis (DMSO): λ_{max} [nm] (ε [M^{-1} cm^{-1}]) = 339 (14), 532 (9). − Molar conductance (DMSO): Λ_M [Ω^{-1} cm^2 mol^{-1}] = 70. − $C_{22}H_{44}Cl_2N_{10}NiO_{10}$ (738.3): calcd. C 35.79, H 6.01, N 18.97; found C 35.38, H 5.62, N 19.27.

$[Ni(C_{20}H_{32}N_8)(isonicotinate)_2]$ (2): To an MeCN/H_2O (v/v; 1:1, 20 mL) solution of **A** (0.50 g, 0.74 mmol), was added dropwise an MeCN solution (10 mL) containing isonicotinic acid (0.18 g, 1.48 mmol) and excess triethylamine (0.30 g, 2.96 mmol) at room temperature. The color of the solution turned from yellow to pale pink. The solution was allowed to stand at room temperature. The pale pink crystals formed, which were filtered off, washed with water, and dried in air. Yield: 85%. − FT IR (Nujol mull, cm^{-1}): $\tilde{\nu}$ = 3213 (s), 3140 (s), 1596 (s), 1565 (s), 1547 (s). − UV/Vis (diffuse reflectance): λ_{max} [nm] = 260, 510, 650. − $C_{32}H_{40}N_{10}NiO_4$ (687.4): calcd. C 55.91, H 5.87, N 20.38; found C 55.24, H 5.87, N 20.58.

$[Ni(C_{20}H_{32}N_8)(BQDC)] \cdot 3\,H_2O$ (3): To an MeCN/H_2O (v/v; 1:1, 20 mL) solution of **A** (0.50 g, 0.74 mmol), was added dropwise an aqueous solution (10 mL) containing potassium 2,2′-biquinoline-4,4′-dicarboxylate ($K_2BQDC \cdot 3\,H_2O$) (0.35 g, 0.74 mmol) at room temperature. The color of the solution turned from yellow to pale yellow. The solution was allowed to stand at room temperature. The pale yellow crystals formed, which were filtered off, washed with water, and dried in air. Yield: 79%. − FT IR (Nujol mull, cm^{-1}): $\tilde{\nu}$ = 3392 (s), 3277 (s), 3183 (s), 3074 (m), 1600 (s), 1579 (s), 1546 (m), 1492 (m), 1026 (s). − UV/Vis (diffuse reflectance): λ_{max} [nm] = 257, 334, 502, 682. − $C_{40}H_{42}N_{10}NiO_7$ (833.5): calcd. C 57.22, H 5.76, N 16.68; found C 56.41, H 5.68, N 16.76.

X-ray Diffraction Measurements: Single crystals of **1** (0.5 × 0.5 × 0.2 mm), **2** (0.2 × 0.2 × 0.06 mm), and **3** (0.6 × 0.7 × 0.08 mm) were mounted on an Enraf−Nonius CAD4 diffractometer. The unit cell parameters were determined from 25 machine-centered reflections with 22° ≤ 2θ ≤ 28° for **1**, 19° ≤ 2θ ≤ 29° for **2**, and 22° ≤ 2θ ≤ 28° for **3**). Intensities were collected with graphite-monochromated Mo-K_α radiation, using the ω-2θ scan mode. For **1**, among 5835 reflections measured in the range 3.30° ≤ 2θ ≤ 49.96°, 4460 were assumed to be observed [$F > 4\sigma(F)$]. For **2**, among 2206 reflections measured in the range 3.84° ≤ 2θ ≤ 50.16°, 1278 were assumed to be observed [$F > 4\sigma(F)$]. For **3**, among 3404 reflections measured in the range 3.80° ≤ 2θ ≤ 49.90°, 1322 were assumed to be observed [$F > 4\sigma(F)$]. Three standard reflections were measured every 2 h as orientation and intensity control and no significant intensity decay was observed. Lorentz and polarization corrections were made. No absorption correction was made. The crystal structure was solved by direct methods[16] for **1** and **3** and by Patterson synthesis[16] for **2**, and refined by full-matrix least-squares methods using the SHELXL97 computer program.[17] For **1**−**3**, the positions of all non-hydrogen atoms were refined with anisotropic displacement factors. In **1**, all hydrogen atoms were located and refined with isotropic thermal parameters except those of the lattice water molecules. In **2** and **3**, all hydrogen atoms were allowed to ride on their bonded atoms with the isotropic displacement factors fixed with values of 1.2 times those of the bonded atoms, except those of the lattice water molecules. The crystallographic data of **1**−**3** are summarized in Table 2. Crystallographic data (excluding structure factors) for the structures reported in this paper have been deposited with the Cambridge Crystallographic Data Centre as supplementary publication nos. CCDC-143549 to -143551. Copies of the data can be obtained free of

Table 2. Crystallographic data for **1**−**3**

	1	**2**	**3**
Empirical formula	$C_{22}H_{44}Cl_2N_{10}NiO_{10}$	$C_{32}H_{40}N_{10}NiO_4$	$C_{40}H_{42}N_{10}NiO_7$
Molecular mass	738.25	687.42	839.60
Crystal system	triclinic	triclinic	orthorhombic
Space group	$P\bar{1}$	$P\bar{1}$	*Pccn*
a [Å]	9.287(1)	8.386(3)	13.451(5)
b [Å]	12.363(2)	8.856(1)	14.662(5)
c [Å]	14.598(2)	10.941(4)	21.393(9)
α [°]	94.84(1)	103.37(2)	90
β [°]	93.75(1)	93.11(3)	90
γ [°]	91.12(1)	92.27(2)	90
V [Å^3]	1666.0(4)	788.3(4)	4219(3)
Z	2	1	4
$D_{calcd.}$ [g cm^{-3}]	1.472	1.448	1.322
T [K]	293(2)	293(2)	293(2)
λ [Å]	0.71069	0.71069	0.71069
μ [mm^{-1}]	0.808	0.671	0.520
F(000)	776	362	1768
Collected	6348	2375	3426
Unique	5835	2103	3404
Observed	4460	1411	1322
Parameters	566	214	264
GOF	1.033	1.020	0.954
R_1[a] (4σ data)	0.0468	0.0607	0.0731
wR_2[b] (4σ data)	0.1284	0.1473	0.1380

[a] $R_1 = \Sigma||F_o| - |F_c||/\Sigma|F_o|$. − [b] $wR_2 = [\Sigma w(F_o^2 - F_c^2)^2/\Sigma w(F_o^2)^2]^{1/2}$.

charge on application to CCDC, 12 Union Road, Cambridge CB2 1EZ, UK [Fax: (internat.) + 44-1223/336-033; E-mail: deposit@ccdc.cam.ac.uk].

Acknowledgments

This work was supported by the Basic Research Institute Program (BSRI98−3415) and the Korea Science and Engineering Foundation through the Center for Molecular Catalysis.

[1] S. Subramanian, M. J. Zaworotko, *Coord. Chem. Rev.* **1994**, *137*, 357.
[2] [2a] W. L. Jorgensen, D. L. Severance, *J. Am. Chem. Soc.* **1990**, *112*, 4768. − [2b] J. Harrowfield, *J. Chem. Soc., Dalton Trans.* **1996**, 3165. − [2c] B. F. Abrahams, P. A. Jackson, R. Robson, *Angew. Chem.* **1998**, *110*, 2801; *Angew. Chem. Int. Ed. Engl.* **1998**, *37*, 2656. − [2d] T. Yamamoto, D. Komarudin, M. Arai, B.-L. Lee, H. Suganuma, N. Asakawa, Y. Inoue, K. Kubota, S. Sasaki, T. Fukuda, H. Matsuda, *J. Am. Chem. Soc.* **1998**, *120*, 2047.
[3] [3a] L. R. Hanton, C. A. Hunter, D. H. Purvis, *J. Chem. Soc., Chem. Commun.* **1992**, 1134. − [3b] H.-C. Weiss, D. Bläser, R. Boese, B. M. Doughan, M. M. Haley, *Chem. Commun.* **1997**, 1703. − [3c] K. Jitsukawa, K. Iwai, H. Masuda, H. Ogoshi, H. Einaga, *J. Chem. Soc., Dalton Trans.* **1997**, 3691. − [3d] K. Biradha, M. J. Zaworotko, *J. Am. Chem. Soc.* **1998**, *120*, 6431.
[4] [4a] G. R. Desiraju, *Crystal Engineering: the Design of Organic Solids*, Elsevier, New York, **1989**, chapter 4. − [4b] M. Munakata, L. P. Wu, T. Kuroda-Sowa, *Bull. Chem. Soc. Jpn.* **1997**, *70*, 1727.
[5] [5a] L.-M. Lehn, *Angew. Chem.* **1990**, *102*, 1347; *Angew. Chem. Int. Ed. Engl.* **1990**, *29*, 1304. − [5b] J. E. Cochran, T. J. Parrott, B. J. Whitlock, H. W. Whitlock, *J. Am. Chem. Soc.* **1992**, *114*, 2269. − [5c] C. A. Hunter, *Chem. Soc. Rev.* **1994**, *23*, 101.
[6] [6a] T. R. Kelly, G. J. Bridger, C. Zhao, *J. Am. Chem. Soc.* **1990**, *112*, 8024. − [6b] R. Laatikainen, J. Ratilainen, R. Sebastian, H. Santa, *J. Am. Chem. Soc.* **1995**, *117*, 11006.
[7] [7a] S. K. Burley, G. A. Petsko, *Science* **1985**, *229*, 23. − [7b] A. S. Shetty, J. Zhang, J. S. Moore, *J. Am. Chem. Soc.* **1996**, *118*, 1019.
[8] [8a] J. A. Real, E. Andréz, M. C. Muñoz, M. Julve, T. Granier, A. Bousseksou, F. Varret, *Science* **1995**, *268*, 265. − [8b] K. Miyamura, A. Mihara, T. Fujii, Y. Goshi, Y. Ishii, *J. Am. Chem. Soc.* **1995**, *117*, 2377. − [8c] Z. J. Zhong, J.-Q. Tao, Z. Yu, C.-Y. Dun, Y.-J. Liu, X.-Z. You, *J. Chem. Soc., Dalton Trans.* **1998**, 327.
[9] W. J. Geary, *Coord. Chem. Rev.* **1971**, *7*, 81.
[10] F. L. Urbach, *Coordination Chemistry of Macrocyclic Compounds* (Ed.: G. A. Melson), Plenum Press, New York, **1979**, pp. 350−355.
[11] H. J. Choi, T. S. Lee, M. P. Suh, *Angew. Chem.* **1999**, *111*, 1490; *Angew. Chem. Int. Ed.* **1999**, *38*, 1405.
[12] [12a] K. E. Brancato-Buentello, W. R. Scheidt, *Angew. Chem.* **1997**, *109*, 1608; *Angew. Chem. Int. Ed. Engl.* **1997**, *36*, 1456. − [12b] E. Kimura, T. Ikeda, M. Shionoya, M. Shiro, *Angew. Chem.* **1995**, *107*, 711; *Angew. Chem. Int. Ed. Engl.* **1995**, *34*, 663.
[13] [13a] R. Hunter, R. H. Haueisen, A. Irving, *Angew. Chem.* **1994**, *106*, 588; *Angew. Chem. Int. Ed. Engl.* **1994**, *33*, 566. − [13b] J. A. Swift, R. Pal, J. M. McBride, *J. Am. Chem. Soc.* **1998**, *120*, 96.
[14] A. L. Spek, PLATON, *A Multipurpose Crystallographic Tool*, Utrecht University, Utrecht, The Netherlands, **1999**.
[15] K. S. Min, M. P. Suh, *Chem. Eur. J.*, in press.
[16] G. M. Sheldrick, *Acta Crystallogr.* **1990**, *A46*, 467.
[17] G. M. Sheldrick, *SHELXL-97*, *Program for the refinement of crystal structures*, University of Göttingen: Göttingen, Germany, **1997.**

Received May 2, 2000
[I00170]

An Accidental Discovery of a New Mixed-Valent Iodine Compound – Crystal Structure of Difluoroiodato(V) Iodine(III) Dichloride [$Cl_2IOI(O)F_2$]

Rolf Minkwitz*[a] and Michael Berkei[a]

Keywords: Iodine / Mixed-valent compounds / Vibrational spectroscopy / Structure elucidation / Halogens

The crystal structure of the novel iodine compound $Cl_2IOI(O)F_2$ is described. $Cl_2IOI(O)F_2$ contains iodine in two different oxidation states (III) and (V) and can formally be described as $ICl_2^+IF_2O_2^-$, linked by an unsymmetrical, nonlinear I–O–I bridge, with I–O bond lengths of 1.84(1) Å and 2.32(1) Å, and a bond angle of 122.5(5)°. It was accidentally obtained by the uncontrolled reaction between CF_3I, CF_3OCl, CF_2O, and Cl_2 at –70 °C over a period of about six months and finally two days at room temperature. $Cl_2IOI(O)F_2$ crystallises in the monoclinic space group $P2_1/c$ with four formula units per unit cell with the dimensions a = 12.910(1), b = 6.987(1), c = 7.550(1) Å, and β = 94.890(1)°. The molecule was additionally characterised by its Raman and IR spectra.

Introduction

Compounds containing iodine in different oxidation states are rather rare, and in most cases limited to polyiodide anions and cations. In neutral compounds, comproportionation to give the more stable oxidation state often takes place. An example of a stable mixed-valent iodine compound is $I(OSO_2F)_2I$.[1] It formally contains an iodine(III) and an iodide(−I). The I−I bond has a length of 2.676(1) Å and shows no ionic character, as might be expected.[1] Another example was reported by Kraft and Jansen in 1996.[2] The authors described the synthesis and characterisation of iodine trioxide I_4O_{12} which contains iodine in the oxidation states (V) and (VII).[2] In 1992, Rehr and Jansen determined the crystal structure of $(IO_2)_3HSO_4$ and reported a complex iodoxo polycation with iodine(III) and (V).[3] It seems that oxygen stabilises these compounds by secondary bonding, so that the tendency to comproportionation becomes negligible.

In this work we report the accidental preparation and crystal structure of difluoroiodato(V) iodine(III) dichloride [$Cl_2IOI(O)F_2$], a singular example of an iodine oxofluoride chloride with mixed-valent iodine atoms.

Results and Discussion

Formation of $Cl_2IOI(O)F_2$

$Cl_2IOI(O)F_2$ was accidentally obtained by the uncontrolled reaction between CF_3I, CF_3OCl, CF_2O, and Cl_2. These compounds were stored in a closed Pyrex ampoule at −70 °C over a period of about six months. After this time the formation of a yellow-orange solid beneath a yellow liquid was observed. The solid was thought to be I_2Cl_6 and so the ampoule was broken and introduced into an outlet at room temperature. Two days later, orange and red crystals were observed in the ampoule, which also contained a yellow gas. The ampoule was then stored under nitrogen at −70 °C, because on exposure to air the crystals were observed to decompose.

All solids were characterised by single crystal X-ray diffraction. The red solid was identified as α-ICl and the orange one as a mixture of I_2Cl_6 and $Cl_2IOI(O)F_2$. We think that the formation of $Cl_2IOI(O)F_2$ involves a complex mechanism, which is still unknown. Bearing in mind that the reaction between CF_3I and excess CF_3OCl yields IF_5, it is likely that IF_5 or a related iodine(V) oxofluoride is one possible intermediate in the formation of $Cl_2IOI(O)F_2$.[4−6] Attempts to repeat the synthesis of $Cl_2IOI(O)F_2$ failed. We decided to try to obtain an X-ray crystal structure and measure the Raman and IR spectra first, and used all the available material. Because of the small quantity of $Cl_2IOI(O)F_2$ obtained we were not able to perform further investigations.

Crystal Structure of $Cl_2IOI(O)F_2$

$Cl_2IOI(O)F_2$ crystallises in the monoclinic system in the space group $P2_1/c$ with a = 12.910(1) Å, b = 6.987(1) Å, c = 7.550(1) Å, β = 94.890(1)°, and four formula units per unit cell. The crystal structure was solved by direct methods and successive difference Fourier syntheses. For refinement full-matrix least-squares methods were applied. A final refinement with anisotropic thermal parameters gave values of $R1$ = 0.0558 and $wR2$ = 0.1297. For the data reduction, structure solution, and refinement, programs in the SHELXTL package, PLATON, MISSYM, and PARST were used.[7−11] The crystal data are summarised in Table 1.

$Cl_2IOI(O)F_2$ can be described as two pseudo-trigonal bipyramids linked by one edge over an unsymmetrical I−O−I bridge with lengths of I(1)−O(1) 1.84(1) Å, I(2)−O(1) 2.32(1) Å and an angle I(1)−O(1)−I(2) of 122.5(5)° (Figure 1). The bridging I(2)−O(1) bond is about 20% longer than the sum of the covalent radii (1.94 Å) and

[a] Contribution from Fachbereich Chemie der Universität Dortmund,
D-44221 Dortmund, Germany

 © WILEY-VCH Verlag GmbH, 69451 Weinheim, 2001 1434−1948/01/0202−0457 $ 17.50+.50/0

Table 1. X-ray diffraction data of $Cl_2IOI(O)F_2$

Space group	$P2_1/c$
Crystal system	monoclinic
a, Å	12.910(1)
b, Å	6.987(1)
c, Å	7.550(1)
α, °	90
β, °	94.89(1)
γ, °	90
Volume, Å^3	678.6(1)
Density (calculated), g cm^{-3}	3.864
Z	4
Formula weight, g mol^{-1}	394.70
Absorption coefficient, mm^{-1}	10.012
Temperature, K	173(2)
F(000)	696
Wavelength, Å	0.71069
Theta range for data collection, °	$3.32 \le \theta \le 25.68$
Index ranges	$-14 \le h \le 13$, $-7 \le k \le 7$, $-6 \le l \le 8$
Reflections collected/independent	3309/1071 [$R(int) = 0.0818$]
Parameters	74
Goodness-of-fit on F^2	1.201
Final R indices [$I < 2\sigma(I)$]	$R1 = 0.0558$, $wR2 = 0.1297$
R indices (all data)	$R1 = 0.0725$, $wR2 = 0.1557$
Largest diff. peak and hole, e. Å^{-3}	1.685 and −2.066
Refinement method	full matrix, least-squares on F^2

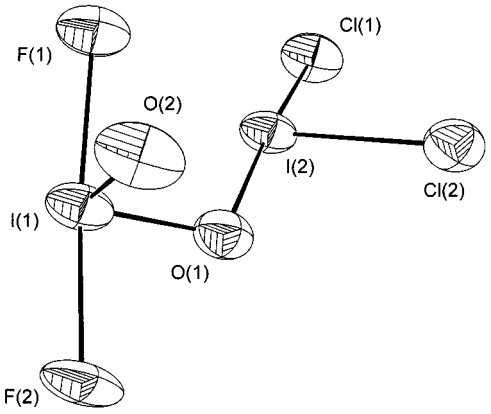

Figure 1. View of a $Cl_2IOI(O)F_2$ molecule; thermal ellipsoids are drawn at the 50% level

34% below the sum of the van der Waals radii (3.50 Å), as published by Bondi.[12] This secondary bond results in a distorted square planar environment around iodine.[13] We think that this description for $Cl_2IOI(O)F_2$ is more reasonable than formulating it as $ICl_2^+IO_2F_2^-$. The molecule contains iodine in two different oxidation states (III) and (V). The axial positions in the iodine(V) group are occupied by fluorine and the equatorial ones by a lone pair, a double bond oxygen, and the bridging oxygen.[14] In agreement with the Gillespie-Nyholm model of molecular geometry, the iodine(III) unit contains chlorine and oxygen in the apical positions, and one chlorine and two lone pairs in the equatorial plane.[15,16] Bond lengths and selected angles for $Cl_2IOI(O)F_2$ are listed in Table 2.

Table 2. Bond lengths [Å] and angles [°] of $Cl_2IOI(O)F_2$ and lengths [Å] and angles [°] of selected intermolecular contacts[a]

I(1)−O(1)	1.84(1)	O(1)−I(1)−O(2)	100.7(5)
I(1)−O(2)	1.81(1)	O(1)−I(1)−F(1)	90.1(4)
I(1)−F(1)	1.969(8)	O(1)−I(1)−F(2)	88.6(5)
I(1)−F(2)	1.917(8)	O(2)−I(1)−F(1)	85.2(4)
I(2)−Cl(1)	2.343(4)	O(2)−I(1)−F(2)	87.4(4)
I(2)−Cl(2)	2.352(5)	F(1)−I(1)−F(2)	172.2(4)
I(2)−O(1)	2.32(1)	Cl(1)−I(2)−Cl(2)	94.1(2)
		O(1)−I(1)−Cl(1)	175.5(3)
I(1)···F(1a)	3.038(8)	O(1)−I(1)−Cl(2)	84.2(3)
I(1)···F(1b)	3.259(9)	I(1)−O(1)−I(2)	122.5(5)
I(1)···F(2c)	3.10(1)		
I(1)···O(2a)	3.32(1)	O(1)−I(1)−O(2d)	170.0(4)
I(1)···O(2d)	2.77(1)	O(2)−I(1)−O(2a)	144.4(4)
I(2)···O(1a)	3.36(1)	O(2)−I(1)−F(1a)	167.3(4)
I(2)···O(2a)	2.50(1)	O(2)−I(1)−F(1b)	117.7(4)
		O(2)−I(1)−F(2c)	115.9(5)
		Cl(2)−I(2)−O(1a)	127.1(2)
		Cl(2)−I(2)−O(2a)	166.0(3)

[a] Symmetry transformations: *a*: x, $1/2 - y$, $-1/2 + z$; *b*: $1 - x$, $1/2 + y$, $1/2 - z$; *c*: $1 - x$, $-1/2 + y$, $1/2 - z$; *d*: $1 - x$, $1 - y$, $1 - z$; *e*: x, $1/2 - y$, $1/2 + z$.

The I−F bonds have lengths of 1.969(8) and 1.917(8) Å and are comparable to those found in IF_3O [1.91(3) and 1.89(3) Å] and in $IF_2(O)OCH_3$ [1.929(3) and 1.964(3) Å].[17,18] The angle between iodine and the two fluorine atoms is 172.2(4)° and shows a difference from the ideal value of 180° due to the steric activity of the lone pair. In $Cl_2IOI(O)F_2$ there is an axial as well as an equatorial I−Cl bond, whose lengths of 2.343(4) and 2.352(5) Å are only slightly larger than the sum of the covalent radii (2.27 Å).[12] The I(2)−O(1) bond, with oxygen as the most electronegative ligand of I(2), has a length of 2.32 (1) Å and is significantly longer than the sum of the covalent radii of 1.94 Å, as published by Bondi.[12] This is in agreement with the principle reported by Varvoglis that, in iodine(III) compounds with axial ligands of different electronegativities, the distance between iodine and the more electronegative ligand is longer than the sum of the covalent radii, while the bond to the less electronegative ligand is comparable with the sum of covalent radii.[19] The bridging angle I(1)−O(1)−I(2) [122.5(5)°] is similar to those found in I_4O_{12} [102.1(4)−129.2(4)°] and $(IO_2)_3HSO_4$ [122.7(7)−133.4(9)°].[2,3]

The molecules are involved in a strong intermolecular linkage containing I−O and I−F contacts. Each I(1) of the iodine(V) unit has five intermolecular contacts, three I−F contacts with lengths between 3.038(8) and 3.259(9) Å, one I−O contact with a length of 3.32(1) Å, and one short I−O contact of 2.77(1) Å that shows along the I(1)−O(1) bond. A distorted octahedral environment for iodine results, similar to that in IF_5.[20] The lone pair occupies one position of the octahedron and four intermolecular contacts are arranged beside it, due to the tendency of the incoming lone pairs to avoid the domains of the other electrons in the valence shell of iodine. As expected, the iodine(III) atom I(2) undergoes only one very short intermolecular I−O contact with a length of 2.50(1) Å, about 1 Å below the sum of the van der Waals radii of 3.50 Å, which results in a

distorted square-planar environment around iodine.[12] The weak I(2)−O(1a) contact of 3.36(1) Å is probably caused by steric effects. All these contacts result in the formation of double layers stacked to the *a*-axis, with chlorine occupying the side positions (Figure 2). Between these layers no interactions below the sum of the van der Waals radii are found.

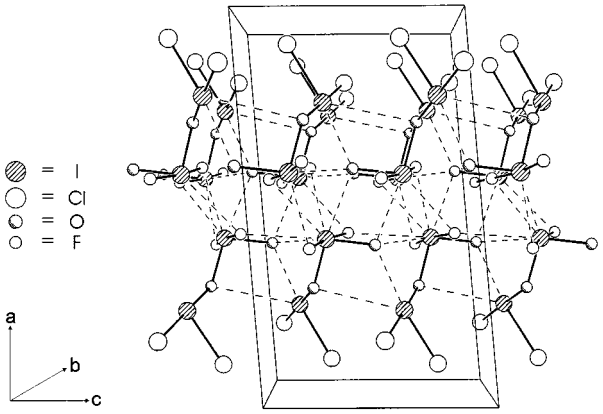

Figure 2. View of the unit cell of $Cl_2IOI(O)F_2$ in the *b*-orientation with a part of its environment; the molecules are arranged in double layers stacked on the *a*-axis and show a strong intermolecular linkage

Table 3. Vibrational frequencies of $Cl_2IOI(O)F_2$

Raman (T = 20 °C)	IR[a] (T = 20 °C)	Assignment
811(4)		
786(14)	776vs	ν I=O
767(9)	752vs	ν I=O
723(14)	723vs	ν I=O
	590w	
537(3)	542m	ν_{as} IF_2
521(5)	521m	ν_s IF_2
507(3)		ν I−O
	468m	ν I−O
412(4)	406m	ν I−O
389(7)	372m	δ IO_2
360(100)	354sh	ν_s ICl_2
342(17)	343m,sh	ν_s ICl_2 (I_2Cl_6)
327(67)	332/323s	ν_{as} ICl_2
	314m, sh	ν_{as} ICl_2 (I_2Cl_6)
264(7)	260vw	δ IF_2
	246vw	
228(7)	232m	δ O−I−F
218(6)	213w	δ O−I−Cl
182(3)		δ O−I−Cl
144(25)		δ ICl_2
121(25)		ν I···O
82(36)		δ I−O−I
68(44)		lattice modes
62(32)		lattice modes
52(48)		lattice modes
33(42)		lattice modes

[a] vs = very strong, s = strong, m = medium, w = weak, vw = very weak, sh = shoulder.

Vibrational Spectra

The observed Raman and IR frequencies of $Cl_2IOI(O)F_2$ are summarised in Table 3 and the spectra are shown in Figure 3. The vibrational spectrum is assigned according to C_1 symmetry for $Cl_2IOI(O)F_2$, with 18 fundamental vibrations expected. The assignment has been made in comparison to known spectra of I_2Cl_6, ICl_2^+, IO_2F, IF_3O, $IO_2F_2^-$, and $(IO_2)_3HSO_4$.[21−23,3]

In the Raman spectrum, the ICl_2 stretching modes are the strongest lines and occur at 327 cm^{-1} (ν_{as} ICl_2) and 360 cm^{-1} (ν_s ICl_2). According to the relative intensities in the Raman and IR spectra, we have assigned the higher frequency to the symmetrical stretching mode. This is in agreement with the assignment for I_2Cl_6 (314 cm^{-1} ν_{as} ICl_2; 344 cm^{-1} ν_s ICl_2) and ICl_2^+ (364 cm^{-1} ν_{as} ICl_2; 371 cm^{-1} ν_s ICl_2).[21,22] The corresponding bending mode is observed at 144 cm^{-1}. The fundamental vibrations of the IF_2 group are assigned to the lines at 264 cm^{-1} (δ IF_2), 521 cm^{-1} (ν_s IF_2), and 537 cm^{-1} (ν_{as} IF_2). The stretching modes exhibit only weak intensities in the Raman spectrum, but they are observed in a typical range for axial IF_2 groups. For comparison, in KIO_2F_2 the I−F stretching modes are found at 472 and 434 cm^{-1} and in IF_3O at 515 and 550 cm^{-1}.[23] A similar behaviour is observed for the I−O stretching modes. In the Raman spectrum these have only low intensities but in the IR spectrum they are assigned to very strong bands. The stretching vibration of the I=O double bond is assigned to the bands at about 723−786 cm^{-1}, the stretching mode for the single bond I(1)−O(1) to the lines between 406 and 507 cm^{-1} and the secondary bond I(2)−O(1) to the line at 121 cm^{-1}. The complexity of the spectra in the range for the I−O stretching modes is typical for this kind of molecule and so the assignment can be made only tentatively.

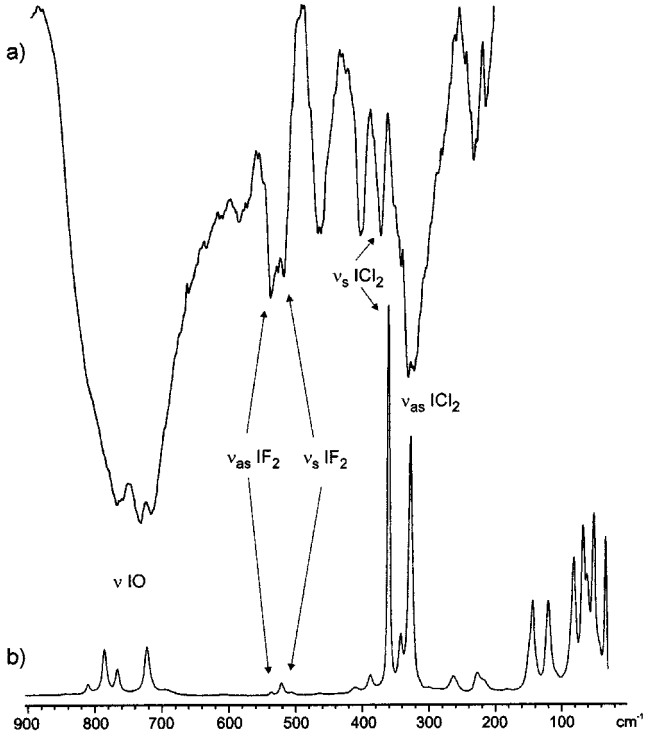

Figure 3. a) IR spectrum and b) Raman spectrum of $Cl_2IOI(O)F_2$

Experimental Section

Caution! CF_3OCl is a highly reactive oxidising agent and potentially explosive when brought into contact with organic material. Avoid contact with CF_3OCl and the other compounds described in this paper because their hydrolysis leads to the formation of HF or HCl, which cause burns and in some cases irreparable damage. Safety precautions should be taken in using and handling these materials.

All synthetic work and sample handling was performed using a standard glass vacuum line and standard Schlenk techniques. Non-volatile materials were handled under dry nitrogen. $Cl_2IOI(O)F_2$ was obtained by the uncontrolled reaction between CF_3I, CF_3OCl, CF_2O, and Cl_2 as described above. We decided to obtain first X-ray, Raman and IR data and in the course of these studies the very small quantity of $Cl_2IOI(O)F_2$ was used up and we were not able to perform NMR spectroscopic or mass spectrometric measurements, or an elemental analysis.

The Raman spectra were recorded on a Jobin Yvon T64000 spectrometer using a Kr^+ laser (647.1 nm) from Spectra Physics. The spectra were obtained in a glass cell at room temperature.[24] Infrared spectra were recorded on a Bruker IFS 113v spectrophotometer. Spectra were obtained from a coated CsBr plate in a special IR cell.[25]

Single crystals were placed in Lindemann capillaries in a cooled stream of dry nitrogen at about −70 °C, and an X-ray diffraction study at −100 °C was carried out using a Nonius Kappa CCD diffractometer. 360 frames via ω-rotation and two times 100s per frame were measured. The crystal-to-detector distance was 3.1 cm. Crystal decay was monitored by repeating the initial frames at the end of data collection. Analysis of the duplicate reflections gave no indications of any decay.

Acknowledgments

This work was supported by the Fonds der Chemischen Industrie.

[1] T. Birchall, G. Denes, R. Faggiani, C. S. Frampton, R. J. Gillespie, R. Kapoor, J. E. Vekris, *Inorg. Chem.* **1990**, *29*, 1527−1530.
[2] T. Kraft, M. Jansen, *Z. Anorg. Allg. Chem.* **1996**, *622*, 167−172.
[3] A. Rehr, M. Jansen, *Z. Anorg. Allg. Chem.* **1992**, *608*, 159−165.
[4] R. Minkwitz, R. Bröchler, H. Preut, Z. Anorg. Allg. *Chem.* **1995**, *621*, 1247−1250.
[5] R. Minkwitz, R. Bröchler, M. Schütze, Z. Anorg. Allg. *Chem.* **1995**, *621*, 1727−1730.
[6] E. E. Aynsley, R. Nichols, P. L. Robinson, *J. Chem. Soc.* **1953**, 623−626.
[7] G. M. Sheldrick, *SHELXTL PLUS An Integrated System for Solving, Refining and Displaying Structures from Diffration Data*, University of Göttingen, Germany **1987**.
[8] A. L. Spek, The EUCLID Package, in: Computational Crystallography (Ed.: D. Sayre), Claredon Press, Oxford, 528, **1982**.
[9] Y. Le Page, *J. Appl. Crystallogr.* **1987**, *20*, 264−269.
[10] M. Nardelli, *Comput. Chem.* **1983**, *7*, 95−98.
[11] Further details of the crystal-structure investigation may be obtained from the Fachinformationszentrum Karlsruhe, D-76344 Eggenstein-Leopoldshafen, Germany, on quoting the depository number CSD-411237.
[12] A. Bondi, *J. Phys. Chem*. **1964**, *68*, 441−451.
[13] N. W. Alcock, *Adv. Inorg. Chem. Radiochem*. **1972**, *15*, 1−58.
[14] H. A. Bent, *Chem. Rev.* **1961**, *61*, 275−311.
[15] R. J. Gillespie, R. S. Nyholm, *Quart. Rev., Chem. Soc.* **1957**, *11*, 339−380.
[16] R. J. Gillespie, *J. Chem. Educ.* **1963**, *40*, 295−301.
[17] A. J. Edwards, P. Taylor, *J. Fluorine. Chem.* **1974**, *4*, 173−179.
[18] R. Minkwitz, M. Berkei, M. Studentkowski, R. Ludwig, *Inorg. Chem.* in press.
[19] A. Varvoglis, *The Organic Chemistry of Polycoordinated Iodine*, VCH, Weinheim, **1992**.
[20] R. D. Burbank, G. R. Jones, *Inorg. Chem.* **1974**, *13*, 1071−1074.
[21] R. Forneris, J. Hiraishi, F. A. Miller, *Spectrochim. Acta*. **1970**, *26A*, 581−591.
[22] R. Forneris, Y. Tavares-Forneris, *J. Mol. Struct.* **1974**, *23*, 241−252.
[23] H. A. Carter, F. Aubke, *Inorg. Chem.* **1971**, *10*, 2297−2301.
[24] A. Werner, Dissertation, University of Dortmund, Germany, **1988.**
[25] L. Bayersdorfer, R. Minkwitz, J. Jander, *Z. Anorg. Allg. Chem.* **1972**, *392*, 137−142.

Received April 17, 2000
[I00152]

Time-Dependent Solution Speciation of the Al^{III}–Citrate System: Potentiometric and NMR Studies

Andrea Lakatos,[a] István Bányai,[b] Patrick Decock,[c] and Tamás Kiss*[a]

Keywords: Aluminum / Citric acid / Oligomerizations / NMR spectroscopy

Time-dependent potentiometric and NMR spectroscopic measurements were carried out in the Al^{III}–citric acid system in an equimolar solution and at an excess of ligand in order to monitor the changes in speciation as a function of time. In fresh solutions, the mononuclear 1:1 species $[AlLH]^+$, $[AlL]$, $[AlLH_{-1}]^-$ and $[AlLH_{-2}]^{2-}$ and the 1:2 complexes $[AlL_2]^{3-}$, $[AlL_2H_{-1}]^{4-}$ and $[AlL_2H_{-2}]^{5-}$ are formed. In agreement with earlier findings (*Inorg. Chem.* **1988**, *27*, 2565), these complexes are converted to a large extent into a thermodynamically more stable trinuclear species as the solutions age. Depending on the composition of the initially formed mononuclear species, the formation of the trinuclear species is accompanied either by the consumption or by the liberation of hydroxide ions. NMR spectroscopy was used to confirm the considerable time dependence of the species distribution. The ^1H, ^{27}Al and ^{13}C NMR spectra indicated that at equilibrium the trinuclear species $[Al_3(LH_{-1})_3(OH)]^{4-}$ predominates in the pH range 4–7. Oligomerization of the mononuclear species takes place through at least one intermediate complex. At equilibrium, the ligand-exchange reactions between the trinuclear species, the mononuclear species and free citrate are slow on the NMR time scale.

Introduction

Citrate is one of the most extensively investigated ligands for Al^{III} in aqueous solution. The reason for this is that citrate is widely found in biological systems and in natural waters. As a powerful complexing agent, citrate may solubilize the neurotoxic Al^{III}, which prefers the coordination of oxygen donor containing ligands, thus permitting the absorption of Al^{III} from the environment to the human body.[1] Since citrate occurs at about 0.1 mM in blood plasma,[2] it can also be a good low molecular mass (l.m.m.) carrier of the absorbed Al^{III} in the blood stream.

Although the Al^{III}–citrate system has previously been studied by several techniques,[3–10] there are still contradictions in the proposed equilibrium model and binding modes of the complexes. The divergence is partly due to the numerous coordination possibilities and protonation states of the donor groups (citrate contains four potential donor groups, but only three can coordinate simultaneously to the same metal ion), and partly due to the rather slow oligomerization reactions that take place in solution. An early potentiometric study by Motekaitis and Martell led to a simple model involving only the mononuclear 1:1 species $[AlLH]^+$, $[AlL]$ and $[AlLH_{-1}]^-$, both in an equimolar solution and at an excess of citrate.[6] In contrast, Gregor and Powell suggested bis(complexes) as the predominant species at a ligand excess. Besides 1:1 complexes, they proposed the formation of $[AlL_2H]^{2-}$ and $[AlL_2]^{3-}$ in slightly acidic solutions and $[AlL_2H_{-1}]^{4-}$ and $[AlL_2H_{-2}]^{5-}$ in neutral and slightly alkaline solutions.[8] From these bis(complexes), $[AlL_2H_{-2}]^{5-}$ and $[AlL_2H_{-1}]^{4-}$ were recently isolated from slightly alkaline solutions as the first mononuclear Al^{III}–citrate complexes, and characterized by X-ray crystallography and NMR spectroscopy.[11,12] In a time-dependent potentiometric study, Öhman demonstrated that in an equimolar solution the monomeric species transform into trimeric complexes $[Al_3L_3H_{-4}]^{4-}$ and $[Al_3L_3H_{-7}]^{7-}$ in very slow processes.[10] One of these trimeric complexes was crystallized in the form of $[NH_4]_4[Al_3(LH_{-1})_3(OH)(H_2O)]$ from a neutral solution and was identified unambiguously and characterized in detail by ^1H, ^{13}C and ^{27}Al NMR spectroscopy and X-ray crystallography.[13]

Such time-dependent studies may furnish a more accurate speciation description of metal-ligand systems in biology, because thermodynamic equilibrium is never reached in biological fluids as a result of the continuous influx and efflux of the components. Thus, nonequilibrium models of metal–ligand interactions may provide more relevant information.[14]

In the present work, a time-dependent speciation study of the Al^{III}–citric acid system was made both under equimolar conditions and at an excess of citrate. The oligomerization reactions of the mononuclear species were followed by ^1H, ^{13}C and ^{27}Al NMR spectroscopy, and the formation of a trinuclear complex through intermediate species was clearly demonstrated.

[a] Department of Inorganic and Analytical Chemistry, University of Szeged,
P. O. Box 440, 6701 Szeged, Hungary
[b] Department of Physical Chemistry, University of Debrecen,
P. O. Box 19, 4010 Debrecen, Hungary
[c] Laboratoire de Chimie Analitique Appliquée, Université du Littoral,
59379 Dunkerque Cedex 1, France
Supporting information for this article is available on the WWW under http://www.wiley-vch.de/home/eurjic or from the author.

 © WILEY-VCH Verlag GmbH, 69451 Weinheim, 2001 1434–1948/01/0202–0461 $ 17.50+.50/0

Results and Discussion

Time-Dependent Potentiometric Measurements

Potentiometric titrations indicate an overlapping stepwise dissociation of three protons from the three carboxylic groups of the ligand. The protonation constants are reported in Table 1.

Table 1. Stability constants of proton (log K)and Al^{III} complexes (log β) of citric acid at 25 °C and I = 0.2 M (KCl)

	This work	log K[a] /log β Ref.[4] [b]	Ref.[8] [c]
$K([HL]^{2-})$	5.57(2)	5.22	5.70
$K([H_2L]^{-})$	4.27(2)	4.08	4.35
$K([H_3L])$	2.87(3)	2.77	2.91
$[AlLH]^{+}$	10.18(8)	9.39	10.81
$[AlL]$	7.85(5)	7.15	8.10
$[AlLH_{-1}]^{-}$	4.27(27)	3.54	–
$[AlLH_{-2}]^{2-}$	−1.77(5)	−2.64	–
$[AlL_2H]^{2-}$	–	–	16.84
$[AlL_2]^{3-}$	12.73(31)	11.61	12.90
$[AlL_2H_{-1}]^{4-}$	7.81(19)	–	6.8
$[AlL_2H_{-2}]^{5-}$	0.4	–	−0.37
$[Al_3L_3H_{-4}]^{4-}$	16.34(8)	14.44	–
$[Al_3L_3H_{-7}]^{7-}$	–	−10.90	–
Fitting (Δ cm^3)[d]	0.0074		
No. of "batch" points[e]	78		

[a] log K values are the logarithm of the stepwise protonation constants, which are numerically equal to the negative logarithm of the acidity constants, pK_a values, of the corresponding species; ±3 s.d. values are given in parentheses. – [b] I = 0.6 M (NaCl); T = 25 °C. – [c] I = 0.1 M (KCl); T = 25 °C. – [d] Average difference between the experimental and the calculated titration curves, expressed in mL of the titrant. – [e] See Experimental Section.

In the Al^{III}–citrate system data collection runs into difficulties because of a pronounced drift in pH due to the slow complexation reactions. Öhman and Sjöberg[4] reported equilibration requiring up to 6 h in slightly acidic solutions at low Al^{III}/citrate ratios. They demonstrated that this pH drift is due to the formation of the trinuclear species $[Al_3(LH_{-1})_3(OH)]^{4-}$ during the slow oligomerization process of the mononuclear complexes.[10] Gregor and Powel minimized this drift by working at Al^{III}/citrate ratios < 1:5. The equilibrium model found at such large excesses of ligand included only the mononuclear species $[AlLH]^{+}$, $[AlL]$, $[Al(HL)L]^{2-}$, $[AlL_2]^{3-}$, $[AlL_2H_{-1}]^{4-}$ and $[Al(LH_{-1})_2]^{5-}$. In earlier work,[19] a series of titrations were carried out at Al^{III}/citric acid ratios of 1:2, 1:3, 1:4 and 1:8. Evaluation of the titration curves obtained at high ligand excesses (ratios of 1:4 and 1:8) led to a model involving only mononuclear mono- and bis(complexes). However, when the titration curves for Al^{III}/citrate ratios > 1:4 were also included in the calculation, a much better fit was obtained if, besides the mononuclear complexes, the trinuclear species $[Al_3(LH_{-1})_3(OH)]^{4-}$ was also assumed. The stability constants obtained in this way, however, cannot be regarded as fully reliable, as equilibration was not definitely attained at each titration point in the pH range 5–7. Moreover, even a slight drift in the electrode response during the very long titration process (up to 4–6 h) may cause a significant error in pH, especially near the end of the titration, when the pH increases sharply (see Figure 2).

In order to acquire an accurate speciation description of the Al^{III}–citrate system in the equilibrium state even at a small ligand excess, and to obtain qualitative information concerning the kinetic route to true thermodynamic equilibrium, the "batch method" described in the Experimental Section was used instead of the normal titration procedure. Measurements were performed at Al^{III}/citrate ratios of 1:1 and 1:3 in the pH range 2.0–8.0 (Figure 1).

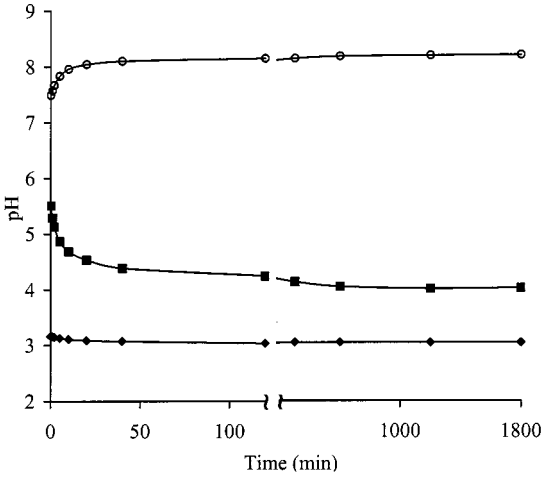

Figure 1. The change of pH as a function of time in solutions of the Al^{III}–citric acid system at a ratio 1:1, c_{Al} = 0.004 M, and at various starting pH values: (◆) 3.16, (■) 5.51, (○) 7.49

The time course of the pH changes of some selected batch solutions at different starting pH values is depicted in Figure 1. The pH changes are seen to be significant in the first 2 h; and complete equilibration can be attained in ca. 30 h. Interestingly, the direction of the pH change is dependent upon the starting pH; at pH < 6.5, the concentration of hydrogen ion increases with time, while above this pH it decreases. It has already been established[10] that this drift in pH is due to slow oligomerization reactions. Depending on the starting pH, the protonation state of the mononuclear complexes varies and their oligomerization may be accompanied by either the liberation or the consumption of protons (vide infra).

Titration curves created by using pH values relating to the same times are depicted in Figure 2. At a metal ion/ligand ratio of 1:1 the titration curves become steeper and steeper as the solution "ages". The differences between the consecutive curves are significant only in the early hours after mixing. At a metal/ligand ratio of 1:3, the differences between the titration curves are smaller than in equimolar solution, since the pH effect of the oligomerization processes is strongly buffered by the proton-dissociation reactions of the free citric acid. The 30-h titration curve represents the equilibrium state. On the basis of earlier literature reports,[4,8,10,15] the equilibrium titration data were evaluated by a speciation model including mononuclear mono- and bis(complexes) in different protonation states, i.e. $[AlLH]^{+}$, $[AlL]$, $[AlLH_{-1}]^{-}$, $[AlLH_{-2}]^{2-}$, $[AlL_2]^{3-}$,

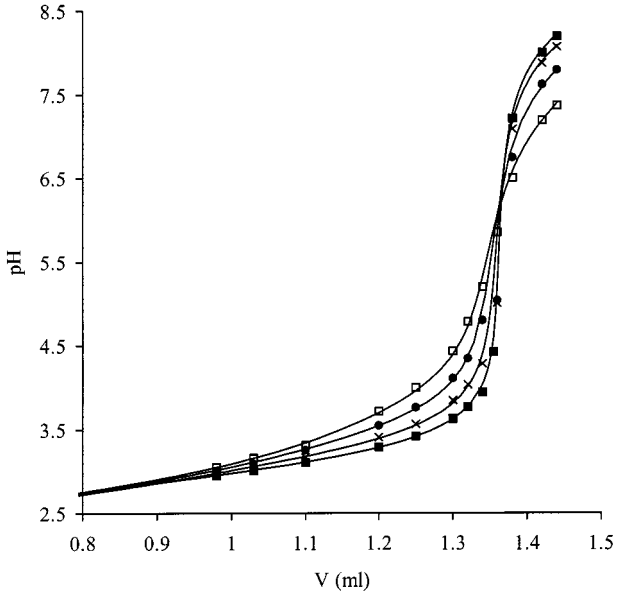

Figure 2. Titration curves (plotted as mL titrant KOH versus pH) of the Al^{III}−citric acid system at a ratio 1:1, $c_{Al} = 0.004$ M and at different times after mixing the reactants: (□) 1 min, (●) 10 min, (×) 40 min (■) at equilibrium (after 30 h)

$[AlL_2H_{-1}]^{4-}$ and $[AlL_2H_{-2}]^{5-}$, and the trinuclear complex $[Al_3L_3H_{-4}]^{4-}$, or more precisely $[Al_3(LH_{-1})_3(OH)]^{4-}$. The stability constants of the complexes, together with some literature data, are listed in Table 1. It can be seen from Table 1 that there is a better agreement in the stability constants of the mono(complexes) (especially the stepwise deprotonation data agree well), while there is a much higher uncertainty in the stability of bis(complexes). Our model is in reasonable good agreement with that proposed by Öhman,[4,10] except that he did not consider the species $[AlL_2H_{-1}]^{4-}$ and $[AlL_2H_{-2}]^{5-}$, and we did not find another trinuclear complex $[Al_3L_3H_{-7}]^{7-}$ or more precisely $[Al_3(LH_{-1})_3(OH)_4]^{7-}$. This latter species, however, is not formed in a significant quantity below pH ≈ 8, the upper limit of our studies. The differences in the stability constants can be explained by the rather large differences in the experimental conditions ($I = 0.6$ M, NaCl and 0.2 M, KCl). The agreement with the stability data of the mononuclear mono- and bis(complexes) reported by Gregor and Powell[8] is much better, as they used much closer experimental conditions ($I = 0.1$ M, KCl).

In order to obtain information about the complexation route of citric acid with Al^{III}, we evaluated the titration curves relating to the same times by using the same speciation model (vide supra). Species distribution curves at different times after the mixing of the components are depicted in Figure 3 and Figure 4. We are aware that the stability data calculated from the non-equilibrium titration points are not real thermodynamic constants (for this reason we do not report their values), but they can provide a roughly qualitative picture regarding the time course of the complex formation processes. Figure 3 clearly indicates that, shortly after mixing, mononuclear complexes predominate in the system, which then transform slowly to the trinuclear complex, $[Al_3(LH_{-1})_3(OH)]^{4-}$, probably through intermediate species. The concentration of the trinuclear species increases with time at the expense of the mononuclear mono(complexes) $[AlLH_{-1}]^{-}$ and $[AlLH_{-2}]^{2-}$, and also of the bis(complexes) $[AlL_2]^{3-}$, $[AlL_2H_{-1}]^{4-}$ and $[AlL_2H_{-2}]^{5-}$ in the case of an excess of ligand.

At pH ≈ 5, $[AlLH_{-1}]^{-}$, the predominating mononuclear complex, is formed in a fairly fast reaction and is in equilibrium with the trinuclear species. The pH of the solution decreases with time (see Figure 1), due to the slow equilibrium of Equation (1).

$$3\,[AlLH_{-1}]^{-} + H_2O \rightleftarrows [Al_3(LH_{-1})_3(OH)]^{4-} + H^{+} \quad (1)$$

At a ligand excess, bis(complexes) like $[AlL_2]^{3-}$ and $[AlL_2H_{-1}]^{4-}$ are also present and are also involved in the oligomerization processes. Several of the possible reactions are given in Equation (2), Equation (3) and Equation (4).

$$[AlL_2]^{3-} + 2\,[AlLH_{-1}]^{-} + H_2O \rightleftarrows [Al_3(LH_{-1})_3(OH)]^{4-} + HL^{2-} + H^{+} \quad (2)$$

$$[AlL(LH_{-1})]^{4-} + 2\,[AlLH_{-1}]^{-} + H_2O \rightleftarrows [Al_3(LH_{-1})_3(OH)]^{4-} + HL^{2-} \quad (3)$$

$$[AlL_2]^{3-} + [AlL(LH_{-1})]^{4-} + [AlLH_{-1}]^{-} + H_2O \rightleftarrows [Al_3(LH_{-1})_3(OH)]^{4-} + 2\,HL^{2-} \quad (4)$$

When the starting pH is ca. 7, the predominant mononuclear species is $[AlLH_{-2}]^{2-}$, and the pH increases with time according to the equilibrium of Equation (5).

$$3\,[Al(LH_{-1})(OH)]^{2-} \rightleftarrows [Al_3(LH_{-1})_3(OH)]^{4-} + 2\,OH^{-} \quad (5)$$

At a ligand excess the transformations of the species $[AlL_2H_{-1}]^{4-}$ and $[AlL_2H_{-2}]^{5-}$ should also be considered. As an illustration some of the possible oligomerization reactions are given in Equation (6) and Equation (7).

$$[AlL(LH_{-1})]^{4-} + 2\,[Al(LH_{-1})(OH)]^{2-} \rightleftarrows [Al_3(LH_{-1})_3(OH)]^{4-} + L^{3-} + OH^{-} \quad (6)$$

$$[Al(LH_{-1})_2]^{5-} + 2\,[Al(LH_{-1})(OH)]^{2-} + H_2O \rightleftarrows [Al_3(LH_{-1})_3(OH)]^{4-} + L^{3-} + 2\,OH^{-} \quad (7)$$

It must be mentioned here that these equilibria are written in the simplest way. During the oligomerization of the mononuclear complexes, one or more intermediate species are formed, as can be demonstrated by NMR spectroscopy (vide infra).

At pH ≈ 3, there is only a slight pH decrease with time. At this pH, the species [AlL] predominates in the fresh solution and only a small amount is transformed to the trinuclear complex at equilibrium. Thus, the changes in pH are not significant (see Figure 1).

NMR Spectroscopic Measurements in Equimolar Al^{III}−Citrate Solutions

^{1}H, ^{13}C and ^{27}Al NMR spectroscopic measurements were carried out to support the potentiometric results. The spectrum recorded at pH ≈ 2 in a 0.04 M solution (Figure 5a) reveals the AB quadruplet of the free citrate (×) at δ = 3.06, 3.03, 2.89 and 2.86 ($J_{AB} = 15.7$ Hz), two broad signals at δ = 2.95 and 2.92 and two sharper signals at δ = 2.83

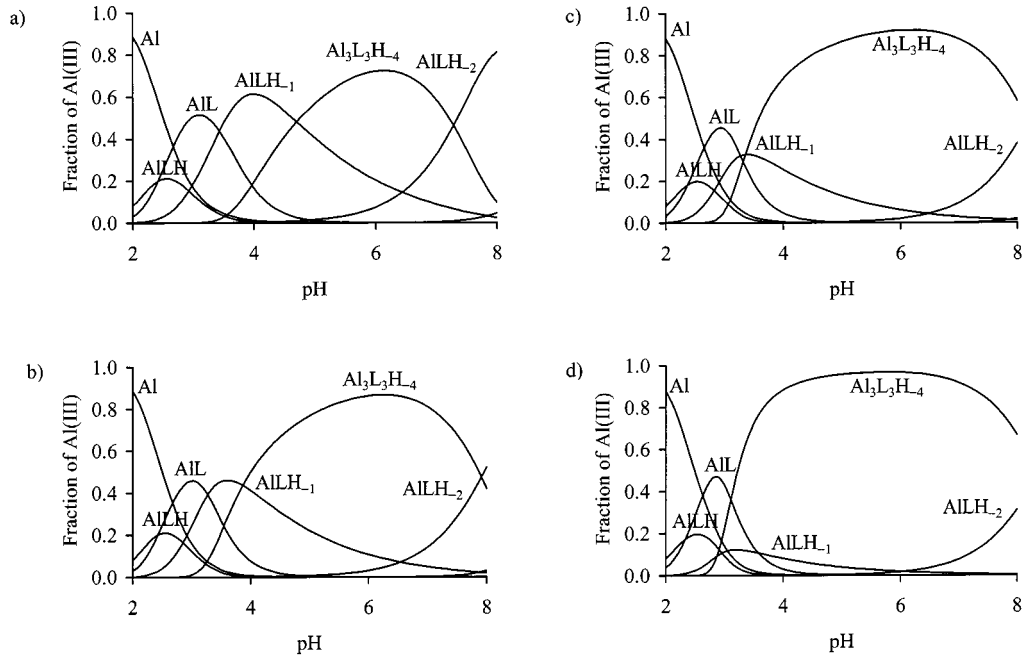

Figure 3. Species distribution curves as a function of pH in the Al^{III}–citric acid system at a ratio 1:1, c_{Al} = 0.004 M and at different times after sample preparation: (a) 1 min, (b) 10 min, (c) 40 min (d) at equilibrium (after 30 h)

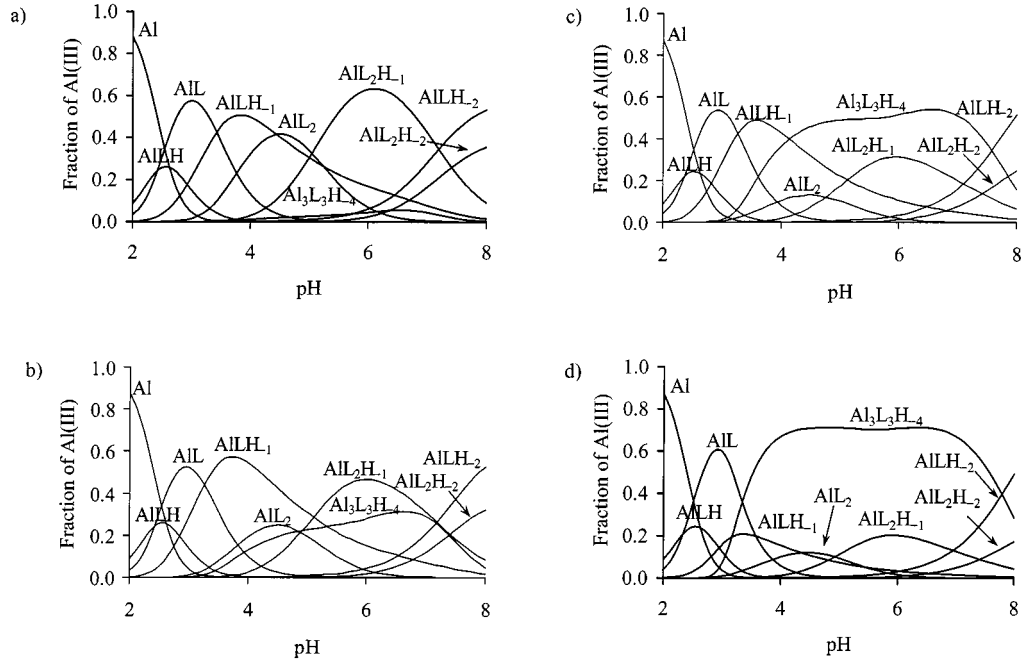

Figure 4. Species distribution curves as a function of pH in the Al^{III}–citric acid system at a ratio 1:3, c_{Al} = 0.004 M and at different times after sample preparation: (a) 1 min, (b) 10 min, (c) 40 min (d) at equilibrium (after 30 h)

and 2.80 which seem to be part of another AB quadruplet. Proton-proton correlation measurements confirm that these four signals form an AB quadruplet (•) with a coupling constant of 17.7 Hz. Potentiometry suggests that these signals belong to the mononuclear species $[AlLH]^+$.

On increasing of the pH to ca. 2.5, the ^1H NMR spectrum (Figure 5b) seems to be more complicated than expected from the speciation curves (Figure 3). From the signals appearing in the spectrum, the AB quadruplet of free citrate can unambiguously be assigned to δ = 3.03, 3.00, 2.87 and 2.84 (×), which is shifted upfield due to the deprotonation of one of the carboxyl groups. The AB quadruplet observed at pH ≈ 2 (•) is also shifted upfield. This indicates the equilibrium of two species, resulting in an average signal due to the fast proton exchange reactions between them. These two mononuclear species are probably $[AlLH]^+$ and [AlL]. The appearance of some low-intensity signals in the spectrum indicates that at 0.04 M, the oligomerization processes have already started at pH ≈ 2.5, while in more dilute solutions (e.g. at 0.004 M, under the conditions of our po-

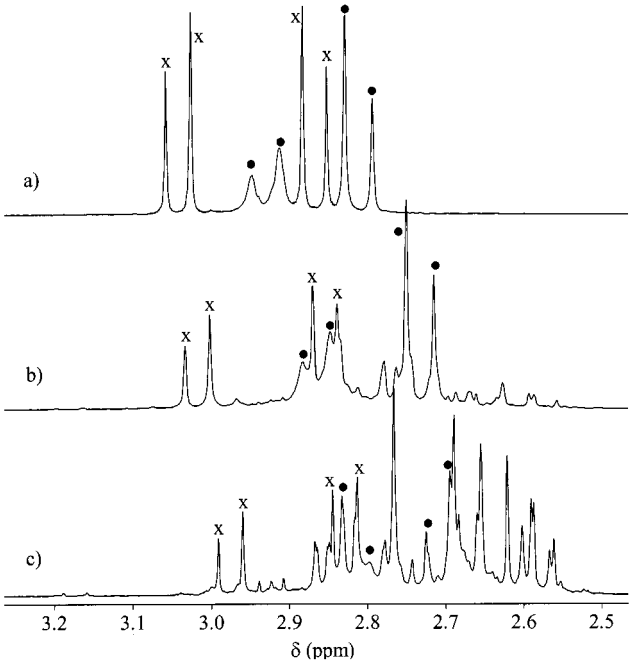

Figure 5. ^1H NMR spectra obtained in the Al^{III}−citric acid system at a ratio 1:1, c_{Al}=0.04 M and at different pH values: (a) pH ≈ 2, (b) pH ≈ 2.5, (c) pH ≈ 3; all spectra were recorded after the thermodynamic equilibrium was reached

tentiometric studies) oligomerization starts only above pH ≈ 3 (Figure 3d). The ^1H COSY NMR spectrum obtained for the same solution (see Supporting Information) indicates that these minor signals form a series of AB quadruplets, suggesting a very asymmetric structure of the oligomeric complex formed at this pH. From these AB quadruplets, three can be clearly identified at δ = 2.86, 2.83, 2.66 and 2.63 (J_{AB} = 16.6 Hz); 2.88, 2.84, 2.63 and 2.59 (J_{AB} = 20.2 Hz) and 2.70, 2.67, 2.59 and 2.56 (J_{AB} = 14.6 Hz). The signal at δ = 2.76 does not couple with any other signal.

At pH ≈ 3, the oligomerization processes are more pronounced. The characteristic AB quadruplet of the mononuclear species that appears at lower concentrations is shifted to δ = 2.83, 2.80, 2.72 and 2.69 (•), and can be assigned to the species [AlL] and $[AlLH_{-1}]^-$ (Figure 5c).

A tridentate chelation of citric acid was assumed, involving the coordination of one of the deprotonated terminal carboxylates, the deprotonated central carboxylate group and the protonated alcoholic OH group in the case of the species $[AlLH]^+$; this latter group is deprotonated in the complex [AlL]. The other terminal carboxylic group is not bound, and protonated in the species $[AlLH]^+$ and [AlL], and deprotonated in the complex $[AlLH_{-1}]^-$. The fact that there is an AB quadruplet in the ^1H NMR spectrum can be explained by a relatively fast intramolecular exchange between the bound and unbound carboxylate moieties, i.e. the citrate molecule behaves fluxionally. A more likely explanation is that one of the methylene proton pairs (e.g. a and a′, see Scheme 1) probably has a spatial arrangement such that its chemical environment changes more than in the case of the protons b and b′ during fluxional motions. For this reason, the signals given by the protons a and a′ are broader than the signals for the protons b and b′. If the rate of fluxionality were lower, separate signals could be observed for the protons a and a′. In our opinion, only this proposed binding mode of the citrate molecule with a 5+6 joined (COO^-, OH, COO^-) chelate system (see Scheme 1) and their fluxional motion can explain the asymmetric pattern of the AB quadruplet assigned to the mononuclear species. Furthermore, participation of the protonated alcoholic OH group in the coordination in the species $[AlAH]^+$ is supported by the observed increase in the stability of this complex as compared with the corresponding complexes of malonic acid (H_2L) or succinic acid (H_2L).[16,17] The basicity adjusted stability constant [log K^* = log $K([AlLH]^+)$ − log $\beta(H_3L)$] characteristic for the equilibrium $Al^{3+} + H_3L \rightleftarrows [AlLH]^+ + 2\ H^+$ is log K^* = −2.53 for Al^{III}−citrate, while it is −5.57 for the corresponding 1:1 complex $[AlL]^+$ formed with succinic acid, which involves a seven-membered (COO^-, COO^-) chelate. The corresponding proton displacement constant for malonic acid, which forms a six-membered (COO^-, COO^-) chelate, is log K^* = −1.51.

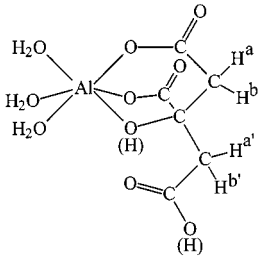

$[AlLH]^+$—[AlL]—$[AlLH_{-1}]^-$

Scheme 1

Similar fluxional behavior was found in the case of the species $[AlL_2H_{-1}]^{4-}$ and $[AlL_2H_{-2}]^{5-}$ in aqueous solution. The solid-state structures of the isolated complexes $[AlL_2H_{-1}]^{4-}$ and $[AlL_2H_{-2}]^{5-}$, determined by X-ray crystallography, indicates asymmetric arrangements of the citrate molecules. Both citric acids bind to Al^{III} through one of the two terminal COO^- groups, the central COO^- group and the deprotonated alcoholate function, while the other terminal carboxylic functions are unbound (one of them is protonated in the species $[AlL_2H_{-1}]^{4-}$, while both are deprotonated in $[AlL_2H_{-2}]^{5-}$).[11,12]

The time-dependent changes in the species distribution in the pH range 3−8, i.e. the slow formation of the trinuclear species $[Al_3(LH_{-1})_3(OH)]^{4-}$ (Figure 3), is clearly demonstrated by NMR spectroscopy too. The required amounts of the stock solutions of Al^{III}, citrate and base were mixed at selected pH values (pH ≈ 5.0 and 7.0) and a series of spectra was taken at predetermined times until pH equilibrium was attained. Equilibrium was considered to be reached when two consecutive spectra coincided.

Figure 6 shows the time-dependence of the ^1H NMR spectra recorded at pH ≈ 5 (similar spectra obtained at pH ≈ 7 are included in the Supporting Information). The signals are initially poorly resolved, broad and merged, indicating dynamic changes in the system. The complexation

processes and/or ligand-exchange reactions between the initially formed mononuclear complexes and intermediate species seem to be fairly fast.

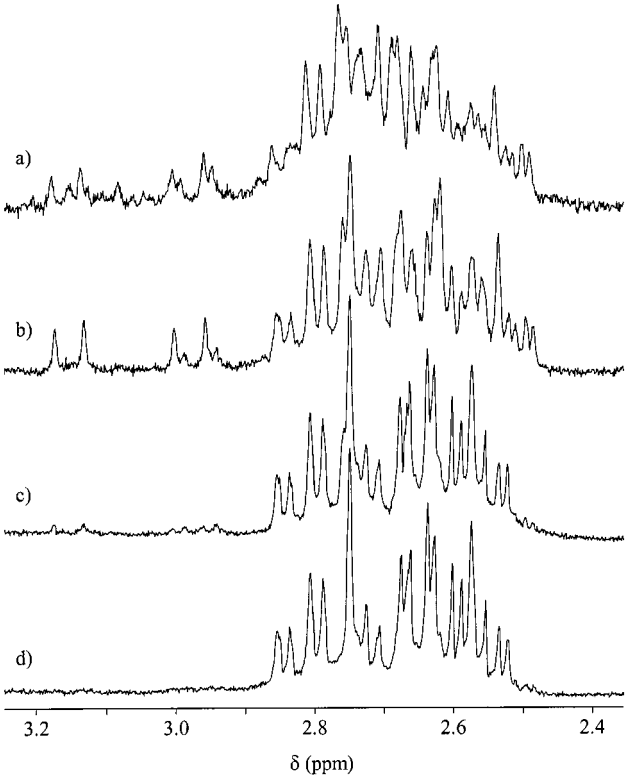

Figure 6. Time dependence of the ^{1}H NMR spectra of the Al^{III}–citric acid system at a ratio 1:1, c_{Al} = 0.04 M at starting pH ≈ 5; (a) 15 min, (b) 40 min, (c) 10 h, (d) 30 h after mixing of the components

At pH ≈ 5 in the equilibrium state, the characteristic but rather complicated spectrum of the trinuclear complex $[Al_3(LH_{-1})_3(OH)]^{4-}$ is obtained (see Figure 6d), as is expected from the potentiometric results. The speciation curves indicate that at this pH the trinuclear complex is the only species present (see Figure 3). The X-ray structure of the isolated trinuclear complex $[Al_3(LH_{-1})_3(OH)]^{4-}$ reveals an asymmetric arrangement of the carboxylate-bridged citrate molecules between the Al^{III} centers.[13] Accordingly, in the ^{13}C NMR spectrum 18 resonances appear: each carbon atom gives a separate signal. Similarly, the ^{1}H NMR spectrum is also complicated as all the methylene protons are chemically and magnetically unequivalent.[13,18] The characteristic ^{1}H resonances of the trinuclear complex are as follows: δ = 2.87, 2.85, 2.82, 2.80, 2.77, 2.74, 2.72, 2.69, 2.68, 2.65, 2.64, 2.62, 2.60, 2.58, 2.57, 2.55 and 2.54. A complete assignment of the signals was achieved by means of 2D carbon–proton correlation measurements and is under publication.[19] The appearance of the weak resonances between δ = 3.0 and 3.2 leads to the conclusion that the trinuclear complex is probably formed through at least one intermediate species. These "extra" resonances may belong to this/these intermediate species, since they reach a maximum intensity in time and are later almost completely absent from the spectrum obtained at equilibrium. It was demonstrated by ^{1}H COSY NMR measurements that they are half of the AB quadruplets, the other half lying under the signals of the trinuclear species.[12]

When the starting pH is ca. 7 (see Supporting Information), the pattern of the spectrum obtained in the equilibrium state clearly indicates the presence of the trinuclear species (the characteristic resonances are listed above), the free citrate (δ = 2.68, 2.63, 2.55 and 2.50; J_{AB} = 15.5 Hz) and a complex which gives broad resonances at δ = 2.49 and 2.45. These latter signals may be half of an AB quadruplet, the other part overlapping with signals of the trinuclear complex. According to potentiometry, this other complex is $[AlLH_{-2}]^{2-}$, which is a mixed hydroxo species with the same citrate binding mode as in the complex $[AlLH_{-1}]^-$. The broadening of the signals is probably due to the presence of the OH^- group in the coordination sphere of the Al^{III}. The appearance of free citrate can be explained by the change in the pH of the samples with time. As discussed above, at this pH the oligomerization is accompanied by a considerable release of OH^-. Thus, the pH at equilibrium is much higher than the starting value, reaching pH > 8.5. At this pH, OH^- starts to displace citric acid from the coordination sphere of Al^{III}, resulting in the parallel formation of $[Al(OH)_4]^-$.

The formation of intermediate complexes during oligomerization is clearly demonstrated by ^{13}C NMR spectroscopy too. To obtain a ^{13}C NMR spectrum of better quality, the concentration of citric acid was increased to 0.2 M and the Al^{III}/citric acid ratio was kept at 1:1. Figure 7 shows the methylene range of the spectra recorded at different times at pH ≈ 5. Spectrum (b) was obtained at equilibrium and the resonances of the six methylene carbon atoms of the asymmetric trinuclear complex are exhibited.[13] Due to the asymmetric structure and kinetically inert nature of the complex (vide extra), each methylene group yields separate signals. The upper spectrum (a) corresponds to a non-equilibrium state. Besides the signals of the trinuclear species, four new resonances can be recognized, at δ = 41.7, 43.6, 43.9 and 47.2. These signals are completely absent from the spectrum at equilibrium. The potentiometric results show that at pH ≈ 5 the complex $[AlLH_{-1}]^-$ oligomerizes to give $[Al_3(LH_{-1})_3(OH)]^{4-}$. This mononuclear complex may give at least 2 signals in the methylene range of the ^{13}C spectrum. Consequently, we cannot assign the "extra" signals in the above discussed spectrum to $[AlLH_{-1}]^-$. They are probably due to some intermediate species which forms during the oligomerization of the mononuclear complex to the final trinuclear species. These intermediate species are presumably oligonuclear complexes which contain at least two molecules of citric acid in an asymmetric arrangement. At pH ≈ 7, the same behavior is observed.

The changes in the Al^{III}–citrate system were also followed by ^{27}Al NMR spectroscopy (see Figure 8). The spectra recorded in a fresh equimolar Al^{III}–citrate solution at pH ≈ 5 and 7 consist of two components; a large peak at δ = 11.5 and a shoulder on the upfield side at about δ = 0. The intensity of the main signal increases with time, while that of the shoulder at δ = 0 initially increases and then undergoes a considerable decrease until equilibrium is re-

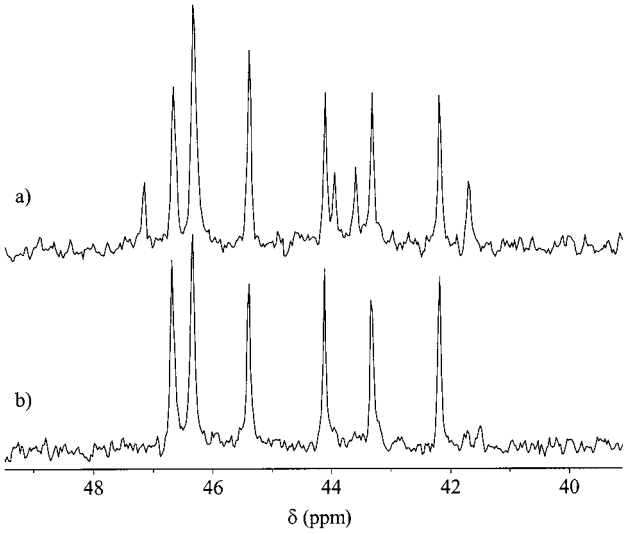

Figure 7. The methylene range of the time-dependent ^{13}C NMR spectra in the Al^{III}−citric acid system at a 1:1 ratio, c_{Al} = 0.2 M, at pH ≈ 5; (a) 12 h after mixing of the components, (b) at equilibrium

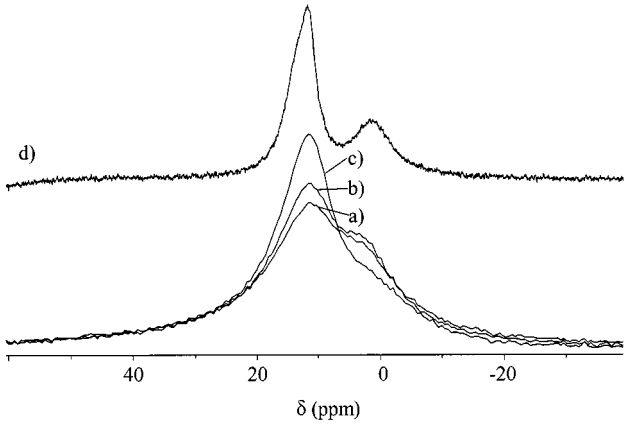

Figure 8. ^{27}Al NMR spectra (measured with a 200 MHz instrument) of the Al^{III}−citric acid system at a 1:1 ratio, c_{Al} = 0.1 M, at pH ≈ 7 and at different times after preparation of the sample; (a) 10 min, (b) 1 h, (c) 30 h, (d) the same spectra as (c) but measured with a 500 MHz instrument

ached. This behavior of the shoulder is probably related to the formation and decomposition of intermediate complexes. The fact that practically the same spectra were recorded at pH ≈ 5 and 7 suggests that a single species, formed fairly slowly, predominates in this pH range. Karlik et al.[5] assigned this spectrum to a mononuclear complex, probably $[AlLH_{-1}]^-$. It is now clear that this spectrum is that of the trinuclear species.

The ^{27}Al NMR spectrum of a sample recorded when the crystalline trinuclear complex was dissolved in water consisted of three signals: at δ = 0.2, at 10.7 and as a downfield shoulder on the latter, at 12.6.[13] In our case, as a result of the lower resolution of the instrument, the signals at δ = 10.7 and 12.6 are merged completely, giving a single broad peak with maximum at δ = 11.5 and the signal at δ = 0.2 becomes a shoulder. The spectral pattern described in the literature[13] was obtained when the same sample, as shown in Figure 8c, was measured with a 500 MHz instrument (see Figure 8d).

NMR Spectroscopic Measurements in the Al^{III}-Citrate System with Ligand Excess

The potentiometric results show that at an excess of ligand, besides the mononuclear 1:1 species, 1:2 complexes are also formed in freshly prepared solutions. These 1:2 and 1:1 complexes undergo slow oligomerization processes which, similarly as in equimolar solutions, result in the predominant formation of the trinuclear species $[Al_3(LH_{-1})_3(OH)]^{4-}$. The solid-state characterization and solution behavior of these 1:2 complexes have already been determined using ^1H and ^{13}C NMR spectroscopy.[11,12] The ^{13}C NMR measurements carried out by Gregor and Powell[8] in a Al^{III}−citrate solution at a 0.25 M Al^{III} and a metal ion/ligand ratio of 1:4, revealed the presence of the 1:2 species and free citrate only. The authors did not mention whether these spectra were taken in fresh solution or in the equilibrium state. In the ^1H NMR spectra measured by us at the same concentration at pH ≈ 5 and 7, but at an Al^{III}/citrate ratio of 1:3 (the ratio used in our potentiometric study), the signals of the trinuclear species could also be unambiguously recognized in the equilibrium state. It was further found that in concentrated solutions the oligomerization processes are slower than at 0.04 M or 0.004 M; equilibrium can be reached in about a week. These results lead to the conclusion that in ref.[8] the spectra were obtained using fresh solutions, and in the equilibrium state the trinuclear complex should also have formed, although in this case (because of the higher ligand excess) in a somewhat lower amount than at a ratio of 1:3. In less concentrated solutions and at higher metal/ligand ratios, the oligomerization processes may truly be negligible.

Conclusions

The time-dependent speciation study of the Al^{III}−citrate system indicates that in fresh solutions mononuclear mono- and bis(complexes) are the predominant species, although the trinuclear complex $[Al_3(LH_{-1})_3(OH)]^{4-}$ is also present, especially under equimolar conditions. However, the concentration of this complex is strongly reduced in the event of a ligand excess. The trinuclear species is formed in slow processes through the oligomerization of mononuclear complexes[10] (see the upper row of Scheme 2). An excess of

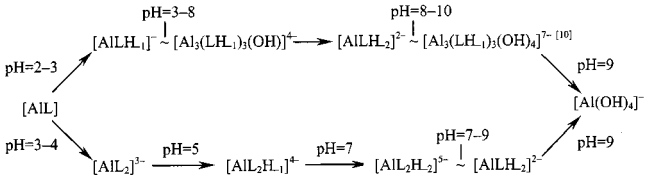

The species $[Al_3(LH_{-1})_3(OH)_4]^{7-}$ was proposed by Öhman at pH > 8[10]

Scheme 2

ligand favors the formation of the bis(complexes) (the reaction steps are indicated in the lower row of Scheme 2); under such conditions these are strongly competitive with the oligomerization processes indicated in the upper row.

These facts may be of importance when speciation model calculations on Al^{III} are performed for biological fluids, e.g. for blood serum, where citric acid may be present in a 100-fold excess as compared with Al^{III}. For the average concentrations of citrate and Al^{III} in serum, Harris[2] estimated 0.1 mM and 3 μM, respectively. However, ca. 80% of the total Al^{III} is bound to transferrin and only 20% is available for the l.m.m. binders.[2,14] As may be seen in Figure 9, under serum conditions the formation of the trinuclear species (even if the complex is very stable) is completely suppressed. In the event of an overload of Al^{III} in the organism, the metal concentration in the serum may increase to 10−100-fold, and this would increase the extent of the formation of the oligomeric species at equilibrium quite considerably. However, its formation is definitely a slow process and our calculations demonstrate that its concentration is still negligible 30 min after absorption.

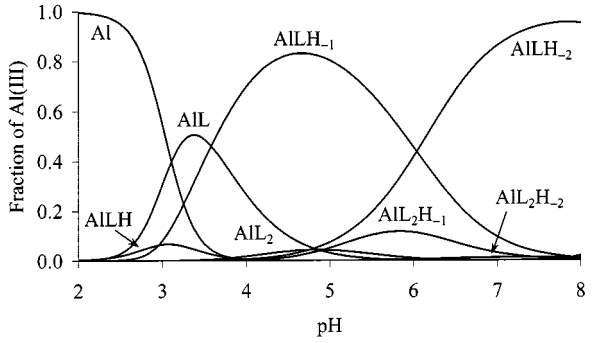

Figure 9. Speciation curves of the Al^{III}−citric acid system, at blood serum conditions, $c_{Al}{}^{III}$ = 0.6 μM, $c_{citrate}$ = 99 μM

As biological fluids are open systems, and by virtue of the continuous metabolic processes, Al^{III} may not spend enough time in the biological fluid for the equilibrium state to be reached. Accordingly, its speciation as calculated with the thermodynamic stability constants may not be totally relevant to the biological conditions. In such cases, only a complete equilibrium and kinetic description of the formation of all complexes can provide the exact biospeciation information. In such a complicated system, however, this can be achieved only in a very long and tedious way. A reasonable estimation of the speciation may be made by using stability constants calculated from measurements under non-equilibrium conditions.

Experimental Section

Reagents: Citric acid, of highest analytical purity (Sigma product), was used without further purification. The exact concentration of the ligand solution was determined by potentiometric titration using the Gran method.[20] The Al^{III} stock solution was prepared from recrystallized $AlCl_3{\cdot}6H_2O$, and its metal concentration was determined gravimetrically through its oxinate. The stock solution contained 0.1 M HCl to prevent hydrolysis of aluminium. The ionic strength of all solutions was adjusted to 0.2 M KCl and the temperature was 25.0±0.1 °C.

Potentiometric Measurements: The stability constants of the proton complexes of the ligands were determined by pH-potentiometric titrations of 10.0 mL samples. The ligand concentration was 0.004 M. The titrations were performed with a 0.2 M carbonate-free KOH solution of known concentration under purified argon. − The time-dependent speciation measurements were performed with the "batch" technique. After the appropriate amounts of stock solutions of Al^{III} were mixed with the ligand and the base, the pH of the solutions was recorded at given times until pH equilibrium was attained in the system (ca. 30 h). The procedure was repeated at different starting pH values, whereby titration curves relating to different times were obtained. The measurements were performed at metal/ligand ratios of 1:1 and 1:3, under intense stirring under argon. The pH range studied was 2−8. The time-dependent changes were monitored in this way for 39 different samples. However, in order to increase the reliability of the speciation description of the system in thermodynamic equilibrium twice as many samples were prepared, but half of them, i.e. every second was measured only 30 h after mixing, when pH equilibrium was surely attained. The stability constants listed in Table 1 were calculated from the total 78 "batch" points. The pH was measured with a Radiometer PHM 84 instrument with a CMAWL Russel combined glass electrode, which was calibrated for hydrogen ion concentration according to Irving et al.[21] − The concentration stability constants $\beta_{pqr} = [M_pL_qH_r]/[M]^p[L]^q[H]^r$ were calculated with the aid of the PSEQUAD computer program.[22] The stability constants used for the hydroxo species of Al^{III} were taken from ref.[23] and corrected to I = 0.2 using the Davies Equation: −5.49 for $[AlH_{-1}]^{2+}$, −13.54 for $[Al_3H_{-4}]^{5+}$, −97.2 for $[Al_{13}H_{-32}]^{7+}$ and −23.40 for $[AlH_{-4}]^{-}$.

NMR Spectroscopy: ^1H and ^{13}C NMR spectra were recorded at 25 °C with a Bruker AM360 spectrometer. In the ^1H and ^{13}C NMR spectra, chemical shifts were referenced to the signal of TMS as an external standard. The samples were prepared in D_2O; the pH was adjusted with concentrated NaOD and DCl, using the relation pH = pD + 0.4. The concentrations of the solutions were 0.04 M or 0.1 M for Al^{III}, and a metal ion/ligand ratio of 1:1 was usually applied. ^{27}Al NMR spectra were recorded with a Bruker AM200 instrument at 25 °C. Chemical shifts were recorded with respect to $[Al(H_2O)_6]^{3+}$. Solutions of 0.1 M Al^{III} and a metal ion/ligand ratio of 1:1 were prepared in water containing 10% of D_2O to provide an NMR lock signal.

Acknowledgments

The work was carried out in the frame of a COST D8 collaboration and was supported by the Hungarian Research Fund (OTKA 23776/97 and T26115) and the Hungarian Ministry of Education (FKFP 0013/97).

[1] R. B. Martin, *Acc. Chem. Res.* **1994**, *27*, 204−210.
[2] W. R. Harris, *Clin. Chem.* **1992**, *38*, 1809−1818.
[3] G. E. Jackson, *S. Afr. Tydskr. Chem.* **1982**, *35*, 89−93.
[4] L. O. Öhman, S. Sjöberg, *J. Chem. Soc., Dalton Trans.* **1983**, 2513−2517.
[5] E. Karlik, E. Tarien, G. A. Elgavish, G. L. Eichhorn, *Inorg. Chem.* **1983**, *22*, 525−529.
[6] R. J. Motekaitis, A .E. Martell, *Inorg. Chem.* **1984**, *23*, 18−23.
[7] M. A. Lopez-Quintela, W. Knoche, J. Veith, *J. Chem. Soc., Faraday Trans.* **1984**, *80*, 2313−2321.
[8] J. E. Gregor, H. K. J. Powell, *Aust. J. Chem.* **1986**, *39*, 1851−1864.
[9] F. T. Greenaway, *Inorg. Chim. Acta* **1986**, *116*, L21−L23.

[10] L. O. Öhman, *Inorg. Chem.* **1988**, *27*, 2565−2570.
[11] M. Matzapetakis, C. P. Raptopoulou, A. Terzis, A. Lakatos, T. Kiss, A. Salifoglou, *Inorg. Chem.* **1999**, *38*, 618−619.
[12] M. Matzapetakis, C. P. Raptopoulou, A. Terzis, A. Lakatos, I. Banyai, T. Kiss, A. Salifoglou, *Inorg. Chem.*, submitted.
[13] T. L: Feng, P. L. Gurian, M. D. Healy, A. R. Barron, *Inorg. Chem.* **1990**, *29*, 408−411.
[14] W. R. Harris, G. Berthon, J. P. Day, C. Exley, T. P. Flaten, W. F. Forbes, T. Kiss, C. Orvig, P. F. Zatta, *J. Toxicol. Environ. Health* **1996**, *48*, 543−568.
[15] E. Kiss, A. Lakatos, I. Bányai, T. Kiss, *J. Inorg. Biochem.* **1998**, *69*, 145−151.
[16] T. Kiss, I. Sóvágó, R. B. Martin, J. Pursiainen, *J. Inorg. Biochem.* **1994**, *55*, 53−57.
[17] T. Kiss, I. Sóvágó, I. Tóth, A. Lakatos, R. Bertani, A. Tapparo, G. Bombi, R. B. Martin, *J. Chem. Soc., Dalton Trans.* **1997**, *11*, 1967−1972.
[18] G. J. Moore, L. O. Sillerud, *J. Magn. Reson.* **1994**, *B103*, 87−90.
[19] A. Bodor, I. Bányai, L. Zékány, I. Tóth, *Inorg. Chem.*, in preparation.
[20] G. Gran, *Acta Chem. Scand.* **1950**, *4*, 559.
[21] H. M. Irving, M. G. Miles, L. D. Pettit, *Anal. Chim. Acta* **1967**, *38*, 475.
[22] L. Zékány, I. Nagypál, G. Peintler, *PSEQUAD for Chemical Equilibria*, Technical Software Distributions, Baltimore, **1991**.
[23] L. O. Öhman, S. Sjöberg, *Acta Chem. Scand.* **1982**, *A36*, 47.
Received April 26, 2000
[I00166]

Iron(III) Complexation by New Aminocarboxylate Chelators – Thermodynamic and Kinetic Studies

Guy Serratrice,*[a] Jean-Baptiste Galey,[c] Eric Saint Aman,[b] and Jacqueline Dumats[c]

Keywords: Iron / Chelates / Thermodynamics / Kinetics / N ligands

The complexation of Fe^{III} by new tetradentate and pentadentate aminocarboxylate chelators, designed to protect cells against iron-catalysed oxidative damage, was investigated. Ferric iron complexes of *N*,*N*′-bis(3,4,5-trimethoxybenzyl)-ethylenediamine-*N*,*N*′-diacetic acid (**L1**), *N*,*N*′-dibenzylethylenediamine-*N*,*N*′-diacetic acid (**L2**) and [*N*-(2-hydroxybenzyl)-*N*′-benzylethylenediamine-*N*,*N*′-diacetic acid] (**L3**) have been characterized in aqueous solution by potentiometric, UV/Vis spectrophotometric and cyclic voltammetric measurements. The parent ligand, ethylenediamine-*N*,*N*′-diacetic acid (**L4**), has also been studied. As expected, the presence of a hard phenolate donor group in **L3** significantly enhances the affinity for iron while decreasing the potential of the Fe^{III}/Fe^{II} redox couple compared to **L1** or **L2**. Kinetics studies have provided the kinetic rate constants related to the formation and the dissociation of the ferric complex with **L3**. The results reveal a fast Fe^{III} uptake, which is a favorable feature for a biological use of this type of ligand. Overall, these results demonstrate the pertinence of the use of such ligands to protect biological tissues against oxidative stress.

Introduction

In recent years there has been an intensive search for new iron ligands with medicinal applications. Several diseases are indeed associated with disturbance of iron homeostasis.[1] One major issue is the treatment of iron-overload-associated situations for people suffering from haematological defects such as β-thalassemia major. Indeed, because man is unable to actively excrete iron, systemic iron overload occurs rapidly when frequent blood transfusions are given.[2] In such situations, treatment with powerful iron chelators is the only effective way to remove excess iron. Currently, the hexadentate siderophore desferrioxamine (DFO) is by far the clinically most used iron chelator. However, DFO lacks oral activity and has a very short biological half life, which results in poor patient compliance.[3] Therefore, considerable effort has been focused on discovering new therapeutically useful iron chelators.

On the other hand, there are also other areas in which iron chelators could be useful. For instance, drugs able to specifically chelate iron from iron-containing enzymes such as ribonucleotide reductase or lipoxygenase could find important applications.[4] Moreover, in addition to systemic iron overload, local iron homeostasis disturbances can occur in several conditions associated with so-called ''oxidative stress'', i.e. when traces of iron are locally released from their normal storage sites and become available to catalyze Fenton chemistry, leading to oxidative damage to surrounding biological molecules.[5] However, there are few reports on the development of iron chelators specifically designed for the treatment of such oxidative stress-associated situations. The main reason is probably that the design of such systems is potentially problematic for medicinal chemists in terms of safety margins owing to the possible interaction of chelators with normal iron metabolism.[6]

We recently developed a new strategy based on the idea that an ''ideal'' iron chelator for use in oxidative stress-related conditions should effectively chelate iron only in pro-oxidant conditions. We therefore explored the possibility of generating pro-drugs that can be oxidatively activated into species with strong iron-binding capacity.[7] Of particular interest in such a strategy is the degree of control exercised by the oxidative stress conditions, whereby a dormant relatively inactive compound is transformed to an active species by the very conditions prevailing at sites where it is most needed.

N,*N*′-Bis(3,4,5-trimethoxybenzyl)ethylenediamine-*N*,*N*′-diacetic acid (**L1**) (Figure 1) is the most extensively studied ligand in this series. In aqueous solutions containing acetate and ferric salts, **L1** forms a μ-acetato μ-oxo diferric iron complex.[8] In the presence of ferrous salts in anaerobic conditions, a mononuclear ferrous complex is formed. Both complexes react with hydrogen peroxide or dioxygen in the presence of ascorbate to form a mononuclear (phenolato)-Fe^{III} complex resulting from the quantitative hydroxylation of **L1** into **L5** (Figure 2). Owing to the well-known affinity of phenolate ligands for ferric iron, **L1** appears to fit the aforementioned prerequisites regarding the generation of a strong iron chelator according to a local oxidative activation process.[9]

[a] Laboratoire de Chimie Biomimétique, LEDSS, UMR CNRS 5616, Université J. Fourier
B. P. 53, 38041 Grenoble, Cedex 9, France
E-mail: Guy.Serratrice@ujf-grenoble.fr
[b] Laboratoire d′Electrochimie Organique et de Photochimie Redox, UMR CNRS 5630, Université J. Fourier,
B. P. 53, 38041 Grenoble, Cedex 9, France
[c] Département Molécules & Matériaux, l'OREAL Recherche Avancée,
1 Avenue Eugène Schueller, 93600 Aulnay sous Bois, France

 © WILEY-VCH Verlag GmbH, 69451 Weinheim, 2001 1434–1948/01/0202–0471 $ 17.50+.50/0

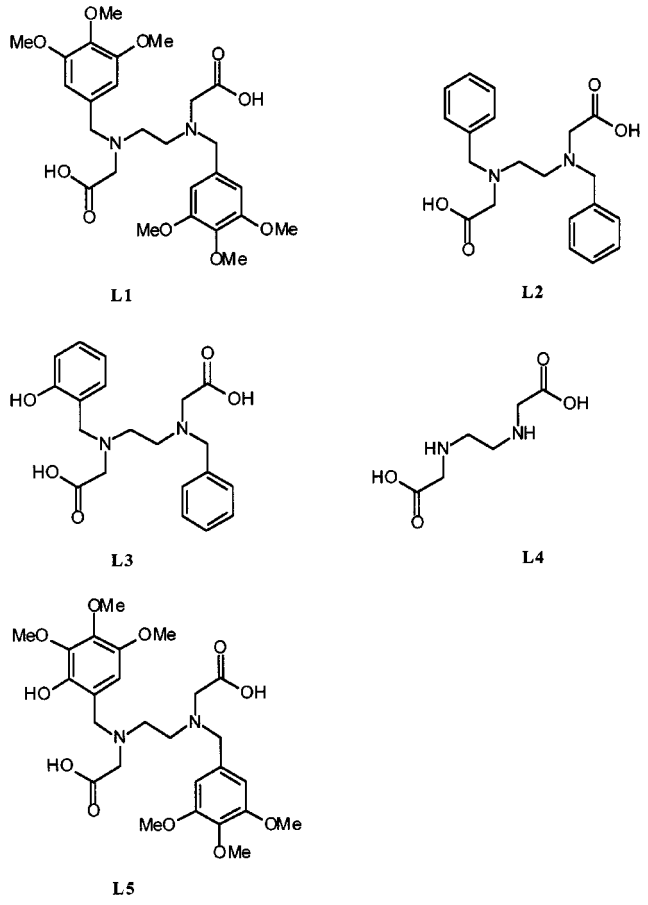

Figure 1. Structure of the ligands **Ln**

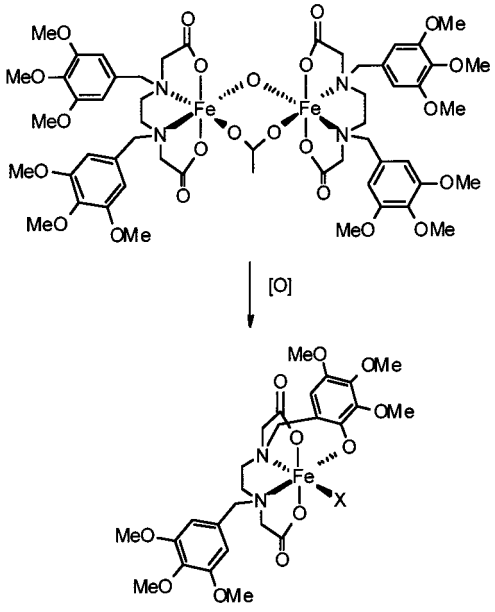

Figure 2. Reaction scheme for the oxidation of $Fe_2(\mathbf{L1})_2$

In the present paper, we extend our previous findings by accurately investigating the physicochemical parameters of Fe^{III} complexation by **L1** and analogs **L2** (*N*,*N*′-dibenzylethylenediamine-*N*,*N*′-diacetic acid) and **L3** [*N*-(2-hydroxybenzyl)-*N*′-benzylethylenediamine-*N*,*N*′-diacetic acid] (Figure 1), i.e. stability constants and redox potentials to demonstrate the pertinence of the use of such ligands to protect biological tissues against iron-catalyzed oxidative damage. The ligand ethylenediamine-*N*,*N*′-diacetic acid (**L4**) was also investigated for comparison and because the stability constants of the ferric complexes are unknown. A detailed kinetic study of the formation and of the dissociation of the ferric complex with **L3** is also described in order to (i) determine the reactivity patterns of this complex containing phenolate and aminoacetate donor groups and (ii) since few data are available in the literature for this type of ligand.

Results and Discussion

Ligand Deprotonation Constants

The deprotonation constants K_a of the ligands investigated in this research were studied by potentiometric titration. Analysis of the potentiometric titration curve (Figure 3a and Figure 3c as examples) by the SUPERQUAD program[10] yielded the pK_{an} values defined by Equation (1) and Equation (2) (charges omitted for clarity) and reported in Table 1.

$$LH_n \rightleftharpoons LH_{n-1} + H^+ \quad (1)$$

$$K_{an} = [LH_{n-1}]\cdot[H^+]/[LH_n] \quad (2)$$

Three pK_a values were determined and these correspond to one carboxylic acid group and the two ammonium groups. By comparison to EDTA the lowest pK_a value for each ligand is attributed to a carboxylic acid and the two highest ones to the ammonium nitrogen atoms. The pK_a values of **L4** are in good agreement with those determined by Harris and Martell [9.67, 6.57 and 2.36 (I = 0.1 M, KNO_3)].[11] The pK_a value of the other carboxylic acid is assumed to be significantly lower than 2.

A fourth pK_a value corresponding to the hydroxy group was determined for the ligand **L3** by spectrophotometric titration. This pK_a cannot be accurately determined by potentiometric titrations since deprotonation occurs at pH > 11. A spectrophotometric titration was carried out over the pH range 10−12. The corresponding UV spectra exhibit an isosbestic point at λ = 270 nm, indicating the presence of only two absorbing species. The data were processed by the LETAGROP SPEFO[12,13] program (absorbance values at 8 wavelengths). The best fit [$\Sigma(A_{exp} - A_{calc})^2 = 10^{-3}$] yielded a p$K_a$ value of 12.0 ± 0.1. The extinction coefficients were determined to be ε_{max} = 3500 $M^{-1}cm^{-1}$ (λ_{max} = 292 nm) and ε_{max} = 10000 $M^{-1}cm^{-1}$ (λ_{max} = 238 nm) for $\mathbf{L3}^{3-}$ and ε_{max} = 50 (λ_{max} = 292 nm) and ε_{max} = 1000 $M^{-1}cm^{-1}$ (λ_{max} = 238 nm) for $\mathbf{L3H}^{2-}$. The pK_a values for **L3** are close to those obtained for the ligands HBIDA [*N*-(2-hydroxybenzyl)iminodiacetic acid][14] and HBED [*N*,*N*′-bis(2-hydroxybenzyl)ethylenediamine-*N*,*N*′-diacetic acid][15] bearing similar donor groups, as indicated in Table 1. The high basicity of the hydroxy group reflects the presence of a hydro-

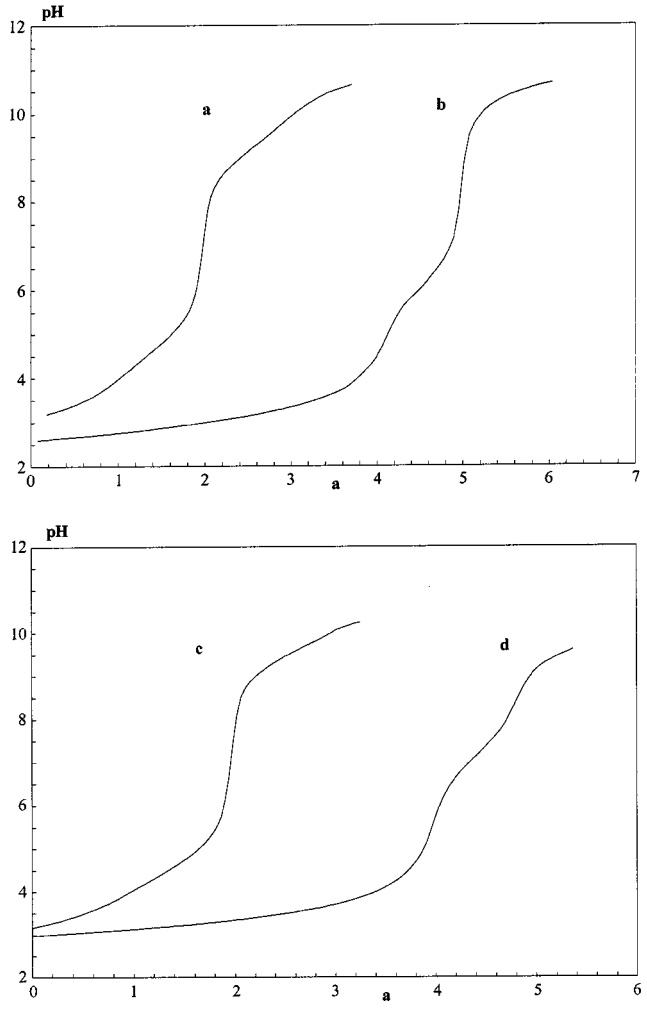

Figure 3. Potentiometric titration curves for (a) 1 mM ligand **L3**; (b) **L3** + Fe^{3+} 1:1, 1 mM; (c) 1 mM ligand **L1**; (d) **L1** + Fe^{3+} 1:1, 1 mM; a = mol of base added per mol of ligand; all solutions were at 25 °C and I = 0.1 M ($NaClO_4$); the data were refined by the SUPERQUAD program (σ_{fit} = 3.5−4.5)

Table 1. Deprotonation constants of the ligands

pK_{an} [a]	L1	L2	L3	L4	HBIDA[b]	HBED[c]
pK_{a1}	9.44(1)	9.68(1)	12.0(1)	9.75(1)	11.71	12.35
pK_{a2}	4.61(2)	4.93(1)	9.11(1)	6.68(2)	8.07	12.08
pK_{a3}	2.87(2)	2.29(3)	4.67(1)	2.64(3)	2.34	8.46
pK_{a4}			2.17(2)			4.76
pK_{a5}						2.18

[a] All values were determined at 25 °C and I = 0.1 M ($NaClO_4$); values in parentheses are standard deviations in the last significant digit. − [b] *N*-(2-Hydroxybenzyl)iminodiacetic acid, ref.[14] − [c] *N*,*N*′-Bis(2-hydroxybenzyl)ethylenediamine-*N*,*N*′-diacetic acid, ref.[15]

gen bond between the amino nitrogen atom and the hydroxy group.

Stability Constants of the Ferric Complexes

The stability constants β_{110} were determined by potentiometric titration for the ferric complexes of ligands **L1**, **L2** and **L4**. The titration curves for a 1:1 ratio of Fe^{III} to ligand (Figure 3d as an example) exhibit two breaks at a = 4 and a = 5, where a is equal to the number of moles of base added per mole of ligand. This clearly indicates the formation of hydroxo complexes Fe(OH)L and $Fe(OH)_2L$ at relatively low pH values. Analysis of the titration curves by the SUPERQUAD program[10] yielded the β_{110} and K^n_{OH} (n = 1 or 2) constants expressed as in Equation (3) and Equation (4).The values are given in Table 2.

$$\beta_{110} = [FeL]/[Fe^{3+}]\cdot[L] \quad (3)$$

$$K^n_{OH} = [Fe(OH)_nL]\cdot[H^+]/[Fe(OH)_{n-1}L] \quad (4)$$

Table 2. Fe^{III}−ligand stability constants and pFe values

Constants[a]	L1	L2	L3	L4
$\log \beta_{110}$	13.95(4)	15.20(9)	27.00(8)[b]	15.50(1)
pK^1_{OH} [c]	3.34(4)	3.52(9)	5.76(8)[b]	3.64(5)
pK^2_{OH} [d]	7.34(5)	7.27(5)		7.18(2)
pFe[e]	17.2	18.1	23.3	18.2

[a] All values were determined at 25 °C and I = 0.1 M ($NaClO_4$); values in parentheses are standard deviations in the last significant digit. − [b] Determined from spectrophotometric titration; K^1_{OH} = 6.02 from potentiometric titration. − [c] $K^1_{OH} = [Fe(OH)L][H^+]/[FeL]$ for the equilibrium $FeL + H_2O \rightleftarrows Fe(OH)L + H^+$. − [d] $K^2_{OH} = [Fe(OH)_2L][H^+]/[Fe(OH)L]$ for the equilibrium $FeLOH + H_2O \rightleftarrows Fe(OH)_2L + H^+$. − [e] Calculated for $[L]_{tot} = 10^{-5}$ M, $[Fe]_{tot} = 10^{-6}$ M at pH = 7.4.

For the tetraprotonated ligand **L3**, the breaks at a = 4 and a = 5 indicate the formation of the FeL and Fe(OH)L complexes (Figure 3b). However, it was not possible to determine the β_{110} value since the formation of the complex is complete at low pH values. Only the value of K^1_{OH} was determined from titration data and this is given in Table 2. The spectrophotometric titration was carried out over the range pH = 1−8 in order to determine the constants β_{110} and K^1_{OH}. The stoichiometric addition of Fe^{III} to a solution of **L3** over the pH range 1−2 led to the formation of a purple complex, the UV/Vis spectrum of which shows a maximum at 525 nm that is attributed to a phenolato-to-Fe^{III} charge transfer transition (Figure 4a). The absorbance data were processed with the LETAGROP-SPEFO program.[12,13] The best fit [$\Sigma(A_{exp} - A_{calc})^2 = 2 \times 10^{-3}$] was obtained by considering the formation of the [FeL] species and provides the values $\log \beta_{110}$ = 27.0 ± 0.08 and ε_{max} = 1950 $M^{-1}cm^{-1}$ (λ_{max} = 520 nm). No spectral change was observed over the pH range 2.5−4.5. As the pH value was increased from 5 to 7, the spectra showed isosbestic points at 394 and 491 nm, indicating that there are only two species with a different absorption in this pH range (Figure 4b). These absorbance data were also refined with the LETAGROP-SPEFO program.[12,13] The best fit [$\Sigma(A_{exp} - A_{calc})^2 = 3 \times 10^{-3}$] showed that deprotonation occurs through a one-proton step yielding a pK^1_{OH} value of 5.76 ± 0.08 and an absorption maximum at λ = 470 nm with ε = 1800 $M^{-1}cm^{-1}$ for the Fe(OH)L species. The value of pK^1_{OH} is in good agreement with the value 6.02 determined by potentiometric titration. The shift of the absorption

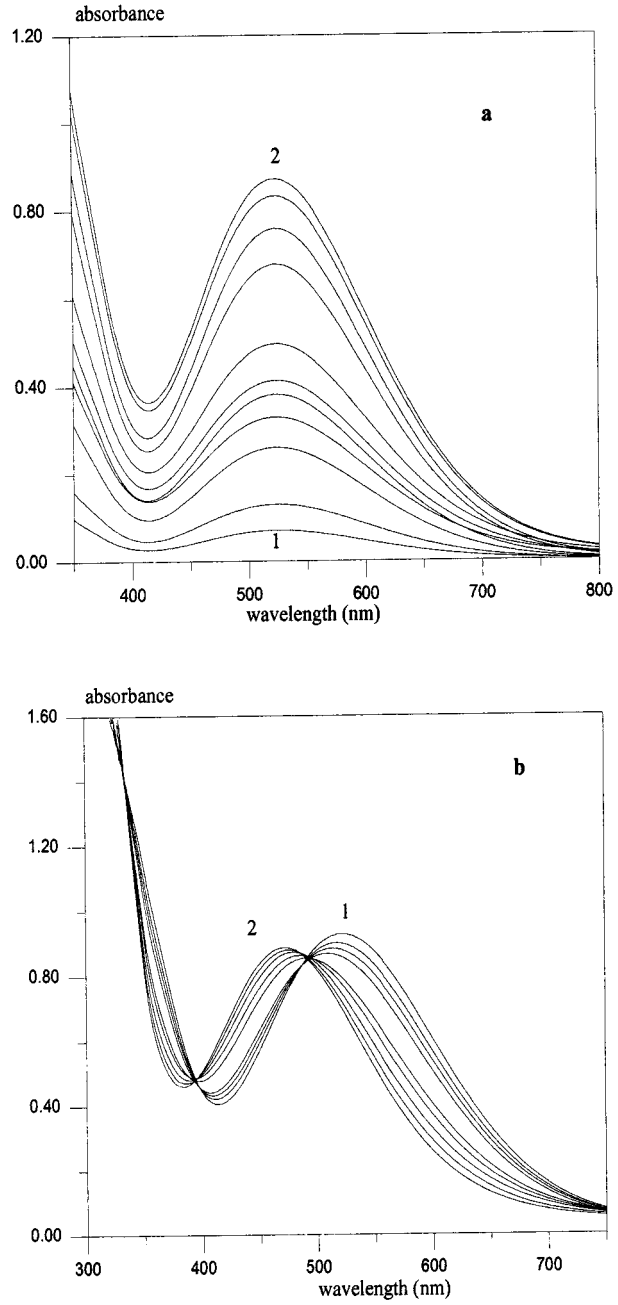

Figure 4. UV/Vis absorption spectra of Fe^{3+}−**L3** as a function of pH; (a) 1: pH = 0.9; 2: pH = 1.8; (b) 1: pH = 4.5; 2: pH = 6.5; $[Fe^{3+}]$ = [**L3**] = 0.5 mM; I = 0.1 M ($NaClO_4$)

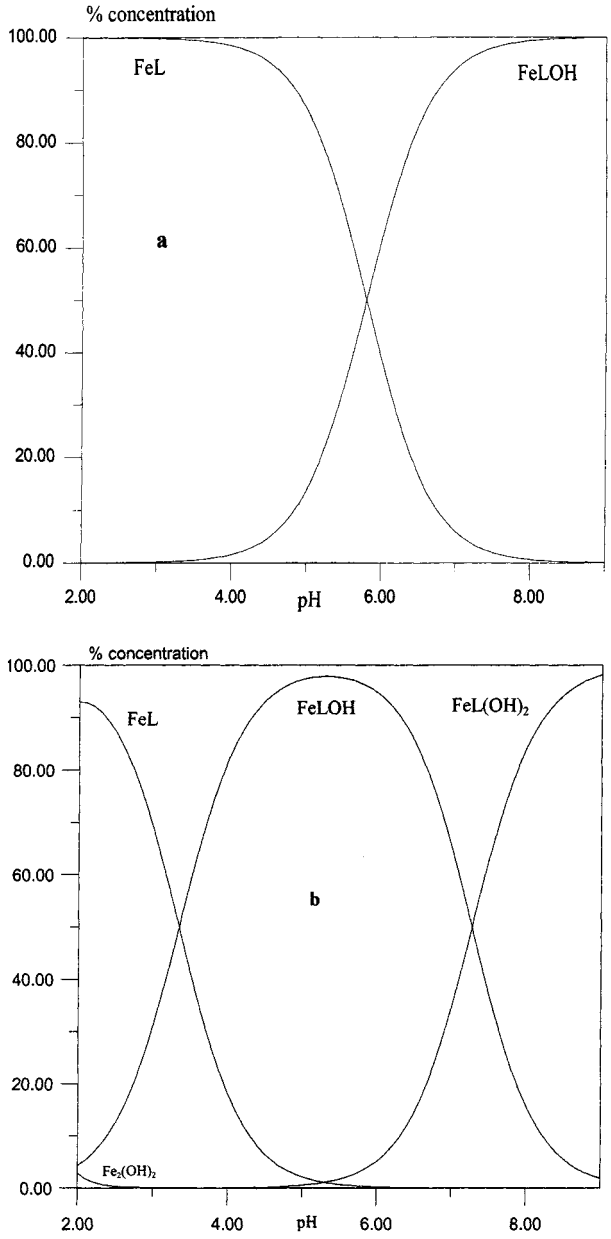

Figure 5. Distribution diagrams of the system Fe^{III}−**L3** (a) and Fe^{III}−**L1** (b) as a function of pH; $[Fe^{3+}]$ = 1 mM, [ligand] = 10 mM

maximum to lower wavelength reflects coordination with the more basic hydroxide ion. A similar spectral change has been observed for the ferric complex with HBIDA[14] [λ_{max} = 518 nm, ε_{max} = 1100 $M^{-1}cm^{-1}$ for FeL, λ_{max} = 460 nm, ε_{max} = 1010 $M^{-1}cm^{-1}$ for Fe(OH)L]. It is worth noting that the extinction coefficient is about half the value for Fe-HBED[15] (λ_{max} = 485 nm, ε_{max} = 3935 $M^{-1}cm^{-1}$), a system that has two phenolate donors and the same framework as **L3**. The distribution curves are shown in Figure 5 for ligands **L1** and **L3**.

The ferric complexes of the tetradentate ligands **L1**, **L2** and **L4** exhibit relatively low stability constants β_{110}, in agreement with those of tetradentate *N*,*N*′-diethylenediamine diacetic acid derivatives. Consequently, low values for pK^1_{OH} are observed (over the range 3.2−3.6). This reflects the high Lewis acid character of the ferric ion in FeL resulting from the low basicity of these ligands. A more reliable parameter for comparison of ligand effectiveness is the pFe^{III} value (= −log $[Fe^{3+}]$). The larger the pFe value, the more effective the ligand. The pFe^{III} values were calculated for $[L]_{tot} = 10^{-5}$ M, $[Fe]_{tot} = 10^{-6}$ M at pH = 7.4 and are reported in Table 2. The pFe values for **L2** and **L4** are very similar, indicating that substitution with benzyl groups does not influence the complexation. The lower ferric affinity of **L1** in comparison to **L2** and **L4** is probably due to steric effects of the methoxy substituents. A higher metal ion affinity is observed for **L3** and this fact is related to the

phenolate donor, as one would expect. An increase in the pFe value of 5.2 from **L2** (18.1) to **L3** (23.3) is observed. A comparison with the hexadentate ligand HBED (pFe = 26.97),[15] which contains two phenolate donors with an EDTA-type framework, shows that incorporation of one phenolate donor increases the pFe value by about 4−5 units. Furthermore, the pFe value for **L3** is higher than that of the tetradentate ligand HBIDA (19.95), which has one phenolate donor, one nitrogen donor and two carboxylate donors. The pK^1_{OH} values are very close, being 5.76 for **L3** and 5.75 for HBIDA. This indicates that the Lewis acidity of Fe^{III} is similar in both complexes.

Electrochemistry

The electrochemical behavior of the Fe^{III} + **L(1−3)** complexes was studied by cyclic voltammetry in an aqueous solution over the pH range 3−10.5 in order to investigate the ability of these complexes to undergo redox cycling under physiological conditions and to catalyze Fenton chemistry. In order to be able to catalyze the formation of hydroxyl radicals in the presence of hydrogen peroxide, an iron complex has to meet two conditions simultaneously: (i) the ferric chelate has to be reducible by physiological reductants, i.e. its standard redox potential must be higher than −0.534 V vs. Ag/AgCl (NADPH/$NADP^+$ redox couple) and (ii) single electron transfer from the ferrous chelate to hydrogen peroxide must be possible, i.e. its redox potential must lie below 0.25 V vs. Ag/AgCl (H_2O_2/HO˙, OH^-). The electrochemical response of the Fe^{III} + **L3** electrolytic solution is characterized in the 3−5 pH range by a quasi-reversible redox wave at $E_{1/2}$ = −0.21 V vs. Ag/AgCl (ΔE_p = 0.12 V, v = 0.1 V s^{-1}) corresponding to the Fe^{III}/Fe^{II} redox couple (Figure 6, curve 1). Increasing the pH value from 5 to 8 results in the progressive appearance of a new redox peak system at $E_{1/2}$ = −0.48 V (ΔE_p = 0.31 V), which grows at the expense of the original one at $E_{1/2}$ = −0.21 V (Figure 6, curves 2−4). Above pH = 8, the original wave disappears and the new peak system reaches full development (Figure 6, curves 5 and 6). This result is in agreement with the pK^1_{OH} value of 5.76 found for the Fe**L3**/Fe(OH)**L3** system and the distribution curve in Figure 5 (see above), i.e. the wave at $E_{1/2}$ = −0.48 V can be attributed to the Fe^{III}(OH)**L3**/Fe^{II}**L3** redox couple. Therefore, at pH = 7.4, the **L3** ferric chelate appears to be mainly in a form that is reducible by physiological reductants. However, the small difference between the $E_{1/2}$ values of NADPH and the **L3** ferric chelate could explain the fact that **L3**−iron is not a catalyst of reductant-driven Fenton reaction under physiological conditions.[7] In addition, a small proportion of the complex remains in the Fe**L3** form, which could be reduced by physiological reductants. This process would allow potential redox cycling of iron, especially during acidosis, which is generally associated with cell oxidative stress. Therefore, it is likely that additional parameters, such as the kinetics of complex formation, compensate for the thermodynamic factor that is favorable for the catalysis of Fenton chemistry.

In contrast, the electrochemical behavior of **L(1−2)** + Fe^{III} complexes appears more complicated, possibly due to the presence of several species in solution at basic pH values, including the μ-oxo binuclear species already characterized by ESI-MS.[8] At pH values above 8, an ill-behaved peak system is seen in the CV curves (Figure 7, curves 1 and 2) (E_{pc} = −0.80 and −0.72 V, E_{pa} = −0.15 and −0.04 V for the complexes **L2** + Fe^{III} and **L1** + Fe^{III}, respectively). For pH values lower than 4.5 (Figure 7,

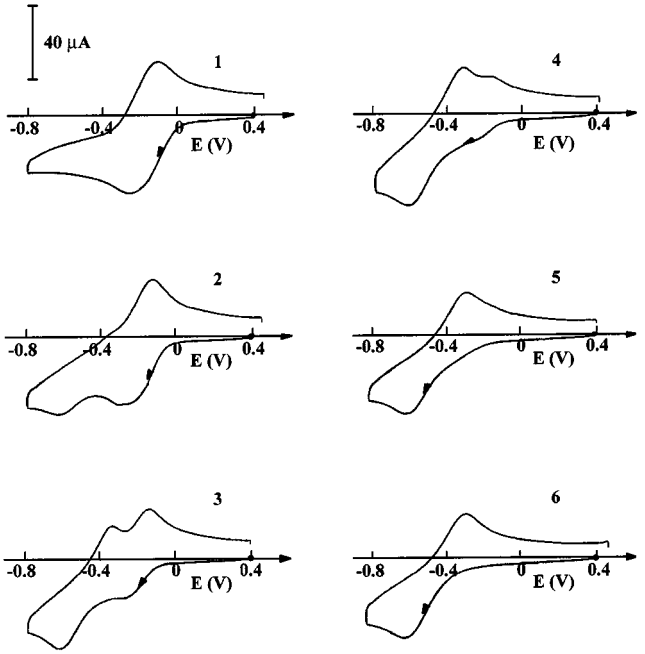

Figure 6. CV curves of Fe^{III} + **L3** (2.9 mM) in H_2O + $NaClO_4$ 0.1 M at a GC electrode (5 mm diameter); scan rate 0.1 Vs^{-1}; E vs. Ag/AgCl, aqueous NaCl (3 M) (+ 0.21 V vs. NHE); pH = 4.2 (1), 5.4 (2), 6.3 (3), 7.0 (4), 8.3 (5), 9.2 (6) (adjusted with $HClO_4$ or NaOH)

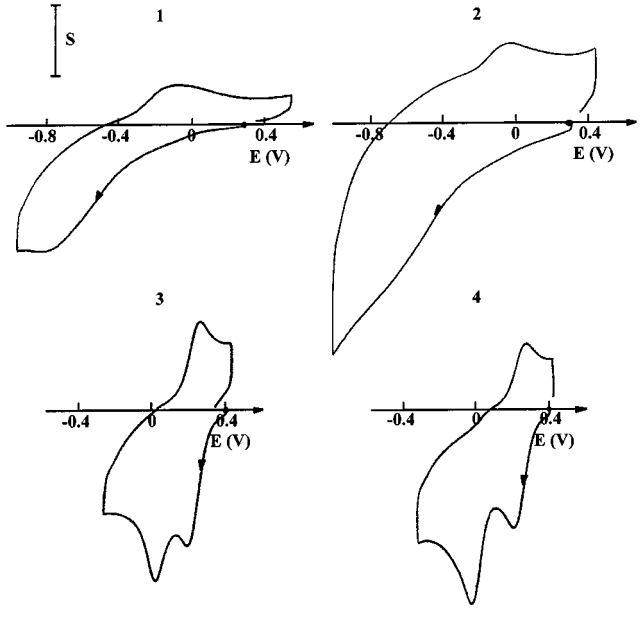

Figure 7. CV curves of Fe^{III} + **L2** (1, 3) and Fe^{III} + **L1** (2, 4), 0.5 mM in H_2O + $NaClO_4$ 0.1 M at a GC electrode (5 mm diameter); scan rate 0.1 V s^{-1}; E vs. Ag/AgCl, aqueous NaCl (3 M) (+0.222 V vs. NHE); pH = 8.3 (1, 2), 3.0 (3, 4) (adjusted with $HClO_4$ or NaOH); scale (S) = 10 μA (1, 2), 4 μA (3, 4)

curves 3 and 4), a reversible redox wave is seen at $E_{1/2}$ = 0.21 and 0.22 V (ΔE_p = 0.06 and 0.08 V, respectively) in the CV curves recorded in the presence of **L2** + Fe^{III} and **L1** + Fe^{III}, respectively. At lower potentials, a fully irreversible peak at 0 V (**L2** + Fe^{III}) or −0.04 V (**L1** + Fe^{III}) is observed, confirming the presence in solution of two different Fe^{III} species in a frozen equilibrium, i.e. the interconversion of these species is slow on the time scale of voltammetry. Between pH = 5 and 8, the CV curves consist of the overlapped electrochemical signals observed in basic and acidic media. These results are in agreement with pK^1_{OH} and pK^2_{OH} values of ca. 3 and 7 found for both **L2** + Fe^{III} and **L1** + Fe^{III} complexes, i.e. in basic media only the $Fe^{III}(OH)_2L$ complex is present in solution whereas in acidic media an equilibrium between $Fe^{III}L$ and $Fe^{III}(OH)L$ occurs. Taking into account the negative shift in potential for the redox couple $Fe^{III}(OH)L/Fe^{II}L$ in comparison to Fe^{III}**L3**/Fe^{II}**L3**, it can be assumed that the reversible wave at around 0.2 V is attributable to the $Fe^{III}L/Fe^{II}L$ redox couple (where L signifies **L1** or **L2**) when the irreversible electron transfer corresponds to the cathodic process characteristic of Fe^{III}(OH)**L3**. The irreversibility of the electron transfer is likely to be due to a change in the coordination sphere around the Fe center upon reduction. Comparing **L1** and **L2**, it must be noted that the substitution of **L1** with electron-donating methoxy groups does not influence significantly the potential characteristic of the iron-localized electron transfer. In addition, under the same experimental conditions, $E_{1/2}$ for the Fe^{III}EDTA/Fe^{II}EDTA redox couple is found at −0.10 V, showing that **L3** stabilizes the Fe^{III} form of the complex by ca. 0.12 V while **L1** and **L2** stabilize the Fe^{II} form of the complex by ca. 0.31 V. This is in agreement with the presence of the hard coordinating hydroxo site on **L3**.

Formation and Acid Hydrolysis Kinetics of the FeL3 Complex

The capacity of a chelator to protect against the formation of damaging oxidizing species is influenced not only by several thermodynamic factors, but also by kinetic factors. Therefore, the kinetics of formation of the Fe**L3** complex was investigated by a stopped-flow spectrophotometric method under pseudo-first-order conditions: [Fe^{III}] and [H^+] >> [L] and at ionic strength I = 2 M, 25 °C. The absorbance change vs. time of the phenolato-to-Fe^{III} charge transfer band at λ = 525 nm showed a single exponential curve indicating that the complex formation reaction proceeds through a single rate-limiting step. The spectra recorded with time using a diode array device were similar to those shown in Figure 4a. It was found that the pseudo first-order rate constants k_{obs} at a given acidity level ([H^+] varied from 0.05 to 0.15 M) have a linear variation as a function of [Fe^{3+}] with a significant intercept (Figure 8) that indicates a contribution of the reverse reaction. The slopes of these plots decrease as [H^+] increases. In addition, the intercepts of the plots increase as [H^+] increases.

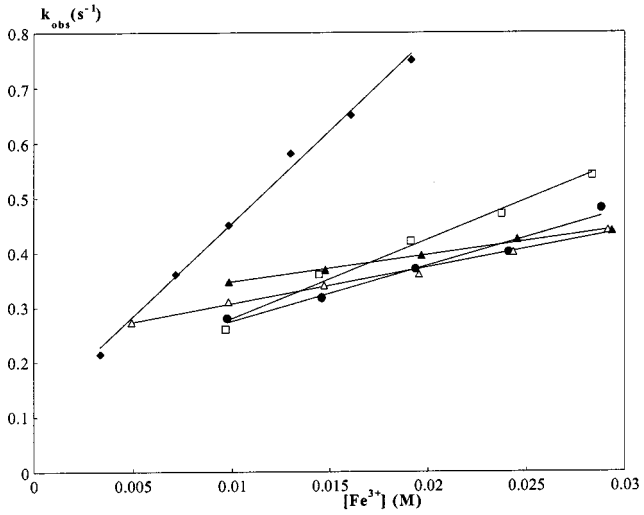

Figure 8. Variation of the experimental rate constant k_{obs} (s^{-1}) for the formation of the Fe^{III}−**L3** complex as a function of [Fe^{3+}] (M) at various [H^+] (M): (◆) 0.05, (□) 0.08, (●) 0.10, (Δ) 0.125, (▲) 0.15; [**L3**] = 0.4 mM; solvent: water, I = 2.0 M ($HClO_4$ + $NaClO_4$), T = 25 °C

The acid hydrolysis kinetics of the Fe−**L3** complex was studied in aqueous solution (ionic strength I = 2 M, 25 °C) by the pH jump method. The pH jump reactions were performed under pseudo-first-order conditions with respect to [H^+] (varying over the range 0.02−0.9 M) for solutions containing Fe^{III} and **L3** in a 1:1 molar ratio at an initial pH value of 4. The UV/Vis spectra recorded as a function of the time resemble the spectra recorded for the formation reaction study and for the equilibrium study at pH < 2 (Figure 4a) and indicate a total dechelation at the iron center. The exponential absorbance decay vs. time recorded at 520 nm indicates that the dissociation occurs through a single determining step. The plot of the k_{obs} rate constants vs. [H^+] is linear over the [H^+] range 0.2−1.0 M and slightly curved at low [H^+] (Figure 9).

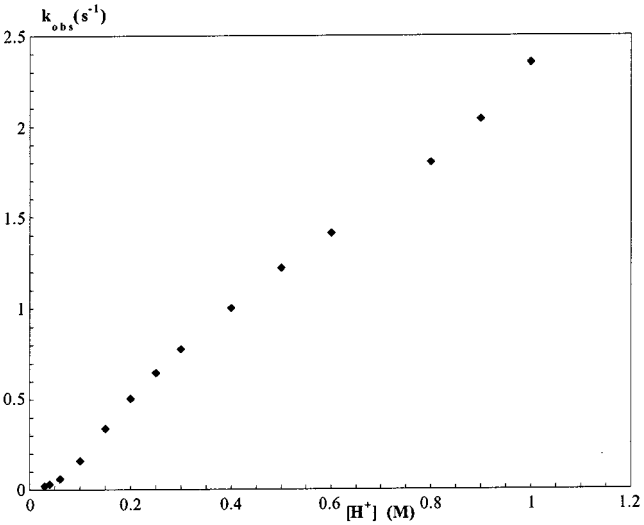

Figure 9. k_{obs} (s^{-1}) as a function of [H^+] (M) in the acid hydrolysis kinetics of the Fe^{III}−**L3** complex, [Fe**L3**] = 0.5 mM; solvent: water; I = 2.0 M ($HClO_4$ + $NaClO_4$), T = 25 °C

By taking into account the equilibria existing in solution under the experimental conditions and after analyzing the kinetics results from both the formation and the hydrolysis reactions, the reaction scheme shown in Equation (5) to Equation (14) can be proposed ($[FeOH]^{2+}$ for $[Fe(OH)(OH_2)_5]^{2+}$, Fe^{3+} for $[Fe(OH_2)_6]^{3+}$ and L for **L3**).

$$Fe^{3+} \rightleftharpoons FeOH^{2+} + H^+ \qquad K_{Fe} \qquad (5)$$

$$LH_5^{2+} \rightleftharpoons LH_4^+ + H^+ \qquad K_{a5} \qquad (6)$$

$$LH_4^+ \rightleftharpoons LH_3 + H^+ \qquad K_{a4} \qquad (7)$$

$$Fe^{3+} + LH_5^{2+} \rightleftharpoons FeLH_2^{3+} + 3\,H^+ \qquad k_0, k_{-0} \qquad (8)$$

$$FeOH^{2+} + LH_5^{2+} \rightleftharpoons FeLH_2^{3+} + 2\,H^+ + H_2O \qquad k_1, k_{-1} \qquad (9)$$

$$Fe^{3+} + LH_4^+ \rightleftharpoons FeLH_2^{3+} + 2\,H^+ \qquad k_2, k_{-2} \qquad (10)$$

$$FeOH^{2+} + LH_4^+ \rightleftharpoons FeLH_2^{3+} + H^+ + H_2O \qquad k_3, k_{-3} \qquad (11)$$

$$Fe^{3+} + LH_3 \rightleftharpoons FeLH_2^{3+} + H^+ \qquad k_4, k_{-4} \qquad (12)$$

$$FeOH^{2+} + LH_3 \rightleftharpoons FeLH_2^{3+} + H_2O \qquad (13)$$

$$FeLH_2^{3+} \rightleftharpoons FeL^+ + 2\,H^+ \qquad K_{FeLH2} \qquad (14)$$

It was assumed that the rate-determining pathway involves the formation of the $[FeLH_2^{3+}]$ complex since the reaction proceeds through the coordination of Fe^{3+} with the phenolato oxygen atom and releases only one H^+ in the reaction according to Equation (12).

The pseudo-first-order kinetic according to Equation (15) can be obtained by neglecting terms from reactions according to Equation (8) to Equation (10), in agreement with the experimental results, where $[Fe^{3+}] = [Fe^{3+}]_{tot} - [FeOH^{2+}] - 2\,[Fe_2(OH)_2^{4+}]$ and $[H^+]$ takes into account the protons involved in formation of $[FeOH]^{2+}$ and $[Fe_2(OH)_2]^{4+}$ ($2\,Fe^{3+} \rightleftarrows [Fe_2(OH)_2]^{4+} + 2\,H^+$, K_{DFe}).

$$k_{obs} = \frac{[Fe^{3+}]}{[H^+]([H^+]^2 + [H^+]K_{a5} + K_{a4}K_{a5})}\{(k_3K_{Fe}K_{a5} + k_4K_{a4}K_{a5})[H^+] + k_5K_{Fe}K_{a4}K_{a5}\} + \{(k_{-3} + k_{-4})[H^+] + k_{-5}\}\left(\frac{[H^+]^2}{[H^+]^2 + K_{FeLH2}}\right) \qquad (15)$$

The values of K_{Fe} and K_{DFe} in 2.0 M $NaClO_4$ are 1.5×10^{-3} M and 2.4×10^{-3} M.[16] Since pK_{a5} was not determined, the fit of the data was performed using the value 1.17, which was obtained for the corresponding deprotonation of HBED.[15] The variation of the pseudo-first-order kinetic rate constant of the hydrolysis reaction is consistent with the last term of Equation 15.[17] The results of the nonlinear least-squares fit to Equation (15) of the combined formation and dissociation data are:

$(k_3K_{Fe}K_{a5} + k_4K_{a4}K_{a5}) = 0.078 \pm 0.018\ M^{-1}s^{-1}$ $k_5 = 13300 \pm 1400\ M^{-1}s^{-1}$

$(k_{-3} + k_{-4}) = 1.83 \pm 0.09\ M^{-1}s^{-1}$ $k_{-5} = 0.42 \pm 0.08\ s^{-1}$ $K_{FeLH2} = 0.026 \pm 0.005\ M^2$

The rate constants of the Fe^{3+} pathways have been found to be generally almost three orders of magnitude lower than those of the $[FeOH]^{2+}$ pathways.[18] So, if we assume a value of about $10\ M^{-1}s^{-1}$ for k_4, it seems reasonable to neglect the $k_4K_{a4}K_{a5}$ term with respect to $k_3K_{Fe}K_{a5}$. Thus, we can obtain $k_3 = 770 \pm 180\ M^{-1}s^{-1}$. From the values of k_5 and k_{-5}, $k_4/k_{-4} = K_{Fe}\,k_5/k_{-5}$ is calculated to be 47.5. An upper limit of k_{-4} is thus estimated to be 0.2 if $k_4 < 10$ and so we can obtain $k_{-3} = 1.6\ s^{-1}$.

In summary, we were able to determine the following rate constants:

$k_5 = 13300 \pm 1400\ M^{-1}s^{-1}$; $k_{-5} = 0.42 \pm 0.08\ s^{-1}$

$k_3 = 770 \pm 180\ M^{-1}s^{-1}$; $k_{-3} = 1.6 \pm 0.1\ s^{-1}$

Ligand substitution reactions at an iron center were assumed to be controlled by water exchange from the inner coordination shell. The rate constants may be described according to the Eigen−Wilkins mechanism[19] with a fast formation step of an outer-sphere complex (K_{os}) followed by a rate-limiting step involving the water substitution of the $[FeOH]^{2+}$ species (k_{ex}) according to Equation (16); k_f stands for k_3 or k_5, S is a statistical coefficient that accounts for the solvent shell composition and can be assigned an approximate value of 1/6.

$$k_f = K_{os} \cdot S \cdot k_{ex} \qquad (16)$$

Since k_{ex} does not change significantly with different ligands, variations in the rate constants are mainly due to the constant K_{os}. The charge of the ligand is one of the factors that influences the value of K_{os}. The constant can be estimated with the Fuoss equation[20] to be 0.2 for reactions of $[FeOH]^{2+}$ with a neutral ligand and ca. 0.02 for a ligand bearing a global positive charge. Accordingly, the value of k_5, which refers to the $[FeOH]^{2+} - LH_3$ pathway, is larger than the value of k_3, which refers to the $[FeOH]^{2+} - LH_4^+$ pathway ($k_5/k_3 \approx 17$). Furthermore, a comparison with the literature data indicates that k_5 is much higher than the rate constants determined for the $[FeOH]^{2+}$ − neutral ligand pathway for phenol, catechol and hydroxamate ligands (about 1×10^3 to $3 \times 10^3\ M^{-1}s^{-1}$). This finding can be explained by taking into account the zwitterionic character of the ligand **L3**. The two carboxylate anions are assumed to increase the K_{os} constant with respect to a ligand bearing no charges. The values of k_5 fall within the range for a ligand containing one or two aminoacetate donor groups,[21] such as H_4EDTA ($30000\ M^{-1}s^{-1}$) and H_3NTA ($15000\ M^{-1}s^{-1}$).

Kinetic data for the dissociation of ferric complexes with this type of ligand are not available in the literature. A comparison can be made with dissociation rate constants obtained for catecholate and hydroxamate ligands, which are the most widely reported in the literature. The dissociation rate of Fe**L3** by the $[FeOH]^{2+}$ pathway (1.6 and $0.42\ s^{-1}$) is close to that of the (monocatecholato)Fe−Tiron (1,2-dihydroxy-3,5-benzenedisulfonate) complex ($1.2\ s^{-1}$)[22] but significantly faster than those of the monohydroxamato

complexes (0.08 s^{-1} for acetohydroxamic acid and 0.0071 s^{-1} for *N*-methylacetohydroxamic acid).[23,24] A comparison with the last step of the dissociation of hexadentate chelates shows that **L3** releases Fe^{III} much faster than the tricatecholate TRENCAMS[25] (0.018 s^{-1}) and than the siderophores pyoverdin[26] ($> 6\ 10^{-5}\ s^{-1}$) and ferrioxamine B[27,28] (0.0021 s^{-1}).

Conclusion

In summary, this work has shown that the bis(aminocarboxylate)benzyl chelators of the present series have a relatively low affinity for Fe^{III}. It must be emphasized that these chelators (except **L3**) should be thermodynamically unable to compete for iron in most metalloproteins and especially for transferrin. For this reason side-effects can be expected to be limited, a situation in contrast to strong iron chelators, which can inhibit enzymes by removal of metal from active sites, by formation of a ternary complex or by depriving the apoenzyme of its normal source of iron. Under prooxidant conditions, e.g. in the presence of hydrogen peroxide, these chelators are hydroxylated to give species with strong iron affinity, as shown by the complexation stability constants and pFe value for **L3**, which are consistent with the presence of a hard phenolate donor group. Moreover, this dramatic increase of affinity for iron is associated with a large decrease in redox potential of Fe^{III}/Fe^{II}, which tends to inhibit iron reduction by physiological reductants thereby avoiding redox cycling of iron. However, it should be kept in mind that such a consideration refers to equilibrium conditions, which is generally not the case in biological systems, and these results agree with previous data showing that the **L3** iron complex is not a catalyst of reductant-driven Fenton reactions.[7] In addition, both the formation and dissociation kinetics of the ferric complex with **L3** were measured and were found to give consistent data. It should be emphasized that an interesting feature of **L3** is the fast uptake of Fe^{III} and its fast release under acidic conditions. The results presented here are in good agreement with biological data showing a very efficient protection of cultured cells by **L3** or **L1** prodrugs against hydrogen peroxide toxicity.[29,9]

Experimental Section

Materials and Equipment: Ligands **L1** and **L2** were prepared according to the procedure described previously.[8] All other compounds were of reagent grade and were used without further purification. Fe^{III} stock solutions were prepared by dissolving appropriate amounts of ferric perchlorate hydrate (Aldrich) in standardized $HClO_4$ and $NaClO_4$ solutions. The solutions were calibrated spectrophotometrically for ferric ions by using a molar extinction coefficient of 4160 $M^{-1}cm^{-1}$ at 240 nm.[30] Mass spectra were obtained by HPLC/MS with a Fisons Platform mass spectrometer equipped with an atmospheric pressure ion source in the electrospray ionization (ESI) mode. ^1H NMR spectra were recorded with a Bruker 500 MHz spectrometer.

Synthesis of L3

(a) *N*-(2-Hydroxybenzyl)-*N*′-benzylethylenediamine: A mixture of 8.05 g (66 mmol) of 2-hydroxybenzaldehyde and 10 g (66.6 mmol) of *N*-benzylethylenediamine was heated in 100 mL of MeOH at 50 °C for 30 min. The mixture was concentrated, the residue suspended in 150 mL of EtOH and 34 mmol of $NaBH_4$ was added. The reaction mixture was stirred at room temperature for 1 h and the solvent evaporated. 100 mL of water was added and concentrated HCl was used to acidify the solution to pH = 1−2. The crystalline dihydrochloride was collected by filtration, washed with cold ethanol and vacuum-dried over P_2O_5 to yield 13.85 g (81%) of *N*-(2-hydroxybenzyl)-*N*′-benzylethylenediamine. − MS (ESI^+); *m*/*z*: 256 $[M + H]^+$, 91 $[C_7H_7^+]$.

(b) *N*-(2-Hydroxybenzyl)-*N*′-benzylethylenediamine Diacetic Acid: A mixture of 12.8 g (50 mmol) of *N*-(2-hydroxybenzyl)-*N*′-benzylethylenediamine, 13.9 g (100 mmol) of bromoacetic acid, 2 g (50 mmol) of NaOH and 8.4 g (100 mmol) of $NaHCO_3$ in 150 mL of water was heated at 40 °C for 6 h while the pH value of the solution was maintained in the range of 11.5−12.5 by the addition of NaOH. Concentrated HCl was added to the reaction mixture until the pH value was lowered to 2. The white precipitate was filtered off and recrystallized from 2-propanol to yield 10 g of *N*-(2-hydroxybenzyl)-*N*′-benzylethylenediamine diacetic acid hydrochloride as a white powder (m.p. 190 °C, yield 46%). − ^1H NMR ([D$_6$]DMSO): δ = 3.14 (t, 2 H), 3.31 (t, 2 H), 3.42 (s, 2 H), 3.90 (2 × s, 4 H), 4.27 (s, 2 H), 6.85 (td, 1 H), 6.95 (d, 1 H), 7.23 (m, 7 H). − $C_{20}H_{25}ClN_2O_5$ (+ 0.05 NaCl) (411.8): calcd. C 58.33, H 6.08, Cl 9.06, N 6.80, O 19.45; found C 58.21, H 6.09, N 6.53, O 19.86, Cl 9.20.

Potentiometric Titrations: All the measurements were made at 25 °C and the solutions were prepared with deionized water that had been distilled twice. The ionic strength was fixed at $I = 0.1$ M with sodium perchlorate (PROLABO puriss). The potentiometric titrations were performed using an automatic titrator system, DMS 716 Titrino (Metrohm), equipped with a combined glass electrode (Metrohm, filled with saturated NaCl solution) and connected to an IBM Aptiva microcomputer. The electrodes were calibrated to read p[H] according to the classical method[31] (from titration of 0.1 M $HClO_4$ by 0.1 M NaOH). The ligand and its iron(III) complex of ca. 0.001 M were titrated with standardized 0.025 M sodium hydroxide. Argon was bubbled through the solutions to exclude CO_2 and O_2. Sodium hydroxide was prepared from 0.1 M NaOH (Prolabo) and was standardized. The titration data (120 points collected over the pH range 2.5−10.5 for the ligand solution and 100 points collected over the pH range 2.5−10 for the Fe^{III}−ligand solution) were refined by the nonlinear least-squares refinement program SUPERQUAD[10] to determine the deprotonation constants (σ_{fit} in the range 3−4). The pK_{an} values were calculated from the cumulative constants determined with the above program. The uncertainties in the pK_{an} values correspond to the standard deviations (1σ) in the cumulative constants.

Spectrophotometric Experiments: UV/Vis absorption spectra were recorded with a Perkin−Elmer Lambda 2 spectrometer using 1.000-cm path-length quartz cells and connected to a microcomputer; the acquisition was made with UV Winlab software (Perkin−Elmer). The temperature was maintained at 25 °C with a Perkin−Elmer PTP-1 variable temperature unit. The ferric complex with **L3** was studied by spectrophotometry. The UV/Vis spectrum of a solution containing equal amounts of ligand and Fe^{III} (10^{-4} M) was recorded as a function of pH over the range 1−8 (adjusted with $HClO_4$ or NaOH). An aliquot was taken from the solution

after each adjustment of the pH value and its spectrum was recorded. The pH measurements were made with a 713 Metrohm digital pH meter equipped with a microelectrode. The ionic strength was fixed at $I = 0.1$ M with $NaClO_4/HClO_4$. The spectrophotometric data were analyzed using the LETAGROP-SPEFO program.[12,13] The program uses a nonlinear least-squares method to calculate the thermodynamic constants of the absorbing species and their corresponding electronic spectra. The calculations were performed using absorbance values from about 6−8 wavelengths (between 400 and 600 nm). The range of values for the residual-squares sum $[\Sigma(A_{exp} - A_{calc})^2]$ of the fits was $10^{-2}-10^{-3}$.

Electrochemical Measurements: Electrochemical experiments were carried out using a PAR model 273 potentiostat equipped with a Kipp−Zonen x-y recorder. All experiments were run at room temperature under argon in a glove-box. A standard three-electrode cell was used. Potentials are referenced to Ag/AgCl, 3 M NaCl, aqueous reference electrode (+0.21 V vs. NHE). A glassy carbon disc electrode, used as a working electrode (5 mm diameter), was polished with 1 μm diamond paste. The electrochemical behavior of the Fe^{III}−ligand complex was studied by cyclic voltammetry (CV) in an aqueous solution containing 0.1 M $NaClO_4$ as a supporting electrolyte and buffered with tris-buffer for the experiments performed at pH = 7. For the experiments performed at pH ≠ 7, the pH value was adjusted following controlled additions of concentrated NaOH or $HClO_4$ aqueous stock solutions. The Fe^{III}−ligand solutions were prepared by dissolving stoichiometric amounts of ferric perchlorate and ligand in the electrolytic solutions.

Kinetics Studies: Kinetic measurements were performed with a KINSPEC UV (BIO-LOGIC Company, Claix, France) stopped-flow spectrophotometer equipped with a diode array detector (J & M) and connected to a TANDON microcomputer. The kinetic data were treated online with the commercial BIO-KINE program (BIO-LOGIC Company, Claix, France). The ionic strength was fixed at $I = 2$ M ($NaClO_4$, $HClO_4$) owing to the H^+ concentrations up to 1 M and allowing comparisons with literature data. − Formation kinetic studies were carried out under pseudo-first-order conditions at 25 °C with Fe^{III} in excess with respect to the ligand. The Fe^{III} concentration spanned the range $5 \times 10^{-3}-3 \times 10^{-2}$ M for each H^+ concentration, which was over the range 0.05−0.15 M. A solution containing Fe^{III} and H^+ and a solution containing the ligand **L3** (2×10^{-4} M) at the same ionic strength were mixed on the stopped-flow apparatus. In each case, first-order kinetics were observed. The reported rate constants are the average of about 8 replicate determinations (standard deviation in the range 1−2%). − The acid hydrolysis kinetics of the Fe^{III}−**L3** complex was studied under pseudo-first-order conditions in the presence of excess protons ($[H^+]$ range 0.02−1.0 M) at 25 °C. The initial pH value of the Fe^{III}−**L3** solution (7×10^{-4} M) was 4.

Acknowledgments

The authors thank Céline Carresi for performing the potentiometric measurements and Arnaud Pierra for performing the UV/Vis spectrophotometric and kinetic measurements with ligand **L3**. We are grateful to Dr. Alain Deronzier (LEOPR, Grenoble, France) for the use of the laboratory facilities, to Professor C. Béguin (LEDSS, Grenoble, France), Professor M. Fontecave and Dr. S. Ménage (CBCRB, CEA, Grenoble, France) for their interest in these studies.

[1] R. C. Hider, S. Singh, *Proc. R. Soc. Edimburgh, Sect. B* **1992**, *99*, 137−168.
[2] R. C. Crichton, In *Inorganic Biochemistry of Iron Metabolism*, Ellis Horwood Ltd., New York, **1991**, p. 173.
[3] C. Herschko, *Mol. Aspects Med.* **1992**, *13*, 114.
[4] J. B. Porter, E. R. Huens, R. C. Hider, *Bailliere's Clin. Haematol.* **1989**, *2*, 257.
[5] B. Halliwell, J. M. C. Gutteridge, *Free Radicals in Biology and Medicine*, 2nd ed., Clarendon Press, Oxford, **1989**.
[6] J.-B. Galey, *Adv. Pharmacol.* **1996**, *38*, 167.
[7] J.-B. Galey, J. Dumats, S. Génard, O. Destrée, P. Pichaud, P. Catroux, L. Marrot, I. Beck, B. Fernandez, G. Barre, M. Seite, G. Hussler, M. Hocquaux, *Biochem. Pharmacol.* **1996**, *51*, 103.
[8] S. Ménage, J.-B. Galey, J. Dumats, G. Hussler, M. Seité, I. Gautier-Luneau, G. Chottard, M. Fontecave, *J. Am. Chem. Soc.* **1998**, *120*, 13370.
[9] J.-B. Galey, O. Destrée, J. Dumats, S. Génard, P. Tachon, *J. Med. Chem.* **2000**, *43*, 1418.
[10] P. Gans, A. Sabatini, A. Vacca, *J. Chem. Soc., Dalton Trans.* **1985**, 1195.
[11] W. R. Harris, A. E. Martell, *Inorg. Chem.* **1976**, *14*, 713.
[12] L. G. Sillen, B. Warsquist, *Ark. Kemi* **1969**, *31*, 377.
[13] M. Meloun, J. Havel, E. Hogfeldt, *Computation of Solution Equilibria*, Ellis Horwood, Chichester, **1988**.
[14] W. R. Harris, A. E. Martell, *Inorg. Chem.* **1975**, *14*, 974.
[15] R. J. Motekaitis, Y. Sun, A. E. Martell, M. J. Welch, *Inorg. Chem.* **1991**, *30*, 2737.
[16] R. M. Milburn, W. C. Vosburgh, *J. Am. Chem. Soc.* **1955**, *77*, 1352.
[17] The term arising from the reverse reaction is negligible under the experimental conditions of the hydrolysis reaction.
[18] M. Birus, N. Kujundzic, M. Pribanic, *Prog. React. Kinet.* **1993**, *18*, 171.
[19] M. Eigen, R. G. Wilkins, *Adv. Chem. Ser.* **1965**, 55.
[20] R. M. Fuoss, *J. Am. Chem. Soc.* **1958**, *80*, 5059.
[21] E. Mentasti, E. Pelizetti, G. Saini, *J. Chem. Soc., Dalton Trans.* **1974**, 1944.
[22] Z. Zhang, R. B. Jordan, *Inorg. Chem.* **1996**, *35*, 1571.
[23] M. Birus, Z. Bradlic, N. Kujundzic, M. Pribanic, P. C. Wilkins, R. G. Wilkins, *Inorg. Chem.* **1985**, *24*, 3980.
[24] M. T. Caudle, A. L. Crumbliss, *Inorg. Chem.* **1994**, *33*, 4077.
[25] F. Thomas, C. Béguin, J.-L. Pierre, G. Serratrice, *Inorg. Chim. Acta* **1999**, *291*, 148.
[26] A.-M. Albrecht-Gary, S. Blanc, N. Rochel, A. Z. Ocaktan, M. A. Abdallah, *Inorg. Chem.* **1994**, *33*, 6391.
[27] B. Monzyk, A. L. Crumbliss, *J. Am. Chem. Soc.* **1982**, *104*, 4921.
[28] M. Birus, Z. Bradlic, G. Krznaric, N. Kujundzic, M. Pribanic, P. C. Wilkins, R. G. Wilkins, *Inorg. Chem.* **1987**, *26*, 1000.
[29] J.-B. Galey, O. Destrée, J. Dumats, P. Pichaud, J. Marché, S. Génard, G. Bracciolli, L. Le Capitaine, H. Plessix, L. Brambilla, O. Cantoni, *Free Rad. Biol. Med.* **1998**, *25*, 881.
[30] R. Bastian, R. Weberling, F. Palilla, *Anal. Chem.* **1956**, *28*, 459.
[31] A. E. Martell, R. J. Motekaitis, *Determination and Use of Stability Constants*, 2nd ed., VCH Publishers, New York, **1992**.

Received May 3, 2000
[I00179]

Reaction of the (Dichloromethyl)oligosilanes $R(Me_3Si)_2Si-CHCl_2$ (R = Me, Ph, Me_3Si) with Organolithium Reagents and the Synthesis of Novel Kinetically Stabilized Silenes

Kathleen Schmohl,[a] Helmut Reinke,[a] and Hartmut Oehme*[a]

Keywords: Lithium / Silaethene / Silanes / Silenes / Silicon

The dichloromethyloligosilanes $R^1(Me_3Si)_2Si-CHCl_2$ (**1a**,**b**) (**1a**: R^1 = Me; **1b**: R^1 = Ph), prepared by treatment of methylbis(trimethylsilyl)silane or phenylbis(trimethylsilyl)silane respectively, with chloroform and potassium *tert*-butoxide, treated with the organolithium reagents R^2Li (R^2 = Me, Ph) to produce the intermediate organolithium derivatives $R^1R^2_2Si-CLi(SiMe_3)_2$ (**10**). Hydrolysis of **10** during the aqueous workup afforded the [bis(trimethylsilyl)methyl]silanes $R^1R^2_2Si-CH(SiMe_3)_2$ (**2**); quenching of the reaction mixture with chlorotrimethylsilane gave the [tris(trimethylsilyl)methyl]silanes $R^1R^2_2Si-C(SiMe_3)_3$ (**11**). The formation of **10** is discussed as proceeding through a remarkable series of isomerization processes involving the transient silenes $R^1R^2Si=C(SiMe_3)_2$ (**7**), which in the presence of an effective excess of R^2Li are immediately trapped to give **10**. By the use of sterically congested organolithium derivatives, the nucleophilic addition of R^2Li to the Si=C bond of **7** can be prevented and kinetically stabilized silenes obtained. Thus, Ph(2,4,6-iPr$_3$C$_6$H$_2$)Si=C(SiMe$_3$)$_2$ (**8b**) was synthesized by the reaction of **1b** with 2,4,6-triisopropylphenyllithium (molar ratio 1:2). Similarly, (Me$_3$Si)(2,4,6-iPr$_3$C$_6$H$_2$)Si=C(SiMe$_3$)$_2$ (**8c**) and (Me$_3$Si)(2-tBu-4,5,6-Me$_3$C$_6$H)Si=C(SiMe$_3$)$_2$ (**9c**) were prepared from (dichloromethyl)tris(trimethylsilyl)silane (**1c**) and 2,4,6-triisopropylphenyllithium or **1c** and 2-*tert*-butyl-4,5,6-trimethylphenyllithium (1:2), respectively, but due to difficulties in the separation of starting material and side products, **8b**, **8c**, and **9c** were obtained in impure form only. Despite the steric congestion, the compounds are reactive and exhibit the usual behavior of silenes. Thus **8b**, **8c**, and **9c** were chemically characterized by the reaction with water to give silanols, by the addition of methanol to give methoxysilanes and by formal [2+2] cycloadditions with benzaldehyde to afford stable 1,2-oxasiletanes. 1-Methyl-1-(2,4,6-triisopropylphenyl)-2,2-bis(trimethylsilyl)silene (**8a**), produced as intermediate from **1a** and 2,4,6-triisopropylphenyllithium (1:2), proved to be unstable in the presence of excess aryllithium compound. Thus, only the addition product Me(2,4,6-iPr$_3$C$_6$H$_2$)$_2$SiCH(SiMe$_3$)$_2$ (**14**) was isolated (after hydrolysis).

Introduction

Silenes are known to be extremely labile compounds which can be isolated and handled under normal conditions only in those cases where structural influences cause an efficient stabilization of the Si=C system.[1] In numerous reactions transient silenes occur as reactive intermediates, but until now the number of synthetic methods affording stable, isolable silenes is rather limited. Brook and co-workers introduced the photochemical isomerization of acyloligosilanes as a versatile method for the generation of silenes, and in 1982 they were the first to isolate a stable silene, $(Me_3Si)_2Si=C(OSiMe_3)Ad$ (Ad = 1-adamantyl), and to perform an X-ray analysis of the compound.[2] In 1983 Wiberg and his group succeeded in applying the classical 1,2 salt elimination to the synthesis of the stable silene $Me_2Si=C(SiMe$*t*$Bu_2)SiMe_3$ and provided the results of its X-ray analysis.[3] Elimination of lithium chloride after addition of *tert*-butyllithium to the carbon−carbon double bond of chloro(vinyl)silanes is also the crucial step in establishing Si=C bonds in a method developed by the groups of Jones and Auner, which was successfully used by Couret et al. in 1994 in the preparation of the stable 1,1-dimesityl-2-neopentylsilene.[4] A further method, which has proved to be an efficient general route to silenes, is the sila Peterson reaction. We were able to contribute to the development of the process and generated a number of transient silenes and studied their mode of dimerization,[5] and in 1996 Apeloig and co-workers succeeded in preparing the stable derivative (tBuMe$_2$Si)$_2$Si=CAd′ (Ad′ = 2-adamantylidene) by this method.[6] A few further stable silenes have been isolated by the groups mentioned.[1] Of course, the structures of these compounds are related to their methods of preparation, and extension of the substitution pattern by introducing new synthetic pathways is desirable.

Recently we reported the reaction of (dichloromethyl)-tris(trimethylsilyl)silane (**1c**) with organolithium reagents RLi (R = Me, *n*Bu, Ph, Mes).[7] As the result of a remarkable sequence of isomerization and addition steps, and a complete reorganization of the substitution pattern of the starting compound, [bis(trimethylsilyl)methyl]silanes **2** were formed as end products [Equation (1)].

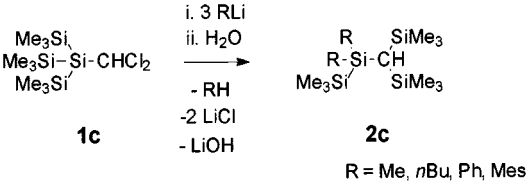

[a] Fachbereich Chemie der Universität Rostock,
18051 Rostock, Germany
Fax: (internat.) + 49-(0)381/498-1765
E-mail: hartmut.oehme@chemie.uni-rostock.de

 © WILEY-VCH Verlag GmbH, 69451 Weinheim, 2001 1434−1948/01/0202−0481 $ 17.50+.50/0

As outlined in Scheme 1 for the behavior of the (dichloromethyl)oligosilanes **1a−c** towards methyllithium or phenyllithium respectively, in the course of this reaction transient silenes occurred as intermediates, which in the presence of excess organolithium reagent were trapped to give the products mentioned. Increasing the bulkiness of the substituents of the organolithium derivatives used in this reaction is expected to afford kinetically stabilized silenes, sufficiently protected against the attack of excess lithium compound and stable with respect to dimerization. Thus, this paper describes the extension of the conversion depicted in Equation (1) for **1c** to (dichloromethyl)methylbis(trimethylsilyl)silane (**1a**) and (dichloromethyl)phenylbis(trimethylsilyl)silane (**1b**), as well as the generation of novel stable silenes along this new synthetic pathway.

Results and Discussion

Reaction of (Dichloromethyl)methylbis(trimethylsilyl)silane (1a) and (Dichloromethyl)phenylbis(trimethylsilyl)silane (1b) with Organolithium Derivatives

The dichloromethylsilanes **1a** and **1b** were prepared adapting a procedure reported by Weidenbruch et al. for the preparation of (dichloromethyl)tri-*tert*-butylsilane.[8] Thus, treatment of methylbis(trimethylsilyl)silane with chloroform in the presence of potassium *tert*-butoxide afforded **1a** in a yield of 36%. Compound **1b** was similarly obtained from phenylbis(trimethylsilyl)silane, $HCCl_3$ and KO*t*Bu (yield 41%) [Equation (2)]. The dichloromethylsilane **1a** has already been described by Sakurai et al., who obtained the compound from 2-chloroheptamethyltrisilane and dichloromethyllithium.[9]

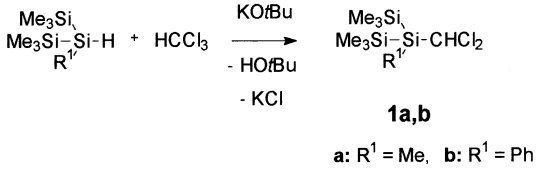

In agreement with the described reaction of **1c** with organolithium compounds,[7] **1a** reacted with methyllithium at room temperature (molar ratio 1:3) to give, after hydrolytic workup, tris(trimethylsilyl)methane (**2ax**). Under the same conditions **1a** and phenyllithium afforded methyldiphenyl[bis(trimethylsilyl)methyl]silane (**2ay**). Similarly, reaction of **1b** with the same organolithium derivatives gave dimethylphenyl[bis(trimethylsilyl)methyl]silane (**2bx**) and triphenyl[bis(trimethylsilyl)methyl]silane (**2by**), respectively (Scheme 1). The structures of the compounds obtained were elucidated on the basis of NMR and MS data (see Experimental Section).

The conversion of **1a−c** to **2** by the means of organolithium compounds is a complex process. Two trimethylsilyl groups migrate from the central silicon atom to the neighboring carbon atom, formally replacing the two chlorine substituents, and the two organic groups introduced by the lithium derivatives occupy the former positions of the two trimethylsilyl substituents. Despite the unexpected outcome of the reaction, the conversion can be rationalized as a clear sequence of known steps. Our proposal for the reaction mechanism is outlined in Scheme 1, which also includes the formerly described conversion of **1c**.[7]

The dichloromethylsilanes **1a−c** are deprotonated by the organolithium reagents with generation of the silylcarbenoids **3**. Elimination of lithium chloride and migration of one trimethylsilyl group from the central silicon atom to the carbene carbon atom affords the intermediate silene **5**.

Rearrangements of silylcarbenes to silenes involving the shift of one substituent from the silicon atom to the neighboring carbene carbon atom are well-documented reactions and a standard method for the generation of transient silenes.[10] Hydrogen, alkyl, aryl, and silyl groups have been found to be suitable migrating substituents in this isomerization process; the migrating ability of the silyl groups exceeds that of the other groups mentioned.[11] In the presence of excess organolithium reagent the silenes **5** are immediately trapped to give the new carbenoids **6**. Repeated elimination of LiCl and a further 1,2-Si,C shift of one trimethylsilyl group affords the silenes **7**, which again undergo nucleophilic addition of a third equivalent of R^2Li, producing **10**. Hydrolysis during the aqueous workup affords **2**.

The intermediate existence of the chlorosilylcarbene **4** could not be proved and an intramolecular Me_3Si/Li exchange in **3**, followed by a 1,2 lithium chloride elimination, might be an alternative route to the silene **5**. Trapping experiments of the carbene **4** were abandoned, since it is well known that silylcarbenes, generated photochemically or thermally from the corresponding diazo compounds, very rapidly rearrange to the respective silenes, and in numerous experiments with different scavenger reagents only the silenes were detected.[11,12] The carbenoids **6** proved to be moderately stable at low temperatures. As described previously, we succeeded in trapping **6cy**, generated from **1c** and phenyllithium, with chlorotrimethylsilane to give $Ph(Me_3Si)_2Si-CCl(SiMe_3)_2$ and by quenching with water, affording $Ph(Me_3Si)_2Si-CHClSiMe_3$.[7] The intermediate organolithium compounds **10**, formed by addition of methyllithium or phenyllithium to the silene double bond of **7**, are suitable precursors for highly congested tris(silyl)-methyl-substituted silanes. Thus, addition of chlorotrimethylsilane to the product mixture obtained after the reaction of **1a**,**b** with MeLi or PhLi produced the [tris(trimethylsilyl)methyl]silanes **11**. Similarly, quenching of **10** with Me_2SiHCl gave the [dimethylsilylbis(trimethylsilyl)-methyl]silanes **12**.

Independent of the molar ratio **1a−c**/RLi, we found the reaction to proceed through all intermediates outlined in Scheme 1 to give the final products **2**, **11**, or **12**, respectively. Attempts to isolate dimers of the silenes **5** or **7** by reducing the ratio of the reactants to 1:2 or 1:1 were unsuccessful. We assume that the deprotonation of **1a−c**, producing the carbenoids **3**, is a slow process compared with the subsequent steps, and the transient silenes **5** and **7**, formed during the course of the reaction, always meet an effective ex-

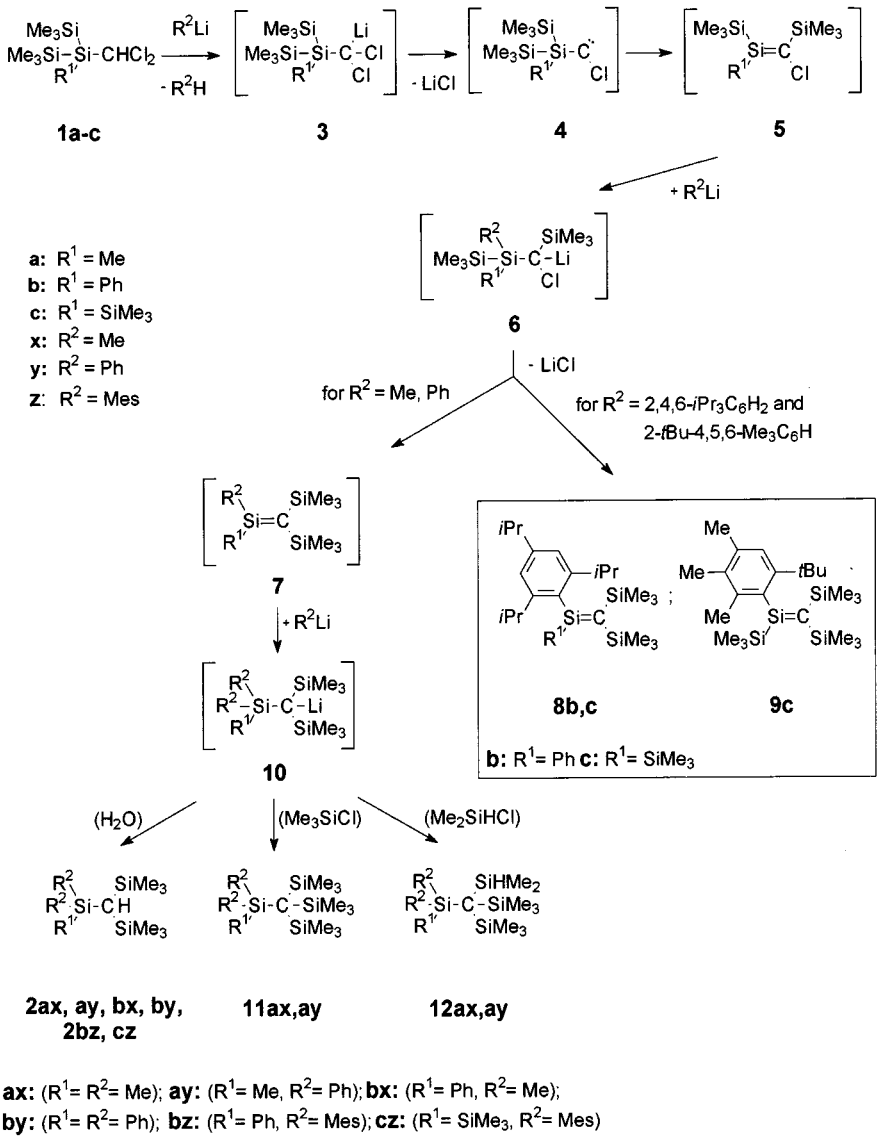

Scheme 1. Reaction of the dichloromethyloligosilanes **1a−c** with organolithium reagents R^2Li

cess of the organolithium reagent, finally producing the congested silanes.

Reaction of the Dichloromethylsilanes 1a−c with 2,4,6-Triisopropylphenyllithium and of 1c with 2-*tert*-Butyl-4,5,6-trimethylphenyllithium − Synthesis and Behavior of the Stable Silenes 8b, 8c, and 9c

As discussed above, in the course of the reaction of the dichloromethylsilanes **1a−c** with methyllithium or phenyllithium, the transient silenes **5** and **7** occur as intermediates. As expected, in the presence of excess organolithium reagent, the almost unprotected, reactive silenes are immediately trapped to give the addition products **6** or **10**, respectively. However, if organolithium reagents are chosen with groups R^2, which, when introduced to the silene Si atom of **7**, provide sufficient stabilization of the silaethene by means of their steric bulk or by intramolecular donor-acceptor interactions, the reaction may stop at this stage and the resulting silenes may be expected to be stable. The high reactivity of silenes of type **5** also allows the addition of extremely congested organolithium derivatives to produce carbenoids **6**, which after loss of LiCl and subsequent isomerization may result in the formation of kinetically stabilized Si=C systems. Thus, we consider (dichloromethyl)oligosilanes and their reaction with organometallic bases as a promising tool in the synthesis of stable silenes.

Following this concept we studied the reaction of **1c** with 8-dimethylamino-1-naphthyllithium and obtained **13** in a straightforward one-pot reaction as a yellow, crystalline compound in a yield of 79% [Equation (3)].[13] The X-ray analysis of **13** confirmed the expected picture of an intramolecularly donor-stabilized silene with fourfold coordination at the silene silicon atom. Obviously, the 8-dimethylaminonaphthyl substituent dramatically decreases the electrophilic character of the silicon center and prevents further attack of organolithium reagent at the silene double bond. Thus, **13** is stable and can be isolated, and the reaction is highly recommended as an efficient and versatile method

for the synthesis of further intramolecularly donor-stabilized silenes.

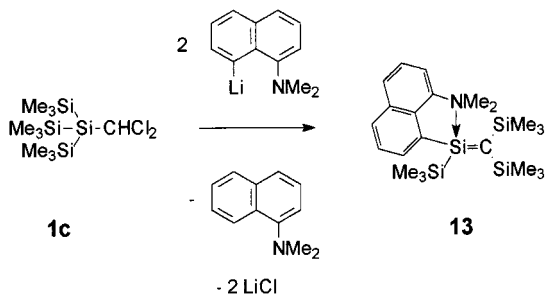

For the synthesis of kinetically stabilized silenes of type **7** two options were taken into consideration. Firstly, bulky groups R^1 may be introduced at the silene Si atom by starting with appropriately substituted (dichloromethyl)silanes **1**, or secondly, space-demanding substituents R^2 may be introduced by the respective organolithium derivatives R^2Li in the reaction with **1a**−**c**. Concerning the first alternative, we tried to synthesize (dichloromethyl)mesitylbis(trimethylsilyl)silane following the standard method described above. Unfortunately, mesitylbis(trimethylsilyl)silane was recovered unchanged after treatment with chloroform and potassium *tert*-butoxide. No reaction between the H-silane and CCl_2 occurred, probably due to steric reasons. On the other hand, **1b** and **1c**, which were chosen for some preliminary experiments, reacted with mesityllithium (1:2) to give after hydrolysis the "normal" silene addition products $PhMes_2Si-CH(SiMe_3)_2$ (**2bz**) and $Me_3SiMes_2Si-CH(SiMe_3)_2$ (**2cz**),[7] respectively, (Scheme 1). Obviously, one *Si*-mesityl substituent and one *Si*-phenyl or *Si*-trimethylsilyl group at the silene silicon atom of **7** provides insufficient protection to the Si=C system against the attack of mesityllithium. Replacement of the mesityl group in **7** by a 2,4,6-tri-*tert*-butylphenyl substituent is expected to increase the kinetic stability of the silene. But 2,4,6-tri-*tert*-butylphenyllithium did not react with the (dichloromethyl)-silane **1c**. The components remained unchanged, i.e. no deprotonation of **1c** occurred, very likely due to the steric congestion in both the dichloromethylsilane and the organolithium compound. Also, the reaction of **1c** with *tert*-butyllithium in pentane gave unsatisfactory results. We obtained a complex mixture of products. Neither a silene, nor any product resulting from a silene, could identified.

However, treatment of **1b** and **1c** with 2,4,6-triisopropylphenyllithium (molar ratio 1:2) afforded in a clean reaction the indefinitely stable silenes **8b** and **8c**, respectively. Similarly, **1c** and 2-*tert*-butyl-4,5,6-trimethylphenyllithium (1:2) gave the silene **9c** (Scheme 1). The compounds were obtained by a straightforward one-pot reaction of the components in ether at room temperature. Unfortunately, we did not succeed in crystallizing the compounds, and in all cases complete separation of starting materials or side products from the oily silenes failed. In particular the quality of **8b** and **9c** did not allow an unambiguous assignment of e.g. their NMR signals, and therefore no spectroscopic data of the compounds are given. The silene **8c** was obtained as a pale yellow oil, only slightly contaminated with 1,3,5-triisopropylbenzene, after reaction of the components, removal of the solvent and extraction of the residue with pentane. Triisopropylbenzene, formed as by-product, was separated by repeated concentration of the pentane solution in vacuo, finally at 100 °C. Furthermore, under these conditions no silene dimerization or uncontrolled decomposition was observed. Compound **8c** could be characterized by its NMR and MS data (see Experimental Section). Indicative of the proposed structure is the ^{29}Si chemical shift of the silene silicon atom of **8c** (δ = 79.6). Silenes with comparable substitution patterns are unknown, but similarly structured derivatives, such as (*E*)-$(Me_3Si)TipSi=C(OSiMe_3)Ad$ ($\delta^{29}Si$ = 40.3; Ad = 1-adamantyl),[14] $Mes_2Si=CHCH_2tBu$ ($\delta^{29}Si$ = 77.6)[4] or $(Me_3Si)(tBuMe_2Si)Si=Ad'$ ($\delta^{29}Si$ = 51.7, Ad′ = 2-adamantylidene)[6] also show characteristic downfield shifts of the Si=C signals in their ^{29}Si NMR spectra. Unfortunately, the ^{13}C NMR signal of the silene carbon atom of **8c**, which is expected to appear with very low intensity, could not be assigned unambiguously.

To our surprise, the reaction of **1a** with 2,4,6-triisopropylphenyllithium (molar ratio 1:2) did not give the stable silene **8a**, but led after aqueous workup to methylbis(2,4,6-triisopropylphenyl)[bis(trimethylsilyl)methyl]silane (**14**) [Equation (4)]. Obviously, replacement of a phenyl group or a trimethylsilyl group in **8b** or **8c**, respectively, by the smaller methyl substituent, decreases the steric protection of the Si=C system and in the presence of excess organolithium reagent a second 2,4,6-triisopropylphenyl substituent is introduced at the silene silicon atom. Compound **14** is an extremely congested silane and structural data would be of particular interest. However, due to the poor crystal quality, the accuracy of the X-ray structural analysis was not very high. Thus, the connectivity of the structure proposed was

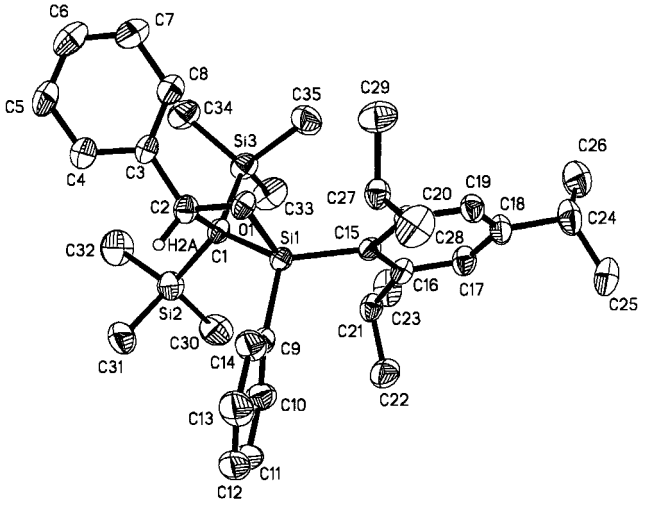

Figure 1. Molecular structure of **19b** in the crystal (H atoms omitted); selected bond lengths [Å] and angles [°]: Si1−O1 1.679(2), O1-C2 1.461(4), C2−C1 1.607(5), C1−Si1 1.924(3), Si1−C15 1.900(3), Si1−C9 1.890(3), C1−Si2 1.912(3), C1−Si3 1.915(4), C2−C3 1.495(5); Si1−O1−C2 112.6(2), O1−C2−C1 99.3(2), C2−C1−Si1 79.11(18), C1−Si1−O1 80.72(13), C9−Si1−C15 107.71(14), Si2−C1−Si3 111.86(17), torsion angle C1−C2−O1−Si1 25.9(2)

confirmed unambiguously, but a detailed discussion of bond parameters is excluded.

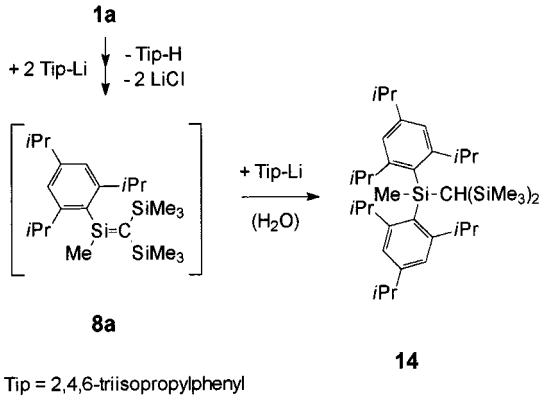

Despite the steric congestion, which prevents the dimerization of **8b**, **8c**, and **9c**, the compounds are reactive and exhibit the typical behavior of silenes. Thus, treatment with water led to the expected formation of the silanols **15b**, **15c**, and **16c** (Scheme 2). Similarly, methanol was added to the silene group to afford the methoxysilanes **17b**, **17c**, and **18c**. The results of the nucleophilic addition of methyllithium or phenyllithium to the Si=C unit, a reaction which we generally used for the characterization of transient silenes,[15] were unclear in case of **8b**, **8c**, and **9c**. We obtained complex mixtures of products, from which no compounds could be isolated. Further, reactions with 2,3-dimethyl-1,3-butadiene, which were intended to give [2+2] or [2+4] cycloadducts,[1] produced unsatisfactory results. The components were recovered unchanged. Both unsuccessful attempts at characterization are interpreted as an indication of the extreme steric shielding of the silene group.

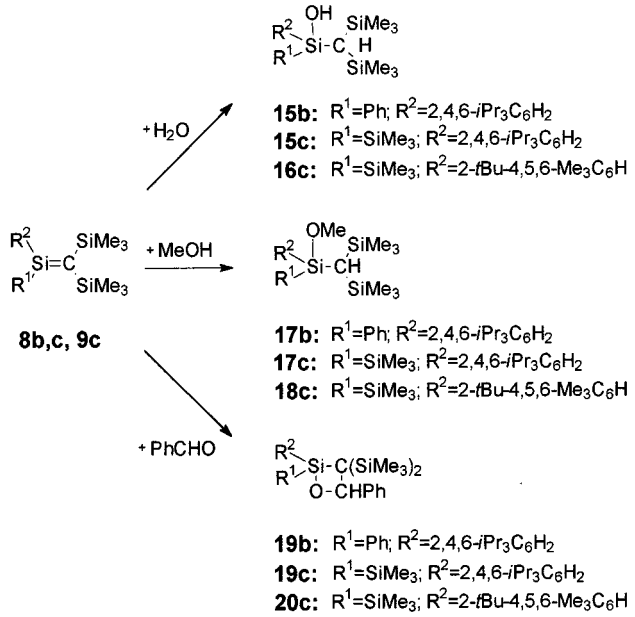

Scheme 2. Conversion of the stable silenes **8b**, **8c**, and **9c** with water into the silanols **15b**, **15c**, and **16c**, with methanol into the methoxysilanes **17b**, **17c**, and **18c**, and with benzaldehyde into the 1,2-oxasiletanes **19b**, **19c**, and **20c**

Benzaldehyde adds to the Si=C functionality of **8b**, **8c**, and **9c** in a formal [2+2] reaction to afford the 1,2-oxasiletanes **19b**, **19c**, and **20c** (Scheme 2). 1,2-Oxasiletanes, generated as intermediates in the reaction of transient silenes with carbonyl compounds in most cases undergo rapid decyclizations to give oligomers of the respective silanones and an olefin.[16] But in case of relatively stable silenes of the "Brook-type",[1b] the formation of stable 1,2-oxasiletanes is common.[17] Compounds **19b**, **19c**, and **20c** were formed in low yields (besides large quantities of unidentified material), but could be isolated in crystalline form, and for all three compounds X-ray structural analyses were performed. The molecular structure of **19b**, which was chosen as an example of the comparable 1,2-oxasiletane systems, is shown in Figure 1. In all three structures the ring bonds are slightly longer than the usual acyclic values [Si−C: **19b**: 1.924(3), **19c**: 1.944(3), **20c**: 1.939(3); C−C: **19b**: 1.607(5), **19c**: 1.603(4), **20c**: 1.600(5); C−O: **19b**: 1.461(4), **19c**: 1.440(4), **20c**: 1.446(4); Si−O: **19b**: 1.679(2), **19c**: 1.684(2), **20c**: 1.680(2) Å]. These data are comparable with those reported for 1,2-oxasiletanes.[17] The four-membered rings in **19c** and **20c** are nearly planar, in **19b** the ring is folded, the torsion angle C1−C2−O1−Si1 being 25.9°.

Experimental Section

General: All reactions involving organometallic reagents were carried out under purified argon. − NMR: Bruker AC 250 or Bruker ARX 300, tetramethylsilane as internal standard. − IR: Nicolet 205 FT-IR. − MS: Intectra AMD 402. − $Me(Me_3Si)_2SiH$, $Ph(Me_3Si)_2SiH$, and $(Me_3Si)_3SiH$ were prepared using the method described by Marschner.[18] − The syntheses and structures of **1c**, **2cx**, **2cy**, and **2cz** were described previously.[7] − Due to the formation of SiC, the results of the elemental analyses of some compounds were unsatisfactory. In these cases HRMS data are given.

(Dichloromethyl)methylbis(trimethylsilyl)silane (1a):[9] At room temperature, KO*t*Bu (1.42 g, 12.6 mmol) and chloroform (1.51 g, 12.6 mmol) were added gradually to a solution of methylbis(trimethylsilyl)silane (2.2 g, 11.5 mmol) in pentane (30 mL). After stirring for 12 h, water was added, the organic layer separated and the aqueous phase extracted with pentane. The collected extracts were dried and concentrated and the residue purified by kugelrohr distillation (50 °C/1.4·10^{-2} mbar) to give 1.14 g (36%) of **1a**. Colorless oil. − ^{1}H NMR ([D$_6$]benzene): δ = 0.16 [s, Si(CH$_3$)$_3$; 18 H], 0.20 (s, SiCH$_3$; 3 H), 5.28 (s, CH; 1 H). − ^{13}C NMR ([D$_6$]benzene): δ = −0.7 [Si(CH$_3$)$_3$], −8.4 (SiCH$_3$), 64.8 (CH). − ^{29}Si NMR ([D$_6$]benzene): δ = −23.2 (*Si*SiMe$_3$), −15.8 (SiMe$_3$). − $C_8H_{22}Cl_2Si_3$ (273.4): calcd. C 35.14, H 8.11, Cl 25.93; found C 35.35, H 8.39, Cl 24.94.

(Dichloromethyl)phenylbis(trimethylsilyl)silane (1b): As described for **1a**, phenylbis(trimethylsilyl)silane (2.2 g, 8.71 mmol), KO*t*Bu (1.1 g, 9.81 mmol) and chloroform (1.17 g, 9.81 mmol) afforded after kugelrohr distillation at 110 °C/2.2·10^{-1} mbar 1.2 g (41%) of a colorless oil. − ^{1}H NMR ([D$_6$]benzene): δ = 0.24 (s, SiCH$_3$; 18 H), 5.63 (s, CH; 1 H), 7.11−7.45 (m, arom. CH; 5 H). − ^{13}C NMR ([D$_6$]benzene): δ = −0.0 (SiCH$_3$), 63.6 (CH), 128.3, 129.2, and 135.3 (arom. CH), 133.8 (arom. C). − ^{29}Si NMR ([D$_6$]benzene): δ = −24.2 (*Si*SiMe$_3$), −15.2 (Si*Si*Me$_3$). − MS (70 eV); *m*/*z* (%): 334 (1) [M]$^+$, 319 (3) [M − CH$_3$]$^+$, 299 (100) [M − Cl]$^+$. − $C_{13}H_{24}Cl_2Si_3$ (335.5): calcd. C 46.54, H 7.20, Cl 21.13; found C 46.79, H 7.13, Cl 21.38.

Tris(trimethylsilyl)methane (2ax): To a solution of **1a** (0.5 g, 1.83 mmol) in ether (30 mL), a threefold molar quantity of methyllithium was gradually added at room temperature. After stirring for 12 h, the mixture was hydrolyzed and the organic layer separated, dried and concentrated. Compound **2ax** was separated by column chromatography (silica gel, heptane) as a colorless oil, yield 0.3 g (70%). The spectral data measured for **2ax** agree with those described in the literature.[19]

Methyldiphenyl[bis(trimethylsilyl)methyl]silane (2ay): Similarly, **1a** (0.5 g, 1.83 mmol) and ethereal phenyllithium solution (5.5 mmol) afforded 0.45 g (68%) of **2ay**. Colorless crystals, m.p. 66−69 °C. − ^{1}H NMR ([D$_6$]benzene): δ = 0.02 [s, Si(CH$_3$)$_3$, 18 H], 0.04 (s, CH, 1 H), 0.74 (s, SiCH$_3$, 3 H), 7.13−7.52 (m, arom. CH, 10 H). − ^{13}C NMR ([D$_6$]benzene): δ = −2.2 (CH), 1.3 (SiCH$_3$), 3.4 [Si(CH$_3$)$_3$], 128.3, 129.0, and 134.8 (arom. CH), 140.4 (arom. C). − ^{29}Si NMR ([D$_6$]benzene): δ = −9.6 (SiMe$_3$), −0.1. −(SiMe). − MS (70 eV); *m/z* (%): 356 (2) [M]$^+$, 341 (100) [M − CH$_3$]$^+$, 279 (5) [M − Ph]$^+$. − C$_{20}$H$_{32}$Si$_3$ (356.7): calcd. C 67.34, H 9.04; found C 67.04, H 9.07.

Dimethylphenyl[bis(trimethylsilyl)methyl]silane (2bx): As described for **2ax**, **1b** (0.5 g, 1.49 mmol), and MeLi (4.50 mmol) gave after chromatographic separation (silica gel, heptane) 0.73 g (84%) of **2bx**. Colorless oil. − ^{1}H NMR ([D$_6$]benzene): δ = −0.38 (s, CH, 1 H), 0.08 [s, Si(CH$_3$)$_3$, 18 H], 0.38 [s, Si(CH$_3$)$_2$, 6 H], 7.18−7.49 (m, arom. CH, 5 H). − ^{13}C NMR ([D$_6$]benzene): δ = −1.0 (CH), 1.8 [Si(CH$_3$)$_3$], 3.4 [Si(CH$_3$)$_2$], 128.8, 133.7, and 134.7 (arom. CH), 142.5 (arom. C). − ^{29}Si NMR ([D$_6$]benzene): δ = − 16.2 (SiMe$_2$Ph), − 0.3 (SiMe$_3$). − MS (70 eV); *m/z* (%): 279 (100) [M − CH$_3$]$^+$. − C$_{15}$H$_{30}$Si$_3$ (294.7): calcd. C 61.14, H 10.26; found C 61.16, H 10.26.

Triphenyl[bis(trimethylsilyl)methyl]silane (2by): As described for **2ax**, **1b** (0.5 g, 1.49 mmol), and PhLi (4.50 mmol) gave after chromatographic separation (silica gel, heptane) and recrystallization from methanol 0.44 g (70%) of **2by**. Colorless crystals, m.p. 82−84 °C. − ^{1}H NMR ([D$_6$]benzene): δ = 0.07 (s, SiCH$_3$, 18 H), 0.31 (s, CH, 1 H), 7.15−7.71 (m, arom. CH, 15 H). − ^{13}C NMR ([D$_6$]benzene): δ = 1.3 (CH), 3.8 (SiCH$_3$), 127.9, 129.4, and 136.7 (arom. CH), 137.9 (arom. C). − ^{29}Si NMR ([D$_6$]benzene): δ = −10.0 (SiPh$_3$), −0.0 (SiMe$_3$). − MS (70 eV); *m/z* (%): 419 (2) [M + H]$^+$, 403 (48) [M − CH$_3$]$^+$, 341 (100) [M − Ph]$^+$, 264 (6) [M − Ph$_2$]$^+$, 259 (11) [M − CH(SiMe$_3$)$_2$]$^+$. − C$_{25}$H$_{34}$Si$_3$ (418.8): calcd. C 71.70, H 8.18; found 70.84, 8.05. HRMS calcd. for C$_{24}$H$_{31}$Si$_3$ (M − CH$_3$): 403.17337; found 403.17013.

Dimesitylphenyl[bis(trimethylsilyl)methyl]silane (2bz): At room temperature, a twofold molar excess of mesityllithium was added to a solution of **1b** (0.56 g, 1.65 mmol) in ether (30 mL). After stirring for 12 h, water was added and the organic phase was separated, dried and concentrated. Column chromatography of the residue (silica gel, heptane) and recrystallization of the product from methanol gave 0.1 g (12%) colorless crystals, m.p. 45−50 °C. − ^{1}H NMR ([D$_6$]benzene): δ = −0.07 and 0.05 (2 s, SiCH$_3$, 2 × 9 H), 0.33 (s, CH, 1 H), 2.09 and 2.22 (2 s, Mes-CH$_3$, 2 × 6 H), 2.33 and 2.34 (2 s, Mes-CH$_3$, 2 × 3 H), 6.70−7.86 (m, arom. CH, 9 H). − ^{13}C NMR ([D$_6$]benzene): δ = −0.4 and 4.7 (SiMe$_3$), 4.7 (CH), 20.9, 21.0, 21.1, 25.8, and 26.1 (aryl-CH$_3$), 127.4, 128.2, 128.9, 129.2, 130.0, 130.6, 136.3, 138.1, 138.5, 143.8, and 144.5 (arom. C). − ^{29}Si NMR ([D$_6$]benzene): δ = −16.0 (aryl$_3$Si), 0.3 and 1.1 (SiMe$_3$). − MS (70 eV); *m/z* (%): 502 (1) [M]$^+$, 487 (5) [M − CH$_3$]$^+$; HRMS calcd. for C$_{31}$H$_{46}$Si$_3$ 502.25965, found 502.29074.

1-(2,4,6-Triisopropylphenyl)-1,2,2-tris(trimethylsilyl)silene (8c): To a solution of **1c** (0.5 g, 1.5 mmol) in ether (30 mL) a twofold molar excess of 2,4,6-triisopropylphenyllithium was gradually added at room temperature. After stirring for 12 h, the mixture was concentrated and the residue extracted with pentane. After filtration, the solution was repeatedly concentrated (with further addition of pentane) in vacuo, finally at 100 °C/10^{-2} mbar, to give 0.4 g (58%) of a pale yellow oil, which proved to be a mixture of **8c** and 1,3,5-triisopropylbenzene. − **8c:** ^{1}H NMR ([D$_6$]benzene): δ = 0.17, 0.24, and 0.49 (3 s, SiCH$_3$, 3 × 9 H), 1.17, 1.25, and 1.38 (3 d, ^3J = 6.7 Hz, *i*Pr-CH$_3$, 3 × 6 H), 2.72 (sept, ^3J = 6.7 Hz, *i*Pr-CH, 1 H), 3.33 (sept, ^3J = 6.7 Hz, *i*Pr-CH, 2 H), 7.00 (s, arom. CH, 2 H). − ^{13}C NMR ([D$_6$]benzene): δ = 1.3, 4.8, and 6.3 (SiCH$_3$), 24.1, 24.2, and 24.7 (*i*Pr-CH$_3$), 34.7 and 38.1 (*i*Pr-CH), 121.0 (arom. CH), 136.0, 151.7, and 152.4 (arom. C), the signal of the Si=C atom could not be assigned unambiguously. − ^{29}Si NMR ([D$_6$]benzene): δ = −15.4 (Si*Si*Me$_3$), −6.8 and −5.7 (CSiMe$_3$), 79.6 (Si=C). − MS (70 eV); *m/z* (%): 463 (88) [M + H]$^+$, 390 (5) [M − SiMe$_3$]$^+$; HRMS calcd. for C$_{25}$H$_{50}$Si$_4$ 462.29285, found 462.29895. − 1,3,5-*i*Pr$_3$C$_6$H$_3$: ^{1}H NMR ([D$_6$]benzene): δ = 1.24 (d, ^3J = 7.5 Hz, CCH$_3$, 18 H), 2.82 (sept, ^3J = 7.5 Hz, CHMe$_2$, 3 H), 6.99 (s, arom. CH, 3 H). − ^{13}C NMR ([D$_6$]benzene): δ = 24.4 (CH$_3$), 34.8 (CH), 122.4 (arom. CH), 149.1 (arom. C).

Tetrakis(trimethylsilyl)methane (11ax): To a solution of **1a** (0.5 g, 1.83 mmol) in ether (30 mL), MeLi (5.5 mol) was added at room temperature. The mixture was stirred for 12 h and subsequently chlorotrimethylsilane (0.5 g, 4.5 mmol) was added. Stirring was continued for further 12 h. After the addition of water, separation of the organic layer and concentration, the residue was purified by column chromatography (silica gel, heptane). Colorless crystals, yield 0.46 g (82%), m.p. 129−135 °C. The spectral data obtained for **11ax** are identical with those of authentic material.[20]

Methyldiphenyl[tris(trimethylsilyl)methyl]silane (11ay): Following the procedure for the synthesis of **11ax**, **1a** (0.5 g, 1.83 mmol), PhLi (5.5 mmol) and chlorotrimethylsilane (0.5 g, 4.5 mmol) gave after chromatography (silica gel, heptane) and recrystallization from ethanol gave colorless crystals (0.44 g), which proved to be a mixture of **11ay** and approx. 10% of **2ay**. The two compounds could not be cleanly separated, therefore only the NMR and MS data of **11ay** are given. − ^{1}H NMR ([D$_6$]benzene): δ = 0.10 (s, SiCH$_3$, 27 H), 0.32 (s, SiCH$_3$, 3 H), 7.13−7.79 (m, arom. H). − ^{13}C NMR ([D$_6$]benzene): δ = 0.8 (SiCH$_3$), 3.5 [Si(CH$_3$)$_3$], Si$_4$C could not be assigned unambiguously, 128.3, 128.9, and 136.3 (m, arom. CH), 140.1 (arom. C). − ^{29}Si NMR ([D$_6$]benzene): δ = −13.1 (SiMePh$_2$), 2.2 (SiMe$_3$). − MS (70 eV); *m/z* (%): 413 (2) [M − CH$_3$]$^+$, 351 (1) [M − Ph]$^+$, 192 (100) [M − C(SiMe$_3$)$_3$]$^+$.

Dimethyl[tris(trimethylsilyl)methyl]silane (12ax): The preparation of **12ax** followed the procedure given for **11ax**, but chlorodimethylsilane was used instead of chlorotrimethylsilane. Thus, **1a** (0.5 g, 1.83 mmol), MeLi (5.5 mmol) and Me$_2$SiHCl (0.5 g, 5.5 mmol) gave after purification by column chromatography (silica gel, heptane) colorless crystals, yield 0.43 g (82%), m.p. 97−103 °C. − IR (KBr): $\tilde{\nu}$ = 2099 cm^{-1} (SiH). − ^{1}H NMR ([D$_6$]benzene): δ = 0.25 (s, SiCH$_3$, 27 H), 0.21 (d, ^3J = 3.0 Hz, SiCH$_3$, 3 H), 0.30 (d, ^3J = 3.0 Hz, SiCH$_3$, 3 H), 4.31 (br. q, ^3J = 3.0 Hz, SiH, 1 H). − ^{13}C NMR ([D$_6$]benzene): δ = −4.1 (quat. C), 1.6 (HSiCH$_3$), 4.5 [Si(CH$_3$)$_3$]. − ^{29}Si NMR ([D$_6$]benzene): δ = −16.9 (SiH), −1.3 (SiMe$_3$). − MS (70 eV): *m/z* (%): 289 (1) [M − H]$^+$, 275 (100) [M − CH$_3$]$^+$. − C$_{12}$H$_{34}$Si$_4$ (290.7): calcd. C 49.57, H 11.79; found C 49.50, H 11.58.

Methyldiphenyl[(dimethylsilyl)bis(trimethylsilyl)methyl]silane (12ay): Similarly, **1a** (0.5 g, 1.83 mmol), PhLi (5.5 mmol), and Me$_2$SiHCl (0.5 g, 5.5 mmol) afforded 0.3 g (40%) of **12ay**. Colorless crystals, m.p. 93−97 °C. − IR (KBr): $\tilde{\nu}$ = 2122 cm^{-1} (SiH). − ^{1}H

NMR ([D$_6$]benzene): δ = 0.18 [d, ^3J = 3.8 Hz, Si(CH$_3$)$_2$, 6 H], 0.22 [s, Si(CH$_3$)$_3$, 18 H], 0.91 (s, PhSiCH$_3$, 3 H), 5.08 (sept, ^3J = 3.8 Hz, SiH, 1 H), 7.14−8.01 (m, arom. CH, 10 H). − ^{13}C NMR ([D$_6$]benzene): δ = −1.8 (quat. C), 1.8 [Si(CH$_3$)$_2$], 5.6 [Si(CH$_3$)$_3$], 127.5, 129.2, and 136.8 (arom. CH), 139.6 (arom. C). − ^{29}Si NMR ([D$_6$]benzene): δ = −16.0 and −15.5 (SiPh$_2$ and SiH), −0.8 (SiMe$_3$). − MS (70 eV); *m/z* (%): 399 (1) [M − H]$^+$, 336 (50) [M − C$_6$H$_5$, − H]$^+$, 321 (100) [M − C$_6$H$_5$, − CH$_3$, − H]$^+$, 264 (10) [M − C$_6$H$_5$, − SiMe$_3$]$^+$. − $C_{22}H_{38}Si_4$ (414.9): calcd. C 63.69, H 9.23; found C 63.65, H 9.13.

Methylbis(2,4,6-triisopropylphenyl)[bis(trimethylsilyl)methyl]silane (14): At room temperature a threefold molar excess of 2,4,6-triisopropylphenyllithium was added to **1a** (0.5 g, 1.8 mmol) in ether (30 mL). After stirring for 12 h, water was added and the organic layer separated, dried and concentrated. Chromatographic separation of the residue (silica gel, heptane) gave 0.42 g (44%) of **14**. Single crystals were obtained by recrystallization from heptane, m.p. 151−156 °C. − ^{1}H NMR ([D$_6$]benzene): δ = 0.11 and 0.38 (2 s, SiCH$_3$, 2 × 9 H), 0.22 (br. s, SiCH$_3$, 3 H), 0.46 (s, CH, 1 H), 1.40 (br. signal) and 1.12−1.23 (m, *i*Pr-CH$_3$, 36 H), 2.73 (m, *i*Pr-CH, 2 H), 3.23, 3.32, 3.59, and 3.73 (4 br. signals, *i*Pr-CH, 4 × 1 H), 6.90−7.20 (2 m, arom. CH, 4 H). − ^{13}C NMR ([D$_6$]benzene): δ = 4.3 and 5.7 [Si(CH$_3$)$_3$], 8.2 (CH), 9.2 (SiCH$_3$), 22.3, 23.0, 23.7, 23.9, 24.9, 25.7, 26.5, and 27.0 (*i*Pr-CH$_3$), 31.7, 32.4, 33.2, 34.1, and 35.3 (*i*Pr-CH), 122.7 (arom. CH), 138.1, 148.8, and 149.4 (arom. C). − ^{29}Si NMR ([D$_6$]benzene): δ = −13.0 (SiMe), −1.4 and 0.6 (SiMe$_3$). − MS (70 eV); *m/z* (%): 608 (1) [M]$^+$, 593 (16) [M − CH$_3$]$^+$, 535 (1) [M − SiMe$_3$]$^+$, 449 (9) [M − CH(SiMe$_3$)$_2$]$^+$, 404 (89) [M − Tip, − H]$^+$, 201 (100) [M − 2 Tip, − H]$^+$. − $C_{38}H_{68}Si_3$ (609.2): calcd. C 74.92, H 11.25; found C 74.10, H 11.01.

General Procedure for the Preparation of the Silanols 15b, 15c, and 16c: To an ethereal solution of the dichloromethylsilane **1b** or **1c** a 2.2-fold molar excess of the respective organolithium compound was added at room temperature. After stirring for 12 h, the product was hydrolyzed by addition of water. The resulting silanols were extracted with ether and the solutions dried and concentrated. The residues were purified by chromatography (silica gel, heptane).

15b: Compound **1b** (0.5 g, 1.5 mmol) and 2,4,6-triisopropylphenyllithium (3.3 mmol) gave 0.4 g (55%) of silanol **15b**. Colorless oil. − IR (cap.): $\tilde{\nu}$ = 3682 cm^{-1}(OH). − ^{1}H NMR ([D$_6$]benzene): δ = 0.17 and 0.20 (2 s, SiCH$_3$, 2 × 9 H), 0.31 (s, CH, 1 H), 1.20 (d, ^3J = 6.7 Hz, *i*Pr-CH$_3$, 12 H), 1.23 (d, ^3J = 6.7 Hz, *i*Pr-CH$_3$, 6 H), 1.89 (s, OH, 1 H), 2.75 (sept, ^3J = 6.7 Hz, *i*Pr-CH, 1 H), 3.65 (sept, ^3J = 6.7 Hz, *i*Pr-CH, 2 H), 7.10−7.70 (m, arom. CH, 7 H). − ^{13}C NMR ([D$_6$]benzene): δ = 3.5 and 3.7 (SiCH$_3$), 7.8 (CH), 24.0, 24.8, and 25.7 (*i*Pr-CH$_3$), 33.3 and 34.5 (*i*Pr-CH), 121.9, 127.4, 129.4, and 133.1 (arom. CH), 135.1, 142.5, 150.5, and 155.3 (arom. C). − ^{29}Si NMR ([D$_6$]benzene): δ = −2.8 (SiOH), −0.4 and 0.7 (SiMe$_3$). − MS (70 eV); *m/z* (%): 469 (70) [M − CH$_3$]$^+$, 467 (100) [M − OH]$^+$, 407 (20) [M − SiMe$_3$]$^+$. − $C_{28}H_{48}Si_3O$ (484.9): calcd. C 69.35, H 9.98; found C 66.87, H 9.80; HRMS calcd. for $C_{27}H_{45}OSi_3$ [M − CH$_3$] 469.26051, found 469.27783.

15c: Compound **1c** (0.5 g, 1.5 mmol) and 2,4,6-triisopropylphenyllithium (3.3 mmol) afforded 0.35 g (49%) of **15c**, colorless crystals, m.p. 54−57 °C (heptane). − IR (KBr): $\tilde{\nu}$ = 3681 cm^{-1} (OH). − ^{1}H NMR ([D$_6$]benzene): δ = 0.02 (s, CH, 1 H), 0.06, 0.20 and 0.30 (3 s, SiCH$_3$, 3 × 9 H), 1.35 (s, OH, 1 H), 1.21, 1.32 and 1.37 (3 d, ^3J = 6.7 Hz, *i*Pr-CH$_3$, 3 × 6 H), 2.77 (sept, ^3J = 6.7 Hz, *i*Pr-CH, 1 H), 3.50 (sept, ^3J = 6.7 Hz, *i*Pr-CH, 2 H), 7.09 (s, arom. CH, 2 H). − ^{13}C NMR ([D$_6$]benzene): δ = 0.7, 3.4, and 3.7 (SiCH$_3$), 9.2 (CH), 24.1, 25.6, and 26.0 (*i*Pr-CH$_3$), 32.5 and 32.4 (*i*Pr-CH), 121.7 (arom. CH), 134.9, 149.9, and 154.5 (arom. C). − ^{29}Si NMR ([D$_6$]benzene): δ = −19.3 (Si*Si*Me$_3$), −0.6 and 1.8 (CSiMe$_3$), 7.6 (SiOH). − MS (70 eV); *m/z* (%): 465 (3) [M − CH$_3$]$^+$, 390 (1) [M − SiMe$_3$, − OH, − H]$^+$, 203 (100) [M − Tip, − SiMe$_3$, − H]$^+$. − $C_{25}H_{52}OSi_4$ (481.6): calcd. C 62.42, H 10.89; found C 62.14, H 10.87.

16c: Compound **1c** (0.5 g, 1.5 mmol) and 2-*tert*-butyl-4,5,6-trimethylphenyllithium (3.3 mmol) gave 0.3 g (44%) **16c**, colorless crystals, m.p. 50−56 °C. − IR (nujol): $\tilde{\nu}$ = 3695 cm^{-1} (OH). − ^{1}H NMR ([D$_6$]benzene): δ = −0.03, 0.19, and 0.38 (3 s, SiCH$_3$, 3 × 9 H), 0.32 (s, CH, 1 H), 1.48 (s, *t*Bu-CH$_3$, 9 H), 1.62 (s, OH, 1 H), 1.93, 2.12, and 2.16 (3 s, aryl-CH$_3$, 3 × 3 H), 7.23 (s, arom. CH, 1 H). − ^{13}C NMR ([D$_6$]benzene): δ = 0.2, 3.6, and 4.4 (SiCH$_3$), 6.1 (CH), 15.1, 21.1, and 24.0 (aryl-CH$_3$), 34.2 (*t*Bu-CH$_3$), 36.6 (*t*Bu-C), 127.0 (arom. CH), 132.4, 135.9, 136.3, 141.2, and 153.7 (arom. C). − ^{29}Si NMR ([D$_6$]benzene): δ = −18.2 (Si*Si*Me$_3$), 0.5 (CSiMe$_3$), 1.5 (SiOH). − MS (70 eV); *m/z* (%): 437 (5) [M − CH$_3$]$^+$, 379 (37) [M − SiMe$_3$]$^+$; HRMS calcd. for $C_{23}H_{48}OSi_4$ 437.24907, found 437.25476.

General Procedure for the Preparation of the Methoxysilanes 17b, 17c, and 18c: At room temperature a 2.2-fold molar excess of the respective organolithium reagent was added to the ethereal solution of **1b** or **1c**, respectively After stirring for 12 h, excess methanol was added and stirring was continued for 2 h. The ethereal phases were separated and concentrated, and the residues were purified by chromatography (silica gel, heptane).

17b: Compound **1b** (0.5 g, 1.5 mmol) and 2,4,6-triisopropylphenyllithium (3.3 mmol) gave 0.45 g (60%) of **17b**, colorless oil. − IR (cap.): $\tilde{\nu}$ = 1103 cm^{-1} (SiOC). − ^{1}H NMR ([D$_6$]benzene): δ = 0.05 and 0.12 (2 s, SiCH$_3$, 2 × 9 H), 0.15 (s, CH, 1 H), 1.04, 1.07 and 1.13 (3 d, ^3J = 6.7 Hz, *i*Pr-CH$_3$, 3 × 6 H), 2.63 (sept, *i*Pr-CH, 1 H), 3.18 (s, OCH$_3$, 3 H), 3.45 (sept, *i*Pr-CH, 2 H), 7.04 (s, Tip-CH, 2 H), 6.95 and 7.54 (2 m, Ph-CH, 5 H). − ^{13}C NMR ([D$_6$]benzene): δ = 3.6 and 4.2 (SiCH$_3$), 8.4 (CH), 24.4, 24.6, and 26.3 (*i*Pr-CH$_3$), 32.3 and 34.5 (*i*PrCH), 51.8 (OCH$_3$), 121.9, 127.5, 129.6, and 132.3 (arom. CH), 136.5, 138.3, 150.5, and 155.6 (arom. C). − ^{29}Si NMR ([D$_6$]benzene): δ = −0.8 and −0.7 (SiMe$_3$), 0.9 (SiOMe). − MS (70 eV): *m/z* (%): 497 (4) [M − H]$^+$, 483 (25) [M − CH$_3$]$^+$, 425 (8) [M − SiMe$_3$]$^+$, 295 (100) [M − Tip]$^+$. − $C_{29}H_{50}OSi_3$ (499.1): calcd. C 69.81, H 10.10; found C 70.09, H 10.11.

17c: Compound **1c** (0.5 g, 1.5 mmol) and 2,4,6-triisopropylphenyllithium (3.3 mmol) gave 0.3 g (40%) of **17c**, colorless crystals, m.p. 58−65 °C. − IR (nujol): $\tilde{\nu}$ = 1114 cm^{-1} (SiOC). − ^{1}H NMR ([D$_6$]benzene): δ = 0.02 (s, SiCH$_3$, 9 H), 0.10 (s, CH, 1 H), 0.33 (s, SiCH$_3$, 18 H),1.23 (d, ^3J = 6.7 Hz, *i*Pr-CH$_3$, 6 H), 1.36 (d, ^3J = 6.7 Hz, *i*Pr-CH$_3$, 12 H), 2.80 (sept, ^3J = 6.7 Hz, *i*Pr-CH, 1 H), 3.18 (sept, ^3J = 6.7 Hz, *i*Pr-CH, 2 H), 3.47 (s, OCH$_3$, 3 H), 7.09 (s, arom. CH), 2 H). − ^{13}C NMR ([D$_6$]benzene): δ = 2.1, 3.3, and 3.8 (SiCH$_3$), 9.9 (CH), 24.1, 25.9, and 26.2 (*i*Pr-CH$_3$), 33.3 and 34.4 (*i*Pr-CH), 52.2 (OCH$_3$), 121.9 (arom. CH), 135.9, 149.9, and 155.1 (arom. C). − ^{29}Si NMR ([D$_6$]benzene): δ = −21.7 (Si*Si*Me$_3$), −0.2 and 1.8 (CSiMe$_3$), 10.4 (SiOMe). − MS (70 eV); *m/z* (%): 494 (8) [M]$^+$, 479 (59) [M − CH$_3$]$^+$, 291 (100) [M − Tip]$^+$; HRMS calcd. for $C_{26}H_{54}OSi_4$ 479.29319, found 479.30170. − $C_{26}H_{54}OSi_4$ (495.1): calcd. C 63.08, H 10.99; found C 63.00, H 10.85.

18c: Compound **1c** (0.5 g 1.5 mmol) and 2-*tert*-butyl-4,5,6-trimethylphenyllithium (3.3 mmol) afforded 0.3 g (43%) of **18c**, colorless crystals, m.p. 86−89 °C. − IR (nujol): $\tilde{\nu}$ = 1124 cm^{-1} (SiOC). − ^{1}H NMR ([D$_6$]benzene): δ = −0.05, 0.28, and 0.35 (3 s, SiCH$_3$, 3 × 9 H), 0.05 (s, CH, 1 H), 1.54 (s, *t*Bu-CH$_3$, 9 H), 1.92, 2.14, and 2.17 (3 s, aryl-CH$_3$, 3 × 3 H), 3.55 (s, OCH$_3$, 3 H), 7.26 (s, arom.

CH, 1 H). – ^{13}C NMR ([D$_6$]benzene): δ = 2.1, 3.5, and 4.3 (SiCH$_3$), 7.1 (CH), 15.1, 21.0, and 25.3 (aryl-CH$_3$), 33.5 (*t*Bu-CH$_3$), 37.4 (*t*Bu-CH), 52.8 (OCH$_3$), 127.3 (arom. CH), 128.3, 132.3, 135.8, 140.8, and 154.3 (arom. C). – ^{29}Si NMR ([D$_6$]benzene): δ = −18.6 (Si*Si*Me$_3$), −0.3 and 0.6 (CSiMe$_3$), 3.8 (SiOMe). – MS (70 eV); *m*/*z* (%): 466 (1) [M]$^+$, 451 (10) [M − CH$_3$]$^+$, 393 (100) [M − SiMe$_3$]$^+$; HRMS calcd. for $C_{23}H_{47}OSi_4$ [M − CH$_3$] 451.27550, found 451.27042. – $C_{24}H_{50}OSi_4$ (467.0): calcd. C 61.73, H 10.79; found C 61.90, H 10.58.

General Procedure for the Preparation of the 1,2-Oxasiletanes 19b, 19c, and 20c: At room temperature a 2.2-fold molar excess of the respective organolithium reagent was added to the ethereal solution of **1b** or **1c**, respectively. After stirring for 12 h, an equimolar quantity of benzaldehyde was added, stirring was continued for 2 h and the reaction quenched with water. The organic layer was separated, dried and concentrated and the residue was purified by chromatography (silica gel, heptane). Single crystals of the oxasiletanes were obtained by recrystallization from acetone.

19b: Compound **1b** (0.5 g, 1.5 mmol), 2,4,6-triisopropylphenyllithium (3.3 mmol) and benzaldehyde (0.16 g, 1.5 mmol) gave 0.1 g (12%) of **19b**, colorless crystals, m.p. 114−119 °C. – IR (cap.): $\tilde{\nu}$ = 1101 cm^{-1} (SiOC). – ^{1}H NMR ([D$_6$]benzene): δ = −0.07 and 0.17 (2 s, SiCH$_3$, 2 × 9 H), 1.17 (d, ^3J = 6.5 Hz, *i*Pr-CH$_3$, 6 H), 1.08, 1.37, 1.49, and 1.69 (4 d, ^3J = 6.5 Hz, *i*Pr-CH$_3$, 4 × 3 H), 2.84, 3.26, and 4.37 (3 sept, ^3J = 6.5 Hz, *i*Pr-CH, 3 × 1 H), 6.28 (s, PhCH, 1 H), 7.00−8.07 (m, arom. CH, 12 H). – ^{13}C NMR ([D$_6$]benzene): δ = 2.8 and 4.0 (SiCH$_3$), 23.9, 25.3, 25.5, 25.9, and 28.1 (*i*Pr-CH$_3$), 31.2, 34.5, and 36.5 (*i*Pr-CH), 36.2 (C(SiMe$_3$)$_2$), 81.3 (CH), 121.0, 123.3, 126.9, 128.2, 129.7, 132.4, and 134.5 (arom. CH), 134.8, 139.8, 151.4, 153.0, and 157.0 (arom. C). – ^{29}Si NMR ([D$_6$]benzene): δ = −2.2 and −0.4 (SiMe$_3$), 8.4 (ring-Si). – MS (70 eV); *m*/*z* (%): 572 (4) [M]$^+$, 557 (5) [M − CH$_3$]$^+$, 495 (2) [M − Ph]$^+$, 325 (100) [M − PhCC(SiMe$_3$)$_2$]$^+$; HRMS calcd. for $C_{35}H_{52}OSi_3$ 572.31011, found 572.33258.

19c: Compound **1c** (0.5 g, 1.5 mmol), 2,4,6-triisopropylphenyllithium (3.3 mmol) and benzaldehyde (0.16 g, 1.5 mmol) afforded 0.3 g (35%) of **19c**, colorless crystals, m.p. 153−155 °C. – IR (nujol): $\tilde{\nu}$ = 1009 cm^{-1} (SiOC). – ^{1}H NMR ([D$_6$]benzene): δ = 0.04, 0.20, and 0.29 (3 s, SiCH$_3$, 3 × 9 H), 1.22 (d, ^3J = 6.7 Hz, *i*Pr-CH$_3$, 6 H), 1.25, 1.39, 1.44, and 1.52 (4 d, ^3J = 6.7 Hz, *i*Pr-CH$_3$, 4 × 3 H), 2.75 (sept, ^3J = 6.7 Hz, *i*Pr-CH, 2 H), 4.13 (sept, ^3J = 6.7 Hz, *i*Pr-CH, 1 H), 6.26 (s, PhCH, 1 H), 7.03 and 7.24 (2 s, Tip-CH, 2 × 1 H), 7.11−7.82 (m, arom. CH). – ^{13}C NMR ([D$_6$]benzene): δ = 1.1, 2.6, and 3.4 (SiCH$_3$), 31.4 [C(SiMe$_3$)$_2$], 82.5 (PhCH), 24.1, 25.3, 25.9, 26.2, and 26.8 (*i*Pr-CH$_3$), 31.8, 34.5, and 35.0 (*i*Pr-CH), 120.3, 122.7, 126.6, and 127.1 (arom. CH), 135.9, 145.6, 150.8, 151.8, and 155.6 (arom. C). – ^{29}Si NMR ([D$_6$]benzene): δ = −15.0 (Si*Si*Me$_3$), −2.6 and 0.9 (CSiMe$_3$), 36.5 (ring-Si). – MS (70 eV); *m*/*z* (%): 553 (10) [M − CH$_3$]$^+$, 495 (69) [M − SiMe$_3$]$^+$; HRMS calcd. for $C_{31}H_{53}OSi_4$ [M − CH$_3$] 553.30991, found 553.31738.

20c: Compound **1c** (0.5 g, 1.5 mmol), 2-*tert*-butyl-4,5,6-trimethylphenyllithium (3.3 mmol), and benzaldehyde (0.16 g, 1.5 mmol) afforded 0.1 g (12%) of **20c**, colorless crystals, m.p. 170−175 °C. – IR (nujol): $\tilde{\nu}$ = 999 cm^{-1} (SiOC). – ^{1}H NMR ([D$_6$]benzene): δ = 0.04, 0.08, and 0.34 (3 s, SiCH$_3$, 3 × 9 H), 1.60 (s, *t*Bu-CH$_3$, 9 H), 1.93, 2.14, and 2.34 (3 s, aryl-CH$_3$, 3 × 3 H), 6.21 (s, PhCH, 1 H), 7.08−7.84 (m, arom. CH, 6 H). – ^{13}C NMR ([D$_6$]benzene): δ = 1.2, 2.9, and 4.7 (SiCH$_3$), 14.7, 21.1, and 23.3 (aryl-CH$_3$), 29.9 [C(SiMe$_3$)$_2$], 33.4 (*t*Bu-CH$_3$), 37.1 (*t*Bu-C), 79.8 (PhCH), 126.9, 127.3, 127.7, and 127.8 (arom. CH), 128.3, 131.6, 136.5, 137.2, 138.6, and 144.9 (arom. C). – ^{29}Si NMR ([D$_6$]benzene): δ = −16.2

Table 1. Crystal data and structure refinement data for compounds **19b**, **19c**, and **20c**

Compound	**19b**	**19c**	**20c**
Empirical formula	$C_{35}H_{52}OSi_3$	$C_{32}H_{56}OSi_4$	$C_{30}H_{52}OSi_4$
Molecular mass	573.04	569.13	541.08
Crystal system	triclinic	monoclinic	monoclinic
Space group	$P\bar{1}$	$P2_1/c$	$P2_1/c$
Unit cell dimensions	a = 9.440(2) Å b = 11.112(3) Å c = 18.440(6) Å α = 83.47(3)° β = 81.43(3)° γ =65.600(10)°	a = 20.740(4) Å b = 9.7790(10) Å c = 18.695(2) Å α = 90° β = 109.260(10)° γ = 90°	a = 21.048(4) Å b = 9.516(2) Å c = 16.667(6) Å α = 90° β = 100.31(2)° γ = 90°
Volume [Å^3]	1738.9(8)	3579.4(9)	3284.4(15)
Z	2	4	4
Density (calcd.) [Mg/m^3]	1.094	1.056	1.094
Absorption coeff. [mm^{-1}]	0.161	0.187	0.201
F(000)	624	1248	1184
Crystal size [mm^3]	0.82×0.52×0.36	0.66×0.46×0.32	0.80×0.40×0.35
Θ range for data coll.[°]	2.02 to 22.00	2.20 to 22.00	1.97 to 22.00
Index ranges	$-9 \le h \le 1$, $-11 \le k \le 11$, $-19 \le l \le 19$	$-21 \le h \le 20$, $-10 \le k \le 1$, $-1 \le l \le 19$	$-22 \le h \le 22$, $-10 \le k \le 1$, $-1 \le l \le 17$
Reflections collected	5219	5578	5170
Independent reflections	4261	4395	4018
[R(int)]	0.0322	0.0362	0.0400
Completeness to Θ = 22.00°	99.9%	99.9%	99.9%
Data/restraints/param.	4261/0/352	4395/0/334	4018/0/318
Goodness-of-fit on F^2	1.020	1.021	1.011
Final R indices [$I > 2\sigma(I)$]	$R1$ = 0.0565 $wR2$ = 0.1512	$R1$ = 0.0493 $wR2$ = 0.1227	$R1$ = 0.0484 $wR2$ = 0.1225
R indices (all data)	$R1$ = 0.0691 $wR2$ = 0.1615	$R1$ = 0.0694 $wR2$ = 0.1354	$R1$ = 0.0679 $wR2$ = 0.1348
Largest diff. peak/hole [e·Å^{-3}]	0.390/−0.267	0.220/−0.174	0.226/−0.193

($Si\mathit{Si}Me_3$), −1.7 and 1.1 ($CSiMe_3$), 21.6 (ring-Si). − MS (70 eV); *m/z* (%): 525 (2) $[M - CH_3]^+$, 467 (11) $[M - SiMe_3]^+$; HRMS calcd. for $C_{29}H_{49}OSi_4$ $[M - CH_3]$ 525.27594, found 525.28607.

X-ray Structure Determinations of 19b, 19c, and 20c: Suitable crystals of the compounds were selected under a microscope and sealed onto a glass fiber. Afterwards rotational photos were taken and 13 reflections chosen to find reasonable reduced cells for the data collections. These data collections were done with a Siemens P4 four-circle diffractometer equipped with a graphite monochromator and using Mo-K_α radiation in a routine ω-scan. The structures were solved by direct methods (*SHELXTL*, Siemens Analytical X-ray Inst. Inc., **1990**) and refined by the full-matrix least-squares method of SHELXL-97 (G. M. Sheldrick, Universität Göttingen, **1997**). All non-hydrogen atoms were refined anisotropically . The H atoms were put into theoretical positions and refined using the riding model. Further details see Table 1. Crystallographic data (excluding structure factors) for the structures in this paper have been deposited with the Cambridge Crystallographic Data Centre as supplementary publication no. CCDC-143201 (**19b**), -143202 (**19c**), and -143203 (**20c**). Copies of the data can be obtained, free of charge, on application to CCDC, 12 Union Road, Cambridge CB2 1EZ, UK [Fax: (internat.) + 44-1223/336-033; E-mail: deposit@ccdc.cam.ac.uk].

Acknowledgments

We gratefully acknowledge the support of our work by the Deutsche Forschungsgemeinschaft and the Fonds der Chemischen Industrie. We thank Prof. M. Michalik, Dr. W. Baumann, and Prof. N. Stoll for recording the NMR and mass spectra.

[1] [1a] A. G. Brook, M. A. Brook, *Adv. Organomet. Chem.* **1996**, *39*, 71−158. − [1b] T. Müller, W. Ziche, N. Auner, in: *The Chemistry of Organic Silicon Compounds* (Eds.: Z. Rappoport, Y. Apeloig), Wiley, New York, **1998**, vol. 2, p. 857−1062.

[2] A. G. Brook, S. C. Nyburg, F. Abdesaken, B. Gutekunst, G. Gutekunst, R. K. M. R. Kallury, Y. C. Poon, Y.-M. Chang, W. Wong-Ng, *J. Am. Chem. Soc.* **1982**, *104*, 5667−5672.

[3] N. Wiberg, G. Wagner, *Angew. Chem.* **1983**, *95*, 1027−1028; *Angew. Chem. Int. Ed. Engl.* **1983**, *22*, 1005−1006. − N. Wiberg, G. Wagner, G. Müller, *Angew. Chem.* **1985**, *97*, 220−221; *Angew. Chem. Int. Ed. Engl.* **1985**, *24*, 229−230. − N. Wiberg, G. Wagner, J. Riede, G. Müller, *Organometallics* **1987**, *6*, 32−35.

[4] G. Delpon-Lacraze, C. Couret, *J. Organomet. Chem.* **1994**, *480*, C14−C15. − G. Delpon-Lacraze, C. deBattisti, C. Couret, *J. Organomet. Chem.* **1996**, *514*, 59−66.

[5] K. Schmohl, M. Blach, H. Reinke, R. Kempe, H. Oehme, *Eur. J. Inorg. Chem.* **1999**, 1667- 1672 and literature cited therein.

[6] Y. Apeloig, M. Bendikov, M. Yuzefovich, M. Nakash, D. Bravo-Zhivotovskii, *J. Am. Chem. Soc.* **1996**, *118*, 12228−12229.

[7] K. Schmohl, T. Gross, H. Reinke, H. Oehme, *Z. Anorg. Allg. Chem.*, **2000**, *626*, 1100−1104.

[8] M. Weidenbruch, H. Flott, B. Ralle, K. Peters, H. G. von Schnering, *Z. Naturforsch.* **1983**, *38b*, 1062−1068.

[9] H. Sakurai, H. Yamamori, M. Kumada, *J. Org. Chem.* **1968**, *33*, 1527−1530.

[10] G. Maas, in: *The Chemistry of Organic Silicon Compounds* (Eds.: Z. Rappoport, Y. Apeloig), Wiley, New York, **1998**, vol. 2, p. 703−778.

[11] A. Sekiguchi, W. Ando, *Chem. Lett.* **1983**, 871−874. − A. Sekiguchi, W. Ando, *Organometallics* **1987**, *6*, 1857−1862.

[12] W. Ando, A. Sekiguchi, T. Migita, *Chem. Lett.* **1976**, 779−782. − R. L. Kreeger, H. Shechter, *Tetrahedron Lett.* **1975**, 2061−2064. − W. Ando, A. Sekiguchi, J. Ogiwara, T. Migita, *J. Chem. Soc., Chem. Commun.* **1975**, 145−146. − W. Ando, A. Sekiguchi, A. J. Rothschild, R. R. Gallucci, M. Jones, T. J. Barton, J. A. Kilgour, *J. Am. Chem. Soc.* **1977**, *99*, 6995−6999. − T. J. Barton, S. K. Hoekman, *J. Am. Chem. Soc.* **1980**, *102*, 1584−1591.

[13] M. Mickoleit, K. Schmohl, R. Kempe, H. Oehme, *Angew. Chem.* **2000**, *112*, 1679−1681; *Angew. Chem. Int. Ed. Engl.* **2000**, *39*, 1610−1612.

[14] P. Lassacher, A. G. Brook, A. J. Lough, *Organometallics* **1995**, *14*, 4359−4365

[15] C. Krempner, H. Reinke, H. Oehme, *Chem. Ber.* **1995**, *128*, 143−149.

[16] G. Raabe, J. Michl, in: *The Chemistry of Organic Silicon Compounds* (Eds.: S. Patai, Z. Rappoport), Wiley, New York, **1989**, part 2, chapter 17, p. 1044−1102.

[17] A. G. Brook, W. J. Chatterton, J. F. Sawyer, D. W. Hughes, K. Vorspohl, *Organometallics* **1987**, *6*, 1246−1256.

[18] C. Marschner, *Eur. J. Inorg. Chem.* **1998**, 221−226.

[19] R. L. Merker, M. J. Scott, *J. Organomet. Chem.* **1965**, *4*, 98−100.

[20] H. Gilman, C. L. Smith, *J. Organomet. Chem.* **1967**, *8*, 245−253.

Received May 9, 2000
[I00188]

Tuning the Reversible Binding of NO to Iron(II) Aminocarboxylate and Related Complexes in Aqueous Solution

Thorsten Schneppensieper,[a] Stefan Finkler,[a] Almut Czap,[a] Rudi van Eldik,*[a] Martin Heus,[b] Peter Nieuwenhuizen,[b] Carel Wreesmann,[b] and Wiebe Abma[c]

Keywords: Iron / Chelates / Thermodynamics / Nitric oxide / Stability constants

Chelate complexes of Fe^{II} were investigated with respect to their reactivity against nitric oxide and dioxygen. Through a systematic variation of the structure of the polyaminocarboxylate EDTA, a series of 38 potential chelate ligands were selected for Fe^{II}. The nitrosyl complexes were prepared from the Fe^{II} chelates with NO gas and examined spectroscopically by UV/Vis and ATR-IR techniques, and themodynamically by determining the overall binding constants for NO. In addition, the reversibility of NO binding to these Fe^{II} chelates and the rate of the competing oxidation by dioxygen were studied qualitatively. Whereas the studied complexes all form more or less stable nitrosyl complexes with a characteristic band pattern in the UV/Vis spectra and only slightly diverging frequencies for the NO stretching vibration in the IR spectra, they differ considerably in the reversibility of NO binding, the overall NO binding constants and the sensitivity towards dioxygen. It was found that an increasing number of donor groups on the chelate ligand causes a stronger coordination to Fe^{II}, and increases the tendency of the Fe^{II} chelates to transfer electron density from iron to substrates like dioxygen or nitric oxide. This results in an accelerated oxidation of Fe^{II} to Fe^{III} by dioxygen and a more pronounced tendency of the corresponding nitrosyl complexes to slowly decompose to Fe^{III} and N_2O. In addition, the overall binding constant for NO (K_{NO}), which spans a range from $1 \cdot 10^3$ to $2 \cdot 10^7$ M^{-1}, increases in the same direction as a result of the inductive effect of the chelate ligand.

Introduction

Chelate complexes of Fe^{II} in aqueous solution have been suggested as homogeneous catalysts for the selective binding and subsequent reduction of NO to dinitrogen in denitrification processes.[1–9] An essential aspect of this process is the efficient binding of NO by a metal chelate in order to increase its solubility in aqueous solution. Although a number of studies have dealt with the binding of NO to chelate complexes of Fe^{II}, none have undertaken a systematic investigation of the chelate properties in order to optimize the efficiency and reversibility of the binding process.[1,10–14] In this study we undertook a systematic variation of the donor number and donor atoms of multidentate chelates, and determined the overall binding constants for NO to the corresponding Fe^{II} complexes. In addition, we studied the reversibility of the binding process, as well as the UV/Vis and IR spectral changes associated with these reactions. Parallel to this, the competing reaction with dioxygen was also investigated quantitatively. An interesting correlation between the binding ability for NO and the oxygen sensitivity of the Fe^{II} complexes was found. The observed trends are reported in a qualitative way, and the most important factors that control the efficiency and reversibility of the binding of NO to Fe^{II} chelates are discussed.

In order to establish an extended series of chelate ligands that are able to bind NO more or less reversibly in the form of Fe^{II} complexes, we used the polyaminocarboxylate EDTA as a reference and starting point for nearly all structural modifications. The seven-coordinate $[Fe^{II}(EDTA)(H_2O)]^{2-}$ complex[15] certainly belongs to the hitherto best examined systems for NO binding in aqueous solution, and detailed kinetic and thermodynamic data are available in the literature.[16–18] Furthermore, EDTA is an inexpensive industrial product and its structure offers nearly unlimited possibilities for modification. Through a systematic variation of the EDTA structure we obtained a set of altogether 38 chelate ligands summarized in Figure 1. Apart from direct EDTA derivatives (**Series 1**), we also studied a considerable number of MIDA analogues as indirect EDTA derivatives (**Series 2**) in order to investigate the influence of a reduction in the molecular size of the chelate ligand on the NO binding characteristics of the corresponding Fe^{II} complexes.

Since a systematic treatment enables more specific conclusions to be reached on the relation between structure and function of the examined systems, it was advantageous to further divide the EDTA and MIDA analogues in different subgroups. Within the series of EDTA analogues (**Series 1**), the ethylene spacer between the two EDTA nitrogens was varied through branching or elongation (**subgroup a**), or some or all of the four acetic acid end groups were replaced without

[a] Institute for Inorganic Chemistry, University of Erlangen-Nürnberg,
Egerlandstraße 1, 91058 Erlangen, Germany
Fax: (internat.) +49−9131/8527387
E-mail: vaneldik@chemie.uni-erlangen.de
[b] Akzo Nobel Chemical Research Arnhem, Department RPH, P. O. Box 9300, 6800 SB Arnhem, The Netherlands
[c] Paques Bio Systems BV, P.O. Box 52, 8560 AB Balk, The Netherlands

 © WILEY-VCH Verlag GmbH, 69451 Weinheim, 2001 1434−1948/01/0202−0491 $ 17.50+.50/0

affecting the central ethylenediamine component (**subgroup b**). The MIDA analogues (**Series 2**) are divided into three subgroups. Whereas in **subgroup a** the methyl group of MIDA is exchanged by another non-coordinating group, it is exchanged in **subgroup b** by a further coordinating function. **Subgroup c** summarizes derivatives in which the nitrogen donor of MIDA is replaced by oxygen, sulfur, a methylene group, or an aromatic nitrogen.

Chelate ligands, which cannot be related directly to either MIDA or EDTA analogues, are compiled in a third main group (**Series 3**). These include the phosphonates ATMP, EDTMP, and DTPMP (derivatives of NTA, EDTA, and DTPA), nitrogen-free hydroxycarboxylic acids like TARTRATE and CITRATE, and the aromatic aminocarboxylate APTA.

Results and Discussion

Preliminary Observations

In the following sections, Fe^{II} chelate complexes and the corresponding nitrosyl complexes are indicated by the formulae $[Fe^{II}(L)_x]$ and $[Fe^{II}(L)_x(NO)]$, respectively, where L = chelate ligand. Although the number of bound chelate molecules are only precisely known in a few cases, especially for L = EDTA (x = 1) and MIDA (x = 1 and 2),[19] it is safe to assume that all EDTA analogues form 1:1, and MIDA analogues with three donor groups form either 1:1 or 1:2 complexes with Fe^{II}. In general, the 1:1 complexes are quite stable species in solution as judged from their stability constants reported in the literature.[19] Typical examples are

Series 1: Analogues of EDTA

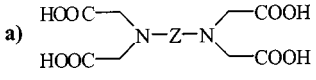

Z = spacer

EDTA: Z = -$(CH_2)_2$-
1,2-PDTA: Z = -$CH(CH_3)$-CH_2-
1,3-PDTA: Z = -$(CH_2)_3$-
HPDTA: Z = -CH_2-$CH(OH)$-CH_2-
1,4-BDTA: Z = -$(CH_2)_4$-
1,6-HDTA: Z = -$(CH_2)_6$-
EGTA: Z = -$(CH_2)_2$-O-$(CH_2)_2$-O-$CH_2)_2$-
CDTA: Z =

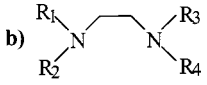

$R_{1\text{-}4}$ = end groups

EDDA: $R_1 = R_3 = H$; $R_2 = R_4 = CH_2$-COOH
α-EDDADP: $R_1 = R_3 = CH_2$-COOH; $R_2 = R_4 = CH(CH_3)$-COOH
β-EDDADP: $R_1 = R_3 = CH_2$-COOH; $R_2 = R_4 = CH_2$-CH_2-COOH
EDTP: $R_1 = R_2 = R_3 = R_4 = CH_2$-$CH_2$-COOH
EDDHPA: $R_1 = R_3 = H$; $R_2 = R_4 = CH(o\text{-}C_6H_4OH)$-COOH
HEDTRA: $R_1 = R_2 = R_3 = CH_2$-COOH; $R_4 = CH_2$-CH_2OH
EDDS: $R_1 = R_3 = H$; $R_2 = R_4 = CH(COOH)$-CH_2-COOH
DTPA: $R_1 = R_2 = R_3 = CH_2$-COOH; $R_4 = (CH_2)_2$-$N(CH_2$-COOH$)_2$

Figure 1. Survey of tested chelate ligands

In order to check these numbers, pH titrations were performed for the complexes $[Fe^{II}(L)_x]$ (L = MIDA, EDTA). Calculations relating to the determination of protonation and complex formation constants were performed using the computer program PSEQUAD.[20] The measured stability constants, $3.39 \cdot 10^{11}$ M^{-2} (L = MIDA) (see Table 1) and $2.29 \cdot 10^{14}$ M^{-1} (L = EDTA) are in good agreement with those reported in the literature.[21] Speciations (see Figure 2) were calculated with the computer program SPECIES.[22] The results for the Fe−MIDA system indicate that below pH 3 no complex formation occurs. Between pH 3 and 5, the 1:1 [Fe(MIDA)] complex is generated, and above pH 5 the 1:2 complex is partially present. At pH 8 the iron is totally complexed and at pH > 10 the 1:2 complex is the dominating species. This species distribution indicates that at pH 5, where most of the experiments were performed, mainly the 1:1 complex will exist. The 1:2 complex will only be present

Series 2: Analogues of MIDA

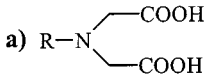

R = non-coordinating group

IDA: R = H
MIDA: R = CH_3
EIDA: R = CH_2-CH_3
^{t}BIDA: R = $C(CH_3)_3$
AIDA: R = C(O)-CH_3
SMIDA: R = CH_2-SO_3H

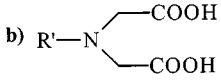

R' = coordinating group

EDG: R' = CH_2-CH_2OH
HPIDA: R' = CH_2-$CH(OH)$-CH_3
NTA: R' = CH_2-COOH
BADA: R' = CH_2-CH_2-COOH
ADA: R' = CH_2-$CONH_2$
CEIDA: R' = CH_2-CH_2-S-CH_2-COOH

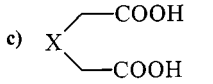

X = hetero atom

ODA: X = O
TDA: X = S
GLUTAR: X = CH_2
DIPIC: X = $N_{arom.}$

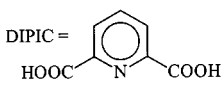

Figure 1. *(Continued)*

Table 1. Stability constants

	log K_1	log K_2	K
$[Fe^{II}(MIDA)_x]$	6.18 ± 0.08	5.35 ± 0.08	$3.39 \cdot 10^{11}$ M^{-2}
$[Fe^{II}(MIDA)_xNO]$	6.86 ± 0.07	4.63 ± 0.09	$3.09 \cdot 10^{11}$ M^{-2}

as the major species when a large excess (ca. 20 fold) of MIDA is used. A similar conclusion was reached on the basis of ^{1}H NMR spectra recorded for the uncoordinated ligand in solution.

Net charges for these complexes are only given when the composition of the complex can be specified, e.g. $[Fe^{II}(EDTA)]^{2-}$. A coordinated water molecule was detected in the crystal structure of the EDTA complex,[15] which can therefore be presented by the formula $[Fe^{II}(EDTA)(H_2O)]^{2-}$. Preliminary water exchange studies on several $[Fe^{II}(L)_x]$ complexes using ^{17}O NMR techniques, indicated that they in general have at least one water molecules bound to the Fe^{II} center.[23] In the absence of further details and for reason of uniformity, water molecules will be omitted in all following formulae. However, it should be kept in mind that some of the complexes are seven-coordinate species, such that the reaction with NO is probably not a simple addition of NO to $[Fe^{II}(L)_x]$ but rather substitution of a labile bound water molecule by NO.

Whereas the coordination stoichiometry of $[Fe^{II}(MIDA)_x]^{(2x-2)-}$ and analogues can now be predicted for the selected experimental conditions in terms of pH and metal to ligand concentration ratio as outlined above, the composition of the corresponding NO complex, viz.

Series 3: Other ligands

ATMP

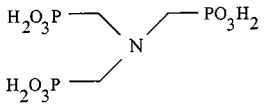

DTPMP

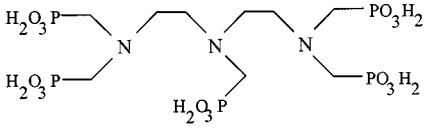

EDTMP

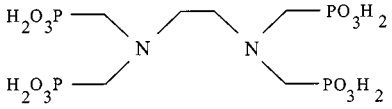

L-TARTRATE

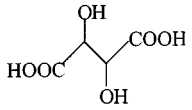

CITRATE

APTA

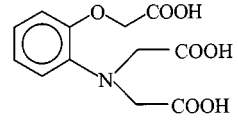

Figure 1. *(Continued)*

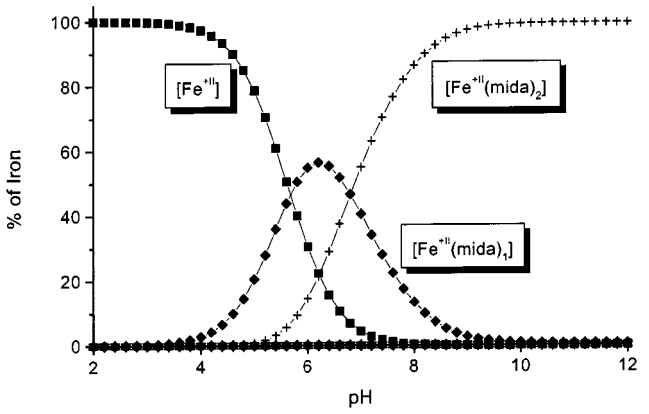

Figure 2. Species distribution curves for the $[Fe^{II}(MIDA)_x]^{(2x-2)-}$ complex [experimental conditions: $[Fe^{II}(MIDA)] = 4 \cdot 10^{-3}$ M, $T = 25$ °C, $I = 0.5$ M ($NaClO_4$)]

$[Fe^{II}(MIDA)_xNO]^{(2x-2)-}$, remains to be determined. For this purpose a potentiometric titration of the NO complex was done. From the speciation diagram it was possible to confirm that under the selected conditions the 1:1 complex is the dominating species in solution (see Figure 3).

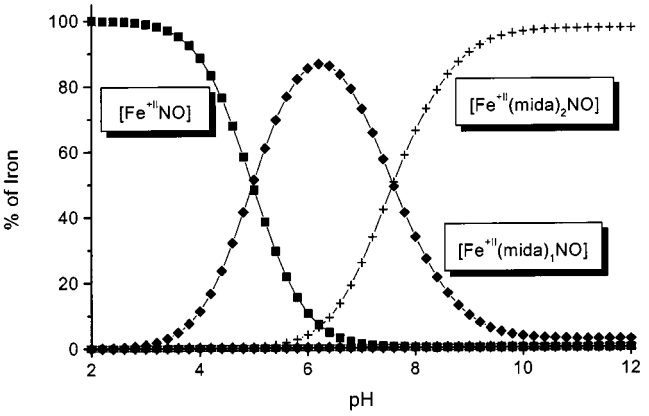

Figure 3. Species distribution curves for the $[Fe^{II}(MIDA)_xNO]^{(2x-2)-}$ complex [experimental conditions: $[Fe^{II}(MIDA)NO] = 4 \cdot 10^{-3}$ M, $T = 25$ °C, $I = 0.5$ M ($NaClO_4$)]

pH titrations of the $[Fe^{II}(MIDA)_xNO]$ complex resulted in a stability constant of $3.09 \cdot 10^{11}$ M^{-2} (Table 1) and show that there is nearly no change in the overall stability constant between $[Fe^{II}(MIDA)_x]$ and $[Fe^{II}(MIDA)_xNO]$. The addition of NO caused a small but significant change in the logK_1 and logK_2 values in favor of the 1:1 complex.

The species distribution (Figure 3) clearly indicates that the reaction with NO significantly stabilizes the 1:1 complex in a manner that at pH 5 more of the 1:1 [Fe(MIDA)NO] complex is generated than found for the speciation in the absence of NO. In fact, the increase in the 1:1 complex is approximately twice the decrease in the 1:2 complex concentration during the introduction of NO into the solution.

It can be concluded from the above described experiments that MIDA and analogous chelates mainly form 1:1 complexes with Fe^{II} and NO. $[Fe(MIDA)_2NO]^{2-}$ can only be prepared in solution in the presence of a large, at least 20 fold, excess of MIDA.

General Features in the UV/Vis and ATR-IR Spectra of Fe^{II} Nitrosyl Complexes

UV/Vis spectra

The identification and spectral characterization of metal−NO complexes has received much attention from researchers over the last few decades, and the results are summarized in some selected publications.[10,11,16,24−27] In the majority of cases, especially when the chelate ligand L is a polyaminocarboxylate, the UV/Vis spectra of the nitrosyl complexes $[Fe^{II}(L)_x(NO)]$ are characterized by three absorption bands: two strong *charge-transfer (C-T)* bands around 340 and 440 nm, respectively, and one weaker *d-d* band between 580 and 640 nm (data are summarized in Table 2). Whereas the position of the high energy *C-T* band at about 340 nm is almost not affected by the nature of the bound chelate ligand, the low energy *C-T* band around 440 nm shows a small, and the *d-d* band a strong dependence on the selected chelate. In addition, a correlation exists between the positions of the *C-T* and *d-d* bands: with decreasing wavelength of the low energy *C-T* band, the wavelength of the *d-d* band increases (see Figure 4).

The two extreme cases are on the one hand the non-chelated iron complex, $[Fe^{II}(H_2O)_5(NO)]^{2+}$, with absorption bands at 451 nm and 585 nm (similar values were also found in the presence of potential ligands such as ^{t}BIDA, EDTP, and glutaric acid which do not coordinate efficiently to Fe^{II}), and on the other hand complexes with coordinated EDTA, DTPA, or HEDTRA, which have absorption bands at about 434 ± 1 nm and 635 ± 2 nm. Most of the other nitrosyl complexes exhibit an intermediate position with respect to their UV/Vis spectra.

Some preliminary observations led us to believe that the shift in the C-T band to lower and that of the *d-d* band to higher wavelengths may be associated with a systematic displacement of electron density between the iron metal center and NO. This is particularly indicated by the chemical features of the corresponding $[Fe^{II}(L)_x]$ complexes

Table 2. Survey of UV/Vis data, IR data, and Stability constants K_{NO} for $[Fe^{II}(L)_x(NO)]$ complexes with different chelate ligands L

Ligand	Fe^{II}/Lig.[a]	K_{NO} values [M^{-1}][b] with exp. errors	UV data [nm][b]	IR data [cm^{-1}][c]
H_2O		(1.15 ± 0.05) ×10^3	336 (440), **451** (265), **585** (85)	**1810** (pH 3.1)
edta	1:1.25	(2.05 ± 0.15) ×10^6	342 (1080), **435** (820), **633** (130)	**1777** (pH 4.2)
cdta	1:1	-	**430**, **628**	**1774** (pH 3.7)
1.2-pdta	1:1.25	(7.4 ± 0.6) ×10^5	343 (1130), **436** (860), **628** (140)	**1775** (pH 4.7)
1,3-pdta	1:1.2	(1.4 ± 0.3) ×10^4	343 (1065), **446** (845), **621** (135)	**1762** (pH 4.7)
hpdta	1:1.25	(1.1 ± 0.2) ×10^5	336 (1050), **437** (740), **619** (160)	**1792** (pH 5.0)
1,4-bdta	1:1.2	(3.75 ± 0.05) ×10^3	340 (980), **444** (650), **598.5** (135)	**1784** (pH 4.3)
1,6-hdta	1:1.1	(7.6 ± 0.4) ×10^3	340 (970), **443** (640), **597** (130)	**1783** (pH 5.4)
egta	1:1.25	(7.7 ± 0.6) ×10^3	341 (1120), **440** (680), **613** (130)	**1783** and **1802** (pH 5.4)
edda	1:1.25	(3.3 ± 0.5) ×10^5	341 (975), **437** (920), **620** (135)	**1765** (pH 5.7)
α-eddadp	1:1	-	**430**, **626**	**1781** (pH 3.5)
β-eddadp	1:1.1	(8.6 ± 0.4) ×10^5	346 (1065), **443** (950), **628** (140)	**1764** (pH 4.9)
edtp	1:1.5	(1.4 ± 0.1) ×10^3	337 (620), **452** (400), **580 s** (105)	**1755** (pH 6.3)
eddhpa	1:1.25, pH = 8.0	> 1 × 10^7	**442** (2450)	not soluble
hedtra	1:1.25	(1.5 ± 0.2) ×10^7	344 (1080), **434** (815), **634** (130)	**1777** (pH 5.0)
(*s,s*)-edds	1:1.3	(9.0 ± 1.0) ×10^5	345 (955),**439**(960), **638** (135)	**1766** (pH 4.5)
rac-edds	1:1.3	(1.9 ± 0.2) ×10^6	344.5 (950), **439** (975), **635** (135)	**1765** (pH 4.8)
dtpa	1:1.25	(3.0 ± 0.3) ×10^6	344 (1200), **433** (830), **636** (130)	**1778** (pH 5.5)
ida	1:3	(1.2 ± 0.1) ×10^4	339 (1050), **440** (815), **604** (140)	**1769** (pH 7.3)
mida	1:3	(9.5 ± 0.7) ×10^3	341 (1065), **444** (740), **598** (145)	**1777** (pH 6.4) **1783** (pH 4.9)
eida	1:3	(7.6 ± 0.3) ×10^3	340 (1020), **443.5** (640), **596.5** (130)	**1783** (pH 7.9)
^{t}bida	1:3	(1.30 ± 0.05) ×10^3	337 (605), **448.5** (360), **584.5** (110)	**1809** (pH 4.2)
aida	1:3	(4.3 ± 0.2) ×10^3	338 (775), **443** (540), **594** (115)	**1810** (pH 3.4)
smida	1:3	(1.1 ± 0.2) ×10^4	339 (1005), **440.5** (800), **605** (140)	**1779** (pH 7.1)
edg	1:3	(1.6 ± 0.2) ×10^5	340 (1230), **437** (810), **610.5** (135)	**1762** (pH 9.2)
hpida	1:3	(2.4 ± 0.2) ×10^5	341 (1250), **436** (835), **614** (140)	**1798** and **1763** (pH 8.6)
nta	1:2.5	(1.75 ± 0.15) ×10^6	342 (1230), **439** (870), **600** (150)	**1793** (pH 6.9)
bada	1:2.5	(4.7 ± 0.4) ×10^5	343.5 (1295), **446** (930), **612** (150)	**1782** (pH 5.4)
ada	1:3	(5.15 ± 0.15) ×10^5	342.5 (1270), **439** (780), **593** (150)	**1801** (pH 8.0)
ceida	1:1.3	(1.2 ± 0.3) ×10^6	**432** (730), **624** (125)	**1791** (pH 4.2)
glutaric acid	1:4	(1.1 ± 0.1) ×10^3	335 (470), **450.5** (290), **584** (95)	
oda	1:3	(4.6 ± 0.1) ×10^3	337 (815), **446.5** (500), **537 s** (210)	not soluble
tda	1:3	(2.1 ± 0.1) ×10^3	340.5 (980), **451** (480), **575 s** (140)	not soluble
dipic	1:1	(1.1 ± 0.1) ×10^4	338 (1170), **433** (880), **600** (160)	not soluble
dipic	1:2.2	not determined	336 (860), **446** (990)	not soluble
atmp	1:3.0	(1.4 ± 0.2) ×10^6	344 (1470), **452** (790), **585** (190)	
edtmp	1:1.5	(1.3 ± 0.2) ×10^6	345 (1320), **444.5** (695), **602** (130)	
dtpmp	1:1.5	(1.35 ± 0.15) ×10^6	346 (1250), **451** (670), **578 s** (175)	
L-tartrate	1:2.5	(1.3 ± 0.1) ×10^3	336 (815), **444** (375), **567** (110)	
citrate	1:2.3	(2.1 ± 0.3) ×10^4	338 (1120), **443** (710), **575** (175)	
apta	1:1.3	(4.5 ± 0.2) ×10^4	344 (950), **444** (600), **542** (240)	**1795** (pH 6.5)

[a] Fe^{II}/Lig. indicates the ratio beween Fe^{II} and chelate ligand L which was used to prepare the $[Fe^{II}(L)_x(NO)]$ complexes for UV/Vis spectra and determination of K_{NO} values. − [b] Conditions (*if not otherwise indicated*): 1 mM Fe^{II} ($FeSO_4$); 100 mM acetic acid/acetate buffer, pH = 5.0; I = 0.5 (adjusted with $NaClO_4$); $T \approx 23$ °C; molar extinction coefficients are quoted in brackets in M^{-1} cm^{-1}. − [c] Conditions (only for IR): 200 mM Fe^{II}; excess of chelate ligand L: 10 to 25%; unbuffered solutions.

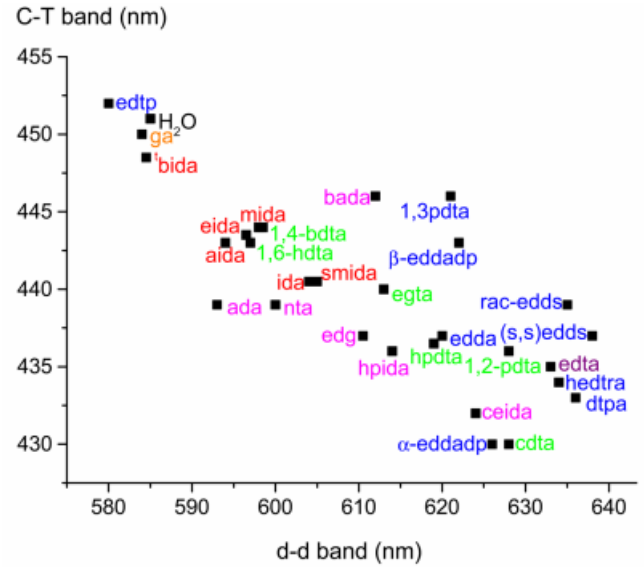

Figure 4. Correlation between the *C-T* and *d-d* band positions in the UV/Vis spectra of $[Fe^{II}(L)_x(NO)]$ complexes with L = polyaminecarboxylates.

which show, as described in detail below, in the direction from L = H_2O to L = EDTA, HEDTRA, or DTPA an increase in oxygen sensitivity accompanied by a decrease in the reversibility of the binding of NO·. Along these lines it could be favorable to consider the pentaaqua and MIDA nitrosyl complexes formally as $[Fe^{II}(H_2O)_5(NO^{\cdot})]^{2+}$ and $[Fe^{II}(MIDA)(NO^{\cdot})]$, respectively, compared to the EDTA nitrosyl complex as $[Fe^{III}(EDTA)(NO^{-})]^{2-}$.[27,28] This would indicate that in the former case the bound NO has more a radical, whereas in the latter case NO has more an anionic character. However, in the selected systems the difference in the distribution of electron density between Fe^{II} and NO seems to be very small, which is most evident from the ATR-IR spectra discussed in the following section.

Fe^{II} nitrosyl complexes which deviate in their UV/Vis data from the common features described above, were in general formed by chelate ligands other than polyaminocarboxylates (Figure 1, **Series 2 subgroup c** and **Series 3**). The most pronounced deviation in the UV/Vis spectrum is exhibited by the Fe^{II} complex of DIPIC. In contrast to all other studied $[Fe^{II}(L)_x]$ complexes, the complexes with L = DIPIC show strong bands associated with the aromatic ring at 459 nm (x = 1) or 482 nm (x = 2). Recently, several structures of iron(II/III) complexes with DIPIC have been reported, and structures with different stoichiometries could be characterized.[29−32] Even the seven-coordinate complex $[Fe^{II}(DIPIC)_2H_2O]^{2-}$ was characterized, which underlines our assumption that in the 1:2 complexes a water molecule can be coordinated in the seventh position.[31]

ATR-IR Spectroscopy

IR spectroscopy is considered to be an useful tool for the determination of the binding mode and oxidation state of NO in metal based complexes.[25,33] Efforts to distinguish between NO bound to the metal center in a linear mode as NO^+ or in a bent mode as NO^- on the basis of the NO stretching frequencies, revealed a considerable overlap in the range between 1600 and 1800 cm^{-1}.[33−35] It seems that there is a gradual change from the extreme NO^- form at lower frequency to the extreme NO^+ form at higher values. On this basis, changes in the electron delocalization for different $Fe^{II}(L)-NO$ complexes should be accompanied by characteristic shifts in the NO stretching frequencies.

Since only a few IR spectra of polyaminocarboxylate−Fe−NO complexes are known from the literature,[18] an extended series of $[Fe^{II}(L)_x]$ and $[Fe^{II}(L)_x(NO)]$ complexes were investigated by IR spectroscopy using the ATR technique.[36] The series was limited to those complexes which could be synthesized at a concentration level required to produce undistorted spectra with a satisfactory intensity and resolution (see Table 2). The values for example, obtained for $[Fe^{II}(EDTA)]^{2-}$ and $[Fe^{II}(EDTA)(NO)]^{2-}$, viz. ν(COO⁻, asym.) = 1588 cm^{-1}, ν(COO⁻, sym.) = 1406, 1325 cm^{-1}, and ν(COO⁻, asym.) = 1611 cm^{-1}, ν(COO⁻, sym.) = 1398, 1317 cm^{-1}, ν(NO) = 1777 cm^{-1}, respectively, are in good agreement with literature data.[37]

In the series of the complexes $[Fe^{II}(H_2O)_5(NO)]^{2+}$, $[Fe^{II}(MIDA)(NO)]$, and $[Fe^{II}(EDTA)(NO)]^{2-}$, the shift in the NO band from 1810 to 1783 to 1777 cm^{-1}, respectively, could suggest a gradual change from a partially more positive (NO^+) to a partially more negative (NO^-) binding character of NO. However, the frequencies of the NO vibrations for the MIDA and EDTA complexes hardly differ from each other, with the result that the deviation is too small to predict a significantly different binding mode. It follows that although the reported IR data do not reveal detailed information on the nature of the Fe-NO bond, the spectra do supplement the UV/Vis data and provide direct evidence for the reversible coordination of NO to the Fe^{II} centers.

Qualitative Characteristics of Fe^{II}-L Complexes During the Reactions with NO and O_2

The influence of the chelate ligand on the chemical features of the Fe^{II} complexes is clearly reflected by the reversibility of NO binding and the oxidation rate of $[Fe^{II}(L)_x]$. There are two extreme cases in which way both substrates (O_2 and NO) react with Fe^{II} chelates: in the first case they bind reversibly to the Fe^{II} center, whereas in the second case a shift of electron density from iron to the substrate, accompanied by the irreversible formation of the corresponding Fe^{III} complex, occurs. These opposite cases are illustrated on the one hand by iron complexes of water (aqua complexes) or several MIDA analogues (reversible substrate binding), and on the other hand by iron complexes of several EDTA analogues (irreversible substrate binding). In the following, MIDA and EDTA were selected as typical chelate ligands in order to examine the opposite features of both groups of complexes in more detail.

Reversibility of the Binding of NO to $[Fe^{II}(L)_x]$ Complexes

The main characteristic of $[Fe^{II}(MIDA)]$ is its ability to bind NO completely reversibly.

This is evident from the UV/Vis spectra in Figure 5, which show the mutual conversion between the $[Fe^{II}(MIDA)]$ complex (traces a, c, and e) and the corresponding nitrosyl complex $[Fe^{II}(MIDA)(NO)]$ (traces b, d, and f) by bubbling alternately NO or an inert gas through the complex solution. Obviously, the inert gases remove low concentrations of free NO from the solution, which are formed by a partial dissociation of the nitrosyl complex. In this way the equilibrium is driven back to the left side of Equation (1) to regenerate finally the pure starting complex $[Fe^{II}(MIDA)]$, from which the nitrosyl complex can be formed again.

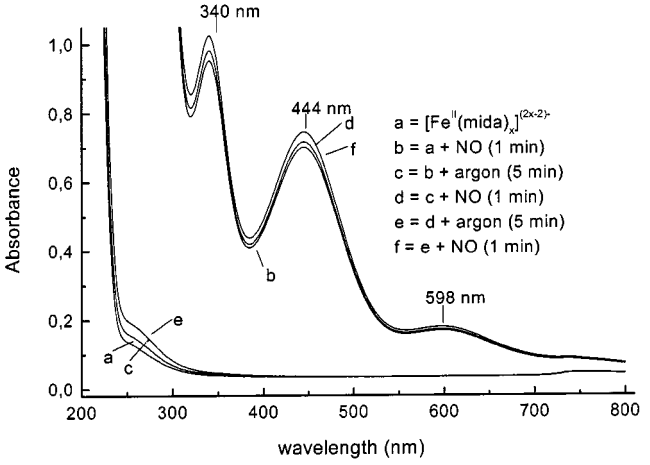

Figure 5. Reversibility of the NO binding to $[Fe^{II}(MIDA)]$ (exp. conditions: 1 mM $FeSO_4 \cdot 7\ H_2O$; 2.5 mM MIDA; 100 mM acetate buffer; pH = 5.0; T = 23 °C)

$$[Fe^{II}(MIDA)] + NO \rightleftharpoons [Fe^{II}(MIDA)(NO^{\cdot})] \quad (1)$$

The complete reversibility of the binding of NO to $[Fe^{II}(MIDA)]$ indicates that practically no electron transfer between Fe^{II} and NO occurs, which means that NO is presumably bound as radical to the Fe^{II} center. A similar behavior was found for the ligand free system (i.e. $[Fe^{II}(H_2O)_6]^{2+}$ species) and in the case of all MIDA analogues which are compiled in Figure 1, **Series 2** under **subgroups a** and **c**.

In comparison to the analogous MIDA complex, the NO chemistry of $[Fe^{II}(EDTA)]^{2-}$ is somewhat more complex.[16–18] As shown in Figure 6, there is to a certain extent a reversible binding of NO to $[Fe^{II}(EDTA)]^{2-}$ that can be observed when the whole experiment is performed within a time period of less than one hour. The fact that from the partially decomposed nitrosyl complex (trace d) the initial nitrosyl complex (trace e) can be restored completely, indicates that no irreversible electron transfer from Fe^{II} to NO occurred during the release of NO. Obviously, an equilibrium between $[Fe^{II}(EDTA)]^{2-}$ and the corresponding nitrosyl complex must exist [Equation (2)], which differs from the corresponding equilibrium for the MIDA system [see Equation (1)] only with respect to the position of the equilibrium, which lies more on the right side and leads to the observed poorer release of NO from the complex (Figure 6, traces c and d).

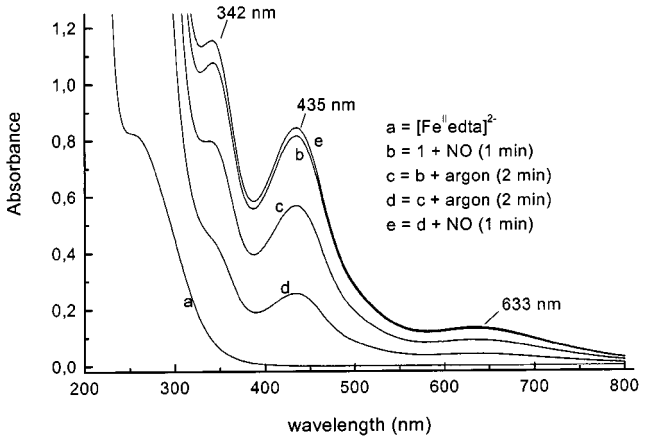

Figure 6. Reversibility of the NO binding to $[Fe^{II}(EDTA)]^{2-}$ (exp. conditions: 1 mM $FeSO_4 \cdot 7\ H_2O$; 1.25 mM EDTA; 100 mM acetate buffer; pH = 5.0; 23 °C)

$$[Fe^{II}(EDTA)]^{2-} + NO \rightleftharpoons [Fe^{II}(EDTA)(NO)]^{2-} \quad (2)$$

An irreversible electron transfer from Fe^{II} to NO occurs in the case of the EDTA system on a time scale of several hours, which is followed by the dissociation of the complex according to Equation (3) into $[Fe^{III}(EDTA)]^{-}$ and NO^{-} (nitroxyl anion). $[Fe^{III}(EDTA)]^{-}$ is identified in the UV/Vis spectrum (Figure 6) by its very intense absorption band below 400 nm,[38] whereas the unstable nitroxyl anion reacts immediately to nitrous oxide (N_2O). The latter product was detected mass spectrometrically in the form of N_2O in the gas phase.[39] As shown in Figure 7, the predominant part of $[Fe^{II}(EDTA)(NO)]^{2-}$ decomposes at room temperature within about 20 h.

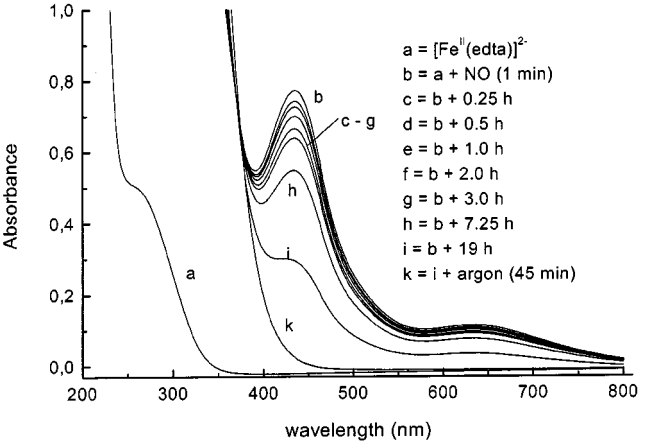

Figure 7. Thermal decomposition of $[Fe^{II}(EDTA)(NO)]^{2-}$ to $[Fe^{III}(EDTA)]^{-}$ and N_2O (exp. conditions: 1 mM $FeSO_4 \cdot 7\ H_2O$; 1 mM EDTA; 100 mM acetate buffer; pH = 5.0; T = 23 °C)

$$[Fe^{II}(EDTA)(NO)]^{2-} \xrightarrow{slow} \underset{(unstable)}{\{Fe^{III}(EDTA)(NO^{-})\}^{2-}} \rightarrow [Fe^{III}(EDTA)]^{-} + \underset{(unstable)}{\{NO^{-}\}} \quad (3)$$

In summary, for the $[Fe^{II}(EDTA)]^{2-}$/NO system a rapid equilibrium between $[Fe^{II}(EDTA)]^{2-}$ and $[Fe^{II}(EDTA)(NO)]^{2-}$

exists, which is followed by a slow and irreversible redox process accompanied by the dissociation of the complex to form $[Fe^{III}(EDTA)]^-$ and N_2O. The slow electron transfer process can be considerably accelerated when instead of EDTA, CDTA, or α-EDDADP are used as chelating ligands. In these cases the dissociation of the nitrosyl complexes to $[Fe^{III}(L)]^-$ and N_2O occurs on a time scale of some minutes. Obviously, small steric and electronic effects may control in a very sensitive way the rate of this irreversible electron transfer process.

Oxygen Sensitivity of $[Fe^{II}(L)_x]$ Complexes

In analogy to the reaction of $[Fe^{II}(MIDA)]$ with nitric oxide, the chemical behavior in the presence of air oxygen indicates that almost no electron transfer reaction from Fe^{II} to O_2 occurs. Consequently, solutions of $[Fe^{II}(MIDA)]$ are not oxidized to $[Fe^{III}(MIDA)]^+$ by air [Equation (4)].

$$[Fe^{II}(MIDA)] + O_2 \not\longrightarrow [Fe^{III}(MIDA)]^+ \quad (4)$$

In contrast to this, $[Fe^{II}(EDTA)]^{2-}$ is highly oxygen sensitive. Its transformation to the corresponding $[Fe^{III}(EDTA)]^-$ complex [Equation (5)] is complete in less than 1 minute. This oxidation reaction proceeds according to a complex multistep mechanism which was extensively studied in the literature.[40−43]

$$2\,[Fe^{II}(EDTA)]^{2-} + {}^1/_2\,O_2 + 2\,H^+ \xrightarrow{\text{fast}} 2\,[Fe^{III}(EDTA)]^- + H_2O \quad (5)$$

Besides EDTA, a similarly high oxidation rate of Fe^{II} complexes is observed when the EDTA analogues 1,2-PDTA, CDTA, HEDTRA, EDDS, and α-EDDADP are used (see Figure 1, **Series 1**).

Comparison Between the Fe^{II} Complexes of MIDA and EDTA Analogues

A final comparison between the MIDA system, and the EDTA, CDTA, and α-EDDADP systems, show that the $[Fe^{II}(MIDA)]$ complex can reversibly bind NO and probably also O_2, but does not tend to undergo any electron transfer process, neither to NO, nor to O_2. In contrast, Fe^{II} complexes of the above mentioned EDTA analogues undergo electron transfer processes both to O_2 and NO. The final products of these reactions are $[Fe^{III}(L)]^-$ and either H_2O or N_2O. Whereas the electron transfer from $[Fe^{II}(L)]^{2-}$ to dioxygen is always very fast, the redox reaction with NO is much slower, especially in the case of EDTA.

Stability Constants (K_{NO}) for $[Fe^{II}(L)_x(NO)]$ Complexes

Measurement of the K_{NO} Values

Stability constants for nitrosyl complexes are based on the equilibrium between $[Fe^{II}(L)_x]$ and $[Fe^{II}(L)_x(NO)]$ complexes [Equation (6)] and are therefore defined by Equation (7).

$$[Fe^{II}(L)_x] + NO \underset{k_{off}}{\overset{k_{on}}{\rightleftharpoons}} [Fe^{II}(L)_x(NO)] \quad (6)$$

$$K_{NO} = k_{on} / k_{off} = \frac{[Fe^{II}(L)_x(NO)]}{[Fe^{II}(L)_x]\cdot[NO]} \quad (7)$$

In general, quite vague and rather divergent K_{NO} data for only a few Fe^{II}−polyamino−carboxylate complexes exist in the literature, especially for the chelating ligands EDTA, NTA, and DTPA and for aquated Fe^{II}, $[Fe^{II}(H_2O)_5(NO)]^{2+}$. A comprehensive survey of literature data is given in the review of Demmink et al.[16] These data were often determined indirectly, e.g. from kinetic measurements according to the relationship $K_{NO} = k_{on}/k_{off}$. The disadvantage of such indirect methods is especially the low degree of accuracy of the calculated values.

In our work, we successfully adopted a direct approach to obtain the equilibrium constant K_{NO} by utilizing the recently developed possibility to measure the concentration of free NO in solution with a NO electrode.[44] The remaining unknown equilibrium concentrations in Equation (7), viz. $[Fe^{II}(L)_x(NO)]$ and $[Fe^{II}(L)_x]$, could be easily determined by UV/Vis spectroscopy.

Influence of the Chelate Ligands on the Magnitude of the K_{NO} Values

The K_{NO} values for the $[Fe^{II}(L)_x(NO)]$ complexes are summarized on a logarithmic scale in Figure 8**a**, in which the different groups and subgroups of chelate ligands are presented in different colors (the corresponding numerical K_{NO} values with their relative error limits are given in Table 2). The scale in Figure 8**a** extends a range from $1\cdot10^3$ M^{-1} to $2\cdot10^7$ M^{-1}. In general, coordination of a chelate ligand to Fe^{II} considerably stabilizes the NO binding on the complex.

A detailed analysis of the magnitude of K_{NO} as a function of the chemical structure of the chelate ligand suggests that both electronic and steric effects have a pronounced influence. The highest K_{NO} values are found for ligands such as EDTA, DTPA, HEDTRA, EDDS, EDTMP, NTA, CEIDA, and ATMP, which have at least four strong donor groups and can bind effectively to the Fe^{II} center. A reduction in the number of strong chelating groups as well as an increased steric hindrance, or elongation of the distances between the chelate groups, lead to a remarkable decrease in the K_{NO} values.

Figure 9 shows a correlation between the K_{NO} values and the position of the *C-T* band for nearly the complete series of nitrosyl complexes. The shift in the *C-T* band to lower wavelengths is probably caused by a more pronounced ligand to metal charge transfer from NO to Fe. The synchronous increase in the band energy and the K_{NO} values in Figure 9 indicates that charge transfer seems to play an important role in the stabilization of the Fe−NO bond. For the very stable $[Fe(EDTA)NO]^{2-}$ complex, the Fe−NO bond is suggested to have significant $Fe^{III}-NO^-$ character and the *LMCT* band occurs at 435 nm, i.e. it has a high energy barrier. On the other hand, for the less stable $[Fe(H_2O)_5(NO)]^{2+}$ complex the *LMCT* band occurs at significantly lower energy (451 nm), with the result that the Fe−NO bond is suggested to have more of a $Fe^{II}-NO$

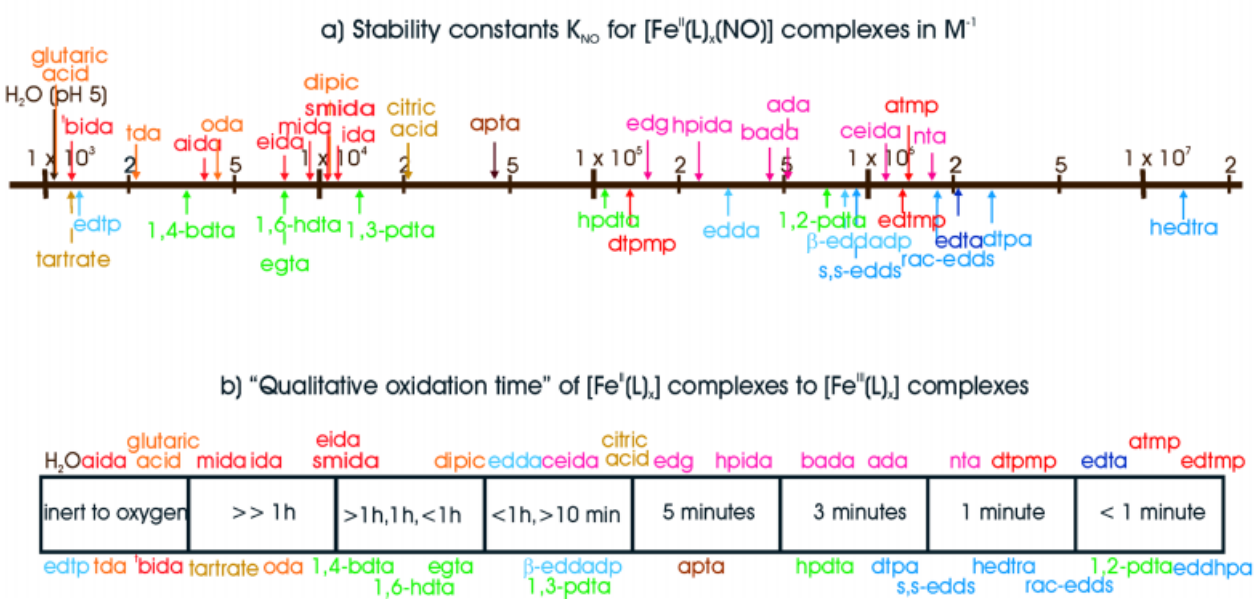

Figure 8. Correlation between K_{NO} and qualitative oxidation time of $[Fe^{II}(L)_x]$ complexes

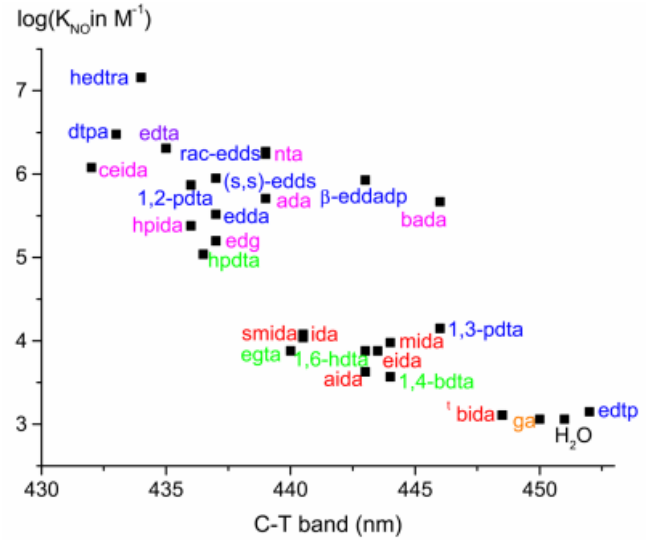

Figure 9. Correlation between the logarithmic K_{NO} values and the position of the *C-T* band in the UV/Vis spectra of $[Fe^{II}(L)_x(NO)]$ complexes with L = polyaminecarboxylates

character. Thus the position of the *LMCT* band is a measure of the charge distribution in the Fe−NO band and correlates directly with the stability of the Fe(L)NO complex.

Following this more general interpretation of the influence of the chelate ligand on the magnitude of K_{NO}, different types of ligands are discussed in more detail.

Stability Constants of $[Fe^{II}(L)(NO)]$ Complexes for EDTA Analogues

For the stability constant of the EDTA complex, $[Fe^{II}(EDTA)(NO)]^{2-}$, a value of approx. $2{\cdot}10^6$ M^{-1} was found, which lies far on the right end of the scale in Figure 8**a** and is in good agreement with literature data ranging between $1.5{\cdot}10^6$ and $3{\cdot}10^6$ M^{-1} at 20 to 25 °C.[14] The high formation constant of the EDTA complex is probably caused by the tailor-made structure of EDTA, which tightly binds all six donor groups to the Fe^{II} center forming five sterically favored five-member rings.

The tuning of the EDTA structure as outlined in Figure 1, **Series 1** (indicated by blue and green colours in Figure 8**a**), clearly demonstrates that the formation of such five-member rings between the donor groups of the ligand and the Fe^{II} center is the most crucial factor for the stabilization of the Fe^{II}−NO bond in the complex. Whereas in 1,2-PDTA the branching of the ethylene spacer of EDTA by a methyl group has only a quite minor influence on the K_{NO} value, both the elongation of the ethylene spacer in the ligands 1,3-PDTA, 1,4-BDTA, 1,6-HDTA, and EGTA, and the substitution of all acetate groups in EDTP by propionate cause a drastic decrease or even a complete loss in the tendency of the ligand to bind to the iron center. This is reflected by K_{NO} values that shift more and more to the value for the pentaaqua nitrosyl complex on the left end of the scale in Figure 8**a**. Obviously, the formation of higher than five-member chelate rings on Fe^{II} is very unfavorable. Therefore, it is not surprising that EDTP with its four elongated carboxylate arms completely looses its binding ability, whilst in 1,3-PDTA, 1,4-BDTA, 1,6-HDTA, and EGTA a coordination of one of both the aminodiacetate units of the ligand to Fe^{II} should still be possible. The exceptional position of the K_{NO} value for the HPDTA complex, which is about ten-fold higher than the value for the 1,3-PDTA complex, is probably caused by coordination of the hydroxyl group to the iron center.

In comparison to the above mentioned ligands, a less pronounced reduction in the K_{NO} constants was observed when only two acetate groups of EDTA were either omitted (EDDA) or substituted by propionate (β-EDDADP) groups. This indicates that in the EDTA structure, besides the ethylene spacer, only two of the four acetate groups are most essential to stabilize the binding of NO. In addition, the deviations between the K_{NO} values of the EDDA and β-ED-

DADP complexes suggest that the propionate groups do not completely loose their ability to bind to Fe^{II}.

The Fe^{II} complexes of EDDS and DTPA have similar K_{NO} values as the EDTA complex, indicating that neither the substitution of the four acetate groups by two succinate groups (EDDS) nor the elongation of the system by an additional ethyleneaminediacetate unit (DTPA) considerably affect the binding characteristics. From the three possible stereoisomers of EDDS, the (*s*,*s*)-form, a natural product synthesized by *Amycolatopsis orientalis*,[45] shows a two-fold lower K_{NO} value than the optical inactive "racemate". It is reasonable to expect that the content of the *meso*-form in the racemate is responsible for the higher K_{NO} value.

Among the EDTA analogues, HEDTRA forms a nitrosyl complex with the highest stability constant. K_{NO} ($1.45 \cdot 10^7$ M^{-1}) exceeds more than five times the value for the EDTA complex. It is not easy to account for this high value, since the molecular structure of the HEDTRA complex is unknown in solution. Probably the hydroxyl group is not (or only weakly) coordinated to the metal center, such that the change in geometry of the complex enhances the stability of the $Fe^{II}-NO$ bond. This suggestion is supported by preliminary kinetic data, which indicate that especially the dissociation rate of NO from the complex (k_{off}) is much slower than in the case of the EDTA complex.[46]

Stability Constants of $[Fe^{II}(L)_x(NO)]$ Complexes for MIDA Analogues

In comparision to $[Fe^{II}(H_2O)_5(NO)]^{2+}$, complexes of MIDA and other three-dentate MIDA analogues stabilize the binding of NO only by a maximum factor of 10, i.e. the K_{NO} values hardly exceed 10^4 M^{-1} (Figure 8**a**, red and orange colors). Under the assumption that, as it was shown in the case of L = MIDA, these ligands selectively form 1:1 nitrosyl complexes with Fe^{II}, the at least 200 times lower stabilization of the $Fe^{II}-NO$ bond in comparison to the EDTA complex can be accounted for in terms of the different coordination geometry of the donor groups. The crystal structure of $[Fe^{II}(EDTA)H_2O]^{2-}$ shows a labile coordinated water molecule as a seventh donor group which is bound nearly opposite to both nitrogens of the mono-capped trigonal-prismatic structure.[15] In the nitrosyl complex, NO most probably substitutes the labile water molecule and as a consequence the $Fe^{II}-NO$ bond is considerably polarized by the strong inductive effect of both opposite nitrogens, and therefore has a high stability.

For the series of three-dentate MIDA analogues, the lower stabilization of the $Fe^{II}-NO$ bond by coordinated ODA, TDA, and AIDA is obviously due to a reduced donor capacity of either the hetero atoms, oxygen (ODA) and sulfur (TDA), or the nitrogen lone pair of AIDA which is delocalized by the acetyl group.

Four-dentate MIDA analogues, which have an additional coordinating group bound to the IDA nitrogen (Figure 1, **Series 2**, **subgroup b**), show in comparison to the three-dentate ligands a strong increase in the K_{NO} values (Figure 8**a**, pink colour). Whereas a hydroxyl group (EDG, HPIDA) increases the stability constant by a factor of about 20, a third carboxylate group (NTA, BADA, CEIDA) can cause a larger than 100 fold enhancement. The most pronounced effect was found in the case of NTA ($K_{NO} = 1.75 \cdot 10^6$ M^{-1}), which likely coordinates to the iron center by creating three sterically favoured five-membered rings. As shown before, both the elongation of an acetate to a propionate group (BADA) and the amide delocalization of ADA, lower the ability to coordinate NO to Fe^{II} and decrease the K_{NO} value by a factor of about 3 in comparison to the NTA complex. The high K_{NO} value of the CEIDA complex ($1.2 \cdot 10^6$ M^{-1}) is probably caused by the fact that the third ligand arm of this chelate coordinates to the Fe^{II} center with both the sulfur and the carboxylate group by forming two five-member rings.

Stability Constants of $[Fe^{II}(L)_x(NO)]$ Complexes for L ≠ Polyaminocarboxylates

The phosphonates ATMP, EDTMP, and DTPMP represent derivatives of the polyaminocarboxylates NTA, EDTA, and DTPA, in which the carboxylate groups are substituted by phosphonate groups. Although the positions of the absorption bands in the UV/Vis spectra differ considerably for the $Fe^{II}-NO$ complexes of both groups (Table 2), the K_{NO} values are in the case of ATMP and EDTMP amazingly similar to the constants for the corresponding NTA and EDTA complexes. This demonstrates that phosphonate is comparable to carboxylate in coordinating to Fe^{II} and stabilizing the $Fe^{II}-NO$ bond. Of both the nitrogen-free compounds, L-tartrate and citrate, only citrate binds strongly to Fe^{II} and causes in comparison to $[Fe^{II}(H_2O)_5(NO)]^{2+}$ a considerably enhanced stability of the Fe^{II}-NO bond with a value of about $2 \cdot 10^4$ M^{-1}.

Correlation Between the Oxygen Sensitivity of $[Fe^{II}(L)_x]$ and the Stability Constants of the Corresponding Nitrosyl Complexes

By comparing the oxygen sensitivity of the $[Fe^{II}(L)_x]$ complexes with the stability constants of the nitrosyl complexes, an interesting correlation was found which enables a more detailed understanding of the chemical nature of these systems. In order to examine the oxygen sensitivity of $Fe^{II}-$ligand complexes, we preferred not to perform detailed quantitative kinetic measurements, due to the complex nature and demanding analysis of the multistep reactions between $[Fe^{II}(L)_x]$ and O_2.[43−46] However, it was as a first approximation sufficient to obtain a set of qualitative data, on which basis the different complexes could be compared. We could realize such a comparison by simply introducing air into solutions of $[Fe^{II}(L)_x]$ complexes and recording UV/Vis spectra before and during the bubbling period in time sequences of 1, 3, 5, 10, 15, 30, 60 ... minutes. The degree of oxidation could easily be followed by the increase in absorbance below 400 nm. The time in which more than approx. 80% of the $[Fe^{II}(L)_x]$ complex was converted into the $[Fe^{III}(L)_x]$ complex was taken as "qualitative oxidation time" and entered for comparison purposes in the qualitative time scale of Figure 8**b**. It can be seen from

Figure 8**b** that the range of "qualitative oxidation time" varies from the totally inert hexaaqua complex to the extremely oxygen sensitive complexes of EDTA, 1,2-PDTA, which are oxidized within a few seconds and can no more be determined accurately by this qualitative method.

A good correlation exists between the oxygen sensitivity of $[Fe^{II}(L)_x]$ complexes and the stability constants of their nitrosyl complexes, which is clearly seen from the comparison in Figure 8**a** and 8**b**. In general, the higher the K_{NO} value for the nitrosyl complex, the shorter the "qualitative oxidation time". Obviously, an increasing inductive effect of the chelate ligand causes both an increasing stability of the $Fe^{II}-NO$ bond in the nitrosyl complexes, and also an enhanced electron transfer from Fe^{II} to O_2 in the corresponding $[Fe^{II}(L)_x]$ complexes. The two extreme cases are on the one hand "naked" $[Fe^{II}(H_2O)_6]^{2+}$ with its very low affinity for both dioxygen and NO, and on the other hand the $[Fe^{II}(EDTA)]^{2-}$ complex with its very high affinity for both dioxygen and NO. Thus the stability of the Fe(L)NO complex directly correlates with the oxygen sensitivity of the $Fe^{II}(L)$ complex, i.e. with the ability to form $Fe^{III}-O_2^-$. This again suggests that the stability of the Fe(L)NO complex is also controlled by its ability to bind NO as $Fe^{III}-NO^-$, which correlates with the position of the *LMCT* band observed in Figure 9. These trends should then also correlate with the redox potentials of the $Fe^{II/III}(L)$ complexes (see Table 3).

Table 3. Redox potentials vs. NHE

$[Fe^{III}(H_2O)_6]^{3+}/[Fe^{II}(H_2O)_6]^{2+}$	$E_{1/2} = 0.771$ V	(ref.[47])
$[Fe^{III}(1,3\text{-PDTA})]^-/[Fe^{II}(1,3\text{-pdta})]^{2-}$	$E_{1/2} = 0.309$ V	(this work)
$[Fe^{III}(EDTA)]^-/[Fe^{II}(EDTA)]^{2-}$	$E_{1/2} = 0.129$ V	(this work)
$[Fe^{III}(DTPA)]^-/[Fe^{II}(DTPA)]^{2-}$	$E_{1/2} = 0.110$ V	(ref.[48])

It is seen from the quoted values that the tendency of $Fe^{II}(L)$ to be oxidized (as reflected by the lower redox potential) correlates directly with the oxygen sensitivity of $Fe^{II}(L)$ and its ability to bind NO. In these cases $Fe^{II}(L)$ is formally oxidized to effectively bind O_2 and NO as $Fe^{III}-O_2^-$ and $Fe^{III}-NO^-$, respectively.

Conclusion

The results reported in this study clearly demonstrate that the correlation found between the oxygen sensitivity and the K_{NO} values for the investigated complexes, makes it very difficult to find suitable $[Fe^{II}(L)_x]$ complexes that will show a low oxygen sensitivity and a high affinity to bind NO (i.e. $K_{NO} > 1\cdot10^6$ M^{-1}). The exceptionally high K_{NO} value for the HEDTRA complex and the more favorable relation between the oxygen sensitivity and K_{NO} values for the DTPA, CEIDA, and β-EDDADP complexes, suggest that these ligands are promising candidates for technical applications. However, so far no kinetic details are available, and the conclusions are based on thermodynamic stability constants for the binding of NO and qualitative observations on the oxygen sensitivity of the complexes. A detailed kinetic analysis of the "on" and "off" reactions for the interaction of $Fe^{II}(L)$ with NO is presently underway[46] and may reveal significant differences that will enable a kinetic control and further tuning of the overall process.

Experimental Section

General Remarks: All experiments were performed under strict exclusion of air oxygen. Buffer solutions were deaerated for extended periods (in general 1 minute per mL solution) with pure N_2 or Ar, or in some cases freeze-thaw cycles were performed under vacuum in order to completely remove the dissolved dioxygen in solution, before they were brought in contact with Fe^{II} salts or nitric oxide.

NO gas, purchased from Messer Griesheim or Rießner Gase in a purity of at least 99.5 vol%, was cleaned from trace amounts of higher nitrogen oxides like N_2O_3 and NO_2 by passing it through an Ascarite II column (NaOH on silica gel, Sigma–Aldrich). NO from a gas tank should not be used after six months following the date of its industrial preparation, since decomposition causes a drastic decrease in the purity of the gas. The decomposition is pressure dependent, which led us to only use bottles filled with a maximum pressure of 20 bar, and resulted in a longer life-time of the NO gas.

The chelate ligands AIDA, ATMP, BADA, 1,4-BDTA, ^{t}BIDA, DTPMP, *rac.* EDDS, (*s,s*)-EDDS,[49] EDG, EDTMP, EIDA, HPDTA, HPIDA, MIDA, NTA, 1,3-PDTA, and SMIDA were supplied by Akzo Nobel. All other ligands and chemicals were purchased from Arcos Chimica, Fluka, Lancaster Synthesis, or Sigma–Aldrich with the highest available purity (at least 97%). APTA was synthesized according to a procedure described in the literature.[50]

UV/Vis spectra were recorded on a Cary 1G UV/Vis spectrophotometer from Varian using a 1 cm quartz cuvette directly attached to a round flask with a sideway gas connection. This enabled the performance of different physical or chemical operations, like bubbling the solution with NO or N_2, and the measurement of spectra under exclusion of dioxygen in the same vessel.

IR spectra were recorded with the use of a two mirror ATR cell on a ATI Mattson FTIR *Infinity* spectrophotometer. The reflection instrument utilizes a Ge crystal as an internal reflection plate with a size of 50 × 20 × 2 mm and 45° angle of incidence. For each complex two independent measurements of 100 scans were performed under inert gas atmosphere.

The concentration of free nitric oxide in solution was determined with an ISO-NOP electrode connected to an ISO-NO Mark II nitric oxide sensor from World Precision Instruments. The NO electrode consists of a membrane covered anode which selectively oxidizes NO to NO_3^- ions. The resulting current is proportional to the concentration of NO in solution. The NO electrode was calibrated daily with fresh solutions of sodium nitrite and potassium iodide according to the method suggested by the manufacturers. The calibration factor nA/μM was determined with a linear fit program.

Potentiometric measurements were performed on a METROHM 702 SM Titrino in a jacketed, air-tight glass titration cell equipped with a combined pH glass electrode (METROHM 6.0203.100), N_2 inlet and outlet, and a graduated 10 mL microburet (METROHM 6.1518.210). The electrode was calibrated with strong acid and strong base so as to read directly in hydrogen ion concentration.

The ion product of water, i.e. $pK_W = -\log[H^+][OH^-] = 13.85$, was determined experimentally. A carbonate-free 0.10 M sodium hydroxide solution was prepared with boiled distilled water and was standardized by titrations with potassium hydrogen phthalate. Gran's method[51] was used to confirm the absence of carbonate in the sodium hydroxide standard solution. The NaOH solution was stored under nitrogen. All solutions were adjusted to an ionic strength of 0.5 M with $NaClO_4$. The temperature was maintained at 25.0 ± 0.1 °C by circulating thermostated water through the outer jacket of the cell. All measurements were carried out while bubbling N_2 through the solution.

pH measurements were performed with the aid of a Mettler Delta 340 pH-meter. The reference electrode was filled with NaCl instead of KCl to prevent precipitation of $KClO_4$.

Cyclic voltammogramms were recorded with an EG&G PARC potentiostat-galvanostat Model 263 controlled by a PC. The electrochemical cell was a conventional one with three electrodes. The reference electrode was Ag/AgCl, the counter electrode was a platinum sheet and a glassy carbon electrode was used as the working electrode (all from BAS). Solutions for cyclic voltammetry were fully deoxygenated with nitrogen for at least 1 h. Following deoxygenation, the behavior of the electrode was studied in the buffer solution and checked by measurements on the redox couple of $K_3[Fe(CN)_6]$. Reported $E_{1/2}$ values are corrected to the NHE scale. The concentration of the solutions was 5 mM for $[Fe^{II}(EDTA)]^{2-}$ and $[Fe^{II}(1,3\text{-PDTA})]^{2-}$. Solutions were prepared by dissolving the respective ligand and $Fe_2(SO_4)_3 \cdot 5\,H_2O$ in 0.1 M acetate buffer at pH 5. The ionic strength was adjusted to 0.5 M ($NaClO_4$).

In all UV/Vis experiments, solutions of 1 mM of Fe^{II} chelates in 100 mM acetate buffer at pH 5.0 were used. The Fe^{II} complexes were prepared from $FeSO_4 \cdot 7\,H_2O$ and the chelate in an excess of 10 to 50% over the required stoichiometric amount, i.e. between 1.1 and 1.5 mM in the case of the EDTA analogues, and between 2.2 and 3.0 mM in the case of the MIDA analogues. In each buffer solution the ionic strength was adjusted to a value of 0.5 M by addition of calculated amounts of sodium perchlorate. For ATR-IR measurements, unbuffered solutions of Fe^{II} chelates at a concentration of up to 200 mM were used.

Acknowledgments

The authors gratefully acknowledge financial support from Akzo Nobel Functional Chemicals, Paques Bio Systems, Fonds der Chemischen Industrie and the Max-Buchner-Forschungsstiftung.

[1] S. G. Chang, D. Littlejohn, S. Lynn, *Environ. Sci. Technol.* **1983**, *17*, 649.
[2] W. Weisweiler, B. Retzlaff, L. Raible, *Chem. Eng. Proc.* **1984**, *18*, 85.
[3] E. Sada, H. Kumazawa, Y. Takada, *Ind. Eng. Chem. Fundam.* **1984**, *23*, 60.
[4] E. Sada, H. Kumazawa, H. Hikosaka, *Ind. Eng. Chem. Fundam.* **1986**, *25*, 386.
[5] E. Sada, H. Kumazawa, H. Machida, *Ind. Eng. Chem. Res.* **1987**, *26*, 2016.
[6] S. S. Tsai, S. A. Bedell, L. H. Kirby, D. J. Zabick, *Environ. Prog.* **1989**, *8*, 126.
[7] V. Zang, R. van Eldik, *Dechema-Monographien* **1989**, *118*, 143.
[8] P. Harriott, K. Smith, L. B. Benson, *Environ. Prog.* **1993**, *12*, 110.
[9] E. K. Pham, S. G. Chang, *Nature* **1994**, *369*, 139.
[10] Y. Hishinuma, R. Kaji, H. Akimoto, F. Nakajima, T. Mori, T. Kamo, Y. Arikawa, S. Nozawa, *Bull. Chem. Soc. Jpn.* **1979**, *52*, 2863.
[11] D. Littlejohn, S. G. Chang, *J. Phys. Chem.* **1982**, *86*, 537.
[12] N. Lin, D. Littlejohn, S. G. Chang, *Ind. Chem. Proc. Des. Dev.* **1982**, *21*, 725.
[13] 1. M. S. Ward and R. E. Shepherd, *Inorg. Chim. Acta* **1999**, *286*, 197.
[14] R. E. Shepherd, M. A. Sweetland, D. E. Junker, *J. Inorg. Biochem.* **1997**, *65(1)*, 1.
[15] [15a] T. Mizuta, J. Wang, K. Miyoshi, *Bull. Chem. Soc. Jpn.* **1993**, *66*, 2547. – [15b] T. Mizuta, J. Wang, K. Miyoshi, *Inorg. Chim. Acta* **1995**, *230*, 119.
[16] J. F. Demmink, I. C. F. van Gils, A. A. C. M. Beenackers, *Ind. Eng. Chem. Res.* **1997**, *36*, 4914 and cit. lit.
[17] V. Zang, M. Kotowski, R. van Eldik, *Inorg. Chem.* **1988**, *27*, 3279.
[18] V. Zang, R. van Eldik, *Inorg. Chem.* **1990**, *29*, 4462.
[19] G. Schwarzenbach, G. Anderegg, W. Schneider, H. Senn, *Helvetia Chim. Acta* **1955**, *132*, 1147.
[20] [20a] L. Zélány, I. Nagypál, G. Peintler, *PSEQUAD*, L. Kossuth University of Debrecen, **1983**; – [20b] L. Zélány, I. Nagypál, *Computational Methods for the Determination of Formation Constants*, Plenum Press, New York, **1985**.
[21] R. M. Smith, A. E. Martell, *Critical Stability Constants*, No. 6, Plenum Press, New York, **1989.**
[22] K. J. Powell, *Soleq: Mini-SCDatabase*, Academic Software, **1999**.
[23] T. Schneppensieper, A. Zahl, R. van Eldik, unpublished results.
[24] C. A. Brown, M. A. Pavlosky, T. E. Westre, Y. Zhang, B. Hedman, K. O. Hodgson, E. I. Solomon, *J. Am. Chem. Soc.* **1995**, *117*, 715.
[25] J. A. McCleverty, *Chem. Rev.* **1979**, *79*, 53.
[26] K. Ogura, M. Watanabe, *Electrochim. Acta* **1982**, *27*, 111.
[27] R. J. P. Williams, *Chem. Soc. Rev.* **1996**, *25*, 77.
[28] C. Hauser, T. Glaser, E. Bill, T. Weyhermüller, K. Wieghardt, *J. Am. Chem. Soc.* **2000**, *122*, 4352.
[29] P. Lainé, A. Gourdon, J.-P. Launey, *Inorg. Chem.* **1995**, *34*, 5129.
[30] P. Lainé, A. Gourdon, J.-P. Launey, *Inorg. Chem.* **1995**, *34*, 5138.
[31] P. Lainé, A. Gourdon, J.-P. Launey, J.-P. Tuchagues, *Inorg. Chem.* **1995**, *34*, 5150.
[32] P. Lainé, A. Gourdon, J.-P. Launey, *Inorg. Chem.* **1995**, *34*, 5156.
[33] D. M. P. Mingos, D. J. Sherman, *Adv. Inorg. Chem.* **1989**, *34*, 293.
[34] J. S. Stamler, D. J. Singel, J. Loscalzo, *Science* **1992**, *258*, 1898.
[35] Y.-M. Chiou, L. Jr. Que, *Inorg. Chem.* **1995**, *34*, 3270.
[36] R. G. J. Miller, B. C. Stace, *Laboratory Methods in Infrared Spectroscopy, Hayden, London* **1972**, *Chapter 14*, 205.
[37] V. Zang, Dissertation, Universität Witten-Herdecke **1990**.
[38] Y. Kurimura, R. Ochiai, N. Matsuura, *Bull. Chem. Soc. Jpn.* **1968**, *41*, 2234.
[39] T. Schneppensieper, Diplomarbeit, Universität Erlangen-Nürnberg **1997**.
[40] E. Sada, H. Kumazawa, H. Machida, *Ind. Eng. Chem. Res.* **1987**, *26*, 1468.
[41] V. Zang, R. van Eldik, *Inorg. Chem.* **1990**, *29*, 1705.
[42] H. J. Wubs, A. A. C. M. Beenackers, *Ind. Eng. Chem. Res.* **1993**, *32*, 2580.
[43] S. Seibig, R. van Eldik, *Inorg. Chem.* **1997**, *36*, 4115.
[44] S. Kudo, J. L. Bourassa, S. E. Boggs, Y. Sato, P. C. Ford, *Anal. Biochem.* **1997**, *247*, 193.
[45] I. Cebulla, Dissertation, Universität Tübingen **1995**.
[46] A. Wanat, T. Schneppensieper, R. van Eldik, unpublished results.
[47] J. Burgess, *Ions in Solution*, Ellis Horwood Series In Inorganic Chemistry, New York, **1988**.
[48] E. R. Brown, J. D. Mazzarella, *J. Electroanal. Chem.* **1987**, *222*, 173.
[49] N. Zwicker, *GIT-Labor-Fachzeitschrift* **1999**, *10*, 1044.
[50] Z. Hualin, L. Peiyi, W. Boyi, W. Jianhua, Z. Peiju, *Polyhedron* **1990**, *9*, 2873.
[51] G. Gran, *Analyst* **1952**, *77*, 661.

Received May 23, 2000
[I00210]

Thermodynamic and Kinetic Studies on Complex-Formation Reactions of a Cobalt(II) Tripodal Tetraamine Complex

Zhong-Lin Lu,[a][‡] Mohamed S. A. Hamza,[a][‡‡] and Rudi van Eldik*[a]

Keywords: Cobalt / Thermodynamics / Kinetics / Tripodal ligands / N ligands

Complex-formation constants were determined for the reaction of $[Co(Me_6tren)(H_2O)]^{2+}$ with different pyridine- and imidazole-based nucleophiles, and the kinetics of these reactions was studied as a function of entering ligand concentration, temperature, and pressure. The steric hindrance associated with the methyl substituents on the trigonal-bipyramidal complex induces a sensitive control over the substitution mechanism from dissociative for the weaker and more bulky entering nucleophiles, to associative for the stronger and less bulky nucleophiles. A changeover in mechanism can be observed as a function of nucleophile concentration, in the case of 2-MeImH as the entering ligand. The mechanistic assignments are based on the observed rate laws, and the activation parameters determined under limiting concentration conditions.

Introduction

The thermodynamics and kinetics of complex-formation and ligand-substitution reactions of octahedral transition metal complexes have been studied in much detail by many groups, and a number of reviews have appeared on this topic, of which a few typical examples are referenced.[1a−1d] In contrast, the formation, stability, and mechanistic behaviour of five-coordinate square-pyramidal or trigonal-bipyramidal first-row transition metal complexes have received significantly less attention.[2] Such five-coordinate complexes can exhibit significantly different ligand substitution behaviour since they are, in principle, able to coordinate an additional nucleophile in the transition state. In contrast, six-coordinate complexes usually undergo dissociative ligand substitution reactions. Thus, the study of their behaviour is of fundamental importance to the understanding of complex-formation and ligand-substitution reactions in general.

By way of a typical example, the introduction of a tripodal tetraamine ligand such as tren [tris(2-aminoethyl)-amine] into the coordination sphere of copper(II) leads to the formation of a trigonal-bipyramidal complex, $[Cu(tren)(H_2O)]^{2+}$. This complex exhibits significantly slower water-exchange and complex-formation reactions than the parent $[Cu(H_2O)_6]^{2+}$ ion due to the absence of Jahn−Teller distortion.[3,4] Not only are the reactions much slower, their mechanism has also changed from the I_d to the I_a type as clearly indicated by the significantly different volumes of activation reported for these reactions.[3,4] Furthermore, the mechanistic behaviour of these complexes can be systematically tuned by the introduction of steric hindrance on the tripodal ligand, viz. tren, trimethylated (Me_3tren, i.e. one methylation per primary amine group of tren) and hexamethylated tren (Me_6tren, i.e. fully methylated primary amine groups).[5] The substitution reactions of $[Cu(Me_3tren)(H_2O)]^{2+}$ are more than two orders of magnitude slower than those of $[Cu(tren)(H_2O)]^{2+}$, but still follow an I_a mechanism. However, in the case of the $[Cu(Me_6tren)(H_2O)]^{2+}$ complex, a further decrease in the substitution rate and a changeover back to a dissociative reaction mechanism is observed. Only at high entering nucleophile concentrations, could evidence for a parallel associative reaction path be observed.[5] The introduction of steric hindrance on the tripodal tetraamine chelate controls the substitution behaviour of these complexes, and the extension of the chelate rings from ethyl to propyl causes a geometric changeover from trigonal-bipyramidal to square-pyramidal which is accompanied by a change in lability.[6]

Based on this experience, we have begun a study on the corresponding behaviour of cobalt(II) complexes. Our interest lies in the activation of dioxygen reported for the $[Co(tren)(H_2O)]^{2+}$ complex [7] and the details of the underlying reaction mechanism, which can then be compared with that previously found for an octahedral cobalt(II) complex.[8] However, since the activation of dioxygen in general involves the combination of ligand substitution and subsequent redox processes, it is at first essential to understand the ligand substitution behaviour of these systems. Due to the extreme oxygen sensitivity of the $[Co(tren)(H_2O)]^{2+}$ complex,[7] we first turned to the almost oxygen-insensitive $[Co(Me_6tren)(H_2O)]^{2+}$ complex and studied its complex-formation reactions in more detail. The

[a] Institute for Inorganic Chemistry, University of Erlangen-Nürnberg,
Egerlandstraße 1, 91058 Erlangen, Germany
E-mail: vaneldik@chemie.uni-erlangen.de
[‡] On leave from the Institute of Physical Chemistry, School of Chemistry and Chemical Engineering, Zhongshan University, Guangzhou, 510275, China
[‡‡] On leave from the Department of Chemistry, Ain Shams University, Cario, Egypt

 © WILEY-VCH Verlag GmbH, 69451 Weinheim, 2001 1434−1948/01/0202−0503 $ 17.50+.50/0

results of this study show that the ligand-substitution mechanism can be controlled by the concentration and nucleophilicity of the entering ligand.

Results and Discussion

Determination of Complex-Formation Constants

The stability constant (log K) of the cobalt(II) complex with the chelate Me_6tren is 8.53, which is smaller than that of the corresponding copper(II) complex (viz. 15.65), and the pK_a of the corresponding aqua complex, $[Co(Me_6tren)(H_2O)]^{2+}$, is 8.6.[9]

The complex-formation constants for substitution of water on $[Co(Me_6tren)(H_2O)]^{2+}$ by pyridine, 4-methylpyridine, and imidazole were determined in the following manner. The complex concentration was kept constant at $3.4 \cdot 10^{-3}$ M and different concentrations of the ligands L were added.

$$[Co(Me_6tren)(H_2O)]^{2+} + L \rightleftharpoons [Co(Me_6tren)(L)]^{2+} + H_2O \quad K$$

On increasing the ligand concentration, the characteristic peak at 470 nm is incrementally reduced and almost disappears completely at high ligand concentrations. A typical example of the spectral changes observed for the substitution reaction with ImH is shown in Figure 1. The spectra in general show clean isosbestic points at low entering nucleophile concentrations, but a shift in isosbestic points occur at high added nucleophile concentrations. In the case of the reaction with ImH this effect is not very strong, but in the case of the reaction with 4-Mepy the deviations in isosbestic points are very significant. This indicates that different substitution products, in which the Me_6tren ligand is displaced in a stepwise manner by the entering nucleophile, can be formed depending on the concentration and nature of the added nucleophile. In fact it was possible to isolate and characterise $[Co(L)_4(H_2O)_2](ClO_4)_2$ (L = 4-MePy) and $[Co(L)_6](ClO_4)_2$ (L = ImH) as reaction products at high concentrations of 4-Mepy and ImH (see Experimental Section). From the molar conductivity measurements it is clear that the two isolated complexes are 2:1 electrolytes. The plot of absorbance at 470 nm versus ligand concentration for the reaction with ImH is shown in Figure 2. The latter data were used to estimate the complex-formation constant (K) in the usual manner.[10] Plots of $\log\{(A_x - A_i)/(A_\infty - A_x)\}$ versus log[nucleophile] showed a linear dependence with unity slope at low nucleophile concentrations, but deviations occurred at higher concentrations due to the formation of 1:2 and higher substituted complexes.

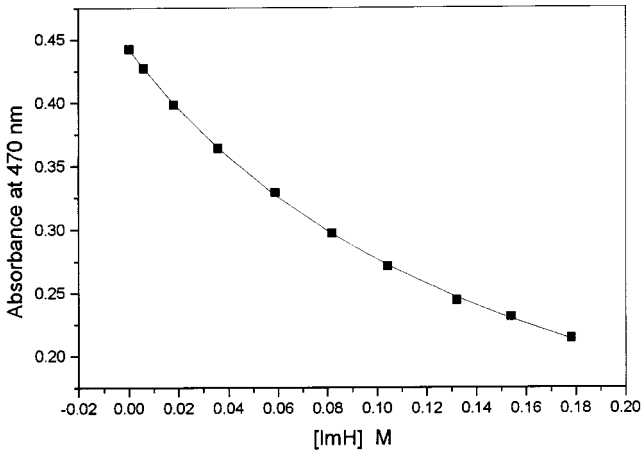

Figure 2. Absorbance at 470 nm versus concentration of ImH for the reaction of $[Co(Me_6tren)(H_2O)]^{2+}$ with ImH at 25.0 °C, pH = 7.92 ± 0.02, I = 1.0 M, 0.05 M Tris buffer, $[Co^{II}] = 3.21 \cdot 10^{-3}$ M

The 1:1 complex-formation constants for pyridine (py), 4-methylpyridine (4-Mepy), and imidazole (ImH) were found to be 1.0 ± 0.3 , 1.8 ± 0.4, and 7.4 ± 1.8 M^{-1} at 25 °C, respectively. A plot of the complex-formation constants (log K) versus the pK_a values of the ligands is shown in Figure 3. It can be seen that log K increases linearly with increasing pK_a, which is consistent with that expected in terms of the basicity of the entering nucleophiles. Such linear correlations between log K and pK_a have also been reported in the literature.[11]

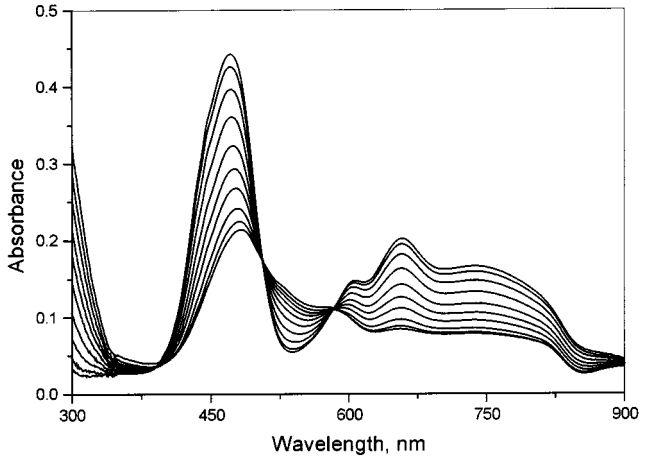

Figure 1. Absorption spectra for the complex formation between $[Co(Me_6tren)(H_2O)]^{2+}$ and ImH ([ImH] from 0.0 to 0.18 M) at 25.0 °C, pH = 7.92 ± 0.02, I = 0.2 M, 0.05 M Tris buffer, $[Co^{II}] = 3.21 \cdot 10^{-3}$ M

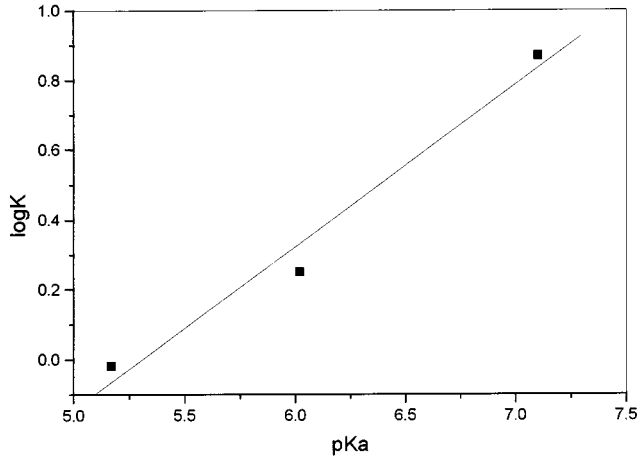

Figure 3. Plot of log K (from thermodynamic method) versus pK_a of the ligands for the reaction between $[Co(Me_6tren)(H_2O)]^{2+}$ and Py, 4-MePy, and ImH

A comparison of the K value for the formation of the pyridine complex, viz. 1.0 ± 0.3 M^{-1}, with that for the corresponding $[Cu(Me_6tren)(H_2O)]^{2+}$ complex, viz. 6.6 ± 0.3 M^{-1},[5] indicates that the copper(II) complex is more stable. This is in agreement with the higher stability constant (log K) reported for $[Cu(Me_6tren)(H_2O)]^{2+}$ as compared with that for $[Co(Me_6tren)(H_2O)]^{2+}$, viz. 15.65 and 8.53, respectively.[9]

Kinetic Analysis

Preliminary Observations

Preliminary kinetic experiments for the reaction of $[Co(Me_6tren)(H_2O)^{2+}]$ with the selected organic bases at a pH < 7.9, revealed kinetic traces in the absence of an added nucleophile as a result of the dilution of the complex solution in the stopped-flow instrument. This effect could be correlated with the dissociation of the complex on dilution. For this reason all kinetic measurements were performed at pH = 7.9 where this effect is negligible. Under this condition a small fraction of the complex exists in the inert hydroxo form due to the pK_a value of 8.6. Further experiments demonstrated that the observed pseudo first-order rate constants measured in the presence of an excess of the nucleophile also depended on the concentration of the cobalt(II) complex; the effect being much stronger at lower pH due to the partial dissociation of the complex under such conditions. All kinetic measurements were therefore performed at a fixed cobalt(II) concentration and a pH of 7.9.

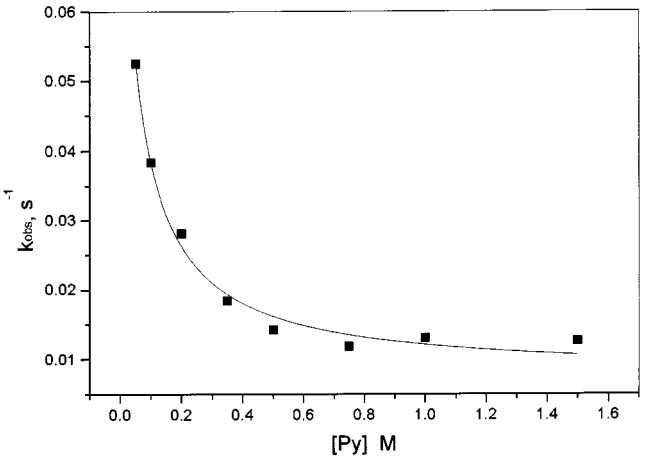

Figure 4. Kinetic data for the reaction of $[Co(Me_6tren)(H_2O)]^{2+}$ with pyridine at 25°C, pH = 7.92 ± 0.02, I = 1.0 M, 0.05 M Tris buffer, $[Co^{II}] = 3.61 \cdot 10^{-3}$ M

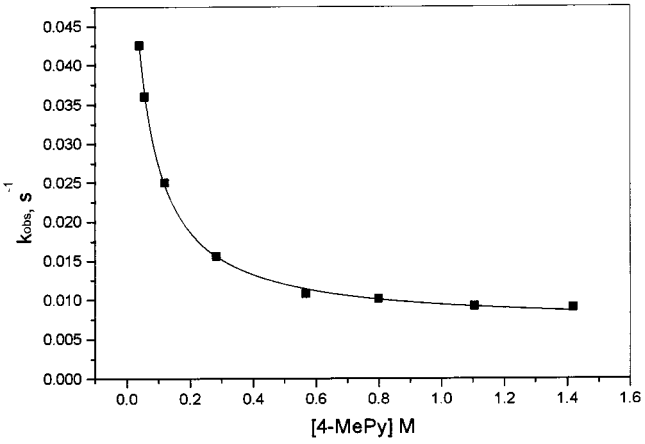

Figure 5. Kinetic data for the reaction of $[Co(Me_6tren)(H_2O)]^{2+}$ with 4-MePy at 25.0 °C, pH = 7.92 ± 0.02, I = 1.0 M, 0.05 M Tris buffer, $[Co^{II}] = 3.2 \cdot 10^{-3}$ M

Reactions of Pyridine and 4-Methylpyridine with $[Co(Me_6tren)(H_2O)]^{2+}$

The reactions of pyridine and 4-methylpyridine with $[Co(Me_6tren)(H_2O)]^{2+}$ are very similar. Kinetic measurements on the reaction were performed using total ligand concentrations in the range of 0.05−1.5 M at a pH = 7.92 and ionic strength of 1.0 M ($NaClO_4$), and thus always at least in 10-fold excess of the $[Co(Me_6tren)(H_2O)]^{2+}$ concentration. When k_{obs} is plotted versus the entering ligand concentration, k_{obs} decreases with increasing ligand concentration over the whole ligand concentration range (see Figure 4 and Figure 5). This is very characteristic for a dissociative mechanism involving an efficient back reaction. A similar nucleophile concentration dependence has been reported for several reversible dissociative ligand substitution reactions in the literature.[12a−12e] However, it should be noted that the observed trends differ significantly from that observed for the substitution reaction of $[Cu(Me_6tren)(H_2O)]^{2+}$ with pyridine [4] (see further Discussion).

On the basis of the observed kinetics, we propose the following reversible two-step mechanism [Equation (1) and Equation (2)].

$$[Co(Me_6tren)(H_2O)]^{2+} \rightleftharpoons [Co(Me_6tren)]^{2+} + H_2O \quad k_1, k_{-1} \qquad (1)$$

$$[Co(Me_6tren)]^{2+} + L \rightleftharpoons [Co(Me_6tren)(L)]^{2+} \quad k_2, k_{-2} \qquad (2)$$

(L = Py and 4-MePy) The rate law for this mechanism can be expressed as shown in Equation (3).

$$k_{obs} = (k_1k_2[L] + k_{-1}k_{-2})/(k_{-1} + k_2[L]) \qquad (3)$$

A non-linear least-squares fit of the data according to Equation (3) reveals that k_1 = 0.0076 ± 0.0025 s^{-1}, k_{-2} = 0.094 ± 0.015 s^{-1}, and k_2/k_{-1} = 18 ± 6 M^{-1} for pyridine, and those for 4-methylpyridine are k_1 = 0.0066 ± 0.0009 s^{-1}, k_{-2} = 0.077± 0.004 s^{-1}, and k_2/k_{-1} = 24 ± 2 M^{-1} at 25 °C. Thus the complex-formation constant K (= $k_1k_2/k_{-1}k_{-2}$) from the kinetic data for the reaction with pyridine is 1.5 ± 0.7 M^{-1} and that for 4-methylpyridine is 2.1 ± 0.3 M^{-1}, whereas the formation constant from the thermodynamic measurements are 1.0 ± 0.3 and 1.8 ± 0.4 M^{-1}, re-

spectively. It follows that the data from the two independent methods are similar within the experimental error limits.

The temperature dependence of the substitution reactions of $[Co(Me_6tren)(H_2O)]^{2+}$ with pyridine and 4-methylpyridine was studied under limiting conditions at pyridine and 4-methylpyridine concentrations of 1.0 and 1.105 M, respectively, i.e. where k_{obs} reaches a minimum and $k_{obs} \approx k_1$. The results are summarised in Table 1, from which it follows that the activation enthalpy and activation entropy are 74 ± 4 kJ mol^{-1} and -35 ± 12 J K^{-1} mol^{-1} for the reaction with pyridine, and 71 ± 2 kJ mol^{-1} and -47 ± 5 J K^{-1} mol^{-1}, respectively, for substitution by 4-methylpyridine. Both the activation entropies are negative and are not in line with the concept of a limiting dissociative mechanism as suggested by the observed rate law. This is not unusual since activation entropies are inherently subjected to large error limits as a result of the way in which they are determined, viz. by extrapolation of rate constants measured over a limited temperature range to $1/T = 0$. For this reason the effect of pressure on the reaction with 4-methylpyridine was studied under similar experimental conditions. It was, however, difficult to obtain accurate data due to turbidity problems that occurred during mixing in the high-pressure stopped-flow system (see Experimental Section). For this reason the ionic strength of the solutions was decreased to almost zero and the temperature was raised to 45.0 ± 0.1 °C, which significantly improved the quality of the data. The results indicate that the observed rate constant (practically k_1) decreases with increasing pressure. The average activation volume calculated from the slope of $\ln(k)$ versus pressure ($= -\Delta V^{\neq}/RT$) for four series of measurements is $+15 \pm 7$ cm^3 mol^{-1}. The large error limits is a result of the unfavourable time scale of the reaction and the small absorbance change associated with the reaction under these conditions. The value in principle supports the operation of a dissociative mechanism.

Reaction of Imidazole with $[Co(Me_6tren)(H_2O)]^{2+}$

The kinetics of the substitution reaction of $[Co(Me_6tren)(H_2O)]^{2+}$ with imidazole differed significantly from that reported above for pyridine and 4-methylpyridine. When k_{obs} is plotted versus the ligand concentration (see Figure 6), it is clear that k_{obs} increases linearly with increasing imidazole concentration in the lower concentration range, but increases almost exponentially in the higher concentration range. The data can be interpreted in terms of a two-step associative substitution mechanism in which imidazole first displaces the coordinated water molecule in Equation (4), followed by either the binding of a second imidazole molecule to form a six-coordinate complex, or the stepwise dechelation of the Me_6tren ligand to form a five-coordinate disubstituted product in Equation (5).

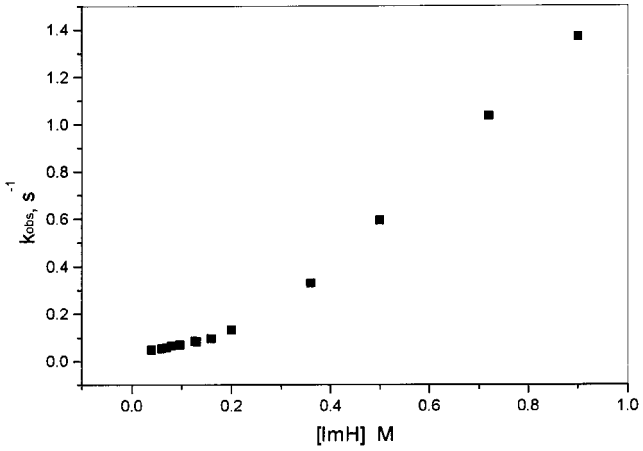

Figure 6. Kinetic data for the reaction of $[Co(Me_6tren)(H_2O)]^{2+}$ with ImH at 25.0 °C, pH = 7.92 ± 0.02, I = 0.2 M, 0.05 M Tris buffer, $[Co^{II}] = 3.21 \cdot 10^{-3}$ M

On the basis of these arguments we propose the following mechanism for the substitution of $[Co(Me_6tren)(H_2O)]^{2+}$ by imidazole (ImH).

Table 1. Kinetic data for the substitution of $[Co(Me_6tren)(H_2O)]^{2+}$ by an organic ligand L at pH = 7.92 ± 0.02, 0.05 M Tris buffer and I = 1.0 M

Ligand (L)	Temp. [°C]	k_{obs} [s^{-1}]	$\Delta H^{\neq}$ [kJ mol^{-1}] and $\Delta S^{\neq}$ [J mol^{-1} K^{-1}]
Pyridine	20.0	0.006 ± 3.0E−4	$\Delta H^{\neq} = 74 \pm 4$
[Py] = 1.0 M	25.0	0.01131 ± 2.9E−4	$\Delta S^{\neq} = -35 \pm 12$
	30.0	0.0158 ± 7.0E−4	
	35.0	0.0277 ± 2.0E−4	
	40.0	0.0471 ± 5.0E−4	
4-Methylpyridine	20.0	0.00575 ± 1.9E−4	$\Delta H^{\neq} = 71 \pm 2$
[4-MePy] = 1.105 M	25.0	0.009152 ± 3.1E−4	$\Delta S^{\neq} = -47 \pm 5$
	30.0	0.01536 ± 1.9E−4	
	35.0	0.02552 ± 7.6E−5	
	40.0	0.0378 ± 6.2E−4	
Imidazole[a]	15.0	0.02935 ± 1.0E−3	$\Delta H^{\neq} = 59 \pm 1$
[ImH] = 0.0964 M	20.0	0.04287 ± 3.2E−3	$\Delta S^{\neq} = -71 \pm 4$
	25.0	0.06872 ± 4.4E−4	
	30.0	0.09986 ± 3.6E−4	
	35.0	0.1524 ± 7.4E−4	
[ImH] = 0.5 M	15.0	0.3056 ± 1.0E−3	$\Delta H^{\neq} = 48 \pm 1$
	20.0	0.4311 ± 3.2E−3	$\Delta S^{\neq} = -87 \pm 4$
	25.0	0.5845 ± 3.8E−3	
	30.0	0.8404 ± 9.1E−3	
	35.0	1.224 ± 6.0E−2	

[a] I = 0.2 M.

$$[Co(Me_6tren)(H_2O)]^{2+} + ImH \rightleftharpoons [Co(Me_6tren)(ImH)]^{2+} + H_2O \quad k_3, k_{-3} \tag{4}$$

$$[Co(Me_6tren)(ImH)]^{2+} + ImH \rightarrow [Co(Me_6tren)(ImH)_2]^{2+} \quad k_4 \tag{5}$$

This leads to rate law (6) for the formation of the substitution products:

$$k_{obs} = k_{-3} + k_3[ImH] + (k_4k_3/k_{-3})[ImH]^2 \tag{6}$$

At lower concentrations of ImH, the rate law Equation (6) reduces to

$$k_{obs} = k_{-3} + k_3[ImH] \tag{7}$$

At higher concentrations of ImH, the rate law Equation (6) can be rewritten as

$$(k_{obs} - k_{-3})/[ImH] = k_3 + (k_4k_3/k_{-3})[ImH] \tag{8}$$

k_{-3} can be obtained directly from the plot of k_{obs} versus [ImH] at lower concentrations (Figure 6), and all other rate constants can then be obtained from the plot of $(k_{obs} - k_{-3})/[ImH]$ versus [ImH] for all the data points (see Figure 7). This results in $k_{-3} = 0.031 \pm 0.002$ s^{-1}, $k_3 = 0.27 \pm 0.03$ M^{-1} s^{-1}, and $k_4(k_3/k_{-3}) = 1.46 \pm 0.08$ M^{-2} s^{-1}, from which it follows that $k_4 \approx 0.17 \pm 0.02$ M^{-1} s^{-1}, i.e. ca. two times as slow as k_3. These data account for the initial linear dependence of k_{obs} on the imidazole concentration in the lower concentration range and the exponential behaviour due to the contribution of the second-order term in imidazole concentration at higher concentrations.

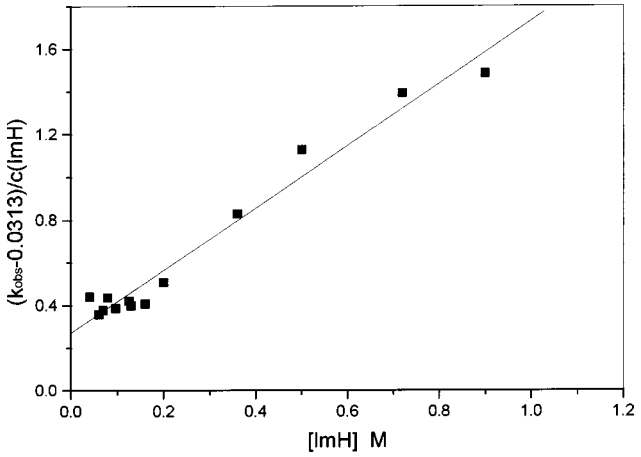

Figure 7. Fit of the kinetic data for the reaction of $[Co(Me_6tren)(H_2O)]^{2+}$ with ImH according to Equation (8) at 25.0 °C, pH = 7.92 ± 0.02, I = 0.2 M, 0.05 M Tris buffer, $[Co^{II}] = 3.21 \cdot 10^{-3}$ M

The temperature dependence of the reaction was studied at imidazole concentrations of 0.096 and 0.50 M, in order to cover the low and high concentration ranges, respectively. The results are included in Table 1 and the activation enthalpies are 48 ± 1 and 59 ± 1 kJ mol^{-1}, respectively. The significantly negative activation entropies of −87 ± 4 and −71 ± 4 J K^{-1} mol^{-1}, respectively, support the associative nature of the substitution process. The effect of pressure on the reaction was studied at an imidazole concentration of 0.16 M, and the pressure dependence of k_{obs} (see Figure 8) results in a $\Delta V^{\neq}$ value of −2.61 ± 0.07 cm^3 mol^{-1}. This small and negative value suggests that substitution by imidazole follows an associative interchange (I_a) mechanism.[3]

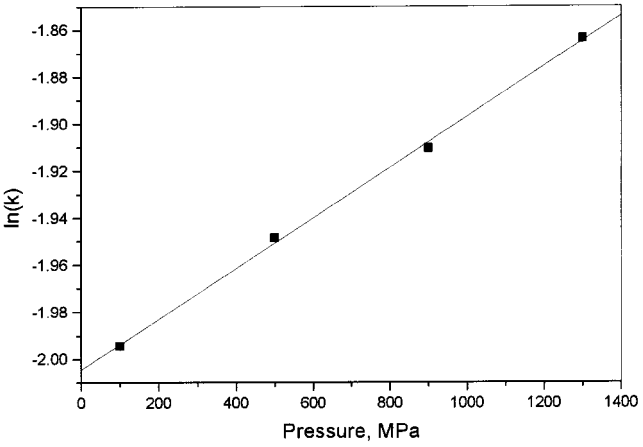

Figure 8. High pressure kinetic data for the reaction between $[Co(Me_6tren)(H_2O)]^{2+}$ and ImH at 25.0 °C, pH = 7.92 ± 0.02, I = 0.2 M, 0.05 M Tris buffer, $[Co^{II}] = 3.21 \cdot 10^{-3}$ M and [ImH] = 0.16 M

Reaction of 2-Methylimidazole with $[Co(Me_6tren)(H_2O)]^{2+}$

The reaction of 2-methylimidazole with $[Co(Me_6tren)(H_2O)]^{2+}$ is again different from that reported above for the reactions with pyridine, 4-methylpyridine and imidazole. In this case a combination of the dependencies reported in Figures 4 to 6 is observed. When k_{obs} is plotted versus the 2-methylimidazole concentration, it first decreases with increasing 2-methylimidazole concentration in the lower concentration range, and then increases with increasing concentration in the higher concentration range (see Figure 9). k_{obs} passes through a minimum at a 2-methylimidazole concentration of ca. 0.2 M and then depends linearly on the 2-methylimidazole concentration as shown in Figure 9. This concentration dependence is very similar to that reported for the substitution reaction of $[Cu(Me_6tren)(H_2O)]^{2+}$ with pyridine.[4] According to the literature and the results reported above, we propose the following mechanism for the substitution reaction of $[Co(Me_6tren)(H_2O)]^{2+}$ with 2-methylimidazole.

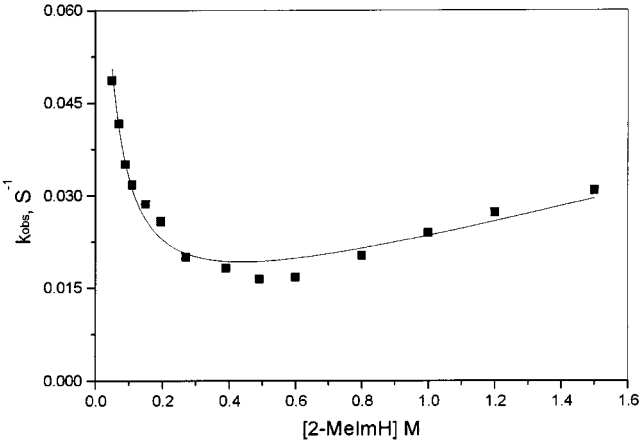

Figure 9. Kinetic data for the reaction of $[Co(Me_6tren)(H_2O)]^{2+}$ with 2-MeImH at 25.0 °C, pH = 7.92 ± 0.02, I = 1.0 M, 0.05 M Tris buffer, $[Co^{II}] = 3.23 \cdot 10^{-3}$ M

The mechanism consists of two parallel competing reaction paths. The displacement of coordinated water proceeds according to a dissociative mechanism that results in a rate law similar to Equation (3), and can account for the decrease in k_{obs} with increasing 2-methylimidazole concentration. The parallel dechelation reaction path can exhibit a linear dependence on the 2-methylimidazole concentration similar to Equation (7), with an intercept for the reverse reaction under conditions where dechelation is a pre-equilibrium step. The combination of these concentration dependencies will result in the curved dependence observed in Figure 9. At low 2-methylimidazole concentration the reaction will proceed mainly by the displacement of coordinated water, whereas at higher 2-methylimidazole concentration the parallel dechelation path will become more important since a linear concentration dependence is exhibited. The reactions can be summarised as described below.

At lower concentrations of 2-MeImH

$$[Co(Me_6tren)(H_2O)]^{2+} \rightleftharpoons [Co(Me_6tren)]^{2+} + H_2O \quad k_1, k_{-1} \qquad (1)$$

$$[Co(Me_6tren)]^{2+} + L \rightleftharpoons [Co(Me_6tren)(L)]^{2+} \quad k_2, k_{-2} \qquad (2)$$

(L = 2-MeImH)

The rate law is the same as given in Equation (3). At higher concentrations of 2-methylimidazole a significant contribution of the parallel associative displacement of the Me_6tren chelate, involving a dechelation pre-equilibrium, is suggested to account for the observed data [Equation (9) and Equation (10)].

$$[Co(Me_6tren)(H_2O)]^{2+} \rightleftharpoons [Co(Me_6tren')(H_2O)]^{2+} \quad K_5 \qquad (9)$$

$$[Co(Me_6tren')(H_2O)]^{2+} + L \rightarrow [Co(Me_6tren')(H_2O)(L)]^{2+} \quad k_6 \qquad (10)$$

(Me_6tren′ represents 3-coordinated Me_6tren; L = 2-MeImH) This mechanism leads to the rate law $k_{obs} = k_6K_5[L]$, and combined with Equation (3) results in the combined rate law

$$k_{obs} = (k_1k_2[L] + k_{-1}k_{-2})/(k_{-1} + k_2[L]) + k_6K_5[L] \qquad (11)$$

At high concentrations of 2-MeImH, Equation (11) reduces to

$$k_{obs} = k_1 + k_6K_5[L] \qquad (12)$$

From a fit of the data in Figure 10 (a) using Equation (3), $k_1 = 0.012 \pm 0.006$ s^{-1}, $k_{-2} = 0.12 \pm 0.04$ s^{-1} and $k_2/k_{-1} = 37 \pm 23$ M[4]$^{-1}$. With these values and using $k_1k_2/k_{-1} = 0.42$ M^{-1} s^{-1}, the experimental data in Figure 9 were fitted to Equation (11), which resulted in $k_1 = 0.007 \pm 0.001$ s^{-1}, $k_{-2} = 0.18 \pm 0.03$ M^{-1} s^{-1}, $k_2/k_{-1} = 60 \pm 10$ M^{-1}, and $k_6K_5 = 0.014 \pm 0.001$ M^{-1} s^{-1}. From a fit of the higher concentration data in Figure 10 (b) using Equation (12), $k_1 = 0.0076 \pm 0.0010$ s^{-1} and $k_6K_5 = 0.0158 \pm 0.001$ M^{-1} s^{-1}. It follows that the experimental data reported in Figure 9 is well described by the mechanism outlined in the reactions represented by Equations (1), (2), (9), and (10).

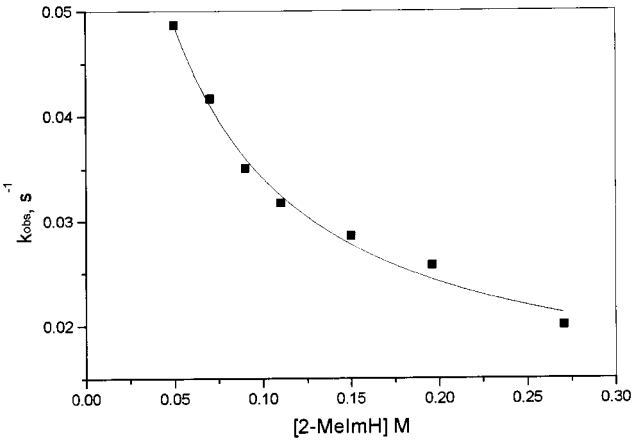

(a)

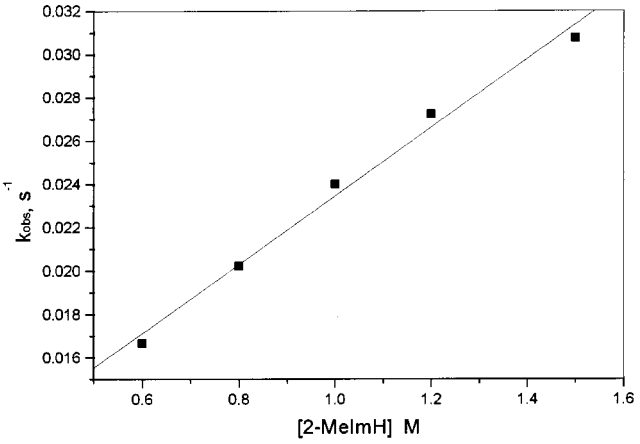

(b)

Figure 10. Fit of the kinetic data reported for the reaction of $[Co(Me_6tren)(H_2O)]^{2+}$ with 2-MeImH in Figure 9; (a) for data at [2-MeImH] < 0.3 M; (b) for data at [2-MeImH] from 0.5 to 1.6 M

Overall Comparison of Kinetic Data

According to the kinetic data for the substitution reaction of $[Co(Me_6tren)(H_2O)^{2+}]$ with pyridine and 4-methylpyridine, the reactions proceed according to a dissociative mechanism, which is controlled by the release of H_2O, i.e. k_1. The limiting rate constants reached at high nucleophile concentrations represent k_1 and are indeed close for the two ligands studied (0.0076 s^{-1} for pyridine as compared with 0.0066 s^{-1} for 4-methylpyridine). On increasing the nucleophilicity, the substitution reaction with imidazole shows an associative character, and a second imidazole ligand can enter the coordination sphere at high ligand concentration.

The steric hindrance associated with 2-methylimidazole prevents an associative reaction at low ligand concentration, and evidence for a dissociative reaction is observed. On increasing the ligand concentration further, a concentration range is reached where an associative process contributes to the overall reaction sequence. Again it can be seen that the limiting (minimum) value reached is that for k_1

(viz. 0.008 s^{-1}), which is close to that found for pyridine and 4-methylpyridine, and is consistent with the same rate-determining step.

For the substitution reaction with imidazole, k_3 (viz. 0.27 M^{-1} s^{-1}) is larger than k_4 (viz. 0.17 M^{-1} s^{-1}), which is in agreement with the difficulty of the second imidazole molecule in entering the coordination sphere. By way of comparison, the second-order rate constant for the reaction with 2-methylimidazole, viz. $k_6K_5 = 0.014$ M^{-1} s^{-1}, is significantly smaller presumably due to steric reasons.

Within the context of a limiting dissociative mechanism, the entering nucleophile must compete with the solvent for the intermediate [Co(Me_6tren)] species, as expressed by the ratio k_2/k_{-1}. This ratio increases from pyridine (18 M^{-1}), to 4-methylpyridine (24 M^{-1}), to 2-methylimidazole (60 M^{-1}), which follows the order of the increase in nucleophilicity of the ligands.

For the aquation of the substituted complex, it can be seen that k_{-2} for pyridine (viz. 0.09 s^{-1}) is similar to that for 4-methylpyridine (viz. 0.08 s^{-1}), and both are larger than the corresponding data (k_{-3}) for imidazole (viz. 0.031 s^{-1}), which is again consistent with the order of nucleophilicity of the ligands. These values are all smaller than that for 2-methylimidazole (viz. 0.18 s^{-1}), which can be ascribed to the steric hindrance associated with the 2-methylimidazole ligand which will accelerate the aquation of the complex.

For the complex-formation constants K, there is a small difference between the thermodynamically and kinetically determined values. For the ligands pyridine, 4-methylpyridine and imidazole, K_{td} is 1.0, 1.8, and 7.4 M^{-1}, respectively, whereas K_{kin} for these ligands is 1.5, 2.1, and 8.7 M^{-1}, respectively. It can be seen that the values of K from the thermodynamic analysis are slightly smaller than those from the kinetic treatment, but are in good agreement considering the error limits involved.

Conclusions

The results of this study have demonstrated how the nature and mechanism of ligand substitution reactions of [Co(Me_6tren)(H_2O)]$^{2+}$ can be controlled in a rather sensitive manner by the nature, concentration, and nucleophilicity of the entering ligand. We are presently in the process of extending this study systematically to the substitution behaviour of the sterically less hindered and more oxygen-sensitive [Co(Me_3tren)(H_2O)]$^{2+}$ and [Co(tren)(H_2O)]$^{2+}$ complexes. Finally, we plan to investigate the activation of dioxygen by both complexes in more detail.

Experimental Section

Materials: The compounds used were of commercially available reagent quality (Acros), except for the preparation reported below. Ultra pure water was used for the preparation of the aqueous solutions. *WARNING: Perchlorate salts are potentially explosive; they should be handled in small amounts and with caution!* − The ligand Me_6tren was prepared according to a literature method and characterised by ^{13}C and ^1H NMR spectroscopy.[13] The spectra were in agreement with those reported in the literature.[13] [Co(Me_6tren)]-(ClO_4)$_2$ was prepared according to the literature and characterised by elemental analysis and spectral data.[14] Solutions of the complex for the thermodynamic and kinetic studies were prepared by dissolving the solid product in the buffer (0.05 M Tris and pH ≈ 7.9) [I = 1.0 M for reactions with pyridine, 4-methylpyridine and 2-methylimidazole; and I = 0.2 M for imidazole ($NaClO_4$)], adding 50% excess of the Me_6tren chelate to stabilise the complex, and adjusting the final pH of the solution with 1.0 M $HClO_4$ to 7.92 ± 0.02.

Physical Measurements: Conductance measurements were made with a HANNA instrument HI1281 at room temperature. − Electronic spectra were measured with a Shimadzu 240 spectrophotometer. − IR spectra were recorded with an ATJ Mattson FT-IR 60 AR spectrophotometer in KBr pellets in the 4000−400 cm^{-1} range. − ESR spectra were recorded with a Bruker DXP 300 AVANCE spectrometer.

Characterisation of [Co(L)$_4$(H_2O)$_2$](ClO_4)$_2$ (L = 4-MePy) and [Co(L)$_6$](ClO_4)$_2$ (L = ImH): In the study of the complex-formation reactions in the presence of a large excess of entering nucleophile, precipitates were formed during the reaction of [Co(Me_6tren)(H_2O)]$^{2+}$ with 4-methylpyridine and imidazole. These were isolated and characterised.

[Co(4-MePy)$_4$(H_2O)$_2$](ClO_4)$_2$: $C_{24}H_{32}Cl_2CoN_4O_{10}$ (666.4): calcd. C 43.26, H 4.84, N 8.41; found C 43.11; H 4.49, N 8.07. − Molar conductivity: 124 cm^2/ohm mol (DMF, 1.03·10^{-3} M, 25 °C). − 151 cm^2/ohm mol [$CH_3CH_2NO_2$, 4.4·10^{-3} M, 25 °C, ref.[15] 157−201 cm^2/ohm mol for Co(4-MePy)$_4$(ClO_4)$_2$]. − Electronic spectrum (in $CHCl_2$/$CHCl_3$, 1:1): λ (ε) = 20700 (sh), 19700 (600) [ref.[15] 18000−23000 cm^{-1} two peaks in CH_2Cl_2 for Co(4-MePy)$_4$(ClO_4)$_2$; 18900 (sh), 17900 (611) in $CHCl_2$/$CHCL_3$ (1:1) for Co(4-MePy)$_4$(PF_6)$_2$[16]]. − IR (cm^{-1}): $\tilde{\nu}$ = 630, 935, 1018, 1092, 1111, 1141 [for ν(ClO_4^-), ref.[17] 625, 925, 1020, 11371]; 1231, 1505, 1618 [for ν(4-MePy), ref.[16] 1240, 1511, 1622]; 3434 [br. for ν(H_2O)]. − ESR: g = 4.25.

[Co(ImH)$_6$](ClO_4)$_2$: $C_{18}H_{24}Cl_2CoN_{12}O_8$ (666.3): calcd. C 32.47, H 3.63, N 25.25; found C 32.47, H 3.50, N 25.42. − Molar conductivity: 154 cm^2/ohm mol (DMF, 1.0·10^{-3} M, 25 °C); 150 cm^2/ohm mol ($CH_3CH_2NO_2$, 6.0·10^{-3} M, 25 °C, ref.[18] 180 cm^2/ohm mol, 23 °C). − Electronic spectrum (in DMF with 10% excess ImH): λ (ε) = 20120 (25), 18940 (sh) cm^{-1} [ref.[18] 20230 (20), 18900 (sh) cm^{-1}]. − IR (cm^{-1}): $\tilde{\nu}$ = 1057, 1089, 1115 [for ν(ClO_4^-), ref.[18] 1000−1120 vs)]; 938, 1537, 3149, 3368 [for ν(NH), ref.[18] 935, 1530, 3100, 3300]. − ESR: g = 4.15 {ref.[19] 4.20 for [Co(ImH)$_6$](NO_3)$_2$}.

Methods

Thermodynamic Studies: Spectral and thermodynamic measurements were carried out at 25.0 ± 0.1 °C in 0.05 M Tris buffer and 1.0 M $NaClO_4$ for pyridine and 4-methylpyridine, and 0.2 M $NaClO_4$ for imidazole. UV/Vis spectra were recorded with a Varian Cary 5 spectrophotometer using a 1-cm quartz cuvette. The pH of the solutions was measured by employing a Mettler Delta pH meter with a Mettler Toledo Inlab 412 combined glass electrode. The electrode calibration for the H^+ concentration was such that pH is defined as −log[H^+]. All test solutions were kept under nitrogen. Details on the experimental method and treatment of the data have been reported before.[20,21]

Kinetic Studies: An Applied Photophysics, Model SX 18MV, stopped-flow spectrophotometer with an observation path length

of 1.0 cm was used to monitor the kinetics of the substitution reaction of $[Co(Me_6tren)](ClO_4)_2$ with organic bases at ambient pressure. In each case the pH values of the complex and ligand solutions were adjusted to 7.92 ± 0.02 using 0.05 M Tris and $HClO_4$. The ionic strength was kept constant at 1.0 M ($NaClO_4$) for the reactions with pyridine, 4-methylpyridine, and 2-methylimidazole, and at 0.2 M for the reaction with imidazole. Temperature control was achieved by circulation of a thermostated fluid (25.0 ± 0.1 °C). The substitution kinetics were monitored at 470 nm, and kinetic traces as a function of concentration and temperature were recorded with an online computer and subsequently processed to yield kinetic parameters using the OLIS KINFIT program (Bogart, GA). A minimum of at least five kinetic traces were recorded for each set of experimental conditions. The kinetic traces fitted well to a single exponential function. − Kinetic measurements at elevated pressure for the substitution reactions of $[Co(Me_6tren)(H_2O)]^{2+}$ with imidazole and 4-methylpyridine were performed with a home-built stopped-flow unit which can be immersed in a high-pressure chamber.[22] For the reaction with imidazole, the solutions were identical to those used in the ambient pressure experiments and the monitoring wavelength was 470 nm. The temperature was controlled by circulation of a thermostated fluid at 25.0 ± 0.1 °C. For the reaction with 4-methylpyridine, the ionic strength of the solutions was reduced to almost zero and the temperature was increased to 45.0 ± 0.1 °C in order to prevent turbidity problems encountered during the mixing of concentrated solutions. The kinetic data was also checked under ambient conditions at low ionic strength, in order to justify the selected conditions.

Acknowledgments

The authors gratefully acknowledge financial support from the Deutsche Forschungsgemeinschaft, Fonds der Chemischen Industrie, and the Alexander von Humboldt Foundation for fellowships to Z. L. L. and M. S. A. H.

[1] [1a] S. F Lincoln, A. E. Merbach, *Adv. Inorg. Chem.* **1995**, *42*, 1−88. [1b] A. Roodt, A. Abou-Hamdan, H. P. Engelbrecht, A. E. Merbach, *Adv. Inorg. Chem.* **1999**, *49*, 60−126. [1c] R. van Eldik, C. Dücker-Benfer, F. Thaler, *Adv. Inorg. Chem.* **1999**, *49*, 1−58. [1d] H. Elias, *Coord. Chem. Rev.* **1999**, *187*, 37−73.

[2] E. A. Ambundo, M. V. Deydier, A. J. Grall, N. Aguera-Vega, L. T. Dressel, T. H. Cooper, M. J. Heeg, L. A. Ochrymowycz, D. B. Rorabacher, *Inorg. Chem.* **1999**, *38*, 4233−4242, and references cited therein.

[3] D. H. Powell, A. E. Merbach, I. Fabian, S. Schindler, R. van Eldik, *Inorg. Chem.* **1994**, *33*, 4468−4473.

[4] D. H. Powell, P. Furrer, P. A. Pittet, A. E. Merbach, *J. Phys. Chem.* **1995**, *99*, 16622−16629.

[5] F. Thaler, C. D. Hubbard, F. W. Heinemann, R. van Eldik, S. Schindler, I. Fabian, A. M. Dittler-Klingemann, F. E. Hahn, C. Orvig, *Inorg. Chem.* **1998**, *37*, 4022−4029.

[6] A. M. Dittler-Klingemann, C. Orvig, F. E. Hahn, F. Thaler, C. D. Hubbard, R. van Eldik, S. Schindler, I. Fabian, *Inorg. Chem.* **1996**, *35*, 7798−7803.

[7] H. Mäcke, *Helv. Chim. Acta* **1981**, *64*, 1579−1598.

[8] M. Zhang, R. van Eldik, J. H. Espenson, A. Bakac, *Inorg. Chem.* **1994**, *33*, 130−133.

[9] G. Anderegg, V. Gramlich, *Helv. Chim. Acta* **1994**, *77*, 685−689.

[10] H. M. Marques, J. C. Bradley, K. L. Brown, H. Brooks, *Inorg. Chim. Acta* **1993**, *209*, 161−169.

[11] M. S. A. Hamza, J. M. Pratt, *J. Chem. Soc., Dalton Trans.* **1994**, 1367−1371.

[12] [12a] H. E. Toma, J. M. Malin, E. Giesbrecht, *Inorg. Chem.* **1973**, *12*, 2084−2089. [12b] J. M. Malin, H. E. Toma, E. Griesbrecht, *J. Chem. Educ.* **1977**, *54*, 385−386.[12c] W. Byers, J. A. Cossham, J. O. Edwards, A. T. Gordon, J. G. Jones, E. T. P. Kenny, A. Mahamed, J. McKnight, D. A. Sweigart, G. A. Tondreau, T. Wright, *Inorg. Chem.* **1986**, *25*, 4767−4774. [12d] K. J. Schneider, R. van Eldik, *Organometallics* **1990**, *9*, 92−96. [12e] R. A. Henderson, K.E. Oglieve, *J. Chem. Soc., Chem. Commun.* **1994**, 1961−1962.

[13] J. H. Coates, P. R. Collins, S. F. Lincoln, *Aust. J. Chem.* **1980**, *33*, 1381−1389.

[14] M. Clampolini, N. Nardi, *Inorg. Chem.* **1966**, *5*, 41−44.

[15] W. C. Jones, W. E. Bull, *J. Chem. Soc. A* **1968**, 1849−1852.

[16] R. M. Morrison, R. C. Thompson, *Can. J. Chem.* **1978**, *56*, 985−991.

[17] D. H. Brown, R. H. Nuttall, J. Mcavoy, D. W. A. Sharp, *J. Chem. Soc. A* **1966**, 892−896.

[18] W. J. Davis, J. Smith, *J. Chem. Soc. A* **1971**, 317−324.

[19] A. Bencini, C. Benelli, D. Gatteschi, C. Zanchini, *Inorg. Chem* **1983**, *22*, 2123−2126.

[20] S. F. Lincoln, C. D. Hubbard, *J. Chem. Soc., Dalton. Trans.* **1974**, 2513−2516.

[21] I. Fábián, H. Diebler, *Inorg. Chem.* **1987**, *26*, 925−928.

[22] R. van Eldik, W. Gaede, S. Wieland, J. Kraft, M. Spitzer, D. A. Palmer, *Rev. Sci. Instrum.* **1993**, *64*, 1335−1357.

Received June 2, 2000
[I00223]

Synthesis, Characterisation and Electrochemical Behaviour of Rhodium(III) Complexes Containing 1,2-Naphthoquinone-2-oxime and Formation of Imine Complexes through N−O Bond Cleavage

Xiao-Xia Liu[a] and Wing-Tak Wong*[a]

Keywords: Rhodium / N ligands / Electrochemistry

The new rhodium(III) complexes [Rh(η^2-nqo)L_2Cl_2] **(1a–1d)** and [Rh(η^2-nqo)$_2$LCl] **(2b–2d)** [**1a**, L = PPh_3; **1b,2b**, L = pyridine (py); **1c,2c**, L = 4-phenylpyridine (ppy); **1d,2d**, L = 4-acetylpyridine (apy)] have been prepared by treatment of the reaction mixture of $RhCl_3 \cdot 3H_2O$ and 1,2-naphthoquinone-2-oxime (nqo) in ethanol by P or N donor ligands. Cyclic voltammetric studies show that the new complexes display an irreversible metal-localised two-electron reduction from Rh^{III} to Rh^{I}, accompanied by the loss of the chloride ligands. The 1,2-naphthoquinone-2-imine (nqi) complexes [Rh(η^2-nqo)(η^2-nqi)Cl_2]·L **(3b–3d)** (**3b**, L = py; **3c**, L = ppy; **3d**, L = apy), [Rh(η^2-nqo)(η^2-nqi)Cl_2] **(4)** and [Rh(η^2-nqo)$_2$(nqi)Cl] **(5)** were obtained by deoxygenation of the oxime group in which N–O bond cleavage is observed. The molecular structures of **1a**, **2b**, **4** and **5** were established by single crystal X-ray analyses.

Introduction

Rhodium(III) complexes containing chloride ligands have attracted much attention. They have been shown to be active in processes such as the photochemical[1] and the electrochemical[2−5] reduction of protons or water to dihydrogen, the electrocatalytic hydrogenation of organics,[2−4] and the electrochemical regeneration of NADH from NAD^+.[6,7] Most of the complexes mentioned above contain 2,2-bipyridine type ligands. 1,2-Naphthoquinone-monooximes are another kind of donor ligand with a π-accepting ability.[8,9] In ruthenium 1,2-naphthoquinone-1-oxime complexes, the MLCT from ruthenium(II) to the ligand occurs with comparatively low energy.[10] The existence and the number of this ligand in 2,2-bipyridine-containing ruthenium complexes influence the electrochemical property of the metal centre.[11] Metal complexes containing 1,2-naphthoquinone-monooximes are of interest as they are widely used for analytical purposes[12,13] and are potentially useful for the preparation of a wide variety of organic compounds.[14−17] However, most of the studies have been concerned with first-row transition metals.[14−20] Reports dealing with these ligands involving complexes of second-row transition metals are very limited.[9,11,21,22] As a continuation of our studies on 1,2-naphthoquinone-monooxime complexes of second row transition metals,[10,23−25] we herein present the formation of a series of chloro rhodium(III) complexes containing 1,2-naphthoquinone-2-oxime (abbreviated as nqoH).

[a] Department of Chemistry, The University of Hong Kong, Pokfulam Road, Hong Kong
Fax: (internat.) +852-2547-2933, or -2857-1586
E-mail: wtwong@hkucc.hku.hk

Supporting information for this article is available on the WWW under http://www.wiley-vch.de/home/eurjic or from the author.

Results and Discussion

Synthesis and Characterisation of Rhodium(III) Complexes [Rh(η^2-nqo)L_2Cl_2] (1a−1d) and [Rh(η^2-nqo)$_2$LCl] (2b−2d)

The new rhodium(III) complexes [Rh(η^2-nqo)L_2Cl_2] **(1a−1d)** and [Rh(η^2-nqo)$_2$LCl] **(2b−2d)** [**1a**, L = PPh_3; **1b,2b**, L = pyridine (py); **1c,2c**, L = 4-phenylpyridine (ppy); **1d,2d**, L = 4-acetylpyridine (apy)] were synthesised by the treatment of a reaction mixture of $RhCl_3 \cdot 3H_2O$ and 1,2-naphthoquinone-2-oxime in refluxing ethanol with PPh_3, pyridine, 4-phenylpyridine or 4-acetylpyridine (Scheme 1). Characterisation of the new complexes by spectroscopic methods (^{1}H NMR, FAB MS) reveals that **1a−1d** contain one nqo and two P or N donor ligands coordinated to the metal centre (Table 1). In order to establish the molecular structure of complex **1a**, a single-crystal X-ray diffraction analysis was carried out. The molecular structure of **1a** is depicted in Figure 1, while bond lengths and angles are available in the Supporting Information. The molecule of **1a** contains a pseudo octahedrally coordinated rhodium centre. The nqo ligand coordinates to the metal centre through its oximato N and naphthoquinonic O atoms to form a five-membered metallocyclic ring [O(1)−Rh−N(1) 81.3(2)°]. This coordination mode is very common for 1,2-naphthoquinone-monooxime ligands.[9,10,16,19−25] The molecule also contains two chloride atoms [Cl(1) and Cl(2)], which are *trans* to the oximato N and naphthoquinonic O atoms, respectively ([N(1)−Rh−Cl(1) 170.8(1)°], [O(1)−Rh−Cl(2) 176.5(1)°]), forming an equatorial plane with the nqo ligand. The two phosphane ligands occupy the perpendicular positions to complete the six coordination configuration of the Rh metal centre ([P(1)−Rh−P(2) 178.32(5)°]). The mean Rh−P distance is 2.3945(1)Å, which is similar to other Rh complexes with phosphane coordinated to their metal centre, such as in [Rh(Hdmg)(bdio)(PEt_3)]$^+$[Rh(Hdmg)$_2Cl_2$]$^-$·H_2O (dmg = dimethylglyoximato; bdio = 2,3-butanedione 2-imino 3-oxi-

 © WILEY-VCH Verlag GmbH, 69451 Weinheim, 2001 1434−1948/01/0202−0511 $ 17.50+.50/0

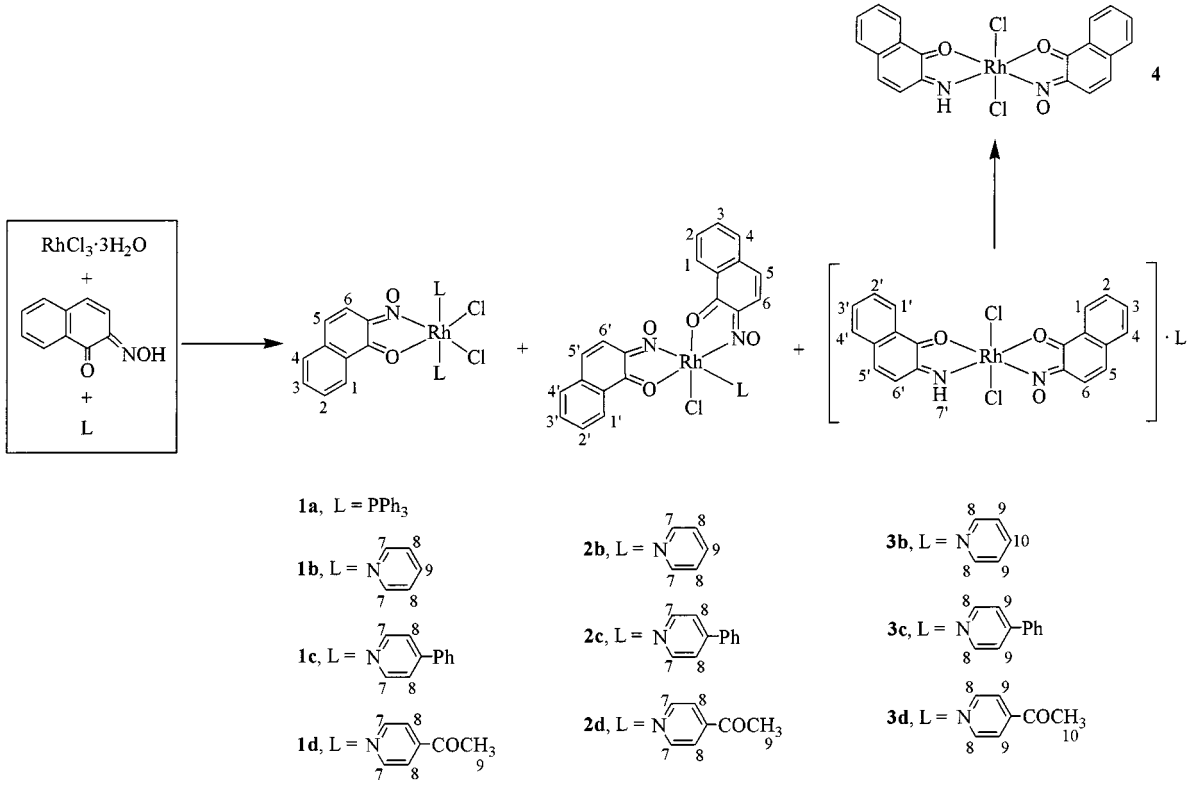

Scheme 1. Reaction of $RhCl_3 \cdot 3H_2O$ with nqoH followed by treatment with the pyridyl ligand

mato), where the corresponding bond length is 2.3817(8)Å.[26] In the ^{1}H NMR spectra of the pyridine complexes **1b**−**1d**, the chemical shifts of the nqo proton signals are very similar to those in **1a**, showing that the nqo ligands have very similar chemical environments. Thus, complexes **1b**−**1d** are proposed to have similar molecular structures to **1a**, with the bidentate nqo ligand and the two chloride atoms occupying the equatorial plane, and the two pyridyl ligands occupying the perpendicular sites.

Characterisation of complexes **2b**−**2d** by spectroscopic methods (Table 1) reveals that they contain two nqo ligands, one pyridyl ligand and one chloride atom. A single crystal X-ray analysis was conducted on **2b**. The molecular structure of [Rh(η^2-nqo)$_2$(py)Cl] **(2b)** is depicted in Figure 2, while the bond parameters can be obtained from the Supporting Information. A distorted octahedral coordination of the rhodium metal centre is observed. The nqo ligands chelate to the metal centre in a similar way as in **1a** [O(1)−Rh−N(1) = 81.3(2)° and O(3)−Rh−N(2) 81.8(2)°]. The oximato N and the naphthoquinonic O atoms adopt a mutually *cis* geometry as in the ruthenium 1,2-naphthoquinone-2-oxime complexes *cis*,*cis*-[Ru(η^2-nqo)$_2$L$_1$L$_2$] (L$_1$, L$_2$ = CO or pyridyl ligands).[10,24] Pyridine is coordinated to the Rh centre through its N atom and is *trans* to the oximato N of an nqo ligand, as in *cis*,*cis*-[Ru(η^2-nqo)$_2$(CO)L] (L = pyridyl ligands).[10,24] The chloride atom is *trans* to the naphthoquinonic O atom of another nqo ligand, with a Rh−Cl bond length of 2.332(2)Å. This is consistent with the Rh−Cl distance in other rhodium complexes such as [Rh(Hdmg)(bdio)(PEt$_3$)]$^+$[Rh(Hdmg)$_2$Cl$_2$]$^-\cdot$H$_2$O [2.3320(9) Å].[26] The nqo ligands of **2b**−**2d** exist in a similar chemical environment, since they display very similar chemical shifts in their ^{1}H NMR spectra. The spatial arrangement of the ligands in complexes **2b**−**2d** should be the same. The asymmetry of the nqo ligands gives rise to the possibility for the presence of structural isomers other than **2b**−**2d**; in fact, we observe some other minor bands in the reaction mixture from TLC. Unfortunately, we could not isolate or characterise these compounds.

Electrochemistry of Complexes 1a−1d and 2b−2d

Cyclic voltammetry of complexes **1a**−**1d** and **2b**−**2d** was performed at a standard scan rate of 100 mV s^{-1} in CH_2Cl_2/0.1 M tetrabutylammonium hexafluorophosphate (TBAH). The redox potentials are listed in Table 2 and the representative cyclic voltammogram of **1a** is shown in Figure 3.

The electrochemical behaviour of [Rh(η^2-nqo)(PPh$_3$)$_2$Cl$_2$] **(1a)** resembles that of other chloro rhodium(III) complexes with 2,2′-bipyridyl ligands, such as [RhL(P)$_2$(Cl)$_2$]$^+$ [2,27] and [RhL$_2$(Cl)$_2$]$^+$,[3,28,29] and some complexes containing π-coordinated ligands [Rh(C$_5$Me$_5$)LCl]$^+$ (P = PPh$_2$Et or PPh$_3$; L = 2,2-bipyridyl ligands).[1,4−6,30−32] This behaviour is characterised by an irreversible, metal-localised two-electron reduction at peak potential E_{c1}, which is associated with the loss of the two chloride ligands (EC mechanism) yielding the Rh^I complex [Scheme 2, Equation (1)]. A controlled-potential electrolysis at a potential slightly negative to this wave, consumes two electrons per molecule of com-

Table 1. Spectroscopic data for compounds **1a−1d**, **2b−2d**, **3b−3d** and **4−7**

Complex	^{1}H NMR spectra (δ, *J*/Hz)	^{31}P NMR spectra (δ, *J*/Hz)	Mass spectra[a] (*m*/*z*)
1a	8.01 (d, J = 7.9, 1 H, H^1), 7.72−7.66 (m, phenyl, 12 H), 7.52 (m, 1 H, H^3), 7.37 (m, 1 H, H^4), 7.35 (m, 1 H, H^2), 7.30−7.25 (m, 6 H, phenyl), 7.22−7.17 (m, 12 H, phenyl), 6.48 (d, J = 9.5, 1 H, H^5), 6.32 (d, J = 9.5, 1 H, H^6)[b]	18.26 [d, J(Rh,P) = 90.7]	834 (870)[c]
1b	8.99 (m, 2 H, H^7), 8.80 (m, 2 H, H$^{7'}$), 8.64 (m, 1 H, H^1), 7.98 (tt, J = 7.6, 1.5, 1 H, H^9), 7.90 (tt, J = 7.6, 1.5, 1 H, H$^{9'}$), 7.66 (m, 1 H, H^3), 7.60 (m, 1 H, H^4), 7.53 (m, 2 H, H^8), 7.51 (m, 1 H, H^2), 7.41 (m, 2 H, H$^{8'}$), 7.40 (d, J = 9.5, 1 H, H^6), 6.94 (d, J = 9.5, 1 H, H^5)	–	504 (504)
1c	9.04 (br.d, J = 6.5, 2 H, H^7), 8.84 (m, 2 H, H$^{7'}$), 8.65 (d, J = 7.7, 1 H, H^1), 7.73 (m, 2 H, H^8), 7.74−7.68 (m, 4 H, phenyl), 7.67 (m, 1 H, H^3), 7.61 (m, 3 H, H$^{4,8'}$), 7.58−7.54 (m, 6 H, phenyl), 7.53 (m, 1 H, H^2), 7.42 (d, J = 9.5, 1 H, H^6), 6.95 (d, J = 9.5, 1 H, H^5)[b]	–	621 (656)[c]
1d	9.19 (br.d, J = 6.6, 2 H, H^7), 9.00 (m, 2 H, H$^{7'}$), 8.61 (d, J = 7.9, 1 H, H^1), 7.95 (dd, J = 5.2, 2 H, 1.5, H^8), 7.82 (dd, J = 5.4, 2 H, 1.5, H$^{8'}$), 7.68 (m, 1 H, H^3), 7.61 (br.d, J = 7.2, 1 H, H^4), 7.52 (m, 1 H, H^2), 7.38 (d, J = 9.5, 1 H, H^6), 6.96 (d, J = 9.5, 1 H, H^5), 2.72 (s, 3 H, H^9 or H$^{9'}$), 2.70 (s, 3 H, H$^{9'}$ or H^9)	–	552 (588)[c]
2b	8.99 (br.d, J = 5.3, 2 H, H^7), 8.75 (d, J = 7.7, 1 H, H^1), 8.42 (d, J = 7.9, 1 H, H$^{1'}$), 7.89 (m, 1 H, H^9), 7.71 (m, 1 H, H^3), 7.63 (m, 1 H, H$^{3'}$), 7.62 (m, 1 H, H^4), 7.56 (m, 2 H, H$^{2,4'}$), 7.50 (m, 2 H, H^8), 7.42 (m, 1 H, H$^{2'}$), 7.33 (m, 1 H, H$^{6'}$), 7.18 (d, J = 9.5, 1 H, H^6), 6.90 (d, J = 9.5, 1 H, H$^{5'}$), 6.89 (d, J = 9.5, 1 H, H^5)[b]	–	562 (562)
2c	8.99 (br.d, J = 6.6, 2 H, H^7), 8.77 (d, J = 8.0, 1 H, H^1), 8.44 (d, J = 7.8, 1 H, H$^{1'}$), 7.71 (m, 1 H, H^3), 7.67 (m, 2 H, H^8), 7.63 (m, 1 H, H$^{3'}$), 7.63−7.55 (m, 3 H, H^4, 2H of phenyl), 7.58 (m, 1 H, H^2), 7.52−7.49 (m, 4 H, H$^{4'}$, 3H of phenyl), 7.43 (m, 1 H, H$^{2'}$), 7.35 (d, J = 9.5, 1 H, H$^{6'}$), 7.20 (d, J = 9.5, 1 H, H^6), 6.91 (d, J = 9.5, 1 H, H$^{5'}$), 6.89 (d, J = 9.5, 1 H, H^5)[b]	–	638 (638)
2d	9.20 (br.d, J = 6.5, 2 H, H^7), 8.73 (d, J = 7.9, 1 H, H^1), 8.41 (d, J = 8.4, 1 H, H$^{1'}$), 7.92 (dd, J = 5.1, 1.7, 2 H, H^8), 7.72 (m, 1 H, H^3), 7.63 (m, 1 H, H$^{3'}$), 7.62 (m, 1 H, H^4), 7.57 (m, 1 H, H^2), 7.56 (d, J = 7.8, 1 H, H$^{4'}$), 7.43 (m, 1 H, H^2), 7.31 (d, J = 9.5, 1 H, H$^{6'}$), 7.18 (d, J = 9.5, 1 H, H^6), 6.91 (d, J = 9.5, 1 H, H$^{5'}$), 6.89 (d, J = 9.5, 1 H, H^5), 2.64 (s, 3 H, H^9)[b]	–	568 (604)[c]
3b	11.46 (br., 1 H, H$^{7'}$), 9.13 (m, 2 H, H^8), 8.64 (d, J = 8.1, 1 H, H^1), 8.24 (d, J = 7.6, 1 H, H$^{1'}$), 8.00 (t, J = 7.6, 1 H, H^{10}), 7.67 (m, 2 H, H$^{3,3'}$), 7.60 (m, 2 H, H^9), 7.57 (m, 1 H, H^4), 7.51 (m, 1 H, H^2), 7.48 (m, 1 H, H$^{2'}$), 7.39 (d, J = 9.5, 1 H, H^6), 7.32 (br.d, J = 7.6, 1 H, H$^{4'}$), 7.09 (br.d, J = 10.2, 1 H, H$^{6'}$), 6.96 (br.d, J = 10.2, 1 H, H$^{5'}$), 6.94 (d, J = 9.5, 1 H, H^5)	–	582 (582)
3c	11.50 (br., 1 H, H$^{7'}$), 9.13 (br.d, J = 6.6, 2 H, H^8), 8.66 (d, J = 7.9, 1 H, H^1), 8.25 (d, J = 7.6, 1 H, H$^{1'}$), 7.77 (br.d, J = 6.6, 1 H, H^9), 7.75−7.72 (m, 2 H, phenyl), 7.67 (m, H, H$^{3'}$), 7.65 (m, 1 H, H^3), 7.61 (br.d, J = 7.1, 1 H, H^4), 7.58−7.54 (m, 3 H, phenyl), 7.51 (m, 1 H, H^2), 7.49 (m, 1 H, H$^{2'}$), 7.40 (d, J = 9.5, 1 H, H^6), 7.32 (br.d, J = 7.5, 1 H, H$^{4'}$), 7.11 (br.d, J = 10.2, 1 H, H$^{6'}$), 7.03 (br.d, J = 10.2, 1 H, H$^{5'}$), 6.95 (d, J = 9.5, 1 H, H^5)[b]	–	658 (658)
3d	11.40 (br., 1 H, H$^{7'}$), 9.34 (br.d, J = 6.5, 2 H, H^8), 8.61 (d, J = 7.9, 1 H, H^1), 8.25 (d, J = 7.8, 1 H, H$^{1'}$), 7.99 (dd, J = 5.2, 1.5, 1 H, H^9), 7.68 (m, 1 H, H$^{3'}$), 7.66 (m, 1 H, H^3), 7.61 (br.d, J = 7.1, 1 H, H^4), 7.52 (m, 1 H, H^2), 7.49 (m, 1 H, H$^{2'}$), 7.38 (d, J = 9.5, 1 H, H^6), 7.33 (br.d, J = 7.4, 1 H, H$^{4'}$), 7.11 (dd, J = 10.1, 1.3, 1 H, H$^{6'}$), 6.98 (br.d, J = 10.1, 1 H, H$^{5'}$), 6.96 (d, J = 9.5, 1 H, H^5), 2.71 (s, 3 H, H^{10})[b]	–	624 (624)
4	–	–	331 (503)[d]
5	10.30 (br., 1 H, H$^{7''}$), 8.82 (d, J = 7.9, 2 H, H$^{1,1'}$), 7.98 (d, J = 7.4, 1 H, H$^{1''}$), 7.75 (br.d, J = 10.1, 1 H, H$^{5''}$), 7.67 (m, 1 H, H^3 or H$^{3'}$), 7.65 (m, 1 H, H$^{3'}$ or H^3), 7.60 (m, 1 H, H$^{3''}$), 7.57 (m, 2 H, H$^{2,2'}$), 7.56 (br.d, J = 7.2, 2 H, H$^{4,4'}$), 7.39 (m, 1 H, H$^{6''}$), 7.37 (m, 1 H, H$^{2''}$), 7.34 (d, J = 9.5, 2 H, H$^{6,6'}$), 7.30 (br.d, J = 7.7, 1 H, H$^{4''}$) 6.86 (d, J = 9.5, 2 H, H$^{5,5'}$)	–	639 (640)
6	8.58 (d, J = 8.0, 3 H, H$^{1,1',1''}$), 7.69 (m, 3 H, H$^{3,3',3''}$), 7.60 (br.d, J = 7.4, 3 H, H$^{4,4',4''}$), 7.49 (m, 3 H, H$^{2,2',2''}$), 7.20 (d, J = 9.5, 3 H, H$^{6,6',6''}$), 6.92 (d, J = 9.5, 3 H, H$^{5,5',5''}$)[b]	–	620 (619)[e]
7	8.59 (d, J = 8.0, 1 H, H^1), 8.50 (d, J = 8.0, 2 H, H$^{1',1''}$), 7.70−7.64 (m, 3 H, H$^{3,3',3''}$), 7.60−7.57 (m, 3 H, H$^{4,4',4''}$), 7.51−7.45 (m, 3 H, H$^{2,2',2''}$), 7.27 (m, 1 H, H^6 or H$^{6'}$ or H$^{6''}$), 7.25 (m, 1 H, H^6 or H$^{6''}$), 7.20 (d, J = 9.5, 1 H, H^6, or H$^{6'}$ or H$^{6''}$), 6.95 (d, J = 9.5, 1 H, H$^{5'}$ or H$^{5''}$), 6.93 (d, J = 9.5, 2 H, H$^{5,5'or5''}$)[b]	–	620 (619)[e]

[a] Calculated values in parentheses. – [b] By ^{1}H,^{1}H COSY NMR spectroscopy. – [c] Only [M − Cl]$^+$ is observed. – [d] Only [M − nqo]$^+$ is observed. – [e] By ESI MS.

plex and leads to a purple-coloured solution. We failed to isolate the purple product as it was not stable enough under our experimental conditions. The colour of the solution slowly changed to red on removing the applied potential. The reverse process, the reoxidation of the Rh^I complex, is also a two-electron step (E_{a1}), with subsequent completion of the coordination sphere of the d^6 metal centre by addition of the chloride ligands [Equation (2)].

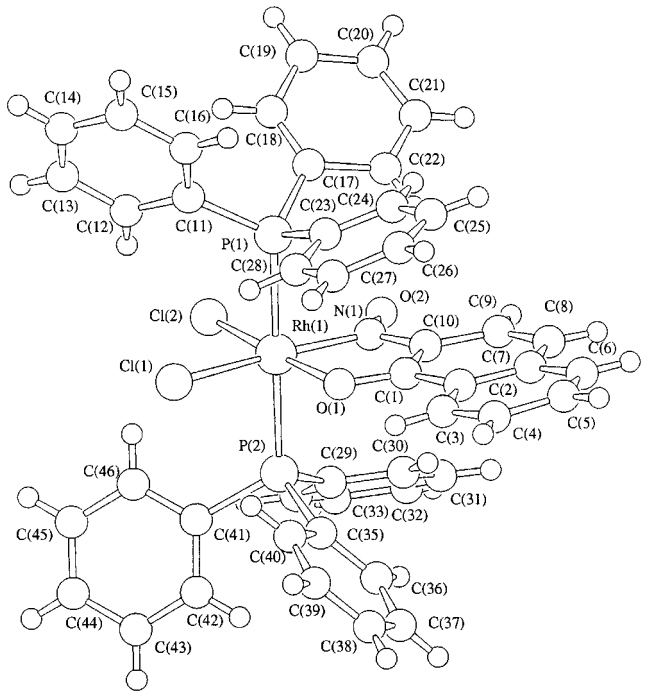

Figure 1. The molecular structure of $[Rh(\eta^2\text{-nqo})(PPh_3)_2Cl_2]$ **(1a)** with the atom numbering scheme

The Rh^I complex can be further reduced at a more negative potential with an apparently reversible (E_{c2}, E_{a2}) single-electron step. The 2,2-bipyridyl complexes displayed similar reversible redox couples, which have been attributed to the reduction of the pyridyl ligand, leading to the coordinated radical anion $L^{\cdot -}$. Lund reported the cyclic voltammetric study of fluorenone oxime (F1=NOH), which displayed a nearly reversible reduction at −1.67 V vs. SCE to its radical anion $F1{=}NOH^{\cdot -}$.[33] The reduction of the oxime group in a copper(II) complex $[Cu(H_2L)(H_2O)_2]Cl_2$ [L is a tripodal ligand containing an oxime group, such as *N*,*N*-(2-hydroxyacetophenyl)-(3-butane-2-oxime)-*N*′-(2-hydroxyacetophenyl)-1,2-diaminoethane] appeared around −1.5 V vs. SCE.[34] Similarly, the one-electron reduction of our nqo complex **1a** is oximato-ligand centred [Equation (3)] and leads to the radical anion. Compared with the free ligand (Table 2), the coordinated nqo is more difficult to reduce due to the π back-donation from the metal centre to the ligand.[30,35] This reduction process for complexes **1b**−**1d** appears at a more negative potential than that of **1a**. As the phosphane is a π-acceptor ligand, the degree of metal-to-nqo-ligand electron shift is smaller in **1a** than in **1b**−**1d**. This ligand-based reduction in complexes **1b**−**1d** is irreversible, and the reoxidation peak of Rh^I to Rh^{III} is not detected. In complexes **2b**−**2d**, apart from the irreversible metal-centred processes, two *quasi*-reversible one-electron reductions of the nqo ligands (E_{c2} for one nqo and E_{c3} for another) at less-negative potentials are observed. Since there are two nqo ligands in each of the **2b**−**2d** complexes,

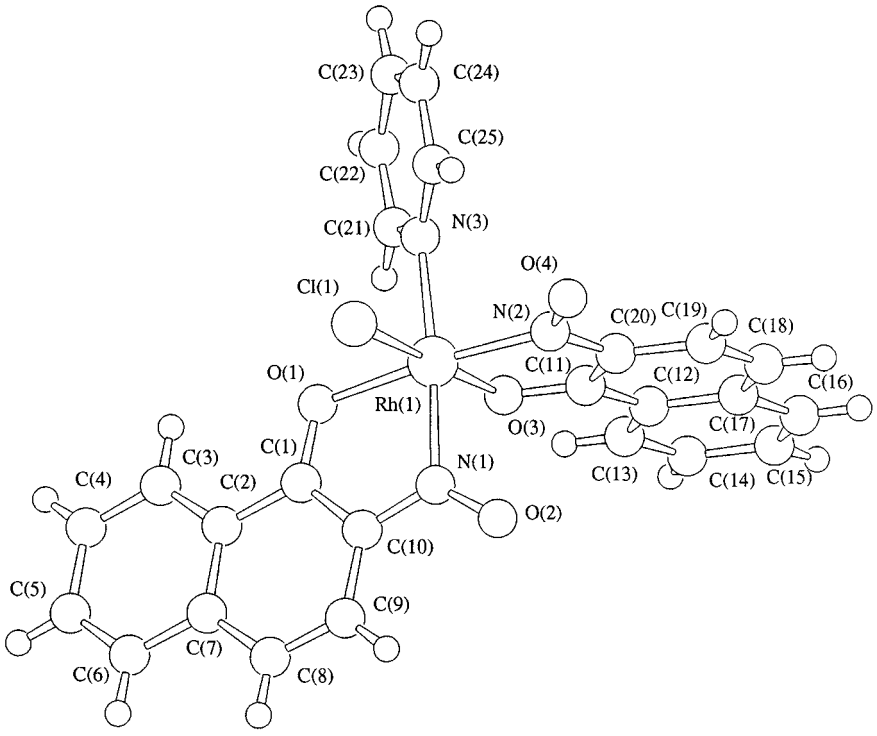

Figure 2. The molecular structure of $[Rh(\eta^2\text{-nqo})_2(py)Cl]$ **(2b)** with the atom numbering scheme

Table 2. Electrochemical data for the free ligand nqoH and complexes **1a**−**1d** and **2b**−**2d**

Compound	E_{c1} [a]	E_{a1}	E_{c2}	E_{a2}	$E_{a2}-E_{c2}$	E_{c3}	E_{a3}	$E_{a3}-E_{c3}$
nqoH	–	–	−1.08[b]	−0.87	0.21	–	–	–
1a	−1.23[b]	0.14	−1.61[c]	−1.51	0.10	–	–	–
1b	−1.12[b]	–	−1.81[b]	–	–	–	–	–
1c	−1.18[b]	–	−1.83[b]	–	–	–	–	–
1d	−1.19[b]	–	−1.81[b]	–	–	–	–	–
2b	−1.09[b]	−0.78	−1.26[d]	−1.15	0.11	−1.43[d]	−1.31	0.12
2c	−1.14[b]	−0.75	−1.31[d]	−1.15	0.16	−1.52[d]	−1.34	0.18
2d	−1.11[b]	−0.72	−1.23[d]	−1.12	0.11	−1.49[d]	−1.32	0.17

[a] Peak potentials in volts vs. $Fc^{0/+}$ obtained from cyclic voltammetry at 100 mV s^{-1} in CH_2Cl_2/0.1 mol dm^{-3} TBAH. – [b] Irreversible. – [c] Apparently reversible. – [d] *Quasi*-reversible.

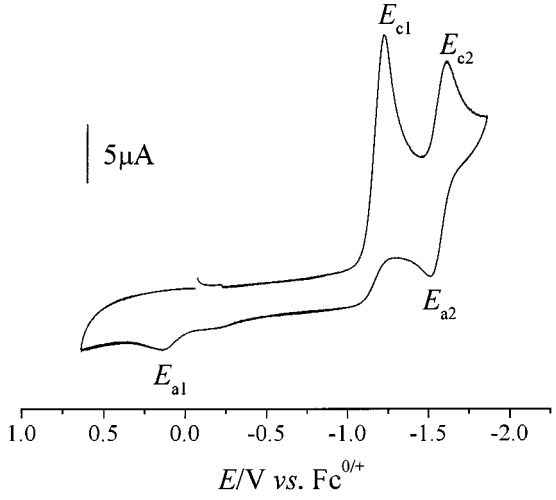

Figure 3. Cyclic voltammogram of $[Rh(\eta^2\text{-nqo})(PPh_3)_2Cl_2]$ **(1a)** in CH_2Cl_2 containing 0.1 mol dm^{-3} TBAH; scan rate, 100 mV s^{-1}

$$[Rh^{III}(nqo)(PPh_3)_2Cl_2] + 2e^- \xrightarrow{E_1} [Rh^{I}(nqo)(PPh_3)_2] + 2Cl^- \quad (1)$$

$$[Rh^{I}(nqo)(PPh_3)_2] - 2e^- + 2Cl^- \xrightarrow{E_2} [Rh^{III}(nqo)(PPh_3)_2Cl_2] \quad (2)$$

$$[Rh^{I}(nqo)(PPh_3)_2] + e^- \underset{E_4}{\overset{E_3}{\rightleftharpoons}} [Rh^{I}(nqo^{\cdot-})(PPh_3)_2]^- \quad (3)$$

Scheme 2. Electrochemical reactions of $[Rh(\eta^2\text{-nqo})(PPh_3)_2Cl_2]$ **1a**

the π back-donation from the metal centre to each nqo ligand will be less than that in complexes **1b**−**1d** with only one nqo ligand present.

Formation of 1,2-Naphthoquinone-2-imine Complexes

The orange-red complexes **3b**−**3d** are also afforded in the reactions with pyridyl ligands (Scheme 1). Their ^1H NMR spectra show the signals for the naphthalene ring and pyridyl protons with an integration ratio of 2:1, and also a broad peak near δ = 11.4, assigned to the NH proton, which disappears after D_2O exchange. In the $^1H,^1H$ COSY spectra of **3c** and **3d**, this peak is coupled with proton $H^{6'}$ of the nqo-derived ring. It can be assigned to the proton on the imino N atom. Slow evaporation of a $CHCl_3$ solution of complexes **3b**−**3d** gave a red crystalline product **4**. An X-ray diffraction analysis was carried out on a single crystal to elucidate the molecular structure. The molecular structure of **4** is shown in Figure 4, and the corresponding bond parameters are available from the supplementary material. The molecule contains two chloride atoms, one nqo ligand and one oximato deoxygenated nqo ligand. There is no pyridyl ligand. The central metal atom also adopts a distorted octahedral coordination mode, as in **1a** and **2b**. The two chloride atoms are *trans* to each other [Cl(1)−Rh−Cl(2) = 178.5(2)°] and the two naphthalene-derived rings occupy the equatorial plane. The nqo and the nqo-derived ligands adopt a chelate mode to the metal centre. The C−O bond length O(3)−C(11) in the nqo-derived ligand is 1.24(2)Å, which is comparable with the corresponding bond length for the quinonic group [C−O = 1.247(5)Å] in 3-hydroxy-2-methyl-1,4-benzoquinone 4-oxime,[36] and is smaller than the corresponding one [O(1)−C(1) = 1.32(1)Å] for the nqo ligand in the same molecule. The C−N bond length ([N(2)−C(20) = 1.27(1) Å]) is of a similar length to the imino C−N bond length [1.294(5)Å] in $[Rh(Hdmg)(bdio)(PEt_3)_2]^+[Rh(Hdmg)_2Cl_2]^-\cdot H_2O$[26] and also to that in $[TcCl(dmg)_2(bdio)BEt]$ [av. C−N = 1.29(1)Å].[37] This bond length is shorter than the corresponding one [N(1)−C(10) = 1.43(2)Å] for the nqo ligand, similar to the situation for the naphthoquinonic group. Complex **4** can be obtained from all three orange-red complexes **3b**−**3d** (based on X-ray single crystal analyses and FAB MS data) under very mild conditions (prolonged standing in $CHCl_3$ solution at room temperature for one day or at −20 °C for a few days). In addition, the pyridyl ligands in **3b**−**3d** can be exchanged with one another, provided that an excess of the pyridyl ligand of the desired complex is added (see below). We suggest that **3b**−**3d** are formed through interaction of the pyridyl ligands with part of a surrounding ligand in **4**. The nqo ligand is believed to undergo N−O bond cleavage of the oximato moiety to give the 1,2-naphthoquinone-2-imino (nqi) ligand, and complex **4** can be formulated as $[Rh(\eta^2\text{-nqo})(\eta^2\text{-nqi})Cl_2]$. Unfortunately, due to the extremely low solubility of **4** in common solvents, we failed to get satisfactory ^1H NMR spectroscopic data. The MS data of **3b**−**3d** conform to the stoichiometry of a molecule containing two chloride atoms, one nqo ligand, one nqi ligand and a pyridine or derived ligand. These complexes can be formulated as $[Rh(\eta^2\text{-nqo})(\eta^2\text{-nqi})Cl_2]\cdot L$ (**3b**, L = py; **3c**, L = ppy; **3d**, L = apy).

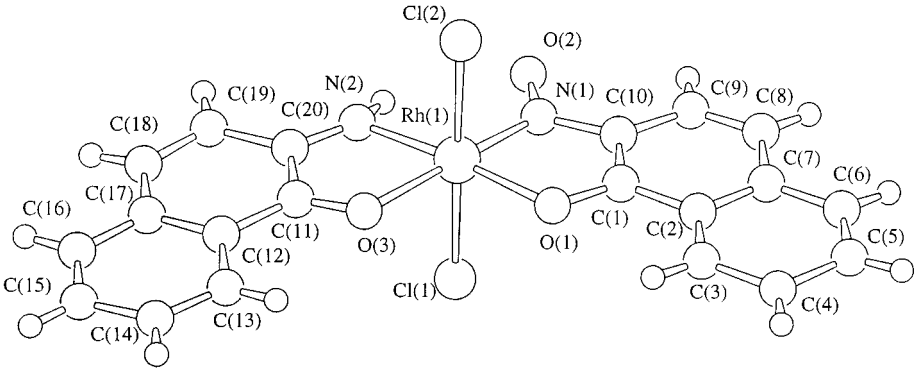

Figure 4. The molecular structure of $[Rh(\eta^2\text{-nqo})(\eta^2\text{-nqi})Cl_2]$ **(4)** with the atom numbering scheme

Conversion Among 3b−3d Through Pyridyl Ligand Exchange

Pyridyl ligand exchange of **3d** by a tenfold excess of pyridine or 4-phenylpyridine at 30 °C was conducted in $CDCl_3$. The reaction mixture was continuously monitored by ^1H NMR spectroscopy and a change in the spectrum observed after 1 h. The proton resonances due to **3d** gradually decrease, accompanied by an increase in the intensities of other proton signals. The proton resonances of **3d** completely disappear after one day. A single product **3b** or **3c** is formed in the two reaction mixtures. The identity of **3b** and **3c** are confirmed by both ^1H NMR spectroscopy and their chromatographic properties. Pyridyl ligand exchange of **3b** by a tenfold excess of 4-acetylpyridine similarly gives **3d** after one day at 30 °C. No crystals of **4** are obtained in these reaction mixtures, even when they stand at room temperature for a long time. This ligand-exchange reaction rate is found to be sensitive to the amount of pyridyl ligand added. A substantial increase in the amount of ligand added results in a faster ligand exchange. This result, along with the isolation of **4** from the $CHCl_3$ solution of **3b−3d**, supports the hypothesis that **3b−3d** are adducts of **4** and the corresponding pyridyl ligand through comparatively loose interaction.

Other Routes for N−O Bond Cleavage of the Oxime Group in 1,2-Naphthoquinone-2-oxime and the Formation of Tris(1,2-naphthoquinone-2-oximato)rhodium(III) Complexes

A low yield (10%) of the N−O bond cleavage product $[Rh(\eta^2\text{-nqo})_2(nqi)Cl]$ **(5)** was obtained from the reaction of nqoH with $[Rh^I(\mu\text{-Cl})(CO)_2]_2$ in benzene. The reaction also affords the tris(1,2-naphthoquinone-2-oximato)-rhodium(III) complexes, *fac*-$[Rh(\eta^2\text{-nqo})_3]$ **(6)** in a 40% yield and *mer*-$[Rh(\eta^2\text{-nqo})_3]$ **(7)** in a 10% yield (Scheme 3). The molecular structure of complex **5** was confirmed by X-ray single crystal analysis. The structure of **5** is shown in Figure 5, while the bond parameters are available from the Supporting Information. The central metal atom adopts an essentially octahedral geometry with three naphthalene-derived rings and one chloride atom. Two of the naphthalene rings are nqo ligands, which occupy the equatorial plane and chelate to the Rh centre in a similar way to other nqoH complexes[10,20,24] including **1a**, **2b** and **4**. The oximato groups, as well as the naphthoquinonic O atoms, adopt a *cis* geometry relative to each other. This differs from our previously determined ruthenium complex *trans,trans*-$[Ru\{\eta^2\text{-(1-nqo)}\}_2(PBu_3)_2]$ (1-nqo = 1,2-naphthoquinone-1-oximato), where both of the oximato N and the naphthoquinonic O atoms in the two equatorial 1-nqo ligands adopt a mutual *trans* geometry.[10] One of the perpendicular positions in **5** is occupied by a chloride atom and the other by an imino N atom of the 1,2-naphthoquinone-2-imino ligand, obtained through the deoxygenation of the oxime group in 1,2-naphthoquinone-2-oxime. The naphthoquinonic O atom of nqi is left pendant with a C−O bond length of 1.26(2)Å, which is comparable with the corresponding ones in complex **4** [1.24(2)Å] and 3-hydroxy-2-

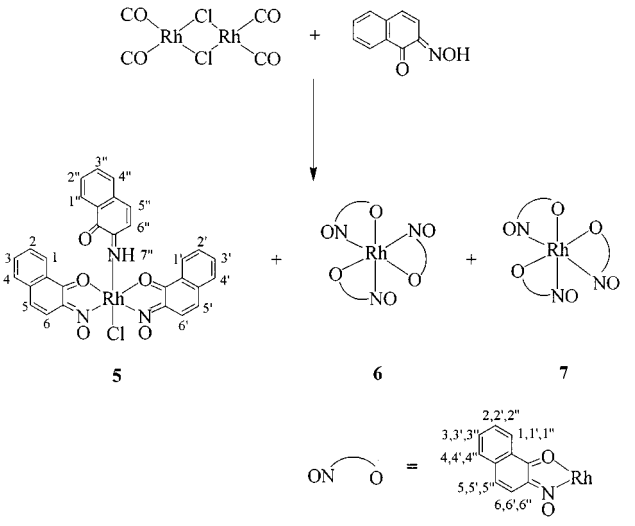

Scheme 3. Reaction of $[Rh^I(\mu\text{-Cl})(CO)_2]_2$ and nqoH

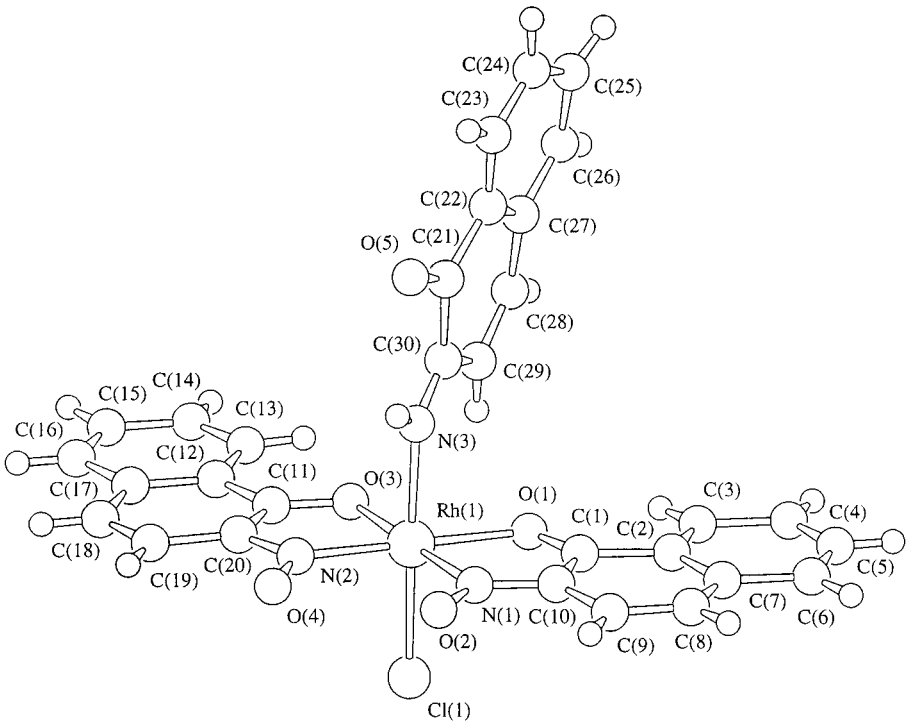

Figure 5. The molecular structure of $[Rh(\eta^2\text{-nqo})_2(nqi)Cl]$ **(5)** with the atom numbering scheme

methyl-1,4-benzoquinone-4-oxime [1.247(5)Å].[36] The C−N bond length of the nqi ligand is [N(3)−C(30) = 1.26(2)Å], which is in good agreement with that in the imino group [N(2)−C(20) = 1.27(1)Å] in **4**. The proton of the NH group appears as a broad peak at δ = 10.30 in the ^{1}H NMR spectrum (Table 1) and also disappears after D_2O exchange.

Previously, there were two other reports on the reduction of the oxime group to imine in rhodium complexes.[26,38] In both cases, $NaBH_4$ was used as the reducing agent. $[Rh^{III}(Hdmg)(H_2dmg)Cl_2]$[26] was first reduced to the Rh^I complex and, upon addition of phosphanes of small size and good donor ability, Rh^I was reoxidised to Rh^{III}, accompanied by the reduction of one of the equatorial oxime groups to imine. We have demonstrated a ruthenium carbonyl-induced deoxygenation of 1,2-naphthoquinone-1-oxime, leading to a coordinated 1,2-naphthoquinone-1-imine intermediate.[23] The ruthenium cluster with naphthoquinone-imino ligands was obtained in low yield through the following coupling reaction. The formation of 1,2-naphthoquinone-2-imine in complex **5** may be caused by the reduction of the oxime group by Rh^I to imine, which is stabilised towards hydrolysis by coordination to the Rh^{III} metal centre. However, in the reaction with $RhCl_3{\cdot}3H_2O$ as the starting material and in the presence of pyridine-type ligands, we have no reducing agent in the system. There are some other reports on the metal-induced deoxygenation of 1,2-naphthoquinone-mono-oxime,[14−18] however, they are all concerned with first-row transition metals. Treatment of the 1,2-naphthoquinone-2-oxime copper(II) complex with PPh_3 gave 2-amino-N^4-(1-hydroxy-2-naphthyl)-1,4-naphthoquinone 4-imine,[16] while 2-amino-1,4-naphthoquinone 4-*N*-phenylimine was obtained on treatment with aniline.[17] Both indicated the formation of nitrene/quinone imine intermediates obtained through the deoxygenation of the oximato group of the ligand. Direct evidence for the imine formation was given by the imine complexes $[Fe(qo{-}A)_2]$ (where qo−A = 4-phenylamino-1,2-naphthoquinone-mono-imine) obtained through the interaction of pentacarbonyl iron(0) with 1,2-naphthoquinone-mono-oxime in the presence of aniline.[18] The reaction between $[Cu\{\eta^2\text{-(1-nqo)}\}_2]$ and aniline gave an imine complex, bis(4-phenylimino-1,2-naphthoquinone-1-imino)bis(aniline)copper(II).[17] The mechanism for the formation of the nqi ligand in **3b**−**3d** and **4** is not certain at this point; however, we believe it occurs as a result of the modification of the coordinated nqo ligand as in the Cu^{II} analogue.[17]

The molecular formulae of **6** and **7**, as established by electrospray ionisation (ESI) mass spectrometry, are consistent with the calculated experimental isotopic patterns for $C_{30}H_{18}N_3O_6Rh$, and reveal their isomeric nature. The isomerism of **6** and **7** was confirmed by ^{1}H NMR spectroscopy in $CDCl_3$. Complex **6** gives rise to the same ^{1}H NMR signals for the three ligands showing that it has a highly symmetrical *fac* geometry as in a very recently structurally characterised ruthenium 1-nqo analogue $[Ru\{\eta^2\text{-(1-nqo)}\}_3]^-$, in which only one set of 1-nqo signals is present for the three ligands.[22] A nickel complex anion $[Ni(4\text{-Clqo})_3]^-$ (4-Clqo = 4-chloro-1,2-benzoquninone-2-oximato)[39] and a naturally occurring pigment ferroverdin[40] *fac*-$[Fe^{II}\{4\text{-}[p\text{-}(CH_2{=}CH)C_6H_4OC(=O)]\text{-1,2-benzoquninone-2-oximato}\}_3]^-$ are other examples of *fac* geometry based on X-ray evidence. Although without X-ray analysis, the geometry of $[Fe^{II}(RQ)_3]^-$ (RQ = 4-R-1,2-benzoquninone-2-ox-

imato, R = Me, *t*Bu, Cl, Br[41] and 3,4-benzo[42]) were also deduced to be *fac*, since the three ligands in the molecule are equivalent (shown by ^{1}H NMR spectroscopy). The three naphthalene rings of complex **7** give rise to different ^{1}H NMR signals, although some of them merge together to give intensified peaks. Thus, complex **7** is proposed to have *mer* geometry as in $[Mn^{III}L_3]$ (L = 4-chloro-1,2-benzoquinone-2-oximato)[43] and $[Ni^{III}(RQ)_3]$ (RQ = 4-R-1,2-benzoquninone-2-oximato, R = Me, *t*Bu and Cl).[44] However, when $[Mn^{III}L_3]$ is electrochemically reduced to anionic $[Mn^{II}L_3]^-$, it exists as a mixture of *fac* and *mer* isomers, both in solution (by ^{1}H NMR spectroscopy) and in the solid state (by X-ray analysis).[43] It was suggested that the favourable *mer* geometry for neutral complexes is partially due to a steric factor, the pendant oximato oxygen atoms are further apart than in the *fac* form. The origin of the *fac* form could be the effect of electrostatic stabilisation.[44] Nevertheless, the complexes are neutral in our system, the *fac* isomer is very favourable and there is no isomerisation observed after separation. This *fac* geometry is also favoured in the tris(arylazooximato)rhodium(III) complexes,[45] whereas the cobalt(III) analogues[46] exist exclusively in the *mer* form. This was explained by an increase in the facial area in going from the Co^{III} to the Rh^{III} chelate.[45]

Experimental Section

All manipulations were carried out under nitrogen with standard Schlenk techniques. Chemicals were purchased from commercial sources and used as received. Preparative thin-layer chromatographic (TLC) plates were prepared from silica (Merck Kieselgel 60 GF_{254}). – ^{1}H NMR spectra were obtained on a Bruker DPX-300 spectrometer using deuterated chloroform as the lock and reference. – Fast atom bombardment (FAB) mass spectra were recorded on a Finnigan MAT 95 mass spectrometer. Electrospray ionisation quadropole ion trap mass spectra were obtained on a Finnigan LCQ™ LC/MS^n system. – Electrochemical measurements were conducted on a PAR 273A potentiostat in CH_2Cl_2 containing 0.1 mol dm^{-3} *n*-tetrabutylammonium hexafluorophosphate (TBAH), using a conventional argon gas sealed three-electrode cell. The working electrode was a glassy carbon disc for cyclic voltammetry and a carbon plate for large-scale electrolysis. Potentials are reported vs. ferrocene internal standard ($Fc^{0/+}$).

Synthesis of $[Rh(\eta^2\text{-nqo})(PPh_3)_2Cl_2]$ (1a): Solid samples of $RhCl_3{\cdot}3H_2O$ (53 mg, 0.2 mmol) and 1,2-naphthoquinone-2-oxime (69 mg, 0.4 mmol) were dissolved in 100 mL ethanol and refluxed for 2 h. PPh_3 (105 mg, 0.4 mmol) in hot ethanol was then added and the solution refluxed for another 10 h. The solvent was then removed and the residue chromatographed by TLC, with a solvent mixture of *n*-hexane/CH_2Cl_2 (1:4, v/v) as the eluent to afford the complex $[Rh(\eta^2\text{-nqo})(PPh_3)_2Cl_2]$ (**1a**; 80%, 139 mg). Red crystals of **1a** were grown by slow evaporation of an *n*-hexane/$CHCl_3$ solution at room temperature. $C_{46}H_{36}Cl_2NO_2P_2Rh$ (870.56): calcd. C 63.5, H 4.2, N 1.6; found C 63.2, H 4.5, N 1.5.).

Synthesis of $[Rh(\eta^2\text{-nqo})L_2Cl_2]$ (1b–1d), $[Rh(\eta^2\text{-nqo})_2LCl]$ (2b–2d), $[Rh(\eta^2\text{-nqo})(\eta^2\text{-nqi})Cl_2]{\cdot}L$ (3b–3d) and the Formation of $[Rh(\eta^2\text{-nqo})(\eta^2\text{-nqi})Cl_2]$ (4): A procedure analogous to the above was followed, adding pyridine (py), 4-phenylpyridine (ppy) or 4-acetylpyridine (apy), respectively, instead of PPh_3. Upon TLC separation with a solvent mixture of *n*-hexane/CH_2Cl_2 (1:5–1:6, v/v), the complexes $[Rh(\eta^2\text{-nqo})L_2Cl_2]$ **(1b–1d)**, $[Rh(\eta^2\text{-nqo})_2LCl]$ **(2b–2d)** and $[Rh(\eta^2\text{-nqo})(\eta^2\text{-nqi})Cl_2]{\cdot}L$ **(3b–3d)** (**1b–3b**, L = py; **1c–3c**, L = ppy; **1d–3d**, L = apy) were isolated. Upon standing in a $CHCl_3$ solution of **3b–3d** at room temperature for one day, red crystals of $[Rh(\eta^2\text{-nqo})(\eta^2\text{-nqi})Cl_2]$ **4** were obtained. Red crystals of **2b** were grown by slow evaporation of *n*-hexane/$CHCl_3$ solution at –20 °C.
1b: $C_{20}H_{16}Cl_2N_3O_2Rh$ (504.1805): calcd. C 47.6, H 3.2, N 8.3; found C 47.8, H 3.1, N 8.1.
1c: $C_{32}H_{24}Cl_2N_3O_2Rh$ (656.3757): calcd. C 58.6, H 3.7, N 6.4; found C 58.3, H 3.9, N 6.3.
1d: $C_{24}H_{20}Cl_2N_3O_4Rh$ (588.2541): calcd. C 49.0, H 3.4, N 7.1; found C 48.7, H 3.2, N 7.3.
2b: $C_{25}H_{17}ClN_3O_4Rh$ (561.7884): calcd. C 53.4, H 3.1, N 7.5; found C 53.5, H 2.9, N 7.2.
2c: $C_{31}H_{21}ClN_3O_4Rh$ (637.8860): calcd. C 58.4, H 3.3, N 6.6; found C 58.7, H 3.4, N 6.4.
2d: $C_{27}H_{19}ClN_3O_5Rh$ (603.8252): calcd. C 53.7, H 3.2, N 7.0; found C, 53.6, H 2.9, N 7.2.
3b: $C_{25}H_{18}Cl_2N_3O_3Rh$ (582.2503): calcd. C 51.6, H 3.1, N 7.2; found C 51.8, H 2.9, N 7.5.
3c: $C_{31}H_{22}Cl_2N_3O_3Rh$ (658.3479): calcd. C 56.6, H 3.4, N 6.4; found C 56.7, H 3.4, N 6.4.
3d: $C_{27}H_{20}Cl_2N_3O_4Rh$ (624.2871): calcd. C 51.9, H 3.2, N 6.7; found C, 51.6, H 2.9, N 7.0.
4: $C_{20}H_{13}Cl_2N_2O_3Rh$ (503.1491): calcd. C 47.7, H 2.6, N 5.6; found C 47.8, H 2.4, H 5.5.

Pyridyl Ligand Exchange of 3d and 3b: Complex **3d** (6 mg, 0.01 mmol) and $CDCl_3$ (1 cm^3) were placed in an oven-dried NMR tube. A tenfold excess of pyridine was added. After warming the tube in a thermostat at 30 °C for 1 h, ^{1}H NMR spectra were recorded at time intervals of 1 h until no **3d** was detected. After 20 h, all **3d** had been converted into **3b** according to the ^{1}H NMR spectroscopic data. The single metal-containing product of **3b** was obtained by TLC separation with a solvent mixture of *n*-hexane/CH_2Cl_2 (1:10, v/v) as the eluent.

The single metal-containing products **3c** and **3d** were obtained by a similar procedure of ligand exchange with **3d** and **3b** and 4-phenylpyridine and 4-acetylpyridine, respectively.

Reaction Between $[Rh^I(\mu\text{-Cl})(CO)_2]_2$ and 1,2-Naphthoquinone-2-oxime: $[Rh^I(\mu\text{-Cl})(CO)_2]_2$ (39 mg, 0.1 mmol) and 1,2-naphthoquinone-2-oxime (104 mg, 0.6 mmol) was dissolved in benzene (50 mL) and stirred at room temperature for 3 h. The solvent was removed from the dark red solution and the residue chromatographed by TLC with *n*-hexane/CH_2Cl_2 (1:5, v/v) as the eluent. Three red products were isolated as $[Rh(\eta^2\text{-nqo})_2(nqi)Cl]$ (**5**; 10%, 13 mg), *fac*-$[Rh(\eta^2\text{-nqo})_3]$ (**6**; 40% yield, 49 mg) and *mer*-$[Rh(\eta^2\text{-nqo})_3]$ (**7**; 10% yield, 12 mg). Single crystals of **5** were grown by slow evaporation of a *n*-hexane/CH_2Cl_2 solution at –20 °C.
5: $C_{30}H_{19}ClN_3O_5Rh$ (639.86): calcd. C 56.3, H 3.0, N 6.6; found C 56.0, H 2.7, N 6.6.
6: $C_{30}H_{18}N_3O_6Rh$ (619.40): calcd. C 58.2, H 2.9, N 6.8; found C 58.0, H 2.6, N 6.8.
7: $C_{30}H_{18}N_3O_6Rh$ (619.40): calcd. C 58.2, H 2.9, N 6.8; found C 58.2, H 3.0, N 7.0.

Crystallography:
Single crystals of **1a**, **2b**, **4** and **5** were obtained as described above. A crystal of **1a** was mounted on a glass fibre by means of epoxy resin, while crystals of **2b**, **4** and **5** were sealed in Lindemann glass capillaries. Crystal intensity data were collected for **1a**, **2b** and **4** on

Table 3. Crystal data and data collection parameters for compounds **1a**, **2b**, **4** and **5**

	1a	**2b**	**4**	**5**
Empirical formula	$C_{46}H_{36}Cl_2NO_2P_2Rh$	$C_{26}H_{18}Cl_4N_3O_4Rh$	$C_{21}H_{14}Cl_5N_2O_3Rh$	$C_{34}H_{27}Cl_9N_3O_5Rh$
M	870.55	681.16	622.52	979.59
Crystal colour, habit	Red, block	Red, block	Orange-red, block	Red, block
Crystal dimensions/mm	0.12 × 0.12 × 0.17	0.22 × 0.16 × 0.18	0.24 × 0.26 × 0.31	0.13 × 0.12 × 0.14
Crystal system	Monoclinic	Triclinic	Monoclinic	Monoclinic
Space group	$P2_1/n$ (no. 14)	$P\bar{1}$(no.2)	$P2_1/n$ (no.14)	$P2_1/n$ (no.14)
a/Å	11.506(1)	7.719(2)	9.088(1)	11.883(1)
b/Å	18.713(1)	12.881(2)	17.651(1)	15.026(2)
c/Å	19.574(1)	15.271(3)	15.154(1)	22.833(1)
α/°	–	111.636(3)	–	–
β/°	106.62(2)	91.619(3)	106.22(2)	96.35(1)
γ/°	–	98.801(3)	–	–
U/Å^3	4038.5(6)	1388.8(4)	2334.1(4)	4051.9(6)
Z	4	2	4	4
D_c/g cm^{-3}	1.432	1.629	1.771	1.606
μ(Mo-K_α)/cm^{-1}	6.73	10.35	13.28	10.56
Reflections collected				38432
Unique reflections	9355	6236	5405	3295
Observed reflectons [$I > 1.5\sigma(I)$]	5568	5092	2635	1885
R	0.051	0.058	0.092	0.094
R'	0.047	0.072	0.077	0.098
Goodness of fit, *S*	1.00	2.51	2.06	2.14

a Siemens Smart CCD and for **5** on a MAR research image-plate scanner, using graphite-monochromated Mo-K_α radiation (λ = 0.71073 Å) for unit-cell determination and data collection. Intensity data were corrected for Lorentz and polarisation effects. An approximation to absorption correction by inter-image scaling was also applied. Summaries of the crystallographic data, structure solution and refinement are given in Table 3. Scattering factors were taken from part a in ref.[47] and anomalous dispersion effects were included in *Fc* (part b). The structures were solved by direct methods (SIR 92[48] for **1a**, **4** and **5**; SHELXS 86[49] for **2b**). The remaining non-hydrogen atoms were determined by subsequent Fourier and Fourier-difference techniques. The structures were refined by full-matrix least-squares analysis on *F*, with all non-hydrogen atoms refined anisotropically until convergence was reached. The hydrogen atoms of the organic moieties were generated in their ideal positions (C−H, 0.95Å). They were included in the structure factor calculations on a Silicon-Graphics computer using the program package TEXSAN.[50]

Crystallographic data (excluding structure factors) for the structures **1a**, **2b**, **4** and **5** reported in this paper have been deposited with the Cambridge Crystallographic Data Centre as supplementary publication no. CCDC-144600 to -144603, respectively. Copies of the data can be obtained free of charge on application to CCDC, 12 Union Road, Cambridge CB2 1EZ, UK [Fax: (internat.) +44-1223/336-033; E-mail: deposit@ccdc.cam.ac.uk].

Acknowledgments

We gratefully acknowledge financial support from the Hong Kong Research Grants Council and the University of Hong Kong. X.-X. Liu acknowledges the receipt of a demonstratorship administered by the Department of Chemistry, University of Hong Kong.

[1] U. Kolle, M. Grutzel, *Angew. Chem. Int. Ed. Engl.* **1987**, *26*, 567−570.
[2] H. C.-Y. Bettega, J.-C. Moutet, S. Tingry, *J. Electroanal. Chem.* **1995**, *391*, 51−61.
[3] I. M. F. De Oliveira, J.-C. Moutet, N. Vlachopoulos, *J. Electroanal. Chem.* **1990**, *291*, 243−249.
[4] C. Caix, S. Chardon-Noblat, A. Deronzier, J.-C. Moutet, S. Tingry, *J. Organomet. Chem.* **1997**, *540*, 105−111.
[5] S. Cosnier, A. Deronzier, N. Vlachopoulos, *J. Chem. Soc., Chem. Commun.* **1989**, 1259−1261.
[6] S. Cosnier, H. Gunther, *J. Electroanal. Chem.* **1991**, *315*, 307−312.
[7] R. Ruppert, S. Herrmann, E. Steckhan, *Tetrahedron Lett*. **1987**, *28*, 6583−6586.
[8] B. Foretic, N. Burger, V. Hankonyi, *Polyhedron* **1995**, *14*, 605−609.
[9] J. Charalambous, W. C. Stoten, K. Henrick, *Polyhedron* **1989**, *8*, 103−107.
[10] X.-X. Liu, W.-T. Wong, *Polyhedron* **2000**, *19*, 7−21.
[11] N. Ghatak, S. Bhattacharya, *Transition Met. Chem*. **1996**, *21*, 423−427.
[12] O. K. Borggaard, H. E. M. Christensen, S. P. Lund, *Analyst* **1984**, *109*, 1179−1182.
[13] O. K. Borggaard, H. E. M. Christensen, T. K. Nielsen, M. Willems, *Analyst* **1982**, *107*, 1479−1483.
[14] H. Barjesteh, E. G. Brain, J. Charalambous, P. Gaganatsou, T. A. Thomas, *J. Chem. Res. (S)* **1995**, 454−454.
[15] A. McKillop, T. S. B. Sayer, *J. Org. Chem.* **1976**, *41*, 1079−1080.
[16] R. G. Buckley, J. Charalambous, M. J. Kensett, M. McPartlin, D. Mukerjee, E. G. Brain, J. M. Jenkins, *J. Chem. Soc., Perkin Trans. 1* **1983**, 693−697.
[17] R. G. Buckley, J. Charalambous, E. G. Brain, *J. Chem. Soc., Perkin Trans. 1* **1982**, 1075−1078.
[18] J. Charalambous, L. I. B. Haines, J. S. Morgan, D. S. Peat, M. J. M. Champbell, J. Bailey, *Polyhedron* **1987**, *6*, 1027−1032.
[19] H. Saarinen, J. Korvenranta, *Acta Chem. Scand.* **1975**, *A29*, 409−413.
[20] J. Korvenranta, H. Saarinen, *Acta Chem. Scand.* **1975**, *A29*, 861−865.
[21] J. Charalambous, K. Henrick, Y. Musa, R. G. Rees, R. N. Whiteley, *Polyhedron* **1987**, *6*, 1509−1512.
[22] A. K. Das, A. Rueda, L. R. Falvello, S.− M. Peng, S. Bhattacharya, *Inorg. Chem*. **1999**, *38*, 4365−4368.
[23] K. K.-H. Lee, W.-T. Wong, *J. Chem. Soc., Dalton Trans.* **1997**, 2987−2995.
[24] K. K.-H. Lee, W.-T. Wong, *J. Organomet. Chem.* **1997**, *547*, 329−335.
[25] X.-X. Liu, W.-T. Wong, *Inorg. Chim. Acta.* **2000**, *299*, 16−27.
[26] R. Dreos, G. Tauzher, S. Geremia, L. Randaccio, F. Asaro, G. Pellizer, C. Tavagnacco, G. Costa, *Inorg. Chem.* **1994**, *33*, 5404−5410.
[27] H. C.-Y. Bettega, J.-C. Moutet, *J. Electroanal. Chem.* **1994**, *364*, 271−275.
[28] I. M. F. De Oliveira, J.-C. Moutet, *J. Electroanal. Chem.* **1993**, *361*, 203−210.

[29] G. Kew, K. DeArmond, K. Hanck, *J. Phys. Chem*. **1974**, *78*, 727−734.
[30] M. Ladwig, W. Kaim, *J. Organomet. Chem.* **1991**, *419*, 233−243.
[31] S. Chardon-Noblat, S. Cosnier, A. Deronzier, N. Vlachopoulos, *J. Electroanal. Chem.* **1993**, *352*, 213−228.
[32] U. Kolle, B.-S. Kang, P. Infelta, P. Comte, M. Gratzel, *Chem. Ber*. **1989**, *122*, 1869−1880.
[33] B. Soucaze-Guillous, H. Lund, *Acta Chem. Scand*. **1998**, *52*, 417−424.
[34] S. Djebbar-Sid, O. Benali-Baitich, J. P. Deloume, *Polyhedron* **1997**, *16*, 2175−2182.
[35] W. Kaim, R. Reinhardt, M. Sieger, *Inorg. Chem*. **1994**, *33*, 4453−4459.
[36] P. C. Christidis, A. Dodd, N. D. Pathirana, J. Charalambous, M. McPartlin, N. Talee, *Acta Cryst*. **1991**, C*47*, 2640−2642.
[37] K. E. Linder, D. P. Nowotnik, M. F. Malley, J. Z. Gougoutas, A. D. Nunn, *Inorg. Chim. Acta* **1991**, *190*, 249−255.
[38] D. Steinborn, M. Rausch, C. Bruhn, *J. Organomet. Chem.* **1998**, *561*, 191−197.
[39] P. W. Carreck, J. Charalambous, M. J. Kensett, M. McPartlin, R. Sims, *Inorg. Nucl. Chem. Lett*. **1974**, *10*, 749−751.
[40] S. Candeloro, D. Grdenic, N. Taylor, B. Thompson, M. Viswamitra, D. C. Hodgkin, *Nature* **1969**, *224*, 589−591.
[41] P. Basu, S. B. Choudhury, S. Pal, A. Chakravorty, *Inorg. Chem.* **1989**, *28*, 2680−2686.
[42] P. Basu, S. Pal, A. Chakravorty, *J. Chem. Soc., Chem. Commun.* **1989**, 977−978.
[43] P. Basu, A. Chakravorty, *J. Chem. Soc., Chem. Commun.* **1992**, 809−810.
[44] D. Ray, A. Chakravorty, *Inorg. Chem.* **1988**, *27*, 3292−3297.
[45] K. C. Kalia, A. Chakravorty, *Inorg. Chem.* **1969**, *8*, 2586−2590.
[46] K. C. Kalia, A. Chakravorty, *Inorg. Chem.* **1968**, *7*, 2016−2020.
[47] D. T. Cromer, J. T. Waber, *International Tables for X-ray Crystallography*, Kynoch Press, Birmingham, **1974**, Vol. 4; (a) Table 2.2.B; (b) Table 2.3.1.
[48] SIR 92, A. Altomare, M. C. Burla, M. Camalli, M. Cascarano, C. Giacovazzo, A. Guagliardi, G. Polidori, *J. Appl. Crystallogr.* **1994**, *27*, 435−442.
[49] G. M. Sheldrick, in *Crystallographic Computing 3*, G. M. Sheldrick, C. Kruger, R. Goddard, Eds., Oxford University Press, **1985**, 175−189.
[50] TEXSAN, Crystal Structure Analysis Package, Molecular Structure Corporation, Houston, TX, **1985** and **1992**.

Received May 24, 2000
[I00215]

Monoanionic *N,N,O*-Scorpionate Ligands and their Iron(II) and Zinc(II) Complexes: Models for Mononuclear Active Sites of Non-Heme Iron Oxidases and Zinc Enzymes

Alexander Beck,[a] Bernhard Weibert,[a] and Nicolai Burzlaff*[a]

Keywords: Scorpionates / Zinc / Iron / Oxidases / Enzymes

The chemical behavior of two bis(3,5-dialkylpyrazol-1-yl)-acetic acids and their coordination properties towards $ZnCl_2$ and $FeCl_2$ was studied. Reaction of bis(3,5-dimethylpyrazol-1-yl)acetic acid (bdmpza) (**1**) with $ZnCl_2$ and $FeCl_2$ gave the 2:1 complexes [$(bdmpza)_2Zn$] (**4**) and [$(bdmpza)_2Fe$] (**5**). Crystal structures of both complexes were obtained. In contrast, the sterically more hindered ligand bis(3,5-di-*tert*-butylpyrazol-1-yl)acetic acid (bdtbpza) (**3**) coordinates only once to zinc(II) resulting in the complex [(bdtbpza)ZnCl] (**6**). This provides a structural model complex for the active sites of zinc enzymes such as thermolysin or carboxypeptidase. The good agreement with these active sites was demonstrated by a crystal structure of **6**. To the best of our knowledge, this is the first report of zinc complexes with a monoanionic *N,N,O*-tridentate ligand using a carboxylate *O*-donor. Substitution of benzylthiolate for the chloride ligand **6** yielded [(bdtbpza)Zn(SCH_2Ph)] (**8**) indicating that the bulky *tert*-butyl groups do not prevent access to the zinc atom. Reaction of bdtbpza (**3**) with $FeCl_2$ led to [(bdtbpza)FeCl] (**7**), which might serve as a structural model complex for the active sites of mononuclear non-heme iron oxidases and oxygenases such as IPNS, DAOCS or CAS.

Introduction

In recent years, there has been a significant progress in the structural characterization of mononuclear non-heme iron enzymes involved in dioxygen activation.[1] The facial motif of the three metal binding amino acids histidine, histidine and aspertate or glutamate is thought to be essential in many of these enzymes.[2] This has caused a growing interest in model complexes for the active sites of these enzymes. The so called facial 2-His-1-carboxylate triad, a term introduced by Que Jr.,[2] is found, for example, in enzymes such as tyrosine hydroxylase (TyrH),[3] 2,3-dihydroxy-biphenyl 1,2-dioxygenase (extradiol catechol dioxygenase) (BphC),[4] isopenicillin N synthase (IPNS)[5–7] or α-ketoglutarate-dependent enzymes such as deacetoxycephalosporine C synthase (DAOCS)[8] and clavaminic acid synthase (CAS).[9]

Due to the lack of suitable monoanionic *N,N,O* ligands that mimic this facial triad, model complexes with *N,N,N* tripod ligands were used to study these enzymatic reactions. The work of Que, Kitajima or Moro-oka often focused on tris(pyrazol-1-yl)borate (Tp) and tris(2-pyridylmethyl)amine (TPA) ligands.[10]

Furthermore, zinc complexes with such *N,N,O* ligands could serve as models for the active site of several zinc enzymes, binding the metal with two histidines and one glutamate. Examples are carboxypeptidase A and thermolysin.[11] Bioinorganic experiments with zinc complexes by Vahrenkamp, Moro-oka and Parkin are again often based on *N,N,N* ligands such as Tp and TPA.[12] Parkin accessed *N,N,O* model complexes indirectly by insertion of formaldehyde or carbon dioxide into a borohydride bond of zinc bis(pyrazol-1-yl)hydroborate complexes.[13,14] Recently, Carrano published the scorpionate ligand (3-*tert*-butyl-2-hydroxy-5-methylphenyl)-bis(3,5-dimethylpyrazol-1-yl)-methane to generate model complexes of zinc enzymes.[15,16] Instead of a carboxylate *O*-donor, this ligand contains a phenolate *O*-donor. Last year Otero et al. introduced for the first time with bis(3,5-dimethylpyrazol-1-yl)acetate (bdmpza, **1**) (Figure 1) and the resulting niobium complex [$NbCl_2$(bdmpza)(PhCCMe)], a scorpionate ligand with a carboxylate and two pyrazole donor groups.[17]

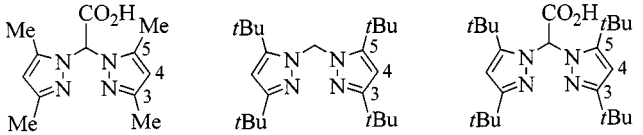

Figure 1. Bispyrazol-1-yl ligands

Herein we report on model complexes of zinc and iron with the scorpionate ligand bis(3,5-dimethylpyrazol-1-yl)acetate (bdmpza, **1**) and the new, sterically more hindered bis(3,5-di-*tert*-butylpyrazol-1-yl)acetate (bdtbpza, **3**).

Results

In our quest to find suitable *N,N,O* ligands as models for the active sites of the facial 2-His-1-carboxylate triad in iron- and zinc-containing enzymes, scorpionate ligands like bis(3,5-dimethylpyrazol-1-yl)acetate (bdmpza, **1**) seemed to be suitable as a mimic for this facial triad.

[a] Fachbereich Chemie der Universität Konstanz,
Universitätsstraße 10, Fach M728, 78457 Konstanz, Germany
Fax: (internat.) +49-(0)7531/883-251
E-mail: nicolai@chemie.uni-konstanz.de

 © WILEY-VCH Verlag GmbH, 69451 Weinheim, 2001 1434–1948/01/0202–0521 $ 17.50+.50/0

In addition to the multistep ligand synthesis published by Otero et al., we found a simple one-step synthesis for bdmpza (**1**) starting from commercially available reagents [Equation (1)].

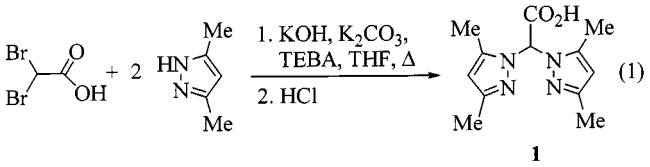

1

Treatment of dibromoacetic acid with two equivalents of 3,5-dimethylpyrazole and an excess of potassium hydroxide, potassium carbonate and a small portion of phase-transfer catalyst gave bdmpza (**1**) in reasonable yield. Unreacted 3,5-dimethylpyrazole could be recycled by extraction with diethyl ether at neutral pH value. The ^{1}H and ^{13}C NMR spectra exhibit resonances similar to those reported by Otero et al. for 0.25 [{Li(H_2O)(bdmpza)}$_4$].[17] Compound **1** is slightly soluble in water. In D_2O a resonance $\delta(^{1}H) = 14.02$ was detected that disappeared after 30 minutes and was assigned to the carboxylate proton.

Reaction of bdmpza (**1**) with the biologically relevant metals iron and zinc afforded the 2:1 complexes **4** and **5**. The double coordination of bdmpza to the metals demonstrated too small a steric hindrance of the ligand bdmpza (**1**). Even equimolar amounts of bdmpza (**1**), base and water-free $ZnCl_2$ or $FeCl_2$ yielded only coordination compounds with two scorpionate ligands bound to the metals. The target compounds [(bdmpza)ZnCl] and [(bdmpza)-FeCl] could not be detected. The formation of small amounts of them should be detectable by MS from the typical isotopic fingerprint of the chlorine atom.

The infrared spectra of both complexes [(bdmpza)$_2$Zn] (**4**) and [(bdmpza)$_2$Fe] (**5**) show an intense $\nu_{as}(CO_2^-)$ absorption at 1659 cm^{-1} and medium intensity bands at 1558 cm^{-1} due to ν(C=N). These values fit those reported for the niobium complex [$NbCl_2$(bdmpza)(PhCCMe)].[17] Complex **4** was characterized spectroscopically. Due to four equivalent pyrazolyl rings, only one set of resonances was detected for these rings. For the paramagnetic complex **5** a ^{1}H NMR spectrum was recorded that shows four single signals at $\delta(^{1}H) = 1.2$, 7.0, 14.4 and 55.7. These resonances were assigned to H^4 of the pyrazolyl groups, the two methyl groups and the proton at the bridging carbon atom, respectively.

The iron compound **5** is stable and can be handled in solution for short periods of time in air. Attempts to exchange one of the bdmpza ligands in **5** with a thiolate ligand have not been successful. X-ray structure determinations of the complexes [(bdmpza)$_2$Zn] (**4**) and [(bdmpza)$_2$Fe] (**5**) finally confirmed their identity (Figure 2 and 3). Selected distances and angles are summarized in Table 1.

The coordination spheres around the zinc and iron atoms are almost octahedral with the scorpionate "clamp" causing a deviation of 4−6° from the 90° angle. The good correspondence of both structures in distances and angles emphasizes the similarity of zinc(II) and iron(II) according to their coordination reactions.

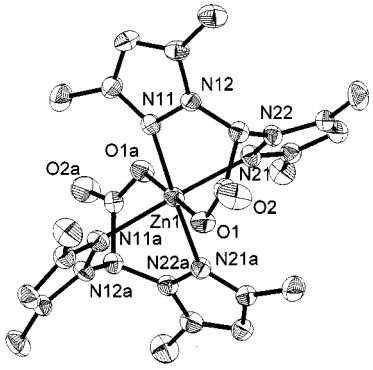

Figure 2. Molecular structure of [(bdmpza)$_2$Zn] (**4**); thermal ellipsoids are drawn at the 50% probability level

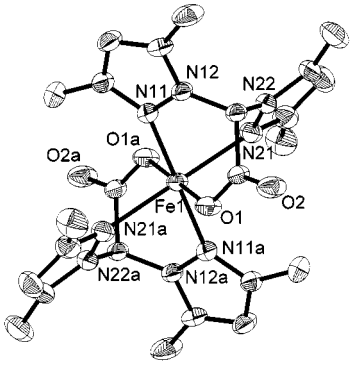

Figure 3. Molecular structure of [(bdmpza)$_2$Fe] (**5**); thermal ellipsoids are drawn at the 50% probability level

Table 1. Selected distances and angles of complexes 4 and 5

Distance [Å]	4	5	Angle [°]	4	5
M−N(11)	2.178(3)	2.169(3)	N(11)−M−N(21)	84.23(12)	84.05(10)
M−N(21)	2.180(3)	2.212(3)	O(1)−M−N(11)	84.42(11)	84.35(10)
M−O(1)	2.119(3)	2.080(3)	O(1)−M−N(21)	86.12(10)	86.36(11)

The chemical workup of iron(II) compounds under anaerobic conditions is much more difficult than with zinc complexes, and the NMR analyses are restricted to paramagnetic ^{1}H NMR spectroscopy because of the high-spin character. Therefore, the chemical similarity is useful to test possible synthetic routes firstly with zinc(II) and to later transfer this knowledge to reactions with iron(II). One might say that the zinc(II) serves as a "Trojan Horse".

The former studies of Moro-oka et al. with model complexes of the trispyrazolylborate ligands Tp^{tBu,iPr} und Tp$^{iPr}{}_2$ have already shown that sterically more hindered pyrazoles can prevent the Tp ligands from coordinating twice to the metal.[10b] We therefore tried to prevent double coordination by introducing substituents R larger than the methyl group at the pyrazole rings.

In analogy to the synthesis of bis(3,5-dimethylpyrazol-1-yl)methane,[18] 3,5-*tert*-butylpyrazole reacted with dichloromethane, base and phase-transfer catalyst to give bis(3,5-*tert*-butylpyrazol-1-yl)methane (bdtbpzm) (**2**). 5-*tert*-Butyl-

3-methylpyrazole proved to be unsuitable for this reaction because three inseparable isomers were obtained in the bis(pyrazol-1-yl)methane formation. Therefore, we used a pyrazole with two identical substituents, R, in positions 3 and 5 [Equation (2)].

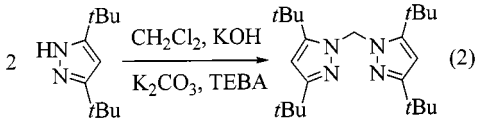

2

As in the synthesis of bdmpza by Otero et al., the scorpionate ligand bis(3,5-di-*tert*-butylpyrazol-1-yl)acetate (bdtbpza) (**3**) could be synthesized from bis(3,5-*tert*-butylpyrazol-1-yl)methane (bdtbpzm) (**2**) by deprotonation with *n*-butyllithium and subsequent addition of carbon dioxide [(Equation (3)].

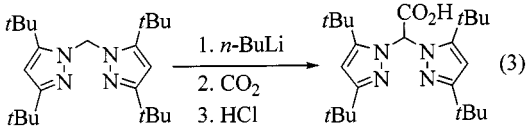

2 **3**

The spectroscopic properties of bdtbpza (**3**) are very similar to bdmpza (**1**), with two high-field signals in the ^{1}H NMR spectrum that are due to the *tert*-butyl groups. Compound **3** was also characterized by an X-ray structure determination (Figure 4 and Table 2).

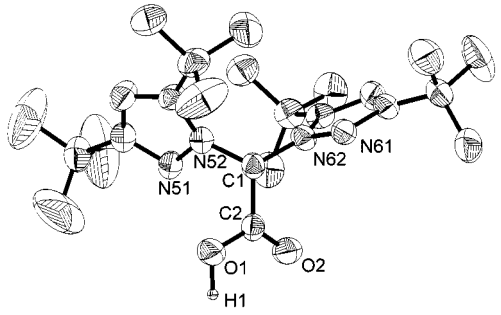

Figure 4. Molecular structure of the bdtbpza ligand (**3**); thermal ellipsoids are drawn at the 50% probability level

Table 2. Selected distances and angles of ligand **3**

Distance [Å]	**3**	Angle [°]	**3**
C(1)−C(2)	1.523(7)	O(1)−C(2)−O(2)	124.6(5)
C(2)−O(1)	1.334(5)	C(2)−C(1)−N(52)	112.5(4)
C(2)−O(2)	1.212(6)	C(2)−C(1)−N(62)	112.1(4)
C(1)−N(52)	1.448(7)	N(52)−C(1)−N(62)	116.0(4)
C(1)−N(62)	1.511(6)		

As in the previous reaction with bdmpza (**1**) the ligand bdtbpza (**3**) was treated with base and water-free $ZnCl_2$ or $FeCl_2$. Fortunately, bdtbpza (**3**) coordinates only once to zinc(II) and iron(II), so that compounds [(bdtbpza)ZnCl] (**6**) and [(bdtbpza)FeCl] (**7**) could be isolated, characterized and tested according to their chemical reactivity.

Both complexes display $\nu_{as}(CO_2^-)$ absorptions around 1680 cm^{-1}. The conformation of the complex [(bdtbpza)-ZnCl] (**6**) could be confirmed by X-ray structure determination (Figure 5). Selected distances and angles are summarized in Table 3.

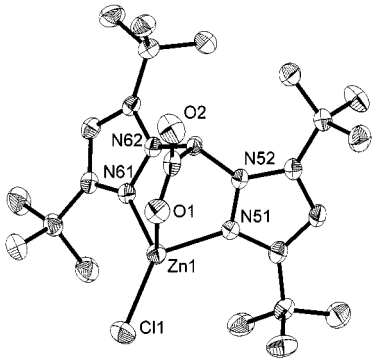

Figure 5. Molecular structure of [(bdtbpza)ZnCl] (**6**); thermal ellipsoids are drawn at the 50% probability level

Table 3. Selected distances and angles of complex **6**

Distance [Å]	**6**	Angle [°]	**6**
Zn−N(51)	2.067(3)	N(51)−Zn−N(61)	87.55(8)
Zn−N(61)	2.053(2)	O(1)−Zn−N(51)	93.85(9)
Zn−O(1)	1.990(2)	O(1)−Zn−N(61)	93.21(9)
Zn−Cl(1)	2.170(2)	N(51)−Zn−Cl(1)	130.62(7)
		N(61)−Zn−Cl(1)	127.18(7)
		O(1)−Zn−Cl(1)	114.64(7)

Compared with the structures of **4** and **5**, the angle O−Zn−N in **6** is widened by 8−9°. As expected, the distance Zn−Cl and the angles O−Zn−N and N−Zn−N are in good agreement with those in the structure of [η^3-$(HCO_2)Bp^{tBu,iPr}$]ZnCl published by Parkin.[14] Similar to this structure, the tetrahedral coordination at zinc is distorted, causing the zinc atom to stack only 0.45 Å out of the N(51)−N(61)−Cl(1) plane. Parkin observed a Zn−O distance of 2.065(4) Å. In **6** the equivalent distance is significantly shorter [1.990(2) Å], due to the fact that one of the donor groups is a carboxylate.

[(Bdtbpza)FeCl] (**7**), in contrast to [$(bdmpza)_2$Fe] (**5**), is not stable to air or moisture: it has to be handled under an atmosphere of argon or nitrogen. Although a dimer $[(bdtbpza)FeCl]_2$ cannot be ruled out completely by our data, an [M$^+$] peak for [(bdtbpza)FeCl] (**7**) can be detected by MS. This indicates that the product [(bdtbpza)FeCl] (**7**) might be isostructural to [(bdtbpza)ZnCl] (**6**). A final answer to this question has to be postponed until a structure determination of **7** is available.

[(Bdtbpza)ZnCl] (**6**) can be treated with benzylthiol and base to yield the benzylthiolate complex [(bdtbpza)-$ZnSCH_2Ph$] (**8**). This reaction is quantitative but it proved to be difficult to remove excess thiol. The spectroscopic properties of **8** are nearly the same as those of **6**, apart from

Table 4. Comparison of Zn−N and Zn−O distances in thermolysin and carboxypeptidase with [(bdmpza)$_2$Zn] (**4**) and [(bdtbpza)ZnCl] (**6**)

	Thermolysin [19]	Carboxypeptidase [20]	[(bdmpza)$_2$Zn]	[(bdtbpza)ZnCl]
d(Zn−N)/Å	2.08, 1.9	2.2	2.178(3)	2.067(3)
d(Zn−N)/Å	2.10, 2.0	2.2	2.180(3)	2.053(2)
d(Zn−O)/Å	2.08, 1.9	2.2	2.119(3)	1.990(2)

additional ^{1}H and ^{13}C NMR spectroscopic signals due to the benzylthiolate ligand. Particularly characteristic for this thiolate ligand is a single resonance at $\delta(^1H) = 3.93$, assigned to the methylene group. A $\nu_{as}(CO_2^-)$ absorption was found at 1677 cm^{-1} in the IR spectrum.

Discussion

The aim of the experiments was to create new structural model complexes for mononuclear non-heme iron oxidases and zinc enzymes. As shown in Table 4 and 5, the distances of the M−N and M−O bonds in [(bdmpza)$_2$Zn] (**4**) and [(bdmpza)$_2$Fe] (**5**) are in good agreement with those of the active sites of thermolysin,[19] carboxypeptidase,[20] IPNS,[5−7] DAOCS[8] and CAS.[9]

Table 5. Comparison of Fe−N and Fe−O distances in IPNS and DAOCS with [(bdmpza)$_2$Fe] (**5**)

	IPNS [6][7]	DAOCS [8]	CAS [9]	[(bdmpza)$_2$Fe]
d(Fe−N)/Å	2.19, 2.09	2.2	2.15, 2.14, 2.25	2.169(3)
d(Fe−N)/Å	2.20, 2.24	2.2	2.12, 2.12, 2.28	2.212(3)
d(Fe−O)/Å	2.06, 2.09	2.2	2.06, 2.07, 2.16	2.080(3)

These data already show that sterically more hindered derivatives of bispyrazolyl acetate should be suitable ligands for model complexes. By using the new ligand bdtbpza (**3**) we implemented this steric hindrance.

With [(bdtbpza)ZnCl] (**6**) a tetrahedral zinc complex with a monoanionic *N,N,O*-tridentate ligand using a carboxylate *O*-donor was synthesized for the first time. A comparison of the X-ray structure determination of **6** with the coordination environment of the enzymes, according to the distances Zn−N and Zn−O (Table 4) indicates their significance as structural models for these active sites. [(Bdtbpza)ZnCl] (**6**) might be the best structural analogue for the enzymes thermolysin and carboxypeptidase.

For future biomimetic studies, a coordination of possible enzymatic substrates to the bdmpza model complexes is essential. In the case of model complexes for the active site of thermolysin or carboxypeptidase, this could be a small peptide. For models of IPNS or α-ketoglutarate-dependent enzymes as CAS or DAOCS, this might be a thiolate or α-ketoglutarate or even a dioxygen. The reactivity of **6** towards an exchange of the chloro ligand by a thiolate clearly shows the potential of the chloro complexes **6** and **7** in the synthesis of zinc(II) and iron(II) model complexes. Therefore, our future work will focus on the synthesis of model complexes for non-heme iron enzymes activating dioxygen, such as IPNS, as well as their chemical reactivity.

As shown recently by Moro-oka et al., the steric hindrance of a Tp^{tBu,iPr} ligand might prevent access of substrates to the metal of the complexes.[10c] Thus, the model complex [Tp^{tBu,iPr}Fe^{II}(O$_2$CMe)] shows no affinity to O$_2$, in contrast to the sterically less-hindered [Tp$^{iPr}{}_2$Fe^{II}(O$_2$CMe)] complex. We propose that this affinity to dioxygen, essential for our further experiments with iron complexes, might be guaranteed by the much smaller carboxylate donor groups in future model complexes [(bdtbpza)FeR].

Conclusions

Two bis(3,5-dialkylpyrazol-1-yl)acetic acids **1** and **3** were introduced as new ligands for synthetic structural analogues of zinc or non-heme iron enzymes. The steric hindrance of bis(3,5-dimethylpyrazol-1-yl)acetic acid is too small, causing the ligand to coordinate twice to zinc(II) or iron(II). With bis(3,5-di-*tert*-butylpyrazol-1-yl)acetic acid the steric hindrance of this new *N,N,O* ligand was improved. The structural model complexes of zinc(II) and iron(II) obtained mimic the so called facial 2-His-1-carboxylate triad; this is especially important in mononuclear non-heme iron enzymes. We are sure that the obtained model complexes represent a good starting point to investigate the reactivity of such enzymes, especially with respect to dioxygen activation.

Experimental Section

All experiments involving iron(II) were carried out in Schlenk tubes under an atmosphere of argon using suitable purified solvents. Microcrystalline precipitates were separated by centrifugation with a Hettich Rotina 46 R Schlenk tube centrifuge. − IR: Biorad FTS 60, CaF_2 cuvets (0.5 mL). − ^{1}H NMR and ^{13}C NMR: Bruker WM 250, Bruker AC 250, JEOL GX 400, δ values relative to TMS; in some cases the ^{13}C NMR spectroscopic signals of quaternary carbon atoms were to weak to be detected. − EI-MS and FAB MS: modified Finnigan MAT 312. − Elemental analyses: Analytical Laboratory of the Fachbereich Chemie. − A modified Siemens P4 diffractometer was used for X-ray structure determinations.

3,5-Dimethylpyrazole, 2,2,6,6-tetramethyl-3,5-heptandione, dibromoacetic acid and $ZnCl_2$ were used as purchased. Water-free $FeCl_2$ was synthesized from $FeCl_3$.[21] 3,5-Di-*tert*-butylpyrazole was obtained by standard literature methods from 2,2,6,6-tetramethyl-3,5-heptandione and hydrazine hydroxide.[22]

Ligand Syntheses

Synthesis of Bis(3,5-dimethylpyrazol-1-yl)acetic Acid (bdmpza) (1): Dibromoacetic acid (5.45 g, 25.00 mmol), 3,5-dimethylpyrazole

(4.81 g, 50.00 mmol), KOH (5.05 g, 90.00 mmol), K_2CO_3 (12.44 g, 90.00 mmol) and benzyltriethylammonium chloride (1.00 g), serving as phase-transfer catalyst, were dissolved in tetrahydrofuran (100 mL) and heated under reflux for 5 to 6 hours. The solvent was removed in vacuo, the residue dissolved in water (100 mL) and acidified to a pH value of 7 with half-concentrated HCl. To remove excess pyrazole, the solution was extracted with diethyl ether (2 × 150 mL). The water phase was further acidified to a pH value of 1 and extracted again with diethyl ether (5 × 150 mL). To improve the extraction of the water-soluble bdmpza **1** tetrahydrofuran can be added. The organic layer was dried (Na_2SO_4) and the solvent was removed in vacuo. The residue was recrystallized from acetone yielding bdmpza (1) as colorless microcrystalline needles and dried in vacuo over SICAPENT©. In an analogous reaction of dichloroacetic acid chloride with three equivalents of 3,5-dimethylpyrazole, bdmpza (**1**) can be obtained in a slightly lower yield. Yield 2.79 g (45%); m.p. 171 °C (dec.). – ^{1}H NMR ($CDCl_3$, 250 MHz): δ = 2.20 (s, 6 H, CH_3), 2.24 (s, 6 H, CH_3), 5.90 (s, 2 H, H_{pz}), 6.76 (s, 1 H, CH). – ^{1}H NMR (D_2O, 250 MHz): δ = 2.09 (s, 6 H, CH_3), 2.18 (s, 6 H, CH_3), 5.99 (s, 2 H, H_{pz}), 6.79 (s, 1 H, CH), 14.03 (s, CO_2H). – ^{13}C NMR ($CDCl_3$, 62.5 MHz): δ = 11.0 (CH_3), 13.3 (CH_3), 69.9 (CH), 107.8 (C_{pz}), 141.7 (C_{pz}), 148.9 (C_{pz}), 165.1 (CO_2H). – EI MS (70 eV, 170 °C): *m*/*z* (%) = 248 (6) [M^+], 204 (20) [$M^+ - CO_2$], 109 (100) [$M^+ - CO_2 - C_5H_7N_2$], 96 (50) [$C_5H_8N_2$]. – IR (THF): $\tilde{\nu}$ = 1758 cm^{-1} (CO_2H), 1563 (C=N). – $C_{12}H_{16}N_4O_2$ (248.28): calcd. C 58.05, H 6.50, N 22.57; found C 58.38, H 6.54, N 22.09.

Synthesis of Bis(3,5-di-*tert*-butylpyrazol-1-yl)methane (bdtbpzm) (2): 3,5-Di-*tert*-butylpyrazole (3.00 g, 16.64 mmol), KOH (3.60 g, 64.16 mmol), K_2CO_3 (9.00 g, 65.12 mmol) and benzyltriethylammonium chloride (0.5 g) were dissolved in dichloromethane (100 mL) and heated under reflux for 5 hours. Salts were removed by filtration and the filtrate was concentrated in vacuo to dryness. The white residue was dissolved in water and extracted with pentane (2 × 150 mL). The organic layer was dried ($MgSO_4$) and the solvent removed in vacuo. The white residue was recrystallized from pentane to give bdtbpzm (**2**) as a white powder, which was dried in vacuo. Yield 2.40 g (77%), m.p. 132 °C. – ^{1}H NMR ($CDCl_3$, 250 MHz): δ = 1.21 (s, 18 H, CH_3), 1.25 (s, 18 H, CH_3), 5.90 (s, 2 H, CH_2), 6.52 (s, 2 H, H_{pz}). – ^{13}C NMR ($CDCl_3$, 62.5 MHz): δ = 29.8 (CH_3), 30.4 (CH_3), 31.9 (C-*t*Bu), 66.7 (CH_2), 101.9 (C_{pz}), 153.0 (C_{pz}), 159.1 (C_{pz}). – EI MS (70 eV, 125 °C): *m*/*z* (%) = 372 (10) [M^+], 315 (1) [$M^+ - C_4H_9$], 193 (100) [$M^+ - C_{11}H_{19}N_2$], 57 (18) [C_4H_9]. – IR (THF): $\tilde{\nu}$ = 1542 cm^{-1} (C=N). – $C_{23}H_{40}N_4$ (372.60): calcd. C 74.14, H 10.82, N 15.04; found C 74.12, H 10.79, N 14.90.

Synthesis of Bis(3,5-di-*tert*-butylpyrazol-1-yl)acetic Acid (bdtbpza) (3): A solution of bis(3,5-di-*tert*-butylpyrazol-1-yl)methane (bdtbpzm) (**2**) (2.30 g, 6.17 mmol) in tetrahydrofuran (50 mL) was treated with *n*BuLi (≈1.6 M solution in hexane, 4 mL, 6.40 mmol) at −70 °C. The solution is allowed to warm to −45 °C during a period of 4 h and finally poured onto 200 g of crushed dry ice. After reaching room temperature, the solvent was removed in vacuo and the white residue dissolved in water (100 mL). The aqueous solution was acidified with half concentrated HCl to a pH value of 1 and extracted with diethyl ether (3 × 100 mL). The combined organic layers were dried (Na_2SO_4) and concentrated in vacuo to give a honey-like yellow oil. The product crystallized within two days when stored at room temperature under air. The white crystalline substance was washed with pentane to remove unchanged bis(3,5-di-*tert*-butylpyrazol-1-yl)methane (bdtbpzm) (**2**), which gave bdtbpza (**3**) as a colorless powder. Upon recrystallization from acetone, cubic crystals suitable for an X-ray structure determination were obtained. Yield 2.25 g (88%), m.p. 92 °C. – ^{1}H NMR ($CDCl_3$, 250 MHz): δ = 1.21 (s, 18 H, CH_3), 1.24 (s, 18 H, CH_3), 6.01 (s, 2 H, H_{pz}), 7.27 (s, 1 H, CH). – ^{13}C NMR ($CDCl_3$, 62.5 MHz): δ = 30.0 (CH_3), 30.1 (CH_3), 31.9 (C-*t*Bu), 32.2 (C-*t*Bu), 72.7 (CH), 103.1 (C_{pz}), 154.0 (C_{pz}), 159.6 (C_{pz}), 166.2 (CO_2H). – EI MS (70 eV, 145 °C): *m*/*z* (%) = 372 (8) [$M^+ - CO_2$], 315 (1) [$M^+ - CO_2 - C_4H_9$], 193 (100) [$M^+ - C_{11}H_{19}N_2 - CO_2$], 57 (20) [$C_4H_9$]. – IR (THF): $\tilde{\nu}$ = 1767 cm^{-1} (CO_2H), 1542 (C=N). – $C_{24}H_{40}N_4O_2 \cdot 0.5\ C_4H_{10}O$ (453.67): calcd. C 68.84, H 10.00, N 12.35; found C 68.48, H 9.76, N 12.36.

Synthesis of Model Compounds

Synthesis of [(bdmpza)$_2$Zn] (4): A solution of bdmpza ligand (**1**) (500 mg, 2.01 mmol) in MeOH (20 mL) was deprotonated with the subsequent addition of NaOH (80 mg, 2.01 mmol). A solution of $ZnCl_2$ (137 mg, 1.01 mmol) in MeOH (10 mL) was then added. The initially clear solution was stirred at room temperature for 1 h. The white precipitate that formed was separated by centrifugation, washed with MeOH (15 mL) and dried in vacuo to afford **4** as a white powder. Colorless prism-like crystals suitable for an X-ray structure determination were obtained by recrystallization from MeOH/H_2O (20:1) at 4 °C. Treatment of bdmpza (**1**) with equimolar amounts of NaOH and $ZnCl_2$ yielded the identical compound. Yield 517 mg (92%), m.p. 280−300 °C (dec.). – ^{1}H NMR ($CDCl_3$, 250 MHz): δ = 1.97 (s, 12 H, CH_3), 2.45 (s, 12 H, CH_3), 5.87 (s, 4 H, H_{pz}), 6.57 (s, 2 H, CH). – ^{13}C NMR ($CDCl_3$, 62.5 MHz): δ = 10.9 (CH_3), 12.7 (CH_3), 67.1 (CH), 106.7 (C_{pz}), 139.7 (C_{pz}), 150.2 (C_{pz}), 166.3 (CO_2^-). – FAB MS (NBOH-matrix): *m*/*z* (%) = 873 (10) [2 M − bdmpza], 559 (20) [MH^+], 419 (40) [$MH^+ - CO_2 - C_5H_7N_2$], 375 (20) [$MH^+ - 2\ CO_2 - C_5H_7N_2$], 361 (20) [$MH^+ - 2\ CO_2 - (C_5H_7N_2)CH_2$], 203 (60) [$(C_5H_7N_2)_2CH^+$], 109 (100) [$(C_5H_7N_2)CH_2^+$], 95 (75) [$C_5H_7N_2$]. – IR ($CH_2Cl_2$): $\tilde{\nu}$ = 1659 cm^{-1} (CO_2^-), 1558 (C=N). – $C_{24}H_{30}N_8O_4Zn$ (559.93): calcd. C 51.48, H 5.40, N 20.01; found C 51.23, H 5.36, N 19.25 or C 51.21, H 5.66, N 20.09.

Synthesis of [(bdmpza)$_2$Fe] (5): A solution of bdmpza ligand (**1**) (500 mg, 2.01 mmol) in MeOH (15 mL) was deprotonated with the subsequent addition of NaOH (80 mg, 2.01 mmol). A solution of water-free $FeCl_2$ (128 mg, 1.01 mmol) in MeOH (10 mL) was then added. The initially clear solution was stirred at room temperature for 2 h. The tan to white precipitate that formed was separated by centrifugation, washed with MeOH (15 mL) and dried in vacuo to yield **5** as a colorless crystal powder. Recrystallization from acetonitrile/dichloromethane (1:1) yielded greenish prism-like crystals suitable for an X-ray structure determination. [(Bdmpza)$_2$Fe] (**5**) was also obtained by treatment of bdmpza (**1**) with equimolar amounts of potassium *tert*-butoxide and $FeCl_2$ in dichloromethane. Yield 512 mg (92%), m.p. 305−315 °C (dec.). – ^{1}H NMR ($CDCl_3$, 250 MHz): δ = 1.2 (s, 2 H, CH), 7.0 (s, 12 H, CH_3), 14.4 (s, 12 H, CH_3), 55.7 (s, 4 H, H_{pz}). – EI MS (70 eV, 340 °C): *m*/*z* (%) = 550 (8) [M^+], 398 (35) [$M^+ - CO_2 - (C_5H_7N_2)CH_2$], 204 (30) [$(C_5H_7N_2)_2CH_2^+$], 109 (78) [$(C_5H_7N_2)CH_2^+$], 96 (40) [$C_5H_8N_2$]. – IR ($CH_2Cl_2$): $\tilde{\nu}$ = 1659 cm^{-1} (CO_2^-), 1558 (C=N). – $C_{24}H_{30}FeN_8O_4$ (550.40): calcd. C 52.35, H 5.50, N 20.36; found C 52.26, H 5.42, N 19.52.

Synthesis of [(bdtbpza)ZnCl] (6): To a solution of bis(3,5-di-*tert*-butylpyrazol-1-yl)acetic acid (bdtbpza) (**3**) (1.00 g, 2.40 mmol) in acetonitrile (30 mL) was added $ZnCl_2$ (380 mg, 2.79 mmol) and the solution stirred vigorously at ambient temperature. After 5 min potassium *tert*-butoxide (268 mg, 2.39 mmol) was added. Within 1 min a white precipitate was formed. After 2 h the solvent was removed in vacuo. The residue was dissolved in dichloromethane (25 mL) and

salts were separated by centrifugation. Dichloromethane was removed in vacuo, the residue washed with diethyl ether (2 × 10 mL) and dried in vacuo to afford [(bdtbpza)ZnCl] (**6**) as a white crystal powder. Recrystallization from acetone at room temperature yielded prism-like colorless crystals within 5 days that were suitable for an X-ray structure determination. Yield 1.06 g (86%), m.p. 239 °C. − ^{1}H NMR ($CDCl_3$, 250 MHz): δ = 1.44 (s, 18 H, CH_3), 1.56 (s, 18 H, CH_3), 6.16 (s, 2 H, H_{pz}), 7.42 (s, 1 H, CH). − ^{13}C NMR ($CDCl_3$, 62.5 MHz): δ = 30.2 (CH_3), 31.2 (CH_3), 32.2 (C-*t*Bu), 32.6 (C-*t*Bu), 72.3 (CH), 103.8 (C_{pz}), 156.4 (C_{pz}), 164.4 (C_{pz}), 165.3 (CO_2^-). − EI MS (70 eV, 240 °C): *m*/*z* (%) = 514 (1) [M^+], 470 (12) [$M^+ - CO_2$], 413 (100) [$M^+ - CO_2 - C_4H_9$], 279 (21) [$M^+ - CH_2 - C_{11}H_{19}N_2 - CO_2$], 193 (7) [$M^+ - Zn - Cl - C_{11}H_{19}N_2 - CO_2$], 57 (54) [$C_4H_9$]. − IR ($CH_2Cl_2$): $\tilde{\nu}$ = 1681 cm^{-1} (CO_2^-), 1547 (C=N). − $C_{24}H_{39}ClN_4O_2Zn$ (516.43): calcd. C 55.82, H 7.61, N 10.85; found C 55.52, H 7.72, N 10.70.

Synthesis of [(bdtbpza)ZnSCH$_2$Ph] (8): A solution of [(bdtbpza)ZnCl] (**6**) (500 mg, 0.97 mmol) in acetonitrile (20 mL) was treated at ambient temperature with benzylthiol (158 mg, 2.79 mmol) and potassium *tert*-butoxide (109 mg, 0.97 mmol). After 3 h the solvent was evaporated, the residue dissolved in dichloromethane (25 mL) and salts removed by centrifugation. The solution was concentrated to dryness in vacuo and the residue was washed with pentane to yield [(bdtbpza)ZnSCH$_2$Ph] (**8**) as a colorless powder. Yield 550 mg (91%), m.p. 88 °C. − ^{1}H NMR ($CDCl_3$, 250 MHz): δ = 1.38 (s, 18 H, CH_3), 1.56 (s, 18 H, CH_3), 3.93 (s, 2 H, SCH_2), 6.13 (s, 2 H, H_{pz}), 7.10−7.39 (m, 5 H, Ph), 7.42 (s, 1 H, CH). − ^{13}C NMR ($CDCl_3$, 62.5 MHz): δ = 29.7 (SCH_2), 30.3 (CH_3), 31.2 (CH_3), 32.2 (C-*t*Bu), 32.5 (C-*t*Bu), 72.2 (CH), 103.6 (C_{pz}), 125.6 (CPh), 128.1 (CPh), 128.5 (CPh), 144.6 (CPh), 155.9 (C_{pz}), 164.0 (C_{pz}), 166.0 (CO_2^-). − EI MS (70 eV, 300 °C): *m*/*z* (%) = 602 (7) [M^+], 557 (2) [$M^+ - CO_2$], 501 (75) [$M^+ - CO_2 - C_4H_9$], 366 (20) [$M^+ - CH_2 - C_{11}H_{19}N_2 - CO_2$], 244 (20) [Zn + $C_{11}H_{19}N_2$], 194 (100) [$C_{11}H_{20}N_2 + CH_2$], 91 (90) [C_7H_7], 57 (30) [C_4H_9]. − IR (CH_2Cl_2): $\tilde{\nu}$ = 1677 cm^{-1} (CO_2^-), 1543 (C=N). − $C_{31}H_{46}N_4O_2SZn$ (604.17): calcd. C 61.63, H 7.67, N 9.27; found C 61.33, H 7.56, N 8.53.

Synthesis of [(bdtbpza)FeCl] (7): To a solution of bis(3,5-di-*tert*-butylpyrazol-1-yl)acetic acid (bdtbpza) (**3**) (500 mg, 1.20 mmol) in acetonitrile (20 mL) was added water-free $FeCl_2$ (150 mg, 1.18 mmol) and the reaction mixture stirred at ambient temperature for 10 min. Potassium *tert*-butoxide (135 mg, 1.20 mmol) was added and stirred for 3 h. The solvent was evaporated and the residue was dissolved in dichloromethane (25 mL). Salts were removed by centrifugation and the solution concentrated to dryness in vacuo. The residue was washed with diethyl ether (2 × 10 mL) and dried in vacuo to afford [(bdmpza)FeCl] (**7**) as a colorless powder. Yield 520 mg (87%), m.p. 203 °C (dec.). − ^{1}H NMR ($CDCl_3$, 250 MHz): δ = −21.4 (s, 18 H, CH_3), 3.2 (s, 2 H, H_{pz}), 11.3 (s, 18 H, CH_3). − EI MS (70 eV, 280 °C): *m*/*z* (%) = 506 (4) [M^+], 462 (11) [$M^+ - CO_2$], 405 (100) [$M^+ - CO_2 - C_4H_9$], 271 (12) [$M^+ - CH_2 - C_{11}H_{19}N_2 - CO_2$], 57 (44) [$C_4H_9$]. − IR ($CH_2Cl_2$): $\tilde{\nu}$ = 1684 cm^{-1} (CO_2^-). − $C_{24}H_{39}ClFeN_4O_2$ (506.90): calcd. C 56.87, H 7.75, N 11.05; found C 56.57, H 7.86, N 10.91.

X-ray Structure Determinations: Single crystals of **3**, **4**, **5** and **6** were sealed in glass capillaries at room temperature. A modified Siemens P4-Diffractometer was used for data collection (Wyckhoff technique, graphite monochromator, Mo-K_α radiation, λ = 0.71073 Å, scan rate 4−30°min^{-1} in ω). Compound **4** was measured at room

Table 6. Structure determination details of compounds **3**, **4**, **5** and **6**

	3	**4**	**5**	**6**
Empirical formula	$C_{24}H_{40}N_4O_2 \cdot 0.5\ Et_2O$	$C_{12}H_{15}N_4O_2Zn_{0.5} \cdot 1.5\ H_2O$	$C_{12}H_{15}Fe_{0.5}N_4O_2 \cdot 0.5\ CH_2Cl_2$	$C_{24}H_{39}ClN_4O_2Zn$
Formula weight	453.66	305.98	317.67	516.41
Crystal color/Habit	colorless prism	colorless prism	green prism	colorless column
Crystal system	tetragonal	monoclinic C	monoclinic C	monoclinic P
Space group	$P4_2/n$	$C2/c$	$C2/c$	$P2_1/n$
a [Å]	19.773(24)	16.228(15)	8.003(3)	10.586(7)
b [Å]	19.773(24)	13.421(12)	18.700(7)	16.170(9)
c [Å]	14.863(17)	14.050(14)	20.147(11)	16.255(9)
α [°]	90.00	90.00	90.00	90.00
β [°]	90.00	108.28(5)	98.62(6)	107.96(7)
γ [°]	90.00	90.00	90.00	90.00
V [Å^3]	5810.9(119)	2905.5(47)	2981.0(23)	2647.0(27)
θ [°]	2.00−23.00	2.01−26.99	2.18−27.00	2.04−27.01
h	−1 to 21	−20 to 20	−10 to 10	−1 to 12
k	−1 to 21	−11 to 17	−23 to 23	−20 to 1
l	−1 to 16	−17 to 17	−24 to 25	−20 to 20
F(000)	1992	1288	1320	1096
Z	8	8	8	4
μ(Mo-K_α) [mm^{-1}]	0.067	0.901	0.730	1.055
Crystal size [mm]	0.55 × 0.5 × 0.5	0.35 × 0.3 × 0.3	0.55 × 0.5 × 0.5	0.55 × 0.55 × 0.6
D_c [gcm^{-1}]	1.037	1.399	1.416	1.296
T [K]	241(2)	293(2)	243(2)	241(2)
Reflections collected	4234	4623	6434	6423
Independent reflections	3159	3176	3179	5134
Obs. reflections (>2σ*I*)	1764	2182	2725	4165
Parameter	301	204	186	289
Restraints	0	3	0	0
Wt. parameter a	0.0907	0.0494	0.1231	0.0388
Wt. parameter b	3.5702	1.6697	6.7913	1.4264
R_1 (obs.)	0.0755	0.0477	0.0623	0.0352
R_2 (overall)	0.1432	0.0865	0.0710	0.0492
wR_1 (obs.)	0.1796	0.0999	0.1927	0.0849
wR_2 (overall)	0.2225	0.1232	0.2062	0.0937
Diff. peak/hole [e/Å^3]	0.227/−0.161	0.429/−0.298	0.535/−1.100	0.267/−0.458

temperature and the others at −30 °C. Structures were solved using direct methods {Siemens SHELXS-93 (VMS)[23]} and refined with full-matrix least-squares against F^2 {Siemens SHELXL-96 (VMS)[24]}. A weighting scheme was applied in the last steps of the refinement with $w = 1/[\sigma^2(F_o^2) + (aP)^2 + bP]$ and $P = [2F_c^2 + \mathrm{Max}(F_o^2,0)]/3$. Hydrogen atoms were included in their calculated positions and refined in a riding model.

The metal atoms in structures of **4** and **5** are in special positions, causing the asymmetric unit to be filled by only half a molecule. Compound **4** crystallized as a solvate with 1.5 water molecules, one of which interacts with the carboxylate group. In the asymmetric unit of structure **5**, half a molecule of dichloromethane was found and refined in a special position.

Compound **3** crystallized with half a molecule of diethyl ether in the asymmetric unit in a special position. The proton of the carboxylic acid was found. The poor *R*-factors of compound **3** are caused by a weak diffraction of the crystal. So the θ-range of the measurement was only up to 23° causing a low reflection/parameter ratio. Nevertheless, anisotropic refinement was applied to all non-hydrogen atoms.

All details and parameters of the measurements are summarized in Table 6. Structure pictures were prepared with the program Diamond 2.1c.[25] Crystallographic data (excluding structure factors) for the structures reported in this paper have been deposited with the Cambridge Crystallographic Data Centre as supplementary publication no. CCDC-145052 (**4**), CCDC-145053 (**5**), CCDC-145054 (**6**) and CCDC-145055 (**3**). Copies of the data can be obtained free of charge on application to CCDC, 12 Union Road, Cambridge CB2 1EZ, UK [Fax: (internat.) + 44-1223/336-033; E-mail: deposit@ccdc.cam.ac.uk].

Acknowledgments

N. B. thanks the Fonds der Chemie for a Liebig-Fellowship and Prof. Dr. H. Fischer for support and discussion. We are indebted to Mrs Quelle and Mr Hägele for recording mass spectra.

[1] A. L. Feig, S. J. Lippard, *Chem. Rev.* **1994**, *94*, 759−805; R. H. Holm, P. Kennepohl, E. I. Solomon, *Chem. Rev.* **1996**, *96*, 2239−2314; L. Que Jr., R. Y. N. Ho, *Chem. Rev.* **1996**, *96*, 2607−2624; C. A. Townsend, *Chem. & Biol.* **1997**, *4*, 721−730; A. L. Nivorozhkin, J.-J. Girerd, *Angew. Chem. Int. Ed. Engl.* **1996**, *35*, 609−611.

[2] E. L. Hegg, L. Que Jr., *Eur. J. Biochem.* **1997**, *250*, 625−629; S. J. Lange, L. Que Jr., *Curr. Op. Chem. Biol.* **1998**, *2*, 159−172; L. Que Jr., *Nature Struct. Biol.* **2000**, *7*, 182−184.

[3] T. Flatmark, R. C. Stevens, *Chem. Rev.* **1999**, *99*, 2137−2160.

[4] T. Senda, K. Sugiyama, H. Narita, T. Yamamoto, K. Kimbara, M. Fukuda, M. Sato, K. Yano, Y. Mitsui, *J. Mol. Biol.* **1996**, *255*, 735−752.

[5] P. L. Roach, I. J. Clifton, V. Fülöp, K. Harlos, G. J. Barton, J. Hajdu, I. Andersson, C. J. Schofield, J. E. Baldwin, *Nature* **1995**, *375*, 700−704.

[6] P. L. Roach, I. J. Clifton, C. M. H. Hensgens, N. Shibata, C. J. Schofield, J. Hajdu, J. E. Baldwin, *Nature* **1997**, *387*, 827−830.

[7] N. I. Burzlaff, P. J. Rutledge, I. J. Clifton, C. M. H. Hensgens, M. Pickford, R. M. Adlington, P. L. Roach, J. E. Baldwin, *Nature* **1999**, *401*, 721−724.

[8] K. Valegård, A. C. Terwisscha van Scheltinga, M. D. Lloyd, T. Hara, S. Ramaswamy, A. Perrakis, A. Thompson, H.-J. Lee, J. E. Baldwin, C. J. Schofield, J. Hajdu, I. Andersson, *Nature* **1998**, *394*, 805−809.

[9] Z. Zhang, J. Ren, D. K. Stammers, J. E. Baldwin, K. Harlos, C. J. Schofield, *Nature Struct. Biol.* **2000**, *7*, 127−133.

[10] [10a] N. Kitajima, H. Fukui, Y. Moro-oka, *J. Am. Chem. Soc.* **1990**, *112*, 6402−6403; H. G. Jang, D. D. Cox, L. Que Jr., *J. Am. Chem. Soc*. **1991**, *113*, 9200−9204; Y.-M. Chiou, L. Que Jr., *J. Am. Chem. Soc*. **1992**, *114*, 7567−7568; N. Kitajima, N. Tamura, H. Amagai, H. Fukui, Y. Moro-oka, Y. Mizutani, T. Kitagawa, R. Mathur, K. Heerwegh, C. A. Reed, C. R. Randall, L. Que Jr., K. Tatsumi, *J. Am. Chem. Soc.* **1994**, *116*, 9071−9085; Y. Zang, L. Que Jr., *Inorg. Chem*. **1995**, *34*, 1030−1035; C. R. Randall, L. Shu, Y.-M. Chiou, S. Hagen, M. Ito, N. Kitajima, R. J. Lachicotte, Y. Zang, L. Que Jr., *Inorg. Chem*. **1995**, *34*, 1036−1039; Y.-M. Chiou, L. Que Jr., *Inorg. Chem*. **1995**, *34*, 3577−3578; Y.-M. Chiou, L. Que Jr., *J. Am. Chem. Soc*. **1995**, *117*, 3999−4013; S. K. Mandal, L. Que Jr., *Inorg. Chem*. **1997**, *36*, 5424−5425. − [10b] M. Ito, H. Amagai, H. Fukui, N. Kitajima, Y. Moro-oka, *Bull. Chem. Soc. Jpn*. **1996**, *69*, 1937−1945; S. Hikichi, T. Ogihara, K. Fujisawa, N. Kitajima, M. Akita, Y. Moro-oka, *Inorg. Chem*. **1997**, *36*, 4539−4547. − [10c] T. Ogihara, S. Hikichi, M. Akita, T. Uchida, T. Kitagawa, Y. Moro-oka, *Inorg. Chim. Acta* **2000**, *297*, 162−170.

[11] W. N. Lipscomb, N. Sträter, *Chem. Rev.* **1996**, *96*, 2375−2433.

[12] [12a] R. Alsfasser, A. K. Powell, H. Vahrenkamp, *Angew. Chem. Int. Ed. Engl.* **1990**, *29*, 898−899; R. Alsfasser, S. Trofimenko, A. Looney, G. Parkin, H. Vahrenkamp, *Inorg. Chem.* **1991**, *30*, 4098−4100; A. Looney, G. Parkin, R. Alsfasser, M. Ruf, H. Vahrenkamp, *Angew. Chem. Int. Ed. Engl.* **1992**, *31*, 92−93; R. Alsfasser, M. Ruf, S. Trofimenko, H. Vahrenkamp, *Chem. Ber.* **1993**, *126*, 703−710; M. Ruf, H. Vahrenkamp, *Inorg. Chem.* **1996**, *35*, 6571−6578; M. Ruf, H. Vahrenkamp, *Chem. Ber.* **1996**, *129*, 1025−1028; M. Ruf, F. A. Schell, R. Walz, H. Vahrenkamp, *Chem. Ber.* **1997**, *130*, 101−104; Review: H. Vahrenkamp, *Acc. Chem. Res.* **1999**, *32*, 589−596. − [12b] S. Hikichi, M. Tanaka, Y. Moro-oka, N. Kitajima, *J. Chem. Soc., Chem. Commun.* **1992**, 814−815. − [12c] A. Looney, R. Han, K. McNeill, G. Parkin, *J. Am. Chem. Soc.* **1993**, *115*, 4690−4697.

[13] C. Dowling, G. Parkin, *Polyhedron* **1996**, *15*, 2463−2465.

[14] P. Ghosh, G. Parkin, *J. Chem. Soc., Dalton Trans.* **1998**, 2281−2283.

[15] B. S. Hammes, C. J. Carrano, *Inorg. Chem.* **1999**, *38*, 3562−3568.

[16] B. S. Hammes, C. J. Carrano, *Inorg. Chem.* **1999**, *38*, 4593−4600.

[17] A. Otero, J. Fernández-Baeza, J. Tejeda, A. Antiñolo, F. Carrillo-Hermosilla, E. Diez-Barra, A. Lara-Sánchez, M. Fernández-López, M. Lanfranchi, M. A. Pellinghelli, *J. Chem. Soc., Dalton Trans.* **1999**, 3537−3539.

[18] S. Juliá, P. Sala, J. del Mazo, M. Sancho, C. Ochoa, J. Elguero, J.-P. Fayet, M.-C. Vertut, *J. Heterocycl. Chem.* **1982**, *19*, 1141−1145.

[19] M. A. Holmes, B. W. Matthews, *J. Mol. Biol.* **1982**, *160*, 623−639.

[20] W. R. Kester, B. W. Matthews, *J. Biol. Chem.* **1977**, *252*, 7704−7710.

[21] P. Kovacic, N. O. Brace, *Inorg. Synth.* **1960**, *6*, 172−173.

[22] N. Kitajima, K. Fujisawa, C. Fujimoto, Y. Moro-oka, S. Hashimoto, T. Kitagawa, K. Toriumi, K. Tatsumi, A. Nakamura, *J. Am. Chem. Soc.* **1992**, *114*, 1277−1291.

[23] G. M. Sheldrick, *SHELXS-93, Program for Crystal Structure Solution*, University of Göttingen, Germany, **1986**.

[24] G. M. Sheldrick, *SHELXL-96, Program for Crystal Structure Refinement*, University of Göttingen, Germany, **1993**.

[25] K. Brandenburg, M. Berndt, Diamond − Visual Crystal Structure Information System, Crystal Impact GbR, Bonn, Germany, **1999**; for Software Review see: W. T. Pennington, *J. Appl. Cryst.* **1999**, *32*, 1028−1029.

Received June 2, 2000
[I00224]

Photochemically Induced Isomerisation of Ruthenium Polypyridyl Complexes

Stefano Fanni,[a] Frances M. Weldon,[a] Leif Hammarström,[b] Emad Mukhtar,[b] Wesley R. Browne,[a] Tia E. Keyes,[c] and Johannes G. Vos*[a]

Keywords: Ruthenium / Coordination modes / Photochemistry / Electrochemistry / Heterocycles

The synthesis and characterisation of a series of ruthenium polypyridyl complexes containing pyridyltriazole ligands in different coordination modes are described. The electrochemical and electronic properties of the compounds with respect to the coordination mode of the pyridyltriazole ligand are reported. Upon photolysis of the complex containing the 1-methyl-3-(pyridin-2-yl)-1,2,4-triazole ligand, irreversible ligand isomerisation is observed.

Introduction

During the last number of years we have been actively involved in the study of ruthenium and osmium polypyridyl complexes containing ligands with 1,2,4-triazole moieties such as pyridyl-[1] and pyrazyltriazoles.[2] These studies have shown that for dinuclear compounds containing anionic triazolate bridges, strong intercomponent interactions are observed.[3] In addition, mononuclear complexes containing negatively charged triazole rings were found to be photostable.[4] Of further interest in these studies is the inherent asymmetry of the ligands. The nitrogen atoms of the pyridine or pyrazine rings have significantly different electronic properties to the triazole-based nitrogen atoms. In addition the N1 (or N2) and N4 atoms of the triazole ring are nonequivalent, as shown by differences between the acid−base properties of complexes containing N2- and N4-bonded ligands.[1,2] With *N*-substituted triazole ligands, either N2- or N4-coordination of the ligands is observed, depending on the position of the substituent.[5] Furthermore, it has been shown that for complexes containing neutral pyridyltriazole ligands, photochemically induced isomerisation of the pyridyltriazole ligand can occur.[4,6]

Recently we developed a new synthetic route towards complexes containing *N*-substituted triazole ligands as shown in Scheme 1.[7]

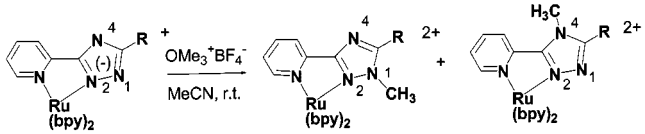

Scheme 1

In this method, the N2 isomer of a 3-(pyridin-2-yl)-1,2,4-triazole (L1) ruthenium polypyridyl precursor complex (**RuL1*N2***) was directly methylated yielding complexes which then contain the ligands 1-methyl-3-(pyridin-2-yl)-1,2,4-triazole (L2) and 4-methyl-3-(pyridin-2-yl)-1,2,4-triazole (L3). Surprisingly, the sterically least favoured complex, **RuL2*N2***, methylated at the N2 position; was obtained as the main product, with a yield of about 90%, whereas in the reaction between L2 and $[Ru(bpy)_2Cl_2]\cdot 2H_2O$ only the N4 isomer of the complex, **RuL2*N4***, could be obtained in appreciable amounts. This new synthetic strategy provided us with the first opportunity to compare their photophysical and photochemical properties and to investigate the role played by steric hindrance. In this paper we report the photochemical and photophysical properties of ruthenium bis(bipyridyl) complexes with the *N*-substituted triazole ligands L2, L3 and 1,4-bis[1-methyl-3-(pyridin-2-yl)-1,2,4-triazol-5-yl]benzene (L4) (see Figure 1). In the latter ligand, both the N2 and N4 sites are sterically hindered. The effect of the benzene and the methyl groups on the composition of the compounds and on their photophysical and photochemical properties were investigated. Emission lifetime, UV/Vis and NMR studies indicate that an irreversible

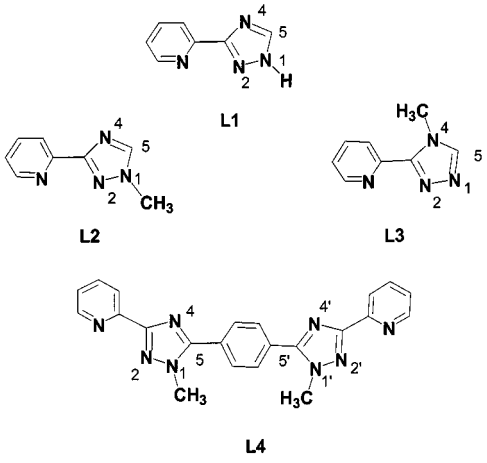

Figure 1. Ligand structures

[a] National Centre for Sensor Research, School of Chemical Sciences, Dublin City University
Dublin 9, Ireland
E-mail: han.vos@dcu.ie
[b] Department of Physical Chemistry, University of Uppsala, Box 532, 75121, Uppsala, Sweden
E-mail: leif.hammarstrom@fki.uu.se
[c] School of Chemistry, Dublin Institute of Technology, Dublin 8, Ireland
E-mail: tia.keyes@dit.ie

 © WILEY-VCH Verlag GmbH, 69451 Weinheim, 2001 1434−1948/01/0202−0529 $ 17.50+.50/0

photoisomerisation takes place, in which the sterically hindered N2-bonded L2 complex is transformed into the N4 species. For the mono- and dinuclear L4 complexes, a less clear picture was obtained, but photoinduced reactions were also observed. The results obtained are discussed with respect to the electronic properties of the compounds.

Results and Discussion

General

An important issue to be addressed first is the coordination mode of the triazole rings in the obtained products, in particular in the L4 complexes. For L2 and L3, the coordination of the triazole ring is known from earlier studies.[1,7] From the reaction mixture of the mononuclear L4 complex, two isomers were isolated by semi-preparative HPLC. In the dinuclear complex, coordination of the two metal units may occur to N2/N2′, N4/N4′ or N2/N4′ of the triazole ring. HPLC analysis of the reaction mixture showed the presence of different isomers. One main isomer was isolated in a pure form by recrystallisation.

^{1}H NMR Spectroscopy

The position of the methyl signals in the ^{1}H NMR spectra is diagnostic for the type of isomer obtained (see Table 1). For L2 and L4, the methyl substituent is expected to resonate significantly further upfield than in the free ligand when the ligand is bonded through the N2 atom. This is a consequence of the steric interaction between the methyl group and a neighbouring bpy ligand. For the N4 isomer a smaller shift is expected since no interaction between the methyl group and the bpy ligands is possible.[1,5,8] The methyl resonances recorded for the complexes fall clearly into two groups. The first set of signals at $\delta \approx 3.2$ is indicative of the presence of steric hindrance, since the values are shifted upfield by about 0.7 ppm, with respect to the free ligand. Such a shift indicates N2 coordination for L2 and L4 complexes. The resonances found at $\delta \approx 4$ point to coordination modes where the methyl group does not interact with the neighbouring bpy ligands and are indicative of N4 coordination in the L2 and L4 ligands and of N2 coordination in the L3 complex. For the dinuclear L4 complex, only one methyl signal was obtained at $\delta = 3.23$, clearly indicating that both centres are bonded in the same manner, namely through N2.

Table 1. Chemical shifts (ppm) for methyl groups; measurements were carried out in DMSO unless otherwise stated

Compound	CH_3
RuL2*N2*	3.15 (3.54[a])
RuL2*N4*	3.97 (4.17[a])
RuL3*N4*	4.21
RuL4*N4* (f)	4.07
(b)	3.82
RuL4*N2* (f)	4.10
(b)	3.27
RuRuL4*N2N2*	3.23
(in CD_3CN)	3.17

[a] Measured in acetone; (f) and (b) refer to the free and bound pyridyltriazole ring, respectively.

Redox Properties

All complexes show well-behaved electrochemistry (see Table 2). The redox processes are reversible, with peak-to-peak separations of 60−100 mV. **RuRuL4*N2N2′*** exhibits a single, two-electron, metal-based oxidation, without any sign of splitting, indicating that the interaction between the metal centres is at best very weak. The N4-coordinated complexes exhibit somewhat lower $Ru^{II/III}$ potentials than the N2 compounds possibly indicating improved π-acceptor properties of ligands coordinated in the N2 mode. The similarity of the reduction potentials of the compounds reported in this work and those observed for $[Ru(bpy)_3]^{2+}$ suggests that the first reduction process is bpy based. This is further confirmed by the first reduction potential observed for **$[Ru(L2N4)_3]^{2+}$** (L2 coordinated through N4) of −1.75 V vs. SCE,[9] approximately 400 mV more negative than that observed for $[Ru(bpy)_3]^{2+}$. This value suggests that the lowest unoccupied molecular orbital (LUMO) in the L2 complex is about 3300 cm^{-1} higher than in the homoleptic bpy complex.

Table 2. Electrochemical data for the triazole complexes; all measurements were carried out in acetonitrile with 0.1 M TEAP; all redox potentials measurements were performed using ferrocene as an internal reference

Complex	Oxidation potential [V vs. SCE]	Reduction potential [V vs. SCE]
RuL2*N2*	1.30	−1.36, −1.57
RuL2*N4*	1.20	−1.39, −1.61
RuL3*N2*	1.19	−1.39, −1.61
RuL4*N2*	1.31	−1.35, −1.56
RuL4*N4*	1.20	−1.35, −1.58
RuRuL4*N2N2′*	1.29	−1.38, −1.59
$[Ru(bpy)_3]^{2+}$	1.26	−1.35, −1.55, −1.80

Electronic Properties

The absorption spectra bands observed in the 400−460 nm region are associated with dπ−π* MLCT bands. The MLCT bands for complexes containing a *N*4-coordinated triazole ring are found at about the same energy as that of $[Ru(bpy)_3]^{2+}$. In agreement with the electrochemical data, the N2-bonded isomers have an MLCT band at higher energy suggesting that in this coordination mode the σ-donor properties of the L2 and L4 ligands are reduced.

All the compounds show emission at room temperature and at 77 K. The emission lifetimes of the complexes in acetonitrile, measured by time-correlated single-photon counting, are given in Table 3. For **RuL2*N4*** and **RuL4*N4***, the major decay component shows a lifetime of 9.0 ns and 35 ns, respectively. A minor (< 5%), faster component has a lifetime of approximately 1 ns. In contrast, for **RuL2*N2*** and **RuL4*N2*** the 1 ns component was dominant. In these samples, a second slower component was present, and its magnitude varied between 15% and 50% for different meas-

Table 3. UV/Vis absorption and emission data for the complexes; all measurements were carried out in acetonitrile unless otherwise stated

Complex	Absorption λ_{max} [nm] (ε [10^4 $M^{-1}cm^{-1}$])	Emission λ_{max} [nm] 300 K	77 K[a]	$\tau_{300\ K}$ [ns]
RuL2*N2*	435 (1.15)	615	566	1.0
RuL2*N4*	452 (1.07)[a]	600[a]	585	9.0
RuL3*N2*	440 (1.44)[a]	600[a]	584	14.0
RuL4*N2*	415 (1.33)	611	570	1
RuL4*N4*	453 (0.90)	614	584	35
RuRuL4*N2N2′*	414 (2.60)	603	573	1
$[Ru(bpy)_3]^{2+}$	452 (1.30)	615	582	950[b]

[a] Measured in ethanol/methanol (4:1, v/v). – [b] Deaerated solution.

urements. The lifetime of this component matched that of the corresponding N4 isomer. The dimeric **RuRuL4*N2N2′*** also has a dominant 1 ns component, with a minor slower (32 ns) component that matches the lifetime of **RuL4*N4***.

The results obtained from the lifetime measurements for the N2 isomers of L2 and L4 were at first hard to explain, since an impurity level as high as 50% would certainly have been detected by the other characterisation techniques. The formation of a photoproduct seems a more likely explanation for the behaviour observed. For the compounds under investigation, the occurrence of photoinduced ligand processes is not unexpected. It is generally assumed that upon excitation of ruthenium polypyridyl complexes, an electron is transferred from the metal-based ground state to a singlet metal-to-ligand charge-transfer (^{1}MLCT) state. From this singlet state, the emitting ^{3}MLCT state is populated efficiently by intersystem crossing. Population of the nearby antibonding triplet metal-centred state (^{3}MC) then explains the photoinduced reactivity of the compounds, and in the literature both ligand exchange and rearrangements have been reported.[4,10,11]

To investigate this hypothesis further, a photolysis was carried out in which ^{1}H NMR spectra were taken after various irradiation times. After irradiating for 6 h in acetonitrile, analysis of the CH_3 resonance suggested that up to 70% of the complex underwent photoinduced isomerisation to the corresponding **RuL2*N4*** complex. Further irradiation (up to 12 h) resulted mainly in decomposition of the complex **RuL2*N2***. This decomposition probably occurs by the formation of a photoinduced intermediate where the pyridyltriazole ligand is coordinated in a monodentate fashion. Such behaviour in strongly coordinating solvents has been reported before for other complexes containing neutral pyridyltriazole ligands.[6b] Under the same conditions, **RuL2*N4*** shows a remarkable photostability and decomposition becomes noticeable only after 24 h of irradiation. The same experiment was carried out in a weakly coordinating solvent, namely acetone, in an effort to reduce the formation of secondary photoproducts (see Figure 2). Analysis of the methyl region of the spectra shows that the resonance originally obtained for the N2 isomer at $\delta = 3.54$ is replaced by a signal at $\delta = 4.17$ after photolysis. This is indicative of the formation of the N4 isomer, and in acetone typically a 100% photoisomerisation of **RuL2*N2*** to **RuL2*N4*** was obtained after irradiation for 30 h. No evidence for the formation of a solvated metal complex was observed. No changes were observed in the ^{1}H NMR spectra of **RuL2*N4*** after irradiating for 24 h. These results suggest that irreversible photoinduced isomerisation of **RuL2*N2*** to **RuL2*N4*** is taking place as shown in Scheme 2.

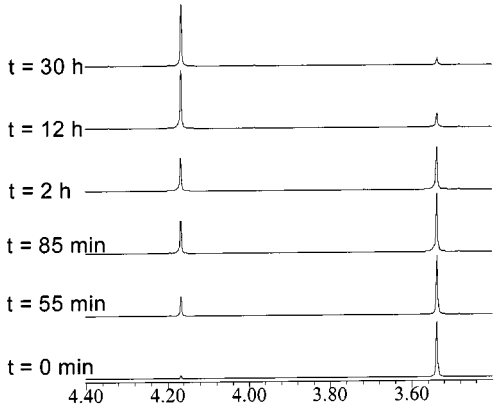

Figure 2. ^{1}H NMR spectra of the methyl region taken during photolysis of **RuL2*N2*** in [D_6]acetone

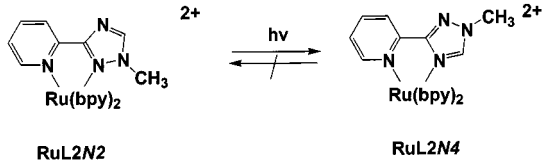

Scheme 2

This photoisomerisation process can also be observed using UV/Vis absorption spectroscopy. As can be seen in Figure 3, irradiation of **RuL2*N2*** in acetone causes a gradual decrease in intensity of the band at 415 nm and a concomitant growth of bands at 355 nm and 455 nm, which are associated with the **RuL2*N4*** complex (Table 3). The UV/Vis spectra show isosbestic points at 448 nm and 372 nm, indicating that photoproducts are formed directly without the production of long-lived intermediates. Upon complete photolysis, no further changes in the absorption spectrum occur, which further indicates the photostability of **RuL2*N4***.

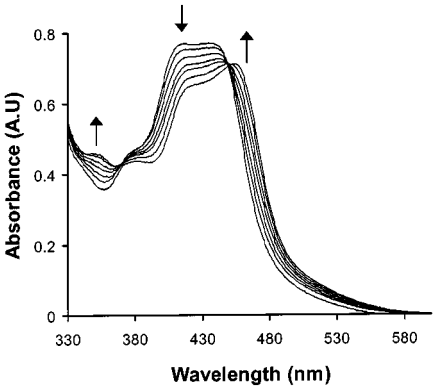

Figure 3. UV/Vis absorption spectra of **RuL2*N2*** in acetone upon irradiation for (a) 0 min, (b) 2.5 min, (c) 5 min, (d) 10 min, (e) 17.5 min, (f) 27.5 min, (g) 120 min

The conclusions drawn from the NMR and UV/Vis studies were further corroborated by emission lifetime measurements on **RuL2*N2*** in acetonitrile exposed to varying amounts of light. The results are shown in Figure 4. To minimise exposure of the sample to light during the lifetime measurements, these were continued for only 2−3 min (giving 1000 counts in the peak channel). In the first measurement, the contribution from the longer lived N4 isomer emission was only 15%. However, after only a few minutes of subsequent irradiation with a 450-W Xe lamp (using a water heat filter and a $\lambda > 385$ nm cut-off), this contribution had increased to 80%, indicating an almost complete conversion into the N4 isomer. When irradiation was continued, an instrument-response limited component ($\tau < 150$ ps) started to appear (not shown), and after 100 min of irradiation very little of the N4 isomer remained. We attribute the very short-lived component to the photolysed complex in which the L2 ligand had presumably been replaced by acetonitrile.

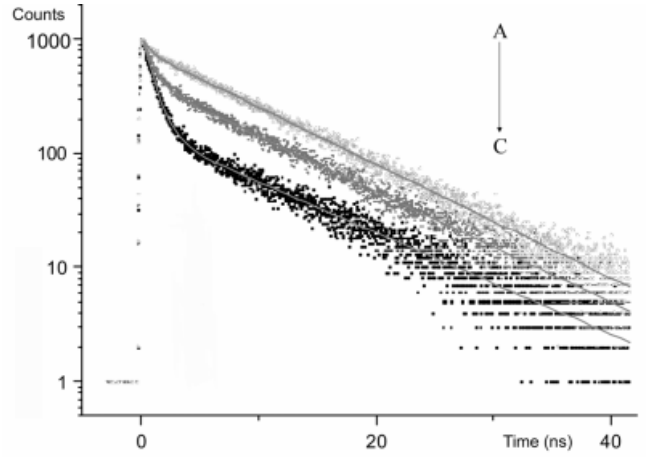

Figure 4. Emission decays for the same sample of **RuL2*N2*** in acetonitrile; curve A: sample prepared in the dark; curve B: after 1.5 min of irradiation with an Xe lamp; curve C: after 6.5 min of irradiation; the lines are double-exponential fits to the data, with lifetimes of 1.0 ns and 9.0 ns; the contribution from the slower component increased from 15% in A to 40% in B and 80% in C

Since **RuL4*N2* and RuRuL4*N2N2′*** also showed a double-exponential emission decay, NMR experiments were also carried out for the L4 compounds. For all three complexes, irradiation in acetone resulted in a complex mixture of products, which could be attributable to partial isomerisation and decomposition of the starting material and products. The results obtained from these experiments were not further analysed.

Concluding Remarks

The results obtained in this investigation demonstrate the importance of steric factors in the photochemical properties of ruthenium polypyridyl compounds. Earlier studies[4] have shown that for the protonated L1 complexes, a *reversible* N2/N4 photoinduced isomerisation is taking place. The results obtained for the L2 complex indicate that sterically hindered complexes (i.e. **RuL2*N2***), have the tendency to release the steric congestion upon photolysis by converting into the corresponding unhindered isomer (i.e. **RuL2*N4***). The presence of a steric constraint in the compound therefore leads to an *irreversible* photoisomerisation.

Pyridyltriazoles are mainly σ-donor ligands and have only limited π-acceptor properties. Therefore it seems likely that the small differences observed in the electronic spectra and in the $Ru^{II/III}$ redox potentials of the different isomers can be explained by a reduced σ-donor capability of the N2 isomer owing to steric hindrance. This leads to a lower excited-state ^{3}MC level in the N2 isomer than in the N4 isomer and facilitates the photochemically induced isomerisation of the N2 isomer by a photochemically driven process.

When substituents are present at both the N1 and C5 positions (as in the three L4 complexes), neither of the possible isomers is sterically unhindered. Hence, irradiation of these complexes results in a mixture of different isomers of similar stability (or, in other words, ''photochemical instability'').

Experimental Section

Materials: All synthetic reagents were of commercial grade and no further purification was employed, unless otherwise stated. All solvents employed in spectroscopic and electrochemical measurements were of HPLC or spectroscopic grade.

Experimental Methods: ^{1}H NMR spectra were recorded with a Bruker AC400 (400 MHz) instrument. For NMR-scale photochemical experiments, 5−10 mg of a given complex was dissolved in [D_3]acetonitrile or [D_6]acetone (0.5 mL), placed in a borosilicate NMR tube and irradiated using a 150-W halogen lamp. NMR spectra were taken at regular intervals and the degree of isomerisation checked by integration of the CH_3 resonance signals. − UV/Vis spectra (accuracy ± 2 nm) were obtained using a Shimadzu UV3100 UV/Vis−NIR spectrophotometer interfaced to an Elonex PC433 personal computer. The estimated error of the extinction coefficients is 5%. − Emission spectra (accuracy ± 5 nm) were obtained with a Perkin−Elmer LS50B luminescence spectrometer

equipped with a red-sensitive Hamamatsu R928 detector, interfaced with an Elonex PC466 personal computer employing Perkin−Elmer FL WinLab custom-built software. At room temperature, unless otherwise indicated, acetonitrile was the solvent used, and excitation and emission slit widths of 10 nm, were employed. At 77 K measurements were carried out in ethanol/methanol (4:1, v/v) using excitation and emission slit widths of 5 nm. The spectra were not corrected for the photomultiplier response. − For electrochemical measurements, HPLC grade acetonitrile dried with molecular sieves was employed. Potentials are ± 50 mV. The electrolyte used was 0.1 M tetraethylammonium perchlorate (TEAP). The electrochemical cell used was a conventional three-compartment cell with glass frits. The reference electrode used was a saturated calomel electrode. The working electrode was a 3-mm diameter teflon shrouded glassy carbon electrode and a platinum gauze was employed as the counter electrode. Prior to reduction measurements, the solutions were degassed for 15 min with nitrogen. Cyclic voltammetry (100 mVs^{-1}) was carried out using a CH instruments Model 660 electrochemical workstation interfaced to an Elonex 486 PC. Analytical HPLC experiments were carried out using a Waters HPLC system, consisting of a model 501 pump, a 20-μL injector loop, a Partisil SCX radial PAK cartridge mounted in a radial compression *Z* module and a Waters 990 photodiode array detector. An NEC APCIII computer controlled the system. The detection wavelength used was 280 nm and the flow rate was 2.0 mL/min. The mobile phase was CH_3CN/H_2O (80:20) containing 0.1 M $LiClO_4$. Semipreparative HPLC was carried out using an ACS pump, a 1-mL injection loop and a Waters Partisil SCX 10 μm cation exchange column (25 × 100 mm). The mobile phase used was $CH_3CN:H_2O$ (80:20) containing KNO_3 (0.12−0.20 M). The flow rate used varied between 1.50 and 2.0 mL/min.

Single-Photon Counting: Fluorescence lifetimes were determined using time-correlated single-photon counting. The excitation source had a tuneable output of a 200 kHz and a 120 femtosecond optical parametric amplifier (OPA, Coherent Radiation Inc). This device was pumped by a regenerative amplifier (700 μJ, 150 fs, 200 kHz) seeded by the 80 fs output of a Ti:Sapphire oscillator. The frequency-doubled fundamental generated in the OPA was used to excite the samples at 400 nm. A polariser was located before the sample to define the vertical polarisation of the excitation light and all fluorescence measurements were carried out with an analysing polariser before the detector was oriented at the magic angle (54.7°), relative to the excitation polarisation, to remove anisotropy effects. Fluorescence was observed through an interference filter centred at 600 nm (Oriel, USA) with a full-width at half-maximum of 10 nm. A microchannel plate multiplier (Hamamatsu) was used for the detection. Instrumental response curves were measured by exchanging the 600 nm interference filter after the sample with a 400 nm filter and recording the scattering from a scatter solution. The instrumental response (FWHM) was ca. 100 ps. The fluorescence decay data were analysed with a nonlinear least-squares program using a modified Levenberg−Marquardt algorithm with iterative reconvolution. The reduced χ^2 and residual plots were used to judge the quality of the fits. The samples for emission lifetime measurements were dissolved in spectroscopic grade acetonitrile (Merck) to an optical density of ca. 0.3 at the excitation wavelength. The solvents were not degassed since quenching by O_2 had negligible effect on the short lifetimes measured. Lifetimes are ± 10%.

Ligand Synthesis

Synthesis of 1,4-Bis[1-methyl-3-(2-pyridyl)-1,2,4-triazol-5-yl]benzene (L4)

Step 1. Synthesis of *N2*-methyl-2-pyridylamidrazone: 2-Cyanopyridine (36 g, 0.35 mol) and excess methylhydrazine (18.43 g, 0.40 mol) were mixed in a minimum amount of ethanol and allowed to stir overnight. The pale yellow crystalline product was filtered, washed with diethyl ether and air dried. Yield 26.7 g (50%). − M.p. 108−110 °C (ref.[12] 109−110 °C). − ^{1}H NMR ($CDCl_3$): δ = 7.24 (1 H, dd, pyridyl H^5), 7.67 (1 H, dd, pyridyl H^4), 8.08 (1 H, d, pyridyl H^3), 8.50 (1 H, d, pyridyl H^6), 5.24 (2 H, br. s, NH), 2.98 (3 H, s, CH_3). − ^{13}C NMR ($CDCl_3$): δ = 38.48, 119.60, 123.32, 136.02, 146.41, 147.77, 150.72.

Step 2. Synthesis of *N*,*N*′-Terephthaloylbis[(*N2*-methyl-2-pyridyl)hydrazidine]: This intermediate was prepared by the dropwise addition of a THF solution (30 cm^3) of terephthaloyl dichoride (5.08 g, 0.025 mol) to a solution of *N2*-methyl-2-pyridylamidrazone (7.50 g, 0.05 mol) and triethylamine (10 cm^3) in THF while maintaining the reaction mixture at 0°C. The reaction mixture was then reduced to approximately 25 mL and an equal volume of water was added. The yellow product was filtered, washed with water, hot methanol and diethyl ether, dried under vacuum and then left in an oven at 60 °C for 24 h. Yield 7.00 g (65%). − M.p. 178−180 °C. − ^{1}H NMR ($CDCl_3$): δ = 8.15 (2 H, s, phenyl), 8.10 (1 H, d, pyridyl H^3), 7.65 (1 H, dd, pyridyl H^4), 7.43 (1 H, dd, pyridyl H^5), 8.60 (1 H, d, pyridyl H^6), 10.30 (1 H, br. s, NH), 4.11 (3 H, s, CH_3). − ^{13}C NMR ($CDCl_3$): δ = 38.50, 120.82, 124.67, 128.85, 129.10, 136.89, 148.24, 150.26, 153.79, 161.2.

Step 3. Cyclization of *N*,*N*′-Terephthaloylbis[(*N2*-methyl-2-pyridyl)hydrazidine] to Form L3: *N*,*N*′-Terephthaloylbis[(*N2*-methyl-2-pyridyl)hydrazidine] (7.00 g, 0.017 mol) was suspended in a minimum volume (ca. 30 mL) of ethylene glycol and heated at reflux for 2 h. A white crystalline precipitate was obtained upon cooling of the solution. Further precipitation of the product was induced by the addition of a small amount of water to the mother liquor. The ligand was recrystallised from boiling methanol, filtered and dried under vacuum overnight. Yield 4.20 g (66%). − M.p. 278−280 °C. − ^{1}H NMR ($CDCl_3$): δ = 8.07 (2 H, s, phenyl), 8.10 (1 H, d, pyridyl H^3), 7.92 (1 H, dd, pyridyl H^4), 7.45 (1 H, dd, pyridyl H^5), 8.67 (1 H, d, pyridyl H^6), 4.12 (3 H, s, CH_3). − ^{13}C NMR ($CDCl_3$): δ = 37.65, 121.58, 124.15, 129.00, 129.13, 137.16, 149.45, 149.71, 154.26, 159.88. − MS; *m*/*z*: 395 $[M + 1]^+$. − $C_{22}H_{18}N_8$: calcd. C 66.98, H 4.60, N 28.41; found C 66.69, H 4.61, N 27.95.

Synthesis of Metal Complexes: *cis*-$[Ru(bpy)_2Cl_2]\cdot 2H_2O$[13] was prepared as reported in the literature. **RuL2*N4*** and **RuL3*N2*** were prepared as reported before.[1] **RuL2*N2*** was prepared by direct methylation[7] of **RuL1*N2***.[1]

Synthesis of $[Ru(bpy)_2L4](PF_6)_2$: L4 (0.789 g, 2 mmol) was dissolved in hot methanol/water (2:1, v/v). To the solution was added *cis*-$[Ru(bpy)_2Cl_2]\cdot 2H_2O$ (0.312 g, 0.6 mmol) and the mixture was heated at reflux for 6 h. Following the removal of most of the solvent by rotary evaporation and the addition of saturated aqueous NH_4PF_6 solution, the resulting precipitate was filtered and dried. HPLC analysis revealed the presence of two isomers in a 30:70 ratio (isomer 1/isomer 2). These were obtained in a pure form by semipreparative HPLC using acetonitrile/water (80:20) containing 0.11 M KNO_3 as the mobile phase and a flow rate of 1.7 mL/min. Total yield after purification (isomer 1 + isomer 2): 0.20 g (30%).

Isomer 1 (RuL4*N4*): $C_{42}H_{34}F_{12}N_{12}P_2Ru\cdot 3H_2O$: calcd. C 45.78, H 3.50, N 14.58; found C 45.24, H 3.12, N 14.14.

Isomer 2 (RuL4*N2*): $C_{42}H_{34}F_{12}N_{12}P_2Ru\cdot H_2O$: calcd. C 45.19, H 3.23, N 15.06; found C 45.41, H 3.15, N 14.93.

Synthesis of [(Ru(bpy)$_2$)$_2$L4](PF$_6$)$_4$·3H$_2$O (RuRuL4*N2N2′*): *cis*-[Ru(bpy)$_2$Cl$_2$]·2H$_2$O (0.624 g, 1.2 mmol) and L4 (0.197 g, 0.5 mmol) were heated at reflux in ethanol/water (2:1, v/v) for 6 h. Upon cooling of the reaction mixture, a few drops of a saturated aqueous solution of ammonium hexafluorophosphate were added, whereupon a bright orange precipitate was obtained. This was filtered and recrystallised from acetone/water (2:1, v/v). HPLC analysis of the product showed the presence of only one isomer. Yield 0.30 g (33%). − $C_{62}H_{50}F_{24}N_{16}P_4Ru_2$·3H$_2$O: calcd. C 40.11, H 3.04, N 12.07; found C 40.27, H 3.08, N 12.02.

Acknowledgments

The authors thank the EC TMR programme (Grant number CT96−0031) for financial assistance.

[1] [1a] R. Hage, R. Prins, J. G. Haasnoot, J. Reedijk, J. G. Vos, *J. Chem. Soc., Dalton Trans.* **1987**, 1381.[1b] B. E. Buchanan, J. G. Vos, M. Kaneko, W. J. M. van der Putten, J. M. Kelly, R. Hage, R. A. G. de Graaff, R. Prins, J. G. Haasnoot, J. Reedijk, *J. Chem. Soc., Dalton Trans.* **1990**, 2425.

[2] [2a] R. Hage, J. G. Haasnoot, H. A. Nieuwenhuis, J. Reedijk, R. Wang, J. G. Vos, *J. Chem. Soc. Dalton Trans.* **1991**, 3271. − [2b] H. A. Nieuwenhuis, J. G. Haasnoot, R. Hage, J. Reedijk, T. L. Snoeck, D. J. Stufkens, J. G. Vos, *Inorg. Chem.* **1991**, *30*, 48. − [2c] T. E. Keyes, C. M. O'Connor, U. O'Dwyer, C. G. Coates, P. Callaghan, J. J. McGarvey, J. G. Vos, *J. Phys. Chem. A* **1999**, *103*, 8915.

[3] R. Hage, J. G. Haasnoot, H. A. Nieuwenhuis, J. Reedijk, D. J. A. De Ridder, J. G. Vos, *J. Am. Chem. Soc.* **1990**, *112*, 9245.

[4] R. Wang, J. G.Vos, R. H. Schmehl, R. Hage, *J. Am. Chem. Soc.* **1992**, *114*, 1964.

[5] E. M. Ryan, R. Wang, J. G. Vos, R. Hage, J. G. Haasnoot, *Inorg. Chim. Acta* **1993**, *208*, 49.

[6] [6a] B. E. Buchanan, H. Hughes, J. H. van Diemen, R. Hage, J. G. Haasnoot, J. Reedijk, J. G. Vos, *J. Chem. Soc, Chem Commun.* **1991**, 300. − [6b] B. E. Buchanan, P. Degn, J. M. Pavon Velasco, H. Hughes, B. S. Creaven, C. Long, J. G. Vos, R. A. Howie, R. Hage, J. H. van Diemen, J. G. Haasnoot, J. Reedijk, *J. Chem. Soc., Dalton Trans.* **1992**, 1177.

[7] S. Fanni, S. Murphy, J. S. Killeen, J. G. Vos, *Inorg. Chem.* **2000**, *39*, 1320.

[8] P. J Steel, F. Lahousse, D. Lerner, C. Marzin, *Inorg. Chem.* **1983**, *22*, 1488.

[9] R. Hage, Ph. D Thesis, Leiden University, **1991**.

[10] [10a] S. Tachiyashiki, H. Ikezawa, K. Mizumachi, *Inorg. Chem.* **1994**, *33*, 623. − [10b] R.Arakawa, S. Tachiyaskiki, T. Matsuo, *Anal. Chem.* **1995**, *67*, 4138.

[11] A. Juris, V. Balzani, F. Barigelletti S. Campagna, P. Belser, A. von Zelewsky, *Coord Chem. Rev.* **1988**, *84*, 85.

[12] S. Kubota, M. Uda, T. Nakagawa, *J. Heterocycl. Chem.* **1975**, *12*, 855.

[13] B. P. Sullivan, D. J. Salmon, T. J. Meyer, *Inorg. Chem.* **1978**, *17*, 3334.

Received June 15, 2000
[I00231]

Protonation of the Heterocyclic Cp-Anion Equivalent [Pyrrolyl-B(C_6F_5)$_3$]Li − Formation of a Useful Neutral Brønsted Acid for the Generation of Homogeneous Metallocene Ziegler Catalysts

Gerald Kehr,[a] Rolf Roesmann,[a] Roland Fröhlich,[a][‡] Christiane Holst,[a][‡] and Gerhard Erker*[a]

Keywords: Protonations / Heterocycles / Homogeneous catalysis / Brønsted acids / Zirconium

N-pyrrolyllithium (**1**) adds to B(C_6F_5)$_3$ to yield [(C_4H_4N)B(C_6F_5)$_3$]Li (**3**). The corresponding monoetherate (**3**·OEt_2) was characterized by X-ray diffraction and shows an η^5 coordination of the pyrrolyl moiety to the lithium cation. Treatment of **3** with HCl in ether leads to H^+ addition at a pyrrolyl α-position to yield the neutral dipolar Brønsted acid system [(C_4H_5N)B(C_6F_5)$_3$] (**4**). The reagent **4** can be used to protonate $Cp_2Zr(CH_3)_3$ to yield [$Cp_2Zr(CH_3)^+$(C_4H_4N)B(C_6F_5)$_3^-$] (**6**) and methane. H^+ transfer from **4** to (butadiene)-zirconocene results in the formation of the (π-allyl)metallocene salt [(C_4H_7)ZrCp_2^+(C_4H_4N)B(C_6F_5)$_3^-$] **(8)**. In analogous reactions, the neutral Brønsted acid was employed as a protonating activator component for the generation of homogeneous Ziegler catalysts derived from a variety of (butadiene)- or (dimethyl)*ansa*-metallocenes. The systems generated by treatment with **4** show comparable activities in ethene or propene polymerization reactions as conventionally generated Group 4 metallocene Ziegler catalysts.

Introduction

The generation of homogeneous Group 4 metallocene Ziegler catalysts and related early and late transition metal catalyst systems is mostly carried out by treatment of the respective metal complex catalyst precursors with methylaluminoxane.[1] Alternatively, alkyl anion abstraction from, for example, ^{R}Cp$_2$MR$_2$ species, with the trityl cation[2] or with B(C_6F_5)$_3$ has also been reported,[3] as has the use of single component catalysts derived from ^{R}Cp$_2$M(butadiene) complexes by addition of B(C_6F_5)$_3$ or the related (pyrrolyl)B(C_6F_5)$_2$ Lewis acids.[4,5] In principle, formation of the active [^{R}CpMR$^+$] catalyst species by protonation with a suitable Brønsted acid would be an alternative, provided sufficiently non-nucleophilic conditions could be maintained throughout the reaction. Ammonium salts have been successfully employed for this purpose, especially dimethylanilinium reagents such as [PhNMe$_2$H$^+$] with [BPh$_4^-$] or [B(C_6F_5)$_4^-$] anions.[6] Sometimes low solubilities and the stoichiometric formation of a tertiary amine have complicated this protonation route for the generation of active homogeneous Ziegler catalysts. We here report the formation and some features of a neutral dipolar Brønsted acid reagent that may make the protonation route in some cases an attractive alternative to the activation methods presently used in homogeneous organometallic Ziegler catalyst formation and the chemistry of reactive organometallic cation systems.[7]

[a] Organisch-Chemisches Institut der Universität Münster, Corrensstraße 40, D-48149 Münster, Germany
Fax: (internat.) +49-251/833-6503
E-mail: erker@uni-muenster.de
[‡] X-ray crystal structure analyses.

Results and Discussion

N-pyrrolyllithium (**1**) was treated with B(C_6F_5)$_3$ (**2**)[8] to yield the [(*N*-pyrrolyl)B(C_6F_5)$_3$]Li reagent **3** (Scheme 1). Complex **3** shows symmetrical pyrrolyl ^{1}H/^{13}C NMR resonances at δ = 6.72 (2,5-H) and 5.84 (3,4-H)/125.0 (C2,5) and 108.9 (C3,4), and a ^{11}B NMR signal at δ = −8.2 (in [D_6]benzene) indicating tetracoordinated boron. A ^{7}Li NMR resonance (in [D_8]THF) at δ = −2.6 points to a mononuclear geometry of the lithium compound **3** in this coordinating solvent.[9] Single crystals of **3**·OEt_2 were obtained from pentane/ether solution at 8 °C that allowed for characterization by an X-ray crystal structure analysis.

The structure shows that the pyrrolyl unit is bonded to a tetravalent boron atom [N1−B: 1.576(4) Å]. The pyrrolyl moiety of the [(C_4H_4N)−B(C_6F_5)$_3^-$] anion exhibits a distorted η^5 coordination to the lithium atom.[10] The Li−N1 bond is short at 2.281(7) Å, the Li−C5 [2.350(8) Å]/Li−C2 [2.423(8) Å], and Li−C4 [2.492(9) Å]/Li−C3 [2.533(9) Å] linkages become increasingly longer, but all heavy atoms of the planar pyrrolyl framework are clearly within bonding

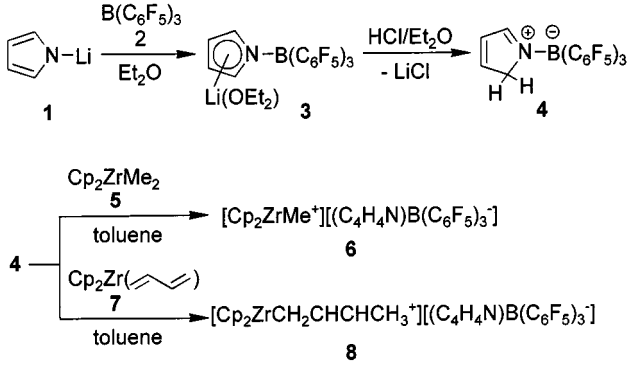

Scheme 1

 © WILEY-VCH Verlag GmbH, 69451 Weinheim, 2001 1434−1948/01/0202−0535 $ 17.50+.50/0

distance of the lithium atom. Extensive bond delocalization is observed inside the C_4H_4N moiety (see Figure 1). The lithium atom in **3** is further coordinated to an ether molecule [O42−Li: 1.830(7) Å] and, remarkably, to two fluorine atoms from the *ortho* F−C bonds of two of the boron bound -C_6F_5 substituents [Li−F16: 2.041(7) Å, Li−F26: 2.467(8) Å]. This additional lithium-fluorine interaction,[11] which is in the same range of bond lengths as the Li−C(pyrrolyl) unit, makes the coordination geometry of the lithium atom in complex **3** distorted tetrahedral [bond angles O42−Li−pyrrolyl (centroid): 136.0°; O42−Li−F16: 105.4(3)°; O42−Li−F26: 118.5(4)°; F16−Li−F26: 81.2(3)°].

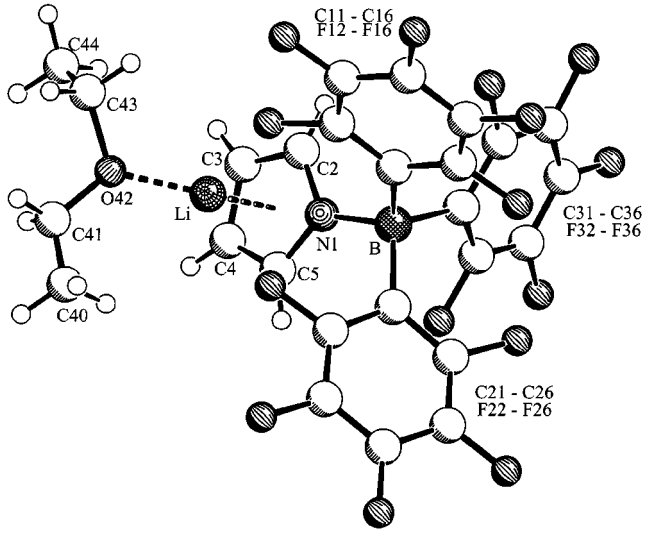

Fjgure 1. Molecular structure of complex **3**; selected bond lengths (Å) and angles (°): B−C21 1.637(5), B−C31 1.647(5), B−C11 1.656(5); C16−F16−Li 136.4(3), C26−F26−Li 136.4(2), N1−B−C21 109.4(3), N1−B−C31 102.5(2), N1−B−C11 112.6(3), C21−B−C31 115.8(3), C21−B−C11 104.1(3), C31−B−C11 112.7(3), C2−N1−B 125.0(3), C2−N1−C5 106.8(3), C5−N1−B 127.1(3); for additional values see text

Treatment of **3** with anhydrous HCl in ether resulted in protonation at an α-carbon atom of the pyrrol ring with formation of **4**. The neutral dipolar product was isolated in 57% yield after recrystallization from toluene. It shows four characteristic ^{1}H NMR resonances of the *N*-borylated pyrrolium ring system at δ = 7.35, 6.34, 5.45 and 3.53 in a 1:1:1:2 ratio {^{13}C NMR signals at δ = 171.1 (C2), 155.5 (C4), 127.2 (C3), 65.3 (C5) in [D_6]benzene; ^{15}N NMR resonance at δ = −145; ^{11}B NMR signal at δ = −7.6 in [D_8]toluene}.

The X-ray crystal structure analysis of **4** (single crystals from toluene at −18 °C; Figure 2) shows a planar pyrrolium ring system bonded to boron [N1−B6: 1.608(2) Å] that exhibits alternating double and single bonds [N1−C2: 1.298(2) Å; C2−C3: 1.431(3) Å; C3−C4: 1.318(3) Å; C4−C5: 1.474(3) Å; N1−C5: 1.449(2) Å; hydrogen atoms at the C_4H_5N ring were located from difference Fourier maps].

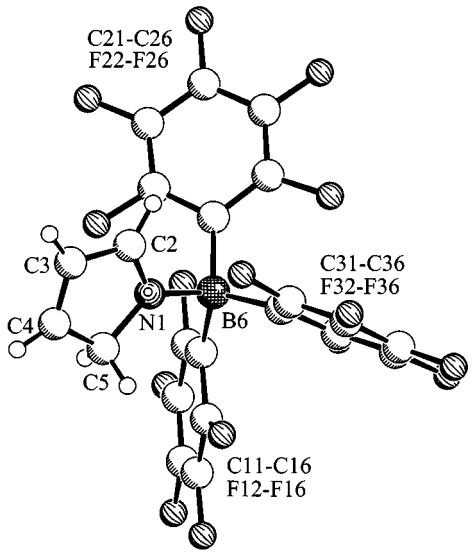

Figure 2. Molecular structure of **4**; selected bond lengths (Å) and angles (°): B6−C21 1.640(2), B6−C31 1.647(2), B6−C11 1.653(2); N1−B6−C21 105.13(12), N1−B6−C31 109.01(12), N1−B6−C11 106.37(12), C21−B6−C31 112.79(13), C21−B6−C11 114.36(13), C31−B6−C11 108.83(12), C2−N1−C5 107.61(14), C2−N1−B6 126.36(14), C5−N1−B6 125.98(13), N1−C2−C3 112.22(17), C4−C3−C2 106.83(18), C3−C4−C5 109.18(18), N1−C5−C4 104.05(16); for additional values see text

The neutral Brønsted acid **4** turns out to be well suited for the generation of group 4 metallocene cation complexes by protonation reactions of a variety of organometallic precursors. Two typical examples are the proton transfer reactions of **4** with dimethylzirconocene (**5**) and (η^4-butadiene)-zirconocene (**7**, see Scheme 1). Compound **4** reacts with $Cp_2Zr(CH_3)_2$ (**5**) in toluene at ambient temperature during 1 h to yield cleanly the organometallic salt [$Cp_2ZrCH_3^+$][$(C_4H_4N)B(C_6F_5)_3^-$] (**6**). The proton transfer reaction in this case results in the liberation of one equivalent of methane. Compound **4** rapidly transfers a proton to the butadiene ligand of **7** to yield a single [Cp_2Zr(*trans*-crotyl)$^+$][$(C_4H_4N)B(C_6F_5)_3^-$] isomer (**8**).

Both reactions were used for the generation of active homogeneous metallocene Ziegler catalysts for ethene polymerization in situ. In addition, the Brønsted acid **4** was employed in the generation of active ethene and propene polymerization catalysts from dimethyl- or η^4-butadiene complexes of a series of *ansa*-metallocene frameworks (see Scheme 2).[12,13] The resulting catalysts were compared with their conventionally generated analogues [i.e. obtained by MAO treatment of the respective metallocene dichlorides, or $B(C_6F_5)_3$ treatment of the respective metallocene dimethyl complexes or -η^4-butadiene complexes], and found to be comparable in activity and selectivity with these established procedures (see Table 1).[13] These reactions demonstrate that H^+ transfer from this new, readily available neutral proton source [$(C_4H_5N)B(C_6F_5)_3$] (**4**) provides an attractive alternative for the formation of reactive organometallic cations and related active catalyst systems, with concurrent generation of the essentially non-nucleophilic counter anion [$(C_4H_4N)B(C_6F_5)_3^-$]. A variety of interesting applications of the neutral Brønsted acid **4** and related sys-

tems in organometallic chemistry and catalysis can be envisioned. Further examples are being actively investigated in our laboratory.

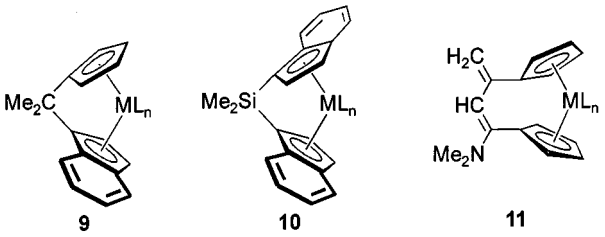

9 **10** **11**

ML_n = $ZrCl_2$ (**a**), $ZrMe_2$ (**b**), Zr(allyl) (**c**);

Scheme 2

Table 1. A comparison of selected data concerning 1-alkene polymerization reactions at homogeneous metallocene Ziegler catalysts using different activation procedures

a) Ethene polymerization[a]

Precursor	µmol	Activator	µmol	t (min)	g PE	Act[b]	mp
5	59.5	$B(C_6F_5)_3$	58.6	60	9.9	169	128
5	35.7	**4**	36.3	30	6.4	359	127
7	33.6	$B(C_6F_5)_3$	35.2	30	10.0	583	128
7	33.6	**4**	34.5	30	8.6	501	130
9a[c]	34.0	MAO	36000	40	18.2	411[d]	[e]
9b	35.6	$B(C_6F_5)_3$	43.0	40	16.2	341[d]	[e]
9b[c]	29.3	**4**	29.4	40	13.8	354	129
9c[c]	27.4	**4**	27.6	60	36.9	673	[e]
11b[c]	29.0	**4**	29.4	15	5.6	386	129

b) Propene polymerization[c]

Precursor	µmol	Activator	µmol	t (min)	g PP	act[b]	%mmmm[f]
9a	34.0	MAO	36200	60	15.1	222	10[d]
9c	35.6	$B(C_6F_5)_3$	43.0	60	31.8	446	10[d]
9c	30.1	**4**	38.0	90	10.2	113	12
10a	22.6	MAO	36200	45	201.8	6700	69[d,g]
10c	39.3	$B(C_6F_5)_3$	43.0	45	63.6	1200	77[d,g]
10c	28.8	**4**	32.8	45	81.9	1900	88[g]

[a] Reactions at 20 °C, 1 bar, if not otherwise noted. – [b] In g polymer/mmol[Zr]·bar·h. – [c] 40 °C, 2 bar. – [d] From ref. 13. – [e] Not determined. – [f] From ^{13}C NMR pentade analysis. – [g] These reactions were not carried out under completely isothermal conditions because of their high exothermicities; that is probably the cause of the slightly different isotacticities observed.

Experimental Section

All reactions were carried out in an inert atmosphere (argon) using Schlenk-type glassware or in a glovebox. Solvents were dried and distilled under argon prior to use. For additional general information including a description of the instrumentation used for physical characterization of the compounds see refs. 5 and 11a.

Preparation of $[(C_4H_4N)B(C_6F_5)_3]Li$ (3): Solid *N*-pyrrolyllithium[14] (0.53 g, 7.27 mmol) was mixed with solid $B(C_6F_5)_3$ (3.72 g, 7.27 mmol). Then, 50 mL of diethyl ether was added and the suspension stirred for 3 h at ambient temperature. Solvent was removed in vacuo and the residue suspended in pentane. The solid product was collected by filtration, washed with pentane (3 × 20 mL) and dried in vacuo to yield **3**·Et_2O (4.5 g, 91%), m.p. 137 °C, decomp. at 204 °C. – ^1H NMR (600 MHz, [D$_6$]benzene, 298 K): δ = 6.72 (m, 2 H, 2,5-H), 5.84 (m, 2 H, 3,4-H), 2.80 (q, 4 H, CH_2 of Et_2O), 0.68 (t, 6 H, CH_3 of Et_2O). – ^{13}C NMR (150.7 MHz, [D$_6$]benzene, 298 K): δ = 148.2 ($^1J_{FC}$ = 234 Hz), 139.8 ($^1J_{FC}$ = 250 Hz), 137.6 ($^1J_{FC}$ = 249 Hz), 121.3 (br., *o*-, *p*-, *m*-, *ipso*-C of C_6F_5), 125.0 (C2,5), 108.9 (C3,4), 65.9, 14.0 (Et_2O). – ^{11}B NMR (64.2 MHz, [D$_6$]benzene, 300 K): δ = −8.2 ($\nu_{1/2} \approx 50$ Hz). – ^7Li NMR (77.8 MHz, [D$_8$]THF, 300 K): δ = −2.6 ($\nu_{1/2} \approx 2$ Hz). – ^{19}F NMR (282 MHz, [D$_6$]benzene, 300 K): δ = −134.9, −157.5, −162.7 (*o*-, *p*-, *m*-F of C_6F_5). – $C_{26}H_{14}BF_{15}LiNO$ (659.1): calcd. C 47.38, H 2.14, N 2.13; found C 47.63, H 2.95, N 1.90.

X-ray Crystal Structure Analysis of 3: $C_{26}H_{14}BF_{15}LiNO$, M = 659.13, yellow crystal 0.20 × 0.20 × 0.10 mm, a = 11.478(2), b = 15.266(6), c = 15.539(2) Å, β = 93.66(1)°, V = 2717.2(12) Å^3, $\rho_{calcd.}$ = 1.611 g cm^{-3}, μ = 15.22 cm^{-1}, empirical absorption correction by ψ scan data ($0.751 \le T \le 0.863$), Z = 4, monoclinic, space group $P2_1/n$ (No. 14), λ = 1.54178 Å, T = 223 K, ω/2θ scans, 5820 reflections collected ($+h$, $-k$, $\pm l$), [(sinθ)/λ] = 0.62 Å^{-1}, 5540 independent (R_{int} = 0.029) and 2856 observed reflections [$I \ge 2\sigma(I)$], 408 refined parameters, R = 0.062, $wR2$ = 0.166, max. residual electron density 0.40 (−0.35) e Å^{-3}, hydrogens calculated and refined as riding atoms.

Preparation of $[(C_4H_5N)B(C_6F_5)_3]$ (4): A 1 M solution of HCl in diethyl ether (3.00 mL, 3.00 mmol) was added dropwise with rapid stirring to a solution of **3**·Et_2O (1.50 g, 2.56 mmol) in 60 mL of ether. Volatiles were removed in vacuo after 30 min. and the residue stirred with pentane (20 mL). The solid was collected by filtration and extracted three times with toluene. Solvent was removed from the combined toluene phases in vacuo. The residue was recrystallized from toluene at -18 °C to yield **4** (852 mg, 57%), m.p. 178 °C. – ^1H NMR (600 MHz, [D$_6$]benzene, 298 K): δ = 7.35 (br., $^1J_{CH}$ = 184 Hz, 1 H, 2-H), 6.34 (m, $^1J_{CH}$ = 180 Hz, 1 H, 4-H), 5.45 (m, $^1J_{CH}$ = 182 Hz, 1 H, 3-H), 3.53 (br., $^1J_{CH}$ = 143 Hz, 2 H, 5-H). – ^{13}C NMR (150.7 MHz, [D$_6$]benzene, 298 K): δ = 171.1 (C2), 155.5 (C4), 148.2 ($^1J_{FC}$ = 241 Hz), 140.6 ($^1J_{FC}$ = 253 Hz), 137.6 ($^1J_{FC}$ = 249 Hz), 118.5 (br., *o*-, *p*-, *m*-, *ipso*-C of C_6F_5), 127.2 (C3), 65.5 (C5). – ^{11}B NMR (192.2 MHz, [D$_6$]benzene, 298 K): δ = −7.6 ($\nu_{1/2} \approx 90$ Hz). – ^{19}F NMR (563.7 MHz, [D$_8$]toluene, 298 K): δ = −132.3, 155.7, −162.6 (*o*-, *p*-, *m*-F of C_6F_5). – ^1H,^{15}N-GHMBC (600/60.7 MHz, [D$_8$]toluene, 213 K): δ = 6.93, 6.07, 5.20/−145 (2-, 4-, 3-H/N). – $C_{22}H_5BF_{15}N$ (579.1): calcd. C 45.63, H 0.87, N 2.42; found C 45.50, H 1.11, N 2.27.

X-ray Crystal Structure Analysis of 4: $C_{22}H_5BF_{15}N$, M = 579.08, light yellow crystal 0.30 × 0.10 × 0.10 mm, a = 10.415(1), b = 11.079(1), c = 18.160(1) Å, β = 98.54(1)°, V = 2072.2(3) Å^3, $\rho_{calcd.}$ = 1.856 g cm^{-3}, μ = 2.04 cm^{-1}, empirical absorption correction by SORTAV ($0.941 \le T \le 0.980$), Z = 4, monoclinic, space group $P2_1/n$ (No. 14), λ = 0.71073 Å, T = 198 K, ω and φ scans, 8760 reflections collected ($\pm h$, $\pm k$, $\pm l$), [(sinθ)/λ] = 0.65 Å^{-1}, 4722 independent (R_{int} = 0.022) and 3772 observed reflections [$I \ge 2\sigma(I)$], 367 refined parameters, R = 0.042, $wR2$ = 0.091, max. residual electron density 0.30 (−0.21) e Å^{-3}, hydrogens from difference Fourier maps and refined as riding atoms.

Data sets were collected with Enraf−Nonius CAD4 and Nonius Kappa-CCD diffractometers, the latter one equipped with a rotating anode generator Nonius FR591. Programs used: data collection EXPRESS (Nonius B.V., **1994**) and COLLECT (Nonius B.V., **1998**), data reduction MolEN (K. Fair, Enraf−Nonius B.V., **1990**) and Denzo-SMN (Z. Otwinowski, W. Minor, *Methods in Enzymology* **1997**, *276*, 307−326), absorption correction for CCD data SORTAV (R. H. Blessing, *Acta Cryst.* **1995**, *A51*, 33−37; R.H.

Blessing, *J. Appl. Cryst.* **1997**, *30*, 421−426), structure solution SHELXS-97 (G. M. Sheldrick, *Acta Cryst.* **1990**, *A46*, 467−473), structure refinement SHELXL-97 (G. M. Sheldrick, Universität Göttingen, 1997), graphics SCHAKAL (E. Keller, Universität Freiburg, 1997).

Crystallographic data (excluding structure factors) for the structures reported in this paper have been deposited with the Cambridge Crystallographic Data Centre as supplementary publications CCDC-144532 (**3**) and CCDC-144533 (**4**). Copies of the data can be obtained free of charge on application to The Director, CCDC, 12 Union Road, Cambridge CB2 1EZ, UK [Fax: (internat.) +44-1223/336-033, E-mail: deposit@ccdc.cam.ac.uk].

Reaction of $Cp_2Zr(CH_3)_2$ (5) with $[(C_4H_5N)B(C_6F_5)_3]$ (4); Generation of 6: Toluene (5 mL) was added to a solid mixture of **5** (101 mg, 0.40 mmol) and **4** (233 mg, 0.40 mmol). Pentane (80 mL) was added to the reaction mixture after 1 h to precipitate the product **6**, which was collected by filtration, washed with pentane (10 mL) and dried in vacuo. Yield of **6**: 210 mg, 64%. − ^{1}H NMR (600 MHz, [D$_8$]toluene, 298 K): δ = 6.98 (br., 2 H, pyrrolyl 2-H, 5-H), 5.27 (s, 10 H, Cp), 5.06 (m, 2 H, pyrrolyl 3-H, 4-H), -0.02 (s, 3 H, Zr−CH$_3$). − ^{13}C NMR (150.7 MHz, [D$_8$]toluene, 223 K): δ = 148.1 ($^1J_{CF}$ = 242 Hz), 139.7 ($^1J_{CF}$ = 249 Hz), 137.3 ($^1J_{CF}$ = 248 Hz), 120.7 (br., *o*-, *p*-, *m*-, *ipso*-C of C$_6$F$_5$), 137.2 ($^1J_{CH}$ = 189 Hz) and 101.8 ($^1J_{CH}$ = 166 Hz, pyrrolyl C2,5 and C3,4), 113.0 ($^1J_{CH}$ = 176 Hz, Cp), 40.2 ($^1J_{CH}$ = 120 Hz, ZrCH$_3$) (assignments confirmed by ^{1}H,^{1}H-GCOSY, ^{1}H,^{13}C-GHSQC and ^{1}H,^{13}C-GHMBC experiments). − ^{11}B NMR (64.2 MHz, [D$_8$]toluene, 298 K): δ = −8.7 ($\nu_{1/2}$ = 110 Hz). − ^{19}F NMR (563.7 MHz, [D$_8$]toluene, 223 K): δ = −130.9, −157.3, −163.2 (*o*-, *p*-, *m*-F of C$_6$F$_5$).

Reaction of (Butadiene)zirconocene (7) with 4; Generation of 8: Toluene (5 mL) was added at ambient temperature to a solid mixture of (*s-cis*-/*s-trans*-η^4-butadiene)ZrCp$_2$ (1:1) (**7**, 51 mg, 0.19 mmol) and **4** (107 mg, 0.19 mmol). The mixture was stirred for 30 min., then the solvent was removed in vacuo. The viscous residue was solidified by stirring with 50 mL of pentane. The product was collected by filtration, washed with pentane (2 × 10 mL) and dried in vacuo, yield of **8**: 106 mg (67%). − ^{1}H NMR (600 MHz, [D$_8$]toluene, 253 K): δ = 7.24, 4.87 (br., each 2 H, pyrrolyl), 4.66 (s, 10 H, Cp), 4.30 (dt, ^3J = 11 Hz, ^3J = 16 Hz, 1 H, =CH−), 3.37 (dq, ^3J = 6 Hz, ^3J = 16 Hz, 1 H, =C*H*−CH$_3$), 1.52 (d, ^3J = 11 Hz, 2 H, =CH$_2$), 1.28 (d, ^3J = 6 Hz, 3 H, CH$_3$). − ^{13}C NMR (150.7 MHz, [D$_8$]toluene, 253 K): δ = 148.3 ($^1J_{CF}$ = 244 Hz), 139.7 ($^1J_{CF}$ = 256 Hz), 137.4 ($^1J_{CF}$ = 249 Hz, *o*-, *p*-, *m*-C of C$_6$F$_5$), *ipso*-C of −C$_6$F$_5$ and pyrrolyl-C not observed, 123.2 ($^1J_{CH}$ = 150 Hz, =CH−), 108.0 ($^1J_{CH}$ = 177 Hz, Cp), 104.1 ($^1J_{CH}$ = 152 Hz, =*C*H−CH$_3$), 47.0 ($^1J_{CH}$ = 155 Hz, =CH$_2$), 18.6 ($^1J_{CH}$ = 126 Hz, CH$_3$) (assignment supported by ^{1}H,^{13}C-GHSQC). − ^{11}B NMR (64.2 MHz, [D$_8$]toluene, 298 K): δ = −8.8 ($\nu_{1/2}$ = 130 Hz). − ^{19}F NMR (563.7 MHz, [D$_8$]toluene, 223 K): δ = −130.8, −157.9, −163.5 (*o-, p-, m*-F of C$_6$F$_5$).

Polymerization Reactions with 4 as an Activator

a) Ethene Polymerization: A glass autoclave was charged with 300 mL of toluene and 2 mL of triisobutylaluminum, then thermostated for 1 h and the solution saturated with ethene (at 1 or 2 bar, see Table 1) for another hour. The catalyst was generated by treatment of the respective metallocene precursor with **4** in toluene, and this toluene solution was injected into the autoclave. The polymerization reaction was stopped by quenching with 50 mL aqueous HCl/methanol (1:5 v/v). The resulting polymer was washed subsequently with HCl, water, methanol and acetone and dried.

b) Propene Polymerization: Reactions were carried out analogously (at 2 bar). After quenching with HCl/CH$_3$OH, water (100 mL) was added. Stereoregular polypropylene samples were then collected by filtration and washed with HCl, water, methanol and acetone. Atactic polypropylene was extracted twice with toluene (200 mL); solvent was removed from the combined organic phases and the polymer dried in vacuo.

Acknowledgments

Financial support from the Fonds der Chemischen Industrie and the Deutsche Forschungsgemeinschaft is gratefully acknowledged.

[1] H. Sinn, W. Kaminsky, *Adv. Organomet. Chem*. **1980**, *18*, 99−149; H.-H. Brintzinger, D. Fischer, R. Mülhaupt, B. Rieger, R. M. Waymouth, *Angew. Chem*. **1995**, *107*, 1255−1283; *Angew. Chem. Int. Ed. Engl*. **1995**, *34*, 1143−1171.

[2] J. C. W. Chien, W.-M. Tsai, M. D. Rausch, *J. Am. Chem. Soc.* **1991**, *113*, 8570−8571.

[3] X. Yang, C. L. Stern, T. J. Marks, *J. Am. Chem. Soc.* **1994**, *116*, 10015−10031.

[4] B. Temme, G. Erker, J. Karl, H. Luftmann, R. Fröhlich, S. Kotila, *Angew. Chem*. **1995**, *107*, 1867−1869; *Angew. Chem. Int. Ed. Engl*. **1995**, *34*, 1755−1757.

[5] G. Kehr, R. Fröhlich, B. Wibbeling, G. Erker, *Chem. Eur. J.* **2000**, *6*, 258−266.

[6] [6a] M. Bochmann, A. J. Jaggar, J. C. Nicholls, Angew. *Chem*. **1990**, *102*, 830−832; *Angew. Chem. Int. Ed. Engl*. **1990**, *29*, 780−782. − [6b] For remotely related systems see, for example: D. Röttger, G. Erker, R. Fröhlich, S. Kotila, *J. Organomet. Chem*. **1996**, *518*, 17−19; B. Wrackmeyer, B. Schwarze, *J. Organomet. Chem*. **1997**, *534*, 181−186; B. Wrackmeyer, B. Schwarze, W. Milius, R. Boese, O. G. Parchment, G. A. Webb, *J. Organomet. Chem*. **1998**, *552*, 247−254; L. H. Doerrer, M. L. H. Green, *J. Chem. Soc., Dalton Trans.* **1999**, 4325−4329; P. Jutzi, C. Müller, A. Stammler, H.-G. Stammler, *Organometallics* **2000**, *19*, 1442−1444.

[7] R. F. Jordan, *Adv. Organomet. Chem*. **1991**, *32*, 325.

[8] A. G. Massey, A. J. Park, F. G. A. Stone, *Proc. Chem. Soc. London* **1963**, 212; A. G. Massey, A. J. Park, *J. Organomet. Chem*. **1964**, *2*, 245−250; A. G. Massey, A. J. Park, *Organometallic Syntheses* (Eds.: R. B. King, J. J. Eisch), Elsevier, New York, **1986**, Vol. 3, p. 461−462.

[9] L. A. Paquette, W. Bauer, M. R. Sivik, M. Bühl, M. Feiger, P. v. R. Schleyer, *J. Am. Chem. Soc.* **1990**, *112*, 8776−8789, and references cited therein.

[10] For examples of (η^5-pyrrolyl) transition metal complexes see: T. Dube, D. Freckmann, S. Conoci, S. Gambarotta, G. P. A. Yap, *Organometallics* **2000**, *19*, 209−211; J. R. Perera, M. J. Heeg, H. B. Schlegel, C. H. Winter, *J. Am. Chem. Soc.* **1999**, *121*, 4536−4537, and references cited therein.

[11] [11a] J. Karl, G. Erker, R. Fröhlich, *J. Am. Chem. Soc*. **1997**, *119*, 11165−11173, and references cited therein. − [11b] See also: H.-J. Buschmann, J. Hermann, M. Kaupp, H. Plenio, *Chem. Eur. J.* **1999**, *5*, 2566−2572; review: H. Plenio, *Chem. Rev.* **1997**, *97*, 3363.

[12] P. C. Wailes, H. Weigold, A. B. Bell, *J. Organomet. Chem*. **1972**, *34*, 155−164; E. Samuel, M. D. Rausch, *J. Am. Chem. Soc.* **1973**, *95*, 6263−6267; G. Erker, J. Wicher, K. Engel, C. Krüger, *Chem. Ber.* **1982**, *115*, 3300−3311; G. Erker, K. Engel, C. Sarter, in *Organometallic Synthesis* (Eds.: R. B. King, J. J. Eisch), Academic Press, New York, **1986**, Vol. 3, p. 32; M. L. H. Green, N. Ishihara, *J. Chem. Soc., Dalton Trans.* **1994**, 657−665; W. J. Gauthier, J. F. Corrigan, N. J. Taylor, S. Collins, *Macromolecules* **1995**, *28*, 3771−3778; S. Knüppel, G. Erker, R. Fröhlich, *Angew. Chem*. **1999**, *111*, 2048−2051; *Angew. Chem. Int. Ed.* **1999**, *38*, 1923−1926.

[13] M. Dahlmann, G. Erker, R. Fröhlich, O. Meyer, *Organometallics* **2000**, *19*, 2956−2967.

[14] A. Franzel, M. Gluth, R. Herbst-Irmer, U. Klingebiel, *J. Organomet. Chem*. **1996**, *514*, 281−286.

Received July 4, 2000
[I00268]

Characterization of Calcined and Reduced Multi-Component Co−Ni−Mg−Al-Layered Double Hydroxides

Didier Tichit,*[a] Solange Ribet,[a] and Bernard Coq[a]

Keywords: Clays / Cobalt / Nickel / Reductions / Spinel phases

Several Co–Ni–Mg–Al-layered double hydroxides (LDH) have been synthesized by coprecipitation at constant pH = 9. All samples present well crystallized, layered structures, no excess phases were detected by X-ray diffraction, and the lattice *a* parameter followed the Vegard correlation. The cations thus belong to the same, brucite-like, lattice. Calcined samples exhibit XRD patterns of the crystallographic phase preferentially adopted by the major cation in the LDH: i.e., a mixed oxide of the rock salt type in the case of Ni or Mg, and a spinel-like structure for Co. Surface areas reached maximum values in the range of 200–300 m^2g^{-1} after calcination at 573 K. They were stabilized with increasing Ni or Mg content, as higher amounts of mixed oxide phase were formed. Programmed temperature reduction showed two domains of H_2 consumption, assigned to reduction of $Co_{3-x}Ni_xO_4$ species below 720 K, and to NiMg(Al)O and $Co_{3-x-y}Ni_xMg_yAlO_6$, of rock salt type and spinel-like structures respectively, above this temperature. These assignments are in agreement with the XRD patterns and show that Ni and Co are associated in the same crystallographic phases.

Introduction

Layered double hydroxides (LDHs) or anionic clays of the general formula $[M_{1-x}^{2+}M_x^{3+}(OH)_2]^{x+}[A^{m-}]_{x/m}\cdot n\,H_2O$ are increasingly used as precursors of catalysts with varying divalent and trivalent cations in their layers.[1] These two cations are distributed inside brucite-like sheets in an octahedral environment. The structure is based on the stacking of these positively charged layers, with hydrated compensating anions in the interlamellar domain.[1,2] Interest in LDHs is undoubtedly increasing because not only two but, more frequently, several cations may be accommodated in the structure, thus leading to a wide variety of multi-component catalyst precursors. Therefore, the intrinsic properties of the resulting catalysts − like acido-basicity and hydrogenating or oxidizing capabilities − might be tuned through the nature and the relative quantities of the cations and the activation conditions. We previously reported that highly active and selective catalysts for the hydrogenation of acetonitrile into ethylamine were obtained when using Co/Ni/Mg/Al LDH precursors.[3] Improvements of these catalysts, which require Ni or Co metals deposited on poorly acidic supports, resulted from adjustment of the Mg content and of alloying Ni, the active metal, with Co.[3,4]

This work is aimed at the study of the synthesis and activation of quaternary Co−Ni−Mg−Al LDHs. Their decomposition has been followed under oxidizing and reducing atmospheres. Special attention has been paid to temperature programmed reduction (TPR) experiments to support XRD in the identification of the nature of phases present in the precursor.

[a] Laboratoire de Matériaux Catalytiques et Catalyse en Chimie Organique, CNRS, UMR 5618, E.N.S.C.M 8,
Rue Ecole Normale, 34296 Montpellier Cedex 5, France
Fax: (internat.) + 33-4/67144349
E-mail: tichit@cit.enscm.fr

Results

Synthesis of the LDH Precursors

Cationic contents of the synthesis solutions and formula of the solids as deduced from their chemical analysis are given in Table 1. It is assumed that all cobalt is in the form of Co^{2+}. The water content is evaluated from TG analysis. As can be seen, Co and Ni content in the layers is close to the corresponding levels in solution. In contrast, the Mg content is always slightly lower than expected. This behavior is in accordance with the respective precipitation pHs of Co, Ni, and Mg in their hydroxide forms, occurring from pH = 9 for the first two elements, but at pH above 10 for the last.

The slight variations described above obviously dictate that the layer charges of the different samples are not strictly identical, since $x = Al^{3+}/(\Sigma M^{2+}+Al^{3+})$ is in the range of 0.25−0.28.

Both nitrate and carbonate anions are present in the structures, always with an excess of anionic charge. This probably results from the presence not only of CO_3^{2-} but also of HCO_3^-, very often formed at pH ≈ 9. The presence of CO_3^{2-} is consistent with contamination by air during synthesis.

XRD profiles of the samples, dried at 353 K, are reported in Figure 1. They show that a single hydrotalcite-like phase is present in all cases, with several (00*l*) reflections. The (003) reflection is usually sharp; in contrast, the (006) and higher reflections are broad in the samples containing Co, Ni, and Mg concomitantly. Such features provide evidence of structures poorly ordered along the *c* axis.

 © WILEY-VCH Verlag GmbH, 69451 Weinheim, 2001 1434−1948/01/0202−0539 $ 17.50+.50/0

Table 1. Proportion of cations in the synthesis solutions and elemental composition of the various Co−Ni−Mg−Al samples

Samples	Synthesis solutions ($M^{2+}/\Sigma M^{n+}$)				Composition of solids	*a* (nm)	*c* (nm)
	Co^{2+}	Ni^{2+}	Mg^{2+}	Al^{3+}			
Co(3)Al	0.75	0.00	0.00	0.25	$[Co_{0.75}Al_{0.25}(OH)_2](CO_3^{2-})_{0.07}(NO_3^-)_{0.12}$, 0.6 H_2O	0.308(8)	2.335(0)
Co(2)Mg(1)Al	0.50	0.00	0.25	0.25	$[Co_{0.53}Mg_{0.18}Al_{0.28}(OH)_2](CO_3^{2-})_{0.07}(NO_3^-)_{0.14}$, 0.6 H_2O	0.307(4)	2.402(2)
Co(1.5)Ni(0.5)Mg(1)Al	0.37	0.12	0.25	0.25	$[Co_{0.40}Ni_{0.13}Mg_{0.19}Al_{0.28}(OH)_2](CO_3^{2-})_{0.05}(NO_3^-)_{0.23}$, 0.6 H_2O	0.306(4)	2.511(1)
Co(1)Ni(1)Mg(1)Al	0.25	0.25	0.25	0.25	$[Co_{0.27}Ni_{0.26}Mg_{0.21}Al_{0.26}(OH)_2](CO_3^{2-})_{0.04}(NO_3^-)_{0.19}$, 0.6 H_2O	0.305(7)	2.511(1)
Co(0.5)Ni(1.5)Mg(1)Al	0.12	0.37	0.25	0.25	$[Co_{0.14}Ni_{0.38}Mg_{0.21}Al_{0.28}(OH)_2](CO_3^{2-})_{0.07}(NO_3^-)_{0.19}$, 0.6 H_2O	0.305(0)	2.455(4)
Ni(2)Mg(1)Al	0.00	0.50	0.25	0.25	$[Ni_{0.53}Mg_{0.19}Al_{0.28}(OH)_2](CO_3^{2-})_{0.05}(NO_3^-)_{0.22}$, 0.6 H_2O	0.304(1)	2.520(6)
Co(1.5)Ni(1.5)Al	0.38	0.37	0.00	0.25	$[Co_{0.36}Ni_{0.36}Al_{0.28}(OH)_2](CO_3^{2-})_{0.04}(NO_3^-)_{0.23}$, 0.5 H_2O	0.305(3)	2.620(0)
Co(0.8)Ni(0.8)Mg(1.4)Al	0.30	0.30	0.15	0.25	$[Co_{0.32}Ni_{0.33}Mg_{0.10}Al_{0.26}(OH)_2](CO_3^{2-})_{0.12}(NO_3^-)_{0.21}$, 0.6 H_2O	0.305(9)	2.428(5)
Co(1.2)Ni(1.2)Mg(0.6)Al	0.20	0.20	0.35	0.25	$[Co_{0.20}Ni_{0.20}Mg_{0.31}Al_{0.28}(OH)_2](CO_3^{2-})_{0.10}(NO_3^-)_{0.12}$, 0.6 H_2O	0.305(9)	2.530(2)

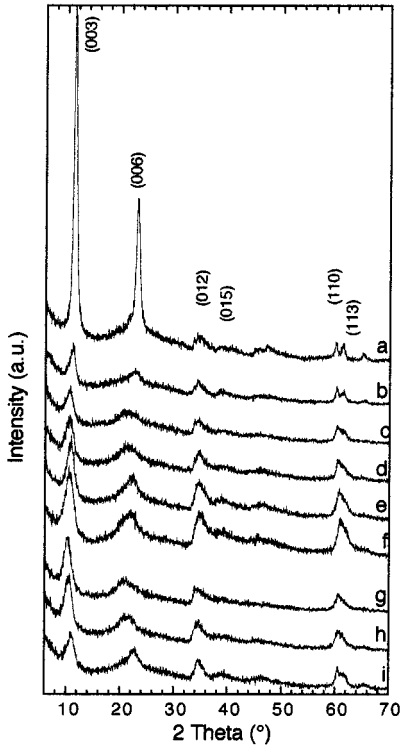

Figure 1. X-ray diffraction patterns of the different samples: (a): Co(3)Al, (b): Co(2)Mg(1)Al, (c): Co(1.5)Ni(0.5)Mg(1)Al, (d): Co(1)Ni(1)Mg(1)Al, (e): Co(0.5)Ni(1.5)Mg(1)Al, (f): Ni(2) Mg(1)Al, (g): Co(1.5)Ni(1.5)Al, (h): Co(1.2)Ni(1.2)Mg(0.6)Al, (i): Co(0.8)Ni(0.8)Mg(1.4)Al

Some peculiar characteristics can otherwise be quoted:

(1) for the series of materials of identical Mg content ($Mg^{2+}/\Sigma M^{2+}$ = 1:3), the (003) and (006) peaks become progressively sharper and the (11*l*) peaks vanish as the Ni content increases. Stacking order between the layers thus increases at the expense of that within the layers.

(2) Mg content has a lesser influence on the shape of the XRD patterns. Its smaller ionic size (0.065 nm) compared to Ni (0.069 nm) or Co (0.074 nm) induces less distortion of the layers.

Therefore, the orders along the *a* and *c* crystallographic directions of the multi-component LDHs mainly depend on their Co and Ni content. Accordingly, the lattice *a* parameter follows the Vegard correlation with the Co or Ni content (Figure 2), but is independent of the Mg content (Table 1). No clear relationship exists between the lattice *c* parameter and Co and Ni content, while a small decrease is noted with Mg content at similar Ni/(Co+Ni) ratio (Table 1). This could not reasonably be assigned to a variation of the layer charge. To sum up, the existence of a unique (003) line and the evolution of the lattice *a* parameter, in agreement with the Vegard correlation, show that all cations belong to the same brucite-like lattice class. Moreover, a low crystallinity of the samples is in line with this assumption, if one considers that up to four cations are accommodated in the layers.

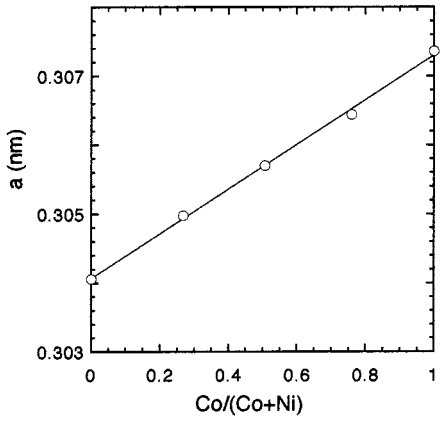

Figure 2. Variation of the lattice *a* parameter of the Co−Ni−Mg−Al samples as a function of Co/(Co+Ni) ratio for $Mg^{2+}/\Sigma M^{2+}$ = 1:3

Results of TG-DTG analysis are given in Table 2. Mass losses occur in two steps up to 973 K, as classically found with Mg−Al and M−Mg−Al samples (M = Ni, Co).[5−10] The low-temperature weight loss originates from the removal of water molecules in the interlayer space and weakly bonded CO_3^{2-} species.[5,7] Dehydroxylation of the layers with concomitant H_2O release, and decomposition of the anions result in the weight loss at 540−600 K. Total weight losses, in the range of 33−39 wt%, increase significantly with Mg content. This is due to the greater water release at ca 350 K in the Mg-containing samples, owing to the higher hydration ability of Mg compared to Ni and Co.

The first peak is at about 393 K in all cases, while there is a systematic shift of the second peak from 543 to 623 K when the Ni/(Co+Ni) molar ratio increases with similar Mg content.

Table 2. Weight losses and temperatures of maximum rates in the thermogravimetric analysis of the various samples

Samples	Total weight loss (%)	1st weight loss T_1 (K)	wt (%)	2nd weight loss T_2 (K)	wt (%)
Co(3)Al	28	463	10	503	18
Co(2)Mg(1)Al	35	393	11	543	24
Co(1.5)Ni(0.5)Mg(1)Al	37	393	10	563	27
Co(1)Ni(1)Mg(1)Al	37	393	10	583	27
Co(0.5)Ni(1.5)Mg(1)Al	38	403	11	603	27
Ni(2)Mg(1)Al	39	383	10	623	29
Co(1.5)Ni(1.5)Al	33	383	8	583	25
Co(1.2)Ni(1.2)Mg(0.6)Al	35	393	9	583	26
Co(0.8)Ni(0.8)Mg(1.4)Al	38	383	13	583	25

Calcination of the LDH Precursors

Calcination of LDH precursors leads to one or several phases. Their number and nature depend on the cations involved in the structure and on the temperature. However, some general tendencies can be expected, considering that below 1100 K, Ni and Mg probably form mixed oxides of NiO and MgO type on the one hand,[9,11,12] while, on the other hand, Co easily forms spinel-like structures.[7,8] The results from TG experiments prompted us to study the samples calcined at 573 and 773 K, since the main structural transformations of LDHs occur in this temperature range.

XRD patterns of the materials calcined at 773 K (Figure 3) look very different, depending on cation composition. For a given sample, the only change observed when the calcination temperature increases from 573 to 773 K is a better crystallinity.

For Ni(2)Mg(1)Al, the (111), (200), and (220) reflections of the NiO-like structure are recorded at 0.2422, 0.2087, and 0.1473 nm. These values are slightly shifted toward lower values than in the pure rock salt type single oxide (04-0835 ICDD data file), due to the presence of smaller ionic radius Al^{3+} within the lattice. For Co(2)Mg(1)Al, reflections at 0.4679, 0.2875, 0.2448, 0.2025, 0.1647, 0.1561, and 0.1432 nm can be assigned to the (111), (220), (311), (400), (422), (511), and (440) planes, respectively, of $CoAl_2O_4$ or Co_3O_4 spinel phases, which are indistinguishable. Such an assignment assumes that Co_3O_4 is thermodyamically more stable under air than CoO.[13] Moving now to quaternary LDHs, the case of Co(1)Ni(1)Mg(1)Al is archetypal, since the most intense peaks both of the rock salt type and of the spinel-like phases are detected. Actually, calcined LDHs exhibit XRD patterns of the crystallographic phases preferentially adopted by the major cation in the structure. Accordingly, Co(0.5)Ni(1.5)Mg(1)Al, Co(0.8)Ni(0.8)Mg(1.4)Al, on the one hand, and Co(1.5)-Ni(0.5)Mg(1)Al, Co(1.2)Ni(1.2)Mg(0.6)Al, on the other hand, present profiles of mixed oxide and spinel-like phases, respectively.

Several relevant features concern the textural properties of the different samples, either non-calcined, or calcined at 573 and 773 K (Table 3). Specific surface areas are generally low, from 20 to 90 m^2g^{-1} for the non-calcined samples, only outgassed at 473 K. This is due to still remaining compensating anions, as shown by the temperatures of the second

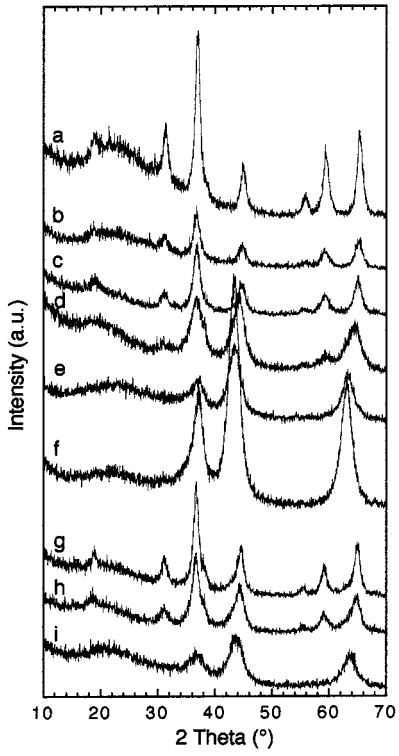

Figure 3. X-ray diffraction patterns of the samples calcined at 773 K: (a): Co(3)Al, (b): Co(2)Mg(1)Al, (c): Co(1.5)Ni-(0.5)Mg(1)Al, (d): Co(1)Ni(1)Mg(1)Al, (e): Co(0.5)Ni(1.5)-Mg(1)Al, (f): Ni(2)Mg(1)Al, (g): Co(1.5)Ni(1.5)Al, (h): Co(1.2)Ni-(1.2)Mg(0.6)Al, (i): Co(0.8)Ni(0.8)Mg(1.4)Al

DTG peaks in the range 540−620 K, except for Co(2)-Mg(1)Al. The adsorption isotherms of the calcined samples are of type II (Figure 4) and the full adsorption−desorption isotherms exhibit type H3 hysteresis loops. Nonetheless, although a hysteresis loop is observed, the isotherms are classified as type IIb (according to Rouquerol et al.[14]) rather than as type IV, because no plateau is observed at high P/P_0. Such adsorption−desorption isotherms are characteristic of aggregates of plate-like particles, classically found with clays. Specific surface areas go through maximum values after calcination at 573 K (Table 3). Their decrease above this temperature is in line with the enhancement of crystallinity shown by XRD. It should be pointed out that, after calcination at 773 K, the specific surface area is higher when Ni

Table 3. Specific surface areas and porous volumes of the various samples

Samples	non-calcined[a] S_{BET} (m^2g^{-1})	V_{por}[b] (cm^3g^{-1})	calcined 573 K S_{BET} (m^2g^{-1})	V_{por}[b] (cm^3g^{-1})	calcined 773 K S_{BET} (m^2g^{-1})	V_{por}[b] (cm^3g^{-1})
Co(3)Al	–	–	166	0.307	145	0.330
Co(2)Mg(1)Al	174	0.175	230	0.309	149	0.236
Co(1.5)Ni(0.5)Mg(1)Al	17	0.030	209	0.199	163	0.201
Co(1)Ni(1)Mg(1)Al	20	0.042	235	0.193	199	0.231
Co(0.5)Ni(1.5)Mg(1)Al	30	0.058	254	0.266	204	0.293
Ni(2)Mg(1)Al	20	0.060	251	0.211	192	0.237
Co(1.5)Ni(1.5)Al	13	0.020	201	0.169	144	0.173
Co(1.2)Ni(1.2)Mg(0.6)Al	15	0.264	234	0.187	127	0.175
Co(0.8)Ni(0.8)Mg(1.4)Al	96	0.023	296	0.435	270	0.489

[a] Outgassed at 473 K. – [b] Porous volume determined from N_2 uptake at $P/P_0 = 0.95$.

progressively substitutes for Co in samples of similar Mg content, or when Mg content increases in samples of similar Co/(Co+Ni) ratio. Indeed well crystallized spinel-like phases result in lower specific surface areas than rock salt-like structures. Microporosity increases with Mg content: i.e., when mixed oxide becomes the major phase. A limited degree of microporosity sometimes appears even though a type II isotherm is found.[14] A slightly higher microporous volume in Mg-containing samples than in Ni-containing counterparts is in agreement with the results reported for Mg(Al)O and Ni(Al)O mixed oxides.[10]

Reduction of the Calcined Materials

TPRs have been performed on the calcined samples. Some profiles are presented in Figure 5, and H_2 uptakes listed in Table 4. Two distinct domains of H_2 consumption – at low (LT) and high (HT) temperature – always appear as previously reported for Co–Al and Co–Mg–Al LDHs.[3] In the LT domain, one can observe a shoulder at about 473 K, then a highly intense peak with its maximum increasing with Co content, going from 533 K for Co(0.5)Ni(1.5)Mg(1)Al to 638 K for Co(2)Mg(1)Al. Both peaks may be assigned to the reduction of Co species, since they are not detected on Ni(2)Mg(1)Al; moreover, their intensities regularly increase with the Co content of Co–Ni–Mg–Al LDHs. For Co–Al and Co–Mg–Al samples, the shoulder at about 473 K in the LT domain was not identified so unequivocally, and was assigned to reduction of Co_3O_4.[6] These propositions will be discussed more extensively later for Co–Ni–Mg–Al LDHs.

In the HT domain, TPR profiles of the ternary LDHs containing only one reducible cation are very distinct. They differ in a narrow and intense peak extending over 100 K

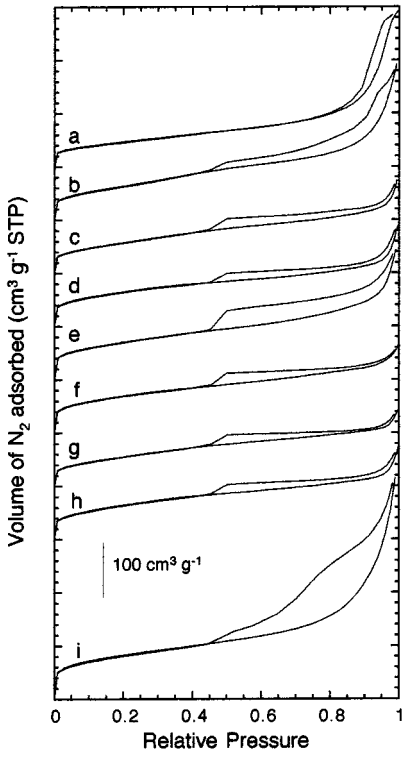

Figure 4. Nitrogen adsorption–desorption isotherms at 77 K of the samples calcined at 573 K: (a): Co(3)Al, (b): Co(2)Mg(1)Al, (c): Co(1.5)Ni(0.5)Mg(1)Al, (d): Co(1)Ni(1)Mg(1)Al, (e): Co(0.5)-Ni(1.5)Mg(1)Al, (f): Ni(2)Mg(1)Al, (g): Co(1.5)Ni(1.5)Al, (h): Co(1.2)Ni(1.2)Mg(0.6)Al, (i): Co(0.8)Ni(0.8)Mg(1.4)Al

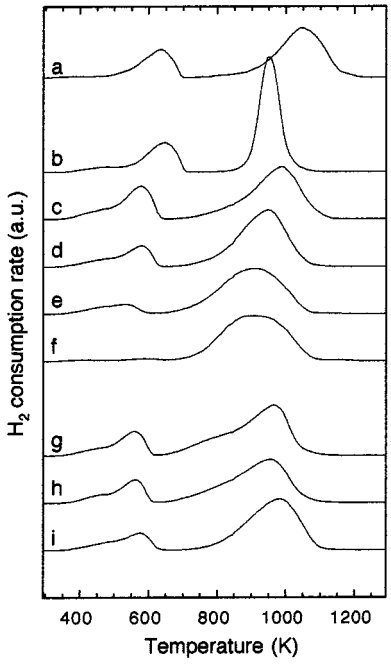

Figure 5. Temperature programmed reduction profiles of the samples calcined at 773 K: (a): Co(3)Al, (b): Co(2)Mg(1)Al, (c): Co(1.5)Ni(0.5)Mg(1)Al, (d): Co(1)Ni(1)Mg(1)Al, (e): Co(0.5)-Ni(1.5)Mg(1)Al, (f): Ni(2)Mg(1)Al, (g): Co(1.5)Ni(1.5)Al, (h): Co(1.2)Ni(1.2)Mg(0.6)Al, (i): Co(0.8)Ni(0.8)Mg(1.4)Al

Table 4. H_2 uptakes (H_2/Co+Ni), mol/mol) in TPR experiments

Samples	calcined at 623 K			calcined at 773 K		
	total	LT	HT	total	LT	HT
Co(3)Al	0.99	0.29	0.70	0.99	0.28	0.71
Co(2)Mg(1)Al	1.23	0.42	0.81	1.11	0.33	0.78
Co(1.5)Ni(0.5)Mg(1)Al	1.23	0.41	0.82	1.17	0.35	0.82
Co(1)Ni(1)Mg(1)Al	1.13	0.33	0.80	1.06	0.22	0.84
Co(0.5)Ni(1.5)Mg(1)Al	1.14	0.25	0.89	1.01	0.12	0.89
Ni(2)Mg(1)Al	1.07	0.15	0.92	0.93	0.00	0.93
Co(1.5)Ni(1.5)Al	1.22	0.31	0.91	1.11	0.24	0.87
Co(1.2)Ni(1.2)Mg(0.6)Al	1.30	0.38	0.92	1.01	0.23	0.78
Co(0.8)Ni(0.8)Mg(1.4)Al	1.23	0.41	0.82	1.04	0.20	0.84

for Co(2)Mg(1)Al, and a large and broad feature extending over 400 K for Ni(2)Mg(1)Al. For Co(1.5)Ni(1.5)Al, with two reducible cations, maxima at 820 and 960 K reflect the presence of Co and Ni reducible phases respectively.

Finally, in the quaternary LDHs, several remarks may be made concerning the influence of Co/(Co+Ni) ratio:

(1) The shape of the TPR peak moves progressively from that characteristic of Co(2)Mg(1)Al to that characteristic of Ni(2)Mg(1)Al upon Ni substitution.

(2) Compared to the Ni free sample [Co(2)Mg(1)Al], a shift of 30 K toward higher temperature is noted when Ni is introduced in low amount [Co(1.5)Ni(0.5)Mg(1)Al]; after that the temperature of maximum H_2 consumption rate is shifted toward lower values when the Ni content becomes higher.

(3) The temperatures of maximum H_2 consumption rates are rather insensitive to the Mg content.

(4) The TPR profiles of samples at identical Co and Ni content [Co/(Co+Ni) = 0.5] are not the simple averaging of those of Co(2)Mg(1)Al and Ni(2)Mg(1)Al samples.

This last remark demands a more detailed discussion, which is emphasized when looking carefully at the H_2 consumption values of samples calcined at 773 K (Table 4). For Co(2)Mg(1)Al, H_2 consumption in the LT and HT domains represents 30 and 70% of the total, respectively. The total H_2/Co molar ratio of 1.11 for this sample is thus consistent with the presence of Co^{3+} in Co_3O_4; this is normally reduced to Co^0 at low temperature, as proposed by Arnoldy and Moulijn.[13] In the TPR of Ni(2)Mg(1)Al, all H_2 was taken up above 600 K; this was previously assigned to NiO-type phase reduction to Ni^0 in similar materials.[5] On the basis of simple combination of the H_2 consumption values for Ni and Co, one might expect that the H_2 taken up in the LT and HT domains for Co(1.5)Ni(1.5)Al would be 15% and 85%, respectively. However, the actual distribution is 22% and 78%. This is a general behavioral pattern, and significantly higher values for H_2 consumption in the LT range persist when Mg is present and/or the Co/(Co+Ni) ratio modulated.

Discussion

The goal when preparing these LDHs was to develop new bimetallic hydrogenation catalyst precursors, particularly active and selective for the hydrogenation of acetonitrile into ethylamine.[3] In this respect it was of utmost importance to identify the kind of intimate vicinity and of interaction between Ni and Co at the different stages of catalyst elaboration. On that account, we will pay special attention in the following discussion to the nature of the phases obtained upon calcination and their evolution during TPR experiments.

As a first step, TG and XRD analysis of the "as-prepared" materials have shown that a unique LDH phase exists. This is, moreover, clearly highlighted in Figure 6, which shows a correlation appearing between the temperature of maximum weight loss from DTG plots (Table 2) and the *a* parameter (Table 1) for samples of various Co/(Co+Ni) ratios and similar Mg content. The temperature of anion decomposition derived from DTG plots reflects the strength of electrostatic interaction between the layers and the anions. When Ni is substituted for Co, the lattice *a* parameter decreases and the positive charges thus become more localized, enhancing the electrostatic attraction with the anions.

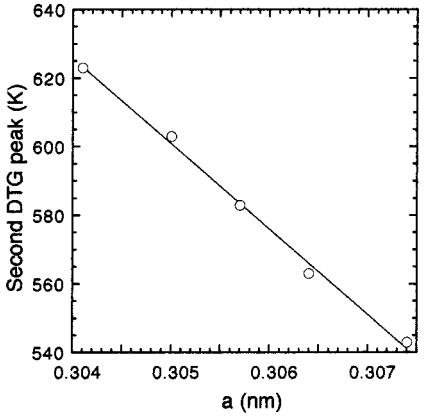

Figure 6. Correlation between the temperature of the second DTG peak and the *a* parameter for the Co−Ni−Mg−Al samples with $Mg^{2+}/\Sigma M^{2+}$ = 1:3

Upon calcination of LDH precursors, one obtains Ni- and Co-containing oxide phases of complex nature and composition. Co-containing LDHs give rise to a crystalline Co_3O_4 phase after calcination at 573 K. In the case of multi-component Co−Ni−Mg−Al LDHs, this behavior might be clarified by examination of the chemical compositions, XRD patterns, and reduction processes in TPR experiments. The reduction of calcined supported Ni catalysts has shown that the prevailing species belong to the NiO-type phase.[15−17]

In contrast, several studies on cobalt or cobalt-magnesium silica gels,[18,19] CoO/Al_2O_3,[13] or Co/SiO_2[20] catalysts reveal the complexity of the reduction process and the multiplicity of phases involved. For example, reduction of Co species, belonging to up to eight sub-phases, occurs within four different temperature domains for Co/Al_2O_3 materials.[13]

As far as the reduction processes in Co−Ni−Mg−Al LDHs are concerned, the main difficulties come from the multiplicity of possible occurring phases. A first remarkable

feature is that the shapes of the reduction profiles above 723 K are unchanged for Co−Mg−Al and Co−Ni−Mg-Al LDHs calcined at 573 or 773 K. This is consistent with the invariance in this temperature range of the crystalline phases detected by XRD. Hence, probably only weak diffusion of the cations is taking place during calcination or reduction processes.

We shall first discuss the reduction processes occurring in the LT domain (< 720 K). There is no peak of hydrogen consumption in the LT domain for the Co-free sample. On that account, the group of peaks appearing at LT for Co-containing materials must correspond to reduction of Co species. This peak was generally a broad feature arising from unresolved contributions. Compared to Co(3)Al, the reduction of Co is made easier in ternary or quaternary compounds containing Co and Ni. At variance with this, reduction of Co is more difficult in Co(2)Mg(1)Al than in Co(3)Al. The hydrogen consumption peak maxima at LT coincide with those generally found for reduction of bulk Co_3O_4[13] in the sequence $Co_3O_4 \rightarrow CoO \rightarrow Co$. Two reduction peaks have indeed been reported for bulk Co_3O_4, silica-supported Co catalysts[20] and promoted cobalt-Kieselguhr Fischer−Tropsch catalysts.[21] However, the reduction of Co_3O_4 to Co^0 on alumina-supported catalyst exhibits only one broad reduction peak,[13] which looks like that observed for reduction of Co(3)Al (Figure 5). The decrease of reducibility of Co upon addition of Mg can be discussed in parallel with the effect of MgO addition, which delayed the reduction of CoO in Kieselguhr-supported Co catalysts.[21] This behavior was ascribed to the formation of CoO−MgO solid solution. On the other hand, a better reducibility of CoO species has been reported upon Ni addition, and accounted for a decrease in their particle sizes.[22] This process may be initiated by formation of a solid solution of CoO and NiO, both exhibiting a rock salt-like structure. According to this proposal, it is a little puzzling why Ni acts as a diluent but Mg does not. For this reason, another process may be postulated, assuming that Ni^{2+} would substitute tetrahedral Co^{2+} in the Co_3O_4 spinel lattice. This would lead to $Co(Co_{2-x}Ni_x)O_4$ phases.[23] The broad peak of H_2 consumption at LT on Co−Ni−Mg−Al materials is very probably composed of two contributions (Figure 5), corresponding to the reduction of these phases in two steps. We previously pointed out the increase in reducibility of Co_3O_4 species with Co loading in Co−Ni−Mg−Al LDHs. A similar phenomenon has, in the case of Co/Al_2O_3, been assigned to a better nucleation process of the metallic nuclei.[24]

In the reduction processes in the HT domain (> 720 K) of the catalysts, several relevant features can be highlighted:

(1) The XRD patterns of the calcined Co- and Ni-rich samples exhibit characteristic lines of spinel and rock salt-like structures, respectively.

(2) Unlike in the LT domain, the reducibility of Co in samples in which Mg and/or Ni are present is higher than in Co(3)Al.

(3) Reduction of the spinel $CoAl_2O_4$ phase, giving rise to a straight and intense peak, was previously reported at least 100 K above the HT reduction peak of Co(3)Al.[13]

(4) Finally, the total H_2 consumption, not exceeding 1.17 [H_2/(Co+Ni)], shows that in multi-cationic samples the cations are not fully reduced. However, it is worth noting that the H_2 consumption relative to that observed for Co(3)Al, increases only slightly upon Mg addition, but more significantly upon Ni addition,.

We can tentatively estimate the H_2 consumption in the LT and HT domains for Co(3)Al, assuming that it would be decomposed into Co_3O_4 and $CoAl_2O_4$ spinel phases upon calcination at 773 K:

$$[Co_{0.75}Al_{0.25}(OH)_2][(CO_3^{2-})_{0.07}(NO_3^-)_{0.12}] \cdot 0.63\ H_2O \rightarrow 0.21\ Co_3O_4 + 0.125\ CoAl_2O_4 + 0.07\ CO_2 + 0.12\ NO + 1.63\ H_2O + 1.15\ O_2 \quad (1)$$

Theoretical H_2 consumption of 1.33 and 1 (H_2/Co) corresponds to the reduction of Co_3O_4 and $CoAl_2O_4$, respectively: close to the experimental values of 1.39 and 1.06 found when these phases are deposited on alumina.[13] This will result in H_2 consumption in the LT and HT domains of 1.11 and 0.17 for Co(3)Al. A large discrepancy is thus noted with the experimental values of 0.29 and 0.71 H_2/Co. Therefore, one should consider that Co_3O_4, reduced in the LT domain, exists in much lower quantities than would be expected from Equation (1). In contrast, a larger amount of a second phase more easily reducible than $CoAl_2O_4$ is formed in the HT domain; this phase might be Co_3AlO_6, as proposed by Arnoldy and Moulijn.[13] It could not be differentiated from $CoAl_2O_4$ by XRD, thanks to their similar patterns. When considering Co(2)Mg(1)Al, we might hypothesize that a $Co_{3-x}Mg_xAlO_6$ phase could probably exist.

When Co, Ni, Mg, and Al are present simultaneously, several phases are involved, because different mixed oxides and spinel-like structures could be formed. Anyway, the reduction profile is clearly modified when Ni content increases: i) the reduction starts at a lower temperature than in the Ni-free sample, ii) the peak becomes less asymmetric, with a progressive increase in intensity of the shoulder observed on the lower temperature side, iii) H_2 consumption increases. In contrast, the reducibility of Ni and Co seems almost insensitive to Mg content. However, as the reducibility of Co increases while that of Ni decreases with Mg content,[5] a compensating effect cannot be ruled out. Therefore, the presence of Ni(Mg)AlO- and $Co_{3-x-y}Ni_xMg_yAlO_6$-type phases can be postulated, with, of course, several other minor phases like, for example, alumina, depending of the nominal compositions of the samples.

To sum up: in Co−Ni−Mg−Al LDHs, the species reduced below 723 K (LT domain) would be a $Co_{3-x}Ni_xO_4$ mixed oxide with a spinel structure. Above 723 K (HT domain), mixed oxides of the NiMg(Al)O type, and a spinel phase containing both Co and Ni − tentatively assigned to $Co_{3-x-y}Ni_xMg_yAlO_6$ − can be proposed. The XRD pat-

tern has the aspect of the rock salt-like structure of the major NiMg(Al)O phase. The existence of a phase containing both Co and Ni is supported by recent results obtained in the hydrogenation of acetonitrile, in which the catalysts obtained from reduction of Co−Ni−Mg−Al LDHs were most active and selective for ethylamine than the catalysts prepared from Ni−Mg−Al and Co−Mg−Al LDHs.[3]

Conclusion

It was possible to obtain multi-component LDHs, accommodating Co, Ni, Mg, and Al cations in the same brucite-like sheet, without identifiable excess phase, in a wide range of compositions. The progressive substitution of Ni for Co decreases the lattice *a* parameter, inducing a stronger electrostatic attraction with the anions, the decomposition of which is thus shifted toward higher temperatures. The thermally decomposed samples are a mixture of Ni- and Mg-containing rock salt-type, and Co-containing spinel-like phases. Accordingly, the surface areas increase with the Ni or Mg content, accounting for the decreasing proportion of spinel-like phase in the mixture. The two distinct temperature domains observed in TPR are in agreement with the well known behavior of Co, giving spinel phases reduced below 720 K, while complex phases containing Co, Ni, and Mg are reduced above this temperature. The two maxima observed in the first domain and the enhancement of reducibility with Ni content suggest that a $Co_{3-x}Ni_xO_4$ phase is formed. H_2 consumption, shapes of the reduction profiles, and also XRD patterns make it plausible to propose that NiMg(Al)O and $Co_{3-x-y}Ni_xMg_yAlO_6$ phases are reduced above 720 K, in relative amounts depending on the stoichiometry of the LDHs. It is worth noting that the reducible Co and Ni cations are in close interaction in these phases, resulting in interesting properties when these materials are used as catalyst precursors.

Experimental Section

Preparation of the LDH Precursors: A solution containing the appropriate amounts of cobalt, nickel, magnesium, and aluminium nitrates (Aldrich) dissolved in 250 cm^3 of deionized water was delivered into a polypropylene reactor by a chromatography-type pump at a constant flow of 1 cm^3min^{-1} at room temperature and ambient atmosphere. A second aqueous solution of 1 M NaOH (SdS) was fed by a pH-stat apparatus (718 Stat Titrino, Metrohm) at a constant pH value of ca. 9.0 ± 0.2. After precipitation, the suspension was aged at 373 ± 5 K for 15 h with stirring. The solid product was isolated by centrifugation, washed thoroughly with deionized water, and dried overnight at 353 K in an oven. Nine samples were synthesized following this procedure, varying the ratio between the divalent cations and maintaining the ratio $M^{2+}/Al^{3+} \approx 3$ (Table 1).

These samples belong to two different families, with molar ratios in solution corresponding on the one hand to $Mg^{2+}/\Sigma M^{2+} = 1:3$ and variable $Ni^{2+}/\Sigma M^{2+}$ and, on the other hand to $Ni^{2+}/(Co^{2+}+Ni^{2+}) = 1:2$ and variable $Mg^{2+}/\Sigma M^{2+}$.

As an example, the multi-component Co−Ni−Mg−Al sample labeled Co(1.5)Ni(0.5)Mg(1)Al corresponds to a compound prepared from $M^{2+}/\Sigma M^{2+} = 1.5:3$, 0.5:3 and 1:3 for Co^{2+}, Ni^{2+}, and Mg^{2+}, respectively.

Characterization of the Solids: Chemical analyses of the samples were performed at the Service Central d'Analyse du C.N.R.S. (Solaize, France). Powder X-ray diffraction (XRD) patterns were recorded on a Philips instrument (40 kV, 20 mA) using Cu*K*α radiation (λ = 0.154 nm). The 2θ angle ranged from 6° to 70°. A monochromator was applied, to avoid fluorescence phenomena. Thermogravimetric experiments (TG) were carried out on a Setaram TG 85 1000 °C microbalance in air (80 cm^3min^{-1}) from 293 to 973 K (ramp: 2 K min^{-1}). Specific surface areas were determined by N_2 adsorption at 77 K with a Micromeritics ASAP 2000 instrument and using the BET equation. The samples were outgassed in vacuum ($2\cdot10^{-4}$ Pa) at 523 K overnight before N_2 adsorption. The calcination of the samples was carried out in an air flow at 573 or 773 K (ramp 2 K min^{-1}). The final temperature was maintained for 5 h.

The reducibility of the samples was examined by temperature programmed reduction by hydrogen (TPR). The experimental setup was derived from that proposed classically.[25] Detection was carried out with the thermal conductivity detector of a Shimadzu GC8 chromatograph. The experimental parameters were carefully selected to meet the recommendations of Monti and Baiker.[26] An aliquot of the catalyst (20−30 mg) was activated first at 623 K or 773 K for 4 h in air (ramp: 2 K min^{-1}, flow: 50 cm^3min^{-1}) and then cooled to room temperature. After flushing with He, the TPR was started in H_2/Ar gas (3:97 vol/vol, purity of both gases > 99.995%) from 293 to 1293 K (ramp: 10 K min^{-1}, flow: 20 cm^3min^{-1}).

[1] D. Tichit, A. Vaccari, *Appl. Clay Sc.* **1998**, *13*, 311−315.
[2] W. T. Reichle, *Chem. Technol.* **1986**, *16*, 58−63.
[3] B. Coq, D. Tichit, S. Ribet, *J. Catal.* **2000**, *189,* 117−128.
[4] F. Medina Cabello, D. Tichit, B. Coq, A. Vaccari, N. T. Dung, *J. Catal.* **1997**, *167*, 142−152.
[5] D. Tichit, F. Medina, B. Coq, R. Dutartre, *Appl. Catal. A: Gen.* **1997**, *159*, 241−258.
[6] S. Ribet, D. Tichit, B. Coq, B. Ducourant, F. Morato, *J. Solid State Chem.* **1999**, *142*, 382−392.
[7] S. Kannan, S. Velu, V. Ramkumar, C. S. Swamy, *J. Mater. Sci.* **1995**, *30*, 1462−1468.
[8] S. Kannan, A. Narayanan, C. S. Swamy, *J. Mater. Sci.* **1996**, *31*, 2353−2360.
[9] M. A. Ulibarri, J. M. Fernandez, F. M. Labajos, V. Rives, *Chem. Mater.* **1991**, *3*, 626−630.
[10] O. Clause, B. Rebours, E. Merlen, F. Trifiro, A. Vaccari, *J. Catal.* **1992**, *133*, 231−246.
[11] B. Rebours, J. B. d'Espinose de la Caillerie, O. Clause, *J. Am. Chem. Soc.* **1994**, *116*, 1707−1717.
[12] B. Basavalingu, J. A. K. Tareen, G. T. Bhandage, *J. Mater. Sci. Lett.* **1986**, *5*, 1227−1231.
[13] P. Arnoldy, J. A. Moulijn, *J. Catal.* **1985**, *93*, 38−54.
[14] F. Rouquerol, J. Rouquerol, K. Sing, *Adsorption by Powders & Porous Solids. Principles, Methodology and Applications*, Academic Press, London, **1999**.
[15] F. Trifiro, A. Vaccari, O. Clause, *Catal. Today* **1994**, *21*, 185−195.
[16] M. K. Titulaer, J. B. H. Jansen, J. W. Geus, *Clays Clay Min.* **1994**, *42*, 249−258.
[17] C. V. Rode, M. Arai, M. Shirai, Y. Nishiyama, *Appl. Catal. A: Gen.* **1997**, *148*, 405−413.
[18] H. Ming, B. C. Baker, *Appl. Catal. A: Gen.* **1995**, *123*, 23−36.
[19] M. K. Niemelä, A. O. I. Krause, *Catal. Lett.* **1995**, *34*, 75−84.

[20] E. Van Steen, G. S. Sewell, R. A. Makhothe, C. Micklethwaite, H. Manstein, M. de Lange, C. T. O'Connor, *J. Catal.* **1996**, *162*, 220−229.
[21] B. A. Sexton, A. E. Hughes, T. W. Turney, *J. Catal.* **1986**, *97*, 390−406.
[22] A. Y. Khodakov, J. Lynch, D. Bazin, B. Rebours, N. Zanier, B. Moisson, P. Chaumette, *J. Catal.* **1997**, *168*, 16−25.
[23] Y. E. Roginskaya, O. V. Morozova, E. N. Lubnin, Y. E. Ulitina, G. V. Lopukhova, S. Trasatti, *Langmuir* **1997**, *13*, 4621−4627.
[24] W. J. Wang, Y. W. Chen, *Appl. Catal. A: Gen.* **1991**, *77*, 223−233.
[25] J. L. Lemaitre, *Characterization of Heterogeneous Catalysts*, Marcel Dekker, New York, **1984**, p.34.
[26] D. A. M. Monti, A. Baiker, *J. Catal.* **1983**, *83*, 323−335.
Received March 3, 2000
[I00113]

Copper(II)- and Proton-Assisted Condensation Reactions of a Tetrapodal Pentaamine with Acetone: Formation of "Podand-cum-Macrocycle" Copper Complexes and a Protonated Bis(aminal)

Christopher Zimmermann,[a] Frank W. Heinemann,[a] and Andreas Grohmann*[a]

Dedicated to Professor Dieter Sellmann on the occasion of his 60th birthday

Keywords: N ligands / Copper / Template synthesis / Schiff bases / Macrocycles

The tetrapodal pentaamine 2,6-$C_5H_3N[CMe(CH_2NH_2)_2]_2$ (pyN_4, **1**) forms mononuclear complexes with Cu^{II}, as shown for a series of compounds of the type $[(\mathbf{1})Cu]X_2$ (X = Br, SCN, PF_6, ClO_4). The coordination environment of the copper ion is square-pyramidal, with the pyridine nitrogen atom of **1** in the apical position. The axial bond $Cu–N_{py}$ is significantly longer than the four Cu–N bonds at the base of the pyramid, average values being 2.16 Å and 2.03 Å, respectively. When $[(\mathbf{1})Cu]X_2$ (X = PF_6, ClO_4) is refluxed with an excess of acetone in methanol in the absence of base, the corresponding bis(isopropylideneimine) complexes $[\{(nac)_2pyN_4\}Cu]X_2$ are obtained, in which two diametrically opposite primary amino groups of **1** have condensed with the ketone. The complex cations, which are now chiral, again have square-pyramidal coordinated Cu^{II}. In the presence of sodium methoxide, the condensation of $[(\mathbf{1})Cu]X_2$ with acetone proceeds further, leading to the formation of one diacetone-amine-imine linkage in the product. A 12-membered 1,5,9-triazamacrocycle, incorporating the 2,6-disubstituted pyridine unit, is thus formed. Two podand nitrogen donors of the NN_4 set (which retains its square pyramidal topology) remain: a primary amine and an isopropylidene imine group. The product forms as a mixture of both conceivable isomers (azomethine groups at the base of the pyramid *cis* or *trans*), which were separated and structurally characterised as the tribromocuprate(I) and hexafluorophosphate salts, respectively. The condensation of metal-free **1** with acetone in the presence of two equivalents of HBr yields the bis(aminal) salt (2,6-$C_5H_3N\{CMe[cyclo\text{-}CH_2NH_2C(CH_3)_2NHCH_2\text{-}]\}_2)Br_2$, in which one of the secondary amino groups in each diazacyclohexane ring is protonated, as ascertained by X-ray crystallography. The aminal is a metal-free tautomer of the bis(isopropylideneimine) ligand $(nac)_2pyN_4$, to which it converts upon reaction with Cu^{II} under suitable conditions, providing an alternative synthetic route to complexes of the type $[\{(nac)_2pyN_4\}Cu]X_2$.

Introduction

The tetrapodal pentaamine **1** (pyN_4) forms mononuclear complexes with cobalt(III), nickel(II), and iron(II/III) in which all four arms of the ligand as well as the apical donor atom are coordinated to the metal centre.[1,2] A monodentate additional ligand completes the coordination octahedron. We are currently exploring ways to introduce a functional periphery into such complexes,[3,4] appended to the basal donor atoms of **1**, that will engage in secondary interactions with the monodentate ligand, so as to control its binding and reactivity. Ligand derivatives with: (a) one, (b) two, or (c) four modified sidearms have been obtained by Schiff base condensation with carbonyl compounds, such as: (a) salicylaldehyde, (b) acetone, or (c) cinnamaldehyde, and isolated in the form of their nickel(II) complexes, which are mononuclear.[4]

The spatial orientation of the secondary donor groups in the ligand periphery has to enable noncovalent interactions

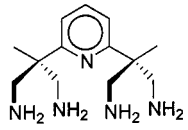

1

with the monodentate ligand; at the same time, the coordination of peripheral groups to the apical site (which would hinder the binding of an exogenous ligand) is to be precluded, and the periphery should not interfere with mononuclear NN_4 complex formation. These difficulties are illustrated by two derivatives of **1**: 1) the mono(salicylaldehyde) derivative, as obtained under (a), above, is hexadentate, its NN_4O donor set occupying all coordination sites in an octahedral complex;[4] 2) a related symmetrical ligand, with four uniformly modified sidearms and a potential NN_4O_4 donor set, adopts a dinucleating coordination mode in the case of nickel(II) and copper(II): each metal ion uses a square-planar disposed N_2O_2 donor subset, and the pyridine nitrogen atom remains uncoordinated.[5]

A strategy to enforce a mononucleating NN_4 donor set in derivatives of **1** irrespective of the nature of the ligand periphery is to increase the rigidity ("juxtapositional fixedness"[6,7]) of the coordination cap. One possibility is to tie

[a] Institut für Anorganische Chemie, Universität Erlangen-Nürnberg,
Egerlandstraße 1, 91058 Erlangen, Germany
E-mail: grohmann@anorganik.chemie.uni-erlangen.de

 © WILEY-VCH Verlag GmbH, 69451 Weinheim, 2001 1434–1948/01/0202–0547 $ 17.50+.50/0

the 1,3-diaminoprop-2-yl sidearms together by bridges between equatorial amino groups, to give a macrocyclic ring "capped" by a pyridine unit. At a later stage, the bridges could carry donor groups pointing towards the sixth coordination site. In order to probe the viability of this approach, we chose a reaction known to furnish acetone-derived C_3 linkages between adjacent NH_2 groups in transition metal amine complexes (the Curtis reaction, Scheme 1).[8,9] In this contribution, we describe the copper(II) complex of **1**, and its reactivity, and that of partially protonated **1**, towards acetone.

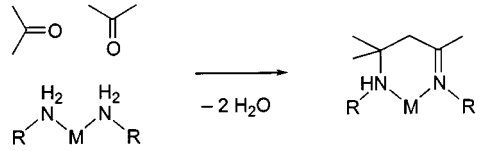

Scheme 1. Condensation of adjacent primary amino groups in a metal complex with acetone to produce a diacetone-amine-imine linkage (Curtis reaction)

Results and Discussion

[(1)Cu]X_2 (X = Br, SCN, PF_6, ClO_4)

The bromide salt [(**1**)Cu]Br_2 formed in good yield as a microcrystalline purple solid upon refluxing a methanolic solution of equivalent amounts of the pentaamine **1**, prepared by neutralisation of **1**·4HBr·MeOH with four equivalents of LiOMe, and $CuCl_2·2H_2O$. Recrystallisation from methanol or methanol/water yielded the solvates [(**1**)Cu]Br_2·0.5MeOH (**2**), [(**1**)Cu]Br_2·2MeOH (**3**), and [(**1**)Cu]Br_2·$3H_2O$ (**4**), and recrystallisation in the presence of NH_4SCN or NH_4PF_6 gave the thiocyanate and hexafluorophosphate salts [(**1**)Cu]$(SCN)_2$·H_2O (**5**) and [(**1**)Cu]$(PF_6)_2$ (**7**). The perchlorate [(**1**)Cu]$(ClO_4)_2$ (**8**), which is soluble in acetone, was obtained directly from the reaction of **1** and $[Cu(DMF)_6](ClO_4)_2$ in methanol (see Experimental Section). The magnetic moment determined for **2** (Gouy balance, 1.7 μB) conforms to one unpaired electron, as expected for Cu^{II}, and a quasi-reversible redox wave in the cyclic voltammogram of this compound at $E_{1/2} = -0.62$ V (vs. NHE) is assigned to the [Cu^{II}/Cu^{I}] couple.[10]

X-ray structural data have been obtained for several compounds of composition [(**1**)Cu]X_2, showing the copper(II) ion to be present in a square-pyramidal coordination environment in all cases. The pyridine nitrogen atom of the pentaamine ligand occupies the axial position, while the primary amino groups are at the base of the pyramid. Without exception, the axial bond Cu−N_{py} is significantly longer than the basal copper−nitrogen bonds, average values being 2.16 Å and 2.03 Å, respectively. While pentacoordinate Cu^{II} is not susceptible to first-order Jahn−Teller effects, such differences, which have been ascribed to a "plasticity effect", are a common feature in the structural chemistry of this ion.[11,12] The following discussion pertains to the cation in [(**1**)Cu]$(SCN)_2$·H_2O (**5**), whose structure is shown in Figure 1. The complex has crystallographic C_1 symmetry. The basal Cu−N bond lengths are similar (Table 1), averaging 2.039(3) Å, while the axial Cu−N bond length is 2.207(2) Å. These values are similar to those determined for the corresponding bonds in the pentaammine copper(II) complex $K[Cu(NH_3)_5](PF_6)_3$.[13] All N_{ax}−Cu−N_{bas} angles in **5** are close to 90°. A distortion of the ligand framework from ideal square-pyramidal geometry, which is probably due, in large measure, to crystal packing effects,[2] causes the pyridine ring to be tilted from the normal on the basal CuN_4 plane by 27.3(1)°, and the nonbonded distances C16···C21 and C17···C20 to be lengthened and shortened

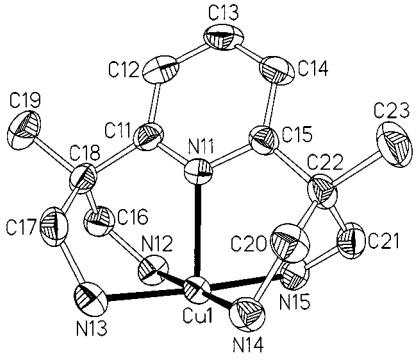

Figure 1. Molecular structure of the cation in **5** with thermal ellipsoids at the 50% probability level; hydrogen atoms have been omitted for clarity

Table 1. Selected bond lengths [Å] and angles [°] for compounds **5**, **9**, **11**, and **12** with estimated standard deviations in parentheses; see also Table 2

Bond or angle	**5**	**9**	**11**	**12**
Cu1−N11	2.207(2)	2.105(4)	2.101(4)	2.141(7)
Cu1−N12	2.069(3)	2.008(2)	2.028(3)	2.001(7)
Cu1−N13	2.019(3)	2.046(2)	1.996(3)	2.022(8)
Cu1−N14	2.024(3)	–	2.028(3)	2.036(7)
Cu1−N15	2.045(3)	–	2.006(3)	2.038(7)
N12−C2	–	1.269(5)	–	–
N12−C5	–	–	–	1.32(1)
N12−C7	–	–	1.473(5)	–
N13−C2	–	–	1.277(5)	1.25(1)
N15−C5	–	–	1.290(5)	–
N15−C7	–	–	–	1.46(1)
N11−Cu1−N12	89.7(1)	94.8(1)	93.2(2)	89.3(3)
N11−Cu1−N13	91.5(1)	89.8(1)	94.0(2)	91.4(3)
N11−Cu1−N14	91.0(1)	–	93.2(2)	90.8(3)
N11−Cu1−N15	85.7(1)	–	90.0(2)	92.7(3)
N12−Cu1−N13	82.3(1)	84.99(9)	85.0(2)	86.8(3)
N14−Cu1−N15	87.0(1)	–	85.1(2)	86.3(3)
N13−Cu1−N14	97.2(1)	–	95.3(2)	92.8(3)
N12−Cu1−N15	93.6(1)	–	94.2(2)	94.1(3)
N12−Cu1−N13A	–	95.04(9)	–	–
N12−Cu1−N14	179.1(1)	–	173.6(2)	179.6(3)
N13−Cu1−N15	175.0(1)	–	176.0(2)	175.8(3)
N12−Cu1−N12A	–	170.3(2)	–	–
N13−Cu1−N13A	–	179.6(3)	–	–
Cu1−N11−C11	116.2(2)	118.7(2)	116.9(3)	116.5(7)
Cu1−N11−C15	116.3(2)	–	117.1(3)	114.7(6)
Cu1−N12−C2	–	126.0(3)	–	–
Cu1−N12−C5	–	–	–	123.4(6)
Cu1−N12−C7	–	–	119.1(3)	–
Cu1−N12−C16	117.0(2)	114.4(2)	114.0(2)	116.2(5)
Cu1−N13−C2	–	–	127.1(3)	128.8(8)
Cu1−N13−C17	112.2(2)	114.5(2)	112.6(3)	112.5(6)
Cu1−N15−C5	–	–	122.3(3)	–
Cu1−N15−C7	–	–	–	120.4(6)
Cu1−N15−C21	–	–	116.9(2)	113.7(5)

to 5.301(5) Å and 4.516(5) Å, respectively (Table 2). In the crystal lattice of **5**, one of the SCN^- counterions is oriented parallel to the basal CuN_4 plane of the cation; its sulfur atom approaches the copper ion to within 2.991(1) Å (sum of the van-der-Waals radii of Cu^{II} and S: 3.20 Å[14]), which may be the underlying reason why **5** has a different colour in the solid state (blue) than those complexes of the [(**1**)Cu]X_2 series where such Cu^{II}/anion contacts are not observed (purple).

Table 2. Intramolecular angles [°] and distances [Å] quantifying the distortions of the ligand cap in complexes **5**, **11** and **12** (with estimated standard deviations in parentheses); compound **9** does not show these distortions owing to crystallographically imposed symmetry; see footnote and text for definitions of angles

Angle or distance	**5**	**11**	**12**
ε[a]	30.7(2)	24.1(3)	29.9(6)
ζ[b]	9.3(1)	7.4(2)	9.0(5)
η[c]	24.6(2)	20.2(2)	25.9(4)
d(C16···C21)[d]	5.301(5)	5.238(6)	5.37(2)
d(C17···C20)[d]	4.516(5)	4.585(7)	4.50(2)

[a] Angle ε between the least-squares planes defined by the pyridine ring (N11, C11, C12, C13, C14, C15) and the quaternary and methyl carbon atoms C18/C19/C22/C23. – [b] Angle ζ between the least-squares planes defined by the equatorial nitrogen atoms N12/N13/N14/N15 and the methylene carbon atoms C16/C17/C20/C21. – [c] Angle η subtended by the lines N11···C13 and N11–Cu1 at N11. – [d] The corresponding distance is 4.965(5) Å in **9.**

[{(nac)$_2$pyN$_4$}Cu](PF$_6$)$_2$

When a suspension of [(**1**)Cu](PF$_6$)$_2$ (**7**) in methanol is refluxed with a large excess of acetone in the absence of base, a mononuclear copper(II) complex is obtained cleanly and in good yield as a blue-violet solid which contains the bis(acetoneimine) derivative of the ligand, as verified by an X-ray structure analysis, i.e. [{(nac)$_2$pyN$_4$}Cu](PF$_6$)$_2$·Me$_2$(C=O) (**9**).[15] Heating the mixture to reflux is essential for the reaction to take place; in a separate experiment under otherwise identical conditions, stirring a solution of **7** in acetone at room temperature led to quantitative re-isolation of the starting material upon workup.

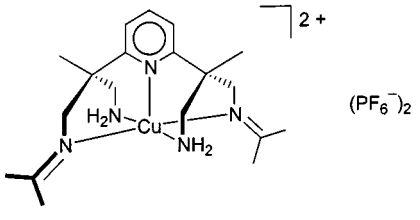

9

The IR spectrum of **9** has absorptions between 3400 and 3000 cm^{-1} (ν_{N-H} str) and at 1582 cm^{-1} (ν_{N-H} def), characteristic of coordinated primary amine groups, and a new strong absorption at 1658 cm^{-1} assigned to the C=N stretching vibration. The spectrum is similar to that of a nickel(II) complex of the same ligand previously isolated from *basic* mixtures of **1** and acetone upon addition of a suitable nickel(II) salt.[4] In the same manner as has been observed for the nickel(II) complex, reacting [(**1**)Cu](PF$_6$)$_2$ (**7**) in neat acetone does not lead to more highly condensed products. The generation of **9** parallels the formation of a copper(II) bis(isopropylideneimine) complex from bis(1,3-propanediamine)copper(II) perchlorate and acetone under base-free conditions, as reported by Curtis and House.[16] A *trans* arrangement of the coordinated *N*-isopropylidene groups was inferred on the basis of circumstantial evidence for this complex, whose hydrolytic instability, however, precluded structural characterisation. The complex was isolated as an intermediate from a reaction which, upon prolonged standing and without added base, produced a square planar 16-membered macrocyclic copper(II) species. Contrary to these observations, compound **9**, which is remarkably stable towards hydrolysis, shows no further reaction with acetone in the absence of base.

The structure of the cation in **9** is shown in Figure 2. The molecule is C_2-symmetrical, with the metal ion, the pyridine nitrogen atom N11, and the pyridine carbon atom C13 lying on the rotation axis. The pyridine, primary amine, and isopropylidene-imine nitrogen atoms define a square pyramid, which is distorted slightly in the sense that, while one basal *trans* N–Cu–N unit is strictly linear [∠(N13–Cu1–N13A) = 179.6(3)°], the other is bent at an angle of ∠(N12–Cu1–N12A) = 170.3(2)° (Table 1). Of the basal Cu–N bonds, those involving the sp^2 nitrogen atoms are shorter [d(Cu1–N12) = 2.008(2) Å], as expected, than those involving the primary amine groups [d(Cu1–N13) = 2.046(2) Å]. Again, the axial Cu–N bond is longer [d(Cu1–N11) = 2.105(4) Å] than the bonds at the base of the pyramid. Overall, the structure resembles that of a related pentacoordinate nickel(II) complex of the same ligand, except that in the latter the M–N_{ax} bond is the shortest of all metal–nitrogen bonds.[4] Complexes of this topology are chiral, the aliphatic quaternary carbon atoms being stereogenic centres as a consequence of asymmetric substitution of the basal N_4 donor set. Compound **9** crystallises in the noncentrosymmetric space group *C*2, which indicates spontaneous resolution of enantiomers upon crystallisation.[17]

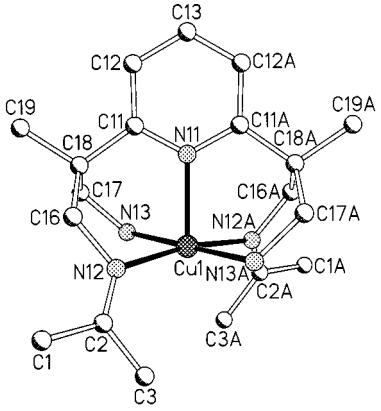

Figure 2. Molecular structure of the cation in **9**; for clarity, ball-and-stick representations have been chosen, and hydrogen atoms have been omitted

Copper(II) Pentaamine Complexes Containing an Acetone-Derived C_3 Bridge and an Isopropylidene-Imine Unit

Whereas refluxing mixtures of [(**1**)Cu]X_2 and acetone in methanol, in the absence of base, yield the *trans*-bis(isopropylideneimine) derivative (compounds **9** and **10**, above), an excess of sodium methoxide in such solutions causes the condensation to proceed further, leading to the formation of one diacetone-amine-imine linkage. A 12-membered 1,5,9-triazamacrocycle, incorporating the pyridine nitrogen atom, is thus formed. Two "podand" nitrogen donors remain of the NN_4 set, viz. a primary amine and an isopropylidene imine group (podand-cum-macrocycle). The condensation parallels the formation of an isolable intermediate in the Ni^{II}/ethylenediamine system, which also contains one diacetone-amine-imine bridge beside an isopropylideneimine and an NH_2 group.[16] In our case, with Cu^{II}, complete cyclisation involving all basal N donors, in a manner similar to the formation of a 16-membered tetraazamacrocycle from the Cu^{II} complex of 1,3-diaminopropane,[8] has so far not been observed. Two regioisomeric forms are possible for the condensation product of **1**, depending on whether the C=N double bonds are *cis* or *trans* with respect to the pyridine ring plane. Indeed, the product initially forms as a mixture of both isomers, which have been separately obtained as the hexafluorophosphate (*trans*, **11**) and tribromocuprate(I) salts (*cis*, **12**), by a combination of fractional crystallisation and temperature-induced isomerisation (see Experimental Section). In the case of **12**, the reducing agent responsible for the formation of $[Cu^{I}Br_3]^{2-}$ is as yet unidentified. However, the pentaamine **1** has been shown to act partially as a reducing agent in the case of some cobalt(III) complexes.[1]

Figure 3 shows the crystal structures of the cations in **11** and **12**. Both complexes, which are chiral, crystallise in centrosymmetric space groups (Table 3). The coordination geometry of the Cu^{II} ion is square-pyramidal in both cases, with a similar tilt of the pyridine ring (Table 2). The Cu−N_{ax} and Cu−N_{bas} bond lengths do not differ markedly from those determined for the bis(isopropylideneimine) complex **9** (Table 1). The diacetone-amine-imine linkage runs alongside the pyridine ring, spanning a pair of *cis*-positioned nitrogen atoms of both 1,3-diaminoprop-2-yl sidearms. The conformation of the bridge is the same in both structures, only its orientation is inverted on going from **11** (C=N *trans*) to **12** (C=N *cis*). Isomerism at the secondary amine centres due to restricted inversion is not observed. Neither structure is significantly strained, as judged from the bond lengths and angles in the ligand framework; in particular, the bond angles in the 12-membered triazamacrocycle incorporating the acetone-derived bridge and the *ortho*-disubstituted pyridine unit are within the range for sp^2- and sp^3-hybridised carbon and nitrogen atoms. The conformation of the triazamacrocycle in **11** and **12** is similar to that found in Cu^{II} and Ni^{II} complexes of 2,4,4-trimethyl-1,5,9-triazacyclododec-1-ene, which may be obtained by the metal-templated condensation of dipropylenetriamine with acetone.[18,19] It therefore seems unlikely that the formation of a second diacetone-amine-imine linkage in **11** or **12** is inhibited purely for reasons of ring strain that would otherwise ensue; rather, the nucleophilicity of the last remaining primary amino group appears to be significantly reduced, and a stronger base may be required to produce an amido ligand in sufficient concentration to allow the second ring closure to proceed.[20]

A Bis(aminal) Derivative From the Reaction of 1·2HBr with Acetone

Beside transition metal ions such as Ni^{II} and Cu^{II}, protons have also been used as a templating agent (and acid catalyst) in macrocyclisations involving C=N bond formation.[3,21] Metal-free condensation products are attractive as they provide indirect access to macrocyclic complexes not otherwise accessible, either by a metal-template reaction or by transmetallation. In the case of 1,2-diaminoethane, with acetone as the carbonyl component, the formation of a macrocyclic product is observed only when the diamine is employed in its monoprotonated form, $H_2NCH_2CH_2NH_2{\cdot}HX$.[22,23] The macrocycle, which separates as the diprotonated salt, is assembled from two equivalents of diamine and four equivalents of acetone, containing two diacetone-amine-imine bridges. The same product forms when mesityloxide (4-methyl-3-pentene-2-one) is used as the carbonyl component. In the case of monoprotonated 1,3-diaminopropane, instead of macrocycle formation, the reaction with acetone may lead preferentially to the aminal derivative, which is a six-membered hexahydropyrimidine ring.[24−27] The intermediate formation of aminals has been invoked as the controlling process in the assembly of a Schiff base tetramacrocycle from **1** and a difunctional aldehyde in the presence of protons,[3] and a bis(aminal) product has been isolated from the reaction of **1** with two equivalents of ferrocenecarbaldehyde.[5] In view

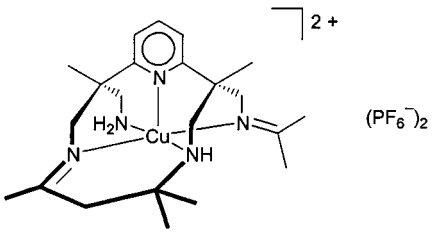

11

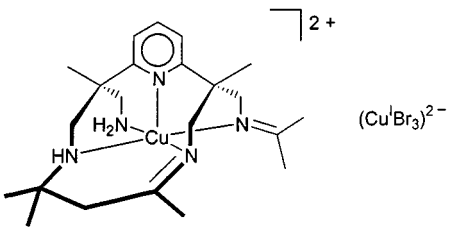

12

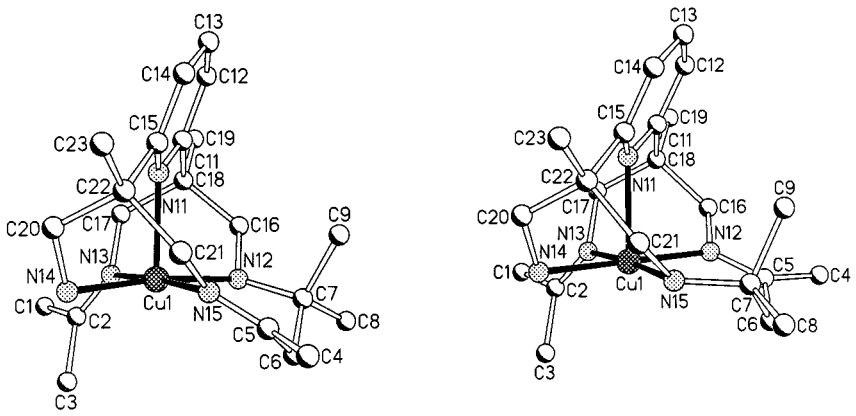

Figure 3. Molecular structures of the two isomeric complexes arising from the condensation of [(**1**)Cu]X_2 with acetone in the presence of base; the orientation of the C=N double bonds is *trans* in **11** (left), and *cis* in **12** (right)

Table 3. Crystallographic data for compounds **5**, **9**, **11**, **12** and **13**

	5	**9**	**11**	**12**	**13**
Empirical formula	$C_{15}H_{25}CuN_7S_2{\cdot}H_2O$	$C_{19}H_{33}CuF_{12}N_5P_2{\cdot}C_3H_6O$	$C_{22}H_{37}CuF_{12}N_5P_2$	$C_{22}H_{37}Br_3Cu_2N_5{\cdot}CH_4O$	$C_{19}H_{35}Br_2N_5{\cdot}CH_4O$
Molecular weight	449.10	743.06	725.05	770.42	525.38
Crystal system	monoclinic	monoclinic	orthorhombic	triclinic	monoclinic
Space group (no.)	$P2_1/n$ (no. 14)	$C2$ (no. 5)	$Pbca$ (no. 61)	$P\bar{1}$ (no. 2)	$P2_1/n$ (no. 14)
a [Å]	14.466(3)	14.367(4)	13.496(3)	9.824(2)	11.977(2)
b [Å]	9.242(2)	10.829(3)	12.663(3)	9.989(2)	12.514(1)
c [Å]	15.102(4)	11.269(4)	34.491(8)	15.404(5)	16.680(3)
α [°]	90	90	90	103.50(2)	90
β [°]	90.69(2)	114.52(2)	90	98.97(2)	104.52(1)
γ [°]	90	90	90	95.72(2)	90
Z	4	2	8	2	4
V [Å^3]	2018.9(8)	1595.1(8)	5895(2)	1437.2(6)	2420.2(6)
$\rho_{calcd.}$ [g cm^{-3}]	1.478	1.547	1.634	1.780	1.442
Diffractometer	Nicolet R3m/V	Nicolet R3m/V	Siemens P4	Nicolet R3m/V	Siemens P4
λ[a] [Å]	0.71073	0.71073	0.71073	0.71073	0.71073
Crystal size [mm^3]	0.45 × 0.32 × 0.20	0.50 × 0.38 × 0.32	0.76 × 0.60 × 0.36	0.28 × 0.24 × 0.12	0.55 × 0.50 × 0.40
T [°C]	298(2)	298(2)	200(2)	298(2)	210(2)
Absorption correction	Psi-scan	Psi-scan	Psi-scan	Psi-scan	Psi-scan
T_{min}/T_{max}	0.334/0.403	0.589/0.665	0.214/0.255	0.077/0.138	0.029/0.084
Scan	ω	ω	ω	ω	ω
2Θ range	$4 \le 2\Theta \le 54$	$4 \le 2\Theta \le 54$	$4 \le 2\Theta \le 54$	$4 \le 2\Theta \le 54$	$4 \le 2\Theta \le 54$
Measured reflections	5525	2760	7834	6986	6610
Unique reflections	4412	2212	6425	6266	5289
Observed reflections[b]	2706	2051	4733	2292	3825
μ(Mo-K_α) [mm^{-1}]	1.308	0.881	0.949	5.675	3.369
Refined parameters	310	238	379	309	254
Data/parameter ratio	14.2	9.3	17.0	20.3	20.8
$wR2$ (all data)[c]	0.0778	0.0737	0.1493	0.1784	0.1228
R 1 (obs. data)[d]	0.0368	0.0316	0.0611	0.0647	0.0500
ρ_{fin}(max/min.) [e Å^{-3}]	0.334/−0.362	0.292/−0.217	1.116/−0.766	1.014/−0.773	0.611/−0.610
Weighting scheme[e]	$k = 0.0340/l = 0$	$k = 0.0489/l = 0$	$k = 0.0523/l = 19.0627$	$k = 0.0803/l = 0$	$k = 0.0536/l = 2.2687$
Abs. struct. parameter	−	0.013(14)	−	−	−

[a] Mo-K_α, graphite monochromator. − [b] with $F_o \ge 4\sigma(F)$. − [c] $wR2 = (\{\Sigma[w(F_o^2 - F_c^2)^2]\}/\{\Sigma[w(F_o^2)^2]\})^{0.5}$. − [d] $R1 = \Sigma||F_o| - |F_c||/\Sigma|F_o|$ for $F > 4\sigma(F)$. − [e] $w = 1/[\sigma^2(F_o^2) + (k{\cdot}P)^2] + l{\cdot}P$and $P = (F_o^2 + 2F_c^2)/3$.

of the fact that the pentaamine **1** contains two 1,3-diaminopropyl residues in close proximity, thereby perhaps favouring macrocyclisation, we studied the reactivity of **1** towards acetone in the presence of two equivalents of hydrogen bromide.

When a methanolic solution of **1**·2 HBr, prepared in situ from the pentaamine tetrahydrobromide by addition of the required amount of LiOMe, is refluxed with an excess of acetone, the mixture soon deposits a colourless precipitate (52% isolated yield). Bands characteristic of a C=N stretching vibration are absent in the IR spectrum of this product, ruling out Schiff base formation. Instead, the combined elemental analysis, NMR and mass spectroscopic data show the material to be a bis(aminal) dihydrobromide/methanol solvate (**13**), formed by condensation of **1**·2HBr with two equivalents of acetone, by the classical mechanism shown in Scheme 2. The same product is obtained, again exclusively, when reacting **1**·2HBr with mesityloxide (4-methyl-3-

pentene-2-one), H^+ apparently catalysing hydrolysis of the latter after its carbonyl group has formed the Schiff base, with concomitant liberation of water.

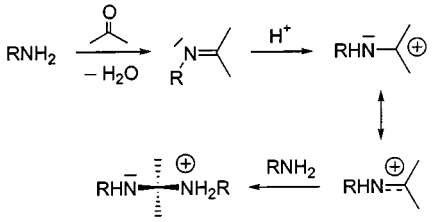

Scheme 2. Formation of the protonated aminal moiety in **13**, involving acetone and two equivalents of primary amine

Single crystals of **13** were of sufficient quality to allow the determination of its solid-state structure, and in particular the hydrogen atom positions, all of which could be deduced from a difference Fourier synthesis. The structure of the dication, which has crystallographic C_1 symmetry, is shown in Figure 4. Each diazacyclohexane ring contains one nitrogen atom carrying two protons and hence a formal positive charge (N13, N15), and one nitrogen atom with a single proton (N12, N14). The diazacyclohexane rings both have a chair conformation, and are held in relative proximity by weak intramolecular/interionic hydrogen bonded contacts between aminal NH/NH_2 groups and one bromide counterion [Figure 4; d(N13−H13B···N14) = 3.230(5) Å, ∠(NHN) = 141.3(4)°, van der Waals radius of N: 1.55 Å;[14] d(N13−H13A···Br1) = 3.223(3) Å, ∠(NHBr) = 160.1(4)°; d(N14−H14B···Br1) = 3.587(3) Å, ∠(NHBr) = 150.8(4)°, sum of van der Waals radii of N and Br: 3.4 Å[14]]. As a consequence of the intramolecular contacts, the "single" proton H14B adopts an equatorial position, while H12B is in an axial position. The nitrogen−carbon bonds involving the NH_2^+ groups are slightly but significantly longer than the corresponding bonds involving NH (see the legend to Figure 4), as has been found for other amine/ammonium pairs.[28] The nitrogen atom N12 has a hydrogen-bonded contact with the OH group of the solvate methanol molecule. Bond lengths and angles in the diazacyclohexane and pyridine rings are in the normal range.

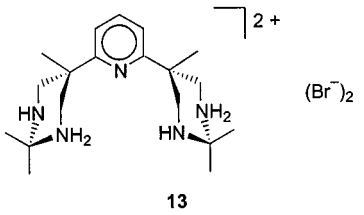

13

The bis(aminal) **13**, when deprotonated, is a metal-free tautomer of the bis(isopropylideneimine) ligand as found in complexes **9** or **10**. Indeed, the reaction of **13** with $[Cu(DMF)_6](ClO_4)_2$, after addition of two equivalents of LiOMe, yields **10** as the exclusive product, as identified by elemental analysis and IR spectroscopy. Compound **13** may thus serve as a metal-free equivalent of this chiral ligand, and work is currently under way to extend its coordination chemistry to other transition metals.

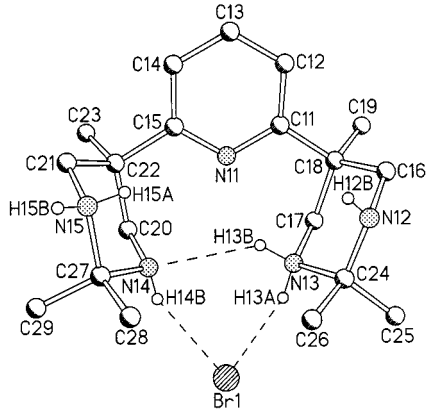

Figure 4. Molecular structure of the doubly protonated bis(aminal) which forms as the dibromide salt **13** when condensing **1**·2HBr with acetone. The positions of all hydrogen atoms have been located in a difference Fourier synthesis, but only the nitrogen-bonded protons are shown for clarity; some structural parameters are: N12−C16 = 1.468(6) Å, N12−C24 = 1.461(6) Å, N13−C17 = 1.501(5) Å, N13−C24 = 1.533(6) Å; C16−N12−C24 = 114.9(4)°, C17−N13−C24 = 114.0(3)°, N12−C24−N13 = 109.2(3)°

Conclusion

Reaction of the copper(II) template $[(\mathbf{1})Cu]^{2+}$ with acetone does not furnish a symmetrical condensation product in which all basal N donors have been incorporated into a macrocyclic ring, spanned by a 2,6-disubstituted pyridine unit, to give a reinforced coordination cap as outlined in the Introduction. The $[(\mathbf{1})Cu]^{2+}$/acetone system may, however, be controlled to provide the chiral bis(isopropylideneimine) ligand $\{(nac)_2pyN_4\}$ exclusively, and other transition metal complexes of this ligand should be accessible by an indirect route, via the diprotonated bis(aminal) of **1** formed in the reaction of **1**·2HBr with acetone. Current work addresses the question whether the metal-free condensation reaction can be extended to other carbonyl compounds, to give a series of chiral square pyramidal coordination caps derived from **1** with two substituted sidearms.

Experimental Section

CAUTION! Although no problems were encountered in this work, transition metal perchlorate complexes with organic ligands are potentially explosive and should be handled with due precautions.

Materials and Instrumentation: Manipulations were performed under dinitrogen using standard Schlenk techniques and freshly dried solvents. Reagents were AR grade or better and were purchased from Merck, Fluka, and Aldrich. **1**·4HBr·MeOH and $[Cu(DMF)_6](ClO_4)_2$ were prepared as described previously.[29,30] IR (KBr discs) and UV/Vis spectra (solvent: DMSO) were recorded on Perkin−Elmer 16PC FT-IR and Shimadzu UV-3101 PC instruments. Cyclic voltammograms were recorded using an EG & G potentiostat PAR model 264A and a conventional three-electrode configuration consisting of a glassy carbon working electrode, a platinum auxiliary electrode and a Ag/AgCl reference electrode (room temperature; solvent: DMSO; scan rate: 50 mV s^{-1}; supporting electrolyte: NBu_4PF_6 [10^{-1} M]; internal standard: ferrocene,

$E(Fc/Fc^+)$ = +0.4 V vs. NHE[31]). NMR spectra were measured on a JEOL JNM-EX 270 spectrometer, and mass spectra were obtained on JEOL MSTATION 700 and Micromass ZABSpecE spectrometers. Magnetic moments were measured using a Johnson-Matthey Gouy balance, with diamagnetic corrections calculated from Pascal's constants.[32] Elemental analyses were performed using Carlo Erba Elemental Analysers 1106 and 1108.

X-ray Crystallography: Crystal data for compounds **5**, **9**, **11**, **12** and **13** are given in Table 3, and selected distances and angles are listed in Table 1 and 2. Cation structures are presented in Figure 1−4. Structural data for other compounds containing the copper complex $[Cu(\mathbf{1})]^{2+}$ have been deposited with the Cambridge Crystallographic Data Centre {$[Cu(\mathbf{1})](Br)_2\cdot 2MeOH$ (**3**), $[Cu(\mathbf{1})](Br)_2\cdot 3H_2O$ (**4**), $[Cu(\mathbf{1})](Br)(PF_6)\cdot MeOH$ (**6**), $[Cu(\mathbf{1})](ClO_4)_2$ (**8**), $[\{(nac)_2pyN_4\}Cu](ClO_4)_2$ (**10**)}; the cation parameters resemble those determined for **5**. All structures discussed in this contribution were solved by direct methods and refined by full-matrix least-squares procedures on F^2 using SHELXTL NT 5.10 (Bruker AXS, 1998). All non-hydrogen atoms were refined anisotropically.

Treatment of Hydrogen Atoms: All hydrogen atom positions in compounds **5**, **11**, **13** were obtained from a difference Fourier synthesis. For the structure of **5**, the positional H atom parameters were refined while a common isotropic displacement parameter was kept constant. In the case of the solvate water molecule in **5** and for the entire structures of **11** and **13**, both positional and common isotropic displacement parameters were kept constant during refinement.

The hydrogen atoms in compounds **9**, **12** were geometrically positioned and allowed to ride on their carrier atoms during refinement; their isotropic displacement parameters were tied to those of the adjacent atoms by a factor of 1.2 or 1.5.

Other Remarks: The disorder of the hexafluorophosphate anions in compound **9** could be resolved into two preferred orientations [occupancy factors 0.86(2) and 0.14(2)].

The maximum of the residual electron density in compound **11** is located within the ligand framework, indicating that a small percentage of the other isomer is present in the crystal structure. In preliminary X-ray structural analyses of product used "as-obtained" (no treatment subsequent to synthesis; see details below), the presence of both isomers in approximately equal amounts led to the determination of identical C−N single and C=N double bond lengths. In the structure of **11**, these distances are distinctly different [N12−C7: 1.473(5) Å, N15−C5: 1.290(5) Å]; for this reason, no allowance was made for the possible presence of the other isomer.

The structure of **12** is unremarkable in this respect, the maximum of the residual electron density being located at the copper atom.

Crystallographic data (excluding structure factors) for the structures reported in this paper have been deposited with the Cambridge Crystallographic Data Centre as supplementary publication nos. CCDC-149662−149665 (**3**−**6**) and CCDC-149666−149671 (**8**−**13**). Copies of the data can be obtained free of charge on application to CCDC, 12 Union Road, Cambridge CB2 1EZ, UK [Fax: (internat.) +44-1223/336-033; E-mail: deposit@ccdc.cam.ac.uk].

$[(\mathbf{1})Cu](X)_2\cdot$solv (X = Br, solv = 0.5MeOH; 2): To a stirred suspension of **1**·4HBr·MeOH (1.24 g, 2.04 mmol) in methanol (20 mL) was added a solution of LiOMe (0.310 g, 8.16 mmol) in MeOH (5 mL) in one portion, to give a clear solution after ca. 15 min. at room temperature. To this was added a solution of $CuCl_2\cdot 2H_2O$ (0.347 g, 2.04 mmol) in methanol (15 mL), and the mixture refluxed overnight. The solution changed colour from brown through blue to purple, and deposited a purple microcrystalline precipitate, which was collected on a glass frit, washed with methanol (3 × 10 mL), and dried in vacuo (0.65 g, 65%). Recrystallisation from methanol or methanol/water, with or without an added anion source (NH_4SCN, NH_4PF_6) and/or diethyl ether, yielded the compounds $[(\mathbf{1})Cu](Br)_2\cdot 2MeOH$ (**3**), $[(\mathbf{1})Cu](Br)_2\cdot 3H_2O$ (**4**), $[(\mathbf{1})Cu](SCN)_2\cdot H_2O$ (**5**), $[(\mathbf{1})Cu](Br)(PF_6)\cdot MeOH$ (**6**), and $[(\mathbf{1})Cu](PF_6)_2$ (**7**), in most cases as single crystals. All compounds are purple, with the exception of compound **5**, which is blue. The following analytical data were obtained for compound **2**: $C_{13}H_{25}Br_2CuN_5\cdot 0.5CH_4O$ (490.8): calcd. C 33.04, H 5.55, N 14.27; found C 33.14, H 5.95, N 14.53. − IR (KBr): $\tilde{\nu}$ = 3442 cm^{-1}, 3432, 3303, 3213, 2982, 2926, 1600, 1584, 1470, 1455, 1250, 1088, 1011, 822, 768, 624. − MS (FAB, *p*-NBA): *m/z* (%) = 314 $[(\mathbf{1})Cu]^+$ (100), 395 $\{[(\mathbf{1})Cu]Br\}^+$ (65). − μ_{Eff} (spin only) = 1.71 BM. − Cyclic voltammetry (room temp., 10^{-3} M soln. in abs. DMSO): $E_{1/2}$ (Cu^{II}/Cu^{I}) = −0.62 V. − UV/Vis: λ_{max} (ε) = 530 nm (61 $dm^3\cdot mol^{-1}\cdot cm^{-1}$).

$[(\mathbf{1})Cu](ClO_4)_2$ (8): In contrast to the bromide salts **2**, **3** and **4**, the perchlorate salt **8** is soluble in acetone. It was prepared from the free pentaamine ligand **1** as follows: A suspension of **1**·4 HBr·MeOH (1.20 g, 1.98 mmol) in MeOH was neutralised by addition of 4 equiv. LiOMe. The resulting solution was taken to dryness, extracted with CH_2Cl_2 to remove LiBr, and the dichloromethane extract taken to dryness to leave **1** as a pale yellow oil. Addition of MeOH (15 mL) gave a clear solution, to which was added in one portion a faint blue solution of $[Cu(DMF)_6](ClO_4)_2$ in MeOH (15 mL). A purple solution formed immediately, which was refluxed for 1 h and subsequently reduced in volume to ca. 20 mL by applying a stream of dry dinitrogen. When crystallisation set in, the mixture was filtered, and diethyl ether allowed to diffuse into the filtrate. The single crystals obtained in this manner were separated by filtration, washed with MeOH, and dried in a stream of dinitrogen (0.21 g, 21%). Additional crops of **8** were obtained by allowing the mother liquor to stand in air. − $C_{13}H_{25}Cl_2CuN_5O_8$ (513.8): calcd. C 30.39, H 4.90, N 13.63; found C 30.68, H 4.96, N 13.75. − IR (KBr): $\tilde{\nu}$ = 3303 cm^{-1}, 3216, 3137, 2963, 2927, 2881, 1601, 1585, 1471, 1456, 1399, 1261, 1084 (br), 1012, 822, 802, 769, 625. − MS (FD): *m/z* (%) = 315 $[(\mathbf{1})Cu]^+$ (100), 413 $\{[(\mathbf{1})Cu](ClO_4)\}^+$ (80).

$[\{(nac)_2pyN_4\}Cu](X)_2$ (X = PF_6: 9): To a suspension of $[(\mathbf{1})Cu](PF_6)_2$ (0.20 g, 0.33 mmol) in methanol (30 mL) was added acetone in large excess (1 mL), and the mixture refluxed overnight to give a purple solution. Diffusion of diethyl ether into this solution produced single crystals of the acetone solvate $[\{(nac)_2pyN_4\}Cu](PF_6)_2\cdot H_3C(C=O)CH_3$ (0.15 g, 62%). − $C_{19}H_{33}CuF_{12}N_5P_2\cdot C_3H_6O$ (743.1): calcd. C 35.56, H 5.29, N 9.43; found C 35.26, H 5.64, N 9.32. − IR (KBr): $\tilde{\nu}$ = 3371 cm^{-1}, 3316, 3214, 3113, 2958, 1729 (acetone), 1658 (C=N), 1582, 1469, 1374, 1265, 1122, 1014, 836 (PF_6), 557. − MS (FAB, *p*-NBA): *m/z* (%) = 394 $[\{(nac)_2\text{-}pyN_4\}Cu]^+$ (100), 475 $\{[\{(nac)_2\text{-}pyN_4\}Cu]Br\}^+$ (35). − μ_{Eff} (spin only) = 1.60(3) BM. − UV/Vis: λ_{max} (ε) = 528 nm (125 $dm^3\cdot mol^{-1}\cdot cm^{-1}$).

X = ClO_4 (10): The perchlorate salt $[(\mathbf{1})Cu](ClO_4)_2$ (**8**), when treated in a similar manner with an excess of acetone in MeOH/acetone at reflux under base-free conditions, gave the corresponding bis(isopropylideneimine) complex **10** as an unsolvated solid. − $C_{19}H_{33}Cl_2CuN_5O_8$ (594.0): calcd. C 38.42, H 5.60, N 11.79; found C 37.92, H 5.95, N 11.70. − IR (KBr): $\tilde{\nu}$ = 3321 cm^{-1}, 3273, 3214, 3113, 2981, 1661 (C=N), 1592, 1469, 1374, 1266, 1088 (br, ClO_4), 818, 624. − MS (FD): *m/z* (%) = 395 $[\{(nac)_2\text{-}pyN_4\}Cu]^+$ (20), 494 $\{[\{(nac)_2\text{-}pyN_4\}Cu]ClO_4\}^+$ (100). Compound **10** may also be

obtained by first reacting a methanolic solution of **1** with acetone under reflux, followed by addition of $[Cu(DMF)_6](ClO_4)_2$ in MeOH. Finally, **10** was obtained from the diprotonated bis(aminal) **13** (see below) as follows: To a solution of **13** in methanol was first added LiOMe (2 equiv.), then $[Cu(DMF)_6](ClO_4)_2$ (1 equiv.) in MeOH, and the mixture refluxed overnight to give a purple solution. Isothermal diffusion of ether into this solution produced a purple crystalline precipitate identified as **10** by IR spectroscopy and elemental analysis.

Preparation of Copper(II) Complexes of 1 Containing an Acetone-Derived C_3 Bridge and an Isopropylidene-Imine Unit: To a stirred suspension of **1**·4HBr·MeOH (0.766 g, 1.26 mmol) in methanol (20 mL) was added a slight excess of sodium metal (0.125 g, 5.23 mmol). After the evolution of H_2 had ceased, acetone (5 mL) was added to the clear solution, and the mixture refluxed for 1 h. After cooling to room temperature, $CuCl_2·2H_2O$ (0.215 g, 1.26 mmol) was added as a solid in one portion, and the mixture refluxed overnight to give a purple solution. To this was added solid $NaPF_6$ to produce a purple precipitate, which was isolated and dried in vacuo (A). Preliminary X-ray data of this material indicated a mixture of two structural isomers (see text and X-ray Crystallography, above) originating from the condensation of $[(\mathbf{1})Cu]^{2+}$ with three equivalents of acetone. Elemental analysis data are in agreement with this formulation: $C_{22}H_{37}CuF_{12}N_5P_2$ (725.0): calcd. C 36.45, H 5.14, N 9.66; found C 36.50, H 5.33, N 9.62. The mother liquor of this preparation was taken to dryness, leaving a reddish-brown solid (B). Both isomers were obtained separately as follows:

Isomer with *trans*-Oriented C=N Double Bonds (11): The crystalline solid obtained under (A), above, was taken up in an acetone/methanol mixture (1:1, 20 mL), and the mixture refluxed overnight to give an intensely coloured purple solution. Cooling to room temperature produced a purple precipitate of single crystals and a faintly pink supernatant. Elemental analysis, although as yet unsatisfactory, and mass spectrometric data indicate a compound of composition $C_{22}H_{37}CuF_{12}N_5P_2$ [bis(hexafluorophosphate) salt, 725.0]: calcd. C 36.45, H 5.14, N 9.66; found C 35.57, H 5.04, N 8.92. − ESI: *m/z* (%) = 434 $[C_{22}H_{37}N_5Cu]^+$ (100). − IR (KBr): $\tilde{\nu}$ = 3356 cm^{-1}, 3307, 3270, 2983, 2939, 2357, 2338, 1660 (C=N), 1589, 1471, 1375, 1243, 1127, 1020, 984, 843 (PF_6), 556.

Isomer with *cis*-Oriented C=N Double Bonds (12): The solid obtained under (B) above was likewise taken up in an acetone/methanol mixture (1:1, 20 mL), and the mixture refluxed overnight. The purple solution, upon cooling to room temperature, deposited reddish-purple single crystals, leaving a strongly coloured purple supernatant. Elemental analysis data best agree with the solid being a monomethanol solvate of composition $C_{22}H_{37}Br_3Cu_2N_5·CH_4O$ (tribromocuprate salt, 770.4): calcd. C 35.86, H 5.36, N 9.09; found C 34.60, H 6.11, N 8.73. − FAB: *m/z* (%) = 434 $[C_{22}H_{37}N_5Cu]^+$ (100). − IR (KBr): $\tilde{\nu}$ = 3442 cm^{-1}, 3212, 3136, 2969, 2368, 2344, 1645 (C=N), 1585, 1572, 1466, 1446, 1420, 1372, 1356, 1241, 1219, 1152, 1095, 1012, 834, 821, 764, 659, 597, 416.

Preparation of the Bis(aminal)dihydrobromide 13: Solid **1**·4HBr·MeOH (0.67 g, 1.1 mmol) was treated with 2 equivalents of LiOMe (1 M solution in methanol, 2.2 mL, 2.2 mmol), giving a clear solution after stirring at room temperature for 5 min. To this was added a large excess of anhydrous acetone (30 mL), and the mixture heated to reflux. A colourless precipitate began to form after a few minutes. Refluxing was continued for 1 h; the mixture was then allowed to cool to room temperature, filtered (G4 glass frit), the obtained solid washed with acetone (2 × 8 mL), and dried in vacuo overnight (0.30 g, 52%). Single crystals of **13** (methanol solvate) were obtained by allowing diethyl ether to diffuse into a methanolic solution of the salt at room temperature. − $C_{19}H_{35}Br_2N_5·CH_4O$ (525.4): calcd. C 45.72, H 7.48, N 13.33; found C 45.92, H 7.30, N 13.25. − ^{1}H NMR ([D$_6$]DMSO, room temp.): δ = 8.35 (br. s, 6 H, NH), 7.84 [AB_2, 3 lines, ^3J(HH) = 7.9 Hz, 1 H, py-H^4], 7.45 [AB_2, 2 lines, ^3J(HH) = 7.9 Hz, 2 H, py-H^{3,5}], 4.12 [br. s, 1 H, OH (methanol)], 3.47 (br. m, 4 H, −C*H*H−), 3.15 [s, 3 H, CH_3 (methanol)], 3.11 (br. m, 4 H, −CH*H*−), 1.52 [s, 6 H, $C(CH_3)_2$], 1.42 [s, 6 H, $C(CH_3)_2$], 1.37 (s, 6 H, py−C−CH_3). − ^{13}C NMR ([D$_6$]DMSO, room temp.): δ = 161.86 (s, C2/6), 138.19 (s, C4), 119.23 (s, C3/5), 69.63 (s, aminal *C*Me$_2$), 48.58 (s, CH_3OH), 46.94 (s, $-CH_2-$), 37.00 (s, py-*C*−Me), 25 [br, aminal C(*C*H$_3$)$_2$], 23.01 (py−C-*C*H$_3$). − FD: *m/z* (%) = 253 $[py(NH_2)_2(NH_3)_2]^+$ (25), 293 $[py(NH_2)(NH_3)(NHC(CH_3)_2NH_2)]^+$ (30), 333 $[py\{NHC(CH_3)_2NH_2\}_2]^+$ (50). − IR (KBr): $\tilde{\nu}$ = 3244 cm^{-1}, 2961, 1585, 1566, 1500, 1470, 1390, 1238, 1123, 1034, 983, 944, 914, 900, 883, 813, 761, 715, 643, 632, 525, 496, 484, 442. A similar reaction of **1**·2HBr in methanol with two equivalents of mesityloxide (4-methyl-3-pentene-2-one, $C_6H_{10}O$), after stirring at room temperature for 3 days, produced **13** as the exclusive product, as identified by elemental analysis and mass spectrometry. Further, mass spectra show the bis(aminal) (*m/z* = 333) to form also when reacting unprotonated **1**, prepared by addition of 4 equiv. of LiOMe to a suspension of **1**·4HBr·MeOH in methanol, with acetone or mesityloxide (3 days, room temperature).

Acknowledgments

We thank Professor D. Sellmann for generous support of this work and Mr. W. Donaubauer and Mr. H.-G. Köhler for mass spectral measurements. Financial support from the Deutsche Forschungsgemeinschaft is gratefully acknowledged.

[1] S. Schmidt, F. W. Heinemann, A. Grohmann, *Eur. J. Inorg. Chem.* **2000**, 1657−1667.
[2] C. Dietz, F. W. Heinemann, J. Kuhnigk, C. Krüger, M. Gerdan, A. X. Trautwein, A. Grohmann, *Eur. J. Inorg. Chem.* **1998**, 1041−1049.
[3] S. Schmidt, W. Bauer, F. W. Heinemann, H. Lanig, A. Grohmann, *Angew. Chem.* **2000**, *112*, 950−953; *Angew. Chem. Int. Ed.* **2000**, *39*, 913−916.
[4] C. Dietz, F. W. Heinemann, A. Grohmann, *Eur. J. Inorg. Chem.* **1999**, 2147−2156.
[5] C. Dietz, F. W. Heinemann, A. Grohmann, *Z. Naturforsch.* **2000**, *55b*, 1037−1044.
[6] D. H. Busch, A. L. Vance, A. G. Kolchinski, in *Comprehensive Supramolecular Chemistry, Vol. 9: Templating, Self-Assembly, and Self-Organization* (Eds.: J. L. Atwood, J. E. D. Davies, J.-M. Lehn, D. D. MacNicol, F. Vögtle, J.-P. Sauvage, M. W. Hosseini), Pergamon, Oxford, **1996**, vol. 9, 1−42.
[7] D. H. Busch, *Chem. Rev.* **1993**, *93*, 847−860.
[8] The reaction is most effective for polyamine complexes of Cu^{II} and Ni^{II}. In the case of 1,3-diaminopropane ligands, it leads to the formation of 16-membered tetraazamacrocycles. The C_3 linkage is a diacetone-amine-imine, and the reaction is the aza analogue of an aldol reaction: N. F. Curtis, *Coord. Chem. Rev.* **1968**, *3*, 3−47.
[9] N. V. Gerbeleu, V. B. Arion, J. Burgess, *Template Synthesis of Macrocyclic Compounds*; Wiley-VCH, Weinheim, **1999**.
[10] J. A. Goodwin, D. M. Stanbury, L. J. Wilson, C. W. Eigenbrot, W. R. Scheidt, *J. Am. Chem. Soc.* **1987**, *109*, 2979−2991.
[11] D. Reinen, *Comments Inorg. Chem.* **1983**, *2*, 227−246.
[12] B. J. Hathaway, *Struct. Bonding* **1984**, *57*, 55−118.
[13] M. Duggan, N. Ray, B. Hathaway, G. Tomlinson, P. Brint, K. Pelin, *J. Chem. Soc., Dalton Trans.* **1980**, 1342−1348.
[14] A. Bondi, *J. Phys. Chem.* **1964**, *68*, 441−451.
[15] $[(\mathbf{1})Cu](ClO_4)_2$ (**8**) gives the same reaction, yielding the corresponding perchlorate salt $[\{(nac)_2\text{-}pyN_4\}Cu](ClO_4)_2$ (**10**), as

long as base-free conditions are maintained and the mixture is heated to reflux.
[16] D. A. House, N. F. Curtis, *J. Am. Chem. Soc.* **1964**, *86*, 223−225.
[17] Racemic crystals (space group *C*2/*c*) are isolated in the case of the perchlorate complex [{(nac)$_2$-pyN_4}Cu](ClO_4)$_2$ (**10**); see Experimental Section for deposition details.
[18] M. D. Santana, A. Rufete, G. Sánchez, G. García, G. López, J. Casabó, E. Molins, C. Miravitlles, *Inorg. Chim. Acta* **1997**, *255*, 21−27.
[19] P. Bradford, R. C. Hynes, N. C. Payne, C. J. Willis, *J. Am. Chem. Soc.* **1990**, *112*, 2647−2654.
[20] R. W. Hay, A. Danby, S. Miller, P. Lightfoot, *Inorg. Chim. Acta* **1996**, *246*, 395−399.
[21] A. J. Atkins, A. J. Blake, M. Schröder, *J. Chem. Soc., Chem. Commun.* **1993**, 353−355.
[22] N. F. Curtis, R. W. Hay, *J. Chem. Soc., Chem. Commun.* **1966**, 524−525.
[23] M. Green, J. Smith, P. A. Tasker, *Inorg. Chim. Acta* **1971**, *5*, 17−24.
[24] K. N. Zelenin, V. V. Alekseyev, I. V. Ukraintsev, I. V. Tselinsky, *Org. Prep. Proc. Int.* **1998**, *30*, 53−61.
[25] R. F. Evans, *Aust. J. Chem.* **1967**, *20*, 1643−1661.
[26] E. Matter, *Helv. Chim. Acta* **1947**, *30*, 1114−1123.
[27] D. StC. Black, D. C. Craig, O. Giitsidis, R. W. Read, A. Salek, M. A. Sefton, *J. Org. Chem.* **1989**, *54*, 4771−4779.
[28] F. H. Allen, O. Kennard, D. G. Watson, L. Brammer, A. G. Orpen, R. Taylor, *J. Chem. Soc., Perkin Trans. 2* **1987**, S1−S19.
[29] S. Schmidt, L. Omnès, F. W. Heinemann, J. Kuhnigk, C. Krüger, A. Grohmann, *Z. Naturforsch.* **1998**, *53b*, 946−954.
[30] J. R. Röper, PhD Thesis, Darmstadt, **1990**.
[31] H.-M. Koepp, H. Wendt, H. Strehlow, *Z. Elektrochem.* **1960**, *64*, 483−491.
[32] O. Kahn, *Molecular Magnetism*; VCH, New York, **1993**.

Received September 20, 2000
[I00352]

Recent Developments in the Reactivity of Allenylidene and Cumulenylidene Complexes

Victorio Cadierno,[a] M. Pilar Gamasa,[a] and José Gimeno*[a]

Dedicated to Prof. Dr. José Barluenga on the occasion of his 60th birthday

Keywords: Allenylidene complexes / Cumulenylidene complexes / Carbene complexes / Vinylidene complexes / Alkynyl complexes

Allenylidene and higher cumulenylidene complexes [M]=C(=C)$_n$=CR^{1}R^2 (n = 1, 2, 3) have continuously gained significance in the context of transition metal carbene chemistry. Important developments which have been disclosed during the last two years are reviewed. These include a variety of stoichiometric and catalytic reactions of allenylidene complexes and their utility in organic synthesis. The related chemistry of butatrienylidene (n = 2) and pentatetraenylidene (n = 3) complexes as well as theoretical studies are also reviewed.

I. Introduction

The chemistry of transition metal carbene complexes has reached such a state of development so as to allow its wide use as one of the most powerful tools in modern organic synthesis.[1] Allenylidene (propadienylidene) complexes [ML$_n$]=C=C=CR^{1}R^2, which belong to the series of unsaturated carbene derivatives [ML$_n$]=C(=C)$_n$=CR^{1}R^2 ($n > 0$; cumulenylidene complexes), have received increasing interest during the last few years. Although the utility of these carbene complexes is still not comparable to that of the classical Fischer-type, both experimental and theoretical studies have been the subject of special attention.

The continuous growth of this chemistry stems mainly from:

a) The presence of an unsaturated carbon chain. Similar to the analogous polyinyl derivatives [ML$_n$]−(C≡C)$_n$−R, cumulenylidenes are potentially useful as precursors of molecular wires or polymers related to polyacetylene of interest in the field of novel materials with opto-electronic properties.[2]

b) The search for novel carbene complexes bearing unsaturated carbon moieties and/or other types of functional groups which can provide multifaceted reactive sites of interest in organic synthesis.

[a] Departamento de Química Orgánica e Inorgánica, Facultad de Química, Instituto Universitario de Química Organometálica "Enrique Moles" (Unidad Asociada al CSIC), Universidad de Oviedo,
33071 Oviedo, Spain
Fax: (internat.) + 34-985/103/446
E-mail: jgh@sauron.quimica.uniovi.es

Victorio Cadierno, born in Oviedo (Spain) in 1969, studied chemistry at the University of Oviedo and received his Ph.D. in 1996 working under the supervision of Prof. J. Gimeno. He then joined the group of Prof. J. P. Majoral at the Laboratoire de Chimie de Coordination du CNRS (Toulouse, France) for a two-year postdoctoral stay. Thereafter, he returned to the University of Oviedo where he is currently "Profesor Asociado". His research interests cover the activation of alkynes by transition metal complexes as well as the coordination chemistry of hemilabile phosphane ligands.

M. Pilar Gamasa, born in Pamplona (Spain), studied chemistry at the University of Zaragoza (Spain) and received her Ph.D. under the supervision of Prof. R. Usón. After two years of postdoctoral studies at the Georgia Institute of Technology (Atlanta, U.S.A.) with Prof. E. C. Ashby, she moved to the University of Oviedo (Spain) and became Associate Professor in 1985. Her research has been focused on the chemistry of transition metal carbonyl complexes and on the activation of alkynes and polyynes by transition metal complexes.

José Gimeno studied chemistry at the University of Zaragoza where he received his Ph.D. in 1973 and was promoted to Assistant Professor of Inorganic Chemistry in 1978. He has spent postdoctoral periods at the University of Athens, Georgia (1975−1977) and University of Regensburg (1981), working with Prof. R. B. King and Prof. W. A. Herrmann, respectively. In 1982 he became Professor of Inorganic Chemistry at the University of Oviedo. Since then his research work has been devoted to the study of the activation of terminal alkynes by transition metal complexes mainly of Group 8, including stoichiometric and catalytic processes of alkynyl, vinylidene, allenylidene and other unsaturated carbene complexes.

MICROREVIEWS: This feature introduces the readers to the authors' research through a concise overview of the selected topic. Reference to important work from others in the field is included.

 © WILEY-VCH Verlag GmbH, 69451 Weinheim, 2001 1434−1948/01/0303−0571 $ 17.50+.50/0

c) The recent discovery of the catalytic activity of allenylidene ruthenium(II) complexes in ring-closing metathesis (RCM) of olefins. These are more accessible catalysts than the classical Schrock-type and Grubbs' alkylidene derivatives.[3]

d) The synthetic accessibility of the cumulenylidene complexes $[ML_n]=C(=C)_n=CR^1R^2$ with higher unsaturation (n = 2, 3) which have also provided further reactivity patterns, albeit in a limited number.

The chemistry of allenylidene complexes and related species have been the subject of two general reviews[4a][4b] which cover the literature up to June 1998 including other specific surveys on rhodium, iridium[4c] and ruthenium complexes.[4d−4f] Brief accounts of the particular aspects of dinuclear and cluster species containing bridging allenylidene moieties have also appeared.[4g−4i] Since the discovery of the first allenylidene complexes $[M\{=C=C=CPh(NEt_2)\}(CO)_5]$ (M = Cr, W)[5a] and $[Mn(=C=C=Ct Bu_2)(\eta^5\text{-}C_5H_5)(CO)_2]$[5b] in 1976 several synthetic approaches have been reported.[4a,4b] Those with the greatest use follow essentially the strategy first used by Selegue for the preparation of $[Ru(=C=C=CPh_2)(\eta^5\text{-}C_5H_5)(PMe_3)_2][PF_6]$ which is based on the spontaneous dehydration of the hydroxyvinylidene species formed, either via **A** or via **B** (see Scheme 1), after the coordination of 2-propyn-1-ols at the metal center.[6]

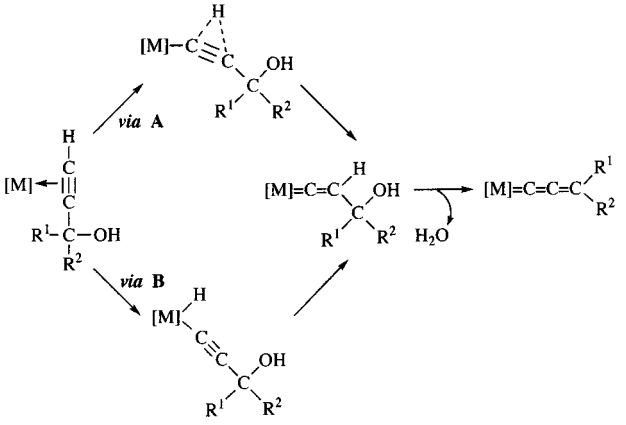

Scheme 1. Mechanism of the isomerization of 2-propyn-1-ols into allenylidene ligands

Large series of mono- and dinuclear derivatives containing half-sandwich (**A**) as well as octahedral (**B**) or square-planar (**C**) electron-rich metal fragments of Groups 6, 7, 8, and 9 have now been isolated (see Figure 1).[7] They are obtained in generally good yields as stable solids and have been fully characterized through the usual spectroscopic and/or diffractometric techniques. Octahedral Group 6 metal carbonyl derivatives $[M(=C=C=CR^1R^2)(CO)_5]$ are generally thermally unstable and the stabilization of the carbene moiety requires the presence of electron-releasing substituents ($R^1 = R^2 = p\text{-}NR'_2C_6H_4$, $p\text{-}OR'C_6H_4$, etc.). Furthermore, a short number of dinuclear and cluster complexes containing bridging allenylidene groups $[(M_nL_m)(\mu\text{-}\eta^x=C=C=CR^1R^2)_y]$ are also known.[4] More recently, cumulenylidene complexes of the type: (*i*) buta-1,2,3-trienylidenes $[ML_n]=C(=C)_2=CR^1R^2$ with $[ML_n]$ = *trans*-$[RuClL_2]^+$ [L_2 = bis(diphenylphosphanyl)methane (DPPM), bis(diethylphosphanyl)methane (DEPM), 1,2-bis(diphenylphosphanyl)ethane (DPPE)}, $[Ru(\eta^5\text{-}C_5H_5)L_2]^+$ {L = PPh_3, $P(OMe)_3$}, $[Fe(\eta^5\text{-}C_5Me_5)L_2]^+$ [L_2 = DPPE, 1,2-bis(diisopropylphosphanyl)ethane (DIPPE)], and (*ii*) penta-1,2,3,4-tetraenylidenes$[ML_n]=C(=C)_3=CR^1R^2$ with $[ML_n]$ = *trans*-$[RuCl(DPPE)_2]^+$, *trans*-$[RhCl(PiPr_3)_2]$, *trans*-$[IrCl(PiPr_3)_2]$, $[Cr(CO)_5]$, $[W(CO)_5]$ have also been described, the latter being prepared through the intermediate formation of $[M\{=C(=C)_5=CR^1R^2\}(CO)_5]$ (M = Cr, W).[4b]

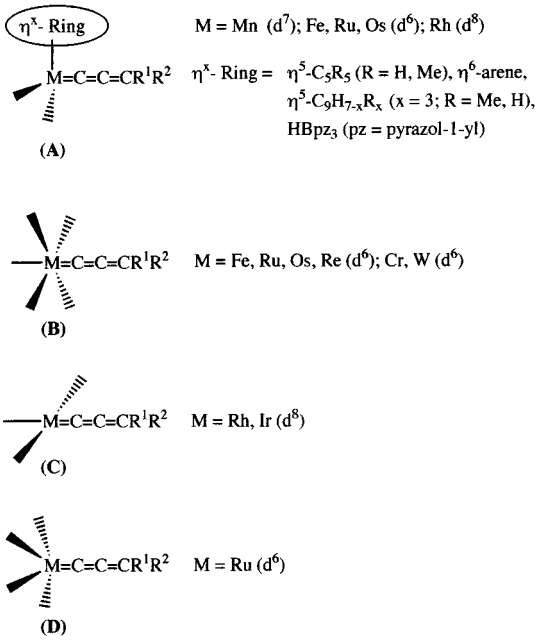

Figure 1. Stereochemistry of mononuclear allenylidenes

Although the first reactivity studies of allenylidene and higher cumulenylidene derivatives emerged simultaneously to their synthesis, their chemistry has grown rapidly and important developments have been disclosed after the period covered in the above-mentioned reviews. The present review will focus mainly on the reactivity studies of allenylidene complexes including stoichiometric and catalytic processes. Special attention will be devoted to the regioselective nucleophilic additions and the utility of these species in organic synthesis. It is worth mentioning the first coordinatively unsaturated Group 8 allenylidene complexes **D** (see Figure 1), some of them showing catalytic activity in RCM (ring-closing metathesis) of olefins.[8] Furthermore, recent advances in theoretical studies which shed light on the chemical behavior as well as a short account of novel structural and spectroscopic properties will be also discussed. Recent developments in the chemistry of related cumulenylidene complexes are also mentioned. This review covers the literature up to May 2000.

II. Structural and Spectroscopic Properties

II.1 X-ray Diffraction Studies

Structural parameters of novel allenylidene complexes studied by X-ray diffraction confirm the previously known features of the metal−allenylidene bonding. Thus, metal−carbon, $C_\alpha-C_\beta$, and $C_\beta-C_\gamma$ bond lengths are in accordance with the well-known description of the bonding as a resonance of metal−carbene and metal−alkynyl mesomers, the latter being the dominant contribution to the observed structures (zwitterionic species $[M]^- - C{\equiv}C-C^+R^1R^2$ for neutral allenylidene complexes):

$$[M]^+{=}C{=}C{=}CR^1R^2 \rightleftarrows [M]-C{\equiv}C-C^+R^1R^2$$

The first coordinatively unsaturated 16-electron allenylideneruthenium complexes, namely $[RuCl_2(=C=C=CPh_2)(PCy_3)_2]$ and $[RuCl_2(=C=C=CPh_2)(PCy_3)(IMes)]$ [IMes = 1,3-bis(2,4,6-trimethylphenyl)imidazol-2-ylidene], have now been described.[8] The crystal structures show that the allenylidene moiety is located at the apex and the ruthenium atom at the bottom of a square pyramid. The most relevant structural feature in both structures is the almost equal bond lengths Ru−C_α (ca. 1.79 Å) which are in the usual range found in other 16-electron carbeneruthenium complexes (1.76−1.84 Å).[9] These values contrast with the larger bond lengths shown by cationic 18-electron species $[Ru]^+{=}C{=}C{=}CR^1R^2$ (see below) indicating that the metal−allenylidene bond is stronger for the former complexes. This structural property is related to the lower catalytic activity of these complexes relative to that observed in the cationic 18-electron (arene)ruthenium complexes in ring-closing metathesis (RCM) reactions (see below). The bond lengths along the allenylidene chain are in the usual range for ruthenium complexes (see below). The allenylidene chain in $[RuCl_2(=C=C=CPh_2)(PCy_3)_2]$ shows an unusual bending [$C_\alpha-C_\beta-C_\gamma$ = 167.20(18)°] which is attributed to a C−H interaction with hydrogen atoms of the PCy_3 ligands.

The rest of the structures reported show M−C_α bond lengths in the 1.858(7)−1.943(8) Å range and $C_\alpha-C_\beta$ in the 1.221(9)−1.267(3) Å range, which compare well with those found previously (1.84−1.94 and 1.24−1.27 Å, respectively).[4a,4b] The allenylidene chain also shows the expected slightly bent linear arrangement (ca. 170−176°).[4a,4b] It should be noted that the *trans*-$[Ru(C{\equiv}CPh)(=C=C=CPh_2)(DPPE)_2][PF_6]$ complex shows bond lengths Ru−C_α [2.11(1) Å] and $C_\alpha-C_\beta$ [1.14(2) Å], unusually larger and shorter, respectively, than those found in analogous mononuclear ruthenium(II) complexes.[10]

Other X-ray crystal-structure determinations include:

A) Mononuclear Derivatives

a) Cationic complexes: (*i*) hexacoordinated ruthenium(II) complexes $[Ru(=C=C=CPh_2)(\eta^5\text{-}C_5Me_5)(PEt_3)_2][BF_4]$,[11] $[Ru\{=C=C=C(Me)(C_4H_3NMe\text{-}2)\}(\eta^5\text{-}C_5H_5)(PPh_3)_2][PF_6]$,[12] $[RuCl(=C=C=CPh_2)(\eta^6\text{-}p\text{-cymene})(IMes)][PF_6]$,[13] $[Ru(=C=C=CPh_2)(\eta^5\text{-TRIPOD})][PF_6]$ (TRIPOD = $CH_3C(CH_2\text{-}\eta^5\text{-}C_5H_4)(CH_2\text{-}\eta^1\text{-}PPh_2)_2$),[14] $[Ru(=C=C=CPh_2)\{HB(pz)_3\}(PPh_3)_2][PF_6]$ (pz = pyrazol-1-yl)[15] and $[RuCl(=C=C=CPh_2)(PPh_3)\{\kappa^3\text{-}N,N,N\text{-}(S,S)\text{-}i\text{Pr-PYBOX}\}][PF_6]$ {(*S,S*)-*i*Pr-PYBOX = 2,6-bis[4′-(*S*)-isopropyloxazolin-2′-yl]pyridine},[16] and (*ii*) the tetra-coordinated rhodium(I) complex *trans*-$[Rh(=C=C=CPh_2)(O=CMe_2)(P\textit{i}Pr_3)_2][PF_6]$.[17]

b) Neutral octahedral ruthenium(II) *fac,cis*-$[RuCl_2(=C=C=CPh_2)(PNP)]$ {PNP= $MeCH_2CH_2N(CH_2CH_2PPh_2)_2$},[18] $[RuCl_2(=C=C=CPh_2)(CO)(Sb\textit{i}Pr_3)_2]$[19] and square-planar iridium(I) *trans*-$[IrF(=C=C=CPh_2)(P\textit{i}Pr_3)_2]$[20] complexes.

B) Polynuclear Derivatives

a) Dinuclear cationic complexes of three types (Figure 2): (*i*) the osmium(II) derivative $[(\eta^5\text{-}C_5H_5)(PPh_3)_2Os\{=C=C=C(H)-C{\equiv}C-Os(\eta^5\text{-}C_5H_5)(PPh_3)_2\}][BF_4]$ (**A**);[21] (*ii*) the mixed-valence ruthenium(II)−ruthenium(III) complex $[Ru(=C=C=Rc)(\eta^5\text{-}C_5H_5)(DPPE)][BF_4]_2$ [Rc = $(\mu^2\text{-}\eta^6\text{:}\eta^5\text{-}C_5Me_4)Ru(\eta^5\text{-}C_5H_5)$] containing a half-sandwich ruthenium(III) fragment bonded to a (cyclopentadienylidene)ethylidene group which acts as the bridging chain to the (η^5-C_5H_5)Ru moiety (**B**).[22] Another example of this type is the dimetallic iron(II)−chromium(0) complex $[(CO)_2(\eta^5\text{-}C_5H_5)Fe(\mu\text{-}\eta^1\text{:}\eta^7\text{-}C_2C_7H_6)Cr(CO)_3][BF_4]$ (**C**) although structural parameters of the Fe−$C_\alpha-C_\beta-C_\gamma$ chain indicate that the bridging moiety can be better described as a substituted tropylium alkynyl group;[23] and (*iii*) the bis(allenylidene)dirhodium(I) complex $\{[(P\textit{i}Pr_3)_2\{Ph(o\text{-Tol})C=C=C=\}Rh]_2(\mu\text{-}1,3\text{-}N_3)\}^+$ (**D**) in which the two allenylidene groups, both rhodium atoms and the bridging azide ligand form an unusual eleven-membered chain.[24]

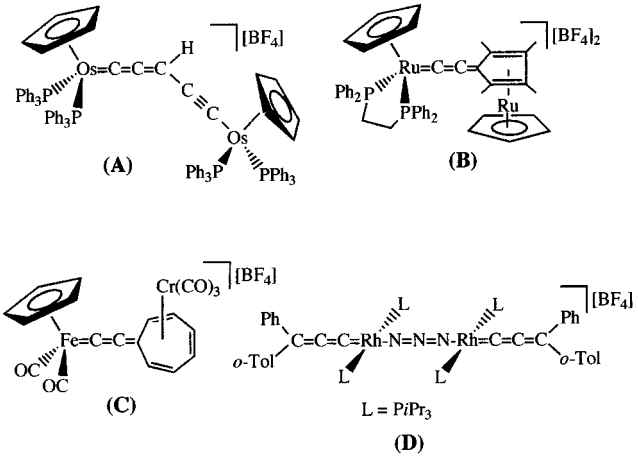

Figure 2. Some structures of dinuclear allenylidene complexes

b) Bridging cumulenylidene complexes (Figure 3): (*i*) The polynuclear complex $[Re(\eta^5\text{-}C_5Me_5)(NO)(PPh_3)(CCC)Os_3(CO)_9(\mu\text{-OMe})]$ (**A**) showing a bridging moiety Re=C=C−C in which the terminal carbon atom is bonded to the three osmium atoms and the center carbon atom binds to the osmium atom that is not methoxide-bridged. The ReCCC chain is highly distorted;[25] (*ii*) bridging butatrien-

ylidene pentanuclear ruthenium complexes $[Ru_5(\mu_5\text{-}CCCCH_2)(\mu_3\text{-}SMe)(\mu\text{-}SMe)(\mu\text{-}PPh_2)_2(CO)_{10}]$ (**B**) and $[Ru_5(\mu_5\text{-}CCCCH_2)(\mu\text{-}SMe)_2(\mu\text{-}PPh_2)_2(CO)_{11}]$ (**C**) in which the cumulenylidene ligand is attached to the cluster by three of its four carbon atoms;[26] (*iii*) trinuclear ruthenium clusters containing bridging μ_3-allenylidene ligands of the type **D**.[27] The X-ray crystal structures of a series of analogous derivatives containing Ru_3 and Ru_3Au cores have been also reported;[27] (*iv*) the Fe,Co mixed metal cluster of composition $[(\eta^5\text{-}C_5Me_5)Fe_2Co_4(\mu\text{-}C_4H)(CO)_{17}]$ (**E**) which consists of two triangular Fe_2Co and Co_3 cluster fragments linked by a C_4H bridge.[28] This moiety acts as a bridging allenylidene interacting with the Fe_2Co fragment as a μ_3-η^1(Fe):η^1(Fe):η^2(Co) ligand.

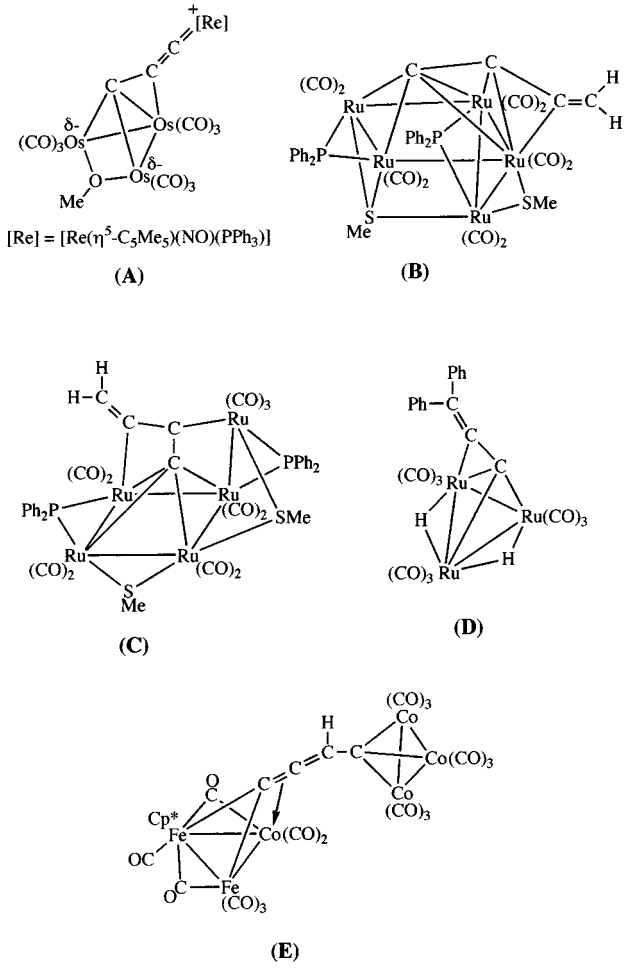

Figure 3. Some structures of polynuclear cumulenylidene complexes

Furthermore, the structures of the dinuclear complexes $[(DMPE)_2IMn{=}C{=}C{=}C{=}C{=}MnI(DMPE)_2][BPh_4]$ [DMPE = 1,2-bis(dimethylphosphanyl)ethane],[29a] $[(\eta^5\text{-}C_5Me_5)(DIPPE)Fe{=}C{=}C{=}C{=}C{=}Fe(DIPPE)(\eta^5\text{-}C_5Me_5)][PF_6]_3$[29b] and $[(\eta^5\text{-}C_5Me_5)(NO)(PPh_3)Re{=}C{=}C{=}C{=}Mn(CO)_2(\eta^5\text{-}C_5H_5)][BF_4]$[30] have also been determined by X-ray diffraction. They consist of a linear arrangement of the bridging cumulenylidene ligand with almost equal C=C distances (ca. 1.27−1.33 Å).

II.2 Spectroscopic Properties

II.2.1 IR and ^{13}C NMR

The infrared spectra of novel allenylidene complexes show the characteristic ν(C=C=C) strong absorption in the 1870−1971 cm^{-1} region. A lower frequency is observed (1803−1825 cm^{-1}) for the dinuclear $Ru^{III}-Ru^{II}$ complexes $[Ru(=C=C=Rc)(\eta^5\text{-}C_5H_5)L^1L^2][BF_4]_2$ [Rc = $(\mu^2\text{-}\eta^6{:}\eta^5\text{-}C_5Me_4)Ru(\eta^5\text{-}C_5H_5)$; $L^1 = L^2 = PPh_3$, L^1L^2 = DPPE] which seems to indicate that the unsaturated chain is intermediate between that of a vinylidene and an allenylidene moiety.[22] C_α chemical shifts and coupling constants *J*(CP) in the ^{13}C NMR spectra have been widely reported and generally used as one of the most relevant data to support the existence of the metal−carbene bond. As expected, typical low field signals are found in the range $\delta \approx 255-320$. The following features deserve to be mentioned: a) although the resonance for the dinuclear iron(II) complex $[(\eta^5\text{-}C_5H_5)(PPh_3)_2Fe\{=C=C=CH-C\equiv C-Fe(PPh_3)_2(\eta^5\text{-}C_5H_5)\}][BF_4]$ appears as usual ($\delta_{C\alpha}$ = 223.3), an high field chemical shift is shown by the corresponding resonance in the analogous osmium derivative ($\delta_{C\alpha}$ = 196.2);[21] b) a significant shielding effect on the C_α nucleus is observed in allenylidenes containing donor groups of the type *trans*-$[RuX\{=C=C=CR^1R^2\}(DPPE)_2][PF_6]$, i.e. X = Cl; R^1 = H; R^2 = *p*-$NMe_2C_6H_4$ ($\delta_{C\alpha}$ = 265.7) vs. X = Cl; R^1 = H; R^2 = Ph ($\delta_{C\alpha}$ = 321.07), X = Cl; $R^1 = R^2$ = *p*-$OMeC_6H_4$ ($\delta_{C\alpha}$ = 288.4) vs. X = Cl; $R^1 = R^2$ = Ph ($\delta_{C\alpha}$ = 308.58), and R^1 = H; R^2 = CH=CH(*p*-$NO_2C_6H_4$) ($\delta_{C\alpha}$ = 322.77);[10] c) although the order $\delta_{C\alpha} > \delta_{C\beta} > \delta_{C\gamma}$ is usually found for most of the allenylidene complexes, an inversion of the sequence of the chemical shifts has been reported in several cases, i.e. *trans*-$[IrX(P\mathit{i}Pr_3)_2]$ (X = OH, OPh, F; $\delta_{C\alpha}$ = 202.7−205.8, $\delta_{C\beta}$ = 252.8−273.9).[20]

II.2.2 Mössbauer Spectroscopy

^{57}Fe Mössbauer spectroscopic studies have been performed for mono- and dinuclear iron−allenylidene complexes by Lapinte et al.[31] The spectrum of the complex $[Fe\{=C=C=C(OMe)Me\}(\eta^5\text{-}C_5Me_5)(DPPE)][BPh_4]$ displays a quadrupole doublet at δ = 0.160 mm s^{-1} with a quadrupole splitting of ΔE_Q= 1.451 mm s^{-1}. These parameters are well-differentiated from those of analogous complexes containing iron−carbon single bonds with the conclusion that by using this spectroscopic technique, it is possible to identify the metal−carbon bonding order. The spectra of the bridging butatrienylidene complexes $[(\eta^5\text{-}C_5Me_5)L^1L^2Fe\{=C=C=C=C(H)Fe(\eta^5\text{-}C_5Me_5)(CO)_2\}][BF_4]$ (L^1L^2 = DPPE, DIPPE) at 80 K show two quadrupole doublets δ = 0.161−0.257 and 0.029 mm s^{-1} (ΔE_Q= 1.973−1.264 and 1.974−1.778 mm s^{-1}, respectively) which are characteristic of iron dinuclear species with two different coordination environments around the metal atoms.[32] The doublet with the larger isomeric shift was assigned to the $[(\eta^5\text{-}C_5Me_5)L^1L^2Fe]$ fragment. These values are consistent with a weak Fe=C π-bond which is in agreement with the electron delocalization along the cumulenylidene chains

in which significant contributions of the mesomers [Fe]−C^+=C=C=C(R)−[Fe] and [Fe]−C≡C−C^+=C(R)−[Fe] are present.

III. Theoretical Studies

Since the early studies by Hoffman[33] using the half-sandwich complex [Mn(=C=C=CH_2)(η^5-C_5H_5)(CO)$_2$] as a model, a series of theoretical calculations on allenylidene complexes involving several metallic fragments have now been reported. These studies, performed using the Extended Hückel Molecular Orbital (EHMO) methodology, generally confirm the initial results obtained on the electronic structure[33] and on the reactivity[34] which establish: (*i*) the most stable conformation of the allenylidene group =C=C=CR^1R^2 is that contained in the molecular plane, (*ii*) the allenylidene fragment is a σ-donor π-acceptor ligand with a dominant contribution to the bonding of the latter component, and (*iii*) the carbon atoms of the unsaturated chain are alternatively electron-poor and electron-rich, starting from the metal center. Hence, electrophilic centers are located at the C_α and C_γ atoms while the C_β atom is a nucleophilic site.

Table 1 collects quantitative data of the LUMO and HOMO distribution, as well as net charges at the carbon atoms of the allenylidene chain on a series of cationic ruthenium and osmium(II) as well as the neutral [OsCl(=C=C=CH_2)(η^5-C_5H_5)(PH_3)] models. On the basis of these data, the following points deserve to be highlighted: (*i*) the LUMO distribution along the C_3 chain (20−28% C_α; 30−37% C_γ) is similar, regardless of the nature of the metal (Ru or Os) and the auxiliary ligands, (*ii*) total charge transfer from the metallic fragments [OsCl(η^5-C_5H_5)(PH_3)] and [Os(η^5-C_5H_5)(PH_3)$_2$]$^+$ is similar and higher (ca. 57−60%) than that of [Os(η^5-C_5H_5)(CO)(PH_3)]$^+$, (*iii*) the fragment [Ru(η^5-C_9H_7)(PH_3)$_2$]$^+$ shows total charge-transfer values which are notably higher (ca. 69−86%) than those of [Ru(η^5-C_9H_7)(CO)(PH_3)]$^+$ and [Ru(η^5-1,2,3-$Me_3C_9H_4$)(CO)(PH_3)]$^+$, respectively.

These results allow the rationalization of the reactivity of these species which can be classified, depending on the type of addition, as electrophilic and nucleophilic allenylidenes. It is worth mentioning the versatile chemical behavior of [Os(=C=C=CPh_2)(η^5-C_5H_5)(P*i*Pr$_3$)$_2$][PF_6], which probably arises from the particular total charge-transfer value and its cationic character which is able to undergo both electrophilic and nucleophilic additions (see below).[38] As a general trend, it can be observed that the cationic complexes undergo orbitally controlled nucleophilic additions at either C_α and C_γ atoms, and that the regioselectivity depends on the steric and/or electronic properties of the ancillary ligands (see below).

EHMO calculations have also been performed for a bridging (allenylidene)dirhodium(I) complex, using [Rh_2(μ-OOCH)(μ-σ,σ-C=C=CH_2)(CO)$_2$(PH_3)$_2$]$^+$ as a model, showing that the allenylidene ligand also behaves as a good π-acceptor ligand, the highest negative charge being located at the C_α atom.[39] This charge is found to decrease towards the C_γ atom. Brief accounts of theoretical calculations on the dinuclear complexes [(η^5-C_5H_5)(PH_3)$_2$Ru{=C=C=C(H)−C≡C−Ru(PH_3)$_2$(η^5-C_5H_5)}]$^+$ [21] and [(PH_3)$_4$IMn=C=C=C=C=MnI(PH_3)$_4$][29a] have also been reported. More recently,[40] density-functional calculations have been performed on the metallacumulenylidene complexes [Cr{(=C)$_n$$H_2$}(CO)$_5$] ($n$ = 2−9) showing, as for the above-mentioned examples, that the electrophilic and nucleophilic attacks are frontier orbital controlled. Dissociation energies have been calculated and found to be essentially independent of the chain length.

IV. Reactivity of Cationic Allenylidene Complexes

As shown in previous theoretical and experimental studies,[4a,4b] the reactivity of novel cationic transition-metal allenylidene derivatives is mainly governed by the electron-deficient character of the C_α and C_γ carbon atoms in the cumulene chain, which are therefore subject to nucleophilic attacks. The regioselectivity of the nucleophilic additions seems to be controlled by the electronic and steric properties both of the substituents on the unsaturated hydrocarbon chain and the ancillary ligands on the metal atom and the nucleophile used (see below). Additions of electrophiles at the nucleophilic C_β atom of neutral allenylidene derivatives are scarce,[4a−4b] the protonation of the diphenylallenylidene osmium(II) complex [Os(=C=C=CPh_2)(η^5-C_5H_5)(P*i*Pr$_3$)$_2$][PF_6] with HPF_6 to give the alkenylcarbyne [Os{≡C−C(H)=CPh_2}(η^5-C_5H_5)(P*i*Pr$_3$)$_2$][PF_6]$_2$ being the only example of an electrophilic addition in a cationic complex reported to date.[38]

Table 1. LUMO and HOMO distribution and net charges of the allenylidene chain on half-sandwich Ru^{II} and Os^{II} complexes

Model	HOMO (%)			LUMO (%)			Net charges			Ref.
	C_α	C_β	C_γ	C_α	C_β	C_γ	C_α	C_β	C_γ	
[Ru(η^5-C_9H_7)(PH_3)$_2$]$^+$	3	21	0	20	6	34	−0.352	−0.151	−0.048	[35]
[Ru(η^5-C_9H_7)(CO)(PH_3)]$^+$	4	21	0	24	4	37	−0.267	−0.118	0.033	[36a]
[Ru(η^5-1,2,3-$Me_3C_9H_4$)(CO)(PH_3)]$^+$	4[a]	21[a]	0[a]	23	4	36	−0.281	−0.118	0.023	[36b]
[Ru(η^5-C_5H_5)(CO)(PH_3)]$^+$	[b]	20	[b]	23	6	31	−0.36	−0.13	−0.05	[37]
[OsCl(η^5-C_5H_5)(PH_3)]	4	22	0	24	5	30	−0.46	−0.07	−0.17	[38]
[Os(η^5-C_5H_5)(PH_3)$_2$]$^+$	4	25	0	24	5	31	−0.41	−0.10	−0.15	[38]
[Os(η^5-C_5H_5)(CO)(PH_3)]$^+$	5	23	0	28	3	33	−0.33	−0.08	−0.09	[38]

[a] Next HOMO. − [b] C_α + C_γ = 6%.

IV.1 Additions of Neutral Nucleophiles

IV.1.1 Alcohols

One of the most remarkable reactions of cationic allenylidene complexes is the nucleophilic addition of alcohols to afford Fischer-type α,β-unsaturated alkoxycarbene derivatives of general formula $[M]^+=C(OR^1)-C(H)=CR^2R^3$.[4a−4b] The regioselectivity of the addition is in agreement with the formation of allenyl species $[M]-C(HO^+R^1)=C=CR^2R^3$ as intermediates or transition states. This oxygen−C_α interaction labilizes the O−H bond, favoring the migration of the hydrogen atom to C_β. The ability of the allenylidene ligand to undergo these nucleophilic attacks is clearly dependent on the electronic and steric nature of the ancillary ligands on the metal atom.[4a−4b] This is nicely illustrated by the behavior of indenylruthenium(II)−allenylidene complexes. Thus, while the disubstituted derivatives $[Ru(=C=C=CR^2R^3)(\eta^5\text{-}1,2,3\text{-}R^1_3C_9H_4)L^1L^2]^+$ (R^1 = H, $L^1 = L_2 = PPh_3$, L^1L^2 = DPPE, DPPM, $R^2 = R^3$ = Ph, $R^2R^3 = C_{12}H_8$; R^1 = Me, L^1L^2 = DPPM, $R^2 = R^3$ = Ph) are unreactive towards alcohols,[41,42] the diphenylallenylidene complexes $[Ru(=C=C=CPh_2)(\eta^5\text{-}1,2,3\text{-}Me_3C_9H_4)(CO)(PR_3)]^+$ (PR_3 = PPh_3, P*i*Pr$_3$, PCy_3) containing the less sterically demanding and more π-accepting CO/PR_3 combination react with methanol or ethanol to yield the alkenyl(alkoxy)carbene derivatives $[Ru\{=C(OR^1)-C(H)=CPh_2\}(\eta^5\text{-}1,2,3\text{-}Me_3C_9H_4)(CO)(PR_3)][BF_4]$ (**1**) (Scheme 2).[42,43] It should be noted that the diphenylallenylidenes $[RuCl(=C=C=CPh_2)(\eta^6\text{-}p\text{-cymene})(PR_3)][PF_6]$ (PR_3 = PCy_3, P*i*Pr$_3$, PPh_3), used recently by Dixneuf and co-workers as active catalysts for the RCM of olefins, are also unreactive towards alcohols.[44]

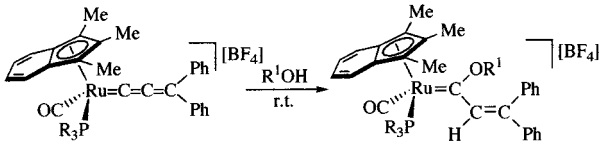

R^1 = Me, PR_3 = PPh_3, P*i*Pr$_3$, PCy_3 **1**
R^1 = Et, PR_3 = PPh_3, P*i*Pr$_3$

Scheme 2. Synthesis of (1,2,3-trimethylindenyl)ruthenium(II)−(alkenyl)(alkoxy)carbene complexes

There is also an influence of the allenylidene substituents in the reactivity of the corresponding complexes towards alcohols. This fact is clearly shown in the formation of the Fischer-type carbene complexes $[Ru\{=C(OMe)-C(H)=C(H)R\}(\eta^5\text{-}C_9H_7)L^1L^2][PF_6]$ (R = Ph, L^1L^2 = DPPE, DPPM; R = H, L^1L^2 = DPPM) which are readily obtained by the reaction of $[RuCl(\eta^5\text{-}C_9H_7)L^1L^2]$ with HC≡CCH(OH)R and $NaPF_6$ in methanol by nucleophilic attack of the alcohol on the unstable allenylidene intermediates $[Ru\{=C=C=C(H)R\}(\eta^5\text{-}C_9H_7)L^1L^2][PF_6]$.[41] The related methoxycarbene derivatives $[Ru\{=C(OMe)-C(H)=CMe_2\}(\eta^6\text{-}C_6Me_6)(MDMPP\text{-}P,O)][PF_6]$[MDMPP-*P*,*O* = P(2-*O*-6-MeOC$_6$H$_3$)Ph$_2$],[45] $[RuCl\{=C(OMe)-C(H)=CPh_2\}(PPh_3)\{\kappa^3\text{-}N,N,N(PYBOX)\}][PF_6]$ [PYBOX = 2,6-bis(dihydrooxazolin-2′-yl)pyridine],[16] and $[Re\{=C(OMe)-C(H)=C(H)Me\}(TRIPHOS)(CO)_2][CF_3SO_3]$ [TRIPHOS = 1,1,1-tris(diphenylphosphanylmethyl)ethane][46] have recently been obtained following this simple synthetic procedure. In addition, the methoxy(methoxyethyl)carbene complex $[Re\{=C(OMe)CH_2CH_2(OMe)\}(TRIPHOS)(CO)_2][CF_3SO_3]$ has been prepared by treatment of hydroxyvinylidene $[Re\{=C=C(H)CH_2(OH)\}(TRIPHOS)(CO)_2][CF_3SO_3]$ with methanol, through a concerted dehydration followed by a double addition of MeOH to the C_α and C_γ atoms of the transient allenylidene $[Re(=C=C=CH_2)(TRIPHOS)(CO)_2][CF_3SO_3]$.[46]

The reaction of $[Ru(=C=C=CPh_2)(\eta^5\text{-}C_5H_5)(CO)(P\text{-}iPr_3)][BF_4]$ with propargyl alcohol is of particular interest. The addition gives the α,β-unsaturated (propargyloxy)carbene complex $[Ru\{=C(OCH_2C{\equiv}CH)-C(H)=CPh_2\}(\eta^5\text{-}C_5H_5)(CO)(PiPr_3)][BF_4]$ (**2**) which reacts with bases to afford a mixture of rare cycloaddition products including **6**, **8**, **9**, and **10** (Scheme 3),[47] the main components of the mixture being dependent on the nature of the base used. The following mechanism is proposed: (*i*) formation in the first step of the (allenyloxy)carbene intermediate **3** by a base-catalyzed isomerization of the propargylic unit into an allenic moiety, (*ii*) an intramolecular Diels−Alder reaction within complex **3** to give the unstable tricyclic alkoxycarbene **4** (the $C_\beta-C_\gamma$ double bond and one of the phenyl groups of the alkenyl unit act as an inner-outer ring diene and the $C=CH_2$ fragment of the alkoxy group acts as a dienophile) and (*iii*) subsequent 1,3-hydrogen shift from the methylene group of the central ring to the OCH= carbon atom on **4** would give carbene intermediate **5** which by aromatization should yield the stable complex **6**. Formation of **8** and **9** has been explained by taking into account that a deprotonation process occurs on **5** to produce the tricyclic alkenyl derivative **7**, which could evolve both by a 1,3- or 1,5-hydrogen shift, respectively. Complex **10** seems to be the result of a concerted intramolecular proton-transfer reaction within the heterocycle of **9**.

IV.1.2 Amines

By analogy with the above-mentioned reactions, the addition of primary or secondary amines to a cationic allenylidene ligand should afford aminocarbene complexes $[M]^+=C(NR^1R^2)-C(H)=CR^3R^4$. In this context, Esteruelas and co-workers have recently described the reactivity of $[Ru(=C=C=CPh_2)(\eta^5\text{-}C_5H_5)(CO)(PiPr_3)][BF_4]$ towards secondary and primary amines.[48] As expected, addition of the N−H bond of the amines to the $C_\alpha-C_\beta$ double bond of the allenylidene group takes place, yielding complexes **11** and **12** (Scheme 4). Nevertheless, structural studies as well as theoretical calculations seem to indicate that these complexes are better described as azoniabutadienyl species, where the contribution of the aminocarbene resonance form is not relevant. Once again, the regioselectivity of these nucleophilic attacks seems to be governed by the steric bulk of the ligands present at the metal center, since the cationic alkynyl derivative $[Ru\{C{\equiv}CCPh_2(NHMe_2)\}(\eta^5\text{-}C_5H_5)(PPh_3)_2][PF_6]$ was quantitatively obtained when

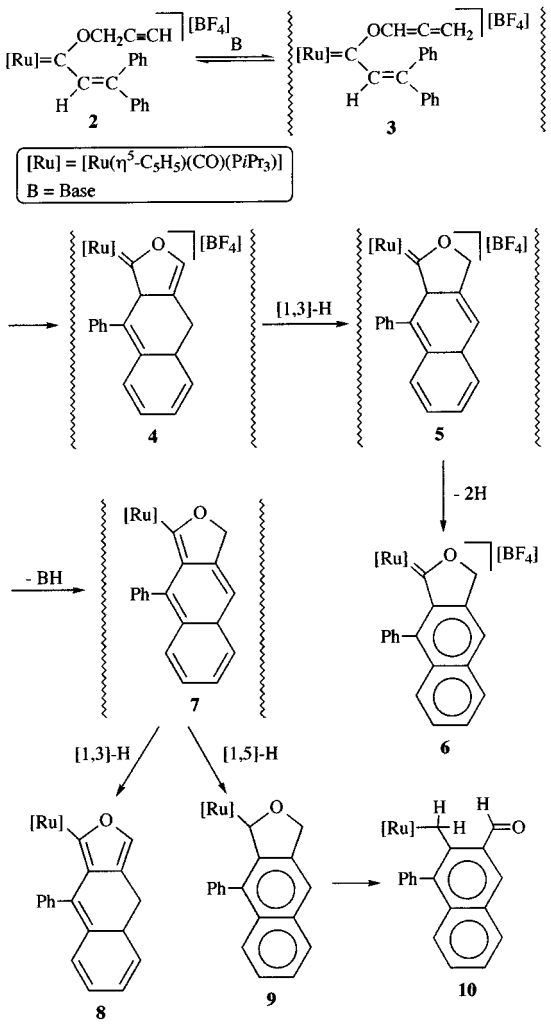

Scheme 3. Synthesis of polycyclic ruthenium(II) complexes starting from $[Ru(=C=C=CPh_2)(\eta^5\text{-}C_5H_5)(CO)(P\mathit{i}Pr_3)][BF_4]$

$[Ru(=C=C=CPh_2)(\eta^5\text{-}C_5H_5)(PPh_3)_2][PF_6]$ was dissolved in neat dimethylamine.[49] The marked difference in behavior between the tertiary and secondary azoniabutadienyl complexes **11** and **12** should be noted. Thus, while deprotonation of **11** takes place on the $CH{=}CPh_2$ group to yield aminoallenyl derivatives **13**, deprotonation of **12** occurs selectively at the nitrogen atom affording azabutadienyl complexes **14** (Scheme 4).[48]

The reactivity of the cationic Rh^I−diphenylallenylidene derivative *trans*-$[Rh(=C=C=CPh_2)(O=CMe_2)(P\mathit{i}Pr_3)_2][PF_6]$ towards pyridine and ammonia has also been explored.[17] Surprisingly, in this case no addition of the amine on the allenylidene chain was observed, giving instead acetone substitution products i.e. *trans*-$[Rh(=C=C=CPh_2)(Py)(P\mathit{i}Pr_3)_2][PF_6]$ and *trans*-$[Rh(=C=C=CPh_2)(NH_3)(P\mathit{i}Pr_3)_2][PF_6]$. In addition, treatment of complexes *trans*-$[RuCl\{=C=C=C(OMe)CH_2Ph\}(DPPE)_2][PF_6]$[50] and $[Re\{=C=C=C(Me)Ph\}(TRIPHOS)(CO)_2][CF_3SO_3]$,[46] containing an acidic hydrogen atom at C_δ, with triethylamine exclusively yields neutral enynyl derivatives *trans*-$[RuCl\{C{\equiv}C{-}C(OMe){=}C(H)Ph\}(DPPE)_2]$ and $[Re\{C{\equiv}C{-}C(Ph){=}CH_2\}(TRIPHOS)(CO)_2]$, respectively, as the result of a deprotonation process.

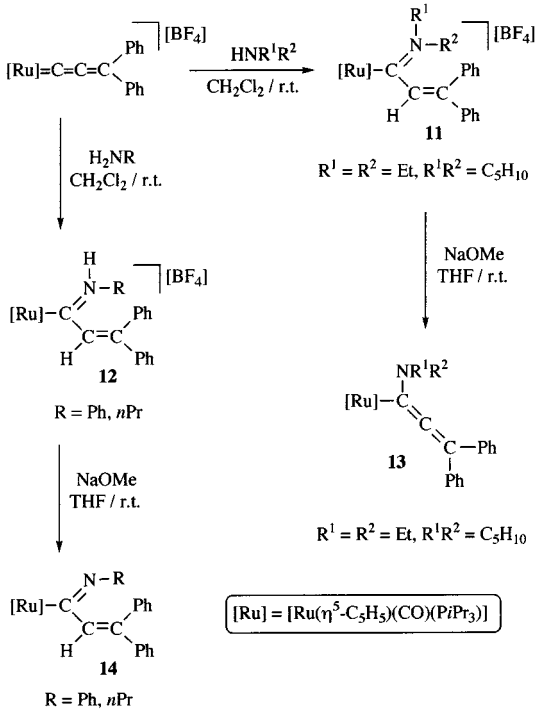

Scheme 4. Preparation of (azoniabutadienyl)-, (aminoallenyl)- and (azabutadienyl)Ru^{II} complexes

IV.1.3 Phosphanes

a) Phosphonioalkynyl and -allenyl Complexes: The nucleophilic attack of phosphanes on allenylidene complexes is a well-documented reaction.[4a−4b] Thus, we have found that indenylruthenium(II)−allenylidene complexes $[Ru\{=C=C=C(R^2)Ph\}(\eta^5\text{-}1,2,3\text{-}R'_3C_9H_4)L^1L^2]^+$ (R^1 = H, R^2 = Ph, $L^1 = L^2 = PPh_3$, L^1L^2 = DPPE, DPPM, L^1 = CO, $L^2 = P\mathit{i}Pr_3$; R^1 = H, R^2 = H, $L^1 = L^2 = PPh_3$; R^1 = Me, R^2 = Ph, L^1 = CO, $L^2 = PPh_3$, $P\mathit{i}Pr_3$) undergo regioselective additions of tertiary phosphanes at the C_γ atom, affording cationic phosphonioalkynyl complexes **15** in excellent yields (Scheme 5).[43,51] The related phosphonioalkynyl derivatives $[Ru\{C{\equiv}CCR^1R^2(PPh_3)\}(\eta^5\text{-}C_9H_7)(PPh_3)_2][PF_6]$ (R^1 = R^2 = H; CR^1R^2 = cyclopentyl, cyclohexyl) and $[Ru\{C{\equiv}CC(H)Ph(PPh_3)\}(\eta^5\text{-}1,2,3\text{-}Me_3C_9H_4(CO)(PPh_3)][BF_4]$ were obtained in a one-pot synthesis by reaction of halide complexes $[RuCl(\eta^5\text{-}C_9H_7)(PPh_3)_2]$ and $[RuBr(\eta^5\text{-}1,2,3\text{-}Me_3C_9H_4)(CO)(PPh_3)]$ with the corresponding propargyl alcohol in the presence of $NaPF_6$ or $AgBF_4$ and a large excess of PPh_3.[43,52,53] These nucleophilic additions seem to be controlled not only by the steric properties of the metallic fragments but also both by the cone angle of the phosphane and the size of the allenylidene substituents. Thus, complexes $[Ru\{C{\equiv}CCPh_2(PMe_3)\}(\eta^5\text{-}C_9H_7)(DPPM)][PF_6]$ and $[Ru\{C{\equiv}CCPh_2(PMe_3)\}(\eta^5\text{-}1,2,3\text{-}Me_3C_9H_4)(CO)(PPh_3)][BF_4]$ slowly isomerize at room temperature to give the thermodynamically more stable phosphonioallenyl derivatives $[Ru\{C(PMe_3){=}C{=}CPh_2\}(\eta^5\text{-}C_9H_7)(DPPM)][PF_6]$[51] and

[Ru{C(PMe$_3$)=C=CPh$_2$}(η^5-1,2,3-Me$_3$C$_9$H$_4$)(CO)(PPh$_3$)][BF$_4$],[43] respectively, while [Ru{C(PMe$_2$Ph)=C=CPh$_2$}(η^5-C$_9$H$_7$)(DPPM)][PF$_6$][51] and [Ru{C(PR$_3$)=C=CPh$_2$}(η^5-C$_5$H$_5$)(CO)(P*i*Pr$_3$)][BF$_4$] (PR$_3$ = PPh$_3$, PMePh$_2$, PHPh$_2$)[54] were obtained regioselectively when allenylidenes [Ru(=C=C=CPh$_2$)(η^5-C$_9$H$_7$)(DPPM)][PF$_6$] and [Ru(=C=C=CPh$_2$)(η^5-C$_5$H$_5$)(CO)(P*i*Pr$_3$)][BF$_4$] were treated with the appropriate phosphane. Related phosphanylalkynyl complexes [Ru{C≡CCR^{1}R^2(PEt$_3$)}(η^5-C$_5$Me$_5$)(PEt$_3$)$_2$][BPh$_4$] (R^1 = R^2 = Me; CR^{1}R^2 = cyclohexyl) were recently synthesized in low yields, by the direct activation of HC≡CC(OH)R^{1}R^2 by [RuCl(η^5-C$_5$Me$_5$)(PEt$_3$)$_2$] without an external source of PEt$_3$.[11] Apparently, phosphane dissociation occurs to some extent in solution, reacting with transient [Ru(=C=C=CR^{1}R^2)(η^5-C$_5$Me$_5$)(PEt$_3$)$_2$][BPh$_4$] species.

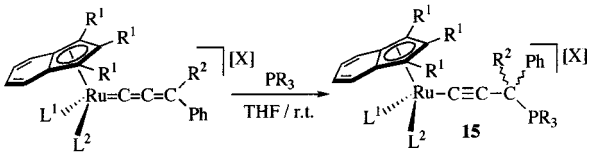

R^1 = H, R^2 = H, L^1 = L^2 = PPh$_3$, PR$_3$ = PMe$_3$, PMe$_2$Ph, PMePh$_2$, PPh$_3$, X = PF$_6^-$
R^1 = H, R^2 = Ph, L^1 = L^2 = PPh$_3$, PR$_3$ = PMe$_3$, PMe$_2$Ph, X = PF$_6^-$
R^1 = H, R^2 = Ph, L^{1}L^2 = DPPE, DPPM, PR$_3$ = PMe$_3$, X = PF$_6^-$
R^1 = H, R^2 = Ph, L^1 = CO, L^2 = P*i*Pr$_3$, PR$_3$ = PMe$_3$, X = BF$_4^-$
R^1 = Me, R^2 = Ph, L^1 = CO, L^2 = PPh$_3$, P*i*Pr$_3$, PR$_3$ = PMe$_3$, X = BF$_4^-$

Scheme 5. Synthesis of indenylruthenium(II)−phosphanylalkynyl complexes

b) Synthetic Utility of Phosphonioalkynyl Complexes: We have exploited the synthetic utility of the readily available indenylruthenium(II)−phosphonioalkynyl complexes [Ru{C≡CC(R^1)H(PR$_3$)}(η^5-C$_9$H$_7$)(PPh$_3$)$_2$][PF$_6$] (R^1 = H, PR$_3$ = PPh$_3$; R = Ph, PR$_3$ = PMe$_3$) containing an acidic hydrogen atom at C$_\gamma$. These complexes are suitable precursors for the high-yield preparation of a wide series of neutral enynyl and polyenynyl complexes **16** (Scheme 6) by means of Wittig-type processes with carbonyl compounds.[55,56] When aldehydes are used, inseparable mixtures of the corresponding (*E*) and (*Z*) stereoisomers are obtained. The polyenynyl skeleton in complexes **16** should be an excellent pathway for electron delocalization between the electron-rich metal fragment [Ru(η^5-C$_9$H$_7$)(PPh$_3$)$_2$] and terminal functional groups. We therefore carried out a series of Wittig reactions using unsaturated aldehydes and ketones bearing strong electron-accepting end groups (e.g. *p*-NO$_2$C$_6$H$_4$, *p*-CNC$_6$H$_4$) or efficient bridging groups (e.g. C≡N, pyridine), capable of coordinating metallic acceptor fragments [e.g. Cr(CO)$_5$, W(CO)$_5$]. As expected, the resulting donor−acceptor enynyl and polyenynyl complexes are of interest as materials with good second-order nonlinear optical (NLO) properties exhibiting high values of the molecular quadratic hyperpolarizability coefficient (β).[52]

We have also shown that protonation of these polyunsaturated alkynyl derivatives proceeds regioselectively at the C$_\beta$ atom of the alkynyl group affording unprecedented cationic

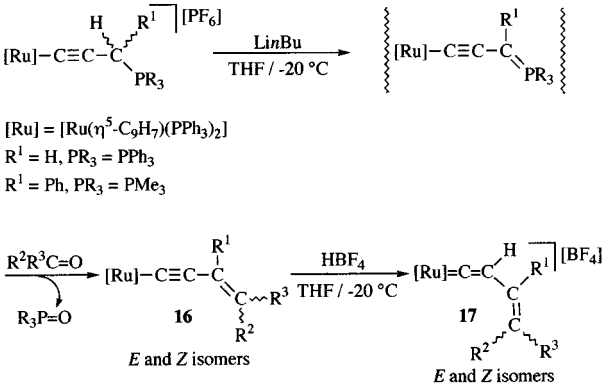

Scheme 6. Synthesis of indenylruthenium(II)−enynyl, −polyenynyl, −vinylvinylidene, and −polyenylvinylidene complexes

vinylvinylidene and polyenylvinylidene species **17** (Scheme 6).[55,56] Vinylvinylidene complexes **17** are of interest in organic synthesis. Heating at reflux in acetonitrile stereoselectively generates the corresponding terminal (*E*)-1,3-enynes **19** and the cationic nitrile complex [Ru(η^5-C$_9$H$_7$)(N≡CMe)(PPh$_3$)$_2$][BF$_4$] (**20**) (Scheme 7).[56] This reaction can be explained taking into account that vinylvinylidenes **17** are in equilibrium with their η^2-coordinated 1,3-enyne tautomers [Ru{η^2-HC≡CC(R^1)=CR^{2}R^3}(η^5-C$_9$H$_7$)(PH$_3$)$_2$][BF$_4$] (**18**). The rapid substitution of the labile coordinated enyne by the more basic acetonitrile ligand favors the displacement of the equilibrium to afford the final species **19** and **20**. Ab initio molecular orbital (MO) calculations on the model [Ru(=C=CH$_2$)(η^5-C$_9$H$_7$)(PH$_3$)$_2$]$^+$ are consistent with the experimental results.

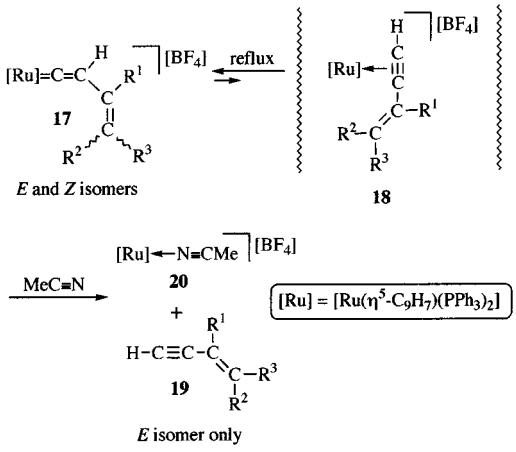

Scheme 7. Synthesis of terminal (*E*)-1,3-enynes starting from indenylruthenium(II)−vinylvinylidene complexes

In summary, it was shown that indenylruthenium(II)−allenylidene complexes are useful precursors for the syn-

thesis of functionalized terminal alkynes. Schemes 6 and 7 show a systematic synthetic approach which allows the isolation of free alkynes in good yields, recovering the metallic fragment quantitatively.

IV.2 Additions of Anionic Nucleophiles: Synthesis of Neutral Alkynyl Complexes [M]−C≡C−C(Nu)R^1R^2

IV.2.1 Heteroanions

In marked contrast to alcohols, alcoholates $[R^1O]^-$ add regioselectively at the C_γ atom of cationic allenylidene complexes to afford neutral alkynyl derivatives of general formula [M]−C≡C−C(OR^1)R^2R^3.[4a−4b] Complexes [Ru{C≡CC(OR)Ph_2}(η^5-C_5H_5)L^1L^2] [L^1 = L^2 = PPh_3, R = Me; L^1 = PPh_3, L^2 = $PPh_2CH_2C(=O)tBu$, R = Me, Et; L^1 = CO, L^2 = P*i*Pr_3, R = Me],[49,54,57] [Ru{C≡CC(OMe)Ph_2}(η^5-C_9H_7)L^1L^2] [L^1 = L^2 = PPh_3; L^1L^2 = DPPE, DPPM; L^1 = CO, L^2 = P*i*Pr_3; L^1 = PPh_3, L^2 = $PPh_2CH_2C(=O)t$-Bu],[43,51,57] [Ru{C≡CC(OMe)Ph_2}(η^5−1,2,3-$Me_3C_9H_4$)(CO)(PPh_3)],[42] [Ru{C≡CC(OMe)$C_{13}H_{20}$}(η^5-C_9H_7)(PPh_3)$_2$],[58] [Ru{C≡CC(OMe)Ph_2} {HB(pz)$_3$}(PPh_3)$_2$],[15] *trans*-[Ru{C≡CC(OMe)Ph_2}(C≡CR)(DPPE)$_2$] (R = Ph, *p*-$OMeC_6H_4$)[10] and [Os{C≡CC(OMe)Ph_2}(η^5-C_5H_5)(P*i*Pr_3)$_2$][38] have recently been synthesized in high yields by treatment of the appropriate allenylidene complex with the corresponding sodium or potassium alkoxide. No isomerization of these alkynyl derivatives into alkoxyallenyl species [M]−C(OR^1)=C=CR^2R^3 has been reported. The inverse regioselectivity observed with these hard nucleophiles seems to be charge-controlled (see Table 1). In agreement with this, theoretical calculations carried out by Esteruelas and co-workers on the model complexes [Ru{C≡CC(OMe)H_2}(η^5-C_5H_5)(CO)(PH_3)] and [Ru{C(OMe)=C=CH_2}(η^5-C_5H_5)(CO)(PH_3)] indicate that the former is approximately 9.29 kcal/mol more stable than the latter.[54] Although neutral alkynyl derivatives usually react with electrophiles at the β-position to produce cationic vinylidene complexes,[4a] protonation of these methoxyalkynyl species regenerates the starting allenylidenes in almost quantitative yields.

The related alkynyl complexes [Ru{C≡CC(OH)Ph_2}(η^5-C_5H_5)(CO)(P*i*Pr_3)] and *trans*-[Ru{C≡CC(H)Ph_2}(C≡CPh)(DPPE)$_2$] have also been regioselectively obtained by the reaction of [Ru(=C=C=CPh_2)(η^5-C_5H_5)(CO)(P*i*Pr_3)][BF_4] and *trans*-[Ru(C≡CPh){=C=C=CPh_2}(DPPE)$_2$][PF_6] with KOH and $NaBH_4$, respectively.[10,54] The cationic (diphenylallenylidene)rhodium(I) derivative *trans*-[Rh(=C=C=CPh_2)(O=CMe_2)(P*i*Pr_3)$_2$][PF_6] also undergoes substitution of the labile acetone ligand when treated with sodium acetate or potassium hydroxide, yielding neutral allenylidenes *trans*-[Rh(=C=C=CPh_2){κ^1(*O*)-COOMe}(P*i*Pr_3)$_2$] and *trans*-[Rh(=C=C=CPh_2)(OH)(P*i*Pr_3)$_2$], respectively.[17]

In our laboratory we have explored the reactivity of indenylruthenium(II)−allenylidene compounds towards N-donor hard nucleophiles such as amides or azides and we have found that complexes [Ru(=C=C=CPh_2)(η^5-1,2,3-$R^1_3C_9H_4$)(CO)L][BF_4] (R^1 = H, L = P*i*Pr_3; R^1 = Me, L = PPh_3, P*i*Pr_3) react with lithium (*S*)-α-methylbenzylamide or lithium (*S*)-1-cyclohexylethylamide to afford alkynyl derivatives **21** in a regioselective manner (Scheme 8).[43] These complexes were obtained as equimolecular mixtures of diastereoisomers. It should be noted that, in marked contrast to the above-mentioned methoxyalkynyl derivatives, complexes **21** are thermodynamically unstable and slowly generate azoniabutadienyl compounds **23** both in solution and in the solid state. Formation of **23** probably involves an initial migration of the amide group from the C_γ to C_α to yield allenyl complexes **22**, followed by protonation on the central carbon atom of the allenic moiety.

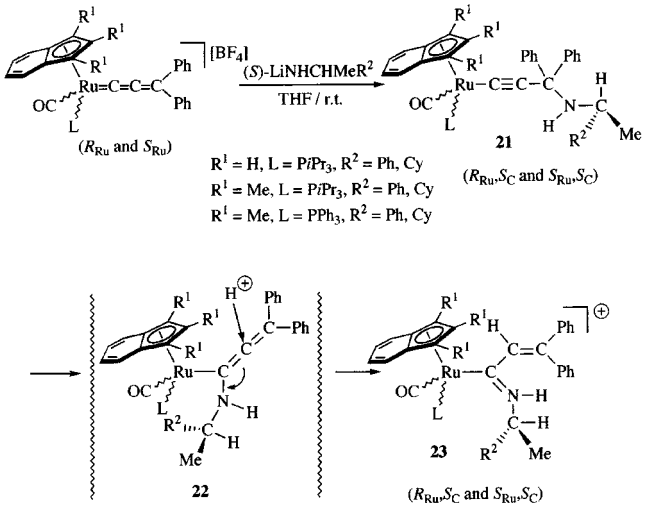

Scheme 8. Reactivity of indenylruthenium(II)−allenylidene complexes towards chiral amides

Treatment of indenyl complexes [Ru(=C=C=CPh_2)(η^5-C_9H_7)L^1L^2][PF_6] (L^1 = PPh_3, L^2 = PPh_3, $PMePh_2$; L^1 = CO, L^2 = PCy_3) with sodium azide in methanol does not afford stable alkynyl species. Instead, the reaction gives the cationic nitrile complexes **27** (Scheme 9).[59] We propose that, although initially the expected alkynyl derivatives **24** are formed, they are readily protonated by the protic solvent (we note that no reaction was observed in the absence of methanol) to generate vinylidene intermediates **25**. Intramolecular attack of the terminal nitrogen atom of the azide group at the electrophilic C_α atom on vinylidenes **25**[4a] and subsequent rearrangement gives the α,β-unsaturated carbene complexes **26**. The reaction ends with the extrusion of N_2 and the migration of the metallic fragment to the nitrogen atom to give the observed products. Complexes **27** can be easily demetalated by treatment with a second equivalent of NaN_3 to yield free diphenylacrylonitrile and the azide complexes [Ru(N_3)(η^5-C_9H_7)L^1L^2].

IV.2.2 Carbanions

Cationic allenylidene complexes can be used as suitable starting materials for carbon−carbon coupling reactions through the nucleophilic addition of carbanions to the unsaturated hydrocarbon chain. In this context we have reported that complexes [Ru(=C=C=CR^1R^2)(η^5-C_9H_7)-

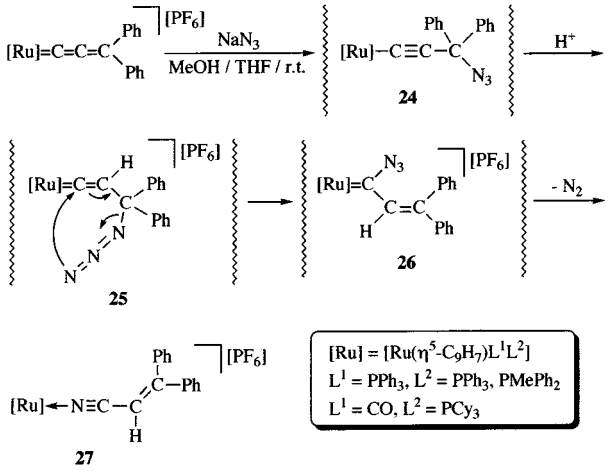

Scheme 9. Reactivity of (indenyl)Ru^{II}−allenylidene complexes towards sodium azide

$L^1L^2][PF_6]$ ($L^1 = L^2 = PPh_3$, $R^1 = R^2 = Ph$, $R^1R^2 = C_{13}H_{20}$; L^1L^2 = DPPE, $R^1 = R^2 = Ph$) regioselectively react with alkyllithium reagents or sodium cyanide under mild conditions to yield $[Ru\{C{\equiv}CC(R^3)R^1R^2\}(\eta^5\text{-}C_9H_7)L^1L^2]$ ($L^1 = L^2 = PPh_3$, $R^1 = R^2 = Ph$, R^3 = Me, *n*Bu, C≡N; $L^1 = L^2 = PPh_3$, $R^1R^2 = C_{13}H_{20}$, R^3 = C≡N; L^1L^2 = DPPE, $R^1 = R^2 = Ph$, R^3 = Me, *n*Bu).[51,58,60] Related cyclopentadienyl complexes $[Ru\{C{\equiv}CC(R)Ph_2\}(\eta^5\text{-}C_5H_5)(PPh_3)_2]$ (R = Me, C≡N, C_5H_5)[49] and $[Os\{C{\equiv}CC(Me)Ph_2\}(\eta^5\text{-}C_5H_5)(P\textit{i}Pr_3)_2]$[38] have recently been obtained using this synthetic methodology. Highly functionalized alkynyl complexes $[Ru\{C{\equiv}CC(C{\equiv}CR^4)R^2R^3\}(\eta^5\text{-}1,2,3\text{-}R^1_3C_9H_4)L^1L^2]$ (R^1 = H, $L^1 = L^2 = PPh_3$, $R^2 = R^3 = Ph$, R^4 = H, Ph, *n*Pr; R^1 = H, L^1L^2 = DPPE, $R^2 = R^3 = Ph$, R^4 = H, Ph, *n*Pr; R^1 = H, $L^1 = L^2 = PPh_3$, $R^2R^3 = C_{13}H_{20}$, R^4 = H; R^1 = H, L^1 = CO, $L^2 = P\textit{i}Pr_3$, $R^2 = R^3 = Ph$, R^4 = H; R^1 = Me, L^1 = CO, $L^2 = PPh_3$, $R^2 = R^3 = Ph$, $R^4 = Ph$) have been prepared in our group using acetylides as nucleophiles.[42,43,51,56]

Some of these alkynyl species have proved to be of interest in both organometallic and organic synthesis. Using $[Ru\{C{\equiv}CC(C{\equiv}CH)Ph_2\}(\eta^5\text{-}C_9H_7)(PPh_3)_2]$ as starting material, and taking advantage of the presence of a triple bond functionality at the end of the alkynyl chain, we carried out a series of Pauson-Khand cyclization reactions.[61] For instance, the unprecedented alkynyl and vinylidene derivatives **28** and **29** containing tricyclic cyclopentenone fragments (Figure 4) have been isolated from the strained cyclic alkenes norbornadiene and norbornene.

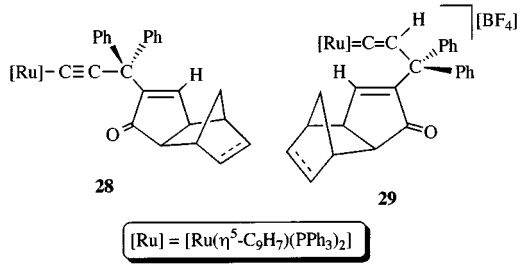

Figure 4. Structure of organometallic cyclopentenones

In addition, using the demetalation approach shown in Scheme 7, the unprecedented diyne $(HC{\equiv}C)_2CC_{13}H_{20}$ (**31**) can be easily prepared by demetalation of vinylidene $[Ru\{{=}C{=}C(H)C(C{\equiv}CH)C_{13}H_{20}\}(\eta^5\text{-}C_9H_7)(PPh_3)_2][BF_4]$ (**30**) with acetonitrile (Scheme 10).[56]

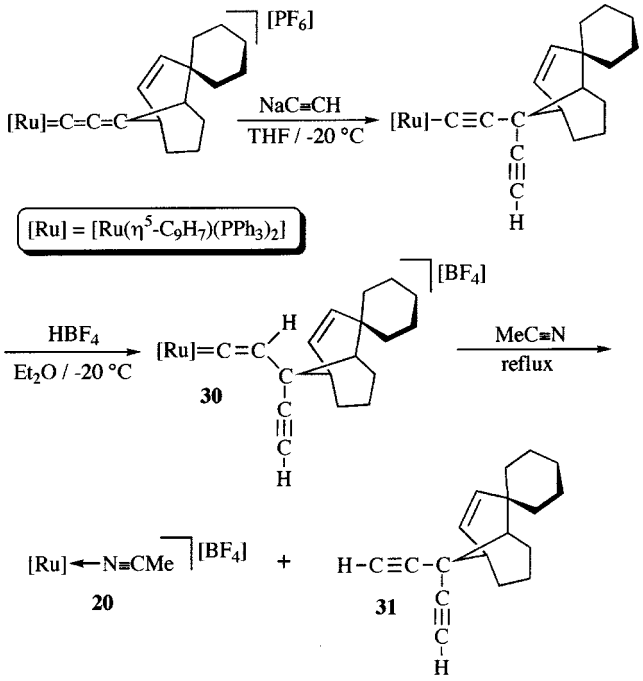

Scheme 10. Demetalation of allenylidene complex $[Ru\{{=}C{=}C{=}C(C_{13}H_{20})\}(\eta^5\text{-}C_9H_7)(PPh_3)_2][PF_6]$

The utility of transition metal allenylidenes in organic synthesis is also demonstrated in the synthesis of terminal oxoalkynes $HC{\equiv}CC(R^1)Ph(CH_2COR^2)$ (**34**), starting from $[Ru\{{=}C{=}C{=}C(R^1)Ph\}(\eta^5\text{-}C_9H_7)(PPh_3)_2][PF_6]$ (R^1 = H, Ph) and lithium enolates ($LiCH_2COR^2$) (Scheme 11).[62] The process is based on the regioselective nucleophilic attack of the enolate moiety at the C_γ atom of the cumulene chain to afford neutral oxo-functionalized alkynyl derivatives **32**. These derivatives are subsequently transformed into vinylidenes **33** and demetalated[62b] with MeC≡N as previously described. Regio- and diastereoselective nucleophilic additions of lithium enolates derived from the chiral ketones (−)-carvone and (+)-pulegone to $[Ru(={C=C=}CPh_2)(\eta^5\text{-}C_9H_7)(PPh_3)_2][PF_6]$ allowed us to prepare chiral alkynyl complexes (*R*,*R*)-**35** and (*R*,*R*)-**36** (see Figure 5).[62a] We note that the related osmium(II)−oxoalkynyl complex $[Os\{C{\equiv}CC(CH_2COMe)Ph_2\}(\eta^5\text{-}C_5H_5)(P\textit{i}Pr_3)_2]$ has recently been obtained by Esteruelas and co-workers.[38]

Chiral oxoalkynes **40** have been obtained by the same methodology from the optically active allenylidene **37** (Scheme 12).[59] The initial formation of alkynyl derivatives **38**, which involves the generation of a new stereogenic center at C_γ, is diastereoselective since only one diastereoisomer is detected by NMR spectroscopy. The configuration of this new chiral carbon atom in both alkynyl (**38**), vinylidene (**39**), or free alkyne (**40**) derivatives is presently unknown.

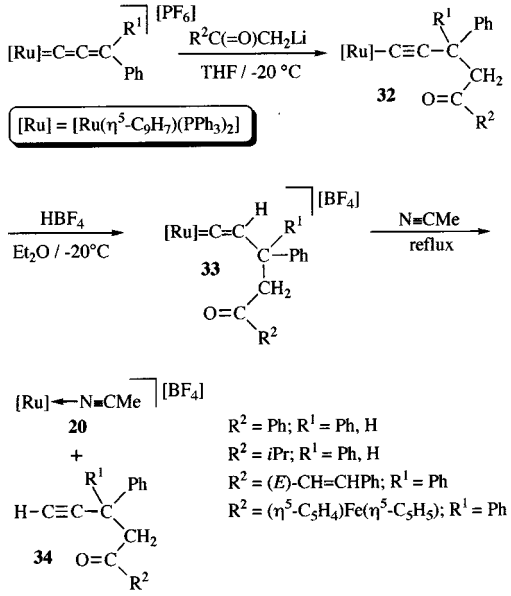

Scheme 11. Synthesis of terminal oxoalkynes from alkynylruthenium(II) complexes

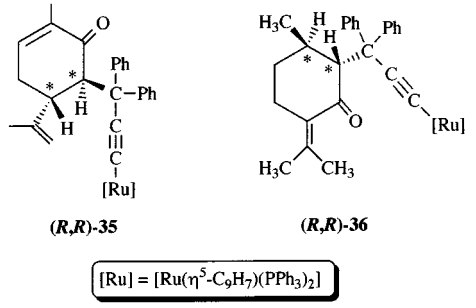

Figure 5. Structure of optically active alkynylruthenium(II) complexes

Cationic indenylruthenium(II)−allenylidene derivatives are also suitable starting materials for the preparation of dimetallic species containing hydrocarbon bridges through carbon−carbon coupling reactions with organometallic anionic nucleophiles. We have reported that [Ru{=C=C=C(R)Ph}(η^5-C_9H_7)(PPh_3)L][PF_6] (R = Ph, L = PPh_3, $PMePh_2$, PMe_2Ph; R = H, L = PPh_3, $PMePh_2$) reacts regioselectively with anionic Fischer-type methoxycarbene derivatives [$(CO)_5M${=C(OMe)CH_2}]$^-$ (M= Cr, Mo, W) to yield unprecedented neutral alkynylcarbene complexes **41** (Scheme 13).[60] Protonation of these compounds leads to the formation of **42**, which represent the first examples of dimetallic complexes containing a vinylidenecarbene type hydrocarbon bridge. In addition, the novel tungsten−methoxycarbenes **43**, bearing a terminal alkyne functionality, could be prepared by selective demetalation of the ruthenium fragment in refluxing acetonitrile.

Nucleophilic additions of carbanions at C_α of cationic allenylidenes to afford neutral allenyl species are also known.[4a−4b] As an example, we have described the synthesis of allenylmetallacyclic derivatives **44** and **45** (Scheme 14) by deprotonation of an auxiliary phosphane

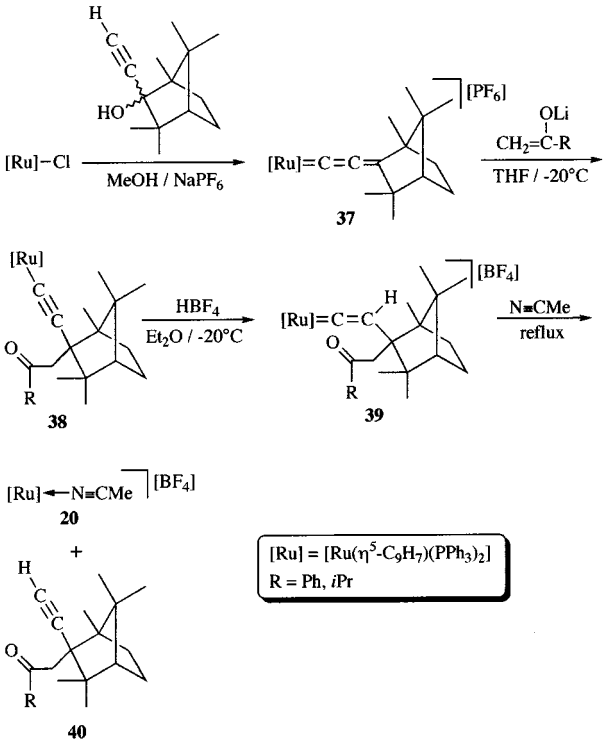

Scheme 12. Synthesis of optically active alkynyl and vinylidene complexes, and terminal alkynes derived from (−)-fenchone

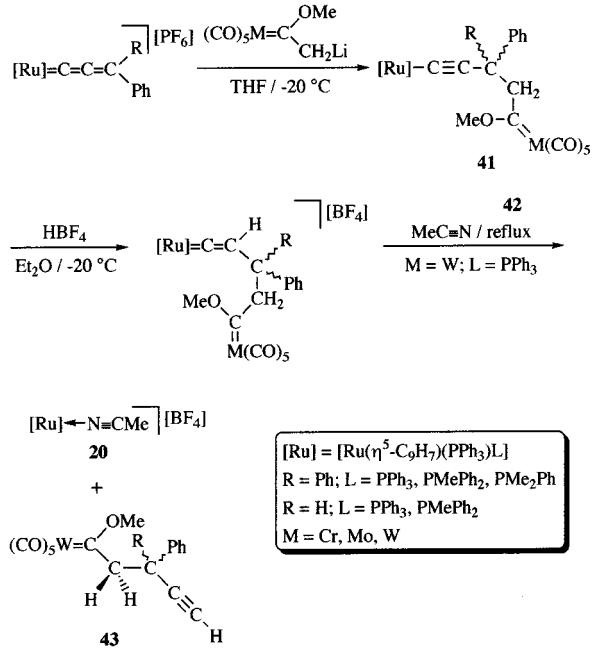

Scheme 13. Preparation of dimetallic complexes containing alkynylcarbene and vinylidenecarbene bridges

ligand and subsequent carbon−carbon coupling between the electrophilic C_α and the initially generated carbanion.[51,57] We note that formation of **44** is diastereoselective since only one pair of enantiomers S_{Ru},R_C/R_{Ru},S_C is

obtained as confirmed by X-ray crystal structure determinations.[57]

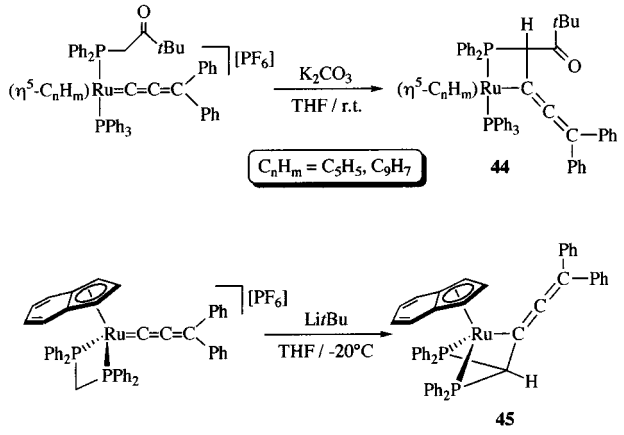

Scheme 14. Intramolecular C−C coupling reactions between allenylidene and phosphane ligands

IV.3 Cyclization Reactions

Cationic transition metal allenylidene complexes are useful starting materials to generate unsaturated cyclic structures by the reaction of their highly polarized unsaturated chain with organic substrates.[4a−4b] In this context, Esteruelas and co-workers have recently reported[63] that $[Ru(=C=C=CPh_2)(\eta^5\text{-}C_5H_5)(CO)(P\textit{i}Pr_3)][BF_4]$ reacted with dicyclohexylcarbodiimide to afford the unprecedented iminium azetidinylidenemethyl complex **48** which was isolated as a mixture of the corresponding (*Z*) (**48a**) and (*E*) (**48b**) stereoisomers (Scheme 15). Formation of **48** can be rationalized as the result of a [2+2] cycloaddition between the $C_\beta-C_\gamma$ double bond of the allenylidene ligand and one of the two carbon−nitrogen double bonds of the carbodiimide group. Thus, intermediate **46** was formed and rapidly evolved into carbene **47**, probably as a mixture of isomers, through an Alder-ene type process. A final charge redistribution within **47** gave the observed species **48**. Complex **48** was used as a suitable precursor for the preparation of other heterocyclic species such as **49−52** (Scheme 15).

The doubly α,β-unsaturated oxygen-containing cyclic carbene complex **53** has been prepared by the addition of ethyl diazoacetate to $[Ru(=C=C=CPh_2)(\eta^5\text{-}C_5H_5)(CO)(P\textit{i}Pr_3)][BF_4]$ (Scheme 16).[64] In this case, a formal 1,3-addition of the organic reagent at the $C_\alpha-C_\beta$ double bond takes place.

Since allenylidenes have two electrophilic and one nucleophilic centers, the reactions of these compounds with organic molecules containing two nucleophilic heteroatoms and one electrophilic hydrogen atom give rise to 1,2,3-diheterocyclization processes. Following the previously reported reactions with the allenylidene complex $[Ru(=C=C=CPh_2)(\eta^5\text{-}C_5H_5)(CO)(P\textit{i}Pr_3)][BF_4]$,[65a] Bianchini and coworkers have similarly found that the cationic (diphenylallenylidene)rhenium(I) complex $[Re(=C=C=CPh_2)(TRIPHOS)(CO)_2][CF_3SO_3]$ reacts with N,S- and N,N-heterocycles to generate heterobicyclic compounds **54−57** (Scheme 17).[65b] All these species are formed by the initial addition of the heteroatom−H bond to the $C_\alpha-C_\beta$ double bond of the allenylidene ligand, to produce intermediate α,β-unsaturated carbenes which undergo a further nucleophilic attack of the second heteroatom at C_γ of the unsaturated chain.[65c]

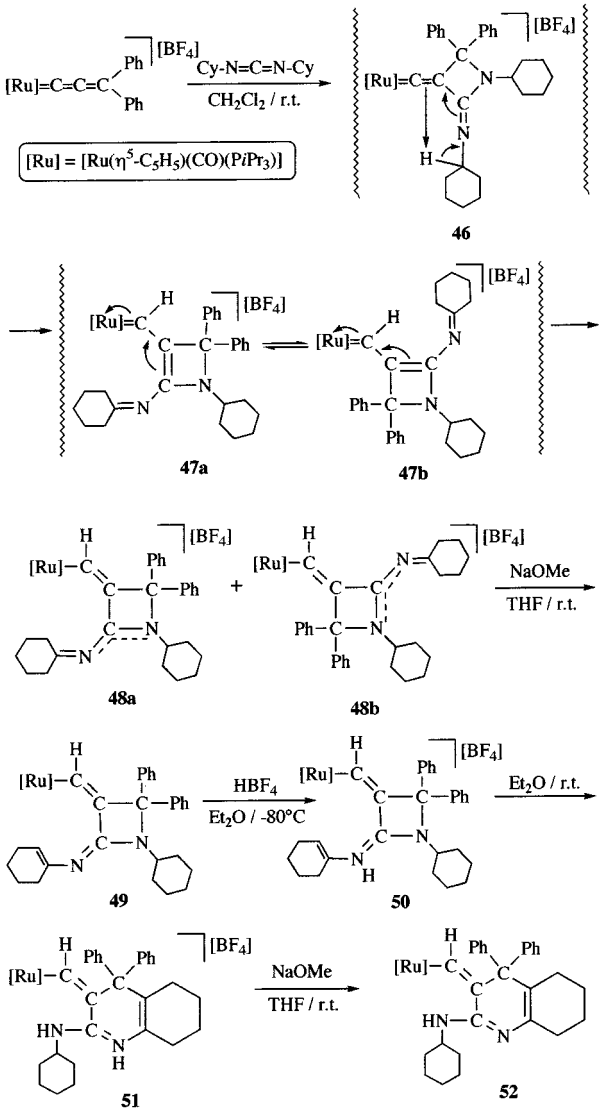

Scheme 15. Reactivity of $[Ru(=C=C=CPh_2)(\eta^5\text{-}C_5H_5)(CO)(P\textit{i}Pr_3)][BF_4]$ towards dicyclohexylcarbodiimide

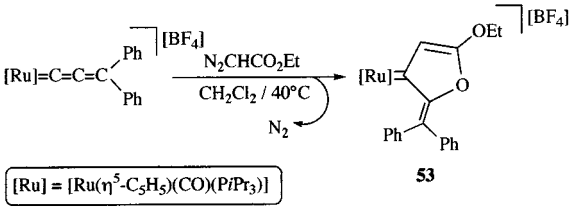

Scheme 16. Cyclization of $[Ru(=C=C=CPh_2)(\eta^5\text{-}C_5H_5)(CO)(P\textit{i}Pr_3)][BF_4]$ with ethyl diazoacetate

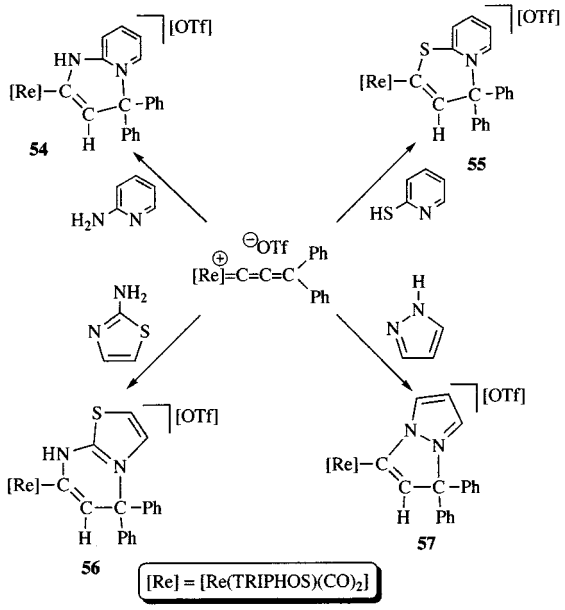

Scheme 17. 1,2,3-diheterocyclizations on [Ru(=C=C=CPh$_2$)(TRIPHOS)(CO)$_2$][OTf]

Other cyclization processes involving direct metal−carbon double-bond additions are also known. Hill and co-workers have recently reported the preparation of metallacyclic allenyl complexes **58** and **60** by the addition of sodium dimethyldithiocarbamate to diphenylallenylidenes [Ru(=C=C=CPh$_2$)(S$_2$CNMe$_2$)(CO)(PPh$_3$)$_2$][PF$_6$] and [Ru(=C=C=CPh$_2$){HB(pz)$_3$}(PPh$_3$)$_2$][PF$_6$], respectively (Scheme 18).[66] Complex **58** is not stable and slowly generates the thermodynamically stable isomer **59**. A plausible mechanism to explain the formation of **58** and **60** may involve the initial attack of dimethyldithiocarbamate at C_α, followed by the substitution of a triphenylphosphane ligand with the C=S group.

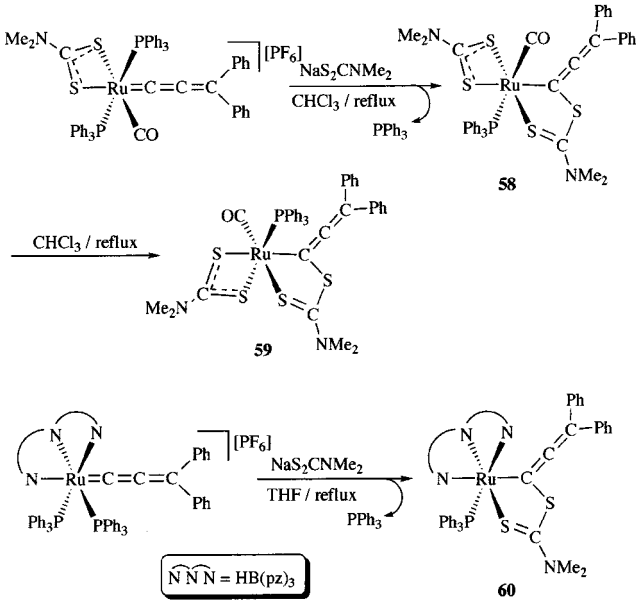

Scheme 18. Coupling of allenylidene ligands with dithiocarbamate

A related intramolecular coupling between an acetate ligand and a transient diphenylallenylidene moiety also occurs when hydroxyalkynyl complex [Ru{C≡CC(OH)Ph$_2$}{κ^1-(*O*)-COOMe}(CO)$_2$(PPh$_3$)$_2$] is treated with HPF$_6$, affording metallacycle **61** (Scheme 19).[67]

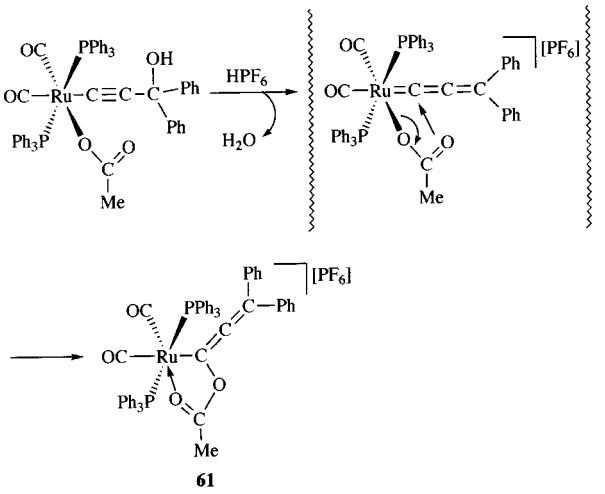

Scheme 19. Intramolecular coupling of an allenylidene ligand with acetate

Finally, dinuclear cyclic complexes **62** and **63** (Scheme 20) have been prepared by Bianchini and co-workers through direct activation of 2-methyl-3-butyn-2-ol or propargyl alcohol by [Re(OTf)(TRIPHOS)(CO)$_2$].[46] In the first case, carbene vinylidene complex **62** seems to be formed by the coupling of transient allenylidene [Re(=C=C=CMe$_2$)(TRIPHOS)(CO)$_2$][CF$_3$SO$_3$] and alkenylvinylidene [Re{=C=C(H)−C(Me)=CH$_2$}(TRIPHOS)(CO)$_2$][CF$_3$SO$_3$] species which are simultaneously generated in the initial dehydration process.[68] An unprecedented coupling between the allenylidene [Re(=C=C=CH$_2$)(TRIPHOS)(CO)$_2$][CF$_3$SO$_3$] and its hydroxyvinylidene precursor [Re{=C=C(H)CH$_2$(OH)}(TRIPHOS)(CO)$_2$][CF$_3$SO$_3$] was proposed in the formation of complex **63**.

V. Reactivity of Neutral Allenylidene Complexes

The reactions of several square-planar (allenylidene)rhodium(I) and -iridium(I) chloride complexes with nucleophiles do not proceed through the typical addition, but instead result in substitution products. For instance, the iridium complex *trans*-[IrCl(=C=C=CPh$_2$)(P*i*Pr$_3$)$_2$] reacts with KOH to give the hydroxo derivative *trans*-[Ir(OH)(=C=C=CPh$_2$)(P*i*Pr$_3$)$_2$].[20] The rhodium complexes *trans*-[RhX{=C=C=CPh(R)}(P*i*Pr$_3$)$_2$] (X = OH, NCO, N$_3$) have been prepared in a similar fashion.[24][69] The fluoride complexes obtained by the treatment of the hydroxo complexes with NEt$_3$·3HF have been used as appropriate starting materials for the preparation of mononuclear (**64**, **65**) and dinuclear (**66**, **67**) alkynyl derivatives (Scheme 21).[70] Alternatively, complexes **66** and **67** can be prepared directly by treatment of the hydroxo derivatives with (Ph$_3$Sn)$_2$C$_4$.

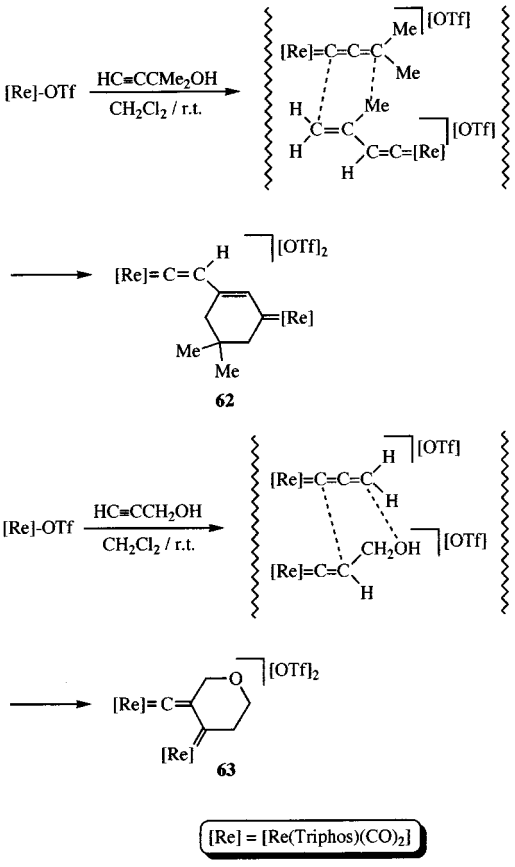

Scheme 20. Couplings between allenylidene and alkenylvinylidene or hydroxyvinylidene ligands

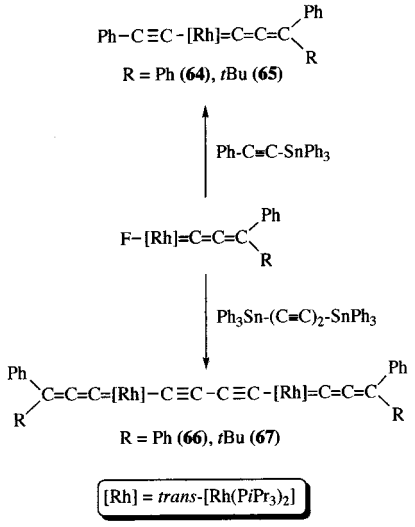

Scheme 21. Substitution reactions on square-planar (allenylidene)-rhodium(I) complexes

The reactions of rhodium azide complexes with CO lead either to the formation of the azidoalkynyl complex **68** or of the cyanoalkenyl derivatives **70** and **71** (Scheme 22).[24] A formal addition of the azide anion to C_α or C_γ is postulated as a possible route to the intermediates which give **70** and **71** by elimination of nitrogen. The azidoalkynyl complex **69** was characterized by NMR at low temperature. No electrophilic addition product was observed in the reaction of the rhodium azide derivatives with $[Me_3O][BF_4]$ leading instead to the formation of the dinuclear bis(allenylidene) complexes **72−75** (Scheme 22).[24]

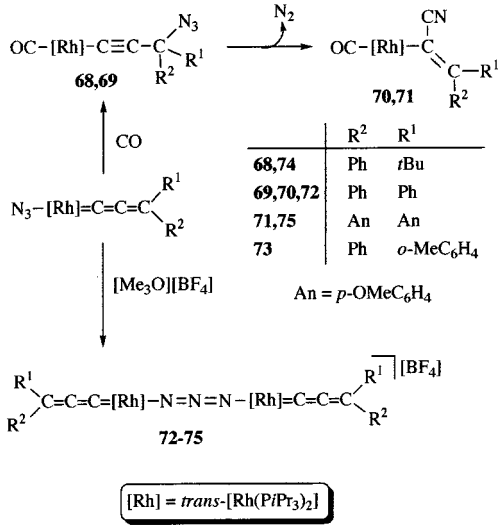

	R²	R¹
68,74	Ph	*t*Bu
69,70,72	Ph	Ph
71,75	An	An
73	Ph	*o*-MeC$_6$H$_4$

Scheme 22. Reactivity of (allenylidene)rhodium(I) azide complexes

New metal-assisted C−C coupling reactions have been described. *trans*-[Ir(OH)(=C=C=CPh$_2$)(P*i*Pr$_3$)$_2$] reacts with an excess of the terminal alkynes RC≡CH (R = Ph, CO_2Me) to give complexes **76** (Scheme 23). The formation of **76** presumably involves the substitution of OH by C_2R, followed by the oxidative addition of a second molecule of the alkyne to give the iridium hydride intermediate [IrH(C≡CR)$_2$(=C=C=CPh$_2$)(P*i*Pr$_3$)$_2$]. This intermediate could undergo a rearrangement to form a metal−allenyl species followed by a C−C coupling process with a third molecule of alkyne.[20]

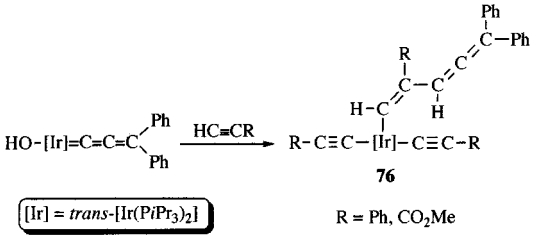

Scheme 23. C−C coupling reactions promoted by *trans*-[Ir(OH)-(=C=C=CPh$_2$)(P*i*Pr$_3$)$_2$]

An unprecedented triple coupling [C_2+C_1+C_1] of alkynyl, allenylidene, and carbonyl groups has been described by Werner and co-workers.[70] This coupling involves the reaction of complex **65** with CO leading to the formation of **77**, a complex containing a highly unsaturated cyclobutenone ligand in the coordinating sphere of the rhodium atom. A possible mechanism for this conversion is shown in the Scheme 24. The proposed intermediate complex **78** was isolated as a thermally unstable solid.

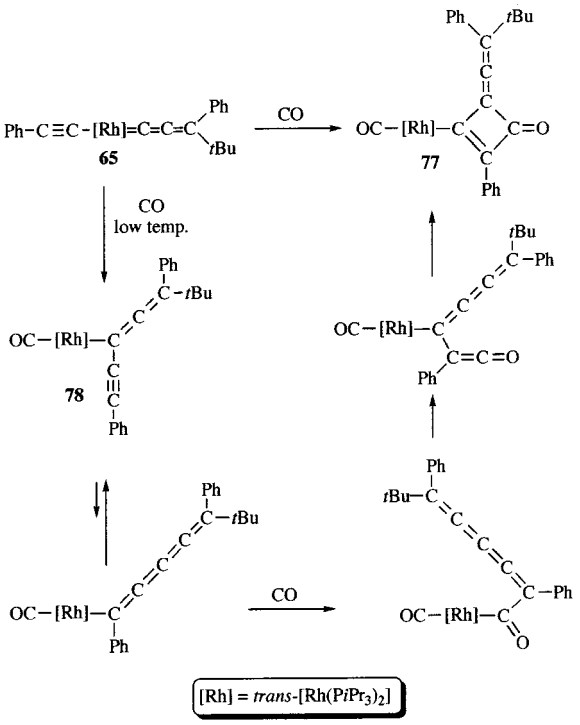

Scheme 24. Unprecedented [C_2+C_1+C_1] coupling of an allenylidene, an alkynyl and a CO ligand

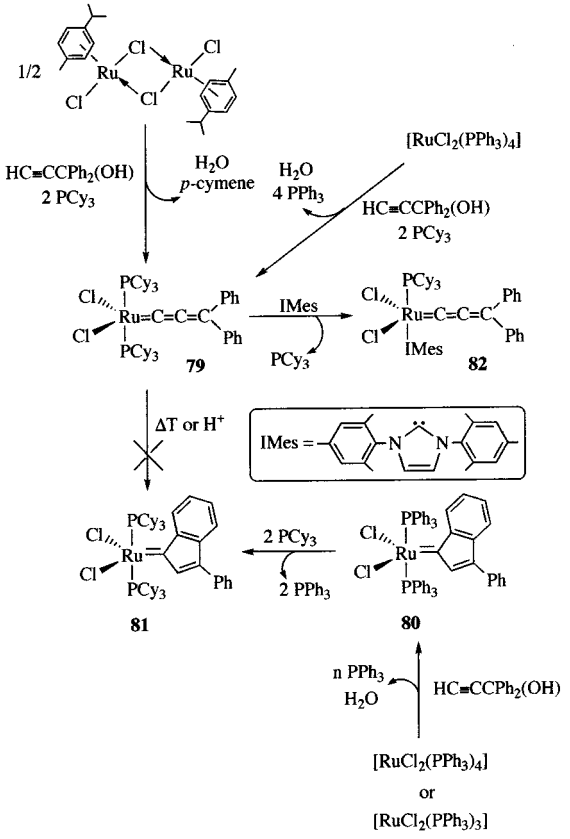

Scheme 25. Synthesis and reactivity of 16-electron ruthenium(II)−allenylidene complexes

A series of 16-electron ruthenium(II)−allenylidene species have been described as the first unsaturated allenylidene complexes (Scheme 25). The parent complex [$RuCl_2$(=C=C=CPh_2)(PCy_3)$_2$] (**79**) is obtained in good yield from the reaction of [$RuCl_2(PPh_3)_4$] or 0.5 equiv. of [$RuCl_2(\eta^6$-*p*-cymene)]$_2$ with 1,1-diphenyl-2-propyn-1-ol and 2 equiv. of PCy_3. However, the reaction of either [$RuCl_2(PPh_3)_3$] or [$RuCl_2(PPh_3)_4$] with HC≡CC(OH)Ph_2 leads only to the 3-phenyl-1-indenylidene complex **80** which then undergoes phosphane exchange with PCy_3 to provide complex **81**. The allenylidene complex **79** is stable at elevated temperatures and towards protic acids, and no conversion into 3-phenyl-1-indenylidene complex **81** was observed.[8,71] The exchange of one PCy_3 ligand for IMes affords the allenylidene complex **82** in high yield (Scheme 25). The similar 16-electron complex [$OsCl_2$(=C=C=CPh_2)(PPh_3)$_2$] has been isolated and is stable in methanol at room temperature.[72]

An intramolecular nucleophilic addition at the allenylidene chain has been described[15][66] in the reaction of the trispyrazolylborate neutral complex [RuCl(=C=C=CPh_2){HB(pz)$_3$}(PPh_3)] with Na[S_2CNMe_2] resulting in the metallacyclic allenyl complex **60** (see Scheme 18). Another type of intramolecular addition was observed in the reaction of [OsCl(=C=C=CPh_2)(η^5-C_5H_5)(P*i*Pr_3)] (**83**) with CH_2=CHMgBr which gives the pentatrienyl complex [Os(η^3-CH_2CHC=C=CPh_2)(η^5-C_5H_5)(P*i*Pr_3)] (**84**) (Scheme 26).[73] This complex is formed by migratory insertion of the allenylidene ligand into the Os−CH=CH_2 bond of the vinylosmium intermediate which cannot be isolated. Complex **83** also reacts with KI to give the iodo derivative **85**.

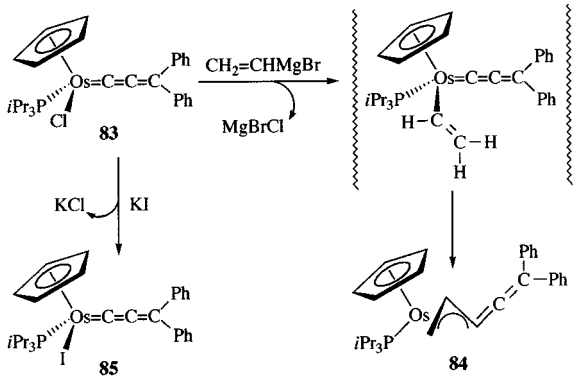

Scheme 26. Reactivity of the neutral allenylidene [OsCl(=C=C=CPh_2)(η^5-C_5H_5)(P*i*Pr_3)]

Nucleophilic addition of water to the allenylidene chain in the complex *fac*,*cis*-[$RuCl_2$(=C=C=CPh_2)(PNP)] (**86**) has been reported to occur both in THF or CH_2Cl_2 at room temperature, to give the carbonyl derivative *fac*,*cis*-[$RuCl_2$(CO)(PNP)] and the corresponding free alkene H_2C=CPh_2 (Scheme 27).[18] The reaction proceeds by regioselective cleavage of the $C_\alpha-C_\beta$ bond. The use of D_2O gives the corresponding deuterated alkene D_2C=CPh_2.

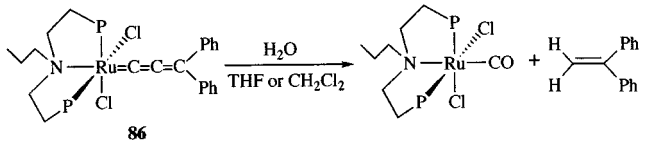

Scheme 27. Selective $C_\alpha-C_\beta$ bond cleavage by water in a ruthenium(II)−allenylidene complex

Dötz and co-workers[74] have reported the synthesis of a series of sugar-derived or (disaccharide)metal−(alkenyl)-(methoxy)carbene complexes obtained from the reactions of sugar-based propargylic alcohols and $[W(CO)_5(THF)]$. The formation of these carbene species is rationalized through the typical addition of alcohols to the transient allenylidene species generated from the propargylic alcohols.

A series of neutral carbonylruthenium trinuclear clusters containing bridging allenylidene groups of type **D** shown in Figure 3 have been reported.[27] These derivatives undergo substitution reactions of the carbonyl groups by phosphane ligands. The formation of a tetranuclear Ru_3Au cluster is also described. Furthermore, a C−C coupling between an allenylidene bridging moiety and a phenyl group of a coordinated dppm ligand in a related Ru_3 cluster to give a 1,3-diphenylindenyl ligand has been also reported.[75]

VI. Reactivity of Complexes Containing Higher Cumulenylidene Ligands

Although the chemistry of higher cumulenylidene complexes $[M]=C(=C)_n=CR^1R^2$ ($n > 1$) has not received as much attention as that of allenylidenes ($n = 1$), theoretical[40] and experimental[4b,4e] evidence point also to the alternating electron deficiency and richness of the carbon atoms of the unsaturated chain as one moves along the chain from the metal atom. Therefore nucleophilic additions at the odd-numbered carbon atoms and electrophilic additions at the even-numbered carbon atoms can be expected.

VI.1 Butatrienylidene Complexes

Mononuclear transition metal complexes containing butatrienylidene ligands $[M]=C(=C)_2=CR^1R^2$ have usually been reported as highly reactive intermediates in different reactions.[4b][4e] Indeed, complexes $[(\eta^5\text{-}C_5Me_5)L^1L^2Fe\{=C=C=C=C(R)Fe(CO)_2(\eta^5\text{-}C_5Me_5)\}]^+$ (L^1L^2 = DPPE, DIPPE; R = H, Me), obtained by protonation or methylation at C_δ of neutral dimetallic butadiynes $[(\eta^5\text{-}C_5Me_5)L^1L^2Fe\{C\equiv CC\equiv CFe(CO)_2(\eta^5\text{-}C_5Me_5)\}]$, are the only butatrienylidene complexes stable enough to be isolated and spectroscopically characterized to date.[32] These stable species have been studied by cyclic voltammetry (CV). Thus, while tertiary butatrienylidenes $[(\eta^5\text{-}C_5Me_5)L^1L^2Fe\{=C=C=C=C(Me)Fe(CO)_2(\eta^5\text{-}C_5Me_5)\}][CF_3SO_3]$ display a reversible one-electron oxidation process and an irreversible reduction process, complexes $[(\eta^5\text{-}C_5Me_5)L^1L^2Fe\{=C=C=C=C(H)Fe(CO)_2(\eta^5\text{-}C_5Me_5)\}][BF_4]$ show a more complicated pattern, owing to the acidic character of the hydrogen atom on C_δ, and signals assigned to $[(\eta^5\text{-}C_5Me_5)L^1L^2Fe\{C\equiv CC\equiv CFe(CO)_2(\eta^5\text{-}C_5Me_5)\}]$ are also observed in the voltammograms. In fact, these monosubstituted complexes can be readily deprotonated with DBU or traces of water to afford the starting butadiynes $[(\eta^5\text{-}C_5Me_5)L^1L^2Fe\{C\equiv CC\equiv CFe(CO)_2(\eta^5\text{-}C_5Me_5)\}]$.

Activation of trimethylsilyl-1,3-butadiyne $HC\equiv CC\equiv CSiMe_3$ by $[FeCl(\eta^5\text{-}C_5Me_5)(DPPE)]$ in methanol has been reported to yield the methoxyallenylidene $[Fe\{=C=C=C(OMe)CH_3\}(\eta^5\text{-}C_5Me_5)(DPPE)][BPh_4]$ (**88**) (Scheme 28).[31] Formation of **88** involves the generation of the unstable butatrienylidene derivative $[Fe(=C=C=C=CH_2)(\eta^5\text{-}C_5Me_5)(DPPE)][BPh_4]$ (**87**), by an initial 1,4-H shift and subsequent desilylation of the intermediate $[Fe\{=C=C=C=C(H)SiMe_3\}(\eta^5\text{-}C_5Me_5)(DPPE)][BPh_4]$, which readily undergoes addition of methanol to the $C_\gamma-C_\delta$ double bond.

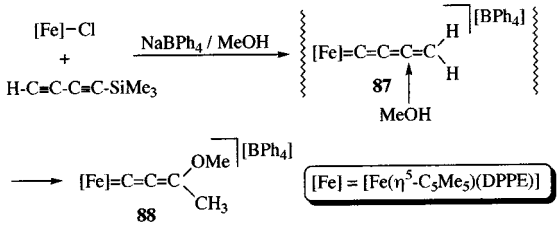

Scheme 28. Synthesis of the iron(II)−allenylidene $[Fe\{=C=C=C(OMe)CH_3\}(\eta^5\text{-}C_5Me_5)(DPPE)][BPh_4]$

Protonation of the neutral diynylruthenium(II) complex *trans*-$[RuCl(C\equiv CC\equiv CPh)(DPPE)_2]$ or direct activation of 1,3-butadiyne $HC\equiv CC\equiv CPh$ by *cis*-$[RuCl_2(DPPE)_2]$ allows the formation of the cationic buta-1,2,3-trienylidene derivative *trans*-$[RuCl\{=C=C=C=C(H)Ph\}(DPPE)_2]^+$.[50] This complex is a very reactive species which cannot be isolated since it adds water or methanol from the reaction media to the electrophilic C_γ atom to yield the acylvinylidene *trans*-$[RuCl\{=C=C(H)C(=O)CH_2Ph\}(DPPE)_2]^+$ or the methoxyallenylidene *trans*-$[RuCl\{=C=C=C(OMe)CH_2Ph\}(DPPE)_2]^+$, respectively.[50]

Treatment of *cis*-$[RuCl_2(DPPM)_2]$ with an excess of butadiyne ($HC\equiv CC\equiv CH$) in the presence of a halide-abstracting reagent ($NaPF_6$ or $NaSbF_6$), allows the generation of *trans*-$[RuCl(=C=C=C=CH_2)(DPPM)_2]^+$, which can be trapped in situ by the addition of tertiary amines to C_γ, to yield stable 2-ammoniobutenynyl complexes **89** (Scheme 29).[76] When 4-(dimethylamino)pyridine is used, this ambident nucleophile binds regioselectively to the unsaturated carbon chain through the pyridine nitrogen atom to give **90**.[76] The reaction of *trans*-$[RuCl(=C=C=C=CH_2)(DPPM)_2]^+$ with (ferrocenylmethyl)dimethylamine has been also reported.[77] In this case the initially generated 2-ammoniobutenynyl derivative **91** evolves into the iminium alkynyl complex **92** by migration of the resonance-stabilized

ferrocenylcarbenium ion from the quaternary nitrogen atom to the neighboring nucleophilic C_δ atom (Scheme 30).

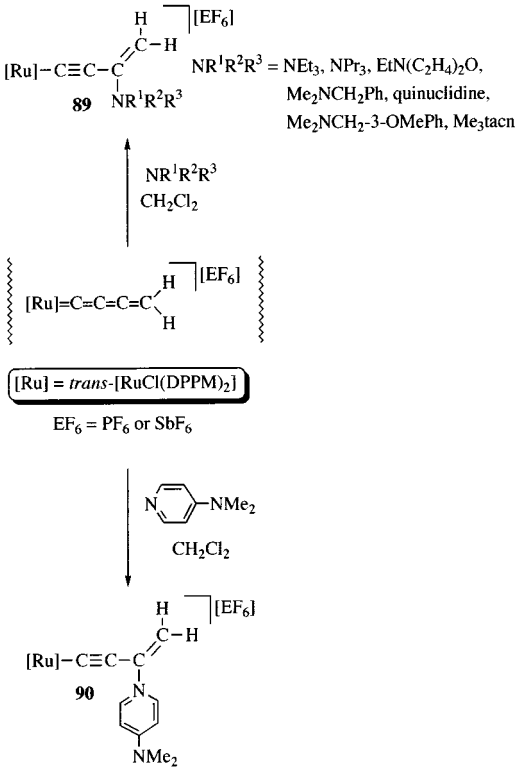

Scheme 29. Reactivity of *trans*-[RuCl(=C=C=C=CH_2)$(DPPM)_2$][EF_6] towards tertiary amines

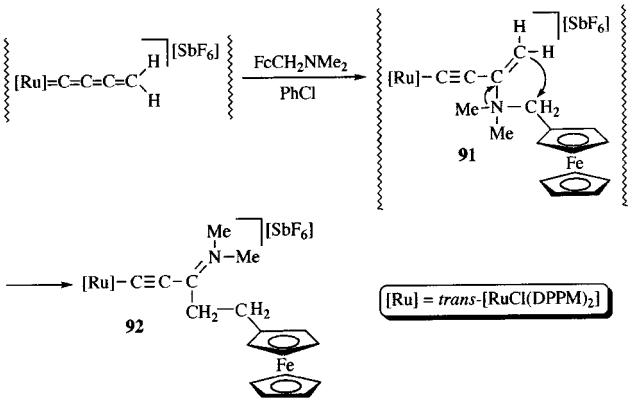

Scheme 30. Reactivity of *trans*-[RuCl(=C=C=C=CH_2)-$(DPPM)_2$][SbF_6] towards (ferrocenylmethyl)dimethylamine

Addition of sulfur nucleophiles at *trans*-[RuCl(=C=C=C=CH_2)$(DPPM)_2$][SbF_6] has been reported to yield thioallenylidene derivatives.[78] Thus, while the reaction with ethanethiol produces *trans*-[RuCl{=C=C=C(SEt)CH_3}-$(DPPM)_2$][SbF_6], by addition of the S−H bond to the $C_\gamma-C_\delta$ double bond of the cumulene chain, thioallenylidene **94** is obtained when allyl methyl sulfide is used (Scheme 31). Formation of **94** involves the initial nucleophilic attack of the sulfide at the electrophilic C_γ atom to generate the unstable enynyl derivative **93** which undergoes a [3,3] thia-Claisen-type rearrangement. In a similar way, thioallenylidene **95** has been prepared from the butatrienylidene *trans*-[RuCl(=C=C=C=CH_2)$(DPPE)_2$][CF_3SO_3] generated in situ and diallyl sulfide (Scheme 31).

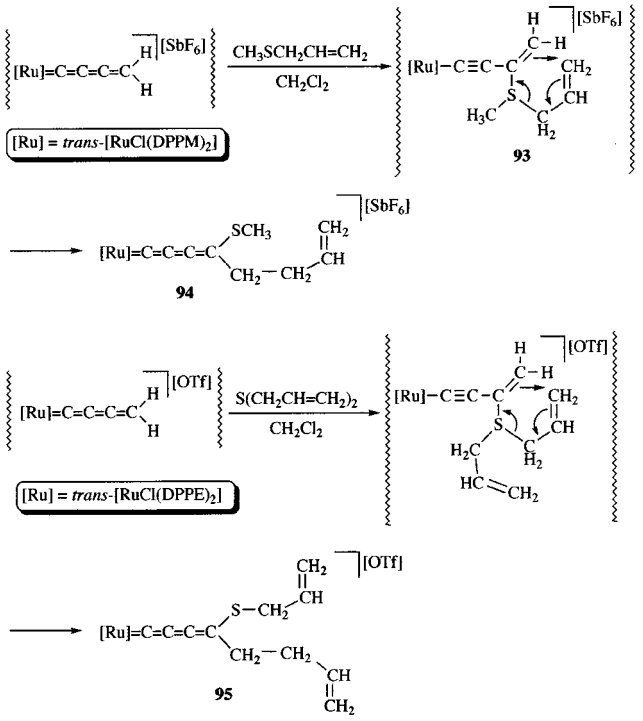

Scheme 31. Synthesis of thioallenylidene complexes from ruthenium(II)−buta-1,2,3-trienylidene intermediates

Full details on the reactivity of the highly reactive butatrienylidene[Ru(=C=C=C=CH_2)(η^5-C_5H_5)$(PPh_3)_2$][PF_6], formed from butadiyne and [Ru(η^5-C_5H_5)(THF)$(PPh_3)_2$]-[PF_6], have recently been reported.[12][79] Complexes [Ru{C≡CC(PPh_3)=CH_2}(η^5-C_5H_5)$(PPh_3)_2$][PF_6], [Ru-{=C=C=C(NPh_2)Me}(η^5-C_5H_5)$(PPh_3)_2$][PF_6], [Ru{C≡CC-(=O)Me}(η^5-C_5H_5)$(PPh_3)_2$], and [Ru{=C=C=C(C_4H_3NMe-2)Me}(η^5-C_5H_5)$(PPh_3)_2$][PF_6] were prepared by trapping this cumulenylidene derivative with triphenylphosphane, diphenylamine, water, and *N*-methylpyrrole, respectively.[12] In addition, a wide series of functionalized alkynyl derivatives containing either quinoline **96** or 1-aza-buta-1,3-diene fragments **97** (Figure 6) can be obtained when complexes [Ru(=C=C=C=CH_2)(η^5-C_5H_5)-L^1L^2][PF_6] [L^1 = L^2 = PPh_3, $P(OMe)_3$] are treated with an excess of aromatic imines.[79]

The synthesis and reactivity of Ru_4−butatrienylidene clusters of type **B−C** (Figure 3) have also been reported.[26]

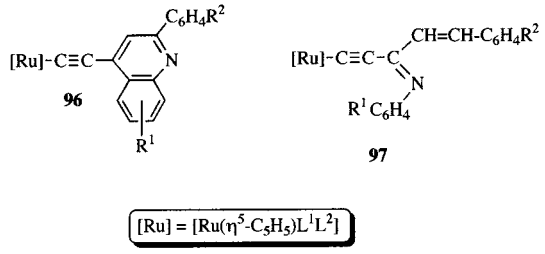

Figure 6. Structures of alkynyl complexes containing quinoline and 1-azabuta-1,3-diene fragments

VI.2 Pentatetraenylidene Complexes

The dimetallic complex $[(\eta^5\text{-}C_5Me_5)(PPh_3)(NO)Re{=}C{=}C{=}C{=}C{=}Mn(CO)_2(\eta^5\text{-}C_5Cl_5)][BF_4]$, obtained by treatment of $[(\eta^5\text{-}C_5Me_5)(PPh_3)(NO)Re{-}C{\equiv}C{-}C{\equiv}C{-}C(OMe){=}Mn(CO)_2(\eta^5\text{-}C_5Cl_5)]$ with an excess of BF_3 gas, is the only pentatetraenylidene derivative reported during the period covered by this review.[30] This cumulenylidene complex is stable towards dimethyl sulfide, ethylene or tetracyanoethylene, but readily reacts with trimethylphosphane, even at −80 °C, to afford complicated mixtures of products which have not been identified.

VII. Catalytic Studies

The role of allenylidene species in catalytic processes has been previously described for ruthenium(II) complexes, albeit in a small number of organic transformations.[80] Remarkably, Fürstner, Dixneuf and co-workers have reported for the first time the catalytic activity of an allenylidene complex, namely $[RuCl(=C=C=CPh_2)(\eta^6\text{-}p\text{-cymene})(PR_3)][PF_6]$ (PR_3 = PCy_3, $PiPr_3$), in ring-closing metathesis of olefins which proves to be comparable in efficiency to the alkylidene derivatives developed by Grubbs.[44] Similarly, the allenylidene complex $[RuCl(=C=C=CPh_2)(\eta^6\text{-}p\text{-cymene})(PCy_3)][PF_6]$ is also a good catalyst for the yne-ene ring-closing metathesis of the mixed propargylic allyl ethers $HC{\equiv}C{-}CR^1R^2OCH_2{-}CH{=}CH_2$ into 3-vinyl-2,5-dihydrofurans.[81] It was shown that an initial photochemical irradiation of the catalyst efficiently promotes the catalytic activity. Following these pioneering works, Dixneuf and co-workers studied the scope of these catalytic transformations.[82] It was demonstrated that the efficiency of these cationic 18-electron allenylidene precatalysts depends on the nature of the counter-anion. The use of $[CF_3SO_3]^-$ improves the activity, which leads to high-yield transformations of *N*,*N*-diallyltosylamine into *N*-tosyldihydropyrrole at room temperature, while the metathesis of the ene-yne ether $HC{\equiv}C{-}C(Me)(Ph)OCH_2{-}CH{=}CH_2$ was completed in a shorter time. New catalytic reactions are produced by using $[BF_4]^-$. Although mechanistic studies have not yet been explored, these preliminary results seem to suggest that the dissociation of the *p*-cymene ligand takes place in the precatalyst complex (either thermally or photochemically), generating a 14-electron allenylidene species $[RuCl(=C=C=CPh_2)(PR_3)]^+$ which effectively acts as the active catalyst.

The catalytic activity of the novel 16-electron allenylidene complexes $[RuCl_2(=C=C=CPh_2)L^1L^2]$ (L^1 = PCy_3, L^2 = PCy_3, IMes) in RCM reactions involving diethyl allylmalonate and *N*,*N*-diallyltosylamine has been investigated[8] showing that the catalytic activity is much poorer than that shown by the above-mentioned cationic 18-electron (allenylidene)ruthenium(II) complexes.[44] This behavior probably arises from the significantly higher bonding energy of the allenylidene moiety at the metal center (see X-ray discussion above). Catalytic studies by Fürstner, Hill, and co-workers in the RCM of α,ω-dienes and -dienynes using mononuclear and dinuclear (allenylidene)ruthenium(II) complexes as catalysts have been also reported.[83] However, the actual nature of the catalysts was recently revisited and reformulated as indenylidene species after full characterization (see complexes **80**−**81** in Scheme 25).[71,84] The first example of a water-soluble allenylidene complex, the dinuclear salt $[(TPPMS)_4Ru_2Cl_4(=C=C=CPh_2)_2]$ (TPPMS = $[Na][Ph_2P\text{-}\{2\text{-}OSO_2C_6H_4\}]$) which shows catalytic activity in ROM and ROMP of olefins, was recently prepared.[85]

Concluding Remarks

Studies on the reactivity of allenylidene and higher cumulenylidene complexes have been widely developed since the discovery of the first derivatives by Fischer and Berke. Both experimental and theoretical studies on allenylidene complexes $[M]{=}C{=}C{=}CR^1R^2$ are now well established, indicating that the electrophilic centers are located at C_α and C_γ, while the C_β atom is a nucleophile site. Nucleophilic attacks dominate the reactivity of allenylidene complexes relative to the electrophilic additions which usually occur in neutral complexes. Recently, an unusual protonation of the cationic complex $[Os(=C=C=CPh_2)(\eta^5\text{-}C_5H_5)(PiPr_3)_2][PF_6]$ with HPF_6 to give the alkenylcarbyne $[Os\{{\equiv}C{-}C(H){=}CPh_2\}(\eta^5\text{-}C_5H_5)(PiPr_3)_2][PF_6]_2$ was reported. Recent theoretical calculations on higher cumulenylidene chains $=C(=C)_n{=}CH_2$ (n = 0−7) also confirm that the electrophilic and nucleophilic attacks are frontier orbital controlled, showing that the carbon atoms are alternatively electron-poor and electron-rich, starting from the metal. Reactivity studies on butatrienylidene and pentatetraenylidene complexes, which are now emerging, seem to agree with these expectations.

Most of the results on the reactivity of allenylidene complexes continue to reveal the potential utility in selective C−C and C−heteroatom bond formation. Relevant developments which have been disclosed are: (*i*) regio- and stereoselective additions at the C_γ atom which provide a valuable methodology for the synthesis of functionalized alkynyl complexes, some of them being of interest for the synthesis of polyen(yn)yl chains; (*ii*) inter- and intramolecular cyclization reactions involving $C_\alpha{-}C_\beta$ and $C_\beta{-}C_\gamma$ double bonds; (*iii*) intramolecular C−C coupling reactions with alkynes, alkenyl and alkynyl groups, leading to the selective formation of highly unsaturated hydrocarbon moieties.

Although the utility of allenylidene complexes in catalytic processes are still scarce, studies of the catalytic activity in ring-closing metathesis (RCM) of olefins have been reported for the first time. Provided that the efficiency is comparable to that of Grubbs' alkylidene complexes, it is apparent that this achievement would enhance the rapid progress of this field in the near future.

Acknowledgments

The authors wish to thank to Profs. M. I. Bruce, M. A. Esteruelas, H. Fischer, S. P. Nolan, M. Peruzzini, H. Werner, and R. F. Winter for kindly providing information on their unpublished work. Financial support of the authors' research provided by the Dirección General de Investigación Científica y Técnica of Spain (DGICYT, Project PB96-0558) and the EU (Human Capital Mobility programme, Project ERBCHRXCT 940501) is also gratefully acknowledged.

Note Added in Proof: (i) Novel examples of catalytic ring-closing olefin metathesis using the 18-electron allenylidene complexes $[RuCl(=C=C=CR_2)(\eta^6\text{-}p\text{-cymene})(PR_3)]_+$ (PR_3 = PPh_3, PCy_3, $PiPr_3$) have been described.[86] – (ii) The allenylidene derivative $[Ru(=C=C=CPh_2)(\eta^5\text{-}C_5H_5)(CO)(PiPr_3)][BF_4]$ reacts with 2-aminopyridine and thioisonicotinamide to afford unprecedented pyrido-[1,2-*a*]pyrimidinyl and 1,3-thiazinyl complexes, respectively, which are formed through 1,2,3-diheterocyclization processes.[87]. In addition, novel functionalised [alkenyl(methoxy)carbene]Ru^{II}, -Cr^0 and -W^0 derivatives have been synthesized by addition of methanol on unstable allenylidene complexes.[88]. – (iii) The isolation and structural characterization of the butatrienylidene complex *trans*-$[IrCl(=C=C=C=CPh_2)(PiPr_3)_2]$,[89] as well as the preparation of pentatetraenylidene derivatives of general formula $[Re(=C=C=C=CAr_2)(\eta^5\text{-}C_5Me_5)(NO)(PPh_3)][BF_4]$ (CAr_2 = 9-fluorenylidene moieties),[90]) have been described. – (iv) The zwitterionic μ-but-2-yn-1-ylidene-4-ylidyne complex $[Ru_3(CO)_{10}(\mu_3\text{-}C\text{-}C{\equiv}C\text{-}\mu\text{-}C)\text{-}Fe_2(\eta^5\text{-}C_5Me_5)_2(CO)_3]$ and its dimerized product containing a cumulenic μ-C_8 ligand $[\{(\eta^5\text{-}C_5Me_5)Fe\}_4\{\mu\text{-}C_8\text{-}C(=O)\}\text{-}\{Ru_2(CO)_{13}\}]$ have been prepared.[91]

[1] For recent reviews see: [1a] W. D. Wulff, in: *Comprehensive Organic Synthesis* (Eds.: B. M. Trost, I. Fleming, L. A. Paquette), Pergamon Press, Oxford, **1991**, vol. 5, p. 1065–1113. – [1b] M. J. Winter, in: *Comprehensive Organometallic Chemistry II* (Eds.: E. W. Abel, F. G. A. Stone, G. Wilkinson), Pergamon Press, Oxford, **1995**, vol. 5, p. 155–214. – [1c] M. P. Doyle, in: *Comprehensive Organometallic Chemistry II* (Eds.: E. W. Abel, F. G. A. Stone, G. Wilkinson), Pergamon Press, Oxford, **1995**, vol. 5, p. 387–468. – [1d] W. D. Wulff, in: *Comprehensive Organometallic Chemistry II* (Eds.: E. W. Abel, F. G. A. Stone, G. Wilkinson), Pergamon Press, Oxford, **1995**, vol. 12, p. 469–547. – [1e] L. S. Hegedus, in: *Comprehensive Organometallic Chemistry II* (Eds.: E. W. Abel, F. G. A. Stone, G. Wilkinson), Pergamon Press, Oxford, **1995**, vol. 12, p. 549–576. – [1f] D. F. Harvey, D. M. Sigano, *Chem. Rev.* **1996**, *96*, 271–288. – [1g] F. Zaragoza Dörwald, in: *Metal Carbenes in Organic Synthesis*, Wiley-VCH, Weinheim, **1999**.

[2] For recent reviews see: [2a] W. Beck, B. Niemer, M. Wieser, *Angew. Chem. Int. Ed. Engl.* **1993**, *32*, 923–949. – [2b] H. Lang, *Angew. Chem. Int. Ed. Engl.* **1994**, *33*, 547–550. – [2c] U. H. F. Bunz, *Angew. Chem. Int. Ed. Engl.* **1996**, *35*, 969–973. – [2d] F. Paul, C. Lapinte, *Coord. Chem. Rev.* **1998**, *178–180*, 431–509. – [2e] See also: R. Dembinski, T. Bartik, B. Bartik, M. Jaeger, J. A. Gladysz, *J. Am. Chem. Soc.* **2000**, *122*, 810–822 and references cited therein.

[3] For recent reviews see: [3a] R. H. Grubbs, S. J. Miller, G. C. Fu, *Acc. Chem. Res.* **1995**, *28*, 446–452. – [3b] M. Schuster, S. Blechert, *Angew. Chem. Int. Ed. Engl.* **1997**, *36*, 2036–2056. – [3c] R. H. Grubbs, S. Chang, *Tetrahedron* **1998**, *54*, 4413–4450.

[4] [4a] M. I. Bruce, *Chem. Rev.* **1991**, *91*, 197–257. – [4b] M. I. Bruce, *Chem. Rev.* **1998**, *98*, 2797–2858. – [4c] H. Werner, *Chem. Commun.* **1997**, 903–910. – [4d] H. Le Bozec, P. H. Dixneuf, *Russ. Chem. Bull.* **1995**, *44*, 801–812. – [4e] D. Touchard, P. H. Dixneuf, *Coord. Chem. Rev.* **1998**, *178–180*, 409–429. – [4f] M. I. Bruce, *Coord. Chem. Rev.* **1997**, *166*, 91–119. – [4g] S. Doherty, J. F. Corrigan, A. J. Carty, E. Sappa, *Adv. Organomet. Chem.* **1995**, *37*, 39–130. – [4h] H. El Amouri, M. Gruselle, *Chem. Rev.* **1996**, *96*, 1077–1103. – [4i] G. Jia, C. P. Lau, *J. Organomet. Chem.* **1998**, *565*, 37–48.

[5] [5a] E. O. Fischer, H. J. Kalder, A. Frank, F. H. Kohler, G. Huttner, *Angew. Chem. Int. Ed. Engl.* **1976**, *15*, 623–624. – [5b] H. Berke, *Angew. Chem. Int. Ed. Engl.* **1976**, *15*, 624.

[6] [6a] J. P. Selegue, *Organometallics* **1982**, *1*, 217–218. – [6b] A. F. Hill, in: *Comprehensive Organometallic Chemistry II* (Eds.: E. W. Abel, F. G. A. Stone, G. Wilkinson), Pergamon Press, Oxford, **1995**, vol. 7, p. 348–356.

[7] An example of Group 4 allenylidene complex, namely $[Ti(=C=C=CPh_2)(\eta^5\text{-}C_5H_5)(PMe_3)]$, is known: P. Binger, P. Müller, R. Wenz, R. Mynott, *Angew. Chem. Int. Ed. Engl.* **1990**, *29*, 1037–1038.

[8] H. J. Schanz, L. Jafarpour, E. D. Stevens, S. P. Nolan, *Organometallics* **1999**, *18*, 5187–5190.

[9] See for example: [9a] J. Huang, E. D. Stevens, S. P. Nolan, J. L. Petersen, *J. Am. Chem. Soc.* **1999**, *121*, 2647–2678. – [9b] J. Huang, H.-J. Schanz, E. D. Stevens, S. P. Nolan, *Organometallics* **1999**, *18*, 2370–2375.

[10] D. Touchard, P. Haquette, A. Daridor, A. Romero, P. H. Dixneuf, *Organometallics* **1998**, *17*, 3844–3852.

[11] E. Bustelo, M. Jiménez Tenorio, M. C. Puerta, P. Valerga, *Organometallics* **1999**, *18*, 4563–4573.

[12] M. I. Bruce, P. Hinterding, P. J. Low, B. W. Skelton, A. H. White, *J. Chem. Soc., Dalton Trans.* **1998**, 467–473.

[13] L. Jafarpour, J. Huang, E. D. Stevens, S. P. Nolan, *Organometallics* **1999**, *18*, 3760–3763.

[14] K. Urtel, A. Frick, G. Huttner, L. Zsolnai, P. Kircher, P. Rutsch, E. Kaifer, A. Jacobi, *Eur. J. Inog. Chem.* **2000**, 33–50.

[15] B. Buriez, I. D. Burns, A. F. Hill, A. J. P. White, D. J. Williams, J. D. E. T. Wilton-Ely, *Organometallics* **1999**, *18*, 1504–1516.

[16] V. Cadierno, M. P. Gamasa, J. Gimeno, L. Iglesias, S. García-Granda, *Inorg. Chem.* **1999**, *38*, 2874–2879.

[17] B. Windmüller, O. Nürnberg, J. Wolf, H. Werner, *Eur. J. Inorg. Chem.* **1999**, 613–619.

[18] C. Bianchini, M. Peruzzini, F. Zanobini, C. Lopez, I. de los Rios, A. Romerosa, *Chem. Commun.* **1999**, 443–444.

[19] H. Werner, C. Grünwald, P. Steinert, O. Gevert, J. Wolf, *J. Organomet. Chem.* **1998**, *565*, 231–241.

[20] K. Ilg, H. Werner, *Organometallics* **1999**, *18*, 5426–5428.

[21] H. P. Xia, W. S. Ng, J. S. Ye, X.-Y. Li, W. T. Wong, Z. Lin, C. Yang, G. Jia, *Organometallics* **1999**, *18*, 4552–4557.

[22] M. Sato, A. Iwai, M. Watanabe, *Organometallics* **1999**, *18*, 3208–3219.

[23] M. Tamm, A. Grzegorzewski, I. Brüdgam, H. Hartl, *J. Chem. Soc., Dalton Trans.* **1998**, 3523–3528.

[24] M. Laubender, H. Werner, *Chem. Eur J.* **1999**, *5*, 2937–2946.

[25] S. B. Falloon, S. Szafert, A. M. Arif, J. A. Gladysz, *Chem. Eur J.* **1998**, *4*, 1033–1042.

[26] C. J. Adams, M. I. Bruce, B. W. Skelton, A. H. White, *J. Organomet. Chem.* **1999**, *584*, 254–264.

[27] M. I. Bruce, B. W. Skelton, A. H. White, N. N. Zaitseva, *J. Chem. Soc., Dalton Trans.* **2000**, 881–890.

[28] M.-C. Chung, A. Sakurai, M. Akita, Y. Moro-oka, *Organometallics* **1999**, *18*, 4684–4691.

[29] [29a] S. Kheradmandan, K. Heinze, H. W. Schmalle, H. Berke, *Angew. Chem. Int. Ed.* **1999**, *38*, 2270–2273. – [29b] M. Guillemot, L. Toupet, C. Lapinte, *Organometallics* **1998**, *17*, 1928–1930.

[30] T. Bartik, W. Weng, J. A. Ramsden, S. Szafert, S. B. Falloon, A. M. Arif, J. A. Gladysz, *J. Am. Chem. Soc.* **1998**, *120*, 11071–11081.

[31] V. Guillaume, P. Thominot, F. Coat, A. Mari, C. Lapinte, *J. Organomet. Chem.* **1998**, *565*, 75–80.

[32] F. Coat, M. Guillemot, F. Paul, C. Lapinte, *J. Organomet. Chem.* **1999**, *578*, 76−84.
[33] B. E. R. Schilling, R. Hoffmann, D. L. Lichtenberger, *J. Am. Chem. Soc.* **1979**, *101*, 585−591.
[34] [34a] H. Berke, G. Huttner, J. von Seyerl, *Z. Naturforsch.* **1981**, *36b*, 1277−1288. − [34b] N. E. Kolobova, L. L. Ivanov, O. S. Zhvanko, O. M. Khitrova, A. S. Batsanov, Y.-T. Struchkov, *J. Organomet. Chem.* **1984**, *262*, 39−47. − [34c] N. E. Kolobova, L. L. Ivanov, O. S. Zhvanko, O. M. Khitrova, A. S. Batsanov, Y.-T. Struchkov, *J. Organomet. Chem.* **1984**, *265*, 271−281.
[35] E. Pérez-Carreño, Ph. D. Thesis, University of Oviedo, **1996**.
[36] [36a] J. Díez, M. P. Gamasa, J. Gimeno, C. Gónzalez-Bernardo, E. Pérez-Carreño, unpublished results. − [36b] C. Gónzalez-Bernardo, M. P. Gamasa, J. Gimeno, L. Iglesias, unpublished results.
[37] M. A. Esteruelas, A. V. Gómez, A. M. López, J. Modrego, E. Oñate, *Organometallics* **1997**, *16*, 5826−5835.
[38] M. Baya, P. Crochet, M. A. Esteruelas, E. Gutiérrez-Puebla, A. M. López, J. Modrego, E. Oñate, N. Vela, *Organometallics* **2000**, *19*, 2585−2596.
[39] A. J. Andrews, M. A. Esteruelas, F. J. Lahoz, J. Modrego, L. A. Oro, J. Schrickel, *Organometallics* **1996**, *15*, 3556−3562.
[40] N. Re, A. Sgamellotti, C. Floriani, *Organometallics* **2000**, *19*, 1115−1122.
[41] V. Cadierno, M. P. Gamasa, J. Gimeno, M. González-Cueva, E. Lastra, J. Borge, S. García-Granda, *Organometallics* **1996**, *15*, 2137−2147.
[42] M. P. Gamasa, J. Gimeno, C. González-Bernardo, J. Borge, S. García-Granda, *Organometallics* **1997**, *16*, 2483−2485.
[43] C. González-Bernardo, Ph. D. Thesis, University of Oviedo, **2000**.
[44] A. Fürstner, M. Picquet, C. Bruneau, P. H. Dixneuf, *Chem. Commun.* **1998**, 1315−1316.
[45] Y. Yamamoto, T. Tanase, C. Sudoh, T. Turuta, *J. Organomet. Chem.* **1998**, *569*, 29−37.
[46] C. Bianchini, N. Mantovani, A. Marchi, L. Marvelli, D. Masi, M. Peruzzini, R. Rossi, A. Romerosa, *Organometallics* **1999**, *18*, 4501−4508.
[47] M. A. Esteruelas, A. V. Gómez, A. M. López, M. Oliván, E. Oñate, N. Ruiz, *Organometallics* **2000**, *19*, 4−14. For related cyclizations using allyl alcohol instead of propargyl alcohol see: M. A. Esteruelas, A. V. Gómez, A. M. López, E. Oñate, N. Ruiz, *Organometallics* **1998**, *17*, 2297−2306.
[48] D. J. Bernad, M. A. Esteruelas, A. M. López, J. Modrego, M. C. Puerta, P. Valerga, *Organometallics* **1999**, *18*, 4995−5003.
[49] M. I. Bruce, P. J. Low, E. R. T. Tiekink, *J. Organomet. Chem.* **1999**, *572*, 3−10.
[50] P. Haquette, D. Touchard, L. Toupet, P. Dixneuf, *J. Organomet. Chem.* **1998**, *565*, 63−73.
[51] V. Cadierno, M. P. Gamasa, J. Gimeno, M. C. López-González, J. Borge, S. García-Granda, *Organometallics* **1997**, *16*, 4453−4463.
[52] V. Cadierno, S. Conejero, M. P. Gamasa, J. Gimeno, I. Asselberghs, S. Houbrechts, K. Clays, A. Persoons, J. Borge, S. García-Granda, *Organometallics* **1999**, *18*, 582−597.
[53] V. Cadierno, M. P. Gamasa, J. Gimeno, J. Borge, S. García-Granda, *Organometallics* **1997**, *16*, 3178−3187.
[54] M. A. Esteruelas, A. V. Gómez, A. M. López, J. Modrego, E. Oñate, *Organometallics* **1998**, *17*, 5434−5436.
[55] V. Cadierno, M. P. Gamasa, J. Gimeno, *J. Chem. Soc., Dalton Trans.* **1999**, 1857−1866.
[56] V. Cadierno, M. P. Gamasa, J. Gimeno, E. Pérez-Carreño, S. García-Granda, *Organometallics* **1999**, *18*, 2821−2832.
[57] P. Crochet, B. Demerseman, M. I. Vallejo, M. P. Gamasa, J. Gimeno, J. Borge, S. García-Granda, , *Organometallics* **1997**, *16*, 5406−5415.
[58] V. Cadierno, M. P. Gamasa, J. Gimeno, E. Lastra, *J. Chem. Soc., Dalton Trans.* **1999**, 3235−3243.
[59] S. Conejero, M. P. Gamasa, J. Gimeno, unpublished results.
[60] V. Cadierno, S. Conejero, M. P. Gamasa, J. Gimeno, *J. Chem. Soc., Dalton Trans.* **2000**, 451−457.
[61] V. Cadierno, M. P. Gamasa, J. Gimeno, J. M. Moretó, S. Ricart, A. Roig, E. Molins, *Organometallics* **1998**, *17*, 697−706. Related cyclizations using (*E*,*Z*)-[Ru{C≡C−C(H)=CH−C≡CPh}(η^5-C_9H_7)(PPh_3)$_2$] are also reported.
[62] [62a] V. Cadierno, M. P. Gamasa, J. Gimeno, E. Pérez-Carreño, A. Ienco, *Organometallics* **1998**, *17*, 5216−5218. − [62b] V. Cadierno, M. P. Gamasa, J. Gimeno, unpublished results.
[63] M. A. Esteruelas, A. V. Gómez, A. M. López, E. Oñate, N. Ruiz, *Organometallics* **1999**, *18*, 1606−1614.
[64] M. A. Esteruelas, A. V. Gómez, A. M. López, M. C. Puerta, P. Valerga, *Organometallics* **1998**, *17*, 4959−4965.
[65] [65a] M. A. Esteruelas, A. V. Gómez, A. M. López, E. Oñate, *Organometallics* **1998**, *17*, 3567−3573. − [65b] C. Bianchini, M. Peruzzini, R. Rossi, personal communication. − [65c] The allenylidene complex [Re(=C=C=CPh_2)(TRIPHOS)$(CO)_2$]-[CF_3SO_3] also reacts with amines (NH_2Ph, $NH_2CH_2C{\equiv}CH$, NH_3, etc.) and thiols (SHPh, SHEt, etc.) to form amino- and thiocarbenes, respectively.
[66] B. Buriez, D. J. Cook, K. J. Harlow, A. F. Hill, T. Welton, A. J. P. White, D. J. Williams, J. D. E. T. Wilton-Ely, *J. Organomet. Chem.* **1999**, *578*, 264−267.
[67] K. J. Harlow, A. F. Hill, T. Welton, *J. Chem. Soc., Dalton Trans.* **1999**, 1911−1912.
[68] Related cyclizations are also known for ruthenium(II)−allenylidene complexes. See ref.[4b]
[69] M. Laubender, H. Werner, *Angew. Chem. Int. Ed.* **1998**, *37*, 150−152.
[70] J. Gil-Rubio, B. Weberndörfer, H. Werner, *Angew. Chem. Int. Ed.* **2000**, *39*, 786−789.
[71] A. Fürstner, B. Gabor, A. F. Hill, L. Jafarpour, M. Liebl, R. Mynott, S. P. Nolan, E. D. Stevens, J. D. E. T. Wilton-Ely, personal communication.
[72] K. J. Harlow, A. F. Hill, J. D. E. T. Wilton-Ely, *J. Chem. Soc., Dalton Trans.* **1999**, 285−291.
[73] P. Crochet, M. A. Esteruelas, A. M. López, N. Ruiz, J. I. Tolosa, *Organometallics* **1998**, *17*, 3479−3486.
[74] K. H. Dötz, D. Paetsch, H. Le Bozec, *J. Organomet. Chem.* **1999**, *589*, 11−20.
[75] M. I. Bruce, B. W. Skelton, A. H. White, N. N. Zaitseva, *Inorg. Chem. Commun.* **1999**, *2*, 17−20.
[76] R. F. Winter, F. M. Hornung, *Organometallics* **1999**, *18*, 4005−4014.
[77] R. F. Winter, *Chem. Commun.* **1998**, 2209−2210.
[78] R. F. Winter, *Eur. J. Inorg. Chem.* **1999**, 2121−2126. − Related Cope-type rearrangements have been reported with allylic amines. See: R. F. Winter, F. M. Hornung, *Organometallics* **1997**, *16*, 4248−4250.
[79] M. I. Bruce, M. Ke, B. D. Kelly, P. J. Low, M. E. Smith, B. W. Skelton, A. H. White, *J. Organomet. Chem.* **1999**, *590*, 184−201.
[80] (Allenylidene)ruthenium(II) complexes have been proposed as key intermediates in the catalytic cyclization-reconstituent addition of propargyl alcohols with allyl alcohols. − [80a] B. M. Trost, J. A. Flygare, *J. Am. Chem. Soc.* **1992**, *114*, 5476−5477. − [80b] B. M. Trost, J. A. Flygare, *Tetrahedron Lett.* **1994**, *35*, 4059−4062. − [80c] B. M. Trost, *Chem. Ber.* **1996**, *129*, 1313−1322.
[81] M. Picquet, C. Bruneau, P. H. Dixneuf, *Chem. Commun.* **1998**, 2249−2250.
[82] M. Picquet, D. Touchard, C. Bruneau, P. H. Dixneuf, *New. J. Chem.* **1999**, *23*, 141−143.
[83] A. Fürstner, A. F. Hill, M. Liebl, J. D. E. T. Wilton-Ely, *Chem. Commun.* **1999**, 601−602.
[84] Nevertheless, these species show very high catalytic activity, even at room temperature. − [84a] L. Jafarpour, H.-J. Schanz, E. D. Stevens, S. P. Nolan, *Organometallics* **1999**, *18*, 5416−5419. − [84b] A. Fürstner, J. Grabowski, C. W. Lehmann, *J. Org. Chem.* **1999**, *64*, 8275−8280. − [84c] M. T. Reetz, M. H. Becker, M. Liebl, A. Fürstner, *Angew. Chem. Int. Ed.* **2000**, *39*, 1236−1239.
[85] M. Saoud, A. Romerosa, M. Peruzzini, *Organometallics* **2000**, *19*, 4005−4007.
[86] [86a] A. Fürstner, M. Liebl, C. W. Lehmann, M, Picquet, R. Kunz, C. Bruneau, D. Touchard, P. H, Dixneuf, *Chem. Eur. J.* **2000**, *6*, 1847−1857. − [86b] A. Fürstner, O. R. Thiel, *J. Org. Chem.* **2000**, *65*, 1738−1742.
[87] D. J. Bernad, M. A. Esteruelas, A. M. López, M. Oliván, E. Oñate, M. C. Puerta, P. Valerga, *Organometallics* **2000**, *19*, 4327−4335.
[88] K. Ulrich, E. Porhiel, V. Péron, V. Ferrand, H. Le Bozec, *J. Organomet. Chem.* **2000**, *601*, 78−86.

[89] K. Ilg, H. Werner, *Angew. Chem. Int. Ed.* **2000**, *39*, 1632−1634.
[90] S. Szafert, P. Haquette, S. B. Falloon, J. A. Gladysz, *J. Organomet. Chem.* **2000**, *604*, 52−58.
[91] M. Akita, M. C. Chung, A. Sakurai, Y. Moro-oka, *Chem. Commun.* **2000**, 1285−1286.

Received May 18, 2000
[I00205]

Metal-Assisted P−H Bond Formation: A Step towards the Hydrogenation of White Phosphorus

Maurizio Peruzzini,*[a] Isaac de los Rios,[a] Antonio Romerosa,[b] and Francesco Vizza[a]

Dedicated to the memory of our unforgettable friend Professor José Antonio Ramírez (1957−2000)

Keywords: P−H bond formation / Phosphanes / Phosphorus / Transition metals

An overview of the chemistry of transition metal complexes containing P–H bonds is presented. Central to this microreview are those compounds in which the P–H bond is assembled by reactions entailing the transfer of one or more hydrogen atoms to white phosphorus or to P_x fragments resulting from P_4 activation and degradation within the coordination sphere of a transition metal complex. The relevance of these processes to the as yet unaccomplished hydrogenation of white phosphorus is briefly discussed.

Contents

1. Introduction
2. Formation of P−H Bonds from Naked P Atoms and Units Bonded to Transition Metal Complexes
2.1 A Survey of Transition Metal Complexes Incorporating P−H Bonds
2.2 Reaction of White Phosphorus with Transition Metal Hydrides
2.2.1 Reaction with Hydrido-Metallocenes
2.2.2 Reactions with Hydrido-Polyphosphanes
2.3 Electrophilic Hydrogenation of P_x Units Incorporated into Transition Metal Complexes
2.4 Nucleophilic Hydrogenation of P_x Units Incorporated into Transition Metal Complexes
3. Concluding Remarks

[a] ISSECC CNR,
Via Jacopo Nardi, 39, 50132 Firenze, Italy
Fax: (internat.) + 39-055/247-8366
E-mail: peruz@fi.cnr.it
[b] Área de Química Inorgánica, Facultad de Ciencias, Universidad de Almería,
04071 Almería, Spain

Maurizio Peruzzini (second from left) was born in Florence, Italy, in 1955. After his "Laurea" cum laude at the University of Florence in 1979 under the supervision of Luigi Sacconi and Piero Stoppioni, he joined the team led by Claudio Bianchini at ISSECC-CNR in 1986, where he is currently Senior Research Associate. He obtained the "Raffaele Nasini" gold medal prize awarded by the Inorganic Chemistry Division of the Societá Chimica Italiana in 1993 in recognition of his contribution to the chemistry of non-classical hydrides. His research interests are primarily in the field of organometallic chemistry and catalysis, as well as the activation and functionalization of pnicogen and chalcogen elements, mediated by transition metals. He has authored over 160 papers and patents and made more than 120 presentations at national and international meetings.

Isaac de los Rios (second from right) was born in Jerez de la Frontera, Spain, in 1970. He received his PhD from the University of Cadiz in 1997 under the guidance of M. Carmen Puerta. He is currently working on the activation and functionalization of white phosphorus in Florence at ISSECC-CNR in the group of Maurizio Peruzzini, with a Spanish Government grant. He has published about 15 papers in organometallic chemistry.

Antonio Romerosa (first from right) was born in Granada, Spain, in 1964. He graduated from the Universidad de Granada with a B.S. in Coordination Chemistry in 1987, and received his Ph.D. in organometallic borane chemistry from the Universidad Autónoma de Barcelona in January 1992. In the same year he undertook a postdoctoral research with Claudio Bianchini and Maurizio Peruzzini at ISSECC-CNR, Florence (Italy), before becoming Assistant Professor and then Associate Professor (1996) at the Universidad de Almería (Spain). He has performed postdoctoral research at ISSECC-CNR (Florence, Italy), Queen's University of Belfast (UK), the Instituto de Química (UNAM, México-DF), and Durham University (UK). His research interests cover fundamental aspects of both organometallic and bioinorganic chemistry. He has authored over 50 papers.

Francesco Vizza (first from left) was born in Cirò (KR), Italy, in 1957 and received his "laurea" in Biology from the University of Florence in 1982 under the supervision of Mario Ciampolini. He was then assistant researcher at the Department of Chemistry of the University of Florence, working in the field of macrocycle complexes. In 1986 he joined ISSECC-CNR, where he is presently Researcher and responsible for a catalysis laboratory. His current research interests are in the fields of homogeneous and heterogeneous catalysis (HDS, HDN, polymerization and copolymerization of olefins), chemistry of white phosphorus, transition metal complexes in therapy and diagnostics, and high-pressure NMR spectroscopy. He has authored about 85 papers and patents.

MICROREVIEWS: This feature introduces the readers to the authors' research through a concise overview of the selected topic. Reference to important work from others in the field is included.

 © WILEY-VCH Verlag GmbH, 69451 Weinheim, 2001 1434−1948/01/0303−0593 $ 17.50+.50/0

1. Introduction

During the second part of the twentieth century there has been a spectacular renaissance of phosphorus chemistry, which has had a profound impact on a broad range of disciplines.[1] Few other branches of chemistry have had a greater influence on chemistry, biology, and material sciences, nor offer greater potential for addressing future needs and opportunities in far-reaching areas of science and engineering.

In keeping with the renowned interest of phosphorus chemistry, the coordination chemistry of elemental phosphorus, which was virtually unexplored until 1970, has now become a mature province of inorganic chemistry and has contributed important results to the resurgence of main group chemistry.[2] It begins from the reporting of $[(PPh_3)_2ClRh(\eta^2\text{-}P_4)]$ by Ginsberg and Lindsell in 1971,[3] and proceeds through an as yet unfinished string of key discoveries. Milestones in this story include, among others, Sacconi's reporting of $[(NP_3)Ni(\eta^1\text{-}P_4)]$ [$NP_3 = N(CH_2CH_2PPh_2)_3$], the first coordination compound exhibiting an intact *tetrahedro*-tetraphosphorus ligand,[4] and the spectacular complexes $[\{Cp^*Mo\}_2(\mu,\eta^6\text{:}\eta^6\text{-}P_6)]$[5] and $[Cp^*Fe(\eta^5\text{-}P_5)]$[6] prepared by Scherer and co-workers. These compounds, respectively containing the unprecedented hexaphosphabenzene and pentaphosphacyclopentadienyl ligands, bolstered confidence in the hypothesized approach based on building up polyphosphorus ligands through the well-known isolobal relationship between P atoms and CH groups.[7] Of course, there were many other breakthroughs in the coordination chemistry of naked phosphorus atoms and units, and dozens of other relevant contributions from the groups led by Sacconi,[8] Scherer,[9] Scheer,[10] Dahl,[11] Markó,[11a,12] Goh,[13] Wachter,[14] Huttner,[15] Stoppioni,[16] Schrock,[17] Cummins,[18] and others[19] have contributed to the rapid metamorphosis of white phosphorus coordination chemistry. Outstanding reviews describing the coordination chemistry of white phosphorus have also appeared in recent literature.[20]

In contrast, studies addressing the reactivity of these complexes have until recently seldom been considered, and remain quite rare in the literature. In addition, many of these early studies have been limited to the straightforward addition of electrophilic metal fragments − generally $M(CO)_5$ (M = Cr, Mo, W) − to the residual electron pair of the unsubstituted phosphorus atom.[21] An excellent recent survey by Whitmire deals with the chemistry of main group/transition metal cluster compounds, but addresses the reactivity of these complexes only to a limited extent,[20b] and does not cover the chemistry related to the metal-mediated hydrogenation of white phosphorus. This microreview is intended to fill this gap and focuses on the metal-mediated formation of P−H bonds, with particular emphasis on those reactions in which the P−H bond is produced starting from the P_4 molecule or fragments thereof.

2. Formation of P−H Bonds from Naked P Atoms and Units Bonded to Transition Metal Complexes

2.1. A Survey of Transition Metal Complexes Incorporating P−H Bonds

Unlike that of nitrogen, the reaction of white phosphorus with hydrogen has received comparably little attention, and the possibility that H_2 might directly react with P_4 is still a matter of debate.[22] Thus, the sparse reports on this subject, indicating that a reaction could take place only under high H_2 pressure at elevated temperature (> 360 °C), should be carefully considered.[23]

Although a bewildering variety of binary phosphorus-hydrogen compounds (phosphanes) have been described in the last thirty years,[24−26] transition metal complexes containing phosphorus hydrides are practically limited to the numerous complexes containing primary (**1**) and secondary (**2**) phosphanes (or phosphites) or their simple derivatives, particularly bridging phosphido species (**3**).[27,28] There also exist a small number of transition metal complexes incorporating one or more PH_3 ligands,[29] but homoleptic species, such as $[Ni(PH_3)_4]$ (**4**), are extremely rare.[30] PH_3 complexes are in turn a suitable starting point for the preparation of terminal and bridging phosphido (PH_2) complexes,[31] and some μ-phosphinidene derivatives, such as $[\{Cp^*Mn(CO)_2\}_2(\mu\text{-}PH)]$ (**5**)[32] and $[\{Co(CO)_4\}_2\{Cr(CO)_3\}(\mu_3\text{-}PH)]$ (**6**)[33] have also been prepared from PH_3 precursors.

Clusters featuring μ_3-PH or μ_4-PH capping phosphinidene ligand are also well known.[33,34] Such compounds can be prepared by direct interaction of PH_3 with polymetallic clusters[34c] or by treating a preformed PH_3 metal complex with a carbonyl cluster.[33] However, the best synthetic approach to phosphinidene clusters is the hydrolysis of silylphosphinidene clusters. A neat application of this preparative methodology has recently been reported by Schauer and co-workers, who synthesized the biphosphinidene cluster $[Fe_3(CO)_9(\mu_3\text{-}PH)_2]$ (**7**) by controlled hydrolysis of P−Si bonds.[35] The reactivity of **7**, which is largely centered on the P−H functionality, has been investigated thoroughly. Remarkably, the reaction chemistry at one P−H functional site is effectively transferred to the second P−H site through the trimetallic $Fe_3(CO)_9$ core.

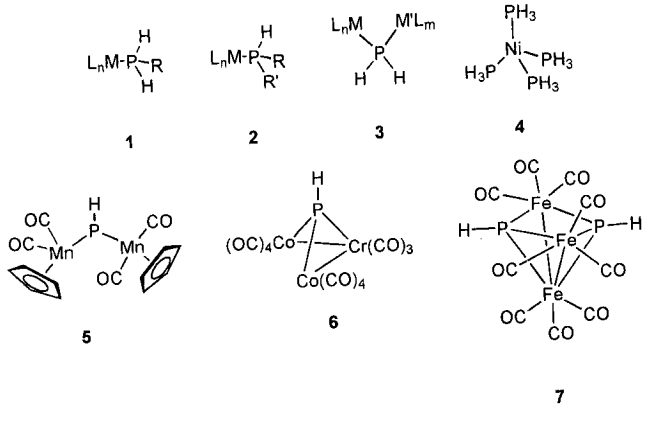

Stable triorganometallic phosphonium salts of formula $[\{Cp(CO)_2Fe\}_3(\mu_3\text{-}PH)]_n$ X (**8**) (n = 1, X = halide; n = 2, X = $FeCl_4$) have been prepared by Lorenz and co-workers by in situ methanolysis of P−Si bonds. Thus, **8** has readily been obtained as reddish brown microcrystals by treatment of $[CpFe(CO)_2X]$ (**9**) with $P(SiMe_3)_3$ at room temperature in toluene followed by crystallization in the presence of methanol.[36] UV irradiation induced the transformation of the tetrachloroferrate salt $[\{Cp(CO)_2Fe\}_3(\mu_3\text{-}PH)]_2[FeCl_4]$ into the *closed-Fe,Fe*-triferriophosphonium derivative $[\{Cp(CO)_2Fe\}\{(\mu\text{-}CO)[Cp(CO)_2Fe]_2\}(\mu_3\text{-}PH)]_2[FeCl_4]$ (**10**) by means of elimination of one CO ligand and formation of an Fe−Fe bond supporting a bridging carbonyl ligand.[37] Notably, the PH protons in both the triferriophosphonium derivatives **8** and **10** can easily be removed with DBU (1,8-diazabicyclo[5.4.0]undecene) in THF. Scheme 1 summarizes these transformations.

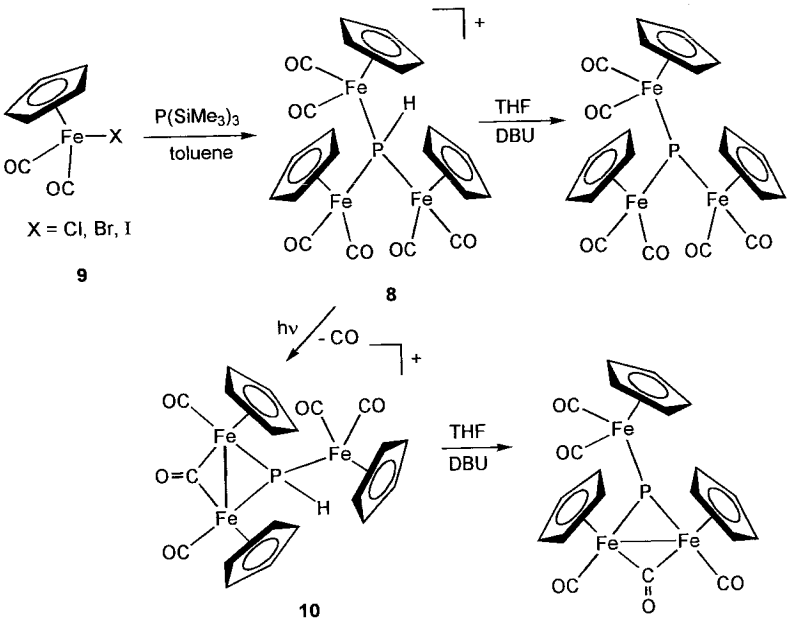

Scheme 1

Of the other phosphanes, including the long-known P_2H_4, no transition metal derivative has yet been reported; unsurprising in view of the hyperreactivity of these molecules and their marked tendency to disproportionate.[24−26] However, complexes of substituted diphosphanes are known, and some of them, such as the dinuclear silver complex $[\{(PH_2Ph)Ag\}_2(\mu,\eta^1\text{:}\eta^1\text{-}P,P'\text{-}P(H)PhP(H)Ph)_2](AsF_6)_2$ (**11**), featuring two bridging diphenyldiphosphane ligands, have been authenticated by X-ray methods.[38] The coordination chemistry of substituted diphosphenes (P_2R_2) has also been studied, but the stabilization of diphosphene complexes usually requires bulky substituents. An outstanding review by Weber highlights the coordination chemistry of these ligands, also including the very few compounds containing P−H bonds.[39] At present, four complexes containing the parent diphosphene ligand (P_2H_2) have been reported. Two of these, $[Cp_2Mo(\eta^2\text{-}P_2H_2)]$ (**12**) and $[Cp_2TaH(\eta^2\text{-}P_2H_2)]$ (**13**), were prepared from direct treatment of metal hydrides with white phosphorus[40,41] and will be discussed in detail in the next section. The formation of the kinetic intermediate $[(dcpe)Ni(\eta^2\text{-}P_2H_2)]$ (**14**) (dcpe = $Cy_2PCH_2CH_2PCy_2$) during the methanolysis of $[(dcpe)Ni(\eta^2\text{-}P_2(SiMe_3)_2)]$ (**15**) en route to the formation of the diphosphorus dimetallic species $[\{(dcpe)Ni\}_2\text{-}(\mu,\eta^2\text{:}\eta^2\text{-}P_2)]$ (**16**) (Scheme 2) was briefly mentioned by Schäfer and co-workers.[42] Although **14** was not stable enough to be isolated, it was observed at low temperature and its ^{31}P and ^1H NMR spectra were recorded. At 0 °C in toluene, it slowly decomposed, yielding **16** and phosphane (PH_3). However, no details about this intriguing decomposition reaction, in which both P−P and P−H bonds were broken and reassembled, were provided.

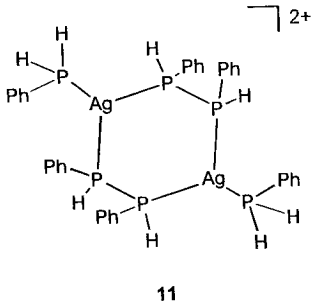

The only other known diphosphene complex was prepared by Stephan and co-workers by treatment of $[\{Cp^*_2Zr(N_2)\}_2(\mu\text{-}N_2)]$ (**17**) with the primary phosphane $PH_2(2,4,6\text{-}t\text{Bu-}C_6H_2)$.[43] The reaction proceeded smoothly in benzene at room temperature to afford the diphosphene complex $[Cp^*_2Zr(\eta^2\text{-}P_2H_2)]$ (**18**) and 2,4,6-tBu$_3$-C_6H_3 in excellent yield (Scheme 3). The formation of **18** was associated with a P−C bond activation reaction at the sterically congested Zr−P system, which forms in the presence of a bulky primary phosphane. Such P−C bond activation

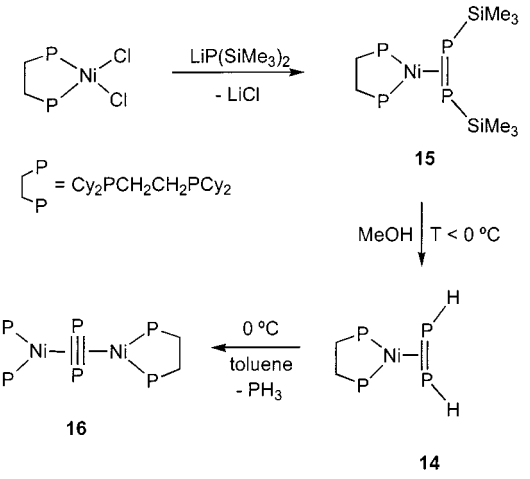

Scheme 2

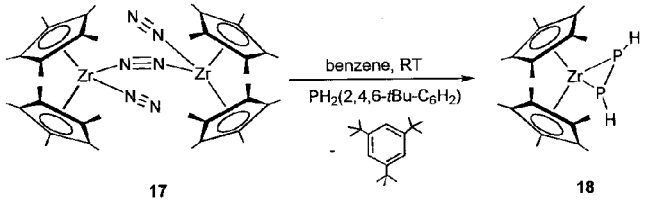

Scheme 3

methodology has successfully been used to synthesize several substituent-free P_x complexes of zirconium.[43]

It is worth mentioning that the parent diphosphene (P_2H_2) molecule, which in the four derivatives mentioned above was stabilized by complexation with low-valent organometallic metallocenes, has never been isolated in the free state. Such a molecule represents the lightest member of the P_nH_n family of phosphorus hydrides, the heavier members of which ($n > 2$) are known in the form of monocyclic phosphanes,[24−26,44] or, for $n = 2$, have been isolated by stabilization with bulky organic substituents. Theoretical investigations of P_2H_2 model complexes, such as $[(PH_3)_2Pd(P_2H_2)]$[45] and $[(CO)_5Cr(P_2H_2)]$[46] predict that the side-on η^2-coordination mode is the preferred one, with a short elongation of the diphosphene ligand P−P bond relative to that in the free molecule.[47]

Also relevant to this survey are the thioxophosphane and selenoxophosphane osmium complexes [Os(η^2-PHE)(CO)$_2$(PPh$_3$)$_2$] (E = S, **19**; Se, **20**), which were elegantly prepared by Roper and co-workers by stepwise addition of triflic acid and DBU to the thiophosphido and selenophosphido derivatives [Os{PH$_2$(E)}(η^1-*O*-OOCCH$_3$)(CO)$_2$(PPh$_3$)$_2$] (E = S, **21**; Se, **22**) (Scheme 4).[48]

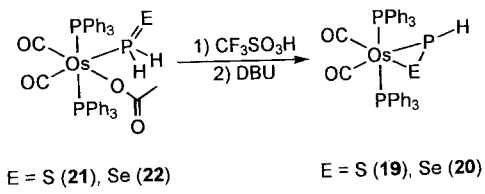

Scheme 4

Apart from these sparse examples, there does not exist any other homogeneous group of low-valent phosphorus transition metal complexes hosting the P−H functionality. This is particularly surprising if one considers that the number of known phosphorus hydrides is only exceeded by that of hydrocarbons[25] and that, notwithstanding the difficulties of directly utilizing higher phosphorus hydrides as starting reagents for preparative purposes, there should be at least three reliable synthetic strategies for incorporation of P−H bonds within the coordination polyhedron of a transition metal complex:

(a) the direct reaction of white phosphorus with transition metal hydrides,

(b) the electrophilic hydrogenation (addition of protic acids) of neutral transition metal species incorporating P_x units,

(c) the nucleophilic hydrogenation (addition of hydride reagents) of transition metal complexes incorporating P_x units.

Although the above strategies should be broadly useful for the synthesis of transition metal complexes with P−H ligands in several preparative contexts, these methods have only been exploited to a very limited extent.

Treatment of white phosphorus with organometallic complexes may sometime result in the direct formation of P−H species even in the absence of suitable hydrogen donor sources. Adventitious water is generally considered to be responsible for the formation in these unpredictable reactions of species containing P−H. A pleasing example of this chemistry is provided by the study of the reaction of the sterically demanding rhenium metallocene [(1,2,3,4-*i*Pr$_4$C$_5$H)Re(CO)$_2$(thf)] (**23**) with excess P_4.[49a] After prolonged reflux in decalin and chromatographic workup, a mixture was obtained, from which the tetraphosphacyclobutane [(1,2,3,4-*i*Pr$_4$C$_5$H)Re(CO)(η^4-P$_4$)] (**24**) and μ-phosphinidene [{(1,2,3,4-*i*Pr$_4$C$_5$H)Re(CO)$_2$}$_2$(μ-PH)] (**25**) complexes were separated (Scheme 5). A similar phosphinidene complex [{Cp*Re(CO)$_2$}$_2$(μ-PH)] (**26**) was obtained by treatment of [{Cp*Re(CO)$_2$}$_2$(μ−H)$_2$] (**27**) with P_4 in toluene. However, no details of the mechanism leading to **26** were given.[49b] The two dirhenium phosphinidenes exhibit NMR resonances shifted strongly to low field (^{31}P: δ = 505/512, and ^{1}H: δ = 15.5/14.8), with direct P−H coupling constants (191/187 Hz) typical of $^1J_{PH}$ couplings.[50]

2.2. Reaction of White Phosphorus with Transition Metal Hydrides

2.2.1. Reactions of White Phosphorus with Hydrido-Metallocenes

The reaction of white phosphorus with a transition metal complex was first described as early as 1974, by Green and co-workers. In a short note it was reported that the molybdenum dihydride [Cp$_2$MoH$_2$] (**28**) reacted smoothly with P_4 in hot toluene at 90 °C to yield, after chromatographic workup on alumina, deep red crystals; these were assigned the stoichiometry [Cp$_2$Mo(η^2-P$_2$H$_2$)] (**12**) on the basis of MS analysis, molecular mass determination, and ^{1}H and

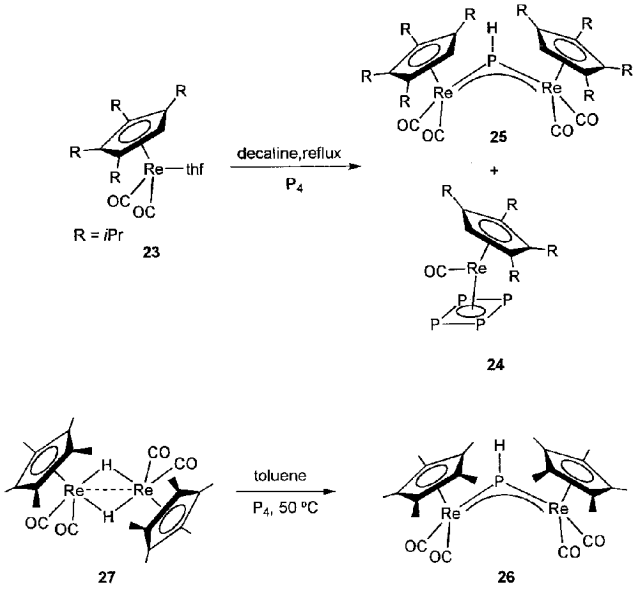

Scheme 5

^{31}P NMR spectroscopy (Scheme 6).[40] However, spectroscopic methods alone were not capable of distinguishing between the two possible stereoisomers of the diphosphene ligand in **12** [*trans* (I) or *cis* (II)], which were preferred to the planar arrangement because of stereochemical arguments. The P_2H_2 ligand in **12** is believed to supply two electrons to the Mo^{II} complex, thus paralleling the bonding behavior of ethene in the related $[Cp_2Mo(C_2H_4)]$.

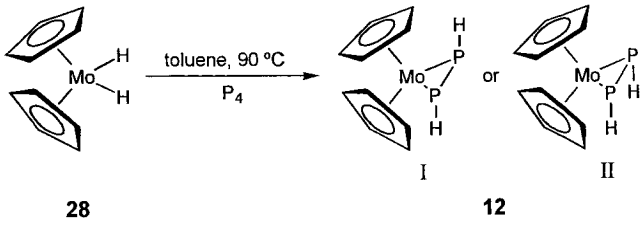

Scheme 6

Confirmation of Green's formulation of **12**, was provided soon after by Cannillo et al., who determined the molecular structure of **12** using X-ray methods. A view of the structure of Green's complex is presented in Figure 1.[51]

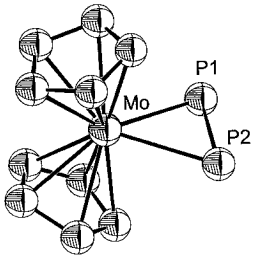

Figure 1. Crystal structure of $[Cp_2Mo(\eta^2\text{-}P_2H_2)]$ (**12**)

The most intriguing feature of the structure is the presence of a *quasi*-isosceles, triangular MoP_2 moiety, featuring a P−P separation of 2.146 Å, shorter than that found in black or white allotropes of phosphorus and in the diphosphane P_2H_4, but longer than the P=P bond length measured for P_2 molecules in the gas phase by electron diffraction.[52] The two P−H hydrogen atoms could not be located in the electron density map, but their presence was confidently inferred from spectroscopic measurements. In particular, the ^{1}H NMR spectrum exhibited an AA′XX′ multiplet at $\delta = 0.19$ with a $J_{PH} + J_{PH'}$ separation of ca. 160 Hz, while the corresponding multiplet in the proton-coupled ^{31}P NMR spectrum appeared at $\delta \approx 203$.[53] A sharp band at 2240 cm^{-1} in the IR spectrum was assigned to the stretching mode of the P−H bond.

No convincing information about the process which results in the assembling of the $Mo(P_2H_2)$ moiety from MoH_2 and excess P_4 has been provided, and the whole mechanism transforming the MoH_2 unit into the $Mo(P_2H_2)$ unit remains obscure. In situ monitoring of the originally reported "one-pot synthesis" of **12** by $^{31}P\{^1H\}$ and ^{1}H NMR spectroscopy was not informative in retrospect.[54] The initial formation of **12** was already observed at 40 °C, but the transformation of **28** into the diphosphene complex was completed within a reasonable time only at temperatures higher than 60 °C. No intermediate species en route to the diphosphene was observed. In our hands, the formation of **12** was confirmed by the appearance in the $^{31}P\{^1H\}$ NMR spectrum ([D$_8$]toluene) of a singlet resonance at $\delta = -194.6$, paralleled by the rising in the proton spectrum of a doublet of doublets at $\delta \approx 0.44$ [^1J(H,P) = 91.5 Hz, ^2J(H,P) = 67.7 Hz].[53] These NMR spectroscopic data, which confirm those given by Green with a lower field instrument, differ from those reported by Stephan and coworkers for $[Cp^*_2Zr(\eta^2\text{-}P_2H_2)]$,[55] but are in line with the NMR spectroscopic data given by Schäfer et al. for the thermally unstable $[(Cy_2PCH_2CH_2PCy_2)Ni(\eta^2\text{-}P_2H_2)]$.[56]

The reaction of primary phosphanes with $[Cp_2MH_3]$ (M = Nb, **29**; Ta, **30**) was thoroughly studied by Stephan and co-workers, who synthesized a variety of hydrido-diphosphene complexes $[Cp_2MH(\eta^2\text{-}P_2R_2)]$ (R = Ph, Cy) using this procedure.[41] In order to prepare unsubstituted diphosphene species, the reaction of white phosphorus with the tantalum trihydride **30** was successfully investigated. Thus, **30** and white phosphorus reacted in toluene at 85 °C to yield colorless crystals of $[Cp_2TaH(\eta^2\text{-}P_2H_2)]$ (**13**) after workup (Scheme 7).

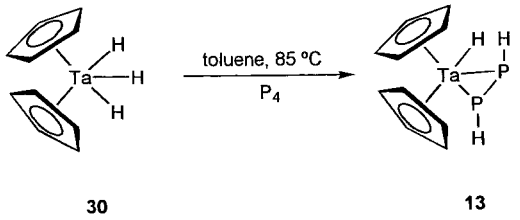

Scheme 7

Compound **13** was characterized by NMR spectroscopy and X-ray crystallography; the structural data revealed geometric features similar to those of **12**, with two cyclopentadienyl rings and a diphosphene ligand coordinated to the metal center. The three-membered MP_2 ring is tightly bonded to tantalum, with P−Ta−P angles ranging from 47.6 to 48.4°. A crystallographically located, but stereo-

chemically inactive, hydride ligand completes the coordination sphere about the metal center. As for **12**, the two diphosphene hydrogen atoms were not located by X-ray methods and their disposition in the complex remains unclear. Theoretical calculations and analogy with the *transoid* disposition adopted by other crystallographically characterized disubstituted diphosphenes of formula $[Cp_2MH(\eta^2\text{-}P_2R_2)]$ (M = Nb, Ta; R = Ph, Cy), gave credence to the view that the P_2H_2 ligand in **13** also adopts a *transoid* disposition. In particular, an energy difference of only 1−2 kcal mol^{-1} for the two optimized structures was computed by EHMO methods. A series of variable-temperature NMR experiments were consistent with the *transoid* structural assignment. Particularly informative was the analysis of the NOE enhancements observed at 193 K between the two P_2H_2 protons and the protons of the two inequivalent Cp rings. Compound **13** is stereochemically non-rigid, but the occurrence of a fluxional process exchanging *cisoid* and *transoid* isomers by inversion of both diphosphene ligand PH moieties could not be confirmed from analysis of the low-temperature NMR spectra. As with the molybdenum derivative **12**, no mechanism for the formation of **13** was provided.

2.2.2 Reactions of White Phosphorus with Hydrido-Polyphosphanes

Notwithstanding Green's breakthrough in metal-assisted P−H chemistry and the continuous and impressive burgeoning of P_4-coordination chemistry during the last two decades,[57] studies dealing with the reactivity of transition metal hydrides with white phosphorus remained almost ignored until a couple of years ago, when we decided to investigate the reactivity of white phosphorus with transition metal hydrides stabilized by tripodal polyphosphanes. Our attention focused first on the known trihydrides [(triphos)RhH_3] (**31**)[58] and [(triphos)IrH_3] (**32**),[59] which had been successfully used by Bianchini and co-workers as hydrogenating catalysts for a variety of organic unsaturated substrates such as alkenes,[60] alkynes,[61] and thiophene derivatives,[62] including the highly HDS-resistant dibenzothiophene.[63] One of the most important reasons for choosing these hydrides at the very beginning of our investigation, apart from the general knowledge of their chemistry and the effectiveness of their catalytic performances in hydrogenation processes, was that the reactivity of both (triphos)Rh and (triphos)Ir systems towards white phosphorus was well known from Sacconi's studies, dating back to 1979.[64] Indeed, irrespective of the rhodium(I) or iridium(I) precursor,[65] the combination of triphos, M^I and white phosphorus resulted in the formation of the air- and moisture-stable complexes [(triphos)M(η^3-P_3)] as lemon yellow (M = Rh, **33**) or off-white (M = Ir, **34**), crystalline materials in moderate yields (Scheme 8).[64][66] Complexes **33** and **34** belong to the extensively studied family of *cyclo*-triphosphorus complexes $[(triphos)M(\eta^3\text{-}P_3)]^{n+}$ (n = 0, M = Co, Rh, Ir; n = 1, M = Ni, Pd, Pt) containing the P_3 unit *trihapto*-coordinated to the transition metal center.[67] The reactivity of these complexes has been widely investigated.[21,68]

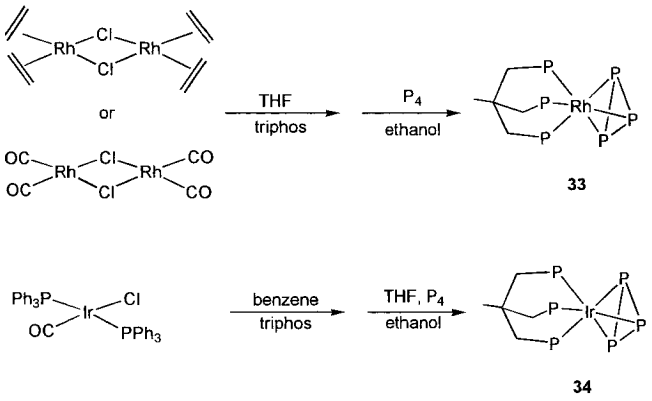

Scheme 8

The generally accepted mechanism that governs the chemistry of both **31** and **32** involves the thermal reductive elimination of dihydrogen to produce the highly reactive species [(triphos)MH]. Once formed, the 16-electron fragment may be blocked by two-electron donor ligands, such as CO, or may reform an M^{III} complex by promoting the oxidative addition of different addends. In no case was removal of the residual hydride observed, although in a few instances it might selectively be delivered onto one of the oxidatively added atoms.[69] On all of these premises, it was of interest to see how the thermally generated fragments [(triphos)MH] would react with white phosphorus.

In keeping with our expectations, treatment of **31** with white phosphorus in THF at about 70 °C under nitrogen did not produce, at least directly, the *cyclo*-triphosphorus species **33**, but afforded an orange solution from which dark yellow microcrystals of the novel complex [(triphos)Rh(η^1:η^2-HP_4)] (**35**) were obtained after solvent removal under reduced pressure (Scheme 9).[70]

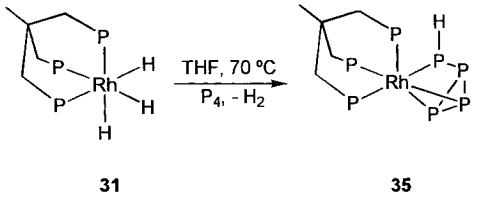

Scheme 9

Although the solid structure of **35** has not yet been verified by X-ray crystallography, the solution structure of the complex was substantiated by intensive multinuclear and multidimensional NMR experiments, which unequivocally demonstrated the presence of the rhodium-bonded η^1:η^2-HP_4 ligand, acting as a six-electron donor towards the (triphos)Rh fragment.

Key points of the NMR spectroscopic characterization lending credence to the proposed structure for **35** were the temperature-invariant $^{31}P\{^1H\}$ NMR spectrum, exhibiting a well-resolved ABCDEFGX spin system (confirmed by computer simulation and fitting), and the ^{31}P,^{31}P-2D COSY NMR spectrum. In particular, it was possible to disentangle the not trivial pattern of P,P connectivities from an analysis

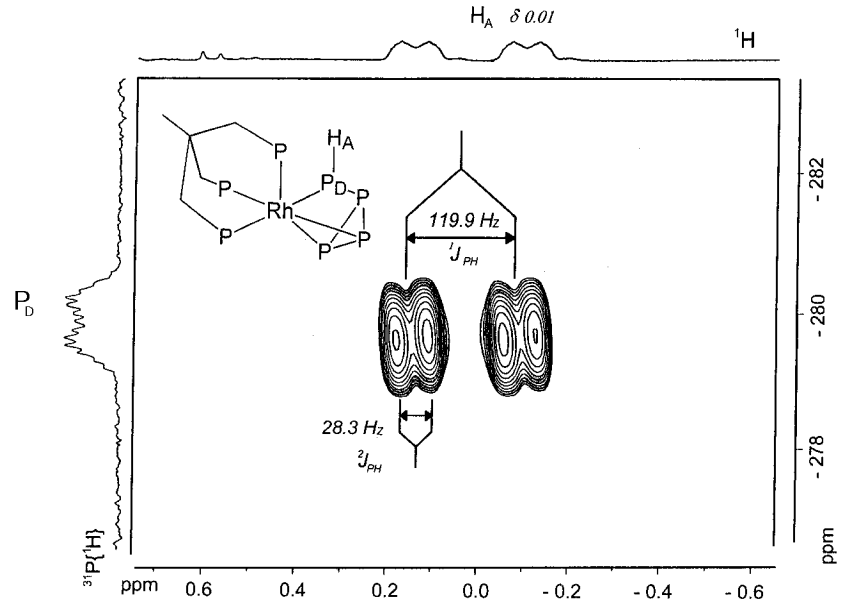

Figure 2. Contour plot of a section of the $^{1}H,^{31}P$-2D NMR spectrum of [(triphos)Rh(η^1:η^2-HP_4)] (**35**), showing the relevant cross peak between the P_D atom and the P−H hydrogen atom

of the homonuclear correlation spectrum, and eventually to confirm the proposed structure for the phosphorus skeleton originating from the P_4 tetrahedron. The presence of the P−H ligand was underscored by a weak absorption at 2213 cm^{-1} in the IR spectrum (disappearing in the deuterated isotopomer [D_1]-**35**), by ^{31}P-DEPT NMR polarization transfer experiments (DEPT-90 and DEPT-135), and by $^{1}H,^{31}P$-HMQC heteronuclear correlation NMR experiments. Inspection of the heterocorrelated spectrum made evident the presence of a cross-peak signal correlating the phosphorus multiplet centered at $\delta = -280.22$ and a doublet of broad doublets resonating at $\delta \approx 0.01$ in the ^{1}H NMR spectrum. A relevant section of the contour-plot diagram, illustrating the one-bond P−H correlation, is presented in Figure 2.

Although the assemblage of the HP_4 ligand from white phosphorus and a transition metal hydride and its incorporation into a metal complex framework is unprecedented, the existence of an HP_4 anion had previously been demonstrated by Baudler and co-workers, who in 1988 prepared the alkaline salts M(HP_4) (**36**: M = Li, Na, K) by treatment of white phosphorus with metal naphthalenide as reducing reagent in 1,2-dimethoxyethane at −78 °C.[71] Unlike **35**, which is stable at room temperature under nitrogen or argon in both solid state and in solution, Baudler's derivatives could not be stored even at low temperature, decomposing in a few days at −78 °C, thus indicating that stabilization of highly reactive intermediates, even in phosphorus hydrido chemistry, can be achieved by means of metal coordination. A comparison of the NMR parameters of **35** with those of Baudler's salt reflects the substantial spectroscopic differences occurring upon stabilization of the tetraphosphorus monohydrido anion by metal coordination, but, noticeably, shows an almost identical value for the two one-bond P−H coupling constants [119.9 Hz for **35** vs. 129 Hz for K(HP_4)]. The P_4H units in both **35** and **36** can be formally considered as monodeprotonated anions derived from the known tetraphosphorus dihydride P_4H_2. This phosphane, which has been identified by mass spectrometry, is the simplest member of the low-hydrogen phosphanes of formula P_nH_{n-2}.[72] These exhibit structural motifs based on condensed polyphosphorus ring systems, and in the case of P_4H_2 a bicyclo[1.1.0]tetraphosphane structure (**37**) has been proposed.[24−26,72] In terms of their structural layouts, both the tetraphosphane **37** and the derivatives **35** and **36** can be traced back to the few known derivatives containing the tetraphosphabicyclobutane skeleton (P_4^{2-}). Complexes of

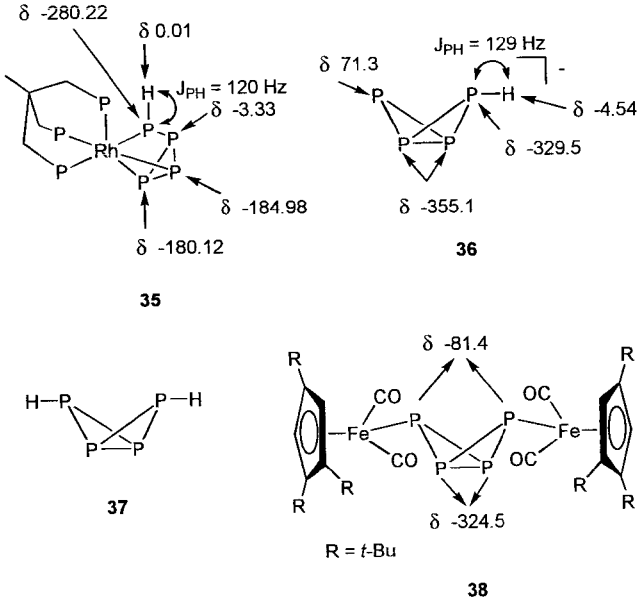

this class, featuring a butterfly MP_4M array, have been directly obtained either by cothermolysis of P_4 with $[\{Cp'(CO)_2Fe\}_2]$ − one example is $[\{Cp'(CO)_2Fe\}_2(\mu,\eta^1{:}\eta^1\text{-}P_4)]$ (**38**) (Cp' = 1,2,4-tBu$_3$-C_5H_2)[73] − or by reaction of the diphosphene complex $[Cp^*(CO)_2Fe(P{=}PCp^*)]$ with $[\{Cp^*(CO)_2Fe\}_2]$ − one example is $[\{Cp^*(CO)_2Fe\}_2\text{-}(\mu,\eta^1{:}\eta^1\text{-}P_4)]$ (**39**).[74]

Now the task at hand was to understand the mechanism leading to **35** and to explore the chemical reactivity of the HP_4 ligand. To address the first point, we decided to follow the reaction of P_4 and **31** by in situ NMR spectroscopy in order to observe some intermediates preceding the formation of the HP_4 ligand. Thus, when a 5-mm NMR tube (sealed under nitrogen) containing a [D$_8$]THF solution of **31** and white phosphorus (1:2) was heated in the NMR probe, a slow reaction took place at ca. 40 °C, selectively producing **35** as the only phosphorus-containing complex, without providing any evidence for intermediate species. The transformation was very slow at this temperature; after 4 h, less than 25% of **31** had been converted into the HP_4 compound. Inspection of the ^{1}H NMR spectrum revealed that dihydrogen had also been released (singlet at $\delta \approx 4.75$). Heating the probe-head to ca. 70 °C resulted in the fast (2 h) disappearance both of the **31** doublet at $\delta \approx 29$ and of the set of resonances due to **35**, and led to the formation of a doublet of quadruplets at $\delta \approx -269$, which was attributed to the *cyclo*-triphosphorus complex **33** by comparison with an authentic specimen.[64] The formation of **33**, which is almost quantitative after 2 h at 70 °C, was accompanied by the disappearance of the H_2 resonance in the proton spectrum and by the progressive development in the $^{31}P\{^1H\}$ NMR spectrum of a singlet resonance at $\delta = -244.77$, which was attributed to the formation of PH_3. In agreement with this assignment, this singlet transformed into a narrow quadruplet, with $^1J(H,P) = 186.9$ Hz, in the proton-coupled NMR spectrum. Figure 3 illustrates these transformations and highlights these experiments.

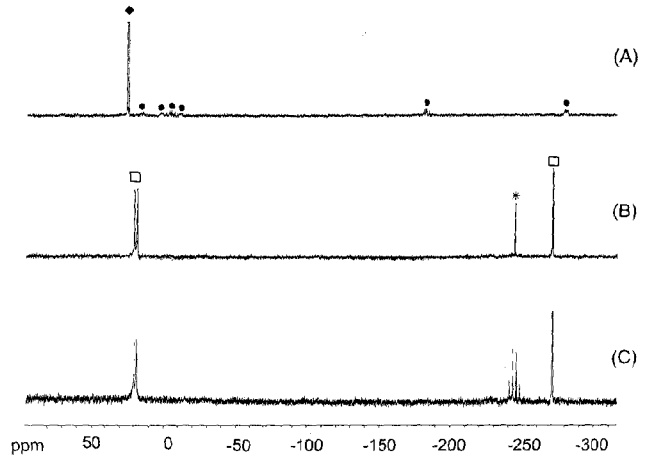

Figure 3. Monitoring of the reaction of $[(triphos)RhH_3]$ (**31**) with P_4 (2:1) in [D$_8$]THF: (A) $^{31}P\{^1H\}$ spectrum after 1 h heating at 40 °C; (B) $^{31}P\{^1H\}$ spectrum after 2 h heating at 70 °C; (C) ^{31}P spectrum after 2 h heating at 70 °C; (◆) $[(triphos)RhH_3]$ (**31**); (•) $[(triphos)Rh(\eta^1{:}\eta^2\text{-}HP_4)]$ (**35**); (□) $[(triphos)Rh(\eta^3\text{-}P_3)]$ (**33**); (*) PH_3

The reaction described above is remarkable because it provides the first evidence that *at least one of the four P atoms of white phosphorus can be hydrogenated to phosphane by a metal-assisted reaction*. It is also worth mentioning that all of the three hydride ligands in **31** are selectively transferred to the same phosphorus atom, while the three remaining phosphorus units in the P_4 molecule are efficiently scavenged in the form of the thermally robust *cyclo*-triphosphorus moiety in complex **33**. A separate NMR experiment carried out with the perdeuterated trihydride [D$_3$]-**31** confirmed the total incorporation of deuterium into the phosphane molecule, thus indicating that the three hydrogen atoms were transferred from the rhodium center to the same phosphorus atom. Addition of H_2 (1 atm) to a [D$_8$]THF solution of **35** at 70 °C transformed the HP_4 species into PH_3 and **33** (Scheme 10), but under N_2 the thermal reaction was difficult to control and the formation of **33** (< 70%) was accompanied by extensive decomposition. No compound arising from the formally produced "phosphinidene" (PH) species was identified and, because of the complexity of the reaction mixture, no experiment aimed at trapping this highly reactive fragment was attempted.

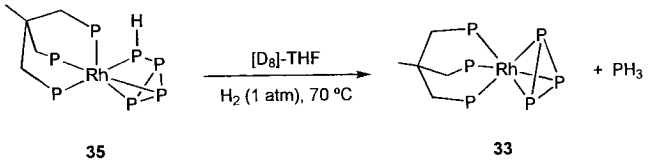

Scheme 10

As NMR monitoring of the reaction of **31** with P_4 did not provide definitive mechanistic information, we turned our attention to the kinetically more inert and thermally more robust iridium complex **32.** As expected, and in keeping with the general behavior of **32**, the reaction of the iridium trihydride with P_4 did not differ from that of its rhodium congener. However, the reaction needed a greater degree of activation to start, taking place only at temperatures higher than 115 °C. At this temperature, the formation of PH_3 and **34** from the undetected complex $[(triphos)Ir(\eta^1{:}\eta^2\text{-}HP_4)]$ (**40**) should occur very rapidly, and thus did not allow for the detection of any intermediate species during an in situ NMR experiment (sealed NMR tube) (Scheme 11). However, having established that the [(triphos)IrH] fragment is well suited as a platform for carrying out the hydrogenation reaction of P_4 to PH_3 and *cyclo*-P_3, it was an obvious step to look through the variety of organometallic complexes available in our laboratory and therefore to turn our attention to the cognate iridium complex $[(triphos)Ir(H)_2Et]$ (**41**).[75] Compound **41** thermally eliminates ethane, rather than H_2, under milder conditions (ca. 70 °C) and, irrespective of the solvent medium (benzene, THF, acetone, acetonitrile, etc), gives the fragment [(triphos)IrH]. This, in the absence of any external reagent, brings about C−H bond activation of the solvent, yielding octahedral Ir^{III} complexes of formula $[(triphos)Ir(H)_2R]$ [R = C_6H_5, C_4H_7O, $CH_2C(O)CH_3$, CH_2CN, etc.]. However, when a solution of **41** in THF or benzene was brought to reflux in the presence

of elemental phosphorus (Ir/P_4 = 1:2), no solvent activation took place, and a bright yellow solution was obtained, from which pale yellow microcrystals of the novel compound [(triphos)IrH(η^2-P_4)] (**42**) separated.[76] Compound **42** was characterized by elemental analysis, mass spectrometry and IR spectroscopy [IR: medium-intensity ν(Ir−H) band at 2061 cm^{-1}], as well as by multinuclear NMR spectroscopy.

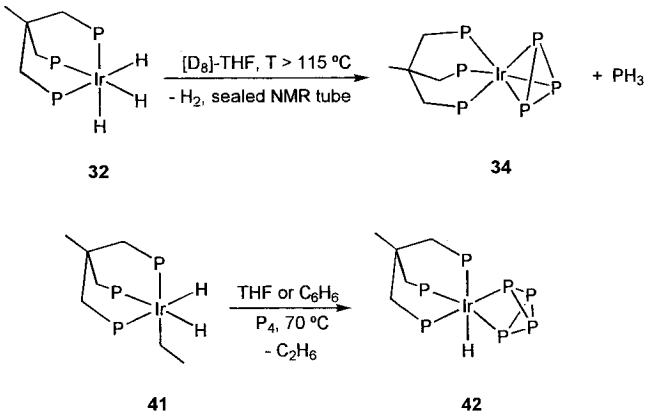

Scheme 11

Complex **42** is a member of the well-known family of transition metal complexes containing the bicyclotetraphosphane ligand[77] and, in keeping with this hypothesized structure, it shows in the $^{31}P\{^1H\}$ NMR spectrum a slightly second-order-perturbed ABB′CDEE′ spin system. Probably, **42** forms by oxidative addition of P_4 to the unsaturated [(triphos)IrH] fragment. This can reasonably be assumed as the first basic step of the reaction of P_4 with both **31** and **32**. In contrast to the easy synthesis of **42**, no analogous rhodium compound could be detected in the reaction of **31** with P_4. However, a species showing NMR parameters in line with that of the anticipated [(triphos)RhH(η^2-P_4)] (**43**) was generated in a 5-mm NMR tube by treating a cold [D_8]THF solution of the hydrido-carbonyl complex [(triphos)RhH(CO)] (**44**)[58] with one equivalent of P_4, dissolved in the same solvent. At room temperature, the transformation of **43** into **35** is sufficiently slow to allow the hydrido-bicyclotetraphosphane complex to be isolated. On standing of the solution at room temperature, **43** was transformed quantitatively into **35** within 3 h (Scheme 12).[78] On the basis of this finding, it is quite probable that **43**, which initially forms at the temperature required to eliminate H_2 thermally from **31**, undergoes a quick transformation into **35** without being observable by NMR experiments.

Compound **42** is kinetically stable and could be isolated in the solid state in pure form. Nevertheless, in a THF solution standing at room temperature in a sealed NMR tube, it spontaneously tautomerized within days into the HP_4 derivative [(triphos)Ir(η^1:η^2-HP_4)] (**40**) (Scheme 13). The reaction was not selective and a number of unknown iridium species and some decomposition products accompanied the formation of **40**, which could not be obtained in a yield higher than 25%. Hydrogenation of **40**, in a [D_8]THF solution heated at about 70 °C, cleanly produced PH_3 and the iridium *cyclo*-P_3 complex **34**. Remarkably, when pressurized with dihydrogen, **42** did not produce PH_3 and **34**, because the reductive elimination of P_4 became competitive with the hydrogenation reaction of the activated P_4 ligand. Thus, after exposure of **42** to H_2 and heating at ca. 70 °C, the trihydride **32** was quantitatively recovered (Scheme 13). Nevertheless, this result is valuable from a mechanistic viewpoint as it underlines that *the functionalization of the activated P_4 ligand by selective delivery of one hydride from the metal center to the phosphorus atom is mandatory for accomplishing the complete hydrogenation of one P atom to PH_3*.

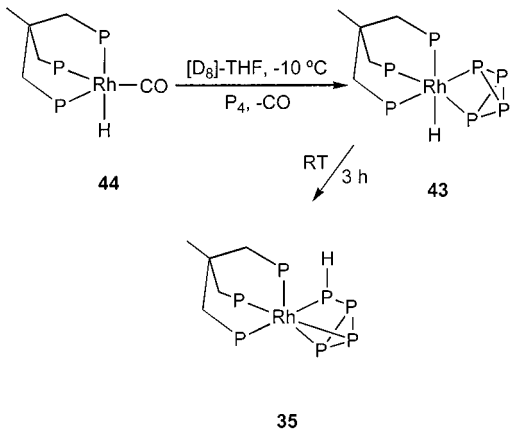

Scheme 12

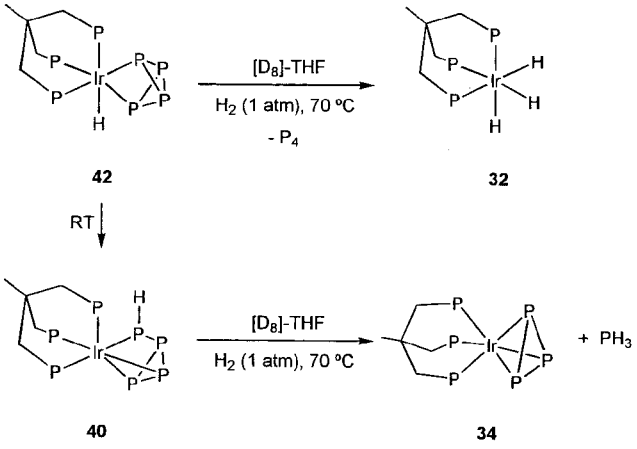

Scheme 13

A perusal of the large body of collected experimental information about the reaction with white phosphorus of **31** and **32** provides convincing evidence with which to propose a plausible mechanism for the hydrogenation of one phosphorus atom in white phosphorus to phosphane. Fundamental key points of the proposed mechanism, which is depicted in Scheme 14 are:

(**A**) the thermal elimination of H_2 from the rhodium or iridium trihydride is the preparative step necessary to generate the highly reactive fragment [(triphos)MH],

(**B**) the P_4 oxidative addition occurs by P−P bond activation and results in the formation of the octahedral hydrido-bicyclotetraphosphanes **42** and **43**. The iridium complex **42** is endowed with enough stability to be isolated in the solid state, but the rhodium analogue **43** could not be intercepted

under the experimental conditions used. It has been synthesized at lower temperature by alternative routes,[78]

(**C**) the unprecedented HP_4 complexes **35** and **40** are obtained from the irreversible intramolecular tautomerization $M(H)(\eta^2\text{-}P_4) \rightarrow M(\eta^1{:}\eta^2\text{-}HP_4)$ by hydride migration from the metal to one of the proximal P atoms of the η^2-P_4 ligand. This step is a prerequisite for the following hydrogenation reaction,

(**D**) in the absence of H_2, the reaction stops at the HP_4 complex, but when dihydrogen is added, or when the reaction is carried out in a closed system, complete hydrogenation of the hydrogenated phosphorus atom in the HP_4 ligand takes place. Notably, the hydrogenation step is accompanied by concomitant P−P bond cleavage with release of PH_3.

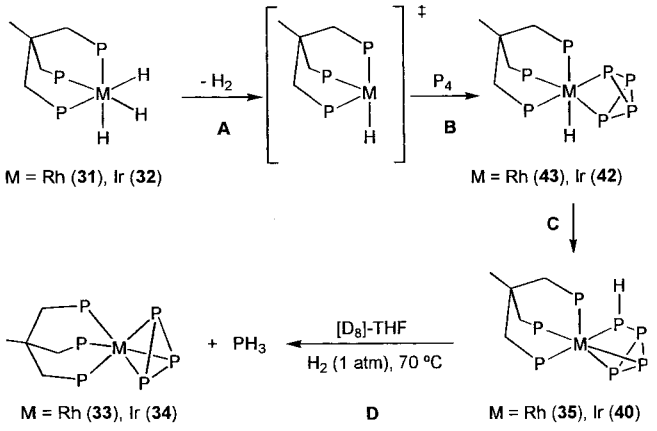

Scheme 14

The final hydrogenation step, conveying two hydrogen atoms to the PH group in the HP_4 ligand, is currently under study. A possible mechanism accounting for the formation of PH_3 involves the metal-mediated, heterolytic splitting of a molecular hydrogen ligand, followed by stepwise addition of H^+ and H^- to the hydridotetraphosphorus ligand. Convincing chemical evidence supporting the heterolytic mechanism comes from the observation that electrophiles like H^+ and Me^+ selectively attack the hydrogen-substituted P atom in **35** (vide infra),[79] and that both (triphos)Rh and (triphos)Ir systems are capable of coordinating H_2, forming the highly fluxional, nonclassical hydrides $[(triphos)Rh(\eta^2\text{-}H_2)(H)_2]^+$ [80] and $[(triphos)Ir(\eta^2\text{-}H_2)(H)_2]^+$.[81]

Now there remains the crucial point of turning the stoichiometric hydrogenation of white phosphorus into a catalytic process. In this regard, we think that the formation of **33**, which accompanies the assemblage of PH_3 from **35** and H_2, represents a dead-end, because the triphos *cyclo*-triphosphorus complexes are extremely robust and cannot return the rhodium precursor to the reaction system under any realistic conditions. Experimentally, we have not yet been able to observe any catalytic reaction, and only a stoichiometric amount of phosphane was produced when a solution of **31** and white phosphorus (Rh/P_4 = 1:10) in $[D_8]$THF was pressurized with up to 30 atm of H_2 in a sapphire NMR tube and heated up to 90 °C (high-pressure NMR experiment). Harsher reaction conditions caused extensive decomposition of the rhodium complexes without increasing the PH_3 yield.[82]

Nonetheless, we think it possible to accomplish the catalytic hydrogenation of P_4, providing that hydrogen transfer from the transition metal hydride to phosphorus is carried out using a metal hydride capable of coordinating and activating P_4, but unable to form stable complexes with the released P_x fragment (i.e. *cyclo*-P_3 in the case at hand). In order to verify this hypothesis, we are currently expanding the range of transition metal hydrides to be treated with white phosphorus. Particularly, we are looking at hydrides stabilized by polydentate ligands capable of easily dissociating one arm (hemilabile ligands), which should make coordination of H_2 to the intermediate P_4-activated complexes possible.[82]

2.3. Electrophilic Hydrogenation of P_x Units Incorporated into Transition Metal Complexes

Electrophilic hydrogenation (addition of protic acids) of neutral transition metal species incorporating P_x units is a simple method for generating the P−H bond functionality in a metal-stabilized polyphosphorus P_x unit. However, this synthetic procedure has scarcely been used and the only well-documented literature example related to such reaction was reported by Stoppioni and co-workers in 1991.[83] By straightforward addition of two equivalents of triflic acid to a suspension of $[(triphos)Co(\eta^3\text{-}P_3)]$ (**45**) in dichloromethane, a rapid dissolution of the starting compound occurred, giving an orange solution from which orange crystals of composition $[(triphos)Co(\eta^3\text{-}HP_3)](OSO_2CF_3)_2\cdot(H_5O_2)$ (**46**) were obtained after layering with benzene at room temperature (Scheme 15).

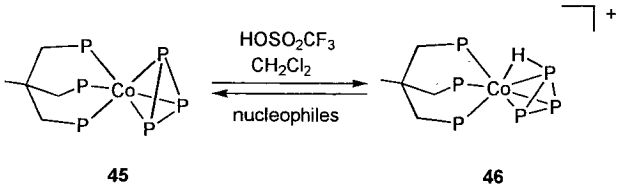

Scheme 15

The reaction is reversible, and even mild nucleophiles such as acetone, ether and ethanol can deprotonate **46**, giving back the *cyclo*-triphosphorus complex **45**. NMR analysis of the complex did not clarify the solution structure of the $[(triphos)Co(\eta^3\text{-}HP_3)]^+$ cation. However, the observation in the ^1H NMR spectrum of a temperature-invariant broad hump at $\delta \approx -13.7$ points to the presence of a hydrogen atom with a rather prominent hydride character.[84] The solid-state structure of **46** consists of triflate anions, $H_5O_2^+$ and $[(triphos)Co(\eta^3\text{-}HP_3)]^+$ cations in a 2:1:1 ratio. Noticeably, the co-crystallized molecules of triflic acid and adventitious water found by the X-ray diffraction analysis do not show any short contacts with the complex cation. The addition of a proton to the tetrahedral array of the parent CoP_3 cluster causes only moderate distortions, resulting in a slight lengthening of the Co−P bonds from 2.301 Å in **45**

to 2.396 Å [d(Co−P)$_{ave}$ = 2.343 Å] in **46** (Figure 4). A rationale for the location of the crystallographically undetected proton was obtained, in view of the distorted solid-state geometry, by theoretical analysis using both a semiempirical extended Hückel approach and ab initio DFT calculations.[85]

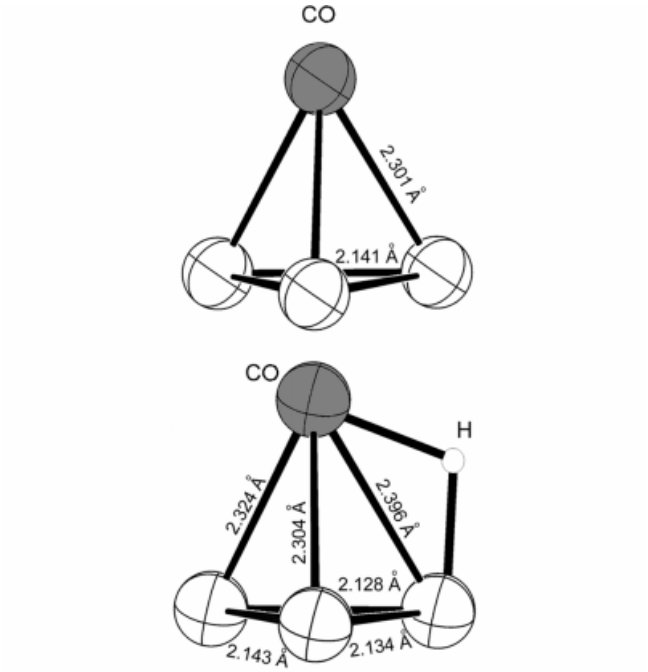

Figure 4. Comparison of the inner cores of [(triphos)Co(η^3-P_3)] (**45**) (top) and [(triphos)Co(η^3-HP_3)]$^+$ (**46**) (bottom); the H atom in **46** has been inserted in a calculated position

Among the four different preferential sites of attack of the H^+ to the CoP_3 moiety, the optimized structure for the $CoHP_3^+$ cation entails the added H atom forming a bridge between one of the phosphorus atoms of the P_3 ring and cobalt. The calculated minimized geometry was found to be in very good agreement with that proposed on the basis of the experimentally observed crystallographic distortions for **46** and has been attributed to the minimal steric requirements of the H^+. In keeping with the existence of slightly higher minima in the energy profile associated with the electrophilic alkylation of **45**,[85] the electrophilic addition of sterically more demanding fragments to **45** results in the formation of geometrically distinct Co(η^3-P_3R)$^{n+}$ (n = 0, 1) adducts, in which the added electrophile may bind one CoP_3 core phosphorus atom as an exocyclic ligand, such as in [(triphos)Co(η^3-P_3{M(CO)$_5$})] (**47**),[21b,86] and [(triphos)-Co(η^3-P_3Me)]PF_6 (**48**),[87] or may be bound to a pair of phosphorus atoms of a slightly elongated P−P edge, such as in the mononuclear mercury adduct [(triphos)Co(η^3-P_3{HgPh})]PF_6 (**49**),[68e] or in the binuclear species with a coinage metal cation bridging two CoP_3 fragments, [{(triphos)Co(η^3-P_3)}$_2$(μ_4-M)]PF_6 (M = Cu, Ag, Au) (**50**).[68d,68g]

The protonated complex **46** was successfully used by Di Vaira and Stoppioni as the starting material for the construction of an unprecedented open-chain P_6H_2 ligand by reaction with [$(PPh_3)_2Pt(C_2H_4)$] (**51**).[88] Thus, addition of **51** to a dichloromethane solution of **46** gave dark brown crystals of [{(triphos)Co}$_2$(η^3,η^3,η^3-P_6H_2){Pt(PPh_3)}]-$(OSO_2CF_3)_2$·$2C_6H_6$ (**52**), authenticated by X-ray methods (Scheme 16).

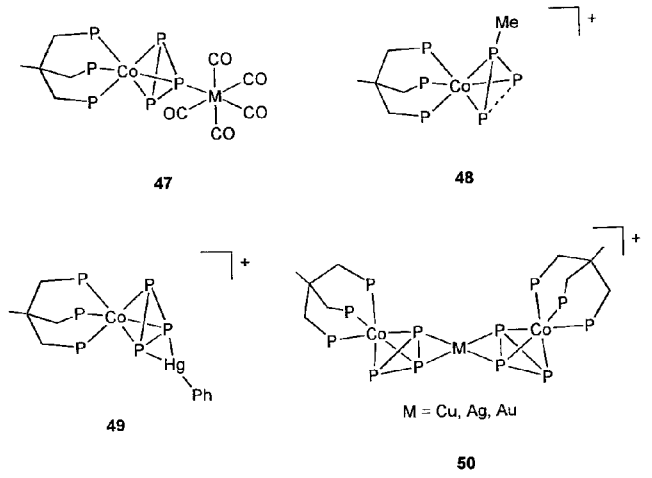

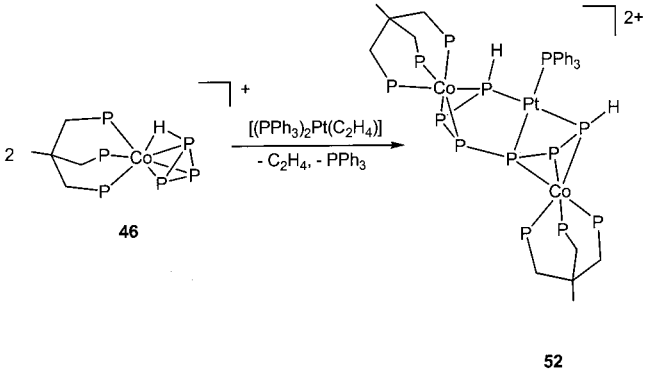

Scheme 16

The cationic complex **52** results from the coming together of two [(triphos)Co(η^3-HP_3)]$^+$ cations and a Pt(PPh_3) moiety. The P_6H_2 fragment is generated by P−P bond formation from two different Co(HP_3)$^+$ units, while during the reaction the labile ethene and one triphenylphosphane ligand are removed from the platinum center. This metal center exhibits the usual square-planar geometry, formed by the residual PPh_3 ligand and by three phosphorus atoms of the assembled P_6H_2 fragment. Although the presence of two triflate anions implies the existence of two protons, as required for charge balance, these could not be located either by structural investigation, or by spectroscopic techniques (IR and ^{1}H NMR). However, the narrow distribution of the six Co−P bonds in **52** [d(Co−P)$_{ave}$ = 2.305 Å] would rule out a bridging Co−H−P location for the skeletal hydrogen atoms in **52**. Similarly, theoretical EH calculations do not indicate any electrophilic privileged target between the six P atoms of the P_6H_2 ligand, but rather point to an appreciable amount of negative charge spread over the six positions in the hexaphosphorus chain.[88]

Addition of electrophiles to [(triphos)Rh(η^1:η^2-HP_4)] (**35**) was briefly considered in order to shed some light on

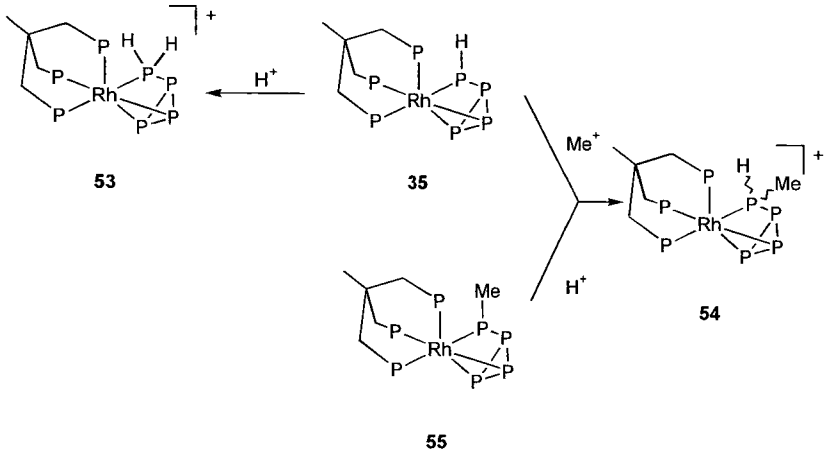

Scheme 17

the reaction mechanism that transforms **35** into PH_3 and **33** (vide supra).[79] Thus, in a series of dedicated in situ experiments, it was demonstrated that the phosphorus atom bearing the P−H functionality is the selected target of electrophilic reagents H^+ or Me^+. As a result, the cationic derivatives [(triphos)Rh(η^1:η^2-H_2P_4)](BF_4) (**53**) and [(triphos)Rh(η^1:η^2-H(Me)P_4)](OSO_2CF_3) (**54**), which were characterized by NMR spectroscopy, were synthesized. Notably, the signal of the phosphorus atom, that underwent the addition of the second substituent, experienced a significant downfield shift, moving − for example − from $\delta = -280.22$ in **35** to -172.83 in **54**. Conclusive evidence confirming the regioselectivity of the electrophilic attack on the RP_4 ligands was obtained by comparing the reaction of **35** with $MeOSO_2CF_3$ and the cross reaction in which one equivalent of HBF_4 or $HOSO_2CF_3$ was added to a solution of the methylated complex [(triphos)Rh(η^1:η^2-MeP_4)] (**55**).[78,79] Irrespective of the starting [(triphos)Rh(RP_4)] substrate and the electrophile used, the final products of the cross reactions exhibited identical NMR properties, and may therefore be assigned as the cationic [(triphos)Rh(η^1:η^2-H(R)P_4)]Y (R = H, **53**; R = Me, **54**). Scheme 17 summarizes these reactions.

2.4 Nucleophilic Hydrogenation of P_x Units Incorporated into Transition Metal Complexes

The "nucleophilic hydrogenation"[89] of transition metal complexes incorporating P_x units is a synthetic methodology that can be successfully used to introduce a P−H functionality into the framework of a transition metal complex. This route to species containing P−H was first adopted by Mays and co-workers, who have recently undertaken a thorough investigation of the reactivity of transition metal complexes featuring a bridging diphosphorus ligand. As a provisional result of these ongoing studies, it has been demonstrated that transition metal species with bridging P_2 ligands have a high synthetic potential as precursors to very unusual and frequently otherwise inaccessible organophosphorus ligands.[90]

As a key contribution to this chemistry, the Cambridge team investigated the reactivity of the easily accessible M_2P_2 tetrahedranes [{$CpM(CO)_2$}$_2$(μ,η^2,η^2-P_2)] [M = Mo (**56**); W (**57**)], originally prepared by Scherer et al., by cothermolysis of white phosphorus and [$CpM(CO)_2$]$_2$ [M = Mo (**58**); W (**59**)] in refluxing toluene.[91] Thus, treatment of **56** (or **57**) with a large excess of NaOH or KOH in wet THF afforded the new anionic phosphido complexes [{$CpM(CO)_2$}$_2$(μ-PH_2)]$^-$ [M = Mo (**60**); W (**61**)] as air-sensitive, purple solutions.[92] The two complexes were not isolated as solids, but after addition of a slight excess of HBF_4·OEt_2, orange crystals of the new neutral derivatives

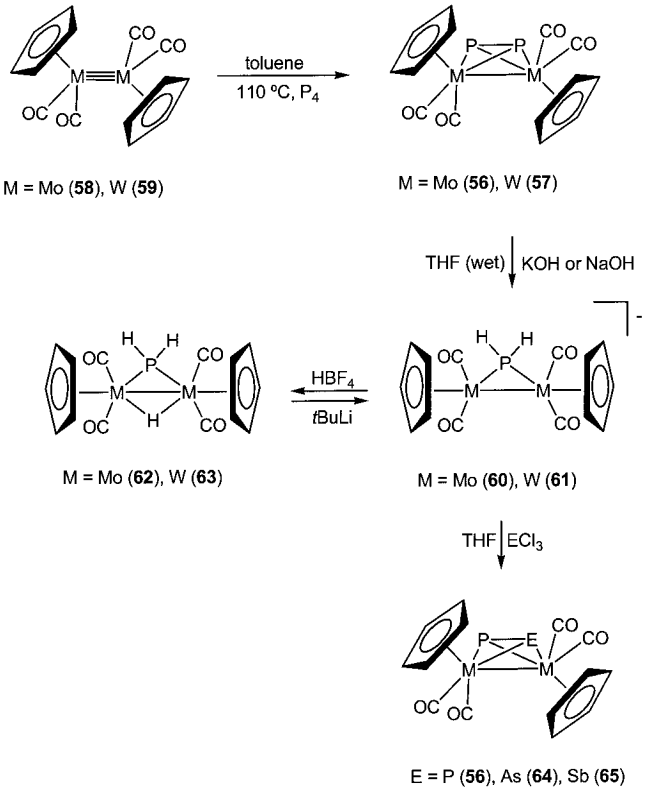

Scheme 18

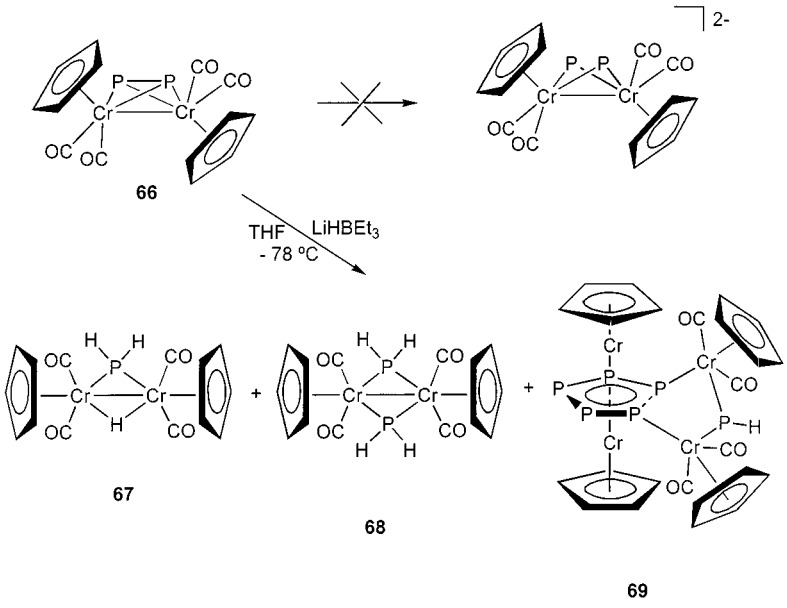

Scheme 19

[{CpM(CO)$_2$}$_2$(μ-PH$_2$)(μ-H)] [M = Mo (**62**); W (**63**)] were obtained in fairly good yield (Scheme 18). As well as by straightforward spectroscopic and FABMS characterization, the molybdenum derivative **62** was authenticated by X-ray diffraction analysis, confirming the presence of an essentially planar MoHMoP core.

The formation of **62** was reversible and the purple color of **60** could be restored by adding one equivalent of *t*BuLi in THF. Solutions of **60** were extremely reactive towards halogenated compounds.[93] Quite remarkable is the reaction with ECl$_3$ (E = P, As, Sb), which immediately produced orange solutions from which the air-stable tetrahedranes [{CpMo(CO)$_2$}$_2$(μ,η^2,η^2-PE)] [E = P (**56**); As (**64**); Sb (**65**)] were obtained. Crystallographic analysis of **64** and **65** confirmed the presence of rare examples of hetero-μ,η^2:η^2-PAs and -μ,η^2:η^2-PSb ligands.

A relevant breakthrough in this chemistry has recently been provided by the German group led by Scheer, which has studied the reactivity of the chromium derivative [{CpCr(CO)$_2$}$_2$(μ,η^2:η^2-P$_2$)] (**66**) towards main-group hydrides.[94] The work of Scheer et al. was aimed at breaking the P−P bond of the Cr$_2$P$_2$ tetrahedrane to generate a dianionic moiety (Cr$_2$P$_2^{2-}$) suitable for use as building block for the formation of new metal-bridged oligomers (a P atom is isolobal with a CH group[7]) (Scheme 19). Surprisingly, the addition of two equivalents of "superhydride" to a THF solution of **66** did not afford the expected dianion,[95] but yielded a mixture of P−H compounds which were separated by column chromatography on silica gel.[96]

The major product was the dichromium complex [{CpCr(CO)$_2$}$_2$(μ-H)(μ-PH$_2$)] (**67**), which shares most of its spectroscopic and structural parameters with Mays' derivatives **62** and **63**. The chromium dimer [{CpCr(CO)$_2$}$_2$(μ-PH$_2$)$_2$] (**68**) and a singular tetrachromium derivative [{CpCr(CO)$_2$}$_2$(μ-PH)}{(CpCr)$_2$(μ,η^1:η^1:η^5:η^5-P$_5$)}] (**69**) were also formed as minor products. Complex **68** consists of two CpCr(CO)$_2$ units held together by two phosphido (μ-PH$_2$) bridges, while the paramagnetic complex **69** exhibits a unique triple-decker sandwich structure in which the middle *cyclo*-P$_5$ ligand additionally coordinates the chromium metal center of an external [{CpCr(CO)$_2$}$_2$(μ-PH)] moiety with two contiguous P atoms. The *cyclo*-P$_5$ ligand is unusually distorted in comparison to other triple-decker complexes with the *cyclo*-P$_5$ ligand,[97] and its bonding properties have been interpreted by supposing a partition of the P$_5$ ligand into a allylic P$_3$ and a P$_2$ subunit.[98]

3. Concluding Remarks

This review summarizes the chemistry of transition metal complexes containing P−H bonds, and specifically highlights the possibility of establishing one or more P−H bonds in a transition metal center by hydrogenation of white phosphorus or polyphosphorus ligands. In examining the wealth of knowledge so far collected about reactions involved in the metal-assisted formation of P−H bonds from P$_4$ or P$_x$ ligands, it has become evident that a first step has been made in the direction of metal-assisted P$_4$ hydrogenation, but it is also evident that there remain many unresolved questions requiring additional synthetic efforts in order to accomplish a second, more important and probably definitive, step in such a direction. Clearly, further studies aimed at unraveling the intimate mechanism of the stoichiometric hydrogenation reactions of white phosphorus described here would be highly desirable in view of the industrial relevance associated with the as yet unaccomplished hydrogenation of the P$_4$ molecule.

The first industrial production of synthetic ammonia from nitrogen and hydrogen was begun at BASF in Ludwigshafen, Germany, in 1913, using a revolutionary catalytic process combining N$_2$ and H$_2$ at high pressure. At present,

we do not yet know when the catalytic production of PH_3 from white phosphorus and hydrogen will be written about in future chemical textbooks, but certainly we now know that transition metal complexes can bring about such intriguing processes.

Acknowledgments

This work was supported by the EU through the inco Copernicus project ERB IC15CT960746 and COSTD17 Action. The authors wish to express their gratitude to their colleagues, H. Butenschön (Hannover, Germany), L. Y. Goh (Singapore), H. Grützmacher (ETH, Zürich, Switzerland), O. J. Scherer (Kaiserslautern, Germany), R. R. Schrock (MIT, MA, USA), D. W. Stephan (Windsor, Canada) and P. Stoppioni (Florence, Italy) for preprints of unpublished results or for answering specific questions about their researches in this area. The authors are indebted to colleagues H. M. Lee (Hong Kong) and M. Ehses (INM, Saarbrücken, Germany) for reading the manuscript and for the helpful suggestions and P. Barbaro (Florence, Italy) for running ^{2}D-NMR spectra. I. R. thanks the Spanish "Ministerio de Educacion y Cultura" for the postdoctoral fellowship granted.

[1] [1a] D. E. C. Corbridge, *Phosphorus: an Outline of its Chemistry, Biochemistry and Technology,* 5th ed., Elsevier, Amsterdam, NL, **1995**. – [1b] K. B. Dillon, F. Mathey, J. F. Nixon, *Phosphorus: The Carbon Copy*, Wiley, Chichester, UK, **1998**.

[2] N. N. Greenwood, *J. Chem. Soc., Dalton Trans.* **1991**, 565.

[3] A. P. Ginsberg, W. E. Lindsell, *J. Am. Chem. Soc.* **1971**, *93*, 2082. For complete characterization of this compound, see: A. P. Ginsberg, W. E. Lindsell, K. J. McCullough, C. R. Sprinkle, A. J. Welch, *J. Am. Chem. Soc.* **1986**, *108*, 403.

[4] P. Dapporto, S. Midollini, L. Sacconi, *Angew. Chem.* **1979**, *91*, 510; *Angew. Chem. Int. Engl. Ed.* **1979**, *18*, 469.

[5] O. J. Scherer, H. Sitzmann, G. Wolmershäuser, *Angew. Chem.* **1985**, *97*, 358; *Angew. Chem. Int. Ed. Engl.* **1985**, *24*, 351.

[6] O. J. Scherer, T. Brück, *Angew. Chem.* **1987**, *99*, 59; *Angew. Chem. Int. Ed. Engl.* **1987**, *26*, 59.

[7] [7a] R. Hoffmann, *Angew. Chem.* **1982**, *94*, 725; *Angew. Chem. Int. Ed. Engl.* **1982**, *21*, 711. – [7b] F. G. A. Stone, *Angew. Chem.* **1984**, *96*, 85; *Angew. Chem. Int. Ed. Engl.* **1984**, *23*, 89. – [7c] W. Tremel, R. Hoffmann, M. Kertesz, *J. Am. Chem. Soc.* **1989**, *111*, 2030.

[8] [8a] F. Cecconi, P. Dapporto, S. Midollini, L. Sacconi, *Inorg. Chem.* **1978**, *17*, 3292. – [8b] L. Fabbrizzi, L. Sacconi, *Inorg. Chim. Acta.* **1979**, *36*, L407. – [8c] M. Di Vaira, S. Midollini, L. Sacconi, *J. Am. Chem. Soc.* **1979**, *101*, 1757. – [8d] M. Di Vaira, C. A. Ghilardi, S. Midollini, L. Sacconi, *J. Am. Chem. Soc.* **1978**, *100*, 2550. – [8e] C. Bianchini, M. Di Vaira, A. Meli, L. Sacconi, *J. Am. Chem. Soc.* **1981**, *103*, 1448. – [8f] P. Dapporto, L. Sacconi, P. Stoppioni, F. Zanobini, *Inorg. Chem.* **1981**, *20*, 3834. – [8g] C. Bianchini, M. Di Vaira, A. Meli, L. Sacconi, *Inorg. Chem.* **1981**, *20*, 1169.

[9] [9a] M. Detzel, G. Friedrich, O. J. Scherer, G. Wolmershäuser, *Angew. Chem.* **1995**, *107*, 1454; *Angew. Chem. Int. Ed. Engl.* **1995**, *34*, 1321. – [9b] M. Detzel, T. Mohr, O. J. Scherer, G. Wolmershäuser, *Angew. Chem.* **1994**, *106*, 1142; *Angew. Chem. Int. Ed. Engl.* **1994**, *33*, 1110. – [9c] O. J. Scherer, H. Sitzmann, G. Wolmershäuser, *Angew. Chem.* **1984**, *96*, 979; *Angew. Chem. Int. Ed. Engl.* **1984**, *23*, 968. – [9d] O. J. Scherer, T. Hilt, G. Wolmershäuser, *Angew. Chem. Int. Ed.* **2000**, *39*, 1426. – [9e] O. J. Scherer, S. Weigel, G. Wolmershäuser, *Chem. Eur. J.* **1998**, *4*, 1910. – [9f] O. Scherer, J. Braun, P. Walther, G. Heckmann, G. Wolmershäuser, *Angew. Chem.* **1991**, *103*, 861; *Angew. Chem. Int. Ed. Engl.* **1991**, *30*, 852. – [9g] O. J. Scherer, T. Mohr, G. Wolmershäuser, *J. Organomet. Chem.* **1997**, *529*, 379. – [9h] O. J. Scherer, J. Vondung, G. Wolmershäuser, *Angew. Chem.* **1989**, *101*, 1395; *Angew. Chem. Int. Ed. Engl.* **1989**, *28*, 1355. – [9i] O. J. Scherer, *Angew. Chem. Int. Ed. Engl.* **2000**, *39*, 1029. – [9j] O. J. Scherer, M. Swarowsky, H. Swarowsky, G. Wolmershäuser, *Angew. Chem.* **1988**, *100*, 738; *Angew. Chem. Int. Ed. Engl.* **1988**, *27*, 694. – [9k] O. J. Scherer, M. Ehses, G. Wolmershäuser, *Angew. Chem.* **1998**, *110*, 530; *Angew. Chem. Int. Ed. Engl.* **1998**, *37*, 507. – [9l] O. J. Scherer, M. Swarowsky, G. Wolmershäuser, *Angew. Chem.* **1988**, *100*, 423; *Angew. Chem. Int. Ed. Engl.* **1988**, *27*, 405. – [9m] O. J. Scherer, T. Brück, G. Wolmershäuser, *Chem. Ber.* **1989**, *122*, 2049. – [9n] O. J. Scherer, B. Höbel, G. Wolmershäuser, *Angew. Chem.* **1992**, *104*, 1042; *Angew. Chem. Int. Ed. Engl.* **1992**, *31*, 1027. – [9o] O. J. Scherer, G. Berg, G. Wolmershäuser, *Chem. Ber.* **1996**, *129*, 53. – [9p] O. J. Scherer, B. Werner, G. Heckmann, G. Wolmershäuser, *Angew. Chem* **1991**, *103*, 562; *Angew. Chem. Int. Ed. Engl.* **1991**, *30*, 553. – [9q] O. J. Scherer, H. Swarowsky, G. Wolmershäuser, W. Kaim, S. Kohlmann, *Angew. Chem.* **1987**, *99*, 1178; *Angew. Chem. Int. Ed. Engl.* **1987**, *26*, 1153.

[10] [10a] M. Scheer, M. Dargatz, P. G. Jones, *J. Organomet. Chem.* **1993**, *447*, 259. – [10b] M. Scheer, E. Herrmann, J. Sieler, M. Oehme, *Angew. Chem.* **1991**, *103*, 1023; *Angew. Chem. Int. Ed. Engl.* **1991**, *30*, 969. – [10c] M. Scheer, M. Dargatz, K. Schenzel, *J. Organomet. Chem.* **1992**, *435*, 123. – [10d] M. Scheer, U. Becker, M. H. Chisholm, J. C. Huffman, F. Lemoigne, O. Eisenstein, *Inorg. Chem.* **1995**, *34*, 3117. – [10e] M. Scheer, U. Becker, *Chem. Ber.* **1996**, *129*, 1307. – [10f] T. Gröer, G. Baum, M. Scheer, *Organometallics* **1998**, *17*, 5916. – [10g] M. Scheer, K. Schuster, A. Krug. H. Hartung, *Chem. Ber.* **1997**, *130*, 1299. – [10h] M. Scheer, G. Friedrich, K. Schuster, *Angew. Chem.* **1993**, *105*, 641; *Angew. Chem. Int. Ed. Egl.* **1993**, *32*, 593. – [10i] P. Kramkowski, M. Scheer, *Angew. Chem. Int. Ed.* **2000**, *39*, 928.

[11] [11a] C. F. Campana, A. Vizi-Orosz, G. Pályi, L. Markó, L. F. Dahl, *Inorg. Chem.* **1979**, *18*, 3054.[11b] G. L. Simon, L. F. Dahl, *J. Am. Chem. Soc.* **1973**, *95*, 2175. – [11c] M. E. Barr, L. F. Dahl, *Organometallics* **1991**, *10*, 3991. – [11d] M. E. Barr, B. R. Adams, R. R. Weller, L. F. Dahl, *J. Am. Chem. Soc.* **1991**, *113*, 3052.

[12] [12a] A. Vizi-Orosz, G. Pályi, L. Markó, *J. Organomet. Chem.* **1985**, *288*, 179. – [12b] A. Vizi-Orosz, G. Pályi, L. Markó, *J. Organomet. Chem.* **1973**, *60*, C25. – [12c] A. Vizi-Orosz, V. Galamb, G. Pályi, L. Markó, G. Bor, G. Natile, *J. Organomet. Chem.* **1985**, *288*, 179.

[13] [13a] L. Y. Goh, *Coord. Chem. Rev.* **1999**, *185/186*, 257. – [13b] L. Y. Goh, C. K. Chu, R. C. S. Wong, T. W. Hambley, *J. Chem. Soc., Dalton Trans.* **1989**, 1951. – [13c] L. Y. Goh, R. C. S. Wong, E. Sinn, *J. Chem. Soc., Chem. Commun.* **1990**, 1484. – [13d] L. Y. Goh, C. K. Chu, R. C. S. Wong, T. W. Hambley, J. Chem. Soc., *Dalton Trans.* **1990**, 977. – [13e] L. Y. Goh, R. C. S. Wong, E. Sinn, *Organometallics* **1993**, *12*, 888. – [13f] L. Y. Goh, R. C. S. Wong, T. C. W. Mak, *J. Organomet. Chem* **1989**, *373*, 71.

[14] J. Wachter, *Angew. Chem.* **1998**, *110*, 782; *Angew. Chem. Int. Ed. Engl.* **1998**, *37*, 751 and references therein.

[15] [15a] H. Lang, G. Huttner, L. Zsolnai, G. Mohr, B. Sigwarth, U. Weber, O. Orama, I. Jibril, *J. Organomet. Chem.* **1986**, *304*, 157. – [15b] H. Lang, G. Huttner, B. Sigwarth, I. Jibril, L. Zsolnai, O. Orama, *J. Organomet. Chem.* **1986**, *304*, 137. – [15c] G. Huttner, U. Weber, B. Sigwarth, O. Scheidstieger, H. Lang, L. Zsolnai, *J. Organomet. Chem.* **1985**, *282*, 331.

[16] M. Di Vaira, P. Stoppioni, *Coord. Chem. Rev.* **1992**, *120*, 259 and references therein.

[17] N. M. Mösch-Zanetti, R. R. Schrock, W. M. Davis, K. Wanninger, S. W. Seidel, M. B. O'Donoghue, *J. Am. Chem. Soc.* **1997**, *119*, 11037.

[18] C. C. Cummins, *Chem. Commun.* **1998**, 1777 and references therein.

[19] [19a] M. Peruzzini, L. Marvelli, A. Romerosa, R. Rossi, F. Vizza, F. Zanobini, *Eur. J. Inorg. Chem.* **1999**, 931. – [19b] M. Driess, J. Aust, K. Merz, C. van Wüllen, *Angew. Chem.* **1999**, *111*, 3967; *Angew. Chem. Int. Ed.* **1999**, *38*, 367. – [19c] S. Charles, J. C. Fettinger, S. G. Bott, B. W. Eichhorn, *J. Am. Chem. Soc.* **1996**, *118*, 4713. – [19d] J. Foerstner, F. Olbrich, H. Butenschön, *Angew. Chem.* **1996**, *108*, 1323; *Angew. Chem. Int. Ed. Engl.* **1996**, *35*, 1234. – [19e] M. H. Chisholm, K. Folting, J. W. Pasterczyk, *Inorg. Chem.* **1988**, *27*, 3057. – [19f] M. Baudler, S. Akpapoglou, D. Ouzonis, F. Wasgestian, B. Meinigke, H. Budzikiewicz, H. Münster, *Angew. Chem.* **1988**, *100*, 288; *Angew. Chem. Int. Ed. Engl.* **1988**, *27*, 280. – [19g] E. Hey, M. F. Lappert, J. L. Atwood, S. G. Bott, *J. Chem. Soc., Chem. Commun.* **1987**, 597. – [19h] F. Cecconi, C. A. Ghilardi, S. Mi-

dollini, A. Orlandini, *Inorg. Chem.* **1986**, *25*, 1766. – [19i] M. Peruzzini, S. Mañas, A. Romerosa, A. Vacca, *Mendeleev Commun.* **2000**, 134.

[20] [20a] O. J. Scherer, *Acc. Chem. Res.* **1999**, *32*, 751. – [20b] K. H. Whitmire, *Adv. Organomet. Chem.* **1998**, *42*, 2. – [20c] M. Scheer, *Coord. Chem. Rev.* **1997**, *163*, 271. – [20d] W. Wang, A. J. Carty, *New J. Chem.* **1997**, *21*, 773. – [20e] M. Scheer, E. Herrmann, *Z. Chem.* **1990**, *29*, 41. – [20f] O. J. Scherer, *Angew. Chem.* **1990**, *102*, 1137; *Angew. Chem. Int. Ed. Engl.* **1990**, *29*, 1104. – [20g] O. J. Scherer, in *Multiple Bonds and Low Coordination in Phosphorus Chemistry*, (Eds.: M. Regitz, O. J. Scherer), Thieme Verlag, Stuttgart, D, **1990**. – [20h]O. J. Scherer, *Angew. Chem.* **1985**, *97*, 905; *Angew. Chem. Int. Ed. Engl.* **1985**, *24*, 924. – [20i] O. J. Scherer, *Comments Inorg. Chem.* **1987**, *6*, 1. – [20j] M. Di Vaira, P. Stoppioni, M. Peruzzini, *Polyhedron* **1987**, *6*, 351.

[21] [21a] S. Midollini, A. Orlandini and L. Sacconi, *Angew. Chem.* **1979**, *91*, 93; *Angew. Chem. Int. Ed. Engl.* **1979**, *18*, 81. – [21b] M. Di Vaira, M. P. Ehses, M. Peruzzini, P. Stoppioni, *Inorg. Chem.* **2000**, *39*, 2199 and references therein.

[22] See for example: *A Comprehensive Treatise on Inorganic and Theoretical Chemistry*, J. W. Mellor, Longmans, Green and Co., London, UK, **1958**, vol. 7, pp. 782−784.

[23] [23a] V. Ipatieff, V. Nikolajeff, *Ber. Dtsch. Chem. Ges.* **1926**, *59*, 595. – [23b] A. Delique, *Bull. Soc. Chim. Fr.* **1933**, *53*, 603.

[24] M. Baudler, *Angew. Chem.* **1982**, *94*, 520; *Angew. Chem. Int. Ed. Engl.* **1982**, *21*, 492.

[25] M. Baudler, *Z. Chem.* **1984**, *24*, 352.

[26] M. Baudler, *Angew. Chem.* **1987**, *99*, 429; *Angew. Chem. Int. Ed. Engl.***1987**, *26*, 419.

[27] See for example: C. A. McAuliffe, *P, As, Sb, and Bi Ligands*, in *Comprehensive Coordination Chemistry* (Ed.: G. Wilkinson), Pergamon, UK, **1987**, vol. 2.

[28] For selected recent references on metal complexes of primary phosphanes see: [28a] I. V. Kourkine, S. V. Maslennikov, R. Ditchfield, D. S. Glueck, G. P. Y. A. Yap, L. M. Liable-Sands, A. L. Rheingold, *Inorg. Chem.* **1996**, *35*, 6708. – [28b] N. J. Goodwin, W. Henderson, B. K. Nicholson, J. Fawcett, D. R. Russell, *J. Chem. Soc., Dalton Trans.* **1999**, 1785.

[29] A search in the Cambridge Data System (April 2000) gave the following X-ray authenticated PH_3 complexes: [29a] N. I. Kirillova, A. I. Gusev, A. A. Pasynskii, Yu. T. Struchkov, *J. Organomet. Chem.* **1973**, *63*, 311. – [29b] W. A. Herrmann, B. Koumbouris, E. Herdtweck, M. L. Ziegler, P. Weber, *Chem Ber.* **1987**, *120*, 931 – [29c] G. Huttner, S. Schelle, *J. Organomet. Chem.* **1973**, *47*, 383 – [29d] G. Huttner, S. Schelle, *J. Cryst. Mol. Struct.* **1971**, *1*, 69. – [29e] J. Bould, P. Brint, X. L. R. Fontaine, J. D. Kennedy, M. Thornton-Pett, *J. Chem. Soc., Chem. Commun.* **1989**, 1763. – [29f] A. J. Deeming, S. Doherty, J. E. Marshall, J. L. Powell, A. M. Senior, *J. Chem. Soc., Dalton Trans.* **1993**, 1093. – [29g] E. J. Ditzel, G. B. Robertson, *Aust. J. Chem.* **1995**, *48*, 1277. – [29h] H.-J. Haupt, O. Krampe, U. Florke, *Z. Anorg. Allg. Chem.* **1996**, *622*, 807.

[30] M. Trabelsi, A. Loutellier, M. Bigorgne, *J. Organomet. Chem.* **1972**, *40*, C45.

[31] See for example: D. Scott Bohle, G. R. Clark, C. E. F. Rickard, W. R. Roper, *J. Organomet. Chem.* **1990**, *393*, 243.

[32] W. A. Herrmann, B. Koumboris, E. Herdtweck, M. L. Ziegler, P. Weber, *Chem. Ber.* **1987**, *120*, 931.

[33] R. G. Austin, G. Urry, *Inorg. Chem.* **1977**, *16*, 3359.

[34] For cluster complexes with μ_3- or μ_4-PH capping ligands see: [34a] U. Honrath, L. Shu-Tang, H. Vahrenkamp, *Chem. Ber.* **1985**, *118*, 132. – [34b] D. J. Brauer, G. Hasselkuss, S. Hietkamp, H. Sommer, O. Stelzer, *Z. Naturforsch., B* **1985**, *40*, 961. – [34c] S. B. Colbran, B. F. G. Johnson, J. Lewis, R. M. Sorrell, *J. Organomet. Chem.* **1985**, *296*, C1. – [34d] E. A. V. Ebsworth, A. P. McIntosh, M. Schröder, *J. Organomet. Chem.* **1986**, *312*, C41. – [34e] S. B. Colbran, F. J. Lahoz, P. R. Raithby, J. Lewis, B. F. G. Johnson, C. J. Cardin, *J. Chem. Soc., Dalton Trans.* **1988**, 173. – [34f] B. F. G. Johnson, J. Lewis, E. Nordlander, P. R. Raithby, *J. Chem. Soc., Dalton Trans.* **1996**, 755.

[35] C. C. Borg-Breen, M. T. Bautista, C. K. Schauer, P. S. White, *J. Am. Chem. Soc.* **2000**, *122*, 3952.

[36] G. Effinger, W. Hiller, I.-P. Lorenz, *Z. Naturforsch., B* **1987**, *42*, 1315.

[37] I.-P. Lorenz, W. Pohl, K. Polborn, *Chem. Ber.* **1996**, *129*, 11.

[38] P. G. Jones, H. W. Roesky, H. Grützmacher, G. M. Sheldrick, *Z. Naturforsch., B* **1985**, *40*, 590.

[39] L. Weber, *Chem Rev.* **1992**, *92*, 1839.

[40] J. C. Green, M. L. H. Green, G. E. Morris, *J. Chem. Soc., Chem. Commun.* **1974**, 212.

[41] N. Etkin, M. T. Benson, S. S. Courtenay, M. J. McGlinchey, A. D. Bain, D. W. Stephan, *Organometallics* **1997**, *16*, 3504.

[42] [42a] H. Schäfer, D. Binder, D. Fenske, *Angew. Chem.* **1985**, *97*, 523; *Angew. Chem. Int. Ed. Engl.* **1985**, *24*, 522. – [42b] H. Schäfer, D. Binder, *Z. Anorg. Allg. Chem.* **1988**, *557*, 45.

[43] [43a]M. C. Fermin, J. Ho, D. W. Stephan, *J. Am. Chem. Soc.* **1994**, *116*, 6033. – [43b] D. W. Stephan, *Angew. Chem. Int. Ed. Engl.* **2000**, *39*, 314.

[44] Ab initio calculations and ring-chain rearrangements of P_3H_3 have recently been reported: M. T. Nguyen, A. Dransfeld, L. Landuyt, L. G. Vanquickenborne, P. v. R. Schleyer, *Eur. J. Inorg. Chem.* **2000**, 103.

[45] [45a] A. L. Rizoupolos, M. P. Sigalas, *New J. Chem.* **1994**, *18*, 197. – [45b] N. Russo, M. Toscano, A. L. Rizoupolos, M. P. Sigalas, *Inorg. Chim. Acta* **1998**, *273*, 72.

[46] K. A. Shugart, R. F. Fenske, *J. Am. Chem. Soc.* **1985**, *107*, 3384.

[47] Theoretical ab initio calculations on free diphosphene (P_2H_2) yielded a P−P separation of 2.004 Å. T. Busch, Ph. D. Thesis, Bielefeld, Germany, **1990** (quoted in ref.[20g]). The P−P length reproduced by ab initio density functional calculations in the model complex $[(PH_3)_2Pd(\eta^2\text{-}P_2H_2)]$ ranges from 2.118 to 2.147 Å.[45b]

[48] [48a] D. Scott Bohle, C. E. F. Rickard, W. R. Roper, *Angew. Chem.* **1988**, *100*, 308; *Angew. Chem. Int. Ed. Engl.* **1988**, *27*, 302. – [48b] D. Scott Bohle, C. E. F. Rickard, W. R. Roper, P. Schwerdtfeger, *Organometallics* **1990**, *9*, 2068.

[49] [49a] G. Schmidt, O. J. Scherer, personal communication, April **2000**. – [49b] M. Ehses, Ph. D. Thesis, Kaiserlautern, Germany, **1998**.

[50] J. F. Brazier, D. Houalla, M. Loenig, R. Wolf, *Top. Phosphorus Chem.* **1976**, *8*, 99.

[51] E. Cannillo, A. Coda, K. Prout, J.-C. Daran, *Acta Crystallogr., B* **1977**, *33*, 2608.

[52] A. B. Burg, W. Mahler, *J. Am. Chem. Soc.* **1961**, *83*, 2388.

[53] Because of a misunderstanding of the reference scale in the original literature,[40] the resonance due to the P_2H_2 ligand in **12** was erroneously reported to be positioned at lower field with respect to H_3PO_4.[39,40] Correctly, it resonates at $\delta = -194.60$, and therefore at higher field with respect to 85% H_3PO_4.[54]

[54] I. de los Rios, M. Peruzzini, unpublished observations.

[55] $[Cp^*_2Zr(\eta^2\text{-}P_2H_2)]$ (**18**) exhibits a singlet resonance at δ = 134.3 in the $^{31}P\{^1H\}$ NMR spectrum and a PH proton signal at δ = 4.68 [dd, J(H,P) = 310.0 and 21.3 Hz].[43]

[56] The signal of the P_2H_2 ligand in $[(dcpe)Ni(\eta^2\text{-}P_2H_2)]$ (**14**) appears as a singlet at $\delta = -120$.[42]

[57] Curiously, Green's report on P_4 functionalization mediated by $[Cp_2MoH_2]$ was published shortly after the first report on metal-mediated P_4 activation by Lindsell and Ginsberg.[3]

[58] J. Ott, L. M. Venanzi, C. A. Ghilardi, S. Midollini, A. Orlandini, *J. Organomet. Chem.* **1985**, *291*, 89.

[59] P. Janser, L. M. Venanzi, F. J. Bachechi, *J. Organomet. Chem.* **1985**, *296*, 229.

[60] C. Bianchini, A. Meli, M. Peruzzini, F. Vizza, A. Albinati, *Organometallics* **1990**, *9*, 2283.

[61] C. Bianchini, A. Meli, M. Peruzzini, F. Vizza, P. Frediani, *Organometallics* **1990**, *9*, 226.

[62] C. Bianchini, J. A. Casares, A. Meli, V. Sernau, F. Vizza, R. A. Sánchez-Delgado, *Polyhedron* **1997**, *16*, 3099.

[63] C. Bianchini, M. V. Jimenez, A. Meli, F. Vizza, V. Herrera, R. A. Sánchez-Delgado, *Organometallics* **1995**, *14*, 2342.

[64] C. Bianchini, C. Mealli, A. Meli, L. Sacconi, *Inorg. Chim. Acta* **1979**, *37*, L54.

[65] The M^1 reagents originally used by Sacconi and co-workers to prepare **31** and **32** were $[RhCl_2(C_2H_4)_2]_2$ and $[(PPh_3)_2Ir(\text{-}CO)Cl]$, respectively.

[66] M. Di Vaira, P. Stoppioni, L. Sacconi, *J. Organomet. Chem.* **1983**, *250*, 183.

[67] M. Di Vaira, L. Sacconi, *Angew. Chem.* **1982**, *94*, 338; *Angew. Chem. Int. Ed. Engl.* **1982**, *21*, 330.

[68] [68a] C. Mealli, S. Midollini, S. Moneti, L. Sacconi, *Cryst. Struct. Commun.* **1980**, *9*, 1017. – [68b] F. Cecconi, C. A. Ghilardi, S. Midollini, A. Orlandini, *J. Chem. Soc., Chem. Commun.*

1982, 229. – [68c] F. Cecconi, C. A. Ghilardi, S. Midollini, A. Orlandini, *Angew. Chem.* **1983**, *95*, 554; *Angew. Chem. Int. Ed. Engl.* **1983**, *22*, 554; *Angew. Chem. Suppl.* **1983**, 718. – [68d] M. Di Vaira, P. Stoppioni, M. Peruzzini, *J. Chem. Soc., Dalton Trans.* **1990**, 109. – [68e] M. Di Vaira, D. Rovai, P. Stoppioni, *Polyhedron* **1990**, *9*, 2477. – [68f] M. Di Vaira, P. Stoppioni, *Polyhedron* **1994**, *13*, 3045. – [68g] M. Di Vaira, M. P. Ehses, M. Peruzzini, P. Stoppioni, *Polyhedron* **1999**, *18*, 2331. – [68h] M. Di Vaira, M. P. Ehses, M. Peruzzini, P. Stoppioni, *J. Organomet. Chem.* **2000**, *593*/*594*, 127.

[69] See, for example, the reaction of [(triphos)RhH_3] with thiophene: C. Bianchini, A. Meli, M. Peruzzini, F. Vizza, P. Frediani, V. Herrera, R. Sánchez-Delgado, *J. Am. Chem. Soc.* **1993**, *115*, 2731 and unpublished observations from this laboratory.

[70] M. Peruzzini, J. A. Ramirez, F. Vizza, *Angew. Chem.* **1998**, *110*, 2376; *Angew. Chem. Int. Ed. Engl.* **1998**, *37*, 2255.

[71] M. Baudler, C. Adamek, S. Opiela, H. Budzkiewicz, D. Ouzounis, *Angew. Chem.* **1988**, *100*, 1110; *Angew. Chem. Int. Ed. Engl.* **1988**, *27*, 1059.

[72] [72a] M. Baudler, H. Ständeke, M. Borgardt, H. Strobel, *Naturwissenschaften* **1965**, *52*, 345. – [72b] M. Baudler, H. Ständeke, M. Borgardt, J. Dobbers, *Naturwissenschaften* **1966**, *53*, 106.

[73] O. J. Scherer, T. Hilt, G. Wolmershäuser, *Organometallics* **1998**, *17*, 4110.

[74] L. Weber, U. Sonnenberg, *Chem. Ber.* **1991**, *124*, 725.

[75] P. Barbaro, C. Bianchini, A. Meli, M. Peruzzini, F. Vizza, *Organometallics* **1991**, *10*, 2227.

[76] Monitoring the reaction between **41** and P_4 in [D_6]-C_6H_6 showed that C–D bond activation from the solvent, giving [(triphos)IrD_2(Ph)], takes place before reaction with P_4. Prolonged heating transforms the dideuteridophenyl complex into the monodeuterated bicyclotetraphosphane derivative [D_1]-**42**.

[77] Complexes containing the bicyclotetraphosphane ligand include: Zr/Hf: [77a] See ref.[9j]. – Fe: [77b] O. J. Scherer, G. Schwarz, G. Wolmershäuser, *Z. Anorg. Allg. Chem.* **1996**, *622*, 951. Co: – [77c] O. J. Scherer, M. Swarowsky, G. Wolmershäuser, *Organometallics* **1989**, *8*, 841. – [77d] M. Scheer, U. Becker, J. C. Huffman, M. C. Chisholm, *J. Organomet. Chem.* **1993**, *461*, C1. – Rh: [77e] A. P. Ginsberg, W. E. Lindsell, K. J. McCullough, C. R. Sprinkle, A. J. Welch, *J. Am. Chem. Soc.* **1986**, *108*, 403. – [77f] M. Scheer, C. Troitzsch, P. G. Jones, *Angew. Chem.* **1992**, *104*, 1137; *Angew. Chem. Int. Ed. Engl.* **1992**, *31*, 1377 – [77g] M. Scheer, C. Troitzsch, L. Hilfert, M. Dargatz, E. Kleinpeter, P. G. Jones, J. Sieler, *Chem. Ber.* **1995**, *128*, 251. – [77h] M. Di Vaira, M. P. Ehses, M. Peruzzini, P. Stoppioni, *Eur. J. Inorg. Chem.*, in press. – Ir: [77i]M. Scheer, U. Becker, E. Matern, *Chem. Ber.* **1996**, *129*, 721. – Pt: [77j] M. Scheer, M. Dargatz, A. Rufinska, *J. Organomet. Chem.* **1992**, *440*, 327.

[78] P. Barbaro, M. Peruzzini, J. A. Ramirez, F. Vizza, *Organometallics* **1999**, *18*, 4237.

[79] P. Barbaro, M. Peruzzini, G. Schmidt, F. Vizza, unpublished results.

[80] V. I. Bakhmutov, C. Bianchini, M. Peruzzini, F. Vizza, E. V. Vorontsov, *Inorg. Chem.* **2000**, *39*, 1655.

[81] C. Bianchini, S. Moneti, M. Peruzzini, F. Vizza, *Inorg. Chem.* **1997**, *36*, 5818.

[82] M. Peruzzini, F. Vizza, unpublished observations.

[83] M. Di Vaira, P. Stoppioni, S. Midollini, F. Laschi, P. Zanello, *Polyhedron* **1991**, *10*, 2123.

[84] For a known example of triphos cobalt hydride, see: C. Bianchini, D. Masi, C. Mealli, A. Meli, M. Sabat, *Gazz. Chim. Ital.* **1986**, *116*, 201.

[85] A. Bencini, M. Di Vaira, P. Stoppioni, M. G. Uytterhoeven, *Theor. Chim. Acta* **1995**, *91*, 187.

[86] C. A. Ghilardi, S. Midollini, A. Orlandini, L. Sacconi, *Inorg. Chem.* **1980**, *19*, 301.

[87] C. Capozzi, L. Chiti, M. Di Vaira, M. Peruzzini, P. Stoppioni, *J. Chem. Soc., Chem. Commun.* **1986**, 1799.

[88] M. Di Vaira, P. Stoppioni, *Polyhedron* **1994**, *13*, 3045.

[89] The term "nucleophilic hydrogenation" is used here in a broad sense to indicate any reaction leading to the formation of a P–H bond through addition of a nucleophile (OH^-, H^-, etc.) to a metal-coordinated P_x unit.

[90] J. E. Davies, N. Feeder, M. J. Mays, P. K. Tompkin, A. D. Woods, *Organometallics* **2000**, *19*, 984 and references therein.

[91] O. J. Scherer, H. Sitzmann, G. Wolmershäuser, *J. Organomet. Chem.* **1984**, *268*, C9.

[92] J. E. Davies, M. J. Mays, P. R. Raithby, G. P. Shields, P. K. Tompkin, *Chem. Commun.* **1997**, 361.

[93] J. E. Davies, L. C. Kerr, M. J. Mays, P. R. Raithby, P. K. Tompkin, A. D. Woods, *Angew. Chem.* **1998**, *110*, 1473; *Angew. Chem. Int. Engl. Ed.* **1998**, *37*, 1428.

[94] P. Sekar, M. Scheer, A. Voigt, R. Kirmse, *Organometallics* **1999**, *18*, 2833.

[95] Formation of a dimetallic-based dianion upon addition of $LiHBEt_3$ is a common feature in both disulfido and diselenido iron complexes: [95a] D. Seyferth, R. S. Henderson, C. Li, *Organometallics* **1982**, *1*, 125. – [95b] D. Seyferth, R. S. Henderson, *J. Organomet. Chem.* **1981**, *294*, 333.

[96] The two complexes **68** and **69** could not be separated by chromatography and were obtained as pure samples by manual separation of their crystals in a glovebox.[94]

[97] [$(Cp^*Cr)_2(\mu,\eta^5{:}\eta^5\text{-}P_5)$]: O. J. Scherer, J. Schwalb, G. Wolmershäuser, W. Kai, R. Gross, *Angew. Chem.* **1986**, *98*, 349; *Angew. Chem. Int. Ed. Engl.* **1986**, *4*, 363. [$(Cp^*Cr)_2(\mu,\eta^5{:}\eta^5\text{-}P_5)$]$SbF_6$: A. K. Hughes, V. J. Murphy, D. O'Hare, *J. Chem. Soc., Chem. Commun.* **1994**, 163.

[98] A similar allylic P_3/P_2 distortion has been found in the *cyclo*-As_5 sandwich complex [$\{Cp^*Mo\}_2(\mu,\eta^5{:}\eta^5\text{-}As_5)$], see: A. L. Rheingold, M. J. Foley, P. J. Sullivan, *J. Am. Chem. Soc.* **1982**, *104*, 4727.

Received June 16, 2000
[I00237]

Metal-Mediated Self-Assembly of Molecular Squares of Porphyrins Rimmed with Coordination Compounds

Elisabetta Iengo,[a] Romina Minatel,[a] Barbara Milani,[a] Luigi G. Marzilli,[b] and Enzo Alessio*[a]

Keywords: Porphyrinoids / Supramolecular chemistry / N ligands / Self-assembly / Ruthenium

Partially coordinated *meso*-tetra(4′-pyridyl)porphyrin, in which two out of four peripheral 4′-(N)py sites are bound to inert Ru^{II} complexes, self assembles with cationic square-planar Pd^{II} or neutral octahedral Ru^{II} 90° angular units to yield a new family of molecular squares, in which the periphery of the porphyrins is rimmed with coordination compounds.

Introduction

The metal-mediated self-assembly of bi- and polydentate *N*-donor ligands is a widely used approach to the efficient construction of discrete two- and three dimensional supramolecular architectures.[1] The same self-assembly principle has been applied to the construction of multiporphyrin assemblies[2] which can either mimic naturally occurring multichromophore aggregates, such as the photosynthetic reaction center and the light harvesting complex of purple bacteria,[3] or can be used as electron- and/or energy-transfer molecular devices for advanced technological tasks.[1a,2] In such supramolecular architectures the position and relative orientation of the chromophores is essentially dictated by the nature and geometry of the metal auxiliaries.[4] In particular, there has been substantial recent interest in the construction of cyclic multiporphyrin assemblies (molecular squares) which lock the chromophores in a mutually coplanar geometry.[1a,5]

In general, the relatively few examples of molecular squares of porphyrins based on homonuclear metal corners or edges have been prepared by coordination of *meso*-di(4′-pyridyl)porphyrins *basic* building blocks,[6] either *cis* (90° angular, A_b) or *trans* (180° linear, L_b), with suitable coordination compounds, precursors for angular (90°, A_a) or linear (180°, L_a) *acidic* building blocks.[7,8] Recently, we described an efficient approach to heterobimetallic cyclic porphyrin assemblies featuring different diagonally opposed metal ions.[9]

Here we report the stepwise construction of a new class of molecular squares of porphyrins comprising two types of metal centers: the nuclei of one metal have a structural role (corners of the square, either Pd or Ru), while those of the other metal (Ru) rim the periphery of the chromophores.

[a] Dipartimento di Scienze Chimiche, Università di Trieste, 34127 Trieste, Italy
Fax: (internat.) +39-040/676-3903
E-mail: alessi@univ.trieste.it
[b] Department of Chemistry, Emory University, Atlanta, Georgia 30322, USA
Supporting information for this article is available on the WWW under http://www.wiley-vch.de/home/eurjic or from the author.

Results and Discussion

In the first step of this synthetic approach two out of four peripheral 4′-(N)py sites of 4′-TPyP[6] were coordinated to metal centers. We reported that treatment of *meso*-(4′-pyridyl)porphyrins with the Ru^{II} complex *cis,fac*-$[RuCl_2(DMSO)_3(CO)]$ (**1**) leads to the selective coordination of *cis,cis,cis*-$[RuCl_2(DMSO\text{-}S)_2(CO)]$ fragments ([**Ru**]) to the peripheral basic sites of the chromophores.[10] The 4′-(N)py−[**Ru**] bonds are both stable and inert. Thus, reaction of 4′-TPyP with two equivalents of **1** yielded a mixture of the five possible adducts (plus unchanged 4′-TPyP):[11] the two bis-ruthenated isomeric products, *cis*-4′-TPyP([**Ru**])$_2$ (**2**) and *trans*-4′-TPyP([**Ru**])$_2$ (**3**), were obtained in pure form by chromatography. The nature and geometry of **2** and **3** were unambiguously established from a combination of ^{1}H NMR spectroscopy (Figure 1) and mass spectrometry. The number of NMR signals for the eight pyrrole protons (β-H) proved to be particularly important in distinguishing between the *cis* and *trans* isomers, since the other resonances are only marginally different: *trans*-4′-TPyP([**Ru**])$_2$ (**3**) gives two doublets of the same intensity (4β-H each), while *cis*-4′-TPyP([**Ru**])$_2$ (**2**) shows two doublets plus two singlets of the same intensity (2β-H each).

The sulfoxide resonances (four equally intense singlets in the region for *S*-bonded DMSO which may overlap partially or completely in pairs) confirm through integration that two [**Ru**] fragments are bound to each 4′-TPyP and are always consistent with the *cis,cis,cis* geometry of each ruthenium unit.[13] Electrospray mass spectrometry (ES-MS) analysis of **2** and **3** gave peaks corresponding to MH^+ (m/z = 1332.0, calculated 1332.2) and MH_2^{2+} (m/z = 667.4, calculated 666.6), plus fragmentation peaks deriving from the loss of one or both [**Ru**] units; the isotopic distribution

 © WILEY-VCH Verlag GmbH, 69451 Weinheim, 2001 1434−1948/01/0303−0609 $ 17.50+.50/0

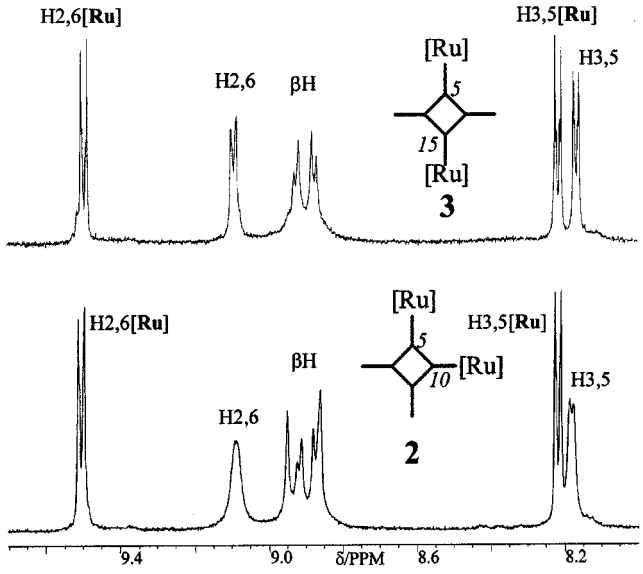

Figure 1. Downfield region of the ^{1}H NMR spectrum of *cis*-4′-TPyP([**Ru**])$_2$ (**2**)[12] (bottom) and *trans*-4′-TPyP([**Ru**])$_2$ (**3**) (top) with the corresponding schematic building block representations; see Figure 2 for labeling scheme; [**Ru**] = *cis,cis,cis*-[RuCl$_2$(DMSO-*S*)$_2$(CO)]

patterns were also consistent with the calculated isotopic envelope expected for such isomers.

We demonstrated that coordination of one (or more) [**Ru**] unit(s) to 4′-PyPs[6] does not affect significantly the further reactivity of the uncoordinated 4′-(N)py ring(s).[11] Compounds **2** and **3**, with two residual unbound 4′-(N)py rings either at 90° or 180°, are thus described as A_b and L_b building blocks, respectively, and are suitable for the construction of molecular squares. As examples, we investigated the reactivity of **2** towards [Pd(dppp)(OTf)$_2$] (**4**) [dppp = 1,3-bis(diphenylphosphanyl)propane, OTf = triflate] and *trans*-[Ru^{II}Cl$_2$(DMSO-*S*)$_4$] (**5**), which are precursors for the double-charged square-planar [Pd(dppp)]$^{2+}$,[7,8] and for the neutral octahedral *trans,cis*-[RuCl$_2$(DMSO-*S*)$_2$] (***t*Ru**) A_a units,[9−11] respectively. The reaction of **2** with **4** or **5** was monitored by ^{1}H NMR spectroscopy in CDCl$_3$ solution, which established that titration of **4** into a CDCl$_3$ solution of **2** led readily to the quantitative formation of [Pd(dppp){*cis*-4′-TPyP([**Ru**])$_2$}]$_2$(OTf)$_4$ (**6**) (Figure 2).

Complex **6** is an example of a new type of heterobimetallic [2+2] molecular square of porphyrins in which the Pd^{II} ions form two corners of the square, while the four Ru^{II} complexes rim the outside of the assembly. Integration of the NMR resonances confirmed the 2:1:1 ratio between [**Ru**], 4′-TPyP, and dppp expected for **6**. ES-MS analysis of **6** gave an [M − 3OTf] peak of *m/z* = 1240.0 (calculated 1240.3) resulting from a loss of three triflate anions from a total of four (and also a series of fragmentation peaks corresponding to the loss of [**Ru**] units and neutral ligands). Coordination of the Pd−bisphosphane fragment to **2** induced characteristic shifts of NMR signals; these included mainly the ^{1}H NMR resonances of the previously unbound 4′-N(py) rings (Figure 3) and the proton-decoupled ^{31}P NMR signal (upfield shift of ca 10 ppm relative to **4**, as is

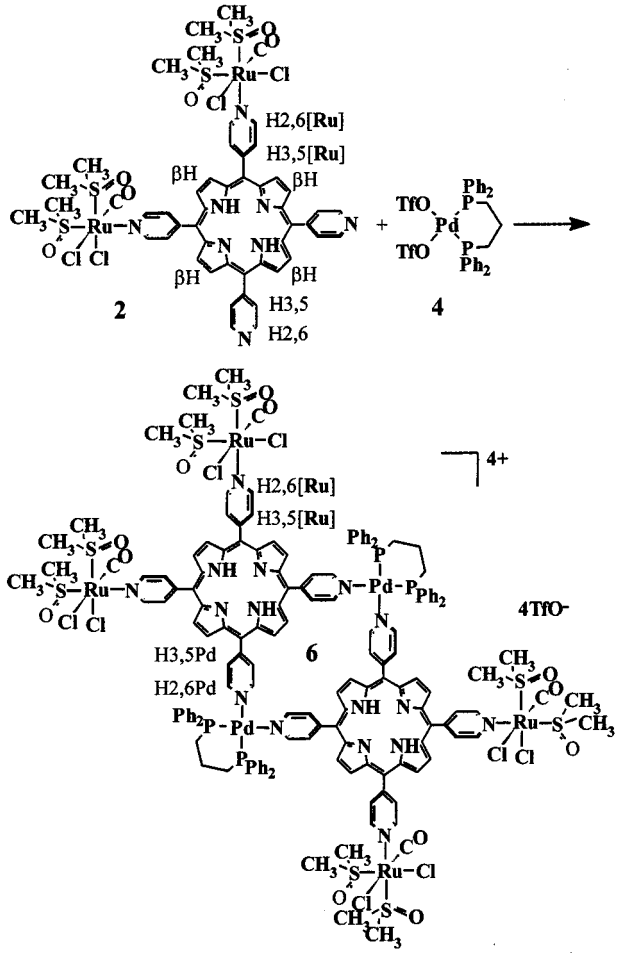

Figure 2. Schematic synthesis of [Pd(dppp){*cis*-4′-TPyP([**Ru**])$_2$}]$_2$(OTf)$_4$ (**6**) with labeling scheme

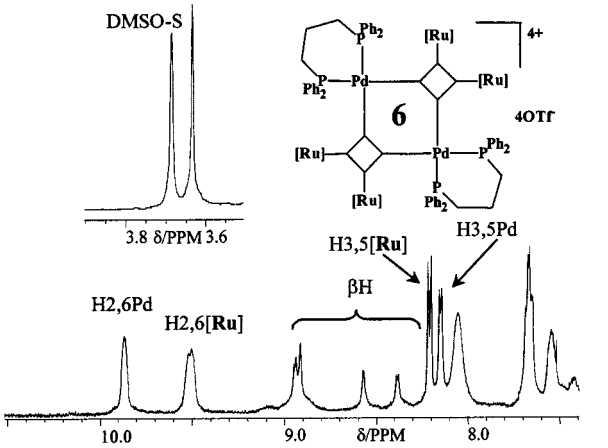

Figure 3. Downfield region, and DSMO-*S* region (insert), of the ^{1}H NMR spectrum of [Pd(dppp){*cis*-4′-TPyP([**Ru**])$_2$}]$_2$(OTf)$_4$ (**6**) with its schematic representation; see Figure 2 for labeling scheme

the case in similar compounds[7,9]). In **6** the resonances of the 4′(N)py−Pd rings are well resolved from those of the 4′(N)py−[**Ru**] rings, which were almost unshifted upon formation of the square. The most downfield H2,6 and the most upfield H3,5 signals (correlated in the COSY spec-

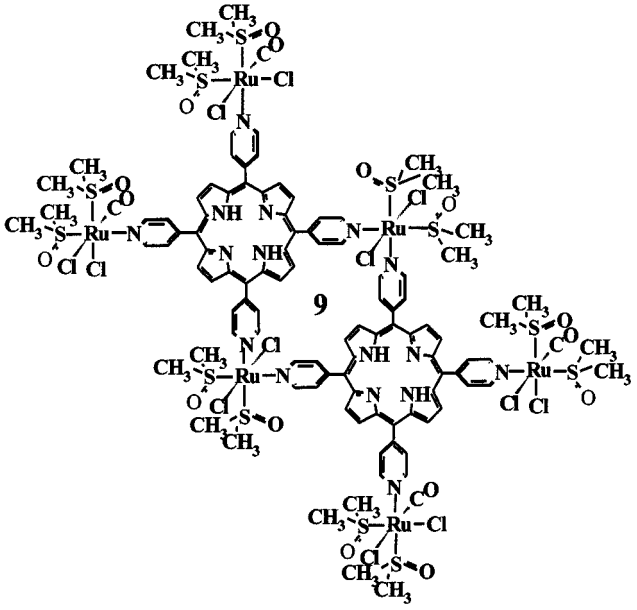

Figure 4. Schematic representation of *trans,cis,cis*-[$RuCl_2$(DMSO-*S*)$_2${*cis*-4′-TPyP([**Ru**])$_2$}]$_2$ (**9**)

trum) were thus attributed to the 4′(N)py−Pd rings; these assignments also agree well with those reported by Stang and co-workers for the corresponding [2+2] molecular square, [Pd(dppp)(4′-*cis*DPyP)]$_2$(OTf)$_4$] (**7**), prepared by reaction of equimolar amounts of 4′-*cis*DPyP and **4**.[7] It should be noted that formation of [Pd(dppp){*cis*-4′-TPyP([**Ru**])$_2$}]$_2$(OTf)$_4$ (**6**) involves a slight upfield shift of the H3,5 resonance of the previously unbound 4′(N)py rings in **2**. Moreover, in **6** one singlet and, in particular, one doublet of the β-H resonances on each porphyrin are remarkably upfield shifted also; these signals are correlated by clear NOE cross-peaks to the H3,5 4′(N)py−Pd signal in the NOESY spectrum. Similar anomalously upfield resonances for the protons closest to Pd were found in the ^{1}H NMR spectra of **7**[7] and of the heterobimetallic Ru^{II}−Pd^{II} cyclic assemblies [Pd(dppp){*trans,cis,cis*-$RuCl_2$(X)(Y)(4′-*cis*DPyP)$_2$}](OTf)$_2$ (X, Y = DMSO-*S*, CO)[9] and were attributed by us to the shielding cone of the phenyl rings of the dppp ligand rather than to the Pd^{II} center.[9] This hypothesis is confirmed here by the NMR spectrum of the [2+2] square of rimmed porphyrins [Pd(PEt_3)$_2${*cis*-4′-TPyP([**Ru**])$_2$}]$_2$(OTf)$_4$ (**8**), closely related to **6** and prepared by treatment of **2** with one equivalent of *cis*-[Pd(PEt_3)$_2$(OTf)$_2$]. In **8**, which lacks the shielding phenyl rings on the phosphanes, the resonances of the pyrrole protons closest to Pd and those of the 4′(N)py−Pd rings are remarkably more downfield-shifted than in **6** (e.g. δ H3,5 = 8.62 in **8** vs. 8.16 in **6**).

Finally, the neutral molecular square of porphyrins rimmed with ruthenium coordination compounds *trans,cis,cis*-[$RuCl_2$(DMSO-*S*)$_2${*cis*-4′-TPyP([**Ru**])$_2$}]$_2$ (**9**, Figure 4) was prepared by treatment of **2** with one equivalent of *trans*-[$Ru^{II}Cl_2$(DMSO-*S*)$_4$] (**5**). Metallacycle **9** features two types of Ru^{II} centers with different coordination environments and roles: ***t*Ru** moieties are located at the two corners of the square, while four [**Ru**] units rim the periphery of the square. Coordination of **2** to the ***t*Ru** moiety affected mainly the H2,6 and H3,5 resonances of the 4′-N(py) ring involved in the new bonds, which experienced downfield shifts similar to those found in the corresponding *trans,cis,cis*-[$RuCl_2$(DMSO-*S*)$_2$(4′-MPyP)$_2$] complexes.[9−11]

Conclusion

In conclusion, we have demonstrated that new families of cationic and neutral multiporphyrin metallacycles, in which the porphyrins are externally decorated with Ru^{II} complexes, are readily assembled through the formation of coordination bonds between partially ruthenated 4′-TPyP and either square planar Pd^{II} or octahedral Ru^{II} auxiliaries, respectively.

The higher degree of complexity of the new molecular squares of porphyrins rimmed with coordination compounds compared to the previously known multichromophore cyclic assemblies requires a more demanding synthetic approach (mainly in terms of purification of the partially metalated porphyrins) but also offers exciting perspectives: in future a proper choice of the external and of the structural metal centers (corners of the square) might favor electron and/or charge transfer from one site to another within the assembly. Moreover, the external metal centers might be exploited for incorporating special properties (e.g. chirality, luminescence, ...) into the multiporphyrin cyclic assembly and for its further functionalization. For the time being, since the main focus of the present work was directed towards the establishment of a synthetic approach for such novel cyclic assemblies, only metal compounds with a well-known and tested chemistry were used both as structural and rimming units.

Experimental Section

^{1}H and ^{31}P{^{1}H} NMR spectra were recorded on a Jeol EX400 spectrometer at 400 and 161.9 MHz, respectively. The ^{1}H NMR signals were referenced to the signal of residual $CHCl_3$ (δ = 7.26) and assignments were made with the aid of 2D COSY experiments, as detailed in the text; ^{31}P NMR spectra were referenced to external H_3PO_4. ES-MS data were obtained on a Perkin−Elmer AP1 spectrometer. Samples were dissolved in chloroform; the spectra were recorded in the positive ion mode at 5.6 kV accelerating potential; 2% trifluoroacetic acid was added to the solutions of **2** and **3**. The UV/Vis spectra were obtained on a Jasco V−550 spectrophotometer. All reagents were analytical grade.

Preparation of *cis*-4′-TPyP([Ru])$_2$ (2) and *trans*-4′-TPyP([Ru])$_2$ (3): The reaction between 4′-TPyP and *cis,fac*-$RuCl_2$(DMSO)$_3$(CO) (**1**) was performed as reported in ref.[11] Components of the mixture were separated by column chromatography on silica gel;[11] the two bis-ruthenated isomeric products, *cis*-4′-TPyP([**Ru**])$_2$ (**2**) and *trans*-4′-TPyP([**Ru**])$_2$ (**3**), were obtained as a mixture from the column and their separation required further preparative-scale TLC on silica gel plates (CH_2Cl_2/EtOH mixture 90:10; R_f **2** = 0.81, R_f **3** = 0.84). The products were extracted from the silica with an acetone/MeOH mixture (80:20). 100 mg of 4′-TPyP yielded, on average, 11 mg each of isolated **2** and **3** (5%). Elemental analyses for **2** and

3 were not reliable because they were affected by the presence of variable amounts of solvent molecules of crystallization.

Selected data for **2:** ^{1}H NMR ($CDCl_3$): δ = −2.96 (s, 2 H, NH), 3.62 (s, 6 H, DMSO-*S*), 3.64 (s, 6 H, DMSO-*S*), 3.69 (s,12 H, DMSO-*S*), 8.19 [m, 4 H, H3,5(py)], 8.22 (m, 4 H, H3,5[**Ru**]), 8.86 (s, 2 H, β-H), 8.88 (d, ^3J = 8 Hz, 2 H, β-H), 8.91 (d, ^3J = 8 Hz, 2 H, β-H), 8.95 (s, 2 H, β-H), 9.09 [m, 4 H, H2,6(py)], 9.51 (m, 4 H, H2,6[**Ru**]). − UV/Vis (CH_2Cl_2): λ (ε × 10^4/M^{-1} cm^{-1}) = 419 (28), 514 (1.5), 549 (0.6), 589 (0.5), 645 (0.2) nm.

Selected data for **3:** ^{1}H NMR ($CDCl_3$): δ = −2.97 (s, 2 H, NH), 3.62 (s, 6 H, DMSO-*S*), 3.64 (s, 6 H, DMSO-*S*), 3.69 (s, 12 H, DMSO-*S*), 8.17 [m, 4 H, H3,5(py)], 8.22 (m, 4 H, H3,5[**Ru**]), 8.88 (d, ^3J = 4 Hz, 4 H, β-H), 8.92 (d, ^3J = 4 Hz, 4 H, β-H), 9.09 [m, 4 H, H2,6(py)], 9.50 (m, 4 H, H2,6[**Ru**]). − UV/Vis (CH_2Cl_2): λ (ε × 10^4/M^{-1} cm^{-1}) = 419 (38.5), 515 (2.2), 549 (0.8), 589 (0.7), 645 (0.3) nm.

Preparation of [Pd(dppp){*cis*-4′-TPyP([Ru])$_2$}]$_2$(OTf)$_4$ (6), [Pd(PEt$_3$)$_2${*cis*-4′-TPyP([Ru])$_2$}]$_2$(OTf)$_4$ (8), and *trans,cis,cis*-[RuCl$_2$(DMSO-*S*)$_2${*cis*-4′-TPyP([Ru])$_2$}]$_2$ (9): Owing to the very low amounts of precursor **2** (few mg), reactions leading to molecular squares **6**, **8**, and **9** were performed exclusively in an NMR tube. The formation of **6** and **8** occurred rapidly, while the formation of **9** required three hours at ambient temperature. The electronic spectra of **8** and **9** are qualitatively very similar to that of **6** (see below) in terms of the shape and position of the absorption bands, but the purity of the products isolated from the NMR solutions upon removal of the solvent (established by NMR spectroscopy) was not deemed high enough for quantitative measurements (determination of absorption coefficients).

Selected data for **6:** ^{1}H NMR ($CDCl_3$): δ = −3.16 (s, 4 H, NH), 3.63 (s, 12 H, DMSO-*S*), 3.69 (s,12 H, DMSO-*S*), 8.16 (m, 8 H, H3,5Pd), 8.21 (m, 8 H, H3,5[**Ru**]), 8.38 (d, ^3J = 4 Hz, 4 H, β-H), 8.58 (s, 4 H, β-H), 8.92 (s, 4 H, β-H), 8.94 (d, ^3J = 4 Hz, 4 H, β-H), 9.52 (m, 8 H, H2,6[**Ru**]), 9.86 (m, 8 H, H2,6Pd). − ^{31}P NMR ($CDCl_3$): δ = 6.1. − UV/Vis (CH_2Cl_2): λ (ε × 10^4/ M^{-1} cm^{-1})= 424 (52.0), 518 (3), 553 (1), 592 (0.6), 646 (0.1) nm.

Selected data for **8:** ^{1}H NMR ($CDCl_3$): δ = −2.98 (s, 4 H, NH), 3.65 (s, 12 H, DMSO-*S*), 3.70 (s, 6 H, DMSO-*S*), 3.71 (s, 6 H, DMSO-*S*), 8.22 (m, 8 H, H3,5[**Ru**]), 8.56 (d, ^3J = 4 Hz, 4 H, β-H), 8.62 (m, 8 H, H3,5Pd), 8.87 (s, 4 H, β-H), 8.94 (d, ^3J = 4 Hz, 4 H, β-H), 9.01 (s, 4 H, β-H), 9.52 (m, 8 H, H2,6[**Ru**]), 10.18 (m, 8 H, H2,6Pd). − ^{31}P NMR ($CDCl_3$): δ = 21.5.

Selected data for **9:** ^{1}H NMR ($CDCl_3$): δ = −2.89 (s, 4 H, NH), 3.71, 3.70, 3.66, 3.64 (s, 72 H, DMSO-*S*), 8.25 (m, 8 H, H3,5[**Ru**]), 8.39 (m, 8 H, H3,5*t***Ru**), 8.96 (m, 8 H, H-β), 9.00 (m, 4 H, H-β), 9.03 (s, 4 H, H-β), 9.55 (m, 8 H, H2,6[**Ru**]), 10.10 (m, 8 H, H2,6*t***Ru**).

Acknowledgments

We thank Italian MURST for financial support and the Mass Spectrometry Facility of the University of Trieste (Prof. F. Benedetti and Dr. F. Hollan) for recording the ES MS spectra. This work was performed in the frame of EU program COST Action D11, project no. D11/0004/98.

[1] [1a] S. Leininger, B. Olenyuk, P. J. Stang, *Chem. Rev.* **2000**, *100*, 853−908. − [1b] M. Fujita, *Chem. Soc. Rev.* **1998**, *27*, 417−425. − [1c] P. J. Stang, *Chem. Eur J.* **1998**, *4*, 19−27.

[2] For a comprehensive recent review see: J.-C. Chambron, V. Heitz, J.-P. Sauvage, *The Porphyrin Handbook* (Eds.: K. M. Kadish, K. M. Smith, R. Guillard), Academic Press, **2000**, Vol. 6, Chapter 40.

[3] [3a] S. E. Webber, *Chem. Rev.* **1990**, *90*, 1469−1482. − [3b] M. R. Wasielewski, *Chem. Rev.* **1992**, *92*, 435−461. − [3c] J. Seth, V. Palaniappan, T. E. Johnson, S. Prathapan, J. S. Lindsey, D. F. Bocian, *J. Am. Chem. Soc.* **1994**, *116*, 10578−10592. − [3d] V. S.-Y. Lin, S. G. DiMagno, M. J. Therien, *Science* **1994**, *264*, 1105−1111. − [3e] H. Kurreck, M. Huber, *Angew. Chem. Int. Ed. Engl.* **1995**, *34*, 849−866. − [3f] A. Harriman, J.-P. Sauvage, *Chem. Soc. Rev.* **1996**, 41−48.

[4] For recent examples, see: [4a] C. C. Mak, N. Bampos, J. K. M. Sanders, *Chem. Commun.* **1999**, 1085−1086. − [4b] E. Alessio, S. Geremia, S. Mestroni, I. Srnova, M. Slouf, T. Gianferrara, A. Prodi, *Inorg. Chem.* **1999**, *38*, 2527−2529. − [4c] A. K. Burrell, D. L. Officer, D. C. W. Reid, K. Y. Wild, *Angew. Chem. Int. Ed.* **1998**, *37*, 114−117. − [4d] C. M.Drain, F. Nifiatis, A.V-asenko, J. D. Batteas, *Angew. Chem. Int. Ed.* **1998**, *37*, 2344−2347.

[5] R. W. Wagner, J. Seth, S. I. Yang, D. Kim, D. F. Bocian, D. Holten, J. S. Lindsey, *J. Org. Chem.* **1998**, *63*, 5042−5049 and references therein.

[6] Abbreviations: *meso*-4′-pyridylporphyrins (4′-PyPs); 5,10-bis(4′-pyridyl)-15,20-diphenylporphyrin (4′-*cis*DPyP); 5,15-bis(4′-pyridyl)-10,20-diphenylporphyrin (4′-*trans*DPyP); 5,10,15,20-tetra(4′-pyridyl)porphyrin (4′-TPyP).

[7] J. Fan, J. A. Whiteford, B. Olenyuk, M. D. Levin, P. J. Stang, E. B. Fleisher, *J. Am. Chem. Soc.* **1999**, *121*, 2741−2752.

[8] [8a] M. Schmitz, S. Leininger, J. Fan, A. M. Arif, P. J. Stang, *Organometallics* **1999**, *18*, 4817−4824. − [8b] P. J. Stang, J. Fan, B. Olenyuk, *Chem. Commun.* **1997**, 1453−1454. − [8c] R. V. Slone, J. T. Hupp, *Inorg. Chem.* **1997**, *36*, 5422−5423. − [8d] C. M. Drain, J.-M. Lehn, *J. Chem. Soc., Chem. Commun.* **1994**, 2313−2315.

[9] E. Iengo, B. Milani, E. Zangrando, S. Geremia, E. Alessio, *Angew. Chem. Int. Ed.* **2000**, *39*, 1096−1099.

[10] E. Alessio, M. Macchi, S. L. Heath, L. G. Marzilli, *Inorg. Chem.* **1997**, *36*, 5614−5623.

[11] E. Alessio, E. Ciani, E. Iengo, V. Yu. Kukushkin, L. G. Marzilli, *Inorg. Chem.* **2000**, *39*, 1434−1443.

[12] As it is often the case with pyridylporphyrins, the broadening of the H2,6 and H3,5 resonances in the ^{1}H NMR spectrum of compound **2** is due to the presence in solution of small amounts of Lewis acids, in this case very likely silica from the chromatographic purification of **2**. The weak and labile interaction between the uncoordinated pyridyl rings of compound **2** and the Lewis acid induces a broadening (and a very small shift) of the proton resonances of such rings.

[13] Since the [**Ru**] moiety is chiral, both **2** and **3** must exist as mixtures of stereoisomers (with *C* or *A* [**Ru**] units), with potentially different NMR signals. However, at the field used, the ^{1}H NMR signals were not distinct for the diastereoisomers.

Received September 4, 2000
[I00332]

A Novel Organometallic Polymer of Osmium(0), $[Os(2,2'\text{-bipyridine})(CO)_2]_n$: Its Electrosynthesis and Electrocatalytic Properties Towards CO_2 Reduction

Sylvie Chardon-Noblat,*[a] Alain Deronzier,*[a] František Hartl,*[b] Joris van Slageren,[b] and Taasje Mahabiersing[b]

Keywords: Osmium / Electrochemistry / Polymers / Carbon dioxide / Reductions

A new kind of organometallic polymer of osmium(0) $[Os^0(bpy)(CO)_2]_n$ (bpy = 2,2′-bipyridine) has been prepared as a thin film on an electrode surface by electrochemical reduction of the mononuclear *trans*(Cl)-$[Os^{II}(bpy)(CO)_2Cl_2]$ precursor complex. This modified electrode proves to be a good electrocatalyst for the reduction of CO_2 in aqueous media.

Introduction

It is now well established that the two-electron reduction of a mononuclear ruthenium(II) complex precursor such as *trans*(Cl)-$[Ru(bpy)(CO)_2Cl_2]$ (bpy = 2,2′-bipyridine) leads to the facile formation of thin films of $[Ru(bpy)(CO)_2]_n$ on conductive electrode surfaces.[1,2] This new kind of organometallic polymer, containing Ru−Ru chains, proved to be a highly selective and efficient catalyst for the electroreduction of carbon dioxide in aqueous media[3,4] and for the water-gas shift (WGS) reaction.[5] It also exhibits interesting photochemical properties.[6] We could reasonably expect formation of an analogous Os^0 organometallic polymer by the electrochemical reduction of the parent mononuclear osmium(II) complex *trans*(Cl)-$[Os(bpy)(CO)_2Cl_2]$ (**1**), which has recently been synthesized but only superficially characterized.[7]

We present here a preliminary electrochemical study of **1** which confirms that films of the $[Os(bpy)(CO)_2]_n$ polymer can indeed be prepared effectively. Their capability to act as an electrocatalyst for CO_2 reduction has been briefly evaluated.

Results and Discussion

Synthesis of Complex 1

The complex *trans*(Cl)-$[Os(bpy)(CO)_2Cl_2]$ (**1**) was synthesized in two steps according to a modified literature procedure[7] (see Experimental Section). The ^1H NMR spectroscopic data reveal that the bpy ligand coordinates in a symmetrical environment, with the chloride ligands occupying the axial positions as schematically depicted in Figure 1.

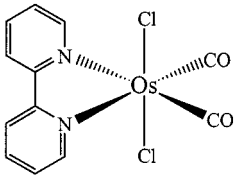

1

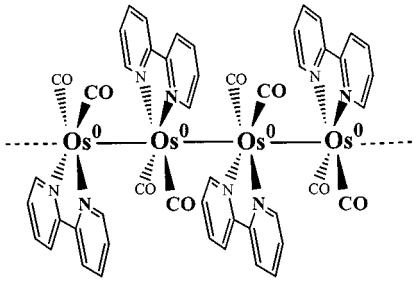

2

Figure 1. Schematic molecular structures of **1** and **2**

The IR spectrum of **1** displays two intense CO-stretching bands (2022 and 1943 cm^{-1}) shifted to lower frequencies relative to the corresponding *trans*(Cl)-$[Ru(bpy)(CO)_2Cl_2]$ complex.[8] It is noteworthy that the ν(CO) band shifts of 41/56 cm^{-1} in the solid state (CsI pellet or nujol) are much larger than the values of 23/31 cm^{-1} in CH_3CN and 24/33 cm^{-1} in THF. The lower ν(CO) frequencies for **1** reflect a stronger Cl→Os σ- and, in particular, π-donation inducing a stronger Os→CO π-back-donation. At the same time the Os−Cl bonds in **1** are stronger and less readily split upon electrochemical reduction than in the Ru derivative, as shown by the radical anion $[Os(bpy^{\cdot-})(CO)_2Cl_2]^-$ detectable by cyclic voltammetry (CV) in THF at moderate scan rates (see below). A similar difference in ν(CO) frequencies and stability of the M−Cl bond was observed, for example,

[a] Laboratoire d'Electrochimie Organique et de Photochimie Rédox, UMR CNRS 5630, Université Joseph Fourier
Grenoble 1, BP 53 38041 Grenoble cedex 9, France
Fax: (internat.) +33-(0)4/7651-4267
E-mail: alain.deronzier@ujf-grenoble.fr
[b] Institute of Molecular Chemistry, Universiteit Van Amsterdam, Nieuwe Achtergracht 166, 1018 WV Amsterdam, The Netherlands
Fax: (internat.) +31-(0)20/525-6456
E-mail: hartl@anorg.chem.uva.nl

 © WILEY-VCH Verlag GmbH, 69451 Weinheim, 2001 1434−1948/01/0303−0613 $ 17.50+.50/0

in the [M(bpy)(CO)$_3$Cl] complex series (M = Re[9] and Mn[10]).

Electrochemical Behaviour of Complex 1

The CV of **1** in CH_3CN (with added 0.1 M TBAP) exhibits an irreversible nearly two-electron cathodic peak at $E_{pc} = -1.61$ V[11] along with small anodic peaks between -0.80 V and 0 V on the reverse scan [Figure 2(a)]. This behaviour is typical of an electrodeposition-redissolution phenomenon, as previously observed for the parent mononuclear Ru^{II} complex.[1,2]

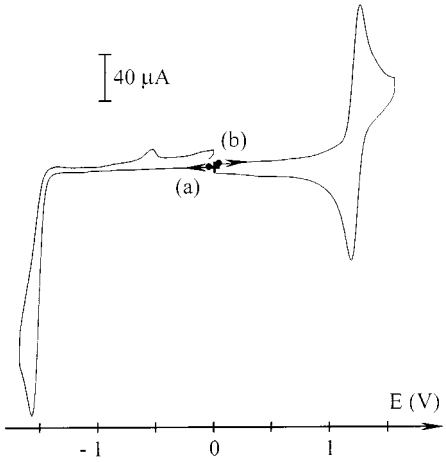

Figure 2. Cyclic voltammograms (ν = 100 mV s^{-1}) of **1** (2.2 mM) in CH_3CN + 0.1 M TBAP at a Pt disc electrode (r = 2.5 mm) recorded between: (a) 0 V and -1.70 V, and (b) 0 V and 1.60 V vs. Ag/Ag$^+$

The negative potential shift observed for the reduction of **1** compared to the corresponding Ru^{II} complex ($\Delta E_{pc} = -0.11$ V)[8] is in agreement with the stronger Os→bpy π-back-donation induced by the Cl→Os donation along with the increased Os→CO π-back-donation, as revealed by the IR ν(CO) data (see above).

The reductive electrochemical polymerization of **1**, monitored by iterative CV or by applied potential electrolysis, leads to a dark green-blue coloured electroactive polymer [Os^0(bpy)(CO)$_2$]$_n$ (**2**) adherent to the working electrode surface. Equation (1) summarizes the overall process of electropolymerization.

$$n\,[Os^{II}(bpy)(CO)_2Cl_2] + 2n\,e^- \rightarrow [Os^0(bpy)(CO)_2]_n + 2n\,Cl^- \quad (1)$$

The electroactivity and electropolymerization properties of the osmium complex **1** are consistent with the mechanism proposed for the electropolymerization of *trans*(Cl)-Ru(bpy) equivalent complex in acetonitrile.[12] The electroreduction of **1** produces ultimately the polymer **2** by an electrochemical propagation process [Equation (2)−(5)]. The initial formation of the one-electron reduced [Os(bpy$^{\bullet-}$)(CO)$_2$Cl$_2$]$^-$ (**1**$^-$) species containing the 2,2′-bipyridine radical anion [Equation (2)] is followed by rapid loss of one chloride ligand to give an Os^I complex [Equation (3)]. This formally 17e$^-$ species readily dimerizes [Equation (4)]. Details of this step will be published in a forthcoming article. The similar or even more facile reducibility of the dimer, and further tetramer and oligomer intermediates compared to that of **1**, allows the growth of a polymeric chain [Equation (5)].

$$[Os^{II}(bpy)(CO)_2Cl_2] + e^- \rightarrow [Os^{II}(bpy^{\bullet-})(CO)_2Cl_2]^- \quad (2)$$

$$[Os^{II}(bpy^{\bullet-})(CO)_2Cl_2]^- \rightarrow [Os^{I}(bpy)(CO)_2Cl] + Cl^- \quad (3)$$

$$2\,[Os^{I}(bpy)(CO)_2Cl] \rightarrow [Os^{I}(bpy)(CO)_2Cl]_2 \quad (4)$$

$$n/2\,[Os^{I}(bpy)(CO)_2Cl]_2 + n\,e^- \rightarrow \text{dimers} \rightarrow \text{oligomers} \rightarrow [Os^0(bpy)(CO)_2]_n + n\,Cl^- \quad (5)$$

Experiments conducted in a less dissociating and coordinating solvent like THF support this overall mechanism. In this solvent the electrogenerated radical anion [Os(bpy$^{\bullet-}$)(CO)$_2$Cl$_2$]$^-$ is remarkably stable, the cyclic voltammogram exhibiting now a nearly reversible one-electron couple at $E_{1/2} = -1.64$ V ($\Delta E_p = 0.17$ V; $I_{pa}/I_{pc} = 0.93$) at a scan rate of 100 mVs^{-1} (Figure 3). However, decreasing the scan rate to 20 mVs^{-1} turns the reduction of **1** almost totally irreversible; an exhaustive electrolysis carried out at -1.80 V then furnished the polymer **2** after two electrons per precursor **1** had been passed (see below). In addition, some UV/Vis, IR and EPR spectroelectrochemical experiments, conducted at low temperatures, are in progress and confirm the localization of the odd electron in the radical anion of **1** on the bpy ligand.

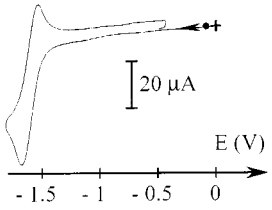

Figure 3. Cyclic voltammogram (ν = 100 mV s^{-1}) of **1** (1.6 mM) in THF + 0.2 M TBAP at a Pt disc electrode (r = 2.5 mm) recorded between 0 V and -1.85 V vs. Ag/Ag$^+$

The growth of the electroactive Os^0 polymeric film **2** can be more conveniently documented by iterative CV carried out in CH_3CN (+ 0.1 M TBAP). Two clear reversible redox systems, characteristic of the polymer electroactivity, appear at $E_{1/2} = -0.80$ V (anodic) and -1.55 V (cathodic) and increase in size continuously as the potential is repeatedly scanned from -0.60 to -1.75 V (Figure 4A). When the resulting modified electrode is transferred into a fresh electrolyte solution in the absence of **1** [Figure 4B(a)], the electroactivity persists and remains unaffected, provided the potential scan is limited to -0.60 V.

The redox properties of **2**, immobilized on the electrode surface, strongly resemble those of [Ru(bpy)(CO)$_2$]$_n$.[2] Their comparison allows us to attribute the reversible anodic system to oxidation of the osmium centre ($Os^{I/0}$) and the reversible cathodic system to the reduction of the bpy ligand (bpy$^{0/\bullet-}$) in the polymer **2**. The complete electropolymerization of **1** (2 mM) can be achieved by its exhaustive controlled-potential electrolysis at a large-surface working electrode at -1.60 V. A quantitative electrical yield (two mol of electron are needed for one mol of precursor complex) is obtained. During this electropolymerization experiment

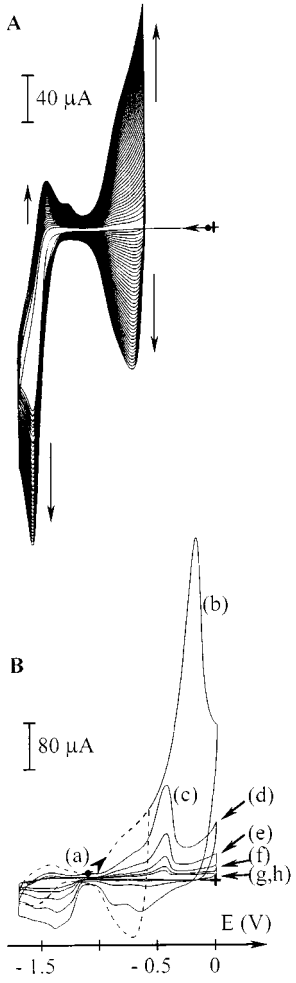

Figure 4. (A) Cyclic voltammograms (ν = 100 mV s^{-1}) of **1** (2.2 mM) in CH_3CN + 0.1 M TBAP at a Pt disc electrode (r = 2.5 mm) from the 1st to the 40th successive scans between −0.60 V and −1.75 V; (B) cyclic voltammograms recorded with the same Pt working electrode modified with surface-deposited **2**, transferred into neat CH_3CN +0.1 M TBAP; scan range: (a) −0.6 V and −1.75 V; (b) − (h) 0 V and −1.75 V vs. Ag/Ag^+

two molar equivalents of chloride ligand were liberated in solution, as revealed by voltammetry on a rotating disk electrode.[13] A comparison of the intensity of the wave at $E_{1/2}$ = 0.60 V (Cl^- oxidation system) with that of a standard solution of chloride confirms the overall stoichiometry of the polymerization process [Equation (1)]. It should be noted that a large anodic peak located at −0.21 V is observed when the potential is scanned back to 0 V [Figure 4B(b)]. This peak corresponds to the oxidation-desorption of the polymer **2** that induces cleavage of the Os−Os bonds, as was also demonstrated for the corresponding Ru^0(bpy) polymer.[8] In fact, successive potential scans in this range of potentials induce the complete disappearance of the polymer film electroactivity [Figure 4B(b)-(h)].

A full physicochemical characterization of the $[Os(bpy)(CO)_2]_n$ polymeric film is not easy to achieve since it is unstable at potentials higher than −0.40 V and cannot be handled in air. However, the molecular structure of **2** presented in Figure 1 is strongly supported by the close resemblance of the physicochemical properties of **2** with those of the corresponding Ru^0 polymer as well as by the following arguments:[2] (a) The insolubility of **2** is in favour of a polymeric structure; (b) The electronic absorption spectrum of the film deposited on optically transparent electrode (OTE) doped with indium tin oxide (ITO) exhibits two broad and intense absorption bands in the visible region (λ_{max} = 554 and 664 nm), consistent with a polymeric structure containing metal−metal bonds and possessing an Os→bpy charge transfer transition;[4] (c) Electropolymerization of **1** consumes exactly two electrons per Os(bpy) moiety and results in decoordination of both Cl^- ligands; (d) The ν(CO) wavenumbers and band pattern of **2** [1958 (vs), 1900 (m) and 1872 (s) cm^{-1}], recorded in THF at 293 K during in situ IR spectroelectrochemical experiments, are close to those of the Ru^0 polymer [1966 (vs), 1908 (s) and 1885 (vs)]. The smaller difference in the ν(CO) wavenumbers between the Os and Ru polymers observed for the parent dichloro complexes (see above), is understandable, as the Cl^- ligands are already dissociated and the metal→CO π-back-donation is therefore not affected.

In the positive potential region, the CV of **1** exhibits a reversible one-electron anodic wave (I_{pa}/I_{pc} = 1) formally corresponding to the Os^{II}/Os^{III} redox couple [Figure 2(b)]. The lower oxidation potential of **1** ($E_{1/2}$ = 1.23 V) than for the corresponding Ru^{II} dichloro complex ($E_{1/2}$ = 1.45 V),[14] again reflects the stronger Cl→Os σ/π-donation. The absence of any associated peak on the reverse cathodic scan on the scale of the CV indicates the stability of the oxidized osmium(III) cationic complex. However, bulk electrolysis at 1.30 V, consuming one electron per mol of **1**, produces a new species which is soluble in the electrolyte and reversibly reducible at a lower potential ($E_{1/2}$ = 0.47 V). Investigation of this novel complex is in progress.

Electrocatalytic Reduction of CO_2 with $[Os(bpy)(CO)_2]_n$ (2)

The electrocatalytic properties of the $[Os(bpy)(CO)_2]_n$ polymer, deposited on the cathode surface as described above, were investigated with CV experiments carried out in CO_2-saturated organic solvents containing ca. 10% water, and pure aqueous media. The initial electroactivity of the polymer in pure CO_2-saturated organic electrolyte [Figure 5(a)] completely changed after addition of 5% water [Figure 5(b)]. In particular, a strong enhancement of the cathodic current at −1.30 V was observed. In addition, repeated voltammetric scanning between −0.70 V and −1.50 V shows that this catalytic effect is persistent. Preparative scale electrolyses, using carbon felt electrodes (10 × 10 × 4 mm^3) modified with electrodeposited $[Os(bpy)(CO)_2]_n$ ($\tau_{Os} = 5 \times 10^{-7}$ mol cm^{-2}), confirm the catalytic activity of this molecular cathode towards CO_2 electroreduction. For instance, preliminary experiments have revealed that electrolysis conducted at −1.23 V vs. SCE in pure aqueous electrolyte (H_2O + 0.1 M $LiClO_4$) produces $HCOO^-$ and CO with 10% and 60% current efficiency, respectively, after 60 C had been consumed. The difference between the $[M(bpy)(CO)_2]_n$ (M = Ru^0 or Os^0) catalysts in the selectivity of the product formation towards formate is noteworthy. It should be recalled that under the same elec-

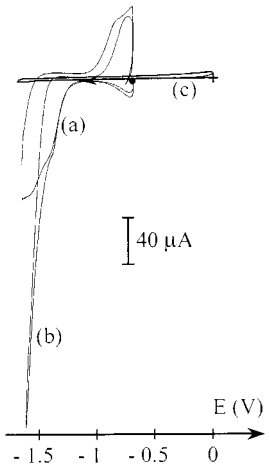

Figure 5. Cyclic voltammograms (ν = 100 mV s^{-1}) in CO_2-saturated CH_3CN + 0.1 M TBAP recorded with a vitreous carbon working electrode (r = 1.5 mm) pre-modified with **2**, deposited during electrolysis of **1** (1.2 mM) at −1.60 V (Q = 5 mC), conditions: (a) before addition of water; (b) after addition of 5% water; (c) zero electroactivity of the naked VC electrode after addition of 5% water

trocatalytic conditions the Ru(bpy) polymer conducts almost quantitative transformation of CO_2 into CO with a current efficiency higher than 97%, whereas the yield of $HCOO^-$ is less than 1%.[3] These results nicely correspond with the different electrocatalytic properties of related mononuclear $[M(bpy)_2(CO)H]^+$ complexes (M = Os^{II} [15] and M = Ru^{II}).[16] In CO_2-saturated CH_3CN with added water the latter Os and Ru complexes act as homogeneous catalysts for the electrochemical reduction of CO_2 to formate with 22% and 17% yield, and to CO with 46% and 57% yield, respectively. Further research to improve the stability and catalytic performance of **2** is in progress.

Conclusion

The strong Cl→Os σ/π-donation makes the axial Os−Cl bonds in *trans*(Cl)-[Os(bpy)$(CO)_2Cl_2$] (**1**) less prone to cleavage upon reduction than the Ru−Cl bonds in the corresponding Ru^{II} complex. Nevertheless, dissociation of the Cl^- ligands is still rapid and produces ultimately the same kind of insoluble, redox-active polymer $[Os^0(bpy)(CO)_2]_n$ (**2**) as reported for Ru. Electrocatalytic reduction of CO_2 in aqueous media, initiated by reduction of **2** deposited on the cathode surface, results in a higher yield of formate production than achieved previously with $[Ru^0(bpy)(CO)_2]_n$. Further investigation of **1**, **2** and closely related complexes is in progress to understand the catalytic mechanism and to improve the catalyst performance.

Experimental Section

General Remarks: K_2OsCl_6 (Alfa) and NH_4Cl (Fluka), formaldehyde and formic acid (both Acros) were used as received. Acetone, hexane, 2-propanol, THF and dichloromethane (all purchased from Acros) were dried by conventional procedures. All syntheses and measurements were performed under an atmosphere of dry nitrogen or argon, using standard Schlenk techniques. Silica gel (kieselgel 60, Merck, 70−230 mesh) for column chromatography was dried and activated by heating in vacuo at 160 °C overnight. The solutions of slightly light-sensitive *trans*(Cl)-[Os(bpy)$(CO)_2Cl_2$] were kept in the dark to avoid photochemical decomposition.

Electrochemical measurements were carried out using an EG & G Princeton Applied Research Model 173 potentiostat-galvanostat equipped with a Sefram TGM 164 X-Y recorder. The cyclic voltammograms were obtained in a conventional three-electrode cell under an argon atmosphere in a dry box (Jaram). The working electrodes for cyclic voltammetry were platinum or vitreous carbon discs (0.19 or 0.07 cm^2) polished with a 2 μm diamond paste (Mecaprex Presi). All potentials are reported relative to Ag|10 mM Ag^+ in CH_3CN + 0.1 M nBu_4NClO_4 (TBAP).[11] The supporting electrolyte, from Fluka, was dried under vacuum at 80° C for 3 days before use. Acetonitrile from Rathburn (HPLC grade) was used as received. THF was freshly distilled from Na/benzophenone.

All preparative-scale electrocatalytic experiments were run under a CO_2 atmosphere on carbon felt pieces (RVC 2000 from Le Carbone Lorraine) modified by a polymer film in a conventional three-electrode cell made air-tight with vacuum grease (M. Apiezon). All experiments were stopped after a predetermined number of coulombs had been passed. The current efficiency corresponds to the theoretical number of mol calculated from the experimental number of coulombs (100% yield)/calculated number of mol after analysis (CO_2 reduction into CO or $HCOO^-$ is a two-electron reduction process). CO was analysed on a Delsi Model 30 gas chromatograph with a FID, with a 120-cm long 5 Å molecular sieve column, followed by a catalytic oven. H_2 was used as carrier gas. Formate ions were analysed on a Waters Associate HPLC with a Bio-Rad HPX-87H cation exchange resin column eluted with 10^{-2} M H_2SO_4 solution. A UV detector at 224 nm was used.

Electronic absorption spectra were recorded with a Hewlett-Packard HP 8452 A diode array spectrophotometer controlled with a Compaq 286 computer. UV/Vis spectroelectrochemical experiments were conducted in a dry box under an argon atmosphere. The cells were inserted into an optical translator connected to the spectrophotometer by an optical fibre system (Photonetics spectrofip system). The optical fibres pass through the wall of the dry box by means of seals. UV/Vis spectroelectrochemical measurements on polymer films were made by using a conventional sandwich-type cell.[17] The optical transparent electrode (OTE) (1.1 cm diameter) was doped with indium tin oxide (ITO) (Balthracon Z 20 from Balzers).

IR spectra were recorded with Perkin−Elmer Spectrum GX FTIR or Bio-Rad FTS-7 FTIR spectrometers. IR spectroelectrochemical experiments at room temperature were carried out with a previously described OTTLE cell equipped with a Pt minigrid working electrode (32 wires/cm) and with CaF_2 windows.[18]

^1H NMR spectra were recorded at room temperature on Bruker AMX 300 or AC-250 spectrometers; the chemical shifts (in ppm) are relative to the solvent $CDCl_3$ (δ = 7.25) or CD_3CN (δ = 1.96).

Synthesis of *trans*(Cl)-[Os(bpy)$(CO)_2Cl_2$] (1) $[Os(CO)_2Cl_2]_n$: K_2OsCl_6 (1 g; 2.1 mmol) was added to an N_2-purged (20 min.) mixture of formaldehyde (15 mL) and formic acid (90%, 50 mL) and refluxed for 3 days. The colour changed from red to green within 3 h and ultimately to light yellow (NB: further reflux produces a brownish solution presumably due to organic decomposition products). Next, the solution was cooled to room temperature and the solvents evaporated. The brownish residue was

extracted with acetone to remove KCl. After evaporation of the acetone the solid was washed with CH_2Cl_2/hexane (1:1) to remove any organic side products. The product was obtained with a yield in the range of 800−900 mg and is a white, occasionally pinkish/yellowish powder. − IR (THF): ν(CO) = 2116 cm^{-1} (m) and 2022 (vs).

***trans*(Cl)-[Os(bpy)(CO)$_2$Cl$_2$] (1):** Polymeric $[Os(CO)_2Cl_2]_n$ (200 mg) and an excess of bpy (5 equiv.) were dissolved in 2-propanol (50 mL) and heated at reflux temperature until the IR spectra showed complete conversion [two intense ν(CO) bands arose at 2040 and 1972 cm^{-1}]. In order to obtain exclusively the desired dichloro complex, the crude product was redissolved in NH_4Cl-saturated CH_2Cl_2 and stirred overnight. The solution was filtered and the resulting complex **1** was purified by column chromatography (activated silica, using CH_2Cl_2/hexane gradient elution) to yield a light yellow powder. Yield: 100 mg (50%). The use of *n*-propanol instead of 2-propanol should be avoided, as it results in significantly lower yields (ca 20%). − IR (THF): ν(CO) = 2032 cm^{-1}(vs), 1962 (vs); in *n*PrOH: ν(CO) = 2041 (vs), 1972 (vs); in CH_2Cl_2: ν(CO) = 2040 (vs), 1971 (vs); in CH_3CN: ν(CO) = 2038 (vs), 1968 (vs); in CsI pellet: ν(CO) = 2022 (vs), 1943 (vs), ν(Os−Cl) 317 (w). − ^{1}H NMR ($CDCl_3$): δ = 9.13 (d, ^3J = 7.2 Hz, 2 H, $H_{6,6'}$), 8.23 (d, ^3J = 10.8 Hz, 2 H, $H_{3,3'}$), 8.13 (t, ^3J = 10.8 Hz, 2 H, $H_{4,4'}$), 7.67 (t, ^3J = 8.0 Hz, 2 H, $H_{5,5'}$). − UV/Vis (THF): λ_{max} = 362 nm; in CH_3CN: λ = 350. − MS (FD^+): *m*/*z* = 474 [M + H]$^+$; (FAB^+): *m*/*z* = 474 [M + H]$^+$, 446 [M + H − CO]$^+$, 439 [M + H − Cl]$^+$, 418 [M + H − 2CO]$^+$, 411 [M + H − 2Cl]$^+$, 383 [M + H − CO − 2Cl]$^+$.

Acknowledgments

We thank the Netherlands Organization for Scientific Research (NWO) and Ministères des Affaires Etrangères for the financial support regarding the bilateral Dutch-French Van Gogh Programme.

[1] M.-N. Collomb-Dunand-Sauthier, A. Deronzier, R. Ziessel, *J. Electroanal. Chem.* **1993**, *350*, 43−55.
[2] C. Caix-Cecillon, S. Chardon-Noblat, A. Deronzier, M. Haukka, T. A. Pakkanen, R. Ziessel, D. Zsoldos, *J. Electroanal. Chem.* **1999**, *466*, 187−196.
[3] M.-N. Collomb-Dunand-Sauthier, A. Deronzier, R. Ziessel, *Inorg. Chem.* **1994**, *33*, 2961−2967.
[4] S. Chardon-Noblat, A. Deronzier, R. Ziessel, D. Zsoldos, *J. Electroanal. Chem.* **1998**, *444*, 253−260.
[5] S. Luukkanen, P. Homanen, M. Haukka, T. A. Pakkanen, A. Deronzier, S. Chardon-Noblat, D. Zsoldos, R. Ziessel, *Applied Catalysis A. General* **1999**, *185*, 157−164.
[6] E. Eskilen, M. Haukka, T. Venäläinen, T. A. Pakkanen, M. Wasberg, S. Chardon-Noblat, A. Deronzier, *Organomettallics* **2000**, *19*, 163−169.
[7] E. Z. Jandrasics, F. R. Keene, *J. Chem. Soc., Dalton Trans.* **1997**, 153−159.
[8] S. Chardon-Noblat, P. Da Costa, A. Deronzier, M. Haukka, T. A. Pakkanen, R. Ziessel, *J. Electroanal. Chem.* **2000**, *490*, 62.
[9] F. P. A. Johnson, M. W. George, F. Hartl, J. J. Turner, *Organometallics* **1996**, *15*, 3374−3387.
[10] F. Hartl, B. D. Rossenaar, G. J. Stor, D. J. Stufkens, *Recl. Trav. Chim. Pays-Bas* **1995**, *114*, 565−570.
[11] [11a] The apparent number of electrons transferred during the reduction of **1** scanned with ν = 100 mV s^{-1}, *n*(app) = 1.84 ± 0.08, has been determined separately by the literature method: C. Amatore, M. Azzabi, P. Calas, A. Jutand, C. Lefrou, Y. Rolin, *J. Electroanal. Chem.* **1990**, 288, 45−63. − [11b] All electrode potentials are referenced to Ag/10^{-2} M Ag^+ in CH_3CN containing 0.1 M TBAP. They can be converted to Fc/Fc^{+} redox system by adding −0.150 V.
[12] S. Chardon-Noblat, A. Deronzier, D. Zsoldos, R. Ziessel, M. Haukka, T. A. Pakkanen, T. Venäläinen, *J. Chem. Soc., Dalton Trans.* **1996**, 2581−2583.
[13] G. Cauquis, A. Deronzier, B. Sillion, B. Damin, J. Garapon, *J. Electroanal. Chem.* **1981**, *117*, 139−146.
[14] M.-N. Collomb-Dunand-Sauthier, A. Deronzier, R. Ziessel, *J. Organomet. Chem.* **1993**, *444*, 191−198.
[15] M. R. M. Bruce, E. Megehee, B. P. Sullivan, H. H. Thorp, T. R. O'Toole, A. Downard, J. R. Pugh, T. J. Meyer, *Inorg. Chem.* **1992**, *31*, 4864−4873.
[16] J. R. Pugh, M. R. M. Bruce, B. P. Sullivan, T. J. Meyer, *Inorg. Chem.* **1991**, *30*, 96−91.
[17] S. Cosnier, A. Deronzier, J.-C. Moutet, *J. Phys. Chem.* **1985**, *23*, 4895−4897.
[18] M. Krejčík, M. Daněk, F. Hartl, *J. Electroanal. Chem.* **1991**, *317*, 179−187.

Received September 27, 2000
[I00367]

Synthesis and Solid-State Structure of $(Li_4Am_3)^+\cdot\{Li[(\mu\text{-}Me)_2Al(Me)tBu]_2\}^-$ {Am = [PhNC(Ph)NPh]$^-$}: A Polymeric Species Incorporating a Lithium-Nitrogen Cluster Cation

Robert P. Davies,[a] David J. Linton,[b] Paul Schooler,[b] Ronald Snaith,[b][†] and Andrew E. H. Wheatley*[b]

Keywords: Aluminum / Cluster compounds / Cations / Lithium

The sequential reaction of PhN(H)C(Ph)NPh (AmH) with $AlMe_3$ and *t*BuLi leads to the isolation of both the cluster $(Li_4Am_3)^+\cdot\{Li[(\mu\text{-}Me)_2Al(Me)tBu]_2\}^-$ **(5)** and the aluminium tris(amidinate) $AlAm_3$ **(6)**. In the solid state, **5** has a polymeric structure based on tetranuclear Li_4-cluster cations and lithium bis(aluminate) anions which associate by the formation of weak Li···MeAl bonds.

Introduction

The current interest being shown in the structures and reactivities of synthetically useful[1] lithium-containing heterobimetallic species[2] led us to synthesise lithium aluminate monomers $Me_2Al(\mu_2\text{-}OAr)_2Li$ (Ar = aryl), species which may play a role in conjugate additions to α,β-unsaturated ketones.[3] Moreover, it has recently been shown that *t*BuLi reacts with $Me_2AlN(Me)C(O)Ph$ to give a lithium aluminate which, in turn, yields a unique heterobimetallic mixed-anion ladder upon introduction of oxygen to the reaction mixture.[4] Whereas this chemistry utilised a reagent containing the $Me_2AlN(R)C(=X)$ fragment (X = O), the use of species in which X = N has also been fruitful. Accordingly, whereas the 1:1 lithium[5] and sodium[6] salts of 2-pyridylamine reagents [(2-Pyr)N(H)R] have been characterised, it has lately been reported that BuLi isomers react with the amidoalane $Me_2AlN(2\text{-}Pyr)Ph$ **(1)** to afford the hydride-containing compounds[7] $[Li(Me_2AltBu_2)_2]^-\{Li_8(H)[N(2\text{-}Pyr)Ph]_6\}^+$ **(2)** and $Li_7(H)[N(2\text{-}Pyr)Ph]_6$ **(3)** both of which incorporate cationic lithium-nitrogen clusters. In seeking to extend this new type of chemistry we have tested the reactivity of BuLi reagents towards Group 13 amidinates — species which have been extensively studied in both neutral[8] and cationic[9] contexts. Accordingly, we have employed $AmAlMe_2$ **(4)** {Am = [PhNC(Ph)NPh]$^-$}. Although simple lithiation[2b,10] has been reported for amidine reagents, as indeed have the syntheses of sodium[10c] and potassium[11] derivatives, we report here the isolation and characterisation of a more complex intermetallic amidinate compound. Reaction of *t*BuLi with **4** affords the tetralithium cluster $(Li_4Am_3)^+\cdot\{Li[(\mu\text{-}Me)_2Al(Me)tBu]_2\}^-$ **(5)** and also the aluminium tris(amidinate) $AlAm_3$ **(6)** (Scheme 1).

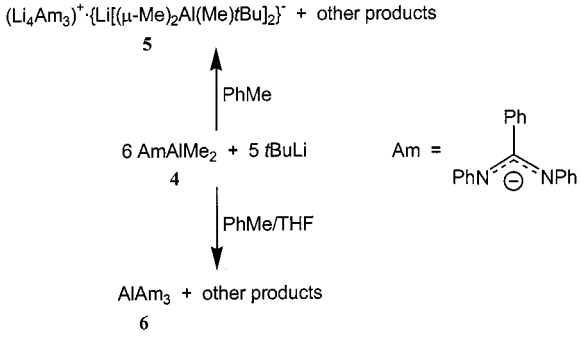

Scheme 1

Results and Discussion

Reaction of a solution of *N*,*N*′-diphenylbenzamidine[12] in toluene with $AlMe_3$ yields the aluminium amidinate $AmAlMe_2$ **(4)**, the treatment of which with *t*BuLi affords a solution from which crystals of **5** can be obtained (see Experimental Section). X-ray crystallography shows that in the solid state **5** is a mixed aggregate composed of an unusual lithium bis(aluminate) anion weakly bonded to a superlithiated cluster cation (Figure 1). The $\{Li[Me_2Al(Me)tBu]_2\}^-$ ion contains two Al centres arranged such that two methyl substituents on each are disposed tetrahedrally about Li(1). The resulting $Li[(\mu\text{-}C)_2Al]_2$ motif indicates some generality for the single previous report of this unit in a molecular context.[7] To the best of our knowledge the only close relative of this anion is present in the solvent-separated ion pair $[Li(DME)_3]^+\{Li[(\mu\text{-}OPh)_2AlEt_2]_2\}^-$.[13] Furthermore, the $\{Li[Me_2Al(Me)tBu]_2\}^-$ ion also constitutes part of a group of only a few characterised Group 1 metal-containing anions.[13,14] The mean M−(μ-C) distances (2.234 and 2.034 Å for M = Li and Al, respectively)

[a] Department of Chemistry, Imperial College of Science, Technology and Medicine,
Exhibition Road, London SW7 2AY, U.K.
[b] Department of Chemistry, University of Cambridge,
Lensfield Road, Cambridge, CB2 1EW, U.K.
Fax: (internat.) +44-1223/336-362
E-mail: aehw2@cam.ac.uk
[†] Deceased.

 © WILEY-VCH Verlag GmbH, 69451 Weinheim, 2001 1434−1948/01/0303−0619 $ 17.50+.50/0

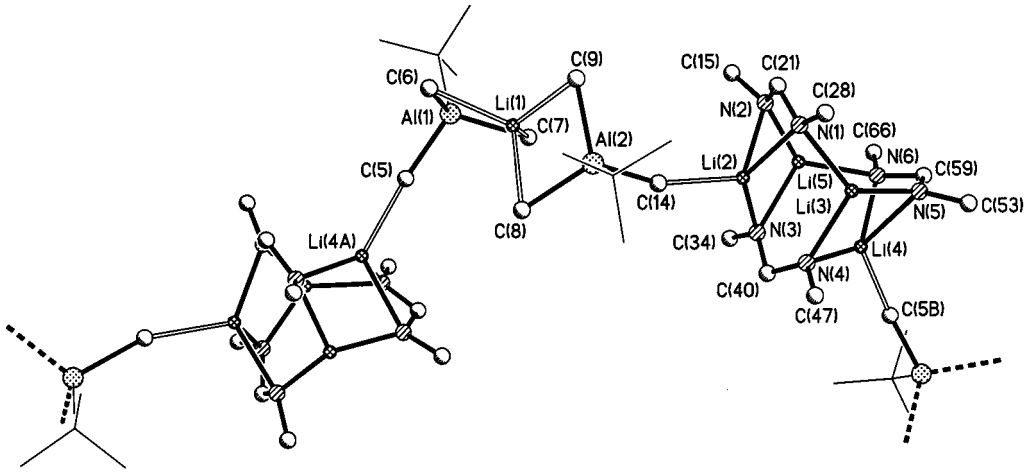

Figure 1. Polymeric structure of **5**; hydrogen atoms, phenyl rings (except the *ipso* atoms of the *N*-bonded rings) omitted for clarity; selected bond lengths (Å) and angles (°): N(1)−Li(3) 2.016(6), Li(3)−N(5) 1.992(6), N(6)−Li(5) 2.016(6), Li(5)−N(2) 1.996(6), N(2)−Li(2) 2.191(6), N(1)−Li(2) 2.089(7), N(4)−Li(3) 2.109(6), N(5)−Li(4) 2.199(6), N(6)−Li(4) 2.064(7), N(3)−Li(5) 2.124(6), Li(2)−N(2) 2.191(6), Li(4)−N(4) 2.130(6); N(2)−Li(5)−N(6) 127.0(3), N(1)−Li(3)−N(5) 125.5(3), N(1)−Li(2)−N(2) 63.7(2), Li(2)−N(2)−Li(5) 75.8(2), N(2)−Li(2)−N(3) 98.5(3), N(2)−Li(5)−N(3) 104.7(3), Li(2)−N(3)−Li(5) 74.9(2), N(5)−Li(4)−N(6) 64.0(2), N(5)−Li(3)−N(4) 105.2(3), N(5)−Li(4)−N(4) 97.7(3), Li(3)−N(5)−Li(4) 76.0(2), Li(3)−N(4)−Li(4) 75.2(2)

correlate accurately with those reported previously both in the molecular anion $[Li(Me_2Al\textit{t}Bu_2)_2]^-$ (2.25 and 2.07 Å)[7] and also in $LiAlEt_4$ (2.30 and 2.02 Å),[15] the polymeric structure of which is based on the same motif.

The cationic fragment of **5**, $(Li_4Am_3)^+$, takes the form of a lithium-nitrogen cluster. Whereas the lithium amide dication cluster recently reported to encapsulate a hydride ion exhibits $Li_8(amide)_6$ stoichiometry,[7] that of the monocationic moiety in **5** is $Li_4(amidinate)_3$. Thus the Li:organic ratio is retained, with the steric requirements of the *N*,*N*′-diphenylbenzamidinate ligand apparently requiring the formation of a smaller aggregate. The cationic component of **5** contains two types of charge-delocalised amidinate ligand, each of which interacts with the alkali metal centres through both of its sp^2-hybridised *N*-centres [C⩬N⩬C(Ph) = 121.6(3)−124.3(3)°]. Two amidinate ions, one on either side of the cluster, incorporate N(1)⩬C(21)⩬N(2) and N(5)⩬C(59)⩬N(6). These ligands both bond to Li(3) and Li(5), affording a concave eight-membered $(NCNLi)_2$ ring.[5e][6b,16] The Li−N interactions within this ring are short [1.992(6)−2.016(6) Å] in comparison to those between these nitrogen atoms and the remaining two lithium centres in the cluster cation [Li(2) and Li(4), 2.064(7)−2.199(6) Å]. Each of the two ligands which form this upper eight-membered ring interact individually with the Group 1 metal centres in the lower tier in an asymmetrically bidentate fashion. Thus, Li(2)−N(1) and Li(4)−N(6) average to 2.077 Å, while Li(2)−N(2) and Li(4)−N(5) average to 2.195 Å. This lengthening of the latter Li−N interactions is consistent with the bonding pattern observed in the eight-membered $(NCNLi)_2$ ring: N(1) and N(6) form relatively short bonds to Li(2) and Li(4) (mean Li−N = 2.016 Å) but interact more weakly with both Li and C centres within the ring [mean N⩬C(Ph) = 1.342 Å]. Conversely, N(2) and N(5) form stronger bonds with both Li and C centres in this ring [mean Li−N = 1.994 Å; mean N⩬C(Ph) = 1.325 Å] at the expense of short interactions with the two basal cations. These last two Li^+ centres are straddled by the third ligand [Li(2)−N(3) and Li(4)−N(4) = 2.113(6) and 2.130(4) Å, respectively]. However, this basal anion is orientated such that both Li(2)···N(4) and Li(4)···N(3) are extended (mean 2.583 Å) so as to be of no bonding significance. Thus, the basal tier of the cluster can be viewed as a four-membered $(LiN)_2$ ring which has undergone the fracture of two *trans*-edges to afford a pair of LiN fragments.[17] The remaining interactions between cluster base and upper $(NCNLi)_2$ ring involve the stabilisation of Li(3) and Li(5) by N(4) and N(3), respectively (mean Li−N = 2.117 Å).

The solid-state structure of **5** reveals a polymer by virtue of weak interactions between Li(2) and the terminal Me group [C(14)] in the anion and between C(5) in this anion and the analogous alkali metal centre [Li(4A)] in the adjoining cationic unit [mean Li···C(Me) = 2.295 Å] (Figure 1). These interactions raise the coordination of the otherwise low-valent Li centres in the cleaved $(LiN)_2$ ring (see above) at the base of the cluster cation. This positively charged component of **5** contrasts with normally observed ion-separated species in which otherwise isolated Li^+ centres are coordinated by a neutral Lewis base,[18] and with the recent observation of $(Li_2)^{2+}$ clusters.[19] Aggregated and charged lithium-containing clusters have also been reported in the lithium "ate" complex $(Li{\cdot}HMPA)^+{\cdot}[Li_5(N{=}CPh_2){\cdot}HMPA]^-$ $[HMPA = O{=}P(NMe_2)_3]$[14b] and $Ta(4\text{-}Me\text{-}C_6H_4)_6^-$ $[Li_4Br_3(Et_2O)_7]^+$,[20] as well as in both **2** and **3**.[7]

Attempts to understand the mechanism of formation of **5** are ongoing. The observation that the amorphous solid obtained by removing the solvent from a 1:1 mixture of *N*,*N*′-diphenylbenzamidine and $AlMe_3$ is $AmAlMe_2$ **(4)**[21] points to the first stage intermediate in the synthesis of **5** being the aluminium mono(amidinate). However, the treatment of this species with *t*BuLi initiates a complex reaction which requires further elucidation. The isolation (see Ex-

perimental Section) and structural characterisation of the aluminium tris(amidinate) $AlAm_3$ **(6)** may also be instructive — attempts to recrystallise THF-solvated (i.e. oligomerised) **5** afforded only a co-crystalline mixture which ^1H NMR spectroscopy suggests contains **5** (or its solvated and deaggregated analogue) and **6**. Mechanical separation of the crystals allows the characterisation of pure $AlAm_3$, for which formulation the solid-state structure (Figure 2) revealed one molecule of lattice toluene.

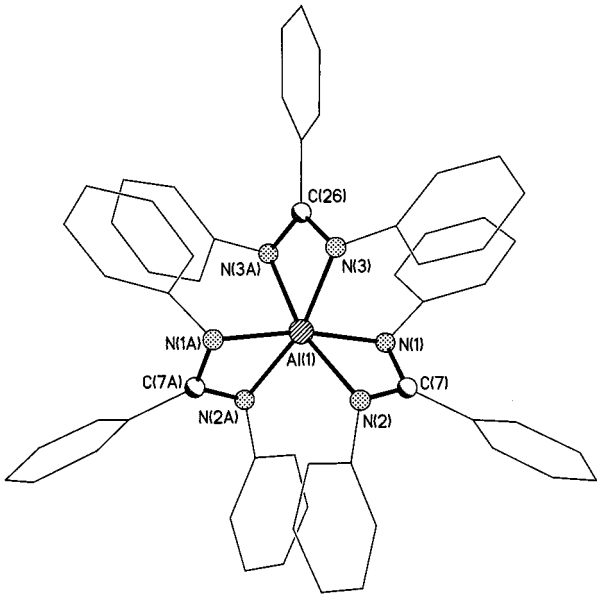

Figure 2. Molecular structure of monomeric **6**·PhMe; hydrogen atoms and lattice toluene molecule omitted for clarity; selected bond lengths (Å) and angles (°): Al(1)−N(1) 1.997(3), Al(1)−N(2) 1.981(3), Al(1)−N(3) 1.985(3); N(1)−Al(1)−N(2) 66.7(1), N(3)−Al(1)−N(3A) 66.8(2)

While the isolation and characterisation of **4**, the novel polymer **5** and also of **6** cast some light on the complex processes occurring in systems of the type discussed here, further mechanistic investigations are clearly required and will be reported subsequently. More generally, we are seeking to vary the choice of *N*-centred organic residue and organoaluminium reagent in an attempt to generate new compounds related to **5**, and so investigate the extent of this chemistry.

Experimental Section

General: All operations were carried out using standard Schlenk techniques. *N*,*N*′-diphenylbenzamidine was used as received from Lancaster. Toluene (freshly distilled from sodium), hexane and THF (freshly distilled from sodium-potassium alloy) and trimethylaluminium and *tert*-butyllithium were added direct to the nitrogen-filled Schlenk tube using standard syringe techniques. − NMR spectroscopy: Bruker DRX 400 (400.137 MHz for ^1H). For ^1H NMR spectroscopy, [D_6]benzene and [D_8]THF as solvents, TMS at 25 °C as external standard.

Dimethylaluminium *N*,*N*′-Diphenylbenzamidinate, 4·$^1/_3$PhMe: *N*,*N*′-diphenylbenzamidine (0.272 g, 1 mmol) was dissolved in toluene (2 mL) and cooled to −78 °C, whereupon $AlMe_3$ (0.5 mL, 1 mmol, 2 M in toluene) was added. The resultant mixture was warmed to room temperature and stirred for 30 minutes. Reflux afforded a yellow solution from which **4**·$^1/_3$PhMe was deposited as an amorphous solid upon removal of the solvent. Yield 73%, m.p. 176−178 °C. − $C_{70}H_{71}Al_3N_6$ (1076): calcd. C 78.07, H 6.60, N 7.81; found C 76.53, H 6.43, N, 8.35. − ^1H NMR (400 MHz, C_6D_6): δ = 7.19−6.49 (m, 16 H, Ph + $^1/_3$*Ph*Me), 2.15 (s, 1 H, $^1/_3$Ph*Me*), −0.01, −0.28 (m, 6 H, AlMe).

Compound 5: As for **4** but after stirring at room temperature for 30 minutes the solution was returned to −78 °C and treated with *t*BuLi (0.49 mL, $^5/_6$ mmol, 1.7 M in pentane). The resultant suspension was warmed to room temperature and dissolved at reflux with the addition of toluene (20 mL). The yellow solution was stored at +70 °C for two days whereupon colourless cubes of **5** were deposited. Yield 35% (based on *t*BuLi consumed), m.p. decomp. from 220 °C. − $C_{71}H_{81}Al_2Li_5N_6$ (1107): calcd. C 76.96, H 7.32, N 7.59; found C 77.95, H 6.69, N, 7.18. − ^1H NMR (400 MHz, [D_8]THF): δ = 7.05, 7.02 (br. m, 18 H, Ph), 6.83 (br. s, 12 H, Ph), 6.48 (br. s, 15 H, Ph), 0.70 (m, $^3J_{H-Al}$ = 5.0 Hz, 18 H, *t*Bu), −1.33 (sext., $^2J_{H-Al}$ = 5.7 Hz, 18 H, AlMe).

Aluminium Tris(*N*,*N*′-diphenylbenzamidinate), 6·PhMe: As for **5** utilising an initial solvent mixture of 5:1 toluene/THF (1:0.2 mL). The suspension produced after *t*BuLi addition and reflux was filtered and the resultant solution stored at room temperature for 1 week, whereupon a complex co-crystalline mixture was obtained. Mechanical separation allowed the characterisation of **6**·PhMe. M.p. 298−300 °C. − $C_{64}H_{53}Al_3N_6$ (933): calcd. C 82.31, H 5.68, N 9.00; found C 80.29, H 5.55, N 9.27. − ^1H NMR (400 MHz, C_6D_6): δ = 7.34−6.89 (m, 16 H, Ph + $^1/_3$*Ph*Me), 2.32 (s, 1 H, $^1/_3$Ph*Me*).

Crystal Data for 5: $C_{71}H_{81}Al_2Li_5N_6$, M = 1107.08, monoclinic, space group *Cc*, a = 13.7160(3), b = 23.9360(7), c = 20.6990(6) Å, β = 90.5220(19)°, U = 6795.3(3) Å^3, Z = 4, D_c = 1.082 g cm^{-3}, Mo-K_α (λ = 0.71070 Å), μ = 0.086 mm^{-1}, T = 180(2) K. 26396 reflections (10837 unique, θ < 50.10°, R_{int} = 0.0481). Refinement on F^2 values of all data gave $wR2$ = 0.1453, conventional R = 0.0547 on F values of 8799 reflections with $F^2 > 2\sigma(F^2)$, 754 parameters. Residual electron density extrema 0.49 and −0.28 e Å^{-3}.

Crystal Data for 6·PhMe: $C_{64}H_{53}AlN_6$, M = 933.10, monoclinic, space group *C*2/*c*, a = 18.2750(12), b = 18.7770(11), c = 16.2890(9) Å, β = 112.547(3)°, U = 5162.3(5) Å^3, Z = 4, D_c = 1.201 g cm^{-3}, Mo-K_α (λ = 0.71070 Å), μ = 0.086 mm^{-1}, T = 180(2) K. 8348 reflections (4517 unique, θ < 49.94°, R_{int} = 0.0358). Refinement on F^2 values of all data gave $wR2$ = 0.2166, conventional R = 0.0707 on F values of 3185 reflections with $F^2 > 2\sigma(F^2)$, 307 parameters. Residual electron density extrema 0.69 and −0.64 e Å^{-3}.

Crystallographic data (excluding structure factors) for the structures reported in this paper have been deposited with the Cambridge Crystallographic Data Centre as supplementary publication nos. CCDC-145946 (**5**) and -145945 (**6**·PhMe). Copies of the data can be obtained free of charge on application to CCDC, 12 Union Road, Cambridge CB2 1EZ, UK [Fax: (internat.) +44-1223/336-033; E-mail: deposit@ccdc.cam.ac.uk].

Acknowledgments

We thank the U.K. EPSRC (D. J. L., P. S.) for financial assistance and St. Catharine's (R. P. D.) and Gonville & Caius (A. E. H. W.) Colleges for Research Fellowships.

[1] T.-L. Ho, *Fiesers' Reagents for Organic Synthesis: Vol. 18*, John Wiley & Sons Inc., New York, **1999**, pp. 204−223 and 257−263.

[2] [2a] A. R. Kennedy, R. E. Mulvey R. B. Rowlings, *Angew. Chem.* **1998**, *110*, 3321−3323; *Angew. Chem. Int. Ed.* **1998**, *37*, 3180−3183. − [2b] A. R. Kennedy, R. E. Mulvey, R. B. Rowlings, *J. Am. Chem. Soc.* **1998**, *120*, 7816−7824. − [2c] A. R. Kennedy, R. E. Mulvey, C. L. Raston, B. A. Roberts, R. B. Rowlings, *Chem. Commun.* **1999**, 353−354.

[3] W. Clegg, E. Lamb, S. T. Liddle, R. Snaith, A. E. H. Wheatley, *J. Organomet. Chem.* **1999**, *573*, 305−312.

[4] R. P. Davies, D. J. Linton, R. Snaith, A. E. H. Wheatley, *Chem. Commun.* **2000**, 193−194.

[5] [5a] D. Barr, W. Clegg, R. E. Mulvey, R. Snaith, *J. Chem. Soc., Chem. Commun.* **1984**, 469−470. − [5b] D. Barr, W. Clegg, R. E. Mulvey, R. Snaith, *J. Chem. Soc., Chem. Commun.* **1984**, 700−701. − [5c] L. M. Engelhardt, G. E. Jacobsen, P. C. Junk, C. L. Raston, B. W. Skelton, A. H. White, *J. Chem. Soc., Dalton Trans.* **1988**, 1011−1020. − [5d] M. Polamo, M. Leskela, *J. Chem. Soc., Dalton Trans.* **1996**, 4345−4349. − [5e] N. Feeder, R. Snaith, A. E. H. Wheatley, *Eur. J. Inorg. Chem.* **1998**, 879−883.

[6] [6a] P. C. Andrews, W. Clegg, R. E. Mulvey, *Angew. Chem.* **1990**, *102*, 1480−1481; *Angew. Chem. Int. Ed. Engl.* **1990**, *29*, 1440−1441. − [6b] P. C. Andrews, D. R. Baker, R. E. Mulvey, W. Clegg, P. A. O'Neil, *Polyhedron* **1991**, *10*, 1839−1841.

[7] D. R. Armstrong, W. Clegg, R. P. Davies, S. T. Liddle, D. J. Linton, P. R. Raithby, R. Snaith, A. E. H. Wheatley, *Angew. Chem.* **1999**, *111*, 3568−3570; *Angew. Chem. Int. Ed.* **1999**, *38*, 3367−3370.

[8] [8a] M. P. Coles, D. C. Swenson, R. F. Jordan, V. G. Young, Jr., *Organometallics* **1997**, *16*, 5183. − [8b] M. P. Coles, D. C. Swenson, R. F. Jordan, V. G. Young, Jr., *Organometallics* **1998**, *17*, 4042. − [8c] S. Dagorne, R. F. Jordan, V. G. Young, Jr., *Organometallics* **1999**, *18*, 4619.

[9] [9a] M. P. Coles, R. F. Jordan, *J. Am. Chem. Soc.* **1997**, *119*, 8125−8126. − [9b] S. Dagorne, I. A. Guzei, M. P. Coles, R. F. Jordan, *J. Am. Chem. Soc.* **2000**, *122*, 274−289.

[10] [10a] T. Chivers, A. Downard, G. P. A. Yap, *J. Chem. Soc., Dalton Trans.* **1998**, 2603−2605. − [10b] C. Averbuj, E. Tish, M. S. Eisen, *J. Am. Chem. Soc.* **1998**, *120*, 8640−8646. − [10c] D. Stalke, M. Wedler, F. T. Edelmann, *J. Organomet. Chem.* **1992**, *431*, C1−C5. − [10d] I. Cragg-Hine, M. G. Davidson, F. S. Mair, P. R. Raithby, R. Snaith, *J. Chem. Soc., Dalton Trans.* **1993**, 2423−2424. − [10e] T. Gebauer, K. Dehnicke, H. Goesmann, D. Fenske, *Z. Naturforsch. B* **1994**, *49*, 1444−1447. − [10f] M. S. Eisen, M. Kapon, *J. Chem. Soc., Dalton Trans.* **1994**, 3507−3510. − [10g] J. Barker, D. Barr, N. D. R. Barnett, W. Clegg, I. Cragg-Hine, M. G. Davidson, R. P. Davies, S. M. Hodgson, J. A. K. Howard, M. Kilner, C. W. Lehmann, I. Lopez-Solera, R. E. Mulvey, P. R. Raithby, R. Snaith, *J. Chem. Soc., Dalton Trans.* **1997**, 951−955. − [10h] W. M. Boesveld, P. B. Hitchcock, M. F. Lappert, *J. Chem. Soc., Chem. Commun.* **1997**, 2091−2092.

[11] P. B. Hitchcock, M. F. Lappert, M. Layh, *J. Chem. Soc., Dalton Trans.* **1998**, 3113−3117.

[12] [12a] J. Barker, M. Kilner, *Coord. Chem. Rev.* **1994**, *133*, 219−300. − [12b] F. T. Edelmann, *Coord. Chem. Rev.* **1994**, *137*, 403−481.

[13] H. Bock, R. Beck, Z. Havlas, H. Schödel, *Inorg. Chem.* **1998**, *37*, 5046−5049.

[14] See for example: [14a] C. Eaborn, P. B. Hitchcock, J. D. Smith, A. C. Sullivan, *J. Chem. Soc., Chem. Commun.* **1983**, 827−828. − [14b] D. Barr, W. Clegg, R. E. Mulvey, R. Snaith, *J. Chem. Soc., Chem. Commun.* **1984**, 226−227. − [14c] H. Gornitzka, D. Stalke, *Angew. Chem.* **1994**, *106*, 695−698; *Angew. Chem. Int. Ed. Engl.* **1994**, *33*, 693−695. − [14d] S. S. Al-Juaid, C. Eaborn, P. B. Hitchcock, K. Izod, M. Mallien, J. D. Smith, *Angew. Chem.* **1994**, *106*, 1336−1338; *Angew. Chem. Int. Ed. Engl.* **1994**, *33*, 1268−1270. − [14e] W. Clegg, L. Horsburgh, R. E. Mulvey, M. J. Ross, *J. Chem. Soc., Chem. Commun.* **1994**, 2393−2394. − [14f] W. Clegg, M. R. J. Elsegood, L. Horsburgh, R. E. Mulvey, M. J. Ross, *Chem. Ber./Recueil* **1997**, *130*, 621−631.

[15] R. L. Gerteis, R. E. Dickerson, T. L. Brown, *Inorg. Chem.* **1964**, *3*, 872−875.

[16] D. R. Armstrong, F. A. Banbury, I. Cragg-Hine, M. G. Davidson, F. S. Mair, E. Pohl, P. R. Raithby, R. Snaith, *Angew. Chem.* **1993**, *105*, 1801−1803; *Angew. Chem. Int. Ed. Engl.* **1993**, *32*, 1769−1771.

[17] W. Clegg, S. T. Liddle, R. E. Mulvey, A. Robertson, *Chem. Commun.* **1999**, 511−512.

[18] *Lithium Chemistry: A Theoretical and Experimental Overview* (Eds.: A.-M. Sapse, P. von R. Schleyer), Wiley, New York, **1995**.

[19] [19a] D. R. Armstrong, A. H. Khandelwal, L. C. Kerr, S. Peasey, P. R. Raithby, G. P. Shields, R. Snaith, D. S. Wright, *Chem. Commun.* **1998**, 1011−1012. − [19b] D. Stalke, D. S. Wright, unpublished results.

[20] S. Kleinhenz, M. Schubert, K. Seppelt, *Chem. Ber./Recueil* **1997**, *130*, 903−906.

[21] [21a] H. D. Hausen, F. Gerstner, W. Schwarz, *J. Organomet. Chem.* **1978**, *145*, 277−284. − [21b] J. Barker, N. C. Blacker, P. R. Phillips, N. W. Alcock, W. Errington, M. G. H. Wallbridge, *J. Chem. Soc., Dalton Trans.* **1996**, 431−437. − [21c] J. Barker, D. R. Aris, N. C. Blacker, W. Errington, P. R. Phillips, M. G. H. Wallbridge, *J. Organomet. Chem.* **1999**, *586*, 138−144.

Received October 2000
[I00386]

Synthesis and X-ray Structures of $[Os_3Pt(CO)_9(\mu_4\text{-}\eta^2\text{-}C{\equiv}CPh)(\eta^1\text{-}C{\equiv}CPh)(L)]$ (L = 4,4′-Dimethyl-2,2′-bipyridine, 4,4′-bis(*tert*-butyl)-2,2′-bipyridine): New Heterometallic Clusters with a μ_4-η^2- and an η^1-Acetylide Group on a Spiked-Triangular Metal Core

Wai-Yeung Wong,*[a] Fai-Lung Ting,[a] and Wai-Lim Lam[a]

Keywords: Osmium / Platinum / Alkyne ligands / Cluster compounds

Treatment of $[Os_3(CO)_{10}(NCMe)_2]$ with platinum bis(alkynyl) complexes *cis*-$[Pt(C{\equiv}CPh)_2(L)]$ [L = 4,4′-dimethyl-2,2′-bipyridine (Me_2bipy), 4,4′-bis(*tert*-butyl)-2,2′-bipyridine (tBu$_2$bipy)] at room temperature readily affords the novel, spiked-triangular heterometallic cluster complexes $[Os_3Pt(CO)_9(\mu_4\text{-}\eta^2\text{-}C{\equiv}CPh)(\eta^1\text{-}C{\equiv}CPh)(L)]$ (L = Me_2bipy **1**, tBu$_2$bipy **2**) in moderate yields. X-ray analysis of both complexes reveals that one alkynyl moiety is coordinated to the metal atoms in a μ_4-η^2(⊥) mode, accompanied by a concomitant transfer of an η^1-C≡CPh group from the platinum centre to the osmium atom to give a metal framework with an osmium atom apically bonded to an Os_2Pt triangle.

Introduction

There is continuing interest in transition metal σ-alkynyl complexes and polymers stemming from their possible applications in materials science.[1,2] Within this field, rigid-rod polymers based on metals linked by alkynyl groups in a *trans*-configuration have proved particularly fruitful, and a number of new materials with novel electronic properties have been prepared, the nature of which depends on the metals, the ancillary ligands and the spacer units.[3−10] Likewise, *cis*-platinum bis(alkynyl) complexes have recently been exploited as novel precursors for the synthesis of a series of homo- or heterobimetallic complexes in which the second metal is linked to the bis(alkynyl) molecule by coordination to the alkynyl C≡C triple bonds.[11−16] The use of alkynyl platinum species as alkynylating agents is also known.[15] These bimetallic complexes have been shown to exhibit a range of interesting chemical and physical properties.[17] In an effort to extend this chemistry to other multimetallic systems, we have studied the reactions of some *cis*-$[Pt(C{\equiv}CPh)_2$(diimine)] complexes with $[Os_3(CO)_{10}(NCMe)_2]$. To our surprise, we have discovered that this leads to new heterometallic complexes formed by transformations involving η^1-acetylide transfer, opening of the Os_3 triangle and formation of two Pt−Os bonds. We describe herein the characterization of two new compounds $[Os_3Pt(CO)_9(\mu_4\text{-}\eta^2\text{-}C{\equiv}CPh)(\eta^1\text{-}C{\equiv}CPh)(L)]$ [L = 4,4′-dimethyl-2,2′-bipyridine (Me_2bipy), 4,4′-bis(*tert*-butyl)-2,2′-bipyridine (tBu$_2$bipy)] showing two distinct bonding modes for the alkynyl fragment.

Results and Discussion

The mixed-metal cluster compounds $[Os_3Pt(CO)_9(\mu_4\text{-}\eta^2\text{-}C{\equiv}CPh)(\eta^1\text{-}C{\equiv}CPh)(L)]$ (L = Me_2bipy **1**, tBu$_2$bipy **2**) were readily prepared by the room temperature reactions of the molecular tweezers *cis*-$[Pt(C{\equiv}CPh)_2(L)]$ with one molar equivalent of $[Os_3(CO)_{10}(NCMe)_2]$ in CH_2Cl_2 (Scheme 1). Complexes **1** and **2** were isolated by preparative TLC as stable red solids in moderate yields and characterized by satisfactory IR and NMR spectroscopy and FAB mass spectrometry. X-ray crystallography established the full details of their molecular structures and the coordination modes of the alkynyl moiety.

Crystals of **1** and **2** were grown from hexane/CH_2Cl_2 at room temperature. Complex **1** crystallized in an asymmetric unit possessing two crystallographically independent molecules. Perspective drawings of **1** and **2** are depicted in Figure 1 and 2, respectively. The structural features of both **1** and **2** are very similar and they will not be discussed separately. The molecular structures of **1** and **2** reveal that the Os_3 triangle has opened out with Os−Os−Os angles of 112.31(2) and 111.41(3)° in **1** and **2**, respectively. This is accompanied by the formation of two Pt−Os bonds. Three carbonyl groups are bound to each osmium atom. The metal core of **1** and **2** consists of an essentially isosceles Os_2Pt triangle, with a third osmium atom, Os(2), apically bonded to Os(1) to give an "out-of-plane" spiked-triangular metal framework. The Pt centre adopts a pseudo square planar geometry. Although there are several known examples of Os_3Pt clusters containing a closed Os_3 triangle with a spiked Pt atom,[18,19] complexes comprising an open triangular cluster of three osmium atoms with a Pt(diimine) moiety spanning one of the two Os−Os bonds are very rare. To the best of our knowledge, structurally characterized examples of such a metal core have only been encountered in $[Os_3Pt(CO)_{11-n}(L)_n(\mu_3\text{-}S)_2]$ (n = 1, 2; L = PPh_3, PMe_2Ph) with phosphane ligands on the Pt atom.[20,21] The Pt−Os distances range from 2.6397(6) to 2.6770(6) Å in **1** and **2**, and are somewhat shorter than those in previously reported Os_3Pt clusters {2.712(1) Å in $[Os_3Pt(\mu\text{-}H)(\mu_4\text{-}\eta^2\text{-}C{\equiv}CPh)(CO)_{10}(PCy_3)]$,[18] 2.714(1)−2.811(1) Å in

[a] Department of Chemistry, Hong Kong Baptist University, Waterloo Road, Kowloon Tong, Hong Kong, P.R. China
E-mail: rwywong@net1.hkbu.edu.hk

 © WILEY-VCH Verlag GmbH, 69451 Weinheim, 2001 1434−1948/01/0303−0623 $ 17.50+.50/0

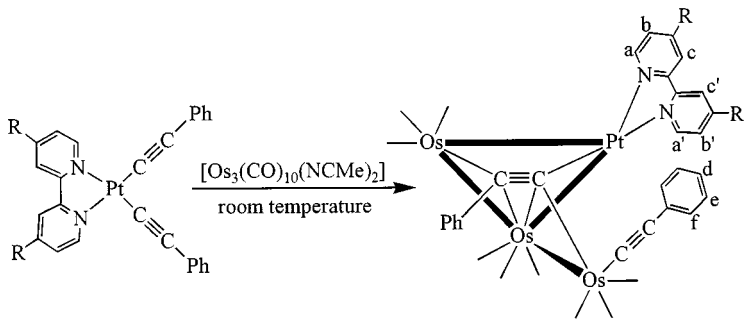

Scheme 1. Synthesis of complexes **1** and **2**

$[Os_3Pt(\mu\text{-}H)_2(\mu\text{-}CO)(CO)_9(COD)]$,[22] 2.764(1) Å in $[Os_3Pt(\mu\text{-}H)_2(\mu_4\text{-}C)(CO)_{10}\{P(cyclo\text{-}C_6H_{11})_3\}]$,[19] 2.789(1)-2.936(1) Å in $[Os_3Pt(CO)_9(PMe_2Ph)_2(\mu_3\text{-}S)_2]$[20]}. The spiked Os(1)−Os(2) edge [2.8909(6) Å in **1**, 2.914(1) Å in **2**] is notably longer than the other Os(1)−Os(3) bond [2.8032(7) Å in **1**, 2.810(1) Å in **2**] in both cases. The Pt−N bond [2.148(7)−2.174(7) Å] is also lengthened after coordination to the cluster motif relative to those observed in other *cis*-platinum bis(alkynyl) diimine complexes [2.04−2.07 Å],[13,14] probably due to the electron-withdrawing nature of the Os_3 fragment.

Another remarkable feature in the formation of **1** and **2** is the activation of a phenylacetylide unit in the starting platinum complex and its facile transfer from the platinum centre to the spiked osmium atom, resulting in a terminal alkynyl group on the Os(2) atom. The −C≡CPh group is σ-bonded to Os(2) in an η^1 mode with the C≡C bond length [average 1.21(2) Å] and Os(2)−C−C bond angle [average 175(1)°] typical of a metal−acetylide bond. The presence of an η^1-acetylide ligand is a relatively rare phenomenon in osmium cluster chemistry, although terminal acetylides are common in mononuclear osmium complexes.[23−25] A similar feature is only found in the homometallic $[Os_3(CO)_6(\mu\text{-}\eta^2\text{-}C{\equiv}CPh)(\eta^1\text{-}C{\equiv}CPh)(\mu\text{-}PPh_2)_2(NH_2Et)_2]$[26] and the heterometallic $[(\eta^5\text{-}C_5Me_5)W(O)(\mu\text{-}O)Os_3(\eta^1\text{-}C{\equiv}CPh)(CO)_{11}]$[27] complexes.

The remaining Pt-alkynyl unit is coordinated to the Os_3 chain with a $\mu_4\text{-}\eta^2(\|)$-C≡CPh moiety (Figure 3), in a manner similar to $[CpWOs_3(CO)_{11}(\mu_4\text{-}\eta^2\text{-}C{\equiv}CPh)]$ involving an alkynyl transfer and formation of two W−Os bonds.[28] The

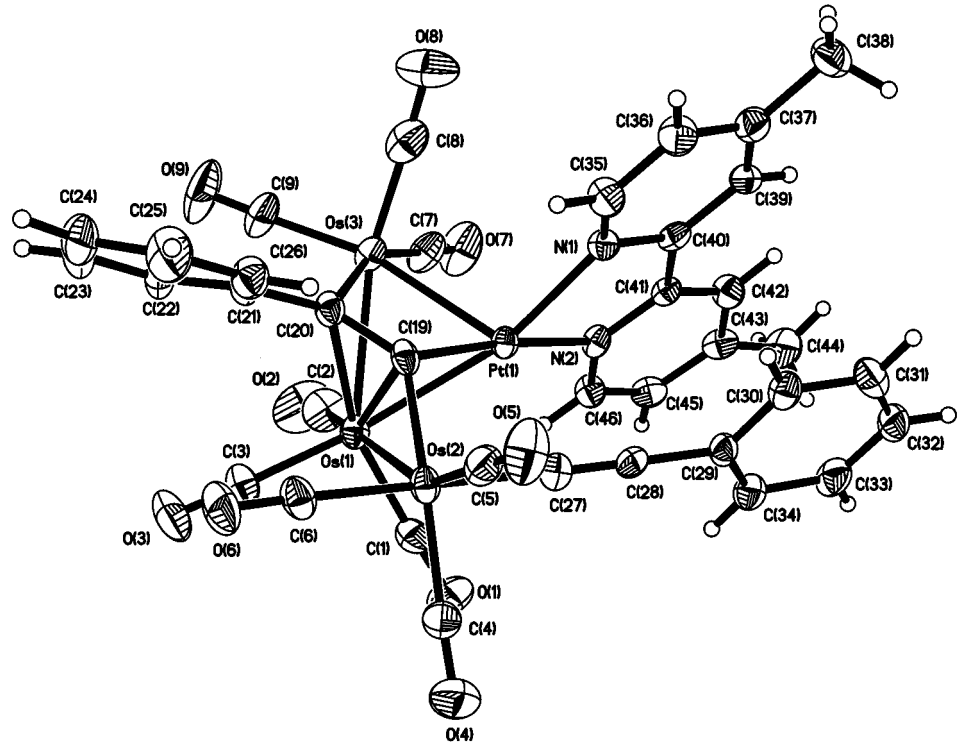

Figure 1. Molecular structure of **1**; important bond lengths (Å) and angles (°): Pt(1)−Os(1) 2.6732(6), Pt(1)−Os(3) 2.6397(6), Os(1)−Os(2) 2.8909(6), Os(1)−Os(3) 2.8032(7), Pt(1)−C(19) 2.011(9), Os(1)−C(19) 2.169(9), Os(1)−C(20) 2.30(1), Os(2)−C(19) 2.06(1), Os(3)−C(20) 2.16(1), Os(2)−C(27) 2.08(1), C(19)−C(20) 1.37(1), C(27)−C(28) 1.21(1); Os(1)−Pt(1)−Os(3) 63.69(2), Pt(1)−Os(1)−Os(3) 57.58(2), Pt(1)−Os(3)−Os(1) 58.74(2), Pt(1)−Os(1)−Os(2) 71.58(1), Os(2)−Os(1)−Os(3) 112.42(2), Pt(1)−C(19)−C(20) 112.1(7), Os(3)−C(20)−C(19) 103.5(6), C(19)−Os(1)−C(20) 35.6(4), Os(2)−C(27)−C(28) 174.0(9)

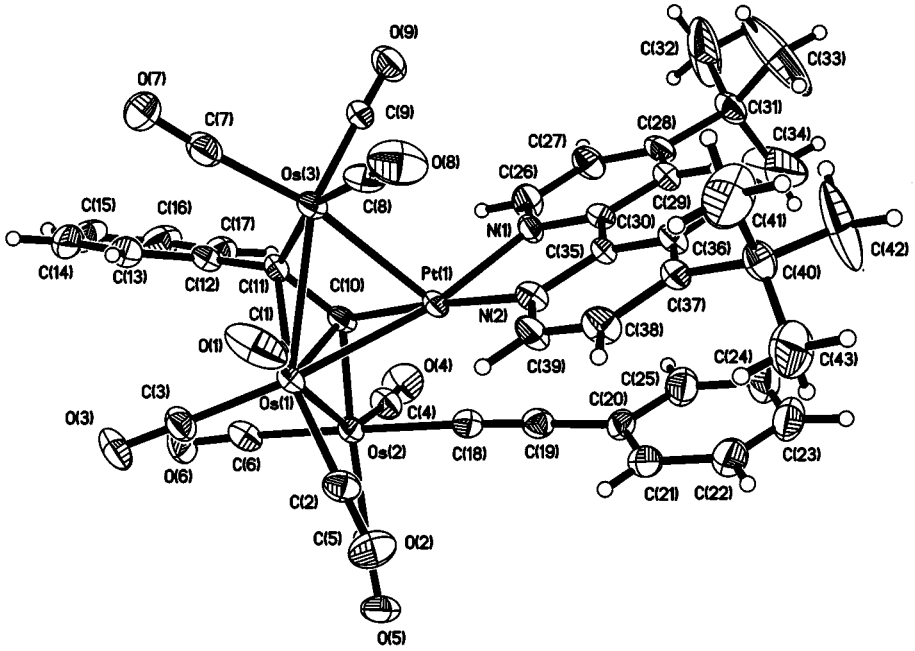

Figure 2. Molecular structure of **2**; important bond lengths (Å) and angles (°): Pt(1)−Os(1) 2.6604(8), Pt(1)−Os(3) 2.6500(9), Os(1)−Os(2) 2.914(1), Os(1)−Os(3) 2.810(1), Pt(1)−C(10) 2.018(9), Os(1)−C(10) 2.196(9), Os(1)−C(11) 2.326(9), Os(2)−C(10) 2.04(1), Os(3)−C(11) 2.075(9), Os(2)−C(18) 2.10(1), C(10)−C(11) 1.42(1), C(18)−C(19) 1.21(2); Os(1)−Pt(1)−Os(3) 63.90(3), Pt(1)−Os(1)−Os(3) 57.87(2), Pt(1)−Os(3)−Os(1) 58.23(3), Pt(1)−Os(1)−Os(2) 71.95(3), Os(2)−Os(1)−Os(3) 111.41(3), Pt(1)−C(10)−C(11) 109.1(6), Os(3)−C(11)−C(10) 105.9(6), C(10)−Os(1)−C(11) 36.4(3), Os(2)−C(18)−C(19) 176(1)

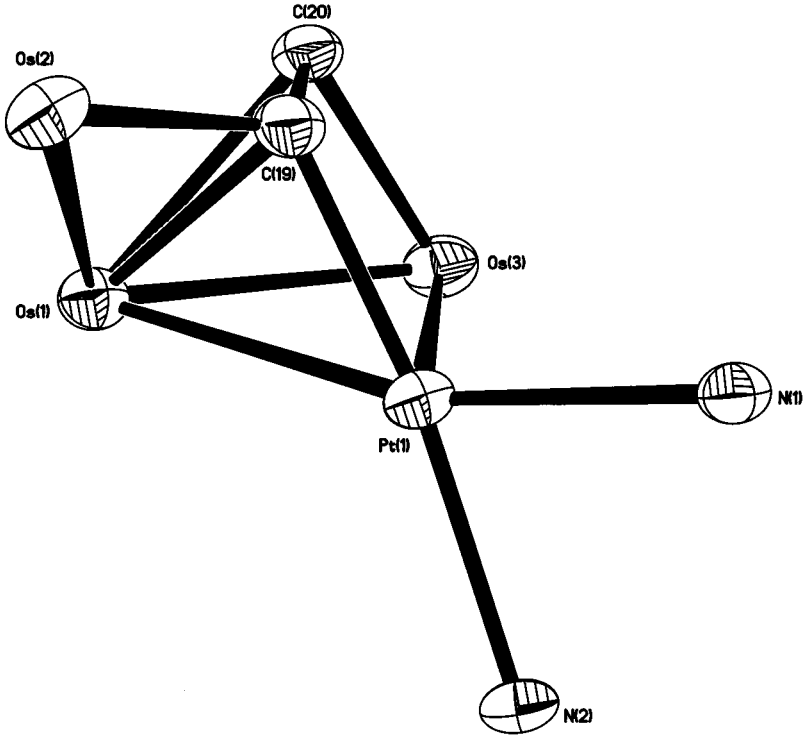

Figure 3. A perspective view of **1** showing the metal core and alkynyl coordination

vectors Pt(1)−Os(3) and C(19)−C(20) in **1** as well as Pt(1)−Os(3) and C(10)−C(11) in **2** are nearly parallel. Although $\mu_4\text{-}\eta^2(\perp)$ bonding modes have been documented for acetylides in spiked tetrametallic systems such as $[Os_3Pt(\mu\text{-}H)(\mu_4\text{-}\eta^2\text{-}C{\equiv}CPh)(CO)_{10}(PCy_3)]$,[18] $[(\eta^5\text{-}C_5H_5)FeRuCo_2(CO)_9(\mu\text{-}CO)(\mu_4\text{-}\eta^2\text{-}C{\equiv}CPh)]$,[29] $[(\eta^5\text{-}C_5H_5)_2Ni_2Fe_2(CO)_5(\mu\text{-}PPh_2)(\mu_4\text{-}\eta^2\text{-}C{\equiv}CPh)]$[30] and $[Ru_3Pt(\mu\text{-}H)\{\mu_4\text{-}\eta^2\text{-}C{\equiv}C(t\text{Bu})\}(CO)_9(COD)]$,[31] clusters with a $\mu_4\text{-}\eta^2(\parallel)$-C≡CPh group are, to the best of our knowledge, not common. The C(19)−C(20)−Os(3)−Pt(1) mean plane makes a

dihedral angle of 57.2° with the triangular Os_2Pt plane in **1** [58.2° in **2**]. Formally, the μ_4-η^2-C≡CPh ligand forms a π bond with Os(1) and three separate σ bonds to Os(2), Os(3) and Pt(1) in each case. Assuming that the μ_4-η^2-C≡CPh and η^1-C≡CPh moieties act as a five- and one-electron donor, respectively, each of the complexes **1** and **2** has 62 cluster valence electrons (CVE) which is consistent with a 16-electron Pt centre. This apparent low CVE count is commonly observed in clusters containing Pt atoms.[32]

Experimental Section

Preparation of $[Os_3Pt(CO)_9(\mu_4\text{-}\eta^2\text{-}C{\equiv}CPh)(\eta^1\text{-}C{\equiv}CPh)(Me_2bipy)]$ (1): A CH_2Cl_2 solution of $[Os_3(CO)_{10}(NCMe)_2]$ (0.050 g, 0.054 mmol) was stirred at room temperature with *cis*-$[Pt(C{\equiv}CPh)_2(Me_2bipy)]$[14,33] (0.031 g, 0.054 mmol) under nitrogen. After 30 min. the solvent was evaporated under vacuum, and the crude product was purified by preparative TLC, eluting with *n*-hexane/CH_2Cl_2 (3:2, v/v) to afford an orange band (R_f = 0.30) which was identified as complex **1** (0.023 g, 30%). – IR (CH_2Cl_2): ν(CO) = 2084 w, 2065 w, 2048 vs, 2012 s, 1998 m, 1973 m and 1960 sh cm^{-1}. – ^1H NMR ($CDCl_3$): δ = 2.33 (s, 3 H, Me), 2.49 (s, 3 H, Me), 6.08 (d, J = 7.3 Hz, 2 H, H_f), 6.58 (t, J = 7.3 Hz, 2 H, H_e), 6.79 (t, J = 7.3 Hz, 1 H, H_d), 7.16–7.49 (m, 9 H, H_b, $H_{b'}$, H_c, $H_{c'}$ and Ph), 8.67 (d, J = 6.8 Hz, 1 H, H_a or $H_{a'}$), 8.85 (d, J = 5.4 Hz, 1 H, H_a or $H_{a'}$). – FAB MS: m/z = 1404 [M^+]. – $C_{37}H_{22}N_2O_9Os_3Pt$ (1404.27): calcd. C 31.51, H 1.57, N 1.99; found C 31.40, H 1.45, N 1.78.

Preparation of $[Os_3Pt(CO)_9(\mu_4\text{-}\eta^2\text{-}C{\equiv}CPh)(\eta^1\text{-}C{\equiv}CPh)(t\text{Bu}_2bipy)]$ (2): A mixture of $[Os_3(CO)_{10}(NCMe)_2]$ (0.050 g, 0.054 mmol) and $[Pt(C{\equiv}CPh)_2(t\text{Bu}_2bipy)]$ (0.036 g, 0.054 mmol) was stirred at room temperature under nitrogen for 30 min. The resulting orange-red solution was evaporated to dryness and the residue was subjected to TLC with *n*-hexane/CH_2Cl_2 (3:2, v/v) as eluent to give complex **2** as an orange band (R_f = 0.50) in 28% yield (0.022 g). – IR (CH_2Cl_2): ν(CO) = 2083 w, 2064 w, 2048 vs, 2011 s, 1998 m, 1972 m and 1958 sh cm^{-1}. – ^1H NMR ($CDCl_3$): δ = 1.30 (s, 9 H, *t*Bu), 1.43 (s, 9 H, *t*Bu), 6.02 (d, J = 7.6 Hz, 2 H, H_f), 6.53 (t, J = 7.6 Hz, 2 H, H_e), 6.78 (t, J = 7.6 Hz, 1 H, H_d), 7.18–7.60 (m, 9 H, H_b, $H_{b'}$, H_c, $H_{c'}$ and Ph), 8.74 (d, J = 5.4 Hz, 1 H, H_a or $H_{a'}$), 8.91 (d, J = 5.7 Hz, 1 H, H_a or $H_{a'}$). – FAB MS: m/z = 1488 [M^+]. – $C_{43}H_{34}N_2O_9Os_3Pt$ (1488.43): calcd. C 34.70, H 2.30, N 1.88; found C 34.49, H 2.20, N 1.75.

Crystallographic Data for $1{\cdot}CH_2Cl_2$: $C_{38}H_{24}Cl_2N_2O_9Os_3Pt$, M = 1489.18, triclinic, space group $P\bar{1}$, a = 9.317(1), b = 17.843(2), c = 25.672(3) Å, α = 73.857(2), β = 87.260(2), γ = 86.020(2)°, U = 4087.8(8) $Å^3$, Z = 4, T = 293 K, μ(Mo-K_α) = 128.91 cm^{-1}, 24218 reflections measured, 17554 unique, R(int) = 0.0370, final $R1$ = 0.0408, w$R2$ = 0.0894 (based on F^2) for 17554 [$I > 2\sigma(I)$] observed reflections.

Crystallographic Data for $2{\cdot}CH_2Cl_2$: $C_{44}H_{36}Cl_2N_2O_9Os_3Pt$, M = 1573.34, triclinic, space group $P\bar{1}$, a = 11.420(2), b = 13.972(3), c = 16.438(3) Å, α = 111.92(3), β = 101.84(3), γ = 90.69(3)°, U = 2370.1(8) $Å^3$, Z = 2, T = 293 K, μ(Mo-K_α) = 111.23 cm^{-1}, 13770 reflections measured, 10007 unique, R(int) = 0.0484, final $R1$ = 0.0553, w$R2$ = 0.1639 (based on F^2) for 10007 [$I > 2\sigma(I)$] observed reflections.

Crystallographic data (excluding structure factors) for the structures reported in this paper have been deposited with the Cambridge Crystallographic Data Centre as supplementary publication nos. CCDC-151605 (**1**) and CCDC-151606 (**2**). Copies of the data can be obtained free of charge on application to The Director, CCDC, 12 Union Road, Cambridge CB2 1EZ, UK [Fax: (internat.) +44-1223/336-033; E-mail: deposit@ccdc.cam.ac.uk].

Acknowledgments

W.-Y. W. thanks the Hong Kong Baptist University for financial support and F.-L. T. acknowledges the receipt of a studentship administered by the Hong Kong Baptist University.

[1] I. Manners, *Angew. Chem. Int. Ed. Engl.* **1996**, *35*, 1602–1621.
[2] R. P. Kingsborough, T. M. Swager, *Prog. Inorg. Chem.* **1999**, *48*, 123–231.
[3] N. J. Long, A. J. Martin, R. Vilar, A. J. P. White, D. J. Williams, M. Younus, *Organometallics* **1999**, *18*, 4261–4269.
[4] T. J. McKay, J. A. Bolger, J. Staromlynska, J. R. Davy, *J. Chem. Phys.* **1998**, *108*, 5537–5541.
[5] N. Chawdhury, A. Köhler, R. H. Friend, M. Younus, N. J. Long, P. R. Raithby, J. Lewis, *Macromolecules* **1998**, *31*, 722–727.
[6] C. J. Adams, S. L. James, P. R. Raithby, *Chem. Commun.* **1997**, 2155–2156.
[7] N. Chawdhury, A. Köhler, R. H. Friend, W. Y. Wong, J. Lewis, M. Younus, P. R. Raithby, T. C. Corcoran, M. R. A. Al-Mandhary, M. S. Khan, *J. Chem. Phys.* **1999**, *110*, 4963–4970.
[8] J. Lewis, P. R. Raithby, W. Y. Wong, *J. Organomet. Chem.* **1998**, *556*, 219–228.
[9] W. Y. Wong, W. K. Wong, P. R. Raithby, *J. Chem. Soc., Dalton Trans.* **1998**, 2761–2766.
[10] W. Y. Wong, S. M. Chan, K. H. Choi, K. W. Cheah, W. K. Chan, *Macromol. Rapid Commun.* **2000**, *21*, 453–457.
[11] S. Yamazaki, A. J. Deeming, *J. Chem. Soc., Dalton Trans.* **1993**, 3051–3057.
[12] D. Zhang, D. B. McConville, C. A. Tessier, W. J. Youngs, *Organometallics* **1997**, *16*, 824–825.
[13] C. J. Adams, P. R. Raithby, *J. Organomet. Chem.* **1999**, *578*, 178–185.
[14] C. J. Adams, S. L. James, X. Liu, P. R. Raithby, L. J. Yellowlees, *J. Chem. Soc., Dalton Trans.* **2000**, 63–67.
[15] J. R. Berenguer, E. Eguizábal, L. R. Falvello, J. Forniés, E. Lalinde, A. Martin, *Organometallics* **2000**, *19*, 490–496.
[16] S. Back, H. Lang, *Organometallics* **2000**, *19*, 749–751.
[17] J. Forniés, E. Lalinde, *J. Chem. Soc., Dalton Trans.* **1996**, 2587–2599.
[18] P. Ewing, L. J. Farrugia, *J. Organomet. Chem.* **1987**, *320*, C47–C50.
[19] L. J. Farrugia, A. D. Miles, F. G. A. Stone, *J. Chem. Soc., Dalton Trans.* **1985**, 2437–2447.
[20] R. D. Adams, I. T. Horvãth, S. Wang, *Inorg. Chem.* **1986**, *25*, 1617–1623.
[21] R. D. Adams, T. S. A. Hor, I. T. Horvãth, *Inorg. Chem.* **1984**, *23*, 4733–4738.
[22] P. Ewing, L. J. Farrugia, *J. Organomet. Chem.* **1988**, *347*, C31–C34.
[23] M. A. Esteruelas, F. J. Lahoz, A. M. López, E. Oñate, L. A. Oro, *Organometallics* **1995**, *14*, 2496–2500.
[24] A. J. Hodge, S. L. Ingham, A. K. Kakkar, M. S. Khan, J. Lewis, N. J. Long, D. G. Parker, P. R. Raithby, *J. Organomet. Chem.* **1995**, *488*, 205–210.
[25] M. C. B. Colbert, J. Lewis, N. J. Long, P. R. Raithby, A. J. P. White, D. J. Williams, *J. Chem. Soc., Dalton Trans.* **1997**, 99–104.
[26] A. A. Cherkas, N. J. Taylor, A. J. Carty, *J. Chem. Soc., Chem. Commun.* **1990**, 385–387.
[27] C. W. Shiu, Y. Chi, A. J. Carty, S. M. Peng, G. H. Lee, *Organometallics* **1997**, *16*, 5368–5371.

[28] Y. Chi, G.-H. Lee, S.-M. Peng, C.-H. Wu, *Organometallics* **1989**, *8*, 1574−1576.
[29] E. Roland, H. Vahrenkamp, *Organometallics* **1983**, *2*, 1048−1049.
[30] C. Weatherell, N. J. Taylor, A. J. Carty, E. Sappa, A. Tiripicchio, *J. Organomet. Chem.* **1985**, *291*, C9−C12.
[31] P. Ewing, L. J. Farrugia, *Organometallics* **1989**, *8*, 1246−1260.
[32] E. Sappa, A. Tiripicchio, A. J. Carty, G. E. Toogood, *Prog. Inorg. Chem.* **1987**, *35*, 437−525.
[33] S. L. James, M. Younus, P. R. Raithby, J. Lewis, *J. Organomet. Chem.* **1997**, *543*, 233−235.

Received November 2, 2000
[I00415]

Supramolecular Assembling of Dizinc Macrocyclic Complexes with Thymine and Uracil — The Role of Intra- and Intermolecular Hydrogen Bonding

Carla Bazzicalupi,[a] Andrea Bencini,*[a] Emanuela Berni,[a] Antonio Bianchi,*[a] Samuele Ciattini,[a] Claudia Giorgi,[a] Piero Paoletti,*[a] and Barbara Valtancoli*[a]

Keywords: Macrocycles / Supramolecular chemistry / Zinc / Nucleobases / Hydrogen bonds

A binuclear Zn^{II} complex with an oxa-aza macrocyclic ligand can bind two deprotonated thymine or uracil moieties, giving versatile building blocks for the assembly of supramolecolar structures, by hydrogen bond pairing of the nucleobases.

Introduction

In the last few years a great deal of interest has been devoted to the recognition of nucleobases, nucleosides and nucleotides by synthetic receptors in aqueous solutions,[1−11] due both to their use as mimic systems for enzymes and to their potential medical application. Particular attention has been focused on the role of nucleobases in the recognition process, since these molecules possess several functions which can be used for hydrogen bonding and/or metal binding. Metal complexes are often chosen as receptors for these substrates. Recent work by Kimura[8−11] has shown that thymine derivatives containing an imide CO−NH−CO moiety (such as AZT or thymidine), are strongly bound by Zn^{II} complexes with cyclen-based macrocycles (cyclen = 1,4,7,10-tetraazacyclododecane), through a recognition process which involves deprotonation of the imide function, metal binding by the deprotonated nitrogen and hydrogen bonding between the CO functions and two complementary amine groups of the macrocyclic unit. This "three-point" binding mode accounts for the selective binding of thymine derivatives with respect to cytosine ones, which don't contain an "imide" moiety.

Several zinc enzymes, however, contain two Zn^{II} ions in their active site. At the same time, binuclear metal complexes with macrocyclic ligands are potential receptors for nucleobases.[10] The particular topology of these ligands, in fact, may force the two metal centres into close proximity where they can act as multipoint binding sites for substrate molecules or anions.[12,13] Ligand **L** presents two almost independent binding moieties — the two triamine chains — separated by two weakly coordinating polyoxa chains.[14] In its dizinc complex each metal is bound by a triamine unit and presents an unsaturated coordination sphere. This complex, therefore, may be a promising receptor for nucleobases, such as thymine (TH) or uracil (UH).

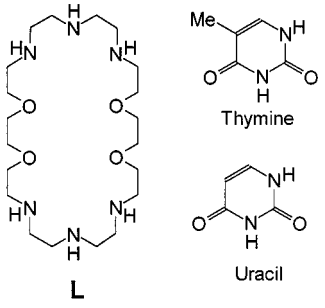

Results and Discussion

Thymine and uracil binding to the dizinc complex $[Zn_2\mathbf{L}]^{4+}$ was studied by means of potentiometric measurements in aqueous solutions. This complex displays similar binding features towards thymine and uracil. We found, in fact, that it forms stable 1:1 and 1:2 complexes with both deprotonated thymine and uracil at neutral or slightly alkaline pH's. Deprotonation and simultaneous binding of thymine and uracil to the $[Zn_2\mathbf{L}]^{4+}$ complex takes place at neutral pH, to give the 1:1 complexes $[Zn_2\mathbf{LT}]^{3+}$ or $[Zn_2\mathbf{LU}]^{3+}$ {log K = 5.3(1) and 5.0(1) for the equilibria $[Zn_2\mathbf{L}]^{4+}$ + T^- = $[Zn_2\mathbf{LT}]^{3+}$ and $[Zn_2\mathbf{L}]^{4+}$ + U^- = $[Zn_2\mathbf{LU}]^{3+}$, respectively}. These complexes are formed in the pH range 6.5−9, with a maximum percentage of ca. 20% at pH 7.5 in solutions containing $[Zn_2\mathbf{L}]^{4+}$ and TH or UH in a 1:1 molar ratio. This process is followed at slightly alkaline pH's by deprotonation and binding of a second nucleobase, leading to the assembly of the $[Zn_2\mathbf{LT}_2]^{2+}$ and $[Zn_2\mathbf{LU}_2]^{2+}$ complexes {log K = 5.0(1) and 4.7(1) for the equilibria $[Zn_2\mathbf{LT}]^{3+}$ + T^- = $[Zn_2\mathbf{LT}_2]^{2+}$ and $[Zn_2\mathbf{LU}]^{3+}$ + U^- = $[Zn_2\mathbf{LU}_2]^{2+}$, respectively}, which contain two deprotonated nucleobases. These species are formed in the pH range 7−10.5 (maximum percentage ca. 60% at pH 9). It is of interest to note that, for both thymine and uracil, the constant for the addition of the first deprotonated nucleobase is almost equal to that for the addition of the second one, suggesting that each nucleobase is coordinated, almost independently, by one Zn^{II} ion of the $[Zn_2\mathbf{L}]^{4+}$ complex.

[a] Department of Chemistry, University of Florence,
Via Maragliano 77, 50144 Florence, Italy
Fax: (internat.) +39-055/354-845
E-mail: benc@chim1.unifi.it

Supporting information for this article is available on the WWW under http://www.wiley-vch.de/home/eurjic or from the author.

 © WILEY-VCH Verlag GmbH, 69451 Weinheim, 2001 1434−1948/01/0303−0629 $ 17.50+.50/0

The crystal structure of the $[Zn_2\mathbf{L}T_2]^{2+}$ cation (Figure 1a) shows that two deprotonated thymine units are coordinated to the two metal centers and lie on opposite sides with respect to an ideal plane containing the macrocycle oxygen atoms. The metals are symmetry related [Zn···Zn′ = 7.667(5) Å] and present a distorted trigonal bipyramidal coordination geometry, with the equatorial plane defined by the "lateral" N(1) and N(3) amine groups of the macrocycle and the deprotonated N(3t) nitrogen of thymine, with a rather short Zn−N(3t) bond length [1.948(6) Å], due to the anionic nature of this donor. The "central" nitrogen N(2) of the triamine unit and an oxygen [O(1)] of the polyoxa chain occupy the apical positions and are bound at longer distances [Zn(1)−N(2) = 2.143(9) Å, Zn(1)−O(1) = 2.398(7) Å] than the other three coordinated nitrogens. The Zn^{II} ion and the two lateral amine groups lie on the plane of the thymine ring [max. deviation 0.325(7) Å for N(1)]. Such a complementary disposition allows the formation of two rather strong hydrogen bonds between the two carbonyl oxygens of thymine and the coordinated N(1) and N(3) amine groups of the macrocycle [N(1)···O(2t) = 3.02(1) Å; N(3)···O(4t) = 3.39(2) Å]. Furthermore, deprotonation of the imide nitrogen develops negative charges at the carbonyl functions, which become better acceptors for the N−H hydrogens. The match of the complementary binding sites of receptor and substrate allows the formation of a tight $(CO)_2N(3t)-ZnN(1)N(3)$ unit and may account for the remarkably high stability in aqueous solution of the present dizinc complex with deprotonated thymine.

Thymine, however, possesses another binding site, the N(1t) nitrogen, which can be used for hydrogen bonding. Besides intramolecular hydrogen bonding, inspection of the crystal packing revealed the formation of hydrogen-bond pairing between the thymine units of different $[Zn_2\mathbf{L}T_2]^{2+}$ complexes. The ORTEP drawing of the crystal packing for the $[Zn_2\mathbf{L}T_2]^{2+}$ complex (Figure 1b) clearly shows that each thymine unit is associated through two symmetry-related strong hydrogen bonds [N(1t)···O(2t) 2.769(9) Å] with a thymine moiety of a different binuclear complex. Consequently, the $[Zn_2\mathbf{L}T_2](ClO_4)_2$ complexes are assembled into infinite pillars of $[Zn_2\mathbf{L}T_2]^{2+}$ units, joined together through a centrosymmetrical hydrogen bond network.

The assembly of this supramolecular architecture can also be ascribed to the macrocyclic structure of **L**, which keeps two Zn-thymine units at rather close distance. At the same time, the well-known ability of thymine to give hydrogen bonds with other nucleobases (a different thymine unit in the present case) allows the formation of the pillared structure presented by the $[Zn_2\mathbf{L}T_2](ClO_4)_2$ complex.

The crucial role played by both intra- and intermolecular hydrogen bonding in this assembling process is confirmed by the crystal structure of the dinuclear Zn^{II} complex with uracil, which presents the same binding sites as with thymine (Figure 2).

In the $[Zn_2\mathbf{L}U_2]^{2+}$ complex, each metal displays a trigonal bipyramidal coordination geometry, very similar to that found in the thymine complex. The N(3u), N(1) and N(3) nitrogens define the basal plane, while the N(2) and

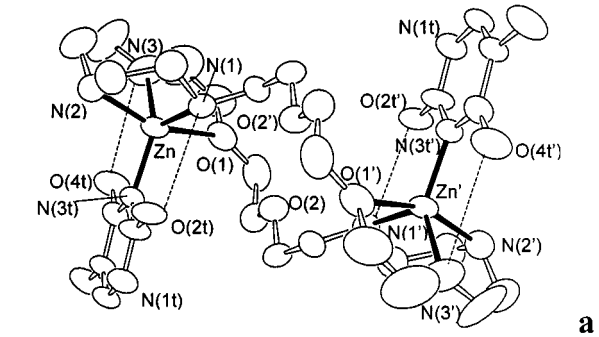

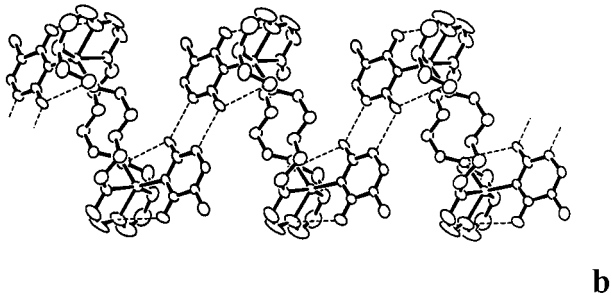

Figure 1. (a) ORTEP drawing of the $[Zn_2\mathbf{L}T_2]^{2+}$ cation; (b) crystal packing for $[Zn_2\mathbf{L}T_2](ClO_4)_2$ displaying the intramolecular hydrogen bonds and the hydrogen bond pairing between thymine units of different $[Zn_2\mathbf{L}T_2]^{2+}$ complexes (perchlorate anions are omitted for clarity); selected bond lengths (Å) and angles (°): Zn−N(3t) 1.948(6), Zn−N(3) 2.034(9), Zn−N(1) 2.070(7), Zn−N(2) 2.143(9), Zn−O(1) 2.398(7); N(3t)−Zn−N(3) 129.0(4), N(3t)−Zn−N(1) 119.2(3), N(3)−Zn−N(1) 111.5(4), N(3t)−Zn−N(2) 105.0(3), N(3)−Zn−N(2) 83.6(4), N(1)−Zn−N(2) 84.7(3), N(3t)−Zn−O(1) 94.5(3), N(3)−Zn−O(1) 74.5(4), N(1)−Zn−O(1) 96.5(3), N(2)−Zn−O(1) 156.9(3), Zn···Zn′ 7.667(5)

O(1) donors, at the apical positions, are coordinated at longer distances. Figure 2 clearly shows the optimal matching between the N(1)−Zn−N(3) unit of the receptor and the $CO-N(3u)^{-}-CO$ imide function, leading, once again, to an enhanced receptor-substrate interaction through the formation of a strong Zn−N(3u) bond [1.93(1) Å] and two N(1)···O(2u) and N(3)···O(4u) hydrogen bonds [3.05(2) and 3.16(2) Å, respectively]. As in the case of thymine, intermolecular hydrogen bond pairing between two symmetry related uracil units of two different dizinc clusters [N(1u)···O(2u), 2.84(2) Å] leads to the formation of infinite pillars of $[Zn_2\mathbf{L}U_2]^{2+}$ complexes (Figure 2b).

To the best of our knowledge, the $[Zn_2\mathbf{L}T_2](ClO_4)_2$ and $[Zn_2\mathbf{L}U_2](ClO_4)_2$ complexes are the first structurally characterized dizinc assemblies containing two thymine or uracil units.

The present structures suggest that binuclear Zn^{II} macrocyclic complexes with nucleobases may be used as building blocks for supramolecular structures, due to the versatile hydrogen bonding ability of these molecules. Intramolecular hydrogen bonds, in fact, give a significant contribution to the stability of the binuclear dithymine or diuracil adducts. At the same time, intermolecular hydrogen bonding of different binuclear complexes contributes to generate the as-

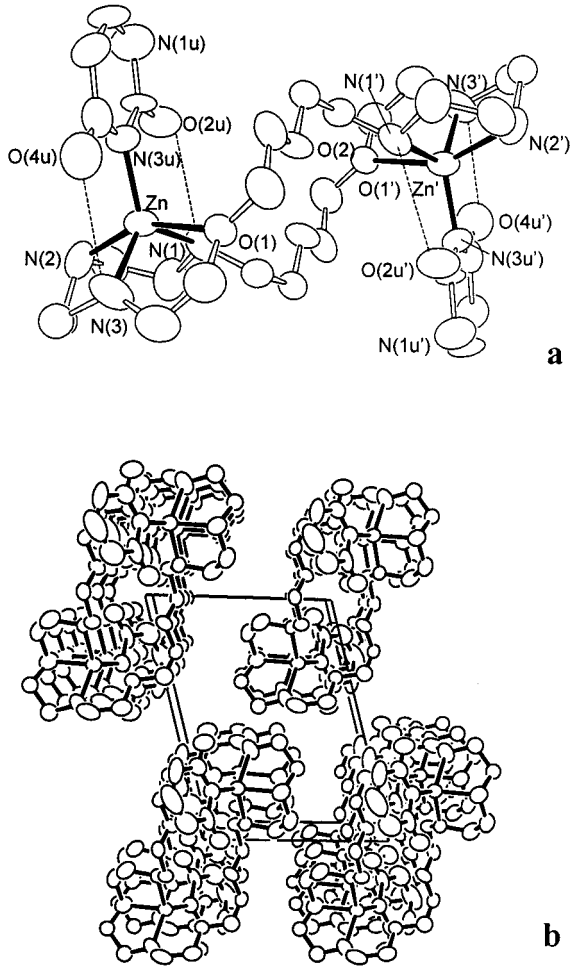

Figure 2. (a) ORTEP drawing of the $[Zn_2\mathbf{L}U_2]^{2+}$ cation; (b) crystal packing for $[Zn_2\mathbf{L}U_2](ClO_4)_2$ [view normal to (011)], displaying the pillared structure of $[Zn_2\mathbf{L}U_2]^{2+}$ cations (perchlorate anions are omitted for clarity); selected bond lengths (Å) and angles (°): Zn−N(3u) 1.93(1), Zn−N(3) 2.04(1), Zn−N(1) 2.08(1), Zn−N(2) 2.11(1), Zn−O(1) 2.462(8); N(3u)−Zn−N(3) 121.9(5), N(3u)−Zn−N(1) 120.0(4), N(3)−Zn−N(1) 117.0(5), N(3u)−Zn−N(2) 111.2(4), N(3)−Zn−N(2) 83.5(5), N(1)−Zn−N(2) 84.9(4), N(3u)−Zn−O(1) 94.1(4), N(3)−Zn−O(1) 73.4(4), N(1)−Zn−O(1) 92.1(3), N(2)−Zn−O(1) 152.3(4), Zn···Zn′ 7.799(2)

sembly of supramolecular architectures based on infinite pillars of $[Zn_2\mathbf{L}T_2]^{2+}$ or $[Zn_2\mathbf{L}U_2]^{2+}$ units.

Further investigations on different nucleobases are in progress.

Experimental Section

General Remarks: Compound **L** and $[Zn_2\mathbf{L}](ClO_4)_4$ were prepared as previously described.[14]

$[Zn_2LT_2](ClO_4)_2$: Crystals of the $[Zn_2\mathbf{L}T_2](ClO_4)_2$ complex were obtained in 82% yield by slow evaporation of an aqueous solution containing $[Zn_2\mathbf{L}](ClO_4)_4$ (0.001 M) and TH (0.002 M) at pH 8. − $C_{30}H_{56}Cl_2N_{10}O_{16}Zn_2$ (1014.49): C 35.52, H 5.56, N 13.81; found C 35.7, H 5.7, N 14.0.

$[Zn_2LU_2](ClO_4)_2$: This compound was prepared in 87% yield in a similar manner as already described for $[Zn_2\mathbf{L}T_2](ClO_4)_2$. − $C_{28}H_{52}Cl_2N_{10}O_{16}Zn_2$ (986.44): C 34.09, H 5.31, N 14.20; found C 34.2,H 5.3, N 14.1.

Potentiometric Measurements: All potentiometric measurements (pH = −log[H^+]) were carried out in 0.1 M NMe_4NO_3 (pK_w = 13.83 at 298.1 K) at 298.1 K, by using the method and procedure from ref.[14] The nucleobase:[Zn^{II} complex] molar ratio was varied from 0.3 to 5 in order to better ascertain the stoichiometry of the adducts. The computer program HYPERQUAD[15] was used to calculate the addition constants from e.m.f. data.

X-ray Crystallographic Study: $[Zn_2\mathbf{L}T_2](ClO_4)_2$: $C_{30}H_{56}Cl_2N_{10}O_{16}Zn_2$, M = 1014.48, triclinic, $P\bar{1}$, a = 9.305(6) Å, b = 9.612(4) Å, c = 13.170(5) Å, α = 103.17(3)°, β = 100.94(4)°, γ = 100.53(4)°, V = 1094.2(9) Å^3, T = 298 K, Z = 1, calculated density 1.540 Mg/m^3. Data collection with an Enraf Nonius CAD4 diffractometer, graphite-monochromated Mo-K_α radiation, crystal size 0.3 × 0.25 × 0.1 mm, θ-2θ scan, $2\theta_{max}$ = 50°, μ = 1.295 mm^{-1}, 4500 reflections collected, 3719 unique (R_{int} = 0.1355) which were used in all calculations, absorption correction by psi-scan method, transmission factors 0.72−0.82, data/parameters 3719/272, final R indices $R1$ = 0.0838 [$I > 2\sigma(I)$], $wR2$ = 0.2711. All hydrogen atoms were introduced in calculated positions.

$[Zn_2\mathbf{L}U_2](ClO_4)_2$: $C_{28}H_{52}Cl_2N_{10}O_{16}Zn_2$, M = 986.44, triclinic, $P\bar{1}$, a = 9.405(1) Å, b = 9.443(1) Å, c = 12.457(2) Å, α = 103.46(1)°, β = 96.81(1)°, γ = 100.53(1)°, V = 1042.7(2) Å^3, T = 298 K, Z = 1, calculated density 1.571 Mg/m^3. Data collection with a Siemens P4 diffractometer equipped with a rotating anode, graphite-monochromated Cu-K_α radiation, crystal size 0.15 × 0.1 × 0.1 mm, θ-2θ scan, $2\theta_{max}$ = 110°, μ = 3.280 mm^{-1}, 2688 reflections collected, 2173 unique (R_{int} = 0.0684) which were used in all calculations, absorption correction by psi-scan method, transmission factors 0.61−0.72, data/parameters 2173/261, final R indices $R1$ = 0.0810 [$I > 2\sigma(I)$], $wR2$ = 0.2278. All hydrogen atoms were introduced in calculated positions.

Both structures were solved using the direct methods of the SIR97 program[16] and refined by full-matrix least-squares on F^2 by means of the SHELXL-97 program.[17]

Crystallographic data (excluding structure factors) for the structure(s) reported in this paper have been deposited with the Cambridge Crystallographic Data Centre as supplementary publications no. CCDC-149822 {$[Zn_2LT_2](ClO_4)_2$} and -149823 {$[Zn_2LU_2](ClO_4)_2$}. Copies of the data can be obtained free of charge on application to CCDC, 12 Union Road, Cambridge CB2 1EZ, UK [Fax: (internat.) + 44-1223/336-033; E-mail: deposit@ccdc.cam.ac.uk].

Acknowledgments

Financial support by the Italian Ministero dell'Università e della Ricerca Scientifica e Tecnologica, within the program COFIN 98, and by Italian research Council (CNR) is gratefully acknowledged.

[1] M. W. Hosseini, A. J. Blaker, J.-M. Lehn, *J. Am. Chem. Soc.* **1990**, *112*, 3896−3904.
[2] J. A. Aguilar, E. Garcia-España, J. A. Guerrero, S. V. Luis, J. M. Llinares, M. F. Miravet, J. A. Ramirez, C. Soriano, *Chem. Commun.* **1995**, 2237−2238.
[3] J. A. Aguilar, B. Celda, V. Fusi, E. García-España, S. V. Luis, M. C. Martínez, J. A. Ramírez, C. Soriano, R. Tejero, *J. Chem. Soc., Perkin Trans. 2* **2000**, 1323−1328.
[4] E. Kimura and T. Koike, *Chem. Commun.* **1998**, 1495−1500.
[5] A. V. Eliseev and H.-J. Schneider, *J. Am. Chem. Soc.* **1994**, *116*, 6081−6088 and references therein.

[6] C. Bazzicalupi, A. Bencini, A. Bianchi, V. Fusi, C. Giorgi, A. Granchi, P. Paoletti and B. Valtancoli, *J. Chem. Soc., Perkin Trans. 2* **1997**, 775−781.
[7] G. Papoyan, K. Gu, J. Wiorkiewicz-Kuczera, K. Kuczera, K. Bowman-James, *J. Am. Chem. Soc.* **1996**, *118*, 1354−1364 and references therein.
[8] M. Shionoya, E. Kimura, M. Shiro, *J. Am. Chem. Soc.* **1993**, *115*, 6730−6737.
[9] M. Shionoya, T. Ikeda, E. Kimura, M. Shiro, *J. Am. Chem. Soc.* **1994**, *116*, 3848−3859.
[10] E. Kimura and M. Kikuchi, H. Kitamura, T. Koike, *Chem. Eur. J.* **1999**, *5*, 3113−3123.
[11] E. Kikuta, M. Murata, N. Katsube, T. Koike, E. Kimura, *J. Am. Chem. Soc.* **1999**, *121*, 5426−5436.
[12] A. J. Blake, N. R. Champness, P. Hubberstey, W.S. Li, M. Schröder, M. A. Withersby, *Coord. Chem. Rev.* **1999**, *183*, 117−138.
[13] J. Nelson, V. McKee, G. Morgan, in *Progr. Inorg. Chem.* (Ed.: K. D. Karlin), Wiley, New York, **1998**, *47*, p 167−316.
[14] C. Bazzicalupi, A. Bencini, A. Bianchi, V. Fusi, C. Giorgi, P. Paoletti, B. Valtancoli, D. Zanchi, *Inorg. Chem* **1997**, *36*, 2784−2790.
[15] P. Gans, A. Sabatini, A. Vacca, *J. Chem. Soc., Dalton Trans.* **1985**, 1195−1200
[16] A. Altomare, M. C. Burla, M. Camalli, G. L. Cascarano, C. Giacovazzo, A. Guagliardi, A. G. G. Moliterni, G. Polidori, R. Spagna, *J. Appl. Crystallogr.* **1999**, *32*, 115.
[17] G. M. Sheldrick, SHELXL-97, University of Göttingen, Göttingen, **1997**.

Received September 21, 2000
[I00355]

Self-Assembly of Fourteen Components into a Soluble, Neutral, Metalloprismatic Cage

Bala Manimaran,[a] T. Rajendran,[a,c] Yi-Long Lu,[a] Gene-Hsiang Lee,[b] Shie-Ming Peng,[b] and Kuang-Lieh Lu*[a]

Keywords: Cage compounds / Rhenium / Solvatochromism / Self assembly / N ligands

A novel one-pot synthesis of rhenium-based triangular prismatic cages has been accomplished in excellent yields by a self-assembly strategy. Reaction of $Re_2(CO)_{10}$ with 2,4,6-tri-4-pyridyl-1,3,5-triazine (tpt) in the presence of an aliphatic alcohol (1-butanol, 1-octanol or 1-dodecanol) afforded molecular prisms, $[\{(CO)_3Re(\mu_2\text{-}OR)_2Re(CO)_3\}_3(\mu_3\text{-}tpt)_2]$ (**1**, R = C_4H_9; **2**, R = C_8H_{17}; **3**, R = $C_{12}H_{25}$) by solvothermal methods. Fine tuning of the solubility is achieved by tailoring the length of the alkyl chain of the alcohol. Compounds **1**–**3** reported here are the first Re-containing molecular prisms of the $M_6L_2L'_6$ type. In addition, they are the first neutral, prismatic cages without counterions that are highly air and moisture stable. Compounds **2** and **3** are soluble in most common organic solvents and they exhibit a large solvatochromism: the value of λ^{ab}_{max} could be tuned over 125 nm simply by changing the polarity of the solvent.

Introduction

The fabrication of nanometer-scale macrocycles by metal-directed, self-assembled cage compounds is an important component of supramolecular chemistry.[1] There is an upsurge of interest in this area due to the potential applications of these molecules in host-guest chemistry and molecular recognition.[2] Since the construction of larger cages by conventional covalent synthetic procedures is a tedious process, self-assembly techniques have been employed by several groups to obtain the metal-directed assembly of cage compounds.[3−5] The nanosized, spherical-cage Pd^{II} complexes constructed by the metal-induced self-assembly strategy using an exotridentate ligand 2,4,6-tri-4-pyridyl-1,3,5-triazine (tpt) exhibit remarkable thermodynamic stability with a large spherical void.[6] Recently, we have initiated a systematic approach for the design of rhenium-containing, neutral, cage-like supramolecules to explore their applications. In this communication we report the synthesis and characterization of the prismatic cages of the type $M_6L_2L'_6$, $[\{(CO)_3Re(\mu_2\text{-}OR)_2Re(CO)_3\}_3(\mu_3\text{-}tpt)_2]$ (**1**, R = C_4H_9; **2**, R = C_8H_{17}; **3**, R = $C_{12}H_{25}$) made from fourteen components, including the octahedrally coordinated Re metal center, the tpt ligand and an aliphatic alcohol. The advantage here is that the product is obtained in excellent yield in a one-pot synthesis by a self-assembly strategy using solvothermal methods, where the alcohol that is used as solvent also serves as one of the reagents. It is noteworthy that the currently known prismatic supramolecules are either highly charged or encapsulated with counterions.[1h,1i,4d,5d] On the other hand, compounds **1**−**3** are the first neutral, prismatic cages without counterions that are highly air and moisture stable. Compounds **2** and **3** are soluble in most common organic solvents and they show a large solvatochromism.

Results and Discussion

Treatment of $Re_2(CO)_{10}$ with tpt in $CH_3(CH_2)_nOH$ (n = 3, 7, 11) using solvothermal methods at elevated temperatures leads to the formation of the thermodynamically stable cage structures **1**, **2**, and **3**, respectively, in excellent yields (Scheme 1). Compound **1** has been spectroscopically and crystallographically characterized. The ORTEP drawing of **1** (Figure 1) reveals a prismatic cage architecture, where two planar tpt ligands coordinate to six rhenium atoms, which are themselves connected by six butoxy bridges, thereby forming a triangular prismatic cage. Each rhenium atom occupies a corner of the triangular prism and is bonded to one nitrogen atom of the pyridyl group of the tpt ligand, two butoxy groups and three carbonyl groups, maintaining a distorted octahedral geometry. The maximum and minimum rhenium−rhenium distances in the molecule are 13.5 and 3.4 Å, respectively. The three pyridyl rings of the tpt moiety are canted slightly (ca. 15°) from the plane containing the triazine ring. Some groups of researchers have experienced difficulty in growing X-ray quality single crystals of metallomacromolecules containing two to twelve metal centers.[7] In contrast, our synthetic strategy has led to the formation of single crystals of good quality. The electroneutrality of the cage compounds **1**−**3** mitigates

[a] Institute of Chemistry, Academia Sinica,
Taipei 115, Taiwan
Fax: (internat.) +886-2/2783-1237
E-mail: lu@chem.sinica.edu.tw
[b] Department of Chemistry, National Taiwan University,
Taipei 107, Taiwan
[c] Permanent address: Department of Chemistry,
Vivekananda college,
Tiruvedakam West, Madurai, 625 217, India

 © WILEY-VCH Verlag GmbH, 69451 Weinheim, 2001 1434−1948/01/0303−0633 $ 17.50+.50/0

interference of the counterions inside the cavity, which creates problem in most of the sensor studies. The extraordinary affinity of oxygen with rhenium is capitalized in this synthetic approach by utilizing oxo-bridges bearing long, hydrophobic tails. The ^1H and ^{13}C NMR spectral measurements and the FAB-MS data of the cage compounds are in agreement with the proposed structures.

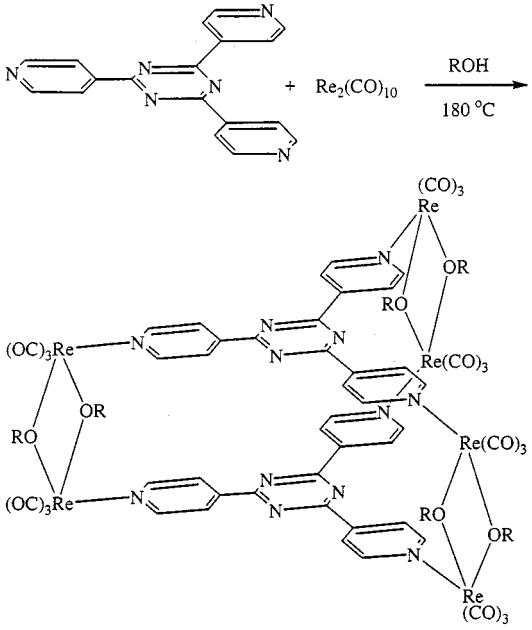

Scheme 1

It has been a challenge to synthesize highly soluble multimetal supramolecules and it is obvious that the solubility of such molecules is of paramount importance for their potential applications. Lees and co-workers have recently reported that complexes with more metal centers have lower solubility; a square complex with four metal components displayed lower solubility than a related triangular complex with three metal components.[7b] Interestingly the solubility of compounds **1**−**3** has been improved enormously by changing the length of the alkyl moiety from butyl to octyl and then to dodecyl. An increase in the chain length of the alkoxo moiety increases the hydrophobicity of the cage, thereby increasing the solubility of the compound in organic solvents. Compounds **2** and **3** are readily soluble in CH_2Cl_2, $(CH_3)_2CO$ and other common organic solvents, whereas **1** is much less soluble. Because of the greater solubility of compounds **2** and **3** they were used for further studies.

Compounds **2** and **3** display an identical CO stretching pattern in their infrared spectra which is similar to that observed for previously reported compounds.[8] The UV/Vis spectra of **2** and **3** in CH_2Cl_2 show an intense, high-energy band at 243 nm and a broad low-energy band at 488 nm. In agreement with previous reports on related systems, the former absorption is assigned to the intraligand $\pi-\pi^*$ transition and the low energy absorption to a metal-to-ligand charge transfer (MLCT) transition.[9] In addition, there is a shoulder at about 265 nm, which may be assigned

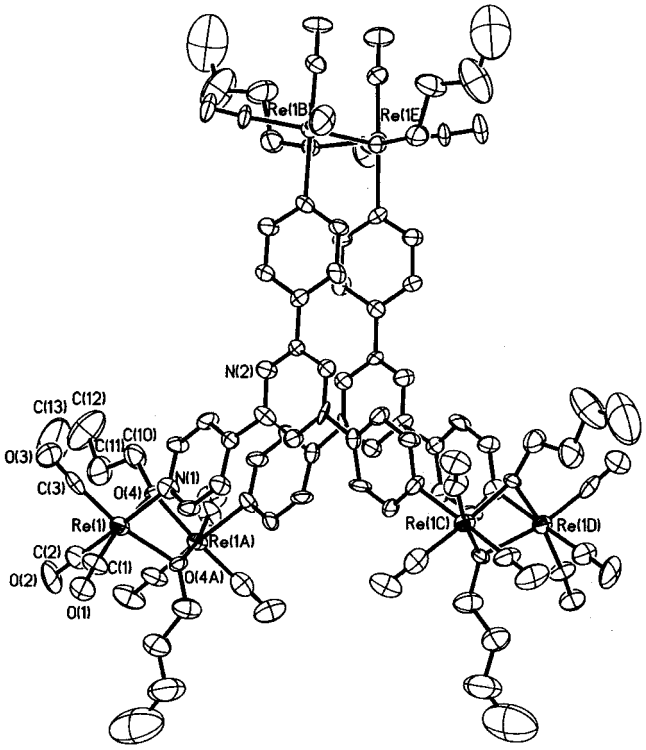

Figure 1. ORTEP diagram of $[\{(CO)_3Re(\mu_2\text{-}OC_4H_9)_2Re(CO)_3\}_3(\mu_3\text{-}tpt)_2]$ (**1**); selected bond lengths (Å) and angles (°): Re(1)−N(1) 2.216(12), Re(1)−O(4) 2.122(10), Re(1)−O(4A) 2.144(9), Re(1)−C(1) 1.98(2), Re(1)−C(2) 1.91(2), Re(1)−C(3) 1.89(2), O(4)−C(10) 1.44(2); O(4)−Re(1)−N(1) 83.1(4), O(4A)−Re(1)−N(1) 82.0(4), Re(1)−O(4)−Re(1A) 105.5(4), O(4)−Re(1)−O(4A) 71.7(4), C(10)−O(4)−Re(1) 124.8(10), C(10)−O(4)−Re(1A) 122.6(10)

to another $\pi-\pi^*$ transition as suggested by Tapolsky et al.[10] The interesting feature that deserves further attention is the observation of the MLCT at a comparatively long wavelength (488 nm), indicating the readily reducible nature of the ligand.[11] We have recorded the absorption spectra of **2** and **3** in a large number of solvents and it is interesting to point out that they show substantial solvatochromism: the value of λ^{ab}_{max} could be tuned over 125 nm, with a corresponding change in the color of the solution from yellow to red, simply by changing the polarity of the solvent (λ^{ab}_{max} values for **2** in DMSO and CCl_4 are 424 and 549 nm, respectively).[12]

In summary we have succeeded in the one-pot, high yield synthesis and characterization of neutral prismatic cages containing hexanuclear rhenium centers linked by six alkoxy bridges bearing lengthy alkyl chains. The presence of the lengthy alkyl chain dramatically increases the hydrophobic nature of the cage-like compounds and hence the solubility, which is a major problem in many of the supramolecular motifs. The interesting photophysical properties and solvatochromism of these supramolecular cage-like structures promise many applications. We are currently extending the metal-induced, self-assembly by solvothermal methods to the synthesis of molecular cages of new architecture from different sets of molecular components, and these results will be reported in a future publication.

Experimental Section

A suspension consisting of a mixture of $Re_2(CO)_{10}$ (98 mg, 0.15 mmol) and tpt (32 mg, 0.10 mmol) in 1-butanol (10 mL) in a 30 mL Teflon flask was placed in a steel bomb. The bomb was placed in an oven maintained at 180 °C for 48 h and then cooled to 25 °C. Good quality, maroon-colored, single crystals of **1** were obtained. The crystals were separated by filtration and washed with 1-butanol. Compounds **2** and **3** were also synthesized by following a similar procedure. The solvent from the reaction mixture was removed by vacuum distillation and the residue was redissolved in CH_2Cl_2 and passed through a short silica gel column to get pure **2** and **3**. Yield: **1**, 109 mg, 81%; **2**, 124 mg, 82%; **3**, 142 mg, 85%.

[{(CO)$_3$Re(μ$_2$-OC$_4$H$_9$)$_2$Re(CO)$_3$}$_3$(μ$_3$-tpt)$_2$] (1): $C_{78}H_{78}N_{12}O_{24}Re_6$ (2684.79): calcd. C 34.89, H 2.93, N 6.26; found C 35.06, H 2.94, N 6.40. − Crystal data ($C_{78}H_{78}N_{12}O_{24}Re_6$): Crystal dimensions 0.20 × 0.10 × 0.03 mm, rhombohedral, space group *R*3(bar)*c*, $a = b = 23.4486(9)$, $c = 27.6604(11)$ Å, $\alpha = \beta = 90°$, $\gamma = 120°$, $V = 13171.1(9)$ Å^3, $Z = 6$, $T = 150(1)$ K, $\rho_{calcd.} = 2.031$ Mg/m^3, $\mu = 8.316$ mm^{-1}, 9628 total reflections, 2539 independent reflections which were used in refinement. The structure was solved to $R1 = 0.0865$ and $wR2 = 0.1166$.

[{(CO)$_3$Re(μ$_2$-OC$_8$H$_{17}$)$_2$Re(CO)$_3$}$_3$(μ$_3$-tpt)$_2$] (2): IR (CH_2Cl_2): ν_{CO} = 2022 (s), 2009 (m), 1913 (m), 1890 (vs) cm^{-1}. − ^{1}H NMR (300 MHz, $CDCl_3$): δ = 8.72 (d, ^3J = 6.5 Hz, 12 H, H^3), 8.24 (d, ^3J = 6.5 Hz, 12 H, H^2), 4.43 (t, ^3J = 8.0 Hz, 12 H), 2.15 (m, 12 H), 1.49 (m, 36 H), 1.25 (m, 24 H), 0.94 (t, ^3J = 6.7 Hz, 18 H). − ^{13}C NMR (75 MHz, $CDCl_3$): δ = 197.2 (s, CO), 170.1 (C, triazine), 153.5 (C^3), 142.2 (C^1), 123.2 (C^2), 82.9 (CH_2), 34.2 (CH_2), 31.9 (CH_2), 29.7 (CH_2), 29.4 (CH_2), 25.3 (CH_2), 22.7 (CH_2), 14.2 (CH_3). − UV/Vis (CH_2Cl_2): λ_{max} (nm) = 488 (MLCT), 243 (LIG). − $C_{108}H_{126}N_{12}O_{24}Re_6$ (3021.43): calcd. C 40.55, H 4.20, N 5.56; found C 40.56, H 4.23, N 5.53. − MS (FAB, ^{187}Re): *m*/*z* = 3024 [M$^+$].

[{(CO)$_3$Re(μ$_2$-OC$_{12}$H$_{25}$)$_2$Re(CO)$_3$}$_3$(μ$_3$-tpt)$_2$] (3): IR (CH_2Cl_2): ν_{CO} = 2022 (s), 2009 (m), 1913 (m), 1890 (vs) cm^{-1}. − ^{1}H NMR (300 MHz, $CDCl_3$): δ = 8.72 (d, ^3J = 6.5 Hz, 12 H, H^3), 8.24 (d, 12 H, H^2), 4.42 (t, ^3J = 8.0 Hz, 12 H), 2.15 (m, 12 H), 1.48 (m, 24 H), 1.29 (m, 84 H), 0.88 (t, ^3J = 6.2 Hz, 18 H). − ^{13}C NMR (75 MHz; $CDCl_3$): δ = 197.2, 197.1 (s, 1:2 CO), 170.1 (C, triazine), 153.5 (C^3), 142.1 (C^1), 123.2 (C^2), 82.8 (CH_2), 34.1 (CH_2), 31.9 (CH_2), 31.5 (CH_2), 29.7 (2 CH_2), 29.6 (2 CH_2), 29.3 (CH_2), 25.2 (CH_2), 22.7 (CH_2), 14.1 (CH_3). − UV/Vis (CH_2Cl_2): λ_{max} (nm) = 488 (MLCT), 242 (LIG). − $C_{126}H_{174}N_{12}O_{24}Re_6$ (3358.08): calcd. C 44.99, H 5.22, N 5.00; found C 45.52, H 5.30, N 4.92. − MS (FAB, ^{187}Re): *m*/*z* = 3360 [M$^+$].

Crystallographic data (excluding structure factors) for the structure reported in this paper have been deposited with the Cambridge Crystallographic Data Centre as supplementary publication no. CCDC-149282 and -149283 (**1**). Copies of the data can be obtained free of charge on application to CCDC, 12 Union Road, Cambridge CB2 1EZ, UK [Fax: (internat.) +44-1223/336-033; E-mail: deposit@ccdc.cam.ac.uk].

Acknowledgments

We thank Academia Sinica and the National Science Council of Taiwan for financial support. We are also grateful to Professor Sunney I. Chan for valuable discussions.

[1] [1a] P. N. W. Baxter, J. -M. Lehn, G. Baum, D. Fenske, *Chem. Eur. J.* **1999**, *5*, 102−112. − [1b] B. Olenyuk, J. A. Whiteford, A. Fechtenkotter, P. J. Stang, *Nature* **1999**, *398*, 796−799. − [1c] N. Takeda, K. Umemoto, K. Yamaguchi, M. Fujita, *Nature* **1999**, *398*, 794−796. − [1d] R. W. Saalfrank, B. Demleitner, *Ligand and Metal Control of Self-Assembly in Supramolecular Chemistry*, in *Perspectives in Supramolecular Chemistry* (Ed.: J. P. Sauvage). Vol. *5* (*Transition Metals in Supramolecular Chemistry*), Wiley-VCH, Weinheim, **1999**, pp 1−51. − [1e] B. F. Abrahams, S. J. Egan, R. Robson, *J. Am. Chem. Soc.* **1999**, *121*, 3535−3536. − [1f] P. J. Stang, B. Olenyuk, *Organometallics* **1997**, *16*, 3094−3096. − [1g] P. Jacopozzi, E. Dalcanale, *Angew. Chem.* **1997**, *109*, 665−667; *Angew. Chem. Int. Ed. Engl.* **1997**, *36*, 613−615. − [1h] M. Fujita, S. Nagao, K. Ogura, *J. Am. Chem. Soc.* **1995**, *117*, 1649−1650. − [1i] P. Baxter, J. -M. Lehn, A. DeCian, J. Fischer, *Angew. Chem.* **1993**, *105*, 92; *Angew. Chem. Int. Ed. Engl.* **1993**, *32*, 69−72.

[2] [2a] L. R. MacGillivray, J. L. Atwood, *Angew. Chem.* **1999**, *111*, 1080−1096. *Angew. Chem. Int. Ed. Engl.* **1999**, *38*, 1018−1033. − [2b] T. Kusukawa, M. Fujita, *J. Am. Chem. Soc.* **1999**, *121*, 1397−1398. − [2c] F. Ibukuro, T. Kusukawa, M. Fujita, *J. Am. Chem. Soc.* **1998**, *120*, 8561−8562. − [2d] D. L. Caulder, R. E. Powers, T. N. Parac, K. N. Raymond, *Angew. Chem.* **1998**, *110*, 1940−1943; *Angew. Chem. Int. Ed. Engl.* **1998**, *37*, 1840−1843. − [2e] S. Mann, G. Huttner, L. Zsolnai, K. Heinze, *Angew. Chem.* **1996**, *108*, 2983−2984; *Angew. Chem. Int. Ed. Engl.* **1996**, *35*, 2808−2809.

[3] [3a] J. Yoon, D. J. Cram, *J. Am. Chem. Soc.* **1997**, *119*, 11796−11806. − [3b] J. Yoon, D. J. Cram, *Chem. Commun.* **1997**, 497−498. − [3c] B. -H. Huisman, D. M. Rudkevich, F. C. J. M. van Veggel, D. N. Reinhoudt, *J. Am. Chem. Soc.* **1996**, *118*, 3523−3524. − [3d] J. R. Fraser, B. Borecka, J. Trotter, J. C. Sherman, *J. Org. Chem.* **1995**, *60*, 1207−1213. − [3e] P. Timmerman, W. Verboom, F. C. J. M. van Veggel, J. P. M. van Duynhoven, D. N. Reinhoudt, *Angew. Chem.* **1994**, *106*, 2437; *Angew. Chem. Int. Ed. Engl.* **1994**, *33*, 2345−2348. − [3f] D. J. Cram, *Nature* **1992**, *356*, 29−36.

[4] [4a] S. Leininger, B. Olenyuk, P. J. Stang, *Chem. Rev.* **2000**, *100*, 853−908. − [4b] E. Uller, B. Demleitner, I. Bernt, R. W. Saalfrank, *Synergistic Effect of Serendipity and Rational Design in Supramolecular Chemistry* (Eds.: M. Fujita), Vol. *96*, **2000**, pp 149−175. − [4c] G. F. Swiegers, T. J. Malefetse, *Chem. Rev.* **2000**, *100*, 3483−3538. − [4d] P. N. W. Baxter, J. -M. Lehn, B. O. Kneisel, G. Baum, D. Fenske, *Chem. Eur. J.* **1999**, *5*, 113−120. − [4e] D. L. Caulder, K. N. Raymond, *Acc. Chem. Res.* **1999**, *32*, 975−982. − [4f] M. Fujita, *Acc. Chem. Res.* **1999**, *32*, 53−61. − [4g] M. Fujita, *Chem. Soc. Rev.* **1998**, *27*, 417−425. − [4h] M. Fujita, K. Ogura, *Bull. Chem. Soc. Jpn.* **1996**, *69*, 1471−1482.

[5] [5a] J. S. Fleming, K. L. V. Mann, C. -A. Carraz, E. Psillakis, J. C. Jeffery, J. A. McCleverty, M. D. Ward, *Angew. Chem.* **1998**, *110*, 1315−1318; *Angew. Chem. Int. Ed. Engl.* **1998**, *37*, 1279−1281. − [5b] S. L. James, D. M. P. Mingos, A. J. P. White, D. J. Williams, *Chem. Commun.* **1998**, 2323−2324. − [5c] S. Roche, C. Haslam, H. Adams, S. L. Heath, J. A. Thomas, *Chem. Commun.* **1998**, 1681−1682. − [5d] P. Jacopozzi, E. Dalcanale, *Angew. Chem.* **1997**, *109*, 665−667; *Angew. Chem. Int. Ed. Engl.* **1997**, *36*, 613−615. − [5e] C. M. Hartshorn, P. J. Steel, *Chem. Commun.* **1997**, 541−542. − [5f] R. W. Saalfrank, R. Burak, A. Breit, D. Stalke, R. H. Irmer, J. Daub, M. Porsch, E. Bill, M. Muther, A. X. Trautwein, *Angew. Chem.* **1994**, *106*, 1697; *Angew. Chem. Int. Ed. Engl.* **1994**, *33*, 1621−1623. − [5g] R. W. Saalfrank, A. Stark, M. Bremer, H. -U. Hummel, *Angew. Chem.* **1990**, *102*, 292; *Angew. Chem. Int. Ed. Engl.* **1990**, *29*, 311−314.

[6] [6a] M. Fujita, D. Ogura, M. Miyazawa, H. Oka, K. Yamaguchi, K. Ogura, *Nature* **1995**, *378*, 469−471. − [6b] M. Fujita, S. -Y. Yu, T. Kusukawa, H. Funaki, K. Ogura, K. Yamaguchi, *Angew. Chem.* **1998**, *110*, 2192−2196; *Angew. Chem. Int. Ed. Engl.* **1998**, *37*, 2082−2085. − [6c] M. Fujita, N. Fujita, K. Ogura, K. Yamaguchi, *Nature* **1999**, *400*, 52−55. − [6d] T. Kusukawa, M. Fujita, *Angew. Chem.* **1998**, *110*, 3327−3329; *Angew. Chem. Int. Ed. Engl.* **1998**, *37*, 3142−3144.

[7] [7a] S. -S. Sun, A. S. Silva, I. M. Brinn, A. J. Lees, *Inorg. Chem.* **2000**, *39*, 1344−1345. − [7b] S. -S. Sun, A. J. Lees, *Inorg. Chem.* **1999**, *38*, 4181−4182. − [7c] E. C. Constable, E. Schofield, *Chem. Commun.* **1998**, 403−404. − [7d] J. Manna, C. J. Kuehl, J. A. Whiteford, P. J. Stang, D. C. Muddiman, S. A. Hofstadler, R. D. Smith, *J. Am. Chem. Soc.* **1997**, *119*, 11611−11619.

[8] [8a] K. D. Benkstein, J. T. Hupp, C. L. Stern, *Inorg. Chem.* **1998**, *37*, 5404−5405. − [8b] C. Jiang, Y. -S. Wen, L. -K. Liu, T. S. A. Hor, Y. K. Yan, *Organometallics* **1998**, *17*, 173−181. − [8c] M. A. El-Sayed, H. D. Kaesz, *Inorg. Chem.* **1963**, *2*, 158−162.
[9] [9a] A. J. Lees, *Chem. Rev.* **1987**, *87*, 711−743. − [9b] T. Rajendran, B. Manimaran, F. -Y. Lee, G. -H. Lee, S. -M. Peng, C. W. Wong, K. -L. Lu, *Inorg. Chem.* **2000**, *39*, 2016−2017.
[10] [10a] G. Tapolsky, R. Duesing, T. J. Meyer, *J. Phys. Chem.* **1991**, *95*, 1105−1112. − [10b] G. Tapolsky, R. Duesing, T. J. Meyer, *Inorg. Chem.* **1990**, *29*, 2285−2297. − [10c] G. Tapolsky, R. Duesing, T. J. Meyer, *J. Phys. Chem.* **1989**, *93*, 3885−3887.
[11] [11a] S. Belanger, M. Gilbertson, D. I. Yoon, C. L. Stern, X. Dang, J. T. Hupp, *J. Chem. Soc., Dalton Trans.* **1999**, 3407−3412. − [11b] S. M. Woessner, J. B. Helms, J. F. Houlis, B. P. Sullivan, *Inorg. Chem.* **1999**, *38*, 4380−4381. − [11c] K. D. Benkstein, J. T. Hupp, C. L. Stern, *J. Am. Chem. Soc.* **1998**, *120*, 12982−12983. − [11d] S. M. Woessner, J. B. Helms, Y. Shen, B. P. Sullivan, *Inorg. Chem.* **1998**, *37*, 5406−5407. − [11e] R. V. Slone, D. I. Yoon, R. M. Calhoun, J. T. Hupp, *J. Am. Chem. Soc.* **1995**, *117*, 11813−11814. − [11f] P. J. Giordano, M. S. Wrighton, *J. Am. Chem. Soc.* **1979**, *101*, 2888−2897.
[12] C. Reichardt, *Chem. Rev.* **1994**, *94*, 2319−2358.

Received November 3, 2000
[I00426]

Oxa- and Azacalixarenes as Ligands for Uranyl Ions − Evidence for Two Different Complexation Modes

Pierre Thuéry,*[a] Martine Nierlich,[a] Jacques Vicens,[b] Bernardo Masci,[c] and Hiroyuki Takemura[d]

Keywords: Uranium / Calixarenes / Zwitterion / Crystal structure

The first crystal structures are reported for uncomplexed parent tetrahomodioxa- and tetrahomodiazacalix[4]arene compounds and their 1:1 uranyl complexes. A 1:1 uranyl complex is also reported for a hexahomotriazacalix[3]arene. While analogous features are observed for the uncomplexed dioxa- and diazacalixarenes, completely different coordination modes are observed in their uranyl complexes. The complex of *p-tert*-butyltetrahomodioxacalix[4]arene is obtained in the presence of triethylamine and consists of an anionic core in which the cation is located at the centre of the lower rim, as is frequently observed. Both *p*-chloro-*N*-benzyl-hexahomotriazacalix[3]arene and *p*-methyl-*N*-benzyl-tetrahomodiazacalix[4]arene react with uranyl nitrate without adding a basic agent. The resulting 1:1 complexes are neutral, the cation being located outside the macrocycle and bound to two phenoxide groups of its zwitterionic form and to the nitrate counter-ions. The difference in coordination mode between homooxa- and homoazacalixarene complexes is attributed to the electrostatic repulsion between the uranyl ions and the ammonium groups located around the lower rim in the latter case, which prevents a close approach of the complexed cation.

Introduction

The work of Shinkai et al., who demonstrated about ten years ago the "uranophile" potential of water-soluble calixarenes, generated an interest that led to the investigation of uranyl complexes of calixarenes.[1] Unfortunately, the crystal structures of the complexes involved have never been elucidated due to the difficulties encountered in growing single crystals. However, since then a lot of structural information has been gathered about the uranyl complexes of parent calix[*n*]arenes (*n* between 5 and 9 and *n* = 12) and homooxacalixarenes,[2] whereas only one crystal structure involving coordinating pendent arms grafted on a calix[4]arene has been reported.[3] Parent calixarenes and homooxacalixarenes readily form uranyl complexes in a basic medium. These are either mononuclear with the smallest calixarenes in cone conformation (*p-tert*-butyldihomooxacalix[4]arene,[2a] *p-tert*-butylhexahomotrioxacalix[3]arene,[2i] *p-tert*-butylcalix[5]arene[2e]) or polynuclear with larger, flattened calixarenes (*p-tert*-butylcalix[8]arene,[2b,2c,2k] *p-tert*-butylcalix[9]arene,[2k] *p-tert*-butylcalix[12]arene[2j]). *p-tert*-Butylcalix[6]arene gives only external complexes with a 2:1,[2g] 2:2[2d] or 3:3[2k] metal:ligand stoichiometry. Calix[7]arene is another peculiar case, being able to engage in complexation only one of its two (trimeric and tetrameric) subunits,[2f] or both.[2h] The complex formed by *p-tert*-butylhexahomotrioxacalix[3]arene (ligand **1** in Scheme 1) is of particular interest since it constitutes the first and, up to now, the only example of a pseudo-trigonal equatorial coordination for the uranyl ion.[2i]

The homooxa- and homoazacalixarenes are less rigid than calixarenes, as shown by ^{1}H NMR spectroscopic measurements in the case of the former.[4] Furthermore, they possess two different kinds of potential binding sites, and homoazacalixarenes, which were first synthesized some years ago,[5] can bear various substituents on the amine nitrogen atom. The metal-ion complexes of homooxacalixarenes thus far reported have been obtained classically in a basic medium.[2a,2i,6] In order to further investigate the complexing properties of these ligands, we synthesized, in the presence of triethylamine, the uranyl complex of another oxacalixarene, *p-tert*-butyltetrahomodioxacalix[4]arene (**2**), the structure of which is reported herein as well as that of the uncomplexed ligand. We have recently begun the investigation of azacalixarenes as ligands and reported the crystal structures of *p*-chloro-*N*-benzylhexahomotriazacalix[3]arene (**3**) and of its mononuclear complex with neodymium nitrate.[7] This work demonstrated a peculiarity of the homoazacalixarenes as ligands in that they are able to com-

[a] CEA/Saclay, SCM (CNRS URA 331)
Bât. 125, 91191 Gif-sur-Yvette, France
Fax: (internat.) +33-1/6908-6640
E-mail: thuery@drecam.cea.fr
[b] ECPM, Laboratoire de Chimie des Interactions Moléculaires Spécifiques (CNRS UMR 7512)
25 rue Becquerel, 67087 Strasbourg, France
Fax: (internat.) +33-3/8813-7813
E-mail: vicens@chimie.u-strasbg.fr
[c] Dipartimento di Chimica and Centro CNR di Studio sui Meccanismi di Reazione, Università "La Sapienza"
Box 34, Roma 62, P.le Aldo Moro 5, 00185 Roma, Italy
Fax: (internat.) +39-06/490-631
E-mail: bmasci@axrma.uniroma1.it
[d] Department of Chemistry, Faculty of Science, Kyushu University
Ropponmatsu 4-2-1, Chuo-ku, Fukuoka 810−8560, Japan
Fax: (internat.) +81-92/726-4755
E-mail: takemura@rc.kyushu-u.ac.jp

 © WILEY-VCH Verlag GmbH, 69451 Weinheim, 2001 1434−1948/01/0303−0637 $ 17.50+.50/0

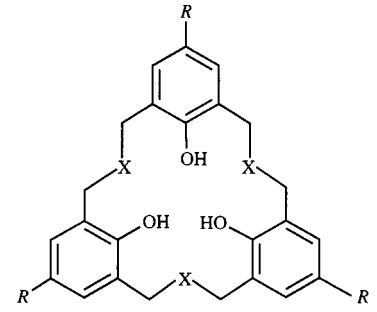

1 X = O, *R* = *tert*-butyl

3 X = N-benzyl, *R* = Cl

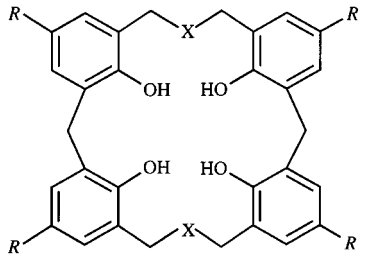

2 X = O, *R* = *tert*-butyl

4 X = N-benzyl, *R* = methyl

Scheme 1. The homooxa- and homoazacalixarenes under study

plex lanthanide ions without the addition of a basic agent such as the commonly used triethylamine or 1,4-diazabicyclo[2.2.2]octane (DABCO), owing to the displacement of the protons from oxygen to nitrogen atoms (zwitterionic or amphiionic form) upon complexation. We report herein the synthesis in a neutral medium as well as the crystal structures of the uranyl complexes of two azacalixarenes, **3** and *p*-methyl-*N*-benzyltetrahomodiazacalix[4]arene (**4**), and the crystal structure of the uncomplexed molecule **4**. Unfortunately, we have not succeeded in growing single crystals of the complex species obtained with **3** and **4** in a basic medium, for comparative purposes. To the best of our knowledge, the crystal structures reported herein are the first ones for parent tetrahomodioxa- and tetrahomodiazacalix[4]arenes and their complexes.

Results and Discussion

Uncomplexed Calixarenes

The asymmetric unit in **2**·2CH_3CN (**5**) is composed of half a molecule, located around a binary axis perpendicular to its mean plane (Figure 1). The overall shape is that of a very distorted cone, and is determined by an intramolecular hydrogen bonding array which links both phenolic and ether groups (Table 1). The two ether links, which give the molecule its high flexibility, are positioned so as to bring the ether atom O(2) and its symmetry-related equivalent O(2′) close to the protons of the phenolic atoms O(3) and O(3′). However, the macrocycle is not large enough to prevent the formation of a cyclic hydrogen bonding array link-

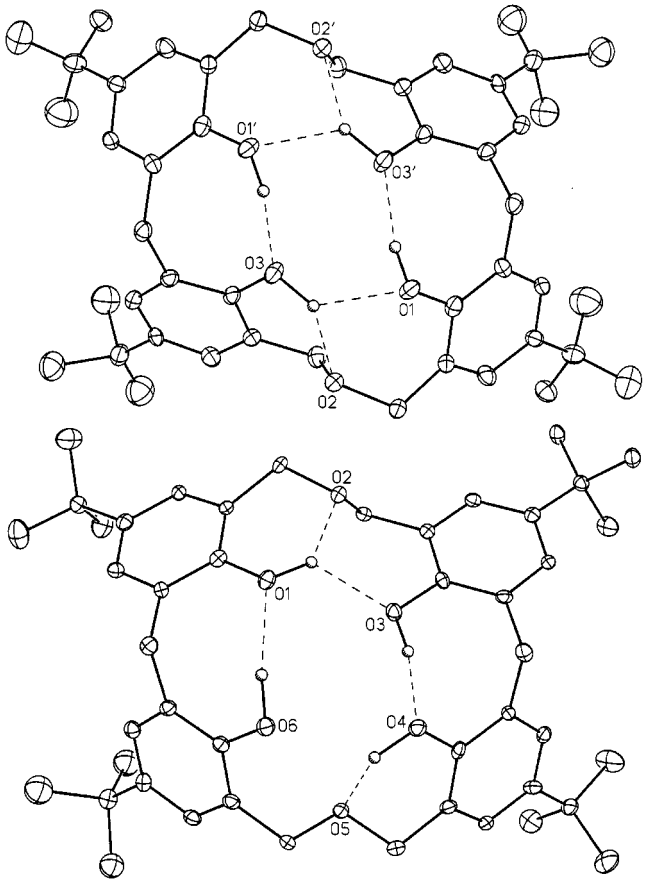

Figure 1. View of *p-tert*-butyltetrahomodioxacalix[4]arene **2** in **5** (top) and in **6** (bottom), showing the difference in hydrogen bonding patterns; hydrogen bonds in dashed lines; hydroxyl protons represented as small spheres of arbitrary radii; other hydrogen atoms and solvent molecules omitted for clarity; symmetry code: ′ = *y*, *x*, −*z*

ing the four phenolic oxygen atoms, with O(3) and O(3′) giving a bifurcated hydrogen bond, the O(3)···O(2) bond being stronger than O(3)···O(1). The calixarene shape can be characterized by the values of the dihedral angles between the phenolic rings and the mean plane defined [± 0.339(4) Å] by the phenolic oxygen atoms, which are 38.8(2) and 47.2(2)° [mean value 43(6)°]. The cup shape is sufficiently deep for the two acetonitrile molecules (not involved in hydrogen bonding) to be included in the cavity: such a situation has already been observed in the case of *p-tert*-butylcalix[6]arene,[8] which confirms the similarity between the two ligands in terms of cavity size.[9]

The asymmetric unit in **2**·2.5C_5H_5N (**6**) is composed of one molecule, represented in Figure 1, the overall features of which are analogous to those in **5**. However, the calixarene conformation is different in the surroundings of atom O(5), which results in a slight enlargement of the macrocycle and the breaking of one of the hydrogen bonds. The interest of this structure is to show that, depending upon the solvent, it is possible to observe conformations of the ether bridge which do not allow bifurcate hydrogen bonds. The values of the dihedral angles between the phenolic rings and the mean plane defined [± 0.188(2) Å] by the phenolic

Table 1. Selected bond lengths (Å) and angles (°)

Uranium environment							
8							
U−O(1)	2.272(4)	U−O(6)	2.333(4)	O(1)−U−O(3)	94.4(2)	O(6)−U−O(1)	84.8(2)
U−O(3)	2.252(4)	U−O(7)	1.795(4)	O(3)−U−O(4)	87.5(2)	O(7)−U−O(8)	178.3(2)
U−O(4)	2.269(4)	U−O(8)	1.804(4)	O(4)−U−O(6)	93.3(2)		
9							
U−O(1)	2.284(7)	U−O(5)	1.772(7)	U−O(9)	2.578(7)	O(6)−U−O(7)	49.2(2)
U−O(3)	2.278(7)	U−O(6)	2.576(7)	U−O(10)	2.586(7)	O(9)−U−O(10)	49.3(2)
U−O(4)	1.771(8)	U−O(7)	2.586(9)	O(1)−U−O(3)	75.1(3)	O(4)−U−O(5)	175.0(3)
10							
U−O(1)	2.234(9)	U−O(6)	1.758(9)	U−O(10)	2.398(10)	O(5)−U−O(6)	176.4(4)
U−O(2)	2.269(8)	U−O(7)	2.530(9)	O(1)−U−O(2)	78.9(3)		
U−O(5)	1.757(8)	U−O(8)	2.504(10)	O(7)−U−O(8)	50.3(4)		
Hydrogen bonds[a]							
5							
O(1)···O(3′)	2.787(7)	O(1)−H	0.94	H···O(3′)	1.91	O(1)−H···O(3′)	155
O(3)···O(1)	2.915(7)	O(3)−H	1.09	H···O(1)	2.08	O(3)−H···O(1)	131
O(3)···O(2)	2.753(7)			H···O(2)	1.89	O(3)−H···O(2)	133
6							
O(1)···O(2)	2.743(5)	O(1)−H	1.11	H···O(2)	1.81	O(1)−H···O(2)	139
O(1)···O(3)	2.989(5)			H···O(3)	2.16	O(1)−H···O(3)	129
O(3)···O(4)	2.763(5)	O(3)−H	1.05	H···O(4)	1.74	O(3)−H···O(4)	166
O(4)···O(5)	2.657(5)	O(4)−H	1.09	H···O(5)	1.79	O(4)−H···O(5)	133
O(6)···O(1)	3.147(5)	O(6)−H	1.09	H···O(1)	2.23	O(6)−H···O(1)	140
7							
O(1)···O(4)	2.861(4)	O(1)−H	0.88	H···O(4)	1.99	O(1)−H···O(4)	177
O(2)···O(1)	2.903(3)	O(2)−H	1.08	H···O(1)	2.49	O(2)−H···O(1)	102
O(2)···N(1)	2.692(4)			H···N(1)	1.64	O(2)−H···N(1)	165
O(3)···O(2)	2.820(3)	O(3)−H	0.94	H···O(2)	1.89	O(3)−H···O(2)	173
O(4)···O(3)	2.946(3)	O(4)−H	1.05	H···O(3)	2.48	O(4)−H···O(3)	106
O(4)···N(2)	2.713(4)			H···N(2)	1.85	O(4)−H···N(2)	137
8							
N(1)···O(8)	2.728(7)	N(1)−H	0.99	H···O(8)	1.77	N(1)−H···O(8)	163
N(2)···O(6)	2.715(7)	N(2)−H	1.05	H···O(6)	1.72	N(2)−H···O(6)	157
9							
N(1)···O(1)	2.95(1)	N(1)−H	0.92	H···O(1)	2.44	N(1)−H···O(1)	116
N(1)···O(2)	2.64(1)			H···O(2)	1.91	N(1)−H···O(2)	136
N(2)···O(2)	2.61(1)	N(2)−H	1.11	H···O(2)	1.74	N(2)−H···O(2)	132
N(2)···O(3)	2.97(1)			H···O(3)	2.20	N(2)−H···O(3)	124
N(3)···O(1)	2.91(1)	N(3)−H	1.05	H···O(1)	2.37	N(3)−H···O(1)	111
N(3)···O(3)	2.84(1)			H···O(3)	1.92	N(3)−H···O(3)	145
10							
N(1)···O(1)	2.88(1)	N(1)−H	0.99	H···O(1)	2.21	N(1)−H···O(1)	124
N(1)···O(2)	2.86(1)			H···O(2)	2.14	N(1)−H···O(2)	128
N(2)···O(3)	2.78(1)	N(2)−H	0.97	H···O(3)	2.07	N(2)−H···O(3)	128
N(2)···O(4)	2.79(1)			H···O(4)	1.97	N(2)−H···O(4)	141
O(3)···O(2)	2.62(1)	O(3)−H	1.09	H···O(2)	1.66	O(3)−H···O(2)	145
O(4)···O(1)	2.69(1)	O(4)−H	1.03	H···O(1)	1.81	O(4)−H···O(1)	145

[a] Symmetry code: $' = y, x, -z$.

oxygen atoms are 38.5(2), 22.7(2), 46.8 (2) and 70.6(1)°, which indicate a strong deviance with respect to a regular cone shape. Two pyridine molecules, roughly orthogonal to each other and not involved in hydrogen bonding, are located in the calixarene cavity.

The asymmetric unit in **4**·CH_3CN (**7**) comprises one molecule, without any crystallographic symmetry (Figure 2). The conformation of the calixarene is strikingly similar to that observed in **5**, with a similar hydrogen bonding pattern. The hydrogen bonds linking the phenolic oxygen atoms between them [O(1)···O(2) and O(3)···O(4)] are however much weaker than their counterparts in **5**: such a predominance of OH···N bonds over OH···O ones has already been encountered in **3**, but was less pronounced.[7] The values of the dihedral angles between the four phenolic rings and the mean plane defined [± 0.321(1) Å] by the phenolic oxygen atoms are 41.1(1), 43.0(1), 30.0(1) and 41.1(1)°, [mean value 39(6)°] comparable to those in **5**. However, in the present case, the cavity, which is not as deep as in **5** and **6**, due to the replacement of *tert*-butyl by methyl substituents, is empty. The benzyl substituents are directed towards the exterior of the macrocycle, on the lower rim side.

If the uncomplexed oxa- and azacalixarenes present closely related features, the basic nature of the nitrogen atoms in the latter results in different complexing behaviours, exemplified hereafter in the case of uranyl ions.

Uranyl Ion Complexes

The complexation of one uranyl ion by **2** in the presence of NEt_3 to give $[UO_2(\mathbf{2} - 4H)]^{2-}(HNEt_3^+)_2$·$CHCl_3$·

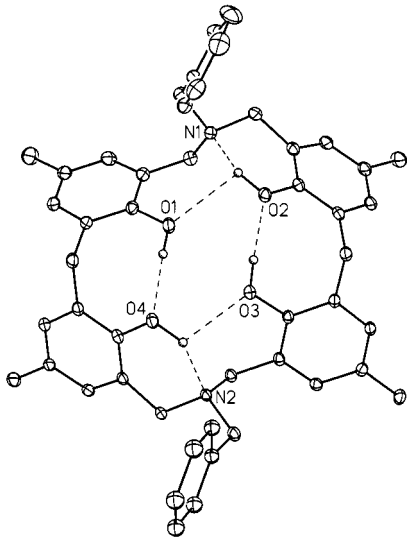

Figure 2. View of *p*-methyl-*N*-benzyltetrahomodiazacalix[4]arene **4** in **7**; hydrogen bonds in dashed lines; hydroxyl protons represented as small spheres of arbitrary radii; other hydrogen atoms and solvent molecule omitted for clarity; only the main component of disordered atoms is represented

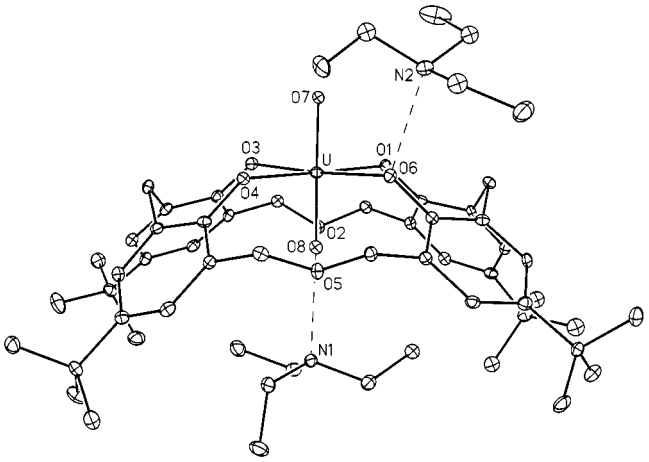

Figure 3. View of the "internal" uranyl ion complex of *p-tert*-butyltetrahomodioxacalix[4]arene **8**; hydrogen bonds in dashed lines; hydrogen atoms and solvent molecules omitted for clarity; only the main component of disordered atoms is represented

CH_3CN (**8**) is accompanied by a conformational change of the macrocycle. As illustrated in Figure 3, the cation is located at the centre of the lower rim, with its main axis perpendicular to it, and bound to the four deprotonated oxygen atoms [mean U−O distance 2.28(3) Å, as observed previously for phenoxide groups[2]]. The molecule presents two orthogonal non-crystallographic symmetry planes with the uranyl axis at their intersection and passing through either the methylene or the ether bridges. Such a square planar equatorial geometry is rather common in calixarene complexes, having been observed in the complexes of *p-tert*-butyldihomooxacalix[4]arene,[2a] *p-tert*-butylcalix[7]arene[2f] and *p*-benzylcalix[7]arene,[2h] but it is rarely so regular [mean $O_{phenol}-U-O_{phenol}$ angle between adjacent phenolic units 90(5)°, mean $O_{uranyl}-U-O_{phenol}$ angle 90(2)°]. In particular, with respect to *p-tert*-butyldihomooxacalix[4]arene, the presence of a second ether link in **2** permits a more symmetrical geometry around the cation. The ether oxygen atoms were not coordinated in the two other uranyl complexes of oxacalixarenes reported.[2a,2i] Also, in the present case, the two ether oxygen atoms are clearly non bonding, being at distances of 3.832(4) and 3.820(4) Å from the uranium atom [values larger than in the previous cases: 3.534(8)[2a] and 3.1(1)[2i] Å] and at distances of 1.812(6) and 1.893(6) Å from the mean plane defined [± 0.027(2) Å] by the four coordinating oxygen atoms. The disruption of the hydrogen bonding pattern of **2** and the location of the four phenolic oxygen atoms in a plane result in a conformation different from those observed in **5** and **6**. The values of the dihedral angles between the four phenolic rings and the mean plane defined by the phenolic oxygen atoms are 47.9(2), 40.0(1), 48.3(1) and 42.9(2)° [mean value 45(4)°]. The two triethylammonium counter-ions in **8** are located as frequently observed, one of them hydrogen bonded to an uranyl oxo atom and included in the calixarene cavity and the other hydrogen bonded to a phenoxide group. We have mentioned above the similarity in size between *p-tert*-butyltetrahomodioxacalix[4]arene and *p-tert*-butylcalix[6]arene; however, these ligands appear very different from equivalent towards uranyl complexation, since the latter gives "external" complexes only.[2d,2g,2k]

Whereas the uranyl ion is located at the centre of the lower rim in the three complexes of oxacalixarenes presently reported, the coordination mode in the complex of the azacalixarene **3**, obtained without a basic agent being added, is completely different. The asymmetric unit in $[UO_2(NO_3)_2\mathbf{3}]\cdot C_5H_5N\cdot CHCl_3$ (**9**) comprises one molecule (Figure 4), which does not possess any true symmetry element, but presents a pseudo symmetry plane containing the atom O(2) and the uranyl ion. The cation is located outside the lower rim array and is bound to two phenoxide ions

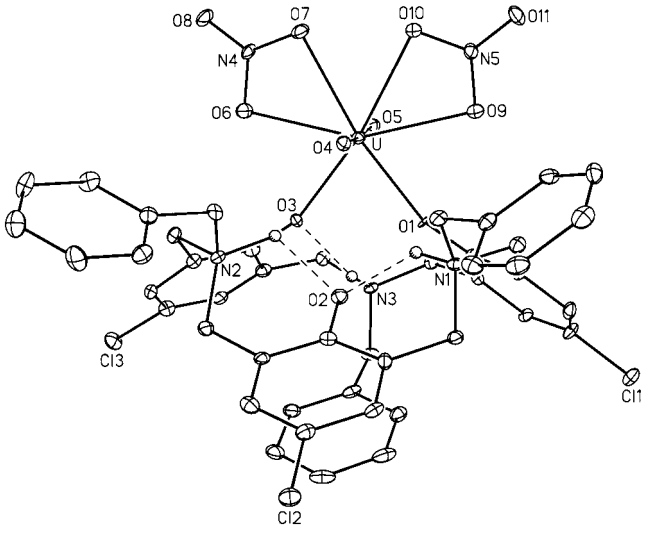

Figure 4. View of the "external" uranyl ion complex of *p*-chloro-*N*-benzylhexahomotriazacalix[3]arene **9**; hydrogen bonds in dashed lines; protons of the ammonium groups represented as small spheres of arbitrary radii; other hydrogen atoms and solvent molecules omitted for clarity

only, with its axis roughly parallel to the mean plane of the molecule. The coordination sphere is completed by two bidentate nitrate ions. Such a six-coordinate environment is unusual in uranyl complexes of calixarenes and is due to the small-bite nature of nitrate ions. The uranium atom is located at 1.556(7) Å from the mean plane defined by the three phenoxide oxygen atoms, a value comparable to that of the neodymium(III) complex of **3** [1.591(2) Å][7] which presents many similarities with **9** (an obvious difference being that the neodymium ion is bound to the three phenoxide oxygen atoms). In both complexes, the three phenolic protons have been transferred to the amine groups upon complexation. An asymmetric array of hydrogen bonds links the ammonium and phenoxide groups in **9**, as in the Nd^{3+} complex. The values of the three dihedral angles between the phenolic rings and the mean plane defined by the three phenolic oxygen atoms are 64.6(3), 2.23(9) and 60.2(3)°: those values are different from those in both the uncomplexed molecule **3** and its Nd^{3+} complex. In the latter case, one of the rings was nearly parallel to the mean plane, as the one corresponding to the non-coordinated phenolic group in **9**, but the two other rings are much more "vertical" in **9**. Two benzyl substituents are located on the lower rim side and directed towards the exterior of the macrocycle whereas the third one is on the upper rim side and directed towards the cavity, in which it occupies a position nearly parallel to that of the uncomplexed phenolic ring.

The question arises as to the role of the acid-enhancing *p*-chlorine substituent in the auto-deprotonation process leading to complex **9** as well as to the Nd^{3+} complex of **3**. Complex **10** brings an answer as well as an interesting point of comparison with complex **8**. The complexation by ligand **4** occurs also without a basic agent being added, giving $[UO_2(NO_3)_2\mathbf{4}]\cdot 0.5CH_3OH\cdot H_2O$ (**10**) in which the complex molecule is neutral. This reaction indicates that the presence of chlorine atoms is not necessary to promote the protons transfer. The asymmetric unit in **10** comprises one complex molecule lacking any symmetry element (Figure 5). The uranyl ion is bound to two phenoxide groups, as in **9**, and its distance from the mean plane defined [± 0.030(5) Å] by the four calixarene oxygen atoms is 1.543(8) Å. The two nitrate counter-ions behave differently: one is bidentate and the other monodentate. This difference with **9** may be ascribed to an $O_{phenol}-U-O_{phenol}$ angle slightly larger in **10** [78.9(3)° to be compared with 75.1(3)° in **9**], which could make the available space insufficient for two bidentate nitrate ions. The two coordinated phenolic groups are deprotonated and the two amine groups are turned into ammonium cations. Hydrogen bonds are formed between each ammonium group and its two neighbouring oxygen atoms, and also between the two non-coordinated, protonated, oxygen atoms O(3) and O(4) and the two phenoxide groups. The modification of the hydrogen bonding pattern with respect to **7** results in a different calixarene conformation. The values of the dihedral angles between the four phenolic rings and the mean oxygen atoms plane are 61.7(3), 59.1(3), 21.0(4) and 16.1(5)°, the two uncomplexed phenolic moieties being closer to the mean plane. Two half-cones are defined on each side of the N(1)···N(2) axis, but their junction does not give an overall cone conformation: the usual terms defining the conformation of classical small calixarenes are of no practical use in the present case, which is reminiscent of larger, flattened calixarenes.

The question arises of the origins of the difference in coordination mode between the uranyl complex of *p*-*tert*-butylhexahomotrioxacalix[3]arene and **8** on the one hand and **9** and **10** on the other. The main reason is likely to be the electrostatic repulsion between the uranyl cation and the two or three ammonium groups in the latter cases, which prevents the cation from being located in the mean plane

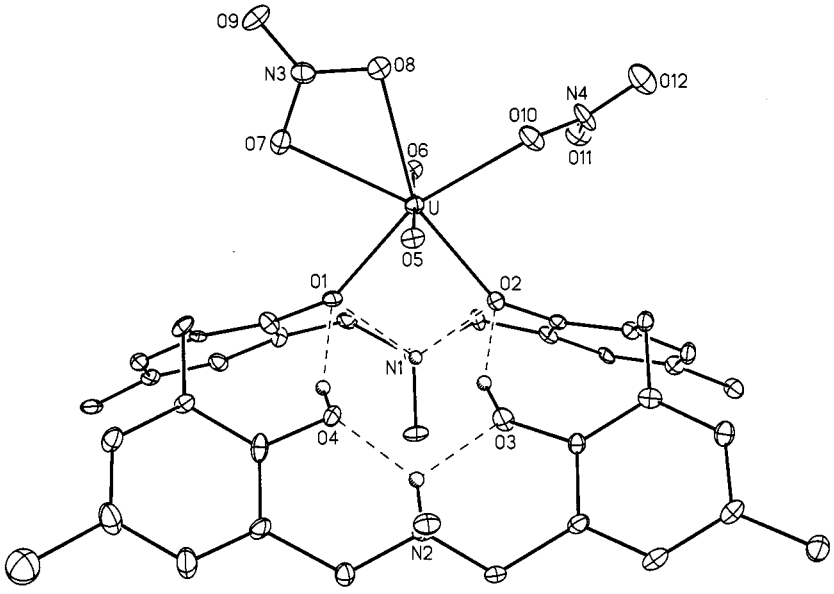

Figure 5. View of the "external" uranyl ion complex of *p*-methyl-*N*-benzyltetrahomodiazacalix[4]arene **10**; hydrogen bonds in dashed lines; protons of the hydroxyl and ammonium groups represented as small spheres of arbitrary radii; other hydrogen atoms, benzyl groups and solvent molecules omitted for clarity

defined by the lower rim. An influence of the steric hindrance associated with the benzyl groups occupying the cavity is not likely, due to the high flexibility of these substituents and the high affinity of phenoxide groups for uranyl ions. In spite of repeated attempts, we did not succeed in growing single crystals of the complex species obtained with azacalixarenes in a basic medium (NEt_3 or DABCO), for comparative purposes. It may be assumed that the deprotonation of the ligand by the base could lead to an anionic complex with a coordination mode closer to that observed with other calixarenes. It must be noted that, by contrast with all the uranyl complexes of calixarenes reported up to now, the azacalixarene complexes **9** and **10** are neutral and not anionic, since the ligand itself is neutral and the metal cation is bound to its counter-ions.

The interest of zwitterions for the simultaneous solvent extraction of cations and anions has recently been pointed out and exemplified by a Schiff base bearing morpholine groups.[10] In this case, the Schiff base with deprotonated hydroxyl groups complexes the metal ion while the protonated morpholine groups complex the counter-ion. The situation is somewhat different in the case of azacalixarenes since the cationic part of the ligand is not directly involved in complexation, but simply pushes the cation into an "external" position in which it cannot reach its usual coordination number from the calixarene and must remain bound to its counter-ions.

Experimental Section

Synthesis

***p-tert*-Butyltetrahomodioxacalix[4]arene (2):** This compound was synthesized as previously reported.[11] Slow evaporation of a solution of **2** in $CHCl_3/CH_3CN$ (1:1) gave colourless single crystals of **2**·$2CH_3CN$ (**5**) suitable for X-ray crystallography, whereas slow evaporation of a solution in pyridine gave colourless single crystals of **2**·$2.5C_5H_5N$ (**6**) of lower quality.

***p*-Methyl-*N*-benzyl-tetrahomodiazacalix[4]arene (4):** A solution of 2,2′-methylenebis(4-methyl-6-hydroxymethyl)phenol (8.00 g, 27.8 mmol) and benzylamine (3.4 g, 31.7 mmol) in 100 mL of xylene was heated under reflux for 34 h. After removal of the solvent under reduced pressure, the resultant oily material was subjected to silica-gel column chromatography with CH_2Cl_2 as an eluent. **4** was obtained as a colourless powder (5.81 g, yield 58.3%). The analytical sample was recrystallized from CH_2Cl_2/C_2H_5OH. M.p. 146−148 °C. − ^1H NMR (270 MHz, $CDCl_3$): δ = 2.17 (s, 12 H, Ar−CH_3), 3.43, 3.60, 4.25 (3bs, 16 H, Ar−CH_2−), 6.69 (d, *J* = 2 Hz, 4 H, Ar−H), 7.03 (d, *J* = 2 Hz, 4 H, Ar−H), 7.34 (br. s, 10 H, side arm Ar−H), 10.6 (br. s, 4 H, Ar−OH). − $C_{48}H_{50}N_2O_4$·$0.5C_2H_5OH$ (741.93): calcd. C 79.32, H 7.20, N 3.78; found C 79.11, H 7.35, N 3.67. Concentration of the mother liquor also afforded 0.31 g (3.3%) of *p*-methyl-*N*-benzyldihomoazacalix-[4]arene. Slow evaporation of a solution of **4** in $CHCl_3/CH_3CN$ (1:1) gave colourless single crystals of **4**·CH_3CN (**7**) suitable for X-ray crystallography.

$[UO_2(2-4H)]^{2-}(HNEt_3^+)_2$·$CHCl_3$·$CH_3CN$ (8): Compound **2** (0.02 g, 0.03 mmol) was dissolved in 6 mL of $CH_3CN/CHCl_3$ (1:1) and 1 mL of NEt_3; a solution of $UO_2(NO_3)_2$·$6H_2O$ (0.03 g, 0.06 mmol) in 2 mL of CH_3CN was then added dropwise, immediately giving an orange solution, which was allowed to slowly evaporate. A few orange single-crystals suitable for X-ray crystallography deposited in three days together with a microcrystalline powder. Microanalysis results including both crystals and powder were unsatisfactory due to the heterogeneous nature of the latter.

$[UO_2(NO_3)_2 3]$·C_5H_5N·$CHCl_3$ (9): Compound **3** (0.15 g, 0.19 mmol) was dissolved in 30 mL of $CH_3CN/CHCl_3$ (1:1) and a solution of $UO_2(NO_3)_2$·$6H_2O$ (0.3 g, 0.6 mmol) in 30 mL of CH_3CN was added dropwise, immediately giving an orange solution. Orange single crystals, unstable out of their mother solution but suitable for X-ray crystallography, were obtained upon recrystallization from pyridine. − $[UO_2(NO_3)_2 3]$·$CHCl_3$·H_2O, $UC_{46}H_{45}Cl_6N_5O_{12}$ (1310.60): calcd. C 42.16, H 3.46; found C 42.06, H 3.35. − FAB-MS $[UO_2$·$C_{45}H_{42}Cl_3N_3O_3]$: *m*/*z* = calcd. 1047.26; found 1048.2.

$[UO_2(NO_3)_2 4]$·$0.5CH_3OH$·H_2O (10): Compound **4** (0.04 g, 0.055 mmol) was dissolved in 3 mL of $CHCl_3$ and a solution of $UO_2(NO_3)_2$·$6H_2O$ (0.04 g, 0.08 mmol) in 5 mL of CH_3OH was added dropwise, immediately giving an orange solution. Orange single crystals suitable for X-ray crystallography were obtained in a few hours. − $UC_{48.5}H_{54}N_4O_{13.5}$ (1146.99): calcd. C 50.79, H 4.75; found C 50.28, H 4.28.

Crystallography

The data were collected on a Nonius Kappa-CCD area detector diffractometer[12] using graphite-monochromated Mo-K_α radiation (0.71073 Å). The crystals were introduced in Lindemann glass capillaries with a protecting "Paratone" oil (Exxon Chemical Ltd.) coating. The data were processed with DENZO-SMN.[13] The structures were solved by direct methods with SHELXS-97[14] and subsequent Fourier-difference synthesis and refined by full-matrix least-squares on F^2 with SHELXL-97.[15] No absorption correction was done for **5**, **6** and **7**, the product μ<d> being lower than 0.1. Absorption effects in **8**, **9** and **10** were corrected empirically with the program MULABS from PLATON.[16] Hydroxyl and ammonium protons, as well as those of chloroform molecules, were introduced as found on the Fourier difference maps whereas all other hydrogen atoms in all compounds were introduced at calculated positions (except in the disordered parts). All hydrogen atoms were treated as riding atoms with a displacement parameter equal to 1.2 (OH, NH, CH, CH_2) or 1.5 (CH_3) times that of the parent atom. All non-hydrogen atoms were refined anisotropically, except the disordered ones. Special features for each compound are indicated in the following.

2·$2CH_3CN$ (5): The data were recorded at ambient temperature since the crystals deteriorate at low temperature, which is seemingly due to a phase transition phenomenon. Some soft restraints have been applied on the badly resolved acetonitrile molecules. The absolute structure could not be determined from the value of the Flack parameter.[17]

2·$2.5C_5H_5N$ (6): One *tert*-butyl substituent was found disordered over two positions, which have been refined with occupation factors constrained to sum to unity. The nitrogen atoms were not located in the pyridine molecules (one of them disordered around a symmetry centre).

4·CH_3CN (7): One of the two benzyl substituents was disordered over two positions sharing two carbon atoms, which have been refined with occupation factors constrained to sum to unity.

$[UO_2(2-4H)]^{2-}(HNEt_3^+)_2$·$CHCl_3$·$CH_3CN$ (8): Some disorder was present on one *tert*-butyl group and one triethylammonium

Table 2. Crystal data and structure refinement details

	5	**6**	**7**	**8**	**9**	**10**
Empirical formula	$C_{50}H_{66}N_2O_6$	$C_{58.5}H_{72.5}N_{2.5}O_6$	$C_{50}H_{53}N_3O_4$	$UC_{61}H_{92}Cl_3N_3O_8$	$UC_{51}H_{48}Cl_6N_6O_{11}$	$UC_{48.5}H_{54}N_4O_{13.5}$
M/g mol^{-1}	791.02	906.69	759.95	1339.76	1371.68	1146.99
T/K	293(2)	120(2)	293(2)	100(2)	100(2)	100(2)
Crystal system	Tetragonal	Monoclinic	Triclinic	Orthorhombic	Monoclinic	Tetragonal
Space group	$P4_12_12$	$C2/c$	$P\bar{1}$	$P2_12_12_1$	Cc	$P4_32_12$
a/Å	17.329(2)	34.380(4)	10.943(2)	12.4313(3)	9.3345(5)	13.882(1)
b/Å	17.329(2)	9.2515(5)	13.132(2)	16.7223(4)	25.283(2)	13.882(1)
c/Å	15.594(2)	36.161(4)	16.485(2)	30.4446(8)	22.924(1)	48.292(5)
α / °	90	90	79.026(10)	90	90	90
β / °	90	116.936(3)	74.077(9)	90	94.634(4)	90
γ / °	90	90	72.397(7)	90	90	90
V/Å^3	4683(1)	10254(2)	2156.4(6)	6328.8(3)	5392.5(5)	9306(2)
Z	4	8	2	4	4	8
μ/mm^{-1}	0.072	0.075	0.074	2.744	3.372	3.560
Reflections collected	27912	34044	15878	43757	18296	20655
Independent reflections	4010	9194	7319	11953	9392	6748
Observed reflections [$I > 2\sigma(I)$]	1230	4252	3940	10505	8301	4812
R_{int}	0.124	0.184	0.064	0.088	0.068	0.121
R_1	0.083	0.101	0.080	0.042	0.050	0.060
wR_2	0.169	0.206	0.201	0.090	0.122	0.111

ion, which was modelled with two positions refined with occupation factors constrained to sum to unity. The absolute structure was determined from the value of the Flack parameter [−0.015(6)].

$[UO_2(NO_3)_2]\cdot C_5H_5N\cdot CHCl_3$ (9): The absolute structure was determined from the value of the Flack parameter [−0.013(7)].

$[UO_2(NO_3)_2]\cdot 0.5CH_3OH\cdot H_2O$ (10): The two benzyl substituents were found disordered over two positions each. These four positions, which have been refined with occupation factors constrained to sum to unity for each benzyl moiety, overlap between neighbouring molecules and share one or two atomic positions. The occupation parameters have been chosen so as to take into account the impossibility of a simultaneous occupation of overlapping positions. The methanol solvent molecule was also found disordered over two sites symmetrically related, each affected with a 0.5 occupation. The structure was refined as corresponding to a racemic twin, the fractional contribution of the two components being x and $(1 - x)$, with $x = 0.504(14)$.

Crystal data and structure refinement parameters are given in Table 2. The molecular plots were drawn with SHELXTL.[18] All calculations were performed on a Silicon Graphics R5000 workstation.

Crystallographic data (excluding structure factors) for the structures reported in this paper have been deposited with the Cambridge Crystallographic Data Centre as supplementary publication no. CCDC-144187−144192 (**5**−**10**). Copies of the data can be obtained free of charge on application to CCDC, 12 Union Road, Cambridge CB2 1EZ, UK [Fax: (internat.) +44-1223/336-033; E-mail: deposit@ccdc.cam.ac.uk].

[1] See, for example: S. Shinkai, in *Calixarenes: a Versatile Class of Macrocyclic Compounds* (Eds.: J. Vicens and V. Böhmer), Kluwer, Dordrecht, **1991**, pp. 173−198, and references therein; T. Nagasaki, S. Shinkai, T. Matsuda, *J. Chem. Soc., Perkin Trans. 1* **1990**, 2617−2618; T. Nagasaki, S. Shinkai, *J. Chem. Soc., Perkin Trans. 2* **1991**, 1063−1066; T. Nagasaki, K. Kawano, K. Araki, S. Shinkai, *J. Chem. Soc., Perkin Trans. 2* **1991**, 1325−1327; K. Araki, N. Hashimoto, H. Otsuka, T. Nagasaki, S. Shinkai, *Chem. Lett.* **1993**, 829−832.

[2] [2a] J. M. Harrowfield, M. I. Ogden, A. H. White, *J. Chem. Soc., Dalton Trans.* **1991**, 979−985. − [2b] P. Thuéry, N. Keller, M. Lance, J. D. Vigner, M. Nierlich, *Acta Crystallogr., Sect. C* **1995**, *51*, 1570−1574. − [2c] P. Thuéry, N. Keller, M. Lance, J. D. Vigner, M. Nierlich, *New. J. Chem.* **1995**, *19*, 619−625. − [2d] P. Thuéry, M. Lance, M. Nierlich, *Supramol. Chem.* **1996**, *7*, 183−185. − [2e] P. Thuéry, M. Nierlich, *J. Inclusion Phenom.* **1997**, *27*, 13−20. − [2f] P. Thuéry, M. Nierlich, M. I. Ogden, J. M. Harrowfield, *Supramol. Chem.* **1998**, *9*, 297−303. − [2g] P. C. Leverd, P. Berthault, M. Lance, M. Nierlich, *Eur. J. Inorg. Chem.* **1998**, 1859−1862. − [2h] P. Thuéry, M. Nierlich, B. Souley, Z. Asfari, J. Vicens, *J. Chem. Soc., Dalton Trans.* **1999**, 2589−2594. − [2i] P. Thuéry, M. Nierlich, B. Masci, Z. Asfari, J. Vicens, *J. Chem. Soc., Dalton Trans.* **1999**, 3151−3152. − [2j] P. C. Leverd, I. Dumazet-Bonnamour, R. Lamartine, M. Nierlich, *Chem. Commun.* **2000**, 493−494. − [2k] For a review, see: J. Harrowfield, *Gazz. Chim. Ital.* **1997**, *127*, 663−671.

[3] P. D. Beer, M. G. B. Drew, D. Hesek, M. Kan, G. Nicholson, P. Schmitt, P. D. Sheen, G. Williams, *J. Chem. Soc., Dalton Trans.* **1998**, 2783−2785.

[4] C. D. Gutsche, L. J. Bauer, *J. Am. Chem. Soc.* **1985**, *107*, 6052−6059.

[5] H. Takemura, K. Yoshimura, I. U. Khan, T. Shinmyozu, T. Inazu, *Tetrahedron Lett.* **1992**, *33*, 5775−5778; I. U. Khan, H. Takemura, M. Suenaga, T. Shinmyozu, T. Inazu, *J. Org. Chem.* **1993**, *58*, 3158−3161; H. Takemura, T. Shinmyozu, H. Miura, I. U. Khan, T. Inazu, *J. Inclusion Phenom.* **1994**, *19*, 193−206; H. Takemura, T. Shinmyozu, T. Inazu, *Coord. Chem. Rev.* **1996**, *156*, 183−200.

[6] C. E. Daitch, P. D. Hampton, E. N. Duesler, *Inorg. Chem.* **1995**, *34*, 5641−5645; C. E. Daitch, P. D. Hampton, E. N. Duesler, T. M. Alam, *J. Am. Chem. Soc.* **1996**, *118*, 7769−7773.

[7] P. Thuéry, M. Nierlich, J. Vicens, H. Takemura, *J. Chem. Soc., Dalton Trans.* **2000**, 279−283.

[8] P. Thuéry, N. Keller, M. Lance, J. D. Vigner, M. Nierlich, *J. Inclusion Phenom.* **1995**, *20*, 373−379.

[9] D. M. Roundhill, in *Progress in Inorganic Chemistry* (Ed.: K. D. Karlin), vol. 43, John Wiley & Sons, **1995**, pp. 533−592.

[10] D. J. White, N. Laing, H. Miller, S. Parsons, S. Coles, P. A. Tasker, *Chem. Commun.* **1999**, 2077−2078.

[11] B. Dhawan, C. D. Gutsche, *J. Org. Chem.* **1983**, *48*, 1536−1539.

[12] *Kappa-CCD Software*, Nonius B.V., Delft, **1998**.

[13] Z. Otwinowski, W. Minor, *Methods Enzymol.* **1997**, *276*, 307−326.

[14] G. M. Sheldrick, *Acta Crystallogr., Sect. A* **1990**, *46*, 467−473.

[15] G. M. Sheldrick, SHELXL-97, Program for the Refinement of Crystal Structures, University of Göttingen, **1997**.

[16] A. L. Spek, PLATON, University of Utrecht, **1998**.

[17] H. D. Flack, *Acta Crystallogr., Sect. A* **1983**, *39*, 876−881.

[18] G. M. Sheldrick, SHELXTL, Version 5.1, University of Göttingen, distributed by Bruker AXS, Madison, WI, **1999**.

Received May 22, 2000
[I00212]

Nickel(II) Tetraazamacrocyclic Complexes with Two Pendant Amino Groups: Electrochemical and Kinetic Studies

Bohdan Korybut-Daszkiewicz,*[a] Joanna Taraszewska,[b] and Bohdan Kamieński[a]

Keywords: Electrochemistry / Kinetics / Macrocyclic ligands / N ligands / Nickel

Isomeric 2,9-bis(amionmethyl)-5,7,7,12,14,14-hexamethyl-1,4,8,11-tetraazacyclotetradecanenickel(II) and -4,11-dienenickel(II) complexes (**1**–**4**) were studied by cyclic voltammetry. The thermodynamic stability of Ni^{III} was the greatest in complex **4** with a *trans* configuration of the pendant amino groups. On acidification, the Ni^{II}/Ni^{III} redox process was not observed. After alkalisation the redox process was only recovered in complex **4**. The kinetics of the two-step macrocyclic ring isomerisation in 1 M HCl and DCl was studied, as a function of temperature, by UV/Vis and ^1H NMR techniques. The energies of activation for the isomerisation of the cyclam ring from *trans*-V (**5α**) to *trans*-II (**5β**) and from *trans*-II to *trans*-I (**5γ**) were equal to 22.6 and 26.9 kcal mol^{-1}, respectively.

Introduction

Tetraazamacrocyclic polyamines bearing pendant amine groups are especially interesting for studying the influence of axial coordination on the properties of the coordinated metal ion. It was found that such intramolecular donors can profoundly alter the properties of the complexed metal ions.[1,2] The first examples of such ligands were synthesised by Kaden.[1] Complexes of this type found application in the electrocatalysis of processes such as the reduction of CO_2 to CO[3] and hydrogen evolution.[4] They can be also linked to monoclonal antibodies, allowing the specific labelling of macrocycle-conjugated antibodies with radioisotopes,[5,6] and their consequent use as targeting agents in the diagnosis and therapy of cancers and other diseases.

The behaviour of metal complexes with such ligands is spectacular due to the internal pH-dependent equilibrium between the open and chelated forms of the pendant arm. When the pendant amine group is protonated, the diamagnetic, square-planar Ni^{II} complexes are formed. However, at higher pH values, coordination of the amine group leads to the paramagnetic, octahedral complexes. Such a change of structure gives a colour variation that may find analytical application. Due to the active role of the flexible side-chain, the above class of molecules was named scorpiands.[7] The pH-dependent electrochemical behaviour of Ni^{II} tetraazamacrocyclic complexes containing one pendant amino group was studied by Fabbrizzi et al.,[7] by Kimura et al.,[3] and by us.[8]

Nickel(II) complexes of cyclam derivatives substituted with two pendant amino groups are also the subjects of the pH-dependent equilibria. Cyclam dienes functionalised with two pendant arms – *trans*-2,9-bis(aminomethyl)-5,7,7,12,14,14-hexamethyl-1,4,8,11-tetraazacyclotetradeca-4,11-dienenickel(II) diperchlorate and its folded *cis* analogue were first synthesised by Korybut-Daszkiewicz,[9,10] and their crystallographic structure determined.[10,11] Recently, Korybut-Daszkiewicz et al.[12] synthesised and characterised isomeric Ni^{II} complexes of *cis*-2,9-bis(aminomethyl)-5,7,7,12,14,14-hexamethyl-1,4,8,11-tetraazacyclotetradecane. The coordination of the two pendant amino groups located on the same side of the tetraazamacrocyclic ring forces the ring to adopt a folded conformation. Protonation of the pendant amino groups resulted in the change of the macrocyclic conformation from folded to planar, and further isomerisation.

This paper is devoted to the study of the pH-dependent electrochemical behaviour of both groups of complexes, and the kinetics of their isomerisation by UV/Vis and ^1H NMR spectroscopy. The schematic structures of studied complexes and their protonated forms are presented in Figure 1.

Results and Discussion

Redox Properties of Complexes

The voltammetric behaviour of complexes **1**–**4** was studied in aqueous solutions containing 0.1 M NaCl as supporting electrolyte. In the negative potential range, reduction of Ni^{II} to Ni^{I} was not observed. The cyclic voltammograms recorded in the positive potential range on the glassy carbon (GC) electrode are shown in Figure 2. In each complex, Ni^{II} was oxidised to Ni^{III} at a potential corresponding to peak *a* and Ni^{III} was reduced to Ni^{II} at a potential corresponding to peak *b*. The redox process Ni^{II}/Ni^{III} in all complexes was reversible. The values of formal potentials E_f, calculated as midpoints between corresponding anodic and cathodic peaks, were 0.70V, 0.66V, 0.60V, and 0.43V for complexes **1**, **2**, **3**, and **4**, respectively.

The voltammetric behaviour of complex **1** at various pH values is shown in Figure 3A. After addition of HCl (pH = 2, curve 2) the current diminished about 25%, in comparison with that in neutral solution, and did not change with time (measurements up to 40 min). The value of E_f shifted

[a] Institute of Organic Chemistry, Polish Academy of Sciences, Kasprzaka 44/52, 01-224 Warsaw, Poland
Fax: (internat.) + 48-22/6326681
E-mail: bkd@icho.edu.pl
[b] Institute of Physical Chemistry, Polish Academy of Sciences, Kasprzaka 44/52, 01-224 Warsaw, Poland

 © WILEY-VCH Verlag GmbH, 69451 Weinheim, 2001 1434–1948/01/0303–0645 $ 17.50+.50/0

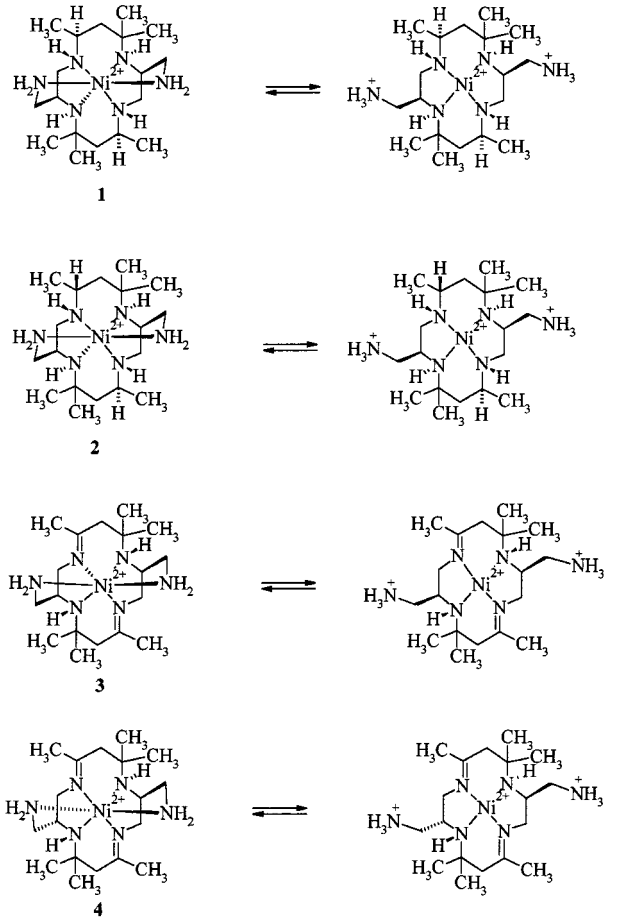

Figure 1. Structures of studied octahedral complexes **1**−**4** and their square-planar protonated forms; the macrocycle in complexes **1**−**3** adopts a folded conformation, and in complex **4** co-planar conformation

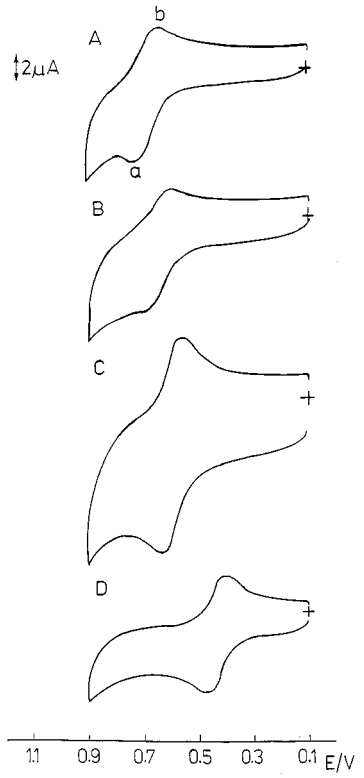

Figure 2. Cyclic voltammograms of $5\cdot10^{-4}$ M complexes **1** (A), **2** (B), **3** (C), and **4** (D) at a GC electrode in aqueous 0.1 M NaCl solution; scan rate 0.05 Vs^{-1}

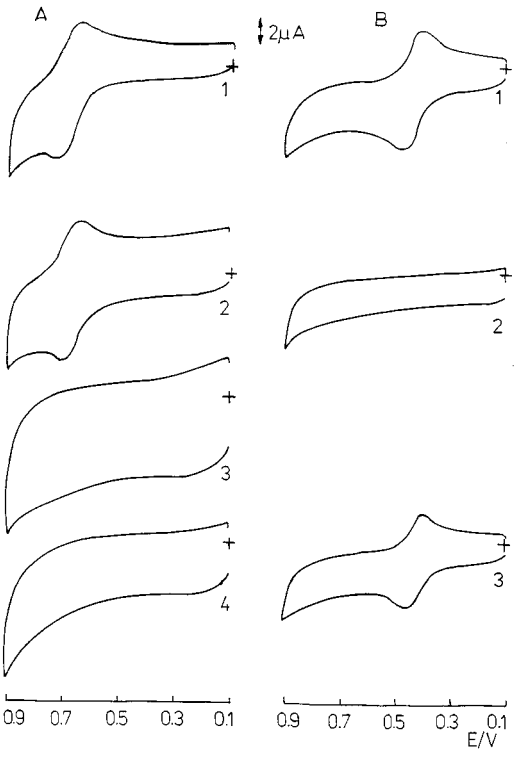

Figure 3. Cyclic voltammograms of $5\cdot10^{-4}$ M complexes **1** (A) and **4** (B) in 0.1 M NaCl as a function of the pH; (A) curve 1: pH = 7; curve 2: pH = 2; curve 3: pH = 1; curve 4: pH = 7; (B) curve 1: pH = 7; curve 2: pH = 3; curve 3: pH = 7

to 0.67 V. Further acidification (pH = 1) caused a rapid decrease of current with time, ultimately resulting in the disappearance of the redox process (curve 3). A subsequent alkalisation of solution did not change the picture even after 2 d (curve 4). The same behaviour was observed for complex **3**. In complex **2** the redox process Ni^{II}/Ni^{III} disappeared already at pH = 3, and did not recover after alkalisation. In complex **4** (Figure 3B) the redox process Ni^{II}/Ni^{III} disappeared at pH = 3, (curve 2) however, it was recovered after the subsequent alkalisation of solution (curve 3).

A comparison of E_f values for the redox process Ni^{II}/Ni^{III} in tetraazamacrocyclic complexes with one and with two pendant amino groups in neutral solutions is presented in Table 1. In tetraazamacrocyclic complexes with one pendant amino group, the most favourable access to the trivalent state was in 6-aminocyclam and the relative stabilization of Ni^{III} was the lowest in *N*-(aminomethyl)cyclam. This is based on the fact that the secondary amines are intrinsically more basic than the tertiary amines, and the interactions of tertiary nitrogen atoms with the metal ion are weaker than those of the secondary amine nitrogen atoms.[13,14]

Table 1. Formal potentials E_f of Ni^{II} tetraazamacrocyclic complexes with one and two pendant amino groups

Complex	E_f ([V] vs.MCE)	Ref.
Ni^{II}-5-AmMe-5,12-diMe-cyclam	0.655	[8]
Ni^{II}-1-AmEt-cyclam	0.740	[7]
Ni^{II}-6-Am-cyclam	0.560	[3]
1	0.700	this work
2	0.660	this work
3	0.600	this work
4	0.430	this work

In complexes **1**−**3**, with two pendant amino groups that are in a folded conformation, the potential of the Ni^{II}/Ni^{III} couple (Table 1) was similar to that in *N*-(aminoethyl)cyclam and 5-aminomethyl-5,12-dimethylcyclam. However, in complex **4**, which is in the *trans* conformation, it was much less positive. From the point of view of the structure of the coordination sphere one can conclude that the thermodynamic stabilization of Ni^{III} is more effective in the *trans* complex, where the macrocycle surrounds the metal ion in a square-planar manner, than in the *cis* analogues with a folded conformation of the amine. A similar effect has been observed by Taraszewska et al.[15] for other nickel azamacrocyclic complexes.

In acidic solutions the behaviour of complexes with two pendant amino groups was different to those with one pendant group. For 5-aminomethyl-5,12-dimethylcyclam studied by us previously[8] at pH = 0.8 we recorded two anodic peaks at potentials 0.65 V and at 0.85 V corresponding to the Ni^{II} oxidation from the complex with a deprotonated and with a protonated amino group, respectively. In more acidic solutions, only a peak at 0.85 V was recorded. Similar behaviour has been described by Fabbrizzi et al.[7] Applying CV with fast scan rates we could record the reduction peak of Ni^{III} from the square-planar complex.[8] In this way we proved experimentally for the first time the existence of Ni^{III} in tetraazamacrocyclic complex in the square-planar form, which is unusual for this type of complex, and has only been observed in some anionic tetraazamacrocyclic complexes.[16] On the basis of the stop-flow experiments we estimated the rate constant of the decoordination of the pendant amino group as equal to 815 s^{-1} (at 25 °C). We observed the reduction of Ni^{II} to Ni^{I}, but the complex of Ni^{I} was not stable.

In complexes with two pendant amino groups studied here, the oxidation of Ni^{II} from the protonated forms was not observed. It may be connected with the presence of many methyl groups in the macrocyclic rings, which forbid the access of axial substituents (solvent or anions), therefore Ni^{III} cannot be formed.

The lack of the redox couple Ni^{II}/Ni^{III} after alkalisation of solutions containing protonated forms of complexes **1**−**3** highlights the fact that the macrocyclic ring cannot be refolded, and coordination of the pendant NH_2 groups to Ni^{II} ion is impossible. It was only possible in complex **4**, which in deprotonated and protonated forms has a planar conformation of the macrocyclic ring with pendant arms in the *trans* configuration. Nevertheless, the octahedral folded complexes **1**−**3** could be regenerated in a basic sodium perchlorate solution.[9,11,12]

Kinetic Studies

As has been described in a previous paper,[12] protonated complex **1** undergoes isomerisation connected with inversion of configuration of N(1) and N(8) nitrogen atoms and simultaneous conformation changes of the six-membered chelate rings. The isomerisation pathway is shown in Scheme 1. The kinetics of isomerisation was followed by UV/Vis and ^1H NMR spectroscopy.

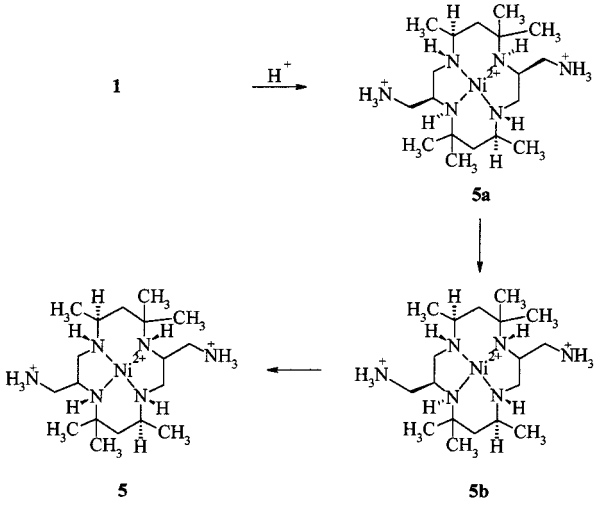

Scheme 1

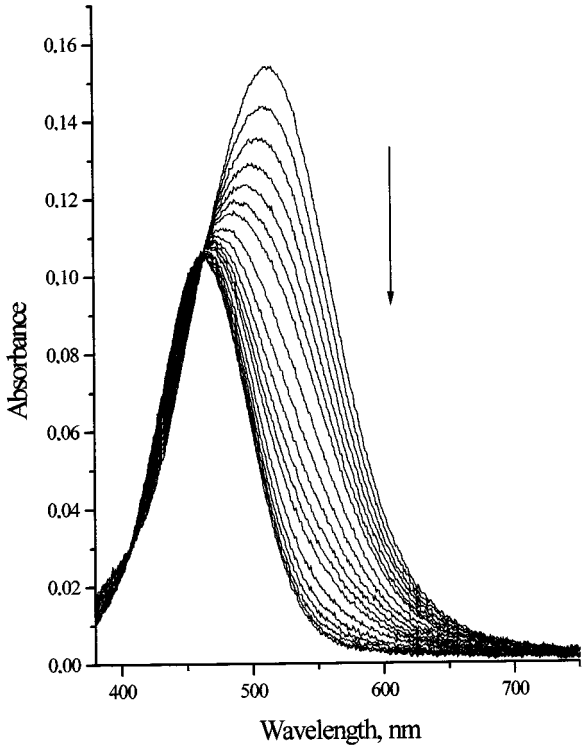

Figure 4. Monitoring of the isomerisation of **5α** into **5β** by UV/Vis spectroscopy; changes of absorption with time recorded for $1 \cdot 10^{-3}$ M complex **1** dissolved in 1 M HCl at 35°C

UV/Vis Studies

Measurements were carried out in solutions of $1 \cdot 10^{-3}$ M of complex **1** dissolved in 1 M HCl in the temperature range 20−45 °C. Changes of absorption with time at 35 °C are shown in Figure 4. The absorption maximum gradually changed from 515 nm, characteristic for complex **5α** (formed from **1** upon protonation) to 462 nm, which is characteristic for isomer **5β**. The steady state was reached after 2.5 h. Absorption changes connected with this isomerisation process were monitored at the wavelength 580 nm. Plots of the absorbance changes vs. time were approximated by the relationship $A(t)/A_o = \exp(-kt)$ for up to 3 half-times, which means that this isomerisation process followed a first-order kinetics. The same procedure was adopted at other temperatures.

Kinetics of isomerisation depended on the acid concentration. A similar experiment carried out in solution acidified with 2 M HCl showed that the kinetics of isomerisation was three times slower ($k = 0.38\ h^{-1}$, 35 °C). In 0.1 M HCl a fast isomerisation to the isomer **5γ** was observed. Such dependence on the acid concentration suggests that the proton dissociation at N(1) and N(8) is the rate determining step in these isomerisation processes. At 35 °C in 0.1 M HCl the inversion of configuration at N(1) and N(8) is fast, and isomer **5γ** is formed in a short time. In 1 M HCl the inversion at the first nitrogen atom is much faster than at second one, therefore we were able to follow the pathway **5α** to **5β**. The isomerisation of **5β** to **5γ** in this medium was followed at higher temperatures by ^{1}H NMR technique (Figure 5).

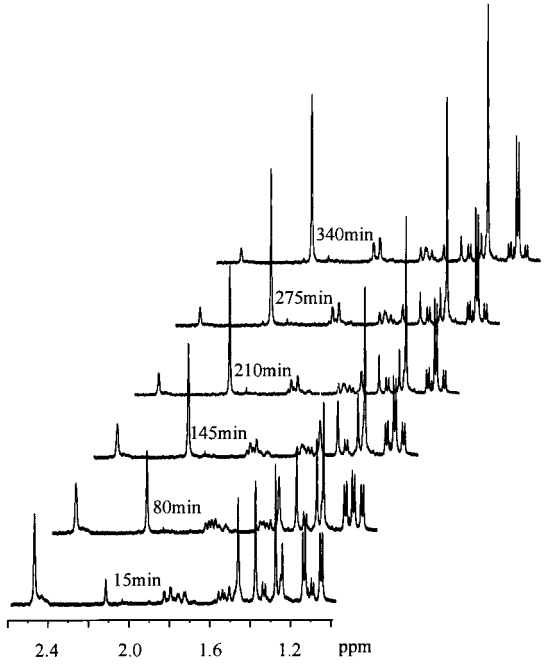

Figure 5. Monitoring of the isomerisation of **5β** into **5γ** by ^{1}H NMR spectroscopy; the methyl group absorption region of the 500 MHz spectra in 1 M DCl solution at 55°C

^{1}H NMR Measurements

The ^{1}H NMR measurements were carried out in $1 \cdot 10^{-3}$ M solutions of complex **5β** in 1 M DCl in the temperature range 40−60 °C. The first spectrum was collected 15 min after dissolution of the sample and the following spectra were measured every 62.5, 32.5, 42.5, 32.5, and 18 min up to 3 half-times at 40, 45, 50, 55, and 60 °C, respectively. The concentrations of the isomer **5β** was followed by integration of 4 proton signal at δ = 2.40−2.53 (overlapping 1 proton multiplet and methyl group singlet) (I_β), and that of the isomer **5γ** by integration of 6 proton methyl group singlet at δ = 2.09−2.16 (I_γ). Plots of the concentration changes vs. time followed a first-order kinetics approximated by the relationship $c(t)/c_0 = \exp(-kt)$ where $c(t)/c_0 = 3I_\beta/(3I_\beta + 2I_\gamma)$.

The values of rate constant k as a function of temperature for both processes are collected in Table 2. The activation energies E_a calculated from this relationship (Figure 6)

Table 2. Dependence of the rate constants of isomerisation on temperature for pathways **5α**−**5β** and **5β**−**5γ** in 1 M HCl and DCl solutions, respectively

Temp. [°C]	**5α**−**5β** k [h^{-1}][a]	**5β**−**5γ** k [h^{-1}][b]
20	0.164	
25	0.336	
30	0.531	
35	1.031	
40	1.785	0.050
45	3.638	0.113
50		0.204
55		0.359
60		0.651

[a] UV/Vis. − [b] ^{1}H NMR.

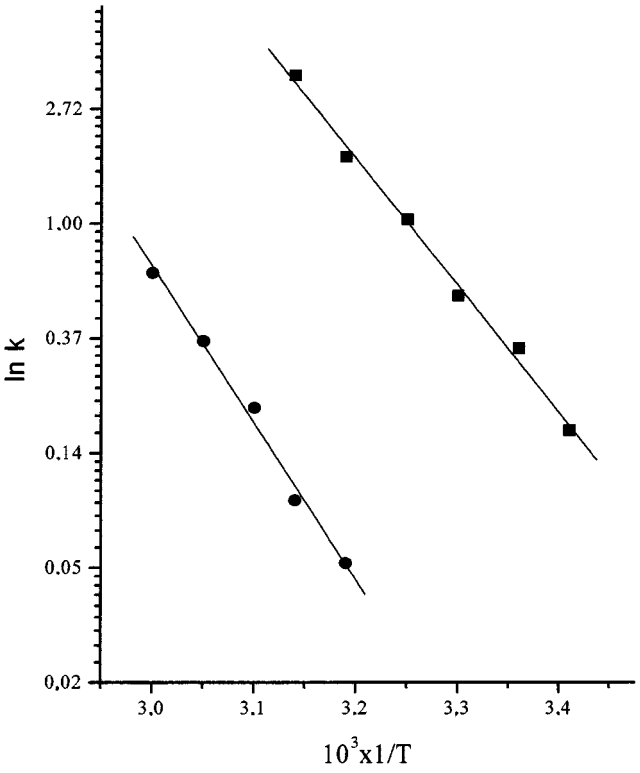

Figure 6. Plots of ln k vs $10^3 \times 1/T$ for the isomerisation of **5α** into **5β** (■) and **5β** into **5γ** (•)

are equal to 22.6 ± 0.7 and 26.9 ± 1.0 kcal mol^{-1} for isomerisation of **5α** into **5β** and **5β** into **5γ**, respectively.

Conclusion

The redox potentials of the Ni^{II}/Ni^{III} couple in complexes **1**−**3**, which are in a folded conformation, were similar to those of complexes with one pendant amino group. However, the thermodynamic stability of Ni^{III} was significantly higher in complex **4**, which exists in a *trans* configuration with a planar conformation of macrocyclic ring. This observation seems to be a general one. The redox process Ni^{II}/Ni^{III} disappeared in acidic solutions and after subsequent alkalisation was recovered only in complex **4** in *trans* configuration.

Protonation of folded complex **1** led to the formation of thermodynamically unstable complex **5α** with a *trans*-V conformation of the macrocyclic ring. Studies in 1 M HCl enabled us to follow the kinetics of stepwise isomerisation of the ring from **5α** through **5β** (*trans*-II) to **5γ** (*trans*-I). The kinetics of isomerisation was followed by UV/Vis and ^{1}H NMR techniques as a function of temperature. The rate constants of the pathway **5α**−**5β** were much higher than those of **5β**−**5γ**. The corresponding activation energies are 22.6 and 26.9 kcal·mol^{-1}, respectively.

Experimental Section

Materials: Complexes **1**−**4** and **5β** were synthesized as described in ref.[12,9,10], respectively. All chemicals were p.a. grade reagents. Triply distilled water was used. The third distillation was carried out from an all-quartz still.

Instrumentation: Cyclic voltammograms of complexes **1**−**4** were measured at a glassy carbon (GC-20) electrode. The counter electrode was a Pt plate. A 1 M aqueous calomel electrode (MCE) was used as the reference electrode. It was connected to the electrolytic cell via an intermediate vessel filled with the solution under investigation. Solutions were deaerated by flushing with pure argon. A measuring system consisting of EPA-20A potentiostat, an EG-20 functions generator (ELPAN Poland) and an *x*,*y* recorder. − The UV/Vis spectra were measured by a Cary 1E (Varian) spectrophotometer. − The 500 MHz ^{1}H NMR spectra were measured in 1 M DCl solutions with a Bruker DRX500 Avance spectrometer.

Acknowledgments

The authors are grateful to Mrs. S. Pawłowska for her great help in electrochemical and UV/Vis measurements. We are indebted to Prof. P. Sobota from Wrocław University for help in estimation of rate constant of de-coordination of a pendant arm by stop-flow method.

[1] T. A. Kaden, *Top. Curr. Chem.* **1984**, *121*, 157−180.
[2] P. V. Bernhardt, G. L. Lawrance, *Coord. Chem. Rev.* **1990**, *104*, 297−343.
[3] E. Kimura, M. Haruta, T. Koike, M. Shionoya, K. Takenouchi, Y. Iitaka, *Inorg. Chem.* **1993**, *32*, 2779−2784.
[4] P. V. Bernhardt, L. A. Jones, *Inorg. Chem.* **1999**, *38*, 5086−5090.
[5] T. A. Kaden, *Pure Appl. Chem.* **1988**, *60*, 1117−1122.
[6] D. Parker, *Chem. Soc. Rev.* **1990**, *19*, 271−291.
[7] P. S. Pallavicini, A. Perotti, A. Poggi, B. Seghi, L. Fabbrizzi, *J. Am. Chem. Soc.* **1987**, *109*, 5139−5144.
[8] J. Taraszewska, G. Rosłonek, B. Korybut-Daszkiewicz, *J. Electroanal. Chem.* **1991**, *297*, 245−255.
[9] B. Korybut-Daszkiewicz, *J. Chem. Soc., Dalton Trans.* **1992**, 1673−1679.
[10] P. Gluziński, J. W. Krajewski, R. A. Koliński, B. Korybut-Daszkiewicz, A. Mishnev, A. Kemme, *Pol. J. Chem.* **1995**, *69*, 350−360.
[11] P. Gluziński, J. W. Krajewski, R. A. Koliński, B. Korybut-Daszkiewicz, A. Mishnev, A. Kemme, *Pol. J. Chem.* **1994**, *68*, 2567−2587.
[12] B. Korybut-Daszkiewicz, P. Gluziński, J. Krajewski, A. Kemme, A. Mishniev, *Eur. J. Inorg. Chem.* **1999**, 263−268.
[13] E. K. Barefield, G. M. Freeman, D. G. Van Derveer, *Inorg. Chem.* **1986**, *25*, 552−558.
[14] M. Ciampolini, L. Fabbrizzi, M. Licchelli, A. Perotti, F. Pezzini, A. Poggi, *Inorg. Chem.* **1986**, *25*, 4131−4135.
[15] J. Taraszewska, G. Rosłonek, Ya. D. Lampeka, I. M. Maloshtan, *J. Electroanal. Chem.* **1998**, *452*, 49−56.
[16] F. V. Lovecchio, E. S. Gore, D. H. Busch, *J. Am. Chem. Soc.* **1974**, *96*, 3109−3118.

Received June 5, 2000
[I00225]

A Novel Redox-Active Conjugated Palladium Homobimetallic Complex

Toshiyuki Moriuchi,[a] Seiji Bandoh,[a] Manabu Miyaishi,[a] and Toshikazu Hirao*[a]

Keywords: Coordination modes / Molecular dynamics / N ligands / Palladium / Redox chemistry

The π-conjugated molecule *N,N′*-bis(4′-dimethylaminophenyl)-1,4-benzoquinone diimine (L^2) was incorporated into the palladium(II) complex **1** bearing the *N,N′*-bis(2-phenylethyl)-2,6-pyridinedicarboxamide ligand, to afford the redox-active conjugated palladium(II) homobimetallic complex **2**. An X-ray crystal structure determination of **2** reveals that two palladium complex units are bridged by the quinone diimine moiety to form the C_2-symmetrical 2:1 complex with an *anti* configuration, and that the bridging π-conjugated spacer moieties are aligned along a straight line almost parallel to the *a* axis, to form the columns of the π-conjugated molecules in the molecular packing. Variable temperature ^{1}H NMR studies of the conjugated complex **2** indicate that the *syn* configuration is enthalpically more favorable than the *anti* configuration in CD_2Cl_2 by 1.0 kcal/mol, but entropically less favorable by 4.5 cal/mol from the van't Hoff plot. The redox function of the quinone diimine moiety is modulated by complexation with the palladium complex **1**. The conjugated complex **2** shows three separate redox waves assignable to the successive one-electron reduction of the quinone diimine moiety and one-electron oxidation process of the two terminal dimethylamino groups. Chemical reduction of **2** in THF with $CoCp_2$ resulted in the appearance of ESR signals with weak ^{105}Pd coupling centered around g = 2.0041. The added electrons are considered to be delocalized over the Pd^{II}-quinone diimine d-π* system in the complex.

Introduction

Quinone diimines can exist in three redox forms: the reduced phenylenediamide dianions, the partially reduced semiquinone diimine radical anions, and the oxidized neutral quinone diimines. The combination of this redox behavior and complexation with transition metals provides an efficient redox system. *o*-Benzoquinone diimines have attracted much attention as a redox-active compound in this context.[1] However, transition metal complexes with *p*-benzoquinone diimine ligands have been investigated in only a few cases and the coordination behavior of *p*-benzoquinone diimine has hitherto remained unexplored.[2] In a previous paper, the emeraldine base form of polyanilines as π-conjugated polymers, which contains a *p*-benzoquinone diimine unit, has been revealed to coordinate to transition metals, affording conjugated complex systems.[3] The polymer complex can effectively serve as an oxidation catalyst,[4] in which the quinone diimine moiety is considered to contribute to a reversible redox process in the catalytic cycle of a transition metal. These results prompted us to investigate the redox properties of the transition metal complexes with *p*-benzoquinone diimines and to characterize the complexes structurally. We herein report the synthesis of the palladium(II) homobimetallic complex with a bridging π-conjugated *p*-benzoquinone diimine.

[a] Department of Applied Chemistry, Faculty of Engineering, Osaka University, Yamada-oka, Suita, Osaka 565−0871, Japan
E-mail: hirao@ap.chem.eng.osaka-u.ac.jp

Results and Discussion

The construction of a conjugated complex system was demonstrated by use of a redox-active π-conjugated molecule, *N,N′*-bis(4′-dimethylaminophenyl)-1,4-benzoquinone diimine (L^2).[5] Complexation with a palladium complex bearing a tridentate ligand, which has one open coordination site, is expected to provide the bimetallic conjugated complex. In this context, the palladium(II) complex [(L^1)Pd(MeCN)] (**1**) bearing one interchangeable coordination site was prepared by treatment of $Pd(OAc)_2$ with the *N*-heterocyclic tridentate podand ligand, *N,N′*-bis(2-phenylethyl)-2,6-pyridinedicarboxamide (L^1H_2),[6] in acetonitrile. The X-ray crystal structure of **1**[7] indicates that the open coordination site is occupied by an ancillary acetonitrile, presenting the complex **1** with one labile ligand.[8] Treatment of the palladium(II) complex **1** with L^2 in acetonitrile led to the formation of the 2:1 complex [(L^1)Pd(L^2)Pd(L^1)] (**2**, Scheme 1).

The structure of the conjugated complex **2** was confirmed by X-ray crystallography. The solid-state molecular structure reveals that the two [(L^1)Pd] units are bridged by the quinone diimine moiety of L^2 to form the C_2-symmetrical 2:1 complex ***anti*-2** with a Pd−Pd separation 8.17 Å, as depicted in Figure 1. Crystallographic data for ***anti*-2** can be found in Table 1, with selected bond lengths and bond angles listed Table 2. Each nitrogen atom of the quinone diimine moiety of L^2 is deviated from the least-squares plane of C(37)−C(38)−C(39*)−C(37*)−C(38*)−C(39) by 4.7° in the same direction, probably due to coordination to a palladium atom which is deviated from the plane by 10.7°. One phenyl ring of the podand moiety of [(L^1)Pd] is oriented in a near face-to-face arrangement at a distance of ca. 3.9 Å with the phenyl ring of another [(L^1)Pd], suggesting a weak π-stacking interaction. This interaction might cause

 © WILEY-VCH Verlag GmbH, 69451 Weinheim, 2001 1434−1948/01/0303−0651 $ 17.50+.50/0

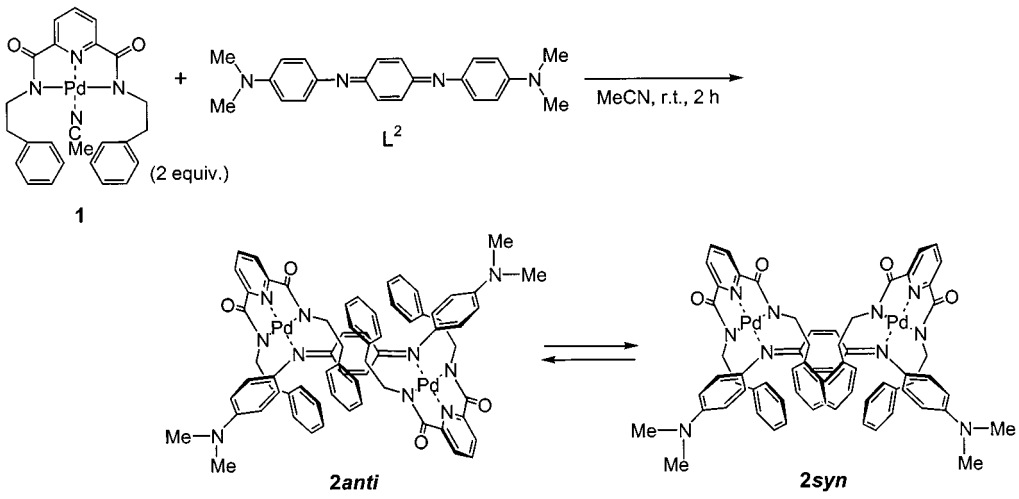

Scheme 1

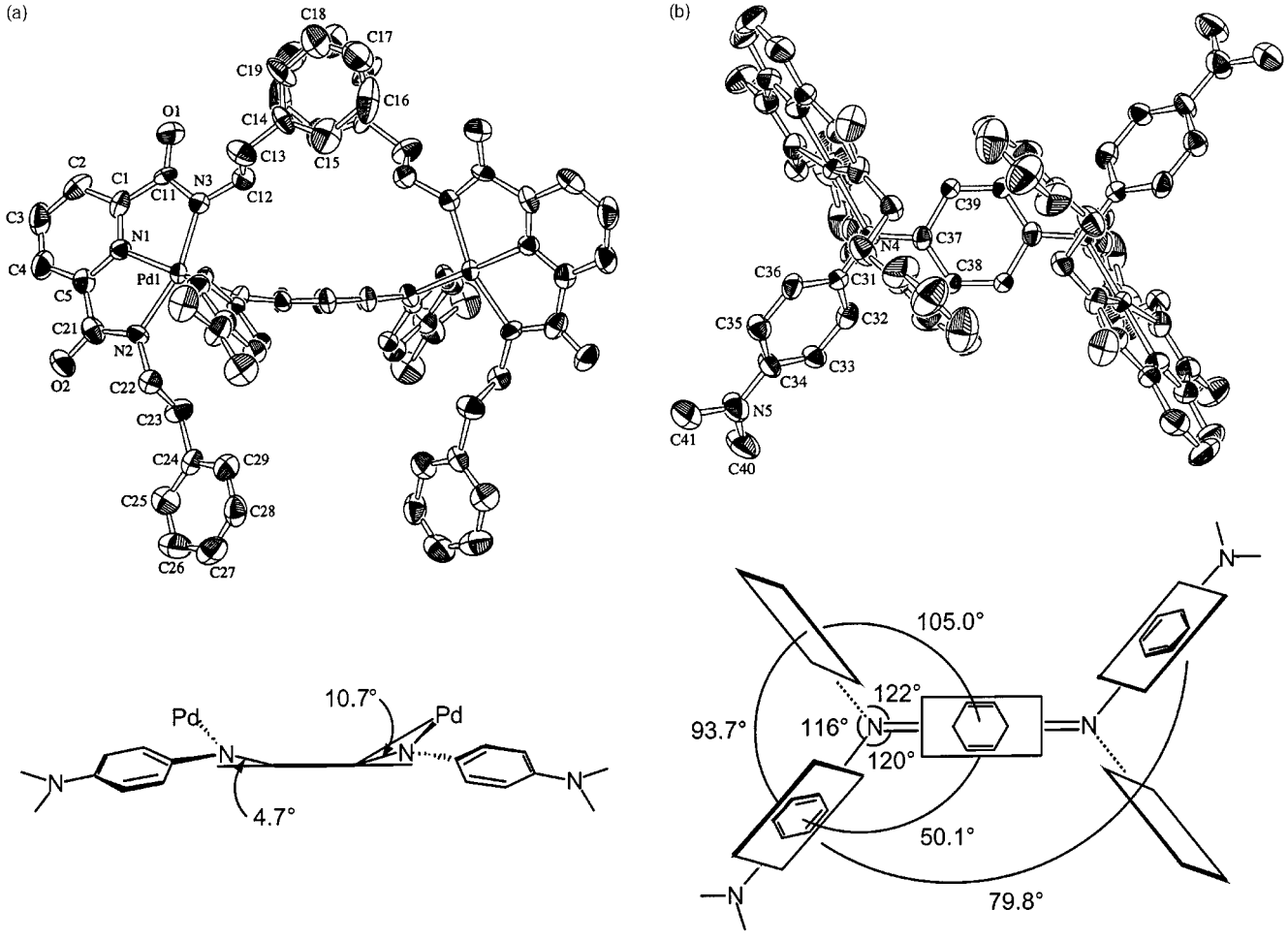

Figure 1. (a) Top view and (b) side view of the X-ray crystal structure of ***anti*-2** (40% probability ellipsoids; hydrogen atoms are omitted for clarity)

Table 1. Crystallographic data for ***anti*-2**

Empirical formula	$C_{68}H_{66}N_{10}O_4Pd_2$
Formula mass	1300.13
Crystal system	monoclinic
Space group	*C*2/*c* (No. 15)
a [Å]	15.858(4)
b [Å]	23.955(8)
c [Å]	18.994(3)
β [°]	112.13(2)
V [Å^3]	6683(2)
Z	4
$D_{calcd.}$ [g cm^{-3}]	1.292
μ(Mo-K_α) [cm^{-1}]	5.91
T [°C]	23
λ(Mo-K_α) [Å]	0.71069
R[a]	0.081
R_w [b]	0.0112

[a] $R = (|F_o| - |F_c|)/|F_o|$. – [b] $R_w = [w(|F_o| - |F_c|)^2/w|F_o|^2]^{1/2}$.

Table 2. Selected bond lengths [Å] and bond angles [deg] for ***anti*-2**

Bond lengths			
Pd–N(1)	1.93(2)	C(37)–C(38)	1.40(2)
Pd–N(2)	2.02(1)	C(37)–C(39)	1.45(2)
Pd–N(3)	2.03(2)	C(38)–C(39*)	1.33(2)
Pd–N(4)	2.05(1)	C(31)–C(36)	1.39(2)
N(4)–C(31)	1.42(2)	C(31)–C(32)	1.40(2)
N(4)–C(37)	1.35(2)		
Bond angles			
N(1)–Pd–N(2)	80.1(7)	N(3)–Pd–N(4)	98.5(6)
N(1)–Pd–N(3)	80.7(7)	Pd–N(4)–C(31)	116(1)
N(1)–Pd–N(4)	179.0(6)	Pd–N(4)–C(37)	122(1)
N(2)–Pd–N(3)	160.8(6)	C(31)–N(4)–C(37)	120(1)
N(2)–Pd–N(4)	100.7(6)		

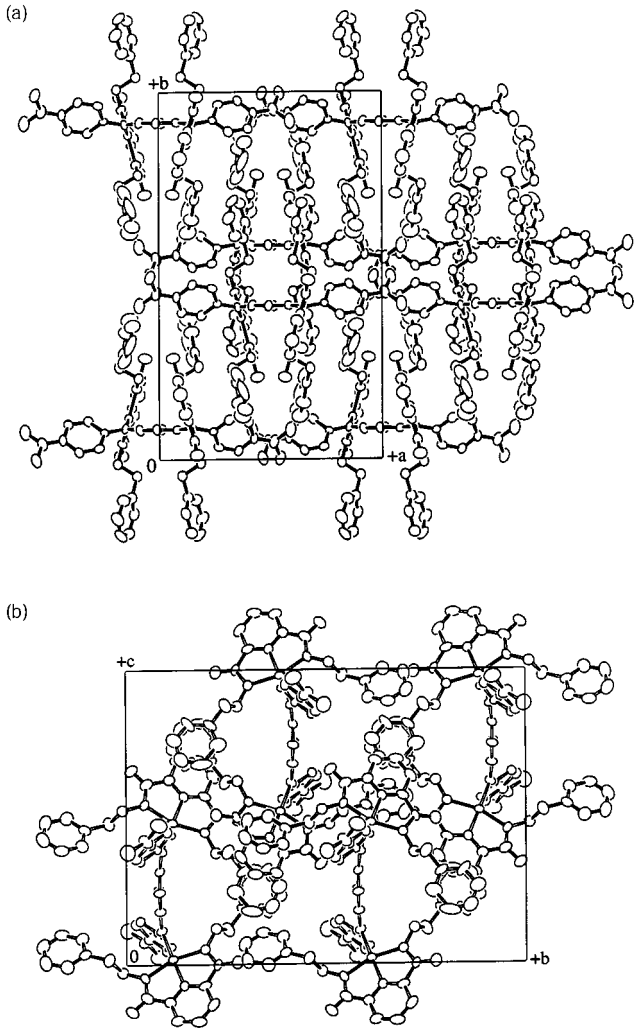

Figure 2. (a) Projection down the *c* axis and (b) projection down the *a* axis of the molecular packing of ***anti*-2**

the above-mentioned deviation of the palladium atoms. Due to π-conjugation of L^2, the orientation of each phenylene ring should be within a limited range of locations parallel to the quinone diimine moiety. The steric interaction between the hydrogen atom at C(32) and the hydrogen atom at C(38), however, causes the phenylene ring of L^2 to rotate away from this orientation, resulting in a conformation with a dihedral angle of 50.1° between the phenylene and quinone planes. Each phenylene ring of L^2 has an opposite dihedral angle with respect to the quinone plane, causing a propeller twist of 79.8° between the planes of the two phenylene rings. The least-squares plane of N(1)–N(2)–N(3)–Pd is at an angle of 109.7° instead of 90° from the plane of C(31)–N(4)–C(37) as a result of the twist of the π-conjugated plane of L^2. Another interesting feature is that the bridging π-conjugated molecules L^2 are aligned along a straight line almost parallel to the *a* axis in the molecular packing (Figure 2a). The coordination planes of palladium composed of the pyridyl and two amide moieties occupy nearly the *bc* plane (Figure 2b).

Variable temperature ^{1}H NMR studies of the conjugated complex **2** indicated interesting molecular dynamics in solution (Figure 3). As the temperature was lowered, the peaks of the *syn* conformer ***syn*-2** appeared and increased gradually. It should be noted that the conjugated complex **2** prefers the *anti* configuration at temperatures above 220 K and the *syn* configuration below this temperature. The equilibrium constant K_{eq} between ***anti*-2** and ***syn*-2** was calculated from variable temperature ^{1}H NMR spectra (Scheme 2). The temperature dependence of K_{eq} is used to construct the van't Hoff plot of $\ln K_{eq}$ vs. T^{-1} (Figure 4). The *syn* configuration is enthalpically more favorable than the *anti* configuration in CD_2Cl_2 by 1.0 kcal/mol, but entropically less favorable by 4.5 cal/mol from the van't Hoff plot.

The interesting redox properties of **2** were disclosed by cyclic voltammetry. The conjugated complex **2** in CH_2Cl_2 shows three separate redox waves ($E_{1/2}$ = –1.49 V, –0.85 V, and 0.20 V vs. Fc/Fc^+) as depicted in Figure 5. The waves at –1.49 V and –0.85 V are assigned to the successive one-electron reduction of the quinone diimine moiety to give

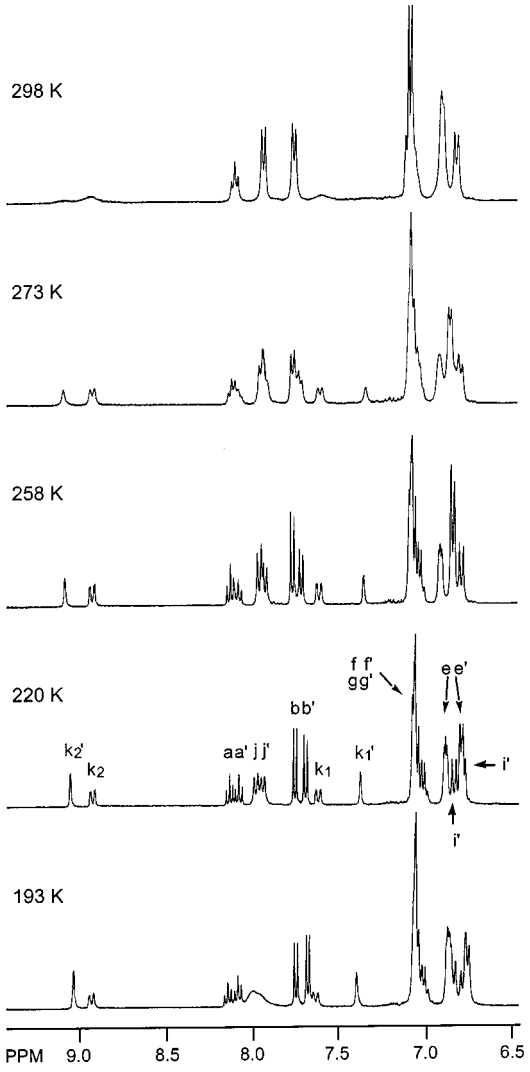

Figure 3. Variable temperature ^{1}H NMR spectrum of **2** in CD_2Cl_2

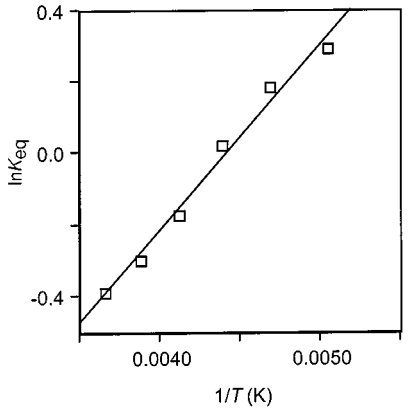

Figure 4. Plot of $\ln K_{eq}$ vs. T^{-1} for **2** in CD_2Cl_2

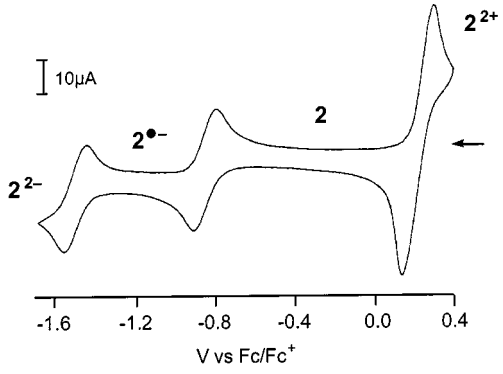

Figure 5. Cyclic voltammogram of **2** (1.0×10^{-3} M) in CH_2Cl_2 (0.1 M nBu$_4$NClO$_4$) at a glassy carbon working electrode with scan rate = 100 mV/s under Ar

the corresponding reduced species. This result is in sharp contrast to the redox behavior of L^2 in CH_2Cl_2, in which an irreversible reduction wave is observed at −1.67 V. Generally, the generated radical anion appears to be unstable, although this depends on the availability of a proton source.[9] In the case of reduction of the complex **2**, the added electrons are considered to be delocalized over the Pd^{II}-quinone diimine d-π* system. Compared with the uncomplexed one, the complexed quinone diimine becomes stabilized as an electron sink. Accordingly, the redox properties of the quinone diimine moiety are modulated by complexation with the palladium complex **1**, affording a multiredox complex system. Furthermore, the most positive anodic peak with twice height ($E_{1/2}$ = 0.20 V) is attributable to a one-electron oxidation process of the two terminal dimethylamino groups.[10] A substantial positive shift of this

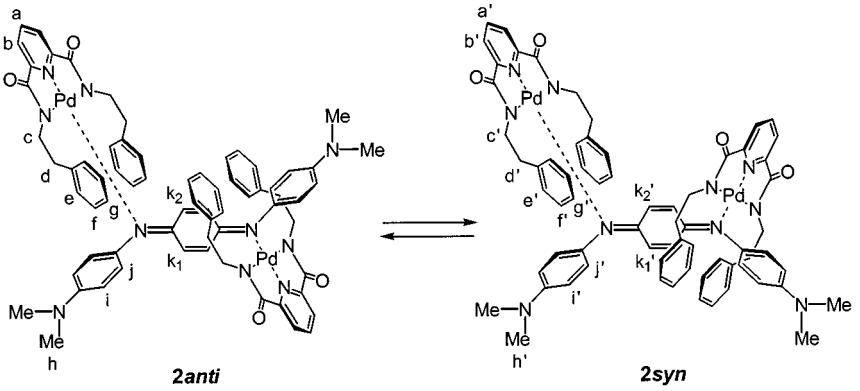

Scheme 2. Numbering of carbon atoms of the conjugated complex **2**; the left palladium complex moiety in each isomer is moved for labelling

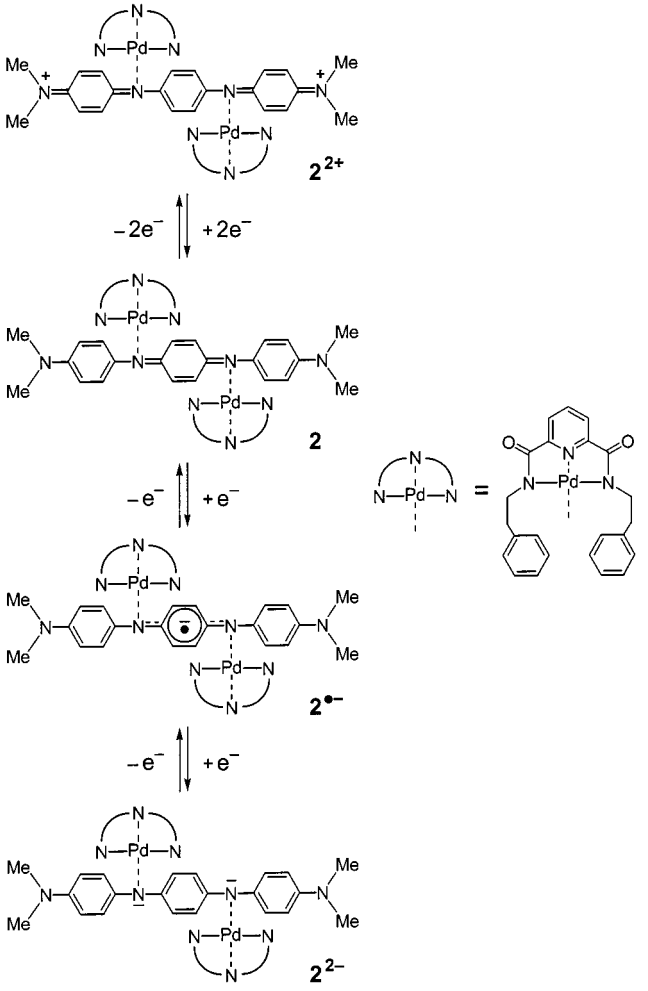

Scheme 3. Schematic representation of the redox behavior of the conjugated complex **2**

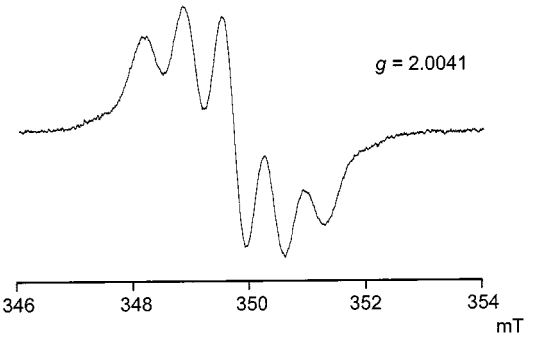

Figure 6. ESR spectrum of $\mathbf{2}^{\bullet-}$ in THF at 290 K

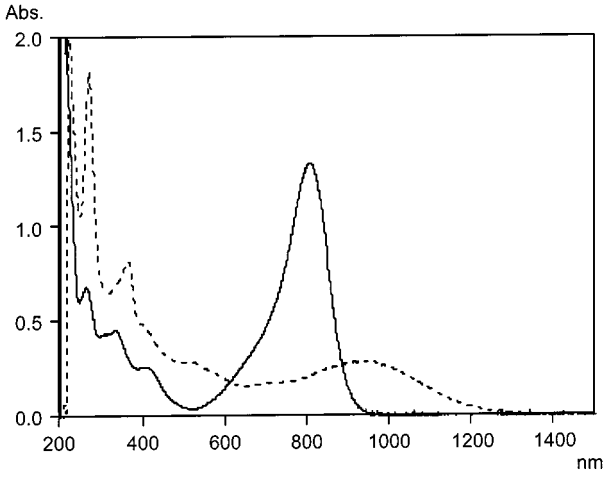

Figure 7. Electronic spectra of **2** (−) and $\mathbf{2}^{\bullet-}$ (− −) (2.0×10^{-5} M) in THF

oxidation wave compared with the free quinone diimine L^2 ($E_{1/2} = -0.08$ V) is consistent with the coordination of L^2 to palladium. The redox behavior of the conjugated complex **2** is depicted schematically in Scheme 3.

To gain insight into the redox properties of the conjugated complex **2**, the redox behavior was investigated spectroscopically. The chemical reduction of **2** in THF with $CoCp_2$ resulted in the appearance of the ESR signals centered around $g = 2.0041$, with hyperfine coupling to two equivalent nitrogen nuclei and four equivalent protons and weak coupling to the ^{105}Pd nucleus (natural abundance 22.2%, $I = 5/2$) as shown in Figure 6, indicating that the unpaired electron is located mostly on the quinone diimine moiety. Some delocalization onto the metal is revealed by the weak satellite lines due to ^{105}Pd coupling. The ESR signal could be approximately simulated by assuming the following parameters: $A_N = 6.6$ G; $A_H = 1.6$ G; $A_{Pd} = 3.4$ G.

The electronic spectrum of a solution of **2** in THF exhibits a strong broad absorption around 806 nm ($\log \varepsilon = 4.82$), probably assignable to a low-energy charge-transfer transition with significant Pd content (Figure 7). The generated semiquinone diimine complex $\mathbf{2}^{\bullet-}$ could be characterized by a broad absorption around 931 nm ($\log \varepsilon = 4.16$) as illustrated in Figure 7. This broad absorption, the assignment of which is not yet clear, might be a charge-transfer transition or an internal transition with significant Pd content.

Conclusion

Two palladium atoms were demonstrated to be bridged by the quinone diimine moiety of the π-conjugated molecule L^2 to afford the novel redox-active conjugated homobimetallic complex system, in which the complexed quinone diimine becomes stabilized as an electron sink. The *syn* configuration of the conjugated complex **2** is enthalpically more favorable than the *anti* one in CD_2Cl_2, but entropically less favorable. These results are related to the conjugated complexes with polyanilines. Bimetallic complexes composed of π-conjugated bridging spacers and terminal redox-active transition metals have currently received much attention as functional materials.[11] From this point of view, the potential use of the present bimetallic complex characterized by the redox-active π-conjugated bridging spacer appears to be promising.

Experimental Section

General Methods: All reagents and solvents were purchased from commercial sources and were further purified by the standard

methods, if necessary. Melting points were determined on a Yanagimoto Micromelting Point Apparatus and were uncorrected. Infrared spectra were obtained with a Perkin−Elmer Model 1605 FT-IR. ^{1}H NMR spectra were recorded on a JEOL JNM-GSX-400 (400 MHz) spectrometer with tetramethylsilane as an internal standard. Mass spectra were run on a JEOL JMS-DX303HF mass spectrometer. Electronic spectra were obtained using a Hitachi U-3500 spectrophotometer.

N,N′-Bis(2-phenylethyl)-2,6-pyridinedicarboxamide (L^1H_2) was prepared according to the method reported in a previous paper.[6b] *N,N′*-Bis(4′-dimethylaminophenyl)-1,4-benzoquinone diimine (L^2) was prepared by the literature method.[5]

Preparation of [(L^1)Pd(MeCN)] (1): A mixture of L^1H_2 (18.7 mg, 0.05 mmol) and $Pd(OAc)_2$ (11.2 mg, 0.05 mmol) in acetonitrile (5 mL) was stirred under argon at room temperature for 2 h. After evaporation of the solvent, the palladium complex **1** was isolated in 96% yield (24.9 mg) as yellow crystals by recrystallization from acetonitrile. M.p. 165−167 °C (uncorrected). − IR (KBr): $\tilde{\nu}$ = 1590, 1388 cm^{-1}. − ^{1}H NMR (400 MHz, CD_3CN, 298 K): δ = 2.78 (t, *J* = 7.3 Hz, 4 H), 3.40 (t, *J* = 7.3 Hz, 4 H), 7.19−7.33 (m, 10 H), 7.56 (d, *J* = 7.7 Hz, 2 H), 8.01 (t, *J* = 7.7 Hz, 1 H). − MS (FAB): *m*/*z* = 478 [(M − CH_3CN)$^+$ + 1]. − $C_{25}H_{24}N_4O_2Pd$ (518.91): calcd. C 57.87, H 4.66, N 10.80; found C 57.83, H 4.75, N 10.76.

Preparation of [(L^1)Pd(L^2)Pd(L^1)] (2): A mixture of **1** (20.8 mg, 0.04 mmol) and L^2 (6.9 mg, 0.02 mmol) was stirred in acetonitrile (20 mL) under argon at room temperature for 2 h. After evaporation of the solution, the conjugated palladium complex **2** was isolated in 73% yield as dark green crystals by recrystallization from chloroform/hexane. M.p. 227−229 °C (decomp.). − IR (KBr): $\tilde{\nu}$ = 1588, 1359, 1161 cm^{-1}. − UV/Vis (THF): λ_{max} (log ε) = 806 (4.82) nm. − ^{1}H NMR (400 MHz, CD_2Cl_2, 220 K, *anti*/*syn* = 1:1): δ = 2.15−2.30 (m, 8 H, *syn* and *anti*), 2.38−2.50 (m, 8 H, *syn* and *anti*), 2.76−2.90 (m, 8 H, *syn* and *anti*), 3.00−3.10 (m, 8 H, *syn* and *anti*), 3.13 (s, 12 H, *anti*), 3.20 (s, 12 H, *syn*), 6.75−6.92 (m, 24 H, *syn* and *anti*), 6.97−7.10 (m, 24 H, *syn* and *anti*), 7.38 (s, 2 H, *syn*), 7.62 (dd, *J* = 10.3, 2.2 Hz, 2 H, *anti*), 7.70 (d, *J* = 8.1 Hz, 4 H, *syn*), 7.76 (d, *J* = 8.1 Hz, 4 H, *anti*), 7.95 (d, *J* = 8.8 Hz, 4 H, *syn*), 7.99 (d, *J* = 8.8 Hz, 4 H, *anti*), 8.10 (t, *J* = 8.1 Hz, 2 H, *syn*), 8.15 (t, *J* = 8.1 Hz, 2 H, *anti*), 8.95 (dd, *J* = 10.3, 2.2 Hz, 2 H, *anti*), 9.08 (s, 2 H, *syn*). − MS (FAB): *m*/*z* = 1301 [M$^+$ + 1]. − $C_{68}H_{66}N_{10}O_4Pd_2$ (1300.18): calcd. C 62.82, H 5.12, N 10.77; found C 62.50, H 5.11, N 10.60.

Generation of [(L^1)Pd(L^2)$^{\bullet-}$Pd(L^1)] (2$^{\bullet-}$): For spectroscopic purposes, **2**$^{\bullet-}$ was generated by treatment of **2** with 1 equiv. of cobaltocene in THF. The cobaltocene and cobaltocenium ion present in the reaction mixture did not significantly interfere with the electronic spectrum because of their low extinction coefficient below 400 nm.

Equilibrium Measurement for 2: Measurement of the equilibrium constants at various temperatures was carried out by integration of the appropriate peaks during ^{1}H NMR spectroscopy. Spectra were taken in CD_2Cl_2 at 15 K intervals from 198 to 273 K. The thermodynamic parameters were determined from the van't Hoff plot of $\ln K_{eq}$ vs. T^{-1}.

Electrochemical Experiments: The cyclic voltammetry measurements were performed on a BAS CV-50 W voltammetry analyzer in deaerated acetonitrile containing 0.1 M *n*Bu_4NClO_4 as a supporting electrolyte at 298 K with a three-electrode system consisting of a highly polished glassy carbon working electrode (BAS), a platinum auxiliary electrode (BAS), and an Ag/AgCl (0.01 M) reference electrode (BAS) at 100 mV/s scan rate. Potentials are given vs. Fc/Fc^+.

X-ray Crystal Structure Determination of *anti*-2: A dark green crystal of the conjugated palladium complex ***anti*-2** with approximate dimensions of 0.20 × 0.20 × 0.30 mm was mounted on a glass fiber. The measurement was made on a Rigaku AFC5R diffractometer with graphite monochromated Mo-K_α radiation and a rotating anode generator. The cell constants and an orientation matrix for data collection were obtained from a least-squares refinement using the setting angles of 25 carefully centered reflections in the range 22.81 < 2θ < 27.12°. The data were collected at a temperature of 23 ± 1 °C using the ω-2θ scan technique to a maximum 2θ value of 55.1°. Totals of 8202 independent reflections were obtained and 7912 were unique. The structure was solved by heavy-atom Patterson methods and expanded using Fourier techniques. The non-hydrogen atoms were refined anisotropically. The final cycle of full-matrix least-squares refinement was based on 2875 observed reflections [$I > 3\sigma(I)$] and 379 variable parameters. R = 0.081, R_w = 0.112. Crystallographic details are given in Table 1. Crystallographic data (excluding structure factors) for the structure reported in this paper have been deposited with the Cambridge Crystallographic Data Centre as supplementary publication no. CCDC-152467 for *anti*-**2**. Copies of the data can be obtained free of charge on application to CCDC. 12 Union Road, Cambridge CB2 1EZ, UK [Fax: (internat.) +44-1223/336-033; E-mail: deposit@ccdc.cam.ac.uk].

Acknowledgments

We thank Professor M. Haga at Chuo University for helpful discussions. We are indebted to Professor Y. Wei for the preparation of L^2. This work was financially supported in part by a Grant-in-Aid for Scientific Research on Priority Areas from the Ministry of Education, Science, and Culture, Japan. Thanks are also due to the Analytical Center, Faculty of Engineering, Osaka University for the use of their facilities.

[1] [1a] A. L. Balch, R. H. Holm, *J. Am. Chem. Soc.* **1966**, *88*, 5201. − [1b] G. G. Christoph, V. L. Goedken, *J. Am. Chem. Soc.* **1973**, *95*, 3869. − [1c] L. F. Warren, *Inorg. Chem.* **1977**, *16*, 2814. − [1d] A. Vogler, H. Kunkely, *Angew. Chem. Int. Ed. Engl.* **1980**, *19*, 221. − [1e] P. Belser, A. von Zelewsky, M. Zehnder, *Inorg. Chem.* **1981**, *20*, 3098. − [1f] M. E. Gross, J. A. Ibers, W. C. Trogler, *Organometallics* **1982**, *1*, 530. − [1g] E. J. Miller, T. B. Brill, *Inorg. Chem.* **1983**, *22*, 2392. − [1h] A. M. Pyle, J. K. Barton, *Inorg. Chem.* **1987**, *26*, 3820. − [1i] H. Masui, A. B. P. Lever, P. R. Auburn, *Inorg. Chem.* **1991**, *30*, 2402. − [1j] H. Masui, A. B. P. Lever, E. S. Dodsworth, *Inorg. Chem.* **1993**, *32*, 258. − [1k] K. N. Mitra, S. Goswami, *Chem. Commun.* **1997**, 49. − [1l] R. A. Metcalfe, A. B. P. Lever, *Inorg. Chem.* **1997**, *36*, 4762. − [1m] T. Jüstel, J. Bendix, N. Metzler-Nolte, T. Weyhermüller, B. Nuber, K. Wieghardt, *Inorg. Chem.* **1998**, *37*, 35. − [1n] K. N. Mitra, S.-M. Peng, S. Goswami, *Chem. Commun.* **1998**, 1685. − [1o] J. Rall, A. F. Stange, K. Hübler, W. Kaim, *Angew. Chem. Int. Ed.* **1998**, *37*, 2681.

[2] [2a] E. F. G. Herington, *J. Chem. Soc.* **1959**, 3633. − [2b] K. Rieder, U. Hauser, H. Siegenthaler, E. Schmidt, A. Ludi, *Inorg. Chem.* **1975**, *14*, 1902. − [2c] H.-Y. Cheng, G.-H. Lee, S.-M. Peng, *Inorg. Chim. Acta* **1992**, *191*, 25.

[3] M. Higuchi, D. Imoda, T. Hirao, *Macromolecules* **1996**, *29*, 8277.

[4] [4a] T. Hirao, M. Higuchi, I. Ikeda, Y. Ohshiro, *J. Chem. Soc., Chem. Commun.* **1993**, 194. − [4b] T. Hirao, M. Higuchi, B. Hatano, I. Ikeda, *Tetrahedron Lett.* **1995**, *36*, 5925. − [4c] M. Higuchi, S. Yamaguchi, T. Hirao, *Synlett* **1996**, 1213. − [4d] M. Higuchi, I. Ikeda, T. Hirao, *J. Org. Chem.* **1997**, *62*, 1072.

[5] Y. Wei, C. Yang, T. Ding, *Tetrahedron Lett.* **1996**, *37*, 731.

[6] The series of *N*-heterocyclic multidentate podand ligands have

been used as complex catalysts in oxygenation with molecular oxygen: [6a] T. Hirao, T. Moriuchi, S. Mikami, I. Ikeda, Y. Ohshiro, *Tetrahedron Lett.* **1993**, *34*, 1031. – [6b] T. Hirao, T. Moriuchi, T. Ishikawa, K. Nishimura, S. Mikami, Y. Ohshiro, I. Ikeda, *J. Mol. Catal. A: Chemical* **1996**, *113*, 117.

[7] T. Moriuchi, S. Bandoh, Y. Miyaji, T. Hirao, *J. Organomet. Chem.* **2000**, *599*, 135.

[8] [8a] W. T. S. Huck, R. Hulst, P. Timmerman, F. C. J. M. van Veggel, D. N. Reinhoudt, *Angew. Chem. Int. Ed. Engl.* **1997**, *36*, 1006. – [8b] J. E. Kickham, S. J. Loeb, S. L. Murphy, *Chem. Eur. J.* **1997**, *3*, 1203. – [8c] B. R. Cameron, S. J. Loeb, G. P. A. Yap, *Inorg. Chem.* **1997**, *36*, 5498.

[9] G. E. Wnek, *Synth. Met.* **1986**, *15*, 213.

[10] A slightly larger cathodic peak than for the anodic peak suggests that the complete oxidation results in the sorption onto the electrode surface and on the reverse scan the complex might redissolve as it is reduced.

[11] [11a] M. Haga, T. Ano, K. Kano, S. Yamabe, *Inorg. Chem.* **1991**, *30*, 3843. – [11b] J.-P. Sauvage, J.-P. Collin, J.-C. Chambron, S. Guillerez, C. Coudret, V. Balzani, F. Barigelletti, L. De Cola, L. Flamigni, *Chem. Rev.* **1994**, *94*, 993. – [11c] W. Weng, T. Bartik, J. A. Gladysz, *Angew. Chem. Int. Ed. Engl.* **1994**, *33*, 2199. – [11d] M. D. Ward, *Chem. Soc. Rev.* **1995**, 121. – [11e] N. Le Narvor, L. Toupet, C. Lapinte, *J. Am. Chem. Soc.* **1995**, *117*, 7129. – [11f] A. Harriman, R. Ziessel, *Chem. Commun.* **1996**, 1707. – [11g] O. Lavastre, J. Plass, P. Bachmann, S. Guesmi, C. Moinet, P. H. Dixneuf, *Organometallics* **1997**, *16*, 184. – [11h] N. D. Jones, M. O. Wolf, D. M. Giaquinta, *Organometallics* **1997**, *16*, 1352. – [11i] M. M. Richter, A. J. Bard, W. Kim, R. H. Scmehl, *Anal. Chem.* **1998**, *70*, 310. – [11j] J. A. Mccleverty, M. D. Ward, *Acc. Chem. Res.* **1998**, *31*, 842. – [11k] M. Hissler, A. El-ghayoury, A. Harriman, R. Ziessel, *Angew. Chem. Int. Ed.* **1998**, *37*, 1717. – [11l] T. Bartik, W. Weng, J. A. Ramsden, S. Szafert, S. B. Falloon, A. M. Arif, J. A. Gladysz, *J. Am. Chem. Soc.* **1998**, *120*, 11071. – [11m] E. C. Constable, C. E. Housecroft, E. R. Schofield, S. Encinas, N. Armaroli, F. Barigelletti, L. Flamigni, E. Figgemeier, J. G. Vos, *Chem. Commun.* **1999**, 869.

Received June 21, 2000
[I00248]

A First Series of Dimeric Porphyrins Electrochemically Linked with Diphosphonium Bridges

Laurent Ruhlmann[b] and Alain Giraudeau*[a]

Keywords: Electrochemistry / Oxidation / Phosphorus / Synthetic methods / Porphyrins

The synthesis of dimeric porphyrins with a diphosphonium bridge in a direct one-pot electrochemical reaction is reported. The variation in the yields of this coupling reaction depends on the conditions of the electrolysis, and was examined mainly with respect to the detected by-products. An interpretation of this selective formation of dimers is proposed. Monomers and trimers were also obtained. These new compounds were characterized by ^{1}H NMR, ^{31}P NMR, UV/Vis spectroscopy and microanalysis. Important excitonic interactions were observed when the two porphyrin chromophores were linked with a short diphosphonium bridge. The NMR-spectroscopic data suggest that isomers are present in solution. Electrochemical data indicate that the two phosphonium groups of the bridge are not electrochemically independent in the zinc dimers.

Introduction

The synthesis of porphyrin dimers is being extensively pursued as these compounds provide models for the study of electron-transfer processes. Over the years, many models with various extended porphyrin structures have been prepared and studied with a particular interest in the dependence of the geometric factors on their physical properties.[1−8] The structural flexibility of the models is largely determined by the nature of the bridge. The totally rigid, covalently linked bis(porphyrins)[9−13] have chromophores fixed at well-defined distances and orientations, whereas conformational effects can be observed with less rigid systems.[14−16] To observe efficient interactions between the different chromophores, a large variety of bridging chains have been used as spacers in the building of dimers, but only a few reports[17−20] have been devoted to phosphanylporphyrins. Electrochemistry has been shown to be an appropriate synthetic tool in the coupling of porphyrins.[21−25] Recently, we reported a dimeric porphyrin,[23] with a diphosphonium bridge, which was synthesized by controlled potential electrolysis, a method that readily provides a convenient access to a large variety of new homometallated porphyrin dimers and trimers in a direct one-pot electrochemical reaction. This paper demonstrates the power of this approach and describes the efficient synthesis of various diphosphonium-bridged porphyrins using more or less rigid diphosphanes with variable length (Figure 1).

[a] Laboratoire d'Electrochimie et de Chimie Physique du Corps Solide, U.M.R. C.N.R.S. no. 7512, Université Louis Pasteur, 4 rue Blaise Pascal, 67000 Strasbourg, France
[b] Laboratoire de Chimie Physique, Equipe d'Electrochimie et de Photoélectrochimie, U.M.R. C.N.R.S. no. 8000, Université Paris-Sud
Bâtiment 420, 91405 Orsay Cedex, France

Physical characteristics of the synthesized porphyrins have been analyzed to identify the interactions between the different moieties in the dimers and the trimers.

Results

Electrosynthesis

The starting point for the synthesis is the electrochemical oxidation of (*meso*-tetraphenylporphyrin)zinc (ZnTPP) in the presence of various di- and triphosphanes. The oxidation waves of ZnTPP are reversible one-electron reactions in CH_3CN/1,2-$Cl_2C_2H_4$ (1:4).[26−28] In the presence of diphosphanes or ARPHOS, the second oxidation step became irreversible (Figure 2) and a new cathodic peak appeared, as observed in the reduction of electrochemically generated isoporphyrins.[28−31] Only the first oxidation step of ZnTPP was taken into account in this work.

In a typical experiment, a solution of the metalloporphyrin ZnTPP (1 equiv.) and bis(diphenylphosphanyl)methane (0.5 equiv.) was oxidized in the presence of 2,6-lutidine (2,6-Lut). 2,6-Lut was used to trap protons liberated during the course of porphyrin oxidation[23] and to prevent diphosphane-induced demetallation of ZnTPP before electrolysis. After maintaining the working potential at +0.85 V vs. SCE for 3 h, the initial violet solution turned green. The decrease in the oxidation current was not exponential with time. When this current reached the residual current measured in the absence of electroactive moieties, the electrolysis was stopped. The number of Coulombs consumed calculated from the recorded current−time curve $i = f(t)$ indicated that 2 Faradays per mol of ZnTPP were consumed in the reaction. After extraction and purification (see Exp. Sect.) the dimer **1-Zn-Zn** was characterized as the only new bis(porphyrin), obtained in 81% yield.

Increasing the diphosphane concentration caused a drastic decrease in the yield of the dimer, even in the presence

 © WILEY-VCH Verlag GmbH, 69451 Weinheim, 2001 1434−1948/01/0303−0659 $ 17.50+.50/0

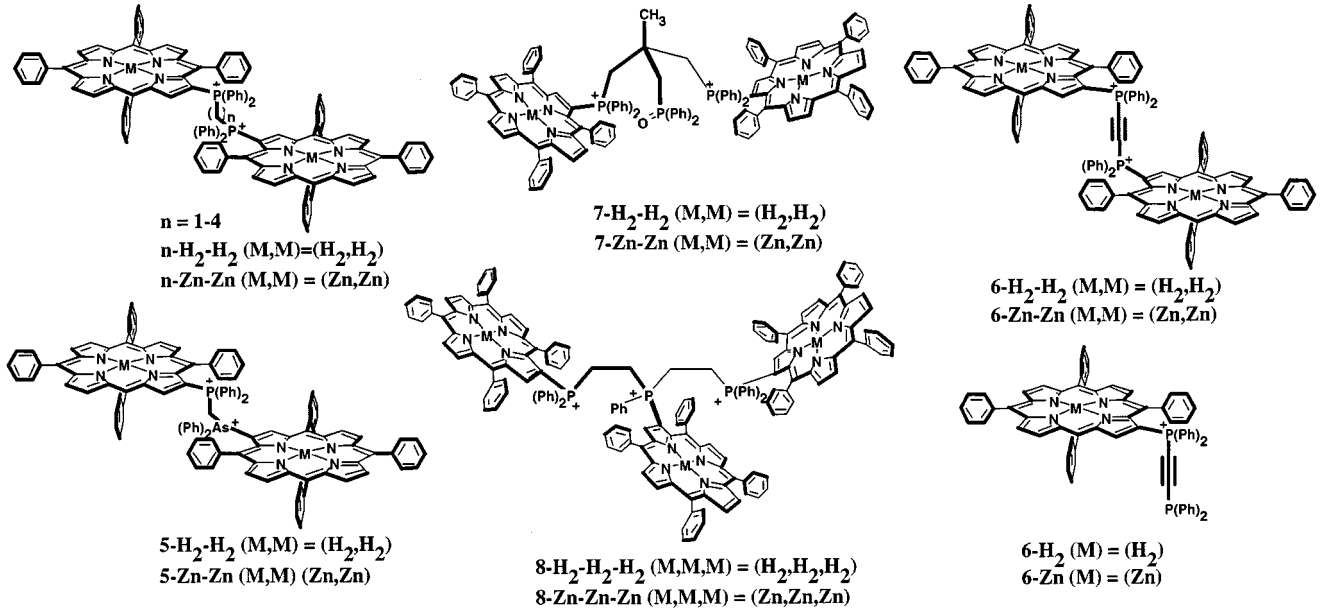

Figure 1. Porphyrins synthesized in this study

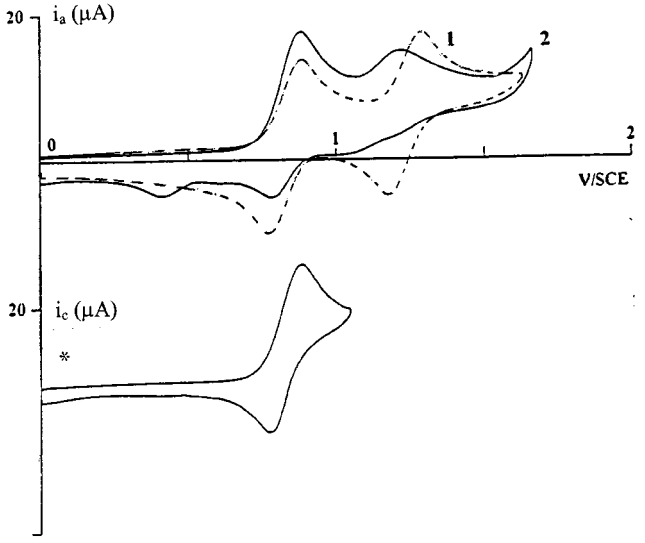

Figure 2. Cyclic voltammetry of ZnTPP in the absence of [1) dotted line] and in the presence of [2) full line] 1,2-bis(diphenylphosphanyl-ethane) (10 equiv.); *: first oxidation step only, in both cases; $CH_3CN/1,2\text{-}Cl_2C_2H_4$ (1:4) + T.E.A.PF_6 (0.1 M); working electrode Pt (v = 100 mV·s^{-1})

of a large excess of 2,6-Lut. No dimer was obtained when more than 10 equiv. of diphosphanes were used. This unexpected feature is interpreted in the discussion on the analysis of the side-products of the reaction. Diphosphane oxide and/or violin were recovered in these experiments; the overall yields of these compounds were high when using high concentrations of diphosphane and 2,6-lutidine.

By using 0.5 mol-equiv. of diphosphane (0.33 mol-equiv. of triphosphane in the case of the trimer **8-Zn-Zn-Zn**), only the desired dimers (or trimer) were produced in good yield.

In the present electrosynthesis, the formation of the dimers is described by Equation (1).

$$2\ P + Nu\text{-}\square\text{-}Nu \xrightarrow{E^1_{ox}} (P\text{-}\beta\text{-}Nu\text{-}\square\text{-}Nu\text{-}\beta\text{-}P)^{2+} + 4\ e^- + 2\ H^+ \quad (1)$$

(P = ZnTPP, Nu-□-Nu = diphosphane)

β-Monosubstituted porphyrin was also formed during the synthesis of the dimer **6-Zn-Zn**, in the presence of more than 0.5 equiv. of bis(diphenylphosphanyl)acetylene, as already described.[23]

UV/Vis Absorption Spectra

All the synthesized porphyrins exhibit a red shift of the Soret (B) and visible (Q) bands relative to the porphyrin subunits ZnTPP and H_2TPP. Complete UV/Vis data are reported in the Exp. Sect. for the electrosynthesized porphyrins. This bathochromic shift results from the electron-withdrawing effect of the positive charge located on the phosphonium cation(s). In the case of the metallated dimers, the Soret band shows significant broadening and its extinction coefficient is less intense than expected. These results suggest the presence of excitonic interactions between the two porphyrin rings in the dimers. These effects are greatly enhanced in the short-bridged **1-M-M** dimers (M = Zn and Cu) as shown in Figure 3 by the large red shift and by the splitting of the Q bands associated with a broad Soret band, with an extinction coefficient that is the lowest of those observed in the case of the **1-Zn-Zn** dimer.

This is clearly the result of exciton coupling which has been reported to become important when two porphyrin moieties are brought into close proximity[32−34] and/or when going from the nonmetallated porphyrin to the metallated parent.[34]

^{1}H NMR Spectra

The ^{1}H NMR spectra of the monomers, dimers and trimers show the well-known downfield shift of the aro-

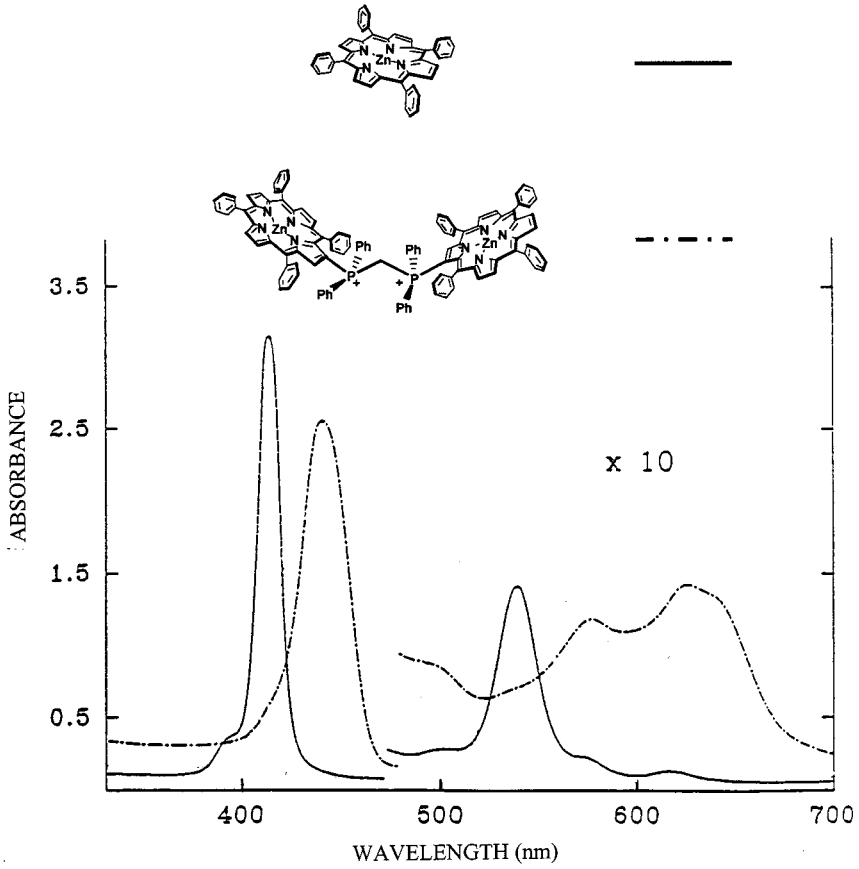

Figure 3. UV/Vis absorption spectra of the bis(porphyrin) **1-Zn-Zn** and of its monomeric subunit in CH_2Cl_2

matic proton signals of the porphyrin ring which characterizes the β-substitutions.[35] In the porphyrin rings of the dimers, the two β-H protons adjacent to the spacer give two distinct well-separated singlets, whereas the other β-proton signals appear as six doublets. The signals for the alkyl protons of the spacers are further downfield than those of the neutral ligands as owing to the presence of a positive charge on the phosphonium group. (For a full assignment, see Exp. Sect.) These protons coalesce into broadened signals or complex multiplets, with a splitting of the signal for the protons of the $-CH_2-$ groups bearing the phosphonium cations. A typical spectrum,[36] illustrated for the dimer **3-H_2-H_2** (Figure 4) shows a broad peak at $\delta \approx 2.42$, corresponding to the internal $-CH_2-$ of the linker and two distinct multiplets at $\delta = 2.80$ and 3.00, corresponding to the external $-CH_2-$ groups.

Such a distinct pair of multiplets is not observed in the corresponding neutral diphosphane which gives a triplet at $\delta = 2.25$. The appearance of two sets of resonances for the protons of the CH_2 groups bearing the phosphorus atoms as well as for the adjacent β-H protons, whose corresponding resonance signals are separated by $\Delta\delta = 0.03$ in the synthesized dimers and trimers, indicates the presence of a mixture of two isomers (Table 1). This is in agreement with previous studies of dimeric porphyrin systems[32,37–39] which connect two rings through their β-pyrrole positions. In particular, conformational analysis predicts a great conformational freedom when the two phenyl groups of the porphyrin unit are not substituted.[39] Furthermore, one of the β-H resonance doublets is shifted significantly downfield from the others. This could suggest that it experiences more shielding than the others, and may indicate the position of the phosphorus-linked phenyl groups.

The signals for the inner N−H protons of all the free-base porphyrins appear upfield as singlets and ruled out a cofacial conformation of the dimers which would induce a large upfield shift of the internal N−H protons[40] that is not observed.

^{31}P NMR Spectra

In the different neutral diphosphanes, the two phosphorus atoms are equivalent and their signals appear upfield as a singlet. In the bis(2-diphenylphosphanylethyl)-phenylphosphane, the signals of the two lateral phosphorus atoms appear as a doublet at $\delta = -13.15$, whereas the central atom gives a triplet at $\delta = -17.15$.

As expected, the two phosphonium cations of the dimers give rise to signals further downfield. Two well-separated signals are observed. A clear-cut evolution of these signals is depicted by the increase in the relative chemical shift $\Delta\delta$ (Table 1) between the two phosphonium groups which correlates with the increase in the length of the bridge linking the porphyrin subunits. These two signals indicate that the two phosphonium cations are in different environments. This result is not surprising because it is energetically not

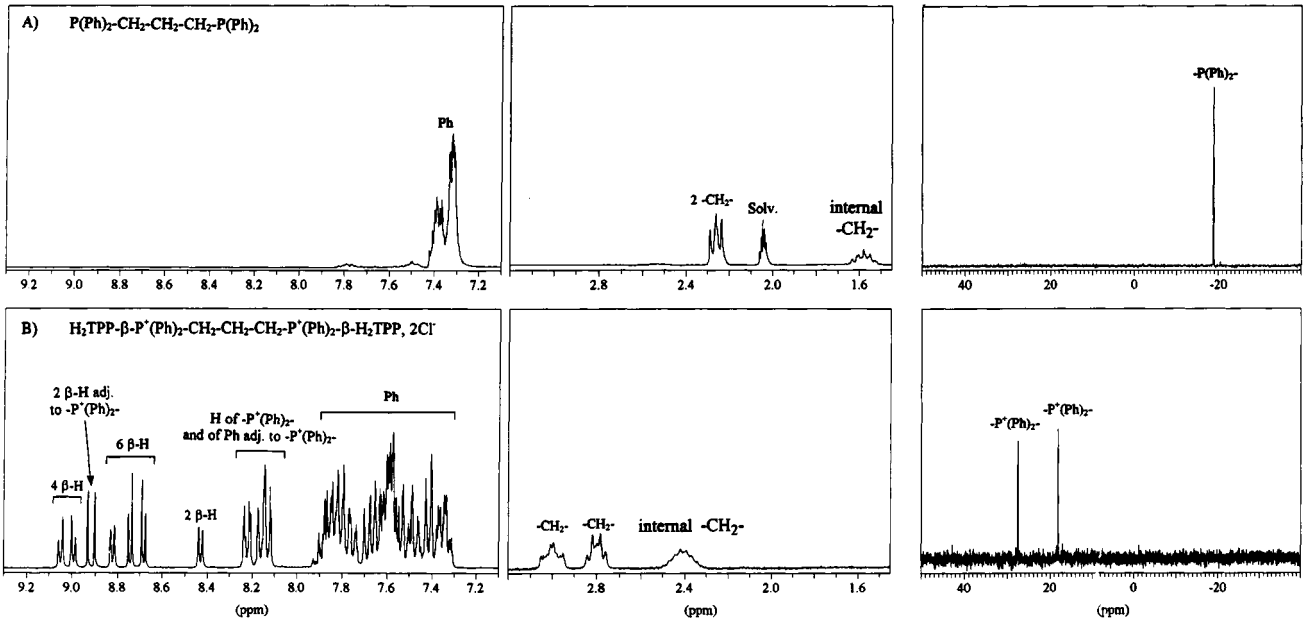

Figure 4. ^{1}H NMR and ^{31}P NMR spectra of A) 1,3-bis(diphenylphosphanyl)propane in [D_6]acetone; B) the bis(porphyrin) **3-H_2-H_2** in [D_6]acetone; for the region $\delta = 3.2-1.5$, see ref.[36]

Table 1. ^{31}P NMR: chemical shifts ($\Delta\delta$) of the phosphonium and phosphane* in the series; ^{1}H NMR: chemical shifts ($\Delta\delta$) of the β-H protons adjacent to the phosphonium in the series

Porphyrins	δ $P^+(Ph)_2$	or δ $P(Ph)_2$	$\Delta\delta$	δ β-H adj.		$\Delta\delta$
1-Zn-Zn	20.02	18.64	1.38	9.08	9.05	0.03
2-Zn-Zn	31.55	25.11	6.44	8.82	8.79	0.03
3-Zn-Zn	28.19	18.68	9.51	8.91	8.88	0.03
4-Zn-Zn	29.67	18.52	11.15	8.94	8.91	0.03
5-Zn-Zn	23.03		–	9.10	9.07	0.03
6-Zn	4.64	3.51*	–	7.80		–
6-Zn-Zn	14.03	13.62	0.41	8.80	8.79	0.01
7-Zn-Zn	26.43	15.88	10.55	9.71	9.68	0.03
1-H_2-H_2	19.83	18.08	1.75	9.08	9.04	0.04
2-H_2-H_2	29.70	26.81	2.89	8.76	8.73	0.03
3-H_2-H_2	27.66	18.08	9.58	8.96	8.93	0.03
4-H_2-H_2	30.02	21.02	9.00	9.01	8.98	0.03
5-H_2-H_2	23.54		–	9.13	9.10	0.03
6-H_2	18.95	3.81*	–	8.93		–
6-H_2-H_2	24.80	16.51	8.29	9.06	9.02	0.04
7-H_2-H_2	25.87	15.61	10.24	9.82	9.79	0.03

favorable to have a dimer when the two phosphorus atoms are in identical environments.

There is clear evidence that this is the case: Both the $(Ph)_2P(CH_2)P(Ph)_2$ and $(Ph)_2P(CH_2)_2P(Ph)_2$ linkages show doublets in the ^{31}P spectra (see Exp. Sect.) indicating the coupling of the phosphorus atoms in different environments. It is quite likely that this is true for the longer congeners, but that the coupling is too small to show it.

Electrochemistry

All electrochemical data are collated in Table 2. Owing to adsorption phenomena that occurred at the Pt electrode and inhibited the reduction signals, the cathode redox behavior of the different synthesized porphyrins was examined on an Hg electrode. The number of exchanged electrons for each system was determined by exhaustive coulometry, and by comparing the limiting currents of the different waves characterizing a given system.

The observed electron transfers were assigned to the π-systems of the porphyrins[41–42] or to the phosphonium cations,[43] based on their known general redox characteristics. This assignment was also achieved by the use of the recorded spectroelectrochemical data. All the spectra show typical features of porphyrin π-cation or π-anion radical complexes: broad α,β bands and a Soret band with decreased intensity as illustrated in Figure 5.

Redox behavior of the substituted monomers has previously been reported.[23] The dimers and trimers exhibit three distinct electroactive sites, namely the spacer and the two or three lateral porphyrin units. The electrochemical ring oxidations and reductions of the porphyrin subunits occur on both sides of the electroactivity range of the spacer. The oxidation potentials of the porphyrins in the dimers and trimers are more positive than the corresponding ones in the unsubstituted subunits. This positive shift may be ascribed to the electron-withdrawing effect of the positively charged spacer.[44] The close values observed between the reduction potentials of the dimers and trimers, and those of the corresponding porphyrin subunits were expected because this reduction occurred in neutral molecules,

Table 2. All potentials in V/SCE obtained from stationary (RDE) or cyclic voltammetry in $CH_3CN/1,2\text{-}Cl_2C_2H_4$ (1:4), T.E.A.PF_6 (0.1 M) medium; transfers are reversible one-electron steps, except when noted; working electrode: Pt

Porphyrins	Ring oxidation			Reduction of $P(Ph)_2^+$ and/or $As(Ph)_2^+$		Ring reduction		
	$E^{II}_{1/2}$		$E^{I}_{1/2}$	$E^{II}_{1/2}$	$E^{I}_{1/2}$	$E^{I}_{1/2}$		$E^{II}_{1/2}$
H_2TPP	1.34		1.10			−1.10		−1.48
ZnTPP	1.16		0.80			−1.37		−1.75
CuTPP	1.33		1.06			−1.22		−1.68
Violine	1.52^{irr}		1.08^{irr}			−0.82		-1.30^{irr}
1-H_2-H_2			$1.22^{2e,irr}$	$-0.74^{2e\ [a]}$		$-1.10^{2e[a]}$		$-1.55^{2e[a]}$
1-Zn-Zn	1.17^{2e}		0.97^{2e}	$-1.04^{[a]}$	$-1.16^{[a]}$	$-1.42^{2e[a]}$		$-1.77^{2e[a]}$
1-Cu-Cu	1.22^{2e}		0.98^{2e}	$-0.97^{[a]}$	$-1.14^{[a]}$	−		$-1.72^{2e[a]}$
2-H_2-H_2			$1.28^{2e,irr}$	$-0.74^{2e[a]}$		$-1.10^{2e[a]}$		$-1.55^{2e[a]}$
2-Zn-Zn	1.23^{2e}		1.02^{2e}	$-0.99^{[a]}$	$-1.17^{[a]}$	$-1.38^{2e[a]}$		$-1.76^{2e[a]}$
3-H_2-H_2			$1.32^{2e,irr}$	$-0.73^{2e[a]}$		$-1.08^{2e[a]}$		
3-Zn-Zn	1.40^{2e}		1.10^{2e}	$-1.00^{[a]}$	$-1.11^{[a]}$	$-1.37^{2e[a]}$		$-1.75^{2e[a]}$
4-H_2-H_2			$1.31^{2e,irr}$	$-0.70^{2e[a]}$		$-1.05^{2e[a]}$		$-1.73^{2e[a]}$
4-Zn-Zn	1.19^{2e}		0.90^{2e}	$-0.94^{[a]}$	$-1.10^{[a]}$	$-1.35^{2e[a]}$		$-1.68^{2e[a]}$
5-H_2-H_2			$1.34^{2e,irr}$	$-0.63^{2e[a]}$		$-0.98^{2e[a]}$		$-1.38^{2e[a]}$
5-Zn-Zn	1.32^{2e}		1.07^{2e}	$-0.97^{[a]}$	$-1.12^{[a]}$	$-1.34^{[a]}$	$-1.66^{[a]}$	$-2.08^{2e[a]}$
6-H_2			1.11^{irr}	$-0.93^{[a]}$		$-1.18^{[a]}$		
6-Zn	1.18		0.89	$-1.04^{[a]}$		$-1.22^{[a]}$		$-1.41^{[a]}$
6-H_2-H_2			$1.32^{2e,irr}$	$-0.73^{[a]}$	$-1.02^{[a]}$	$-1.30^{2e[a]}$		$-1.52^{2e[a]}$
6-Zn-Zn	1.35	1.25	1.03^{2e}	$-0.73^{[a]}$	$-1.12^{[a]}$	$-1.30^{2e[a]}$		
7-H_2-H_2			$1.34^{2e,irr}$	$-0.62^{2e[a]}$		$-1.01^{2e[a]}$		
7-Zn-Zn	1.29^{2e}		1.00^{2e}	$-0.92^{[a]}$	$-1.10^{[a]}$	$-1.38^{2e[a]}$		$-1.68^{2e[a]}$
8-H_2-H_2-H_2			$1.27^{3e,irr}$	$-0.67^{3e[a]}$		$-0.94^{3e[a]}$		
8-Zn-Zn-Zn	$1.37^{3e,irr}$		1.02^{3e}	$-0.93^{3e[a]}$		$-1.27^{3e[a]}$		$-1.65^{3e[a]}$

[a] Potentials obtained by polarography (dropping mercury electrode).

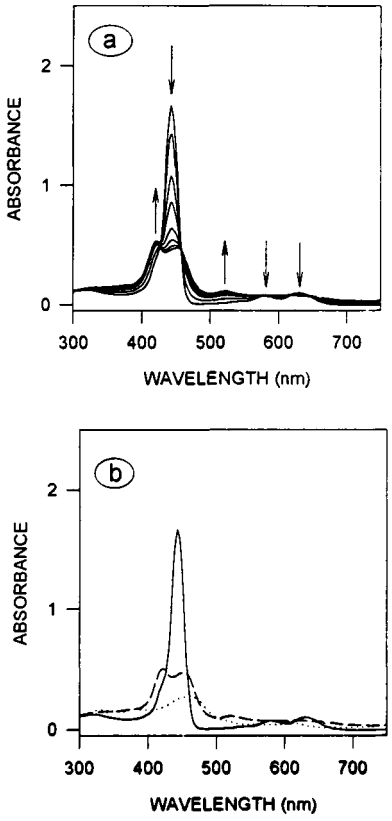

Figure 5. a) UV/Vis absorption spectra recorded during the oxidation of **4-Zn-Zn** in $CH_3CN/1,2\text{-}Cl_2C_2H_4$ (1:4) + T.E.A.PF_6 (0.1 M) at 1.0 V vs. SCE; b) UV/Vis absorption spectra of **4-Zn-Zn**: (− − − −) unoxidized form, (------) two-electron oxidized species (first wave, 1.00 V), and (·····) four-electron oxidized species (second wave, 1.27 V)

and the positively charged spacers become neutral before the reduction of the side porphyrin rings. In the synthesized porphyrins, each of the different oxidation and reduction steps observed appears as reversible or quasi-reversible, with an exchange of one electron per porphyrin subunit, except for the oxidation step of the nonmetallated complexes. The irreversible two-electron transfer observed in the free-base porphyrins may be explained by the instability of the radical cation.[24]

The reduction signal of the phosphonium cations appeared in CV at −0.70 V vs. SCE for the free bases and −1.1 V vs. SCE for the zinc complexes. This cathode signal corresponds to a two-electron reduction step. Two distinct reduction peaks are observed in all the zinc dimers and in the **6-H_2-H_2** dimer, each corresponding to a reversible electron transfer. This feature indicates that the two phosphonium cations are not independent.

By analyzing both the redox and UV/Vis results of the synthesized dimers, a common behavior appeared that depended on the nature (metallated or not) of these compounds. While the free-base dimers showed only minimal excitonic effects, the corresponding metallated dimers showed significant interactions between the chromophores. Similarly, the two phosphonium cations appeared as independent electroactive centers in the free-base dimers, but showed an interaction in their metallated homologs. This behavior could be analyzed as a consequence of δ−π interactions present in the metalloporphyrins. These interactions would thus favor a coupling between the different subunits (spacer, porphyrin). Consequences of these δ−π interactions have already been reported with the redox behavior of substituted metalloporphyrins.[44]

Discussion

Previous results on the electrochemical preparation of porphyrin dimers with a viologen as a spacer have established that the synthesis is achieved by means of a two-electron reaction per mol of porphyrin.[24] This sequence was also validated in the synthesis of the above porphyrins.

Nevertheless, a large increase in the diphosphane present in solution somewhat limits the range of the experiments. When a large excess of diphosphanes is added, the concentration of the 2,6-lutidine has to be increased to prevent the diphosphane-induced demetallation of ZnTPP. Owing to the lengthy electrolysis and the hygroscopic nature of 2,6-lutidine, an increase in its concentration leads to the introduction of significant amounts of water in the coulometric solution. Thus, if the hydroxide ions become the main nucleophile present in solution and if they react with the generated π-cation radical of the porphyrin, then, hydroxyisotetraphenylporphyrin is produced. Further α-attack of the OH^- ions would lead to violin formation, as already described by Dolphin et al.[45] The final purple complex isolated as a by-product exhibited electronic and ^1H NMR spectra similar to violins, in which only three of the pyrrole rings are conjugated. When phosphanes are the main nucleophiles in solution, phosphonium isoporphyrin would be formed before further α-attack of the OH^- ions would take place. This α-attack would give betaine and a four-membered ring transition state[46] (intermediate in the Wittig reaction), leading to the formation of (*meso*-tetraphenylporphyrin)zinc and phosphane oxide. This reaction would explain the drastic decrease in the yield of the dimers and of the characterized side-products collected when the concentration of 2,6-lutidine and/or of the diphosphanes was increased.

The most intriguing feature in this synthesis is the selective formation of dimers even with excess nucleophile. This was not observed with the rigid linear 4,4′-bipyridine linker. This result may be explained if one considers that the phosphorous atoms act as more efficient nucleophiles than the nitrogen atoms in these experiments, and that the phosphorus ligands used as linkers are flexible chains. The fact that both monomers and dimers are formed when the more rigid acetylene chain is used agrees with this hypothesis. This is also supported by the higher yield of desired dimer observed in the case of the long flexible diphosphane: 1,4-bis(diphenylphosphanyl)butane chain. Steric hindrance is most probably the reason why only two porphyrin units are linked with 1,1,1-tris(diphenylphosphanylmethyl)ethane, while the trimer **8-Zn-Zn-Zn** is formed when using the stretched bis(2-diphenylphosphanylethyl)phenylphosphane chain.

Conclusion

The results presented in this paper clearly illustrate that phosphorus ligands act as powerful nucleophiles which allow electrochemical β-substitutions on *meso*-tetraphenylporphyrins. When 0.5 mol-equiv. of diphosphanes is used, only the dimers are produced in good yields (> 60%). Selective dimer formation in a one-pot electrochemical step is particularly noteworthy when considering that only the monomer was generated in the case of the 4,4′-bipyridine nucleophiles.

Evidence for excitonic coupling is observed in the dimers. This effect is particularly enhanced in the metallated **1-M-M** dimers and demonstrates that bridging with the short 1,2-bis(diphenylphosphonium)methane chain keeps the two porphyrin chromophores in an interactive proximity. Isomers are therefore possible because of the two different electrophilic β-sites. Both ^1H NMR and ^{31}P NMR spectroscopy results suggest that geometric factors modulate the mutual interactions of the two porphyrin units in the dimers. The preparation of the trimer further validates this electrochemical method as a direct route to oligomeric porphyrins linked by phosphonium bridges.

Experimental Section

I. Materials: All solvents and chemicals were of reagent-grade quality, purchased commercially and used without further purification unless otherwise stated. CH_2Cl_2, for use in exhaustive electrolysis or UV/Vis spectrophotometry, was heated at reflux in the presence of CaH_2 and then distilled off. The supporting electrolyte tetraethylammonium hexafluorophosphate (T.E.A.PF_6) was used without further purification. All the diphosphanes and triphosphanes were purchased from Strem Chemical Inc. Thin-layer chromatography (TLC) was performed on commercially prepared alumina or silica gel plates purchased from Roth Sochiel.

II. Apparatus: All electrochemical measurements were carried out under argon at 25 °C on a dropping mercury electrode or on a disk electrode. Voltammetric data were obtained with a standard three-electrode system using a Bruker E 130 M potentiostat and a high-impedance millivoltmeter (minisis 6000, Tacussel). Current−potential curves were obtained from an Ifelec If 3802 X-Y recorder. The working electrode was a platinum disk (E.D.I. type, Solea Tacussel) with a surface area of 3.14 mm^2. A platinum wire was used as the auxiliary electrode. The reference electrode was a saturated calomel electrode (SCE) that was electrically connected to the studied solution by a junction bridge filled with the corresponding solvent/supporting electrolyte solution. − For polarographic and differential pulse polarographic experiments, a signal generator (GSATP from Solea-Tacussel) was associated with a potentiostatic device (Solea-Tacussel), comprising of a potentiostat (PRT 20−2X) and a voltage pilot unit (Servovit 2). − Coulometric measurements and quantitative electrochemical synthesis were performed either in a standard 50-mL cell or in a large 300-mL cell. In the standard cell, the working electrode was a platinum wire (Ø = 0.8 mm) with a length of 60 cm. In the large cell, the working electrode was a cylindrical platinum grid (Ø = 5 cm, h = 7 cm). For the controlled-potential electrolysis, the anodic and cathodic compartments were separated by a fritted glass disk to prevent diffusion of the electrogenerated species. − The spectrophotometric analyses were performed with a Hewlett−Packard 8452 A diode array spectrometer. The thin-layer spectroelectrochemical cell has been described previously.[47] − UV/Vis spectra were recorded with a Shimazu UV-260 spectrophotometer and a Hewlett−Packard 8452 A diode array spectrometer. − ^1H and ^{31}P NMR spectra were

obtained in [D_6]acetone with a Bruker AC 300 spectrometer (300 MHz and 120 MHz, respectively). − Elemental analyses were performed by the microanalysis services of the Chemical Department of I.U.T. Sud (Strasbourg).

III. Synthesis: Compounds H_2TPP, ZnTPP and CuTPP were prepared and purified by known procedures.[48,49]

Electrochemical Synthesis. − General Procedure: Prior to electrolysis, the corresponding mixtures were stirred and degassed by bubbling argon through the solution for 10 min. The desired working potential was then applied. During anodic oxidation, the electrolyzed solution was continuously stirred and maintained under argon. The course of the reaction was monitored by TLC (silica gel/1% CH_3OH in CH_2Cl_2) and UV/Vis spectrophotometry. Electrolysis was stopped when the current reached the residual current measured in the absence of electroactive material (i.e., 0.1 M solution of T.E.A.PF_6). After electrolysis, the solvents were removed in a rotary evaporator. The residue was dissolved in a minimum amount of CH_2Cl_2; the mixture was then poured into water, and the organic layer was washed three times. The organic solution was dried with $CaSO_4$, concentrated (to 5 mL), and then purified by chromatography. Typical preparation and characterization of a dimer **1-Zn-Zn**, **1-H_2-H_2** and **1-Cu-Cu** are reported below.

1-Zn-Zn: ZnTPP (200 mg, 2.95×10^{-4} mol), 2,6-Lut (50 μL, 4.30 10^{-4} mol) and $(Ph)_2P-CH_2-P(Ph)_2$ (57 mg, 1.475×10^{-4} mol) were dissolved in a solution of T.E.A.PF_6 (0.1 M, 300 mL) in 1,2-$Cl_2C_2H_4$/CH_3CN (4:1). The electrolysis was carried out for 6 h at +0.85 V vs. SCE. After the workup, as described above, the organic extract (5 mL) was purified by chromatography on silica gel. The first fraction (eluted with CH_2Cl_2) was unchanged ZnTPP (32 mg, 0.47×10^{-4} mol). The desired product was eluted with a mixture of CH_2Cl_2/CH_3OH (99:1). After evaporation of the solvent, **1-Zn-Zn** was recrystallized from CH_2Cl_2/*n*-hexane to afford the product as green crystals (242 mg, 1.19×10^{-4} mol, 81%). − UV/Vis (CH_2Cl_2): λ_{max} (ε, $M^{-1}cm^{-1}$): = 442 (186900), 580 (9100), 624 (10800), 644 nm (10700). − ^{1}H NMR [300 MHz, $(CD_3)_2CO$, 25 °C]: δ = 9.08 [s, 1 H, β-H adj. to $-P(Ph)_2-^+$], 9.05 [s, 1 H, β-H adj. to $-P(Ph)_2-^+$], 8.85 (d, J_{cis} = 4.77 Hz, 2 H, β-H), 8.83 (d, J_{cis} = 4.80 Hz, 4 H, β-H), 8.79 (d, J_{cis} = 4.77 Hz, 2 H, β-H), 8.64 (d, J_{cis} = 4.77 Hz, 2 H, β-H), 8.17 [dt, J_o = 7.71 Hz, J_m= 1.47 Hz, 4 H, *o*-H of $-P(Ph)_2-^+$], 8.15 (d, J_{cis} = 4.77 Hz, 2 H, β-H), 8.13 [dt, J_o= 7.71 Hz, J_m = 1.47 Hz, 4 H, *o*-H of $-P(Ph)_2-^+$], 8.02 [dt, J_o = 7.71 Hz, J_m = 1.47 Hz, 4 H, *o*-H of Ph adj. to $-P(Ph)_2^+$], 7.84−7.49 (m, 36 H, H of Ph), 7.40 (t, J_o = 7.71 Hz, 3 H, *p*-H of Ph), 7.39 [t, J_o = 7.71 Hz, 3 H, *p*-H of Ph], 7.13 [t, J_o = 7.71 Hz, 2 H, *p*-H of Ph adj. to $-P(Ph)_2^+$], 7.00 [t, J_o = 7.71 Hz, 4 H, *p*-H of $-P(Ph)_2-^+$], 3.71 (d, ^1J = 12.12 Hz, 1 H, $-CH_2$), 3.65 (d, ^1J = 12.12 Hz, 1 H, $-CH_2-$). − ^{31}P NMR [120 MHz, $(CD_3)_2CO$, 25 °C]: δ = 20.02 [d, $^2J_{P-P}$ = 15.01 Hz, $-P(Ph)_2^+$], 18.64 [d, $^2J_{P-P}$ = 15.01 Hz, $-P(Ph)_2-^+$], −145.44 (sept, $^1J_{P-F}$ = 700.80 Hz, PF_6^-). − $C_{113}H_{76}F_{12}N_8P_4Zn_2$ (2028.54): calcd. C 66.91, H 3.77, N 5.52, P 6.11; found C 66.80, H 3.87, N 5.61, P 6.08. − M.p. > 300 °C.

1-H_2-H_2: Hydrochloric acid (25%, 100 mL) was added to a solution of **1-Zn-Zn** in acetone, and the mixture was stirred for 30 min at room temperature. After the addition of water (200 mL), the organic layer was separated, washed with water and neutralized with saturated sodium acetate solution. The solution was again washed with water, dried with $CaSO_4$ and concentrated. Recrystallization of the residue with CH_2Cl_2/*n*-hexane gave **1-H_2-H_2** in almost quantitative yield. − UV/Vis (CH_2Cl_2): λ_{max} (ε, $M^{-1}cm^{-1}$) = 432 (461600), 530 (22600), 560 (8200), 604 (8300), 670 nm (16000). − ^{1}H NMR [300 MHz, $(CD_3)_2CO$, 25 °C]: δ = 9.08 [s, 1 H, β-H adj. to $-P(Ph)_2-^+$], 9.04 [s, 1 H, β-H adj. to $-P(Ph)_2-^+$), 9.04 (d, J_{cis} = 4.41 Hz, 2 H, β-H), 9.02 (d, J_{cis} = 4.41 Hz, 2 H, β-H), 8.82 (d, J_{cis} = 4.41 Hz, 2 H, β-H), 8.76 (d, J_{cis} = 4.41 Hz, 2 H, β-H), 8.71 (d, J_{cis} = 4.41 Hz, 2 H, β-H), 8.40 (d, J_{cis} = 4.41 Hz, 2 H, β-H), 8.24 [d, J_o = 7.35 Hz, 4 H, *o*-H of $-P(Ph)_2-^+$], 8.18 [d, J_o = 7.35 Hz, 4 H, *o*-H of $-P(Ph)_2-^+$], 8.11 [d, J_o = 7.35 Hz, 4 H, *o*-H of Ph adj. to $-P(Ph)_2-^+$], 7.85−7.39 (m, 42 H, H of Ph), 7.21 [t, J_o = 6.99 Hz, 2 H, *p*-H of Ph adj. to $-P(Ph)_2-^+$], 7.05 (t, J_o = 6.99 Hz, 4 H, *p*-H of Ph), 3.72 (d, ^1J = 12.12 Hz, 1 H, $-CH_2-$), 3.67 (d, ^1J = 12.12 Hz, 1 H, $-CH_2-$), −2.47 (s, 4 H, N−H). − ^{31}P NMR [120 MHz, $(CD_3)_2CO$, 25 °C]: δ = 19.83 [d, $^1J_{P-C}$ = 14.18 Hz, $-P(Ph)_2^+$], 18.08 [d, $^2J_{P-P}$ = 14.18 Hz, $-P(Ph)_2$]. − $C_{113}H_{80}Cl_2N_8P_2$ (1682.80): calcd. C 80.65, H 4.79, N 6.66, P 3.68; found C 80.81, H 4.83, N 6.52, P 3.60. − M.p. > 300 °C.

1-Cu-Cu: 1-H_2-H_2 was dissolved in a CH_2Cl_2/CH_3OH (1:1) mixture with an excess of $Cu^{II}(CH_3COO)_2 \cdot H_2O$ (10 equiv.). The mixture was heated at reflux for 3 h, and after cooling, was treated with tetraethylammonium hexafluorophosphate (100 equiv.). After evaporation of the solvent, the residue was dissolved in a minimum amount of CH_2Cl_2, washed with water (4 times) and dried with $CaSO_4$ for 6 h. The solution was concentrated to 5 mL in a rotary evaporator and then purified on a silica gel column (CH_2Cl_2) to afford black−violet crystals of **1-Cu-Cu** in more than 90% yield. − UV/Vis (CH_2Cl_2): λ_{max} (ε, $M^{-1}cm^{-1}$) = 440 (246500), 576 (13600), 625 (16500), 643 nm (15000). − $C_{113}H_{76}Cu_2F_{12}N_8P_4$ (2024.89): calcd. C 66.97, H 3.78, N 5.53, P 6.11; found C 66.81, H 3.82, N 5.48, P 6.01. − M.p. > 300 °C.

2-Zn-Zn: The same procedure as described for **1-Zn-Zn** was applied using ZnTPP (200 mg, 29.5 mmol, 1 equiv.), 2,6-Lut (50μL, 43 mmol) and $(Ph)_2P-CH_2-CH_2-P(Ph)_2$ (57 mg, 14.8 mmol, 0.5 equiv.). The product **2-Zn-Zn** (196 mg; 9.6 mmol) was obtained in 65% yield. − UV/Vis (CH_2Cl_2): λ_{max} (ε, $M^{-1}cm^{-1}$) = 436 (420800), 568 (18500), 614 nm (22100). − ^{1}H NMR [300 MHz, $(CD_3)_2CO$), 25 °C]: δ = 9.04 (d, J_{cis} = 4.80 Hz, 2 H, β-H), 8.91 (d, J_{cis} = 4.80 Hz, 2 H, β-H), 8.82 [s, 1 H, β-H adj. to $-P^+(Ph)_2-$], 8.79 [s, 1 H, β-H adj. to $-P^+(Ph)_2-$], 8.76 (d, J_{cis} = 4.80 Hz, 2 H, β-H), 8.68 (d, J_{cis} = 4.77 Hz, 2 H, β-H), 8.66 (d, J_{cis} = 4.77 Hz, 2 H, β-H), 8.16 (d, J_{cis} = 4.80 Hz, 2 H, β-H), 8.12 [d, J_o = 6.60 Hz, 4 H, *o*-H of $-P^+(Ph)_2-$], 8.04 [d, J_o = 7.70 Hz, 4 H, *o*-H of $-P^+(Ph)_2-$], 8.00 [d, J_o = 6.60 Hz, 4 H, *o*-H of Ph adj. to $-P^+(Ph)_2$], 7.83−7.35 (m, 48 H, H of Ph), 2.40−2.17 (m, 4 H, $-CH_2-$). − ^{31}P NMR [120 MHz, $(CD_3)_2CO$, 25 °C]: δ = 31.55 [d, $^3J_{P-P}$ = 53.00 Hz, $-P^+(Ph)_2-$], 24.11 [d, $^3J_{P-P}$ = 53.0 Hz, $-P^+(Ph)_2-$], −145.35 (sept, $^1J_{P-F}$ = 700.70 Hz, PF_6^-). − $C_{114}H_{78}F_{12}N_8P_4Zn_2$ (2042.57): calcd. C 67.03, H 3.84, N 5.49; found C 67.17, H 3.80, N 5.53.

2-H_2-H_2: The same procedure as described for **1-H_2-H_2** was used to obtain quantitatively **2-H_2-H_2**. − UV/Vis (CH_2Cl_2): λ_{max} (ε, $M^{-1}cm^{-1}$) = 432 (450000), 532 (22400), 560 (8000), 604 (7800), 668 nm (16000). − ^{1}H NMR [300 MHz, $(CD_3)_2CO$), 25 °C]: δ = 9.02 (d, J_{cis} = 5.1 Hz, 2 H, β-H), 8.96 (d, J_{cis} = 5.1 Hz, 2 H, β-H), 8.79 (d, J_{cis} = 5.1 Hz, 2 H, β-H), 8.76 [s, 1 H, β-H adj. to $-P^+(Ph)_2-$], 8.73 [s, 1 H, β-H adj. to $-P^+(Ph)_2-$], 8.72 (d, J_{cis} = 4.8 Hz, 2 H, β-H), 8.67 (d, J_{cis} = 4.8 Hz, 2 H, β-H), 8.41 (d, J_{cis} = 5.1 Hz, 2 H, β-H), 8.20 [dt, J_o = 6.6 Hz, J_m = 1.5 Hz, 4 H, *o*-H to $-P^+(Ph)_2-$], 8.16 [dt, J_o= 6.6 Hz, J_m = 1.5 Hz, 4 H, *o*-H of $-P(Ph)_2-^+$], 8.08 [d, J_o= 6.6 Hz, J_m = 1.5 Hz, 4 H, *o*-H of Ph adj. to $-P^+(Ph)_2$], 7.87−7.45 (m, 44 H, H of Ph), 7.26 [t, J_o = 7.7 Hz, 4 H, *p*-H of $-P^+(Ph)_2-$], 2.35−2.15 (m, 4 H, $-CH_2-$), −2.53 (s, 4 H, N−H internal). − ^{31}P NMR [120 MHz, $(CD_3)_2CO$, 25 °C]: δ = 29.70

[s, $-P^+(Ph)_2-$], 26.81 [s, $-P^+(Ph)_2$]. – $C_{114}H_{82}Cl_2N_8P_2$ (1758.78): calcd. C 80.70, H 4.87, N 6.60; found C 80.72, H 4.92, N 6.55.

3-Zn-Zn: This was prepared by the same method as **1-Zn-Zn** using ZnTPP (200 mg, 29.5 mmol, 1 equiv.), 2,6-Lut (50 μL, 43.0 mmol) and $(Ph)_2P-CH_2-CH_2-CH_2-P(Ph)_2$ (61 mg, 14.8 mmol, 0.5 equiv.). After 5 h of electrolysis at 0.85 V vs. S.C.E., **3-Zn-Zn** (213 mg, 10.4 mmol) was obtained in 70% yield. – UV/Vis (CH_2Cl_2): λ_{max} (ε, $M^{-1}cm^{-1}$) = 438 (308400), 572 (12900), 620 nm (15900). – ^1H NMR [300 MHz, $(CD_3)_2CO$), 25 °C]: δ = 8.91 [s, 1 H, β-H adj. to $-P^+(Ph)_2-$], 8.88 [s, 1 H, β-H adj. to $-P^+(Ph)_2-$], 8.81 (d, J_{cis} = 4.8 Hz, 2 H, β-H), 8.80 (d, J_{cis} = 4.8 Hz, 2 H, β-H), 8.79 (d, J_{cis} = 4.8 Hz, 2 H, β-H), 8.77 (d, J_{cis} = 4.8 Hz, 2 H, β-H), 8.64 (d, J_{cis} = 4.8 Hz, 2 H, β-H), 8.18 (d, J_{cis} = 4.8 Hz, 2 H, *β*-H), 8.18–8.10 [m, 8 H, *o*-H to $-P^+(Ph)_2-$], 8.01 [dt, J_o= 6.2 Hz, J_m = 1.5 Hz, 4 H, *o*-H of Ph adj. to $-P^+(Ph)_2$], 7.86–7.30 (m, 48 H, H of Ph), 2.64 (dt, ^1J = 10.65 Hz, ^3J = 7.35 Hz, 2 H, $-CH_2-$), 2.46 (dt, ^1J = 10.65 Hz, ^3J = 7.35 Hz, 2 H, $-CH_2-$), 1.94 (m, 2 H, $-CH_2-$ internal). – ^{31}P NMR [120 MHz, $(CD_3)_2CO$, 25 °C]: δ = 28.19 (s, $-P^+(Ph)_2-$], 18.68 (s, $-P^+(Ph)_2$], −145.47 (sept, $^1J_{P-F}$ = 700.8 Hz). – $C_{115}H_{80}N_8P_4F_{12}Zn_2$ (2056.60): calcd. C 67.16, H 3.92, N 5.45; found C 67.27, H 4.01, N 5.40.

3-H_2-H_2: 3-H_2-H_2 was obtained quantitatively by the same method described for **1-H_2-H_2**. – UV/Vis (CH_2Cl_2): λ_{max} (ε, $M^{-1}cm^{-1}$) = 432 (427600), 530 (22300), 568 (5700), 612 (6800), 670 nm (17800). – ^1H NMR [300 MHz, $(CD_3)_2CO$), 25 °C]: δ = 9.05 (d, J_{cis} = 4.8 Hz, 2 H, β-H), 9.00 (d, J_{cis} = 4.8 Hz, 2 H, β-H), 8.96 [s, 1 H, β-H adj. to $-P^+(Ph)_2-$], 8.93 [s, 1 H, β-H adj. to $-P^+(Ph)_2-$], 8.84 (d, J_{cis} = 5.1 Hz, 2 H, β-H), 8.74 (d, J_{cis} = 4.8 Hz, 2 H, β-H), 8.69 (d, J_{cis} = 4.8 Hz, 2 H, β-H), 8.44 (d, J_{cis} = 5.1 Hz, 2 H, β-H), 8.22 [dt, J_o = 5.9 Hz, J_m = 1.8 Hz, 4 H, *o*-H of $-P^+(Ph)_2-$], 8.18 [dt, J_o = 5.9 Hz, J_m = 1.8 Hz, 4 H, *o*-H of $-P^+(Ph)_2-$], 8.12 [d, J_o = 6.6 Hz, J_m = 1.8 Hz, 4 H, *o*-H of Ph adj. to $-P^+(Ph)_2$], 7.86–7.58 (m, 44 H, H of Ph), 7.46 [t, J_o = 5.9 Hz, 4 H, *p*-H of Ph adj. to $-P^+(Ph)_2-$], 7.41 [tt, J_o = 5.9 Hz, J_m = 1.8 Hz, 4 H, *p*-H of $-P^+(Ph)_2-$], 7.32 (tt, J_o = 7.0 Hz, J_m = 2.8 Hz, 8 H, *p*-H of Ph), 2.78 (dt, ^3J = 10.68 Hz, ^1J = 7.40 Hz, 2 H, $-CH_2-$), 2.66 (dt, ^3J = 10.68 Hz, ^1J = 7.40 Hz, 2 H, $-CH_2-$), 2.13 (m, 2 H, $-CH_2-$), −2.53 (s, 4 H, N–H internal). – ^{31}P NMR [120 MHz, $(CD_3)_2CO$, 25 °C]: δ = 27.66 [s, $-P^+(Ph)_2-$], 18.08 [s, $-P^+(Ph)_2$]. – $C_{115}H_{84}Cl_2N_8P_2$ (1710.86): calcd. C 80.73, H 4.95, N 6.55; found C 80.74, H 4.93, N 6.48.

4-Zn-Zn: 4-Zn-Zn was prepared by the same method as **1-Zn-Zn** using ZnTPP (200 mg, 29.5 mmol, 1 equiv.), 2,6-Lut (50 μL, 43.0 mmol) and $(Ph)_2P-CH_2-CH_2-CH_2-CH_2-P(Ph)_2$ (63 mg, 14.8 mmol, 0.5 equiv.). After recrystallization, **4-Zn-Zn** was obtained (284 mg; 13.8 mmol, 93%). – UV/Vis (CH_2Cl_2): λ_{max} (ε, $M^{-1}cm^{-1}$) = 444 (293700), 536 (5300), 580 (11200), 638 nm (15800). – ^1H NMR [300 MHz, $(CD_3)_2CO$), 25 °C]: δ = 8.94 [s, 1 H, β-H adj. to $-P^+(Ph)_2-$], 8.91 [s, 1 H, β-H adj. to $-P^+(Ph)_2-$], 8.80 (d, J_{cis} = 4.77 Hz, 2 H, β-H), 8.74 (d, J_{cis} = 4.77 Hz, 2 H, β-H), 8.70 (d, J_{cis} = 4.77 Hz, 2 H, β-H), 8.67 (d, J_{cis} = 4.77 Hz, 2 H, β-H), 8.53 (d, J_{cis} = 4.77 Hz, 2 H, β-H), 8.10–8.02 [m, 10 H, *o*-H of $-P^+(Ph)_2-$ + 2 β-H], 7.97 [d, J_o = 6.00 Hz, 4 H, *o*-H of Ph adj. to $-P(Ph)_2-^+$], 7.84–6.80 (m, 48 H, H of Ph), 2.35–2.25 (m, 2 H, $-CH_2-$), 2.00–1.75 (m, 2 H, $-CH_2-$) 1.30–1.15 (m, 2 H, $-CH_2-$), 0.92–0.80 (m, 2 H, $-CH_2-$). – ^{31}P NMR [120 MHz, $(CD_3)_2CO$, 25 °C]: δ = 29.67 [s, $-P^+(Ph)_2-$], 18.52 [s, $-P^+(Ph)_2-$], −145.35 (sept, $^1J_{P-F}$ = 700.7 Hz, PF_6^-). – $C_{116}H_{82}F_{12}N_8P_4Zn_2$ (2070.63): calcd. C 67.29, H 3.99, N 5.41; found C 67.42, H 4.04, N 5.38.

4-H_2-H_2: 4-H_2-H_2 was obtained quantitatively as described for **1-H_2-H_2**. – UV/Vis (CH_2Cl_2): λ_{max} (ε, $M^{-1}cm^{-1}$) = 432 (418500), 530 (23300), 566 (7000), 612 (7500), 668 nm (16800). – ^1H NMR [300 MHz, $(CD_3)_2CO$), 25 °C]: δ = 9.09 (d, J_{cis} = 4.77 Hz, 2 H, β-H), 9.06 (d, J_{cis} = 4.77 Hz, 2 H, β-H), 9.01 [s, 1 H, β-H adj. to $-P^+(Ph)_2-$], 8.98 [s, 1 H, β-H adj. to $-P^+(Ph)_2-$], 8.87 (d, J_{cis} = 4.77 Hz, 2 H, β-H), 8.79 (d, J_{cis} = 4.77 Hz, 2 H, β-H), 8.74 (d, J_{cis} = 4.77 Hz, 2 H, β-H), 8.42 (d, J_{cis} = 5.16 Hz, 2 H, β-H), 8.28–8.17 [m, 12 H, *o*-H to $-P^+(Ph)_2-$ and *o*-H Ph adj. to $-P^+(Ph)_2-$], 7.90–7.07 (m, 48 H, H of Ph), 2.49–2.38 (m, 2 H, $-CH_2-$), 1.90–1.81 (m, 2 H, $-CH_2-$) 1.37–1.21 (m, 2 H, $-CH_2-$), 0.92–0.75 (m, 2 H, $-CH_2-$), −2.46 (s, 4 H, N–H internal). – ^{31}P NMR [120 MHz, $(CD_3)_2CO$, 25 °C]: δ = 30.02 [s, $-P^+(Ph)_2-$], 21.02 (s, $-P^+(Ph)_2$]. – $C_{116}H_{86}Cl_2N_8P_2$ (1724.87): calcd. C 80.78, H 5.03, N 6.50; found C 80.91, H 5.09, N 6.46.

5-Zn-Zn: This compound was prepared by the same method as **1-Zn-Zn** using ZnTPP (200 mg, 29.5 mmol, 1 equiv.), 2,6-Lut (50 μL, 43.0 mmol) and $(Ph)_2P-CH_2-CH_2-As(Ph)_2$ (65 mg, 1.7 mmol, 0.5 equiv.). The product **5-Zn-Zn** was obtained (184 mg, 0.881 mmol, 60%). – UV/Vis (CH_2Cl_2): λ_{max} (ε, $M^{-1}cm^{-1}$) = 436 (426000), 568 (15500), 614 nm(18300). – ^1H NMR [300 MHz, $(CD_3)_2CO$), 25 °C]: δ = 9.10 [s, 1 H, β-H adj. to $-P^+(Ph)_2-$], 9.07 [s, 1 H, β-H adj. to $-P^+(Ph)_2-$], 8.89 (d, J_{cis} = 4.77 Hz, 1 H, β-H), 8.86 (d, J_{cis} = 4.77 Hz, 1 H, β-H), 8.85 (d, J_{cis} = 4.77 Hz, 1 H, β-H), 8.82 (d, J_{cis} = 4.77 Hz, 1 H, β-H), 8.81 (d, J_{cis} = 4.80 Hz, 2 H, β-H), 8.79 (d, J_{cis} = 4.80 Hz, 2 H, β-H), 8.68 (d, J_{cis} = 4.77 Hz, 2 H, β-H), 8.25 (d, J_{cis} = 4.80 Hz, 1 H, β-H), 8.22 (d, J_{cis} = 4.77 Hz, 1 H, β-H), 8.18–8.03 [m, 12 H, *o*-H of $-P^+(Ph)_2-$ and *o*-H of Ph adj. to $-P^+(Ph)_2$], 7.90–6.50 (m, 48 H, H of Ph), 2.68 (m, 2 H, $-CH_2-$), 2.39 (m, 2 H, $-CH_2-$). – ^{31}P NMR [120 MHz, $(CD_3)_2CO$, 25 °C]: δ = 23.23 [s, $-P^+(Ph)_2-$], −143.39 (sept, $^1J_{P-F}$ = 700.7 Hz, PF_6^-). – $C_{114}H_{78}AsF_{12}N_8P_3Zn_2$ (2086.52): calcd. C 65.62, H 3.77, N 5.37; found C 65.72, H 3.82, N 5.34.

5-H_2-H_2: Compound **5-H_2-H_2** was obtained quantitatively as described for **1-H_2-H_2**. – UV/Vis (CH_2Cl_2), λ_{max} (ε, $M^{-1}cm^{-1}$) = 432 (370000), 500 (21100), 566 (7400), 612 (6700), 670 nm (12800). – ^1H NMR [300 MHz, $(CD_3)_2CO$, 25 °C]: δ = 9.13 [s, 1 H, β-H adj. to $-P^+(Ph)_2-$], 9.10 [s, 1 H, β-H adj. to $-P^+(Ph)_2-$], 9.08 (d, J_{cis} = 5.16 Hz, 2 H, β-H), 9.05 (d, J_{cis} = 5.16 Hz, 2 H, β-H), 8.97 (d, J_{cis} = 5.1 Hz, 2 H, β-H), 8.79 (d, J_{cis} = 4.80 Hz, 2 H, β-H), 8.74 (d, J_{cis} = 4.80 Hz, 2 H, β-H), 8.47 (d, J_{cis} = 5.16 Hz, 1 H, β-H), 8.46 (d, J_{cis} = 5.16 Hz, 1 H, β-H), 8.28–8.12 [m, 12 H, *o*-H of $-P^+(Ph)_2-$ and *o*-H of Ph adj. to $-P^+(Ph)_2$], 7.92–7.20 (m, 48 H, H of Ph), 2.75 (m, 2 H, $-CH_2-$), 2.42 (m, 2 H, $-CH_2$), −2.44 (s, 4 H, N–H internal). – ^{31}P NMR [120 MHz, $(CD_3)_2CO$, 25 °C]: δ = 22.54 [s, $-P^+(Ph)_2-$]. – $C_{114}H_{82}AsCl_2N_8P_3$ (2030.72): calcd. C 75.95, H 4.59, N 6.22; found C 76.11, H 4.64, N 6.20.

6-Zn and 6-Zn-Zn: ZnTPP (20 mg, 29.5 mmol), 2,6-Lut (20 μL, 17.20 × 10^{-5} mol) and $(Ph)_2P-C\equiv C-P(Ph)_2$ (11.6 mg, 2.95 × 10^{-5} mol) were dissolved in a solution of T.E.A.PF_6 (0.1 M) in 1,2-$Cl_2C_2H_4$/CH_3CN (4:1). The stirred reaction mixture was electrolyzed for 3 h at 0.80 V vs. SCE. After workup, the unchanged ZnTPP was separated from the monomeric (**6-Zn**) and dimeric (**6-Zn-Zn**) porphyrins by column chromatography (silica gel), eluting with CH_2Cl_2/0.1% CH_3OH. Further elution did not allow for the effective separation of the two porphyrins (**6-Zn** and **6-Zn-Zn**). Pure monomer and dimer were obtained only after demetallation of the mixture and chromatography as described below. After coulometry, the solvents were evaporated. The residue was dissolved in a minimum amount of CH_2Cl_2/CH_3COCH_3 (1:1) and dilute HCl (25%, 100 mL) was added. This mixture was stirred for 30 min at room temperature. After the addition of water (200 mL), the organic layer was collected, washed again and neutralized with sodium acetate. The porphyrins **6-H_2** and **6-H_2-H_2** were then separ-

ated by column chromatography (CH_2Cl_2/0.1% CH_3OH) to give, after recrystallization from CH_2Cl_2/*n*-hexane, brown powders: **6-H$_2$** (6.8 mg, 22%) and **6-H$_2$-H$_2$** (16.7 mg, 66%).

6-H$_2$: H$_2$TPP-β-P$^+$(Ph)$_2$−C≡C−P(Ph)$_2$, Cl$^-$: UV/Vis (CH_2Cl_2): λ_{max} (ε, $M^{-1}cm^{-1}$) = 426 (269200), 522 (17400), 558 (8400), 598 (7800), 655 nm (8300). − ^{1}H NMR [300 MHz, $(CD_3)_2CO$, 25 °C]: δ = 8.93 (s, 1 H, β-H), 8.77 (d, J_{cis} = 4.8 Hz, 1 H, β-H), 8.76 (d, J_{cis} = 4.8 Hz, 1 H, β-H), 8.73 (d, J_{cis} = 4.8 Hz, 1 H, β-H), 8.56 (d, J_{cis} = 4.8 Hz, 1 H, β-H), 8.42 (d, J_{cis} = 4.8 Hz, 1 H, β-H), 8.25−8.18 [m, 5 H, 4 *o*-H of −P$^+$(Ph)$_2$ − and 1 β-H], 8.06 [dt, J_o = 6.6 Hz, J_m = 1.7 Hz, 2 H, *o*-H of Ph adj. to −P$^+$(Ph)$_2$−], 7.86−7.76 (m, 10 H, *o*-H of Ph), 7.72−7.42 (m, 16 H, H of Ph), 7.36 (t, J_o = 7.7 Hz, 3 H, *p*-H of Ph), 7.35 [t, J_o = 7.0 Hz, 2 H, *p*-H of P(Ph)$_2$], 7.23 [t, J_o = 7.7 Hz, 1 H, *p*-H of Ph adj. to P$^+$(Ph)$_2$], 7.16 [t, J_o = 7.7 Hz, 2 H, *p*-H of −P$^+$(Ph)$_2$−], −2.57 (s, 2 H, N−H). − ^{31}P NMR [120 MHz, $(CD_3)_2CO$, 25 °C]: δ = 18.95 [s, −P$^+$(Ph)$_2$−], 3.51 [s, −P(Ph)$_2$−]. − $C_{70}H_{49}ClN_4P_2$ (1043.60): calcd. C 80.57, H 4.73, Cl 3.40, N 5.37, P 5.94; found C 80.70, H 4.78, Cl 3.40, N 5.41, P 6.02.

6-H$_2$-H$_2$: H$_2$TPP-β-P$^+$(Ph)$_2$−C≡C−P$^+$(Ph)$_2$-β-H$_2$TPP, 2 Cl$^-$: UV/Vis (CH_2Cl_2): λ_{max} (ε, $M^{-1}cm^{-1}$) = 430 (214200), 527 (16600), 564 (4900), 607 (7300), 666 nm (10900). − ^{1}H NMR [300 MHz, $(CD_3)_2CO$, 25 °C]: δ =9.06 (d, J_{cis} = 5.5 Hz, 2 H, β-H), 9.02 (d, J_{cis} = 5.5 Hz, 2 H, β-H), 8.87 (d, J_{cis} = 5.5 Hz, 1 H, β -H), 8.85 (d, J_{cis} = 5.5 Hz, 1 H, β-H), 8.76 [s, 1 H, -H adj. to −P$^+$(Ph)$_2$−], 8.71 [s, 1 H, β-H adj. to −P$^+$(Ph)$_2$−], 8.67 (s, 1 H, β-H), 8.64 (s, 1 H, β-H), 8.46 (d, J_{cis} = 5.5 Hz, 1 H, β-H), 8.41 (d, J_{cis} = 5.5 Hz, 1 H, β-H), 8.26−8.19 [m, 10 H, 8 *o*-H of −P$^+$(Ph)$_2$− and 2 β-H], 8.14−8.05 [m, 4 H, *o*-H of Ph adj. to −P$^+$(Ph)$_2$−], 7.93−7.14 (m, 48 H, H of Ph), −2.48 (s, 2 H, N−H), −2.51 (s, 2 H, N−H). − ^{31}P NMR [120 MHz, $(CD_3)_2CO$, 25 °C]: δ = 24.80 [s, −P$^+$(Ph)$_2$−], 16.51 [s, −P$^+$(Ph)$_2$−]. − $C_{114}H_{78}Cl_2N_8P_2$ (1692.80): calcd. C 80.89, H 4.64, Cl 4.19, N 6.62, P 3.66; found C 80.75, H 4.78, Cl 4.34, N 6.70, P 3.81.

6-Zn: Compound **6-H$_2$** was dissolved in a solution of $(CH_3COO)_2Zn^{II}$ (10 equiv.) in CH_2Cl_2/CH_3OH (1:1). The mixture was maintained at reflux for 3 h. After cooling at room temperature, the mixture was treated with an excess of tetraethylammonium hexafluorophosphate (100 equiv.). After evaporation of the solvent, the residue was dissolved in a minimum amount of CH_2Cl_2. The mixture was then poured into water, and the organic layer was washed (4 times) and dried with $CaSO_4$ for 6 h. The solution was then concentrated (to 5 mL) and purified by chromatography on a silica gel column (elution with CH_2Cl_2/CH_3OH, 99:1) to give a dark green powder of **6-Zn** in 90% yield. − UV/Vis (CH_2Cl_2): λ_{max} (ε, $M^{-1}cm^{-1}$) = 428 (209200), 560 (9400), 603 nm (5000). − ^{1}H NMR [300 MHz, $(CD_3)_2CO$, 25 °C]: δ = 8.84 (d, J_{cis} = 4.8 Hz, 1 H, β-H), 8.800 (d, J_{cis} = 4.8 Hz, 1 H, β-H), 8.798 [s, 1 H, β-H adj. to −P$^+$(Ph)$_2$−], 8.77 (d, J_{cis} = 4.8 Hz, 1 H, β-H), 8.768 (d, J_{cis} = 4.8 Hz, 1 H, β-H), 8.63 (d, J_{cis} = 4.8 Hz, 1 H, β-H), 8.17 (d, J_{cis} = 4.8 Hz, 1 H, β-H), 8.11 [dd, J_o = 8.8 Hz, J_m = 1.8 Hz, 4 H, *o*-H of −P$^+$(Ph)$_2$−], 8.01 [dd, J_o = 8.1 Hz, J_m = 1.5 Hz, 2 H, *o*-H of Ph adj. to −P$^+$(Ph)$_2$−], 7.94−7.55 (m, 26 H, *o*-H and *m*-H of Ph), 7.49 [t, J_o = 7.4 Hz, 2 H, *p*-H of P(Ph)$_2$], 7.41 (t, J_o = 7.4 Hz, 3 H, *p*-H of Ph), 7.31 [t, J_o = 7.4 Hz, 1 H, *p*-H of Ph adj. to −P$^+$(Ph)$_2$], 7.03 [t, J_o = 7.4 Hz, 2 H, *p*-H of −P$^+$(Ph)$_2$], − ^{31}P NMR [120 MHz, $(CD_3)_2CO$, 25 °C]: δ = 4.64 [s, −P$^+$(Ph)$_2$−], 3.51 [s, −P$^+$(Ph)$_2$−], −145.44 (sept, $^1J_{P-F}$ = 700.8 Hz, PF_6^-). − $C_{70}H_{47}F_6N_4P_3Zn$ (1216.47): calcd. C 69.12, H 3.89, N 4.61, P 7.64, Zn 5.37; found C 69.31, H 4.05, N 4.74, P 7.75, Zn 5.56.

6-Zn-Zn: The same procedure described for **6-Zn** was used to obtain **6-Zn-Zn** from **6-H$_2$-H$_2$** in 90% yield. − UV/Vis (CH_2Cl_2): λ_{max} (ε, $M^{-1}cm^{-1}$) = 438 (215600), 569 (10600), 623 nm (11800). − ^{1}H NMR [300 MHz, $(CD_3)_2CO$, 25 °C]: δ= 8.87 (d, J_{cis} = 4.8 Hz, 2 H, β-H), 8.82 (d, J_{cis} = 4.8 Hz, 4 H, β-H), 8.80 [s, 1 H, β-H adj. to −P$^+$(Ph)$_2$−], 8.79 [s, 1 H, β-H adj. to −P$^+$(Ph)$_2$−], 8.78 (d, J_{cis} = 4.8 Hz, 2 H, β-H), 8.65 (d, J_{cis} = 4.8 Hz, 2 H, β-H), 8.18 (d, J_{cis} = 4.8 Hz, 2 H, β-H), 8.16 [d, J_o = 7.7 Hz, 4 H, *o*-H of −P$^+$(Ph)$_2$ −], 8.12 [d, J_o = 7.7 Hz, 4 H, *o*-H of −P$^+$(Ph)$_2$−], 8.03 [d, J_o = 7.7 Hz, 4 H, *o*-H of Ph adj. to −P$^+$(Ph)$_2$−], 7.90−7.10 (m, 48 H, H of Ph), − ^{31}P NMR [120 MHz, $(CD_3)_2CO$, 25 °C]: δ = 14.03 [s, −P$^+$(Ph)$_2$−], 13.62 [s, −P$^+$(Ph)$_2$−], 145.44 (sept, $^1J_{P-F}$ = 700.8 Hz, PF_6^-). − $C_{114}H_{74}F_{12}N_8P_4Zn_2$ (2038.54): calcd. C 67.17, H 3.66, N 5.50, P 6.08, Zn 6.41; found C 67.32, H 3.74, N 5.42, P 6.22, Zn 6.52.

7-Zn-Zn: This was prepared by the same method as **1-Zn-Zn**, using ZnTPP (200 mg, 2.95×10^{-4} mol, 1 equiv.), 2,6-Lut (50 μL, 4.3×10^{-4} mol) and 1,1,1-tris(diphenylphosphanylmethyl)ethane (61 mg, 0.98×10^{-4} mol. 0.33 equiv.). Product **7-ZnZn** was recovered (184 mg, 0.88×10^{-4} mol, 75%). − UV/Vis (CH_2Cl_2): λ_{max} (ε, $M^{-1}cm^{-1}$) = 446 (298000), 582 (12100), 640 nm (19900). − ^{1}H NMR [300 MHz, $(CD_3)_2CO$, 25 °C]: δ = 9.71 [s, 1 H, β-H adj. to −P$^+$(Ph)$_2$−], 9.68 [s, 1 H, β-H adj. to −P$^+$(Ph)$_2$−], 8.90 [d, J_{cis} = 4.80 Hz, 4 H, β-H adj. to −P$^+$(Ph)$_2$−], 8.82 (d, J_{cis} = 4.80 Hz, 2 H, β-H), 8.80 (d, J_{cis} = 4.80 Hz, 2 H, β-H), 8.76 (d, J_{cis} = 4.77 Hz, 2 H, β-H), 8.51 (d, J_{cis} = 4.77 Hz, 2 H, β-H), 8.24 [dt, 4 H, J_m = 1.83 Hz, J_o = 6.99 Hz, *o*-H of Ph adj. to −P$^+$(Ph)$_2$−], 8.20−8.13 [m, 12 H, *o*-H of −P$^+$(Ph)$_2$− and PO(Ph)$_2$], 7.99−6.67 (m, 54 H, H of Ph), 4.60 [d, ^3J = 13.30 Hz, 2 H, −CH$_2$−PO(Ph)$_2$], 2.69 [d, ^1J = 13.30 Hz, 1 H, −CH$_2$−P$^+$(Ph)$_2$−], 2.62 [d, ^1J = 13.30 Hz, 1 H, −CH$_2$−P$^+$(Ph)$_2$−], 1.92 [d, ^1J = 13.30 Hz, 1 H, −CH$_2$−P$^+$(Ph)$_2$−], 1.86 (d, ^1J = 13.30 Hz,1 H, −CH$_2$−), 0.80 (s, 3 H, −CH$_3$−). − ^{31}P NMR (120 MHz, $(CD_3)_2CO$, 25 °C): δ = 26.43 [s,PO(Ph)$_2$- and −P$^+$(Ph)$_2$−], 15.88 [s, −P$^+$(Ph)$_2$−], −143.35 (sept, $^1J_{P-F}$ = 700.7 Hz, PF_6^-). − $C_{129}H_{93}F_{12}N_8OP_5Zn_2$ (2284.83): calcd. C 67.81, H 4.10, N 4.90, P 6.78; found C 68.00, H 4.08, N 4.88, P 6.61.

7-H$_2$-H$_2$: This was prepared by the same method as **1-H$_2$-H$_2$** and was obtained in 93% yield. − UV/Vis (CH_2Cl_2): λ_{max} (ε, $M^{-1}cm^{-1}$) = 438 (308000), 534 (16600), 578 (5300), 620 (5200), 680 nm (14200). − ^{1}H NMR [300 MHz, $(CD_3)_2CO$, 25 °C]: δ = 9.82 [s, 1 H, β-H adj. to −P$^+$(Ph)$_2$−], 9.79 [s, 1 H, β-H adj. to−P$^+$(Ph)$_2$−], 9.13 (d, J_{cis} = 5.16 Hz, 2 H, β-H), 9.10 (d, J_{cis} = 5.16 Hz, 2 H, β-H), 8.92 (d, J_{cis} = 5.13 Hz, 2 H, β-H), 8.79 (d, J_{cis} = 4.77 Hz, 2 H, β-H), 8.72 (d, J_{cis} = 4.77 Hz, 2 H, β-H), 8.63 (d, J_{cis} = 5.13 Hz, 2 H, β-H), 8.34−8.20 [m, 16 H, *o*-H of Ph of −P$^+$(Ph)$_2$− and PO(Ph)$_2$− and *o*-H of Ph adj. to P$^+$(Ph)$_2$−], 8.05−6.79 (m, 48 H, H of Ph), 4.12 [d, ^3J = 13.30 Hz, 2 H,−CH$_2$−PO(Ph)$_2$], 2.61 [d, ^1J = 14.10 Hz, 1 H, −CH$_2$−P$^+$(Ph)$_2$−], 2.59 [d, ^1J = 14.10 Hz, 1 H, −CH$_2$−P$^+$(Ph)$_2$−], 1.85 [m, 2 H, −CH$_2$−P$^+$(Ph)$_2$−], 0.80 (s, 3 H, −CH$_3$−). − ^{31}P NMR [120 MHz, $(CD_3)_2CO$, 25 °C]: δ = 25.87 [s, PO(Ph)$_2$− and −P$^+$(Ph)$_2$−], 15.63 [s, −P$^+$(Ph)$_2$−]. − $C_{129}H_{97}Cl_2N_8OP_3$ (1939.09): calcd. C 79.90, H 5.04, N 5.78, P 4.79; found C 80.20, H 5.10, N 5.80, P 4.31.

8-Zn-Zn-Zn: The method employed in the synthesis of **1-Zn-Zn**, using ZnTPP (200 mg, 2.95×10^{-4} mol, 1 equiv.), 2,6-Lut (50 μL, 4.3×10^{-4} mol) and TRIPHOS (61 mg, 0.976×10^{-4} mol, 0.33 equiv.), led to the formation of product **8-Zn-Zn-Zn** (184 mg, 0.88×10^{-4} mol, 70%). − UV/Vis (CH_2Cl_2): λ_{max} (ε, $M^{-1}cm^{-1}$) = 441 (298000), 583 (12100), 628 nm (19900),. − ^{1}H NMR [300 MHz, $(CD_3)_2CO$, 25 °C]: δ = 9.70 [m, 3 H, β-H adj. to −P$^+$(Ph)$_2$−], 9.88

[d, J_{cis} = 4.77 Hz, 3 H, β-H adj. to $-P^+(Ph)_2-$], 8.82 [d, J_{cis} = 4.77 Hz, 3 H, β-H adj. to $-P^+(Ph)_2-$], 8.77 (d, J_{cis} = 4.77 Hz, 3 H, β-H), 8.63 (d, J_{cis} = 4.77 Hz, 3 H, β-H), 8.22−8.04 [m, 19 H, 16 *o*-H of Ph adj. to $-P^+(Ph)_2-$ + 3 β-H], 7.91−7.06 (m, 69 H, H of Ph), 3.10−2.90 [m, 4 H, $-CH_2-P^+(Ph)_2-$], 2.72−2.36 [m, 12 H, $-CH_2-P^+(Ph)_2-$]. − ^{31}P NMR [120 MHz, $(CD_3)_2CO$, 25 °C]: δ = 29.82 [d, $^3J_{P-P}$ = 45.2 Hz, $-P^+(Ph)_2-$], 27.25 [t, $^3J_{P-P}$ = 45.2 Hz, $-P^+(Ph)_2-$], −143.54 (sept, $^1J_{P-F}$ = 700.7 Hz, PF_6^-). − $C_{166}H_{114}F_{18}N_{12}P_6Zn_3$ (3000.78): calcd. C 66.44, H 3.83, N 5.60, Zn 6.54; found C 66.27, H 3.76, N 5.58, Zn 6.41.

8-H_2-H_2-H_2: This was prepared by the same method as **1-H_2-H_2** and was obtained from **8-Zn-Zn-Zn** in 93% yield. − UV/Vis (CH_2Cl_2): λ_{max} (ε, $M^{-1}cm^{-1}$) = 432 (325100), 530 (18000), 567 (7000), 611 (7900), 667 nm (14400). − ^{1}H NMR [300 MHz, $(CD_3)_2CO$, 25 °C]: δ = 9.88 [s, 3/2 H, β-H adj. to $-P^+(Ph)_2-$], 9.82 [s, 3/2 H, β-H adj. to $-P^+(Ph)_2-$], 8.98 [d, J_{cis} = 4.77 Hz, 3 H, β-H adj. to $-P^+(Ph)_2-$], 8.96 [d, J_{cis} = 4.77 Hz, 3 H, β-H adj. to $-P^+(Ph)_2-$], 8.90 (d, J_{cis} = 4.77 Hz, 3/2 H, β-H), 8.87 (d, J_{cis} = 4.77 Hz, 3/2 H, β-H), 8.76 (d, J_{cis} = 4.77 Hz, 3 H, β-H), 8.74 (d, J_{cis} = 4.77 Hz, 3 H, β-H), 8.69 (d, J_{cis} = 4.77 Hz, 3 H, β-H), 8.26−8.03 [m, 19 H, 16 *o*-H of Ph adj. to $-P^+(Ph)_2-$ + 3 β-H], 7.89−6.63 (m, 69 H, H of Ph), 3.43−3.10. [m, 4 H, $-CH_2-P^+(Ph)_2-$], 2.80−2.39.[m, 12 H, $-CH_2-P^+(Ph)_2-$], −2.67 (s, 4 H, N−H of H_2TPP external), −2.45 (s, 2 H, N−H of H_2TPP internal). − ^{31}P NMR [120 MHz, $(CD_3)_2CO$, 25 °C]: δ = 29.54 [d, $^3J_{P-P}$ = 45.2 Hz, $-P^+(Ph)_2-$], 26.74 [t, $^3J_{P-P}$ = 45.2 Hz, $-P^+(Ph)_2-$], −143.54 (sept, $^1J_{P-F}$ = 700.7 Hz, PF_6^-). − $C_{166}H_{120}Cl_3N_{12}P_3$ (2482.17): calcd. C 80.33, H 4.87, N 6.67, P 3.74; found C 80.47, H 4.69, N 6.74, P 3.93.

Acknowledgments

We warmly thank the Centre National de la Recherche Scientifique for financial support.

[1] M. J. Crossley, P. L. Burn, *J. Chem. Soc., Chem. Commun.* **1991**, 1569−1571.
[2] M.R. Wasielewski, *Chem. Rev.* **1992**, *92*, 435−461.
[3] M. Bixon, J. Fajer, G. Feher, J. H. Freed, D. Gamlich, A. J. Hoff, H. Levanon, K. Möbins, R. Nechushtai, J. R. Norris, A. Scherz, J. L. Sessler, D. Stehlik, *Isr. J. Chem.* **1992**, *32*, 449−467.
[4] S. Prathapan, T. E. Johnson, J. S. Lindsey, *J. Am. Chem. Soc.* **1993**, *115*, 7519−7520.
[5] V. S. Y. Lin, M. J. Therien, *Chem. Eur. J.* **1995**, 1, 645−651.
[6] K. M. Kadish, N. Guo, E. V. Cæmelbecke, A. Froiio, R. Paolesse, D. Monti, P. Tagliatesta, T. Boschi, L. Prodi, F. Bolletta, N. Zaccheroni, *Inorg. Chem.* **1998**, *37*, 2358−2365.
[7] J. L. Sessler, V. L. Capuano, A. Harriman, *J. Chem. Soc., Chem. Commun.* **1999**, 1771−1782.
[8] G. Hungerford, M. V. der Auweraer, J.-L. Chambron, V. Heitz, J.-P. Sauvage, J.-L. Pierre, D. Zurita, *Chem. Eur. J.* **1999**, *5*, 2089−2100.
[9] J. L. Sessler, M. R. Johnson, S. E. Creager, J. C. Fettinger, J. A. Ibers, *J. Am. Chem. Soc.* **1990**, *112*, 9310−9329.
[10] E. J. Atkinson, A. M. Oliver, M. V. Paddon Row, *Tetrahedron Lett.* **1993**, *34*, 6147−6150.
[11] D. P. Arnold, L. J. Nitschinsk, *Tetrahedron Lett.* **1993**, *34*, 693−696.
[12] J. S. Lindsey, S. Prathapan, T. E. Johnson, R. W. Wagner, *Tetrahedron* **1994**, *50*, 8941−8968.
[13] H. L. Anderson, *Inorg. Chem.* **1994**, *33*, 972−981.
[14] P. Krausz, Ch. Giannotti, *J. Chim. Phys.* **1983**, *80*, 299−303.
[15] H. Tamiaki, S. Suzuki, K. Maruyana, *Bull. Chem. Soc. Jpn.* **1993**, *66*, 2633−2697.
[16] S. Matile, N. Berova, K. Nakanishi, J. Fleischhauer, R. W. Woody, *J. Am. Chem. Soc.* **1996**, *118*, 5198−5206.
[17] N. Bampos, V. Marvaud, J. K. M. Sanders, *Chem. Eur. J.* **1998**, *4*, 335−342.
[18] G. Märkl, M. Reiss, P. Kreitmeier, H. Nörth, *Angew. Chem. Int. Ed. Engl.* **1995**, *20*, 2230−2234.
[19] R. H. Jin, S. Aoki, K. Shima, *Chem. Commun.* **1996**, 1939−1940.
[20] A. K. Burrell, D. L. Officer, D. C. W. Reid, K. Y. Wild, *Angew. Chem.* **1998**, *110*, 998−1002.
[21] T. Ogawa, Y. Nishimoto, N. Yoshida, N. Ono, H. Osuka, *J. Chem. Soc., Chem. Commun.* **1998**, 337−338.
[22] T. Ogawa, Y. Nishimoto, N. Yoshida, N. Ono, A. Osuka, *Angew. Chem. Int. Ed.* **1999**, *38*, 176−179.
[23] L. Ruhlmann, A. Giraudeau, *Chem. Commun.* **1996**, 2007−2008.
[24] A. Giraudeau, L. Ruhlmann, L. El Kahef, M. Gross, *J. Am. Chem. Soc.* **1996**, *118*, 2969−2979.
[25] L. Ruhlmann, A. Shulz, A. Giraudeau, C. Messerschmidt, J. H. Fuhrhop, *J. Am. Chem. Soc.* **1999**, *121*, 6664−6667.
[26] D. G. Davis, in *The Porphyrins* (Ed.: D. Dolphin), Academic Press, New York, **1979**, vol. 5, p. 53−125.
[27] A. Giraudeau, L. El Kahef, *Can. J. Chem.* **1991**, *69*, 1161−1165.
[28] A. S. Hinman, B. J. Pavelich, S. Pons, A. E. Kondo, *J. Electroanal. Chem.* **1987**, *234*, 145−162.
[29] A. El-Kasmi, D. Lexa, P. Maillard, M. Momenteau, J. M. Savéant, *J. Am. Chem. Soc.* **1991**, *113*, 1586−1595.
[30] K. M. Kadish, R. K. Rhodes, *Inorg. Chem.* **1981**, *20*, 2961−2996.
[31] K. M. Barkigia, M. W. Renner, H. Xie, K. M. Smith, J. Fajer, *J. Am. Chem. Soc.* **1993**, *115*, 7894−7899.
[32] P. J. Angiolillo, V. S. Y. Lin, J. M. Vanderkoi, M. J. Therien, *J. Am. Chem. Soc.* **1995**, *117*, 12514−12527.
[33] A. Helms, D. Heiler, G. Mc Lendon, *J. Am. Chem. Soc.* **1992**, *114*, 6227−6238.
[34] J. L. Sessler, V. L. Capuano, *Tetrahedron Lett.* **1993**, *34*, 2287−2290.
[35] H. J. Shine, A. G. Padilla, S. M. Wu, *J. Org. Chem.* **1979**, *44*, 4069−4075.
[36] Because the splitting of the signal of the two external $-CH_2-$ was more pronounced in [D_5]pyridine (δ = 3.00−2.80) than in [D_6]acetone (δ = 2.78−2.66), [D_5]pyridine was chosen for the representation of this splitting.
[37] E. E. Bonfantini, D. L. Officer, *Tetrahedron Lett.* **1993**, *34*, 8531−8534.
[38] A. K. Burrell, D. L. Officer, D. C. W. Reid, *Angew. Chem. Int. Ed. Engl.* **1995**, *34*, 900−904.
[39] J. J. Gosper, M. Ali, *J. Chem. Soc., Chem. Commun.* **1994**, 1707−1708.
[40] Y. Le Mest, M. L'Her, N. H. Hendricks, K. Kim, J. P. Collman, *Inorg. Chem.* **1992**, *31*, 835−847.
[41] J. H. Fuhrhop, K. M. Kadish, D. G. Davis, *J. Am. Chem. Soc.* **1973**, *95*, 5140−5147.
[42] A. Giraudeau, H. J. Callot, M. Gross, *Inorg. Chem.* **1979**, *18*, 201−206.
[43] E. V. Nikitin, A. S. Romakhin, V. A. Zagumennov, Y. A. Balokin, *Electrochim. Acta* **1997**, *42*, 2217−2224.
[44] A. Giraudeau, H. J. Callot, J. Jordan, I. Ezahr, M. Gross, *J. Am. Chem. Soc.* **1979**, *101*, 3857−3862.
[45] D. Dolphin, D. J. Halko, E. C. Johnson, K. Rousseau, in *Porphyrin Chemistry Advances* (Ed.: F. R. Longo), Ann Arbor Science, MI, **1979**, chapter 10, p. 123−125.
[46] G. Wittig, *Angew. Chem.* **1956**, *68*, 505−509.
[47] C. Bernard, J. P. Gisselbrecht, M. Gross, E. Vogel, M. Lausmann, *Inorg. Chem.* **1994**, *33*, 2393−2401.
[48] A. D. Adler, F. R. Longo, F. Kampas, K. Kim, *J. Inorg. Nucl. Chem.* **1970**, *32*, 2443−2445.
[49] G. H. Barnett, M. F. Hudson, K. M. Smith, *Tetrahedron Lett.* **1973**, *30*, 2887−2888.

Received June 17, 2000
[I00249]

2-(4′,4′-Dimethyl-3′,4′-dihydrooxazol-2′-yl)phenol: Some First-Row Transition Metal Complexes of This Naturally Occurring Binding Group

Govindasamy Mugesh,[a] Harkesh B. Singh,*[a] and Ray J. Butcher[b]

Dedicated to Prof. B. L. Khandelwal on the occasion of his 63rd birthday

Keywords: Oxazolines / Metal assisted hydrolysis / Hydrogen bonds / Chirality / Siderophores

The synthesis and characterization of monomeric Mn^{III}, Co^{II}, Ni^{II}, Cu^{II}, and Zn^{II} phenolates derived from a biologically relevant ligand, 2-(4′,4′-dimethyl-3′,4′-dihydrooxazol-2′-yl)-phenol (**1**), are described. The addition of $Mn(OAc)_2 \cdot 4\,H_2O$ to an ethanolic solution of **1** affords an unexpected 1:3 complex $[Mn(OR)\{O(Ox)\}_2]$ (**2**) [R = $C_6H_4CONHC(Me_2)CH_2OH$, Ox = 2-(4,4-dimethyl-2-oxazolinyl)phenyl] in which one of the five-membered oxazoline rings is partially hydrolyzed. The complexes $[M\{O(Ox)\}_2]$ [M = Co (**3**), Ni (**4**), Cu (**6**), or Zn (**7**)] were prepared in good yield by the reactions of **1** with the corresponding metal acetates. Novel formation of the six-coordinate Ni^{II} complex **5** with neutral acetic acid was observed during the crystallization process. The complexes were characterized by elemental analysis, magnetic susceptibility, as well as EPR, ^1H NMR, electronic, and mass spectral techniques. Complexes **2**, **3**, **5**, **6**, and **7** were characterized by single crystal X-ray diffraction studies. Complex **2** is six-coordinate whereas complexes **3**, **6**, and **7** are four-coordinate with two oxazoline bidentate ligands. The geometry around the metal center is found to be distorted tetrahedral for all of the four-coordinate complexes. Complex **5** is octahedral with four coordination sites occupied by the two bidentate oxazoline ligands and the other two are occupied by two neutral acetic acid molecules. The hydroxy groups of the coordinated acetic acid are hydrogen-bonded to the phenolate oxygen atoms of the oxazoline ligands. The variable-temperature ^1H NMR spectroscopic studies of complex **7** indicate that the interconversion between the (*M*) and (*P*) helix is slow at low temperatures.

Introduction

Interest in the biochemistry of 2-(2-hydroxyphenyl)-2-oxazoline started with the finding that this ligating moiety is present as a naturally occurring iron chelator in some classes of siderophores such as mycobactine, parabactin, and vibriobactin.[1]

Owing to the strong chelating ability of the oxazoline ligand and its high affinity for Fe^{III}, the siderophores have been shown to be highly potent in the deferration of mammalian cell lines and are potentially useful for chelation therapy.[2] The use of oxazoline ligands in a wide range of catalytic reactions has also been reported in recent years.[3] In this regard much effort has been directed towards the synthesis and catalytic applications of metal complexes containing 2-(2′-hydroxyphenyl)-2-oxazoline ligands.[4] Recently, Ti^{IV} and Zr^{IV} complexes of 2-(2′-hydroxyphenyl)-2-oxazolines have been used for some homogeneous catalytic reactions such as Mukaiyama reaction, allylations, hydrocyanations, Diels–Alder reactions.[4b] In these cases, the bis-(oxazoline)-ligated transition metal Lewis acids displayed activity for almost all commonly encountered Lewis acid promoted reactions. More recently, Ni^{II}, Pd^{II}, and Mn^{III} complexes of chiral oxazoline ligands containing N,O and N,P moieties and Mn^{III} complex of 2-(2′-hydroxyphenyl)-2-oxazoline have been used for the catalytic epoxidation of styrene.[5]

Although a few complexes of 2-(2′-hydroxyphenyl)-2-oxazolines with trivalent and divalent metal ions are known,[6–8] very little information is available about their structural chemistry. As part of our work on intramolecularly coordinated organochalcogens,[9] we have recently described the synthesis and characterization of Group 12 metal chalcogenolates (S, Se, Te) with bidentate oxazoline ligands.[10] Interestingly, the (thiolato)-[10a] and (selenolato)-zinc[10b] complexes were found to be chiral at room temperature and interconversion between the (*M*) and (*P*) helix was slow at room temperature. Replacement of the S or Se by Te led to the faster interconversion between the (*M*) and (*P*) forms. A similar trend was observed when the central metal ion was varied. It was observed that the interconversion of enantiomers at small metal ions, such as zinc, was slower whereas at the larger metal ions, such as mercury, it was much faster even at low temperature. Since the isolation of "helically" chiral metal complexes of zinc with lighter chalcogens (S, Se) was found to be more facile than the complexes with the heavier chalcogen (Te), it was thought worthwhile to extend our approach to the lightest chalcogen (oxygen) as well. Also, in order to generalize our observations, we extended our approach to other transition metals where the isolation of the tetrahedral complexes was

[a] Department of Chemistry, Indian Institute of Technology
Powai, Bombay 400076, India
Fax: (internat.) + 91-22/572-3480
E-mail: chhbsia@chem.iitb.ernet.in
[b] Department of Chemistry, Howard University
Washington, DC 20059, USA

 © WILEY-VCH Verlag GmbH, 69451 Weinheim, 2001 1434–1948/01/0303–0669 $ 17.50+.50/0

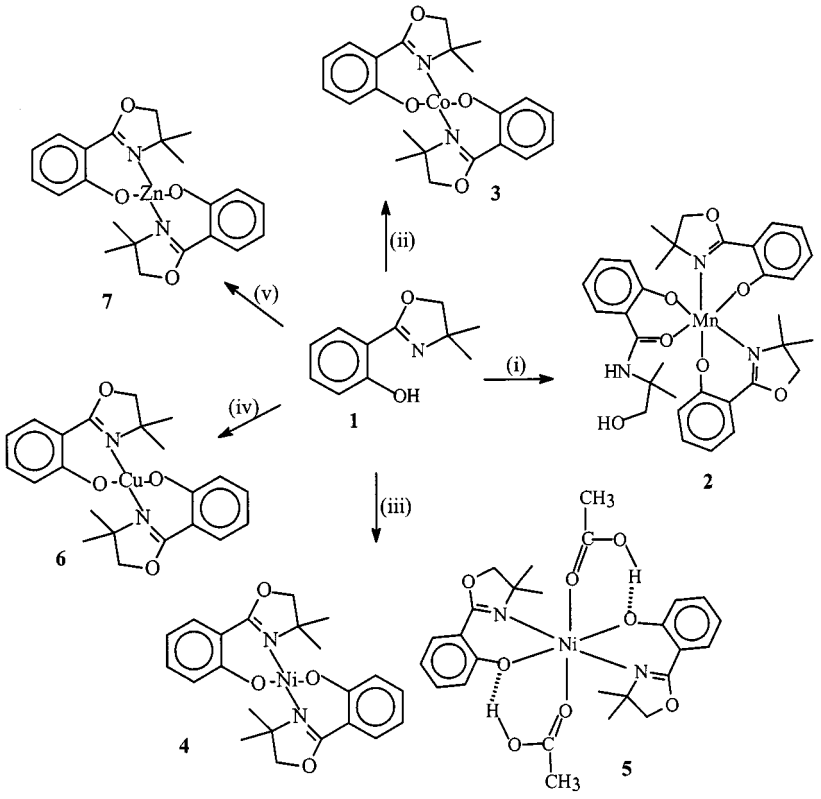

Scheme 1. Synthetic route to the metal complexes **2**–**7**; reagents and conditions: i) $Mn(OAc)_2 \cdot 4\,H_2O$, EtOH, room temp., 24 h; ii) $Co(OAc)_2 \cdot 4\,H_2O$, EtOH, room temp., 12 h; iii) $Ni(OAc)_2 \cdot 4\,H_2O$, EtOH, room temp., 18 h; iv) $Cu(OAc)_2 \cdot H_2O$, EtOH, room temp., 24 h; v) $Zn(OAc)_2$, EtOH, room temp. 24 h

feasible. In this paper we describe the synthesis and characterization of Mn^{III}, Co^{II}, Ni^{II}, Cu^{II}, and Zn^{II} complexes with the naturally occurring 2-(2′-hydroxyphenyl)-2-oxazoline ligating moiety.

Results and Discussion

Synthesis

The ligand 2-(4′,4′-dimethyl-3′,4′-dihydrooxazol-2′-yl)-phenol (**1**) was prepared in a one-pot synthesis by following the published procedure with minor modifications.[5] Since the proton of the hydroxy group in the oxazoline was acidic enough to react with the metal salts containing basic anion acetate, the ligand was treated with various metal acetates in absolute ethanol to obtain the corresponding metal complexes (Scheme 1). The addition of $Mn(OAc)_2 \cdot 4\,H_2O$ to an ethanolic solution of **1** afforded a black-green solution of complex **2**. Elemental analysis of the black-green crystals obtained upon slow evaporation of the solvent did not match with the expected 1:2 complex. Instead, it indicated the formation of a 1:3 complex where manganese was in a +3 oxidation state. Interestingly, one of the oxazoline rings undergoes a metal-assisted hydrolysis (vide infra) in the presence of acetic acid produced during the reaction. However, no hydrolysis of the oxazoline ring was observed with the other metal ions.

The partial hydrolysis of the oxazoline ring in complex **2** is similar to the hydrolysis of the active site of Agrobactin, a siderophore from *Agrobacterium tumefaciens*. The oxazoline ring of the siderophore hydrolyzes in the presence of an acid to give the open-chain form, Agrobactin A (Scheme 2).[1a] It has been further reported by Neilands et al. that the replacement of the −OH group in the 2-position of the benzene ring with −OMe or −OBz groups in Agrobactin led to a facile opening of the oxazoline ring.[1c] Similarly, in ligand **1** the coordination of the nitrogen atom to the metal center probably disturbs the co-planarity of the oxazoline ring leading to hydrolysis of the five-membered ring in the presence of acetic acid. The partial hydrolysis of the oxazoline ring is also noteworthy since acid hydrolysis of the oxazoline ring in complex **2** leads to the formation of an amide instead of the expected acid (−COOH). The mechanism of the hydrolysis involves the formation of the oxazolium ion. The oxazolium ion so formed presumably then

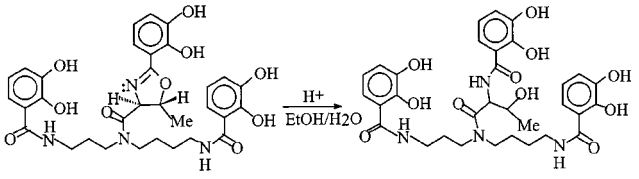

Scheme 2. Acid-catalyzed hydrolysis of the oxazoline ring present in the active site of Acrobactin to the open-chain from, Agrobactin A

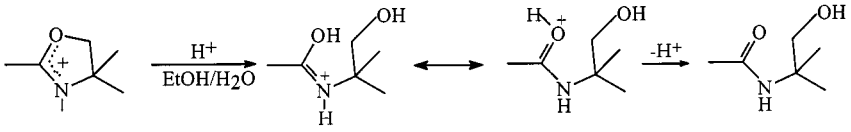

Scheme 3. Proposed mechanism of the hydrolysis of oxazoline ring in complex **2**

opens to afford the cleaved product which then undergoes tautomerization to give the open-chain amide (Scheme 3).[1a]

In order to determine whether the presence of air plays an important role in the ligand hydrolysis, the synthesis of complex **2** was attempted under nitrogen. In this case, a very air-sensitive green-colored gummy solid, presumably the expected Mn^{II} complex, was obtained. All efforts to obtain crystals of the Mn^{II} complex were unsuccessful. Isolation of the Mn^{III} complex under aerobic conditions further demonstrates that both the stability of the Mn^{III} oxidation state and its oxophilicity promote the ligand hydrolysis.

The addition of $Co(OAc)_2 \cdot 4\,H_2O$ to an ethanolic solution of **1** resulted in an immediate formation of Co^{II} complex **3** as a pink-colored solid. The crystals of the complex were obtained from a CH_2Cl_2/methanol (1:1) solution. When an ethanolic solution of **1** was added to a solution of $Ni(OAc)_2 \cdot 4\,H_2O$, an immediate formation of a green precipitate was observed. After 12 h of stirring at room temperature, the pale green solid obtained was filtered and washed with ethanol. Interestingly, the slow concentration of the filtrate afforded dark green crystals which were different from the compound obtained by filtration of the reaction mixture. Elemental analyses of both the products indicated that the pale green solid was the expected 1:2 complex **4** whereas the dark green crystalline solid (**5**) obtained from the filtrate was an acetic acid [produced in the reaction mixture during the reaction of $Ni(OAc)_2 \cdot 4\,H_2O$ with **1**] adduct of **4** (vide infra). The addition of acetic acid to an ethanolic solution of complex **4** also afforded complex **5**. Although four-coordinate Ni^{II} complexes are known to coordinate extra ligands in solution to set up equilibria between four-, five-, and six-coordinate complexes,[11] the strong bonding of the acetic acid molecules in this case is surprising since the recrystallization from methanol did not lead to the expected exchange.[11b] The Cu^{II} and Zn^{II} complexes **6** and **7** were prepared in good yields by the reaction of **1** with the corresponding metal acetates. All the complexes are quite soluble in common organic solvents such as CH_2Cl_2, $CHCl_3$, benzene, etc.

NMR Spectroscopy

Complex **7** was studied in solution by NMR spectroscopy. The ^1H NMR spectrum of **7** in $CDCl_3$ showed only small chemical shift differences compared with the spectrum of **1**. We have recently observed an AB spin behavior of the methylene protons in the corresponding zinc thiolate and selenolate complexes, and used it as a diagnostic probe for their chirality.[10a,10b] For complex **7**, no such behavior was observed at room temperature and the signals for the methyl and methylene protons were observed as singlets. However, the signals due to the methyl and methylene protons were slightly broad and this showed that the complex was probably not rigid at room temperature. At −55 °C, the $-CH_3$ protons gave rise to two singlets and the $-CH_2-$ protons gave an AB quadruplet (Figure 1). When the solution was heated to 50 °C, the two signals observed for the methyl protons and the AB quadruplet for the methylene protons became sharp singlets. This clearly indicates that the interconversion of the (*M*) and (*P*) helix is fast at room temperature and becomes slow at a low temperature on the NMR spectoscopic time scale. A similar behavior was observed at low temperatures for the cadmium thiolate, selenolate, and tellurolate complexes derived from 4,4-dimethyl-2-phenyloxazoline.[10] The ^{13}C NMR spectrum of **7** was re-

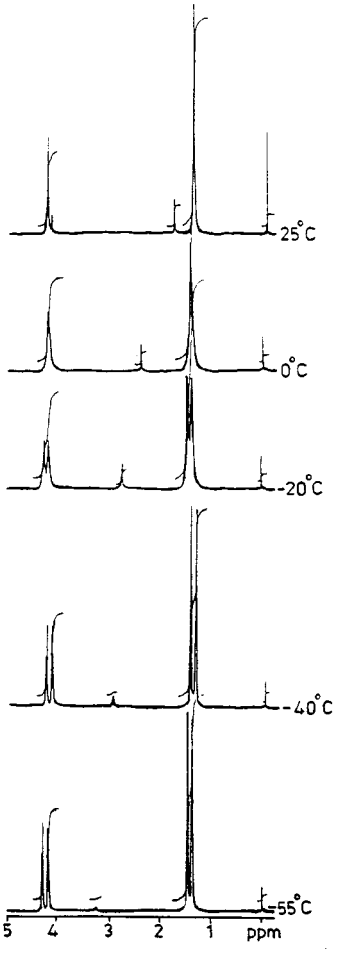

Figure 1. Variable-temperature ^1H NMR ($CDCl_3$, 300 MHz) spectra (in part only) of **7** at −55°C, the signals due to the $-CH_2-$ and $-CH_3$ protons split into an AB quadruplet and two singlets, respectively

corded in $CDCl_3$. The methyl and methylene carbon signal were shifted upfield with respect to those of **1**. The signals for the oxygen-bearing aromatic carbon atom and C(2) of the heterocycle were significantly shifted downfield (δ = 160.2 and 165.3 for **1**, δ = 170.0 and 170.5 for **7**).

Magnetic Properties

The room-temperature magnetic moment of the black-green manganese(III) complex **2** is 3.33 BM which indicates that the complex is low-spin (S = 1). The observed magnetic moment of **2** is considerably larger than the spin-only value of 2.83 BM for two unpaired electrons. This result is attributable to the presence of the orbital angular momentum for the ground term ion. Mn^{III} is known to form low-spin octahedral complexes only with strong donors like cyanides, oximes, or porphyrins. Complex **2** provides a rare example of a low-spin Mn^{III} complex with N and O donors from the oxazoline ligand. Although the effective magnetic moments for the tetrahedral Co^{II} complexes are normally observed close to the spin-only values, the observed magnetic moment for the Co^{II} complex **3** (μ_{eff} = 4.57 BM) is much higher than the spin-only magnetic moment (μ = 3.87 BM) for three unpaired electrons. This discrepancy may again be caused by angular momentum introduced to the ground state (A_2) by mixing of higher T states. The magnetic moment of 3.05 BM determined for the octahedral Ni^{II} complex **5** is very close to the spin-only value for two unpaired electrons, whereas the magnetic moment observed for tetrahedral Ni^{II} complex **4** (3.42 BM) is much higher than the spin-only value. This is in agreement with the general observation that octahedral Ni^{II} complexes have less orbital momentum than the tetrahedral complexes. It is known that the magnetic moment of truly tetrahedral Ni^{II} complexes should be about 4.2 BM because of the ground state, $^3T_1(F)$, which has much inherent orbital angular momentum. However, it is also reported that even slight distortion in the geometry reduces this markedly by splitting the orbital degeneracy. Thus, fairly regular tetrahedral complexes have moments of 3.5−4.0 BM, while for the more distorted ones the moments are 3.0−3.5 BM, i.e. in the same range as for six-coordinate complexes. The magnetic moment observed for **4**, therefore, suggests that the geometry around the metal ion is highly distorted. The magnetic moment of complex **6** (1.76 BM) is very close to the spin only value (1.73 BM) for one unpaired electron. The geometry around the metal center is, therefore, predicated as planar since a higher orbital contribution to the magnetic moment is expected for a tetrahedral Cu^{II} complex than for a planar one.[12]

Electronic Spectra

The solution-phase electronic spectrum (> 200 nm) of the ligand **1** consists of two relatively intense bands centered at 255 nm (ε_{max} = 47500 $M^{-1}cm^{-1}$) and 303 (ε_{max} = 36600 $M^{-1}cm^{-1}$), involving $\pi\rightarrow\pi^*$ transitions, and a low-intensity feature (ε_{max} = 2500 $M^{-1}cm^{-1}$) in the 350−360 nm region, responsible for the yellow color, and presumably involving $n\rightarrow\pi^*$ excitation. The electronic spectrum of **2** is dominated by a peak with medium intensity centering at 303 nm (ε_{max} = 7480 $M^{-1}cm^{-1}$), attributable to the $\sigma(N)\rightarrow Mn^{III}$ ligand-to-metal charge-transfer (LMCT) transition. One broad band at 658 nm (ε_{max} = 191 $M^{-1}cm^{-1}$) may be attributed to the ligand field transition. A broad peak centered at 500 nm (ε_{max} = 357 $M^{-1}cm^{-1}$) is also attributed to d-d transition. Four-coordinate tetrahedral and pseudo-tetrahedral Co^{II} complexes are commonly intense blue or green in color. Complex **3** shows pink color in the solid state as well as in solution. However, this is not surprising since a few complexes with dipivaloylmethane are known to give a pink color in solution.[13,14] In the tetrahedral Co^{II} case, there are three regions of absorption and, therefore, three spin-allowed electronic transitions are expected. Three d-d transition bands were observed as weak features at 501 nm (ε_{max} = 110 $M^{-1}cm^{-1}$), 563 (ε_{max} = 90 $M^{-1}cm^{-1}$), and 619 (ε_{max} = 30 $M^{-1}cm^{-1}$). The splitting of the middle band is probably due to spin-orbit coupling. There are four strong absorption bands in the high-energy region, 244 nm (ε_{max} = 33850 $M^{-1}cm^{-1}$), 281 nm (ε_{max} = 12070 $M^{-1}cm^{-1}$), 312 nm (ε_{max} = 10000 $M^{-1}cm^{-1}$), and 344 nm (ε_{max} = 11750 $M^{-1}cm^{-1}$), which can be assigned to the ligand transitions and charge-transfer transitions. For **4**, two bands, observed at 689 nm (ε_{max} = 15 $M^{-1}cm^{-1}$) and 591 nm (ε_{max} = 12 $M^{-1}cm^{-1}$), can be attributed to d-d transitions. There are three strong absorption bands in the high-energy region, 246 nm (ε_{max} = 12900 $M^{-1}cm^{-1}$), 309 nm (ε_{max} = 4730 $M^{-1}cm^{-1}$), and 336 nm (ε_{max} = 2590 $M^{-1}cm^{-1}$), which may be assigned to charge transfer and intra-ligand transitions. For **5**, there are two intense bands in the region between 200 and 340 nm that may be assigned to the intra-ligand $\pi\rightarrow\pi^*$ transitions. The band at 340 nm (ε_{max} = 1500 $M^{-1}cm^{-1}$) with medium intensity indicates the charge-transfer (CT) character. Finally, a weak feature (ε_{max} = 12 $M^{-1}cm^{-1}$) assigned to d-d transition, is present in the 500−600 nm range. For the Cu^{II} complex **6**, the ligand field transition occurs as a single broad band centering at 653 nm with an ε_{max} of 105 $M^{-1}cm^{-1}$. In addition two intense bands appear at higher energies. The peak that appears at 244 nm (ε_{max} = 30600 $M^{-1}cm^{-1}$) is assigned to the $\sigma(N)\rightarrow Cu^{II}$ LMCT transition.[15−17] The peak with medium intensity at 343 nm (ε_{max} = 11600 $M^{-1}cm^{-1}$) is too low for a charge-transfer transition involving an N donor. For tetrahedral Cu^{II} complexes with phenolate coordination, the $Cu^{II}\rightarrow$phenolate MLCT absorption occurs near 300 nm.[18,19] Therefore, the band at 309 nm (ε_{max} = 10600 $M^{-1}cm^{-1}$) is assigned as the higher energy $Cu^{II}\rightarrow\pi^*$-phenolate transition.

Electrochemistry

The cyclic voltammograms of **2−6** were recorded at room temperature in acetonitrile in the potential range −1.5 to +2.0 V vs. Ag/AgCl reference electrode. Complex **2** exhibits a quasi-reversible one-electron oxidation-reduction corresponding to the Mn^{IV}/Mn^{III} redox process ($E_{1/2}$ = 1.59 V; ΔE_p = 130 mV vs. Fc/Fc^+, $E_{1/2}$ = 0.38 V; ΔE_p = 100 mV at scan rate 50 mVs^{-1}). The Mn^{III}/Mn^{II} couple was not

observed up to −2.2 V, showing high stability of the Mn^{III} state in the present environment. Other complexes do not show any well-defined response in this potential range.

X-ray Crystallography

Crystal Structure of 2

Complex **2** crystallizes in the triclinic space group $P\bar{1}$. As can be seen in Figure 2, one of the five-membered oxazoline rings is partially hydrolyzed to give the open-chain form. The Mn^{III} ion present in the complex is six-coordinate where two nitrogen donor atoms of oxazoline rings and one carbonyl oxygen atom of the hydrolyzed oxazoline are coordinated to the central metal ion in addition to the aryloxo groups. Selected bond lengths and angles are summarized in Table 1. The three Mn−O−(Ar) bond lengths are close to each other but differ significantly from the distance between Mn and the carbonyl oxygen atom. The Mn−O and Mn−N bond lengths are comparable with the corresponding bond lengths reported for other related Mn^{III} pseudo-octahedral complexes.[19] The bond lengths and angles for the oxazoline ring reflect many similarities with the Agrobactin (Table 2).[1c] The intramolecular hydrogen bonds which are very similar to the ones observed in Agrobactin efficiently stabilize the molecular structure in the crystalline state. There are several weak interactions between the atoms in the crystal structure. Of these interactions, the hydrogen bonding between the NH proton and oxygen atom of the hydrolyzed oxazoline ring [O(33)···H−N(3) 2.266(6) Å; O(33)···N(3) 2.697(4) Å] is found to be much stronger than the others.

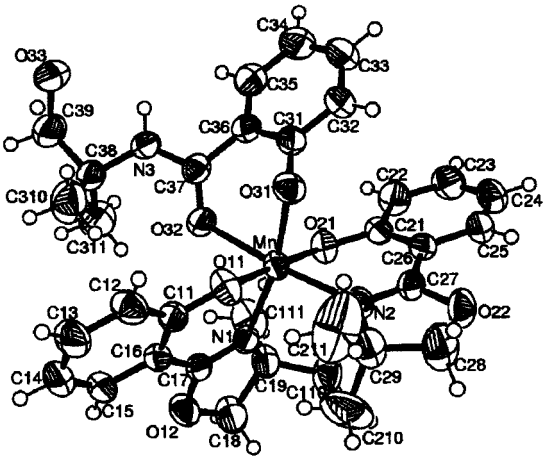

Figure 2. Crystal structure of complex **2**

Table 1. Selected bond lengths [Å] and angles [°] for **2**

Mn−N(1)	2.086(2)	Mn−N(2)	2.250(3)
Mn−O(21)	1.870(2)	Mn−O(11)	1.879(2)
Mn−O(31)	1.931(2)	Mn−O(32)	2.223(2)
O(21)−Mn−O(11)	178.39(10)	O(21)−Mn−O(31)	92.12(10)
O(11)−Mn−O(31)	88.86(10)	O(21)−Mn−N(1)	91.69(10)
O(11)−Mn−N(1)	87.60(9)	O(31)−Mn−N(1)	168.16(9)
O(21)−Mn−O(32)	91.71(9)	O(11)−Mn−O(32)	89.66(10)
O(31)−Mn−O(32)	84.07(9)	N(1)−Mn−O(32)	84.62(9)
O(21)−Mn−N(2)	86.11(9)	O(11)−Mn−N(2)	92.59(10)
O(31)−Mn−N(2)	91.49(10)	N(1)−Mn−N(2)	99.95(10)
O(32)−Mn−N(2)	174.99(9)		

Crystal Structure of 3

A perspective view of the molecule with an atom numbering scheme is shown in Figure 3. Compound **3** crystallizes as a neutral monomer in the $P\bar{1}$ space group of a triclinic system. The geometry around the Co^{II} center is tetrahedral with two bidentate oxazoline ligands. Selected bond lengths and angles are given in Table 3. The average Co−O bond length 1.9052 Å is significantly shorter than those reported for $Co(OAc)_2(imid)_2$ [1.984(1) Å][20] and $Co(OAc)_2$(2-Me-imid)$_2$ [2.098(1) Å].[21] The average Co−N bond lengths 1.9885 Å is also shorter than those observed for $Co(OAc)_2(imid)_2$ [2.0135(1) Å] $Co(OAc)_2$(2-Me-imid)$_2$ [2.062(3) Å]. The average chelate bite angle of O−Co−N is 94.57°. The larger bite angle leads to relatively smaller O−Co−O and N−Co−N angles of 119.23(7)° and 121.25(7)°, respectively. The O−Co−O angle of 119.23(7)° is higher than the corresponding value reported for Co-

Table 2. The bond lengths and angles for the oxazoline ring of complex **2** compared with those of the active site of Agrobactin

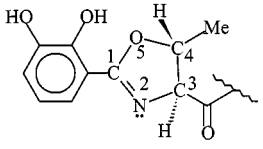

Agrobactin[a]		Complex **2**			
C(1)−N(2)	1.286(5)	N(1)−C(17)	1.288(4)	N(2)−C(27)	1.286(4)
C(3)−N(2)	1.464(5)	N(1)−C(19)	1.503(4)	N(2)−C(29)	1.485(4)
C(1)−O(5)	1.327(5)	O(12)−C(17)	1.353(3)	O(22)−C(27)	1.365(3)
C(4)−O(5)	1.466(5)	O(12)−C(18)	1.442(4)	O(22)−C(28)	1.428(4)
C(3)−C(4)	1.547(5)	C(18)−C(19)	1.526(5)	C(28)−C(29)	1.519(5)
C(1)−O(5)−C(4)	106.6(3)	C(17)−O(12)−C(18)	106.2(2)	C(27)−O(22)−C(28)	106.0(3)
C(1)−N(2)−C(3)	106.6(3)	C(17)−N(1)−C(19)	107.6(2)	C(27)−N(2)−C(29)	108.2(3)
O(5)−C(1)−N(2)	118.9(3)	O(12)−C(17)−N(1)	116.3(3)	O(22)−C(27)−N(2)	116.4(3)

[a] The atom numbering scheme of the active site of Agrobactin.

$(OAc)_2(2\text{-Me-imid})_2$ [105.1(1)°]. The interplanar angle between Co−O(11)−N(1) and Co−O(21)−N(2) is 94.7°.

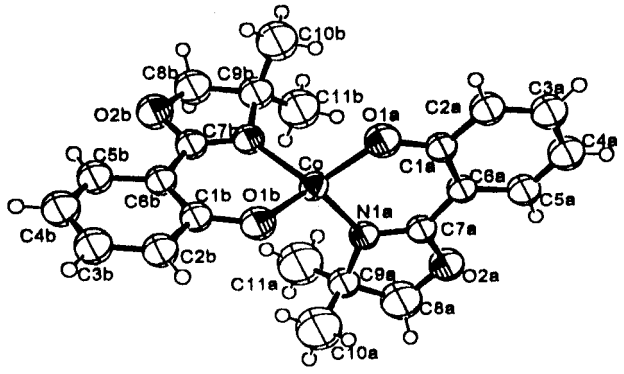

Figure 3. Crystal structure of complex **3**

Table 3. Selected bond lengths [Å] and angles [°] for **3**, **6**, and **7**

Bond lengths/angles	**3** M = Co	**6** M = Cu	**7** M = Zn
M−N(1)	1.9770(16)	1.985(1)	1.9866(19)
M−N(2)	1.9799(16)	1.986(2)	1.992(2)
M−O(11)	1.9025(15)	1.885(2)	1.9026(18)
M−O(21)	1.9075(14)	1.880(2)	1.9187(18)
O(11)−C(11)	1.312(2)	1.308(3)	1.308(3)
(12)−C(17)	1.349(2)	1.353(3)	1.356(3)
O(12)−C(18)	1.442(3)	1.439(3)	1.445(4)
O(21)−C(21)	1.309(2)	1.309(3)	1.302(3)
O(22)−C(27)	1.355(2)	1.347(3)	1.353(3)
O(22)−C(28)	1.451(3)	1.424(4)	1.448(4)
N(1)−C(17)	1.295(2)	1.298(3)	1.287(3)
N(1)−C(19)	1.494(2)	1.509(3)	1.488(3)
N(2)−C(27)	1.288(2)	1.297(3)	1.286(3)
N(2)−C(29)	1.497(2)	1.501(3)	1.497(3)
O(11)−M−O(21)	119.23(7)	156.04(9)	117.73(9)
N(1)−M−N(2)	121.25(7)	160.20(8)	121.14(9)
N(1)−M−O(21)	116.61(6)	92.05(7)	116.75(8)
N(2)−M−O(21)	94.03(6)	91.99(7)	94.16(8)
O(11)−M−N(1)	95.13(6)	91.76(7)	95.90(8)
O(11)−M−N(2)	112.52(7)	92.38(8)	112.90(9)

Crystal Structure of 5

The molecular structure of complex **5** is shown in Figure 4. Selected bond lengths and angles are presented in Table 4. The unit cell of **5** contains two nonsymmetric equivalent molecules. No significant differences between these two molecules are observed. The structure of complex **5** is found to be quite interesting. The Ni atom is six-coordinate and the geometry around the metal center is distorted octahedral. The Ni ion is bonded to two nitrogen and two oxygen atoms [both pairs are in the *cis* position (O−Ni−N angles 88.22−98.37°)] as well as two oxygen atoms of neutral acetic acid molecules. Interestingly, the acidic protons form strong hydrogen bonds with the aryloxo function of the ligand. This observation is similar to the one reported for a binuclear nickel(II) complex in which the neutral acidic acid molecule is involved in a hydrogen bonding with the alkoxo function.[11b] The C−O bond lengths of the coordinated oxygen atoms [C(12a)−O(3a) 1.223(3) Å, C(12b)−O(3b) 1.223(3) Å] are quite short while the distance of the noncoordinated oxygen atoms [C(12a)−O(4a) 1.302(4) Å, C(12b)−O(4b) 1.298(3) Å] are rather long. The bonding situation of the acetic acid molecules then allows for assuming double-bond-coordinated carbonyl groups C(12a)−O(3a) and C(12b)−O(3b) and C−O single bonds C(12a)−O(4a) and C(12b)−O(4b). The molecule has eight rings: two phenyl groups, two oxazoline groups, and four six-membered chelate rings; the latter are connected by the metal atom. The Ni(1)−N(1a) [2.075(2) Å] and Ni(1)−N(1b) [2.074(2) Å] distances are larger than those reported for four-coordinate Ni^{II} complexes with similar oxazoline ligands.[6] From the bond angle values it is observed that the two nitrogen atoms of the oxazoline five-membered rings and the two oxygen atoms of neutral acetic acid molecules form a square planar arrangement and the two phenolate oxygen atoms lie above and below the plane. The O(1a)−Ni(1)−O(1b) bond angle of 169.98(7)° indicates that these two atoms lie in the axial positions. The geometrical isomer isolated is, therefore, defined as the *cis* isomer.

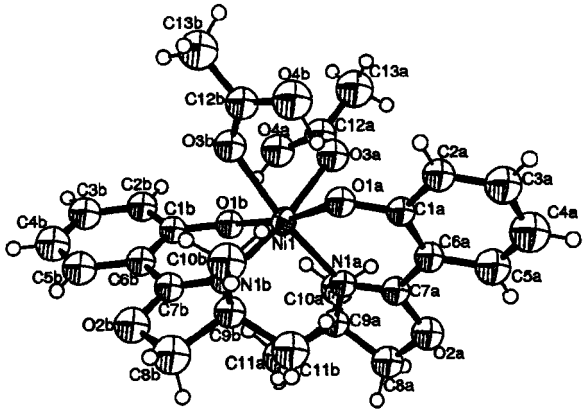

Figure 4. Crystal structure of complex **5**

Table 4. Significant bond lengths [Å] and angles [°] for **5**

Ni(1)−O(1a)	1.998(2)	Ni(1)−O(1b)	2.016(2)
Ni(1)−N(1b)	2.074(2)	Ni(1)−N(1a)	2.075(2)
Ni(1)−O(3b)	2.137(2)	Ni(1)−O(3a)	2.176(2)
O(1a)−Ni(1)−O(1b)	169.98(7)	O(1a)−Ni(1)−N(1b)	97.94(8)
O(1b)−Ni(1)−N(1b)	88.22(8)	O(1a)−Ni(1)−N(1a)	88.57(7)
O(1b)−Ni(1)−N(1a)	98.37(7)	N(1b)−Ni(1)−N(1a)	98.47(8)
O(1a)−Ni(1)−O(3b)	87.06(7)	O(1b)−Ni(1)−O(3b)	85.22(7)
N(1b)−Ni(1)−O(3b)	88.33(8)	N(1a)−Ni(1)−O(3b)	172.37(8)
O(1a)−Ni(1)−O(3a)	85.37(7)	O(1b)−Ni(1)−O(3a)	87.58(7)
N(1b)−Ni(1)−O(3a)	172.23(8)	N(1a)−Ni(1)−O(3a)	87.58(7)
O(3b)−Ni(1)−O(3a)	84.81(8)		
Ni(2)−O(1c)	2.001(2)	Ni(2)−O(1c′)	2.001(2)
Ni(2)−N(1c)	2.074(2)	Ni(2)−N(1c′)	2.074(2)
Ni(2)−O(3c)	2.179(2)	Ni(2)−O(3c′)	2.179(2)
O(1c)−Ni(2)−N(1c)	88.71(9)	O(1c′)−Ni(2)−N(1c)	97.67(8)
O(1c)−Ni(2)−N(1c′)	97.67(8)	O(1c′)−Ni(2)−N(1c′)	88.71(9)
N(1c)−Ni(2)−N(1c′)	100.83(12)	O(1c)−Ni(2)−O(3c)	87.51(9)
O(1c′)−Ni(2)−O(3c)	84.97(9)	N(1c)−Ni(2)−O(3c)	170.34(9)
N(1c′)−Ni(2)−O(3c)	88.49(9)	O(1c)−Ni(2)−O(3c′)	84.97(9)
O(1c′)−Ni(2)−O(3c)	87.51(9)	N(1c)−Ni(2)−O(3c′)	88.49(9)
N(1c′)−Ni(2)−O(3c′)	170.34(9)	O(3c)−Ni(2)−O(3c′)	82.32(14)
O(1c)−Ni(2)−O(1c′)	170.01(12)		

Crystal Structure of 6

An ORTEP view of the copper complex **6** is shown in Figure 5. Complex **6** crystallizes in the monoclinic space group $P2_1/c$. The N atoms of the oxazoline five-membered ring and phenolato O atoms gave a distorted tetrahedral arrangement. Both tetrahedral and planar configurations have been reported for the related bis[*N*-alkylsalicylaldiminato(*O*−*N*)]copper(II) complexes, depending upon the nature of the alkyl groups.[22] For comparison with **6**, the complexes with α-branched *N*-alkyl groups should be considered. In the case of *i*Pr or *t*Bu groups, they were found to be pseudo-tetrahedral in the solid state. For example, bis[*N*-isopropylsalicylaldiminato(*O*−*N*)]copper(II) has a tetrahedral structure with an angle of 60° between the salicylaldiminato planes, whereas, *N*-Ph and *N*-Me substituted complexes are almost planar.[23,24] Lehn and co-workers have reported the crystal structure of a chiral bis(dihydrooxazole)copper(II) complex,[25] with a dihedral angle of 52° between the two N−Cu−N planes. Similar to the salicylaldiminato complexes, the oxazoline complexes also form both tetrahedral and square planar complexes depending upon the nature of the alkyl groups present on the five-membered ring. Bolm et al. have reported a Cu^{II} complex with a chiral oxazoline ligand in which the geometry around the metal center was found to be almost square planar.[6] However, the geometry around the metal center in complex **6** tends more towards tetrahedral which is probably due to the presence of the two methyl groups on the oxazoline ring. Bolm et al. have also reported that there is an interaction between the Cu atom of one molecule and the phenolate O atom of the neighboring molecule which make the Cu atoms pentacoordinate.[6] However, in complex **6** no such interactions were observed. In **6**, the angle between O(11)−Cu−N(1) and O(21)−Cu−N(2) planes is 30.8°, which indicates a distortion from planar geometry. The Cu−O distances [1.880(2) Å and 1.885(2) Å] and the Cu−N distances [1.985(2) Å, 1.986(2) Å] are similar to those reported for the chiral Cu^{II} complex[6] and bis(*N*-alkylsalicylaldiminato)copper(II) complexes.[24] In **6**, the angles of 91.76(7)° and 91.99(7)° for O(11)−Cu−N(1) and O(21)−Cu−N(2) are slightly smaller than the corresponding angles in bis(*N*-alkylsalicylaldiminato)copper(II) (94.4 and 95.0°). Significant bond lengths and angles for **6** are given in Table 3.

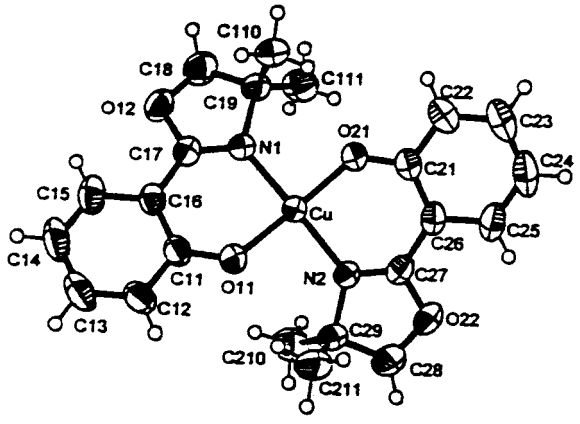

Figure 5. Crystal structure of complex **6**

Crystal Structure of 7

The colorless crystals of Zn^{II} complex **7** belong to the space group $P\bar{1}$ of the triclinic system. An ORTEP view of the structure is shown in Figure 6. Selected bond lengths and angles for **6** are given in Table 3. The Zn atom has a distorted tetrahedral coordination configuration. The interplanar angle between Zn−O(11)−N(1) and Zn−O(21)−N(2) is 86.2°. The planes between the phenyl ring and the heterocyclic ring are only slightly twisted. The dihedral angle between C(15)−C(16)−C(17)−O(12) is −0.9(3)°, that of C(15)−C(16)−C(17)−N(1) is −179.8(2)°. The Zn−O(11), Zn−O(21), Zn−N(1), and Zn−N(2) bond lengths are 1.9026(18), 1.9187(18), 1.9866(19), and 1.992(2) Å. Whereas the Zn−O distances do not differ substantially from values reported for similar Schiff base complexes,[26] the Zn−N distances are relatively short. However, the Zn−N bond lengths are slightly longer than the values reported for a similar oxazoline complex.[6]

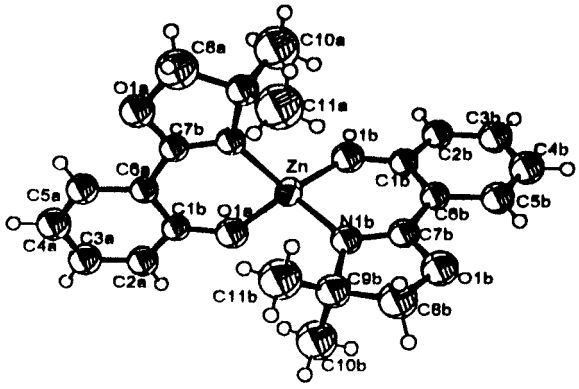

Figure 6. Crystal structure of complex **7**

Conclusion

In conclusion, we have shown that the 2-(4′,4′-dimethyl-3′,4′-dihydrooxazol-2′-yl)phenol ligand can be conveniently used to synthesize tetrahedral complexes of the late first row transition metals. Complexes **3**, **6**, and **7** crystallize as racemates in achiral space group, however, for complex **7**, the interconversion between the (*M*) and (*P*) helix is slow at low temperatures. Since the other complexes (Co, Ni, Cu) are found to be paramagnetic, the variable-temperature NMR spectroscopy of these complexes, which is used to study their low-temperature behavior, could not be attempted. The solid-state structures show that none of these complexes are chiral. Similar to the behavior of Agrobactin, the ligand 2-(4′,4′-dimethyl-3′,4′-dihydrooxazol-2′-yl)-phenol undergoes metal-assisted hydrolysis/oxidation in the presence of oxophilic Mn^{III} ions to give the partially hydrolyzed oxazoline ring as found in Agrobactin A, forming a novel mononuclear complex. The ability of Ni^{II} to form six-coordinate complexes with neutral ligands allows the

isolation of a novel octahedral Ni^{II} complex with a neutral acetic acid ligand.

Experimental Section

General Procedures: Solvents were purified by standard procedures[27] and were freshly distilled prior to use. 2-Amino-1-methyl-1-propanol (Merck) and $ZnCl_2$ were also purified prior to use.[27] 2-Hydroxybenzonitrile (Merck) was used as received. − Melting points were recorded in capillary tubes and are uncorrected. − IR spectra were recorded as KBr pellets with a Nicolet Impact 400 FT-IR spectrometer. − For **1** and **7**, the ^1H, and ^{13}C spectra were obtained at 300 and 75.42 MHz in $CDCl_3$ with a Varian VXR 300S spectrometer. Chemical shifts are cited with respect to $SiMe_4$ as an internal standard. − Elemental analyses were performed with a Carlo−Erba model 1106 elemental analyzer. − Fast atom bombardment (FAB) mass spectra were recorded at room temperature with a JEOL SX 102 DA-6000 mass spectrometer/data system using xenon (6 kV, 10 mV) as the bombarding gas. − Cyclic Voltammetry (CV) experiments were performed with an EPΣG Princeton Applied Research Potentiostat/Galvanostat Model 273A which consisted of a one-compartment cell with platinum working and counter electrodes and an Ag−AgCl electrode (reference electrode). Tetraethylammonium perchlorate was used as the supporting electrolyte. All solutions were purged with argon or nitrogen and retained under these gases while the CV data were recorded. − The EPR spectra of the complexes in chloroform or ethanol were recorded with a Varian E-112 EPR spectrometer using tetracyanoethylene as *g* marker ($g = 2.00277$) at room temperature and liquid-nitrogen temperatures. − Magnetic susceptibilities of powdered samples were determined at room temperature with a Faraday balance, standardized with mercury tetracyanocobaltate(II) [$\chi = 16.44 \cdot 10^{-6}$ cm^3 mol^{-1}]. The molar susceptibilities were corrected for ligand diamagnetism using Pascal's constants. The effective magnetic moments were calculated using the expression $\mu_{eff} = 2.83(\chi_m \times T)^{1/2}$. − Electronic absorption spectra were obtained in $CHCl_3$ at 25 °C in a 1-cm quartz cuvette with a Shimadzu UV-2100 apparatus.

Synthesis of 2-(4′,4′-Dimethyl-3′,4′-dihydrooxazol-2′-yl)phenol (1): This compound was synthesized by following the published procedure with minor modifications.[5] 2-Amino-1-methyl-1-propanol (5.99 g, 6.41 mL, 67.20 mmol), 2-hydroxybenzonitrile (5.35 g, 44.91 mmol), and $ZnCl_2$ (0.31 g, 2.24 mmol) were dissolved in chlorobenzene (90 mL) and refluxed for 24 h under nitrogen. The resulting reaction mixture was filtered to remove the undissolved impurities. The filtrate was concentrated under reduced pressure to give a brown oil which was dissolved in 50 mL of CH_2Cl_2 and washed with water. The organic layer was separated, dried with anhydrous Na_2SO_4, filtered, and concentrated to give the desired compound as a light brown oil.

Synthesis of [Mn(OR){O(Ox)}$_2$] (2): To a solution of $Mn(OAc)_2 \cdot 4\,H_2O$ (0.25 g, 1.02 mmol) in absolute ethanol (20 mL) was added a solution of **1** (0.38 g, 1.99 mmol) in ethanol (10 mL). The reaction mixture was stirred for 24 h at room temperature. The resulting dark green solution was concentrated under reduced pressure to give a dark oil. This was dissolved in dry ether (20 mL) and filtered through Celite to remove the undissolved impurities. Addition of hexane (20 mL) to the ethereal solution followed by cooling of the solution overnight afforded a black-green solid. The solid was filtered off, washed with hexane and dried under reduced pressure to give **2** as a black-green crystalline solid. Compound **2** was recrystallized by slow concentration of a solution of **2** in 1:1 mixture of CH_2Cl_2 (5 mL)/CH_3OH (5 mL) at room temperature to give black-green crystals. Yield: 0.31 g (48%). − M.p. 180−182°C. − $C_{33}H_{38}MnN_3O_7$ (643.6): calcd. C 61.58, H 5.95, N 6.53; found C 61.52, H 5.10, N 6.13. − MS; *m/z*: 453 $[C_{22}H_{26}N_2O_5Mn]^+$, 435 $[C_{22}H_{24}N_2O_4Mn]^+$, 293 $[C_{11}H_{14}NO_5Mn]^+$, 244 $[C_{11}H_{12}NO_2Mn]^+$, 191 $[C_{11}H_{12}NO_2]^+$, 173 $[C_{11}H_{12}NO]^+$. − IR (KBr): $\tilde{\nu}$ = 1580 cm^{-1}(C=O), 1609 cm^{-1}(C=N). − EPR (Solid & $CDCl_3$, 298 K): Silent.

Synthesis of [Co{O(Ox)}$_2$] (3): To a solution of $Co(OAc)_2 \cdot 4\,H_2O$ (0.25 g, 1.01 mmol) in absolute ethanol (20 mL) was added a solution of **1** (0.38 g, 1.99 mmol) in ethanol (10 mL). A pink-colored compound precipitated immediately. The stirring was continued for 12 h at room temperature. The resulting crude solid was filtered and dried under vacuum. Pink-colored needle-shaped crystals of the desired compound **3** were obtained by slow concentration of a CH_2Cl_2(5 mL)/methanol(5 mL) solution of the crude product at room temperature. Yield: 0.37g (85%). − M.p. 234−236°C. − $C_{22}H_{24}CoN_2O_4$ (439.4): calcd. C 60.14, H 5.50, N 6.38; found C 60.23, H 5.35, N 6.22. − MS; *m/z* (%): 439 $[M^+, C_{22}H_{24}N_2O_4Co]^+$ (100), 364 $[C_{22}H_{24}N_2O_3]^+$, 249 $[C_{11}H_{12}NO_2Co]^+$, 190 $[C_{11}H_{12}NO_2]^+$, 177 $[C_{11}H_{12}NO]^+$. − IR (KBr): $\tilde{\nu}$, 1618 cm^{-1} (C=N).

Synthesis of [Ni{O(Ox)}$_2$] (4): To a solution of $Ni(OAc)_2 \cdot 4\,H_2O$ (0.25 g, 1.01 mmol) in absolute ethanol (20 mL) was added a solution of **1** (0.38 g, 1.99 mmol) in ethanol (10 mL). The resulting green solution was stirred for 18 h at room temperature. The pale green solid formed was filtered and washed with ethanol and dried under vacuum. The pale green crystals of **4** were obtained by slow concentration of a CH_2Cl_2(5 mL)/ethanol(5 mL) solution of the crude product. Slow concentration of the filtrate at room temperature afforded the dark green crystals of **5**.

4: Yield: 0.26g (60%). − M.p. 224−226°C. − $C_{22}H_{24}N_2NiO_4$ (439.2): calcd. C 60.17, H 5.51, N 6.38; found C 59.84, H 5.32, N 6.10. − MS; *m/z* (%): 555 $[C_{26}H_{32}N_2O_8Ni]^+$, 496 $[C_{24}H_{28}N_2O_6Ni]^+$, 439 $[C_{22}H_{24}N_2O_4Ni]^+$, 424 $[C_{21}H_{21}N_2O_4Ni]^+$, 367 $[C_{15}H_{20}NO_6Ni]^+$, 352 $[C_{14}H_{17}NO_6Ni]^+$, 248 $[C_{11}H_{12}NO_2Ni]^+$, 176 $[C_{11}H_{12}NO]^+$ (100). − IR (KBr): $\tilde{\nu}$ = 1622 cm^{-1} (C=N). − EPR (Solid, 77 K): $g_{eff} = 2.18$.

5: Yield: 0.17g (30%). − M.p. 198−200°C. − $C_{26}H_{32}N_2NiO_8$ (559.3): calcd. C 55.84, H 5.77, N 5.01; found C 55.54, H 5.45, N 4.87. − MS; *m/z* (%): 555 [M, $C_{26}H_{32}N_2O_8Ni]^+$ (100), 498 $[C_{24}H_{28}N_2O_6Ni]^+$, 439 $[C_{22}H_{24}N_2O_4Ni]^+$, 424 $[C_{21}H_{21}N_2O_4Ni]^+$, 365 $[C_{15}H_{20}NO_6Ni]^+$, 352 $[C_{14}H_{17}NO_6Ni]^+$, 248 $[C_{11}H_{12}NO_2Ni]^+$, 176 $[C_{11}H_{12}NO]^+$. − IR (KBr): $\tilde{\nu}$ = 1617 cm^{-1} (C=N), 1706 cm^{-1} (C=O). − EPR (Solid & $CDCl_3$, 298 K): Silent.

Synthesis of [Cu{O(Ox)}$_2$] (6): To a solution of $Cu(OAc)_2 \cdot H_2O$ (0.20 g, 1.01 mmol) in absolute ethanol (20 mL) was added a solution of **1** (0.38 g, 1.99 mmol) in ethanol (10 mL). The resulting green-colored solution was stirred for 24 h at room temperature and then filtered. The filtrate was concentrated under vacuum to give a green-colored solid. Recrystallization of the solid from CH_2Cl_2(5 mL)/methanol(5 mL) mixture at room temperature afforded the dark green crystals of **6**. Yield: 0.38g (85%). − M.p. 190−192°C. − $C_{22}H_{24}CuN_2O_4$ (443.10): calcd. C 59.52, H 5.45, N 6.31; found C 59.27, H 5.23, N 6.14. − MS; *m/z* (%): 443 [M, $C_{22}H_{24}N_2O_4Cu]^+$ (100), 371 $[C_{22}H_{24}N_2O_3]^+$, 253 $[C_{11}H_{12}NO_2Cu]^+$, 191 $[C_{11}H_{12}NO_2]^+$, 176 $[C_{11}H_{12}NO]^+$. − IR(KBr): $\tilde{\nu}$ = 1614 cm^{-1} (C=N). − EPR ($CHCl_3$, 25 °C): g_{eff} = 2.31.

Synthesis of [Zn{O(Ox)}$_2$] (7): To a solution of $Zn(OAc)_2$ (0.46 g, 2.51 mmol) in absolute ethanol (30 mL) was added a solution of **1** (0.95 g, 4.97 mmol) in ethanol (10 mL). The reaction mixture was stirred for 24 h at room temperature during which time a white solid was formed. The solid was filtered and dried under vacuum. Colorless crystals of the desired compound were obtained by recrystallization from $CHCl_3$(5 mL)/hexane (5 mL). Yield: 0.40 g (90%). − M.p. 210−212 °C. − $C_{22}H_{24}N_2O_4Zn$ (445.8): calcd. C 59.27, H 5.43, N 6.28; found C 59.14, H 5.22, N 6.16. − ^{1}H NMR ($CDCl_3$): δ = 1.38 (s, 12 H, CH_3), 4.16(s, 4 H, CH_2), 6.52−6.56 (dd, 2 H, Ar-H), 6.84−6.88 (d, 2 H, Ar-H) 7.25−7.33 (dd, 2 H, Ar-H), 7.67−7.71 (d, 2 H, Ar-H). − ^{13}C NMR ($CDCl_3$): δ = 28.34, 66.39, 77.77, 108.95, 113.86, 123.14, 130.05, 134.99, 168.11, 170.27. − MS; *m/z* (%): 702 $[C_{33}H_{36}N_3O_6Zn_2]^+$, 445 [M, $C_{22}H_{24}N_2O_4Zn]^+$ (100), 254 $[C_{11}H_{12}NO_2Zn]^+$, 238 $[C_{10}H_9NO_2Zn]^+$, 191 $[C_{11}H_{12}NO_2]^+$. − IR (KBr): $\tilde{\nu}$ = 1645 cm^{-1} (C=N).

X-ray Crystallographic Studies: The diffraction measurements for compounds **2**, **3**, **5**, **6**, and **7** were performed at room temperature (293 K) with a Siemens R3m/V diffractometer using graphite-monochromated Mo-K_α radiation (λ = 0.71073 Å). The unit cell was determined from 25 randomly selected reflections using the automatic search index and least-squares routine. For **2**, the θ range for data collection was from 2.25 to 27.50° whereas for **3**, **5**, **6**, and **7** the ranges were 2.58−27.50°, 1.29−27.50°, 2.40−27.50°, and 2.58−50.59°. The index range for **2** was $-13 \le h \le 0$, $-13 \le k \le 13$, $-19 \le l \le 20$ while for **3**, **5**, **6**, and **7** the ranges were $0 \le h \le 10$, $-13 \le k \le 13$, $-16 \le l \le 17$; $0 \le h \le 41$, $-20 \le k \le 0$, $-21 \le l \le 21$; $-14 \le h \le 0$, $0 \le k \le 12$, $-25 \le l \le 25$, and $0 \le h \le 11$, $-14 \le k \le 14$, $-18 \le l \le 18$. The data for **3**, **6**, and **7** were corrected for Lorentz, polarization, and absorption effects. The maximum and minimum transmission values of the correction factors for compounds **3** (dimensions 0.48 × 0.50 × 0.49 mm), **6** (0.19 × 0.88 × 0.38 mm), and **7** (0.28 × 0.64 × 0.32 mm) were 0.4733 and 0.3904, 0.2873 and 0.2187, and 0.9181 and 0.8319. The data were monitored by measuring two standard reflections every 60 min of X-ray exposure time. The structures were solved by routine heavy-atom (using SHELXS 86[28]) and Fourier methods and refined by full-matrix least squares with the non-hydrogen atoms anisotropic and hydrogen atoms with fixed isotropic thermal parameters of 0.07 Å^2 using the SHELXL 93 program.[29] The hydrogen atoms were partially located from difference electron-density maps and the rest were fixed at calculated positions. Scattering factors were from common sources.[30] Some details of data collection and refinement are given in Table 5 and Table 6. Crystallographic data (excluding structure factors) for the structures reported in this paper have been deposited with the Cambridge Crystallographic Data Centre as supplementary publications nos. CCDC-134052 (**2**), -134053 (**3**), -134054 (**5**), -134055 (**6**), -134056 (**7**). Copies of the data can be obtained free of charge on application to CCDC, 12 Union Road, Cambridge CB21EZ, UK [Fax: (internat.) + 44-1223/336-033; E-mail: deposit@ccdc.cam.ac.uk].

Table 6. Crystal data and structure refinement for **6** and **7**

	6	**7**
Empirical formula	$C_{22}H_{24}CuN_2O_4$	$C_{22}H_{24}N_2O_4Zn$
Molecular mass	443.97	445.80
Crystal system	monoclinic	triclinic
Space group	$P2_1/c$	$P\bar{1}$
a [Å]	11.462(2)	8.0231(8)
b [Å]	9.3919(12)	11.4838(13)
c [Å]	19.628(2)	13.2563(13)
α [°]	90	115.582(7)
β [°]	91.726(8)	96.924(6)
γ [°]	90	94.500(7)
V [Å^3]	2112.0(4)	1081.9(2)
Z	4	2
D(calcd.) [Mg/m^3]	1.396	1.368
Abs. coeff. [mm^{-1}]	1.064	1.164
Obsd. reflexions [$I > 2\sigma$]	4800	5969
Final $R(F)$ [$I > 2\sigma(I)$][a]	0.0358	0.0432
$wR(F^2)$ indices [$I > 2\sigma(I)$]	0.0928	0.1132
Data/restrains/parameters	4799/0/291	5968/0/291
Goodness of fit on F^2	1.03	1.07

[a] Definitions: $R(F_o) = ||F_o| - |F_c||/|F_o|$ and $wR(F_o^2) = \{[w(F_o^2 - F_c^2)^2]/[w(F_c^2)^2]\}^{1/2}$.

Acknowledgments

We are grateful to the Department of Science and Technology (DST), New Delhi and Board of Research in Nuclear Sciences (BRNS), Department of Atomic Energy, Bombay for funding this work. Additional help from the Regional Sophisticated Instrumentation Centre (RSIC), Indian Institute of Technology (IIT),

Table 5. Crystal data and structure refinement for **2**, **3**, and **5**

	2	**3**	**5**
Empirical formula	$C_{33}H_{38}N_3O_7Mn$	$C_{22}H_{24}N_2O_4Co$	$C_{26}H_{32}N_2O_8Ni$
Molecular mass	643.60	439.36	559.25
Crystal system	triclinic	triclinic	monoclinic
Space group	$P\bar{1}$	$P\bar{1}$	$C2/c$
a [Å]	10.095(2)	8.018(2)	31.690(6)
b [Å]	10.646(2)	11.472(3)	15.401(2)
c [Å]	15.734(4)	13.230(3)	16.856(3)
α [°]	94.76(2)	64.581(14	90
β [°]	108.22(2)	79.358(14)	97.083(9)
γ [°]	91.14(2)	85.54(2)	90
V [Å^3]	1598.7(6)	1080.2(5)	8164(2)
Z	2	2	12
D(calcd.) [Mg/m^3]	1.337	1.351	1.365
Abs. coeff. [mm^{-1}]	0.464	0.823	0.763
Obsd. reflexions [$I > 2\sigma$]	7332	4345	9231
Final $R(F)$ [$I > 2\sigma(I)$][a]	0.0558	0.0344	0.0427
$wR(F^2)$ indices [$I > 2\sigma(I)$]	0.1267	0.0917	0.1019
Data/restrains/parameters	7328/0/447	4345/0/291	9228/0/567
Goodness of fit on F^2	1.043	1.09	1.08

[a] Definitions: $R(F_o) = ||F_o| - |F_c||/|F_o|$ and $wR(F_o^2) = \{[w(F_o^2 - F_c^2)^2]/[w(F_c^2)^2]\}^{1/2}$.

Bombay, for EPR and 300-MHz NMR spectroscopy is gratefully acknowledged. R. J. B. wishes to acknowledge the DoD-ONR program for funds to upgrade the diffractometer.

[1] [1a] S. A. Ong, T. Peters, J. B. Neilands, *J. Biol. Chem.* **1979**, *254*, 1860. – [1b] T. Peterson, J. B. Neilands, *Tetrahedron Lett.* **1979**, *50*, 4805. – [1c] T. Peterson, K. -E. Falk, S. A. Leong, M. P. Klein, J. B. Neilands, *J. Am. Chem. Soc.* **1980**, *102*, 7715. – [1d] Y. Nagao, T. Miyasaka, Y. Hagiwara, E. Fujita, *J. Chem. Soc., Perkin Trans. 1* **1984**, 183. – [1e] D. L. Eng-Wilmot, D. van der Helm, *J. Am. Chem. Soc.* **1980**, *102*, 7719.

[2] A. Jacobs, G. P. White, G. H. Tait, *Biochem. Biophys. Res. Commun.* **1977**, *74*, 1626.

[3] [3a] H. Brunner, H. Nishiyama, K. Itoh, in: *Catalytic Asymmetric Synthesis* (Ed.: I. Ojima), VCH Publishers, New York, **1993**, p. 303. – [3b] J. V. Allen, J. M. J. Williams, *Tetrahedron: Asymmetry* **1994**, *5*, 277. – [3c] H. Brunner, D. Henrichs, *Tetrahedron: Asymmetry* **1995**, *6*, 653. – [3d] E. Macedo, C. Moberg, *Tetrahedron: Asymmetry* **1995**, *6*, 549. – [3e] H. Eichelmann, H.-J. Gais, *Tetrahedron: Asymmetry* **1995**, *6*, 643. – [3f] C. J. Richards, D. E. Hibbs, M. B. Hursthouse, *Tetrahedron Lett.* **1995**, *36*, 3745.

[4] [4a] P. G. Cozzi, C. Floriani, A. C. Villa, C. Rizzoli, *Inorg. Chem.* **1995**, *34*, 2921. – [4b] P. G. Cozzi, C. Floriani, *J. Chem. Soc., Perkin Trans.1* **1995**, 2557.

[5] [5a] M. G. Simon, S. Jansat, G. Muller, D. Panyella, M. F. Bardia, X. Soians, *J. Chem. Soc., Dalton Trans.* **1997**, 3755. – [5b] M. Hoogenraad, K. Ramkisoensing, H. Kooijman, A. L. Spek, E. Bouwman, J. G. Haasnoot, J. Reedijk, *Inorg. Chim. Acta* **1998**, *279*, 217.

[6] H. R. Hoveyda, V. Karunaratne, S. J. Rettig, C. Orvig, *Inorg. Chem.* **1992**, *31*, 5408.

[7] C. Bolm, K. Wieghardt, M. Zehnder, D. Glasmacher, *Helv. Chim. Acta* **1991**, *74*, 717.

[8] C. Bolm, K. Wieghardt, M. Zehnder, T. Renff, *Chem. Ber.* **1991**, *124*, 1173.

[9] [9a] H. B. Singh, N. Sudha, *Coord. Chem. Rev.* **1994**, *135–136*, 469. – [9b] R. Kaur, H. B. Singh, R. J. Butcher, *Organometallics* **1995**, *14*, 4755. – [9c] R. Kaur, H. B. Singh. R. P. Patel, S. K. Kulshreshtha, *J. Chem. Soc., Dalton Trans.* **1996**, 461. – [9d] S. C. Menon, H. B. Singh, J. M. Jasinski, J. P. Jasinski, R. J. Butcher, *Organometallics* **1996**, *15*, 1707. – [9e] S. C. Menon, H. B. Singh, R. P. Patel, K. Das, R. J. Butcher, *Organometallics* **1997**, *18*, 563. – [9f] G. Mugesh, A. Panda, H. B. Singh, N. S. Punekar R. J. Butcher, *Chem. Commun.* **1998**, 2227. – [9g] G. Mugesh, H. B. Singh, R. J. Butcher, *Tetrahedron: Asymmetry* **1999**, *10*, 237. – [9h] G. Mugesh, A. Panda, H. B. Singh, R. J. Butcher, *Chem. Eur J.* **1999**, *5*, 1411. – [9i] A. Panda, G. Mugesh, H. B. Singh, R. J. Butcher, *Organometallics* **1999**, *18*, 1986.

[10] [10a] G. Mugesh, H. B. Singh, R. J. Butcher, *Eur. J. Inorg. Chem.* **1999**, 1229. – [10b] G. Mugesh, H. B. Singh, R. P. Patel, R. J. Butcher, *Inorg. Chem.* **1998**, *37*, 2663. – [10c] G. Mugesh, H. B. Singh, R. J. Butcher, *J. Organomet. Chem.* **1999**, *577*, 243.

[11] [11a] M. Schroder, "Nickel: Inorganic and Coordination Chemistry" in: *Encyclopedia of Inorganic Chemistry* (Ed.: R. B. King) John Wiley & Sons, New York, **1994**, vol. 4, p. 2392. – [11b] D. Volkmer, A. Horstmann, K. Griesar, W. Haase, B. Krebs, *Inorg. Chem.* **1996**, *35*, 1132.

[12] B. N. Figgis, *Nature* **1958**, *182*, 1568.

[13] R. L. Carlin Jr., S. L. Holt, *Inorg. Chem.* **1963**, *2*, 849.

[14] F. A. Cotton, D. M. L. Goodgame, M. Goodgame, *J. Am. Chem. Soc.* **1961**, *83*, 4690.

[15] H. Yokoi, T. Isobe, *Bull. Chem. Soc. Jpn.* **1969**, *42*, 2187.

[16] B. P. Kennedy, A. B. P. Lever, *J. Am. Chem. Soc.* **1973**, *95*, 6907.

[17] V. M. Miskowski, J. A. Thich, R. Solomon, H. J. Schugar, *J. Am. Chem. Soc.* **1976**, *98*, 8344.

[18] A. R. Amundsen, J. Whelan, G. Bosnich, *J. Am. Chem. Soc.* **1977**, *99*, 6730.

[19] G. Das, R. Shukla, S. Mandal, R. Singh, P. K. Bharadwaj, J. Van Hall, K. H. Whitmire, *Inorg. Chem.* **1997**, *36*, 323.

[20] W. D. Horrocks, J. N. Ishley, R. R. Whittle, *Inorg. Chem.* **1982**, *21*, 3265.

[21] W. D. Horrocks, J. N. Ishley, R. R. Whittle, *Inorg. Chem.* **1982**, *21*, 3270.

[22] P. L. Orioli, L. Sacconi, *J. Am. Chem. Soc.* **1966**, *88*, 277.

[23] E. C. Lingafelter, G. L. Simmons, B. Morosin, C. Scheringer, C. Freiburg, *Acta Crystallogr.* **1961**, *14*, 1222.

[24] L. Wei, R. M. Stogsdill, E. C. Lingafelter, *Acta Crystallogr.* **1964**, *17*, 1058.

[25] J. Hall, J. -M. Lehn, A. DeCian, J. Fisher, *Helv. Chim. Acta* **1991**, *74*, 1.

[26] R. H. Prince, in: *Comprehensive Coordination Chemistry* (Eds.: G. Wilkinson, R. D. Gilliard, J. A. McCleverty), Pergamon Press, Oxford, **1987**, vol. 5, pp. 925.

[27] D. D. Perrin, W. L. F. Armarego, D. R. Perrin, *Purification of Laboratory Chemicals*, 2nd ed., Pergamon, Oxford, **1980**.

[28] G. M. Sheldrick, *Crystallographic Computing 3*, Oxford University Press, Oxford, **1985**, p. 175.

[29] G. M. Sheldrick, *SHELX 93, Program for Crystal Structure Determination*, University of Göttingen, **1993**.

[30] *International Tables for X-ray Crystallography*, Kynoch Press, Birmingham, **1974**, vol. 4, pp. 99, 149.

Received June 30, 2000
[I00259]

Structural Investigations of Oligomeric Axially Bridged Ruthenium Phthalocyanines by EXAFS Spectroscopy

Achim Weber,[a] Teja S. Ertel,[a] Ulrich Reinöhl,[a] Martin Feth,[a] Helmut Bertagnolli,*[a] Meret Leuze,[b] and Michael Hanack*[b]

Keywords: EXAFS spectroscopy / Ruthenium / Phthalocyanines / Structure elucidation

To obtain more information about the structure of phthalocyaninatoruthenium compounds an EXAFS investigation was carried out on amorphous bisaxially bridged phthalocyaninatoruthenium(II) oligomers, $[PcRu(tz)]_n$ (**1**), $[PcRu(pyz)]_n$ (**2**) and $[PcRu(dib)]_n$ (**3**). Detailed structural models for the three compounds were deduced from the determined atomic distances around the metal center. A bisaxial structure of the ligands could be proven for all compounds and additionally, the structure parameters could be determined.

Introduction

In recent years phthalocyaninatoruthenium(II) complexes have been investigated with particular regard to their preparation, chemistry, and structure.[1−3] Some years ago we reported the first synthesis of pure phthalocyaninatoruthenium(II) $(PcRu)_2$.[4] Later, we developed a convenient method for obtaining $(PcRu)_2$ by thermal decomposition of the corresponding bisisoquinoline or bis-3-chloropyridine complex $PcRu(L)_2$ (L = iqnl; 3-Clpy) at 250 or 270 °C,[5,6] respectively. This provides the basis for the preparation of axially bridged $[PcRu(L)]_n$ oligomers with bidentate bridging ligands L [e.g. L = pyrazine (pyz), *s*-tetrazine (tz), 1,4-diisocyanobenzene (dib)] as a new class of intrinsic semiconductors.[2,4]

An important condition for achieving electrical conductivity in phthalocyaninato compounds is the stacked arrangement of the macrocycles. Assuming a suitably small distance between cofacially arranged planar macrocycles possessing an extended π-electron system, electron delocalization by π-π overlap of the perpendicular orbitals in a stacked arrangement is possible. In particular, oxidation (or less frequently reductive doping) of the macrocycles generates charge carriers leading to semiconducting or conducting quasi-one-dimensional materials.

Phthalocyaninato compounds, however, do not crystallize in this stacked arrangement, except phthalocyaninatolead(II) (PcPb) in its monoclinic modification.[7] Metallophthalocyanines in general crystallize in an α- or β-modification (inclined stacked), which is not favorable for π-orbital overlap and thus for the formation of a conducting band.

[a] Institut für Physikalische Chemie, Universität Stuttgart
Pfaffenwaldring 55, 70569 Stuttgart, Germany
Fax: (internat.) +49-711/685-4443
E-mail: h.bertagnolli@ipc.uni-stuttgart.de
[b] Institut für Organische Chemie, Universität Tübingen,
Auf der Morgenstelle 18, 72076 Tübingen, Germany
Fax: (internat.) +49-7071/295-244
E-mail: hanack@uni-tuebingen.de

Some years ago a route was developed to stacked arrangements of phthalocyaninato transition metal compounds which lead to coordination oligomers and polymers where the macrocycle, the central metal atom and the bridging ligand can be varied systematically. The stacking is achieved by connecting the central transition metal atoms of the macrocycle with bidentate bridging ligands L bisaxially. Such bridged macrocyclic transition metal compounds $[MacM(L)]_n$ have been synthesized and investigated in detail with respect to their physical properties.[8,9] The bridging ligands L are linear π-electron-containing organic molecules, for example pyrazine, 1,4-diisocyanobenzene or substituted 1,4-diisocyanobenzenes, *s*-tetrazine or substituted tetrazines, and others. Many of the bridged macrocyclic metal complexes $[MacM(L)]_n$ (“shish-kebab polymers”) can be prepared in high yields and high purity by treating the metallomacrocycle MacM with the pure ligand or with the ligand in an appropriate solvent. The bridged structure has been confirmed for many compounds using a variety of physical methods[8] including detailed IR investigations,[10] Mössbauer spectroscopy,[11] ^1H and ^{13}C NMR spectroscopy[12] and scanning tunneling microscopy (STM).[13]

$(PcRu)_2$ reacts easily with ligands L such as pyrazine, *s*-tetrazine, 1,4-diisocyanobenzene and others to form the corresponding monomers $PcRu(L)_2$, and under somewhat different conditions to form the bridged systems $[PcRu(L)]_n$.[4,14] Although the monomeric complexes $PcM(L)_2$ (L = pyz, tz, dib; M = Fe, Ru, Os) are all insulators, it can be seen that the ligand (L) has a significant effect on the conductivity of the bridged complexes $[PcM(L)]_n$: as 1,4-diazabicyclo[2.2.2]octane (dabco) is a ligand containing no π-orbitals to interact with the metallomacrocycle the $[PcM(dabco)]_n$ complexes are also insulators,[2] whereas an increase in electrical conductivity is observed for the pyrazine- and 1,4-diisocyanobenzene-bridged compounds. $[PcRu(pyz)]_n$ (**2**) and $[PcRu(dib)]_n$ (**3**) exhibit electrical conductivities ($\sigma_{RT} = 1 \times 10^{-7}$ S cm^{-1} and σ_{RT} =

 © WILEY-VCH Verlag GmbH, 69451 Weinheim, 2001 1434−1948/01/0303−0679 $ 17.50+.50/0

2×10^{-6} S cm^{-1})[4,15] in the low semiconducting region. However, by changing the bridging ligand to *s*-tetrazine or its derivatives the conductivity increases by three to five orders of magnitude without external oxidative doping.[2,16] With *s*-tetrazine as the ligand in $[PcRu(tz)]_n$ (**3**), a powder conductivity of 0.01 S cm^{-1} can be achieved.

Structural investigations on oligomeric phthalocyaninatoruthenium(II) compounds with EXAFS or LAXS spectroscopy have only been performed on oxygen-containing materials up to now.[3] Extended X-ray absorption fine structure (EXAFS) has been considered to be a powerful technique for determining the local atomic environment of a specific atom without regard to the state of the sample. An analysis of the EXAFS provides information on the bond length, the coordination number, the "Debye−Waller"-like factor, and the nature of the scattering atoms surrounding an excited atom.[17,18] In this paper, we have studied (μ-*s*-tetrazine)phthalocyaninatoruthenium(II) (**1**), (μ-pyrazine)phthalocyaninatoruthenium(II) (**2**) and (μ-1,4-diisocyanobenzene)phthalocyaninatoruthenium(II) (**3**) as amorphous solids by transmission EXAFS spectroscopy.

Results and Discussion

(μ-*s*-Tetrazine)phthalocyaninatoruthenium(II) (1)

In the Fourier transforms (see Figure 1b and 1d), several coordination shells are visible. In fitting the EXAFS function to the experiment we fixed the coordination numbers to the known values of the phthalocyanine molecule. Furthermore, the four shells of the phthalocyanine macrocycle were only fitted independently in such a way that the determined distances led to meaningful interatomic distances in the macrocycle itself. Taking these considerations into account the number of parameters decreases from 12 to 9 and is clearly less than the number of independent data points (22).[19]

Five backscatterers are necessary for a good fit of the EXAFS function (see Figure 1c, 1d and Table 1). These are the four backscatterers of the phthalocyanine macrocycle and one nitrogen backscatterer, which can be traced back to the bridging ligand *s*-tetrazine at a distance of 2.22 Å. Without this backscatterer the fit worsens significantly to

Table 1. EXAFS-determined structural data of **1**[a]

1	*N*	R^4, Å	σ^4, Å	R^5, Å	σ^5, Å
$Ru-N_{Indol}$	4	2.02±0.02	0.068±0.011	2.02±0.02	0.058±0.013
Ru−C	8	3.02±0.03	0.081±0.014	3.04±0.03	0.076±0.016
$Ru-N_{Aza}$	4	3.22±0.03	0.088±0.009	3.27±0.03	0.088±0.016
Ru−C	8	3.97±0.04	0.095±0.019	3.98±0.04	0.080±0.014
$Ru-N_{tz}$	2			2.22±0.02	0.075±0.009

[a] Absorber−backscatterer distance *r*, coordination number *N* and Debye−Waller factor σ with their calculated standard deviation. The simulations with four and five backscatterers are marked by the superscripts 4 and 5. The ΔE_0 shift of **1** of EXCURV92 is 19.03 eV and the *R*-factors are 35.8[4] and 28.2[5].

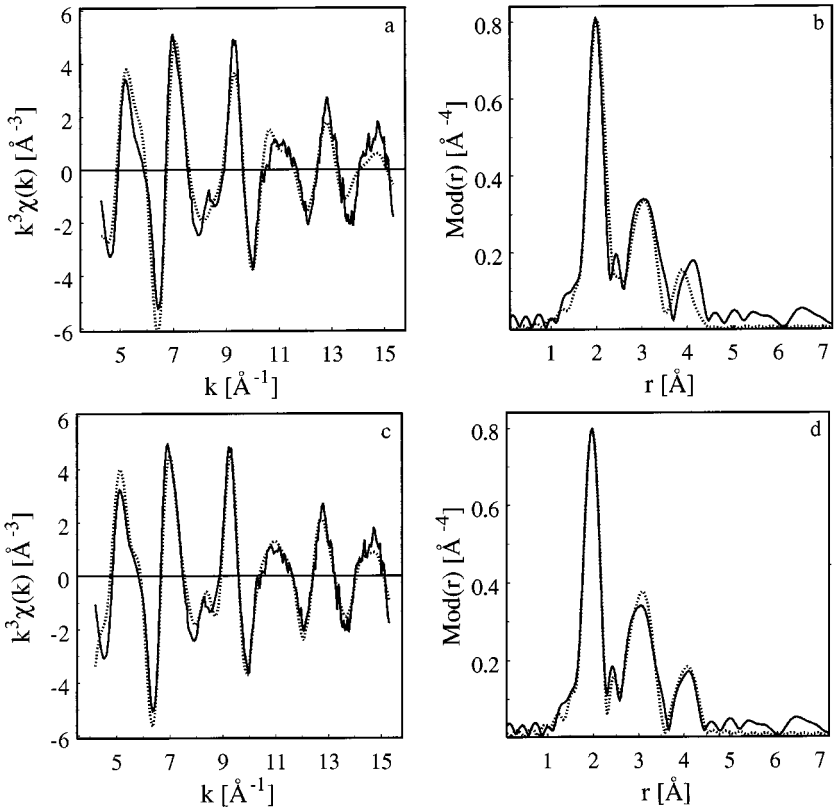

Figure 1. Experimental (solid line) and calculated (dotted line) Ru−K $k^3 \cdot \chi(k)$ functions (a, c) and their corresponding Fourier transforms without phase correction (b, d) of **1** (*k* range: 3.45−15.45 Å^{-1}); simulation with four (a, b) and five (c, d) backscatterers; the corresponding structural data are given in Table 1

about 21%. The difference of the fit with four and five backscatterers can be compared in Figure 1a and 1b (four backscatterers) and Figure 1c and 1d (five backscatterers). The resulting model of **1** with the determined distances can be seen in Figure 2a.

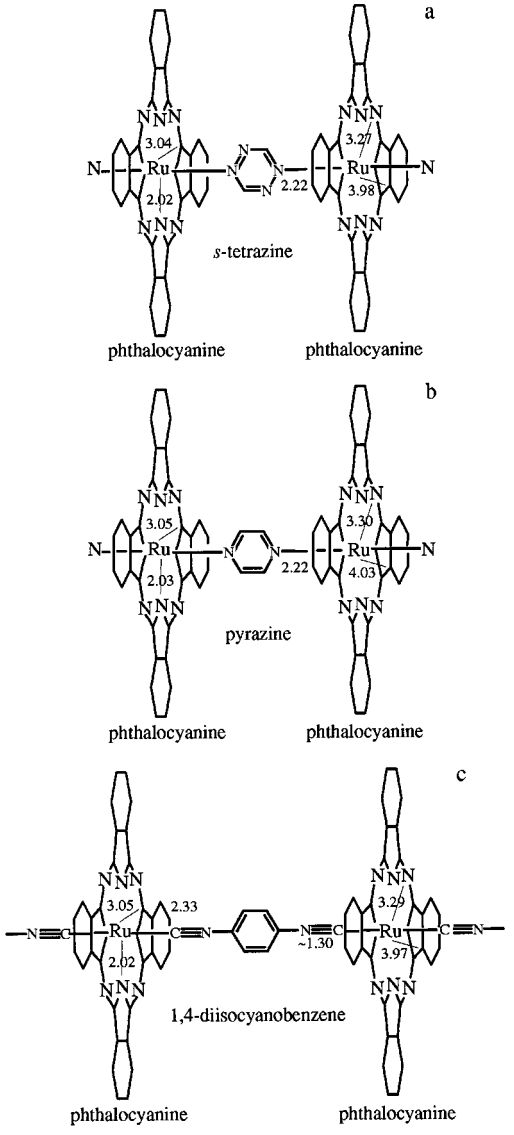

Figure 2. Determined distances and proposed structures of **1** (a), **2** (b) and **3** (c)

Without any knowledge of the structure, one would expect the ruthenium atom to be located in the plane of the phthalocyanine ring. A planar arrangement of the atoms should give rise to a considerable contribution of multiple scattering to the EXAFS spectrum. Defining the multiple scattering unit shown in Figure 3, we found in several calculations that for this geometrical arrangement the relevant maximum order of multiple scattering is three. But in all fits we could not describe the experimental spectrum satisfactorily.

Since only single scattering contributes to the EXAFS function, we are forced to assume that the ruthenium atom

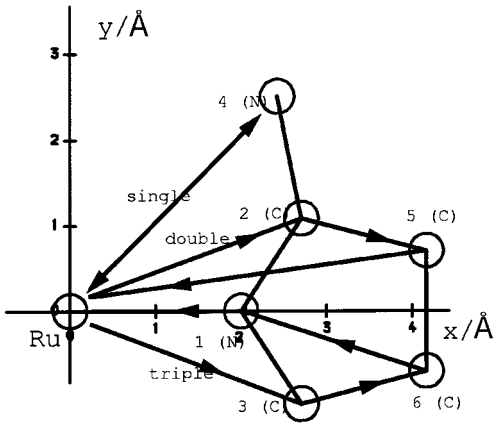

Figure 3. Defined multiple scattering unit illustrating single, double and triple scattering paths; for reasons of clarity the axially coordinated ligand atom is not drawn, but included in our calculations

is not positioned in the plane of the ring, the ring itself is not planar, or both. In order to check the dependence of the amount of multiple scattering from the out-of-plane displacement of the ruthenium atom in an idealized planar macrocycle, we performed systematic calculations. We found the astonishing result that the amount of multiple scattering does not depend very strongly on the out-of-plane position of the ruthenium atom. The contribution of the multiple scattering almost vanishes only when the displacement amounts to 1.75 Å. Since such a large displacement of the ruthenium atom is quite unlikely, we have to conclude that the nonplanarity of the macrocycle is the main cause of the absence of any multiple scattering and that the possible displacement of the ruthenium atom — if it exists — plays only a minor role. From the determined distances, it is not possible to make any structural statements concerning the nonplanarity of the macrocycle.

(μ-Pyrazine)phthalocyaninatoruthenium(II) (2)

For a good simulation of the EXAFS function of compound **2**, at least five shells are necessary (see Table 2 and Figure 4). These are the four shells of the phthalocyanine macrocycle and an additional nitrogen backscatterer at 2.22 Å, which can only be assigned to the ligand pyrazine as there are no ring atoms located in that distance range. The fit index decreases to about 9% if we take five shells of

Table 2. EXAFS-determined structural data of **2**[a]

2	N	R^4, Å	σ^4, Å	R^5, Å	σ^5, Å
$Ru-N_{Indol}$	4	2.04±0.02	0.074±0.009	2.03±0.02	0.066±0.010
Ru−C	8	3.05±0.03	0.073±0.014	3.05±0.03	0.071±0.016
$Ru-N_{Aza}$	4	3.31±0.03	0.088±0.012	3.30±0.03	0.087±0.012
Ru−C	8	4.03±0.04	0.087±0.022	4.03±0.04	0.084±0.021
$Ru-N_{pyz}$	2			2.22±0.03	0.099±0.023

[a] Absorber−backscatterer distance r, coordination number N and Debye−Waller factor σ with their calculated standard deviation. The simulations with four and five backscatterers are marked by the superscripts 4 and 5. The ΔE_0 shift of **2** is 19.60 eV and the R-factors are 38.9[4] and 35.4[5].

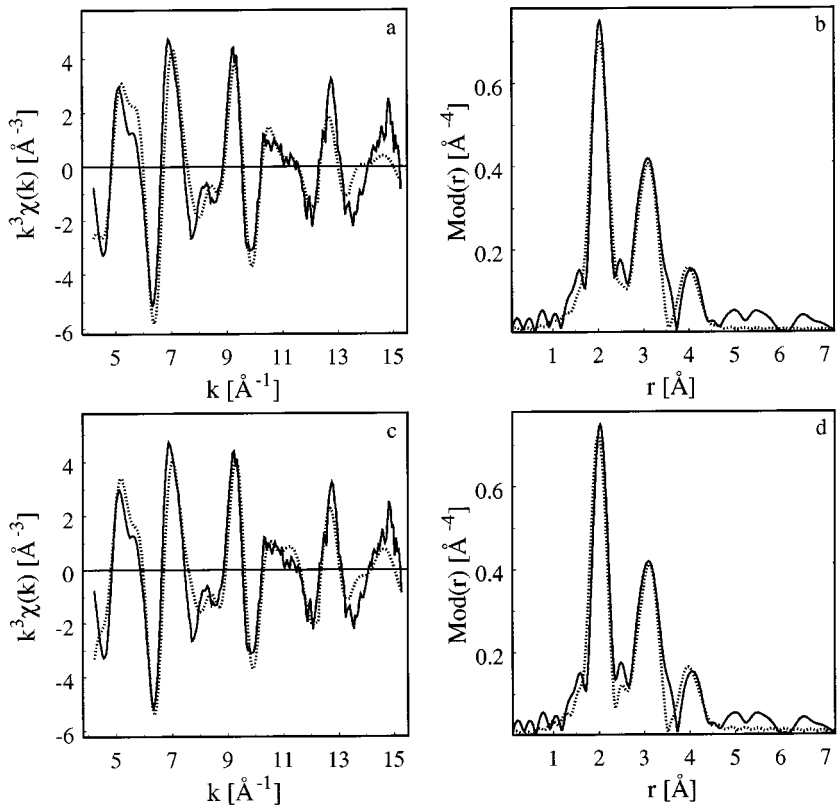

Figure 4. Experimental (solid line) and calculated (dotted line) Ru−K $k^3 \cdot \chi(k)$ functions (a, c) and their corresponding Fourier transforms without phase correction (b, d) of **2** (k range: 3.45−15.45 Å^{-1}); simulation with four (a, b) and five (c, d) backscatterers; the corresponding structural data are given in Table 2

the phthalocyanine macrocycle instead of four into account (compare Figure 4a, 4b and 4c, 4d).

If we make the simplified assumption that the four nitrogen atoms of the phthalocyanine macrocycle that form the first coordination shell lie in a plane, the displacement of the ruthenium atom can be explained in the following way. From crystallographic data we know that the metal−nitrogen distance of planar systems, for example in phthalocyaninatomanganese(tetracyanoethenide), is typically 1.97 ± 0.3 Å.[20−22] As a N−N diagonal distance of 3.94 ± 0.6 Å follows from this value, we can calculate that the ruthenium atom is located 0.4 ± 0.3 Å outside the plane of the macrocycle (see Figure 2). It should be noted that this triangulation depends critically on both the measured Ru−N distance and the assumed N-center distance. It is only given here to get a rough estimation of the amount of the possible displacement. The resulting model of **2** with the determined distances can be seen in Figure 2b.

(μ-1,4-Diisocyanobenzene)phthalocyaninatoruthenium(II) (3)

As in **1**, five shells are required to describe the EXAFS function (see Table 3 and Figure 5). Again, these are the four shells of the phthalocyanine macrocycle and one additional carbon backscatterer at 2.33 Å, which can only be assigned to the ligand 1,4-diisocyanobenzene as in that distance range no ring atoms are located. The fit worsens drastically (nearly 40%) if we do not take this fifth carbon backscatterer into account (compare Figure 5a and 5b with 5c and 5d). Further backscatterers could not be found by EXAFS spectroscopy. The next distance to the nitrogen from the 1,4-diisocyanobenzene should be about 1.3 Å further away than the carbon backscatterer (at about 3.6 Å). A fitting with this backscatterer in this distance range does not increase the agreement of the experimental EXAFS function compared to the fitted function. The resulting model of **3** with the determined distances can be seen in Figure 2c.

Table 3. EXAFS-determined structural data of **3**

3	N	R^4, Å	σ^4, Å	R^5, Å	σ^5, Å
Ru−N_{Indol}	4	2.02±0.02	0.105±0.021	2.03±0.02	0.094±0.020
Ru−C	8	3.04±0.03	0.101±0.023	3.05±0.03	0.092±0.023
Ru−N_{Aza}	4	3.30±0.03	0.069±0.012	3.29±0.03	0.072±0.014
Ru−C	8	3.99±0.04	0.095±0.019	3.97±0.04	0.096±0.020
Ru−C_{dib}	2			2.33±0.03	0.071±0.014

[a] Absorber−backscatterer distance r, coordination number N and Debye−Waller factor σ with their calculated standard deviation. The simulations with four and five backscatterers are marked by the superscripts 4 and 5. The ΔE_0 shift of **3** is 19.05 eV and the R-factors are 49.4[4] and 30.4[5].

Conclusion

It was possible to deduce detailed structural models for (μ-*s*-tetrazine)phthalocyaninatoruthenium(II) (**1**), (μ-pyraz-

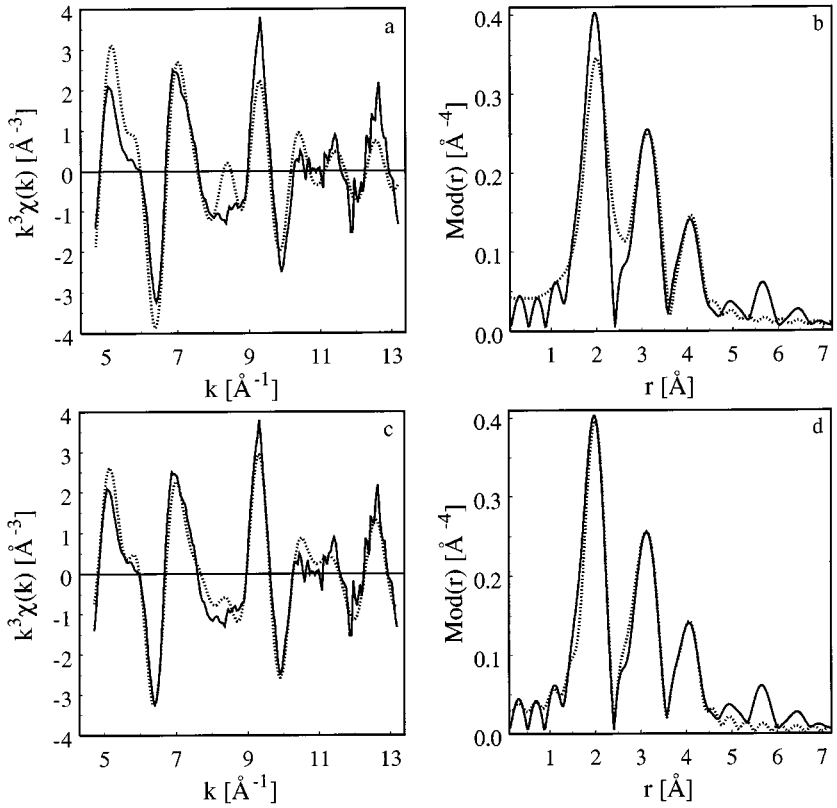

Figure 5. Experimental (solid line) and calculated (dotted line) Ru−K k^3·$\chi(k)$-functions (a, c) and their corresponding Fourier transforms without phase correction (b, d) of **3** (k range: 3.45−13.25 Å^{-1}); simulation with four (a, b) and five (c, d) backscatterers; the corresponding structural data are given in Table 3

ine)phthalocyaninatoruthenium(II) (**2**) and (μ-1,4-diisocyanobenzene)phthalocyaninatoruthenium(II) (**3**) by EXAFS spectroscopy. A sixfold coordination of the ruthenium atom exists in the investigated compounds, where the bridging ligands are located axially in an octahedral arrangement on both sides of the phthalocyanine macrocycle. The differences in the environment around the ruthenium center between the compounds **1**, **2** and **3** are not significant.

Experimental Section

^{1}H NMR: Bruker ARX 250 (250.133 MHz), as internal standard [D$_5$]pyridine was used. − UV/Vis Shimadzu UV−365. − Elemental analyses: Carlo Erba Elemental Analyzer 1104, 1106. Due to the formation of ruthenium nitride and carbide, only hydrogen values were determined by elemental analysis for the oligomeric phthalocyaninatoruthenium complexes **1**−**3**.

Starting Materials and General Methods: Pyrazine was commercially available. 1,4-Diisocyanobenzene[23] and *s*-tetrazine[24] were prepared according to known procedures. Phthalocyaninatoruthenium was prepared according to the method described previously.[5]

(μ-*s*-Tetrazine)phthalocyaninatoruthenium(II) (1): A mixture of phthalocyaninatoruthenium (**1**) (100 mg, 0.16 mmol), *s*-tetrazine (15 mg, 0.18 mmol), and dry tetrahydrofuran (10 mL) was refluxed under an inert gas atmosphere for 6 days. After cooling to room temperature, the reaction mixture was centrifuged. The collected solid was washed several times with acetone and then dried in vacuo at 70 °C. Yield: 87 mg (78%), blue-black powder.

$[C_{34}H_{18}N_{12}Ru]_n$ ($[695.67]_n$): calcd. H 3.1; found H 3.1. − ^{1}H NMR (250 MHz, [D$_5$]pyridine, 25 °C): δ = 7.78−8.13 (m, 1 H, Pc-H$_a$), 8.75−9.44 (m, 1 H, Pc-H$_b$). − UV/Vis (chlorobenzene): λ_{max} = 642, 583 nm.

(μ-Pyrazine)phthalocyaninatoruthenium(II) (2): A mixture of phthalocyaninatoruthenium (100 mg, 0.16 mmol), pyrazine (15 mg, 0.19 mmol), and dry tetrahydrofuran (10 mL) was refluxed under an inert gas atmosphere for 6 days. After cooling to room temperature, the reaction mixture was centrifuged. The collected solid was washed several times with acetone and dried in vacuo at 70 °C. Yield: 67 mg (60%), dark blue powder.

$[C_{36}H_{20}N_{10}Ru]_n$ ($[693.69]_n$): calcd. H 2.9; found H 2.9. − ^{1}H NMR(250 MHz, [D$_5$]pyridine, 25 °C): δ = 5.67 (m, 1H; pyrazine), 7.86−8.01 (m, 4 H, Pc-H$_a$), 9.44−9.55 (m, 4 H, Pc-H$_b$). − UV/Vis (chlorobenzene): λ_{max} = 639, 585 nm.

(μ-1,4-Diisocyanobenzene)phthalocyaninatoruthenium(II) (3): A mixture of phthalocyaninatoruthenium (**1**) (100 mg, 0.16 mmol), 1,4-diisocyanobenzene (22 mg, 0.17 mmol), and dry tetrahydrofuran (10 mL) was refluxed under an inert gas atmosphere for 6 days. After cooling to room temperature, the reaction mixture was centrifuged. The collected solid was washed several times with acetone and then dried in vacuo at 70 °C. Yield: 91 mg (75%), blue-black powder.

$[C_{40}H_{20}N_{10}Ru]_n$ ($[742.09]_n$): calcd. H 2.8; found H 2.8. − ^{1}H NMR (250 MHz, [D$_5$]pyridine, 25 °C): δ = 3.6−3.7 (m, 4 H, 1,4-diisocyanobenzene), 7.88−8.06 (m, 8 H, Pc-H$_a$), 9.36−9.57 (m, 8 H, Pc-H$_b$). − UV/Vis (chlorobenzene): λ_{max} = 640, 582 nm.

EXAFS Measurements: The EXAFS measurements of the oligomeric phthalocyaninatoruthenium complexes **1**−**3** were performed

at the ruthenium K edge at 22118 eV, at the beamline A1, at the Hamburger Synchrotronstrahlungslabor (HASYLAB) at DESY, Hamburg, with a Si<311> double crystal monochromator under ambient conditions (5.4 GeV, beam current 100 mA). The tilt of the second monochromator crystal was set to 30% harmonic rejection. Energy resolution was estimated to be about 10 eV at the ruthenium K edge. Data were collected in transmission mode with ion chambers which were continuously flushed with argon. Energy calibration was monitored with a 20 μm thick ruthenium metal foil. All measurements were performed under an inert gas atmosphere. The samples were embedded in a polyethylene matrix, whose thickness was adjusted to an absorption jump of $\mu = 1.5$. First, background absorption was removed from the experimental absorption spectrum by subtraction of a Victoreen-type polynomial. Then, the spectrum with background subtracted was convoluted with a series of increasingly broader Gaussian functions and the common intersection point of the convoluted spectra was taken as energy E_0.[25,26] To determine the smooth part of the spectrum, corrected for pre-edge absorption, a piecewise polynomial was used. It was adjusted in such a manner that the low-R components of the resulting Fourier transform were minimal. After division of the background-subtracted spectrum by its smooth part, the photon energy was converted into a photoelectron wavenumber scale. The resulting EXAFS function was weighted with k^3. Data analysis in k space was performed according to the curved-wave multiple scattering formalism of the program EXCURV92 with the XALPHA phase and amplitude functions.[27] The mean free path of the scattered electrons was calculated from the imaginary part of the potential (VPI was set to −4.00), the amplitude reduction factor AFAC was fixed at 0.8 and an overall energy shift (E_0) was assumed.

Acknowledgments

We wish to thank HASYLAB (Hamburg) for kind support of synchrotron radiation and the Fonds der Chemischen Industrie for generous financial support. This work has been supported by the DFG (Grant No. Li 154/41−4).

[1] C. C. Leznoff, A. B. P. Lever, *Phthalocyanines, Properties and Applications* (Eds.: C. C. Leznoff, A. B. P. Lever), Vol. 1−4, VCH, New York, **1989−1994**.
[2] M. Hanack, M. Lang, *Adv. Mater.* **1994**, *6*, 819−833.
[3] [3a] A. Capobianchi, A. M. Paoletti, G. Pennesi, G. Rossi, R. Caminiti, C. Ercolani, *Inorg. Chem.* **1994**, *33*, 4635−4640. − [3b] A. Capobianchi, G. Pennesi, A. M. Paoletti, G. Rossi, R. Caminiti, C. Sadun, C. Ercolani, *Inorg. Chem.* **1996**, *35*, 4643−4648. − [3c] L. Alagna, A. Capobianchi, G. Pennesi, T. Prosperi, G. Rossi, *J. Phys. IV* **1997**, *C2*, 1261−1262.
[4] W. Kobel, M. Hanack, *Inorg. Chem.* **1986**, *25*, 103−107.
[5] [5a] M. Hanack, J. Osío-Barcina, E. Witke, J. Pohmer, *Synthesis* **1992**, *1/2*, 211−214. − [5b] M. Hanack, R. Polley, *Synthesis* **1997**, *3*, 295−296.
[6] [6a] M. Hanack, S. Knecht, R. Polley, *Chem. Ber.* **1995**, *128*, 929−933. − [6b] M. Hanack, R. Polley, *Inorg. Chem.* **1994**, *33*, 3201−3204.
[7] K. Ukei, *Acta Crystallogr.* **1973**, *329*, 2290−2292.
[8] H. Schultz, h. Lehmann, M. Rein, M. Hanack, *Struct. Bonding* (Berlin) **1991**, *74*, 41−146.
[9] [9a] M. Hanack, A. Datz, R. Fay, K. Fischer, U. Keppeler, J. Koch, J. Metz, M. Mezger, O. Schneider, H.-J. Schulze, in *handbook of Conducting polymers* (Ed.: T.A. Skotheim), *Vol. 1*, Marcel Dekker, New York **1986**, pp. 133−204. − [9b]M. Hanack, S. Deger, A. Lange, *Coord. Chem. Rev.* **1988** *83*, 115−136.
[10] J. Metz, O. Schneider, M. Hanack, *Spectrochim. Acta* **1982**, *38A*, 1265−1273.
[11] M. Hanack, U. Keppeler, A. Lange, A. Hirsch, R. Dieing, in *Phthalocyanines, Properties and Applications* (Eds.: C.C. Leznoff, A.B.P. Lever), Vol. 2, VCH, Weinheim **1993**, pp. 43−96.
[12] U. Keppeler, W. Kobel, H.-U. Siehl, M. Hanack, *Chem. Ber.* **1985**, *118*, 2095−2104.
[13] R. Aldinger, M. Hanack, K.-H. Hermann, A. Hirsch, K. Kasper, *Synth. Met.* **1993**, *60*, 265−268.
[14] U. Keppeler, S. Deger, A. Lange, M. Hanack, *Angew. Chem.* **1987**, *99*, 349−350; *Angew. Chem. Int. Ed. Engl.* **1987**, *26*, 344−345.
[15] M. Hanack, U. Keppeler, H.-J. Schulze, *Synth. Met.* **1987**, *20*, 347−356.
[16] J. Pohmer, M. Hanack, J. Osío-Barcina, *J. Mater. Chem.* **1996**, *6*, 957−962.
[17] E. A. Stern, *Phys. Rev. B* **1974**, *10*, 3027−3037.
[18] F. W. Lytle, D. E. Sayers, E. A. Stern, *Phys. Rev. B* **1975**, *11*, 4825−4835.
[19] S. S. Hasnain, in *X-ray Absorption Fine Structure: International Workshop on Standards and Criteria in XAFS*, Ellis Horwood, New York, **1991**, 751−770.
[20] L. H. Vogt Jr., A. Zalkin, D. H. Templeton, *Inorg. Chem.* **1967**, *6*, 1725−1730.
[21] J. S. Miller, C. Vazquez, J. C. Calabrese, R. S. McLean, A. Epstein, *J. Adv. Mater.* **1994**, *6*, 217−221.
[22] D. Wöhrle, G. Mayer, *Kontakte (Darmstadt)* **1985**, *3*, 38−48.
[23] I. Ugi, *DAS 1 158 500*, April 6, **1962**.
[24] [24a] G. H. Spencer, P. Cross, K. B. Wiberg, *J. Chem. Phys.* **1961**, *35*, 1939. − [24b] W. Skorianetz, E. sz. Kováts, *Helv. Chim. Acta* **1970**, *53*, 251−263. − [24c] W. Skorianetz, E. sz. Kováts, *Helv. Chim. Acta* **1971**, *54*, 1922−1939; *Beware of heating s-tetrazine with other solids without a solvent:* see: [24d] T. Curtius, A. Darapsky, E. Müller, *Ber. Dtsch. Chem. Ges.* **1908**, *41*, 3161−3172.
[25] T. S. Ertel, H. Bertagnolli, S. Hückmann, U. Kolb, D. Peter, *Appl. Spectrosc.* **1992**, *46*, 690−698.
[26] M. Newville, P. Livins, Y. Yakoby, J. J. Rehr, E. A. Stern, *Phys. Rev. B* **1993**, *47*, 14126−14131.
[27] S. J. Gurman, N. Binsted, I. J. Ross, *Phys. C* **1986**, *19*, 1845−1861.

Received July 17, 2000
[I00279]

Half-Sandwich Chloro Complexes as Ligands for $RuCl_2L_2$ (L = PR_3, alkene): Syntheses, Structures, and Catalytic Activity of New Homo- and Heterobimetallic Complexes

Ana C. da Silva,[a] Holger Piotrowski,[a] Peter Mayer,[a] Kurt Polborn,[a] and Kay Severin*[a]

Keywords: Halides / Catalysis / Heterobimetallic complexes / Oxidations / Ruthenium / Rhodium / Iridium

Homo- and heterobimetallic complexes, in which half-sandwich complexes of ruthenium(II), rhodium(III), and iridium(III) are connected via three chloro bridges to $RuCl_2(PPh_3)_2$, have been synthesized. The complexes were obtained in quantitative yields by reaction of $[(cymene)RuCl(\mu\text{-}Cl)]_2$ or $[Cp^*MCl(\mu\text{-}Cl)]_2$ (M = Rh, Ir) with $[(PPh_3)_2ClRu(\mu\text{-}Cl)_3Ru(Me_2CO)(PPh_3)_2]$ (**2**). The crystal structure of **2** has been determined by X-ray analysis. Evidence that half-sandwich chloro complexes are generally suited for stabilizing $RuCl_2L_2$ fragments is provided by the synthesis of complexes $[(cymene)Ru(\mu\text{-}Cl)_3RuCl(dppb)]$ [dppb = 1,4-bis(diphenylphosphanyl)butane] and $[(cymene)Ru(\mu\text{-}Cl)_3RuCl(cod)]$ (cod = 1,5-cyclooctadiene), both of which have been structurally characterized. The abilities of all the complexes to catalyze the oxidation of secondary alcohols with 2-butanone have been investigated. The complex $[Cp^*Rh(\mu\text{-}Cl)_3RuCl(PPh_3)_2]$ has proved to be highly active, displaying a performance superior to that of previously known catalysts such as $[RuCl_2(PPh_3)_3]$. Using a substrate/catalyst ratio of 500:1, initial turnover frequencies of up to 3400 h^{-1} were observed. The potential of these types of bimetallic complexes to act as catalysts for other reactions is discussed.

Introduction

Inspired by Nature, specifically by the high efficiencies and selectivities of bimetallic metalloenzymes, chemists have tried hard to design polynuclear complexes showing superior performances in catalytic reactions. Despite numerous efforts, often accompanied with elaborate syntheses of suitable ligands, success has hitherto been rare, especially in relation to catalysts with relevance in organic synthesis.[1] Prominent exceptions are the heterometallic lanthanide complexes developed by Shibasaki et al., which are excellent catalysts for asymmetric aldol and nitro-Mannich-type reactions,[2] and a dinuclear rhodium complex that has been used in hydroformylation reactions.[3]

We have investigated the syntheses, structures, and reactivities of dinuclear complexes in which two different metal fragments are connected by halo bridges.[4] A major advantage of this kind of compound is that the synthesis is generally fast and easy. Consequently, a variety of different complexes can be obtained in a short time, allowing an efficient screening of their catalytic properties.

The first convincing evidence that highly active catalysts can be found within this class of compounds was recently provided by the groups of Grubbs and Herrmann. Studying metathesis reactions with well-defined (carbene)ruthenium complexes, they discovered that dinuclear complexes in which ruthenium, osmium, and rhodium complexes are connected by chloro bridges to a ruthenium fragment are exceptionally active.[5] Importantly, the catalytic activity of the carbene complex is modulated by the second metal fragment, which itself does not participate directly in the catalytic reaction.

We describe herein the synthesis and structures of new homo- and heterobimetallic complexes containing $RuCl_2L_2$ fragments (L = PR_3, alkene). The formally unsaturated 14-electron species are coordinated to half-sandwich complexes of ruthenium, rhodium, and iridium via three chloro bridges. The catalytic oxidation of secondary alcohols by 2-butanone with these types of bimetallic complexes is reported.

Results and Discussion

Synthesis of Dinuclear Complexes with $RuCl_2(PR_3)_2$ Fragments

$[RuCl_2(PPh_3)_3]$ is a remarkably versatile catalyst precursor. Catalytic reactions such as hydrogenations, isomerizations, oxidations, and hydrosilylations have been carried out with this complex, in some cases with remarkable efficiency.[6] A major drawback of $[RuCl_2(PPh_3)_3]$, however, is its low solubility in organic solvents. For several reactions, the loss of one triphenylphosphane ligand is assumed to occur prior to catalysis. We were thus interested in ascertaining whether organometallic chloro complexes of the late transition metals could be used to stabilize and solubilize the active $RuCl_2(PPh_3)_2$ fragment. In a first experiment, we investigated the reaction of $[(cymene)RuCl(\mu\text{-}Cl)]_2$ with $[RuCl_2(PPh_3)_3]$ in dichloromethane (Scheme 1).

[a] Department Chemie, Ludwig-Maximilians-Universität München,
Butenandtstraße 5−13, 81377 München, Germany
Fax: (internat.) + 49-(0)89/2180-7866
E-mail: kse@cup.uni-muenchen.de

 © WILEY-VCH Verlag GmbH, 69451 Weinheim, 2001 1434−1948/01/0303−0685 $ 17.50+.50/0

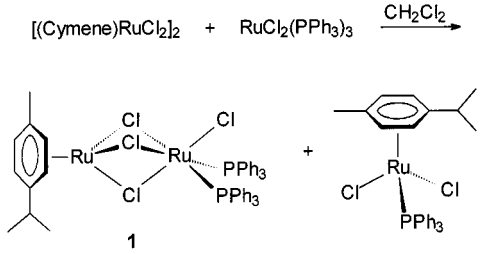

Scheme 1. Synthesis of complex **1**

Equimolar amounts of two products were formed, one of which was identified as [(cymene)$RuCl_2(PPh_3)$] by NMR (^1H, ^{31}P). The second product (**1**) was isolated in pure form by washing the mixture with acetone. Spectroscopic as well as analytical data pointed to a complex of the empirical formula [Ru_2Cl_4(cymene)$(PPh_3)_2$]. The geometry of **1** was established by a single-crystal X-ray analysis, which revealed a structure with three bridging chloro ligands. This geometry is what was expected in view of the high tendency of (arene)-[7] as well as (phosphane)ruthenium(II) complexes[6c] to form (μ-Cl)$_3$ structures. Unfortunately, despite numerous attempts, we were unable to obtain crystallographic data of satisfactory quality and therefore a more detailed analysis of the structure of **1** is not presented.

In a quest for a more suitable source of the $RuCl_2(PPh_3)_2$ fragment, we turned our attention to a complex of the stoichiometry [$RuCl_2(PPh_3)_2(Me_2CO)]_n$ (**2**). Wilkinson first synthesized this compound by heating [$RuCl_2(PPh_3)_3$] in acetone under reflux.[8] Later, a dimeric structure with two bridging chloro ligands was suggested,[9] but problems in reproducing the reaction were also reported.[10] We have found that a complex of this formula can be obtained if [$RuCl_2(PPh_3)_3$] is treated with acetone at room temperature. The heterogeneous reaction is best carried out without stirring. Under these conditions, dark-red crystals of **2** are formed in good yield after several days. The crystals, which can be stored without the need for an inert gas, display very low solubility in all common organic solvents. The molecular structure of **2** in the crystal is shown in Figure 1. The complex is dimeric but, contrary to previous suggestions, three and not two chloro bridges are observed. Consequently, the second molecule of acetone is not coordinated to the ruthenium center. Therefore, complex **2** should be formulated as [$(PPh_3)_2$ClRu(μ-Cl)$_3$Ru(Me_2CO)-$(PPh_3)_2$]Me_2CO.

The geometry about the ruthenium atoms can be described as distorted octahedral. The distortion is mainly due to the sterically demanding phosphane ligands and is manifested in large P−Ru−P angles (98.2 and 99.7°). In agreement with general theoretical investigations,[11] the acetone ligand shows an η^1 and not an η^2 coordination mode. The C−O bond length in the coordinated acetone molecule is slightly longer (1.20 Å) than the C−O bond length in the co-crystallized "free" acetone molecule (1.17 Å). The structural motif found for **2** is common in (phosphane)ruthenium chemistry. Several other complexes of the

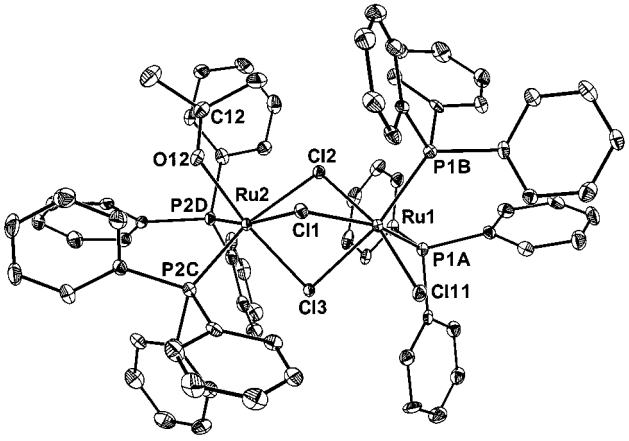

Figure 1. Molecular structure of **2** in the crystal; the solvent molecule and hydrogen atoms are omitted for clarity; selected bond lengths [Å] and angles [°]: Ru1−Cl1 2.540(2), Ru1−Cl2 2.395(2), Ru1−Cl3 2.450(2), Ru2−Cl1 2.446(2), Ru2−Cl2 2.470(2), Ru2−Cl3 2.368(2), Ru1−Cl11 2.400(2), Ru1−P1A 2.268(2), Ru1−P1B 2.293(2), Ru2−P2C 2.300(2), Ru2−P2D 2.316(2), Ru2−O12 2.121(4), O12−C12 1.201(8); Ru1−Cl3−Ru2 83.19(5), P1A−Ru1−P1B 98.23(6), Cl2−Ru1−Cl11 165.04(5), P2C−Ru2−P2D 99.71(6)

general formula [$(PR_3)_2$ClRu(μ-Cl)$_3$Ru(L)$(PR_3)_2$] (L = neutral or anionic ligand) have been described.[6c,12] Structural data for the closely related [$(PPh_3)_2$ClRu(μ-Cl)$_3$Ru(CS)$(PPh_3)_2$] are available.[13]

Complex **2** proved to be an ideal starting material for the synthesis of **1** and the heterobimetallic complexes **3** and **4**. Upon reaction of **2** with [(cymene)RuCl(μ-Cl)]$_2$ or [Cp*MCl(μ-Cl)]$_2$ (M = Rh, Ir) in dichloromethane, the dinuclear compounds were obtained in quantitative yields (Scheme 2).

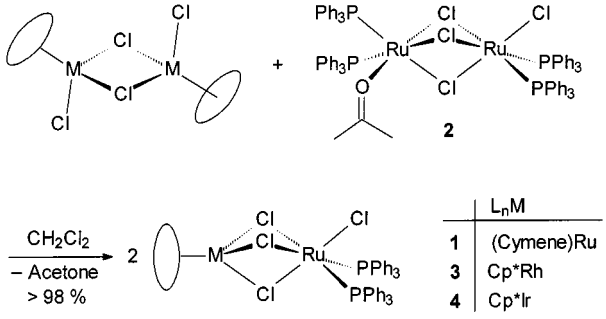

Scheme 2. Synthesis of the homo- and heterobimetallic complexes **1**, **3**, and **4**

Compounds **3** and **4** are among the first heterobimetallic complexes with three chloro bridges to be synthesized.[14] Heterobimetallic $Rh^{III}-Ru^{II}$ complexes with bridging hydrido and carboxylato ligands have been described by Süss-Fink.[15] In contrast to [$RuCl_2(PPh_3)_3$], the new complexes show good solubility in a variety of organic solvents, such as dichloromethane, tetrahydrofuran, and benzene, a prerequisite for applications in homogeneous catalysis. Although they are not very sensitive towards oxygen in the solid state, solutions of **1**, **3**, and **4** readily turn brown upon exposure to air.

For catalytic applications, ruthenium complexes with chelating phosphane ligands are especially interesting since the

accessibility of the active site can be controlled by the bite angle of the chelate. Furthermore, stereochemical information can be introduced using chiral ligands. To demonstrate that half-sandwich chloro complexes are suited for stabilizing $RuCl_2(L-L)$ complexes [L−L = bis(phosphane)], we have synthesized complex **5** by reaction of $[RuCl_2(PPh_3)(dppb)]$ with $[(cymene)RuCl(\mu\text{-}Cl)]_2$; $[(cymene)RuCl_2(PPh_3)]$, which is formed as a side product, can be separated by crystallization from acetone.

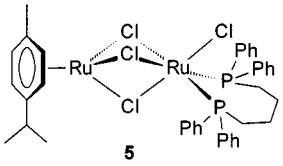

5

The structure of complex **5** in the crystal is shown in Figure 2. As expected, the (η^6-arene)Ru fragment is coordinated via three chloro bridges to the second ruthenium atom, the geometry about which can be described as distorted octahedral. The Ru−Cl bond length to the terminal chloro ligand (2.39 Å) is smaller than the Ru−Cl distances of the bridging chloro ligands (2.41−2.53 Å). The P−Ru−P bond angle (94.2°) is comparable to those found in other Ru(dppb) complexes.[16]

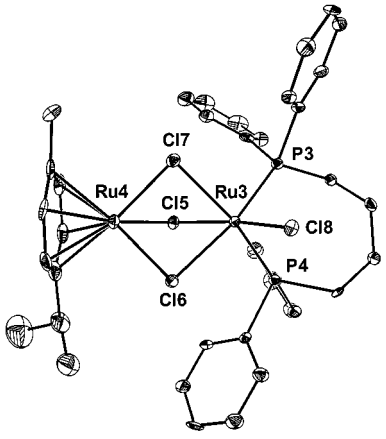

Figure 2. Molecular structure of **5** in the crystal; hydrogen atoms and solvent molecules are omitted for clarity; selected bond lengths [Å] and angles [°]: Ru4−Cl5 2.425(2), Ru4−Cl6 2.410(2), Ru3−Cl6 2.535(2), Ru4−Cl7 2.438(2), Ru3−Cl5 2.407(2), Ru3−Cl7 2.534(2), Ru3−P3 2.240(2), Ru3−P4 2.249(2), Ru3−Cl8 2.387(2); Ru3−Cl5−Ru4 86.17(6), P3−Ru3−P4 94.24(7), Cl8−Ru3−Cl5 166.99(7), P4−Ru3−Cl5 94.63(6)

Synthesis of a Dinuclear Complex with an $RuCl_2(cod)$ Fragment

To investigate whether half-sandwich chloro complexes can form dinuclear complexes with other $RuCl_2L_2$ fragments (L ≠ PR_3), we studied the reaction of $[(cymene)RuCl(\mu\text{-}Cl)]_2$ with $[RuCl_2(cod)(NCCH_3)_2]$. This complex was chosen because the acetonitrile ligands could be expected to be labile. After reaction in refluxing acetone and crystallization from CH_2Cl_2/pentane, we were able to isolate the dimeric complex **6** (Scheme 3).

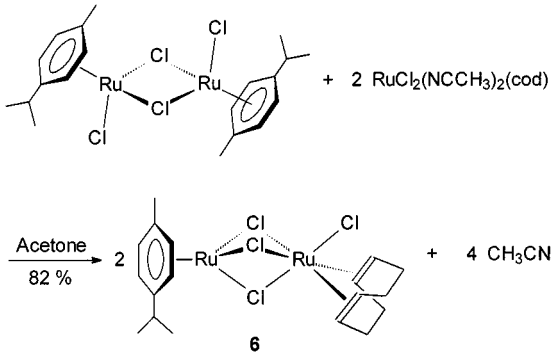

6

Scheme 3. Synthesis of complex **6**

Due to the reduced symmetry of **6** as compared to $[RuCl_2(cod)(NCCH_3)_2]$, four discrete signals due to the C atoms of the cyclooctadiene ligand are observed in its ^{13}C NMR spectrum ($CDCl_3$). Accordingly, two groups of signals are observed for the olefinic protons in the ^1H NMR spectrum. X-ray analysis of **6** reveals a structure similar to that of **5**, with the dppb ligand being substituted by a cod ligand (Figure 3). Again, the Ru−Cl bond length to the terminal chloro ligand (2.39 Å) is shorter than the Ru−Cl distances of the bridging chloro ligands (2.42−2.49 Å). The cyclooctadiene ligand shows the normal tub conformation with Ru−C bond lengths in the expected range.[17]

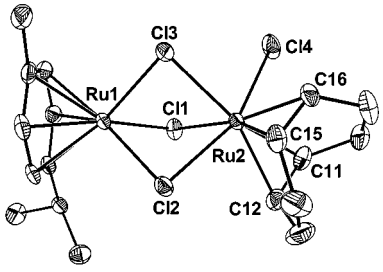

Figure 3. Molecular structure of **6** in the crystal; hydrogen atoms are omitted for clarity; selected bond lengths [Å] and angles [°]: Ru1−Cl1 2.441(1), Ru1−Cl2 2.422(1), Ru1−Cl3 2.441(1), Ru2−Cl1 2.482(1), Ru2−Cl2 2.454(1), Ru2−Cl3 2.485(1), Ru2−Cl4 2.388(1), Ru2−C11 2.177(4), Ru2−C12 2.185(4), Ru2−C15 2.174(4), Ru2−C16 2.181(4); Cl2−Ru1−Cl1 79.02(4), Cl4−Ru2−Cl2 158.06(4), Cl4−Ru2−Cl3 84.31(5), Cl2−Ru2−Cl3 78.54(4), Cl1−Ru2−Cl3 82.00(4), Ru1−Cl3−Ru2 83.53(3)

Catalytic Oxidations of Secondary Alcohols

Various methods are available for the oxidation of alcohols to carbonyl compounds. Especially appealing − both from an economic as well as environmental point of view − are transition metal catalyzed oxidations in which ketones act as both the solvent and the oxidant for the process. One of the most successful catalyst precursors for this Oppenauer-type[18] reaction is $[RuCl_2(PPh_3)_3]$. This was demonstrated by the group of Bäckvall. In the presence of K_2CO_3, hydrogen is catalytically transferred from secondary alcohols to acetone with high efficiency.[19] We have investigated the ability of the aforementioned dinuclear complexes to catalytically oxidize alcohols under conditions similar to those employed by Bäckvall. In a first series of

experiments, we screened the reactivities of **1** and **3−6** in the oxidation of diphenylmethanol. Using 0.2 mol-% of the catalyst precursor, 2-butanone as the hydrogen acceptor, and K_2CO_3 as the base, we were able to obtain benzophenone in 22−94% yield (Table 1, Entries 1−5, Scheme 4). The heterobimetallic Cp*Rh^{III} complex **3** displayed the highest activity. Subsequently, we tested the activities of the metal complexes used in our synthesis. All the half-sandwich complexes displayed activities comparable to that of $[RuCl_2(PPh_3)_3]$, but significantly lower than that of **3** (Table 1, Entries 6−10). The phosphane complexes **1** and **3−5** were also employed in the oxidation of 1-phenylethanol (Table 1, Entries 11−14). Again, the highest yield was obtained with complex **3**, followed by the (cymene)Ru^{II} complex **4**. With acetophenone as the substrate, initial turnover frequencies were determined. For all the dinuclear complexes, values in excess of 1000 h^{-1} were obtained, with a maximum of 3400 h^{-1} for the reactions with complex **3**.

Table 1. Catalytic oxidation of diphenylmethanol and 2-phenylethanol by 2-butanone; the reactions were performed in refluxing 2-butanone (2.00 mL) with 0.40 mmol of the substrate, the appropriate catalyst (0.80 μmol), and K_2CO_3 (0.40 mmol)

Entry	Complex	R	Time [h]	Yield [%][a]
1	**1**	Ph	3	92
2	**3**	Ph	3	94
3	**4**	Ph	3	29
4	**5**	Ph	3	25
5	**6**	Ph	3	22
6	$[(cymene)RuCl_2]_2$[b]	Ph	3	14
7	$[Cp^*RhCl_2]_2$ [b]	Ph	3	15
8	$[Cp^*IrCl_2]_2$ [b]	Ph	3	14
9	$[RuCl_2(PPh_3)_3]$	Ph	3	16
10	$[RuCl_2(dppb)(PPh_3)]$	Ph	3	4
11	**1**	CH_3	1	86
12	**3**	CH_3	1	99
13	**4**	CH_3	1	68
14	**5**	CH_3	1	70

[a] Determined by GC analysis. − [b] Substrate/metal = 500:1.

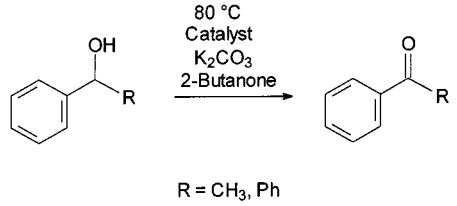

Scheme 4

In order to test the scope of the catalyst precursor **3**, oxidations of several other aromatic and aliphatic (cyclic and linear) alcohols have been carried out. With just 0.2 mol-% of **3**, good to excellent yields were obtained after 1 h (Table 2). Remarkably, even cyclohexanol, a substrate which is known to be problematic,[19] was converted into cyclohexanone in 85% yield within 1 h. With $[RuCl_2(PPh_3)_3]$ under otherwise identical conditions, only 5% of the product was obtained. Oxidation of the primary alcohol $PhCH_2OH$ was not possible with our catalyst system. Deactivation of the catalyst through the formation of carbonyl complexes is a possible explanation. In the oxidation of the unsaturated alcohol cyclohexenol, the isomer cyclohexanone was observed as a side product. Contrary to previous reports concerning reactions with $[RuCl_2(PPh_3)_3]$,[19a] the presence of a small amount of water (0.5%) reduces the activity of **3**. Although catalytic amounts of base are sufficient to initiate the reaction, larger quantities of K_2CO_3 are favorable because the base can bind residual water. No reaction was observed in the absence of base.

Table 2. Oxidation of secondary alcohols by 2-butanone in the presence of the heterobimetallic complex **3**; the reactions were performed as described in the Exp. Sect. with a substrate/catalyst ratio of 500:1

Entry	Substrate	Product	Yield [%][a]
1	1-indanol	1-indanone	> 99
2	1-tetralol	1-tetralone	97
3	cyclopentanol	cyclopentanone	95
4	cyclohexanol	cyclohexanone	85
5	cycloheptanol	cycloheptanone	99
6	2-octanol	2-octanone	86

[a] The yield was determined by GC analysis after 1 h.

The mechanism of this potentially very complicated reaction has still to be elucidated. Most probably, one or more hydrido complexes are formed through reaction of **3** with the deprotonated substrate. This kind of reaction has been described for $[Cp^*RhCl(\mu\text{-}Cl)]_2$[20] as well as for $[RuCl_2(PPh_3)_3]$.[6c] The hydrido complex(es) represent(s) the catalytically active species, being able to transfer hydrogen from the substrate to 2-butanone. Based on the results of our control experiments, which show that $[Cp^*RhCl(\mu\text{-}Cl)]_2$ and $[RuCl_2(PPh_3)_3]$ on their own are less active (Table 1, Entries 7 and 9), and the fact that $RuHX(PPh_3)_2$ (X = Cl, H) is electronically unsaturated,[21] it is reasonable to predict that di- or polynuclear complexes with chloro and/or hydrido bridges play an important role in the catalytic cycle.

Conclusions

We have shown that half-sandwich complexes of ruthenium, rhodium, and iridium can be used to stabilize $RuCl_2(PPh_3)_2$, a metal fragment with special importance in homogeneous catalysis. In the dinuclear complexes formed, the two metal centers are connected by three chloro bridges. With regard to future applications in organic synthesis, it should be emphasized that the synthesis of these complexes is fast and easy: they can be obtained in virtually 100% yield by reaction of commercially available half-sandwich complexes with **2**, which itself can be prepared in crystalline form simply by mixing $[RuCl_2(PPh_3)_3]$ with acetone. Half-sandwich complexes are also suited for stabilizing other $RuCl_2L_2$ fragments. This has been demonstrated by synthesizing complex **5** with a chelating phosphane ligand and complex **6** with a cyclooctadiene ligand. We assume that related complexes can be obtained in a similar fashion.

The heterobimetallic $Rh^{III}-Ru^{II}$ complex **3** represents one of the best catalyst precursors for the Oppenauer-type oxidation of simple secondary alcohols yet found. In the presence of 0.2 mol-% of **3** and a weak base, aromatic and

aliphatic alcohols are converted into the corresponding ketones in good to excellent yield within 1 h. Side reactions are not generally observed.

We are currently exploring the potential of these types of bimetallic complexes to act as catalyst precursors for other reactions. Both metal fragments − the organometallic π-complex[22] as well as the $RuCl_2L_2$ fragment − are known to be essential constituents of catalysts for hydrogenations, the metathesis of olefins, and isomerization reactions, among others. We think that the combination of these two fragments within one molecule can give rise to new catalyst systems with superior characteristics (solubility, activity, selectivity). Further results will be presented in the near future.

Experimental Section

General Remarks: All reactions were performed under dry dinitrogen. The solvents were distilled from appropriate drying agents and stored under dinitrogen. 2-Butanone (> 99.7%) was obtained from Riedel-de Häen and degassed prior to use. The complexes $[RuCl_2(PPh_3)_3]$,[23] $[RuCl_2(PPh_3)(dppb)]$,[24] $[(cymene)RuCl(\mu\text{-}Cl)]_2$,[25] $[Cp^*MCl(\mu\text{-}Cl)]_2$ (M = Rh, Ir),[26] and $[RuCl_2(cod)(NCCH_3)_2]$[27] were prepared according to literature procedures. − NMR spectra were recorded with JEOL EX 400 or GSX 270 spectrometers using the residual protonated solvents as internal standards. − GC-MS analyses were performed with a CP-cyclodextrin-B-2,3,6-M-19 column (50 m) coupled to a Varian 3800 spectrometer.

2: $[RuCl_2(PPh_3)_3]$ (959 mg, 1.00 mmol) was suspended in acetone (60−500 mL) without stirring. After several days, red crystals had formed, which were isolated, washed with acetone (4 × 100 mL), and dried in a stream of dinitrogen. The yields (53−90%) and the reaction times (2−14 d) were found to depend on the amount of acetone. Large amounts of acetone give short reaction times but also reduce the yields. − $C_{39}H_{36}Cl_2OP_2Ru$ (754.6): calcd. C 62.07, H 4.81; found C 61.95, H 4.88.

Synthesis of Complexes 1, 3, and 4: A mixture of **2** (75.5 mg, 0.10 mmol) and the appropriate chloro-bridged complex (0.05 mmol) in CH_2Cl_2 (15 mL) was stirred until a clear solution had been obtained (1−2 h). After removal of the solvent under reduced pressure and drying in vacuo, the products were obtained in quantitative yields.

1: Red powder. − ^{1}H NMR (270 MHz, CD_2Cl_2): δ = 1.19 [d, ^3J = 7 Hz, 6 H, $CH(CH_3)_2$], 2.12 (s, 3 H, CH_3, cymene), 2.75 [s, ^3J = 7 Hz, 1 H, $CH(CH_3)_2$], 5.15 (d, ^3J = 11 Hz, 1 H, $CH{=}CH_2$), 5.22 (d, ^3J = 5 Hz, 2 H, CH, cymene), 5.38 (d, ^3J = 5 Hz, 2 H, CH, cymene), 7.00−7.30 (m, 30 H, Ph). − ^{13}C NMR (68 MHz, CD_2Cl_2): δ = 18.4, 22.0 (CH_3, cymene), 30.9 (CH, cymene), 78.4, 78.5 (CH, cymene), 95.3, 101.4 (C, cymene), 126.8−136.1 (Ph). − ^{31}P NMR (109 MHz, CD_2Cl_2): δ = 50.3. − $C_{46}H_{44}Cl_4P_2Ru_2 \cdot 1/2CH_2Cl_2$ (1045.2): calcd. C 53.43, H 4.34; found C 53.59, H 4.25.

3: Red powder. − ^{1}H NMR (270 MHz, CD_2Cl_2): δ = 1.60 (s, 15 H, Cp*), 7.01−7.32 (m, 30 H, Ph). − ^{13}C NMR (68 MHz, CD_2Cl_2): δ = 9.1 (CH_3, Cp*), 93.7 (d, ^1J = 9 Hz, C, Cp*), 126.6−135.2 (Ph). − ^{31}P NMR (109 MHz, CD_2Cl_2): δ = 50.1. − $C_{46}H_{45}Cl_4P_2RhRu \cdot 1/4CH_2Cl_2$ (1026.8): calcd. C 54.10, H 4.47; found C 54.00, H 4.53.

4: Red powder. − ^{1}H NMR (270 MHz, CD_2Cl_2): δ = 1.56 (s, 15 H, Cp*), 7.02−7.35 (m, 30 H, Ph). − ^{13}C NMR (68 MHz, CD_2Cl_2): δ = 8.9 (CH_3, Cp*), 85.3 (C, Cp*), 126.5−136.1 (Ph). − ^{31}P NMR (109 MHz, CD_2Cl_2): δ = 52.1. − $C_{46}H_{45}Cl_4P_2RhRu \cdot 2/3CH_2Cl_2$ (1151.5): calcd. C 48.68, H 4.06; found C 48.50, H 4.15.

5: A solution of $RuCl_2(dppb)(PPh_3)$ (172 mg, 0.20 mmol) and $[(cymene)RuCl_2]_2$ (122 mg, 0.20 mmol) in acetone (25 mL) was heated under reflux. After 30 min, the heating was stopped and the solution was placed in a freezer (−20 °C). After 7 d, red crystals had formed, which were isolated and dried in a stream of dinitrogen. Yield: 109 mg (60%). − ^{1}H NMR (270 MHz, CD_2Cl_2): δ = 1.17 [d, ^3J = 7 Hz, 6 H, $CH(CH_3)_2$], 1.21−1.32 (m, 2 H, CH_2), 1.75−1.87 (m, 2 H, CH_2), 2.00−2.09 (m, 2 H, CH_2), 2.12 (s, 3 H, CH_3, cymene), 2.71 [s, ^3J = 7 Hz, 1 H, $CH(CH_3)_2$], 3.11−3.20 (m, 2 H, CH_2), 5.18 (d, ^3J = 6 Hz, 2 H, CH, cymene), 5.31 (d, ^3J = 6 Hz, 2 H, CH, cymene), 7.21−7.65 (m, 20 H, Ph). − ^{13}C NMR (68 MHz, CD_2Cl_2): δ = 18.4, 22.0, 22.6 (CH_2, dppb; CH_3, cymene), 29.8, 30.0, 30.3 (m, PCH_2), 30.9 (CH, cymene), 78.3, 78.5 (CH, cymene), 95.0, 101.0 (C, cymene), 127.0−140.7 (Ph). − ^{31}P NMR (109 MHz, CD_2Cl_2): δ = 54.4. − $C_{38}H_{42}Cl_4P_2Ru_2CH_3COCH_3$ (962.7): calcd. C 51.15, H 5.03; found C 51.20, H 5.05.

6: A mixture of $[RuCl_2(cod)(NCCH_3)_2]$ (38.0 mg, 0.10 mmol) and $[(cymene)RuCl(\mu\text{-}Cl)]_2$ (30.6 mg, 0.05 mmol) in acetone (10 mL) was heated under reflux for 1 h. After removal of the solvent under reduced pressure, the product was crystallized from CH_2Cl_2/hexane. Orange crystals, yield 49 mg (82%). − ^{1}H NMR (270 MHz, $CDCl_3$): δ = 1.39 [d, ^3J = 7 Hz, 6 H, $CH(CH_3)_2$], 1.72−1.81 (m, 4 H, CH_2, cod), 2.23−2.31 (m, 2 H, CH_2, cod), 2.32 (s, 3 H, CH_3, cymene), 2.44−2.50 (m, 2 H, CH_2, cod), 2.96 [s, ^3J = 7 Hz, 1 H, $CH(CH_3)_2$], 4.33−4.39 (m, 2 H, CH, cod), 4.44−4.50 (m, 2 H, CH, cod), 5.44 (d, ^3J = 6 Hz, 2 H, CH, cymene), 5.66 (d, ^3J = 6 Hz, 2 H, CH, cymene). − ^{13}C NMR (68 MHz, CD_2Cl_2): δ = 18.8, 22.5, 29.6, 29.9, 31.3 (CH_2, cod; CH, CH_3, cymene), 78.1, 79.6, 84.5, 84.9 (CH, cod + cymene), 97.2, 101.0 (C, cymene). − $C_{18}H_{26}Cl_4Ru_2$ (586.4): calcd. C 36.87, H 4.47; found C 36.87, H 4.43.

Crystal Structure Analyses: The structures of complexes **2** and **5** were determined with a Stoe IPDS. The structure of complex **6** was determined with an Enraf−Nonius diffractometer. Structure solution was performed by direct methods using SHELXS-97 or SHELXS-86.[28] The structures were refined by full-matrix least-squares techniques on F^2 (SHELXL-97, SHELXL-93).[28] For the hydrogen atoms, a riding model was employed. Complex **5** co-crystallized with pentane and dichloromethane. There are three molecules of CH_2CH_2 in the unit cell, the positions of two of which are only partially occupied (Table 3). Crystallographic data (excluding structure factors) for the structures reported in this paper have been deposited with the Cambridge Crystallographic Data Centre as supplementary publication nos. CCDC-144081 (**5**), -144082 (**2**), -144083 (**6**). Copies of the data can be obtained free of charge on application to the CCDC, 12 Union Road, Cambridge CB2 1EZ, U.K. [Fax: (internat.) + 44-(0)1223 336033; E-mail: deposit@ccdc.cam.ac.uk].

General Procedure for the Catalytic Oxidation of Secondary Alcohols: A suspension of K_2CO_3 (55.3 mg, 0.40 mmol) and the substrate (0.40 mmol) in 2-butanone (2.00 mL) was heated under reflux under dry dinitrogen. The reaction was initiated by addition of the catalyst (0.8 μmol), dissolved in CH_2Cl_2 (0.40 mL). After the time indicated, a sample (50 μL) was removed from the reaction vessel, quenched with acetone/acetic acid (3.5:1, 450 μL), and analyzed by capillary GC. The initial turnover frequency for the reduc-

Table 3. Crystallographic data for complexes **2**, **5**, and **6**

	2	**5**	**6**
Empirical formula	$C_{78}H_{72}Cl_4O_2P_4Ru_2$	$C_{83.4}H_{100.8}Cl_{12.8}P_4Ru_4$	$C_{18}H_{26}Cl_4Ru_2$
Molecular mass [g mol^{-1}]	1509.25	2085.26	586.33
Crystal size	0.15 × 0.12 × 0.06	0.23 × 0.05 × 0.04	0.43 × 0.37 × 0.53
Crystal system	monoclinic	triclinic	monoclinic
Space group	*Cc*	$P\bar{1}$	$P2_1/n$
a [Å]	25.4377(17)	16.1765(11)	10.4555(14)
b [Å]	12.2724(6)	17.8665(15)	10.487(2)
c [Å]	22.6572(14)	18.5778(18)	19.063(3)
α [°]	90	109.395(10)	90
β [°]	105.028(8)	94.293(10)	96.843(12)
γ [°]	90	116.366(8)	90
Volume [Å^3]	6831.3(7)	4377.9	2075.3(6)
Z	4	2	4
Density [g cm^{-3}]	1.467	1.582	1.877
Temperature [K]	200(3)	200(3)	295(2)
Absorption coefficient [mm^{-1}]	0.740	1.183	1.969
Θ range [°]	1.66 to 23.98	1.74 to 25.81	2.12 to 23.98
Index ranges	$-28 \le h \le 29$ $-13 \le k \le 13$ $-25 \le l \le 25$	$-18 \le h \le 18$ $-21 \le k \le 21$ $-22 \le l \le 22$	$-11 \le h \le 0$ $0 \le k \le 11$ $-21 \le l \le 21$
Reflections collected	18798	34346	3430
Independent reflections	9825 (R_{int} = 0.0509)	15738 (R_{int} = 0.0899)	3235 (R_{int} = 0.0145)
Absorption correction	numerical	numerical	semi-empirical
Max. and min. transmission	0.9581 and 0.9150	0.9732 and 0.9127	0.9984 and 0.8846
Data/restraints/parameters	8009/2/815	7735/2/898	3109/0/221
Goodness-of-fit on F^2	0.871	0.765	1.156
Final *R* indices [$I > 2\sigma(I)$]	*R*1 = 0.0307, *wR*2 = 0.0589	*R*1 = 0.0456, *wR*2 = 0.0836	*R*1 = 0.0260, *wR*2 = 0.0817
R indices (all data)	*R*1 = 0.0442, *wR*2 = 0.0751	*R*1 = 0.1165, *wR*2 = 0.0968	*R*1 = 0.0270, *wR*2 = 0.0825
Largest diff. peak/hole [eÅ^{-3}]	0.320/−0.511	2.018/−0.767	0.512/−0.527

tion of acetophenone was deduced from the time course of product formation over the first 10 min.

Acknowledgments

K. S. thanks Prof. Dr. W. Beck (LMU München) for his generous support and E. Karaghiosoff for technical assistance. Financial funding from the Bayerischer Habilitations-Förderpreis (K. S.) is gratefully acknowledged.

[1] [1a] E. K. van den Beuken, B. L. Feringa, *Tetrahedron* **1998**, *54*, 12985. – [1b] B. Bosnich, *Inorg. Chem.* **1999**, *38*, 2554. – [1c] H. Steinhagen, G. Helmchen, *Angew. Chem.* **1996**, *108*, 2489; *Angew. Chem. Int. Ed. Engl.* **1996**, *35*, 2339; M. W. Göbel, *Angew. Chem.* **1994**, *106*, 1201; *Angew. Chem. Int. Ed. Engl.* **1994**, *33*, 1141.

[2] [2a] M. Shibasaki, H. Sasai, T. Arai, *Angew. Chem.* **1997**, *109*, 1290; *Angew. Chem. Int. Ed. Engl.* **1997**, *36*, 1236. – [2b] K. Yamada, S. J. Harwood, H. Gröger, M. Shibasaki, *Angew. Chem.* **1999**, *111*, 3713; *Angew. Chem. Int. Ed.* **1999**, *38*, 3504.

[3] [3a] R. C. Matthews, D. K. Howell, W.-J. Peng, S. G. Train, W. D. Treleaven, G. G. Stanley, *Angew. Chem.* **1996**, *108*, 2402; *Angew. Chem. Int. Ed. Engl.* **1996**, *35*, 2253.– [3b] G. Süss-Fink, *Angew. Chem.* **1994**, *106*, 71; *Angew. Chem. Int. Ed. Engl.* **1994**, *33*, 67.– [3c] M. E. Broussard, B. Juma, S. G. Train, W.-J. Peng, S. A. Laneman, G. G. Stanley, *Science* **1993**, *260*, 1784.

[4] [4a] M. Öhm, A. Schulz, K. Severin, *Eur. J. Inorg. Chem.* **2000**, 2623. – [4b] K. Polborn, K. Severin, J. Chem. Soc., *Dalton Trans.* **1999**, 759. – [4c] K. Polborn, K. Severin, *Eur. J. Inorg. Chem.* **1998**, 1187.– [4d] K. Severin, S. Mihan, W. Beck, *Inorg. Chim. Acta* **1995**, *240*, 339.

[5] [5a] T. Weslamp, F. J. Kohl, W. Hieringer, D. Gleich, W. Herrmann, *Angew. Chem.* **1999**, *111*, 2573–2576; *Angew. Chem. Int. Ed.* **1999**, *38*, 2416. – [5b] E. L. Dias, R. H. Grubbs, *Organometallics* **1998**, *17*, 2758. Structurally related allenylidene complexes have been described: A. Fürstner, A. F. Hill, M. Liebl, J. D. E. T. Wilton-Ely, *Chem. Commun.* **1999**, 601.

[6] [6a] T. Naota, H. Takaya, S.-I. Murahashi, *Chem. Rev.* **1998**, *98*, 2599. – [6b] M. A. Bennett, T. W. Matheson, in *Comprehensive Organometallic Chemistry*, vol. 4 (Eds.: G. Wilkinson, F. G. A. Stone, E. W. Abel), Pergamon, Oxford, **1982**, p. 931 ff. – [6c] F. H. Jardine, in *Progress in Inorganic Chemistry*, vol. 31 (Ed. S. J. Lippard), John Wiley & Sons, New York, **1984**, p. 265 ff.

[7] [7a] F. Grepioni, D. Braga, P. J. Dyson, B. F. G. Johnson, F. M. Sanderson, M. J. Calhorda, L. F. Veiros, *Organometallics* **1995**, *14*, 121. – [7b] F. B. McCormick, W. B. Gleason, *Acta Crystallogr.* **1993**, *C49*, 1493. – [7c] D. A. Tocher, M. D. Walkinshaw, *Acta Crystallogr.* **1982**, *B38*, 30383. – [7d] T. Arthur, T. A. Stephenson, *J. Organomet. Chem.* **1981**, *208*, 369. – [7e] D. R. Robinson, T. A. Stephenson, T. Arthur, *J. Organomet. Chem.* **1978**, *162*, 121.

[8] J. D. Gilbert, G. Wilkinson, *J. Chem. Soc. A* **1969**, 1749.

[9] R. A. Head, J. F. Nixon, *J. Chem. Soc., Dalton Trans.* **1978**, 901.

[10] P. R. Hoffman, K. G. Caulton, *J. Am. Chem. Soc.* **1975**, *97*, 4221.

[11] F. Delbecq, P. Sautet, *J. Am. Chem. Soc.* **1992**, *114*, 2446.

[12] M. Schröder, T. A. Stephenson, in *Comprehensive Coordination Chemistry*, vol. 4 (Eds.: G. Wilkinson, R. D. Gillard, J. A. McCleverty), Pergamon, Oxford, **1987**, p. 277 ff.

[13] A. J. Fraser, R. O. Gould, *J. Chem. Soc., Dalton Trans.* **1974**, 1139.

[14] [14a] A.-R. Al-Ohaly, J. F. Nixon, *Inorg. Chim. Acta* **1985**, *103*, 83. – [14b] T. Arthur, T. A. Stephenson, *J. Organomet. Chem.* **1981**, *208*, 369. – [14c] R. A. Head, J. F. Nixon, *J. Chem. Soc., Dalton Trans.* **1978**, 909. For heterobimetallic complexes with a (μ-Br)$_3$ bridge, see: A. C. da Silva, H. Piotrowski, P. Mayer, K. Polborn, K. Severin *J. Chem. Soc., Dalton Trans.* **2000**, 2960.

[15] G. Meister, H. Stoeckli-Evans, G. Süss-Fink, *J. Organomet. Chem.* **1995**, *496*, 197.

[16] [16a] L. R. Dinelli, A. A. Batista, K. Wohnrath, M. P. de Araujo, S. L. Queiroz, M. R. Bonfadini, G. Oliva, O. R. Nascimento, P. W. Cyr, K. S. MacFarlane, B. R. James, *Inorg. Chem.* **1999**, *38*, 5341. – [16b] K. S. MacFarlane, I. S. Thorburn, P. W. Cyr, D. E. K.-Y. Chau, S. J. Rettig, B. R. James, *Inorg. Chim. Acta* **1998**, *270*, 130. – [16c] A. M. Joshi, I. S. Thorburn, S. J. Rettig, B. R. James, *Inorg. Chim. Acta* **1992**, *198–200*, 283.

[17] [17a] K.-M. Frosin, L. Dahlenburg, *Inorg. Chim. Acta* **1990**, *167*, 83. – [17b] T. V. Ashworth, M. J. Nolte, R. H. Reimann, E. Singleton, *J. Chem. Soc., Dalton Trans.* **1978**, 1043. – [17c] R. O. Gould, C. L. Jones, D. R. Robertson, T. A. Stephenson, *J. Chem. Soc., Dalton Trans.* **1977**, 129.
[18] C. F. de Graauw, J. A. Peters, H. van Bekkum, J. Huskens, *Synthesis* **1994**, 1007.
[19] [19a] M. L. S. Almeida, M. Beller, G.-Z. Wang, J.-E. Bäckvall, *Chem. Eur. J.* **1996**, *2*, 1533. – [19b] G.-Z. Wang, J.-E. Bäckvall, *Chem. Commun.* **1992**, 337.
[20] C. White, A. J. Oliver, P. M. Maitlis, *J. Chem. Soc., Dalton Trans.* **1973**, 1901.
[21] K. G. Caulton, *New J. Chem.* **1994**, *18*, 25.
[22] [22a] P. M. Maitlis, *Acc. Chem. Res.* **1978**, *11*, 301. – [22b] A. Fürstner, L. Ackermann, *Chem. Commun.* **1999**, 95. – [22c] A. Hafner, A. Mühlebach, P. A. van der Schaaf, *Angew. Chem.* **1997**, *109*, 2213; *Angew. Chem. Int. Ed. Engl.* **1997**, *36*, 2121.
[23] P. S. Hallman, T. A. Stephenson, G. Wilkinson, *Inorg. Synth.* **1970**, *12*, 237.
[24] C. W. Jung, P. E. Garrou, P. R. Hoffman, K. G. Caulton, *Inorg. Chem.* **1984**, *23*, 726.
[25] M. A. Bennett, T.-N. Huang, T. W. Matheson, A. K. Smith, *Inorg. Synth.* **1982**, *21*, 74.
[26] J. W. Kang, K. Moseley, P. M. Maitlis, *J. Am. Chem. Soc.* **1969**, *91*, 5970.
[27] M. O. Albers, T. V. Ashworth, H. E. Oosthuizen, E. Singleton, *Inorg. Synth.* **1989**, *26*, 68.
[28] G. M. Sheldrick, *SHELXL-97* and *SHELXL-93*, *Programs for Crystal Structure Refinement*, University of Göttingen, **1997** and **1993**; *SHELXS-97* and *SHELXS-86*, *Programs for Crystal Structure Solution*, University of Göttingen, **1997** and **1986**, respectively.

Received July 19, 2000
[I00284]

Paramagnetic Bis(amidinate) Iron(II) Complexes and their Diamagnetic Dicarbonyl Derivatives[‡]

Beatrice Vendemiati,[a] Giansiro Prini,[b] Auke Meetsma,[a] Bart Hessen,*[a] Jan H. Teuben,[a] and Orazio Traverso[b]

Keywords: Iron / N ligands / Magnetic properties / X-ray diffraction / Carbonyl complexes

Reactions of two equivalents of the lithium amidinate salts Li[*t*BuC(NR)$_2$] (R = *i*Pr, cyclohexyl) with $FeCl_2$ have been found to yield paramagnetic bis(amidinate) iron(II) compounds of the type [*t*BuC(NR)$_2$]$_2$Fe. In the case of R = cyclohexyl, the product has been characterized by single-crystal X-ray diffraction analysis as having a distorted tetrahedral geometry. The derivative with R = *i*Pr is an oil, but its ^{1}H and ^{13}C NMR spectra indicate a similar monomeric structure. Both species have been found to react readily with CO to give the new diamagnetic Fe^{II} dicarbonyls [*t*BuC(NR)$_2$]$_2$Fe(CO)$_2$. The compound with R = *i*Pr has been structurally characterized, which showed it to have a strongly distorted octahedral structure with the carbonyls in a *cis* arrangement.

Introduction

The amidinates [RC(NR′)$_2$]$^-$ (R = H, alkyl, aryl; R′ = alkyl, aryl, $SiMe_3$) constitute a class of versatile monoanionic ancillary ligands for transition metals.[1] They can bind in a chelating *N*,*N*′-η^2 fashion to a single metal center, or form *N*,*N*′-μ bridges between two metals. In the latter case, "lantern" complexes of the type {[μ-RC(NR′)$_2$]$_2$M}$_2$ can be formed that may contain very short M−M bonding contacts.[2,3] Amidinates have also found extensive use as ancillary ligands in catalytically active metal complexes, e.g. in Group 4 metal mono- and bis(amidinate) complexes, which can be activated with methylalumoxane (MAO) to give active olefin polymerization catalysts,[4] in cationic aluminum amidinate alkyls,[5] and in neutral (alkyl)bis(amidinate)vanadium ethene oligomerization catalysts.[6] To date, the chemistry of amidinate complexes of iron has yielded only a few well-defined complexes. For Fe^{II}, one type of dimeric bis(amidinate) complex has been reported, {[RC(NPh)$_2$]$_2$Fe}$_2$ (R = H, Ph), which has a "twisted" A-frame structure with two bridging and two dihapto amidinate ligands.[7] In addition, one example of a monomeric bis(amidinate) Fe^{II} complex is known, which contains amidinate ligands bearing ferrocenyl substituents on their backbone carbons, i.e. {[FcC(NCy)$_2$]$_2$Fe} (Fc = ferrocenyl).[8] As yet, no details of the reactivities of these complexes have been reported.

We are interested in the chemistry of iron(II) amidinates, especially with respect to their Lewis acidic behavior, their redox chemistry, and their potential as catalyst precursors. We describe herein the synthesis and characterization of paramagnetic monomeric iron(II) complexes of the highly substituted amidinate ligands [*t*BuC(NR)$_2$]$^-$ (R = *i*Pr, cyclohexyl).[9] The bis(amidinate) species [*t*BuC(NR)$_2$]$_2$Fe has been structurally characterized for R = Cy. These complexes appear to be quite light-sensitive. They react with CO to give the new distorted octahedral dicarbonyls *cis*-[*t*BuC(NR)$_2$]$_2$Fe(CO)$_2$, of which the derivative with R = *i*Pr has also been structurally characterized.

Results and Discussion

The lithium amidinates Li[*t*BuC(NR)$_2$] (R = *i*Pr, Cy) used in this study were readily available from the reaction of the corresponding carbodiimides with *t*BuLi.[9] Reaction of two equivalents of Li[*t*BuC(NCy)$_2$] with $FeCl_2$ in THF solution produced a brown-yellow colored solution, which gradually turned red-brown on exposure to ambient light. When the reaction mixture was worked-up under these conditions, a significant amount of a red-brown oil was recovered, which hampered isolation of the desired product. However, when the reaction and subsequent workup were performed with the exclusion of light, extraction with and crystallization from pentane yielded the bis(amidinate) Fe^{II} complex [*t*BuC(NCy)$_2$]$_2$Fe (**1a**) as yellow crystals in 54% isolated yield (Scheme 1). An analogous procedure with Li[*t*BuC(N*i*Pr)$_2$] resulted in a relatively low yield of a deep-brown/yellow oil that resisted all attempts to crystallize it. NMR spectroscopy (vide infra) indicated that this oil consisted mainly of [*t*BuC(N*i*Pr)$_2$]$_2$Fe (**1b**), although some impurities were present.

[‡] Netherlands Institute for Catalysis Research (NIOK) publication RUG-00-4-3.

[a] Center for Catalytic Olefin Polymerization, Stratingh Institute for Chemistry and Chemical Engineering, University of Groningen,
Nijenborgh 4, 9747 AG Groningen, The Netherlands
E-mail: hessen@chem.rug.nl
[b] Dipartimento di Chimica, Centro di Studio su Fotoreattivitá e Catalisi, Universitá di Ferrara,
Via Borsari 46, 44100 Ferrara, Italy

 © WILEY-VCH Verlag GmbH, 69451 Weinheim, 2001 1434−1948/01/0303−0707 $ 17.50+.50/0

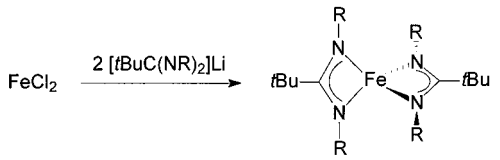

1a [R]=[Cy]
1b [R]=[*i*Pr]

Scheme 1. Formation of the bis(amidinate) iron(II) complexes

A crystal structure determination of **1a** was performed (Figure 1; selected interatomic distances and angles are listed in Table 1). It showed the compound to be monomeric, with two dihapto amidinate ligands and the iron in a distorted tetrahedral environment. The geometry of the two Fe−N−C−N four-membered rings is essentially planar [largest deviation seen in the Fe−N(3)−C(30)−N(4) dihedral angle of 10.3(2)°, Fe−N(1)−C(13)−N(2) = −4.9(2)°]. The angle between these two least-squares planes is 86.4(1)°. The structure is similar to that of the only other known monomeric bis(amidinate) Fe^{II} complex, {[FcC(NCy)$_2$]$_2$Fe},[8] although in the latter the average Fe−N distance is longer (2.037 Å vs. 2.020 Å in **1a**) and the dihapto amidinates are less symmetrically bound (the largest difference between the Fe−N distances for one amidinate ligand is 0.025 Å vs. 0.011 Å in **1a**).

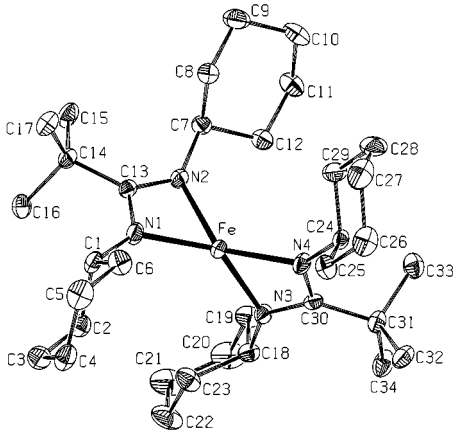

Figure 1. Molecular structure of **1a**; hydrogen atoms are omitted for clarity

Table 1. Selected interatomic distances (Å) and bond angles (°) in **1a**

Fe−N(1)	2.014(2)	N(1)−C(13)	1.336(3)
Fe−N(2)	2.025(2)	N(2)−C(13)	1.340(3)
Fe−N(3)	2.026(2)	N(3)−C(30)	1.328(3)
Fe−N(4)	2.015(2)	N(4)−C(30)	1.347(3)
N(1)−Fe−N(2)	65.38(8)	N(1)−Fe−N(4)	143.41(8)
N(3)−Fe−N(4)	65.15(8)	N(2)−Fe−N(3)	124.71(8)
N(1)−Fe−N(3)	137.38(8)	N(2)−Fe−N(4)	132.90(8)
N(1)−C(13)−N(2)	109.2(2)	N(3)−C(30)−N(4)	108.9(2)
Fe−N(1)−C(1)	135.8(2)	Fe−N(2)−C(7)	133.8(2)
Fe−N(3)−C(18)	133.8(2)	Fe−N(4)−C(24)	137.3(2)

The bis(amidinate) Fe^{II} compounds **1** are paramagnetic. Magnetic susceptibility measurements on solid **1a** showed Curie−Weiss behavior over the temperature range 5−300 K with μ_{eff} = 4.82 and θ = −1.36 K, consistent with a magnetically dilute solid with tetrahedral d^6 ions (S = 2). ^{1}H NMR spectra of the compounds **1** in C_6D_6 (25 °C) consequently show broad resonances, but nevertheless allow assignments to be made. For **1b**, three resonances are observed at δ = 190.4, 8.8, and −2.2 (in a 2:9:12 ratio) which can be attributed to the *i*Pr CH, *t*Bu CH_3, and *i*Pr CH_3 groups, respectively. For **1a**, the first two resonances are also present (at δ = 188.6 and 9.0), but these are accompanied by additional resonances (at δ = 11.9 and 10.7, as well as a group of less-well-resolved resonances in the δ = 4−0 region of the spectrum) that can be attributed to the cyclohexyl methylene protons. NMR spectroscopy thus suggests that complexes **1a** and **1b** have a similar structure in solution. The ^{13}C NMR spectrum of **1b** (C_6D_6, 25 °C) consists of two broad resonances at δ = 336 and 310, most probably attributable to the *t*Bu and *i*Pr methyl groups, respectively, and a third broad feature at δ = 661. The assignment of the latter resonance is ambiguous, as it could feasibly be attributed to the *i*Pr CH group or the *t*Bu quaternary carbon. The ^{13}C NMR spectrum of **1a** shows similar resonances (at δ = 628, 335, and 304), with two additional narrower resonances at δ = 27.9 and 20.1, associated with the δ- and γ-CH_2 groups, respectively, of the cyclohexyl moiety.

Both 14-electron bis(amidinate) Fe^{II} complexes **1** react with CO in hexane solution in the absence of light to give the diamagnetic carbonyl derivatives [*t*BuC(NR)$_2$]$_2$Fe(CO)$_2$ (R = Cy, **2a**; *i*Pr, **2b**), which were obtained in the form of orange crystals (Scheme 2). The IR spectra of these compounds show two carbonyl vibrations [**2a**: ν(CO) = 1999 and 1929 cm^{-1}], indicative of a *cis*-dicarbonyl structure. The ^{1}H and ^{13}C NMR spectra of the derivative with R = *i*Pr (**2b**) show the resonances of one *t*Bu group and two nonequivalent *i*Pr groups, each with two diastereotopic methyl groups. This, together with the IR data, suggests a C_2-symmetric octahedral *cis*-bis(η^2-amidinate)Fe(CO)$_2$ structure for **2b** that is nonfluxional on the NMR time scale at ambient temperature. The ^{1}H NMR spectrum of **2a** is less-well-resolved, but is consistent with the same structure type. For both complexes, the carbonyl ^{13}C NMR resonance is found at δ = 219.

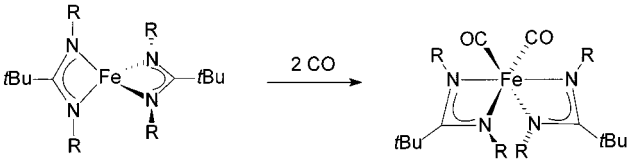

1a [R]=[Cy]
1b [R]=[*i*Pr]

2a [R]=[Cy]
2b [R]=[*i*Pr]

Scheme 2. Formation of the bis(amidinate) iron(II) dicarbonyl complexes

An X-ray crystal structure determination of **2b** corroborated the conclusions drawn from the spectroscopic studies.

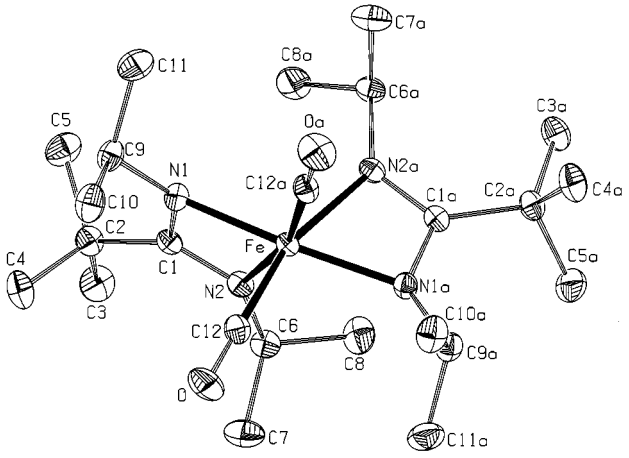

Figure 2. Molecular structure of **2b**; hydrogen atoms are omitted for clarity

Table 2. Selected interatomic distances (Å) and bond angles (°) in **2b**

Fe−N(1)	1.986(1)	N(1)−C(1)	1.342(2)
Fe−N(2)	2.031(1)	N(2)−C(1)	1.324(2)
Fe−C(12)	1.771(2)	O−C(12)	1.143(2)
N(1)−Fe−N(2)s	62.53(5)	N(1)−Fe−N(2a)	104.21(5)
N(1)−Fe−C(12)	90.48(6)	N(2)−Fe−C(12)	90.65(6)
N(1)−Fe−C(12a)	99.85(6)	N(2)−Fe−C(12a)	163.99(6)
N(1)−Fe−N(1a)	165.01(5)	N(2)−Fe−N(2a)	90.01(5)
C(12)−Fe−C(12a)	93.09(7)	Fe−C(12)−O	179.1(1)

The structure is shown in Figure 2, while pertinent interatomic distances and angles are listed in Table 2. The compound crystallizes in the space group C_2/c, with a C_2 symmetry axis passing through the Fe atom. The amidinate ligands are again bound in a dihapto fashion with the FeNCN ring having a planar geometry [the dihedral angle Fe−N(1)−C(1)−N(2) is −4.6(1)°]. The two Fe-amidinate planes, related by C_2 symmetry, are essentially orthogonal [87.49(8)°]. The Fe−N(2) distance is 0.045 Å longer than the Fe−N(1) distance, as a consequence of the *trans*-position of N(2) in relation to the CO ligand. Compared to the two known Fe^{II} *cis*-dicarbonyl complexes with bidentate monoanionic ligands — the phosphanyl-enolate and phosphanyl-carboxylate derivatives $[Ph_2PCHC(Ph)O]_2Fe(CO)_2$ [10] and $[Ph_2PCH_2C(O)O]_2Fe(CO)_2$[11] — complex **2b** has a much more strongly distorted octahedral geometry. This is due to the very small "bite angle" of the dihapto amidinate ligand, i.e. N(1)−Fe−N(2) is just 64.53(5)°, as compared to O−Fe−P angles of 82−86° in the other two complexes. In all three complexes, the C−Fe−C angle is about 93°, and hence this feature would appear to be quite insensitive to changes in the ligand. In the IR spectra, the carbonyl vibrations for **2** are found at noticeably lower wavenumbers than for the phosphanyl-carboxylate and -enolate complexes (2048, 1998 cm^{-1} and 2023, 1969 cm^{-1}, respectively), indicating that the amidinate ligands are better donors.

In conclusion, we have prepared two paramagnetic 14-electron bis(amidinate) iron(II) complexes and their diamagnetic 18-electron dicarbonyl derivatives. ^1H and ^{13}C NMR spectroscopy of the paramagnetic complexes proved helpful in establishing their structural relationship, which was especially useful as **1b** could not be crystallized. We are presently studying the Lewis acidities, electrochemistry, and photochemistry of the new complexes. Preliminary results suggest that the binding of the two CO molecules to the $(amidinate)_2Fe$ moiety can be readily reversed upon irradiation.

Experimental Section

General: All experiments were performed under a nitrogen atmosphere using standard Schlenk, glove-box, and vacuum line techniques. All manipulations involving compounds **1** were performed in the absence of light, the samples being protected by enveloping glassware in a black plastic bag whenever possible. Solvents (pentane, hexane, THF) were distilled from Na/K alloy prior to use. Deuterated benzene was dried over Na/K alloy and vacuum transferred before use. The Li salts Li[*t*BuC(NR)$_2$] (R = Cy, *i*Pr)[9] and anhydrous $FeCl_2$ [12] were prepared according to literature procedures. − NMR spectra were recorded on Varian VXR-300 or Unity 500 spectrometers. The ^1H NMR spectra were referenced to the resonances of residual protons in the deuterated solvent. Chemical shifts (δ) are given relative to tetramethylsilane (downfield shifts are positive). − IR spectra were recorded on a Mattson 4020 Galaxy FT-IR spectrophotometer. − Elemental analyses were performed at the Microanalytical Department of the University of Groningen; all data are the average of at least two independent determinations. − Magnetic susceptibility measurements on solid **1a** were performed on an MPMS-7 Quantum Design instrument under zero-field cooled conditions (1000 T field, 5−300 K temperature range). The EMU and temperature data are the average of three independent determinations; μ_{eff} was calculated from the total spin quantum number $S = 1.96$ obtained from the Curie−Weiss law ($C = 2.90$, $\theta = -1.35$ K).

Preparation of [*t*BuC(NCy)$_2$]$_2$Fe (1a): All manipulations were performed under the exclusion of light (vide supra). To a stirred suspension of $FeCl_2$ (0.653 g, 5.51 mmol) in THF (40 mL), solid Li[*t*-BuC(NCy)$_2$] (2.843 g, 10.5 mmol) was added at ambient temperature. After stirring for 2 h, the solvent was removed in vacuo, and then any residual THF was removed by stirring the mixture with pentane (20 mL) and subsequently pumping off the volatiles. Extraction of the residue with pentane (30 mL), concentration of the extract, and cooling it to −25 °C afforded 1.640 g (2.81 mmol, 54%) of **1a** as analytically pure yellow crystals. − ^1H NMR ([D$_6$]benzene, 25 °C): δ = 188 ($\Delta\nu_{1/2}$ = 280 Hz, 4 H, *i*Pr CH), 11.9 ($\Delta\nu_{1/2}$ = 40 Hz, 8 H, Cy CH$_2$), 10.7 ($\Delta\nu_{1/2}$ = 60 Hz, 8 H, Cy CH$_2$), 9.0 ($\Delta\nu_{1/2}$ = 60 Hz, 18 H, *t*Bu Me), 2.7 ($\Delta\nu_{1/2}$ = 470 Hz, 8 H, Cy CH$_2$), 1.5 ($\Delta\nu_{1/2}$ = 73 Hz, 4 H, Cy CH$_2$), 1.1 ($\Delta\nu_{1/2}$ = 33 Hz, 4 H, Cy CH$_2$), 0.5 ($\Delta\nu_{1/2}$ = 785 Hz, 8 H, Cy CH$_2$). − $^{13}C\{^1H\}$ NMR ([D$_6$]benzene, 25 °C): δ = 628 (assignment uncertain), 335 (*t*Bu Me), 304 (Cy β-CH$_2$), 27.9 (Cy δ-CH$_2$), 20.1 (Cy γ-CH$_2$). − $C_{34}H_{62}N_4Fe$ (582.7): calcd. C 70.08, H 10.72, N 9.61, Fe 9.58; found C 69.74, H 10.79, N 9.39, Fe 9.75.

Preparation of [*t*BuC(N*i*Pr)$_2$]$_2$Fe (1b): Following a similar procedure as described above for **1a**, but using Li[*t*BuC(N*i*Pr)$_2$] (0.934 g, 4.91 mmol) and $FeCl_2$ (0.308 g, 2.43 mmol), 0.26 g (0.61 mmol, 25%) of crude **1b** was obtained as a brown-yellow oil upon evaporation of the solvent from the pentane extract. − ^1H NMR ([D$_6$]ben-

Table 1. Data relating to the crystal structure determinations of **1a** and **2b**

	1a	**2b**
Empirical formula	$C_{34}H_{62}FeN_4$	$C_{24}H_{46}FeN_4O_2$
Formula mass	582.74	478.50
Crystal size (mm)	0.25 × 0.30 × 0.38	0.20 × 0.25 × 0.50
Temperature [K]	130	130
Radiation	Mo-K_α	Mo-K_α
Wavelength [Å]	0.71073	0.71073
Crystal system	monoclinic	monoclinic
Space group	$P2_1/n$	$C2/c$
a [Å]	10.872(2)	17.195(1)
b [Å]	16.962(3)	8.282(1)
c [Å]	18.644(1)	18.779(1)
β [°]	93.69(1)	103.099(7)
Volume [Å^3]	3431.0(9)	2604.7(4)
Z, calcd. density [Mgm^{-3}]	4, 1.128	4, 1.220
μ [mm^{-1}]	0.466	0.605
Scan	ω/2θ	ω/2θ
F(000)	1280	1040
θ range [°]	1.10 to 26.0	1.11 to 27.0
Index ranges	$-13 \le h \le 13$ $0 \le k \le 20$ $-22 \le l \le 0$	$-21 \le h \le 21$ $-10 \le k \le 0$ $-23 \le l \le 23$
Refl. collected/unique	7232/6702	6057/2841
Refl. observed [$I > 4.0\sigma(I)$]	4892	2647
Parameters refined	600	222
$wR(F^2)$[a] (for $F_o^2 > 0$)	0.1004	0.0913
Weighting scheme: a, b	0.0441, 1.234	0.0595, 2.3807
$R(F)$[b] [for $F_o > 4.0\ \sigma(F_o)$]	0.0443	0.0347
Diff. peak and hole (e/Å^3)	−0.30, 0.26(6)	−0.40, 1.90(7)

[a] $wR(F^2) = \{\Sigma[w(F_o^2 - F_c^2)^2]/\Sigma[w(F_o^2)^2]\}^{1/2}$, where $w = 1/[\sigma^2(F_o^2) + (aP)^2 + bP]$ and $P = [\max(F_o^2,0) + 2F_c^2]/3$. − [b] $R(F) = \Sigma(||F_o| - |F_c||)/\Sigma|F_o|$.

zene, 25 °C): δ = 190 ($\Delta\nu_{1/2}$ = 240 Hz, 4 H, *i*Pr CH), 8.8 ($\Delta\nu_{1/2}$ = 55 Hz, 18 H, *t*Bu Me), −2.2 ($\Delta\nu_{1/2}$ = 305 Hz, 24 H, *i*Pr Me). Resonances attributable to a diamagnetic impurity (probably derived from the ligand) are visible in the NMR spectrum at around δ = 3−4 and 0.6−1.6. − $^{13}C\{^1H\}$ NMR ([D$_6$]benzene, 25 °C): δ = 661 (assignment uncertain), 336 (*t*Bu Me), 310 (*i*Pr Me).

Preparation of [*t*BuC(NCy)$_2$]$_2$Fe(CO)$_2$ (2a): A 50 mL flask was charged with **1a** (0.323 g, 0.55 mmol) and hexane (10 mL). The flask was attached to a vacuum line, the solution was degassed by several freeze-pump-thaw cycles, and then CO (140 Torr, 1.2 mmol) was admitted. The mixture was allowed to stand (protected from light) for two days at ambient temperature. It was then concentrated and cooled to −25 °C, whereupon orange bar-shaped crystals were deposited. Yield: 0.244 g (0.38 mmol, 69%) of analytically pure **2a**. − ^{1}H NMR ([D$_6$]benzene, 25 °C): δ = 4.19 (m, 2 H, Cy CH), 3.53 (m, 2 H, Cy CH), 2.2−1.5 (m, 32 H, Cy CH$_2$), 1.26 (s, 18 H, *t*Bu Me), 1.20 (m, 8 H, Cy CH$_2$). − ^{13}C (APT) NMR ([D$_6$]benzene, 25 °C): δ = 219.4 (CO), 176.6 (NCN), 57.4 and 58.0 (NCH), 40.9 [*C*(CH$_3$)], 38.6, 36.3, 35.1, and 32.3 (CH$_2$), 30.5 [C(*C*H$_3$)$_3$], 26.5 (2×), 26.2, 26.1, 25.9, and 25.8 (CH$_2$). − IR (Nujol, KBr): $\tilde{\nu}$ = 1999, 1929 cm^{-1} [ν(CO)]. − $C_{36}H_{62}FeN_4O_2$ (638.8): calcd. C 67.69, H 9.78, N 8.77, Fe 8.74; found C 67.56, H 9.67, N 8.58, Fe 8.60.

Preparation of [*t*BuC(N*i*Pr)$_2$]$_2$Fe(CO)$_2$ (2b): For this preparation, compound **1b** was first generated by reaction of $FeCl_2$ (0.150 g, 1.18 mmol) with Li[*t*BuC(N*i*Pr)$_2$] (0.450 g, 2.36 mmol) in THF (15 mL) as described above, and the product was extracted with hexane (20 mL). A flask charged with this hexane extract was attached to a vacuum line and the solution was degassed; thereafter CO (1 bar) was admitted. After allowing the solution to stand for two days (protected from light), it was filtered, concentrated, and cooled to −25 °C. This led to the deposition of 0.158 g (0.33 mmol, 28% overall) of orange crystalline **2b**; m.p. 112−113 °C. − ^{1}H NMR ([D$_6$]benzene, 25 °C): δ = 4.58 (quint., $^3J_{HH}$ = 5.8 Hz, 2 H, *i*Pr CH), 3.95 (quint., $^3J_{HH}$ = 6.3 Hz, 2 H, *i*Pr CH), 1.50 and 1.19 (d, $^3J_{HH}$ = 5.8 Hz, 6 H each, *i*Pr Me), 1.27 and 1.15 (d, $^3J_{HH}$ = 6.3 Hz, 6 H each, *i*Pr Me), 1.17 (s, 18 H, *t*Bu). − ^{13}C (APT) NMR ([D$_6$]benzene, 25 °C): δ = 219.4 (CO), 177.1 (NCN), 49.6 and 48.5 (NCH), 41.1 [*C*(CH$_3$)], 30.7 [C(*C*H$_3$)$_3$], 27.5, 26.3, 24.7, and 22.8 [CH(*C*H$_3$)$_2$]. − IR (Nujol, KBr): $\tilde{\nu}$ = 2009, 1942 cm^{-1} [ν(CO)].

X-ray Crystal Structure Determinations: Diffraction data were collected on an Enraf−Nonius CAD4-F diffractometer. Pertinent crystallographic data and information concerning the data collection and residuals can be found in Table 3. For **1a**, the cell parameters were derived from the setting angles of 22 reflections in the range 16.37° ≤ θ ≤ 21.54°; for **2b** from 22 reflections in the range 17.95° ≤ θ ≤ 20.39°. Intensity data were corrected for Lorentz and polarization effects, but not for absorption. The structures were solved by Patterson methods and the models were extended by direct methods applied to difference structure factors using the program *DIRDIF*.[13] In both structures, all hydrogen atoms were located and refined with isotropic displacement parameters. Final refinement on F^2 was carried out by full-matrix least-squares techniques. Calculations were performed with the program packages *SHELXL*[14] (least-squares refinement) and *PLATON*[15] (geometric data). Crystallographic data (excluding structure factors) for the structures reported in this paper have been deposited with the Cambridge Crystallographic Data Centre as supplementary publication nos. CCDC-147087 for **1a** and -147086 for **2b**. Copies of the data can be obtained free of charge on application to the CCDC, 12 Union Road, Cambridge CB2 1EZ, U.K. [Fax: (internat.) + 44-1223/336-033; E-mail: deposit@ccdc.cam.ac.uk].

Acknowledgments

The authors wish to thank J. Baas for performing the solid-state susceptibility measurements on **1a**, and Montell Italia S.p.A. and the University of Ferrara for grants (to G.P. and B.V.).

[1] [1a] F. T. Edelmann, *Coord. Chem. Rev.* **1994**, *137*, 403. – [1b] J. Barker, M. Kilner, *Coord. Chem. Rev.* **1994**, *133*, 219–300.

[2] [2a] F. A. Cotton, L. M. Daniels, C. A. Murillo, *Inorg. Chem.* **1993**, *32*, 2881–2885. – [2b] D. I. Arnold, F. A. Cotton, D. J. Maloney, J. H. Matonic, C. A. Murillo, *Polyhedron* **1997**, *16*, 133–141. – [2c] F. A. Cotton, L. M. Daniels, X. Feng, D. J. Maloney, J. H. Matonic, C. A. Murillo, *Inorg. Chim. Acta* **1997**, *256*, 291–301.

[3] [3a] S. Hao, S. Gambarotta, C. Bensimon, J. J. H. Edema, *Inorg. Chim. Acta* **1993**, *213*, 65–74. – [3b] S. Hao, P. Berno, K. M. Ravinder, S. Gambarotta, *Inorg. Chim. Acta* **1996**, *244*, 37–49.

[4] [4a] D. Herskovics-Korine, M. S. Eisen, *J. Organomet. Chem.* **1995**, *503*, 307–314. – [4b] R. Gómes, R. Duchateau, A. N. Chernega, J. H. Teuben, F. T. Edelmann, M. L. H. Green, *J. Organomet. Chem.* **1995**, *491*, 153–158. – [4c] C. Averbuj, E. Tish, M. S. Eisen, *J. Am. Chem. Soc.* **1998**, *120*, 8640–8646. – [4d] V. Volkis, M. Shmulinson, C. Averbuj, A. Lisovskii, F. T. Edelmann, M. S. Eisen, *Organometallics* **1998**, *17*, 3155–3157.

[5] M. P. Coles, R. F. Jordan, *J. Am. Chem. Soc.* **1997**, *119*, 8125–8126.

[6] E. A. C. Brussee, A. Meetsma, B. Hessen, J. H. Teuben, *Chem. Commun.* **2000**, 497–498.

[7] F. A. Cotton, L. M. Daniels, J. H. Matonic, C. A. Murillo, *Inorg. Chim. Acta* **1997**, *256*, 277–282.

[8] J. R. Hagadorn, J. Arnold, *Inorg. Chem.* **1997**, *36*, 132–133.

[9] M. P. Coles, D. C. Swenson, R. F. Jordan, V. G. Young, Jr., *Organometallics* **1997**, *16*, 5183–5194.

[10] P. Braunstein, G. C. Cea, A. DeCian, J. Fischer, *Inorg. Chem.* **1992**, *31*, 4203–4206.

[11] J. Takács, L. Markó, P. Kiprof, E. Herdtweck, W. A. Herrmann, *Polyhedron* **1989**, *8*, 1503–1507.

[12] P. Kovacic, N. O. Brace, *Inorg. Synth.* **1960**, *6*, 172–173.

[13] P. T. Beurskens, G. Beurskens, R. de Gelder, S. García-Granda, R. O. Gould, R. Israël, J. M. M. Smit, *The DIRDIF-99 Program System*, Crystallography Laboratory, University of Nijmegen, The Netherlands, **1999**.

[14] G. M. Sheldrick, *SHELXL-97 – A Program for the Refinement of Crystal Structures*, University of Göttingen, Germany, **1997**.

[15] A. L. Spek, *PLATON – A Program for the Automated Analysis of Molecular Geometry*, University of Utrecht, The Netherlands, **1999**.

Received July 31, 2000
[I00300]

Intercalates of Vanadyl Phosphate with Unsaturated Alcohols

Ludvík Beneš,*[a] Klára Melánová,[a] Vítězslav Zima,[a] Miroslava Trchová,[b] Eva Uhlířová,[b] and Pavel Matějka[c]

Keywords: Vanadium / Phosphorus / Alcohols / Intercalations / Vibrational spectroscopy / X-ray scattering

Intercalates of $VOPO_4$ with several linear unsaturated alcohols (2-propen-1-ol, 2-buten-1-ol, 2-propyn-1-ol, 2-butyn-1-ol, 3-butyn-1-ol 2-pentyn-1-ol, 3-pentyn-1-ol, 4-pentyn-1-ol, 5-hexyn-1-ol, 2-octyn-1-ol, and 10-undecyn-1-ol) have been prepared and characterized by powder X-ray diffractometry, IR and Raman spectrometry, and thermogravimetry. The arrangement of the alcohol molecules with respect to the type and position of the multiple bonds in the carbon chain is proposed. Alcohols with terminal triple bonds form very stable intercalates. It is presumed that these alcohols are anchored to the host layers by donor-acceptor bonds between their oxygen atoms and the vanadium atoms of the host, and by H-bonding between the acetylenic hydrogen of the terminal carbon and the oxygen atoms of the host.

Introduction

The tetragonal layer structure of $VOPO_4$ is made up of distorted VO_6 octahedra and PO_4 tetrahedra which are linked by corner-sharing oxygen atoms (O_{host}).[1−3] Each octahedron is joined to four tetrahedra and the layers are connected along the *c* axis by the sharing of the remaining two trans vertices of the octahedron. One of these two vanadium−oxygen bonds is short indicating the presence of a V=O bond, while the other is much longer and can be ascribed to the coordination of the oxygen atom from the V=O group of an adjacent $(VOPO_4)_\infty$ layer. Interlayer interactions are therefore established through V=O···V bonds in anhydrous $VOPO_4$. In $VOPO_4{\cdot}2H_2O$, the sixth position in the VO_6 octahedron is complemented by the oxygen atom of one water molecule which is then *trans* to the oxygen atom of the V=O bond. The second water molecule is located in the interlayer space and is H-bonded to O_{host} atoms and to the water molecules of the first type. The formation reaction of $VOPO_4{\cdot}2H_2O$ from $VOPO_4$ can be considered as a kind of intercalation reaction, in which the coordination of the guest species to the metal center provides the driving force.[3] Similar reactions have been described for other donor ligands containing oxygen or nitrogen containing functional groups, leading to new materials with interesting properties and structures.[4] Vanadyl phosphate forms a number of intercalation compounds with molecular guests having a Lewis base character.[5] Intercalations of aliphatic and aromatic amines,[6−10] heterocycles,[10−14] carboxylic acids[15] and their derivatives,[16] amino acids,[17] metallocenes,[18,19] alcohols,[20,21] diols,[20,22,23] and poly(oxyethylene) compounds[24] have been studied.

The reaction of solid $VOPO_4{\cdot}2H_2O$ with liquid or melted solid 1-alkanols in a microwave field leads to intercalation compounds with the composition $VOPO_4{\cdot}2C_nH_{2n+1}OH$ (n = 2−18). All the polycrystalline layer complexes retain the structure of the original $(VOPO_4)_\infty$ layers. The alcohol molecules are placed between the host layers in a bimolecular arrangement, that is, in two layers. The guest molecules are anchored to the host layers by donor−acceptor bonds between the oxygen atom of the OH group of the guest (O_{guest}) and the vanadium atom (V_{host}), and also by hydrogen bonds between the OH group and O_{host}. The aliphatic chains of the intercalated alcohol molecules possess an all-*trans* configuration and their axes are perpendicular to the plane of the host layers.[20] In the intercalates of $VOPO_4$ with 1,ω-diols and 1,2-diols, the guest molecules are bonded to the host layers in a similar way as in the alkanol intercalates.[20,22]

Intercalates of vanadyl phosphate with *cis*-2-butene-1,4-diol and 2-butyne-1,4-diol have been prepared. It was presumed from the values found for the basal spacing that the molecules of *cis*-2-butene-1,4-diol and 2-butyne-1,4-diol are arranged in a similar manner to those of 1,4-butanediol in the interlayer space. The observed differences in the basal spacings confirm this proposal because the distances between the terminal oxygen atoms calculated from the bond lengths and bond angles decrease in the order 1,4-butanediol (6.20 Å) > 2-butyne-1,4-diol (5.75 Å) > *cis*-2-butene-1,4-diol (5.62 Å).[23]

The influence of the multiple bond and its position in the alcohol chain on the arrangement of the guest molecules in the interlayer space of the host, and on the properties of the intercalate formed is reported.

[a] Joint Laboratory of Solid State Chemistry of Academy of Sciences of the Czech Republic and University of Pardubice, Studentská 84, 532 10 Pardubice, Czech Republic
Fax: (internat.) +420-40/603-6011
E-mail: ludvik.benes@upce.cz
[b] Faculty of Mathematics and Physics, Charles University, V Holešovičkách 2, 180 00 Prague, Czech Republic
Fax: (internat.) +420-02/2191-2351
E-mail: trchova@mbox.troja.mff.cuni.cz
[c] Department of Analytical Chemistry, Institute of Chemical Technology, Technická 5, 166 28 Prague, Czech Republic

 © WILEY-VCH Verlag GmbH, 69451 Weinheim, 2001 1434−1948/01/0303−0713 $ 17.50+.50/0

Results and Discussion

In contrast to ethanol, propanol and butyl alcohol,[25] no unsaturated alcohol can be intercalated into anhydrous vanadyl phosphate. Only 2-propen-1-ol, 2-buten-1-ol and 2-propyn-1-ol can replace the water molecules in $VOPO_4 \cdot 2H_2O$. The intercalates with longer unsaturated alcohols had to be prepared by reintercalation of propanol-intercalated vanadyl phosphate. The intercalates prepared were yellow, crystalline solids, indicating that the vanadium(V) had not been significantly reduced.

The diffractograms of all intercalates show a series of relatively sharp (00*l*) reflections (see Figure 1 and 2). The *a* parameters of their tetragonal lattices were determined from the (200) and (*h*0*l*) lines, provided they were observed. The values found for the lattice parameters *a* and *c* are presented in Table 1. The number of alcohol molecules per formula unit in $VOPO_4 \cdot x$ROH is hereafter referred to as the stoichiometric quotient *x*. The experimental stoichiometric quotients x_{exp} obtained by the thermogravimetric analyses, and by the elemental analyses for the carbon and hydrogen content are given in Table 1. For comparison, the values of x_{calc}, calculated as a ratio of the volume of the alcohol intercalated and the molar volume of the free alcohol, which was calculated from its density, are also given in this table. The volume of the alcohol intercalated was calculated as the difference between the unit cell volume of the intercalate and anhydrous $VOPO_4$. It is obvious from Table 1 that the packing of the guest molecules is closer in the intercalate than in the free alcohol.

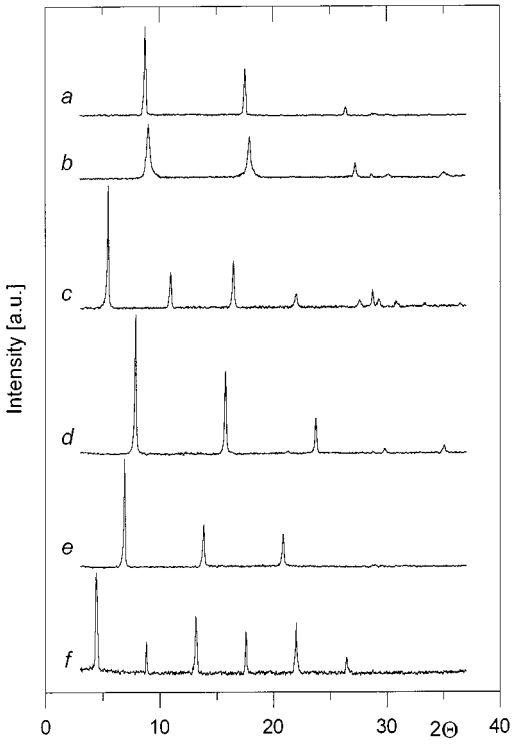

Figure 1. The diffractograms of the vanadyl phosphate intercalates with alcohols with a terminal triple bond: (a) 2-propyn-1-ol; (b) 3-butyn-1-ol (phase formed at laboratory temperature); (c) 3-butyn-1-ol (phase formed at higher temperature); (d) 4-pentyn-1-ol; (e) 5-hexyn-1-ol; (f) 10-undecyn-1-ol

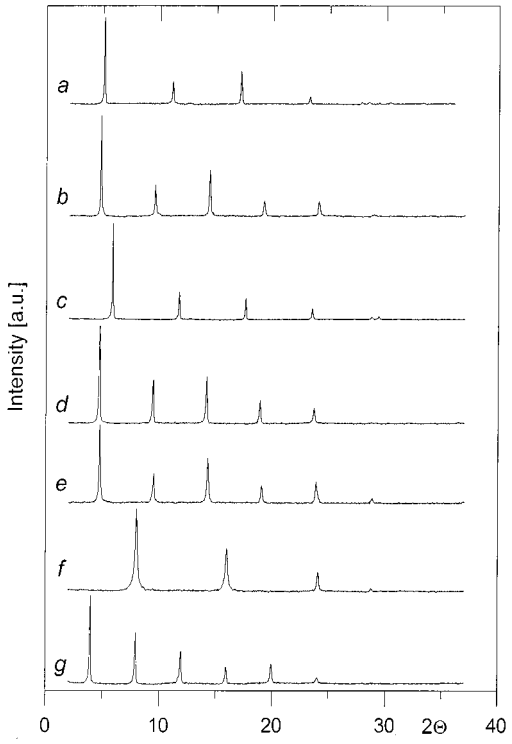

Figure 2. The diffractograms of the vanadyl phosphate intercalates with other unsaturated alcohols: (a) 2-propen-1-ol; (b) 2-buten-1-ol; (c) 2-butyn-1-ol; (d) 2-pentyn-1-ol; (e) 3-pentyn-1-ol (phase formed at laboratory temperature); (f) 3-pentyn-1-ol (phase formed at higher temperature); (g) 2-octyn-1-ol

Table 1. Lattice parameters and the guest contents in $VOPO_4$ intercalated with unsaturated alcohols

Alcohol	*a* [Å]	*c* [Å]	x_{exp}	x_{calc}
2-propen-1-ol	6.22	14.76	1.90	1.82
2-buten-1-ol	6.20	18.51	2.05	1.96
2-propyn-1-ol	6.22	10.15	1.60	1.20
2-butyn-1-ol	6.22	15.07	1.93	1.71
3-butyn-1-ol	6.21	16.15	1.95	1.84
	6.20	9.83	0.91	0.87
2-pentyn-1-ol	6.21	18.80	–	1.84
3-pentyn-1-ol	6.20	18.64	1.92	1.83
	6.21	11.10	1.11	0.89
4-pentyn-1-ol	6.22	11.23	1.08	0.89
5-hexyn-1-ol	6.16	12.76	1.10	0.90
2-octyn-1-ol	6.20	22.26	–	1.47
10-undecyn-1-ol	6.21	19.90	1.05	0.96

The alcohols with a terminal triple bond (4-pentyn-1-ol, 5-hexyn-1-ol and 10-undecyn-1-ol) form intercalates containing one molecule of alcohol per formula unit; they are stable in air at ambient conditions (relative humidity 40–60%). 3-Butyn-1-ol forms an intercalate containing two alcohol molecules per formula unit at room temperature. This intercalate is unstable and slowly loses one molecule of alcohol to form a phase with a lower basal spacing. This transformation is irreversible. The same phase, which is stable at room temperature, is formed when $VOPO_4 \cdot 2C_3H_8OH$ is heated with 3-butyn-1-ol. The transformation is also observed at 38 °C during temperature XRD measurements of the $VOPO_4 \cdot 2$(3-butyn-1-ol) intercal-

ate. 2-Propyn-1-ol forms an intercalate, containing about 1.6 molecules of alcohol per formula unit, which is stable in air.

Alcohols with a triple bond at the second carbon atom (2-butyn-1-ol, 2-pentyn-1-ol and 2-octyn-1-ol) form unstable intercalates which rapidly decompose to $VOPO_4{\cdot}2H_2O$ in air at ambient conditions (relative humidity 40−60%). Therefore, it was not possible to determine the composition for 2-pentyn-1-ol- and 2-octyn-1-ol-intercalated vanadyl phosphate. Phases with lower basal spacing ($d = 10.56$ Å at 74−111 °C for 2-butyn-1-ol, and $d = 15.9$ Å at around 77 °C and 11.6 Å at 87−115 °C for 2-pentyn-1-ol) were found by XRD measurements in situ at the given temperatures. These phases cannot be synthesized by the method described in the Experimental Section at the given temperatures. The number of guest molecules probably increases during the cooling of the reaction mixture after the synthesis; compounds containing two guest molecules are then formed.

3-Pentyn-1-ol forms an intercalate with two alcohol molecules at room temperature. This intercalate slowly loses one molecule of alcohol and transforms to a phase with a lower basal spacing in air (relative humidity ≈ 40−60%). This then slowly decomposes to $VOPO_4{\cdot}2H_2O$. The intercalate with a basal spacing of 11.10 Å can be prepared by heating $VOPO_4{\cdot}2C_3H_7OH$ with 3-pentyn-1-ol at 80 °C. The phase with a higher alcohol content and a higher basal spacing is not formed, which indicates that the high-temperature phase is very stable. The same transformation was observed at about 50 °C during temperature XRD measurements of the $VOPO_4{\cdot}2$(3-pentyn-1-ol) intercalate.

Both alcohols with a double bond (2-propen-1-ol and 2-buten-1-ol) form intercalates with a similar composition and stability as the corresponding saturated alcohols.[20]

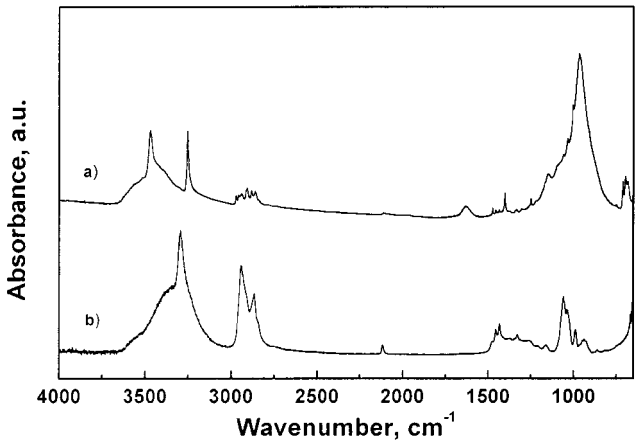

Figure 3. FTIR spectra: (a) 5-hexyn-1-ol-intercalated vanadyl phosphate (in KBr pellet); (b) liquid 5-hexyn-1-ol (ATR on ZnSe crystal)

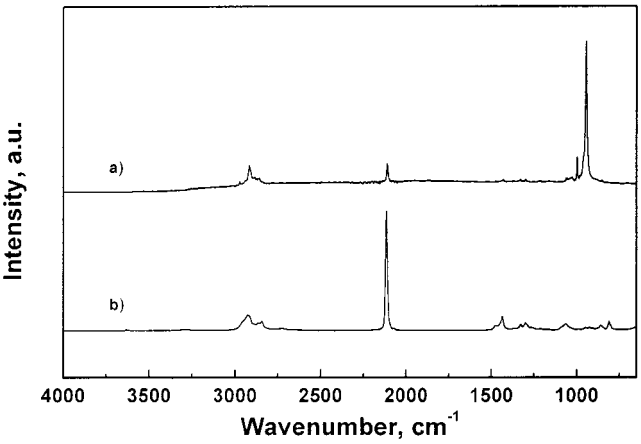

Figure 4. Raman spectra: (a) 5-hexyn-1-ol-intercalated vanadyl phosphate; (b) liquid 5-hexyn-1-ol

Infrared and Raman Spectra

The infrared spectra of 2-propen-1-ol, 2-propyn-1-ol, 4-pentyn-1-ol, 5-hexyn-1-ol and their $VOPO_4$ intercalates were measured in KBr pellets in the transmission mode. The spectra of the corresponding alkynols in the liquid state were measured by the ATR technique on ZnSe crystal.

The infrared spectra of liquid 5-hexyn-1-ol and its $VOPO_4$ intercalate are given in Figure 3. The Raman spectra of these compounds are given in Figure 4. The results for 4-pentyn-1-ol are very similar to that obtained for 5-hexyn-1-ol, and they are not presented here. The positions of the main spectral bands of the host structure in the spectrum of $VOPO_4$ intercalated with 5-hexyn-1-ol differ only slightly from those of anhydrous vanadyl phosphate or its hydrated form.[26] This confirms that the structure of the original $VOPO_4$ layers remains unchanged after the intercalation reaction. The intense band at 948 cm^{-1} in the Raman spectrum corresponds to the symmetric $\nu(PO_4)$ stretching vibration of the phosphate tetrahedron in the $(VOPO_4)_\infty$ layers, and is observed at 966 cm^{-1} in the infrared spectrum. The position of the vanadyl stretching vibration V=O at 1004 cm^{-1} in the Raman spectrum indicates coordination of O_{guest} to V_{host}. This band is observed at 1007 cm^{-1} in the infrared spectrum, allowing us to distinguish this band from other bands belonging to the intercalated alcohol molecules.

The infrared and Raman spectra of pure and intercalated 5-hexyn-1-ol differ in the position, shape and intensity of the corresponding bands as a consequence of the intercalation reaction in the interlayer space. The O−H stretching vibration must be sensitive to a phase change as in the case of 2-propyn-1-ol.[27] The infrared spectrum of liquid 5-hexyn-1-ol shows that the alcohol is completely associated. The ν(O−H) frequencies occur at about 3575 and 3392 cm^{-1}. The higher frequency band results from ν(O−H) of the terminal OH group, where the oxygen atom is hydrogen-bonded to the hydrogen atom of the O−H group of the adjacent guest molecule in the intermolecularly hydrogen-bonded chain. The lower frequency of the ν(O−H) band results from the intermolecularly hydrogen-bonded OH groups within the chain.[27] Remarkable changes are observed in this region upon intercalation into $VOPO_4$. A new sharp band at 3474 cm^{-1} occurs in the intercalated compound. Such bands are usually observed for unassociated hydroxyl groups, absorbing strongly in the region 3670−3580 cm^{-1}.[28] The presence of this new band is likely

to be related to the steric hindrance resulting from the hydrogen bonds. We suggest that it arises as a result of the anchoring of the oxygen atom from the OH group to the vanadium atom by donor−acceptor bonds. The shoulder on the higher frequency side of this band probably results from an association with other alcohol molecules, or from the formation of hydrogen bonds to the oxygen atoms from the layers. A sharp band at about 1404 cm^{-1} corresponds to the O−H bending vibration and strongly supports the assignment of the hindered hydroxyl stretching vibration. The band observed at about 1630 cm^{-1} is probably due to the association of the hydroxyl groups and the water molecules in KBr pellet.

The acetylenic C−H stretching vibration is observed at 3295 cm^{-1} for liquid 5-hexyn-1-ol. This vibration is remarkably constant with respect to the variation of the chemical structure of the rest of the molecule, but is sensitive to its physical state.[29] The acetylenic hydrogen is able to associate freely with proton-accepting groups, which leads to the shift of the vibration up to 120 cm^{-1} in extreme cases.[30] The position of this vibration is shifted to 3254 cm^{-1} after intercalation in $VOPO_4$, reflecting the association with the hydroxyl group of the second alcohol molecule or the formation of hydrogen bonds to the oxygen atoms from the layers. The ≡C−H bending vibration results in one or two strong absorption bands in the 610−680 cm^{-1} region.[29]

The remarkable change in the C−H vibrations is observed when going from liquid 5-hexyn-1-ol to its intercalated form. During the fixation of the intercalated molecules in the interlayer space some new bands arise in the region of the stretching vibrations, where only two bands at 2945 and 2867 cm^{-1} are observed in the infrared spectrum of the liquid alcohol. The interaction of the alcohol molecules with the host in the intercalate leads to the splitting of the bands in the 1150−1490 cm^{-1} region. The four fundamental bands expected to occur in this region are: CH_2 bending δ(C−H), CH_2 wagging ω(C−H), O−H bending δ(O−H) and CH_2 twisting γ(C−H).[27] The C≡C stretching absorption band has appreciable intensity only in hydrocarbons with terminal triple bonds.[30] This band occurs at 2121 cm^{-1} both in the infrared and Raman spectra of the liquid alcohol, and is very intense in the latter. It is shifted to 2114 cm^{-1} in the intercalate.

The infrared spectra of liquid 2-propyn-1-ol and its intercalate in $VOPO_4$ are given in Figure 5. The Raman spectra of these compounds are given in Figure 6. These spectra differ from those of 5-hexyn-1-ol and 4-pentyn-1-ol intercalated in $VOPO_4$. The Raman spectrum of the intercalate with 2-propyn-1-ol is strongly influenced by baseline radiation. The intense broad band centered at about 915 cm^{-1} in this spectrum probably corresponds to the symmetric ν(PO_4) stretching vibration of the phosphate tetrahedron,[26] overlapped by the strong band of 5-hexyn-1-ol. The sharp band at 996 cm^{-1} corresponds to the V=O stretching vibration. Interpretation of this region in the infrared spectrum is rather complicated. The ν(PO_4) stretching vibration, the V=O stretching vibration and the C−O_{guest}H stretching vibration overlap in this part of the spectrum. With the help

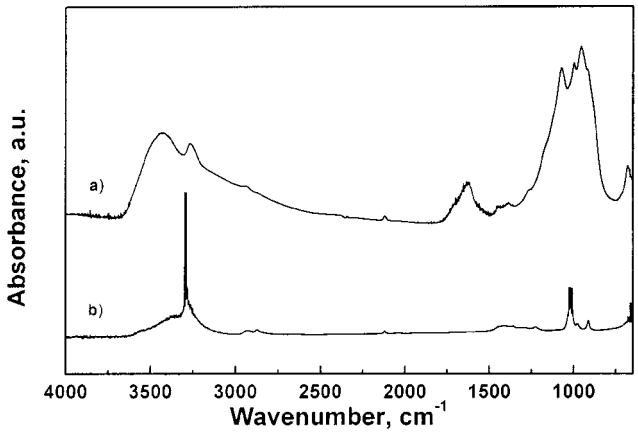

Figure 5. FTIR spectra: (a) 2-propyn-1-ol-intercalated vanadyl phosphate (in KBr pellet); (b) liquid 2-propyn-1-ol (ATR on ZnSe crystal)

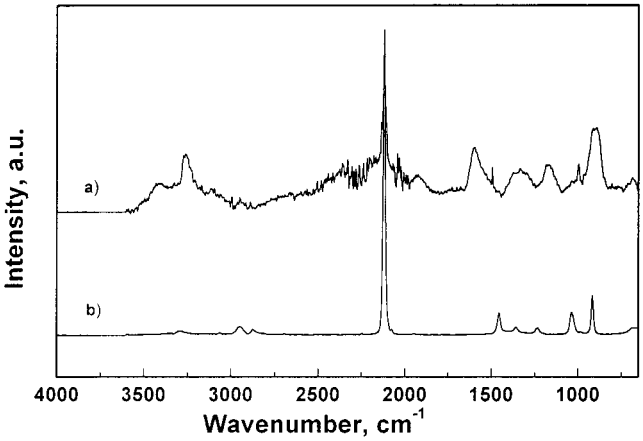

Figure 6. Raman spectra: (a) 2-propyn-1-ol-intercalated vanadyl phosphate; (b) liquid 2-propyn-1-ol

of the Raman spectrum, the band at 959 cm^{-1} in the infrared spectrum is assigned to the symmetric ν(PO_4) stretching vibration which is infrared active due to the distortion of the phosphate tetrahedron in the intercalate. The band at about 1004 cm^{-1} is probably due to the vanadyl V=O stretching vibration corresponding to the anchoring of the hydroxyl oxygen of 2-propyn-1-ol to V_{host}. The C−O_{guest}H stretching band of the alcohol is likely to be overlapped by other bands. The intense band at about 1074 cm^{-1} may be an asymmetric stretching vibration ν(PO_4) of the phosphate tetrahedron. This band is due to the strong interaction between the alcohol hydroxyl and acetylenic groups, and the phosphate oxygen through hydrogen-bonds.

Changes are also observed in the high frequency region of the spectrum of the intercalate relative to that of liquid 2-propyn-1-ol. The strong hydrogen bonding of the alcohol in the intercalate leads to a broad band for the OH stretching vibration centered at about 3434 cm^{-1}. The band at about 1630 cm^{-1} with a shoulder at about 1719 cm^{-1} corresponds to the bending vibrations of the hydrogen-bonded OH groups and of the water molecules in the KBr pellet. The sharp and intense band of the acetylenic CH vibration observed in the spectrum of the liquid alcohol at 3295 cm^{-1}

is shifted to 3270 cm^{-1} in the spectrum of the intercalate. In the Raman spectrum, this band is broadened and observed at 3265 cm^{-1}, which corresponds to the hydrogen bonding of the acetylenic CH group with O_{host}. The position of the C≡C stretching absorption band both in liquid 2-propyn-1-ol and in the intercalate occurs at 2121 cm^{-1} in the infrared spectrum and is very intense in the Raman spectrum at about 2125 cm^{-1}.

The infrared spectra of liquid 2-propen-1-ol and its $VOPO_4$ intercalate are given in Figure 7. The Raman spectra of these compounds are given in Figure 8. The Raman spectrum of the intercalate is only slightly influenced by baseline radiation. The intense band at about 944 cm^{-1} in the Raman spectrum probably corresponds most to the symmetric $\nu(PO_4)$ stretching vibration of the phosphate tetrahedron, and the sharp band at 1000 cm^{-1} to the V=O stretching vibration. The bands of 2-propen-1-ol in the Raman spectrum are at the same positions in the intercalate and in liquid 2-propen-1-ol. With the help of the Raman spectrum, the band at 948 cm^{-1} in the infrared spectrum was assigned to the symmetric $\nu(PO_4)$ stretching vibration. The band at about 996 cm^{-1} is probably the $C-O_{guest}H$ stretching band of the intercalated alcohol. Its position is also not changed in the intercalate as a consequence of the weak interaction between the alcohol and the host layers. The intense band at about 1104 cm^{-1} in the spectrum of the intercalate is assigned to the asymmetric stretching vibration $\nu(PO_4)$ of the phosphate tetrahedron. This band is due to the hydrogen bonds between the alcohol hydroxyl and the phosphate oxygen, analogous to the saturated 1-alkanols.[31] The strong hydrogen bonding of the alcohol in the intercalate leads to broad OH stretching vibration bands centered at about 3403 and 3582 cm^{-1}. The band at about 1630 cm^{-1} is assigned to the bending vibration of the hydrogen-bonded OH groups and the water molecules in the KBr pellet, and is overlapped by the C=C stretching vibration band in 2-propen-1-ol. This band is very strong in the Raman spectra.

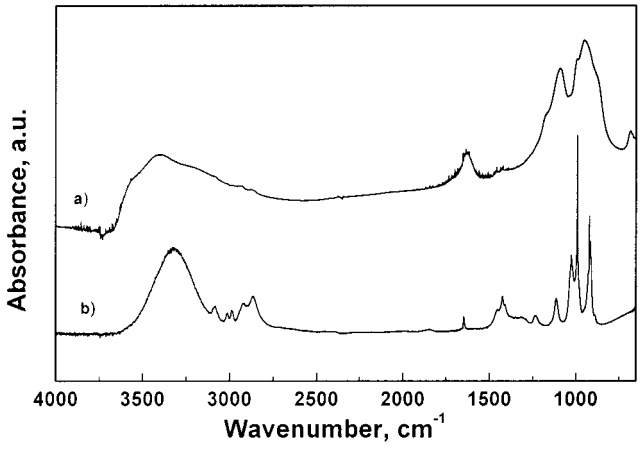

Figure 7. FTIR spectra: (a) 2-propen-1-ol-intercalated vanadyl phosphate (in KBr pellet); (b) 2-propen-1-ol (ATR on ZnSe crystal)

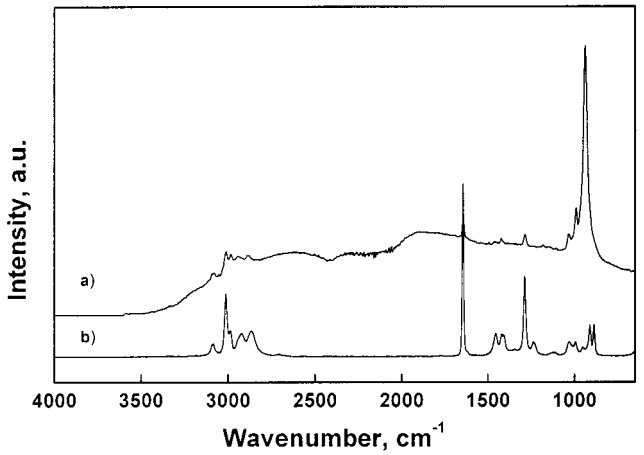

Figure 8. Raman spectra: (a) 2-propen-1-ol-intercalated vanadyl phosphate; (b) liquid 2-propen-1-ol

Suggested Structures

Alcohols with a double bond in their aliphatic chain are placed in the interlayer space of the host in a way similar to that of saturated alcohols with the same chain length (i.e. the distance from C_1 to C_n).[20,31] This means that they are arranged in two layers and the angle, α, at which they are tilted to the plane of the host sheets, increases with an increasing number of carbon atoms, as in the homologous series of ethanol, 1-propanol and 1-butanol intercalates.[31] Half of the guest molecules are anchored to V_{host} by donor−acceptor bonds with O_{guest}. The rest of the guest molecules forms hydrogen bonds between their OH groups and O_{host} or between these OH groups and the guest oxygen atoms coordinated to V_{host}.

The intercalates containing about two molecules of alcohols with a triple bond (2-butyn-1-ol, less stable phase of 3-butyn-1-ol with a higher basal spacing, 2-pentyn-1-ol, and 3-pentyn-1-ol) per formula unit have distinctly lower basal spacings than the intercalates with saturated alcohols with the same chain length.[20] The shortening of the chain length by the triple bond is insignificant irrespective of its position. This means that in the presumed bimolecular arrangement of the guest molecules, the carbon chain must be tilted towards the host layers more (it must have a smaller α value) than the intercalates with saturated alcohols, in which the chains are perpendicular to the host layers.[20,31] With respect to other aspects, it can be presumed that the guest molecules are bonded in a manner similar to that found for the alken-1-ol and 1-alkanol intercalates discussed previously.

Alcohols with terminal triple bonds (except 2-propyn-1-ol) form intercalates which are very stable in air and which contain one guest molecule per formula unit ($x = 1$). Elongating their carbon chain by one atom increases the basal spacing of the intercalate by 1.4 Å, which is more than the value corresponding to adding one carbon atom to a chain perpendicular to the host layer (1.279 Å).[20] On the other hand, the basal spacing of the 3-butyn-1-ol intercalate (9.83 Å) excludes a bimolecular arrangement with slanted alcohol chains, as two alkyl chains placed parallel with $(VOPO_4)_\infty$ sheets in the interlayer space require a basal spacing of 12 Å.[24] An alcohol with a terminal triple bond

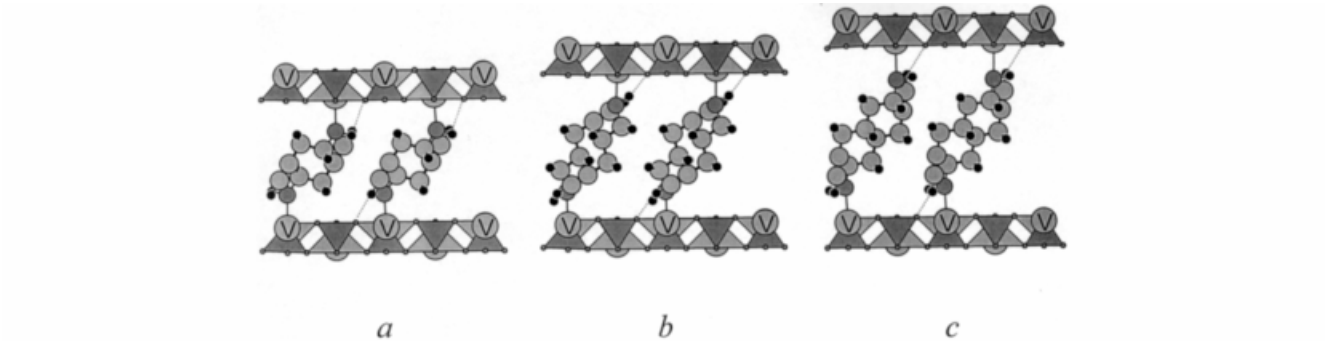

Figure 9. Proposed arrangement of 3-butyn-1-ol (a), 4-pentyn-1-ol (b) and 5-hexyn-1-ol (c) molecules between the host layers; the hydrogen bonds between the acetylenic hydrogen of the guest and O_{host} are depicted as dotted lines

must therefore be arranged in the monomolecular manner depicted in Figure 9. The alcohols with terminal triple bonds are anchored to the $(VOPO_4)_\infty$ layers in two ways. Firstly, by coordination of their O_{guest} from the OH group to V_{host}, and secondly by forming a hydrogen bond between the acidic hydrogen of the guest H−C≡C− group and O_{host} in such a way that the guest molecules generate a pillared structure similar to that found in the 1,ω-diol intercalates,[17] thus increasing the stability of the intercalate. As can be seen in Figure 9 for the 3-butyn-1-ol, 4-pentyn-1-ol and 5-hexyn-1-ol series, α increases with increasing length of the alkyl chain. This increase can be attributed to the increase of guest−guest hydrophobic interactions between the carbon chains. In the case of the 10-undecyn-1-ol intercalate, the alkyl chains are almost perpendicular ($\alpha \approx 90°$) to the host layers (see Figure 10), and the basal spacing of the intercalate is accordingly about 1 Å more than that of the 1,10-decandiol intercalate with a chain that is one carbon atom shorter. In the arrangement described above, the O_{guest} atoms are placed so that they cause a mutual shift of the neighboring host layers. This shift leads to the formation of a turbostratic structure in the intercalate, which explains the absence of (*hkl*) reflections in the diffractograms.

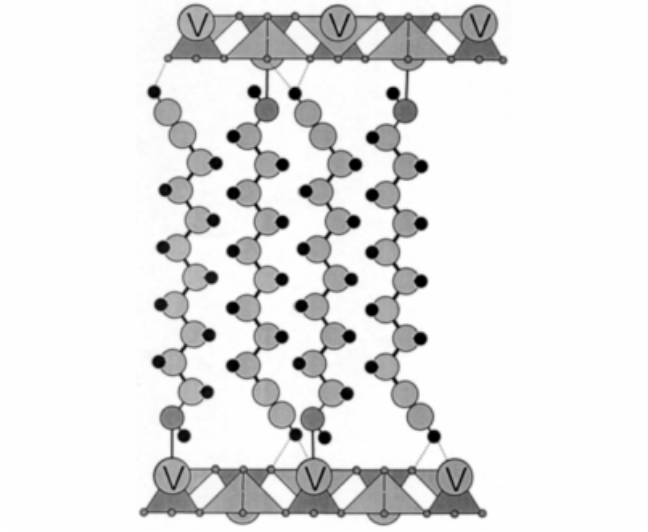

Figure 10. Proposed arrangement of 10-undecyn-1-ol molecules between the $VOPO_4$ layers; the hydrogen bonds between the acetylenic hydrogen of the guest and O_{host} are depicted as dotted lines

The intercalate with 2-propyn-1-ol has a different arrangement of the guest molecules. The number of guest molecules in the intercalate is about 1.6 molecules per vanadium atom. Accordingly, we can propose that one molecule of alcohol is anchored to the host layer by a $V_{host}-O_{guest}$ donor-acceptor bond. The guest molecules are bonded to the adjacent host layer by the hydrogen bond between the H−C≡C− group and O_{host}, as in other alcohols with terminal triple bonds.. The diffractograms of the intercalate correspond to a turbostratic structure, this means that the host layers are mutually shifted. Such an arrangement forms cavities in the interlayer space, in which other alcohol molecules can be placed (Figure 11). These molecules are bonded by hydrogen bonds both to the host layers and to neighboring coordinated alcohol molecules.

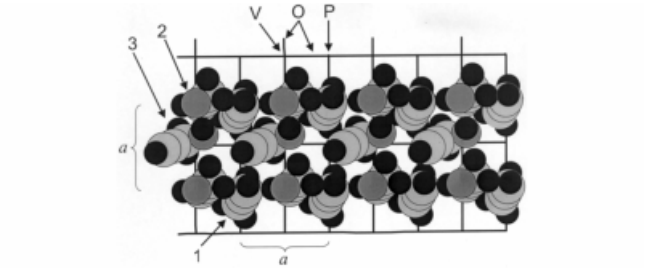

Figure 11. Arrangement of 2-propyne-1-ol molecules between the $VOPO_4$ layers viewed down the *c* axis; the upper $VOPO_4$ layer is not depicted; 1 = guest molecules coordinated to the lower host layer; 2 = guest molecules coordinated to the upper host layer; 3 = H-bonded guest molecules

Experimental Section

Preparation: Intercalates of 2-propen-1-ol, 2-propyn-1-ol and 2-buten-1-ol were prepared by suspending $VOPO_4 \cdot 2H_2O$ (0.3 g) in dry alcohol (7 mL), and subsequent short exposure (0.5−2 min) to a microwave field. Intercalates of the other unsaturated 1-alcohols were obtained by the following reintercalation reaction. The solid propanol-intercalated host ($VOPO_4 \cdot 2C_3H_7OH$) was prepared first and used as the starting material.[20] The reintercalation reactions were carried out by shaking $VOPO_4 \cdot 2C_3H_7OH$ (0.4 g) in the corresponding alcohol (5 mL) for two days. The solid product formed was filtered off. All samples for the X-ray diffraction analyses were left with a small residue of the respective alcohol. The samples for the TG-DTA and elemental analyses were washed with dry ether and dried under dry nitrogen at room temperature.

Analyses: The TGAs of the intercalates were performed with a Derivatograph MOM (Hungary), the measurements were carried out in the temperature range of 30−600 °C in air, at a heating rate of 5 °C/min. The weight of the samples was 100 mg. In some cases the composition was checked by elemental analysis (C, H).

Diffraction Measurements: The powder data of the intercalates with a minor surplus of the guest alcohol were obtained with an X-ray diffractometer (HZG-4, Freiberger Präzisionsmechanik, Germany) using Cu-$K_{\alpha 1}$ radiation (λ = 1.54051 Å) with discrimination of the Cu-K_{β} by a Ni filter. The Cu-$K_{\alpha 2}$ intensities were removed from the original data. Silicon (a = 5.43055 Å) was used as an internal standard. Diffraction angles were measured from 1.5° to 37° (2Θ). The polycrystalline sample containing an excess of the liquid guest was placed in a flat sample holder and protected against moisture by a polyethylene foil. The stability of the intercalate in air was tested by exposing it to air with ambient humidity, on a glass plate. Temperature measurements (from 22 to 240 °C) were carried out on a heated corundum plate with a thermocouple.[32] Each diffractogram was measured at constant temperature and a cycle of heating and measuring lasted about 20 min.

IR Spectra Measurements: Infrared measurements in the range 400−4000 cm^{-1} were made with a fully computerized Nicolet IMPACT 400 FTIR spectrometer (300 scans per spectrum at 2 cm^{-1} resolution). Measurements were performed in the transmission mode as KBr pellets and by the ATR technique on ZnSe crystal.[33] The spectra were corrected for the H_2O and CO_2 content in the optical path.

Raman Spectra Measurements: FT Raman spectra were collected using a Fourier transform near-infrared (FT-NIR) spectrometer Equinox 55/S (Bruker) equipped with an FT Raman module FRA 106/S (Bruker) (128 interferograms were co-added per spectrum in the range 4000−(−1000) cm^{-1} at 4 cm^{-1} resolution).

Acknowledgments

This work was supported by the Grant Agency of the Czech Republic, grant no. 203/97/1010 and the Academy of Sciences of the Czech Republic (Key Project 12).

[1] H. R. Tietze, *Aust. J. Chem.* **1981**, *34*, 2035−2038.
[2] M. Tachez, F. Theobald, J. Bernard, A. W. Hewat, *Rev. Chim. Minerale* **1982**, *19*, 291−300.
[3] A. J. Jacobson, in *Encyclopedia of Organic Chemistry* (Ed.: R. B. King), Wiley, Chichester, **1994**, Vol. 3, p. 1556.
[4] G. Lagaly, *Colloid Polym. Sci.* **1991**, *269*, 1198−1211.
[5] J. Kalousová, J. Votinský, L. Beneš, K. Melánová, V. Zima, *Collect. Czech. Chem. Commun.* **1998**, *63*, 1−19.
[6] K. Beneke, G. Lagaly, *Inorg. Chem.* **1983**, *22*, 1503−1507.
[7] L. Beneš, R. Hyklová, J. Kalousová, J. Votinský, *Inorg. Chim. Acta* **1990**, *177*, 71−74.
[8] H. Nakajima, G. Matsubayashi, *Chem. Lett.* **1993**, 423−426.
[9] N. Kinomura, T. Toyama, N. Kumada, *Solid State Ionics* **1995**, *78*, 281−286.
[10] A. De Stefanis, S. Foglia, A. A. G. Tomlinson, *J. Mater. Chem.* **1995**, *5*, 475−483.
[11] J. W. Johnson, A. J. Jacobson, J. F. Brody, S. M. Rich, *Inorg. Chem.* **1982**, *21*, 3820−3825.
[12] A. De Stefanis, A. A. G. Tomlinson, *J. Mater. Chem.* **1994**, *5*, 319−322.
[13] T. Yatabe, G. Matsubayashi, *J. Mater. Chem.* **1996**, *6*, 1849−1852.
[14] T. Yatabe, M. Nakano, G. Matsubayashi, *J. Mater. Chem.* **1998**, *8*, 699−703.
[15] L. Beneš, J. Votinský, J. Kalousová, K. Handlíř, *Inorg. Chim. Acta* **1990**, *176*, 255−259.
[16] M. Martinez-Lara, L. Moreno-Real, A. Jimenez-Lopez, S. Bruque-Gamez, A. Rodriguez-Garcia, *Mat. Res. Bull.* **1986**, *21*, 13−22.
[17] V. Zima, L. Beneš, K. Melánová, *Solid State Ionics* **1998**, *106*, 285−290.
[18] G. Matsubayashi, S. Ohta, *Chem. Lett.* **1990**, 787−790.
[19] S. Okuno, G. Matsubayashi, *Chem. Lett.* **1993**, 799−802.
[20] L. Beneš, K. Melánová, V. Zima, J. Kalousová, J. Votinský, *Inorg. Chem.* **1997**, *36*, 2850−2854.
[21] K. Melánová, L. Beneš, V. Zima, J. Kalousová, J. Votinský, *J. Incl. Phenom.* **1999**, *33*, 391−402.
[22] K. Melánová, L. Beneš, V. Zima, *J. Incl. Phenom.* **2000**, *36*, 301−309.
[23] L. Beneš, K. Melánová, V. Zima, *J. Solid State Chem.* **2000**, *151*, 225−230.
[24] K. Melánová, L. Beneš, V. Zima, R. Vahalová, M. Kilián, *Chem. Mater.* **1999**, *11*, 2173−2178.
[25] L. Beneš, J. Votinský, J. Kalousová, J. Klikorka, *Inorg. Chim. Acta* **1986**, *114*, 47−50.
[26] M. Trchová, P. Čapková, P. Matějka, K. Melánová, L. Beneš, *J. Solid State Chem.* **1999**, *148*, 197−204.
[27] R. A. Nyquist, *Spectrochim. Acta* **1971**, *27A*, 2513−2523.
[28] G. Socrates, *Infrared Characteristic Group Frequencies*, John Wiley & Sons, Chichester **1980**.
[29] R. A. Nyquist, W. J. Potts, *Spectrochim. Acta* **1960**, *16*, 419−427.
[30] S. Holly, P. Sohár, *Absorption Spectra in the Infrared Region − Theoretical and Technical Introduction*, Akadémiai Kiadó, Budapest **1975**.
[31] P. Čapková, K. Melánová, L. Beneš, H. Schenk, *J. Mol. Model.* **2000**, *6*, 9−15.
[32] L. Beneš, *Sci. Pap. Univ. Pardubice, Ser. A* **1996**, *2*, 151−155.
[33] L. Beneš, K. Melánová, M. Trchová, P. Čapková, P. Matějka, *Eur. J. Inorg. Chem.* **1999**, 2289−2294.

Received July 31, 2000
[I00301]

Multiple Oxidative Addition of $Ph_2(C_5H_4N)PSe$ to $[Ru_3(CO)_{12}]$ − Structural Characterization of $[Ru_3(\mu_3\text{-}Se)(\mu\text{-}PPh_2)_2(\mu\text{-}C_5H_4N)(\mu_3\text{-}C_5H_4N)(CO)_6]$ Containing Two Differently Metalated 2-Pyridyl Fragments

Daniele Cauzzi,[a] Claudia Graiff,[a] Chiara Massera,[a] Giovanni Predieri,*[a] and Antonio Tiripicchio[a]

Keywords: Ruthenium / Selenium / Bridging ligands / N ligands / Carbonyl complexes / Cluster compounds

The ligand $Ph_2(2\text{-}C_5H_4N)PSe$ undergoes multiple fragmentation by reaction with $[Ru_3(CO)_{12}]$ affording the 54-electron trinuclear complex $[Ru_3(\mu_3\text{-}Se)(\mu\text{-}PPh_2)_2(\mu\text{-}C_5H_4N)(\mu_3\text{-}C_5H_4N)(CO)_6]$ (**1**) which does not contain any Ru–Ru bond and is built up by a unique synergism of five bridging ligands. Complex **1** contains two bridging pyridyl groups: the first one connects two ruthenium atoms through σ bonds and lies on the plane defined by the three metals; the second one is also σ-bound to two ruthenium atoms, and is nearly perpendicular to the metal plane in such a way that it appears to be involved in a weak π interaction with the third metal.

Introduction

The chemistry of chalcogenido-carbonyl metal compounds comprises a variety of molecular architectures spanning from dinuclear metal species to giant molecular clusters.[1,2] In this context, systematic investigations carried out by our group on the reactivity of tertiary phosphane and diphosphane selenides, such as Ph_3PSe and $(Ph_2PSe)_2CH_2$ (dppmSe$_2$) towards $[M_3(CO)_{12}]$ (M = Fe or Ru) have shown that these reactions provide simple, sometimes selective synthetic routes to phosphane-substituted, selenido-carbonyl clusters.[3−5] Moreover, these processes lead in some instances to the formation of species not easily achievable by other paths, such as $[Ru_4(\mu_3\text{-}Se)_4(CO)_{10}(dppm)]$, which is the first reported 72-electrons Ru−Se cubane-like cage complex.[6]

As a natural extension of these studies, we have considered the reactions of group-8 carbonyl clusters with tertiary phosphane selenides bearing heterocyclic moieties, such as the 2-pyridyl and 2-thienyl rings. The presence of these groups was expected to lead to new reactivity patterns in cluster growing processes, owing to the coordinating ability of the heteroatoms and to the possible release of heterocyclic fragments. In fact, we have recently found that the reaction of $Ph_2(C_4H_3S)PSe$ with $[Ru_3(CO)_{12}]$ affords the open triangular 50-electron cluster $[Ru_3(\mu_3\text{-}Se)_2(CO)_7\{P(C_4H_3S)Ph_2\}_2]$ and the 48-electron cluster $[Ru_3(\mu_3\text{-}Se)(\mu\text{-}PPh_2)(\mu\text{-}C_4H_3S)(CO)_6\{P(C_4H_3S)Ph_2\}]$ derived from the multiple fragmentation of one phosphane ligand on the metal triangle.[7]

Regarding the pyridyl derivative $Ph_2(2\text{-}C_5H_4N)PSe$, its parent compound $Ph_2(2\text{-}C_5H_4N)P$ (and related ligands) has been extensively used to bridge metal centres in dinuclear and cluster species.[8−10] However, faced with $[Ru_3(CO)_{12}]$ it undergoes a P−C cleavage expelling a phenyl ring,[11] the P−C(Py) bond remaining intact. On the other hand, pyridyl fragments on ruthenium and osmium clusters have been obtained by direct reactions with pyridine and related molecules.[12−15] The organometallic chemistry of nitrogen and sulfur heterocycles is further motivated by its relevance to the hydrodenitrogenation and hydrodesulfurization processes.[16]

Results and Discussion

The reaction between $Ph_2(2\text{-}C_5H_4N)PSe$ and $[Ru_3(CO)_{12}]$ affords the products shown in Scheme 1 (carbonyls omitted), whose distribution depends on the reaction conditions. Cluster **2** [*nido* core, seven skeletal electron pairs (sep)] should be regarded as the primary product of the oxidative attack of two selenide molecules to the metal triangle, whereas cluster **3** (*closo*, 7 sep) should derive from **2** through thermal condensation and ligand exchange processes. Clusters of these two families are generally the main

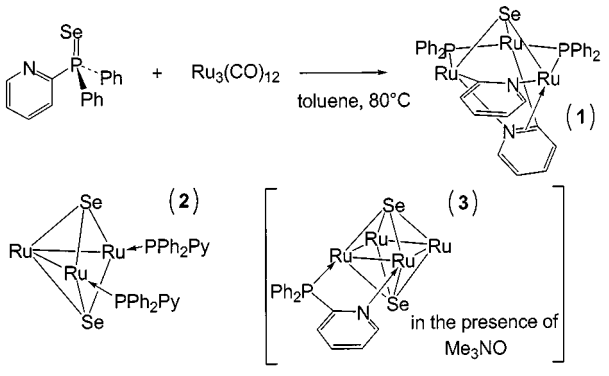

Scheme 1

[a] Dipartimento di Chimica Generale ed Inorganica, Chimica Analitica, Chimica Fisica, Università di Parma, Centro di Studio per la Strutturistica Diffrattometrica del CNR,
Parco Area delle Scienze 17/A, 43100 Parma, Italy
Fax: (internat.) +39-0521/905-557
E-mail: predieri@unipr.it

 © WILEY-VCH Verlag GmbH, 69451 Weinheim, 2001 1434−1948/01/0303−0721 $ 17.50+.50/0

products in the reactions of iron and ruthenium carbonyls with phosphane selenides.[3]

In addition, the starting triruthenium triangle undergoes multiple oxidative attack by two P−C(Py) groups, resulting in the formation of the unprecedented compound $[Ru_3(\mu_3\text{-}Se)(\mu\text{-}PPh_2)_2(\mu\text{-}C_5H_4N)(\mu_3\text{-}C_5H_4N)(CO)_6]$ (**1**), whose molecular structure is shown in Figure 1.

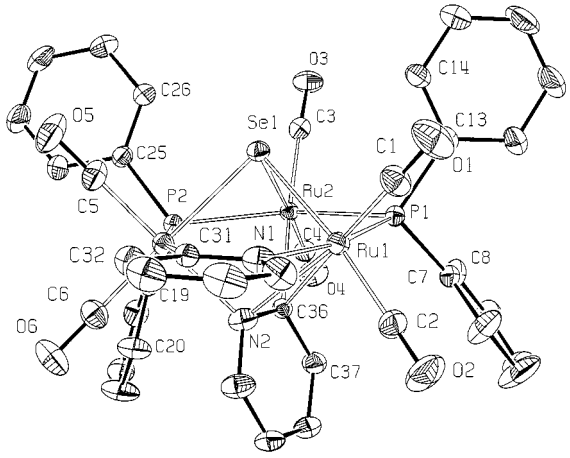

Figure 1. ORTEP diagram (30% probability level) of the molecular structure of **1** showing the atom numbering scheme; selected interatomic distances (Å): Ru(1)−Se(1) 2.515(1), Ru(1)−P(1) 2.433(1), Ru(1)−N(1) 2.173(2), Ru(1)−N(2) 2.619(3), Ru(1)−C(36) 2.822(3), Ru(2)−Se(1) 2.599(1), Ru(2)−P(1) 2.395(1), Ru(2)−P(2) 2.404(1), Ru(2)−C(36) 2.147(2), Ru(3)−Se(1) 2.550(1), Ru(3)−P(2) 2.416(1), Ru(3)−N(2) 2.171(2) Ru(3)−C(31) 2.128(2), N(1)−C(31) 1.348(3), N(2)−C(36) 1.353(3), Ru(1)···Ru(2) 3.351(1), Ru(1)···Ru(3) 3.442(1), Ru(2)···Ru(3) 3.476(1)

The structure of this polynuclear species is characterized by the presence of a nearly planar array of eleven atoms forming two roughly coplanar fused rings, i.e. the heptaatomic RuPRuPRuCN cycle and one pyridyl ring [dihedral angle 6.9(1)°]. The selenido ligand bridges three noninteracting ruthenium(II) atoms, and is elevated over the mean plane defined by the heptaatomic ring by 1.62 Å. This value is significantly lower than the mean distance of the selenium atoms from the Ru_4 plane (1.82 Å) observed in the Ru_4Se_2 octahedral clusters,[3] as a consequence of the rather large Ru···Ru spans (average 3.42 Å). This μ_3-Se bridging mode, connecting three noninteracting metal atoms, has two precedents in another trinuclear ruthenium compound containing a phosphazene ligand[17] and in a triosmium derivative.[18]

Another peculiarity of the structure of **1** is the presence of two different bridging fashions of the 2-pyridyl group. The first one [μ_2-η^1:η^1, concerning the N(1) ring] differs from those usually observed in the triangular Ru or Os clusters containing *N*-heterocyclic fragments, as these ligands currently occupy edge-bridging diaxial sites;[14] the present mode (coplanarity with the Ru_3 ensemble) is rather rare, being paralleled only by that observed in the bridged butterfly cluster $[HRu_5C(CO)_{14}(C_5H_4N)]$.[19] The second bridging mode is adopted by the N(2) ring capping the trimetallic plane opposite to the selenium atom. N(2) and C(36) are σ-bound to Ru(3) and Ru(2), respectively, in such a way that the pyridine ring is nearly perpendicular to the plane defined by the three metal atoms (74°), and seems involved in a weak π interaction with the third metal. Although this interaction with Ru(1) appears quite weak [Ru(1)−N(2) 2.619(3), Ru(1)−C(36) 2.822(3) Å], it could be required to complete the coordination sphere of Ru(1) and is suggested by the orientation of the pyridine ring. In fact, the pyridine plane is inclined towards Ru(1) with respect to the Ru(2)−Ru(3) axis by 11.0°. Moreover, if we consider that the capping pyridyl group donates two π electrons to Ru(1), the whole set of ligands contributes 30 electrons to the structure, attaining the expected count of 54 electrons. This would be an unprecedented type of bridging mode for the pyridyl group, although it has been observed with the piperidyl ligand.[20] There is one other structure where the pyridyl fragment adopts a μ_3-bridging mode, but in a η^1:η^1:η^1 fashion.[21]

As a final remark, it should be emphasized that complex **1** is built up by a unique structural synergism of five bridging ligands. It has been obtained from $Ph_2(2\text{-}C_5H_4N)PSe$ through P=Se and P−C(Py) bond cleavages, the latter process contrasting with the reactivity of $Ph_2(2\text{-}C_5H_4N)P$ towards $[Ru_3(CO)_{12}]$, which undergoes P−C(Ph) rupture,[11] as mentioned in the introduction. The different behaviour observed in this work could be due to the presence of capping selenido ligands, as observed in the case of diphenylthienylphosphane selenide.[7]

Experimental Section

General Remarks: The starting reagents $[Ru_3(CO)_{12}]$, KNCSe, $Ph_2(2\text{-}C_5H_4N)P$ and Me_3NO are pure commercial products (Aldrich and Fluka) and were used as received. The solvents (C. Erba) were dried and distilled by standard techniques before use. All manipulations (prior to the TLC separations) were carried out under dry nitrogen by means of standard Schlenk techniques. Elemental (C, H, N) analyses were performed with a Carlo Erba EA 1108 automated analyzer. IR spectra (KBr discs or CH_2Cl_2 solutions) were recorded on a Nicolet 5PC FT spectrometer. ^1H (300 MHz), ^{31}P (81.0 MHz, 85% H_3PO_4 as external reference) NMR spectra ($CDCl_3$ solutions) were recorded on Bruker instruments, AC 300 (^1H) and CXP 200 (^{31}P).

Synthesis of $Ph_2(2\text{-}C_5H_4N)PSe$: A large excess of KNCSe (1.50 g, 10.4 mmol) was added to an acetonitrile (150 mL) solution of diphenyl-2-pyridylphosphane (0.70 g, 2.7 mmol); the solution was stirred at room temperature for 3 h, then the solvent was removed in vacuo and the residue was washed with water. The rough powder was recrystallized from ethanol, obtaining a white microcrystalline product (yield 85%). $C_{17}H_{14}PNSe$ (342.24): calcd. C 56.7, H 4.1, N 4.1; found C 57.2, H 3.9, N 4.0. − FTIR (KBr): $\tilde{\nu}$ = 569 cm^{-1} (PSe). − ^{31}P NMR ($CDCl_3$): δ = 31.5 [s, ^1J(P,Se) = 720 Hz]. − ^1H NMR ($CDCl_3$): δ = 8.71 [d, ^3J(H,H) = 4 Hz, 1 H, 6-Py], 8.61 [t, ^3J(H,H) = ^3J(H,P) = 6 Hz, 1 H, 3-Py], 7.92−7.34 (mm, 12 H, 2Ph, Py).

Reactions of $Ph_2(C_5H_4N)PSe$ with $[Ru_3(CO)_{12}]$: $[Ru_3(CO)_{12}]$ (150 mg, 0.235 mmol) was reacted 1:2 with $Ph_2(C_5H_4N)PSe$ (161 mg, 0.469 mmol) in toluene at 70 °C for 1 h until the solution turned deep reddish brown. The mixture was evaporated to dryness and the residue was redissolved in a small amount of dichloromethane. TLC separation on silica, with a 1:1 dichloromethane/hexane as

eluent mixture, yielded three products: a red band, a light orange one and a reddish orange one, in order of elution. Two trace products and some decomposition were also observed. The first product was identified as **1** after the solution of its crystal structure (yield 12%). The third reddish orange derivative was identified as $[Ru_3Se_2(CO)_7\{P\text{-}P(C_5H_4N)Ph_2\}_2]$ (**2**) by comparison of its ^{31}P NMR and FT-IR spectra with those of the related cluster $[Ru_3Se_2(CO)_7(PPh_3)_2]$[22] (yield 32%). The identity of the second product is under investigation. Compound **1**: FTIR (CH_2Cl_2): $\tilde{\nu}$ = 2021 s (CO), 2013 sh, 1964 s cm^{-1}. – $^{31}P\{^1H\}$ NMR ($CDCl_3$, 25 °C): δ = 49.0 (d), −18.6 [d, ^2J(P,P) = 166 Hz]. – ^1H NMR ($CDCl_3$, 25 °C): δ = 8.52 [d, ^3J(H,H) = 6 Hz, 1 H Py], 7.91−6.62 (m, 13 H, 2Ph, Py).

The same 1:2 reaction was carried in the presence of Me_3NO (18 mg, 0.24 mmol) and gave a deep red solution; it was processed as in the previous case, yielding, in order of elution, **1** (10%), $[Ru_4Se_2(CO)_9(\mu\text{-}P,N\text{-}Ph_2(C_5H_4N)P)]$ (**3**) (light orange 22%) and **2** (7%), along with an unidentified species and some decomposition. Cluster **3** was identified by comparison of its IR spectral data with those of the analogous dppm derivative.[4] Purification by crystallization (from a CH_2Cl_2/MeOH mixture at 5 °C for some days) gave well-formed crystals of **1** suitable for X-ray analysis.

X-ray Structural Analysis: Cluster **1**, $C_{40}H_{28}N_2O_6P_2Ru_3Se$, M = 1076.75 triclinic, space group $P\bar{1}$, a = 16.619(4) Å, b = 12.494(3) Å, c = 10.214(5) Å, α = 98.49(4)°, β = 111.28(6)°, γ = 106.70(2)°, V = 2000(1) Å^3, Z = 2, D_c = 1.788 g·cm^{-3}, F(000) = 1052, graphite monochromated Mo-K_α radiation, λ = 0.71073 Å, μ = 21.56 cm^{-1}. Philips PW 1100 diffractometer, θ−2θ scan technique at room temperature. 11672 Unique reflections measured (with θ in the range 3−30°) and used in the refinement. The structure was solved by Patterson and Fourier methods and refined by full-matrix least-squares procedures (based on F_o^2), using the SHELX-97 system of crystallographic computer programs.[23] All non-hydrogen atoms were refined anisotropically; all hydrogen atoms were placed at their geometrically calculated positions and refined riding on their parent atoms; final wR_2 = 0.0688 and R_1 [for 8871 reflections with $I > 2\sigma(I)$] 0.0272; weighting scheme used in the last cycles of refinement $w = 1/[\sigma^2F_o^2 + (0.0365\ P)^2]$, where $P = (F_o^2+2F_c^2)/3$. Crystallographic data (excluding structure factors) for the structure(s) included in this paper have been deposited with the Cambridge Crystallographic Data Centre as supplementary publication no. CCDC-147775. Copies of the data can be obtained free of charge on application to CCDC, 12 Union Road, Cambridge CB2 1EZ, UK [Fax: (internat.) + 44-1223/336-033; E-mail: deposit@ccdc.cam.ac.uk].

Acknowledgments

Financial support from the Ministero dell'Università e della Ricerca Scientifica e Tecnologica (Rome, Cofin 98) is gratefully acknowledged. The facilities of the Centro Interdipartimentale di Misure "G. Casnati" (Università di Parma) were used to record the NMR and mass spectra.

[1] L. C. Roof, J. W. Kolis, *Chem. Rev.* **1993**, *93*, 1037.
[2] D. Fenske, in *Clusters and Colloids* (Ed.: G. Schmidt), VCH, Weinheim, **1994**, p. 212.
[3] D. Cauzzi, C. Graiff, G. Predieri, A. Tiripicchio, in *Metal Clusters in Chemistry* (Eds.: P. Braunstein, L. Oro, P. Raithby), VCH, Weinheim, **1999**, vol 1, p. 193.
[4] D. Cauzzi, C. Graiff, G. Predieri, A. Tiripicchio, C. Vignali, *J. Chem. Soc., Dalton Trans.* **1999**, 237.
[5] D. Cauzzi, C. Graiff, C. Massera, G. Predieri, A. Tiripicchio, D. Acquotti, *J. Chem. Soc., Dalton Trans.* **1999**, 3515.
[6] D. Cauzzi, C. Graiff, M. Lanfranchi, G. Predieri, A. Tiripicchio, *J. Chem. Soc., Dalton Trans.* **1995**, 2321.
[7] D. Cauzzi, C. Graiff, C. Massera, G. Predieri, A. Tiripicchio, *Inorg. Chim. Acta* **2000**, *300−302*, 471.
[8] A. J. Deeming, M. B. Smith, *J. Chem. Soc., Chem. Commun.* **1993**, 844.
[9] C. G. Arena, D. Drommi, F. Faraone, M. Lanfranchi, F. Nicolò, A. Tiripicchio, *Organometallics* **1996**, *15*, 3170.
[10] N. D. Jones, K. S. MacFarlane, M. B. Smith, R. P. Schutte, S. J. Rettig, B. R. James, *Inorg. Chem.* **1999**, *38*, 3956, and references therein.
[11] N. Lugan, G. Lavigne, J.-J. Bonnet, *Inorg. Chem.* **1987**, *26*, 585.
[12] C. Choo Yin, A. J. Deeming, *J. Chem. Soc., Dalton Trans.* **1975**, 2091.
[13] P. F. Jackson, B. F. G. Johnson, J. Lewis, W. J. H. Nelson, M. McPartlin, *J. Chem. Soc., Dalton Trans.* **1982**, 2099.
[14] M. P. Cifuentes, M. G. Humphrey, B. W. Skelton, A. H. White, *J. Organomet. Chem.* **1996**, *513*, 201
[15] A. J. Deeming, M. J. Stchedroff, C. Whittaker, A. J. Arce, Y. De Sanctis, J. W. Steed, *J. Chem. Soc., Dalton Trans.* **1999**, 3289.
[16] R. Prins, in *Handbook of Heterogeneous Catalysis* (Eds.: G. Ertl, H. Knözinger, J. Weitkamp), VCH, Weinheim, **1997**, vol. 4, p. 1908.
[17] A. M. Z. Slawin, M. B. Smith, J. D. Woollins, *Chem. Commun.* **1996**, 2095.
[18] A. J. Arce, P. Arrojo, A. J. Deeming, Y. De Sanctis, *J. Chem. Soc., Chem. Commun.* **1991**, 1491.
[19] G. Conole, M. McPartlin, H. R. Powell, T. Dutton, B. F. G. Johnson, J. Lewis, *J. Organomet. Chem.* **1989**, *379*, C1.
[20] M. P. Cifuentes, M. G. Humphrey, B. W. Skelton, H. White, *J. Organomet. Chem.* **1993**, *458*, 211.
[21] C. J. Adams, M. I. Bruce, B. W. Skelton and A. H. White, *J. Organomet. Chem.* **1993**, *445*, 211.
[22] P. Baistrocchi, D. Cauzzi, M. Lanfranchi, G. Predieri, A. Tiripicchio, M. Tiripicchio Camellini, *Inorg. Chim. Acta* **1995**, *235*, 173.
[23] G. M. Sheldrick, *SHELX-97, Program for the Solution of Crystal Structures*, University of Göttingen, **1997**.

Received August 4, 2000
[I00305]

Symmetric and Non-Symmetric Dinuclear Alkenyl-Bridged Carbene Complexes of Chromium and Tungsten

Karine Ulrich,[a] Véronique Guerchais,[a] Karl-Heinz Dötz,[b] Loic Toupet,[c] and Hubert Le Bozec*[a]

Keywords: Binuclear complexes / Carbenes / Bridging ligands / Chromium / Tungsten

Treatment of $(CO)_5W{=}C(NMe_2)CH{=}CH{-}Ar{-}(OH)(H)C{\equiv}CH$ (**1a–b**) [**a**: $-Ar-$ =1,4-C_6H_4–; **b**: $-Ar-$ = 2,5-C_4H_2S–] with $W(CO)_5$(THF) in methanol yields the nonsymmetrical bis(alkenylcarbene)-bridged ditungsten complexes $(CO)_5W{=}C(NMe_2)CH{=}CH{-}Ar{-}CH{=}CH(OMe)C{=}W(CO)_5$ (**3a–b**). Similarly, the symmetrical bis(methoxycarbene)ditungsten derivative $[(CO)_5W{=}C(OMe)CH{=}CH{-}]_2$(1,4-$C_6H_4$–) (**4a**) is obtained in a low yield from the precursor $(CO)_5W{=}C(OMe)$-$CH{=}CH{-}C_6H_4{-}(OH)(H)C{\equiv}CH$ (**2a**). Complexes **3a** and **3b** undergo aminolysis reactions with diamines such as piperazine and ethylenediamine to produce the corresponding bis[alkenyl(amino)carbene]ditungsten complexes **5a–b** and **6a–b**. The reaction of **1a** with $Cr(CO)_5$(THF) affords the heterobimetallic (W–Cr) bis(carbene) complex $(CO)_5W{=}C(NMe_2)CH{=}CH{-}Ar{-}CH{=}CH(OMe)C{=}Cr(CO)_5$ (**3′a**). This complex, as well as the bis(methoxycarbene) derivative **4′a**, can also be obtained by treatment of $(CO)_5W{=}C(XR)CH{=}CH{-}C_6H_4{-}CHO$ [**1c**: XR = NMe_2; **2c**: XR = OMe] with $(CO)_5Cr{=}C(OMe)CH_2^-Li^+$. All the new compounds have been characterized by analytical and spectroscopic methods, and the single-crystal structures of **3a**, **4a–b**, and **4′a** have been established.

Introduction

During the last decade, binuclear transition-metal complexes with unsaturated organic spacers such as polyynes have been the subject of considerable investigations due to their potential applications in molecular electronics or nonlinear optics.[1,2] A wide range of bis(carbene) complexes have also been reported. Thus, symmetrical bis(carbene) complexes of Groups 6 and 7 metals containing aryl[3,4] and thienyl[5,6] bridges are accessible from dilithiated aromatic precursors by the classic Fischer method. A series of alkenyl- or polyenyl-bridged bis(carbene) complexes have been prepared either by condensation reactions of dialdehydes with the methyl group of (alkoxy)methylcarbene complexes,[7,8,9] or by oxidative coupling of $[M]{=}C(OR)CH_2Li$.[10,11] The synthesis of a symmetrical bis(carbene) complex with an ammonium pentadienide bridge has also been described.[12] The formation of bis(aminocarbene)-dichromium complexes[13] has been achieved by reaction of arylbis(amides) with $Cr(CO)_5^{2-}$. Recently, H. Fischer et al. reported an efficient synthesis of symmetrically substituted alkynediyl-bridged aminocarbene complexes by Pd coupling of two $(CO)_5M{=}C(NR_2)(C{\equiv}C)_n$ units (n = 1,2,3).[14] The same precursors were also used to prepare polynuclear complexes of the type $[(CO)_5M{=}C(NR_2)(C{\equiv}C)]_xM'L_n$.[15] By contrast, nonsymmetrical bis(carbene) complexes are scarce. A bis(aminocarbene)chromium−iron complex has been prepared in two steps by the reaction of a diamide with $Cr(CO)_5^{2-}$and $Fe(CO)_4^{2-}$.[13] An ethyne-bridged (alkoxycarbene)(aminocarbene)ditungsten complex was also recently obtained by the Fischer route starting from an ethynylcarbene complex.[14] We have previously described a convenient route to alkenyl(alkoxy)- and -(amino)carbene complexes of Groups 6 and 8 metals, by activation of propargyl alcohol derivatives.[16,17] With the use of dialkynols, this procedure was recently applied to the synthesis of alkenylcarbene complexes **I** containing a free propargyl alcohol substituent (Scheme 1).[18] In this paper we report a new synthetic route to a series of dinuclear π-conjugated bridged carbenechromium(0) and -tungsten(0) complexes. We show that this methodology, which is based on the sequential activation of dialkynols, opens the route to nonsymmetrical bis(carbene) complexes **II**. Preliminary results of this work have already been reported.[19]

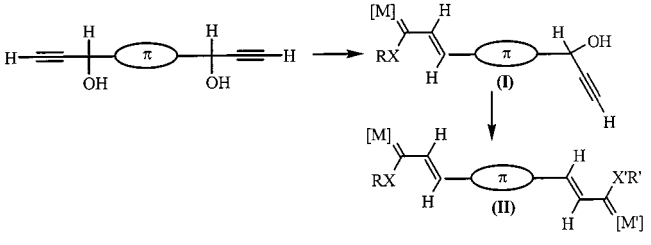

Scheme 1

[a] UMR 6509 CNRS-Université de Rennes 1, Organométalliques et Catalyse, Université de Rennes 1, Campus de Beaulieu, 35042 Rennes Cedex, France
E-mail: lebozec@univ-rennes1.fr
[b] Kekulé-Institut für Organische und Biochemie der Rheinischen Friedrich-Wilhelms-Universität, 53121 Bonn, Germany
[c] UMR 6626 CNRS − Université de Rennes 1, Groupe Matière Condensée, Université de Rennes 1, Campus de Beaulieu, 35042 Rennes Cedex, France

 © WILEY-VCH Verlag GmbH, 69451 Weinheim, 2001 1434−1948/01/0303−0725 $ 17.50+.50/0

Results and Discussion

Synthesis of Bis(carbene)-Bridged Ditungsten Complexes

When solutions of the [alkenyl(dimethylamino)carbene]-tungsten complex **1a** and of the photogenerated $W(CO)_5(THF)$ adduct in methanol/tetrahydrofuran were combined at room temperature, the color gradually changed from red to dark red. The reaction proceeded rather slowly and required 3 d for completion. The bimetallic complex **3a** was obtained in a 60% yield after chromatographic workup (Scheme 2). Under similar conditions, the symmetrical binuclear bis(methoxycarbene) derivative **4a** was isolated from **2a** in a lower yield (30%) as violet microcrystals. This latter complex was already obtained as a by-product (9%) during the synthesis of **2a** from the dialkynol 1,4-[H−C≡CH(OH)]C_6H_4.[18]

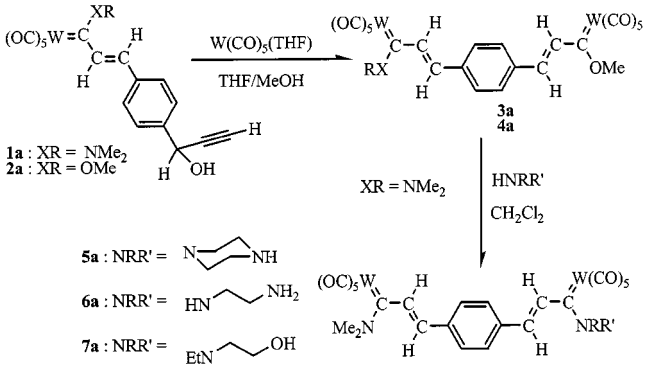

Scheme 2

The same protocol was applied to **1b** to prepare the thienyl-bridged bimetallic complex **3b** in a 61% yield (Scheme 3). The new complexes **3a** and **3b** were unequivocally characterized by means of standard spectroscopic techniques (IR, ^1H and $^{13}C\{^1H\}$ NMR). The structures of **3a**, the symmetrical bis(methoxycarbene) derivative **4a** and its thienyl analog **4b**[18] were also confirmed by X-ray diffraction studies (vide supra). The stereoselective formation of the new CH=CH bond was easily deduced by the coupling constants, $^3J_{H\text{-}H} \approx 16-17$ Hz, which is indicative of an (*E*) configuration. For each alkenyl fragment, the ^1H and ^{13}C shifts of the β-proton and β-carbon atom appear upfield from the shift of the α-proton and α-carbon atom, respectively (Table 1). This trend was previously observed for monometallic alkenyl(alkoxy)- and -(amino)carbene complexes.[16,20] The ^1H and ^{13}C NMR spectra show two N*Me* signals as expected by the restricted rotation around the C(carbene)−NMe_2 bond. The ^{13}C NMR spectra also display two carbene resonances at $\delta \approx 300$ and 250, in the range characteristic for (alkoxycarbene)- and (aminocarbene)tungsten complexes, respectively. Thus, these data suggest that there is apparently no π delocalization occurring along the alkenyl bridges, in contrast to the recently described π-conjugated ethyne-bridged bis(carbene) complex $(CO)_5W{=}C(NMe_2){-}C{\equiv}C{-}(OMe){=}W(CO)_5$ where the carbene resonances were found shifted upfield by more than 60 ppm [δ = 235.9 and 181.7].[14]

Complexes **3a** and **3b** could be easily transformed into bis(aminocarbene) complexes by the classical aminolysis route. For example, addition of excess of piperazine, ethylenediamine or 2-(ethylamino)ethanol (3−5 equiv.) in dichloromethane at room temperature led to the isolation of the bis(aminocarbene) complexes **5a−b**, **6a−b** [(*E*)/(*Z*) ≈ 9:1], or **7a** in good yields (Scheme 2 and Scheme 3).

Spectroscopic data clearly reveal the presence of two alkenyl(amino)carbene fragments (see Table 1 and Exp. Sect.). We note in particular the presence of two characteristic low-field singlet resonances for the carbene carbon atoms (δ ≈ 250). As these complexes contain a free amine site, a second aminolysis reaction was attempted in order to prepare tetrametallic tetrakis(aminocarbene) complexes. However, after stirring a 1:1 mixture of **6b** and **3a** in dichloromethane at room temperature, no reaction occurred, even after 1 d. The starting complexes were recovered.

Synthesis of Bis(carbene)-Bridged Tungsten−Chromium Complexes

Treatment of **1a** with $Cr(CO)_5(THF)$ at room temperature, and after 18 h of stirring, afforded the new heterobimetallic (W−Cr) bis(carbene) complex **3′a** in a modest yield, up to 30% (Scheme 4). Prolonged reaction times were found to decrease the yield. This observation reflects the reduced thermal stability of both $Cr(CO)_5(THF)$ and **3′a**, which slowly decompose in solution. Efforts to prepare the analogous bis(methoxycarbene) complex **4′a** starting from the less reactive compound **2a** failed.

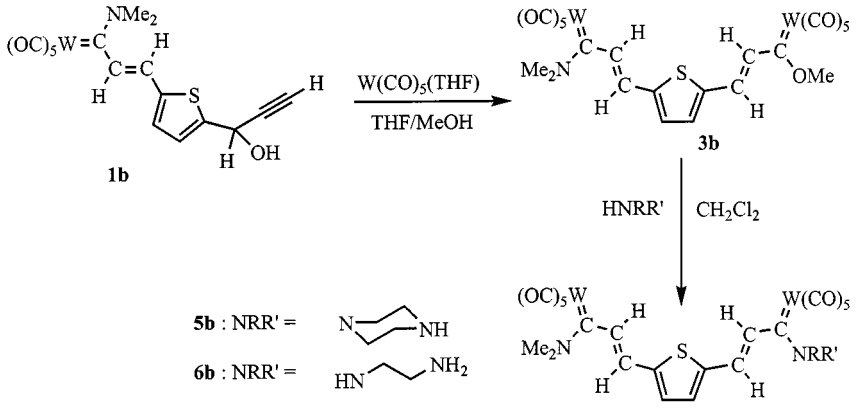

Scheme 3

Table 1. Selected ^1H and ^{13}C NMR spectroscopic data for the bimetallic complexes in $CDCl_3$

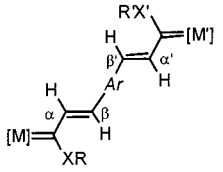

Complex	M	XR	M′	X′R′	−*Ar*−	M=C	M′=C	$C_{\alpha,\alpha'}$ ($H_{\alpha,\alpha'}$)	$C_{\beta,\beta'}$ ($H_{\beta,\beta'}$)
4a	$W(CO)_5$	OMe	$W(CO)_5$	OMe	$-C_6H_4-$	307.0	−	144.2 (7.85)	131.8 (7.10)
4b	$W(CO)_5$	OMe	$W(CO)_5$	OMe	$-C_4H_2S-$	304.2	−	143.6 (7.68)	134.7 (7.22)
−[a]	$Cr(CO)_5$	OMe	$Cr(CO)_5$	OMe	$-C_6H_4-$	333.4	−	140.0 (7.95)	127.4 (6.90)
3a	$W(CO)_5$	OMe	$W(CO)_5$	NMe_2	$-C_6H_4-$	306.5	252.1	143.3 (7.81), 139.6 (7.05)	133.3 (7.12), 122.0 (5.86)
3b	$W(CO)_5$	OMe	$W(CO)_5$	NMe_2	$-C_4H_2S-$	303.1	250.9	139.8 (7.56), 135.4 (6.90)	135.2 (7.28), 117.3 (6.11)
4′a	$W(CO)_5$	OMe	$Cr(CO)_5$	OMe	$-C_6H_4-$	306.9	333.4	144.2 (7.89), 140.0 (7.97)	131.9 (7.12), 127.4 (6.85)
3′a	$Cr(CO)_5$	OMe	$W(CO)_5$	NMe_2	$-C_6H_4-$	332.7	252.3	139.5 (7.93), 139.3 (7.09)	128.6 (6.92), 121.9 (5.93)

[a] Ref.[18]

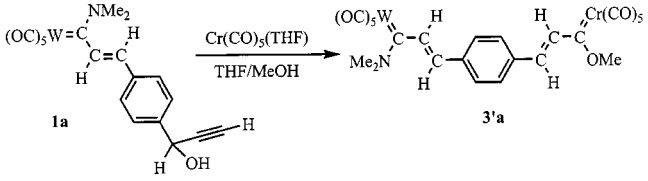

Scheme 4

An alternative synthetic approach to **3′a** and **4′a** is the use of the Aumann's procedure which allows the condensation of aldehydes with the Fischer-type (methoxy)methylcarbene derivative $(CO)_5Cr{=}C(OMe)Me$.[7] The [alkenyl(methoxy)carbene]tungsten complex **2c**, containing a *p*-phenylaldehyde group, was generated in a 40% yield on activation of the propargyl alcohol derivative **c** with $W(CO)_5(THF)$. Subsequent addition of dimethylamine afforded, almost quantitatively, the corresponding (dimethylamino)carbene complex **1c** (Scheme 5).

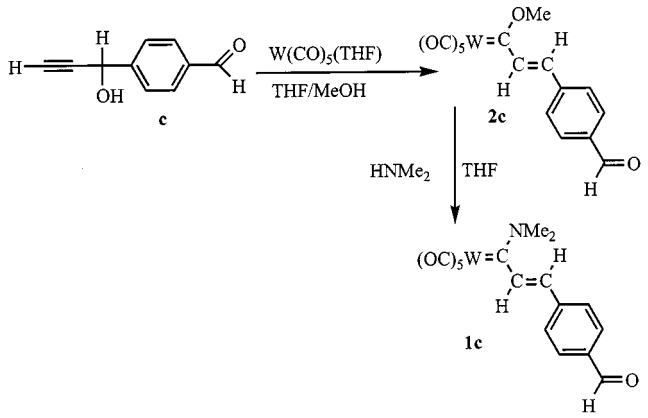

Scheme 5

When complex **2c** was combined with $(CO)_5Cr{=}C(OMe)Me$ and treated with Et_3N/Me_3SiCl the heterobimetallic complex **4′a** was obtained in a 33% yield after chromatographic workup (Scheme 6). The same route was also employed for the synthesis of **3′a**, but the isolated yield was lower (20%).

Spectroscopic data are in agreement with the proposed nonsymmetric structures. The ^1H NMR spectrum of **4′a** exhibits two singlets for the two nonequivalent O*Me* groups, and two AB systems for the α,β- and α′,β′-alkenyl protons, respectively. The ^{13}C NMR spectrum consists of distinct signals for the two alkenyl and methoxy carbon atoms, and the carbene resonances are found in the range typical for [(methoxy)carbene]chromium and -tungsten. The unsymmetrical alkenyl-bridged [(dimethylamino)carbene](methoxycarbene) complex **3′a** also exhibits two distinct sets of proton and carbon atom resonances (Table 1 and Exp. Sect.).

Molecular Structures of 3a, 4a, 4b, and 4′a

The structures of the carbene complexes **3a**, **4a**, **4b**, and **4′a** were determined by single-crystal X-ray diffraction. The molecular structures are displayed in Figures 1−4. Selected bond lengths and angles are listed in Table 2. In all cases, the environment about the metal atoms is octahedral. The (*E*) configuration of the alkenyl double bond in these molecules was confirmed. Moreover, in all cases the carbon chain adopts a *s-trans* stereochemistry with respect to the $C_{carb}-C_\alpha$ bond.

Structure of 4b

The two "$W(CO)_5$" fragments are on the same side of the thiophene bridge, a feature already observed for the dinuclear chromium complex $[Cr(CO)_5(=C(OEt)-]_2(C_4H_2S)$ (Figure 1).[5] However, by contrast to the latter species, the sulfur atom of the ring in **4b** is directed towards the metal units. The W=C bond length [2.166(9) Å] is similar to that found in other W−(alkoxycarbene) complexes.[21] The C−C and S−C bond lengths of the thiophene ring [1.360(12), 1.365(12), 1.368(12); 1.713(9), and 1.719(9) Å] compare well with those of thiophene-containing complexes.[5,22,23] The

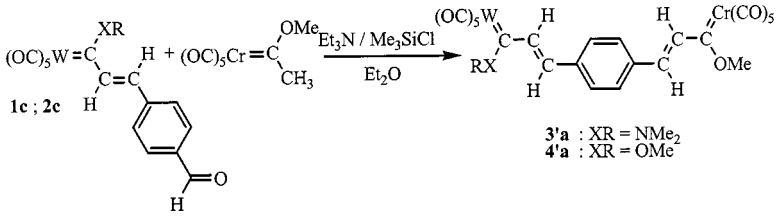

Scheme 6

Table 2. Selected bond lengths [Å] and angles [°] for **4b**,**4a**, **3a**, and **4′a**

4b		**4a**		**3a**		**4′a**	
W1−C7	2.166(9)	W1−C7	2.165(6)	W1−C6	2.256(7)	W(Cr)−C7	2.111(6)
W2−C16	2.190(8)	C7−C8	1.464(7)	W2−C19	2.181(7)	C7−C8	1.438(8)
C7−C8	1.435(11)	C8−C9	1.320(7)	C6−C9	1.489(10)	C8−C9	1.333(8)
C8−C9	1.336(13)	C9−C10	1.433(7)	C9−C10	1.315(10)	C9−C10	1.452(8)
C9−C10	1.453(11)	C7−O6	1.329(7)	C10−C11	1.463(10)		
C13−C14	1.440(12)			C19−C18	1.472(10)		
C14−C15	1.349(12)			C18−C17	1.315(10)		
C15−C16	1.455(11)			C17−C14	1.444(10)		
S1−C10	1.713(9)			C6−N	1.315(9)		
S1−C13	1.719(9)			C19−O6	1.309(9)		
W1−C7−O6	130.6(6)	W1−C7−O6	131.0(4)	W1−C6−N1	130.7(5)	W(Cr)−C7−O6	130.7(4)
W1−C7−C8	121.0(6)	W1−C7−C8	121.2(4)	W1−C6−C9	113.6(5)	W(Cr)−C7−C8	121.3(5)
C7−C8−C9	125.2(8)	C7−C8−C9	124.2(5)	N1−C6−C9	115.7(7)	C7−C8−C9	124.5(6)
O6−C7−C8	108.4(7)	O6−C7−C8	107.8(5)	W2−C19−O6	131.8(5)	O6−C7−C8	107.9(5)
W2−C16−O7	130.6(6)			W2−C19−C18	120.0(5)		
W2−C16−C15	119.6(6)			O6−C19−C18	108.2(6)		
C16−C15−C14	122.6(8)						
O7−C16−C15	109.8(7)						

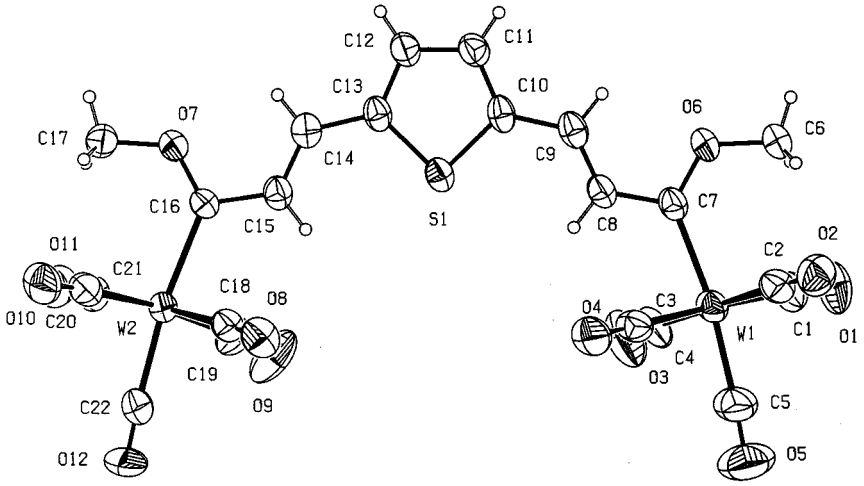

Figure 1. Molecular structure of $(CO)_5W{=}C(OMe)CH{=}CH{-}C_4H_2S{-}CH{=}CH(OMe)C{=}W(CO)_5$ (**4b**)

pattern of bond lengths in **4b** [W−C7 2.166(9), C7−C8 1.435(11), C8−C9 1.336(13), C9−C10 1.453(11) Å], indicates a limited π delocalization in the ground state.[24] Remarkably, the thiophene ring, the alkenyl, the carbene carbon and the tungsten atoms are in a plane (mean deviation from the plane 0.06 Å).

Structure of Complexes 4a, 3a, and 4′a

As observed in **4b**, in all cases the two metal units are in a *cis* configuration with respect to the benzene ring. The W=C(O) bond length [2.165(6) Å] in **4a** (Figure 2) is normal. The alkenyl portion in **4a** exhibits an alternating C−C single-bond, double-bond, and single-bond sequence [1.464(7), 1.320(7), 1.433(7) Å].

Complex **3a** (Figure 3) exhibits a W=C(N) distance of 2.256(7) Å, which is rather long relative to that of typical aminocarbene complexes [W−C 2.186(22) Å in $(CO)_5W{=}C(NHMe)Ph)$].[25,26] The C(carbene)−N bond [1.315(9) Å] is somewhat short indicating a double-bond character.[14] These values compare well with those reported for

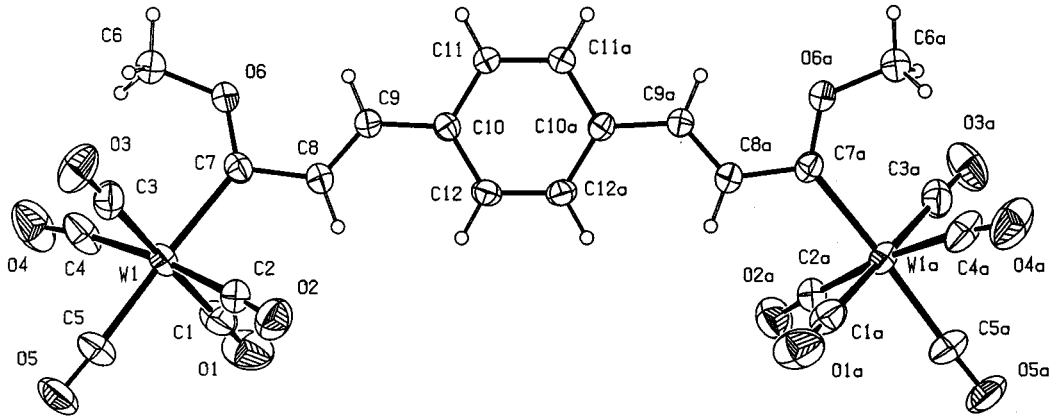

Figure 2. Molecular structure of $(CO)_5W{=}C(OMe)CH{=}CH{-}C_6H_4{-}CH{=}CH(OMe)C{=}W(CO)_5$ (**4a**)

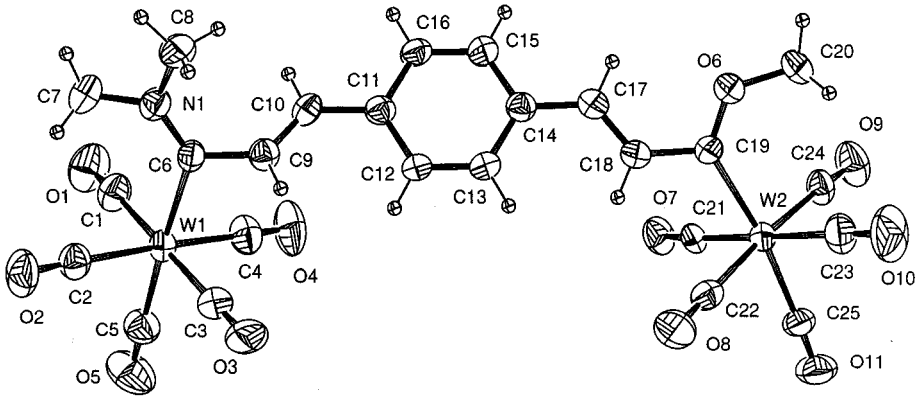

Figure 3. Molecular structure of $(CO)_5W{=}C(NMe_2)CH{=}CH{-}C_6H_4{-}CH{=}CH(OMe)C{=}W(CO)_5$ (**3a**)

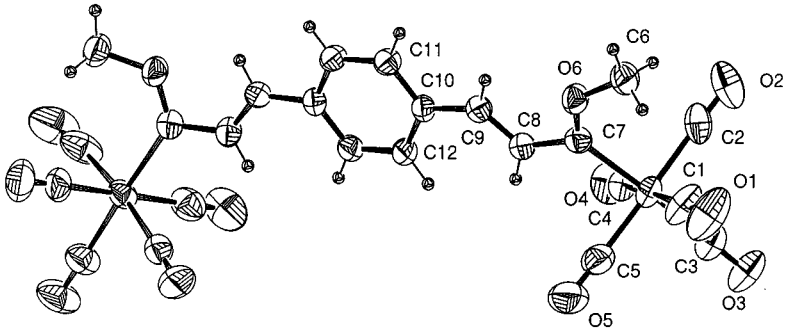

Figure 4. Molecular structure of $(CO)_5W{=}C(OMe)CH{=}CH{-}C_6H_4{-}CH{=}CH(OMe)C{=}Cr(CO)_5$ (**4′a**)

$(CO)_5W{=}C(NMe_2){-}(NMe_2)C{=}W(CO)_5$ [W=C 2.295(7), 2.281(7); C_{carb}–N 1.310(8), 1.314(9) Å],[14] $[(CO)_5W{=}C(NMe_2)C{\equiv}C{-}Hg{-}C{\equiv}CC(NMe_2){=}W(CO)_5]$, and $[(CO)_5W{=}C(NMe_2)C{\equiv}C{-}TiCp_2{-}C{\equiv}CC(NMe_2){=}W(CO)_5]$.[15] This is consistent with the magnetically nonequivalent methyl substituents in the NMR spectra. The W–C(O) distance [2.181(7) Å] is in the range of that of the above structures. As for **4a**, the C–C bond chain is alternated [1.489(10), 1.315(10), 1.463(10); 1.472(10), 1.315(10), 1.444(10) Å]. The bridging carbon chain is planar (mean deviation from the plane 0.087 Å); however, the two metal units deviate from this plane by 23° and 65° for the C(alkoxy)- and C(amino)carbene parts, respectively.

The molecular structure of the heterodimetal (Cr–W) complex **4′a** (Figure 4) is disordered for the metal positions (W,Cr), a feature which is also observed for $(CO)_5Cr\{{=}C(COMe)CH_2CH_2C(OMe)C{=}\}W(CO)_5$.[27] It is worth noting that the orientation of the aromatic ring contrasts with that in the (Cr–Fe) complex $[(CO)_5Cr\{{=}C(NMe_2)(m\text{-}C_6H_4)C(NMe_2){=}\}Fe(CO)_4]$ in which the phenyl bridge is perpendicular to the plane of the metal–carbene bond.[13]

Conclusion

This study shows that binuclear alkenylcarbene-bridged complexes can be conveniently prepared by sequential activation of bis(propargyl alcohol) derivatives. This route allows the synthesis of nonsymmetrical bis(carbene) complexes containing either two different tungsten–carbene fragments (amino- and alkoxycarbene) or two different me-

tallic centers (Cr and W). This opens up an entry to novel "push-pull" heterobimetallic bis(carbene) compounds, for instance with Groups 6 and 8 metals since they are both known to activate propargyl alcohols. Moreover, the reactivity of alkenylcarbene complexes is known to depend on the nature of the metal (Cr vs. W) and the substituent (alkoxy vs. amino) in typical reactions such as annulations and Diels−Alder cycloadditions. Studies on the reactivity of our nonsymmetric complexes, particularly with regard to the ability to discriminate the two metal−carbene fragments, are in progress.

Experimental Section

General: All manipulations were carried out under argon with Schlenk techniques. Solvents were dried and distilled before use by standard techniques. − NMR spectra were recorded with Bruker DPX-200 and Bruker AM-300 spectrometers. − Infrared spectra were obtained with a Nicolet FT-IR spectrometer. − High resolution mass spectra were obtained with Varian MAT 311 and Micromass ZABSpec TOF spectrometers at the C.R.M.P.O., University of Rennes 1. − Microanalyses were performed by the "Centre de Microanalyse du CNRS" at Vernaison, France.

Procedures for the Preparation of Bis(carbene)-Bridged Ditungsten Complexes

$(CO)_5W{=}C(NMe_2)CH{=}CH{-}C_6H_4{-}CH{=}CH(MeO)C{=}W(CO)_5$ (3a): A solution of $W(CO)_6$ (0.421 g, 1.2 mmol) in 60 mL of THF was irradiated for 6 h at room temperature by using a Rayonet and a Pyrex photochemical reactor. The yellow solution of $W(CO)_5$(THF) was then transferred into a Schlenk flask containing a solution of **1a** (0.537 g, 1 mmol) in 30 mL of methanol. The reaction mixture was stirred for 3 d at room temperature. After evaporation of the solvent under vacuum, the red residue was chromatographed on silica gel. Elution with dichloromethane/pentane (1:3) gave the bimetallic complex **3a** as a red solid in a 60% yield (0.525 g). − IR (CH_2Cl_2): ν_{CO} = 2059 (m), 1905 (s); $\nu_{C=C}$ = 1581 (w), 1546 (w) cm^{-1}. − ^1H NMR (300.133 MHz, $CDCl_3$): δ = 7.81 (d, 1 H, $^3J_{HH}$ = 15.4 Hz, C*H*=), 7.54 (d, 2 H, $^3J_{HH}$ = 8.3 Hz, C_6H_4-), 7.36 (d, 2 H, $^3J_{HH}$ = 8.3 Hz, C_6H_4-), 7.12 (d, 1 H, $^3J_{HH}$ = 15.4 Hz, C*H*=), 7.05 (d, 1 H, $^3J_{HH}$ = 16.7 Hz, C*H*=), 5.86 (d, 1 H, $^3J_{HH}$ = 16.7 Hz, C*H*=), 4.57 (s, 3 H, O*Me*), 3.77 [s, 3 H, N*Me* (*Z*)], 3.36 [s, 3 H, N*Me* (*E*)]. − ^{13}C {^1H} NMR (75.469 MHz, $CDCl_3$): δ = 306.5 (W=*C*), 252.1 (W=*C*), 203.9, 203.4 (*C*O), 198.3, 197.6 (*C*O), 143.3 (*C*H=), 139.6 (*C*H=), 138.6, 134.3 (C_6H_4−), 133.3 (*C*H=), 129.9, 127.3 (C_6H_4−), 122.0 (*C*H=), 69.05 (O*Me*), 53.5 [N*Me* (*Z*)], 44.5 [N*Me* (*E*)]. − $C_{27}H_{17}NO_{11}W_2$ (874.98): C 34.31, H 1.96, N 1.60; found C 34.97, H 2.19, N 1.61. − HRMS (FAB^+): calcd. for $C_{27}H_{17}NO_{11}{}^{184}W_2$ 874.9821; found 874.9834.

$(CO)_5W{=}C(OMe)CH{=}CH{-}C_6H_4{-}CH{=}CH(MeO)C{=}W(CO)_5$ (4a): The synthesis followed the method outlined for the synthesis of **3a**. Compound **4a** was obtained from $W(CO)_6$ (0.417 g, 1.1 mmol) and **2a** (0.520 g, 0.99 mmol) as a red dark powder in a 30% yield (0.250 g). − IR (CH_2Cl_2): ν_{CO} = 2065 (m), 1941 (s) cm^{-1}. − ^1H NMR (300.133 MHz, $CDCl_3$): δ = 7.85 (d, 2 H, $^3J_{HH}$ = 15.5 Hz, C*H*=), 7.50 (s, 4 H, C_6H_4−), 7.10 (d, 1 H, $^3J_{HH}$ = 15.5 Hz, C*H*=), 4.55 (s, 6 H, OCH_3). − ^{13}C {^1H} NMR (200.131, $CDCl_3$): δ = 307.0 (W=*C*), 203.8, 197.4 (*C*O), 144.2 (*C*H=), 137.1 (C_6H_4-), 131.8 (*C*H=), 129.0 (C_6H_4−), 69.1 (OCH_3).

$(CO)_5W{=}C(NMe_2)CH{=}CH{-}C_4H_2S{-}CH{=}CH(OMe)C{=}W(CO)_5$ (3b): The synthesis followed the method outlined for the synthesis of **3a**. Compound **3b** was obtained from $W(CO)_6$ (0.320 g, 0.91 mmol) and **1b** (0.370 g, 0.68 mmol)as a red dark oil in a 61% yield (0.370 g). − IR (CH_2Cl_2): ν_{CO} = 2064 (m), 1931 (s) cm^{-1}. − ^1H NMR (200.131 MHz, $CDCl_3$): δ = 7.56 (d, 1 H, $^3J_{HH}$ = 15.0 Hz, C*H*=), 7.28 (d, 1 H, $^3J_{HH}$ = 15.0 Hz, C*H*=), 6.90 (d, 1 H, $^3J_{HH}$ = 16.3 Hz, C*H*=), 7.28 (d, 1 H, $^3J_{HH}$ = 3.7 Hz, C_4H_2S), 6.95 (d, 1 H, $^3J_{HH}$ = 3.7 Hz, C_4H_2S), 6.11 (d, 1 H, $^3J_{HH}$ = 16.3 Hz, C*H*=), 4.57 (s, 3 H, O*Me*), 3.81 [s, 3 H, N*Me* (*Z*)], 3.40 [s, 3 H, N*Me* (*E*)]. − ^{13}C {^1H} NMR (50.322 MHz, $CDCl_3$): δ = 303.1 (W=*C*), 250.9 (W=*C*), 203.8, 203.1 (*C*O), 198.1, 197.5 (*C*O), 146.2, 142.3 (C_4H_2S), 139.8 (*C*H=), 139.4 (*C*H=), 135.4 (*C*H=), 129.0, 126.8 (C_4H_2S), 117.3 (*C*H=), 68.7 (O*Me*), 53.4 [N*Me* (*Z*)], 44.7 [N*Me* (*E*)]. − HRMS (FAB^+): calcd. for $C_{23}H_{15}NO_{11}S^{184}W_2$ 880.9385; found 880.9411.

$(CO)_5W{=}C(NMe_2)CH{=}CH{-}C_6H_4{-}CH{=}CH(MeO)C{=}Cr(CO)_5$ (3′a): In a procedure analogous to the synthesis of **3a**, $Cr(CO)_6$ (0.2 g, 0.9 mmol) was irradiated in THF at −10 °C for 6 h. The yellow solution of $Cr(CO)_5$(THF) was then transferred into a Schlenk flask containing a solution of **1a** (0.3 g, 0.6 mmol) in 30 mL of methanol. The reaction mixture was stirred for 18 h at room temperature. After evaporation of the solvent under vacuum, the red residue was chromatographed on a silica gel column. Elution with dichloromethane/pentane (1:3) gave the bimetallic complex **3′a** as a red oil in a 30% yield (0.132 g). − IR (CH_2Cl_2): ν_{CO} = 2056 (m), 1944 (s), 1928 (s) cm^{-1}. − ^1H NMR (250 MHz, $CDCl_3$): δ = 7.93 (d, 1 H, $^3J_{HH}$ = 15.3 Hz, C*H*=), 7.57 (d, 2 H, $^3J_{HH}$ = 8.3 Hz, C_6H_4−), 7.42 (d, 2 H, $^3J_{HH}$ = 8.3 Hz, C_6H_4−), 7.09 (d, 1 H, $^3J_{HH}$ = 16.7 Hz, C*H*=), 6.92 (d, 1 H, $^3J_{HH}$ = 15.3 Hz, C*H*=), 5.93 (d, 1 H, $^3J_{HH}$ = 16.7 Hz, C*H*=), 4.80 (s, 3 H, O*Me*), 3.83 [s, 3 H, N*Me* (*Z*)], 3.42 [s, 3 H, N*Me* (*E*)]. − ^{13}C {^1H} NMR (75.469 MHz, $CDCl_3$): δ = 332.7 (Cr=*C*′), 252.3 (W=*C*), 216.9, 203.4 (*C*O), 216.6, 197.6 (*C*O), 139.5 (*C*H=), 139.3 (*C*H=), 138.6, 134.1 (C_6H_4-), 129.9 (*C*H=), 128.6, 127.1 (C_6H_4-), 121.9 (*C*H=′), 53.4 (O*Me*), 49.5 [N*Me* (*Z*)], 44.4 [N*Me* (*E*)]. − HRMS (FAB^+): calcd. for $C_{25}H_{17}NO_{11}CrW$ 743; found 742.97.

$(CO)_5W{=}C(OMe)CH{=}CH{-}C_6H_4{-}CHO$ (2c): A solution of $W(CO)_6$ (2.6 g, 7.4 mmol) in 60 mL of THF was irradiated for 6 h at room temperature by using a Rayonet and a Pyrex photochemical reactor. The yellow solution of $W(CO)_5$(THF) was then transferred into a Schlenk flask containing a solution of the dialkynol derivative **c** (1 g, 6.2 mmol) in 30 mL of methanol. The reaction mixture was then stirred for 18 h at room temperature. After evaporation of the solvent under vacuum, the red residue was chromatographed on a silica gel column. Elution with dichloromethane/pentane (1:3) gave the red monometallic complex **2c** as a red oil in a 38% yield (1.19 g). − IR (CH_2Cl_2): ν_{CO} = 2066 (m), 1939 (s) cm^{-1}. − ^1H NMR (200.131 MHz, $CDCl_3$): δ = 10.0 (s, 1 H, C*H*O), 7.91 (d, 1 H, $^3J_{HH}$ = 15.5 Hz, C*H*=), 7.65 (m, 4 H, C_6H_4−) 7.11 (d, 1 H, $^3J_{HH}$ = 15.5 Hz, C*H*=), 4.65 (s, 3 H, O*Me*). − ^{13}C {^1H} NMR (75.46 MHz, $CDCl_3$): δ = 307.8 (W=*C*), 203.7, 197.2 (*C*O), 145.4 (*C*H=), 140.6 (*C*H=), 137.2, 130.5 (C_6H_4−), 129.4 (C_6H_4−), 69.3 (O*Me*). − HRMS (FAB^+): calcd. for $C_{16}H_{10}O_7{}^{182}W$ 497.9939; found 497.9937.

$(CO)_5W{=}C(OMe)CH{=}CH{-}C_6H_4{-}CH{=}CH(MeO)C{=}Cr(CO)_5$ (4′a): Equimolar quantities of **2c** (0.252 g, 0.5 mmol) and the complex $(CO)_5Cr(OCH_3)(CH_3)$ (0.126 g, 0.5 mmol) were dissolved in ether (30 mL) with triethylamine (0.280 mL, 2 mmol) and trimethylsilyl chloride (0.250 mL, 1.5 mmol), and the resulting mixture was stirred for 6 h at room temperature. The solvent was removed under vacuum, and the red-brown residue was chromatographed on a silica gel column. Elution with dichloromethane/pentane (1:3) gave the bimetallic complex **4′a** in a 33% yield (0.012 g). − IR

(CH_2Cl_2): ν_{CO} = 2067, 2057 (m), 1943 (s) cm^{-1}. – ^1H NMR (200.131 MHz, $CDCl_3$): δ = 7.97 (d, 1 H, $^3J_{HH}$ = 15.3 Hz, C*H*=), 7.89 (d, 1 H, $^3J_{HH}$ = 15.3 Hz, C*H*=), 7.59 (m, 4 H, C_6H_4–), 7.12 (d, 1 H, $^3J_{HH}$ = 15.3 Hz, C*H*=), 6.85 (d, 1 H, $^3J_{HH}$ = 15.3 Hz, C*H*=), 4.81 (s, 3 H, O*Me*), 4.63 (s, 3 H, O*Me*). – $^{13}C\{^1H\}$ NMR (50.32 MHz, $CDCl_3$): δ = 333.4 (Cr=*C*), 306.9 (W=*C*), 224.3, 216.5 (*C*O), 203.4, 197.3 (*C*O), 144.2 (*C*H=), 140.0 (*C*H=), 138.6, 134.1 (C_6H_4–), 129.9 (*C*H=), 128.6, 127.1 (C_6H_4–), 121.9 (*C*H=), 69.1 (O*Me*), 66.6 (O*Me*). – HRMS (FAB^+): calcd. for $C_{24}H_{14}O_{12}Cr^{182}W$ 730.21; found 729.8.

General Procedure for the Preparation of Bis[alkenyl(amino)carbene]-ditungsten Complexes: To a solution of **3a** (0.874 g, 1 mmol) in 20 mL of dichloromethane at room temperature was added 3–5 equiv. of amine. The color rapidly changed from red to orange. After stirring for 20 min, the solvent was removed in vacuo and the crude product was chromatographed on a silica gel column using pentane/dichloromethane (1:2) as the eluent. Evaporation of the solvent gave the bis(aminocarbene) complexes as orange solids in good yields.

$(CO)_5W=C[N(-CH_2CH_2-)_2NH]CH=CH-C_6H_4-CH=CH-(Me_2N)C=W(CO)_5$ (5a): Yield 54% (0.501 g). – IR (paraffin): ν_{CO} = 2061 (m), 1894 (s); $\nu_{C=C}$ = 1530 (f) cm^{-1}. – ^1H NMR (300.135 MHz, $[D_6]$acetone): δ = 7.54 (s, 4 H, C_6H_4–), 7.32 (d, 2 H, $^3J_{HH}$ = 16.7 Hz, C*H*=), 6.15 (d, 1 H, $^3J_{HH}$ = 16.7 Hz, C*H*=), 6.10 (d, 1 H, $^3J_{HH}$ = 16.8 Hz, C*H*=), 4.36 and 4.10 (m, 4 H, CH_2), 3.94 [s, 3 H, N*Me* (*Z*)], 3.59 [s, 3 H, N*Me* (*E*)], 3.20 and 3.01 (m, 4 H, CH_2). – $^{13}C\{^1H\}$ NMR (75.469 MHz, $[D_6]$acetone): δ = 248.3, 245.0 (W=*C*), 204.7, 204.5 (*C*O), 199.5, 199.3 (*C*O), 140.3, 139.4 (*C*H=), 136.9, 136.8, 127.9 (C_6H_4–), 124.3, 122.9 (*C*H=), 65.2 and 56.7 (CH_2), 54.3 [N*Me* (*Z*)], 48.5 and 48.2 (CH_2), 44.92 [N*Me* (*E*)]. – $C_{28}H_{23}N_3O_{10}W_2$ (929): C 36.17, H 2.50, N 4.52; found C 36.41, H 2.62, N 4.48. – HRMS (FAB^+): calcd. for $C_{28}H_{23}N_3O_{10}{}^{184}W_2$ 929.0399; found 929.0400.

$(CO)_5W=C[N(-CH_2CH_2-)_2NH]CH=CH-C_4H_2S-CH=CH-(Me_2N)C=W(CO)_5$ (5b): Yield 50% (0.440 g). – IR (CH_2Cl_2): ν_{CO} = 2061 (m), 1925 (s) cm^{-1}. – ^1H NMR (200.135 MHz, $[D_6]$-acetone): δ = 7.02 (d, 2 H, $^3J_{HH}$ = 16.4 Hz, C*H*=), 7.0 (m, 2 H, C_4H_2S), 6.20 (d, 2 H, $^3J_{HH}$ = 16.4 Hz, C*H*=), 4.39 and 4.14 (m, 4 H, CH_2), 3.86 [s, 3 H, N*Me* (*Z*)], 3.52 [s, 3 H, N*Me* (*E*)], 2.94 and 2.88 (m, 4 H, CH_2).

$(CO)_5W=C[N(H)(CH_2-CH_2NH_2)]CH=CHC_6H_4CH=CH-(Me_2N)C=W(CO)_5$ (6a): Yield 75% (0.677 g). – IR (KBr): ν_{CO} = 2062 (m), 1895 (s) cm^{-1}. – ^1H NMR (300.134 MHz, CD_2Cl_2): δ = 7.38 (d, 2 H, $^3J_{HH}$ = 8.2 Hz, C_6H_4–), 7.21 (d, 2 H, $^3J_{HH}$ = 8.2 Hz, C_6H_4–), 7.03 (d, 2 H, $^3J_{HH}$ = 16.7 Hz, C*H*=), 5.95 (d, 2 H, $^3J_{HH}$ = 16.7 Hz, C*H*=), 3.80 [s, 3 H, N*Me* (*Z*)], 3.36 [s, 3 H, N*Me* (*E*)], 2.88 (m, 2 H, CH_2), 2.73 (t, 2 H, CH_2). – $^{13}C\{^1H\}$ NMR (75.469 MHz, $[D_6]$acetone): δ = 248.4 (W=*C*), 204.4, 202.5 (*C*O), 199.3, 199.1 (*C*O), 140.8 (C_6H_4–), 139.8 (*C*H=), 135.4, 129.4, 127.7 (C_6H_4–), 124.7 (*C*H=), 65.2 (NH*C*H_2), 54.3 [N*Me* (*Z*)], 44.9 [N*Me* (*E*)], 33.1 (*C*H_2NH_2). – $C_{26}H_{21}N_3O_{10}W_2$ (903): C 34.55, H 2.34, N 4.65; found C 30.09, H 1.96, N 3.83. – HRMS (FAB^+): calcd. for $C_{26}H_{21}N_3O_{10}{}^{184}W_2$ 903.0246; found 903.0240.

$(CO)_5W=C[N(H)(CH_2-CH_2-NH_2]CH=CH-C_4H_2S-CH=CH(Me_2N)C=W(CO)_5$ (6b): Yield 70% (0.636 g). – IR (CH_2Cl_2): ν_{CO} = 2061 (m), 1924 (s) cm^{-1}. – ^1H NMR (200.131 MHz, $CDCl_3$): δ = 6.84 (d, 1 H, $^3J_{HH}$ = 3.5 Hz, C_4H_2S), 6.74 (d, 1 H, $^3J_{HH}$ = 3.5 Hz, C_4H_2S), 6.67 (d, 2 H, $^3J_{HH}$ = 15.3 Hz, C*H*=), 6.14 (d, 2 H, $^3J_{HH}$ = 15.3 Hz, C*H*=), 3.80 [s, 3 H, N*Me* (*Z*)], 3.40 [s, 3 H, N*Me* (*E*)], 3.09 (m, 2 H, CH_2), 2.82 (m, 2 H, CH_2). – $^{13}C\{^1H\}$ NMR (75.469 MHz, CD_2Cl_2): δ = 204.19, 202.07 (*C*O), 198.8, 198.2 (*C*O), 54.5 [N*Me* (*Z*)], 49.1 [N*Me* (*E*)]. – HRMS (FAB^+): calcd. for $C_{24}H_{19}N_3O_{10}S^{184}W_2$ 908.9810; found 908.9815.

$(CO)_5W=C[N(CH_2CH_2OH)CH_2CH_3]CH=CH-C_6H_4-CH=CH(Me_2N)C=W(CO)_5$ (7a): Yield 81% (0.755 g). – IR (CH_2Cl_2):

Table 3. Crystallographic data for **4b**,**4a**, **3a**, and **4′a**

	4b	**4a**	**3a**	**4′a**
Empirical formula	$C_{22}H_{12}O_{12}SW_2$	$C_{24}H_{14}O_{12}W_2$	$C_{25}H_{17}NO_{11}W_2$	$C_{24}H_{14}CrO_{12}W$
Molecular mass	868.08	862.05	875.10	730.20
Crystal size [mm]	0.45 × 0.33 × 0.33	0.32 × 0.15 × 0.12	0.40 × 0.26 × 0.12	0.47 × 0.34 × 0.22
Crystal system	triclinic	monoclinic	monoclinic	monoclinic
Space group	$P\bar{1}$	*C*2/*c*	$P2_1/n$	$P2_1/n$
a [Å]	7.408(15)	14.792(5)	9.045(2)	14.785(3)
b [Å]	10.313(4)	16.610(5)	13.997(4)	16.478(5)
c [Å]	17.802(4)	12.274(5)	22.425(6)	12.228(4)
α [°]	99.42(2)	90.000(5)	90	90
β [°]	98.92(5)	114.822(5)	92.648(2)	115.04(2)
γ [°]	96.32(7)	90.000(5)	90	90
V [Å^3]	1313(3)	2737.1(17)	2836.0(13)	2699.1(13)
Z	2	4	4	4
$\rho_{calcd.}$ [g cm^{-3}]	2.196	2.092	2.050	1.797
T [K]	293(2)	293(2)	293(2)	293(2)
μ [mm^{-1}] (Mo-K_α)	8.896	8.458	8.163	4.721
Absorption correction	psi scan	psi scan	psi scan	psi scan
F(000)	808	1608	1640	1408
θ_{range} [°]	1.18 to 26.97	1.95 to 26.99	1.72 to 27.84	1.96 to 26.98
Index ranges	$0 \le h \le 9$	$0 \le h \le 18$	$0 \le h \le 11$	$0 \le h \le 18$
	$-13 \le k \le 13$	$0 \le k \le 21$	$-18 \le k \le 17$	$0 \le k \le 21$
	$-22 \le l \le 22$	$-15 \le l \le 14$	$-29 \le l \le 29$	$-15 \le l \le 14$
Number of reflections collected	6170	3097	12043	3049
Number of independent reflections	5718	2984	6706	2936
Numbers of reflections with $I > 2\sigma(I)$	4071	2219	5347	1888
Number of parameters	518	173	353	173
R_1 [$I > 2\sigma(I)$]	0.0476	0.0292	0.0474	0.0473
R_1 (all data)	0.0768	0.0576	0.0659	0.0963
wR_2 (all data)	0.1383	0.0762	0.1289	0.1180
Largest different peak/hole, min./max. [eÅ^{-3}]	1.993/–2.150	0.777/–0.527	1.563/–2.064	0.746/–0.926

ν_{CO} = 2061 (m) 1924 (s) cm^{-1}. – ^1H NMR (200.131 MHz, $CDCl_3$): δ = 7.36 (s, 4 H, C_6H_4–), 7.08 (d, 1 H, $^3J_{HH}$ = 16.7 Hz, C*H*=), 7.02 (d, 1 H, $^3J_{HH}$ = 16.7 Hz, C*H*=), 5.95 (d, 1 H, $^3J_{HH}$ = 16.7 Hz, C*H*=), 5.89 (d, 1 H, $^3J_{HH}$ = 16.7 Hz, C*H*=), 4.23 (q, 2 H, $^3J_{HH}$ = 7.3 Hz, NCH_2CH_3), 4.09 (t, 2 H, CH_2), 3.94 (m, 2 H, CH_2OH), 3.82 [s, 3 H, N*Me* (*Z*)], 3.40 [s, 3 H, N*Me* (*E*)], 1.44 (t, 3 H, $^3J_{HH}$ = 7.2 Hz, CH_3), 1.25 (t, 1 H, O*H*). – ^{13}C {^1H} NMR (75.469 MHz, $CDCl_3$): δ = 254.0, 252.5 (W=*C*), 203.6, 203.5 (*C*O), 198.4, 198.3 (*C*O), 139.2, 138.5 (*C*H=), 135.8, 135.4, 127.0, 126.9 (C_6H_4–), 123.0, 122.1 (*C*H=), 60.2 (O*Me*), 58.1 (NCH_2), 53.5 [N*Me* (*Z*)], 53.3 NCH_2CH_2, 44.3 [N*Me* (*E*)], 14.1 (CH_3), 13.9 (CH_2). – HRMS (FAB^+): calcd. for $C_{28}H_{24}N_2O_{11}{}^{184}W_2$ 932.0399; found 932.0403.

X-ray Crystal Structure Analysis: Crystals, data collection, and refinement parameters for complexes **3a**, **4a**, **4b**, and **4′a** are given in Table 3. Crystals were obtained by slow concentration of a dichloromethane solution. All X-ray data were collected with an automatic diffractometer CAD4 NONIUS (graphite-monochromated Mo-K_α radiation, λ = 0.71073 Å). After Lorentz and polarization corrections, the structures were solved with SIR-97,[27] which reveals the non-hydrogen atoms of the structure and a statistical disorder between Cr and W atoms (complex **4′a**). After anisotropic refinement, a Fourier difference map reveals all the hydrogen atoms. The whole structures were refined with SHELXL97 by the full-matrix least-squares technique (use of *F* square magnitude; *x*, *y*, *z*, β_{ij} for Cr, W, C, and O atoms, *x*, *y*, *z* in riding mode for H atoms).[28] Crystallographic data (excluding structure factors) for the structures reported in this paper have been deposited with the Cambridge Crystallographic Data Centre as supplementary publication no. CCDC-146553 (**4b**), -146554 (**4a**), -146555 (**3a**), -146556 (**4′a**). Copies of the data can be obtained free of charge on application to CCDC, 12 Union Road, Cambridge, CB2 1EZ, UK [Fax: (internat.) + 44-1223/336-033; E-mail: deposit@ccdc.cam.ac.uk].

Acknowledgments

We thank the Région Bretagne and the CNRS for financial support. K. U. is grateful to the D.A.A.D for a fellowship.

[1] F. Paul, C. Lapinte, *Coord. Chem. Rev.* **1998**, *178–180*, 431.
[2] I. R. Whittall, A. M. McDonagh, M. G. Humphrey, M. Samoc, *Adv. Organomet. Chem.* **1999**, *43*, 349.
[3] [3a] N. Hoa Tran Huy, P. Le Floch, F. Robert, Y. Jeannin, *J. Organomet. Chem.* **1987**, *327*, 311.- [3b] E. O. Fischer, W. Röll, N. Hoa Tran Huy, K. Ackermann, *Chem. Ber.* **1982**, *115*, 2951.
[4] T. Albrecht, J. Sauer, H. Nöth, *Tetrahedron Lett.* **1984**, *35*, 561.
[5] Y. M. Terblans, H. M. Roos, S. Lotz, *J. Organomet. Chem.* **1998**, *566*, 133.
[6] S. Maiorana, A. Papagni, E. Licandro, *Gazz. Chim. Ital.* **1995**, *125*, 377.
[7] R. Aumann, H. Heinen, *Chem. Ber.* **1987**, *120*, 537.
[8] O. Briel, A. Fehn, W. Beck, *J. Organomet. Chem.* **1999**, *578*, 247.
[9] C. Mongin, Y. Ortin, N. Lugan, R. Mathieu, *Eur. J. Inorg. Chem.* **1999**, 739.
[10] A. Rabier, N. Lugan, R. Mathieu, G. L. Geoffroy, *Organometallics* **1994**, *13*, 4676.
[11] A. Geisbauer, S. Mihan, W. Beck, *J. Organomet. Chem.* **1995**, *501*, 61.
[12] R. Aumann, B. Jasper, R. Fröhlich, S. Kotila, *J. Organomet. Chem.* **1995**, *502*, 137.
[13] M. Havranek, M. Husak, D. Dvorak, *Organometallics* **1995**, *14*, 5024.
[14] C. Hartbaum, E. Mauz, G. Roth, K. Weissenbach, H. Fischer, *Organometallics* **1999**, *18*, 2619.
[15] C. Hartbaum, G. Roth, H. Fischer, *Eur. J. Inorg. Chem.* **1998**, 191.
[16] C. Cosset, I. Del Rio, H. Le Bozec, *Organometallics* **1995**, *14*, 1938.
[17] D. Pilette, K. Ouzzine, H. Le Bozec, P. H. Dixneuf, C. E. F. Rickard, W. R. Roper, *Organometallics* **1992**, *11*, 809.
[18] K. Ulrich, E. Porhiel, V. Péron, V. Ferrand, H. Le Bozec, *J. Organomet. Chem.* **2000**, *601*,78.
[19] V. Péron, E. Porhiel, V. Ferrand, H. Le Bozec, *J. Organomet. Chem.* **1997**, *539*, 201.
[20] B. A. Anderson, W. D. Wulff, T. S. Powers, S. Tribbitt, A. L. Rheingold, *J. Am. Chem. Soc* **1992**, *114*, 10784.
[21] [21a] C. A. Toledano, H. Rudler, J.-C. Daran, Y. Jeannin, *J. Chem. Soc., Chem. Commun.* **1984**, 574.– [21b] C. A. Toledano, A. Parlier, H. Rudler, J.-C. Daran, Y. Jeannin, *J. Chem. Soc., Chem. Commun.* **1984**, 576.
[22] K. R. J. Thomas, J. T. Lin, Y. S. Wen, *J. Organomet. Chem.* **1999**, *575*, 301.
[23] J. Lewis, N. J. Long, P. R. Raithby, G. P. Shieds, W.-Y. Wong, M. Younus, *J. Chem. Soc., Dalton Trans.* **1997**, 4283.
[24] R. Aumann, I. Göttker-Schnetmann, R. Fröhlich, O. Meyer, *Eur. J. Org. Chem.* **1999**, 2545.
[25] J. T. Guy Jr, D. Bennett, *Transition Met. Chem.* **1984**, *9*, 43.
[26] A. Rahm, W. D. Wulff, A. L. Rheingold, *Organometallics* **1996**, *12*, 597.
[27] A new tool for crystal structure determination and refinement: A. Altomare, M. C. Burla, M. Camalli, G. Cascarano, C. Giacovazzo, A. Guagliardi, A. G. G. Moliterni, G. Polidori, R. Spagna, *J. Appl. Crystallogr.* **1998**, *31*, 74.
[28] G. M. Sheldrick, *SHELXL93, Program for the Refinement of Crystal Structures*, University of Göttingen, Germany, **1993**.

Received August 9, 2000
[I00314]

Mössbauer, Crystallographic, and Density Functional Theoretical Investigation of the Electronic Structure of Bis-Ligated Low-Spin Iron(II) Phthalocyanines

Victor N. Nemykin,[a] Nagao Kobayashi,*[a] Victor Y. Chernii,[b] and Vitaly K. Belsky[c]

Keywords: Iron / Phthalocyanines / Mössbauer spectroscopy / Density functional calculations

We present the crystal structure of pcFe(4-methylpiperidine)$_2$ as a first example of a low-spin iron(II) phthalocyanine (pc) complex bis-axially coordinated by aliphatic amines. It is shown that electronic rather than steric effects are responsible for the elongation of the Fe–N(axial) bond in pcFeL$_2$ complexes. Using density functional theory, the electronic structures as well as Mössbauer isomer shifts and quadrupole splittings have been investigated for a large number of pcFeL$_2$ and pcFeL^{1}L^2 complexes, in which the axial ligands have varying electronic and steric properties. The electron charge densities and electric field gradients at the iron ion were evaluated using a locally dense basis approach with Wachters' all-electron basis set for the iron ion, the 6-311++G(2d) basis set for atoms directly bonded to the iron ion, the 6-31G(d) basis set for atoms two bonds away from the iron ion, and the 3-21G* basis set for all other atoms. A good correlation between the theoretical and experimental isomer shifts and quadrupole splittings has been observed for all the complexes tested. It has also been shown that the proposed model for the calculation of Mössbauer spectral parameters is adequate for the evaluation of the axial ligand conformation in cases of conformational flexibility in pcFeL$_2$ complexes.

Introduction

Iron-containing tetrapyrrole macrocycles and their analogues have been found to be capable of mimicking the active sites of a wide variety of biological enzymes.[1] Tetrabenzotetraazaporphyrin, i.e. phthalocyanine (pc), iron complexes have been the subject of widespread interest, both as homogeneous and heterogeneous catalytic systems with high oxygenating activity,[2] and have also been extensively studied as heme protein models[3] by virtue of their high thermal and chemical stability. The possibility of axial coordination and the stability of iron−axial ligand bonds are key features of these systems that play an important role in catalytic and model biological processes.[1−3] The nature of the central metal−axial ligand bonding in phthalocyanine iron complexes has been qualitatively discussed over the past 30 years. A large number of bis-axially coordinated low-spin iron(II) pcs (pcFeL$_2$ or pcFeL^{1}L^2) with aliphatic and heterocyclic nitrogen bases, isonitriles, phosphanes, and phosphites have been studied.[4−6] In principle, Mössbauer spectroscopy represents one of the most powerful methods for assessing the metal−axial ligand interaction in these systems. However, despite a large amount of experimental data concerning the Mössbauer spectra of iron pcs,[5,6] publications on the theoretical analysis of ^{57}Fe Mössbauer spectral parameters of these complexes are scarce, especially for bis-axially coordinated low-spin iron(II) pcs. This can be mainly attributed to two factors.[6] Firstly, only a few good X-ray crystallographic structures are available for pcFeL$_2$ or pcFeL^{1}L^2 complexes that can be used as initial structures for quantum mechanical calculations.[7] With a view to rectifying this situation, we present herein the first crystal structure of a low-spin iron(II) pc bis-axially coordinated by aliphatic amines. Secondly, the computation of energies, electronic structures, and properties of transition metal complexes requires consideration of electronic correlation effects.[8] However, for calculations of the electronic structures on systems of the size of pcFeL$_2$ or pcFeL^{1}L^2 (containing up to 97 atoms), all the usual electron correlation methods, based, for example, on multiconfigurational interaction, Möller−Plesset perturbation theory, or other algorithms, would require speeds typically as high as ca. N^5 (where N is the number of basis functions) and are still expensive. Fortunately, computational methods based on density functional theory (DFT) can be used as an alternative to conventional ab initio methods for large systems of this type because they include electron correlation effects in the exchange-correlation functional and are computationally very inexpensive. As has recently been shown, the simplest local density approximation (LDA) as well as the more precise B3LYP exchange-correlation functional generally give much better results for the ground-state properties of transition metal compounds, including porphyrins having structures that closely resemble those of pcs, than those obtained at the semiempirical or conventional ab initio Hartree−Fock levels.[9] In this paper, we present Mössbauer

[a] Department of Chemistry, Graduate School of Science, Tohoku University,
Sendai 980-8578, Japan
Fax: (internat.) + 81-22/217-7719
E-mail: nagaok@mail.cc.tohoku.ac.jp
[b] Vernadsky Institute of General and Inorganic Chemistry, Palladina Ave. 32/34, 252680 Kiev, Ukraine
[c] Karpov Institute of Physical Chemistry, Vorontsovo Pole 10, 103064 Moscow, Russia
Supporting information for this article is available on the WWW under http://www.wiley-vch.de/home/eurjic or from the author.

 © WILEY-VCH Verlag GmbH, 69451 Weinheim, 2001 1434−1948/01/0303−0733 $ 17.50+.50/0

spectra and the results of DFT calculations for a large number of bis-axially coordinated iron(II) pcs. In addition, X-ray crystallographic data are presented for a low-spin iron(II) pc coordinated by two aliphatic amines. In order to find the best computational method for the prediction of Mössbauer spectral parameters and to understand the origin of the differences in the spectroscopic data, comparative semiempirical, conventional ab initio, and DFT calculations have also been performed. In particular, we wanted to ascertain whether it is possible to reproduce a large difference in quadrupole splitting (ΔE_Q) among the complexes (from 0.56 to 2.28 mm s^{-1}), and to rationalize the influence of specific effects, such as the conformation of the axial ligands, on the Mössbauer spectral parameters. For these purposes, we chose the following pcs, in which the axial ligands have varying electronic and steric properties: pcFe(14en)$_2$ (**1**), pcFe(mepip)$_2$ (**2**), pcFe($BuNH_2$)$_2$ (**3**), pcFe(mim)$_2$ (**4**), pcFe(mepy)$_2$ (**5**), pcFe(*cyclo*-$C_6H_{11}NC$)$_2$ (**6**), pcFe(CO)(dmf) (**7**), and [pcFe$(CN)_2$]$^{2-}$ (**8**), where 14en, mepip, mim, and mepy are 1,4-diaminobutane, 4-methylpiperidine, *N*-methylimidazole, and 4-methylpyridine, respectively. As described below, the results represent the first successful theoretical analysis and prediction of Mössbauer spectral parameters in bis-axially coordinated low-spin iron(II) pcs.

Results and Discussion

Structural Aspects and Rotational Barriers

The SHELXTL-93 structure of pcFe(mepip)$_2$ (**2**) is shown in Figure 1. Atomic coordinates, as well as selected intramolecular distances and angles for this complex, are summarized in the Supporting Information (Tables 2 and 3) with the numbering scheme indicated in Figure 1. The structure of pcFe(mepip)$_2$ (**2**) is the first X-ray structure of an iron(II) pc to provide unprecedented stereochemical data on the coordination of aliphatic amines to iron pcs. In the recently reported X-ray structure of turnip cytochrome *f*, one of the axial ligands was found to be the α-NH_2 group of *Tyr*-1, and thus pcFe(mepip)$_2$ (**2**) may provide a useful starting point for delineating the role of aliphatic amino acids in biologically relevant amine complexes of iron porphyrins. In the unit cell of pcFe(mepip)$_2$ (**2**), four solvated mepip molecules are present in a chair conformation. The iron ion is coordinated by six nitrogen atoms that form an approximately square-bipyramidal structure. The essentially uniform Fe−N(pc) distance (1.93 Å) is consistent with a low-spin iron(II) configuration and is close to the corresponding distances found in other known bis(amino)-ligated iron(II) pcs such as pcFe(mim)$_2$ (**4**) and pcFe(mepy)$_2$ (**5**) (Table 1).[7a,7b] The Fe−N(mepip) distance (2.12 Å) is longer than that in any of the known iron(II) pcs bis-axially coordinated through the N, C, or O atoms of the ligands.[7] Two factors may be invoked to account for this bond elongation, namely steric interactions between protons of the axial ligand and the pc core, and electronic effects. Both of these are discussed below. The N(pc)−Fe−N(mepip) angles are close to 90° (the largest deviation is 1.85°). The phthalocyanine core is almost planar, keeping the interatomic distances close to those in pcFe(mim)$_2$ (**4**) and pcFe(mepy)$_2$ (**5**).[7] The axial ligands adopt a chair conformation with the intramolecular distances and angles close to those in solvated molecules present in the unit cell. The dihedral planes between the axial ligands are close to zero. This orientation of the axially coordinated mepip planes relative to the phthalocyanine core in the structure of **2** is fixed by the steric requirements imposed by the conformation of the solvated, as well as neighboring, axially coordinated mepip molecules. Any rotation of the axially coordinated ligands about the Fe−N(mepip) axis leads to a reduction in the non-bonding interactions between the carbon or hydrogen atoms of the axial ligands and the axially coordinated ligands of neighboring molecules of pcFe(mepip)$_2$ (**2**) and/or solvated mepip molecules. For example, rotation of the axial ligand about the *z* axis by 90° would result in unacceptably close non-bonding contacts (less that 2 Å) between the carbon atoms of the axial ligand and a nitrogen atom of a solvated mepip molecule. Such steric hindrance to the rotation of axial ligands in the crystal structure of pcFe(mepip)$_2$ (**2**) is well reproduced by rotational barrier calculations at the molecular mechanical and semiempirical levels. The results of calculations at the molecular mechanical level are summarized in Figure 2. Similarly qualitative results were obtained from semiempirical PM3 level calculations. Thus, the procedure described in the Experimental Section leads to estimated barriers for rotation of the axial ligands of 1.92 kcal mol^{-1}, 1.20 kcal mol^{-1}, and 2.54 kcal mol^{-1} at the MM+ level and of 2.07 kcal mol^{-1}, 1.71 kcal mol^{-1}, and 2.95 kcal mol^{-1} at the PM3 level for pcFe(mepip)$_2$ (**2**), pcFe(mim)$_2$ (**4**), and pcFe(mepy)$_2$ (**5**), respectively. Similar results have recently been reported for the barriers to rotation of axial ligands in predominantly planar or slightly distorted bis-axially coordinated iron(II) and iron(III) porphyrins.[9a,10] Thus, it is clear that in the gas phase, or in solution in the absence of any specific interactions between bis-axially coordinated iron(II) pcs and solvent molecules, the rotational barrier for rotations of axial ligands is invariably very small, in agreement with the room-temperature ^{1}H NMR spectral data.[4a−4e] On the other hand, for solvated mepip molecules the height of the rotational barrier of the axial ligand increases by more than two orders of magnitude according to both MM+ and PM3 calculations (Figure 2). Finally, it is important to delineate the factors that are responsible for the elongation of the Fe−N(axial) bond in pcFe(mepip)$_2$ (**2**) as compared with the corresponding distances in the complexes pcFe(mim)$_2$ (**4**) and pcFe(mepy)$_2$ (**5**). If steric interactions were to play a major role, as discussed previously[11] for tppFe(pip)$_2$, which contains an almost planar porphyrin core, the decrease in the Fe−N(axial) bond length would lead to a dramatic increase in the barrier to rotation of the axial ligand in pcFe(mepip)$_2$ (**2**). In order to reproduce this effect, model calculations on pcFe(mepip)$_2$ (**2**) were carried out in which the Fe−N(axial) bond length was shortened to 2.04 Å [as in pcFe(mepy)$_2$ (**5**)]. The results

showed that, in fact, the barrier to rotation of the axial ligand increases by less than 1.0 kcal mol^{-1} and that the total energies differ by less than 7 kcal mol^{-1}, both at the molecular mechanical and semiempirical levels. These results clearly indicate that the elongation of the Fe−N(axial) bond in pcFe(mepip)$_2$ (**2**) must stem from a difference in the electronic structure of the axial ligands in pcFe(mepip)$_2$ (**2**) compared to the situation in other pcFeL$_2$ and pcFeL^{1}L^2 complexes, in particular complexes pcFe(mim)$_2$ (**4**) and pcFe(mepy)$_2$ (**5**). Indeed, the Fe−N(axial) distances are roughly paralleled by the order of the magnitude of the sum of σ-donor and π-acceptor properties of the axial ligands: mepip > mepy > *cyclo*-$C_6H_{11}NC$ > CO.[5b,12]

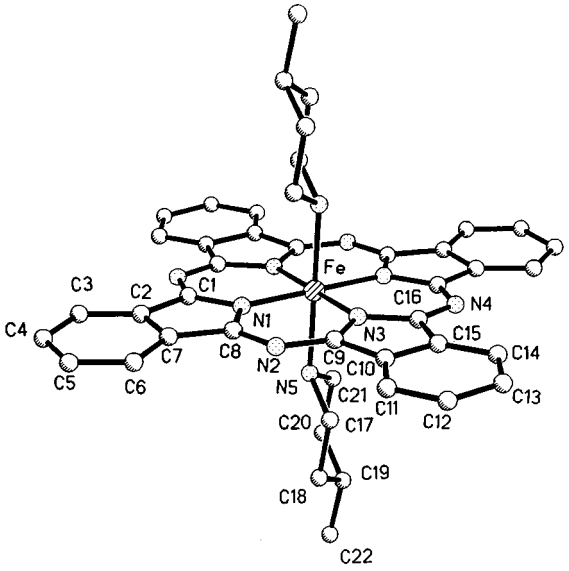

Figure 1. Perspective view of **2**; hydrogen atoms are omitted for clarity

Table 1. Structural data (distances in Å)

	1	**2**[a]	**3**	**4**[b]	**5**[c]	**6**[d]	**7**[e]	**8**[f]
Fe−N_{pc}	1.930	1.930	1.930	1.932	1.934	1.943	1.892	1.941
Fe−L_{ax}	2.080	2.119	2.080	2.012	2.040	1.911	1.72/2.07	1.960
$\|z_{max}\|$[g]	0.0	0.0	0.0	0.0	0.0	0.0	0.04	0.0

[a] This work. – [b] Ref.[7b] – [c] Ref.[7a] – [d] Ref.[7d] – [e] Ref.[7g] Fe−C(CO)/Fe−O(dmf). – [f] Ref.[7c] – [g] $|z_{max}|$ denotes the displacement of iron atom from the phthalocyanine N_4 plane.

Mössbauer Spectra of Bis-axially Coordinated Iron(II) Phthalocyanines

As for other low-spin ($S = 0$) iron(II) inorganic and organometallic compounds,[13] the Mössbauer spectra of bis-axially coordinated iron(II) phthalocyanines consist of one doublet,[5] the example shown in Figure 3 being typical. The quadrupole splitting, ΔE_Q, varies significantly from 0.56 mm s^{-1} in the complex [pcFe(CN)$_2$]$^{2-}$ (**8**) to 2.89 mm s^{-1} in pcFe(dabco)$_2$.[5d] The valence contribution (q_{val}) to ΔE_Q is approximately related to the anisotropy of the Fe(3d) and Fe(4p) shell occupations, as expressed by the Townes−Dailey approximation:[9a,13−16] $q_{val} =$

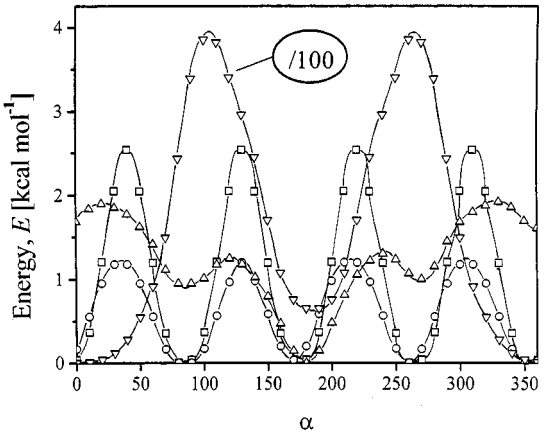

Figure 2. Barriers to axial ligand rotation in **2** (upward triangles), in **2** with solvated mepip molecules (inverted triangles), in **4** (circles), and **5** (squares), computed by a molecular mechanics (MM+) method

$^4/_7(1 - R)\langle r^{-3}\rangle_{3d}\{n(d_{xy}) + n(d_{x^2-y^2}) - n(d_{z^2}) - [n(d_{xz}) + n(d_{yz})]/2\} + {}^4/_5(1 - R)\langle r^{-3}\rangle_{4p}\{[n(p_x) + n(p_y)]/2 - n(p_z)\}$, where n(d) and n(p) are the effective populations of the respective iron orbitals, and $\langle r^{-3}\rangle$ is the expectation value of $1/r^3$ taken over the appropriate iron radial functions. For most bis-axially coordinated low-spin iron(II) macrocyclic complexes, such as pcs, porphyrins, and substituted dioximates, the valence contribution to ΔE_Q dominates[5,6a,9a] and hence the large (> 2.0 mm s^{-1}) quadrupole splitting seen in many pcFeL$_2$ complexes having a formal $(d_{xy})^2(d_{xz},d_{yz})^4$ electronic configuration is difficult to understand. Accordingly, in order to understand this phenomenon and to reproduce the large ΔE_Q values, comparative quantum chemical calculations were performed on the various pcFeL$_2$ and pcFeL^{1}L^2 complexes, as described in the next section.

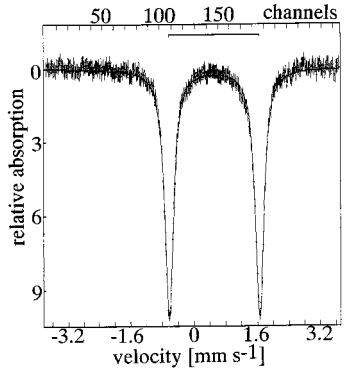

Figure 3. Room-temperature, zero-field Mössbauer spectrum of **2**

Density Functional Theory Calculations

Despite the large amount of experimental data on Mössbauer spectra of low-spin iron(II) pcs, only one theoretical study of quadrupole splittings on the basis of INDO semiempirical calculations has been published, although the parameters were not given.[6a] Moreover, to the best of our knowledge, there has been no report of a successful theoretical analysis of Mössbauer spectral parameters for low-spin

Table 2. Computed total charge electron densities for the ^{57}Fe atoms in complexes **1−8**, together with the calculated and experimental Mössbauer quadrupole splittings (in mm s^{-1}) and asymmetry parameters

		1a	1b	2	3	4	5	6	7	8a	8b
δ	Expt.	0.48[a]		0.53[a]	0.51[a]	0.52[a]	0.52[b]	0.39[c]	0.35[d]	0.38[e]	
ΔE_Q	Expt.	1.84		+2.28[f]	1.97	1.71	+1.96[g]	+0.69[h]	+1.56[i]	0.56	
η	Expt.	0.0		0.0	0.0	0.0	0.0	0.0	0.0	0.0	
ΔE_Q	*Z*/*S*[j]	1.02		0.97	1.09	0.88	0.96	0.40	1.51	0.28	
ΔE_Q	RHF			1.33		0.76					
ΔE_Q	B3LYP	1.92	1.99	2.18	2.02	1.72	1.94	0.55	1.84	−0.02	0.51
η	B3LYP	0.0	0.0	0.0	0.0	0.0	0.0	0.1	0.0	0.0	0.4
ρ(o)	B3LYP G98	11616	11616	11616	11616	11616	11616	11617	11617	11617	11617
ρ(o)	B3LYP GS	11615.94	11615.99	11615.84	11616.03	11615.91	11615.94	11616.51	11616.77	11616.65	11616.66
ΔE_Q	LSDA	2.304		2.69	2.20	2.10	2.24	0.87	1.93	0.26	0.78
η	LSDA	0.1		0.0	0.0	0.0	0.0	0.1	0.0	0.0	0.2
ρ(o)	LSDA G98	11566		11566	11566	11566	11566	11567	11567	11567	11567
ΔE_Q	LDA	1.90		2.46	2.53	2.17	2.30	0.91	2.10	0.28	0.95
η	LDA	0.0		0.0	0.0	0.0	0.1	0.1	0.0	0.0	0.3
ρ(o)	LDA G98	11579		11579	11579	11579	11579	11580	11580	11580	11580

[a] This work. − [b] Ref.[5a] − [c] Ref.[5d] − [d] Ref.[5e] − [e] Ref.[5f] − [f] Based on sign determined for $pcFe(pip)_2$, ref.[5i] − [g] Based on sign determined for $pcFe(py)_2$, ref.[4c] − [h] Based on sign determined for $pcFe(mesNC)_2$, ref.[5d] − [i] Based on sign determined for pcFe(CO)(MeOH), ref.[5i] − [j] Abbreviations: *Z*/*S* is Zerner's INDO-S parameterization; RHF is the ab initio Hartree−Fock level with Wachters' all-electron basis set on iron and the 6−311+G(2d) basis set on all other atoms; G98 is Gaussian-98W; GS is GAMESS (USA).

iron(II) pcs. In view of this, the Mössbauer spectral parameters for the complexes $pcFe(mepip)_2$ (**2**) and $pcFe(mim)_2$ (**4**), for which relatively large quadrupole splittings were observed compared to other low-spin iron(II) pcs, have been analyzed theoretically, and the results have been compared by quantum chemical calculations at the following levels of theory: (i) semiempirical ZINDO/S,[17] (ii) conventional ab initio [with the same basis set as discussed for DFT methods, as well as with Wachters' all-electron basis set for iron and 6-311+G(2d) for all other atoms], (iii) DFT methods with B3LYP, LDA, and LSDA EC functionals. As can be seen from the results presented in Table 2, the electric field gradients obtained from both semiempirical and conventional ab initio methods show a marked deviation from the experimental values, while those obtained from the DFT methods are much closer. As a consequence, in the following we will discuss and compare only the results of the DFT calculations.

Orbital Energies

The order of the orbital energies is shown in Table 3, in the Supporting Information (Tables 4 and 5), and Figure 4 and Figure 5. In general, the order of metal-centered orbitals reflects the splitting pattern of distorted octahedral coordination of the central ion. The "t_{2g}" manifold of the Fe(3d) orbitals is split into an almost degenerate d_{xz} and d_{yz} pair and a d_{xy} orbital, except in the case of $[pcFe(CN)_2]^{2-}$ (**8**), while the "e_g" manifold is split into d_{z^2} and $d_{x^2-y^2}$ orbitals. Furthermore, in all cases the LUMO "e_g" orbitals are pc-centered as in other metal-containing pcs.[21] However, the relative energies of the metal-centered orbitals as well as the pc-centered orbitals were found to be strongly dependent on the EC functional used. Thus, when the B3LYP EC hybrid functional was used (Figure 4), the pc "a_{1u}" (in D_{4h} notation) orbital was found to be the HOMO for all the complexes, except in the case of

Table 3. Calculated orbital energies (eV) for complexes **1−8** using the B3LYP hybrid EC functional

Orbital	1	2	3	4	5	6	7	8
$d_{x^2-y^2}$	1.133	1.250	1.209	1.447	1.184	1.004	0.719	6.600
d_{z^2}	0.365	0.091	−0.065	0.749	0.306	0.478	−0.422	6.598
pc "b_{1u} (π*)"	−0.440	−0.677	−0.676	−0.399	−0.602	−0.602	−0.657	4.224
pc "e_g (π*)"	−1.966	−2.219	−2.230	−1.904	−2.120	−2.128	−2.281	3.056
	−1.974	−2.231	−2.239	−1.904	−2.122	−2.130	−2.278	3.056
pc "a_{1u} (π)"	−4.406	−4.628	−4.663	−4.364	−4.523	−4.591	−4.688	0.548
d_{xz}	−4.853	−5.058	−5.151	−4.841	−5.156	−5.306	−5.898	0.591
d_{yz}	−4.888	−5.120	−5.168	−4.843	−5.167	−5.310	−5.902	0.591
d_{xy}	−5.269	−5.367	−5.415	−5.090	−5.437	−5.498	−6.037	0.037
pc "a_{2u}(π)"	−5.893	−6.252	−6.316	−5.991	−6.193	−5.885	−6.522	0.015
2p(Fe)	702.80	702.73	702.79	702.50	702.97	703.19	703.89	697.49
3s(Fe)	92.14	92.16	92.21	91.89	92.28	92.49	93.26	86.77
Δ_{cf}	5.237	5.180	5.095	5.591	5.468	5.786	5.478	6.007
Δ_{ct}	4.431	4.412	4.484	4.443	4.560	4.706	5.243	3.633
Δ_{Qband}	2.436	2.378	2.428	2.460	2.402	2.462	2.408	2.508
Δ_{Bband}	3.923	4.027	4.071	4.087	4.072	3.756	4.242	3.041
$\Delta_{a1u-a2u}$	1.487	1.624	1.653	1.627	1.670	1.294	1.834	0.533

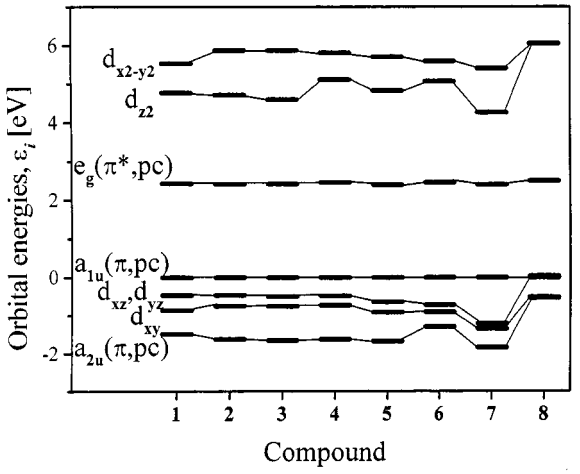

Figure 4. The ground-state MOs of complexes **1**−**8** [relative to "a_{1u}" (pc) orbital] with predominant Fe(3d) character, as well as the most important pc-centered MOs, as obtained by B3LYP DFT calculations

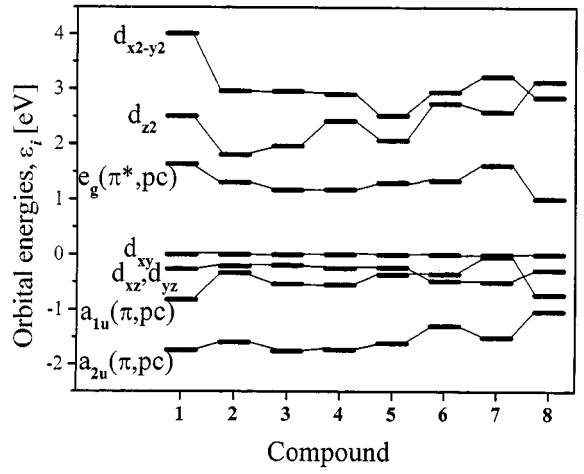

Figure 5. The ground-state MOs of complexes **1**−**8** (relative to d_{xy} orbital) with predominant Fe(3d) character, as well as the most important pc-centered MOs, as obtained by LSDA DFT calculations

$[pcFe(CN)_2]^{2-}$ (**8**) where the d_π orbitals are slightly higher in energy and are thus the HOMOs. For **1**−**8**, the d_{xz} and d_{yz} orbitals are higher in energy compared to d_{xy}, while the $d_{x^2-y^2}$ orbital is always higher in energy than d_{z^2}. When LDA and LSDA EC functionals were employed (Figure 5), the order of the orbital energies was found to be roughly similar, but differed in a few respects. Thus, the near-degenerate "d_π" orbitals are always lower in energy than the d_{xy} orbital, which is the HOMO. The $d_{x^2-y^2}$ orbital is higher in energy than the d_{z^2} orbital for **1**−**7**, while in the case of $[pcFe(CN)_2]^{2-}$ (**8**) the order of these orbitals is reversed. As can be seen in Figure 4 and 5, the splitting between the $d_{x^2-y^2}$ and d_{z^2} orbitals is considerably smaller for the complexes pcFe(*cyclo*-$C_6H_{11}NC)_2$ (**6**) and $[pcFe(CN)_2]^{2-}$ (**8**). The main reason for this is the destabilization of the iron d_{z^2} orbital due to the shorter iron−axial ligand distances as compared to those in the other tested complexes. In the case of $[pcFe(CN)_2]^{2-}$ (**8**), strong electron donation from the negatively charged cyano groups also serves to destabilize the d_{z^2} orbital. In the case of complexes pcFe(*cyclo*-$C_6H_{11}NC)_2$ (**6**) and pcFe(CO)(dmf) (**7**), which contain at least one axial ligand with strong π-back-donating properties, the d_{xz} and d_{yz} orbitals are significantly stabilized and have lower energies than the pc-centered "a_{1u}" orbital.

It is interesting to compare the calculated iron 2p and 3s orbital energies with the experimentally determined ionization potentials (IPs) (XPS experiments) for the $pcFe(im)_2$ ($Fe_{2p3/2}$: 708.0 eV; Fe_{3s}: 92.5 eV) and $pcFe(3mepy)_2$ ($Fe_{2p3/2}$: 708.1 eV; Fe_{3s}: 92.3 eV) complexes.[19] The reverse-signed 2p and 3s iron orbital energies computed for complexes **1**−**8** [Table 3 and Supporting Information (Tables 4 and 5)] parallel the IP values obtained from the XPS data. In particular, the closest values were obtained using the B3LYP EC functional.

The crystal field splittings, Δ_{cf}, defined as the differences between the orbital energies of d_π (average value) and d_{z^2} for the B3LYP EC functional (Figure 4) or d_{xy} and d_{z^2} {$d_{x^2-y^2}$ for $[pcFe(CN)_2]^{2-}$ (**8**)} for the LDA and LSDA EC functionals (Figure 5) are larger than 1.8 eV, in agreement with the observed low-spin ground state for **1**−**8** (in general, the value of Δ_{cf} parallels the values in the spectrochemical series).[20] It is well known that in the electronic spectra of $pcFeL_2$ and $pcFeL^1L^2$ complexes, the band at around 2.95 eV can be assigned as a metal-to-ligand charge transfer (MLCT) band [d_{xz}, d_{yz} → "b_{1u}" (π*, pc)] since it is sensitive to the nature of the axial ligand.[4f,21] Using the LDA and LSDA EC functionals, the estimated energies of the MLCT bands were in qualitative agreement with the available experimental data, while with the B3LYP EC functional, the obtained values reflected a strong overestimation of the MLCT band energies, which is typical of ground-state calculations with hybrid DFT EC functionals.[22] For all the tested EC functionals, the pc "a_{1u}" orbital was found to be higher in energy than the pc "a_{2u}" orbital and the orbital separation was of the order of 1 eV or more {except for complex $[pcFe(CN)_2]^{2-}$ (**8**)}, consistent with the fact that the lowest energy π-π* transition has an essentially pure "a_{1u}" (π, pc) → "e_g"(π*, pc) configuration.[21]

Isomer Shifts and Electric Field Gradients

The following five quantities can be derived from Mössbauer experiments, as well as theoretical calculations using SCF wavefunctions:[13] isomer shift (δ), quadrupole splitting (ΔE_Q), the sign of the principal component, V_{zz}, of the EFG tensor, the direction of V_{zz}, and the asymmetry parameter (η). The isomer shift in Mössbauer spectroscopy depends on the electron charge density, ρ(0), at the nucleus and is proportional to changes in ρ(0) with respect to reference compounds. Thus, $\delta = \alpha[\rho(0) - \rho_r(0)]$, where α is a calibration constant and ρ(0) and $\rho_r(0)$ are the electron charge densities at the nuclei in the sample and reference compounds, respectively.[13] For quantum chemical calculations, the $\rho_r(0)$ value is usually replaced by a constant, β, and thus δ is calculated as $\delta = \alpha[\rho(0) - \beta]$. In the ideal case, β corresponds to the electron charge density at the Mössbauer nucleus in the reference compound.[13,23] A good correlation was found when plotting the isomer shift

values against the calculated total electron charge densities on the iron atoms for complexes **1−8** (Figure 6). The calibration constant, α, was evaluated as −0.192 a_o^3 mm s^{-1} for the eight points, with a correlation coefficient r^2 of 0.980 and an r.m.s. error of 0.016 mm s^{-1}. This obtained value of α is close to that recently published and used for CASSCF ab initio calculations of Mössbauer spectral parameters for iron porphyrins (−0.166 a_o^3 mm s^{-1})[23a] and other iron-containing inorganic and organometallic compounds.[24] Moreover, the value obtained for constant β (Figure 6) is close to the calculated total electron charge density at the iron atom in sodium nitroprusside (11617.77 a_o^{-3}). When the calculated value for sodium nitroprusside ρ(0) was included in the ρ(0)/δ correlation analysis, the correlation coefficient did not change ($r^2 = 0.981$), but α changed significantly from −0.19 to −0.26 a_o^3 mm s^{-1}. The latter value of α is closer to that found by Trautwein et al. for some iron-containing inorganic compounds (−0.31 to −0.38 a_o^3 mm s^{-1}).[25] The calibration constant α can also be written as $\alpha = (4Ze^2R^2c/5E_\gamma)\cdot(\delta R/R) = C\cdot(\delta R/R)$,[13] where R is the average nuclear radius and δR is the change in radius on going from the ground to the excited state. Having estimated α from a ρ(0)/δ correlation analysis and calculated the total electron charge density for sodium nitroprusside, which is used as a reference compound, it is possible to estimate the value of $\delta R/R$ in order to support our isomer shift calculations on $pcFeL_2$ and $pcFeL^1L^2$ complexes. Using the value of $C = 0.3083\cdot10^3$ a_o^3 mm s^{-1} obtained by Alton and Swift,[24c] the $\delta R/R$ values were estimated (average for **1−8**) as $-6.16\cdot10^{-4}$ and $-8.43\cdot10^{-4}$ when α is −0.19 and −0.26 a_o^3 mm s^{-1}, respectively. Both these values are in reasonable agreement with previously published results.[24] Although the computed values of α and $\delta R/R$ estimated from the correlation analysis are different, the present results are very promising because they suggest that Mössbauer isomer shifts in iron pcs, and probably in other iron-containing compounds as well, can be calculated with high accuracy using modern DFT methods.

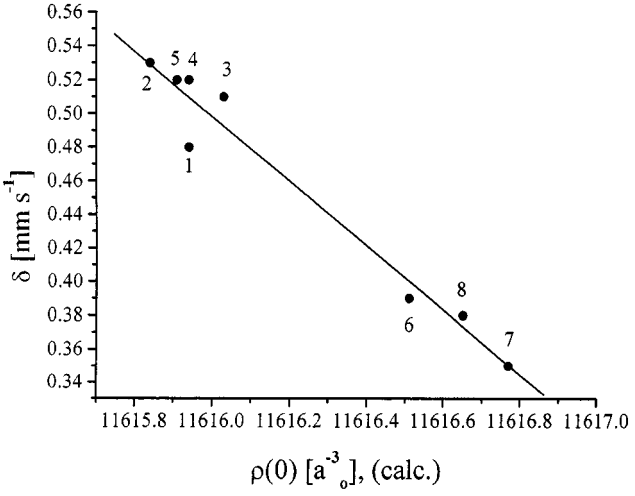

Figure 6. Correlation between the observed Mössbauer isomer shifts and the calculated total electron densities at the ^{57}Fe nucleus by the B3LYP DFT method; numerical values are given in Table 2

The Mössbauer quadrupole splittings and asymmetry parameters, η, for compounds **1−8**, calculated using the locally dense basis set approach in conjunction with the B3LYP, LSDA, and LDA EC functionals are presented in Table 2, while those calculated with the B3LYP EC functional are shown graphically in Figure 7. The results of our DFT calculations using the B3LYP EC functional demonstrate that the magnitude of the ΔE_Q values, the sign and orientation of the principal component of the EFG tensor, and the η values, are all in agreement with the experimental data. A correlation coefficient of $r^2 = 0.982$, with an r.m.s. error of 0.14 mm s^{-1}, has been found between the predicted and experimental ΔE_Q values for complexes **1−8**. These results are very promising, since they suggest that DFT methods can now be applied with some reliability to predicting both Mössbauer quadrupole splittings and Mössbauer isomer shifts in large systems such as phthalocyanines, for which other methods based on semiempirical and conventional ab initio quantum mechanical levels have hitherto proved inadequate. For example, for the complex $pcFe(mepip)_2$ (**2**), we have computed ΔE_Q and δ values of 2.18 and 0.52 mm s^{-1}, respectively, which can be quite favorably compared with the experimental values of 2.28 and 0.53 mm s^{-1}. Similarly, for complex $pcFe(cyclo\text{-}C_6H_{11}NC)_2$ (**6**), even though the EFG is much smaller, there is likewise good accord between the computed (0.55 and 0.35 mm s^{-1}) and experimental (0.69 and 0.39 mm s^{-1})[5d] values. Among complexes **1−8**, the computed and experimental ΔE_Q values only differ significantly in the case of the complex $[pcFe(CN)_2]^{2-}$ (**8**) (marked as **8a** in Table 2 and indicated by an unfilled circle in Figure 7); this large deviation could originate from the uncompensated lattice effects of two positively charged counterions, as well as from deficiencies in the basis sets and the functional used. Indeed, when, for example, two sodium ions were placed in the positions of the cationic nitrogen atoms of PNP counterions, as determined experimentally for $(PNP)_2[pcFe(CN)_2]$,[7c] the calculated ΔE_Q value was found to be in excellent agreement with the experimental data (marked as case **8b** in Table 2). The large η value calculated in the case of **8b** can easily be explained by taking into consideration the fact that in the actual crystal of $(PNP)_2[pcFe(CN)_2]$, the iron pc is symmetrically surrounded by four PNP cations,[7c] whereas in our model calculation only two sodium ions were used in order to compensate for the negative charge of the $[pcFe(CN)_2]^{2-}$ moiety. The observation that V_{zz} is directed along the Na−Na axis supports this explanation. As pointed out in the literature,[4a][5a][5b] the axial ligand in the complex $pcFe(14en)_2$ (**1**) is probably stabilized through intramolecular hydrogen bond formation. It is thus interesting to compare the experimental Mössbauer spectral parameters with those calculated for the open-chain (**1a**) and intramolecularly hydrogen-bonded conformations (**1b**). The calculated Mössbauer spectral parameters for **1a** are close to those calculated for the complex $pcFe(BuNH_2)_2$ (**3**), for which only an open-chain conformation is possible. On the other hand, the calculated Mössbauer spectral parameters for **1b** are in close agreement with the experimental data, sup-

porting the previously proposed hypothesis concerning the possibility of intramolecular hydrogen bonding in this complex. Additional evidence concerning the axial ligand conformation in pcFe(14en)$_2$ (**1**) can be obtained from a comparison of the experimental ^{1}H NMR spectra of pcFe(14en)$_2$ (**1**) and pcFe(BuNH$_2$)$_2$ (**3**) and the computed isotropic shifts for the protons of the axial ligands. It is well known that in the ^{1}H NMR spectra of pcFeL$_2$ complexes the protons of the axial ligands are strongly shielded by the ring current of the pc ring, this effect depending on the electronic structures of the axial ligands and their positions in relation to the pc plane.[4a−4e] The experimental chemical shifts for the coordinated NH$_2$ protons in pcFe(14en)$_2$ (**1**) and pcFe(BuNH$_2$)$_2$ (**3**), as well as the calculated chemical shifts and shieldings are summarized in Table 4, together with the calculated NMR parameters for ^{57}Fe. Again, the calculated chemical shifts for **1a** and pcFe(BuNH$_2$)$_2$ (**3**) are close, while the values for **1b** differ significantly in accord with the experimental data. Finally, the computed ^{57}Fe chemical shifts have reasonable values, as judged on the basis of the available experimental and calculated data for bis-axially coordinated iron(II) porphyrins.[9c,26] Since the calculated η values for complexes **1**−**8** are small, and the direction of V_{zz} corresponds almost exactly with the molecular z axis, in agreement with the experimental data,[4c,4d] the V_{zz} components of the EFG can be divided into the so-called valence, covalence, and lattice contributions.[9a,14,15] The valence contribution is approximately proportional to the anisotropy of the Fe(3d) and Fe(4p) shell occupations. The covalence contribution is almost proportional to the Fe−ligand overlap population, while the ligand contribution arising from the cores and valence electrons of all ligand atoms is roughly proportional to the charge on the atom of the ligand directly coordinated to the iron and the Fe−ligand distance as Z/r^3. Taking all these factors into consideration, it appears possible to discuss the influence of each contribution on the EFG in complexes **1**−**8**. Unfortunately, however, as discussed in the literature,[27,28] the Mulliken population and charge distribution analysis are completely inappropriate for systems containing a large number of diffuse Gaussian-like functions. Thus, considering the fact that for bis-axially coordinated iron pcs and porphyrins, particularly for those with experimentally large ΔE_Q values, the valence contribution usually dominates over the covalent and ligand contributions,[9a] the anisotropy of the Fe(3d) and Fe(4p) shell occupations can be expected to be around 0.3−0.5 electrons for complexes **1**−**5** and **7**. However, a Mulliken population analysis gave an anisotropy of Fe(3d) shell occupation of no more than 0.23 electrons. The covalent contribution, which is based on the Mulliken population analysis, is also inappropriate because the overlap populations have negative (!) values for all the Fe−ligand bonds in all the cases tested and, of course, do not have any physical meaning. The most attractive alternative to the Mulliken population analysis is based on the use of Natural Bond Orbital (NBO) population and charge distribution analysis.[28] However, the NBO package, as implemented in the Gaussian-98 program family and GAMESS (USA) software, is unable to operate with such large and highly covalent systems as found in phthalocyanines. Since the Gaussian-98W program is based on Gaussian-type basis functions, the next questions to be addressed are the influence of various basis sets, particularly on the iron atom, and of the functionals on the calculated EFG components and thus the ΔE_Q values. From our comparative calculations of the EFG components for the complexes pcFe(mepip)$_2$ (**2**) and [pcFe(CN)$_2$]$^{2-}$ (**8**) using the Wachters−Hay all-electron basis set (611111111/51111/311) for the iron ion, with and without the inclusion of diffuse functions, and using the original Wachters' all-electron basis set for the iron ion,[16,17] with and without the inclusion of polarization functions, it can be concluded that the influence of diffuse and polarization functions is small, and that the ΔE_Q values computed with the Wachters−Hay all-electron basis set are in better agreement with the experimental data [Supporting Information (Table 6)]. The ΔE_Q values calculated with pure DFT functionals (LDA and LSDA), as well as those estimated from Gaussian-98W calculations of ρ(0), are presented in Table 2. Inspection of these results reveals that the estimated values of ρ(0) are in good agreement with the expected values, while both functionals are systematically overestimated with respect to the experimentally observed ΔE_Q values for complexes **1**−**7**. However, in both cases, a good correlation between calculated and experimental ΔE_Q values is observed, with correlation coefficients r^2 of 0.957 and 0.993 and r.m.s. errors of 0.18 and 0.09 mm s^{-1} for the LDA and LSDA EC functionals, respectively. One of the advantages of the hybrid DFT B3LYP EC functional is that it is not necessary to take Sternheimer corrections into consideration when ΔE_Q values are computed from the EFG tensor components. On the other hand, for pure DFT methods, Sternheimer corrections must be applied when ΔE_Q values are computed, at least for the LDA functional, as pointed out by the authors.[9a,14,15] Since it is impossible to separate valence, covalence, and lattice contributions to the EFG using the Gaussian-98W

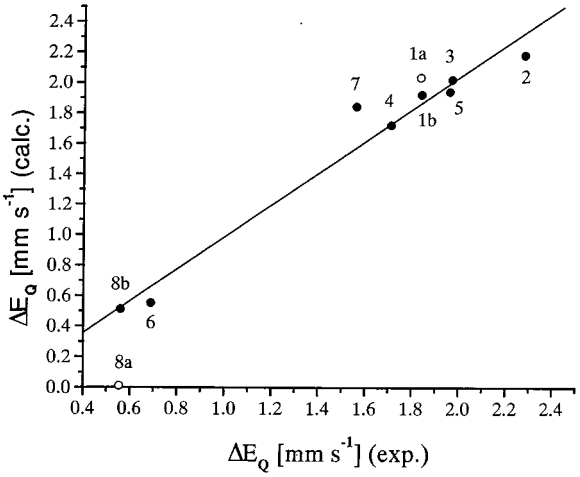

Figure 7. Correlation between the experimental and calculated (by the B3LYP DFT method) Mössbauer quadrupole splittings in complexes **1**−**8**; numerical values are given in Table 2

Table 4. Calculated and experimental ^{1}H (coordinated NH_2 group) and ^{57}Fe NMR shielding (ppm) for complexes **1** and **3**

Complex	Atom	Shielding tensor element. σ_{11}	σ_{22}	σ_{33}	Isotropic shielding σ_i	Isotropic shift δ_i Calcd.	Exp.
1a	Fe[a]	−14435	−14228	−7326	−11996	9084	
	NH_2 [b]	35.4265	38.2657	47.2148	40.3023	−8.38	−6.58
1b	Fe	−13944	−13810	−6634	−11462	8551	
	NH_2	29.9200	37.0061	47.1299	38.0187	−6.10	−6.58
3	Fe	−14635	−14538	−7305	−12159	9247	
	NH_2	36.8145	39.6581	47.2216	41.2314	−9.31	−7.44

[a] The isotropic shifts are obtained from the computed absolute shielding as: $\delta = -2912 - \sigma$, where the value of $\delta = -2912$ refers to the computed absolute shielding in $Fe(CO)_5$. − [b] The isotropic shifts are obtained from the computed absolute shielding as: $\delta = 31.9197 - \sigma$, where the value of $\delta = 31.9197$ refers to the computed absolute shielding of the protons in TMS at the B3LYP/6−31G(d) level.

and GAMESS (USA) programs, we were unable to accurately calculate ΔE_Q values for complexes **1**−**8** applying Sternheimer corrections, even at the limits of the simple Townes−Dailey approximation.[16,29]

Thus, it is concluded that DFT methods, particularly employing the B3LYP EC functional, are now able to reproduce and predict the Mössbauer spectral parameters of bis-axially coordinated iron(II) pcs with high accuracy, in contrast to semiempirical and conventional ab initio methods. The hybrid B3LYP EC functional can be recommended as the best approximation for the evaluation of total electron charge density and electric field gradient on a Mössbauer nucleus using the Gaussian-98W program, while the LDA and LSDA EC functionals are only useful with software implementing an alternative to Mulliken population analysis algorithms.[9a,14,15]

Conclusions

In this paper, we have discussed the relationship between the nature of the axial ligands in bis-axially coordinated iron(II) phthalocyanines and their electronic structures, structural, and Mössbauer spectral parameters. The first example of a crystal structure of a low-spin iron(II) pc bis-axially coordinated by aliphatic amines has been presented, and the reasons for the observed elongation of the Fe−N(ax) bond length have been discussed. The electronic structures of numerous $pcFeL_2$ and $pcFeL^1L^2$ complexes have been assessed on the basis of density functional theory calculations. The results constitute the first accurate calculations of Mössbauer quadrupole splittings and isomer shifts for bis-axially coordinated low-spin iron(II) phthalocyanine complexes by means of density functional theory methods. A good correlation between the experimental and theoretical values has been obtained using the hybrid B3LYP EC functional, while with the pure DFT LDA and LSDA functionals, it has been found that Sternheimer corrections need to be taken into consideration when quadrupole splittings are computed. Of particular interest is the reproduction of the Mössbauer spectral parameters of complexes with conformationally flexible axial ligands.

Experimental Section

Synthesis: Compounds **1**−**4** were synthesized according to standard methods.[4a−4c][5a−5c] All the complexes were characterized by their UV/Vis, ^{1}H NMR, and Mössbauer spectra, as well as by elemental analysis [Supporting Information (Table 1)]. In addition, an experimental geometry for $pcFe(mepip)_2$ (**2**) was determined by an X-ray crystallographic analysis.

X-ray Crystallography: A single crystal of $pcFe(mepip)_2$ (**2**) was obtained by slowly evaporating the solvents from a benzene/heptane (1:3, v/v) solution of the complex over a period of a week. Diffraction data were collected with a CAD-4 diffractometer using Mo-K_α radiation ($\lambda = 0.71073$ Å). The structure was solved by full-matrix least-squares techniques on F^2 for all data, with anisotropic thermal parameters for non-hydrogen atoms and isotropic parameters for hydrogen atoms. All calculations were performed using the SHELXTL-93 software.[30] General information concerning the crystal structural determination is given in Table 5. Crystallographic data (excluding structural factors) for **2** have been deposited at the Cambridge Crystallographic Data Centre (CCDC) as supplementary publication no. CCDC-145879. Copies of the data

Table 5. Crystal data and structure refinement for **2**

Empirical formula	$C_{56}H_{68}FeN_{12}$
Formula mass	965.08
T	293 K
Crystal system	monoclinic
Space group	$P2(1)/a$
Unit cell dimensions	$a = 11.792(2)$ Å
	$b = 17.213(3)$ Å
	$c = 12.645(3)$ Å
	$\beta = 102.58(3)°$
Volume	2505.0(9) Å^3
Z	4
Standards number	3
Standards interval time	60 min
Standards decay	0.01%
Density (calculated)	1.279 mg/m^3
Absorption coefficient	0.352 mm^{-1}
$F(000)$	1028
Crystal size	0.42 × 0.31 × 0.28 mm
θ range for data collection	1.65−22.47°
Index ranges	$-12 \le h \le 12$
	$0 \le k \le 18$
	$0 \le l \le 13$
Reflections collected	2036
Independent reflections	1925 [R(int.) = 0.0124]
Data/restraints/parameters	1925/0/434
Final R indices [$I > 2\sigma(I)$]	$R_1 = 0.0305$ $wR_2 = 0.0843$
R indices (all data)	$R_1 = 0.0305$ $wR_2 = 0.0843$
Extinction coefficient	0.0000(4)
Largest diff. peak and hole	0.244 and −0.232 eÅ^{-3}

can be obtained free of charge on application to the CCDC, 12 Union Road, Cambridge CB2 1EZ, U.K. [Fax: (internat.) + 44-1223/336-033; E-mail: deposit@ccdc.cam.ac.uk].

Mössbauer Spectroscopy: Mössbauer spectra were recorded using a GRS-4M spectrometer in constant acceleration mode. The source was ^{57}Co in a chromium matrix with an initial activity of 50 mCi. Isomer shifts were referenced to sodium nitroprusside at 298 K (the conversion factor from sodium nitroprusside to iron foil is -0.257 mm s^{-1}).

Computational Aspects: Total electron charge density and electric field gradient calculations were carried out using Gaussian-98W software.[31] In order to negate convergence problems, the following procedures were used for the energy convergence and electric field gradient calculations: Step 1: All atoms were represented by a 3-21G* basis set at the Hartree−Fock level. Step 2: As Step 1, but iron was represented by a Wachters−Hay all-electron basis set (611111111/51111/311) using the scaling factors of Raghavachari and Trucks,[32] and the 6-31G* basis set was used for all atoms directly attached to or two bonds away from iron. Step 3: As Step 2, but using the respective exchange-correlation functional. The following exchange-correlation (EC) functionals were used for the DFT calculations: Becke's three-parameter exchange functional with the Lee, Parr, and Yang correlation functional (B3LYP),[33] the Local Density Approximation (LDA) functional,[34] and the Local Spin Density exchange functional with the Vosko, Wilk, and Nusair correlation functional (LSDA).[35] Step 4: As Step 3, but a 6-311++G(2d) basis set was used for all atoms directly attached to iron. Since Raghavachari and Trucks recommended both scaling and the inclusion of diffuse functions when using a Wachters−Hay basis set for the first transition row elements,[32] we compared electric field gradient calculations on the complexes pcFe(mepip)$_2$ (**2**) and [pcFe(CN)$_2$]$^{2-}$ (**8**) using a Wachters−Hay basis set for iron with and without diffuse functions. Moreover, since the Wachters−Hay basis set implemented in the Gaussian-98W program and the set originally reported by Wachters[36] are different, we also compared electric field gradient calculations on the complexes pcFe(mepip)$_2$ (**2**) and [pcFe(CN)$_2$]$^{2-}$ (**8**) using the original Wachters' all-electron basis set for iron (62111111/331211/3111), with and without the inclusion of polarization functions.[37] A more detailed discussion concerning the influence of different Wachters' basis sets at the iron atom on the electric field gradient tensor elements in the complexes pcFe(mepip)$_2$ (**2**) and [pcFe(CN)$_2$]$^{2-}$ (**8**) is given in the Results and Discussion section. The total electron charge densities on the iron atoms were estimated using Gaussian-98W software with the help of the atoms-in-molecules (AIM) algorithm.[21] Since the current codes of AIM included in the Gaussian-98W program can only operate up to five digits when total electron densities are computed (this leads to an error of 0.1−0.2 mm s^{-1} in the isomer shift calculations), the total electron charge densities on the iron atoms were calculated more precisely using GAMESS (USA) software[38] with the help of converged wavefunctions obtained from the previous DFT calculations [DFT is not currently included in GAMESS (USA)]. The components of the electric field gradient tensor (EFG), V_{ii}, were directly calculated using a Gaussian-98W program based on the following expression: $V_{ij} = \partial^2/\partial_{xi}\partial_{xj}[\Sigma Z_A e/(|r_A - r_{Fe}|) - \int e\rho(r)/(|r - r_{Fe}|)dr]$, where r_{Fe} is the position vector of the iron nucleus, ρ(r) is the first-order density matrix of electrons, and r_A and Z_A are the position vector of the nucleus of atom A and the nuclear charge, respectively. The measured ΔE_Q is related to the major component, V_{zz}, of the EFG tensor according to the following expression[33] where e is the electron charge, Q is the quadrupole moment of the $I^* = 3/2$ 14.4 keV excited state, and η is the asymmetry parameter [$\eta = |V_{xx} - V_{yy}|/|V_{zz}|$ ($V_{zz} > V_{yy} > V_{xx}$)].

$$\Delta E_Q = (1/2)eQV_{zz}(1 + \eta^2/3)^{1/2}$$

The magnitude of the nuclear quadrupole moment Q was chosen as 0.16 barn on the basis of the most recently determined value.[9b,39] This value is also close to that used by Trautwein's group (0.15 barn) for calculations of Mössbauer spectral parameters using an LDA EC functional.[9a,14,15] As recently shown[9b−9d] for DFT calculations with a B3LYP hybrid EC functional, Sternheimer corrections do not have to be taken into account when ΔE_Q is predicted on the basis of the DFT calculations. Experimentally determined geometries for pcFe(mepip)$_2$ (**2**), pcFe(mim)$_2$ (**4**), pcFe(mepy)$_2$ (**5**), pcFe(*cyclo*-C$_6$H$_{11}$NC)$_2$ (**6**), pcFe(CO)(dmf) (**7**), and [pcFe(CN)$_2$]$^{2-}$ (**8**) were used,[7] with the modification that C−H and N−H bond lengths were extended to typical values (1.05−1.09 Å); the most important structural parameters are given in Table 1. Since X-ray crystal data are not available for the complexes pcFe(14en)$_2$ (**1**) and pcFe(BuNH$_2$)$_2$ (**3**), the pc core was reproduced from the experimental geometry of pcFe(mepip)$_2$ (**2**), while in each case the axial ligands were placed at an Fe−N distance of 2.08 Å and their geometries were optimized at the semiempirical PM3 level[40] using the Polack−Ribiere algorithm[41] with help of the HyperChem 5.1Pro software.[42] Since the experimental geometries for pcFe(mepip)$_2$ (**2**) and pcFe(mepy)$_2$ (**5**) are quite similar, in spite of the pronounced difference between the axial ligands (mepip is a pure and strong σ-donor, while mepy is a moderate σ-donor and π-acceptor),[5b,12] the structural parameters of the pc core were considered to be representative of those of pcFe(14en)$_2$ (**1**) and pcFe(BuNH$_2$)$_2$ (**3**) as well. The choice of structural parameters for the axial ligands in pcFe(14en)$_2$ (**1**) and pcFe(BuNH$_2$)$_2$ (**3**) was not so straightforward. However, our electronic structural calculations on pcFe(14en)$_2$ (**1**) and pcFe(BuNH$_2$)$_2$ (**3**) showed the geometry of the axial ligands as obtained by optimization at the semiempirical PM3 level to be adequate for the prediction of Mössbauer and ^{1}H NMR spectral parameters. The molecular z axis was defined by the iron atom and the two atoms of the axial ligands directly coordinated to it. The rotation barriers of the axial ligands were calculated using the HyperChem 5.1Pro software at the molecular mechanics (MM+ force field) and semiempirical (PM3) levels. In all such model calculations, the phthalocyanine core and one axial ligand were kept fixed, while the other axial ligand was rotated in steps of 10° about the molecular z axis. The height of rotation barrier was then derived from the variation of the total energy as a function of the rotation angle. The NMR shielding tensor elements were calculated using the gauge-including atomic orbital (GIAO) method[43] with the help of the Gaussian-98W program. The aforementioned basis set with the hybrid B3LYP EC functional (Step 4) was used for the calculations of the NMR isotropic shifts.

Supporting Information Available: Spectroscopic and analytical data for the pcs used in this study. Atomic coordinates, equivalent isotropic displacement parameters, bond lengths and angles for **2**. Calculated orbital energies for complexes **1**−**8** using the LSDA and LDA EC functionals. Calculated, using the B3LYP hybrid EC functional and different basis sets for iron, Mössbauer quadrupole splittings in complexes **2** and **8** (see the note on the first page of this article).

Acknowledgments

The authors are grateful to Dr. E. V. Polshin for assistance in performing the Mössbauer experiments. V. N. N. thanks the JSPS

(grant no. P98418) and INTAS (grant no. 97-0791) for financial support. This research was partly supported by a Grant-in-Aid for Scientific Research (B) No. 11440192 and by funds for the Priority Area "Creation of Novel Delocalized Electron Systems", Award No. 12020206, from the Ministry of Education, Science, Sports, and Culture, Japan, and the Scandinavia−Japan Sasakawa Foundation to N. K.

[1] J. T. Groves, K. Shalyaev, J. Lee, in: *The Porphyrin Handbook*, vol. 4 (Eds.: K. M. Kadish, K. M. Smith, R. Guilard), Academic Press, San Diego, **2000**, pp. 17−40.

[2] O. L. Kaliya, E. A. Luk'yanets, in: *Fundamental Research in Homogeneous Catalysis*, vol. 1 (Ed.: E. A. Shilov), Gordon and Breach Sci. Publ., New York, London, **1986**, pp. 1−35.

[3] S. Neya, in: *Phthalocyanines: Properties and Applications*, vol. 4 (Eds.: C. C. Leznoff, A. B. P. Lever), VCH, New York, **1996**, pp. 447−479.

[4] [4a] V. N. Nemykin, V. Y. Chernii, V. V. Trachevskii, S. V. Volkov, *Ukr. Khim. Zh.* **1997**, *63*, 4. − [4b] N. A. Kostromina, V. Y. Chernii, V. N. Nemykin, I. V. Komarov, *Zh. Neorg. Khim.* **1995**, *40*, 1491. − [4c] B. W. Dale, R. J. R. Williams, P. R. Edwards, C. E. Johnson, *Trans. Faraday Soc.* **1968**, *64*, 3011. − [4d] C. K. Choy, J. R. Mooney, M. E. Kenney, *J. Magn. Reson.* **1979**, *35*, 1. − [4e] J. Maskasky, M. E. Kenney, *J. Am. Chem. Soc.* **1973**, *95*, 1443. − [4f] E. A. Ough, M. J. Stillman, *Inorg. Chem.* **1994**, *33*, 573. − [4g] J. J. Watkins, A. L. Balch, *Inorg. Chem.* **1975**, *14*, 2720. − [4h] D. A. Sweigart, *J. Chem. Soc., Dalton Trans.* **1976**, 1476. − [4i] M. Hanack, A. Hirsch, *Synth. Met.* **1989**, *29*, F9.

[5] [5a] V. N. Nemykin, V. Y. Chernii, E. V. Polshin, S. V. Volkov, *Ukr. Khim. Zh.* **1997**, *63*, 75. − [5b] V. N. Nemykin, A. E. Polshina, V. Y. Chernii, E. V. Polshin, N. Kobayashi, *J. Chem. Soc., Dalton Trans.* **2000**, 1019. − [5c] G. V. Ouedraogo, C. More, Y. Richard, D. Benlian, *Inorg. Chem.* **1981**, *20*, 4387. − [5d] M. Hanack, in: *Phthalocyanines: Properties and Applications*, vol. 2 (Eds.: C. C. Leznoff, A. B. P. Lever), VCH, New York, **1993**, pp. 43−96. − [5e] F. Calderazzo, S. Frediani, B. R. James, G. Pampaloni, K. J. Reimer, J. R. Sams, A. M. Serra, D. Vitalli, *Inorg. Chem.* **1982**, *21*, 2302. − [5f] B. W. Dale, R. J. R. Williams, P. R. Edwards, C. E. Johnson, *Trans. Faraday Soc.* **1968**, *64*, 620. − [5g] D. C. Grenoble, H. G. Drickamer, *J. Chem. Phys.* **1971**, *55*, 1624. − [5h] R. Taube, *Pure Appl. Chem.* **1974**, *38*, 427. − [5i] B. R. James, J. R. Sams, T. B. Tsin, K. J. Reimer, *J. Chem. Soc., Chem. Commun.* **1978**, 746.

[6] [6a] V. Valenti, P. Fantucci, F. Cariati, G. Micera, M. Petrera, N. Burriesci, *Inorg. Chim. Acta* **1988**, *148*, 191. − [6b] R. Taube, *Z. Chem.* **1966**, *6*, 8. − [6c] P. Coppens, L. Li, *J. Chem. Phys.* **1984**, *81*, 1983.

[7] [7a] F. Cariati, F. Marazzoni, M. Zocchi, *J. Chem. Soc., Dalton Trans.* **1978**, 1018. − [7b] C. Ercolani, F. Monacelli, S. Dzugan, V. L. Goedken, G. Pennesi, G. Rossi, *J. Chem. Soc., Dalton Trans.* **1991**, 1309. − [7c] W. Kalz, H. Homborg, H. Kuppers, B. J. Kennedy, K. S. Murray, *Z. Naturforsch.* **1984**, *39b*, 1478. − [7d] M. Hanack, G. Renz, J. Strahle, S. Schmid, *Chem. Ber.* **1988**, *121*, 1479. − [7e] M. Hanack, G. Renz, J. Strahle, S. Schmid, *J. Org. Chem.* **1991**, *56*, 3501. − [7f] F. Calderazzo, G. Pampaloni, D. Vitali, I. Collamati, J. Dessy, V. Fares, *J. Chem. Soc., Dalton Trans.* **1980**, 1965. − [7g] F. Calderazzo, G. Pampaloni, D. Vitali, G. Pelizzi, I. Collamati, S. Frediani, A. M. Serra, *J. Organomet. Chem.* **1980**, *191*, 217.

[8] R. G. Parr, W. Yang, *Density Functional Theory of Atoms and Molecules*, Oxford University Press, New York, **1989**.

[9] [9a] M. Grodzicki, H. Flint, H. Winkler, A. F. Walker, A. X. Trautwein, *J. Phys. Chem.* **1997**, *101*, 4202. − [9b] R. H. Havlin, N. Godbout, R. Salzmann, M. Wojdelski, W. Arnold, C. E. Schulz, E. Oldfield, *J. Am. Chem. Soc.* **1998**, *120*, 3144. − [9c] N. Godbout, R. H. Havlin, R. Salzmann, P. G. Debrunner, E. Oldfield, *J. Phys. Chem.* **1998**, *102*, 2342. − [9d] N. Godbout, L. K. Sanders, R. Salzmann, R. H. Havlin, M. Wojdelski, E. Oldfield, *J. Am. Chem. Soc.* **1999**, *121*, 3829.

[10] M. K. Safo, F. A. Walker, A. M. Raitsimring, W. P. Walters, D. P. Dolata, P. G. Debrunner, W. R. Scheidt, *J. Am. Chem. Soc.* **1994**, *116*, 7760; O. Q. Munro, P. S. Madlala, R. A. F. Warby, T. B. Seda, G. Hearne, *Inorg. Chem.* **1999**, *38*, 4724.

[11] J. P. Collman, J. L. Hoard, N. Kim, G. Lang, C. A. Reed, *J. Am. Chem. Soc.* **1975**, *97*, 2676.

[12] S. S. Fielder, M. C. Osborne, A. B. P. Lever, W. J. Pietro, *J. Am. Chem. Soc.* **1995**, *117*, 6990; V. N. Nemykin, A. E. Polshina, E. V. Polshin, N. Kobayashi, *Mendeleev Commun.* **2000**, 54.

[13] P. Gutlich, R. Link, A. X. Trautwein, *Mössbauer Spectroscopy and Transition Metal Chemistry*, Springer, Berlin, Heidelberg, **1978**; T. E. Cranshaw, B. W. Dale, G. O. Longworth, C. E. Johnson, *Mössbauer Spectroscopy and its Applications*, Cambridge University Press, Cambridge, **1985**.

[14] H. Paulsen, M. Krockel, M. Grodzicki, E. Bill, A. X. Trautwein, G. J. Liegh, J. Silver, *Inorg. Chem.* **1995**, *34*, 6244.

[15] M. Grodzicki, V. Männing, A. X. Trautwein, M. Friedt, *J. Phys. B* **1987**, *20*, 5595; M. Grodzicki, S. Lauer, A. X. Trautwein, A. Vera, *Adv. Chem. Ser.* **1981**, *194*, 3.

[16] C. H. Townes, B. P. Dailey, *J. Chem. Phys.* **1949**, *17*, 782.

[17] J. E. Ridley, M. C. Zerner, *Theor. Chim. Acta* **1976**, *42*, 223; A. D. Bacon, M. C. Zerner, *Theor. Chim. Acta* **1979**, *53*, 21.

[18] M. J. Stillman, T. Nyokong, in: *Phthalocyanines: Properties and Applications*, vol. 1 (Eds.: C. C. Leznoff, A. B. P. Lever), VCH, New York, **1989**, pp. 133−289.

[19] G. V. Ouedraogo, D. Benlian, L. Porte, *J. Chem. Phys.* **1980**, *73*, 642.

[20] A. B. P. Lever, *Inorganic Electronic Spectroscopy*, Elsevier, Amsterdam, **1984**.

[21] J. Cioslowski, A. Nanayakkara, M. Challacombe, *Chem. Phys. Lett.* **1993**, *203*, 137.

[22] *Density Functional Methods in Chemistry and Material Science* (Ed.: M. Springborg), Wiley, New York, **1997**.

[23] [23a] S. Yamamoto, J. Teraoka, H. Kashiwagi, *J. Chem. Phys.* **1988**, *88*, 303. − [23b] S. Obara, H. Kashiwagi, *J. Chem. Phys.* **1982**, *77*, 3155.

[24] [24a] P. S. Bagus, U. I. Walgren, J. Almlöf, *J. Chem. Phys.* **1976**, *64*, 2324. − [24b] A. X. Trautwein, F. E. Harris, A. J. Freeman, J. P. Desclaux, *Phys. Rev. B* **1975**, *11*, 4101. − [24c] L. R. B. Elton, A. Swift, *Proc. Phys. Soc. London* **1964**, *64*, 125.

[25] A. X. Trautwein, F. E. Harris, *Theor. Chim. Acta* **1973**, *30*, 45.

[26] J. R. Polam, J. L. Wright, K. A. Christensen, F. A. Walker, H. Flint, H. Winkler, M. Grodzicki, A. X. Trautwein, *J. Am. Chem. Soc.* **1996**, *118*, 5272.

[27] H. P. Luthi, J. H. Ammeter, J. Almlöf, K. Faergi, *J. Chem. Phys.* **1982**, *77*, 2002; J. B. Collins, A. Streitwieser, *J. Comput. Chem.* **1980**, *1*, 81.

[28] A. E. Reed, R. B. Weinstock, F. Weinhold, *J. Chem. Phys.* **1985**, *83*, 735; F. Weinhold, *Natural Bond Orbital Analysis Programs*, Board of Regents of the University of Wisconsin System, **1999**.

[29] R. Reschke, A. X. Trautwein, *Theor. Chim. Acta* **1978**, *47*, 85.

[30] G. M. Sheldrick, *SHELXTL-93*, *A Program for the Refinement of Crystal Structures*, University of Göttingen, Germany, **1993**.

[31] M. J. Frisch, G. W. Trucks, H. B. Schlegel, G. E. Scuseria, M. A. Robb, J. R. Cheeseman, V. G. Zakrzewski, J. A. Montgomery, R. E. Stratmann, J. C. Burant, S. Dapprich, J. M. Millam, A. D. Daniels, K. N. Kudin, M. C. Strain, O. Farkas, J. Tomasi, V. Barone, M. Cossi, R. Cammi, B. Mennucci, C. Pomelli, C. Adamo, S. Clifford, J. Ochterski, G. A. Petersson, P. Y. Ayala, Q. Cui, K. Morokuma, D. K. Malick, A. D. Rabuck, K. Raghavachari, J. B. Foresman, J. Cioslowski, J. V. Ortiz, B. B. Stefanov, G. Liu, A. Liashenko, P. Piskorz, I. Komaromi, R. Gomperts, R. L. Martin, D. J. Fox, T. Keith, M. A. Al-Laham, C. Y. Peng, A. Nanayakkara, C. Gonzalez, M. Challacombe, P. M. W. Gill, B. G. Johnson, W. Chen, M. W. Wong, J. L. Andres, M. Head-Gordon, E. S. Replogle, J. A. Pople, *Gaussian-98W (Revision A.7)*, Gaussian, Inc., Pittsburgh, PA, **1998**.

[32] P. J. Hay, *J. Chem. Phys.* **1977**, *66*, 4377; K. Raghavachari, G. W. Trucks, *J. Chem. Phys.* **1989**, *91*, 1062.

[33] A. D. Becke, *J. Chem. Phys.* **1993**, *98*, 5648.

[34] W. Kohn, L. J. Sham, *Phys. Rev. A* **1965**, *140*, 1133.

[35] S. H. Vosko, L. Wilk, M. Nusair, *Can. J. Phys.* **1980**, *98*, 1200.

[36] A. J. H. Wachters, *J. Chem. Phys.* **1970**, *52*, 1033.

[37] Basis sets were obtained from the *Extensible Computational Chemistry Environment Basis Set Database, Version 1.0*, as developed and distributed by the Molecular Science Computing Facility, Environment and Molecular Sciences Laboratory, which is a part of the Pacific Northwest Laboratory, P. O. Box 999, Richland, WA 99352, and is funded by the U.S. Depart-

ment of Energy under contract DE-AC06−76RLO 1830. Contact David Feller, Karen Schuchardt, or Don Jones for further information.
[38] M. W. Schmidt, K. K. Baldridge, J. A. Boatz, S. T. Elbert, M. S. Gordon, J. H. Jensen, S. Koseki, N. Matsunaga, K. A. Nguyen, S. J. Su, T. L. Windus, M. Dupuis, J. A. Montgomery, *J. Comput. Chem.* **1993**, *14*, 1347.
[39] P. Dufek, P. Bhala, K. Schwarz, *Phys. Rev. Lett.* **1995**, *75*, 3545.
[40] J. J. P. Stewart, *J. Comp. Aided Mol. Design* **1990**, *4*, 1.
[41] *HyperChem Computational Chemistry*, Hypercube, Inc., Gainesville, FL, **1996**.
[42] *HyperChem 5.1 Pro*, Hypercube, Inc., Gainesville, FL, USA, **1997**.
[43] K. Wolinski, J. F. Hilton, P. Pulay, *J. Am. Chem. Soc.* **1990**, *112*, 8251.

Received August 17, 2000
[I00321]

ε-Caprolactam as a Donor Ligand for Lanthanide Halides: Formation of Cationic $[Ln(C_6H_{11}NO)_6Cl]^{2+}$ and $[Ln(C_6H_{11}NO)_4Cl_2]^{+}$ Complexes

William J. Evans,*[a] Cy H. Fujimoto,[a] Michael A. Greci,[a] and Joseph W. Ziller[a]

Keywords: Lanthanides / Cations / ε-Caprolactam / Halides / O ligands

Examination of the coordination chemistry of ε-caprolactam with lanthanide trichlorides reveals that cationic ε-caprolactam-solvated complexes of two types can be obtained from acetonitrile depending on the size of the metal. The larger lanthanides Ce, Nd, Pr, and Sm form capped octahedral dications, $[Ln(C_6H_{11}NO)_6Cl]^{+2}$, with the chloride ligand in the capping position. The smaller metals Eu, Gd, and Ho form *trans*-octahedral monocations $[Ln(C_6H_{11}NO)_4Cl_2]^{+}$. Chloride ions are the counteranions in both cases.

Introduction

To define the first step in lanthanide-based ring opening polymerization of ε-caprolactone,[1] the coordination chemistry of this substrate with lanthanide trichlorides was previously studied.[2] These investigations showed that this monomer enhances the solubility of the lanthanide trichlorides in THF and generates a wide range of structures. $[YbCl_3(C_6H_{10}O_2)(THF)_2]$ and $[YCl_3(C_6H_{10}O_2)_3]$ were observed as well as ion pairs such as $[TbCl_4(THF)_2]^-[TbCl_2(THF)_5]^+$ and $[Cl_3Ln(\mu\text{-}Cl)_3LnCl_3]^{3-}$-$[Ln(C_6H_{10}O_2)_8]^{3+}$ (Ln = Sm and Nd).[2] This is in contrast to the usual coordination chemistry of yttrium and the lanthanide trichlorides in the presence of oxygen donors, which typically involves formation of seven coordinate pentagonal bipyramidal species of the general formula $LnCl_3L_4$ (L = oxygen donor ligand).[3]

Since metal trichlorides are important starting materials in the chemistry of yttrium and the lanthanides,[4] and since the presence of bridging or nonbridging ligands can have a significant effect on the chemistry of these metals,[5] it was of interest to determine if other neutral ligands similar to ε-caprolactone could likewise modify the chemistry of the lanthanide halides. Accordingly, we have studied the coordination chemistry of the lanthanide chlorides with a nylon-6 precursor, ε-caprolactam, since it is structurally similar to ε-caprolactone (Figure 1).

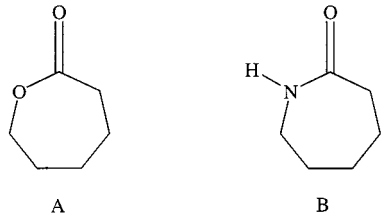

A B

Figure 1. A. ε-Caprolactone; B. ε-Caprolactam

[a] University of California, Irvine, Department of Chemistry, CA 92697−2025, USA
Fax: (internat.) +1-949/824-2210
E-mail: wevans@uci.edu

Since ε-caprolactam is more basic than ε-caprolactone, it has the potential to provide enhanced effects. To the best of our knowledge there is only one structural report of a lanthanide ε-caprolactam complex in the literature, $[Pr(C_6H_{11}NO)_8]^{3+}[OSO_2CF_3^-]_3$, a complex formed from hydrated praseodymium triflate and ε-caprolactam in triethylorthoformate.[6] We report here our synthetic and structural studies on the $LnCl_3$/ε-caprolactam system and the series of cationic complexes which resulted.

Results

ε-Caprolactam differs from ε-caprolactone[2] in that addition of this compound to slurries of the lanthanide trichlorides in THF does not bring the solids into solution. In fact, addition of ε-caprolactam to slurries of the lanthanide trichlorides in THF led to little visible change, except for the metals, neodymium, gadolinium, and holmium which had slight color changes. However, removal of solvent from these $LnCl_3$/ε-caprolactam mixtures, followed by washing with toluene to remove excess ε-caprolactam, gave solids whose IR spectra indicated the presence of coordinated ε-caprolactam. Crystallization from hot THF of the $PrCl_3$/ε-caprolactam product generated the dicationic ε-caprolactam complex $[Pr(C_6H_{11}NO)_6Cl]^{2+}$ as its chloride salt $[Pr(C_6H_{11}NO)_6Cl]Cl_2$ (Figure 2).

Single crystals of $[Ce(C_6H_{11}NO)_6Cl]Cl_2$ and $[Nd(C_6H_{11}NO)_6Cl]Cl_2$ were also obtained in this way, but the approach was not general for the remainder of the lanthanides.

Since THF was not a viable solvent for exploring the coordination chemistry of ε-caprolactam with the entire series of lanthanide trichlorides, an alternative solvent was examined. Acetonitrile proved to be suitable, even though it could have led to acetonitrile-solvated complexes. As with THF, addition of ε-caprolactam to slurries of lanthanide trichlorides in acetonitrile led to only small visible changes except for the Nd, Gd, and Ho systems. Although no obvious changes occurred, ε-caprolactam did become incorporated into the metal-containing solids isolated from these

 © WILEY-VCH Verlag GmbH, 69451 Weinheim, 2001 1434−1948/01/0303−0745 $ 17.50+.50/0

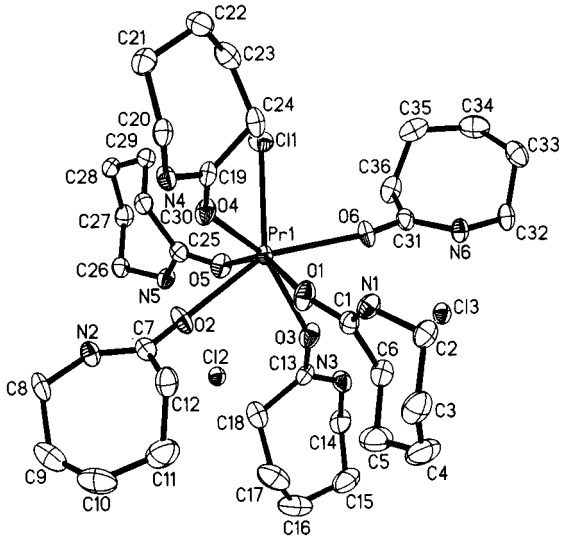

Figure 2. Thermal ellipsoid plot of $[Pr(C_6H_{11}NO)_6Cl)]Cl_2$ **(2)** with the probability ellipsoids drawn at the 50% level; complexes **1**, **3**, and **4** are isomorphous with **2**

systems. Recrystallization of these materials from hot acetonitrile gave single crystals suitable for X-ray diffraction for seven lanthanides ranging in size from Ce to Ho.

Two types of complexes crystallized, neither of which contained acetonitrile. Complexes of the formula $[Ln(C_6H_{11}NO)_6Cl]Cl_2$ (Figure 2) were found for the larger metals Ce **(1)**, Pr **(2)**, Nd **(3)**, and Sm **(4)**. Complexes **1, 2,** and **3** were identical to the ε-caprolactam complexes obtained from THF. Complexes of formula $[Ln(C_6H_{11}NO)_4Cl_2]Cl$ (Figure 3) were found for Eu **(5)**, Gd **(6)**, and Ho **(7)**.

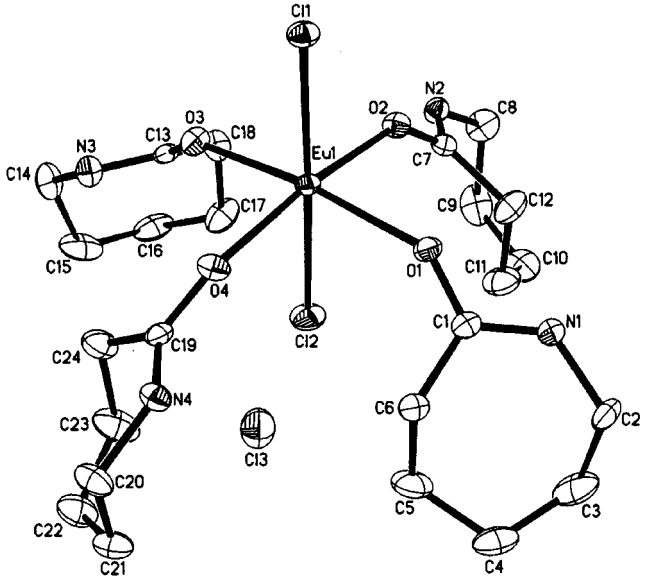

Figure 3. Thermal ellipsoid plot of $[Eu(C_6H_{11}NO)_4Cl_2)]Cl$ **(5)** with the probability ellipsoids drawn at the 50% level; complexes **6** and **7** are structurally similar to **5**

The complexes were characterized by infrared spectroscopy and elemental analysis and were definitively identified by X-ray crystallography. The IR spectra of **5−7** were similar to those of **1−4,** but the two types of spectra could be distinguished from each other in the fingerprint region. Single crystals were not obtained in the lanthanum case, **8**, but the white solid isolated from the analogous synthesis had an infrared spectrum identical to those of **1−4**.

Complexes **1−4** crystallize in the same space group and their unit cell parameters decrease from Ce to Sm, as is consistent with the decreasing size of the metals.[7] Each lanthanide in **1−4** is seven coordinate with a capped octahedral geometry arising from coordination of the carbonyl oxygen atoms of six ε-caprolactam molecules and one chloride, which is in the capping position. The two remaining chloride ions in the structure are separated from the metal at distances over 6 Å. The bond lengths in **1−3** and **5** vary as expected based on the changes in metal size (Table 1).

Only the praseodymium complex **2** will be described in detail since it can be directly compared to the only other lanthanide ε-caprolactam complex in the literature, $[Pr(C_6H_{11}NO)_8]^{3+}[OSO_2CF_3^-]_3$ **(9)**.[6] The degree of distortion in the capped octahedral geometry of **2** can be evaluated from the O−Pr−O angles between the *trans* oxygen atoms of the distorted octahedron, which range from 150.4−153.1(10)° and the adjacent O−Pr−O angles which range from 72.2(2)° to 117.8(2)° with an average angle of 87.6(2)°. The Pr−Cl distance [2.757(2) Å] can be compared to that in the six coordinate analog $PrCl_3(HMPA)_3$ [2.72(1) Å].[8] The average Pr−O bond length in **2** [2.418(3) Å] is comparable to that in **9** [2.449(12) Å] which has a higher coordination number and a higher charge on the cation. Both of these Pr−O(ε-caprolactam) distances are comparable to the Pr−O(HMPA) distance in $PrCl_3(HMPA)_3$ [2.353(2) Å],[8] a complex that also contains a strongly coordinating ligand.

The late metal complexes of formula $[Ln(C_6H_{11}NO)_4Cl_2]Cl$ [Ln = Eu **(5)**; Gd **(6)**; Ho **(7)**] have a six coordinate octahedral geometry with the chloride ligands in the *trans* positions. Complexes **6** and **7** are structurally similar to **5**, but they are not isomorphous. Unfortunately, only connectivity could be determined for both **6** and **7**, so **5** will be described in detail. The structure of **5** is only slightly distorted from a regular octahedral geometry with O−Eu−O *trans* angles of 172.42(7)−177.63(2)° and O−Eu−O *cis* angles of 85.17(5)−94.99(5)°. The Eu−Cl bond length in **5** [2.6505(8) Å] is comparable to the analogous bond length in seven coordinate $EuCl_3(THF)_4$,[3c] [2.628(3) Å]. The Eu−O bond in **5** [2.315(2) Å], is significantly shorter than the Eu−O(THF) distance in $EuCl_3(THF)_4$ [2.435(7) Å],[3c] even when the difference in coordination number is taken into account.[7]

Discussion

ε-Caprolactam differs considerably in its coordination chemistry with the lanthanide trichlorides compared to ε-caprolactone. Although its size and coordination mode, through the carbonyl group, are similar to those of ε-caprolactone, ε-caprolactam does not enhance the solubility of

Table 1. Bond lengths in $[Ln(C_6H_{11}NO)_6Cl]^{2+}$ and $[Ln(C_6H_{11}NO)_4Cl_2]^+$

Compound	Ln	Ln−O	$Ln-Cl_{coordinated}$	(Ln−O) − (Ln radius)[7]	(Ln−Cl) − (Ln radius)[7]
1	Ce	2.437(3)	2.7798(9)	1.37	1.71
2	Pr	2.418(3)	2.757(2)	1.36	1.70
3	Nd	2.407(3)	2.7412(12)	1.36	1.70
5	Eu	2.315(18)	2.6505(8)	1.37	1.71

the metal trichlorides and does not generate a variety of different structures upon coordination. Instead, the greater basicity of ε-caprolactam makes it such a powerful ligand that it displaces one or two chloride ligands from the metal and forms cationic complexes. The formation of these cations explains why ε-caprolactam does not increase solubility in solvents of moderate polarity.

The displacement of chloride ligands by ε-caprolactam leads to two types of crystalline cations, dicationic $[Ln(C_6H_{11}NO)_6Cl]^{2+}$ complexes for the larger metals and monocationic $[Ln(C_6H_{11}NO)_4Cl_2]^+$ compounds for the smaller metals. The existence of just two classes of compounds is typical of many types of lanthanide complexes in which the structural type with a high coordination number is found early in the series and a smaller coordinate variation forms with the later metals.[9]

Conclusion

Although ε-caprolactam is not useful in solubilizing lanthanide trichlorides, it is a powerful coordinating ligand which can displace anionic ligands and stabilize cationic complexes of these large metals.

Experimental Section

All of the compounds described below were handled under nitrogen with rigorous exclusion of air and water using standard Schlenk, vacuum line, and glovebox techniques. Solvents were prepared and physical measurements obtained as previously described.[10] All solvents were dried by distillation from sodium/benzophenone ketyl, except acetonitrile which was purchased anhydrous from Aldrich. ε-Caprolactam was purchased from Aldrich and sublimed before use. The lanthanide trichlorides were dried as previously described.[11] IR spectra were obtained as thin films using an ASI ReactIR 1000 spectrometer. Complete elemental analyses were performed by Desert Analytics, Tucson, Arizona. Complexometric analyses were obtained as previously described.[12]

General Procedures for the Synthesis of $[Ln(C_6H_{11}NO)_6Cl]Cl_2$ and $[Ln(C_6H_{11}NO)_4Cl_2]Cl$. Preparation of $[Ce(C_6H_{11}NO)_6Cl]Cl_2$ (1): In a glovebox, ε-caprolactam (0.36 g, 3.2 mmol) was added to a 15 mL slurry of THF and $CeCl_3$ (0.10 g, 0.41 mmol). After stirring overnight, volatiles were removed by rotary evaporation and the solids were washed with hot toluene (3 × 5.0 mL) to remove any excess ε-caprolactam. The resultant solid was dried under vacuum and was isolated as a white powder (0.20 g, 53%). X-ray quality crystals were grown from a concentrated THF solution. − $Ce(C_6H_{11}NO)_6Cl_3$ (925.43): calcd. C 46.72, H 7.19, N 9.08, Cl 11.49; found C 46.88, H 7.19, N 9.16, Cl 11.28. − IR: $\tilde{\nu}$ = 3177 vs, 2922 s, 2853 s, 1613 vs, 1490 s, 1440 s, 1351 s, 1293 s, 1258 s, 1200 s, 1119 s, 1079 s, 980 s, 822 s, 791 s, 690 s cm^{-1}. Complex **1** was also obtained using an analogous procedure with acetonitrile in place of THF. The composition of the product obtained from acetonitrile was determined by comparing IR spectra and unit cell parameters of single crystals.

$[Ln(C_6H_{11}NO)_6Cl]Cl_2$ [Ln = Pr (2); Nd (3); Sm (4)] and $[Ln(C_6H_{11}NO)_4Cl_2]Cl$ [Ln = Eu (5); Gd (6); Ho (7)]: Compounds **2**−**7** were prepared as described for **1**. Complexes **1**, **2** and **3** gave single crystals in THF and acetonitrile. Complexes **4**−**7** gave single crystals only from acetonitrile. Solvents, reagents, yields and spectroscopic data for individual samples are given below.

$[Pr(C_6H_{11}NO)_6Cl]Cl_2$ (2): In THF, $PrCl_3$ (0.09 g, 0.4 mmol) and ε-caprolactam (0.30 g, 2.7 mmol) were combined and a green solid (0.26, 77%) was isolated. − $Pr(C_6H_{11}NO)_6Cl_3$ (926.23): calcd. Pr 15.21, found Pr 15.0. − IR: $\tilde{\nu}$ = 3177 vs, 2922 s, 2853 s, 1613 vs, 1490 s, 1440 s, 1417 w, 1366 s, 1293 w, 1258 w, 1200 s, 1119 s, 1092 w, 1073 w, 980 s, 868 w, 826 s, 775 s, 690 s cm^{-1}.

$[Nd(C_6H_{11}NO)_6Cl]Cl_2$ (3): ε-Caprolactam (0.60 g, 5.3 mmol) was added to a pale blue-green slurry of $NdCl_3$ (0.17 g, 0.67 mmol) in THF and a light blue solid was isolated (0.42, 67%). − $Nd(C_6H_{11}NO)_6Cl_3$ (929.56): calcd. Nd 15.51, found Nd 15.2. − IR: $\tilde{\nu}$ = 3181 vs, 2922 s, 2853 s, 1610 vs, 1490 s, 1440 s, 1366 s, 1289 s, 1258 s, 1200 s, 1119 s, 1092 w, 1073 w, 980 w, 891 w, 868 w, 826 s, 772 s, 690 s cm^{-1}.

$[Sm(C_6H_{11}NO)_6Cl]Cl_2$ (4): $SmCl_3$ (0.1 g, 0.4 mmol) and ε-caprolactam (0.31 g, 2.7 mmol) were combined in acetonitrile. A white solid (0.29, 80%) was isolated. − $Sm(C_6H_{11}NO)_6Cl_3$ (935.68): calcd. Sm 16.07, found Sm 15.8. − IR: $\tilde{\nu}$ = 3176 vs, 2912 s, 2850 s, 1610 vs, 1487 s, 1438 s, 1417 w, 1366 s, 1293 w, 1258 w, 1200 s, 1119 s, 1092 w, 1073 w, 980 s, 868 w, 826 s, 775 s, 690 s cm^{-1}.

$[Eu(C_6H_{11}NO)_4Cl]Cl_2$ (5): ε-Caprolactam (0.50 g, 4.4 mmol) was added to a slurry of $EuCl_3$ (0.23 g, 0.89 mmol) in acetonitrile . The slurry was stirred overnight and was worked up as described above (0.35 g, 55%). − $Eu(C_6H_{11}NO)_4Cl_3$ (710.96): calcd. Eu 21.37, found Eu 21.5. − IR: $\tilde{\nu}$ = 3177 vs, 2922 s, 2853 s, 1617 vs, 1490 s, 1436 vs, 1200 s, 1119 s, 1089 s, 980 s, 961 s, 822 s, 791 s, 691 s cm^{-1}.

$[Gd(C_6H_{11}NO)_4Cl]Cl_2$ (6): ε-Caprolactam (0.51 g, 4.5 mmol) was added to a white slurry of $GdCl_3$ (0.22 g, 0.83 mmol) in acetonitrile. Immediately after mixing the reagents, a clear solution formed. After approximately 30 min., the mixture deposited a white precipitate. The resultant white solid was isolated as described above and dried under vacuum (0.51 g, 85%). − $Gd(C_6H_{11}NO)_4Cl_3$ (716.25): calcd. Gd 21.96; found Gd 21.4. − IR: $\tilde{\nu}$ = 3165 vs, 2930 s, 2860 s, 1606 vs, 1494 s, 1370 s, 1324 s, 1289 s, 1204 s, 1166 w, 1123 s, 1092 s, 984 s, 961 s, 892 w, 869 s, 826 s, 799 s, 691 s cm^{-1}.

$[Ho(C_6H_{11}NO)_4Cl_2]Cl$ (7): ε-Caprolactam (1.0 g, 8.9 mmol) was added to a pink slurry of $HoCl_3$ (0.44 g, 1.6 mmol) in acetonitrile. A white solid resulted (1.0 g, 85%). − $Ho(C_6H_{11}NO)_4Cl_3$ (723.93):

calcd. Ho 22.78; found Ho 22.0. − IR: $\tilde{\nu}$ = 3165 vs, 2926 s, 2860 s, 1606 vs, 1494 s, 1432 s, 1355 s, 1289 s, 1262 w, 1166 w, 1119 s, 1092 w, 1027 w, 984 w, 961 w, 891 w, 868 w, 822 s, 787 s, 687 s cm^{-1}.

$[La(C_6H_{11}NO)_6Cl]Cl_2$ (8): ε-Caprolactam (1.2 g, 11 mmol) was added to a white slurry of $LaCl_3$ (0.38 g, 1.6 mmol) in acetonitrile and the mixture was stirred overnight. The resultant solid was isolated following the procedures described above (0.53 g, 37%). − $La(C_6H_{11}NO)_6Cl_3$ (924.22): calcd. La 15.03; found La 15.4. − IR: $\tilde{\nu}$ = 3177 vs, 2922 s, 2853 s, 1602 vs, 1490 s, 1440 s, 1351 s, 1293 s, 1258 s, 1200 s, 1119 s, 1092 w, 1073 w, 980 s, 826 s, 776 s, 691 s cm^{-1}.

X-ray Data Collection, Structure Determination, and Refinement for $[Ce(C_6H_{11}NO)_6Cl]Cl_2$ (1): A colorless crystal of approximate dimensions 0.15 × 0.14 × 0.13 mm obtained from a solution of acetonitrile was mounted on a glass fiber and transferred to a Bruker CCD platform diffractometer. The SMART[13] program package was used to determine the unit-cell parameters and for data collection (40 sec/frame scan time for a hemisphere of diffraction data). The raw frame data was processed using SAINT[14] and SADABS[15] to yield the reflection data file. Details are in Table 2.

Subsequent calculations were carried out using the SHELXTL[16] program. The space group was the centrosymmetric monoclinic space group *Cc*. The structure was solved by direct methods and refined on F^2 by full-matrix least-squares techniques. The analytical scattering factors[17] for neutral atoms were used throughout the analysis. Hydrogen atoms were included using a riding model. At convergence, *wR2* = 0.0630 and GOF = 1.147 for 469 variables refined against 7697 unique data. As a comparison for refinement on *F*, *R1* = 0.0291 for those 7416 data with $I > 2\sigma(I)$. The absolute structure was assigned by refinement of the Flack parameter.[18]

$[Pr(C_6H_{11}NO)_6Cl]Cl_2$ (2): All data were collected on a Siemens P4 diffractometer from a crystal of dimensions 0.43 × 0.43 × 0.40 mm. The determination of Laue symmetry, crystal class, unit cell parameters and the crystal's orientation matrix were carried out according to standard procedures. Intensity data were collected at 163 K using a 2θ/ω scan technique with Mo-K_α radiation. The raw data were processed with a local version of CARESS[19] which employs a modified version of the Lehman−Larsen algorithm to obtain intensities and standard deviations from the measured 96-step peak profiles. Subsequent calculations were carried out using the SHELXTL[16] program. All data were corrected for absorption and for Lorentz and polarization effects and were placed on an approximately absolute scale. The space group was the noncentrosymmetric *Cc*. At convergence, *wR2* = 0.0517 and GOF = 1.148 for 470 variables refined against all 5393 unique data. As a comparison for refinement of *F*, *R1* = 0.0218 for those 5152 data with $I > 2\sigma(I)$.

$[Nd(C_6H_{11}NO)_6Cl]Cl_2$ (3): From a solution of THF, a pale violet crystal of approximate dimensions 0.14 × 0.26 × 0.37 mm was mounted on a glass fiber and transferred to the Siemens P4 diffractometer. A total of 3995 intensity data within a limiting Bragg angle of 28.00° were measured. Structure solution and refinement were based upon all 3995 unique reflections. Solution of the structure was accomplished by a combination of direct and heavy-atom methods. Final full-matrix least-squares refinement of 469 structure parameters included anisotropic displacement parameters for all non-hydrogen atoms. Hydrogen atoms were included in idealized positions (C−H = 0.96 Å) and refined by use of the riding model. Computer programs utilized included CARESS[19] for data processing and SHELXTL,[16] Version 5.02, for all other computations.

$[Eu(C_6H_{11}NO)_4Cl_2]Cl$ (5): A colorless crystal of approximate dimensions 0.07 × 0.25 × 0.31 mm was mounted on a glass fiber and handled as described above for **1**. The space group was the centrosymmetric monoclinic $P2_1/n$. At convergence, *wR2* = 0.0700 and GOF = 1.006 for 325 variables refined against 7304 unique data. As a comparison for refinement on F, *R1* = 0.0309 for those 5532 data with $I > 2\sigma(I)$.

Crystallographic data (excluding structure factors) for the structure(s) reported in this paper have been deposited with the Cambridge Crystallographic Data Centre as supplementary publication no. CCDC-147969 (**3**), -147970 (**1**), -147971 (**2**), -147972 (**5**). Copies of the data can be obtained free of charge on application to CCDC, 12 Union Road, Cambridge CB2 1EZ, UK [Fax: (internat.) +44-1223/336-033; E-mail: deposit@ccdc.cam.ac.uk].

Acknowledgments

For support of this research, we thank the Division of Chemical Sciences of the Office of Basic Energy Sciences of the Department of Energy.

Table 2. X-ray crystallographic data for $[Ce(C_6H_{11}NO)_6Cl]Cl_2$ **(1)**, $[Pr(C_6H_{11}NO)_6Cl]Cl_2$ **(2)**, $[Nd(C_6H_{11}NO)_6Cl]Cl_2$ **(3)**, and $[Eu(C_6H_{11}NO)_4Cl_2]Cl$ **(5)**

Compound	**1**	**2**	**3**	**5**
Formula	$C_{36}H_{66}CeCl_3N_6O_6$	$C_{36}H_{66}Cl_3N_6O_6Pr$	$C_{36}H_{66}Cl_3N_6NdO_6$	$C_{24}H_{44}Cl_3EuN_4O_4$
M	925.42	926.21	929.54	710.94
Temp. (K)	158	168	163	158
Crystal system	Monoclinic	Monoclinic	Monoclinic	Monoclinic
Space group	*Cc*	*Cc*	*Cc*	$P2_1/n$
a (Å)	18.3538(10)	18.3487(14)	18.329(2)	12.0849(9)
b (Å)	10.5987(6)	10.5950(8)	10.5861(8)	20.8091(15)
c (Å)	23.4298(13)	23.401.(6)	23.398(2)	12.2285(9)
α (degrees)	90	90	90	90
β (degrees)	105.5350(10)	105.610(9)	105.638(5)	90.6580(10)
γ (degrees)	90	90	90	90
V ($Å^3$)	4391.2(4)	4381.5(12)	4371.9(6)	3075.0(4)
Z	4	4	4	4
$\rho_{calcd.}$ (Mg/m^3)	1.400	1.404	1.412	1.536
μ (mm^{-1})	1.266	1.342	1.418	2.334
Final *R*1[$I>2\sigma(I)$]	0.0290	0.0218	0.0234	0.0309
Final *wR*2 (all data)	0.0630	0.0517	0.0482	0.0700

[1] [1a] S. J. McLain, N. E. Drysdale, U.S. Patent 5028667 (**1991**), assigned to E. I. du Pont de Nemours and Co. – [1b] S. J. McLain, T. M. Ford, N. E. Drysdale, Polymer Prepr., *Am. Chem. Soc., Div. Polym. Chem.* **1992**, *33*, 463. – [1c] S. J. McLain, T. M. Ford, N. E. Drysdale, N. Jones, E. F. McCord, W. J. Evans, J. L. Shreeve, *Polym. Prepr., Am. Chem. Soc., Div. Polym. Chem.* **1994**, *35*, 534. – [1d] W. J. Evans, H. Katsumata, *Macromolecules* **1994**, *27*, 4011. – [1e] J. Feijen, W. M. Stevels, M. J. K. Ankone, P. J. Dijkstra, *Macromolecules* **1996**, *29*, 3332. – [1f] H. Yasuda, H. Tamai, *Prog. Polym. Sci.* **1993**, *18*, 1097. – [1g] H. Yasuda, E. Ihara, M. Yamashita, Y. Takemoto, *Macromolecules* **1996**, *29*, 1798.

[2] W. J. Evans, J. L. Shreeve, J. W. Ziller, R. J. Doedens, *Inorg. Chem.* **1995**, *34*, 576.

[3] [3a] W. J. Evans, T. J. Boyle, J. W. Ziller, *J. Am. Chem. Soc.* **1993**, *115*, 5084. – [3b] W. Gecheng, G. Hanrong, J. Zhongsheng, S. Qi, *J. Struct. Chem. (Jiegou Huaxue)* **1989**, *8*, 61. – [3c] S. H. Lin, Z. C. Dong, J. S. Huang, Q. E. Zhang, X. L. Lu, *Acta Crystallogr.* **1991**, *C47*, 426. – [3d] C. Wenqi, X. Y. Zhongsheng, F. Yuguo, Y. Guangdi, *Inorg. Chim. Acta.* **1987**, *130*, 125 – [3e] J. Zhongsheng, N. Guojin, H. Ninghai, C. Wenqi, *J. Appl. Chem. (Yingyong Huaxue)* **1989**, *6*, 68. – [3f] H. Ninghai, L. Young-Hua, S. Qi, X. Yan, S. En-Dong, *Acta. Chim. Sin. (Huaxue Xuebao)* **1986**, *44*, 388.

[4] [4a] F. T. Edelmann, *Synthetic Methods of Organometallic Inorganic Chemistry* (Ed.: W. A. Herrman), Thieme Medical Publishers, New York, **1997**, Vol. 6. – [4b] H. Schumann, J. A. Meese-Marktscheffel, A. Esser, *Chem. Rev.* **1995**, *95*, 865.

[5] [5a] W. J. Evans, M. S. Sollberger, *Inorg. Chem.* **1988**, *27*, 4417. – [5b] W. J. Evans, J. M. Olofson, J. W. Ziller, *J. Am. Chem. Soc.* **1990**, *112*, 2308. – [5c] W. J. Evans, T. A. Ulibarri, L. R. Chamberlain, D. Alvarez, Jr., *Organometallics* **1990**, *9*, 2124. – [5d] W. J. Evans, *Polyhedron* **1987**, *6*, 803.

[6] P. C. Isolani, H. A. Alvarez, J. R. Matos, G. Vicentini, E. Castellano, J. Zukerman-Schpector, *J. Coord. Chem.* **1998**, *43*, 346.

[7] R. D. Shannon, *Acta. Cryst.* **1976**, *A32*, 751.

[8] L. J. Radonovich, M. D. Glick, *J. Inorg. Nucl. Chem.* **1973**, *35*, 2745–2752.

[9] [9a] T. J. Marks, R. D. Ernst, in *Comprehensive Organometallic Chemistry* (Eds.: G. Wilkinson, F. G. A. Stone, E. W. Abel), Pergamon Press, Oxford, **1982**, Vol. 3, 173–270. – [9b] T. Moeller, *Comprehensive Inorganic Chemistry*, (Eds.: J. C. Bailar, Jr., H. J. Emeléus, R. Nyholm, A. F. Trotman-Dickenson), Pergamon Press, New York, **1973**, Vol. 4, 1–101. – [9c] A. F. Wells, *Structural Inorganic Chemistry, 4th ed.*, Oxford University, London, **1975**. – [9d] A. F. Hart, in *Comprehensive Coordination Chemistry*, (Eds.: G. Wilkinson, R. D. Gillard, M. J. A. McCleverty), Pergamon Press, New York, **1987**, Vol. 3, 1059–1127. – [9e] W. J. Evans, S. E. Foster, *J. Organomet. Chem.* **1992**, *433*, 79. – [9f] E. C. Baker, G. W. Halstead, K. N. Raymond, *Struct. Bonding* **1976**, *25*, 23. – [9g] S. P. Sinha, *Struct. Bonding* **1976**, *25*, 69.

[10] W. J. Evans, L. R. Chamberlain, T. A. Ulibarri, J. W. Ziller, *J. Am. Chem. Soc.* **1988**, *110*, 6423.

[11] M. D. Taylor, C. D. Carter, *J. Inorg. Nucl. Chem.* **1962**, *24*, 387.

[12] J. L. Atwood, W. E. Hunter, A. L. Wayda, W. J. Evans, *Inorg. Chem.* **1981**, *20*, 4115.

[13] *SMART Software Users Guide*, Bruker Analytical X-Ray Instruments, Madison, WI, **1997**.

[14] *SAINT Software User Guide*, Bruker Analytical X-Ray Instruments, Madison, WI, **1997**.

[15] G. M. Sheldrick, *SADABS*, Bruker Analytical Instruments, Inc., Madison, WI, **1997**.

[16] G. M. Sheldrick, *SHELXTL*, Bruker Analytical X-Ray Instruments, Madison, WI, **1997**.

[17] *International Tables for X-Ray Crystallography*, Kluwer Academic Publishers, Dordrecht, **1992**, Vol. C.

[18] H. D. Flack, *Acta. Cryst.* **1983**, *39*, 876.

[19] R. W. Broach, *CARESS*, Argonne National Laboratory, Illinois, **1978.**

Received August 18, 2000
[I00323]

Assembly of Zinc Ions by the New ON_2S_2 Ligand BMIBIP

Claas Sudbrake[a] and Heinrich Vahrenkamp*[a]

Dedicated to Professor Dieter Sellmann on the occasion of his 60th birthday

Keywords: N ligands / S ligands / O ligands / Zinc / Ligand design / Enzyme models

The new ON_2S_2 ligand bis(iminomethyl)-2-6-bis(mercaptoisobutyl)-4-methylphenol (H_3BMIBIP) has been synthesized from 2,6-diformyl-4-methylphenol and 2-mercaptoisobutylamine. Its reaction with diethylzinc in the presence of alcohols yields complexes of composition [(BMIBIP)Zn_2(OR)] (R = CH_3, C_2H_5 and $CH_2C_6H_4CF_3$). A structure determination of the trifluoromethylbenzylate compound has shown it to be a tetranuclear complex consisting of two (BMIBIP)Zn_2 units linked by triply bridging alkoxide ligands to form a double norcubane with a $Zn_4O_4S_2$ framework.

Introduction

The phenomenon of cooperativity in conventional catalysis and the fact that many metalloenzymes have binuclear reaction centers[1] have spurred the investigations of binuclear coordination compounds in recent years. Out of this has emerged a new class of polydentate ligands, the so-called binucleating ligands.[2] A simple construction principle for these consists in the use of a central bridging unit (phenolate, thiophenolate, bipyridine, pyrazole, etc.) to which two polydentate side groups are attached. The functionalization of the binuclear reaction centers that can be achieved with such ligands has been impressively demonstrated recently by modelling iron[3] and copper[4] containing enzymes.

The most common type of binucleating ligand is derived from the basic framework **A** which itself is a variation of the classical salicylic aldimine type. Its thiophenolate analogue **B** is much less developed in coordination chemistry. This is repeated when the hapticity of the ligands is increased: while the Cambridge Crystallographic Database yields more than 130 entries for complexes derived from type **C**, there are just 9 for type **D**, including two zinc complexes.[5] Finally the sulfur-rich type **E** is represented by only four copper complexes containing the sulfur as a thioether donor,[6] while N_2S_3 ligands of type **F**, or complexes thereof, seem to be unknown so far.

As was shown by the pioneering work of Sellmann and co-workers,[7] sulfur-rich polydentate ligands have a high versatility for bioinorganic and catalytic model complex chemistry. We have tried to apply this in the field of zinc chemistry by the design and use of N_2S,[8,9] NS_2,[10] and N_3S_2 [11] ligands which contain sulfur as thiolate. Like others, we soon found that it is difficult to control oligothiolates because the bridging tendency of the thiolate sulfur causes a rich, but unpredictable, chemistry of oligonuclear complexes. However, we were also able to show that the application of multiply chelating ligands reduces the aggregation tendency and allows the formation of mononuclear zinc-bis(thiolate) complexes.[11]

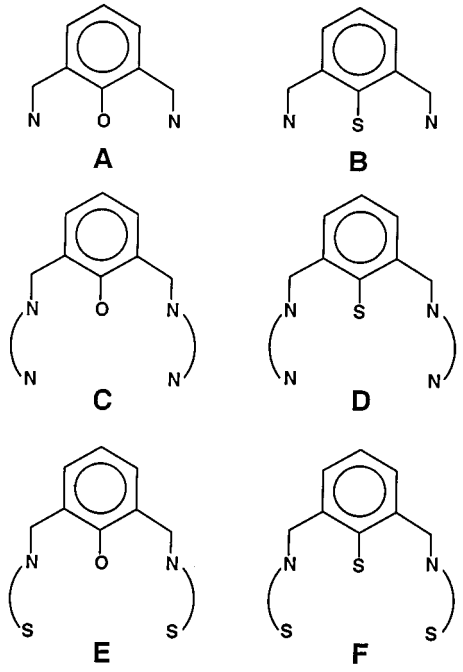

Along these lines we started working on binucleating ligands of type **E**. This paper describes the new ligand H_3BMIBIP and some zinc complexes thereof.

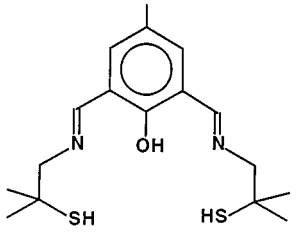

H_3BMIBIP

[a] Institut für Anorganische und Analytische Chemie der Universität Freiburg,
Albertstr. 21, 79104 Freiburg, Germany
Fax: (internat.) + 49-761/203-6001
E-mail: vahrenka@uni-freiburg.de

 © WILEY-VCH Verlag GmbH, 69451 Weinheim, 2001 1434−1948/01/0303−0751 $ 17.50+.50/0

Results and Discussion

Ligand H_3BMIBIP

The ligand synthesis was easy, as both its components 2,6-diformyl-4-methylphenol (**1**) and 2-mercaptoisobutylamine (**2**) are commercially available. Compound **2** was chosen in order to introduce a moderate amount of steric hindrance in the vicinity of sulfur in order to reduce the bridging tendency of the thiolate functions. Schiff base condensation of the two components was straightforward and yielded H_3BMIBIP in moderate yields. The ligand exists as a pale yellow crystalline solid which is easily identified by its simple ^{1}H NMR spectrum (see Experimental Section).

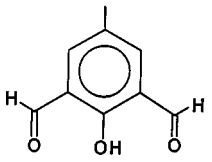

1

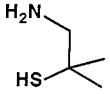

2

Zinc Complexes

In its deprotonated state the ligand BMIBIP is trianionic. Its combination with two divalent metal ions therefore calls for the binding of one additional monoanionic ligand. Ideally, this ligand should have the tendency for bridging, thereby completing the square configuration of both metal ions. In simple cases this might be a halide or thiolate ligand, whereas for bioinorganic model studies it might be, for example, an organophosphate. In the case of zinc binding one would envisage the attachment of additional monodentate ligands to complete a square pyramidal or octahedral coordination.

We tried to verify this for zinc complexes by treating the ligand with base and subsequently with zinc salts. The resulting, probably oligomeric or polymeric, complexes could not be obtained in a pure state. However, using diethylzinc both as the base and as the source of zinc yielded crystalline products in good yields. When alcohols were present, either as a solvent or as a co-reagent, these products had the composition L·Zn(OR). Thus, reaction with methanol, ethanol, or 4-trifluoromethylbenzyl alcohol gave the complexes **3a**, **3b**, and **3c**, respectively. Complexes **3** are soluble in polar aprotic organic solvents and crystallize as yellow solvates from chloroform or dichloromethane. Their ^{1}H NMR spectroscopic data (see Experimental Section) are in accordance with the composition [(BMIBIP)Zn_2(OR)] (**3a**: R = Me, **3b**: R = Et, **3c**: R = 4-$CF_3C_6H_4CH_2$).

Structure of 3c

Triclinic crystals of **3c** were obtained from chloroform. They contain four formula units and four solvent molecules per unit cell, the latter disordered over six positions. The four formula units of **3c** make up two crystallographically independent tetranuclear molecular units. These are quite similar and can both be represented by the simplified drawing of Figure 1. Table 1 lists the relevant bond lengths in the tetranuclear dimers.

Table 1. Zinc-ligand bond lengths (Å) in **3c**

	Molecule 1	Molecule 2
Zn1−O1	2.076(4)	2.088(4)
Zn1−N1	2.001(5)	1.999(5)
Zn1−S1	2.389(2)	2.382(2)
Zn1−O2	2.019(4)	2.014(4)
Zn1−O2′[a]	2.094(4)	2.096(4)
Zn2−O1	2.160(4)	2.156(4)
Zn2−N2	2.079(5)	2.084(5)
Zn2−S2	2.295(2)	2.291(2)
Zn2−O2	2.151(4)	2.172(4)
Zn2−S1′[a]	2.377(2)	2.383(2)

[a] Bonds linking the two dinuclear units.

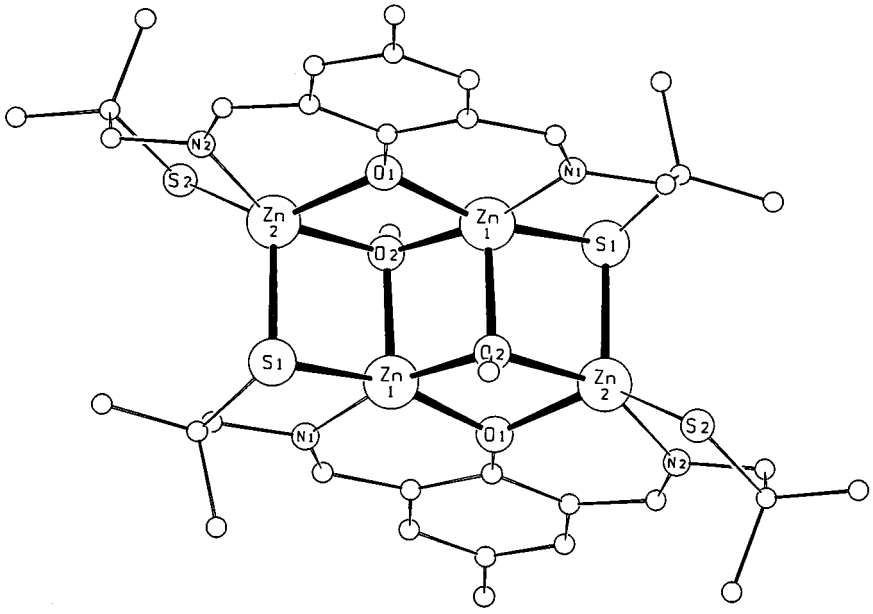

Figure 1. Molecular structure of **3c** (*p*-trifluorobenzylate units at O2 omitted for clarity)

The molecular constitution found for **3c** represents a new type of tetranuclear aggregate which is assembled from two pentadentate ligands. In each of the two dinuclear units, the BMIBIP ligand exerts its expected ligation pattern by giving both zinc ions a square environment. The dimerization of the two dinuclear units is brought about by placing them face to face across a center of symmetry and linking them through the unshared electron pairs of O2 and S1. Thereby the linkage is represented by four rungs of a ladder, and the resulting $Zn_4O_4S_2$ core has the shape of two open cubes sharing a common face.

The coordination of all four zinc ions is square-pyramidal. Both Zn1 and Zn2 have a basal ZnO_2NS coordination, but the apical donor is oxygen for Zn1 and sulfur for Zn2. Accordingly, the BMIBIP ligand uses one of its thiolate functions as a terminal and the other as a bridging ligand. Thus, although the whole tetranuclear complex has inversion symmetry it contains no other symmetry elements.

The observed bond lengths (Table 1) are in their normal ranges (cf. the chemistry of zinc alkoxides or zinc thiolates). The Zn−N bonds are the shortest, corresponding to the fact that N is only terminal. The Zn−S bonds underline this by the clear distinction of the Zn−S2 and Zn−S1 distances. Among the Zn−O bonds it is noticeable that those from Zn1 are significantly shorter than those from Zn2; this may reflect the presence of the very good donor S2 as a terminal ligand on Zn2.

Conclusions

This work has shown that H_3BMIBIP is a good candidate for the assembly of metal ions. It is easy to synthesize, it provides a biorelevant ON_2S_2 donor set able to surround two metal ions in a square-planar fashion, and it can position the two metal ions such that both can coordinate to one and the same additional ligand, i.e. a substrate for a catalytic process. When zinc is present as the divalent metal ion, its tendency to be five-coordinate in the given donor set can easily be met by dimerization of the LZn_2X complexes. It should be worthwhile to find out how other divalent metals, for example with preference for square-planar or octahedral coordination, make use of the donor capacity of BMIBIP.

Experimental Section

General: For general working and measuring procedures, see ref.[12] All reactions were performed under an inert atmosphere. Starting materials were obtained commercially.

H_3BMIBIP: A solution of 2,6-diformyl-4-methylphenol (1.01 g, 6.18 mmol) in methanol (25 mL) was added to a solution of 2-mercaptoisobutylamine hydrochloride (1.75 g, 12.35 mmol) also in methanol (25 mL). Upon stirring and addition of anhydrous sodium acetate (1.02 g, 12.35 mmol) a cloudy precipitate started forming. After refluxing for 30 min. and cooling to room temp. the solvent was removed in vacuo. The residue was redissolved in 20 mL of dichloromethane, filtered and evaporated to dryness again. Crystallization of the residue from 10 mL of methanol at 4 °C yielded H_3BMIBIP (0.84 g, 40%) as a yellow powder, m.p. 99 °C. − $C_{17}H_{26}N_2OS_2$ (338.5): calcd. C 60.31, H 7.74, N 8.27; found C 60.27, H 7.67, N 8.13. − ^{1}H NMR (CD_3COOD): δ = 1.55 (s, 12 H, CH_3), 2.19 (s, 3 H, CH_3), 3.43 (s, 4 H, CH_2), 6.22 (d, J = 6.8 Hz, 2 H, CH=N), 7.28 (d, J = 6.4 Hz, 2 H, Ph).

3a: A 1 M solution of diethylzinc in *n*-hexane (5.00 mL, 5.00 mmol) was slowly dropped with stirring into a solution of H_3BMIBIP (0.84 g, 2.49 mmol) in a mixture of absolute methanol (10 mL) and absolute dichloromethane (30 mL). After stirring for 1 h the volume was reduced in vacuo to 20 mL upon which the product precipitated. After filtration, washing with a small amount of diethyl ether and drying in vacuo **3a** (0.68 g, 51%) was obtained as a pale yellow microcrystalline solid. M.p. 165 °C. − $C_{18}H_{26}N_2O_2S_2Zn_2{\cdot}0.5CH_2Cl_2$ (457.3 + 42.5): calcd. C 41.16, H 5.04, N 5.19, Zn 24.23; found C 41.33, H 4.93, N 5.52, Zn 24.25. − ^{1}H NMR ($CDCl_3$): δ = 1.12 (s, 12 H, CH_3), 1.76 (s, 3 H, CH_3), 2.20 (s, 3 H, CH_3), 3.41 (s, 4 H, CH_2), 5.32 (s, 1 H, CH_2Cl_2), 7.09 (s, 2 H, CH=N), 8.15 (s, 2 H, Ph).

3b: A 1 M solution of diethylzinc in *n*-hexane (2.66 mL, 2.66 mmol) was slowly dropped with stirring into a solution of H_3BMIBIP (0.45 g, 1.33 mmol) in a mixture of absolute ethanol (2 mL) and absolute chloroform (15 mL). After stirring for 30 min. the solvent was removed in vacuo. The residue was redissolved in a few milliliters of chloroform and layered with diethyl ether. After 4 days at 4 °C the resulting precipitate was filtered off, washed with a few milliliters of diethyl ether and dried in vacuo to give **3b** (0.39 g, 47%) as a pale yellow powder. M.p. 195 °C. − $C_{19}H_{28}N_2O_2S_2Zn_2{\cdot}CHCl_3$ (511.4 + 119.4): calcd. C 38.09, H 4.63, N 4.44, Zn 20.73; found C 38.09, H 4.70, N 4.70, Zn 21.25. − ^{1}H NMR ([D_6]DMSO): δ = 1.07 (t, J = 7.0 Hz, 3 H, CH_3), 1.45 (s, 12 H, CH_3), 2.13 (s, 3 H, CH_3), 3.30 (s, 4 H, CH_2), 3.58 (q, J = 7.0 Hz, 2 H, OCH_2), 7.10 (s, 2 H, CH=N), 7.26 (s, 1 H, $CHCl_3$), 8.10 (s, 2 H, Ph).

3c: A 1 M solution of diethylzinc in *n*-hexane (4.03 mL. 4.03 mmol) was dropped slowly with stirring into a solution of H_3BMIBIP (0.68 g, 2.02 mmol) and 4-trifluoromethylbenzyl alcohol (0.53 g, 3.00 mmol) in absolute chloroform (25 mL). After stirring for 1 h the solution was filtered, the filtrate reduced to half its volume in vacuo and layered with diethyl ether. After 1 day at 4 °C the precipitate was filtered off and washed with a few milliliters of hexane to give **3c** (0.56 g, 40%) as a colorless powder. M.p. 188 °C. − $C_{25}H_{29}F_3N_2O_2S_2Zn_2{\cdot}0.5CHCl_3$ (641.4 + 59.7): calcd. C 43.69, H 4.24, N 4.00; found C 43.80, H 4.75, N 4.15. − ^{1}H NMR ($CDCl_3$): δ = 1.47 (s, 12 H, CH_3), 1.66 (s, 2 H, OCH_2), 2.20 (s, 3 H, CH_3), 3.57 (s, 4 H, CH_2), 7.19 (m, 6 H, Ph), 7.24 (s, 0.5 H, $CHCl_3$), 8.08 (s, 2 H, CH=N).

Structure Determination:[13] From a chloroform solution of **3c** layered with diethyl ether crystals of composition $(\mathbf{3c})_2{\cdot}2CHCl_3$ were obtained. Diffraction data were recorded at room temp. with the ω/2θ technique on a Nonius CAD4 diffractometer fitted with a molybdenum tube (K_α, λ = 0.7107 Å) and a graphite monochromator. No absorption corrections were applied. The structures were solved by direct methods and refined anisotropically with the SHELX program suite.[14] Hydrogen atoms were included with fixed distances and isotropic temperature factors 1.5 times those of their attached atoms. Parameters were refined against F^2. The R values are defined as $R_1 = \Sigma|F_o - F_c|/\Sigma F_o$ and $wR_2 = \{\Sigma[w(F_o^2 - F_c^2)^2]\Sigma[w(F_o^2)^2]\}^{1/2}$. Drawings were produced with SCHAKAL.[15] Table 2 lists the crystallographic data.

Table 2. Crystallographic data for **3c**

Empirical formula	$C_{52}H_{60}Cl_6F_6N_4O_4S_4Zn_4$
Molecular mass	1521.4
Crystal size [mm]	0.6 × 0.3 × 0.3
Space group	$P\bar{1}$
Z	2
a [Å]	13.097(3)
b [Å]	14.477(3)
c [Å]	20.547(4)
α [°]	69.53(3)
β [°]	71.92(3)
γ [°]	85.96(3)
V [Å^3]	3466(1)
d(calcd.) [gcm^{-3}]	1.46
μ(Mo-K_α) [mm^{-1}]	1.78
hkl range	h: −16 to 16 k: 0 to 17 l: −23 to 25
Measured reflections	14190
Independent reflections	13622
Observed refl. [$I > 2\sigma(I)$]	10462
Parameters	709
Refined reflections	13622
R_1(obs.refl.)	0.065
wR_2(all refl.)	0.226
Residual electron density [e/Å^3]	+1.0/-1.0

Acknowledgments

This work was supported by the Deutsche Forschungsgemeinschaft.

[1] N. Sträter, W. N. Lipscomb, T. Klabunde, B. Krebs, *Angew. Chem.* **1996**, *108*, 2158−2191; *Angew. Chem. Int. Ed. Engl.* **1996**, *35*, 2024−2055.
[2] D. E. Fenton, H. Okawa, *Chem. Ber.* **1997**, *130*, 433−442, and references cited therein.
[3] Y. Dang, S. Yan, V. G. Young, L. Que, *Angew. Chem.* **1996**, *108*, 674−676; *Angew. Chem. Int. Ed. Engl.* **1996**, *35*, 618−620.
[4] F. Meyer, H. Pritzkow, *Angew. Chem.* **2000**, *112*, 2199−2202; *Angew. Chem. Int. Ed.* **2000**, *39*, 2112−2115, and references cited therein.
[5] S. Brooker, P. D. Croucher, F. M. Roxburgh, *J. Chem. Soc., Dalton Trans.* **1996**, 3031−3037.
[6] O. Kahn, T. Mallah, J. Gouteron, S. Jeannin, Y. Jeannin, *J. Chem. Soc., Dalton Trans.* **1989**, 1117−1126.
[7] D. Sellmann, J. Sutter, *Acc. Chem. Res.* **1997**, *30*, 460−469; D. Sellmann, J. Utz, N. Blum, F. W. Heinemann, *Coord. Chem. Rev.* **1999**, *190−192*, 607−627.
[8] U. Brand, H. Vahrenkamp, *Inorg. Chem.* **1995**, *34*, 3285−3293.
[9] U. Brand, H. Vahrenkamp, *Chem. Ber.* **1996**, *129*, 435−440.
[10] U. Brand, H. Vahrenkamp, *Z. Anorg. Allg. Chem.* **1996**, *622*, 213−218.
[11] U. Brand, R. Burth, H. Vahrenkamp, *Inorg. Chem.* **1996**, *35*, 1083−1086.
[12] M. Förster, R. Burth, A. K. Powell, T. Eiche, H. Vahrenkamp, *Chem. Ber.* **1993**, *126*, 2643−2648.
[13] The crystallographic data of the structures described in this paper were deposited with the Cambridge Crystallographic Data Centre as supplementary publication no. CCDC-149311 Copies of these data are available free of charge from the following address: The Director, CCDC, 12 Union Road, Cambridge UK, CB2 1EZ [Fax: (internat.) +44-1223/336-033; E-mail: deposit@ccdc.cam.ac.uk].
[14] G. M. Sheldrick, *SHELX-86* and *SHELXL-93*, *Programs for Crystal Structure Determination*, Universität Göttingen, **1986** and **1993**.
[15] E. Keller, *SCHAKAL for Windows*, Universität Freiburg, **1998**.
Received September 11, 2000
[I00340]

Methylated Derivatives of Hydrazinium Azide

Anton Hammerl,[a] Gerhard Holl,[b] Klaus Hübler,[c][‡] Manfred Kaiser,[b] Thomas M. Klapötke,*[a] and Peter Mayer[a][‡]

Keywords: Azides / Hydrazine / Hydrazinium azide / Nitrogen

The synthesis and characterization of polymethylated hydrazinium azide species is reported. The crystal structure of methylhydrazinium azide and *N,N′*-dimethylhydrazinium azide was determined. The thermal, shock and friction sensitivity as well as the explosion products of some of the compounds were investigated.

Introduction

Hydrazinium azide, first reported by Curtius in 1891,[1] is a powerful explosive. The explosion of hydrazinium azide produces nitrogen, hydrogen and ammonia.[2]

$$[N_2H_5]^+[N_3]^- \xrightarrow[30\ bar]{\Delta} 2.18\ N_2 + 1.52\ H_2 + 0.65\ NH \quad (1)$$

This encouraged us to investigate hydrazinium azide for use as a nitrogen rich, highly energetic material.[3−8] We replaced the hydrogen atoms in hydrazinium azide step-by-step with methyl groups, characterized these compounds and tested the explosive characteristics of the most promising compounds.

Results and Discussion

Of all possible methyl-substituted hydrazine azide compounds, *N,N*-dimethylhydrazinium azide **(1)** and *N,N,N*-trimethylhydrazinium azide **(2)** have been reported previously.[4,7] Here, we report the syntheses and characterization of methylhydrazinium azide **(3)**, *N,N′*-dimethylhydrazinium azide **(4)**, *N,N,N′*-trimethylhydrazinium azide **(5)**, *N,N,N′,N′*-tetramethylhydrazinium azide tetramethylhydrazinate **(6)**, *N,N,N,N′*-tetramethylhydrazinium azide **(7)** and pentamethylhydrazinium azide **(8)**.

Azides **3**,**4**,**5** and **6** (Table 1) were prepared by adding a solution of HN_3 in ether to the anhydrous hydrazine at 0 °C. Methylhydrazinium azide **(3)** was isolated as a colorless solid and purified by sublimation. *N,N′*-dimethylhydrazinium azide **(4)** and *N,N,N′*-trimethylhydrazinium azide **(5)** were isolated as ether insoluble liquids that were purified by low temperature sublimation.

Table 1. Numbering scheme for methylated hydrazinium derivatives

	R_1	R_2	R_3	R_4
3	CH_3	H	H	H
1	CH_3	CH_3	H	H
4	CH_3	H	CH_3	H
5	CH_3	CH_3	CH_3	H
6	CH_3	CH_3	CH_3	CH_3

The reaction of tetramethylhydrazine with HN_3 is different from the other reactions since a clear solution forms after the addition of HN_3. After distilling off ether and HN_3, it was possible to isolate a yellowish oil that was purified by low temperature sublimation.

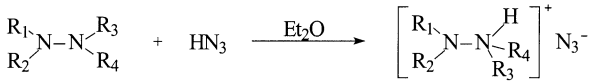

(2)

Compounds **3**−**6** are all sensitive to oxidation. The oxidation is faster in compounds where more methyl groups are present. Methylhydrazinium azide **(3)** is hygroscopic but can be stored in air for several minutes before a color change occurs, while the liquid HN_3 salts turn brown immediately and form black residues in minutes. The HN_3 salts **3**−**6** are very volatile. TG analysis of **3** showed that the compound sublimes at ambient temperature and a drastic increase of sublimation rate occurs at temperatures higher than 50 °C.

Compounds **7** and **8** (Table 2) were made by halogen exchange of the respective iodide salts with silver azide. They were purified by recrystallization from methanol. Compounds **7** and **8** are hygroscopic but not sensitive to oxidation.

[a] Department of Chemistry,
Butenandtstraße 5−13(D), 81377 München, Germany
Fax: (internat.) +49-6221/487-672
E-mail: tmk@cup.uni-muenchen.de
[b] Wehrwissenschaftliches Institut für Werk-, Explosiv- und Betriebsstoffe,
53913 Swisstal, Germany
[c] Institut für Anorganische Chemie,
Pfaffenwaldring 55, 70569 Stuttgart, Germany
[‡] Crystal structure analysis.

 © WILEY-VCH Verlag GmbH, 69451 Weinheim, 2001 1434−1948/01/0303−0755 $ 17.50+.50/0

Table 2. Numbering scheme for methylated hydrazinium azide derivatives with methylated nitrogen atoms

	R_1	R_2
2	H	H
7	CH_3	H
8	CH_3	CH_3

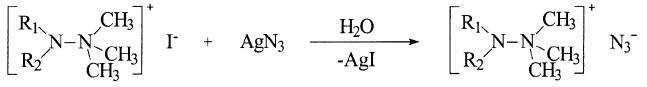

(3)

The vibrational spectra (Table 3) show the characteristic absorptions of the azide anion around 2030 cm^{-1} [$\nu_{as}(N_3^-)$, IR] and around 1330 cm^{-1} [$\nu_s(N_3^-)$, Raman] for all the compounds. *N,N,N′,N′*-tetramethylhydrazinium azide tetramethylhydrazinate **(6)** also shows an absorption at 2131 cm^{-1} (IR) and 2129 cm^{-1} (Raman) that is assigned to the HN_3 moiety. We believe that this band is due to the dissociation of the tetramethylhydrazine−HN_3 adduct, explaining the fierce explosions observed with this compound.

Table 3. Characteristic analytical data for hydrazinium azide derivatives

	N*H* (^{1}H)	^{14}N NMR	$\nu_{as}(N_3^-)$	$\nu_s(N_3^-)$	m.p.
3	6.89	−134 −278 −323	2037	1340	68 °C
4	7.33	−134 −275	2034	1339	−8 °C
5	7.54	−134 −275	−	1336	10 °C
6	6.22	−130 −255	2131 (HN_3) 2018	1331	−20 °C
7	6.49	−131 −278 −301	2037	1332	174 °C
8	−	−132 −278 −291	2009	1321	180 °C

The ^{14}N NMR spectra for **3**,**4**,**5**,**7** and **8** (Table 3) show two signals around δ = −134 and −277, the first corresponding to the terminal nitrogen atoms, and the second to the central nitrogen atom. Compound **6** has two signals at δ = −130 and −258. The shift of δ = −258 suggests that the azide ion is bound differently from that of the other compounds. A similar ^{14}N NMR shift is observed for phenylhydrazinium azide phenylhydrazinate at δ = −255.[9] This compound consists of two phenylhydrazine units that are bridged by a proton via hydrogen bonds. The azide anion is connected through weaker hydrogen bonds to the two phenylhydrazine units. Azide **6** seems to be a similar compound because of the ^{14}N NMR shifts, the easy elimination of HN_3 and because hydrazinium azide salts, in general, are not soluble in ether. Tetramethylhydrazine is the weakest base of the hydrazines[10] used here, which explains this behavior. Hydrogen diazide shows a similar structure with two azide ions being bridged by a proton via hydrogen bonds.[11] This is not possible here because tetramethylhydrazine is more basic than an azide ion. In solution no third signal in the ^{14}N NMR around δ = −320 for HN_3 was detected for **6**. We believe that the bands for HN_3 that were detected in the vibrational spectra display belong to only trace amounts of HN_3 due to their high intensity. Elemental analysis for **4**, **5** and **6** was not performed because of serious security hazards. Compounds **7** and **8** show a third, broad signal at δ = −301 and −306, respectively, for the nitrogen atoms of the hydrazinium ions. The ^{1}H NMR spectra in [D_6]DMSO show signals for the NH protons at around δ = 7. The signals for the CH protons and their ^{13}C NMR resonances are in similar ranges to that of the starting materials.

Crystal Structure of 3

Crystals of **3** are orthorhombic, space group *Pnma* with $Z = 8$ molecules in the unit cell. The bond lengths and angles of the methylhydrazinium ion as indicated in Figure 1 are in good agreement with methylhydrazinium trifluoroacetate.[12] Two pairs of hydrogen bonds connect the methylhydrazinium ion to four adjacent azide ions. The shorter pair connects the protonated central nitrogen atom N4 with two N3 atoms of an azide ion, the longer pair of hydrogen bonds connects the terminal hydrazine nitrogen atom with two N1 atoms of an azide atom. The azide atoms show a small difference in N−N bond lengths. The N1−N2 bond is 1.167(1) Å long, slightly shorter than the N2−N3 bond which is 1.184(1) Å. This is caused by stronger hydrogen bonding of N3 [N4−H4−N3 contact distance 2.8815(7) Å] than N1 [N5−H5−N1 contact distance 3.1018(9) Å].

Crystal Structure of 4

The crystals used for the structure determination of **4** were twinned, monoclinic, with space group *Cc* and $Z = 4$. The bond lengths and angles of the dimethylhydrazinium ion (Figure 2) are in good agreement with the bond lengths of other hydrazinium ions. The torsion angles of the hydrazinium ion are 175.2(3)° and 176.6(3)°, i.e. almost 180°. This conformation is stabilized with hydrogen bonds. The N−N bond lengths of both independent azide ions are different in length, as is the case with the azide ion in **3**. The longer N−N bond length in the azide ion corresponds to two shorter hydrogen bonds to adjacent hydrazinium ions; the shorter N−N bond length corresponds to a longer hydrogen bond to the next hydrazinium ion, as in **3**.

The hydrogen-bonded hydrazinium and azide ions form layers (Figure 3). The methyl groups of the hydrazinium ions are above and below these layers, so that two methyl groups are between each layer. The weak interactions between the layers explain the low melting point of the compound. The structure of compound **5**, which also has a melting point below room temperature, should be similar.

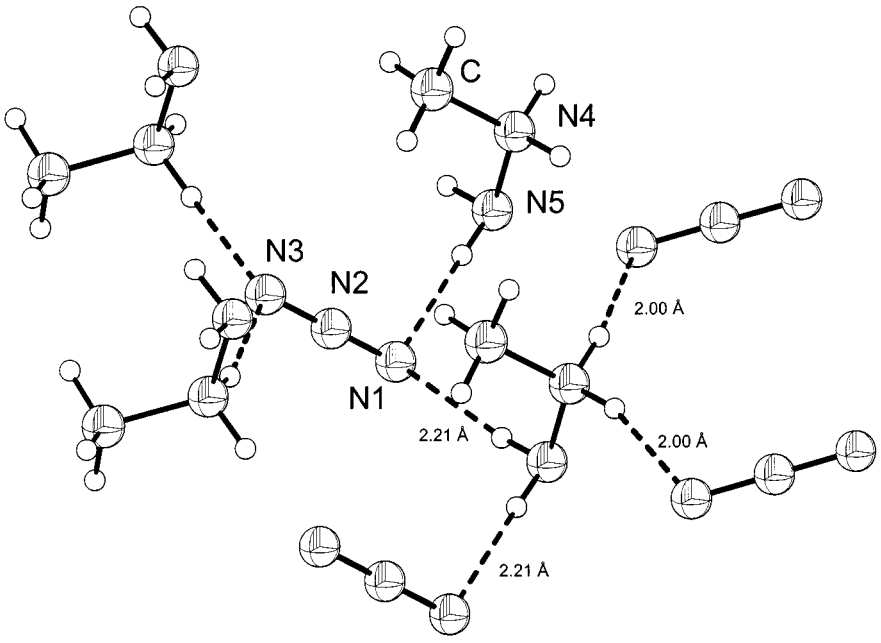

Figure 1. Molecular structure and hydrogen bonds of **3** as an ORTEP plot (thermal ellipsoids represent 25% probability); selected bond lengths [Å] and angles [°]: N1−N2 1.167(1), N2−N3 1.184(1), N4−N5 1.438(1), C−N4 1.484(1),N4−H4 0.91(1), N5−H5 0.89(1); N1−N2−N3 179.6(1), N5−N4−C 116.81(9), N5−N4−H4 105.6(7), C−N4−H4 110.4(7); contact distances [Å]: N4−N5−H5 105.1(8), N4−H4−N1 2.966(1), N4−H4−N3 2.8815(7), N5−H5−N1 3.1018(9)

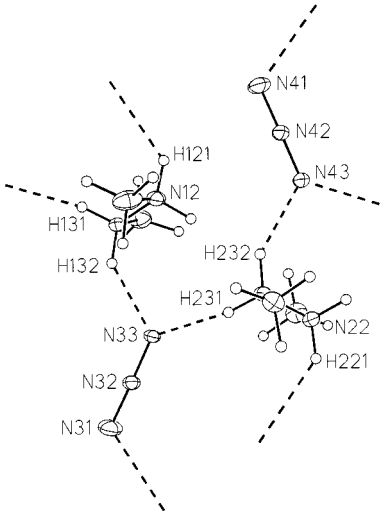

Figure 2. Molecular structure and atom numbering scheme of **4** (thermal ellipsoids represent 25% probability); selected bond lengths [Å] and angles [°]: C11−N12 1.471(5), C21−N22 1.488(4), N12−N13 1.446(3), N22−N23 1.441(3), N13−C14 1.476(4), N23−C24 1.471(4), N31−N32 1.166(4), N41−N42 1.173(4), N32−N33 1.182(4), N42−N43 1.186(4); C11−N12−N13 108.7(3), C21−N22−N23 107.3(2), N12−N13−C14 111.4(3), N22−N23−C24 109.5(2), N31−N32−N33 178.6(4), N41−N42−N43 178.4(3); contact distances [Å]: N12−N31 2.993(5), N22−N41 3.033(4), N12−N23 3.296(4), N13−N33 2.776(3), N23−N43 2.760(4), N13−N22 3.258(4), N13−N43 2.816(4), N23−N33 2.839(3); torsion angles: C11−N12−N13−C14 175.2(3), C21−N22−N23−C24 176.6(3)

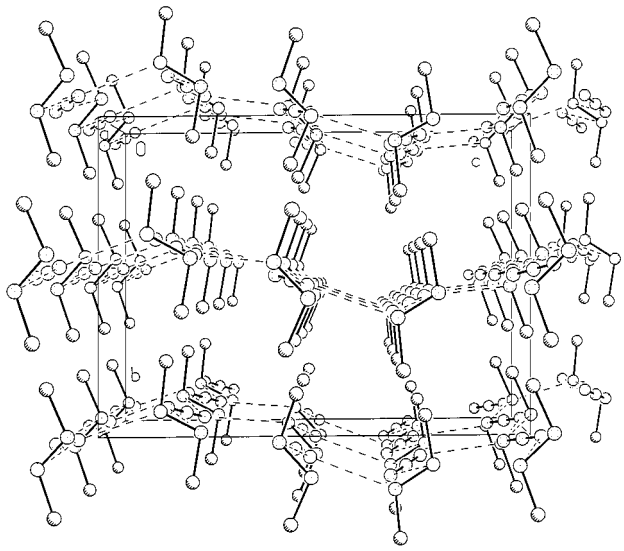

Figure 3. Layers in the crystal structure of **4**

Sensitivity Towards Shock, Friction and Electric Charge, and Thermal Sensitivity

All reported compounds show almost no sensitivity towards shock or friction. No detonation was observed after dropping a weight of 5 kg from 50 cm onto the compounds, nor was any detonation observed when grinding the compounds in a mortar. When exposing the compounds to an electric discharge of about 20 kV from a high frequency brush electrode, all compounds showed no sensitivity. The thermal sensitivity of the HN_3 salts differs from compounds with trimethylated nitrogen atoms. The HN_3 salts **1**, **3**, **4, 5** and **6** do not explode when heated with a heating rate of about 10 °C/min.; they sublime away from the heat source. An explosion can only be started by a strong heat source, for example a hot metal plate or a Bunsen burner. The more methyl groups that are attached to the hydrazinium ion, the fiercer the explosion gets. Methylhydrazinium azide **(3)** and the *N,N*-dimethylhydrazinium azide **(1)** show the same properties, while *N,N′*-dimethylhydrazinium azide **(4)** and compounds **5** and **6** give a much bigger explosion. *N,N′*-

dimethylhydrazinium azide **(4)** exploded in the microanalyser, damaging the glass tubing. In general one would expect less-fierce explosions with an increasing number of methyl groups. In our studies the compounds with more methyl groups are liquids and the bonding of HN_3 to the hydrazine unit is therefore weaker.

The trimethylated compounds **2**, **7** and **8** are less sensitive. While *N,N,N*-trimethylhydrazinium azide **(2)** gives a weak explosion on heating with a Bunsen flame, *N,N,N,N′*-tetramethylhydrazinium azide **(7)** only burns, and pentamethylhydrazinium azide **(8)** burns more sluggishly than **7**.

For methylhydrazinium azide **(3)**, *N,N*−dimethylhydrazinium azide **(1)**, *N,N′*-dimethylhydrazinium azide **(4)**, *N,N,N*-trimethylhydrazinium azide **(2)** and *N,N,N,N′*-tetramethylhydrazinium azide **(7)** the gaseous products were determined after their explosions. The appropriate azide (100 mg) was loaded into a 150 mL evacuated steel vessel. The explosion was started with a red hot metal wire and the gaseous products were analyzed by mass spectrometry and IR spectroscopy.

Explosion Products

After the explosion of methylhydrazinium azide **(3)**, H_2, N_2 and methane were detected. The IR spectrum also showed trace amounts of HN_3. *N,N*-Dimethylhydrazinium azide **(1)** produced dinitrogen as the main product. Small amounts of dihydrogen, methane and methylated amines were also detected.

N,N′-dimethylhydrazinium azide **(4)** produced dinitrogen, dihydrogen and methane as well as trace amounts of methylated amines. *N,N,N*-Trimethylhydrazinium azide **(2)** exploded to dinitrogen, dihydrogen, trimethylamine and trace amounts of methane. *N,N,N,N′*-Tetramethylhydrazinium azide gave dinitrogen, trimethylamine, trace amounts of dihydrogen, and other methylated amines. For all compounds no carbon soot was found after the explosion.

Conclusion

We substituted the hydrogen atoms of hydrazinium azide with methyl groups and the products formed during the explosion of methylhydrazinium azide **(3)**, *N,N′*-dimethylhydrazinium azide **(1)**, *N,N′*-dimethylhydrazinium azide and *N,N,N*-trimethylhydrazinium azide **(2)** include hydrogen.

N,N′-Dimethylhydrazine, *N,N,N′*-trimethylhydrazine and *N,N,N′,N′*-tetramethylhydrazine give salts with HN_3 that are liquid at room temperature and give rise to fiercer explosions than solid compounds.

Hydrazinium azides with a trimethylated nitrogen atom are not sensitive to oxidation and are not volatile, but are very hygroscopic. Due to the increased number of methyl groups the compounds explode only sluggishly.

Experimental Section

General Remarks: *CAUTION: Silver azide, hydrazoic acid and all the reported compounds are explosives. Safety equipment like leather gloves, face-shields and ear-plugs are recommended.* All syntheses were carried out using standard Schlenk techniques under dry nitrogen or argon. Ether was purified by distillation over Na/benzophenone, and methanol by distillation over Na. The distilled solvents were stored under nitrogen. Methylhydrazine and *N,N*-dimethylhydrazine were used as provided by Aldrich, *N,N′*-dimethylhydrazine was prepared by reacting *N,N′*-dimethylhydrazinium chloride from Fluka with sodium hydroxide and was dried over BaO and CaH_2. *N,N,N′*-trimethylhydrazine,[13] *N,N,N′,N′*-tetramethylhydrazine,[14] *N,N,N,N′*-tetramethylhydrazinium iodide[15] and pentamethylhydrazinium iodide[13] were prepared according to known procedures. − NMR: Jeol EX 400, ^1H (400.0 MHz), ^{13}C (100.0 MHz): chemical shifts refer to $\delta_{TMS} = 0.00$; ^{14}N (28.6 MHz): shifts refer to CH_3NO_2. − IR: Nicolet 520 FT-IR (solid compounds as KBr pellets, liquid compounds as film between KBr plates). − Raman: Perkin−Elmer FTIR-2000 spectrometer (Nd-Yag Laser: 1064 nm, Laser power: 100 mW). − CHN analysis: Elementar Vario EL analyzer. − Melting points: Büchi B450. − DSC: Setaram DSC 141. − TG: Setaram DTA-TG 92. − MS: Balzers QMS 420.

Methylhydrazinium Azide (3): A 2 M solution of HN_3 in ether (25 mL) was slowly added to anhydrous methylhydrazine (0.55 g, 12.0 mmol). During the addition a colorless precipitate was formed. After the addition the reaction mixture was stirred for an hour. The precipitate was separated, washed with ether and pentane. Methylhydrazinium azide was sublimed to give colorless crystals. − Yield: 0.91 g (86%). − m.p.: 68 °C. − IR: $\tilde{\nu}$ = 3355 m, 3290 m, 3202 s, 3121 s, 3033 m, 2974s, 2864 m, 2776 m, 2505 m, 2037 s(ν_{as}, N_3), 1605 m, 1591 m, 1486 m, 1454 w, 1402 w, 1339 m, 1333 m, 1112 s, 1009 s, 934 s, 890 m, 802 w, 649 m, 642 m, 515 m, 427 m cm^{-1}. − Raman: $\tilde{\nu}$ = 3167 w, 3018 m, 2953 s, 2795 w, 1459 w, 1340 vs(ν_s N_3), 1290 w, 1013 w, 877 w, 253 w, 181 m, 122 m cm^{-1}. − ^1H NMR ([D$_6$]DMSO): δ = 2.50 (s, 3 H, CH_3), 6.89 (s, 4 H, NH). − ^{13}C NMR ([D$_6$]DMSO): δ = 37.6 (CH_3). − ^{14}N NMR ([D$_6$]DMSO): δ = −134 (*N*N*N*), −278 (N*N*N), −323 (Me*N*H_2*N*H_2). − DSC: 69.3 °C (m.p.), 151.5 °C. − CH_7N_5 (89.10): calcd. C 13.48, H 7.92, N 78.60; found C 13.23, H 7.83, N 78.55.

***N,N′*-Dimethylhydrazinium Azide (4):** A 2 M solution of hydrazoic acid in ether (25 mL) was slowly added to anhydrous *N,N′*-dimethylhydrazine (1.25 g, 20.8 mmol). Two liquid phases formed. The lower phase was separated, washed with ether and pentane and purified by sublimation at −20 °C. − Yield: 1.3 g (61%). − M.p.: −8 °C. − IR: $\tilde{\nu}$ = 3333 m, 3223 m, 2966 m, 2747 m, 2477 m, 2018 s(ν_{as} N_3), 1607 mm, 1463 w, 1408 w, 1332 w, 1248 w, 1190 w, 1108 w, 946 w, 823 w, 640 w, 627 vw, 494 w, 476 w, 397 w cm^{-1}. − Raman: $\tilde{\nu}$ = 3213 w, 2964 m, 2803 w, 1465 w, 1339 (ν_s N_3), 834 w, 464 w, 103 s cm^{-1}. − ^1H NMR ([D$_6$]DMSO): δ = 2.53 (s, 6 H, CH_3), 7.33 (s, 3 H, NH). − ^{13}C NMR ([D$_6$]DMSO): δ = 33.8 (CH_3). − ^{14}N NMR ([D$_6$]DMSO): δ = −134 (*N*N*N*), −275 (N*N*N). − DSC: 137.4 °C (decomp.). − $C_2H_9N_5$ (103.13): calcd. C 23.29, H 8.80, N 67.91; found C 21.66, H 8.84, N 61.09.

***N,N,N′*-Trimethylhydrazinium Azide (5):** A 2 M solution of hydrazoic acid in ether (15 mL) was slowly added to anhydrous *N,N,N′*-trimethylhydrazine (0.50 g, 6.8 mmol). After the addition of 3 mL of the solution the reaction mixture became turbid. After all of the HN_3 had been added to the reaction mixture, two liquid phases formed. The bottom phase was separated and stored at −30 °C. After several days colorless crystals sublimed onto the walls of the reaction vessel. − Yield: 0.36 g (46%). − M.p.: 10 °C. − Raman: $\tilde{\nu}$ = 3152 w, 3026 w, 2964 m, 1580 w, 1456 w, 1336 s(ν_s N_3), 1247 vw, 1181 vw, 1139 vw, 999 vw, 889 vw, 818 m, 474 m, 220 s, 155 s, 99 s cm^{-1}. − ^1H NMR ([D$_6$]DMSO): δ = 2.50 (s, 3 H, CH_3),

2.63 (s, 6 H, $(CH_3)_2$), 7.54 (s, 2 H, NH). − ^{13}C NMR ([D$_6$]DMSO): δ = 34.3 ($NHCH_3$), 46.6 [$N(CH_3)_2$]. − ^{14}N NMR ([D$_6$]DMSO): δ= −134 (*N*N*N*), −275 (N*N*N).

***N,N,N′,N′*-Tetramethylhydrazinium Azide Tetramethylhydrazinate(6):** A 2 M solution of hydrazoic acid in ether (10 mL) was slowly added to anhydrous tetramethylhydrazine (0.77 g, 8.8 mmol). After the addition of 3 mL of the HN_3 solution the reaction mixture became turbid. After all of the HN_3 solution had been added, a clear solution was obtained. HN_3 and ether were distilled off and a syrupy yellow liquid remained. At −78 °C a colorless solid was isolated by fractional sublimation at 10^{-3} Torr. − Yield: 0.57 g (55%) − M.p.: − 22 °C − IR: $\tilde{\nu}$ = 3319 m, 2969 s, 2669 m, 2594 m, 2497 m, 2451 m, 2131 s (HN_3), 2018 s(ν_{as} N_3), 1645 w, 1469 m, 1443 w, 1412 w, 1326 w, 1244 w, 1215 m, 1182 m, 1146 w, 1134 m, 1097 m, 1059 m, 1026 m, 989 w, 962 w, 880 w, 729 w, 639 w, 623 vw, 548 m, 500 m, 439 vw. cm^{-1} − Raman: $\tilde{\nu}$ = 3006 m, 2967 s, 2800 m, 2129 w (ν_{as} N_3, HN_3), 1475 m, 1445 m, 1331 (ν_s N_3), 989 vw, 963 w, 882 w, 732 m, 550 w, 502 w, 97 s cm^{-1}. − ^{1}H NMR ([D$_6$]DMSO): δ = 2.28 (s, 12 H, C*H*$_3$), 7.33 (s, 3 H, N*H*). − ^{13}C NMR ([D$_6$]DMSO): δ = 38.5 (*C*H$_3$). − ^{14}N NMR ([D$_6$]DMSO): δ= −135 (*N*N*N*), −258 (N*N*N).

***N,N,N,N′*-Tetramethylhydrazinium Azide (7):** Silver azide was prepared by adding a solution of silver nitrate (1.60 g, 9.4 mmol) in 20 mL of water to a solution of sodium azide (0.80 g, 12.3 mmol) in 20 mL of water. Silver azide was filtered off and washed with water. The wet product was then added to a solution of *N,N,N,N′*-tetramethylhydrazinium iodide (1.00 g, 4.6 mmol) in water. Yellow silver iodide immediately precipitated. The reaction mixture was stirred overnight and the water removed under vacuum. The product was recrystallized from methanol. − Yield: 0.35 g (58%) − M.p.: 174 °C (decomposition). − IR: $\tilde{\nu}$ = 3429 s, 3194 s, 3055 s, 2989 s, 2037 s(ν_{as}, N_3), 1730 w, 1635 m, 1541 w, 1485 m, 1456 m, 1385 m, 1278 w, 1268 w, 1186 w, 1121 w, 1049 w, 977 w, 939 w, 838 w, 712 w, 649 w, 642 w, 522 w, 451 w cm^{-1}. − Raman: $\tilde{\nu}$ = 3031 m, 2940 m, 2789 w, 1465 w, 1441 w, 1398 w, 1332 s(ν_s N_3), 1247 vw, 947 vw, 847 w, 715 w, 102 s cm^{-1}. − ^{1}H NMR ([D$_6$]DMSO): δ = 2.57 (d, *J* = 3.0 Hz, 3 H, NHC*H*$_3$), 3.21 [s, 9 H, N(C*H*$_3$)$_3$], 6.61 (q, *J* = 6.2 Hz, 1 H, N*H*CH$_3$). − ^{13}C NMR ([D$_6$]DMSO): δ = 30.5 (NCH_3), 53.4 [$N(CH_3)_3$]. − ^{14}N NMR ([D$_6$]DMSO): δ= −131 (*N*N*N*), −278 (N*N*N), −301 [$CH_3NHN(CH_3)_3$]. − $C_4H_{13}N_5$ (131.18): calcd. C 36.62, H 9.99, N 53.38; found C 35.3, H 9.67, N 50.06.

Pentamethylhydrazinium Azide (8): Silver azide was prepared as above. The wet product was then reacted with a solution of pentamethylhydrazinium iodide (0.89 g, 3.8 mmol) in water. Yellow silver iodide immediately precipitated. The reaction mixture was stirred overnight and the water removed under vacuum. The product was washed with CH_2Cl_2 and dried under oil pump vacuum to give **8** as a colorless solid (0.34 g). − Yield: 0.34 g (61%) − M.p. 180 °C (decomposition). − IR: $\tilde{\nu}$ = 3304 s, 3321 s, 3025 s, 2945 m, 2819 m, 2615 w, 2528 w, 2009 s (ν_{as} N_3), 1654 w, 1473 s, 1263 w, 1254 w, 1223 m, 1196 m, 1169 w, 1121 m, 1092 m, 1070 w, 1021 s, 954 s, 929 m, 807 s, 672 m, 632 m, 528 m, 490 m, 408 m cm^{-1}. − Raman: $\tilde{\nu}$ = 3040 m, 3023 m, 2982 m, 2811 w, 1448 w, 1322 s (ν_s N_3), 1248 w, 1124 vw, 949 w, 930 w, 809 w, 675 m, 529 w, 492 w, 467 w, 403 vw, 104 s cm^{-1}. − ^{1}H NMR ([D$_6$]DMSO): δ = 2.64 [s, 6 H, N(C*H*$_3$)$_2$], 3.22 [s, 9 H, N(C*H*$_3$)$_3$]. − ^{13}C NMR ([D$_6$]DMSO): δ = 40.0 [N(*C*H$_3$)$_2$], 50.9 [N(*C*H$_3$)$_3$]. − ^{14}N NMR ([D$_6$]DMSO): δ = −132 (*N*N*N*), −278 (N*N*N), −291 [$H_2NN(CH_3)_3$]. − $C_5H_{15}N_5$ (145.20).

Explosion Results

1: MS (EI): *m*/*z* (%) = 1 (3), 2 (3) [H_2], 13 (0.6), 14 (12), 15 (8), 16 (6), 17 (2), 18 (5), 26 (0.8), 27 (2), 28 (100) [N_2], 29 (2), 30 (3), 35 (0.4), 42 (3), 56 (0.4), 57 (0.6), 71 (0.8), 72 (1). − IR: $\tilde{\nu}$ = 3175−3020 w (CH_4), 3017 m (CH_4), 3002−2750 w (CH_4), 1586 w, 1469 w, 1304 m, 1137 w, 1010 m, 890 w, 783 w cm^{-1}.

2: MS (EI): *m*/*z* (%) = 1(9), 2 (85) [H_2], 12 (1), 13 (3), 14 (17), 15 (46), 16 (27) [CH_4], 17 (2) [NH_3], 18 (4), 25 (0.5), 26 (3), 27 (7), 28 (100) [N_2], 29 (5), 30 (15), 39 (1), 40 (3), 41 (3), 42 (18), 43 (4), 44 (2), 50 (1), 52 (0.6), 56 (0.7), 57 (4), 58 (26), 59 (11) [$N(CH_3)_3$], 60 (0.4), 71 (2), 72 (3), 89 (0.3). − IR: $\tilde{\nu}$ = 3154−3050 m (CH_4), 2965 s [$N(CH_3)_3$], 2823 s [$N(CH_3)_3$], 2775 s [$N(CH_3)_3$], 2185 w (HN_3), 2117 m (HN_3), 2090 m (HN_3), 1583 w, 1459 s [$N(CH_3)_3$], 1283 s [$N(CH_3)_3$], 1185 m [$N(CH_3)_3$], 1042 m [$N(CH_3)_3$], 970 m, 827 m, 585 w cm^{-1}.

3: MS (EI): *m*/*z* (%) = 1 (2), 2 (100) [H_2], 12 (0.3), 13 (0.8), 14 (8), 15 (8), 16 (10) [CH_4], 17 (0.3) [NH_3], 18 (0.3), 27 (0.3), 28 (47) [N_2], 29 (0.6), 30 (0.2), 32 (3), 40 (0.44), 41 (0.2). − IR: $\tilde{\nu}$ = 3344 w, 3316 w, 3175−3020 m (CH_4), 3016 s (CH_4), 3002−2750 m (CH_4), 2192 m (HN_3), 2153 m (HN_3), 2118 s (HN_3), 1342 m, 1304, 1269 m, 1165 m, 1132 m, 1033 m, 816 m cm^{-1}.

4: MS (EI): *m*/*z* (%) = 1 (7), 2 (13) [H_2], 13 (3), 14 (16), 15 (50), 16 (31) [CH_4], 17 (2) [NH_3], 18 (4), 27 (3), 28 (100) [N_2], 29 (3), 43 (6), 44 (1), 58 (2). − IR: $\tilde{\nu}$ = 3175−3020 w (CH_4), 3017 m (CH_4), 3002−2750 w (CH_4), 1384 s, 1282 m, 1195 s, 1159 s, 970 m, 899 w cm^{-1}.

7: MS (EI): *m*/*z* (%) = 1 (7), 2 (6) [H_2], 12 (1), 13 (2), 14 (15), 15 (37), 16 (4), 17 (0.5), 18 (4), 26 (2), 27 (7), 28 (100) [N_2], 29 (5), 30 (22), 31 (0.5), 32 (11), 38 (0.5), 39 (1), 40 (4), 41 (5), 42 (28), 43 (6), 44 (6), 45 (0.9), 47 (0.5), 48 (0.4), 50 (0.6), 51 (0.4), 52 (0.5), 56 (1), 57 (7), 58 (47), 59 (20) [$N(CH_3)_3$], 60 (0.7). − IR: $\tilde{\nu}$ = 2964 m, 2823 m, 2117 w, 1384 m, 1279 m, 1195 s, 1124 s, 969 s, 900 m, 597 w cm^{-1}.

Table 4. Crystallographic data and data related to data acquisition and refinement for compounds **3** and **4**

Compound	**3**	**4**
Chem. formula	CH_7N_5	$C_2H_9N_5$
Formula weight	89.09	103.12
Crystal size [mm]	0.20 × 0.32 × 0.55	0.20 × 0.80 × 0.80
Crystal system	Orthorhombic	Monoclinic
Space group	*Pnma*	*Cc*
a [Å]	9.962(1)	7.982(2)
b [Å]	5.1316(5)	10.175(2)
c [Å]	9.2280(9)	13.745(3)
β [°]	90.00	90.0
V [Å^3]	471.77(9)	1016.4(4)
Z	8	4
ρ(calcd.) [mg/m^3]	1.2545(2)	1.227
μ [mm^{-1}]	0.097	0.091
F(000)	192	448
Temp, [K]	200(2)	173(2)
Refl. collected	4328	4012
Refl. unique	612	2881
Refl. observed (4σ)	545	2653
R (int.)	0.0624	0.0406
No. variables	52	144
GOOF	1.153	1.096
Final *R* (4σ)	0.0310	0.0564
Final *wR*2	0.0844	0.1400
Larg. res. peak [e/Å^3]	0.188	0.42
Twin matrix	−	−1 0 0 0 1 0 0 0 1
Twin scaling factor	−	0.487(3)

X-ray Crystallographic Study: Single crystals of **3** and **4** were submerged in dried perfluoropolyether oil under anaerobic conditions. Suitable crystals were mounted on a glass fiber, transferred to the diffractometer and cooled in the cold gas stream derived from liquid nitrogen. The measurement for **3** was performed on a Stoe IPDS diffractometer equipped with an image-plate area detector and for that of **4** on a Siemens P4 diffractometer, both with graphite monochromated Mo-K_α radiation (λ = 0.71073 Å). All calculations were performed using SIR-97[16] and SHELXL-97. Crystallographic data are reported in Table 4.[17]

Crystallographic data (excluding structure factors) for the structure(s) reported in this paper have been deposited with the Cambridge Crystallographic Data Centre as supplementary publication nos. CCDC-149154 (**3**) and CCDC-149571 (**4**). Copies of the data can be obtained free of charge on application to CCDC, 12 Union Road, Cambridge CB2 1EZ, UK [Fax: (internat.) + 44-1223/336-033; E-mail: deposit@ccdc.cam.ac.uk].

Acknowledgments

Financial support by the Deutsche Forschungsgemeinschaft (KL 636/7−1), the Fonds der Chemischen Industrie and the German Federal Office of Defense Technology and Procurement (BWB) is gratefully acknowledged.

[1] T. Curtius, *Ber.* **1891**, *24*, 3341−3349.
[2] E. P. Kirpichev, A. P. Alekseev, Yu. I. Rubtsov, G. B. Manelis, *Russian Journal of Phys. Chem.* **1973**, *47*, 1654.
[3] H. Holfter, T. M. Klapötke, A. Schulz, *Eur. J. Solid State Inorg. Chem.* **1996**, *33*, 855−864.
[4] T. M. Klapötke, P. S. White, I. C. Tornieporth-Oetting, *Polyhedron* **1996**, *15*, 2579−2582.
[5] W.-H. Walther, T. M. Klapötke, G. Holl, *29th Annual Conference of ICT* **1998**, P134, Fraunhofer Institut für Chemische Technologie (ICT), Karlsruhe.
[6] T. M. Klapötke, H. Nöth, H. Schwenk-Kircher, W.-H. Walther, *Polyhedron* **1999**, *18*, 717−719.
[7] T. Habereder, A. Hammerl, G. Holl, T. M. Klapötke, J. Knizek, H. Nöth, *Eur. J. Inorg. Chem.* **1999**, 849−852.
[8] T. Habereder, A. Hammerl, G. Holl, K. Hübler, T. M. Klapötke, H. Nöth, J. Knizek, *31st Annual Conference of ICT* **2000**, P150, Fraunhofer Institut für Chemische Technologie (ICT), Karlsruhe.
[9] A. Hammerl, T. M. Klapötke, unpublished results.
[10] Houben−Weyl, *Methoden der Organischen Chemie* **1967**, *XI2*, 6−70.
[11] B. Neumüller, F. Schmock, K. Dehnicke, *Z. Anorg. Allg. Chem.* **1999**, *625*, 1243−1245.
[12] V. E. Shklover, Y, T, Struchkov, *Acta Cryst.* **1985**, *C41*, 734−736.
[13] R. T. Beltrami, E. R. Bissel, *J. Am. Chem. Soc.* **1956**, *78*, 2467−2468.
[14] K.-H. Linke, R. Turley, E. Flaskamp, *Chem. Ber.* **1973**, *106*, 1052−1053.
[15] H. Wieland, E. Schamberg, *Chem.Ber.* **1920**, *53*, 1329−1335.
[16] A. Altomare, M. C. Burla, M. Camalli, G. L. Cascarano, C. Giacovazzo, *J. Appl. Crystallogr.* **1999**, *32(1)*, 115−119.
[17] G. M. Sheldrick, SHELXL-97, *Program for Crystal Structure Refinement*, Universität Göttingen, **1997**.

Received September 19, 2000
[I00350]

Lipophilic Metal−Salicylideneimine−Crown Ether Hybrids — Ditopic Carriers in the Facilitated Transport of Amphiphilic Molecules Across Bulk Liquid Membranes

Jay D. Pike,[a] Dell T. Rosa,[a] and Dimitri Coucouvanis*[a]

Keywords: Supramolecular chemistry / Molecular recognition / Manganese / Macrocyclic ligands / Facilitated transport

The crown ether-functionalized Mn^{III} salicylaldimine complexes manganese(III) 4,5-bis(3,5-di-*tert*-butylsalicylideneimine)benzo-18-crown-6-X [X = Cl^-, I^-, CH_3COO^-, $(CH_3)_3CCOO^-$, $B(Ph)_4^-$] have recently been synthesized and studied as effective ditopic transport carriers of hydrophobic amino acids and neurotransmitters through $CHCl_3$ bulk liquid membranes (BLMs). A detailed analysis of the BLM transport of tryptophan and serotonin with these complexes, along with various derivatives, shows the ditopic nature of the mechanism of transport and reveals the importance of the role of both the crown ether function and the metal center. Kinetic data on the BLM transport of tryptophan follow Michaelis–Menten behavior with K_m = 25 mM and $V_m = 6.75 \times 10^{-3} h^{-1}$. Variable temperature studies on the rate of transport of tryptophan (and serotonin) were conducted. From Arrhenius plots, the activation energies, E_a, and pre-exponential factors, A, were determined to be 20 ± 1 (17 ± 5) kJ mol^{-1} and 8200 (947) $M^{-1}h^{-1}$, respectively. From these parameters, values for the thermodynamic activation energies, $\Delta G^{\ddagger}$, $\Delta H^{\ddagger}$, and $\Delta S^{\ddagger}$ were calculated to be 26 ± 4 (32 ± 1) kJ mol^{-1}, 17 ± 1 (14 ± 5) kJ mol^{-1}, and –30 ± 9 (–60 ± 14) J K^{-1} mol^{-1}, respectively. Similar studies with serotonin are reported.

Introduction

Cell membranes that protect the cell and at the same time allow for the transport of solutes across the cell boundary consist of lipid bilayers that contain a hydrophobic interior flanked by hydrophilic surfaces. The transport of biologically important small molecules through cell membranes is an essential process for living organisms.[1] The vast majority of such molecules are water-soluble species that by themselves are insoluble in lipid membranes.

In the absence of sufficient hydrophobicity, facilitated transport by specific carriers is necessary to allow for appreciable partitioning for the transport of hydrophilic molecules.[2] A great number of naturally occurring carriers are known for the transport of amino acids, neurotransmitters, nucleosides, sugars, etc. Often these carriers are proteins of mostly unknown structures that exhibit high specificity in the recognition of substrates.[3] The transporter proteins are difficult to isolate, although several have been obtained from various systems including the *E. coli* glucose transport system,[4] the *E. coli* β-galactoside transport system,[5] the baker's yeast galactose transport system,[6] the *E. coli* leucine binding membrane component,[7] and the *E. coli* arginine transport system.[8]

Other hydrophilic molecules, including most drugs, cannot readily cross lipid bilayer membranes unassisted. Carriers for the facilitated transport of hydrophilic drugs across cell membranes are rare and the design and synthesis of such molecules are of vital concern to pharmacology.

The transport of particles across membranes may be either by simple passive permeation (free diffusion) or by facilitated diffusion. Facilitated transport may be "active" or "passive." In the former, the transport process is coupled with the free energy of a chemical reaction that takes place in the transport region and is converted into "pumping" work. In the latter, the driving force is derived from the concentration gradient across the membrane (electrochemical potential gradient) and is at times assisted by "counterflow". This occurs when concentration gradients of two substances at opposite sites of the membrane accelerate the rate of transport of both substances.[9] An example of this type of amino acid transport is the transport of the essential extracellular serine, glycine, and threonine in *Streptococcus faecium*. The transport of these amino acids into the cell is coupled with the outward transport of alanine, which is synthesized in large quantities inside the cells.[10]

Numerous artificial transport systems with varying degrees of success have been developed, including: a) the effective transport of amino acid derivatives by metal complex carriers across CH_2Cl_2 or $CHCl_3$ bulk liquid membranes (BLMs) using hydrophobic, neutral $LM(Cl)_2$ complexes (M= Co^{2+}, Cu^{2+}, L = a macrocyclic polyamine ligand) in basic aqueous solutions assisted by the concomitant transport of antiport halide ions[11]; b) the pH-gradient driven transport of amino acids by positively or negatively charged hydrophobic carriers;[12] c) the transport of hydrophobic amino acids from aqueous solution at the isoelectric point by Kemp's triacid-acridine 2:1 condensate;[13] d) the transport of phenylalanine in a neutral pH transport system

[a] Department of Chemistry, University of Michigan,
930 N. University Ave, Ann Arbor, MI 48109-1055, USA
Fax: (internat.) +1-734/647-4865
E-mail: dcouc@umich.edu

Supporting information for this article is available on the WWW under http://www.wiley-vch.de/home/eurjic or from the author.

 © WILEY-VCH Verlag GmbH, 69451 Weinheim, 2001 1434−1948/01/0303−0761 $ 17.50+.50/0

facilitated by cooperative ditopic interactions between the amino acid and unbound arylboronic acid and crown ethers;[14] e) the simultaneous transport of anions and cations by a neutral bifunctional receptor that contains calix[4] phosphate and an appended uranyl salophene unit;[15] f) the ditopic fixation and transport of amino acids with a bifunctional metalloporphyrin receptor;[16] g) the proposed ditopic transport of amino acids by lanthanide(III) tris(β-diketonate) complexes,[17] and; h) the use of phenylboronic acid/trioctylmethylammonium bromide as a carrier of amino acids through a dichloroethane BLM.[18] The enantioselective transport of amino acid derivatives also has been reported with chiral organic agents,[19] and several other metal complexes[20] have shown the ability to transport certain amino acids.

Our interest in supramolecules containing individual subunits with unique structural and reactivity properties[21] has led us to the synthesis of crown-functionalized salicylaldimine ligands. These compounds are readily obtained by Schiff-base coupling reactions between an appropriate salicylaldehyde and 1,2-diaminobenzo-crown ethers or 1,2,1′,2′-tetraaminodibenzo-crown ethers. The products that have been obtained thus far contain one tBu$_4$-salphen unit per 18-crown-6 unit (Figure 1A) and, more recently, 15-crown-5 and 12-crown-4 units.[22] With dibenzo-crown ethers, 2:1 tBu$_4$-salphen:crown ether molecules have been obtained with 18-crown-6 (Figure 1B), 24-crown-8, and 30-crown-10 units.[22b] The supramolecular coordination chemistry of crown ether-functionalized complexes[23] has been studied to a considerable extent and includes derivatives of salicylaldimines,[24] porphyrins,[25] and phthalocyanines.[26] The synthesis of derivatives of salphen ligands with 15-crown-5 ethers fused to the salicylidene rings has been reported.[27] The structures of these compounds[28] have not been determined, although their reactions with metal ions and elementary characterization have been reported.[29]

Metal complexes of the dinucleating ligands reported herein can be obtained readily by the incorporation of transition metal ions into the salicylaldimine portion of the ligand and, when available, alkali metal ions into the crown ether subunit. The presence of both electron pair accepting sites (the salicylaldimine-bound metal) and hydrogen bond accepting sites (the crown ether cavity) makes these molecules ideally suited for the recognition of zwitterions and amphiphilic molecules in general.

In previous communications,[30] we reported our studies on tryptophan and serotonin transport across a $CHCl_3$ BLM using crown ether-functionalized Mn^{III} and Ni^{II} complexes. In this paper we report in detail the synthesis and structures of these ditopic receptor molecules and our detailed studies of their use in the passive transport of tryptophan and serotonin across BLMs (Figure 2).

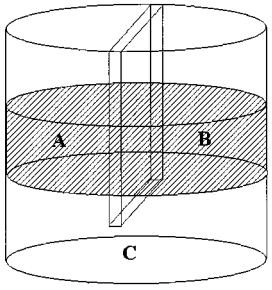

Figure 2. Bulk Liquid Membrane, BLM, transport cell: (A) and (B) source and receiving compartments; (C) $CHCl_3$ BLM

The active uptake of tryptophan is the first step in the synthesis of serotonin in the brain and is facilitated by a carrier that also transports other neutral and branched-chain amino acids. Serotonin is a very important neurotransmitter and influences a multitude of brain functions including sleep, cognition, sensory perception, motor activity, temperature regulation, appetite, sexual behavior, and hormone excretion.[31] Efficient synthetic carriers that facilitate the transport of both tryptophan and serotonin are not known.

Results and Discussion

Synthesis

The synthesis of *N*,*N*′-4,5-dimethoxybenzenebis(3,5-di-*tert*-butylsalicylideneimine) **(4)** and 4,5-bis(3,5-di-*tert*-butylsalicylideneimine)benzo-18-crown-6 **(9)** (Scheme 1) involves

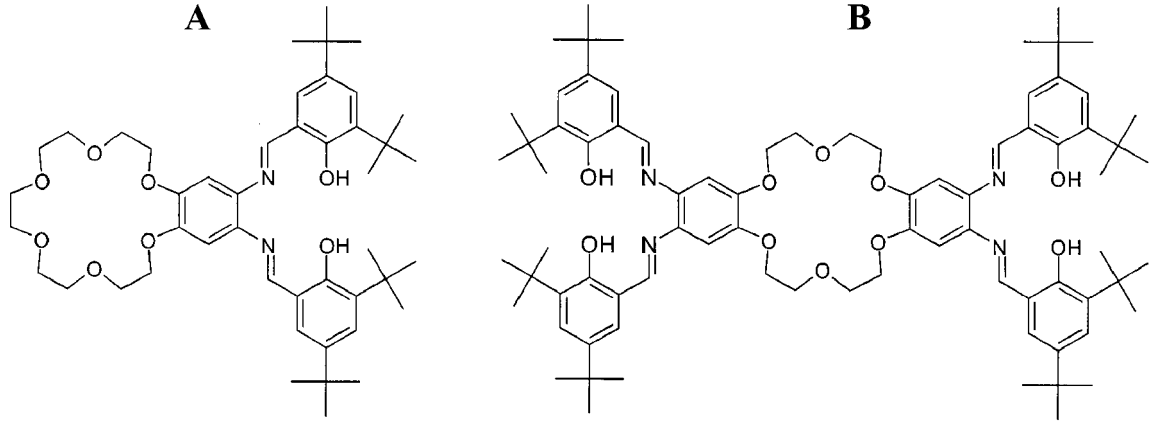

Figure 1. Ditopic Receptor Ligands: (A) tBu$_4$18-C-6; (B) (tBu$_4$)$_2$18-C-6

nitration of benzo-18-crown-6 followed by catalytic hydrogen reduction and Schiff-base condensation with the appropriate salicylaldehyde. The metal complexes of **4** (tBu$_4$M-Veratrole) and **9** (tBu$_4$M18-C-6) are obtained by addition of a methanolic solution of the metal salt to a chloroform solution of the ligand. Addition of "wet" methanolic solutions of alkali metal salts (KI, KCl, CsI, CsCl) to the chloroform solutions of the crown ether complexes allows for the introduction of alkali metal ions to the empty crown ether cavities. Complexes with two different Cs:M ratios were obtained by simply adjusting the CsI:M complex stoichiometry (M = Ni^{2+}, Mn^{3+}). An excess of salt usually yields the 1:1 (Cs^+ or K^+):tBu$_4$M18-C-6 complex.

The 1:2 (Cs^+):tBu$_4$M18-C-6 complexes are obtained when a 2:1 tBu$_4$M18-C-6:CsI ratio is used in the synthesis. The counterions that accompany the cationic Mn^{III} complexes can be exchanged readily with anions of the alkali metal salts. This often presents analytical problems and therefore the use of reagents with different anions is avoided.

Spectroscopic Characterization

The infrared spectra of the tBu$_4$M18-C-6 complexes in the region between 3500 cm^{-1} to 450 cm^{-1} are similar for different metal ions and dominated by the characteristic vibrations of the ligand. The spectra have been previously

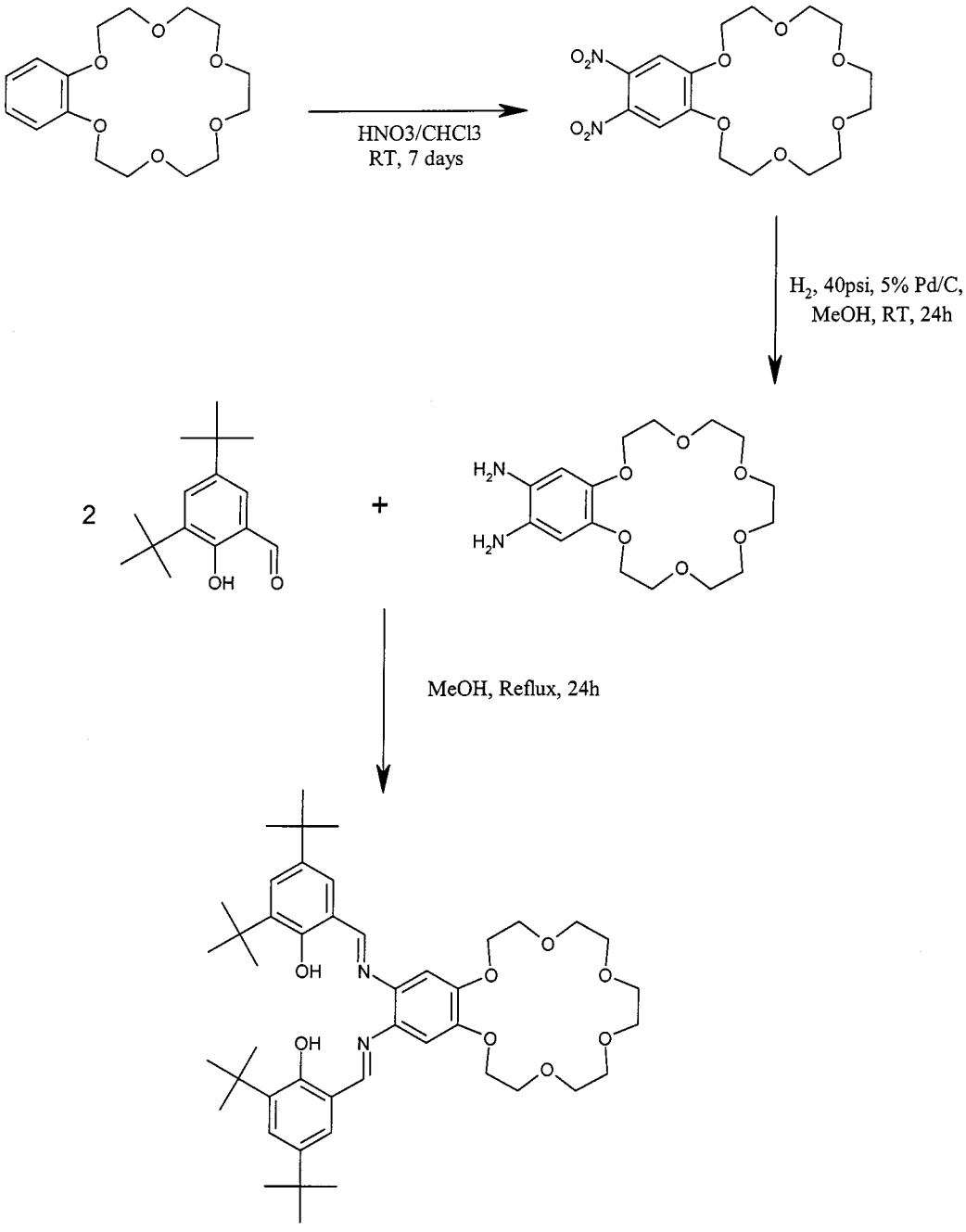

Scheme 1. Synthesis of tBu$_4$H$_2$18-C-6 **(9)**

assigned for the ligand as well as for the complexes. In the spectra of all the tBu$_4$M18-C-6 complexes the C=C stretching vibration occurs between 1595 and 1470 cm^{-1}, and the C=C out-of-plane bending at about 750 cm^{-1}. The C−H stretching of the *tert*-butyl groups is observed at 2960, 2910, and 2868 cm^{-1} and the imine stretch −C=N− is observed between 1620 and 1606 cm^{-1}. A C−O stretch for the phenolic oxygens of the salicylidene subunit is observed at about 1180 cm^{-1}. The out-of-plane C−H bending for the aromatic ring protons is observed at 820 to 846 cm^{-1}. The manganese complexes **5**, **6**, **15−28,** and **33** show the metal−oxygen stretch coupled with ring distortions around 540 cm^{-1}. Only very weak vibrations are observed in the far-IR region of the spectrum with features around 380 cm^{-1} and at times near 340 cm^{-1}.

Electronic Spectra

The electronic spectrum of ligand **9** shows two strong absorptions at 390 nm and 280 nm. The former is associated with an n−π* transition of the C=N group and the latter with a π−π* transition.[32] A shoulder at 239 nm is also due to a π−π* transition.[32] The spectra of the metal derivatives of **9** (tBu$_4$M18-C-6) (Table 1) are quite similar for different metal ions, even when alkali metal ions occasionally occupy the ether cavity. Generally, addition of transition metal ions to the salphen unit produces a change in color from the pale yellow color of the metal-free ligand to a deep red or brown color. In the Ni^{II} complex **10**, a sharp new band appears in the electronic spectrum at 496 nm, assigned to a charge-transfer transition from the ligand to the metal d orbitals (for Ni^{II}Salphen, the absorptions observed at 380−480 nm have previously been assigned[33] as charge transfer bands). The π−π* band at 266 nm in the free ligand also increases in intensity. Solutions of the Mn^{III} complexes **15−28,** and **33** in CH_2Cl_2 (Table 1) show broad bands at 490, 380, and 320 nm, and a sharper π−π* band at 260 nm [in the Mn(salen)X complexes, absorptions have been reported[34] at 588, 481, and 400 nm but only the visible region was scanned from 667−400 nm]. The electronic spectra of the tBu$_4$M18-C-6 complexes and the tBu$_4$MVeratrole complexes are similar.

Magnetic Susceptibility

The magnetic moments for the Mn^{III} complexes (Table 2) are all consistent with $S = 2$ ground states where variations from the spin only value (4.9 BM) may be due to spin-orbit coupling or inter/intramolecular interactions in the solid state. The complex **27**, with a structure similar to **14**, shows a magnetic moment (6.80 BM at 300 K and 6.26 BM at 4 K) less than that expected for two independent Mn^{III} centers (≈9.8 BM for 2 Mn^{III}) and indicative of antiferromagnetic coupling.

Table 2. Magnetics susceptibilities (μ_{eff}^{corr}/mol, in BM) for selected complexes at 300 and 4 K

	5[a]	**15**	**20**	**22**	**27**
300K	5.06	4.41	5.08	5.38	6.80
4K	4.88	4.38	4.84	4.95	6.26

[a] See Table 1 for the numbering scheme of complexes.

^{1}H NMR Spectroscopic Studies

The compounds, **3** and **9**,and their diamagnetic Ni^{II} derivatives, **4**, **10,** and **12−14**, could be characterized by ^{1}H NMR in a satisfactory manner in CD_2Cl_2 using the solvent as a reference. In the spectrum of **3**, the aromatic proton resonances appear at δ = 7.44, 7.28, and 6.87. The resonance for the imine proton is found at δ = 8.71 and for the *tert*-butyl protons at δ = 1.43 and 1.33. The Ni^{II} derivative **4** also shows a similar pattern with a large shift observable

Table 1. UV/Visible absorbances for the tBu$_4$M18-C-6 complexes **10−28** in CH_2Cl_2

	Abbreviated name	≈500	≈410	n-π* ≈390	≈350	≈310	π-π* ≈280	π-π* ≈260	π-π* ≈240
10	tBu$_4$Ni18-C-6	496	407	386	370		297	266	
11	tBu$_4$Ni18Cl· (HexNH$_3$Cl)	498	407	388	371		299	267	240
12	tBu$_4$Ni18-C-6(KI)	498	406	387	371		299	266	236
13	tBu$_4$Ni18-C-6(CsI)	496	406	387	372		296	266	
14	tBu$_4$Ni18-C-6(1/2 CsCl)	496	402	386	369	305	292	270	238
15	tBu$_4$Mn18-C-6Cl	483		380	364	319		263	
16	tBu$_4$Mn18-C-6I	493		379	356	321		262	
17	tBu$_4$Mn18-C-6(BPh$_4$)	471		377		320			
18	tBu$_4$Mn18-C-6(OAc)	485		375	358	318		260	
19	tBu$_4$Mn18-C-6(Piv)	489		374	355	316		262	
20	tBu$_4$Mn18-C-6Cl(KI)	500	419	384	354	326		259	
21	tBu$_4$Mn18-C-6Cl(KCl)	488		379	349	320		262	
22	tBu$_4$Mn18-C-6Cl(CsI)	498		381	356	320		262	
23	tBu$_4$Mn18-C-6Cl(CsCl)	488		376	353	319		262	
24	tBu$_4$Mn18-C-6Cl (1/2 CsCl)	487		379	348	321		262	
25	tBu$_4$Mn18-C-6I(KI)	495		379	349	314		261	
26	tBu$_4$Mn18-C-6I(CsI)	495		379	353	324		260	
27	tBu$_4$Mn18-C-6I (1/2 CsCl)	491		379	354	321		260	
28	tBu$_4$Mn18-C-6I(1/2 CsI)	495		377	348	322		260	

for the imine proton found at δ = 7.99. The remaining proton resonances are only slightly changed.

The ^{1}H NMR resonances of the salphen unit in **9** and its Ni^{II} derivative **10** are similar to those of their salen-veratrole counterparts. The assignment of the resonance peaks (Table 3) follow the numbering in Scheme 2. The protons of the phenol oxygen atoms in **9** readily exchange with water protons present in the solvent. The *tert*-butyl groups in all spectra are found at about δ = 1.3 to 1.4. The salphen unit of **9** shows the aromatic proton resonances at δ = 6.86, 7.22, and 7.44. These resonances, upon Ni^{II} coordination, shift to δ = 7.08, 7.13, and 7.38. The imine proton again shows the greatest shift upon metal complexation from δ = 8.66 to 7.96. The resonances due to the crown ether protons are unaffected by Ni^{II} coordination and are found at δ = 3.62, 3.66, 3.71, 3.90, and 4.23 in both **9** and **10**.

Table 3. ^{1}H NMR results of the *t*$Bu_4$18-C-6 compound **(9)** and its Ni^{II} complexes

	1[a]	2	3	4	5	6	7	8	9	10	11
9[b]	1.32	1.43	7.43	7.25	8.68	6.85	4.23	3.90	3.71	3.67	3.63
10[b]	1.32	1.44	7.39	7.16	8.04	7.14	4.23	3.90	3.72	3.66	3.62
10[c]	1.29	1.39	7.39	7.40	8.61	7.67	4.25	3.83	3.63	3.57	3.54
12[b]	1.32	1.44	7.39	7.16	8.03	7.14	4.23	3.90	3.72	3.67	3.62
12[c]	1.30	1.40	7.32	7.40	8.06	7.73	4.33	3.87	3.69	3.62	3.59
13[b]	1.35	1.47	7.44	7.74	8.61	7.43	4.41	3.57	3.49	3.55	3.57
13[c]	1.28	1.39	7.30	7.38	8.62	7.67	4.27	3.82	3.63	3.58	3.54
14[b]	1.35	1.48	7.45	7.81	8.78	7.35	4.42	3.83	3.62	3.52	3.43
	1.33	1.43	7.42	7.51	8.68	6.92	4.31		3.65	3.55	3.50
14[c]	1.29	1.40	7.32	7.40	8.63	7.68	4.27	3.83	3.65	3.59	3.55
10[d]	1.34	1.47	7.40	7.63	8.49	7.42	4.38	3.62	3.61	3.53	3.58
12[e]	1.32	1.45	7.39	7.16	8.04	7.15	4.24	3.90	3.72	3.67	3.64
13[e]	1.32	1.45	7.39	7.16	8.04	7.15	4.24	3.90	3.72	3.67	3.64

[a] See Table 1 for the numbering scheme of the complexes and Scheme 2 for the proton numbering scheme. − [b] Spectra taken in CD_2Cl_2. − [c] Spectra taken in D_6-DMSO. − [d] Spectrum taken in CD_2Cl_2 after the solution was saturated with a 0.100M CsI in D_2O solution. − [e] Spectrum taken in CD_2Cl_2 after the solution was saturated with D_2O.

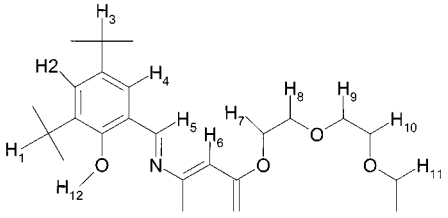

Scheme 2. Proton numbering for NMR spectra of the *t*Bu_4Ni18-C-6 complexes

When an alkali metal ion coordinates to the crown ether cavity, shifts can readily be seen in a non-coordinating solvent such as CD_2Cl_2. The alkali metal complexes show a remarkably different pattern in the crown ether proton resonances compared to those observed for **9** and **10.** Complexes **12**, **13**, and **14** show only three inequivalent sets of protons at around δ = 3.5, 3.6, and 4.3 with the resonance at δ = 3.6 accounting for twelve protons by integration of the areas. In the 1:2 Cs^+:complex **14** twice as many ^{1}H resonances are found as with the monomer **13**. This doubling of resonances reflects the loss of symmetry as a result of dimerization. The protons that point inside the pocket occupied by the Cs^+ ion are differentiated from the protons residing on the same carbon but oriented outside the pocket. This proton inequivalency shows that the "sandwich" complex (Figure 3D) that forms in the solid state stays intact in a noncoordinating environment.

In a coordinating solvent such as [D_6]DMSO, the spectra of the CsI derivatives **13** and **14** are identical and indicate dissociation of the alkali metal ions as a result of competition with the coordinating solvent. A common ^{1}H NMR pattern also is seen when CD_2Cl_2 solutions of the complexes **12**−**14** are saturated with D_2O. The resulting spectra are similar to that of **10**. An equilibrium between the complex **10** and CsI is evident when a saturated aqueous solution of CsI is extracted by a CD_2Cl_2 solution of **10**. The ^{1}H NMR spectrum of this solution of **10** exhibits resonance shifts that are similar to the 1:1 Cs^+:complex **13**. The same experiment with KI does not show any changes and perhaps reflects the insignificant partitioning of KI in CD_2Cl_2.

Description of Structures

[Nickel(II) 4,5-bis(3,5-di-*tert*-butylsalicylideneimine)benzo-18-crown-6] *n*-hexylammonium chloride (11)

The structure of **11** (Figure 3A) shows the benzo-18-crown-6 unit covalently attached to the Ni^{II}-*t*Bu_4Salphen unit. The Ni−O and Ni−N bond lengths (Table 4) are unexceptional and similar to those reported previously for other similar square planar complexes.[35] The *n*-hexylammonium cation that co-crystallizes with the ditopic receptor molecule in **11** shows the aliphatic chain oriented parallel to the *t*Bu_4Salphen unit at a distance of approximately 3.8 Å. The $-NH_3^+$ end is coordinated to the crown ether unit with the N atom nearly equidistant from the six ether oxygen donors. The average N−O distance of 2.92(4) Å is indicative of strong H-bonding interactions [N−O range 2.848(4)−3.032(4) Å]. This distance is slightly longer than the corresponding distance reported for the ammonium bromide "adduct" of 18-crown-6.[36] In **11** the nitrogen of the hexylammonium cation lies 0.901 Å above the plane formed by the crown ether oxygen atoms. The dihedral angle between the best plane defined by the six crown ether oxygen atoms and the NiO_2N_2 Ni^{II}-Salphen plane is 150°. This orientation places the Ni^{II} center approximately 8.5 Å from the crown ether O_6 centroid. In the lattice, pairs of individual **11** units are found nearly parallel to one another with the closest intermolecular Ni^{II}-18-crown-6 distance at 3.507 Å. The hexylammonium cations are located between the loosely held dimers and the Cl^- counterion is located 6.454 Å from the Ni^{II} ion.

[Nickel(II) 4,5-bis(3,5-di-*tert*-butylsalicylideneimine)benzo-18-crown-6]Cl (12-Cl)

In the structure of **12** (Figure 3B) the Ni^{II} coordination is also square planar and nearly identical to that found in **11** (Table 4). The Ni^{II} ion is located 0.0062(1) Å above the plane formed by the salicylidene oxygen and nitrogen donor atoms. A potassium cation resides in the crown ether pocket

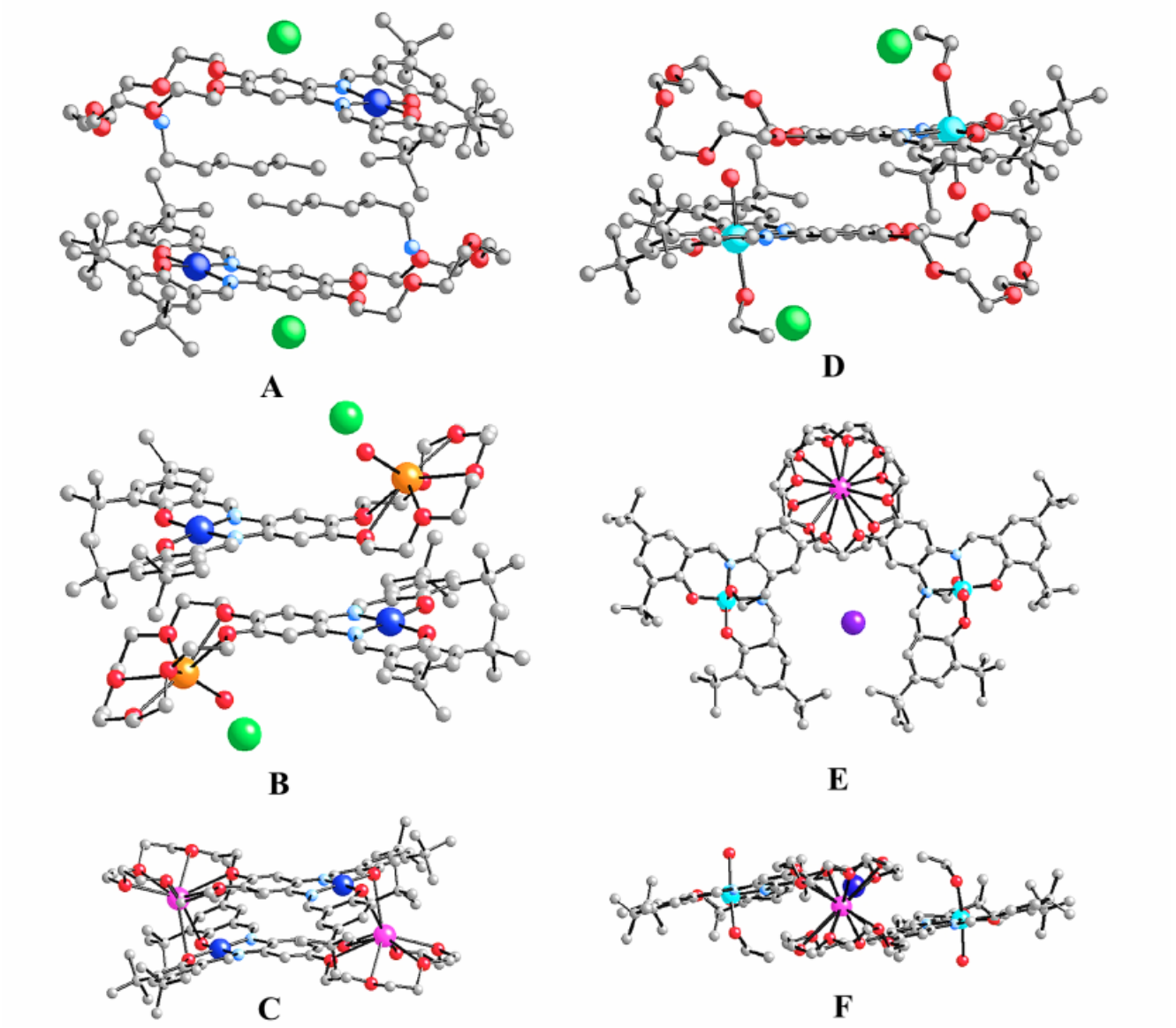

Figure 3. Molecular rendering obtained from Crystal Maker (color scheme: Ni blue; C grey; N light blue; O red; Mn aquamarine blue; K orange; Cs pink) using crystallographic coordinates of: (A) tBu$_4$Ni18-C-6[HexNH$_3$Cl] (**11**); (B) tBu$_4$Ni18-C-6(KI) (**12**); (C) the dimeric complex of tBu$_4$Ni18-C-6(CsI) complex (**13**); (D) tBu$_4$Mn18-C-6Cl (**15**), showing the hydrogen bonding between the H$_2$O ligand and the crown ether; (E) tBu$_4$uMn18-C-6I(1/2 CsI) (**28**); and (F) side view of the sandwich complex tBu$_4$Mn18-C-6I(1/2 CsI) (**28**)

Table 4. Selected bond lengths (in Å) for **11**−**15, 27**

	11[a]	**12**	**13**	**14**	**15**	**27**
M−O	1.843(6), 1.848(8)	1.866(2), 1.847(4)	1.864(4), 1.847(4)	1.90(2), 1.847(14)	1.866(2), 1.874(2)	1.84(2) 1.87(2)
M−N	1.859(2), 1.856(2)	1.868(2), 1.855(2)	1.849(4), 1.856(5)	1.90(2), 1.84(2)	1.992(3), 1.990(2)	1.96(2) 1.98(2)
M−L$_a$					2.214(3)	2.22(2)
M−L$_b$					2.289(3)	2.33(2)
C=N	1.303(3) 1.306(3)	1.307(3) 1.313(3)	1.284(8) 1.286(7)	1.30(3) 1.25(3)	1.302(4) 1.303(4)	1.33(3) 1.38(3)
C−O	1.301(2) 1.309(2)	1.310(3) 1.306(3)	1.331(7) 1.329(7)	1.28(2) 1.26(2)	1.323(3) 1.328(4)	1.43(3) 1.34(3)
C−O(ether)	1.42(3)	1.41(3)	1.42(4)	1.38(4)	1.41(3)	1.42(7)
A−O(ether)[b]		2.83(5)	3.05(9)	3.29(8)		3.34(12)

[a] See Table 1 for the numbering scheme of complexes. − [b] A represents the alkali metal coordinated to the cavity of the crown ether.

at a distance of 7.102(1) Å from the Ni^{II} ion. The K^+ ion is seven coordinate bound to the six oxygen atoms of the crown ether [avg. K−O = 2.83(2) Å; range 2.751(4)−2.899(4) Å] and a water molecule [$K-O_{H_2O}$ = 2.687(4) Å]. The potassium cation in **12** is located 0.747(4) Å above the best plane defined by the six crown ether oxygen atoms. The crown ether−K^+ bonding in **12** is similar to that reported for the potassium thiocyanate complex of 18-crown-6[37] (avg. K−O = 2.805 Å; range 2.770−2.833 Å). The chloride anion is found 3.478(1) Å from the K^+ ion, 7.102(1) Å from the Ni^{2+} ion and is hydrogen bonded to the K^+ bound water molecule at 3.409(3) Å. In the lattice, the closest Ni−Ni distance is 8.098(1) Å and the closest intermolecular contact is between Ni^{II} and O(8) at 3.507(3) Å.

[Nickel(II) 4,5-bis(3,5-di-*tert*-butylsalicylideneimine)benzo-18-crown-6]CsI (13)

In the structure of **13** (Figure 3C) the eight coordinate cesium ion is bound to the crown ether (Table 4) [avg. Cs−O = 3.08(3) Å; range 3.021(4)−3.177(4) Å] and two salicylidene oxygen atoms of another molecule at 3.298(4) Å and 3.266(4) Å. The dimeric arrangement is a consequence of the large ionic radius of Cs^+, which accommodates coordination numbers higher than six when associated with oxygen ligands. The coordination of the cesium in **13** is similar to that reported[38] for cesium thiocyanate with 18-crown-6 (avg. Cs−O = 3.146 Å; range 3.04−3.27 Å). Two nitrogen atoms (ordered thiocyanate anions) at 3.30 and 3.32 Å complete the eightfold coordination. The iodide anion for **13** is found 7.246 Å from the cesium ion and close to five carbon atoms at distances that range from 3.762(4) Å to 3.984(4) Å.

[Nickel(II) 4,5-bis(3,5-di-*tert*-butylsalicylideneimine)benzo-18-crown-6](1/2 CsI) (14)

In **14**, the cationic dimer (Figure 3D) contains two $C_{46}H_{64}N_2NiO_8$ units bound to a single cesium ion "sandwiched" between the two crown ether units. The cesium ion is twelve coordinate [avg. Cs−O = 3.30(3) Å; range 3.168(4)−3.445(4) Å]. In the structure, the two Cs^+-coordinated 18-crown-6 units are nearly parallel (dihedral angle between the two best O_6 planes is 3.1°) and staggered relative to each other. The distance of the cesium ion from the two planes is 1.832(4) Å and 1.741(4) Å. This arrangement is similar to a stack of 18-crown-6 units with cesium ions reported by Domasevitch, et al.[39] [avg. Cs−O = 3.265(8) Å; range 3.152(7)−3.431(8) Å]. In **14**, the iodide counterion is situated nearly equidistant from the two Ni^{2+} ions [6.867(2) Å and 6.952(2) Å] and the cesium ion [7.265(4) Å]. The Ni − Ni distance is 13.137(9) Å. Six solvent molecules are found in the lattice, a water molecule and five methanol molecules. All solvents are found at their sites at half occupancy.

Manganese(III) 4,5-bis(3,5-di-*tert*-butylsalicylideneimine)-benzo-18-crown-6-Cl (15)

In the structure of **15** the Mn^{III} ion occupies the tBu_4-Salphen unit and is octahedral, with the axial positions occupied by a water molecule [$Mn-O_{H_2O}$ = 2.289(3) Å] and an ethanol molecule ($Mn-O_{EtOH}$ = 2.214 Å). Both of these Mn−O bond lengths are in the range 2.21−2.29 Å so the ligands cannot be hydroxide or ethoxide (Figure 3E). The Mn^{III}−L distances, both axial and equatorial, are similar to that reported for the Mn(salen) acetate structure[40] [$Mn-O_{acetate}$ = 2.201(5) Å]. In **15**, the Mn^{III} ion is located 0.012(4) Å above the plane of the salicylidene oxygen and nitrogen atoms toward the ethanol ligand [in Mn(salen)-acetate[40] the Mn^{III} ion is found 0.017(4) Å out of the equatorial plane towards the acetate ligand]. Also found in the asymmetric unit were an additional ethanol molecule of solvation and the chloride anion [Mn−Cl = 4.541(1) Å]. The chloride anion is hydrogen bonded to the hydroxyl proton of the coordinated ethanol ligand [$Cl-O_{EtOH}$ = 3.085(4) Å] and the additional ethanol molecule of crystallization [$Cl-O_{EtOH}$ = 3.025(4) Å]. Short intermolecular hydrogen bonds in the crystal are observed between the Mn-bound H_2O ligand and the 18-crown-6 unit of another molecule. The dimeric arrangement (Figure 3E) again demonstrates the hydrogen bonding abilities of the crown ether units. The distance between the centroid of the crown ether and the manganese is 8.570(1) Å, and indicates that for effective direct crown ether-to-metal ditopic interactions the optimum donor-acceptor site separation within a zwitterionic guest should be around 8 ± 1 Å.

Bis[Manganese(III) 4,5-bis(3,5-di-*tert*-butylsalicylideneimine)benzo-18-crown-6 chloride]CsI (27)

The twelve coordinate Cs^+ cation in the dimeric **27** is located on a crystallographic twofold axis at 0, *y*, 1/4 in the space group *C*2/*c*. The general structure of the dimeric trication in **27** (Figure 3F) is very similar to that found in the structure of **14** (Table 4) and to a previously reported CsCl:benzo-18-crown-6 1:2 complex.[41] The iodide anion in the asymmetric unit is found in two positions with occupancies of 0.20 and 0.30 at 7.038(2) Å and 7.114(2) Å from the Mn^{III} ions and at 7.801(4) Å and 7.526(4) Å from the Cs^+ ion. The Mn−Mn distance at 13.113(9) Å is quite similar to the Ni−Ni distance in **14** of 13.137(9) Å. The chloride ion is also located at a position equidistant from the two Mn^{III} ions [8.14(1) Å]. In a manner similar to that described for **15**, each of the two Mn^{III} ions in **27** are axially coordinated by an ethanol and water molecules with M−O bond lengths of 2.33(2) Å and 2.22(2) Å, respectively.

Transport Properties of the Ditopic Receptors

The salphen-crown ether ditopic receptors are characterized by the availability of both an electron accepting site and an electron donating site within the same molecule. This availability allows the salphen-crown ether ditopic receptors to recognize and interact with amphiphilic guest

molecules. Important molecules of this type include amino acid zwitterions, or bifunctional molecules that contain acidic ammonium or basic carboxylate or hydroxo groups. The effective relative stability of 1:1 host-guest complexes is subject to size "matching" and is expected to be important in determining the selectivity features of host-guest interactions. The relative importance of a particular pair of interactions is difficult to evaluate when multiple interactive sites are present within the host and guest molecules. Generally, the sum of the $\Delta\Delta G$ values for the interactions involving host-guest complexation (following desolvation and/or reorganization events) will determine the thermodynamic feasibility of a given process.

In addition to the thermodynamic driving force required for transport ($\Delta\Delta G < 0$), favorable kinetics must allow for the association or dissociation of a guest molecule with a host carrier. An analysis of tryptophan and serotonin transport data obtained with various carriers leads to certain elementary conclusions and hypotheses regarding the transport properties of the salphen-crown ether ditopic receptors.

Tryptophan was chosen initially for transport experiments due to its hydrophobic nature relative to other amino acids and also its convenient electronic spectrum. It absorbs at 278 nm with an extinction coefficient of 5000 $M^{-1}cm^{-1}$, which permits sensitive detection in the millimolar range. In addition to the ammonium and carboxylate functional groups, tryptophan has additional sites for interaction, principally a phenyl ring that may $\pi-\pi$ stack with the aromatic rings of the salphen crown and the indole N−H group which may hydrogen bond to axial ligands on the metal center. The rate of tryptophan transport by numerous carriers was determined to evaluate the relative importance of the different sites. The benzo-18-crown-6 system was used as a benchmark against which all results could be compared. Transport studies with serotonin were carried out to determine the importance of size compatibility in the transport process.

An analysis of the fluxes[42] for the transport of tryptophan with various carriers (Table 5) shows a wide variation in the abilities of the salphen-crown ether hybrids to serve as carriers. The differences are associated mainly with the type of metal ion coordinated by the salphen ligand and also the type of alkali metal ion that may occupy the crown ether cavity. The role of the salphen-bound metal centers in the transport properties of the ditopic receptor carriers becomes apparent when the rate of tryptophan transport with the positively charged Mn^{III} complex **16** is compared to that of the free ligand **9**, the Ni^{II} complex **10**, the Cu^{II} complex **29**, and the corresponding $Fe^{III}-O-Fe^{III}$ dimeric complex[43] (Figure 4). In **9**, **10**, and **29**, the carrier is neutral and is not subject to significant electrostatic interactions with the tryptophan zwitterion. Furthermore, the ligand field stabilizations of the square Ni^{II} and Cu^{II} centers in **10** and **29** preclude any strong axial interactions with the carboxylate functional group on the amino acid. As a result, **9, 10,** and **29** are inferior carriers relative to **16** and their transport properties are similar to those exhibited by simple crown ethers. The transport of tryptophan by the neutral $Fe^{III}-O-Fe^{III}$ complex, however, is significant and proceeds at approximately 70% the rate observed for the Mn^{III} cation. In **16,** the best carrier in the group, the Mn^{III} ion not only carries a net positive charge but also has a propensity to bind axially coordinated ligands. The superior transporting character of **16** relative to the $Fe^{III}-O-Fe^{III}$ dimer may be due to the electrostatic interactions, which are significant for the former but weak or absent for the latter.

Table 5. Calculated fluxes of the selected complexes (based on 24 h measurement)

Cmpd	Abbrv. Name	Flux[a]	Cmpd	Flux[a]	Cmpd	Flux[a]
Bz18-C-6		2.36	**13**[b]	1.52	**21**[b]	4.94
4	tBu$_4$NiVeratrole	0	**14**[b]	1.52	**22**[b]	40.5
	(tBu$_4$Fe18-C-6)$_2$O	40.2	**15**[b]	32.5	**23**[b]	6.67
5	tBu$_4$MnVeratrole Cl	6.92	**16**[b]	54.9	**24**[b]	6.14
6	tBu$_4$MnVeratrole I	1.12	**17**[b]	109	**25**[b]	20.8
9	tBu$_4$H$_2$18-C-6	2.04	**18**[b]	9.92	**26**[b]	41.5
10[b]		1.48	**19**[b]	62.5	**27**[b]	36.2
12[b]		0.48	**20**[b]	8.70	**28**[b]	29.2

[a] The unit for flux is (mol/second/mol Carrier/m^2) $\times 10^{-4}$ – [b] The abbreviated name for this compound can be found in Table 1.

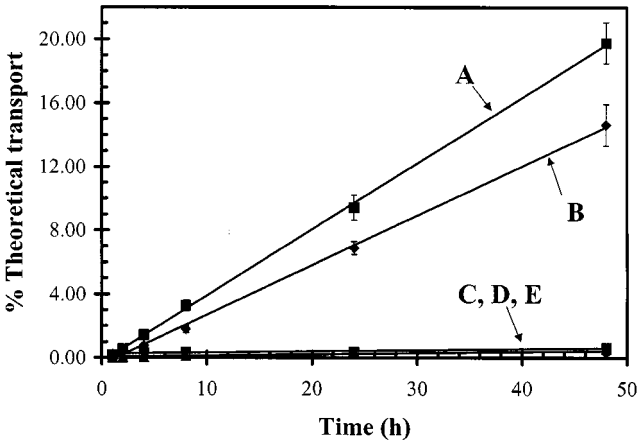

Figure 4. $CHCl_3$ BLM transport of tryptophan by 0.9 mM solutions of the carriers: (A) tBu$_4$Mn18-C-6I **(16)**; (B) [tBu$_4$Fe18-C-6]O, Fe−O−Fe dimer; (C) tBu$_4$Ni18-C-6 **(10)**; (D) tBu$_4$Cu18-C-6 **(29)**; (E) tBu$_4$H$_2$18-C-6 **(9)**; the initial concentration of tryptophan in the source phase was 50 mM

The initial transport rates of tryptophan and serotonin by tBu$_4$Mn18-C-6X (X = I, Cl) were determined as a function of carrier concentration (Figure 5) and showed first order dependence. In this concentration-gradient driven process, the concentrations of tryptophan or serotonin in the source and receiving compartments of the transport cell eventually become equal as the system asymptotically approaches equilibrium. First order rate constants obtained from these plots by linear fits of the data (Figure 5) show a slower rate of transport for serotonin (Figure 5C) than for tryptophan (Figure 5A).

For the facilitated transport of a given solute through a membrane by a membrane-residing carrier, C_m, the flux, J_{solute}, is defined as[44]:

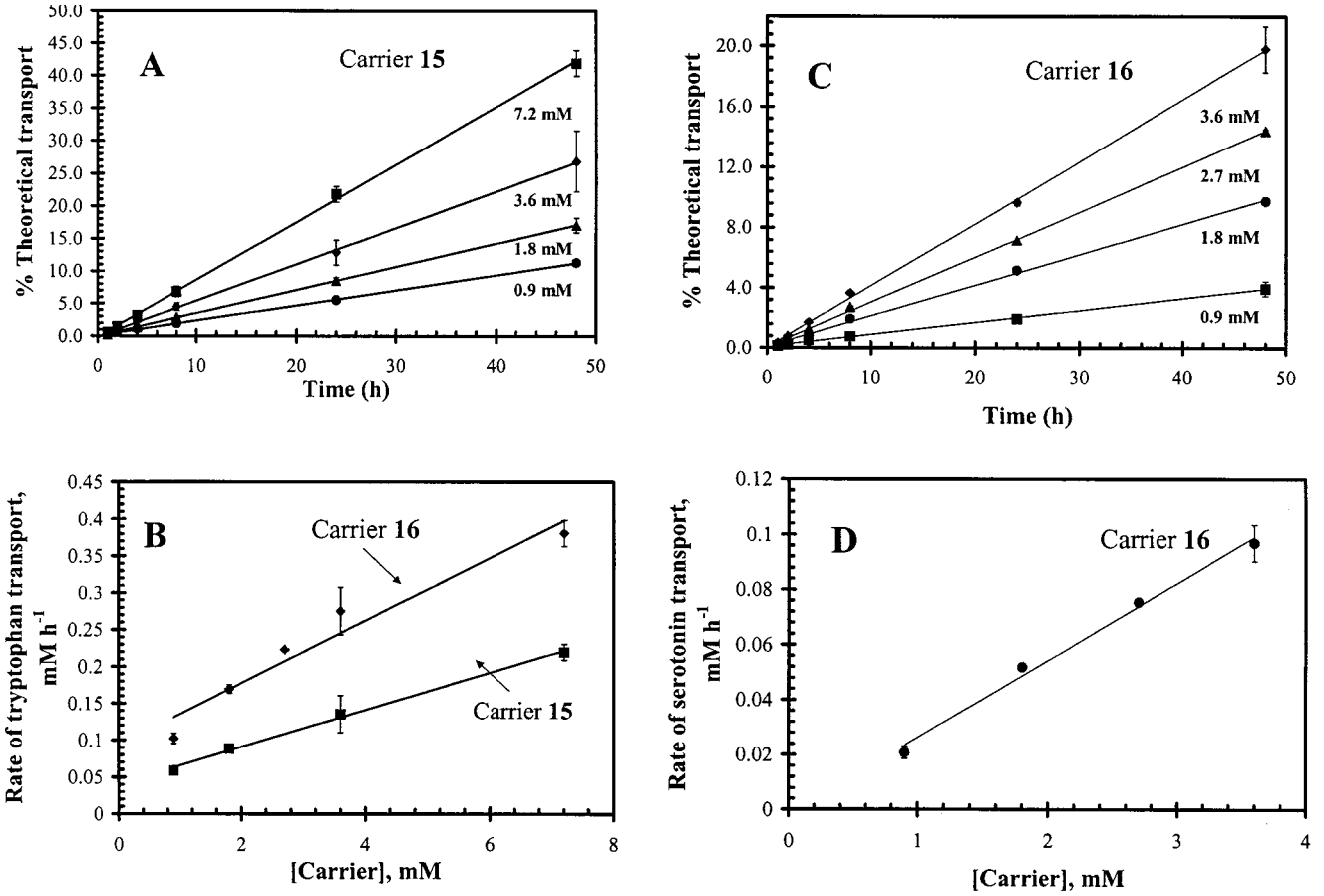

Figure 5. (A) $CHCl_3$ BLM transport of tryptophan as a function of tBu$_4$Mn18-C-6Cl **(15)** carrier concentration; the concentration of carrier varied from 0.9−7.2 mM; (B) plots of the rate of tryptophan transport vs. carrier concentration for tBu$_4$Mn18-C-6I **(16)** and tBu$_4$Mn18-C-6Cl **(15)**; (C) $CHCl_3$ BLM transport of serotonin as a function of tBu$_4$Mn18-C-6I **(16)** carrier concentration; the concentration of carrier varied from 0.9−7.2 mM; (D) plot of the rate of serotonin transport vs. concentration of tBu$_4$Mn18-C-6I; the initial concentration of tryptophan in the source phase was 50 mM

$$J_{solute} = \frac{D_{cs}C_oK_{ex}}{L}\frac{S_s - S_r}{(1+K_{ex}S_s)(1+K_{ex}S_r)}$$

where D_{cs} = carrier−solute diffusion constant, C_0 = total concentration of carrier, S_s = concentration of solute at source interface, S_r = concentration of solute at receiving interface, L = membrane thickness, and $K_{ex} = [CS_m]/[S_s][C_m]$. When K_{ex} is not very small and/or S_s is reasonably large (such as early in the transport process), then $K_{ex}S_r << 1$ and the flux is given by:

$$J_{solute} = \frac{D_{cs}C_oK_{ex}S_s}{L}\frac{S_s}{(1+K_{ex}S_s)}$$

which is of the form of the Michaelis−Menten equation for the process:

$$C_m + S_s \xleftrightarrow{Kex} [CS_m] \rightarrow C_m + S_r$$

The Michaelis−Menten constant K_m ($K_m = [S_s][C_m]/[CS_m] = 1/K_{ex}$) can be obtained from double-reciprocal Lineweaver−Burk plots. The transport of tryptophan and serotonin were followed as a function of substrate concentration and found to follow Michaelis−Menten kinetics. From Lineweaver−Burk plots (Figure 6), K_m values of 25 mM and 245 mM were determined for tryptophan and serotonin transport, respectively. From these apparent Michaelis constants carrier-permeant extraction constants ($K_{ex} = 1/K_m$) of 40 M^{-1} and 4 M^{-1} were determined for the tryptophan and serotonin carrier complexes, respectively. The origin of this difference in K_m and K_{ex} values is difficult to ascertain considering the multitude of interactions that contribute to various extents to the overall free energy of carrier-guest complexation. Practical difficulties in maintaining control of pH and their effects in the transport process also make comparisons difficult. Phenomenologically, one may expect weaker Mn−O bonding with the protonated phenolic oxygen donor of serotonin than with the carboxylate group of tryptophan. In such a case, and considering other events energetically similar, one may attribute the differences to differences in Mn−O interactions.

Kinetic studies as a function of temperature for tryptophan and serotonin transport and Arrhenius plots (Figure 7) yielded activation parameters (Table 6). The energies of activation E_a of 20 ± 1 and 17 ± 5 kJ mol^{-1} indicate diffusion-controlled processes.[44]

Studies were conducted to determine the relative transport efficiency of the ditopic receptors by comparison to

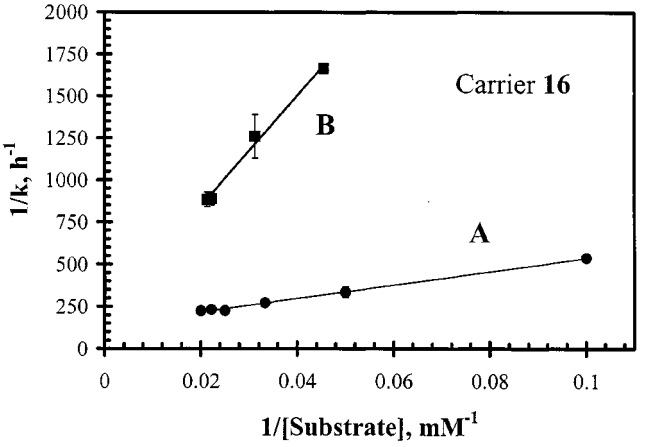

Figure 6. Lineweaver−Burk plots for: (A) tryptophan transport, and (B) serotonin transport with *t*Bu$_4$Mn18-C-6I **(16)** as the carrier; concentrations of tryptophan and serotonin were 10−50 mM and 22−47 mM, respectively

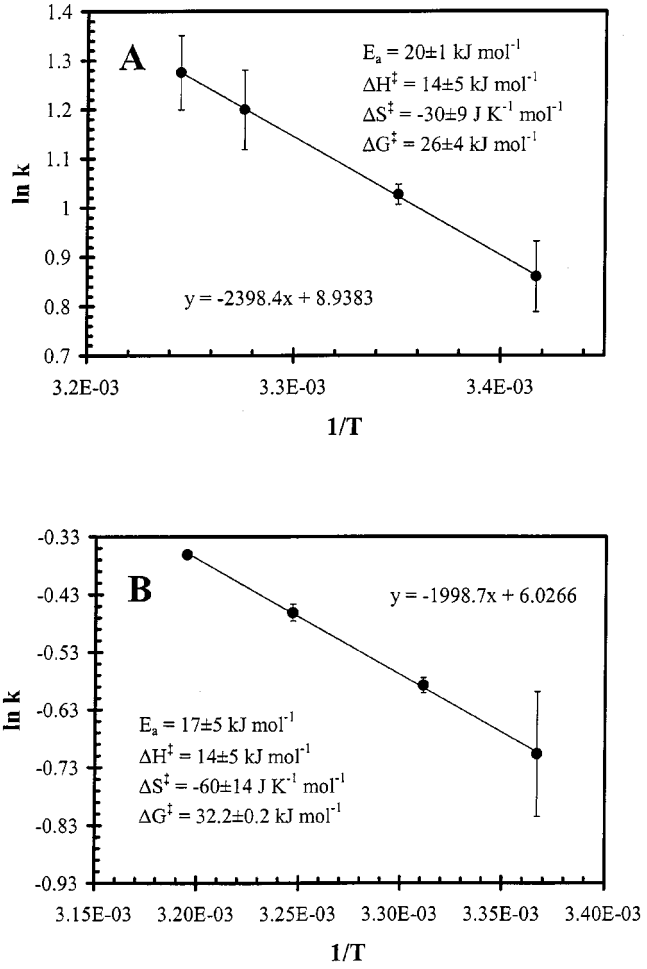

Figure 7. Arrhenius plots for: (A) tryptophan, and (B) serotonin transport with *t*Bu$_4$Mn18-C-6I **(16)** as the carrier; temperature range: 297−315 K

that of an equimolar mixture of two closely related monotopic half-receptors. The transport of tryptophan by a 1:1 mixture of Mn^{III} *N*,*N*′-dimethoxybenzenebis(3,5-di-*tert*-butylsalicylideneimine) iodide **(6)** and benzo-18-crown-6 were compared to those of **16** and also of **6** and benzo-18-crown-6 individually. The results show (Figure 8A) that in an equimolar mixture the two carrier components of **16** function synergistically. The rate of transport observed with **16**, however, is still 30% faster and indicative of moderate ditopic cooperativity. The same experiments carried out with serotonin (Figure 8B) show greater ditopic cooperativity and can be attributed to a better spatial matching between the donor-acceptor pairs within the serotonin-**16** complex. The synergism displayed by the mixture of the two carrier components of **16** in the transport of tryptophan and serotonin (Figure 8) has been reported previously for equimolar mixtures of arylboronic acids and crown ethers in the transport of L-phenylalanine through $CHCl_3$. Similarly, the ditopic cooperativity shown by **16** in the transport of tryptophan, which is more pronounced in the transport of serotonin, has been reported previously for crown ether-functionalized boronic acids in the facilitated transport of catecholamines.[45] The synergism observed in the tryptophan transport by a 1:1 mixture of benzo-18-crown-6 and **6** suggests that the transport of tryptophan by **16** may proceed simultaneously by first and second order reactions. A plot of the tryptophan transport rate as a function of carrier concentration (Figure 5) and an attempted fit with a second degree polynomial did not show evidence for a second order process, where two molecules of **16** act in tandem in the transport process.

The Role of the Crown Ether Unit

The salphen-crown ether ditopic receptors are capable of lowering the kinetic barrier associated with the $H_2O-CHCl_3$ interface transport of the carrier-guest complex. This is due to the ability of the relatively hydrophilic crown ether to "invade" the water solution across the interface. The covalently bound highly hydrophobic salphen unit precludes the partitioning of the carrier into the water. The importance of the crown ether in the transport of tryptophan is apparent when **16** is compared to the *t*Bu$_4$MnVeratrole complex **6** (Figure 9). The latter is a complex similar in most aspects to **16** except that it lacks the crown ether appendage. The electronic structural similarities[46] between **6** and **16** notwithstanding, the rates of tryptophan transport between **6** and **16** differ significantly and indicate that the crown ether unit plays an important role in transport. This undoubtedly derives from the hydrogen-bond-accepting nature of the crown ether cavity and its ability to interact with $-NH_3^+$ groups. This type of interaction has been previously established in various structure determinations[47] and also in the structure of **11** (Figure 3A).

The importance of an unhindered crown ether group in the transport of tryptophan is further demonstrated in the difference in transport rates between the salphen-crown, such as **16**, and the salphen-crown-salphen carriers, such as **33** (Figure 1B). The former shows transport rates (Figure 9) far superior to those observed with the latter with two metal-salphen units. A reason for this counter-intuitive difference may be the additional hydrophobic unit in **33** that effectively blocks the crown ether from penetrating across the interface. Nevertheless, the possibility that this differ-

Table 6. Michaelis–Menten K_m and V_m values and activation parameters for the rate of transport of tryptophan and serotonin

Substrate	K_m(mM)	V_m(h^{-1})	E_a(kJ mol^{-1})	$\Delta H^{\ddagger}$(kJ mol^{-1})	$\Delta S^{\ddagger}$(J mol^{-1})	$\Delta G^{\ddagger}$(kJ mol^{-1})
Tryptophan	25.4	0.00675	20±1	17±1	−30±9	26±4
Serotonin	245	0.00712	17±5	14±5	−60±14	32±1

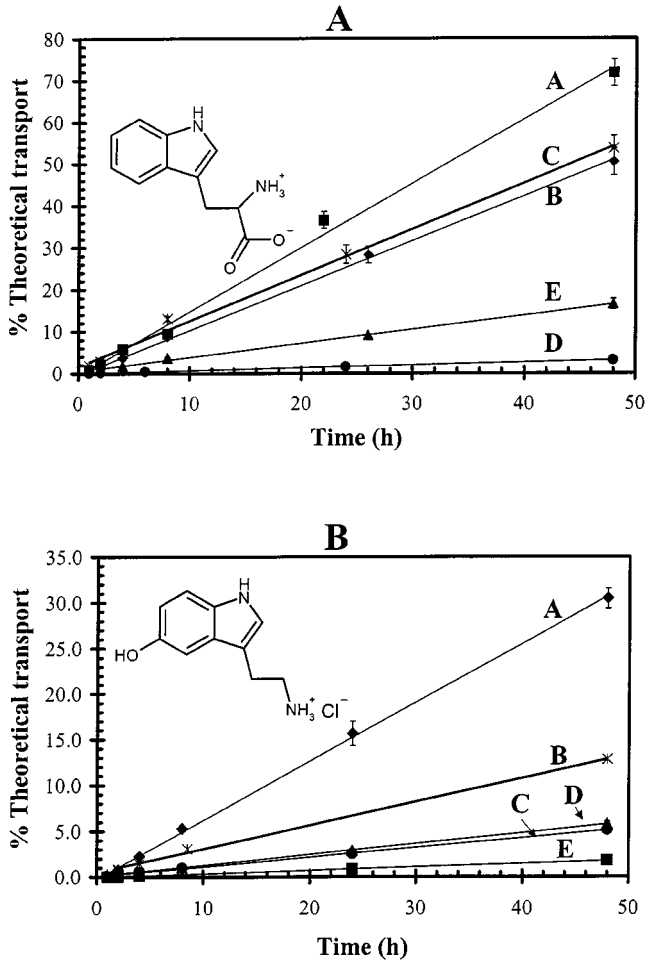

Figure 8. **A:** $CHCl_3$ BLM transport of tryptophan by 7.2 mM solutions of: (A), tBu$_4$Mn18-C-6I; (B), benzo-18-crown-6 + tBu$_4$MnVeratroleI (1:1 molar ratio); (C), tBu$_4$Mn18-C-6I + KI (1:1 molar ratio); (D), tBu$_4$MnVeratroleI; (E), benzo-18-crown-6. The initial concentration of tryptophan in the source phase was 50 mM; **B:** $CHCl_3$ BLM transport of serotonin by 7.2 mM solutions of: (A), tBu$_4$Mn18-C-6I; (B), tBu$_4$Mn18-C-6I + KI (1:1 molar ratio); (C), tBu$_4$MnVeratroleI; (D), benzo-18-crown-6 + tBu$_4$MnVeratroleI (1:1 molar ratio); (E), benzo-18-crown-6

ence still may be partly due to the differences in donor properties between the benzo-18-crown-6 and dibenzo-18-crown-6 units should not be overlooked. In the dibenzo-18-crown-6 units, weaker donor properties may be displayed due to the presence of only two aliphatic ether oxygen donors.[48]

An examination of the transport properties of the tBu$_4$Mn18-C-6X (**15** and **16**) and tBu$_4$MnVeratroleX (**5** and **6**) carriers (X = Cl and I; Figure 10) shows the I^- salt of the former to be better than the Cl^- salt. The opposite is observed with the latter, where **5** shows a faster transport rate than the corresponding I^- salt, **6**. The crown ether unit

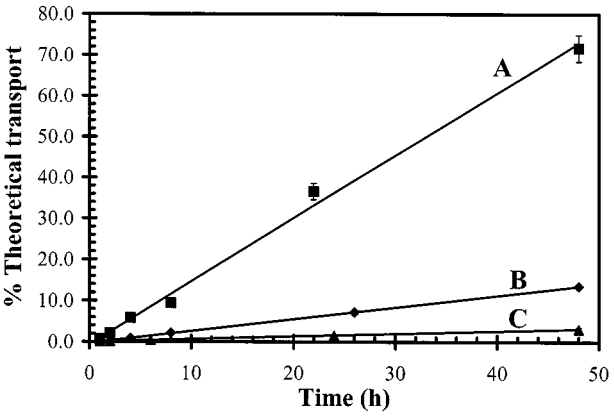

Figure 9. $CHCl_3$ BLM transport of tryptophan by 7.2 mM solutions of: (A) tBu$_4$Mn18-C-6I, (B) (tBu$_4$Mn)$_2$18-C-6I, and (C) tBu$_4$MnVeratroleI; the initial concentration of tryptophan in the source phase was 50 mM

common to **15** and **16** allows the penetration of these carriers across the interface and the higher transport rate of the I^- carrier **16** is very likely due to its higher ionic nature relative to the Cl^- analog, **15** (vide infra). In **5** and **6**, the absence of the crown ether appendix underscores the need for a different kinetic factor for facilitating interface crossing. A possible explanation for the halide effects in the transport properties of **5** and **6** is that the less hydrophobic Cl^- salt is more likely to effectively approach the interface than the I^- salt. It appears that, in transport with the tBu$_4$MnVeratroleX carriers, the ability to approach the interface becomes the rate-determining step.

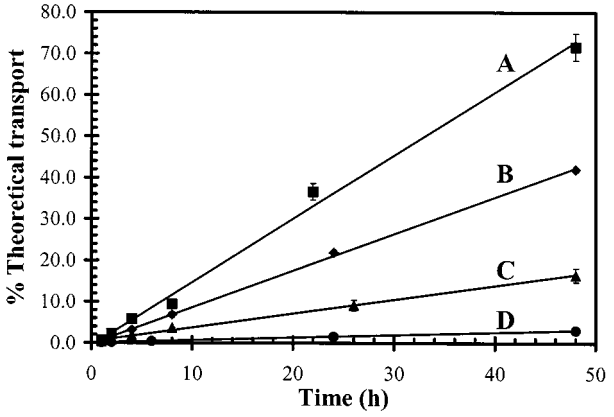

Figure 10. $CHCl_3$ BLM transport of tryptophan by 7.2 mM solutions o: (A) tBu$_4$Mn18-C-6I, (B) tBu$_4$Mn18-C-6Cl, (C) tBu$_4$MnVeratroleCl, and (D) tBu$_4$MnVeratroleI; the initial concentration of tryptophan in the source phase was 50 mM

The Effects of Alkali Metal Ions

The beneficial contributions of the crown ether units in the transport of tryptophan are diminished when alkali metal ions are introduced to the crown ether cavities of **15**

and **16**. Alkali metal ions are well-known to bind strongly to crown ethers in interactions that depend greatly on size matching between the ionic radius of the cation and the crown ether cavity.[49] The effects on the rate of tryptophan transport when alkali metal ions are competing with the $-NH_3^+$ moiety of the amino acid are as expected, and show a decrease in the rate of tryptophan transport when K^+ or CsCl salts are present at various concentrations. With CsI, the rate of transport depends on the concentration of Cs^+ in the $CHCl_3$ phase. With both **26** and **28**, the rate of transport slightly increases relative to that in the absence of the Cs^+ ion. Once a saturated aqueous solution of CsI is used in both the source and receiving compartments, the rate decreases following the behavior of the other alkali metal salts. The alkali metal salt-effect has been studied in the transport of amino acids into cells of *Streptomyces hydrogenans*, where K^+ or Rb^+ salts were introduced into a solution of the amino acid and an increase in the transport rate into the cell was observed.[50] In the present systems, the aqueous source and receiving compartments in transport experiments using carriers **20**−**28** were analyzed for the appropriate alkali metal salt by both conductivity experiments and HPLC analyses. These analyses showed that at least 95% of all K^+ salts and CsCl leached into the aqueous solutions after the first hour of transport. These results support the contention that the alkali metal-induced decrease in the tryptophan transport rate is due to the competition of the alkali metal cations with the $-NH_3^+$ group of tryptophan for the crown ether "tail" of the carrier as it penetrates the interphase. This is not the case with the CsI "adducts" **26** and **28**. The concentration of CsI in the aqueous phases in contact with $CHCl_3$ solutions of **26** and **28** tended to be consistently lower and, at equilibrium, only 75% of the total amount of CsI had leached out. The hydrophobicity of the CsI and its association with the carriers **26** and **28** in $CHCl_3$ solution may be the reason for the transport-rate enhancement found with the complexes **26** and **28**. However, the specific host-guest interactions involved in tryptophan transport with **26** and **28** are not clear and may have their origin in the unique structure of **28**, which persists in $CHCl_3$ solution. The ^1H NMR spectrum of the Ni^{II} complex **10** in CD_2Cl_2 (saturated with CsI) exhibits resonances reminiscent of the spectrum of tBu$_4$Ni18-C-6(CsI) **(13)**. This behavior demonstrates a significant tendency of CsI to partition into the organic phase and interact with the carrier.

Axial Interactions with the Mn^{III} Center

Numerous positively charged Mn^{III} salen complexes are known with the counterions bound to the metal (in noncoordinating solvents), forming square pyramidal complexes.[51] In coordinating solvents, the cationic Mn^{III} complexes form 2:1 solvent adducts with an octahedral geometry. This is also demonstrated in the crystal structures of **15,** which show that when **15** is crystallized from a methanol solution, the metal accepts two axially coordinated solvent molecules, whereas crystallization from ethyl acetate gives a derivative with the chloride counterion coordinated to one of the two axial sites on the metal.[52] The electronic spectra of the complexes **15**−**19** in CH_2Cl_2 solution are all unique and show varying magnitudes of axial ligand−metal ion interactions, as evidenced by the location of an electronic absorption band between 470 and 500 nm (Table 1). The tetraphenylborate salt **17** shows this absorption at the shortest wavelength (470 nm). Taking into account the noncoordinating properties of this anion, the absorbance is probably due to coordination of the MeOH present in the CH_2Cl_2. Indeed, a common band is observed at 460 nm for all complexe **15**−**19**, in MeOH solution (Table 7). The bathochromic shifts of the 470 nm band, caused by coordination of electron donors to the Mn^{III} center in **15**−**19**, indicate that this electronic absorption is very likely due to a metal-to-ligand charge transfer (MLCT) process. The relative substrate transport rates are slower for carriers that show the larger bathochromic shifts of the MLCT band (Table 1). The differences in the bathochromic shift of the CT absorption reflect differences in strength of the Mn^{III}-axial ligand interactions. Generally, the transport data indicate that the less coordinating anions do not compete effectively with the amino acids for the Mn^{III} site. As a result, the efficiency of tryptophan transport follows the order: $B(Ph)_4^- > I^- = Piv^- > Cl^- > Ac^-$ (Figure 11). This is also the order by which Λ_m, the molar conductivity, increases (Table 7). The conductance measurements indicate that hydrophobic $CHCl_3$−ion interactions promote ionic dissociation in $CHCl_3$ solution.

As a consequence, the greater donor properties of the pivalate anion, with an expected superior solubility in nonaqueous media and anticipated stronger interactions with the Mn^{III} center, are not reflected in the transport rate of tryptophan by it; the latter shows a higher transport rate than the acetate salt **18**.

With tetraphenylborate as a counterion for the Mn^{III} carrier, compound **17** shows a considerable increase in the rate of tryptophan transport. This is noteworthy considering the limited solubility of **17** in $CHCl_3$. Indeed, the solubility of **17** is considerably less than that of the other carriers. The origin of this reduced solubility of **17** in nonaqueous media may be due to extensive charge localization in the carrier ion-pair. The bulky tetraphenylborate anion, which is unable to coordinate to the metal ion, leaves a full positive charge on the metal. Similar arguments may be made for the iodide salt **16**, which also shows fast transport rates. In addition to hydrophobicity, another reason for the increase in the rate of transport observed with the tetraphenylborate and iodide salts may be that these weakly interacting anions allow the salphen-bound metal to interact with the aqueous phase and coordinate axial H_2O ligands (vide infra).

Host−Guest Interactions

In the zwitterionic form, amino acids can interact either with the RNH_3^+ group (with the crown ether site in the carrier) or with the $R-COO^-$ group (with the Mn^{III} site). With hosts such as **16**, the host-guest interactions cannot be ditopic due to the short span of the amino acid functional groups relative to the separation between the Mn^{III}

Table 7. Comparison of the electronic spectra and molar conductivity between carrier complexes with different anions in CH_2Cl_2 and MeOH

Complex	λ_{max} of the MLCT band in CH_2Cl_2 (in nm)	λ_{max} of the MLCT band in MeOH (in nm)	Λ_m ($\mu S\ cm^2\ mol^{-1}$)
15[a]	483	460	4
16	498	460	15
17	471	460	325
18	485	460	3
19	489	460	15

[a] The abbreviated name of this compound can be found in Table 1.

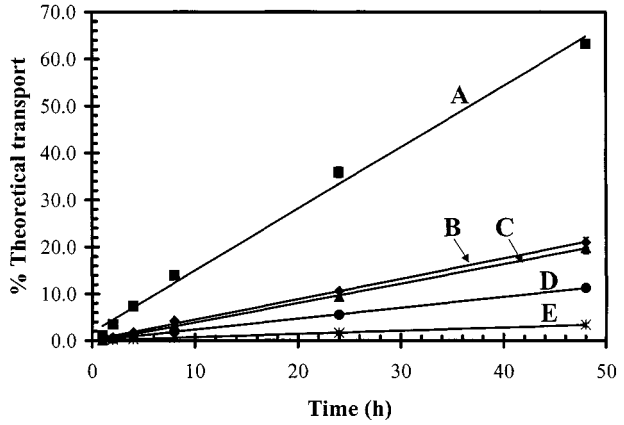

Figure 11. Effect of the anion, X, in the transport of tryptophan by 0.9 mM solutions of the tBu$_4$Mn18-C-6X carriers: (A) tBu$_4$Mn18-C-6(BPh$_4$) **(17)**, (B) tBu$_4$Mn18-C-6(Piv) **(19)**, (C) tBu$_4$Mn18-C-6I **(16)**, (D) tBu$_4$Mn18-C-6Cl **(15)**, and (E) tBu$_4$Mn18-C-6(OAc) **(18)**; the initial concentration of tryptophan in the source phase was 50 mM

center and the crown ether cavity. This distance becomes shorter when H_2O is added axially to the Mn^{III} center and should make it possible for the zwitterionic amino acid guest to hydrogen-bond to the water molecules through the carboxylate group and simultaneously to the crown ether cavity through the ammonium group. The observed ditopic behavior (Figure 8) very likely reflects transport with a water-coordinated Mn^{III} center. Molecular mechanics calculations[53] on the tryptophan-tBu$_4$Mn18-C-6 complex support this suggestion and show (see Figure 12) that, when tryptophan is placed in the pocket of the carrier that contains a water molecule axially coordinated to the Mn^{III} center, the relative energy of the host-guest complex decreases.[53] In the energy-minimized structure, in addition to RNH_3^+ hydrogen bonding with the crown ether appendix ($RNH_3^+\cdots O$, 2.69 Å), short hydrogen bonds are found between the amino acid carboxylate group and the Mn^{III}-bound water molecule($COO^-\cdots H_2O-Mn$, 2.51 Å). In the energy-minimized structure without the Mn^{III}-bound water molecule, the only hydrogen bonding interaction is between the RNH_3^+ unit and the crown ether unit ($RNH_3^+\cdots O$, 2.69 Å; $COO^-\cdots Mn$, 3.79 Å). The same type of calculations was performed with serotonin. With a water molecule axially bound to the Mn^{III} ion in **16** the energy minimized structures (Figure 13) show the relative energy of the serotonin-**16** complex[53] much higher than that of the complex without an axially bound water molecule. The lower energy of the latter is not unexpected considering the favorable spatial disposition of the donor (OH group) and acceptor (NH_3^+ group) sites in the serotonin molecule at a distance of 8.35 Å. This distance is comparable to the Mn^{III}-crown ether centroid distance of 8.72 Å and allows for an optimal host-guest interaction. This interaction accounts for the superior ditopic effect shown in the serotonin transport by **16** (Figure 8B) relative to the transport of tryptophan by the same carrier (Figure 8A).

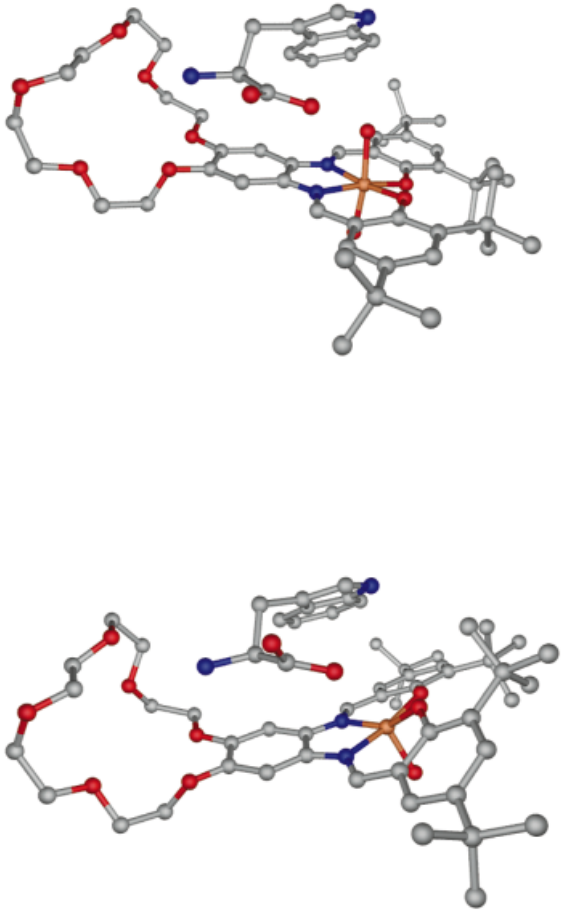

Figure 12. Optimized structures of the tryptophan-tBu$_4$Mn18-C-6 complex: (A) with, and (B) without an Mn-coordinated H_2O ligand

Other modes of interaction are possible with tryptophan and the ditopic carriers. These include a contact between

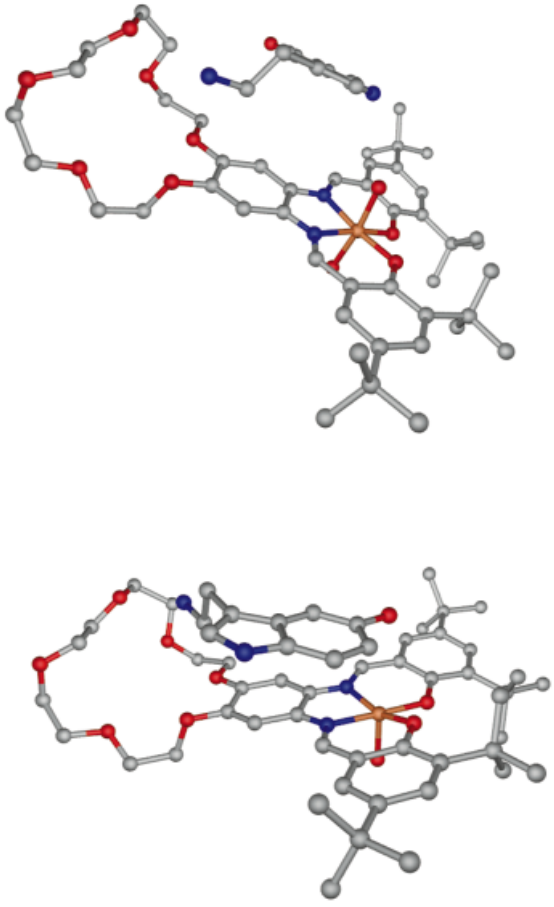

Figure 13. Optimized structure of the serotonin-tBu$_4$Mn18-C-6 complex: (A) with, and (B) without an Mn-coordinated H_2O ligand

the aromatic ring of tryptophan and the "bridging" aromatic ring of the carrier through π-stacking and also simple hydrophobic interactions of tryptophan with the organic phase. The use of leucine and phenylalanine in transport experiments was undertaken to explore the possible importance of these modes of interaction. Solubility data indicate that both are slightly less hydrophobic than tryptophan (11.4 mg TRP/mL H_2O at 23 °C, 24.3 mg LEU/mL H_2O at 25 °C, and 29.7 mg PHE/mL H_2O at 23 °C[54]). The rates of transport of the three amino acids show a dependence on hydrophobicity but not on aromaticity and suggest that the rates depend on the ability of the amino acids to approach and enter the organic solvent-water interface.

Conclusion

A new class of ditopic receptor molecules has been synthesized and structurally characterized. The unique structural features of these molecules are: a) a very lipophilic unit that consists of two 3,5-di-*tert*-butylsalicylideneimine moieties that form a square O_2N_2 coordination site, and b) a relatively hydrophilic benzo-18-crown-6 ether unit capable of binding to alkali metal ions and hydrogen bonding with ammonium functional groups. These molecules, which are totally insoluble in water but very soluble in nonpolar solvents, have been found to be effective in the facilitated transport of hydrophobic amino acids and serotonin across $CHCl_3$ bulk liquid membranes.

The metal ion within the O_2N_2 coordination site, and its affinity for axial ligands, determines transport efficiency. The neutral Ni^{II} derivatives of the ditopic receptors, with little affinity for axial ligands, are poor carriers and their efficiency in the transport of tryptophan is roughly equal to the unmetallated ligands or benzo-18-crown-6 ether. In contrast, the monocationic Mn^{III} derivatives are very efficient carriers in the facilitated transport of tryptophan and serotonin. In these carriers the counterions that can also coordinate to the Mn^{III} ion inhibit transport and the inhibition is roughly correlated to the magnitude of interaction, which is also reflected in the extent of ionic dissociation as determined by equivalent conductance measurements.

The kinetics of tryptophan and serotonin transport are first order in both substrate and carrier. The transport by equimolar mixtures of the individual interacting units (the Mn^{III} complex of the tetra-*tert*-butylsalphenveratrole tetradentate ligand and the benzo-18-crown-6 cyclic ether) shows some synergism. The two units, when covalently bound in the ditopic receptors, are considerably more effective and show ditopic cooperativity, which is moderate for tryptophan and considerably better for serotonin. The results correlate with molecular mechanics calculations and the relative energies associated with the optimized host-guest structures. The slower rate of serotonin transport is attributed to its greater hydrophilicity relative to tryptophan. Tritopic carriers that consist of two hydrophobic salphen units on either side of a dibenzo-18-crown-6 ether bridging unit are not efficient in the transport of tryptophan. This result, and the poor transport properties of the Mn-veratrole complex, have been rationalized in terms of either the blocking or unavailability of the crown ether unit in both of these ineffective carriers.

It is suggested that the interface-invading ability of the sterically unencumbered crown ether in the ditopic carriers lowers the kinetic barrier to interphase transport. The latter is thermodynamically driven by the concentration gradient between the source and receiving phase. The catalytic effect of the crown ether appendage is also apparent in the transport properties of ditopic carriers when alkali metal ions are present. In the latter case, transport is inhibited as the RNH_3^+ group of the tryptophan zwitterion competes with the alkali metal cations and does not have free access to the water-invading crown ether.

Experimental Section

General Remarks: Chemicals/Instrumentation

Details regarding the acquisition and purification of the solvents and reagents used, along with details regarding instruments used and spectroscopic techniques and methods can be found in the Supporting Information.

Synthesis

1,2-Dimethoxy-4,5-dinitrobenzene (1): A modified procedure of Frisch and Bogert[55] for the nitration of 1,2-dimethoxybenzene was carried out and the compound was obtained in 80% yield.[56]

1,2-Diamino-4,5-dimethoxybenzene (2): The reduction of 1,2-dimethoxy-4,5-dinitrobenzene was performed as reported by Weinberger and Day[57] and the product was obtained in 75% yield.

***N,N′*-4,5-Dimethoxybenzenebis(3,5-di-*tert*-butylsalicylideneimine), *t*Bu$_4$Veratrole (3):** Under an inert atmosphere, compound **2** (1.70 g, 10 mmol) was dissolved in MeOH (70 mL) to give a colorless solution. A solution of 3,5-di-*tert*-butylsalicylaldehyde (4.77 g, 20 mmol) in MeOH (50 mL) was added and the resulting bright yellow solution was refluxed for 18 hours. Upon cooling the product precipitated as a yellow crystalline material. The solid was collected by filtration in air and dried overnight under vacuum. Yield 4.2 g (70%).[56]

Nickel(II) *N,N′*-4,5-Dimethoxybenzenebis(3,5-di-*tert*-butylsalicylideneimine), *t*Bu$_4$NiVeratrole (4): Ligand **3** (3.00 g, 5 mmol) was dissolved in $CHCl_3$ (100 mL). Nickel acetate tetrahydrate (1.25 g, 5 mmol) was dissolved in 40 mL of methanol. This solution was slowly added to the solution of **3**. A bright red or orange powder precipitated immediately. Stirring was continued for one hour. The precipitate was collected by filtration, washed with EtOH (10 mL), and dried under vacuum overnight to yield an orange-red powder. Yield 2.96 g (90%). − $C_{38}H_{52}N_2NiO_4$ (659.55): calcd. C 69.41, H 7.66, N 4.26, Ni 8.93; found C 69.65, H 7.57, N 4.17, Ni 8.04. − UV/Vis (CH_2Cl_2): λ (ε × 10^{-3} м$^{-1}$ cm^{-1}) = 496 nm (br, 14.6), 466 (sh, 12.1), 404 (sh, 27.0), 386 (42.1), 371 (sh, 29.1), 298 (25.2), 266 (55.5). − IR (CsI): $\tilde{\nu}$ = 1614 cm^{-1} (vs, C=N), 383 (s). − ^{1}H NMR (300 MHz, CD_2Cl_2): δ = 7.99 (s, 2 H), 7.39 (d, 2 H), 7.26 (d, 2 H), 7.11 (d, 2 H), 4.00 (s, 6 H), 1.47 (s, 18 H), 1.32 (s, 18 H). − ^{13}C NMR (300 MHz, CD_2Cl_2): δ = 97.7, 120, 127, 131, 137, 138, 141, 150, 154, 164.

Manganese(III) *N,N′*-4,5-Dimethoxybenzenebis(3,5-di-*tert*-butylsalicylideneimine)X, *t*Bu$_4$MnVeratroleX [X = Cl (5) or I (6)]: A procedure similar to that described for the synthesis of **4** above was followed for the synthesis of **5** and **6**.[56]

4,5-Dinitrobenzo-18-crown-6 (7): Solid benzo-18-crown-6 (5 g, 16.0 mmol) was added slowly over thirty minutes to concentrated nitric acid (150 mL) with stirring. $CHCl_3$ (100 mL) was added to the yellow solution and the two layers were stirred for seven days. After this time the acid was diluted with an equal volume of distilled water. The product was extracted with chloroform (3 × 100 mL). The chloroform was evaporated to dryness leaving a yellow waxy residue. The product was used without further purification. Yield 5.5 g (85%). − ^{1}H NMR (300 MHz, [D$_6$]DMSO): δ = 7.76 (s, 2 H), 4.30 (m, 4 H), 3.76 (m, 4 H), 3.58 (m, 8 H), 3.50 (s, 4 H).

4,5-Diaminobenzo-18-crown-6 (8): Compound **7** (2 g, 4.95 mmol), 5% palladium on activated carbon (1 g), and methanol (100 mL) were placed into a hydrogenation vessel. The mixture was degassed and allowed to react with hydrogen gas at 40 p.s.i. with agitation for 18 hours. The solution was filtered under Schlenk conditions through a minimal pad of celite and the clear solution was reduced to dryness by removing the solvent under reduced pressure. A pale off-white powder was obtained that readily decomposed in solution when exposed to air but was moderately stable as a solid. The solid was stored under inert atmosphere conditions. Yield 0.85 g (50%).

4,5-Bis(3,5-di-*tert*-butylsalicylideneimine)benzo-18-crown-6, *t*Bu$_4$H$_2$18-C-6 (9): Under an inert atmosphere, compound **8** (1 g, 2.91 mmol) and 3,5-di-*tert*-butylsalicylaldehyde (1.36 g, 5.82 mmol) were dissolved in methanol (50 mL). The resulting solution was refluxed under N_2 for 48 hours. The product precipitated from solution upon cooling as a yellow powder and was isolated by filtration in air. Yield 3.25 g (72%).[56]

Nickel(II) 4,5-Bis(3,5-di-*tert*-butylsalicylideneimine)benzo-18-crown-6, *t*Bu$_4$Ni18-C-6 (10): An amount of nickel acetate tetrahydrate (0.16 g, 0.65 mmol) was dissolved in MeOH (50 mL) and added to a solution of **9** (0.5 g, 0.65 mmol) in CH_2Cl_2 (50 mL) resulting in an intense red solution. The solvent was slowly evaporated to afford fibrous red crystals. Yield 0.38 g (70%).[56]

Nickel(II) 4,5-Bis(3,5-di-*tert*-butylsalicylideneimine)benzo-18-crown-6·*n*-hexylammonium chloride, *t*Bu$_4$Ni18-C-6[HexNH$_3$Cl] (11): This compound was obtained in 40% yield in a manner analogous to that used for the synthesis of **10** in the presence of hexylammonium chloride.[56] The complex crystallized from a dark red MeOH/acetone solution upon slow evaporation of acetone.

[Nickel(II) 4,5-Bis(3,5-di-*tert*-butylsalicylideneimine)benzo-18-crown-6]AX, *t*Bu$_4$Ni18-C-6(AX) [AX = KI (12); CsI (13); 1/2 CsI (14)]: AX (0.60 mmol or 0.30 mmol in the case of **14**) was dissolved in MeOH (50 mL) and added to a solution of **10** (0.5 g, 0.60 mmol) dissolved in acetone (50 mL). The intense red color remained unchanged. The compounds **12**, **13** and **14** were obtained in yields of 80%, 85% and 85%, respectively.[56]

Manganese(III) 4,5-Bis(3,5-di-*tert*-butylsalicylideneimine)benzo-18-crown-6-X, *t*Bu$_4$Mn18-C-6X [X = Cl (15); I (16); B(Ph)$_4$ (17); Acetate (18); Pivalate (19)]: Manganese(II) acetate (0.16 g, 0.65 mmol) was dissolved in MeOH (50 mL) and added to a solution of **9** (0.5 g, 0.65 mmol) in $CHCl_3$ (50 mL), resulting in a dark brown solution. An excess amount of the sodium salt of the anion (2.6 mmol) was added to provide an anionic source for the Mn^{III} center. The ethanol solution of the compound was stirred in air overnight and the solvent removed. The residue was redissolved in chloroform (50 mL) and washed with deionized water (10 × 100 mL) to remove the excess salt and any sodium coordinated by the crown ether. The complex was isolated by evaporation of the remaining solvent. Crystals of **15** were obtained by slow evaporation of an ethanol or ethyl acetate solution of the complex.[56]

15: Yield 0.74 g (80%). − $C_{46}H_{64}MnN_2O_8Cl{\cdot}CH_3CH_2OH{\cdot}H_2O$: calcd. C 62.15, H 7.82, Mn 5.92, N 3.02; found C 61.88, H 8.14, Mn 5.87, N 3.09. − UV/Vis (CH_2Cl_2): λ (ε × 10^{-3} м$^{-1}$ cm^{-1}) = 483 nm (br, 12.2), 380 (20.5), 364 (sh, 19.7), 319 (20.9), 263 (30.4); UV/Vis (MeOH): λ (ε × 10^{-3} м$^{-1}$ cm^{-1}) = 459 nm (br, 12.1), 378 (29.7), 313 (24.0), 258 (35.5). − FAB-MS (3-nitrobenzyl alcohol): *m*/*z* = 827 [M − CH_3CH_2OH − H_2O − Cl]. − IR (CsI): $\tilde{\nu}$ = 1605 (vs, C=N) cm^{-1}, 393, 359. − Magnetic moment, μ_{eff}^{corr} = 4.41 BM/mole (300 K); 4.38 (4 K).

The syntheses and spectroscopic and physical properties of **16**, **17**, **18** and **19**, obtained in 95%, 87%, 95% and 94%, respectively, were similar to those of **15**.[56]

[Manganese(III) 4,5-Bis(3,5-di-*tert*-butylsalicylideneimine)benzo-18-crown-6 chloride]AX, *t*Bu$_4$Mn18-C-6Cl(AX) [AX = K, (20); KCl (21); CsI (22); CsCl (23); 1/2 CsCl (24)]: AX (0.60 mmol or 0.30 mmol in the case of **24**) was dissolved in methanol (50 mL) and added to a methanolic solution of **15** (0.61 g, 0.60 mmol). The compounds were isolated in 90%, 92%, 85% and 88%, respectively for **20**, **21**, **22** and **23**, by slow solvent evaporation.

[Manganese(III) 4,5-Bis(3,5-di-*tert*-butylsalicylideneimine)benzo-18-crown-6 iodide]AX, *t*Bu$_4$Mn18-C-6I(AX) [AX = KI (25); CsI (26);

Table 8. X-ray crystallographic and experimental data for complexes **11**−**15**, **27**

Complex	**11**[a]	**12**	**13**	**14**	**15**	**27**
Formula	$NiC_{52}H_{80}N_3O_8Cl$	$KNiC_{46}H_{66}N_2O_9I$	$CsNiC_{46}H_{64}N_2O_8I$	$CsNi_2C_{92}H_{128}N_4O_{16}I$	$MnC_{48}H_{72}N_2O_{10}Cl$	$CsMn_2C_{96}H_{144}N_4O_{20}ClI_2$
F.W. (g mol^{-1})	969.37	1015.74	1091.52	1923.24	927.51	2114.82
space group	$P2_1/n$	$P\bar{1}$	$P\bar{1}$	$P\bar{1}$	$P\bar{1}$	$C2/c$
a (Å)	10.58880(10)	10.37910(10)	10.0693(2)	18.818(4)	10.9387(2)	24.0961(6)
b (Å)	19.15051(10)	15.9553(2)	16.6268(1)	19.544(4)	14.3794(2)	30.2777(6)
c (Å)	30.9815(4)	18.449	19.2304(3)	20.335(4)	18.4478(4)	18.9944(4)
α (Å)	90	112.16	114.672(1)	106.57(3)	104.958(1)	90
β (Å)	93.7140(10)	102.97	102.098(1)	102.75(3)	104.245(1)	114.1030(10)
γ (Å)	90	96.43	93.290(1)	114.16(3)	99.140(1)	90
Z	4	2	1	2	2	4
V (Å^3)	6269.26(11)	2691.12(4)	2822.39	6033(2)	2639.45(8)	12649.6(5)
$\rho_{calcd.}$ (Mg m^{-3})	1.107	1.324	1.584	1.039	1.225	0.779
T (K)	158(2)	158(2)	173(2)	293(2)	173(2)	158(2)
λ (Å)	0.71073	0.71073	0.71073	0.71073	0.71073	0.71073
μ (mm^{-1})	0.502	0.690	1.860	1.370	0.358	0.829
$R1$[b] (all data)	0.0694	0.0734	0.0753	0.2170	0.0858	0.1725
$wR2$[c] (all data)	0.1755	0.2065	0.1758	0.3413	0.1570	0.4207

[a] See Table 1 for the numbering scheme of complexes. − [b] $R1 = \Sigma||F_o| - |F_c||/\Sigma|F_o|$. − [c] $wR2 = \{\Sigma[w(F_o^2 - F_c^2)^2]/\Sigma[w(F_o^2)^2\}^{1/2}$, $w = 1/[\sigma^2(F_o^2) + (0.0186P)^2 + 17.3751P]$, where $P = [\mathrm{Max}(F_o^2, 0) + 2F_c^2]/3$.

1/2 CsCl (27); 1/2 CsI (28)]: The synthesis of these iodo derivatives, in high yields, was also similar to that of **20**−**24**.[56]

Copper(II) 4,5-Bis(3,5-di-*tert*-butylsalicylideneimine)benzo-18-crown-6, *t*Bu$_4$Cu18-C-6 (29): This compound was obtained from copper acetate in a manner similar to that described for the synthesis of **10**.

4,4′,5,5′-Tetranitrodibenzo-18-crown-6 (30): Solid dibenzo-18-crown-6 (5 g, 13.9 mmol) was added slowly over thirty minutes to 150 mL of concentrated nitric acid and the mixture was stirred until all remaining solids dissolved. The orange solution was then poured over one liter of ice and a yellow solid precipitated. The solid was collected by filtration, washed with deionized water (100 mL), saturated sodium bicarbonate solution until there was no further CO_2 evolution, and then deionized water (3 × 100 mL). The yellow powder was allowed to air dry. Yield 7.2 g (96%). − ^{1}H NMR (300 MHz, [D$_6$]DMSO): δ = 7.73 (s, 4 H), 4.29 (unresolved, 8 H), 3.83 (unresolved, 8 H). − ^{13}C NMR (300 MHz, [D$_6$]DMSO): δ = 150.9 (4 C), 135.8 (4 C), 108.2 (4 C) 69.1 (4 C), 68.2 (4 C).

4,4′,5,5′-Tetraaminodibenzo-18-crown-6, (31): Compound **30** (2 g, 3.70 mmol) was ground to a fine powder and placed into a hydrogenation vessel along with one gram of palladium on activated carbon and distilled methanol (100 mL). The mixture was deoxygenated and allowed to react with hydrogen gas at about 40 p.s.i. with agitation for 18 hours. The solution was filtered under Schlenk conditions through a minimal pad of celite and the pale off-white filtrate was reduced to dryness with a cold trap. Compound **30** was obtained as a pale off white powder. The compound readily decomposed in solution when exposed to air, and was moderately stable as a solid. The material was handled under nitrogen and used immediately. Yield ≈50%.

4,4′,5,5′-Tetra(3,5-di-*tert*-butylsalicylideneimine)dibenzo-18-crown-6, (*t*Bu$_4$H$_2$)$_2$18-C-6 (32): Under an inert atmosphere, compound **31** (1 g, 2.38 mmol) and 3,5-di-*tert*-butylsalicylaldehyde (2.23 g, 9.52 mmol) were dissolved in methanol (50 mL). The solution was refluxed with stirring under N_2 overnight. The product precipitated from solution upon cooling as a yellow powder and was isolated by filtration in air. Yield 2.52 g (53%); m.p. 266−268 °C.

Bis[Manganese(III) 4,4′,5,5′-tetra(3,5-di-*tert*-butylsalicylideneimine)chloride] Dibenzo-18-crown-6, (*t*Bu$_4$Mn)$_2$18-C-6 (33): Manganese(II) chloride (0.10 g, 0.80 mmol) was dissolved in methanol (50 mL) and added to a solution of **32** (0.5 g, 0.39 mmol) in dichloromethane (50 mL). The resulting yellowish-brown solution was refluxed for eighteen hours with stirring under air. The solution was evaporated to dryness and the remaining dark brown residue was dissolved in acetone (50 mL). The brown solution was filtered and methanol (30 mL) was added to the filtrate. The resulting solution was allowed to evaporate to dryness to yield dark brown crystals of **33**. These were collected by filtration and dried under vacuum. Yield 70%.[56]

X-ray Crystallographic Study

Collection and Reduction of X-ray Data: Single crystal, X-ray diffraction data were collected for complexes **11**−**15** and **27**. For structures **11**, **12**, **13**, **15**, and **27** a selected crystal was attached to a glass fiber and mounted on the Siemens SMART system for data collection at 173(2)K (Mo-K_α radiation: λ = 0.71073 Å). Data collection and analysis procedures are described in the Supporting Information for each of the structures. Crystal and refinement data are listed in Table 8. Details concerning structure solution and refinement for each of the structures reported herein have been deposited as Supporting Information.

Acknowledgments

The authors gratefully acknowledge the support of this work by a grant from the National Science Foundation, CHE 9307382.

[1] P. Lauger, *Angew. Chem. Int. Ed. Engl.* **1969**, *8*, 42.
[2] [2a] L. R. DeYoung, K. A. Dill, *Biochemistry* **1988**, *27*, 5281−5289. − [2b] *Mammalian Amino Acid Transport Mechanisms and Control* (Eds.: M. S. Kilberg, D. Haussinger), Plenum Press, New York, **1992**. − [2c] M. S. Kilberg, B. R. Stevens, D. A. Novak, *Annu. Rev. Nutr.* **1993**, *13*, 137−165. − [2d] C. Seel, A. Ganan, J. de Mendoza, *Top. Curr. Chem*. **1995**, *175*, 101. − [2e] J. L. Sessler, A. Andrievsky, *Top. Curr. Chem.* **1996**, *176*, 1119.
[3] [3a] J. C. Skou, *Biochim. Biophysica Acta* **1957**, *23*, 394. − [3b] H. R. Kaback, E. R. Stadtman, *Proc. Nat. Acad. Sci. USA* **1966**, *55*, 920. − [3c] W. R. Penrose, G. E. Nichoalds, J. R. Piperno, D. L. Oxender, *J. Biol. Chem*. **1968**, *243*, 5921−5928.
[4] D. Rogers, *J. Bacteriol*. **1964**, *88*, 279.
[5] [5a] C. F. Fox, E. P. Kennedy, *Proc. Nat. Acad. Sci. USA* **1965**, *54*, 891. − [5b] T. H. D. Jones, E. P. Kennedy, *Federat. Proc*. **1968**, *27*, 644.
[6] C. Haskovec, A. Kotyk, *Europ. J. Biochem.* **1969**, *9*, 343.

[7] [7a] J. R. Piperno, D. L. Oxender, *J. Biol. Chem.* **1966**, 5732. – [7b] W. R. Penrose, G. E. Nichoalds, J. R. Piperno, D. L. Oxender, *J. Biol. Chem*. **1968**, *243*, 5921.

[8] O. H. Wilson, J. D. Holden, *J. Biol. Chem*. **1969**, *244*, 2737.

[9] K. Ring, *Angew. Chem. Int. Ed. Engl*. **1970**, *9*, 345−356.

[10] T. D. Brock, G. Moo-Penn, *Biochem. Biophysics* **1962**, *98*, 183.

[11] [11a] K. Maruyama, H. Tsukube, T. Araki, *Tetrahedron Letters* **1981**, *22*, 2001. – [11b] H. Tsukube, *Angew. Chem. Int. Ed. Engl*. **1982**, *21*, 304−305. – [11c] K. Maruyama, H. Tsukube, T. Araki, *J. Am. Chem. Soc*. **1982**, *104*, 5197−5203.

[12] J. P. Behr, J. M. Lehn, *J. Am. Chem. Soc.* **1973**, *95*, 6108.

[13] J. Rebek, Jr., B. Askew, D. Nemeth, K. Parris, *J. Am. Chem. Soc*. **1987**, *109*, 2432−2434.

[14] M. T. Reetz, J. Huff, J. Rudolph, K. Tollner, A. Deege, R. Goddard, *J. Am. Chem. Soc.* **1994**, *116*, 11588−11589.

[15] F. P. Rudkevich, J. D. Mercer-Chalmers, W. Verboom, R. Ungaro, F. de Jong, D. N. Reinhoudt, *J. Am. Chem. Soc.* **1995**, *117*, 6124−6125.

[16] Y. Aoyama, M. Asakawa, A. Yamagishi, H. Toi, H. Ogoshi, *J. Am. Chem. Soc*. **1990**, *112*, 3145−3151.

[17] H. Tsukube, S. Shinoda, J. Uenishi, T. Kanatani, H. Itoh, M. Shiode, T. Iwachido, O. Yonemitsu, *Inorg. Chem*. **1998**, *37*, 1585−1591.

[18] L. K. Mohler, A. W. Czarnik, *J. Am. Chem. Soc*. **1993**, *115*, 7037.

[19] [19a] M. Newcomb, R. C. Helgeson, D. J. Cram, *J. Am. Chem. Soc*. **1974**, *96*, 7367−7369. – [19b] M. Newcomb, J. L. Toner, R. C. Helgeson, D. J. Cram, *J. Am. Chem. Soc*. **1979**, *101*, 491−4947.

[20] [20a] K. Maruyama, H. Tsukube, T. Araki, *Tetrahedron Letters* **1981**, *22*, 2001−2004. – [20b] K. Maruyama, H. Tsukube, T. Araki, *J. Am. Chem. Soc*. **1982**, *104*, 5197−5203. – [20c] H. Tsukube, *Angew. Chem. Int. Ed. Engl*. **1982**, *21*, 304−305. – [20d] H. Tsukube, S. Shinoda, J. Uenishi, T. Kanatani, H. Itoh, M. Shiode, T. Iwachido, O. Yonemitsu, *Inorg. Chem*. **1998**, *37*, 1585−1591.

[21] [21a] S. Jonasdottir, C. G. Kim, J. Kampf, D. Coucouvanis, *Inorg. Chim. Acta* **1996**, *243*, 255−270. – [21b] S. M. Malinak, D. Coucouvanis, *Inorg. Chem*. **1996**, *35*, 4810−4811.

[22] [22a] D. T. Rosa, D. Coucouvanis, to be published. – [22b] D. T. Rosa, *Ph. D. Thesis*, University of Michigan, **1998**.

[23] F. C. J. M. Van Veggel, W. Verboom, D. N. Reinhoudt, *Chem. Rev.* **1994**, *94*, 279−299.

[24] [24a] D. N. Reinhoudt, J. A. A. de Boer, J. W. H. M. Viterwijik, S. Harkema, *J. Org. Chem*. **1985**, *50*, 4809. – [24b] A. R. van Doorn, R. Schaafstra, M. Bos, S. Harkem, J. van Eerden, W. Verboom, D. N. Reinhoudt, *J. Org. Chem*. **1991**, *56*, 6083−6094. – [24c] W. F. Nijenhuis, A. R. van Doorn, A. M. Reichwein, F. de Jong, D. N. Reinhoudt, *J. Am. Chem. Soc*. **1991**, *113*, 3607. – [24d] C. J. van Staveren, J. van Eerden, F. C. J. M. van Veggel, S. Harkema, D. N. Reinhoudt, *J. Am. Chem. Soc*. **1988**, *110*, 4494.

[25] [25a] N. Kobayashi, T. Osa, *Heterocycles*, **1981**, *15*, 675. – [25b] J. L. Sessler, T. D. Mody, R. Ramasamy, A. D. Sherry, *New J. Chem*. **1992**, *16*, 541−544.

[26] [26a] O. E. Sielcken, W. Dreuth, R. J. M. Nolte, Recl. Trav. Chim. Pays-*Bas.* **1990**, *109*, 425. – [26b] O. E. Sielcken, M. M. van Tilborg, M. F. M. Roks, R. Hendriks, W. Dreuth, R. J. M. Nolte, *J. Am. Chem. Soc*. **1987**, *109*, 4261. – [26c] Z. Gasyna, N. Kobayashi, M. J. Stillman, *J. Chem. Soc., Dalton. Trans.* **1989**, 2397. – [26d] N. Kobayashi, A. B. P. Lever, *J. Am. Chem. Soc*. **1987**, *109*, 7433. – [26e] N. Kobayashi, Y. Nishiyama, *J. Chem. Soc., Chem. Commun.* **1986**, 1462.

[27] S. Can, O. J. Bekaraglou, *J. Chem. Soc., Dalton Trans.* **1988**, 2831.

[28] A. Gul, A. I. Okur, A. Cihan, N. Tan, O. Bekaroglou, Synth. React. Inor. Met.-*Org. Chem*. **1986**, *16*, 871−884.

[29] [29a] S. Karabocek, N. Karabocek, *Polyhedron* **1997**, *16*, 1771−1774. – [29b] Y. Gok, I. Degirmencioglu, S. Karabocek, *Synth. React. Inor. Met.-Org. Chem*. **1997**, *27*, 331−345.

[30] [30a] D. T. Rosa, D. Coucouvanis, *Inorg. Chem*. **1998**, *37*, 2328. – [30b] D. T. Rosa, V. G. Young, D. Coucouvanis, *Inorg. Chem*. **1998**, *37*, 5042−5043.

[31] J. R. Cooper, F. E. Bloom, R. H. Roth, *The Biochemical Basis of Neuropharmacology*, Oxford University Press, Oxford, **1996**.

[32] R. M. Silverstein, G. C. Bassler, T. C. Morrill, *Spectrometric Identification of Organic Compounds*, John Wiley & Sons: New York, **1991**; 5th ed.

[33] S. D. Bella, I. Fragala, M. A. Diaz-Garcia, I. Ledoux, T. J. Marks, *J. Am. Chem. Soc*. **1997**, *119*, 9550−9557.

[34] A. Van der Bergen, K. S. Murray, M. J. O'Connor, B. O. West, *Aust. J. Chem*. **1969**, *22*, 39.

[35] D. Christodoulou, M. G. Kanatzidis, D. Coucouvanis, *Inorg. Chem*. **1990**, *29*, 191−201.

[36] O. Nagano, A. Kobayashi, Y. Sasaki, *Bull. Chem. Soc. Jpn*. **1978**, *51*, 790−793.

[37] P. Seiler, M. Dobler, J. D. Dunitz, *Acta Cryst*. **1974**, *B30*, 2744.

[38] C. J. Pedersen, *J. Am. Chem. Soc.* **1970**, *92*, 386.

[39] K. V. Domasevitch, V. V. Ponomareva, E. B. Rusanov, *J. Chem. Soc., Dalton Trans.* **1997**, 1177−1180.

[40] J. E. Davies, B. M. Gatehouse, K. S. Murray, *J. Chem. Soc., Dalton Trans.* **1973**, 2523.

[41] D. L. Ward, S. B. Dawes, O. Fussa, J. L. Dye, *Am. Cryst. Assoc., Abstr. Paper (Winter)* **1985**, *13*, 25.

[42] The flux values (Table) used for comparison purposes was calculated using the 24 h measurement and is expressed in mol or equivalents and dividing by: the time (in seconds), number of mol of carrier, and the area of $2.2 \times 10^{-3} m^2$. This value was then multiplied by 10^4 to give a reasonably scaled number.

[43] [43a] D. T. Rosa, Dissertation Thesis, University of Michigan, **1998**. – [43b] D. T. Rosa, D. Coucouvanis, manuscript in preparation.

[44] [44a] T.M. Fyles, in *Inclusion Aspects of Membrane Chemistry* (Eds. Y. Osa, J. Atwood), Lluwer: Dordecht, **1991**, Vol. 2, pp. 59−110. – [44b] B. D. Smith, S. Gardiner, *Advances in Supramolecular Chemistry*, **1999**, *5*, 157−202.

[45] M. F. Paugam, J. T. Bien, B. D. Smith, *J. Am. Chem. Soc*. **1996**, *118*, 9820−9825.

[46] The similarity is apparent in the ^{1}H NMR spectra of ligands **3** and **9**. The aromatic protons of **3** appear at δ = 8.71, 7.44, 7.28, and 6.87, and those of **9** at δ = 8.68, 7.43, 7.25, and 6.85. The electronic spectra of **6** and **16** also are very similar.

[47] D. J. Cram, R. N. Trueblood, *Top. Curr. Chem*. **1981**, *98*, 43.

[48] D. J. Cram, J. M. Cram, *Acc. Chem. Res.* **1978**, *11*, 8.

[49] C. J. Pedersen, *Angew. Chem. Int. Ed. Engl*. **1988**, *27*, 1021−1027.

[50] K. Ring, *Angew. Chem. Int. Ed. Engl*. **1970**, *9*, 345−356.

[51] [51a] A. R. Oki, D. J. Hodgson, *Inorg. Chim. Acta* **1990**, *170*, 65−73. – [51b] J. W. Gohdes, W. H. Armstrong, *Inorg. Chem*. **1988**, *27*, 1842−1846.

[52] D. T. Rosa, D. Coucouvanis, to be published.

[53] The program Hyperchem was used for performing mm+ calculations. We feel that the absolute values of the energies obtained for the optimized structures are rather unreliable given the lack of sophistication in these calculations. The relative values of the energies, however, can be used for comparative purposes. These are as follows: carrier with tryptophan interacting with the H_2O, 59.67 kcal/mol; carrier with tryptophan interacting with the metal, 73.3 kcal/mol; carrier with serotonin interacting with H_2O, 31.4 kcal/mol; carrier with serotonin interacting with the metal, 27.2 kcal/mol.

[54] *The Merck Index, 11th Ed.* (Ed.: S. Budavari), Merck & Co., Rahway, NJ, **1989**.

[55] J. Frisch, M. T. Bogert, *J. Org. Chem.* **1943**, *8*, 331.

[56] The detailed synthesis, spectroscopic characterization and analytical data for the compound(s) have been deposited as Supporting Information.

[57] L. Weinberger, A. R. Day, *J. Org. Chem*. **1959**, *24*, 1451−1455.

Received August 30, 2000
[I00351]

Dioxo- and Oxovanadium(V) Complexes of Biomimetic Hydrazone *ONO* Donor Ligands: Synthesis, Characterisation, and Reactivity

Mannar R. Maurya,*[a] Shilpa Khurana,[a] Carola Schulzke,[b] and Dieter Rehder[b]

Keywords: Vanadium / Oxo complexes / NMR spectroscopy / Hydrazones / N ligands / O ligands

The dioxovanadium(V) complexes M[VO_2(L)*solv*] (**2**, **5**, **6**) have been isolated along with dimeric, oxo-bridged monooxovanadium complexes with the formula [{VOL}$_2$μ-O] (**1**, **4**), and characterised by their spectral and thermogravimetric properties and reactivity patterns. H_2L is the hydrazone H_2{(R-sal)-iNH} [sal derives from salicylaldehyde (R = H) or *p*-Cl-salicylaldehyde (R = Cl)] or H_2hap-iNH, where hap is the *o*-hydroxyacetophenone moiety, and iNH stands for isonicotinic acid hydrazide. In the isolated potassium (M = K) complexes **2a**, **5** and **6**, *solv* is a water molecule, which was exchanged for methanol or DMSO in the respective solutions as shown by ^{51}V NMR. Treatment of the dimeric (**1** and **4**) or anionic complexes (**2a** and **5**) with H_2O_2 yielded (unstable) oxoperoxovanadium complexes K[$VO(O_2)$L] (**7**, **8**). Acidification of **1** and **4** afforded oxohydroxo complexes. When compound **2a** is dissolved in methanol, it is partly deoxygenated to form [VO(OMe)(HOMe)L] (**9**), the crystal and molecular structures of which have been determined, confirming the *ONO* binding mode of L in its enolate form.

Introduction

The coordination chemistry of vanadium with multidentate ligands has achieved a special status in the last decade because of its catalytic[1,2] and medicinal[3−5] input. Structural and/or functional models for vanadate-dependent haloperoxidases, for vanadium nitrogenases and other biologically active vanadium compounds have further stimulated vanadium coordination chemistry.[6,7] The active site structures of the vanadate-dependent haloperoxidases have been revealed by X-ray diffraction studies. Accordingly, the vanadate ion is distorted towards a trigonal pyramid, thus providing a fifth coordination site which is occupied by N^{ε} of a histidine, covalently linking the vanadate ion to the protein.[8−10] These enzymes lose their activity upon reduction or removal of vanadium; re-oxidation or reconstitution with vanadate fully restores their activity,[11] demonstrating that V^V (VO^{3+} or VO_2^+) is essential for catalytic activity. Various types of oxovanadium(V) complexes such as [VO(OR)(HOR)L],[12−16] [VO(OR)L][17,18] [{VOL}$_2$μ-O],[19−22] [VOL(DD)],[23−30] [VO_2L][29,31−42] [H_2L is an *ONO* (hydrazone, azo or Schiff base) ligand, and DD a monobasic, bidentate *OO* or *ON* donor], [VO_2-(picolinate)$_2$]$^-$,[43] and [VO_2(nitrilotriacetate)]$^{2-}$[44] have been studied in this context.

Dioxovanadium(V) complexes are commonly synthesised by the reaction of (i) vanadates with *ONO*-functional ligands in aqueous solution,[33−38] or (ii) [VO(acac)$_2$] (acacH = acetylacetone) or $VOSO_4$ with the ligands in non-aqueous or mixed solvent media followed by oxidation with O_2.[37−40] Pecoraro et al. have prepared dioxovanadium(V) complexes by the reaction of [$VO(OEt)_3$] with appropriate ligands[41] or by oxidation of oxovanadium(IV) complexes with KNO_2 in H_2O/MeOH.[42] The present series of dioxovanadium complexes containing *ONO*-functional ligands[37−42,45] is comparatively limited. We present here the preparation and characterisation of VO_2^+ complexes of *N*-isonicotinamidosalicylaldimines (aroylhydrazones; Scheme 1). These ligands possess five potential donor sites, three of which are used, namely the phenolate and enolate oxygen atoms, and the imine nitrogen atom originating from the condensation of the hydrazine and salicylaldehyde. Coordination compounds of aroylhydrazones have been reported to act as inhibitors of enzymes,[46a] and antifungal/antibacterial agents.[46b] Spectral and structural aspects, reactivity patterns of the compounds, and the crystal structure of a deoxygenation product are reported.

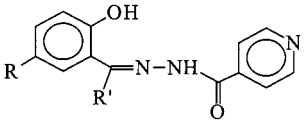

R' = H, R = H: **H_2sal-iNH**
R' = H, R = Cl: **H_2Clsal-iNH**
R' = Me, R = H: **H_2hap-iNH**

Scheme 1

Results and Discussion

Synthesis and Solid-State Characteristics of Dioxovanadium Complexes

Structures of the dioxovanadium complexes **2**, **5** and **6**, based on spectroscopic data, thermogravimetric studies, elemental analyses and the X-ray diffraction analysis of **9** (the deoxygenation product of **5**) are shown in Scheme 2. The structures are formulated for the solid samples isolated as described in the Exp. Sect. As shown by ^{51}V NMR spectro-

[a] Department of Chemistry, University of Roorkee, Roorkee 247 667, India
E-mail: rkmanfcy@rurkiu.ernet.in
[b] Institut für Anorganische und Angewandte Chemie, Universität Hamburg, Martin-Luther-King-Platz 6, 20146 Hamburg, Germany
E-mail: rehder@xray.chemie.uni-hamburg.de

 © WILEY-VCH Verlag GmbH, 69451 Weinheim, 2001 1434−1948/01/0303−0779 $ 17.50+.50/0

scopy (see below), the water ligand is possibly replaced by a solvent molecule in methanol and DMSO.

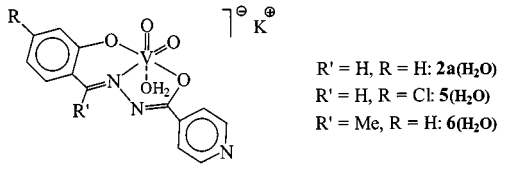

R' = H, R = H: **2a(H_2O)**
R' = H, R = Cl: **5(H_2O)**
R' = Me, R = H: **6(H_2O)**

Scheme 2

A solution of potassium vanadate(V), generated in situ by dissolving V_2O_5 in aqueous KOH, reacts with the potassium salt of the ligands H_2Rsal-iNH (Scheme 1) at pH = 7.5 to give two types of vanadium(V) complexes, namely the neutral, oxo-bridged dimeric monooxovanadium complexes [{VO(Rsal-iNH}$_2$μ-O] (**1**: R = H; **4**: R = Cl), and potassium salts of the anionic dioxovanadium complexes K[VO_2(Rsal-iNH)H_2O)] [**2a(H_2O)**: R = H; **5(H_2O)**: R = Cl]. Using $NH_4[VO_3]$ and the sodium salt of the ligands results in the formation of the corresponding ammonium salts NH_4[VO_2(Rsal-iNH)H_2O)] [**2b(H_2O)**: R = H] along with the dimers. The final pH value of the reaction mixture plays an important role in that a decrease (to pH = 6.5) increases the yield of the dimeric complex. Neutral dimeric and anionic complexes can be separated by fractional crystallisation from methanol, where the dimers crystallise first. The ligand H_2hap-iNH only yields the dioxovanadium complex K[VO_2(hap-iNH)H_2O] [**6(H_2O)**]. Complex **1** was also synthesised by allowing equimolar amounts of [$VO(acac)_2$] and H_2sal-iNH to react in acetone, followed by aerial oxidation [Equations (1) and (2)].

$$[VO(acac)_2] + H_2\text{sal-iNH} \rightarrow \underset{\mathbf{3}}{[VO(\text{sal-iNH})]} + 2\text{acacH} \quad (1)$$

$$2\underset{\mathbf{3}}{[VO(\text{sal-iNH})]} + 1/2O_2 \rightarrow \underset{\mathbf{1}}{[\{VO(\text{sal-iNH})\}_2\mu\text{-O}]} \quad (2)$$

The intermediate complex **3** can be isolated as a stable solid. Furthermore, **1** is obtained from the reaction of $VO(OEt)_3$ with H_2sal-iNH in absolute ethanol under aerobic conditions. The most probable reaction pathways for this reaction are given by Equations (3) and (4), based on the analogy of the formation of the dimeric complex [{VO(sal-L-pheala)}$_2$μ-O] (H_2sal-L-pheala = *N*-salicylidene-L-phenylalaninato) by exposure of CH_2Cl_2 solutions of [VO(OMe)(MeOH)(sal-L-pheala)] to air.[21] The underlying reaction is probably an exchange of OR by OH (from moisture), followed by condensation to form the dimeric compound.

$$VO(OEt)_3 + H_2\text{sal-iNH} \xrightarrow{\text{EtOH}} [VO(OEt)(EtOH)(\text{sal-iNH})] \quad (3)$$

$$[VO(OEt)(EtOH)(\text{sal-iNH})] \xrightarrow{(H_2O)} [\{VO(\text{sal-iNH})\}_2\mu\text{-O}] \quad (4)$$

The brown, dimeric complexes **1** and **4** are poorly soluble in methanol, ethanol, DMF and DMSO, while the yellow to yellow-orange dioxo complexes **2, 5** and **6** are soluble in all these solvents.

As shown by, inter alia, thermogravimetric analysis, **2**, **5** and **6** contain one molecule of water. Thermogravimetric data are collated in Table 1. The dioxo complexes lose water in the temperature range 90−200 °C, indicative of covalently, though not particularly strongly bonded water. This is expected if the water is coordinated in the *trans* position to one of the doubly bonded oxygen atoms (cf. Scheme 2). The remaining anhydrous complexes **2a**, **5** and **6** decompose at higher temperatures (loss of the ligand less one oxygen atom) to form potassium metavanadate $K[VO_3]$. The decomposition pattern is different for the anhydrous ammonium salt **2b**: Between 205 and 330 °C, a weight loss of 7.5% corresponding to the loss of NH_3 and H_2O occurs, possibly by the reaction sequence represented by Equations (5) and (6).

$$NH_4[VO_2(\text{sal-iNH})] \rightarrow H[VO_2(\text{sal-iNH})] + NH_3 \quad (5)$$

$$2H[VO_2(\text{sal-iNH})] \rightarrow [\{VO(\text{sal-iNH})\}_2\mu\text{-O}] + H_2O \quad (6)$$

On further heating, [{VO(sal-iNH)}$_2$μ-O] decomposes to yield V_2O_5 as the final product. The decomposition pattern of **4** is interesting because it undergoes elimination of oxy-

Table 1. Thermogravimetric analyses

Compound	Temperature range (°C)	% Weight loss obs. (calcd.)	Group lost	(Expected) residue	% Residue obs. (calcd.)
2a	100-200	5.2 (4.8)	H_2O	K[VO_2(sal-iNH)]	
	350-750	59.0 (58.8)	L − 1O	K[VO_3]	35.8 (36.4)
2b	110-185	5.0 (5.0)	H_2O	NH_4[VO_2(sal-iNH)]	
	205-330[a]	7.5 (7.3)	NH_3 + 1/2H_2O	1/2[V_2O_3(sal-iNH)$_2$]	
	340-600	63.0 (62.3)	L − 1O	V_2O_5	24.5 (25.4)
4	160-225	2.5 (2.3)	1/2O_2	2[VO(Clsal-iNH)]	
	255-730	71.5 (71.4)	2L − 3O	V_2O_5	26.0 (26.0)
5	90-185	4.5 (4.4)	H_2O	K[VO_2(Clsal-iNH)]	
	63.0 (62.3)		L − 1O	K[VO_3]	33.5 (33.4)
6	4.5 (4.6)		H_2O	K[VO_2(hap-iNH)]	
	61.0 (60.3)		L − 1O	K[VO_3]	34.5 (35.1)

[a] See text for additional details.

gen by the rupture of the μ-$O(VO)_2$ fragment with the concomitant thermally induced reduction of V^V to V^{IV} and the formation of **3** [Equation (7)].

$$\underset{\mathbf{1}}{[\{VO(sal\text{-}iNH)\}_2\mu\text{-}O]} \rightarrow 2\underset{\mathbf{3}}{[VO(sal\text{-}iNH)]} + 1/2O_2 \quad (7)$$

The poor stability of **3** did not allow for its isolation, in contrast to the corresponding Mo and W systems, where the intermediately formed species have been isolated and characterised.[47]

The IR spectra of the ligands exhibit bands in the regions 1678−1680 and 3100−3180 cm^{-1} due to ν(C=O) and ν(NH) stretches, respectively. These bands disappear on complexation, indicating the transformation of the carbonyl moiety owing to enolisation and consequent replacement of H by the metal ion. A new band appearing in the 1210−1250 cm^{-1} region was assigned to the ν(C−O) (enolato) mode. The ν(C=N) (azomethine) stretch of the ligands appears at 1609−1629 cm^{-1}, and this band is shifted to a lower wavenumber by 10−15 cm^{-1} in the complexes, thereby indicating the coordination of the azomethine nitrogen atom. In the dimeric complexes **1** and **4**, this band is doubled, suggesting a nonequivalence of the two halves of the molecule, e.g. because of an asymmetric bridge. A ligand band at 900−1000 cm^{-1} due to the ν(N−N) stretch undergoes a 10−40 cm^{-1} shift to a higher wavenumber upon complexation. The high frequency shift of the ν(N−N) band is expected because of diminished repulsion between the lone pairs of adjacent nitrogen atoms.[48] A broad band for the ligands at approximately 2800 cm^{-1} was assigned to intramolecular hydrogen bonds involving the phenolic OH group; the absence of this band in the dioxo complexes indicates the deprotonation of the phenol and subsequent coordination of the oxygen atom to the metal centre. However, the presence of a broad band at approximately 3400 cm^{-1} is possibly due to coordinated water in these complexes. The dimeric complexes exhibit weak combination bands covering the region 2300−2700 cm^{-1}. This again suggests extensive intermolecular hydrogen bonding in the complexes.

All dioxovanadium(V) complexes exhibit two sharp bands in the 900−950 cm^{-1} region, indicative of the *cis*-$\{VO_2\}^+$ structural unit. In the dimeric complexes, two sharp bands arise at ca. 960 cm^{-1}, assigned to ν(V=O), and a broad band is observed at ca. 860 cm^{-1} due to ν[V−(μ-O)−V]. The presence of two ν(V=O) in the dimers **1** and **4** supports the nonequivalence of the two oxo-bridged halves[22] already noted above.

Solution Studies

The electronic absorption spectra of all the ligands and complexes were recorded in methanol, and the absorption maxima with their extinction coefficients (wherever possible) are listed in Table 2. The UV spectra of the ligands exhibit three spectral bands at 214.5−219.5, 284−289.5 and 330−342 nm. The most probable assignments for these bands are $\Phi \rightarrow \Phi^*$, $\pi \rightarrow \pi^*$ and $n \rightarrow \pi^*$ transitions, respectively. A weak shoulder associated with the second band, due to hydrogen bonding and association, is absent in the dioxo complexes. This indicates that the hydrogen bonds are broken after complex formation. In dimeric complexes, however, this band is still present, therefore indicating the existence of hydrogen bonding in solution as well. Other intra-ligand bands are still present in the complexes, with significant shifts in the band positions towards lower wavelengths. Dioxovanadium(V) complexes have a $3d^0$ configuration, and d−d bands are therefore not expected. All the complexes display an intense to medium electronic spectral band in the visible region at 403−410 nm. This was assigned to a ligand-to-metal charge-transfer (LMCT) transition from the phenolate oxygen atom to an empty d-orbital of the vanadium atom.

Table 2. Electron absorption spectra

Compound	λ_{max}/nm (ε/$M^{-1}cm^{-1}$)
H_2sal-iNH	333(16240), 289(18800), 214(25930)
$[\{VO(sal\text{-}iNH)\}_2\mu\text{-}O]$, **1**	402.5, 322, 279(sh), 226
$K[VO_2(sal\text{-}iNH)H_2O]$, **2a**	403.5(3746), 321(6245), 277(6790), 225(13890)
$NH_4[VO_2(sal\text{-}iNH)H_2O]$, **2b**	402.5(3000), 323(5070), 280(5410), 229(10140)
H_2Clsal-iNH	342.5(8025), 289.5(10475), 219.5(14875)
$[\{VO(Clsal\text{-}iNH)\}_2\mu\text{-}O]$, **4**	408.5, 321.5, 277(sh), 237
$K[VO_2(Clsal\text{-}iNH)H_2O]$, **5**	410.5(6100), 316.5(9600), 279(10085), 235(20730)
H_2hap-iNH	330(4860), 284.5(6350), 215(11960)
$K[VO_2(hap\text{-}iNH)H_2O]$, **6**	387(6200), 310(9500), 279(10800), 228(21900)
$K[VO(O_2)(sal\text{-}iNH)H_2O]$, **7**	412, 321, 222
$K[VO(O_2)(Clsal\text{-}iNH)H_2O]$, **8**	410, 322, 225

Further evidence for the coordination mode of the ligands was obtained from the ^1H and ^{13}C NMR spectra. The relevant spectral data are collected in Tables 3 and 4. They confirm the IR and UV/Vis evidence. A significant downfield shift of the azomethine (−CH=N−) proton signal in the complexes relative to the corresponding free ligands demonstrates the coordination of the azomethine nitrogen atom. In the ^1H NMR spectrum of the complexes, the absence of the ligand signals arising from the phenolic −OH and the hydrazone −NH protons in the δ = 11.08−13.19 region further indicates that bonding occurs through the phenolate and enolate groups. The methyl protons of H_2hap-iNH resonate at δ = 3.36, and this signal

Table 3. ^{1}H chemical shifts; see numbering scheme below

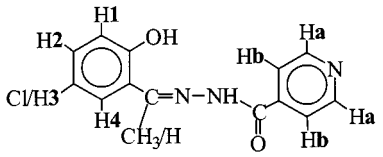

Compound[a,b]	-OH	-NH	-CH=N-	H_a	H_b	H4	H2	H1, H3
H_2sal-iNH	12.30	11.08	8.67(s)	8.79(d)	7.84(d)	7.59(d)	7.31(td)	6.94(d), 6.90(d)
[{VO(sal-iNH)}$_2\mu$-O], **1**			9.04(s)	8.77(br)	8.00(d)	7.65(d)	7.42(t)	ca. 6.88(m)
($\Delta\delta$)			(0.37)	(-0.02)	(0.16)	(0.06)	(0.11)	(-0.04)
K[VO_2(sal-iNH)H_2O], **2a**			9.05(s)	8.68(br)	7.86(d)	7.59(d)	7.37(t)	6.81(d)
($\Delta\delta$)			(0.38)	(-0.09)	(0.02)	(0)	(0.06)	(-0.11)
H_2Clsal-iNH	12.36	11.11	8.65(s)	8.79(d)	7.83(d)	7.65(dd)	7.32(td)	6.95(d)
[{VO(Clsal-iNH)}$_2\mu$-O], **4**			9.05(s)	8.80(br)	8.06(br)	7.76(br)	7.42(d)	6.95(d)
($\Delta\delta$)			0.40	(0.01)	(0.23)	(0.11)	(0.10)	(0)
K[VO_2(Clsal-iNH)H_2O], **5**			9.05(s)	8.68(br)	7.87(br)	7.58(br)	7.37(br)	6.80(d)
($\Delta\delta$)			(0.40)	(0.11)	(0.04)	(-0.07)	(0.05)	(-0.15)
H_2hap-iNH[c]	13.19	11.59	-	8.81(d)	7.84(d)	7.65(dd)	7.32(td)	6.89, 6.92(d)
K[VO_2(hap-iNH)H_2O][d], **6**				8.68(d)	7.90(d)	7.78(d)	7.32(t)	6.80(d), 6.83(d)
($\Delta\delta$)			-	(-0.13)	(0.06)	(0.13)	(0)	(-0.09) (-0.21)

[a] Letters given in parentheses indicate the signal structure: s = singlet, d = doublet, t = triplet, dd = doublet of doublets, td = triplet of doublets, m = multiplet, br = broad (unresolved). – [b] ($\Delta\delta$) = δ(complex) – δ(ligand). – [c] Methyl proton signals at δ = 3.36. – [d] Methyl proton signals at δ = 3.14 and 3.16.

appears as two independent signals of equal intensity at δ = 3.14 and 3.16 for complex **6**. Aromatic protons appear in the expected regions in spectra of the ligands as well as of the complexes, with slight shifts in their positions. All these data are consistent with what has previously been observed in dioxo molybdenum(VI)[49] and dioxotungsten(VI)[50] complexes with these ligands, and supports their dibasic tridentate *ONO* coordination mode.

^{13}C NMR spectra (Table 4 and Figure 1) also provide useful diagnostic tools for the elucidation of the structures of the complexes. Assignments were based on the chemical shift and intensity patterns, and on the coordination-induced shifts $\Delta\delta$ = [δ(complex) – δ(free ligand)] of the signals for carbon atoms in the vicinity of the coordinating functions.[51] Large coordination shifts were observed for the carbon atoms bearing the phenolate and enolate oxygen atoms (C3 and C8) and for the azomethine carbon atom (C1). The ^{13}C NMR spectra of the dimeric, neutral complexes are nearly identical to those of the anionic dioxo complexes. The nonequivalence of the two halves of the molecules in solutions of dimers **1** and **4** is reflected in a broadening of the respective resonances. The solubility of the ammonium complex **2b** is too low to obtain high quality spectra. The spectral pattern of **2b** is, however, identical to that of the potassium salts **2a** and **5**. Heating the solutions to improve the solubility, causes slow demetallation of the complexes.

To further characterise the complexes, we recorded ^{51}V NMR spectra; δ(^{51}V) values of specific compounds are presented in the Exp. Sect. Owing to the quadrupole moment (spin 7/2) of the ^{51}V nucleus, the resonances are somewhat broadened; the line widths at half-height are typically approximately 200 Hz, which is still relatively narrow in ^{51}V NMR spectroscopy.[52] The dioxovanadium complexes **2**, **5** and **6** all show one strong resonance between δ = –530 and –550, which is what one would expect for a dioxovanadium complex containing a mixed *O*/*N* donor set.[52,53] For **2** and **5**, there is a distinct solvent dependence: In [D_6]DMSO, the signal appears at δ = –532, in methanol between δ = –539 and –541, and in deuterated methanol (CD_3OD) at δ = –549, hinting at participation of the solvent in coordination. The solvent dependence is less pronounced for **6** (δ = –533 and –538 in [D_6]DMSO and CD_3OD, respectively), which may be explained by steric hindrance imparted by the methyl group on the azomethine carbon atom, preventing effective binding of the solvent to the sixth coordination site. The approximately 10 ppm upfield shift of the signals in deuterated with respect to nondeuterated methanol can be traced back to a deuterium isotope effect $^n\Delta^D$ through two bonds ($DOCD_3$) plus three bonds ($DOCD_3$), [($^2\Delta$ + $3^3\Delta$)^D]: The heavier isotope gives rise to a more pronounced shielding of the metal nucleus as a consequence of a diminished paramagnetic deshielding term in the overall shielding.[52a]

Reactivity Patterns of 1 to 6, and the Structure of 9

cis-Dioxovanadium(V) complexes commonly generate oxomonoperoxo species in solution on treatment with

Table 4. ^{13}C NMR chemical shifts; for atom labelling see scheme below

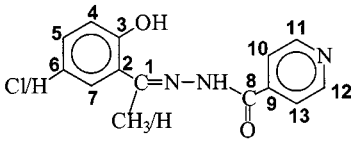

Compound	C1	C8	C3	C9	C11, C12	C10, C13	C2, C4, C5, C6, C7
H_2sal-iNH	148.94	161.35	157.47	139.99	150.40	131.76	116.45, 118.70, 119.45, 121.52, 129.19
[{VO(sal-iNH)}$_2$μ-O], **1** (Δδ)[a]	156.50 (7.56)	167.20 (5.85)	164.30 (6.83)	141.80	148.00	134.20	116.20, 118.40, 118.80, 122.50, 133.20
K[VO_2(sal-iNH)H_2O], **2a** (Δδ)	157.37 (8.43)	167.82 (6.37)	164.96 (7.49)	140.13	150.04	133.68	116.85, 119.94, 121.55, 132.88
H_2Clsal-iNH	146.49	161.52	156.02	139.92	150.41	131.14	118.28, 120.72, 121.54, 123.10, 127.23
[{VO(Clsal-iNH)}$_2$μ-O], **4** (Δδ)	156.66 (10.17)	168.32 (6.80)	163.94 (7.92)	143.41	148.22	131.14	119.08, 122.54, 123.89, 132.35
K[VO_2(Clsal-iNH)H_2O], **5** (Δδ)	157.38 (10.89)	167.82 (6.30)	164.96 (8.90)	140.09	150.07	133.68	116.85, 119.94, 121.56, 123.89
H_2hap-iNH[b]	159.50	162.98	158.73	140.10	150.15	131.58	117.35, 118.62, 119.42, 122.01, 128.74
K[VO_2(hap-iNH)H_2O][c], **6** (Δδ)	163.90 (4.40)	167.30 (4.32)	161.33 (2.60)	149.26	150.26	133.39	116,52, 120.32, 121.89, 122.56, 130.28

[a] Δδ = δ(complex) − δ(free ligand). − [b] Methyl carbon signal at δ = 14.30. − [c] Methyl carbon signal at δ = 16.95.

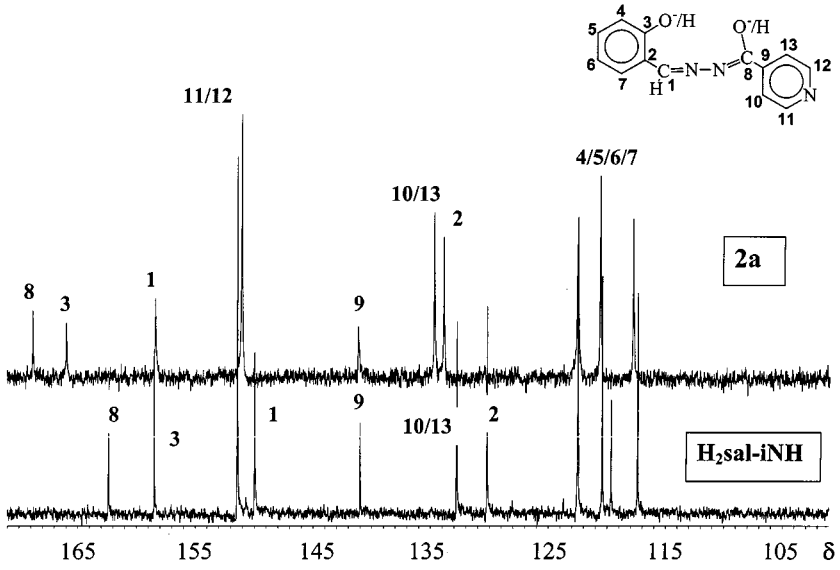

Figure 1. 90.56 MHz $^{13}C\{^1H\}$ NMR spectra of H_2sal-iNH (below) and its dioxovanadium complex **2a** in [D_6]DMSO (above); the inset shows the enol(ate) form of the ligand

H_2O_2,[14,54,55] and a corresponding reaction was also accomplished with **2a** and **5** with 30% H_2O_2 in methanol in an ice bath to yield **7** and **8** [cf. Equations (8) and (9)], which can also be obtained from the dimeric compounds **1** and **4.** The reaction, as monitored by electron absorption spectroscopy (Figure 2), exhibits an increase in intensity and shift of the band at 402.5 nm for **1** to 412 nm for **7**. Correspondingly, the 403.5 nm band of **2a** is shifted to 410 nm. This new band remains constant for several hours at approximately 10 °C. The rate at which peroxo complex formation occurs, seems to be dependent on the amount of H_2O_2 added. In both cases, the bands of the starting products at 322 and 226 nm remain almost unchanged, while the band at 279 nm gradually disappears. A similar spectral pattern was observed for **8**, in which these bands appear at 410, 322 and 225 nm. The relative stability of the peroxo

species at approximately 10 °C in the presence of excess of H_2O_2 enabled us to isolate complexes **7** and **8** (see Exp. Sect.), which showed a UV/Vis spectrum similar to that observed during spectroscopic studies. The peroxo complexes **7** and **8** show three IR-active modes associated with the $\{V(O_2)\}^{2+}$ moiety, namely the symmetric $V(O_2)$ stretch (ν_2) at ca. 580 cm^{-1}, the antisymmetric $V(O_2)$ (ν_3) at ca. 740 cm^{-1}, and the O−O (ν_1) stretch at ca. 895 cm^{-1}, characteristic of η^2-coordination of the peroxo group.[56] In addition, complexes **7** and **8** display the ν(V=O) mode at 950 (**7**) and 954 cm^{-1} (**8**). The isolated peroxo complexes are unstable and lose oxygen even at ambient temperature within a day. The species obtained in this way have spectral patterns (IR as well as electronic) similar to those of the dimers. The overall reaction may thus be represented as shown by the coupled (through **7**) [Equations (8) and (9)].

$$\underset{\mathbf{2a}}{[VO_2(\text{sal-iNH})]^-} + H_2O_2 \leftrightarrows \underset{\mathbf{7}}{[VO(O_2)(\text{sal-iNH})]^-} + H_2O \quad (8)$$

$$2\underset{\mathbf{7}}{[VO(O_2)(\text{sal-iNH})]^-} + 2H^+ \leftrightarrows \underset{\mathbf{1}}{[\{VO(\text{sal-iNH})\}_2\mu\text{-O}]} + H_2O_2 + \tfrac{1}{2}\,O_2 \quad (9)$$

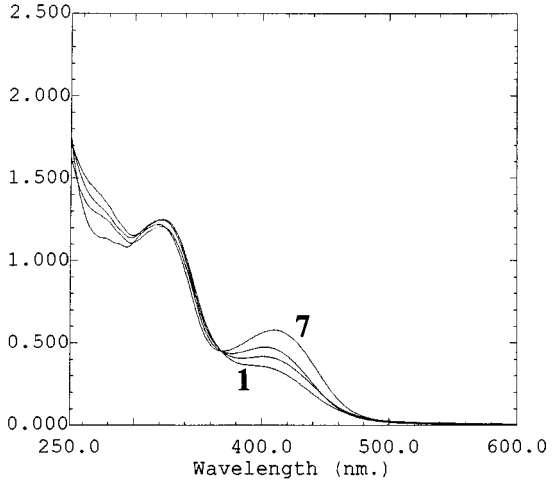

Figure 2. Titration of $[\{VO(\text{sal-iNH})\}_2\mu\text{-O}]$ (**1**) with 30% H_2O_2; the spectra were recorded after the successive addition of 2-drop portions of H_2O_2 to 5 mL of ca. 10^{-4} M solutions of **1** in MeOH

At ambient temperature, the ^{51}V NMR spectrum of **1** after addition of H_2O_2 in CD_3OD showed five resonances at δ = −616, −658, −678, −687 and −692. All these resonances are further upfield than those of the starting products and should indicate the formation of peroxo species.[57] The signal at δ = −692 corresponds to the diperoxovanadate $[VO(O_2)_2OH]^{2-}$, which is formed by partial decomposition of the peroxo complex.[58]

A solution of dimers **1** and **4** in methanol was treated with methanolic KOH at pH ≈ 8.5 and stirred for 1−2 h to provide $K[VO_2L(H_2O)]$-type complexes. The reaction is reversible, i.e. treatment of the monomeric complexes **2a** and **5** with HCl in methanol at pH ≈ 6.5 provides $[\{VOL\}_2\mu\text{-O}]$.

Addition of methanol *saturated* with HCl gas to a methanolic solution of **4** results in a colour change from orange-red to dark red with a gradual shift of the bands at 321.5 and 408.5 nm to 337 and 428 nm, respectively, as illustrated in Figure 3a. A similar behaviour has also been observed for **1**; the bands at 322 and 402.5 nm gradually shifted to 341 and 425 nm on acidification. Based on literature reports[42,59] on similar reactions, the species formed on acidification is most probably $[VO(OH)(\text{Clsal-iNH})H_2O]$. A hydroxooxo complex, viz. $[VO(OH)(HL)]^+$, H_2L = *N*-[(*o*-hydroxyphenyl)methyl]-*N*′-(2-hydroxyethyl)ethylenediamine, has been generated by Pecoraro et al.[33] in solution from the respective dioxovanadium(V) dimer, and the hydroxovanadium(IV) complex $[TpVO(OH)(H_2O)]$ [Tp = tris(pyrazolyl)borate] has recently been structurally characterised.[60] The formation of a hydroxo complex is further corroborated by an upfield shift of the ^{51}V NMR resonance from $\delta(^{51}V) = -533$ for **4** to δ = −554 for the species formed on acidification. The dependence of the ^{51}V shielding on protonation is well documented for vanadates(V)[57] and peroxovanadates.[57a,61] IR and electronic spectra of the compound isolated from the solution under study match well with those of **4**, indicating that on isolation, deprotonation and recovery of the starting material occurs. The reversibility of the reaction is also pertinent in solution (Figure 3b), when the acidified solution is treated with KOH dissolved in methanol. These results are of some interest in the context of the active-site structure and the function of vanadate-dependent haloperoxidases, for which a hydroxo ligand in an apical position has been noted on the basis of X-ray diffraction data[8−10] and proposed as an intermediate on the basis of kinetic studies.[42] Interestingly, no isosbestic points were observed during the progress of the reaction, which indicates complete conversion of $[(VOL)_2\mu\text{-O}]$ into the new species. A further increase in the HCl concentration does not cause changes in the LMCT band positions; excess HCl finally results in decomposition.

The formation of the neutral, monomeric monooxovanadium complex $[VO(OMe)(HOMe)(\text{Clsal-iNH})]$ (**9**) from the dioxo complex **5** by exposing methanolic solutions to low temperatures for a couple of weeks is of interest in the context of oxovanadium complexes used as oxo-transfer reagents both in catalytic and stoichiometric oxygenation reactions.[62,63] We have not been able to isolate bulk amounts of **9**; the predominant species in the mother liquor remains **5**, suggesting an equilibrium of the kind shown in Equation (10), from which **9** is gradually removed by crystallisation. The presence of small amounts of **9** in solution is also indicated by ^{51}V NMR (minor signal at −543).

$$\underset{\mathbf{5}}{K[VO_2(\text{Clsal-iNH})]} + 2\text{MeOH} \leftrightarrows \underset{\mathbf{9}}{[VO(OMe)(HOMe)(\text{Clsal-iNH})]} + \text{KOH} \quad (10)$$

Figure 4 shows an ORTEP drawing of the molecule, and a section from the unit cell of **9**, and Table 5 contains selected structure parameters. The basic structure is that of a tetragonal pyramid with the doubly bonded oxygen atom in the apex, and the phenolate and enolate oxygen atoms O2 and O3, the methoxide oxygen atom O4 and the imine nitrogen atom N1 in the plane. The vanadium atom devi-

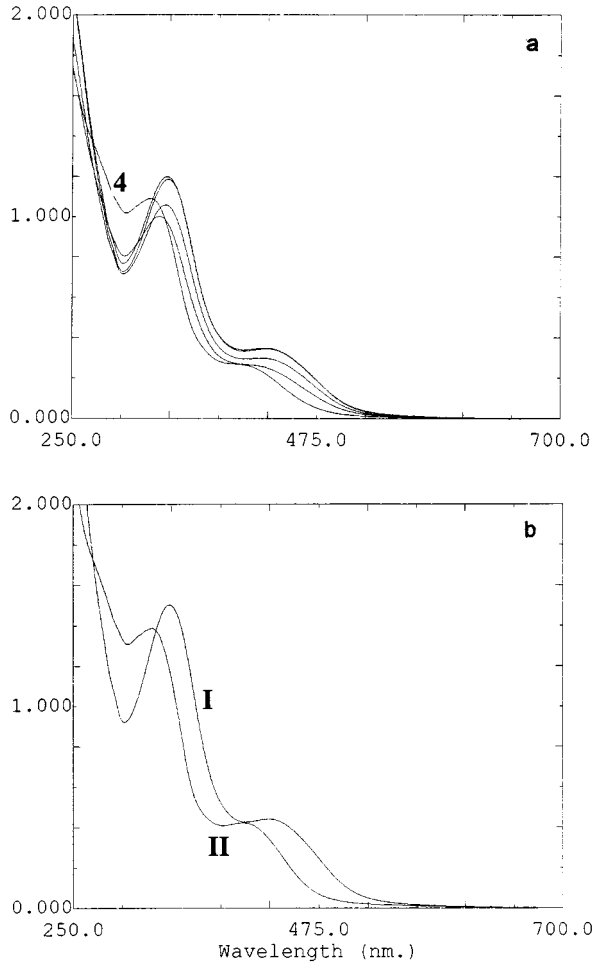

Figure 3. (a): Titration of [{VO(Clsal-iNH}$_2$μ-O] (**4**) with a saturated solution of HCl methanol; the spectra were recorded after the successive addition of 5-drop portions of methanol/HCl to 10 mL of a ca. 10^{-4} M solution of **4**; (b) electronic absorption spectra of **4** in methanol/HCl (I) and at pH ≈ 8.0 after addition of methanolic KOH to this solution (II)

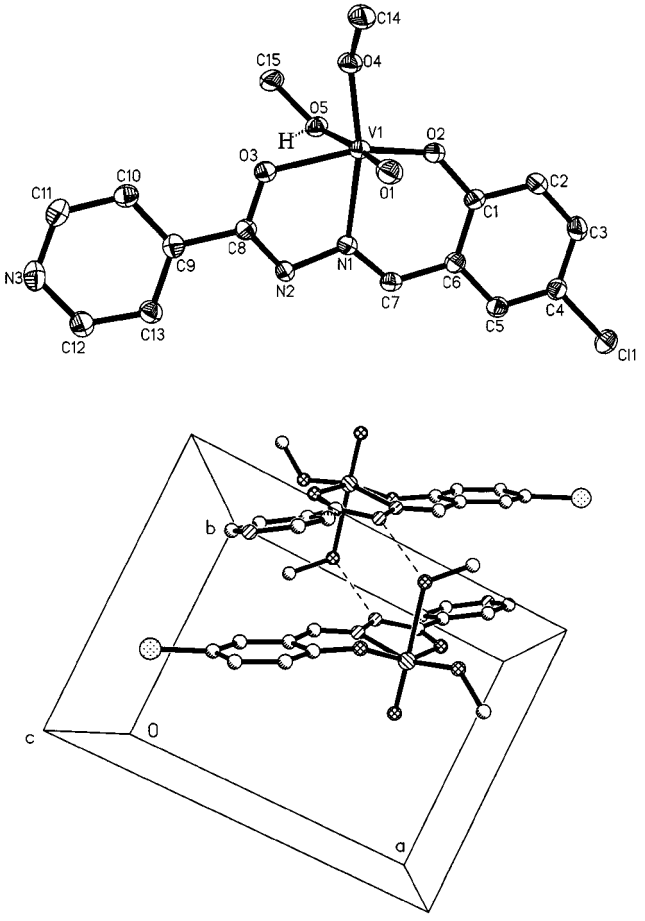

Figure 4. ORTEP plot (at the 50% probability level) of [VO(OMe)-(HOMe)(Clsal-iNH)] (**9**) (top), and a representation of the unit cell showing the interatomic hydrogen bonds (bottom)

Table 5. Selected bond lengths [pm] and bond angles [°] for **9**

V1-O1	1.558(2)	O1-V1-O5	175.84(9)
V1-O2	1.867(2)	O2-V1-O4	101.74(9)
V1-O3	1.971(2)	O3-V1-O4	95.44(9)
V1-O4	1.769(2)	O2-V1-N1	83.33(9)
V1-O5	2.327(2)	O3-V1-N1	74.18(8)
V1-N1	2.130(2)	O1-V1-O3	101.09(10)
O2-C1	1.341(3)	O1-V1-O2	100.13(10)
O3-C8	1.300(3)	O1-V1-O3	97.76(10)
O4-C14	1.426(3)	O2-V1-O5	81.99(9)
O5-C15	1.431(3)	O3-V1-O5	78.97(8)
O5-H5	0.82(4)	O4-V1-O5	81.88(8)
N2···H5	2.052	N1-V1-O5	82.15(8)
Cl1-C4	1.747(3)	V1-N1-N2	116.13(16)
N1-N2	1.402(3)	V1-N1-C7	127.23(17)
N1-C7	1.294(4)	N2-N1-C7	116.4(2)
N2-C8	1.309(3)	N1-N2-C8	108.0(2)

ates from this plane by 0.23 Å. The position *trans* to the oxo group is occupied by a weakly bonded methanol molecule [V−O5 = 2.327(2) Å]. The elongation of this bond is due to the strong *trans* influence of the oxo group and has previously been observed in other complexes containing the {VO(*ONO*)HOR}[12−16,29] or {VO(*ONO*)H_2O}[64] moieties. The other bond lengths *d* are similar to those observed in similar complexes;[12,25,28,29] the distances *d*(O3−C8) [1.300(3) Å] and *d*(N2−C8) [1.309(3) Å] support the enolate mode of coordination. With 175.84(9)°, the O=V−(HOMe) axis is almost linear. In the tetragonal plane, the two "open" angles O2−V−O4 and O3−V−O4 amount to 101.7 and 95.4°, while the bite angles of the tridentate ligand are 74.2° for the 5-membered ring, and 83.3° for the 6-membered ring. The ligand system is practically planar. The only angle that deviates significantly from sp^2 planarity is the angle of 108.0(2)° at the (noncoordinating) N2. This nitrogen atom is involved in intermolecular hydrogen bonding to the proton of the coordinated methanol, as shown in Figure 4, bottom; the N2···H−O5 distance amounts to 2.87 Å.

Conclusion

Oxovanadium(V) complexes show in vitro and in vivo activity in oxidation and oxygen-transfer reactions.[62,65] In the native systems (vanadate-dependent haloperoxidases) which have also been shown to exhibit oxo-transferase activity,[66] vanadium is in an O_4N-coordination environment. Intermediates formed during catalytic turnover, containing protonated {VO_2} [{VO(OH)}, {VO(H_2O)}] and {VO(O_2)}

cores have been postulated.[42,62,67,68] The dioxovanadium compounds described here model the active site in vanadate-dependent haloperoxidases in that they contain an O_4N-donor set (as well as a weakly bonded water molecule), including a doubly bonded oxo group which can be protonated to form a hydroxooxo complex, or replaced by peroxide to form an oxoperoxo complex. Furthermore, the ability of vanadium compounds to transfer oxo groups is modelled by the formation of a structurally characterised monooxo complex [VO(OMe)(HOMe)L] (**9**) by deoxygenation of the dioxo complex K[VO_2L(HOMe)] [**2a(MeOH)**].

Experimental Section

General Remarks: V_2O_5, NH_4VO_3, salicylaldehyde (sal), isonicotinic acid hydrazide (iNH) and *o*-hydroxyacetophenone (hap) were purchased from Loba Chemie, India. 5-Chlorosalicylaldehyde was prepared according to a literature procedure.[69] H_2sal-iNH,[70a] H_2Clsal-iNH,[70a] H_2hap-iNH[70b] (cf. Scheme 1) and [VO(acac)$_2$][71] were prepared as described previously. − Elemental analyses were carried out by the Central Drug Research Institute, Lucknow, India. − IR spectra were recorded as KBr pellets with a Perkin−Elmer model 1600 FT-IR. − UV/Vis spectra (in methanol) were recorded with a UV-1601 PC UV/Vis spectrophotometer. − ^{1}H NMR spectra were obtained with a Bruker 200 MHz spectrometer, ^{13}C and ^{51}V NMR spectra with a Bruker AM 360 spectrometer at 90.56 and 94.73 MHz, respectively, in rotating 10-mm diameter vials with the common parameter settings. All δ(^{51}V) values are quoted relative to $VOCl_3$ as external standard. − Thermogravimetric analyses of the complexes were carried out on a simple manually operated thermobalance constructed in our laboratory. The instrument was calibrated using crystallised $CuSO_4 \cdot 5H_2O$. Samples were run under a dynamic air atmosphere, with a heating rate of 3 to 5 °C min^{-1}.

Crystal Structure Determination: Data were collected with a Syntex $P2_1$ diffractometer in the 2θ-scan mode using a graphite monochromator and Cu-K_α radiation. Crystal data and details of the data collection and refinement are collated in Table 6. The program systems SHELXS 86 and SHELXL 93 were used throughout.[72] The methanolic hydrogen atom (H5O on O5) was found explicitly; all other hydrogen atoms were placed into calculated positions and included with common thermal parameters in the last cycles of refinement. An absorption correction (DIFABS) was carried out. Crystallographic data for the structure reported in this paper have been deposited with the Cambridge Crystallographic Data centre as supplementary publication no. CCDC-148428. Copies of the data can be obtained free of charge on application to CCDC,12 Union Road, Cambridge CB2 1EZ, UK [Fax: (internat.)+ 44-1223/336-033; E-mail: deposit@ccdc.cam.ac.uk].

Table 6. Crystal data and structure refinement for [VO(OMe)(HOMe)(Clsal-iNH)] (**9**)

Empirical formula	$C_{15}H_{15}ClN_3O$ V
Molecular mass, g mol^{-1}	403.69
Temperature, K	173(2) K
Wavelength, Å	1.54178
Crystal system, space group	monoclinic, *P*2(1)/*c*
Unit cell dimensions,	
a, Å	10.730(2)
b, Å	7.9047(13
c, Å	19.902(4)
β, °	105.188(16)
Cell volume, Å^3	1629.2(5)
Z	4
Calculated density, g cm^{-3}	1.646
Absorption coefficient, mm^{-1}	6.908
F(000)	824
Crystal size, mm	0.50 × 0.40 × 0.40
θ range for data collection, °	4.27–76.42
Index ranges	$-13 \le h \le 4, -3 \le k \le 9, -24 \le l \le 25$
Reflections collected/unique	3626/3401 [*R*(int) = 0.0285]
Data/restraints/parameters	3401/0/247
Goodness-of-fit	1.032
Final *R* indices [$I > 2\sigma(I_0)$]	*R*1 = 0.0465, *wR*2 = 0.1266
R indices (all data)	*R*1 = 0.0576, *wR*2 = 0.1346
Extinction coefficient	0.0024(3)
Largest diff. peak and hole, eÅ^{-3}	0.871 and –0.935

Preparation of Complexes: For thermogravimetric analyses and UV/Vis, ^{1}H and ^{13}C NMR spectroscopic data, cf. Tables 1−4 in the Discussion; IR and ^{51}V NMR spectroscopic data are included in the Exp. Sect.

[{VO(sal-iNH)}$_2$μ-O] (1), K[VO_2(sal-iNH)H_2O] (2a) and [VO(sal-iNH)] (3): Vanadium(V) oxide (0.50 g, 5 mmol) was dissolved in aqueous KOH (0.30 g, 5 mmol in 10 mL) and stirred for 2 h. The resulting solution was filtered. A filtered solution of H_2sal-iNH (1.20 g, 5 mmol), dissolved in aqueous KOH (0.60 g, 10 mmol in 20 mL), was added to the above solution with stirring, and the pH value of the reaction mixture was slowly adjusted to 7.5 with HCl (4 M). After 2 h of stirring, the precipitated orange solid was filtered, washed with cold water followed by acetone, and dried. On recrystallisation from methanol (ca. 40 mL), **1** precipitated as a brown solid, which was filtered off and dried in vacuo over silica gel. After reducing the volume of the filtrate to ca. 10 mL and keeping it at ca. 10 °C, yellow crystalline **2a** separated within 2−4 d. This was filtered off, washed with acetone and dried as above. Yield of **1**: 256 mg (15%); **2a**: 820 mg (40%). − **Data for 1:** $C_{26}H_{18}N_6O_7V_2$ (628.4): calcd. C 49.69, H 2.87, N 13.38; found C 49.79, H 3.12, N 13.11. − IR (KBr): $\tilde{\nu}_{max}$ = 1635 cm^{-1}, 1605 (C=N), 1212 (C−O, enolic), 1045(N−N), 970, 955(V=O), 864 [V-(μ-O)−V], 477, 461, 406(V−O, V−N). − ^{51}V NMR: δ = −541 ([D$_6$]DMSO), −549 and a minor signal at −541 (CD_3OD/CH_3OH). − **Data for 2a:** $C_{13}H_{11}KN_3O_5V$ (379.3) calcd. C 41.17, H 2.90, N 11.08; found C 41.00, H 3.13, N 10.86. − IR (KBr): $\tilde{\nu}_{max}$ = 1603 (C=N) cm^{-1}, 1213 (C−O, enolic), 1025 (N−N), 928, 907 (sym and asym VO_2), 595, 405 (V−O, V−N). − ^{51}V NMR: δ = −532 ([D$_6$]DMSO), −541 and minor signal at −549 (CH_3OH/CD_3OD).

Alternative Preparation of 1: A solution of H_2sal-iNH (1.20 g, 5 mmol) in acetone (20 mL) was added with stirring to an equimolar amount of [VO(acac)$_2$], dissolved in acetone (10 mL), and the resulting yellowish green suspension was heated at reflux in a water bath for 4 h. After cooling to room temperature, a green precipitate of [VO(sal-iNH)] (**3**) was filtered off, washed with acetone and dried. Compound **3** was suspended in acetone (30 mL), and air was slowly passed through the suspension at ca. 40 °C for ca. 20 h with occasional shaking, or until the yellowish green suspension had completely disappeared and crystalline orange-red solid **1** separated instead. This was filtered, washed with acetone, recrystallised from methanol and dried. Yield (based on [VO(acac)$_2$]) 60%. For the preparation of **1**, it is not necessary to isolate intermediate **3**. − **Data for 3:** $C_{13}H_9N_3O_4V$ (322.2): calcd. C 50.99, H 2.94, N 13.73; found C 50.68, H 3.08, N 13.60. − IR (KBr): $\tilde{\nu}_{max}$ = 1606(C=N) cm^{-1}, 994(V=O). − Complex **1** was also prepared in almost the same yield from the reaction of VO(OEt)$_3$ and H_2sal-iNH in absolute ethanol under aerobic conditions: A solution of H_2sal-iNH (1.20 g, 5 mmol) in absolute ethanol (20 mL) was added to VO(OEt)$_3$ (equiv. to 5 mmol, prepared[41] in situ) in absolute ethanol (10 mL), and the reaction mixture was heated at reflux for

6 h. After reducing the volume to ca. 10 mL, the flask was kept open to air at room temp., yielding orange-red **1** within 24 h. This was filtered, washed with ethanol and dried in vacuo.

$NH_4[VO_2(sal\text{-}iNH)H_2O]$ (2b): $NH_4[VO_3]$ (0.59 g, 5 mmol) was dissolved in water (10 mL) by heating in a water bath. This solution was added to a filtered solution of H_2sal-iNH (1.20 g, 5 mmol), dissolved in aqueous NaOH (0.40 g, 10 mmol), with stirring, and the pH value was adjusted to 7.5 with HCl (4 M). After 2 h, stirring was stopped, and the orange solid, which had separated, was filtered off, washed with water, followed by acetone, and dried. The crude mass was dissolved by heating in a minimum amount of methanol, and filtered. On standing overnight at ambient temperature, brown solid **1** precipitated. This was filtered off and dried in vacuo. After reducing the filtrate to ca. 10 mL, it was kept at 10 °C for a few days, whereupon yellow crystals of **2b** separated. These were filtered off and dried in vacuo at ambient temperature. Yield of **1**: 317 mg (20%); **2b**: 808 mg (45%). − **Data for 2b:** $C_{13}H_{13}N_4O_5V$ (356.2): calcd. C 43.82, H 3.65, N 15.73; found C 43.61, H 3.83, N 15.56. − IR (KBr): $\tilde{\nu}_{max}$ = 1605 cm^{-1} (C=N), 1225 (C−O, enolic), 1063 (N−N), 946, 927 (sym and asym VO_2), 477, 463, 420 (V−O, V−N).

$[\{VO(Clsal\text{-}iNH)\}_2\mu\text{-}O]$ (4) and $K[VO_2(Clsal\text{-}iNH)H_2O]$ (5): Complexes **4** (25% yield) and **5** (40% yield) were prepared analogously to **1** and **2a**, replacing H_2sal-iNH with H_2Clsal-iNH. − **Data for 4:** $C_{26}H_{16}Cl_2N_6O_7V_2$ (646.30): calcd. C 44.77, H 2.30, N 12.05; found C 44.47, H 2.51, N 11.83. − IR (KBr): $\tilde{\nu}_{max}$ = 1625 cm^{-1}, 1602 (C=N), 1288 (C−O, enolic), 1087 (N−N), 952 (V=O), 846 [V−(μ-O)−V], 462, 427 (V−O, V−N). − ^{51}V NMR: δ = −539 ([D_6]DMSO), −548 and a minor signal at −543 (CD_3OD/CH_3OH). − **Data for 5:** $C_{13}H_{10}ClKN_3O_5V$ (413.7): calcd. C 37.73, H 2.42, N 10.16; found C 37.85, H 2.61, N 10.04. − IR (KBr): $\tilde{\nu}$ = 1607 cm^{-1} (C=N), 1288 (C−O, enolic), 1038 (N−N), 938, 904 (sym and asym VO_2), 462, 416 (V−O, V−N). − ^{51}V NMR: δ = −532 ([D_6]DMSO), −541 (CH_3OH/CD_3OD).

$K[VO_2(hap\text{-}iNH)H_2O]$ (6): The potassium salt of the ligand H_2hap-iNH was prepared in situ by treating H_2hap-iNH (1.27 g, 5 mmol) with KOH (0.60 g, 10 mmol) in water (15 mL). This solution was added dropwise to stirred aqueous potassium vanadate (5 mmol, prepared from V_2O_5 and KOH). The pH value of the reaction mixture was adjusted to 7.5 by slow addition of HCl (4 M). After 2 h, the yellow solid, which had separated, was filtered off, washed with acetone and dried in vacuo. Yield 1080 mg (55%). $-C_{14}H_{13}KN_3O_5V$ (393.3): calcd. C 42.75, H 3.30, N 10.68; found C 42.55, H, 3.63, N 10.74. − IR (KBr): $\tilde{\nu}_{max}$ = 1587 cm^{-1} (C=N), 1248 (C−O, enolic), 1058 (N−N), 943, 907 (sym and asym VO_2), 473 (V−O, V−N). − ^{51}V NMR: δ = −533 ([D_6]DMSO), −538 and a minor signal at −547 (CH_3OH/CD_3OD).

$K[VO(O_2)(sal\text{-}iNH)H_2O]$ (7) and $K[VO(O_2)(Clsal\text{-}iNH)H_2O]$ (8): $K[VO_2(sal\text{-}iNH)\cdot H_2O]$ (**2a**, 0.150 g) was dissolved in methanol (10 mL) and the clear, yellow solution was cooled with ice. H_2O_2 (30%, 4 mL) was added dropwise to the stirred solution. The resulting orange-red solution was stirred for 2 h, and the red solid **7**, which separated was filtered off, washed with cold methanol and dried in vacuo. Additional, impure peroxo complex **7** was obtained from the filtrate on cooling it overnight to 5 °C. Complex **8** was prepared similarly, using $K[VO_2(Clsal\text{-}iNH)\cdot H_2O]$ (**5**, 0.150 g) and H_2O_2 (30%, 4 mL). Satisfactory elemental analyses were not obtained owing to the instability of the peroxo complexes. Further characteristics are discussed in the text.

[VO(OMe)(HOMe)(Clsal-iNH)] (9): Crystals of **9** suitable for X-ray analysis were grown in a saturated solution of **5** in methanol, standing at 4 °C for a few weeks.

Acknowledgments

This work was supported by the Deutsche Forschungsgemeinschaft and the Fonds der Chemischen Industrie. M. R. M. and S. K. are thankful to the Council of Scientific and Industrial Research, New Delhi, for financial support of the work. We also acknowledge C,H,N analyses carried out by RSIC, Central Drug Research Institute, Lucknow.

[1] A. Butler, M. J. Clague, G. E. Meister, *Chem Rev.* **1994**, *94*, 625.
[2] C. Slebodnick, B. J. Hamestra, V. L. Pecoraro, *Struct. Bond. (Berlin)* **1997**, *89*, 51.
[3] C. Djordjevic, G. L. Wampler, *J. Inorg. Biochem.* **1985**, *25*, 51.
[4] J. H. McNeil, V. G. Yuen, H. R. Hoveyda, C. Orvig, *J. Med. Chem.* **1992**, *35*, 1489.
[5] K. H. Thompson, J. H. McNeil, C. Orvig, *Inorg. Chem.* **1999**, *38*, 2288.
[6] [6a] D. Rehder, *Bioinorganic Chemistry: Transition Metals in Biology and Their Coordination Chemistry*, (Ed.: A. X. Trautwein), Wiley-VCH, Weinheim, **1997**, chapter D6. − [6b] D. Rehder, *Metal Ions in Biological Systems; Vanadium and Its Role in Life* (Eds.: H. Sigel, A. Sigel), Marcel Dekker Inc., New York, **1995**, chapter 1.
[7] D. Rehder, *Coord. Chem. Rev.* **1999**, *182*, 297
[8] M. Weyand, H.-J. Hecht, M. Kieß, M.-F. Liaud, H. Vilter, D. Schomburg, *J. Mol. Biol.* **1999**, *293*, 595.
[9] A. Messerschmidt, L. Prade, R. Wever, *Biol. Chem.* **1997**, *378*, 309.
[10] S. Macedo-Ribeiro, W. Hemrika, R. Renirie, R. Wever, A. Messerschmidt, *J. Biol. Inorg. Chem.* **1999**, *4*, 209.
[11] A. Butler, C. J. Carrano, *Coord. Chem. Rev.* **1991**, *109*, 61
[12] K. Nakajima, M. Kojima, K. Toriumi, K. Saito, J. Fujita, *Bull. Chem. Soc. Jpn.* **1989**, *62*, 760.
[13] V. Vergopoulos, W. Priebsch, M. Fritzsche, D. Rehder, *Inorg. Chem.* **1993**, *32*, 1844.
[14] M. J. Clague, N. L. Keder, A. Butler, *Inorg. Chem.* **1993**, *32*, 4754.
[15] H. Schmidt, D. Rehder, *Inorg. Chim. Acta* **1998**, *267*, 229.
[16] R. Fulwood, H. Schmidt, D. Rehder, *J. Chem. Soc., Chem. Commun.* **1995**, 1443.
[17] M. Bashirpoor, H. Schmidt, C. Schulzke, D. Rehder, *Chem. Ber./Receuil* **1997**, *130*, 651.
[18] W. Wang, F.-L. Zeng, X. Wang, M.-Y. Tan, *Polyhedron* **1996**, *15*, 1699.
[19] C. J. Carrano, C. M. Nunn, R. Quan, J. A. Bonadies, V. L. Pecoraro, *Inorg. Chem.* **1990**, *29*, 944.
[20] J. Costa Pessoa, J. A. L. Silva, A. L. Vieira, L. Vilas. Boas, P. O'Brien, P. Thornton, *J. Chem. Soc., Dalton Trans.* **1992**, 1745.
[21] S. Mondal, P. Ghosh, A. Chakravorty, *Inorg. Chem.* **1997**, *36*, 59.
[22] [22a] H. Schmidt, M. Bashirpoor, D. Rehder, *J. Chem. Soc., Dalton. Trans.* **1996**, 3865. − [22b] C. Grüning, H. Schmidt, D. Rehder, *Inorg. Chem. Commun.* **1999**, *2*, 57.
[23] [23a] J. Chakravarty, S. Dutta, S. K. Chandra, P. Basu, A. Chakravorty, *Inorg. Chem.* **1993**, *32*, 4249. − [23b] S. Dutta, P. Basu, A. Chakravorty, *Inorg. Chem.* **1993**, *32*, 5343.
[24] J. Chakravarty, S. Dutta, A. Day, A. Chakravorty, *J. Chem. Soc., Dalton. Trans.* **1994**, 557.
[25] [25a] S. Mondal, S. P. Rath, S. Dutta, A. Chakravorty, *J. Chem. Soc., Dalton. Trans.* **1996**, 99. − [25b] S. Mondal, S. P. Rath, K. K. Rajak, A. Chakravorty, *Inorg. Chem.* **1998**, *37*, 1713.
[26] S.-X. Liu, S. Gao, *Polyhedron* **1998**, *17*, 81.
[27] S. Gao, Z.-Q. Weng, S.-X. Liu, *Polyhedron* **1998**, *17*, 3595.
[28] S.-X. Liu, S. Gao, *Inorg. Chim. Acta* **1998**, *282*, 149.
[29] K. K. Rajak, S. P. Rath, S. Mondal, A. Chakravorty, *Indian J. Chem.* **1999**, *38A*, 405.
[30] S. Bhattacharya, T. Ghosh, K. R. Sur, *J. Indian Chem. Soc.* **2000**, *77*, 59.
[31] C. Djordjevic, M. Lee, E. Sinn, *Inorg. Chem.* **1989**, *28*, 719.

[32] D. C. Crans, P. K. Shin, *J. Am. Chem. Soc.* **1994**, *116*, 1305.
[33] G. J. Colpas, B. J. Hamstra, J. W. Kampf, V. L. Pecoraro, *Inorg. Chem.* **1994**, *33*, 4669.
[34] D. C. Crans, A. D. Keramidas, M. Mahroof-Tahir, O. P. Anderson, M. M. Miller, *Inorg. Chem.* **1996**, *35*, 3599.
[35] M. Mahroof-Tahir, A. D. Keramidas, R. B. Goldfarb, O. P. Anderson, M. M. Miller, D. C. Crans, *Inorg. Chem.* **1997**, *36*, 1657.
[36] D. C. Crans, A. D. Keramidas, S. S. Amin, O. P. Anderson, S. M. Miller, *J. Chem. Soc., Dalton Trans.* **1997**, 2799.
[37] V. Vergopoulos, W. Priebsch, M. Fritzsche, D. Rehder, *Inorg. Chem.* **1993**, *32*, 1844.
[38] X. Li, M. S. Lah, V. L. Pecoraro, *Inorg. Chem.* **1988**, *27*, 4657.
[39] [39a] G. Asgedom, S. Sreedhara, J. Kivikoski, J. Valkonen, C. P. Rao, *J. Chem. Soc., Dalton Trans.* **1995**, 2459. – [39b] G. Asgedom, S. Sreedhara, J. Kivikoski, E. Kolehmainen, C. P. Rao, *J. Chem. Soc., Dalton Trans.* **1996**, 93.
[40] N. Julien-Cailhol, E. Rose, J. Vaisserman, D. Rehder, *J. Chem. Soc., Dalton Trans.* **1996**, 2111.
[41] C. A. Root, J. D. Hoeschele, C. R. Cornman, J. W. Kampf, V. L. Pecoraro, *Inorg. Chem.* **1993**, *32*, 3855.
[42] B. J. Hamstra, G. J. Colpas, V. L. Pecoraro, *Inorg. Chem.* **1998**, *37*, 949.
[43] M. Melchior, K. H. Thompson, J. M. Jong, S. J. Rettig, E. Shuter, V. G. Yuen, Y. Zhou, J. H. McNeill, C. Orvig, *Inorg. Chem.* **1999**, *38*, 2288.
[44] M.-H. Lee, N. H. Heo, S. Hayashi, *Polyhedron* **1998**, *17*, 55.
[45] J. A. Bonadies, C. J. Carrano, *J. Am. Chem. Soc.* **1986**, *108*, 4088.
[46] [46a] J. C. Craliz, J. C. Rub, D. Willis, J. Edger, *Nature* **1955**, *34*, 176. – [46b] M. J. M. Campbell, *Coord. Chem. Rev.* **1975**, *15*, 279.
[47] M. R. Maurya, S. A. Bhakare, *J. Chem. Res. (S)* **1996**, 390.
[48] S. P. Perlepes, D. Nicholls, M. R. Harrison, *Inorg. Chim. Acta* **1985**, *102*, 137.
[49] M. R. Maurya, *J. Chem. Res. (S)* **1995**, 248.
[50] M. R. Maurya, C. Gopinathan, *Indian J. Chem.* **1996**, *35A*, 701.
[51] A. D. Keramidas, A. B. Papaioannou, A. Vlahos, T. A. Kabanos, G. Bonas, A. Makriyannis, C. P. Rapropoulou, A. Terzis, *Inorg. Chem.* **1996**, *35*, 357.
[52] [52a] D. Rehder, C. Weidemann, A. Duch, W. Priebsch, *Inorg. Chem.* **1988**, *27*, 584. – [52b] D. Rehder, *Transition Metal Nuclear Magnetic Resonance* (Ed.: P. S. Pregosin), Elsevier, New York, **1991**, p. 1.
[53] O. W. Howarth, *Progr. Magn. Reson. Spectrosc.* **1990**, *22*, 453.
[54] R. Schwendt, P. Svancárek, L. Kuchta, J. Marek, *Polyhedron* **1998**, *17*, 2161.
[55] F. W. B. Einstein, R. J. Batchelor, S. J. Angus-Dunne, A. S. Tracey, *Inorg. Chem.* **1996**, *35*, 1680.
[56] A. D. Westland, F. Haque, J.-M. Bouchard, *Inorg. Chem.* **1980**, *19*, 2255.
[57] [57a] H. Schmidt, I. Andersson, D. Rehder, L. Pettersson, *J. Inorg. Biochem.* **2000**, *80*, 149. – [57b] M. Casný, D. Rehder, H. Schmidt, H. Vilter, V. Conte, *J. Inorg. Biochem.* **2000**, *80*, 157.
[58] The species observed by Rao et al.[39a] in the reaction between H_2O_2 and [HAMP][VO_2(Brsal-amp)] (HAMP is 2-amino-2-methylpropanol, and H_2Brsal-amp is the Schiff base derived from 5-bromosalicylaldehyde and 2-amino-2-methylpropanol) in acetonotrile is probably also $[VO(O_2)_2OH]^{2-}$, since the IR spectrum showed peaks due to the peroxovanadium group only and no indication of the coordination of the ligand.
[59] B. S. Parajon-Costa, A. C. Gonzales-Baro, E. J. Baran, *J. Coord. Chem.* **1999**, *47*, 417.
[60] M. Kosugi, S. Hickichi, M. Akita, Y. Moro-oka, *Inorg. Chem.* **1999**, *38*, 2567.
[61] A. T. Harrison, O. W. Howarth, *J. Chem. Soc., Dalton Trans.* **1985**, 1173.
[62] Y. Zhang, R. H. Holm, *Inorg. Chem.* **1990**, *29*, 911.
[63] T. Hirao, *Chem. Rev.* **1997**, *97*, 2707.
[64] D. Rehder, C. Schulzke, H. Dau, C. Meinke, J. Hanss, M. Epple, *J. Inorg. Biochem.* **2000**, *80*, 115, and references cited therein.
[65] I. W. C. E. Arends, M. P. Birelli, R. A. Sheldon, *Stud. Surf. Catal.* **1997**, *110*, 1031.
[66] [66a] M. A. Andersson, S. G. Allenmark, *Tetrahedron* **1998**, *54*, 15293. – [66b] H. B. ten Brink, A. Tuyman, H. L. Dekker, W. Memrika, Y. Izumi, T. Oshiro, H. E. W. Schoemaker, R. Wever, *Inorg. Chem.* **1998**, *37*, 6780.
[67] A. Butler, A. H. Baldwin, *Struct. Bond.* **1997**, *89*, 109.
[68] V. Conte, F. Di Furia, G. Licini, *Appl. Catal.* **1977**, *157*, 335.
[69] F. J. Welcher, *Organic Analytical Reagents*, van Nostrand Co., New York, **1947**, vol. 3, p. 254.
[70] [70a] K. N. Srivastava, S. Das, R. A. Lal, *Indian J. Chem., A* **1986**, *25*, 85. – [70b] C. P. Prabhakaran, B. G. Nair, *Trans. Met Chem.* **1983**, *8*, 368.
[71] R. A. Rowe, M. M. Jones, *Inorg. Synth.* **1957**, *5*, 113.
[72] [72a] G. M. Sheldrick, *SHELXS 86*, University of Göttingen, **1986**. – [72b] G. M. Sheldrick, *SHELXL 93*, University of Göttingen, **1993**.

Received July 24, 2000
[I00291]

Antimony-Substituted Keggin-Type Polyoxomolybdates: Polar Crystals and Catalytic Oxidative Dehydrogenation of Alcohols

Alexander M. Khenkin,[a] Linda J. W. Shimon,[b] and Ronny Neumann*[a]

Keywords: Antimony / Polyoxometalates / Alcohols / Molybdenum / Dehydrogenations

An antimony-substituted polyoxomolybdate, $[PSb^{III}(H_2O)Mo_{11}O_{39}]^{4-}$, of the α-Keggin structure, has been synthesized. Although the molecular structure is typical, we have found from the analysis of the X-ray diffraction data that the crystal is anisotropic with alignment of the molecular units so that the substituted antimony atoms are all directed along the polar *c* axis and on the same side of the molecular unit. UV/Vis, ESR and magnetic susceptibility data support a formulation of $[PSb^{III}(H_2O)Mo_{11}O_{39}]^{4-}$ whereby there is partial electron delocalization with some formation (10–20%) of Mo^{V}. Oxidation of $[PSb^{III}(H_2O)Mo_{11}O_{39}]^{4-}$ with ozone or bromine yields the oxidized species $[PSb^{V}(O)Mo_{11}O_{39}]^{4-}$ and $[PSb^{V}(Br)Mo_{11}O_{39}]^{3-}$. In the anaerobic oxydehydrogenation of alcohols, $[PSb^{V}(O)Mo_{11}O_{39}]^{4-}$ is more active than $[PSb^{V}(Br)Mo_{11}O_{39}]^{3-}$. Catalytic aerobic oxidation of benzylic alcohols to aldehydes was also possible with no over-oxidation and formation of carboxylic acids.

Introduction

Mixtures of metal oxides containing both main group and transition metal elements are very important materials used as catalysts for heterogeneous, gas phase oxidative transformations. Such oxidative transformations include oxydehydrogenation, oxygenation and ammonoxidation reactions. Conceptually, polyoxometalates or heteropolyanions may be considered to be soluble analogs of such metal oxides and have been shown to be of general interest as catalysts for low temperature, homogeneous, liquid phase oxidation reactions.[1−6] Essentially, research carried out to date in this context can be divided into two main groups. In one research area, transition metal-substituted polyoxotungstates are used as catalysts. Here, it has been convenient to picture the catalytic process by proposing the activation of an oxidant such as iodosobenzene,[7−9] hydroperoxide,[10−18] periodate,[19−22] *N*-oxide,[23] or molecular oxygen[24−26] at the transition metal center which is "ligated" by a lacunary polyoxotungstate. In the second set of investigations, polyoxomolybdates and polyoxovanadomolybdates of the Keggin structure with high redox potentials, almost invariably $[PV_xMo_{12-x}O_{40}]^{q-}$ ($x = 0, 1, 2$), are used as catalysts. Significant applications of these compounds include their use in place of copper salts in Wacker-type reactions,[27−28] in oxydehydrogenation reactions[29−33] and most recently in the oxygenation of hydrocarbons.[34]

Since mixed metal oxides containing antimony oxide often play an important role in heterogeneous oxidation catalysis, we sought to prepare and characterize the first polyoxomolybdates of the Keggin structure substituted in the addenda position by Sb^{III} and Sb^{V} atoms. The catalytic activity of these polyoxoantinomatomolybdates was investigated and compared to the well-known polyoxovanadomolybdates. The literature that describes antimony-containing polyoxometalates is rather scant. Originally little was known about the compositions and structures of Sb^{III}-containing polyoxotungstates.[35−37] More recently, large clusters of polyoxotungstates containing Sb^{III} in the heteroatom but not addenda positions have been prepared and structurally determined.[38−39] Also, it has been shown that antimony *counter cations* have a stabilizing effect on polyoxometalates at high (>400 °C) temperatures.[40−42]

Results and Discussion

Synthesis, Structure Determination and Characterization of $[PSb^{III}(H_2O)Mo_{11}O_{39}]^{4-}$

The first approach taken to prepare phosphomolybdates with antimony substitution in the addenda position was by the classical synthesis whereby an acidified solution of molybdate, antimonate, and phosphate is extracted with diethyl ether. For example, Sb_2O_5 (5 mmol) in 50 mL concentrated HCl was refluxed until dissolution, followed by addition of Na_2HPO_4 (5 mmol in 10 mL H_2O), $Na_2MoO_4{\cdot}2H_2O$ (55 mmol in 40 mL H_2O) and 2.5 mL concentrated H_2SO_4 and heating at 90 °C for 1 h. The isolated polyoxometalate was shown by ICP-MS to contain only a very small amount of antimony with a P/Sb/Mo ratio of 1:0.04:12. Increasing the amount of Sb_2O_5 was to no avail. However, preparation of the antimony(III)- and antimony(V)-substituted phosphomolybdate is straightforward in nonaqueous media by insertion of $Sb(OAc)_3$ into the lacunary position of $[Q_4H_3PMo_{11}O_{39}]$ [$Q = (n\text{-}C_4H_9)_4N^+$], Equation (1).[43]

$$Q_4H_3PMo_{11}O_{39} + Sb(OAc)_3 \xrightarrow[CH_3CN]{} Q_4Sb(L)^{III}PMo_{11}O_{39}$$

[a] Department of Organic Chemistry, Weizmann Institute of Science, Rehovot, Israel 76100
[b] Chemical Services Division, Weizmann Institute of Science, Rehovot, Israel 76100

 © WILEY-VCH Verlag GmbH, 69451 Weinheim, 2001 1434−1948/01/0303−0789 $ 17.50+.50/0

The reaction yielded, after recrystallization, dark green prisms of $Q_4PSb^{III}(H_2O)Mo_{11}O_{39}$ which were used for X-ray diffraction measurements. The compound crystallizes in the monoclinic space group C_c (No. 9) with two molecular formula units per asymmetric unit. For details of the structural analysis, see the Experimental Section, Table 1 and Supporting Information. The polyoxoanion itself has the usual α-Keggin-type structure. For one molecule of the asymmetric unit, the central phosphate moiety was well defined whereas for the other phosphate there was disordered oxygen coordination. Also there is coordination of a simple oxygen-containing ligand (assumed to be water) at the antimony position. Generally, in most monosubstituted Keggin structures, XMW_{11}, the substituted metal atom positions are fully disordered due to the cubic crystal structure.[44] Here, the lower monoclinic symmetry has allowed us to determine that the compound crystallizes anisotropically with the antimony atoms aligned along the polar *c* axis (Figure 1). The anisotropic antimony positions originally determined from the Patterson solution were confirmed by the observation that isotropic substitution into the structure at other positions, or assuming positional disorder of the antimony atom, led to statistically significantly poorer *R* values without the addition of extra parameters. Inspection of the packing revealed the anisotropic arrangement of the molecule with respect to the polar *c* axis. Importantly, this anisotropy is observed despite the fact that the larger Sb^{III} cation (0.80 Å vs. 0.60 Å for Mo^{VI})[45] is well accommodated in the addenda position of the Keggin compound without significantly distorting the molecular structure. The average bond lengths are $Mo-O_t$ = 1.686 (range 1.65−1.74, s = 0.038), $Mo-O_c$ = 1.992 (range 1.76−2.08, s = 0.104) and $Mo-O_e$ = 1.926 (range 1.81−2.09, s = 0.091). The average bond lengths for the antimony position are $Sb-O_t$ = 1.72, $Sb-O_c$ = 1.86 and $Sb-O_e$ = 1.85 and are not statistically different from those associated with molybdenum: that is, the Sb−O bonds lengths are within one standard deviation of those of the respective Mo−O bond lengths. In the past in mono-substituted Keggin compounds, such anisotropy has been observed only in two cases. In the first example, it was observed for the $[GaPbW_{11}O_{39}]^{7-}$ compound.[46] This Keggin species has a significantly distorted structure because of the much larger size of the Pb^{2+} cation[45] (W^{VI} = 0.58 Å vs. Pb^{II} = 1.18 Å), which might explain the anisotropic crystals formed. In the second instance, alignment is attained by formation of chains in manganese- and cobalt-substituted phosphotungstates. Bonds are formed due to displacement of the labile aquo ligand of the transition metal leading to chainlike polymeric structures with molecular units bridging oxo moieties, WO_t-M.[47−48] To reiterate, in this case the structure is not distorted, nor is there indication of intermolecular bonding.

Several additional lines of evidence support the substitution of Sb^{III} into the lacunary position of the polyoxomolybdate. First, the IR spectrum of $[PSb^{III}(H_2O)Mo_{11}O_{39}]^{4-}$ (Figure 2b) is similar to that of $[PMo_{12}O_{40}]^{3-}$ and significantly different from the spectrum of the lacunary species

Table 1. Crystallographic data for $[Q_4PSb^{III}(H_2O)Mo_{11}O_{39}]$

Space group	*Cc* (No. 9)
a, Å	45.6230 (7)
b, Å	14.1800 (2)
c, Å	26.4390 (4)
β, deg	95.8933 (8)
V, Å^3	17013.9 (4)
Z	4
$\rho_{calcd.}$, g cm^{-3}	1.821
μ(Mo-K_α), mm^{-1}	1.965
No. of unique reflections	10857
No. of reflections [$I \geq 2\sigma(I)$]	10443
R [$I \geq 2\sigma(I)$]	0.065
R (all data)	0.067

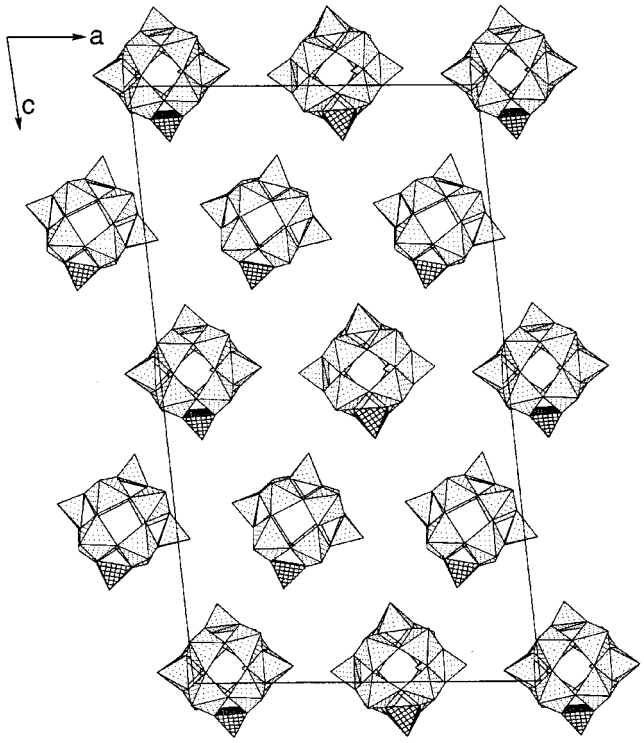

Figure 1. Structure of the inorganic sub-lattice in the *ac* plane; the Sb-containing polyhedra are hashed and the Mo-containing polyhedra are dotted

(Figure 2a). The four peak spectrum of the complete polyoxometalate is typical for Keggin structures of T_d symmetry. Second, the ^{31}P NMR spectrum of $[Q_4PSb^{III}(H_2O)Mo_{11}O_{39}]$ has a single peak at δ = −1.20, whereas the peak for the lacunary $[Q_4H_3PMo_{11}O_{39}]$ is at δ = −4.82. The cyclic voltammogram of $[PSb^{III}(H_2O)Mo_{11}O_{39}]^{4-}$ {0.5 mM $[Q_4PSb^{III}(H_2O)Mo_{11}O_{39}]$, 1 M QBF_4 in CH_3CN} shows a well-defined one- or two-electron Mo (VI → V) process that is very similar to that of $[PMo_{12}O_{40}]^{3-}$. No oxidation of antimony(III) to antimony(V) or reduction of antimony(V) to antimony(III) in the polyoxomolybdate was observed in the cyclic voltammograms in the interval +1.1 to −0.3 V.

We have formulated the Sb^{III}-substituted species as $[PSb^{III}(H_2O)Mo_{11}O_{39}]^{4-}$ indicating localization of the valence electrons on the antimony atom. This formulation is worthy of further comment. Thus, it is important to stress that upon addition of $Sb(OAc)_3$ to the lacunary substrate

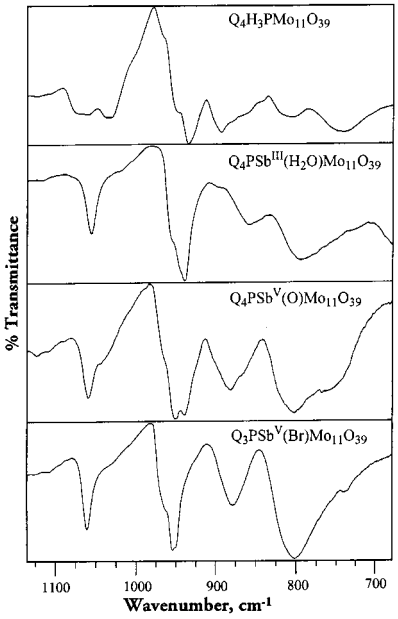

Figure 2. IR spectra of the various phosphoantimonatomolybdates

the solution became deep green, indicating reduction of the polyoxomolybdate and electron transfer (delocalization) from Sb^{III} (5s electrons) to Mo^{VI} (4d). In the UV/Vis spectrum of $[Q_4PSb^{III}(H_2O)Mo_{11}O_{39}]$ in acetonitrile the typical absorbance at ≈750 nm is observed. Importantly, however, the molar extinction coefficient ($\varepsilon = 0.17\ mM^{-1}cm^{-1}$) is one order of magnitude less than a one-electron-reduced $[PMo_{12}O_{40}]^{4-}$ ion prepared by addition of one equivalent of hydrazine to $[PMo_{12}O_{40}]^{3-}$. The intensity of the peak at ≈750 nm is a well-known measure of the degree of reduction of polyoxometalates.[49] Second, the ESR spectrum of $[Q_4PSb^{III}(H_2O)Mo_{11}O_{39}]$ in CH_3CN at 25 °C showed only a weak isotropic signal at the expected field,[50] $g = 1.937$, $A = 75$ G, which had about ≈5−10% of the intensity of $[PMo_{12}O_{40}]^{4-}$. Finally, the magnetic susceptibility was measured and found to be approximately 0.45 μ_B. A value of ≈1.8 μ_B for a d^1 state is to be expected. Our interpretation of the UV/Vis, ESR and magnetic susceptibility spectroscopic data is that upon addition of $Sb(OAc)_3$ to the lacunary species there is no electron transfer from Sb^{III} to Mo^{VI} with formation of Sb^{IV} or Sb^{V} and one or more Mo^{V} centers; rather, there is only partial electron delocalization with some formation of Mo^{V}.[51] Complete transfer of one electron and localization of an electron at a molybdenum center, i.e. formation (formally) of $[PSb^{IV}Mo^{V}Mo^{VI}_{10}O_{39}]^{4-}$, should have yielded both more intense UV/Vis and ESR spectra, and a magnetic susceptibility for a d^1 state of ≈1.8 μ_B. Since Sb^{IV} is an uncommon oxidation state, a transfer of two electrons could be contemplated to form $[PSb^{V}Mo^{V}_2Mo^{VI}_9O_{39}]^{4-}$; this, however, should have yielded a yet more intense absorbance at 750 nm and no or a weak ESR signal due to antiferromagnetic coupling.

Oxidation of $[Q_4PSb^{III}(H_2O)Mo_{11}O_{39}]$

The Sb^{III}-substituted polyoxomolybdate can conveniently be oxidized to a Sb^{V} analog by either molecular bromine or ozone. Addition of one equivalent of Br_2 to $[Q_4PSb^{III}(H_2O)Mo_{11}O_{39}]$ immediately forms a yellow compound. Similarly, bubbling ozone though a CH_3CN solution of $[Q_4PSb^{III}(H_2O)Mo_{11}O_{39}]$ for five minutes also yielded a yellow solution with a slight greenish tint. Both treatments gave ESR-silent compounds and appeared to be diamagnetic from the magnetic susceptibility measurements, suggesting that all the Sb^{III} atoms were oxidized to Sb^{V}. The IR spectra of the products resulting from the two treatments were somewhat different. The oxidation with bromine gave a compound whose IR spectrum (Figure 2d) was essentially unchanged from that of the original Sb^{III} compound(Figure 2b). On the other hand, treatment with ozone gave a product whose IR spectrum was slightly different (Figure 2c). Most notable is the split peak at 951 and 939 cm^{-1}. The ^{31}P NMR spectra of the two compounds are also different: treatment with Br_2 gave a compound with a peak at $\delta = -5.00$, whereas with ozone a peak at $\delta = -5.25$ was obtained. As will be discussed below, the resulting Sb^{V}-containing compounds can also be differentiated based on their activity in the stoichiometric oxidation of alcohols (Table 2). Based on the IR spectra and elementary analysis, we assume that oxidation by bromine yielded $[Q_3PSb^{V}(Br)Mo_{11}O_{39}]$while with ozone $[Q_4PSb^{V}(O)Mo_{11}O_{39}]$was obtained according to the reaction pathways in Equation (2) and Equation (3).

$$Q_4PSb^{III}Mo_{11}O_{39} + Br_2 \longrightarrow Q_3PSb^{V}(Br)Mo_{11}O_{33} + QBr$$

$$Q_4PSb^{III}Mo_{11}O_{39} + O_3 \longrightarrow Q_4PSb^{V}(O)Mo_{11}O_{39} + O_2$$

The appearance of an additional peak in the IR spectra of $[Q_4PSb^{V}(O)Mo_{11}O_{39}]$ at 939 cm^{-1} is most likely explained by the Sb = O_t vibration — a Sb−Br absorption would be expected at lower out-of-range energies (<400 cm^{-1}).

Anaerobic and Catalytic Aerobic Oxidation of Alcohols by Sb-POM

In Table 2 we have summarized the results for the anaerobic oxidation (under argon) of various alcohols by phosphoantimonato(V)molybdates in benzonitrile at 135 °C: primary alcohols are oxidized selectively to aldehydes and secondary alcohols to the corresponding ketones. From these results it is easy to determine that $[Q_4PSb^{V}(O)Mo_{11}O_{39}]$ is a more active oxidant than $[Q_3PSb^{V}(Br)Mo_{11}O_{39}]$. The order of activity is benzylic > allylic ≈ cycloaliphatic > secondary aliphatic > primary aliphatic alcohols. These results indicate that the C−H bond strength determines the reactivity of the alcohol. During the reaction the yellow color of $[Q_4PSb^{V}(O)Mo_{11}O_{39}]$ and $[Q_3PSb^{V}(Br)Mo_{11}O_{39}]$ was changed to the deep-green color of a reduced polyoxometalate. The reaction stoichiometry and the extinction coefficient measured at 750 nm indicate that a two-electron-reduced polyoxometalate was formed.

Aerobic catalytic oxidation of alcohols and other substrates by $[Q_4PSb^{V}(O)Mo_{11}O_{39}]$ as catalyst was also invest-

Table 2. Anaerobic oxidation of alcohols by phosphoantimonato(V) molybdates

Substrate	Product	Yield of polyoxometalate[a] $[Sb(O)PMo_{11}O_{39}]^{4-}$	$[SbBrPMo_{11}O_{39}]^{3-}$
Benzyl alcohol	benzaldehyde	100 (100)[b]	100 (80)[b]
1-Phenylethanol	acetophenone	100	100
Cinnamyl alcohol	cinnamaldehyde	100	100
1-Hexanol	1-hexanal	70	0
2-Hexanol	2-hexanone	98	50
Cyclohexanol	cyclohexanonone	100 (38)[b]	85 (0)[b]
cis-2-Hexanol	*cis*-2-hexanal	100	45
trans-2-Hexanol	*trans*-2-hexanal	100	40
cis-3-Hexanol	*cis*-3-hexanal	80	15

[a] Reaction conditions: alcohol (40 mM) and polyoxometalate (5 mM) were treated with 1 mL of PhCN at 135 °C under Ar for 20 h. – [b] In acetonitrile at 80 °C.

Table 3. Aerobic oxidation catalyzed by $[Q_4PSb^{V}(O)Mo_{11}O_{39}]$

Substrate	Product	Conversion, mol-%[a]
Benzyl alcohol	benzaldehyde	76 (5)[b]
1-Phenylethanol	acetophenone	80 (9)[c]
Cinnamyl alcohol	cinnamaldehyde	100
4-Methoxybenzyl alcohol	4-methoxybenzaldehyde	62
4-Methylbenzyl alcohol	4-methylbenzaldehyde	78
4-Nitrobenzyl alcohol	4-nitrobenzaldehyde	100 (62)[d]
Benzylamine	$PhCH_2N{=}CHPh$	40
Dihydroanthracene	anthracene	7 (62)[c]

[a] Reaction conditions: substrate (100 mM) and $[Q_4PSb^{V}(O)Mo_{11}O_{39}]$ (1 mM) were reacted in 1 mL of PhCN at 135 °C under 2 atm. O_2 for 20 h. – [b] Catalyst: $Q_4PSb^{III}(H_2O)Mo_{11}O_{39}$. – [c] Catalyst: $Q_5PV_2Mo_{10}O_{40}$. – [d] 4-Nitrobenzyl alcohol, 300 mM.

igated (Table 3) in pressure tubes at 135 °C under two atmospheres of oxygen with PhCN as solvent. Of the alcohols tested only benzylic alcohols were oxidized in appreciable yields. Cyclohexanol, 2-hexanol, and *cis*-2-hexenol all gave less than 5 mol-% conversion in this catalytic system with $[Q_4Sb(O)PMo_{11}O_{39}]$ as catalyst. Interestingly, the electron-donating methoxy substituent reduced the yield whereas the electron-withdrawing nitro substituent increased the yield significantly (up to 186 turnovers were measured). It is notable that benzoic acids as overoxidation products were not detected under the reaction conditions. Benzylamine was also oxidatively dehydrogenated to the corresponding Schiff base imine, $PhCH{=}NCH_2Ph$, in a reaction that has been observed in the past for $[PV_2Mo_{10}O_{40}]^{5-}$. In fact, the use of the better known oxidation catalyst $[Q_5PV_2Mo_{10}O_{40}]$ gave an activity about one order of magnitude less than for the oxidation of benzylic alcohols. On the other hand, in the oxydehydrogenation of dihydroanthracene to anthracene, $[Q_4PSb^{V}(O)Mo_{11}O_{39}]$ was significantly less active than $[Q_5PV_2Mo_{10}O_{40}]$ (7 mol-% conversion vs. 65 mol-%). Also interesting is to note that the antimony(III) compound $[Q_4PSb^{III}(H_2O)Mo_{11}O_{39}]$ showed little catalytic activity. Finally, in a competitive oxidation of benzyl alcohol and [D_7]benzyl alcohol a kinetic isotope effect of 2.8 ± 0.1 was measured. It would be premature and presumptuous to present a mechanistic pathway for oxydehydrogenation catalyzed by $[Q_4PSb^{V}(O)Mo_{11}O_{39}]$. However, the low kinetic isotope effect, the higher activity of 4-nitrobenzyl alcohol vs. 4-methoxybenzyl alcohol and the relative inactivity compared to $[Q_5PV_2Mo_{10}O_{40}]$ for dihydroanthracene oxidation, where mechanistic research has indicated an electron-transfer-initiated process,[33–34] all indicate that for $[Q_4PSb^{V}(O)Mo_{11}O_{39}]$ a different mechanism is to be expected.

Experimental Section

Synthesis of $Q_4PSb^{III}(H_2O)Mo_{11}O_{39}$: $[Q_4H_3PMo_{11}O_{39}]$ (Q^+ = tetra-*n*-butylammonium cation) was prepared by the literature procedure,[43] and its purity ≈99% was determined by ^{31}P NMR, infrared and UV/Visible spectroscopic analysis. $[Q_4PSb^{III}(H_2O)Mo_{11}O_{39}]$ was synthesized as follows: antimony(III) acetate (0.116 g, 0.39 mmol, 1.5 equiv.) was added to a solution of $Q_4H_3PMo_{11}O_{39}$ (0.7 g, 0.26 mmol) in acetonitrile (30 mL). The color slowly changed from yellow-green to deep-green. After 2 hours of stirring the reaction mixture was filtered. The solution was placed in a crystallizing dish and allowed to evaporate slowly at room temperature. The crude, deep green crystalline product was separated by filtration and recrystallized from acetonitrile to give green crystals of $[Q_4PSb^{III}(H_2O)Mo_{11}O_{39}]$ (0.6 g, 84%). $C_{64}H_{146}Mo_{11}N_6O_{40}PSb$ (2819.91): calcd. C 27.26, H 5.15, N 1.99; found C 27.45, H 5.36, N 1.72. ICP-MS ratio P:Sb:Mo = 1:1:11. The UV/Vis spectrum was measured on an HP 8452 diode array instrument. – λ_{max} (CH_3CN) = 218 nm (ε = 830 mM^{-1} cm^{-1}), 316 (ε = 18), 750 (ε = 0.17). The ^{31}P NMR was measured on a Bruker DPX 250 spectrometer at 101.254 MHz with H_3PO_4 as external standard, a single peak at δ = −1.20 was observed. The IR spectrum was measured on a Nicolet Protégé 460 with a sample deposited on a KBr disk by evaporation of an CH_3CN solution. Peaks at $\tilde{\nu}$ = 1061, 955, 862, 802 cm^{-1} were observed. Cyclic voltammetry was measured on a BAS −1 instrument fitted with a glass carbon working electrode. A 0.5 mM solution of $[Q_4PSb^{III}(H_2O)Mo_{11}O_{39}]$ in acetonitrile with 1 M QBF_4 was used for the measurements. $E_{1/2}$ = −0.14, +0.2 and an irreversible anodic wave at +0.9 V vs. SCE (similar to $Q_3PMo_{12}O_{40}$). The ESR spectra were

measured at room temperature on a Bruker ER-200 spectrometer with DPPH as reference. The spectrum of 1 mM $[Q_4PSb^{III}(H_2O)Mo_{11}O_{39}]$ in CH_3CN at 25 °C showed a weak isotropic signal at $g = 1.937$, width 75 G. The average magnetic susceptibility was measured on a Sherwood Scientific Magnetic Susceptibility Balance as a neat powder at 22 °C. Pascal's constants were used to obtain the final diamagnetic correction. To avoid errors in our estimates of the diamagnetic correction the susceptibility of the lacunary $[Q_4H_3PMo_{11}O_{39}]$ was measured as reference. The difference between the magnetic susceptibility of $[Q_4H_3PMo_{11}O_{39}]$ and $[Q_4H_3PMo_{11}O_{39}]$ allowed us to calculate the effective magnetic moment of the delocalized blue electron[52] which was 0.45 μ_B. Slow concentration of the acetonitrile solution gave emerald-green prisms which were used for the single-crystal X-ray diffraction investigation.

Crystal Structure Determination of $[Q_4PSb^{III}(H_2O)Mo_{11}O_{39}]$: Data were collected on dark-green prisms 0.2 × 0.2 × 0.1 mm using a Nonius−Kappa CCD diffractometer with Mo-K_α ($\lambda = 0.71073$ Å) radiation. 43215 reflections and 10857 independent reflections were collected with $-40 \le h \le 39$, $0 \le k \le 12$, $-23 \le l \le 24$, frame scan width of 1.0°, scan speed 1° per 20 sec and a typical mosaicity of 0.5°. Data were processed with Denzo−Scalepack.[53] The crystallographic data are presented in Table 1. The structure was solved by Patterson methods with SHELXS-97. Full-matrix least-squares refinement was based on F^2 with SHELX-97. Refinement proceeded to convergence by minimizing $\Sigma||F_o| - |F_c||/\Sigma|F_o|$. 1229 parameters with 580 restraints yielded a final $R = 0.0651$ for data with $I > 2\sigma(I)$ and $R = 0.0673$ for all 10857 reflections. A final difference-Fourier synthesis map showed several peaks less than 2.008 e/Å^3 scattered about the unit cell without significant features. The goodness-of-fit on F^2 was 1.062. As is common for these polyoxometalate structures the counter cations were mostly disordered and therefore also incomplete but are equally distributed throughout the cell.

Crystallographic data (excluding structure factors) for the structure reported in this paper have been deposited with the Cambridge Crystallographic Data Centre as supplementary publication no. CCDC-149090. Copies of the data can be obtained free of charge on application to CCDC, 12 Union Road, Cambridge CB2 1EZ [Fax: (internat.) +44-1223/336-033; E-mail: deposit@ccdc.cam.ac.uk].

Oxidation of $[Q_4PSb^{III}(H_2O)Mo_{11}O_{39}]$: A solution of $[Q_4PSb^{V}(O)Mo_{11}O_{39}]$ was prepared by bubbling an oxygen stream (250 mL/min) containing 9 μg/mL of ozone through a 1.6 mM solution of $[Q_4PSb^{III}(H_2O)Mo_{11}O_{39}]$ in acetonitrile. After 5 min the color changed from green to yellow. UV (CH_3CN): $\lambda_{max} = 218$ nm, 302 (sh). − ^{31}P NMR: $\delta = -5.25$. − IR: $\tilde{\nu} = 1059$, 951, 939, 881 and 804 cm^{-1}. A solution of $[Q_3PSb^{V}(Br)Mo_{11}O_{39}]$ was prepared by addition of one equivalent Br_2 as a 0.4 mM solution of Br_2 in acetonitrile to a 1.6 mM solution of $[Q_4PSb^{III}(H_2O)Mo_{11}O_{39}]$ in acetonitrile. The color immediately changed from green to yellow. UV: $\lambda_{max} = 270$ nm. − ^{31}P NMR: $\delta = -5.00$. − IR: $\tilde{\nu} = 1061$, 954, 879 and 802 cm^{-1}.

Oxidation Reactions with Phosphoantimonato(V) Molybdates: Typically, oxidation reactions were carried out in 13 mL glass pressure tubes by loading the vial with the appropriate amounts of substrate, polyoxometalate and solvent. The tube was purged and loaded with the desired gas (argon or oxygen) by using three freeze, pump and thaw cycles. The reaction tube was placed in a thermostated oil bath and the mixture stirred magnetically. Aliquots were removed at the appropriate time intervals for analysis by gas chromatography. Oxidation reaction products were characterized using reference compounds, when available, by use of GLC (HP-6890 gas chromatograph) with a flame ionization detector and a 15 m × 0.32 mm 5% phenylmethylsilicone (0.25 μm coating) capillary column and helium carrier gas. Products whose initial identity was questionable were unambiguously identified using a gas chromatograph equipped with a mass-selective detector (GC-MS HP 5973) equipped with the same column.

[1] N. Mizuno, M. Misono, *J. Mol. Catal.* **1994**, *86*, 319−342.
[2] T. Okuhara, N. Mizuno, M. Misono, *Adv. Catal.* **1996**, *41*, 113−252.
[3] C. L. Hill, D. C. Duncan, M. K. Harrup, *Comments Inorg. Chem.* **1993**, *14*, 367−384.
[4] C. L. Hill, C. M. Prosser-McCartha, *Coord. Chem. Rev* **1995**, *143*, 407−455.
[5] R. Neumann, *Prog. Inorg. Chem.* **1998**, *47*, 317−370.
[6] I. V. Kozhevnikov, *Chem. Rev.* **1998**, *98*, 171−198.
[7] C. L. Hill, R. B. Brown, *J. Am. Chem. Soc.* **1986**, *108*, 536−538.
[8] D. Mansuy, J.-F. Bartoli, P. Battioni, D. K. Lyon, R. G. Finke, *J. Am. Chem. Soc.* **1991**, *113*, 7222−7226.
[9] H. Weiner, Y. Hayashi, R. G. Finke, *Inorg. Chem.* **1999**, *38*, 2579−2591.
[10] M. Faraj, C. L. Hill, *J. Chem. Soc., Chem. Commun.* **1987**, 1487−1488.
[11] R. Neumann, A. M. Khenkin, *Inorg. Chem.* **1995**, *34*, 5753−5760.
[12] A. M. Khenkin, C. L. Hill, *Mendeleev Commun.* **1993**, 140−141.
[13] R. Neumann, M. Gara, *J. Am. Chem. Soc.* **1994**, *116*, 5509−5510.
[14] R. Neumann, M. Gara, *J. Am. Chem. Soc.* **1995**, *117*, 5066−5074.
[15] R. Neumann, A. M. Khenkin, *J. Mol. Catal.* **1996**, *114*, 169−180.
[16] R. Neumann, D. Juwiler, *Tetrahedron* **1996**, *47*, 8781−8788.
[17] R. Neumann, A. M. Khenkin, D. Juwiler, H. Miller, M. Gara, *J. Mol. Catal.* **1997**, *117*, 169−183.
[18] N. Mizuno, C. Nozaki, I. Kiyoto, M. Misono, *J. Am. Chem. Soc.* **1998**, *120*, 9267−9272.
[19] R. Neumann, C. Abu-Gnim, *J. Chem. Soc., Chem. Commun.* **1989**, 1324−1326.
[20] R. Neumann, C. Abu-Gnim, *J. Am. Chem. Soc.* **1990**, *112*, 6025−6031.
[21] M. Bressan, A. Morvillo, G. Romanello, *J. Mol. Catal.* **1992**, *77*, 283−288.
[22] X. Zhang, K. Sasaki, C. L. Hill, *J. Am. Chem. Soc.* **1996**, *118*, 4809−4816.
[23] R. Neumann, A. M. Khenkin, M. Dahan, *Angew. Chem.* **1995**, *107*, 1740−1742; *Angew. Chem. Int. Ed. Engl.* **1995**, *34*, 1587−1589.
[24] R. Neumann, M. Dahan, *Nature* **1997**, *388*, 353−355.
[25] R. Neumann, M. Dahan, *J. Am. Chem. Soc.* **1998**, *120*, 11969−11976.
[26] H. Weiner, R. G. Finke, *J. Am. Chem. Soc.* **1999**, *121*, 9831−9842.
[27] K. I. Matveev, *Kinet. Catal.* **1977**, *18*, 716−730.
[28] J. R. Grate, D. R. Mamm, S. Mohajan, *Mol. Eng.* **1993**, *3*, 205−229.
[29] R. Neumann, M. Lissel, *J. Org. Chem.* **1989**, *54*, 4607−4610.
[30] R. Neumann, M. Levin, *J. Org. Chem.* **1991**, *56*, 5707−5710.
[31] O. A. Kholdeeva, A. V. Golovin, R. A. Maksimovskaya, I. V. Kozhevnikov, *J. Mol. Catal.* **1992**, *75*, 235−244.
[32] M. Lissel, H. Jansen van de Wal, R. Neumann, *Tetrahedron Lett.* **1992**, *33*, 1795−1798.
[33] R. Neumann, M. Levin, *J. Am. Chem. Soc.* **1992**, *114*, 7278−7286.
[34] A. M. Khenkin, R. Neumann, *Angew. Chem.* **2000**, *112*, 4088−4090; *Angew. Chem. Int. Ed.* **2000**, *39*, 4254−4256.
[35] J. Fisher, L. Ricard, R. Weiss, *J. Am. Chem. Soc.* **1976**, *98*, 3050−3052.

[36] T. Yamase, H. Naruke, Y. Sasaki, *J. Chem. Soc., Dalton Trans.* **1990**, 1687−1696.
[37] Y. Ozawa, Y. Sasaki, *Chem. Lett.* **1987**, 923−926.
[38] M. Bösing, I. Loose, H. Pohlmann, B. Krebs, *Chem. Eur. J.* **1997**, *3*, 1232−1237.
[39] I. Loose, E. Droste, M. Bösing, H. Pohlmann, M.H. Dickman, C. Rosu, M. T. Pope, B. Krebs, *Inorg. Chem.* **1999**, *38*, 2688−2694.
[40] F. Cavani, M. Koutyrev, F. Trifiro, *Catal. Today* **1996**, *28*, 319−333.
[41] F. Cavani, M. Koutyrev, F. Trifiro, *Catal. Today* **1995**, *24*, 365−368.
[42] S. Albonetti, F. Cavani, M. Koutyrev, F. Trifiro, *Catal. Lett.* **1995**, *30*, 253−262.
[43] L. A. Combs-Walker, C. L. Hill, *Inorg. Chem.* **1991**, *30*, 4016−4026.
[44] H. T. Evans, Jr., *Perspect. Struct. Chem.* **1971**, *4*, 1−59.
[45] R. D. Shannon, C. T. Prewitt, *Acta Cryst.* **1969**, *B25*, 925−929.
[46] G. F. Tourné, C. M. Tourné, A. Schouten, *Acta Cryst.* **1982**, *B38*, 1414−1418.
[47] J. R. Galán-Mascarós, C. Giménez-Saiz, S. Triki, C. J. Gómez-Garcia, E. Coronado, L. Ouahab, *Angew. Chem. Int. Ed. Engl.* **1995**, *34*, 1460−1462; *Angew. Chem.* **1995**, *107*, 1601−1603.
[48] H. T. Evans, Jr., T. J. R. Weakley, G. B. Jameson, *J. Chem. Soc., Dalton Trans.* **1996**, 2537−2540.
[49] J. N. Barrows, M. T. Pope, *Adv. Chem.* **1990**, *226*, 403−414.
[50] T. Yamase, M. Suga, *J. Chem. Soc., Dalton Trans.* **1989**, 661−669.
[51] C. Sanchez, J. Livage, J. P. Launay, M. Fournier, Y. Jeannin, *J. Am. Chem. Soc.* **1992**, *104*, 3194−3202.
[52] N. Casan-Pastor, L. C. W. Baker, *J. Am. Chem. Soc.* **1992**, *114*, 10384−10394.
[53] Z. Otwinowski, W. Minor, *Method Enzymol.* **1997**, *276*, 307−326.

Received September 8, 2000
[I00339]

Photochemically Induced Silicon−Carbon Bond Cleavage in a Dimethylsilyl-Bridged Dicyclopentadienyl Diruthenium Complex

Thomas Fox[a] and Peter Burger*[a]

Keywords: Cyclopentadienes / Ruthenium / IR spectroscopy / Photochemistry / Rearrangements / Thermodynamics / Density functional calculations

The synthesis and X-ray crystal structure of the novel permethylated dimethylsilyl-bridged diruthenium complex $Me_2Si[(C_5Me_4)Ru(CO)_2]_2$ **(1)** is reported. The molecular structure displays a metal–metal bond of 2.7121(4) Å, which is supported by two symmetrical μ-bridging CO groups and, in addition, two terminal carbonyl ligands. In solution, exchange of these carbonyl groups is observed, as shown by ^{13}C NMR EXSY and VT IR-measurements. It is suggested that the exchange process proceeds via the energetically disfavoured intermediate **1a**, which displays four terminal CO ligands. This view is supported by density functional calculations, which indicate a C_2-symmetrical structure for **1a**. Photochemically induced cleavage of the silicon–carbon and Ru–Ru bonds in **1** results in complex **3**, which is thermodynamically uphill from **1** according to our DFT calculations. The molecular structure of complex **3** was unambiguously confirmed by X-ray crystallography.

Introduction

Thermal or photochemical skeletal rearrangements of dicyclopentadienyl ligands in dinuclear complexes with bridging cyclopentadienyl groups have recently received significant attention.[1−5] Perhaps the most exciting result in this area is the fulvalenediyl diruthenium system recently reported by Vollhardt and co-workers.[5] These complexes undergo photochemically induced C−C bond cleavage to give *energetically less-stable* products. Since this process can be thermally reversed, it has been anticipated that these systems might be potential light energy storage systems. As part of our research into oxidation catalysis, we have considered dicyclopentadienyl-bridged ditungsten complexes with metal−metal multiple bonds.[6] Recently, we have extended our research program to include the group 8 transition metals ruthenium and osmium. In the course of these studies, we observed facile, and quantitative, photochemically induced Si−C bond cleavage in the dimethylsilyl-bridged permethylated complex $Me_2Si[(C_5Me_4)Ru(CO)_2]_2$ (**1**). While this work was in progress, Bitterwolf et al. reported similar results in the parent complex $Me_2Si[(C_5H_4)Ru(CO)_2]_2$ (**2**),[7] which was shortly followed by an alternative synthesis for **2** and a short discussion on fluxionality in the parent compound by Zhou and coworkers.[8] In this paper, we will focus on kinetic and thermodynamic aspects of the fluxional processes in the metal−metal bonded complex **1** and its photochemical Si−C bond cleavage product **3**.'

Results and Discussion

In analogy to the parent complex **2** and the methano-bridged congener $CH_2[(C_5Me_4)Ru(CO)_2]_2$ (**4**), the dinuclear complex **1** was obtained from the treatment of the permethylated dimethylsilyl-bridged ligand with 0.66 equiv. $Ru_3(CO)_{12}$ in refluxing octane [Equation (1)].[8,9]

When the reaction according to Equation (1) was carried out under rigorously oxygen-free conditions, the ^1H NMR spectrum of the crude reaction mixture displayed, along with the signals of the major product **1**, additional peaks for a C_{2v} symmetrical minor product. The most prominent resonance of the minor product was a singlet at $\delta = -10.0$ in [D$_6$]benzene, indicative of a ruthenium hydride complex. In analogy with the hydride resonance in the unbridged pentamethyl cyclopentadienyl (Cp*) compound Cp*Ru(CO)$_2$H, which displays a singlet for the Ru hydride at $\delta = -10$,[10] we tentatively assigned these resonances to the presumed initial dihydride product $SiMe_2[(C_5Me_4)Ru(CO)_2H]_2$ (**5**). Complex **5** could then convert into the final product **1** with concomitant H_2 loss. Attempts to isolate the presumed dihydride complex **5**, either exclusively or as a major product, failed. We therefore carried out the reaction with few measures to exclude O_2 (see Experimental Section for details).[11]

Initial attempts to isolate the dinuclear product **1** from the reaction mixture by chromatography proved to be cumbersome, since, on alumina (Al_2O_3, neutral, act II−III), partial decomposition to give $[(C_5Me_4H)Ru(CO)_2]_2$ (**6**), by reaction of **1** with the alumina support, was observed. The identification of complex **6** was facilitated through its diagnostic ^1H NMR resonance of the unique Cp ring proton ($C_5Me_4\mathit{H}$), observed as singlet at $\delta = 4.46$ in [D$_6$]benzene. Formation of compound **6** from **1** during this workup procedure was later confirmed when pure complex **1** was subjected to column chromatography on alumina. The isolation of **1** was, however, accomplished by sublimation at 190 °C in high vacuum, after which compound **1** was obtained as an analytically pure, orange, air-stable solid in ca. 50% yield.

[a] Anorganisch-Chemisches Institut der Universität Zürich, Winterthurerstrasse 190, 8057 Zürich, Switzerland
E-mail: chburger@aci.unizh.ch

 © WILEY-VCH Verlag GmbH, 69451 Weinheim, 2001 1434−1948/01/0303−0795 $ 17.50+.50/0

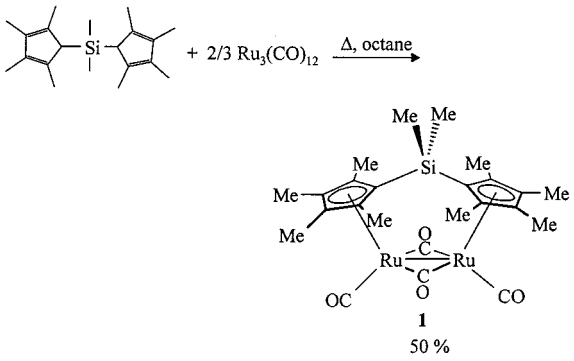

It should be noted at this point that in the X-ray crystal structure of the related parent complex $Me_2Si[(C_5H_4)Ru(CO)_2]_2$ (**2**), two bridging and two terminal CO groups were observed.[8] Differences in the solution and the IR spectra of **2** in KBr, however, suggested an equilibrium between the structure found in the solid state and another isomer, with four terminal CO groups, in solution. These results contrasted with the findings for the related methano-bridged diruthenium complex $CH_2[(C_5H_4)Ru(CO)_2]_2$ (**4**), for which four terminal CO groups were observed in the X-ray crystal structure, with just minor amounts of the corresponding bridged carbonyl complex $CH_2[(C_5H_4)Ru(\mu\text{-}CO)(CO)]_2$ in solution.[9]

The latter findings for the parent complex **2**, together with investigations by Angelici et al. into analogous CH_2- and C_2H_4-bridged complexes,[12] as well as a number of experimental and theoretical studies dedicated to the structural isomerism of CO ligands in the unbridged ruthenium and iron complexes $[CpFe,Ru(CO)_2]_2$, prompted us to look in detail at the solution structure of complex **1** and, in particular, consider the fluxional processes shown in Equation (2).[13–16] Before we address the solution behaviour of **1**, we will discuss the solid-state structure of compound **1** as observed in the single-crystal X-ray structure.

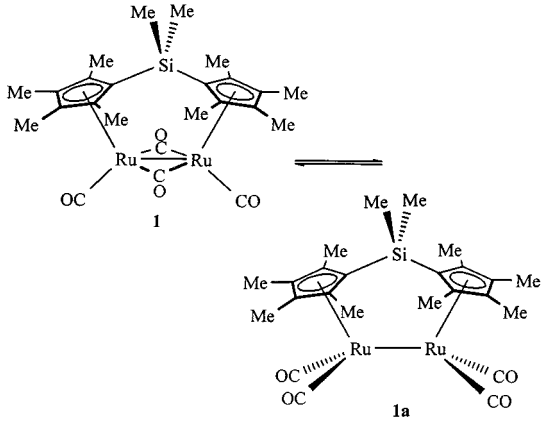

X-ray Crystal Structure of 1

The molecular structure of **1**, presented in Figure 1, illustrates that there are two types of carbonyl groups: i.e., two bridging and two terminal carbon monoxide ligands. This parallels findings from the X-ray crystal structure of the parent complex **2**. Details of data collection are summarized in Table 4; selected distances and angles are given in Table 1.

The molecule is located on a crystallographic C_2 axis passing through the Si atom and the midpoint of the Ru–Ru vector. A Ru–Ru single bond is indicated by a metal–metal distance of 2.7121(4) Å, with two symmetrical μ-bridging carbonyl groups [Ru1–C10 2.031(3), Ru1–C10A 2.032(3) Å] supporting the metal–metal bond. The metal–metal bond length is thus in the usual range observed for other cyclopentadienyl-bridged ruthenium complexes with μ-bridging carbonyl groups.[4,7,8,12] The remaining terminal CO groups [Ru1–C11 1.869(3) Å] are contained within the plane of the Ru metal centres and the centroids of the cyclopentadienyl rings. The ruthenium centres and the bridging carbonyl groups form a puckered four-membered ring, with a pucker angle of ca. 29°. A similar observation has been made for the ethano-bridged complex $C_2H_4[(C_5H_4)Ru(\mu\text{-}CO)(CO)]_2$ by Angelici et al.,[12] and has been rationalized on electronic grounds in a study by Hoffmann and co-workers.[16] From the top view of the molecular structure of complex **1** presented in Figure 1, it becomes immediately apparent that the molecular symmetry is close to idealized C_{2v} symmetry.

IR Data

In the IR spectrum of **1** in CH_2Cl_2 at room temperature, three absorptions in the ν(CO) range were detected: at 1980 (vs, terminal), 1940 (w, terminal), and 1757 (s, bridging) cm^{-1}. The band at 1757 cm^{-1} clearly demonstrates the presence of a μ-bridging carbonyl ligand consistent with the molecular structure of complex **1** observed in the solid state. Since we could detect just *two* terminal CO stretches in the terminal IR range, as would have been predicted for the μ-CO bridged complex **1**, there was initially no evidence for an additional isomer, such as the unbridged complex **1a**.

However, in the less polar solvent pentane, an additional *third* band could be observed in the terminal CO range [1992(vs), 1966(w), 1942(w)] in the IR spectrum. The presence of this additional vibration provided strong evidence for the presence of a further species, which was tentatively assigned as the isomer **1a**. In order to obtain further evidence for an exchange equilibrium between the bridging and presumed nonbridging complexes **1** and **1a**, we attempted variable temperature (VT) FT-IR measurements on **1** in pentane. Due to the quite low solubility of **1** in this solvent, however, these experiments proved to be difficult. While changes in the relative intensities of the absorptions consistent with a change in equilibrium concentrations were observed, no quantitative interpretation of the data was possible. We have therefore turned to VT NMR spectroscopic measurements on complex **1**; these are described in the following sections.

NMR Spectroscopic Analysis

The ^1H NMR spectrum of **1** in CD_2Cl_2 solution is temperature-*independent* (−95 °C to 35 °C) and displays three

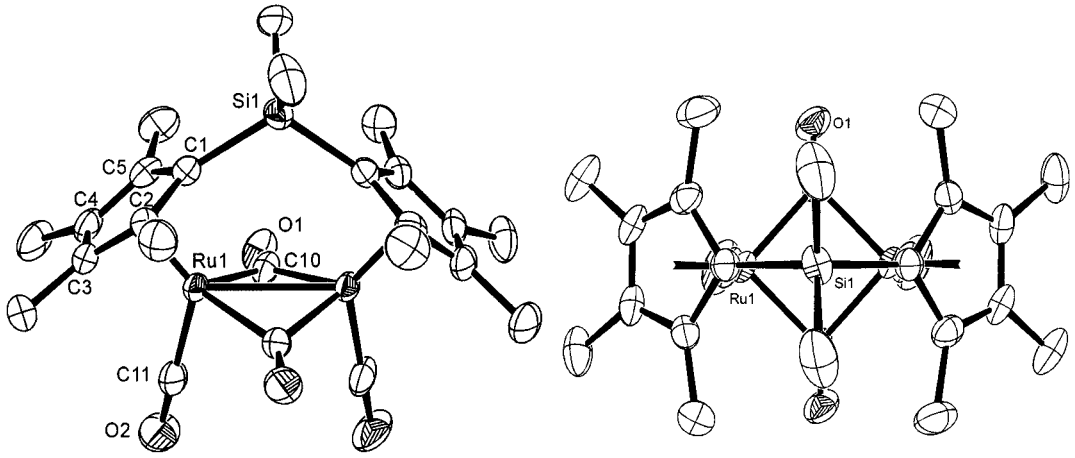

Figure 1. Ortep plots [side (left) and top (right)] of complex **1**; thermal ellipsoids are shown at the 50% probability level

Table 1. Selected distances [Å] and angles [°] with ESDs for complex **1**; Z1 is the midpoint of carbon atoms C1 to C5; "A" indicates symmetrically equivalent positions

Ru1−Ru1A	2.7121(4)	Ru1−C1	2.259(3)
Ru1−C2	2.283(3)	Ru1−C3	2.248(3)
Ru1−C4	2.248(3)	Ru1−C5	2.278(3)
Ru1−C10	2.031(3)	Ru1−C10A	2.032(3)
Ru1−C11	1.869(3)	C10−O1	1.180(4)
C11−O2	1.149(4)	Si1−C1	1.896(3)
$C-C(Cp)_{avg}$	1.44	Ru1−Z1	1.906
C10−Ru1−C10A	93.5(1)	C10−Ru1−C11	88.4(1)
C10−Ru1−Ru1A	48.7(1)	C11−Ru1−Ru1A	101.6(1)
Ru1−C10−Ru1A	83.2(1)	C1−Si1−C1A	110.7(1)
Ru1−C10−O1	136.6(2)	Ru1A−C10−O1	139.9(2)
Ru1−C11−O2	179.0(3)	C10−Ru1−Z1	121.5
C11−Ru1−Z1	130.1	Z1−Ru1−Ru1A	128.3
Z1−Ru1−Ru1A−Z1A	5.0	C11A−Ru1A−Ru1−Z1	182.7

sharp, well-resolved singlets for the ring methyl and dimethylsilyl groups, with a 2:2:1 integration ratio consistent with a C_{2v} symmetrical structure. In sharp contrast to this, we observed a strong temperature dependence for the ^{13}C NMR resonances of the CO ligands in **1**. At −95 °C, the 75.3 MHz ^{13}C NMR spectrum of **1** in CD_2Cl_2 solution displays two well-resolved resonances for two chemically inequivalent carbon monoxide ligands: at δ = 201.5 and 259.9, respectively. Upon warming, the ^{13}CO NMR resonances start to broaden at −85 °C and shift towards each other, until they completely disappear at −50 °C. For the Cp and dimethylsilyl groups, on the other hand, only sharp resonances with small temperature shifts were observed, which corresponds with the temperature independence of the ^1H NMR spectrum. Overall, the process was found to be completely reversible, which suggested an equilibrium between an *energetically preferred structure*, with two terminal and two bridging CO ligands (at lower temperature) as observed in the X-ray crystal structure, and an energetically *less favourable* complex with four terminal CO groups. This scenario is identical to the proposed exchange in the unsubstituted parent complex **2**.[8] In the fast-exchange regime, at higher temperatures, just one ^{13}C NMR CO resonance was therefore predicted in the time-averaged ^{13}C NMR spectrum. This was confirmed through ^{13}C NMR in $[D_{18}]$decahydronaphthalene at 100 °C and 50.3 MHz, with a single, sharp resonance at δ = 223.6 observed for the CO groups.

In order to provide unambiguous evidence for an equilibrium exchange between the terminal and bridging CO groups in complex **1**, through the intermediacy of isomer **1a** [Equation (2)], we resorted to 2D-^{13}C EXSY experiments. Thanks to the excellent solubility of **1** in CD_2Cl_2 even at low temperatures, this experiment appeared feasible for natural ^{13}C abundance in the CO ligands. From inspection of the line widths of the two chemically inequivalent ^{13}CO resonances at 75.3 MHz in the temperature range between −95 and −50 °C, a temperature of −65 °C was deemed a reasonable compromise between the line shape and exchange rate. The measurement was performed using a standard 2D EXSY pulse sequence over two days. The 2D EXSY spectrum is presented in Figure 2.

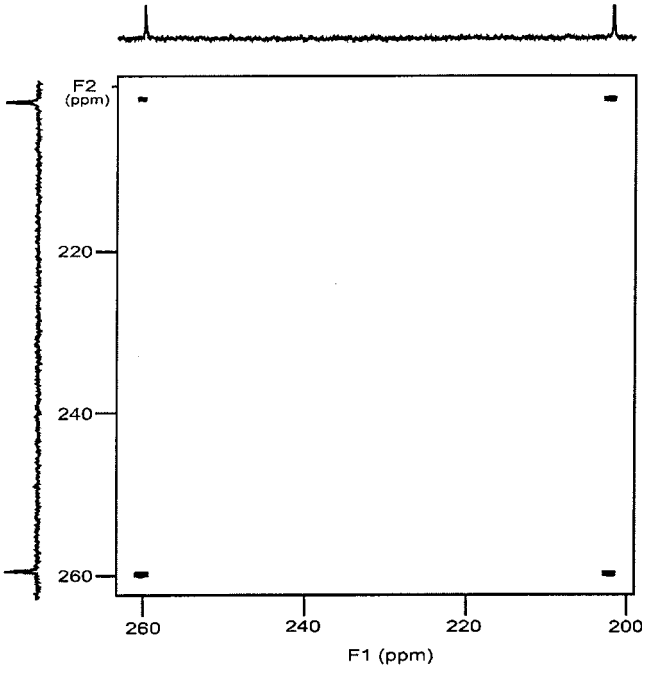

Figure 2. EXSY ^{13}C NMR spectrum (carbonyl range)

The substantial cross peaks between the two chemically inequivalent ^{13}CO resonances in the 2D EXSY spectrum provide excellent supporting evidence for the exchange of the bridging and terminal carbonyl groups, and clearly substantiate the exchange mechanism presented in Equation (2).

Subsequently, the determination of the activation parameters for the exchange process was attempted from a lineshape analysis of the temperature-dependent natural abundance ^{13}C NMR CO resonances. Unfortunately, this procedure turned out to be unreliable because of the strong dependence of the derived activation parameters on the natural line width in the slow-exchange regime, which could not be determined with sufficient accuracy. While the experimental and simulated ^{13}C NMR spectra were in excellent agreement, fits of the Eyring plot showed a large dependence on this parameter with derived $\Delta H^{\ddagger}$ values, varying by as much as 14 ± 4 kcal/mol. Further attempts to determine the rate of exchange by coalescence measurements were thwarted by difficulties in detecting the coalesced ^{13}C NMR carbonyl resonance, due to its extreme broadness. Further support for the observed exchange was therefore sought from DFT calculations, which are presented below. Prior to the discussion of these results, however, we will discuss a further reaction that was observed in the course of our investigations.

Photochemical Reaction of 1

In the course of studying photochemical CO ligand substitution reactions in **1**, we noticed the formation of a new compound in which the CO ligands had *not* been substituted. We hence studied the UV irradiation (medium pressure Hg lamp) of complex **1** by itself; i.e, in the absence of any added ligand [Equation (3)]. Conversion into the novel photochemical product **3** was also observed under these conditions and appeared to be clean (95% isolated yield) and fast. Essentially identical rates for the photochemical conversion were observed when a 1 M $NaNO_2$ solution as a UV/Vis cutoff filter (400 nm cutoff) was used in the photolysis experiments, implying that the lowest energy transition at 460 nm (broad band) in the UV/Vis spectrum of **1** in toluene is crucial to the photochemical process(es). The ^1H and ^{13}C NMR spectra of this product displayed five singlets (1:1:1:1:1 ^1H NMR integration ratio) for the methyl resonances of the Cp-methyl and the $SiMe_2$ groups and suggested a significant structural change compared to complex **1**. In the IR spectrum, the absence of bands in the expected range for μ-bridging CO groups was particularly noteworthy, and *four* bands for terminal CO groups at 2009 (vs), 1983 (vs), 1948 (vs), and 1922 (vs) cm^{-1} were observed in CH_2Cl_2 solution. The aforementioned spectroscopic data were consistent with the proposed structure for complex **3** shown in Equation (3), in which Si−C bond cleavage has occurred.

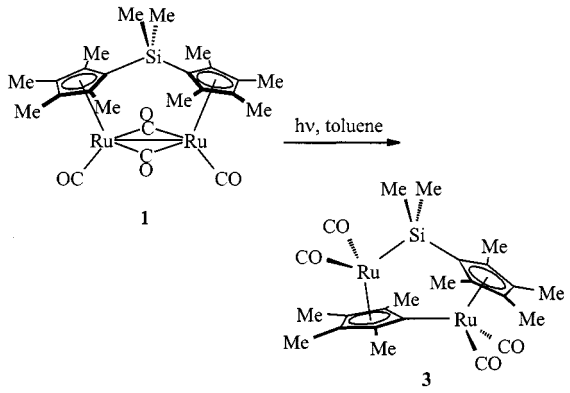

The structural assignment was unambiguously confirmed by the results of an X-ray crystal structure analysis (Figure 3). Details of data collection and selected distances and angles are summarized in Table 2 and 4.

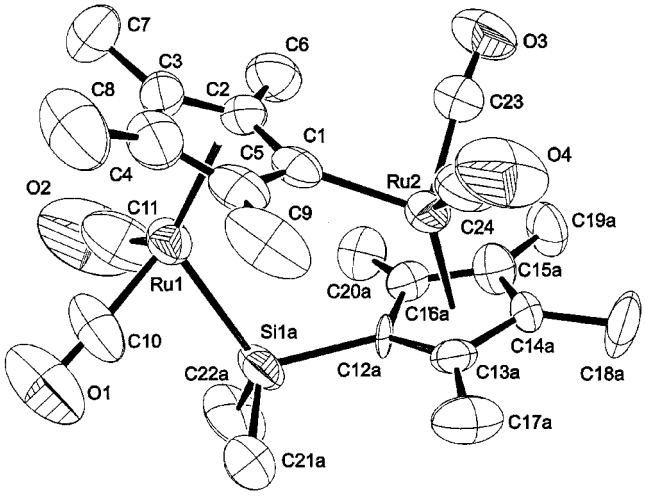

Figure 3. Ortep plot of the photochemical Si−C cleavage product, complex **3**; thermal ellipsoids are shown at the 50% probability level; only one of the disordered cyclopentadienyl rings (denoted by affix a) is shown

Since disordering of the $SiMe_2$ group and one of the attached Cp rings caused severe problems in the refinement, we will refrain from the discussion of bond angles and distances and instead briefly inspect the bond topology in complex **3**. In addition to the cleavage of the Si−C bond in the starting material, the Ru−Ru single bond observed in the starting material (complex **1**) is no longer present in the product, and new ruthenium−carbon and ruthenium−silicon bonds have been formed. There are four terminal carbonyl ligands, which explains the absence of bands in the μ-CO bridging ligand range in the IR spectrum.

Photochemical silicon-carbon cleavage in **1** parallels observations by Bitterwolf et al. in the unsubstituted parent complex **2**.[1] In the latter case, however, the reaction has been found to be more complicated, and competition between Si−C and, in addition, C−H activation of the cyclopentadienyl ring C−H group in the position *ortho* to the bridgehead atom was noticed. The apparent difference be-

Table 2. Selected bond lengths [Å] and angles [°] with ESDs for complex **3**; Z1 and Z2 are the midpoints of carbon atoms C1 to C5 and C12A,B to C16A,B, respectively; "A" and "B" indicate disordered positions

Ru1−Si1A,B$_{avg.}$	2.41(1)	Ru2−C1	2.146(11)
Ru1−C10	1.827(10)	Ru1−C11	1.820(13)
Ru2−C23	1.874(4)	Ru2−C24	1.838(11)
C10−O1	1.148(10)	C11−O2	1.189(13)
C23−O3	1.159(10)	C24−O4	1.176(12)
Ru1−Z1	1.91	Ru2−Z2$_{avg.}$	1.92
Ru1····Ru2	3.96		
C10−Ru11−C11	93.2(5)	C10−Ru−Si1A,B$_{avg.}$	87.8
C11−Ru1−Si1A,B$_{avg.}$	85.0	C10−Ru1−Z1	128.3
C11−Ru1−Z1	127.7	Si1A,B−Ru1−Z1$_{avg.}$	121.0
Ru1−C10−O1	176.6(11)	Ru1−C11−O2	175.7(12)
C23−Ru2−C24	90.7(5)	C1−Ru2−C23	90.4(4)
C1−Ru2−C24	90.8(4)	C23−Ru1−Z2$_{avg.}$	127.3
C24−Ru2−Z2$_{avg.}$	124.8	C1−Ru2−Z2$_{avg.}$	122.3
Ru2−C23−O3	174.3(8)	Ru2−C24−O4	176.2(11)
Z1−Ru1−C22−Si1−C12$_{avg.}$	−23	Z2−Ru2−C1−Ru1$_{avg.}$	0

tween the outcome of the photochemical reactions of complexes **1** and its unsubstituted congener **2** is best explained with a more difficult C−H activation step (higher activation barrier) at the sp^3-hybridized methyl group in **1**, as compared to the aromatic C−H group in **2**; there is ample evidence for this in the literature.[17,18] The higher barrier would thus lead to a preference for the Si−C activation step over its C−H counterpart. In an attempt to shed some light on the mechanism of this transformation, we have attempted to investigate this reaction thermally in a kinetic study. However, even under very harsh conditions (i.e. at temperatures of 180 °C and after an extended period of time), we could not detect thermal formation of the Si−C cleavage product **3**, and only unchanged starting material **1** was recovered, quantitatively. Prior to our DFT-calculations, which are detailed in the next section, we anticipated that complex **3** might not be obtained from **1** under thermal control, due to a thermally inaccessible barrier for the thermal transformation ($\Delta G^{\ddagger} > 40$ kcal/mol).

DFT Calculations

In view of the fact that complexes **1** and **3** might be interesting systems for light energy storage, we turned to DFT calculations to establish the thermodynamic preferences of this system. In addition, we wanted to assess the relative thermodynamic stabilities of the μ-CO bridged complex **1**, and its isomer **1a** with four terminal CO groups.

The molecular geometries found in the X-ray crystal structures of **1** and **3** were used as starting points for the geometry optimizations. A Becke−Perdew (BP86) functional[19,20] and TZVP basis-sets including a relativistic pseudopotential (Stuttgart−Dresden, ecp-28-mwb)[21] for the Ru centres and an SVP basis for the residual atoms were used at the initial stage in these calculations (basis I). After convergence of the optimizations at this level, TZVP-basis sets were applied for all atoms and the optimizations pursued further (basis II). Typically, this procedure required just a few optimization cycles to converge with the larger basis sets. An excellent agreement of the optimized geometries for complexes **1** and **3** with their X-ray crystal structures, with few deviations, was observed. As previously noticed in metal carbonyl complexes by others,[22,23] the unscaled calculated ν(CO) vibrational data were also in good agreement with the observed experimental IR data. The final calculated total energies are depicted graphically in Figure 4; selected calculated angles and ν(CO) vibrations of the optimized geometries, along with their experimentally determined values, are given in Table 3.

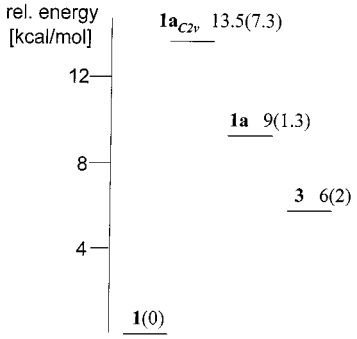

Figure 4. Relative energies of complexes **1**, **1a**, **1a$_{C2v}$**, and **3** as determined by DFT calculations using the BP86 functional; relative energies (kcal/mol) for B3LYP optimized geometries are included in parentheses (not on scale)

The results of the DFT calculations for complexes **1** and **1a** clearly provide supporting evidence for the higher thermodynamic stability of the μ-bridged carbonyl isomer **1**, with a preference of ca. 9 kcal/mol for **1**. However, on the basis of the fact that both isomers are present in comparable concentrations in pentane, as determined by IR spectroscopy, the theoretically predicted energy difference between the isomers **1** and **1a** is deemed to be too large. In view of this consideration, we have also included entropic contributions to this equilibrium; these are quite likely to be in favour of the unbridged isomer **1a**. This apparent unsatisfactory agreement may be attributed to solvation effects, which are not included in the (gas phase) calculations. It deserves special mention that strongly polar solvents were found to have a remarkable influence on the equilibrium position of such isomers.[13] However, since both isomers **1**

Table 3. Calculated and experimental distances, angles and ν(CO) vibrational data; DFT (BP-86) calculated vibrational data are unscaled and are given in cm^{-1}; Z denotes the centroid of a Cp ring; indexes b and t denote bridging and terminal; for essentially identical values, only averaged (avg.) data are given; rounded distances are given in [Å], angles in [°]; selected experimental data are included in parentheses

	Complex **1**	Complex **1a**	Complex $\mathbf{1a_{C2v}}$	Complex **3**
ν(CO)	1987w (1980)	2003 (s)		2008 (2009) (s)
ν(CO)	1955s (1940s)	1958 (w)		1990 (1983) (vs)
ν(CO)	1816s	1944 (s)		1953 (1948) (vs)
ν(CO)	1794s (1757s)	1932 (w)		1938 (1922) (vs)
d(Ru1−Ru2)	2.73(2.71)	2.87	2.97	
$d(Ru-Z)_{avg}$	1.96(1.91)	1.95	1.95	1.96 (1.92)
$d(Ru-CO_t)_{avg}$	1.86(1.87)	1.86	1.86	1.87 (1.84)
$d(Ru-CO_b)_{avg.}$	2.05(2.03)			
$d(Si-C_{Cp})$	1.92(1.90)	1.91	1.90	1.95
$d(Ru-\eta^1C_{Cp})$				2.13 (2.15)
d(Ru−Si)				2.44 (2.41)
Z−Ru1−Ru2	127.7(128.3)	120.7	123.6	
OC_t-Ru-Z	128.3(130.1)	127.0, 129.9	126.0	
$OC_t-Ru1-Ru2$	104.1(101.6)	85.7, 90.6	89.4	
$OC_t-Ru-CO_t$		90.4	91.6	90.0, 91.7
$OC_t-Ru-CO_b$	89.8(88.4)			
$OC_b-Ru-CO_b$	93.5(87.9)			
$Ru-C-O_b$	138.2(139.9)			
Si−Ru1−Z1				118.5
$Z2-Ru2-\eta^1C_{Cp}$				121.1
$OC_t-Ru2-\eta^1C_{Cp}$				91.2, 91.7
$OC_t-Ru1-Si$				86.9, 90.3
$OC_t-Ru1-CO_t$				91.7
$OC_t-Ru1-CO_t$				90.0
Z1−Ru1−Ru2−Z2	0.0	50.0	0.0_f	178.3
OC−Ru1−Ru2−CO		50.2, 140.6		

and **1a** are present even in the low-polarity solvent pentane, which can be quite confidently deemed compatible with the DFT calculations in the gas phase, it is suspected that the energetics of this system might not be appropriately represented by the applied BP86 functional. In addition, we have therefore performed calculations with the B3LYP hybrid functional,[24] which has been deemed to give excellent thermodynamic data not only for organic compounds but also for organometallic species. These calculations were performed with the large basis set (basis II) and the BP86-optimized geometries for the geometry optimizations. In general, the B3LYP-calculated relative energy differences (Figure 4) are appreciably smaller, while the energetic order of the isomers is unchanged. On the basis of the calculated difference of 1.3 kcal/mol between **1** and **1a**, a ca. 1:10 mixture in favour of the bridged isomer **1** would be predicted. Note that this is in good agreement with our temperature-dependent ^{13}C NMR and IR spectroscopic data.

It is worth mentioning that the geometry of the unbridged complex with four terminal CO groups (i.e. **1a**), converged at a structure that displays approximate C_2 symmetry, rather than C_{2v}. This can easily be seen from a plot along the metal-metal bond of **1a**, which is presented in Figure 5.

When the geometry optimizations were performed with C_{2v} symmetry constraints (complex $\mathbf{1a_{C2v}}$), the energy was found to lie 4.5 (BP86, 6 kcal/mol B3LYP) kcal/mol above that of **1a**. The presence of several imaginary frequencies in the range from −500 to $-64\ cm^{-1}$ nevertheless clearly showed that the optimized geometry for $\mathbf{1a_{C2v}}$ is not a stationary point (local minimum). Analysis of the latter frequencies showed that the major driving force behind the distortion to **1a** is due to the fact that it allows elongation of the $Si-C_{bridgehead}$ bond and shortening of the Ru−Ru bond. While we have no conclusive explanation for the energy differences between the two functionals, it should be noted that, in high level calculations on a nickel olefin system, an excellent agreement between these two functionals was observed, and also with calculations performed at the CASPT2 level.[25] It is noteworthy that we also observed negligible energy differences between B3LYP and BP86 functional in a related dicyclopentadienyl-bridged diruthenium system containing a CMe_2 rather than a dimethylsilyl

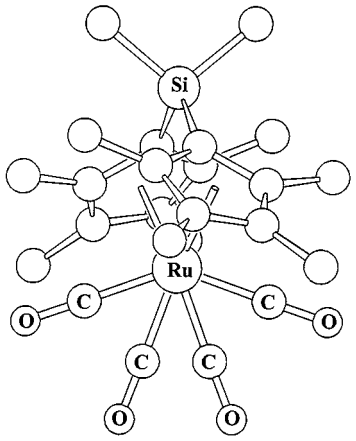

Figure 5. View along the metal−metal bond of the DFT-optimized structure of complex **1a**

bridge {i.e., $Me_2C[(C_5H_4)Ru(CO)_2]_2$}.[26] Furthermore, an inspection of the deviations between experimental and theoretical enthalpies for silicon-containing neutral compounds of the G2 test set[27] revealed large errors for both the BP86 (−7, +11 kcal/mol) and the B3LYP (−20, +3 kcal/mol) functionals, with the latter being more accurate for less-polar compounds. Hence, on the basis of these data, no clear judgement can be made as to either the appropriateness or the accuracy of these two widely applied functionals. Nevertheless, it is thought that despite the heavy usage of the B3LYP functional as the "ultima ratio" for DFT-derived energies in organometallic systems, some doubts seem appropriate and further calibration studies are definitely required.

Nevertheless, the most interesting result from the DFT calculations is the fact that the photochemically rearranged product **3** is estimated to be *6 kcal/mol less thermodynamically stable* (BP-86-functional, 2 kcal/mol for the B3LYP functional) than the metal-metal bonded starting material **1**. This view is further supported by single-point MP2 calculations (for details see Experimental Section) of the BP-86 optimized geometries **1** and **3**, which also showed a pronounced thermodynamic preference of 7 kcal/mol for complex **1** over **3**. For the unsubstituted parent complex $Me_2Si[(C_5H_4)Ru(CO)_2]_2$ (**2**), and its Si−C cleavage product **6** (the unsubstituted analogue of complex **3**), we calculate a similar thermodynamic situation, with compound **2** being energetically favoured by 6 kcal/mol (BP-86 functional, basis II). This sparked the idea that the photochemical transformation might be *reversed* thermally (**3** → **1**). We have therefore studied the thermolysis of **3** in toluene, which is described in the next section.

Thermolysis Experiments on Complex 3

The thermolysis experiments involving **3** were performed at temperatures up to 170 °C in sealed NMR tubes in [D_8]toluene and monitored by ^{1}H NMR spectroscopy. However, under these conditions thermal reconversion of complex **3** into **1** was *not* observed, even after extended reaction times (2 weeks) and at the highest possible temperatures. At present, it is therefore unclear whether large kinetic barriers account for the absence of a thermal reaction or whether the applied DFT methodology might not be accurate enough to make such predictions. However, it is especially noteworthy that we have observed an excellent agreement between experimentally determined (by DSC) energy differences and DFT calculations (within 1 kcal/mol) between constitutional isomers in the aforementioned, closely related C_1-bridged diruthenium system, $Me_2C[(C_5H_4)Ru_2(CO)_2]_2$.[26] At present, we therefore favour the notion that thermally unaccessible kinetic barriers (> 40 kcal/mol) prevent thermal reconversion of **3** to **1**.

Conclusion

The DFT calculations suggest that, in analogy to Vollhardt's fulvalenediyl diruthenium system,[5] rather inert, energetically disfavoured, photochemically rearranged products can also be obtained with other X-bridged (e.g., X = $SiMe_2$ here) dicyclopentadienyl systems. While the photochemical reaction could not be reversed for complexes **1** and **1a**, we will report on related functional systems in due course.

Experimental Section

The dimethylsilyl-bridged dicyclopentadiene ligand $Me_2Si(C_5Me_4H)_2$ was prepared according to published methods.[28] $Ru_3(CO)_{12}$ was used as received from Alfa. − ^{1}H NMR and ^{13}C NMR spectra were recorded on Varian Gemini 200 and 300 spectrometers operating at 200, 300 and 50.1, 75.4 MHz respectively. Chemical shifts are given in ppm and are referenced to the residual H solvent shift or ^{13}C NMR solvent shift. The assignment of ^{1}H NMR and ^{13}C NMR resonances is based on NOE and DEPT experiments. − IR spectra were measured on a Biorad-FTS 45 Fourier IR-spectrometer. − X-ray crystal structure analyses were performed on a STOE-IPDS image plate system with monochromated Mo-K_α (0.70713 Å) beam. − Elemental analysis were performed with a LECO CHNS-900 analyzer in our institute.

Synthesis of $SiMe_2[C_5Me_4Ru(CO)_2]_2$ (1): $SiMe_2(C_5Me_4H)_2$ (1 g, 3.33 mmol) and $Ru_3(CO)_{12}$ (1.4 g, 2.22 mmol) were refluxed for 5 days in 80 mL of *non-deoxygenated* octane. After this period, the resulting dark brown mixture was allowed to come to room temperature and the solvent removed in high vacuum. The solid residue was then sublimed at 190 °C and 10^{-2} Torr, with the product collected as an orange solid at the water-cooled sublimation finger, and finally recrystallized from CH_2Cl_2/ether at −30 °C. ***Caution:*** *The solid remainder of the sublimation is highly pyrophoric.* Yield: 1.04 g, 1.67 mmol, 50%. − ^{1}H NMR (25 °C, C_6D_6): δ = 1.93 (s, 12 H, $SiMe_2[\alpha$-$C_5Me_4]$), 1.80 (s, 12 H, $SiMe_2[\beta$-$C_5Me_4]$), 0.28 (s, 6 H, $SiMe_2[C_5Me_4]$). − ^{13}C{^{1}H} NMR (CD_2Cl_2, −65 °C): δ = 260.3(s, *C*O), 202.1 (s, *C*O) 110.6 (s, C_5Me_4), 103.8 (s, C_5Me_4), 78.9 (s, bridgehead C_5Me_4), 13.1 (s, C_5Me_4), 11.3 (s, C_5Me_4), 2.8 (s, $SiMe_2$). − $C_{10}D_{14}$, 100 °C: δ = 223.6 (s, *C*O), 110.1 (s, C_5Me_4), 105.1 (s, C_5Me_4), 79.1 (s, bridgehead C_5Me_4), 14.8 (s, C_5Me_4), 12.5 (s, C_5Me_4), 5.5 (s, $SiMe_2$). − IR (carbonyl range, CH_2Cl_2): $\tilde{\nu}$ = 1980(vs), 1940(w), 1757(s) cm^{-1}; IR (carbonyl range, KBr): $\tilde{\nu}$ = 1978(vs), 1934(w), 1768(s) cm^{-1}. − MS(EI, 70 eV): *m*/*z* (%) = 612 (100) [$M^{+\cdot}$], 584 (30) [$M^{+\cdot}$ − CO], 556 (100) [$M^{+\cdot}$ − 2 CO], 528 (100) [$M^{+\cdot}$ − 3 CO]. − $C_{24}H_{30}O_4Ru_2Si$ (612.7): calcd: C 47.05, H 4.94; found C 46.79, H 4.81.

Synthesis of Complex 3: Compound **1** (100 mg, 0.295 mmol) was dissolved in a Teflon-tap-sealed Pyrex Schlenk tube in 100 mL dry, thoroughly deoxygenated toluene, to give an orange solution. The Schlenk tube was immersed in a water bath kept at 10 °C and with the tube placed in close proximity to a medium pressure Hg lamp (HPK 125 W). An almost colourless (faintly yellowish) solution indicated the end of the photolysis reaction (usually 6 h). The solvent was removed in high vacuum and the product recrystallized from a toluene/pentane (1:1) mixture at −35 °C to give a colourless microcrystalline solid. Yield: 95 mg, 0.28 mmol, 95%. − ^{1}H NMR (25 °C, C_6D_6): δ = 2.14 (s, 6 H, C_5Me_4), 2.00 (s, 6 H, C_5Me_4), 1.88 (s, 46 H, C_5Me_4), 1.53 (s, 6 H, C_5Me_4), 0.78 (s, 6 H, $SiMe_2$). − ^{13}C{^{1}H} NMR (C_6D_6): δ = 205.9, 203.1 (*C*O), 129.4, 110.8, 105.3 104.7, 101.1, 76.4 ($Me_2SiC_5Me_4$, RuC_5Me_4), 16.4, 12.9, 11.9, 10.4, 8.3(s, C_5Me_4, $SiMe_2$). − MS (EI, 70 eV): *m*/*z* (%) = 612 (15) [$M^{+\cdot}$],

Table 4. Crystal and data collection parameters for compounds **1** and **3**

	1	**3**
Empirical formula	$C_{24}H_{30}O_4Ru_2Si$	$C_{24}H_{30}O_4Ru_2Si$
Formula mass	612.7	612.7
Habit	orange cube	colourless rect., parallelepiped
Crystal size [mm]	0.2 × 0.2 × 0.2	0.1 × 0.1 × 0.15
Crystal system	tetragonal	monoclinic
Space group	$P4_32_12$ (no. 96)	$P2_1/n$ (no. 14)
a [Å]	8.3800(3)	9.009(1)
b [Å]		16.551 (2)
c [Å]	32.1153(14)	16.963 (3)
β [°]		95.18 (2)
V [Å^3]	2508.5 (2)	2519.0(8)
Z	4	4
$\rho_{calcd.}$ [g/cm^3]	1.622	1.616
abs. coeff. [mm^{-1}]	1.28	1.28
F(000)	1232	1232
Temp [K]	183	183
abs. corr.	numerical	numerical
T_{min}, T_{max}	0.55, 0.99	0.30, 0.44
λ [Å], Mo-$K\alpha$	0.707173	0.707173
Scan type	Image Plate/-rotation	Image Plate/-rotation
2 Θ range [°]	4−52	4−52
No. of refl. meas. Total, unique	17008, 2429	18963, 4636
No. of parameters	141	280
$R_1(F^2 > 2\sigma(F^2))$	0.0198	0.0451
$wR_2(F^2 > 2\sigma(F^2))$	0.0540	0.0731
GooF, S	1.035	1.022
Res. el. dens. [e$^-$/Å^3]	0.30, −0.27	0.65, −1.1

584 (70) [$M^{+\cdot}$ − CO], 556 (100) [$M^{+\cdot}$ − 2 CO], 528 (80) [$M^{+\cdot}$ − 3 CO]. − IR (carbonyl range, CH_2Cl_2): $\tilde{\nu}$ = 2009(vs), 1983 (vs), 1948 (vs), 1922 (vs) cm^{-1}. − $C_{24}H_{30}O_4Ru_2Si$ (612.7): C 47.05, H 4.94; found C 46.67, H 4.68.

DFT and MP2 Calculations: The applied methodology is described in the text. The DFT calculations were performed with the Turbomole program suite[29] and using the RI-J-DFT (BP-86 functional) implementation (RIDFT) for the geometry optimizations and the calculation of the second derivatives.[30] Essentially identical energy differences were obtained with the BP-86 functional using the *pure* DFT rather than the RI-J-DFT method. The parallelized version of the Turbomole program package was used on our 12 CPU Linux cluster in all cases.[31] The single-point MP2 calculations on **1** and **3** were carried out using the geometry optimized with the BP-86 functional using the basis set described below. The RI implementation of MP2 available in Turbomole was used for these calculations (RIMP2),[32] with molecular orbitals possessing eigenvalues lower than −3 Hartrees treated as frozen core (MOs 1−35 for both **1** and **1a**). Final total energies in Hartree with unscaled zero-point energies in parentheses (in kJ/mol) for the optimized geometries using a Becke−Perdew (BP86) functional (RI-DFT method), TZVP basis sets[33] for all atoms and a Stuttgart−Dresden pseudopotential (ECP-28-mwb)[21] for the ruthenium centres are: **1**: −1713.84199(1232); **1a**: −1713.83043(1232); $\mathbf{1a_{C2v}}$: −1713.82021; **3**: −1713.83285(1236). Second derivatives were obtained numerically from finite differences. Using the same basis sets and ECPs, but the hybrid functional B3LYP instead, the following total energies were obtained for optimized geometries (cartesian gradients < 10^{-3} Hartree/Bohr): **1:** −1712.59622; **1a**: −1712.59412; $\mathbf{1a_{C2v}}$: −1712.58449; **3:** −1712.59309 [Hartree]. In the latter case, the BP86 optimized geometries were used as starting geometries. The MP2 total single point energies for compounds **1** and **3** with the HF energies and MP2 energy corrections in parentheses are: **1**: −1708.47894 [−1703.30867 (HF), −5.17028 (MP2)]; **3** −1708.46803 [−1703.33175 (HF), −5.13628 (MP2)]. The total energies in Hartrees for the optimized geometries (cartesian gradients < $2{\cdot}10^{-4}$ Hartree/Bohr) using the BP-86 functional with its RI-implementation in Turbomole, TZVP basis sets for all atoms and a Stuttgart−Dresden pseudopotential for Ru (ECP-28-mwb) of the unsubstituted parent complex **2** and the Si−C cleavage product **6** derived from it (the analogue of **3**), are: **2**: −1399.21427; **6**: −1399.20464.

X-ray Crystal Structure Analyses. − General Remarks: Suitable single crystals of complexes **1** and **3** were mounted on glass fibres in Paratone-N (oil) and were transferred on the goniometer head to the diffractometer and the crystal cooled to −80 °C in a N_2 cryostream. The data sets were collected with graphite monochromated Mo-K_α radiation (0.707173 Å) on a Stoe IPDS image plate diffractometer. Intensities were corrected for Lorentz and polarization effects and absorption corrections performed numerically with the faces and corresponding crystal dimensions determined using the STOE Faceit-Video CCD camera microscope system. The structures were solved using direct methods with the SHELXS-86 program package.[34] The refinements were carried out with SHELXL-93 using all unique F_o^2.[35] Except for complex **3**, all non-hydrogen atoms were refined anisotropically. The positions of the hydrogen atoms were calculated in idealized positions (C−H bonds fixed at 0.96 Å) and refined as a riding model with a fixed isotropic displacement factor of U = 0.08 Å^2. The details of the data collection and refinement, including R-values, are summarized in Table 4.

Complex 3: The cyclopentadienyl ring connected to the $SiMe_2$ unit and the dimethylsilyl group itself (atoms C12A,B−C22A,B, Si1A,B) were found to be disordered and were refined with two split positions (labelled A and B) and refined with occupation factors of 0.57 and 0.43. Carbon atoms C12−C22 were refined isotropically and all other non-hydrogen atoms anisotropically.

Crystallographic data for complexes **1** and **3** (excluding structure factors) have been deposited with the Cambridge Crystallographic Data Centre as supplementary publication numbers CCDC-140425 (**1**) and -140426 (**3**). Copies of the data can be obtained free of charge on application to CCDC, 12 Union Road, Cambridge CB2 1EZ, UK [Fax: (internat.) +44-1223/336-033; E-mail: deposit@ccdc.cam.ac.uk].

Acknowledgments

We are indebted to Professor Heinz Berke for his ongoing support.

[1] T. E. Bitterwolf, J. E. Shade, J. A. Hansen, A. L. Rheingold, *J. Organomet. Chem.* **1996**, *514*, 13−21.
[2] W. Xie, B. Wang, X. Dai, X. S., X. Zhou, *Organometallics* **1998**, *17*, 5406−5410.
[3] Y. Zhang, S. Xu, G. Tian, X. Zhou, J. Sun, *Organometallics* **1998**, *17*, 1122−1127.
[4] X. Zhou, Y. Zhang, W. Xie, S. Xu, J. Sun, *Organometallics* **1997**, *16*, 3474−3481.
[5] R. Boese, J. K. Cammack, A. J. Matzger, K. Pflug, W. B. Tolman, K. P. C. Vollhardt, T. W. Weidman, *J. Am. Chem. Soc.* **1997**, *119*, 6757−6773.
[6] C. Cremer, H. Jacobsen, P. Burger, *Chimia* **1997**, *51*, 650−653.
[7] T. E. Bitterwolf, M. B. Leonard, P. A. Horine, J. E. Shade, A. L. Rheingold, D. J. Staley, G. P. A. Yap, *J. Organomet. Chem.* **1996**, *512*, 11−20.
[8] X. Zhou, Y. Zhang, S. Xu, G. Tian, B. Wang, *Inorg. Chim. Acta* **1997**, *262*, 109−112.
[9] S. A. R. Knox, K. Macpherson, A. G. Orpen, M. C. Rendle, *J. Chem. Soc., Dalton Trans.* **1989**, 1807−1813.
[10] G. O. Nelson, *Organometallics* **1983**, *2*, 1474−1475.
[11] A. P. Humphries, S. A. R. Knox, *J. Chem. Soc., Dalton Trans.* **1975**, 1710−1714. O_2 has been recognized to accelerate the reductive elimination of H_2 in $CpRu(CO)_2H$. This fact is used in the improved synthesis of $[CpRu(CO)_2]_2$. N. M. Doherty, S. A. R. Knox, M. J. Morris, C. P. Casey, G. T. Whiteker, *Inorg. Synth.* **1990**, *28*, 189−191.
[12] C. Nataro, L. M. Thomas, R. J. Angelici, *Inorg. Chem.* **1997**, *36*, 6000−6008.
[13] J. G. Bullitt, F. A. Cotton, T. J. Marks, *Inorg. Chem.* **1972**, *11*, 671−676.
[14] F. A. Cotton, G. Yagupsky, *Inorg. Chem.* **1967**, *6*, 15−20.
[15] L. J. Farrugia and L. Mustoo, *Organometallics* **1992**, *11*, 2941−2944.
[16] E. D. Jemmis, A. R. Pinhas, R. Hoffmann, *J. Am. Chem. Soc.* **1980**, *102*, 2576−2585.
[17] A. E. Shilov, G. B. Shul′pin, *Chem. Rev.* **1997**, *97*, 2879−2932.
[18] C. L. Hill, *Activation and Functionalization of Alkanes*, John Wiley & Sons, Inc., New York, Chichester, Brisbane, Toronto, Singapore, **1989**.
[19] A. D. Becke, *Phys. Rev. A* **1988**, *38*, 3098−3100.
[20] J. P. Perdew, *Phys. Rev. B* **1986**, *33*, 8822−8824.
[21] D. Andrae, U. Häußermann, M. Dolg, H. Stoll, H. Preuß, *Theor. Chim. Acta* **1990**, *77*, 123−141.
[22] V. Jonas, W. Thiel, *J. Chem. Phys.* **1995**, *102*, 8474−8484.
[23] V. Jonas, W. Thiel, *J. Chem. Phys.* **1996**, *105*, 3636−3648.
[24] A. D. Becke, *J. Chem. Phys.* **1993**, *98*, 5648−5652.
[25] F. Bernardi, A. Bottoni, M. Calcinari, I. Rossi, M. Robb, *J. Phys. Chem. A* **1997**, *101*, 6310−6314.
[26] P. Burger, manuscript in preparation.
[27] L. A. Curtiss, K. Raghavachari, G. W. Trucks, J. A. Pople, *J. Chem. Phys.* **1991**, *94*, 7221−7230.
[28] C. M. Fendrick, L. D. Schertz, V. W. Day, T. J. Marks, *Organometallics* **1988**, *7*, 1828−1838.
[29] R. Ahlrichs, M. Bär, M. Häser, H. Horn, C. Kölmel, *Chem. Phys. Letters* **1989**, *162*, 165−169.
[30] K. Eichkorn, O. Treutler, H. Oehm, M. Häser, R.Ahlrichs, *Chem. Phys. Lett.* **1995** *242*, 652−660
[31] R. Ahlrichs, M. Bär, M. Häser, H. Horn, C. Kölmel, *Chem. Phys. Letters* **1989**, *162* 165−169. R. Ahlrichs, S. D. Elliott, U. Huniar, *Ber. Bunsen, Phys. Chem.* **1998**, *102*, 795−804; M. von Arnim R. Ahlrichs, *J. Comp. Chem.* **1998**, *19*, 1746−1757.
[32] F. Weigend, M. Häser, *Theor. Chem. Acc.* **1997**, *97*, 331−340; F. Weigend, M. Häser, H. Patzelt, R. Ahlrichs, *Chem. Phys. Lett.* **1998**, *294*, 143−152.
[33] H. Schäfer, H. Horn, R. Ahlrichs, *J. Chem. Phys.* **1992**, *97*, 2571−2577.
[34] G. M. SHELDRICK, *SHELXTL PLUS*, University of Göttingen, Germany, **1988**.
[35] G. M. Sheldrick, *SHELXL 93*, University of Göttingen, Germany, **1993**.

Received March 6, 2000
[I00086]

Synthesis and Properties of Dimetallic Complexes Based on a New Oxalamidine-Derived Ligand System with Pendant Pyridine Functionality

Jörg Wuckelt,[a] Manfred Döring,*[a] Helmar Görls,[a] and Peter Langer*[b]

Keywords: Molybdenum / Cobalt / Hydrogen bonds / Chelates / N ligands

Reaction of sterically hindered bis(imidoyl)chlorides of oxalic acid with picolylamine afforded conformationally locked oxalic acid-derived amidines with pendant pyridine functionalities. Based on this new multivalent ligand system, dimetallic complexes were efficiently prepared.

Introduction

The synthesis of dimetallic complexes, particularly those containing two different transition metals "communicating" with each other, is of considerable current interest for both theoretical and practical reasons.[1] Important properties have been postulated for these compounds, such as cooperative effects in catalysis, intramolecular electron-transfer reactions, molecular-based ferromagnetic and antiferromagnetic interactions and self-organization processes. However, the synthesis of heterodimetallic complexes is associated with severe problems, since two metals exhibiting different demands in terms of their coordination sphere have to be brought close together. Very recently, the preparation of heterodimetallic complexes has been realized using aminopyridines as bridging ligands.[2] Herein, we report an efficient synthesis of heterodimetallic complexes which relies on the use of a new multivalent ligating system.

The ability of amidinates to act as four-electron-donating, bidentate ligands for main group elements, transition metals, and the lanthanides is well established.[3] We and others have studied the coordination chemistry of oxalic acid-derived amidines which can act as four-electron-donor ligands (to give five-membered rings) or as bridging ligands.[4] Very recently, the coordination chemistry of ancillary amidinate ligands with a pendant pyridine functionality has been described by Arnold and co-workers. The metal complexes (Mg, Al, Zr, La) prepared were shown to be monomeric, with the pendant pyridine coordinated intramolecularly.[5] In most cases, the tridentate ligands coordinated meridionally to the metal centre. This work prompted us to disclose our results related to the coordination chemistry of oxalic acid-derived amidines containing pendant pyridine functionalities. The use of this new ligand system allowed the efficient synthesis of a variety of heterodimetallic diazadiene complexes.

Results and Discussion

Unfortunately, our initial attempts to prepare the desired ligands **3** by condensation of 2-aminomethylpyridine with the oxalic acid bis(imidoyl)chlorides **1a–c** (R = Tol, Ph, $MeOC_6H_4$)[4e] in the presence of triethylamine were unsuccessful, since cyclization products were exclusively obtained.[4f] The use of oxalic acid bis(imidoyl)esters, prepared by reaction of the corresponding bis(imidoyl)chlorides with ethanol, was equally disappointing and resulted in formation of complex reaction mixtures. Fortunately, the problem could be eventually solved by the use of the sterically hindered bis(imidoyl)chlorides **1d–f** [R = 2,4,6-$Me_3C_6H_2$, 2,6-$Me_2C_6H_3$, 2,6-(iPr)$_2C_6H_3$] which allowed the preparation of the desired oxalamidines **3a–c**, respectively, in good yields (Scheme 1). During the synthesis of **3c**, the cyclization product **2** was obtained as a side-product in 15% yield. The use of sterically undemanding bis(imidoyl)chlorides was possible in the reaction of 2-aminoethylpyridine with

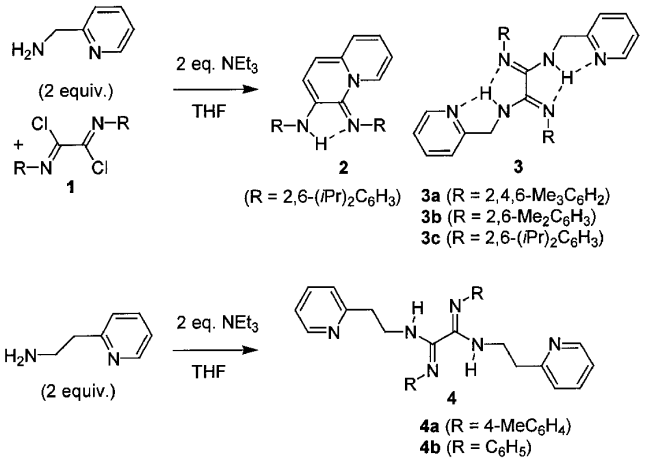

Scheme 1. Preparation of oxalamidines with pendant pyridine functionality

[a] Institut für Anorganische und Analytische Chemie der Universität Jena,
August-Bebel-Straße 2, 07743 Jena, Germany
[b] Institut für Organische Chemie der Georg-August-Universität Göttingen,
Tammannstraße 2, 37077 Göttingen, Germany
Fax: (internat.) +49-(0)551/399-475
E-mail: planger@uni-goettingen.de

 © WILEY-VCH Verlag GmbH, 69451 Weinheim, 2001 1434–1948/01/0303–0805 $ 17.50+.50/0

bis(imidoyl)chlorides to give the amidines **4** (**4a**: R = Tol, **4b**: R = Ph) in good yields.

Amidines represent flexible molecules which usually undergo *E*/*Z* isomerization by a tautomeric rotation mechanism.[6a] In the case of oxalamidines, *two* imino-groups are present and rotation of the central C−C bond can give rise to *s-trans* or *s-cis* conformations.[6b] Therefore, very complex or coalescent ^{1}H NMR spectra are normally observed at room temperature due to the highly flexible structure. Interestingly, *sharp* signals and a low-field NH resonance were observed for compounds **3** which suggested that the latter are conformationally restricted by the presence of intramolecular hydrogen bonds and by the high steric demand of the substituents. Moderately broad signals were observed only for the CH_2 and the NH groups. The location of the NH group was proven by low-temperature ^{1}H NMR measurements: upon cooling to 0 °C, formation of a doublet is observed for the CH_2 groups due to a ^3J coupling of the latter with the adjacent NH group.

The structure of amidine **3a** was independently confirmed by X-ray crystallography (Figure 1). The amidine moiety is planar and shows an *s-trans*-(*Z*/*Z*) configuration. The bulky mesityl groups are twisted out-of-plane by 104.9°. It is noteworthy that the oxalamidines **3** represent rare examples of systems containing intramolecular three-centre ("bifurcated") hydrogen bonds.[7] Two hydrogen bonds (to the amidine nitrogen N1A and to the pyridine nitrogen N3) are observed for the hydrogen atom located at nitrogen N2 (N1A−H 2.18 Å, N3−H 2.41 Å). Bifurcated hydrogen bonds are of great current interest since they play an important role in DNA conformation[8] and in protein hydration.[9] Two types of three-centre interaction can be distinguished, one involving two donors and one acceptor ("HXH"), and the other involving one donor and two acceptors ("XHY"). Very recently, computational studies of a depsipeptide model have shown that addition of a second acceptor (Y) to a hydrogen bond XH has no enthalpic benefit, while addition of a second donor (H) to XH is modestly favourable enthalpically.[10]

Two conformations are, in principle, possible for oxalamidine ligands coordinated to the metal. The ligand can posses an *s-trans*- or an *s-cis* conformation. We have found that oxalamidinate complexes of molybdenum posses the *s-cis* conformation.[4c−4d,12] These compounds are thus 1,4-diazadiene complexes.[11] The reaction of dibenzyldiphenyloxalamidine with $Mo(CO)_4$(nor) resulted in rotation of the central C−C bond and coordination of the aromatic (rather than the aliphatic) imino groups to the metal to give an *s-cis*-configured DAD complex (Scheme 2).[12] The chemoselectivity can be explained by the fact that protonation of the nitrogen atom would result in interruption of the conjugation of the phenyl and the imino group. Interestingly, formation of the *s-trans*-configured complex **5** was observed in the reaction of ligand **3a** with $Mo(CO)_4$(nor) (Scheme 2). The structure of complex **5** was determined by spectroscopic means: whereas only two carbonyl absorptions (IR) are observed for $Mo(CO)_4$(nor), four absorptions are observed for complex **5**. In addition, two sets of signals are

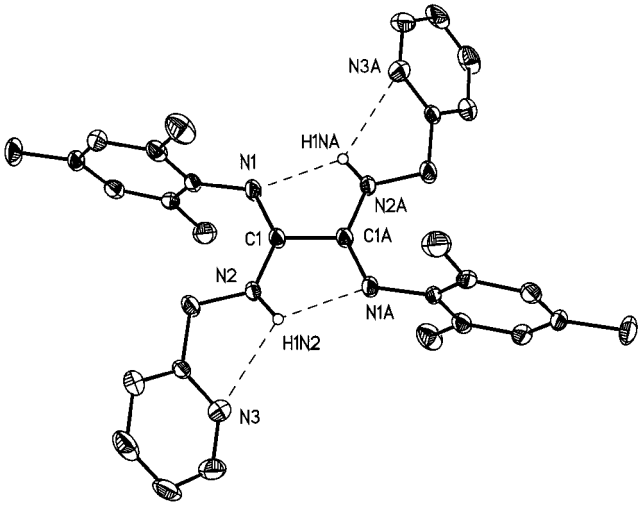

Figure 1. ORTEP plot of **3a** with the atom numbering scheme; the thermal ellipsoids of 50% probability are shown for the non-hydrogen atoms; selected bond lengths [Å] and angles [°]: N1−C1 1.276(3), N2−C1 1.340(3), C1−C1A 1.526(4); N1−C1−C1A 116.5(2), N2−C1−C1A 113.1(2), C1−N2−C2 128.2(2), N2−C2−C3−N3 40.3, C1−N1−C8−C9 104.9

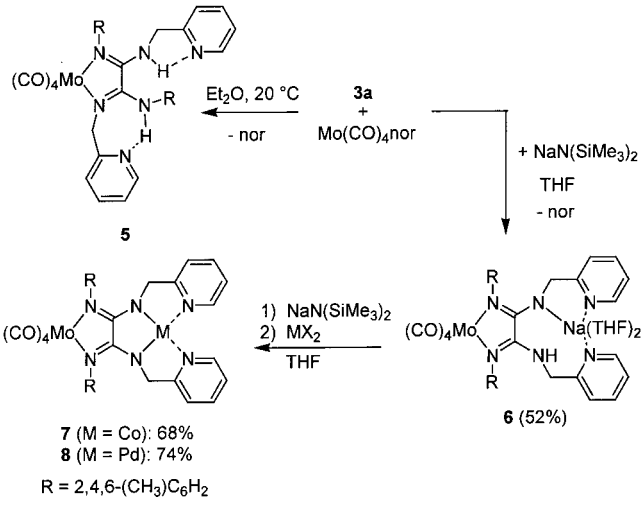

Scheme 2. Synthesis of hetero-dimetallic complexes **5**−**8**

observed in the ^{1}H NMR spectrum. In the ^{13}C NMR spectrum of **5**, separate signals are detected for all carbon atoms which could be assigned to the proposed structure. All spectroscopic data indicate that complex **5** adopts an unsymmetrical structure containing an *s-trans*-configured oxalamidine unit rather than a symmetrical structure containing a *cis*-configured oxalamidine unit. The *s-trans* selectivity can be explained by the assumption that the hydrogen bond involving the pyridine nitrogen is more stable than the hydrogen bond located within the oxalamidine substructure. The 2-aminomethylpyridine subunit is planar due to intramolecular hydrogen bonding. Therefore, coordination of *two aromatic* imino groups to the metal would result in severe steric interactions. Coordination of *two* aliphatic imino groups to the metal would result in cleavage of two relatively stable pyridine hydrogen bonds. In contrast, formation of complex

5 involves a prototropic shift, cleavage of a weak hydrogen bond and formation of a strong one.

To support our hypothesis, compound **3a** was deprotonated with $NaN(SiMe_3)_2$: reaction of the sodium salt of **3a** with $Mo(CO)_4$(nor) gave the *s-cis*-configured heterodimetallic complex **6** (Scheme 2). The structure of complex **6** was independently confirmed by an X-ray structure analysis (Figure 2). The pyridine moieties are located above and below the plane of the chelate system. The mesityl substituents of the ligand are located orthogonal to each other due to steric interactions. The sodium atom is coordinated by two pyridine nitrogens, by an amidinate-derived nitrogen atom and by an oxygen atom of a neighbouring molecule. These atoms define the equatorial square plane of a distorted octahedron. The oxygen atoms of two THF molecules are located at the axial positions. The Mo−C33 bond is shorter than the other Mo−C distances due to the *trans* effect of the nitrogen N1 and the polarizing influence of the sodium ion. The C35−O3 bond is elongated (1.189 Å) and lies in the same range as normal C−O double bonds.[13]

Deprotonation of the NH group of complex **6** and subsequent reaction with one equivalent of $CoBr_2$ or $PdCl_2$ resulted in formation of the heterodimetallic complexes **7** (Mo/Co) and **8** (Mo/Pd). The spectroscopic properties of these products are very similar to those of complex **6**, which suggests that the same type of structure is adopted. For compound **8** only two signals (^{1}H NMR) are observed for the CH_3 groups and only one signal is observed for the CH_2 groups. The chemical shifts are almost identical to those observed for complex **6**. Due to the anionic character of the ligands, bathochromic shifts (IR) are observed for the equatorial carbonyl ligands of complexes **6**−**8**. Whereas examples are known where hydrogen bonding influences the selectivity or the rate of organic transformations, such effects are rare in complexation reactions. However, such processes should play an important role in the binding of transition metals to biomolecules.

The synthesis and properties of *homo*dimetallic complexes were next studied. Reaction of $Cu(OAc)_2$ with the pyridyloxalamidines **3** and **4** resulted in formation of the deeply green to black coloured (Cu/Cu) complexes **9** and **10** (Scheme 3). Reaction of ligands **3** with $PdCl_2(CH_3CN)_2$ resulted in formation of the orange coloured (Pd/Pd) complexes **11**.

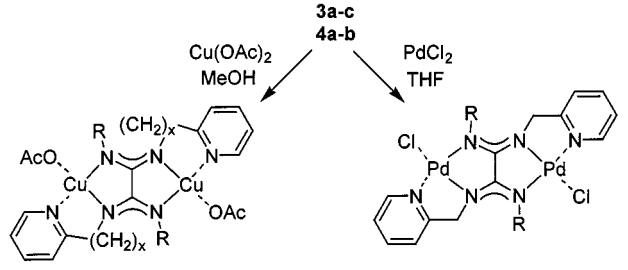

9a (R = 2,4,6-$Me_3C_6H_2$):	34%	**11a** (R = 2,4,6-$Me_3C_6H_2$):	41%
9b (R = 2,6-$Me_2C_6H_2$):	50%	**11b** (R = 2,6-(*i*Pr)$_2C_6H_2$):	50%
9c (R = 2,6-(*i*Pr)$_2C_6H_2$):	72%	**11c** (R = 4-MeC_6H_4):	62%
10a (R = 4-MeC_6H_4):	62%		
10b (R = 2,6-$MeOC_6H_4$):	68%		

Scheme 3. Synthesis of homo-dimetallic complexes **9**−**11**

The structure of the Cu complex **10a** was independently confirmed by an X-ray structure analysis (Figure 3). Deeply green coloured single crystals of **10a** were obtained from a

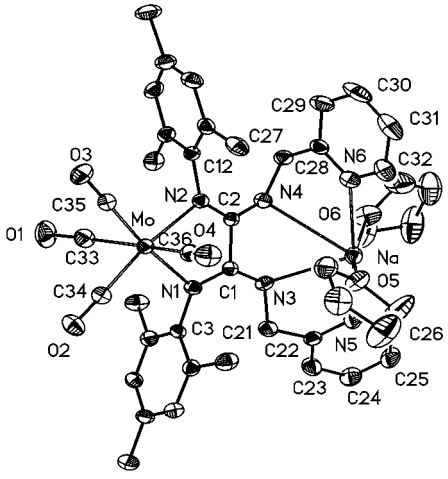

Figure 2. ORTEP plot of **6** with the atom numbering scheme; the thermal ellipsoids of 50% probability are shown for the non-hydrogen atoms; selected bond lengths [Å] and angles [°]: Mo−N1 2.244(3), Mo−C35 1.916(5), N3−C1 1.310(5), N5−Na 2.426(5), O2−C34 117.2(6), Mo−N2 2.271(3), N1−C1 1.348(5), N3−Na 2.652(4), N6−Na 2.518(4), O3−C35 1.184(5), Mo−C33 2.031(5), N2−C2 1.289(5), N4−C2 1.360(5), O3A−Na 2.378(4), C1−C2 1.524(6); N1−Mo−N2 71.52(12), N1−C1−C2 112.5(3), N4−C2−C1 112.4(4), Mo−N1−C1 119.6(3), N2−C2−C1 117.4(4), C1−N3−Na 112.4(3), N3−Na−N6 109.9(13), Mo−N2−C2 118.3(3), N3−C1−C2 113.4(4), N3−Na−N5 66.94(13)

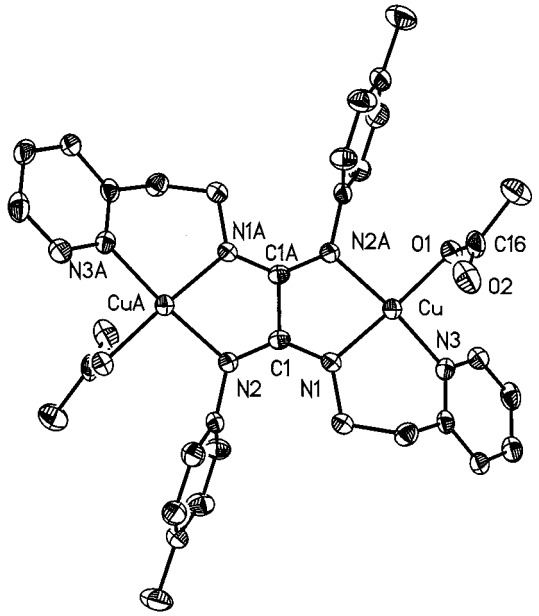

Figure 3. ORTEP plot of **10a** with the atom numbering scheme; the thermal ellipsoids of 50% probability are shown for the non-hydrogen atoms; selected bond lengths [Å] and angles [°]: N1−C1 1.314(6), Cu−N1 1.940(3), Cu−N3 2.008(3), N2−C1 1.316(4), Cu−N2A 1.973(3), Cu−O1 1.953(3), C1−C1A 1.537(3); N1−C1−C1A 113.4(4), N2A−Cu−O1 94.16(11), C1−N1−Cu 115.6(2), N2−C1−C1A 113.9(4), C1−N2−CuA 114.2(2), N1−Cu−N3 94.22(12), N1−Cu−N2A 82.92(12)

1:1 solution of MeOH and water. The ligand shows an *s-trans*-(*E*/*E*) configuration. The square-planar coordination spheres of the Cu^{II} atoms are distorted. The amidine moiety is planar. In contrast, the tolyl groups are twisted out of plane by ca. 90°. The bond lengths C1−N1 and C1−N2 are almost identical, due to delocalization of the π-electrons (N1−C1−N2). Whereas intense (C=N) absorptions (IR) were observed for the free ligands, no respective absorptions were present for the metal complexes **9−11**, again due to delocalization of the π-electrons. In the electron paramagnetic resonance (EPR) spectrum of complex **10b** a signal was detected at $g = 2.082$. Although the hyperfine structure could not be resolved, the value and the anisotropy of the resonance line were typical for the $g_\perp$ signal of Cu^{II}. An antiferromagnetic interaction between the Cu atoms can be anticipated.[14] Quantitative EPR measurements showed that only ca. 15% of Cu^{II} with $s = 0.5$ was present. The magnetic moment of complex **10b** ($\mu_{eff} = 1.55$ BM, T = 296 K) was lower than the spin-only value of the Cu^{II} ion ($\mu_{eff} = 1.73$ BM).

In conclusion, we have reported the synthesis of conformationally locked oxalic acid-derived amidines with pendant pyridine functionalities. Based on this multivalent ligand system, new hetero- and homodimetallic complexes were efficiently prepared.

Experimental Section

General: All solvents were dried by standard methods and all reactions were carried out under an inert atmosphere. Petroleum ether (PE, b.p. 40−70 °C), diethyl ether (E), *tert*-butyl methyl ether (MTBE), toluene and acetone were distilled prior to use. The solvents that were used for the reactions (THF and ether), were distilled from sodium/benzophenone immediately prior to use. The oxalic acid bis(imidoyl)chlorides were prepared according to literature procedures.[4e] NMR: 200 MHz and 50 MHz (for ^1H and ^{13}C, respectively), if not quoted otherwise, on an AC 200 F (Bruker) apparatus. The solvents $CDCl_3$, CD_2Cl_2 and [D_8]THF were used as received. The multiplicity of the carbon atoms was determined by the DEPT 135 technique and quoted as: CH_3, CH_2, CH and C for primary, secondary, tertiary and quaternary carbon atoms. MS: EI, 70 eV; CI, H_2O: chemical ionization with water. Preparative scale chromatography: J. T. Baker silica gel (60−200 mesh). For the EPR measurements, an ESP 300 E apparatus (Bruker, ν = 9.4 GHz, internal standard: diphenylpicrylhydrazyl). Melting points, uncorrected, were measured using a Büchi apparatus. Elemental analyses: Microanalytical laboratory of the Universities of Hannover and Jena.

General Procedure for the Preparation of Oxalic Acid Amidines (3): A THF solution of **1** (2.0 mmol), 2-picolylamine (0.44 mL) and NEt_3 (0.63 mL, 4.5 mmol) was refluxed for 48 h. After cooling, the precipitated $HNEt_3Cl$ was filtered and the solvent of the filtrate was removed in vacuo. The residue was purified by chromatography (toluene → toluene/acetone = 1:1).

***N*,*N*′-Bis(2-pyridylmethyl)-1,2-bis(2,4,6-trimethylphenylimino)-ethane-1,2-diamine (3a):** Yield: 0.73 g of colourless crystals (72%), m.p. 148−150 °C. − ^1H NMR (200 MHz, CD_2Cl_2): δ = 2.10 (s, 12 H, 2- and 6-CH_3), 2.29 (s, 6 H, 4-CH_3), 4.00 (s, 4 H, CH_2), 6.82 (s, 4 H, CH), 7.02 (br. d, 2 H, Pyr-CH), 7.14 (t, 2 H, Pyr-CH), 7.59 (t, 2 H, Pyr-CH), 8.20 (br, 2 H, NH), 8.48 (d, 2 H, Pyr-CH). − ^{13}C NMR (50 MHz, CD_2Cl_2): δ = 18.6 (2,6-CH_3), 20.9 (4-CH_3), 47.6, 121.6, 122.4, 128.3, 128.6, 131.6, 136.7, 144.5, 146.0 (br), 149.5, 158.1. IR (Nujol): $\tilde{\nu}$ = 3309 (m, ν_{NH}), 1648 (s, ν_{CN}), 1607 (m), 1592 (m), 1569 (m) cm^{-1}. − MS [CI (H_2O)]: *m*/*z* (%) = 505 (100) [M^+ + 1], 412 (24), 252 (18) [M^+/2], 93 (19). − $C_{32}H_{36}N_6$ (504.7): calcd. C 76.16, H 7.19, N 16.65; found C 76.21, H 7.11, N 16.33.

1,2-Bis(2,6-dimethylphenylimino)-*N*,*N*′-bis(2-pyridylmethyl)ethane-1,2-diamine (3b): Yield: 1.1 g of colourless crystals (58%), m.p. 136−138 °C. ^1H NMR (200 MHz, CD_2Cl_2): δ = 2.14 (s, 12 H, CH_3), 4.00 (d, J = 4.4 Hz, 4 H, CH_2), 6.87 (t, J = 6.3 Hz, 2 H, Pyr-CH), 7.00 (d, J = 6.7 Hz, 6 H, Ar), 7.13 (t, J = 5.0 Hz, 2 H, Pyr), 7.58 (t, J = 7.7 Hz, 2 H, Pyr), 8.19 (br, 2 H, NH), 8.48 (d, J = 4.8 Hz, 2 H, Pyr). − ^{13}C NMR (50 MHz, CD_2Cl_2): δ = 18.6 (CH_3), 47.5 (CH_2), 121.6, 122.4, 127.6, 128.9, 136.7, 145.6, 147.2, 149.5, 157.9. − IR (Nujol): $\tilde{\nu}$ = 3301 (s, ν_{NH}), 1662 (s, ν_{CN}), 1588 (s), 1569 (m), 1492 (s) cm^{-1}. − MS [CI (H_2O)]: *m*/*z* (%) = 477 (100) [M^+ + 1], 384 (19), 238 (10) [M^+/2], 147 (4), 126 (7), 110 (5), 93 (12). − $C_{30}H_{32}N_6$ (476.6): calcd. C 75.60, H 6.77, N 17.63; found C 75.74, H 7.17, N 17.32.

1,2-Bis(2,6-diisopropylphenylimino)-*N*,*N*′-bis(2-pyridylmethyl)-ethane-1,2-diamine (3c): Yield: 0.85 g of colourless crystals (72%), m.p. 144−146 °C. − ^1H NMR (200 MHz, CD_2Cl_2): δ = 1.19, 1.23 (2 × d, J = 1.9 Hz, 2 × 12 H, *iPr*-CH_3), 3.14 (m, 4 H, *i*Pr-CH), 4.11 (s, 4 H, CH_2), 7.01−7.28 (m, 10 H, Ar, Hetar), 7.58 (t, 2 H, J = 7.7 Hz, Hetar), 8.21 (br, 2 H, NH), 8.46 (d, J = 4.8 Hz, 2 H, Hetar). ^{13}C NMR (50 MHz, CD_2Cl_2): δ = 22.5, 22.6 (*iPr*-CH_3), 29.3 (*iPr*-C), 47.7, 121.4, 122.4, 122.8, 123.0, 136.8, 138.9, 145.2, 149.6, 157.9. − IR (Nujol): $\tilde{\nu}$ = 3289 (s, ν_{NH}), 1658 (s, ν_{CN}), 1592 (s), 1582 (m), 1569 (m) cm^{-1}. − MS [CI (H_2O)]: *m*/*z* (%) = 589 (100) [M^+ + 1], 294 (8) [M^+/2]. − $C_{38}H_{48}N_6$ (588.8): calcd. C 77.51, H 8.22, N 14.27; found C 76.88, H 8.29, N 14.08.

3-(2,6-Diisopropylphenylamino)-4-(diisopropylphenylimino)-4*H*-pyrido[1,2-a]pyrazine (2): During the synthesis of **3c**, **2** was isolated as an orange coloured solid (250 mg, 15%); m.p. 147−148 °C. − ^1H NMR (200 MHz, CD_2Cl_2): δ = 1.12−1.27 (m, J = 6.9 Hz, 12 H, *i*Pr-CH_3), 3.04 (hex, J = 6.9 Hz, 4 H, *i*Pr-CH), 6.14 (t, J = 6.7 Hz, 1 H, Py), 6.43 (t, J = 7.6 Hz, 1 H, Py), 6.92−7,33 (m, 8 H, Ar), 7.42 (s, 1 H, NH), 7.97 (d, J = 7.7 Hz, 1 H, Py). − ^{13}C NMR (50 MHz, CD_2Cl_2): δ = 22.7, 2.8 (*i*Pr-CH_3), 29.1, 29.5 (*i*Pr-CH), 113.3, 117.4, 120.6, 122.8, 123.1, 123.8, 125.8, 126.1, 127.1, 127.8, 129.8, 134.3, 137.9, 145.1, 146.2, 147.3. − IR (Nujol): $\tilde{\nu}$ = 3376 (s, ν_{NH}); 1624 (s, $\nu_{C=N}$); 1586 (m); 1556 (s) u. 1496 (s) cm^{-1}. − MS [CI (H_2O)]: *m*/*z* (%) = 481 (100) [M^+ + 1], 437 (8), 293 (10), 187 (7), 146 (6). − $C_{32}H_{40}N_4$ (480.70): calcd. C 79.96, H 8.39, N 11.66; found C 79.20, H 8.42, N 12.17.

General Procedure for the Preparation of Ligands 4: To a THF solution (100 mL) of 2-(2-aminoethyl)pyridine (20 mmol) and NEt_3 (2.8 mL, 20 mmol) was slowly added a THF solution (50 mL) of **1** (10 mmol) at 0 °C. The mixture was slowly warmed to ambient temperature and was then stirred at 50 °C for 1 h. After cooling, the precipitated $HNEt_3Cl$ was filtered and the solvent of the filtrate was removed in vacuo. The residue was isolated by addition of ether to the crude product and purified by recrystallization from $MeOH/H_2O$.

***N*,*N*′-Bis[(2-aminoethyl)-2-pyridyl]-1,2-bis(4-tolylimino)ethane-1,2-diamine (4a):** Yield: 0.51 g of a brown-yellow solid (53%), m.p. 125−126 °C. − ^1H NMR (200 MHz, [D_8]THF): δ = 2.22 (s, 6 H, Tol-CH_3), 2.98 (br, 4 H, CH_2 to Pyr), 3.60 (br, 4 H, CH_2 to NH),

6.43 (br, 4 H, Ar), 6.80 (d, J = 7.1 Hz, Pyr, 2 H), 7.12 (m, 6 H, Ar, Pyr), 7.58 (t, J = 7.2 Hz, 4 H, Pyr), 8.45 (d, J = 6.5 Hz, 2 H, NH). − ^{13}C NMR (50 MHz, [D$_8$]THF): δ = 20.8 (CH_3), 37.4 (CH_2 to Pyr), 41.2 (CH_2 to NH), 121.7, 122.6, 123.8, 129.0, 130.9, 136.6, 148.2, 149.8, 151.9, 161.3. − IR (Nujol): $\tilde{\nu}$ = 3261 (s, ν_{NH}), 1639 (s, $\nu_{C=N}$), 1622 (s), 1605 (s), 1588 (m), 1536 (s), 1507 (s) cm^{-1}. − MS [EI]: m/z (%) = 476 (8) [M$^+$], 383 (7), 370 (5), 278 (16) [M$^+$/2], 145 (6), 134 (9), 118 (12), 106 (100), 94 (17), 91 (13), 78 (14), 65 (5). − $C_{30}H_{32}N_6$ (476.6): calcd. C 75.60, H 6.77, N 17.63; found C 75.63, H 6.77, N 17.63.

***N*,*N*′-Bis[(2-aminoethyl)-2-pyridyl]-1,2-bis(4-methoxyphenylimino)-ethane-1,2-diamine (4b):** Yield: 3.9 g of a brown-yellow solid (76%), m.p. 85−87 °C. − ^{1}H NMR (200 MHz, [D$_6$]DMSO): δ = 2.96, 3.49 (br, 2 × 4 H, CH_2), 3.65 (s, 6 H, OCH_3), 3.60, 6.57 (2 × d, J = 8.5 Hz, 2 × 4 H, Ar), 7.24 (m, 6 H, Pyr), 7.73 (m, 2 H, Pyr), 8.48 (d, J = 4.5 Hz, 2 H, NH). − ^{13}C NMR (50 MHz, [D$_6$]DMSO): δ = 36.3, 40.8 (CH_2), 55.0 (OCH_3), 112.9, 121.3, 122.5, 123.0, 136.3, 143.0, 148.9, 151.2, 154.2, 159.6. − IR (Nujol): $\tilde{\nu}$ = 3248 (s, ν_{NH}), 1638 (s), 1618 (s), 1566 (s), 1531 (s), 1504(s) cm^{-1}. − MS [CI (H_2O)]: m/z (%) = 509 (100) [M$^+$ + 1], 415 (8), 301 (41), 254 (6) [M$^+$/2], 149 (10), 124 (37), 106 (61), 93 (7). − $C_{30}H_{32}N_6O_2$ (508.6): calcd. C 70.84, H 6.34, N 16.52; found C 70.49, H 6.58, N 16.07.

Synthesis of Tetracarbonyl[*N*,*N*′-bis(2-pyridylmethyl)-1,2-bis(2,4,6-trimethylphenylimino)ethane-1,2-diamine]molybdenum (5): An ether solution of $Mo(CO)_4$(nor) (0.30 g, 1.0 mmol) and **3a** (1.0 mmol) was stirred for 24 h. The product was filtered, washed with a small amount of cold ether and dried in vacuo to give 0.39 g of red crystals (55%). ^{1}H NMR (200 MHz, CD_2Cl_2): δ = 2.22−2.38 (m, 18 H, CH_3), 5.00, 5.26 (2 × s, 2 × 2 H, CH_2), 6.55−8.86 (m, 12 H, Ar), 10.42 (s, 2 H, NH). − ^{13}C NMR (50 MHz, CD_2Cl_2): δ = 18.8, 19.3, 21.0 (CH_3), 121.1, 121.6, 121.8, 122.4, 123.1, 123.2, 128.3, 128.8, 128.9, 129.3, 129.5, 130.3, 132.3, 132.8, 132.9, 136.7, 137.1, 138.0, 138.8, 148.9, 149.6, 152.9, 156.1, 160.1, 161.1, 205.4, 206.9, 221.9; IR (Nujol): $\tilde{\nu}$ = 3400 (w, ν_{NH}), 2006, 1907, 1893, 1862, 1815, 1803, 1781 (s, $\nu_{C\equiv O}$), 1592 (s), 1572 (s), 1561 (s), 1484 (s) cm^{-1}. − $C_{36}H_{36}MoN_6O_4$ (712.7): calcd. C 60.67, H 5.09, N 11.79; found C 60.11, H 5.03, N 11.72.

Synthesis of Bis(tetrahydrofuran)sodium Tetracarbonyl[*N*,*N*′-bis(2-pyridylmethyl)-1,2-bis(2,4,6-trimethylphenylimino)ethane-1,2-diaminato]molybdate (6): To a THF solution (25 mL) of **3a** (0.51 g, 1.0 mmol) was slowly added a THF solution of $NaN(SiMe_3)_2$ (1 mL, 1 M). After stirring for 30 min the solution was warmed to 20 °C and a THF solution (30 mL) of $Mo(CO)_4$(nor) (0.30 g, 1.0 mmol) was added. After stirring for 2 h, the precipitated yellow solid was filtered, washed three times with THF (10 mL) and dried in vacuo to give 0.45 g of yellow crystals (52%). ^{1}H NMR (200 MHz, [D$_6$]DMSO): δ = 2.00, 2.13 (2 × s, 2 × 9 H, CH_3), 5.32, 4.12 (2 × s, 2 × 2 H, CH_2), 6.55−8.27 (m, 12 H, Ar). − IR (Nujol): $\tilde{\nu}$ = 1991, 1877, 1863, 1812, 1769, 1754 (s, $\nu_{C\equiv O}$), 1593 (m), 1566 (m), 1537 (s) cm^{-1}. − $C_{44}H_{51}N_6MoNaO_6$ (878.9): calcd. C 60.13, H 5.85, N 9.56; found C 59.59, H 5.65, N 9.26.

Synthesis of Metal Complexes (7a−b): To a THF solution (25 mL) of **6** (0.51 g, 1.0 mmol) was added a THF solution of $NaN(SiMe_3)_2$ (2 mL, 1 M). After stirring for 30 min a THF solution (30 mL) of $Mo(CO)_4$(nor) (0.30 g, 1.0 mmol) was added. The solution was stirred for 30 min and subsequently a THF solution (25 mL) of $CoBr_2(THF)_2$ or $PdCl_2(CH_3CN)_2$ (1 mmol) was added. After stirring for 4 h the solution was filtered (celite) and the filtrate was concentrated in vacuo. An ether layer was added on the top of the THF solution which resulted in precipitation of the product as greenish crystals.

Cobalt(II) Bis(tetrahydrofuran)[*N*,*N*′-bis(2-pyridylmethyl)-1,2-bis(2,4,6-trimethylphenylimino)ethane-1,2-diaminato]molybdate (7a): Yield: 0.52 g (68%). − IR (Nujol): $\tilde{\nu}$ = 1983, 1929, 1854, 1838, 1805 (s, $\nu_{C\equiv O}$), 1610 (s, $\nu_{C=N}$), 1579 (s), 1558 (s) cm^{-1}. − $C_{44}H_{50}CoMoN_6O_6$ (913.78): calcd. C 57.83, H 5.52, N 9.20, Co 6.45; found C 57.19, H 5.93, N 9.42, Co 6.55.

Palladium(II) Bis(tetrahydrofuran)[*N*,*N*′-bis(2-pyridylmethyl)-1,2-bis(2,4,6-trimethylphenylimino)ethane-1,2-diaminato]molybdate (7b): Yield: 0.71 g (74%). − ^{1}H NMR (200 MHz, [D$_6$]DMSO): δ = 2.04, 2.14 (2 × s, 18 H, CH_3), 4.16 (br, 4 H, CH_2), 6.64, 8.54 (m, 12 H, Ar, Pyr). − IR (Nujol): $\tilde{\nu}$ = 1995, 1914, 1883, 1822, 1745 (s, $\nu_{C\equiv O}$), 1611 (s, $\nu_{C=N}$), 1586 (s), 1562 (s) cm^{-1}. − $C_{44}H_{50}MoN_6O_6Pd$ (961.3): calcd. C 54.98, H 5.24, N 8.74; found C 54.43, H 5.13, N 9.00.

Synthesis of the Dimetallic Cu Complexes (9a−c) and (10a−b): A MeOH solution (25 mL) of $Cu(OAc)_2(H_2O)$ (0.36 g, 2.0 mmol) and of the ligand **3** or **4** (1 mmol) was stirred for 2 h at 50 °C. The deep green solution was filtered and the solvent of the filtrate was removed in vacuo. To the residue was added ether and the precipitate was filtered and dried in vacuo. The crude product was recrystallized from MeOH or H_2O/MeOH (1:1).

Bis(acetato)[*N*,*N*′-bis(2-pyridylmethyl)-1,2-bis(2,4,6-trimethylphenylimino)ethane-1,2-diaminato]dicuprate(II) (9a): Yield: 0.25 g of deep green to black crystals (34%). − IR (Nujol): $\tilde{\nu}$ = 1613 (s), 1595 (s), 1566 (s) cm^{-1}. − $C_{36}H_{40}Cu_2N_6O_4$ (747.8): calcd. C 57.82, H 5.39, N 11.24, Cu 16.99; found C 57.80, H 5.38, N 11.19, Cu 16.41.

Bis(methanol)bis(acetato)[1,2-bis(2,6-dimethylphenylimino)-*N*,*N*′-bis(2-pyridylmethyl)ethane-1,2-diaminato]dicuprate(II) (9b): Yield: 0.40 g of deep green to black crystals (50%). − IR (Nujol): $\tilde{\nu}$ = 3370 (br, $\nu_{OH(MeOH)}$), 1611 (s), 1582 (s), 1567 (s) cm^{-1}. − $C_{36}H_{42}Cu_2N_6O_6$ (781.9): calcd. C 55.30, H 5.41, N 10.75, Cu 16.26; found C 55.06, H 5.38, N 10.87, Cu 15.95.

Bis(acetato)[1,2-bis(2,6-diisopropylphenylimino)-*N*,*N*′-bis(2-pyridylmethyl)ethane-1,2-diaminato]dicuprate(II) (9c): Yield: 0.57 g of deep green to black crystals (69%). − IR (Nujol): $\tilde{\nu}$ = 1625 (s), 1599 (s), 1582 (s), 1567 (s) cm^{-1}. − $C_{42}H_{52}Cu_2N_6O_4$ (832.0): calcd. C 60.63, H 6.30, N 10.10, Cu 15.28; found C 60.71, H 6.42, N 10.11, Cu 14.87.

Bis(methanol)bis(acetato){*N*,*N*′-bis[(2-aminoethyl)-2-pyridyl]-1,2-bis(4-tolylimino)ethane-1,2-diaminato}dicuprate(II) (10a): Yield: 0.49 g of deeply green to black coloured crystals (62%). − IR (Nujol): $\tilde{\nu}$ = 3265 (br, $\nu_{OH(MeOH)}$), 1607 (s), 1571 (s), 1505 (s), 1485 (s) cm^{-1}. − $C_{36}H_{42}Cu_2N_6O_6$ (781.9): calcd. C 55.30, H 5.41, N 10.75, Cu 16.26; found C 55.37, H 5.58, N 10.67, Cu 15.74.

Bis(methanol)bis(acetato){*N*,*N*′-bis[(2-aminoethyl)-2-pyridyl]-1,2-bis(4-methoxyphenylimino)ethane-1,2-diaminato}dicuprate(II) (10b): Yield: 0.53 g of deep green to black crystals (68%). − IR (Nujol): $\tilde{\nu}$ = 3390 (br, ν_{OH}, MeOH), 1606 (s), 1586 (s), 1502 (s), 1486 (s) cm^{-1}. − μ_{eff} = 1.5 BM. − EPR (296 K, solid): $g_\perp$ = 2.0036. − $C_{35}H_{40}Cu_2N_6O_7$ (783.8): calcd. C 53.70, H 5.15, N 10.74, Cu 16.09; found C 53.36, H 5.01, N 10.88, Cu 15.87.

Synthesis of the Dimetallic Pd Complexes (11a−c): A THF solution (30 mL) of $PdCl_2(CH_3CN)_2$ (0.52 g, 2.0 mmol) and of the ligand **3** or **4** (1.0 mmol) was stirred for 24 h at 20 °C. The product, which precipitated as an orange solid, was filtered, washed with THF and dried in vacuo.

Dichloro[*N*,*N*′-bis(2-pyridylmethyl)-1,2-bis(2,4,6-trimethylphenylimino)ethane-1,2-diaminato]dipalladate(II) (11a): Yield: 0.36 g of an

orange solid (41%). − IR (Nujol): $\tilde{\nu}$ = 1633 (s), 1610 (m), 1593 (s), 1577 (s), 1568 (s), 1515 cm^{-1}. − $C_{38}H_{46}Cl_2N_6Pd_2$ (870.6): calcd. C 52.43, H 5.33, N 9.65, Cl 8.14; found C 51.88, H 5.35, N 10.45, Cl 8.12.

Dichloro[1,2-bis(2,6-diisopropylphenylimino)-*N*,*N*′-bis(2-pyridylmethyl)ethane-1,2-diaminato]dipalladate(II) (11b): Yield: 0.50 g of an orange solid (58%). − IR (Nujol): $\tilde{\nu}$ = 1610 (m), 1593 (s), 1577 (s), 1564 (s) cm^{-1}. − $C_{38}H_{46}Cl_2N_6Pd_2$ (870.6): calcd. C 52.43, H 5.33, N 9.65, Cl 8.14; found C 51.88, H 5.35, N 10.04, Cl 8.45.

Dichloro{*N*,*N*′-bis[(2-aminoethyl)-2-pyridyl]-1,2-bis(4-tolylimino)-ethane-1,2-diaminato}dipalladate(II) (11c): Yield: 0.39 g of an orange solid (52%). − ^{1}H NMR (200 MHz, [D$_6$]DMSO): δ = 2.18 (s, 6 H, CH_3), 2.97, 3.31 (2 × br, 2 × 4 H, CH_2), 6.93 (m, 4 H, Ar), 6.85 (t, J = 7.6 Hz, 1 h, Pyr), 6.93 (d, J = 6.9 Hz, 1 H, Pyr), 7.41 (t, J = 8.4 Hz, 1 H, Pyr), 8.40 (d, J = 5.4 Hz, 1 H, Pyr). − IR (Nujol): $\tilde{\nu}$ = 1673 (s), 1605 (m), 1579 (s), 1504 (m) cm^{-1}. − $C_{30}H_{30}N_6Cl_2Pd_2$ (758.4): calcd. C 47.51, H 3.99, N 11.08, Cl 9.35; found C 47.39, H 4.38, N 11.53, Cl 9.51.

Crystal Structure Determinations: The intensity data for the compound were collected on a Nonius Kappa CCD diffractometer, using graphite-monochromated Mo-K_α radiation. Data were corrected for Lorentz and polarization effects, but not for absorption.[15,16]

The structures were solved by direct methods (SHELXS [17]) and refined by full-matrix least-squares techniques against F_o^2 (SHELXL-97[18]). The hydrogen atoms of the structures were included at calculated positions with fixed thermal parameters. All non-hydrogen atoms were refined anisotropically.[18] XP (SIEMENS Analytical X-ray Instruments, Inc.) was used for structure representations.

Crystal Data for 3a:[19] $C_{32}H_{36}N_6$, M_r = 504.67 g mol^{-1}, colourless prism, size 0.40 × 0.38 × 0.32 mm^3, monoclinic, space group $P2_1/n$, a = 6.4164(5), b = 21.157(2), c = 10.3108(6) Å, β = 94.085(2)°, V = 1396.2(2) $Å^3$, T = 183 K, Z = 2, $\rho_{calcd.}$ = 1.200 gcm^{-3}, μ (Mo-K_α) = 0.73 cm^{-1}, F(000) = 540, 3067 reflections, Θ_{max} = 26.27°, 2815 independent reflections, 1724 reflections with $F_o > 4\sigma(F_o)$, 208 parameters, R = 0.0568, R_w = 0.1645, largest difference peak and hole: 0.369 e $Å^{-3}$.

Crystal Data for 6:[19] $C_{44}H_{51}MoN_6NaO_6$, M_r = 878.84 g mol^{-1}, colourless prism, size 0.30 × 0.25 × 0.15 mm^3, monoclinic, space group $P2_1/n$, a = 12.3530(6), b = 20.6111(5), c = 17.2796(8) Å, β = 94.755(1)°, V = 4384.4(3) $Å^3$, T= −90 °C, Z = 4, $\rho_{calcd.}$ = 1.331 gcm^{-3}, μ(Mo-K_α) = 3.62 cm^{-1}, F(000) = 1832, 11681 reflections in h(−13/0), k(−22/21), l(−19/19), measured in the range 3.95° ≤ Θ ≤ 23.31°, completeness Θ_{max} = 98.6%, 6126 independent reflections, R_{int} = 0.036, 5706 reflections with $F_o > 4\sigma(F_o)$, 527 parameters, 0 restraints, $R1_{obs}$ = 0.047, wR^2_{obs} = 0.121, $R1_{all}$ = 0.066, wR^2_{all} = 1.134, GOOF = 1.084, largest difference peak and hole: 0.485/−0.555 e $Å^{-3}$.

Crystal Data for 10a:[19] $C_{36}H_{44}N_6O_6Cu_2$, M_r = 783.85 g mol^{-1}, brown prism, size 0.40 × 0.38 × 0.36 mm^3, orthorhombic, space group $Pbca$, a = 9.173(1), b = 14.853(1), c = 26.275(1) Å, α = β = γ = 90°, V = 3579.9(5) $Å^3$, T = 183 K, Z = 4, $\rho_{calcd.}$ = 1.454 gcm^{-3}, μ(Mo-K_α) = 0.73 cm^{-1}, F(000) = 1632, 3634 reflections, Θ_{max} = 26.31°, 3634 independent reflections, 2228 reflections with $F_o > 4\sigma(F_o)$, 278 parameters, R = 0.0431, R_w = 0.0979, largest difference peak and hole: 0.413 e $Å^{-3}$.

Acknowledgments

P. L. thanks Professor Dr. A. de Meijere for his support. Financial support from the Fonds der Chemischen Industrie (Liebig scholarship and funds for P. L.) and from the Deutsche Forschungsgemeinschaft is gratefully acknowledged.

[1] [1a] D. W. Stephan, *Coord. Chem. Rev.* **1989**, *95*, 41. − [1b] W. A. Herrmann, B. Cornils, *Angew. Chem.* **1997**, *109*, 1074; *Angew. Chem. Int. Ed. Engl.* **1997**, *36*, 1049.

[2] A. Spannenberg, M. Oberthür, H. Noss, A. Tillack, P. Arndt, R. Kempe, *Angew. Chem.* **1998**, *110*, 2190; *Angew. Chem. Int. Ed.* **1998**, *37*, 2079.

[3] [3a] F. T. Edelmann, Coord. *Chem. Rev.* **1994**, *137*, 403. − [3b] J. Barker, M. Kilner, *Chem. Rev.* **1994**, *133*, 219. − [3c] J. R. Hagadorn, J. Arnold, *Angew. Chem.* **1998**, *110*, 1813; *Angew. Chem. Int. Ed.* **1998**, *37*, 1729. − [3d] G. D. Whitener, J. R. Hagadorn, J. Arnold, *J. Chem. Soc., Dalton Trans.* **1999**, 1249.

[4] For the coordination to boron, see: [4a] S. Trofimenko, *J. Am. Chem. Soc.* **1969**, *91*, 2139. − For titanium, see: [4b] M. Pasquali, C. Floriani, A. Chiesi-Villa, C. Guastini, *J. Am. Chem. Soc.* **1979**, *101*, 4740. − [4c] M. Döring, H. Görls, R. Beckert, *Z. Anorg. Allg. Chem.* **1994**, *620*, 551. − [4d] P. Fehling, M. Döring, F. Knoch, R. Beckert, H. Görls, *Chem. Ber.* **1995**, *128*, 405. − For the synthesis of oxalic acid-bis(imidoyl)chlorides, see: [4e] D.Lindauer, R. Beckert, T. Billert, M. Döring, H. Görls, *J. Prakt. Chem.* **1995**, *337*, 143. − [4f] J. Brandenburg, R. Beckert, P. Fehling, M. Döring, H. Görls, *J. Prakt. Chem.* **1996**, *338*, 430.

[5] K. Kincaid, C. P. Gerlach, G. R. Giesbrecht, J. R. Hagadorn, G. D. Whitener, A. Shafir, J. Arnold, *Organometallics* **1999**, *18*, 5360.

[6] [6a] L. M. Jackman, T. Jen, *J. Am. Chem. Soc.* **1975**, *97*, 2811. − [6b] G. Scherer, H.-H. Limbach, *J. Am. Chem. Soc.* **1994**, *116*, 1230.

[7] [7a] A. K. Aggarwal, D. W. Rodgers, M. Drottar, M. Ptashne, S. C. Harrison, *Science* **1988**, *242*, 899. − [7b] M. Sundaralingham, Y. C. Sekharudu, *Science* **1989**, *244*, 1333. − [7c] A. Askew, P. Ballester, C. Buhr, K. S. Jeong, S. Jones, K. Parris, K. Williams, J. Rebek, *J. Am. Chem. Soc.* **1989**, *111*, 1082. − [7d] M. M. Conn, J. Rebek, *Chem. Rev.* **1997**, *97*, 1647.

[8] [8a] H. C. M. Nelson, J. T. Finch, B. F. Luisi, A. Klug, *Nature* **1987**, *330*, 221. − [8b] V. Fritsch, E. Westhof, *J. Am. Chem. Soc.* **1991**, *113*, 8271.

[9] [9a] H. J. Savage, C. J. Elliot, C. M. Freeman, J. L. Finney, *J. Chem. Soc., Faraday Trans.* **1993**, *89*, 2609. − [9b] I. K. McDonald, J. M. Thornton, *J. Mol. Biol.* **1994**, *238*, 777.

[10] J. Yang, S. H. Gellman, *J. Am. Chem. Soc.* **1998**, *120*, 9090.

[11] Diazadiene transition metal complexes represent efficient catalysts for olefin polymerization: [11a] L. K. Johnson, S. Mecking, M. Brookhart, *J. Am. Chem. Soc.* **1996**, *118*, 267. − [11b] A. S. Abu-Surrah, B. Rieger, *Angew. Chem.* **1996**, *108*, 2627; *Angew. Chem. Int. Ed. Engl.* **1996**, *35*, 2475. − [11c] C. M. Killian, L. K. Johnson, M. Brookhart, *Organometallics* **1997**, *16*, 2005. − [11d] A. S. Abu-Surrah, B. Rieger, *Angew. Chem.* **1996**, *108*, 2627; *Angew. Chem. Int. Ed. Engl.* **1996**, *35*, 2475. See also: − [11e] G. van Koten, K. Vrieze, *Adv. Organomet. Chem.* **1982**, *21*, 151.

[12] M. Döring, P. Fehling, H. Görls, W. Imhof, R. Beckert, D. Lindauer, *J. Prakt. Chem.* **1999**, *341*, 748.

[13] F. H. Allen, O. Kennard, D. G. Watson, L. Brammer, A. G. Orpen, R. Taylor, *J. Chem. Soc., Perkin Trans. 2* **1987**, 1.

[14] For molecular-based ferromagnetic interactions in heterodimetallic complexes, see: K. Nakatani, J. Y. Carriat, Y. Journaux, Y., O. Kahn, F. Lloret, J. P. Renard, Y. Pei, J. Sletten, M. Verdaguer, *J. Am. Chem. Soc.* **1989**, *111*, 5739.

[15] COLLECT, Data Collection Software; Nonius B.V., Netherlands, **1998**.

[16] Z. Otwinowski, W. Minor, "Processing of X-ray Diffraction Data Collected in Oscillation Mode", in *Methods in Enzymology*, Vol.- 276, Macromolecular Crystallography, Part A, edited by C.W. Carter, R.M. Sweet, pp. 307−326, Academic Press **1997**.

[17] G.M. Sheldrick, *Acta Crystallogr. Sect. A* **1990**, *46*, 467.

[18] G.M. Sheldrick, SHELXL-97 (Release 97.2), University of Göttingen, Germany, **1997**.

[19] Crystallographic data (excluding structure factors) for the structure(s) included in this paper have been deposited with the Cambridge Crystallographic Data Centre as supplementary publication nos. CCDC-145494 (**3a**), CCDC-140090 (**6**), and CCDC-145493 (**10a**). Copies of the data can be obtained free of charge on application to CCDC, 12 Union Road, Cambridge CB2 1EZ, UK [Fax: (internat.) + 44-1223/336-033; E-mail: deposit@ccdc.cam.ac.uk].

Received June 14, 2000
[I00234]

Formation and Dissociation Kinetics of the Complexes $Gd(DOTP)^{5-}$ and $Gd(DOTPMB)^{-}$

László Burai,[a] Róbert Király,[a] István Lázár,[a] and Ernő Brücher*[a]

Keywords: Gadolinium / Imaging agents / Kinetics / Macrocyclic ligands / Phosphonate complexes

The monobutyl ester of H_8DOTP, the ligand $H_4DOTPMB$, was synthesized, and the protonation constants (K_i^H) and the stability constant of Gd(DOTPMB) were determined by pH-potentiometry (25 °C, 0.1 M Me_4NCl): $\log K_i^H$, (i = 1, 2, and 3) = 10.34(0.02), 7.72(0.025), and 2.42(0.030), respectively, and $\log K_{GdL}$ = 12.19(0.05). The rates of formation of Gd(DOTPMB) and Gd(DOTP) were studied by ^1H relaxometry in the pH range 5.4–7, and also by spectrophotometry in the case of Gd(DOTP) (7 < pH < 8). For both reactions, first-order rate constants were obtained at different concentration ratios of the reactants, which indicated the rapid formation of a reaction intermediate. The compositions of the intermediates are $Gd(H_iDOTPMB)$ (i = 1, 2) and $H_nGd(H_2DOTP)$ (n = 0–4), respectively, where one or two protons are attached to the nitrogen atoms of the ligand. The rate of rearrangement (k_r) of the intermediate $Gd(H_iDOTPMB)$ to the product Gd(DOTPMB) increases with increasing $[OH^-]$: $k_r = k_{OH}[OH^-] + k_{2OH}[OH^-]^2$, where k_{OH} = (1.3±0.25) $\times 10^3$ $M^{-1}s^{-1}$ and k_{2OH} = (7.8±0.2) $\times 10^{11}$ $M^{-2}s^{-1}$. For the formation reaction of Gd(DOTP), only the first term exists and k_{OH} = (7.2±0.1) $\times 10^3$ $M^{-1}s^{-1}$. For the complexation reactions, similar mechanisms were proposed in which deprotonation of the species Gd(HDOTPMB) and $H_nGd(HDOTP)$ plays the rate-determining role. For the deprotonation, general base catalysis was found to be satisfactory. The rate of dissociation of Gd(DOTPMB) in 0.025–1.0 M HCl solution ([HCl] + $[Me_4NCl]$ = 1.0 M) was lower than that of Gd(DOTP) and the first-order rate constants exhibited saturation curves with increasing $[H^+]$. Based on the assumption that the protonated species HGd(DOTPMB) and $H_5Gd(DOTP)$ dissociate, the rate constants (and protonation constants) were found to be (5.4±0.2) $\times 10^{-4}$ $M^{-1}s^{-1}$ (K_{GdL}^H = 1.7±0.1) and (2.1±0.1) $\times 10^{-4}$ $M^{-1}s^{-1}$ (K_{H4GdL}^H = 1.9±0.1), respectively.

Introduction

Complexes of lanthanides with the tri- and tetraacetate derivatives of cyclen (e.g. DOTA; H_4DOTA = 1,4,7,10-tetraazacyclododecanetetraacetic acid) are finding wide-ranging applications in medical diagnosis and therapy. $Gd(DOTA)^-$ is a clinically used contrast agent in magnetic resonance imaging (MRI).[1−5] The radioactive $^{90}Y(DOTA)^-$ attached to proteins or monoclonal antibodies is a potential drug in the therapy of cancer.[4,6] The success of the cyclic tetraazapolycarboxylates in practical use, and also their interesting chemistry, initiated the synthesis and study of the phosphonate analogues. The ligand 1,4,7,10-tetraazacyclododecanetetrakis(methylenephosphonic acid), H_8DOTP, an analogue of H_4DOTA, has also been synthesized.[7−9] The protonation constants of $DOTP^{8-}$ are unusually high because of the large negative charge of the ligand, and the first protonation constant could be determined only by ^1H NMR spectroscopy.[10] The stability constants of the complexes $Ln(DOTP)^{5-}$ [Ln^{3+} = lanthanide(III) ion] are somewhat higher than those of $Ln(DOTA)^-$.[10−12] However, the species $Ln(DOTP)^{5-}$ predominates only at pH > ca. 9, while in the pH range 4−9, protonated complexes are formed: $H_iLn(DOTP)^{(5-i)-}$ (i = 1−4). The successive protonation equilibria have been characterized by determining the protonation constants.[12]

The complex $Gd(DOTP)^{5-}$ cannot be used as a contrasting agent in MRI because of its high negative charge [at physiological pH values, the monoprotonated $GdH(DOTP)^{4-}$ predominates[12]]. However, some complexes $Ln(DOTP)^{5-}$ are used as shift and relaxation reagents in biology.[6,13−16]

The complexes of lanthanides with the monoesters of DOTP are similar to the complexes of DOTA in that they possess a single negative charge, and can be regarded as potential contrast agents in MRI. (The charges of the ligands DOTP and DOTPMB as well as those of the complexes will be written only when absolutely necessary.) The complex formed between Gd^{3+} and the monobutyl ester of

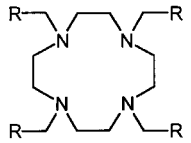

R = COOH	H_4DOTA
R = $PO(OH)_2$	H_8DOTP
R = PO(OBu)OH	$H_4DOTPMB$

Scheme 1

DOTP (= DOTPMB; see Scheme 1) interacts strongly with human serum albumin and is partly excreted through the hepatobiliary system. $Gd(DOTPMB)^-$ can therefore be regarded as a potential liver contrast agent.[17]

It is important for lanthanide complexes used in biological systems to be thermodynamically stable and in particular they should be kinetically inert. Whereas the stability constant of $Gd(DOTP)^{5-}$ is known,[12] that of

[a] Department of Inorganic and Analytical Chemistry, University of Debrecen,
Debrecen 4010, Hungary
Fax: (internat.) + 36-52/489-667
E-mail: ebrucher@delfin.klte.hu

 © WILEY-VCH Verlag GmbH, 69451 Weinheim, 2001 1434−1948/01/0303−0813 $ 17.50+.50/0

$Gd(DOTPMB)^-$ has not been reported.[17] Practically no quantitative data are available on the formation and dissociation rates of the Ln^{3+} complexes of DOTP and its esters. Kim et al. found that both the formation and dissociation of La(F-DOTPME) {F-DOTPME = 1,4,7,10-tetraazacyclododecane-1,4,7,10-tetrakis[methylenephosphonic acid mono-(2′,2′,2′-trifluoroethyl) ester]} were very slow, and that the stability constant of the complex ($\log K_{LaL}$ = 14.9[18]) was much lower than that of $La(DOTP)^{5-}$ ($\log K_{LaL}$ = 27.6[12]). Both this finding and the much lower protonation constants of the ligand F-$DOTPME^{4-}$ indicate that the basicity of the oxygen donors in the phosphonate ester functional groups, −PO(OR)OH, is much lower than that in the phosphonate groups, $-PO(OH)_2$. The values of the protonation constants indicate that the phosphonate ester groups, −PO(OR)OH, similarly to the phosphinate groups, −PO(R)OH, are strongly acidic.[18,19] In spite of the low basicity of the phosphinate oxygen atoms, the kinetic stability of the lanthanide complexes of the tetraazatetraphosphinate derivative ligand is very high. The proton-assisted dissociation rates of the phosphinate complexes in 0.1 M HCl are comparable with those of $Ln(DOTA)^-$.[4,5,19−23] Thus, a high kinetic stability can be expected for the complex $Gd(DOTPMB)^-$.

The rates of formation and dissociation of the complexes Gd(DOTP) and Gd(DOTPMB) were studied in order to obtain useful information about the biological application of the ligands DOTP and DOTPMB, and for a comparison of the kinetic behaviour of complexes formed with DOTP, DOTPMB, and DOTA, which have similar donor atoms but different functional groups and charges.

Results and Discussion

Protonation and Stability Constants

In order to control the purity of the DOTP sample, we re-determined the protonation constants of $DOTP^{8-}$. The K_1^H value was too high to be determined by pH-potentiometry.[10] The log K_i^H values (i = 2−7) obtained were 12.45(0.005), 9.18(0.007), 7.95(0.008), 6.08(0.008), 5.20(0.007), and 1.85(0.15), respectively, which agree well with the data reported earlier by Delgado et al.[10] and Geraldes et al.[8]

Three protonation constants could be determined by pH-potentiometry for the ligand $DOTPMB^{4-}$: $\log K_1^H$ = 10.34(0.020), $\log K_2^H$ = 7.72(0.025) and $\log K_3^H$ = 2.42(0.030). The completely deprotonated $DOTPMB^{4-}$ has only four negative charges, and its first two protonation constants are therefore significantly lower than those of $DOTP^{8-}$. The oxygen donor atoms of the $P(O)(OBu)O^-$ groups are weakly basic, and therefore we obtained only one protonation constant in the low pH range (2 < pH < 5). For the protonation sequence of the 12-membered tetraaza macrocyclic derivatives, which possess methylenephosphonate pendant arms, it was demonstrated that the first two protonations take place on two opposite nitrogen atoms of the ring.[8]

The stability constant of $Gd(DOTPMB)^-$, calculated from the titration data obtained with the "out-of-cell" technique, was found to be $\log K_{GdL}$ = 12.19(0.05). The formation of protonated or dinuclear complexes was not detected

The stability constant of $Gd(DOTPMB)^-$ is much lower than that of $Gd(DOTP)^{5-}$ ($\log K_{GdL}$ = 28.8[12]), because the charge of the $DOTPMB^{4-}$ and the basicity of its donor atoms are much lower than those of $DOTP^{8-}$.

Formation Kinetics of $Gd(DOTP)^{5-}$ and $Gd(DOTPMB)^-$

The reactions between Gd^{3+} and DOTP or DOTPMB in the pH range 5.4−7 are relatively slow and can be studied by measuring the longitudinal relaxation rates of the water protons. The relaxivities of Gd^{3+}·aq and the complexes $Gd(DOTP)^{5-}$ and $Gd(DOTPMB)^-$ differ sufficiently to furnish reliable rate data. In the presence of excess ligand, the formation rates can be expressed as Equation (1), where k_{obs} is a pseudo-first-order rate constant, and $[GdL]_t$ is the total concentration of the complex formed.

$$\frac{d[GdL]_t}{dt} = k_{obs}[Gd^{3+}] \quad (1)$$

Similarly to the results obtained in the study of the formation of the complexes $Ln(DOTA)^-$,[20−23] first-order rate constants were obtained even at comparable concentrations of the reactants. These findings were interpreted by assuming that there is a rapid formation of a reaction intermediate which rearranges to the product in the rate-determining step, characterized by the rate constant, k_r in Equation (2).

$$Gd^{3+} + H_xL \rightleftharpoons (x\text{-}y)H^+ + Gd(H_yL) \xrightarrow{k_r} GdL + yH^+ \quad (2)$$

The values of the rate constants, k_{obs}, increase with increasing ligand concentration, and at a ligand to Gd^{3+} ratio of approximately 2−3 give rise to a saturation value, k_r. In the presence of a 10-fold excess of ligand, we obtained such values (i.e., $k_{obs} = k_r$), which characterize the rate of rearrangement of the intermediate.

In the formation reactions of $Gd(DOTPMB)^-$, the ligand is present in the form of the species $H_2DOTPMB^{2-}$ and $HDOTPMB^{3-}$ (5.4 < pH < 7), since the protonation constants of $DOTPMB^{4-}$ ($\log K_i^H$) are 10.34, 7.72, and 2.42. The reaction intermediates formed by mixing solutions of Gd^{3+} and DOTPMB are probably mono- and diprotonated species, Gd(HDOTPMB) and $Gd(H_2DOTPMB)^+$, since there is practically no pH change at the start of the reaction. The structures of the intermediates are probably not similar to those of $Ce(H_2DOTA)^+$, Ce(HDOTA), and $Eu(H_2DOTA)^+$,[22,23] in which four carboxylate oxygens are coordinated to the Ln^{3+}, which occupies an "out-of-cage" position, while the protons protonate one or two nitrogen atoms. The structure of the ligand DOTPMB is not known and probably only two phosphonate ester groups of the mono- or diprotonated ligand can be coordinated to the Gd^{3+} in the intermediates.

The rate constants k_r are presented in Figure 1 and display a second-order dependence on the OH^- concentration.

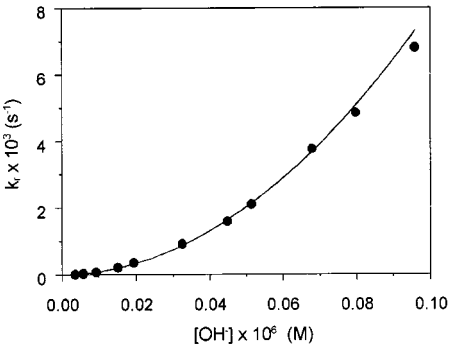

Figure 1. First-order rate constants (k_r) obtained for the formation reaction of $Gd(DOTPMB)^{-}$ {25 °C, 0.1 M $(CH_3)_4NCl$, $[Gd^{3+}]_t = 5\cdot10^{-4}$ M, $[L]_t = 5\cdot10^{-3}$ M}

$$k_r = k_{OH}[OH^-] + k_{2OH}[OH^-]^2 \quad (3)$$

The fit of the k_r data to Equation (3) gave the rate constants k_{OH} and k_{2OH}, presented in Table 1.

Table 1. Rate constants characterizing the formation of complexes with cyclen derivative ligands {25 °C, 0.1 M $(CH_3)_4NCl$}

	Gd(DOTP)	Gd(DOTPMB)	Gd(DOTA)[a]
k_{OH} [$M^{-1}s^{-1}$]	$(7.2\pm0.1)\cdot10^3$	$(1.3\pm0.25)\cdot10^3$	$5.9\cdot10^6$
k_{2OH} [$M^{-2}s^{-1}$]	–	$(7.8\pm0.2)\cdot10^{11}$	–
k_{LnHL} [s^{-1}]	–	$(3.3\pm1.6)\cdot10^{-4}$	18.5[b]
k^{OH}_{LnHL} [$M^{-1}s^{-1}$]	–	$(4.4\pm1.7)\cdot10^5$	$1.9\cdot10^7$[b]

[a] Ref.[26] – [b] Obtained for the formation of Ce(DOTA).[24]

The mechanism of formation of $Gd(DOTPMB)^{-}$ is presumably similar to those of the complexes $Ln(DOTA)^{-}$.[22–24] It is assumed that the diprotonated intermediate is involved in a dissociation equilibrium with the kinetically active monoprotonated intermediate [Equation (4)].

$$Gd(H_2DOTPMB)^+ \rightleftharpoons Gd(HDOTPMB) + H^+ \quad (4)$$

The extent of dissociation is characterized by the protonation constant, $K^H_{GdHL} = [GdH_2L]/([GdHL][H^+])$. With an increase in the pH, the monoprotonated intermediate is produced in increasing amounts in a direct reaction, since $\log K^H_2 = 7.72$. This intermediate undergoes deprotonation in a slow, rate-determining process, presumably with the assistance of an H_2O molecule [Equation (5)] or an OH^- ion [Equation (6)].[24]

$$Gd(HDOTPMB) + H_2O \xrightarrow{k_{GdHL}} Gd(DOTPMB)^- + H_3O^+ \quad (5)$$

$$Gd(HDOTPMB) + OH^- \xrightarrow{k^{OH}_{GdHL}} Gd(DOTPMB)^- + H_2O \quad (6)$$

The slow transfer of a proton is followed by a fast rearrangement of the deprotonated intermediate to furnish the product.

On the basis of the equilibrium reaction [Equation (4)], the concentration of the monoprotonated intermediate is directly proportional to the OH^- concentration, which explains the direct proportionality between the rate constant k_r and the OH^- concentration. The second-order dependence of the k_r values on the OH^- concentration can be interpreted in terms of the OH^--catalyzed deprotonation of the monoprotonated intermediate Gd(HDOTPMB) [Equation (6)].

When Equations (5) and (6) are taken into account, the rate of formation of $Gd(DOTPMB)^{-}$ can be given as in Equation (7).

$$\frac{d[GdL]_t}{dt} = k_{GdHL}[GdHL] + k^{OH}_{GdHL}[GdHL][OH^-] \quad (7)$$

Comparing Equation (1) and Equation (7), and bearing in mind that the formation of the intermediates is practically complete in the presence of excess ligand ($[Gd^{3+}] = [GdHL] + [GdH_2L]$), the concentration of GdH_2L can be expressed in terms of the protonation constant K^H_{GdHL}, when Equation (8) is obtained[24], where K_W ($= 1.66\cdot10^{-14}$) is the ionic product of water. From the fit of the experimental k_r values (Figure 1) to Equation (8), the rate constants k_{GdHL} and k^{OH}_{GdHL}, and the protonation constant K^H_{GdHL} were calculated and are presented in Table 1.

$$k_r = \frac{k_{GdHL}[H^+] + k^{OH}_{GdHL}K_W}{[H^+] + K^H_{GdHL}[H^+]^2} \quad (8)$$

In the postulated reaction mechanisms expressed by Equations (4)–(6), the deprotonation of the monoprotonated intermediate Gd(HDOTPMB) plays an important role. If the reactions according to Equations (5) and (6) are rate-controlling, then general base catalysis must occur in the formation reactions. In this case, deprotonation of the intermediate will take place with the transfer of a proton to any Brönsted base, e.g. to the basic form of the buffer. The rate constants $k_{obs} = k_r$ presented in Figure 2 increase with increasing concentration of the buffer MES, which indicates the validity of the Brönsted equation and the occurrence of general base catalysis.[25] These results demonstrate that the rate-determining step in the formation of $Gd(DOTPMB)^{-}$ is the transfer of a proton from the intermediate Gd(HDOTPMB) to a Brönsted base (H_2O, OH^- or the basic form of the buffer), followed by a fast rearrangement of the deprotonated intermediate, in which the Gd^{3+} enters the coordination cage formed by the four nitrogen and oxygen atoms of the ligand.

The formation kinetics of $Gd(DOTP)^{5-}$ seems simpler than in the case of $Gd(DOTPMB)^{-}$, since the rate of formation is directly proportional to the OH^- concentration in the pH range 5.4–8, as shown in Figure 3. On the basis of the rate constants in Figure 3, the rate law is also simple for the formation of $Gd(DOTP)^{5-}$, since $k_r = k_{OH}[OH^-]$, where $k_{OH} = (7.2\pm0.1)\times10^3$ $M^{-1}s^{-1}$. The k_{OH} values obtained for the formation of Gd(DOTP), Gd(DOTPMB), and Gd(DOTA)[20] are compared in Table 1. It can be seen that the rates of formation of Gd(DOTA) and of some other complexes Ln(DOTA)[20–23] are significantly higher than those of the phosphonate com-

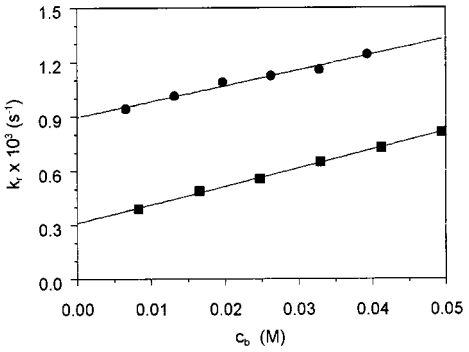

Figure 2. First-order rate constants (k_r) obtained for the formation reaction of $Gd(DOTP)^{5-}$ at pH = 6.82 (■) and of $Gd(DOTPMB)^{-}$ at pH = 6.43 (●) as a function of the concentration of the buffer MES {25 °C, 0.1 M $(CH_3)_4NCl$, $[Gd^{3+}]_t = 5\cdot10^{-4}$ M, $[L]_t = 5\cdot10^{-3}$ M}

plexes, and Gd(DOTP) is formed somewhat faster than Gd(DOTPMB) in this pathway. The simple rate law characterising the formation of Gd(DOTP) is surprising, because the ligand is present in the form of the species H_2L^{6-}, H_3L^{5-}, H_4L^{4-}, H_5L^{3-}, and H_6L^{2-} in the pH range investigated, in which several differently protonated intermediates can be formed in the first stage of the formation reaction.

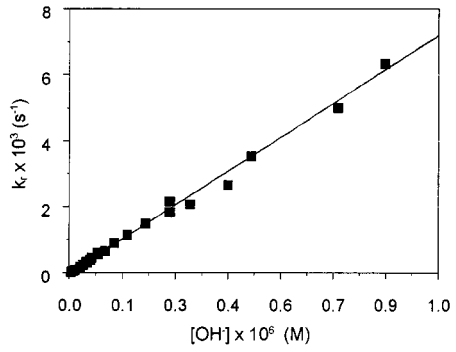

Figure 3. First-order rate constants (k_r) obtained for the formation reaction of $Gd(DOTP)^{5-}$ {25 °C, 0.1 M $(CH_3)_4NCl$, $[Gd^{3+}]_t = 5\cdot10^{-4}$ M, $[L]_t = 5\cdot10^{-3}$ M}

In the reactions of formation of the similar complexes $Ln(DOTA)^{-}$ in the pH range 4−6, a pronounced pH drop was observed at the start of the reactions, which was followed by a slow decrease in the pH value.[20,22] This finding was explained in terms of the formation of the intermediate $Ln(H_2DOTA)^{+}$, which slowly lost the protons.[22,23] In contrast, we did not observe any drop in the pH value when solutions of Gd^{3+} and $H_xDOTP^{(8-x)-}$ were mixed. This indicates that the composition of the intermediate formed is $Gd(H_xDOTP)$, where x is the average number of protons on DOTP at the given pH value. Taking the protonation constants of DOTP into consideration, in the pH range 5.3−8 the average number of protons decreases from $x = 5.7$ to $x = 3.5$. Since two of these protons are attached to two diagonally located nitrogen atoms of the ligand in the pH range investigated, an average of between $n = 3.7$ and 1.5 protons protonate the eight phosphonate oxygen atoms, and thus there are always at least four nonprotonated oxygen atoms $-O^-$ which coordinate to Gd^{3+} in the intermediates $H_nGd(H_2DOTP)$. However, it is not likely that the protonated $H_xDOTP^{(8-x)-}$ is preorganized in a similar way as the ligand $H_xDOTA^{(4-x)-}$. The X-ray crystal structure of H_8DOTP indicates that two diagonally located phosphonate groups are positioned above the plane of the ring nitrogen atoms, while the other two phosphonate groups are orientated away from the ring.[9] It thus seems more probable that only two methylenephosphonate groups are coordinated to Gd^{3+} in the protonated intermediates $H_nGd(H_2DOTP)$. This difference in the structures of the intermediates $H_nGd(H_2DOTP)$ and $Gd(H_2DOTA)$ partly explains the significantly lower rates of formation of the complexes $Ln(DOTP)^{5-}$.

The rearrangement of the intermediate to the product occurs with the loss of protons. The complexes Gd(DOTP) formed are protonated on the noncoordinated oxygen atoms at pH < 9.[12] The protonation constants[12] indicate that the average composition of the protonated complex at pH = 8 is $H_{0.6}Gd(DOTP)$, while at pH = 5.3 it is $H_{2.5}Gd(DOTP)$, i.e. the rearrangement of the intermediate and the entry of Gd^{3+} into the coordination cage occurs with the liberation of 1−2 protons.

The data presented in Figure 2 indicate that the rate constants k_r increase with increasing concentration of the basic form of the buffer, MES, pointing to the validity of general base catalysis. This can be interpreted by assuming the formation of kinetically active intermediates with the dissociation of one of the two protons attached to the nitrogen atoms [Equation (9)] where $n = 0-4$.

$$H_nGd(H_2L) \rightleftharpoons H_nGd(HL) + H^+ \quad (9)$$

The rate-controlling step is presumably the transfer of the proton from the nitrogen atom of $H_nGd(HL)$ to a Brönsted base, e.g. H_2O or the basic form of the buffer. It may be expected that the catalytic effect of OH^- occurs at pH > 8. However, in the formation of $Ce(DOTA)^{-}$, the effect of OH^- catalysis was observed at pH > ca. 7.5.[24] The direct dependence of the formation rates on $[OH^-]$ (Figure 3) is a consequence of the equilibrium according to Equation (9). The concentration of the intermediate $H_nGd(HL)$, which plays a crucial role in the rate-determining step, is directly proportional to $[OH^-]$.

On the basis of the direct proportionality between the rates of formation (k_r) and the concentration of OH^-, it can be assumed that the rate-controlling proton transfer is not influenced by the presence of various numbers of protons attached to the phosphonate oxygen atoms in the intermediates $H_nGd(HL)$. Based on this assumption, the rate of formation of Gd(DOTP) can be expressed as $\Sigma k_{H_nGd(HL)}[H_nGd(HL)]$. To calculate of the rate constants $k_{H_nGd(HL)}$, it is necessary to know the stability constants of the intermediates $H_nGd(H_2L)$. Unfortunately, these stability constants are not available and their pH-potentiometric determination would be difficult, because of the very low solubilities of some protonated species. The rate of

formation of $Gd(DOTP)^{5-}$ can thus be characterized by the rate constant k_{OH} presented in Table 1.

Table 2. Rate constants and protonation constants characterizing the dissociation and protonation of the complexes {25 °C, 1.0 M $(CH_3)_4NCl$ − HCl}

	Gd(DOTP)	Gd(DOTPMB)	Gd(DOTA)[a]
$k_{HGdL} \times 10^4$ [$M^{-1}s^{-1}$]	5.4±0.2	2.1±0.1	0.006
K^H_{HiGdL}[b]	1.7±0.1	1.9±0.1	14[c]

[a] Ref.[20] − [b] $i = 4$ for Gd(DOTP) and $i = 0$ for Gd(DOTPMB) and Gd(DOTA). − [c] Determined by pH-potentiometry.[22]

The k_{OH} values obtained for the formation of $Gd(DOTP)^{5-}$ and $Gd(DOTPMB)^{-}$ are significantly lower than the value of the rate of formation of Gd(DOTA) (Table 1). These differences can be interpreted by assuming a more preorganised structure of the ligand DOTA than of DOTP and DOTPMB. The structures of the intermediates $Gd(H_2DOTPMB)$ and $H_nGd(H_2DOTP)$ probably differ more significantly from the structures of the products $Gd(DOTPMB)^{-}$ and $Gd(DOTP)^{5-}$ than in the case of the complexes of DOTA. The deprotonation and rearrangement of Gd(HDOTPMB) with the assistance of an H_2O molecule are particularly slow if we take into account that this intermediate is present in a macroscopic concentration, owing to the low value of $\log K_2^H$. The extremely slow formation of $Gd(DOTPMB)^{-}$ through this pathway is particularly evident if the $k_{Ln(HL)}$ value ($3.3 \cdot 10^{-4}$ s^{-1}) is compared with that obtained for $Ce(DOTA)^{-}$ ($k_{Ln(HL)} = 18.5$ s^{-1}). This large difference in the rate constants is indicative of the difficulties connected with the deprotonation and rearrangement of the intermediate Gd(HDOTPMB).

Kinetic Stability of $Gd(DOTP)^{5-}$ and $Gd(DOTPMB)^{-}$

It is known from the literature that the dissociation of the Ln^{III} complexes of tetraaza macrocyclic derivative ligands is very slow, because of their rigid structures.[19−22,26] ^1H, ^{13}C and ^{31}P NMR spectroscopic studies indicate that the structures of the complexes $Ln(DOTP)^{5-}$ are even more rigid than that of $Ln(DOTA)^{-}$.[27] The kinetic stability of $Gd(DOTP)^{5-}$ and $Gd(DOTPMB)^{-}$ was therefore studied in the presence of a large excess of HCl. The reaction according to Equation (10) was observed.

$$GdL + xH^+ \rightleftharpoons Gd^{3+} + H_xL \quad (10)$$

The progress of the dissociation was monitored by measuring the changes in the longitudinal relaxation rates of water protons in solutions with different HCl concentrations. The rate of the dissociation reaction is as shown in Equation (11) where $[GdL]_t$ is the total concentration of the Gd^{3+} complex.

$$-\frac{d[GdL]_t}{dt} = k_d[GdL]_t \quad (11)$$

The first-order rate constants (k_d) are shown in Figure 4. The k_d values increase with increasing $[H^+]$, showing saturation curves. Similar results were obtained in the study of the rates of dissociation of some DOTA and DOTA-derivative complexes.[20,22,26] This led us to assume that rapid formation of protonated complexes occurs at the beginning of the reaction. The protonation occurs on the phosphonate oxygen atom(s), but the resulting protonated complex cannot dissociate directly because the Gd^{3+} is in the "coordination cage". For dissociation, at least one proton must be transferred to a ring nitrogen atom, after which the metal ion moves out from the "in-cage" position and the dissociation may take place. Either the transfer of the proton(s) or the structural rearrangement or both processes occur slowly. The protonation equilibria of $Gd(DOTP)^{5-}$, which forms the thermodynamically stable protonated species $HGd(DOTP)^{4-}$, $H_2Gd(DOTP)^{3-}$, $H_3Gd(DOTP)^{2-}$, and $H_4Gd(DOTP)^{-}$ in the pH range 4−8,[12] suggest that species that can dissociate [e.g. $H_5Gd(DOTP)$, etc.] are formed at lower pH values, as a consequence of further protonation. This assumption was supported by the ^1H NMR spectra of $La(DOTP)^{5-}$ solutions, recorded after the addition of increasing amounts of DCl. When 1−4 equiv. of DCl had been added to the solution, the spectrum was similar to that shown in Figure 5C, even after a few weeks. After the addition of 5 equiv. of DCl, the spectrum slowly changed, as shown in Figure 6. The multiplet pattern of the spectrum at the beginning of the reaction (Figure 5C and Figure 6A) was transformed into two broad bands, characteristic of the ligand (Figure 5A). The conversion was almost complete after 4 months. This reveals that the attachment of the fifth proton plays a crucial role in the kinetic stability of the complex. This proton must be attached to a binding $P-O^-$ oxygen atom since the four noncoordinated oxygen atoms are protonated when the rigid, symmetrical structure of the complex is no longer evident. When a noncoordinated phosphonate group is formed, one of the protons can be transferred to the nitrogen atom, after which the Ln^{3+} ion moves out of the coordination cage, and dissociation occurs.

Since the complex $Gd(DOTPMB)^{-}$ involves only four coordinated P−O donor groups, formation of the monoprotonated complex HGd(DOTPMB) results in the breaking

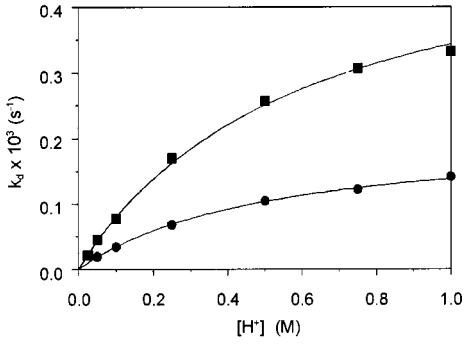

Figure 4. Rate constants of dissociation (k_d) of $Gd(DOTP)^{5-}$ (■) and of $Gd(DOTPMB)^{-}$ (●) as a function of the H^+ concentration {25 °C, 1.0 M $(CH_3)_4NCl$ − HCl, $[GdL]_t = 1 \times 10^{-3}$ M}

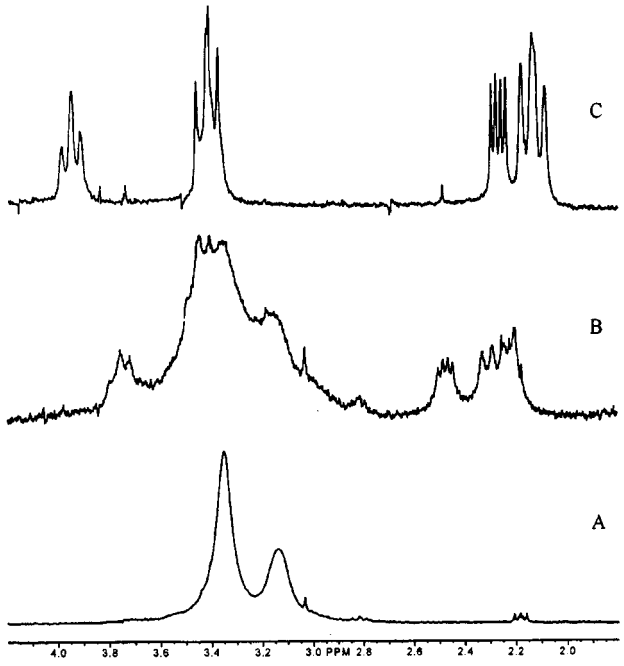

Figure 5. ^{1}H NMR spectra of DOTP at pD = 6 (A), and of La(DOTP)$^{5-}$ at pD = 4.5 (B) and at pD = 10.2 (C)

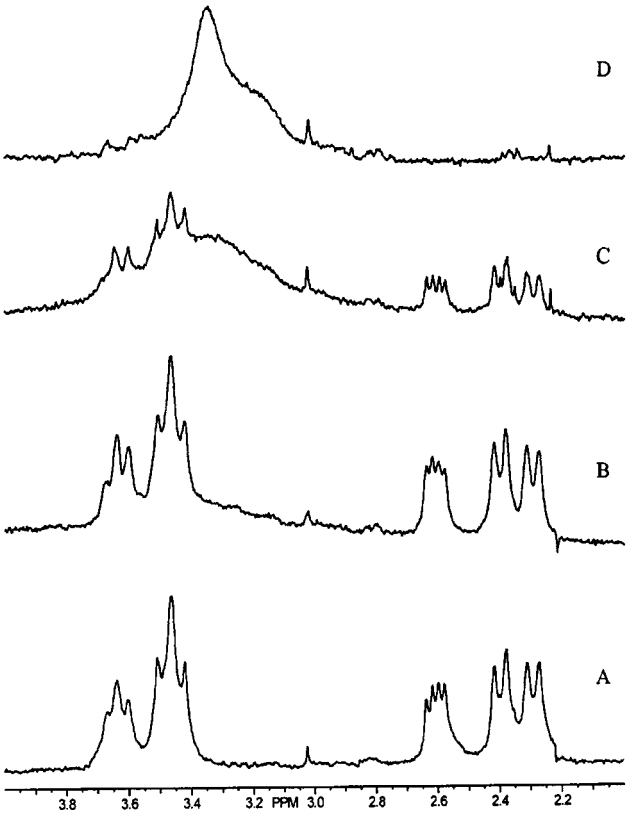

Figure 6. ^{1}H NMR spectra of La(DOTP)$^{5-}$ immediately after the addition of 5 equiv. of DCl (A), 1 d later (B), 1 week later (C), and 4 months later (D)

of a Gd^{3+}−O−P bond, after which a nitrogen atom can be protonated and the complex dissociates.

If dissociation of the protonated species HGd(DOTPMB) and H_5Gd(DOTP) is assumed, the rate of dissociation can be given as Equation (12) where $i = 1$ for Gd(DOTPMB) and $i = 5$ for Gd(DOTP).

$$-\frac{d[GdL]_t}{dt} = k_{HiGdL}[H_iGdL] \quad (12)$$

The total concentration of the complexes is $[GdL]_t = [H_{i-1}GdL] + [H_iGdL]$, since formation of the tetraprotonated H_4Gd(DOTP)$^-$ is practically complete at pH < 3. From Equations (11) and (12), and by using the expression for the total concentration of the complexes, we obtain Equation (13) where K^H_{HiGdL} is the first protonation constant of Gd(DOTPMB) ($i = 0$) and the fifth protonation constant ($i = 4$) of Gd(DOTP): $K^H_{HiGdL} = [H_{i+1}GdL)]/([H_iGdL][H^+])$.

$$k_d = \frac{k_{HiGdL}K^H_{HiGdL}[H^+]}{1 + K^H_{HiGdL}[H^+]} \quad (13)$$

The experimental k_d data (Figure 4) were fitted to Equation (13), and the rate constants k_{HiGdL} and protonation constants K^H_{HiGdL} were calculated (Table 2). The low value of K^H_{H4GdL} for Gd(DOTP)$^{5-}$ indicates that further protonation of H_4Gd(DOTP)$^-$, in which all the oxygen donors are bonded or protonated, is much more difficult than the protonation of e.g. H_3Gd(DOTP)$^{2-}$ ($\log K^H_{H3GdL} = 4.0$[12]). It is surprising that the kinetic stability of Gd(DOTP) is somewhat lower than that of Gd(DOTPMB) (Table 2) in spite of the much higher thermodynamic stability of Gd(DOTP)$^{5-}$ ($\log K_{Gd(DOTP)} = 28.8$[12] and $\log K_{Gd(DOTPMB)} = 12.19$). This unexpected result is probably a consequence of the practical unavailability of protonation sites in Gd(DOTPMB)$^-$. The negatively charged phosphonate oxygen atoms are coordinated to Gd^{3+}, while the oxygen atoms of the ester cannot be protonated under such conditions. Furthermore, the basicity of the P−O$^-$ oxygen atoms is very low; the third protonation constant of DOTPMB is $\log K^H_3 = 2.42$.

These results permit some general conclusions to be made about the kinetic stability of the Gd^{3+} complexes. The kinetic stability depends on the availability of basic protonation sites on the complex. The complex is appreciably inert against proton-assisted dissociation if the basicity of the donor atoms of some functional groups is low. In this case, the stability constant is also low, but the low ligand basicity means that the extent of protonation of the complex is very low, and thus the proton-assisted dissociation occurs slowly. Similar findings on the kinetic stabilities of the complexes of phosphinate and amide derivatives of DOTA and DTPA were reported earlier.[19,28,29]

Owing to its high kinetic stability, Gd(DOTPMB)$^-$ can be regarded as a safe contrast agent (it is more inert than Gd(DTPA)$^{2-}$), in spite of its relatively low stability constant.

Table 2 gives the rate constant k_{HGdL} which characterizes the proton-assisted dissociation of Gd(DOTA)$^-$.[20] On the basis of Equation (13), at low [H$^+$] $k_d = k_{HiGdL}K^H_{HiGdL}[H^+] = k_1[H^+]$. Wang et al.[20] reported the k_1 value and k_{HGdL} was calculated with the use of the protonation constant of Gd(DOTA)$^-$.[22] A comparison of the

data reveals that the rates of dissociation of the Gd^{3+} complexes with the phosphonate and phosphonate ester ligands are larger by about three orders of magnitude. The protonation constant of $Gd(DOTA)^{-}$ is about ten times larger than that of $H_4Gd(DOTP)$ or Gd(DOTPMB). However, $Gd(DOTA)^{-}$ is known to be protonated on a non-coordinated carboxylate oxygen atom[30] and thus even the protonated complex is relatively inert.[30] The formation of $HGd(DOTPMB)$ or $H_5Gd(DOTP)$ occurs at low pH values where the complex is thermodynamically unstable and protonation results in decoordination of a functional group and gradual dissociation of the complex.

Conclusions

The ligand DOTP and its monobutyl ester, DOTPMB, are significantly more sluggish than their tetraacetate analogue, DOTA, in their reactions with Gd^{3+}. However, the proton-assisted dissociation of the complexes $Gd(DOTP)^{5-}$ and $Gd(DOTPMB)^{-}$ is approximately one thousand times faster than that of $Gd(DOTA)^{-}$.

The basicities of the nitrogen and particularly of the oxygen donor atoms and the charge of $DOTPMB^{4-}$ are much lower than those of $DOTP^{8-}$, and the stability constants of $Gd(DOTPMB)^{-}$ and $Gd(DOTP)^{5-}$ are $\log K_{GdL} = 12.19$ and $\log K_{GdL} = 28.8$, respectively. In spite of this large difference in stability, the proton-assisted dissociation of $Gd(DOTP)^{5-}$ is somewhat faster than the similar reaction of $Gd(DOTPMB)^{-}$. The high inertness of $Gd(DOTPMB)^{-}$ is a result of the low basicities of the donor atoms. $Gd(DOTP)^{5-}$ forms protonated complexes in neutral media, while $Gd(DOTPMB)^{-}$ is protonated only in acidic solutions.

The complexes $Gd(DOTP)^{5-}$ and $Gd(DOTPMB)^{-}$ are formed slowly through the formation of protonated intermediates, $H_nGd(H_2DOTP)$ and $Gd(H_2DOTPMB)$, in which presumably only two functional groups are coordinated to the Gd^{3+} and two nitrogen atoms are protonated. The rearrangement of the intermediates to the product is a general base-catalyzed process, with the release of the last proton from the ring nitrogen atoms as the rate-determining step.

Experimental Section

Synthesis of H_8DOTP: The ligand H_8DOTP was synthesized according to a published method.[9] The purity of the ligand was checked by ^{1}H NMR spectroscopy and was found to be higher than 99.5%.

Synthesis of Na_4DOTPMB: Into a 100-mL round-bottomed flask were placed cyclen (2.66 g, 15.41 mmol), benzene (15 mL), glacial acetic acid (6 mL), paraformaldehyde (3.20 g), and dibutyl phosphite (13.0 g), dissolved in benzene (15 mL), and the mixture was stirred at room temperature for 3 d. From the reaction mixture, an azeotropic mixture of benzene and water (20 mL) was distilled off, then benzene (30 mL) was added to the residue and distilled off again. This latter procedure was repeated once more, and the solution was then concentrated under reduced pressure to give a dark brown viscous oil. This oil was redissolved in diethyl ether (150 mL), and water (50 mL) was added. Solid sodium bicarbonate was added until the evolution of gas had ceased. The organic phase was separated and dried with anhydrous sodium sulfate for 8 h. The drying agent was filtered off and the filtrate was concentrated under reduced pressure, furnishing the dibutyl ester DOTPDB as a viscous, dark brown oil. DOTPDB was suspended in water (50 mL), sodium hydroxide pellets (14 g) were added and the two-phase mixture was vigorously stirred and boiled for 30 min, and then left to stand at room temperature for 2 d. The aqueous layer was removed, water (50 mL) and sodium hydroxide (10 g) were added, and the mixture was boiled with vigorous stirring for 30 min. The mixture was then cooled to room temperature, and the aqueous layer was separated. The semisolid residue was redissolved in boiling water (approx. 28 mL), sodium hydroxide solution (4.8 M, 3 mL) was added and the clear solution was heated at reflux for 3 h. NaOH pellets were then added until a significant amount of solid had precipitated. Additional NaOH (2 g) was added and, after cooling, the precipitate was filtered off, washed thoroughly with acetone and dried to constant weight under reduced pressure, resulting in a brownish hygroscopic powder, which proved to be pure Na_4DOTPMB (8.69 g). – ^{1}H NMR (D_2O, DSS): δ = 3.88 (q, 8 H, O–CH_2), 2.89 (d, 8 H, N–CH_2–P), 2.75 (s, 16 H, ring CH_2), 1.63 (m, 8 H, CH_2), 1.38 (m, 8 H, CH_2), 0.92 (t, 12 H, CH_3).

Equilibrium Measurements: The concentrations of ligand solutions were determined by pH-potentiometry, from the titration curves obtained in the absence and in the presence of excess $CaCl_2$. – $LnCl_3$ (Ln = Gd and La) solutions were prepared by dissolving Ln_2O_3 (99.9%, Fluka) in 6 M HCl, after which the excess HCl was evaporated. The concentrations of $LnCl_3$ solutions were determined by complexometry with standardized K_2H_2EDTA, and xylenol orange was used as indicator. – The pH-potentiometric titrations were carried out in jacketed vessels kept at a constant temperature of 25 °C (thermostat), with a Radiometer PHM85 pH-meter, an ABU80 autoburette and PHG211 glass and K401 calomel electrodes. The ionic strength of the solutions was maintained constant (0.1 M Me_4NCl, $pK_W = 13.90$). For the titrations, an Me_4NOH solution (0.1 M) was used. Hydrogen ion concentrations were calculated from the measured pH values by a known procedure.[24,31] For the determination of the protonation constants of the ligands, the concentrations of the samples were 0.010 M for DOTP and 0.0038 M for DOTPMB. Three parallel titrations (60–90 points) were performed for each ligand in the pH range 2.0–12.2. The protonation constants are defined as $K_i^H = [H_iL]/([H_{i-1}L][H^+])$. – The compositions of the intermediates formed in the reaction between Gd^{3+} and H_xDOTP were studied by measuring the pH changes that occurred after the reactants were mixed. The concentrations of Gd^{3+} and H_xDOTP in the samples were $3\cdot10^{-4}$ M and $5\cdot10^{-3}$ M, respectively. The initial pH values of the samples (which were slightly buffered owing to the presence of a small excess of ligand) were 5.37, 6.07, 6.88, and 7.82. The decrease in the pH value was measured until equilibrium was reached. For the determination of the amount of protons released in the reactions, similar samples containing only H_xDOTP (0.1 M KCl) were titrated with HCl of known concentration until the equilibrium pH was established. – The stability constant of $Gd(DOTPMB)^{-}$ was determined by an "out-of-cell" technique. In the pH range 2.7–5.0, 15 solution samples (5 mL) were prepared in which the concentrations of DOTPMB and $GdCl_3$ were 0.0038 M each. The equilibrium pH values were measured three weeks after the preparation of the samples.

Kinetic Measurements: The rates of formation of the complexes were studied by relaxometry in the pH range 5.4−7.0. The formation of $Gd(DOTP)^{5-}$ was also investigated by spectrophotometry ($7.0 < pH < 8.0$). For the formation reactions, pseudo-first-order conditions were maintained with a 10-fold ligand excess, while the concentration of Gd^{3+} was $5\cdot10^{-4}$ M. All measurements were performed at constant temperature (25±0.2 °C) and constant ionic strength (0.1 M Me_4NCl). − The rates of formation reactions at $pH < 7.0$ were studied by measuring the longitudinal relaxation rates ($1/T_1$) of water protons. The pseudo-first-order rate constants (k_{obs}), were calculated from the values of the proton relaxation rates measured at the start, at time t and at equilibrium of the reactions. The proton relaxation times were measured at 9 MHz with an MRS-4 NMR spectrometer (Institute Jozef Stefan, Ljubljana, Slovenia). The temperature of the sample holder was kept constant with the use of an air stream. The T_1 values were measured by using the inversion recovery method (180° − τ − 90°), with an average of 4−6 measurements at 6−8 different τ values. A constant pH value was maintained by using 0.05 M MES as a buffer. − In the spectrophotometric measurements, the indicator method[32] was applied. In slightly buffered solutions (0.01 M HEPES, pH = 7.0−8.0), an approximate decrease of 0.1 in the pH value was monitored at 573 nm by using cresol red as indicator ($c_{ind} = 2.5\cdot10^{-5}$ M). The measurements were carried out with a Cary 1E UV/Vis spectrophotometer, using tandem cells for mixing the reagents. − The rates of dissociation of the complexes were studied by relaxometry (25 °C) in 0.025−1.0 M HCl. The ionic strength of the solutions was kept constant. The sum of the concentrations of HCl and Me_4NCl was 1.0 M. The concentrations of $Gd(DOTP)^{5-}$ and $Gd(DOTPMB)^{-}$ were each 0.001 M. For calculation of the first-order rate constant, k_d, the relaxation rates were used, measured at the start, at time t and at equilibrium of the reaction. − The ^1H NMR spectra were recorded in D_2O with a Bruker AM 360 spectrometer, DSS being used as internal standard. The pD values were calculated from the measured pH values by using the known equation[33] pD = pH + 0.4. − The protonation constants and the stability constants were calculated from the equilibrium measurement data through the use of the PSEQUAD program.[34] All calculations with kinetic data were made with least-squares fitting by the program SCIENTIST® for WINDOWS™ by MICROMATH®, version 2.0. The reported errors correspond to the standard deviation calculated by the programs.

Acknowledgments

This research was supported in part by the Hungarian Ministry of Education (FKFP 0448/1997) and by the Hungarian Science Foundation (OTKA 23810).

[1] R. B. Lauffer, *Chem. Rev.* **1987**, *87*, 901.
[2] M. F. Tweedle, in: *Lanthanide Probes in Life, Chemical and Earth Sciences* (Eds.: J.-C. G. Bünzli, G. R. Choppin), Elsevier, Amsterdam, **1989**, p. 127.
[3] G. R.Choppin, K. M. Schaab, *Inorg. Chim. Acta* **1996**, *252*, 299.
[4] D. Parker, J. A. G. Williams, *J. Chem. Soc., Dalton Trans.* **1996**, 3613.
[5] P. Caravan, J. J. Ellison, T. J. McMurry, R. B. Lauffer, *Chem. Rev.* **1999**, *99*, 2293.
[6] W. A. Volkert, T. J. Hoffmann, *Chem. Rev.* **1999**, *99*, 2269.
[7] M. I. Kabachnik, T. Ya. Medved, F. I. Belskij, S. A. Pisareva, *Izv. Acad. Nauk SSSR, Ser. Khim.* **1984**, 844.
[8] C. F. G. C. Geraldes, A. D. Sherry, W. P. Cacheris, *Inorg. Chem.* **1989**, *28*, 3336.
[9] I. Lázár, D. C. Hrncir, W.-D. Kim, G. E. Kiefer, A. D. Sherry, *Inorg. Chem.* **1992**, *31*, 4422.
[10] R. Delgado, L. C. Siegfried, T. A. Kaden, *Helv. Chim. Acta* **1990**, *73*, 140.
[11] W. P. Cacheris, S. K. Nickle, A. D. Sherry, *Inorg. Chem.* **1987**, *26*, 958.
[12] A. D. Sherry, J. Ren, J. Huskens, E. Brücher, É. Tóth, C. F. G. C. Geraldes, M. M. Castro, W. P. Cacheris, *Inorg. Chem.* **1996**, *35*, 4604.
[13] A. D. Sherry, C. R. Malloy, F. M. H. Jeffrey, W. P. Cacheris, C. F. G. C. Geraldes, *J. Magn. Reson.* **1988**, *76*, 528.
[14] D. C. Buster, M. M. C. A. Castro, C. F. G. C. Geraldes, C. R. Malloy, A. D. Sherry, T. C. Siemers, *Magn. Reson. Med.* **1990**, *15*, 25.
[15] N. Bansal, M. J. Germann, V. Seshan, G. T. Shires, C. R. Malloy, A. D. Sherry, *Biochemistry* **1993**, *32*, 5638.
[16] S. Aime, P. Ascenzi, E. Comoglio, M. Fasano, S. Paoletti, *J. Am. Chem. Soc.* **1995**, *115*, 9365.
[17] C.F.G.C. Geraldes, A. D. Sherry, I. Lázár, A. Miseta, P. Bogner, E. Berényi, B. Sümegi, G. E. Kiefer, K. McMillan, F. Maton, R. N. Müller, *Magn. Reson. Med.* **1993**, *30*, 696.
[18] W. D. Kim, G. E. Kiefer, J. Huskens, A. D. Sherry, *Inorg. Chem.* **1997**, *36*, 4134.
[19] K. P. Pulukkody, T. J. Norman, D. Parker, L. Royle, C. J. Broan, *J. Chem. Soc., Perkin Trans. 2.* **1993**, 605.
[20] X. Wang, T. Jin, V. Comblin, A. Lopez-mut, E. Merciny, J. F. Desreux, *Inorg. Chem.* **1992**, *31*, 1095.
[21] K. Kumar, T. Jin, W. Xiangium, J. F. Desreux, M. F. Tweedle, *Inorg. Chem.* **1994**, *33*, 3823.
[22] É. Tóth, E. Brücher, I. Lázár, I. Tóth, *Inorg. Chem.* **1994**, *33*, 4070.
[23] S. L. Wu, Jr. W. D. Horrocks, *Inorg. Chem.* **1995**, *34*, 3724.
[24] L. Burai, I. Fábián, R. Király, E. Szilágyi, E. Brücher, *J. Chem. Soc., Dalton Trans.* **1998**, 243.
[25] J. W. Moore, R. G. Pearson, *Kinetics and Mechanisms*, 3rd ed., J. Wiley and Sons, New York, **1981**, p. 353.
[26] K. Kumar, C. A. Chang, M. F. Tweedle, *Inorg. Chem.* **1993**, *32*, 587.
[27] C. F. G. C. Geraldes, A. D. Sherry, G. E. Kiefer, *Magn. Reson.* **1992**, *97*, 290.
[28] J. R. Morrow, L. A. Buttrey, V. M. Shelton, K. A. Berback, *J. Am. Chem. Soc.* **1992**, *114*, 1903.
[29] G. L. Jr.Rothermel, E. N. Rizkalla, G. R. Choppin, *Inorg. Chim. Acta* **1997**, *262*, 133.
[30] E. Szilágyi, É. Tóth, E. Brücher, A. E. Merbach, *J. Chem. Soc., Dalton Trans.* **1999**, 2481.
[31] H. M. Irving, M. G. Miles, L. Pettit, *Anal. Chim. Acta* **1967**, *38*, 475.
[32] J. C. Cassat, R. G. Wilkins, *J. Am. Chem. Soc.* **1968**, *90*, 6045.
[33] K. Mikkelsen, S. O. Nielsen, *J. Phys. Chem.* **1960**, *64*, 632.
[34] L. Zékány, I. Nagypál, in: *Computational Methods for Determination of Formation Constants* (Ed.: D. J. Leggett), Plenum Press, New York, **1985**, p. 291.

Received June 16, 2000
[I00236]

Effect of Ion Coordination on the Conformational and Electronic Structure of 3,4-Bis(alkylthio)thiophenes

Fransesca Goldoni,[a] Luciano Antolini,[b] Geoffrey Pourtois,[c] Albertus P. H. J. Schenning,[a] René A. J. Janssen,[a] Roberto Lazzaroni,[c] Jean-Luc Brédas,[c] and E. W. Meijer*[a]

Keywords: Sulfur heterocycles / S ligands / Transition metals / Density functional calculations

A joint experimental and theoretical approach is used to study the coordination of soft transition metal ions with 3,4-bis(alkylthio)thiophenes. The synthesis of [$PdCl_2${3,4-bis(3-methylbutylthio)thiophene}], [$PtCl_2${3,4-bis(3-methylbutylthio)thiophene}] and [$PdCl_2${3′,4′-bis[2-(*S*)-methylbutylthio]-2,2′:5′,2′′-terthiophene}] by exchange of the benzonitrile ligands in [$PdCl_2(PhCN)_2$] and [$PtCl_2(PhCN)_2$] for the thiophene derivatives with thioether side chains is described. Changes in the conformational and electronic structure of the molecules were studied by X-ray diffraction, cyclic voltammetry, and optical and NMR spectroscopy; these experimental data are interpreted with the help of quantum mechanical calculations based on density functional theory. The complexes crystallize in a mixture of diastereoisomers, these stereoisomers are in equilibrium in solution, as observed by variable-temperature NMR spectroscopy. The complexation diminishes the electron-donor ability of the sulfur to the thiophene ring, as observed from the blueshift of the absorption maximum and from the absence of an oxidation wave in the positive potential regime for monomeric 3,4-bis(alkylthio)thiophenes. In this way it is possible to tune the properties of thiophene derivatives by ion coordination.

Introduction

Over the past two decades, thiophenes have attracted strong interest, because of the possible applications of the corresponding polymers in secondary batteries, sensors, photo- and electroluminescent devices, etc.[1−4] In particular, the development of side chain-substituted conjugated derivatives has led to the discovery of a number of interesting phenomena that are not observed in the unsubstituted parent polymers. For instance, the introduction of groups that could act as ligands opens possibilities for application in areas such as chemosensors and catalysis, as reported by Swager et al.[5,6] and Reynolds et al.,[7] respectively.

Because complexes with transition metal ions are of general use in fields such as catalysis, we are investigating the synthesis and properties of new conjugated polymers with alkylthio side groups, since thioether ligands are well known for their ability to complex soft transition metal ions.[8,9] Such conjugated polymers could act as probes or modulators of the activity of the catalytic centre. Furthermore, these systems could be used to anchor biomolecules in a reversible fashion by metal coordination. Similarly, Leclerc et al.[10] reported the possibility of fixing avidin to polythiophene through acid-base complexes. Finally, ion coordination can also be envisioned as an interesting approach to modulate the properties of the conjugated polymer in a noncovalent way.

In this paper we describe the synthesis of [$PdCl_2${3,4-bis(3-methylbutylthio)thiophene}] (**5**), [$PtCl_2${3,4-bis(3-methylbutylthio)thiophene}] (**6**) and [$PdCl_2${3′,4′-bis[2-(*S*)-methylbutylthio]-2,2′:5′,2′′-terthiophene}] (**7**) by exchange of the benzonitrile ligands in [$PdCl_2(PhCN)_2$] and *cis*-[$PtCl_2(PhCN)_2$] for the thiophene derivatives with thioether side chains. The complexes **5** and **6** crystallize in a mixture of diastereoisomers and these stereoisomers are in equilibrium in solution, as observed by variable temperature NMR spectrosocpy. The optical and electrochemical properties of the thiophene derivatives are strongly modified by the presence of the transition metal ions. To account for these properties, this paper also reports theoretical calculations on the geometries of the molecules and on their corresponding energies, together with the interpretation of the optical spectra.

[a] Laboratory of Macromolecular and Organic Chemistry, Eindhoven University of Technology,
P. O. Box 513, 5600 MB Eindhoven, The Netherlands
Fax: (internat.) +31-40/245-1036
E-mail: tgtobm@chem.tue.nl
[b] Dipartimento di Chimica, Università di Modena e Reggio Emilia,
Via Campi 183, 41100 Modena, Italy
Fax: (internat.) +39-59/373-543
E-mail: antolini@unimo.it
[c] Service de Chimie des Matériaux Nouveaux, Centre de Recherche en Electronique et Photonique Moléculaires, Université de Mons-Hainaut,
Place du Parc 20, 7000 Mons, Belgium
Fax: (internat.) +32-65/373-861
E-mail: Roberto@averell.umh.ac.be

Results and Discussion

Synthesis of the Complexes

The 3,4-bis(3-methylbutylthio)thiophenes **2** and 3,4-bis[2-(*S*)-methylbutylthio]thiophene **3** were conveniently synthesized by transetherification of 3,4-dimethoxythiophene (**1**) with the corresponding thiols, as we reported

 © WILEY-VCH Verlag GmbH, 69451 Weinheim, 2001 1434−1948/01/0303−0821 $ 17.50+.50/0

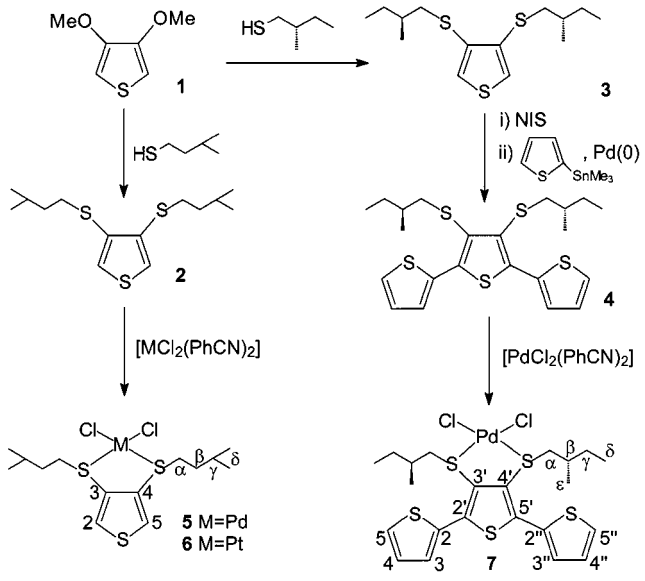

Scheme 1. Synthesis of the complexes **5**−**7**

previously.[11] Stille coupling of the diiodo derivative of **3** with two equivalents of 2-trimethyltinthiophene in the presence of catalytic amounts of Pd^0 produced the desired terthiophene **4**.[12]

The chelate Pd complexes **5** and **7** were obtained by the reaction of an equimolar amount of the dithioether in dichloromethane with $[PdCl_2(PhCN)_2]$, as shown in Scheme 1. The complexes were separated as orange-red solids upon addition of 2-propanol. Using the same conditions as for complex **5**, the corresponding Pt derivative *cis*-$[PtCl_2(PhCN)_2]$ did not react with the ligand at room temperature, as reported for other thioether ligands.[8] However, under UV irradiation in $CHCl_3$, chelate complexation of the dithioether ligand to the platinum centre took place and was completed in a few hours. Addition of hexane led to precipitation of complex **6** as a pale yellow solid. All new compounds **2**−**7** were fully analysed, including NMR spectroscopy and elemental analysis.

Crystal Structure

Both compounds **5** and **6** crystallize in the monoclinic $P2_1/c$ space group, in quasi-identical cells (the axes or

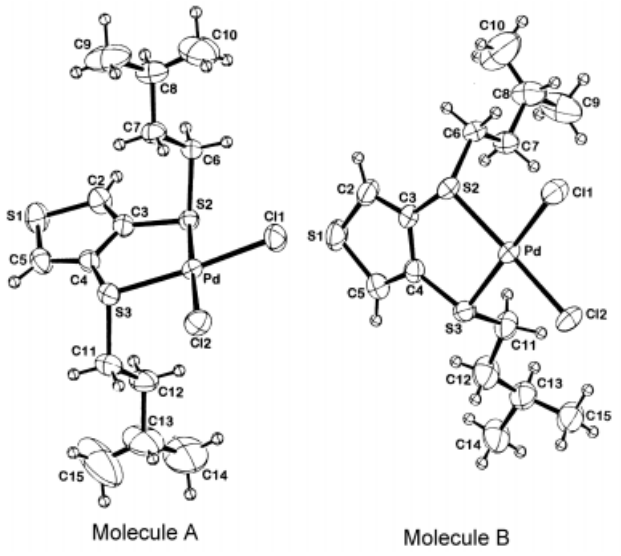

Figure 1. ORTEP drawing of the two independent molecules of compound **5**; thermal ellipsoids for non-H atoms enclose 30% probability

Table 1. X-ray data collection and processing for compounds **5** and **6**

	5	**6**
Empirical formula	$C_{14}H_{24}Cl_2PdS_3$	$C_{14}H_{24}Cl_2PtS_3$
Formula weight	465.81	554.50
Temperature (K)	293(2)	293(2)
Wwavelength (Å)	0.71073	0.71073
Crystal system	monoclinic	monoclinic
Space group	$P2_1/c$	$P2_1/c$
a (Å)	14.305(2)	14.370(1)
b (Å)	16.299(3)	16.283(2)
c (Å)	17.101(3)	17.136(1)
α (°)	90	90
β (°)	100.01(2)	100.199(8)
γ (°)	90	90
V (Å^3)	3926.5(13)	3946.1(6)
Z	8	8
$\rho_{calcd.}$ (Mg/m^3)	1.576	1.867
μ (Mo-K_α, mm^{-1})	1.526	7.689
Crystal size (mm)	0.38 × 0.30 × 0.20	0.25 × 0.20 × 0.15
θ range (°)	2.12−26.96	1.91−26.00
Index ranges	$-18 \le h \le 18$	$-17 \le h \le 17$
	$-1 \le k \le 20$	$-1 \le k \le 20$
	$-1 \le l \le 21$	$-1 \le l \le 20$
Reflns collected	10049	9311
Unique reflns	8528 [R_{int} = 0.0273]	7721 [R_{int} = 0.0260]
Observed reflns [$I>2\sigma(I)$]	5656	5122
Abs. corr. transmission	0.711−1.000	0.657−1.000
Parameters refined	362	361
$R1 = \Sigma\|\|F_o\|-\|F_c\|\|/ \Sigma\|F_o\|$	0.0370	0.0430
(Observed rflns) $wR2$	0.1016	0.0801
Largest diff. peak and hole (e· Å^3)	0.860 and −0.463	0.905 and −0.806

angles do not differ by more than 0.45%, see Table 1).[13] In both compounds the asymmetric unit contains two crystallographically independent *syn* and *anti* isomeric molecules, which are shown in Figure 1 and 2 along with the atom numbering. Selected bond lengths and angles are reported in Table 2.2

A comparison between all structural features of both isomers of complexes **5** and **6**, starting from atomic fractional coordinates, reveals such a close resemblance that the same description can be indifferently applied to either the Pd (**5**) or Pt (**6**) derivative. Most of the corresponding bond lengths, bond angles, and torsion angles in compounds **5** and **6** are equal within one or two standard deviations; moreover, this is equally true for their nonbonded intermolecular contacts. In both complexes, the metal atoms of the two independent molecules display nearly ideal square-planar four-coordination, with the two *cis* Cl atoms and the two sulfanyl S atoms from the substituted thiophene molecule binding in a chelating fashion. As expected, the thiophene rings are nearly coplanar with respect to the coordination planes. The metal atoms are coplanar with their donor atoms in A-labelled molecules, and slightly displaced from the plane in B-labelled ones (Table 2).

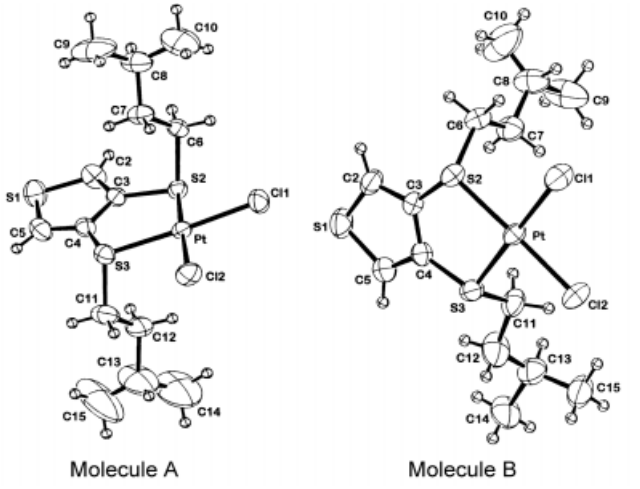

Figure 2. ORTEP drawing of the two independent molecules of compound **6**; thermal ellipsoids for non-H atoms enclose 30% probability

In order to estimate the relative energy of the different structures and to gain information on changes in the electronic density due to complexation, calculations were performed on representative models using a Density Functional Theory (DFT) approach. To keep the computational effort to a reasonable level, the alkylthio side chains were represented by methylthio groups. The theoretical description of the geometry obtained for [$PdCl_2${3,4-bis(methylthio)thiophene}] is fully consistent with the X-ray data of compound **5**. The largest difference between theoretical and experimental data is only about 0.02 Å and 3° for the bond lengths and bond angles, respectively. A comparison between the theoretical structures of 3,4-bis(methylthio)thiophene (Figure 3a) and [$PdCl_2${3,4-bis(methylthio)thiophene}] (Figure 3b,c) is reported in Table 3. These data indicate that the complexation does not lead to significant bond length or angle modifications in the thiophene moiety. The changes are large on the thioether groups where the complexation leads to an increase (0.03 Å) of the bond lengths between the C_β of the thiophene ring and the sulfur atoms.

The nature of the bonds between the thioether groups and the Pd atom is clearly covalent: the calculated Pd−S distances (2.292 Å) are indeed slightly lower than the sum

Table 2. Selected bond lengths and angles in compounds **5** and **6**

	Compound **5** (Me = Pd)		Compound **6** (Me = Pt)	
	Molecule **A**	Molecule **B**	Molecule **A**	Molecule **B**
Bond lengths (Å)				
Me−Cl(1)	2.301(1)	2.291(1)	2.309(2)	2.300(3)
Me−Cl(2)	2.306(1)	2.304(1)	2.314(2)	2.311(2)
Me−S(2)	2.263(1)	2.266(1)	2.248(2)	2.252(2)
Me−S(3)	2.264(1)	2.263(1)	2.254(2)	2.250(2)
S(1)−C(2)	1.688(5)	1.697(6)	1.700(10)	1.693(10)
S(1)−C(5)	1.696(5)	1.690(5)	1.702(11)	1.694(10)
C(3)−S(2)	1.765(4)	1.771(5)	1.774(8)	1.780(9)
S(2)−C(6)	1.816(4)	1.807(4)	1.817(8)	1.810(9)
C(4)−S(3)	1.776(4)	1.782(4)	1.771(9)	1.763(9)
S(3)−C(11)	1.808(4)	1.818(5)	1.813(9)	1.814(9)
Bond angles (°)				
Cl(1)−Me−Cl(2)	92.83(5)	92.05(5)	91.61(10)	90.83(9)
Cl(1)−Me−S(2)	87.18(4)	88.13(4)	87.58(9)	88.69(9)
Cl(1)−Me−S(3)	176.35(5)	179.43(4)	176.63(9)	179.31(9)
Cl(2)−Me−S(2)	176.70(4)	176.53(5)	177.06(8)	176.98(9)
Cl(2)−Me−S(3)	88.46(5)	88.47(5)	88.67(9)	88.50(9)
S(2)−Me−S(3)	91.73(4)	91.36(4)	92.31(8)	91.98(9)
Torsion angles (°)				
Me−S(2)−C(6)−C(7)	−50.5(3)	48.3(4)	−51.1(7)	48.6(8)
C(3)−S(2)−C(6)−C(7)	57.0(3)	−60.7(4)	56.6(7)	−61.0(8)
Me−S(3)−C(11)−C(12)	−49.5(5)	168.2(4)	−47.7(9)	166.8(8)
C(4)−S(3)−C(11)−C(12)	58.8(5)	−84.4(4)	60.6(9)	−86.1(9)
out of plane (Å) of Me atom [a]	0.001(1)	0.032(1)	0.006(1)	0.031(1)

[a] The four donor atoms were used to define the plane.

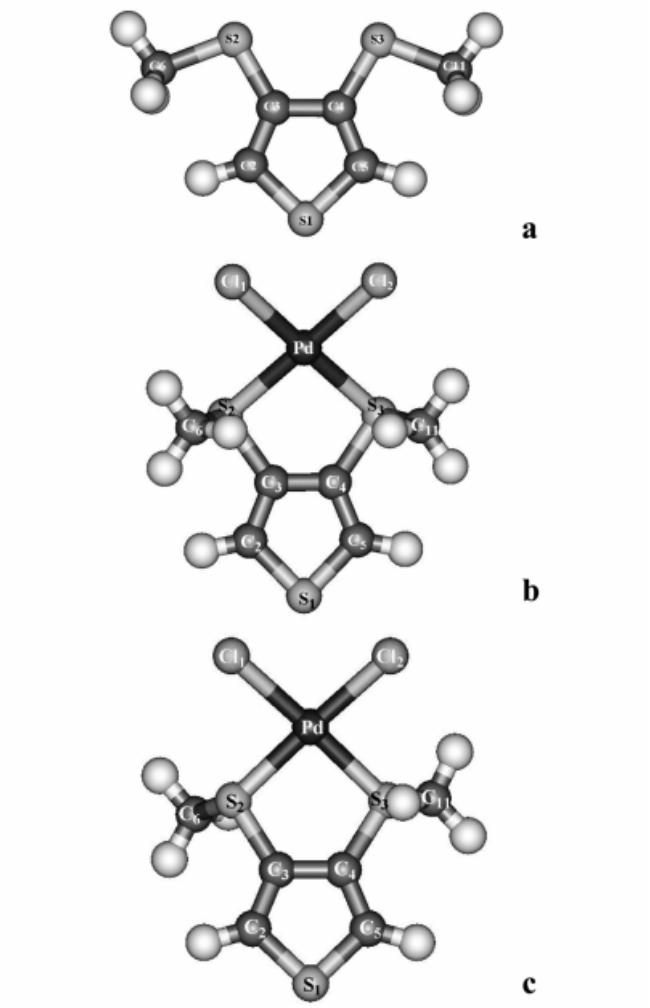

Figure 3. Chemical structure of 3,4-bis(methylthio)thiophene (**a**) and {$PdCl_2$[3,4-bis(methylthio)thiophene]} *syn* (**b**) and *anti* (**c**) isomers

of the covalent radii (2.330 Å).[14] The quasi-equivalent bond lengths to the two Cl atoms (2.304 Å) and to the two sulfanyl S atoms (2.292 Å) and their respective angles (about 90°) form a nearly square planar configuration around the Pd centre, as also observed in the X-ray structure.

From the calculations it is possible to evaluate the stability of the complex, i.e., the binding energy of $PdCl_2$ to 3,4-bis(methylthio)thiophene; this is obtained from the difference in total energy between the complex and the separate partners. The value calculated with a nonlocal-gradient-corrected DFT approach is -181 kJ mol^{-1} and -171 kJ mol^{-1} for the *syn* and *anti* isomers, respectively. We also checked that alternative bonding sites for the Pd atom (the sulfur atom of the thiophene ring and the π system of the thiophene ring) lead to complexes with much lower binding energies (-83 and -52 kJ mol^{-1}, respectively).

In both complexes, the two independent molecules in the crystallographic unit differ only by the absolute configuration around the metal-bonded S atoms, which are stereocentres. Both crystals contain all the diastereoisomeric

Table 3. Comparison of theoretical bond lengths and angles of {3,4-bis(methylthio)thiophene} (**a**) and [$PdCl_2${3,4-bis(methylthio)thiophene}] (**b**) with the experimental data for compound **5** (isomer B)

	a	b	X-ray structure of compound **5**
Bond lengths (Å)			
Pd−Cl(1)		2.304	2.291(1)
Pd−Cl(2)		2.304	2.304(1)
Pd−S(2)		2.292	2.266(10)
Pd−S(3)		2.292	2.262(13)
S(1)−C(2)	1.714	1.708	1.697(6)
C(2)−C(3)	1.371	1.370	1.347(6)
C(3)−C(4)	1.427	1.418	1.415(6)
C(4)−C(5)	1.371	1.370	1.346(6)
C(5)−S(1)	1.714	1.708	1.690(5)
C(3)−S(2)	1.741	1.770	1.771(5)
S(2)−C(6)	1.793	1.801	1.807(4)
C(4)−S(3)	1.741	1.770	1.782(4)
S(3)−C(11)	1.793	1.801	1.818(5)
Bond angles (°)			
Cl(1)−Pd−Cl(2)		95.50	92.05(5)
Cl(1)−Pd−S(2)		86.34	88.13(4)
Cl(1)−Pd−S(3)		178.03	179.43(4)
Cl(2)−Pd−S(2)		178.03	176.53(5)
Cl(2)−Pd−S(3)		86.34	88.47(5)
S(2)−Pd−S(3)		91.79	91.36(4)

forms. The S atoms of the A- and B-labelled molecules display *R,R* and *R,S* configurations, respectively. Due to the presence of an inversion centre (and of a glide plane), the inverted *S,S* and *R,S* configurations are also present, and hence the compounds crystallise in a racemic form. There are no significant differences between the corresponding bond lengths and angles of the two independent molecules, and their values compare well with the mean bond lengths retrieved from the Cambridge Structural Database.[15,16] It is of interest to note that the strong similarities between the two structures also apply to probable disorder problems, which involve, in particular, two terminal methyl groups of the alkyl chains. In both crystals, and in both independent molecules, the C(9) and C(10) atoms are affected by extremely high temperature factors, and, as a consequence, by extremely short (and unrealistic) bond lengths. Nevertheless, to observe this effect in both independent molecules and in both complexes could be of some significance with regard to their molecular packing mode. As reported above, both complexes exhibit the same molecular packing, characterised by only three nonbonded distances lower than 3.60 Å (two C···S and one C···C contacts). These interactions occur only between racemic pairs (A- or B-labelled) of molecules.

Variable Temperature NMR Spectroscopy

The variable temperature ^{1}H NMR spectrum of the palladium complex **5** in chloroform solution is shown in Figure 4. At room temperature the compound shows a singlet for the α-proton of the thiophene, and broad peaks in the aliphatic region, corresponding to the thioether side chains, all deshielded relative to the values for uncomplexed com-

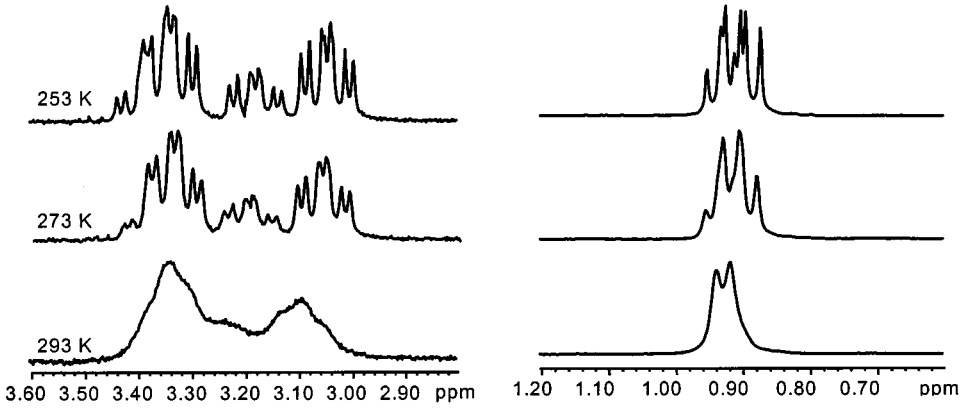

Figure 4. Variable temperature ^{1}H NMR spectrum of compound **5** in $CDCl_3$ in the regions corresponding to the signals of the SCH_2 and CH_3 protons

pound **2**. In the ^{13}C NMR spectrum at room temperature, there are two peaks in the aromatic region at $\delta = 128$ and 135, corresponding to the two α- and β-carbons of the thiophene ring, respectively, while five peaks for the aliphatic region are recorded, including two at $\delta = 21.9$ and 22.2 corresponding to the two methyl end groups, indicating that these groups have a reduced motional freedom. At −20 °C, the thioether side chains resolve into several multiplets. The diastereotopic $SCH_2(\alpha)$ is resolved into two groups of signals, each consisting of two double triplets, as shown in Figure 4. At lower temperatures, we also observe the presence of two doublets of doublets for the CH_3 group at the end of the chain, confirming the presence of two isomers.

The two *syn* and *anti* isomers are in equilibrium in solution, and from the coalescence temperature and the ratio of the integrated signals, we can deduce that one is preferred over the other in a 2:1 ratio. An approximate energy barrier of 68 kJ mol^{-1} can be calculated for the interconversion between the two isomers, and the difference in energy between the two forms is approximately 1.7 kJ mol^{-1}. The theoretical calculations on the corresponding [$PdCl_2${3,4-bis(methylthio)thiophene}] isomers (Figure 3) indicate that the *syn* form is more stable than the *anti* form by about 10 kJ mol^{-1}. Such an overestimation, relative to the experimental value, may be due to the fact that the calculations are performed on single isolated molecules, thereby neglecting the influence of the solvent. The two isomers can be identified with the two couples of diastereoisomeric molecules A and B observed in the crystal.

UV/Vis Spectroscopy

With respect to uncomplexed compound **2**, which presents an absorption maximum at 286 nm, the absorption maximum in complex **5** is blue-shifted by 29 nm, to 257 nm (Figure 5). The spectrum also shows two smaller bands at 315 nm ($\varepsilon = 2800$ dm^3 mol^{-1} cm^{-1}) and 412 nm ($\varepsilon = 1000$ dm^3 mol^{-1} cm^{-1}). INDO/SCI calculations on [$PdCl_2${3,4-bis(methylthio)thiophene}] indicate that the maximum at 257 nm is a HOMO to LUMO+1 transition localised on the thiophene moiety, and that the two bands at 315 nm and 412 nm are due to transitions involving the Pd atoms.

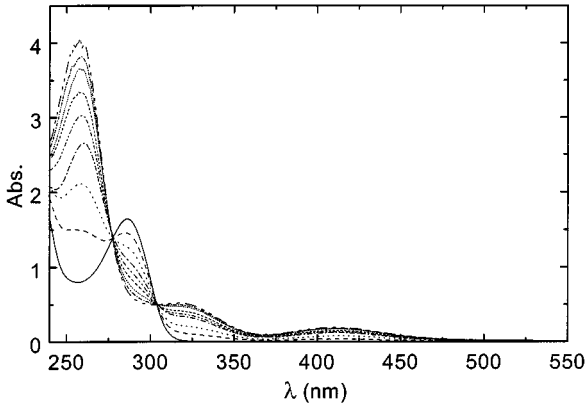

Figure 5. UV/Vis spectra of the titration of 3,4-bis(3-methylbutylthio)thiophene **(2)** with [$Pd(CH_3CN)_2Cl_2$] in acetonitrile

The blue shift of 29 nm found for the main absorption is related to the stabilization of the HOMO due to the diminished electron-donating ability of the S atoms; as a result, the absorption maximum gets closer to that of thiophene itself (231 nm). The absorption coefficient is significantly increased from $\varepsilon = 4800$ dm^3 mol^{-1} cm^{-1} at 286 nm in the uncomplexed compound to 11100 dm^3 mol^{-1} cm^{-1} at 257 nm in compound **5**.

From the titration experiment, we can observe the presence of two clear isosbestic points, indicating the presence of the two species (complexed and uncomplexed) in solution (see Figure 5).

Cyclic Voltammetry and Electropolymerisation.

The electrochemical characterisation of **5** reveals one reversible reduction wave at −0.71 V, while **2** just presents an irreversible oxidation wave at 1.7 V. No oxidation wave is observed for **5** in the positive potential regime ($E \leq 1.8$ V), which is in contrast to what is found in electron-donor-substituted thiophenes.[17−19] Therefore compound **5** cannot be oxidatively electropolymerised.

In order to explain this behaviour, we computed the electronic properties of 3,4-bis(methylthio)thiophene and its $PdCl_2$ complex. The electrophilic character of $PdCl_2$ is

clearly illustrated through the Mulliken charge-transfer analysis (Table 4).

Table 4. Mulliken charge analysis for [$PdCl_2${3,4-bis(methylthio)thiophene}]; the charge variation is defined as the difference between the DFT-calculated electronic charges in the complex and in the isolated compounds; a negative value corresponds to a gain of electronic density

Atoms	Charge variation |e|
Cl(1)	−0.16
Cl(2)	−0.16
Pd	−0.29
C(6)H_3 group	+.008
C(11)H_3 group	+.008
S(3)	+0.11
S(2)	+0.11
C(3)	−0.04
C(4)	−0.04
C(2)H	+0.10
C(5)H	+0.10
S(1)	+0.07

As a consequence of complexation, a partial charge transfer (−0.6 |e|) takes place from 3,4-bis(methylthio)thiophene to $PdCl_2$. The sulfur atoms of the thioether groups and the C_α atoms of the thiophene ring are the most depleted sites, while the alkyl side chains and the C_β atoms of the ring remain almost untouched. Globally, the decrease in electron density on the organic molecule upon complexation is consistent with the fact that oxidation becomes more difficult. Along the same lines, the redox properties can be qualitatively interpreted on the basis of the one-electron electronic structure of the molecule. Indeed, the oxidation process corresponds to the removal of one electron and can thus be roughly connected to the energy of the HOMO.[20] Similarly, the reduction process induces the addition of one electron that must be deposited on the LUMO.

The analysis of the electronic structure of 3,4-bis(methylthio)thiophene (**a**) and its $PdCl_2$ complex (Figure 6) shows two important points. Firstly, the HOMO of [$PdCl_2${3,4-bis(methylthio)thiophene}] is similar to that of 3,4-bis(methylthio)thiophene but is strongly stabilized (Table 5). This implies that oxidation becomes more difficult when going from 3,4-bis(methylthio)thiophene to its $PdCl_2$ complex. Secondly, the complexation leads to the localization of the LUMO on the Pd atom and to a strong energetic stabilization (Table 5). This is fully consistent with the appearance of a reduction peak at −0.71 V.

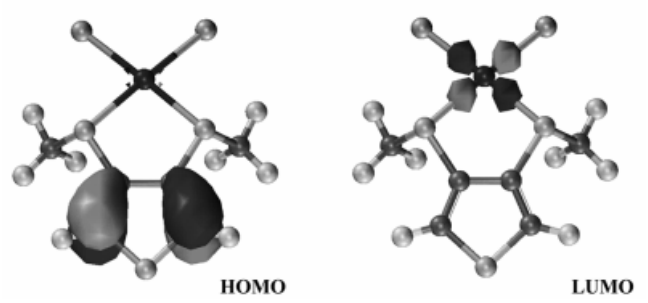

Figure 6. INDO-calculated HOMO and LUMO patterns of [$PdCl_2${3,4-bis(methylthio) thiophene}]

Table 5. Comparison of the INDO energies of the LUMO, and HOMO for 3,4-bis(methylthio)thiophene (**a**), {$PdCl_2$[3,4-bis(methylthio) thiophene]} (**b**), [3′,4′-bis(methylbutylthio)-2,2′:5′,2′′-terthiophene] (**4**), and {$PdCl_2$[3′,4′-bis(methylthio)-2,2′:5′,2′′-terthiophene} (**7**); the energies are in electron volts (eV)

	a	**b**	**4**	**7**
LUMO	0.34	−1.32	−0.88	−1.88
HOMO	−8.17	−9.70	−6.77	−7.75

Since complexation diminishes the electronic density on the α-positions of the thiophene ring (Table 4), electrochemical oxidation and monomer coupling at these positions become more difficult. This explains why the electropolymerisation of compound **5** was not successful. To overcome this problem, we therefore synthesized compound **7**, which possesses both a complexed Pd atom and two pristine C_α sites. This compound also has a reversible redox wave at −0.71 V and, most importantly, shows a highly irreversible oxidation wave at 1.7 V. This behaviour is consistent with the electronic structure of [$PdCl_2${3,4-bis(methylthio)thiophene}] and [$PdCl_2${3′,4′-bis(methylthio)-2,2′:5′,2′′-terthiophene}] (Table 5). The energetic values and the nature of the frontier molecular orbitals are modified when going from the thiophene complex to the terthiophene complex (Figure 7 and Table 5). In the terthiophene complex, both the HOMO and LUMO are mostly localized on the organic backbone, with strong similarities to those of the uncomplexed molecule. The HOMO of [$PdCl_2${3′,4′-bis(methylthio)-2,2′:5′,2′′-terthiophene}] is strongly destabilized (1.95 eV) relative to that of [$PdCl_2${3,4-bis(methylthio)thiophene}]. This destabilization of the HOMO implies that the oxidation process is much easier for [$PdCl_2${3′,4′-bis(methylthio)-2,2′:5′,2′′-terthiophene}] than for [$PdCl_2${3,4-bis(methylthio)thiophene}]. As for [$PdCl_2${3,4-bis(methylthio)thiophene}], complexation leads to the stabilization (1 eV) of the LUMO. However, the LUMO is no longer localized on the Pd atom but on the terthiophene part while the LUMO+1 is found on the Pd atom.

Based on these considerations, it is most likely that the oxidation wave at 1.7 V is due to the oxidation of the terthiophene moiety. Red films of electrochemically active, polymeric material can be grown on the Pt electrode by repetitive cycling, but the polymer is no longer soluble in organic solvents. The results of the electropolymerisation and of the complexation of the preformed polymers will be reported in a forthcoming paper.[21]

Conclusion

Complexes between thiophenes substituted with thioether ligands and transition metal ions were successfully synthesized. We have shown that complexation leads to the freezing of the rotation of the side chains, as the complexes

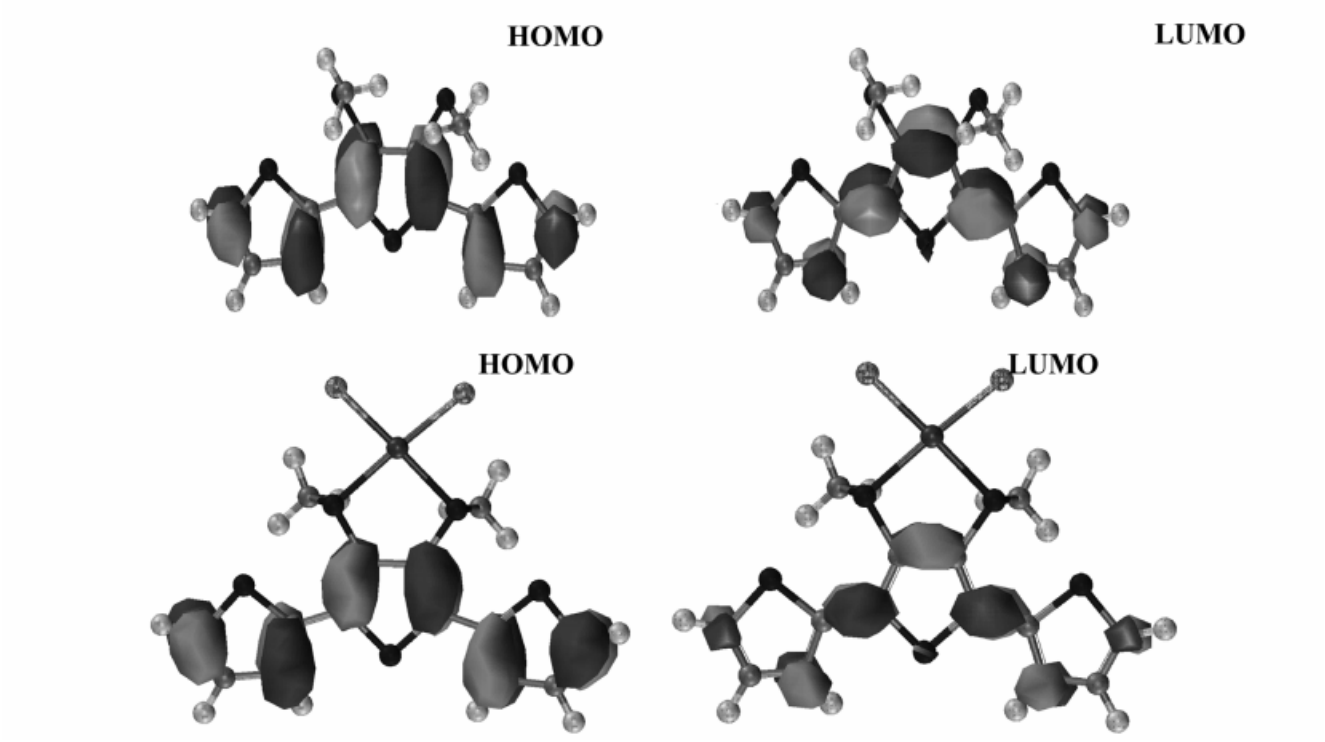

Figure 7. INDO-calculated HOMO and LUMO patterns of [$PdCl_2${3′,4′-bis(methylthio)-2,2′:5′,2′′-terthiophene} and -{3′,4′-bis(methylbutylthio)-2,2′:5′,2′′-terthiophene}]

are crystalline at room temperature. Furthermore, the reversible linkage with the metal ions modifies the optical and electrochemical properties of the thiophene derivatives. Thus, metal complexation can be used as a reversible tool for the modification of the properties in π-conjugated polymers.

Experimental Section

General Remarks: The IR spectra were recorded on a Perkin−Elmer 1600 series FT-IR spectrometer. NMR spectra were recorded on a Varian Gemini 300 spectrometer. Chemical shifts are reported in ppm downfield from TMS. The UV/Vis spectra were recorded on a Perkin−Elmer Lambda 900 spectrophotometer. Cyclic voltammograms were recorded with 0.1 M tetrabutylammonium hexafluorophosphate as supporting electrolyte using a Potentioscan Wenking POS73 potentiostat. The working electrode was a platinum disc (0.2 cm^2), the counterelectrode was a platinum plate (0.5 cm^2) and the reference electrode was a saturated calomel electrode calibrated against a Fc/Fc^+ couple. Electrospray-MS (ESI/MS) measurements were performed on a Perkin−Elmer/Sciex API300 mass spectrometer. Elemental analysis (C, H, N) was obtained by combustion analysis using a Perkin−Elmer 2400. 3,4-Bis(3-methylbutylthio)thiophene (**2**)[11] and 3′,4′-bis[2-(*S*)-methylbutylthio]-2,2′:5′,2′′-terthiophene (**4**)[12] were prepared as previously reported. All other reagents were commercial products and were used as received. Solvents were dried by standard procedures.

[$PdCl_2${3,4-Bis(3-methylbutylthio)thiophene}] (5): The ligand 3,4-bis(3-methyl-butylthio)thiophene[11] (**2**; 75 mg, 0.26 mmol) was added to a solution of [$PdCl_2(PhCN)_2$] (100 mg, 0.26 mmol) in dry dichloromethane (5 mL). After stirring at room temperature for 20 min., 2-propanol was added to give an orange precipitate of **5** which was filtered off and dried in vacuo (115 mg, 95%). − ^{1}H NMR (300 MHz, $CDCl_3$, 20 °C, TMS): δ = 7.6 (s, 2 H, 2-H and 5-H), 3.3 (broad, 4 H, α-H), 2.06 (broad, 2 H, γ-H), 1.8−1.4 (broad, 4 H, β-H), 0.87 (broad, 6 H, CH_3). − ^{13}C NMR (75 MHz, $CDCl_3$, 20 °C): δ = 134 (C_4 and C_5), 128 (C_2 and C_3), 43 (α-C), 38 (δ-C), 27 (β-C), 22.2 (CH_3) and 21.9 (CH_3). − ES-MS; *m/z*: 395 [M − 2Cl]. − $C_{14}H_{24}Cl_2PdS_3$ (465.7): calcd. C 36.11, H 5.15; found C 36.11, H 5.24.

[$PtCl_2${3,4-Bis(3-methylbutylthio)thiophene}] (6): The ligand 3,4-bis(3-methyl-butylthio)thiophene[11] (**2**; 30.5 mg, 0.13 mmol) was added to a solution of [$PtCl_2(PhCN)_2$] (50 mg, 0.13 mmol) in chloroform (10 mL). The solution was irradiated (about 300 nm) at 35 °C for 11 h. The chloroform was evaporated and hexane was added. The solid was stirred in hot hexane, then the solvent was removed by decantation. The solid was then recrystallized from 2-propanol to give **6** (23.6 mg, 48%). − ^{1}H NMR (300 MHz, $CDCl_3$, 20 °C, TMS): δ = 7.56 and 7.54 (s, 2 H, 2-H and 5-H), 3.28 and 3.15 (two multiplets, 4 H, α-H), 2.00 (multiplet, 2 H, γ-H), 1.8−1.4 (three multiplets, 4 H, β-H), 0.95, 0.94, 0.91 and 0.89 (four doublets, 6 H, 2 CH_3). − ^{13}C NMR (75 MHz, $CDCl_3$, 20 °C): δ = 125 (C_2 and C_3), 43 (α-C), 37.7 and 37.6 (δ-C), 27.3 and 27.2 (β-C), 22.4, 22.3 and 22.0 (CH_3). − $C_{14}H_{24}Cl_2PtS_3$ (554.3): calcd. C 30.33, H 4.32; found C 30.70, H 3.99. Probably due to a broadening of the signals, the peaks of the C_4 and C_5 could not be detected, even after an overnight acquisition.

[$PdCl_2${3′,4′-Bis[2-(*S*)-methylbutylthio]-2,2′:5′,2′′-terthiophene}] (7): The ligand 3′,4′-bis[2-(*S*)-methylbutylthio]-2,2′:5′,2′′-terthiophene[12] (**4**; 100 mg, 0.22 mmol) was added to a solution of [$PdCl_2(PhCN)_2$] (84 mg, 0.22 mmol) in dichloromethane (10 mL). After stirring at room temperature for 20 min., the solvent was removed to give **7** (115 mg, 83%). − ^{1}H NMR (300 MHz, $CDCl_3$, 20 °C, TMS): δ = 7.54 (dd, J_{35} = 0.98 Hz, J_{45} = 5 Hz, 2 H, 5-H and 5"-H), 7.40 (broad dd, 2 H, 3-H and 3"-H), 7.16 (dd, J_{34} = 3.7 Hz,

J_{45} = 5 Hz, 2 H, 4-H and 4"-H), 3.4−2.8 (broad multiplets, 4 H, α-H), 2.1−1.6 (broad, 2 H, β-H), 1.4−1.0 (broad, 4 H, γ-H), 0.9−0.6 (broad, 6 H, δ- and ε-CH_3). − ^{13}C NMR (75 MHz, $CDCl_3$, 20 °C): δ = 130.6 (2C, 2-C and 2′′-C), 129.7 (2C, CH), 129.1 (2C, CH), 128.8 (2C, CH), 53.4, 52.8, 50.8, 50.2 [2C, CH_2(α)], 35.7, 34.3 [2C, CH(β)], 29.3, 29.2 [2C, CH_2 (γ)], 19.8, 18.9 [2C, CH_2(ε)], 11.3, 11.2 [2C, CH_2(δ)]. − $C_{22}H_{28}Cl_2PdS_5$ (629.9): calcd. C 41.95, H 4.47; found C 41.01, H 4.51. Probably due to a broadening of the signals, the peaks of the quaternary carbons could not be detected, even after an overnight acquisition.

Crystal Structure Determination for Compounds 5 and 6: Diffraction data for compound **5** were collected on a Enraf−Nonius CAD4 diffractometer, whereas those for compound **6** were obtained with a Siemens P4RA-M18X diffractometer equipped with a rotating anode (52 kV, 130 mA). In both cases, the ω-2θ scan mode was chosen. Crystal data and details of data collections and refinements are summarised in Table 1. The structures were solved by direct methods (SHELXS-86) and were refined by full-matrix least-square calculations based on F^2 (SHELXL-93). All non-hydrogen atoms were refined anisotropically, and H atoms were constrained to remain in ideal positions on the C atoms to which they are bonded. In both compounds, two methyl groups (C_9 and C_{10} in Figure 1 and 2) display unusually high thermal motion parameters and extremely short bond lengths, perhaps indicative of light disorder.

Theoretical Methodology: 3,4-Bis(methylthio)thiophene and [3′,4′-bis(methylthio)-2,2′:5′,2′′-terthiophene] were used as representative models for the 3,4-bis(3-methylbutylthio)thiophene (**2**) and [3′,4′-bis(methylbutylthio)-2,2′:5′,2′′-terthiophene] (**4**), respectively. The geometries of the isolated molecules as well as those of the complexes with $PdCl_2$ were fully optimized at the density functional level of calculation. The main advantage of Density Functional Theory (DFT) with respect to Hartree−Fock is that it allowed us to take electron correlation explicitly into account, which is of the utmost importance in the description of metal-organic interactions. The Vosko-Wilk-Nusair[22] function for the exchange-correlation potential in the local density approximation was used, along with a double numerical precision basis set (DNP) of 6−311 G* quality.[23] A frozen-core approximation equivalent to the use of a pseudopotential was used for the palladium and chlorine atoms. The binding energies and charge distributions calculations were carried out at the nonlocal level of DFT using the Becke-Lee-Yang-Parr gradient-corrected functional[24,25] for the exchange-correlation potential. This methodology has already been successfully applied to metal-organic systems containing aluminum, nickel, copper, and iron.[26,27] The interpretation of the optical spectra of [{$PdCl_2$(3,4-bis(methylthio) thiophene}] (**5**) was performed on the basis of Hartree−Fock INDO semiempirical calculations, coupled to a Single Configuration Interaction description (SCI).[28]

Acknowledgments

The authors are grateful to the Centro Interdipartimentale Grandi Strumenti for X-ray data collection and to the Centro Interdipartimentale di Calcolo Automatico e Informatica Applicata for computing facilities in X-ray structure calculations. This research is carried out in the framework of the European Commission Training and Mobility of Researchers Network SELOA. The work in Mons is also partly supported by the Belgian Federal Government Office of Science Policy (SSTC) program "Pôle d′attraction Interuniversitaire en Chimie Supramoléculaire et Catalyse (PAI 4/11)" FNRS/FRFC. R.L. is Maître de Recherches du Fonds National de la Recherche Scientifique (FNRS-Belgium).

[1] F. Hide, M. A. Díaz-García, B. J. Schwartz, A. J. Heeger, *Acc. Chem. Res.* **1997**, *30*, 430−436.
[2] G. Horowitz, F. Garnier, A. Yassar, R. Hajlaoui, F. Kouki, *Adv. Mater.* **1996**, *8*, 52−54.
[3] A. Dodabalapur, H. E. Katz, L. Torsi, R. C. Haddon, *Science* **1995**, *269*, 1560−1562.
[4] J. H. Burroughes, D. D. C. Bradley, A. R. Brown, R. N. Marks, K. Mackay, R. H. Friend, P. L. Burn, A. B. Holmes, *Nature* **1990**, *347*, 539−541.
[5] M. J. Marsella, T. M. Swager, *J. Am. Chem. Soc.* **1993**, *115*, 12214−12215.
[6] T. M. Swager, *Acc. Chem. Res.* **1998**, *31*, 201−207.
[7] J. L. Reddinger, J. R. Reynolds, *Chem. Mater.* **1998**, *10*, 1236−1243.
[8] S. Gladiali, D. Fabbri, L. Kollàr, C. Claver, N. Ruiz, A. Alvarez-Larena, J. F. Piniella, *Eur. J. Inorg. Chem.* **1998**, 113−118.
[9] M. Diéguez, A. Ruiz, C. Claver, M. M. Pereira, A. M. d′A. Rocha Gonsalves, *J. Chem. Soc., Dalton Trans.* **1998**, 3517−3522.
[10] K. Faïd, M. Leclerc, *J. Am. Chem. Soc.* **1998**, *120*, 5274−5278.
[11] F. Goldoni, B. M. W. Langeveld-Voss, E. W. Meijer, *Synth. Commun.* **1998**, 2237−2244.
[12] F. Goldoni, R. A. J. Janssen, E. W. Meijer, *J. Polym. Sc: Part A: Polym. Chem.* **1999**, *37*, 4629−4639.
[13] Crystallographic data (excluding structure factors) for the structures in this paper have been deposited with the Cambridge Crystallographic Data Centre as supplementary publication nos. CCDC-150830 (**5**), -150831 (**6**). Copies of the data can be obtained, free of charge, on application to CCDC, 12 Union Road, Cambridge CB2 1EZ, UK [Fax: (internat.) +44-1223/336-033; E-mail: deposit@ccdc.cam.ac.uk]
[14] M. Winter, *http://www.webelements.com.*
[15] F. H. Allen, O. Kennard, D. G. Watson, L. Brammer, A. Guy Orpen, R. Taylor, *J. Chem. Soc. Perkin Trans. 2* **1987**, S1−S19.
[16] A. Guy Orpen, L. Brammer, F. H. Allen, O. Kennard, D. G. Watson, R. Taylor, *J. Chem. Soc., Dalton Trans.* **1989**, S1−S83.
[17] A. Smie, A. Synowczyk, J. Heinze, R. Alle, P. Tschuncky, G. Götz, P. Bäuerle, *J. Electronanal. Chem.* **1998**, *452*, 87−95.
[18] J. L. Reddinger, J. R. Reynolds, *Macromolecules* **1997**, *30*, 673−675.
[19] G. Zotti, M. C. Gallazzi, G. Zerbi, S. V. Meille, *Synth. Met.* **1995**, *73*, 217−225.
[20] F. Demanze, J. Cornil, F. Garnier, G. Horowitz, P. Valat, A. Yassar, R. Lazzaroni, J. L. Brédas, *J. Phys. Chem. B* **1997**, *101*, 4553−4558.
[21] F. Goldoni, A. P. H. J. Schenning, E. W. Meijer, unpublished results.
[22] S. H. Vosko, L. Wilk, M. Nusair, *Can. J. Phys.* **1980**, *58*, 1200−1211.
[23] Dmol software package from Biosym/MSI.
[24] C. Lee, W. Yang, R. G. Parr, *Phys. Rev. B* **1988**, *37*, 785−789.
[25] A. D. Becke, *J. Chem. Phys.* **1988**, *88*, 2547−2553.
[26] V. Parente, G. Pourtois, R. Lazzaroni, J. L. Brédas, *Synth. Met.* **1997**, *85*, 1031−1034.
[27] X. Crispin, R. Lazzaroni, V. Geskin, N. Baute, P. Dubois, R. Jérôme, J. L. Brédas, *J. Am. Chem. Soc.* **1999**, *121*, 176−187.
[28] Zindo software package from Biosym/MSI.

Received July 5, 2000
[I00270]

Transition Metal (^{53}Cr, ^{59}Co, ^{91}Zr, and ^{95}Mo) and ^{14}N NMR Spectroscopy of Coordination Compounds Containing Nitrogen Donor Ligands in Low-Viscosity Fluids

Sander Gaemers,[a] Jeroen Groenevelt,[a] and Cornelis J. Elsevier*[a]

Keywords: High-pressure NMR / Low-viscosity solvents / NMR spectroscopy / Quadrupole nuclei / Supercritical fluids / Subcritical fluids / Transition-metal NMR

Appreciable decreases of the line widths of NMR resonances of the quadrupolar nuclei ^{14}N, ^{53}Cr, ^{59}Co, ^{91}Zr, and ^{95}Mo have been obtained in supercritical solvents and in low-viscosity liquefied gases. Several α-diimines $R^1N{=}C(R^2){-}C(R^2){=}NR^1$ and their coordination compounds have been studied. Regarding the solubility of two α-diimines and some Cr, Zr, and Mo complexes it appears that the addition of small amounts of a modifier (acetone, CH_2Cl_2, THF) results in enhanced solubility of compounds without detrimental effects on the line widths. The use of HP NMR tubes (with and without pressure sensor) is very appropriate for measurements of NMR spectra under high pressure in supercritical fluids and liquefied gases of low viscosity. In several cases it appeared that the use of liquefied gases is more straightforward than the use of supercritical fluids, and gives similar or better results in terms of reduction of line widths.

Introduction

Nuclear magnetic resonance in solution plays an essential role in structure elucidation in chemistry, particularly the characterization of organometallic and coordination compounds. The development of transition metal NMR spectroscopy has greatly increased the knowledge of the relation between chemical shift and structure[1,2] in metal-containing compounds, and can help in solving structures and elucidating reaction mechanisms involving transition metal complexes.[3] Unfortunately, approximately 75% of the metal nuclei have a nuclear spin $I > {}^1/_2$, i.e. these nuclei possess a nuclear quadrupole moment. Obtaining NMR spectra of such nuclei can be troublesome due to their short T_1 and T_2, caused by the (extremely) efficient quadrupolar relaxation mechanism, which results in broadened resonance lines.[4,5] Accordingly, the application of nitrogen NMR spectroscopy for the analysis of nitrogen-containing compounds is difficult due to the low natural abundance of ^{15}N (0.36%), and the quadrupole moment of ^{14}N.

If line widths of quadrupolar nuclei could be considerably reduced, their acquisition and analysis would be greatly facilitated.[6,7] The quadrupolar relaxation[4] of a nucleus with $I > {}^1/_2$ is given in Equation (1), where I denotes the nuclear spin, η_s is the asymmetry parameter of the complex, χ is the nuclear quadrupole coupling constant, and τ_c is the rotational correlation time of the molecule in solution.

$$\Delta\nu_{1/2} = \frac{1}{\pi T_1} = \frac{1}{\pi T_2} = \frac{3\pi}{10}\left(\frac{2I+3}{I^2(2I-1)}\right)\left(1+\frac{\eta_s}{3}\right)(\chi)^2\,\tau_c$$

[a] Institute of Molecular Chemistry, Coordination and Organometallic Chemistry, University of Amsterdam, Nieuwe Achtergracht 166, 1018 WV Amsterdam, The Netherlands
E-mail: else4@anorg.chem.uva.nl

The expression for the rotational correlation time is presented in Equation (2), where V is the molecular volume, η_v is the bulk solvent viscosity, k is Boltzmann's constant, and T the temperature.

$$\tau_c = \frac{V\eta_v}{kT}$$

From Equation (1) and Equation (2) it appears that the quadrupolar relaxation rates can be reduced by employing solvents with a low bulk viscosity. For instance, supercritical fluids (SCFs) possess very low viscosities, which is one to two orders of magnitude lower than that of organic solvents,[6] enabling significant reductions of the line widths of quadrupolar broadened resonance lines.[7] Fortunately, the critical temperature and pressure of numerous compounds (see Table 1) are readily accessible by employing versatile yet simple devices like sapphire high-pressure NMR tubes in commercial NMR spectrometers.[8] This fact greatly facilitates the semi-routine acquisition of NMR spectra in supercritical fluids.

The recent and rapid growth in the use of SCFs as reaction media, particularly in catalysis involving transition metal compounds in homogeneous solution, is clearly evident.[9] A major problem is the low solvating power of these

Table 1. Critical values of solvents used in this study

Solvent[a]	T_c[b]	P_c[c]	ρ_c[d]
$CHCl_3$	536.4	54.7	0.667
Acetone	508.1	47.00	0.278
CO_2	304.14	73.75	0.468
CH_2F_2	351.6	58.30	0.545
CHF_3	299.3	48.58	0.526
$CClF_3$	302	38.7	0.581
SF_6	318.69	37.7	0.734

[a] Data taken from ref.[13] – [b] Critical temperature in K. – [c] Critical pressure in bar. – [d] Critical density in g/mL.

 © WILEY-VCH Verlag GmbH, 69451 Weinheim, 2001 1434–1948/01/0303–0829 $ 17.50+.50/0

fluids. Apolar compounds usually dissolve sufficiently in SCFs for catalysis and NMR spectroscopy (e.g. small organic molecules[6a,6c] or metal-carbonyl complexes[6b,6d]). For more polar compounds, there are several options: (i) modification with fluorinated anions[10] or with apolar side chains;[11] (ii) addition of small amounts of a co-solvent to a supercritical fluid;[12] (iii) application of polarizable SCFs, e.g., CHF_3, $CClF_3$, $CHClF_2$. In this study, we have taken recourse to the latter two options.

We have studied a number of nitrogen donor ligands (α-diimines) and transition metal complexes in liquefied gases and supercritical fluids by ^{14}N and transition metal (^{59}Co, ^{91}Zr, ^{95}Mo, ^{53}Cr) NMR spectroscopy. Several of these low-viscosity (supercritical) solvents were used to try to reduce their resonance line width. The solubility of α-diimines in several supercritical solvents has also been assessed. The data have been compared to those in common organic solvents.

Results and Discussion

A. ^{14}N NMR Spectroscopy of α-Diimines

Solubility

The solubility of the α-diimine $Me_3CCH_2N{=}C(Me){-}C(Me){=}NCH_2CMe_3$ [*neo*Pe−DAB(Me)] has been determined in $CDCl_3$, CO_2, CHF_3, and $CClF_3$ at 293 K and 323 K by comparison of the relative integrals of the proton signal of the $CH_2C(CH_3)_3$ moiety in their ^1H NMR spectra in the respective solvents. The sample volume of the HP NMR tube[8] was reduced to 1.7 mL employing an aluminum plug inserted in the high pressure NMR tube in order to reduce convection in the HP NMR tube and to ensure proper thermostatization of the samples during NMR experiments. The relative solubilities, the line widths at half height $\Delta\nu_{1/2}(^{14}N)$ and the ^{14}N and ^1H chemical shifts have been compiled in Table 2.

In liquefied gases and supercritical fluids, saturated solutions of *neo*Pe-DAB(Me) were employed at concentrations ranging from 0.004 to 0.072 M. The maximum achievable concentration in the compressed gasses amounted to 0.072 M in CO_2(l) at 293 K and 55.5 bar; the concentration employed in $CDCl_3$ was 0.091 M. The solubilities at 293 K and at 323 K are graphically shown in Figure 1.

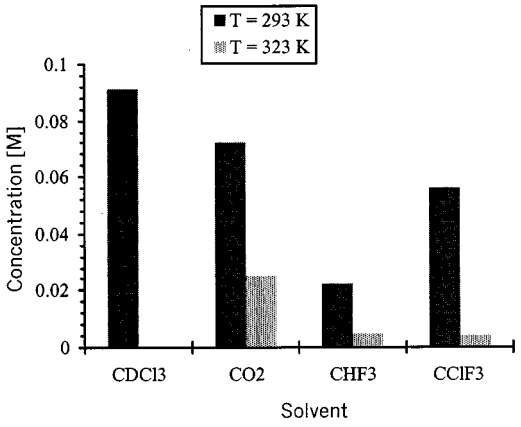

Figure 1. Solubility of $Me_3CCH_2N{=}C(Me){-}C(Me){=}NCH_2CMe_3$ [*neo*Pe-DAB(Me)] in various liquid and supercritical solvents

The solubility of *neo*Pe-DAB(Me) decreases by a factor of about 5 going from $CDCl_3$ to liquefied CHF_3 (293 K), but not very much for liquefied CO_2 or $CClF_3$. Its solubility is much lower (by a factor of between 4 and 20) in the supercritical state for the solvents studied (CO_2, $CClF_3$, CHF_3). This is the result of the low density of the SCFs compared to the density of the liquid state, which leads to a decrease of the solvent−solute interactions. The highest solubility of *neo*Pe-DAB(Me) in the series of pressurized gases studied was observed for CO_2 and $CClF_3$ in the liquid state. Its solubility in CHF_3, either in the liquid or supercritical state, is approximately a factor 4 or 5 lower than its solubility in liquid or supercritical CO_2. The higher solubility of *neo*Pe-DAB(Me) in liquid $CClF_3$ compared to liquid CHF_3 is due to the higher polarizability of the former. The higher solubility of *neo*Pe-DAB(Me) in CO_2 compared to CHF_3 is surprising as the dipole moment of the latter is higher than that of CO_2 [$\mu(CHF_3)$ = 1.65 Debye; $\mu(CHCl_3)$ = 1.01 Debye][13] and the polarizability of CHF_3

Table 2. Solubility and ^{14}N line width of *neo*Pe-DAB in several low-viscosity solvents

[a]	$CDCl_3$		CO_2		CHF_3		$CClF_3$	
T (K)	293	323	293	323	293	323	293	323
P[b]	nd	nd	55.5	97.9	40.3	67.0	31.2	48.6
ρ_c[c]	−	−	ld	0.67	ld	0.64	ld	0.66
Amount/mmol[d]	0.154	0.154	0.126	0.120	0.136	0.125	0.127	0.127
[*neo*Pe-DAB][e]	0.091	n.d.	0.072	0.025	0.022	0.005	0.056	0.004
$\delta(^1H)$[f]	0.95	0.97	−0.6	0.3	−0.4	0.4	−0.6	0.4
$\Delta\nu_{1/2}$[g]	1100±25	670±25	295±10	160±10	280±10	160±10	300±10	140±10
$F_{1/2}$[h]	1.6		1.8		1.8		2.1	
$\delta(^{14}N)$[i]	−40	−39	−41	−40	−42	−41	−41	−40

[a] The experiments were performed in the HP NMR cell described in ref.[8] − [b] Pressure in bar, nd not determined. − [c] Density of the supercritical fluid in g/ mL, ld density of the liquefied gas at its vapour pressure and 293 K. − [d] Amount of *neo*Pe-DAB(Me). − [e] Uncorrected relative integral of the $CH_2C(CH_3)_3$ proton signal, the integral of a 0.091 M $CDCl_3$ solution was arbitrarily calibrated at 1. − [f] Proton chemical shift of $CH_2C(CH_3)_3$ in ppm. − [g] ^{14}N NMR resonance line width at half height in Hz. − [h] Reduction factor $F_{1/2}$= $[\Delta\nu_{1/2}(293\ K)]/[\Delta\nu_{1/2}(323\ K)]$. − [i] ^{14}N chemical shift in ppm.

is slightly higher than that of CO_2 [$\alpha(CHF_3) = 2.80$ Å^3; $\alpha(CO_2) = 2.63$ Å^3].[14]

Chemical Shift

The ^{14}N chemical shifts of *neo*Pe-DAB(Me) vary between $\delta = -39$ and -42 (Table 2), the ^{14}N NMR resonances shift by 1 ppm upon heating the solutions from 293 K to 323 K. The change in ^{14}N chemical shift observed when heating liquefied gases is similar to the change observed when heating a $CDCl_3$ solution. In the case of the compressed gases, the effect of temperature on the chemical shift of the ^{14}N NMR resonance of *neo*Pe-DAB(Me) is not caused by a decrease of the fluid density, but is due to variations in the shielding tensor.

The variation in the ^1H chemical shift is more striking. The proton signals are shifted by approximately -1.5 ppm upon changing the solvent from $CDCl_3$ to the liquefied gases. In $CDCl_3$ no change is observed for the ^1H chemical shift, when heating the solution from 293 K to 323 K, whereas the chemical shift increases by 1 ppm in the case of the liquefied gases. This is explained by the variation of the diamagnetic volume susceptibility of the compressed gases changing from the liquid to the supercritical state.[15]

Line Widths

Line widths of the ^{14}N NMR resonances of *t*Bu-DAB and *neo*Pe-DAB(Me) in CO_2, $CClF_3$, CHF_3, SF_6, and acetone/[D_6]acetone (3:1) have been determined at various temperatures in the range 293−323 K. These data are graphically shown in Figure 2.

The reduction of the ^{14}N line widths in supercritical solvents compared to acetone and $CDCl_3$ is appreciable. [The ^{14}N line width of *neo*Pe-DAB(Me) has also been compared to $CDCl_3$ at 293 K; 1100 ± 25 Hz and at 323 K: 670 ± 20 Hz, see above, Table 2.] This clearly demonstrates the advantageous effect of the low-viscosity fluids on quadrupolar relaxation rates: Indeed much sharper lines are observed in the liquefied gases and supercritical fluids. Although the line widths of the ^{14}N resonances of *t*Bu-DAB (Figure 2, A) and *neo*Pe-DAB(Me) (Figure 2, B) are very different, the variation in line width for each compound spans a similar range, indicating that the values of τ_c in the various liquefied gases and SCFs are comparable. Furthermore, as expected, the observed ^{14}N NMR line widths are lower in the SCFs (at 323 K) than in the liquefied gases (at 293 K). Reduction factors[16] of the line widths of the ^{14}N NMR resonances in liquefied gases at 293 K and in the SCFs at 323 K relative to $CDCl_3$ at 293 K, as well as at 323 K, have been compiled in Table 3.

Not withstanding the fact that acetone has a much lower viscosity than chloroform, the line widths of the ^{14}N resonances in the liquefied gases and SCFs are considerably reduced with respect to acetone solutions. The line widths of the ^{14}N resonances observed in the liquefied gases range from 280 to 300 Hz, the line widths in the SCFs range from 140 to 160 Hz. This indicates similar viscosities of the solvents used (CO_2, $CClF_3$, CHF_3) for each of the domains (liquid and supercritical state, respectively).

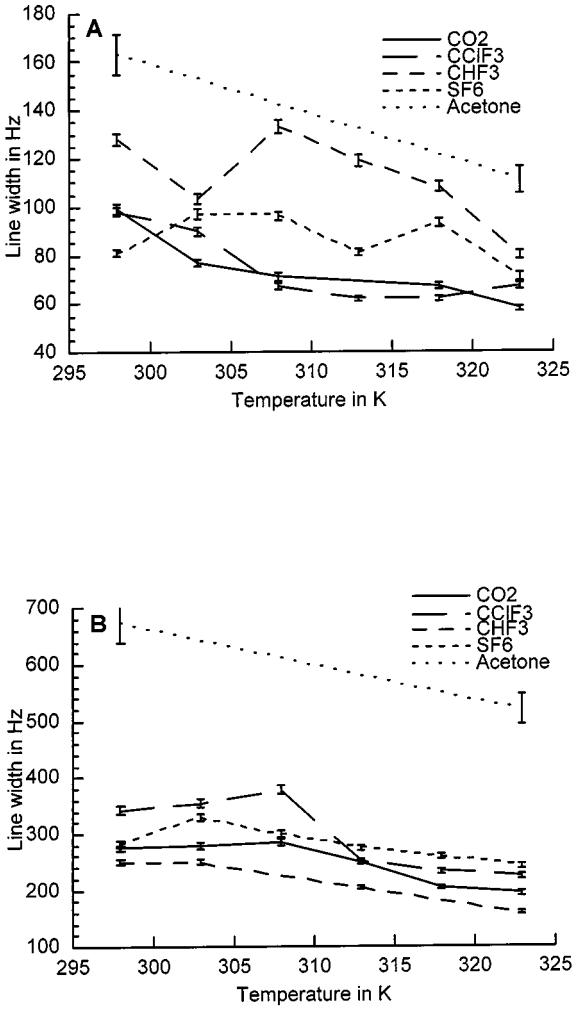

Figure 2. ^{14}N line widths at half height of (A) $Me_3CN{=}C(H){-}C(H){=}NCMe_3$ (*t*Bu-DAB) and (B) $Me_3CCH_2N{=}C(Me){-}C(Me){=}NCH_2CMe_3$ [*neo*Pe-DAB(Me)] in various compressed gasses and acetone; estimated error for the line widths (2%) indicated

Table 3. Reduction factors ($F_{1/2}$) of the ^{14}N line width for *neo*Pe-DAB(Me) in liquefied gases and supercritical fluids

$CDCl_3$[a]	CO_2		CHF_3		$CClF_3$	
T (K)	293	323	293	323	293	323
293	3.7	6.9	3.9	6.9	3.7	7.8
323	2.3	4.2	2.4	4.2	2.2	4.8

[a] Reduction factors [$F_{1/2} = \Delta\nu_{1/2}$(organic solvent)/$\Delta\nu_{1/2}$(compressed gas)] are reported relative to $CDCl_3$ at 293 K and 323 K.

Heating solutions in liquefied gases to above the critical temperature results in a reduction of the ^{14}N line width. The reduction factors associated with these changes range from 1.8 to 2.1. For $CDCl_3$ a reduction factor of 1.6 is observed when heating a solution from 293 K to 323 K. This indicates that the additional line narrowing resulting from the reduced viscosity of the supercritical fluid compared to the liquefied gas is small. The combined temper-

ature and viscosity effect of $CDCl_3$ is similar to that observed for the compressed gases. The fact that only a small viscosity effect is observed points to a significant "free rotor" contribution to the overall rotational correlation time, as has been described for tertiary amines.[17] For *neo*Pe-DAB(Me) the highest reduction of the ^{14}N resonance line width is found in supercritical $CClF_3$ (7.8 and 4.8 relative to $CDCl_3$ at 293 K and 323 K, respectively). The $F_{1/2}$ values found for supercritical CO_2 and CHF_3 are equal: 6.9 and 4.2 relative to $CDCl_3$ at 293 K and 323 K, respectively. This finding indicates that in CO_2 and CHF_3, the values of τ_c are similar under the conditions used.

In some cases the ^{14}N resonances were found to broaden upon heating the solutions from room temperature to the supercritical state, further heating resulted in a decrease of the ^{14}N line width. The initial (inhomogeneous) broadening of the ^{14}N resonances is attributed to the precipitation of solid material and convection.

Finally, we note that the reduction factors within a given solvent increase with temperature, as is seen for the ^{14}N resonances of *t*Bu-DAB and *neo*Pe-DAB(Me) (Table 2, Figure 2). When going from a liquefied gas at 298 K to the supercritical fluid at 323 K, the same or slightly larger reduction factors are observed when compared to the reduction factors for the acetone solutions in the same temperature range. This indicates that the reduced viscosity of the supercritical fluid compared to the liquefied gas contributes only slightly to the reduction of line widths.

B. Transition Metal and ^{14}N NMR Spectroscopy of Selected Coordination Compounds

^{59}Co NMR Spectroscopy

As an initial test of the appropriateness of our HP NMR system for transition metal NMR spectroscopy in SCFs, we have repeated an experiment performed by Rathke et al. in a static probe.[9a] The ^{59}Co NMR spectrum of $Co_2(CO)_8$ has been recorded in $[D_6]$benzene and CO_2(sc) and line widths of 10.4 kHz in $[D_6]$benzene at 296 K and 5.5 kHz in supercritical CO_2 at 310 K were observed. The ^{59}Co resonance recorded in supercritical CO_2 is well in agreement with the previously reported value of 5.1 kHz. The line width observed in $[D_6]$benzene is a factor of three smaller than the line width of 30 kHz reported previously.[9a] Possibly, the much larger line width in that case is due to poor homogeneity.

Further, we investigated the line widths of the ^{59}Co NMR resonances of $Co_4(CO)_{12}$ in $CDCl_3$ and CO_2. Due to its low solubility, the ^{59}Co NMR spectrum could only be recorded in liquid CO_2. The line widths for the apical ^{59}Co resonance of $Co_4(CO)_{12}$ are 4.0 kHz in $CDCl_3$ (296 K) and 3.6 kHz in CO_2 (296 K). The resonances of the cobalt atoms at the basal position were broader: 12.0 kHz in $CDCl_3$ (296 K) and 5.2 kHz in CO_2 (296 K). The variation in line width is the result of differences in the electric field gradient, experienced at the two sites of the cluster. This explanation is in agreement with previous reports concerning substituted cobalt clusters[18] and mixed cobalt−ruthenium clusters.[19] Upon changing from $CDCl_3$ solution to CO_2 solution, the reduction of the line width of the apical resonance is only 10%, whereas the line width of the basal resonance is reduced by more than a factor of two. The reduction of the rotational correlation time upon reducing the solvent viscosity from $CDCl_3$ to liquid CO_2 applies to the whole cluster, therefore one would expect the reduction factors of the line widths of the basal and apical ^{59}Co NMR resonances to be equal. However, it is documented that, due to differences in solvent polarity, the ratio of the line widths of the basal and the apical cobalt nuclei in various solvents varies between 1.9 in pentane and 3.2 in $CDCl_3$.[6] Here, we obtained a calculated ratio of 1.4 which, in agreement with the more apolar character of CO_2, is smaller but close to that observed for pentane.

^{53}Cr and ^{14}N NMR Spectroscopy

The application of supercritical solvents for the reduction of the resonance line width of quadrupolar transition metal nuclei has been further demonstrated for ^{53}Cr NMR spectroscopy. Two chromium isonitrile complexes $Cr(CO)_{6-x}(t\text{BuNC})_x$ (x = 1, 2) were studied by means of ^{14}N and ^{53}Cr NMR. The results have been compiled in Table 4.

Table 4. ^{14}N and ^{53}Cr NMR chemical shifts and line widths of two chromium isocyanide complexes of type $Cr(CO)_{6-x}(t\text{BuNC})_x$ in $[D_6]$acetone and CO_2

x[a]	Nucleus[b]	$[D_6]$Acetone[c]	CO_2(l)[c]	CO_2(sc)[d]	$F_{1/2}$[e]
1	^{14}N	2.5 Hz δ = −171.4	6 Hz δ = −176.1	5 Hz δ = −175.6	0.5
	^{53}Cr	90 Hz δ = 17.9	35 Hz δ = 15.7	35 Hz δ = 36.1	2.6
2	^{14}N	7 Hz δ = −174.5	7.5 Hz δ = −178.6	−	0.9
	^{53}Cr	44 Hz δ = 60.4	34 Hz δ = 52.4	−	1.3

[a] Number of *t*BuNC groups. − [b] Nucleus studied. − [c] Line width in Hz and chemical shift in ppm at T = 295 K. − [d] Line width in Hz and chemical shift in ppm at T = 343 K. − [e] Reduction factor [$F_{1/2} = \Delta\nu_{1/2}$(organic solvent)/$\Delta\nu_{1/2}$(compressed gas)].

The ^{14}N NMR resonances of the chromium complexes are sharp and broadened slightly with respect to uncoordinated *t*BuNC [$\Delta\nu_{1/2}(^{14}N)$ = 0.6 Hz[8]], indicating a small increase in the electric field gradient at the nitrogen atom upon coordination of the isocyanide group to the chromium center. The in this special case already very narrow ^{14}N line widths are found to increase slightly, changing from a $[D_6]$acetone solution to a liquid or supercritical CO_2 solution. This is most likely the result of inhomogeneous broadening as the experiment was performed on an unlocked and non-spinning sample. In addition, the precipitation of some solid material might have occurred in supercritical CO_2. The spectrum of $Cr(CO)_4(t\text{BuNC})_2$ could not be recorded in supercritical CO_2 due to its poor solubility in this medium.

The line widths of the chromium resonances for $Cr(CO)_{6-x}(t\text{BuNC})_x$ were found to decrease by a factor of

2.6 ($x = 1$) and 1.3 ($x = 2$) when changing the solvent from [D_6]acetone to supercritical ($x = 1$) and liquid ($x = 2$) CO_2. The reduction of the line widths of the already narrow ^{53}Cr resonances is relatively modest, especially when compared to ^{53}Cr line widths of many other chromium compounds[5c,20] and to the reduction of the ^{59}Co resonances described above.

To demonstrate the advantageous effect of the use of modifiers, the ^{53}Cr NMR spectrum of a 0.05 M solution of $(CO)_5Cr{=}C(NH_2)(Ph)$ was recorded in CO_2(sc) (critical density: 0.48 g/mL) with the addition of 5% (v/v) [D_6]acetone. This resulted in a ^{53}Cr NMR line width of 432 Hz ±5 Hz at δ = 170 (T = 323 K) after 14 h measuring time. This signal was found to be slightly broadened with respect to the signal recorded in the same mixture at 293 K, which had a line width of 402 ±5 Hz at δ = 169. The addition of a small amount of [D_6]acetone was used to dissolve the otherwise insoluble (in CO_2) chromium complex. Importantly, at the same sample concentration (0.05 M) no signal could be observed in pure [D_6]acetone after 14 h. A line width of $\Delta\nu_{1/2}$ = 1150 Hz at δ = 159 was reported for a highly concentrated sample (0.4 M in [D_6]acetone).[20] The signal observed by us for a 0.05 M sample after 48 h at 298 K in [D_6]acetone had a line width of 1340 Hz at δ = 151, thus a reduction factor $F_{1/2}$ = 3.3 applies.

^{95}Mo and ^{14}N NMR Spectroscopy

Complexes of type $Mo(CO)_4$(R-DAB) [R = *t*Bu, *c*Hex; R-DAB = R−N=C(H)−C(H)=N−R] are virtually insoluble in liquid and supercritical CO_2. The addition of a small amount of a modifier ([D_6]acetone) increases the solubility of these complexes in the low-viscosity liquid and supercritical fluid mixtures to such an extent that their ^{14}N and ^{95}Mo NMR spectra can be recorded. The results for $Mo(CO)_4$(R-DAB) complexes, which readily dissolve in [D_6]acetone and moderately so in CO_2/[D_6]acetone mixtures, have been compiled in Table 5 and Table 6.

Table 5. ^{14}N and ^{95}Mo line widths and chemical shifts of $Mo(CO)_4$(*t*Bu-DAB) in [D_6]acetone and CO_2/[D_6]acetone mixtures (critical density 0.48 ±0.02 g/mL)

R = *t*Bu % [D_6]acetone[a]	Nuc	T = 297 K $\Delta\nu_{1/2}$[b]	δ≅[c]	T = 323 K $\Delta\nu_{1/2}$[b]	δ[c]
7% (0.5 mL)	^{14}N	525	−31.6	390	−28.6
	^{95}Mo	54	−1178	33	−1171.1
11% (0.75 mL)	^{14}N	423	−33.7	428	−30.8
	^{95}Mo	27	1182.0	27	−1173.6
14% (1.00 mL)	^{14}N	494	−33.8	417	−32.1
	^{95}Mo	53	−1189.8	43	−1174.9
100%	^{14}N	669	−33.6	542	−31.2
	^{95}Mo	38	−1204.0	38	−1186.4

[a] Amount of acetone v/v in the supercritical state; volume of the HP NMR tube: 6.9 mL. − [b] Line width in Hz. − [c] Chemical shift in ppm.

In the CO_2/[D_6]acetone mixtures, the line width of the ^{14}N and ^{95}Mo resonances decreases relative to the line width observed in [D_6]acetone, and decreases slightly with decreasing acetone concentration in the CO_2. This was expected, based on the concomitant decrease of the viscosity of the mixture. The line width of the ^{14}N resonance of $Mo(CO)_4$(*t*Bu-DAB) is lower than that of $Mo(CO)_4$(*c*Hex-DAB), and is found at higher frequencies. The smallest line width for $Mo(CO)_4$(*t*Bu-DAB) was 390 Hz, observed in supercritical CO_2/7% [D_6]acetone, for $Mo(CO)_4$(*c*Hex-DAB) 417 Hz in supercritical CO_2/11% [D_6]acetone. Only modest reduction factors are thus obtained for these compounds. A solution of (*t*Bu-DAB)$Mo(CO)_4$ in liquid CCl_2F_2 at 323 K resulted in a ^{14}N line width of 450 Hz. The same compound measured in a $CClF_3/CH_2Cl_2$ (89:11; v/v) mixture at 323 K resulted in a ^{14}N-resonance line-width of 370 Hz, the complex was insoluble in pure $CClF_3$.

Table 6. ^{14}N and ^{95}Mo line widths and chemical shifts of $Mo(CO)_4$(*c*Hex-DAB) in [D_6]acetone and CO_2/[D_6]acetone mixtures (critical density 0.48 ±0.02 g/mL)

R = *c*Hex % [D_6]acetone[a]	Nuc	T = 297 K $\Delta\nu_{1/2}$[b]	δ≅[c]	T = 323 K $\Delta\nu_{1/2}$[b]	δ[c]
7% (0.5 mL)	^{14}N	nd[d]	nd[d]	555	−39.1
	^{95}Mo	nd[d]	nd[d]	38	−1185.9
11% (0.75 mL)	^{14}N	450	−37.0	417	−40.1
	^{95}Mo	30	1199	38	−1188.7
14% (1.00 mL)	^{14}N	745	−43.9	488	−42.2
	^{95}Mo	86	−1208	26	−1191.6
100%	^{14}N	919	−39.3	605	−38.3
	^{95}Mo	43	−1225.9	38	−1204.9

[a] Amount of acetone v/v in the supercritical state; volume of the tube 6.9 mL. − [b] Line width in Hz. − [c] Chemical shift in ppm. − [d] Not determined due to low solubility.

The ^{95}Mo resonances are found at lower frequencies for (*t*Bu-DAB)$Mo(CO)_4$ than for the (*c*Hex-DAB)$Mo(CO)_4$ complex. Raising the temperature of the solutions of the complexes (R-DAB)$Mo(CO)_4$ (R = *t*Bu, *c*Hex) results in an increase of both the ^{14}N and ^{95}Mo chemical shifts. The chemical shifts of the ^{14}N and ^{95}Mo resonances are found to be lowest in the solutions containing a low percentage of [D_6]acetone. Increasing the amount of acetone results in a shift to higher ppm values. These findings are in agreement with a decrease of the metal-centered excitation energy ΔE_{av} at higher temperatures and higher solvent polarity, resulting in a high frequency shift.[5c,21]

Only very small reductions of the line widths (or none at all) of the already narrow ^{95}Mo NMR resonance were observed when changing from [D_6]acetone to low-viscosity CO_2/[D_6]acetone mixtures. This might be due to the coupling of the ^{14}N to the ^{95}Mo, resulting in broadened signals due to unresolved coupling. However, at low viscosity and high temperatures, no resolved couplings between ^{14}N and ^{95}Mo could be observed. Further studies at various magnetic field strengths may shed light on this conjecture.

^{91}Zr NMR Spectroscopy

The generally polar Zr^{IV} compounds are insoluble in liquid or supercritical CO_2, but these complexes can be solubilized in the apolar CO_2 by the addition of a small amount of THF (CO_2/THF = 93:7; v/v), similar to the cases described above. The solubility of Cp_2ZrCl_2 in CO_2/THF mixtures can be increased to such levels that it is possible to

observe the ^{91}Zr resonance in the supercritical mixture at 323 K. The line width of Cp_2ZrCl_2 is reduced from 375 Hz in THF at 296 K to 210 Hz in the supercritical mixture.[22a] However, the acquisition of the ^{91}Zr resonance in the CO_2/THF mixture took 14 h, whereas the ^{91}Zr signal can be acquired in 10 min in pure THF solution. Many ^{91}Zr resonances reported[5b][22b] are much broader, however. For such Zr species there may be an advantage of measuring ^{91}Zr NMR in CO_2/THF mixtures.

Conclusions

The employed HP NMR tubes with[8] and without[23] a pressure sensor are very appropriate and safe to use for measurements of NMR spectra under high pressure in supercritical fluids and liquefied gases of low viscosity. It has been shown that in order to increase the solubility of poorly soluble compounds in liquid or supercritical CO_2, small amounts of a modifier (an organic solvent) may be added, which further enables better shimming and acquisition in the locked mode.

The ^{14}N line widths follow the trend of the solvent viscosities, and are thus considerably reduced (by a factor of up to 7 or 8), even when compared to the line width observed in low-viscosity organic solvents like $CDCl_3$ and acetone. In view of the low solvating power of low-density SCFs, the use of liquefied gases, i.e. liquid CO_2 and $CClF_3$, might be preferred for the reduction of quadrupolar broadened NMR lines, since these combine a relatively high solvating power with large reduction factors. Moreover, the experimental procedure for NMR spectroscopy in liquefied gases is more straightforward than in SCFs and fewer problems with phase separation and precipitation of solid material are expected during NMR experiments.

NMR of quadrupolar transition metal ions in low-viscosity liquefied gases or in supercritical solvents with and without the addition of modifiers results in some cases in an appreciable decrease of their resonance line widths. Enhanced solubilities without detrimental effects on the line widths can easily be achieved by the addition of small amounts of a modifier (acetone, CH_2Cl_2, THF).

Experimental Section

General: All spectra were recorded with a Bruker DRX300 NMR spectrometer, employing a 10-mm broadband probe (^{103}Rh-^{91}Zr)-{^1H}. The solubility experiments were carried out in a 10-mm o.d., 8-mm i.d. sapphire HP NMR tube with pressure sensor as described previously.[8] The HP NMR tube was modified with an aluminum plug to reduce the sample volume to 1.7 mL. Some experiments were performed in a modified HP NMR tube similar to the one described by Roe.[23a] The volume of this 10-mm o.d., 8-mm i.d. tube is 6.0 mL.[23b] – The complexes $Co_4(CO)_{12}$,[24] $(t\text{BuNC})_x\text{Cr}(CO)_{6-x}$ (x = 1,2)[25] (R-DAB)Mo(CO)$_4$ (R = *t*Bu, *c*Hex, DAB = diazabutadiene;[26] and Cp_2ZrBr_2)[27] were synthesized according to literature procedures. A sample of $(CO)_5Cr{=}C(NH_2)(Ph)$ was kindly provided by Prof. Dr. K.-H. Dötz (Universität Bonn). Cp_2ZrCl_2 was obtained from Alfa and used as received.

Sample Preparation: The NMR samples were prepared by charging the HP NMR tube described previously[8] with the appropriate α-diimine, typically 50 mg. The HP NMR tube was flushed three times with the appropriate gas (to suppress the N_2 signal) and filled with the liquefied gas using either the hand driven pump for CO_2, or by condensation of the solvent gas with liquid nitrogen for $CClF_3$, CHF_3, and SF_6. The critical density used varied between ρ_c and ρ_c + 0.1 g/mL. – For the determinations of the solubility in liquefied gases, the HP NMR tube was charged with the appropriate amount of *neo*Pe-DAB(Me). The concentration of *neo*Pe-DAB(Me) amounted to 0.091 M in $CDCl_3$. In other solvents, saturated solutions were obtained with concentrations varying between 0.004 M and 0.071 M (see Table 2). Prior to dissolution of the α-diimines, the tube was flushed three times with the solvent gas. The gas was introduced using the methods described previously,[8] after warming to room temperature the excess solvent was carefully evaporated until the desired level was reached. For the determinations of the solubility in supercritical fluids, the aluminum plug was placed in the HP NMR tube after introduction of the desired compound. The tube was charged with the appropriate liquefied gas and the density of the supercritical state was determined by weight. All of the solutions studied were supercritical at 323 K, except for $CDCl_3$. – Samples for NMR experiments (determinations of line widths) were also prepared as described above[8] for the experiments with diimines. For NMR of metal complexes: A sample of (*t*Bu-DAB)Mo(CO)$_4$ (0.23 g, 0.6 mmol) was dissolved in the appropriate amount of [D_6]acetone (see Table 5 and Table 6), the HP NMR tube was filled with CO_2 employing a hand driven pump;[8] similarly, solutions of (*c*Hex-DAB)Mo(CO)$_4$ were prepared by dissolving a 0.10 g sample (0.25 mmol) in the appropriate amount of [D_6]acetone and filling the HP NMR tube with CO_2. A solution of (*t*Bu-DAB)Mo(CO)$_4$ in CCl_2F_2 was prepared by condensing CCl_2F_2 in an HP NMR tube containing a 0.10 g sample of the complex (0.26 mmol). Similarly $CClF_3$ was condensed in an HP NMR tube containing a solution of 0.10 g (*t*Bu-DAB)Mo(CO)$_4$ (0.26 mmol) in 0.5 mL CH_2Cl_2. A 0.05 M solution of $(CO)_5Cr{=}C(NH_2)(Ph)$ was prepared in CO_2/acetone, 95:5 (v/v). The samples of other metal compounds were prepared as concentrated solutions.

NMR Experiments: All spectra were recorded in the unlocked and non-spinning mode, except for the spectra recorded in $CDCl_3$ or acetone, these were recorded in the locked mode. The NMR experiments at 293 K were performed by cooling the samples with a stream of cold nitrogen using the spectrometers variable-temperature unit. The ^1H NMR spectra were recorded using the decoupler coil of the 10-mm broadband probe. A total of 20 transients were recorded for every spectrum. For each spectrum 32k complex points were sampled over a spectral width of 7585 Hz. An acquisition time of 2.2 s, a pre-acquisition delay of 10 s, and pulse duration of 5 μs were used (ca. 30). Before integration of the ^1H signals, the base line was corrected for small offsets using the spectrometer software in the automatic mode. In the proton spectrum, typically line widths of 2–3 Hz at half-height were found. The ^{14}N NMR spectra were recorded using the broad-band observe coil of the 10-mm broad band probe. An *anti*-ring sequence was used to reduce probe ringing. The number of transients recorded for the ^{14}N NMR experiments was 2000, and 4096 complex points were sampled over a spectral width of 10823 Hz, resulting in an acquisition time of 0.2 s, a pre-acquisition delay of 5 ms and a π/2 pulse duration of 27 μs were used. – The ^{95}Mo π/2 pulse duration was 34 μs, ^{53}Cr

$\pi/2$ pulse duration was 32 μs, and an *anti*-ring sequence was used to reduce rolling base lines. An exponential multiplication one tenth of the natural line width was applied prior to Fourier transformation. The ^{14}N resonances are reported relative to $MeNO_2$, ^{95}Mo relative to 2 M MoO_4Na_2 in D_2O, ^{59}Co relative to a saturated $K_3Co(CN)_6$ solution in D_2O, ^{53}Cr relative to a $Cr(CO)_6$ solution in $CDCl_3$ and ^{91}Zr relative to Cp_2ZrBr_2 in $CDCl_3$.[22b]

Acknowledgments

The authors wish to thank Ing. J. M. Ernsting for skillful technical assistance with the NMR spectrometer and H. Luyten for the construction and maintenance of the high-pressure NMR tube. We thank the Council for Chemical Sciences of the Netherlands Organization for Scientific Research (CW-NWO) and the John van Geuns Foundation for financial support with acquiring the spectrometer and probe.

[1] W. von Philipsborn, *Chem. Soc. Rev.* **1999**, *28*, 95.
[2] [2a]J. G. Donkervoort, M. Bühl, J. M. Ernsting, C. J. Elsevier, *Eur. J. Inorg. Chem.* **1999**, 27. – [2b] W. Leitner, M. Bühl, R. Fornika, C. Six, W. Baumann, E. Dinjus, M. Kessler, C. Krüger, A. Rufinska, *Organometallics* **1999**, *18*, 1196.
[3] I. Banyai, J. Glaser, J. Losonczi, *Inorg. Chem.* **1997**, *36*, 5900.
[4] I. P. Gerothanassis, C. G. Tsanaktsidis, *Concepts Magn. Reson.* **1996**, *8*, 63.
[5] See for instance: [5a] D. Rehder, *Magn. Reson. Rev.* **1984**, *9*, 125. – [5b] D. Rehder, in: *Transition Metal NMR Spectroscopy* (Ed.: P. S. Pregosin), Elsevier, Amsterdam, **1991**, p. 1–58. – [5c] C. Brevard, P. S. Pregosin, R. Thouvenot, in: *Transition Metal NMR Spectroscopy* (Ed.: P. S. Pregosin), Elsevier, Amsterdam, **1991**, p. 59–89. – [5d] S. Gaemers, J. van Slageren, C. M. O'Connor, J. G. Vos, R. Hage, C. J. Elsevier, *Organometallics* **1999**, *18*, 5238.
[6] [6a] J. M. Robert, R. F. Evilia, *J. Am. Chem. Soc.* **1985**, *107*, 3733. – [6b] D. M. Lamb, D. G. vander Velde, J. Jonas, *J. Magn. Reson.* **1987**, *73*, 345. – [6c] J. M. Robert, R. F. Evilia, *Anal. Chem.* **1988**, *60*, 2035. – [6d] J. W. Rathke, R. J. Klingler, T. R. Krause, *Organometallics* **1991**, *10*, 1350. – [6e] R. J. Klingler, J. W. Rathke, *Progr. Inorg. Chem.*, vol. 39 (Ed.: S. J. Lippard), John Wiley & Sons, Inc., New York, **1991**. – [6f] M. P. Waugh, G. A. Lawless, *Advanced Applications of NMR to Organometallic Chemistry* (Eds.: M. Gielen, R. Willem, B. Wrackmeyer), John Wiley & Sons Ltd., Chichester, **1996**. – [6g] J. W. Rathke, R. J. Klingler, R. E. Gerald II, D. E. Fremgen, K. Woelk, S. Gaemers, C. J. Elsevier, in: *Chemical Synthesis in Supercritical Fluids* (Eds.: W. Leitner, P. G. Jessop), Wiley-VCH, Weinheim, **1999**, section 3.2, p. 165–194.
[7] S. Gaemers, C. J. Elsevier, *Chem. Soc. Rev.* **1999**, *28*, 135.
[8] S. Gaemers, H. Luyten, J. M. Ernsting, C. J. Elsevier, *Magn. Reson. Chem.* **1999**, *37*, 25.
[9] [9a] J. W. Rathke, R. J. Klingler, T. R. Krause, *Organometallics* **1991**, *10*, 1350. – [9b] P. G. Jessop, Y. Hsiao, T. Ikariya, R. Noyori, *J. Am. Chem. Soc.* **1996**, *118*, 344. – [9c] A. Fürstner, D. Koch, K. Langemann, W. Leitner, C. Six, *Angew. Chem. Int. Ed. Engl.* **1997**, *36*, 2466. – [9d] R. S. Oakes, A. A. Clifford, K. D. Bartle, M. T. Pett, C. M. Rayner, *Chem. Commun.* **1999**, 247. – [9e] S. Kainz, A. Brinkmann, W. Leitner, A. Pfaltz, *J. Am. Chem. Soc.* **1999**, *121*, 6421.
[10] [10a] M. J. Burk, S. Feng, M. F. Gross, W. Tumas, *J. Am. Chem. Soc.* **1995**, *117*, 8277. – [10b] K. Angermund, W. Baumann, E. Dinjus, R. Fornika, H. Görls, M. Kessler, C. Krüger, W. Leitner, F. Lutz, *Chem. Eur. J.* **1997**, *3*, 755.
[11] [11a] S. Kainz, D. Koch, W. Baumann, W. Leitner, *Angew. Chem. Int. Ed. Engl.* **1997**, *36*, 1628. – [11b] A. M. Kluwer, C. J. Elsevier, work in progress.
[12] [12a] B. A. Benner, *Anal. Chem.* **1998**, *70*, 4594. – [12b] M. Palma, L. T. Taylor, *J. Chromatogr. A* **1999**, *849*, 117.
[13] *Handbook of Chemistry and Physics* (Ed.: R. C. Weast), CRC Press Inc., Boca Raton, **1983**.
[14] C. J. F. Böttcher, P. Bordewijk, *Theory of electric polarisation*, vol. 2, Elsevier, Amsterdam, **1978**.
[15] A. Dardin, J. M. DeSimone, E. T. Samulski, *J. Phys. Chem. B* **1998**, *102*, 1775.
[16] Reduction factor $F_{1/2} = \Delta\nu_{1/2}$(organic solvent)/$\Delta\nu_{1/2}$(compressed gas).
[17] S. Gaemers, C. J. Elsevier, *Magn. Reson. Chem.*, in press.
[18] T. Richert, K. Elbayed, J. Raya, P. Granger, P. Braunstein, J. Rosé, *Magn. Reson. Chem.* **1996**, *34*, 689.
[19] P. Braunstein, J. Rosé, P. Granger, T. Richert, *Magn. Reson. Chem.* **1991**, *29*, S31.
[20] A. Hafner, L. S. Hegedus, G. deWeck, B. Hawkins, K. H. Dötz, *J. Am. Chem. Soc.* **1988**, *110*, 8413.
[21] M. Minelli, J. H. Enemark, R. C. Brownlee, M. J. O'Connor, A. G. Wedd, *Coord. Chem. Rev.* **1985**, *68*, 169.
[22] [22a] Previously, a line width of 276 Hz in THF at 298 K (at 8.37 MHz) has been reported: B. G. Sayer, N. Hao, G. Dénès, D. G. Bickley, M. J. McGlinchey, *Inorg. Chim. Acta* **1984**, *273*, C51. – [22b] M. Bühl, G. Hopp, W. von Philipsborn, S. Beck, M. Prosenc, U. Rief, H.-H. Brintzinger, *Organometallics* **1996**, *15*, 778.
[23] [23a] D. C. Roe, *J. Magn. Reson.* **1985**, *63*, 388. – [23b] C. J. Elsevier, *J. Mol. Catal.* **1994**, *92*, 285.
[24] P. Chini, V. G. Albano, *J. Organomet. Chem.* **1968**, *15*, 433.
[25] M. O. Albers, E. Simpleton, H. J. Coville, *J. Chem. Educ.* **1986**, *63*, 444
[26] H. Bock, H. tom Dieck, *Chem. Ber.* **1967**, *100*, 228.
[27] P. M. Bruce, B. M. Kingston, M. F. Lappert, T. R. Spalding, R. C. Srivastava, *J. Chem. Soc. A* **1969**, 2106.

Received July 17, 2000
[I00283]

On the Influence of the Bite Angle on the Allylic Alkylation of (*E*) and (*Z*) Substrates: Loss and Retention of Double Bond Stereochemistry

Richard J. van Haaren,[a] Gino P. F. van Strijdonck,[a] Henk Oevering,[b] Joost N. H. Reek,[a] Paul C. J. Kamer,[a] and Piet W. N. M. van Leeuwen*[a]

Keywords: Allyl complexes / Homogeneous catalysis / P ligands / Palladium

The bite angle of bidentate phosphane ligands has a pronounced influence on the degree of retention of the double bond geometry of the allylic substrate in the allylic alkylation reaction. To study the effect of the ligand on the regioselectivity, (*Z*)- and (*E*)-pent-2-enyl acetate were used as substrates. The alkylation of substrates with an (*E*) conformation of the double bond results in the preferential formation of the linear (*E*) product. A larger bite angle of the ligand results in an increase of the regioselectivity to >98% for the Sixantphos ligand. Analogously, the alkylation of (*Z*) substrates results in the formation of the linear (*Z*) product. Remarkably, for (*Z*) substrates, a larger bite angle of the ligand leads to an increased regioselectivity for the formation of the branched product instead of the linear product, up to 47.5% for Sixantphos. The observed regioselectivities are rationalized in terms of: a) a competition between *syn-anti* isomerization and alkylation, and b) a combination of steric and electronic effects in the transition state of the reaction. For all ligands tested, the reaction is faster for the (*E*) than for the (*Z*) substrate. However, competition experiments using the Sixantphos ligand show a relatively fast reaction rate for the (*Z*) substrate, which indicates that the coordination of the substrate to palladium is the discriminating, but not the rate-determining, step when both substrates are present.

Introduction

Transition metal-catalyzed allylic alkylation is a useful tool in synthetic organic chemistry.[1] A total control of the stereoselectivity and regioselectivity is required for most applications of this reaction. Whereas the enantioselective alkylation of symmetrically disubstituted allyl moieties (derived from, for example, cyclohexenyl acetate) has received much attention in the literature,[1] the regioselectivity of the reaction with other types of allylic substrates has been studied less extensively.[2−6]

When nonsymmetrically substituted allylic substrates are used,[2−6] regiocontrol is required prior to enantiocontrol (Figure 1). So far, palladium catalysts are the most widely studied, and generally show for such substrates a preference for the formation of the linear product.[1a,2] With bidentate P-N ligands, however, it is possible to obtain a high regioselectivity for the chiral branched product.[3] Catalysts based on other metals,[4] such as tungsten or iridium, also show a preference for the branched product, but the rate of the reaction is much lower than that found for palladium.

Relatively few studies have been reported concerning the influence of the geometry of the starting allylic substrate on the regioselectivity of the palladium catalyzed reaction.[5] Some years ago, Åkermark et al. reported such a study in which phenanthroline-type ligands were used in the allylic alkylation reaction with sodium diethyl 2-methylmalonate as the nucleophile.[5a] It was found that the regioselectivity of the reaction is dependent on the geometry of the double bond [(*E*) or (*Z*)] of the substrate. The (*E*) substrate reacts with the Pd(ligand) fragment to form an allylic complex having a *syn* geometry, which, after reaction with the nucleophile, mainly yields the linear (*E*) product. Analogously, the (*Z*) substrate reacts to form a (ligand)Pd(allyl) complex with an *anti* geometry (see Figure 1), which results in the formation of the linear (*Z*) and the branched product. They also reported that in the catalytic reactions, the regioselectivity is determined by competition between *syn-anti* isomerization and alkylation.

Recently, we have reported on the effect of the bite angle of bidentate *phosphane* ligands on the *syn*/*anti* ratio of cationic (P-P)Pd(crotyl) complexes.[6] It was found that a large bite angle leads to a low *syn*/*anti* ratio as a result of increased steric interactions. *Stoichiometric* alkylation of these complexes showed a correlation between the bite angle and the regioselectivity: the complexes were present as *syn*/*anti* mixtures, which complicated interpretation of the data. Moreover, apart from the C1 to C3 selectivity, the regioselectivity of the *catalytic* reaction was also determined by the competition between *syn-anti* isomerization and alkylation, which obscured structure-selectivity relations.

The *syn-anti* isomerization of the allyl moiety involves a π-σ rearrangement during which the allyl moiety is temporarily σ-bonded to the palladium through the substituted terminal allylic carbon atom (see Figure 2).[7] Rotation about the Pd−C bond and the adjacent C−C bond, followed by σ-π rearrangement then yields the other (*syn* or *anti*) isomer. As a result of increased steric hindrance, this process is slower when the substituent is larger. In order to explore the influence of the size of the allyl substituent on

[a] Institute of Molecular Chemistry, University of Amsterdam, Nieuwe Achtergracht 166, 1018 WV, Amsterdam, Netherlands
[b] DSM Research B. V., Postbus 18, 6160 MD, Geleen, Netherlands

 © WILEY-VCH Verlag GmbH, 69451 Weinheim, 2001 1434−1948/01/0303−0837 $ 17.50+.50/0

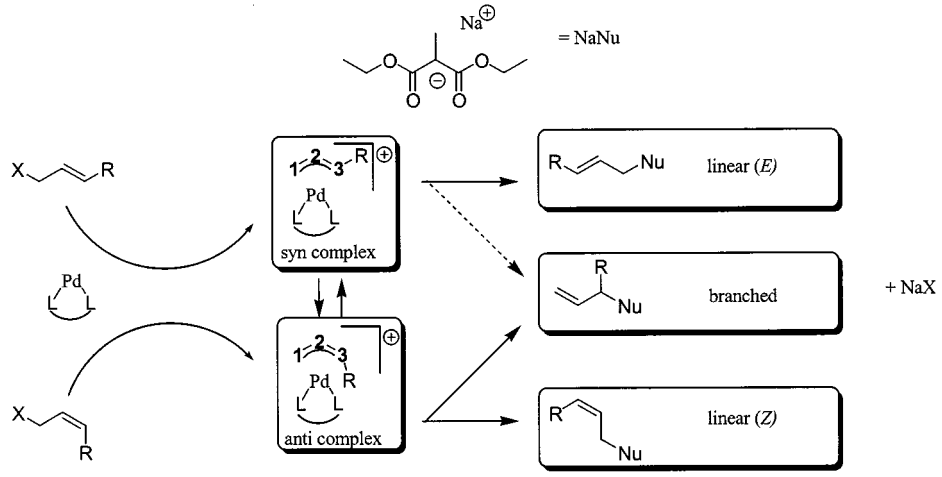

Figure 1. Regioselectivity in the allylic alkylation and numbering scheme

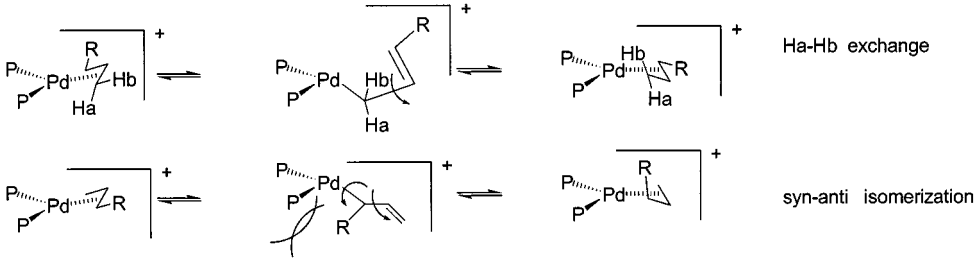

Figure 2. The π-σ rearrangement on different terminal sites of the allyl moiety (top: H_a-H_b exchange does not involve *syn-anti* isomerization of substituent R; bottom: *syn-anti* isomerization of substituent R is hampered by steric hindrance)

the regioselectivity, we have also performed the reaction with methyl-, ethyl- and propyl-substituted allylic substrates. By using (*Z*)- and (*E*)-pent-2-enyl acetate as substrates instead of (*E*)-but-2-enyl acetate, it appeared that a small change in steric size resulted in a relatively slow *syn-anti* isomerization rate (see below). This way, we have been able to study the effects of the ligands on the alkylation of the transient *syn* and *anti* isomeric complexes.

Results

All experiments were carried out with cationic (crotyl)Pd(ligand) complexes as catalyst precursors using four ligands that differ significantly in the calculated bite angle[6] (dppe, dppb, DPEphos and Sixantphos, see Figure 3).

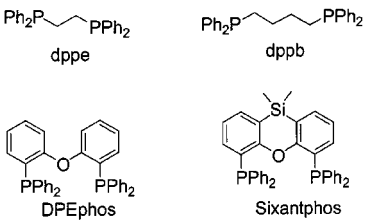

ligand	calculated bite angle[a] (°)
dppe	85
dppb	99
DPEphos	108
Sixantphos	110

Figure 3. The ligands {[a]: the bite angle has been determined by pm3(tm) geometry optimization of the cationic (crotyl)Pd(ligand) complexes that have been employed in the catalytic experiments[6]}

(*Z*) *and* (*E*) *Allylic Substrates*

To study the effect of the double bond geometry of the substrate we performed the allylic alkylation of (*Z*)- and (*E*)-pent-2-enyl acetate with sodium diethyl 2-methylmalonate as the nucleophile (Table 1). Starting from the (*E*) substrate, the linear (*E*) product is formed primarily. When the bite angle of the ligand is larger, the regioselectivity for the formation of this product increases. In contrast, the (*Z*) substrate reacts to form both the linear (*Z*) and the branched product. In this case, a larger bite angle of the ligand results in an increase of the regioselectivity to the branched product. With dppe, the reaction rate is low compared to the other ligands and, remarkably, the linear (*E*) product is formed in high regioselectivity, even starting from the (*Z*) substrate. The fastest reactions are observed using the relatively flexible ligands dppb and DPEphos. For all ligands, the alkylation of the (*Z*) allylic substrate is slower than that of the (*E*) allylic substrate.

Competition Experiments

To gain more insight into the different courses the reaction takes for the (*E*)- and (*Z*)-pent-2-enyl acetate, competition experiments were carried out with the ligands dppb and Sixantphos (Table 2). It was found that in the separate experiments the alkylation of the (*Z*) substrate is much slower than that of the (*E*) substrate. With dppb in the com-

Table 1. Alkylation of (*Z*)- and (*E*)-pent-2-enyl acetate

Substrate geometry	Complex (ligand)	TOF_{ini} [a] (mole/mole/h)	% branched[b]	% linear *E*[b]	% linear *Z*[b]
E	dppe	2100	1.9	94.2	3.9
E	dppb	7200	1.4	96.9	1.7
E	DPEphos	16900	1.1	98.1	0.8
E	Sixantphos	5500	1.0	98.3	0.6
Z	dppe	160	3.1	86.4	10.5
Z	dppb	1400	15.6	7.3	77.1
Z	DPEphos	3200	26.7	1.1	72.3
Z	Sixantphos	950	47.5	0.8	51.7

[a] Determined after 2 minutes reaction time (the reaction conditions are described in the Experimental Section). – [b] Determined after complete conversion.

Table 2. Competition experiment using (*E*)- and (*Z*)-pent-2-enyl acetate

Complex (ligand)	Time (min.)	% *Z* substrate[a]	% *E* substrate[a]	% branched[b]	% linear *E*[b]	% linear *Z*[b]
dppb	2	5	11	7	40	53
dppb	5	12	16	9	43	48
dppb	10	28	33	9	43	48
dppb	30	56	58	9	47	44
dppb	60	75	77	9	48	43
dppb	180	88	92	9	50	41
Sixantphos	2	12	8	36	23	41
Sixantphos	5	36	21	35	26	39
Sixantphos	10	65	38	34	29	37
Sixantphos	30	95	82	28	42	30
Sixantphos	60	100	98	25	48	27
Sixantphos	180	100	100	24	50	26

[a] Percentage of substrate consumed (the reaction conditions are described in the Experimental Section). – [b] Regioselectivity, percentage of total yield.

petition experiments, however, a much smaller difference in conversion rate is observed between the (*E*) and (*Z*) substrates. Furthermore, when Sixantphos is used as the ligand, the (*Z*) substrate is consumed at a higher rate than the (*E*) substrate. The initially predominating consumption of the (*Z*) substrate results in the formation of primarily the linear (*Z*) and the branched product. The regioselectivity of the reaction is dependent on the conversion and, as the reaction proceeds, the fraction of linear (*E*) product increases.

Influence of the Size of the Allyl Substituent

The results with (*E*)-pent-2-enyl acetate show a different regioselectivity than previously found for (*E*)-but-2-enyl acetate.[6] The results of the allylic alkylation of (*E*)-substituted allylic substrates bearing substituents of different size (methyl, ethyl and propyl) are compared in Table 3. In all cases there is a preference for the formation of the linear (*E*) product. The selectivity for the formation of the (*E*)

Table 3. Alkylation of various (*E*)-substituted allylic acetates (but-2-enyl acetate, pent-2-enyl acetate, hex-2-enyl acetate)

Substrate	Complex (ligand)	TOF_{ini} [a] (mole/mole/h)	% branched[b]	% linear *E*[b]	% linear *Z*[b]
Butenyl	dppe	2000	20.0	68.8	11.1
Butenyl	dppb	8900	17.9	79.0	3.1
Butenyl	DPEphos	8700	17.4	80.1	2.5
Butenyl	Sixantphos	9100	12.9	85.7	1.4
Pentenyl	dppe	2100	1.9	94.2	3.9
Pentenyl	dppb	7200	1.4	96.9	1.7
Pentenyl	DPEphos	16900	1.1	98.1	0.8
Pentenyl	Sixantphos	5500	1.0	98.3	0.6
Hexenyl	dppe	150	1.1	97.3	1.7
Hexenyl	dppb	1900	0.8	98.9	0.3
Hexenyl	DPEphos	200	0.6	99.3	0.1
Hexenyl	Sixantphos	700	0.7	99.2	0.1

[a] Determined after 2 minutes reaction time (the reaction conditions are described in the Experimental Section). – [b] Determined after complete conversion.

product increases when ligands with a larger bite angle are used. As expected, the regioselectivity is also influenced by the size of the substituent. The selectivity increases when the substituent is larger, leading to 99.3% linear (*E*) product in the alkylation of (*E*)-hex-2-enyl acetate (R = propyl) by a Sixantphos-ligated palladium complex. The size of the substituent also has a pronounced effect on the rate of the reaction: the larger the substituent, the slower the reaction.

Discussion

Several studies have been devoted to the origin of regioselectivity in the palladium-catalyzed allylic alkylation.[1a,2−6,8−10] Two different effects have been reported: 1) in the case of an *early* transition state, the regioselectivity is determined by the relative electrophilicity of the terminal allylic carbon atoms and steric hindrance is of minor importance;[8] 2) in the case of a *late* transition state, the degree steric hindrance encountered during the nucleophilic attack and the subsequent rotation of the allyl moiety becomes important.[2a,9] The route to the formation of the linear product is then favored over that of the branched product.

From theoretical[10] and experimental studies it is known that the allylic alkylation reaction proceeds by attack of the nucleophile on the cationic (π-allyl)Pd(ligand) species (Figure 4). This results in the formation of a single bond between the attacked allylic carbon atom and the nucleophile (stage **a**). A C=C double bond is then formed between the other two allylic carbon atoms (stage **b**). During these processes, the allyl moiety rotates, forming a transient neutral (olefin)Pd(P-P) complex (stage **b**).

In a recent theoretical study, a combined explanation is presented for the apparent occurrence of either an early or a late transition state.[10c] The nucleophilic attack at the most electrophilic terminal allylic carbon atom (early transition state) results in a lowering of the energy barrier of stage **b** of the reaction.

Influence of the Alkene Geometry

The alkylation of (*E*)-pent-2-enyl acetate does not yield more than 4% of the linear (*Z*) product and 2% of the branched product (Table 1), thus giving almost complete retention of alkene geometry. The linear (*E*) product can only be formed from the *syn* isomer (see Figure 1), indicating that for each of the tested palladium(ligand) complexes, oxidative addition of the (*E*) substrate yields mainly the *syn* isomer. Analogously, the results obtained for (*Z*)-pent-2-enyl acetate (Table 1) indicate that after its oxidative addition to palladium, the *anti* isomer is formed, which then reacts to form the linear (*Z*) product. However, reaction of the (*Z*) substrate leads to the formation of a relatively large amount of the linear (*E*) product. These mixtures of products can only be formed after isomerization from *anti* to *syn* (or vice versa) has occurred. Thus, the regioselectivity is a result of: (i) the *syn*/*anti* equilibrium, (ii) the competition between isomerization and alkylation, and (iii) the C1 to C3 regioselectivity for attack on the *syn* and the *anti* isomer.[5a] These points will be discussed individually below.

Concerning the *syn*/*anti* ratio, we have shown before that for cationic (crotyl)Pd(ligand) complexes (ligand = dppe, dppb, DPEphos and Sixantphos), the *syn* isomer is more stable than the *anti* isomer.[6] The crotyl substrate yields an allyl group with a relatively small methyl substituent. After oxidative addition of a pentenyl substrate, an allyl moiety bearing a larger ethyl group (*syn* or *anti*) is formed which will show more steric interaction of both the *syn* and the *anti* isomer with the ligand. The data obtained from the catalytic experiments (Table 1) indicate that the relatively small difference in size between a methyl and an ethyl substituent has a large effect on the *syn*/*anti* ratio of the transient allyl complexes. Because the results indicate that the *anti*-to-*syn* isomerization prevails over the *syn*-to-*anti* isomerization (Table 1), it is concluded that for larger substituents on the allyl group, the preferred *syn*/*anti* ratio is higher than that previously observed for the methyl substituent.

The occurrence of a competition between *syn*-*anti* isomerization and alkylation is supported by the concurrence

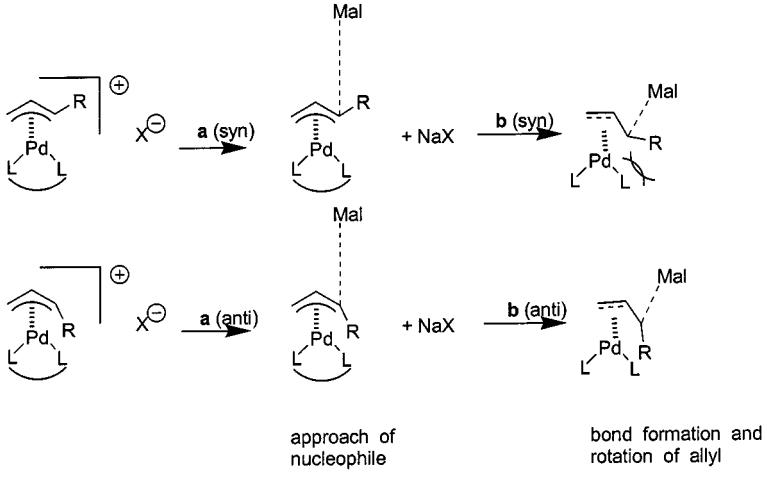

Figure 4. *Syn* and *anti* complexes: comparison of the consecutive steps of the reaction

of a low reaction rate and a low regioselectivity. Thus, the alkylation of the (*Z*) substrate occurs at a lower rate than that of the (*E*) substrate, allowing *anti*-to-*syn* isomerization to take place prior to nucleophilic attack, which lowers the overall regioselectivity. The rate of isomerization is especially fast for dppe relative to the rate of alkylation; the reaction of the (*Z*) substrate leads almost exclusively to the formation of the (*E*) product.

The effect of the bite angle on the C1 to C3 regioselectivity of the alkylation is different for the *syn* and the *anti* isomer. The selectivity of the *syn* isomer to the formation of the linear (*E*) product increases when the bite angle is larger. This can be explained in terms of steric hindrance during both stages **a** and **b** of the reaction. The linear C1 position is more accessible for the approaching nucleophile than the branched C3 position. Furthermore, during the bond formation the substituent has to bend away from the nucleophile in the direction of the sterically crowded Pd(ligand) fragment. Nucleophilic attack on the allyl moiety results in the formation of a transient palladium-olefin complex,[9c] in which the C=C double bond is located in the P−Pd−P plane and the malonate-substituted C3 atom below this plane (see Figure 4). When the branched product has been formed, the substituted C3 site, bearing the ethyl group and the malonate, is rotated out of the P−Pd−P plane (stage **b**). In a *syn*-substituted allyl moiety, the ethyl group points in the direction of the phenyl rings of the ligand. The steric interactions thus encountered are more pronounced when the bite angle of the ligand is larger. So, during both stages **a** and **b** of the reaction, steric hindrance directs the regioselectivity to the formation of the linear (*E*) product.

In contrast, the effect of the bite angle on the regioselectivity of the alkylation of the *anti* isomer shows the opposite trend. It is known that in palladium complexes of disubstituted allylic substrates, the branched *anti* position is relatively electrophilic and consequently more reactive than the branched *syn* position.[5b] The geometrical distortion resulting from steric interactions with the ligand are relatively large for the *anti* compared to the *syn* isomer. An increase of the bite angle will enhance the geometrical distortion of the allyl moiety and thereby[2c][10c] enhance the relative electrophilicity of the allylic carbon atom at the branched C3 position compared to the C1 position. Thus, during the approach of the nucleophile (stage **a** of the reaction) the electronic effects may prevail over the steric hindrance giving the branched product. During the rotation of the allyl moiety after the nucleophilic attack has taken place (stage **b**), the ethyl group of the *anti* isomer will point downward, i.e. not in the direction of the phenyl rings of the ligand, and steric hindrance will be less than in the case of the *syn* isomer (stage **b**). So also for the *anti* isomer, in both stage **a** and **b** of the reaction, the regioselectivity is directed to the formation of the same regioisomer, i.e. the branched product for the *anti* isomer and the linear (*E*) product for the *syn* isomer.

Competition Experiments

The competition experiments carried out to gain more mechanistic insight in the reaction course of the (*E*) and the (*Z*) substrate showed a relatively high reaction rate for the latter. Because the overall reaction rate in the separate experiments is higher for the (*E*) substrate than for the (*Z*) substrate, the discrimination in the competition experiments has to take place in an early stage of the catalytic cycle of the reaction. As a result of the better accessibility of the (*Z*) double bond relative to the (*E*) double bond, the coordination of the substrate to palladium will be faster for the (*Z*) than for the (*E*) substrate. As the (*E*) substrate is found to react faster, we conclude that the next steps of the reaction proceed at a higher rate for the (*E*) substrate than for the (*Z*) substrate (Figure 5).

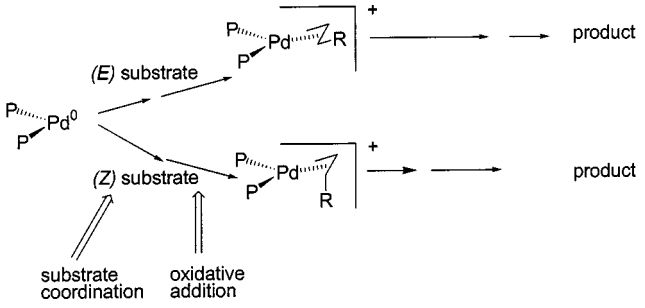

Figure 5. Schematic representation of the origin of kinetic resolution (the size of the arrows indicates the relative rate)

The change in rate difference in the competition experiments compared to the separate experiments is larger for Sixantphos, the ligand with the largest bite angle (Table 2). Upon coordination of the substrate to a Pd^0(Sixantphos) complex, the steric hindrance will be larger than for the analogous complex with the dppb ligand, and therefore the discrimination between the (*E*) and (*Z*) substrate will be more pronounced for Sixantphos. It is possible that, for dppb, the substrate discrimination does take place at this stage, but its effect may be compensated by a rate difference in the next steps of the reaction.

It can be argued that the discriminating step, coordination of the olefin, is not the rate determining step of the reaction. If the coordination of the (*E*) substrate were rate limiting, and thus slower than the coordination of the (*Z*) substrate, the (*E*) substrate would not react faster in the *separate* experiments. Analogously, if the coordination to palladium were the rate determining step for the (*Z*) substrate, it would not be found to react faster in the *competition* experiments.

On the other hand, if the rate determining step for the *E* substrate is indeed the substrate coordination and for the *Z* substrate, the subsequent oxidative addition would be rate determining and the latter being slower than the substrate coordination of the (*E*) substrate, the above arguments are not true. Unfortunately, the coordination of the substrate and the subsequent oxidative addition cannot be distinguished in kinetic experiments.

Effect of the Size of the Substituent

The alkylation of the (*E*) substrates with different substituents all show the same trend (Table 3). Both a larger bite angle of the ligand and a larger substituent on the allyl moiety result in an increase of the regioselectivity to the formation of the linear (*E*) product. As has been described above, the *syn*/*anti* isomer ratio will be lower for small groups, which accounts for the relatively large amount of linear (*Z*) product formed from alkylation of (*E*) but-2-enyl acetate. Furthermore, the relatively large size of the ethyl and propyl groups relative to the methyl group, hinders the attack of the nucleophile on the branched position. This explains the smaller amounts of branched product formed when either the substituent or the bite angle of the ligand is larger.

The rate of the reaction is also affected by the size of the substituent. The lower rate of reaction when larger substrates are used can be explained in terms of steric hindrance. During the oxidative addition and the nucleophilic attack, a larger allylic substrate will experience more steric hindrance than a small allylic substrate and the reaction may therefore proceed at a lower rate. The product dissociation will probably not be rate limiting, but, nevertheless, the coordination of a larger product will be more hindered than that of a small one, and therefore it may dissociate faster than a small product. Which of these effects prevails depends on the nature of the rate limiting step of the reaction, which may be determined by the size and orientation of the substituent and the bite angle of the ligand.

In the absence of significant steric interactions, a larger bite angle of the ligand results in an increase of the rate of reaction. Thus, the alkylation of (*E*)-but-2-enyl acetate occurs at the highest rate when the Sixantphos ligand is used. The rate of alkylation of the larger substrates is the highest for catalysts bearing a flexible ligand favoring a relatively large bite angle, such as dppb or DPEphos.

Conclusion

We separated the effect of the bite angle on the regioselectivity resulting from the *syn* and the *anti* isomeric complex. The regioselectivity of the reaction of the *syn* isomer is determined by steric effects in both the first and the second stage of the reaction, resulting in almost exclusive formation of the linear (*E*) product. The geometry of the allyl moiety in the *anti* isomer is presumably distorted to a large extent and the electrophilicity of the branched position is large relative to the linear position. The regioselectivity of its alkylation is, in the first stage of the reaction, mainly governed by electronic factors, and in the second stage by steric effects. For *syn* complexes of ligands with a large bite angle, the *linear* product is favored both in the first and the second stage of the reaction, whereas for the *anti* isomer, the *branched* product becomes the favored regioisomer in both stages of the reaction.

In competition experiments between the (*E*) and (*Z*) substrates, the (*Z*) substrate is found to react at a rate that is similar to or faster than that of the (*E*) substrate, whereas in separate experiments the reaction with the (*E*) substrate is faster. This effect is more pronounced for Sixantphos than for dppb. The substrate discrimination presumably takes place in the stage of coordination of the olefin to the metal center, prior to oxidative addition and prior to the rate determining step. Therefore, in a system in which both the (*E*) and (*Z*) substrate are present, the latter dominates the reaction rate.

Experimental Section

^{1}H NMR (300 MHz, TMS, $CDCl_3$), $^{31}P\{^1H\}$ (121.5 MHz external 85% H_3PO_4, $CDCl_3$), ^{13}C NMR (75.4 MHz, TMS, $CDCl_3$) were recorded on a Bruker AMX-300 spectrometer. The product distribution of the alkylation experiments was measured on an Interscience Mega2 GC apparatus, equipped with a DB1 column (length 30 m, inner diameter 0.32 mm, film thickness 3.0 μm) and an F.I.D. detector.

All experiments were carried out using standard Schlenk techniques. All solvents and allylic substrates were freshly distilled prior to use. Diethyl 2-methylmalonate, NaH, and (*E*)-hex-2-enyl acetate were obtained from Aldrich.

General Synthetic Procedures: Sodium diethyl 2-methylmalonate (0.5 M in THF) was prepared from diethyl 2-methylmalonate (20 mmol, 3.48 g) and NaH (20 mmol, 0.48 g) in THF at 273 K. The synthesis and characterization of all complexes,[6] crotyl acetate,[6] and the alkylation products of the coupling of crotyl acetate and (*E*)-hex-2-enyl acetate to sodium diethyl 2-methylmalonate are described elsewhere.[5a]

Alkylation Reactions: The *catalytic* reactions were performed at 292 K in THF (5 mL), using 0.05 mol-% of catalyst (0.25 μmol), 0.5 mmol of substrate (0.064 g) and 1.0 mmol of sodium diethyl 2-methylmalonate (0.20 g). All reagents were added from stock solutions. The reaction was monitored by taking samples from the reaction mixture which, after aqueous work up, were analyzed by GC using decane (0.0142 g) as the internal standard. − NMR spectroscopic data were obtained in $CDCl_3$ (δ in ppm).

Diethyl 2-Methyl-[(2*E*)-pent-2-en-4-yl]malonate (linear *E*): ^{1}H: δ = 0.90 (t, ^3J = 7.3 Hz, 3 H, C*H*$_3$−CH$_2$−CH=), 1.22 (t, ^3J = 7.0 Hz, 6 H, O−CH$_2$−C*H*$_3$), 1.32 (s, 3 H, C$_{quat.}$−CH$_3$), 2.0 (m, 2H, CH$_3$−C*H*$_2$−CH=), 2.50 (d, ^3J = 6.9 Hz, 2 H, C$_{quat.}$−C*H*$_2$−CH=), 4.12 (q, ^3J = 7.0 Hz, 4 H, O−C*H*$_2$−CH$_3$), 5.25 (m, 1 H, olefinic H), 5.50 (m, 1 H, olefinic H). − $^{13}C\{^1H\}$: δ = 14.1 (*C*H$_3$−CH$_2$−CH=), 14.5 (O−CH$_2$−*C*H$_3$), 20.1 (C$_{quat.}$−*C*H$_3$), 26.0 (CH$_3$−*C*H$_2$−CH=), 39.2 (C$_{quat.}$−*C*H$_2$−CH=), 54.3 (*C*$_{quat.}$−CH$_3$), 61.5 (O−*C*H$_2$−CH$_3$), 123.1 (CH$_3$−CH$_2$−*C*H=), 137.4 (CH$_3$−CH$_2$−CH=*C*H), 172.5 (C=O).

Diethyl 2-Methyl-[(2*Z*)-pent-2-en-4-yl]malonate (linear *Z*): ^{1}H: δ = 0.90 (t, ^3J = 7.5 Hz, 3 H, C*H*$_3$−CH$_2$−CH=), 1.20 (t, ^3J = 7.0 Hz, 6 H, O−CH$_2$−C*H*$_3$), 1.33 (s, 3H, C$_{quat.}$−CH$_3$), 2.05 (m, 2H, CH$_3$−C*H*$_2$−CH=), 2.56 (d, ^3J = 7.5 Hz, 2 H, C$_{quat.}$−C*H*$_2$−CH=), 4.12 (q, ^3J = 7.0 Hz, 4 H, O−C*H*$_2$−CH$_3$), 5.15 (m, 1H, CH$_3$−CH$_2$−CH=C*H*), 5.45 (m, 1H, CH$_3$−CH$_2$−C*H*=CH). − $^{13}C\{^1H\}$: δ = 13.9 (*C*H$_3$−CH$_2$−CH=), 14.4 (O−CH$_2$−*C*H$_3$), 17.4 (C$_{quat.}$−*C*H$_3$), 20.0 (CH$_3$−*C*H$_2$−CH=), 33.4 (C$_{quat.}$−CH$_2$-CH=), 51.3 (*C*$_{quat.}$−CH$_3$), 61.6 (O−*C*H$_2$−CH$_3$), 122.7 (CH$_3$−CH$_2$−*C*H=), 135.9 (CH$_3$−CH$_2$−CH=*C*H), 172.5 (C=O).

3-(Diethyl 2-Methyl [(1*E*)-pent-1-ene malonate) (branched): ^{1}H: δ = 0.82 (t, ^3J = 7.5 Hz, 3 H, C*H*$_3$−CH$_2$−CH=], 1.20 (t, ^3J = 7.0 Hz, 6 H, O−CH$_2$−C*H*$_3$), 1.21 (m, 2H, CH$_3$−C*H*$_2$−CH), 1.32 (s, 3H, C$_{quat.}$−CH$_3$), 3.38 (m, 1H, CH$_3$−CH$_2$−C*H*), 4.12 (q, ^3J = 7.0 Hz, 4 H, O−C*H*$_2$−CH$_3$), 5.01 (d, ^3J = 16.8 Hz, 1 H, *E*−CH=C(H)*H*), 5.05 (d, *J* = 10.2 Hz, 1 H, *Z*−CH=C(H)*H*), 5.6 (m, 1H −C*H*=C(H)H). − ^{13}C{^{1}H}: δ = 12.8 (*C*H$_3$−CH$_2$−CH), 14.4 (O−CH$_2$−*C*H$_3$), 17.4 (C$_{quat.}$−*C*H$_3$), 21.0 (CH$_3$−*C*H$_2$−CH), 46.5 (CH$_3$−CH$_2$−*C*H), 51.3 (*C*$_{quat.}$−CH$_3$), 61.6 (O−*C*H$_2$−CH$_3$), 118.9 (−CH−CH=*C*H$_2$), 137.2 (−CH−*C*H=CH$_2$), 172.5 (C=O).

Acknowledgments

This research was carried out with financial support from DSM Research B.V. and with a subsidy from the Ministerie van Onderwijs, Cultuur en Wetenschappen as part of the E. E. T. program for clean chemistry.

[1] [1a] B. M. Trost, D. V. van Vranken, *Chem. Rev.* **1996**, *96*, 395−422. − [1b] M. Yamaguchi, K. Ohba, H. Tomonaga, T. Yamagishi, *J. Mol. Cat. A: Chem.* **1999**, *140*, 255−258. − [1c] J. F. Bower, R. Jumnah, A. C. Williams, J. M. J. Williams, *J. Chem. Soc., Perkin Trans. 1* **1997**, 1411−1420. − [1d] S. Schleichl, G. Helmchen, *Eur. J. Inorg. Chem.* **1999**, 2515−2521.

[2] [2a] G. E. Oosterom, R. J. Van Haaren, J. N. H. Reek, P. C. J. Kamer, P. W. N. M. Van Leeuwen, *Chem. Commun.* **1999**, 1119−1120. − [2b] M. Kranenburg, P. C. J. Kamer, P. W. N. M. van Leeuwen, *Eur. J. Inorg. Chem.* **1998**, 25−27. − [2c] J. D. Oslob, B. Akermark, P. Helquist, P.-O. Norrby, *Organometallics* **1997**, *16*, 3015−3021. − [2d] R. Kuwano, Y. Ito, *J. Am. Chem. Soc.* **1999**, *121*, 3236−3237.

[3] [3a] R. J. van Haaren, C. J. M. Druijven, G. P. F. van Strijdonck, H. Oevering, J. N. H. Reek, P. C. J. Kamer, P. W. N. M. van Leeuwen, *J. Chem. Soc., Dalton Trans.* **2000**, *10*, 1549−1554. − [3b] R. Pretot, A. Pfaltz, *Angew. Chem. Int. Ed.* **1998**, *37*, 323−325. − [3c] S. Vyskocil, M. Smrcina, V. Hanus, M. Polasek, P. Kocovsky, *J. Org. Chem.* **1998**, *63*, 7738−7748.

[4] Iridium: [4a] R. Takeuchi, M. Kashio, *J. Am. Chem. Soc.* **1998**, *120*, 8647−8655. − [4b] B. Bartels, G. Helmchen, *Chem. Commun.* **1999**, 741−742. − [4c] K. Fuji, N. Kinoshita, K. Tanaka, T. Kawabata, *Chem. Commun.* **1999**, 2289−2290; Molybdenum: [4d] M. P. T. Sjogren, H. Frisell, B. Åkermark, P.-O. Norrby, L. Eriksson, A. Vitagliano, *Organometallics* **1997**, *16*, 942−950; Rhodium: [4e] P. A. Evans, J. D. Nelson, *J. Am. Chem. Soc.* **1998**, *120*, 5581−5582; Platinum: [4f] A. J. Blacker, M. L. Clark, M. S. Loft, J. M. J. Williams, *Chem. Commun.* **1999**, 913−914. − [4g] A. J. Blacker, M. L. Clarke, M. S. Loft, M. F. Mahon, M. E. Humphries, J. M. J. Williams, *Chem. Eur. J.* **2000**, *6*, 353−360. − [4h] Tungsten: R. Pretot, G. C. Lloyd-Jones, A. Pfaltz, *Pure Appl. Chem.* **1998**, *70*, 1035−1040.

[5] [5a] M. P. T. Sjogren, S. Hansson, B. Åkermark, A. Vitagliano, *Organometallics* **1994**, *13* **19**63−1971. − [5b] U. Kazmaier, F. L. Zumpe, *Angew. Chem. Int. Ed.* **2000**, *39*, 802−804.

[6] R. J. Van Haaren, H. Oevering, B. B. Coussens, G. P. F. Van Strijdonck, J. N. H. Reek, P. C. J. Kamer, P. W. N. M. Van Leeuwen, *Eur. J. Inorg. Chem.* **1999**, 1237−1241.

[7] K. Vrieze, P. W. N. M. van Leeuwen, *Dynamic Nuclear Magnetic Resonance Spectroscopy*, Academic Press, New York, **1975**.

[8] F. Robert, F. Delbecq, C. Nguefack, D. Sinou, *Eur. J. Inorg. Chem.* **2000**, 351−358.

[9] [9a] P. Dierkes, S. Ramdeehul, L. Barloy, A. de Cian, J. Fischer, P. C. J. Kamer, P. W. N. M. van Leeuwen, J. A. Osborn, *Angew. Chem. Int. Ed.* **1998**, *37*, 3116−3118. − [9b] A. Pfaltz, *Acc. Chem. Res.* **1993**, *26*, 339−345. − [9c] H. Steinhagen, M. Reggelin, G. Helmchen, *Angew. Chem. Int. Ed. Engl.* **1997**, *36*, 2108−2110.

[10] [10a] P. E. Blochl, A. Togni, *Organometallics* **1996**, *15*, 4125−4132. − [10b] H. Hagelin, B. Akermark, P.-O. Norrby, *Chem. Eur. J.* **1999**, *5*, 902−909. − [10c] V. Blanchadell, M. Moreno-Manas, F. Pajuelo, R. Pleixats, *Organometallics* **1999**, *18*, 4934−4941. − [10d] T. Suzuki, H. Fujimoto, *Inorg. Chem* **1999**, *38*, 370−382.

Received July 28, 2000
[I00299]

On the Stabilisation of a Singlet Nitrene by the Phosphaniminato and Related Imine-Type Substituents, a Quantum Chemical Investigation

W. Schoeller*[a] and A. B. Rozhenko[a]

Dedicated to Prof. K. Dehniche on the occasion of his 70th birthday

Keywords: Density functional calculations / Nitrenes / Substituent effects / Radicals

The substituent effects on the singlet–triplet energy separations are explored for phosphanylnitrenes and related congeners from the Group 14 to Group 16 elements. Imine-type substituents (e.g. phosphaniminato, methyleneimine etc.) are more effective than amino groups in lowering the energy of a singlet below that of a triplet state. It is due to an effective stabilisation of the singlet and a destabilisation of the triplet.

Introduction

Nitrenes **A** are highly unstable species.[1−3] They become more stable in the case of phosphanylnitrenes **B** (X = N) that are substituted with bulky amino groups at the phosphorus atom (R^1,R^2 = NR'_2, R′= alkyl) (Scheme 1). It opens a wide field for the syntheses of new types of structures in low-coordination phosphorus chemistry.[4−9] Similarly, amino-substituted phosphanylphosphinidenes are considered as useful intermediates.[10−12] Consequently, the particular role of the amino group as a stabilising factor on a singlet ground state of a nitrene has been addressed by a variety of quantum chemical investigations.[13−21]

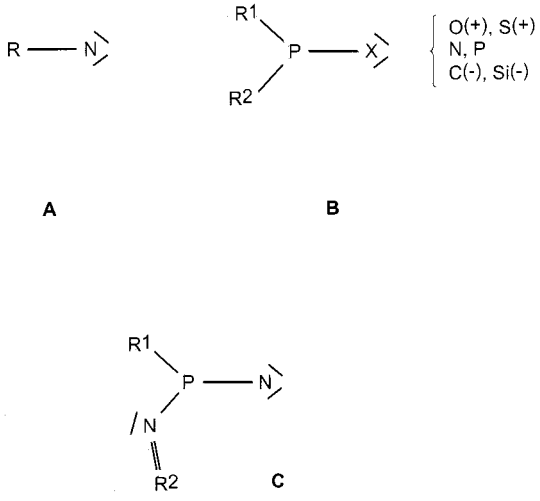

Scheme 1

These investigations indicate that nitrenes and especially phosphinidenes possess small energy separations between the singlet and the lowest-energy triplet state. On this basis, nitrenes are reminiscent of carbenes[22] as was recently summarised.[23,24]

Despite the wealth of investigations into nitrenes, important aspects that have hitherto not been investigated remain open: (1) The electronic structures of valence isoelectronic nitrene homologues of type **B**, with X originating from Group 16 ($X = O^{(+)}$, $S^{(+)}$) or from Group 14 ($X = C^{(-)}$, $Si^{(-)}$). In the present quantum chemical study, it will be shown that the Group 16 homologues possess singlet ground states and that the Group 14 homologues possess triplet ground states. (2) The effect of an imino function of type **C** in which a lone-pair is adjacent to the phosphorus atom. Evidence is given that these types of substituents [R^2= PH_3, $C(NH_2)_2$, CH_2, PH] are essentially more effective than amino groups in moving the energy of the singlet below that of the triplet, thus making it the ground state. A peculiar π-donating effect of methyleneimine-substituted iminophosphanes has been found.[25,26] The status of oxo- and thioxophosphonium ions has also been summarised recently.[6] The details of the calculations are given in the Theoretical Section at the end of this publication.

Results and Discussion

a. Qualitative Considerations

According to EH calculations,[27] the relevant molecular-orbital system of the parent phosphanylnitrene (C_{2v} symmetry imposed) is as follows (Figure 1).

The frontier orbitals are the p-orbital of the nitrogen atom (HOMO), in plane with the residual atoms, and the π* molecular orbital (LUMO) of the P−N bond. Phosphorus is much less electronegative than nitrogen,[28] hence the larger coefficient in the π* molecular orbital is at the phosphorus atom. In the π molecular orbital (HOMO-1), the opposite is true: the larger coefficient is located at the more electronegative nitrogen atom.

The two relevant lowest-energy electronic states (singlet and triplet) are constructed from these orbitals. The re-

[a] Fakultät für Chemie der Universität
Postfach 100131, 33501 Bielefeld, Germany
Fax: (internat.) + 49-(0)521/106-6146
E-mail: wolfgang@tc3.chemie.uni-bielefeld.de

 © WILEY-VCH Verlag GmbH, 69451 Weinheim, 2001 1434−1948/01/0303−0845 $ 17.50+.50/0

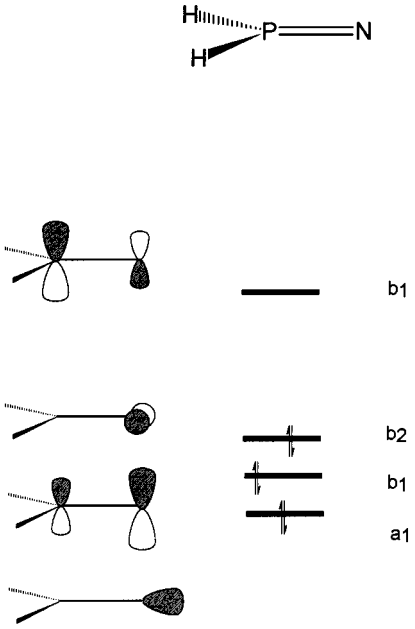

Figure 1. Frontier orbital system of the parent phosphanylnitrene

sulting Slater determinants for these states (C_{2v} symmetry) are as follows:

$\Psi\ (^1A_1) = ...(a_1)^2(b_1)^2(b_2)^2>$

$\Psi\ (^3A_2) = ...(a_1)^2(b_1)^2(b_2)^1(b_1)^1>$

MCSCF calculations[29] on the parent phosphanyl nitrene indicate that the given Slater determinants describe both states well. Geometry optimisation results in a planar structure (C_{2v} symmetry) for the singlet, while the triplet adopts a pyramidal structure at the phosphorus atom (C_s symmetry). The equilibrium structures are illustrated in Molden plots[30] shown in Figure 2 for the equilibrium singlet (top) and triplet (bottom) structures. The findings agree with the previous considerations of phosphanyl nitrenes.[14]

From the one-electron considerations, the following tendencies of the stabilities of the nitrenes and their valence isoelectronic homologues are observed: (a) π-Donating substituents raise the energy of the LUMO (π*), owing to conjugation with this molecular orbital. The HOMO (p) is generally not affected by substituents at the phosphorus atom.

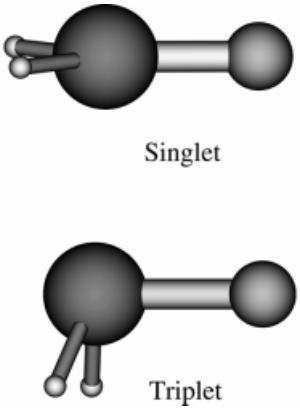

Figure 2. Molden plots of equilibrium singlet ($^1A_1$, C_{2v} symmetry) and triplet states ($^3A''$, C_s symmetry) of the parent phosphanylnitrene

Consequently, π-donating substituents increase the energy difference between the HOMO and the LUMO, and a singlet ground state is pronounced. (b) On the other hand, π-electron-attracting substituents favour a triplet ground state. The ability to enhance a singlet ground state should become more pronounced with increasing polarity of the P−X π-bond, i.e., in the order $X = O^{(+)} > N > C^{(-)}$. (c) When the terminal main group element X is less electronegative, the energy of the HOMO raises stronger than the energy of the LUMO. In other words the energy gap between these orbitals decreases and a triplet ground state is facilitated. It corresponds to the hypothesis that a singlet ground state is expected for these species in the order $X = C^{(-)} < N < O^{(+)}$. As will be shown below, a further effect is important for the strength of the resulting P−N π-bond in the singlet state of the nitrene. Strong σ-electron-withdrawing substituents at the phosphorus atom strengthen the P−N bond.

b. Phosphanylnitrene and Substituent Effects

We first investigated the parent systems, i.e., the phosphanylnitrene and its related valence isoelectronic homologues. The corresponding Group 14 and Group 16 congeners of various elements X were considered. The most relevant bonding parameters for the investigated species in their lowest-energy singlet and triplet states are collected in Table 1. The various electronic states were evaluated at the density functional level [B3LYP/6-31+g(d)] and at the more sophisticated CCSD(t) level. For the latter, a valence triple-zeta basis set augmented by diffuse functions was used. The more elaborate CCSD(t) calculations parallel the trends already observed at the density functional level. However, in general they tend to enhance more the stabilities of the singlet species. In the case of the nitrenes, the results also agree

Table 1. Relevant bonding parameters (bond lengths in Å, bond angles in degrees) and singlet−triplet energy differences (in kcal/mol) of phosphanylnitrenes and element homologues H_2PX; the first entry is the singlet ($^1A_1$, C_{2v} symmetry), the second entry is the triplet ($^3A''$, C_s symmetry), electron affinities and/or ionisation potentials (in eV) are given in parentheses

X	P−X	XPH	HPH	ΔE (DFT)[a]	ΔE [CCSD(t)][b]
$C^{(-)}$	1.646	131.8	96.3	−0.3 [1.2][c]	0.0
	1.833	128.0	104.0	0.0	1.8
$Si^{(-)}$	2.125	131.7	96.7	−6.8 [0.9][c]	−7.0
	2.393	102.8	92.4	0.0	0.0
N	1.522	127.6	104.9	0.0 [9.4;1.3][d]	0.0
	1.718	98.9	95.9	6.9	13.3
P	1.962	128.3	103.3	0.0 [8.1;1.6][d]	0.0
	2.209	98.7	94.6	−2.4	−0.3
$O^{(+)}$	1.462	122.1	115.9	0.0 [9.1][e]	0.0
	1.609	102.5	109.1	39.8	49.9
$S^{(+)}$	1.822	123.9	112.2	0.0 [8.7][e]	0.0
	2.070	102.7	103.7	18.3	25.5

[a] B3LYP/6-31+g(d) plus zero-point vibrational energy (*ZPE*) correction. − [b] CCSD(t)/aug-cc-pVTZ//B3LYP/6-31+g(d). − [c] Ionisation potentials (in eV) for the formation of the corresponding cation doublet states, with *ZPE* correction. − [d] The first entry is the ionisation potential, the second entry is the electron affinities. − [e] Electron affinities (in eV) towards anion doublets, with *ZPE* correction.

with the quantum chemical investigations already presented (see ref.[21] and cited work).

On the contrary, the species with X = $C^{(-)}$ or $Si^{(-)}$ are most likely to be found in a triplet ground state. At the very least, the singlet−triplet energy separations are fairly small. When X is more electronegative than nitrogen, a strong preference for a singlet ground state is observed. One may of course question whether the carbide or silicide analogues may exist at all, in the sense that in the corresponding singlet state, the negative charge will be kept in the structure or it undergoes spontaneous ionisation with the loss of an electron. In order to obtain a deeper insight into this aspect, we have also examined the corresponding lowest-energy doublet states ($^2B_2$, C_{2v} symmetry). The corresponding energy quantities (energy values obtained at the density functional level, in eV) are shown in the table in parentheses. Accordingly, the corresponding radicals have only a small tendency to add a further electron in the formation of a carbide or a silicide, but alternatively a rather large electron affinity is obtained for the Group 15 and Group 16 congeners.

Next we studied the effect of a typical π-donor (R^1, R^2 = NH_2) or π-acceptor (SiH_3) on the phosphanylnitrene and its valence isoelectronic homologues. The results of these investigations are collected in Table 2. Since the more elaborate CCSD(t) calculations parallel those at the density functional level, the following discussion will be based on the results calculated at the density functional level.

In accordance with the qualitative considerations, amino groups at the phosphorus atom tend to stabilise a singlet rather than a triplet ground state. Silyl groups do the opposite. The π-donation is most effective for the Group 16 congeners (X = $O^{(+)}$ > $S^{(+)}$) and least effective for X = $C^{(-)}$ and $Si^{(-)}$. For the latter species the ground state is a triplet.

In all cases, the resulting P−X bonds are shorter than those of corresponding double bond systems, for example, in iminophosphanes (ca. 1.54 Å)[31] or methylenephosphanes (ca. 1.64 Å).[32,33] Simultaneously, the bonds towards the trigonal phosphorus atom are significantly elongated. The most striking example is the diaminophosphanyl carbide, in which the P−N bonds become 1.803 Å, which is longer than a P−N single bond (1.76 Å).[28] An NBO population analysis[34] (Wiberg bond orders in italics) gives the results shown in Scheme 2.

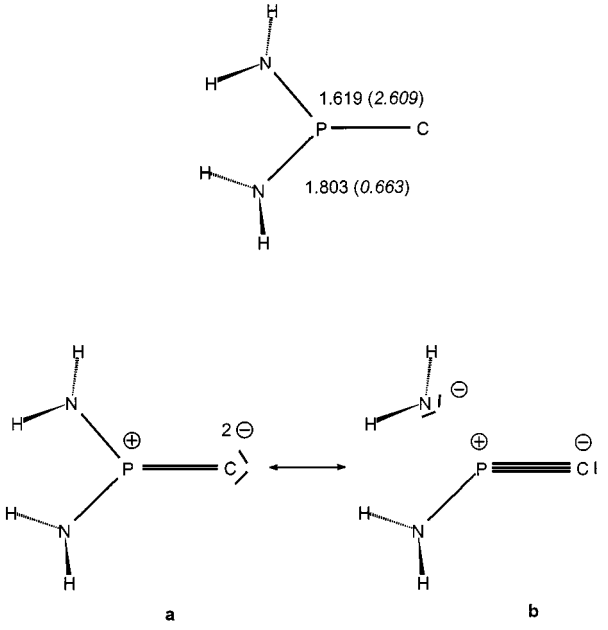

Scheme 2

The weakening of the P−N (amino) bonds is compensated by the strengthening of the P−C bond. It can be attributed to the participation of the limiting structures **b** versus **a**, because the negative charge is shifted from the less electronegative carbon atom to the more electronegative nitrogen atoms.

We have also probed the effect of push-pull substitution at the phosphorus atom, i.e., R^1 = NH_2, R^2 = SiH_3. The effect on the singlet−triplet energy separation (17.4 kcal/mol) is similar to the effect of the monoamino-substituted nitrene (17.5 kcal/mol). In addition, we have investigated the case where the two amino groups are incorporated into a five-membered ring system *cyclo*-[N(H)CH=CHN(H)PN]. The singlet−triplet energy separation (18.0 kcal/mol) is similar to that found with monoamino substitution, but less than with diamino substitution (21.8 kcal/mol).

Table 2. Substituent effects on the singlet−triplet energy separations (in kcal/mol) in nitrene homologues R^1R^2PX, at the B3LYP/6-31+g(d) level

R^1	R^2	X	Symmetry[a]	P−N [Å][a]	Δ*E* [kcal/mol]
NH_2	NH_2	$C^{(-)}$	C_2	1.619	0.7
SiH_3	SiH_3	$C^{(-)}$	C_1	1.660	−2.6
NH_2	NH_2	$Si^{(-)}$	C_2	2.065	−4.4
SiH_3	SiH_3	$Si^{(-)}$	C_1	2.148	−8.1
NH_2	NH_2	N	C_2	1.504	21.8
SiH_3	SiH_3	N	C_1	1.542	5.1
NH_2	NH_2	P	C_2	1.934	9.5
SiH_3	SiH_3	P	C_1	1.996	−2.0
NH_2	NH_2	$O^{(+)}$	C_2	1.459	55.0
SiH_3	SiH_3	$O^{(+)}$	C_1	1.489	28.5
NH_2	NH_2	$S^{(+)}$	C_2	1.879	37.1
SiH_3	SiH_3	$S^{(+)}$	C_1	1.923	17.9

[a] Singlet states.

c. Amine- versus Imine-Type Substituents

A significant shortening of the P−X bond is observed for the nitrenes (X = N), in cases where strongly electronegative substituents are attached to the phosphorus atom

Table 3. Singlet−triplet energy separations (in kcal/mol) in various substituted nitrenes R^1R^2PN, at the B3LYP/6-31+g(d) level

R^1	R^2	Symmetry[a]	P−N [Å][a]	ΔE [kcal/mol]
NH_2	H	C_2	1.508	17.5
SiH_3	NH_2	C_1	1.517	17.4
F	H	C_s	1.499	18.2
F	F	C_{2v}	1.495	3.4
OH (*E*)	H	C_s	1.504	21.6
cyclo-[N(H)CH=CHN(H)]		C_2	1.508	18.0
H_3PN (*Z*)	H	C_1	1.516	24.8
H_3PN (*Z*)	H_3PN (*Z*)	C_1	1.523	32.6
H_3PP (*Z*)	H	C_1	1.531	18.1
H_2CN (*Z*)	H	C_1	1.517	15.2
$(H_2N)CN$ (*Z*)	H	C_1	1.521	25.5
HPN (*Z*)	H	C_1	1.520	15.5

[a] Singlet states.

(Table 3), for R^1, R^2 = F or OH. These substituents are capable of polarising the phosphorus atom, i.e., to withdraw p-electron density from it. As a consequence, the σ-bond of P−N experiences more s-character and is shortened. In essence, it increases the stability of the P−N multiple bond.

At first glance, one would expect an increased singlet−triplet energy separation. However, electronegative substituents at the phosphorus atom have another effect, too. It is known that electronegative substituents increase the inversion barrier at a phosphane group.[35,36] Thus, electronegative substituents also favour a pyramidal triplet state. The calculated data (see Table 3) confirm this assertion. Fluorine, which is a poor π-donor but a strong electron-withdrawing σ-acceptor, tends to shorten the P−N bond (relative to the parent phosphanylnitrene). One fluorine atom (R^1/R^2 = F/H) shortens the P−N bond and increases the singlet-triplet energy separation, but the introduction of a second fluorine atom (R^1/R^2 = F/F) further reduces the P−N distance and simultaneously decreases the singlet−triplet energy difference. The special effect of fluorine substitution on the P−N bond length in the phosphanylnitrene is in agreement with the analogous limiting structure **a** and **b**, as has previously been noted[21].

The amino group is a strong π-donor (p-orbital) but on the other hand is also a strong σ-acceptor (sp^2-orbital). It is thus not the most suitable substituent for singlet stabilisation. A more appropriate substituent for singlet stabilisation should be a stronger π-donor as well as weaker σ-acceptor than the amino group. The latter aspect is of importance, otherwise the pyramidal triplet is equally well stabilised. A substituent that is more suitable for this purpose was therefore sought.

It has been well established that a phosphaniminato ligand can coordinate to a transition-metal fragment with a strong variation of the valence angle at the nitrogen atom.[37] More generally, it indicates that an imino function exerts σ-effects which are *dynamically* operative. This means that the σ-inductive effect of the same substituent can act differently in the lowest-energy singlet or triplet state. The two extreme bonding features (Scheme 3), **c** versus **d** are considered.

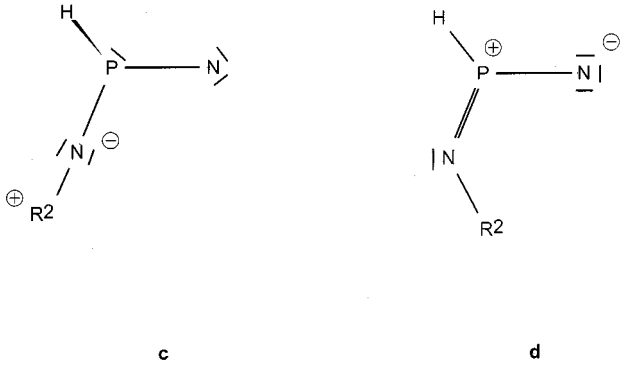

Scheme 3

In **c**, the nitrogen atom is sp-hybridised, while in the bent structure **d** it is sp^2-hybridised (PNP = 120°) [or sp^3 (109°)]. In **c** two lone pairs at the imino nitrogen atom are present, thus destabilising the triplet (with a pyramidal phosphorus atom, see Figure 2) by lone-pair repulsion (N vs. P). On the other hand, π-conjugation of the imino nitrogen atom with the phosphorus atom is present in **d**, and a singlet ground state is favoured. It should be noted that in the case of an amino group, lone-pair repulsion can be avoided in the triplet state by rotation of the amino group. Based on the present considerations, one can predict that substituents at the phosphorus atom that have an imino rather than an amino functional group are more likely to stabilise singlet ground states in the nitrenes and related species.

In order to strengthen these arguments, quantum chemical calculations [at the B3LYP/6-31+g(d) level] were performed on a variety of substituents with imino functions in the α-position to the phosphorus atom, namely, the phosphaniminato (H_3P-N), phosphanephosphinato (H_3P-P), methyleneimino (H_2C-N), diamino(methyleneimino) [$(H_2N)_2C-N$], and iminophosphane (HP=N) substituents (Table 3). Corresponding Molden plots of the equilibrium lowest-energy singlet and triplet states are shown representatively for the phosphaniminato ligand in Figure 3.

The structures preferentially adopt (*Z*) conformations. The P−N multiple bonds are significantly longer than in

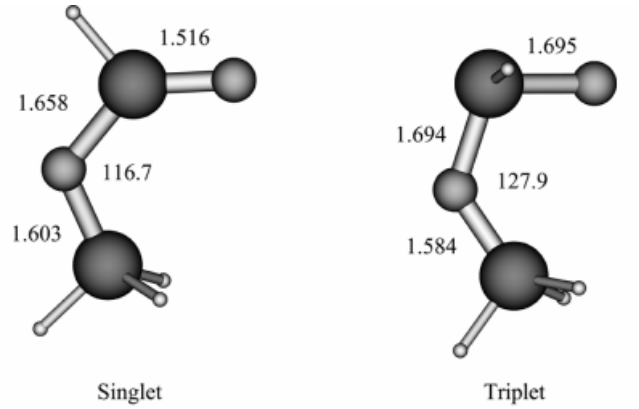

Figure 3. Molden plots of monosubstituted phosphaniminatonitrene; singlet state (left), lowest-energy triplet state (right)

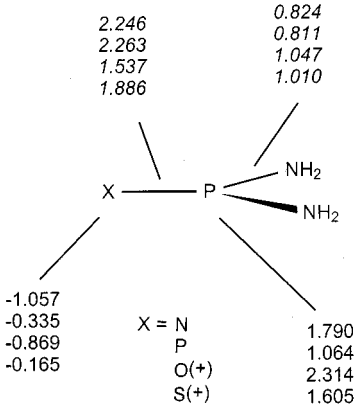

Scheme 4

the amino-substituted nitrenes (see Table 2), and the singlet−triplet separations are enlarged. Similar trends, shown here only for the phosphaniminato ligand, were observed for the other imino-type substituents, type **C**. For the phosphaniminato ligand we have also probed the case of disubstitution. The trend in mono- vs. disubstitution is not additive. It is worth noting the peculiar role of the phosphaniminato ligand which has also recently been shown to stabilise the singlet of phosphanylcarbenes.[38] Imine-type functional groups are also predicted to lengthen the strained P−P bond in 1,2-diphosphacyclobutene.[39]

Based on the singlet−triplet energy separations (see Table 1) the diamino-substituted oxo- and thioxophosphonium species should be fairly stable. In their planar singlets, the central phosphorus atom is surrounded by electronegative substituents. Results from the NBO population analysis for the case of **B** ($R^1 = R^2 = NH_2$ and X = , N, P, $O^{(+)}$, $S^{(+)}$) are shown in Scheme 4 (Wiberg bond orders are italicised).

The central atom (P) gains a large positive charge in the cations since the electron density is withdrawn to the peripheral atoms which are more electronegative than the central phosphorus atom. It is known that the thioxophosphonium cations and the nitrenes spontaneously dimerise to form four-membered ring systems.[6]

Conclusion

The results of our investigations can be summarised as follows:

(1) Singlet nitrenes are stabilised by π-donors. The stabilisation effects increase for the Group 16 and decrease for the Group 14 congeners. The opposite is true for π-attracting substituents. The carbides and silicides possess triplet ground states.

(2) Substituents which bear an imino function in an α-position to the phosphorus atom, e.g., the phosphaniminato ligand, promote a singlet ground state even more strongly than an amino group. Our investigations have thus revealed a new type of substituent for the stabilisation of species which were hitherto considered as being short-lived intermediates. In the experiment, however, the structures are encumbered by bulky substituent effects which in addition affect the kinetic stabilities of these species.

Theoretical Section

All calculations were performed with the Gaussian-98 set of programs.[40] The various structures were fully optimised at the B3LYP level by using the 6-31+g(d) basis set.[41−43] The density functional is built with Becke's three-parameter exchange functional[44,45] and the nonlocal correlation functional of Lee, Yang, and Parr.[46] The energy optimisations were conducted by analytically determined nuclear coordinate gradients. All the investigated structures were characterised by vibrational analysis within the harmonic approximation. The population analysis at the given optimised geometries were carried out according to the Weinhold−Reed partitioning scheme.[34] Further correlation corrections were obtained at the CCSD(t) level[47−49] by using triple-zeta valence basis sets[50,51] augmented with diffuse functions. One may note that the singlet−triplet energy separations within density functional theory depend on the shape of the chosen functional.[52] Nevertheless, the chosen density functional method is expected to predict correct trends for the substituent effects.

Acknowledgments

This work was supported by the Deutsche Forschungsgemeinschaft and the Fonds der Chemischen Industrie. The computer time was allocated by the computation centre at the University at Bielefeld and the University at Aachen.

[1] W. Lwoski, *Nitrenes*, Wiley-Interscience, New York, **1970**.
[2] S. Patai, *The Chemistry of the Azido Group*, Wiley-Interscience, New York, **1971**.
[3] E. F. V. Scriven, *Azides and Nitrenes: Reactivity and Utility*, Academic Press, New York, **1984**.
[4] J. P. Majoral, G. Bertrand, E. Ocando-Mavarez, A. Baceiredo, *Bull. Soc. Chim. Belg.* **1986**, *95*, 945−957.
[5] G. Alcarez, A. Baceiredo, F. Dahan, G. Bertrand, *J. Am. Chem. Soc.* **1994**, *116*, 1225−1229.
[6] O. Guerret, G. Bertrand, *Acc. Chem. Res.* **1997**, *30*, 486−493.
[7] D. Bourissou, G. Bertrand, *Adv. Organomet. Chem.* **1999**, *44*, 175.
[8] S. Goumri-Magnet, O. Polishchuk, H. Gornitzka, C. J. Marsden, A. Baceiredo, G. Bertrand, *Angew. Chem.* **1999**, *111*, 3938−3941; *Angew. Chem. Int. Ed. Engl.* **1999**, *38*, 3727.
[9] T. Kato, H. Gornitzka, A. Baceiredo, A. Savin, G. Bertrand, *J. Am. Chem. Soc.* **2000**, *122*, 998−999.
[10] G. Fritz, T. Vaahs, H. Fleischer, E. Matern, *Angew. Chem.* **1989**, *101*, 324−325; *Angew. Chem. Int. Ed. Engl.* **1989**, *28*, 315.
[11] G. Fritz, T. Vaahs, H. Fleischer, E. Matern, *Z. Anorg. Allg. Chem.* **1989**, *570*, 54−66.
[12] W. Frank, V. Petry, E. Gerwaling, G. J. Reiß, *Angew. Chem.* **1996**, *108*, 1616−1618; *Angew. Chem. Int. Ed. Engl.* **1996**, *35*, 1512.
[13] M. T. Nguyen, M. A. McGinn, A. F. Hegarty, *J. Am. Chem. Soc.* **1985**, *107*, 8029−8033.
[14] T. L. Allen, A. C. Scheiner, Y. Yamaguchi, H. F. Schaefer III, *Chem. Phys. Lett.* **1985**, *121*, 154−158.
[15] M. T. Nguyen, T. K. Ha, *Chem. Phys. Lett.* **1989**, *158*, 135−141.
[16] G. Trinquier, *J. Am. Chem. Soc.* **1982**, *104*, 6969−6977.
[17] K. Ito, S. Nagase, *Chem. Phys. Lett.* **1986**, *126*, 531−536.

[18] R. Ahlrichs, H. Schiffer, *J. Am. Chem. Soc.* **1985**, *107*, 6494−6498.
[19] G. Trinquier, *J. Am. Chem. Soc.* **1986**, *108*, 568−577.
[20] W. W. Schoeller, V. Staemmler, *Inorg. Chem.* **1984**, *23*, 3369−3372.
[21] M. T. Nguyen, A. Van Keer, T.-K. Ha, L. G. Vanquickenborne, *J. Mol. Struct. (Theochem)* **1994**, *310*, 125−134.
[22] C. R. Kemnitz, W. L. Karney, W. T. Borden, *J. Am. Chem. Soc.* **1998**, *120*, 3499−3503; and cited literature.
[23] D. Bourissou, O. Guerret, F. P. Gabbai, G. Bertrand, *Chem. Rev.* **2000**, *100*, 39−91.
[24] C. Buron, H. Gornitzka, V. Romanenko, G. Bertrand, *Science* **2000**, *288*, 834−836.
[25] E. Niecke, M. Nieger, C. Gärtner-Winkhaus, B. Kramer, *Chem. Ber.* **1990**, *123*, 477−479.
[26] U. Krüger, H. Pritzkow, H. Grützmacher, *Chem. Ber.* **1991**, *124*, 329−331.
[27] [27a] R. Hoffmann, *J. Chem. Phys.* **1963**, *39*, 1397−1412; and subsequent publications. − [27b] The EH program was written by G. A. Landrum: *YAeHMOP-Hückel Molecular Orbital Package*, Version 2.0, Cornell University, **1997**, URL: http://overlap.chem.cornell.edn:8080/yaehmop.html.
[28] L. Pauling, *The Nature of the Chemical Bond*, 3rd edition, Cornell University Press, New York, **1960**.
[29] W. W. Schoeller, unpublished results.
[30] Program *Molden* written by G. Schaftonaar: www.caos.kun.nl/schaft/molden/molden.html
[31] E. Niecke, D. Gudat, *Angew. Chem.* **1991**, *103*, 251−270; *Angew. Chem. Intern. Ed. Engl.* **1991**, *30*, 217−237.
[32] R. Appel, F. Knoll, *Adv. Inorg. Chem.* **1989**, *33*, 259−375.
[33] R. Appel, I. Ruppert, *Angew. Chem.* **1981**, *93*, 771−784; *Angew. Chem. Int. Ed. Engl.* **1981**, *20*, 731−744.
[34] A. E. Reed, L. A. Curtiss, F. Weinhold, *Chem. Rev.* **1988**, *88*, 899−926. E. D. Glendening, A. E. Reed, J. E. Carpenter, F. Weinhold, *NBO Version 3.1*.
[35] A. Rauk, L. C. Allen, K. Mislow, *Angew. Chem.* **1970**, *82*, 453−468; *Angew. Chem. Int. Ed. Engl.* **1970**, *9*, 400.
[36] J. M. Lehn, *Fortschr. Chem. Forsch.* **1970**, *15*, 311.
[37] K. Dehnicke, M. Krieger, W. Massa, *Coord. Chem. Rev.* **1999**, *182*, 19−65.
[38] W. W. Schoeller, *Eur. J. Inorg. Chem.* **2000**, 369−374.
[39] W. W. Schoeller, U. Tubbesing, A. B. Rozhenko, *Eur. J. Inorg. Chem.* **1998**, 951−955.
[40] M. J. Frisch, G. W. Trucks, H. B. Schlegel, G. E. Scuseria, M. A. Robb, J. R. Cheeseman, V. G. Zakrzewski, J. A. Montgomery, R. E. Stratmann, J. C. Burant, S. Dapprich, J. M. Millam, A. D. Daniels, K. N. Kudin, M. C. Strain, O. Farkas, J. Tomasi, V. Barone, M. Cossi, R. Cammi, B. Mennucci, C. Pomelli, C. Adamo, S. Clifford, J. Ochterski, G. A. Petersson, P. Y. Ayala, Q. Cui, K. Morokuma, D. K. Malick, A. D. Rabuck, K. Raghavachari, J. B. Foresman, J. Cioslowski, J. V. Ortiz, B. B. Stefanov, G. Liu, A. Liashenko, P. Piskorz, I. Komaromi, R. Gomperts, R. L. Martin, D. J. Fox, T. Keith, M. A. Al-Laham, C. Y. Peng, A. Nanayakkara, C. Gonzalez, M. Challacombe, P. M. W. Gill, B. G. Johnson, W. Chen, M. W. Wong, J. L. Andres, M. Head-Gordon, E. S. Replogle and J. A. Pople, *Gaussian 98* (Revision A.1), Gaussian Inc., Pittsburgh, PA, **1998**.
[41] R. Ditchfield, W. J. Hehre, J. A. Pople, *J. Chem. Phys.* **1971**, *54*, 724−728. W. J. Hehre, R. Ditchfield, J. A. Pople, *J. Chem. Phys.* **1972**, *56*, 2257−2261.
[42] The diffuse functions were chosen according to: T. Clark, J. Chandrasekhar, G. W. Spitznagel, P. v. R. Schleyer, *J. Comput. Chem.* **1983**, *4*, 294−301.
[43] Exponents for the polarisation functions: M. J. Frisch, J. A. Pople, J. S. Binkley, *J. Chem. Phys.* **1984**, *80*, 3265−3269.
[44] A. D. Becke, *Phys. Rev. A* **1988**, *38*, 3098−3100. A. D. Becke, *J. Chem. Phys.* **1993**, *98*, 5648−5653. A. D. Becke, *J. Chem. Phys.* **1996**, *104*, 1040−1046.
[45] J. K. Labanowski, J. W. Andzelm (Eds.), *Density Functional Methods in Chemistry*, Springer Verlag, New York, **1991**.
[46] C. Lee, W. Yang, R. G. Parr, *Phys. Rev. B* **1988**, *37*, 785.
[47] J. Cizek, *Adv. Chem. Phys.* **1969**, *14*, 35−89.
[48] G. D. Purvis, R. J. Bartlett, *J. Chem. Phys.* **1982**, *76*, 1910−1918.
[49] G. E. Scuseria, H. F. Schaefer III, *J. Chem. Phys.* **1989**, *90*, 3700−3703.
[50] D. E. Woon, T. H. Dunning, Jr., R. J. Harrison, *J. Chem. Phys.* **1993**, *98*, 1358−1371.
[51] R. E. Kendale, T. H. Dunning, Jr., R. J. Harrison, *J. Chem. Phys.* **1992**, *96*, 6796−6806.
[52] H. Nagao, M. Nishino, Y. Shigeta, T. Soda, Y. Katagawa, T. Onishi, Y. Yoshioka, K. Yamaguchi, *Coord. Chem. Rev.* **2000**, *198*, 265−295; and cited references.

Received August 1, 2000
[I00303]

The Metalation of (*tert*-Butyldimethylsilyl)(2-pyridylmethyl)amine with Dimethylzinc and Subsequent Zinc-Mediated Carbon−Carbon Coupling Reaction

Matthias Westerhausen,*[a] Tobias Bollwein,[a] Nikolaos Makropoulos,[a] Thomas M. Rotter,[a] Tassilo Habereder,[a] Max Suter,[a] and Heinrich Nöth[a]

Keywords: Amides / Zinc / C−C coupling / Metalations / Metallacycles / N ligands

The lithiation of 2-(aminomethyl)pyridine and the subsequent reaction with $ClSiMe_2tBu$ yields (*tert*-butyldimethylsilyl)(2-pyridylmethyl)amine (**1**). The metalation of **1** with dimethylzinc gives colorless dimeric methylzinc 2-pyridylmethyl(*tert*-butyldimethylsilyl)amide (**2**), which crystallizes in the triclinic space group $P\bar{1}$. The solvent-free thermal decomposition of **2** at 150 °C leads to the evolution of methane, the precipitation of zinc metal and the formation of amine **1**, bis(methylzinc)—1,2-dipyridyl-1,2-bis(*tert*-butyldimethylsilylamido)ethane (**3**), and bis[(*tert*-butyldimethylsilyl)(2-pyridylmethyl)amido]zinc (**4**). Compound **3** can be obtained in good yield by reacting **2** with dimethylzinc at elevated temperatures in toluene. During this reaction, zinc metal precipitates and methane is evolved. The C–C coupling product **3** crystallizes in the tetragonal space group $I4_1cd$. The lithiation of **1** and the subsequent metathesis reaction with anhydrous $ZnCl_2$ yields complex **4** almost quantitatively.

Introduction

Pyridine complexes of zinc compounds are a well-known class of substance. On the one hand pyridine, as well as its derivatives such as 2,2′-bipyridine, are able to stabilize dialkylzinc[1−3] or even a geminal biszincated alkane but,[4] on the other hand, these coligands support homolytic Zn−C bond cleavage upon irradiation.[5] Furthermore, multi-dentate azaligands such as, for example, trispyrazolylborate anions enable reactions at the metal centers that can serve as model systems for enzymes.[6]

The reaction of dialkylzinc with 1,4-di(*tert*-butyl)-1,4-diazabutadiene (DAB) or *N*-*tert*-butylpyridine-2-carbaldimine (PYCA) yields the corresponding 1:1 complexes, which are red in color.[7] Subsequent to the adduct formation these compounds have three possible reaction pathways depending on the zinc-bonded alkyl substituent and on the reaction conditions: *C*-alkylation (**A**), *N*-alkylation (**B**) and homolytic Zn−C bond cleavage (**C**) (Scheme 1).[7,8,9] During all these reactions, one alkylzinc moiety remains unchanged and can be regarded as a spectator because the coordination of this metal fragment to the nitrogen atoms of the chelating ligand remains unchanged. Precipitation of zinc metal was not reported to occur during the course of the reactions.

Complex **C** shows a monomer-dimer equilibrium. The dimerization occurs through C−C bond formation as shown in Scheme 2. The newly formed C−C bond is longer than a C−C single bond, as exemplified by [Et−Zn(PYCA)]$_2$ with 156.9(8) pm and [Me_3SiCH_2−Zn(DAB)]$_2$ with a longer distance of 162 pm.[10]

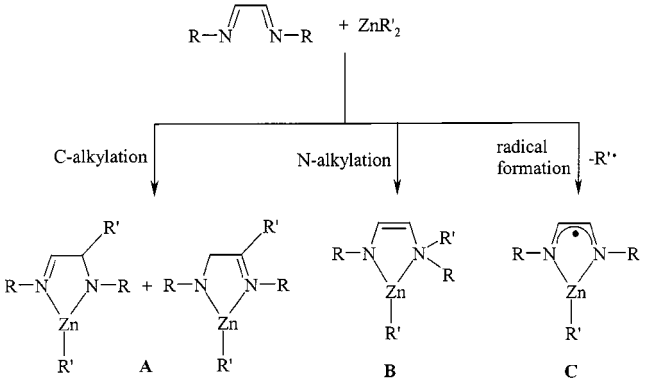

Scheme 1. Possible reaction pathways of dialkylzinc with 1,4-di(*tert*-butyl)-1,4-diazabutadiene.

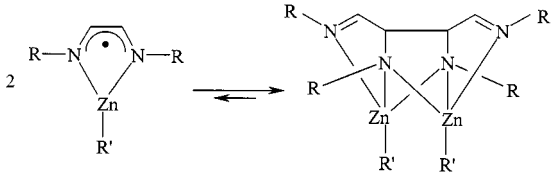

Scheme 2. Monomer-dimer equilibrium through C−C bond cleavage and formation.

The reduction of 1,4-di(*tert*-butyl)-1,4-diazabutadiene with lithium and the subsequent metathesis reaction with (DAB)$ZnCl_2$ yields $Zn(DAB)_2$, which can easily be reduced with potassium or oxidized in a comproportionation with (DAB)$Zn(O_3S-CF_3)_2$.[11] During all these reaction sequences, which were reported by van Koten and co-workers, the oxidation state of +2 for zinc remains unchanged.

Here we report on the synthesis of (*tert*-butyldimethylsilyl)(2-pyridylmethyl)amine, which can easily be metalated

[a] Department Chemie der Ludwig-Maximilians-Universität, Munich,
Butenandtstraße 9 (House D), 81377 Munich, Germany
Fax: (internat.) + 49-(0)89/2180−7867
E-mail: maw@cup.uni-muenchen.de

 © WILEY-VCH Verlag GmbH, 69451 Weinheim, 2001 1434−1948/01/0303−0851 $ 17.50+.50/0

by dimethylzinc. The thermal decomposition as well as the reaction of this product with excess dimethylzinc leads to C−C bond formation and the precipitation of an equimolar amount of zinc metal. This unusual oxidative carbon−carbon coupling under formation of Zn^0 is irreversible and evidence for a monomer−dimer equilibrium by homolytic C−C bond cleavage was not found. The zincation of 2-(*N*-*tert*-butylaminomethyl)-1-methylbenzimidazole also uses the chelate effect and a zinc atom with a coordination number of 3 can be stabilized.[12] However, C−C bond formation was not observed during this reaction.

Results and Discussion

Synthesis

The lithiation of 2-pyridylmethylamine and the subsequent metathesis reaction with *tert*-butyldimethylsilyl chloride quantitatively yields (*tert*-butyldimethylsilyl)(2-pyridylmethyl)amine (**1**). Zincation of **1** with dimethylzinc in toluene gives colorless dimeric methylzinc—(*tert*-butyldimethylsilyl)(2-pyridylmethyl)amide (**2**) according to Scheme 3.

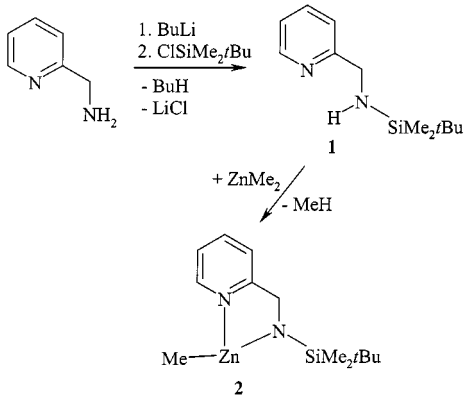

Scheme 3. Synthesis of **1** and **2**

The thermal decomposition of molten **2** at approximately 150 °C (Scheme 4) leads to the evolution of methane, as confirmed by mass spectrometry. During the course of this reaction the precipitation of zinc metal is observed and the NMR spectroscopic data also indicate the formation of **1**. In addition to these substances two new compounds are formed, namely the C−C coupling product bis(methylzinc)—1,2-bis(*tert*-butyldimethylsilylamido)-1,2-dipyridylethane (**3**) and bis[(*tert*-butyldimethylsilyl)(2-pyridylmethyl)-amido]zinc (**4**). Complex **4** forms due to zincation of (*tert*-butyldimethylsilyl)(2-pyridylmethyl)amine (**1**) by derivative **2** under elimination of methane, as shown in Scheme 5. The C−C coupling product and the elemental zinc are formed in an equimolar ratio. Scheme 4 represents the reaction sequence of this thermolysis of **2** and the ^1H NMR spectrum of the thermolysis reaction is presented in Figure 1. The subsequent addition of dimethylzinc leads to the metalation of **1** and to dismutation reactions with **4**, both of which lead to **2**. The isolation of analytically pure **4** by fractional crystallization was not possible due to co-precipitation of minor amounts of **2** and/or **3** in the sample. For the sake of comparison, compound **4** was prepared by the metathesis reaction of anhydrous $ZnBr_2$ with lithium 2-pyridylmethyl-(*tert*-butyldimethylsilyl)amide, which was generated in situ by lithiation of **1**.

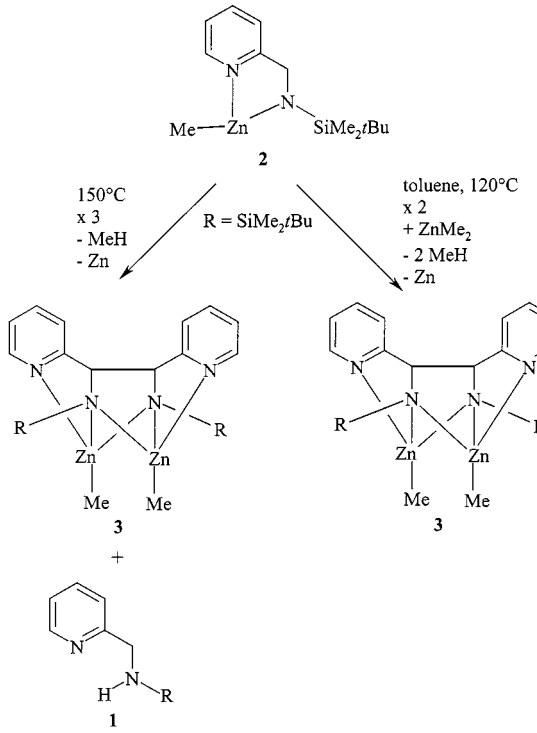

Scheme 4. Synthesis of the C−C coupling product **3** by reaction of **2** with dimethylzinc and as a result of thermal decomposition of **2** at 150 °C, which also gives complex **4** due to the metalation of **1** with **2** in the melt.

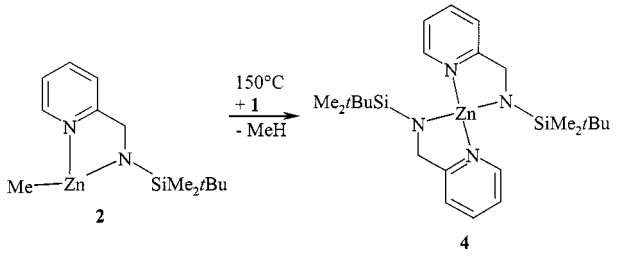

Scheme 5

In order to avoid the formation of bis[2-pyridylmethyl-(*tert*-butyldimethylsilyl)amido]zinc (**4**) and to obtain quantitatively the C−C coupling product **3**, dimethylzinc is added prior to the thermolysis of **2** in refluxing toluene. In this case neither amine **1** nor complex **4** are detectable by NMR spectroscopy, as shown in Figure 1. The zincation of the CH_2 group and the oxidative C−C coupling reaction lead to the precipitation of zinc metal, as confirmed by X-ray powder diffraction methods (Figure 2). The use of a molar ratio of 3:2 for dimethylzinc and (*tert*-butyldimethylsilyl)(2-pyridylmethyl)amine (**1**) gives **3** and elemental zinc in a 1:1 molar ratio.

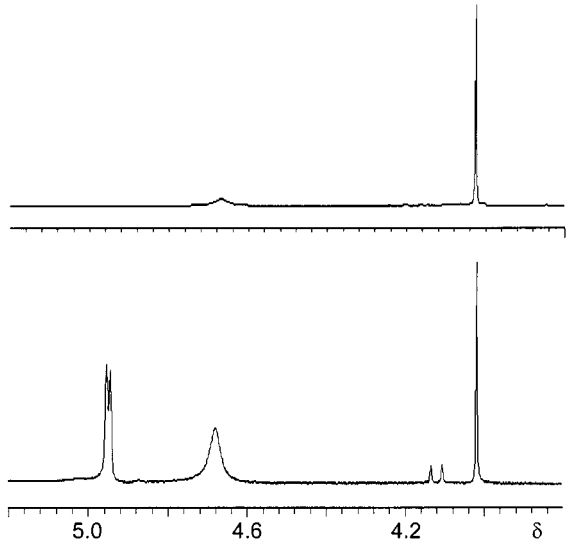

Figure 1. ^{1}H NMR spectroscopic monitoring of the progress of the C−C coupling reaction shown in the region of δ = 4.0 to 5.1 at 30 °C. Upper spectrum: Reaction of **2** with dimethylzinc in toluene; only compounds **2** and **3** are observed. Lower spectrum: Spectrum after thermal decomposition of **2** at 150 °C for 2 hours; after dissolving the residue in toluene compounds **1**, **3**, and **4** are detected (see also Table 2).

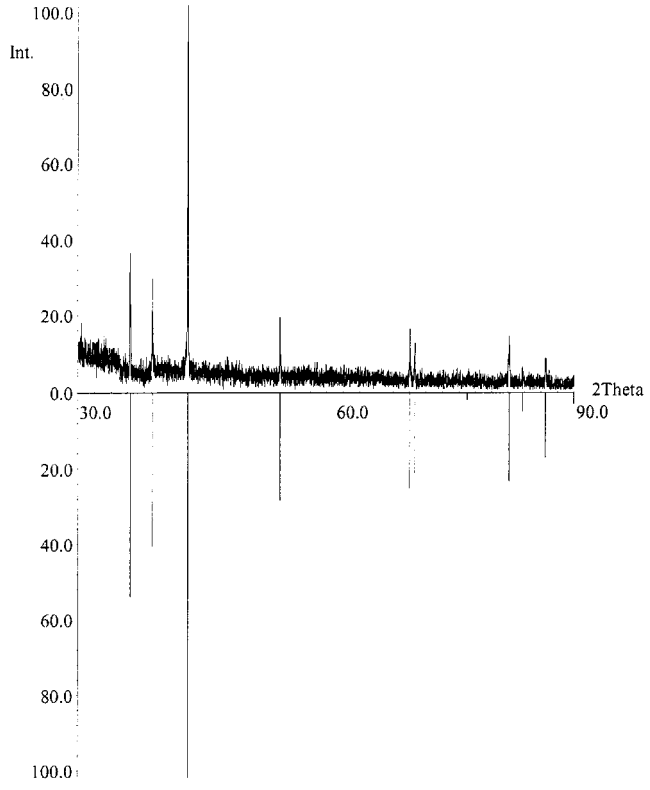

Figure 2. X-ray powder diffractogram of zinc that precipitated during the C−C coupling reactions (upper spectrum) and the reference line spectrum (below).

The stereoselective C−C coupling reaction leads to the formation of the *R*,*R* and *S*,*S* enantiomers, whereas a *meso*-diastereomer was not observed. A similar product with *tert*-butyl substituents at the nitrogen atoms was obtained by metalation of the corresponding amine and was already reported by van Koten and co-workers.[10] However, this complex dissociates into monomeric radicals through a homolytic C−C bond cleavage, as shown in Scheme 2. The presence of trialkylsilyl substituents seems to prevent this monomerization process. The colorless C−C coupling product **3** is EPR silent and its solution is colorless. In order to investigate the influence of the C−C coupling reaction on the coordination spheres of zinc and the amide nitrogen atoms the crystal structure determinations of **2** and **3** were performed.

Molecular Structures of 2 and 3

The molecular structure of **2** is shown in Figure 3 along with the numbering scheme. The second half of the molecule is generated by inversion symmetry and these atoms are marked with apostrophes. The zinc atom Zn1 is coordinated tetrahedrally by three nitrogen atoms and a methyl group. Selected bond lengths and angles are given in Table 1.

Due to the inversion symmetry the central Zn_2N_2 cycle is planar with an N1−Zn1−N1′ angle of 94°. The Zn−C distances lie within a characteristic range and there is no sign of steric strain in this dimer, although the Zn−N bonds are slightly longer than those in the aminomethylpyridine complexes of the zinc dihalides[13] and much longer than those in homoleptic zinc bis(amides).[14]

Figure 4 shows the molecular structure and the numbering scheme of the C−C coupling product **3**. The second half of the molecule is generated by crystallographic C_2 symmetry and the generated atoms are marked with apostrophes. Selected structural data are presented in Table 2. For the sake of comparison the numbering schemes of **2** and **3** are alike.

A tetradentate aza ligand is formed in the C−C coupling. Therefore, the methyl groups at the zinc atoms are at the same side of the Zn_2N_2 cycle. The C7 atom is chiral. Due to the molecular C_2 symmetry and the noncentrosymmetric

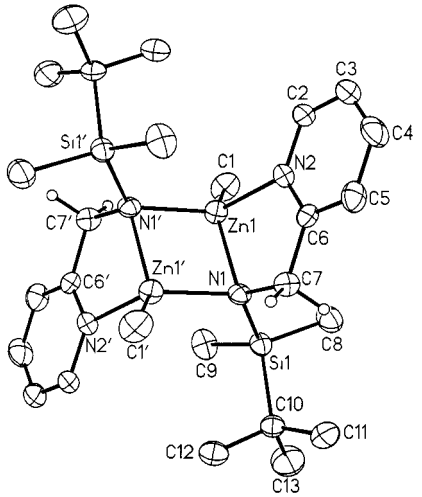

Figure 3. Molecular structure of **2**. The ellipsoids represent a probability of 40%. Atoms generated by the crystallographic inversion symmetry (−*x*, −*y*, −*z* + 1) are marked with apostrophes. The hydrogen atoms are omitted for clarity (with the exception of those at C7/C7′).

Table 1. Selected bond lengths [pm] and angles [°] of **2** and **3**

	2	3
Zn1−C1	199.1(9)	196.4(3)
Zn1−N2	208.2(7)	211.1(2)
Zn1−N1	211.7(6)	215.7(2)
Zn1−N1′	209.7(6)	208.8(2)
N1−Si1	174.0(6)	172.4(2)
N1−C7	145(1)	145.7(3)
N2−C2	136.3(9)	134.3(3)
N2−C6	135(1)	134.9(3)
C2−C3	137(1)	136.7(4)
C3−C4	137(2)	136.5(4)
C4−C5	139(1)	139.2(3)
C5−C6	139(1)	137.8(3)
C6−C7	152(1)	153.8(3)
C7−C7′	-	156.7(4)
C1−Zn1−N1	131.9(3)	135.5(1)
C1−Zn1−N1′	119.1(3)	131.1(1)
C1−Zn1−N2	112.4(4)	121.1(1)
N1−Zn1−N1′	94.0(2)	75.10(8)
N1−Zn1−N2	82.4(2)	81.55(7)
N1′−Zn1−N2	111.1(2)	96.56(8)
Si1−N1−Zn1	110.8(3)	120.9(1)
Si1−N1−Zn1′	124.8(3)	122.8(1)
Si1−N1−C7	113.6(5)	120.3(2)
Zn1−N1−Zn1′	86.0(2)	79.73(7)
Zn1−N1−C7	110.0(4)	94.9(1)
Zn1′−N1−C7	107.9(5)	108.3(1)

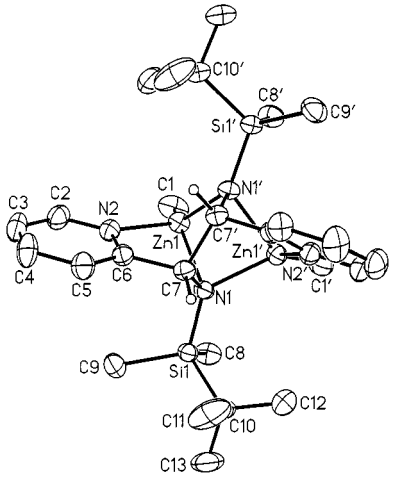

Figure 4. Molecular structure and numbering scheme of **3**. The ellipsoids represent a probability of 40%. Atoms generated by the crystallographic C_2 symmetry ($-x + 1 - 1$, $-y + 1$, $z + 1 - 1$) are marked with apostrophes. The hydrogen atoms are omitted for clarity (with the exception of those at C7/C7′).

tetragonal space group $I4_1cd$, the crystalline compound of this material consists of the *R*,*R* enantiomer. The arrangement of the molecules in the solid state is shown in Figure 5 and it can be seen that the molecules are orientated in the same direction.

The newly formed C7−C7′ bond of **3** is rather long, a situation also observed for $[Et-Zn(PYCA)]_2$ and $[Me_3SiCH_2-Zn(DAB)]_2$.[10] The tetradentate aza ligand enforces strong deviations from planarity in the Zn_2N_2 cycle. The angle between the normals of the planes N1/Zn1/N1′ and N1/Zn1′/N1′ amounts to 72.1°. This leads to short transannular Zn1Zn1′ contacts [287.5(2) pm for **2** and 272.11(5) pm for **3**] and small endocyclic angles at Zn1 and N1 (Table 1). The environment of C7 shows only insignificant deviations from the tetrahedral geometry.

Table 2. Selected NMR spectroscopic data of (*tert*-butyldimethylsilyl)(2-pyridylmethyl)amine (**1**), the metalation product **2**, the C−C coupling product **3**, and bis[2-pyridylmethyl(*tert*-butyldimethylsilyl)amido]zinc (**4**).

Compound	1	2	3	4
^{1}H :				
δ(H1)	–	−0.25	−0.51	–
δ(H2)	8.47	8.25	7.98	7.95
δ(H3)	6.68	6.47	6.48	6.38
δ(H4)	7.17	6.85	6.97	6.84
δ(H5)	7.06	6.52	6.77	6.64
δ(H7)	4.09	4.65	4.03	4.93[a]
δ(H8)	0.01	−0.11	0.40	0.34
δ(H9)	0.01	−0.11	0.15	0.28
δ(CMe_3)	0.87	1.10	0.82	1.27
^{13}C{^{1}H}				
δ(C1)	–	−12.64	−14.07	–
δ(C2)	148.88	145.44	146.66	145.64
δ(C3)	121.03	121.67	122.38	122.03
δ(C4)	135.71	137.54	138.36	136.16
δ(C5)	120.45	121.49	119.89	121.10
δ(C6)	163.24	165.49	168.49	166.44
δ(C7)	48.21	54.09	67.27	54.39
δ(C8)	−5.04	−3.57	−2.06	−3.03
δ(C9)	−5.04	−3.57	−3.23	−3.30
δ(C10)	18.47	20.83	20.59	20.84
δ(CMe_3)	26.25	28.59	27.68	28.08
^{29}Si{^{1}H}				
δ(Si)	9.04	10.32	8.66	3.92

[a] Mean value of an AB spin system, δ = 4.91; δ = 4.95; $^2J(H_A,H_B)$ = 19.9 Hz.

NMR Spectroscopy

The NMR parameters of these compounds are listed in Table 2. The numbering scheme is taken from the X-ray structures presented in Figure 3 and 4 for **2** and **3**, respectively. The hydrogen atoms carry the same numbers as the corresponding carbon atoms. A similar numbering scheme is applied to **1** and **4**.

The C−C coupling and the resulting higher steric strain on the zinc centers lead to a high-field shift of the signals due to the zinc-bonded methyl groups in both the ^{1}H and the ^{13}C{^{1}H} NMR spectra. The signals due to the silicon-bonded methyl substituents of **2** are shifted to higher field compared to **1**, whereas the methyl groups of **3** are more deshielded. Furthermore, two singlets are observed for the methyl groups at the Si atoms for **3** and **4**. Compounds **2** and **4**, which both contain the bidentate (*tert*-butyldimethylsilyl)(2-pyridylmethyl)amide substituent, are easily identified by their δ(^{29}Si{^{1}H}) values.

The most sensitive NMR probe for these molecules is the C7/H7 moiety and therefore this region was chosen to monitor the thermal decomposition of **2** (Figure 1). The AB spin system for the methylene group in **4** results from the tetrahedral geometry at the zinc atom: One hydrogen atom at C7 is at the same side as the pyridyl group of the opposite ligand, whereas the other H atom is oriented to the side of the trialkylsilyl group. The geminal coupling constant has a

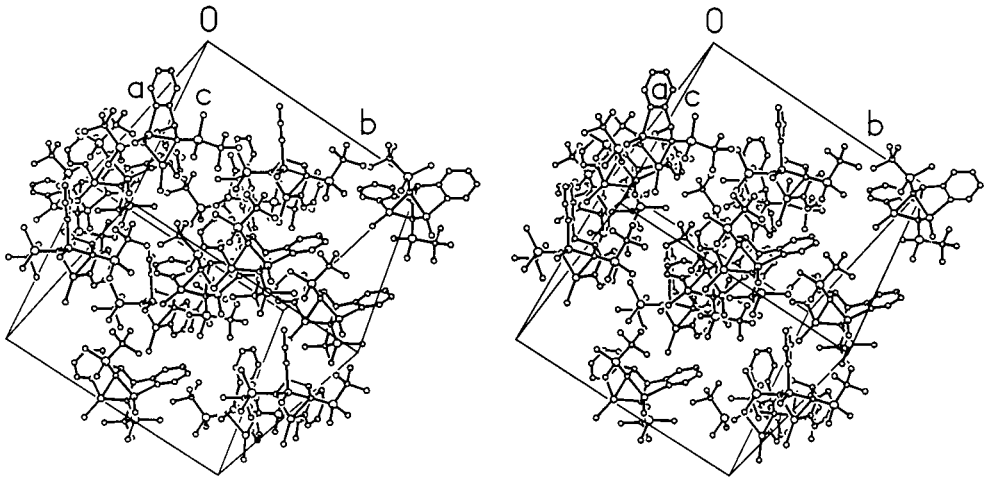

Figure 5. Stereoscopic view of the arrangement of the molecules of **3** in the elementary cell. All atoms are drawn with arbitrary radii, the H-atoms are omitted for clarity.

value of approximately 20 Hz and lies in the expected range. The ^{13}C chemical shifts of C7 vary between $\delta = 48.2$ for (*tert*-butyldimethylsilyl)(2-pyridylmethyl)amine (**1**) and $\delta = 67.3$ for the C−C coupling product **3**.

Conclusion and Prospects

The zincation of (*tert*-butyldimethylsilyl)(2-pyridylmethyl)-amine (**1**) quantitatively yields **2**. The thermolysis of this compound, as well as the reaction of **2** with dimethylzinc, leads to oxidative C−C bond formation and yields **3**. At the same time the precipitation of an equimolar amount of zinc metal is observed. The synthetic approach to compound **3** is different to the synthesis of (PYCA)ZnEt reported by van Koten and co-workers. In contrast to bis(alkylzinc)—1,2-bis(*tert*-butylamido)-1,2-dipyridylethane, a monomer-dimer equilibrium is not observed for **3**. This allows the investigation of the reactivity of two zinc atoms that are in close contact with each other without considering the chemistry of radicals, which would form due to the homolytic C−C bond cleavage.

Experimental Section

General Remarks: All experiments and manipulations were carried out under an argon atmosphere. Reactions were performed using standard Schlenk techniques and the solvents were dried and thoroughly deoxygenated prior to use. − NMR spectra were recorded on Jeol GSX270 and EX400 spectrometers. − A Nicolet 520 FT-IR spectrophotometer was used to record the IR spectra; solid substances were analysed in nujol between KBr plates (vs very strong, s strong, m medium strong, w weak, vw very weak, sh shoulder). − The low carbon and nitrogen values in the elemental analyses result from the presence of carbide and carbonate as well as nitride formation during combustion of the compounds.

(*tert*-Butyldimethylsilyl)(2-pyridylmethyl)amine (1): A 2.5 M solution of *n*-butyllithium in hexane (40 mL, 100 mmol) was added slowly to a precooled solution (−78 °C) of 10.8 g of 2-aminomethylpyridine (100 mmol) in 100 mL of tetrahydrofuran. After 5 minutes of stirring, a solution of 15.1 g of *tert*-butyldimethylsilyl chloride (100 mmol) in 25 mL of tetrahydrofuran was added at −78 °C. The reaction solution was allowed to warm up and stirred at room temperature for an additional 2 h. The solvent was removed in vacuo at room temperature. The residue was dissolved in pentane and any insoluble materials were filtered off. The volatile components were removed at 120 °C to leave **1** as an oil which is an only slightly air-sensitive oil; yield: 19.54 g (87.9 mmol), 88%. − NMR spectroscopic data are listed in Table 2. − IR: $\tilde{\nu} = 3370$ cm^{-1} br, 3084 sh, 3069 w, 3010 w, 2953 s, 2928 s, 2896 s, 2883 s, 2855 s, 1593 s, 1571 m, 1471 s, 1463 s, 1434 s, 1406 s, 1388 s, 1360 m, 1344 w, 1254 s, 1216 w, 1145 sh, 1125 s, 1093 m, 1085 m, 1047 m, 1006 m, 995 m, 955 w, 938 m, 884 sh, 832 s, 812 m, 776 s, 752 m, 726 w, 680 w, 662 m, 628 w, 595 w, 565 w, 456 w, 403 w, 374 br, 358 br. − $C_{12}H_{22}N_2Si$ (222.406): calcd. C 64.80, H 9.97, N 12.59; found C 63.88, H 9.62, N 12.56.

Methylzinc—2-Pyridylmethyl(*tert*-butyldimethylsilyl)amide (2): A 2.0 M solution of dimethylzinc in toluene (4.8 mL, 9.6 mmol) was added slowly at 0 °C to a solution of (*tert*-butyldimethylsilyl)(2-pyridylmethyl)amine (**1**) (2.12 g, 9.53 mmol) in 10 mL of toluene. After 15 h stirring at room temperature the volume of the dark solution was reduced to a few milliliters. Storage at 5 °C led to the precipitation of colorless crystals of **2**; yield: 2.13 g (3.53 mmol of dimeric **2**), 74%. − M.p. 136 °C. − NMR spectroscopic data are listed in Table 2. − IR: $\tilde{\nu} = 1641$ cm^{-1} vw, 1606 vs, 1593 s, 1572 vs, 1553 sh, 1485 vs, 1474 s, 1431 vs, 1408 vs, 1387 s, 1355 s, 1320 w, 1283 s, 1253 vs, 1208 m, 1154 s, 1148 s, 1125 s, 1105 m, 1084 m, 1059 s, 1045 vs, 1022 s, 1007 s, 994 s, 960 s, 936 m, 886 sh, 829 vs, 814 sh, 771 vs, 719 s, 675 sh, 661 vs, 637 s, 617 s, 564 m, 499 s, 460 s, 446 s, 415 s, 403 m, 389 s, 364 m, 327 w, 286 vw. − $[C_{13}H_{24}N_2SiZn]_2$ (603.624): calcd. C 51.73, H 8.02, N 9.28; found C 51.09, H 7.90, N 9.34.

Zinc Complex 3. − Method A (Thermal Decomposition of 2): Compound **2** was heated without a solvent for 2 h at 150 °C. The evolving gas was collected and identified as methane by mass spectrometry. During the thermal decomposition reaction zinc metal precipitated. The NMR spectroscopic investigation confirmed the formation of **1**, **3**, and **4**, and small amounts of unchanged **2** were still

present. Compounds **1** to **4** were dissolved in hydrocarbons and separated from the insoluble materials. X-ray powder diffraction analysis of the residue verified the elimination of zinc metal, which was formed in an equimolar amount to the C−C coupling product **3**.

Method B (C−C Coupling Reaction): To a solution of 3.57 g of (*tert*-butyldimethylsilyl)(2-pyridylmethyl)amine (**1**) (16.1 mmol) in 20 mL of toluene was added 12.0 mL of a 2.0 M solution of dimethylzinc in toluene. The quantitative formation of **2** was confirmed by ^{1}H NMR measurements. The reaction mixture was heated under reflux for 5 h. During this time zinc metal precipitated. The solution was filtered and the volume of was reduced to a few milliliters. On cooling the solution to −18 °C colorless crystals of **3** precipitated in the shape of small grains of rice; yield: 6.49 g (10.79 mmol), 67%. − Physical data: M.p. 191 °C. − NMR spectroscopic data are listed in Table 2. − IR: $\tilde{\nu}$ = 1642 cm^{-1} vw, 1631 vw, 1602 vs, 1495 vw, 1474 vs, 1463 s, 1441 vs, 1408 m, 1386 m, 1357 m, 1348 m, 1331 w, 1290 m, 1279 m, 1249 vs, 1229 sh, 1212 w, 1186 vw, 1154 vs, 1106 m, 1060 vs, 1045 vs, 1020 vs, 1007 s, 936 vs, 890 m, 870 m, 844 s, 827 vs, 807 vs, 771 vs, 753 vs, 730 sh, 675 vs, 664 vs, 641 vs, 606 s, 573 vw, 557 sh, 544 m, 528 vs, 462 s, 437 s, 410 m, 378 w, 314 vw, 292 w, 274 w. − $C_{26}H_{46}N_4Si_2Zn_2$ (601.608): calcd. C 51.90, H 7.71, N 9.32; found C 52.01, H 7.81, N 9.32.

Zinc Complex 4: A 1.6 M solution of *n*-butyllithium (4.89 mL) in diethyl ether was added slowly at −78 °C to a solution of (*tert*-butyldimethylsilyl)(2-pyridylmethyl)amine (**1**) (1.74 g, 7.82 mmol) in 10 mL of tetrahydrofuran. A solution of zinc dibromide (0.88 g, 3.91 mmol) in 5 mL of tetrahydrofuran was added to the reaction solution at 0 °C. The mixture was stirred for 10 h, the solvent was removed and the residue was extracted with pentane. Recrystallization yielded colorless **4**; yield: 0.70 g (1.37 mmol), 35%. − M.p. 114 °C. − NMR spectroscopic data are listed in Table 2. − IR: $\tilde{\nu}$ = 3414 cm^{-1} w, 3377 w, 1636 vw, 1604 s, 1594 sh, 1570 m, 1481 s, 1471s 1433 s, 1406 m, 1386 w, 1348 m, 1280 s, 1246 s, 1220 sh, 1211 w, 1151 m, 1122 vs, 1102 s, 1045 s, 1018 m, 1005 m, 994 sh, 982 sh, 927 s, 830 vs, 813 sh, 777 sh, 764 vs, 754 sh, 721 m, 671 sh, 657 m, 645 w, 614 w, 566 vw, 513 w, 486 vw, 469 vw, 454 vw, 429 sh, 407 w, 375 w, 351 w, 297 vw. − $C_{24}H_{42}N_4Si_2Zn$ (508.176): calcd. C 56.72, H 8.33, N 11.03; found C 56.72, H 8.33, N 11.03.

X-ray Structure Determinations of 2 and 3: Data were collected on a Siemens P4 diffractometer with a Siemens SMART−CCD area detector with graphite monochromated Mo-K_α radiation (λ = 71.073 pm) using oil-coated, rapidly cooled single crystals.[15] Crystallographic parameters and details of data collection and refinement procedures are summarized in Table 3.

The structures were solved by direct methods and refined with the software packages SHELXL-93 and SHELXL-97.[17] Neutral scattering factors were taken from Cromer and Mann[18] and for the hydrogen atoms from Stewart et al.[19] The non-hydrogen atoms were refined anisotropically. The H-atoms were considered with a riding model under restriction of ideal symmetry at the corresponding carbon atoms. Crystallographic data (excluding structure factors) for the structures of **2** and **3** has been deposited with the Cambridge Crystallographic Data Centre as supplementary publication no. CCDC-147824 for **2** and -147825 for **3**. Copies of the data can be obtained on application to CCDC, 12 Union Road, Cambridge CB2 1EZ, UK [E-mail: deposit@ccdc.cam.ac.uk].

Table 3. Crystallographic data of **2** and **3** as well as details of the structure solution and refinement procedures

Compound	2	3
Empirical formula	$C_{13}H_{24}N_2SiZn$	$C_{13}H_{23}N_2SiZn$
Formula mass [gmol^{-1}]	301.80	300.79
T [K]	193(2)	193(2)
Crystal system	triclinic	tetragonal
Space group[16]	$P\bar{1}$ (No. 2)	$I4_1cd$ (No. 110)
a [pm]	858.3(2)	1873.6(1)
b [pm]	986.1(2)	1873.6(1)
c [pm]	1060.7(2)	1781.6(1)
α [°]	72.413(3)	90
β [°]	83.311(4)	90
γ [°]	68.207(3)	90
V [nm^3]	0.7946(2)	6.2542(6)
Z	2	16
$d_{calcd.}$ [gcm^3]	1.261	1.278
μ [mm^{-1}]	1.604	1.630
F(000)	320	2544
Scan range [°]	$4.0 < 2\theta < 58.5$	$4.3 < 2\theta < 58.6$
Measured data	4588	17200
Unique data (R_{int})	2431 (0.0223)	3277 (0.0356)
Absorption. corr.	semiempirical	semiempirical
Max./min. transmission	0.7397/0.5662	0.7363/0.6405
Parameters	160	160
Restraints	0	1
wR_2[a] (all data, on F^2)	0.2061	0.0593
R_1[a] (all data)	0.0706	0.0307
Flack parameter	−	0.007(9)
Data with $I > 2\sigma(I)$	2157	2952
R_1 [$I > 2\sigma(I)$]	0.0652	0.0247
Gof s[b] on F^2	1.126	1.025
Residual dens. [enm^{-3}]	1303/−708	301/−277
CCDC number	CCDC-147824	CCDC-147825

[b] $s = \{\Sigma[w(F_o^2 - F_c^2)^2]/(N_o - N_p)\}^{1/2}$.

Acknowledgments

This work was financially supported by the Deutsche Forschungsgemeinschaft, Bonn, and the Fonds der Chemischen Industrie, Frankfurt/Main. We thank Mr. S. Correll for performing the X-ray powder diffraction experiments. T. Bollwein wishes to express his gratitude to the Fonds der Chemischen Industrie for a Ph. D. scholarship.

[1] For examples see: K.-H. Thiele, J. Köhler, *Z. Anorg. Allg. Chem.* **1965**, *337*, 260−267; K.-H. Thiele, H. Rau, *Z. Anorg. Allg. Chem.* **1967**, *353*, 127−134; H. Rau, K.-H. Thiele, *Z. Anorg. Allg. Chem.* **1967**, *355*, 253−264; K. J. Fisher, *Inorg. Nucl. Chem. Lett.* **1973**, *9*, 921−925; J. Behm, S. D. Lotz, W. A. Herrmann, *Z. Anorg. Allg. Chem.* **1993**, *619*, 849−852; J. Pickard, B. Straub, *Z. Naturforsch.* **1995**, *50b*, 1517; H. Gornitzka, C. Hemmert, G. Bertrand, M. Pfeiffer, D. Stalke, *Organometallics* **2000**, *19*, 112−114.

[2] J. G. Noltes, J. Boersma, *J. Organomet. Chem.* **1967**, *9*, 1−4; A. J. de Koning, J. Boersma, G. J. M. van der Kerk, *J. Organomet. Chem.* **1980**, *186*, 159−172; E. Wissing, M. Kaupp, J. Boersma, A. L. Spek, G. van Koten, *Organometallics* **1994**, *13*, 2349−2356.

[3] M. Westerhausen, B. Rademacher, W. Schwarz, *J. Organomet. Chem.* **1992**, *427*, 275−287; M. Westerhausen, B. Rademacher, *J. Organomet. Chem.* **1993**, *443*, 25−33.

[4] P. C. Andews, C. L. Raston, B. W. Skelton, A. H. White, *Organometallics* **1998**, *17*, 779−782.

[5] W. Kaim, *Chem. Ber.* **1981**, *114*, 3789; M. Westerhausen, B. Rademacher, in *The Chemistry of the Copper and Zinc Triads* (Eds.: A. J. Welch, S. K. Chapman), The Royal Society of Chemistry, Cambridge, **1993**, pp. 148−151.

[6] E. Kimura, *Prog. Inorg. Chem.* **1994**, *41*, 443. For recent examples see: A. Looney, G. Parkin, R. Alsfasser, M. Ruf, H. Vahrenkamp, *Angew. Chem.* **1992**, *104*, 57−58; *Angew. Chem. Int. Ed. Engl.* **1992**, *31*, 92−93; M. Ruf, F. A. Schell, R. Walz, H.

Vahrenkamp, *Chem. Ber./Recueil* **1997**, *130*, 101−104; M. Rombach, C. Maurer, K. Weis, E. Keller, H. Vahrenkamp, *Chem. Eur J.* **1999**, *5*, 1013−1027.
[7] G. van Koten, J. T. B. H. Jastrzebski, K. Vrieze, *J. Organomet. Chem.* **1983**, *250*, 49−61.
[8] J. T. B. H. Jastrzebski, J. M. Klerks, G. van Koten, K. Vrieze, *J. Organomet. Chem.* **1981**, *210*, C49−C53.
[9] M. Kaupp, H. Stoll, H. Preuss, W. Kaim, T. Stahl, G. van Koten, E. Wissing, W. J. J. Smeets, A. L. Spek, *J. Am. Chem. Soc.* **1991**, *113*, 5606−5618; E. Wissing, M. Kaupp, J. Boersma, A. L. Spek, G. van Koten, *Organometallics* **1994**, *13*, 2349−2356; E. Wissing, E. Rijnberg, P. A. van der Schaaf, K. van Gorp, J. Boersma, G. van Koten, *Organometallics* **1994**, *13*, 2609−2615; E. Wissing, K. van Gorp, J. Boersma, G. van Koten, *Inorg. Chim. Acta* **1994**, *220*, 55−61.
[10] A. L. Spek, J. T. B. H. Jastrzebski, G. van Koten, *Acta Cryst.* **1987**, *C43*, 2006−2007; E. Wissing, S. van der Linden, E. Rijnberg, J. Boersma, W. J. J. Smeets, A. L. Spek, G. van Koten, *Organometallics* **1994**, *13*, 2602−2608.
[11] E. Rijnberg, B. Richter, K.-H. Thiele, J. Boersma, N. Veldman, A. L. Spek, G. van Koten, *Inorg. Chem.* **1998**, *37*, 56−63.
[12] M. S. Chinn, J. Chen, *Inorg. Chem.* **1995**, *34*, 6080−6084.
[13] M. Westerhausen, T. Bollwein, K. Polborn, *Z. Naturforsch.* **2000**, *55b*, 51−59.
[14] A. Haaland, K. Hedberg, P. P. Power, *Inorg. Chem.* **1984**, *23*, 1972−1975; P. P. Power, K. Ruhlandt-Senge, S. C. Shoner, *Inorg. Chem.* **1991**, *30*, 5013−5015; W. S. Rees, D. M. Green, W. Hesse, *Polyhedron* **1992**, *11*, 1697−1699; M. A. Putzer, A. Dashti-Mommertz, B. Neumüller, K. Dehnicke, *Z. Anorg. Allg. Chem.* **1998**, *624*, 263−266; W. S. Rees, O. Just, H. Schumann, R. Weimann, *Polyhedron* **1998**, *17*, 1001−1004; H. Schumann, J. Gottfriedsen, S. Dechert, F. Girgsdies, *Z. Anorg. Allg. Chem.* **2000**, *626*, 747−758.
[15] T. Kottke, D. Stalke, *J. Appl. Crystallogr.* **1993**, *26*, 615−619; D. Stalke, *Chem. Soc. Rev.* **1998**, *27*, 171−178.
[16] *International Tables for Crystallography* (Ed.: T. Hahn), Vol. A, *Space Group Symmetry*, 2nd Ed., D. Reidel, Dordrecht, **1984**.
[17] G. M. Sheldrick, *SHELXL-93*, Universität Göttingen, **1993**; *SHELXL-97*, Universität Göttingen, **1997**.
[18] D. T. Cromer, J. B. Mann, *Acta Crystallogr.* **1968**, *24*, 321−324.
[19] R. F. Stewart, E. R. Davidson, W. T. Simpson, *J. Chem. Phys.* **1965**, *42*, 3175−3187.

Received August 4, 2000
[I00308]

Dinuclear Zinc(II) Complexes of *N*,*N*′-Bis[2-(hydroxyphenyl)methyl]-*N*,*N*′-bis(2-pyridylmethyl)-1,*n*-alkanediamines

Harry Adams,[a] Darren Bradshaw,[a] and David E. Fenton*[a]

Keywords: Zinc / N ligands / O ligands / Structure elucidation

Neutral homodinuclear zinc(II) complexes [ZnL]·$ZnCl_2$ have been obtained from the reactions of the proligands *N*,*N*′-bis(2-hydroxybenzyl)-*N*,*N*′-bis(2-methylpyridyl)-1,2-ethanediamine (H_2L^1) and *N*,*N*′-bis(2-hydroxybenzyl)-*N*,*N*′-bis(2-methylpyridyl)-1,3-propanediamine (H_2L^2) with zinc chloride. Crystals of [ZnL^1]·$ZnCl_2$ (**3**) are triclinic, of space group *P*1(bar), with *a* = 9.2240(7), *b* = 10.4005(9), and *c* = 15.6418(13) Å, α = 91.634(2), β = 91.566(2), γ = 112.625(2)° and *Z* = 2, and those of [ZnL^2]·$ZnCl_2$ (**2**) are monoclinic, of space group $P2_1/c$, with *a* = 19.249(4), *b* = 17.275(4), and *c* = 16.546(3) Å, β = 92.742(5)° and *Z* = 8. The structures were refined by full-matrix least-squares procedures to R_1 = 0.0589 for **3** and R_1 = 0.085 for **2** for 4080 and 3786 independent reflections with $I \geq 4\sigma(I)$ respectively. The Zn in the [ZnL] moiety is coordinated in a distorted octahedral geometry [$N_2N'_2O_2$] and this unit serves as a chelating ligand, through the pair of phenolic O atoms, towards the $ZnCl_2$. The second zinc atom is in a distorted tetrahedral geometry. The structure of **2** shows a racemic mixture of two enantiomers, in which the pendant pyridinyl N atoms are *trans* to each other, whereas the structure of **3** reveals a new stereoisomer in which the pendant pyridinyl N atoms are *cis* to each. ^{1}H NMR spectroscopic data for the complexes shows a rigid solution structure for **2** and fluxional behaviour for **3**.

Introduction

An interest in generating models for manganese-containing metallobiosites led Neves et al. to synthesise mononuclear manganese(III) complexes of the *N*,*N*′-bis(2-hydroxybenzyl)-*N*,*N*′-bis(2-methylpyridyl)-1,*n*-alkanediamine ligands H_2L^1 (*n* = 2) and H_2L^2 (*n* = 3).[1] The crystal structure of [MnL^1]PF_6 revealed that the manganese(III) is present in a pseudo-octahedral geometry with each of the two halves of the hexadentate ligand providing a facial N_2O donor set. The phenolic O-atoms were found to be *cis* to each other and, with the N-atoms of the ethylenic spacer, provided the equatorial donor array.

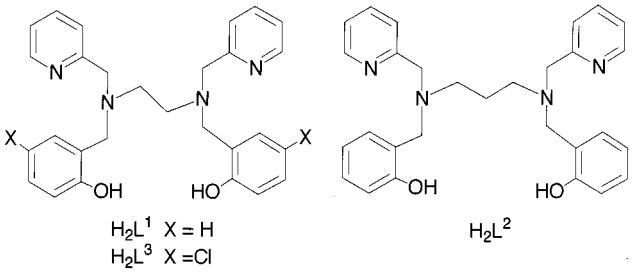

The pyridinyl N-atoms are in the apical sites and so are *trans* to each other. Similar pseudo-octahedral geometries and ligand dispositions have been found for gallium(III) and indium(III) in the closely related mononuclear complexes [ML^3]ClO_4 (M = Ga, In),[2] and for vanadium(III) in the complex [VL^1]PF_6.[3] The hexadentate ligands [O^(N^N_{pyr})^(N^N_{pyr})^O] have the capability to produce stereoisomers (Figure 1) but only (**1a**) has been crystallographically characterised in the above-mentioned complexes.

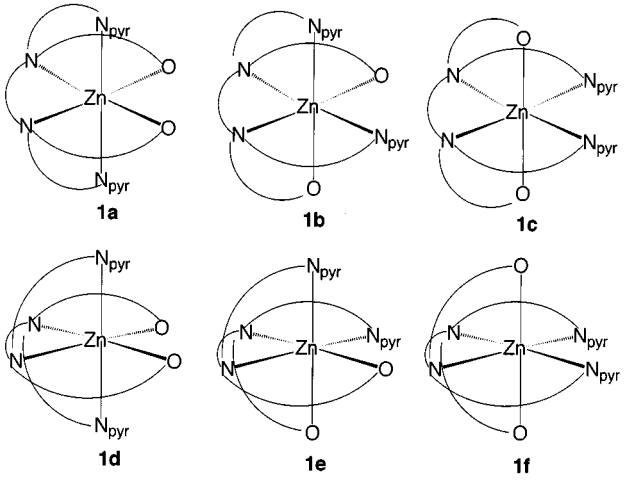

Figure 1. Octahedral stereoisomers derived from the ligands [O^(N^N_{pyr})^(N^N_{pyr})^O]

During the course of an investigation into the complexation of zinc(II) by tripodal and linked polypodal ligands bearing phenolic and pyridinyl groups[4–6] we have found that, in contrast to the above generation of mononuclear trivalent metal complexes, the reaction of zinc(II) chloride with H_2L^2 and H_2L^1 gives the homodinuclear complexes **2** and **3**, respectively, in which the anticipated neutral hexadentate zinc(II) complexes are not isolated but act as ligands towards a zinc chloride entity. In this paper we report this reactivity together with the crystal structures of

[a] Department of Chemistry, Dainton Building, The University of Sheffield,
Sheffield S3 7HF, UK
Fax: (internat.) +44-114/278-673
E-mail: d.fenton@sheffield.ac.uk

 © WILEY-VCH Verlag GmbH, 69451 Weinheim, 2001 1434–1948/01/0303–0859 $ 17.50+.50/0

the resulting complexes. Prior to this report, studies of H_2L^1 and H_2L^2 with divalent metals have been restricted to those on the application of H_2L^1 in the extraction of divalent first row transition metals into $CHCl_3$ in which the speciation revealed that the ligand could act not only in a hexadentate mode but also in tri- and tetradentate modes to give positively charged species.[7]

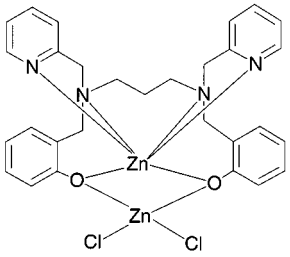

2

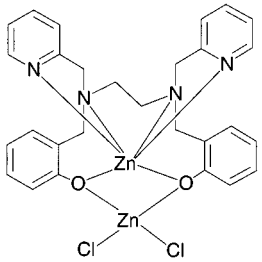

3

Results and Discussion

The Complex $[ZnL^2]\cdot ZnCl_2$ (2)

Reaction of the ligand H_2L^2 with two equivalents of $ZnCl_2$ in acetonitrile solution in the presence of NEt_3 gave colourless crystals suitable for X-ray analysis. The analytical data suggested that a complex with a molecular formula $[Zn_2L^2Cl_2]$ had formed and it was noted that changing the ratio of the starting materials from 1:2 to 1:1 did not change the stoichiometry of the reaction product. As a dinuclear product had not been expected the crystal structure was determined in order to establish the bond connectivity. There are two enantiomeric molecules in the asymmetric unit. The molecular structure of each, depicted in Figure 2, revealed that one Zn atom is completely encapsulated by the deprotonated ligand in a pseudo-octahedral coordination environment similar to that found in $[MnL^1]PF_6$, and in contrast to the structure found for $Zn(L^4)_2\cdot 2H_2O$, in which there is no steric constraint imposed by an alkane linker joining the secondary amines and the phenolate-O atoms are *trans* to each other, as are the pyridinyl-N atoms.[8] This octahedral complex $[ZnL^2]$ acts as a ligand with the *cis*-phenolate O-atoms chelating to the second zinc atom to give the product $[ZnL^2]\cdot ZnCl_2$ (**2**).

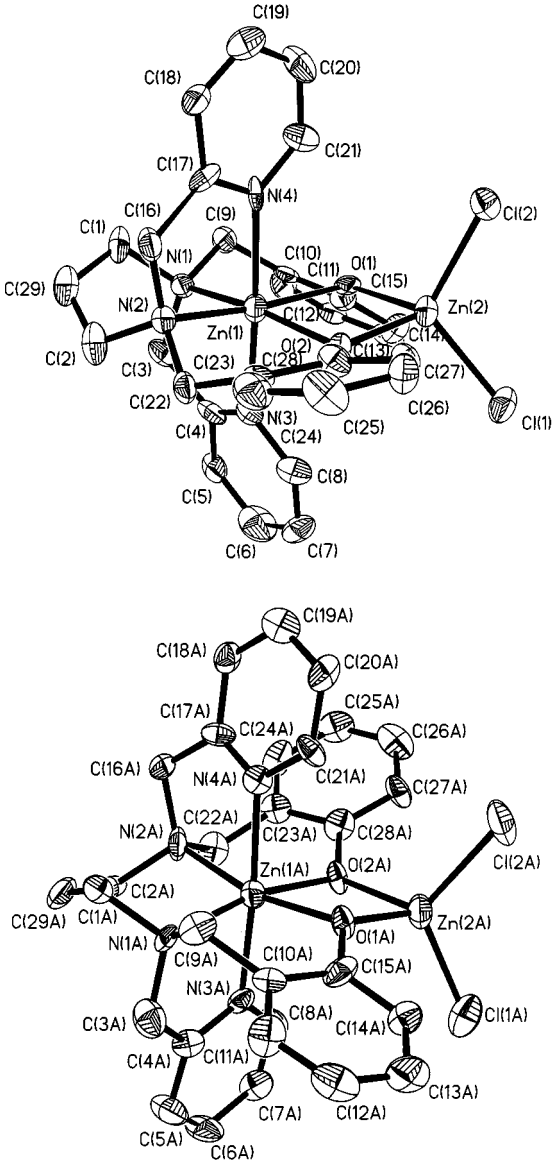

Figure 2. ORTEP drawings of the enantiomers of $[ZnL^2]\cdot ZnCl_2$ [Δ-**2** (a) and Λ-**2** (b)] showing the crystallographic labelling; thermal ellipsoids for the non-hydrogen atoms are drawn at the 50% probability level

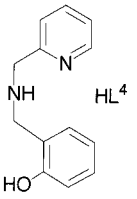

HL^4

The reaction of H_2L^2 with zinc(II) acetate yields the related complex $[ZnL^2]\cdot Zn(OAc)_2]$ in which the octahedral $[ZnL^2]$ unit, derived from stereoisomer **1a**, coordinates to the $Zn(OAc)_2$ through the *cis*-phenolato O atoms. The two acetato groups are monodentate and the second Zn atom is in a distorted T_d environment.[9]

The second zinc atom has a distorted tetrahedral coordination environment with two Cl atoms completing the coordination sphere. The Δ enantiomer (**1d**) is that containing Zn(1) and Zn(2), and the Λ enantiomer (**1a**) is that containing Zn(1A) and Zn(2A) (Figure 3); the designations Λ and Δ have been assigned assuming the species are tris-chelates with atom sequences O(1)Zn(2)O(2), N(2)C(16)C(17)N(4), and N(1)C(3)C(4)N(3) serving as chelating ligands.

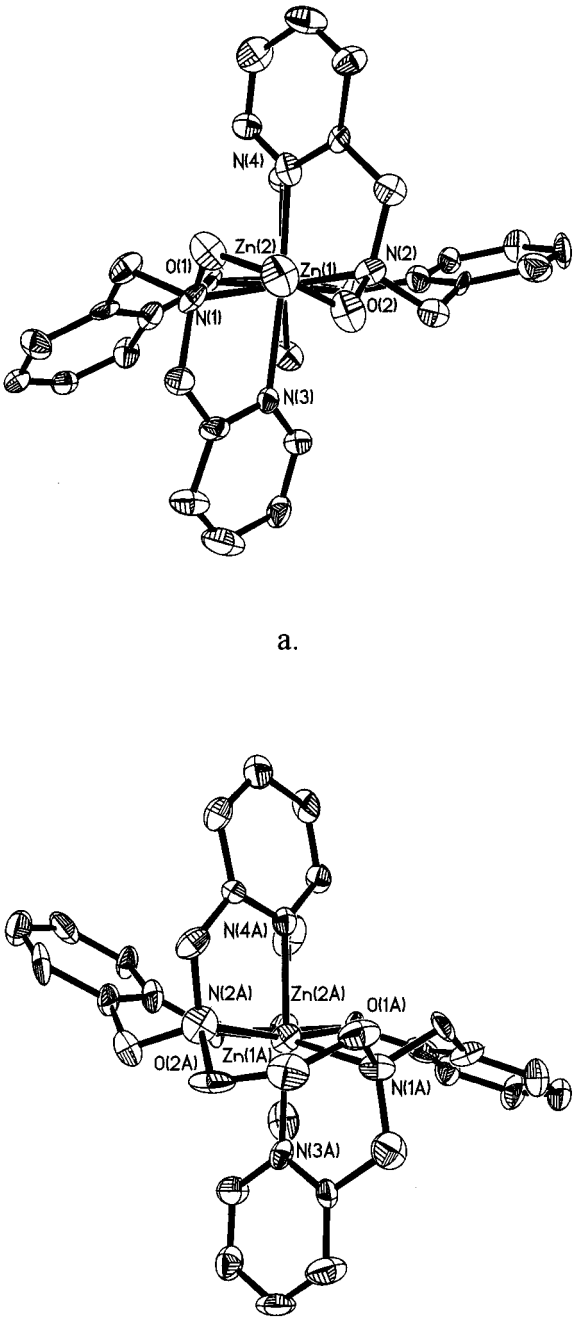

Figure 3. ORTEP drawings of the enantiomers of $[ZnL^2]\cdot ZnCl_2$ [Δ-**2** (a) and Λ-**2** (b)] viewed along the equatorial plane [(N(1)−N(2)−O(1)−O(2)]; thermal ellipsoids for the non-hydrogen atoms are drawn at the 50% probability level

Bond lengths and angles relating to the coordination at the metals are given in Table 1. The three *trans* angles in the octahedral sector of the Δ enantiomer, N(3)−Zn(1)−N(4), N(1)−Zn(1)−O(2), and N(2)−Zn(1)−O(1) are 175.2(3), 168.6(3), and 169.2(3)° respectively, and those in the Λ enantiomer, N(4A)−Zn(1A)−N(3A), N(1A)−Zn(1A)−O(2A), and N(2A)−Zn(1A)−O(1A) are 174.8(3), 167.6(3), and 167.1(3)° respectively, indicating some distortion from a pure octahedral geometry. The Zn−O bond lengths for Zn-phenolate interactions average 2.08 Å and are shorter than those for the Zn-amine interactions (average length = 2.17 Å) and those for the Zn−pyridyl interactions (average length = 2.14 Å).

Table 1. Selected bond lengths[Å] and bond angles [deg] for complexes **2** and **3**

	Δ-2	**Λ-2**[a]	**3**
Zn(1)−O(1)	2.101(6)	2.083(6)	2.084(3)
Zn(1)−O(2)	2.070(6)	2.059(6)	2.172(3)
Zn(1)−N(1)	2.176(7)	2.177(8)	2.181(4)
Zn(1)−N(2)	2.155(8)	2.162(8)	2.200(4)
Zn(1)−N(3)	2.133(8)	2.127(8)	2.169(4)
Zn(1)−N(4)	2.156(8)	2.136(8)	2.122(4)
Zn(1)−Zn(2)	3.0540(18)	3.0474(18)	3.1171(8)
Zn(2)−O(1)	1.997(6)	1.979(6)	1.992(3)
Zn(2)−O(2)	1.997(6)	1.998(6)	1.969(3)
Zn(2)−Cl(1)	2.224(3)	2.221(3)	2.2163(14)
Zn(2)−Cl(2)	2.231(3)	2.233(3)	2.2483(13)
N(1)−Zn(1)−O(2)	168.6(3)	167.6(3)	109.18(13)
N(2)−Zn(1)−O(1)	169.2(3)	167.1(3)	160.50(14)
N(3)−Zn(1)−N(4)	175.2(3)	174.8(3)	90.47(15)
N(2)−Zn(1)−N(1)	94.2(3)	94.9(3)	81.93(15)
N(2)−Zn(1)−O(2)	93.4(3)	93.5(3)	87.11(14)
N(1)−Zn(1)−O(1)	93.1(3)	93.0(3)	91.67(14)
O(1)−Zn(1)−O(2)	80.6(2)	80.5(2)	77.57(12)
N(3)−Zn(1)−N(2)	100.9(3)	96.9(3)	108.72(15)
N(3)−Zn(1)−N(1)	78.8(3)	80.1(3)	78.43(14)
N(3)−Zn(1)−O(2)	91.4(3)	89.8(3)	163.52(13)
N(3)−Zn(1)−O(1)	88.3(3)	94.4(3)	87.79(14)
N(4)−Zn(1)−N(2)	79.7(3)	77.9(3)	79.53(15)
N(4)−Zn(1)−N(1)	96.4(3)	99.5(3)	154.04(15)
N(4)−Zn(1)−O(2)	93.3(3)	91.2(3)	87.92(14)
N(4)−Zn(1)−O(1)	91.6(3)	90.8(3)	111.49(14)
O(2)−Zn(2)−O(1)	85.0(2)	84.6(3)	84.63(13)
Cl(1)−Zn(2)−Cl(2)	113.98(13)	117.22(13)	116.63(5)
O(2)−Zn(2)−Cl(1)	110.9(2)	113.2(2)	111.99(10)
O(2)−Zn(2)−Cl(2)	115.12(19)	115.1(2)	116.92(10)
O(1)−Zn(2)−Cl(1)	119.88(19)	114.0(2)	115.79(10)
O(1)−Zn(2)−Cl(2)	108.90(19)	108.1(2)	106.66(10)
Zn(1)−O(1)−Zn(2)	96.3(3)	97.2(3)	99.72(14)
Zn(1)−O(2)−Zn(2)	97.3(2)	97.4(3)	97.54(14)

[a] The atomic labelling sequence for **Λ-2** in Figures 2 and 3 is 1A, 2A, 3A etc. corresponding directly to that for **Δ-2** of 1, 2, 3 etc.

The coordination environment of the second zinc atom in each enantiomer is a distorted tetrahedron. The bond angles for the chelated O−Zn−O are 85.0(2)° [O(1)−Zn(2)−O(2)] and 84.6(3)° [O(1A)−Zn(2A)−O(2A)], and 113.98(11)° and 117.22(13)° for the Cl−Zn−Cl angles Cl(1)−Zn(2)−Cl(2) and Cl(1A)−Zn(2A)−Cl(2A) respectively. The remaining O−Zn−Cl angles are closer to the expected tetrahedral values. The Zn−O bonds (average length = 1.99 Å) are shorter than those at Zn(1) and Zn(1A) and the Zn−Cl bond lengths average 2.23 Å. The

intermetallic separations are 3.0540(18) [Zn(1)···Zn(2)] and 3.0474(18) Å [Zn(1A)···Zn(2A)].

Although the role of transition metal complexes as ligands has been well established for complexes of tetradentate salicylaldimines such as salen (salen = *N*,*N*′-ethylenebis(salicylideneimine)[2,2′-{1,2-ethanediylbis(nitrilomethylidyne)phenol}])[10] the above complex is a novel example of a hexadentate metal complex acting as a donor ligand towards a second metal atom. Previously, dinuclear zinc(II) complexes of the type $Zn(TSB)ZnX_2$ (X = Cl, ClO_4; TSB = tetradentate Schiff base), in which both zinc atoms were regarded as four-coordinate with a square coplanar Zn atom from the Schiff base adjacent to a tetrahedral Zn atom in the inorganic salt (Type 1), have been reported but no X-ray structural characterisation was made.[11,12] Homo- and heterodinuclear complexes in which a square coplanar Schiff base complex acts as a bidentate ligand towards a coordinatively unsaturated bis(1,1,1,5,5,5-hexafluoropentane-2,4-dionato)metal(II) (Type 2) have also been reported.[13–18]

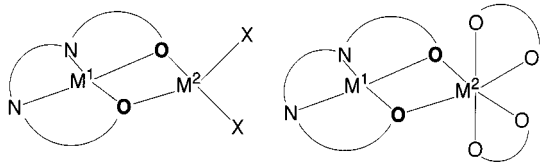

In contrast the current compounds have a six-coordinated metal complex acting as a ligand towards an inorganic salt and resemble the coordination pattern found in the complex $[L^5Zn(OH_2)ZnCl_2]\cdot 0.5\,CH_3CN$.[19] In this compound one of the zinc atoms is octahedrally coordinated by the pentadentate dianionic macrocyclic ligand (L^5) and a water molecule, whilst the second zinc atom is tetrahedrally coordinated to two bridging phenolate oxygen atoms and to two chloride ions. The Zn···Zn separation was given as 3.08 Å but further details on bonds and angles were not released as the poor crystallinity of the crystals inhibited an accurate structure determination.

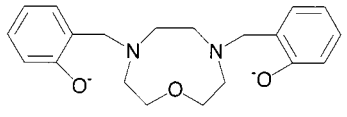

L^5

The Complex $[ZnL^1]\cdot ZnCl_2$ (3)

The reaction of $ZnCl_2$ with H_2L^1 gave the complex $[ZnL^1]\cdot ZnCl_2$ (**3**). Intriguingly the crystal structure revealed that a different spatial arrangement of donor atoms was present (Figure 4). Instead of the pyridine N-atoms being *trans* to each other they are now *cis* [N(3)–Zn(1)–N(4), 90.47(15)°, **1b**] and so give rise to a previously unreported stereoisomer for this class of compounds. There are two molecules, an enantiomeric pair, in the triclinic unit cell, with only one molecule in the asymmetric unit; the opposite enantiomer is generated by the inversion centre of the *P*1(bar) space group.

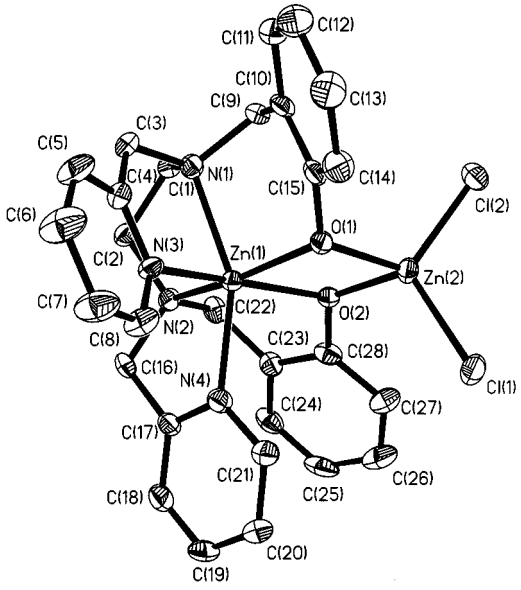

Figure 4. ORTEP drawing of $[ZnL^1]\cdot ZnCl_2$ (**3**) showing the crystallographic labelling; thermal ellipsoids for the non-hydrogen atoms are drawn at the 50% probability level

Bond lengths and angles relating to the coordination at the metals are given in Table 1. The three *trans* angles in the octahedral sector of the molecule, N(1)–Zn(1)–N(4), N(3)–Zn(1)–O(2), and N(2)–Zn(1)–O(1) are 154.04(15), 163.52(13), and 160.50(14)°, respectively, and are indicative of a larger distortion of the octahedral coordination geometry at Zn(1). The Zn–O bond lengths for Zn–phenolate interactions are 2.084(3) [(Zn(1)–O(1)] and 2.172(3) Å [Zn(1)–O(2)], and are again shorter than those for the Zn–amine interactions, 2.181(4) [Zn(1)–N(1)] and 2.200(4) Å [Zn(1)–N(2)], and those for the Zn–pyridyl interactions of 2.169(4) [Zn(1)–N(3)] and 2.122(4) Å [Zn(1)–N(4)]. The five-membered ring ($ZnNC_2N$) formed by the ethylenediamine linker has a skew conformation with a torsion angle N(1)–C(1)–C(2)–N(2) of −59.4° and the two carbon atoms of the linker, C(1) and C(2), are displaced by 0.43 and −0.30 Å on opposite sides of the ZnNN plane.

The second zinc atom is again in a tetrahedrally distorted coordination environment. The bond angle for the chelated O–Zn–O is 84.63(13)° [O(1)–Zn(2)–O(2)] and 113.63(5)° for the Cl–Zn–Cl angle [Cl(1)–Zn(2)–Cl(2)]. The remaining O–Zn–Cl angles are slightly more divergent [106.66(10)–116.92(10)°] from the expected tetrahedral values than in **2**. The Zn–O bonds (average length = 1.98 Å) are shorter than those at Zn(1) and the Zn–Cl bond lengths average 2.23 Å introducing further asymmetry to the tetrahedral site. The intermetallic separation of 3.1171(8) Å [Zn(1)···Zn(2)] is longer than that found in **2**.

Solution Studies

The ^{1}H NMR spectra of the metal complexes were recorded in [D$_6$]DMSO. The spectrum of **2** was sharp, as had been noted for the spectra of the closely related mononuclear gallium(III) and indium(III) complexes [ML]ClO$_4$ (L = L^1, L^3).[2] The spectra of these complexes did not undergo significant changes on raising the temperature from room temperature to 120 °C, indicating the intact and rigid nature of the octahedral complexes in solution. The structure is possibly stabilised by the presence of six-membered chelate rings, formed by the phenolic arms, in their preferred equatorial configuration.[1,20] The minor shifts of the ^{1}H resonance signals and slight broadenings of the signals were attributed to thermal vibrations of the coordinated ligands at elevated temperatures.[2] In contrast, although the resonances of **3** are close in value to those reported for the corresponding gallium and indium complexes some of them showed significant broadening at room temperature. An enhancement of the broadening and changes in chemical shifts occurred as the temperature was raised to 100 °C. This suggests that there are dynamic processes occurring over this temperature range. It was not possible to freeze any molecular motions due to the solution range of [D$_6$]DMSO, nor was it possible to obtain a limiting high temperature spectrum. It is proposed that the stereoisomer found in the solid state (**1b**), in which one of the six-membered chelate rings formed by the phenolic arms is in an equatorial configuration and the other is in an axial configuration, is less rigid than the stereoisomer **1a** in which both six-membered chelate rings formed by the phenolic arms are equatorial. Interconversion of the arms together with accompanying movement of the ethane linker would lead to the resonance broadening that is observed.

Conclusions

In contrast to the reactions of H$_2$L^1 and H$_2$L^2 with trivalent metals, which gave discrete mononuclear complex cations, zinc chloride reacts with H$_2$L^2 and H$_2$L^1 to give the dinuclear zinc(II) complexes **2** and **3**. In these complexes one zinc(II) atom is fully encapsulated by the deprotonated hexadentate ligand in a pseudo-octahedral geometry and this moiety then acts as a ligand towards ZnCl$_2$ through the *cis*-phenolato-O atoms. The second zinc(II) atom is in a distorted tetrahedral coordination environment. The structure of **2**, in which the pyridinyl N donors are *trans* to each other, is similar to those found for the trivalent metal complexes of L^1 in which the stereoisomer **1a** is found, but the structure of **2** further showed the presence in the asymmetric unit of a racemic mixture of the two enantiomers Λ (**1a**) and Δ (**1d**). The structure of **3** revealed a previously unreported second stereoisomer **1b** in which the pyridinyl N donors are *cis* to each other; in this case only one enantiomer was present in the asymmetric unit with the opposite enantiomer being generated from an inversion centre [$P\bar{1}$ space group].

Experimental Section

Measurements: Elemental analyses were carried out by the University of Sheffield microanalytical service. ^{1}H NMR spectra were recorded using a Bruker WH-400 spectrometer. Positive ion fast atom bombardment (FAB) mass spectra were recorded using a VG PROSPEC spectrometer (the matrix used was 4-nitrobenzyl alcohol).

Materials: Reagent or AR grade chemicals were used in this study. *N*,*N*′-bis(2-hydroxybenzyl)-*N*,*N*′-bis(2-methylpyridyl)-1,2-ethanediamine (H$_2$L^1) and the *N*,*N*′-bis(2-hydroxybenzyl)-*N*,*N*′-bis(2-methylpyridyl)-1,3-propanediamine (H$_2$L^2) were prepared by the published methods.[1,2]

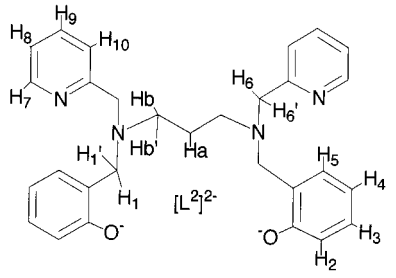

Synthesis of Complexes

[Zn(L^2)·ZnCl$_2$] (2): *N*,*N*′-bis(2-hydroxybenzyl)-*N*,*N*′-bis(2-methylpyridyl)-1,3-propanediamine (100 mg, 0.21 mmol) was dissolved in warm acetonitrile (10 mL) containing a trace amount of NEt$_3$. ZnCl$_2$ (60 mg; 0.44 mmol) was added and the solution was gently refluxed for 1 hour. After cooling and standing the solution afforded colourless crystals suitable for X-ray analysis. Yield: 84 mg, 60%. − ^{1}H NMR ([D$_6$]DMSO): δ = 8.85 (d, 2 H, 7-H), 7.71 (t, 2 H, 8-H), 7.27 (t, 2 H, 9-H), 7.04 (d, 2 H, 10-H), 6.95 (d, 2 H, 5-H), 6.81 (t, 2 H, 4-H), 6.64 (d, 2 H, 2-H), 6.45 (t, 2 H, 3-H), 4.33 (d, 2 H, 6′-H), 4.15 (d, 2 H, 1′-H), 3.73 (d, 2 H, 6-H), 3.36 (d, 2 H, 1-H), 2.79 (m, 2 H, b′-H), 2.64 (m, 2 H, b-H), 2.21 (bd, 2H, a-H). − MS (FAB; *m*NBA): *m*/*z* = 531 [Zn(L^2) + H]$^+$. − C$_{29}$H$_{30}$Cl$_2$N$_4$O$_2$Zn$_2$ (668.2): calcd. C 52.12, H 4.52, N 8.38, Cl 10.61; found C 52.03, H 4.56, N 8.23, Cl 10.90.

Table 2. Crystallographic data for **2** and **3**

	2	**3**
Formula	C$_{29}$H$_{30}$Cl$_2$N$_4$O$_2$Zn$_2$	C$_{28}$H$_{28}$Cl$_2$N$_4$O$_2$Zn$_2$
Formula mass	668.21	654.18
Space group, *Z*	$P2_1/c$, 8	$P\bar{1}$, 2
Wavelength [Å]	0.71073	0.71073
a [Å]	19.249(4)	9.2240(7)
b [Å]	17.275(4)	10.4005(9)
c [Å]	16.546(3)	15.6418(13)
α [deg]	90	91.634(2)
β [deg]	92.742(5)	91.566(2)
γ [deg]	90	112.625(2)
V [Å^3]	5496(5)	1386.3(2)
T [K]	150(2)	150(2)
ρ_{calc} [mg·m^{-3}]	1.615	1.567
μ [mm^{-1}]	1.976	1.956
Final *R*[a]	R_1 = 0.085	R_1 = 0.0589
	wR_2 = 0.1604	wR_2 = 0.1256

[a] $R_1 = \Sigma||F_o| - |F_c||/\Sigma|F_o|$ with $I > 4\sigma(I)$ and $wR_2 = \{\Sigma[w(F_o^2 - F_c^2]/\Sigma[w(F_o^2)]\}^{1/2}$.

[$Zn(L^1)\cdot ZnCl_2$] (3): *N*,*N*′-bis(2-hydroxybenzyl)-*N*,*N*′-bis(2-methylpyridyl)-1,2-ethanediamine (100 mg; 0.22 mmol) was dissolved in warm acetonitrile (8 mL) containing a trace amount of NEt_3 and $ZnCl_2$ (60 mg; 0.44 mmol) was added. The solution was gently refluxed for 1 hour. After cooling and standing the solution gave colourless crystals suitable for X-ray analysis. Yield, 107 mg; 74.6%. − ^{1}H NMR ([D$_6$]DMSO); aromatics at δ = 8.80 (d), 7.75 (bd), 7.32 (t), 7.06 (bd), 6.98 (d), 6.77 (t), 6.42 (t), 6.15 (bd); aliphatics at δ = 4.25 (bd), 4.08 (d), 3.96 (bd), 3.55 (d), 3.05 (bd), 2.70 (bd). − MS (FAB; *m*NBA): *m*/*z* = 517 [$Zn(L^1)$ + H]$^+$. − $C_{28}H_{28}Cl_2N_4O_2Zn_2$ (654.2): calcd. C 51.41, H 4.31, N 8.56, Cl 10.84; found C 51.48, H 4.28, N 8.37, Cl 10.92.

X-ray Crystallography: Relevant X-ray crystal data are given in Table 2. Measurements were made on a Siemens SMART CCD area diffractometer using graphite-monochromatised Mo-K_α radiation, λ = 0.71073 Å. The programs used were Siemens SMART and SAINT for control and integration software and SHELXTL as implemented on the Viglen Pentium computer.[21]

Crystallographic data (excluding structure factors) for the structures reported in this paper have been deposited with the Cambridge Crystallographic Data centre as supplementary publication nos. CCDC-148463 (**2**) and -148464 (**3**). Copies of the data can be obtained free of charge on application to CCDC, 12 Union Road, Cambridge CB12 1EZ, UK [Fax: (internat.) +44-1223/336-033; E-mail: deposit@ccdc.cam.ac.uk].

Acknowledgments

We thank the BBSRC for a studentship (to D.B.) and the EPSRC for funds towards the purchase of the diffractometer.

[1] A. Neves, S. M. D. Erthal, I. Vencato, A. S. Cecinto, *Inorg. Chem.* **1992**, *31*, 4749−4755.
[2] E. Wong, S. Liu, S. J. Rettig, C. Orvig, *Inorg. Chem.* **1995**, *34*, 3057−3064.
[3] A. Neves, A. S. Ceccato, S. M. D. Erthal, I. Vencato, B. Nuber, J. Weiss, *Inorg. Chim. Acta* **1991**, *187*, 119−121.
[4] H. Adams, N. A. Bailey, D. E. Fenton, Q-Y. He, *J. Chem. Soc., Dalton Trans.* **1996**, 2857 -2865.
[5] C. O. Rodriguez de Barbarin, N. A. Bailey, D. E. Fenton, Q.-Y. He, *J. Chem. Soc., Dalton Trans.* **1997**, 161−166.
[6] H. Adams, N. A. Bailey, D. E. Fenton, Q-Y. He, *J. Chem. Soc., Dalton Trans.* **1997**, 1533−1539.
[7] N. Hirayama, N. Ichitani, K. Kubono, Y. Matsuoka, H. Kokusen, T. Honjo, *Talanta.* **1997**, *44*, 2019−2025.
[8] A. Neves, I. Vencato, C. N. Verani, *J. Braz. Chem. Soc.* **1997**, *8*, 265−270.
[9] D. Bradshaw, unpublished results **2000**.
[10] E. Sinn, C. M. Harris, *Coord. Chem. Revs.* **1968**, *4*, 391−422.
[11] S. J. Gruber, C. M. Harris, E. Sinn, *J. Inorg. Nuclear Chem.* **1968**, *30*, 1805−1830.
[12] G. E. Batley, D. P. Graddon, *Austr. J. Chem.* **1968**, *21*, 1473−1485.
[13] D. E. Fenton, N. Bresciani-Pahor, M. Calligaris, G. Nardin, L. Randaccio, *J. Chem. Soc., Chem. Commun.* **1979**, 39−40.
[14] N. Bresciani-Pahor, M. Calligaris, G. Nardin, L. Randaccio, D. E. Fenton, *Transition Met. Chem.* **1980**, *5*, 180−183.
[15] N. B. O'Bryan, T. O. Maier, I. C. Paul, R. S. Drago, *J. Am. Chem. Soc.* **1973**, *95*, 6640−664.
[16] K. A. Leslie, R. S. Drago, G. D. Stucky, D. J. Kitko, J. A. Breese, *J. A. Inorg. Chem.* **1979**, *18*, 1885−1891.
[17] L. Banci, C. Benelli, D. Gatteschi, *Inorg. Chem.* **1981**, *20*, 2734−2735.
[18] L. Banci, C. Benelli, D. Gatteschi, *Inorg. Chem.* **1981**, *20*, 4397−4400.
[19] C. Flassbeck, K. Wieghardt, E. Bill, C. Butzlaff, A. X. Trautwein, B. Nuber, J. Weiss, *Inorg. Chem.* **1992**, *31*, 21−26.
[20] K. Bernauer, *Top. Curr. Chem.* **1976**, *65*, 1−35.
[21] *SHELTXL.* An integrated system for solving and refining crystal structures from diffraction data (Revision 5.1). Bruker AXS Ltd., Madison, Wis., USA, **1997**.

Received August 22, 2000
[I00326]

Investigation of the Cu^{II}/NCS^{-}/dpk Reaction System in CH_3OH [dpk = Di(2-pyridyl) Ketone]: Isolation, Structural Analysis and Magnetic Properties of a Dimer and a 1D Polymer with the Same Empirical Formula $[Cu(NCS)_2(dpk{\cdot}CH_3OH)]$

Zurine E. Serna,[a] Roberto Cortés,*[b] M. Karmele Urtiaga,[c] M. Gotzone Barandika,[b] Luis Lezama,[a] M. Isabel Arriortua,[c] and Teófilo Rojo*[a]

Keywords: N ligands / Copper / Coordination chemistry / EPR spectroscopy / Magnetic properties

Two polymorphous compounds with the general formula $[Cu(NCS)_2(dpk{\cdot}CH_3OH)]_n$ (dpk = di-2-pyridyl-ketone) have been synthesised and have been characterised both structurally and magnetically. The $dpk{\cdot}CH_3OH$ ligand is the result of the metal-promoted solvolysis of dpk in methanol and acts as a neutral donor. X-ray analysis carried out on single crystals for both compounds revealed that compound **1** is dimeric exhibiting double (*N*,*S*)-thiocyanate bridges, while compound **2** is 1D consisting of chains in which the metallic centres are connected through single *end-to-end* NCS^- groups. Magnetic susceptibility data showed that both compounds are antiferromagnetic, the values for the exchange constant *J* are –0.9 (**1**) and –0.3 cm^{-1} (**2**). The low values of *J* are consistent with the (N_{eq},S_{ax})-disposition of the thiocyanate bridges in the octahedral coordination sphere.

Introduction

High-dimensional arrangements exhibit potential applications in a great number of fields from heavy constructions to micro-circuitry.[1] Coordination polymers, in particular, have been the focus of attention of a great number of works devoted to the correlation between structural features and magnetic properties.[2] In this context, it is worth mentioning that the *N*,*N*′-type voluminous organic ligands have been extensively used, either as spacers or as coordination-site blockers.

Among the *N*,*N*′-donors, the di(2-pyridyl) ketone (dpk) ligand can be pointed out. This ligand exhibits certain singularities that explain its tendency to give rise to clusters[3] rather than infinite extended lattices when polynuclear systems are formed. The ligand dpk has three potential donor sites, however, when the ketocarbonyl group of dpk undergoes metal-promoted solvation (Scheme 1), four donor sites are exhibited. The resulting hydrated ($dpk{\cdot}H_2O$) or "alcoholated" (dpk·ROH) derivative can chelate either in a protonated or deprotonated state. As a consequence, the coordination possibilities of dpk are multiple and have been widely reported in the literature.[3,4] For instance, Tsohos et al.[3d] have reported a nonanuclear Co^{II}-dpk compound that clearly illustrates the capabilities of dpk. In this nonamer, the hydrated dpk derivative acts as a tetradentate ligand that is bonded to five different atoms of cobalt. This concentration of metallic ions around an organic molecule is obviously due to the proximity of the four potential donor atoms.

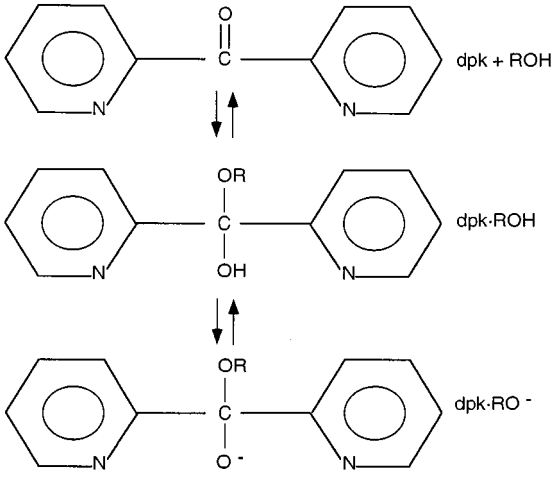

Scheme 1

The versatility of dpk could also be useful for the preparation of infinite arrays. To prevent cluster formation, pseudohalides could be used in combination with the organic ligand (as commonly carried out for other *N*,*N*′-

[a] Departamento de Química Inorgánica, Facultad de Ciencias, Universidad del País Vasco (UPV/EHU), Aptdo. 644, 48080 Bilbao, Spain
E-mail: QIPROAPT@lg.ehu.es
[b] Departamento de Química Inorgánica, Facultad de Farmacia, Universidad del País Vasco (UPV/EHU), Aptdo. 450, 01080 Vitoria, Spain
E-mail: QIPCOMOR@lg.ehu.es
[c] Departamento de Mineralogía y Petrología, Facultad de Ciencias, Universidad del País Vasco (UPV/EHU), Aptdo. 644, 48080 Bilbao, Spain

 © WILEY-VCH Verlag GmbH, 69451 Weinheim, 2001 1434–1948/01/0303–0865 $ 17.50+.50/0

groups). With this aim, we have been working on Ni^{II}-dpk-L systems (L = N_3, NCO, NCS). However, our first results have confirmed the tendency of dpk to concentrate metallic ions around it, through the characterisation of some tetramers.[4j,4k]

In order to explore the possibility of obtaining infinite polynuclear systems with other metals, this work was focused on Cu^{II}-systems. For this metallic cation a 1D arrangement has been synthesised. In particular, the results herein reported concern the magnetic and structural characterisation of two polymorphs with the general formula $[Cu(NCS)_2(dpk{\cdot}CH_3OH)]_n$. Compound **1** is a dimer exhibiting double (*N*,*S*)-thiocyanate bridges, while compound **2** consists of chains in which the metallic centres are connected through single *end-to-end* NCS^- groups. In both cases, the alcoholated dpk-derivative, dpk·CH_3OH, acts as a tridentate ligand and bonds to a single copper atom.

Results and Discussion

Structural Analysis

The structures of **1** and **2** are shown in Figure 1 and Figure 2, respectively. As observed, compound **1** consists of Cu^{II} dimers in which the metallic cations are connected through di-μ-(1,3)-NCS bridges, while compound **2** consists of chains in which the metallic cations are connected through single *end-to-end* thiocyanate bridges. The intermetallic distances through the thiocyanate bridges are 5.393 (**1**) and 5.994 (**2**) Å.

The octahedral coordination sphere around the Cu^{II} cations is similar for both polymorphous compounds. Thus, in both compounds the axial positions are occupied by S and O atoms: S1 corresponding to a bridging thiocyanate group and O1 belonging to the dpk·CH_3OH group. The formation of the dpk·CH_3OH is as a result of the solvolysis of the original dpk in methanol. At the equatorial positions, four N-atoms can be found, N3 and N4 atoms corresponding to a bridging and a terminal thiocyanate, respectively, and N1 and N2 belonging to the organic ligand. Thus, the main difference between **1** and **2** lies in the fact that in **1** each copper centre is connected to another copper centre through the S1 and N3 atoms, while in **2** each copper centre is connected to two other copper centres, one through the S1 atom and the other through the N3 atom. In this way, Cu^{II}-chains extend along the y direction for **2**.

The coordination sphere around the Cu^{II} cations in both compounds is noticeably distorted. This distortion can be attributed to the *N*,*O*,*N*′-terdentate coordination of dpk·CH_3OH and the long Cu−S distances. As can be seen in Table 1, the axial distances [Cu−S1 = 2.852(2) Å and Cu−O1 = 2.487(4) Å for **1**, and Cu−S1 = 2.837(1) Å and Cu−O1 = 2.503(2) Å for **2**] are remarkably higher than the equatorial ones [Cu−N average distances are 1.987 (**1**) and 1.991(**2**) Å]. The terdentate chelation of dpk·CH_3OH results in an angle of 109.8° (**1**) and 115.5° (**2**) between both pyridyl rings, as well as in important deviations from the ideal octahedral angles.

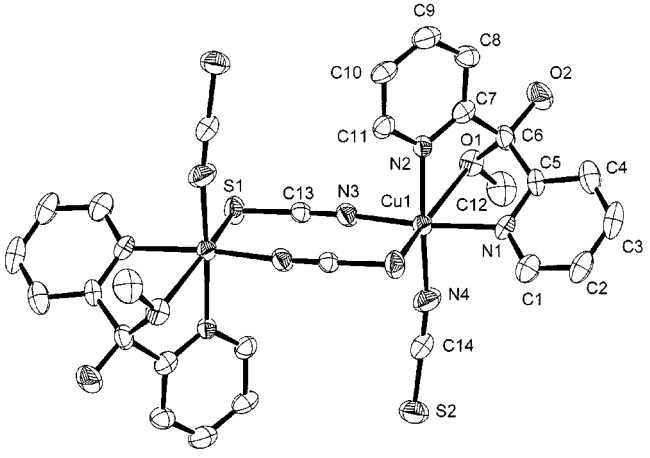

Figure 1. ORTEP view (50% probability) of the structure for compound **1** (H atoms are omitted for clarity)

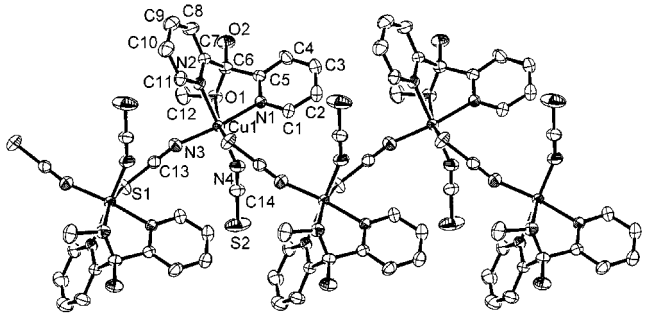

Figure 2. ORTEP view (50% probability) of the structure for compound **2** (H atoms are omitted for clarity)

Table 1. Selected bond lengths (Å) and angles (°) for compounds **1** and **2**

	1[a]	**2**[b]
Cu(1)−N(1)	2.026(5)	2.026(5)
Cu(1)−N(2)	2.022(4)	2.032(2)
Cu(1)−N(3)	1.945(5)	1.969(3)
Cu(1)−N(4)	1.956(5)	1.945(3)
Cu(1)−S(1i)	2.852(2)	2.837(1)
Cu(1)−O(1)	2.487(4)	2.503(2)
N(3)−C(13)	1.145(7)	1.145(4)
C(13)−S(1)	1.632(6)	1.637(3)
N(4)−C(14)	1.157(7)	1.143(4)
C(14)−S(2)	1.626(7)	1.620(3)
S(1i)−Cu(1)−O(1)	154.4(1)	162.78(5)
S(1i)−Cu(1)−N(1)	90.7(1)	96.76(7)
S(1i)−Cu(1)−N(2)	88.9(1)	91.90(7)
S(1i)−Cu(1)−N(3)	97.7(1)	93.45(9)
S(1i)−Cu(1)−N(4)	93.3(2)	92.3(1)
O(1)−Cu(1)−N(1)	72.1(1)	72.03(8)
O(1)−Cu(1)−N(2)	71.2(1)	74.62(8)
O(1)−Cu(1)−N(3)	98.2(2)	97.1(1)
O(1)−Cu(1)−N(4)	106.0(2)	101.2(1)
N(1)−Cu(1)−N(2)	87.1(2)	85.88(9)
N(3)−Cu(1)−N(2)	90.2(2)	90.0(1)
N(3)−Cu(1)−N(4)	92.0(2)	90.3(1)
N(4)−Cu(1)−N(1)	90.3(2)	93.1(1)
C(13)−N(3)−Cu(1)	171.9(5)	164.4(3)
N(3)−C(13)−S(1)	178.7(5)	179.6(3)
C(14)−N(4)−Cu(1)	167.0(6)	154.8(3)
N(4)−C(14)−S(2)	178.1(6)	179.1(3)

[a] *i* for this compound = 1 − *x*, −*y*, 1 − *z*. − [b] *i* for this compound = −*x*, 1/2 + *y*, 1/2 − *z*.

The structural features concerning the intermetallic connections are typical for thiocyanate bridges in octahedral systems.[5] Thus, both compounds exhibit the common $Cu-N_{eq}-C-S_{ax}-Cu$ coordination for the *end-to-end* thiocyanate bridge. On the other hand, the bridge-angles (N−C−S = 178.4°, C−S−Cu = 91.4°, S−Cu−N = 95.5° and Cu−N−C = 169.5° for **1**, and N−C−S = 179.3°, C−S−Cu = 91.4 °, S−Cu−N = 92.9° and Cu−N−C = 159.5° for **2**) show a slight deviation from the ideal ones.

It is worth mentioning that a great number of intermolecular and intramolecular H-bonds are present for both compounds (Table 2). As a result, the dimers (**1**) and the chains (**2**) are packed as displayed in Figure 3 and 4, respectively. As observed in Figure 3, there are magnetically nonequivalent ions which are related by the following operation of symmetry: x, $1/2 - y$, $1/2 + z$. The distance between these Cu atoms is 8.644(2) Å and the angle formed by the normals to their equatorial planes is 70.7(1)°. The presence of magnetically nonequivalent atoms in the unit cell will be used below in the EPR discussion. On the other hand, as seen in Figure 4, the packing of the chains in **2** allows π-π interactions between the pyridyl rings [inter-ring distance is 3.96(5) Å].

In summary, even if the dpk derivative in **2** acts as a tridentate ligand, the preparation of an extended dpk system has been possible as the organic ligand does not act as a bridging group but as a coordination-site blocker. In this sense, the role played by thiocyanate as the only intermetallic linker seems to be crucial to prevent the formation of clusters, as desired.

Table 2. Intermolecular[a] H-bond lengths (Å) and angles (°) for **1** and **2**

Compound 1

Donor−H	Donor···Acceptor	H.···Acceptor	Donor−H···.Acceptor
O2−H13	O2···S2(i)	H13···S2(i)	O2−H13···S2(i)
0.820(4)	3.330(4)	2.547(2)	160.4(3)
C8−H8	C8···N3(ii)	H8···N3(ii)	C8−H8···N3(ii)
0.930(6)	3.531(8)	2.912(5)	125.2(4)
(i) $2 - x$, $-y$, $2 - z$		(ii) x, $1/2 - y$, $1/2 + z$	

Compound 2

Donor−H	Donor···Acceptor	H···Acceptor	Donor−H···Acceptor
C8−H8	C8···O2(i)	H8···O2(i)	C8−H8···O2(i)
0.930(4)	3.489(5)	2.606(4)	158.7(2)
(i) $-x + 1$, $-y$, $-z$			

[a] The intramolecular ones can be found in the Supporting Information.

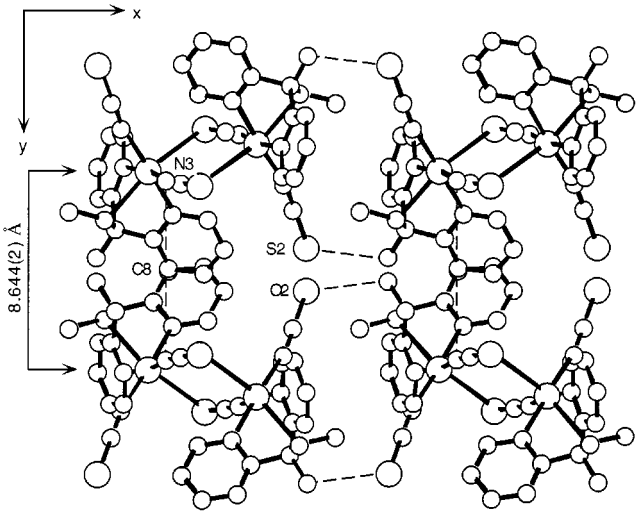

Figure 3. View of the packing of the dimers for **1** on the xy plane; discontinuous lines represent H-bonds (see Table 2); the magnetically nonequivalent atoms are located at 8.644(2) Å

IR Spectroscopy

A summary of the most important IR bands corresponding to compounds **1** and **2**, together with their tentative assignments[6] are given in Table 3. As can be seen, both compounds exhibit a split absorption at about 2100 cm^{-1} that corresponds to the asymmetric stretching mode of the C=N bond for the *N*,*S*-bonded thiocyanate.

In relation to the absorptions caused by the organic ligand, it is worth mentioning that the band at 1680 cm^{-1}, assigned to the C=O bond in conjugation with the pyridyl rings in dpk, is shifted to lower frequencies after solvolysis due to the presence of the C−O bond.[7] The bands assigned to the pyridyl ring stretching modes in **1** and **2** are also remarkably shifted, relative to the free dpk ligand, due to the loss of coplanarity between the pyridyl rings after rehybridisation from sp^2 to sp^3. The IR spectra also revealed the bands corresponding to the skeleton vibrations of the coordinated dpk·CH_3OH, which appear at slightly shifted frequencies relative to the free dpk.

EPR Spectroscopy

X- and Q-band powdered EPR spectra for **1** were recorded at room temp. down to 4.2 K. The spectra do not significantly change with temperature; a slight narrowing of the linewidth with decreasing temperature is observed. Q-band spectra, however, are better resolved than X-band ones. Figure 5 shows the Q-band spectrum for **1** at room temp. The signal seems to be rhombic, as is usually related to an exchange *g*-tensor. Additionally, there is a weak, broad signal at about 10750 G that must also be considered.

In order to interpret the spectrum in Figure 5 some structural features should be taken into account. The Cu^{II} octahedra in **1** are axially elongated suggesting that the molecular *g*-tensor is axial. However, it is also worth noting that compound **1** exhibits magnetically nonequivalent ions (Figure 3) that could involve interdimeric interactions. If the exchange interaction between nonequivalent centres were higher than the difference between the relative Zeeman energies, the EPR spectrum would not reveal the characteristics of the molecular *g*-tensor, but would show the ones corresponding to an average exchange *g*-tensor, g^{ex}. In that case, the components of the g^{ex} tensor could be expressed as a function of the components of the molecular *g*-tensor and the angles between them:[8] $(g_1^{ex})^2 = g_{\parallel}^2\cos^2\alpha + g_{\perp}^2\mathrm{sen}^2\alpha$ $(g_2^{ex})^2 = g_{\parallel}^2\mathrm{sen}^2\alpha + g_{\perp}^2\cos^2\alpha$ $g_3^{ex} = g_{\perp}$

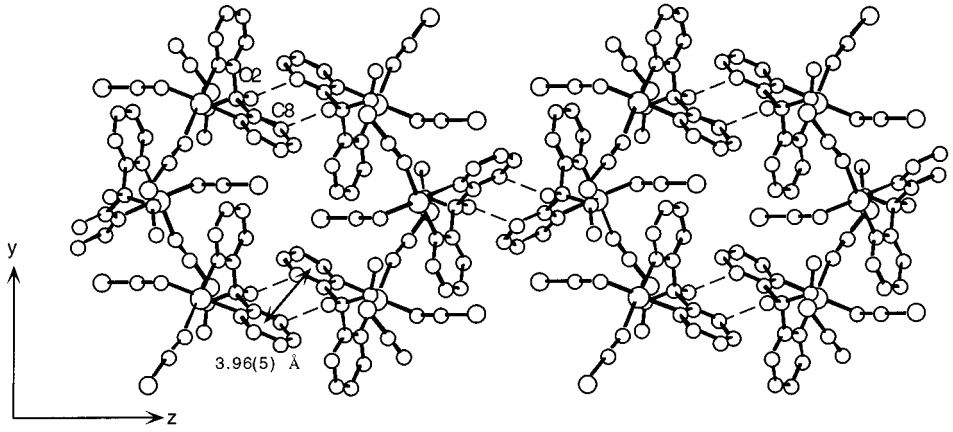

Figure 4. Packing of the dimers for **2** on the yz plane showing the H-bonds as discontinuous lines (see Table 2); the distance between parallel pyridyl rings is 3.96(5) Å

Table 3. Selected IR bands (cm^{-1}) for free dpk and the title compounds, together with their assignments

	free dpk[a]	Compound **1**	Compound **2**
Thiocyanate, ν(CN)	-	2121s, 2095s	2122s, 2074s
ν(CO)	1680s	1605	1597
Pyridyl ring stretching	1578s	1441	1381
Pyridyl ring breathing	998	1057	1057
Pyridyl C−H out of plane bending	753s, 742s	774	774
Pyridyl ring in plane vibration	662	673	650

[a] s: strong.

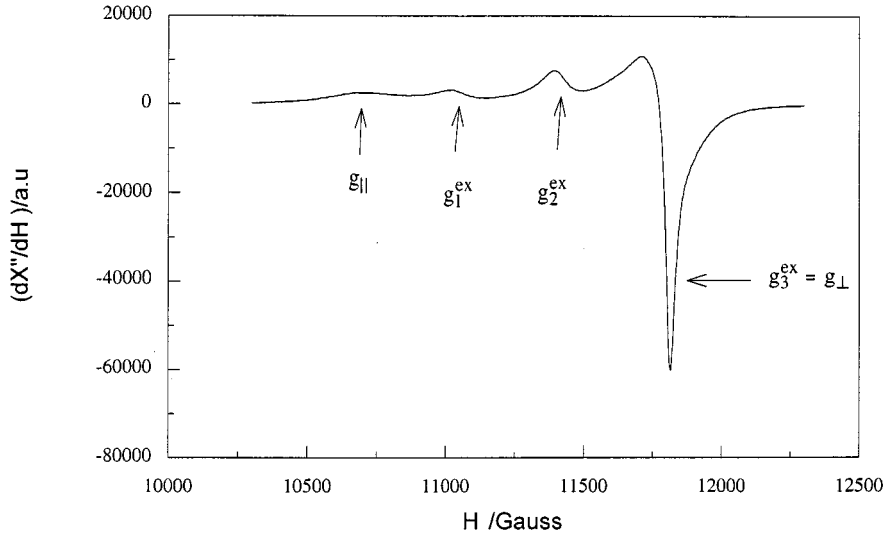

Figure 5. Q-band EPR powder spectrum at room temp. for **1**

where 2α is the angle formed by the magnetically non-equivalent chromophores; i.e. the canting angle between the normals to the equatorial planes of two interacting polyhedra [Equation (1)]:

$$\cos 2\alpha = \frac{g_1^{ex} - g_2^{ex}}{g_1^{ex} + g_2^{ex} - 2g_3^{ex}} \quad (1)$$

The observed values are $g_1^{ex} = 2.214$, $g_2^{ex} = 2.133$, $g_3^{ex} = 2.063$. Accordingly, $g_{\|} = 2.280$ and $g_{\perp} = 2.063$ have been calculated. The sequence $g_{\|} = 2.280 > g_{\perp} = 2.063 > 2.04$[8] agrees with the topology of the elongated [CuN_4SO] chromophores for **1**, as it corresponds to an ideal D_{4h} symmetry (d_x^2-$_y^2$ ground state). A calculated value of $2\alpha = 68°$ compares excellently with the crystallographic value of 70.7(1)°.

At this point, it is worth noting that the weak, broad signal on the spectrum that does not correspond to the rhombic tensor (ca. 10750 Gauss), but completely coincides with the $g_{\|}$ value deduced from g^{ex}. In other words, the spectrum seems to be the sum of two signals: those corresponding to the exchange and the molecular *g*-tensors. This unusual fact which has already been reported for two other

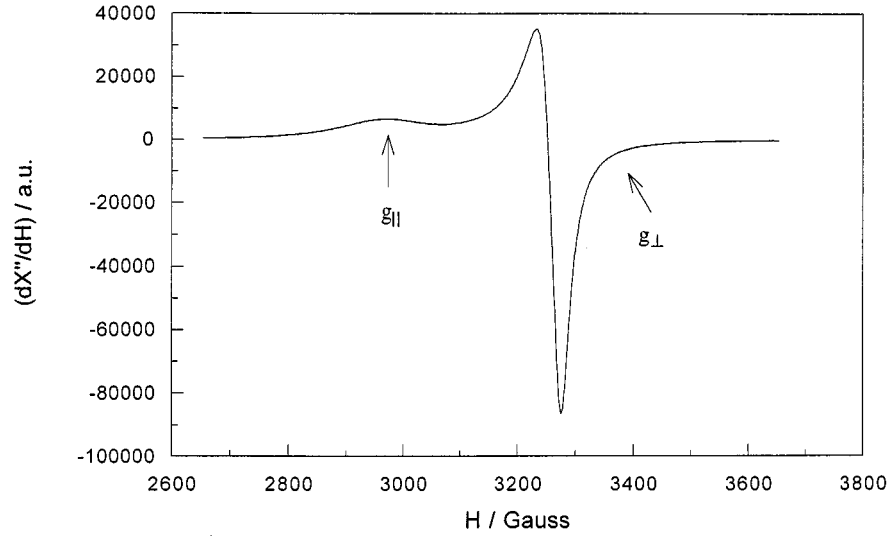

Figure 6. X-band EPR powder spectrum at room temp. for **2**

Cu^{II} compounds,[9] can only take place if the value of the exchange constant for the intermolecular coupling is similar to the Q-band energy-gap.

Figure 6 displays the X-band powdered EPR spectrum at room temp. for compound **2**. As observed, the signal is characteristic of an axial *g*-tensor with $g_{\|} = 2.258$ and $g_{\perp} = 2.052$. As for **1**, a slight narrowing of the linewidth is observed when the temperature is lowered from room temp. to 4.2 K. The *g* values account for a $d_{x^2-y^2}$ ground state, with an elongated octahedral copper(II) centre. They are in accordance with the $[CuN_4SO]$ chromophore corresponding to **2**.

Magnetic Properties

Compounds **1** and **2** were magnetically characterised through measurements of the thermal variation of the magnetic susceptibility, χ_m. Both polymorphous compounds exhibit similar magnetic behaviour. Thus, for both, χ_m continuously increases upon cooling (from 2.03×10^{-3} and 1.31×10^{-3} cm^3mol^{-1} at room temp. for **1** and **2**, respectively), the increase becoming exponential at temperatures tending to zero.

Figure 7 and 8 show the thermal variation of the $\chi_m T$ product and χ_m^{-1} for **1** and **2,** respectively. As can be seen, the $\chi_m T$ magnitude remains practically constant down to 25 K (**1**) and 50 K (**2**), temperatures below which the $\chi_m T$ values rapidly decrease towards zero. On the other hand, the Curie−Weiss law is followed over the whole measured temperature range in both cases. The calculated values of C_m and *g* (0.432 (**1**) and 0.429 (**2**) cm^3 K mol^{-1} and 2.146 (**1**) and 2.138 (**2**), respectively) are typical for an octahedrally-coordinated Cu^{II}.[10] The Weiss temperature, θ, has been observed to be −0.71 and −0.40 K, for **1** and **2**, respectively.

The above-mentioned aspects are indicative of the occurrence of antiferromagnetic exchange coupling which should take place through the thiocyanate intermetallic bridges. In order to evaluate the extension of these magnetic interactions, Equation (2) and (3) were used for **1** and **2**, respectively.

$$\chi_m = \frac{Ng^2\beta^2}{3kT}\frac{1}{1+\frac{exp(-2J/kT)}{3}} \quad (2)$$

$$\chi_m = \frac{Ng^2\beta^2}{kT}\frac{A+Bx+Cx^2}{1+Dx+Ex^2+Fx^3} \quad (3)$$

$A = 0.25,\quad B = 0.14995,\quad C = 0.30094,\quad D = 1.9862,\quad E = 0.68854,\quad F = 6.0626$

$x = J/kT$

where *N* and *k* are the Avogadro and Boltzmann constants, respectively, and β is the Bohr magneton.

The first of the expressions [Equation (2)][11] evaluates χ_m as a function of the exchange constant *J* for dimers with $S = 1/2$. The best fit parameters for **1** have been observed to be $J = -0.9$ cm^{-1} and $g = 2.145$. As observed in Figure 7, where the calculated $\chi_m T$ curve is displayed, there is an excellent agreement between both the theoretical and experimental data. On the other hand, the second expression [Equation (3)][12] accounts for the antiferromagnetic coupling for a Heisenberg chain with $S = 1/2$. Thus, the best fit parameters for **2** have been calculated to be $J = -0.3$ cm^{-1} and $g = 2.142$. As observed in Figure 8, the theoretical $\chi_m T$ curve reproduces the experimental data quite well.

Magnetic and Structural Correlations

Table 4 summarises the *J* values found in the literature for other (*N*,*S*)−NCS-bridged octahedral systems.[5,13] As observed, all but one exhibit low values for the magnetic

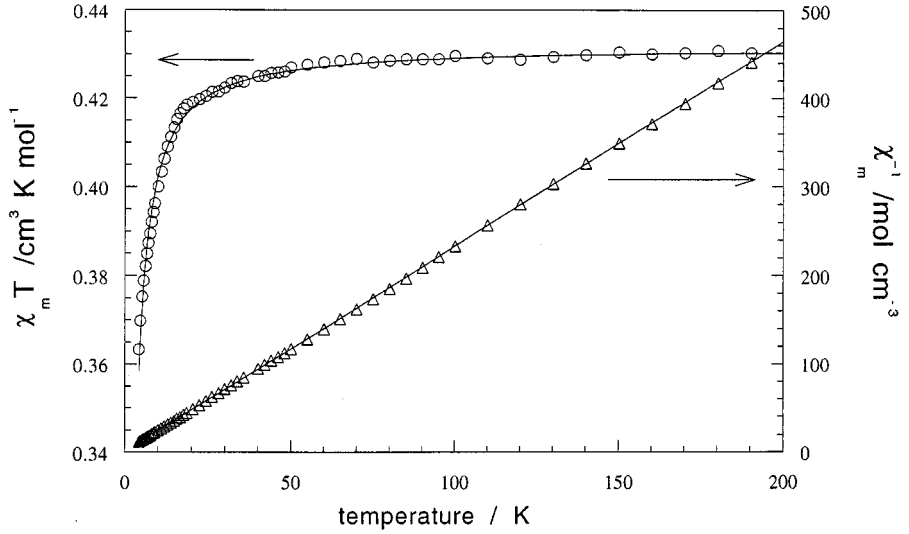

Figure 7. Thermal evolution of $\chi_m T$ and χ_m^{-1} for compound **1** and their corresponding theoretical curves

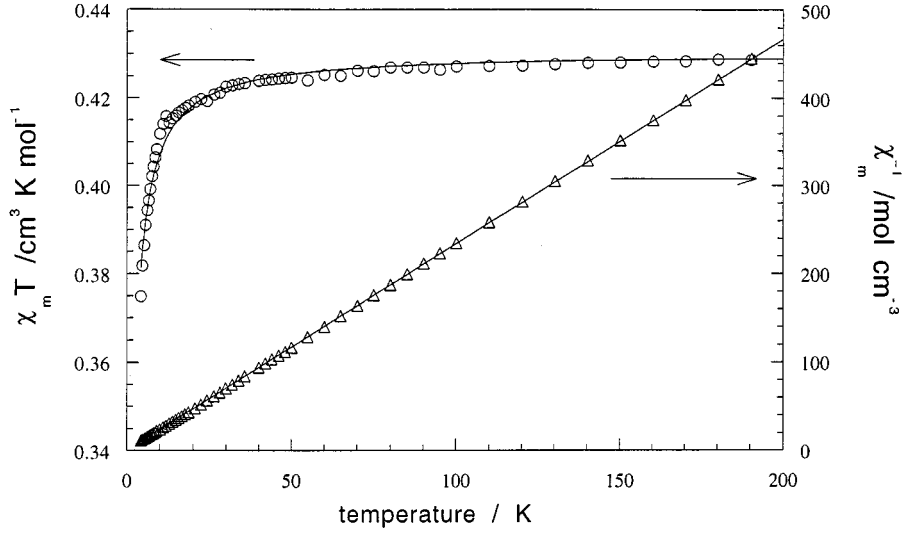

Figure 8. Thermal evolution of $\chi_m T$ and χ_m^{-1} for compound **2** and their corresponding theoretical curves

Table 4. Magnetic exchange constant J (cm^{-1}) for μ-(1,3)-NCS bridged Cu^{II} systems; N_e-S_a = N(equatorial)−S(axial) bridge; N_e-S_e = N(equatorial)−S(equatorial) bridge; Et_3dien = 1,4,7-triethyldiethylenetriamine; ept = *N*-(2-aminoethyl)-1,3-propanediamine; bheg = *N*,*N*-bis(2-hydroxyethyl)glycinato; bmp = 2,2′-bipyrimidine; Hmtpo = 4*H*,7*H*,5-methyl-7-oxo[1,2,4]triazolo[1,5-*a*]-pyrimidine; neg = negligible

Compound	Bridging mode	J	Reference
$[Cu(bpm)(NCS)_2]_n$	N_e-S_a	−0.6	[5a]
$[Cu(bheg)(NCS)]_n$	N_e-S_a	neg	[5b]
$[Cu_2(NCS)_2(Et_3dien)_2](ClO_4)_2$	N_e-S_a	+7.7	[5c]
$[Cu_2(NCS)_2(ept)_2](ClO_4)_2$	N_e-S_a	+1.3	[5c]
$[Cu(4\text{-bromopyridine})_2(NCS)_2]_n$	N_e-S_a	−	[5d]
1	N_e-S_a	−0.9	this work
2	N_e-S_a	−0.3	this work
$\{[Cu(NCS)_2(Hmtpo)\text{-}(H_2O)]_2\}_n$	N_e-S_a $+N_e-S_e$	−148	[13]

exchange constant. It is worth noting that the common feature for the majority is the $N_{eq}-S_{ax}$ disposition of the bridge, while for the strongly antiferromagnetic compound[13] the "rare" $N_{eq}-S_{eq}$ bridge-mode can also be found. As discussed below this is in total agreement with the theoretical predictions.

On theoretical bases,[14] the $N_{eq}-S_{ax}$ disposition leads to the accidental orthogonality of the MO arising from the e_g metallic orbitals, minimising the antiferromagnetic component of the global J constant (as experimentally confirmed for octahedral systems). Therefore, the fact that the strongly antiferromagnetic compound in Table 4 cannot be described by this disposition confirms this theoretical analysis (which is obviously valid for both single and double *end-to-end* thiocyanate bridges).

Conclusions

The use of the pseudohalide thiocyanate in combination with the blocking ligand dpk has led to the preparation of two polymorphous Cu^{II}-compounds: a 1D polymer and a

Table 5. Crystal data and structure refinements for **1** and **2**

Compound	**1**	**2**
Formula	$C_{14}H_{12}CuN_4O_2S_2$	$C_{14}H_{12}CuN_4O_2S_2$
M_w	395.95	395.95
Crystal system	Monoclinic	Monoclinic
Space group	$P2_1/c$	$P2_1/c$
a [Å]	11.673(2)	9.080(1)
b [Å]	17.215(3)	8.942(2)
c [Å]	8.295(2)	20.653(4)
β [°]	108.13(2)	103.54(2)
V [Å^3]	1584.1(5)	1630.3(5)
Z	4	4
$\rho_{cald.}$ [g.cm^{-3}]	1.660	1.613
μ (Mo-K_α) [cm^{-1}]	16.55	16.0
T [K]	20	20
λ (Mo-K_α) [Å]	0.71070	0.71070
Reflections collected	4878	5033
Unique data measured	4588	4746
Observed data with $I \geq 2.5\sigma(I)$	1771	3036
Number of parameters refined	211	211
R[a]	0.0627	0.0392
wR^2[b]	0.0954	0.1054

[a] $R(F_o) = (\Sigma||F_o| - |F_c||)/(\Sigma|F_o|)$. – [b] $wR(F_o^2) = \{\Sigma[w(F_o^2 - F_c^2)^2]/\Sigma[w(F_o^2)^2]\}^{1/2}$.

dimer. In both cases, the metallic cations are coordinated in a similar way to dpk·CH_3OH as well as to terminal and *end-to-end* thiocyanate groups. The dpk·CH_3OH is the result of the metal-promoted solvolysis of dpk in methanol. Both compounds are weakly antiferromagnetic as expected for the (N_{eq},S_{ax})-type intermetallic bridges.

Experimental Section

Synthesis

The synthesis of the title compounds was carried out by mixing an aqueous solution of $CuCl_2·2H_2O$ (0.5 mmol, 10 mL) with an aqueous solution of NaNCS (1 mmol, 10 mL). After stirring for one hour, a solution of dpk (15 mmol, 50 mL) in methanol was added. A green precipitate immediately appeared. Methanol was then added until this precipitate dissolved. The resulting solution was left to stand at room temperature. After several days, two types of green X-ray quality single crystals were obtained: (**1**) elongated prismatic crystals (yield 17%) and (**2**) regular prismatic crystals (yield 23%). Elemental analysis and ICP results were in good agreement with the $C_{14}H_{12}CuN_4O_2S_2$ stoichiometry for both compounds. – **1:** calcd. C 42.47, H 3.05, Cu 16.05, N 14.15, S 16.19; found C 42.5, H 3.1, Cu 15.9, N 14.2, S 16.1. – **2:** calcd. C 42.47, H 3.05, Cu 16.05, N 14.15, S 16.19; found C 42.4, H 3.0, Cu 16.0, N 14.1, S 16.1.

Physical Measurements

Microanalyses were performed with a LECO CHNS-932 analyser. Analytical measurements were carried out in an ARL 3410 + ICP with a Minitorch equipment. IR spectroscopy was performed on a Nicolet 520 FTIR spectrophotometer in the 400−4000 cm^{-1} region. EPR spectra were recorded on powdered samples at X- and Q-band frequencies, with a Bruker ESP300 spectrometer equipped with a standard OXFORD low-temperature device calibrated by the NMR probe for the magnetic field, the frequency measured by using a Hewlett−Packard 5352B microwave frequency computer. Magnetic susceptibilities of powdered samples were carried out in the temperature range 1.8−300 K (at a value of 1000 Gauss of the magnetic field) using a Quantum Design Squid MPM5−7 magnetometer, equipped with a helium continuous-flow cryostat. The experimental susceptibilities were corrected for the diamagnetism of the constituent atoms (Pascal tables).

Crystal Structure Determination

Single-crystal X-ray measurements for compounds **1** and **2** were carried out at room temperature on an Enraf−Nonius CAD-4 diffractometer with graphite-monochromated Mo-K_α radiation, operating in ω/2θ scanning mode using suitable crystals for data collection. Accurate lattice parameters were determined from least-squares refinement of 25 well-centred reflections. Intensity data were collected in the θ range 1−30°. During data collection, two standard reflections periodically observed showed no significant variation. Corrections for Lorentz and polarisation factors were applied to the intensity values.

The structures were solved by heavy-atom Patterson methods using the program SHELXS-97[15] and refined by a full-matrix least-squares procedure on F^2 using SHELXL-97.[16] Non-hydrogen atom scattering factors were taken from the International Tables of X-ray Crystallography.[17] In Table 5, crystallographic data and processing parameters for compounds **1** and **2** are shown.

Crystallographic data (excluding structure factors) for the structures reported in this paper have been deposited with the Cambridge Crystallographic Data Centre as supplementary publication nos. CCDC-143208 (**1**) and CCDC-143207 (**2**). Copies of the data can be obtained free of charge on application to The Director, CCDC, 12 Union Road, Cambridge CB2 1EZ UK [Fax: (internat.) +44-1223/336-033; E-mail: deposit@ccdc.cam.ac.uk].

Acknowledgments

This work has been carried out with the financial support of the Universidad del País Vasco/Euskal Herriko Unibertsitatea (Grant UPV 130310-EB201/1998), the Gobierno Vasco/Eusko Jaurlaritza (Project PI96/39) and the Ministerio de Educación y Cultura (Project PB97−0637). Z. E. S. also thanks the Ministerio de Educación y Ciencia for the grant AP96 20174323.

[1] [1a] G. R. Desiraju, in *Crystal Engineering: Design of Organic Solids*, Elsevier, Amsterdam, **1989**; *Angew. Chem. Int. Ed. Engl.* **1995**, *34*, 2311−2313. – [1b] R. Robin, B. F. Abrahams, R. R. Barten, R. W. Gable, B. F. Huskiness, J. Lieu, *Supramolecular Architecture*, ACS, Washington DC, **1992**, Ch. 19.M.

[2] M. Turnbull, T. Sugimoto, L. K. Thomson, *Molecule-Based Magnetic Materials*, American Chemical Society, Washington, DC, **1996**.

[3] [3a] V. Tangoulis, C. P. Raptopoulou, A. Terzis, S. Paschalidou, S. P. Perlepes, E. G. Bakalbassis, *Inorg. Chem.* **1997**, *36*, 3996−4006. − [3b] V. Tangoulis, C. P. Raptopoulou, S. Paschalidou, A. E. Tsohos, E. G. Bakalbassis, A. Terzis, S. P. Perlepes, *Inorg. Chem.* **1997**, *36*, 5270−5277. − [3c] V. Tangoulis, C. P. Raptopoulou, S. Paschalidou, E. G. Bakalbassis, S. P. Perlepes, A. Terzis, *Angew. Chem. Int. Ed. Engl.* **1997**, *36*, 1083−1085. − [3d] A. E. Tsohos, S. Dionyssopoulou, C. P. Raptopoulou, A. Terzis, E. G. Bakalbassis, S. P. Perlepes, *Angew. Chem. Int. Ed.* **1999**, *38*, 983−985.

[4] [4a] A. C. Deveson, S. L. Heath, C. J. Harding, A. K. Powell, *J. Chem. Soc., Dalton Trans.* **1996**, 3173−3178. − [4b] A. Basu, T. G. Kasar, N. Y. Sapre, *Inorg. Chem.* **1988**, *27*, 4539−4542. − [4c] A. N. Papadopoulos, V. Tangoulis, C. P. Raptopoulou, A. Terzis, D. P. Kessissoglou, *Inorg. Chem.* **1996**, *35*, 559−565. − [4d] M. L. Tong, H. K. Lee, S. L. Zheng, X. M. Chen, *Chem. Lett.* **1999**, 1087−1088. − [4e] O. S. Sommerer, W. P. Jensen, R. A. Jacobson, *Inorg. Chim. Acta* **1990**, *172*, 3−11. − [4f] G. Alonzo, N. Bertazzi, F. Maggio, F. Benetollo, G. Bombieri, *Polyhedron* **1996**, *15*, 4269−4273. − [4g] S. L. Wang, J. W. Richardson, S. J. Brigg, R. A. Jacobson, W. P. Jensen, *Inorg. Chim. Acta* **1986**, *111*, 67−72. − [4h] C. A. Kavounis, C. Tsiamis, C. J. Cardin, Y. Zubavichus, *Polyhedron* **1996**, *15*, 385−390. − [4i] Z. Serna, M. G. Barandika, R. Cortés, M. K. Urtiaga, M. I. Arriortua, *Polyhedron* **1998**, *18*, 249−255. − [4j] Z. E. Serna, M. G. Barandika, R. Cortés, M. K. Urtiaga, G. E. Barberis, T. Rojo, *J. Chem. Soc. Dalton Trans.* **2000**, 29−34. − [4k] Z. E. Serna, L. Lezama, , M. K. Urtiaga, M. I. Arriortua, M. G. Barandika, R. Cortés, T. Rojo, *Angew. Chem. Int. Ed.* **2000**, *39*, 344−347. − [4l] A. D. Q. Ferreira, A. Bino, D. Gibson, *Inorg. Chim. Acta* **1997**, *265*, 155−161. − [4m] S. O. Sommerer, B. L. Westcott, A. J. Jircitano, K. A. Abboud, *Acta Cryst.* **1996**, *C52*, 1426−1428. − [4n] S. R. Breeze, S. N. Wang, J. E. Greedan, N. P. Raju, *Inorg. Chem.* **1996**, *35*, 6944−6951. − [4o] M. A. S. Goher, F. A. Mautner, *Polyhedron* **2000**, *19*, 601−606.

[5] [5a] M. Julve, M. Verdaguer, G. DeMunno, J. A. Real, G. Bruno, *Inorg. Chem.* **1993**, *32*, 795−802. − [5b] H. Yamaguchi, Y. Inomata, T. Takeuchi, *Inorg. Chim. Acta* **1990**, *172*, 105−112. − [5c] R. Vicente, A. Escuer, E. Peñalba, X. Solans, M. Font-Bardía, *Inorg. Chim. Acta* **1997**, *255*, 7−12. − [5d] M. Kabesova, M. Dunaj-Jurco, J. Soldánová, *Inorg. Chim. Acta* **1987**, *130*, 105−111.

[6] K. Nakamoto, *Infrared Spectra of Inorganic and Coordination Compounds*, John Wiley & Sons: New York, **1997**.

[7] R. R. Osborne, W. R. Mc Whinnie, *J. Chem. Soc. A* **1967**, 2075−2096.

[8] B. Hathaway, D. E. Billing, *Coord. Chem. Rev.* **1970**, 143−163.

[9] [9a] W. Henke, S. Kremer, D. Reinen, *Inorg. Chem.* **1983**, *22*, 2858−2863. − [9b] T. Rojo, M. Insausti, L. Lezama, J. L. Pizarro, M. I. Arriortua, R. Calvo, *J. Chem. Soc., Faraday Trans.* **1995**, *91*, 423−429.

[10] F. E. Mabbs, D.J. Machin, *Magnetism and Transition Metal Complexes*, Chapman and Hall: London, **1973**.

[11] B. Bleany, K. D. Bowers, *Proc. R. Soc. London Ser. A* **1952**, *214*, 451−463.

[12] [12a] J. W. Hall, Ph. D. Université de Caroline Nord, (USA), **1977**. − [12b] W. E. Hatfield, *J. Appl. Phys.* **1981**, *52*, 1985−1992.

[13] J. A. R. Navarro, M. A. Romero, J. M. Salas, M. Quirós, E. R. T. Tiekink, *Inorg. Chem.* **1997**, *36*, 4988−4991.

[14] [14a] M. Kabesova, R. Boca, M. Melnik, D. Valigura, M. Dunaj-Jurco, *Coord. Chem. Rev.* **1995**, *140*, 112−118. − [14b] A. P. Ginsberg, R. L. Martin, R. W. Brookes, R. C. Sherwood, *Inorg. Chem.* **1972**, *11*, 2884−2889.

[15] G. M. Sheldrick, *SHELXS-97. Program for the Solution of Crystal Structures*, University of Göttingen, Germany, **1997**a.

[16] G. M. Sheldrick, *SHELXL-97. Program for the Refinement of Crystal Structures*, University of Göttingen, Germany, **1997**b.

[17] *International Tables for X-ray Crystallography, Vol. IV*, Kynoch Press, Birmingham, **1974**.

Received July 17, 2000
[I00277]

Importance of the Presence of Chloride Ions in the First Steps of Palladium-Catalyzed Nucleophilic Allylic Substitutions

Christian Amatore,*[a] Anny Jutand,*[a] Mohamed A. M'Barki,[a] Gilbert Meyer,[a] and Loïc Mottier[a]

Keywords: Palladium / Halides / Allyl complexes / NMR spectroscopy / Cyclic voltammetry

$[Pd(\eta^3\text{-}C_3H_5)(\mu\text{-}Cl)]_2 + 4PPh_3$ and $[(\eta^3\text{-}C_3H_5)PdCl(PPh_3)] + 1PPh_3$ do not produce the cationic (π-allyl)palladium(II) complex $[(\eta^3\text{-}C_3H_5)Pd(PPh_3)_2]^+Cl^-$ but a neutral (σ-allyl)palladium(II) chloride complex $[(\eta^1\text{-}CH_2{=}CH{-}CH_2)PdCl(PPh_3)_2]$ in DMF and THF. This latter complex is also formed when one equivalent of chloride ion is added to $[(\eta^3\text{-}C_3H_5)Pd(PPh_3)_2]^+(BF_4)^-$, leading to the conclusion that $[Pd(\eta^3\text{-}C_3H_5)(\mu\text{-}Cl)]_2 + 4PPh_3$ and $[(\eta^3\text{-}C_3H_5)Pd(PPh_3)_2]^+(BF_4)^-$ are not equivalent precursors for the palladium-catalyzed allylic substitutions when they are performed in the absence of added chloride ions. The (σ-allyl)palladium(II) chloride complex $[(\eta^1\text{-}CH_2{=}CH{-}CH_2)PdCl(PPh_3)_2]$ is also formed instead of $[(\eta^3\text{-}C_3H_5)Pd(PPh_3)_2]^+(AcO)^-$ when the oxidative addition of allylic acetate to palladium(0) complexes, such as $[Pd^0(dba)_2] + 2PPh_3$, is performed in the presence of chloride anions. A cationic (π-allyl)palladium(II) complex is thus not formed in the presence of chloride ions, which are either delivered by the catalytic precursor or deliberately added.

Introduction

Palladium(0) complexes catalyze nucleophilic substitutions of allylic acetates (Tsuji−Trost reaction, Equation (1)).[1]

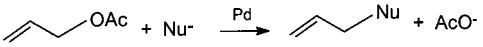

(1)

The main precursors of the palladium(0) catalyst are: **A**: $[Pd^0L_4]$; **B**: $[Pd^0(dba)_2]$ (or $[Pd^0_2(dba)_3] + nL$); **C**: $[(\eta^3\text{-}C_3H_5)PdL_2]^+(BF_4)^-$, a cationic (π-allyl)palladium(II) complex which provides a palladium(0) complex in situ after reaction with the nucleophile; or **D**: $[Pd(\eta^3\text{-}C_3H_5)(\mu\text{-}Cl)]_2 + 4$ L, a dimeric (π-allyl)palladium(II) chloride whose reaction with phosphane ligands is supposed to afford $[(\eta^3\text{-}C_3H_5)PdL_2]^+Cl^-$ and eventually a palladium(0) complex after reaction with the nucleophile.[1] These four different catalytic precursors are often considered to be equivalent, leading to the same active $[Pd^0L_2]$ catalyst and to the same cationic (π-allyl)palladium(II) complex $[(\eta^3\text{-}C_3H_5)PdL_2]^+(AcO)^-$ formed through oxidative addition of $[Pd^0L_2]$ to the allylic acetate. However, recent papers point out that Pd-catalyzed nucleophilic allylic substitutions strongly depend on the precursor of the palladium(0) catalyst in terms of reactivity, regioselectivity and enantioselectivity.[2]

We have already established that $[Pd^0L_4]$ or $[Pd^0(dba)_2]$ associated with phosphane ligands effectively provide the same species $[Pd^0L_2]$, which is active in oxidative additions but is present in low and nonidentical concentrations relative to the precursor concentration because of its endergonic equilibrium with the nonreactive $[Pd^0L_3]$ or $[Pd^0(dba)L_2]$ complexes, respectively.[3] Consequently, $[Pd^0(PPh_3)_4]$ was found to be more efficient than $\{[Pd^0(dba)_2] + 2PPh_3\}$ in allylic nucleophilic substitutions.[4] Conversely, the nucleophilic attack on precursor **C**, the cationic (π-allyl)palladium(II) complex $[(\eta^3\text{-}C_3H_5)PdL_2]^+(BF_4)^-$ is expected to provide $[Pd^0L_2]$ in stoichiometric amounts relative to the precursor. Therefore, the three precursors **A**, **B** and **C** should behave differently in terms of the kinetics of their oxidative addition to an allylic acetate, but should give the same cationic complex $[(\eta^3\text{-}C_3H_5)PdL_2]^+(AcO)^-$, the key intermediate prone to react with the nucleophile.

When considering precursor **D**, i.e., $\{[Pd(\eta^3\text{-}C_3H_5)(\mu\text{-}Cl)]_2 + 4L\}$, one equivalent of chloride ion is now present although its role is very often neglected. However, this chloride ion may introduce a change in the mechanism. Indeed, we have already established the influence of anions, chloride or acetate, delivered by the precursors of the Pd^0 catalyst on the mechanism of palladium-catalyzed cross-coupling[5a−5c] and Heck reactions.[5b−5d] In this context, it has been observed that deliberately added chloride ions induce stereocontrol in palladium-catalyzed substitutions of cyclic allylic acetates.[6] Recent papers report the beneficial effect of added halides on the regioselectivity of the allylic nucleophilic substitution,[7] as well as on its enantioselectivity.[7b,8] In other cases, a negative effect of added chloride ions on the enantioselectivity has been reported and interpreted as a partial destruction of the memory effect due to the formation of asymmetric ion-pairs between the cationic (π-allyl)palladium(II) complex and acetate anion.[2]

We report here an investigation on the effect of chloride ions on the first steps in the mechanism of palladium-catalyzed allylic substitution, leading to the conclusion that pre-

[a] Ecole Normale Supérieure, Département de Chimie, UMR CNRS 8640,
24, Rue Lhomond, 75231 Paris, Cedex 5, France
Fax: (internat.) + 33-1/4432-3325
E-mail: Anny.Jutand@ens.fr
E-mail: amatore@ens.fr

 © WILEY-VCH Verlag GmbH, 69451 Weinheim, 2001 1434−1948/01/0303−0873 $ 17.50+.50/0

cursor **D** behaves quite differently from precursors **A**, **B**, and **C**. Cationic (π-allyl)palladium intermediates are not formed from **D** or when chloride anions are voluntary added to any catalytic system **A**, **B** or **C**.

Results and Discussion

Reaction of $[Pd(\eta^3\text{-}C_3H_5)(\mu\text{-}Cl)]_2$ (1) with $4PPh_3$ in DMF

When four equivalents of PPh_3 (2 equiv. of L per Pd) were added to a solution of the dimeric (π-allyl)palladium(II) chloride **1** in $CDCl_3$, the three ^1H NMR signals observed for the free complex **1** (Table 1) totally disappeared.

Neither the five signals of $[(\eta^3\text{-}C_3H_5)PdCl(PPh_3)]$ **(7)** (Table 1) nor the three signals of a cationic (π-allyl)palladium(II) $[(\eta^3\text{-}C_3H_5)Pd(PPh_3)_2]^+Cl^-$ (Table 1) were detected. Instead, a main set of two signals was observed: a quintet (1 H, J = 10 Hz) and a broad doublet (4 H, J = 10 Hz). They are characteristic of the (σ-allyl)palladium chloride complex $[(\eta^1\text{-}CH_2{=}CH{-}CH_2)PdCl(PPh_3)_2]$ **(2)** (Table 1, Scheme 1, route a) as already observed by Shaw et al.[9] Such an NMR pattern is characteristic of a fast equilibrium between two σ forms of **2** [Equation (2)] responsible for the magnetic equivalence of the four CH_2 protons.[9,10]

$$CH_2{=}CH\text{-}C^*H_2\text{-}Pd\text{-}Cl(PPh_3)_2 \rightleftharpoons C^*H_2{=}CH\text{-}CH_2\text{-}Pd\text{-}Cl(PPh_3)_2 \quad (2)$$

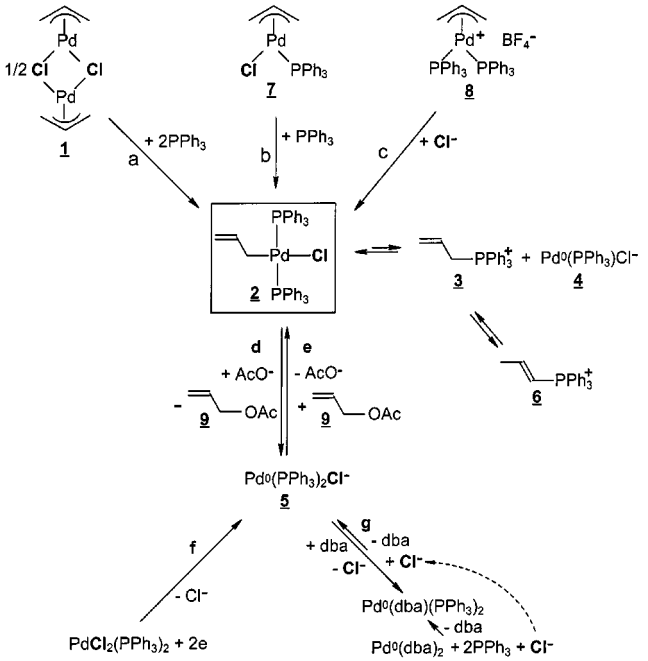

Scheme 1. Formation of a (σ-allyl)palladium chloride complex

The ^{31}P NMR spectrum exhibits a single, broad major signal at δ = 20.75 ($\Delta\nu_{1/2}$ = 50 Hz) in DMF and δ = 19.85 ($\Delta\nu_{1/2}$ = 67 Hz) in $CDCl_3$, which is characteristic of the (σ-allyl)palladium chloride complex **2**.

Extra ^1H NMR signals were also observed and assigned to the allytriphenylphosphonium cation **3** (Table 1, Scheme 1) by comparison with an authentic sample of the

Table 1. Characterization of $C_3H_5{-}Pd^{II}$ complexes and $C_3H_5{-}PPh_3^+$ cations (Scheme 1)

	^1H NMR (ppm)[a]	^{31}P NMR (ppm)[b] DMF	THF	E^p_{Red} (volts)[c] DMF
1[d]	3.04 (d, J = 12 Hz, 2 H) 4.12 (d, J = 6.7 Hz, 2 H) 5.46 (t of t, J = 12 and 6.7 Hz, 1 H)	-	-	n.o.
2[e][f][g]	3.72 (br.d, J = 10 Hz, 4 H) 5.62 (quintet, J = 10 Hz, 1 H)	20.75 (br. s)[e] 20.50 (br. s)[f] 20.24 (br. s)[g]		−2.03[g] −2.04[h]
2[e][i]	3.61 (d, J = 10 Hz, 4 H) 5.73 (quintet, J = 10 Hz, 1 H)		11.85 (br. s)[e]	
3[e,f,g]	4.92 (dd, J = 15 and 7 Hz, 2 H) 5.38 (dd, J = 9.5 and 4.5, 1 H) 5.56 (dd, J = 17 and 4.5, 1 H)	22.00 (s)[e] 21.72 (s)[f] 21.74 (s)[g]		−1.54[g] −1.53[h]
6[e,f,g]	2.37 (ddd, J = 6.5, 1.9 and 1.9 Hz, 3 H) 6.60 (ddq J = 22, 16 and 6.5 Hz, 1H) 8.02 (ddq J = 24, 16 and 1.9 Hz, 1H)	19.35 (s)[e] 19.10 (s)[f] 19.12 (s)[g]		
7[d]	2.83 (d, J = 14 Hz, 1 H) 3.11 (d, J = 7 Hz, 1 H) 3.77 (dd, J = 14 and 10 Hz, 1 H) 4.76 (ddd, J = 7, 7 and 1 Hz, 1 H) 5.61 (ddt, J = 14, 14 and 7 Hz, 1 H)	22.77 (s)	22.43 (s)	−1.88
8[d]	3.58 (m, 2 H) 3.97 (bd, J = 6.7 Hz, 2 H) 5.97 (tt, J = 13.5 and 6.7 Hz, 1 H)	23.99 (s)	24.53 (s)	−1.25

[a] 250 MHz; shifts are referred to TMS. Solvent: $CDCl_3$ except [i]. For simplification, aromatic protons are voluntarily omitted. − [b] 163 MHz; shifts are referred to H_3PO_4. The solvent contains 10% [D_6]acetone. − [c] Peak potentials at a gold disk electrode are relative to SCE. Scan rate: 0.2 Vs^{-1} at 20 °C. − [d] Authentic sample. − [e] Formed in reaction of **1** with 4 equiv. PPh_3. − [f] Formed in reaction of **7** with 1 equiv. PPh_3. − [g] Formed in reaction of **8** with 1 equiv. nBu_4NCl. − [h] Formed in the oxidative addition of the electrogenerated $Pd^0(PPh_3)_2Cl^-$ to the allylic acetate **9**. − [i] Solvent: [D_8]THF.

chloride salt **3**·Cl.[12] However, a slight shift of the CH_2-P^+ signal to higher field suggested that chloride was not the counter anion of **3**.[13] Considering that the phosphonium cation **3** was generated from the (σ-allyl)palladium complex **2** by a kind of reductive elimination [Equation (3)], this implies that a palladium(0) complex **4** is also formed concomitantly.

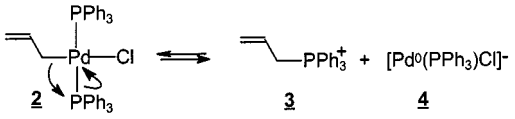

(3)

This interpretation is confirmed by voltammetric data. Indeed, performing cyclic voltammetry in DMF on a solution of **1** (2 mM) and 4 equivalents of PPh_3, revealed the presence of an oxidation peak at −0.03 V which characterizes a palladium(0) complex: it disappeared in the presence of PhI. Moreover, Equation (3) has to be an equilibrium since the ratio **2:3**, (initially equal to 3, as determined from the ^1H NMR spectroscopic data) decreases in the presence of increasing amounts of PPh_3 or dba. The effect of extra PPh_3 or dba is to stabilize the low ligated palladium(0) complex formed in Equation (3) as a more stable complex $[Pd^0(PPh_3)_nCl]^-$ (n = 2, 3)[14] or $[Pd(dba)(PPh_3)_2]$[3] inducing then a shift of the equilibrium in Equation (3) towards its right-hand side.

The conductivity of a solution of **1** (2 mM) and 4 equivalents of PPh_3 was measured in DMF at 20 °C and found to be 78 μS. This shows the formation of ionic species in DMF in agreement with the formulation in Equation (3). The conductivity increases upon successive additions of PPh_3 because of the shift of the equilibrium towards its right hand-side by stabilization of the palladium(0) complex **4** (vide supra). A conductivity of only 2 μS was measured for the same solution in $CDCl_3$, indicating that **4** and **3** (whose ^1H NMR signals are detected in $CDCl_3$) are ion-paired in this less polar solvent.

After two hours, a set of three ^1H NMR signals appeared and were assigned to the 3-propenyltriphenylphosphonium cation **6** by comparison with an authentic sample of **6**·Cl[12] (Table 1, Scheme 1). This cation was formed by the slow isomerization of **3**. The ^{31}P NMR signals of **6** and **3** were also detected in DMF (Table 1) and $CDCl_3$. The stability of **2** strongly depends on the phosphane ligand. The thermodynamic ability of **2** to form phosphonium salts is higher when the phosphane is more basic, consequently the stability of **2** follows the order:

$(p\text{-}CF_3C_6H_4)_3P > (p\text{-}ClC_6H_4)_3P > (p\text{-}HC_6H_4)_3P > (p\text{-}CH_3C_6H_4)_3P$

This set of experiments establishes that addition of four equivalents of PPh_3 per mol of **1** (precursor **D**) does not lead to the expected cationic π-allylpalladium complex $[(\eta^3\text{-}C_3H_5)PdL_2]^+Cl^-$ but to the σ-allylpalladium complex $[(\eta^1\text{-}CH_2{=}CH{-}CH_2)PdCl(PPh_3)_2]$ **(2)** (Scheme 1, route a). This main complex is involved in an equilibrium with a palladium(0) complex, an allylphosphonium salt and a 3-propenylphosphonium salt at longer times (1 h).

The mechanism of the formation of the (σ-allyl)palladium complex $[(\eta^1\text{-}CH_2{=}CH{-}CH_2)PdCl(PPh_3)_2]$ **(2)** cannot be established since no intermediate was observed as its formation from **1** and $4PPh_3$ is too fast. It is known, however, that when only two equivalents of PPh_3 are added to **1**, a neutral (π-allyl)palladium chloride complex $[(\eta^3\text{-}C_3H_5)PdCl(PPh_3)]$ **(7)** is formed.[9] Compound **7** is thus a possible intermediate in the formation of **2**. We have therefore investigated the reaction of **7** with one equivalent of added PPh_3.

Reaction of $[(\eta^3\text{-}C_3H_5)PdCl(PPh_3)]$ (7) with PPh_3 in DMF

Analysis of a solution of **7** containing one equivalent of PPh_3 in $CDCl_3$ or DMF by ^1H and ^{31}P NMR spectroscopy and conductivity measurements showed the same chemical behavior as for the mixture {**1** + $4PPh_3$} (Table 1), i.e., no formation of the cationic (π-allyl)palladium complex $[(\eta^3\text{-}C_3H_5)PdL_2]^+Cl^-$ but formation of the (σ-allyl)palladium chloride complex $[(\eta^1\text{-}CH_2{=}CH{-}CH_2)PdCl(PPh_3)_2]$ **(2)** involved in the equilibrium in Equation (3) (Scheme 1, route b).

Since the cationic (π-allyl)palladium complex $[(\eta^3\text{-}C_3H_5)PdL_2]^+Cl^-$ was not generated, it was of interest to test the reactivity of chloride ions with the cationic (π-allyl)palladium complex $[(\eta^3\text{-}C_3H_5)PdL_2]^+(BF_4)^-$ **(8)**.

Reaction of $[(\eta^3\text{-}C_3H_5)Pd(PPh_3)_2]^+(BF_4)^-$ 8 with Chloride Ions in DMF

Addition of one equivalent of nBu$_4$NCl to a solution of the cationic (π-allyl)palladium complex $[(\eta^3\text{-}C_3H_5)PdL_2]^+(BF_4)^-$ **(8)** in $CDCl_3$ or DMF induced the complete disappearance of **8** with formation of the (σ-allyl)palladium chloride complex $[(\eta^1\text{-}CH_2{=}CH{-}CH_2)PdCl(PPh_3)_2]$ **(2)** by attack of the chloride ion at the cationic Pd^{II} center (Scheme 1, route c; Table 1). In agreement with the above results, the allyltriphenylphosphonium cation **3** was also formed in this process [Equation (3)].

When less than one equivalent of chloride ion (0.2 equiv.) was added to **8**, the three signals of **8** became broad and overlapped the two signals of **2**. This suggests that the reaction c in Scheme 1 is a dynamic equilibrium lying towards **2** so that it is totally shifted towards the (σ-allyl)palladium chloride **2** as soon as one equivalent of chloride ions are added to **8**.

Reaction of $[(\eta^1\text{-}CH_2{=}CH{-}CH_2)PdCl(PPh_3)_2]$ (2) with Acetate Ions in DMF

Acetate anions are continuously released in a palladium-catalyzed substitution at allylic acetates [Equation (1)]. These released acetate ions may conceivably compete with chloride ions for the stabilization of Pd^{II} complexes. We have thus investigated the reaction of acetate ions with the σ-allylpalladium chloride, $[(\eta^1\text{-}CH_2{=}CH{-}CH_2)PdCl(PPh_3)_2]$ **(2)**. When one equivalent of nBu$_4$NOAc was added to **2** (preliminarily formed by reaction of **8** with one equiva-

lent of nBu$_4$NCl), the allylic acetate **9** (19%) was observed on the ^{1}H NMR spectrum performed in $CDCl_3$. It was checked independently that nBu$_4$NOAc did not react with commercial **3**·Cl to produce the allylic acetate by a direct nucleophilic substitution. Note, however, that AcO^- catalyzes the isomerization of **3**·Cl to **6**·Cl, but without formation of **9**. This shows that the (σ-allyl)palladium chloride complex **2** is attacked by the acetate ion to produce allylic acetate (Scheme 1, route d), probably by reaction of the acetate anion at the allyl ligand by an S_N2' reaction [Equation (4)].

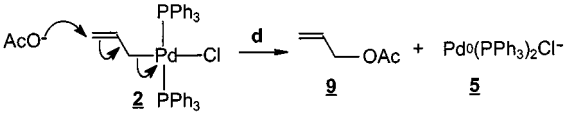

(4)

This reaction affords an anionic species $[Pd^0(PPh_3)_2Cl]^-$ **(5)**.[14] Such an anionic Pd^0 complex can be generated by reduction of $[PdCl_2(PPh_3)_2]$ (Scheme 1, route f).[14] It was thus of interest to investigate the oxidative addition of **5** to allylic acetate **9**, which is the backward reaction of Equation (4).

Oxidative Addition of $[Pd^0(PPh_3)_2Cl]^-$ to Allylic Acetate in DMF

The electrochemical bielectronic reduction of $[PdCl_2(PPh_3)_2]$ (2 mM in DMF) at −0.88 V produced $[Pd^0(PPh_3)_2Cl]^-$ **(5)** characterized by its oxidation peak at +0.10 V. In the presence of the allylic acetate **9** (4 mM) the oxidation peak current of the electrogenerated palladium(0) decreased, showing a partial reaction of **5** with **9**. This also released AcO^- in solution as characterized by the observation of its oxidation peak at +0.68 V. If the cationic $[(\eta^3\text{-}C_3H_5)Pd(PPh_3)_2]^+(AcO)^-$ **(10)** complex were formed in the oxidative addition, its reduction should be observed at around −1.25 V, which is the reduction potential of an authentic sample of $[(\eta^3\text{-}C_3H_5)Pd(PPh_3)_2]^+(BF_4)^-$ **(8)**. Such a reduction peak was not observed, but instead, two reduction peaks were present at more negative potentials, −1.53 V and −2.04 V, showing that the formation of **10** was bypassed. The same couple of reduction peaks was also observed when two equivalents of chloride ions were added to $[(\eta^3\text{-}C_3H_5)Pd(PPh_3)_2]^+(BF_4)^-$ **(8)**, a reaction which affords the (σ-allyl)palladium chloride **2** and the phosphonium cation **3** with $Pd^0(PPh_3)Cl^-$ as the counter-anion [Equation (3]. The reduction peak at −1.53 V was then assigned to the reduction of **3** by comparison with an authentic sample of **3**·Cl, whereas the reduction peak at −2.02 V was assigned to the reduction peak of the (σ-allyl)palladium chloride complex **2**.

This establishes that the oxidative addition of $[Pd^0(PPh_3)_2Cl]^-$ to allylic acetate takes place (backward reaction of Equation (4), route e in Scheme 1) and does not afford the cationic (π-allyl)palladium complex $[(\eta^3\text{-}C_3H_5)Pd(PPh_3)_2]^+(AcO)^-$ **(10)** but the (σ-allyl)palladium chloride $[(\eta^1\text{-}CH_2{=}CH{-}CH_2)PdCl(PPh_3)_2]$ **(2)** by the reversible overall reaction shown in Equation (5) (Scheme 1, route f,e,d).[15]

$$Pd^0(PPh_3)_2Cl^- + CH_2{=}CH\text{-}CH_2\text{-}OAc \rightleftharpoons (\eta^1\text{-}C_3H_5)PdCl(PPh_3)_2 + AcO^- \quad (5)$$

However, $[PdCl_2(PPh_3)_2]$ is not often used as a precursor of Pd^0 in allylic substitutions because most nucleophiles active in the allylic substitutions are not able to reduce the Pd^{II} precursor to Pd^0. We have thus investigated the effect of chloride ions on the oxidative addition to allylic acetate starting from another catalytic system: $\{[Pd^0(dba)_2] + 2PPh_3\}$ often used as a precursor of Pd^0 catalysts.[1,16]

Oxidative Addition of $\{[Pd^0(dba)_2] + 2PPh_3\}$ to Allylic Acetate in the Presence of Chloride Ions in DMF

We have established that the oxidative addition of $[Pd^0(dba)_2] + 2PPh_3$ to the allylic acetate **9** is reversible and provides a cationic (π-allyl)palladium complex $[(\eta^3\text{-}C_3H_5)PdL_2]^+(AcO)^-$ **(10)** in DMF (free ions) and in THF (ion pairs) (Equations 6−8).[17] This gives rise to the overall equilibrium in Equation (9) which may be monitored by UV spectroscopy.[17]

$$Pd^0(dba)_2 + 2\,PPh_3 \longrightarrow Pd^0(dba)(PPh_3)_2 + dba \quad (6)$$

$$Pd^0(dba)(PPh_3)_2 \rightleftharpoons Pd^0(PPh_3)_2 + dba \quad (7)$$

$$Pd^0(PPh_3)_2 + CH_2{=}CH\text{-}CH_2\text{-}OAc \rightleftharpoons (\eta^3\text{-}C_3H_5)Pd(PPh_3)_2^+ + AcO^- \quad (8)$$

$$Pd^0(dba)(PPh_3)_2 + CH_2{=}CH\text{-}CH_2\text{-}OAc \rightleftharpoons (\eta^3\text{-}C_3H_5)Pd(PPh_3)_2^+ + AcO^- + dba \quad (9)$$

When nBu$_4$NCl (750 equiv.) was added to a solution of $[Pd^0(dba)_2]$ (1 mM) and $2PPh_3$ in DMF, the absorbance of $[Pd^0(dba)(PPh_3)_2]$ at 396 nm decreased and reached a limiting value (70% of the initial absorbance) establishing the interference of chloride ions in the equilibrium in Equation (7), which is in agreement with the known stability of the anionic complex $Pd^0(PPh_3)_2Cl^-$ [14] [Equation (10)]. It is worthwhile to note that a large amount of nBu$_4$NCl is required to observe a significant decrease of the $[Pd^0(dba)(PPh_3)_2]$ concentration. This indicates that dba is a better ligand for $[Pd^0(PPh_3)_2]$ than Cl^-, and that at low chloride concentration, $[Pd^0(PPh_3)_2Cl]^-$ is only present at trace levels.

$$Pd^0(dba)(PPh_3)_2 + Cl^- \rightleftharpoons Pd^0(PPh_3)_2Cl^- + dba \quad (10)$$

When 60 equivalents of $CH_2{=}CH{-}CH_2{-}OAc$ were added to a solution of $[Pd^0(dba)_2] + 2PPh_3$ in DMF, the absorbance of $[Pd^0(dba)(PPh_3)_2]$ at 396 nm decreased and reached a limiting value corresponding to the thermodynamic

concentration of $[Pd^0(dba)(PPh_3)_2]$ imposed by the equilibrium in Equation (9) (Figure 1a, $t < 70$ s).

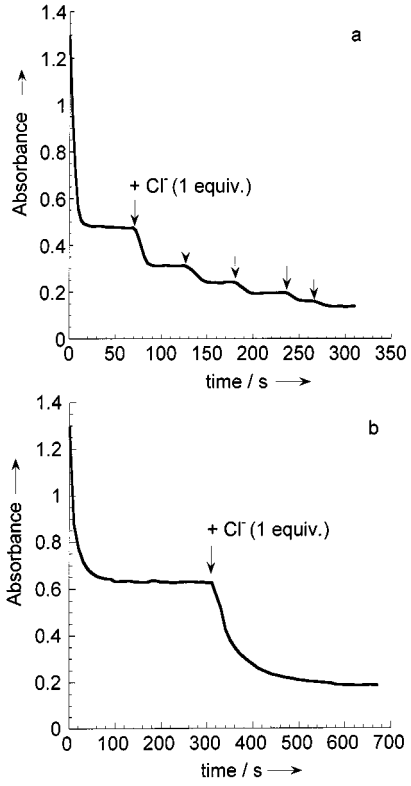

Figure 1. a) Variation of the absorbance ($\lambda = 396$ nm) of the UV spectrum performed in DMF at 20 °C in a 1 mm path cell of a solution of $[Pd^0(dba)_2]$ (1 mmol dm^{-3}) and PPh_3 (2 mmol dm^{-3}) after addition of 60 equivalents of $CH_2{=}CH{-}CH_2{-}OAc$ ($t < 70$ s), followed by successive additions of nBu$_4$NCl (one equivalent at each addition as indicated by the arrows; b) same experiment performed in THF ($\lambda = 394$ nm) after addition of 72 equivalents of $CH_2{=}CH{-}CH_2{-}OAc$ ($t < 300$ s), followed by addition of one equivalent of nBu$_4$NCl as indicated by the arrow

When one equivalent of nBu$_4$NCl was added, the limiting absorbance decreased to a lower value; it again decreased by successive additions of one equivalent of nBu$_4$NCl (Figure 1a). This shows that the chloride anion reacts with $[(\eta^3\text{-}C_3H_5)PdL_2]^+(AcO)^-$ **(10)** formed in the oxidative addition [Equation (9)], shifting this equilibrium to give the total disappearance of $[Pd^0(dba)(PPh_3)_2]$. This reaction gave the (σ-allyl)palladium complex $[(\eta^1\text{-}CH_2{=}CH{-}CH_2)PdCl(PPh_3)_2]$ **(2)** [Equation (11)], which was characterized by performing ^{1}H NMR spectroscopy on a solution of $[Pd^0(dba)_2] + 2PPh_3$ in $CDCl_3$ after addition of **9** (3 equiv.) followed by nBu$_4$NCl (3 equiv.).

$$[(\eta^3\text{-}C_3H_5)Pd(PPh_3)_2]^+(AcO)^- + Cl^- \longrightarrow (\eta^1\text{-}C_3H_5)PdCl(PPh_3)_2 + AcO^- \quad (11)$$

However, AcO^- anions are released in reaction (11), so that a reaction similar to route d of Scheme 1 should operate, giving rise to the formation of $[Pd^0(dba)(PPh_3)_2]$ as the main Pd^0 complex [Equation (12)] instead of $[Pd^0(PPh_3)_2Cl]^-$.

$$(\eta^1\text{-}C_3H_5)PdCl(PPh_3)_2 + AcO^- + dba \longrightarrow Pd^0(dba)(PPh_3)_2 + CH_2{=}CH\text{-}CH_2\text{-}OAc + Cl^- \quad (12)$$

This has been checked independently by addition of nBu$_4$NOAc (1 equiv.) and dba (2 equiv.) to complex **2** (preliminary formed by reaction of **8** and one equivalent of nBu$_4$NCl). The formation of 19% of allylic acetate was then observed in the ^{1}H NMR spectrum performed in $CDCl_3$, together with $[Pd^0(dba)(PPh_3)_2]$, characterized by its two ^{31}P NMR signals in $CDCl_3$ and DMF[18] [Equation (12)].

Therefore, the oxidative addition of allylic acetate to the palladium(0) generated from $[Pd(dba)_2] + 2PPh_3$ and performed in the presence of chloride ions in DMF is a reversible reaction which affords a (σ-allyl)palladium chloride complex [Equation (13)] and not a cationic (π-allyl)palladium(II) complex $[(\eta^3\text{-}C_3H_5)PdL_2]^+X^-$ (X = Cl or AcO).[19]

$$Pd^0(dba)(PPh_3)_2 + CH_2{=}CH\text{-}CH_2\text{-}OAc + Cl^- \rightleftharpoons (\eta^1\text{-}C_3H_5)PdCl(PPh_3)_2 + AcO^- + dba \quad (13)$$

Formation of $[(\eta^1\text{-}CH_2{=}CH{-}CH_2)PdCl(PPh_3)_2]$ in THF

The reaction of the dimeric (π-allyl)palladium(II) chloride **1** with four equivalents of PPh_3 in [D$_8$]THF afforded the (σ-allyl)palladium chloride complex $[(\eta^1\text{-}CH_2{=}CH{-}CH_2)PdCl(PPh_3)_2]$ **(2)** (Table 1, Scheme 1, route a) characterized by its two signals, a quintet (1 H, $J = 10$ Hz) and a doublet (4 H, $J = 10$ Hz) (Table 1) as observed in DMF (vide supra). The ^{31}P NMR spectrum performed in THF exhibited a single, broad major signal ($\Delta\nu = 135$ Hz, Table 1) whose shift strongly depended on the solvent. Indeed, when DMF was added (THF:DMF = 1:1), the ^{31}P NMR signal shifted from $\delta = 11.85$ to 15.35. The phosphonium cation **3** was not observed in pure THF, even at longer times (over 1 h). It is only after addition of two equivalents of dba that the phosphonium cations **3** and **6** could be detected on the ^{31}P NMR spectrum, together with $[Pd^0(dba)(PPh_3)_2]$ ($\delta = 27.34$ and 25.57). This shows that the equilibrium shown in Equation (3) is still operating in THF but is considerably less shifted towards its right-hand side than in DMF, probably because THF is a weaker ligand than DMF for $[Pd^0PPh_3)Cl^-]$ and a weaker solvent for the phosphonium cations **3** and **6**.

Reaction of $[(\eta^3\text{-}C_3H_5)PdCl(PPh_3)]$ **(7)** with one equivalent of PPh_3 or $[(\eta^3\text{-}C_3H_5)Pd(PPh_3)_2]^+(BF_4)^-$ **(8)** with one equivalent of nBu$_4$NCl in THF afforded the (σ-allyl)palladium chloride complex **2** (Scheme 1, route b and c, respectively). As in DMF, no cationic (π-allyl)palladium is formed in THF from **1**, **7**, and **8**, in the presence of chloride ions delivered either by the precursors (**1** or **7**) or deliberately added (to **8**). The three precursors provide the same (σ-allyl)palladium chloride complex **2** (Scheme 1a,b,c).

When 72 equivalents of $CH_2{=}CH{-}CH_2{-}OAc$ were added to a solution of $[Pd^0(dba)_2] + 2PPh_3$ in THF, the absorbance of $[Pd^0(dba)(PPh_3)_2]$ at 394 nm decreased and reached a limiting value corresponding to the thermodynamic concentration of $[Pd^0(dba)(PPh_3)_2]$ imposed in the equilibrium shown in Equation (14) (Figure 1b, $t < 300$ s).[17] This equilibrium is similar to that observed in DMF [Equation (9)] except for the ionic species' ion-pairing.

$$Pd^0(dba)(PPh_3)_2 + CH_2{=}CH{-}CH_2{-}OAc \rightleftharpoons (\eta^3\text{-}C_3H_5)Pd(PPh_3)_2{}^+AcO^- + dba \quad (14)$$

When one equivalent of nBu$_4$NCl was added, the absorbance decreased to almost zero (Figure 1b). This shows that the reaction of one chloride ion with $[(\eta^3\text{-}C_3H_5)PdL_2]^+(AcO)^-$ **(10)** formed in the oxidative addition [Equation (14)] was more efficient than in DMF, shifting this equilibrium to give the total disappearance of $[Pd^0(dba)(PPh_3)_2]$ as soon as one equivalent of Cl^- were added (compare Figure 1a and 1b). This establishes that the reversible overall reaction in Equation (13) is shifted more towards its right-hand side in THF than in DMF.

Formation of $[(\eta^1\text{-Ph}-CH{=}CH-CH_2)PdCl(PPh_3)_2]$

When four equivalents of PPh_3 were added to a solution of the dimeric (π-cinnamyl)palladium(II) chloride $[Pd(\eta^3\text{-}Ph-C_3H_4)(\mu\text{-}Cl)]_2$ **(11)** in $CDCl_3$, the four nonaromatic ^{1}H NMR signals characteristic of complex **11** (Table 2) totally disappeared and three new ^{1}H NMR signals were observed and assigned to the (σ-cinnamyl)palladium(II) chloride complex **12** $[(\eta^1\text{-Ph}-CH{=}CH-CH_2)PdCl(PPh_3)_2]$ (Scheme 2, route a).

Table 2. Characterization of cinnamyl−Pd^{II} complexes (Scheme 2)

	^{1}H NMR (ppm)[a]
11[b]	2.97 (d, J = 12 Hz, 1 H) 3.90 (d, J = 6.7 Hz, 1 H) 4.55 (d, J = 11.5 Hz, 1 H) 5.73 (ddd, J = 12, 11.5 and 6.7 Hz, 1 H)
12[c][d]	3.22 (d, J = 10 Hz, 2 H) 5.45 (d, J = 13 Hz, 1 H) 6.10 (dt, J = 10 and 13 Hz, 1 H)
13[b]	3.68 (t, J = 6.5 Hz, 1 H) 3.80 (pseudo t, J = 10 Hz, 1 H) 5.45 (pseudo t, J = 12 Hz, 1 H) 6.41 (m, 1 H)

[a] 250 MHz; shifts are referred to TMS. Solvent: $CDCl_3$. For simplification, aromatic protons are voluntarily omitted. − [b] Authentic sample. − [c] Formed in reaction of **11** with 4 equiv. PPh_3. − [d] Formed in reaction of **13** with 1 equiv. nBu$_4$NCl.

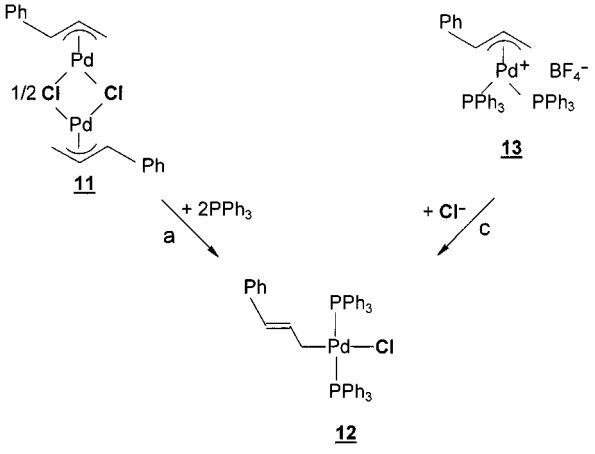

Scheme 2. Formation of a (σ-cinnamyl)palladium chloride complex

This reaction also gives the phosphonium cation $Ph-CH{=}CH-CH_2-PPh_3^+$ (24%) as in the allyl series (see above, Scheme 1). In contrast to the (σ-allyl)palladium(II) chloride complex **2**, which was found to be involved in a fast equilibrium between two σ-forms [Equation (2)], the (σ-cinnamyl)palladium(II) chloride complex **12** is not involved in such an equilibrium (or the equilibrium is very slow) because of the phenyl substituent. Indeed, the ^{1}H NMR spectrum (three different types of non aromatic ^{1}H with an integration of 1:1:2, Table 2) is clearly consistent with a complex of structure $Ph-CH{=}CH-CH_2-PdClL_2$ and not with the isomerized form $Ph-CH(PdClL_2)-CH{=}CH_2$ whose ^{1}H NMR spectrum should exhibit four different non aromatic signals with the same integration.

Complex **12** was also formed when one equivalent of nBu$_4$NCl was added to a solution of the cationic (π-cinnamyl)palladium complex **13** in $CDCl_3$ (Scheme 2, route b) whose four ^{1}H NMR signals were no longer detected (Table 2).

About the Permanence of the Cl^- Effect in the Presence of Increasing Amounts of AcO^- Produced During a Catalytic Reaction

In the case where a catalytic reaction is initiated by the precursor mixture $[Pd(\eta^3\text{-}C_3H_5)(\mu\text{-}Cl)]_2$ **(1)** + 4PPh_3, the chloride ion concentration is low compared to that of the acetate ions, which are progressively released from the allylic acetate when the catalytic reaction proceeds. One may think that our present results might be affected as a function of the conversion. However, this is not the case. Indeed, it is important to stress that the relative concentration of the (σ-allyl)palladium(II) chloride complex **2** versus the (π-allyl)palladium(II) complex **8** is not affected by the acetate concentration but only depends on the chloride concentration [Scheme 3, reaction (15)].

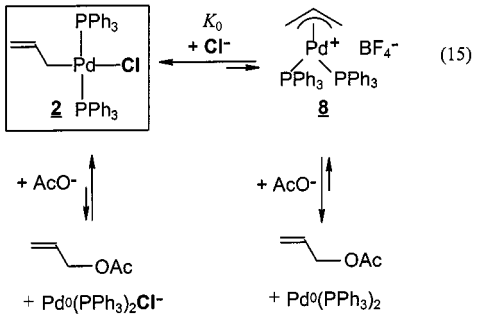

Scheme 3

The (σ-allyl)palladium(II) chloride complex **2** is quantitatively formed from {**1** + 4PPh_3}, and as well as when one equivalent of Cl^- is added to the cationic complex **8** (see above) so that the equilibrium between **2** and **8** [Scheme 3, Equation (15)] lies considerably in favor of **2** with $K_0\times[Cl^-] >> 100$. The nucleophile may then react with either **2** and **8**, or with both complexes in parallel. In the presence of AcO^-, two competitive reversible reactions occur, which lead to the formation of the allylic acetate (Scheme 3). But provided that reaction (15) in Scheme 3 remains at equilibrium, these reactions do not affect the relative concentration of **2** and **8**, since it only depends on Cl^- concentration

and not on $[Cl^-]/[AcO^-]$. One therefore has: $[\mathbf{2}]/[\mathbf{8}] = K_0 \times [Cl^-] >> 100$, whatever the AcO^- concentration. The effect of AcO^- concentration is only to decrease the absolute concentrations of **2** and **8** but not their ratio, so that the nature of the reactive species, which reacts with the nucleophile, will not be affected by the acetate concentration but will only depend on the intrinsic reactivity of the nucleophile with **2** or **8** and on K_0 and the Cl^- concentration, which determine the respective concentrations of **2** and **8**. When reaction (15) is displaced from its equilibrium by the combined actions of OAc^- and the nucleophile, the kinetic situation becomes much more intricate. The comparative reactivity of a nucleophile with cationic $[(\eta^3\text{-allyl})PdL_2]^+(BF_4)^-$ [20] complexes or with the related complexes $[(\eta^1\text{-allyl})PdClL_2$ is under investigation.

Conclusion

In DMF or THF, the cationic (π-allyl)palladium complex $[(\eta^3\text{-}C_3H_5)Pd(PPh_3)_2]^+Cl^-$ is not formed from $[Pd(\eta^3\text{-}C_3H_5)(\mu\text{-}Cl)]_2 + 4PPh_3$, $[(\eta^3\text{-}C_3H_5)PdCl(PPh_3)] + 1PPh_3$ or $[(\eta^3\text{-}C_3H_5)Pd(PPh_3)_2]^+(BF_4)^- + 1Cl^-$. Instead, these three precursors lead to the formation of the same (σ-allyl)palladium chloride complex $[(\eta^1\text{-}CH_2{=}CH{-}CH_2)PdCl(PPh_3)_2]$ (Scheme 1a,b,c). Moreover, the latter complex is also formed instead of $[(\eta^3\text{-}C_3H_5)Pd(PPh_3)_2]^+(AcO)^-$ when the oxidative addition of palladium(0) complexes to the allylic acetate is performed in the presence of chloride ions, either already ligated to the palladium(0) complex (when $[PdCl_2(PPh_3)_2]$ is the Pd^0 precursor) or deliberately added to a chloride-free palladium(0) complex (when $[Pd(dba)_2] + 2PPh_3$ is the Pd^0 precursor) (Scheme 1f,g,d,e).

This emphasizes the crucial role of presumably "innocent", ligands such as chloride ions, which do not behave as simpler counter-anions of cationic (π-allyl)palladium(II) complexes[2][7b] but modify the chemical structure of reactive intermediates by formation of neutral (σ-allyl)palladium(II) chloride complexes. This also shows that the catalytic precursors of Tsuji–Trost reactions, i.e., $[Pd(\eta^3\text{-}C_3H_5)(\mu\text{-}Cl)]_2 + 4PPh_3$ or $[(\eta^3\text{-}C_3H_5)Pd(PPh_3)_2]^+(BF_4)^-$ are not equivalent since the former system does not lead to the latter complex due to the presence of chloride in its structure. They become equivalent only when chloride ions are added to $[(\eta^3\text{-}C_3H_5)Pd(PPh_3)_2]^+(BF_4)^-$ but then both provide a neutral (σ-allyl)palladium(II) chloride.

Therefore, among the four catalytic precursors **A**: $[Pd^0L_4]$, **B**: $[Pd^0(dba)_2] + nL$, **C**: $[(\eta^3\text{-}C_3H_5)PdL_2]^+(BF_4)^-$, and **D**: $[Pd(\eta^3\text{-}C_3H_5)(\mu\text{-}Cl)]_2 + 4PPh_3$, the precursor **D** behaves quite differently. Indeed, the intermediate prone to react with the nucleophile is not a cationic (π-allyl)palladium(II) complex, as usually assumed, but a neutral (σ-allyl)palladium(II) chloride. Consequently, this may affect the regioselectivity of the reaction as well as its enantioselectivity in the case of substituted allylic acetates and chiral ligands. The formation of a neutral (σ-allyl)palladium(II) chloride should then be taken into consideration when chloride anions are purposely added to any Pd-catalyzed nucleophilic allylic substitution.

Experimental Section

General Remarks: ^{31}P NMR spectra were recorded on a Bruker spectrometer (101 MHz) using H_3PO_4 as an external reference. – ^1H NMR spectra were recorded on a Bruker spectrometer (250 MHz) using TMS as an internal reference. – UV spectra were recorded on a DU 7400 Beckman spectrophotometer. – Cyclic voltammetry was performed with a home made potentiostat and a wave form generator Tacussel GSTP4. The cyclic voltammograms were recorded on a Nicolet 301 oscilloscope. – Conductivity was measured on a Tacussel CDM210 conductivity meter (cell constant = 1 cm^{-1}).

Chemicals: DMF was distilled from calcium hydride under vacuum and THF from sodium/benzophenone. Commercial allylic acetate $CH_2{=}CH{-}CH_2{-}OAc$ (Acros) was used after filtration through alumina. Commercial (π-allyl)palladium(II)chloride dimer complex, $[Pd(\eta^3\text{-}C_3H_5)(\mu\text{-}Cl)]_2$ (Acros) was used without any purification. $[(\eta^3\text{-}C_3H_5)PdCl(PPh_3)]$,[9] $[(\eta^3\text{-}C_3H_5)Pd(PPh_3)_2][BF_4]$,[17] $[Pd(\eta^3\text{-Ph}{-}C_3H_4)(\mu\text{-}Cl)]_2$ [21] $[Pd(\eta^3\text{-Ph}{-}C_3H_4)(PPh_3)]_2$ [20] and $[Pd(dba)_2]$[22] were prepared according to published procedures.

UV Experiments: These were performed in a thermostated 1 mm path length cell on solutions of $[Pd(dba)_2]$ (11 mg, 0.02 mmol, 1 mmol dm^{-3}) and 2 equivalents of PPh_3 (10 mg, 0.04 mmol) in 20 mL of DMF or THF with the appropriate amount of $CH_2{=}CH{-}CH_2{-}OAc$ and nBu_4NCl (see text and Figure 1).

Electrochemical Set-up and Procedure for Voltammetry: Experiments were carried out in a three-electrode cell connected to a Schlenk line. The counter electrode was a platinum wire of ca. 1 cm^2 apparent surface area; the reference was a saturated calomel electrode (Tacussel) separated from the solution by a bridge filled with 3 mL of DMF containing nBu_4NBF_4 (0.3 g, 0.3 mol dm^{-3}). Cyclic voltammetry was performed at a steady gold disk electrode (diameter 0.5 mm) with a scan rate of 0.2 V s^{-1} from a solution of $[Pd(\eta^3\text{-}C_3H_5)(\mu\text{-}Cl)]_2$ (9 mg, 0.024 mmol) and 4 equivalents of PPh_3 (25 mg, 0.096 mmol) in 12 mL of DMF containing nBu_4NBF_4 (1.2 g, 0.3 mol dm^{-3}).

Acknowledgments

This work has been supported by the Centre National de la Recherche Scientifique (CNRS, UMR 8640) and the Ministère de la Recherche (Ecole Normale Supérieure). We thank Professor H. J. Cristau from Montpellier University for a helpful discussion on the isomerization of allyltriphenylphosphonium cations.

[1] [1a] J. Tsuji, *Palladium Reagents and catalysts*, John Wiley & Sons, Chichester, **1996**, p. 290. – [1b] S. A. Godleski, in *Comprehensive Organic Synthesis, Vol. 4* (Eds: B. M. Trost, I. Flemming), Pergamon, Oxford, **1991**. – [1c] C. G. Frost, J. Howard, J. M. J. Williams, *Tetrahedron: Asymmetry* **1992**, *3*, 1089–1122. – [1d] G. Consiglio, R. Waymouth, *Chem. Rev.* **1989**, *89*, 257–276. – [1e] A. Pfaltz, *Acc. Chem. Rev.* **1993**, *26*, 339–345. – [1f] T. Hayashi, in *Catalytic Asymmetric Synthesis* (Ed: I. Ojima), VCH, New York, **1993**, p. 325. – [1g] B. M. Trost, D. L. Van Vranken, *Chem. Rev.* **1996**, *96*, 395–422. – [1h] B. M. Trost, *Acc. Chem. Res.* **1996**, *29*, 355–364.

[2] [2a] G. C. Lloyd-Jones, S. C. Stephen, *Chem. Commun.* **1998**, 2321–2322. – [2b] G. C. Lloyd-Jones, S. C. Stephen, *Chem. Eur. J.* **1998**, *4*, 2539–2549.

[3] [3a] C. Amatore, A. Jutand, F. Khalil, M. A. M'Barki, L. Mottier, *Organometallics* **1993**, *12*, 3168−3178. − [3b] C. Amatore, A. Jutand, G. Meyer, *Inorg. Chim. Acta.* **1998**, *273*, 76−84. − [3c] C. Amatore, A. Jutand, *Coord. Chem. Rev.* **1998**, *178−180*, 511−528.

[4] [4a] D. Ferroud, J. P. Genêt, J. Muzart, *Tetrahedron Lett* **1984**, *25*, 4379−4382. − [4b] W. Oppolzer, J. M. Gaudin, *Helvetica Chim. Acta* **1987**, *70*, 1477. − [4c] S. I. Murahashi, Y. Taniguchi, Y. Imada, Y. Tanigawa, *J. Org. Chem.* **1989**, *54*, 3292−3303.

[5] [5a] C. Amatore, A. Jutand, A. Suarez, *J. Am. Chem. Soc.* **1993**, *115*, 9531−9541. − [5b] C. Amatore, A. Jutand, *J. Organomet. Chem.* **1999**, *576*, 254−278. − [5c] C. Amatore, A. Jutand, *Acc. Chem. Res.* **2000**, *33*, 314−321. − [5d] C. Amatore, E. Carré, A. Jutand, A. M. M'Barki, G. Meyer, *Organometallics.* **1995**, *14*, 5605−5614.

[6] R. E. Nordberg, J-E. Bäckvall, *J. Organomet. Chem.* **1985**, *285*, C24−C26.

[7] [7a] M. Kawatsura, Y. Uozumi, T. Hayashi, *Chem. Commun.* **1998**, 217−218. − [7b] B. M. Trost, F. D. Toste, *J. Am. Chem. Soc.* **1999**, *121*, 4545−4555.

[8] U. Burckhardt, M. Baumann, A. Togni, *Tetrahedron: Asymmetry* **1997**, *8*, 155−159.

[9] J. Powell, B. L. Shaw, *J. Chem. Soc. A* **1967**, 1839−1851

[10] A similar NMR pattern was observed when the ^{1}H NMR spectrum of **1** was measured in DMSO in the absence of ligand[11a] as well as for allylmagnesium bromide.[11b]

[11] [11a] J. C. W. Chien, H. C. Dehm, *Chem. Ind.* **1961**, 745−746. − [11b] J. E. Nordlander, J. D. Roberts, *J. Am. Chem. Soc.* **1959**, 1769−1770.

[12] G. Büchi, H. Wüest, *Helv. Chim. Acta* **1971**, *188−189*, 1681−1687.

[13] For commercial **3**·Cl: $\delta(CH_2{-}P^+) = 4.95$ in $CDCl_3$. Since ion pairs were formed in $CDCl_3$, the ^{1}H NMR shift of **3**·Cl is very sensitive to the ionic strength and varies from $\delta = 4.95$ to 4.67 and 4.33 after addition of nBu$_4$NBF$_4$ (0.5 and 2.7 equiv. respectively). The signal position is also sensitive to the counteranion as observed for authentic samples of **3**·Br in $CDCl_3$: $\delta(CH_2{-}P^+) = 4.60$.

[14] C. Amatore, M. Azzabi, A. Jutand, *J. Am. Chem. Soc.* **1991**, *113*, 8375−8384.

[15] This oxidative addition proceeds in two successive reversible steps via a Pd^0 complex ligated to the double bond of the allylic acetate: [15a] C. Amatore, A. Jutand, M. A. M'Barki, L. Mottier, unpublished results. − [15b] M. A. M'Barki, PhD thesis, Paris, **1992**. − [15c] L. Mottier, PhD thesis, Paris **1995**.

[16] For the seminal use of [(Pd(dba)$_2$] with bidentate and then monodentate phosphane ligands in allylic nucleophilic substitutions see: J. C. Fiaud A. Hibon de Gournay, M. Larchevêque, *J. Organomet. Chem.* **1978**, *154*, 175−185 and ref.[4a]

[17] C. Amatore, A. Jutand, G. Meyer, L. Mottier, *Chem. Eur. J.* **1999**, *5*, 466−473.

[18] $\delta = 27.05$ and 24.66 in $CDCl_3$; $\delta = 27.20$ and 25.29 in DMF, see ref. [3]

[19] The (σ-allyl)palladium(II) chloride complex [(η^1-CH_2=CH−CH_2)PdCl(PPh$_3$)$_2$] is also formed in the irreversible oxidative addition of the allylic chloride CH_2=CH−CH_2−Cl to a solution of [Pd(dba)$_2$] and two equivalents of PPh$_3$.

[20] O. Kuhn, H. Mayr, *Angew. Chem. Int. Ed.* **1999**, *38*, 343−346.

[21] P. R. Auburn, P. B. Mackenzie, B. Bosnich, *J. Am. Chem. Soc.* **1985**, *107*, 2033−2046.

[22] Y. Takahashi, T. Ito, S. Sakai, Y. Ishii, *J. Chem. Soc., Chem. Commun.* **1970**, 1065−1066.

Received July 24, 2000
[I00289]

Characterization of Calcined and Reduced Multi-Component Co−Ni−Mg−Al-Layered Double Hydroxides

Didier Tichit,* Solange Ribet, Bernard Coq

Eur. J. Inorg. Chem. **2001**, 539−546

Due to a data transmission error, Figure 5 does not appear on page 542 of the printed version and is therefore reproduced below; the electronic versions (PDF, HTML) are not affected.

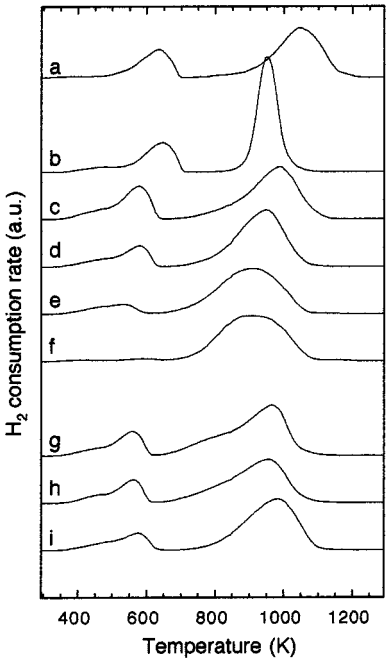

Figure 5. Temperature programmed reduction profiles of the samples calcined at 773 K: (a): Co(3)Al, (b): Co(2)Mg(1)Al, (c): Co(1.5)Ni(0.5)Mg(1)Al, (d): Co(1)Ni(1)Mg(1)Al, (e): Co(0.5)-Ni(1.5)Mg(1)Al, (f): Ni(2)Mg(1)Al, (g): Co(1.5)Ni(1.5)Al, (h): Co(1.2)Ni(1.2)Mg(0.6)Al, (i): Co(0.8)Ni(0.8)Mg(1.4)Al

The Editors
[C I00113]

 © WILEY-VCH Verlag GmbH, 69451 Weinheim, 2001 1434−1948/01/0303−0881 $ 17.50+.50/0

Heterocyclopentadienyl Complexes of Group-3 Metals

François Nief[a]

Keywords: Lanthanides / Actinides / Coordination modes / Heteroelements / Cyclopentadienes

Heterocyclopentadienyl complexes of group-3 metals (scandium, yttrium, lanthanum and the lanthanides, and uranium) are compounds in which one or more –CH units of a cyclopentadienyl-like ligand have been replaced by a heteroelement (nitrogen, phosphorus, arsenic, or antimony). These ligands can have very diverse substitution patterns, notably with bridged and cavitand-like structures. In addition to the classical η^5-coordination behaviour, the heterocyclopentadienyl ligand can adopt a very large array of coordination patterns. Some complexes have a very promising chemistry since they have been found to activate small molecules such as nitrogen and ethylene.

I. Introduction

Cyclopentadienyl π-complexes of group-3 metals (including scandium, yttrium, lanthanum and the lanthanides, and the actinides) have received a tremendous amount of attention in the past few years.[1] These metals can achieve very high coordination numbers (c.n.) (up to 12), but it is possible to obtain stable complexes with lower coordination numbers by increasing the steric bulk on the cyclopentadienyl ligand. For instance, introduction of the η^5-pentamethylcyclopentadienyl (Cp*) ligand, which has become ubiquitous in this chemistry, has allowed for the isolation of stable complexes such as $Cp^*_2LnX_2^-$ (X = halogen, c.n. = 8), Cp^*_2LnR (R = alkyl, c.n. = 7), or even the divalent lanthanide complexes Cp^*_2Ln (Ln = Sm, Eu, c.n. = 6). In addition, some of these complexes are highly efficient homogeneous catalysts.[2]

Another possibility for modifying a cyclopentadienyl ligand is the replacement of one or several carbon atoms of this ring by a group-15 heteroelement; an isoelectronic heterocyclopentadienyl ligand is thus obtained.

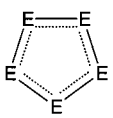

E = CH, N, P, As, Sb, Bi

Several such heterocyclopentadienyl ligands have been used in group-3 metal chemistry. They include the pyrrolyl, phospholyl, and arsolyl ring systems with one heteroelement in the ring, the pyrazolyl ligand with two heteroelements and the 1,2,4-triphospholyl and 1,2,4-stibadiphospholyl ligands with three heteroelements. Like the cyclopentadienyl anion, all these ligands, in the anionic form, formally derive from the corresponding pyrrole, phosphole, arsole, pyrazole, 1,2,4-triphosphole and 1,2,4-stibadiphosphole ring systems, respectively, by deprotonation.

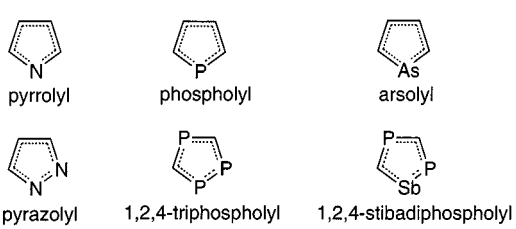

Of course many types of substituents have been introduced on these rings, notably by benzoannelation such as in

[a] Laboratoire Hétéroéléments et Coordination, CNRS UMR 7653, DCPH, Ecole Polytechnique,
91128 Palaiseau Cedex, France
Fax: (internat.) + 33-1/69333990
E-mail: nief@poly.polytechnique.fr

François Nief was born, raised, and educated in Paris. He graduated as Docteur ès Sciences from the University of Paris in 1981. After a one-year post-doctoral stay in 1982 at the University of Wisconsin, Madison, with Professor C. P. Casey, he joined the research group of Professor F. Mathey where he currently holds joint appointments at CNRS as chargé de recherche (senior researcher) and at Ecole Polytechnique as maître de conférences (associate professor). His main research interests include the applications of phosphorus ligands in the organometallic chemistry of the early transition metals, especially the lanthanides.

MICROREVIEWS: This feature introduces the readers to the authors' research through a concise overview of the selected topic. Reference to important work from others in the field is included.

 © WILEY-VCH Verlag GmbH, 69451 Weinheim, 2001 1434–1948/01/0404–0891 $ 17.50+.50/0

indolyl, phosphindolyl, carbazolyl, and dibenzophospholyl ligands. Bridged ligands have also been used: Complexes with chelating or cavitand-like pyrrolyl ligands such as bipyrrolyl or calix[4]tetrapyrrolyl (porphynogen) have recently been prepared (it is worth noting that a cavitand structure based on cyclopentadienyl has not been made yet).

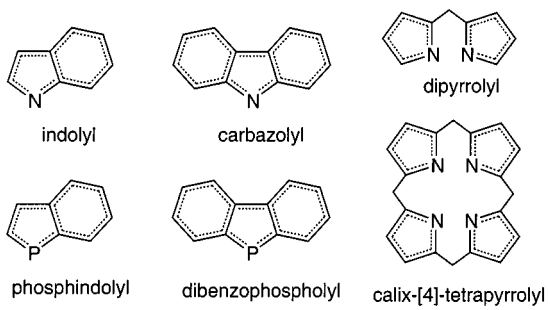

All these 5-membered ring systems, except for pyrazolyl, have been shown to behave as "true" heterocyclopentadienyl ligands in the sense that complexes displaying the η^5-coordination mode (A), which is typical of the cyclopentadienyl group, have been isolated. Since the heteroatom in the ring still possesses a lone pair of electrons, other coordination patterns are possible, namely the η^1-mode (B, planar or bent), in which there is a σ bond with the group-3 metal, the $\mu{:}\eta^5,\eta^1$-mode (C), in which both the ring and the lone pair are coordinated, and the $\mu{:}\eta^1$-bridging mode (D).

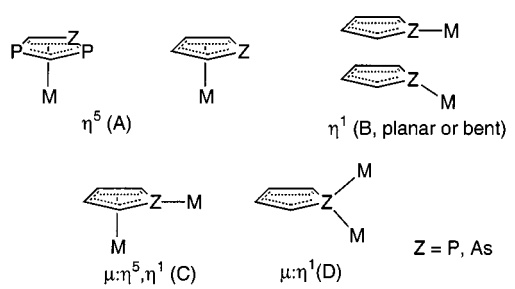

The proximity of two heteroatoms in the pyrazolyl, 1,2,4-triphospholyl, and 1,2,4-stibadiphospholyl ligands can give rise to other coordination modes: η^2-(E, planar or bent), $\mu{:}\eta^2$-(F) and $\mu{:}\eta^1$-(G).

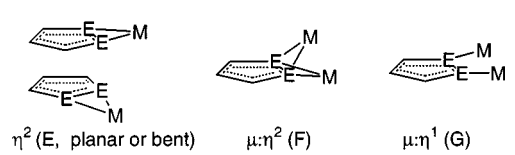

Heterocyclopentadienyl complexes of group-3 metals have been studied less than the cyclopentadienyl complexes. However, many references have appeared in the past few years and so this field is rapidly expanding.

Interest in the structure and reactivity of these complexes stems from:

a) coordination mode A and comparison with analogous cyclopentadienyl complexes,

b) the additional possibilities offered by coordination modes C and E for mononuclear complexes,

c) coordination modes D, F, and G which give rise to polynuclear complexes,

d) heterocyclopentadienyl complexes based on pyrrolyl ligands with bridging or cavitand structures, and

e) synthetic pathways possibly different from those of cyclopentadienyl complexes.

This review will tentatively cover the complexes of group-3 metals (scandium, yttrium, lanthanum and the lanthanides, and uranium) with heterocyclopentadienyl ligands as described above. Group-3 metal complexes with ligands that have extended delocalised structures, such as porphyrin, or with pyrazolylborates, in which the formal negative charge does not reside on the heterocyclic ring, will not be considered in this survey.

II. Complexes with Nonbridged Ligands

A. Monocyclic Pyrrolyl, Phospholyl and Arsolyl Complexes

1. Pyrrolyl Complexes

In contrast to the cyclopentadienyl ligand, there is a dissymmetry in the ligand ring electron density of the heterocyclopentadienyl ligand, owing to the fact that the heteroatom bears a larger part of the overall electronic density than the carbon atoms. This effect is more important for the pyrrolyl ligand because of the higher electronegativity of the nitrogen atom. Considering the strong electrophilicity of group-3 metals, one would thus expect mostly the η^1-bonding mode between the pyrrolyl ligand and these elements. As an illustration, Schumann et al. have prepared a series of complexes containing both the Cp or Cp* ligand and the pyrrolyl (pyr) or the 2,5-dimethylpyrrolyl (Dmpyr) ligand:[3] $[(\eta^5\text{-Cp})_2(\eta^1\text{-L})\text{Lu(THF)}]$ (L = pyr, Dmpyr) and $[(\eta^5\text{-Cp*})_2(\eta^1\text{-pyr})\text{Y(THF)}]$. X-ray data on $[(\eta^5\text{-Cp})_2(\eta^1\text{-Dmpyr})\text{Lu(THF)}]$ (**1**) and NMR evidence show that in these complexes, the pyrrolyl ligand is indeed σ-bonded to the group-3 metal.

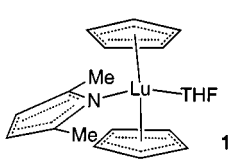

1

However, π-coordination of the pyrrolyl ligand can be also achieved. In a seminal paper, Marks[4] prepared $[\text{U(Dmpyr)}_4]$ by reaction of KDmpyr with UCl_4. Although no structural data are available for this compound, a VT NMR study suggests that the low-temperature structure of this fluxional complex is that of $[\text{U}(\eta^1\text{-Dmpyr})_3(\eta^5\text{-Dmpyr})]$. Presumably, $[\text{U(Dmpyr)}_4]$ with all the Dmpyr ligands σ-bonded would be sterically too unsaturated (c.n. =

4) and so one of the ligands is π-bonded in order to decrease this unsaturation.

Schumann et al. then introduced the 2,5-di-*tert*-butylpyrrolyl ligand (Dtpyr) in group-3 metal chemistry. It was expected that for steric reasons, the two *tert*-butyl groups would inhibit coordination with the nitrogen lone pair and indeed mostly η^5-coordinated complexes have been obtained with this ligand, such as the bis(pyrrolyl)Ln^{II} complexes $[(\eta^5\text{-Dtpyr})_2Ln(THF)]$ (Ln = Sm, Yb),[5] the (pyrrolyl)Yb^{III} compound $[(\eta^5\text{-Dtpyr})YbCl_2(THF)_2]$[6] (**2**), and the mixed (cyclooctatetraenyl/pyrrolyl)Ln^{III} complexes $[(\eta^8\text{-COT})(\eta^5\text{-Dtpyr})Sm(THF)]$ (**3**) and $[(\eta^8\text{-COT})(\eta^5\text{-Dtpyr})Ln]$ (Ln = Tm, Lu).[7] However, σ,π complexation of the Dtpyr ligand is also possible since the nitrogen lone pair of this ligand is coordinated with sodium in the neodymate(III) dimer $[\{(\eta^5\text{-Dtpyr})(\mu{:}\eta^5,\eta^1\text{-Dtpyr})(\mu^2\text{-Cl})(\mu^3\text{-Cl})Na(THF)\}_2]$[5] (**4**).

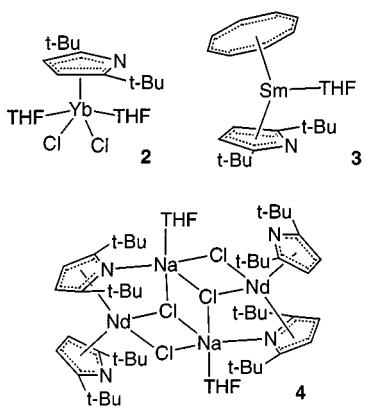

2. Phospholyl and Arsolyl Complexes

In contrast to pyrrolyl, one would expect mostly η^5- or $\mu{:}\eta^5,\eta^1$-bonding modes of the phospholyl (or arsolyl) ligand owing to the close electronegativities of the =CH− and =P− (or =As−) entities (the so-called diagonal analogy).[8] We will see that this is not always so. The following phospholyl and arsolyl ligands have been used.

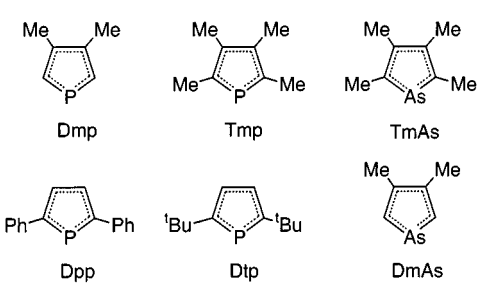

With the Tmp and TmAs ligands, one can usually obtain the same types of η^5-complexes as those described with the Cp* ligand. For instance, classical Ln^{III} ate complexes such as $[(\eta^5\text{-Tmp})_2LnCl_2Li(solv)_2]$[9] [Ln = Y, Lu, solv = Et_2O, dimethoxyethane (DME)] or $[(\eta^5\text{-Tmp})_2LnCl_2K]$ (Ln = Nd, Sm)[10] have been prepared by the reaction of the appropriate alkali metal phospholide with $LnCl_3$. In the case of $[(\eta^5\text{-Tmp})_2YCl_2Li(Et_2O)_2]$, it has been possible to observe the coupling of ^{31}P with ^{89}Y by NMR. From the small value of this coupling and from the triplet pattern in the ^{89}Y spectrum, it has been suggested that this complex retains the η^5-structure in solution. The polymeric crystal structure of $[\{(\eta^5\text{-Tmp})(\mu{:}\eta^5,\eta^1\text{-Tmp})Ln(\mu_3\text{-Cl})_2K(Et_2O)\}_n]$ (**5**), while similar to that of $[\{(\eta^5\text{-Cp*})_2Ce(\mu_3\text{-Cl})_2K(THF)\}_n]$,[11] shows additional coordination of the lone pair of one Tmp ligand to potassium. As was the case with their Cp* analogues, $[(\eta^5\text{-Tmp})_2LnCl_2K]$ could be transformed into the neutral alkyl complexes $[(\eta^5\text{-Tmp})_2LnCH(SiMe_3)_2]$ (Ln = Nd, Sm) by reaction with $LiCH(SiMe_3)_2$.

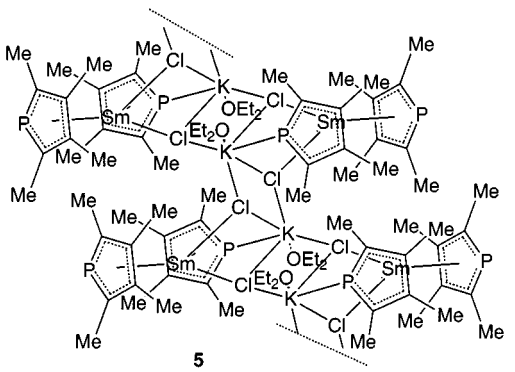

Divalent lanthanide chemistry with phospholyl ligands is also similar to that observed with the Cp* ligand. Thus, $[(\eta^5\text{-L})_2Ln(THF)_2]$ (Ln = Yb, Sm, L = Tmp, TmAs, Dpp)[12] could be obtained by the classical metathesis reaction of the potassium phospholides with $LnI_2(THF)_2$. More interestingly, these molecules could also be prepared by insertion of metallic ytterbium or samarium (in the form of the commercial powders) into the P−P bond of a 1,1′-biphospholyl or -biarsolyl.[13] Once again, investigation of the ytterbium complexes by multinuclear (^{31}P, ^{171}Yb) NMR suggests π-complexation of the phospholyl ligand with Yb. The structure of $[(\eta^5\text{-Dpp})_2Yb(THF)_2]$ (**6**) has been determined by X-ray crystallography.

In $[(\eta^5\text{-L})_2Ln(THF)_2]$ (L = Tmp, TmAs, Ln = Sm, Yb), THF is very easily lost under vacuum, with the formation of decomposition products L_2Ln, which are insoluble in nonpolar solvents.[13] In contrast, it is known that $[(\eta^5\text{-Cp*})_2Sm(THF)_2]$ sublimes by heating under high vacuum, to give unsolvated toluene-soluble $[(\eta^5\text{-Cp*})_2Sm]$.[14] Although the structures of L_2Ln are still unknown, it is suspected that these materials are polymers, with Ln−P or Ln−As σ-bonds. However, L_2Ln compounds are reactive in nonpolar solvents: $[Tmp_2Yb]$ reacts in toluene with a stable nucleophilic carbene such as *N*,*N*-diisopropyl-2,3-dimethylimida-

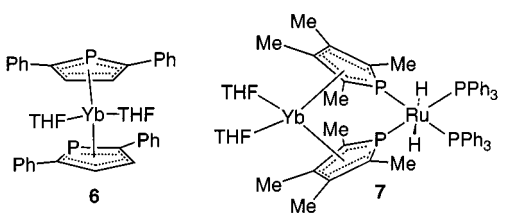

zolylidene (carb) to give the adduct $[(\eta^5\text{-Tmp})_2\text{Yb(carb)}]$.[15] Since the Tmp_2Yb moiety still possesses two lone pairs at the phosphorus atoms, it can act as a chelating ligand in the heterobimetallic Yb/Ru complexes, $[(L)_2\text{Yb}(\mu{:}\eta^5,\eta^1\text{-Tmp})_2\text{RuH}_2(\text{PPh}_3)_2]$ [L = THF (**7**), Carb].[15,16]

The use of zerovalent Yb as a precursor to phospholyl complexes could be extended to the synthesis of monophospholyl Yb complexes. Insertion of Yb metal into the P−Cl bond of 1-chloro-2,3,4,5-tetramethylphosphole or the P−S bond of 1-phenylthio-2,3,4,5-tetramethylphosphole afforded the corresponding Yb^{II} dimers $[\{(\eta^5\text{-Tmp})\text{Yb}(\mu\text{-E})(\text{THF})_2\}_2]$ [E = Cl (**8**), SPh (**9**)].[17]

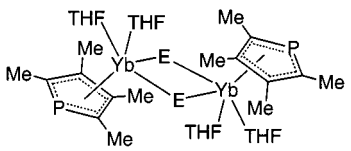

E = Cl (**8**), SPh (**9**)

The following examples illustrate how the substitution pattern on the heterocyclopentadienyl ring can influence its coordination chemistry. Compounds such as $[(\eta^5\text{-Cp*})_3\text{M}]$ (M = Nd, Sm, U)[18] exist but they cannot be synthesised by the metathesis reaction of MX_3 (X = halogen) with the appropriate alkali metal salts, because these reactions often require donor solvents such as THF which can react with the sterically overcrowded $Cp*_3M$ intermediates. However, removal of just one methyl group on the Cp* ring allows for the easy synthesis of $[(\eta^5\text{-}C_5Me_4H)_3\text{Ln}]$ (Ln = La, Sm, Tb) by the metathesis route.[19] In a way, the Tmp ligand may be regarded as looking more like C_5Me_4H than Cp*: The lone pair on the phosphorus atom in the Tmp ligand is sterically more similar to a C−H bond in Cp than to a $C-CH_3$ bond in Cp*. However, reaction of three equivalents of KTmp with $SmCl_3$ in toluene did not give $[(\eta^5\text{-Tmp})_3\text{Sm}]$. An ate complex of polymeric two-dimensional structure, which retains KCl, was obtained instead. Its X-ray structure has been determined and is that of $[\{(\eta^5\text{-Tmp})\text{Sm}(\mu{:}\eta^5,\eta^1\text{-Tmp})_2(\mu\text{-Cl})\text{K}(\eta^6\text{-toluene})\}_n]$[20] (**10**).

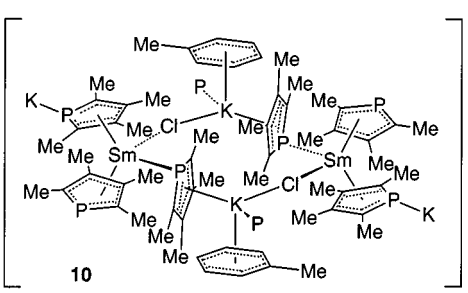

This complex looks like a reaction intermediate towards a hypothetical $[(\eta^5\text{-Tmp})_3\text{Sm}]$ since the Sm atom in **10** is complexed with three Tmp ligands, but KCl has not been eliminated. Under the same conditions with the Dmp ligand, a neutral tris(Dmp) dimer, $[\{(\eta^5\text{-Dmp})_2(\mu{:}\eta^5,\eta^1\text{-Dmp})\text{Sm}\}_2]$ (**11**), was obtained[20]. In this case, since the Dmp ligand is smaller, the Sm atom can achieve a c.n. of 10.

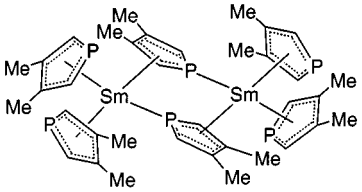

11

It thus seemed interesting to study the coordination of the phospholyl ligand around Sm in complexes of composition $Cp*_2\text{Sm(L)}$ (L = phospholyl, arsolyl), that is, when the Sm atom is in a very crowded environment imposed by two Cp* ligands. $Cp*_2\text{Sm(L)}$ (L = Tmp, Dmp, Dmas, Dtp) was prepared by reductive cleavage of the P−P or As−As bonds of the corresponding 1,1′-biphospholyls or -biarsolyls by $Cp*_2Sm$.[21] Three types of structures were obtained.

With Tmp as ligand, the structure is that of $[(\eta^5\text{-Cp*})_2(\eta^1\text{-Tmp})]$ (**12**). The Tmp ligand is only σ-bonded to Sm, but since this atom is still coordinatively unsaturated (c.n. = 7), it will look for additional electronic density through an interaction with one of the α-methyl groups of the σ-Tmp ligand, which thus becomes unsymmetrically bonded to Sm.

With Dmp or Dmas as ligands, the structure is that of an unsymmetrical dimer, $[(\eta^5\text{-Cp*})_4\text{Sm}_2(\eta^1\text{-L})(\mu{:}\eta^5,\eta^1\text{-L})]$ [L = Dmp (**13**), Dmas (**14**)]. Apparently, there is enough room around the Sm atom to achieve π-coordination with the less bulky Dmp or Dmas. However, the lone pair on this π-ligand is still available for complexation with another $Cp*_2Sm$ unit, which then only needs σ-coordination with another Dmp or Dmas ligand to achieve the optimum c.n. of 8. With Dtp as ligand, the lone pair is sterically hindered, so only π-coordination is possible and the structure is that of $[(\eta^5\text{-Cp*})_2(\eta^5\text{-Dtp})]$ (**15**).

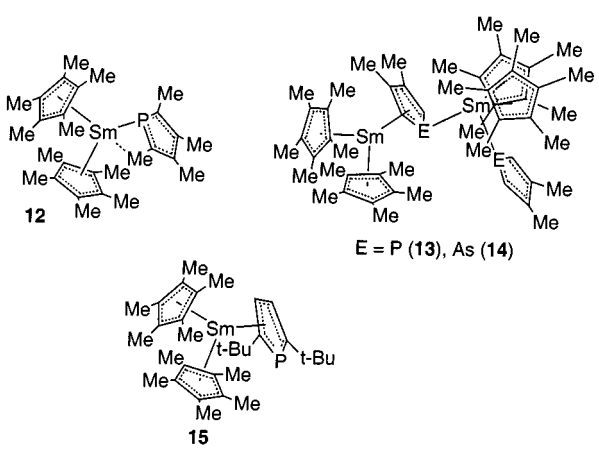

The Tmp ligand has been extensively used in actinide chemistry, in which most of its chemistry parallels that observed with the Cp* ligand. Mono- or bis(phospholyl)U^{IV} complexes such as $[(\eta^5\text{-Tmp})\text{UCl}_3(\text{DME})]$[22] (**16**), $[(\eta^5\text{-Tmp})_2\text{UCl}_2]$,[22] $[(\eta^5\text{-Tmp})_2\text{U}(\text{BH}_4)_2]$[23] (**17**), and $[(\eta^5\text{-}$

Tmp)U(BH$_4$)$_3$][24] could be prepared by reaction of UCl$_4$ or U(BH$_4$)$_4$ with KTmp. A mixed Tmp/Cp* complex, [(η^5-Tmp)(η^5-Cp*)U(BH$_4$)$_2$],[22,25] could also be obtained from KTmp and [(η^5-Cp*)U(BH$_4$)$_3$]. These Tmp complexes could, in turn, be converted into [(η^5-Tmp)UX$_3$(DME)], [(η^5-Tmp)(η^5-Cp*)UX$_2$], and [(η^5-Tmp)$_2$UX$_2$] (X = alkyl, alkoxy) by reaction with the appropriate nucleophiles.[22] However, contrary to the case with the Cp* ligand, tris(phospholyl)U^{IV} complexes can be obtained: [(η^5-Tmp)$_3$UCl] (**18**) was prepared from KTmp and UCl$_4$ and this compound was transformed into [(η^5-Tmp)$_3$UMe] and [(η^5-Tmp)$_3$UH].[26] Here, the Tmp ligand behaves similarly to the C$_5$Me$_4$H ligand since [(η^5-C$_5$Me$_4$H)$_3$UCl][27] has been prepared and its structure determined by X-ray.

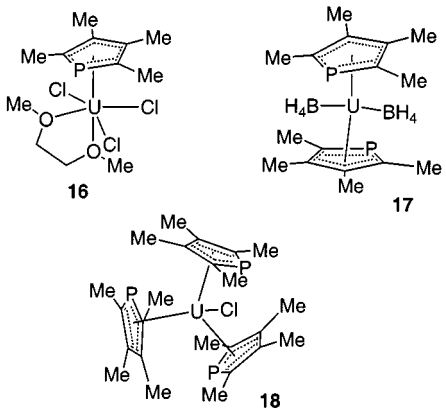

Low-valent (phospholyl)U^{III} complexes could also be obtained either by reduction of the corresponding U^{IV} complexes with sodium amalgam or by reaction of TmpK with the U^{III} precursor [(η^6-mesitylene)U(BH$_4$)$_3$].[23] When these reactions were performed in THF, U^{III} ate complexes such as [{(η^5-Tmp)$_2$U(BH$_4$)$_2$}(M)] and [{(η^5-Tmp)U(BH$_4$)$_3$}(M)] (M = Na, K) were obtained. However, reduction of [(η^5-Tmp)$_2$U(BH$_4$)$_2$] or [(η^5-Tmp)(η^5-Cp*)U(BH$_4$)$_2$] in toluene led to the precipitation of NaBH$_4$ and to the isolation of neutral U^{III} dimers [{(η^5-Tmp)(μ:η^5,η^1-Tmp)U(BH$_4$)}$_2$] (**19**) and [{(η^5-Cp*)(μ:η^5,η^1-Tmp)U(BH$_4$)}$_2$], respectively. In these compounds, the ^{31}P NMR signal of the bridging Tmp ligand was detected very far downfield (δ ≈ 3500−3900). The structure of **19** has been determined by an X-ray crystal structure analysis.[25]

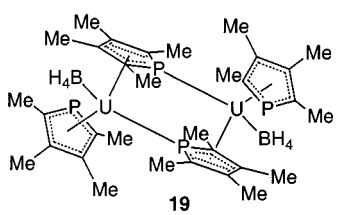

A comparison of the electronic properties of the Tmp and Cp* ligand has been made by electrochemical measurements. The following one-electron reversible potentials (vs. ferrocene/ferricinium) were found for [(η^5-Tmp)$_2$U(BH$_4$)$_2$] (−1.49 V), [(η^5-Tmp)(η^5-Cp*)U(BH$_4$)$_2$] (−1.66 V), and [(η^5-Cp*)$_2$U(BH$_4$)$_2$] (−1.83 V). These results clearly show that the Tmp ligand is less electron-rich than the Cp* ligand. An additional piece of evidence for this is the fact that only [(η^5-Tmp)$_2$U(BH$_4$)$_2$] was reduced when an equimolar mixture of [(η^5-Tmp)$_2$U(BH$_4$)$_2$] and [(η^5-Cp*)$_2$U(BH$_4$)$_2$] was treated with 0.5 equivalents of sodium amalgam. The chemistry of (phospholyl)uranium complexes is therefore not only influenced by steric but also by electronic factors.[22]

Finally, further evidence for the accessibility of the phosphorus lone pairs was found by the X-ray characterisation of two U−Ni heterobimetallic compounds: [Cl$_2$U(μ:η^5,η^1-Tmp)$_2$Ni] (**20**) and [{Cl$_2$U(μ:η^5,η^1-Tmp)$_2$(μ-Tmp)Ni}$_2$][28] (**21**).

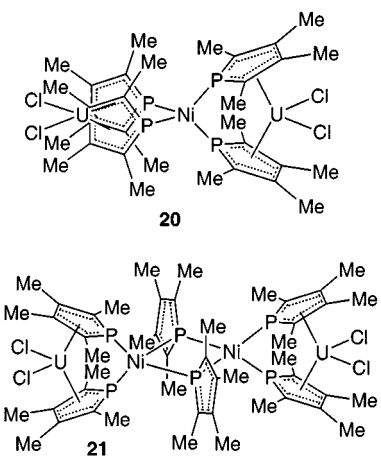

B. Ring-Fused Pyrrolyl and Phospholyl Complexes

Another opportunity for comparing the phospholyl and pyrrolyl ligands is the study of the effect of benzoannelation on the coordinating properties of these ligands. The following ligands have been used, mostly in Ln^{II} chemistry.

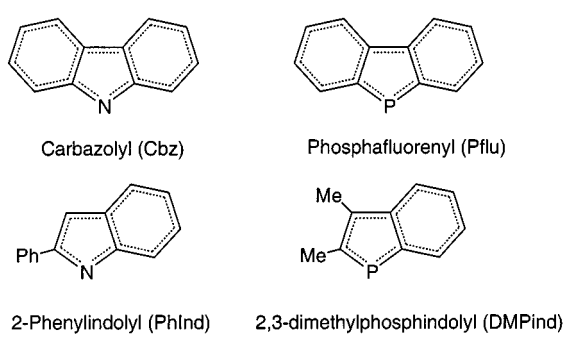

In general, the Ln^{II} complexes are 6-coordinate octahedral or distorted octahedral complexes of general formula [(η^1-L)$_2$Ln(D)$_4$] (L = PhInd, Cbz; Ln = Sm, Eu, Yb; D = donor). Planarity or near-planarity at the nitrogen atom is achieved and thus coordination of type B (planar) is present. The ligands L can be either axial, e.g. in [(η^1-Cbz)$_2$Sm(*N*-MeIm)$_4$][29] (**21**, *N*-MeIm = *N*-Methylimidazole) and [(η^1-PhInd)$_2$Yb(THF)(diglyme)][30] (**23**) or equat-

orial, e.g. in $[(\eta^1\text{-Cbz})_2Ln(THF)_4]$ [Ln = Eu[31] (**24**), Sm[29] (**25**)] and $[(\eta^1\text{-Cbz})_2Yb(THF)_2(DME)]$[32] (**26**). The steric bulk of the PhInd ligand probably causes the lability of the THF ligand in $[(PhInd)_2Yb(THF)_4]$. Heating this compound in toluene in the presence of DME produced a five-coordinate dimer, $[\{(\eta^1\text{-PhInd})(\mu{:}\eta^1\text{-PhInd})Yb(DME)\}_2]$ (**27**), in which there is an unprecedented coordination of type E for one of the PhInd ligands.[30] A single Sm^{III} complex, $[(PhInd)_3Sm(THF)]$, has been mentioned but its structure is unknown.[31]

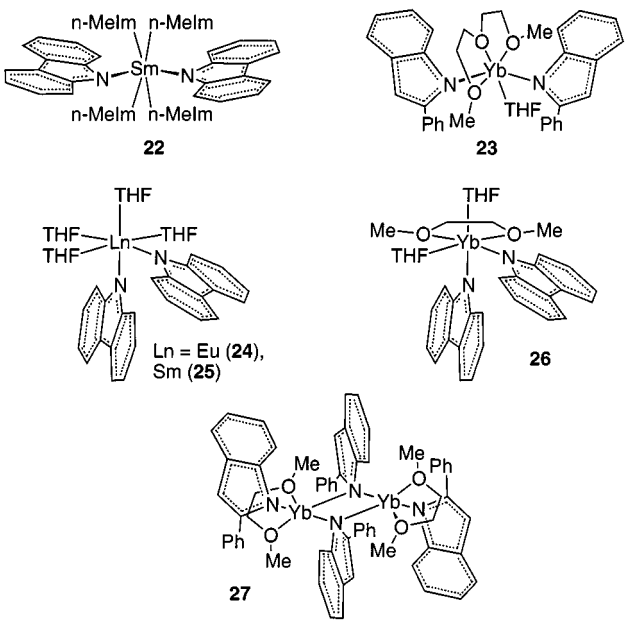

The phosphorus analogues of the indolyl and carbazolyl ligands have a completely different behaviour. The DMPind (2,3-dimethylphosphindolyl) ligand is still π-complexed with the Sm atom in $[(\eta^5\text{-DMPind})_2Sm(THF)_2]$[33] (**28**) while this is no longer the case in the octahedral phosphafluorenyl complexes, $[(\eta^1\text{-Pflu})_2Ln(THF)_4]$ [Ln = Sm[33] (**29**), Yb[34] (**30**)], which display type B (bent) coordination. Remarkably, the Pflu ligands in **29** are axial while in **30** they are equatorial, which points to a probable small energy difference between the two forms.

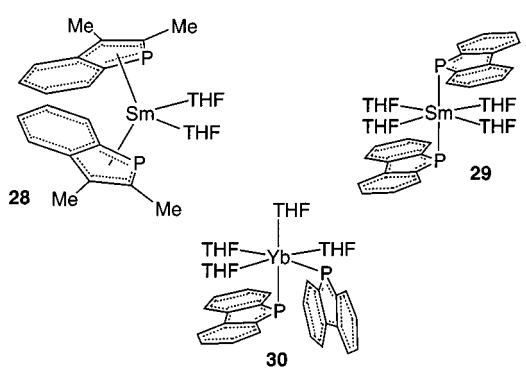

The difference in coordination behaviour between the phosphindolyl and phosphafluorenyl ligands is due to the weaker electron density of the 5-membered ring in the phosphafluorenyl ligand (because of the double benzoannelation), that prevents π-coordination by this ring, so only σ-coordination of the phosphafluorenyl ligand is possible. However, unlike the carbazolyl ligand, the phosphafluorenyl ligand is bent at the phosphorus atom because of the greater tendency of phosphorus to form pyramidal compounds. However, indenyl and fluorenyl complexes of Sm^{II} are both η^5-coordinated.[35]

C. Pyrazolyl, Triphospholyl and Stibadiphospholyl Complexes

Raymond and Eigenbrodt, Jr. were the first to demonstrate the planar η^2-coordination mode of the pyrazolyl ligand (mode E) in uranium chemistry. The metathesis reactions of $[Cp_3UCl]$ and $[Cp^*_2UCl_2]$ with potassium pyrazolate afforded $[Cp_3U(pz)]$[36] (**31**, pz = pyrazolate) and $[Cp^*_2U(pz)_2]$[37] (**32**) or $[Cp^*_2U(Cl)(pz)]$[37] (**33**), respectively (depending on the stoichiometry).

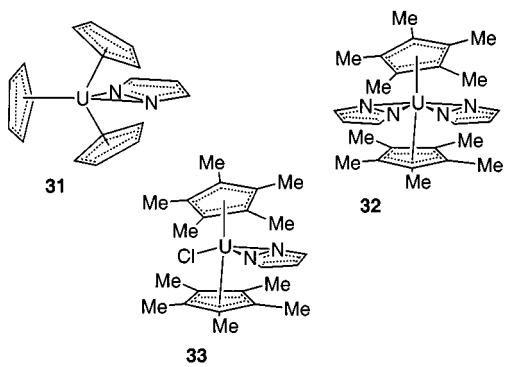

Early experiments involved the reaction of lanthanide halides with sodium pyrazolate or 3,5-dimethylpyrazolate (Dmpz). Polynuclear sodium pyrazolyllanthanoidates such as $[Ln_3(\mu\text{-Dmpz})_6(\eta^2\text{-Dmpz})_2(\mu^3\text{-O})Na_2(THF)_2]$ (Ln = Y, Ho, Yb, Lu) were obtained, in which the interstitial oxygen atom most likely originated from water present as an impurity in the solvents. Here, the Dmpz ligand can be found in coordination modes E and G.[38]

In almost all other group-3 pyrazolate metal complexes, coordination mode E is present for at least one of the pyrazolyl ligands. In $[LnL_3(D)_n]$ (L = substituted pyrazolyl; D = donor ligand), the coordination mode of the remaining pyrazolyl ligands depends on the substitution pattern of the pyrazolyl ring. With ligands possessing a group with relatively low steric bulk, such as Dmpz, both coor-

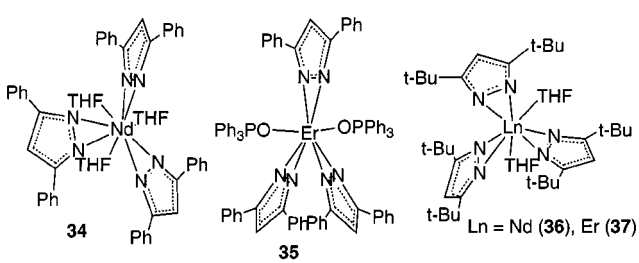

dination modes E and G can be found, e.g. in [{(η^2-Dmpz)$_2$(μ:η^1-Dmpz)Nd(μ-THF)}$_2$].[39] With bulkier pyrazoyls such as 3,5-diphenylpyrazolyl (Dppz) or 3,5-di-*tert*-butylpyrazolyl (Dtpz), only type E is encountered in [(η^2-Dppz)$_3$Nd(THF)$_3$] (**34**), [(η^2-Dppz)$_3$Ln(OPPh$_3$)$_2$] [Ln = La, Nd, Er (**35**)],[40] and [(η^2-Dtpz)$_3$Ln(THF)$_2$] [Ln = Y, La, Nd (**36**), Sm, Gd, Dy, Er (**37**), Yb, Lu].[41]

It should be noted that because Dppz is sterically less bulky than Dtpz, the coordination number for the Nd atom in **34** (c.n. = 9) is greater than in **36** (c.n. = 8). Likewise, there are two DME ligands (one chelating and one η^1) in 9-coordinate [(η^2-Dppz)$_3$Ln(η^2-DME)(η^1-DME)] [Ln = Er[42] (**38**), Nd[43] (**39**)] while the structure of 8-coordinate [{(η^2-Dtpz)$_3$Nd(μ-DME)}$_n$] is polymeric, with one bridging DME ligand[42] (**40**).

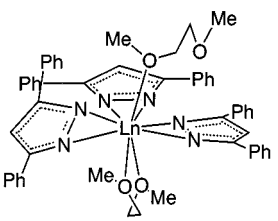

Ln = Er (**38**), Nd (**39**)

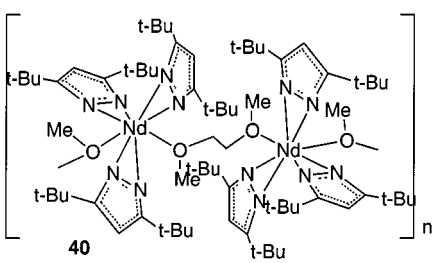

40

In the absence of donor solvents, the reaction of erbium chloride with KDtpz in toluene gave polymeric [{K(μ-Dtpz)$_3$Er}$_n$] (**41**) displaying an unprecedented η^3-interaction of the Dtpz ligand with the potassium atom. Adding 18-C-6 and DME to this polymer resulted in the isolation of a homoleptic 8-coordinate erbate complex, [{K(18-C-6)(DME)(Toluene)}$^+$ · {(η^2-Dtpz)$_4$Er}$^-$] (**42**).[44]

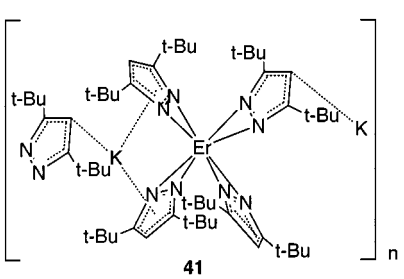

41

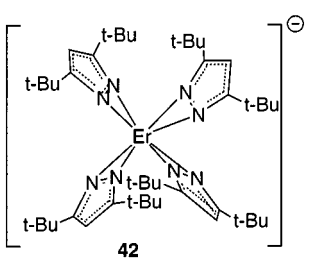

42

Neutral homoleptic complexes could be obtained under harsher conditions: Reaction of neat neutral HDtpz with the lanthanide metal in the presence of Hg metal at 220 °C had a different outcome, depending on the metal. The following compounds were obtained: complexes of Nd^{III} and Sm^{III}, [Ln(Dtpz)$_3$] (Ln = Sm, Nd), an Eu^{II} complex, [Eu(Dtpz)$_2$], and an interesting mixed valence Yb^{II,III} complex, [(η^2-Dtpz)$_3$(μ:η^2-Dtpz)$_2$Yb$_2$] (**43**) with coordination modes E and F. Coordination mode F is also present in [(η^2-Dtpz)$_4$(μ:η^2-Dtpz)$_2$Nd$_2$][45]

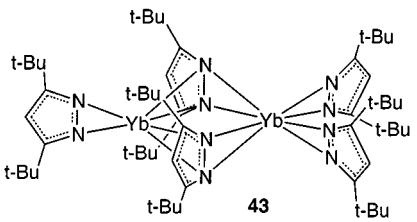

43

Ln^{II} complexes could be prepared by several routes, notably by redox-transmetallation reactions involving lanthanide powders and mild oxidants such as thallium or mercury pyrazolates or even diphenylmercury in the presence of pyrazoles. With DME as donor ligand, all complexes have the structure of 8-coordinate [(η^2-L)$_2$Ln(DME)$_2$] {Ln = Sm, Eu (**44**), Yb, L = Dtpz, Dppz, and 4,5-dihydro-2*H*-benz[*g*]indazolyl (**45**)}. The pyrazolyl ligands generally have the *cis* configuration, except in [(η^2-Dppz)$_2$Eu(DME)$_2$] in which they are *trans*.[46]

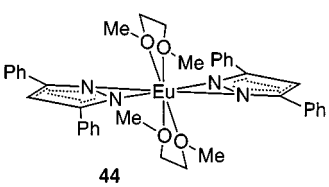

44

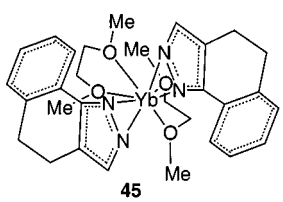

45

In the case of Yb and with THF as donor ligand, there is only one coordinated THF, and both coordination types E and F are present in [(η^2-Dtpz)$_2$(μ:η^2-Dtpz)$_2$Yb$_2$(THF)$_2$][47] (**46**).

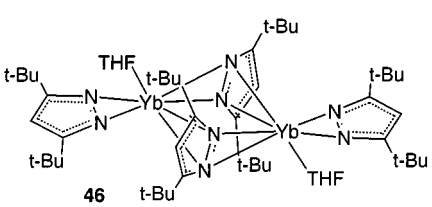

46

Organolanthanide complexes containing the pyrazolyl ligand have also been prepared. The reaction of [(η^5-MeC$_5$H$_4$)$_3$Ln] with Dmpz gave [(MeC$_5$H$_4$)Ln(Dmpz)$_2$] (Ln = Nd, Gd, Dy, Yb). These compounds reacted with silicone grease, and insertion of a dimethylsilanone unit into an Ln−N bond took place, thus affording dimeric [{(η^5-MeC$_5$H$_4$)(η^2-Dmpz)(μ:η^1,η^2-OSiMe$_2$-Dmpz)Ln}$_2$] [Ln = Yb[48a] (**47**), Dy[48b]]. In this oxygen-bridged dimer, both

Dmpz moieties display the type F (planar) coordination mode.[48]

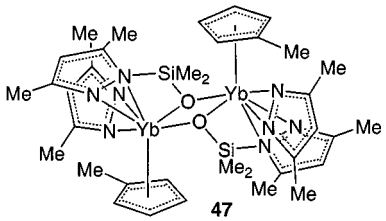
Me Me
SiMe2
Yb
O
N
Me
Me
Me

Almost all compounds described so far with this type of ligand display σ,π-complexation of both pyrrolyl rings to a lanthanide metal centre, and thus polynuclear complexes are obtained, frequently in cyclic structures. Generally, the two π-complexing rings belong to two different bridged ligands, but there is one example in which the lanthanide metal centre is π-complexed to two rings belonging to the same ligand.

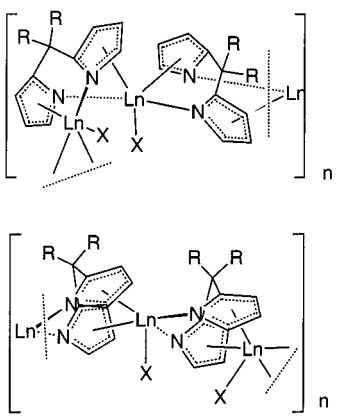

The proximity of the metal centres in these polynuclear complexes allow for the cooperative behaviour of the metallic centres: Reaction of K_2Dpdp with $SmI_2(THF)_2$ in the presence of nitrogen irreversibly gave a tetranuclear Sm^{III}−nitrogen (formally N_2^{4-}) complex, [{(μ:η^5,η^1-Dpdp)Sm}$_4$(μ:η^1,η^1,η^2,η^2-N_2)] (**57**). In the absence of nitrogen, a compound of global composition [{(Dpdp)Sm}$_7$ · SmI_2] was obtained; it is in fact a zwitterionic Sm^{II} species, [{(μ:η^5,η^1-Dpdp)Sm}$_5$(μ$_5$-I)$^-$ · {(μ:η^5,η^1-Dpdp)}$_2$Sm$_3$(THF)$_3$(μ$_3$-I)$^+$] (**58**). Reduction of this zwitterion with KH in the presence of N_2 yielded the nitrogen compound **57**.[53]

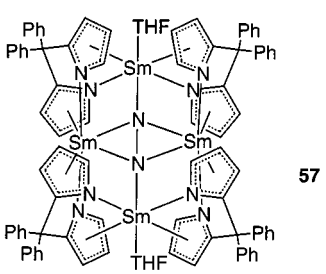

57

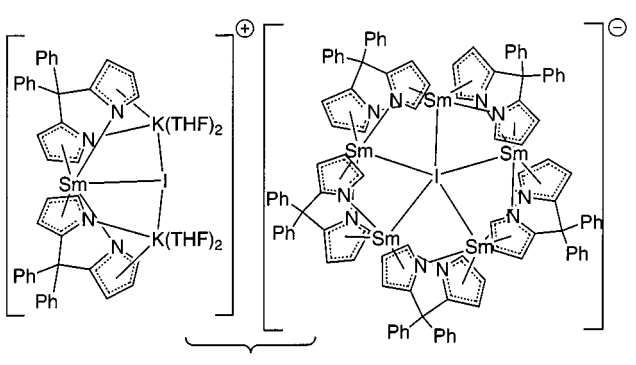

58

The reaction of K_2Dpdp with $SmCl_3(THF)_3$ gave a yellow compound (presumably [DpdpSmCl]) which was further reduced with alkali metals under argon; surprisingly, the outcome of this reduction was different, depending on the alkali metals used. With potassium, a tetrameric samarium(II) compound, [{(μ:η^5,η^1-Dpdp)Sm}$_4$(μ$_4$-Cl)K(THF)$_2$] (**59**), was obtained, which displays η^5-coordination of potassium with one pyrrolyl ring. With lithium and sodium, the reduction was not complete and mixed-valent $Sm^{II,III}$ octameric anionic complexes **60**, [{(μ:η^5,η^1-Dpdp)Sm}$_8$(μ$_4$-Cl)$_4$Li}$^{2-}$ · {$Li_2Cl(THF)_4$}$^+$ · {$Li(THF)_4$}$^+$], and **61**, [{(μ:η^5,η^1-Dpdp)Sm}$_8$(μ$_4$-Cl)$_4$Na}$^-$ · {$Na(THF)_5$}$^+$], respectively, were obtained. While the overall structures of **60** and **61** are similar, the reduction surprisingly occurred to a greater extent with lithium than with sodium since **60** displays one Sm^{III} and seven Sm^{II} atoms whereas in **61** there are two Sm^{III} and six Sm^{II} atoms. The reaction of **60** and **61** with KH in the presence of N_2 gave the above-mentioned tetranuclear Sm nitrogen complex **57**.[54]

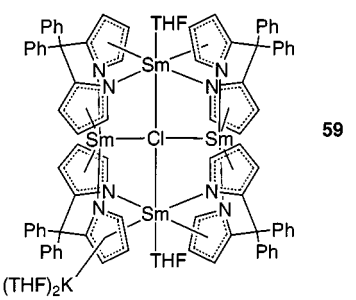

59

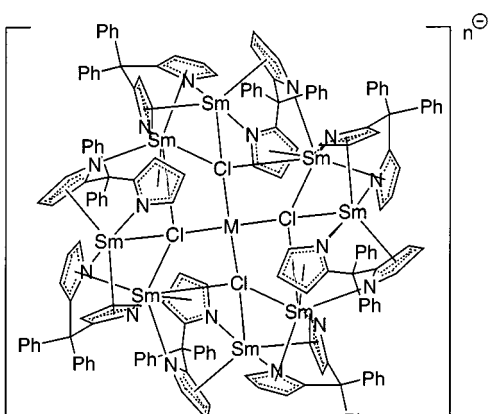

M = Li, n = 2 (**60**)
M = Na, n = 1 (**61**)

The reaction of Li_2Dpdp with $YbCl_3(THF)_3$ gave a yellow-orange compound (presumably [DpdpYbCl]) that was further reduced to Yb^{II} complexes with alkali metals. With lithium an octameric ytterbium(II) dianionic species, [{(μ:η^5,η^1-Dpdp)Yb}$_8$(μ$_3$-Cl)$_2$Li}$^{2-}$ · {[$Li(THF)_4$]$^+$}$_2$] (**62**) was obtained, whereas with sodium a monomeric ytterbate(II) complex, [(μ:η^5,η^1-Dpdp)$YbNa_2(THF)_4$] (**63**), was isolated displaying μ:η^5,η^1-type coordination both to ytterbium and to sodium.[55]

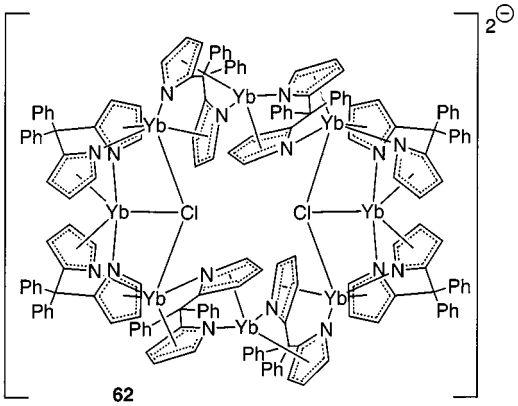

62

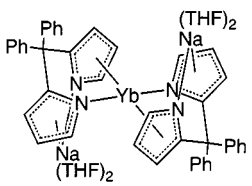

63

Structural variations of the dipyrrolyl ligand included the use of the Dpch and Dpet ligands in samarium chemistry. The reaction of K_2Dpet with $SmI_2(THF)_2$ gave a pentanuclear μ-iodo anionic complex, $[\{(\mu{:}\eta^5,\eta^1\text{-Dpet})Sm\}_5(\mu_5\text{-}I)^- \cdot K(THF)_6^+]$ (**64**), similar to that observed with the Dpdp ligand. Each metal centre is now π-bonded to pyrrolyl rings belonging to the same ligand. The results obtained with the Dpch ligands are different since reaction of K_2Dpch with $SmI_2(THF)_2$ or of Na_2Dpch with $SmCl_3(THF)_3$ followed by reduction with sodium metal afforded a mixed-valence complex, $[\{(\mu{:}\eta^5,\eta^1\text{-Dpch})Sm\}_4(\mu_2\text{-}O)(THF)_2]$ (**65**). Presumably, the oxygen atom comes from a THF molecule. It thus seems that the modifications on the ligand greatly affect the redox potential of the coordinated metal centres.[56]

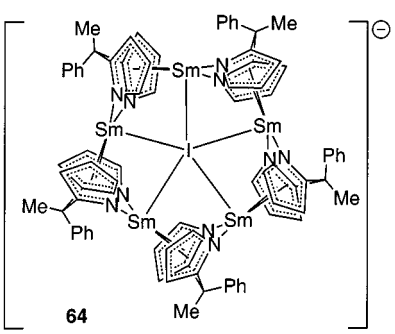

64

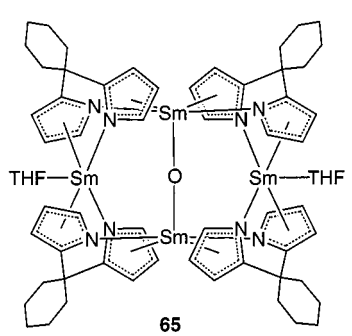

65

B. Macrocyclic Tetrapyrrolyl Complexes

Cyclic calix[4]tetrapyrrolyl (also called porphynogen) macrocyclic ligands have been used in lanthanide chemistry. These ligands provide a rather rigid environment in which the lanthanide metal centre can use most of its coordination sites, often in an $\eta^5,\eta^1,\eta^5,\eta^1$-coordination mode with the pyrrolyl rings, one or two coordination sites on the metal centre then being left for chemical transformations. In addition, the very electron-rich environment (up to four negative charges on the tetrapyrrolide anion) enhances the reactivity of the metal centre towards the activation of small molecules, as reported hereafter. Two ligands have been used, mainly octaethylporphynogen (Oepg) as well as cyclohexylporphynogen (Chpg) (Scheme 1).

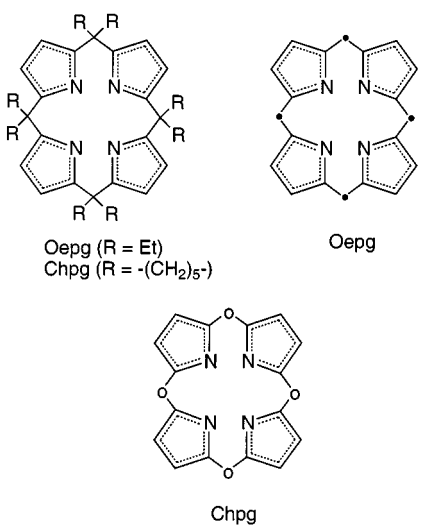

Oepg (R = Et)
Chpg (R = -(CH$_2$)$_5$-)

Oepg

Chpg

Scheme 1. For clarity, the following abbreviations are used in the subsequent schemes: • = C(Et)$_2$, o = C [−(CH$_2$)$_5$−]

The outcome of the reaction of $LnCl_3$ with porphynogen anions depends very much on the nature of the counterion; the reactions of the lithium salts are described first.

The reaction of $OepgLi_4$ with $YCl_3(THF)_{3.5}$ gave an enolate complex, $[Li(THF)_2(Oepg)Y(\mu\text{-}OCH{=}CH_2)Li(THF)]$ (**66**), in which the yttrium atom is $\eta^5,\eta^1,\eta^1,\eta^1$-bonded to the Oepg ligand. The enolate moiety probably arises from THF cleavage. Attempted substitution of this enolate with an alkyl or hydride group was unsuccessful and instead a lithium salt of the Oepg ligand, $[\{(Oepg)[Li(THF)]_4\}\{(THF)Li(OCH{=}CH_2)\}_2]$, was isolated[57].

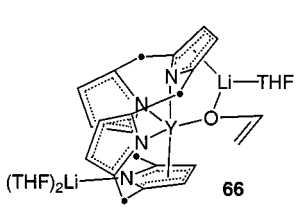

66

The reaction of $SmCl_3(THF)_3$ with $OepgLi_4$ or $ChpgLi_4$ gave $[(Oepg)ClSm(\mu_3\text{-}Cl)Li_3(THF)_4]$ (**67**) and $[(Chpg)ClSm(\mu_3\text{-}Cl)Li_3(THF)_4]$, respectively. In this case, the Sm atom displays $\eta^5,\eta^1,\eta^5,\eta^1$-coordination with the pyrrolyl ligands, and the lithium atoms are also bonded to the pyrrolyl groups. These compounds have a very rich chemistry: The reaction of $[(Oepg)ClSm(\mu_3\text{-}Cl)Li_3(THF)_4]$ with RLi gave the σ-bonded $[(Oepg)RSm(\mu_3\text{-}Cl)Li_3(THF)_4]$ [R = Me, vinyl (**68**)]. Treatment of $[(Oepg)RSm(\mu_3\text{-}Me)Li_3(THF)_4]$ with H_2 or phenylsilane afforded an Sm^{III} hydride, $[(Oepg)(THF)Sm(\mu_3\text{-}H)Li_2(THF)_2]$ (**69**), which could also be conveniently obtained from $[(Oepg)RSm(\mu_3\text{-}Cl)Li_3(THF)_4]$ by reaction with $LiAlH_4$. Compound **68** was thermally unstable and decomposed into an Sm^{II} complex, $[(Oepg)(THF)Sm(\mu_3\text{-}Cl)Li_3(THF)_4]$.[58]

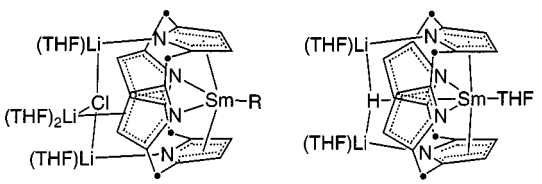

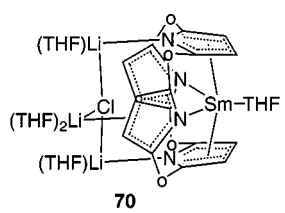

Similar μ_3-chloro−Sm^{II} complexes are also available by lithium reduction of the appropriate chloro−Sm^{III} complexes: Reaction of lithium with $[(Chpg)ClSm(\mu_3\text{-}Cl)Li_3(THF)_4]$ under argon gave $[(Chpg)(THF)Sm(\mu_3\text{-}Cl)Li_3(THF)_4]$ (**70**) while reduction of $[(Oepg)ClSm(\mu_3\text{-}Cl)Li_3(THF)_4]$ resulted in an μ_3-enolato−Sm^{II} complex, $[(Oepg)(Et_2O)Sm(\mu_3\text{-}OCH{=}CH_2)Li_3(THF)_2]$ (**71**), in which the enolate moiety is again likely to arise from THF cleavage. This complex **71** reversibly added ethylene to give an Sm^{III} dimer, $[\{(Oepg)Sm(\mu_3\text{-}OCH{=}CH_2)Li_3(THF)_2\}_2(\mu\text{-}CH_2CH_2)]$ (**72**), in which the ethylene has been formally reduced to its dianion as suggested by the long C−C bond (1.49 Å).[59] The reaction of lithium with $[(Oepg)ClSm(\mu_3\text{-}Cl)Li_3(THF)_4]$ [formed in situ by reaction of $SmCl_3(THF)_3$ and $OepgLi_4$] under nitrogen resulted in nitrogen reduction and the formation of an Sm^{III} complex containing a tetralithium hydrazide, $[\{(Oepg)SmLi\ (THF)_2\}_2(N_2Li_4)]$ (**73**), presumably through a transient Sm^{II} species which is reoxidized to Sm^{III} by means of an electron transfer to N_2.[60]

A different series of complexes was obtained when the reaction stoichiometry of Sm and Oepg is 2:1. The reaction of 2 equivalents of $SmCl_3(THF)_3$ with one equivalent of $OepgLi_4$ gave the dinuclear $[(Oepg)\{Sm(\mu\text{-}Cl)_2Li(THF)_2\}_2]$ (**74**) in which both Sm atoms are $\eta^5,\eta^1,\eta^5,\eta^1$-coordinated to the Oepg ligand. Permethylation of this complex with MeLi afforded $[(Oepg)\{Sm(\mu\text{-}Me)_2Li(THF)_2\}_2]$ (**75**). Hydrogenolysis of **75** did not give the expected result (replacement of the two μ-Me ligands by two μ-H ligands) but instead yielded the above-mentioned monosamarium hydride complex **69**. This complex **69** was also obtained by reduction of **74** with phenylsilane, but in this case a bis(μ-enolate) intermediate, $[(Oepg)(THF)Sm(\mu_3\text{-}H)Li_2(\mu_3\text{-}OCH{=}CH_2)_2Li_2(THF)_2]$ (**76**), was isolated.[61]

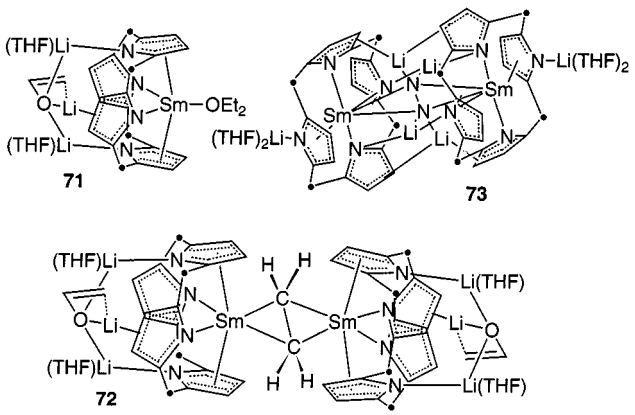

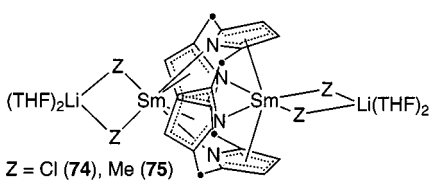

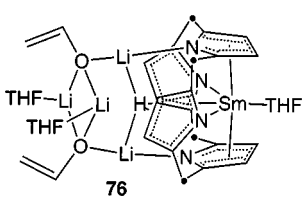

The reaction of **74** with $LiAlH_4$ did not give the expected dihydride either but instead reduction to Sm^{II} occurred. This reduction could be performed stepwise. Depending on the reaction conditions, a mixed-valent $Sm^{II,III}$ complex, $[(THF)_2Sm(Oepg)Sm(\mu\text{-}Cl)_2Li(THF)_2]$ (**77**), or a fully reduced Sm^{II} complex, $[(Oepg)Sm_2(THF)_4]$ (**78**), was obtained. This latter complex could also be made by lithium reduction of **74** or by the metathesis reaction of $OepgLi_4$ with $SmI_2(THF)_2$. The closely related $[(Oepg)Sm_2(Et_2O)_2]$ (**79**) could be prepared by the acid−base reaction of the Sm^{II} precursor, $[\{(TMS)_2N\}_2Sm(Tmeda)]$, with $OepgH_4$.[60b] All bimetallic Oepg−Sm complexes described above display a remarkably short Sm−Sm distance (3.30−3.40 Å), with the consequence that the magnetic moments of **78** and **79** (1.98 and 1.95 μ_B, respectively) are much lower than expected, presumably because of a magnetic interaction between the two Sm atoms.[61]

The reaction of the sodium salt of Oepg ($OepgNa_4$) with lanthanide halides provides an entry into yet another class of compounds. Here, the structure of the isolated products

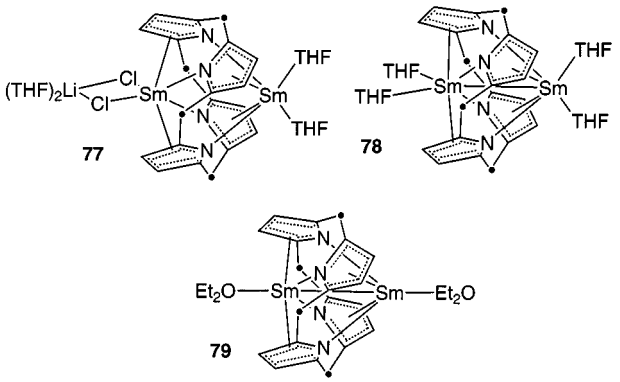

is very much dependent on the reaction conditions and in particular on the solvent used in the reaction and/or for recrystallisation. In all cases there are no anionic ligands other than the Oepg macrocycle bonded to the Ln metal centre (such as chloride or enolate as described above when $OepgLi_4$ was used as the precursor). In THF, the reaction of $OepgNa_4$ with $LnCl_3(THF)_n$ gave [(Oepg)Ln(THF)Na(THF)$_2$] [Ln = Pr, Nd, Sm, Eu, Gd (**80**), Yb], in which the ligand is $\eta^5,\eta^1,\eta^5,\eta^1$-coordinated to the lanthanide metal centre and the sodium is η^3-ligated to one of the pyrrolyl rings and η^1-bonded to a nitrogen atom on another. By recrystallisation from DME, striking structural changes occur and $[\{(Oepg)_2Ln_2\}^{2-} \cdot 2\ \{Na(DME)_3\}^+]$ [Ln = Pr, Nd, Sm (**81**) Eu, Gd] were obtained. In these compounds, the macrocyclic ring bonded to the lanthanide centre has dimerised, with the formation of an Ln−C(pyrrole) σ-bond owing to C−H activation by the Ln metal centre. Further recrystallisation of these complexes in THF, THF/DME, or THF/dioxane mixtures only affects the coordination mode of the sodium atom and the $(Oepg)_2Ln_2$ dimeric structure in $[\{(Oepg)_2Ln_2\}\{Na(S)_2\}_2]$ (Ln = Pr, Nd, Sm, Gd; S = DME or THF) (**82**: Ln = Pr, S = DME) and in the polymeric $[(\{(Oepg)_2Ln_2\}\{Na(THF)\}_2\{\mu\text{-Dioxane}\})_n]$ (Ln = Nd, Gd) is left intact. Thus, it appears that the Oepg dimerisation by C−H activation is essentially irreversible.[62]

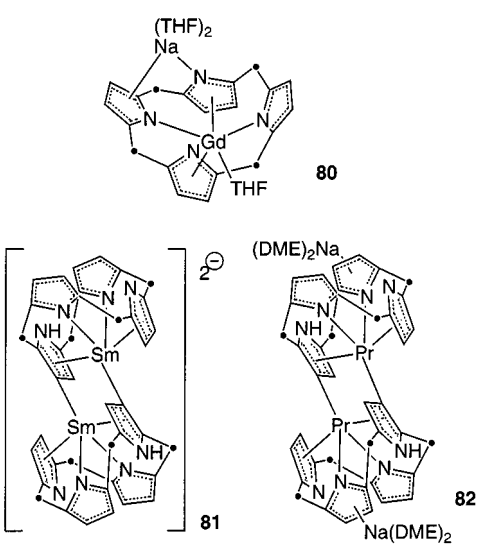

The reaction of [(Oepg)Ln(THF)Na(THF)$_2$] with sodium naphthalenide in the presence of N_2 resulted in the reduction and formation of a diazenide dianion (N_2^{2-}) complexed to two OepgLn entities, $[\{[Na(THF)_2]_2(Oepg)Ln\}_2(\mu{:}\eta^2,\eta^2\text{-}N_2)]$ (Ln = Pr, Nd). Again, recrystallisation from donor solvents resulted in structural variations concerning the bonding properties of the sodium cation: In dioxane two sodium atoms are also bonded to the diazenide ligand in $[\{[Na(Dioxane)_2(Oepg)Nd(Dioxane)Na]_2(\mu{:}\eta^1\mathit{Na},\eta^2\mathit{Nd},\eta^1\mathit{Na}',\eta^2\mathit{Nd}'\text{-}N_2)]$ (**83**), while in DME only one sodium atom is bonded to the Oepg moiety in the anionic complex $[\{[Na(THF)_2(Oepg)Pr]_2(\mu{:}\eta^2,\eta^2\text{-}N_2)\}^{2-} \cdot 2\ \{Na(DME)_3\}^+]$ (**84**). Evidence for a diazenide is provided by the N=N bond length (1.24 Å).[63]

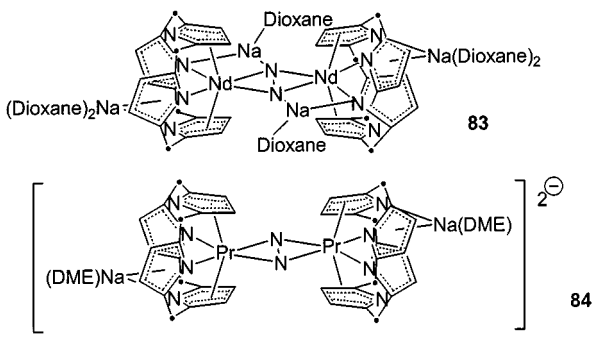

Similarly, reduction of [(Oepg)Ln(THF)Na(THF)$_2$] (Ln = Pr, Nd) with sodium naphthalenide in the presence of ethylene yielded $[\{[Na(THF)_2(Oepg)Ln]_2(\mu{:}\eta^2,\eta^2\text{-}CH_2CH_2)\}^{2-} \cdot \{Na_2(THF)(18\text{-}C\text{-}6)_2(\mu\text{-Dioxane})\}^{2+}]$ [Ln = Pr, Nd (**85**)] in which the ethylene has been reduced to ($CH_2CH_2^{2-}$) as indicated by the C−C single-bond length of 1.49 Å. Interestingly, these compounds could also be obtained from the above-mentioned diazenide complexes **83** and **84** simply by reaction with ethylene in the presence of [18-C-6]. The behaviour of [(Oepg)Ln(THF)Na(THF)$_2$] in the presence of sodium naphthalenide has been attributed to a reduction of these complexes to transient Pr^{II} and Nd^{II} species which are then able to activate small molecules such as N_2 or C_2H_4 by electron transfer.

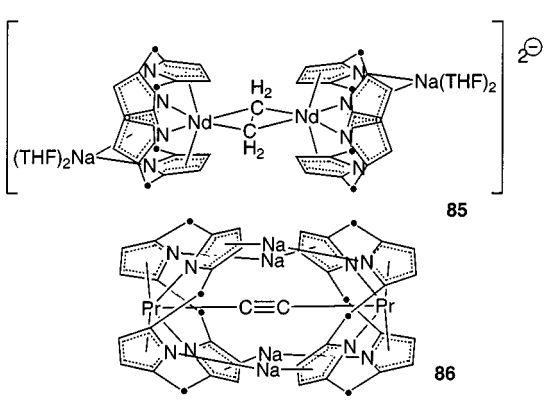

When the [(Oepg)Ln(THF)Na(THF)$_2$] (Ln = Pr, Nd)/sodium naphthalenide methodology was applied to acetylene,

deprotonation occurred (not reduction) and the resulting acetylide led to the formation of $[\{(Oepg)LnNa_2\}_2(\mu\text{-}C{\equiv}C)]$ (**86**) in which four unsolvated sodium atoms and the C≡C unit are inserted as "spacers" between the two OepgLn units.[64]

Conclusion

The use of heterocyclopentadienyl ligands in group-3 metal chemistry has led to the formation of compounds with several coordination modes. Some of them exhibit remarkable reactivity, for instance, in the activation of small molecules (N_2 and ethylene) and in achieving transient uncommon low-valent oxidation states [Pr^{II}, Nd^{II}]. From here, there are some obvious challenges that for some of them will, undoubtedly, be met in the future.

The relatively electron-poor π-phospholyl ligand might be used to stabilise uncommon lanthanide(II) oxidation states such as Tm^{II}. There is also a clear synthetic challenge to include the phospholyl or other phosphorus-based ligands in the bridged or cavitand-like structures such as those used with the pyrrolyl ligand.

As far as nitrogen-based ligands are concerned, there still remains the objective of preparing a complex with an η^5-coordinated pyrazolyl ligand. The reactivity of the bridged or cavitand-like pyrrolyl complexes with other small molecules such as CO and CO_2 will certainly be investigated.

The actinide chemistry is relatively underrepresented, especially in the domain of the nitrogen-based ligands.

Finally, several reported complexes have great potential in catalytic applications.[65]

Acknowledgments

Financial support of this work by CNRS and Ecole Polytechnique is acknowledged. The author also wishes to thank Professor Nixon for permission to disclose unpublished results.

[1] [1a] F. T. Edelmann, in: *Comprehensive Organometallic Chemistry II* (Eds.: E.W. Abel, F. G. A. Stone), vol.4 (Scandium, Yttrium, Lanthanides, Actinides, and Titanium group), Pergamon Press, Oxford, **1995**, p. 11. – [1b] H. Schumann, J. A. Meese-Marktscheffel, L. Esser, *Chem. Rev.* **1995**, *95*, 865–986. – [1c] C.J. Schavieren, *Adv. Organomet. Chem.* **1995**, *36*, 283–362.

[2] [2a] H.Yasuda, H. Tamai, *Prog. Polym. Sci.* **1993**, *18*, 1097–1139. – [2b] G. A. Molander, E. D. Dowdy, in: *Topics in Organometallic Chemistry*, vol. 2 (Lanthanides: Chemistry and Use in Organic Synthesis) (Ed.: S. Kobayashi), Springer-Verlag, Heidelberg, Germany, **1999**, p. 120. – [2c] R. Anwander, in: *Applied Homogeneous Catalysis with Organometallic Compounds*, vol. 2 (Eds.: B. Cornils, W. A. Herrmann), VCH Publishers, New York, **1996**, sect. 3.2.5, p. 866.

[3] H. Schumann, P. R. Lee, A. Dietrich, *Chem. Ber.* **1990**, *123*, 1331–1334.

[4] T. J. Marks, J. R. Kolb, *J. Organomet. Chem.* **1974**, *82*, C35–C39.

[5] H. Schumann, J. Winterfeld, H. Hemling, N. Kuhn, *Chem. Ber.* **1993**, *126*, 2657–2659.

[6] H. Schumann, E. C. E. Rosenthal, J. Winterfeld, G. Kociok-Köhn, *J. Organomet. Chem.* **1995**, *495*, C12–C14.

[7] H. Schumann, E. C. E. Rosenthal, J. Winterfeld, R. Weimann, J. Demtschuk, *J. Organomet. Chem.* **1996**, *507*, 287–289.

[8] K. B. Dillon, F. Mathey, J. F. Nixon, *Phosphorus: the Carbon Copy*, Wiley, Chichester, **1998**.

[9] F. Nief, F. Mathey, *J. Chem. Soc., Chem. Commun.* **1989**, 800–801.

[10] F. Nief, P. Riant, L. Ricard, P. Desmurs, D. Baudry-Barbier, *Eur. J. Inorg. Chem.* **1999**, 1041–1045.

[11] W. J. Evans, J. M. Olofson, H. Zhang, J. L. Atwood, *Organometallics* **1988**, *7*, 629–633.

[12] F. Nief, L. Ricard, F. Mathey, *Polyhedron* **1993**, *12*, 19–26.

[13] F. Nief, F. Mathey, *Synlett* **1991**, 745–746.

[14] W. J. Evans, L. A. Hughes, T. P. Hanusa, *J. Am. Chem. Soc.* **1984**, *106*, 4270–4272.

[15] P. Desmurs, A. Dormond, F. Nief, D. Baudry, *Bull. Soc. Chim. Fr.* **1997**, *134*, 683–688.

[16] P. Desmurs, M. Visseaux, D. Baudry, A. Dormond, F. Nief, L. Ricard, *Organometallics* **1996**, *15*, 4178–4181.

[17] F. Nief, L. Ricard, *J. Chem. Soc., Chem. Commun.* **1994**, 2723–2724.

[18] [18a] W. J. Evans, K. J. Forrestal, J. T. Leman, J. W. Ziller, *Organometallics* **1996**, *15*, 527–531. – [18b] W. J. Evans, C. A. Seibel, J. W. Ziller, *J. Am. Chem. Soc.* **1998**, *120*, 6745–6752. – [18c] W. J. Evans, K. J. Forrestal, J. W. Ziller, *Angew. Chem. Int. Ed. Engl.* **1997**, *36*, 774.

[19] H. Schumann, M. Glanz, H. Hemling, *J. Organomet. Chem.* **1993**, *445*, C1–C3.

[20] H.-J. Gosink, F. Nief, L. Ricard, F. Mathey, *Inorg. Chem.* **1995**, *34*, 1306–1307.

[21] F. Nief, L. Ricard, unpublished results.

[22] P. Gradoz, D. Baudry, M. Ephritikhine, M. Lance, M. Nierlich, J. Vigner, *J. Organomet. Chem.* **1994**, *466*, 107–118.

[23] D. Baudry, M. Ephritikhine, F. Nief, L. Ricard, F. Mathey, *Angew. Chem. Int. Ed. Engl.* **1990**, *29*, 1485–1486.

[24] P. Gradoz, D. Baudry, M. Ephritikhine, F. Nief, F. Mathey, *J. Chem. Soc., Dalton. Trans.* **1992**, 3047–3051.

[25] P. Gradoz, M. Ephritikhine, M. Lance, J. Vigner, M. Nierlich, *J. Organomet. Chem.* **1994**, *481*, 69–73.

[26] P. Gradoz, C. Boisson, D. Baudry, M. Lance, M. Nierlich, J. Vigner, M. Ephritikhine, *J. Chem. Soc., Chem. Commun.* **1992**, 1720–1721.

[27] F. G. N. Cloke, S. A. Hawkes, P. B. Hitchcock, P. Scott, *Organometallics* **1994**, *13*, 2895–2897.

[28] T. Arliguie, M. Ephritikhine, M. Lance, M. Nierlich, *J. Organomet. Chem.* **1996**, *524*, 293–297.

[29] W. J. Evans, G. W. Rabe, J. W. Ziller, *Organometallics* **1994**, *13*, 1641–1645.

[30] C. T. Abrahams, G. B. Deacon, C. M. Forsyth, W. C. Patalinghug, B. W. Skelton, A. H. White, *Aust. J. Chem.* **1995**, *48*, 1933–1947.

[31] G. B. Deacon, C. M. Forsyth, B. M. Gatehouse, P. A. White, *Aust. J. Chem.* **1990**, *43*, 795–806.

[32] C. T. Abrahams, G. B. Deacon, B. M. Gatehouse, G. N. Ward, *Acta Crystallogr., Sect. C (Cryst. Struct. Commun.)* **1994**, *50*, 504–507.

[33] F. Nief, L. Ricard, *J. Organomet. Chem.* **1994**, *464*, 149–154.

[34] F. Nief, L. Ricard, unpublished results.

[35] W. J. Evans, T. S. Gummersheimer, T. J. Boyle, J. W. Ziller, *Organometallics* **1994**, *13*, 1281–1284.

[36] C. N. Eigenbrot, Jr., K. N. Raymond, *Inorg. Chem.* **1981**, 1553–1556.

[37] C. N. Eigenbrot, Jr., K. N. Raymond, *Inorg. Chem.* **1982**, 2653–2660.

[38] H. Schumann, P. K. Lee, J. Löbel, *Angew. Chem. Int. Ed. Engl.* **1989**, *28*, 1033–1035.

[39] G. B. Deacon, B. M. Gatehouse, S. Nickel, S. N. Platts, *Aust. J. Chem.* **1991**, *44*, 613–621.

[40] J. E. Cosgriff, G. B. Deacon, B. M. Gatehouse, *Aust. J. Chem.* **1993**, *46*, 1881–1896.

[41] [41a] J. E. Cosgriff, G. B. Deacon, B. M. Gatehouse, H. Hemling, H. Schumann, *Angew. Chem. Int. Ed. Engl.* **1993**, *32*, 874–875. – [41b] J. E. Cosgriff, G. B. Deacon, B. M. Gatehouse, H. Hemling, H. Schumann, *Aust. J. Chem.* **1994**, *47*, 1223–1235.

[42] J. E. Cosgriff, G. B. Deacon, G. D. Fallon, B. M. Gatehouse, H. Schumann, R. Weimann, *Chem. Ber.* **1996**, *126*, 953–958.

[43] G. B. Deacon, E. E. Delbridge, G. D. Fallon, C. Jones, D. E. Hibbs, M. B. Hursthouse, B. W. Skelton, A. H. White, *Organometallics* **2000**, *19*, 1713–1721.

[44] G. B. Deacon, E. E. Delbridge, C. M. Forsyth, *Angew. Chem. Int. Ed.* **1999**, *38*, 1766−1767.
[45] G. B. Deacon, A. Gitlits, B. W. Skelton, A. H. White, *Chem. Commun.* **1999**, 1213−1214.
[46] [46a] G. B. Deacon, E. E. Delbridge, B. W. Skelton, A. H. White, *Eur. J. Inorg. Chem.* **1998**, 543−565. − [46b] G. B. Deacon, E. E. Delbridge, B. W. Skelton, A. H. White, *Eur. J. Inorg. Chem.* **1999**, 751−761.
[47] G. B. Deacon, E. E. Delbridge, B. W. Skelton, A. H. White, *Angew. Chem. Int. Ed.* **1998**, *37*, 2251−2252.
[48] [48a] X. Zhou, H. Ma, X. Yuang, X. You, *J. Chem. Soc., Chem. Commun.* **1995**, 2483−2484. −[48b] X. Zhou, W. Ma, Z. Huang, R. Cai, X. You, X. Huang, *J. Organomet. Chem.* **1997**, *545−546*, 309−314.
[49] H. Schumann, J. Loebel, J. Pickart, C. Quian, Z. Xie, *Organometallics* **1991**, *10*, 215−219.
[50] G. K. B. Clentsmith, F. G. N. Cloke, P. B. Hitchcock, M. D. Francis, J. F. Nixon, A. G. Avent, unpublished results.
[51] G. K. B. Clentsmith, F. G. N. Cloke, P. B. Hitchcock, M. D. J. Hanks, J. F. Nixon, unpublished results.
[52] P. L. Arnold, F. G. N. Cloke, P. B. Hitchcock, *Chem. Commun.* **1997**, 481−482.
[53] T. Dubé, S. Conoci, S. Gambarotta, G. P. A. Yap, G. Vasapollo, *Angew. Chem. Int. Ed.* **1999**, *38*, 3657−3659.
[54] T. Dubé, S. Gambarotta, G. P. A. Yap, S. Conoci, *Organometallics* **2000**, *19*, 115−117.
[55] T. Dubé, D. Freckmann, S. Conoci, S. Gambarotta, G. P. A. Yap, *Organometallics* **2000**, *19*, 209−211.
[56] T. Dubé, S. Conoci, S. Gambarotta, G. P. A. Yap, *Organometallics* **2000**, *19*, 1182−1185
[57] J. Jubb, S. Gambarotta, R. Duchateau, J. H. Teuben, *J. Chem. Soc., Chem. Commun.* **1994**, 2641−2642.
[58] T. Dubé, S. Gambarotta, G. P. A. Yap, *Organometallics* **2000**, *19*, 121−126.
[59] T. Dubé, S. Gambarotta, G. P. A. Yap, *Angew. Chem. Int. Ed.* **1999**, *38*, 1432−1435.
[60] [60a] J. Jubb, S. Gambarotta, *J. Am. Chem. Soc.* **1994**, *116*, 4477−4478. − [60b] J.-I. Song, S. Gambarotta, *Angew. Chem. Int. Ed. Engl.* **1995**, *34*, 2141−2143.
[61] T. Dubé, S. Gambarotta, G. P. A. Yap, *Organometallics* **2000**, *19*, 817−823.
[62] E. Campazzi, E. Solari, R. Scopelliti, C. Floriani, *Inorg. Chem.* **1999**, *38*, 6240−6245.
[63] E. Campazzi, E. Solari, C. Floriani, R. Scopelliti, *Chem. Commun.* **1998**, 2603−2604.
[64] E. Campazzi, E. Solari, R. Scopelliti, C. Floriani, *Chem. Commun.* **1999**, 1617−1618.
[65] Phospholyl complexes of the group-4 metals have already been tested in catalysis, e. g. see: E. J. M. de Boer, I. J. Gilmore, F. M. Korndorfer, A. D. Horton, A. van der Linden, B. W. Royan, B. J. Ruisch, L. Schoon, R. W. Shaw, *J. Mol. Catal. A: Chem.* **1998**, *128*, 155−165.

Received July 3, 2000
[I00262]

Stability of the Metal Configuration in Chiral-at-Metal Half-Sandwich Compounds

Henri Brunner[a]

Keywords: Chirality / Half-sandwich complexes / Metal configuration / Configuration determination / Fluxionality

Half-sandwich compounds with a three-legged piano-stool geometry are prominent examples of optically active chiral-at-metal complexes. In these compounds, the configuration at the metal atom may be stable or labile in solution. Configurationally stable compounds can be used for the elucidation of the stereochemical course of substitution reactions and for organic synthesis in ligand transformation reactions. With configurationally labile compounds, the rate of change of the metal configuration can be measured, which sets an upper limit with regard to the handling of the compounds in solution. Surprisingly, in a number of recent papers the lability of the metal configuration has been overlooked resulting in misinterpretations and wrong conclusions.

Introduction

Organometallic compounds of the transition elements with chiral metal atoms can be resolved with respect to the metal configuration for many different ligand combinations and geometries.[1−21] As discussed in a recent review,[1] pseudo-tetrahedral half-sandwich complexes with a three-legged piano stool geometry, as in $\boldsymbol{R}_{\mathrm{Mn}}$-**1** and $\boldsymbol{S}_{\mathrm{Mn}}$-**1**,[22,23] are prominent examples. For the specification of the metal configuration, see refs.[24,25]

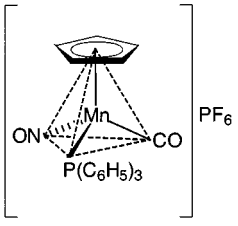

$\boldsymbol{R}_{Mn}$-1

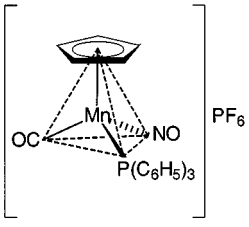

$\boldsymbol{S}_{Mn}$-1

[a] Institut für Anorganische Chemie der Universität, D-93040 Regensburg, Germany
Fax: (internat.) +49-(0)941/943-4439
E-mail: henri.brunner@chemie.uni-regensburg.de

In a classical resolution procedure, a racemic mixture is converted into a pair of diastereomers by introducing an enantiomerically pure auxiliary. The auxiliary is then removed from the separated diastereomers to give the resolved enantiomers. The ultimate goal of such a resolution is to obtain both enantiomers in pure form. Enantiomers have mirror image chiroptical properties but give identical NMR spectra; their NMR differentiation is only possible with the help of chiral shift-reagents.

Diastereomers differ in their physical properties, such as solubility, and usually also in their ^{1}H NMR spectra. Therefore, the progress of the diastereomer separation can be monitored by NMR spectroscopy and the diastereomer ratio can be determined by the integration of suitably resolved signals. Thus, the NMR spectrum of a given diastereomer shows whether the "other" diastereomer is present or absent, without the need for the addition of a chiral shift-reagent. As far as NMR differentiation is concerned, diastereomers thus contain more information than enantiomers.

In most of the organometallic compounds described herein, the optically active auxiliary is part of one of the ligands. Usually, it is not easy to remove the chiral auxiliary after diastereomer separation. Therefore, resolution proced-

Henri Brunner was born in 1935 and studied chemistry at the University of Munich. He obtained his Ph. D. (1963) under the supervision of E. O. Fischer. After a postdoctoral year at the University of California, Los Angeles, with Prof. H. D. Kaesz, he completed his "habilitation" at the TU Munich in 1969. In 1970, he became Chair of Inorganic Chemistry at the University of Regensburg, a position which he still occupies. His research fields concern the stereochemistry of organometallic compounds and reactions, enantioselective catalysis, and the use of platinum complexes in the chemotherapy of cancer. He has received several awards, most recently the German−French Alexander von Humboldt Award (1993), the Max Planck Award for International Cooperation (1997), and the Horst Pracejus Award of the German Chemical Society (1999).

MICROREVIEWS: This feature introduces the readers to the authors' research through a concise overview of the selected topic. Reference to important work from others in the field is included.

 © WILEY-VCH Verlag GmbH, 69451 Weinheim, 2001 1434−1948/01/0404−0905 $ 17.50+.50/0

ures frequently stop after separation of the diastereomers, which differ only in the configuration at the metal atom.

In solution, the chiral-at-metal compounds behave differently. Some of them prove to be configurationally stable; their metal configuration does not change even at higher temperatures. Others are labile with respect to the metal configuration; the isomers interconvert at various rates. The solution behavior is in contrast to the behavior in the solid state. All of the organometallic compounds discussed herein are configurationally stable at the metal atom in the solid state, even those which are configurationally labile in solution. This fact was already emphasized in the very first study.[22] It is the configurational stability at the metal center in organometallic compounds in solution which is the key aspect of this Microreview. The configurational stability sets an upper limit with regard to the handling of a given compound in solution and to the conditions for its reactions in which the stereochemical course with respect to the metal center is to be elucidated. It also determines the accessible temperature range for measuring the kinetics of the change of the metal configuration. Another reason for taking up the issue of the stability of the metal configuration in this Microreview is its misinterpretation in a number of recent papers, which has led to wrong conclusions (see later).

Measurement of the Change of Configuration at the Metal Atom

The configurational change at the metal atom can be monitored by polarimetric measurements. In such measurements, enantiomeric complexes that contain only chiral metal atoms approach the 1:1 racemization equilibrium. Figure 1 shows the decrease in the optical activity and the approach to the racemization equilibrium $\boldsymbol{R}_{Mn}$-**2** $\leftrightharpoons$ $\boldsymbol{S}_{Mn}$-**2**.[26]

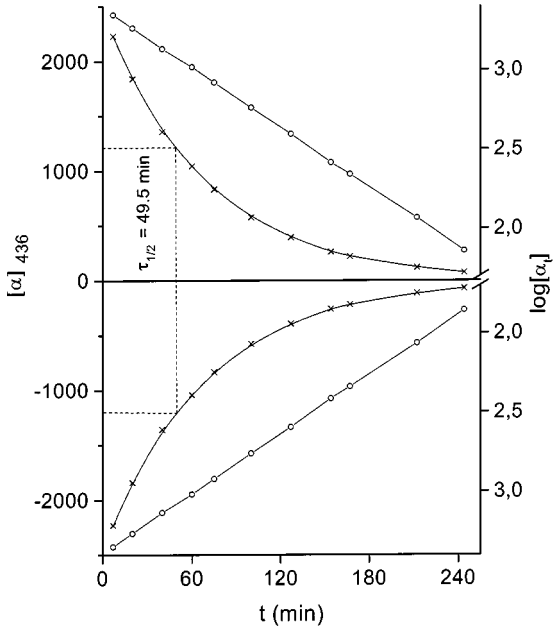

Figure 1. Racemization of $\boldsymbol{R}_{Mn}$-**2** and $\boldsymbol{S}_{Mn}$-**2** in toluene solution at 20 °C

$\boldsymbol{R}_{Mn}$-**2** $\boldsymbol{S}_{Mn}$-**2**

If the diastereomers which are used in such polarimetric studies contain, besides the configurationally labile metal atom, configurationally stable asymmetric carbon atoms, the epimerization at the metal atom results in equilibria with nonzero optical rotations and equilibrium ratios displaced from 1:1. Under these circumstances, the equilibrium ratio of two diastereomers that differ only in the metal configuration gives a measure of the chiral induction of the enantiomerically pure ligand on the metal configuration under thermodynamic control.[15]

Because organometallic complexes of the transition elements are generally colored and absorb strongly in the visible region, the transparency in the polarimetric measurements is usually limited. Therefore, only dilute solutions can be studied, the air-sensitivity of which represents a possible source of error in such measurements.

Diastereomers such as $\boldsymbol{R}_{Ru}\boldsymbol{S}_{C}$-**3** and $\boldsymbol{S}_{Ru}\boldsymbol{S}_{C}$-**3** differ in their ^{1}H NMR spectra.[27,28] Thus, the kinetics of the configurational change at the metal atom can be followed by time-dependent integration of suitable signals. In this technique, the quantities to be used are larger, the possibilities for the exclusion of air are better and, therefore, the results are more reliable than those obtained from polarimetry. Figure 2 shows the change in the concentration of the complexes $\boldsymbol{R}_{Ru}\boldsymbol{S}_{C}$-**3** and $\boldsymbol{S}_{Ru}\boldsymbol{S}_{C}$-**3** as a function of time, as measured by ^{1}H NMR spectroscopy, during approach of the epimerization equilibrium $\boldsymbol{R}_{Ru}\boldsymbol{S}_{C}$-**3**/$\boldsymbol{S}_{Ru}\boldsymbol{S}_{C}$-**3** = 95.8:4.2 in $CDCl_3$ solution, and its interpretation according to first-order kinetics.[27,28]

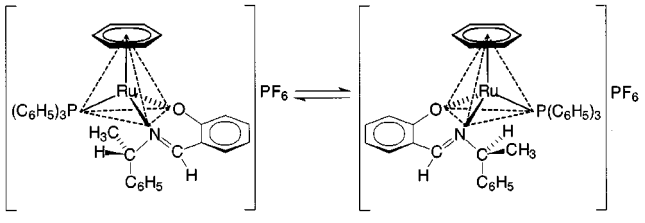

$\boldsymbol{R}_{Ru}\boldsymbol{S}_{C}$-**3** $\boldsymbol{S}_{Ru}\boldsymbol{S}_{C}$-**3**

In most cases, the configurational change at the metal atom is a first-order process. Therefore, a convenient measure of the configurational stability is given by the half-life $\tau_{1/2}$. The half-life for the approach to the racemization equilibrium of complexes $\boldsymbol{R}_{Mn}$-**2** and $\boldsymbol{S}_{Mn}$-**2** in toluene at 20 °C is 49.5 min,[26] while the half-life for the approach to the epimerization equilibrium of complexes $\boldsymbol{R}_{Ru}\boldsymbol{S}_{C}$-**3** and $\boldsymbol{S}_{Ru}\boldsymbol{S}_{C}$-**3** (Figure 2) in $CDCl_3$ at 12 °C is 25 min.[27] Thus, a

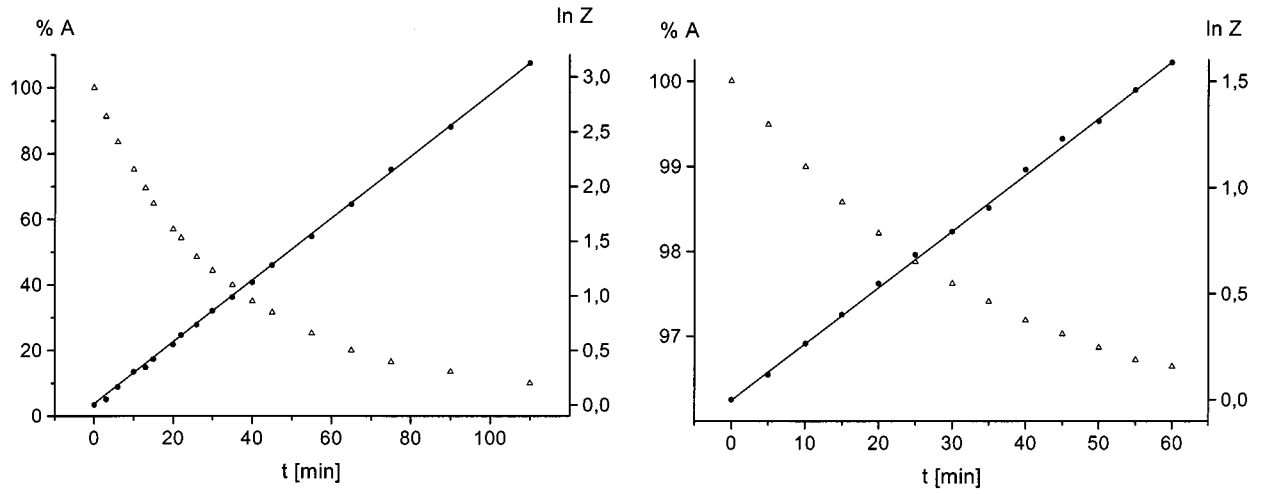

Figure 2. Epimerization of $\boldsymbol{R}_{Ru}\boldsymbol{S}_{C}$-**3** (left side) and $\boldsymbol{S}_{Ru}\boldsymbol{S}_{C}$-**3** (right side) in $CDCl_3$ solution at 12 °C; left ordinates: $[A_t]$ by ^1H NMR integration; right ordinates: ln$Z$, where $Z = ([A_o] - [A_\infty])/([A_t] - [A_\infty])$

change in the configuration at the metal atom takes place in solution in both cases, although this is much faster for $\boldsymbol{R}_{Ru}\boldsymbol{S}_{C}$-**3** and $\boldsymbol{S}_{Ru}\boldsymbol{S}_{C}$-**3** than for $\boldsymbol{R}_{Mn}$-**2** and $\boldsymbol{S}_{Mn}$-**2**.

As first-order reactions are not concentration dependent, the study of the racemization or epimerization kinetics is not restricted to pure enantiomers or diastereomers. Even samples only partly resolved, or those already partly racemized or epimerized, can be used to measure the change of a labile metal configuration, provided that the composition is sufficiently displaced from the equilibrium composition. The rate constant k, and from it the half-life $\tau_{1/2}$, are obtained from the function $\ln[(A_o - A_\infty)/(A_t - A_\infty)] = kt$, where A_o = starting concentration, A_t = concentration at time t, and A_∞ = equilibrium concentration after ten half-lives. By virtue of proportionality, instead of the concentrations A, the measured optical rotations of the sample or the integrals of suitable NMR signals can be used directly. For enantiomers, $A_\infty = 0$ and for diastereomers, $A_\infty \neq 0$. In order to dissect the first-order rate constant k for approach to equilibrium for diastereomers into k_1 and k_{-1} for the forward and backward reactions, respectively, and to determine the equilibrium constant K from the equilibrium optical rotation, the optical rotations of the pure diastereomers must be known. If the diastereomers differ in their ^1H or ^{31}P NMR spectra, these quantities can be directly determined by integration of the spectrum of an equilibrated sample. Thus, information concerning the change of the metal configuration can be obtained through studies of both the racemization of enantiomers and the epimerization of diastereomers.

Half-Sandwich Complexes with Stable and Labile Metal Configurations

The first resolved organometallic compounds $\boldsymbol{R}_{Mn}$-**1**/$\boldsymbol{S}_{Mn}$-**1** are configurationally stable at the metal atom and do not undergo racemization in solution. They can be kept in CH_2Cl_2 for weeks without any decrease in the optical rotation.[23] On the other hand, the benzoyl compounds $\boldsymbol{R}_{Mn}$-**2**/$\boldsymbol{S}_{Mn}$-**2**, which are formed in the reaction of $\boldsymbol{R}_{Mn}$-**1**/$\boldsymbol{S}_{Mn}$-**1** with phenyllithium, are configurationally labile at the Mn atom (Figure 1).[26] Thus, compounds $\boldsymbol{R}_{Mn}$-**1**/$\boldsymbol{S}_{Mn}$-**1** and $\boldsymbol{R}_{Mn}$-**2**/$\boldsymbol{S}_{Mn}$-**2**, which were involved in the early studies of optically active organotransition metal compounds, are representative examples of the two alternatives, having stable and labile metal configurations, respectively. This makes it even more surprising that so many ambiguities have recently arisen regarding the stability of the metal configuration in similar compounds (see later).

The configurational stability of the benzoyl complexes $\boldsymbol{R}_{Mn}$-**2** and $\boldsymbol{S}_{Mn}$-**2** can be tuned by *para*-substitution of the phenyl ring of the benzoyl ligand[26] and by *para*-substitution of the phenyl rings of the triphenylphosphane ligand.[29] An NMe_2 substituent on the benzoyl ligand reduces the half-life at 20 °C in toluene to 3.6 min, whereas a CF_3 substituent increases it to 418 min.[26] The same *para*-substituents have the opposite effect if they are attached to the phenyl rings of the triphenylphosphane ligand. As the benzoyl and triphenylphosphane ligands are on different sides of the critical bond, this indicates that it is the Mn−P bond that undergoes dissociation in the rate-determining step. CF_3 substituents in the *para*-position of the phenyl rings of the phosphane ligand give a half-life of 5.9 min, while OCH_3 substituents extend it to 337 min.[29] Hammett plots have been constructed for both series of compounds. Thus, a combination of an NMe_2 substituent on the benzoyl ligand and a CF_3 substituent on the triphenylphosphane ligand would give an extremely labile metal configuration, whilst the opposite combination should give the most stable compound in this series.[18] Obviously, knowledge of the half-life for the change of the metal configuration is important with regard to the handling of solutions of optically active compounds without appreciable loss of enantiomeric purity.

The aminophosphanes (*S*)-$Ph_2P-NH-CH(Me)(Ph)$ and (*S*)-$Ph_2P-N(Me)-CH(Me)(Ph)$ have proved to be versatile chiral phosphane ligands[30] akin to triphenylphosphane.[31]

The complex $\boldsymbol{R}_{Mo}\boldsymbol{S}_{C}$-**4**, containing (*S*)-$Ph_2P-N(Me)-CH(Me)(Ph)$ as the optically active auxiliary, is configurationally stable in solution even at higher temperatures.[32,33] In contrast, the chloro complex $\boldsymbol{R}_{Fe}\boldsymbol{S}_{C}$-**5**, a derivative of the same optically active aminophosphane ligand, is configurationally labile at the Fe atom. $\boldsymbol{R}_{Fe}\boldsymbol{S}_{C}$-**5** has a half-life of 181 min. at 20 °C in benzene solution, while the corresponding bromo compound epimerizes in the same solvent with a half-life of 185 min. at 45 °C.[34] With a half-life of 51 min. at 70 °C, the corresponding iodo compound has the highest configurational stability of the compounds CpFe(CO)Hal(aminophosphane).[35] The analogous compound CpFe(CO)Me(aminophosphane) epimerizes with respect to the iron configuration in benzene solution with a half-life of 70 min. at 70 °C.[36] However, the thermal epimerization of CpFe(CO)Me(aminophosphane) has to be distinguished from the epimerization induced by electron transfer (reaction with $[Cp_2Fe]PF_6$), which, at room temperature, is complete within five minutes.[36]

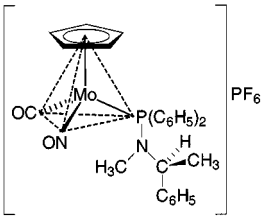

$R_{Mo}S_{C}$-**4**

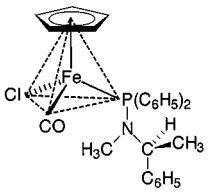

$R_{Fe}S_{C}$-**5**

The enantiomeric acetyl complexes $\boldsymbol{R}_{Fe}$-**6** and $\boldsymbol{S}_{Fe}$-**6**, which are configurationally stable at room temperature, have been developed as optically active auxiliaries for enantioselective organic synthesis.[7–11,37–40] These highly selective stoichiometric reagents are commercially available and allow the synthesis of a variety of compounds by virtue of the enolate chemistry of the acetyl substituent. Most of the $[CpRe(PPh_3)(NO)X]$ compounds[2,4,5] described by Gladysz, for example $\boldsymbol{S}_{Re}$-**7**,[41] are configurationally stable at the metal atom, even at higher temperatures. However, it cannot be ruled out that one or other of the compounds, reported to be configurationally stable, will start to racemize or epimerize at higher temperatures before decomposition occurs.

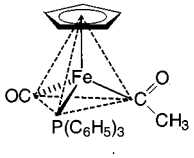

R_{Fe}-**6**

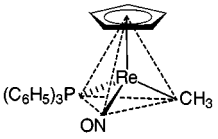

S_{Re}-**7**

Whereas half-sandwich complexes of the three-legged piano-stool type racemize or epimerize through ligand dissociation, half-sandwich complexes of the four-legged piano-stool type, which are notoriously labile at the metal center, do so by intramolecular rearrangements without ligand dissociation.[1,3,14,17–19] These isomerizations at the metal atom can sometimes be investigated by ^1H NMR spectroscopy with the help of diastereotopic probes, a resolution with respect to the metal configuration being unnecessary. Such coalescence measurements are, however, restricted to relatively rapid reactions, in contrast to those that can be followed by time-dependent integration of suitable diastereomer signals. Half-sandwich complexes of the four-legged piano-stool type will not be considered further in this review.

Half-Sandwich (η^6-Arene)ruthenium Complexes

Recently, half-sandwich (η^6-arene)ruthenium(II) complexes have attracted much interest as catalyst precursors for organic transformations.[42] In 1991, Mandal and Chakravarty synthesized chiral-at-metal half-sandwich ruthenium compounds of the type $[(\eta^6\text{-cymene})Ru(LL^*)L']ClO_4$ and $[(\eta^6\text{-cymene})Ru(LL^*)Hal]$, with cymene = 1-isopropyl-4-methylbenzene and LL* = the anion of (*S*)-(1-phenylethyl)salicylaldimine. L′ was a unidentate ligand, such as triphenylphosphane or 4-methylpyridine, and Hal a halide ligand.[43] The complexes $\boldsymbol{R}_{Ru}\boldsymbol{S}_{C}$-**8** and $\boldsymbol{R}_{Ru}\boldsymbol{S}_{C}$-**9** are representative examples.

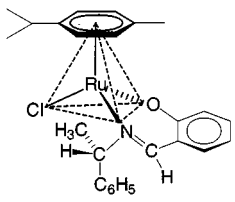

$R_{Ru}S_{C}$-**8**

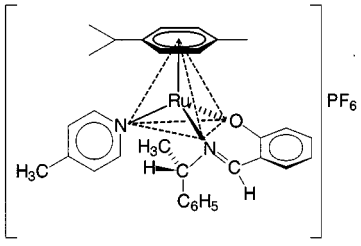

$R_{Ru}S_{C}$-**9**

In subsequent studies, the stereochemistry of the substitution of the chloro ligand in $\boldsymbol{R}_{Ru}\boldsymbol{S}_{C}$-**8** by other ligands was investigated,[44,45] for example, by 4-methylpyridine in the reaction $\boldsymbol{R}_{Ru}\boldsymbol{S}_{C}$-**8** → $\boldsymbol{R}_{Ru}\boldsymbol{S}_{C}$-**9**. Through not taking into account the configurational instability of their compounds, Mandal and Chakravarty made serious misassignments. What they referred to as "retention or inversion stereochemistry of substitution reactions" had actually nothing to do with the substitution reactions themselves. It only reflected the different stabilities of the diastereomers in the diastereomer equilibria, which were rapidly established before and after the slow substitution reactions. The terms "retention" and "inversion" imply that the reactions under consideration are kinetically controlled and that there is no prior or subsequent epimerization. However, compounds of the type $\boldsymbol{R}_{Ru}\boldsymbol{S}_{C}$-**8** and $\boldsymbol{R}_{Ru}\boldsymbol{S}_{C}$-**9** are configurationally labile at the metal center. Thus, the diastereomers $\boldsymbol{R}_{Ru}\boldsymbol{S}_{C}$-**10** and $\boldsymbol{S}_{Ru}\boldsymbol{S}_{C}$-**10** of the benzene derivative $[(\eta^6\text{-}C_6H_6)Ru(LL^*)4\text{-Mepy}]PF_6$ interconvert through a change in the Ru configuration. The approach to the equilibrium $\boldsymbol{R}_{Ru}\boldsymbol{S}_{C}$-**10** ⇆ $\boldsymbol{S}_{Ru}\boldsymbol{S}_{C}$-**10** at −35 °C in acetone solution has a half-life of $\tau_{1/2}$ = 82 min.[46]

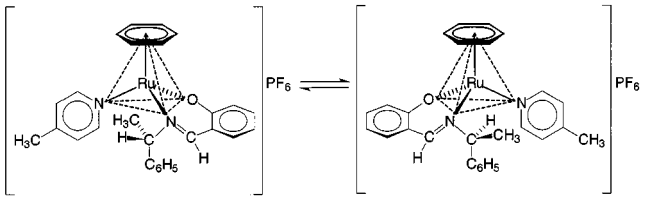

$R_{Ru}S_C$-10 $S_{Ru}S_C$-10

A similar equilibration is observed for [(η^6-cymene)Ru(LL*)4-Mepy]PF_6, the $\boldsymbol{R_{Ru}S_C}$-**9**/$\boldsymbol{S_{Ru}S_C}$-**9** equilibrium distribution at room temperature being 76:24 in [D_6]-acetone and 82:18 in $CDCl_3$.[47] These values do not prove predominant retention of configuration in the substitution of the chloro ligand by the 4-methylpyridine ligand in the reaction $\boldsymbol{R_{Ru}S_C}$-**8** → $\boldsymbol{R_{Ru}S_C}$-**9** as claimed by Mandal and Chakravarty. They give instead a measure of the different stabilities of the diastereomers in diastereomer equilibria such as $\boldsymbol{R_{Ru}S_C}$-**10** ⇆ $\boldsymbol{S_{Ru}S_C}$-**10**. After having uncovered these mistakes, the author's group published a corrigendum[47] including an appeal for the proper use of stereochemical terminology. Note that on going from $\boldsymbol{R_{Ru}S_C}$-**8** to $\boldsymbol{R_{Ru}S_C}$-**9** there is a change in the relative Ru configuration and simultaneously a change in the priority sequence of the ligands from cymene > Cl > O > N in $\boldsymbol{R_{Ru}S_C}$-**8** to cymene > O > N(imine) > N(4-methylpyridine) in $\boldsymbol{R_{Ru}S_C}$-**9**.

In 1995, Nelson and co-workers synthesized the compounds [(η^6-arene)Ru(LL*)Cl], with η^6-arene = benzene, toluene, cymene, and LL* = *ortho*-metalated (*S*)-*N*,*N*-dimethyl-1-phenylethylamine.[48] The parent compounds, from which all the other cymene complexes were derived, were the chloro complexes $\boldsymbol{R_{Ru}S_C}$-**11**/$\boldsymbol{S_{Ru}S_C}$-**11**.

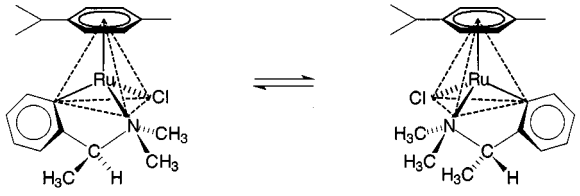

$R_{Ru}S_C$-11 $S_{Ru}S_C$-11

The chloro complexes were obtained in a diastereomer ratio $\boldsymbol{R_{Ru}S_C}$-**11**/$\boldsymbol{S_{Ru}S_C}$-**11** = 87:13. Erroneously, the diastereomers $\boldsymbol{R_{Ru}S_C}$-**11** and $\boldsymbol{S_{Ru}S_C}$-**11** were described as being configurationally stable at the ruthenium center:[48] "the ^{1}H NMR spectra obtained in $CDCl_3$, [D_6]acetone, and CD_3NO_2 solutions.....are independent of time (days) and temperature (−20 to 50 °C), indicating their configurational stability". The authors must have used equilibrated samples for their NMR experiments at −20 °C, otherwise they would have noticed that it is in this temperature range that the Ru configuration starts to change. The author's group demonstrated that the half-life for approach to the equilibrium $\boldsymbol{R_{Ru}S_C}$-**11** ⇆ $\boldsymbol{S_{Ru}S_C}$-**11** at 4 °C in CD_2Cl_2 is 108 min. The half-life was found to be 9 min. at 11 °C, showing that solutions of the complexes cannot be handled at room temperature without rapid change of the metal configuration.[49]

The wrong assumption of configurational stability was repeated by Nelson's group in a paper published in 1996[50] and in three papers published in 1999.[51−53] Fatally, it was used as a basis for stereochemical assignments in substitution reactions, which were inevitably wrong. The authors cited our warning in ref.[47] but did not take it into account. For example, on addition of NaI to complexes $\boldsymbol{R_{Ru}S_C}$-**11**/$\boldsymbol{S_{Ru}S_C}$-**11** the iodo complexes $\boldsymbol{R_{Ru}S_C}$-**12**/$\boldsymbol{S_{Ru}S_C}$-**12** are formed in a reaction for which "predominant retention of configuration at ruthenium", was claimed.[50] This is true only in a strictly formal sense. However, as the authors presented associative, dissociative, and ring-slippage mechanisms at length, they definitely addressed the substitution reaction itself, which was as unjustified as it was in the case of Mandal and Chakravarty's work.

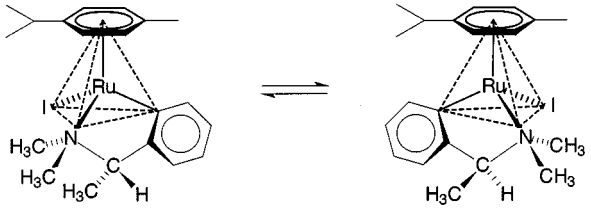

$R_{Ru}S_C$-12 $S_{Ru}S_C$-12

The iodo complexes turned out to be even more configurationally labile than the chloro complexes. Their half-lives were found to be 62 min. at −15 °C and 15 min. at −4 °C in CD_2Cl_2.[49] Therefore, no conclusions regarding the stereochemistry of the substitution reaction $\boldsymbol{R_{Ru}S_C}$-**11**/$\boldsymbol{S_{Ru}S_C}$-**11** → $\boldsymbol{R_{Ru}S_C}$-**12**/$\boldsymbol{S_{Ru}S_C}$-**12** can be drawn, because the diastereomer ratios of the starting material (chloro complexes $\boldsymbol{R_{Ru}S_C}$-**11**/$\boldsymbol{S_{Ru}S_C}$-**11**) and the products (iodo complexes $\boldsymbol{R_{Ru}S_C}$-**12**/$\boldsymbol{S_{Ru}S_C}$-**12**) have nothing to do with it. The diastereoselectivities only reflect the different stabilities of the diastereomers in the respective diastereomer equilibria. Arguments such as those invoking total retention of configuration in the reaction of the major diastereomer $\boldsymbol{R_{Ru}S_C}$-**11** and partial retention and inversion in the reaction of the minor diastereomer $\boldsymbol{S_{Ru}S_C}$-**11** to account for the observed diastereoselectivities are inherently flawed.[50,51]

A single-crystal X-ray structure analysis had been carried out for the diastereomer $\boldsymbol{R_{Ru}S_C}$-**11**. It was assigned to the major diastereomer of the 87:13 pair $\boldsymbol{R_{Ru}S_C}$-**11**/$\boldsymbol{S_{Ru}S_C}$-**11** because "the crystals of this species have a higher chance of being isolated from a mixture" assuming "that each bulk-crystallized sample is a solid mixture of the two diastereomers in a ratio equal to that observed in their solutions" — a strange argument implying a 13% statistical chance of being wrong![48,51] The author's group dissolved the crystals obtained from the 87:13 mixture of $\boldsymbol{R_{Ru}S_C}$-**11**/$\boldsymbol{S_{Ru}S_C}$-**11** at −80 °C and showed by ^{1}H NMR spectroscopy that they consisted of the pure diastereomer $\boldsymbol{R_{Ru}S_C}$-**11**.[49] It was only in the temperature range around 0 °C that the minor dias-

tereomer $S_{Ru}S_C$-**11** began to appear due to the onset of epimerization. Thus, from an 87:13 mixture of diastereomers under the aforementioned crystallization conditions, a single diastereomer crystallized exclusively and was removed from the equilibrium. Through re-establishment of the equilibrium, all the material was converted into a single pure diastereoisomer, a process referred to as an asymmetric transformation of the second kind.[54] If the Ru configuration were stable, the composition of the solid obtained on evaporation of the solvent would have been the same as that in solution (Nelson's conclusion).[48,51] However, after recognition of the configurational lability at the Ru center, the formation of a single pure isomer on crystallization can be understood. Consequently, there was no danger of picking a crystal of the minor diastereomer and of making a wrong configurational assignment.

In recent papers by Nelson's group,[52,53] further chiral-at-metal (η^6-arene)ruthenium complexes have been reported as being obtained through substitution of the chloride ligand in compounds of the type $R_{Ru}S_C$-**11**/$S_{Ru}S_C$-**11** by azide, nitrite, thiocyanate, cyanate, and other ligands. It will have to be checked whether these compounds really are "configurationally rigid in solution under mild conditions" and whether or not "these ligand substitution reactions proceed with predominant retention of configuration at ruthenium".

CpCo Complexes

At the end of 1999, a paper was published by Pfeffer et al.[55] concerning a series of cobaltacyclic compounds of the type [(η^5-C_5H_5)Co(LL′)I] differing in the configuration at the metal. With the optically active ligands LL′H = (R_C)-(+)- and (S_C)-(−)-*N*,*N*-dimethyl-1-phenylethylamine, a mixture of the two diastereomers, $R_{Co}R_C$-**13**, $S_{Co}R_C$-**13** and $S_{Co}S_C$-**13**, $R_{Co}S_C$-**13**, respectively, in a 19:1 ratio (91% *de*) was obtained. This ratio "could not be improved by fractional crystallization or column chromatography" and "^{1}H NMR studies indicate that the compounds are configurationally stable at the cobalt center". Moreover, "no epimerization could be observed in solution, for instance, over a period of seven days at room temperature in either $CDCl_3$ or [D_6]acetone". Although the diastereomers "displayed comparable crystallization rates so that the bulk sample from which X-ray quality crystals were obtained contained the same ratio of both diastereomers as determined above", the crystal structure of $R_{Co}R_C$-**13** was assigned to the major diastereomer on the basis that "the crystals of this species have a higher statistical chance of being isolated from a mixture of diastereomers". Thus, the same (wrong) argumentation was used as for the (η^6-arene)ruthenium complexes discussed above.[48,50−53]

The author's group synthesized the complexes $R_{Co}R_C$-**13**/$S_{Co}R_C$-**13** according to the published procedure[55] using [(η^5-C_5H_5)CoI_2]$_2$ and *ortho*-lithiated (R_C)-(+)-*N*,*N*-dimethyl-1-phenylethylamine. Dark-green needles were obtained, the ^{1}H NMR spectrum of which in CD_2Cl_2 solution at room temperature exhibited signals due to both diastereomers $R_{Co}R_C$-**13** and $S_{Co}R_C$-**13** in a 96:4 ratio (92% *de*), in agreement with ref.[55] However, when a sample of crystals was dissolved in CD_2Cl_2 and the ^{1}H NMR spectrum was recorded at −40 °C, only the signals of the major diastereomer were seen.[49] Measurements at −20 °C, 0 °C, and +21 °C revealed that the minor diastereomer $S_{Co}R_C$-**13** was formed only at higher temperatures.

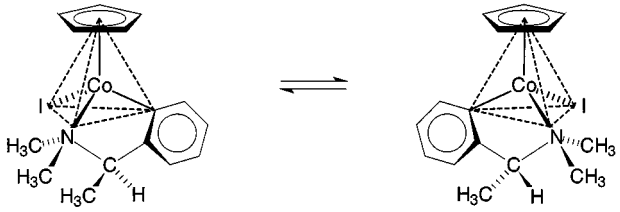

$R_{Co}R_C$-13 $S_{Co}R_C$-13

The half-life for the conversion of $R_{Co}R_C$-**13** into the equilibrium mixture $R_{Co}R_C$-**13** ⇆ $S_{Co}R_C$-**13** was estimated to be between 20 and 25 min. in CD_2Cl_2 solution at +1.4 °C. The accuracy of these measurements is limited by the fact that the equilibration of the major diastereomer involves only a small concentration change to give the equilibrium mixture major diastereomer/minor diastereomer = 96:4. Clearly, the major diastereomer $R_{Co}R_C$-**13** cannot be handled at room temperature without a rapid change in the metal configuration. The measurements leading to the postulation of configurational stability at the cobalt center[55] were thus most probably carried out with epimerized samples. Interestingly, it has been demonstrated previously that the configuration at cobalt is labile in compounds $R_{Co}S_C$-**14** and $R_{Co}S_C$-**15**.[56] However, the latter compounds, which are very similar to compounds $R_{Co}R_C$-**13**/$S_{Co}R_C$-**13** and are subject to the same stereochemical problem of the cobalt configuration, were not mentioned in ref.[55]

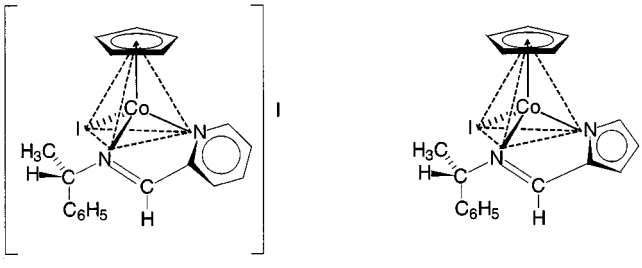

$R_{Co}S_C$-14 $R_{Co}S_C$-15

Cp*Rh and Cp*Ir Complexes

In 1997, Loza, Parr, and Slawin synthesized the compounds [Cp*M(ON)Cl] ($R_{Rh}S_C$-**16**/$S_{Rh}S_C$-**16** and $R_{Ir}S_C$-**17**/$S_{Ir}S_C$-**17**), where ON was the anion of (+)-*N*-[(*S*)-1-phenylethyl]salicylaldimine.[57] A high diastereomeric excess was claimed as, in the room-temperature ^{1}H NMR spectra, only one isomer was seen in each series. The compound $R_{Ir}S_C$-**17** was characterized by X-ray structure analysis, as a result

of which the (R_{Ir},S_C)-configuration was assigned to the only diastereomer observed in solution. These conclusions turned out to be wrong or unreliable because the authors had overlooked the configurational instability at the metal center in these complexes.[58]

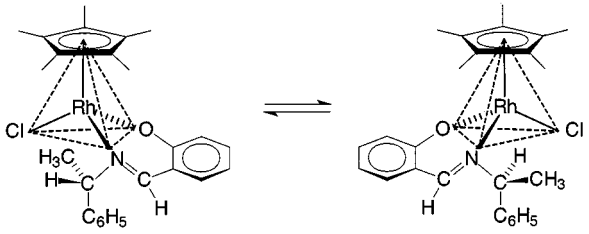

***R*$_{Rh}$*S*$_C$-16** **S*$_{Rh}$S$_C$-16**

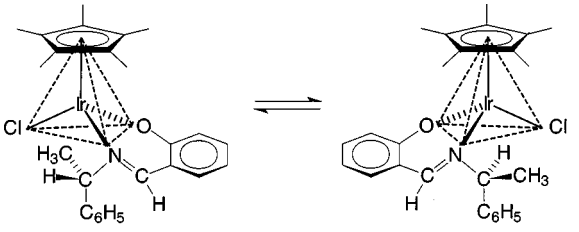

***R*$_{Ir}$*S*$_C$-17** **S*$_{Ir}$S$_C$-17**

The author's group confirmed that the ^{1}H NMR spectra of ***R***$_{Rh}$***S***$_C$**-16**/***S***$_{Rh}$***S***$_C$**-16** and ***R***$_{Ir}$***S***$_C$**-17**/***S***$_{Ir}$***S***$_C$**-17** featured only one set of signals. However, it was found that the room temperature ^{1}H NMR spectra were the averaged high temperature limiting spectra (fast-exchange regime of two diastereoisomers in their diastereomer equilibria). At low temperatures, interconversion of the two diastereomers of each pair became so slow that the diastereomers gave separate signals that could be integrated. The ratios were found to be 81:19 at −80 °C in CD_2Cl_2 in the rhodium series ***R***$_{Rh}$***S***$_C$**-16**/***S***$_{Rh}$***S***$_C$**-16** and 85:15 at −50 °C in $CDCl_3$ in the iridium series ***R***$_{Ir}$***S***$_C$**-17**/***S***$_{Ir}$***S***$_C$**-17**. As equilibration with respect to the metal center in these compounds is fast even at −80 °C, the transfer of the absolute configuration found in the solid state to the major isomer in solution, as assumed in ref.[57], does not have any sound basis.

It cannot be taken for granted that it is always the *major* isomer that crystallizes from a dynamic diastereomer equilibrium. In the series of chloro complexes ***R***$_{Rh}$***S***$_C$**-18**/***S***$_{Rh}$***S***$_C$**-18**, the diastereomer equilibrium distribution in CD_2Cl_2 was found to be ***R***$_{Rh}$***S***$_C$**-18**/***S***$_{Rh}$***S***$_C$**-18** = 87:13 at room temperature. In this case, it was definitely the *minor* diastereomer (13% content only!) that crystallized. This was proven by X-ray crystallography and low-temperature NMR spectroscopic analysis of the crystals dissolved at −80 °C. For the iodo system ***R***$_{Rh}$***S***$_C$**-19**/***S***$_{Rh}$***S***$_C$**-19**, the reverse was found to be true. From the 87:13 equilibrium mixture, the *major* isomer crystallized in a diastereomerically pure state. Due to the rapid isomerization of the compounds ***R***$_{Rh}$***S***$_C$**-16**/***S***$_{Rh}$***S***$_C$**-16** and ***R***$_{Ir}$***S***$_C$**-17**/***S***$_{Ir}$***S***$_C$**-17**, the NMR test at −80 °C is not available. Therefore, no unequivocal configurational assignment of the diastereomers in solution can be made.

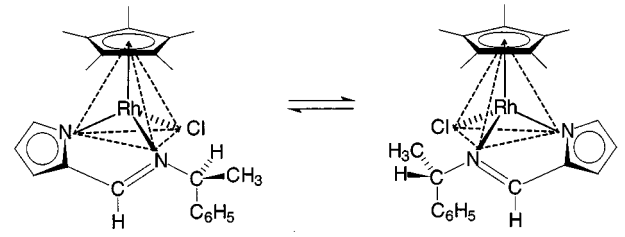

***R*$_{Rh}$*S*$_C$-18** **S*$_{Rh}$S$_C$-18**

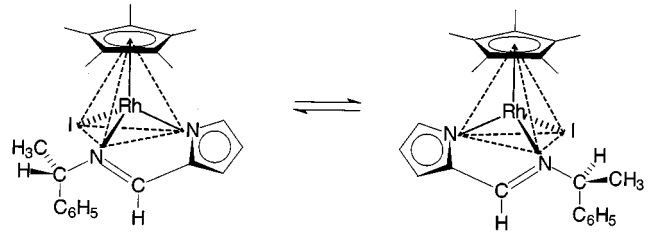

***R*$_{Rh}$*S*$_C$-19** **S*$_{Rh}$S$_C$-19**

Low Temperature NMR Spectra in Solution — A Solution for the Aforementioned Problems

Diastereomers differing only in the metal configuration may be formed under kinetic control or under thermodynamic control.[15] In both cases, the diastereomer ratios can be close to 1:1 or may reach high values.[15] Irrespective of the ratio, the isolation of diastereomerically pure samples or at least diastereomerically enriched samples (relative to the starting composition) should be possible by means of fractional crystallization or chromatography including zone cutting, provided that the diastereomers are configurationally stable at the metal center. If a diastereomer mixture resists separation or enrichment whatever its composition (as in refs.[48,55] etc.), the reason may be configurational instability at the metal atom. In such cases, the configurational stability/lability should be checked by all the available techniques, including the dissolution of samples crystallized at low temperatures and the measurement of low-temperature NMR spectra without prior warming. Provided that the equilibration between the two diastereoisomers is slow under the conditions of dissolution, this technique shows whether a crystallized sample consists of a pure diastereoisomer or a mixture of the two diastereomers. Depending on the crystallization conditions and the epimerization rate, both situations may be encountered.

In the previous paragraphs, several publications by different groups in good journals have been discussed, where the conclusions drawn were either partly or wholly wrong. At present, there are high standards as far as the publication of preparative work and X-ray structure analyses is concerned.

However, with respect to stereochemistry and mechanisms the quality standards are not so high, as demonstrated herein for the narrow field of half-sandwich ruthenium, cobalt, rhodium, and iridium complexes. Confusion results and corrections are required. In the worst case reinvestigations are necessary some time later to avoid contradictions. In most of the cases discussed, low temperature NMR experiments, easily available with modern equipment, would have proved or disproved the ideas, assumptions, and conclusions put forward. Why is this technique not used more frequently?

[1] H. Brunner, *Angew. Chem.* **1999**, *111*, 1248; *Angew. Chem. Int. Ed.* **1999**, *38*, 1194.
[2] J. A. Gladysz, B. J. Boone, *Angew. Chem.* **1997**, *109*, 566; *Angew. Chem. Int. Ed. Engl.* **1997**, *36*, 550.
[3] H. Brunner, in *Chemical Synthesis: Gnosis to Prognosis* (Eds.: C. Chatgilialoglu, V. Snieckus), Kluwer Academic Publishers, Dordrecht, **1996**, p. 91.
[4] O. Meyer, P. C. Cagle, K. Weickhardt, D. Vichard, J. A. Gladysz, *Pure Appl. Chem.* **1996**, *68*, 79.
[5] G. A. Stark, M. A. Dewey, G. B. Richter-Addo, D. A. Knight, A. M. Arif, J. A. Gladysz, in *Stereoselective Reactions of Metal-Activated Molecules* (Eds.: H. Werner, J. Sundermeyer), Vieweg-Verlag, Braunschweig, **1995**, p. 51.
[6] H. Brunner, in *Chirality − From Weak Bosons to the α-Helix* (Ed.: R. Janoschek), Springer-Verlag, Berlin, Heidelberg, **1991**, p. 166.
[7] H. Brunner, *Angew. Chem.* **1991**, *103*, A-310.
[8] S. G. Davies, *Aldrichimica Acta* **1990**, *23*, 31.
[9] B. K. Blackburg, S. G. Davies, M. Whittacker, in *Stereochemistry of Organometallic and Inorganic Compounds, Vol. 3* (Ed.: I. Bernal), Elsevier, Amsterdam, **1989**, p. 141.
[10] S. G. Davies, *Pure Appl. Chem.* **1988**, *60*, 13.
[11] S. G. Davies, I. M. Dordor-Hedgecock, R. J. C. Easton, S. C. Preston, K. H. Sutton, J. C. Walker, *Bull. Soc. Chem. Fr.* **1987**, 608.
[12] G. Consiglio, F. Morandini, *Chem. Rev.* **1987**, *87*, 761.
[13] H. Brunner, *Angew. Chem.* **1983**, *95*, 921; *Angew. Chem. Int. Ed. Engl.* **1983**, *22*, 879.
[14] H. Brunner, *Adv. Organomet. Chem.* **1980**, *18*, 151.
[15] H. Brunner, *Acc. Chem. Res.* **1979**, *12*, 250.
[16] H. Brunner, in *The Organic Chemistry of Iron*, Vol. 1 (Eds.: E. A. Koerner von Gustorf, F.-W. Grevels, I. Fischler), Academic Press, New York, **1978**, p. 299.
[17] H. Brunner, *Chem. Unserer Zeit* **1977**, *11*, 157.
[18] H. Brunner, *J. Organomet. Chem.* **1975**, *94*, 189.
[19] H. Brunner, *Top. Stereochem.* **1975**, *56*, 67.
[20] H. Brunner, *Ann. N. Y. Acad. Sci.* **1974**, *239*, 213.
[21] H. Brunner, *Angew. Chem.* **1971**, *83*, 274; *Angew. Chem. Int. Ed. Engl.* **1971**, *10*, 249.
[22] H. Brunner, *Angew. Chem.* **1969**, *81*, 395; *Angew. Chem. Int. Ed. Engl.* **1969**, *8*, 382.
[23] H. Brunner, H.-D. Schindler, *J. Organomet. Chem.* **1970**, *24*, C7.
[24] C. Lecomte, Y. Dusausoy, J. Protas, J. Tirouflet, A. Dormond, *J. Organomet. Chem.* **1974**, *73*, 67.
[25] H. Brunner, *Enantiomer* **1997**, *2*, 133.
[26] H. Brunner, M. Langer, *J. Organomet. Chem.* **1975**, *87*, 223.
[27] H. Brunner, R. Oeschey, B. Nuber, *Angew. Chem.* **1994**, *106*, 941; *Angew. Chem. Int. Ed. Engl.* **1994**, *33*, 866.
[28] H. Brunner, R. Oeschey, B. Nuber, *J. Chem. Soc., Dalton Trans.* **1996**, 1499.
[29] H. Brunner, J. A. Aclasis, *J. Organomet. Chem.* **1976**, *104*, 347.
[30] H. Brunner, W. Rambold, *Angew. Chem.* **1973**, *85*, 1118; *Angew. Chem. Int. Ed. Engl.* **1973**, *12*, 1013.
[31] H. Brunner, W. Steger, *Z. Naturforsch.* **1976**, *31b*, 1493.
[32] H. Brunner, J. Doppelberger, *Bull. Soc. Chim. Belg.* **1975**, *84*, 923.
[33] H. Brunner, J. Doppelberger, *Chem. Ber.* **1978**, *111*, 673.
[34] H. Brunner, G. Wallner, *Chem. Ber.* **1976**, *109*, 69.
[35] H. Brunner, F. Rackl, *J. Organomet. Chem.* **1976**, *118*, C19.
[36] H. Brunner, K. Fisch, P. G. Jones, J. Salbeck, *Angew. Chem.* **1989**, *101*, 1558; *Angew. Chem. Int. Ed. Engl.* **1989**, *28, 1521.*
[37] H. Brunner, E. Schmidt, *J. Organomet. Chem.* **1970**, *21*, P53.
[38] H. Brunner, E. Schmidt, *J. Organomet. Chem.* **1972**, *36*, C18.
[39] G. M. Reisner, I. Bernal, H. Brunner, M. Muschiol, *Inorg. Chem.* **1978**, *17*, 783.
[40] I. Bernal, H. Brunner, M. Muschiol, *Inorg. Chim. Acta* **1988**, *142*, 235.
[41] F. Agbossou, E. J. O'Connor, C. M. Garner, N. Quirós Méndez, J. M. Fernández, A. T. Patton, J. A. Ramsden, J. A. Gladysz, *Inorg. Synth.* **1992**, *29*, 211.
[42] R. Noyori, S. Hashiguchi, *Acc. Chem. Res.* **1997**, *30*, 97.
[43] S. K. Mandal, A. R. Chakravarty, *J. Organomet. Chem.* **1991**, *417*, C59.
[44] S. K. Mandal, A. R. Chakravarty, *J. Chem. Soc., Dalton Trans.* **1992**, 1627.
[45] S. K. Mandal, A. R. Chakravarty, *Inorg. Chem.* **1993**, *32*, 3851.
[46] H. Brunner, R. Oeschey, B. Nuber, *J. Chem. Soc., Dalton Trans.* **1996**, 1499.
[47] H. Brunner, R. Oeschey, B. Nuber, *Inorg. Chem.* **1995**, *34*, 3349.
[48] S. Attar, J. H. Nelson, J. Fischer, A. de Cian, J.-P. Sutter, M. Pfeffer, *Organometallics* **1995**, *14*, 4559.
[49] H. Brunner, T. Zwack, *Organometallics* **2000**, *19*, 2423.
[50] S. Attar, V. J. Catalano, J. H. Nelson, *Organometallics* **1996**, *15*, 2932.
[51] N. Gül, J. H. Nelson, *Polyhedron* **1999**, *18*, 1835.
[52] H. D. Hansen, K. Maitra, J. H. Nelson, *Inorg. Chem.* **1999**, *38*, 2150.
[53] N. Gül, J. H. Nelson, *Organometallics* **1999**, *18*, 709.
[54] E. E. Turner, M. M. Harris, *Quart. Rev.* **1947**, *1*, 299.
[55] M. R. Meneghetti, M. Grellier, M. Pfeffer, J. Dupont, J. Fischer, *Organometallics* **1999**, *18*, 5560.
[56] H. Brunner, G. Riepl, R. Benn, A. Rufińska, *J. Organomet. Chem.* **1983**, *253*, 93.
[57] M. L. Loza, J. Parr, A. M. Z. Slawin, *Polyhedron* **1997**, *16*, 2321.
[58] H. Brunner, A. Köllnberger, T. Burgemeister, M. Zabel, *Polyhedron* **2000**, *19*, 1519.

Received May 12, 2000
[I00175]

First Examples of a New Family of Redox-Functionalised Chelate Complexes Based on a 1,1′-Ferrocenediyl-Bridged Di(amido) Ligand

Ulrich Siemeling,*[a] Oliver Kuhnert,[b] Beate Neumann,[b] Anja Stammler,[b] Hans-Georg Stammler,[b] Benno Bildstein,[c] Michael Malaun,[c] and Piero Zanello[d]

Keywords: Amides / Sandwich compounds / Polymerisation / Titanium / Zirconium

Treatment of $Fe[(C_5H_4)NHPh]_2$ (**1**H_2) with $M(NMe_2)_4$ (**3a**: M = Ti, **3b**: M = Zr) in benzene afforded the chelates (**1**)$Ti(NMe_2)_2$ (**4**) and (**1**)$Zr(NMe_2)_2(HNMe_2)$ (**5**), respectively. Chelate **5** was cleanly oxidised by ferrocenium hexafluorophosphate in acetonitrile. Treatment of **5** with two equivalents of $[Me_2NH_2]Cl$ (**6**) in benzene afforded (**1**)$ZrCl_2(HNMe_2)$ (**7**). The chelates **5** and **7** were characterised by X-ray structure analyses. The new redox-active chelate complexes are precatalysts for the polymerisation of ethylene.

The search for new generation nonmetallocene catalysts for the polymerisation of α-olefins is of continuing interest.[1] Complexes of the Group 4 metals containing chelating di(amido) ligands represent a very promising class of (pre-)catalysts in this context. This has been demonstrated in recent years by the groups of Bochmann,[2] Eisen,[3] Gibson,[4] McConville,[5] Schrock,[6] and others,[7] building on earlier work by Bürger et al.[8] Ziegler and co-workers, using quantum-chemical methods, have rationalised the factors governing the ethylene polymerisation activity of such catalysts.[9]

We decided to utilise the novel 1,1′-ferrocenediyl-bridged ligand system $Fe[(C_5H_4)NPh]_2$ (**1**) in this context. This ligand is related to **2**, recently reported by Kempe and coworkers.[10] They found that, because of the high flexibility of **2**, complexes of the type **2**TiXY (X = Y = NMe_2; X = NMe_2, Y = Cl) are unstable. Not surprisingly, therefore, catalytically active complexes of **2** are unknown. In contrast, **1** would be expected to provide a fairly rigid ligand framework and should furthermore exhibit excellent π-donor qualities (beneficial for olefin insertion),[9] since the amido nitrogen atoms are directly connected to the electron-rich ferrocene moiety.[11]

We note that the electronic properties of our redox-active ligand system can be changed quite dramatically by oxidation. In fact, the development of redox-active ligands which allow the electrochemical control of stoichiometric and catalytic reactivities of transition metal centres is of great current interest.[12]

[a] Fachbereich 18 (Physik) der Universität Gesamthochschule Kassel,
Heinrich-Plett-Straße 40, 34132 Kassel, Germany
Fax: (internat.) +49-561/804-4777
E-mail: siemeling@uni-kassel.de
[b] Fakultät für Chemie der Universität Bielefeld,
Universitätsstraße 25, 33615 Bielefeld, Germany
[c] Institut für Allgemeine, Anorganische und Theoretische Chemie der Universität Innsbruck,
Innrain 52a, 6020 Innsbruck, Austria
[d] Dipartimento di Chimica, Università di Siena,
Via Aldo Moro, 53100 Siena, Italy

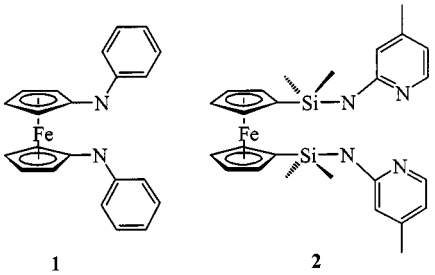

1 **2**

Metathesis of **1**H_2 [13] with one equivalent of $Ti(NMe_2)_4$ (**3a**) afforded (**1**)$Ti(NMe_2)_2$ (**4**). Analogously, treatment of **1**H_2 with $Zr(NMe_2)_4$ (**3b**) gave (**1**)$Zr(NMe_2)_2(HNMe_2)$ (**5**), and treatment of this with two equivalents of $[Me_2NH_2]Cl$ (**6**) furnished (**1**)$ZrCl_2(HNMe_2)$ (**7**) (Scheme 1). Di(amido)-zirconium(IV) complexes may be viewed as relatives of zirconocene derivatives[4] and hence ours are akin to the ferrocenediyl-bridged zirconocene dichloride $\{Fe[(C_5H_4)$-$C_5Me_4]_2\}ZrCl_2$ reported by Brintzinger and co-workers.[14]

Cyclic voltammetric studies have shown that the ligand precursor **1**H_2 undergoes a chemically reversible, one-electron oxidation at $E^{\circ\prime} = -0.06$ V (vs. SCE) in dichloromethane solution. Such an easy oxidation matches well the corresponding process exhibited by the related species $Fe[(C_5H_4)NMe_2]_2$ and $Fe[(C_5H_4)NPh_2]_2$.[15,16] Complexation of the metal-ligand fragment causes the ferrocenediyl-centred oxidation of the zirconaferrocenophane (**1**)$Zr(NMe_2)_2(HNMe_2)$ (**5**) to become slightly more difficult, by about 40 mV ($E^{\circ\prime} = -0.02$ V), indicating that the $Zr(NMe_2)_2(HNMe_2)$ fragment withdraws electron density from the ferrocene subunit. Chemical oxidation of **5** was cleanly achieved with one equivalent of ferrocenium hexafluorophosphate in acetonitrile.

Single crystal X-ray diffraction studies have been performed for both new zirconium compounds. The zirconium atom in **5** is coordinated by five nitrogen atoms in a distorted trigonal bipyramidal arrangement (Figure 1). The axial positions are occupied by the amino ligand and the

 © WILEY-VCH Verlag GmbH, 69451 Weinheim, 2001 1434−1948/01/0404−0913 $ 17.50+.50/0

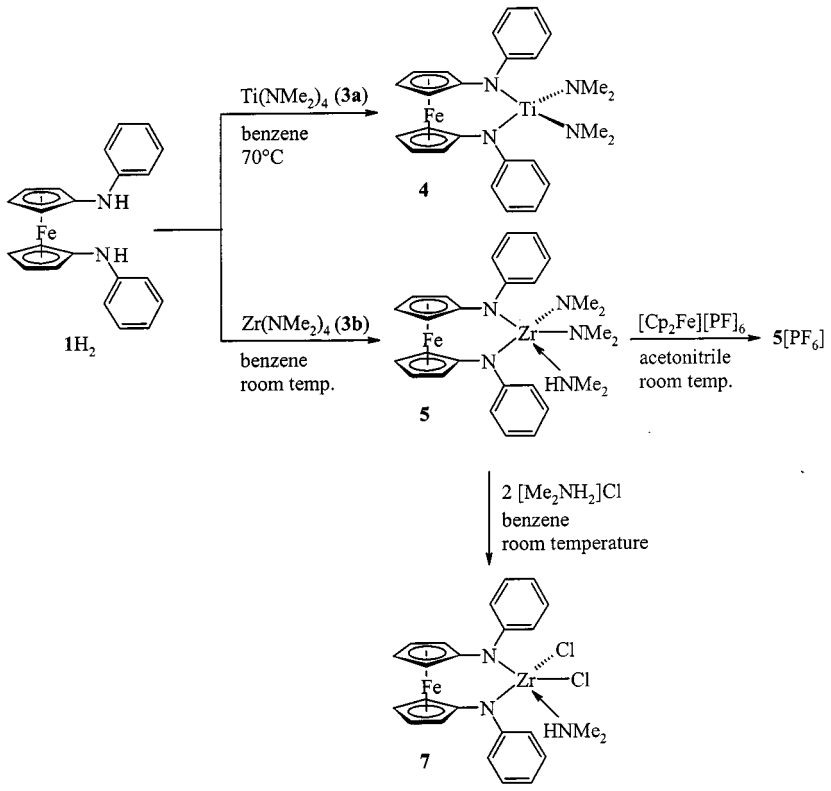

Scheme 1. Synthesis of the chelate complexes **4**, **5**, **5**[PF_6], and **7**

amido ligand *trans* to it, their ligating atoms forming an angle of 171.4(3)° with the Zr atom. The N(1)−Zr(1)−N(2) bite angle of the chelating ligand **1** is 132.9(3)°. The amino nitrogen−zirconium distance is 243.8(8) pm — consistent with a Zr−N(sp^3) single bond — while, thanks to their partial double-bond character, the four amido nitrogen−zirconium bonds are much shorter, ranging from 205.7(7) to 215.4(7) pm. These bond lengths are similar to those found for the related compound [Ph_2Si(N-Ar)$_2$]Zr(NMe_2)$_2$($HNMe_2$) (Ar = 2,6-$Me_2C_6H_3$).[4] The cyclopentadienyl rings of the ferrocene unit are in an eclipsed orientation. The parallel sandwich structure is slightly distorted and opens up towards the zirconium centre with a cyclopentadienyl ring tilt angle of 11.4°. The Fe−Zr distance of 333.9 pm precludes a significant bonding interaction between the two metal atoms.

The core geometry of **7** is also best described as distorted trigonal bipyramidal (Figure 2). Again, the amino ligand is in an axial position, the second axial position being occupied by a chloro ligand [N(3)−Zr(1)−Cl(1) 172.12(10)°]. In related systems containing linked amido-cyclopentadienyl ligands,[17] the amino ligand is positioned between the two chloro ligands. The N(1)−Zr(1)−N(2) bite angle is essentially identical to that in **5**, while the corresponding zirconium−nitrogen bond lengths are slightly shorter, resulting in a smaller cyclopentadienyl tilt angle of 9.4° and a shorter Fe−Zr distance of 331.0 pm. In both compounds, all amido nitrogen atoms are trigonal planar and the phenyl rings lie approximately in the plane defined by the zirconium atom and the amido nitrogen atoms of the chelating ligand **1**.

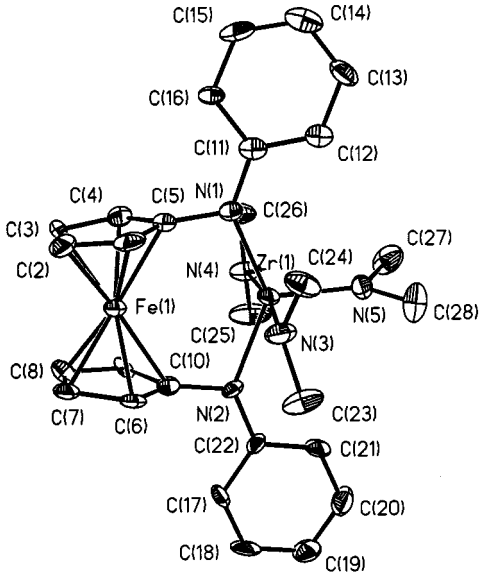

Figure 1. Molecular structure of **5** in the crystal; selected bond lengths (pm) and angles (°): Zr(1)−N(1) 212.8(7), Zr(1)−N(2) 215.3(7), Zr(1)−N(4) 215.4(7), Zr(1)−N(5) 205.7(7), N(1)−C(5) 142.3(11), N(1)−C(11) 139.5(10), N(2)−C(10) 141.3(10), N(2)−C(22) 138.9(9); N(3)−Zr(1)−N(5) 92.5(3), N(4)−Zr(1)−N(5) 96.0(3)

Preliminary investigations have shown that these new compounds are precatalysts for the polymerisation of ethylene.[18] The results of a detailed study, which also addresses the aspect of redox-tuning of catalyst activity, will be reported in due course.

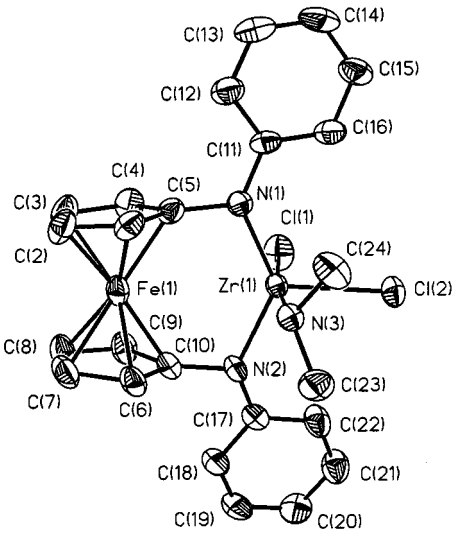

Figure 2. Molecular structure of **7** in the crystal; selected bond lengths (pm) and angles (°): Zr(1)−N(1) 206.0(4), Zr(1)−N(2) 207.6(4), Zr(1)−N(3) 238.3(4), Zr(1)−Cl(1) 245.95(16), Zr(1)−Cl(2) 241.76(14), N(1)−C(5) 141.6(6), N(1)−C(11) 141.4(6), N(2)−C(10) 141.9(6), N(2)−C(17) 139.4(6); N(3)−Zr(1)−Cl(2) 81.56(10), Cl(1)−Zr(1)−Cl(2) 91.02(5)

Experimental Section

General: All manipulations were performed under an inert atmosphere (purified argon or dinitrogen), using standard Schlenk and cannula techniques or a conventional glovebox. Solvents and reagents were dried and purified by standard procedures. − NMR spectra were recorded at 300 K with a Bruker DRX 500 spectrometer operating at 500.13 MHz for ^{1}H; TMS was used as external reference. − The materials and apparatus used for the electrochemical investigations have been described elsewhere.[19] − Elemental analyses were performed by the Microanalytical Laboratory of Universität Bielefeld.

Complex 4: A solution of **1**H_2 (0.87 g, 2.35 mmol) and **3a** (0.53 g, 2.35 mmol) in benzene (1 mL) was kept at 70 °C for 2 h. The volatile components were then removed in vacuo. The residue was extracted with *n*-hexane (20 mL) and the extract filtered. The filtrate was reduced to dryness in vacuo, leaving the product as a brownish yellow solid. Yield 0.90 g (76%). − ^{1}H NMR ($CDCl_3$): δ = 3.24 (s, 12 H, NMe_2), 3.63 (s, 4 H, C_5H_4), 4.54 (s, 4 H, C_5H_4), 6.71 ("t", apparent J = 6.9 Hz, 2 H, Ph), 6.78 ("d", apparent J = 7.9 Hz, 4 H, Ph), 7.16 ("t", apparent J = 7.2 Hz, 4 H, Ph). − ^{13}C{^{1}H} NMR ($CDCl_3$): δ = 45.1 (NMe_2), 68.9, 71.0, 87.3 (C_5H_4), 115.4, 118.1, 128.9, 154.5 (Ph). − $C_{26}H_{30}FeN_4Ti$ (502.3): calcd. C 62.17, H 6.02, N 11.15; found C 61.18, H 5.88, N 11.71.

Complex 5: Benzene (7 mL) was added to **1**H_2 (0.87 g, 2.35 mmol) and **3b** (0.60 g, 2.35 mmol), affording a light yellow precipitate. The mixture was stirred for 1 h at room temperature. Crystallisation from a minimal quantity of hot benzene afforded the product as light yellow crystals. Yield 0.99 g (71%). − ^{1}H NMR ($CDCl_3$): δ = 2.39 (br. s, 6 H, HNMe_2), 3.05 (s, 12 H, NMe_2), 3.70 (t, J = 1.9 Hz, 4 H, C_5H_4), 4.62 (t, J = 1.9 Hz, 4 H, C_5H_4), 6.66 ("t", apparent J = 7.2 Hz, 2 H, Ph), 6.74 ("d", apparent J = 7.8 Hz, 4 H, Ph), 7.17 ("t", apparent J = 7.7 Hz, 4 H, Ph). − ^{13}C{^{1}H} NMR ($CDCl_3$): δ = 39.1 ($HNMe_2$), 43.2 (NMe_2), 68.5, 70.5, 89.9 (C_5H_4), 115.3, 117.0, 129.1, 153.9 (Ph). − $C_{28}H_{37}FeN_5Zr$ (590.7): calcd. C 56.93, H 6.31, N 11.86; found C 56.69, H 6.11, N 11.20.

Complex 5[PF_6]: A solution of **5** (59 mg, 0.10 mmol) and ferrocenium hexafluorophosphate (33 mg, 0.10 mmol) in acetonitrile (5 mL) was stirred at room temperature for 5 h. The volatile components (solvent and ferrocene) were then removed in vacuo, leaving the product as a brown solid. Yield 73 mg (99%). − $C_{28}H_{37}F_6FeN_5PZr$ (735.6): calcd. C 45.72, H 5.07, N 9.52; found C 45.69, H 5.02, N 8.87.

Complex 7: A solution of **5** (0.28 g, 0.47 mmol) and **6** (77 mg, 0.94 mmol) in benzene (10 mL) was stirred at room temperature for 15 h. The resulting yellow precipitate was then filtered off. Crystallisation from a minimal quantity of chloroform afforded the product as yellow needles. Yield 59 mg (22%). − ^{13}C{^{1}H} NMR ($CDCl_3$): δ = 39.1 ($HNMe_2$), 43.2 (NMe_2), 68.9, 71.0, 87.3 (C_5H_4), 115.4, 118.1, 128.9, 154.5 (Ph). − $C_{24}H_{25}Cl_2FeN_3Zr{\cdot}2CHCl_3$ (812.2): calcd. C 38.45, H 3.35, N 5.17; found C 39.04, H 3.23, N 5.20.

Crystal Structure Determinations of 5 and 7:[20] A yellow single crystal of **5** (dimensions 0.5 × 0.5 × 0.25 mm) and **6** (dimensions 0.8 × 0.4 × 0.4 mm), respectively, was used for data collection at 173 K on a Siemens $P2_1$ four-circle diffractometer with graphite-mono-

Table 1. X-ray structure analysis data of **5** and **7**

Chem. formula	$C_{28}H_{37}FeN_5Zr$	$C_{24}H_{25}Cl_2FeN_3Zr{\cdot}2\ CHCl_3$
Mol. wt.	590.70	812.18
Space group	Monoclinic, $P2_1/c$	Orthorhombic, *Pbcn*
a [Å]	12.771(5)	15.029(6)
b [Å]	12.605(5)	17.751(6)
c [Å]	17.149(11)	24.766(10)
β [°]	98.03(4)	
V [Å^3]	2734(2)	6607(4)
Z	4	8
ρ(calcd.) [g/cm^3]	1.435	1.633
μ [mm^{-1}]	0.937	1.424
F(000)	1224	3248
Index ranges	$0 \le h \le 15$, $0 \le k \le 14$, $-20 \le l \le 20$	$0 \le h \le 20$, $0 \le k \le 23$, $0 \le l \le 33$
θ range [°]	1.6−25.0	1.6−28.5
Reflections collected	5046	8388
Independent reflections	4814 [R(int.) = 0.0701]	8388
Data/restraints/parameters	4814/0/322	8388/0/360
Goodness-of-fit on F^2	1.052	1.013
Final $R1$[a] [$I > 2\sigma(I)$]/$wR2$[b]	0.0814/0.1911	0.0609/0.1348
Larg. diff. peak/hole [e/Å^3]	1.041/−0.901	1.041/−1.182

[a] $R1 = \Sigma||F_o| - |F_c||/\Sigma|F_o|$. − [b] $wR2 = \{\Sigma[w(F_o^2-F_c^2)^2]/\Sigma[w(F_o^2)^2]\}^{0.5}$.

chromated Mo-K_α radiation (λ = 0.71073 Å). The structure was solved by direct methods. Programs used were Siemens SHELXTL PLUS[21] and SHELXL-97.[22] Full-matrix, least-squares refinement on F^2 was carried out anisotropically for the non-hydrogen atoms. Hydrogen atoms were included at calculated positions, using a riding model. Further X-ray structure analysis data are given in Table 1.

Acknowledgments

This work was generously supported by the Deutsche Forschungsgemeinschaft and the Fonds der Chemischen Industrie. P. Z. gratefully acknowledges financial support by the University of Siena (PAR 1999). Jens Vor der Brüggen and Giuliana Opromolla are thanked for electrochemical measurements.

[1] Review: G. J. P. Britovsek, V. C. Gibson, D. F. Wass, *Angew. Chem.* **1999**, *111*, 448−468; *Angew. Chem. Int. Ed.* **1999**, *38*, 428−447.

[2] N. A. H. Male, M. Thornton Pett, M. Bochmann, *J. Chem. Soc., Dalton Trans.* **1997**, 2487−2491.

[3] H. Mack, M. S. Eisen, *J. Organomet. Chem.* **1996**, *525*, 81−87.

[4] V. C. Gibson, B. S. Kimberley, A. J. P. White, D. J. Williams, P. Howard, *Chem. Commun.* **1998**, 313−314.

[5] See, for example: J. D. Scollard, D. H. McConville, N. C. Payne, J. J. Vidal, *Macromolecules* **1996**, *29*, 5241−5243.

[6] See, for example: T. H. Warren, R. R. Schrock, W. M. Davis, *Organometallics* **1998**, *17*, 308−321.

[7] See, for example: [7a] Z. Ziniuk, I. Goldberg, M. Kol, *Inorg. Chem. Commun.* **1999**, *2*, 549−551. − [7b] Y.-M. Jeon, S. J. Park, J. Heo, K. Kim, *Organometallics* **1998**, *17*, 3161−3163. − [7c] F. Jäger, H. W. Roesky, H. Dorn, S. Shah, M. Noltemeyer, H.-G. Schmidt, *Chem. Ber./Recl.* **1997**, *130*, 399−403. − [7d] S. Tinkler, R. J. Deeth, D. J. Duncalf, A. McCamley, *Chem. Commun.* **1996**, 2623−2624. − [7e] A. D. Horton, J. de With, A. J. van der Linden, H. van de Weg, *Organometallics* **1996**, *15*, 2672−2674.

[8] See, for example: [8a] H. Bürger, K. Wiegel, *Z. Anorg. Allg. Chem.* **1976**, *419*, 157−162. − [8b] H. Bürger, K. Wiegel, *Z. Anorg. Allg. Chem.* **1976**, *426*, 301−308. − [8c] H. Bürger, K. Wiegel, *J. Organomet. Chem.* **1977**, *124*, 279−292. − [8d] D. J. Brauer, H. Bürger, K. Wiegel, *J. Organomet. Chem.* **1978**, *150*, 215−231. − [8e] H. Bürger, D. Beiersdorf, *Z. Anorg. Allg. Chem.* **1979**, *459*, 111−118. − [8f] H. Bürger, W. Geschwandtner, G. R. Liewald, *J. Organomet. Chem.* **1983**, *259*, 145−156.

[9] [9a] P. Margl, L. Deng, T. Ziegler, *J. Am. Chem. Soc.* **1998**, *120*, 5517−5525. − [9b] P. Margl, L. Deng, T. Ziegler, *Organometallics* **1998**, *17*, 933−946.

[10] A. Spannenberg, P. Arndt, M. Oberthur, R. Kempe, *Z. Anorg. Allg. Chem.* **1997**, *623*, 389−393.

[11] See, for example: H. Plenio, D. Burth, *Organometallics* **1996**, *15*, 4054−4062.

[12] Review: A. M. Allgeier, C. A. Mirkin, *Angew. Chem.* **1998**, *110*, 936−952; *Angew. Chem. Int. Ed.* **1998**, *37*, 894−908.

[13] B. Bildstein, M. Malaun, unpublished results.

[14] P. Scott, U. Rief, J. Diebold, H. H. Brintzinger, *Organometallics* **1993**, *12*, 3094−3101.

[15] K.-P. Stahl, G. Boche, W. Massa, *J. Organomet. Chem.* **1984**, *277*, 113−125.

[16] W. E. Britton, R. Kashyap, M. El-Hashash, M. El-Kady, M. Herberhold, *Organometallics* **1986**, *5*, 1029−1031.

[17] See, for example: [17a]D. W. Carpenetti, L. Kloppenburg, J. T. Kupec, J. L. Petersen, *Organometallics* **1996**, *15*, 1572−1581. − [17b] A. K. Hughes, A. Meetsma, J. H. Teuben, *Organometallics* **1993**, *12*, 1936−1945.

[18] U. Siemeling, O. Kuhnert, M. O. Kristen, G. Hauck, unpublished results.

[19] A. Togni, M. Hobi, G. Rihs, G. Rist, A. Albinati, P. Zanello, D. Zech, H. Keller, *Organometallics* **1994**, *13*, 1224−1234.

[20] Crystallographic data (excluding structure factors) for the structures reported in this paper have been deposited with the Cambridge Crystallographic Data Centre as supplementary publication nos. CCDC-149674 (for **5**) and CCDC-149675 (for **7**). Copies of the data can be obtained free of charge on application to CCDC, 12 Union Road, Cambridge CB2 1EZ, UK [Fax: (internat.) +44-1223/336-033; E-mail: deposit@ccdc.cam.ac.uk].

[21] G. M. Sheldrick, *SHELXTL PLUS*, Siemens Analytical Instruments, Madison, WI, USA, **1990**.

[22] G. M. Sheldrick, *SHELXL-97*, University of Göttingen, Germany, **1997**.

Received September 25, 2000
[I00366]

Palladium and Rhodium Complexes with Planar-Chiral Carborane Ligands[‡]

Henri Brunner,*[a] Andreas Apfelbacher,[a] and Manfred Zabel[a]

Dedicated to Professor Dr. Dieter Sellmann on the occasion of his 60th birthday

Keywords: Chirality / Carboranes / Palladium / Rhodium / Asymmetric catalysis

Base degradation of the prochiral 1-diphenylphosphanyl-2-phenyl-1,2-dicarba-*closo*-dodecaborane (**1**) affords the planar-chiral 7-diphenylphosphanyl-8-phenyl-7,8-dicarba-*nido*-undecaborate anion (**2**). Resolution of the racemic anion carried out using a well-established procedure, gave the internally diastereomeric palladium complexes **3*R*-*R*** and **3*R*-*S***. These complexes were separated by fractional crystallization. A single-crystal X-ray analysis of **3*R*-*R*** established the *exo*-*nido* bonding of the carborane ligand via the phosphorus atom and the adjacent BH group, and the (*R*) configuration of the carborane ligand. The enantiomerically pure anions of **2** were liberated from the diastereomerically pure palladium complexes **3*R*-*R*** and **3*R*-*S***, respectively, by subsequent addition of HCl and NaCN. The *exo*-*nido*-rhodium–carborane complexes **4**–**8** were prepared by heating **2e*R*** or **2e*S*** with $[Rh(COD)Cl]_2$ and/or a chiral chelating phosphane, such as DIOP and BINAP, under reflux. The chiral complexes were tested under enantioselective catalysis conditions such as hydrogenation of acetamidocinnamic acid, hydrogenation of ketopantolactone, and hydrosilylation of acetophenone.

Introduction

For the realization of planar chirality, the ferrocene system is the most suitable skeleton.[1] Two different substituents in the 1,2- or 1,3-positions of the same cyclopentadienyl ring are sufficient to make the systems chiral. In the cyclopentadienyl anions $[C_5H_3RR']^-$, the symmetry plane is removed on complexation with a metal fragment. In contrast, *nido*-carboranyl anions such as $[B_9C_2H_{10}RR']^-$ or $[B_9C_2H_9RR']^{2-}$, containing two different substituents in the open face, are chiral by themselves, because the cage side and the open face are different. Until recently, there have only been a few attempts to resolve *nido*-carboranyl anions, potential ligands in enantioselective catalysts. Early reports came from the groups of Zakharkin and Hawthorne.[2–5] Meanwhile, a series of optically active boron cage compounds was described, of which four were *nido*-C_2B_9 derivatives.[6] Last year a *nido*-carboranyl anion $[B_9C_2H_{10}RR']^-$ was resolved with a SPh and a CH_2OH substituent at the adjacent carbon atoms.[7]

In this paper we report on the resolution of the chiral carboranylphosphane anion $[B_9C_2H_{10}(PPh_2)(Ph)]^-$ [8] obtained as the racemate in the base degradation of the carborane $[B_{10}C_2H_{10}(PPh_2)(Ph)]$[9] (**1**), the phenyl substituent of which is introduced in the synthesis with phenylacetylene, and the diphenylphosphanyl group by metallation. The racemic anion is incorporated into a palladium complex containing enantiopure *ortho*-metallated *N,N*-dimethyl-(*S*)-1-phenylethylamine. After separation of the diastereomers, the resolved anions are cleaved from the palladium complex and introduced into rhodium complexes. In these metal complexes, the carboranylphosphane anion binds as a chelate ligand in an *exo*-*nido*-mode via the phosphorus atom and the adjacent B–H group. The enantiomers **4*R*** and **4*S***, and the enantiomers/diastereomers **5*RR*-*R***, **5*SS*-*S*** and **5*RR*-*S*** were used as catalysts in the enantioselective hydrogenation of acetamidocinnamic acid and ketopantolactone, and in the enantioselective hydrosilylation of acetophenone with diphenylsilane.[10]

The Planar-Chiral Anion 7-Diphenylphosphanyl-8-phenyl-7,8-dicarba-*nido*-undecaborate

The sequence of syntheses started with the addition of phenylacetylene to decaborane(14)[11] to give 1-phenyl-1,2-dicarba-*closo*-dodecaborane. Metallation of the acidic CH group with BuLi, and reaction with $ClPPh_2$ provided 1-diphenylphosphanyl-2-phenyl-1,2-dicarba-*closo*-dodecaborane[10] (**1**) (Scheme 1), on which a single-crystal X-ray analysis was performed, as shown in Scheme 1. Both carboranes are achiral molecules. Planar chirality only comes into play after the base degradation of **1** with piperidine to yield the salt piperidinium 7-diphenylphosphanyl-8-phenyl-7,8-dicarba-*nido*-undecaborate (**2a**) (Scheme 1).[9] Resolution of the racemic anion of **2a** was attempted by use of enantiomerically pure counter-cations, such as *N,N,N*-trimethyl-(*S*)-1-phenylethylammonium, *N*-methylbrucinium, or *N*-methylquininium as the resolving agents in ethanol. The exchange of the piperidinium ion in **2a** for the enantiomerically pure cations to give **2b**–**d** was carried out according to literature procedures.[9] In the three series **2b**–**d**, mixtures of two diastereomers in ratios of about 1:1 were isolated. It was not possible to separate the diastereomers of the series **2b**–**d** by crystallization. For example, after 15 recrystallizations of **2b** no change in the optical rotation of the diastereomer mixture was observed.

[‡] Enantioselective Catalyses, 136. – Part 135: Ref.[23]

[a] Institut für Anorganische Chemie, Universität Regensburg, 93040 Regensburg, Germany

 © WILEY-VCH Verlag GmbH, 69451 Weinheim, 2001 1434–1948/01/0404–0917 $ 17.50+.50/0

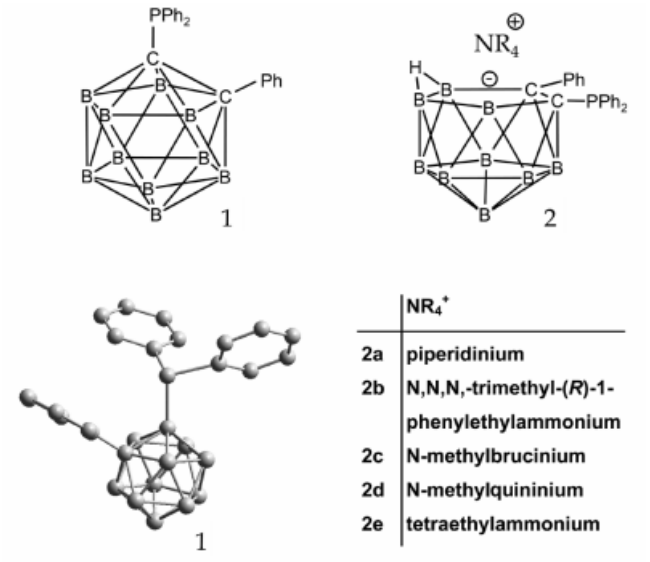

	NR_4^+
2a	piperidinium
2b	N,N,N,-trimethyl-(*R*)-1-phenylethylammonium
2c	N-methylbrucinium
2d	N-methylquininium
2e	tetraethylammonium

Scheme 1. The carborane **1** and the salts **2a−e** (B abbreviates BH); ORTEP diagram of **1**

Resolution of the Anion *rac*-7-Diphenylphosphanyl-8-phenyl-7,8-dicarba-*nido*-undecaborate Via Internally Diastereomeric Palladium Complexes

Using the well-established procedure for the resolution of racemic bis(phosphanes) via internally diastereomeric palladium complexes,[12,13] it was possible to resolve the *rac*-7-diphenylphosphanyl-8-phenyl-7,8-dicarba-*nido*-undecaborate anion. The diastereomers **3*R*-*R*** and **3*R*-*S*** (Scheme 2) were synthesized from **2e** and di-μ-chlorobis{(*R*)-2-[1-(dimethylamino)ethyl]phenyl-*C,N*}palladium[14] in CH_2Cl_2 at 10 °C. To remove the by-product NEt_4Cl the solvent was exchanged for $CHCl_3$ and the solution was stirred for 3 h. During this time, the mixture of the diastereomers **3*R*-*R*** and **3*R*-*S*** precipitated as a yellow-green powder in a ratio 55:45. The NEt_4Cl remained in solution.

The IR spectrum of the mixture **3*R*-*R*/3*R*-*S*** shows an intense absorption at 2570 cm^{-1}, characteristic of the B−H stretching vibrations of *nido*-carboranes. The ^{31}P NMR spectrum of the mixture of the diastereomers exhibits singlets at δ = 28.64 for **3*R*-*R*** and 31.35 for **3*R*-*S***. The ^1H NMR spectrum displays a broad resonance centered at δ = −2.3 confirming the existence of a B−H−B bridge in **3*R*-*R*** and **3*R*-*S***. Two quadruplets at δ = −0.38 for **3*R*-*R*** and 0.35 for **3*R*-*S*** are assigned to the Pd−H−B bridges. The two diastereotopic methyl groups of the $N(CH_3)_2$ groups give two doublets at δ = 2.77 and 2.89 for **3*R*-*R***, and two doublets at δ = 2.61 and 3.08 for **3*R*-*S***. A doublet at δ = 1.83 for **3*R*-*R*** and a doublet at δ = 1.45 for **3*R*-*S*** results from the CCH_3 group, and a doublet of a quadruplet at δ = 3.62 for **3*R*-*R*** and a quadruplet at δ = 4.33 for **3*R*-*S*** from the CH group.

As **3*R*-*R*** and **3*R*-*S*** differ in the chemical shifts of their NMR spectra, the ratio **3*R*-*R*:3*R*-*S*** can be determined by integration of the methyl signals in the ^1H NMR spectrum, or the phosphorus signals in the ^{31}P NMR spectrum. Furthermore, the ^1H and ^{31}P NMR spectra indicate that **3*R*-*R*** and **3*R*-*S*** are the isomers in which PPh_2 and NMe_2 as well as BH and *ortho*-C are *trans* to each other. This is in agreement with the X-ray structure analysis for **3*R*-*R***, given below.

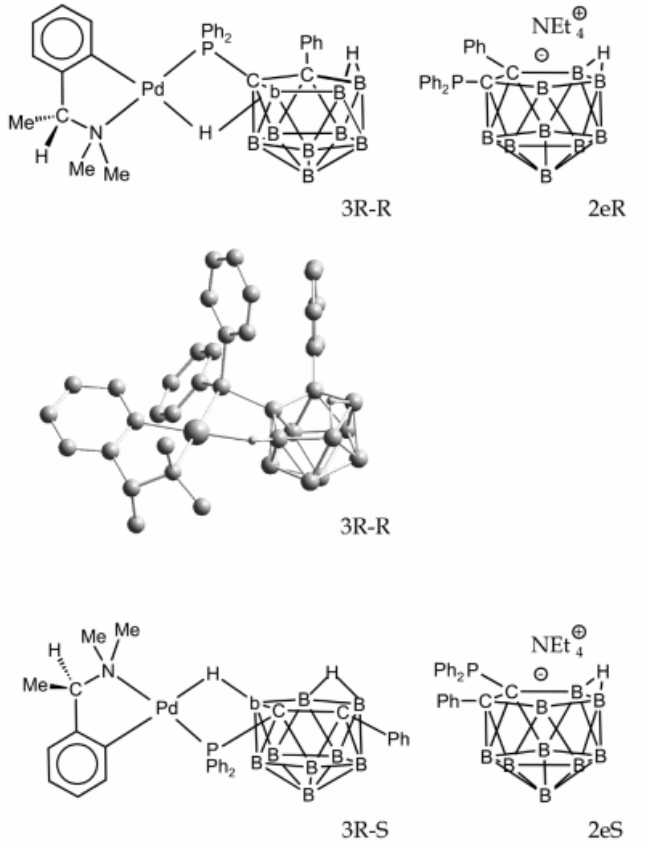

Scheme 2. The diastereomeric Pd complexes **3*R*-*R*** and **3*R*-*S***, and the resolved salts **2e*R*** and **2e*S*** (abbreviations: B = BH and b = B); ORTEP diagram of **3*R*-*R***

The separation of the diastereomers **3*R*-*R*** and **3*R*-*S*** was first attempted by fractional crystallization from toluene/petroleum ether at −20 °C. Yellow needles were isolated containing the diastereomers in a ratio of 1:1. However, in the separation of the diastereomers **3*R*-*R*/3*R*-*S*** from the by-product NEt_4Cl it had been noticed that in a mixture of toluene and pentane the **3*R*-*R*** isomer was enriched. Based on this observation a procedure to separate the diastereomers was developed. The 1:1 mixture **3*R*-*R*/3*R*-*S*** was dissolved in toluene. Dropwise addition of pentane precipitated a light brown powder enriched in **3*R*-*R*** (**3*R*-*R*/3*R*-*S*** = 90:10), whereas the filtrate was enriched in **3*R*-*S*** (**3*R*-*R*/3*R*-*S*** = 33:66). To get the pure diastereomers **3*R*-*R*** and **3*R*-*S***, both fractions were re-dissolved in toluene. Pentane was added and the solutions were crystallized to yield pure **3*R*-*R*** and **3*R*-*S***, respectively, as light brown, rhombic crystals. The separation of the diastereomers **3*R*-*R*** and **3*R*-*S*** can be monitored by ^1H and ^{31}P NMR spectroscopy.

A single-crystal X-ray analysis of **3*R*-*R*** established the (*R*) configuration (see below) of the *nido*-carborane ligand relative to the coordinated *ortho*-metallated *N,N*-dimethyl-(*R*)-1-phenylethylamine ligand (Scheme 2). It also

showed that the carborane ligand coordinated to the palladium atom with the phosphorus atom and the adjacent BH group in an *exo-nido* fashion. Furthermore, the X-ray analysis confirmed the *trans* position of PPh_2, NMe_2, and BH, *ortho*-C in **3*R*-*R***.

The configuration of planar-chiral carborane ligands was specified according to the Schlögl convention[1,2] for planar-chiral ferrocenes. The observer looks onto the open five-membered ring of the carborane. By considering the disposition of the substituents, ordered according to the Cahn−Ingold−Prelog rules, clockwise is assigned to the (*R*) configuration, counterclockwise to the (*S*) configuration. Thus, in complex **3*R*-*R*** (Scheme 2) the priority sequence is $PPh_2 > CPh > BH$, and the carborane ligand has an (*R*) configuration.

The liberation of the enantiomerically pure anions from the separated palladium complexes was performed in two steps. First, boiling solutions of the diastereomerically pure complexes **3*R*-*R*** and **3*R*-*S*** in acetone containing hydrochloric acid removed the *N*,*N*-dimethylamino-(*R*)-1-phenylethylamine ligand from the Pd complexes. Then, the carborane ligand was liberated from the palladium complex by dissolving in CH_2Cl_2 and stirring with an excess of NaCN and NEt_4Cl in water. Pure **2e*R*** and **2e*S*** (Scheme 2) were isolated from the organic phase as white powders, after discarding the water phase.

The IR spectra of **2e*R*** and **2e*S*** show an intense absorption at 2570 cm^{-1}, typical of the B−H stretching vibrations of *nido*-carboranes. The ^1H NMR spectra display a broad resonance at δ = −1.8 to −2.2, assigned to the B−H−B bridge, and a broad absorption at δ = −0.2 to −2.8 originating from the nine BH groups. The $^{31}P\{^1H\}$ NMR spectra exhibit one signal at δ = 9.45 for the PPh_2 group. The $^{11}B\{^1H\}$ NMR spectra show five peaks in a ratio of 1:1:5:1:1 at negative δ values. As expected, the optical rotations of **2e*R*** and **2e*S*** show an image/mirror image relationship. The enantiomeric purity of **2e*R*** seems to be a little higher than that of **2e*S***.

The Rhodium−Carborane Complexes 4−8

For the preparation of the Rh(COD)carborane complexes **4*R*** and **4*S*** (Scheme 3) enantiomerically pure **2e*R*** or **2e*S*** was refluxed with $[Rh(COD)Cl]_2$ in ethanol. The orange clear solution became a yellow suspension. After cooling to room temperature, the solvent was evaporated to a few mL, affording yellow **4*R*** and **4*S***, respectively. Solutions of these complexes in CH_2Cl_2 are air-sensitive. The $^{31}P\{^1H\}$ NMR spectra of **4*R*** and **4*S*** display a doublet centered at δ = 36.78 with a coupling constant $^1J_{Rh,P}$ = 114.6 Hz. Scheme 3 shows the ORTEP plot of the *exo-nido* structure of complex **4*S***.

For the syntheses of the rhodium−bis(phosphane)−carborane complexes **5**−**8** $[Rh(COD)Cl]_2$, **2e*R*** or **2e*S*** and the chelating bis(phosphane) were heated under reflux in ethanol. The rhodium complexes precipitated as orange powders in high purity. The bis(triphenylphosphane)rhodium complex containing the racemic anion 7-diphenylphosphanyl-8-phenyl-7,8-dicarba-*nido*-undecaborate had been described before.[15]

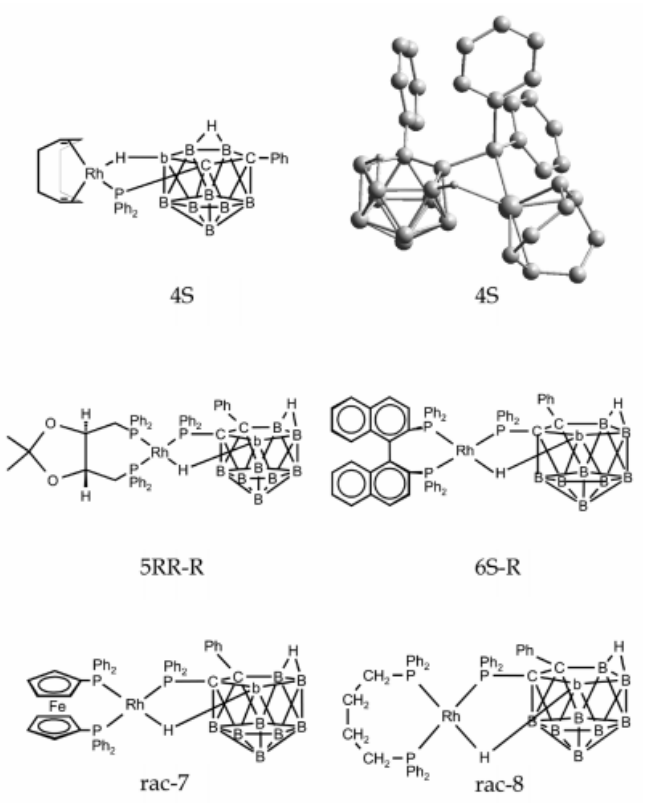

Scheme 3. The Rh(COD) complex **4*S*** and the ORTEP diagram of **4*S***; the [bis(phosphane)]Rh complexes **5**−**8** (abbreviations: B = BH and b = B)

With (*R*,*R*)- or (*S*,*S*)-DIOP as the chelating bis(phosphane), the enantiomers **5*RR*-*R*** and **5*SS*-*S***, as well as their diastereomer **5*RR*-*S*** were formed (Scheme 3). All the complexes were orange powders, slightly soluble, but air-stable in CH_2Cl_2 solution. The ^1H NMR spectra display the signals of the RhHB and BHB bridges at δ = −2.70 and −2.00 to −1.00 for **5*RR*-*R*** and **5*SS*-*S***, and at δ = −3.25 to −2.78 and −2.30 to −2.25 for **5*RR*-*S***, indicating the *exo-nido* structure of the complexes. The ^{31}P NMR spectra show ABX systems. The AB systems (8-line ddd structures for each P atom) are assigned to the two phosphorus atoms of the DIOP ligands, whereas the X parts of the spectra give doublets of a multiplet.

(*S*)-BINAP as the chelating bis(phosphane) afforded a 73% yield of a red-orange powder of **6*S*-*R*** (Scheme 3), for which the ^1H NMR spectrum indicates the *exo-nido* structure. The ^{31}P NMR spectrum shows an ABX system, in which the AB part is assigned to the two PPh_2 groups of BINAP (δ = 6.98 and 34.61) and the X part to the PPh_2 group of the carborane ligand (δ = 43.62).

Using racemic **2e** together with the chelating bis(phosphanes) bis(diphenylphosphanyl)ferrocene and 1,4-bis(diphenylphosphanyl)butane, racemates of the complexes **7** and **8** (Scheme 3) were formed in yields of 84% and 60%, respectively, as orange powders (*exo-nido* types). The $^{31}P\{^1H\}$ NMR spectra of both complexes exhibit ABX sys-

tems in which the AB parts are due to the two PPh_2 groups of the bis(phosphane) ligand (ddd structures) and the X parts, doublets of a multiplet, due to the carborane ligand.

Remarkably, attempts to coordinate bis(phosphanes), which form five-membered rings, such as CHIRAPHOS or NORPHOS, were not successful. Similarly, the chelating ligand (2*R*,3*R*)-1,4-dimercapto-2,3-butanediol and (*S*)-2,2′-diamino-1,1′-binaphthyl did not give the corresponding *exo-nido*-rhodium−carborane complexes. Thus, the preparation of rhodium−carborane complexes with another chelating ligand was confined to bis(phosphanes) forming seven-membered rings.

Enantioselective Catalysis

In order to explore the enantioselectivity of the new complexes **4**−**8** in asymmetric catalyses, the hydrogenation of acetamidocinnamic acid, the hydrogenation of ketopantolactone, and the hydrosilylation of acetophenone were selected for study. In all three systems it was found that only complexes **4** and **5** were catalytically active.

In a methanol solution of (*Z*)-α-*N*-acetamidocinnamic acid, containing the catalysts **4** and **5**, there was no hydrogenation while stirring under 1 atm of H_2 for 48 h at room temperature. However, complete hydrogenation resulted in an autoclave under 50 bar of H_2 at 65 °C in toluene/ethanol mixtures. The product *N*-acetylphenylalanine was converted into its methyl ester[16] in order to measure the *ee* by GC. After the hydrogenation with complexes **4*R*** and **4*S***, a black solution had formed indicating the decomposition of complexes **4*R*** and **4*S***, whereas with complexes **5*RR-R*** and **5*RR-S*** an orange solution resulted.

In 5 mL ethanol/10 mL toluene, **4*R*** gave 60−62% *ee* of *N*-acetyl-L-phenylalanine (Table 1, last column). The enantiomerically less pure **4*S*** afforded the D product in a somewhat reduced enantioselectivity. In **4*R*** and **4*S*** the planar-chiral carborane ligand is the only source of chirality, responsible for the chiral induction in the enantioselective hydrogenation reaction. Complex **5*RR-R***, containing (*R*,*R*)-DIOP in addition to the (*R*)-carborane ligand, produced 60−63% *ee* of *N*-acetyl-D-phenylalanine. Complex **5*RR-S***, containing (*R*,*R*)-DIOP in addition to the opposite (*S*)-carborane ligand, gave 50−57% *ee* with the same *N*-acetyl-D-phenylalanine in excess. Evidently, the configuration of *N*-acetylphenylalanine is controlled by the ligand (*R*,*R*)-DIOP. The small differences produced by the diastereomeric catalysts **5*RR-R*** and **5*RR-S*** could be due to the opposite configurations of the carborane ligand. Another explanation is the dissociation of the carborane ligand from the (*R*,*R*)-DIOP complexes **5*RR-R*** and **5*RR-S*** − a reasonable assumption, because empty coordination sites are needed for the binding of substrate and hydrogen during the catalysis.[17] However, the complete dissociation of the carborane ligands from the complexes **5*RR-R*** and **5*RR-S*** should give identical chiral inductions.

Table 1. Enantioselectivities (% *ee*) obtained with complexes **4** and **5** as catalysts in the hydrogenation of (*Z*)-α-*N*-acetamidocinnamic acid

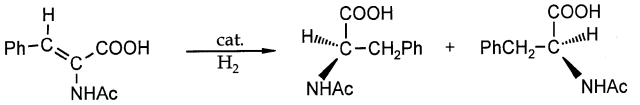

Complex[a]	10 mL of ethanol 5 mL of toluene	5 mL of ethanol 5 mL of toluene	5 mL of ethanol 10 mL of toluene
4*R*	12.7, 12.0 L	48.1, (40.0), 50.1 L	61.9, 60.3, 61.7, 61.3, 62.3 L
4*S*	19.5 D	− −	55.8, 58.0, 54.8, 62.3 D
5*RR-R*	76.1, 79.6 D	(80.5) D	63.0, 60.2 D
5*RR-S*	62.6, 57.1 D	− −	56.6, 50.0, (40.4) D

[a] Ratio catalyst/substrate = 1:100. Substrate quantity 200 mg (0.975 mmol). Reaction conditions: 50 bar H_2 pressure, 65 °C, 48 h. Quantitative hydrogenation according to ^1H NMR spectra. Enantiomeric excess determined by GC on a Chirasil-L-Val column.

It was interesting to investigate the dependence of the enantioselectivity on the composition of the solvent (Table 1, columns 2−4). The limiting factor was the solubility of acetamidocinnamic acid, which is insoluble in toluene and of the rhodium−carborane complexes, which are only sparingly soluble in ethanol. For complexes **4** with the COD/carborane ligand set, the enantioselectivity decreased appreciably with an increasing ethanol/toluene ratio. For complexes **5** the opposite trend was observed. The higher the ratio ethanol/toluene the higher was the chiral induction. For the complex **5*RR-R*** at a ratio ethanol/toluene = 10:5 the enantioselectivity was close to 80%. An *ee* of 80−81% is the value expected from the literature for the Rh(DIOP) catalyst.[18] The observed solvent dependence is therefore in agreement with a dissociation of the carborane ligand from complexes **5** during catalysis.

The hydrogenation of ketopantolactone, catalyzed by complexes **4** and **5**, was carried out in a stirred autoclave under 50 bar H_2 at 50 °C for 48 h in toluene, resulting in a complete reduction to (*R*)- and (*S*)-pantolactone.[19] The achieved enantioselectivities are given in Table 2. Complex **4*R***, consisting of the COD ligand and the enantiomerically pure (*R*)-carborane ligand, afforded (*R*)-pantolactone in 23% *ee*. The enantiomerically less pure enantiomer **4*S*** gave 16.4% *ee* of (*S*)-pantolactone. Again, the carborane ligand is the only chiral information in the complexes **4*R*** and **4*S***. Complexes **5*RR-R*** and **5*SS-S*** are enantiomers, containing the (*R*,*R*)-DIOP/(*R*)-carborane and the (*S*,*S*)-DIOP/(*S*)-carborane ligand set. These systems gave enantioselectivities of 59−66% for (*R*)- and (*S*)-pantolactone, respectively. For comparison, under the same conditions the catalyst [Rh(*R*,*R*)-DIOP-Cl]$_2$ afforded 54.4% of (*R*)-pantolac-

tone,[20] indicating a dissociation of the carborane ligand from the complexes **5*RR*-*R*** and **5*SS*-*S***.

Table 2. Complexes **4** and **5** as catalysts in the hydrogenation of ketopantolactone

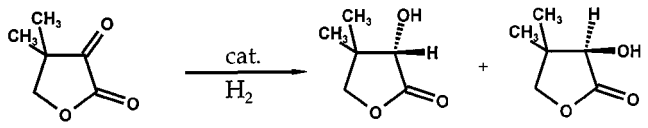

Complex[a]	*ee* [%]	Configuration
4*R*	22.5, 23.0	*R*
4*S*	(16.3)	*S*
5*RR*-*R*	63.6, 58.7, 63.4	*R*
5*SS*-*S*	58.9, 61.1, 66.6	*S*

[a] Ratio catalyst/substrate = 1:200. Ketopantolactone quantity 258 mg (2.01 mmol). Reaction conditions: 50 bar H_2 pressure, 50 °C, 48 h. Quantitative reduction and enantiomeric excess determined by GC on a Chirasil-DEX-CB column.

The hydrosilylation of acetophenone with diphenylsilane (room temperature, 48 h) was catalyzed by the complexes **4*R***, **5*RR*-*S*** and **5*SS*-*S*** to give (*R*)- or (*S*)-1-phenylethanol.[20,21] The enantioselectivities (and in addition the conversion and the enol ether content)[21] are summarized in Table 3. Complex **4*R*** induced an enantiomeric excess of 7−9% of (*R*)-1-phenylethanol, whereas the diastereomers **5*RR*-*S*** and **5*SS*-*S*** both gave 26−27% *ee* of (*R*)- and (*S*)-pantolactone, respectively. The enantioselectivity of [Rh(*R*,*R*)-DIOP-Cl]$_2$ as the chiral catalyst under the same conditions was 27% of (*R*)-1-phenylethanol,[18] compatible with a dissociation of the carborane ligand from **5*RR*-*S*** and **5*SS*-*S*** and a rhodium−DIOP species being the enantioselective catalyst.

Table 3. Complexes **4** and **5** as catalysts in the hydrosilylation of acetophenone with diphenylsilane

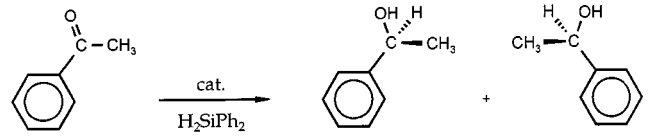

Complex[a]	Conversion [%]	Enol ether [%]	1-Phenylethanol Yield [%]	1-Phenylethanol *ee* [%]
4*R*	75, 83	0, 5	75, 79	8.9, 6.7 (*R*)
5*RR*-*S*	92, 92, 37	16, 9, 0	76, 83, 37	26.0, 26.3, 27.7 (*R*)
5*SS*-*S*	72, 80, 89	17, 45, 48	62, 59, 52	(20.7), 25.7, 27.5 (*S*)

[a] Ratio catalyst/acetophenone/diphenylsilane = 1:400:400. Acetophenone and diphenylsilane quantities 1.0 mL (8.5 mmol) and 1.6 mL (8.6 mmol). Reaction conditions: room temperature, 2 d. Conversion, content of enol ether and silyl ether measured by ^{1}H NMR spectroscopy. Enantiomeric excess determined by GC on a Chirasil-DEX-CB column.

In addition, the complexes **4*R*** and **4*S*** were used as catalysts in the diastereoselective hydrogenation of folic acid showing promising results.[22]

Experimental Section

General: All experiments were conducted under dry nitrogen using Schlenk techniques. Solvents were freshly distilled under nitrogen from appropriate drying agents before use. − NMR measurements: ^{1}H at 400 MHz and ^{13}C at 100.1 MHz referenced to $SiMe_4$, ^{11}B at 128 MHz referenced to external $BF_3{\cdot}OEt_3$, ^{31}P at 162 MHz referenced to external H_3PO_4 using a Bruker ARX 400 instrument (chemical shifts in units of parts per million downfield from $SiMe_4$, coupling constants in Hertz). − IR spectra: Beckman IR 4240. − Specific rotations: Perkin−Elmer polarimeter 241. Decaborane(14),[12] 1-phenylcarborane,[23] 1-diphenylphosphanyl-2-phenylcarborane[10] (**1**), tetraethylammonium 7-diphenylphosphanyl-8-phenyl-7,8-dicarba-*nido*-undecaborate[9] (**2e**), and DIOP[19,24] were synthesized according to literature procedures. BINAP, bis(diphenylphosphanyl)ferrocene, and 1,4-bis(diphenylphosphanyl)butane were commercially obtained.

Synthesis of the Mixture of Diastereomers (*R*)-{2-[1-(Dimethylamino)ethyl]phenyl-*C*,*N*}[*exo*-*nido*-(*R*)-(7-diphenylphosphanyl-8-phenyl-7,8-dicarbaundecaborato)]palladium (3*R*-*R*) and (*R*)-{2-[1-(Dimethylamino)ethyl]phenyl-*C*,*N*}[*exo*-*nido*-(*S*)-(7-diphenylphosphanyl-8-phenyl-7,8-dicarbaundecaborato)]palladium (3*R*-*S*): Compound **2** (7.66 g, 14.6 mmol) and (*R*)-di-μ-chlorobis{2-[1-(dimethylamino)ethyl]phenyl-*C*,*N*}palladium[15] (4.03 g, 7.03 mmol) were stirred in 200 mL of CH_2Cl_2 at −10 °C for 4 h. The solvent was evaporated and the yellow-green product was suspended in 20 mL of $CHCl_3$, while the NEt_4Cl remained in solution. After stirring for 3 h, the yellow-white diastereomers **3*R*-*R*/3*R*-*S*** were precipitated in a ratio of 55:45. The residue was filtered and washed with 3 × 5 mL of $CHCl_3$. Yield 5.48 g (58%). − $[\alpha]_\lambda$ (c = 1.0, CH_2Cl_2) = −6 (578 nm), −8 (546 nm), −24 (436 nm). − IR (KBr): $\tilde{\nu}$ = 2535 cm^{-1} vs (B−H). − MS (FAB-NI-LSIMS): *m*/*z* (%) = 647.7 (100) [M]$^+$, 498.3 (95) [M$^+$ − $C_{10}H_{14}N$]. − $C_{30}H_{39}B_9NPPd$ (647.7): calcd. C 55.44, H 6.06, N 2.15; found C 55.39, H 6.14, N 2.06.

Separation of the Diastereomers 3*R*-*R* and 3*R*-*S*: The diastereomeric mixture **3*R*-*R*/3*R*-*S*** (400 mg, 0.62 mmol) was dissolved in 50 mL of toluene and filtered. At 15−20 °C 150 mL of pentane was added through a dropping funnel within 5−6 h (1 drop per 3 s). 80−90 mg of a brown powder (**3$_{pow}$**) with a ratio **3*R*-*R*/3*R*-*S*** = 90:10 was precipitated and filtered off. The solvent of the filtrate was evaporated to yield 200 mg of a brown powder (**3$_{fil}$**) with a ratio **3*R*-*R*/3*R*-*S*** = 33:66. To obtain the pure diastereomers **3*R*-*R*** and **3*R*-*S***, 350 mg of **3$_{pow}$** or **3$_{fil}$** were dissolved in 50 mL of toluene. Pentane (35 mL) was added, and the solution filtered and crystallized at −20 °C to yield 200 mg (16%) of pure **3*R*-*R*** or 200 mg (23%) **3*R*-*S***.

3*R*-*R*: $[\alpha]_\lambda$ (c = 1.0, CH_2Cl_2) = 21 (578 nm), 30 (546 nm), 120 (436 nm). − ^{1}H NMR (CD_2Cl_2): δ = −2.4 to −2.1 (br., 1 H, BHB), −0.38 (q, $^1J_{H,B}$ = 34.1 Hz, 1 H, PdHB), 1.5−2.5 (br., 8 H, BH), 1.83 (d, $^3J_{H,H}$ = 6.6 Hz, 3 H, $CHCH_3$), 2.77 (d, $^4J_{H,P}$ = 2.0 Hz, 3 H, NCH_3), 2.89 (d, $^4J_{H,P}$ = 4.1 Hz, 3 H, NCH_3), 3.62 (dq, $^3J_{H,H}$ = 6.6 Hz, $^4J_{H,P}$ = 2.2 Hz, 1 H, CH), 6.16−6.25 (m, 1 H, Pd/CH_{ortho}), 6.45−6.55 (m, 1 H, H_{ar}), 6.69−6.91 (m, 9 H, H_{ar}), 6.94−7.09 (m, 1 H, H_{ar}), 7.11−7.19 (m, 2 H, H_{ar}), 7.39−7.63 (m, 3 H, H_{ar}), 7.81−7.92 (m, 2 H, H_{ortho} in PPh_2). − Signals different in ^{1}H{^{31}P} NMR (CD_2Cl_2): δ = 2.77 (s, 3 H, NCH_3), 2.89 (s, 3 H, NCH_3), 3.62 (q, $^3J_{H,H}$ = 6.6 Hz, 1 H, CH). − ^{11}B{^{1}H} NMR (CD_2Cl_2): δ = −34.15 (s, 1 B), −28.07 (s, 1 B), −23.31 (s, 2 B), −13.13 (s, 2 B), −10.91 (s, 1 B), −8.31 (s, 1 B), −2.70 (s, 1 B). − ^{13}C{^{1}H} NMR (CD_2Cl_2): δ = 23.41 (s, $CHCH_3$), 48.55 (s, NCH_3),

52.00 (s, NCH_3), 64.00−67.00 (br., CPh), 74.32 (s, CCH_3), 123.61 (s, C_{ar}), 125.70 (d, J =8.3 Hz, C_{ipso} in CPh, C_{ar}), 126.36 (d, $J_{C,P}$ = 7.6 Hz, C_{meta} in PPh_2), 127.20 (d, $J_{C,P}$ = 14.6 Hz, C_{meta} in PPh_2), 128.55 (m, C_{ipso} in PPh_2, C_{ar}), 129.55 (m, C_{ar}), 131.41 (d, J = 2.5 Hz, C_{ar}), 132.56 (m, C_{ar}), 134.07 (s, C_{ar}), 136.51 (d, J = 13.3 Hz, $CPPh_2$), 136.81 (d, J =13.4 Hz, C_{ar}), 155.66 (d, J =2.6 Hz, CPd). − $^{31}P\{^1H\}$ NMR (CD_2Cl_2): δ = 28.64 (s, PPh_2).

3*R*-*S*: $[\alpha]_\lambda$ (c = 1.0, CH_2Cl_2) = −35 (578 nm), −45 (546 nm), −149 (436 nm). − ^1H NMR (CD_2Cl_2): δ = −2.5 to −2.0 (br., 1 H, BHB), 0.35 (q, $^1J_{H,B}$ = 35.4 Hz, 1 H, PdHB), 1.45 (d, $^3J_{H,H}$ = 6.7 Hz, 3 H, $CHCH_3$), 1.5−2.5 (br., 8 H, BH), 2.61 (d, $^4J_{H,P}$ = 2.7 Hz, 3 H, NCH_3), 3.08 (d, $^4J_{H,P}$ = 3.4 Hz, 3 H, NCH_3), 4.33 (q, $^3J_{H,H}$ = 6.7 Hz, 1 H, CH), 6.20−6.28 (m, 1 H, Pd/CH_{ortho}), 6.50−6.57 (m, 1 H, H_{ar}), 6.78−6.93 (m, 8 H, H_{ar}), 7.01−7.07 (m, 1 H, H_{ar}), 7.11−7.14 (m, 2 H, H_{ar}), 7.39−7.46 (m, 1 H, H_{ar}), 7.49−7.59 (m, 3 H, H_{ar}), 7.84−7.89 (m, 2 H, H_{ortho} in PPh_2). − Signals different in $^1H\{^{31}P\}$ NMR (CD_2Cl_2): δ = 2.61 (s, 3 H, NCH_3), 3.08 (s, 3 H, NCH_3). − $^{11}B\{^1H\}$ NMR (CD_2Cl_2): δ = −35.10 (s, 1 B), −28.22 (s, 1 B), −24.67 (s, 1 B), −22.96 (s, 1 B), −13.77 (s, 1 B), −12.23 (s, 1 B), −10.40 (s, 1 B), −8.93 (s, 1 B), −3.31 (s 1 B). − $^{13}C\{^1H\}$ NMR (CD_2Cl_2): δ = 14.26 (s, $CHCH_3$), 44.70 (s, NCH_3), 50.96 (s, NCH_3), 64.00−67.00 (br., CPh), 71.88 (s, CCH_3), 124.31 (s, C_{ar}), 125.60 (d, J =1.4 Hz, C_{ipso} in CPh, C_{ar}), 126.77 (d, $J_{C,P}$ = 7.6 Hz, C_{meta} in PPh_2), 127.25 (d, $J_{C,P}$ = 13.0 Hz, C_{meta} in PPh_2), 128.55 (m, C_{ipso} in PPh_2, C_{ar}), 129.41 (m, $C_{ipso,}$ C_{ar}), 131.33 (d, J =3.1 Hz, C_{ar}), 132.44 (d, J =2.7 Hz, C_{ar}), 132.68 (d, J =10.7 Hz, C_{ar}), 133.84 (s, C_{ar}), 136.10 (d, J =13.5 Hz, $CPPh_2$), 137.31 (d, J =13.9 Hz, C_{ar}), 153.20 (d, J =2.7 Hz, CPd). − $^{31}P\{^1H\}$ NMR (CD_2Cl_2): δ = 31.35 (s, PPh_2).

The Enantiomerically Pure Salts Tetraethylammonium (*R*)- and (*S*)-7-Diphenylphosphanyl-8-phenyl-7,8-dicarbaundecaborate (2e*R* and 2e*S*): A solution of **3*R*-*R*** or **3*R*-*S*** (1 g, 1.544 mmol) in 50 mL of acetone was heated under reflux for 8 h with 10 mL of conc. HCl. The solvent was removed and the residue was washed with water. The product was dissolved in CH_2Cl_2 (30 mL) and a solution of NaCN (1 g) and NEt_4Cl (1 g) in water (50 mL) was added. After stirring for 24 h, the organic layer was separated, washed with water and dried with $CaCl_2$. After filtering, the solvent was evaporated to yield 0.61 g (76%) of a white powder of **2e*R*** or **2e*S***, respectively.

2e*R*: $[\alpha]_\lambda$ (c = 1.0, CH_2Cl_2) = 149 (578 nm), 182 (546 nm), 513 (436 nm). − IR (KBr): $\tilde{\nu}$ [cm^{-1}] = 2530 vs (B−H). − MS (FAB-NI-LSIMS): m/z (%) = 410.3 (30) $[MO]^+$, 394.3 (50) $[M]^+$, 306.1 (100) [M^+ − CPh]. − ^1H NMR (CD_2Cl_2): δ = −1.8 to −2.2 (br., 1 H, BHB), −0.2 to 2.8 (br., 9 H, BH), 1.33 (t, $^3J_{H,H}$ = 6.9 Hz, 12 H, CH_3), 3.35 (q, $^3J_{H,H}$ = 6.9 Hz, 8 H, CH_2), 7.8−6.9 (m, 15 H, Ph). − $^{11}B\{^1H\}$ NMR (CD_2Cl_2): δ = −34.66 (s, 1 B, BHB), −31.85 (s, 1 B, BHB), −22.55 to −12.65 (br., 5 B), −9.40 (s, 1 B), −6.62 (s, 1 B). − $^{31}P\{^1H\}$ NMR (CD_2Cl_2): δ = 9.45 (s). − $C_{28}H_{45}B_9NP$ (523.2): calcd. C 64.00, H 8.67, N 2.60; found C 63.96, H 8.63, N 2.72.

2e*S*: $[\alpha]_\lambda$ (c = 1.0, CH_2Cl_2) = −138 (578), −152 (546), −482 (436).

(1,5-Cyclooctadiene)[(*R*)-*exo*-*nido*-(7-diphenylphosphanyl-8-phenyl-7,8-dicarbaundecaborato)]rhodium (4*R*) and (1,5-Cyclooctadiene)[(*S*)-*exo*-*nido*-7-diphenylphosphanyl-8-phenyl-7,8-dicarbaundecaborato)]rhodium (4*S*): To a solution of **2e*R*** or **2e*S*** (100 mg, 0.191 mmol) in ethanol (50 mL) was added $[Rh(COD)Cl]_2$ (42 mg, 0.095 mmol). After heating under reflux for 5 h, the clear orange solution had become a yellow suspension. The reaction mixture was concentrated to 10 mL and the yellow powder was isolated. Yield 49 mg (43%) of **4*R*** or **4*S***.

4*R*: $[\alpha]_\lambda$ (c = 1.0, CH_2Cl_2) = −307 (578 nm), −367 (546 nm), −905 (436 nm). − IR (KBr): $\tilde{\nu}$ [cm^{-1}] = 2535 vs (B−H). − MS (FAB-NI-LSIMS): m/z (%) = 605.3 (100) $[M]^+$. − ^1H NMR (CD_2Cl_2): δ = −2.5 to −2.0 (br., 1 H, BHB), −1.00 to −0.10 (br., 1 H, RhHB), 0.50−2.50 (br., 8 H, BH), 1.80 (m, 2 H, CH_2), 2.00 (m, 2 H, CH_2), 2.21 (m, 3 H, CH_2), 2.56 (m, 1 H, CH_2), 3.00 (m, 1 H, CH), 3.57 (m, 1 H, CH), 5.23 (m, 1 H, CH), 5.38 (m, 1 H, CH), 6.62−6.70 (m, 2 H, CPh), 6.71−6.76 (m, 2 H, $CPPh_2$), 6.81−6.86 (m, 2 H, CPh), 6.92−6.97 (m, 1 H, CPh), 6.99−7.06 (m, 2 H, PPh_2), 7.26−7.32 (m, 1 H, PPh_2), 7.37−7.49 (m, 5 H, PPh_2). − $^{31}P\{^1H\}$ NMR (CD_2Cl_2): δ = 36.78 (d, $^1J_{Rh,P}$ = 114.6 Hz, PPh_2). − $C_{28}H_{37}B_9PRh$ (605.3): calcd. C 55.53, H 6.16; found C 55.34, H 6.32.

Synthesis of the Rhodium−Carborane Complexes. − General Procedure: To a solution of **2e*R*** or **2e*S*** (100 mg, 0.191 mmol) in ethanol (50 mL) were added $[Rh(COD)Cl]_2$ (42 mg, 0.095 mmol) and 0.191 mmol of a bis(phosphane). While heating under reflux for 5 h an orange powder precipitated. The product was filtered and washed with 3 × 10 mL of ethanol and 2 × 10 mL of pentane.

[(*R*,*R*)-DIOP][*exo*-*nido*-(*R*)-(7-diphenylphosphanyl-8-phenyl-7,8-dicarbaundecaborato)]rhodium (5*RR*-*R*), [(*S*,*S*)-DIOP][*exo*-*nido*-(*S*)-(7-diphenylphosphanyl-8-phenyl-7,8-dicarbaundecaborato)]rhodium (5*SS*-*S*), and [(*R*,*R*)-DIOP][*exo*-*nido*-(*S*)-(7-diphenylphosphanyl-8-phenyl-7,8-dicarbaundecaborato)]rhodium (5*RR*-*S*)

5*RR*-*R*: This was synthesized from **2e*R*** (120 mg, 0.229 mmol), $[Rh(COD)Cl]_2$ (55.5 mg, 0.113 mmol), and (*R*,*R*)-DIOP (116 mg, 0.233 mmol). Yield 179 mg (78%), orange powder. − $[\alpha]_\lambda$ (c = 1.0, CH_2Cl_2) = −102 (589 nm), −107 (578 nm), −117 (546 nm). − IR (KBr): $\tilde{\nu}$ [cm^{-1}] = 2535 vs (B−H). − MS (FD, CH_2Cl_2): m/z (%) = 995.1 (100) $[M]^+$. − ^1H NMR (CD_2Cl_2): δ = −2.70 to −2.10 (br., 1 H, BHRh), −2.00 to −1.00 (br., 1 H, BHB), 0.15−2.85 (br., 8 H, BH), 1.05 (s, 3 H, CH_3-DIOP), 1.13 (s, 3 H, CH_3-DIOP), 2.15 (m, 1 H, CH_2-DIOP), 2.55 (m, 3 H, CH_2-DIOP), 3.70 (m, 1 H, CH-DIOP), 4.05 (m, 1 H, CH-DIOP), 6.61 (m, 4 H, H_{ar}), 6.76 (m, 2 H, H_{ar}), 6.83 (m, 1 H, H_{ar}), 6.93 (m, 6 H, H_{ar}), 7.05 (m, 4 H, H_{ar}), 7.14 (m, 4 H, H_{ar}), 7.44 (m, 10 H, H_{ar}), 7.61 (m, 2 H, H_{ar}), 7.79 (m, 2 H, H_{ar}). − $^{11}B\{^1H\}$ NMR (CD_2Cl_2): δ = −34.2 (br., 1 B), −28.5 (br., 1 B), −26.2 (d, 1 B), −23.5 (br., 2 B), −13.7 (br., 2 B), −10.5 (br., 1 B), −2.8 (br., 1 B). − $^{13}C\{^1H\}$ NMR (CD_2Cl_2): δ = 26.81 (d, J =17.1 Hz, $C(CH_3)_2$), 30.84 (d, J = 20.2 Hz, CH_2), 34.56 (d, J = 20.2, CH_2), 65−70 (br., CPh), 77.46 (d, J = 6.2, CH), 108.72 (s, $C(CH_3)_2$), 126.54 (m, C_{ar}), 126.87 (m, C_{ar}), 127.43 (d, J =10.8 Hz, C_{ar}), 128.20 (d, J = 9.0 Hz, C_{ar}), 128.41 (m, C_{ar}), 129.60 (m, C_{ar}), 129.71 (s, C_{ar}), 130.22 (s, C_{ar}), 130.78 (m, C_{ar}), 130.90 (m, C_{ar}), 131.05 (m, C_{ar}), 132.10 (m, C_{ar}), 132.33 (d, J = 10.3 Hz, C_{ar}), 132.71 (d, J = 10.3 Hz, C_{ar}), 133.27 (d, J = 9.9 Hz, C_{ar}), 133.40 (s, C_{ar}), 133.92 (d, J = 11.9 Hz, C_{ar}), 134.40 (d, J = 11.9 Hz, C_{ar}), 135.92 (d, J = 14.4 Hz, C_{ar}), 137.51 (d, J = 3.0 Hz, C_{ar}). − $^{31}P\{^1H\}$ NMR (CD_2Cl_2): δ = 12.35 (ddd, $^2J_{P(A),P(B)}$ = 288 Hz, $^2J_{P(A),P(C)}$ = 38.5 Hz, $^2J_{P(A),Rh}$ = 117.9 Hz, 1 P, $P_{(A)}$), 16.22 (ddd, $^2J_{P(B),P(A)}$ = 288 Hz, $^2J_{P(B),P(C)}$ = 41.9 Hz, $^2J_{P(B),Rh}$ = 130.4 Hz, 1 P, $P_{(B)}$), 29.31 (dm, $^1J_{P(C),Rh}$ = 197.2 Hz, 1 P, $P_{(C)}$). − $C_{51}H_{57}B_9O_2P_3Rh$ (995.1): calcd. C 61.50, H 5.73; found C 60.43, H 5.81.

5*RR*-*S*: This was synthesized from **2e*S*** (120 mg, 0.229 mmol), $[Rh(COD)Cl]_2$ (55.5 mg, 0.113 mmol), and (*R*,*R*)-DIOP (116 mg, 0.233 mmol). Yield 179 mg (78%), orange powder. − $[\alpha]_\lambda$ (c = 1.0, CH_2Cl_2) = −158 (589 nm), −169 (578 nm), −216 (546 nm). − IR (KBr): $\tilde{\nu}$ [cm^{-1}] = 2535 vs (B−H). − MS (FD, CH_2Cl_2): m/z (%) = 995.1 (100) $[M]^+$. − ^1H NMR (CD_2Cl_2): δ = −3.25 to −2.78 (br., 1 H, BHRh), −2.30 to −2.25 (br., 1 H, BHB), 0.50−2.50 (br., 8 H,

BH), 1.12 (s, 3 H, CH_3-DIOP), 1.17 (s, 3 H, CH_3-DIOP), 2.25 (m, 1 H, CH_2-DIOP), 2.55 (m, 2 H, CH_2-DIOP), 2.75 (m, 1 H, CH_2-DIOP), 3.75 (m, 1 H, CH-DIOP), 3.90 (m, 1 H, CH-DIOP), 6.52 (m, 4 H, H_{ar}), 6.82 (m, 5 H, H_{ar}), 6.91 (m, 7 H, H_{ar}), 7.20 (m, 9 H, H_{ar}), 7.45 (m, 6 H, H_{ar}), 7.68 (m, 2 H, H_{ar}), 7.88 (m, 2 H, H_{ar}). − $^{11}B\{^1H\}$ NMR (CD_2Cl_2): δ = −34.0 (br., 1 B), −27.9 (br., 1 B), −25.0 (d, 1 B), −23.6 (br., 1 B), −14.1 (br., 2 B), −11.7 (br., 1 B), −8.4 (br., 1 B), −2.8 (br., 1 B). − $^{31}P\{^1H\}$ NMR (CD_2Cl_2): δ = 9.19 (ddd, $^2J_{P(A),P(B)}$ = 288.5 Hz, $^2J_{P(A),P(C)}$ = 39.2 Hz, $^2J_{P(A),Rh}$ = 117.9 Hz, 1 P, $P_{(A)}$), 18.00 (ddd, $^2J_{P(B),P(A)}$ = 288.5 Hz, $^2J_{P(B),P(C)}$ = 42.7 Hz, $^2J_{P(B),Rh}$ = 129.7 Hz, 1 P, $P_{(B)}$), 26.95 (dm, $^1J_{P(C),Rh}$ = 204.5 Hz, 1 P, $P_{(C)}$). − $C_{51}H_{57}B_9O_2P_3Rh$ (995.1): calcd. C 61.50, H 5.73; found C 60.78, H 5.62.

[(*S*)-Binap][*exo-nido*-(*R*)-(7-diphenylphosphanyl-8-phenyl-7,8-dicarbaundecaborato)]rhodium (6*S-R*): This was synthesized from compound **2e*R*** (87 mg, 0.168 mmol), $[Rh(COD)Cl]_2$ (40 mg, 0.082 mmol), and (*S*)-BINAP (100 mg, 0.160 mmol). Yield 131 mg (73%), orange powder. − $[\alpha]_\lambda$ (*c* = 1.0, CH_2Cl_2) = −70 (589 nm), −120 (578 nm), −141 (546 nm). − IR (KBr): $\tilde{\nu}$ [cm^{-1}] = 2530 vs (B−H). − MS (FD, CH_2Cl_2): *m*/*z* (%) = 1119.4 (100) $[M]^+$, 725.4 (33) $[M^+ - C_{20}H_{25}B_9P]$. − ^1H NMR (CD_2Cl_2,): δ = −3.32 to −2.68 (br., 1 H, BHRh), −2.62 to −2.21 (br., 1 H, BHB), 0.05−2.48 (br., 8 H, BH), 6.37 (m, 2 H, H_{ar}), 6.62 (s, 10 H, H_{ar}), 6.74 (m, 3 H, H_{ar}), 6.91 (m, 8 H, H_{ar}), 7.21 (m, 12 H, H_{ar}), 7.59 (m, 10 H, H_{ar}), 7.95 (m, 2 H, H_{ar}). − $^{11}B\{^1H\}$ NMR (CD_2Cl_2): δ = −39.8 (br., 1 B), −28.6 (br., 1 B), −23.4 (br., 2 B), −20.6 (br., 1 B), −13.3 (br., 2 B), −8.8 (br., 1 B), −3.1 (br., 1 B). − $^{31}P\{^1H\}$ NMR (CD_2Cl_2): δ = 6.98 (ddd, $^2J_{P(A),P(B)}$ = 288.9 Hz, $^2J_{P(A),P(C)}$ = 33.3 Hz, $^1J_{P(A),Rh}$ = 119.8 Hz, 1 P $P_{(A)}$), 34.61 (ddd, $^2J_{P(B),P(A)}$ = 288.9 Hz, $^2J_{P(B),P(C)}$ = 37.8 Hz, $^1J_{P(B),Rh}$ = 133.9 Hz, 1 P, $P_{(B)}$), 43.62 (dm, $^1J_{P(C),Rh}$ = 195.3 Hz, 1 P, $P_{(C)}$). − $C_{64}H_{57}B_9P_3Rh$ (1119): calcd. C 60.55, H 5.97; found C 61.60, H 5.80.

[*rac*-1,1-Bis(diphenylphosphanyl)ferrocene][*exo-nido*-(7-diphenylphosphanyl-8-phenyl-7,8-dicarbaundecaborato)]rhodium (7): This was synthesized from *rac*-**2e** (193 mg, 0.368 mmol), $[Rh(COD)Cl]_2$ (90 mg, 0.184 mmol), and 1,1-bis(diphenylphosphanyl)ferrocene (192 mg, 0.368 mmol). Yield 325 mg (84%), orange powder. − IR (KBr): $\tilde{\nu}$ [cm^{-1}] = 2530 vs (B−H). − MS (FD, CH_2Cl_2): *m*/*z* (%) = 1051.1 (100) $[M]^+$, 655.1 (70) $[M^+ - C_{20}H_{25}B_9P]$. − ^1H NMR (CD_2Cl_2): δ = −4.10 to −3.05 (br., 1 H, BHRh), −2.70 to −2.35 (br., 1 H, BHB), 0.45−2.50 (br., 8 H, BH), 3.61 (s, 1 H, fc_{meta}), 3.58 (s, 1 H, fc_{meta}), 4.06 (s, 2 H, fc_{meta}), 4.34 (s, 1 H, fc_{ortho}), 4.42 (s, 1 H, fc_{ortho}), 4.51 (s, 1 H, fc_{ortho}), 4.65 (s, 1 H, fc_{ortho}), 6.71 (m, 5 H, H_{ar}), 7.06 (m, 10 H, H_{ar}), 7.35 (m, 2 H, H_{ar}), 7.68 (m, 8 H, H_{ar}), 7.45 (m, 6 H, H_{ar}), 8.11 (m, 4 H, H_{ortho} in PPh_2). − $^{31}P\{^1H\}$ NMR (CD_2Cl_2): δ = 8.06 (ddd, $^2J_{P(A),P(B)}$ = 297.8 Hz, $^2J_{P(A),P(C)}$ = 30.0 Hz, $^1J_{P(A),Rh}$ = 134.3 Hz, 1 P, $P_{(A)}$), 26.97 (ddd, $^2J_{P(B),P(A)}$ = 297.8 Hz, $^2J_{P(B),P(C)}$ = 42.0 Hz, $^1J_{P(B),Rh}$ = 120.5 Hz, 1 P, $P_{(B)}$), 43.66 (dm, $^1J_{P(C),Rh}$ = 201.4 Hz, 1 P, $P_{(C)}$). − $C_{54}H_{53}B_9FeP_3Rh$ (1051): calcd. C 61.65, H 5.05; found C 61.38, H 5.25.

[*rac*-1,4-Bis(diphenylphosphanyl)butane][*exo-nido*-(7-diphenylphosphanyl-8-phenyl-7,8-dicarbaundecaborato)]rhodium (8): This was synthesized from *rac*-**2e** (200 mg, 0.381 mmol), $[Rh(COD)Cl]_2$

Table 4. Crystal data and structure refinement for **1**, **3*R-R*** and **4*S***

Compound	**1**	**3*R-R***	**4*S***
Empirical formula	$C_{20}H_{25}B_{10}P$	$(C_{30}H_{39}B_9NPPd)\cdot 2(C_7H_8)$	$(C_{28}H_{37}B_9PRh)\cdot 0.5(C_7H_8)$
Molecular mass	404.47	832.55	650.81
Crystal size [mm]	0.94 × 0.72 × 0.12	0.49 × 0.34 × 0.22	0.50 × 0.36 × 0.20
Crystal system	triclinic	orthorhombic	monoclinic
Space group	$P\bar{1}$ (no. 2)	$P2_12_12_1$ (no. 19)	$P2_1/n$ (no. 14)
a [Å]	11.0599(9)	11.7316(6)	10.9388(7)
b [Å]	14.7472(13)	14.3635(8)	21.9488(16)
c [Å]	15.8620(14)	25.6339(8)	14.0388(10)
α [°]	102.948(9)	90	90
β [°]	105.009(9)	90	107.736(8)
γ [°]	104.293(9)	90	90
Volume [Å^3]	2304.0(4)	4319.5(4)	3210.4(4)
Z, $D_{calcd.}$ [Mg/m^3]	4, 1.166	4, 1.280	4, 1.347
μ [mm^{-1}]	0.13	0.50	0.60
F(000)	840	1728	1340
Data Collection			
Measurement device type	STOE-IPDS diffractometer		
Measurement method	rotation		
Temperature [K]	297(2)	123(1)	123(1)
Radiation (monochromated)	Mo-K_α (graphite), 0.71073 [Å]		
Θmin, Θmax [°]	2.09, 25.60	1.91, 25.74	1.86, 25.84
Index ranges	$-11 \le h \le 12$	$-14 \le h \le 14$	$-13 \le h \le 13$
	$-17 \le k \le 17$	$-17 \le k \le 17$	$-26 \le k \le 26$
	$-18 \le l \le 19$	$-31 \le l \le 31$	$-17 \le l \le 17$
No. refl. collected/unique	15640/8030	32170/8209	43841/6086
Reflections $I > 4\sigma(I)$	4643	7715	5342
Absorption correction	none	none	none
Refinement			
Refinement method	Full-matrix least squares on F^2		
Hydrogen treatment	constr.	mixed	all free
Data, parameters	8030, 559	8209, 697	6086, 528
Weighting scheme	$w = 1/[\sigma^2(F_o^2) + (0.0569P)^2]$ $P = (F_o^2 + 2F_c^2)/3$	$w = 1/[\sigma^2(F_o^2) + (0.0270P)^2]$	$w = 1/[\sigma^2(F_o^2) + (0.0512P)^2 + 0.2487P]$
Final *R*, *wR*2, *S* [$I>4\sigma(I)$]	0.0431, 0.0954, 0.813	0.0186, 0.0412, 0.997	0.0270, 0.0693, 1.057
R, *wR*2 (all data)	0.0753, 0.1021	0.0211, 0.0417	0.0318, 0.0710
Absolute structure parameter		−0.037(11)	
Min./max. resd. density [e/Å^{-3}]	−0.156, 0.238	−0.158, 0.387	−0.340, 0.884

(94 mg, 0.184 mmol), and 1,4-bis(diphenylphosphanyl)butane (164 mg, 0.385 mmol). Yield 211 mg (60%), orange powder. − IR (KBr): $\tilde{\nu}$ [cm^{-1}] = 2530 vs, (B−H). − MS (FD, CH_2Cl_2): *m*/*z* (%) = 939.3 (5) $[MO]^+$, 923.4 (100) $[M]^+$. − ^1H NMR (CD_2Cl_2): δ = −2.55 to −2.15 (br., 1 H, BHRh), −1.70 to −0.70 (br., 1 H, BHB), 0.20−2.40 (br., 8 H, BH), 1.84 (m, 4 H, CH_2), 2.20 (m, 4 H, CH_2PPh_2), 6.62 (m, 4 H, H_{ar}), 6.77 (m, 2 H, H_{ar}), 6.91 (m, 9 H, H_{ar}), 7.04 (m, 2 H, H_{ar}), 7.13 (m, 4 H, H_{ar}), 7.23 (m, 3 H, H_{ar}), 7.30 (m, 1 H, H_{ar}), 7.44 (m, 6 H, H_{ar}), 7.67 (m, 4 H, H_{ar}). − $^{31}P\{^1H\}$ NMR (CD_2Cl_2): δ = 13.67 (ddd, $^2J_{P(A),P(B)}$ = 286.0 Hz, $^2J_{P(A),P(C)}$ = 35.1 Hz, $^1J_{P(A),Rh}$ = 119.0 Hz, 1 P, $P_{(A)}$), 26.97 (ddd, $^2J_{P(B),P(A)}$ = 286.0 Hz, $^2J_{P(B),P(C)}$ = 44.3 Hz, $^1J_{P(B),Rh}$ = 130.5 Hz, 1 P, $P_{(B)}$), 41.17 (dm, $^1J_{P(C),Rh}$ = 198.4 Hz, 1 P, $P_{(C)}$). − $C_{48}H_{53}B_9P_3Rh$ (923.4): calcd. C 62.40, H 5.74; found C 61.60, H 5.80.

X-ray Crystal Structure Determination of 1, 3*R*-*R*, and 4*S*: Data collection was performed on a STOE Imaging Plate Diffraction System (IPDS) equipped with an Oxford Cryosystems Cryostream Cooler for low-temperature measurements (Table 4). All data were corrected for Lorentz and polarisation effects. Final unit cell parameters were obtained by a least-squares refinement on a set of either 2000 (**1**) or 8000 (**3*R*-*R***, **4*S***) reflections equally distributed in reciprocal space. The structures were solved by direct methods (SIR-97)[25] and subsequent difference Fourier methods. Refinement on F^2 was carried out by full-matrix least-squares techniques (SHELXL97).[26] All non-H atoms were refined with anisotropic thermal parameters. H atoms were located from difference Fourier syntheses and refined with isotropic thermal parameters in three different ways: all free (**4*S***), some free, some as riding atoms (**3*R*-*R***), and all as riding atoms (**1**) with $U_{iso}(H) = 1.2U_{eq}$(C or B). The crystal structure of **3*R*-*R*** contains two toluene solvent molecules, one of them disordered between two orientations. Crystallographic data (excluding structure factors) for the structures reported in this paper have been deposited with the Cambridge Crystallographic Data Centre as supplementary publication nos. CCDC-147724 (**3*R*-*R***), CCDC-147725 (**4*S***) and CCDC-147726 (**1**). Copies of the data can be obtained free of charge on application to CCDC, 12 Union Road, Cambridge CB2 1EZ, UK [Fax: (internat.) + 44-1223/336-033; E-mail: deposit@ccdc.cam.ac.uk].

[1] K. Schlögl, *Top. Stereochem.* **1967**, *1*, 39.
[2] G. Wagner, R. Herrmann, in: A. Togni, T. Hayashi, *Ferrocenes*, Wiley-VCH, Weinheim, **1995**, p. 173.
[3] L. I. Zakharkin, E. I. Kukulina, L. S. Podvisotskaya, Izv. Akad. Nauk SSSR, *Ser. Khim.* **1966**, 1866.
[4] M. F. Hawthorne, D. C. Young, P. M. Garrett, D. A. Owen, S. G. Schwerin, F. N. Tebbe, P. A. Wegner, *J. Am. Chem. Soc.* **1968**, *90*, 862.
[5] R. T. Baker, M. S. Delaney, R. E. King, C. B. Knobler, J. A. Long, T. B. Marder, T. E. Paxson, R. G. Teller, M. F. Hawthorne, *J. Am. Chem. Soc.* **1984**, *106*, 2965.
[6] P. E. Behnken, D. C. Busby, M. Delaney, R. E. King III, C. W. Kreimendahl, T. B. Marder, J. J. Wilczynski, M. F. Hawthorne, *J. Am. Chem. Soc.* **1984**, *106*, 7444.
[7] J. Plesek, S. Hermanek, B. Stibr., *Pure Appl. Chem.* **1991**, *63*, 399.
[8] F. Teixidor, M. A. Flores, C. Vinas, *Organometallics* **1999**, *18*, 5409.
[9] C. Vinas, R. Nunzez, F. Teixidor, R. Kivekäs, R. Sillanpää, *Organometallics* **1996**, *15*, 3850.
[10] L. I. Zakharin, M. N. Zhubeova, A. V. Kazantsev, *Zh. Obsch. Khim.* **1972**, *42*, 1013
[11] A. Apfelbacher, Ph.D. Thesis, Universität Regensburg, **2000**.
[12] G. B. Dunks, K. Barker, E. Hedaya, C. Hefner, K. Palmer-Ordonez, P. Remec, *Inorg. Chem.* **1981**, *20*, 1692.
[13] N. K. Roberts, S. B. Wild, *J. Chem. Soc., Dalton Trans.* **1979**, 2015.
[14] S. B. Wild, *Coord. Chem. Rev.* **1997**, *166*, 291.
[15] S. Otsuka, A. Nakamura, T. Kano, K. Tani, *J. Am. Chem. Soc.* **1971**, *93*, 4301.
[16] C. Vinas, M. A. Flores, R. Nunzez, F. Teixidor, R. Kivekäs, R. Sillanpää, *Organometallics* **1998**, *17*, 2278.
[17] H. Brunner, L. Wagenhuber, *J. Organomet. Chem.* **1996**, *525*, 259.
[18] H. Brunner, D. Mijolovic, *J. Organomet. Chem.* **1999**, *577*, 346.
[19] H. B. Kagan, T.-P. Dang, *J. Am. Chem. Soc.* **1972**, *94*, 6429.
[20] H. Brunner, T. Tracht, *Tetrahedron: Asymmetry* **1998**, *9*, 3373.
[21] H. Brunner, U. Obermann, *Chem. Ber.* **1989**, *122*, 499.
[22] H. Brunner, R. Störiko, B. Nuber, *Tetrahedron: Asymmetry* **1998**, *9*, 407.
[23] H. Brunner, S. Rosenboem, *Chem. Monthly*, submitted for publication.
[24] M. M. Fein, D. Grafstein, J. E. Paustian, J. Bobinski, B. M. Lichstein, N. Mayes, N. Schwartz, M. S. Cohen, *Inorg. Chem.* **1963**, *2*, 1115.
[25] B. A. Murrer, J. M. Brown, P. A. Chaloner, P. N. Nicholson, D. Parker, *Synthesis* **1979**, 350.
[26] A. Altomare, G. Cascarano, C. Giacovazzo, A. Guagliardi, *J. Appl. Crystallogr.* **1993**, *26*, 343.
[27] G. M. Sheldrick, *SHELXL97, Program for crystal structure refinement*, University of Göttingen, Germany, **1997**.

Received August 22, 2000
[I00325]

New Chiral Cyclopentadienylrhenium Lewis Acids Featuring Fluorinated Triarylphosphanes and Enhanced Acceptor Abilities − An Unusual Carbon−Fluorine Bond Activation in a Metal Coordination Sphere

Wolfgang Mohr,[a] Gene A. Stark,[b] Haijun Jiao,[a] and J. A. Gladysz*[a]

Dedicated to Professor Dr. H.-J. Bestmann on the occasion of his 75th birthday

Keywords: Phosphanes / Chiral Lewis acids / Nucleophilic aromatic substitutions / Rhenium / Carbon−fluorine bond activation / DFT calculations

The acetonitrile complex $[(\eta^5\text{-}C_5H_5)Re(NO)(NCCH_3)(CO)]^+BF_4^-$ (**1**) and $P(4\text{-}C_6H_4CF_3)_3$ slowly react (2 d, room temperature) to give the substitution product $[(\eta^5\text{-}C_5H_5)Re(NO)\{P(4\text{-}C_6H_4CF_3)_3\}(CO)]^+BF_4^-$ (**3**, 85%). The reaction of **1** and less nucleophilic $P(C_6F_5)_3$ must be conducted in a melt at 140 °C, but $[(\eta^5\text{-}C_5H_5)Re(NO)\{P(C_6F_5)_3\}(CO)]^+BF_4^-$ (**11**) is isolated in 90% yield. Reduction of **3** by $NaBH_4$ gives the methyl complex $(\eta^5\text{-}C_5H_5)Re(NO)\{P(4\text{-}C_6H_4CF_3)_3\}(CH_3)$, which is treated with TfOH and $H_3CN{=}C(H)C_6H_5$ to give the imine complex $[(\eta^5\text{-}C_5H_5)Re(NO)(PPh_3)\{N(CH_3){=}C(H)C_6H_5\}]^+TfO^-$ (**9**). Complex **9** was, like the non-fluorinated analog, unreactive towards allyltin nucleophiles. Complex **11** should lead to a more reactive imine complex, but $NaBH_4$ gave a methyl complex that was difficult to purify. However, $NaOCH_3$ or $NaSCH_3$/methanol gave easily purified $(\eta^5\text{-}C_5H_5)Re(NO)\{P(4\text{-}C_6F_4OCH_3)_3\}(CO_2CH_3)$ (85%) or $(\eta^5\text{-}C_5H_5)Re(NO)\{P(4\text{-}C_6F_4SCH_3)_3\}(CO_2CH_3)$ (51%), in which all *para*-fluorine atoms have undergone nucleophilic displacements, and the carbonyl ligands methoxide additions. This suggests that catalytic chemistry of the chiral Lewis acid $[(\eta^5\text{-}C_5H_5)Re(NO)\{P(C_6F_5)_3\}]^+$ (**I**-F_{15}) will be complicated by nucleophilic degradation. Nonetheless, density functional calculations show that **I**-F_{15} is a much stronger σ acceptor and weaker π donor than less fluorinated analogs.

Introduction

Numerous modern catalytic methods for enantioselective organic synthesis make use of chiral transition metal Lewis acids.[1] The optimization of their steric and/or electronic properties is essential for many processes. For example, the fine tuning of donor/acceptor characteristics was critical to the development of chiral cyclopentadienyliron and -ruthenium catalysts for highly enantioselective Diels−Alder cycloadditions.[2] In the same vein, there are a variety of chiral titanium(IV) catalysts that activate aldehydes towards enantioselective additions of allylstannanes.[1] However, more electrophilic, fluorinated titanium(IV) catalysts are required to promote analogous reactions of less nucleophilic but cheaper and more readily available allylsilanes.[3]

We have undertaken extensive studies of adducts of the chiral rhenium Lewis acid $[(\eta^5\text{-}C_5H_5)Re(NO)(PPh_3)]^+$ (**I**) and unsaturated organic ligands such as aldehydes,[4] ketones,[5] alkenes,[6] and imines.[7] These are readily available in enantiomerically pure form, and stoichiometric additions of strong carbon nucleophiles often proceed with high diastereoselectivities.[4−7] However, weaker nucleophiles such as allylstannanes do not give rapid additions. In fact, rate experiments show that **I**, unlike many other transition metal Lewis acids, does not strongly activate unsaturated ligands towards nucleophiles. This has hampered the development of transformations that would be catalytic in rhenium.

The lack of activation can be ascribed to electronic properties of **I**. Most transition metal Lewis acids are best regarded as amphoteres. Except for d^0 systems, they have occupied d orbitals that are usually capable of backbonding to the acceptor orbitals of Lewis bases. The Lewis acid **I** is a strong π base, with the high-lying d donor orbital shown in Figure 1. The importance of this orbital in bonding to unsaturated ligands is evidenced by numerous structural studies.[4a,5,8] These indicate that unsaturated ligands adopt conformations that allow high degrees of overlap of their acceptor orbitals, even in the presence of opposing steric factors.

Accordingly, we sought to prepare analogs of **I** with enhanced σ acidities and diminished π basicities. In principle, any of the three spectator ligands can be modified. However, the nitrosyl group is an outstanding π acceptor, and we know of no other three-electron donor that could further enhance the acidity of the rhenium ion. Cyclopentadienyl ligands can be extensively halogenated, or substituted with electron-withdrawing perfluoroalkyl groups.[9] These would represent viable modification strategies. However, we elected to investigate analogs with fluorinated triarylphosphanes, in part due to our independent interest in highly fluorinated phosphanes for use in fluorous phase catalysis.[10]

In this paper, we describe the synthesis and some surprising reactions of Lewis base adducts of the new chiral rhenium Lewis acids $[(\eta^5\text{-}C_5H_5)Re(NO)\{P(4\text{-}C_6H_4CF_3)_3\}]^+$ [**I**-

[a] Institut für Organische Chemie,
Universität Erlangen-Nürnberg,
Henkestraße 42, 91054 Erlangen, Germany
[b] Department of Chemistry, University of Utah,
Salt Lake City, Utah 84112, USA

 © WILEY-VCH Verlag GmbH, 69451 Weinheim, 2001 1434−1948/01/0404−0925 $ 17.50+.50/0

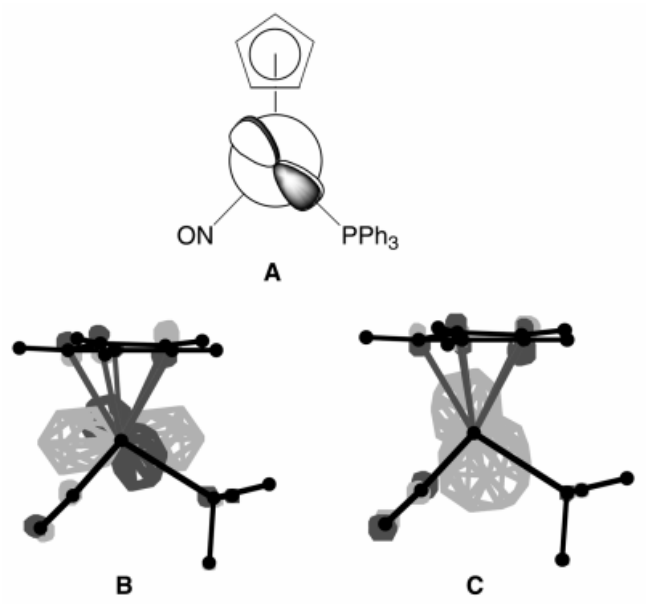

Figure 1. A: idealized d orbital HOMO of the chiral rhenium Lewis acid $[(\eta^5\text{-}C_5H_5)Re(NO)(PPh_3)]^+$ (**I**); B: computed HOMO of the model Lewis acid $[(\eta^5\text{-}C_5H_5)Re(NO)(PH_3)]^+$ (ref.[25]); C: computed LUMO of the model Lewis acid $[(\eta^5\text{-}C_5H_5)Re(NO)(PH_3)]^+$ (ref.[25])

$(CF_3)_3]$ and $[(\eta^5\text{-}C_5H_5)Re(NO)\{P(C_6F_5)_3\}]^+$ (**I**-F_{15}). In the former, the *para* positions of the aryl groups in **I** are substituted with trifluoromethyl groups. A slightly increased σ acidity, and a slightly decreased π basicity, was expected. In the latter, all aryl positions are fluorinated. A greatly enhanced Lewis acidity, and a greatly diminished π basicity, was expected. We also report high-level density functional calculations that allow more quantitative comparisons of the electronic properties of these compounds.

Results

The Nonafluorinated Lewis Acid I-$(CF_3)_3$

The substitution-labile acetonitrile complex $[(\eta^5\text{-}C_5H_5)Re(NO)(NCCH_3)(CO)]^+BF_4^-$ (**1**) and PPh_3 have previously been shown to react in refluxing ethyl methyl ketone to give the non-fluorinated phosphane complex $[(\eta^5\text{-}C_5H_5)Re(NO)(PPh_3)(CO)]^+BF_4^-$ (**2**).[11] As shown in Scheme 1, compound **1** and the commercially available phosphane $P(4\text{-}C_6H_4CF_3)_3$ were similarly allowed to react. Spectroscopic monitoring showed the need for a somewhat longer reaction time, presumably due to reduced nucleophilicity of the phosphane. After 46 h, workup gave the target complex $[(\eta^5\text{-}C_5H_5)Re(NO)\{P(4\text{-}C_6H_4CF_3)_3\}(CO)]^+ BF_4^-$ (**3**) in 85% yield.

Complex **3** was characterized by NMR (^1H, ^{13}C, ^{31}P) and IR spectroscopy, as described in the Exp. Sect. As summarized in Table 1, the IR $\tilde{\nu}_{CO}$ and $\tilde{\nu}_{NO}$ values were 30−12 cm^{-1} greater than those of **2**,[11] consistent with decreased π basicity and increased σ acidity. The ^{13}C NMR CO signal was coupled to the phosphorus signal and upfield of that of **2** (Table 1). All aryl carbon atoms showed coupling to the phosphorus atom, and those *ipso* and *ortho*

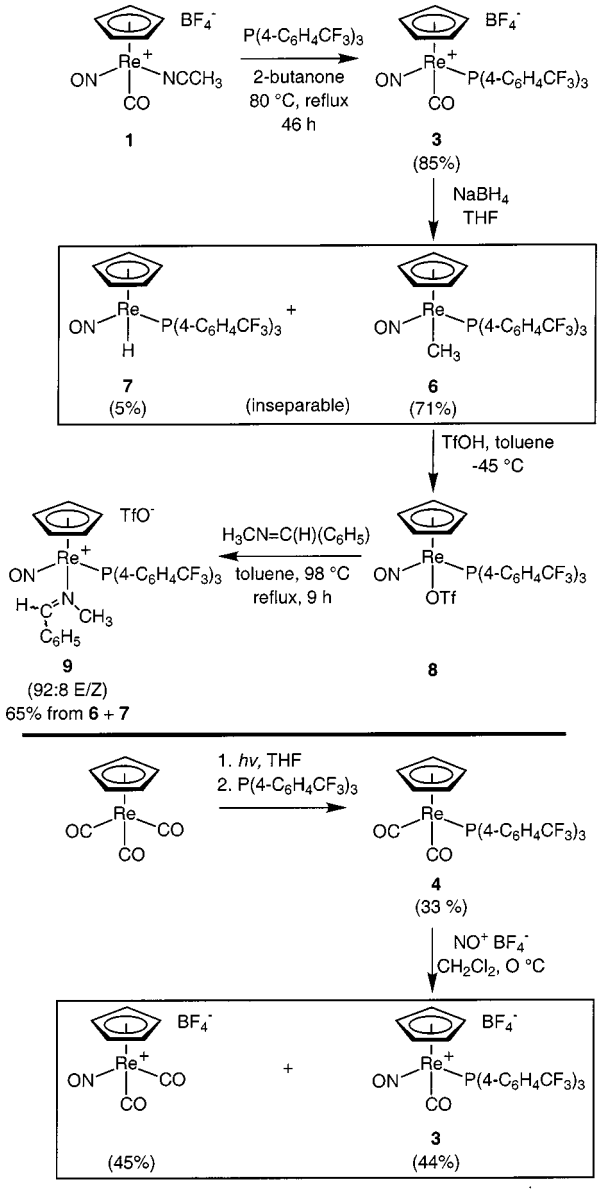

Scheme 1. Syntheses and reactions of nonafluorinated complexes

to the trifluoromethyl group were further coupled to the fluorine atoms. Complex **3** could also be prepared by the reaction of dicarbonyl complex $(\eta^5\text{-}C_5H_5)Re(CO)_2\{P(4\text{-}C_6H_4CF_3)_3\}$ (**4**) and $NO^+BF_4^-$ (Scheme 1, bottom). However, due to a competing phosphane displacement to give $[(\eta^5\text{-}C_5H_5)Re(NO)(CO)_2]^+BF_4^-$,[11] the yield was only 44%. Complex **4** could in turn be prepared from $(\eta^5\text{-}C_5H_5)Re(CO)_3$[11] by a standard photolysis/substitution sequence in THF,[12] but our best yield was only 33%.

The reduction of non-fluorinated **2** by $NaBH_4$ in THF gives the methyl complex $(\eta^5\text{-}C_5H_5)Re(NO)(PPh_3)(CH_3)$ (**5**).[11] As shown in Scheme 1, compound **3** and $NaBH_4$ were analogously treated. Workup gave 97−93:3−7 mixtures of the expected methyl complex $(\eta^5\text{-}C_5H_5)\text{-}Re(NO)\{P(4\text{-}C_6H_4CF_3)_3\}(CH_3)$ (**6**) and the unexpected hydride complex $(\eta^5\text{-}C_5H_5)Re(NO)\{P(4\text{-}C_6H_4CF_3)_3\}(H)$ (**7**), as determined by integration of the cyclopentadienyl ^1H

Table 1. Spectroscopic features that reflect the relative electronic properties of the chiral rhenium Lewis acids

Complex	Lewis acid	Lewis base	IR ν_{NO} [cm^{-1}]	IR ν_{CO} [cm^{-1}]	$^{13}C\{^1H\}$ NMR α- or β-C [δ]	J_{CP} [Hz]	$^{1}P\{^1H\}$ NMR [δ]
2	**I**	CO	1760[a]	2001[a]	196.7[b] [c]	8.8	12.4[d]
3	**I**-$(CF_3)_3$	CO	1772[e]	2031[e]	194.4[b]	8.6	14.4[b]
11	**I**-F_{15}	CO	1794[f]	2046[f]	191.2[d]	6.1	−48.0[d]
5	**I**	CH_3	1630[g]	–	−37.5[a]	6.0	25.5[a]
6	**I**-$(CF_3)_3$	CH_3	1663[h]	–	−37.2[b]	7.0	28.9[b]
14	**I**-F_{15}	CH_3	1687[f]	–	−33.1[d]	7.1	−26.5[d]
8	**I**	$C_6H_5(H)C{=}NCH_3$	1679[e]	–	178.2[b]	2.7	18.4[b]
9	**I**-$(CF_3)_3$	$C_6H_5(H)C{=}NCH_3$	1703[e]	–	180.0[d]	3.6	22.8[d]

[a] CH_2Cl_2. – [b] CD_3CN. – [c]Redetermined as part of this study for the purpose of obtaining the previously unresolved coupling constant. – [d] [D_6]Acetone. – [e] KBr. – [f] Powder film. – [g] THF. – [h] Hexane.

NMR signals. The combined yield was 76%. Extensive attempts to separate hexane-soluble **6** and **7** by crystallization or TLC were unsuccessful. Hence, they were characterized as a mixture. Similar reductions have been effected with a variety of phosphane ligands,[13,14] but a hydride complex by-product has not been noted earlier. Both **6** and **7** exhibited diagnostic spectroscopic features,[11,15] such as $ReCH_3$ and ReH ^{1}H NMR signals (δ = 0.97 and −9.70) that were coupled to the phosphorus signal (J_{HP} = 6 and 29 Hz). The IR $\tilde{\nu}_{NO}$ value of **6** was greater than that of the non-fluorinated analog **5** (Table 1).[11]

The methyl complex **5** can be converted by various strong acid/solvent combinations into several functional equivalents of the chiral Lewis acid **I**. One of the most convenient is the corresponding triflate,[16] which can be isolated or treated directly with Lewis bases such as imines or thioethers to give adducts of the formula $[(\eta^5\text{-}C_5H_5)Re(NO)(PPh_3)(L)]^+\ TfO^-$.[17,18] Based upon available data,[19] there would be a reasonable chance that related rhenium hydride complexes would behave similarly. Accordingly, the methyl complex **6** was used as a mixture with **7**.

As shown in Scheme 1, compound **6/7** and TfOH were combined in toluene at −45 °C to generate the new triflate complex $(\eta^5\text{-}C_5H_5)Re(NO)\{P(4\text{-}C_6H_4CF_3)_3\}(OTf)$ (**8**). Complex **8** was not isolated, but directly treated with the imine $H_3CN{=}C(H)C_6H_5$. Since the analogous reaction of the non-fluorinated triflate is very slow at room temperature,[17] the sample was kept at 98 °C for 9 h. Workup gave the imine complex $[(\eta^5\text{-}C_5H_5)Re(NO)\{P(4\text{-}C_6H_4CF_3)_3\}\{N(CH_3){=}C(H)C_6H_5\}]^+TfO^-$ (**9**) as a 92:8 mixture of (*E*)/(*Z*) C=N isomers in 65% yield. Complex **9** was characterized analogously to **3** and **6/7**. The IR $\tilde{\nu}_{NO}$ value was greater than that of the non-fluorinated analog $[(\eta^5\text{-}C_5H_5)Re(NO)(PPh_3)\{N(CH_3){=}C(H)C_6H_5\}]^+TfO^-$ (**10**; Table 1),[17] which would logically correlate with an enhanced imine carbon electrophilicity. An (*E*) C=N isomer (larger phenyl and bulky rhenium substituents *trans*) also dominated with **10**.[17] These assignments were supported, among other factors, by the relative magnitudes of the $^4J_{HH}$ values of the $H_3CN{=}CH$ linkages (1.7 vs. 1.2 Hz).[20]

The imine complex **9** was combined with the allylstannane $H_2C{=}CHCH_2Sn(n\text{Bu})_3$ in CD_2Cl_2 and THF. The former sample was unchanged after 3 d at ambient temperature, as assayed by ^{1}H and ^{31}P NMR. The latter sample was unchanged after 1 d at 60 °C, as assayed by ^{31}P NMR. Carbon−carbon bond-forming reactions of imines and allylstannanes are readily catalyzed by titanium, palladium, and copper Lewis acids.[21] Hence, the modified rhenium Lewis acid **I**-$(CF_3)_3$ remained insufficiently activating, and a more reactive species was sought.

The Pentadecafluorinated Lewis Acid I-F_{15}

A $ClCH_2CH_2Cl$ solution of the acetonitrile complex **1** and the commercially available phosphane $P(C_6F_5)_3$ was kept at 88 °C for 11 h. No reaction occurred, as monitored by IR spectroscopy. A $Cl_2CHCHCl_2$ solution of **1** and $P(C_6F_5)_3$ was similarly kept at 129 °C for 14 h. An IR spectrum indicated that several products had formed. However, the ^{31}P NMR spectrum showed mainly $P(C_6F_5)_3$ (δ = −74.2; 73%), and one new signal that was assigned to the oxide $O{=}P(C_6F_5)_3$ (δ = −7.9; 27%) based upon the close agreement with the chemical shift in the literature (δ = −7.8).[22]

Reactions were attempted in the absence of solvent. Complex **1** and $P(C_6F_5)_3$ melt at 119 and 107 °C, respectively, and were kept at 140 °C (1.0:1.3 molar ratio) for 10 h. During this time, some of the $P(C_6F_5)_3$ sublimed to the top part of the flask not immersed in the oil bath. Thus, the reaction did not go to completion. Nevertheless, unchanged **1** could be separated from the desired substitution product $[(\eta^5\text{-}C_5H_5)Re(NO)\{P(C_6F_5)_3\}(CO)]^+\ BF_4^-$ (**11**), which was isolated as a yellow powder in 32% yield. Modified reaction vessels were then assayed. The operationally most simple protocol involved starting with 1.5 equivalents of $P(C_6F_5)_3$, inserting some glass wool into the neck of the flask, immersing the flask *completely* in an oil bath (gas release bubbler protruding), and adding a second charge of $P(C_6F_5)_3$ (0.5 equiv.) halfway through the 50 h reaction. This gave **11** in 90% yield on a 3.5-g scale.

Complex **11** was characterized analogously to the other new compounds above. The IR $\tilde{\nu}_{CO}$ and $\tilde{\nu}_{NO}$ values were greater than the $P(4\text{-}C_6H_4CF_3)_3$ analog **3** (Table 1), indicating a further enhancement of σ acidity and diminution of backbonding into the NO and CO ligands. The ^{13}C NMR CO signal was upfield of that of **3** (Table 1). The ^{31}P NMR

signal was downfield of that of $P(C_6F_5)_3$ ($\delta = -48.0$ vs. -74.2 to -75.5).[22] However, only a broad singlet was observed ($w_{1/2} = 39-40$ Hz), as opposed to the fluorine-coupled pseudoquintuplet ($J_{PF} = 35$ Hz) of the free phosphane.

The enantiomers of the non-fluorinated carbonyl complex **2** are easily resolved.[11] The first step entails reaction with excess $NaOCH_3$ in methanol to generate the isolable methoxycarbonyl complex $(\eta^5\text{-}C_5H_5)Re(NO)(PPh_3)(CO_2CH_3)$.[11] Hence, **11** was similarly treated, as shown in Scheme 2. A product precipitated (**12**), but the ^1H NMR spectrum showed both the expected CO_2CH_3 signal ($\delta = 3.12$, s) and an unanticipated resonance ($\delta = 4.21$, t, $J_{HF} = 2$ Hz). These always appeared in concert, and integrated to a 3:9 ratio. The mass spectrum gave a parent ion consistent with the formula $(\eta^5\text{-}C_5H_5)Re(NO)\{P(C_6F_4OCH_3)_3\}(CO_2CH_3)$, in which a fluorine atom in each aryl ring has been substituted by a methoxy group. The ^{13}C NMR spectrum showed only four aryl signals, requiring a threefold *para* substitution, as well as two types of methoxy signals ($\delta = 62.9$, t, $J_{CF} = 4$ Hz and 48.9, s). Under optimized conditions, **12** could be obtained in 85% yield.

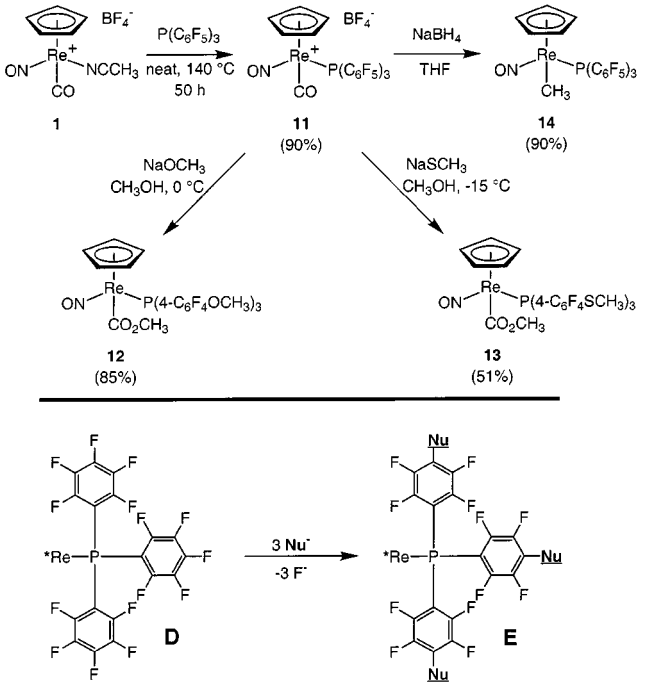

Scheme 2. Synthesis and reactions of pentadecafluorinated complexes

There is abundant precedent for nucleophilic aromatic substitutions of hexafluorobenzene, and the *para*-fluorine atoms of substituted pentafluorobenzenes.[23,24] However, the conversion of **11** to **12** represents one of the few times that this has been observed with a non-ligating arene in a metal coordination sphere.[24b] In a separate experiment, **11** and $NaOCH_3$ were combined in a 1:1 molar ratio in methanol, and the homogeneous reaction monitored by ^{31}P NMR. Several new signals appeared with chemical shifts close to that of **11** ($\delta = -50$ to -51), and several new signals appeared with chemical shifts close to that of **12** ($\delta = -33$ to -35). These were attributed to intermediate levels of *para* substitution. If methoxide addition to the carbonyl group of **11** were *ir*reversible, this would indicate that fluoride substitution occurs both before and after carbonyl addition.

In order to probe the generality of such threefold substitutions, **11** and the thiolate $NaSCH_3$ were allowed to react in methanol. As shown in Scheme 2, workup gave the sulfur-containing complex $(\eta^5\text{-}C_5H_5)Re(NO)\{P(4\text{-}C_6F_4SCH_3)_3\}(CO_2CH_3)$ (**13**) in 51% yield. Interestingly, a methoxy group selectively added to the carbonyl ligand of **11**, whereas thiomethoxy groups selectively displaced fluoride. This structure was supported by a molecular ion peak in the mass spectrum, a correct C/H/N/S microanalysis, and numerous IR and NMR features. For example, the IR $\tilde{\nu}_{CO}$ value of **13** was very similar to that of **12** (1613 vs. 1603 cm^{-1}). Also, the $ArSCH_3$ NMR signals of **13** were distinctly upfield of the $ArOCH_3$ signals of **12** [^1H: $\delta = 2.62$ (br s) vs. 4.21; $^{13}C\{^1H\}$: $\delta = 17.0$ (t, $J_{CF} = 5$ Hz) vs. 62.9].

Although the substitution reactions in Scheme 2 are of interest in their own right, they tempered our enthusiasm for the $P(C_6F_5)_3$ ligand as part of a second-generation chiral rhenium Lewis acid. Even if an enantiomer separation not requiring a methoxide addition could be effected, there would be a high probability that similar substitutions would compromise other target reactions or applications in catalysis. Accordingly, it was decided to pursue only one additional reaction in this series, that of **11** and $NaBH_4$. Under conditions comparable to those in Scheme 1, the methyl complex $(\eta^5\text{-}C_5H_5)Re(NO)\{P(C_6F_5)_3\}(CH_3)$ (**14**) could be isolated as a crude powder in 90% yield by benzene or toluene extraction of the reaction mixture.

Complex **14** exhibited a number of diagnostic spectroscopic features. These included (1) a ^1H NMR spectrum with methyl ($\delta = 0.76$, d, $J_{HP} = 10$ Hz) and cyclopentadienyl signals, both very similar to those of **6**, (2) corresponding ^{13}C NMR signals (Table 1), and (3) an intense molecular ion peak in the mass spectrum. However, NMR spectra showed residual benzene or toluene, even after prolonged periods under high vacuum that routinely removed these solvents from other complexes. Treatments with cold pentane improved the purities, but correct microanalyses could never be obtained. Finally, attempts to generate various functional equivalents of the Lewis acid **I**-F_{15} from **14** gave unusual results that would be difficult to interpret without further intensive study.

Computations

There would be obvious approaches to generating highly fluorinated but less substitution-prone triarylphosphanes. Hence, as a justification for possible continued work, we sought computational support for our intuitive estimation of the relative donor/acceptor properties of the fragments **I**, **I**-$(CF_3)_3$, and **I**-F_{15}. One starting point might be to compare model compounds with PH_3 ligands, several of which have been studied previously,[25] to those with PH_xF_{3-x} ligands. Although such systems would contain fewer atoms and electrons and could be investigated at a very high level of

rigor, they also constitute less satisfying models for triarylphosphanes.

Accordingly, the geometry of the trimethylphosphane complex (η^5-C_5H_5)Re(NO){$P(CH_3)_3$}(CH_3) was optimized at the level of density functional theory (B3LYP) with the LANL2DZ basis set and an additional set of polarization functions (LANL2DZp) as introduced by Hay and Wadt[26] and implemented in the GAUSSIAN98 program.[27] These results are fully described elsewhere.[26] Next, the phosphorus methyl groups were replaced by C_6H_5, 4-C_6H_4F, and C_6F_5 groups, keeping all geometric features of the (η^5-C_5H_5)Re(NO)(P)(CH_3) entity constant. Note that the second series features *para*-fluorine atoms, as opposed to the larger CF_3 groups of the compounds in Scheme 1.

The PPh_3, P(4-C_6H_4F)$_3$, and P(C_6F_5)$_3$ entities were partially optimized at the HF/LANL2DZ level. The rhenium−phosphorus conformations were allowed to vary, but the HCCC and FCCC torsion angles were fixed at 180.0° − in other words, planar arene rings. This approximation is justified by unpublished results with the hydride complex (η^5-C_5H_5)Re(NO)(PPh_3)(H), for which we have done a full structure optimization and find essentially planar phenyl rings. Next, the methyl groups were replaced by a positive charge, and the orbital energies of the resulting rhenium Lewis acids **I**, **I**-F_3 [roughly equivalent to **I**-$(CF_3)_3$], and **I**-F_{15} calculated**.**

Key data are summarized in Table 2. As would have been intuitively predicted, both the HOMO and LUMO energies decrease with increasing numbers of fluorine atoms. The HOMO energies decrease to a greater extent, indicating that major effect of the fluorine atoms is to diminish π basicity. However, the LUMO energy decrease is still significant, indicating a large enhancement of σ acidity. A mathematical consequence is that the HOMO/LUMO gap steadily *in*creases. Not surprisingly, the energies of other orbitals decrease with increasing fluorine substitution.

Table 2. Frontier orbital energies [eV] (HF/LANL2DZp) of the chiral Lewis acids

Orbital	Lewis acid		
	I	**I**−$(CF_3)_3$	**I**−F_{15}
LUMO+1	−1.15	−1.82	−2.19
LUMO	**−3.50**	**−4.09**	**−4.28**
HOMO	**−11.87**	**−12.67**	**−13.42**
HOMO−1	−11.93	−12.86	−13.53
HOMO−2	−12.21	−13.02	−13.80
Δ(LUMO − HOMO)	**8.37**	**8.58**	**9.14**

Discussion

A number of conclusions can be drawn from the above data. With regard to the original objective of this study, the chiral rhenium Lewis acid **I** will clearly require *more* than three highly electronegative aryl substituents in order to activate unsaturated ligands to a broader range of nucleophilic additions. The IR and computational data indicate that **I**-F_{15} should be much more activating than **I**-$(CF_3)_3$, where we had only negative results. However, Scheme 2 shows that this system is prone to nucleophilic displacement of the *para*-fluorine atoms in the aryl rings, a process with much precedent in the organofluorine literature.[23,24] One solution would be to seek substitution-resistant analogs, perhaps with *para*-CF_3 or -$C(CF_3)_3$ groups. The bulk of the latter might help to retard the possible nucleophilic displacement of fluorine atoms at other positions (*ortho*, *meta*).

Despite its markedly attenuated basicity, the perfluorinated phosphane P(C_6F_5)$_3$ has an extensive coordination chemistry.[28] However, to the best of our knowledge, none of these complexes has ever been observed to undergo nucleophilic aromatic substitution. Nonetheless, threefold substitutions do occur with the free ligand.[24a] As shown in Scheme 3, P(C_6F_5)$_3$ and hydrazine cleanly react in refluxing ethanol to give a tris(hydrazino) product. Under analogous conditions, substituted hydrazines gave only partial substitution. Reactions with alkoxides occur at room temperature, but are much more complex. In the case of $NaOCH_3$, the major products are derived from phosphorus−carbon bond cleavage, although the threefold substitution product P(4-$C_6F_4OCH_3$)$_3$ can be isolated in 20% yield.[24a] Thus, the rhenium Lewis acid **I**-F_{15} activates the *para*-fluorine atoms of P(C_6F_5)$_3$ towards substitution.

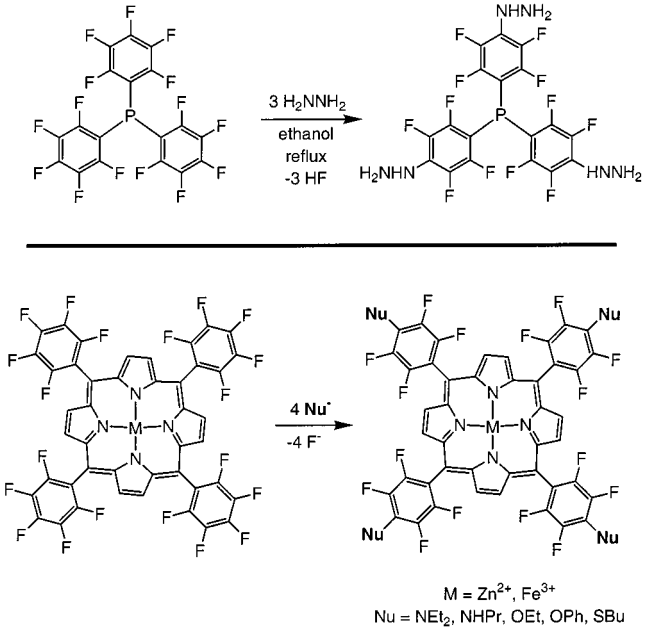

Scheme 3. Some relevant previously reported reactions

Metal-mediated carbon−fluorine bond activation is of particular current interest.[29] We are aware of only one other paper describing nucleophilic aromatic substitutions of σ-pentafluorophenyl groups in metal coordination spheres. The (porphyrin)zinc and -iron compounds illustrated in Scheme 3 (bottom) undergo clean fourfold substitutions with a variety of nucleophiles.[24b] The successful application of sulfur nucleophiles in both this system and ours suggests new ways by which metal complexes might be anchored to thiophilic gold surfaces.

If problems with nucleophilic aromatic substitution can be solved, there are potential advantages associated with perfluorinated triarylphosphanes in chiral transition metal Lewis acids. For instance, many examples of strongly attractive π-stacking interactions between perfluoroarenes and non-fluorinated analogs have recently been documented.[30] This might be a very effective control element for some types of enantioselective reactions. Indeed, Ojima has investigated transformations of various adducts the pentafluorinated iron Lewis acid $[(\eta^5\text{-}C_5H_5)Fe(CO)\{P(C_6H_5)_2C_6F_5\}]^+$.[31] This is approximately isostructural to our Lewis acids **I** and **I**-F_{15}, but with just one pentafluorophenyl ring. He often found improved stereoselectivities as compared to the non-fluorinated homolog $[(\eta^5\text{-}C_5H_5)Fe(CO)\{P(C_6H_5)_3\}]^+$. This was attributed to π interactions involving the fluorinated ring.

As noted in the introduction, the Lewis acid **I** might also be modified on the cyclopentadienyl ligand. Indeed, we have reported a number of more electron-rich alkylated derivatives.[32] From a synthesis standpoint, it would be relatively straight-forward to pursue a "tandem activation" strategy. Regardless, this paper concludes our investigations of new types of chiral rhenium Lewis acids that were begun in the USA. Future publications will describe new initiatives that were conceived and fully executed in our new laboratory in Franconia.

Experimental Section

General Data: All reactions were carried out under dry nitrogen using conventional Schlenk techniques. Analytical data were recorded with standard instruments, some of which were described in a previous paper.[17] Rather than enumerate the many small differences between the two locations in which this work was conducted, readers are referred to two dissertations.[33] − Solvents were treated as follows: acetone, distilled from P_2O_5; CH_3CN distilled from P_2O_5; CH_2Cl_2, distilled from Sicapent® (Fluka); ether, distilled from CaH_2; hexane, distilled from K; methanol, distilled from Mg; [D_6]acetone, stored over molecular sieves (4 Å). The imine $H_3CN{=}C(H)C_6H_5$ (Aldrich) was vacuum-distilled, $NaSCH_3$ was used as received (Fluka), and $P(4\text{-}C_6H_4CF_3)_3$ and $P(C_6F_5)_3$ were used as received (Strem) or prepared by literature procedures.[33b,34] Other solvents and reagents were used as received from common commercial sources.

$[(\eta^5\text{-}C_5H_5)Re(NO)\{P(4\text{-}C_6H_4CF_3)_3\}(CO)]^+BF_4^-$ (3). − A: A Schlenk flask was charged with $[(\eta^5\text{-}C_5H_5)Re(NO)(NCCH_3)(CO)]^+BF_4^-$ (**1**;[11] 0.194 g, 0.429 mmol) and fitted with a condenser that was joined to an N_2 line/oil bubbler. Ethyl methyl ketone (20 mL) was added. The solution was refluxed (oil bath) with stirring for 46 h, and allowed to cool. Hexane (ca. 200 mL) was added. The yellow solid was collected by filtration, washed with pentane (20 mL), and dried by oil pump vacuum to give **3** (0.313 g, 0.363 mmol, 85%). − **B:** A Schlenk flask was charged with $(\eta^5\text{-}C_5H_5)Re(CO)_2\{P(4\text{-}C_6H_4CF_3)_3\}$ (preparation below; 1.121 g, 1.449 mmol) and CH_2Cl_2 (50 mL), and cooled to 0 °C. Solid $NO^+BF_4^-$ (0.204 g, 1.74 mmol; freshly washed with 20 mL of CH_2Cl_2) was added with stirring. The ice bath was allowed to warm. After 30 h, solvent was removed by rotary evaporation. THF (250 mL) was added. The bright yellow powder was collected on a frit to give $[(\eta^5\text{-}C_5H_5)Re(NO)(CO)_2]^+ BF_4^-$ (0.274 g, 0.647 mmol, 45%).[11] The filtrate was concentrated (ca. 2 mL), and hexane (50 mL) was added. The yellow solid was collected on a frit, washed with CH_2Cl_2/hexane (20 mL, 20:80 v/v) and pentane (20 mL), and dried by oil pump vacuum to give **3** (0.545 g, 0.632 mmol, 44%), m.p. 236−237 °C (dec.). − $C_{27}H_{17}BF_{13}NO_2PRe$ (862.4): calcd. C 37.60, H 1.99; found C 37.04, H 2.01. − IR (cm^{-1}, CH_2Cl_2/KBr): $\tilde{\nu}_{CO}$: 2027/2031 (s); $\tilde{\nu}_{NO}$: 1772/1772 (s). − NMR (δ, CD_3CN):[35] ^1H: 7.95−7.86 (m, 6 H of 3 C_6H_4), 7.63−7.52 (m, 6 H of 3 C_6H_4), 5.96 (s, C_5H_5); $^{13}C\{^1H\}$: 194.4 (d, $^2J_{CP}$ = 8.6, CO), 135.2 (d, $^2J_{CP}$ = 12.3, *o*-C_6H_4), 135.1 (d, $^1J_{CP}$ = 58.9, *i*-C_6H_4), 134.6 (qd, $^2J_{CF}$ = 33, $^4J_{CP}$ = 3, *p*-C_6H_4), 127.6 (qd, $^3J_{CF}$ = 3.9, $^3J_{CP}$ = 11.9, *m*-C_6H_4), 124.5 (q, $^1J_{CF}$ = 272, CF_3), 96.1 (s, C_5H_5); $^{31}P\{^1H\}$: 14.4 (s).

Reduction of 3: A Schlenk flask was charged with **3** (0.114 g, 0.132 mmol), THF (20 mL), and $NaBH_4$ (0.015 g, 0.40 mmol). The mixture was stirred for 2 h, and solvent was removed by oil pump vacuum. Benzene (100 mL) was added, and the sample was filtered through silica gel. Solvent was removed by rotary evaporation. The residue was dissolved in hexane (50 mL), and the solution was slowly concentrated by rotary evaporation. An orange powder formed, which was collected on a frit and dried under oil pump vacuum to give a 93:7 mixture (0.078 g) of $(\eta^5\text{-}C_5H_5)Re(NO)\{P(4\text{-}C_6H_4CF_3)_3\}(CH_3)$ (**6**) (0.073 g, 0.093 mmol, 71%) and $(\eta^5\text{-}C_5H_5)Re(NO)\{P(4\text{-}C_6H_4CF_3)_3\}(H)$ (**7**) (0.005 g, 0.007 mmol, 5%), m.p. 165−166 °C. − IR (cm^{-1}, THF/hexane): $\tilde{\nu}_{NO}$: 1645/1663 (s). − MS:[36] 763 [**6**$^+$] (100%), 749 [**7**$^+$] (6%), 748 [**6**$^+$ − CH_3] (23%). − NMR (**6**; δ, $CDCl_3$):[35] ^1H: 7.77−7.67 (m, 6 H of 3 C_6H_4), 7.59−7.48 (m, 6 H of 3 C_6H_4), 5.00 (s, C_5H_5), 0.97 (d, $^3J_{CP}$ = 6.1, CH_3); $^{13}C\{^1H\}$: 139.9 (d, $^1J_{CP}$ = 48.6, *i*-C_6H_4), 133.8 (d, $^2J_{CP}$ = 11.1, *o*-C_6H_4), 132.4 (qd, $^2J_{CF}$ = 33, $^4J_{CP}$ = 2, *p*-C_6H_4), 125.5 (qd, $^3J_{CF}$ = 3.7, $^3J_{CP}$ = 10.1, *m*-C_6H_4), 123.5 (q, $^1J_{CF}$ = 273, CF_3), 90.0 (s, C_5H_5), −37.2 (d, $^2J_{CP}$ = 7.0, CH_3); $^{31}P\{^1H\}$: 28.9 (s). − NMR (**7**, partial; δ, $CDCl_3$): ^1H: 5.02 (s, C_5H_5), −9.70 (d, $^2J_{CP}$ = 29.3, ReH); $^{13}C\{^1H\}$: 85.8 (s, C_5H_5); $^{31}P\{^1H\}$: 31.6 (s).

$[(\eta^5\text{-}C_5H_5)Re(NO)\{P(4\text{-}C_6H_4CF_3)_3\}\{N(CH_3){=}C(H)C_6H_5\}]^+TfO^-$ (9): A Schlenk flask was charged with a **6/7** mixture (0.070 g, 0.092 mmol) and toluene (10 mL), and cooled to −45 °C (CH_3CN/CO_2). Then TfOH (0.008 mL, 0.09 mmol) was added dropwise with stirring. After 10 min, $H_3CN{=}C(H)C_6H_5$ (0.056 mL, 0.46 mmol) was added. The flask was placed in a 98 °C bath, and a precipitate began to form. After 9 h, the mixture was cooled to room temperature and hexane (50 mL) was added. The yellow-orange powder was collected by filtration, washed with hexane (10 mL), and dried by oil pump vacuum to give **9** as a 92:8 (*E*)/(*Z*) mixture (0.060 g, 0.059 mmol, 65%), m.p. 238−239 °C (dec.).[37] − $C_{35}H_{26}BF_{12}N_2O_4PReS$ (1026.6): calcd. C 41.38, H 2.58; found C 40.76, H 2.66. − IR (cm^{-1}, CH_2Cl_2/KBr): $\tilde{\nu}_{NO}$: 1701/1703 (s). − MS:[36] 866.8 (100) $[(C_5H_5)Re(NO)\{P(C_6H_4CF_3)_3\}\{N(CH_3) = C(H)\text{-}C_6H_5\}]^+$, 747.9 (62) $[(C_5H_5)Re(NO)\{P(C_6H_4CF_3)_3\}]^+$. − NMR (δ, [$D_6$]acetone):[35] ^1H: 8.45/8.69 (d/br s, $^4J_{HH}$ = 1.7, *E*/*Z* =CH), 8.05−7.92 (m, 5 H of 3 C_6H_4 + C_6H_5), 7.85−7.71 (m, 6 H of 3 C_6H_4 + C_6H_5), 7.61−7.40 (m, 4 H of 3 C_6H_4 + C_6H_5), 7.19−7.12 (2 H of C_6H_5), 6.03/6.09 (2 s, *E*/*Z* C_5H_5), 4.01/3.65 (2 d, $^4J_{HH}$ = 1.7/1.2, *E*/*Z* NCH_3);[20] $^{13}C\{^1H\}$: 180.0 (d, $^3J_{CP}$ = 3.6, C=N), 136.1 (d, $^1J_{CP}$ = 53.0, *i*-C_6H_4), 135.5 (d, $^2J_{CP}$ = 11.9, *o*-C_6H_4), 133.7 (dq, $^4J_{CP}$ = 2.4, $^2J_{CF}$ = 32.8, *p*-C_6H_4), 127.4 (dq, $^3J_{CP}$ = 11.1, $^3J_{CF}$ = 3.8, *m*-C_6H_4), 132.8, 130.5, 129.4, 129.0 (4s, C_6H_5), 94.2/94.7 (2 s, *E*/*Z* C_5H_5), 56.1 (s, CH_3). $^{31}P\{^1H\}$: 22.8/20.8 (2 s, *E*/*Z*).

$[(\eta^5\text{-}C_5H_5)Re(NO)\{P(C_6F_5)_3\}(CO)]^+BF_4^-$ (11): A 5-mL flask was charged with **1** (1.800 g, 4.12 mmol), $P(C_6F_5)_3$ (3.397 g,

6.39 mmol), and a stir bar. The neck was fitted with a glass wool plug and a nitrogen bubbler. The flask was placed beneath the surface of a 140 °C oil bath (bubbler protruding). After 27 h, additional $P(C_6F_5)_3$ (1.103 g, 2.07 mmol) was added. After another 23 h, the bath was removed. The solid that formed upon cooling was extracted with CH_3CN (70 mL). The extract was filtered through Celite and concentrated to 5 mL by rotary evaporation. A hexane/ether mixture (70 mL, 1:1 v/v) was added. The yellow precipitate was collected on a glass frit (G3) and washed with hexane (40 mL) and CH_2Cl_2/hexane (ca. 200 mL, 4:5 v/v) until the filtrate was colorless. The yellow powder was dried by oil pump vacuum to give **11** (3.453 g, 3.72 mmol, 90%), m.p. 246−248 °C. − $C_{25}H_5BF_{18}NO_2PRe$ (921.3): calcd. C 31.05, H 0.54, N 1.51; found C 31.41, H 0.54, N 1.89. − IR (cm^{-1}, CH_2Cl_2/CH_3CN/powder film): $\tilde{\nu}_{CO}$: 2043/2047/2046 (s); $\tilde{\nu}_{NO}$: 1794/1794/1794 (s). − MS:[36] 842 (100) $[(C_5H_5)Re(NO)\{P(C_6F_5)_3\}(CO)]^+$, 814 (15) $[(C_5H_5)Re(NO)\{P(C_6F_5)_3\}]^+$, 310 (15) $[(C_5H_5)Re(NO)(CO)]^+$. − NMR (δ):[35] ^1H ([D$_6$]acetone/CD_3CN): 6.33/5.94[38] (s, C_5H_5); $^{13}C\{^1H\}$ ([D$_6$]acetone/CD_3CN): 191.2/191.3 (d, $^2J_{CP}$ = 6.1/6.8, CO), 148.1/148.3 (dm, $^1J_{CF}$ = 249.1/247, *m*-C_6F_5), 146.1/146.5 (dm, $^1J_{CF}$ = 260.0/261, *p*-C_6F_5), 139.3/139.6 (dm, $^1J_{CF}$ = 258.6/252, *o*-C_6F_5), 104/− (dm, $^1J_{CP}$ = 58.5/−, *i*-C_6F_5),[39] 97.2/97.1 (s, C_5H_5); $^{31}P\{^1H\}$ ([D$_6$]acetone/CD_3CN): −48.0/−48.5 (br s, $w_{1/2}$ = 40/39 Hz); $^{19}F\{^1H\}$ ([D$_6$]acetone):[39] −129.0 (m, *o*-C_6F_5), −144.3 (tt, $^3J_{FF}$ = 20, $^4J_{FF}$ = 8, *p*-C_6F_5), −152.2 (s, BF_4), −158.8 (t, $^3J_{FF}$ = 20, *m*-C_6F_5).

(η^5-C_5H_5)Re(NO){P(4-$C_6F_4OCH_3$)$_3$}(CO_2CH_3) (12): A Schlenk flask was charged with **11** (0.8830 g, 0.951 mmol) and methanol (10 mL) and cooled to 0 °C. Then $NaOCH_3$ (5.4 M in methanol; 1.232 mL. 6.65 mmol) was added. The sample was stirred for 2 h at 0 °C. The yellow precipitate was collected on a glass frit (G3), washed with methanol (15 mL) and water (20 mL), and dried by oil pump vacuum to give **12** (0.7345 g, 0.808 mmol, 85%), m.p. 131−134 °C (dec.). − $C_{28}H_{17}F_{12}NO_6PRe$ (908.6): calcd. C 37.01, H 1.89; N 1.54; found C 36.73, H 1.93; N 1.35. − IR (cm^{-1}, powder film): $\tilde{\nu}_{CO}$: 1613 (s); $\tilde{\nu}_{NO}$: 1695 (s). − MS:[36] 909 (5) [**12**$^+$], 878 (100) [**12**$^+$ − OCH_3], 850 (8) [**12**$^+$ − CO_2CH_3], 568 (3) $[P(C_6F_4OCH_3)_3]^+$. − NMR (δ, [D$_6$]acetone):[35] ^1H: 5.44 (s, C_5H_5), 4.21 (t, $^5J_{HF}$ = 2, 3 $C_6F_4OCH_3$), 3.12 (s, CO_2CH_3); $^{13}C\{^1H\}$: 189.1 (d, $^2J_{CP}$ = 12.9, CO_2CH_3), 148.4 (dm, $^1J_{CF}$ = 248.7, *m*-C_6F_4), 141.3 (dm, $^1J_{CF}$ = 228.6, *o*-C_6F_4), 142.2 (t, *p*-C_6F_4),[40] 106.0 (m, *i*-C_6F_4), 94.9 (s, C_5H_5), 62.9 (t, $^4J_{CF}$ = 4.1, $C_6F_4OCH_3$), 48.9 (s, CO_2CH_3); $^{31}P\{^1H\}$: −36.4 (br s, $w_{1/2}$ = 23 Hz).

(η^5-C_5H_5)Re(NO){P(4-$C_6F_4SCH_3$)$_3$}(CO_2CH_3) (13): A Schlenk flask was charged with **11** (0.2000 g, 0.215 mmol) and methanol (8 mL). The sample was stirred to dissolve all **11**, and then cooled to −15 °C (ice/NaCl bath). Then $NaSCH_3$ (0.1056 g, 1.507 mmol) was added with stirring. After 10 min, the yellow precipitate was collected on a glass frit (G3) and dried by oil pump vacuum to give **13** (0.1040 g, 0.108 mmol, 51%), m.p. 140−141 °C (dec.). − $C_{28}H_{17}F_{12}NO_3PReS_3$ (956.8): calcd. 35.15, H 1.79; N 1.46, S 10.05; found C 35.44, H 1.71, N 1.16, S 10.32. − IR (cm^{-1}, powder film): $\tilde{\nu}_{CO}$: 1603 (s); $\tilde{\nu}_{NO}$: 1718 (s). − MS:[36] 958 (2) [**13**$^+$ + H], 926 (100) [**13**$^+$ − OCH_3], 898 (20) [**12**$^+$ − CO_2CH_3], 616 (10) $[P(C_6F_4SCH_3)_3]^+$. − NMR (δ, $CDCl_3$):[35] ^1H: 5.40 (s, C_5H_5), 3.25 (s, OCH_3), 2.62 (br. s, $w_{1/2}$ = 4 Hz, 3 SCH_3); $^{13}C\{^1H\}$: 190.1 (d, $^2J_{CP}$ = 13, CO_2CH_3), 146.3 (dm, $^1J_{CF}$ = 254.2, *m*-C_6F_4), 146.1 (dm, $^1J_{CF}$ = 253.4, *o*-C_6F_4), 121.6 (t, $^2J_{CF}$ = 18.1, *p*-C_6F_4), 111.0 (m, *i*-C_6F_4), 94.0 (s, C_5H_5), 49.5 (s, OCH_3), 17.0 (t, $^4J_{CF}$ = 4.8, SCH_3); $^{31}P\{^1H\}$: −34.1 (br s, $w_{1/2}$ = 26 Hz).

(η^5-C_5H_5)Re(NO){P(C_6F_5)$_3$}(CH_3) (14): A Schlenk flask was charged with **11** (0.300 g, 0.323 mmol) and THF (15 mL) and (as an extra precaution) freeze-pump-thaw degassed (3 ×). Then $NaBH_4$ (0.026 g, 0.69 mmol) was added with stirring. After 10 min, the THF was removed by oil pump vacuum. Benzene (10 mL) was added, and the sample was filtered through a short silica gel plug on a glass frit (G3). Solvent was removed from the filtrate by rotary evaporation and oil pump vacuum to give **14** as an orange powder (0.241 g, 0.291 mmol, 90%) that still contained benzene (see text). The sample was suspended in cold pentane (10 mL), and analogously collected by filtration and dried. This gave **14** with less but still detectable residual solvent (0.225 g, 0.175 mmol, 84%), m.p. 141−143 °C (dec.). − $C_{24}H_8F_{15}NOPRe$ (828.5): calcd. C 34.79, H 0.97, N 1.69; found C 35.79, H 1.32, N 1.75. − IR (cm^{-1}, powder film): $\tilde{\nu}_{NO}$: 1687 (s). − MS:[36] 829 (100) [**14**$^+$], 297 (90) $[(C_5H_5)Re(NO)(CH_3)]^+$. − NMR (δ, [D$_6$]acetone):[35] ^1H: 5.28 (s, C_5H_5), 0.76 (d, $^3J_{HP}$ = 9.5, CH_3); $^{13}C\{^1H\}$: 147.9 (dm, $^1J_{CF}$ = 254.8, *m*-C_6F_5), 144.2 (dm, $^1J_{CF}$ = 250.3, *p*-C_6F_5), 138.6 (dm, $^1J_{CF}$ = 254.7, *o*-C_6F_5), 109.7 (m, *i*-C_6F_5),[39] 93.3 (s, C_5H_5), −33.1 (d, J_{CP} = 7.1, CH_3); $^{31}P\{^1H\}$: −26.5 (br s, $w_{1/2}$ = 16 Hz).

(η^5-C_5H_5)Re(CO)$_2${P(4-$C_6H_4CF_3$)$_3$} (4): A quartz tube was charged with (η^5-C_5H_5)$Re(CO)_3$ (0.584 g, 1.74 mmol)[11] and THF (250 mL), and placed in an ice/water bath. The solution was irradiated with a 450-W Hanovia high-pressure mercury-vapor lamp. The sample was continuously stirred and purged with N_2. The formation of (η^5-C_5H_5)$Re(CO)_2(THF)$[12a] was verified by IR ($\tilde{\nu}_{CO}$: 1908, 1836 cm^{-1}). After 3 h, the lamp was turned off and P(4-$C_6H_4CF_3$)$_3$ (1.01 g, 2.17 mmol) was added to the brown solution. After 72 h, solvent was removed by oil pump vacuum. Hexane (ca. 200 mL) was added, and the mixture was filtered through Celite. The filtrate was slowly concentrated by rotary evaporation. Off-white crystals formed, which were collected by filtration, washed with pentane, and dried by oil pump vacuum to give **4** (0.442 g, 0.580 mmol, 33%), m.p. 187−188 °C (dec.). − $C_{28}H_{17}F_9O_2PRe$ (773.6): calcd. C 43.47, H 2.21; found C 43.27, H 2.26. − IR (cm^{-1}, THF/CH_2Cl_2): $\tilde{\nu}_{CO}$: 1938/1937 (s), 1874/1869 (s). − NMR (δ, $CDCl_3$):[35] ^1H: 7.72−7.65 (m, 6 H of 3 C_6H_4), 7.58−7.47 (m, 6 H of 3 C_6H_4), 5.00 (s, C_5H_5); $^{13}C\{^1H\}$: 200.8 (d, $^2J_{CP}$ = 8.5, 2CO), 141.3 (d, $^1J_{CP}$ = 50.0, *i*-C_6H_4), 132.2 (d, $^2J_{CP}$ = 10.0, *o*-C_6H_4), 132.2 (qd, $^2J_{CF}$ = 33, $^4J_{CP}$ = 2, *p*-C_6H_4), 125.3 (qd, $^3J_{CF}$ = 3.7, $^3J_{CP}$ = 10.5, *m*-C_6H_4), 123.5 (q, $^1J_{CF}$ = 273, CF_3), 83.8 (s, C_5H_5); $^{31}P\{^1H\}$: 33.9 (s).

Acknowledgments

We thank the Deutsche Forschungsgemeinschaft (DFG; GL 300-1/4), the Fonds der Chemischen Industrie, and the US NIH for support of this research.

[1] *Comprehensive Asymmetric Catalysis I−III* (Eds.: E. N. Jacobsen, A. Pfaltz, H. Yamamoto), Springer-Verlag, Berlin, Germany, **1999**.

[2] [2a] E. P. Kündig, B. Bourdin, G. Bernardinelli, *Angew. Chem. Int. Ed. Engl.* **1994**, *33*, 1856−1858; *Angew. Chem.* **1994**, *106*, 1931−1934. − [2b] M. F. Bruin, E. P. Kündig, *Chem. Commun.* **1998**, 2635−2636. − [2c] E. P. Kündig, C. M. Saudan, G. Bernardinelli, *Angew. Chem. Int. Ed.* **1999**, *38*, 1220−1223; *Angew. Chem.* **1999**, *111*, 1298−1301.

[3] [3a] D. R. Gauthier Jr., E. M. Carreira, *Angew. Chem. Int. Ed. Engl.* **1996**, *35*, 2363−2365; *Angew. Chem.* **1996**, *108*, 2521−2523. − [3b] B. L. Pagenkopf, E. M. Carreira, *Chem. Eur. J.* **1999**, *5*, 3437−3442.

[4] [4a] C. M. Garner, N. Quirós Méndez, J. J. Kowalczyk, J. M. Fernández, K. Emerson, R. D. Larsen, J. A. Gladysz, *J. Am. Chem. Soc.* **1990**, *112*, 5146−5160. − [4b] D. M. Dalton, C. M. Garner, J. M. Fernández, J. A. Gladysz, *J. Org. Chem.* **1991**,

56, 6823−6829. − [4c] D. P. Klein, J. A. Gladysz, *J. Am. Chem. Soc.* **1992**, *114*, 8710−8711.

[5] D. M. Dalton, J. M. Fernández, K. Emerson, R. D. Larsen, A. M. Arif, J. A. Gladysz, *J. Am. Chem. Soc.* **1990**, *112*, 9198−9212.

[6] T.-S. Peng, A. M. Arif, J. A. Gladysz, *J. Chem. Soc., Dalton Trans.* **1995**, 1857−1865.

[7] [7a] G. A. Stark, M. A. Dewey, G. B. Richter-Addo, D. A. Knight, A. M. Arif, J. A. Gladysz, in: *Stereoselective Reactions of Metal-Activated Molecules* (Eds.: H. Werner, J. Sundermeyer), Vieweg-Verlag: Braunschweig, Germany, **1995**, p. 51−72, and references therein. − [7b] G. A. Stark, J. A. Gladysz, *Inorg. Chim. Acta* **1998**, *269*, 167−180.

[8] J. A. Gladysz, B. J. Boone, *Angew. Chem. Int. Ed. Engl.* **1997**, *36*, 550−583; *Angew. Chem.* **1997**, *109*, 566−602.

[9] Lead references to an extensive literature: [9a] K. Sünkel, *Chem. Ber./Recueil* **1997**, *130*, 1721−1730. − [9b] R. P. Hughes, S. M. Maddock, A. L. Rheingold, L. M. Liable-Sands, *J. Am. Chem. Soc.* **1997**, *119*, 5988−5989.

[10] [10a] L. J. Alvey, D. Rutherford, J. J. J. Juliette, J. A. Gladysz, *J. Org. Chem.* **1998**, *63*, 6302−6308. − [10b] A. Klose, J. A. Gladysz, *Tetrahedron: Asymmetry* **1999**, *10*, 2665−2674. − [10c] L. J. Alvey, R. Meier, T. Soós, P. Bernatis, J. A. Gladysz, *Eur. J. Inorg. Chem.* **2000**, 1975−1983.

[11] F. Agbossou, E. J. O′Connor, C. M. Garner, N. Quirós Méndez, J. M. Fernández, A. T. Patton, J. A. Ramsden, J. A. Gladysz, *Inorg. Synth.* **1992**, *29*, 211−225.

[12] [12a] I. S. Butler, N. J. Coville, D. Cozak, *J. Organomet. Chem.* **1977**, *133*, 59−71. − [12b] M. Wrighton, *Chem. Rev.* **1974**, *74*, 401−430.

[13] P(*p*-tol)$_3$: M. A. Dewey, G. A. Stark, J. A. Gladysz, *Organometallics* **1996**, *15*, 4798−4807.

[14] See also: W. E. Meyer, A. J. Amoroso, M. Jaeger, J. Le Bras, W.-T. Wong, J. A. Gladysz, *J. Organomet. Chem.* **2000**, *616*, 44−53.

[15] G. L. Crocco, J. A. Gladysz, *J. Am. Chem. Soc.* **1988**, *110*, 6110−6118.

[16] J. H. Merrifield, J. M. Fernández, W. E. Buhro, J. A. Gladysz, *Inorg. Chem.* **1984**, *23*, 4022−4029.

[17] D. A. Knight, M. A. Dewey, G. A. Stark, B. K. Bennett, A. M. Arif, J. A. Gladysz, *Organometallics* **1993**, *12*, 4523−4534.

[18] P. C. Cagle, O. Meyer, K. Weickhardt, A. M. Arif, J. A. Gladysz, *J. Am. Chem. Soc.* **1995**, *117*, 11730−11744.

[19] J. M. Fernández, J. A. Gladysz, *Organometallics* **1989**, *8*, 207−219.

[20] [20a] R. A. Abramovitch, E. P. Kyba, *J. Am. Chem. Soc.* **1974**, *96*, 480−488. − [20b] D. A. Nelson, R. L. Atkins, *Tetrahedron Lett.* **1967**, *51*, 5197−5200.

[21] [21a] Y. Yamamoto, N. Asao, *Chem. Rev.* **1993**, *93*, 2207−2293. − [21b] H. Nakamura, H. Iwama, Y. Yamamoto, *J. Am. Chem. Soc.* **1996**, *118*, 6641−6647. − [21c] X. Fang, M. Johannsen, S. Yao, N. Gathergood, R. G. Hazell, K. A. Jørgensen, *J. Org. Chem.* **1999**, *64*, 4844−4849.

[22] M. Fild, I. Hollenberg, O. Glemser, *Z. Naturforsch., B* **1967**, *22*, 253−256.

[23] T. B. Patrick, in: *Chemistry of Organic Fluorine Compounds II* (Eds.: M. Hudlický, A. E. Pavlath), ACS Monograph 187, American Chemical Society, Washington, D. C., **1995**, pp. 501−524.

[24] Additional literature: [24a] H. R. Hanna, J. M. Miller, *Can. J. Chem.* **1979**, *57*, 1011−1017. − [24b] P. Battioni, O. Brigaud, H. Desvaux, D. Mansuy, T. G. Traylor, *Tetrahedron Lett.* **1991**, *32*, 2893−2896. − [24c] P. A. Deck, M. J. Lane, J. L. Montgomery, C. Slebodnick, F. R. Fronczek, *Organometallics* **2000**, *19*, 1013−1024. − [24d] Nucleophilic substitutions of π-fluoroarene complexes are well known, see: M. F. Semmelhack, G. Hilt, J. H. Colley, *Tetrahedron Lett.* **1998**, *39*, 7683−7686, and references to earlier work therein. This paper also describes a nucleophilic substitution of P(C$_6$F$_5$)$_3$, which was evaluated as linker ligand for solid-phase synthesis.

[25] J. Le Bras, H. Jiao, W. E. Meyer, F. Hampel, J. A. Gladysz, *J. Organomet. Chem.* **2000**, *616*, 54−66.

[26] [26a] P. J. Hay, W. R. Wadt, *J. Chem. Phys.* **1985**, *82*, 299−310. − [26b] T. H. Dunning, Jr., P. J. Hay, in: *Modern Theoretical Chemistry* (Ed.: H. F. Schaefer III), Plenum, New York, **1976**, p. 1. For polarization functions (ζ = 0.6 for C; ζ = 0.34 for P, and ζ = 0.073 for Re) see: S. Huzinaga, J. Anzelm, M. Klobukowski, E. Radzio-Andzelm, Y. Sakai, H. Tatewaki, in: *Gaussian Basis Sets for Molecular Calculations*, Elsevier, Amsterdam, **1984**.

[27] M. J. Frisch, G. W. Trucks, H. B. Schlegel, G. E. Scuseria, M. A. Robb, J. R. Cheeseman, V. G. Zakrzewski, J. A. Montgomery, Jr., R. E. Stratmann, J. C. Burant, S. Dapprich, J. M. Millam, A. D. Daniels, K. N. Kudin, M. C. Strain, O. Farkas, J. Tomasi, V. Barone, M. Cossi, R. Cammi, B. Mennucci, C. Pomelli, C. Adamo, S. Clifford, J. Ochterski, G. A. Petersson, P. Y. Ayala, Q. Cui, K. Morokuma, D. K. Malick, A. D. Rabuck, K. Raghavachari, J. B. Foresman, J. Cioslowski, J. V. Ortiz, B. B. Stefanov, G. Liu, A. Liashenko, P. Piskorz, I. Komaromi, R. Gomperts, R. L. Martin, D. J. Fox, T. Keith, M. A. Al-Laham, C. Y. Peng, A. Nanayakkara, C. Gonzalez, M. Challacombe, P. M. W. Gill, B. Johnson, W. Chen, M. W. Wong, J. L. Andres, C. Gonzalez, M. Head-Gordon, E. S. Replogle, J. A. Pople, *GAUSSIAN98, Revision A.5*, Gaussian, Inc., Pittsburgh, PA, **1998**. − For computational methods and applications see: [27a] W. J. Hehre, L. Radom, P. v. R. Schleyer, J. A. Pople, *Ab initio Molecular Orbital Theory*, New York, **1986**. − [27b] J. B. Foresman, A. Frisch, *Exploring Chemistry with Electronic Structure Methods: A Guide to Using Gaussian*, 2nd ed., Gaussian, Inc., Pittsburgh, PA, **1996**.

[28] Representative references from the many that are easily retrieved by data base searches: [28a] R. D. W. Kemmitt, D. I. Nichols, R. D. Peacock, *J. Chem. Soc. A* **1968**, 1898−1902. − [28b] K. Jacob, F. Voigt, K. Merzweiler, C. Pietzsch, *J. Organomet. Chem.* **1997**, 545−546, 421−433. − [28c] M. Selke, W. L. Karney, S. I. Khan, C. S. Foote, *Inorg. Chem.* **1995**, *34*, 5715−5720. − [28d] C. Corcoran, J. Fawcett, S. Friedrichs, J. H. Holloway, E. G. Hope, D. R. Russell, G. C. Saunders, A. M. Stuart, *J. Chem. Soc., Dalton Trans.* **2000**, 161−172, and earlier papers cited therein.

[29] [29a] J. L. Kiplinger, T. G. Richmond, C. E. Osterberg, *Chem. Rev.* **1994**, *94*, 373−431. − [29b] J. Burdeniuc, B. Jedlicka, R. H. Crabtree, *Chem. Ber./Recueil* **1997**, *130*, 145−154. − [29c] T. G. Richmond, in: *Topics in Organometallic Chemistry*, vol. 3 (Ed.: S. Murai), Springer, New York, **1999**, pp. 243−269. − [29d] T. G. Richmond, *Angew. Chem. Int. Ed.* **2000**, *39*, 3241−3244; *Angew. Chem.* **2000**, *112*, 3378−3380.

[30] [30a] F. Ponzini, R. Zagha, K. Hardcastle, J. S. Siegel, *Angew. Chem. Int. Ed.* **2000**, *39*, 2323−2325; *Angew. Chem.* **2000**, *112*, 2413−2326, and references therein. − [30b] G. W. Coates, A. R. Dunn, L. M. Henling, J. W. Ziller, E. B. Lobkovsky, R. H. Grubbs, *J. Am. Chem. Soc.* **1998**, *120*, 3641−3649. − [30c] M. L. Renak, G. P. Bartholomew, S. Wang, P. J. Ricatto, R. J. Lachicotte, G. C. Bazan, *J. Am. Chem. Soc.* **1999**, *121*, 7787−7798. − [30d] C. Dai, P. Nguyen, T. B. Marder, A. J. Scott, W. Clegg, C. Viney, *Chem. Commun.* **1999**, 2493−2494.

[31] I. Ojima, H. B. Kwon, *J. Am. Chem. Soc.* **1988**, *110*, 5617−5621.

[32] Representative examples: [32a] J. J. Kowalczyk, A. M. Arif, J. A. Gladysz, *Chem. Ber.* **1991**, *124*, 729−742. − [32b] T.-S. Peng, C. H. Winter, J. A. Gladysz, *Inorg. Chem.* **1994**, *33*, 2534−2542. − [32c] See also: K. Kromm, B. D. Zwick, O. Meyer, F. Hampel, J. A. Gladysz, *Chem. Eur. J.*, in press.

[33] [33a] G. A. Stark, Ph. D. Thesis, University of Utah, **1997**. − [33b] W. Mohr, Diplom Thesis, University of Erlangen-Nürnberg, **1999**.

[34] L. A. Wall, R. E. Donaldio, W. J. Pummer, *J. Am. Chem. Soc.* **1960**, *82*, 4846−4848.

[35] NMR spectra were recorded on > 300 MHz instruments. All *J* values are in Hz, and the *i*/*o*/*m*/*p* positions of *para*-disubstituted benzene rings are defined with respect to the phosphorus atom. The relative areas of ^{1}H NMR signals are defined by the assignments (e.g., 3 CH_3 = 9 H) unless noted. Spectra were referenced as follows (δ): ^{1}H: Si(CH$_3$)$_4$ (0.00) or residual CD_2HCN (1.93) or CD_2HCOCD_3 (2.04); ^{13}C: CD_3CN (1.3), CD_3COCD_3 (29.8), $CDCl_3$ (77.0), or CD_2Cl_2 (53.8); ^{31}P: external 85% H_3PO_4 (0.00); ^{19}F: $CFCl_3$ (0.00).

[36] (+)-FAB, 3-NBA/CH_2Cl_2 or 3-NBA matrix, *m*/*z* (%) for most intense peak of isotope envelope.

[37] Some preparations gave small amounts of a by-product believed to be the methylamine complex [(η^5-C$_5$H$_5$)Re(NO){P(4-C$_6$H$_4$CF$_3$)$_3$}{N(CH$_3$)H$_2$}]$^+$TfO$^-$, presumably derived from inadvertent hydrolysis of the C=N linkage at some stage (PPh_3 analog: M. A. Dewey, D. A. Knight, D. P. Klein, A. M. Arif, J. A. Gladysz, *Inorg. Chem.* **1991**, *30*, 4995−5002). This more-

soluble species could be separated from **9** by crystallization from acetone/hexanes. − MS:[36] 778.7 (100) $[(C_5H_5)Re(NO)\{P(C_6H_4CF_3)_3\}\{N(CH_3)H_2\}]^+$, 747.8 (65) $[(C_5H_5)Re(NO)\{P(C_6H_4CF_3)_3\}]^+$. − NMR (δ, CD_3COCD_3, partial): ^1H: 5.79 (s, C_5H_5); $^{13}C\{^1H\}$: 93.3 (s, C_5H_5); $^{31}P\{^1H\}$: 22.3.

[38] This larger than usual solvent dependency has been duplicated with different samples.

[39] These signals were assigned by analogy to those of $P(C_6F_5)_3$: [39a] M. G. Hogben, W. A. G. Graham, *J. Am. Chem. Soc.* **1969**, *91*, 283−291. − [39b] H. J. Frohn, H. Maurer, *J. Fluorine Chem.* **1986**, *34*, 129−145.

[40] This value represents one line of an obscured triplet.

Received September 20, 2000
[I00353]

Vanadium(IV and V) Complexes Containing *SNO* (Dithiocarbonylhydrazone; Thiosemicarbazone) Donor Sets

Dongren Wang,[a] Martin Ebel,[a] Carola Schulzke,[a] Cerstin Grüning,[a] Saroj K. S. Hazari,[b] and Dieter Rehder*[a]

Keywords: Vanadium / Thiosemicarbazones / Thiohydrazones / Sulfur coordination / Biomimetic compounds

The VO^{2+} complexes [VOCl(*ONS*)] (**3**) and [VO(*ONS*)′] (**4**), and the VO^{3+} complexes [VO(OEt)(*ONS*)′] (**5**) {*ONS* = (*R*)-salicylaldehyde thiosemicarbazonate(1–) R = 5,6-C_4H_4 (**3a**) or 3-OMe (**3b**); (*ONS*)′ = (*R*)-salicylaldehyde[benzylmercaptothiocarbonylhydrazonate(2–)], R = H, (**4a/5a**) or 3-OMe (**4b/5b**)} have been prepared and characterised by IR, EPR, ^{1}H-, and ^{51}V-NMR spectroscopy. In (*S*)-*s*BuOH, **4a** converts to [VO{(*S*)-O*s*Bu}(*ONS*)′] (**5c**) and [VO(OH)(*ONS*)′] (or a condensation product thereof). Solutions of **5c** show three ^{51}V NMR signals, two of which are due to two diastereomers. The EPR spectra of **3** and **4** in THF reveal the presence of octahedral species in solution. The crystal and molecular structures of complexes **3a**·$OCMe_2$, **5a**, and **5b** have been obtained, revealing basically a tetragonal pyramid, and coordination of the sulfur function in the thiocarbonyl (**3**) or enethiolate mode (**5**). The relevance of the compounds to bioinorganic aspects is addressed.

Introduction

Vanadium coordination chemistry has attracted increasing interest during the last few years, due to the model character of many vanadium complexes for the biological function of vanadium,[1–5] the use of (oxo)vanadium complexes in oxidation and oxo transfer catalysis,[6,7] and potential medicinal applications such as the treatment of diabetes types I (insulin deficiency) and II (insulin resistance).[8,9] In its biogenic compounds, and in its interactions with biogenic ligand systems, vanadium coordinates to *O*, *N*, and *S* functions. Among the *O* functionalities are phenolate from tyrosine, as in the insulin-mimetic action of vanadium (possibly as a result of the inhibition of a protein tyrosine-phosphatase),[10] as well as dopa and hydroxy-dopa of tunichrome fragments in the vanadocytes of certain species of *Ascidiaceae* (sea squirts).[11] The imine nitrogen atom of histidine is coordinated to vanadate(V) (HVO_4^{2-}) in vanadate-dependent haloperoxidases from marine brown algae such as *Ascophyllum nodosum* (knobbed wrack),[12] and from the mould *Curvularia inaequalis*,[13,14] as well as to $V^{IV/II}$ in the VFe cofactor of the *M* cluster of vanadium-nitrogenase from *Azotobacter*.[15] In the latter case, the coordination sphere of vanadium is complemented by homocitrate and three bridging sulfides. Sulfur coordination, through cysteinate, has also been observed in vanadate-derivatised tyrosine phosphatase,[16] and is likely to be the initiating step in redox inhibition by V^V of enzymes containing cysteine in their active centre.[17] This process has been simulated by the in vitro oxidation of thiolates to disulfides.[18,19] As far as the use of vanadium-based catalyst systems in oxidation/oxygenation reactions is concerned, the conversion of sulfides (thioethers) RR′S to sulfoxides RR′S=O by peroxides is noteworthy, a process that is catalysed in vivo by vanadate-dependent peroxidases,[20,21] and in vitro by vanadium complexes containing *ONO* donor sets,[22–24] where *N* is an amine or imine function, and *O* a phenolic or alcoholic oxygen atom. The enantioselectivity of these reactions suggests an intermediate coordination of the sulfide to the vanadium centre, thus giving rise to an intermediate coordination sphere comprising *S*, *N*, and *O*.

Against this background, we are investigating vanadium complexes with *SNO* functional ligands such as thiosemicarbazones and mercaptothiocarbonylhydrazones with salicylaldehydes as the carbonyl component (Scheme 1). Sulfur coordination of these ligand systems occurs through the doubly bonded thio group in the case of the semicarbazones **1**, and through the thiolate group of the enthiol tautomer in the case of the hydrazones **2**, providing, in the latter case, rare examples[25–30] of redox-stable V^V complexes with thiolate coordination. The hydrazones **2** with a "masked" thiolate function are employed advantageously for coordination to vanadium(V), since they resist the otherwise common oxidation of thiolates to disulfides by V^V.

Thio coordination to vanadium is additionally of interest with respect to the insulin-mimetic potential of vanadyl dithiocarbamates.[31] More generally, metal complexes of thiosemicarbazones have also been discussed in the context of their antibacterial and antifungal properties.[32,33]

Results and Discussion

Preparation and Characteristics

The vanadium complexes were prepared as described by Equations (1) to (3) in THF [**3**; Equation (1)] and in eth-

[a] Institut für Anorganische und Angewandte Chemie, Universität Hamburg,
20146 Hamburg, Germany
E-mail: rehder@xray.chemie.uni-hamburg.de
[b] Department of Chemistry, University of Chittagong, Chittagong, Bangladesh
E-mail: tapashi@ctgu.edu

 © WILEY-VCH Verlag GmbH, 69451 Weinheim, 2001 1434–1948/01/0404–0935 $ 17.50+.50/0

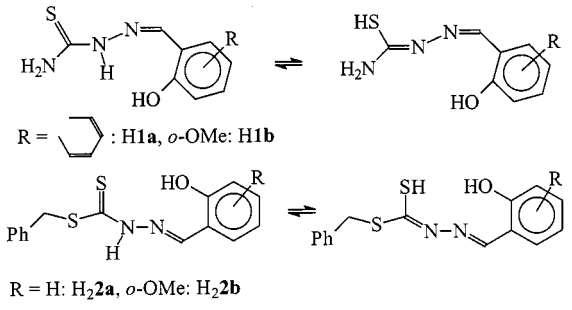

Scheme 1

anol/water [**4**, Equation (2), and **5**, Equation (3)], respectively, under either an inert gas (**3** and **4**) or under aerobic conditions (**5**). An acetate buffer was used to capture the protons generated in Equation (2).

$$[VOCl_2(thf)_2] + H\mathbf{1} \rightarrow \underset{\mathbf{3}}{[VOCl(\mathbf{1})]} + [Hthf]Cl \quad (1)$$

$$VO^{2+} + H_2\mathbf{2} \rightarrow \underset{\mathbf{4}}{[VO(\mathbf{2})]} + 2H^+ \quad (2)$$

$$2[VO(\mathbf{2})] + \tfrac{1}{2}O_2 + 2EtOH \rightarrow \underset{\mathbf{5a/b}}{2[VO(\mathbf{2})OEt]} + H_2O \quad (3)$$

The green complexes **3a** and **3b** were isolated as the THF and water adducts (**3a**·$^3/_4$THF and **3b**·$^1/_2H_2O$·$^1/_2$THF), respectively, the complexes **4a** and **4b** with varying amounts of solvent, viz. **4a**·EtOH, **4a**·$^1/_4H_2O$, and **4b**·H_2O. Crystals of **3a** were obtained as **3a**·$OCMe_2$ from acetone. Complexes **5a** and **5b** were free of coordinated solvent or solvent of crystallisation, and thus differ from the related hydrazone complex [VO(OMe)(*SNO*)′′(HOMe)], where (*SNO*)′′ is salicylaldehyde-thiobenzoylhydrazone.[34] Spectroscopic data are summarised in Table 1 and Table 2. All of the complexes show the IR bands characteristic of ν(−HC=N−) (around 1600 cm^{-1}) and ν(V=O) (998−962 cm^{-1}), with the latter usually doubled; cf. Table 1. An additional sharp and intense band observed for the crystals of **3a**·$OCMe_2$ at 1696 cm^{-1} is assigned to ν(C=O) of acetone of crystallisation. The bathochromic shift with respect to free acetone is due to the involvement of the carbonyl group in H bonding interaction with N−NH and C−NH_2 of the semicarbazone ligand, as identified by the X-ray structure analysis (see below). Complex **3a** still shows the ν(NH) (3276 and 3137 cm^{-1}) also present in the free ligand **1a** (3263 and 3165 cm^{-1}), indicating the coordination of the sulfur function in the thiocarbonyl form, a fact that is again corroborated by the structure determination. The corresponding ν(NH) for **1b** and **3b** are 3343 and 3167 cm^{-1}(**1b**), and 3291 and 3189 cm^{-1} (**3b**). The ν(C=S), 1192 in **1a** and 1185 cm^{-1} in **1b**, are slightly weakened on coordination, and thus experience a bathochromic shift to 1148 (**3a**) and 1162 cm^{-1} (**3b**). The complexes **4** and **5** show two resolved ν(C=N) bands, which we attribute to the presence of two C=N double bonds in the enthiolate framework of the hydrazone ligand (see the respective tautomeric form in Scheme 1).

The methine group is also clearly visible by its ^{1}H NMR feature (Table 2) of the diamagnetic complexes **5** (δ = 9.08); the methine proton resonances (δ = 7.98 in the free ligands **2**) are thus shifted to low (magnetic) field on coordination of the imine nitrogen atom. The protons of the methylene group of the benzyl substituent on the noncoordinating sulfur atom are only marginally affected. A feature of particular interest is the occurrence of two resonances, for the methylene and methyl protons of the ethyl group, in an intensity ratio of approximately 1:2 for uncoordinated ethanol and coordinated ethanolate, suggesting an equilibrium between ethoxide and hydroxo complex (or its condensation product) as depicted in Equation (4).

$$\begin{aligned} &[VO(OEt)\mathbf{2}] + H_2O \leftrightarrows [VO(OH)\mathbf{2}] + EtOH \\ &\quad\mathbf{5} \\ &2[VO(OH)\mathbf{2}] \leftrightarrows [\{VO(\mathbf{2})\}_2\mu\text{-}O] + H_2O \end{aligned} \quad (4)$$

This situation is also reflected in the ^{51}V NMR spectra, which show two resonances, separated by 51 ppm (**5a**) and 56 ppm (**5b**), with the less intense low-field signal corresponding to the hydroxo (or dimeric, μ-O-bridged) form. This assignment is carried out on the basis of the spectrum obtained after treatment of **4a** with (*S*)-*s*BuOH, which gives rise to the formation of [VO{(*S*)-O*s*Bu}**2a**] (**5c**) with two centres of chirality (V and C_α of the butoxide group) in equilibrium with [VO(OH)**2a**]. Of the two resonances, the less intense one at δ = −347 is a singlet belonging to the

Table 1. Selected IR, δ(^{51}V) and EPR data

	ν(N=CH)[a]	ν(V=O)[a]	δ(^{51}V)[b]	g_0	A_0[c]
3a	1618	995[d]		1.979	98.7, 101.0[e] (THF)
3b	1605	998/973[f]		1.971	94.3, 100.7 (CH_2Cl_2)
4a	1603, 1588	988, 966		1.972	93.7, 100.9[g] (THF)
4b	1603, 1590	991, 977		1.98	99.8[h]
5a	1602, 1590	984, 962 *sh*	−348[i], −399	1.98	99.6
5b	1600, 1589	985, 976 *sh*	−340[i], −396		
5c	1601, 1590	986	−347[i], −411/−414		

[a] In KBr; in cm^{-1}. − [b] In $CDCl_3$. − [c] A in 10^{-4} cm^{-1}. − [d] In THF solution, the ν(V=O) is at 976 cm^{-1}. − [e]Two components (*1* and *2*, not resolved in *g*) are present; $A_0 = 93.7 \cdot 10^{-4}$ cm^{-1} corresponds to the main component *1*. Parameters under anisotropic conditions (100 K): *g* values (obtained from a fitting procedure) are $g_{xy}^{(1)} = 1.99$, $g_z^{(1)} = 1.956$; $g_{xz}^{(2)} = 1.981$, $g_z^{(2)} = 1.950$; $A_{xy}^{(1)} = 60$, $A_z^{(1)} = 161$; $A_{xy}^{(2)} = 65$, $A_z^{(2)} = 173 \cdot 10^{-4}$ cm^{-1}. Cf. also Figure 1 and Equation (5). − [f] Broad resonance with two maxima. − [g] The ratio of components *1* and *2* is reversed with respect to **3a**, i.e the smaller A corresponds to the minor species. Anisotropic coupling constants of main component: $A^{(2)}{}_z = 160$, $A^{(2)}{}_{xy} = 61 \cdot 10^{-4}$ cm^{-1}. − [h] $g_z = 1.96$, $g_{xy} = 1.99$; $A_z = 176.5$, $A_{xy} = 63.4 \cdot 10^{-4}$ cm^{-1}. − [i] This signal corresponds to [VO(*SNO*)OH] or [{VO(*SNO*)}$_2$μ-O].

Table 2. δ(^{1}H) NMR spectroscopic data

Ligand[a]	−NH−	−N=CH−	$PhCH_2S$−	$-OCH_3$	$-OCH_2CH_3$	$-OCH_2CH_3$
2a	9.98	7.98	4.60			
2b	9.89	7.98	4.56	3.91		
5a	−	9.08	4.47		1.25, 1.63[b]	3.72, 5.42[b]
5b	−	9.08	4.48	3.95	1.24, 1.64[b]	3.75, 5.45[b]

[a] In $CDCl_3$. For the ligands **1a** and **1b**, see Exp. Sect. − [b] Intensity ratio ca.1:2; the first signal corresponds to free ethanol.

butoxide-free complex, while the more intense to higher field is doubled and belongs to **5c**. The separation between the two components of this signal, δ = −411.3 and −414.2, is within the range expected for the signal splitting for a vanadium compound being present as two diastereomeric pairs of enantiomers.[35,36] The ^{51}V chemical shifts are in the range expected for a donor set containing one sulfur function, i.e. to low field by about 150 to 200 ppm with respect to complexes with O_xN_y donor sets.[37]

The EPR spectrum of crystals of **3a**·$OCMe_2$ dissolved in THF exhibits the isotropic eight-line pattern typical of VO^{2+} complexes [$S = {}^1/_2$, $I(^{51}V) = {}^7/_2$]. Along with the main species in this spectrum, characterised by a hyper-fine coupling constant $A_0 = 93.7\cdot10^{-4}$ cm^{-1}, there is a second species with a rather high value ($A_0 = 101.0\cdot10^{-4}$ cm^{-1}). This situation is also revealed by the anisotropic spectrum in frozen THF solution (Figure 1), which is a superposition of the parallel (*z*) and perpendicular (*xy*) parts of the main (*1*) and the minor component (*2*). The A_z values are $A_z^{(1)} = 161\cdot10^{-4}$ and $A_z^{(2)} = 173\cdot10^{-4}$ cm^{-1}. Based on the additivity relationship $A_z = \Sigma n_i A_{zi}$ (n_i denotes the nature of the four equatorial ligand functions, and A_{zi} are the corresponding contributions to A_z),[38] a value of $161\cdot10^{-4}$ cm^{-1} is in agreement with an equatorial *ClONS* donor set in **3a**, while a value of $173\cdot10^{-4}$ cm^{-1} should indicate addition of an oxygen-functional ligand L in solution, such as THF, possibly accompanied by a rearrangement of the tridentate ligand so as to place the sulfur donor atom into an axial position.

Taking 45.7 and $33.9\cdot10^{-4}$ cm^{-1} as the contributions of a relatively weak *O* donor such as THF[39] and the thiocarbonyl function, respectively, a calculated value of $A_z^{(2)} = 172.8\cdot10^{-4}$ cm^{-1} is obtained, in very good agreement with the found coupling constant of $173\cdot10^{-4}$ cm^{-1}. We hence suggest an equilibrium as depicted in Equation (5), where species *1* is represented by **3a** and species *2* by *trans*-**3a(L)**, where *trans* denotes the position of S in the axial position (*trans* to the doubly bonded oxo ligand). In THF solutions, L would presumably be THF.

Since the same pattern arises in the isotropic spectrum of a solution of **3a**·$OCMe_2$ in CH_2Cl_2, where the compound is but sparingly soluble, L appears to be acetone in this solvent. In principal, the EPR of the vanillin derivative **3b** compares well with that of **3a**, in that there are two components *1* and *2* present in the spectrum. The ratio is, however inverse, i.e. compound *2* corresponding to the species with the larger coupling constant, **3b(L)**, is the major component. The A_0 and A_z values for **4a** and **4b** are somewhat larger (Table 1) than those for the tetragonal-pyramidal species *1* of **3a** and **3b**, in accord[40] with an octahedral coordination in solution and the equatorial plane dominated by strongly electronegative ligand functions in the case of **4**, which thus corresponds to **3(L)**. Again, the sixth position in the coordination polyhedron of THF solutions of **4** is supposed to be occupied by THF.

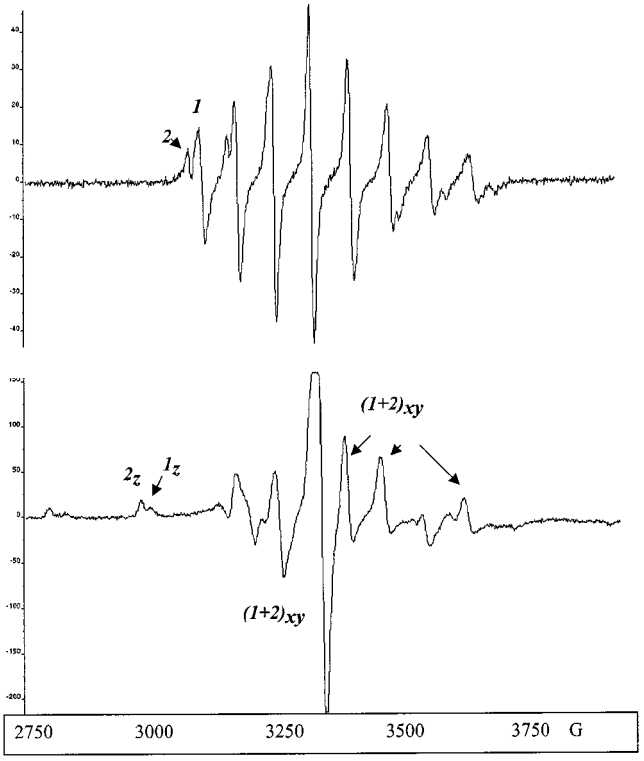

Figure 1. EPR spectrum of **3a** in THF solution at room temperature (top) and at 100 K; the *z* (parallel) and *xy* (perpendicular) components are indicated, as are the two species *1* and *2* present in solution; cf. Equation (4)

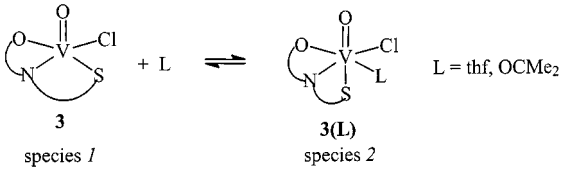

(5)

Structure Descriptions

Selected bond lengths and bond angles are given in Table 3. In the V^{IV} (VO^{2+}) thiosemicarbazone complex **3a**, vanadium is basically in a tetragonal-pyramidal environment (Figure 2) with the doubly bonded oxo group O1 of the vanadyl moiety in the apical position, and the chloro

ligand, O2, N1, and S3 of the tridentate thiosemicarbazone ligand in the plane. There is a sizeable distortion towards a trigonal bipyramid, quantified by a τ value of 0.28, where τ is defined by $\tau = [(O2-V-N1) - (O3-V-S2)]/60$; $\tau = 0$ for ideal tetragonal pyramids, and $\tau = 1$ in the case of an ideal trigonal bipyramid. The S3−C12 bond [1.708(3) Å] is significantly shorter than in most structurally characterised Ni and Cu complexes with comparable ligands (ca. 1.73−1.76 Å[39,41−44]), indicating coordination of the ligand through a thiocarbonyl rather than through an enthiolate in the case of **3a**, and is thus in agreement with thiosemicarbazones coordinated to early transition metals such as Cr[45] and Mo.[46] This view is corroborated by the localisation of the hydrogen atom on the nonbonding N2, which is linked by an intermolecular hydrogen bond to the carbonyl oxygen atom O3 of acetone of crystallisation; *d*(O3···H−N2) = 2.154 Å. Further intermolecular hydrogen bonds exist between the hydrogen atoms on the primary amine group (N3) and O3 [*d*(O3···H−N3) = 2.02] and the phenolate oxygen atom O2 [*d*(O2···H−N3) = 2.019 Å]. The hydrogen bonding network is shown in Figure 2 (bottom).

Other bonding parameters within the ligand system are comparable to those in thiosemicarbazone complexes of other metals.[38−46] The bond lengths between the vanadium centre and the three ligand functions also compare to those of the vanadium-*ONS* complex [V(nap-amtph)$_2$], where nap-amtph is the Schiff base formed between *o*-hydroxynaphthaldehyde and *o*-aminothiophenol,[47] and to [V(mpg)*o*-phen] [H_3mpg = *N*-(2-mercaptopropionyl)glycine]. In all these complexes [as in the hydrazone complexes **5** (see below)] the V−S bond lengths [**3a**: 2.358(1), [V(nap-amtph)$_2$]: 2.306(2) and 2.351(2), [V(mpg)*o*-phen]: 2.3820(14) Å] fall at the short end of the range for *d*(V−S);[47−49] they are also significantly shorter than in the complex [VO(H_2O)L], where H_2L is thiosemicarbazone-diacetate; [*d*(V−S) = 2.435, *d*(V−N) = 2.362 Å].[50] On the other hand, V−S bonds in V^V complexes containing the tetrafunctional trithiolate N($CH_2CH_2S^-$)$_3$ are still shorter (averaging around 2.25 Å[29,30]) than in the aforementioned complexes with *ONS* donor sets. The V−Cl bond in **3a** [2.341(1) Å] again compares to that in other chlorovanadium complexes.[35,51,52]

A tetragonal pyramid is also the basic structure for the V^V (VO^{3+}) thiohydrazone complexes **5a** and **5b** (Figure 3), in which the chloro ligand of the V^{IV} complex **3a** is replaced by an ethanolate moiety, and the tridentate *ONS* acts as a dianionic ligand. The vanadium ion is 0.49 (**5a**) and 0.52 Å (**5b**) above the plane spanned by S2, N1, O2, and O3 (i.e. the tridentate ligand and the ethoxy group). The distortion towards a trigonal bipyramid compares with that of **3a**, i.e. τ = 0.28 (**5a**) and 0.27 (**5b**). As expected for enthiolate (**5**) vs. thiocarbonyl coordination (**3**), the bond lengths *d*(S−C2) in **5** are substantially longer than *d*(S−C12) in **3a**, the *d*(N2−C2) in **5** substantially shorter than *d*(N2−C12) in **3a** (Table 3). In line with this view are the bond angles at N2: (N1−N2−C12) = 118.7(2)° in **3a** is close to the tet-

Table 3. Selected structure parameters

	[VOCl(**1a**)], **3a**	[VO(OEt)(**2a**)], **5a**	[VO(OEt)(**2b**)], **5b**[a]
Bond lengths [Å]			
V−Cl	2.341(1)		
V=O (V1−O1)	1.590(2)	1.594(3)	1.608(6)
V−O(phenolate)	1.914(2) (V−O2)	1.828(3) (V−O3)	1.859(4)
V−O(ethanolate)		1.754(3) (V−O2)	1.771(6)
V−S	2.358(1)	2.343(2) (V−S2)	2.345(3)
V−N1	2.087(3)	2.152(3)	2.098(5)
S(coord.)−C12/2	1.708(3) (S−C12)	1.731(4) (S2−C2)	1.750(6)
N2−C12/2	1.334(4) (N2−C12)	1.290(6) (N2−C2)	1.289(7)
N1−N2	1.391(3)	1.393(5)	1.402(6)
N1=CH−	1.303(4) (N1−C11)	1.287(6) (N1−C3)	1.301(7)
O(phenolate)−C	1.334(4) (O2−C1)	1.344(6) (O3−C6)	1.339(7)
S1−C2		105.0(2) (O1−V−O2)	101.6(4)
Bond angles [°]			
O1−V−Cl	105.78(9)		
O1−V−O(phenolate)	111.03(11) (O1−V−O2)	108.5(2) (O1−V−O3)	110.1(4)
O1−V−O(ethanolate)		105.0(2) (O1−V−O2)	101.6(4)
O1−V−N1	99.57(11)	95.5(2)	95.0(3)
O1−V−S	110.58(9)	107.30(14) (O1−V−S2)	107.0(2)
Cl−V−O(phenolate)	89.71(7)		
Cl−V−S	87.15(3)		
O(eth.)−V−O(phen.)		99.4(2) (O2−V−O3)	95.2(3)
O(ethanolate)−V−S2		87.14(13) (O2−V−S2)	86.1(2)
O(phenolate)−V−S	137.50(7)	140.39(13) (O3−V−S2)	140.67(16)
N1−V−S	80.69(7)	77.28(11) (N1−V−S2)	78.81(15)
S−C(carbonyl)−N2	120.7(2) (S−C12−N2)	127.7(3) (S2−C2−N2)	125.6(4)
C(carbonyl)−N2−N1	118.7(2) (C12−N2−N1)	112.5(3) (C2−N2−N1)	112.2(5)
N2−N1=CH	116.3(2) (N2−N1−C11)	112.2(3) (N2−N1−C3)	112.4(5)
N1=CH−C(Ph)	124.1(3) (N1−C11−C10)	125.3(4) (N1−C3−C11)	125.0(6)
V1−O(phen.)−C(Ph)	126.78(18)	132.5(3) (V1−O3−C6)	132.0(4)
C2−S1−C1		102.2(2)	102.3(3)

[a] Same numbering scheme as for **5a**.

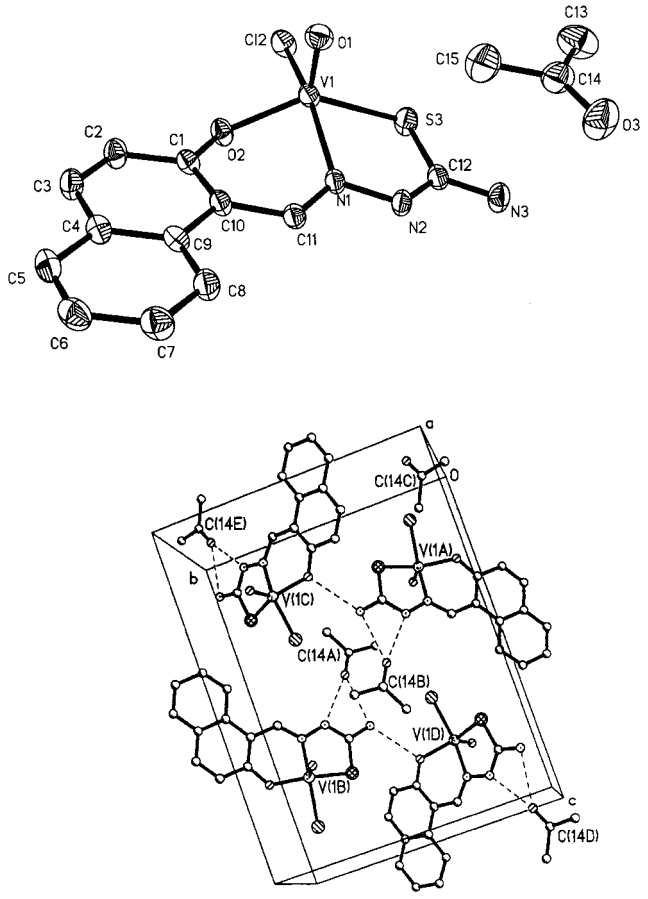

Figure 2. ORTEP plot (at the 50% probability level) and numbering scheme of **3a**·acetone (top), and a representation of the unit cell (bottom) showing the hydrogen bonding network (dashed lines)

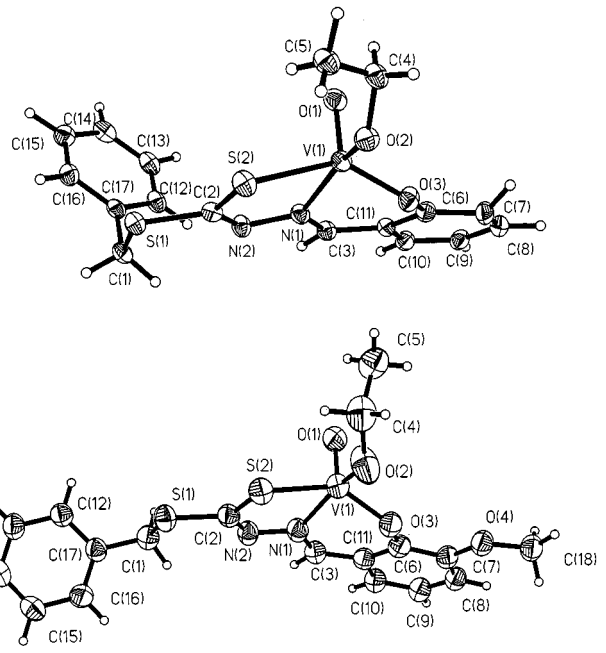

Figure 3. ORTEP plots (50% probability level) and numbering schemes for **5a** (top) and **5b** (bottom)

rahedral angle, while the angles (N1−N2−C2) = 112.5(3) (**5a**) and 112.2(5)° (**5b**) are close to that for trigonal planar geometry. The exchange of chloride in **3a** for ethanolate in **5** does not effect *d*(V−N1) *trans* to the negatively charged ligand, while the V−O(phenolate) bond is clearly shorter in **5** than in **3a**, and also shorter than in other structurally characterised early transition metal (Cr and Mo) complexes with a similar donor set,[45,46] or in Schiff base oxovanadium complexes with a salicylaldehyde moiety.[53] The reason for these unprecedentedly short V−O(phenolate) bonds, which approach the lengths otherwise observed with V−O(alcoholate) bonds [1.80 to 1.74 Å,[54] cf. also the respective data for *d*(V−O2) in Table 3], may be traced back to a strengthening of this bond as a result of comparatively weak bonding interaction between V^V and the soft thiolate opposite the hard phenolate oxygen.

The bicyclic system formed between the vanadium centre and the tridentate ligand is slightly folded along the V−N1 axis: The angles between the planes V−O3−C6−C11−C3−N1 and V−N1−N2−C2−S2 amount to 16.92(15) (**5a**) and 20.41(22)° (**5b**). The planes by themselves are not ideal, with the largest deviations encountered with V1 (−0.228) and O3 (0.252 Å) in the plane V−O3−C6−C11−C3−N1 of **5a**. Despite of the similarities between **5a** and **5b**, the only difference being the presence of a methoxy substituent on the aldehyde component in **5b**, the arrangement of the outer spheres of these complexes exhibits specific differences; Figure 3. While, in **5b**, the benzyl moiety stretches towards the periphery and the ethanolate is bent off the V=O group, the benzyl and ethoxide groups in **5a** are arranged so as to provide a large open cavity approximately 8.3 Å across.

Experimental Section

Starting materials were obtained from commercial sources [thiosemicarbazone, salicylaldehyde, 2-hydroxynaphthalenecarbaldehyde, *o*-vanillin, hydrazine hydrate (99−100%), and oxovanadium sulfate pentahydrate]. $[VOCl_2(thf)_2]$ was prepared according to a literature procedure.[55]

Physical Measurements: IR spectra were obtained as KBr pellets with a Perkin−Elmer spectrometer 1720 FT. − NMR spectra were recorded with a Bruker AM 360 or Varian Gemini 200 BB spectrometer with the usual spectrometer settings. All $\delta(^{51}V)$ values are referenced against $VOCl_3$. − EPR spectra were measured with a Bruker ESP 300E spectrometer at 9.74 GHz in 1−5 mM solutions. ^1H and ^{51}V NMR, EPR, and selected IR data for the complexes are collated in Table 1 and Table 2 in the Discussion. − X-ray structure analyses were carried out in the θ/2θ scan mode with an Enraf−Nonius CAD4 diffractometer with monochromated (graphite monochromator) Cu-K_α irradiation (λ = 1.54178 Å). The hydrogen atoms on N2 and N3 of **3a**·$OCMe_2$ were located; all other hydrogen atoms were placed into calculated positions and included with isotropic displacement factors in the last cycles of the structure refinements. The program packages SHELXS 86[56] and SHELXL 93[57] were used throughout. Absorption corrections (DIFABS) were carried out. Crystal data and data for the structure solutions and refinements are collated in Table 4. Crystallographic data (excluding structure factors) for the structures reported in this

Table 4. Structure and refinement parameters

	3a·OCMe$_2$	**5a**	**5b**
Empirical formula	$C_{15}H_{16}ClN_3O_3SV$	$C_{17}H_{17}N_2O_3S_2V$	$C_{18}H_{19}N_2O_4S_2V$
Molecular mass [g mol^{-1}]	404.76	412.39	442.41
Temperature [K]	173(2)	293(2)	173(2)
Crystal system	monoclinic	triclinic	triclinic
Space group	$P2_1/c$	$P\bar{1}$	$P\bar{1}$
a [Å]	7.7413(17)	10.069(2)	8.319(12)
b [Å]	13.219(2)	10.170(4)	10.515(4)
c [Å]	17.044(4)	10.241(4)	12.244(13)
α [°]		90.87(3)	72.51(7)
β [°]	98.28(2)	115.56(3)	71.02(11)
γ [°		107.63(3)	81.30(6)
Cell volume [Å^3]	1725.9(7)	888.6(3)	964.3(18)
Z	**4**	**2**	**2**
Density (calcd.) [g cm^{-3}]	1.558	1.541	1.524
Absorption coeff. [mm^{-1}]	7.53	7.03	6.56
F(000)	828	424	456
Crystal size [mm]	0.6 × 0.3 ×0.2	1.1 × 0.3 ×0.1	0.9 × 0.25 × 0.1
θ range [°]	4.25−76.32	4.63−76.39	5.08−76.36
Index ranges	$-9 < h < 3$	$-11 < h < 12$	$0 < h < 10$
	$0 < k < 16$	$-12 < k < 12$	$-13 < k < 13$
	$-21 < l < 21$	$-12 < l < 5$	$-14 < l < 15$
Reflections collected	3937	3986	4387
Unique reflections	3626	3727	4046
R(int)	0.0307	0.0324	0.0366
Number of param.	233	295	247
R indices, $I > 2\sigma(I_0)$:			
$R1$, $wR2$	0.0561, 0.1446	0.0809, 0.2125	0.0805, 0.2226
R indices, all data	0.0650, 0.1577	0.0913, 0.2259	0.1378, 0.2606
$R1$, $wR2$			
Diff. peak/hole [e Å^{-3}]	1.205/−1.224	1.772/−1.040	0.680/−0.525

paper have been deposited with the Cambridge Crystallographic Data Centre as supplementary publication no. CCDC-152692 (**5b**), -152693 (**5a**) and -152694 (**3a**·OCMe$_2$). Copies of the data can be obtained free of charge on application to CCDC, 12 Union Road, Cambridge CB2 1EZ, UK [Fax: int. code + 44-1223/336-033; E-mail: deposit@ccdc.cam.ac.uk].

2-Hydroxynaphthalene-1-carbaldehyde Thiosemicarbazone (H1a), and 6-Methoxysalicylaldehyde Thiosemicarbazone (H1b): These ligands were synthesised in analogy to the procedure of Poruhit et al.[58] For the preparation of H**1a**, a hot solution of thiosemicarbazone (2.25 g, 25 mmol) in 20 mL of ethanol was treated with 2-hydroxynaphthalenecarbaldehyde (4.31 g, 25 mmol) in 20 mL of ethanol, and the mixture was gently heated under reflux for 4 h. It was then cooled down to room temp., the precipitate collected by filtration, washed with ethanol and dried in vacuo. Yield 3.44 g (60%). − $C_{12}H_{12}N_3OS$ (246.31): calcd. C 58.76, H 4.52, N 17.14; found C 58.44, H 4.63, N 17.09. − H**1b** was obtained with a yield of 7.14 g (74%) in an analogous manner from thiosemicarbazone (4.50 g, 50 mL, dissolved in 20 mL of ethanol) and *o*-vanillin (7.60 g, 50 mmol, dissolved in 10 mL of ethanol) after 2 h of heating under reflux. − $C_9H_{11}N_3O_2S$ (225.27): calcd. C 47.99, H 4.90, N 18.66; found C 47.60, H 5.22, N 18.21. − ^{1}H NMR: δ (THF) [multiplicity, J Hz] = 10.71 and 10.57 (NH, NH$_2$); 9.03 (N=CH); 8.15 [d, 8.5], 7.807 [d, 9.0] and 7.79 [dd, 6.8], 7.51 [tt, 7.7 and 1.3], 7.37 [tt, 7.1], 7.14 [d, 9.0] (aromatic H).

Salicylaldehyde- and 6-Methoxysalicylaldehyde [(Benzylmercapto)-thiocarbonyl]hydrazone ($H_2$2a and $H_2$2b): The ligands were prepared by condensation of benzylmercaptothiocarbonylhydrazine (benzyl dithiacarbazate) and salicylaldehyde or *o*-vanillin.[59] Benzylmercaptothiocarbonylhydrazine (3.97 g, 20 mmol) and salicylaldehyde/vanillin (2.0 mL/3.05 g, 20 mmol), dissolved in 100/150 mL of ethanol, were heated under reflux for 90 min. The ligands separated in the form of pale yellow crystals on cooling the solution to room temp. Yield for H_2**2a**/H_2**2b** after recrystallisation from ethanol: 4.65/4.31 g (75/65%). The precursor benzylmercaptothiocarbonylhydrazine was prepared as follows: KOH (22.9 g) was dissolved in 140 mL of 90% ethanol and treated with 20 mL of hydrazine hydrate. The mixture was cooled in an ice bath to 8−10 °C, and 25 mL of CS_2 was added dropwise with stirring. The orange-yellow oil that formed was separated with a separating funnel and redissolved in 120 mL of precooled 40% ethanol, and the solution placed in an ice bath. Benzoyl chloride (50 mL) was then added with vigorous stirring. The ester separated as a white solid, which was filtered off and recrystallised from toluene and ethanol to yield 11.11 g of dry product. Additional 4.46 g of the compound was obtained by adding water to the filtrate and workup of the resulting precipitate. Overall yield 19%.

[VOCl(1a)] (3a) and [VOCl(1b)] (3b). − 3a: To a stirred solution of H**1a** (0.25 g, 1.0 mmol) in 20 mL of THF was added [$VOCl_2$(thf)$_2$] (0.28 g, 1.0 mmol) in 15 mL of THF. The resulting green solution was stirred at room temp. for 2 h. The green compound that separated was filtered off, washed with THF and then with *n*-pentane, and dried in vacuo. Yield 0.19 g (50%). − Analysis for **3a**·$^3/_4$THF: $C_{12}H_{10}ClN_3O_2SV\cdot{}^3/_4$THF (400.76): calcd. C 44.96, H 4.02, N 10.48, V, 12.71; found C 44.74, H 4.26, N 10.32, V 12.68. − IR (KBr): $\tilde{\nu}$/cm^{-1} = 3131, (NH), 1618 (C=N), 1541 (NH), 995 (V=O). −Crystals of **3a**·acetone suitable for the X-ray analysis were obtained by allowing an acetone solution of **3a** to slowly concentrate at room temperature. − **3b** was prepared in an analogous manner to **3a** from [$VOCl_2$(thf)$_2$] (0.28 g, 1.0 mmol) and H**1b** (0.23 g, 1.0 mmol) with a yield of 0.24 g (70%). − $C_9H_{10}ClN_3O_3SV\cdot{}^1/_2$THF·$^1/_2H_2O$ (371.70): calcd. C 35.53, H 4.07, N 11.30; found C 35.38, H 4.06, N 11.14. − IR (KBr): $\tilde{\nu}$/cm^{-1} = 3186 (NH), 1605 (C=N), ca. 980 (V=O).

[VO(2a)]·EtOH (4a·EtOH): The hydrazone H_2**2a** (0.79 g, 2.61 mmol), vanadyl sulfate (0.66 g, 2.61 mmol) and sodium acet-

ate trihydrate (0.71 g, 5.2 mmol) were dissolved in 60 mL of ethanol and stirred under N_2 over night. The green solution was then treated dropwise with 150 mL of N_2-saturated water. A green precipitate of **4a**·EtOH formed, which was filtered off, washed with water and pentane, and dried in vacuo. Yield 0.75 g (70%). − $C_{17}H_{18}N_2O_3S_2V$ (413.40): calcd. C 49.39, H 4.39, N 6.78; found C 49.43, H 4.59, N 6.74. − IR (KBr): $\tilde{\nu}/cm^{-1}$ = 3057/3026 (ArH), 2972 (CH_2), 1625, 1603/1588 (HC=N), 1546 (Ph−C=N), 1280, 1029, 985/967 (V=O), 823, 754, 698 [δ(CH)], 631, 567, 519, 459.

[VO(2a)]·$^1/_4H_2O$ (4a·$^1/_4H_2O$): To a suspension of H_2**2a** (0.76 g, 2.5 mmol) and sodium acetate trihydrate (0.68 g 5 mmol) in 60 mL of ethanol was added (under N_2) dropwise within 5 min a solution of oxovanadium sulfate pentahydrate (0.64 g (2.5 mmol) in 30 mL of water, and the mixture stirred at room temp. until all of the H_2**2a** had been taken up by the green solution (ca. 90 min). Water (90 mL) was added dropwise to precipitate **4a** as a microcrystalline product, which was filtered off, washed thoroughly with water followed by a few mL of pentane, and dried in vacuo. According to the elemental analysis, the green product contained $^1/_4$ mol percent of water. − $C_{15}H_{12}N_2O_2S_2V·^1/_4H_2O$ (371.84): calcd. C 48.45, H 3.39, N 7.53; found C 48.52, H 3.50, N 7.58. − The IR shows essentially the same features as that of **4a·EtOH**.

[VO(2b)]·H_2O (4b·H_2O): The hydrazone H_2**2b** (1.66 g, 5.0 mmol), vanadyl sulfate (1.28 g, 5 mmol), and sodium acetate trihydrate (1.37 g, 10.0 mmol) were dissolved in 50 mL of ethanol and stirred under N_2 overnight. The solution initially turned orange-brown, and a brown precipitate formed. (In more dilute solutions, the amount of precipitate that formed decreased, and the solution exhibited a brown-green colour.) To this suspension, 100 mL of water, degassed and saturated with N_2, was added dropwise and with stirring. The precipitate turned green; it was filtered off, washed with water and pentane, and dried in vacuo. Yield 1.40 g (69%). − $C_{16}H_{16}N_2O_4S_2V$ (415.38): calcd. C 46.27, H 3.88, N 6.74; found C 46.65, H 3.76, N 6.77. − IR (KBr): $\tilde{\nu}/cm^{-1}$ = 3084, 3061, 3030 (ArH), 2848 (OMe), 1602/1686 (HC=N), 1553 (Ph−C=N), 1299, 1255, 1110, 991/977 (V=O), 768, 735, 693, 606, 515.

[VO(OEt)2a] (5a), and [VO(OEt)2b] (5b): Complex **4a**·EtOH or **4b**·H_2O was heated under reflux in ethanol for 3−4 h (no inert gas). The brown to dusky brown products were separated and dried in vacuo. − **5a**: $C_{17}H_{18}N_2O_3S_2V$ (413.40): calcd. C 49.39, H 4.39, N 6.78; found C 49.43, H 4.59, N 6.74. − IR (KBr): $\tilde{\nu}/cm^{-1}$ = 3023 (ArH), 2974, 2922, 2860 (CH_2), 1602/1590 (HC=N), 1550 (Ph−C=N), 1275, 1028, 1004, 984/962 (V=O), 914, 909, 834, 765, 696 [δ(CH)], 645, 537, 519, 459. − **5b**: $C_{18}H_{19}N_2O_4S_2V$ (442.42): calcd. C 48.87, H 4.33, N 6.33; found C 45.99, H 4.14, N 6.45. − IR (KBr): $\tilde{\nu}/cm^{-1}$ = 3028 (ArH), 2983, 2934, 2832 (CH_2), 1600/1589 (HC=N), 1555 (Ph−C=N), 1285, 1257, 1227, 1108, 985/976 (V=O), 969, 776, 738, 699, 605, 447. − Black-brown rhombohedral crystals of **5a** and **5b** suitable for an X-ray diffraction analysis were obtained by allowing hot ethanol solutions to slowly cool down to room temperature.

Acknowledgments

This work was supported by the Deutsche Forschungsgemeinschaft (grant Re 431/13−3), the Fonds der Chemischen Industrie, the Deutsche Akademische Austauschdienst (stipend for S. K. S. H.), and a fellowship donated by the P. R. China (D. W.). We thank Prof. T. Kabanos, University of Ioannina, for his support in interpreting the EPR spectra.

[1] *Vanadium Compounds, Chemistry, Biochemistry and Therapeutic Applications* (Eds.: A. S. Tracey, D. C. Crans), ACS Symp. Ser. 711, **1998**.
[2] *J. Inorg. Biochem.* **2000**, *80* (Special Issue on Biological Aspects of Vanadium; Guest Eds.: D. Rehder, V. Conte).
[3] *Vanadium and Its Role in Life* (vol. *31* of *Metal Ions in Biological Systems*; Eds.: H. Sigel, A. Sigel), Marcel Dekker, New York, **1995**.
[4] D. Rehder, *Coord. Chem. Rev.* **1999**, *182*, 297.
[5] *Vanadium in the Environment* (Ed.: J. O. Nriagu), Wiley, New York, **1998**.
[6] T. Hirao, *Chem. Rev.* **1997**, *97*, 2707.
[7] J. W. C. E. Arends, M. Pellizon, R. A. Sheldon, *Stud. Surf. Sci. Catal.* **1997**, *110*, 1031.
[8] K. H. Thompson, J. H. McNeill, C. Orvig, *Chem. Rev.* **1999**, *99*, 2561.
[9] Y. Shechter, J. Li, J. Meyerovitch, D. Gefel, R. Bruck, G. Elberg, D. S. Miller, A. Shisheva, *Mol. Cell Biochem.* **1995**, *153*, 39.
[10] H. V. Strout, P. P. Vicario, R. Saperstein, E. E. Slater, *Endocrinology* **1989**, *124*, 1918.
[11] S. W. Taylor, B. Kammerer, E. Bayer, *Chem. Rev.* **1997**, *97*, 333.
[12] M. Weyand, H.-J. Hecht, M. Kieß, M.-F. Liaud, H. Vilter, D. Schomburg, *J. Mol. Biol.* **1999**, *293*, 595.
[13] A. Messerschmidt, L. Prade, R. Wever, *Biol. Chem.* **1997**, *378*, 309.
[14] S. Macedo-Ribeiro, W. Hemrika, R. Renirie, R. Wever, A. Messerschmidt, *J. Biol. Inorg. Chem.* **1999**, *4*, 209.
[15] R. R. Eady, *Chem. Rev.* **1996**, *96*, 3013.
[16] M. Zhang, M. Zhou, R. L. van Etten, C. V. Stauffacher, *Biochemistry* **1997**, *36*, 15.
[17] J. E. Banabe, L. A. Echegoyen, B. Pastrona, M. Martinez-Maldonado, *J. Biol. Chem.* **1987**, *262*, 9555.
[18] W. Tsagkalidis, D. Rehder, *J. Biol. Inorg. Chem.* **1996**, *1*, 507.
[19] W. Tsagkalidis, D. Rodewald, D. Rehder, *Inorg. Chem.* **1995**, *34*, 1943.
[20] H. B. ten Brink, A. Tuynman, H. L. Dekker, W. Hemrika, Y. Izumi, T. Oshiro, H. E. Shoemaker, R. Wever, *Inorg. Chem.* **1998**, *37*, 6780.
[21] M. A. Andersson, S. G. Allenmark, *Tetrahedron* **1998**, *54*, 15293.
[22] H. Schmidt, M. Bashirpoor, D. Rehder, *J. Chem. Soc., Dalton Trans.* **1996**, 3865.
[23] C. Bolm, F. Bienewald, *Angew. Chem. Int. Ed. Engl.* **1995**, *34*, 2883.
[24] K. Nakajima, K. Kojima, J. Fujita, *Bull. Chem. Soc. Jpn.* **1990**, *63*, 2620.
[25] D. C. Crans, C. M. Simone, *Biochemistry* **1991**, *30*, 6734.
[26] C. R. Cornman, T. C. Stauffer, P. D. Boyle, *J. Am. Chem. Soc.* **1997**, *119*, 5986.
[27] A. J. Tasiopoulos, A. T. Vlahos, A. D. Keramidas, T. A. Kabanos, Y. G. Deligiannakis, C. P. Raptopoulos, A. Terzis, *Angew. Chem. Int. Ed. Engl.* **1996**, *35*, 2531.
[28] S. C. Sendlinger, J. R. Nicholson, E. B. Lobkovsky, J. C. Huffman, D. Rehder, G. Christou, *Inorg. Chem.* **1993**, *32*, 204.
[29] K. K. Nanda, E. Sinn, A. W. Addison, *Inorg. Chem.* **1996**, *35*, 2.
[30] S. C. Davies, D. L. Hughes, Z. Janas, L. B. Jerzykiewicz, R. L. Richards, J. R. Sanders, J. E. Silverston, P. Sobota, *Inorg. Chem.* **2000**, *39*, 3485.
[31] H. Sakurai, H. Watanabe, H. Tamura, H. Yasui, R. Matsushita, J. Takada, *Inorg. Chim. Acta* **1998**, *283*, 175.
[32] D. X. West, S. B. Padhye, P. B. Sonawane, R. C. Chikate, *Asian J. Chem. Rev.* **1990**, *1*, 125.
[33] M. E. Hossain, M. N. Alam, M. A. Ali, M. Nazimuddin, F. E. Smith, R. C. Hynes, *Polyhedron* **1996**, *15*, 973.
[34] W. Bansse, E. Ludwig, E. Uhlemann, F. Weller, K. Dehnicke, W. Herrmann, *Z. Anorg. Allg. Chem.* **1992**, *613*, 36.
[35] C. Weidemann, W. Priebsch, D. Rehder, *Chem. Ber.* **1989**, *122*, 235.
[36] D. Rehder, in: *Transition Metal NMR* (vol. *13* of *Studies in Inorganic Chemistry*; Ed.: P. S. Pregosin), Elsevier, Amsterdam, **1991**, p. 1.
[37] D. Rehder, C. Weidemann, A. Duch, W. Priebsch, *Inorg. Chem.* **1988**, *27*, 584.

[38] A. J. Tasiopoulos, A. N. Troganis, A. Evangelou, C. R. Raptopoulou, A. Terzis, Y. Deligiannakis, T. A. Kabanos, *Chem. Eur. J.* **1999**, *5*, 910.
[39] M. E. Hossain, M. N. Alam, M. A. Ali, M. Nazimuddin, F. E. Smith, R. C. Hynes, *Polyhedron* **1996**, *15*, 973.
[40] G. R. Hanson, Y. Sun, C. Orvig, *Inorg. Chem.* **1996**, *35*, 6507.
[41] D. X. West, Y. Yang, T. L. Klein, K. I. Goldberg, A. E. Liberta, J. Valdes-Martinez, R. A. Toscano, *Polyhedron* **1995**, *14*, 1681.
[42] Z. Lu, C. White, A. L. Rheingold, R. H. Crabtree, *Inorg. Chem.* **1993**, *32*, 3991.
[43] P. Souza, A. I. Matesanz, V. Fernandez, *J. Chem. Soc., Dalton Trans.* **1996**, 3011.
[44] J. Valdez-Martinez, R. A. Toscano, A. Zentella-Dehesa, M. M. Salberg, G. A. Brain, D. X. West, *Polyhedron* **1996**, *15*, 427.
[45] M Soriano-Garcia, J. Valdés-Martínez, R. A. Toscano, J. Gómez-Lara, *Acta Crystallogr. C* **1985**, *41*, 500.
[46] G. Argay, A. Kálmán, V. M. Leovac, V. I. Cesljevic, B. Ríbar, *J. Coord. Chem.* **1996**, *37*, 165.
[47] M. Farahbakhsh, H. Nekola, H. Schmidt, D. Rehder, *Chem. Ber./Recueil* **1997**, *130*, 1129.
[48] P. R. Klich, A. T. Daniher, P. R. Challen, D. B. McConville, W. J. Youngs, *Inorg. Chem.* **1996**, *35*, 347.
[49] H. Maeda, K. Kanamori, H. Michibata, T. Tonno, K. Okamoto, J. Hidaka, *Bull. Chem. Soc. Jpn.* **1993**, *66*, 790.
[50] N. V. Gerbeleu, I. F. Burshtein, G. A. Kiosse, I. G. Filippova, O. A. Bologa, V. I. Lozan, T. I. Malinovskii, *Dokl. Akad. Nauk SSSR* **1985**, *284*, 155.
[51] H. Schmidt, D. Rehder, *Inorg. Chim. Acta* **1998**, *267*, 229.
[52] V. Vergopoulos, S. Jantzen, N. Julien, E. Rose, D. Rehder, *Z. Naturforsch. B* **1994**, *49*, 1127.
[53] D. Rehder, C. Schulzke, H. Dau, C. Meinke, J. Hanss, M. Epple, *J. Inorg. Biochem.* **2000**, *80*, 115, and literature cited therein.
[54] M. Bashirpoor, H. Schmidt, C. Schulzke, D. Rehder, *Chem. Ber./Recueil* **1997**, *130*, 651.
[55] H. Tietz, K. Schmetlick, G. Kreisel, *Z. Chem.* **1985**, *25*, 290.
[56] G. M. Sheldrick, *SHELXS 86*, University of Göttingen, **1986**.
[57] G. M. Sheldrick, *SHELXL 93*, University of Göttingen, **1993**.
[58] S. Purohit, A. P. Koley, L. S. Prasad, P. T. Manoharan, S. Ghosh, *Inorg. Chem.* **1989**, *28*, 3735.
[59] M. Busch, M. Starke, *J. Prakt. Chem.* **1916**, *93*, 59.

Received September 13, 2000
[I00344]

The Complexation Behaviour of Crown Ethers with Some Divalent Transition Metal and Silver Ions in a 40%(v/v) Ethanol + Water Medium

Vijaykumar S. Ijeri[a] and Ashwini K. Srivastava*[a]

Keywords: Crown compounds / Transition metals / Electrochemistry / Stability constants / Silver

The stability constants in 40%(v/v) ethanol + water mixture were evaluated for complexes of Ni^{II}, Co^{II}, Cu^{II}, Zn^{II}, Mn^{II} and Ag^{I} with the macrocyclic polyethers 15-crown-5, benzo-15-crown-5, 18-crown-6 and dicyclohexano-18-crown-6 by conductometric titrations. In addition, a potentiometric study of the Cu^{II} and Ag^{I} complexes was undertaken to compare the results with those obtained by conductivity measurements. The complexation studies indicate 1:1 complex formation between the metal ion and crown ether and the log $K_{ML^{n+}}$ values are in the range 1.0–3.0. The limiting molar conductivities of the metal ions and their crown ether complexes were also determined.

Introduction

The complexation of alkali cations by neutral molecules was quite uncommon till the discovery of crown ethers by Pedersen,[1] who prepared and studied several crown ether complexes of alkali and alkaline earth metal ions.[2,3] Until now the complexation behaviour of alkali and alkaline earth metal ions with crown ethers has been extensively studied[4−8] in various solvents. The complexation of transition metal ions has been studied mainly with respect to aza and thia crown ethers,[4,8−12] as they are softer ligands. Little attention, however, has been given to the complexation behaviour of transition metal ions with oxygen-containing crown ethers.[7,13−16]

The object of the present work was to study the complexation behaviour of Ni^{II}, Co^{II}, Cu^{II}, Zn^{II}, Mn^{II} and Ag^{I} perchlorates with 15-crown-5 (15C5), benzo-15-crown-5 (B15C5), 18-crown-6 (18C6) and dicyclohexano-18-crown-6 (DCH18C6) in a 40%(v/v) ethanol + water medium by conductometry. The complexation of Cu^{II} and Ag^{I} has been studied by potentiometry as well in order to compare these results with those obtained by conductometric measurements. Aqueous alcohol is widely used as a physiological substrate. Also, as this particular composition ensured the solubility of B15C5 and DCH18C6, and, interestingly, lies on the maxima of the viscosity curve of ethanol + water mixtures, it was chosen for the present study.

Theory

The conductance data of the divalent metal perchlorates were treated by the Fuoss and Edelson method as used in previous studies.[6] The method consists of evaluating the limiting equivalent conductance (Λ_0) and the first step association constant (K_A) of an electrolyte MX_2 in 40% ethanol + water based on the following equilibrium:

$$M^{2+} + ClO_4^- \overset{K_A}{\rightleftharpoons} MClO_4^+ \quad (1)$$

where M = Ni, Co, Cu, Zn, Mn. The equilibrium leading to the neutral species $M(ClO_4)_2$ is neglected in this method.

The treatment of conductance data for silver perchlorate was done by using the Shedlovsky function.[17] The equations[6,7,18] used for the calculation of the stability constants are described briefly in the following sections.

Conductometric Study of Crown Ether Complexation with Metal Perchlorates

The complexation of a metal ion (M) with a crown ether (L) may be represented as:

$$\begin{array}{ccccc} M^{n+} & + & L & \rightleftharpoons & ML^{n+} \\ \alpha[M]_t & & [L]_t - (1-\alpha)[M]_t & & (1-\alpha)[M]_t \end{array} \quad (2)$$

where $[M]_t$, $[L]_t$ and α are the total concentration of cation, the total concentration of crown ether and the fraction of uncomplexed cation, respectively. Accordingly the thermodynamic stability constant $K'_{ML^{n+}}$ is given by:

$$K'_{ML^{n+}} = [ML]\cdot f_{ML^{n+}}/[M]\cdot f_{M^{n+}}[L]\cdot f_L \quad (3)$$

Where [ML], [M] and [L] are the concentrations of complexed cation, uncomplexed cation and uncomplexed crown ether, respectively, and $f_{ML^{n+}}$, $f_{M^{n+}}$ and f_L are the corresponding activity coefficients. The concentration stability constant $K_{ML^{n+}}$, which is reported, since $f_{ML^{n+}}$ and $f_{M^{n+}}$ are unknown, is given by:

$$K_{ML^{n+}} = K'_{ML^{n+}}\cdot f_{M^{n+}}/f_{ML^{n+}} = [ML]/[M][L] = (1-\alpha)/\alpha[L] \quad (4)$$

The conductivity (κ) of a solution containing metal perchlorate and crown ether is written as:

$$\kappa = \kappa_{MClO_4} + \kappa_{MClO_4} \quad (5)$$

[a] Department of Chemistry, University of Mumbai, Vidyanagari, Santacruz (E),
Mumbai − 400098, Maharashtra, India
Fax: (internat.) +91-022/652-8547
E-mail: aks@chem.mu.ac.in
akschbu@yahoo.com

 © WILEY-VCH Verlag GmbH, 69451 Weinheim, 2001 1434−1948/01/0404−0943 $ 17.50+.50/0

where κ_{MClO_4} and κ_{MClO_4} are the conductivities of metal perchlorate and metal crown ether perchlorate, respectively. The respective molar conductivities are given by:

$$\Lambda_{MClO_4} = \kappa_{MClO_4}/[M] = \kappa_{MLClO_4}/\alpha[M]_t \quad (6)$$

and

$$\Lambda_{MLClO_4} = \kappa_{MLClO_4}/[ML] = \kappa_{MLClO_4}/(1 - \alpha)[M]_t \quad (7)$$

Equation (5) may be written in terms of molar conductance (Λ) by considering the total concentration $[M]_t$ from Equation (6) and (7), to give:

$$\Lambda = \kappa/[M]_t = \alpha\Lambda_{MClO_4} + (1 - \alpha)\Lambda_{MLClO_4} \quad (8)$$

The correction for the viscosity changes is neglected, as the crown ether concentration was kept low. From Equation (4) and (8) one obtains:

$$K_{ML^{n+}} = (\Lambda_{MClO_4} - \Lambda)/(\{\Lambda - \Lambda_{MLClO_4}\}[L]) \quad (9)$$

where $[L] = [L]_t - \{[[M]_t \cdot (\Lambda_{MClO_4} - \Lambda)]/(\Lambda_{MClO_4} - \Lambda_{MLClO_4})\}$. The Λ_{MLClO_4} value is estimated from the Λ values at the point of a large $[L]_t$-to-$[M]_t$ ratio. With this value of Λ_{MLClO_4}, the $K_{ML^{n+}}$ value in Equation (9) can be calculated.

The procedure for obtaining the limiting ionic conductivity is as follows. From the principle of mass balance, the total concentration can be written as:

$$[M]_t = [M] + [ML] \quad (10)$$

$$[L]_t = [L] + [ML] \quad (11)$$

Combining Equation (4) with Equation (10) and (11), the following quadratic equation is obtained:

$$K_{ML^{n+}} \cdot [ML]^2 - \{1 - K_{ML^{n+}}([M]_t + [L]_t)\}[ML] + K_{ML^{n+}} \cdot [M]_t[L]_t = 0 \quad (12)$$

The [M] value is obtained from Equation (10) using the [ML] value calculated from Equation (12) at a particular concentration of metal perchlorate $[M]_t$ and crown ether $[L]_t$. The κ_{MClO_4} value in Equation (5) at this [M] point can be obtained from the Λ_{MClO_4} vs. $[MClO_4]^{1/2}$ plot. Then, the Λ_{MLClO_4} value at the corresponding [ML] point can be calculated from Equation (5) and (7) using this κ_{MClO_4} value and organised in the form of a Λ_{MLClO_4} vs. $[MClO_4]^{1/2}$ plot. The limiting molar conductance (Λ_0) of the metal−crown ether perchlorate is determined by extrapolation of the plot generated in the above manner. The limiting ionic conductance ($\lambda^0_{ML^{n+}}$) value of the metal−crown ether complex is obtained by using the value $\lambda^0_{ClO_4^-} = 26.8$ S cm^2 mol^{-1}. This value was obtained indirectly from the limiting molar conductivities of $AgClO_4$, $AgNO_3$, KCl and KNO_3.

Potentiometric Study of Crown Ether Complexation with Silver and Copper Perchlorates

The stability constant ($K_{ML^{n+}}$) for Ag^I with crown ether, from Equation (2) and (4), is given by:

$$K_{ML^{n+}} = (1 - \alpha)/(\alpha\{[L]_t - [M]_t(1 - \alpha)\}) \quad (13)$$

The determination of α is based on the measurement of the emf of the cell:

Ag/AgCl reference electrode // $AgClO_4$ + L /Ag in 40% ethanol + water

The conductance and potentiometric studies on $AgClO_4$ in 40% ethanol + water show that it is completely dissociated and the silver electrode behaves linearly over the range 1×10^{-1} M − 1×10^{-5} M. Therefore, the difference (ΔV) between the emf of the salt solution and that of the salt + crown ether solution can be taken to reflect the concentration ratios. The Nernst equation is used to give the following relation:

$$\alpha = 10^{-\Delta V/59.16mV} \quad (14)$$

Putting this value of α in Equation (13), $K_{ML^{n+}}$ is obtained.

Equation (15) was used to determine α for Cu^{II}:

$$\alpha = 10^{-\Delta V/29.58\ mV} \quad (15)$$

Results and Discussion

On treatment of the conductance data of the divalent metal perchlorates and silver perchlorate with the Fuoss−Edelsen and Shedlovsky equations, respectively, it was found that none of them showed any association in this solvent mixture. Similar observations were made by earlier workers[17,19] i.e. measurable association was found in cases where the ethanol percentage was greater than about 45% (v/v) for salts like potassium picrate, potassium chloride, cesium chloride, lithium chloride, etc. The values of the limiting molar conductivities, $\lambda^0_{M^{n+}}$ of the metal ions derived from the Fuoss−Edelson and Shedlovsky plots are given in Table 1 along with the limiting molar conductivities of the complexes.

Table 1. Limiting molar conductivities of M^{n+} and ML^{n+}

$\lambda^0_{M^{n+}}$/S cm^2 mol^{-1}		$\lambda^0_{ML^{n+}}$/S cm^2 mol^{-1}			
Metal ion	Solvated metal ion	15C5	B15C5	18C6	DCH18C6
Ni^{II}	50.8	80.7	86.2	82.6	86.4
Co^{II}	46.1	49.1	47.4	48.2	48.2
Cu^{II}	54.7	57.7	56.7	65.1	63.5
Zn^{II}	47.0	74.6	49.0	65.6	70.5
Mn^{II}	41.0	42.8	43.0	44.6	46.2
Ag^{I}	28.7	24.4	23.5	22.8	18.0

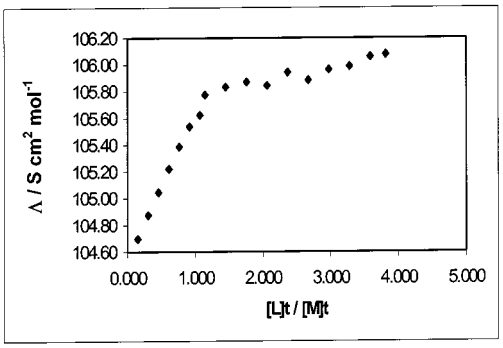

Figure 1. Plot of Λ vs. $[L]_t/[M]_t$ for 15C5−$Cu(ClO_4)_2$ system

Figure 1 and 2 show plots of Λ vs. $[L]_t/[M]_t$ for Cu^{II} and Ag^{I} with 15-crown-5, respectively, and they are representative of other metal ions and crown ethers.

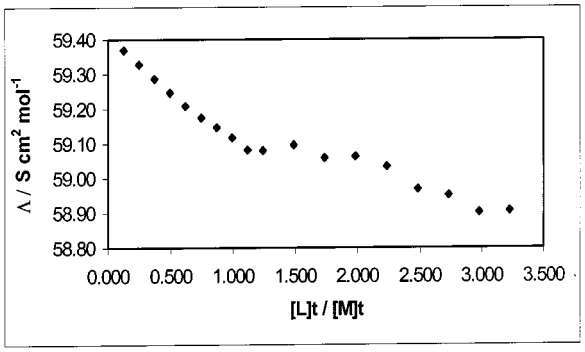

Figure 2. Plot of Λ vs. $[L]_t/[M]_t$ for 15C5−$AgClO_4$ system

It was observed that the Λ value increases with an increase in the $[L]_t/[M]_t$ ratio for all the systems involving the divalent transition metal ions, whereas a decrease in Λ values was observed in systems involving silver ions. This can be explained on the basis of the solvation sphere. The divalent transition metal ions have a high charge-to-radius ratio, on account of which they are highly solvated. On complexation, however, the crown ether molecule replaces the solvation sheath around the metal ion and, as a result, the moving entity becomes less bulky and more mobile. The silver ion, on the other hand, is relatively large and has a lower charge-to-radius ratio; hence it is solvated to a lesser extent. When complexed with crown ether it becomes bulkier causing a decrease in its mobility and also in the Λ values. The curves show a break point at $[L]_t/[M]_t \approx 1$, which indicates the formation of 1:1 complexes between the crown ethers and the metal ions. In the case of Ag-15C5 and Ag-B15C5 a slight break is also observed at $[L]_t/[M]_t \approx 2$, which hints at the formation of 2:1 sandwich complexes. However, in this paper we are confining our discussions to 1:1 complexes.

The values of the stability constants as log $K_{ML^{n+}}$ for the divalent metal ions (arranged in the order of increasing ionic radii) and silver complexes, obtained by conductometry and potentiometry, are given in Table 2 and 3, respectively.

Table 2. Stability constants (log $K_{ML^{n+}}$) for the metal ion−crown ether complexes by conductometry; figures in brackets indicate standard deviations ($6 \leq n \leq 9$)

Metal ion	15C5[a]	B15C5[a]	18C6[a]	DCH18C6[a]
Ni^{II}	1.95 (0.05)	2.01 (0.05)	1.65 (0.03)	1.74 (0.03)
Co^{II}	1.90 (0.08)	2.01 (0.06)	1.80 (0.06)	1.82 (0.09)
Cu^{II}	2.10 (0.05)	2.33 (0.08)	1.88 (0.07)	1.95 (0.04)
Zn^{II}	1.82 (0.04)	2.01 (0.08)	1.59 (0.04)	1.60 (0.04)
Mn^{II}	1.97 (0.03)	1.98 (0.03)	2.76 (0.03)	2.88 (0.05)
Ag^{I}	1.35 (0.04)	1.16 (0.01)	2.06 (0.02)	1.89 (0.01)

[a] Log ($K_{ML^{n+}}$/mol dm^{-3}).

Table 3. Stability constants (log $K_{ML^{n+}}$) for the metal ion−crown ether complexes by potentiometry; figures in brackets indicate standard deviation ($6 \leq n \leq 9$)

Metal ion	15C5[a]	B15C5[a]	18C6[a]	DCH18C6[a]
Cu^{II}	2.04 (0.04)	2.32 (0.10)	1.85 (0.04)	1.95 (0.08)
Ag^{I}	1.37 (0.03)	1.15 (0.01)	2.07 (0.02)	1.87 (0.01)

[a] Log ($K_{ML^{n+}}$/mol dm^{-3}).

Among the divalent ions it is observed that copper happens to form more stable complexes, which may be explained on the basis of its larger size relative to the other ions. However, the lower stability of zinc complexes remains unexplained. Also, as there is not much difference in the ionic radii of the divalent metal ions studied, one cannot establish a clear relationship based on the cavity sizes and the ionic radii alone. Other factors such as extent of solvation, entropy changes, changes in the conformations, etc. also need to be considered. Among the crown ethers studied, it is observed that the substituent bearing crown ethers forms more stable complexes with the divalent ions. This may be due to the contraction of the cavity size, making it closer to the diameter of the ions. As a result, the most stable complexes are formed with B15C5, the order being B15C5 > 15C5 > DCH18C6 > 18C6. In the case of silver the opposite trend is observed, mainly because the diameter of the silver ion is much larger, the order being 18C6 > DCH18C6 > 15C5 > B15C5.

It is clear that the log $K_{ML^{n+}}$ values for copper and silver complexes in this medium are low relative to those in pure propylene carbonate (PC) and 20wt% propylene carbonate + ethylene carbonate (EC). For example, in PC log $K_{ML^{n+}}$ values for Ag−18C6 and Ag−DCH18C6 are 5.78 and 4.86, respectively,[6] and in 20wt% PC + EC they are 4.92 and 4.93, respectively.[7] The copper complexes in 20wt% PC + EC, with 15C5 and B15C5 show a log $K_{ML^{n+}}$ of 4.20 and 3.78, respectively.[7] This can be attributed to the strong solvating properties and hydrogen bonding capability of water and ethanol molecules. The hydrogen bonds of these molecules and the ether oxygen atoms decrease the complexing ability of crown ethers, whereas the log $K_{ML^{n+}}$ values for the divalent metal ions in 40% ethanol + water are nearly the same as those observed in methanol,[14] which has hydrogen bonds and a lower dielectric constant. The stability constants for Ag-B15C5 and Ag-18C6 complexes in a 90% (v/v) ethanol + water mixture[20] were found to be 3.47 and 3.58, respectively, whereas in pure ethanol[21] the values for Ag-15C5 and Ag-18C6 are 3.12 and 3.36, respectively. A comparison of these values shows the effect of hydrogen bonding. Water, being a strongly hydrogen bonding solvent, decreases the stability of the complexes, and as the percentage of water decreases, the stability increases. Similar observations were found in dioxane + water mixtures.[22] As the ratio of dioxane/water was increased from 2:8 (v/v) to 8:2 (v/v), the stability of the K-18C6 complex increased from 2.47 to 4.21. However, the transition metal complexes are less stable than the alkali metal complexes in

a similar medium (e.g. methanol)[8] and this can be explained on the basis of the "Hard and Soft, Acid-Base" (HSAB) concept.[12,23,24] The transition metal ions being soft acids would form stronger coordination bonds with sulfur/nitrogen-containing polyethers, which are softer bases than oxygen.

The limiting molar conductivities (Table 1) of the transition metal ion complexes do not show any particular trend, except that they are higher than those of the solvated ions, whereas in the case of silver complexes they are lower than those of the solvated ions.

Conclusion

The results obtained show that crown ethers form complexes with transition metal ions, although weak ones, in protic polar media and it is observed that the stabilities are not solely dependent on the ion/cavity sizes. The close agreement between the results obtained by conductometry and potentiometry is remarkable as it gives an accurate indication of the stabilities of the complexes.

Experimental Section

Solvents: Double distilled, deionised water was used for the preparation of all solutions. Triple distilled ethanol (over molecular sieves), containing less than 0.2% water (as determined by Karl Fischer titration), was used to prepare the ethanol-water mixtures. Both the solvents were stored in sealed containers to prevent atmospheric contamination. Appropriate volumes of ethanol and water were mixed to give the 40% (v/v) solvent mixture.

Reagents: Silver perchlorate was prepared as described in the literature[25] and standardized by titration against sodium chloride on a DL 53 autotitrator. The other metal perchlorates were prepared from their respective carbonates by the general methods described elsewhere[26] and were standardized by titration against EDTA on a DL 53 autotitrator. The crown ethers, 15-crown-5 (Fluka), benzo-15-crown-5 (Aldrich), 18-crown-6 (Aldrich) and dicyclohexano-18-crown-6 (Fluka) were used as received.

Apparatus: A Mettler Toledo DL53 autotitrator with automatic temperature compensation (ATC) was used for the standardization of metal salt solutions and potentiometric and conductivity measurements. The probes used were: silver electrode with Ag/AgCl reference electrode (DM 141-SC) and conductometric sensor (Inlab 710). An Elico, digital pH-mV meter (model LI-120) was used for emf measurements of cells involving Cu^{II}, in conjunction with a saturated calomel electrode (SCE).

Procedure for Conductometry: All measurements were done at 25 ± 0.1 °C, using a conductometric sensor Inlab 710 (with ATC), which was calibrated regularly with Mettler Toledo standard solutions. All molar conductivities were calculated after correcting for the solvent conductivity.

Method 1. Determination of K_A of the Transition Metal Perchlorates: Pure solvent mixture was placed in the cell and the conductance was measured. A step-by-step increase in the metal ion concentration was effected by means of the autotitrator. The conductivity was measured after each addition, followed by mixing, and the most stable reading over a span of 10 minutes was taken.

Method 2. Determination of $K_{ML^{n+}}$: The metal perchlorate solution ($\approx 1 \times 10^{-3}$ M) was placed in the cell and the conductivity was measured. The crown ether solution (≈0.02 M) was added to the cell in small increments until the total concentration of the crown ether was approximately 2−3 times as large as that of the metal perchlorate. The conductivity was measured after each addition as above.

Method 3. Determination of Λ_0 of $MLClO_4$: A crown ether solution ($\approx 2 \times 10^{-3}$ M) was placed in the cell and the conductance of the solution was measured. Then, a step-by-step increase in the concentration of metal perchlorate was effected as mentioned above until the concentration of metal perchlorate became approximately twice as large as that of the crown ether.

Procedure for Potentiometry: The silver indicator electrode (DM 141- SC) with an inbuilt Ag/AgCl reference element was used for all measurements involving Ag^{I} ions. As a general procedure, the emfs were recorded every 2 minutes. The potentials recorded were the average of the last two observations, which normally agreed to within ±0.1 mV; the measured cell potentials were reproducible to ±0.5 mV.

A pure copper wire (purity >99.95%) in conjunction with the SCE was used for measurement of emfs along with an Elico, digital pH-millivoltmeter. As a general procedure, the emfs were recorded every 2 minutes. The potentials recorded were the average of the last two observations, which normally agreed to within ±1 mV; the measured cell potentials were reproducible to ±3 mV.

Stock solutions of silver/copper perchlorates and crown ethers were prepared in a 40% ethanol + water mixture. The experimental solutions were prepared by appropriate dilution of the stock solutions to the required concentrations.

The dielectric constant and viscosity of 40%(v/v) ethanol + water were interpolated from previous data[17,27] using data fitting software (Numerical Methods Toolkit)[28] and were found to be 58.41 and 2.29 cP, respectively.

[1] C. J. Pedersen, *J. Am. Chem. Soc.* **1967**, *89*, 7017−7036.
[2] C. J. Pedersen, *J. Am. Chem. Soc.* **1970**, *92*, 386−391.
[3] C. J. Pedersen, *J. Am. Chem. Soc.* **1970**, *92*, 391−394.
[4] R. M. Izatt, K. Pawlak, J. S. Bradshaw, *Chem. Rev.* **1995**, *95*, 2529−2586.
[5] H. P. Hopkins Jr., A. B. Norman, *J. Phys. Chem.* **1980**, *84*, 309−314.
[6] A. K. Srivastava and B. Tiwari, *J. Electroanal. Chem.* **1992**, *325*, 301−311.
[7] R. A. Samant, Ph.D. Thesis, University of Mumbai, India, **1998**.
[8] R. M. Izatt, J. S. Bradshaw, S. A. Nielsen, J. D. Lamb, J. J. Christensen, D. Sen, *Chem. Rev.* **1985**, *85*, 271−339.
[9] L. S. W. L Sokol, L. A. Ochrymowycz, D. B. Rorabacher, *Inorg. Chem.* **1981**, *20*, 3189−3195.
[10] M. Kodama, E. Kimura, *J. Chem. Soc., Dalton Trans.* **1980**, 2536−2538.
[11] H. J. Buschmann, *Inorg. Chim. Acta* **1985**, *108*, 241−245.
[12] D. Siswanta, K. Nagatsuka, H. Yamada, K. Kumakura, H. Hisamoto, Y. Shichi, K. Toshima, K. Suzuki, *Anal. Chem.* **1996**, *68*, 4166−4172.

[13] M. D. Hampton, C. A. Peters, L. A. Wellington, *Anal. Chim. Acta* **1987**, *194*, 171−176.
[14] L. Chen, M. Bos, P. D. J. Grootenhuis, A. Christenhusz, E. Hoogendam, D. N. Reinhoudt, W. E. Van der Linden, *Anal. Chim. Acta* **1987**, *201*, 117−125.
[15] S. M. Khalifa, H. F. Aly, J. D. Navratil, *Talanta* **1989**, *36*, 406−408.
[16] V. S. Ijeri and A. K. Srivastava, *Fresenius J. Anal. Chem.* **2000**, *367*, 373−377.
[17] A. J. Dill, O. Popovych, *J. Chem. Eng. Data* **1969**, *14*, 156−160.
[18] Y. Takeda, K. Katsuta, Y. Inoue, T. Hakushi, *Bull. Chem. Soc. Jpn.* **1988**, *61*, 627−632.
[19] J. L. Hawes, R. L. Kay, *J. Phys. Chem.* **1965**, *69*, 2420−2430.
[20] C. Luca, H. A. Azab, *Anal. Lett.* **1984**, *17*, 1937−1946.
[21] H. R. Pouretedal, M. Shamsipur, *J. Chem. Eng. Data* **1998**, *43*, 742−744.
[22] V. P. Solov′ev, N. N. Strakhova, O. A. Raevsky, V. Rudiger, H. J. Schneider, *J. Org. Chem.* **1996**, *61*, 5221−5226.
[23] R. G Pearson, *J. Chem. Educ.* **1968**, *45*, 643−648.
[24] R. G. Pearson, *J. Am. Chem. Soc.* **1963**, *85*, 3533−3539.
[25] A. K. Srivastava, R. A Samant, S. D. Patankar, *J. Chem. Eng. Data* **1996**, *41*, 431−435.
[26] A. I. Popov, D. H. Geske, *J. Am. Chem. Soc.***1957**, *79*, 2074−2079.
[27] G. Akerlof, *J. Am. Chem. Soc.* **1932**, *54*, 4125−4139.
[28] R. P. Canale, S. C. Chapra, *Numerical Methods for Engineers*, 3rd ed., Mc Graw Hill, **1998**.

Received September 25, 2000
[O00359]

Synthesis and Coordination Chemistry of Chelate Ligands Containing Cyclopentadienyl, Indenyl and Fluorenyl Donors − Diastereoselectivity and NMR Structure Analysis

Joachim Vogelgesang,[a] Axel Frick,[a] Gottfried Huttner,*[a] and Peter Kircher[a]

Dedicated to Prof. Dr. Heinrich Vahrenkamp on the occasion of his 60th birthday

Keywords: Cyclopentadienes / Tripodal ligands / NMR spectroscopy / Distance geometry / Ruthenium / Phosphorus

The functionalised oxetane $O(CH_2)_2C(CH_2Br)(CH_2OMs)$ (**1**) is transformed into *tripod* ligands $ROCH_2C(CH_2PPh_2)(CH_2PR'_2)(CH_2Cp^{\#})$ (R = H, $SiMe_3$; R′ = Ph, Et; $Cp^{\#}$ = indenyl, fluorenyl) (**4**) in a few steps. Epichlorohydrin $O(CH_2)CH(CH_2Cl)$ (**5**) allows for diastereoselective one-pot syntheses of the Cp-functionalised chelate ligands $(Cp^{\#}CH_2)C(H)OH(CH_2PPh_2)$ ($Cp^{\#}$ = Cp, indenyl, fluorenyl) (**6**). The $SiMe_3$-protected derivatives of these ligands react with $RuCl_2(PPh_3)_3$ to produce $\{Me_3SiOCH(CH_2\text{-}\eta^1\text{-}PPh_2)(CH_2\text{-}\eta^5\text{-}Cp^{\#})Ru(PPh_3)(Cl)\}$ ($Cp^{\#}$ = Cp, indenyl) (**15**) with high diastereoselective preference. With the same starting material, *tripod* ligands **4** form $Me_3SiOCH_2C(CH_2\text{-}\eta^1\text{-}PPh_2)(CH_2\text{-}\eta^1\text{-}PR_2)(CH_2\text{-}\eta^5\text{-}Indenyl)RuCl$ (R = Ph, Et) (**16**). As shown by complete NMR spectroscopy based structure analyses (DG methods) of **16**, the formation of **16** (R = Et) is diastereoselective. The only diastereomer which is observed is the one in which the PEt_2 donor and the phenylene part of the indenyl ligand are juxtaposed. In addition to quantitative NMR spectroscopy structure analyses, traditional analytical techniques, including X-ray analyses, were used to confirm the results.

Introduction

Cyclopentadienyl ligands which are linked to additional donor groups by side-chains of appropriate lengths are a special class of chelate ligands and hold quite some promise in catalytic applications. Whereas the chemistry of *ansa* Cp ligands, so elegantly developed by H. Brintzinger and his group,[1] has boomed in recent years, the chemistry of Cp-based chelate ligands bearing functionalities other than Cp groups is only in its early state of development. This is especially surprising in the case of Cp derivatives containing additional phosphane donor groups, since the chemistry of $CpM(PR_3)_n$ metal templates is so well developed. The only possible reason for this fact appears to be the lack of suitable methods for the synthesis of the ligands. It has been shown that tripodal ligands $CH_3C(CH_2PR_2)(CH_2PR'_2)(CH_2Cp^{\#})$ ($Cp^{\#}$ = Cp, indenyl, fluorenyl) are accessible by different routes[2] and some coordination chemistry of such ligands has been reported.[3]

Since it has been shown that *tripod* ligands $H_3CC(CH_2X)(CH_2Y)(CH_2Z)$ (X, Y, Z = donor groups with at least one of them being a Cp derivative) are accessible via appropriately functionalised oxetanes in fair yields,[2] the development of the synthesis of hydroxy-functionalised *tripod* ligands $(HOCH_2)C(CH_2PR_2)(CH_2PR'_2)(CH_2Cp^{\#})$ via oxetane precursors appears to be worthwhile. In this paper ligands of this type ($Cp^{\#}$ = indenyl, fluorenyl; PR_2, PR'_2 = PPh_2, PEt_2) (**3**, **4**) as well as some of their coordination chemistry, are described.

Yet another way to hydroxy-functionalised chelate ligands containing phosphorus donor groups and $Cp^{\#}$ ligands linked by a three-carbon chain may be based on the use of epichlorohydrin as the starting material. It has been shown that the enantioselective synthesis of bidentate and tridentate chelate ligands containing up to three different phosphorus donors $HC(CH_2PR_2)(CH_2PR'_2)(OPR''_2)$ may be achieved in this way.[4] In this paper we show that $Cp^{\#}$ donor groups may also be introduced, leading to compounds $HC(CH_2Cp^{\#})(CH_2PPh_2)(OPPh_2)$ (**12**) and $ROCH(CH_2Cp^{\#})(CH_2PPh_2)$ (**6**, **9**). Some coordination compounds of these novel ligands are also described.

Results and Discussion

Ligand Syntheses

Starting from Neopentane Derivatives

The functionalized oxetane **1**, which has been shown to undergo selective exchange of its functional groups by two

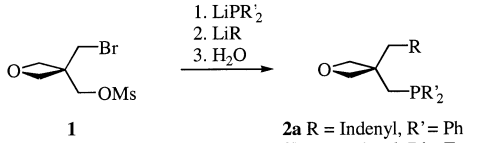

1

2a R = Indenyl, R' = Ph
2b R = Indenyl, R' = Et
2c R = Fluorenyl, R' = Ph

Scheme 1

[a] Anorganisch-Chemisches Institut der Universität Heidelberg, Im Neuenheimer Feld 270, 69120 Heidelberg, Germany
Fax: (internat.) + 49-(0)6221/545707
E-mail: g.huttner@indi.aci.uni-heidelberg.de

 © WILEY-VCH Verlag GmbH, 69451 Weinheim, 2001 1434−1948/01/0404−0949 $ 17.50+.50/0

Table 1. NMR spectroscopic data of compounds **2**−**4**[a]

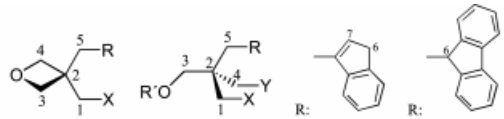

No.	R[b] X[b] Y, R'[b]	1[c] $CH_{2a,b}$ [2H]	2[c] C_q	3[c] $CH_{2a,b}$ [2H]	4[c] $CH_{2a,b}$ [2H]	5[c] $CH_{2a,b}$ [2H]	6[c] $-CH_n-$ (n = 1–2)	7[c] −CH= [1H]	CH aromatic	X	Y
2a	Indenyl	2.93 (d)	—	4.67, 4.77 (2d)		3.25 (s)	3.47 (s) [2H]	6.27 (s)	7.33–7.67 (m) [14H]		—
	PPh_2	$^2J_{HP}$ = 2.6 Hz		$^2J_{HH}$ = 6.0 Hz							
	O (Oxetane)	37.3 (d)	43.1 (d)	82.4 (d)		35.4 (d)	38.7 (s)		119.7–146.3		—
		$^1J_{CP}$ = 15.6 Hz	$^2J_{CP}$ = 15.6 Hz	$^3J_{CP}$ = 11.0 Hz		$^3J_{CP}$ = 10.6 Hz				{−25.6 (s)}	—
2b	Indenyl	2.06 (d)	—	4.58, 4.70 (2d)		3.07 (s)	3.41 (s) [2H]	6.18 (s)	7.25–7.52 (m) [4H]	1.06 (m) [6H] 1.46 (m) [4H]	—
	PEt_2	$^2J_{HP}$ = 4.4 Hz		$^2J_{HH}$ = 5.8 Hz							
	O (Oxetane	35.2 (d)	42.6 (d)	82.5 (d)		35.1 (d)	38.5 (s)		119.5–146.3	9.9 (d) $^2J_{CP}$ = 12.1 Hz 20.0 (d) $^3J_{CP}$ = 11.6 Hz	—
		$^1J_{CP}$ = 16.6 Hz	$^2J_{CP}$ = 15.6 Hz	$^3J_{CP}$ = 10.6 Hz		$^3J_{CP}$ = 11.0 Hz				{−31.2 (s)}	—
3a	Indenyl	2.53, 2.63 (2dd)	—	3.66 (s)	2.53, 2.63 (2dd)	3.09 (s)	3.40 (s) [2H]	6.39 (s)	7.26–7.59 (m) [24H]		
	PPh_2	$^2J_{HH}$ = 14.4 Hz			$^2J_{HH}$ = 14.4 Hz						
	PPh_2, H	$^2J_{HP}$ = 2.8, 3.4 Hz			$^2J_{HP}$ = 2.8, 3.4 Hz						
		37.2 (dd)	44.5 (t)	69.5 (t)	37.2 (dd)	34.7 (t)	38.6 (s)		120.3–146.9		
		$^1J_{CP}$ = 16.6 Hz $^3J_{CP}$ = 8.8 Hz	$^2J_{CP}$ = 11.6 Hz	$^3J_{CP}$ = 8.4 Hz	$^1J_{CP}$ = 16.6 Hz $^3J_{CP}$ = 8.8 Hz	$^3J_{CP}$ = 8.5 Hz				{−28.4 (s)}	
3b	Indenyl	2.57 (d)	—	3.66 (s)	1.75 (d)	2.96 (s)	3.39 (s) [2H]	6.38 (s)	7.21–7.64 (m) [14H]		0.91–1.13 (m) [6H] 1.38–1.50 (m) [4H]
	PPh_2	$^2J_{HP}$ = 3.6 Hz			$^2J_{HP}$ = 4.8 Hz						
	PEt_2, H	37.3 (dd)	43.7 (pt)	69.7 (pt)	35.4 (dd)	34.8 (pt)	38.5 (s)		120.2–146.9		9.8 (d) $^2J_{CP}$ = 11.2 Hz 19.9, 20.0 (2d)
		$^1J_{CP}$ = 16.3 Hz $^3J_{CP}$ = 8.4 Hz	$^2J_{CP}$ = 11.4 Hz	$^3J_{CP}$ = 8.3 Hz	$^1J_{CP}$ = 16.9 Hz $^3J_{CP}$ = 8.7 Hz	$^3J_{CP}$ = 8.2 Hz				{−27.5 (s)}	$^1J_{CP}$ = 10.4 Hz {−35.0 (s)}
4a	Indenyl	2.58 (m)	—	3.47 (s)	2.58 (m)	2.96 (s)	3.33 (s) [2H]	6.25 (s)	7.20–7.60 (m) [24H]		
	PPh_2	36.7 (dd)	44.2 (t)	68.8 (pt)	36.7 (dd)	34.5 (t)	38.5 (s)		120.3–147.2		
	PPh_2, TMS	$^1J_{CP}$ = 17.0 Hz $^3J_{CP}$ = 10.0 Hz	$^2J_{CP}$ = 12.0 Hz	$^3J_{CP}$ = 9.3 Hz	$^1J_{CP}$ = 17.0 Hz $^3J_{CP}$ = 10.0 Hz	$^3J_{CP}$ = 8.5 Hz				{−27.8 (s)}	
4b	Indenyl	2.60, 2.70 (2dd)	—	3.55, 3.60 (2d)	1.83 (d)	2.99 (s)	3.40 (s) [2H]	6.35 (s)	7.23–7.65 (m) [14H]		1.10 (m) [6H] 1.44 (m) [4H]
	PPh_2	$^2J_{HH}$ = 14.0 Hz		$^2J_{HH}$ = 9.7 Hz	$^2J_{HP}$ = 5.0 Hz						
	PEt_2, TMS	$^2J_{HP}$ = 3.8, 4.0 Hz									
		36.3 (dd)	43.5 (pt)	68.8 (pt)	34.8 (dd)	34.4 (pt)	38.5 (s)		120.4–147.3		10.0 (d) $^2J_{CP}$ = 11.0 Hz 20.1, 20.2 (2d)
		$^1J_{CP}$ = 16.0 Hz $^3J_{CP}$ = 9.0 Hz	$^2J_{CP}$ = 12.0 Hz	$^3J_{CP}$ = 9.2 Hz	$^1J_{CP}$ = 16.0 Hz $^3J_{CP}$ = 9.0 Hz	$^3J_{CP}$ = 8.6 Hz				{−27.2 (s)}	$^1J_{CP}$ = 11.0 Hz {−36.1 (s)}
2c	Fluorenyl	2.99 (d)	—	4.41, 4.51 (d)		2.53 (d)	4.07 (t) [1H]	—	7.30–7.86 (m) [18H]		—
	PPh_2	$^2J_{HP}$ = 2.2 Hz		$^2J_{HH}$ = 6.1 Hz		$^3J_{HH}$ = 7.2 Hz	$^3J_{HH}$ = 7.2 Hz				
	O (Oxetane)	36.9 (d)	43.4 (d)	83.5 (d)		42.8 (d)	44.8 (s)	—	120.2–147.3		—
		$^1J_{CP}$ = 16.6 Hz	$^2J_{CP}$ = 14.1 Hz	$^3J_{CP}$ = 11.1 Hz		$^3J_{CP}$ = 9.1 Hz				{−26.7 (s)}	—
3c	Fluorenyl	2.39 (m)	—	3.39 (m)	2.39 (m)	2.72 (d)	4.25 (t)	—	7.24–7.86 (m) [28H]		
	PPh_2	$^2J_{HH}$ = 14.5 Hz			$^2J_{HH}$ = 14.5 Hz	$^3J_{HH}$ = 4.6 Hz	$^3J_{HH}$ = 4.6Hz				
	PPh_2, H	37.9 (dd)	44.9 (t)	69.7 (t)	37.9 (dd)	39.3 (t)	45.7 (s)	—	120.4–148.9		
		$^1J_{CP}$ = 17.0 Hz $^3J_{CP}$ = 9.2 Hz	$^2J_{CP}$ = 11.0 Hz	$^3J_{CP}$ = 8.2 Hz	$^1J_{CP}$ = 17.0 Hz $^3J_{CP}$ = 9.2 Hz	$^3J_{CP}$ = 8.3 Hz				{−29.2 (s)}	
4c	Fluorenyl	2.37 (m)	—	3.25 (s)	2.37 (m)	2.69 (d)	4.20 (m)	—	7.20–7.85 (m) [28H]		
	PPh_2	$^2J_{HH}$ = 15.0 Hz			$^2J_{HH}$ = 15.0 Hz	$^3J_{HH}$ = 6.0 Hz					
	PPh_2, TMS	37.4 (dd)	44.6 (t)	69.3 (t)	37.4 (dd)	38.7 (t)	45.6 (s)	—	120.2–149.2		
		$^1J_{CP}$ = 16.3 Hz $^3J_{CP}$ = 10.0 Hz	$^2J_{CP}$ = 11.3 Hz	$^3J_{CP}$ = 9.0 Hz	$^1J_{CP}$ = 16.3 Hz $^3J_{CP}$ = 10.0 Hz	$^3J_{CP}$ = 8.4 Hz				{−29.0 (s)}	

[a] For ease of comparison the sequence of entries in this table does not follow the numbering scheme; sequence of entries for each compound: ^1H NMR, $^{13}C\{^1H\}$ NMR, $^{31}P\{^1H\}$ NMR spectroscopic data are embedded in curly brackets; solvent: $CDCl_3$; $CH_{2a;b}$ designates CH_2 groups whose protons may be diastereotopic depending on the symmetry of the compound; lines adjacent to individual column entries indicate that signals referring to the columns to which these lines extend are within the range given in each case or are mapped to one and the same signal. − [b] This column refers to the composition of the individual compounds with reference to the graphical illustration (Footnote[c]). − [c] Designators of the individual groups as used in the header of the table: see graphics on top of the table.

different PR_2 donors,[5] has also been shown to allow for the introduction of one phosphorus and one Cp donor.[6] The reaction of **1** with one equivalent of $LiPPh_2$ followed by the reaction with one equivalent of LiInd or LiFlu (Ind = indenyl, Flu = fluorenyl) yields compounds **2** after hydrolysis and chromatographic workup (Scheme 1).

Compounds **2a** (colourless oil) and **2c** (waxy solid) were produced in fair yields (74%/64%) while **2b** (oil) was obtained in a yield of only 10%. The yield of **2b** was lower than that of **2a** because $LiPEt_2$ is much more basic than $LiPPh_2$. Instead of replacing the OMs group, PEt_2^- deprotonated the methyl group of the mesylate function such that upon hydrolysis, the CH_2OMs function was transformed into the CH_2OH function from which the mesylate was prepared.[7] Similar problems have been observed with tosylate-activating groups where even the *p*-methyl group is acidic

enough to be deprotonated.[8] The use of phenylsulfonate might be an alternative solution, but has not yet been tested with the problem at hand. The sequence in which the nucleophiles are added in the synthesis of **2** from **1** is important, since selective monosubstitution, which results when $LiPR_2$ is added first, is not achieved when $LiCp^{\#}$ is added as the first reagent. Compounds **2** were fully characterised by their spectroscopic and analytical data (Table 1 and Table 10).

All the NMR (^1H, ^{13}C, ^{31}P) signals, except for those in the aromatic region, have been unambiguously assigned (Table 1). As had already been observed in the synthesis of indenyl-containing *tripod* ligands,[2a] the indenyl residue was selectively bonded at its 3-position.[9]

Compounds **2** reacted with $LiPR_2$ by the nucleophilic ring opening of the oxetane cycle to produce **3** after hydrolysis. After chromatographic workup, **3a** and **3c** were obtained as waxy solids, while **3b** formed an oil (Scheme 2).

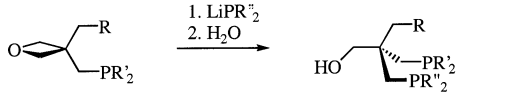

2a R = Indenyl, R' = Ph
2b R = Indenyl, R' = Et
2c R = Fluorenyl, R' = Ph

3a R = Indenyl, R' = R" = Ph
3b R = Indenyl, R' = Et, R" = Ph
3c R = Fluorenyl, R' = R" = Ph

Scheme 2

The transformation of **2** into **3** occurred in yields between 62% and 73%. Analytical (Table 10) and spectroscopic data (Table 1) of **3** are in full agreement with the assigned structure. An almost complete assignment of the NMR peaks (except for those in the aromatic regions) is reported in Table 1.

Preliminary experiments into the coordination chemistry of **3** indicated that the presence of the OH group might cause problems: Deprotonation of **3a** by one equivalent of *n*BuLi and subsequent reaction with $FeCl_2$ or $FeCl_2(PPh_3)_2$ [10] resulted in insoluble, brown products of unknown composition. The same protocol, however, yields $HOCH_2C(CH_2\text{-}\eta^1\text{-}PPh_2)_2(CH_2\text{-}\eta^5\text{-}Cp)FeCl$ when the Cp analogue of **3a** is used.[6] It appears that because the indenyl moiety is less acidic than the Cp moiety, deprotonation of the OH group of **3a** is a concomitant or even dominant reaction when **3a** is treated with *n*BuLi. The use of two equivalents of *n*BuLi did not improve the situation: Insoluble, brown products were again obtained. It was hoped to overcome this problem by protection of the hydroxy group as an ether derivative. It is known that transforming the CH_2OH groups of *neo*-pentane-based *tripod* ligands into ether functional groups is problematic.[11] Special protocols have been developed in specific cases which overcome these problems, one of these special protocols being based on rigid temperature control under Williamson conditions.[12]

Deprotonation of **3a** by *n*BuLi may be performed as a kind of titration, since a slight excess of *n*BuLi deprotonates the indenyl residue. The anion formed by deprotonation of the indenyl moiety is of an intense violet colour. The alkoxide which is obtained when **3a** is treated with one equivalent of *n*BuLi was allowed to react with methyl iodide or ethyl iodide in THF at temperatures from −15 °C up to 30 °C in different experiments (Scheme 3).

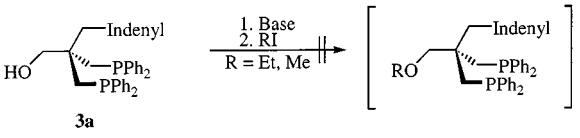

3a

Scheme 3

The selective formation of just one product was not observed in any of the experiments. TLC analyses as well as mass spectrometric and NMR spectroscopic analyses revealed the formation of a mixture of many products in each case. A tentative explanation for this observation may be a proton-transfer equilibrium activating the indenyl part of the ligand with the resulting indenyl anion being far more reactive towards alkyl iodides than the alkoxide function. Alkyl substitution may therefore occur at the indenyl group.

This hypothesis was not further investigated, since it was found that the protection of the alcohol group of **3** is easily achieved by its reaction with trimethylchlorosilane, leading to the siloxy derivatives **4** (Scheme 4), which are obtained as colourless oils of high viscosity. The analytical and spectroscopic data of compounds **4** (Table 10 and Table 1) are in full agreement with the assigned structures.

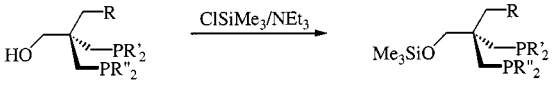

3a R = Indenyl, R' = R" = Ph
3b R = Indenyl, R' = Et, R" = Ph
3c R = Fluorenyl, R' = R" = Ph

4a R = Indenyl, R' = R" = Ph
4b R = Indenyl, R' = Et, R" = Ph
4c R = Fluorenyl, R' = R" = Ph

Scheme 4

Starting from Epichlorohydrin

Epichlorohydrin (**5**) has been shown to be an efficient starting material for the synthesis of bidentate and tridentate chelate ligands.[4] The tandem-type process of ring-opening and ring-closing steps occurring upon treating epichlorohydrin with phosphorus nucleophiles has been analysed in detail.[4b,4c] An essential step in this synthetic approach is the nucleophilic opening of the oxirane ring by phosphide nucleophiles which has also been observed with some related oxirane starting materials.[13] In the case of epichlorohydrin as the ligand precursor, this ring-opening step has also been shown to work with nitrogen and sulfur nucleophiles.[4a] In view of this proven tolerance of the reaction, it appeared appealing to study the reactivity of **5** towards Cp nucleophiles.

It had already been shown by B. Rieger et al. that functionalised oxiranes may be attacked by Cp nucleophiles, with substitution at one of the oxirane carbon atoms and concomitant opening of the oxirane ring.[14] With respect to the nucleophilic ring-opening reaction of oxiranes, the Cp nucleophiles show the same type of reactivity as phosphorus, nitrogen and sulfur nucleophiles. This type of reaction works as well with **5** as the starting compound. When **5** was treated with one equivalent of $LiPPh_2$, attack occurred at the unsubstituted oxirane carbon atom. The phos-

phane-substituted alkoxide resulting from this reaction may be characterised as an intermediate at low temperatures.[4b,4c] At higher temperatures, the alkoxide oxygen atom attacks the CH_2Cl functional group with the formation of an oxirane, which may then be further attacked by nucleophiles at its unsubstituted carbon atom.[4]

This sequence of steps, when performed with CpMgCl as the second nucleophile, led to the formation of **6a** in which a Cp unit and a PPh_2 unit are connected by a 2-hydroxy-1,3-propanediyl chain (Scheme 5). Compound **6a** was obtained as a mixture of two double-bond isomers (Table 2, ^{13}C NMR). Its formation was always accompanied by the formation of some 1,3-bis(diphenylphosphanyl)-2-propanol, even when lower than stoichiometric quantities of $LiPPh_2$ were used. This by-product could not be separated from **6a** such that on first inspection, C,H analysis (Table 10) appeared to be inconsistent with the given formula. The relative content of this by-product was judged from the ^1H NMR spectrum of **6a** where the methine proton (at the 2-position of the C_3 chain) at the hydroxy-substituted carbon atom resonates at $\delta = 3.97$ (Table 2) while the $HOCH(CH_2PPh_2)_2$ proton gives rise to a signal at $\delta = 3.73$.[4b,4c] Chromatographic separation of the products was not possible. It was, however, possible to obtain an analytically pure derivative of **6a** (**9a**, see below). When LiInd or LiFlu were used as the nucleophiles in the second preparation step, minor quantities of the corresponding diphosphanes were also obtained, but could be separated by chromatography such that **6b**/**6c** were obtained as analytically pure substances. Compounds **6a** and **6b** are colourless oils, and **6c** is a colourless solid. The composition of **6** is evident from microanalytical and mass spectrometric data (Table 10). The structure is unequivocally clear from their NMR spectra (Table 2).

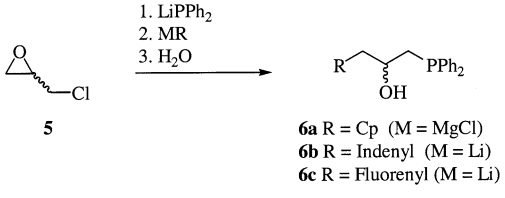

5

6a R = Cp (M = MgCl)
6b R = Indenyl (M = Li)
6c R = Fluorenyl (M = Li)

Scheme 5

The sequence in which the nucleophiles are added to **5** is important. It had already been observed that spiro cyclisation may occur when an electrophilically activating group is present at the 4-position relative to a Cp carbon atom.[2a] This type of reaction corresponds to the dominant reaction pathway when **5** is treated with Cp nucleophiles and this is apparent from the reaction of **5** with LiInd. When **5** was treated with five equivalents of LiInd, the disubstitution product **7** was obtained in only 4% yield while the spiro derivatives *syn*-**8**/*anti*-**8** were formed in 40% overall yield (Scheme 6).

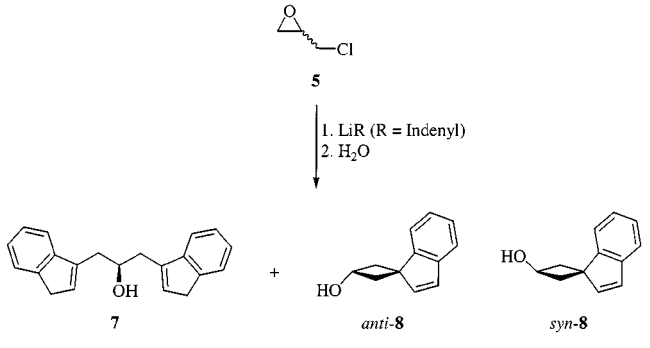

7 *anti*-**8** *syn*-**8**

Scheme 6

The assignment of *syn* and *anti* configurations to the two components of the product mixture followed the arguments explicitly described for closely analogous cases which were observed during indenyl substitution of *neo*-pentane-derived *tripod* ligands and was based on ^1H NMR spectroscopic data (Table 3).[2a]

The isomers of **8** might in principle be separated by crystallisation as is demonstrated by the fact that upon crystallisation, single crystals of *anti*-**8** suitable for X-ray analysis were obtained. The structure of *anti*-**8** is shown in Figure 1 together with the structure of **7** from which single crystals could also be grown. There is nothing peculiar about the molecular structure of *anti*-**8**. Distances and angles are in the normal ranges (Table 4).

While the molecular symmetry of *anti*-**8** is C_s (Figure 1), the molecules aggregate in space group $P4_1$ to form a chiral crystal. The hydrophilic and hydrophobic parts of the molecule are embedded in specific compartments of the crystal with the hydroxy groups forming an infinite hydrogen-bonded spiral around a 4_1 axis of the $P4_1$-symmetric unit cell (Figure 2). The O···O distance between neighbouring oxygen atoms is only 265 pm. The position of the bridging hydrogen atoms has been determined by diffraction methods (H−O 83 pm, H···O 183pm). The O···H−O angle is 174°. The hydrogen bonds are hence almost linear. The H−O···H angle is approximately 110°. A view of this interesting arrangement in the direction of the 4_1 axis is shown in Figure 2, giving an impression of the infinite hydrophilic channels along the crystal.

The structure of **7** (Figure 1) shows no peculiarities in the bond lengths and angles (Table 5). The position of the indenyl substituents is such that they are as far apart as possible with respect to the three-carbon linker between them. This type of orientation of indenyl and fluorenyl substituents linked by a three-carbon chain had already been observed for *tripod* ligands containing these groups.[2a] The solid-state structure is again an interesting one. As already observed for *anti*-**8**, hydrophobic and hydrophilic compartments are well separated in the crystal. Compound **7** crystallises in the achiral space group $P2_1/n$. The hydroxy groups form hydrogen-bonded zigzag chains around the 2_1 axes of the unit cell. The O···O distances between the hydrogen-bonded oxygen atoms is only 274 pm. The H−O···H angle is 129°, the O−H distances were found to be 92 pm and 183 pm, with the O−H···O group being almost linear (168°).

It has been found that the transformation of enantiomerically pure epichlorohydrin into its disubstituted products $HOCH(CH_2PR_2)(CH_2PR'_2)$ follows a completely enantioselective pathway.[4] In order to find out if enantioselectiv-

Table 2. NMR spectroscopic data of compounds **6**−**7**, **9**−**12**[a]

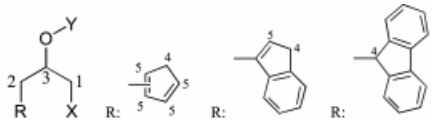

No.	R[b] X[b] Y[b]	1[c] $CH_{2a,b}$ [2H]	2[c] $CH_{2a,b}$ [2H]	3[c] CH [1H]	4[c] $-CH_n-$ (n = 1–2)	5[c] −CH=	CH aromatic	X	Y
6a	Cp	2.41 (m)	2.75 (m)	3.97 (m)	2.92, 3.02 (2m) [2H]	6.17–6.50 (m) [3H]	7.35–7.55 (m) [10H]	———	2.21 (bs) [1H]
	PPh_2	37.2, 37.4 (2d)	39.4, 40.3 (2d)	69.1, 69.7 (2d)	42.0, 44.3 (2s)	———	128.8–146.3	———	—
	H	$^1J_{CP}$ = 13.0 Hz	$^3J_{CP}$ = 8.1 Hz	$^2J_{CP}$ = 16.2 Hz				{–24.6 (s)}	—
6b	Indenyl	2.59 (d)	2.95, 3.13 (2dd)	4.27 (m)	3.45 (bs) [2H]	6.41 (s) [1H]	7.30–7.65 (m) [14H]	———	2.53 (bs) [1H]
	PPh_2	$^3J_{HH}$ = 6.6 Hz	$^2J_{HH}$ = 14.3 Hz						
	H		$^3J_{HH}$ = 7.9, 3.0 Hz						
		37.6 (d)	37.6 (d)	68.5 (d)	38.5 (s)	———	119.8–145.5	———	—
		$^1J_{CP}$ = 13.4 Hz	$^3J_{CP}$ = 8.1 Hz	$^2J_{CP}$ = 16.6 Hz				{–24.5 (s)}	—
6c	Fluorenyl	2.32 (m)	2.22, 2.45 (2m) [3H]	4.05 (m)	4.30 (m) [1H]	—	7.30–7.88 (m) [18H]	———	2.22 (m) [2H]
	PPh_2								
	H	38.8 (d)	42.6 (d)	68.1 (d)	45.2 (s)	—	120.4–147.8	———	—
		$^1J_{CP}$ = 12.8 Hz	$^2J_{CP}$ = 7.8 Hz	$^2J_{CP}$ = 14.9 Hz				{–25.6 (s)}	—
7	Indenyl	3.02 (m) ———		4.52 (m)	3.52 (s) [4H]	6.53 (s) [2H]	7.30–7.65 (m) [8H]	———	2.24 (s) [1H]
	Indenyl	36.4 (s) ———		69.2 (s)	38.5 (s)	———	119.7–145.7	———	—
	H								
9a	Cp	2.44 (pt)	2.82 (m)	4.05 (m)	3.00 (m) [2H]	6.16–6.54 (m) [3H]	7.36–7.56 (m) [10H]		0.08 (s) [9H]
	PPh_2	J_{HH} = 5.8 Hz							
	TMS	37.7, 37.8 (2d)	39.6, 40.3 (2d)	71.1, 71.6 (2d)	41.8, 44.9 (2s)	———	128.7–145.9	———	0.7 (s)
		$^1J_{CP}$ = 14.2 Hz	$^2J_{CP}$ = 8.4 Hz	$^2J_{CP}$ = 17.6 Hz				{–23.2 (s)}	—
9b	Indenyl	2.50 (m)	2.93, 3.14 (2dd)	4.24 (m)	3.40 (s) [1H]	6.35 (s) [1H]	7.28–7.59 (m) [14H]	———	–0.01 (s) [9H]
	PPh_2		$^2J_{HH}$ = 14.1 Hz						
	TMS		$^3J_{HH}$ = 7.0, 4.5 Hz						
		38.3 (d)	37.7 (d)	70.3 (d)	38.3 (s)	———	119.8–145.9	———	0.6 (s)
		$^1J_{CP}$ = 14.4 Hz	$^3J_{CP}$ = 8.6 Hz	$^2J_{CP}$ = 18.1 Hz				{–23.5 (s)}	—
12a	Cp	2.47, 2.68 (2dd)	2.80–3.00 (m)	4.31 (m)	3.00 (m) [2H]	6.10–6.49 (m) [3H]	7.37–7.58 (m) [20H] ———		
	PPh_2	$^2J_{HH}$ = 13.9 Hz							
	PPh_2	$^3J_{HH}$ = 7.2, 6.1 Hz							
		36.2 (dd)	37.9, 38.7 (2dd)	79.0 (m)	41.8, 44.5 (2s)	———	128.5–146.2 ———		
		$^1J_{CP}$ = 15.3 Hz	$^3J_{CP}$ = 5.5, 8.3 Hz					{–24.7, –24.8 (2d)}	{106.7, 106.8 (2d)}
		$^3J_{CP}$ = 14.4 Hz						{$^4J_{PP}$ = 5.9 Hz}	{$^4J_{PP}$ = 5.9 Hz}
12b	Indenyl	2.55, 2.71 (2dd)	3.17 (d)	4.52 (m)	3.22 (s) [2H]	6.20 (s) [1H]	7.24–7.58 (m) [24H] ———		
	PPh_2	$^2J_{HH}$ = 13.9 Hz	$^3J_{HH}$ = 6.2 Hz						
	PPh_2	$^3J_{HH}$ = 6.7, 5.9 Hz							
		36.8 (dd)	36.4 (dd)	78.2 (dd)	38.4 (s)	———	119.9–144.5 ———		
		$^1J_{CP}$ = 15.6 Hz	$^3J_{CP}$ = 8.7, 6.0 Hz	$^2J_{CP}$ = 20.1, 17.0 Hz				{–24.9 (d)}	{107.0 (d)}
		$^3J_{CP}$ = 5.5 Hz						{$^4J_{PP}$ = 5.6 Hz}	{$^4J_{PP}$ = 5.6 Hz}
12c	Fluorenyl	2.42, 2.79 (2m) ———		4.54 (m)	4.25 (m) [1H]	—	7.28–7.89 (m) [28H] ———		
	PPh_2	37.5 (dd)	42.2 (m)	77.4 (dd)	44.7 (s)	—	120.3–148.1 ———		
	PPh_2	$^1J_{CP}$ = 15.6 Hz		$^2J_{CP}$ = 15.7, 18.8 Hz				{–25.8 (d)}	{105.8 (d)}
		$^3J_{CP}$ = 5.9 Hz						{$^4J_{PP}$ = 5.9 Hz}	{$^4J_{PP}$ = 5.9 Hz}
10	Cp	2.4–3.0 (m) [7H] ———		4.18 (m)	2.4–3.0 (m) [7H]	6.12–6.49 (m) [3H]	7.43–7.77 (m) [10H] ———		2.4–3.0 (m)
	PPh_2BH_3						0.4–1.9 (bs) [3H]		[7H]
	H	33.72, 33.77 (2d)	39.4, 40.3 (2d)	67.5 (d)	42.0, 44.2 (2s)	———	129.2–135.0 ———		—
		$^1J_{CP}$ = 36.3 Hz	$^3J_{CP}$ = 11.4 Hz	$^2J_{CP}$ = 24.1 Hz				{9.7, 10.5 (2s)}	—
11	Cp	2.58 (m) [4H] ———		5.19 (m)	2.97 (m) [5H]	6.18–6.47 (m) [3H]	7.46–7.86 (m) [10] ———		2.97 (m) [5H]
	PPh_2BH_3						0.7–1.9 (bs) [3H]		
	Ms	31.3, 32.0 (2d)	36.9, 37.9	79.1, 79.2 (2d)	42.0, 44.4 (2s)	———	129.2–142.3 ———		
		$^1J_{CP}$ = 13.1, 12.7 Hz	$^3J_{CP}$ = 5.1, 5.5 Hz	$^2J_{CP}$ = 4.5, 5.0 Hz				{10.3 (bs)}	38.3, 38.6 (2s)

[a] For ease of comparison, the sequence of entries in this table does not follow the numbering scheme; sequence of entries for each compound: ^{1}H NMR, ^{13}C{^{1}H} NMR, ^{31}P{^{1}H} NMR spectroscopic data are embedded in curly brackets; solvent: $CDCl_3$; $CH_{2a;b}$ designates CH_2 groups whose protons may be diastereotopic depending on the symmetry of the compound; lines adjacent to individual column entries indicate that signals referring to the columns to which these lines extend are within the range given in each case or are mapped to one and the same signal. − [b] This column refers to the composition of the individual compounds with reference to the graphical illustration (Footnote[c]). − [c] Designators of the individual groups as used in the header of the table: see graphics on top of the table.

ity could also be achieved when Cp nucleophiles were used in the second step of the transformation, the one-pot synthesis of **6b** was performed with enantiomerically pure *S*-(+)-**5** as well as with *R*-(−)-**5** (Scheme 7).

Compound *R*-(−)-**6b** was obtained from *S*-(+)-**5** in a yield of 42%, showing a specific rotation of $[\alpha]_D^{20} = -18.73 \pm 0.53$. Compound *S*-(+)-**6b** was obtained from *R*-(−)-**5** in the same yield. The optical rotation for this product was

Table 3. NMR spectroscopic data of compound **8**[a]

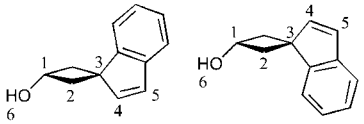

	No.	1[b] CH [1H]	2[b] $CH_{2a;b}$ [4H]	3[b] C_q	4[b] –CH= [1H]	5[b] –CH= [1H]	CH aromatic [4H]	6[b] OH [1H]
^{1}H-NMR	*syn*-**8**	4.77 (dt) $^3J_{HH}$ = 15.1, 7.4 Hz	2.75 (m)	—	6.73, 6.82 (2d) $^3J_{HH}$ = 5.4 Hz		7.30–7.73 (m)	3.57 (bs)
	anti-**8**	5.02 (dt) $^3J_{HH}$ = 14.6, 7.3 Hz	2.75 (m)	—	6.56, 6.78 (2d) $^3J_{HH}$ = 5.4 Hz		7.30–7.73 (m)	3.57 (bs)
^{13}C{^{1}H}-NMR	*syn*-**8**	62.8 (s)	41.3 (s)	46.8 (s)	———	———	121.5–152.1	—
	anti-**8**	63.8 (s)	41.1 (s)	47.6 (s)	———	———	121.5–152.1	—

[a] Solvent $CDCl_3$. – [b] Designators of the individual groups as used in the header of the table: see graphics on top of the table.

Table 4. Selected bond lengths [pm], bond angles [°], and torsion angles [°] for *anti*-**8**

[a]

C1–O	141.5(3)	O–C1–C3	120.0(3)
C1–C2	152.9(4)	O–C1–C2	118.7(2)
C1–C3	154.2(4)	C5–C4–C8	101.7(2)
C2–C4	155.5(4)	C3–C4–C8	115.5(2)
C3–C4	156.6(4)	C2–C4–C8	116.2(2)
C4–C5	151.3(3)	C3–C4–C5	119.3(2)
C5–C6	133.3(4)	C2–C4–C5	117.9(2)
C6–C7	146.8(4)	O–C1–C2–C4	143.9(3)
C7–C8	140.3(4)	O–C1–C3–C4	–142.7(3)
C4–C8	151.2(4)	C1–C3–C4–C2	19.5(2)
C_{ar}–C_{ar}	138.1(4)–139.3(4)	C2–C1–C3–C4	–19.8(2)
		C1–C3–C4–C8	–98.3(2)
C1–C2–C4	89.0(2)	C1–C2–C4–C8	97.5(3)
C1–C3–C4	88.1(2)	C1–C3–C4–C5	140.0(3)
C2–C1–C3	88.9(2)	C1–C2–C4–C5	–141.5(3)
C2–C4–C3	87.1(2)		

[a] The numbering scheme used refers to the scheme shown in Figure 1; it is different from the scheme used to label individual atoms in the deposited data; C_{ar}–C_{ar} designates the distances within the anellated cycles excluding C7–C8 which is given explicitly.

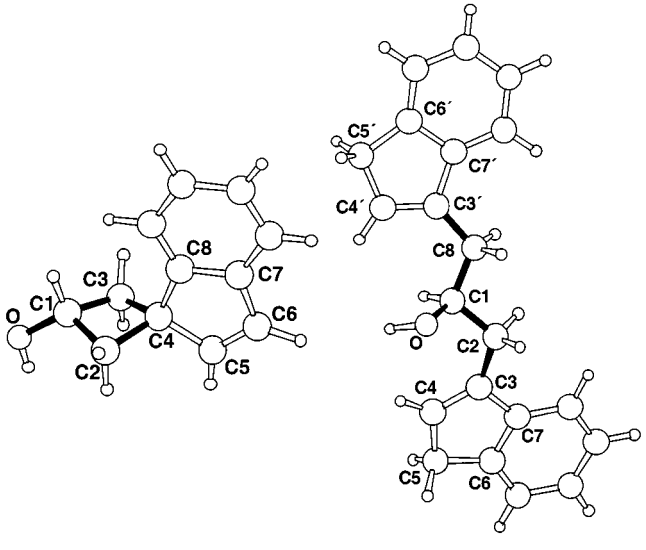

anti-**8** **7**

Figure 1. Structures of **7** and *anti*-**8**

$[\alpha]_D^{20}$ = 17.28 ± 0.48. The optical rotations are thus opposite in sign but equal in size (within the limits of error). While this is no proof for complete enantioselectivity, it agrees with the observations that the reaction is completely enantioselective when using phosphorus nucleophiles.[4] It also agrees with the results of similar reactions with other types of oxiranes in which complete enantioselectivity is observed.[14]

Since the hydroxy groups in **6** might complicate the coordination of these ligands, protection of these groups was considered to be important. As already experienced with **3**, ether formation under Williamson conditions was not successful with **6**; only inseparable mixtures of compounds were obtained. In contrast, protection with chlorotrimethylsilane did not cause any problems and the siloxy derivatives **9** were prepared (Scheme 8).

Silylation of **6a** proceeded in close to quantitative yields and is also a good method to purify **6a**, since **9a** is easily separated from $Me_3SiOCH(CH_2PPh_2)_2$ by chromatography. Both compounds **9** were fully characterised by their analytical and spectroscopic data (Table 2 and Table 10).

In order to activate the hydroxy group of **6** it was not protected but instead the mesylate **11** was synthesised. For this purpose, the phosphane group had to be protected. Addition of BH_3·THF led to the formation of **10** (Scheme 9).

Compound **10** was obtained as an analytically pure, colourless oil after chromatographic workup (Table 10). In contrast to the other Cp derivatives containing phosphorus

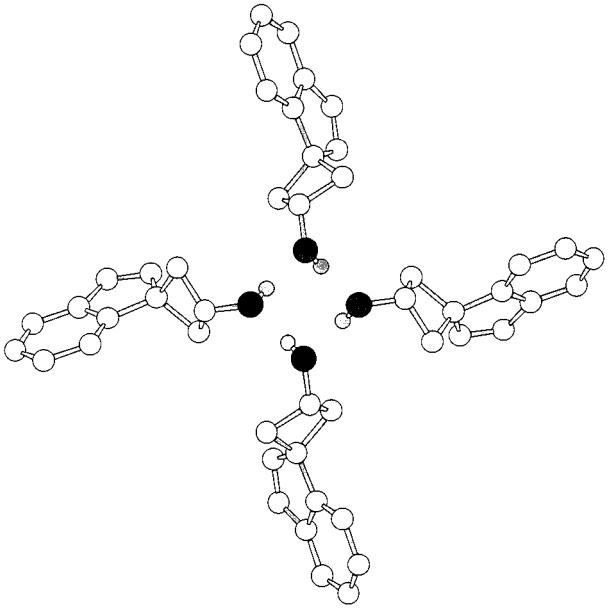

Figure 2. The hydrogen-bonded spiral formed by *anti*-**8** in the crystal in a projection along its 4_1 axis

Table 5. Selected bond lengths [pm], bond angles [°], and torsion angles [°] of **7**

[a]

C1−O	144.3(2)	C3−C7	147.6(3)
C1−C2	152.5(3)	C3′−C7′	147.9(3)
C1−C8	152.3(3)	$C_{ar}-C_{ar}$	138.5(3)−
C2−C3	150.0(0)		139.2(3)
C8−C3′	149.3(3)	O−C1−C2	117.2(2)
C3−C4	134.5(3)	O−C1−C8	109.9(2)
C3′−C4′	135.0(3)	C2−C1−C8	110.2(2)
C4−C5	150.2(3)	C1−C2−C3	117.2(2)
C4′−C5′	150.1(3)	C1−C8−C3′	117.2(2)
C5−C6	150.6(3)	O−C1−C2−C3	71.5(2)
C5′−C6′	150.3(3)	O−C1−C8−C3′	−65.0(2)
C6−C7	140.3(3)	C1−C2−C3−C4	−15.2(3)
C6′−C7′	140.7(3)	C1−C8−C3′−C4′	4.9(3)

[a] The numbering scheme used refers to the scheme shown in Figure 1; it is different from the scheme used to label individual atoms in the deposited data; $C_{ar}-C_{ar}$ designates the distances within the anellated cycles excluding C6−C7 and C6′−C7′ which are given explicitly.

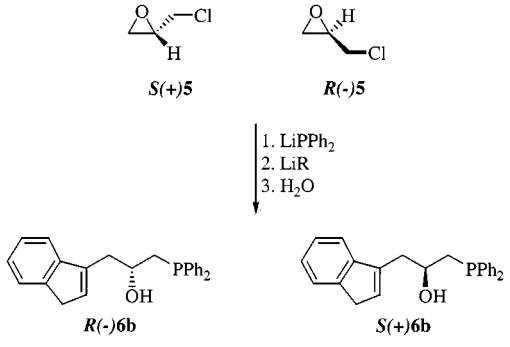

Scheme 7

donor groups described in this paper, the double bond isomers of **10** are resolved in its ^{31}P NMR spectrum (Table 2). This is consistent with earlier findings reported for some

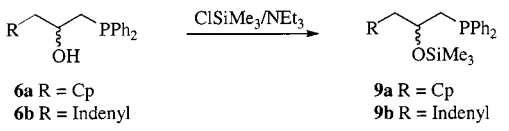

Scheme 8

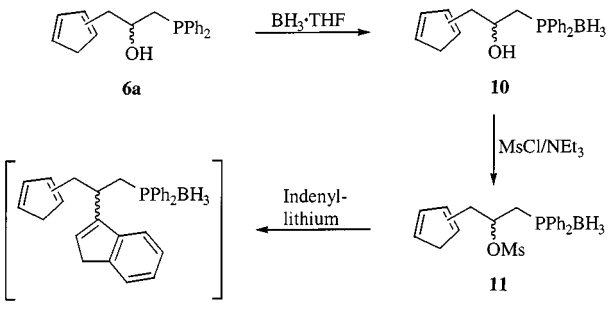

Scheme 9

ligands containing Cp and PPh_2BH_3 substituents.[2b] Mesylation of **10** by standard methods led to **11**, which was obtained as a colourless oil after chromatography. Analytical and spectroscopic data (Table 10 and Table 2) confirmed its identity. To test the reactivity of the mesylate functional group in this compound, **11** was treated with two equivalents of indenyllithium. Hydrolysis and chromatographic workup gave only a mixture of products, among which the expected product was clearly present as shown by mass spectrometry (prominent signal at m/z = 420 [M^+]). Further purification was not possible.

Compounds **6** are also suitable starting materials for the synthesis of tripodal ligands. Their reaction with $ClPPh_2$ produced **12** containing one $CH_2Cp^{\#}$, one CH_2PPh_2 and one $OPPh_2$ group. Compounds **12a** and **12b** were obtained as colourless oils while **12c** was a waxy solid (Scheme 10).

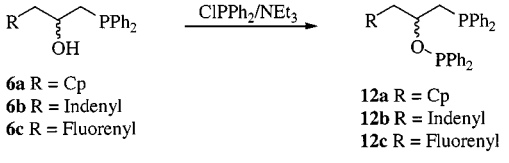

Scheme 10

Mass spectra, elemental analyses and NMR spectra are consistent with the given structures (Table 10 and Table 2). The double-bond isomers of **12a** give rise to separate peaks in the ^{31}P NMR spectrum (Table 2). The impurity of **6a** [$HOCH(CH_2PPh_2)_2$, see above] was transformed into its $OPPh_2$ derivative.[4] This derivative was present as an impurity in **12a** and could not be separated by chromatography (but compare **9a**, see above). Its elemental composition was determined by HRMS while **12b** and **12c** gave highly satisfying C,H analyses (Table 10). The NMR spectroscopic data (Table 2) were consistent with the given formulas; **12b** and **12c** also showed two separate peaks for their double-bond isomers in the ^{31}P NMR spectra (Table 2).

Coordination Chemistry

Tripodal ligands $RCH_2C(CH_2PR'_2)(CH_2PR_2'')(CH_2Cp)$ have been shown to form *tripod* metal templates $RCH_2C(CH_2\text{-}\eta^1\text{-}PR'_2)(CH_2\text{-}\eta^1\text{-}PR_2'')(CH_2\text{-}\eta^5\text{-}Cp)M$ with iron, manganese, molybdenum and ruthenium.[2,3,6,15] The procedures leading to manganese and molybdenum derivatives are complicated multi-step reactions and therefore were not suitable to test the coordination capabilities of Cp-containing *tripod* ligands.[2b,3a] In contrast, derivatives of the type $RCH_2C(CH_2\text{-}\eta^1\text{-}PR'_2)(CH_2\text{-}\eta^1\text{-}PR_2'')(CH_2\text{-}\eta^5\text{-}Cp)MCl$ have been obtained for M = Fe and Ru by convenient one-step procedures.[2a,3b,6,15] The different classes of ligands described in this paper were therefore initially tested for their reactions with $FeCl_2$ or $FeCl_2(PPh_3)_2$.[10] Compounds **4** did, after deprotonation with *n*BuLi, react with these reagents to yield deep-brown THF solutions from which no pure compounds could be isolated. In contrast, compounds **9** reacted with $FeCl_2(PPh_3)_2$ [10] under similar conditions to yield the ferrocene derivatives **13** instead of the corresponding $CpLFePPh_3Cl$ compounds. These ferrocene derivatives were obtained in good yields when $FeCl_2$ was used as the starting material (Scheme 11).

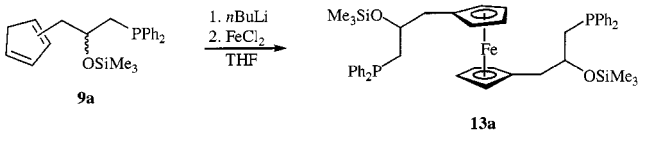

9a **13a**

Scheme 11

Compound **13a** was obtained from **9a** as a yellow, waxy material in analytically pure form (Table 11). With two stereogenic centres, **13a** must exist as a mixture of *meso* and *racemic* forms. The interaction of the chiral groups is, however, too small to make this differentiation recognisable in its NMR spectra. Only one set of signals was observed for each group (see Experimental Section). One sharp ^{31}P NMR resonance is observed at $\delta = -23.6$. The Cp protons give rise to one unresolved signal at $\delta = 4.01$. Regarding the diastereotopic methylene protons, the pair at the CH_2Cp group gives rise to a well-resolved pattern at $\delta = 2.77$ with $^2J_{HH} = 14.0$ Hz and $^3J_{HH} = 6.0$ Hz (see Experimental Section) while those of the CH_2PPh_2 group appear as an unresolved multiplet at $\delta = 2.26$ (see Experimental Section). The ^{13}C NMR spectra show well-resolved peaks for the individual types of carbon atoms and allowed for the complete assignment of the Cp carbon atoms as well as of the carbon atoms of the side chains (see Experimental Section). As is characteristic for ferrocene and its derivatives **13a** shows a reversible oxidation in its cyclovoltammogram. The electronic influence of the side chains in **13a** is small, since oxidation occurs at $E_{1/2} = 325$ mV (vs. SCE), while ferrocene − under the same conditions − is oxidised at $E_{1/2} = 367$ mV.

The presence of free phosphane donors in **13a** is also apparent from its ^{31}P NMR signal at $\delta = -23.6$ (see Experimental Section). Additional evidence came from the reaction of **13a** with $Cr(CO)_5THF$ which resulted in a yellow, waxy substance. The mass spectrum of this yellow material shows a peak at $m/z = 1198$ [M^+, **13b**·2 $Cr(CO)_5$], which by consecutive loss of CO groups and one Cr atom, leads to a prominent signal at $m/z = 866$. Reaction of **9b** with $FeCl_2$ gave **13b** as a dark red, viscous oil (Scheme 12).

The number of stereoisomers is increased by a factor of two with respect to the number of isomers of **13a**, the reason being the loss of symmetry on going from the monosubstituted Cp ligand in **13a** to the monosubstituted indenyl ligand in **13b**. Nevertheless, only one sharp ^{31}P NMR signal is observed for **13b** at $\delta = -23.5$. The ^1H NMR spectrum of **13b**, on the other hand, clearly shows two different sets of signals with an intensity ratio of approximately 1:1. Thus, two signals are observed for the TMS protons, one at $\delta = -0.25$ and the other at $\delta = -0.20$. Two well-separated signals are also observed for the protons at the 3-position of the indenyl ligands, one at $\delta = 4.48$ and the other one at $\delta = 4.36$. The signals relating to the other protons partly overlap. COSY experiments,[16] nevertheless, allowed for their unambiguous assignment. It followed that there are two classes of isomers of **13b** which are discernible by ^1H NMR spectroscopic data. ^{13}C NMR spectroscopic data are in agreement with these findings (see Experimental Section). Since it had been shown with **13a** as the example that the chirality of the substituents does not lead to separate signals for the corresponding diastereomers, the two classes of isomers observed for **13b** must be due to the two sets of diastereomers which result by formally adding the R−IndFe entity to either of the two sides of the second R−Ind ligand. Compound **13b** shows a reversible oxidation, as one would expect for a ferrocene derivative with $E_{1/2} = 106$ mV (vs. SCE). It is more readily oxidised than ferrocene which shows its oxidation peak at 470 mV in the same experiment.

The reactions of **4** and **9** with $FeCl_2$ and $FeCl_2(PPh_3)_2$ [10] did not produce compounds in which the Cp-type donor and the phosphorus donors bind in a chelate mode. To test whether $CoCl_2$ might be an appropriate precursor for the formation of such chelate compounds, the prototype ligand

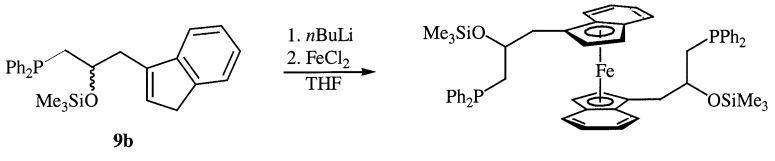

9b **13b**

Scheme 12

$CH_3C(CH_2PPh_2)_2(CH_2Cp)$[2b] was treated with $CoCl_2$·THF (Scheme 13).

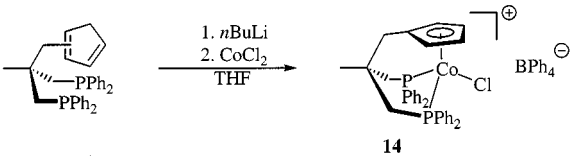

14

Scheme 13

From the dark brown reaction mixture, the violet chelate compound was separated by chromatography and isolated as its analytically pure BPh_4 salt **14**. The ^{31}P NMR resonance of **14** occurs at $\delta = 25.4$. The ^1H NMR spectrum, as well as the ^{13}C NMR spectrum, confirm the assigned structure (see Experimental Section). The isolation of **14** showed that $CoCl_2$ might be a suitable starting material to obtain the desired chelate compounds. Since the yield of **14** was lower than the yields of the corresponding iron compounds,[2a][3b,6] $RuCl_2(PPh_3)_3$ was tested as an alternative precursor. It had been found that its reaction with $CH_3C(CH_2PPh_2)_2(CH_2Cp)$ produces $CH_3C(CH_2$-η^1-$PPh_2)_2(CH_2$-η^5-Cp)RuCl in yields of up to 41% and it had also been observed that this compound, once formed, is quite stable.[15] Thus, the coordination capabilities of the ligands **9** were tested once again with $RuCl_2(PPh_3)_3$ as the starting coordination compound.

When **9a** was deprotonated by *n*BuLi in THF, a yellow, oily product remained after evaporation of the solvent. Addition of a solution of this residue in 1,2-dichloroethane to a solution of $RuCl_2(PPh_3)_3$ in 1,2-dichloroethane produced a slightly brown reaction mixture. Keeping this reaction mixture at 90 °C for 1 h resulted in the formation of **15a** as a yellow crystalline powder in yields of 50% after chromatographic workup (Scheme 14, Table 11). The chirality at the siloxy-substituted carbon atom and the metal-centred chirality result in **15a** existing as two diastereomers, each comprising of an enantiomeric pair. The ^{31}P NMR spectrum of **15a** shows two well-resolved doublets of high intensity and two equally well-resolved doublets with about $^1/_{10}$ of the intensity of the two major doublets (Experimental Section). The assumption that these two patterns arise from two diastereomers present in a ratio of 10:1 was justified by the ^1H NMR spectrum of **15a**. Four well-separated signals are observed for the Cp protons of the major isomer. Two of the four Cp protons of the minor isomer give rise to well-separated signals, while the other two are hidden under the signals of the methine protons and of one of the Cp protons of the major isomer (see Experimental Section). The diastereomeric ratio, as inferred from the corresponding integrals, was 13:1.

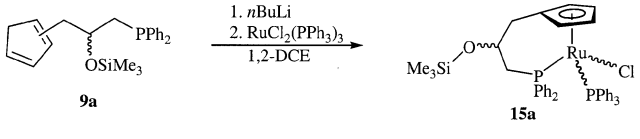

9a **15a**

Scheme 14

Diastereomeric discrimination has already been observed in the preparation of other similar compounds. B. Trost et al. have tested a series of chelate ligands which contain a Cp moiety covalently linked to a PPh_2 entity by a chiral spacer. When these ligands were used in the preparation of compounds of type **15a**, diastereomeric ratios of up to 5:1 were observed with $-(CH_2)_3-(H)(CH_2Ph)C-$ as the chiral linker, the stereogenic centre being bonded to the phosphorus atom.[17] Single crystals of **15a** were obtained in about 80% yield by slow evaporation of the solvent from saturated CH_2Cl_2/PE (boiling range 40−60 °C) solutions.

X-ray analysis showed them to contain the racemate of **15a** with two independent molecules **15a** in the asymmetric unit of the centrosymmetric unit cell (Table 6 and Figure 3). The configuration at the stereogenic centres of the analysed diastereomer was *R*,*R* and *S*,*S*. Based on the high yield with which single crystals were obtained, it was assumed that the major isomer was the diastereomer contained in the crystal. The chelate cycle formed by C4, C3, C2, C1, P1 and Ru1 adopts an approximate chair conformation (Figure 3; Table 6, torsion angles). The $OSiMe_3$ group is in an equatorial position (Figure 3 and Table 6) of this cycle. The PPh_3 ligand occupies an axial position, with the Cl ligand lying in an equatorial position with respect to this idealised description (Figure 3 and Table 6). The coordination around the ruthenium centre (Figure 3) is similar to that observed in other derivatives of the type $CpRuL_2Cl$.[15] The rotational position of the phenyl groups of the PPh_2 moiety of the chelate ligand corresponds to the generally observed position in *tripod* metal compounds $H_3CC(CH_2$-η^1-$PPh_2)_2(CH_2$-η^5-Cp)RuCl.[15] The phenyl groups of the PPh_3 ligand adopt the usual propeller-type arrangement (Figure 3). Bonding to the Cp ligand is symmetric, and all the $Ru-C^{Cp}$ distances are similar (Table 6). The Cp ligand is planar to within ± 1 pm. The carbon atom of the chelate chain which bonds to the Cp entity (Figure 3, C3) deviates from this plane by 16 pm (14 pm in the other independent molecule) in a direction opposite to the ruthenium centre.

Table 6. Selected bond lengths [pm], bond angles [°], and torsion angles [°] of **15a**

[a]

Ru1−P1	228.3(2)/227.9(2)	C6−C7	142.6(9)/140.8(8)
Ru1−P2	231.1(2)/231.3(2)	C7−C8	144.1(9)/141.8(8)
Ru1−C4	219.1(6)/218.8(6)	P1−Ru1−P2	99.5(1)/98.5(1)
Ru1−C5	221.1(6)/223.3(6)	P1−Ru1−Z	119.1/119.8
Ru1−C6	222.6(6)/223.7(6)	P2−Ru1−Z	124.6/124.5
Ru1−C7	224.8(6)/222.0(6)	P1−Ru1−Cl1	95.1(1)/94.8(1)
Ru1−C8	218.3(6)/218.6(6)	P2−Ru1−Cl1	89.9(1)/91.4(1)
Ru1−Z	184.9/185.1	Z−Ru1−Cl1	121.4/120.7
Ru1−Cl1	244.4(2)/244.8(2)	C2−C1−P1−Ru1	−58.6(5)/53.1(5)
C3−C4	151.4(9)/150.1(8)	C1−C2−C3−C4	−63.2(7)/59.1(7)
C4−C5	143.8(9)/145.2(9)	C2−C3−C4−Ru1	46.1(8)/−45.3(7)
C4−C8	142.1(9)/143.1(8)	C3−C4−C5−C6	173.1(6)/173.3(6)
C5−C6	140.9(9)/140.9(9)	C3−C4−C8−C7	171.7(5)/−173.1(6)

[a] Atom identifiers refer to Figure 3; Z designates the centre of the Cp ligand. There are two independent molecules **15a** in the crystal; the data referring to the second molecule are given following the slash in each case.

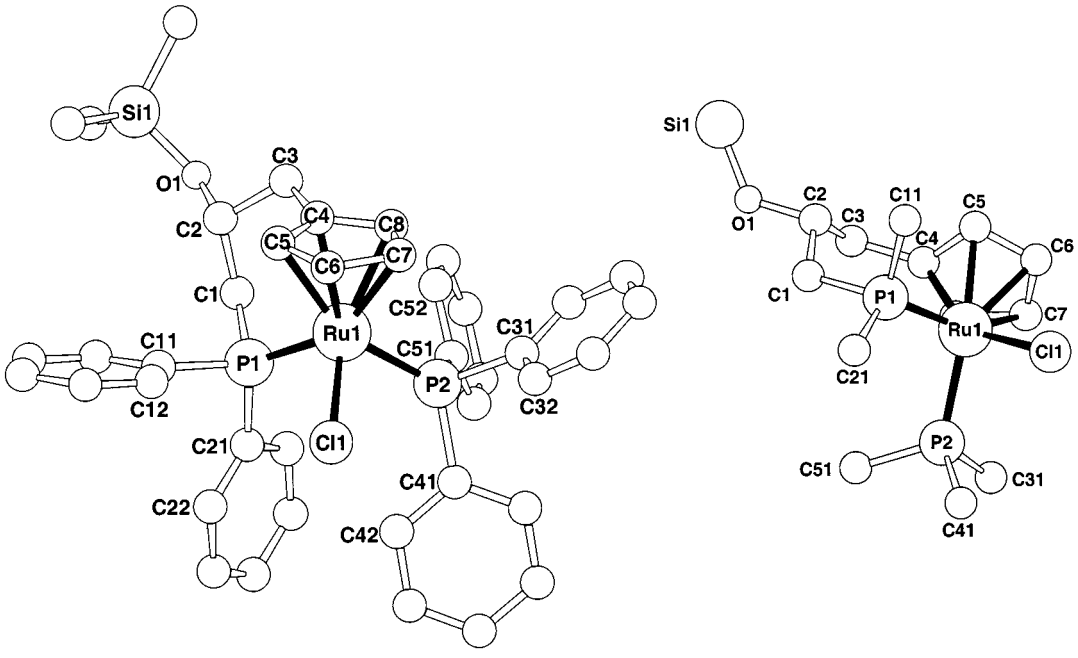

Figure 3. Structure of **15a**; left-hand side: general view and labelling scheme; right-hand side: view showing the chair conformation of the chelate cycle

The structure of the second diastereomer, which is formed in only 7% relative to the major isomer, must correspond to the one in which the positions of the PPh_3 and the Cl ligands are exchanged. Inspection of Figure 3 shows that steric crowding should increase by this exchange.

The number of possible isomers (four in the case of **15a**) occurring as two diastereomeric pairs will be increased by a factor of two when **9b** acts as a ligand in **15b**, due to the additional chirality introduced by anellating the Cp moiety.

The reaction of **9b** with $RuCl_2(PPh_3)_3$ under similar conditions used in the preparation of **15a** might thus, in principle, lead to the formation of four diastereomeric forms of **15b** (Scheme 15), each of them comprising of an enantiomeric pair, and the results of such a reaction might therefore be difficult to analyse. On the other hand, the diastereomeric discrimination already observed in the formation of **15a** might even be enhanced by the additional steric congestion introduced by the anellated benzene ring in the indenyl derivative compared to the Cp derivative. This is, in fact, found in the experimental results. Only two sharp and well-resolved doublets are observed for **15b** in its ^{31}P NMR spectrum. The ^{1}H NMR spectrum shows sets of signals which can unequivocally be assigned to only one diastereomer, with no indication of any contamination by other diastereomers. The signals for the methylene and the methine protons of the chelate cycle as well as the resonances of the two Cp protons are observed in the range between $\delta = 2.4$ and $\delta = 4.5$ (see Experimental Section). Assignment of the individual resonances was possible by analysis of the individual coupling constants, as well as by ^{31}P decoupling. In the ^{13}C NMR spectrum of **15b**, the corresponding resonances can unambiguously be assigned. The *ipso*-carbon atoms of the indenyl moiety were also identified by their corresponding signals. No attempt was made to assign the signals in the arene region.

All these NMR spectra show that only one diastereomer was formed by the reaction of **9b** with $RuCl_2(PPh_3)_3$. Based on the known structure of **15a**, it appears that anellation of the Cp moiety at the side of the chelate chain would lead to less steric crowding than anellation at the PPh_3 side. Replacing the Cp moiety in **15a** by the indenyl group, as in **15b**, resulted in an increase in diastereomeric differentiation and **15b** was formed exclusively in one diastereomeric form.

With *tripod* ligands such as **4b**, which have a stereogenic carbon centre by virtue of their two different phosphorus donors, diastereomeric differentiation might also be expected in their tripodal-coordinated derivatives. In order to test the coordination capabilities of **4**, the achiral ligand **4a** was deprotonated with *n*BuLi and treated with $RuCl_2(PPh_3)_3$. Chromatographic workup led to **16a** (Scheme 16). The yield of **16a** (42%) (Table 11) appeared sufficient to also test the less easily accessible ligand **4b** in this type of reaction. A modest yield of 16% of **16b** was obtained (Table 11, Scheme 17).

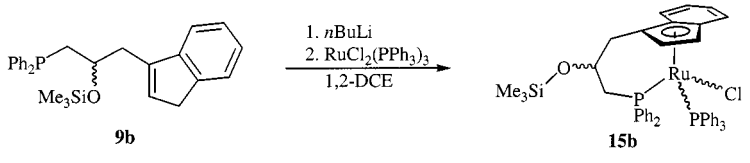

Scheme 15

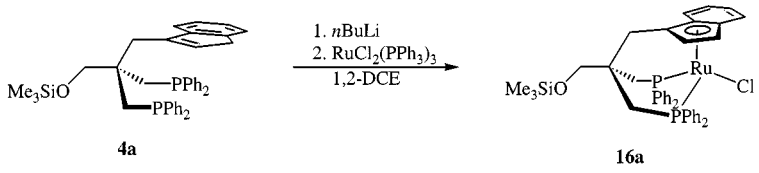

4a **16a**

Scheme 16

Table 7. ^{1}H and $^{31}P\{^{1}H\}$ NMR spectroscopic data of compounds **16**

Atom[a][b]	**16a**	**16b**	Atom[b]	**16a**	**16b**	Atom[b]	**16a**	**16b**
H^{1a}	2.40 (dd) [1H] $^{2}J_{HH}$ = 15.5 Hz, $^{2}J_{HP}$ = 10.3 Hz	1.15 (m)	**H^{11}**	7.27 (m)	–	**H^{4}**	4.66 (dd) [1H] $^{3}J_{HH}$ = 2.7 Hz J_{HP} = 7.2 Hz	4.53 (dd) $^{3}J_{HH}$ = 2.5 Hz J_{HP} = 8.4 Hz
			H^{21}	7.33 (m)	–			
			H^{31}	7.36 (m)	7.80 (m)			
H^{1b}	2.55 (dd) [1H] $^{2}J_{HH}$ = 15.5 Hz, $^{2}J_{HP}$ = 9.4 Hz	1.55 (m)	**H^{41}**	8.06 (dd) $^{3}J_{HH}$ = 6.6 Hz, $^{3}J_{HP}$ = 7.8 Hz	8.10 (dd) $^{3}J_{HH}$ = 6.6 Hz, $^{3}J_{HP}$ = 8.5 Hz	**H^{5}**	5.73 (dd) [1H] $^{3}J_{HH}$ = 2.7 Hz J_{HP} = 3.3 Hz	5.59 (m) $^{3}J_{HH}$ = 2.5 Hz
H^{2a}	2.91 (dd) [1H] $^{2}J_{HH}$ = 15.4 Hz, $^{2}J_{HP}$ = 10.7 Hz	2.98 (dd) [1H] $^{2}J_{HH}$ = 15.1 Hz, $^{2}J_{HP}$ = 11.4 Hz	**H^{11a}**	–	1.55 (m)	**H^{6}**	7.60 (d) [1H] $^{3}J_{HH}$ = 8.2 Hz	7.58 (d) [1H] $^{3}J_{HH}$ = 7.4 Hz
			H^{11b}	–	1.97 (m)			
			H^{12}	–	0.38 (m)	**H^{7}**	7.04 (t) $^{3}J_{HH}$ = 7.3 Hz	7.26 (m)
H^{2b}	2.01 (m) [1H]	1.75 (m)	**H^{21a}**	–	0.15 (m)			
H^{3a}	2.06 (d) [1H] $^{2}J_{HH}$ = 14.4 Hz	1.92 (m)	**H^{21b}**	–	1.15 (m)	**H^{8}**	6.23 (t) $^{3}J_{HH}$ = 7.6 Hz	7.58 (m)
			H^{22}	–	0.65 (dt)			
H^{3b}	1.84 (d) [1H] $^{2}J_{HH}$ = 14.4 Hz	1.92 (m)			$^{3}J_{HH}$ = 7.4 Hz $^{3}J_{HP}$ = 7.2 Hz	**H^{9}**	6.07 (d) $^{3}J_{HH}$ = 8.2 Hz	7.21 (m)
CH_2O	3.85 (br. s) [2H]	3.63 (br. s) [2H]						
$SiCH_3$	0.36 (s) [9H]	0.28 (s) [9H]						
P^{1}	30.4 (d) $^{2}J_{PP}$ = 80.2 Hz	33.8 (d) $^{2}J_{PP}$ = 77.1 Hz						
P^{2}	54.0 (d) $^{2}J_{PP}$ = 80.2 Hz	56.3 (d) $^{2}J_{PP}$ = 77.1 Hz						

[a] Solvent $CDCl_3$. – [b] For designation of the atoms refer to Figure 6 (**16a**) and Figure 9 (**16b**).

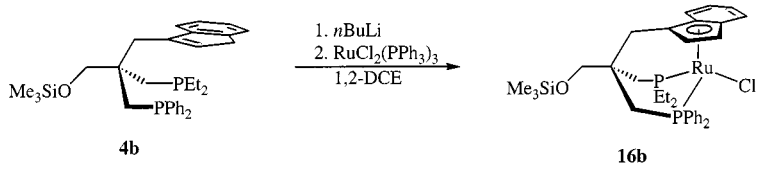

4b **16b**

Scheme 17

Both compounds **16** were obtained as red, microcrystalline powders. Two sharp doublets are observed in the ^{31}P NMR spectrum of **16a** (δ = 30.4, 54.0, $^{2}J_{PP}$ = 80.2 Hz, Table), as is expected owing to its lack of symmetry. One of the phosphorus atoms is close to the anellated benzene moiety of the indenyl ligand, while the other one is further away, on the less congested side of the compound. ^{1}H NMR spectroscopic data (Table 7) and ^{13}C NMR spectroscopic data (see Experimental Section) are in agreement with the given formula (Table 11). By an extensive series of NMR experiments, it was proved (see below) that the signal at δ = 30.4 can be assigned to the phosphorus nucleus which lies below the anellated benzene ring.

With **4b** as the ligand constituent of **16b**, two diastereomeric forms of **16b** could be expected: one with the anellated ring on the side of the PPh_2 group and a second with the PEt_2 group and the anellated ring close to each other. From the ^{31}P NMR spectroscopic data of **16b**, it appeared that only one of these isomers was formed (Table 7). In order to find out which of the two possible isomers was formed, since it was not possible to grow single crystals of **16**, the structures of **16a** and **16b** were elucidated by NMR experiments.

NMR Analysis

Compound **16a** shows a well-resolved ^{1}H NMR spectrum (Figure 4 and Table 7). Filtering this spectrum by means of long-range phosphorus coupling led to the lower traces shown in Figure 4. The signals of the methylene protons, as well as the signals of the aromatic protons are clearly differentiated by these traces. $^{2}J_{HP}$ coupling leads to prominent signals for the methylene groups which are directly bonded to the phosphorus nuclei. The protons of the methylene groups are diastereotopic owing to the lack of symmetry of the compound as a whole. This diastereotopicity is apparent from the characteristic doublet of doublets for each of the protons of the methylene groups linked to the phosphorus atom. The signals labelled H^{1A}/

H^{1B} (Figure 4 and Figure 6) are therefore assigned to the methylene group at P^1, the ones labelled H^{2A}/H^{2B} (Figure 4 and Figure 6) originate from the methylene group at P^2. The remaining signals H^{3A}/H^{3B} (Figure 4 and Figure 6) must therefore be due to the CH_2Cp group. The CH_2O-$SiMe_3$ group (Figure 4 and Figure 6) gives rise to signals at $\delta = 3.85$ and 0.36.

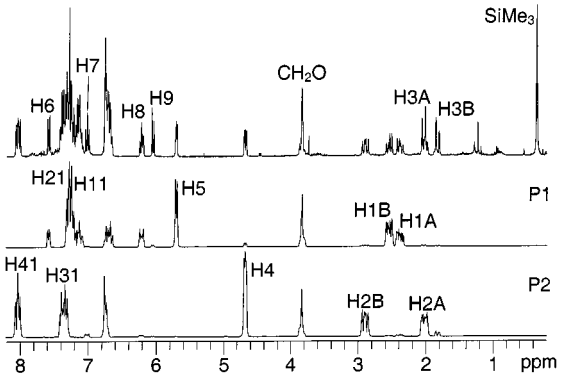

Figure 4. ^1H NMR spectrum (top) and cross-sections of the $\{^1H,^{31}P\}$-HMBC spectrum of **16a**; centre trace: filtering by long-range coupling to P^1; bottom trace: filtering by long-range coupling to P^2

The parts of the spectrum assigned to the protons of the Cp moiety are less conclusive: There are different pathways along which ^{31}P coupling to these protons may occur, while for the methylene protons $^2J_{HP}$ coupling is the dominant pathway. It is interesting to note that one of the Cp protons (H^5; Figure 4 and Figure 6) correlates strongly with P^1, while the other shows a strong correlation with P^2 (H^4; Figure 4 and Figure 6).

The aromatic protons are as well differentiated by their different correlations with P^1 and P^2 (Figure 4 and Figure 6). Unambiguous assignment was not possible from this experiment alone and the assignment given in Figure 4 was based on additional experimental grounds. A plausible argument for assigning the signal H^{41} (Figure 4 and Figure 6) comes from comparison with the NMR spectroscopic behaviour of other tripod metal compounds:[15,18] In the aryl region of the ^1H NMR spectra of such compounds, the signals with the greatest downfield shift have always been found to be due to the *ortho*-protons of phosphorus-bonded phenyl rings, wherever assignment was possible. The well-separated signal observed for H^{41} in the aromatic region (Figure 4 and Figure 6) together with its downfield shift allowed for its assignment to an *ortho*-proton of a phenyl

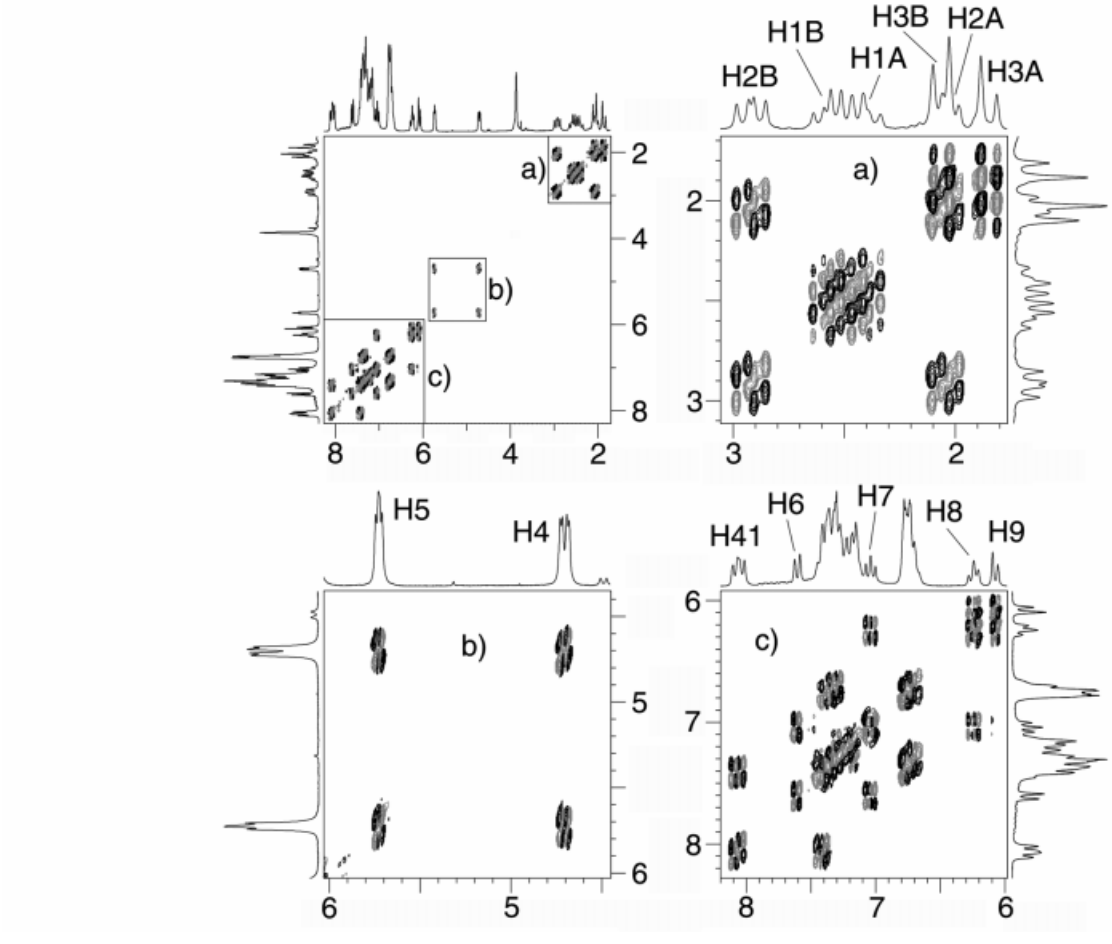

Figure 5. DQF-COSY spectrum of **16a**; the individual regions labelled a, b, and c in the complete spectrum (top left) are shown in magnified form under these labels

ring bonded to P^2. ^{31}P-decoupling reduced the doublet of doublet structure of this signal (Figure 4) to a well-resolved doublet, as expected.

The assignment of the individual signals in the methylene region was confirmed by COSY experiments. These experiments revealed the individual methylene groups by their $^2J_{HH}$ coupling (Figure 5a).

COSY data were important for the unambiguous assignment of resonances to the indenyl part of the molecule. While the Cp part of the indenyl ligand was clearly apparent even from 1D NMR experiments (Figure 4, see above), the signals of the protons H^6-H^9 (Figure 4, Figure 5 and Figure 6) in the anellated benzene ring of the indenyl fragment, while apparent as individual patterns, could not be assigned with respect to their mutual sequence. The COSY spectrum shown in Figure 5 (5c) enabled the sorting of the signals into a sequence of mutually neighbouring protons. The only ambiguity remaining was the question as to which of the protons, H^6 or H^9, was at the back or the front of the molecule (Figure 6). This ambiguity was resolved by NOE

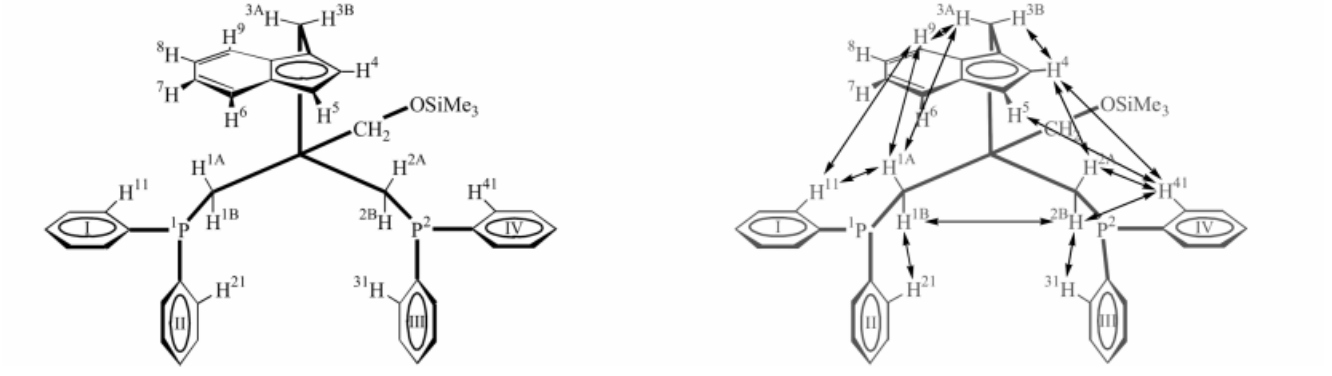

Figure 6. Numbering scheme used in the NMR analysis of **16a**; the right hand side shows the conformationally relevant and experimentally accessible NOE contacts as double-headed arrows

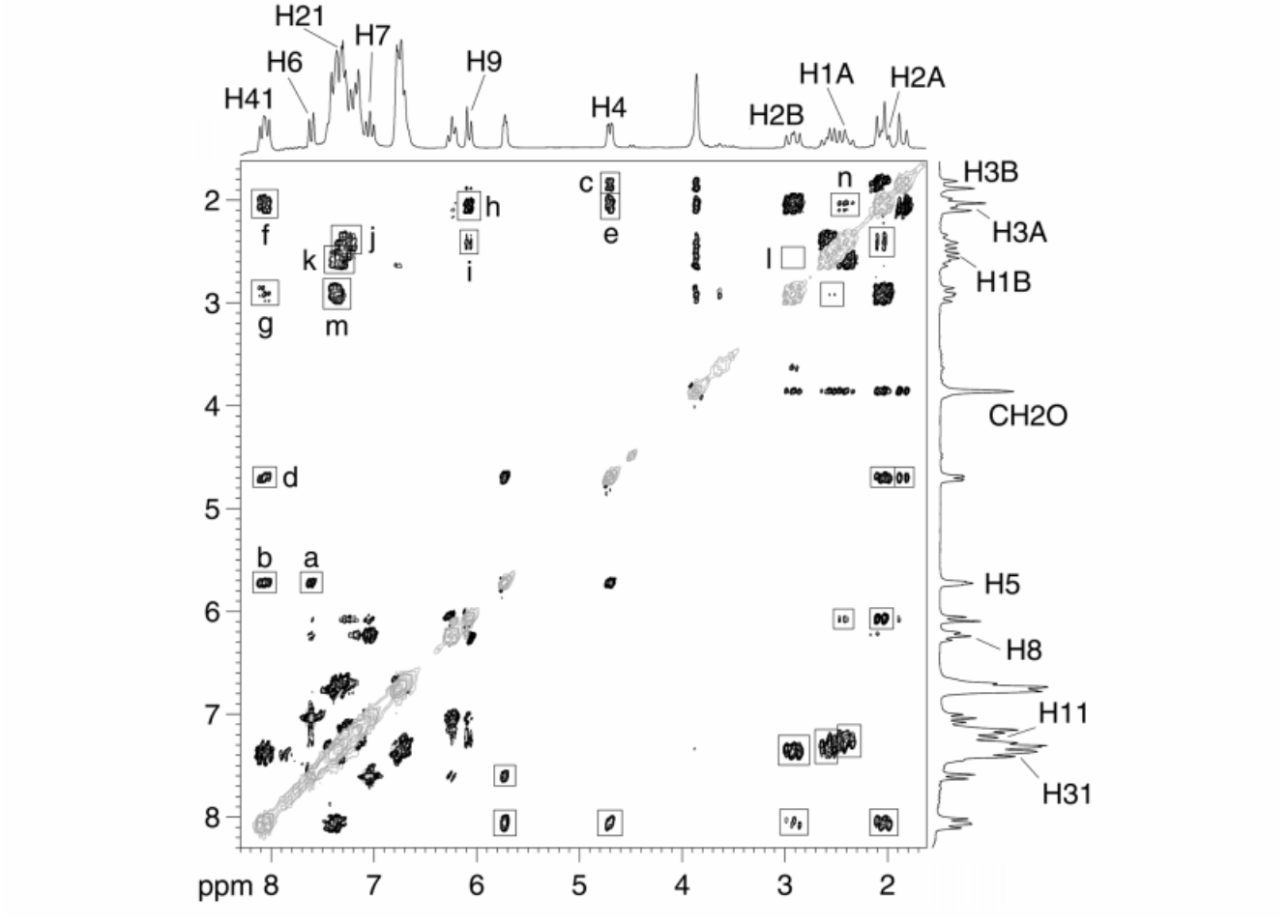

Figure 7. NOESY spectrum of **16a**; the labels designating individual conformationally relevant cross-peaks are used as an abbreviated reference in the text; the origin of the cross-peaks follows from the labelling of the spectral traces

experiments (Figure 7),[19] which finally allowed for the unambiguous assignment of all the conformationally relevant protons labelled in Figure 6. The ambiguity about the position of the protons H^6/H^9 was resolved by the observation of a strong cross-peak (Figure 7; labelled a) between one of the protons of the Cp part of the ligand (H^5) and one of the protons of the anellated benzene moiety (H^6). The position of both protons (referring to Figure 6) is clear from this observation.

H^5 shows a correlation with H^{41} (Figure 7; b) while H^4 shows correlations with H^{3b}, H^{41} and H^{2A} (Figure 7; c, d, e). H^{2A} itself correlates with H^{41} (Figure 7; f) and H^{41} shows a cross-peak with H^{2B} (Figure 7; g), which also correlates with H^{31} (Figure 7; m). These correlations built up a framework which unambiguously differentiated between the two sides of the compound and showed that the phosphorus atom labelled P^2 was at the side of the molecule opposite to that containing the anellated benzene ring (Figure 6).

The mutual orientation of the constituents at the other side of the molecule may be inferred from cross-peaks between H^9 and the methylene protons H^{3A} and H^{1A} (Figure 7; h, i). H^{1A} correlates with H^{11} and with H^{3A} (Figure 7; j, n). The second proton of this methylene group H^{1B}, shows a cross-peak with H^{21} as well as with H^{2b} (Figure 7; k, l). Some additional correlations involving *meta*-protons are also observed (Table 8). A scaffolding was thus apparent from the NOE experiments which qualitatively completely defined the conformation of **16a** (Figure 6, right-hand side).

A quantitative insight into the conformational manifold adopted by **16a** in solution was provided by a molecular modelling approach. To this end, a model representation was constructed. The basic geometry may be taken from the experimental structures of similar compounds such as $H_3CC(CH_2\text{-}\eta^1\text{-}PPh_2)_2(CH_2\text{-}\eta^5\text{-}Cp)RuCl$[15] with the anellated benzene moiety and the TMS group being added by modelling procedures.[20] The model thus generated was locally optimised with respect to energy as a template for any further calculations. Alternatively, the model may be constructed without explicit reference to similar molecules by using the parameters of the modelling package (Discover 3.0, ESFF force field) alone. Both these approaches led to basically the same conformations of the model template.

As was also observed in the structures of Cp derivatives $H_3CC(CH_2\text{-}\eta^1\text{-}PPh_2)_2(CH_2\text{-}\eta^5\text{-}Cp)RuCl$, the chelate cage itself is chiral.[15] The torsion angles $Ru-P-CH_2-C_{ipso}$ never conform to a mirror symmetric arrangement, even in the case of Cp derivatives.[2,3,6,15] With the indenyl ligand of **16a**, additional side differentiation was imposed on the molecules such that conformational diastereomers may exist. To cope with this problem, starting from the model compound, a second model was constructed leaving everything unchanged besides the orientation of the indenyl group which was rotated around its $C-CH_2$ axis by 180°. These two diastereomeric model templates, together with the quantitative information of the inter-proton distances were used for distance-geometry (DG) calculations.[21] From these procedures, a set of conformations resulted, which were in agreement with the restraints imposed by the distances pertaining to the model and by the inter-proton distances from the NOE data.

Table 8. NOE contacts in **16a**

No.[a]	**16a**		d_{NOE} [pm]	$d_{calcd.}$ [pm]	σ^2 [pm^2]
1	H1A	H1B	251	177	5476
2	H2A	H2B	206	176	900
3	H3A	H3B	218	176	1764
4	H4	H5	253	265	144
5	H5	H6	278	295	289
6	H6	H7	230	242	144
7	H7	H8	234	256	484
8	H8	H9	245	240	25
9	H41	H42	201	247	2116
10	CH_2OSi	H1A	289	245	1936
11	CH_2OSi	H1B	300	308	64
12	CH_2OSi	H2B	302	291	121
13	CH_2OSi	H3A	270	246	576
14	CH_2OSi	H3B	281	239	1764
15	H1A	H3A	304	254	2500
16	H1A	H11	226	209	289
17	H1A	H9	318	319	1
18	H1B	H2B	361	274	7517
19	H1B	H21	229	232	9
20	H2A	H4	260	268	64
21	H2A	H41	247	247	0
22	H2B	H41	305	265	1600
23	H2B	H31	226	213	169
24	H3A	H9	256	245	121
25	H3B	H4	290	278	144
26	H4	H41	280	296	256
27	H4	H42	370	437	4489
28	H5	H41	259	245	196
29	H8	H12	289	363	5476
30	H9	H11	298	318	400
Contacts No.		1−9	1−30	10−30	15−30
RMS [pm]		35	36	36	38

[a] Atom labels refer to Figure 6 throughout. H42 (No. 27) and H12 (No. 29) designate protons in the *meta* position of the aryl rings IV and I, respectively. Contacts No. 1−9 refer to distances which are fixed by the covalent framework. In the final calculations, contacts No. 2 and 4 were used as reference distances to transform the NOE volume integrals into distances. Contacts No. 10−14 designate distances which are not fixed by the covalent framework but refer to CH_2 protons of the CH_2OSi fragment which are diastereotopically not differentiated in the spectra. The "dummy atom" approach was used to incorporate these contacts in the calculations.[29] Contacts No. 15−30 are also not fixed by the covalent framework and build up a tight scaffolding to which the conformation has to adopt. The *ortho* and *meta* protons of the aryl groups show no diastereotopic differentiation in the spectra. For the purpose of distance-geometry calculations, each pair of these protons was replaced by a dummy atom.[29] For the purpose of energy minimisation and rms calculation, the protons were assigned individually with respect to whichever one gave the shorter distance. The rms values given refer to inter-proton distances exclusively. The set of contacts to which they refer is indicated by the appropriate range in terms of their numeric labels. Since contacts No. 1−9 refer to distances which are fixed by covalent bonding, the respective rms value presents an expected value for the overall accuracy. The rms values referring to all contacts (No. 1−30) or only to conformationally relevant subsets (No. 10−30, No. 15−30) are well within the expected range.

Figure 8 shows the results obtained for **16a**. The ten conformations (grey) with the lowest distance violations (with the best overall agreement) are shown. While it is clear from the NMR observations that the phenyl groups are free to

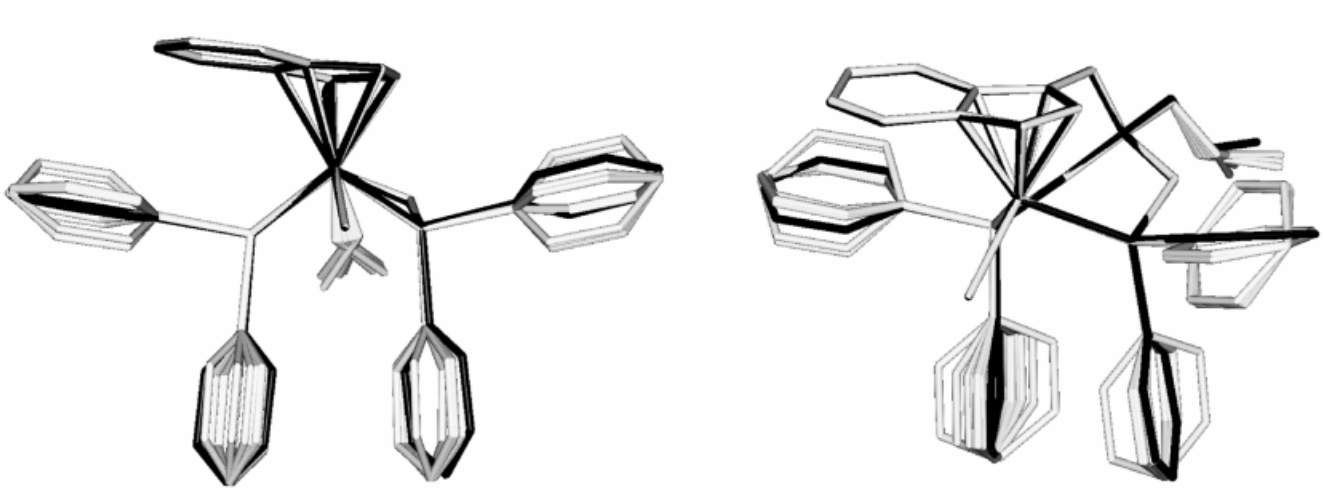

Figure 8. NMR-derived conformations characterising **16a** in solution; the conformation shown in black represents the optimal single conformation

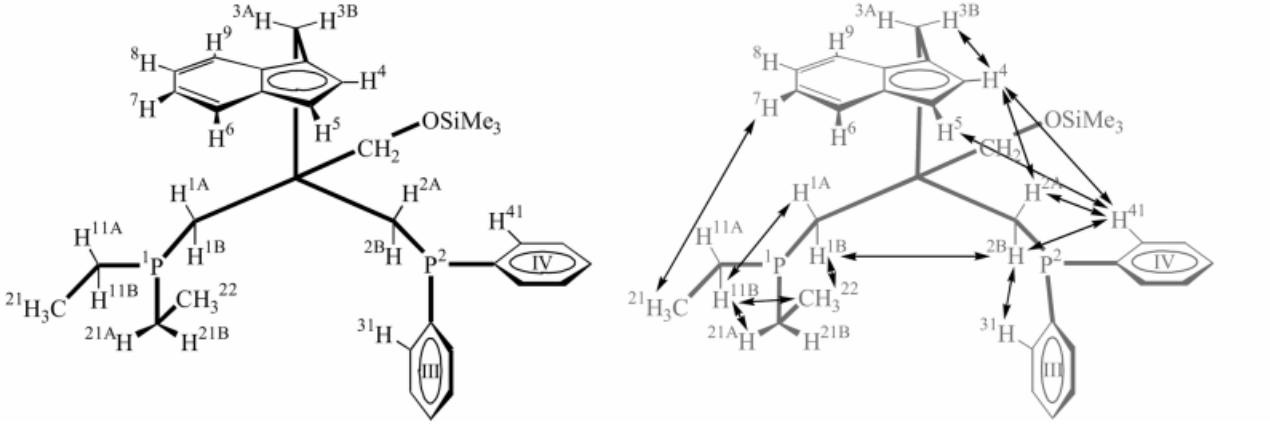

Figure 9. Numbering scheme used in the NMR analysis of **16b**; the right-hand side shows the conformationally relevant and experimentally accessible NOE contacts as double-headed arrows

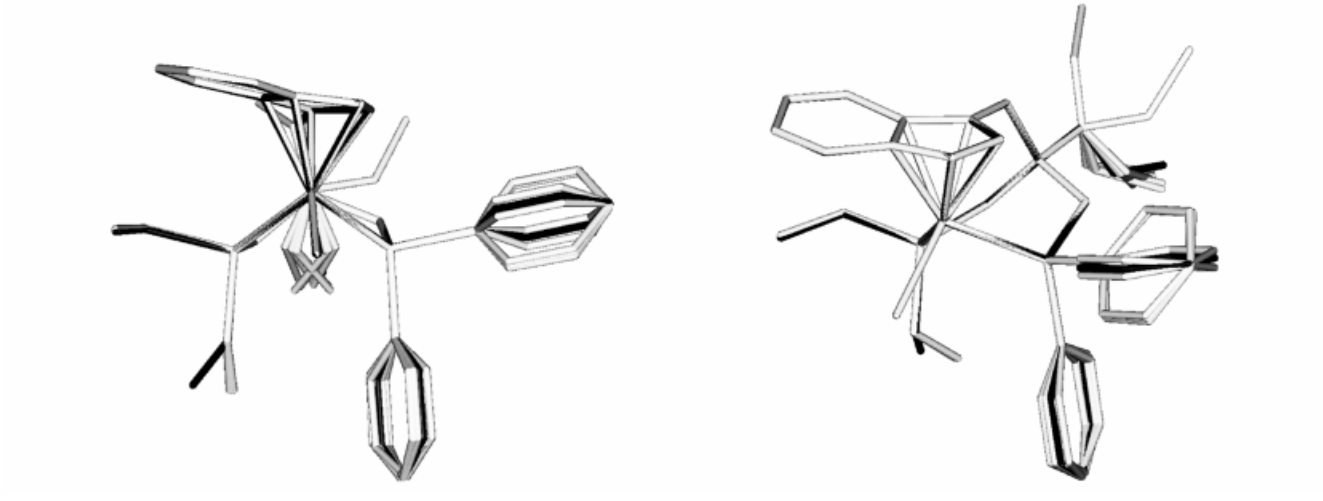

Figure 10. NMR-derived conformations characterising **16b** in solution; the conformation shown in black represents the optimal single conformation

rotate (only one H_{ortho} signal for each of the four phenyl groups was observed) a rotational preference is apparent from the distance-geometry results (Figure 8). From this set of conformations, obtained by distance-geometry calculations, the one with the best agreement was used to define the starting structure for geometry optimisation on the ba-

Table 9. NOE contacts in **16b**

No.[a]	**16b**		d_{NOE} [pm]	$d_{calcd.}$ [pm]	σ^2 [pm^2]
1	H1A	H1B	185	177	64
2	H2A	H2B	195	176	350
3	H3A	H3B	272	176	9293
4	H4	H5	250	265	237
5	H5	H6	277	295	310
6	H6	H7	233	242	74
7	H11A	H11B	197	176	458
8	H11B	H12	271	248	520
9	H21A	H21B	183	175	66
10	H21A	H22	265	248	292
11	H41	H42	210	246	1332
12	CH_2OSi	H1A	270	243	708
13	CH_2OSi	H1B	296	315	372
14	CH_2OSi	H2A	272	257	210
15	CH_2OSi	H2B	274	289	219
16	CH_2OSi	H3B	237	236	1
17	H1A	H11B	242	267	650
18	H1B	H2B	295	272	506
19	H1B	H22	282	223	3505
20	H2A	H4	230	246	262
21	H2A	H41	247	249	5
22	H2B	H41	269	258	130
23	H2B	H31	220	209	121
24	H3B	H4	299	285	196
25	H4	H41	280	314	1156
26	H5	H41	251	242	79
27	H7	H12	296	337	1706
28	H11B	H21A	239	310	5055
29	H11B	H22	263	224	1552
Contacts No.		1−11	1−29	12−29	17−29
RMS [pm]		34	32	30	34

[a] Atom labels refer to Figure 9 throughout. The meaning of columns and designations is analogous to the one explicitly described for **16a** in Table 8. Contacts No. 1, 2, 4, and 7 were used as the distance reference.

sis of energy minimisation. The resulting minimised conformation is shown in black in Figure 8.

With the best model from distance-geometry alone, the rms deviation between the observed and calculated distances is only approximately 3 pm. This traditional measure of quality of agreement between calculated conformations and NOE distances is quite biased, since the distances determined by the covalent framework and the distances referring to NOE contacts are measured by the same ruler. It appears more appropriate to consider the difference between NOE-derived distances and their computationally generated counterparts alone to derive a measure of quality. For the model generated by distance-geometry, this measure results in an rms of 48 pm. With the optimal conformation obtained after energy minimisation, this rms deviation is approximately 36 pm and thus corresponds to the error estimated for the accuracy of the NOE distances (Table 8).

The procedure as described for the NMR analysis of **16a** was also applied to **16b**. ^{1}H,^{31}P-HMBC[22] and ^{1}H,^{1}H-COSY experiments together with other 2D NMR spectroscopic data did allow for the complete assignment of an extensive subset of signals (Table 7, Figure 9 and Experimental Section).

The measured NOE contacts built up a tight scaffolding which the conformation of **16b** had to adopt (Figure 9, right-hand side). The NMR spectroscopic data also clearly showed that **16b** was diastereomerically pure. If there were another diastereomer present, its concentration must be below the NMR detectable limit (< 1%). It is clear from these experiments that the phosphorus nucleus of the PEt_2 group resonates upfield (P^1, δ = 33.8, Table 7) from that of the PPh_2 group (P^2, δ = 56.3, Table 7). It is also clear that the PEt_2 group is located on the same side as the anellated benzene ring. Refinement of the structure by the same procedures applied to **16a** led to the set of conformations shown in Figure 10.

The optimal single conformation is shown in black in Figure 10. The rms deviation between the calculated and experimental values of 18 conformationally relevant interproton distances (Figure 9) is only 30 pm (Table 9). This single conformation is therefore in optimal agreement with the NOE data. The most important result of this NMR analysis is that it proves that chiral indenyl-containing *tripod* ligands form their *tripod* metal derivatives under complete diastereoselective control.

Conclusion

Functionalised tripod ligands of the type $ROCH_2C(CH_2PPh_2)(CH_2PR'_2)(CH_2Cp^{\#})$ ($Cp^{\#}$ = indenyl, fluorenyl) are accessible from the oxetane precursor $O(CH_2)_2C(CH_2Br)(CH_2OMs)$ in a few steps. These tripod ligands form ruthenium complexes of the $CpRuL_2Cl$ type with the $Cp^{\#}$ group and the phosphorus donor groups linked by a *neo*-pentane scaffolding.

Epichlorohydrin is a suitable starting material to prepare chelate ligands $(Cp^{\#}CH_2)CHOH(CH_2PPh_2)$ in fully diastereoselective one-pot syntheses. These chelate ligands coordinate highly diastereoselectively to $Ru(PPh_3)(Cl)$.

The formation of the complex $Me_3SiOCH_2C(CH_2$-η^1-$PPh_2)(CH_2$-η^1-$PEt_2)(CH_2$-η^5-Indenyl)RuCl is completely diastereoselective, with the six-membered cycle of the indenyl constituent lying on the same side to which the PEt_2 group is coordinated.

A complete and unambiguous structure analysis of the *tripod* compounds $Me_3SiOCH_2C(CH_2$-η^1-$PPh_2)(CH_2$-η^1-$PR_2)(CH_2$-η^5-Indenyl)RuCl (R = Ph, Et) by a combination of NMR spectroscopy methods as well as distance-geometry modelling is reported, which documents the power of NMR methods for the quantitative analysis of structures of coordination compounds.

Experimental Section

General Remarks: All manipulations involving phosphanes were carried out under argon by means of standard Schlenk techniques and were monitored by TLC (Macherey−Nagel Co., Polygram SIL G/UV_{254}). All solvents were dried by standard methods[23] and distilled under argon. The solvents $CDCl_3$ and CD_2Cl_2 used for NMR spectroscopic measurements were degassed by three successive

"freeze-pump-thaw" cycles and dried over 4-Å molecular sieves. − MS: Finnigan MAT 8320; EI (70 eV); FAB (Xenon; matrix: 4-nitrobenzyl alcohol). − HR-MS(EI): Jeol JMS-700. − HR-MS(FAB): VG ZAB 2F − Melting points: Gallenkamp MFB-595 010; uncorrected values. − Optical rotations: Jasco DIP310, 10-cm cell, Na-D line (λ = 589 nm) − Cyclovoltammetry: EG&G Princeton Applied Research model 273; potentials in mV versus SCE at a glassy carbon electrode at 25 °C; solutions of compounds: 10^{-3} M in 0.1 M Bu_4NPF_6 in CH_2Cl_2. − Elemental analyses: Microanalytical Laboratory of the Organisch-Chemisches Institut, Universität Heidelberg.

Materials: Silica gel (Kieselgel z. A. 0.06−0.2 mm, J. T. Baker Chemicals B. V.) used for chromatography was degassed at 1 mbar for 24 h and saturated with argon. A solution of *n*BuLi in hexane (2.5 M) was used for deprotonations. *S*-(+)- and *R*-(−)-epichlorohydrin (**5**) (97% *ee*) were degassed and checked for optical purity by measurement of their specific rotations ($|[\alpha]_D^{20}| = 34.3$[24]). $HPEt_2$,[25] $HPPh_2$,[26] 3-(bromomethyl)-3-(methanesulfonoxymethyl)oxetane (**1**),[5] 1,1-bis(diphenylphosphanylmethyl)-1-(cyclopentadienylmethyl)ethane,[2b] $(PPh_3)_2FeCl_2$ [10] and $(PPh_3)_3RuCl_2$ [27] were prepared according to or by adaptation of literature procedures. All other chemicals were obtained from commercial suppliers and used without further purification.

NMR: Spectra were recorded at 298 K with a Bruker Avance DPX200 spectrometer at 200.13 MHz (^{1}H), 50.323 MHz (^{13}C), 81.014 MHz (^{31}P) and with a Bruker Avance DRX300 spectrometer at 300.13 MHz (^{1}H), 121.495 MHz (^{31}P); chemical shifts (δ) are reported in ppm with $CHCl_3$ (^{1}H: δ = 5.32; ^{13}C: δ = 53.5) as internal standard; ^{31}P chemical shifts (δ) are reported in ppm with 85% H_3PO_4 (^{31}P: δ = 0) as external standard. Acronyms of pulse programmes refer to pulse sequences supplied under these names for the BRUKER series of instruments; relaxation delays for 2D NMR experiments were set at around 1.5 s if not stated otherwise. ^{1}H-^{31}P-HMBC: pulse sequence inv4gslrnd; instruments DRX300 (**16a**), DPX200 (**16b**); spectral width F_2 = 2588 Hz, F_1 = 3888 Hz (**16a**), F_2 = 1717 Hz, F_1 = 2755 Hz (**16b**), mixing time 70 ms. ^{1}H,^{13}C-HMBC: pulse sequence inv4gslrnd; instrument DPX200; spectral width F_2 = 1380 Hz, F_1 = 6542 Hz (**16a**), F_2 = 1717 Hz, F_1 = 7348 Hz (**16b**), mixing time 70 ms. ^{1}H,^{13}C-HSQC: pulse sequence invieagssi; instrument DPX200; spectral width F_2 = 1380 Hz, F_1 = 6542 Hz (**16a**), F_2 = 1717 Hz, F_1 = 7046 Hz (**16b**). ^{1}H,^{1}H-DQFCOSY: pulse sequence cosygsmftp; instrument DPX200; spectral width 1380 Hz (**16a**), 1717 Hz (**16b**) in both dimensions. ^{1}H,^{1}H-NOESY: pulse sequence noesytp; instrument DPX200; spectral width 1380 Hz (**16a**), 1717 Hz (**16b**) in both dimensions; relaxation delay 2.0 s; mixing time 500 ms.

NOE Analysis: The NOE peaks were integrated by standard methods (volume integration, Felix software package from MSI).[20,28] The peak volumes were transformed to distances by assuming the initial rate approximation to be valid. For bringing the distances to an absolute scale, the known inter-proton distances of H^4/H^5 (265 pm) and H^{2A}/H^{2B} (178 pm) (**16a**) and H^{1A}/H^{1B}, H^{2A}/H^{2B}, H^{11A}/H^{11B} (178 pm) and H^4/H^5 (265 pm) (**16b**) were used. Other combinations of reference distances were also tested; different sets of references did not cause changes greater than 10%. Owing to the fact that only one mixing time was used, the overall accuracy of the NOE-derived distances will not be much better than 30 pm.

Distance-Geometry Calculations: The NOE-derived distances were used to build the distance matrix, together with the distance limits derived from covalent bonding. Upper and lower boundaries for NOE distances were set at 10%. The distance restraints derived from covalent bonding were defined by the DGII programme package (DGII package of NMR Refine module, InsightII, 98.0).[20b] Some of the protons, the *ortho*- and *meta*-protons of the phenyl groups and the protons of the CH_2OSiMe_3 group had to be replaced by dummy atoms since no diastereotopic differentiation was apparent for these protons. The upper boundary of the distance interval referring to these dummy protons was appropriately increased by 100 pm.[29] Distance-geometry calculations were used to produce a total of 200 conformations for each of the compounds **16a** and **16b**. The starting models were based on the structures obtained in each case by energy minimisation. In order to efficiently cope with the problem caused by the conformational chirality of the cage, the mirror image of this model with respect to the torsions within this cage was also incorporated as a starting point. Each of these two starting structures for each of the compounds **16a** and **16b** was allowed to adapt to the NOE restraints (DGII package of NMR Refine module, Insight98.0).[20b] The number of different conformations resulting from this procedure was limited to 100 for each starting geometry. It was observed that the minimisation procedure was able to converge from one sense of skew of the scaffolding to its opposite. Repetitive runs, however, showed that the degree of skewness of the chelate cage of the resulting structures was highly biased by the degree of skewness of the starting structure. This problem was overcome by the technique described above. With respect to the torsion angles $Ru-P-CH_2-C_{ipso}$, the DGII runs produce solutions which are close to being either symmetric with respect to the idealised mirror plane (bisecting the P−Ru−P angle and vertical to the P−Ru−P plane) or are antisymmetric with respect to this plane. With respect to energy minimisation calculations (see below) the best solutions for these torsional arrangements were used as a starting point. From the 200 conformations generated for both **16a** and **16b**, the 10 with the best overall agreement were selected to produce the superposition graphs shown in Figure 8 and Figure 10. In order to construct a model which best approximates the NOE distances and at the same time corresponds to a local minimum of the force field generated molecular hypersurface, the following procedure was adopted. Energy minimisation of the best structures generated by distance-geometry was done with the distances determined by NOE measurements constrained by corresponding high-force constants (harmonic potential force constants: 100 kcal·mol^{-1}·Å^{-2}). After reaching convergence, the NOE-derived constraints were removed and the conformation was allowed to relax on the basis of the molecular force field alone. The rms deviation between the model with NOE restraints and the one without was found to be 37 pm (**16a**) and 26 pm (**16b**) (based on all atoms). The resulting conformations are shown in black in Figure 8 and Figure 10. Generating an optimal model by the alternative procedure of taking the best solutions from the DGII runs as the starting points for the force-field refinement (no additional NOE restraints) led to similar results. The optimal solution derived by constrained refinement was again found. The minima derived by both methods were the same for **16a** (rms = 1.6 pm, based on all atoms) and **16b** (rms = 1.7 pm, based on all atoms). As a measure of agreement between the models and the experimental values, the rms deviation between the distance estimates from the model and from the experiment was calculated. Different subsets of inter-proton distances were included in these calculations. As is seen in Table 8 and Table 9, the individual error estimates were very similar to each other, independent of which subset was chosen for their calculation.

Synthetic Procedures: The analytical data are collected in Table 10 and 11. NMR spectroscopic data, if not explicitly given in the experimental protocols are presented in Table 1−3, and Table 7.

Table 10. Analytical data of compounds **2**−**12**

No.	Empirical formula (M)	Eluent[a] (R_f)	MS (EI) m/z (%) [Frag.]	$C_{calcd.}$, $H_{calcd.}$, $P_{calcd.}$ C_{found}, H_{found}, P_{found}	M.p.[b] [°C]	HR-MS $M^+_{calcd./found}$	Yield (%)
2a	$C_{26}H_{25}OP$ (384.46)	PE/Et_2O, 7:3 (0.33)	384 (100) [M^+]; 353 (52) [$M^+ - CH_2O$]; 199 (24) [$M^+ - PPh_2$]	81.23, 6.55 80.64, 6.49	–	–	74
2b	$C_{18}H_{25}OP$ (288.37)	PE/Et_2O, 7:3 (0.37)	288 (100) [M^+]; 259 (66) [$M^+ - Et$]; 258 (82) [$M^+ - CH_2O$]	74.97, 8.74 73.24, 8.53	–	–	10
2c	$C_{30}H_{27}OP$ (434.52)	PE/Et_2O, 1:1 (0.47)	434 (89) [M^+]; 404 (2) [$M^+ - CH_2O$]; 269 (4) [M^+ − Fluorenyl]; 255 (3) [$M^+ - CH_2$Fluorenyl]	82.93, 6.26, 7.13 83.00, 6.58, 6.53	78	–	64
3a	$C_{38}H_{36}OP_2$ (570.65)	PE/Et_2O, 3:2 (0.40)	571 (34) [M^+]; 494 (45) [$M^+ - Ph$]; 385 (100) [$M^+ - PPh_2$]	79.98, 6.36, 10.86 79.18, 6.37, 10.84	80 (dec.)	–	73
3b	$C_{30}H_{36}OP_2$ (474.56)	PE/Et_2O, 3:2 (0.48)	474 (12) [M^+]; 445 (100) [$M^+ - Et$]; 397 (7) [$M^+ - Ph$]; 385 (5) [$M^+ - PEt_2$]; 289 (28) [$M^+ - PPh_2$]	75.93, 7.65, 13.05 74.56, 7.50, 12.59	–	–	68
3c	$C_{42}H_{38}OP_2$ (620.71)	PE/Et_2O, 6.5:3.5 (0.37)	620 (16) [M^+]; 544 (80) [$M^+ - Ph$]; 467 (30) [$M^+ - 2Ph$]; 435 (34) [$M^+ - PPh_2$]	81.27, 6.17, 9.98 80.86, 6.40, 9.65	96	–	62
4a	$C_{41}H_{44}OP_2Si$ (642.83)	PE/Et_2O, 9:1 (0.44)	642 (59) [M^+]; 566 (55) [$M^+ - Ph$]; 458 (100) [$M^+ - PPh_2$]	76.60, 6.90, 9.65 75.75, 7.25, 9.76	–	–	86
4b	$C_{33}H_{44}OP_2Si$ (546.74)	PE/Et_2O, 9:1 (0.41)	547 (6) [M^+]; 518 (100) [$M^+ - Et$]; 362 (15) [$M^+ - PPh_2$]	72.49, 8.12, 11.34 72.38, 8.29, 11.26	–	–	84
4c	$C_{45}H_{46}OP_2Si$ (692.89)	PE/Et_2O, 9:1 (0.49)	693 (31) [M^+]; 617 (85) [$M^+ - Ph$]; 405 (38) [$M^+ - CH_2OTMS - PPh_2$]; 343 (19) [$M^+ - PPh_2$ − Fluorenyl]; 329 (100) [$M^+ - PPh_2$ − Fluorenyl − CH_2]	78.01, 6.69, 8.94 78.02, 7.17, 8.77	–	–	38
6a	$C_{20}H_{21}OP$ (308.36)	PE/Et_2O, 3:2 (0.37)	308 (63) [M^+]; 307 (24) [$M^+ - H$]	77.89, 6.87 74.02, 6.80	–	308.13300/ 308.13394	82
6b	$C_{24}H_{23}OP$ (358.42)	PE/Et_2O, 1:1 (0.39)	358 (92) [M^+]	80.43, 6.47, 8.64 79.99, 6.50, 8.95	–	–	49
6c	$C_{28}H_{25}OP$ (408.48)	PE/Et_2O, 3:2 (0.3)	408 (32) [M^+]	82.33, 6.17, 7.58 82.45, 6.13, 7.01	44	–	82
7	$C_{21}H_{20}O$ (288.39)	PE/Et_2O, 1:1 (0.43)	288 (53) [M^+]; 270 (46) [$M^+ - H_2O$]; 159 (85) [$M^+ - CH_2$Indenyl]	87.46, 6.99 86.93, 7.00	61	–	4
8	$C_{12}H_{12}O$ (172.22)	PE/Et_2O, 1:1 (0.22)	172 (22) [M^+]; 143 (13) [$M^+ - COH$]; 128 (100) [$M^+ - CH_2CHOH$]	83.69, 7.02 83.54, 7.13	–	–	30
9a	$C_{23}H_{29}OPSi$ (380.54)	PE/Et_2O, 9:1 (0.72)	381 (62) [M^+]; 292 (13) [$M^+ - OTMS$]	72.59, 7.68, 8.14 71.01, 7.84, 8.16	–	380.1725/ 380.1729	96
9b	$C_{27}H_{31}OPSi$ (430.60)	PE/Et_2O, 9:1 (0.56)	431 (66) [M^+]; 314 (100) [$M^+ - Indenyl$]	75.31, 7.26, 7.19 75.14, 7.41, 7.36	–	–	77
10	$C_{20}H_{24}BOP$ (322.20)	PE/Et_2O, 3:2 (0.32)	321 (25) [M^+]; 308 (60) [$M^+ - BH_3$]; 242 (10) [$M^+ - CH_2Cp$]; 108 (63) [$M^+ - CH_2PPh_2BH_3$]	74.50, 7.51, 9.61 73.24, 7.54, 9.49	–	–	71
11	$C_{21}H_{26}BO_3PS$ (400.29)	PE/Et_2O, 2:3 (0.37)	402 (5) [M^+]; 385 (4) [$M^+ - BH_3$]; 370 (70) [$M^+ - CH_3 - BH_3$]; 305 (18) [$M^+ - OSO_2CH_3$]; 291 (14) [$M^+ - BH_3 - OSO_2CH_3$]	62.98, 6.55, 7.74 60.63, 6.66	–	–	70
12a	$C_{32}H_{30}OP_2$ (492.54)	PE/Et_2O, 9:1 (0.48)	492 (10) [M^+]; 307 (28) [$M^+ - PPh_2$]; 291 (59) [$M^+ - OPPh_2$]	78.03, 6.14, 12.58 75.92, 6.27	–	492.17719/ 492.18007	45
12b	$C_{36}H_{32}OP_2$ (542.59)	PE/Et_2O, 4:1 (0.63)	542 (6) [M^+]; 357 (38) [$M^+ - PPh_2$]; 341 (48) [$M^+ - OPPh_2$]	79.69, 5.94, 11.42 79.49, 6.09, 11.36	–	–	51
12c	$C_{40}H_{34}OP_2$ (592.65)	PE/Et_2O, 4:1 (0.59)	592 (12) [M^+]; 515 (20) [$M^+ - Ph$]; 427 (26) [$M^+ - Fluorenyl$]; 413 (94) [$M^+ - CH_2$Fluorenyl]; 391 (100) [$M^+ - OPPh_2$]; 407 (29) [$M^+ - PPh_2$]	81.07, 5.78, 10.45 81.07, 5.78, 9.90	97	–	61

[a] PE = petroleum ether (boiling range 40−60 °C). − [b] dec. = decomposition.

Ligand Syntheses

General Procedure for the Synthesis of Compounds 2: The corresponding phosphane R_2PH (10 mmol) for the generation of the nucleophile **I** was dissolved in THF (50 mL) and deprotonated by the dropwise addition of *n*BuLi (10 mmol) at 0 °C. This solution was stirred for 1 h at 25 °C. Meanwhile, nucleophile **II** (22 mmol, 2.2 equiv.) (indene or fluorene) was dissolved in THF (50 mL) and deprotonated in the same manner as nucleophile **I**. 3-(Bromomethyl)-3-(methanesulfonoxymethyl)oxetane (**1**) (10 mmol) was dissolved in THF (50 mL) and cooled to −10 °C. At this temperature, the previously prepared phosphide (nucleophile **I**) solution was added dropwise over a period of 2 h. After the addition was completed, the mixture was allowed to warm to 25 °C and stirring was continued for another 30 min. Meanwhile the solution of nucleophile **II** was heated to 60 °C and the oxetane solution was added dropwise over a period of 1 h. The mixture was then heated at reflux for 2 h. After cooling to 25 °C, the mixture was hydrolysed by the addition of water (30 mL). The organic phase was separated, and the aqueous layer was extracted with diethyl ether (3 × 30 mL). The combined organic phases were washed with saturated NaCl solution until a neutral pH was achieved, and then dried with Na_2SO_4. The solvent was evaporated in vacuo and the residue was purified by column chromatography (silica gel; eluent, R_f, yields, and analytical data as given in Table 10).

General Procedure for the Synthesis of Compounds 3: Phosphane R_2PH (6 mmol, 1.2 equiv.) for the generation of the nucleophile was dissolved in THF (40 mL) and deprotonated by the dropwise addition of *n*BuLi (6 mmol) at 0 °C. This solution was stirred for 1 h at 25 °C. Meanwhile, oxetane **2** (5 mmol) was dissolved in THF (40 mL) and deprotonated in the same manner as the phosphane. The solution of the phosphide was added dropwise to the solution of the oxetane **2** over a period of 45 min at 25 °C. The resulting mixture was stirred for 3 h. The mixture was then heated at reflux for 2 h. After cooling to 25 °C the mixture was hydrolysed by the addition of water (30 mL). The organic phase was separated, and the aqueous layer was extracted with diethyl ether (3 × 30 mL). The combined organic phases were washed with saturated NaCl solution until a neutral pH was achieved, and then dried with Na_2SO_4. The solvent was evaporated in vacuo and the residue was purified by column chromatography (silica gel; eluent, R_f, yields, and analytical data as given in Table 10).

General Procedure for the Synthesis of Compounds 4 and 9: The starting material (**3** or **6**) (4 mmol) was dissolved in CH_2Cl_2 (20 mL) and triethylamine (6 mmol, 1.5 equiv.) was added. The solution was cooled to 0 °C and trimethylsilyl chloride (5.2 mmol, 1.3 equiv.) was added dropwise. Stirring was continued for 1.5 h and then all volatiles were removed in vacuo. The remaining residue was further purified by column chromatography (silica gel; eluent, R_f, yields, and analytical data as given in Table 10).

General Procedure for the Synthesis of Compound 6a: Diphenylphosphane (10 mmol, 1 equiv.) was dissolved in THF (30 mL) and deprotonated by the dropwise addition of *n*BuLi (10 mmol) at 0 °C. This solution was stirred for 1 h at 25 °C. Meanwhile, epichlorohydrin (10 mmol) was dissolved in THF (30 mL) and cooled to −70 °C. At this temperature, the phosphide solution was added dropwise over a period of 45 min. After warming to 25 °C, the solution was stirred for 30 min and added dropwise over a period of 20 min to a solution of CpMgCl·2THF (23 mmol, 2.3 equiv.) in THF (40 mL). The resulting mixture was stirred for 15 h at 25 °C. The mixture was hydrolysed by the addition of an NH_4Cl solution (10%, 50 mL). The organic phase was separated, and the aqueous layer was extracted with diethyl ether (3 × 30 mL). The combined organic phases were washed with a saturated NaCl solution until a neutral pH was achieved and then dried with Na_2SO_4. The solvent was evaporated in vacuo and the residue was purified by column chromatography (silica gel; eluent, R_f, yields, and analytical data as given in Table 10).

General Procedure for the Synthesis of Compounds 6b/6c: Diphenylphosphane (10 mmol, 1 equiv.) for the generation of the nucleophile **I** was dissolved in THF (30 mL) and deprotonated by the dropwise addition of *n*BuLi (10 mmol) at 0 °C. This solution was stirred for 1 h at 25 °C. Meanwhile, epichlorohydrin (10 mmol) was dissolved in THF (30 mL) and cooled to −70 °C. At this temperature, the solution of the phosphide was added dropwise over a period of 45 min. After warming to 25 °C, the solution was stirred for 30 min and added dropwise over a period of 20 min to a solution of nucleophile **II** (indenyllithium or fluorenyllithium, prepared in the same manner as nucleophile **I**) (23 mmol, 2.3 equiv.) in THF (40 mL). The resulting mixture was stirred for 15 h at 25 °C. The mixture was hydrolysed by the addition of water (30 mL). The organic phase was separated, and the aqueous layer was extracted with diethyl ether (3 × 30 mL). The combined organic phases were washed with a saturated NaCl solution until a neutral pH was achieved, and then dried with Na_2SO_4. The solvent was evaporated in vacuo and the residue was purified by column chromatography (silica gel; eluent, R_f, yields, and analytical data as given in Table 10). The same procedure was used for the synthesis of *R*-(−)-**6b** from *S*-(+)-**5** and *S*-(+)-**6b** from *R*-(−)-**5**.

Procedure for the Synthesis of Compounds 7, 8: Indene (108 mmol) was dissolved in THF (40 mL). This solution was cooled to 0 °C and treated with *n*BuLi (108 mmol). The solution was allowed to warm to 20 °C and stirred for 1.5 h. Meanwhile, epichlorohydrin (2.16 mmol) was dissolved in THF (20 mL) at −40 °C. The freshly prepared solution of LiInd was added to this solution through a Teflon® capillary under a slight overpressure of Argon over 1 h. The resulting solution was stirred for 15 h at 20 °C. After hydrolysis with H_2O (30 mL), the organic phase was separated and the aqueous phase extracted with diethyl ether (3 × 30 mL). The combined organic phases were washed with a saturated NaCl solution until a neutral pH was achieved, and dried with $NaSO_4$. After evaporation of all volatiles in vacuo, the remaining material was dissolved in CH_2Cl_2 and separated by column chromatography (silica gel; eluent, R_f, yields, and analytical data as given in Table 10).

Procedure for the Synthesis of Compound 10: Compound **6a** (6.0 mmol) was dissolved in THF (40 mL). BH_3/THF (7.8 mL, 16.2 mmol) were added dropwise at 0 °C over 5 min. After stirring the solution for 1 h at 0 °C, the volatiles were removed in vacuo. The remaining colourless oil was dissolved in CH_2Cl_2 and purified by column chromatography (silica gel; eluent, R_f, yields, and analytical data as given in Table 10).

Procedure for the Synthesis of Compound 11: Compound **10** (6.0 mmol) was dissolved in CH_2Cl_2 (30 mL). After the addition of triethylamine (9 mmol), the solution was cooled to 0 °C. MsCl (7.8 mmol) was added over 2 min and the solution was stirred for 6 h at 20 °C. After hydrolysis with H_2O (10 mL), the organic phase was separated. The aqueous phase was extracted with CH_2Cl_2 (3 × 20 mL). The combined organic phases were washed with a saturated NaCl solution until a neutral pH was achieved, and dried with $NaSO_4$. After evaporation of the solvent, the viscous oily residue was dissolved in CH_2Cl_2 and purified by column chromatograph (silica gel; eluent, R_f, yields, and analytical data as given in Table 10).

General Procedure for the Synthesis of Compounds 12: Compound **6** (4 mmol) was dissolved in CH_2Cl_2 (20 mL) and triethylamine (5.6 mmol, 1.4 equiv.) was added. The solution was cooled to 0 °C and chlorodiphenylphosphane (4.8 mmol, 1.2 equiv.) was added dropwise. Stirring was continued for 2 h at 25 °C, and then all volatiles were removed in vacuo. The remaining residue was further purified by column chromatography (silica gel; eluent, R_f, yields, and analytical data as given in Table 10).

Syntheses of Coordination Compounds

General Procedure for the Synthesis of Compounds 13: Compound **9** (1 mmol) was dissolved in THF (20 mL) and deprotonated by the dropwise addition of *n*BuLi (1 mmol) at 0 °C. The solution was stirred for 1.5 h at 25 °C. Meanwhile, $FeCl_2$ (0.6 mmol) was suspended in THF (15 mL) and stirred for 30 min. This solution was added dropwise to the solution of the deprotonated ligand over a period of 10 min. The mixture was stirred for 1 h. After this time, the mixture was heated, in the case of **13a**, for 4 h at reflux, and in the case of **13b**, for 2 h at 50 °C. All volatiles were removed in vacuo and the remaining residue was further purified by column chromatography. In the case of **13a**, the remaining residue was taken up in diethyl ether and purified by chromatography on neutral Al_2O_3 (Brockmann activity grade III). On evaporation of the solvent from the eluate, the purified compound **13a** was obtained in oily form. Further purification could be achieved by washing with petroleum ether (boiling range 40−60 °C) and resulted in a microcrystalline solid (Table 11). In the case of **13b**, the remaining residue was purified by chromatography on neutral Al_2O_3 (Brockmann activity grade III). The contaminants were eluted with petroleum ether (boiling range 40−60 °C) and mixtures of petroleum ether/toluene. Subsequently, compound **13b** was eluted with toluene. On evaporation of the solvent from the eluate, the purified compound **13b** was obtained in microcrystalline form (Table 11).

^{1}H NMR: 13a ($CDCl_3$): δ = −0.03 (s, 18 H, SiCH_3), 2.26 (m, 4 H, CH_2P), 2.58 (dd, 2 H, CH_{2a}Cp, $^2J_{HH}$ = 14.0 Hz, $^3J_{HH}$ = 6.0 Hz), 2.77 (dd, 2 H, CH_{2b}Cp, $^2J_{HH}$ = 14.0 Hz, $^3J_{HH}$ = 6.0 Hz), 3.72 (m, 2 H, C*H*OSi), 4.01 (br. s, 8 H, Cp*H*), 7.30−7.50 (m, 20 H, aromatic C*H*). − **13b** ($CDCl_3$): δ = −0.25, −0.20 (2 s, 18 H, SiCH_3), 2.10−2.40 (m, 4 H, CH_2P), 2.55−3.40 (m, 4 H, CH_2Indenyl), 3.67 (m, 2 H, C*H*OSi), 3.80−4.10 (m, 2 H, Indenyl five-membered ring C*H*), 4.36 (m, 1 H, Indenyl five-membered ring C*H*), 4.48 (m, 1 H, Indenyl five-membered ring C*H*), 6.85−7.19 (m, 8 H, Indenyl six-membered ring C*H*), 7.19−7.55 (m, 20 H, aromatic *H*).

^{13}C{^{1}H} NMR: 13a ($CDCl_3$): δ = 0.6 (s, Si*C*H_3), 37.4 (d, *C*H_2P, $^1J_{CP}$ = 14.6 Hz), 39.6 (d, *C*H_2Cp, $^3J_{CP}$ = 8.5 Hz), 68.6, 68.7 (2 s, CpH (3, 4), 70.4, 71.0 [2 s, CpH (2, 5)], 72.3 (d, *C*HOSi, $^2J_{CP}$ = 17.6 Hz), 84.9 (s, *ipso*-C_q-Cp), 128.7−139.8 (aromatic *C*). − **13b** ($CDCl_3$): δ = 0.5 (s, Si*C*H_3), 36.0−38.1 (m, *C*H_2P and *C*H_2Indenyl), 60.7 (m, Indenyl five-membered ring *C*H), 61.5 (s, Indenyl five-membered ring *C*H), 71.7 (m, *C*HOSi), 73.4 (m, Indenyl five-membered ring *C*H), 75.8 (m, *ipso*-C_q-Indenyl five-membered ring), 87.1 (m, Indenyl five-membered ring C_q), 122.8−140.1 (aromatic and olefinic *C*H).

Table 11. Analytical data of compounds **13**−**16**

No.	Empirical formula (*M*)	MS *m/z* (%) [Frag.]	$C_{calcd.}$, $H_{calcd.}$, $P_{calcd.}$ C_{found}, H_{found}, P_{found}	M.p.[a] [°C]	HR-MS $M^+_{calcd./found}$	Cyclovoltammetry Potential [mV] (SCE)	Yield (%)
13a	$C_{46}H_{56}FeO_2P_2Si_2$ (814.90)	*EI* 814 (18) [M$^+$]; 435 (100) [M$^+$ − $C_{23}H_{29}OPSi$]	67.80, 6.93, 7.60 68.00, 7.06, 7.84	−	−	$E_{1/2}$ = 325; ΔE = 70	86
13b	$C_{54}H_{60}FeO_2P_2Si_2$ (915.02)	*EI* 915 (8) [M$^+$]; 485 (100) [M$^+$ − $C_{27}H_{31}OPSi$]; 430 (54) [$C_{27}H_{31}OPSi$]	70.88, 6.61 69.70, 6.65	−	914.2956/ 914.2947	$E_{1/2}$ = 107; ΔE = 283	47
14	$C_{58}H_{53}BClCoP_2$ (917.20)	*FAB* 597 (100) [M$^+$ − BPh_4]; 562 (28) [M$^+$ − BPh_4 − Cl]; 503 (22) [M$^+$ − BPh_4 − Cl − Co]	75.95, 5.82, 6.75 73.31, 6.76, 6.14	−	−	−	38
15a	$C_{41}H_{43}ClOP_2RuSi$ (778.33)	*EI* 778 (4) [M$^+$]; 517 (18) [M$^+$ − PPh_3]; 481 (17) [M$^+$ − PPh_3 − Cl]	63.27, 5.57, 7.96 62.71, 5.90, 7.84	190 dec.	−	$E_{1/2}$ = 531; ΔE = 160	51
15b	$C_{45}H_{45}ClOP_2RuSi$ (828.39)	*FAB* 828 (80) [M$^+$]; 793 (100) [M$^+$ − Cl]	65.21, 5.48 64.60, 5.93	176 dec.	828.1447/ 793.1758, 828.1443/ 793.1777	$E_{1/2}$ = 429; ΔE = 92	36
16a	$C_{41}H_{43}ClOP_2SiRu$ (778.32)	*FAB* 778 (70) [M$^+$]; 743 (100) [M$^+$ −Cl]	63.22, 5.57 61.61, 5.67	160 dec.	778.1290/ 743.1602, 778.1306/ 743.1642	$E_{1/2}$ = 276; ΔE = 73	42
16b	$C_{33}H_{43}ClOP_2RuSi$ (682.25)	*FAB* 682 (100) [M$^+$]	−	154 dec.	682.1290/ 647.1602, 682.1266/ 647.1589	$E_{1/2}$ = 231; ΔE = 99	16

[a] dec. = decomposition.

$^{31}P\{^1H\}$ NMR: 13a ($CDCl_3$): δ = −23.6 (s). − **13b** ($CDCl_3$): δ = −23.5 (s).

General Procedure for the Synthesis of Compound 14: 1,1-Bis-(diphenylphosphanylmethyl)-1-(cyclopentadienylmethyl)ethane (1 mmol) was dissolved in THF (20 mL) and deprotonated by the dropwise addition of *n*BuLi (1 mmol) at 0 °C. The solution was stirred for 1.5 h at 25 °C. Meanwhile, $CoCl_2$ (1 mmol) was suspended in THF (20 mL) and cooled to −30 °C. The deprotonated ligand was added dropwise to this solution over a period of 5 min. After addition was completed, the mixture was allowed to warm to 20 °C and stirred for another 45 min. All volatiles were removed in vacuo. The remaining residue was dissolved in ethanol (20 mL) and $NaBPh_4$ (1 mmol) was added. After stirring for 2 h, all volatiles were removed in vacuo and the remaining residue was further purified by column chromatography. Compound **14** was eluted with THF/CH_2Cl_2 mixtures. On evaporation of the solvent from the eluate, the purified compound **14** was obtained in microcrystalline form (Table 11).

^1H NMR: 14 (CD_2Cl_2): δ = 1.26 (br. s, 2 H,CH_2Cp), 1.52 (br. s, 3 H, C_qCH_3), 2.29 (m, 2 H, CH_{2a}P, $^2J_{HH}$ = 15.7 Hz), 2.59 (m, 2 H, CH_{2b}P, $^2J_{HH}$ = 15.7 Hz), 4.68 (br. s, 2 H, Cp), 5.99 (br. s, 2 H, Cp), 6.75−7.95 (m, 60 H, aromatic C*H*).

$^{13}C\{^1H\}$ NMR: 14 (CD_2Cl_2): δ = 31.3 (m, *C*H_2P), 33.3 (t, C_qCH_3, $^3J_{CP}$ = 12.9 Hz), 35.1 (s, *C*H_2Cp), 47.3 (s, C_q), 76.7, 97.9, 100.5 (3 s, Cp), 121.6−135.8 and 162.3−165.3 (m, aromatic *C*H).

$^{31}P\{^1H\}$ NMR: 14 (CD_2Cl_2): δ = 23.3 (s).

General Procedure for the Synthesis of Compounds 15 and 16: The appropriate ligand (**4** or **9**) (1 mmol) was dissolved in THF (20 mL) and deprotonated by the dropwise addition of *n*BuLi (1 mmol) at 0 °C. This solution was stirred for 1.5 h at 25 °C. All volatiles were then removed in vacuo and the remaining residue was dissolved in 1,2-dichloroethane (1,2-DCE) (15 mL). This solution was added dropwise over a period of 10 min at 25 °C to a solution of $RuCl_2(PPh_3)_3$ (1 mmol) in 1,2-DCE (30 mL). The mixture was stirred for 30 min. After this time, the mixture was heated for 2 h (**16**)/1.5 h (**15**) at 90 °C. All volatiles were removed in vacuo and the remaining residue was further purified by column chromatography. − **16** [solid phase neutral Al_2O_3 (Brockmann activity grade III)]: The excess triphenylphosphane and other contaminants were eluted with diethyl ether and the compounds **16** were subsequently eluted with Et_2O/CH_2Cl_2 mixtures. − **15** (solid phase silica gel): The excess triphenylphosphane and other contaminants were eluted with petroleum ether (boiling range 40−60 °C) (PE) and PE/Et_2O mixtures. The compounds **15** were eluted with PE/Et_2O 1:1. − On evaporation of the solvent from the eluate, the purified compounds **15** and **16** were obtained in microcrystalline form (Table 11).

^1H NMR: 15a ($CDCl_3$): Major product: δ = −0.03 (s, 9 H, SiCH_3), 1.73 (dd, 1 H, CH_{2a}Cp, $^2J_{HH}$ = 12.0 Hz, $^3J_{HH}$ = 14.0 Hz), 2.05 (dd, 1 H, CH_{2b}Cp, $^2J_{HH}$ = 12.0 Hz, $^3J_{HH}$ = 12.0 Hz), 2.55 (m, 2 H, CH_2P), 3.68 (m, 1 H, C*H*OSi), 3.73 (br. s, 1 H, Cp), 3.88 (br. s, 1 H, Cp), 4.52 (br. s, 1 H, Cp), 5.40 (br. s, 1 H, Cp), aromatic C*H*: 6.55−6.70 (m, 2 H), 6.86−6.94 (m, 2 H), 6.95−7.50 (m, 19 H), 8.05−8.20 (m, 2 H). − Minor product: δ = 4.97 (s, 0.08 H, Cp), 5.18 (s, 0.08 H, Cp). − **15b** ($CDCl_3$): δ = 0.14 (s, 9 H, SiCH_3), 2.78 (m, 2 H, CH_2P), 3.23 (m, 1 H, Indenyl five-membered ring C*H*, $^3J_{HH}$ = 2.2 Hz), 3.28 (m, 1 H, CH_{2a}Indenyl), 3.70 (m, 1 H, CH_{2b}Indenyl, J_{HP} = 7.6 Hz), 4.08 (m, 1 H, C*H*OSi), 4.34 (m, 1 H, Indenyl five-membered ring C*H*, $^3J_{HH}$ = 2.2 Hz), 6.80−7.70 (m, 29 H, aromatic and olefinic C*H*).

$^{13}C\{^1H\}$ NMR: 15a ($CDCl_3$): Major product: δ = 0.5 (s, Si*C*H_3), 33.2 (s, *C*H_2Cp), 37.0 (d, *C*H_2P, $^1J_{CP}$ = 28.1 Hz), 68.6 (d, *C*HOSi, $^2J_{CP}$ = 12.5 Hz), 74.4 (d, Cp, J_{CP} = 10.0 Hz), 76.6 (s, Cp), 78.2 (d, Cp, J_{CP} = 11.0 Hz), 84.7 (s, *ipso*-C_q-Cp), 99.8 (s, Cp), 127.6−135.9 (aromatic *C*H). **15b** ($CDCl_3$): δ = 0.6 (s, Si*C*H_3), 32.5 (s, *C*H_2Indenyl), 39.2 (d, *C*H_2P, $^1J_{CP}$ = 29.7 Hz), 65.0 (s, Indenyl five-membered ring *C*H), 69.1 (d, *C*HOSi, $^2J_{CP}$ = 9.5 Hz), 73.6 (d, *ipso*-C_q-Indenyl five-membered ring, J_{CP} = 13.6 Hz), 83.9 (s, Indenyl five-membered ring *C*H), 104.7 (d, Indenyl five-membered ring C_q,

Table 12. Crystal data for compounds **7**, **8**, and **15a**

Compound	**7**	*anti*-**8**	**15a**·2 CH_2Cl_2
Empirical formula	$C_{21}H_{20}O$	$C_{12}H_{12}O$	$C_{84}H_{90}Cl_6O_2P_4Ru_2Si_2$
Molecular mass	288.370	172.220	431.615
Crystal size [mm]	0.05 × 0.1 × 0.2	0.07 × 0.07 × 0.2	0.15 × 0.1 × 0.03
Crystal system	monoclinic	tetragonal	triclinic
Space group (No.)[31c]	$P2_1/n$ (14)	$P4_1$ (76)	$P\bar{1}$ (2)
Lattice constants:			
a [pm]	1645.0(3)	1260.6(2)	1001.3(2)
b [pm]	502.2(1)	1260.6(2)	1668.1(3)
c [pm]	1971.9(4)	604.4(1)	2473.6(5)
α [°]	90	90	100.69(3)
β [°]	109.63(3)	90	90.51(3)
γ [°]	90	90	101.10(3)
V [10^6 pm^3]	1534	960.5	3980
Z	4	4	4
d_x [g cm^{-3}]	1.248	1.191	1.441
T [K]	200	200	200
Scan range	2.8° ≤ 2Θ ≤ 52.1°	3.2° ≤ 2Θ ≤ 52.1°	2.8° ≤ 2Θ ≤ 52.0°
Method	ω scan, Δω = 1.0°	ω scan, Δω = 1.0°	ω scan, Δω = 2.0°
Scan speed	40 s frame^{-1}	30 s frame^{-1}	25 s frame^{-1}
No. of measured rflns.	11122	6580	57851
No. of unique rflns.	3003	1876	15570
No. of observed rflns.	2162	982	9344
Observation criterion	$I \geq 2\sigma$	$I \geq 2\sigma$	$I \geq 2\sigma$
No. of param. refined	259	154	911
Resid. el. density [10^{-6} e pm^{-3}]	0.28	0.14	1.65
R_1/R_w [%] (refinement on F^2)	5.7/17.1	4.7/8.0	6.8/15

J_{CP} = 8.0 Hz), 112.7 (s, Indenyl five-membered ring C_q), 122.4−138.8 (aromatic and olefinic *C*H). − **16a** ($CDCl_3$): δ = 0.16 (s, Si*C*H$_3$), 28.6 (dd, *C*H$_2$P^1, $^1J_{CP}$ = 34.0 Hz, $^3J_{CP}$ = 5.5 Hz), 30.0 (dd, *C*H$_2$P^2, $^1J_{CP}$ = 39.0 Hz, $^3J_{CP}$ = 4.1 Hz), 31.4 (s, *C*H$_2$Indenyl), 55.4 (dd, C_qCH$_2$O, $^2J_{CP}$ = 7.8 Hz and 4.1 Hz), 58.9 (s, C_qCH^4), 73.9 (t, C_q*C*H$_2$O, $^3J_{CP}$ = 13.0 Hz), 75.9 (d, *C*H^5, $^2J_{CP}$ = 13.6 Hz), 97.5 (s, *C*H^4), 113.4 (m, C_qCH^5), 117.0 (s, *C*H^9), 118.0 (s, C_qCH^9), 125.3 (s, *C*H^6), 125.6 (s, *C*H^7), 128.2 (s, *C*H^8), 127.6−143.0 (aromatic *C*H). For designation of protons see Figure 6. − **16b** ($CDCl_3$): δ = 0.0 (s, Si*C*H$_3$), 7.8 (d, PCH$_2$*C*H$_3$, $^2J_{CP}$ = 32.1 Hz), 8.0 (d, PCH$_2$*C*H$_3$, $^2J_{CP}$ = 26.6 Hz), 15.9 (d, P*C*H$_2$CH$_3$, $^1J_{CP}$ = 21.1 Hz), 25.7 (d, P*C*H$_2$CH$_3$, $^1J_{CP}$ = 24.8 Hz), 28.4 (m, *C*H$_2$PEt$_2$), 29.1 (m, *C*H$_2$PPh$_2$), 30.3 (s, *C*H$_2$Indenyl), 54.7 (dd, C_qCH$_2$O, $^2J_{CP}$ = 6.4 Hz and 3.7 Hz), 57.8 (s, C_qCH^4), 71.8 (d, *C*H^5, J_{CP} = 12.8 Hz), 73.8 (pt, C_q*C*H$_2$O, $^3J_{CP}$ = 12.8 Hz), 94.1 (s, *C*H^4), 116.2 (m, C_qCH^5, J_{CP} = 3.7 Hz and 4.5 Hz), 118.5 (s, *C*H^9), 119.4 (m, C_qCH^9, J_{CP} = 2.7 Hz and 4.5 Hz), 124.7 (s, *C*H^6), 125.2 (s, aromatic *C*H), 126.0 (s, *C*H^7), 128.5−141.9 (aromatic *C*H and *C*H^8). For designation of protons see Figure 9.

^{31}P{^{1}H} NMR: 15a ($CDCl_3$): Main product: δ = 23.3 (d, $^2J_{PP}$ = 41.0 Hz), 43.2 (d, $^2J_{PP}$ = 41.0 Hz). − Minor product: 25.5 (d, $^2J_{PP}$ = 39.9 Hz), 40.4 (d, $^2J_{PP}$ = 39.9 Hz). − **15b** ($CDCl_3$): δ = 35.7 (d, $^2J_{PP}$ = 35.5 Hz), 40.0 (d, $^2J_{PP}$ = 35.5 Hz).

X-ray Crystallographic Study: Suitable crystals were taken directly out of the mother liquor, immersed in perfluorinated polyether oil and fixed to a glass capillary at 200 K. The measurements were carried out with a Nonius−Kappa CCD diffractometer (low-temperature unit, graphite-monochromated Mo-K_α radiation). The data was processed by the standard Nonius software.[30] All calculations were performed using the SHELX software package.[31] Structures were solved by direct methods with the SHELXS-97 programme[31a] and refined with the SHELXL-97 programme.[31b] Graphic handling of the structural data during solution and refinement was performed with XPMA.[32] Atomic coordinates and anisotropic thermal parameters of the non-hydrogen atoms were refined by full-matrix least-squares calculations. Data for the structure determinations are compiled in Table 12. The figures of the structures (Figure 1−3) were made with WinRay-32.[33] Crystallographic data (excluding structure factors) for the structures reported in this paper have been deposited with the Cambridge Crystallographic Data Centre as supplementary publication no. CCDC-140087 (**7**), -140086 (*anti*-**8**) and -140088 (**15a**). Copies of the data can be obtained free of charge on application to CCDC, 12 Union Road, Cambridge CB2 1EZ, UK [Fax: (internat.) + 44-1223/336-033; E-mail: deposit@ccdc.cam.ac.uk].

Acknowledgments

We are indebted to the German Science Foundation (DFG), SFB 247, the VW Foundation (Stiftung Volkswagenwerk) and the Fonds der Chemischen Industrie for financial support. A generous loan of ruthenium(III) chloride by the DEGUSSA AG is gratefully acknowledged. We wish to thank T. Jannack (mass spectrometry), the Microanalytical Laboratory and the Mass spectrometry department (high resolution mass spectra) of the Institute of Organic Chemistry.

[1] S. Martin, H. H. Brintzinger, *Inorg. Chim. Acta* **1998**, *280*, 189−192, and references cited therein.
[2] [2a] J. Vogelgesang, G. Huttner, E. Kaifer, P. Kircher, P. Rutsch, S. Cunskis, *Eur. J. Inorg. Chem.* **1999**, 2187−2199. − [2b] B. Antelmann, U. Winterhalter, G. Huttner, B. C. Janssen, J. Vogelgesang, *J. Organomet. Chem.* **1997**, *545*−*546*, 407−420.
[3] [3a] B. Antelmann, G. Huttner, U. Winterhalter, *J. Organomet. Chem.* **1998**, *555*, 119−125. − [3b] B. Antelmann, G. Huttner, J. Vogelgesang, O. Walter, U. Winterhalter, *J. Organomet. Chem.* **1997**, *549*, 139−148.
[4] [4a] J. Karas, G. Huttner, K. Heinze, P. Rutsch, L. Zsolnai, *Eur. J. Inorg. Chem.* **1999**, 405−420. − [4b] J. Scherer, G. Huttner, M. Büchner, *Chem. Ber.* **1996**, *129*, 697−713. − [4c] J. Scherer, G. Huttner, M. Büchner, J. Bakos, *J. Organomet. Chem.* **1996**, *129*, 45−58. − [4d] H. Brunner, A. Sicheneder, *Angew. Chem.* **1988**, *100*, 730−731; *Angew. Chem. Int. Ed. Engl.* **1988**, *27*, 718−719.
[5] T. Seitz, A. Muth, G. Huttner, *Z. Naturforsch., Teil B* **1995**, *50*, 1045−1049.
[6] B. Antelmann, G. Huttner, U. Winterhalter, *J. Organomet. Chem.* **1998**, *553*, 433−441.
[7] T. Seitz, Ph. D. Dissertation, University of Heidelberg, **1994**.
[8] H. Heidel, Ph. D. Dissertation, University of Heidelberg, **1994**.
[9] K. L. Gibis, Ph. D. Dissertation, University of Heidelberg, **1994**.
[10] L. H. Pignolet, D. Forster, W. d. W. Horrocks, *Inorg. Chem.* **1968**, *7*, 828−830.
[11] [11a] T. Seitz, A. Asam, G. Huttner, O. Walter, L. Zsolnai, *Z. Naturforsch., Teil B* **1995**, *50*, 1287−1306. − [11b] T. Seitz, A. Muth, G. Huttner, T. Klein, O. Walter, M. Fritz, L. Zsolnai, *J. Organomet. Chem.* **1994**, *469*, 155−162.
[12] P. Schober, R. Soltek, G. Huttner, L. Zsolnai, K. Heinze, *Eur. J. Inorg. Chem.* **1998**, 1407−1415.
[13] [13a] K. L. Marsi, M. E. Co-Sarno, *J. Org. Chem.* **1977**, *42*, 778−781. − [13b] K. Issleib, H. M. Möbius, *Chem. Ber.* **1961**, *94*, 102−106.
[14] [14a] G. Jany, R. Fawzi, M. Steimann, B. Rieger, *Organometallics* **1997**, *16*, 544−550. − [14b] B. Rieger, G. Jany, M, Steimann, R. Fawzi, *Z. Naturforsch.* **1994**, *49b*, 451−458. − [14c] B. Rieger, G. Jany, R. Fawzi, M. Steimann, *Organometallics* **1994**, *13*, 647−653. − [14d] B. Rieger, G. Jany, *Chem. Ber.* **1994**, *127*, 2417−2419. − [14e] B. Rieger, *J. Organomet. Chem.* **1991**, *420*, C17−C20.
[15] K. Urtel, A. Frick, G. Huttner, L. Zsolnai, P. Kircher, P. Rutsch, E. Kaifer, A. Jacobi, *Eur. J. Inorg. Chem.* **2000**, 33−50.
[16] [16a] U. Piantini, O. W. Sørensen, R. R. Ernst, *J. Am. Chem. Soc.* **1982**, *104*, 6800−6801. − [16b] M. Rance, O. W. Sørensen, G. Bodenhausen, G. Wagner, R. R. Ernst, K. Wüthrich, *Biochem. Biophys. Res. Commun.* **1983**, *117*, 479−485.
[17] B. M. Trost, B. Vidal, M. Thommen, *Chem. Eur. J.* **1999**, *5*, 1055−1069.
[18] [18a] S. Beyreuther, J. Hunger, S. Cunskis, T. Dierks, A. Frick, E. Planker, G. Huttner, *Eur. J. Inorg. Chem.* **1998**, 1641−1653. − [18b] S. Beyreuther, A. Frick, J. Hunger, G. Huttner, B. Antelmann, P. Schober, R. Soltek, *Eur. J. Inorg. Chem.*, in press.
[19] J. Jeener, B. H. Meier, P. Bachmann, R. R. Ernst, *J. Chem. Phys.* **1979**, *71*, 4546−4563.
[20] [20a] *Felix 98*, Molecular Simulations Inc., http://www.msi.com. − [20b] *Insight II 98.0*, Molecular Simulations Inc., http://www.msi.com.
[21] [21a] A. E. Torda, W. F. v. Gunsteren, in *Reviews in Computational Chemistry*, vol. III (Eds.: A. E. Torda, W. F. V. Gunsteren), VCH Publishers Inc., New York, **1996**, chapter 3 and references therein. − [21b] J. M. Blaney, J. S. Dixon, in *Reviews in Computational Chemistry*, vol. V (Eds.: A. E. Torda, W. F. V. Gunsteren), VCH Publishers Inc., New York, **1996**, chapter 6 and references therein.
[22] A. Bax, M. F. Summers, *J. Am. Chem. Soc.* **1986**, *108*, 2093−2094.
[23] *Organikum*, Deutscher Verlag der Wissenschaften, Berlin, **1990**.
[24] J. Baldwin, A. Raab, K. Mensler, B. Arison, D. McClure, *J. Org. Chem.* **1978**, *43*, 4876−4878.
[25] K. Issleib, A. Tzschach, *Chem. Ber.* **1959**, *92*, 704−711.
[26] [26a] R. E. Ireland, D. M. Walba, *Org. Synth. Coll. Vol.* **1988**, *6*, 567−570. − [26b] K. Issleib, H. O. Fröhlich, *Z. Naturforsch., Teil B* **1959**, *14*, 349−350.
[27] P. S. Hallmann, T. A. Stephenson, G. Wilkinson, *Inorg. Synth.* **1970**, *12*, 237−240.
[28] B. A. Borgias, M. Gachin, D. Kerwood, T. L. James, *Progr.*

NMR Spectrosc. **1990**, *22*, 83−100.
[29] M. Reggelin, H. Hoffmann, M. Köck, D. F. Mierke, *J. Am. Chem. Soc.* **1992**, *114*, 3272−3277.
[30] *DENZO-SMN, Data processing software*, Nonius, **1998**, http://www.nonius.com.
[31] [31a] G. M. Sheldrick, *SHELXS-97, Programme for Crystal Structure Solution*, University of Göttingen, **1997**, http://shelx.uni-ac.gwdg.de/shelx/index.html. − [31b] G. M. Sheldrick, *SHELXL-97, Programme for Crystal Structure Refinement*, University of Göttingen, **1997**, http://shelx.uni-ac.gwdg.de/shelx/index.html. − [31c] *International Tables for X-ray Crystallography*, vol. 4, Kynoch Press, Birmingham, U.K., **1974**.
[32] L. Zsolnai, G. Huttner, *XPMA*, University of Heidelberg, **1994**, http://www.uni-heidelberg.de/institute/fak12/AC/huttner/htmlsoftware.html.
[33] R. Soltek, G. Huttner, *WinRay-32*, University of Heidelberg, **1998**, http://www.uni-heidelberg.de/institute/fak12/AC/huttner/htmlsoftware.html

Received March 3, 2000
[I00240]

Efficient Syntheses of the Complete Set of Compounds $[\{(OC)_5M\}_6E_6]^{2-}$ (M = Cr, Mo, W; E = Ge, Sn) − Structure and Redox Behaviour of the Octahedral Clusters $[Ge_6]^{2-}$ and $[Sn_6]^{2-}$

Gerd Renner,[a] Peter Kircher,[a] Gottfried Huttner,*[a] Peter Rutsch,[a] and Katja Heinze[a]

Dedicated to Professor Dieter Sellmann on the occasion of his 60th birthday

Keywords: Main-group elements / Cluster compounds / Carbonyl ligands / NMR spectroscopy / Germanium / Tin

Improved syntheses of the known clusters $[\{(OC)_5Cr\}_6Ge_6]^{2-}$ (**1**) and $[\{(OC)_5Cr\}_6Sn_6]^{2-}$ (**4**) are reported. The new synthetic procedures also allow for the preparation of the molybdenum and tungsten derivatives $[\{(OC)_5M\}_6Ge_6]^{2-}$ (M = Mo: **2**; M = W: **3**) and $[\{(OC)_5M\}_6Sn_6]^{2-}$ (M = Mo: **5**; M = W: **6**). Compounds **1**–**6** were obtained as crystalline $[Ph_4P]$ salts, whose structures were determined for the whole series **1**–**6** by single-crystal X-ray analyses. All six $[Ph_4P]$ salts crystallise in tetragonal space groups, with the site group symmetries of the cluster core ranging from C_{4h} to D_{4h}. The average octahedral symmetry of the cluster core in solution is evident from ^{119}Sn NMR spectroscopic data. Reversible one-electron oxidation of the dianions is suggested by cyclovoltammograms, while reduction is irreversible throughout. Electronic transitions which could be due to the cluster core were not found in the experimentally accessible energy range above 300 nm (below 4 eV). These findings indicate a high intrinsic stability of the precise electron clusters $[Ge_6]^{2-}$ and $[Sn_6]^{2-}$.

Introduction

The main group clusters $[Sn_6]^{2-}$ and $[Ge_6]^{2-}$ have been characterised in the form of their organometallic derivatives $[\{(OC)_5Cr\}_6Sn_6]^{2-}$ (**4**) and $[\{(OC)_5Cr\}_6Ge_6]^{2-}$ (**1**).[1,2] While octahedral aggregates are a common type of arrangement for transition-metal clusters and a common motif in the structural chemistry of boranes and carboranes, they are by no way the preferred motif for the aggregation of other main-group elements, either in molecular compounds or in solid-state phases.[3] Thus anionic aggregates of the heavier group-14 elements $[E_m]^{n-}$ of tetrahedral shape e.g. $[Ge_4]^{2-}$, of trigonal-bipyramidal shape $[E_5]^{n-}$ [4,5] or of a shape somewhere between a monocapped archimedian antiprism (*nido*) and a tricapped trigonal prism (*closo*) $[E_9]^{n-}$ [6−11] are well-characterised species known as components of solid-state structures.[3,12] They are also, to a lesser extent, known in molecular anions in solution or in salt-type molecular compounds. No aggregate of the type $[E_6]^{n-}$ [13,14] has ever been observed until now, and it is only in an organometallic environment that such species are persistent in molecular anions. The compounds $[\{(OC)_5Cr\}_6Sn_6]^{2-}$ (**4**)[1] and $[\{(OC)_5Cr\}_6Ge_6]^{2-}$ (**1**)[2] are the only ones thus far characterised. Their octahedral structures are well documented,[1,2] but their chemical properties could not yet be studied in detail as they are difficult to prepare in large amounts. Analysing the properties of these prototype species would be interesting for the following reasons:

Simple MO models predict that the clusters $[E_6]^{2-}$ (E = Ge, Sn), which form the core of their organometallic derivatives $[(L_nM)_6E_6]^{2-}$ (L_nM = 16 electron transition metal template), should be especially stable in view of their large HOMO−LUMO gap. This is in agreement with the accepted electron-counting rules[15,16] which state that *closo* octahedral species are stable, with seven skeleton electron pairs which is just the number of such pairs in $[E_6]^{2-}$ (E = group-14 element). On the basis of this model, it can be deduced that oxidation as well as reduction of such species should be difficult, and reduction might well lead to rearrangements, producing more open forms of the clusters.[15,16] A large HOMO−LUMO gap, as expected on the basis of such models, would also mean that electronic absorptions arising from transitions within the cluster framework should have a relatively high energy. Furthermore, the structures of the $[E_6]^{2-}$ entities should be close to octahedral in each case, largely independent of the type of organometallic protecting group L_nM. This octahedral arrangement should also persist in solution.

With all these questions in mind, it appears necessary to search for better synthetic strategies to produce the compounds $[(L_nM)_6E_6]^{2-}$. It had recently been found that the digermanium derivative $[\{(OC)_5Cr\}_2Ge_2I_4]^{2-}$, which is itself obtained by the reduction of GeI_2 with $Na_2[Cr_2(CO)_{10}]$, is a suitable precursor from which $[\{(OC)_5Cr\}_6Ge_6]^{2-}$ (**1**) is obtained in up to 40% yield by further reduction.[17] This result stimulated a more systematic screening of the reactions of $[M_2(CO)_{10}]^{2-}$ [18,19] (M = Cr, Mo, W) with $EHal_2$ (GeI_2, $SnCl_2$). In this way, feasible procedures for the syntheses of $[\{(OC)_5M\}_6E_6]^{2-}$ (E = Ge, Sn; M = Cr, Mo, W) have been developed such that the cyclovoltammetric and spectroscopic behaviour of these

[a] Anorganisch-Chemisches Institut der Universität Heidelberg
Im Neuenheimer Feld 270, 69120 Heidelberg, Germany
Fax: (internat.) + 49-(0)6221/545707
E-mail: g.huttner@indi.aci.uni-heidelberg.de

 © WILEY-VCH Verlag GmbH, 69451 Weinheim, 2001 1434−1948/01/0404−0973 $ 17.50+.50/0

compounds, as well as their solid-state and solution structures, could now be studied in detail. The results of these preparative efforts and the spectroscopic, cyclovoltammetric, and structural studies are reported in this paper.

Results and Discussion

Preparation of Ge_6 Clusters

It had been shown that $K_2[Cr(CO)_5]$ reacts with $SnCl_2$ to produce $[\{(OC)_5Cr\}_6Sn_6]^{2-}$ (**4**) which could be isolated in the form of its $K(crypt)_2$ salt.[1] The straightforward transfer of this synthetic approach to the chemistry of germanium did, however, not result in an analogous $[\{(OC)_5Cr\}_6Ge_6]^{2-}$ cluster. Only when $Na_2[Cr_2(CO)_{10}]$ was treated with GeI_2 in the presence of bipy (bipy = 2,2′-bipyridine), did the cluster $[\{(OC)_5Cr\}_6Ge_6]^{2-}$ (**1**) result (Scheme 1), which was isolated as its Ph_4P salt.[2]

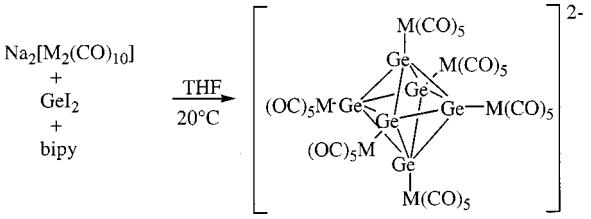

1 (M = Cr, yield: 11%)
2 (M = Mo, yield: 9%)
3 (M = W, yield: 9%)

Scheme 1. Syntheses and yields of **1**–**3** from a 1:1:1 mixture of the reagents

This type of procedure was now found to work with the decacarbonyldimetallates of molybdenum and tungsten as well, to produce **2** and **3**, respectively. The yields obtained in this route are modest throughout, with a maximum of 11% in the case of chromium and approximately 9% in the case of molybdenum and tungsten.

It has now been found that changing the stoichiometry of the reactants by increasing the amount of the dimetallate to a threefold molar excess with respect to GeI_2, produces the desired clusters in fair yields, without any addition of bipy (Scheme 2).

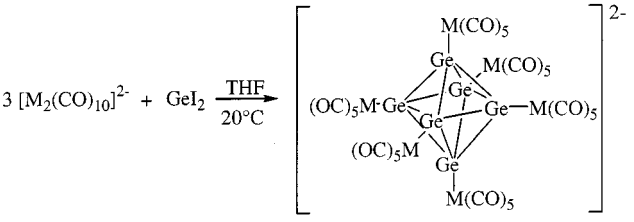

2 (M = Mo, yield: 47%)
3 (M = W, yield: 60%)

Scheme 2. Syntheses and yields of **2**, **3** from a 1:3 mixture of the reagents

It appears therefore that the only function of bipy in the reported synthesis of **1**[2] is to reduce the amount of GeI_2 by complexation, such that the stoichiometric excess of the dimetallate relative to the germanium iodide is appropriately increased.[20]

For the reaction of $[Cr_2(CO)_{10}]^{2-}$ with GeI_2, it has been shown that $[\{(OC)_5Cr\}I_2Ge-GeI_2\{Cr(CO)_5\}]^{2-}$ is obtained when the stoichiometric ratio of $[Cr_2(CO)_{10}]^{2-}$ and GeI_2 is 1:1.[17] This digermanium compound is an intermediate in the reductive pathway from GeI_2 to the $[Ge_6]^{2-}$ core of **1**: Further reduction of $[\{(OC)_5Cr\}I_2Ge-GeI_2\{Cr(CO)_5\}]^{2-}$ with 2 equiv. of $[Cr_2(CO)_{10}]^{2-}$ produces **1** in fair yields (Scheme 3).[17]

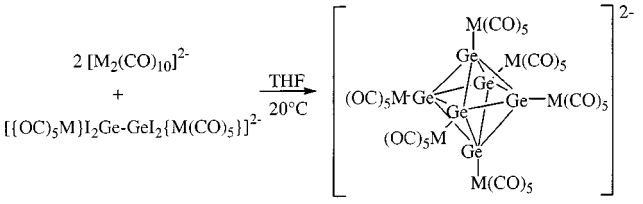

1 (M = Cr, yield: 40%)
3 (M = W, yield: 60%)

Scheme 3. Syntheses of **1** and **3** from tetraiododigermanate(2−)-precursors in a ratio 2:1

This type of reaction has been reported for compound **1**.[17] It has now been found that **3** can be obtained in good yields (60%) from $[\{(OC)_5W\}I_2Ge-GeI_2\{W(CO)_5\}]^{2-}$ [17] and 2 equiv. of $[W_2(CO)_{10}]^{2-}$. The decacarbonyldimetallates may be used as their sodium[18] or potassium salts,[19] without a significant change in reactivities and yields. The tetraiododigermanate derivatives $[\{(OC)_5M\}I_2Ge-GeI_2\{M(CO)_5\}]^{2-}$ are easily accessible for M = Cr, W, while for M = Mo the corresponding compound could not be isolated in a pure state. Its production is always accompanied by the formation of **2**, and it was not yet possible to separate the digermanate derivative from this cluster. For M = Cr and W, on the other hand, the compounds $[\{(OC)_5M\}I_2Ge-GeI_2\{M(CO)_5\}]^{2-}$ are ideal starting materials for the syntheses of **1** and **3**. Their reduction to these cluster compounds by KC_8 (Scheme 4) is a clean reaction from which the clusters are easily obtained in a pure state.

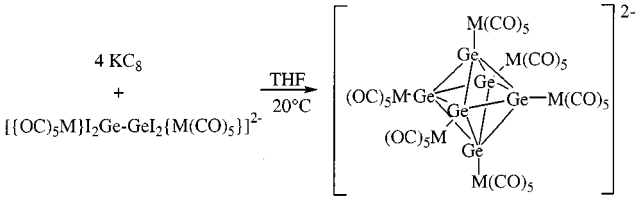

1 (M = Cr, yield: 42%)
3 (M = W, yield: 60%)

Scheme 4. Syntheses and yields of **1** and **3** by KC_8 reduction

Preparation of Sn_6 Clusters

The first compound of the series (**4**) was obtained from the reaction of $K_2[Cr(CO)_5]$ with $SnCl_2$.[1] It has now been found that the reaction of $Na_2[Cr_2(CO)_{10}]$ with $SnCl_2$ in a

1:1 molar ratio also leads to the formation of **4** (Scheme 5, Table 1).

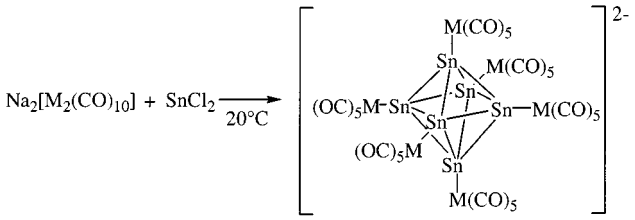

4 (M = Cr, yield: 11%)
5 (M = Mo, yield: 36%)
6 (M = W, yield: 9%)

Scheme 5. Syntheses and yields of **4**–**6**

Table 1. Complexes of type **1**–**6**

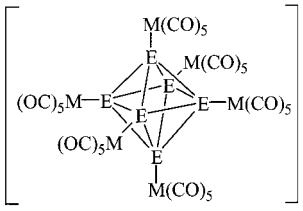

	E	M	Cation
1	Ge	Cr	$[Ph_4P^+]$
2	Ge	Mo	$[Ph_4P^+]$
3	Ge	W	$[Ph_4P^+]$
4	Sn	Cr	$[Ph_4P^+]$
5	Sn	Mo	$[Ph_4P^+]$
6	Sn	W	$[Ph_4P^+]$

The reaction is sensitive to the molar ratio of the reactants: When $Na_2[Cr_2(CO)_{10}]$ and $SnCl_2$ are used in a 3:1 ratio, the star-type compound $[Sn\{Cr(CO)_5\}_3]^{2-}$ is the main product.[21] With $Na_2[Mo_2(CO)_{10}]$ or $Na_2[W_2(CO)_{10}]$ used in the same molar ratio, mixtures of products are obtained which do not contain any **5** or **6**, as judged from their IR absorptions. When a ratio of 1:1 is used, the isolated yield of **4** (as its Ph_4P salt) is approximately 10%, along with other products in the reaction mixture. $[\{(OC)_5Cr\}SnCl_3]^-$ and $[\{(OC)_5Cr\}_2SnCl_2]^{2-}$ (both isolated as their Ph_4P salts) were found to be formed in substantial amounts ($[Ph_4P][\{(OC)_5Cr\}SnCl_3]$, 26% and $[Ph_4P]_2[\{(OC)_5Cr\}_2SnCl_2]$, 42%). The same type of reaction has already been used to synthesise $[\{(OC)_5M\}_2SnCl_2]^{2-}$ (M = Cr, Mo, W).[22,23] These compounds were, in fact, the main products from which the clusters had to be separated by chromatography. In the case of **5**, the use of ethanol as the solvent instead of THF greatly improved the yield. In this solvent, **5** is precipitated by the addition of Ph_4PCl, while the $[Ph_4P]$ salts of the by-products remain in solution. Traces of $[Ph_4P]_2[\{(OC)_5Mo\}_2SnCl_2]$, which are precipitated together with $[Ph_4P^+]_2$·**5**, are easily washed out with ethanol such that analytically pure $[Ph_4P^+]_2$·**5** is obtained in 36% yield, without the necessity of chromatographic purification.

Structures and Properties

The structures of **1** and **4** have been reported for the phosphonium salt $[Ph_4P^+]_2$·**1**[2] and for the potassium salt $[K^+(crypt)]_2$·**4**.[1] In order to unequivocally prove the constitution of the phosphonium salts **2**–**6**, the structures were determined by X-ray analysis. Crystals of the tin compounds **4**–**6** were obtained by layering THF solutions of the salts with ethanol and the germanium compounds **2** and **3** were crystallised by layering DMA (*N*,*N*-dimethylacetamide) solutions of their salts with ethanol. From the crystals obtained this way, those of **4** contain 1 equiv. of THF per formula unit as a solvate, whereas the other compounds crystallise as such. The high symmetry of the phosphonium cation (S_4) and of the cluster anions are in agreement with tetragonal space groups, which are found for the phosphonium salts of all six compounds **1**–**6** (Table 6). The phosphorus centre of the phosphonium cation occupies a special position in each case such that its crystallographic point-group symmetry is S_4. The centres of the anionic clusters are also located at special positions. Owing to steric influence, the $M(CO)_5$ moieties have to be rotated around their Sn–M or Ge–M axes in such a way that they cannot conform to an arrangement which would be symmetric with respect to the idealised mirror planes of the "octahedron" formed by the main-group elements. The tilt imposed on these groups maximally allows for D_4 symmetry. This is the crystallographic symmetry apparent for the anions in $[Ph_4P^+]_2$·**1** and $[Ph_4P^+]_2$·**2** (space group *P*4/*nnc*). The phosphonium salts of **3**, **5**, and **6** crystallise in space group *I*4/*mmm*, which implies apparent D_{4h} symmetry of the anions. This apparent symmetry is fulfilled by a statistical 1:1 disorder of each $M(CO)_5$ group over two mirror-symmetric rotational positions. The $[Ph_4P]$ salt of **4** contains 1 equiv. of THF solvate per formula unit, its space-group symmetry is *I*4/*m*, with the crystallographic site-group symmetry of the cluster corresponding to C_{4h}. Again, this symmetry, which is exact for the Sn_6 core results from the superposition of two rotational positions of the $Cr(CO)_5$ units at the C_4 axis around their Cr–Sn bonds. The crystallographically determined symmetry of the "octahedron" formed by the main-group elements corresponds to the site-group symmetry in each case, and is, in fact, D_{4h} throughout. Therefore the main-group clusters have a tetragonally distorted octahedral symmetry. The observed distortion corresponds to a slight elongation of the octahedra along the C_4 axis (Table 2, Figure 1).

As the quantitative data (Table 2) show, there is a slight variation of the Ge–Ge distances from **1**–**3**, with **3** having $W(CO)_5$ groups showing the longest, and **1** having the $Cr(CO)_5$ groups showing the shortest distances. For the tin compounds **4**–**6**, no such variation is apparent (Table 2). The angles within and subtended by the main-group octahedra are fairly constant throughout and are in each case close to the values expected for an ideal octahedron (E–E–E: 60°, 90°; M–E–E: 135°; Table 2). The angles

Table 2. Selected bond lengths [pm] and angles [°] of compounds $[Ph_4P^+]_2$·**1**−**6** (labels refer to Figure 1 throughout, with E1 on the tetragonal axis in each case)

	$[Ph_4P^+]_2$·**1**	$[Ph_4P^+]_2$·**2**	$[Ph_4P^+]_2$·**3**	$[Ph_4P^+]_2$·**4**	$[Ph_4P^+]_2$·**5**	$[Ph_4P^+]_2$·**6**
E1−E2	254.1(1)	258.0(4)	259.2(4)	293.0(1)	292.8(1)	292.8(3)
E2−E2A	252.5(2)	256.7(5)	259.2(5)	291.7(1)	290.2(1)	289.2(3)
E1−M1	242.6(2)	257.3(6)	255.7(5)	262.6(2)	271.1(3)	269.4(4)
E2−M2	239.5(2)	254.8(4)	251.8(3)	258.3(1)	273.5(1)	273.2(2)
M1−E1−E2	135.4(3)	135.3(1)	135.0(1)	135.3(1)	135.5(1)	135.7(5)
M2−E2−E2A	135.00	135.00	135.00	139.5(1)	134.5(1)	134.3(5)
M2−E2−E1	134.7(1)	134.7(1)	135.0(1)	134.6(1)	135.00	135.00
E1−E2−E2A	60.2(1)	60.2(1)	60.0(1)	60.2(1)	60.3(1)	60.4(3)
E2−E1−E2A	59.6(1)	59.7(1)	60.0(1)	59.7(1)	59.4(3)	59.2(6)
	89.3(1)	89.4(2)	90.0(2)	89.5(1)	89.00(5)	88.6(1)
E1−E2−E1A	90.7(1)	90.6(2)	90.0(2)	90.5(1)	91.0(5)	91.4(1)
E2−E2A−E2B	90.00	90.00	90.00	89.5(1)	90.00	90.00
E1−M1−C(ax)	180.0	180.0	180.0	180.0	180.0	180.0
E2−M2−C(ax)	180.0(3)	180.0(6)	180.0(1)	180.0(2)	180.0(4)	180.0(9)
E−M−C(eq)	86.7(3)−88.9(2)	87.1(7)−89.1(6)	86.0(9)−88.9(9)	87.7(2)−88.8(2)	86.3(5)−88.4(5)	87.2(6)−89.9(9)
C(ax)−M−C(eq)	91.1(2)−93.3(2)	91.0(6)−92.9(7)	91.1(9)−94.0(9)	91.2(2)−91.5(2)	91.5(5)−92.3(7)	90.1(9)−92.8(6)
C(eq)−M−C(eq)	89.0(3)−90.8(3)	89.2(9)−91.0(6)	89.0(1)−90.7(1)	89.2(3)−90.0(1)	88.7(6)−89.9(1)	86.4(5)−90.0(1)
	173.4(5)−177.8(4)	174.2(9)−177.0(6)	175.9(2)−177.7(2)	175.3(3)−177.6(4)	175.3(9)−176.8(9(	174.4(9)- 179.9(9)
M1−C(ax)−O(ax)	180.0	180.0	180.0	180.0	180.0	180.0
M2−C(ax)−O(ax)	180.0(9)	180.0(9)	180.0(1)	180.0(5)	180.0(1)	180.0(9)
M−C(eq)−O(eq)	176.9(7)−179.8(6)	174.2(9)−178.1(9)	176.2(3)−178.0(3)	178.1(5)−179.3(5)	177.4(9)−179.2(9)	176.7(9)−179.5(9)

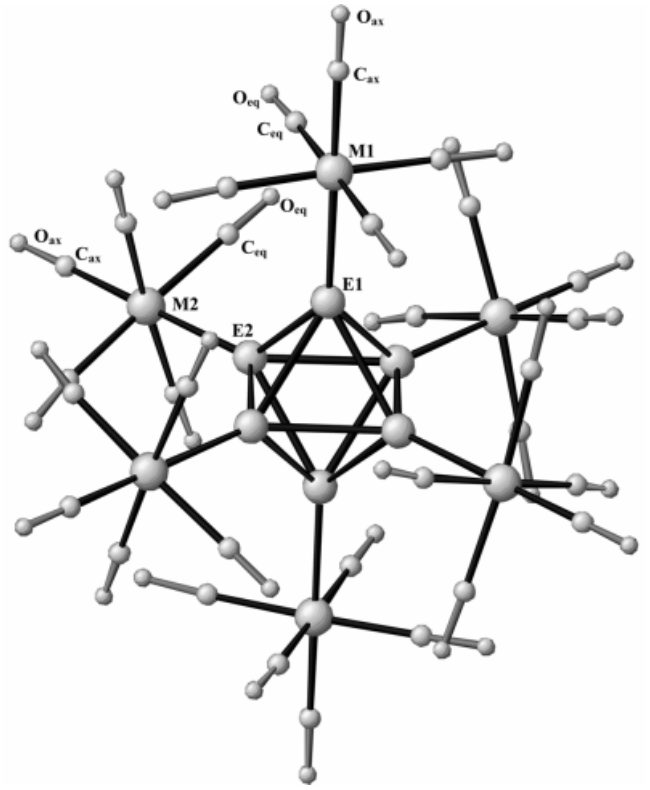

Figure 1. Structure of **2** as a representative of the architecture of **1**−**6**; labels refer to Table 2; the tetragonal axis is vertical in Figure 1, with E1 lying on this axis

describing the geometry of the $M(CO)_5$ fragments (Table 2) indicate a slight umbrella effect with the equatorial carbonyl groups bending towards the main-group centre. An overview of the geometric parameters characterising the $[E_6]^{2-}$ core of the clusters given in Table 2 makes it clear that neither the kind of the protective groups $M(CO)_5$ (M = Cr, Mo, W), nor the specific crystal environment, have a strong influence on the structure of the cluster core. It appears therefore that the observed geometry corresponds to a well-defined energy minimum on the corresponding hypersurface.

The idealised *closo* octahedral structure of the $[E_6]^{2-}$ core should therefore also characterise the structure of the compounds in solution. The pattern of $\tilde{\nu}$(CO) infrared bands observed for **1**−**6** (Table 3) is simple enough to substantiate this expectation. With two $M(CO)_5$ groups in slightly different chemical environments, a maximum of six absorptions should be expected. A maximum of five absorptions is observed (Table 3), and only four bands are apparent in most cases.

Table 3. $\tilde{\nu}$(CO) − IR spectroscopic data of compounds $[Ph_4P^+]_2$·**1**−**6**

	$\tilde{\nu}$(CO) − IR [cm^{-1}]				
$[Ph_4P^+]_2$·**1**[a]	–	2043s	2010w	1951vs	1910s
$[Ph_4P^+]_2$·**2**[a]	–	2056s	2029m	1957vs	1907vs
$[Ph_4P^+]_2$·**3**[a]	–	2056s	2031m	1952vs	1910s
$[Ph_4P^+]_2$·**4**[b]	2052m	2037s	–	1943vs	1912vs
$[Ph_4P^+]_2$·**5**[b]	2070w	2052s	2013w	1951vs	1907vs
$[Ph_4P^+]_2$·**6**[b]	2068w	2052s	2017m	1945vs	1905vs

[a] DMA. − [b] THF.

This indicates that the high symmetry found in the anions in the solid state is also preserved in solution. A more direct indication of a cluster geometry that is octahedral on average, comes from NMR spectroscopy. The ^{119}Sn resonances of **4**−**6** (Table 4) show clear tin satellites in each case, with coupling constants of approximately 1800 Hz, characteristic of tin−tin contacts.[24] The integral ratio of the main signal to the satellites is as expected for an arrangement in which the observed tin nucleus is surrounded by four other nuclei, each of them in an abundance of 7.6% (calculated: 30.4%; observed 28%).[25] The ^{119}Sn NMR spectrum of $[Ph_4P^+]_2$·**6**

shows ^{183}W coupling with $^1J_{W-Sn} = 700$ Hz for the main signal, as well as for the satellites. In agreement with the overall octahedral geometry, there is only one ^{13}C resonance for the equatorial CO groups of compounds **1−6**, and one for the axial carbonyl groups, wherever these could be measured (solubility) (Table 4).

The $[E_6]^{2-}$ octahedra acting as the ligand core in compounds **1−6** are electron-precise *closo* clusters.[15,16] As a result of a low-lying HOMO and a high-energy LUMO, these clusters should be difficult to oxidise and reduce. Cyclic voltammetry reveals (Table 5) that despite the charge of −2 on these clusters, their oxidation occurs only at approximately +0.3 V (vs. SCE). This oxidation is reversible in some cases (Table 5). It thus follows that removing an electron from the filled t_{1u} HOMO does not induce a strong distortion of the cluster. Further irreversible oxidation of the cluster core is observed in the range up to approximately +0.8 V (vs. SCE) (Table 5). At higher potentials, the $M(CO)_5$ groups are oxidised. The peaks corresponding to an oxidation of the $M(CO)_5$ groups are roughly six times larger than the peaks that correspond to electron-transfer processes involving the cluster core. Polarograms also show an approximate 1:6 ratio of the corresponding step heights. This must mean that electron transfer involving the cluster core includes the whole $[E_6]^{2-}$ entity and not just one individual main-group centre, while electron transfer involving the $M(CO)_5$ entities involves each such group individually. Reduction of compounds **1−6** is irreversible throughout and occurs between −0.6 and −0.9 V (vs. SCE) (Table 5). Reduction of the $M(CO)_5$ entities is observed from approximately −1.4 V (vs. SCE) towards lower potentials and is also irreversible (Table 5).

The reversible oxidation of the cluster core documented by the cyclovoltammetric experiments would suggest that the cluster dianions could also be oxidised to the monoanions by chemical means. However, it was found that mild oxidants (sulfur, propylene sulfide, Fc^+), applied in solvents such as CS_2, DMA, THF, or mixtures of these, leave the dianions unchanged (IR control) for hours. Strong oxidants such as I_2 and tetrabromoorthoquinone lead to fragmentation of the clusters. The sodium salts of the cluster dianions are also stable against chemical reduction: Their THF solutions may be in contact with KC_8 without any sign of change, even after several days.

The cyclovoltammetric data indicate that the HOMO−LUMO separation within the clusters should be roughly 1.5 eV. Hence, if electronic HOMO−LUMO transitions were allowed, these would be expected to occur in the

Table 4. ^1H, $^{31}P\{^1H\}$, and $^{13}C\{^1H\}$ NMR spectroscopic data of compounds $[Ph_4P^+]_2$·**1−6**

	^1H $H_{arom.}$[c]	$^{31}P\{^1H\}$	$^{119}Sn\{^1H\}$	$^{13}C\{^1H\}$[d] CO_{ax}	CO_{eq}	C_{para}	C_{ortho}	C_{meta}	C_{ipso}
$[Ph_4P^+]_2$·**1**[a]	8.01−7.67	23.6	–	222.2	217.0	136.2	135.4	131.3	118.8
$[Ph_4P^+]_2$·**2**[a]	7.97−7.69	23.6	–	–	206.4	135.2	134.3	130.3	117.5
$[Ph_4P^+]_2$·**3**[a]	7.97−7.69	23.6	–	–	197.6	135.2	134.4	130.3	117.6
$[Ph_4P^+]_2$·**4**[b]	7.87	24.3	508 ($^1J_{Sn-Sn}$ = 1848 Hz)	–	218.0	136.4	135.6	131.4	118.9
$[Ph_4P^+]_2$·**5**[b]	7.87	26.3	561 ($^1J_{Sn-Sn}$ = 1780 Hz)	–	–	136.2	135.5	131.2	188.8
$[Ph_4P^+]_2$·**6**[b]	8.03−7.87	24.3	198 ($^1J_{Sn-Sn}$ = 1803 Hz, $^1J_{W-Sn}$ = 700 Hz)	204.7	198.8	136.4	135.7	131.4	119.0

[a] $[D_6]$DMSO. − [b] $[D_6]$acetone. − [c] Unresolved multiplets. − [d] C_{para} [d, $^4J(^{31}P,^{13}C)$ = 3 Hz]; C_{ortho} [d, $^2J(^{31}P,^{13}C)$ = 10 Hz]; C_{meta} [d, $^3J(^{31}P,^{13}C)$ = 13 Hz]; C_{ipso} [d, $^1J(^{31}P,^{13}C)$ = 89 Hz]; $[Ph_4P^+]$.

Table 5. Analytical data of compounds $[Ph_4P^+]_2$·**1−6**

	M.p. [°C]	UV/nm (THF/DMA) λ_{max} (ε [l mol^{-1} cm^{-1}])	Empirical formula (mol. mass)	Elemental analysis	CV (CH_3CN)[a] [V]
$[Ph_4P^+]_2$·**1**	104−105 (dec.)	276 (12000); 301 (12000); 365 (3000)	$C_{78}H_{40}O_{30}P_2Cr_6Ge_6$ (2266.62)	calcd. C 41.33 H 1.78 found C 41.27 H 2.01	Ox: +0.34rev., +0.81, + 1.12 Red.: −0.92, −1.54, −1.75, −1.94
$[Ph_4P^+]_2$·**2**	160−163 (dec.)	298 (12400); 325 (12000); 377 (6400)	$C_{78}H_{40}O_{30}P_2Mo_6Ge_6$ (2530.27)	calcd. C 37.03 H 1.59 found C 37.20 H 1.92	Ox.: +0.29rev., +0.70, +0.82, +1.08 Red.: −1.44, −1.74, −1.93
$[Ph_4P^+]_2$·**3**	228−229 (dec.)	276 (16000); 329 (4500); 375 (3000)	$C_{78}H_{40}O_{30}P_2W_6Ge_6$ (3057.81)	calcd. C 30.64 H 1.32 found C 28.69 H 1.72	Ox.: +0.62, +0.86, +1.10 Red.: −0.90, −1.44, −1.62, −1.93
$[Ph_4P^+]_2$·**4**	207−208 (dec.)	329 (30800); 392 (7000)	$C_{78}H_{40}O_{30}P_2Cr_6Sn_6$ (2543.22)	calcd. C 37.66 H 1.85 found C 38.00 H 2.08	Ox.:[b] +0.39rev., +0.69, +0.83, +1.01, +1.32 Red.:[b] −0.60, −1.40, −1.48
$[Ph_4P^+]_2$·**5**	184−186 (dec.)	295 (36000); 328 (31000); 404 (12000)	$C_{78}H_{40}O_{30}P_2Mo_6Sn_6$ (2806.88)	calcd. C 33.38 H 1.44 found C 32.67 H 1.93	Ox.: +0.33, +0.48, +0.67, +0.81, +1.10 Red.: −1.39, −1.89
$[Ph_4P^+]_2$·**6**	200−201 (dec.)	295 (33000); 320 (30000); 381 (10000); 423 (8000)	$C_{78}H_{40}O_{30}P_2W_6Sn_6$ (3334.34)	calcd. C 28.10 H 1.21 found C 27.76 H 1.65	Ox.: +0.24, +0.40, +0.55, +0.87, +1.11 Red.: −1.27, −1.94

[a] Potentials were measured vs. SCE with the exception of $[Ph_4P^+]_2$·**4** (see footnote[b]). The working electrode was a glassy-carbon electrode in each case, with a platinum wire used as the counter electrode. Redox processes were judged to be reversible if the separation of their anodic and cathodic peaks was similar to the one observed for the Fc/Fc^+ redox couple in the same experiment. A square-root dependence of peak height on scan speed was taken as the second criterion. The data given for the other electrode processes refer to peak potentials E_P^R or E_P^C throughout. − [b] The potentials refer to a platinum wire as the reference electrode and are thus on a deliberate absolute scale. Whenever an SCE electrode was immersed into the solution, the compound was found to disintegrate.

visible range. MO analysis of the cluster core on the other hand reveals that these transitions are symmetry-forbidden since the HOMO has t_{1u} symmetry and the LUMO has t_{2u} symmetry. The transition from the HOMO (t_{1u}) to the LUMO+1 (t_{1g}) would be symmetry-allowed. The energy difference between the corresponding orbitals is however quite large, and owing to the shape of the orbitals, the transition moment should be small. In agreement with this, UV/Vis spectra of the $[Ph_4P]$ salts **1**−**6** (Table 5) do not show a spectroscopic pattern that could be assigned to transitions within the cluster core. The high-energy absorptions above 350 nm are characteristic of $M(CO)_5$ derivatives as a whole (see for instance ref.[21]); the lower energy absorptions at approximately 400 nm are interpreted as LMCT absorptions. In agreement with germanium having a higher electronegativity than tin, these CT bands occur at higher energy for the germanium compounds than for the tin analogues (Table 5).

Experimental Section

General: All manipulations were carried out under argon by means of standard Schlenk techniques at 20 °C unless otherwise mentioned. All solvents were dried by standard methods, and distilled under argon. $[D_6]$DMSO and $[D_6]$acetone used for the NMR spectroscopic measurements were degassed by three successive "freeze-pump-thaw" cycles and dried with 4 Å molecular sieves. Silica gel (Kieselgel z. A. 0.06−0.2 mm, J. T. Baker Chemicals B. V.) used for chromatography and Kieselgur (Kieselgur, gereinigt, geglüht, Erg. B.6, Riedel-de Haën AG) used for filtration were degassed at 1 mbar at 130 °C for 12 h and saturated with argon. − NMR: Bruker Avance DPX 200 at 200.13 MHz (^{1}H), 50.323 MHz (^{13}C{^{1}H}), 81.015 MHz (^{31}P{^{1}H}), 74.631 MHz (^{119}Sn{^{1}H}); chemical shifts (δ) in ppm relative to $[D_6]$DMSO (^{1}H: δ = 2.50; ^{13}C: δ = 39.4) and $[D_6]$acetone (^{1}H: δ = 2.05; ^{13}C: δ = 206.2) as internal standards and to 85% H_3PO_4 (^{31}P: δ = 0) and $(CH_3)_4Sn$ (^{119}Sn: δ = 0) as external standards, respectively. − IR: Bruker FT-IR IFS-66; CaF_2 cells. − UV/Vis/NIR: Perkin−Elmer Lambda 19; cells (0.2 cm; Hellma 110 suprasil). − Cyclic voltammetry: Methrom "Universal Meß- und Titriergefäß", Methrom GC electrode RDE 628, platinum electrode, SCE electrode, Princeton Applied Research Potentiostat Model 273, 10^{-3} M in 0.1 M nBu$_4$NPF$_6$/CH_3CN. − Elemental analysis: Microanalytical laboratory of the Organisch-Chemisches Institut, Universität Heidelberg. − Melting points: Gallenkamp MFB-595 010; the values are not corrected.

Preparation of $[Ph_4P]_2[\{(OC)_5M\}_6Ge_6]$, $[Ph_4P^+]_2$·1, $[Ph_4P^+]_2$·2, $[Ph_4P^+]_2$·3 (M = Cr, Mo, W)

Method 1, the "bipy Method" (Suitable for the Preparation of $[Ph_4P^+]_2$·1−3): To a stirred orange solution of $Na_2[M_2(CO)_{10}]$[18] (M = Cr: 430 mg, 1 mmol; M = Mo: 518 mg, 1 mmol; M = W: 694 mg, 1 mmol) in THF (50 mL), solid GeI_2 (326 mg, 1 mmol) and solid 2,2′-bipyridine (156 mg, 1 mmol) were added in one portion. After stirring for 30 min, the deep red solution was filtered through Kieselgur (3 cm, Ø = 3 cm), concentrated in vacuo (3 mL) and purified by chromatography on silica gel (15 cm, Ø = 3 cm; THF). With THF as the eluent all by-products could be removed.[2,17,22] After elution with ethanol, the solutions of the sodium salts of **1**, **2**, and **3**, respectively, were obtained, which were reduced to 10 mL in vacuo. Addition of solid $[Ph_4P]Cl$ (750 mg, 2 mmol) led to the red-brown $[Ph_4P]$ salts of **1**, **2**, and **3**, which were separated from the mother liquor by filtration, washed with ethanol (2 × 5 mL) and diethyl ether (2 × 5 mL), and dried in vacuo. Yields: $[Ph_4P^+]_2$·**1**: 43 mg, 0.02 mmol, 11%; $[Ph_4P^+]_2$·**2**: 42 mg, 0.02 mmol, 9% $[Ph_4P^+]_2$·**3**: 50 mg, 0.02 mmol, 9% (with respect to GeI_2).

Method 2, Reduction with $K_2[M_2(CO)_{10}]$ (Suitable for the Preparation of $[Ph_4P^+]_2$·2, $[Ph_4P^+]_2$·3): KC_8 [811 mg, 6 mmol, freshly prepared by dry heating of graphite powder (577 mg, 48 mmol) with potassium (235 mg, 6 mmol) by a heat gun (650 °C) in a Schlenk tube under vacuum] and $M(CO)_6$ (M = Mo: 6 mmol = 1.58 g, M = W: 2.11 g, 6 mmol) in THF (50 mL) were stirred for 12 h at 20 °C, during which time CO evolution had ceased. After this period of time, solid GeI_2 (326 mg, 1 mmol) was added to the dark green heterogeneous mixture, causing a colour change to deep brown. After stirring for 1 h, the reaction mixture was filtered through Kieselgur (3 cm, Ø = 3 cm) and concentrated in vacuo (3 mL). Further workup was carried out as in Method 1. Yields: $[Ph_4P^+]_2$·**2**: 220 mg, 0.08 mmol, 47% $[Ph_4P^+]_2$·**3**: 320 mg, 0.10 mmol, 60% (with respect to GeI_2).

Method 3, Reduction of Tetraiododigermanates by Decacarbonyldimetallate (Suitable for the Preparation of $[Ph_4P^+]_2$·1, $[Ph_4P^+]_2$·3): To a solution of $Na_2[\{(OC)_5M\}I_2Ge-GeI_2\{M(CO)_5\}]$[17] (M = Cr, W) in THF (30 mL), a solution of $Na_2[M_2(CO)_{10}]$[18] in THF (30 mL) was added in 10-mL portions during a period of 3 h. The colour of the solution gradually turned to red-brown. Further workup was carried out as in Method 1. Yields: $[Ph_4P^+]_2$·**1**: 151 mg, 0.07 mmol, 40%; $[Ph_4P^+]_2$·**3**: 310 mg, 0.10 mmol, 60% (with respect to GeI_2).

Method 4, Reduction of Tetraiododigermanates with KC_8 (Suitable for the Preparation of $[Ph_4P^+]_2$·1, $[Ph_4P^+]_2$·3): To solid KC_8 [540 mg, 4 mmol; freshly prepared from graphite powder (384 mg, 32 mmol) and potassium (156 mg, 4 mmol) as above], a solution of $Na_2[\{(OC)_5M\}I_2Ge-GeI_2\{M(CO)_5\}]$[17] (M = Cr, W) in THF (50 mL) was added and stirred for 1 h. Further workup was carried out as in Method 1. Yields: $[Ph_4P^+]_2$·**1**: 164 mg, 0.07 mmol, 42%; $[Ph_4P^+]_2$·**3**: 306 mg, 0.10 mmol, 60% (with respect to GeI_2). Single crystals suitable for X-ray structure analysis were obtained by layering concentrated DMA solutions of $[Ph_4P^+]_2$·**1**, $[Ph_4P^+]_2$·**2**, and $[Ph_4P^+]_2$·**3** with ethanol.

Preparation of $[Ph_4P]_2[\{(OC)_5M\}_6Sn_6]$, $[Ph_4P^+]_2$·4 (M = Cr), $[Ph_4P^+]_2$·6 (M = W): To a stirred orange solution of $Na_2[M_2(CO)_{10}]$[18] (M = Cr: 430 mg, 1 mmol; M = W: 694 mg, 1 mmol) in THF (50 mL), solid $SnCl_2$ (190 mg, 1 mmol) was added in one portion. The orange solution turned deep red immediately. After stirring for 30 min, the reaction mixture was filtered through Kieselgur (3 cm, Ø = 3 cm). The resulting red solution was concentrated in vacuo (3 mL) and purified by chromatography on silica gel (15 cm, Ø = 3 cm; THF). A mixture of THF/ethanol (15:1) was used until the elute was colourless. A red band remained on top of the column and could be eluted with ethanol. $[Na^+]_2$·**4** and $[Na^+]_2$·**6** were obtained as deep red ethanolic solutions, which were concentrated to 10 mL in vacuo. Addition of solid $[Ph_4P]Cl$ (750 mg, 1 mmol) led to the corresponding deep red $[Ph_4P]$ salts of **4** and **6**, respectively, which precipitated immediately. The solids were separated from the mother liquor by filtration, washed with ethanol (2 × 5 mL), diethyl ether (2 × 10 mL), and dried in vacuo. Yields: $[Ph_4P^+]_2$·**4**: 46 mg, 0.02 mmol, 11%; $[Ph_4P^+]_2$·**6**: 50 mg, 0.02 mmol, 9% (with respect to $SnCl_2$). For growing single crystals of $[Ph_4P^+]_2$·**4** and $[Ph_4P^+]_2$·**6**, the deep-red solids were dissolved in

Table 6. Crystal structure data of compounds $[Ph_4P^+]_2$·**1**−**6**

Compound	$[Ph_4P^+]_2$·**1**	$[Ph_4P^+]_2$·**2**	$[Ph_4P^+]_2$·**3**	$[Ph_4P^+]_2$·**4**·thf	$[Ph_4P^+]_2$·**5**	$[Ph_4P^+]_2$·**6**
Empirical formula	$C_{78}H_{40}Cr_6Ge_6O_{30}P_2$	$C_{78}H_{40}Ge_6Mo_6O_{30}P_2$	$C_{78}H_{40}Ge_6O_{30}P_2W_6$	$C_{82}H_{40}Cr_6O_{31}P_2Sn_6$	$C_{78}H_{40}Mo_6O_{30}P_2Sn_6$	$C_{78}H_{40}O_{30}P_2Sn_6W_6$
Molecular mass [g/mol]	2266.56	2530.27	3057.81	2607.22	2806.88	3334.34
Crystal dimension [mm]	0.20·0.20·0.25	0.15·0.15·0.15	0.10·0.10·0.10	0.35·0.35·0.25	0.30·0.30·0.20	0.35·0.35·0.25
Crystal system	tetragonal	tetragonal	tetragonal	tetragonal	tetragonal	tetragonal
space group (no.)	*P4/nnc* (126)	*P4/nnc* (126)	*I4/mmm* (139)	*I4/m* (87)	*I4/mmm* (139)	*I4/mmm* (139)
a [pm]	1462.1(6)	1514.4(3)	1499.8(2)	1294.7(1)	1594.5(1)	1573.3(1)
b [pm]	1462.1(6)	1514.4(3)	1499.8(2)	1294.7(1)	1594.5(1)	1573.1(1)
c [pm]	1970.0(6)	1971.3(5)	1971.8(4)	2815.7(5)	1912.2(2)	1897.3(1)
Cell volume [10^6pm^3]	4211(3)	4521(2)	4435(1)	4720(1)	4862(1)	4696(1)
Molecular units/cell	2	2	2	2	2	2
Density (calculated) [g cm^{-3}]	1.787	1.859	2.787	1.835	1.890	2.329
Temperature [K]	200	200	200	200	210	200
No. of reflns. for cell parameter refinement	32	28		41	25	31
Scan range	$4.1° \le 2\Theta \le 50°$	$3.4° \le 2\Theta \le 51°$	$3.4° \le 2\Theta \le 52°$	$3.5° \le 2\Theta \le 49°$	$5.1° \le 2\Theta \le 54°$	$4.3° \le 2\Theta \le 54°$
Scan speed (ω) [° min^{-1}]	10	8		10	10	6
Integration time [s/frame]			10			
No. of rflns. measured	4251	4101	12416	2738	2948	2809
No. of unique rflns.	1864	2117	1284	2009	1548	1486
No. of rflns. observed ($\ge 2\sigma$)	1067	807	986	1719	1036	1016
No. of parameters refined	144	132	97	159	134	109
residual electron density [·10^{-6} e pm^{-3}]	0.85/−0.91	1.63/−1.56	4.00/−1.60	0.89/−0.44	0.49/−0.83	1.74/−2.30
R_1/R_w [%] (refinement on F^2)	4.2/13.4	8.9/33.6	7.0/18.9	3.3/9.3	5.3/12.9	5.3/14.8

THF (5 mL) and layered with ethanol (20 mL). Within one week at 20 °C, deep-red crystals suitable for X-ray analysis were obtained.

Preparation of $[Ph_4P]_2[\{(OC)_5Mo\}_6Sn_6]$, $[Ph_4P^+]_2$·5: To a stirred ethanolic solution (50 mL) of $Na_2[Mo_2(CO)_{10}]$[18] (518 mg, 1 mmol), solid $SnCl_2$ (190 mg, 1 mmol) was added in one portion. After 30 min of stirring, the deep red solution was filtered through Kieselgur (3 cm, Ø = 3 cm), reduced to a volume of 10 mL in vacuo. Upon addition of solid $[Ph_4P]Cl$ (750 mg, 1 mmol), the red $[Ph_4P]$ salt of **5** precipitated immediately and was separated from the mother liquor by filtration. After washing the red solid with ethanol (2 × 5 mL) and diethyl ether (2 × 10 mL), the residue was dried in vacuo. Yield: $[Ph_4P^+]_2$·**5**: 171 mg, 0.06 mmol, 36% (with respect to $SnCl_2$). For growing single crystals of $[Ph_4P^+]_2$·**5**, the red solid was dissolved in THF (5 mL) and layered with ethanol (20 mL). Within one week at 20 °C, red crystals suitable for X-ray analysis were obtained.

X-ray Structure Determinations: The measurements for $[Ph_4P^+]_2$·**1**, **2**, **4**, **5**, **6** were carried out with a Siemens P4 four-circle diffractometer. Data for $[Ph_4P^+]_2$·**3** were collected with a Nonius Kappa CCD diffractometer, all using Mo-K_α radiation. In the case of the data collection with the Siemens P4 four-circle diffractometer, the intensities of three check reflections (measured every 100 reflections) remained constant throughout, thus indicating crystal and electronic stability. The data collected using a scintillation counter measuring device (Siemens P4) were corrected as usual including experimental absorption correction. The data from the CCD device (Nonius Kappa CCD) were processed by the standard Nonius software.[26] All calculations were performed using the SHELXT PLUS software package. Structures were solved by direct methods with the SHELXS-86 program and refined with the SHELXL-93 program.[27−29] The program XPMA[30] and WinRay32[31] were used for graphical handling of the data. The structures were refined in fully or partially anisotropic models by full-matrix least-squares calculations. Hydrogen atoms were introduced at calculated positions. The data for the structure determinations is presented in Table 6. Crystallographic data for the structures reported in this paper (except for $[Ph_4P^+]_2$·**1**: CSD-408093[2]) have been deposited with the Cambridge Crystallographic Data Centre as supplementary publications no. CCDC-149568 ($[Ph_4P^+]_2$·**2**), -149565 ($[Ph_4P^+]_2$·**3**), -149564 ($[Ph_4P^+]_2$·**4**), -149566 ($[Ph_4P^+]_2$·**5**), and -149567 ($[Ph_4P^+]_2$·**6**). Copies of the data can be obtained free of charge on application to CCDC, 12 Union Road, Cambridge CB2 1EZ, UK [Fax: (internat.) + 44-1223/336-033; E-mail: deposit@ccdc.cam.ac.uk].

[1] B. Schiemenz, G. Huttner, *Angew. Chem.* **1993**, *105*, 295−296; *Angew. Chem. Int. Ed. Engl.* **1993**, *32*, 297−298.

[2] P. Kircher, G. Huttner, K. Heinze, G. Renner, *Angew. Chem.* **1998**, *110*, 1754−1755; *Angew. Chem. Int. Ed.* **1998**, *37*, 1664−1665.

[3] J. D. Corbett, *Angew. Chem.* **2000**, *112*, 682−704; *Angew. Chem. Int. Ed.* **2000**, *39*, 670−690.

[4] R. W. Rudolph, W. L. Wilson, R. C. Taylor, *J. Am. Chem. Soc.* **1981**, *103*, 2480−2481.

[5] S. C. Critchlow, J. D. Corbett, *J. Chem. Soc., Chem. Commun.* **1981**, 236−237.

[6] C. H. E. Belin, J. D. Corbett, A. Cisar, *J. Am. Chem. Soc.* **1977**, *99*, 7163−7169.

[7] C. Belin, H. Mercier, V. Angilella, *New J. Chem.* **1991**, *15*, 931−938.

[8] V. Queneau, S. C. Sevov, *Angew. Chem.* **1997**, *109*, 1818−1820; *Angew. Chem. Int. Ed. Engl.* **1997**, *36*, 1754−1756.

[9] T. F. Fässler, M. Hunziker, *Inorg. Chem.* **1994**, *33*, 5380−5381.

[10] C. Downie, Z. Tang, A. M. Guloy, *Angew. Chem.* **2000**, *112*, 346−348; *Angew. Chem. Int. Ed.* **2000**, *39*, 337−340.

[11] D. Kummer, L. Diehl, *Angew. Chem.* **1970**, *82*, 881−882; *Angew. Chem. Int. Ed. Engl.* **1970**, *9*, 895−896.

[12] H. G. von Schnering, *Angew. Chem.* **1981**, *93*, 44−63; *Angew. Chem. Int. Ed. Engl.* **1981**, *20*, 33−52.

[13] An organic derivative containing a trigonal prismatic Ge_6 core of heteroprismane-type structure has been reported: A. Sekiguchi, C. Kabuto, H. Sakurai, *Angew. Chem.* **1989**, *101*, 97−98; *Angew. Chem. Int. Ed. Engl.* **1989**, *28*, 55−56.

[14] A Ge_6 arrangement, possibly octahedral in shape, is inferred for the series of gas-phase clusters $[Ge_6Cl_n]^{m-}$: P. Jackson, K. J. Fischer, G. E. Gadd, I. G. Dance, D. R. Smith, G. D. Willett, *Int. J. Mass Spectrom. Ion Process* **1997**, *164*, 45−69.

[15] K. Wade, *Adv. Inorg. Chem. Radiochem.* **1976**, *18*, 1−66.

[16] D. M. P. Mingos, R. L. Johnston, *Struct. Bond.* **1987**, *68*, 29−87.

[17] G. Renner, P. Kircher, G. Huttner, P. Rutsch, *Eur. J. Inorg. Chem.* **2000**, 879−887.
[18] E. Lindner, H. Behrens, S. Birkle, *J. Organomet. Chem.* **1968**, *15*, 165−175.
[19] L. B. Handy, J. K. Ruff, L. F. Dahl, *J. Am. Chem. Soc.* **1970**, *92*, 7312−7326.
[20] This is in contrast to the idea put forward in ref.[2] that bipy is essential as an electron-transfer reagent in the synthesis of **1**.
[21] P. Kircher, G. Huttner, K. Heinze, *J. Organomet. Chem.* **1998**, *562*, 217−227.
[22] P. Kircher, G. Huttner, B. Schiemenz, K. Heinze, L. Zsolnai, O. Walter, A. Jacobi, A. Driess, *Chem. Ber./Recueil* **1997**, *130*, 687−699.
[23] P. Kircher, G. Huttner, K. Heinze, B. Schiemenz, L. Zsolnai, M. Büchner, A. Driess, *Eur. J. Inorg. Chem.* **1998**, 703−720.
[24] R. W. Rudolph, W. L. Wilson, F. Parker, R. C. Taylor, D. C. Young, *J. Am. Chem. Soc.* **1978**, *100*, 4629−4630.
[25] In comparing the integrals of the peaks it is assumed that in agreement with the symmetry of the compound, the relaxation times of the nuclei are equal and therefore the integrals are affected by the measurement technique to the same extent.
[26] Collect datacollection software, Nonius, **1998**; http://www.nonius.com
[27] G. M. Sheldrick, *SHELXS-86 − Program for Crystal Structure Solution*, University of Göttingen, **1986**; http://www.shelx.uni-ac.gwdg.de/shelx/index.html
[28] G. M. Sheldrick, *SHELXL-93 − Program for Crystal Structure Refinement*, University of Göttingen, **1993**; http://www.shelx.uni-ac.gwdg.de/shelx/index.html
[29] *International Tables for X-ray Crystallography*, Kynoch-Press, Birmingham, **1974**, vol. 4.
[30] L. Zsolnai, G. Huttner, *XPMA*, University of Heidelberg, **1998**; http://www.rzuser.uni-heidelberg.de/~il1/laszlo/xpm.html
[31] R. Soltek, *WinRay32*, University of Heidelberg, **2000**; http://www.uni-heidelberg.de/institute/fak12/AC/huttner/frame/frame_soft.html

Received September 18, 2000
[I00348]

Monomer−Dimer Equilibria of Oxo/Imido Complexes of Heptavalent Rhenium: Theoretical and Spectroscopic Investigations

Philip Gisdakis,[a] Notker Rösch,*[a] Éva Bencze,[b,c] Janos Mink,[c,d] Isabel S. Gonçalves,[e] and Fritz E. Kühn*[b]

Keywords: Density-functional calculations / Imido ligands / Oxygen bridges / Rhenium / Transition states

Mixed oxo/imido derivatives of methyltrioxorhenium(VII) form dimers in the solid state at ambient temperature. Density-functional calculations show that the dimerization is exothermic. The most stable derivatives were calculated to display a pseudo trigonal-bipyramidal coordination with two bridging oxygen centers and the methyl groups in a *trans* arrangement. This configuration is energetically more favored than a *cis* arrangement of the methyl groups and a pseudo square-pyramidal structure at the metal centers. In the case of methyltrioxorhenium(VII), the dimerization is slightly endothermic, even for the optimal dimeric structure, so that dimers cannot be isolated. However, there is evidence for the transient existence of oxygen bridges between methyltrioxorhenium(VII) in solution. For mixed imido/oxo species, oxygen bridging is observed in all cases of dimerization; results of thermogravimetric/mass spectrometric studies demonstrate that these bridging dimers are weakly bound. From vibrational spectroscopic analysis, there is no evidence for nitrogen-bridged homologues. The density-functional calculations show that imido groups form bridges only in the case of sterically undemanding ligands. However, these complexes are too unstable to be isolated.

Introduction

Organorhenium(VII) oxides have been studied in great detail in recent years. The use of some derivatives, most prominently methyltrioxorhenium(VII), as catalysts in a broad range of reactions[1] triggered a significant amount of investigations,[2] among them several theoretical studies.[3] However, far less investigations have been devoted to organorhenium(VII)imido compounds. Very few studies concerning their synthesis, structures, and spectroscopic properties have been carried out in the last two decades.[2a,4] Recently, we discovered a temperature-dependent monomer−dimer equilibrium that occurs in solution in the case of mixed oxo/imido Re^{VII} complexes.[5] However, the ability of mixed oxo/imido complexes to form dimers may provide more insight into the propensity of methyltrioxorhenium(VII) to polymerize. It is important to remember that the first polymeric organometallic oxide ever described was formed from methyltrioxorhenium(VII).[6] To date, the manner in which the polymerization of methyltrioxorhenium(VII) starts or which intermediates are formed remain open to discussion since dimeric or oligomeric units have never been isolated or observed in situ. Therefore, it is of interest to compare methyltrioxorhenium(VII) with closely related complexes in which some or all of the oxygen ligands are replaced by imido groups, in order to examine conditions that would enable dimeric methylrhenium(VII) oxo complexes to be isolated. The energy differences between oxo/imido complexes and pure oxo complexes are of particular interest in this respect.

It is worth noting that isolated dimeric methylrhenium(VII) oxo/imido complexes have been observed to exhibit structural features[5] that differ from those predicted for hypothetical dimeric methyltrioxorhenium(VII) based on Hartree−Fock self-consistent field calculations using a relativistic effective core potential.[6c] In this context, a recent computational study focused on the thermochemistry of the Re−oxo bond cleavage in complexes of the type $LReO_3$, with L = Cp, Cp*, CH_3, C_6H_5, and others.[7] The Re−O bond-dissociation energy was found to depend quite strongly on the nature of the ligand L. A comparison of the calculated results with experimental data demonstrated the convincing accuracy of the applied computational method, a hybrid density-functional approach, and hence the opportunity for a computational study of organometallic thermochemistry.

Another point of interest in recent literature reports is the ability of methyltrioxorhenium(VII) and related complexes to easily exchange their terminal oxygen ligands. This has been shown by ^{17}O NMR spectroscopic studies[8] and it has been assumed that this process proceeds through oxy-

[a] Institut für Physikalische und Theoretische Chemie, Technische Universität München,
Lichtenbergstraße 4, 85747 Garching, Germany
[b] Anorganisch-Chemisches Institut der Technischen Universität München,
Lichtenbergstraße 4, 85747 Garching bei München, Germany
[c] Institute of Isotope and Surface Chemistry of the Hungarian Academy of Sciences,
P. O. Box 77, 1525 Budapest, Hungary
[d] Department of Analytical Chemistry, University of Veszprém, Egyetem UTCA 10, P. O. Box 158, 8203 Veszprém, Hungary
[e] Departamento de Química, Universidade de Aveiro, Campus de Santiago, 3800 Aveiro, Portugal

 © WILEY-VCH Verlag GmbH, 69451 Weinheim, 2001 1434−1948/01/0404−0981 $ 17.50+.50/0

gen bridges. However, the existence of energetically accessible dimeric states that allow oxygen exchange through such bridges is still unclear.

In the present work, we perform a detailed theoretical study of the monomer−dimer equilibria that occur in the case of mixed methylrhenium(VII) oxo/imido species and we compare them to dimers of pure oxo and imido derivatives. The theoretical study is supplemented by thermogravimetric/mass spectrometric investigations of the sublimation behavior of selected complexes of this type and a detailed IR/Raman study of monomeric and dimeric oxo/imido methylrhenium(VII) complexes.

Results and Discussion

Dimer Systems

We start with an overview of the various monomers and dimers to be studied. From the monomeric compound CH_3ReO_3 (**1**) one can derive the monomers of interest if one successively substitutes oxo functions by imido groups to yield $CH_3ReO_2(NR)$ (**2**), $CH_3ReO(NR)_2$ (**3**), and $CH_3Re(NR)_3$ (**4**). In the computational investigation, we used two imido groups with R = H (**a**) and CH_3 (**b**), while for the experimental characterization we employed the (2,6-diisopropylphenyl)imido ligand (**c**) (see Scheme 1). Such a relatively bulky ligand is required to guarantee the sufficient stability of the product complexes. Accordingly, the hydrogen compound $CH_3ReO_2(NH)$ is referred to as **2a**, whereas **2b** designates the corresponding methylated compound $CH_3ReO_2(NCH_3)$. We proceeded in the same way with the bis- and tris(imido) complexes $CH_3ReO(NR)_2$ and $CH_3Re(NR)_3$. The experimentally characterized and therefore most stable dimer structures of the monomers **2c** and **3c** are denoted as **5c** and **6c**, respectively. We will begin by analyzing different isomeric structures of the analogous H- and CH_3-ligated systems **5a/b** and **6a/b** and later on will introduce a more detailed nomenclature for describing these different structures.

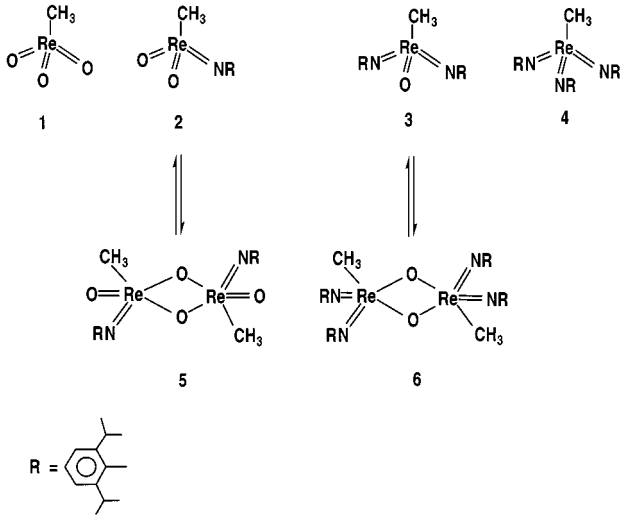

Scheme 1

In the computational study we focused on homogenous dimers, i.e. dimers that consist of two equal monomeric units of **1**, **2a/b**, and **3a/b**. We also studied two mixed dimers, composed of two different monomers. The complexes can only dimerize as two fundamental structural types: a pseudo trigonal-bipyramidal coordination [**A**, see Figure 1, (a) and (b)] and a pseudo square-pyramidal coordination of the rhenium center [**B**, see Figure 1, (c) and (d)]. In the latter case, two terminal and two bridging ligands form the basis of a square pyramid, while the methyl ligand defines its top. Structures **A** and **B** may each occur with a *cis* and *trans* orientation of the CH_3 ligand. Furthermore, we need

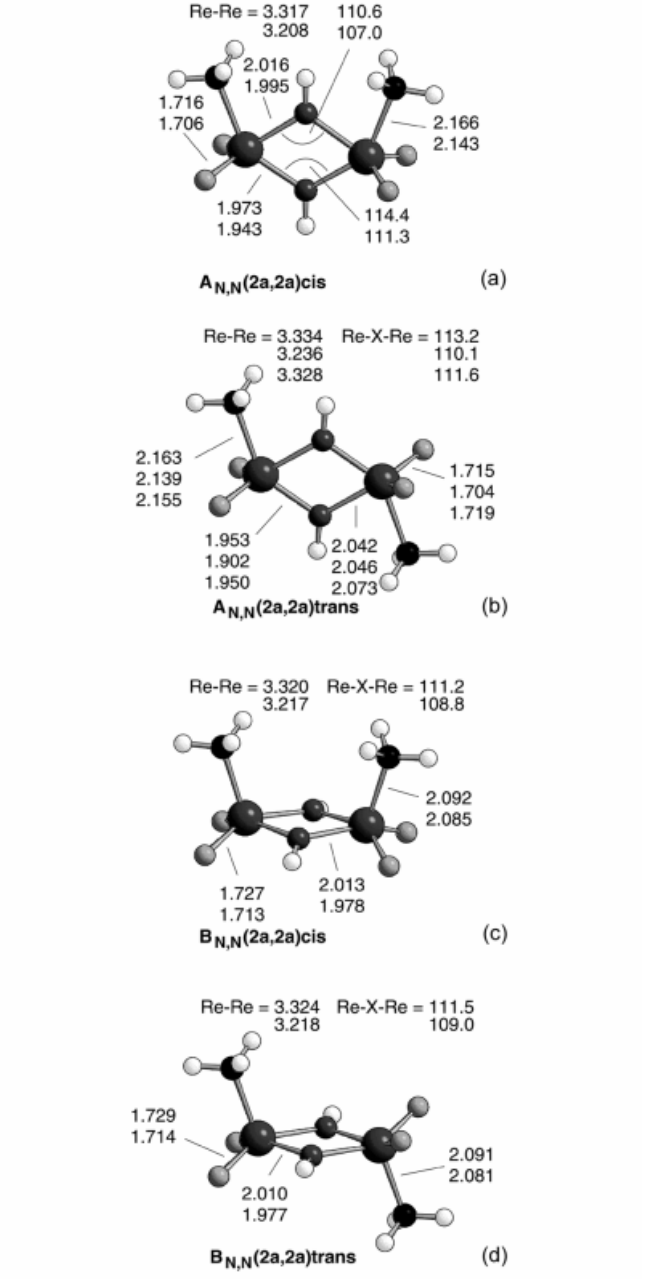

Figure 1. Calculated structures of homogeneous dimers of **2a** with bridging nitrogen centers; pertinent calculated structure parameters (bond lengths in Å, angles in °) of the corresponding dimers of **2a**, **1**, and **2b** listed in columns in that order

to indicate the bridging atoms X (O and/or N) of the imido complexes **2** and **3** and of the mixed dimers. For this purpose, we add the bridging atoms as subscripts. For instance,

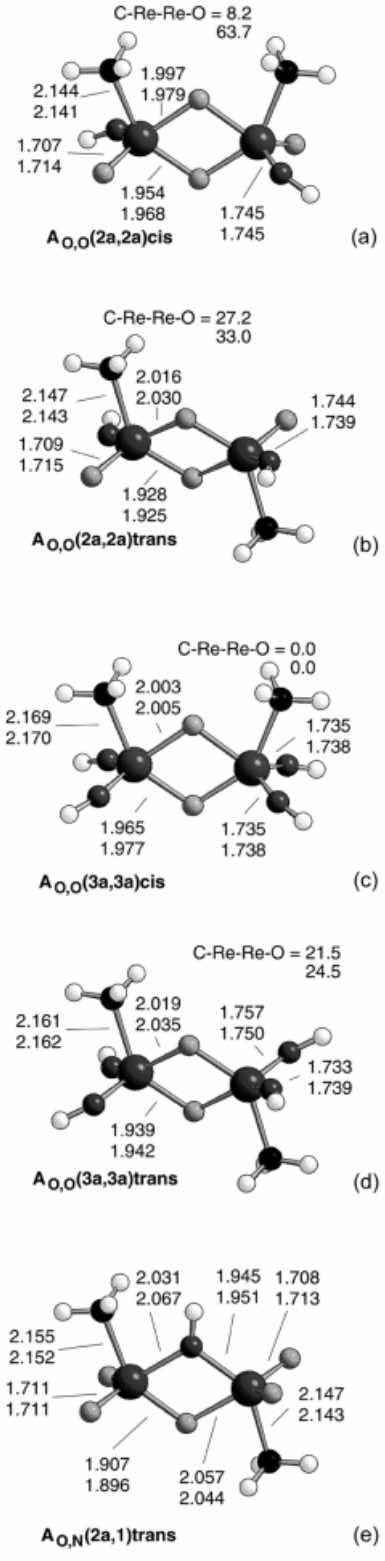

Figure 2. Calculated structures of homogeneous dimers of **2a** and **3a** with bridging oxygen centers and of the mixed O-bridged/N-bridged dimer (**2a**,**1**); pertinent calculated structure parameters (bond lengths in Å, angles in °) of the corresponding dimers of **2a** and **2b** or **3a** and **3b** in columns in that order

complex $\mathbf{A_{N,N}(2a-2a)cis}$ exhibits a trigonal-bipyramidal conformation (structure **A**) with two N atoms bridging two **2a** monomers in which the two methyl groups adopt a *cis* orientation.

In Figure 1 and Figure 2 we display various structures of dimers (**2a**,**2a**), (**3a**,**3a**), and (**2a**,**1**). Inspection of the calculated vibrational data reveals that, with one (partial) exception, all structures **A** correspond to local minima, whereas structures **B** represent transition structures (see below). The exceptional case $\mathbf{A_{N,N}(2b-2b)trans}$ features two vibrational modes with imaginary frequencies that correspond to rotational motions of the methyl substituents at the nitrogen centers; thus, even in this case, the remaining framework of the dimer represents a local-minimum structure.

Structural Properties

In Figure 1, featuring the homogeneous dimer of **2a** with bridging imido groups, we also present characteristic bond lengths and angles of dimers of **1** and **2b** in compact column form: values in the first line of each column refer to dimers with bridging NH groups (monomer **2a**). Values in the second line refer to dimers of the monomer **1**. Where present, values in the third line refer to dimers with bridging NCH_3 groups (monomer **2b**). To facilitate the calculations, symmetry constraints have been employed, resulting in idealized dimer structures (see below). The *cis* complexes [C_{2v} symmetry for **1** and **2a**; Figure 1, (a) and (c)] exhibit a mirror plane perpendicular to the carbon−rhenium plane, containing the bridging atoms, while the *trans* structures feature an inversion center [C_{2h} symmetry for **1** and **2a**; Figure 1, (b) and (d)]. In type **B** structures, the Re−X bonds are equivalent by symmetry, while type **A** structures exhibit two shorter and two longer Re−X bonds. Each bridging atom of complex $\mathbf{A_{X,X}(Y-Y)cis}$ is symmetrically located between the rhenium atoms and both Re−X bonds are of equal length. In complexes $\mathbf{A_{X,X}(Y-Y)trans}$ with two different Re−X bond lengths, each bridging atom X may be assigned to one of the two rhenium centers; the Re−X bond located closer to the methyl ligand is shorter.

Energetics

One goal of the computational study was to determine the most stable dimeric structures of MTO and of related imido complexes (Table 1). As models for the whole class of systems, we first calculated the formation energies of the dimers of MTO **1** and of the N-bridged dimers of the mono(imido) derivative **2a** of MTO, for both fundamental structure types **A** and **B** and different orientations of the methyl groups. In the next step, the most stable structures determined in this way were then also studied for the dimers of **2b**, **3a**, and **3b**. To assist in assessing the relative energies of the various configurations, the dimerization energies are compared in Figure 3. The formation of dimers $\mathbf{B_{O,O}(1-1)cis}$ and $\mathbf{B_{O,O}(1-1)trans}$, displaying a square-pyramidal coordination, from two MTO monomers is more endothermic (by 35.5 and 32.2 kcal/mol, respectively) than that of the corresponding type **A** dimers $\mathbf{A_{O,O}(1-1)cis}$ and

$A_{O,O}$(1−1)trans with a trigonal-bipyramidal coordination (by 5.8 and 1.7 kcal/mol, respectively). The *trans* configurations are more stable than the corresponding *cis* forms by 3−4 kcal/mol. It is worth noting that the differences in stability between the **A** and **B** forms are very similar for both *cis*/*trans* isomers. **$A_{O,O}$(1−1)cis** is more stable than **$B_{O,O}$(1−1)cis** by 29.7 kcal/mol; the corresponding energy difference of the *trans* complexes is 30.5 kcal/mol. For the most stable dimer **$A_{O,O}$(1−1)trans**, we also calculated that the enthalpy of formation (at T = 298.15 K) is larger than the dimerization energy by 1.7 kcal/mol (Table 1).

Table 1. Calculated results of dimerization energies ΔE and selected dimerization enthalpies ΔH (in kcal/mol)

	ΔE	ΔH
MTO dimers:		
$A_{O,O}$(1−1)cis	5.78	
$A_{O,O}$(1−1)trans	1.74	3.47
$B_{O,O}$(1−1)cis	35.54	
$B_{O,O}$(1−1)trans	32.21	
N-Bridged mono(imido) dimers:		
$A_{N,N}$(2a−2a)cis	−7.68	
$A_{N,N}$(2a−2a)trans	−9.34	−5.07
$B_{N,N}$(2a−2a)cis	17.97	
$B_{N,N}$(2a−2a)trans	20.08	
$A_{N,N}$(2b−2b)trans	12.38	13.39
Terminal mono(imido) dimers:		
$A_{O,O}$(2a−2a)cis	4.19	
$A_{O,O}$(2a−2a)trans	−1.15	4.10
$A_{O,O}$(2b−2b)cis	−0.33	
$A_{O,O}$(2b−2b)trans	−2.50	−1.04
Terminal bis(imido) dimers:		
$A_{O,O}$(3a−3a)cis	5.43	
$A_{O,O}$(3a−3a)trans	1.44	3.04
$A_{O,O}$(3b−3b)cis	0.68	
$A_{O,O}$(3b−3b)trans	−1.81	0.36
N-Bridged tris(imido) dimers:		
$A_{N,N}$(4a−4a)trans	−5.03	
$A_{N,N}$(4b−4b)trans	10.30	
Mixed dimers:		
$A_{O,N}$(1−2a)trans	−4.85	
$A_{O,N}$(1−2b)trans	4.23	

A similar stability trend was found for the N-bridged dimers of **2a**. Type **A** structures are more stable than type **B** structures. For **A**, the *trans* orientation of the methyl group is also more stable than the *cis* configuration: the dimerization energy was calculated to be −9.3 kcal/mol for **$A_{N,N}$(2a−2a)trans** and −7.7 kcal/mol for **$A_{N,N}$(2a−2a)cis.** However, the *cis*/*trans* energy difference, 1.6 kcal/mol, is only half as large as for the corresponding dimers of MTO. Note that for type **B** structures (square-pyramidal coordination of Re), the *cis*/*trans* preference is reversed. **$B_{N,N}$(2a−2a)cis** is less endothermic than **$B_{N,N}$(2a−2a)trans** with dimerization energies of 18.0 and 20.1 kcal/mol, respectively. This finding is a consequence of the symmetry constraints employed in the calculations. In the *trans* complex (C_{2h} symmetry), the imido H atom is unable to bend outside the Re−N−Re plane, as it can in the case of the *cis* orientation in which the H atom bends downwards (Figure 1). However, the **A**/**B** energy difference for the *trans* isomers (29.4 kcal/mol) is very similar to that of MTO dimers (29.7 kcal/mol for *cis* and 30.5 kcal/mol for *trans*). For the *cis* dimers of **2a**, the **A**/**B** energy difference is significantly reduced (25.7 kcal/mol) since **$B_{N,N}$(2a−2a)cis** is more stable than **$B_{N,N}$(2a−2a)trans**.

In contrast to the results obtained for the MTO dimers, the N-bridged dimers of **2a** feature exothermic dimerization energies for type **A** structures. For the most stable isomer **$A_{N,N}$(2a−2a)trans** we also calculated the enthalpy of dimerization (−5.1 kcal/mol, Table 1), which is less exothermic than the corresponding dimerization energy by 4.3 kcal/mol. Substitution of the bridging imido H atom by a methyl group in the most stable dimer **$A_{N,N}$(2a−2a)trans** leads to the congener **$A_{N,N}$(2b−2b)trans** and renders the dimerization endothermic (12.4 kcal/mol). This is due to steric hindrance, but electronic effects are also probably involved since the energy difference due to methylation (21.7 kcal/mol) seems to be too high to be caused by steric hindrance only. The dimerization enthalpy of **$A_{N,N}$(2b−2b)trans** is larger than the corresponding energy difference (1 kcal/mol, Table 1).

The fundamental structure type **A** (trigonal-bipyramidal coordination) with a *trans* orientation of the methyl groups yields the most stable structures of the O-bridged [**$A_{O,O}$(1−1)trans**] as well as of the N-bridged dimers [**$A_{N,N}$(2a−2a)trans**] of MTO and its imido derivatives. While the energy differences between corresponding complexes of structures **A** and **B** is about 30 kcal/mol, the *cis*/*trans* energy difference is approximately only 1−3 kcal/mol. Therefore, in the following we will focus on trigonal-bipyramidal complexes **A**, but we will continue to compare *cis* and *trans* isomers.

Substitution of two terminal oxo groups (one per monomer) in MTO dimers **$A_{O,O}$(1−1)cis/trans** by imido groups (NH in the case of monomer **2a** and NCH_3 in the case of monomer **2b**) leads to **$A_{O,O}$(2a−2a)cis/trans** and **$A_{O,O}$(2b−2b)cis/trans** (see Figure 2). The *cis* compounds were calculated with C_2 symmetry, while the *trans* configurations may be studied with a C_i-symmetry constraint. This substitution results in dimer formation becoming exothermic or at least less endothermic [**$A_{O,O}$(2a−2a)cis**]; in the case of the **2a** dimers, the dimerization energies change by −1.6 and −2.9 kcal/mol for *cis* and *trans* configurations, respectively, and even more so in the case of the **2b** dimers, by −6.1 and −4.2 kcal/mol for *cis* and *trans* configurations, respectively (Table 1). The energy preference between the more stable *trans* isomers is reversed at the enthalpy level: **$A_{O,O}$(2b−2b)trans** is estimated to be the only stable homogeneous dimer with terminal mono(imido) complexes.

Substitution of all four terminal oxo groups of **$A_{O,O}$(1−1)cis/trans** by imido ligands leads to the O-bridged dimers of the bis(imido) derivatives of MTO, **$A_{O,O}$(3a−3a)cis/trans** and **$A_{O,O}$(3b−3b)cis/trans**. The *cis* dimers were calculated with C_{2v} symmetry, while the *trans* compounds were calculated with C_i symmetry. Among these oxygen-bridged dimers with two terminal amido group, **$A_{O,O}$(3b−3b)trans** is estimated to exhibit the least endothermic enthalpy of formation (Table 1). In general, the formation energies of these dimers are larger than those of the corresponding mono(imido) compound dimers, but still lower than those of the corresponding dimers of MTO

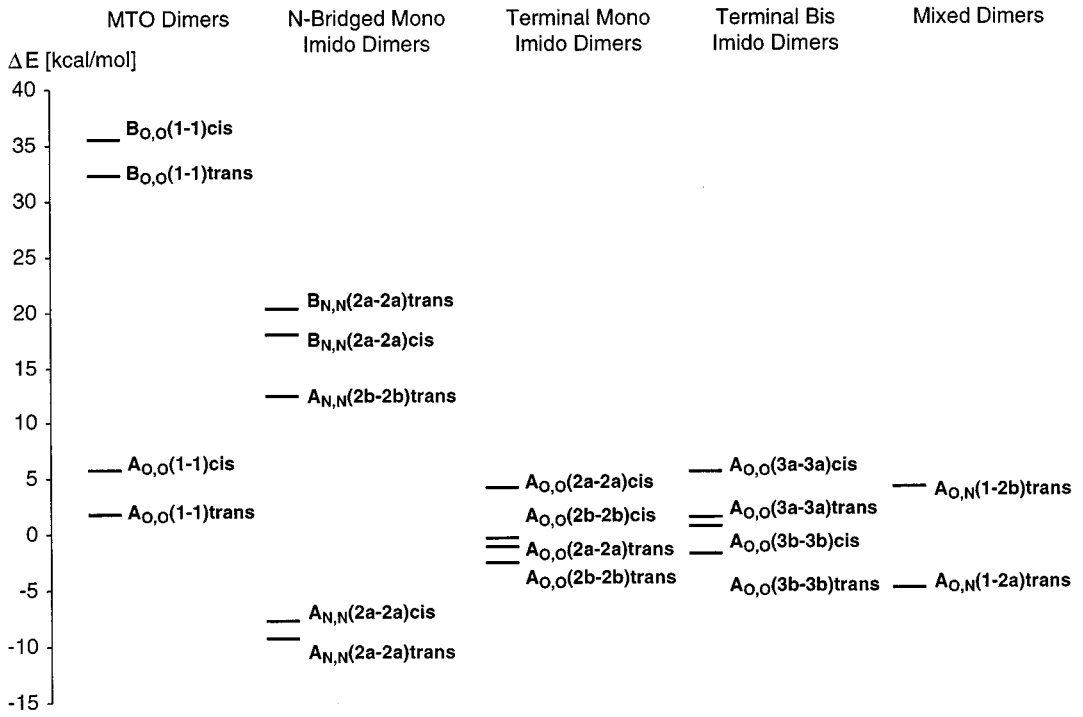

Figure 3. Calculated dimerization energies ΔE of various structures [MTO = methyltrioxorhenium(VII)]

(Figure 3). Just as in the case of the mono(imido) compounds, methyl substituents at the N atoms render dimer formation less endothermic. Substitution of the bridging oxygen centers of $\mathbf{A_{O,O}(3a-3a)trans}$ by NH groups leads to $\mathbf{A_{N,N}(4a-4a)trans}$; in this way, the dimerization energy is reduced by 6.5 kcal/mol, rendering the process exothermic (Table 1). On the other hand, the analogous substitution by NCH_3, resulting in the dimer $\mathbf{A_{N,N}(4b-4b)trans}$, changes the dimerization energy by 12.1 kcal/mol and renders the dimerization notably endothermic.

Mixed dimers provide more insight into the energy situation, since they feature one O and one NH bridge and are therefore intermediate between the dimeric structures of **1** and **2**. In these mixed dimers MTO, dimerizes with **2a** to form O,N-bridged $\mathbf{A_{O,N}(1-2a)trans}$ or with **2b** to form $\mathbf{A_{O,N}(1-2b)trans}$. Stated differently, if one substitutes one bridging oxygen center of the MTO dimer $\mathbf{A_{O,O}(1-1)trans}$ by NH, the dimerization energy changes by −6.6 kcal/mol and dimer formation becomes exothermic by −4.9 kcal/mol. Further substitution of the second bridging oxygen atom, leading to $\mathbf{A_{N,N}(2a-2a)trans}$ renders the formation even more exothermic with a change in the energy of dimer formation of −4.5 kcal/mol. In the case of NCH_3 the situation is reversed: substitution of the first imido renders dimer formation more endothermic by 2.5 kcal/mol and substitution of the second one even more so, by 8.2 kcal/mol.

In summary, substitution of one terminal oxo group of each monomer by an imido group renders dimer formation less endothermic or even exothermic. Substitution of the second terminal oxo group leads to a dimer stability in between that of MTO dimers and its mono(imido) derivatives. Compounds containing terminal NCH_3 groups always yield more stable dimers than NH imido complexes. Mixed O- and NH-bridged dimers exhibit dimer formation energies between those of purely O-bridged and purely NH-bridged complexes, while the mixed O- and NCH_3-bridged dimer forms more readily than the purely NCH_3-bridged dimer. These results suggest that NH groups in bridging positions render dimer formation more favorable, while NCH_3 imido complexes do so in terminal positions. In fact, imido groups with larger carbon substituents will not assume bridging positions.

Structurally, the dimerization reaction is an addition of two Re=O (Re=NR) bonds, resulting in a substitution of one Re=O (Re=NR) double bond by two Re−O (Re−NR) single bonds. One thus expects that the dimerization energy is controlled by the strength of the Re=O (Re=NR) bond.[7] To analyze this effect, we calculated the reaction energy for the monomeric compounds **1**, **2a/b**, and **3a/b**, when water is added to the rhenium−oxo bond, resulting in $Re(OH)_2$ moieties. In addition to model N-bridged dimerization, we calculated the energy of the addition of water to the Re=NR units of **2a/b**, which results in the formation of Re(OH)(NHR) moieties. Figure 4 demonstrates a linear correlation of these reaction energies of water addition with the most endothermic (or least exothermic) dimerization energies; only $\mathbf{A_{N,N}(2b-2b)trans}$ and $\mathbf{A_{N,N}(4b-4b)trans}$ give rise to exceptions. The more stable the product of water addition, the more exothermic is the dimerization. In $\mathbf{A_{N,N}(2b-2b)trans}$, the large endothermicity is due to the steric repulsion between the *N*-methyl groups and the methyl groups coordinated at the rhenium centers. As judged by the energy of water addition, the intrinsic dimerization energy should be comparable to that of MTO [$\mathbf{A_{O,O}(1-1)trans}$].

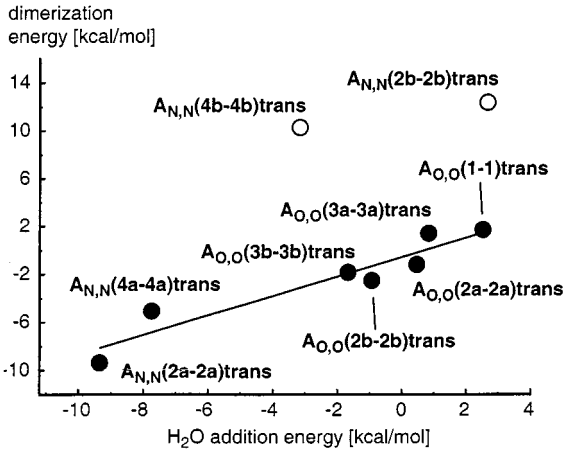

Figure 4. Calculated dimerization energies as function of the calculated energies of the addition of H_2O to an Re=X bond of the corresponding monomers

Thermogravimetry and Mass Spectrometry (TG-MS)

We now turn to a discussion of the dimerization process based on experimental information. We anticipated that two different features should influence the sublimation points of the complexes **1**−**4**: (i) the dimerization of compounds **2c** and **3c** by oxygen bridges (to yield **5c** and **6c**); and (ii) the increasing weight of the monomers due to successive replacement of terminal oxo ligands by bulky imido groups. The relative importance of these independent factors can be convincingly demonstrated by TG-MS examinations. The thermal behavior of CH_3ReO_3 (**1**) has already been reported.[9] This compound already begins to sublime below 50 °C; no decomposition is evident even after complete sublimation. These compounds are less volatile because of the weight increase due to the bulky imido ligands, and the dimerization to form compounds **5c** and **6c** at ambient temperatures. Therefore, they sublime at significantly higher temperatures than compound **1**. For **5c** and **6c**, sublimation is observed to start at 76.75 and 157.08 °C, respectively. The complexes sublime completely, and no residues remain. Mass spectrometry of the gas phase shows no traces of the dimeric species **5c** and **6c**, only the monomers **2c** and **3c** are observed. The sublimed compounds crystallize immediately on colder parts of the thermobalance. NMR and IR spectroscopy of the crystallized compounds clearly shows that dimers **5c** and **6c** have been reformed. The onset of the sublimation of complex **4c** is at 193.48 °C. As expected, no dimer is observed in the gas phase, whereas NMR and IR spectroscopy of the sublimed complex indicates the presence of the original dimer complex. No residue remains after the sublimation, confirming that decomposition does not take place. The changes in the temperature at which sublimation of complexes **1**, **4c**, **5c**, and **6c** starts evidently depends only on the molecular mass of the monomer and increases in accordance with the increasing number of the heavy imido ligands from < 50°C in **1** to nearly 200 °C in **4c**. These observations show that the energy which is necessary to monomerize complexes **5c** and **6c** must be relatively small and that the Re−O−Re bridges are weak. This is in good agreement with the computational results on the Re−O−Re bond strength described above and with observations made in solution.[5] Since all compounds examined display a dimerization energy of less then 5 kcal/mol, it is not surprising that Re−O−Re bonds break readily at the observed temperatures.

Vibrational Properties of the Dimers

The structures of the monomers under investigation belong to the C_{3v} (**1** and **4c**) and C_{2h} (**5c** and **6c**) symmetry groups or can be idealized such that these symmetry assignments hold. Characteristic vibrations are given in Table 2. Complex **4c** shows a strong analogy with compound **1**.[10] The only important difference in this context is observed for the $Re(=N)_3$ stretching vibrations which are assigned to the bands at 1333 cm^{-1} and 1290 cm^{-1} for the asymmetric and symmetric modes, respectively (calculated at 1268 cm^{-1} and 1311 cm^{-1} for **4b** and at 943 cm^{-1} and 971 cm^{-1} for **4a**, see below). The vibrations of the $[CH_3-Re]$ moiety are characteristic for all species examined. It is clear that the IR and Raman bands alternate, especially for the Re−O−Re and the $Re-CH_3$ skeletal stretching modes. This finding indicates the existence of an inversion center for the dimeric compounds. The mutual-exclusion rule is even more pronounced for low-frequency skeletal deformational modes (below 500 cm^{-1}, see Table 2).

There is no strong Raman band in the low-frequency region that can be assigned unambiguously to an Re−Re stretching mode. Accordingly, the dimeric compounds should have a bridging structure. The Re−Re bond lengths of **5c** and **6c** were determined experimentally to be 3.090(1) Å and 3.1190(3) Å, respectively;[5] the corresponding calculated values of the analogous methyl-ligated dimers of **2b** and **3b** [actually in configurations **$A_{O,O}$(2b−2b)trans** and **$A_{O,O}$(3b−3b)trans**, see below] are 3.18 Å and 3.20 Å, respectively. Therefore, the Re−Re interaction cannot be fully ignored, but the metal−metal interaction are probably very weak. For comparison, we mention that the Re−Re distance in the hypothetical dimer $(CH_3ReO)_2(\mu\text{-}O)_2$ of the Re^V species CH_3ReO_2 was calculated to be 2.59 Å. The metal−metal distance in the corresponding dimer $(CpReO)_2(\mu\text{-}O)_2$ of the species $CpReO_3$ was calculated to be 3.14 Å.[7] On the other hand, the Re−Re distance of the experimentally characterized dimer $[(CH_3)_2Re^{VI}O]_2(\mu\text{-}O)_2$ is 2.593(<1) Å[11] and that of $(Cp^*ReO)_2(\mu\text{-}O)_2$ is 3.143(<1) Å.[12]

On the basis of experimental IR and Raman spectroscopy, and the calculated dimerization energies, we conclude that there are no N-bridged dimers with bulky substituents on the nitrogen atom. All dimers are expected to feature bridging oxygen atoms. Experimental characterization of the vibrations of N-bridged dimers is thus not possible. For the oxygen-bridged dimers, two characteristic bands near 725 cm^{-1} and 695 cm^{-1} were assigned to Re−O−Re stretching modes. These Re−O−Re stretching vibrations have a lower intensity in solution spectra. There are no indications pointing to the formation of Re−N−Re bridges, neither in the solid state, nor in solution. However,

Table 2. Selected structurally characteristic IR and Raman frequencies in the range 3000−500 cm^{-1}, and full spectra below 500 cm^{-1}

CH_3ReO_3 (**1**)[a]		$[CH_3ReO_2(NR)]_2$ (**5c**)		$[CH_3ReO(NR)_2]_2$ (**6c**)		$CH_3Re(NR)_3$ (**4c**)		Assignments	Sym. spec.	
IR	Raman	IR	Raman	IR	Raman[b]	IR	Raman		C_{3v}	C_{2h}
2989 m	2984 m	2961 m	2966 m	2968 m	2961 m	2961 m	2962 s	Re−CH_3 asym. str.	e	
2900 m	2902 w	–	2905 s	–	2914 sh	–	2907 s	Re−CH_3 sym. str.	a_1	
			2899 sh		2902 s					
1374 w	1375 w,dp					1378 s	1379 w, sh	CH_3 asym. def.	e	
					1382 w, dp			CH_3 asym. def.		a_g/b_g
		1378 s		1378 s				CH_3 asym. def.		a_u/b_u
		1378 s						Re=N asym. str.		b_u
			1338 vs					Re=N sym. str.		a_g
						1333 s	1333 vs	$Re(=N)_3$ asym. str.	e	
				1333 s	1333 sh, dp			$Re(=N)_2$ asym. str.		a_g/b_u
						1290 m	1291 s	$Re(=N)_3$ sym. str.	a_1	
					1298 m, p			$Re(=N)_2$ sym. str.		a_g
				1290 s				$Re(=N)_2$ asym. str.		b_u
1207 w	1206 vw.p					1229 w	1227 w, m	CH_3 sym. def.	a_1	
		1227 m		1229 m				CH_3 sym. def.		b_u
			1225 m		1227 m, p			CH_3 sym. def.		a_g
998 vs	995 vvs,p							ReO_3 sym. str.	a_1	
959 vvs	960 m,dp							ReO_3 asym. str.	e	
		950 vs						ReO asym. str.		b_u
			948 w					ReO sym. str.		a_g
740 m	736 w					748 s	745 sh	CH_3 rock	e	
			740vw		759 w, dp			CH_3 rock		a_g/b_g
		746 s		749 s				CH_3 rock		a_u/b_u
			725 m		725 w,dp			Re−O−Re str.		a_g
		703 vs		681 vs				Re−O−Re str.		b_u
567 w	572 w,p					538 w, m	537 m	Re−CH_3 str.	a_1	
		541 w		539 w, m				Re−CH_3 str.		b_u
			533 w, m		524 m, p			Re−CH_3 str.		a_g
		461 sh	461 sh		463 w, dp		464 wm	*6c* imido ligand		
		450 w	457 w	456 w		456 w				
			439 w	439 w	439wm, p	439 w	437 m	*6a* imido ligand		
				426 w		425 w				
				394 w						
		370 vw	387 sh		370 sh					
		357 w		355 w		359 w		*18b* imido ligand		
				347 vw						
325 w	315 s, dp	333 w						ReO_3, ReO_2 deform.	e	b_u
						330 vw	329 m	ReN_3 deform.	e	
		302 w	305 m	311 w	308 m, p	307 w		ReN, ReN_2, ReN_3 deform	a_1	
							297 s	ReN_3 rock	e	
		291 sh		281 rw	298 sh			(*15* imido ligand)		
								ReN, ReN_2 deform.		
						268 vw				
						256 vw				
				263 w	256 w, p	248 vw	254 m	*9a* imido ligand		
			251 w, m	253 w	251vw			Re−O−Re deform.		
254 s	248 s, dp	243w	239 sh					ReO_3, ReO_2 rock		
		227w			226 m, p	215 vw	224 vw	*10a* imido ligand		
		189 vw	183 vw		196 w			Re−O−Re deform.		
		165 vw		170 vw	169 vw	169 vw	178 vw			
			148 sh	156 vw	156 sh					
				148 w	148 sh					
			134 m	134 w, m	134 m		134 s	*17b* imido ligand		

[a] From ref.[10] − [b] Depolarization ratios from solution Raman spectra, but all other frequencies for solid samples.

to allow for a systematic comparison, we have also calculated the vibrations of N-bridged dimers.

In Figure 5 we present the approximate normal modes ν_1 to ν_4 that involve a movement of the bridging atom; the corresponding calculated vibrational frequencies are collected in Table 3. The frequencies range from 470 to 750 cm^{-1}, and the largest occurs in the oxygen-bridged dimer $\mathbf{A_{O,O}(1-1)trans}$. An exception is vibration ν_4 which is similar for the dimers $\mathbf{A_{O,O}(2b-2b)trans}$, $\mathbf{A_{O,O}(3a-3a)trans}$, and $\mathbf{A_{O,O}(3b-3b)trans}$, but with slightly larger frequencies. N-Bridged dimers tend to exhibit higher frequencies than their O-bridged congeners. For $\mathbf{A_{N,N}(2a-2a)trans}$, ν_2 has a higher frequency than ν_1, in contrast to the other complexes. The frequencies ν_2 and ν_4 of $\mathbf{A_{N,N}(2a-2a)trans}$ couple to a N−CH_3 stretching mode, thus splitting into higher and lower frequency modes.

The experimental IR and Raman bands observed for compound **5c** at 950 cm^{-1} and 948 cm^{-1} demonstrate the presence of terminal oxygen atoms bonded to the rhenium center. It was not possible to assign a band to an Re−N−Re bridging structure of compounds **5c** and **6c**. Also for **4c** we were unable to identify a bridging NR unit, thus indicating the absence of such dimers. This is in agreement with the calculated results that the formation of N-

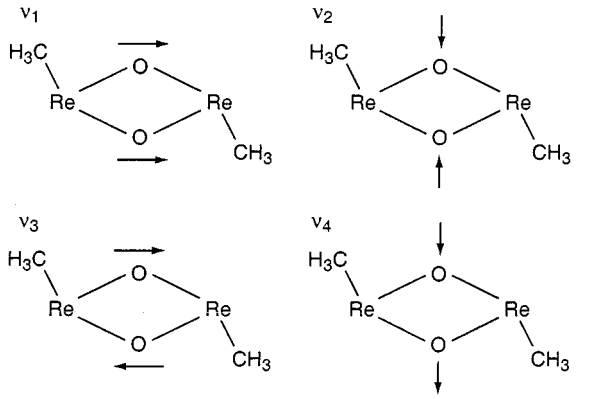

Figure 5. Sketch of the characteristic normal modes of the bridging unit Re−X−Re

Table 3. Calculated Re−X−Re frequencies $\nu_1-\nu_4$ of various dimers (in cm^{-1})

	ν_1[a]	ν_2[a]	ν_3[a]	ν_4[a]
$A_{O,O}$(1−1)trans	738.8	723.2	596.0	522.7 471.5[b]
$A_{N,N}$(2a−2a)trans	744.7	756.5	640.1	567.0
$A_{N,N}$(2b−2b)trans	753.2	480.5 1122.3[c]	679.3	395.7 1056.8[c]
$A_{O,O}$(2a−2a)trans	708.3	694.9	572.0	485.5
$A_{O,O}$(2b−2b)trans	718.5	687.4	557.5	535.9 493.8[b]
$A_{O,O}$(3a−3a)trans	728.6	679.6	563.8	520.7 479.9[b]
$A_{O,O}$(3b−3b)trans	700.4	667.8	541.5	527.0 575.6[b]
$A_{C,C}$(7−7)trans	639.7	548.2	644.5	467.4

[a] See Figure 6 for sketches of the corresponding normal modes. − [b] Vibration couples to Re−C stretching vibration, and thus splits into symmetric and antisymmetric contributions. − [c] Vibration coupled to the N−CH_3 stretching vibration; the modes with higher frequencies exhibit a larger N−CH_3 contribution.

bridged dimers with bulky substituents is endothermic. In a nitrogen-bridging structure, compound **6c** should show strong stretching features for Re=O bonding. However, such features are completely missing from the vibrational spectra (Table 2).

We also did not observe a mixture of monomeric and dimeric molecules in the case of complexes **5c** and **6c** in the solid state. Only dimeric compounds seem to be present under these particular conditions. This question had remained unsettled since our first synthesis of these complexes and their identification as dimers by X-ray crystallography.[5] It had not been possible to exclude the simultaneous presence of both monomeric and dimeric forms in the solid state, but only dimers crystallize easily. Previously, we showed that a temperature-dependent monomer−dimer equilibrium can be observed by NMR spectroscopy in solution.[5]

Assignment of the spectral region below 500 cm^{-1} is rather complicated since a number of features are characteristic of 1,2,3-substituted aromatic ring vibrations. The imido ligand exhibits local C_{2v} symmetry, and therefore the polarized Raman bands have a_1 character. Consequently the polarized lines of compound **6c** at 439, 256, and 226 cm^{-1} can be assigned to modes *6a*, *9a*, and *10a*, respectively. This Wilson notation (italicized numbers) of the aromatic ring vibrations of the (2,6-diisopropylphenyl)imido ligand was chosen according to ref.[13]

It is interesting to compare the strengths of Re=O and Re−CH_3 bonds of different complexes[7] using the stretching frequencies as a probe for the bond strength. In CH_3ReO_3, the Re=O stretching frequencies ν(Re=O) are 997 cm^{-1} and 954 cm^{-1} for the symmetric and asymmetric vibrations, respectively. The Re=O bond length is 1.705 Å. For the dimeric compound **5c**, ν(Re=O) is 950 cm^{-1} and 948 cm^{-1} (for the symmetric and antisymmetric vibrations, respectively) and the Re=O bond length is 1.702 Å. According to these values, substitution of an oxo ligand of MTO by an imido group (or several such substitutions), and subsequent dimerization leads to a weakening of the Re=O bonds.

However, not only is the Re=O bond weakened owing to substitution of oxo groups by imido groups, but the Re−C bond also changes. Figure 6a shows how the Re−C stretching frequencies vary with the corresponding bond lengths based on experimental (filled symbols) and calculated data (open symbols). Calculated values differ from the corresponding experimental values (Table 4). For CH_3ReO_3 (**1**), *d*(Re−C) was measured to be 2.060 Å, while we calculated 2.090 Å. In accordance with this longer bond, the corresponding stretching frequency is lower (exp.: 574 cm^{-1}; calcd.: 550 cm^{-1}). For the other complexes investigated experimentally (**4c**, **5c**, and **6c**), we may compare the model systems **4b**, **$A_{O,O}$(2b−2b)trans** and **$A_{O,O}$(3b−3b)trans**. Here also, the calculated bonds tend to be weaker, as judged by an overestimation of the bond lengths [by 0.026 Å in **4b**, 0.008 Å in **$A_{O,O}$(2b−2b)trans**, and 0.021 Å in **$A_{O,O}$(3b−3b)trans**] and an underestimation of the corresponding stretching frequencies. These calculated data fit the same essentially linear relationship between bond lengths and frequencies as the experimental data (Figure 6a). The MTO dimer and the N-bridged imido dimer are the only exceptions (open diamonds, Figure 6a). Figure 6b shows the calculated stretching frequencies as a function of the natural atomic charge of the rhenium center. For the monomers **1**, **2a/b**, **3a/b**, and **4a/b**, we conclude that with increasing electron deficiency at the metal center, i.e. with higher positive charge *q*(Re) (Figure 6b), the Re−C bond becomes shorter and more rigid (higher vibrational frequency). The dimers do not fit that linear correlation. The effect of rehybridization on the metal center due to dimerization causes more complex changes in the electronic structure which, in turn, affects the Re−C bond.

Ligand Exchange between Monomers

Finally, we discuss the energies of group-exchange reactions between two monomers, which occur via a dimer structure. We will start by discussing a possible reaction coordinate. Symmetry is a key point for rationalizing this exchange problem. If we assume a synchronous process, the reaction pathway has to pass a structure where both M−X bonds of each bridging atom X are equivalent by symmetry.

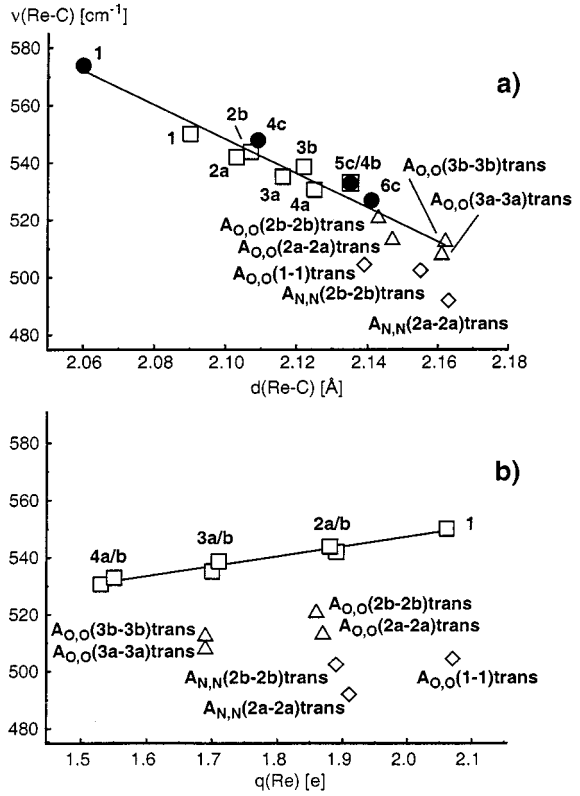

Figure 6. Experimental (filled circles) and calculated (open symbols) Re−C stretching frequencies ν(Re−C) as a function of (a) the Re−C bond length *d*(Re−C); and (b) the calculated natural atomic charges *q*(Re) of Re (in e); for the calculated data, the most stable conformers were used (monomers − open squares, O-bridged dimers − open triangles, MTO dimer and N-bridged dimers − open empty diamonds)

Table 4. Calculated and experimental Re−C bond lengths (in Å) and stretching frequencies (in cm^{-1}) for various monomers and dimers; also shown are the corresponding calculated natural atomic charge *q*(Re) (in e)

	d(Re−C)	ν(Re−C)	*q*(Re)
Monomers:			
1	2.090	550.2	2.06
1[a]	2.060	574	
2a	2.103	542.1	1.89
2b	2.107	544.0	1.88
3a	2.116	535.3	1.70
3b	2.122	538.8	1.71
4a	2.125	530.8	1.53
4b	2.135	533.1	1.55
4c[a]	2.135	541, 533	
Dimers:			
$\mathbf{A_{O,O}(1-1)trans}$	2.139	504.6	2.07
$\mathbf{A_{N,N}(2a-2a)trans}$	2.163	492.1	1.91
$\mathbf{A_{N,N}(2b-2b)trans}$	2.155	502.6	1.89
$\mathbf{A_{O,O}(2a-2a)trans}$	2.147	513.7	1.87
$\mathbf{A_{O,O}(2b-2b)trans}$	2.143	521.3	1.86
$\mathbf{A_{O,O}(3a-3a)trans}$	2.161	508.5	1.69
$\mathbf{A_{O,O}(3b-3b)trans}$	2.162	513.1	1.69
5c[a]	2.141	539, 527	
6c[a]	2.109	548	

[a] Experimental values.

This structure can be a transition state, but it could also be a stable or metastable intermediate (see Figure 7). In the first case the reaction coordinate features one transition structure that interconnects two local equilibrium points of the potential-energy surface (PES). Each of the atoms can be assigned to a certain metal center. The final structure can either be two isolated molecules, or a dimer which has two bridging atoms X with two different M−X bond lengths. If the structure with the symmetry-equivalent M−X bonds is a (meta)stable intermediate, then the reaction path has two saddle points which lie between the symmetric local minimum structure and the structure where each atom X is uniquely assigned to only one metal center.

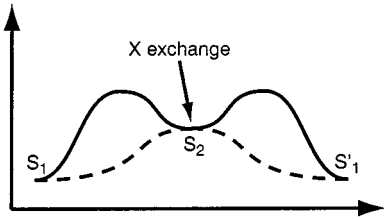

Figure 7. Sketch of the potential-energy surface for the exchange of group X in dimers at the stationary point S_2; the stationary points S_1 and S_1' indicate configurations in which the groups X can be assigned to one of the metal centers, either in the case of two monomers or in the case of a dimer with asymmetric bridges; the solid line represents an energy profile with S_2 as (meta)stable intermediate, the dashed line represents an energy profile with S_2 as transition state

In the following discussion of ligand-exchange reactions, we will restrict ourselves to the special case of oxygen-bridged dimers. For ligand-exchange reactions of MTO and related dimers, we can discriminate four pertinent structures which can be (meta)stable intermediate dimers or transitions states, or stable dimers in which each bridging atom X belongs to one metal center only.

Only structure $\mathbf{A_{O,O}(1-1)trans}$ exhibits two different M−X bonds, while the structures $\mathbf{A_{O,O}(1-1)cis}$, $\mathbf{B_{O,O}(1-1)cis}$ and $\mathbf{B_{O,O}(1-1)trans}$ can either be (meta)-stable intermediates, or transition states. From frequency calculations, one discovers that *cis* and *trans* structures **B** are both third-order saddle points, and thus not proper transition states. On the other hand, *cis* and *trans* configurations of structure **A** are both metastable.

The optimized transition state (see Figure 8) of the oxygen exchange reaction corresponds to a complex reaction coordinate. The barrier height $\Delta E^{\neq}$ is 23.8 kcal/mol ($\Delta H^{\neq}$ = 24.4 kcal/mol). It connects two isolated MTO complexes (lower-energy asymptote in Figure 7) with dimer structure $\mathbf{A_{O,O}(1-1)trans}$, which is thus identified as a metastable intermediate (Figure 7). The dimerization energy ΔE of this intermediate is 1.7 kcal/mol (ΔH = 3.5 kcal/mol, see Table 1). To facilitate the understanding of the three-dimensional structure of the transition state, we display two orientations of this structure in Figure 8. The arrows indicate the motion of the nuclei along the reaction coordinate in the direction in which the metastable intermediate $\mathbf{A_{O,O}(1-1)trans}$ is formed. Note that the order of the Re−O bond lengths in the bridging unit is reversed in comparison to the dimeric compound (see Figure 1). The shorter Re−O bond in the transition state (1.835 Å; Fig-

ure 8) is the one closer to the Re−C bond, which is 2.046 Å in the dimer [see Figure 1, (a)]. The longer bond in the transition structure (2.208 Å, Figure 8) is *trans* to the methyl group; it corresponds to the shorter bridging bond, 1.902 Å (Figure 1), of the dimer. These changes demonstrate the exchange of the two oxygen atoms through the formation of a dimer. In the transition state, the two carbon−rhenium bonds do not fall in one plane, in contrast to the dimer structure; the dihedral angle C−Re−Re−C is 115°. The nuclear motion along the reaction coordinate does not only comprise an exchange of oxygen centers, but also a rotation of each monomer around the shorter Re−O bridging bond in the transition state. However, the transition structure exhibits C_2 symmetry, with the rotation axis perpendicular to the plane that contains the Re−O bridging bonds.

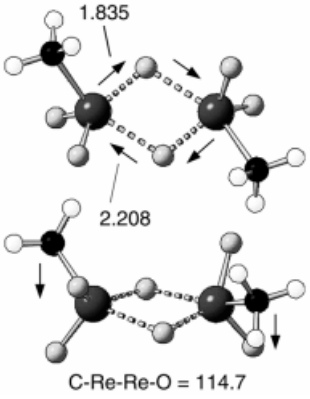

Figure 8. Calculated transition-state structure of oxygen exchange in the dimer $\mathbf{A_{O,O}(1-1)trans}$; top: view onto the Re−O−Re plane; bottom: Re−O−Re plane rotated around the Re−Re axis; arrows indicate motions of the nuclei along the reaction coordinate from the transition state to the metastable intermediate $\mathbf{A_{O,O}(1-1)trans}$; bond lengths in Å, angles in °

Conclusions

The most stable dimers of oxo, imido, and mixed imido/oxo alkylrhenium(VII) complexes display a trigonal-bipyramidal structure at the metal centers, with a *trans* arrangement of the methyl ligands. While the *cis* arrangement of the methyl ligands leads only to slightly higher energies (about 5 kcal/mol), pseudo square-pyramidal arrangements have a considerably higher energy (about 30 kcal/mol) than trigonal-bipyramidal structures. This is in good agreement with published structures, but contrasts with previously published HF calculations concerning the first step of the polymerization of methyltrioxorhenium(VII). In all cases examined, the stabilization gained by the dimerization process is rather small (usually < 5 kcal/mol), explaining the ease of the Re−O−Re bond cleavage and reformation during the sublimation process of the compounds **2** ⇄ **5** and **3** ⇄ **6**. In some cases, most notably for methyltrioxorhenium(VII), the dimerization process is (slightly) endothermic, according to our calculations. Therefore, dimers cannot be isolated but are likely to be present as short-lived species. This explains the ease of reversible oxygen-transfer reactions between O-labeled and -unlabeled organorhenium(VII) oxides which have often been observed,[8] even in water-free solvents. Based on the present results, we suggest that these processes proceed via (short-lived) oxygen bridges.

According to our calculations, N-bridged dimers of the compounds **2**−**4** should be stable. At first glance, this seems to contradict our vibrational spectroscopy results, which show no indication for N-bridged species whatsoever. However, our calculations were performed with N−H and $N-CH_3$ species as bridging groups and have already shown that dimer formation becomes more endothermic when N−H groups are substituted by $N-CH_3$ species. However, imido and mixed imido/oxo complexes with N−H or $N-CH_3$ groups are too unstable to be isolated.[4] The bulky ligands we used in an attempt to isolate imido or oxo/imido species evidently disfavor dimers significantly more than do CH_3 groups, thus resulting in monomers such as **4** becoming the energetically preferred species.

Experimental Section

All preparations and manipulations were performed with standard Schlenk techniques under oxygen- and water-free argon. Solvents were dried by standard procedures: THF, Et_2O, *n*-pentane, and *n*-hexane with Na/benzophenone ketyl. Acetonitrile and dichloromethane were distilled after heating at reflux for several hours over P_2O_5. Acetone was distilled from K_2CO_3 and kept over 4-Å molecular sieves. − The TG/MS studies were carried out with a Perkin−Elmer TGA 7 thermobalance coupled with a Balzers QMG 420 mass spectrometer. The thermolysis experiments were carried out in a dynamic helium environment (purity 5.0, 45 sccm) using a 50−600 °C temperature program at a rate of 10 °C/min. The temperature of the capillary interface was 280 °C. TG studies were additionally performed using a Shimadzu TGA-50 thermobalance. The experiments were carried out under nitrogen at 25−1000 °C, at a rate of 5 °C/min from room temperature to 1000 °C, using a platinum cell. − The Raman spectra were recorded with a Bio-Rad dedicated FT-Raman spectrometer using the near-infrared excitation 1064 nm of a Nd:YAG diode laser. − The infrared spectra in the 4000−200 cm^{-1} region were recorded using a Bio-Rad FTS-175 spectrometer equipped with CsI-based beam splitter, and the far-infrared (400−50 cm^{-1}) measurements were carried out with the same spectrometer, but using a 6-μm Mylar beam-splitter. − The compounds CH_3ReO_3 (**1**), $[CH_3ReO_2(NR)]_2$ (**5c**), $[CH_3ReO(NR)_2]$ (**6c**), and $CH_3Re(NR)_3$ (**4c**) (with R = 2,6-diisopropylphenyl) were prepared according to published procedures.[5,14]

Computational Details: All electronic structure calculations were performed with the hybrid B3-LYP[15] density-functional scheme,[16] using effective-core potentials for rhenium with a partly decontracted basis set for rhenium.[17] Geometry optimizations were carried out using a 6-311G(d,p) basis[18] on all centers (except Re). Enthalpies were calculated at this level following standard procedures.[19] Finally, two f exponents[3e,7] were added to the basis set of Re to evaluate energies in a single-point fashion. Details of this computational strategy have been discussed elsewhere.[7] Transition-state structures were verified to feature only one imaginary frequency in the vibrational spectrum. Additionally, by following

the transition vector, we verified that the reaction products and reactants are directly reached from the transition structure.[20]

Acknowledgments

F. E. K. is greatly indebted to Prof. Dr. W. A. Herrmann for continuous support. This work was supported by the DAAD (Accões Integradas and Keretében Megvalósuló Program), the BMFT/JNICT Protokoll, the Deutsche Forschungsgemeinschaft, and the Fonds der Chemischen Industrie.

[1] W. A. Herrmann, F. E. Kühn, G. M. Lobmeier, in: *Aquous Phase Catalyis* (Eds.: B. Cornils, W. A. Herrmann), VCH-Wiley, Weinheim, New York, **1998**.

[2] Recent reviews: [2a] W. A. Herrmann, F. E. Kühn, *Acc. Chem. Res.* **1997**, *130*, 1169. – [2b] F. E. Kühn, R. W. Fischer, W. A. Herrmann, *Chem. Unserer Zeit* **1999**, *33*, 192. – [2c] F. E. Kühn, W. A. Herrmann, *Struct. Bonding* **2000**, *97*, 211.

[3] [3a]T. Szyperski, P. Schwerdtfeger, *Angew. Chem. Int. Ed. Engl.* **1989**, *28*, 1128. – [3b] R. Wiest, T. Leininger, G. H. Jeung, M. Bénard, *J. Phys. Chem.* **1992**, *96*, 10800. – [3c] S. Köstlmeier, O. D. Häberlen, N. Rösch, W. A. Herrmann, B. Solouki, H. Bock, *Organometallics* **1996**, *15*, 1872. – [3d] S. Köstlmeier, V. A. Nasluzov, W. A. Herrmann, N. Rösch, *Organometallics* **1997**, *16*, 1786. – [3e] P. Gisdakis, S. Antonczak, S. Köstlmeier, W. A. Herrmann, N. Rösch, *Angew. Chem. Int. Ed.* **1998**, *37*, 2211. – [3f] C. Mealli, J. A. Lopez, M. J. Calhorda, C. C. Romão, W. A. Herrmann, *Inorg. Chem.* **1994**, *33*, 1139. – [3g] A. Gobbi, G. Frenking, *J. Am. Chem. Soc.* **1994**, *116*, 9275.

[4] [4a] C. J. Longley P. D. Savage, G. Wilkinson, B. Hussain, M. Hursthouse, *Polyhedron* **1988**, *7*, 1079. – [4b] A. D. Horton, R. R. Schrock, J. H. Freundenberger, *Organometallics* **1987**, *6*, 893. – [4c] D. S. Williams, R. R. Schrock, *Organometallics* **1993**, *12*, 1148. [4d] M. R. Cook, W. A. Herrmann, P. Kiprof, J. Takacs, *J. Chem. Soc., Dalton Trans.* **1991**, 797. – [4e] A. Gutierrez, G. Wilkinson, B. Hussain-Bates, M. B. Hursthouse, *Polyhedron* **1990**, *9*, 2081. – [4f] W. A. Herrmann, G. Weichselbaumer, R. A. Paciello, R. A. Fischer, E. Herdtweck, J. Okuda, D. W. Marz, *Organometallics* **1990**, *9*, 489. – [4g] W. D. Wang, J. H. Espenson, *Organometallics* **1999**, *18*, 5170.

[5] W. A. Herrmann, H. Ding, F. E. Kühn, W. Scherer, *Organometallics* **1998**, *17*, 2751.

[6] [6a] W. A. Herrmann, R. W: Fischer, *J. Am. Chem. Soc.* **1995**, *117*, 3223. – [6b] H. S. Genin, K. A. Lawler, R. Hoffmann, W. A. Herrmann, R. W: Fischer, W. Scherer, *J. Am. Chem. Soc.* **1995**, *117*, 3244. – [6c] S. Köstlmeier, G. Pacchioni, W. A. Herrmann, N. Rösch, *J. Organomet. Chem.* **1996**, *514*, 111. – [6d] W. A. Herrmann, W. Scherer, R. W. Fischer, J. Blümel, M. Kleine, W. Mertin, R. Gruehn, J. Mink, H. Boysen, C. C. Wilson, R. M. Ibberson, L. Bachmann, M. Mattner, *J. Am. Chem. Soc.* **1995**, *117*, 3231.

[7] P. Gisdakis, S. Antonczak, N. Rösch, *Organometallics* **1999**, *18*, 5044.

[8] [8a] W. A. Herrmann, F. E. Kühn, P. W. Roesky, *J. Organomet. Chem.* **1995**, *485*, 243. – [8b] W. A. Herrmann, F. E. Kühn, M. U. Rauch, J. D. G. Correia, G. R. J. Artus, *Inorg. Chem.* **1995**, *34*, 2914. – [8c] W. A. Herrmann, J. D. G. Correia, M. U. Rauch, G. R. J. Artus, F. E. Kühn, *J. Mol. Catal.* **1997**, *118*, 33. – [8d] W. A. Herrmann, W. A. Wojtczak, G. R. J. Artus, F. E. Kühn, M. R. Mattner, *Inorg. Chem.* **1997**, *36*, 465.

[9] W. A. Herrmann, W. Wachter, F. E. Kühn, R. W. Fischer, *J. Organomet. Chem.* **1998**, *553*, 443.

[10] J. Mink, G. Keresztury, A. Stirling, W. A. Herrmann, *Spectrochim. Acta* **1994**, *50A*, 2039.

[11] W. A. Herrmann, J. G. Kuchler, J. K. Felixberger, E. Herdtweck, W. Wagner, *Angew. Chem. Int. Ed. Engl.* **1988**, *27*, 394.

[12] W. A. Herrmann, M. Flöel, J. Kulpe, J. K. Felixberger, E. Herdtweck, *J. Organomet. Chem.* **1988**, *355*, 297.

[13] G. Varsányi, *Assignment for Vibrational Spectra of 700 Benzene Derivatives*, Akadémia Kiadó, Budapest, **1973**, pp. 298.

[14] W. A. Herrmann, R. Kratzer, R. W. Fischer, *Angew. Chem. Int. Ed. Engl.* **1997**, *36*, 2652.

[15] [15a] A. D. Becke, *J. Chem. Phys.* **1993**, *98*, 5648. – [15b] C. Lee, W. Yang, R. G. Parr, *Phys. Rev. B* **1988**, *37*, 785.

[16] M. J. Frisch, G. W. Trucks, H. B. Schlegel, P. M. W. Gill, B. G. Johnson, M. A. Robb, J. R. Cheeseman, T. Keith, G. A. Petersson, J. A. Montgomery, K. Raghavachari, M. A. Al-Laham, V. G. Zakrzewski, J. V. Ortiz, J. B. Foresman, J. Cioslowski, B. B. Stefanov, A. Nanayakkara, M. Challacombe, C. Y. Peng, P. Y. Ayala, W. Chen, M. W. Wong, J. L. Andres, E. S. Replogle, R. Gomperts, R. L. Martin, D. J. Fox, J. S. Binkley, D. J. Defrees, J. Baker, J. P. Stewart, M. Head-Gordon, C. Gonzalez, J. A. Pople, *Gaussian 94, Revision D.4*, Gaussian Inc., Pittsburgh PA, USA, **1995**.

[17] [17a] P. J. Hay, W. R. Wadt, *J. Chem. Phys.* **1985**, *82*, 299. [17b] G. Frenking, I. Antes, M. Böhme, S. Dapprich, A. W. Ehlers, V. Jonas, A. Neuhaus, M. Otto, R. Stegmann, A. Veldkamp, S. F. Vyboishchikov, in: *Reviews in Computational Chemistry*, vol. 8 (Eds.: K. B. Lipkowitz, D. B. Boyd), VCH, New York, **1996**, p. 63.

[18] R. Krishnan, J. Binkley, R. Seeger, J. Pople, *J. Chem. Phys.* **1980**, *72*, 650.

[19] W. J. Hehre, L. Radom, P. v.R. Schleyer, J. A. Pople, *Ab initio Molecular Orbital Theory*, Wiley, New York, **1986**.

[20] Internal reaction coordinate analysis carried out at the LanL2DZ level; cf. ref.[17]; see also: C. Gonzalez, H. B. Schlegel, *J. Chem. Phys.* **1990**, *94*, 5523.

Received September 27, 2000
[I00363]

Stereoselective Synthesis of Hexacoordinated Mononuclear Cyclometalated Rhodium(III) Complexes − Transfer of Chirality from the Metal Center to the Ligand

Liana Ghizdavu,[a] Alex von Zelewsky,*[a] and Helen Stoeckli-Evans[b]

Keywords: Rhodium / Chirality / Cyclometalations / Stereoselective synthesis / Mononuclear complexes

The cleavage of ΔΔ[Rh(th4,5ppy)$_2$(μ-Cl)]$_2$ [th4,5ppy is enantiomerically pure (8*R*,10*R*)-2-(2′-thienyl)-4,5-pinenopyridine(−)] by 5 different diimines and 11 diamines yields monomeric cations Δ[Rh(th4,5ppy)$_2$(*N*∩*N*)]$^+$. In all cases, the cleavage reaction preserves the original Δ configuration at the metal center. When *N*∩*N* is a chiral or a prochiral ligand, various degrees of stereoselectivity is observed, depending on where the stereogenic center is located in *N*∩*N*. The reported results open up a systematic method towards the synthesis of tris(bidentate)Rh^{III} complexes with a completely predetermined stereochemistry.

Introduction

The syntheses of coordination compounds in which the metal atom is a stereogenic center have not often been performed in a stereoselective manner.[1] This is in sharp contrast to the large number of examples known from organic chemistry in which stereoselectivity is the subject of intense study. Stereoselectivity in coordination compounds can be achieved through the use of enantiomerically pure chiral ligands in various ways. Here we describe the formation of mononuclear rhodium(III) complexes comprising of two cyclometalating bidentate ligands plus one bidentate diimine or diamine (Scheme 1).

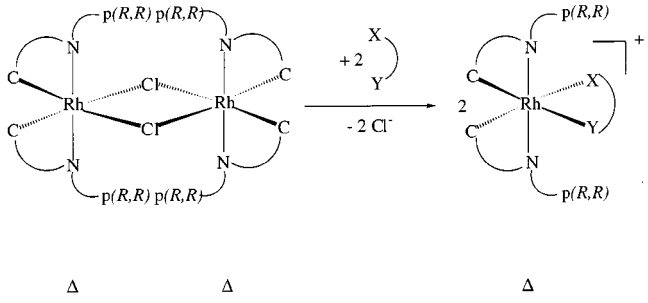

Scheme 1

The reaction step that determines the configuration of the final product is the formation of a homochiral dimer.[2] The latter can be cleaved by achiral, prochiral or chiral bipyridine-type or diamine ligands (Table 1).[3]

This cleavage reaction takes place with the retention of the configuration at the metal centers in the dinuclear species.Thus, a generally applicable method is given for the stereoselective synthesis of compounds that are of high potential interest in various fields, such as enantioselective catalysis, and as intercalators in DNA.[4,5] Generally, the preparation of compounds that are isomerically pure is preferred over the often cumbersome and often inapplicable separation methods sometimes used in coordination chemistry.[6] This is certainly true for highly selective and efficient reactions such as those described in the present work.

[a] Institute of Inorganic Chemistry, University of Fribourg, Pérolles, 1700 Fribourg, Switzerland
Fax: (internat.) + 41-26/300-9738
E-mail: Alexander.vonzelewsky@unifr.ch
[b] Institute of Chemistry, University of Neuchâtel, Avenue de Bellevaux 51, 2000 Neuchâtel, Switzerland

Results and Discussion

The formation of the homochiral dinuclear precursor of the monomers, ΔΔ[Rh(th4,5ppy)$_2$(μ-Cl)]$_2$ (**I**) has been described before.[2] The configuration Δ at the two metal centers is induced by the natural product (−)-myrtenal, used for the synthesis of the thienyl-4,5-pinenepyridine ligand. Complex **I** can be prepared in high isomeric purity. It can be cleaved in a smooth reaction (CH_2Cl_2, 40 °C, ca. 60 min) producing the mononuclear species **I**−**XVII** in high yields (60−80%) as shown in Scheme 2, Scheme 3 and Scheme 4. We discuss the complexes according to the type of bidentate ligand used in the cleavage reaction.

Diimine Ligands

Three different types of diimine ligands can be distinguished: *Achiral* (bpy) → **II** (Scheme 2), *chiral with one pinene group* (4,5-pbpy, 5,6-pbpy) → **V**, **VI**, and *chiral with two pinene groups* (bis-4,5-pbpy, bis-5,6-pbpy) → **III** and **IV**. Complexes **II** and **III** were prepared as PF_6 salts.

The simplest of these species, **II**, has C_2 symmetry. The ^{1}H NMR spectrum clearly shows the equivalence of the corresponding protons in the two 2,2′-thienyl-4,5-pinenepyridine ligands and of those in the coordinated bpy in the complex. It also suggests the retention of configuration at the metal centers after the cleavage reaction, since two dia-

 © WILEY-VCH Verlag GmbH, 69451 Weinheim, 2001 1434−1948/01/0404−0993 $ 17.50+.50/0

Table 1. Ligands and their abbreviations

Ligand name	Formula	Abbreviation
(8*R*,10*R*)-2-(2'-Thienyl)-4,5-pinenopyridine[(-)]	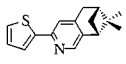	th4,5ppy
2,2'-bipyridine		2,2'-bpy
4,5;4',5'-pinenobipyridine	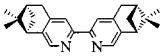	4,5;4',5'pbpy
5,6;5',6'-pinenobipyridine	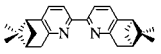	5,6;5',6'pbpy
4,5-pinenobipyridine	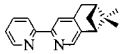	4,5-pbpy
5,6-pinenobipyridine	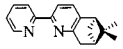	5,6-pbpy
cis-1,2 -Diamino-cyclohexane		rac-chxn
(1*R*,2*R*)-(-)-1,2-diaminocyclohexane		*(R,R)*-chxn
(1*S*,2*S*)-(-)-1,2-diaminocyclohexane		*(S,S)*-chxn
ethylenediamine		en
propylenediamine		rac-pn
1,2-diphenyl-ethylenediamine	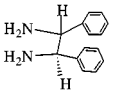	rac-st
(R,R)-diphenyl-ethylenediamine	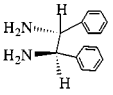	*(R,R)*-st
(S,S)-diphenyl-ethylenediamine	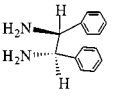	*(S,S)*-st
N,N'-dimethyl-ehylenediamine	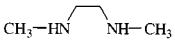	dmen
N-methyl-ehylenediamine	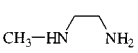	men
N,N'-diphenyl-ehylenediamine	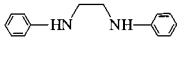	dpen

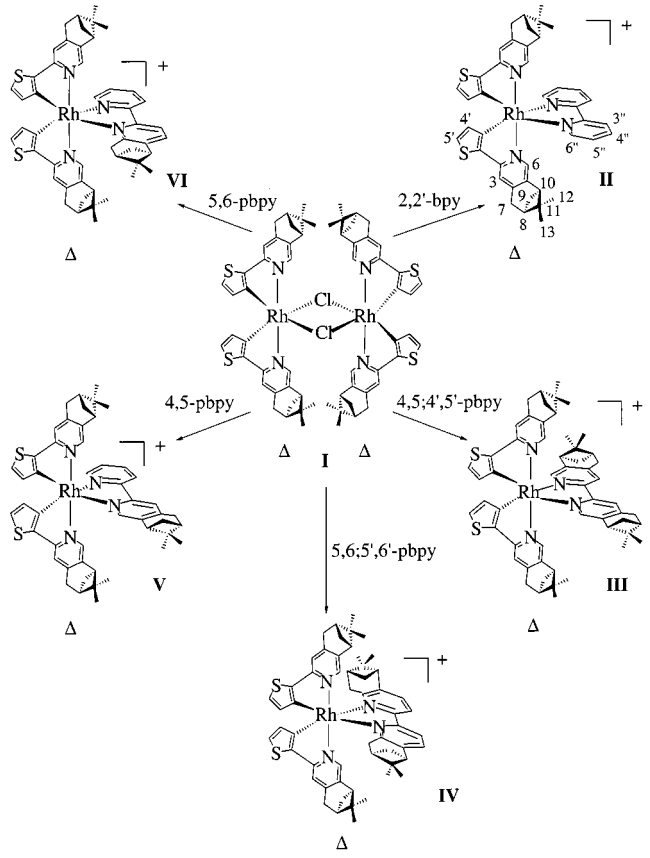

Scheme 2

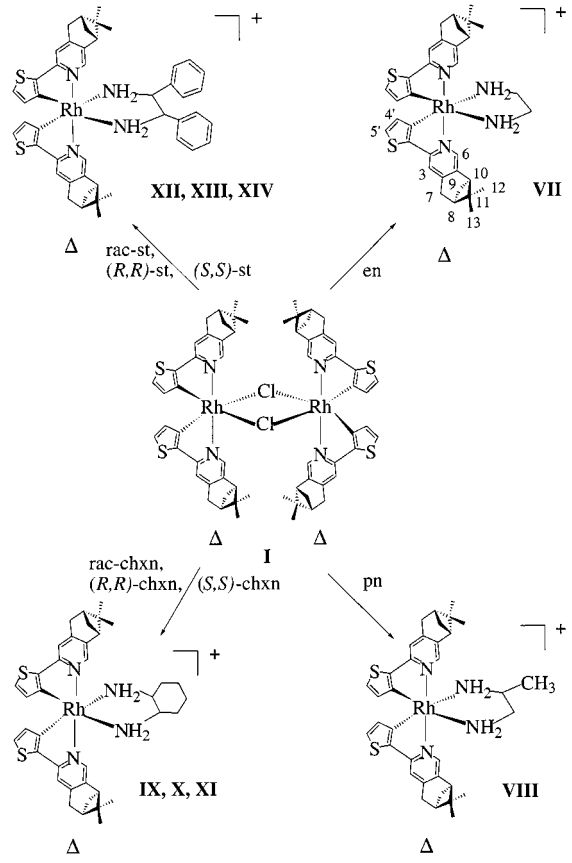

Scheme 3

stereomeric products [(*R*,*R*)Δ and (*R*,*R*)Λ, both C_2-symmetric] would result in two sets of protons. The Δ configuration follows from the CD spectrum (Figure 1), that gives clear indications for this isomer.[7] The strong peak of mass

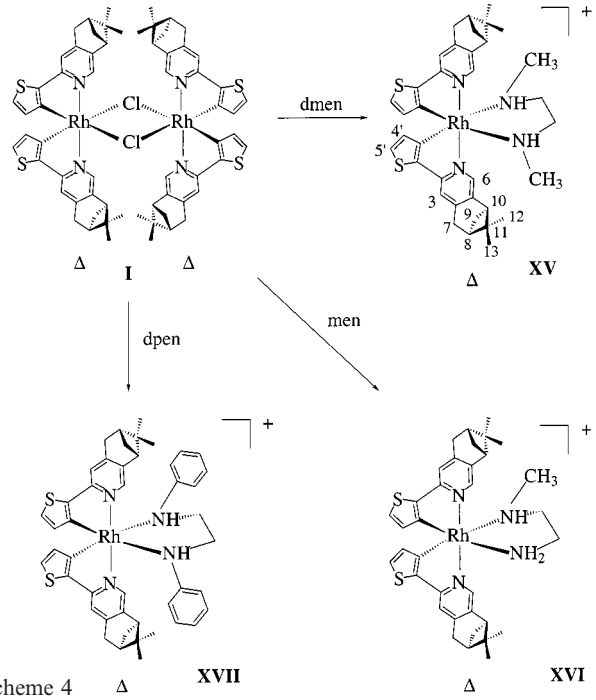

Scheme 4

767 (**II**-PF_6) confirms the mononuclear nature of this complex.

The complexes **III** and **IV** also have C_2 symmetry, as demonstrated by ^{1}H NMR spectroscopy. The aromatic region of the ^{1}H NMR spectra is even more simple than that of **II** owing to the use of "dipineno"-fused 2,2′-bipyridines (bis-4,5-pbpy, bis-5,6-pbpy) ligands. Those spectra show one set of protons, which proves the isomeric purity of the complexes. The CD spectra are similar to those of **II**, again indicating the retention of the Δ configuration. The peaks (100%) at 955 (**III** − PF_6) and 956 (**IV** − Cl) correspond to mononuclear species.The complexes **V** and **VI** with the unsymmetrical ligands 4,5-pbpy and 5,6-pbpy are not C_2-symmetric. The ^{1}H NMR spectra are therefore more complicated. Nevertheless, only one complete set of signals is observed, again showing that the configuration of the metal center is retained. The assignment of the peaks was carried out using a combination of COSY and NOE techniques for **VI**, while **V** was characterised by COSY spectra. The CD spectra (Figure 1) are in agreement with the Δ configuration at the metal center and have the same shape as the spectra of the dinuclear ΔΔ precursor, and as the spectra of the complexes **II**, **III** and **IV**. The MS spectra show mass peaks 861 (**V**, **VI** − Cl), indicating that the complexes are mononuclear.

Diamine Ligands

Several 1,2-diamine-type ligands have been used: *Achiral diamines* (en) → **VII** (Scheme 3 and Scheme 4), *chiral and prochiral diamines with one stereogenic center* (pn and men) → **VIII**, **XVI** and *chiral and prochiral diamines with two stereogenic centers* (chxn, st, dmen, dpen) → **IX** → **XI**, **XII** → **XIV**, **XV**, **XVII**.

Δ[Rh(th4,5ppy)$_2$(en)]Cl

The cation **VII** shows all characteristic peaks of the th-4,5-pinenopyridine as well as the signals of the NH_2 and CH_2 groups of ethylenediamine in the ^{1}H NMR spectrum. No splitting of these peaks occurs, clearly indicating that only one configuration at the metal center is present. The CD spectrum of **VII** (Figure 2.) shows that the Δ configura-

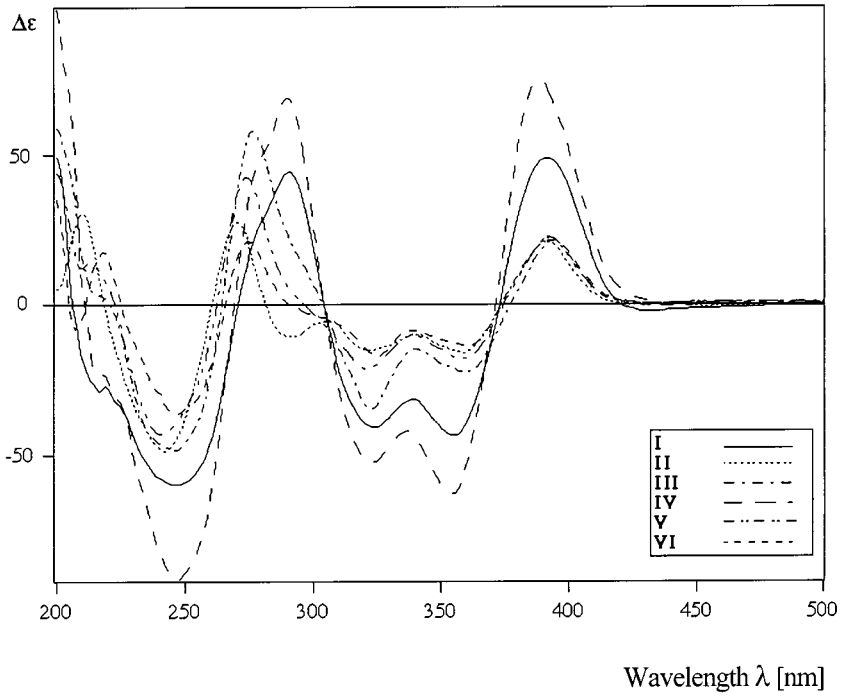

Figure 1. CD spectra of the complexes **I**, **II**, **III**, **IV**, **V** and **VI**

tion of the homochiral dinuclear precursor is preserved in the cleavage reaction.

Δ[Rh(th4,5ppy)$_2$(*rac*-pn)]Cl

The cation **VIII** occurs in two diastereomeric forms. The ^{1}H NMR spectrum shows a splitting of each signal of the th-4,5-pinenopyridine ligands in the aromatic region into four peaks (most easily seen e.g. in the signal of the 6′ proton at δ = 8.33 in the corresponding en complex). The small splitting (Δδ = 0.040 and 0.056, respectively, for 1:1 intensity lines for the 6′ proton) is due to the loss of the C_2 symmetry of the complex, whereas the larger splitting (Δδ = 0.27) is caused by the presence of two diastereoisomers Δ[Rh(th4,5ppy)$_2${(*R*)-pn}]Cl and Δ[Rh(th4,5ppy)$_2${(*S*)-pn}]Cl, respectively. These two diastereoisomers are formed in a ratio of 1:0.85, i.e. with a very low stereoselectivity. The CD spectra (Figure 2), which are mainly due to the disymmetry of the metal center and not to the ligands themselves, again clearly show the retention of the Δ configuration at the metal center.

Δ[Rh(th4,5ppy)$_2$(*rac*-chxn)]Cl (IX), Δ[Rh(th4,5ppy)$_2${(*R,R*)-chxn}]Cl (X), Δ[Rh(th4,5ppy)$_2${(*S,S*)-chxn}]Cl (XI)

Cleavage of the dinuclear complex **I** by *rac*-chxn (*rac*-trans-1,2-diaminocyclohexane) yields a product that shows a doubling of all peaks in the ^{1}H NMR spectrum (Figure 3, **IX**). The splitting is largest for proton 6 (Δδ = 0.32) and becomes smaller for proton 4 (Δδ = 0.038) and proton 3 (Δδ = 0.02), while the signals of protons 5 are superposed. The intensity ratio is nearly 1:1, indicating almost no stereoselectivity for this diamine ligand. An assignment of the two diastereomers is possible by using enantiomerically pure (*R*,*R*)-chxn and (*S*,*S*)-chxn. The two spectra in Figure 3 are obtained for **X** and **XI**.

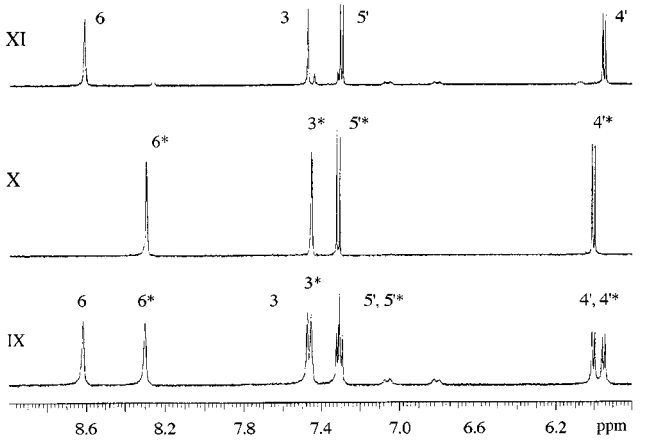

Figure 3. The aromatic region of the ^{1}H NMR spectra of complexes **IX**, **X** and **XI**

The CD spectra of all three complexes again show a retention of the Δ configuration upon cleavage of the dichloro bridge. Despite the fact that the ^{1}H NMR spectra show a relatively large splitting of the corresponding nuclei in the diastereomers, indicating an influence of the relative config-

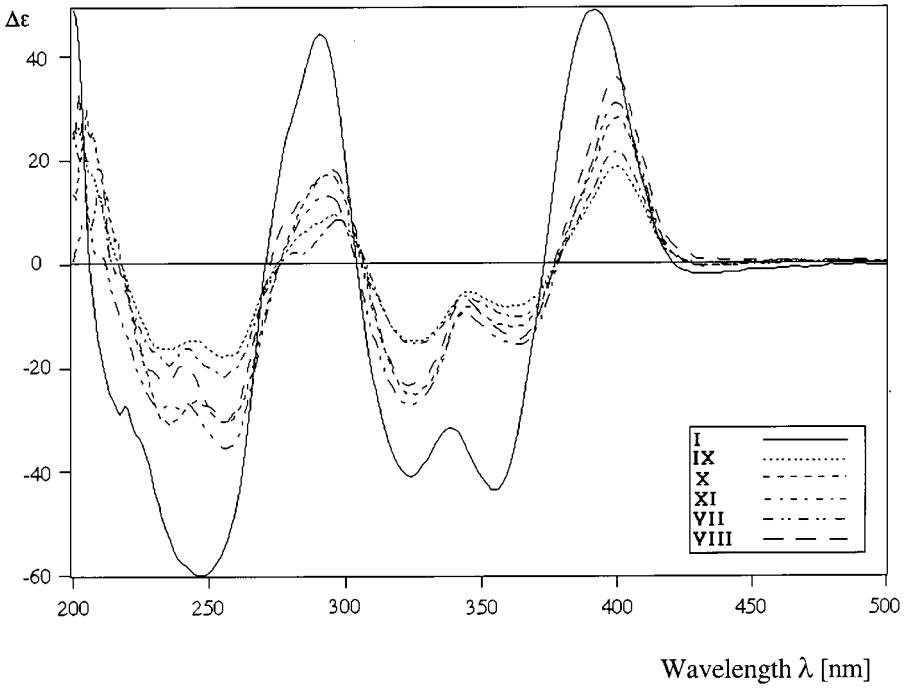

Figure 2. CD spectra of the complexes **I**, **VII**, **VIII**, **IX**, **X** and **XI**

urations of the chirality elements within the complex on the electronic structure, almost no chiral discrimination occurs in the cleavage reaction. Evidently, the differences in thermodynamic stability of the resulting diastereomers are too small to allow for significant stereoselectivity.

Δ[Rh(th4,5ppy)$_2$(*rac*-st)]Cl (XII), Δ[Rh(th4,5ppy)$_2${(*R*,*R*)-st}]Cl (XIII), Δ[Rh(th4,5ppy)$_2${(*S*,*S*)-st}]Cl (XIV)

The enantiomerically pure (*R*,*R*)- and (*S*,*S*)-stilbenediamines cleave the dinuclear complex **I** in a clean reaction, yielding isomerically pure mononuclear species (Figure 4). When the racemate of the ligand is used, both diastereomers, Δ[Rh(th4,5ppy)$_2${(*S*,*S*)-st}]Cl and Δ[Rh(th4,5ppy)$_2$-{(*R*,*R*)-st}]Cl, are observed in a 1:5.5 ratio by the ^{1}H NMR spectroscopy (Figure 4). The diastereomeric ratio was calculated from the signals for the protons at the 6 position in the ^{1}H NMR spectra. Since no separation step was applied to the reaction mixture after the cleavage reaction, this ratio represents the ''true'' stereoselectivity of this step.

In the case of Δ[Rh(th4,5ppy)$_2$[(*S*,*S*)-st}]Cl, crystals suitable for X-ray structure determination could be obtained.

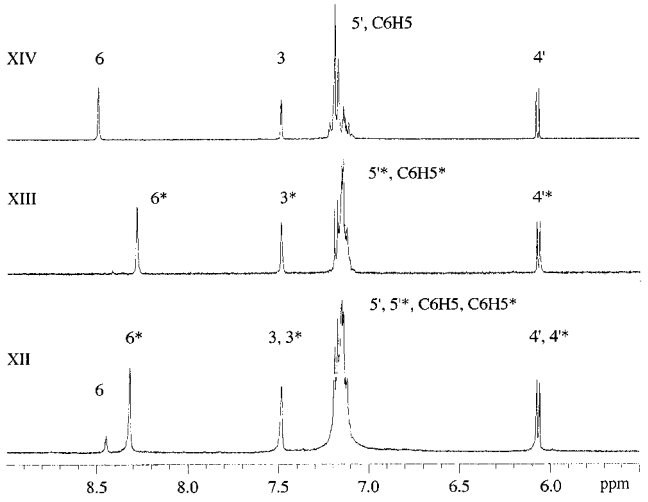

Figure 4. The aromatic region of the ^{1}H NMR spectra of complexes **XII**, **XIII** and **XIV**

Table 2. Crystallographic data

	XIV
Empirical formula	$C_{46}H_{48}ClN_4RhS_2 \cdot 3/4H_2O$
Molecular mass	872.88
Temperature [K]	223(2)
Crystal system	hexagonal
Space group	$P6_522$ (no. 179)
Color of crystal	orange
a [Å]	18.7322(10)
b [Å]	18.7322(10)
c [Å]	48.900(4)
V [Å^3]	14859.9(17)
Z	12
Density (calculated) [g/cm^{-3}]	1.170
Absorption coeff. [mm^{-1}]	0.516
F(000)	5442
Crystal size [mm]	0.45 × 0.25 × 0.15
Independent refls.	7849
Observed refls. [$I < 2\sigma(I)$]	4354
Final *R* indices [$I > 2\sigma(I)$][a]	$R1 = 0.0511$, $R2 = 0.1217$
R indices of all data[a]	$R1 = 0.0908$, $R2 = 0.1364$
Goodness-of-fit (obsd. data)	0.828
Residual density [e/Å^3]	0.529/−0.338

$R1 = \Sigma(F_o - F_c)/\Sigma(F_o)$; $wR2 = [\Sigma(w(F_o^2 - F_c^2)^2\}/\Sigma\{w(F_o^4)\}]^{1/2}$.

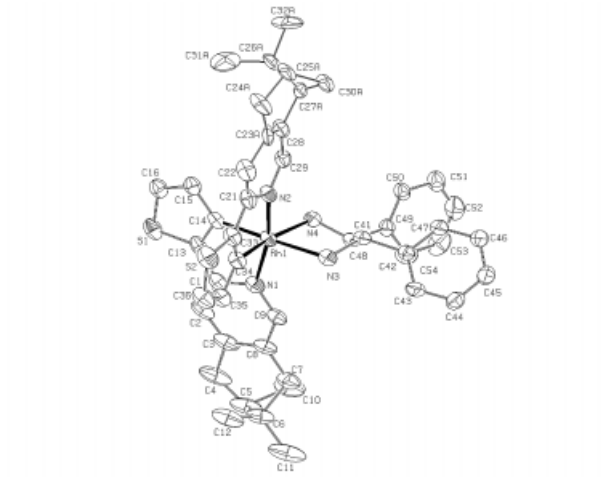

Figure 5. Numbered ORTEP[20] plot, with thermal ellipsoids drawn at the 30% probability level of the molecular structure of the cation Δ[Rh(th4,5ppy)$_2${(*S*,*S*)-st}]$^+$; the hydrogen atoms have been omitted for clarity

Structural Discussion

The X-ray structure (Table 2) of the Δ[Rh(th4,5ppy)$_2${(*S*,*S*)-st}]$^+$ cation (Figure 5) clearly reveals its absolute configuration. It is in agreement with all the other observations in this series of reactions, in which retention of the configuration at the metal center has always been observed. The enantiomerically pure diamine ligand with two (*S*)-configured stereogenic carbon centers adopts a δ conformation (ob) for the 5-membered chelate ring, putting the phenyl groups in equatorial positions.

This is to be expected from a consideration of interligand interactions, which would result in relatively large steric constraints in the axial orientation. The ^{1}H NMR spectrum reveals that this conformation is also strongly preferred in solution, since no broadening of the corresponding signals occur. The other features of the X-ray structure, such as bond lengths and angles, correspond to the expected values.

Δ[Rh{th4,5(*R*,*R*)ppy}$_2$(*N*,*N*′-dmen)]Cl (XV)

This compound is obtained from a smooth cleavage reaction of the dimer with *N*,*N*′-dimethylethylenediamine. Four diastereomers could be obtained, in principle, since the ligating nitrogen centers of the diamine are stereogenic after complexation. They can be designated as Δ[Rh-(th4,5(*R*,*R*)ppy)$_2$(*N*,*N*′-dm(*R*,*R*)en)]Cl (**A**), Δ[Rh{th4,5-(*R*,*R*)ppy}$_2${*N*,*N*′-dm(*S*,*S*)en}]Cl (**B**), Δ[Rh{th4,5-(*R*,*R*)ppy}$_2${*N*,*N*′-dm(*R*,*S*)en}]Cl (**C**), Δ[Rh{th4,5-

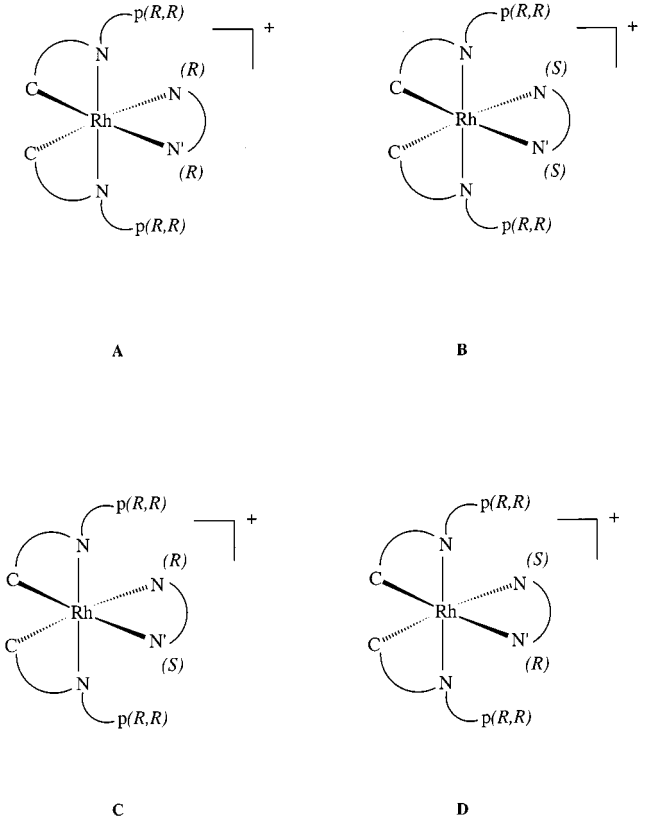

Figure 6. Isomers A, B, C, D

(*R*,*R*)ppy}$_2${*N*,*N*′-dm(*S*,*R*)en}] Cl (**D**). Compounds **A** and **B** are C_2-symmetric species, whereas **C** and **D** show no symmetry (Figure 6).

The ^{1}H NMR spectrum clearly indicates that only one C_2-symmetric complex is formed. Model considerations indicate that the species with a Δ,δ-(*R*,*R*) configuration should have the lowest energy. This corresponds to an axial configuration of the two methyl groups of the diamines.

Δ[Rh{th4,5(*R*,*R*)ppy}$_2$(*N*-men)]Cl (XVI), Δ[Rh{th4,5(*R*,*R*)ppy}$_2$(*N*,*N*′-dpen)]Cl (XVII)

Cleavage of the dinuclear precursor **I** with *N*-men and *N*,*N*′-dpen afforded the expected mononuclear species. These two ligands are prochiral in the sense that one or two ligating nitrogen centers are rendered stereogenic upon coordination to the metal center, as in the case of *N*,*N*′-dmen, described above. The unsymmetrical *N*-men ligand clearly forms one single isomer, within ^{1}H NMR detection limits. In analogy to the Δ[Rh{th4,5(*R*,*R*)ppy}$_2$(*N*,*N*′-dmen)]Cl, this isomer was assigned the configuration Δ-(*R*). The symmetrical *N*,*N*′-dpen again yields one single isomer, as in the case of *N*,*N*′-dmen.

Stereoselectivity

A stereoselective synthesis of coordination compounds has been known since the time of A. Werner.[8] However, it was not developed until recently in a systematic manner.[1] The contents of the present article are a contribution to the field of stereoselective synthesis of Rh^{III} complexes. The first point concerns the regioselectivity in the synthesis of the dinuclear complex from which the mononuclear species are obtained through cleavage reactions. It was shown earlier[9,10] that the cyclometalation is completely regioselective, yielding the *C*,*C*-*cis* isomer.

Owing to the chiral induction by the pinene groups p(*R*,*R*), the Δ diastereomer is strongly preferred over the corresponding Λ form.[2] The cleavage of the dimer always occurs with *complete retention* of configuration at the Rh^{III} centers. Of the 8 possible diastereomers Δ/Λ,A, Δ/Λ,B, Δ/Λ,C, Δ/Λ,D, one single compound, namely Δ,A is obtained from the Δ/Δ dimer, when an unsymmetrical diimine ligand *N*,*N*′ is used in the cleavage reaction. The same is observed for symmetric diimine ligands *N*,*N*′, in which a total of 6 diastereomers (C = D in this case) are possible (see Scheme 2). In cases where several isomers can be obtained by using racemic mixtures of chiral bidentate ligands (pn, chxn, and stilbenediamine), or where stereogenic centers are created at nitrogen donor atoms (*N*,*N*′-dmen, *N*-men, *N*,*N*′-dpen), various degrees of stereoselectivity have been ob-

Table 3. Diastereomeric ratios of complexes obtained by cleavage with racemic (**1**−**3**) or prochiral (**4**−**6**) diamines

Entry	Diastereomers	*de* (%)[a]
1	Δ[Rh(th4,5ppy)$_2${(*R*,*R*)-chxn}]Cl/Δ[Rh(th4,5ppy)$_2${(*S*,*S*)-chxn}]Cl	0
2	Δ[Rh(th4,5ppy)$_2${(*R*,*R*)-pn}]Cl/Δ[Rh(th4,5ppy)$_2${(*S*,*S*)-pn}]Cl	8
3	Δ[Rh(th4,5ppy)$_2${(*R*,*R*)-st}]Cl/Δ[Rh(th4,5ppy)$_2${(*S*,*S*)-st}]Cl	70
4	Δ[Rh(th4,5ppy)$_2${(*R*,*R*)-dmen}]Cl/Δ[Rh(th4,5ppy)$_2${(*S*,*S*)-dmen}]Cl	100
5	Δ[Rh(th4,5ppy)$_2${(*R*,*R*)-men}]Cl/Δ[Rh(th4,5ppy)$_2${(*S*,*S*)-men}]Cl	100
6	Δ[Rh(th4,5ppy)$_2${(*R*,*R*)-dpen}]Cl/Δ[Rh(th4,5ppy)$_2${(*S*,*S*)-dpen}]Cl	100

[a] Determined by ^{1}H NMR spectroscopy from the solution after completion of the reaction. This *de* value did not change appreciably during the course of the reaction.

served. The values of the diastereomeric excess (*de*) are given in Table 3.

In the three cases of chiral bidentate ligands pn, chxn, and stilbenediamine, the stereoselectivity is either absent (chxn), very low (pn) or relatively low (stilbenediamine). This is due to the fact that the stereogenic centers in these ligands are situated relatively far from the stereogenic centers located at the 4,5 positions of the pinene on the pyridine rings. In contrast, in all complexes in which the stereogenic center is created at a ligating nitrogen atom of the incoming diamine in the cleavage reaction, *complete* (within analytical accuracy) stereoselectivity is observed. The coordinating stereogenic nitrogen centers are formed with only one of two possible absolute configurations. Model studies show a strong preference for a Δ-(*R*,*R*) configuration, where (*R*,*R*) designates the absolute configuration of the coordinating nitrogen centers. We can safely assume that for *N*-men, and *N*,*N*′-dpen, the same configurations are present. This result shows that with these cyclometalated Rh^{III} complexes, a cascade of chirality can be realized (Scheme 5).

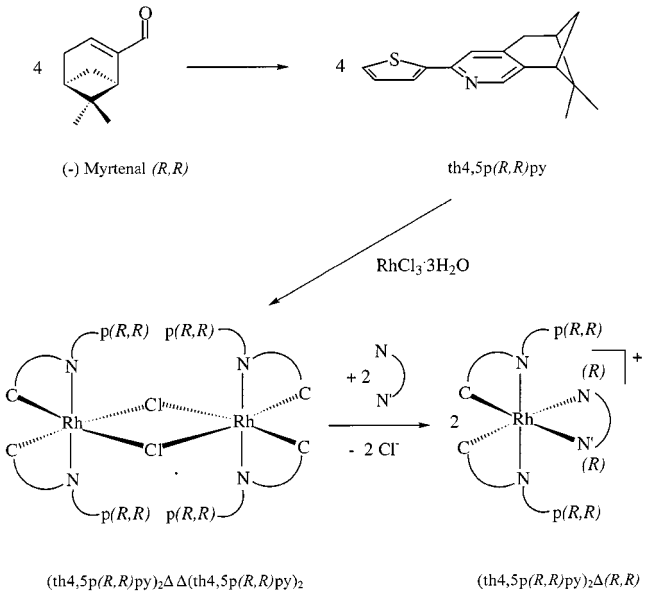

Scheme 5

The origin of the isomeric purity of the final mononuclear complexes, e.g. Δ[Rh{th4,5(*R*,*R*)ppy}$_2$(*N*,*N*′-dmen)]Cl, lies in the natural product (−)-myrtenal, which was synthesised biochemically in the plant myrtle (held sacred to Venus in ancient times).[11] All steps in the reaction scheme leading to the final product are stereoselective. Chirality is thus transferred from a relatively simple organic molecule to the bidentate ligand th4,5p(*R*,*R*)py, From there it is transferred to the metal center Rh^{III}, and then further to another ligand (*N*,*N*′-dmen, *N*-men, *N*,*N*′-dpen), in which two new stereogenic centers are created upon complexation.

Conclusions

The incorporation of a chiral natural compound, which is available in enantiomerically pure form, into a ligand by highly efficient synthetic procedures opens up new possibilities in coordination chemistry. In this contribution we showed that in this way, a family of chiral mononuclear Rh^{III} complexes with a predetermined absolute configuration is easily accessible. Starting with a cyclometalation reaction, the reaction sequence yields isomerically pure mononuclear products that consist of four stereogenic centers located on the ligands, and one on the metal ion. Chirality can be further transferred to prochiral ligands that form stereogenic centers upon complexation, increasing the number of chirality elements in the whole complex by one or two. The stereoselectivity of this last step strongly depends on the distance between the newly created stereogenic centers and the metal ion.

Experimental Section

Measurements and Materials: NMR spectra were obtained with a Varian Gemini-300 spectrometer (300 MHz for ^{1}H and 75.46 MHz for ^{13}C) using the solvent as internal standard relative to TMS; J values are reported in Hz, and δ in ppm. Definitive assignments of NMR spectra was achieved with a combination of NOE and COSY experiments, and APT techniques; qr = quaternary, te = tertiary, se = secondary, pr = primary carbon. − UV/Vis spectral data were recorded with Perkin−Elmer Lambda 5 and Perkin−Elmer Lambda 40 spectrometers; λ_{max} in nm, ε in M^{-1} cm^{-1}. − CD spectra were recorded with Jobin-Yvon and JASCO J-715 spectropolarimeters; λ_{max} (Δε) in nm. − IR spectral data were obtained with Perkin−Elmer 683 and Perkin−Elmer 16 PC FT-IR spectrometers; using samples (1%) in compressed KBr pellets; $\tilde{\nu}$ in cm^{-1}. − MS: VG-Instruments 7070E mass spectrometer equipped with an FAB inlet system. − Elemental analyses were carried out by CIBA Specialty Chemicals, Marly, Switzerland and in Ecole D'Ingineurs de Fribourg, Switzerland. − Unless otherwise stated, all chemicals and reagent-grade products were obtained from Fluka, Aldrich or Merck and used without further purification. (1*R*)-(−)-Myrtenal was obtained from Fluka, > 97%, [α] = 14.6. − The ligands (8*R*,10*R*)-2-(2′-thienyl)-4,5-pinenopyridine,[12] 4,5-pinenobipyridine,[3,13] 5,6-pinenobipyridine,[14] 4,5;4′,5′-pinenobipyridine,[15] 5,6;5′,6′-pinenobipyridine,[16] and 1,2-diphenylethylendiamine[17] were prepared according to literature methods.

X-ray Structure Determination of Δ[Rh(th4,5ppy)$_2${(*S*,*S*)-st}]Cl: Suitable crystals (yellow/orange cubes) of **XIV** were grown by the slow diffusion of diethyl ether into a solution of CH_2Cl_2. Intensity data were collected at 223 K with a Stoe Image Plate Diffraction system using Mo-K_α graphite-monochromated radiation. Image plate distance 70 mm, φ scans 0−200°, step Δφ = 1°, θ range 2.01−25.86°, $d_{max.}-d_{min.}$ = 12.45−0.81 Å. The structure was solved by direct methods using the program SHELXS-97.[18] The refinement and all further calculations were carried out using SHELXL-97.[19] The H atoms were included in calculated positions and treated as riding atoms using SHELXL-97 default parameters. The non-H atoms were refined anisotropically, using weighted full-matrix least squares on F^2. The Cl anion was disordered over two sites, one being situated on a twofold axis. The second was located at a general position and given an occupancy of 0.5. The coordinates correspond to the correct absolute structure of the molecule in the crystal. For one of the ligands, the pinene group was disordered over two sites (A, B); they were each given occupancies of 0.5. A region of electron density observed in a final difference map

was modeled satisfactorily as three partially occupied water molecules and the SWAT[19] parameter was also refined. The molecular structure and crystallographic numbering scheme are illustrated in the PLATON[20] drawing (Figure 5). The CIF files, including complete tables of bond lengths, bond angles and torsion angles have been deposited with the Cambridge Crystallographic Data Centre as supplementary publication no. CCDC 150465 {Δ[Rh(th4,5ppy)$_2$[(S,S)-st)]Cl}. Copies of the data can be obtained free of charge on applicaton to CCDC, 12 Union Road, Cambridge CB2 1EZ, UK [Fax: (internat.) + 44-1223/336-033; E-mail: deposit@ccdc.cam.ac.uk].

Δ[Rh(th4,5ppy)$_2$(bpy)]PF$_6$ (II): A solution of ΔΔ[Rh(th4,5ppy)$_2$(μ-Cl)]$_2$ (64.73 mg, 0.05 mmol) and 2,2′-bipyridine (15.62 mg, 0.10 mmol) in CH_2Cl_2 (20 mL) was heated at reflux for 90 min under N_2 and protected from light. After cooling, addition of NH_4PF_6 (10% solution in MeOH, 3 mL) gave a white precipitate which was filtered off. Addition of a large excess of Et_2O to the filtrate yielded a yellow-orange precipitate of Δ[Rh(th4,5ppy)$_2$-(bpy)]PF$_6$, which was filtered off. The filtrate {still containing Δ[Rh(th4,5ppy)$_2$(bpy)]PF$_6$} was concentrated and diluted with CH_3CN (1 mL). Addition of H_2O (5 mL) gave the yellow-orange precipitate Δ[Rh(th4,5ppy)$_2$(bpy)]PF$_6$. The solid was filtered, added to the rest of the Δ[Rh(th4,5ppy)$_2$(bpy)]PF$_6$ powder and dried in vacuo. Yield: 57 mg (67%). − ^{1}H NMR (CD_3CN, 300 MHz): δ = 8.47 (d, 2 H, ^3J = 8.2 Hz, H−C(3′′)], 8.13 (dd, 2 H, ^3J = 8.12 Hz, ^3J = 7.69 Hz, ^4J = 1.65 Hz H−C(4′′)], 7.97 (ddd, 2 H, ^3J = 5.3 Hz, ^3J = 0.72 Hz H−C(6′′)], 7.54 (tdd, 2 H, ^3J = 7.6 Hz, ^3J = 5.38 Hz, ^4J = 1.15 Hz, H−C(5′′)], 7.45 (s, 2 H, H−C(6)] 7.43 (d, 2 H, ^3J = 4.8 Hz, H−C(5′)], 6.97 (s, 2 H, H−C(3)], 6.23 (d, 2 H, ^3J = 4.73 Hz, H−C(4′)], 3.04 (d, 4 H, ^3J = 3.02 Hz, H−C(7)], 2.567−2.63 (m, 4 H, H−C(10), H−C(9$_{exo}$)], 2.232 (tdd, 2 H, ^4J = 5.52 Hz, ^3J = 5.68 Hz, ^3J = 2.7 Hz, H−C(8)], 1.3 (s, 6 H, H−C(13)], 0.96 (d, 2 H, ^2J = 9.6 Hz, H−C(9$_{endo}$)], 0.68 (s, 6 H, H−C(12)]. − MS (FAB); *m/z* (%): 767 (100) [M − PF_6^-], 611 (43) [Rh(th4,5ppy)$_2$], 356 (5) [Rh(th4,5ppy]. − UV/Vis (CH_3CN): λ (ε) = 378 (10057), 307 (sh), 286 (34913), 270 (sh). − IR (KBr): ṽ = 3450 (w), 3055 (w), 2937 (m), 1619 (m), 1489 (s), 1469 (m), 1444 (m), 1427 (m), 1385 (w), 1242 (w), 1027 (w), 948 (w), 840 (s), 764 (m), 738 (w), 709 (w), 557 (m). − CD (CH_3CN): λ (Δε) = 391 (21), 358 (−16.1), 321 (−15.2), 270 (27.7), 242 (−49.5), 210 (30.5). − $C_{42}H_{40}F_6N_4PRhS_2\cdot 2H_2O$: calcd. C 53.16, H 4.67, N 5.90; found C 53.45, H 4.63, N 5.99.

Δ[Rh(th4,5ppy)$_2$(4,5;4′,5′pbpy)]PF$_6$ (III): III was prepared as described for II, using ΔΔ[Rh(th4,5ppy)$_2$(μ-Cl)]$_2$ (64.73 mg, 0.05 mmol) and 4,5;4′,5′-pinenobipyridine (34.45 mg, 0.10 mmol) in CH_2Cl_2 (15 mL). Yield: 94 mg (85%) of orange Δ[Rh(th4,5ppy)$_2$-(4,5;4′,5′pbpy)]PF$_6$. − ^{1}H NMR (CD_3CN, 300 MHz): δ = 8.22 (s, 2 H, H−C(3′′)], 7.49 (s, 2 H, H−C(6′′)], 7.41 (s, 2 H, H−C(3)], 7.39 (d, 2 H, ^3J = 4.8 Hz, H−C(5′)], 6.73 (s, 2 H, H−C(6)], 6.22 (d, 2 H, ^3J = 4.8 Hz, H−C(4′)], 3.16 (d, 4 H, ^3J = 2.5 Hz, H−C(7′′)], 3.03 (d, 4 H, ^3J = 3.1 Hz, H−C(7)], 2.687−2.54 (m, 6 H, H−C(10′′), H−C(9′′$_{exo}$), H−C(8′′)], 2.345−2.14 (m, 6 H, H−C(10), H−C(9$_{exo}$), H−C(8)], 1.4 (s, 6 H, H−C(13′′)], 1.3 (s, 6 H, H−C(13)], 1.07 (d, 2 H, ^2J = 9.62 Hz, H−C(9′′$_{endo}$)], 0.97 (d, 2 H, ^2J = 9.83 Hz, H−C(9$_{endo}$)], 0.68 (s, 12 H, H−C(12′′, 12)]. − ^{13}C NMR (CD_3CN, 75 MHz): δ = 168.1 (qr), 160.4 (qr), 154.5 (qr), 150.3 (qr), 149.6 (qr), 148 (qr), 146.9 (te), 144.9 (te), 141.1 (qr), 136.6 (qr), 131.5 (te), 128.9 (te), 124 (te), 119.2 (te), 45.6 (te), 45.5 (te), 40.6 (te), 40.5 (te), 39.9 (qr), 39.8 (qr), 33.9 (se), 33.5 (se), 31.9 (se), 31.6 (se), 25.9 (pr), 25.8 (pr), 21.65 (pr), 21.6 (pr). − MS (FAB); *m/z* (%): 955 (100) [M −PF_6^-], 611 (16) [Rh(th4,5ppy)$_2$], 356 (9) [Rh(th4,5ppy)]. − UV/Vis (CH_3CN): λ (ε) = 378 (10523), 316 (sh), 275 (52754). − IR (KBr): ṽ = 2926 (m), 2364 (w), 2344 (w), 1711 (m), 1619 (m), 1488 (m), 1422 (w), 1407 (w), 1365 (w), 1263 (w), 1220 (w), 1032 (w), 948 (w), 913 (w), 875 (m), 840 (s), 711 (w), 557 (m). − CD (CH_3CN): λ (Δε) = 392 (21.3), 359 (−22.1), 322 (−35), 276 (57.3), 245 (−48.). − $C_{56}H_{60}F_6N_4PRhS_2\cdot 2H_2O$: calcd. C 59.14, H 5.67, N 4.93; found C 59.49, H 6.06, N 4.42.

Δ[Rh(th4,5ppy)$_2$(5,6;5′,6′pbpy)]Cl (IV): A solution of ΔΔ[Rh(th4,5ppy)$_2$(μ-Cl)]$_2$ (64.73 mg, 0.05 mmol) and 5,6;5′,6′-pinenobipyridine (34.45 mg, 0.10 mmol) in CH_2Cl_2 (15 mL) was heated at reflux for 90 min under N_2 and protected from light. The solution was concentrated and the addition of Et_2O yielded Δ[Rh(th4,5ppy)$_2$(5,6;5′,6′pbpy)]Cl as a yellow precipitate (65 mg, 65%). − ^{1}H NMR (CD_3CN, 300 MHz): δ = 8.76 (s, 2 H, H−C(6)], 8.03 (d, 2 H, ^3J = 7.75 Hz, H−C(3′′)], 7.36−7.34 (m, 4 H, H−C(3), H−C(4′′)], 7.13 (d, 2 H, ^3J = 4.8 Hz, H−C(5′)], 5.99 (d, 2 H, ^3J = 4.7 Hz, H−C(4′)], 3.14 (d, 4 H, ^3J = 2.5 Hz, H−C(7′′)], 3.09 (d, 4 H, ^3J = 2.75 Hz, H−C(7)], 2.97 (dd, 2 H, ^3J = 5.42 Hz, H−C(10′′)], 2.84−2.69 (m, 6 H, H−C(10), H−C(9′′$_{exo}$, 9$_{exo}$)], 2.4−2.33 (m, 4 H, H−C(8′′), H−C(8)], 1.44 (s, 6 H, H−C(13′′)], 1.41 (s, 6 H, H−C(13)], 1.32−1.24 (m, 4 H, H−C(9′′, 9$_{endo}$)], 0.78 (s, 6 H, H−C(12′′)], 0.64 (s, 6 H, H−C(12)]. − MS (FAB); *m/z* (%): 956 (100) [M − Cl^-], 611 (62) [Rh(th4,5ppy)$_2$]. − UV/Vis (CH_3CN): λ (ε) = 376 (30171), 282 (90478). − IR (KBr): ṽ = 3436 (m), 2926 (m), 2361 (w), 1618 (s), 1489 (s), 1428 (w), 1261 (w), 1238 (w), 1134 (w), 1012 (w), 946 (w), 873 (m), 705 (w). − CD (CH_3CN): λ (Δε) = 388 (76.6), 354 (−63.3), 323 (−52.9), 289 (69.1), 247 (−97.6.). − $C_{56}H_{60}ClN_4RhS_2\cdot 2CH_2Cl_2\cdot H_2O$: calcd. C 59.06, H 5.64, N 4.75; found C 58.83, H 5.13, N 4.14.

Δ[Rh(th4,5ppy)$_2$(4,5pbpy)]Cl (V): V was prepared as described for IV, using ΔΔ[Rh(th4,5ppy)$_2$(μ-Cl)]$_2$ (64.73 mg, 0.05 mmol) and 4,5-pinenobipyridine (25.04 mg, 0.10 mmol) in CH_2Cl_2 (15 mL). Yield: 87 mg (96%) of yellow Δ[Rh(th4,5ppy)$_2$(4,5pbpy)]Cl. − ^{1}H NMR (CD_3CN, 300 MHz): δ = 8.48 (d, 1 H, ^3J = 8.21 Hz, H−C(3′′′)], 8.37 (s, 1 H, H−C(3′′)], 8.11 (ddd, 1 H, ^3J = 7.94 Hz, ^3J = 7.86 Hz, ^4J = 1.67 Hz, H−C(4′′′)], 7.97 (ddd, 1 H, ^3J = 5.3 Hz, ^4J = 1.6 Hz, H−C(6′′′)], 7.53−7.37 (m, 6 H, H−C(5′′′), H−C(6′′), H−C(3), H−C(3°), H−C(5°), H−C(5′)], 6.99 (s, 1 H, H−C(6°)], 6.71 (s, 1 H, H−C(6)], 6.25 (d, 1 H, ^3J = 4.6 Hz, H−C(4°)], 6.18 (d, 1 H, ^3J = 4.7 Hz, H−C(4′)], 3.17 (d, 2 H, ^3J = 2.5 Hz, H−C(7′′)], 3.05−3.01 (m, 4 H, H−C(7°), H−C(7)], 2.67−2.2 (m, 9 H, H−C(10′′), H−C(10°), H−C(10), H−C(9′′$_{exo}$), H−C(9°$_{exo}$), H−C(9$_{exo}$), H−C(8′′), H−C(8°), H−C(8)], 1.38 (s, 3 H, H−C(13′′)], 1.31 (s, 3 H, H−C(13°)], 1.28 (s, 3 H, H−C(13)], 1.07 (d, 1 H, ^2J = 9.55 Hz, H−C(9′′$_{endo}$)], 0.96 (d, 1 H, ^2J = 9.34 Hz, H−C(9°$_{endo}$)], 0.95 (d, 1 H, ^2J = 9.83 Hz, H−C(9$_{endo}$)], 0.68 (s, 3 H, H−C(12′′)], 0.67(s, 3 H, H−C(12°)], 0.66(s, 3 H, H−C(12)]. − MS (FAB); *m/z* (%): 861 (100) [M − Cl^-], 611 (36) [Rh(th4,5ppy)$_2$]. − UV/Vis (CH_3CN): λ (ε) = 378 (9729), 313 (sh), 301(sh), 287 (sh), 273 (43182), 236 (sh). − IR (KBr): ṽ = 3384 (m), 2923 (m), 1618 (s), 1488 (s), 1473 (m), 1421 (m), 1261 (m), 1240 (w), 1098 (w), 1032 (w), 947 (w), 874 (m), 797 (m), 756 (m), 708 (m). − CD (CH_3CN): λ (Δε) = 391 (23.2), 358 (−18.3), 320 (−21.2), 273 (43.5), 240 (−44.4.), 212 (14.5). − $C_{49}H_{50}ClN_4RhS_2\cdot CH_2Cl_2$: calcd. C 61.13, H 5.33, N 5.70; found C 60.80, H 5.71, N 5.66.

Δ[Rh(th4,5ppy)$_2$(5,6pbpy)]Cl (VI): ΔΔ[Rh(th4,5ppy)$_2$(μ-Cl)]$_2$ (64.73 mg, 0.05 mmol) and 5,6-pinenobipyridine (25.04 mg, 0.10 mmol) in CH_2Cl_2 (15 mL) were heated at reflux for 90 min and treated as described for **IV** to give Δ[Rh(th4,5ppy)$_2$(5,6pbpy)]Cl (70 mg, 78%). − ^{1}H NMR (CD_3CN, 300 MHz): δ = 8.42 (d, 1 H, ^3J = 8.24 Hz, H−C(3′′′)], 8.25 (d, 1 H, ^3J = 8.03 Hz, H−C(3′′)], 8.07 (ddd, 1 H, ^3J = 7.9 Hz, ^3J = 7.89 Hz, ^4J = 1.65 Hz, H−C(4′′′)]:

7.74 (ddd, 1 H, ^3J = 5.5 Hz, ^4J = 1.65 Hz, ^5J = 0.94 Hz, H−C(6′′′)], 7.64 (d, 1 H, J = 8.03 Hz, H−C(4′′)], 7.46 (s, 1 H, H−C(3°)], 7.43−7.38 (m, 4 H, H−C(3), H−C(6°), H−C(5′′′), H−C(5°)], 7.3 (d, 1 H, J = 4.8 Hz, H−C(5′)], 6.89 (s, 1 H, H−C(6)], 6.16 (d, 2 H, ^3J = 4.89 Hz, H−C(4′), H−C(4°)], 3.07−3.03 (m, 4 H, H−C(7′′), H−C(7°)], 2.99 (d, 2 H, ^3J = 2.47 Hz, H−C(7)], 2.89−2.16 (m, 9 H, H−C(10′′), H−C(10°), H−C(10), H−C(9′′), H−C(9°), H−C(9), H−C(8′′), H−C(8°), H−C(8)], 1.33 (s, 3 H, H−C(13′′)], 1.28 (s, 3 H, H−C(13°)], 1.25 (s, 3 H, H−C(13)], 1.2 (d, 1 H, ^2J = 9.73 Hz, H−C(9′′$_{endo}$)], 0.98 (d, 1 H, ^2J = 9.4 Hz, H−C(9°$_{endo}$)], 0.83 (d, 1 H, ^2J = 9.6 Hz, H−C(9$_{endo}$)], 0.7 (s, 3 H, H−C(12′′)], 0.64 (s, 3 H, H−C(12°)], 0.07 (s, 3 H, H−C(12)]. − MS (FAB); *m/z* (%): 861 (100) [M − Cl$^-$], 611 (30) [Rh(th4,5ppy)$_2$]. − UV/Vis (CH_3CN): λ (ε) = 374 (8694), 317 (sh), 305 (sh), 289 (sh), 273 (36225). − IR (KBr): ṽ = 3406 (m), 2929 (m), 2362 (m), 2342 (m), 1706 (m), 1619 (m), 1488 (s), 1433 (m), 1364 (w), 1221 (w), 1035 (w), 873 (w), 793 (w), 710 (w). − CD (CH_3CN): λ (Δε) = 393 (22.1), 360 (−13.7), 324 (−16.7), 274 (21.4), 246 (−37.3), 218 (18.3). − $C_{49}H_{50}ClN_4RhS_2·3H_2O$: calcd. C 61.85, H 5.93, N 5.89; found C 61.65, H 5.69, N 5.53.

Δ[Rh(th4,5ppy)$_2$(en)]Cl (VII): ΔΔ[Rh(th4,5ppy)$_2$(μ-Cl)]$_2$ (48.00 mg, 0.04 mmol) and ethylenediamine (7.00 mg, 0.12 mmol) in CH_2Cl_2 (15 mL) were heated at reflux for 90 min under N_2 and protected from light. The solvent was evaporated and the pale yellow powder was dried in vacuo. Yield: 45 mg (86%) of Δ[Rh(th4,5ppy)$_2$(en)]Cl. − ^{1}H NMR (CD_3CN, 300 MHz): δ = 8.24 (s, 2 H, H−C(6)], 7.42 (s, 2 H, H−C(3)], 7.1 (d, 2 H, ^3J = 4.52 Hz, H−C(5′)], 6.06 (d, 2 H, ^3J = 4.53 Hz, H−C(4′)], 3.748−3.71 (m, NH_2), 3.15 (d, 4 H, ^3J = 2.26 Hz, H−C(7)], 3.01−2.98 (m, 2 H, H−C(10), CH_2), 2.836−2.667 (m, 2 H, H−C(9′$_{exo}$)], 2.36 (tdd, 2 H, ^3J = 2.81 Hz, ^3J = 5.66 Hz, ^3J = 5.63 Hz, H−C(8)], 1.45 (s, 6 H, H−C(13)], 1.26 (d, 2 H, ^2J = 9.67 Hz, H−C(9$_{endo}$)], 0.78 (s, 6 H, H−C(12)]. − MS (FAB); *m/z* (%): 671 (62) [M − Cl$^-$], 611 (95) [Rh(th4,5ppy)$_2$], 356 (12) [Rh(th4,5ppy) − H$^+$]. − UV/Vis (CH_3CN): λ (ε) = 391 (11456), 333 (sh), 302 (sh), 278 (30975). − IR (KBr): ṽ = 3282 (w), 3110 (w), 2928 (m), 1709 (m), 1619 (m), 1485 (s), 1428 (w), 1361 (w), 1219 (w), 1038 (w), 871 (w), 709 (w), 528 (w). − CD (CH_3CN): λ (Δε) = 399 (31), 363 (−15.4), 324 (−27.2), 293 (13.7), 255 (−35.4), 234 (−28). − $C_{34}H_{40}ClN_4RhS_2·2H_2O$: calcd. C 54.94, H 5.97, N 7.54, S 8.63; found C 55.24, H 5.89, N 7.66, S 8.46.

Δ[Rh(th4,5ppy)$_2$(*rac*-pn)]Cl (VIII): As described for **VII**, using ΔΔ[Rh(th4,5ppy)$_2$(μ-Cl)]$_2$ (48.00 mg, 0.04 mmol) and propylenediamine (1,2-diaminopropane) (8.25 mg, 0.09 mmol) in CH_2Cl_2 (15 mL) afforded Δ[Rh(th4,5ppy)$_2$(*rac*-pn)]Cl (49 mg, 91%). − ^{1}H NMR ([D$_6$]DMSO, 300 MHz): δ = 8.64 (s, 1 H, H−C(6*S*)], 8.60 (s, 1 H, H−C(6′′*S*)], 8.33 (s, 1 H, H−C(6*R*)], 8.29 (s, 1 H, H−C(6′′*R*)], 7.48−7.47 (m, 4 H, H−C(3*S*), H−C(3′′*S*), H−C(3*R*), H−C(3′′*R*)], 7.335−7.292 (m, 4 H, H−C(5′*S*), H−C(5′′′*S*), H−C(5′*R*), H−C(5′′′*R*)], 6.035−5.93 (m, 4 H, H−C(4′*R*), H−C(4′′′*R*), H−C(4′*S*), H−C(4′′′*S*)], 4.49−4.23 (NH_2), 3.85−3.79 (CH), 3.625−3.566 (CH_2), 3.349 (s, 3 H, CH_3), 3.194−3.101 (m, 8 H, H−C(7)], 3.01−2.737 (m, 8 H, H−C(10), H−C(9$_{exo}$)], 2.4−2.33 (m, 4 H, H−C(8)], 1.44 (s, 12 H, H−C(13)], 1.27−1.13 (m, 4 H, H−C(9$_{endo}$)], 0.75 (s, 12 H, H−C(12)]. − MS (FAB); *m/z* (%): 685 (65) [M − Cl$^-$], 611 (100) [Rh(th4,5ppy)$_2$], 356 (10) [Rh(th4,5ppy) − H$^+$]. − UV/Vis (CH_3CN): λ (ε) = 391 (11386), 334 (sh), 302 (sh), 278 (30552). − IR (KBr): ṽ = 3292 (w), 3081 (w), 3052 (w), 2918 (m), 1619 (s), 1485 (s), 1366 (w), 1266 (w), 1071 (w), 1041 (w), 871 (m), 709 (m). − CD (CH_3CN): λ (Δε) = 399 (36.6), 363 (−14), 324 (−23.4), 294 (17.8), 256 (−29.9), 233 (−21.5). − $C_{35}H_{42}ClN_4RhS_2·H_2O$: calcd. C 56.86, H 5.99, N 7.58, S 8.67; found C 56.31, H 6.11, N 7.90, S 8.16.

Δ[Rh(th4,5ppy)$_2$(*rac*-chxn)]Cl (IX): A solution of ΔΔ[Rh(th4,5ppy)$_2$(μ-Cl)]$_2$ (64.73 mg, 0.05 mmol) and *rac*-chxn (17.00 mg, 0.15 mmol) in CH_2Cl_2 (15 mL) was heated at reflux for 90 min. The solvent was evaporated and the pale yellow powder was dried in vacuo. Yield: 78 mg (73%) of Δ[Rh(th4,5ppy)$_2$(*rac*-chxn)]Cl. − ^{1}H NMR ([D$_6$]DMSO, aromatic region, 300 MHz): δ = 8.62 (s, 2 H, H−C(6*S,S*)], 8.3 (s, 2 H, H−C(6*R,R*)], 7.47 (s, 2 H, H−C(3*S,S*)], 7.45 (s, 2 H, H−C(3*R,R*)], 7.33−7.29 (m, 4 H, H−C(5′*R,R*), H−C(5′*S,S*)], 6.00 (d, 2 H, ^3J = 4.7 Hz, H−C(4′ *R,R*)], 5.95 (d, 2 H, ^3J = 4.7 Hz, H−C(4′*S,S*)]. − MS (FAB); *m/z* (%): 725 (100) [M − Cl$^-$], 611 (77) [Rh(th4,5ppy)$_2$], 356 (6) [Rh(th4,5ppy) − H$^+$]. − UV/Vis (CH_3CN): λ (ε) = 391 (7785), 336 (sh), 302 (sh), 278 (20021). − IR (KBr): ṽ = 3290 (w), 3275 (w), 3111 (w), 2930 (m), 2861 (w), 2360 (w), 2343 (w), 1709 (w), 1622 (m), 1579 (w), 1546 (w), 1489 (s), 1359 (w), 1293 (m), 1239 (w), 1176 (w), 1132 (w), 1103 (w), 1043 (w), 875 (m), 709 (w). − CD (CH_3CN): λ (Δε) = 399 (18.9), 360 (− 8.43), 325 (−15), 295 (9.47), 256 (−17.9), 234 (−16). − $C_{38}H_{46}ClN_4RhS_2·3H_2O·NH_4OH$: calcd. C 53.66, H 6.75, N 8.23; found C 53.53, H 6.29, N 8.89.

Δ[Rh(th4,5ppy)$_2${(*R,R*)-chxn}]Cl (X): As described for **IV**, using ΔΔ[Rh(th4,5ppy)$_2$(μ-Cl)]$_2$ (129.45 mg, 0.10 mmol) and (*R,R*)-chxn (34.25 mg, 0.29 mmol) in CH_2Cl_2 (20 mL) afforded Δ[Rh(th4,5ppy)$_2${(*R,R*)-chxn}]Cl (125 mg, 82%). − ^{1}H NMR ([D$_6$]DMSO, aromatic region, 300 MHz): δ = 8.29 (s, 2 H, H−C(6)], 7.45 (s, 2 H, H−C(3)], 7.32 (d, 2 H, ^3J = 4.76 Hz, H−C(5′)], 6.00 (d, 2 H, ^3J = 4.76 Hz, H−C(4′)]. − MS (FAB); *m/z* (%): 725 (98) [M − Cl$^-$], 611 (64) [Rh(th4,5ppy)$_2$], 356 (7) [Rh(th4,5ppy) − H$^+$]. − UV/Vis (CH_3CN): λ (ε) = 391 (11237), 334 (sh), 301 (sh), 280 (37247). − IR (KBr): ṽ = 3272 (m), 3205 (w), 3100 (m), 2928 (m), 1709 (m), 1619 (s), 1485 (s), 1366 (w), 1293 (w), 1128 (w), 1047 (w), 1028 (w), 876 (m), 704 (m). − CD (CH_3CN): λ (Δε) = 399.8 (28.2), 360 (−11.6), 324 (−25), 293 (17.5), 256 (−30), 235 (−31). − $C_{38}H_{46}ClN_4RhS_2·H_2O$: calcd. C 58.56, H 6.2, N 7.19; found C 58.91, H 6.2, N 7.84.

Δ[Rh(th4,5ppy)$_2${(*S,S*)-chxn}]Cl (XI): As described for IV, using ΔΔ[Rh(th4,5ppy)$_2$(μ-Cl)]$_2$ (64.73 mg, 0.05 mmol) and (*S,S*)-chxn (17.00 mg, 0.15 mmol) in CH_2Cl_2 (15 mL) afforded Δ[Rh(th4,5ppy)$_2${(*S,S*)-chxn}]Cl (61 mg, 80%). − ^{1}H NMR ([D$_6$]DMSO, aromatic region, 300 MHz): δ = 8.61 (s, 2 H, H−C(6)], 7.47 (s, 2 H, H−C(3)], 7.29 (d, 2 H, ^3J = 4.73 Hz, H−C(5′)], 6.00 (d, 2 H, ^3J = 4.73 Hz, H−C(4′)]. − MS (FAB), *m/z*: 725 (97) [M − Cl$^-$], 611 (85) [Rh(th4,5ppy)$_2$], 356 (7) [Rh(th4,5ppy) − H$^+$]. − UV/Vis (CH_3CN): λ (ε) = 391 (10721), 329 (sh), 279 (33678). − IR (KBr): ṽ = 3282 (w), 3110 (w), 2928 (m), 1700 (w), 1619 (m), 1485 (s), 1238 (w), 1133 (w), 1033 (w), 871 (w), 704 (w). − CD (CH_3CN): λ (Δε) = 399 (21.8), 362 (−10.4), 326 (−15), 296 (8.56), 254 (−21.7), 234 (−19.8). − $C_{38}H_{46}ClN_4RhS_2·2H_2O$: calcd. C 57.24, H 6.32, N 7.03; found C 57.29, H 6.08, N 7.06.

Δ[Rh(th4,5ppy)$_2$(*rac*-st)]Cl (XII): A mixture of ΔΔ[Rh(th4,5ppy)$_2$(μ-Cl)]$_2$ (16.00 mg, 0.012 mmol) and 1,2-diphenylethylendiamine (15.75 mg, 0.075 mmol) in CH_2Cl_2 (15 mL) was stirred for 1 h at room temperature. The yellow-orange solution was heated at reflux for 90 min. After the removal of the solvent, orange Δ[Rh(th4,5ppy)$_2$(*rac*-st)]Cl was obtained (20 mg, 94%). The excess ligand was removed by crystallisation after redissolving the powder obtained after the reaction. − ^{1}H NMR (CD_3CN, 300 MHz): δ = 8.43 (s, 2 H, H−C(6*S,S*)], 8.32 (s, 2 H, H−C(6*R,R*)], 7.48 (s, 4 H, H−C(3*S,S*), H−C(3*R,R*)], 7.28−7.11 (m, 24 H, C_6H_5, H−C(5′*S,S*), H−C(5′*R,R*)], 6.07 (m, 4 H, H−C(4′*S,S*), H−C(5′*R,R*)], 4.25−3.9 (m, 6 H, NH_2, CH), 3.32 (m, 12 H, H−C(7*S,S*), H−C(7*R,R*), H−C(10*S,S*), H−C(10*R,R*)],

2.95−2.87 (m, 4 H, H−C(9_{exo} *S,S*), H−C(9_{exo}*R,R*)], 2.48−2.4 (m, 4 H, H−C(8*S,S*), H−C(8*R,R*)], 1.58−1.502 (m, 12 H, H−C(13*S,S*), H−C(13*R,R*)], 1.44−1.411 (m, 4 H, H−C(9_{endo}*S,S*), H−C(9_{endo}*R,R*)], 0.83 (s, 12 H, H−C(12*S,S*), H−C(12*R,R*)]. − MS (FAB), *m/z*: 823 (90) [M − Cl^-], 611 (95) [Rh(th4,5ppy)$_2$], 356 (9) [Rh(th4,5ppy) − H^+]. − UV/Vis (CH_3CN): λ (ε) = 388 (9894), 331 (sh), 278 (29011). − IR (KBr): ṽ = 3397 (w), 3311 (w), 3052 (w), 2928 (m), 1705 (m), 1619 (s), 1485 (s), 1429 (w), 1367 (w), 1224 (w), 1133 (w), 1019 (w), 871 (w), 762 (w), 700 (m), 562(w). − CD (CH_3CN): λ (Δε) = 400 (29.2), 361 (−11.3), 326 (−16.8), 289 (23), 254 (−21.6 sh), 237 (−28.8). − $C_{46}H_{48}ClN_4RhS_2\cdot H_2O$: calcd. C 62.96, H 5.74, N 6.39; found C 63.05, H 5.99, N 6.72.

Δ[Rh(th4,5ppy)$_2${(*R,R*)-st}]Cl (XIII): As described for **IV**, using ΔΔ[Rh(th4,5ppy)$_2$(μ-Cl)]$_2$ (7.00 mg, 0.005 mmol) and (*R,R*)-st (2.30 mg, 0.01 mmol) in CH_2Cl_2 (15 mL) yielded Δ[Rh(th4,5ppy)$_2${(*R,R*)-st}]Cl (9 mg, 97%). − ^{1}H NMR (CD_3CN, 300 MHz): δ = 8.29 (s, 2 H, H−C(6)], 7.49 (s, 2 H, H−C(3)], 7.2−7.110 (m, 12 H, C_6H_5, H−C(5′)], 6.07 (d, 2 H, ^3J = 4.85 Hz, H−C(4′)], 4.225−4.10 (m, 4 H, NH_2), 3.21 (d, 4 H, ^3J = 2.26 Hz, H−C(7)], 3.09 (dd, 2 H, ^4J = 5.43, ^3J = 5.5 Hz, H−C(10)], 2.9 (ddd, 2 H, ^3J = 5.8 Hz, ^3J = 5.9 Hz, ^2J = 9.73 Hz, H−C(9_{exo})], 2.42 (tdd, 2 H, ^4J = 4.94 Hz, ^3J = 5.8 Hz, ^3J = 2.5 Hz, H−C(8)] 1.501 (s, 6 H, H−C(13)], 1.42 (d, 2 H, ^2J = 9.61 Hz, H−C(9_{endo})], 0.83 (s, 6 H, H−C(12)]. − MS (FAB); *m/z* (%): 823 (85) [M − Cl^-], 611 (100) [Rh(th4,5ppy)$_2$], 356 (8) [Rh(th4,5ppy) − H^+]. − UV/Vis (CH_3CN): λ (ε) = 392 (10299), 331 (sh), 302 (sh), 278 (28651). − CD (CH_3CN): λ (Δε) = 399 (30.7), 362 (−11.33), 326 (−16.5), 290 (26.2), 252 (−23.53 sh), 236 (−31.5). − $C_{46}H_{48}ClN_4RhS_2\cdot CH_3CN\cdot CH_2Cl_2$: calcd. C 59.72, H 5.42, N 7.106, S 6.5; found C 60.155, H 5.45, N 7.13, S 6.31.

Δ[Rh(th4,5ppy)$_2${(*S,S*)-st}]Cl (XIV): As described for **IV**, using ΔΔ[Rh(th4,5ppy)$_2$(μ-Cl)]$_2$ (70.00 mg, 0.054 mmol) and (*S,S*)-st (22.96 mg, 0.11 mmol) in CH_2Cl_2 (15 mL) afforded Δ[Rh(th4,5ppy)$_2${(*S,S*)-st}]Cl (80.86 mg, 87%). − ^{1}H NMR (CD_3CN, 300 MHz): δ = 8.49 (s, 2 H, H−C(6)], 7.49 (s, 2 H, H−C(3)], 7.23−7.12 (m, 12 H, C_6H_5, H−C(5′)], 6.07 (d, 2 H, ^3J = 4.7 Hz, H−C(4′)], 4.15−4.12 (m, 4 H, NH_2), 3.21 (d, 4 H, ^3J = 2.32 Hz, H−C(7)], 3.16 (dd, 2 H, ^4J = 5.34, ^3J = 5.5 Hz, H−C(10)], 2.9 (ddd, 2 H, ^3J = 5.6 Hz, ^3J = 5.98 Hz, ^2J = 10.1 Hz, H−C(9_{exo})], 2.42 (tdd, 2 H, ^4J = 5.7 Hz, ^3J = 5.9 Hz, ^3J = 3.02 Hz, H−C(8)] 1.5 (s, 6 H, H−C(13)], 1.41 (d, 2 H, ^2J = 9.83 Hz, H−C(9_{endo})], 0.83 (s, 6 H, H−C(12)]. − MS (FAB); *m/z* (%): 823 (92) [M − Cl^-], 611 (90) [Rh(th4,5ppy)$_2$], 356 (10) [Rh(th4,5ppy) − H^+]. − UV/Vis (CH_3CN): λ (ε) = 391 (9532), 337 (sh), 278 (26434). − IR (KBr): ṽ = 3406 (w), 2924 (m), 1709 (s), 1621 (m), 1489 (s), 1432 (w), 1384 (m), 1364 (m), 1222 (m), 1013 (w), 874 (w), 842 (w), 758 (w), 700 (m), 564 (w), 530 (w). − CD (CH_3CN): λ (Δε) = 399 (30.2), 365 (−13), 325 (−15.2), 294 (16.6), 279 (sh), 249 (−22.8), 238 (−25.4), 206 (34). − $C_{46}H_{48}ClN_4RhS_2\cdot 3H_2O$: calcd. C 60.48, H 5.96, N 6.13, S 7.02; found C 60.74, H 5.705, N 6.33, S 6.655.

Δ[Rh(th4,5ppy)$_2$(dmen)]Cl (XV): A mixture of ΔΔ[Rh(th4,5ppy)$_2$(μ-Cl)]$_2$ (25 mg, 0.02 mmol) and *N,N′*-dimethylethylenediamine (3.40 mg, 0.04 mmol) in CH_2Cl_2 (15 mL) was heated at reflux for 90 min. The solvent was removed to afford orange Δ[Rh(th4,5ppy)$_2$(dmen)]Cl (26 mg, 92%). − ^{1}H NMR (CD_3CN, 500 MHz): δ = 8.58 (s, 2 H, H−C(6)], 7.432 (s, 2 H, H−C(3)], 7.21 (d, 2 H, ^3J = 4.76 Hz, H−C(5′)], 6.04 (d, 2 H, ^3J = 4.84 Hz, H−C(4′)], 4.71 (2 H, NH), 3.15−3.08 (m, 10 H, CH_2, H−C(7), H−C(10)], 2.81−2.76 (ddd, 2 H, ^3J = 5.76 Hz, ^3J = 5.81 Hz, ^2J = 9.74 Hz, H−C(9_{exo})], 2.43−2.35 (m, 2 H, 2H−C(8)], 1.59 (d, 6 H, ^3J = 5.76 Hz, CH_3), 1.46 (s, 6 H, H−C(13)], 1.30 (d, 2 H, ^2J = 9.7 Hz, H−C(9_{endo})], 0.7857 (s, 6 H, H−C(12)]. − MS (ESI); *m/z* (%): 699 (100) [M − Cl^-]. − UV/Vis (CH_3CN): λ (ε) = 392 (9139), 333 (sh), 278 (25327). − CD (CH_3CN): λ (Δε) = 400 (25.4), 365 (−12.8), 329 (−15.36), 297 (14.7), 279 (10.26), 254 (−23.07.), 234 (−22.8), 204 (13.79). − $C_{36}H_{44}ClS_2N_4Rh\cdot 5H_2O$: calcd. C 52.38, H 6.59, N 6.78; found C 52.04, H 6.56, N 6.28.

Δ[Rh(th4,5ppy)$_2$(men)]Cl (XVI): As described for **XV**, using ΔΔ[Rh(th4,5ppy)$_2$(μ-Cl)]$_2$ (20 mg, 0.015 mmol) and *N*-methylethylenediamine (2.30 mg, 0.03 mmol) in CH_2Cl_2 (5 mL) gave Δ[Rh(th4,5ppy)$_2$(men)]Cl (15 mg, 67%). − ^{1}H NMR (CD_3CN, 300 MHz): δ = 8.54 (s, 1 H, H−C(6)], 8.43 (s, 1 H, H−C(6)], 7.435 (s, 2 H, H−C(3)], 7.42 (s, 2 H, H−C(3)], 7.216−7.17 (m, 2 H, H−C(5′, 5′′′)], 6.1 (d, 1 H, ^3J = 4.74 Hz, H−C(4′)], 5.99 (d, 1 H, ^3J = 4.88 Hz, H−C(4′)], 4.655−4.49 (m, 1 H, NH), 4.014−3.87 (m, 1 H, NH), 3.145−2.93 (m, 8 H, CH_2, H−C(7), H−C(7′), H−C(10), H−C(10′)], 2.834−2.64 (m, 2 H, H−C(9_{exo}), H−C($9'_{exo}$)], 2.365−2.15 (m, 4 H, H−C(8), H−C(8′), CH_2), 1.63 (d, 3 H, ^3J = 5.98 Hz, CH_3), 1.45 (s, 6 H, H−C(13)], 1.322−1.234 (m, 2 H, H−C(9_{endo}), H−C($9'_{endo}$)], 0.78 (s, 6 H, H−C(12)]. − MS (ESI); *m/z* (%): 685 (100) [M − Cl^-]. − UV/Vis (CH_3CN): λ (ε) = 391 (12246), 333 (sh), 278 (33782). − CD (CH_3CN): λ (Δε) = 401 (33.1), 365 (−14.9), 326 (−22.37), 295 (17.6), 281 (10.56) 254 (−29.4.), 234 (−24.35), 207 (13.76). −: $C_{35}H_{42}ClN_4RhS_2\cdot H_2O$: calcd. C 56.86, H 5.99, N 7.58; found C 56.16, H 6.04, N 7.97.

Δ[Rh(th4,5ppy)$_2$(dpen)]Cl (XVII): As described for **XV**, using ΔΔ[Rh(th4,5ppy)$_2$(μ-Cl)]$_2$ (20 mg, 0.015 mmol) and *N,N′*-diphenylethylenediamine (6.56 mg, 0.03 mmol) in CH_2Cl_2 (15 mL) afforded Δ[Rh(th4,5ppy)$_2$(dpen)]Cl (22.4 mg, 84%). − ^{1}H NMR (CD_3CN, 300 MHz): δ = 8.76 (s, 2 H, H−C(6)], 7.36 (s, 2 H, H−C(3)], 7.105 (m, 6 H, C_6H_5), 6.60 (m, 6 H, H−C(5′), C_6H_5), 5.99 (d, 2 H, ^3J = 4.94 Hz, H−C(4′)], 4.51 (m, 2 H, NH), 3.26 (m, 4 H, CH_2), 3.14 (d, 4 H, ^3J = 2.41 Hz, H−C(7)], 2.97 (dd, 2 H, ^4J = 5.49, ^3J = 5.43 Hz, H−C(10)], 2.77 (ddd, 2 H, ^3J = 5.7 Hz, ^3J = 5.84 Hz, ^2J = 9.83 Hz, H−C(9_{exo})], 2.34 (tdd, 2 H, ^4J = 5.62 Hz, ^3J = 5.68 Hz, ^3J = 2.74 Hz, H−C(8)] 1.44 (s, 6 H, H−C(13)], 1.30 (d, 2 H, ^2J = 9.62 Hz, H−C(9_{endo})], 0.77 (s, 6 H, H−C(12)]. − MS (ESI); *m/z* (%): 823 (10) [M − Cl^-], 611 (100) [Rh(th4,5ppy)$_2$]. − UV/Vis (CH_3CN): λ (ε) = 373 (12076), 282 (31405), 254 (33407). − CD (CH_3CN): λ (Δε) = 384 (17.2), 352 (−12.5), 321 (−18. 6), 288 (16.77), 249 (−17.38) 242 (−17.3.), 204 (13.12). − $C_{46}H_{48}ClN_4RhS_2\cdot 3H_2O$: calcd. C 60.48, H 5.95, N 6.133 found C 60.46, H 5.86, N 5.55.

Acknowledgments

The authors wish to thank the Swiss National Science Foundation for financial support.

[1] U. Knof, A. von Zelewsky, *Angew. Chem. Int. Ed.* **1999**, *38*, 302−322.
[2] L. Ghizdavu, B. Kolp, A. von Zelewsky, H. Stoeckli-Evans, *Eur. J. Inorg. Chem.* **1999**, 1271−1279.
[3] P. Hayoz, A. von Zelewsky, *Tetrahedron Lett.* **1992**, *33*, 5165−5168.
[4] N. Y. Sardesai, K. Zimmermann, J. K. Barton, *J. Am. Chem. Soc.* **1994**, *116*, 7502−7508.
[5] B. P. Hudson, C. M. Dupureur, J. K. Barton, *J. Am. Chem. Soc.* **1995**, *117*, 9379−9380.
[6] N. C. Fletcher, P. C. Junk, D. A. Reitsma, F. R. Keene, *J. Chem. Soc., Dalton Trans.* **1998**, 133−138.
[7] M. Ziegler, A. von Zelewsky, *Coord. Chem. Rev.* **1998**, *177*, 257−300.
[8] A. P. Smirnoff, *Helv. Chim. Acta* **1920**, *3*, 177−195.

[9] U. Maeder, T. Jenny, A. von Zelewsky, *Helv. Chim. Acta* **1986**, *69*, 1085−1087.
[10] U. Maeder, A. von Zelewsky, H. Stoeckli-Evans, *Helv. Chim. Acta* **1992**, *75*, 1320−1332.
[11] Webster's, *Webster's New World Dictionary, College Edition*, The World Publishing Company, Library of Congress Catalog Card Number 66-13151, **1966**.
[12] M. Gianini, A. Forster, P. Haag, A. von Zelewsky, H. Stoeckli-Evans, *Inorg. Chem.* **1996**, *35*, 4889−4895.
[13] P. Hayoz, A. von Zelewsky, H. Stoeckli-Evans, *J. Am. Chem. Soc.* **1993**, *115*, 5111−5114.
[14] P. Collomb, A. von Zelewsky, *Tetrahedron: Assymetry* **1995**, *6*, 2903.
[15] M. Tiecco, L. Testaferri, M. Tingoli, D. Chianelli, M. Montanucci, *Synthesis* **1984**, 736−738.
[16] S. Rupprecht, P. Collomb, P. Belser, A. von Zelewky, H. Viebrock, P. Burger, unpublished results.
[17] S. Pikul, E. J. Corey, *Org. Synth.* **1993**, *71*, 22−29.
[18] SHELXS-97, Program for Crystal Structure Determination: G. M. Sheldrick, *Acta Crystallogr.* **1990**, *A46,* 467.
[19] G. M. Sheldrick, *SHELXL-97, Program for Crystal Structure Refinement,* Universität Götingen, Götingen, Germany, **1997**.
[20] PLATON/PLUTON: A. L. Spek, *Acta Crystallogr.* **1990**, *A46*, C34.

Received May 5, 2000
[I00180]

Solid and Solution State NMR Spectra and the Structure of the Gallium Citrate Complex $(NH_4)_3[Ga(C_6H_5O_7)_2]\cdot 4H_2O$

Geoffrey E. Hawkes,*[a] Paul O'Brien,[b][+] Henryk Salacinski,[b] Majid Motevalli,[a] and Isaac Abrahams[a]

Keywords: Gallium / NMR spectroscopy / Structure elucidation / Citrate speciation

A gallium citrate complex $(NH_4)_3[Ga(C_6H_5O_7)_2]\cdot 4H_2O$ (**1**) has been isolated from an aqueous mixture of gallium nitrate and citric acid at pH = 9. In the solid state **1** is monomeric and includes the near centrosymmetric ion $[Ga(C_6H_5O_7)_2]^{3-}$ in the asymmetric unit, with each tridentate citrate coordinating to gallium through an alkoxide oxygen, an oxygen of the central carboxyl group and an oxygen of a terminal carboxyl group. The second terminal carboxyl group is not bound to the metal centre. The two alkoxide oxygen–gallium distances in the asymmetric unit are significantly shorter than the four carboxyl oxygen–gallium distances, indicating a stronger bond for the former. The number and intensities of the resolved resonances in the solid state ^{13}C MAS/NMR spectrum are consistent with the X-ray structure. In aqueous solution near neutral pH (5.5 to 6.4) the complex partially dissociates to give an equilibrium of the 1:1 and 1:2 gallium/citrate species together with free citrate. Two sets of resonances are observed in both the ^1H and ^{13}C NMR spectra of solutions of the complex and these correspond to bound and free citrate; there is no resolution of resonances for the 1:1 and 1:2 species. The relative strength of the alkoxide oxygen–gallium bond in the metal-bound citrate ligand leads to a slow intermolecular chemical exchange situation (rate < ca. 12 s^{-1}) between the bound and free ligand. The carboxylate oxygen–gallium bonds are quite labile and relatively rapid intramolecular chemical exchange occurs (rate > ca. 700 s^{-1}) between the metal-bound and pendant terminal carboxyl groups, averaging their ^1H and ^{13}C NMR signals. The diffusion coefficients for the free and complexed citrate measured from the ^1H NMR spectra do not appear to be complicated by chemical exchange effects and, as expected, the diffusion coefficient for the complexed ligand is smaller than for the free ligand. In solution in the intermediate pH range (4.8 to 6.4) a new ^{71}Ga signal is observed at ca. δ = 27 ($\Delta\nu_{1/2} \approx 10.6$ kHz) which is assigned to the gallium citrate complexed species.

Introduction

Citrate is a an important endogenous ligand which occurs in blood plasma[1] (ca. 10^{-4} mM) and ca. 0.3% w/w in teeth and bone.[2,3] Metal−citrate complexes are involved or implicated in a wide range of physiological functions; for example, ferrous citrate in the activation of catalytic activity of the enzyme aconitase (citrate isocitrate hydrolyase),[4] zinc citrate in the genetic disorder of zinc metabolism *acrodermatitis enteropathica*,[5,6] and aluminium citrate in neurotoxic conditions.[7] Bismuth−citrate complexes have been used[8,9] in the treatment of peptic ulcers; our interest focuses on gallium citrate complexes. Edwards and Hayes[10] reported that ^{67}Ga citrate accumulates in soft tissue tumours and, subsequently, hot gallium citrate has found wide use in a range of imaging systems for tumour localisation and in identifying inflammatory lesions.[11] In addition, Hart et al.[12] reported the use of cold gallium nitrate for the treatment of solid tumours and, more recently, Jonkhoff et al.[13] studied the therapeutic use of gallium citrate on leukaemic patients. Despite the widespread use of gallium citrate very little structural information is available. Banta et al.[14] reported the X-ray structural analysis of the trimethyl (and triethyl) ester complexes bis[(trimethylcitrato)dimethylgallium(III)] and we recently published the X-ray structure of the gallium(III) citrate complex $(NH_4)_3[Ga(C_6H_5O_7)_2]\cdot 4H_2O$ (**1**).[15] Here we present further discussion on the structure, together with a detailed NMR spectroscopic analysis of the structure both in the solid state and in solution around physiological pH.

Our preliminary report[15] showed that the complex anion is comprised of two tridentate citrate ligands giving rise to approximately octahedral coordination around the gallium. Citrate may act as both a chelating and a bridging ligand, and many X-ray structures have shown the metal complexes to be oligomeric with either the carboxyl groups or the hydroxy oxygens bridging more than one metal centre. However, monomeric 2:1 (citrate/metal) structures have been reported for the complex anions in ammonium bis(citrato)cuprate(II),[16] ammonium bis(citrato)zinc(II),[17] pyridinium bis(citrato)chromium(III),[18] and ammonium bis(monomethylcitrato)germanate(IV).[19] Citrate chelation in relation to enzymatic function has been the subject of an earlier review.[3]

Glickson et al.[20] measured the ^{71}Ga and ^1H NMR spectra of solutions of gallium nitrate with citric acid. They concluded that 1:1 citrate/metal complexes were formed in

[a] Structural Chemistry Group, Department of Chemistry, Queen Mary & Westfield College,
Mile End Road, London E1 4NS, United Kingdom
Fax: (internat.) +44-207/882-7794
E-mail: g.e.hawkes@qmw.ac.uk
[b] Department of Chemistry, Imperial College of Science Technology and Medicine,
South Kensington, London SW7 2AY, United Kingdom
[+] Present address: Department of Chemistry,
The University of Manchester,
Oxford Road, Manchester M13 9PL, United Kingdom

 © WILEY-VCH Verlag GmbH, 69451 Weinheim, 2001 1434−1948/01/0404−1005 $ 17.50+.50/0

strongly acidic media, whereas in near neutral solutions the stoichiometry of the complexation was more difficult to determine, although polymeric species were indicated. In a subsequent study of the aqueous gallium nitrate/citric acid system, Chang et al.[21] used both ^{1}H and ^{13}C NMR spectroscopy to show the existence of both 1:1 and 2:1 citrate/gallium complexes (Ga_nCit_n and Ga_nCit_{2n}), and for approximately neutral solutions concluded that n is a small integer. Apparent conditional (pH = 5.80) stability constants for the stepwise complexation were estimated as $K_1 = 48 \pm 1$ M^{-1} and $K_2 = 13 \pm 1$ M^{-1}.

Results and Discussion

The X-ray structure determination of (**1**) has been described in a preliminary communication.[15] As shown in Figure 1, two citrate ligands complex with each gallium to yield an approximately centrosymmetric molecule and the asymmetric unit is one molecule. The molecule is achiral with (*R*)-configuration at C3 and (*S*)-configuration at C9.

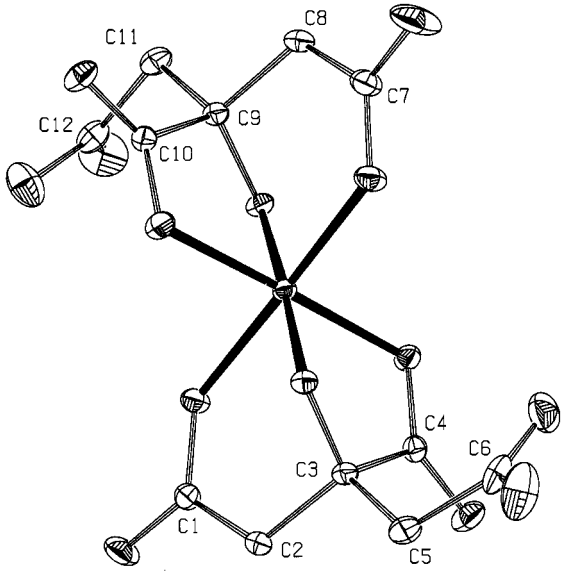

Figure 1. The structure of $[Ga^{III}(citrate)_2]^{3-}$

The high frequency region of the solid state 75.5 MHz ^{13}C magic angle spinning (MAS) NMR spectrum is shown in Figure 2 and summarised in Table 1. There are five well-resolved resonances at δ = 173.9, 179.4, 180.7, 185.6 and 189.9 due to the carboxyl groups, with the resonance at δ = 179.4 being approximately double the intensity of the other four. In addition there are two broader signals to lower frequency at δ = 76.0 due to the nonprotonated carbons C3,9, and at δ ≈ 48 due to the methylene carbons C2,5,8,11. The high frequency region is consistent with the X-ray structure, there being six inequivalent carboxyl groups with the shifts of two being accidentally the same at δ = 179.4. As described below we assign the two highest frequency signals

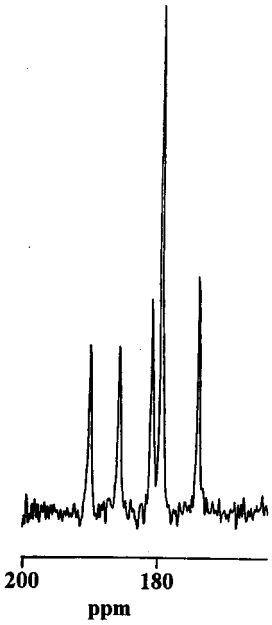

Figure 2. The high frequency region (carbonyl signals) of the 75.5 MHz ^{13}C solid state MAS NMR spectrum of $[Ga^{III}(citrate)_2]^{3-}$

Table 1. ^{13}C Chemical shifts for (**1**) in the solid and in solution

	Solid[a]	Solution[b] pH = 6.4	Solution[b] pH = 1.75
C1,6,7,12	173.9, 179.4,[c] 180.7	179.5	175.5
C4,10	185.6, 189.9	186.5	180.6
C3,9	76.0	74.6	74.7
C2,5,8,10	48	46.5	43.1

[a] Measured at 75.5 MHz. – [b] Measured at 100.6 MHz. – [c] This resonance has double intensity.

(δ = 185.6 and 189.9) to the central carboxyl carbons C4 and C10.

The solution state 122.0 MHz ^{71}Ga spectra of the gallium citrate complex, measured as a function of pH, are shown in Figure 3. The isotope ^{71}Ga has 39.6% natural abundance and the nucleus is quadrupolar with spin $I = {}^3/_2$, and as such it is to be expected that the NMR spectra are dominated by broad signals. The spectrum of the most acidic solution (pH = 1.75) is dominated by a relatively sharp signal at δ ≈ 0 with $\Delta\nu_{1/2}$ < ca. 500 Hz with evidence of a weaker broader ($\Delta\nu_{1/2} \approx$ 12 to 15 kHz) signal to slightly higher frequency (δ ≈ 30 to 40). Similarly, the spectrum of the most basic solution (pH = 9.4) has a sharper signal at δ = 222 with a suggestion of a very weak broad signal at δ ≈ 0. The spectra measured at intermediate pH values showed just a single broad signal: pH = 4.8, at δ ≈ 29 with $\Delta\nu_{1/2} \approx$ 7.7 kHz; pH = 5.5, at δ ≈ 30 with $\Delta\nu_{1/2} \approx$ 11.4 kHz; pH = 6.4, at δ ≈ 27 with $\Delta\nu_{1/2} \approx$ 10.6 kHz.

The ^{1}H and ^{13}C NMR spectra (400 and 100.6 MHz, respectively) show features in common with certain of the ^{1}H spectra reported by Glickson et al.[20] and the ^{13}C spectra reported by Chang et al.,[21] with the expected better resolution here resulting from the use of higher field spectro-

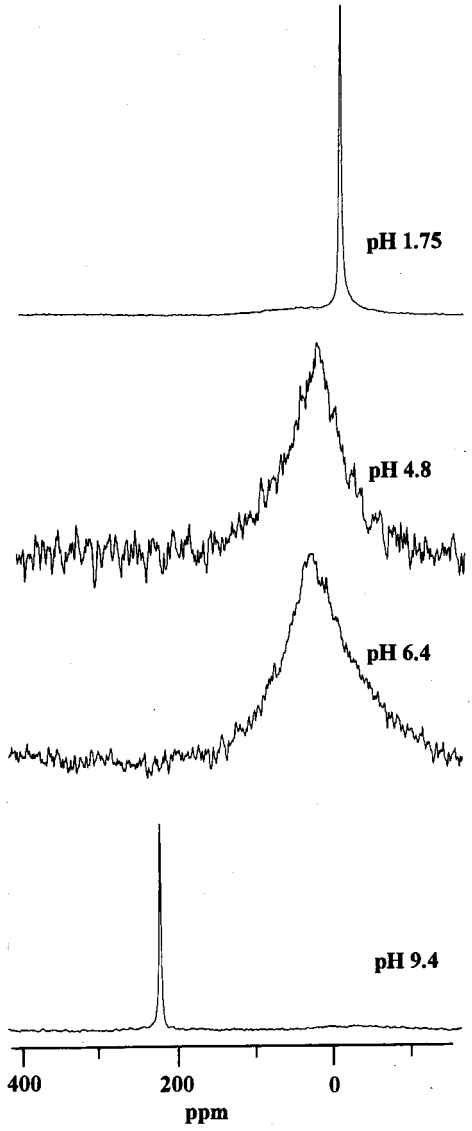

Figure 3. The 122.0 MHz solution state ^{71}Ga spectra of $[Ga^{III}(citrate)_2]^{3-}$ as a function of pH

meters. The ^{13}C spectrum of the complex at pH = 1.75 (Table 1) shows two sets of citrate resonances in an approximate ratio 45:55; the slightly weaker group signals occurring at δ = 43.1 ($-CH_2-$), 74.7 (>C<), 175.5 (terminal $-CH_2CO_2$), and 180.6 (central CO_2) are assigned to citrate in a Ga−citrate complex, whereas the slightly stronger signals at δ = 43.6, 73.7, 173.9 and 177.2 are assigned to free citrate. The assignment between free and complexed citrate for these two groups of signals is confirmed by the ^{13}C shift difference between the two carbonyl signals (3.3 ppm) from a solution of citric acid alone, measured at pH = 1.95. The ^1H spectrum at pH = 1.75 comprises two equally intense multiplets centred at δ = 2.91 and 2.76 due to overlapping signals from the free and complexed citrate methylene protons. At pH = 4.8 the ^{13}C resonances assigned to the complex are more intense than those due to free citrate (in the approximate ratio 65:35), whereas in the range pH = 5.5 to 6.4 the ratio is nearer 80:20. In basic solution at pH = 9.4 only one set of signals is observed due to free citrate. In the intermediate pH range (4.8 to 6.4) the appearance of the ^1H spectra are entirely consistent with the ^{13}C spectra, with two resolved *AB* type splitting patterns (e.g. at pH = 6.4, $\delta_A = 2.58$, $\delta_B = 2.44$, $J_{AB} = 16.9$ Hz for the complex, $\delta_A = 2.54$, $\delta_B = 2.41$, $J_{AB} = 15.2$ Hz for free citrate). The assignment of these *AB* signals between complexed and free citrate is confirmed by the values for J_{AB} across the pH range — Glickson et al.[20] reported J_{AB} values for free citrate in the range 16.2 to 15.4 Hz between pH = 0.75 and 8.71, and for gallium citrate in the range 16.7 (pH = 0.70) to 17.5 Hz (pH = 7.76). In the intermediate pH range many minor signals appeared in both the ^1H and ^{13}C spectra which are probably due to various oligomeric complex species.[20,21] These minor signals were not apparent in either ^1H or ^{13}C spectra measured at extremes of pH (1.75 and 9.4).

The ^{13}C shifts for the complex at pH = 6.4 (Table 1) were δ = 186.5, 179.5, 74.6 and 46.5, with the highest frequency signal due to the central carboxyl carbons C4,10 and the signal at δ = 179.5 due to the carboxyl carbons C1,6,7,12. The average shift for the two highest frequency ^{13}C signals in the solid state (vide supra) is δ = 187.8 and the average for the other carboxyl signals in the solid state is δ = 178.4. These two averages of solid state data compare favourably with the solution state shifts for the carboxyl signals and provide the assignment for the solid state signals.

The diffusion coefficients were measured for 30 mM and 10 mM samples by the ^1H NMR method (see Experimental section). As shown by Stejskal and Tanner,[22] the signal intensities vary according to Equation (1):

$$I_i = I_{0i} \exp(-K^2 \cdot D \cdot \Delta) \quad (1)$$

where $K = \gamma \cdot G_i \cdot \delta$ with γ the nuclear spin gyromagnetic ratio, and G_i and δ are the strength and duration of the field gradient, D is the diffusion coefficient for the molecular species and Δ is the diffusion period. The signal intensities I_i are measured as a function of the gradient strength G_i, and I_{0i} is the signal intensity in the absence of any field gradient. All plots of $\ln(I_i)/K^2$ were linear and the values for the diffusion coefficients obtained are given in Table 2. Deviation from linearity in these plots would have indicated the importance of chemical exchange between the various citrate species, occurring at an intermediate rate on the time-scale of the diffusion period (300 ms). For such complex behaviour a double-exponential dependence of I_i upon K^2 would be expected.[23]

Solid State Structure

Subsequent to our original interpretation[15] of the X-ray crystal structure, we have examined the possibility of alternative distributions of water and ammonium species in the structure refinement.[24] Bearing in mind the relative X-ray scattering of these species with that of the total crystal structure an unambiguous assignment is difficult. A mar-

Table 2. Diffusion coefficients, measured from ^{1}H spectra at 600 MHz, for free and complexed citrate in solutions of (**1**)

Sample[a]	30 mM	10 mM
Free citrate	5.64×10^{-10} m^2 s^{-1}	5.73×10^{-10} m^2 s^{-1}
Complexed citrate	4.34×10^{-10} m^2 s^{-1}	4.24×10^{-10} m^2 s^{-1}

[a] Samples at pH ca. 5.9

ginal improvement in *R* factors is seen with the two half-occupancy water sites changed to ammonium ions. This would suggest a molecular formula of $(NH_4)_4[Ga(C_6H_5O_7)(C_6H_4O_7)]\cdot 3H_2O$, wherein only one of the pendant carboxyl groups is protonated. However, this does not change the coordination geometry at gallium. For what it is worth the elemental analysis (see Experimental Section) supports our original interpretation of three ammonium ions and four water molecules in the molecular formula. An important feature of the previously reported[15] structure are the Ga−O distances. The Ga−O(2) and Ga−O(5) distances are 1.900 and 1.890 Å, and are notably shorter than the Ga−carboxyl oxygen distances which are in the range 1.976−2.054 Å. This feature must reflect the stronger bonding between the gallium and the alkoxide oxygens [O(2) and O(5)] than between gallium and the carboxyl oxygens. The crystal structures of other monomeric 2:1 citrate/metal complexes show the opposite situation, namely the metal−carboxyl bonds are shorter for the bis(citrato)-cuprate(II)[16] and bis(citrato)zinc(II)[17] anions, whereas for the bis(citrato)chromium(III)[18] anion the Cr−O bond lengths are all quite similar. In all three of these latter complexes the integrity of the hydroxyl group is maintained, i.e. it is not deprotonated. On the other hand, in the structure[19] of the bis(citrato)germanate(IV) anion the citrates do coordinate through alkoxide oxygens and the Ge−O(alkoxide) distance is 1.813 Å, with the Ge−O(carboxyl) distances at 1.908 and 1.930 Å. The shortening of the metal−alkoxide oxygen distance relative to the metal−carboxyl oxygen is maintained in other (polymeric) structures where the alkoxide is ligating a single metal, e.g. the complex anions[25] $[Bi_2(citrate)_2]$.

Glusker[3] has reported that the carbon backbone of the citrate ligand (the five carbon fragment including the two terminal carboxyl carbons) typically adopts one of two conformations in metal complexes. These are an extended conformation wherein the two torsion angles about the carbon−carbon bonds are both about 180°, or a folded conformation for which one of the angles is about 180° and the other is about 60°. The two distinct citrate ligands for **1** are both described by extended conformations with the torsion angles[26] for the first ligand C1−C2−C3−C5 and C2−C3−C5−C6 both equal to 176.6°, and for the second ligand C12−C11−C9−C8 equal to 165.2° and C11−C9−C8−C7 equal to −179.5°.

Solution State Structure

The earlier solution-state studies[20,21] used samples prepared by the equilibration of solutions of gallium nitrate and citric acid, in contrast to the samples used here which were prepared by direct dissolution of the crystalline gallium citrate complex **1**. However, it is clear that the main features of the solution structure are similar.

Glickson et al.[20] reported 27.5 MHz ^{71}Ga spectra of gallium nitrate in the presence of citrate in acidic solution. They concluded that the gallium citrate complex partially dissociates in acid medium to give $Ga(D_2O)_6^{3+}$, together with some undissociated complex; however, they did not obtain direct evidence for the presence of the gallium complex since they suggested that the signal due to the complex was broadened beyond detection by quadrupolar relaxation. In highly alkaline aqueous solution a signal due to $Ga(OD)_4^-$ was observed and it was concluded that little of the complex persisted. As indicated below, our analysis of the ^{1}H and ^{13}C NMR spectroscopic data indicate that the gallium citrate complex is the dominant species for a 100 mM solution at about neutral pH, and so our new ^{71}Ga data show the signal due to the complex to occur around $\delta = 27$ with a value for $\Delta\nu_{1/2} \approx 10$ to 12 kHz.

All solution state NMR spectroscopic data on the complex, both from this study and earlier work[20,21] show that in solution the terminal $-CH_2CO_2$ groups in the gallium complex are equivalent. The X-ray structure of the 1:2 complex indicates that in solution there should be at the very least two distinct environments for the $-CH_2CO_2$ groups — two of the groups are bound through oxygen to the gallium, and the other two are not directly bound. However, there are only single ^{13}C signals for the CH_2 and CO_2 groups and only one *AB*-type pattern in the ^{1}H spectrum for the complex. These observations are consistent with rapid intramolecular exchange between the two environments. While we cannot directly quantify the rate of this process, the full spread in ^{13}C shifts from the solid state for the CH_2CO_2 groups is 6.8 ppm (= 680 Hz), and therefore this exchange must occur with a rate greater than ca. 700 s^{-1}. This process cannot be intermolecular since in the intermediate pH range separate ^{13}C and ^{1}H signals are observed for both free and complexed citrate, and so any intermolecular exchange must be relatively very slow — the chemical shift separation for the *B* protons in the two environments is 0.03 ppm (at pH = 6.4), which is 12 Hz, and the rate of intermolecular exchange must be considerably slower than 12 s^{-1}. In solution we cannot specify unequivocally the nature of the gallium citrate complex as a 1:2 or as a 1:1 species. The ^{1}H and ^{13}C shifts for the citrate ligands in the two situations are likely to be very similar and could either be superimposed or coalesced by the intermolecular exchange which, although slow for the free ⇄ complexed citrate process, could be fast with respect to the 1:2 ⇄ 1:1 complexes with the smaller chemical shift difference.

Very slow intermolecular exchange results from the citrate ligands being anchored to the metal by the alkoxide oxygens [O(2) and O(5) in the structure]. The lengths of these metal−oxygen bonds are 1.90 and 1.89 Å, and are significantly shorter than the other four carboxyl oxygen−metal bonds (2.05, 1.98, 2.02 and 1.98 Å); these shorter bonds should also be the least labile.

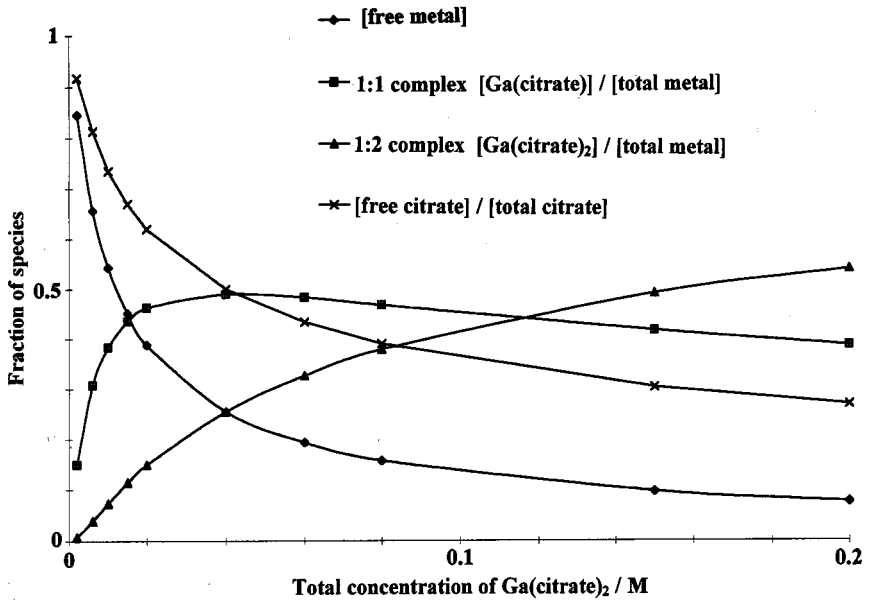

Figure 4. The relative proportions of the species present in a solution of $[Ga^{III}(citrate)_2]^{3-}$, calculated using the stability constants K_1 = 48 ± 1 M^{-1} and K_2 = 13 ± 1 M^{-1}

As indicated above, in the pH range 5.5 to 6.4 the ratio of complexed to free citrate is ca. 4:1, although we are unable to distinguish between complexed citrate in the 1:2 or 1:1 species. Chang et al.[21] were able to estimate conditional stability constants for the stepwise binding of citrate to gallium as K_1 = 48 ± 1 M^{-1} and K_2 = 13 ± 1 M^{-1} at pD = 5.40 (pH = 5.80). With these values we calculate the proportions of the various gallium species present at equilibrium as shown in Figure 4. For a total gallium concentration of 100 mM, as $Ga(citrate)_2$, the proportions of gallium present as the 1:2 complex and the 1:1 complex are 0.41 and 0.45 respectively. This distribution gives a total complexed-to-free citrate ratio as 1.8:1 which is similar to the ratio of 4:1 indicated by the ^{13}C and ^1H NMR spectroscopic data. To further substantiate this suggestion, the 600 MHz ^1H spectrum of a more dilute sample (ca. 30 mM

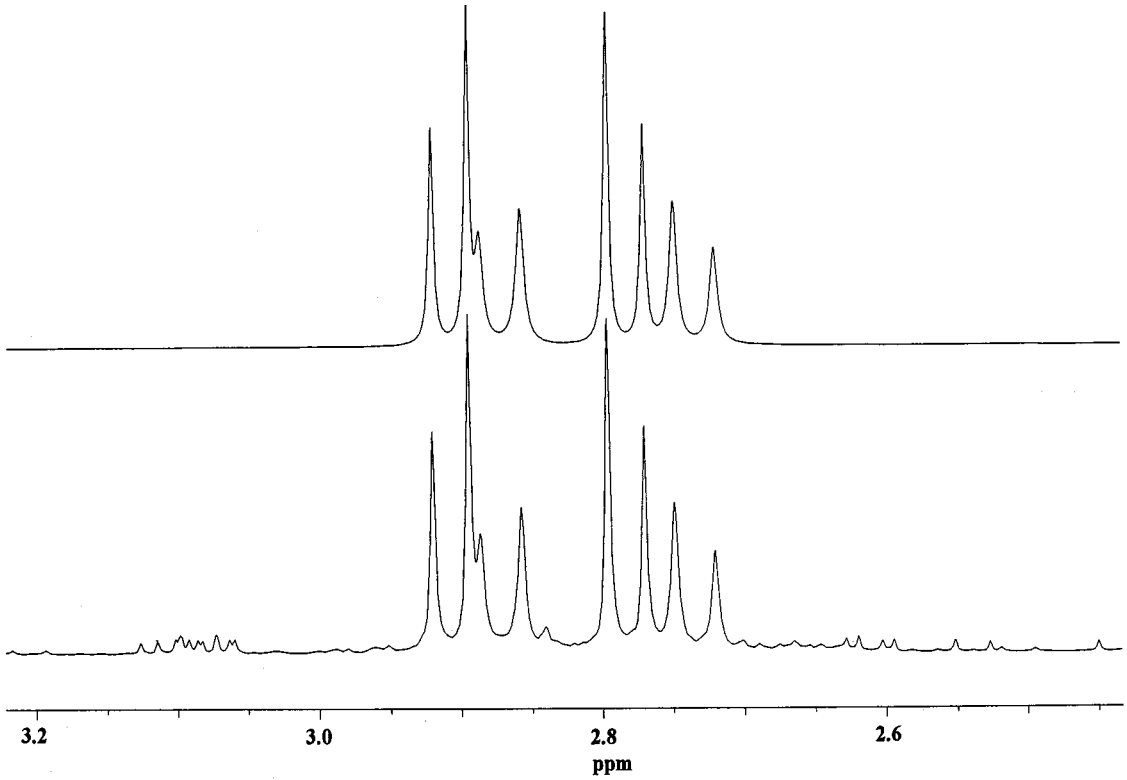

Figure 5. Experimental (lower) and simulated (upper) 600 MHz ^1H NMR spectra of the methylene region of 30 mM $[Ga^{III}(citrate)_2]^{3-}$ at pH 5.9

at pH 5.9) of Ga(citrate)$_2$ was measured (Figure 5) and integration gave a ratio for complexed to free citrate as 1.6:1. Inspection of Figure 5 gives the calculated complexed-to-free citrate ratio 0.8:1 at a total concentration of 30 mM. A third sample of ca. 10 mM gave an experimental ratio for complexed to free citrate as 0.5:1 compared with a calculated ratio (Figure 4) of 0.4:1. In principal our experimental data should allow the calculation of new values for the binding constants K_1 and K_2; however, since our samples were unbuffered solutions, and the concentrations used were approximate, such a calculation was not performed. It is sufficient to note that the complexed-to-free citrate ratios determined here experimentally are in reasonable agreement with those predicted from the conditional stability constant data of Chang et al.[21] in the same pH region.

The calculation for the spectrum shown in Figure 5 employed pure Lorentzian lineshapes and the average linewidth for the four lines of the *AB* pattern due to the complexed citrate was 0.5 greater than the average linewidth for the lines of the free citrate. This observation is fully consistent with the above argument that the ^{1}H NMR signals due to the complexed citrate are a composite of signals from both 1:2 and 1:1 complexes. In the lower field spectra (400 MHz) there was no direct evidence that the signals were due to a superposition of both 1:2 and 1:1 complexes, but at the higher field this additional broadening of the lines could be due to partial resolution of shifts from the two species, or to the higher field pushing the spectrum more towards the coalescence region for intermolecular exchange between the two species.

The diffusion coefficients measured (Table 2) for free citrate average to 5.7×10^{-10} m^2 s^{-1} over the two solutions (10 and 30 mM) and this is to be compared with the value 4.8×10^{-10} m^2 s^{-1} measured[27] for free citrate in human plasma, and 10.2×10^{-10} m^2 s^{-1} measured[28] for free citrate in a ranitidine bismuth citrate solution. It is reasonable that the plasma value should be somewhat lower since plasma is more viscous and contains a multitude of additional endogenous solutes. However, the origin of the larger discrepancy between the value for free citrate found here and that found by Parkinson et al.[28] is not obvious. The pH of the samples may be an important factor and further discussion should await the results of more detailed studies on the effect of the medium on the self diffusion coefficient of citric acid. The average value for the diffusion coefficient of the complexed citrate (Table 2) is 4.3×10^{-10} m^2 s^{-1} and again it is reasonable that this is lower than the free citrate value simply because of the increased molecular weight of the species. These values for the complexed citrate represent a composite of the values for the 1:1 and 1:2 gallium/citrate species which have different relative proportions in the two solutions (10 and 30 mM, vide supra), however the difference in the values for the complexed citrate between the two solutions is not significant (ca. 2%) and should not be interpreted further. The difference in the diffusion coefficients (free − complexed) although not great, is significant; that for the complexed citrate is ca. 25% smaller than that for the free ligand and this similarity helps to reinforce the conclusion that these major complexed species are not oligomeric. Therefore the earlier suggestion by Chang et al.[21] that the major complexed species are Ga_nCit_n and Ga_nCit_{2n} where n is a small integer can be refined to set $n = 1$.

Conclusion

The solid state structure of $(NH_4)_3[Ga(C_6H_5O_7)_2]\cdot 4H_2O$ (**1**) is monomeric and includes the near centrosymmetric ion $[Ga(C_6H_5O_7)_2]^{3-}$ in the asymmetric unit, with each tridentate citrate coordinating to gallium through the alkoxide oxygen, an oxygen of the central carboxyl group and an oxygen of a terminal carboxyl group. The second terminal carboxyl group is protonated and not bound to the metal centre. The two alkoxide oxygen−gallium distances in the asymmetric unit are significantly shorter than the four carboxyl oxygen−gallium distances, indicating a stronger bond for the former case. The number and intensities of resolved resonances in the solid state ^{13}C MAS/NMR spectrum are entirely consistent with the X-ray structure.

The pH-dependent ^{71}Ga NMR spectra of the complex in aqueous solution show a dominant peak due to $Ga(D_2O)_6^{3+}$ at pH = 1.75, and at pH = 9.4 a peak due to $Ga(OD)_4^-$, in agreement with the earlier work of Glickson et al.[20] In the intermediate pH range a new ^{71}Ga signal is observed at $\delta \approx 27$ ($\Delta\nu_{1/2} \approx 10.6$ kHz) which is assigned to the gallium citrate complexed species.

In aqueous solution nearer neutral pH (5.5 to 6.4) the complex partially dissociates to give an equilibrium of the 1:1 and 1:2 gallium/citrate species together with free citrate. For the solution species two sets of resonances are observed in both the ^{1}H and ^{13}C NMR spectra and these correspond to bound and free citrate, with no resolution of resonances for the 1:1 and 1:2 species. The relative strength of the alkoxide oxygen−gallium bond in the metal-bound citrate ligand leads to a slow chemical exchange situation between the metal-bound and free ligand. The carboxylate oxygen−gallium bonds are quite labile and relatively rapid chemical exchange results between the bound and pendant terminal carboxyl groups, thereby averaging their ^{1}H and ^{13}C NMR signals. The diffusion coefficients measured from the ^{1}H NMR spectra do not appear to be complicated by chemical exchange effects and, as expected, that for the complexed ligand is smaller than for the free ligand.

Experimental Section

The preparation of **1** has been previously reported.[15] Typical yields were in the range 60−70%. $C_{12}H_{30}GaN_3O_{18}$: calcd. C 25.11, H 5.27, N 7.32; found C 24.56, H 6.55, N 7.56; {$C_{12}H_{31}GaN_4O_{17}$, i.e. $(NH_4)_4[Ga(C_6H_5O_7)(C_6H_4O_7)]\cdot 3H_2O$: calcd. C 25.15, H 5.45, N 9.78}.

The solid state ^{13}C CP/MAS NMR spectrum was measured at 75.5 MHz using a Bruker MSL-300 spectrometer equipped with a standard Bruker MAS probe with double-bearing rotation mechanism. The sample was studied as a microcrystalline powder in a 4 mm o.d. zirconia rotor at an MAS frequency ca. 8.5 kHz. The spec-

trum was recorded at ambient probe temperature, and the chemical shifts are referenced to external liquid tetramethylsilane. The samples for solution state NMR were prepared by dissolution of the crystalline complex in D_2O at approximate concentrations of 100 mM, 30 mM and 10 mM, and the pH was adjusted by addition of NaOH or HCl solution. pD was measured using a Corning model 7 meter and pH is determined as pD (measured) + 0.40. ^{13}C, ^{71}Ga and ^{1}H solution state NMR spectra were measured at 100.6, 122.0 and 400 MHz, respectively, using a Bruker DRX-400 spectrometer, and additional ^{1}H spectra were obtained with a Bruker AMX-600. Chemical shifts are reported on the high frequency positive scale relative to external TSP (trimethylsilylpropionic acid) (^{1}H and ^{13}C) and a 1.0 M $Ga(NO_3)_3$ solution for ^{71}Ga spectra. The measurements of the diffusion coefficients used the AMX-600 instrument which is equipped with a Bruker B-AFPA30 gradient unit capable of providing gradients up to 2 T m^{-1} along the magnetic field direction (z axis). The diffusion data were acquired using a version of the LED delay pulse sequence[29] with the inclusion of the WATERGATE solvent peak suppression scheme[30] to eliminate the resonance of the water. A series of spectra were measured for values of the gradient strength in the range 1−30% maximum in random order using bipolar sine-shaped gradients (1 ms), a diffusion period of 300 ms and a gradient recovery time of 2 ms. The gradient strength was calibrated in a separate experiment on a water sample assuming a value[31] for the diffusion coefficient of water as 2.37×10^{-9} m^2 s^{-1}. Peak areas were measured by iterative simulation of the spectra using the Bruker WIN-1D and WIN-FIT programs, assuming pure Lorentzian lineshapes, and the intensities for each of the four lines of the *AB* patterns for the free and for the complexed citrate were summed for each value of the gradient strength used.

Acknowledgments

We thank the University of London Intercollegiate Research Service (ULIRS) for provision of the MSL-300 facility at University College, and for the AMX-600 spectrometer at QMW. We thank Mr. R.N Sheppard at IC for the measurement of the solution state spectra with the DRX-400 spectrometer, and the Microanalytical Service at IC for the elemental analysis. Finally we also thank one of the referees for pointing out the possibility that the pendant carboxyl groups might not be protonated.

[1] R. B. Martin, *J. Inorg. Biochem.* **1986**, *28*, 181−187.
[2] J. P. Glusker, *Acc. Chem. Res.* **1980**, *13*, 345−352.
[3] S. B. Etcheverry, M. C. Apella, E. J. Baran, *J. Inorg. Biochem.* **1984**, *20*, 269−274.
[4] [4a]J. J. Villafranca, A. S. Mildvan, *J. Biol. Chem.* **1971**, *246*, 5791−5798. − [4b] J. J. Villafranca, A. S. Mildvan, *J. Biol. Chem.* **1972**, *247*, 3454−3463.
[5] N. Danbolt, K. Closs, *Acta Dermatol. Venereol.* **1942**, *23*, 127−169.
[6] D. Lonnerdal, A. G. Stanislowski, L. S. Hurley, *J. Inorg. Biochem.* **1980**, *12*, 71−78.
[7] [7a] C. T. Driscol, J. P. Baker, J. J. Bisogni, C. L. Schofield, *Nature* **1980**, *284*, 161−164. − [7b] A. C. Alfrey, *Adv. Clin. Chem.* **1983**, *23*, 69−91.
[8] C. F. Baxter, *Chem. Br.* **1992**, *28*, 445−448.
[9] P. J. Sadler, H. Sun, *J. Chem. Soc., Dalton Trans.* **1995**, 1395−1401.
[10] [10a] C. L. Edwards, R. L. Hayes, *J. Nucl. Med.* **1969**, *10*, 103−105. − [10b] C. L. Edwards, R. L. Hayes, *J. Am. Med. Assoc.* **1970**, *212*, 1182−1190.
[11] For a review see R. B. Grove, *Proc. Annu. Meet. Contin. Educ. Lect.* 18th, Winston-Salem, N.C., **1977**, paper no. 9.
[12] [12a] M. M. Hart, R. H. Adamson, *Proc. Nat. Acad. Sci. USA* **1971**, *68*, 1623−1626. − [12b] M. M. Hart, C. F. Smith, S. T. Yancy, R. H. Adamson, *J. Nat. Cancer Inst.* **1971**, *47*, 1121−1127.
[13] A. R. Jonkhoff, M. A. B. D. Plaizier, G. J. Ossenkoppele, G. J. J. Teule, P. C. Huijgens, *Br. J. Cancer* **1995**, *72*, 1541−1546.
[14] G. A. Banta, S. J. Rettig, A. Storr, J. Trotter, *Can. J. Chem.* **1985**, *63*, 2545−2549.
[15] P. O'Brien, H. Salacinski, M. Motevalli, *J. Am. Chem. Soc.* **1997**, *119*, 12695−12696.
[16] R. C. Bott, D. S. Sagatys, D. E. Lynch, G. Smith, C. H. L. Kennard, T. C. W. Mak, *Aust. J. Chem.* **1991**, *44*, 1495−1498.
[17] R. Swanson, W. H. Ilsley, A. G. J. Stanislowski, *Inorg. Biochem.* **1983**, *18*, 187−194.
[18] M. Quiros, D. M. L. Goodgame, D. J. Williams, *Polyhedron* **1992**, *11*, 1343−1348.
[19] H.-C. Chiang, K.-C. Yang, C.-H. Ueng, *J. Chinese Chem. Soc.* **1994**, *41*, 59−63.
[20] J. D. Glickson, T. P. Pitner, J. Webb, R. A. Gams, *J. Am. Chem. Soc.* **1975**, *97*, 1679−1683.
[21] C. H. F. Chang, T. P. Pitner, R. E. Lenkinski, J. D. Glickson, *J. Am. Chem. Soc.* **1977**, *99*, 5858−5863.
[22] E. O. Stejskal, J. E. Tanner, *Chem. Phys.* **1965**, *42*, 288−292.
[23] C. T. W. Moonen, P. van Gelderen, G. W. Vuister, P. C. M. van Zijl, *J. Magn. Reson.* **1992**, *97*, 419−425.
[24] A referee questioned our original interpretation that both protonated pendant carboxyl groups are protonated, and this prompted our re-evaluation of the X-ray data.
[25] [25a] W. A. Hermann, E. Herdtweck, L. Pajdla, *Z. Kristallogr.* **1992**, *198*, 257−264. − [25b] E. Asato, K. Katsura, M. Mikuriya, T. Fujii, J. Reedijk, *Inorg. Chem.* **1993**, *32*, 5322−5329. − [25c] P. J. Barrie, M. I. Djuran, M. A. Mazid, M. McPartlin, P. J. Sadler, I. J. Scowen, H. Sun, *J. Chem. Soc., Dalton Trans.* **1996**, 2417−2422.
[26] The ± sign convention for the torsion angles is that given by F.H. Allen, D. Rogers, *Acta Cryst.* **1969**, *B25*, 1326−1330.
[27] J. C. Lindon, J. K. Nicholson, personal communication.
[28] J. A. Parkinson, H. Sun, P. J. Sadler, *Chem. Commun.* **1998**, 881−882.
[29] S. J. Gibbs, C. S. Johnson, Jr., *J. Magn. Reson.* **1991**, *93*, 395−402.
[30] M. Piotto, V. Saudek, V. Sklenar, *J. Biomol. NMR* **1992**, *2*, 661−665.
[31] M. I. Hrovat, C. G. Wade, *J. Magn. Reson.* **1981**, *44*, 62−75.

Received February 21, 2000
[I00066]

Crystal Structures and ^{29}Si NMR Calculations of Amino-Functionalized Silyllithium Compounds

Carsten Strohmann,*[a] Oliver Ulbrich,[a] and Dominik Auer[a]

Keywords: Ab initio calculations / Lithium / NMR spectroscopy / Silanes / Si ligands

X-ray structural analysis of the amino-functionalized silyllithium compounds tris(tetrahydrofuran)[bis(diethylamino)phenylsilyl]lithium (**4**·3THF) and tris(tetrahydrofuran)[(diethylamino)bisphenylsilyl]lithium (**7**·3THF) are presented. Both compounds are monomeric in the solid state as well as in solution. Despite the formal negative charge at the silicon atom, the nitrogen centres are flattened. No Li–N interactions were observed, in contrast to the homologous (lithiomethyl)amines. RI-DFT calculations give an explanation for the variation of experimental Si–Li bond lengths of 2.627(4) Å (**4**·3THF), 2.682(8) Å (**7**·3THF) and 2.732(7) Å {tris(tetrahydrofuran)[bis(diphenylamino)phenylsilyl]lithium} (**1**·3THF). N–Si orbital interactions, influenced by the type of substituents located at the nitrogen centre, affect these structural parameters as well as the ^{29}Si NMR chemical shifts. The apparently unusual experimental values of the ^{29}Si NMR resonance signals at δ = 20.3 (for **7**·3THF) and δ = 28.4 (for **4**·3THF) can be explained by DFT-IGLO calculations and are a consequence of the combination of electronegative and electropositive substituents at the silicon centre.

Introduction

Silyllithium compounds are useful and important reagents for silyl-group transfer reactions to organic molecules or organometallic systems.[1a,1b] Generally, silyllithiums can be prepared by reaction of a chlorosilane with lithium metal and cleavage of the disilane intermediate (Scheme 1),[2a−2c] although that method is limited to systems bearing at least one aryl group.[2c]

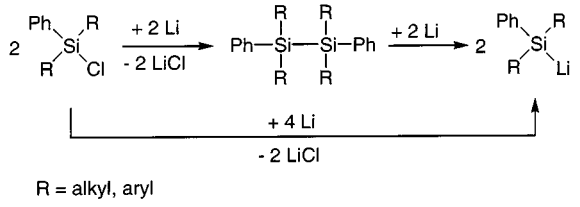

Scheme 1.

In contrast to alkyl- and arylsilyllithiums, functionalized silyllithium species have been studied less extensively. Some dialkylamino-functionalized silyllithium compounds with phenyl substituents at the central silicon atom have been developed by Tamao et al.[3a−3c] These compounds, especially **4** and **7**, can be prepared according to Scheme 1 and are stable in solution at room temperature. Nevertheless, structural information about these dialkylamino-functionalized silyllithium compounds is scarce.[4a,4b,5] Tamao and co-workers were able to prove that dialkylamino-functionalized silyllithiums are monomeric in solution by observation of ^{29}Si−^{7}Li coupling (quadruplet) in the ^{29}Si NMR spectra in the temperature range of −100 to −110 °C.[5] However, the nature of the unusual ^{29}Si NMR chemical shifts of such compounds is still not well understood. More structural information about dialkylamino-functionalized silyllithiums can be concluded from the solid state structure of tris(tetrahydrofuran)[(diphenylamino)bisphenylsilyl]-lithium (**1**·3THF) (Figure 1).[5]

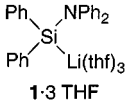

1·3 THF

Figure 1. Structural formula of **1**·3THF

The crystal structure shows a monomeric silyllithium system with the lithium centre being coordinated by three THF molecules. A closer look at the structural parameters reveals a quite long Si−Li bond of 2.732(7) Å and a planar nitrogen centre. The phenyl substituents at the nitrogen centre enhance the planarisation of this centre, and therefore it is not clear if this system is comparable to the synthetically useful dialkylamino-functionalized silyllithiums. Elongation of the Si−Li and Si−N bonds in compound **1**·3THF should be caused by the additional interaction of the lone pair at the amino group with the phenyl substituents.

We attach importance to the clarification of the structural facts of dialkylamino-functionalized silyllithiums in order to study structure/reactivity patterns. The most important questions are: i) What are the structures of bis(diethylamino)phenylsilyllithium (**4**) or (diethylamino)bisphenylsilyllithium (**7**) in the solid state? and ii) How can we explain the unusual downfield shifts of the ^{29}Si NMR resonance signals?[3a,5]

Results and Discussion

The silyllithium compound **4** was prepared starting from chlorosilane **2** and lithium metal in THF, as described by

[a] Institut für Anorganische Chemie, Universität Würzburg
Am Hubland, 97074 Würzburg, Germany
Fax: (internat.) +49-931/888-4605
E-mail: c.strohmann@mail.uni-wuerzburg.de

 © WILEY-VCH Verlag GmbH, 69451 Weinheim, 2001 1434−1948/01/0404−1013 $ 17.50+.50/0

Tamao and co-workers (Scheme 2).[3c] In the ^{29}Si NMR spectrum of the reaction mixture of **2** with lithium metal at temperatures above 0 °C we observe a resonance signal for the disilane **3** (main product), as well as a signal for **4**. Furthermore we also found chlorosilane **2** at shorter reaction times, allowing us to conclude that the reaction of **2** with **4** to give **3** is slow. Disilane **3** is not cleaved by lithium to give the silyllithium compound **4**. We assume the following reaction pathway: the silyllithium compound **4** is the primary product of the reaction of chlorosilane **2** with lithium metal, compound **4** reacts to form the disilane **3** at temperatures above 0 °C and a cleavage of the disilane by lithium is not observed. Reaction of **2** at low temperatures (< 0 °C) leads to **4**, which is stable and does not react with chlorosilane **2** at that temperature.

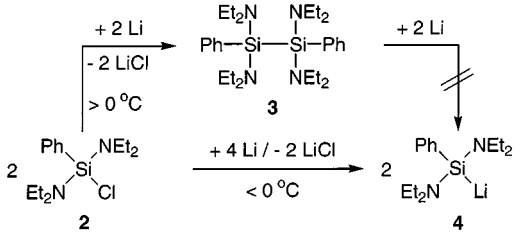

Scheme 2.

The analogous synthesis of the silyllithium species **7**, also described by Tamao and co-workers,[3c] follows a different reaction path (Scheme 3). The primary product of the reaction of chlorosilane **5** with lithium metal at temperatures of −40 to −20 °C is the disilane **6**. Raising the temperature of the reaction mixture to 0 °C results in the cleavage of the Si−Si bond and the formation of the silyllithium species **7**. This can also be recognized by a change of colour during the reaction or from the analogous synthesis of **7** starting from **6**.

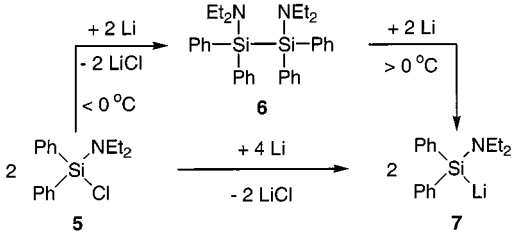

Scheme 3.

Compounds **4** and **7** were isolated as crystalline THF adducts. The amino-functionalized silyllithium compound **4**·3THF crystallized from *n*-pentane at −90 °C in the triclinic crystal system, space group $P\bar{1}$ (Figure 2 and Table 2). The crystals melt at temperatures above −20 °C. **4**·3THF is monomeric in the solid state with the lithium centre being surrounded by three THF molecules in a tetrahedral geometry. Neither an intramolecular coordination of the lithium centre by the nitrogen atoms nor a chelating effect could be observed. This is not unusual but *is* in contrast to (lithiomethyl)amines.[6] Nevertheless the Si−Li bond length is relatively short [2.627(4) Å] compared to other silyllithium species [2.732(7) Å in **1**·3THF;[5] 2.70 Å in $(Me_3SiLi)_2$·3 $(Me_2NCH_2CH_2NMe_2)_3$;[7] 2.66 Å in $(Me_3Si)_3SiLi$·3THF;[8] 2.67 Å in Ph_3SiLi·3THF;[9] 2.65 Å in $(Me_3SiLi)_6$].[10a,10b] The two nitrogen centres in **4**·3THF show an almost planar environment; the deviations from the plane are 0.057 and 0.088 Å. The total sum of the bond angles at the nitrogen centres are 354.9° and 358°, respectively (360° in **1**·3THF[5]). The Si−N bond lengths in **4**·3THF are relatively long [1.772(2) and 1.781(2) Å] compared to other aminosilanes [1.73 and 1.72 Å in $(Et_2N)_2PhSiSiPh(NEt_2)_2$],[11] but shorter than the corresponding bonds of 1.824(3) Å in **1**·3THF (see Table 1).

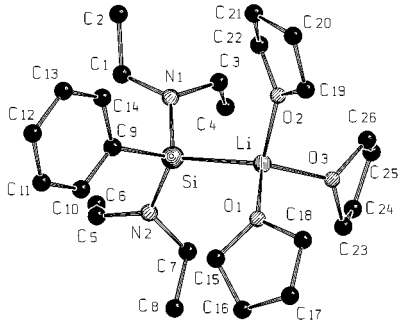

Figure 2. Molecular structure of tris(tetrahydrofuran)[bis(diethylamino)phenylsilyl]lithium (**4**·3THF) in the crystal; selected bond lengths [Å] and angles [°]: Si−Li 2.627(4), Si−N(1) 1.781(2), Si−N(2) 1.772(2), Si−C(9) 1.926(2), Li−O(1) 1.987(5), Li−O(2) 1.972(5), Li−O(3) 1.971(4); N(2)−Si−N(1) 112.66(11), N(2)−Si−C(9) 100.14(11), N(1)−Si−C(9) 100.01(11), N(2)−Si−Li 120.05(13), N(1)−Si−Li 110.26(13), C(9)−Si−Li 111.39(12), C(1)−N(1)−C(3) 113.4(2), C(1)−N(1)−Si 124.9(2), C(3)−N(1)−Si 116.6(2), C(7)−N(2)−C(5) 114.2(2), C(7)−N(2)−Si 119.0(2), C(5)−N(2)−Si 124.8(2)

Crystals from the amino-functionalized silyllithium compound **7**·3THF could be obtained by fast crystallization from a solution in *n*-pentane at −30 °C. The compound crystallises in the monoclinic crystal system, space group $P2_1/c$ with two molecules in the asymmetric unit (Figure 3 and 4, and Table 2). The structure analysis was performed at −10 °C, because single crystals of **7**·3THF are very sensitive to strong cooling, which results in a slow decomposition and bad quality of the collected reflection data. Like **4**·3THF the silyllithium species **7**·3THF is monomeric in the solid state and no intramolecular coordination of the lithium centre by the nitrogen atom was found. The lithium centres are surrounded by three THF molecules in a tetrahedral geometry. The Si−Li bond lengths [2.682(8) and 2.678(8) Å] are longer than in the comparable compound **4**·3THF. An elongation of the Si−N bond relative to other aminosilanes can also be observed. The nitrogen centre shows an almost planar environment, as in compound **4**·3THF, with deviations from the plane of 0.061 and 0.095 Å and a sum of angles of 357.6° and 354.1°, respectively.

The structure of **4**·3THF in [D_8]toluene solution is also monomeric, which is confirmed by an observed $^{29}Si-^{7}Li$ coupling [quadruplet for the resonance signal, $^{1}J(^{29}Si,^{7}Li)$= 56.8 Hz] in the ^{29}Si NMR spectrum at −40 °C. Further cooling causes an asymmetric spreading and a splitting of the signal set at −75 °C indicating a freezing of a dynamic process. Compound **7**·3THF also shows monomeric behavi-

Table 1. Selected data taken from crystal structure analysis and quantum chemical calculations

	Crystal structure analysis			Calculated values[a]		
	1·3THF[5]	**4**·3THF	**7**·3THF	**1**·3THF	**4**·3THF	**7**·3THF
Si−Li [Å]	2.732(7)	2.627(4)	2.682(8) 2.678(8)	2.770	2.680	2.732
Si−N [Å]	1.824(3)	1.781(2) 1.772(2)	1.764(4) 1.763(4)	1.873	1.837 1.827	1.824
N (Sum of angles) [°]	360.0	354.9/358	357.6/354.1	360.0	354.8/357.9	354.0

[a] Values taken from RI-DFT calculations at the BP86/TZVP level.

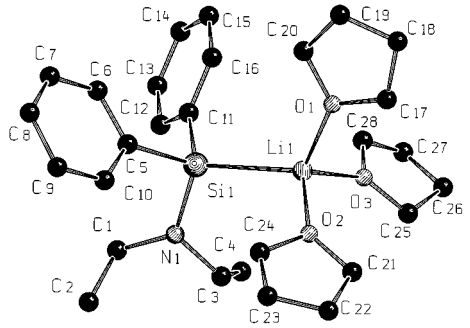

Figure 3. Molecular structure of tris(tetrahydrofuran)[(diethylamino)bisphenylsilyl]lithium (**7**·3THF) (molecule 1) in the crystal; selected bond lengths [Å] and angles [°]: Si(1)−Li(1) 2.682(8), Si(1)−N(1) 1.764(4), Si(1)−C(5) 1.909(5), Si(1)−C(11) 1.917(5), Li(1)−O(1) 1.966(10), Li(1)−O(2) 1.944(9), Li(1)−O(3) 1.978(10); N(1)−Si(1)−C(5) 100.7(2), N(1)−Si(1)−C(11) 106.3(2), N(1)−Si(1)−Li(1) 109.2(2), C(5)−Si(1)−Li(1) 123.4(2), C(11)−Si(1)−Li(1) 115.2(2), C(5)−Si(1)−C(11) 100.1(2), C(1)−N(1)−C(3) 112.8(5), C(1)−N(1)−Si(1) 125.8(4), C(3)−N(1)−Si(1) 119.0(4)

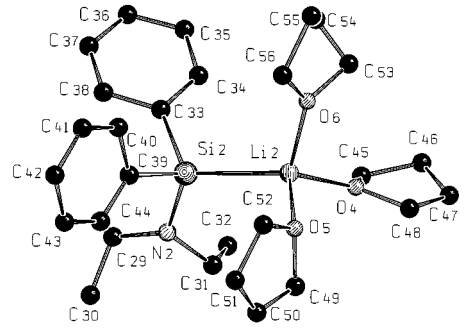

Figure 4. Molecular structure of tris(tetrahydrofuran)[(diethylamino)bisphenylsilyl]lithium (**7**·3THF) (molecule 2) in the crystal; selected bond lengths [Å] and angles [°]: Si(2)−Li(2) 2.678(8), Si(2)−N(2) 1.763(4), Si(2)−C(33) 1.926(4), Si(2)−C(39) 1.916(5), Li(2)−O(4) 1.954(9), Li(2)−O(5) 1.969(9), Li(2)−O(6) 1.970(9); N(2)−Si(2)−C(33) 106.0(2), N(2)−Si(2)−C(39) 101.6(2), N(2)−Si(2)−Li(2) 116.4(2), C(33)−Si(2)−Li(2) 119.2(2), C(39)−Si(2)−Li(2) 111.4(2), C(33)−Si(2)−C(39) 99.7(2), C(29)−N(2)−C(31) 112.9(4), C(29)−N(2)−Si(2) 122.4(3), C(31)−N(2)−Si(2) 118.8(3)

our in [D_8]toluene solution. At −68 °C a $^{29}Si-^{7}Li$ coupling [quadruplet for the resonance signal, $^{1}J(^{29}Si,^{7}Li) = 50.6$ Hz] can be observed in the ^{29}Si NMR spectrum. Further cooling does not lead to an asymmetric spreading as in compound **4**·3THF. These $^{29}Si-^{7}Li$ couplings do not allow us to reach any definite conclusion about the nature of the Si−Li bond (contribution of covalency), although it is conspicuous that lithiated silanes with coordinating solvents show a directed Si−Li interaction[7−10b] in contrast to the alkyl homologues.[12]

Comparing the structures of the dialkylaminosilyllithium compounds **4**·3THF and **7**·3THF with other structural data from known silyllithium compounds shows, that the Si−Li bonds are among the shortest [2.627 (4) Å for **4**·3THF] and the longest [2.732(7) Å for **1**·3THF] of such systems. In order to distinguish between crystallographic (e.g. packing) and substituent effects at the silicon centre we performed quantum chemical calculations on compounds **1**·3THF, **4**·3THF and **7**·3THF. RI-DFT calculations at the BP86/TZVP level were used for structure optimization of these molecules. The relative values of important structural parameters, such as Si−Li and Si−N distances, are reproduced by these quantum chemical calculations (see Table 1). The performed DFT calculations overestimate the values of the bond lengths, as is common for such methods.[13a,13b]

NBO analyses show that the lone pair of the dialkyamino group interacts with an antibonding orbital located at the silicon centre, resulting in an increase in the charge at this centre compared to triorganosilyllithium compounds. These interactions cause a contraction of the polar Si−Li bond and therefore **4**·3THF has the shortest Si−Li distance of all three systems. Since **7**·3THF has only one dialkylamino group, the Si−Li bond length is longer than in **4**·3THF. The lone pair at the nitrogen centre in **1**·3THF is delocalized onto the phenyl groups; this results in a weaker interaction with the silicon centre and therefore the Si−N and Si−Li bonds are elongated.

Tamao and co-workers observed that the ^{29}Si NMR spectra of (aminosilyl)lithiums and (alkoxysilyl)lithiums show a downfield shift relative to the corresponding chlorosilanes, in contrast to (triorganosilyl)lithiums.[3a,5] In order to understand these downfield shifts and the observed structural parameters we optimized the energy of the simplified model compounds $Ph(Me_2N)_2SiLi$ and $Ph_2(Me_2N)SiLi$ by DFT methods [B3LYP/6−31+G(d)] and calculated the NMR resonance signals using the GIAO method [HF/6−311+G(2d,p)].[14a,14b] The geometrical parameters of the minimized model systems show similar structural characteristics as the molecular structures of **4**·3THF and **7**·3THF in the crystal, but with too short Si−Li bonds [2.476 Å for $Ph(Me_2N)_2SiLi$ and 2.490 Å for $Ph_2(Me_2N)SiLi$]. This effect can be explained by the absence of coordinating solvent molecules. The calculated values for the ^{29}Si NMR resonance signals of our model compounds are δ = 21.0

[$Ph(Me_2N)_2SiLi$] and δ = 18.9 [$Ph_2(Me_2N)SiLi$], close to the experimental values of δ = 28.4 for **4** and δ = 20.3 for **7**. These results confirm the trend of the downfield shift of functionalized silyllithiums compared to (triorgano)silyllithiums, and therefore coordinating solvent molecules can be omitted in model systems for ^{29}Si NMR calculations.

Calculations performed on the simplified model systems Me_3SiLi, $Me_2(H_2N)SiLi$ and $Me(H_2N)_2SiLi$ within the bounds of the DFT-IGLO method allow a thorough analysis of the shielding tensors concerning paramagnetic contributions of localised molecular orbitals (LMO).[15a,15b] The result is that, with the change from Me_3SiLi (calculated chemical shift: δ = −5.7) to $Me_2(H_2N)SiLi$ (calculated chemical shift: δ = 14.9), the significant contribution for the shielding tensors of the remaining two LMOs of the Si−C bond as well as the Si−Li LMO increase considerably. This is caused by the very large induced coupling of these LMOs with the σ*(Si−N) orbital, resulting in a decreased shielding [and increased chemical shift of $Me_2(H_2N)SiLi$]. At the same time the number of Si−C LMOs decreases (Si−N LMOs make a lower paramagnetic contribution than Si−C LMOs). The latter effect predominates with the addition of a second H_2N group [$Me(H_2N)_2SiLi$] causing, in total, an increase of the shielding compared to $Me_2(H_2N)SiLi$ [calculated chemical shift for $Me(H_2N)_2SiLi$: δ = 9.9]. A similar trend was observed for the gradual replacement of the methyl groups of Me_4Si with chloro substituents.[16] That effect can also be observed for other metallated silanes with R_2N or RO substituents and explained by NMR calculations. Further calculations on this topic are in progress.

Experimental Section

General: All preparations were performed using standard Schlenk techniques under an oxygen-free and water-free argon atmosphere. Tetrahydrofuran was dried over Na/benzophenone and freshly distilled under argon. ^{29}Si NMR spectra were recorded on a Bruker DRX-300 (59.6 MHz) spectrometer with an external standard of tetramethylsilane (δ = 0.0).

Synthesis of Tris(tetrahydrofuran)[bis(diethylamino)phenylsilyl]-lithium (4·3THF): The synthesis was performed as described by Tamao and co-workers[3c] but with a reaction temperature of −40 to −20 °C. − $^{29}Si\{^1H\}$ NMR (C_7D_8, 233 K): δ = 28.4 (q, $^1J_{SiLi}$ = 56.8 Hz).

Synthesis of Tris(tetrahydrofuran)[(diethylamino)bisphenylsilyl]-lithium (7·3THF): The synthesis was performed as described by Tamao and co-workers[3c]. − $^{29}Si\{^1H\}$ NMR (C_7D_8, 205 K): δ = 20.3 (q, $^1J_{SiLi}$ = 50.6 Hz).

Computational Methods: All calculations were carried out on gas-phase structures.[17] Structure optimizations of $Ph(Me_2N)_2SiLi$ and $Ph_2(Me_2N)SiLi$ at the B3LYP/6−31+G(d) level were performed using GAUSSIAN 98.[14b] Selected bond lengths [Å] and angles [°] for $Ph(Me_2N)_2SiLi$: Si−Li 2.481, Si−N(1) 1.788, Si−N(2) 1.788, Si−C(5) 1.922, C(5)−Si−N(1) 102.8, C(5)−Si−N(2) 102.8, N (sum over angles) 355.0; absolute SCF energy: −797.855415745 Hartree; − selected bond lengths [Å] and angles [°] for $Ph_2(Me_2N)SiLi$: Si−Li 2.490, Si−N 1.786, Si−C(3) 1.921, Si−C(9) 1.934, C(3)−Si−N 104.3, C(9)−Si−N 108.5, N (sum over angles) 352.4; absolute SCF energy: −894.925802514 Hartree.

The RI-DFT[18] calculations on compounds **1**·3THF, **4**·3THF and **7**·3THF were done with the TURBOMOLE[19] program at the BP86/TZVP level with starting coordinates taken from the crystal structure analyses. Selected bond lengths [Å] and angles [°] for **1**·3THF: Si−Li 2.770, Si−N 1.873, Si−C(1) 1.950, Si−C(7) 1.939, C(1)−Si−N 103.4, C(7)−Si−N 103.9, N (sum over angles) 360.0; absolute SCF energy: −1976.437591873 Hartree; − selected bond lengths [Å] and angles [°] for **4**·3THF: Si−Li 2.688, Si−N(1) 1.827, Si−N(2) 1.837, Si−C(9) 1.948, C(9)−Si−N(1) 100.8, C(9)−Si−N(2) 100.5, N (sum over angles) 357.9; absolute SCF energy: −1653.023345787 Hartree; − selected bond lengths [Å] and angles [°] for **7**·3THF: Si−Li 2.732, Si−N 1.824, Si−C(5) 1.964, Si−C(11) 1.947, C(5)−Si−N 105.8, C(11)−Si−N 101.4, N (sum over angles) 354.0; absolute SCF energy: −1671.469514876 Hartree. The criterion for convergence for these calculations was lowered to a change in absolute SCF energy of 5×10^{-5} Hartree, due to the size of these systems. Minimizing the energy starting from the second conformer of **7**·3THF in the crystal showed no significant differences in the results compared to the calculated values of the other conformer of **7**·3THF.

The GIAO method-based NMR calculations [HF/6−311+G(2d,p)] of $Ph(Me_2N)_2SiLi$ and $Ph_2(Me_2N)SiLi$ were performed with GAUSSIAN 98.[14a,14b] Calculated absolute shieldings σ were converted into relative shifts δ with σ calculated at the same level for TMS [$\sigma_{calcd}(Si)$ = 385.9]; calculated value of σ for $Ph(NMe_2)_2SiLi$: 364.83; calculated value of σ for $Ph_2(NMe_2)SiLi$: 367.18.

The structures of the model systems Me_3SiLi, $Me_2(H_2N)SiLi$ and $Me(H_2N)_2SiLi$ were optimized at the B3LYP/6−31+G(d) level using GAUSSIAN 98.[14b] Selected bond lengths [Å] and angles [°] for Me_3SiLi: Si−Li 2.516, Si−C 1.928, C−Si−C 104.2, C−Si−Li 114.4; absolute SCF energy: −416.770639118 Hartree; selected bond lengths [Å] and angles [°] for $Me_2(H_2N)SiLi$: Si−Li 2.509, Si−C(1) 1.921, Si−C(2) 1.930, Si−N 1.790, C(1)−Si−N 101.9, C(2)−Si−N 109.8; absolute SCF energy: −432.828715216 Hartree; selected bond lengths [Å] and angles [°] for $Me(H_2N)_2SiLi$: Si−Li 2.494, Si−C 1.915, Si−N(1) 1.788, Si−N(2) 1.788, C−Si−N(1) 100.5, C−Si−N(2) 100.6; absolute SCF energy: −448.891440368 Hartree. DFT-IGLO calculations of chemical shifts for Me_3SiLi, $Me_2(H_2N)SiLi$ and $Me(H_2N)_2SiLi$ have been done at the sum-over-states density-functional perturbation theory level (SOS-DFPT),[15b,20] varying the gradient-corrected PW91[21a−21c] exchange-correlation functional. A compromise strategy discussed earlier[15b,22a,22b] was applied to obtain accurate Kohn−Sham MOs with moderate effort, by adding an extra iteration with a larger integration grid and without fit of the exchange-correlation potential after SCF convergence had been reached. FINE[22a,22b] angular grids with 32 points of radial quadrature were used. All of the DFT-IGLO calculations were carried out using the deMon NMR code.[22a,22b,23] IGLO-II all-electron basis sets were used on all atoms with density and exchange-correlation potential fitting auxiliary basis sets of the sizes 5.1 (H), 5.2 (C, Li, N) and 5.4 (Si). Calculated absolute shieldings σ were converted into relative shifts δ with σ calculated at the same level for TMS [$\sigma_{calcd}(Si)$ = 368.1]. Absolute shielding σ and selected contributions of certain LMOs for Me_3SiLi: σ = 373.8, Si−C LMO −100.5, Si−Li LMO −103.7; absolute shielding σ and selected contributions of certain LMOs for $Me_2(H_2N)SiLi$: σ = 353.2, Si−C(1) LMO −116.0, Si−C(2) LMO −111.2, Si−N LMO −91.0, lone pair N LMO 7.4, Si−Li

Table 2. Selected crystallographic data for **4**·3THF and **7**·3THF

	4·3THF	**7**·3THF
Empirical formula	$C_{26}H_{49}LiN_2O_3Si$	$C_{28}H_{44}LiNO_3Si$
Formula weight [g/mol]	472.70	477.67
Temperature [K]	173(2)	263(2)
Wavelength [Å]	0.71073	0.71073
Crystal system	Triclinic	Monoclinic
Space group	$P\bar{1}$	$P2_1/c$
a [Å]	8.981(2)	10.274(2)
b [Å]	10.424(2)	33.791(7)
c [Å]	17.668(4)	17.996(4)
α [°]	74.36(3)	90
β [°]	76.67(3)	103.14(3)
γ [°]	67.16(3)	90
Volume [Å^3]	1453.1(5)	6084.1(22)
Z	2	8
Density (calcd.) [g/cm^3]	1.080	1.043
F(000)	520	2080
Crystal size [mm^3]	0.60 × 0.40 × 0.20	0.80 × 0.80 × 0.50
Theta range for data collection [°]	2.26 to 27.00	2.40 to 24.00
Index ranges (h,k,l)	−11,11; −13,13; −23,23	−13,13; −44,43; −23,23
Reflections collected	10362	30076
Independent reflections	5922 [R(int) = 0.0616]	9344 [R(int) = 0.1266]
Refinement method	Full-matrix least-squares on F^2	
Data/restraints/parameters	5913/0/302	9333/0/618
Goodness-of-fit on F^2	1.008	1.050
Final R indices [$I > 2\sigma(I)$]	$R1$ = 0.0606 $wR2$ = 0.1450	$R1$ = 0.0832 $wR2$ = 0.1927
R indices (all data)	$R1$ = 0.1048 $wR2$ = 0.1680	$R1$ = 0.1701 $wR2$ = 0.2216
Extinction coefficient	–	0.0019(7)
Largest diff. peak and hole [eÅ^{-3}]	0.422 and −0.361	0.306 and −0.300

LMO −120.0; absolute shielding σ and selected contributions of certain LMOs for $Me(H_2N)_2SiLi$: σ = 358.2, Si−C LMO −116.3, Si−N(1) LMO −85.6, lone pair N(1) −3.6, Si−N(2) LMO −100.6, lone pair N(2) LMO 4.5, Si−Li LMO −126.9.

X-ray Crystal Structure Analysis: Suitable crystals of **4**·3THF and **7**·3THF were obtained from *n*-pentane solutions at −30 °C (**7**·3THF) or −90 °C (**4**·3THF) as THF adducts. The crystals were mounted in inert oil on a glass fibre and transferred to the cold gas stream of the diffractometer [Stoe IPDS; graphite monochromated Mo-K_α radiation (λ = 0.71073 Å)]. The structures were solved using direct and Fourier methods (SHELXS-86[24a]); refinement by full-matrix least-squares methods (based on F_o^2, SHELXL-93[24b]); anisotropic thermal parameters for all non-H atoms in the final cycles; the H atoms were refined on a riding model in their ideal geometric positions. Crystal data and refinement details of structures **4**·3THF and **7**·3THF are reported in Table 2.

Crystallographic data (excluding structure factors) for the structures included in this paper have been deposited with the Cambridge Crystallographic Data Centre as supplementary publication nos. CCDC-139102 (**4**·3THF) and -151411 (**7**·3THF). Copies of the data can be obtained free of charge on application to CCDC, 12 Union Road, Cambridge CB2 1EZ, UK [Fax: (internat.) + 44-1223/336-033; Email: deposit@ccdc.cam.ac.uk].

Acknowledgments

We are grateful to the Deutsche Forschungsgemeinschaft (DFG), the Fonds der Chemischen Industrie and Chemetall GmbH for financial support and the donation of chemicals. We thank Prof. Dr. M. Kaupp, Universität Würzburg, for helpful discussions regarding the interpretations of the NMR calculations.

[1] [1a] I. Fleming, R. S. Roberts, S. C. Smith, *J. Chem. Soc., Perkin Trans. 1* **1998**, 1215−1228. − [1b] U. Schubert, A. Schenkel, *Transition Met. Chem.* **1985**, 210−212.

[2] [2a] N. A. Rahman, I. Fleming, A. B. Zwicky, *J. Chem. Res. (S)* **1992**, 292. − [2b] H. Gilman, K. Shiina, D. Aoki, B. J. Gaj, D. Wittenberg, T. Brennan, *J. Organomet. Chem.* **1968**, *13*, 323−328. − [2c] K. Tamao, A. Kawachi, *Adv. Organomet. Chem.* **1995**, *38*, 1−58.

[3] [3a] A. Kawachi, K. Tamao, *Bull. Chem. Soc. Jpn.* **1997**, *70*, 945−955; selected ^{29}Si NMR spectroscopic data of alkylsilyllithium-, aminosilyllithium- and alkoxysilyllithium compounds and the corresponding chlorosilanes: $Ph_2MeSiCl$ (δ = 10.0), $Ph_2MeSiLi$ (δ = −20.5), $(Et_2N)PhMeSiCl$ (δ = 2.3), $(Et_2N)PhMeSiLi$ (δ = 14.4), $(Et_2N)_2PhSiCl$ (δ = −18.8), $(Et_2N)_2PhSiLi$ (δ = 28.7), $(t$BuO$)_2PhSiCl$ (δ = −56.5), $(t$BuO$)_2PhSiLi$ (δ = 41.8). − [3b] K. Tamao, A. Kawachi, Y Ito, *Organometallics* **1993**, *12*, 580−582. − [3c] K. Tamao, A. Kawachi, Y. Tanaka, H. Ohtani, Y. Ito, *Tetrahedron* **1996**, *52*, 5765−5772.

[4] [4a] A. Kawachi, K. Tamao, 12th International Symposium on Organosilicon Chemistry, Sendai, Japan, poster abstracts P 82. − [4b] C. Strohmann, O. Ulbrich, 12th International Symposium on Organosilicon Chemistry, Sendai, Japan, poster abstracts P 81.

[5] A. Kawachi, K. Tamao, *J. Am. Chem. Soc.* **2000**, *122*, 191−196.

[6] C. Bruhn, F. Becke, D. Steinborn, *Organometallics* **1998**, *17*, 2124−2126.

[7] B. Teclé, W. H. Ilsley, J. P. Oliver, *Organometallics* **1982**, *1*, 875−877.

[8] A. Heine, R. Herbst-Irmer, G. M. Sheldrick, D. Stalke, *Inorg. Chem.* **1993**, *32*, 2694−2698.

[9] H. V. R. Dias, M. M. Olmstead, K. Ruhlandt-Senge, P. P. Power, *J. Organomet. Chem.* **1993**, *462*, 1−6.

[10] [10a] T. F. Schaaf, W. Butler, M. D. Glick, J. P. Oliver, *J. Am. Chem. Soc.* **1974**, *96*, 7593−7594. − [10b] W. H. Ilsley, T. F. Schaaf, M. Glick, J. P. Oliver, *J. Am. Chem. Soc.* **1980**, *102*, 3769−3774.

[11] K. Tamao, A. Kawachi, Y. Nakagawa, Y. Ito, *J. Organomet. Chem.* **1994**, *473*, 29−34.

[12] T. Kottke, D. Stalke, *Angew. Chem.* **1993**, *105*, 619−621; *Angew. Chem. Int. Ed. Engl.* **1993**, *32*, 580−582.

[13] [13a] M. Kaupp, *Chem. Ber.* **1996**, *129*, 535−544. – [13b] J. A. Altmann, N. C. Handy, V. E. Ingamells, *Int. J. Quant. Chem.* **1996**, *57*, 533−542.
[14] [14a] K. Wolinski, J. F. Hilton, P. Pulay, *J. Am. Chem. Soc.* **1990**, *112*, 8251−8260. – [14b] Gaussian 98; Revision A.6, M. J. Frisch, G. W. Trucks, H. B. Schlegel, G. E. Scuseria, M. A. Robb, J. R. Cheeseman, V. G. Zakrzewski, J. A. Montgomery, Jr., R. E. Stratmann, J. C. Burant, S. Dapprich, J. M. Millam, A. D. Daniels, K. N. Kudin, M. C. Strain, O. Farkas, J. Tomasi, V. Barone, M. Cossi, R. Cammi, B. Mennucci, C. Pomelli, C. Adamo, S. Clifford, J. Ochterski, G. A. Petersson, P. Y. Ayala, Q. Cui, K. Morokuma, D. K. Malick, A. D. Rabuck, K. Raghavachari, J. B. Foresman, J. Cioslowski, J. V. Ortiz, B. B. Stefanov, G. Liu, A. Liashenko, P. Piskorz, I. Komaromi, R. Gomperts, R. L. Martin, D. J. Fox, T. Keith, M. A. Al-Laham, C. Y. Peng, A. Nanayakkara, C. Gonzalez, M. Challacombe, P. M. W. Gill, B. Johnson, W. Chen, M. W. Wong, J. L. Andres, C. Gonzalez, M. Head-Gordon, E. S. Replogle, and J. A. Pople, Gaussian, Inc., Pittsburgh PA, **1998**.
[15] [15a] W. Kutzelnigg, U. Fleischer, M. Schindler, in *NMR-Basic Principles and Progress*, Vol. 23, Springer, Heidelberg, **1990**, pp. 165ff. – [15b] V. G. Malkin, O. L. Malkina, L. A. Eriksson, D. R. Salahub, in *Theoretical and Computational Chemistry*, Vol. 2 (Eds.: P. Politzer, J. M. Seminario), Elsevier, Amsterdam, **1995**.
[16] S. Berger, W. Bock, G. Frenking, V. Jonas, F. Müller, *J. Am. Chem. Soc.* **1995**, *117*, 3820−3829.
[17] *Landolt−Börnstein, Numerical Data and Functional Relationships in Sciences and Technology*, Vols 7, 15, 21, 23: *Structure Data of Free Polyatomic Molecules*, Springer, Berlin, **1979**, **1987**, **1992**, **1995**.
[18] K. Eichkorn, O. Treutler, H. G. Öhm, M. Häser, R. Ahlrichs, *Chem. Phys. Lett.* **1995**, *240*, 283−289.
[19] Program System TURBOMOLE V 5.1: R. Ahlrichs, M. Bär, M. Häser, H. Horn, C. Kömel, *Chem. Phys. Lett.* **1989**, *162*, 165−169.
[20] V. G. Malkin, O. L. Malkina, M. E. Casida, D. R. Salahub, *J. Am. Chem. Soc.* **1994**, *116*, 5898−5908.
[21] [21a] J. P. Perdew, Y. Wang, *Phys. Rev. B* **1992**, *45*, 13244−13249. – [21b] J. P. Perdew, in *Electronic Structure of Solids* (Eds.: P. Ziesche, H. Eischrig), Akademie Verlag, Berlin, **1991**. – [21c] J. Perdew, J. A. Chevary, S. H. Vosko, K. A. Jackson, M. R. Pederson, D. J. Singh, C. Fiolhais, *Phys. Rev. B* **1992**, *46*, 6671−6687.
[22] deMon program: [22a] D. R. Salahub, R. Fournier, P. Mlynarski, I. Papai, A. St-Amant, J. Ushio, in *Density Functional Methods in Chemistry* (Eds.: J. Labanowski, J. Andzelm), Springer, New York, **1991**. – [22b] A. St-Amant, D. R. Salahub, *Chem. Phys. Lett.* **1990**, *169*, 387−392.
[23] V. G. Malkin, O. L. Malkina, D. R. Salahub, *Chem. Phys. Lett.* **1996**, *261*, 335−345.
[24] [24a] G. M. Sheldrick, *SHELXS-86*, *Program for Crystal Structure Solution*, University of Göttingen, Germany, **1986**. – [24b] G. M. Sheldrick, *SHELXL-93*, *Program for Crystal Structure Refinement*, University of Göttingen, Germany, **1993**.

Received April 5, 2000
[I00132]

Covalently Linked Ruthenium(II)−Manganese(II) Complexes: Distance Dependence of Quenching and Electron Transfer

Katja E. Berg,[a] Anh Tran,[a] Mary Katherine Raymond,[b] Malin Abrahamsson,[b] Juliusz Wolny,[c] Sophie Redon,[a] Mikael Andersson,[b] Licheng Sun,[a] Stenbjörn Styring,[d] Leif Hammarström,*[b] Hans Toftlund,*[c] and Björn Åkermark*[a]

Keywords: Ruthenium / Manganese / N ligands / Electron transfer

Continuing our development of artificial models for photosystem II in green plants, a series of compounds have been prepared in which a $Ru(bpy)_3^{2+}$ photosensitizer is covalently linked to a manganese(II) electron donor. In addition to a trispicolylamine ligand, two other manganese ligands, dipicolylamine and aminodiacetic acid, have been introduced in order to study ligands that are appropriate for the construction of manganese dimers with open coordination sites for the binding of water. Coordination equilibria of the manganese ions were monitored by EPR. The interactions between the ruthenium and manganese moieties were probed by flash photolysis, cyclic voltammetry and steady-state and time-resolved emission measurements. The quenching of the Ru^{II} excited state by Mn^{II} was found to be rapid in complexes with short Ru–Mn distances. Nevertheless, each Ru^{II} species could be photo-oxidized by bimolecular quenching with methylviologen, and the subsequent electron transfer from Mn^{II} to Ru^{III} could be monitored.

Introduction

Considerable efforts have been made to create biomimetic systems for natural photosynthesis.[1] The search for alternative renewable energy sources often underlies this research, and there is a need to understand, at a fundamental level, how nature converts solar energy into chemical forms that can be stored. An important subject involves the structure and function of the manganese cluster in the oxygen-evolving complex (OEC) in photosystem II (PS II).[2−3]

To date, biomimetic systems have focused either on new polynuclear manganese model complexes, or on supramolecular assemblies based on porphyrins and transition metal complexes.[4−5] Our aim has been to use the principles of the natural PS II to construct supramolecular complexes in which a photosensitizer is covalently linked to one or several manganese ions. Ultimately, the idea in this project is to imitate Nature by photochemically oxidizing water to form oxygen, and to use the electrons released in this process to generate fuels, for example, H_2.

As an artificial replacement for the chlorophyll photosensitizer in PS II, we have used Ru^{II} trisbipyridyl complexes because they have favorable photochemical properties and are stable and relatively easy to synthesize. With complex **1b**, it was demonstrated that upon photo-oxidation of the Ru^{II} complex by an external acceptor, electron transfer occurred from Mn^{II} to Ru^{III}.[6] However, the rate of electron transfer in **1b** was rather low: $k_{ET} = 1.8 \cdot 10^5\ s^{-1}$. In an operating system, such a rate would probably be too low to compete with back electron transfer. It is therefore important to prepare complexes where the ET rate from the manganese is higher. An obvious way of increasing the rate relative to

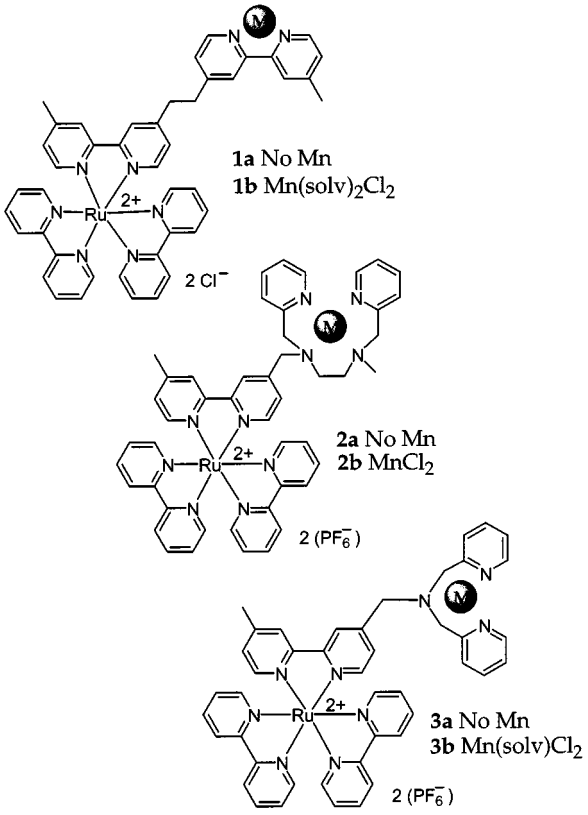

[a] Dept. of Organic Chemistry, Stockholm University, 106 91 Stockholm, Sweden
[b] Dept. of Physical Chemistry, Uppsala University, Box 532, 751 21 Uppsala, Sweden
[c] Dept. of Chemistry, Odense University, Campusvej 55, 5230 Odense M., Denmark
[d] Dept. of Biochemistry, Center for Chemistry and Chemical Engineering, University of Lund, Box 124, 221 00 Lund, Sweden

 © WILEY-VCH Verlag GmbH, 69451 Weinheim, 2001 1434−1948/01/0404−1019 $ 17.50+.50/0

complex **1b** is to decrease the Ru−Mn distance. This was estimated to be ca. 13 Å by using Chem 3D.[6] The bispicene complex **2b**, which has an estimated Ru−Mn distance of ca. 9 Å, was therefore synthesized. However, because of quenching by the manganese, the lifetime of the excited state of this complex became so short, only 7 ns, that we were unable to observe electron transfer to the external acceptor, methylviologen.[6] The Ru−Mn distance thus seemed very important for the functioning of the Ru sensitizer.

A study of the influence of this distance on the lifetime of the excited state of the ruthenium moiety and also on the rate of electron transfer from Mn to the photogenerated Ru^{III} clearly seems interesting. We therefore decided to synthesize a few binuclear Ru−Mn complexes with different Ru−Mn distances. In this paper, we describe complexes **3b**−**7b**, where manganese is coordinated to dipicolylamine (dpa), trispicolylamine (tpa), and aminodiacetic acid (ada).

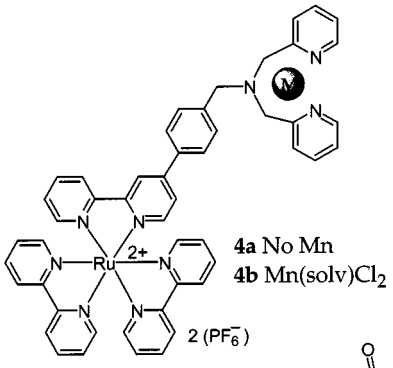

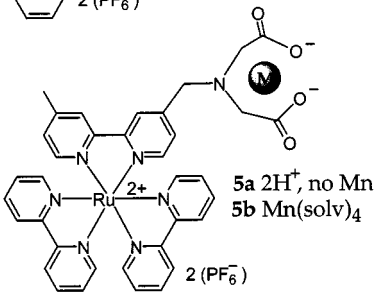

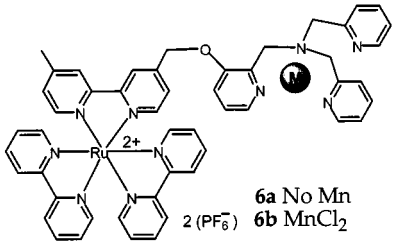

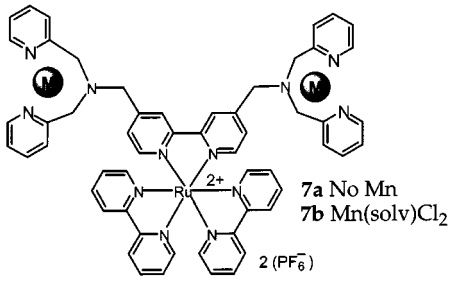

Dpa and tpa are known to bind manganese quite strongly.[7−8] In complex **4b**, a tolyl spacer was inserted between the Mn ligand and the Ru center, and in **6b** a longer link was used. The lifetimes of the excited states, the intramolecular electron transfer rates, as well as the coordinating ability and the stability in solution are discussed and compared to those previously reported for complexes **1b** and **2b**.

Results

Synthesis and Characterization

Two different strategies were used for the preparation of complexes **3b**−**7b**. In the synthesis of **5b**, ligand **8e** was obtained by the reaction of bromomethylbipyridine (**8b**) with iminodiacetic acid dimethyl ester.

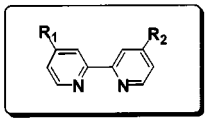

8a $R_1=CH_3$, $R_2=CH_2OH$
8b $R_1=CH_3$, $R_2=CH_2Br$
8c $R_1=R_2=CH_2OH$
8d $R_1=R_2=CH_2Br$
8e $R_1=CH_3$, $R_2=CH_2N(CH_2CO_2CH_3)_2$

The ruthenium part was then introduced to give **10a**, which was hydrolyzed to **5a** and reacted with manganese(II). Complex **5b** could not be obtained in a pure form. In the synthesis of the other complexes, the ruthenium part was introduced before the ligand for manganese. Thus complexes **3b** and **7b** were prepared by the reaction of the ruthenium complexes **9b** and **9c** with dipicolylamine to give **3a** and **7a**, respectively, which were then treated with manganese(II) (Scheme 1). Complex **6b** was prepared in a similar way by the reaction of complex **9b** with the phenolic trispicolylamine **16** (Scheme 2).

In the synthesis of complex **4b**, ligand **14** was first prepared by a classical polypyridine synthesis (Scheme 3). Tolualdehyde and pyruvate were condensed to give the ketoacid **11**, which after a second condensation with 2-pyridacyl pyridinium iodide and treatment with ammonia gave the

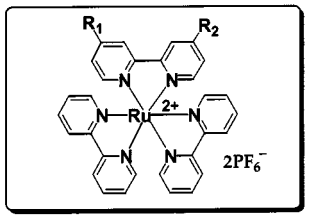

9a $R_1 = R_2 = H$
9b $R_1 = CH_3$, $R_2 = CH_2Br$
9c $R_1 = R_2 = CH_2Br$
10a $R_1 = CH_3$, $R_2 =$ 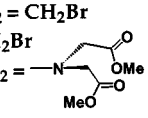

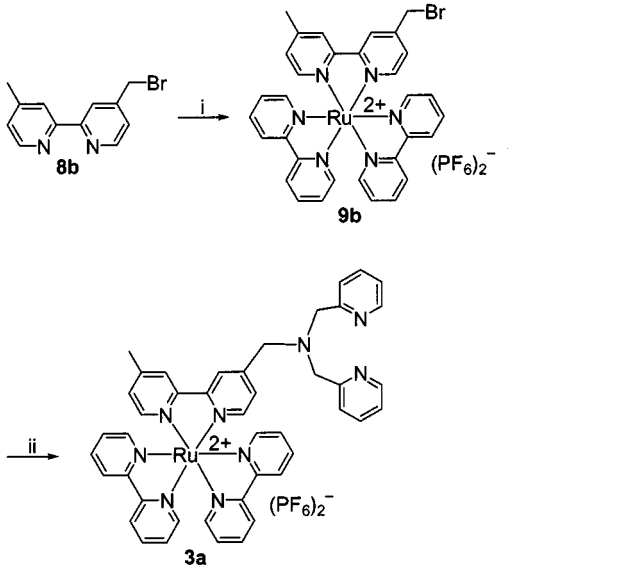

(i) $Ru(bpy)_2Cl_2$, CF_3SO_3Ag, acetone; (ii) dipicolylamine, Et_3N, MeCN

Scheme 1

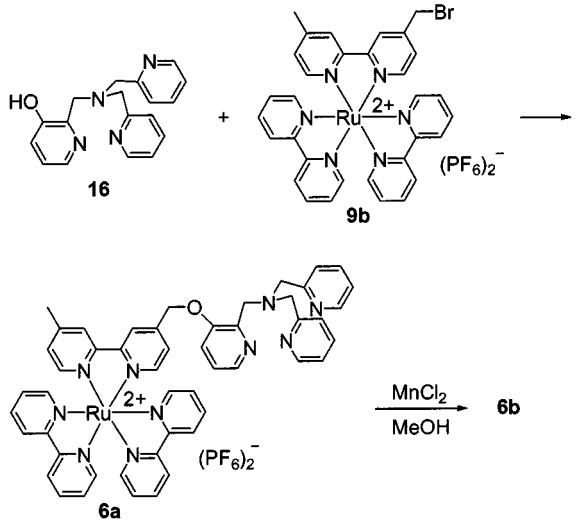

Scheme 2

ammonium carboxylate **12**. Decarboxylation by strong heating of the carboxylate in the absence of solvent gave the bipyridine **13**, which was brominated to give **14**. This was reacted with *cis*-$Ru(bpy)_2Cl_2$ to give the ruthenium complex **15**, then with dipicolylamine to give **4a**, which was converted into the dinuclear Ru−Mn complex **4b** by treatment with $MnCl_2$.

All new complexes in this paper, except **5b**, have been characterized using electrospray ionization mass spectroscopy (ESI-MS), ^1H NMR spectroscopy, and EPR spectroscopy. For manganese complexes, the NMR signals for the ruthenium moiety were generally observed as broadened peaks, whereas the signals for the manganese part could not be detected within a spectral width of 15 ppm.

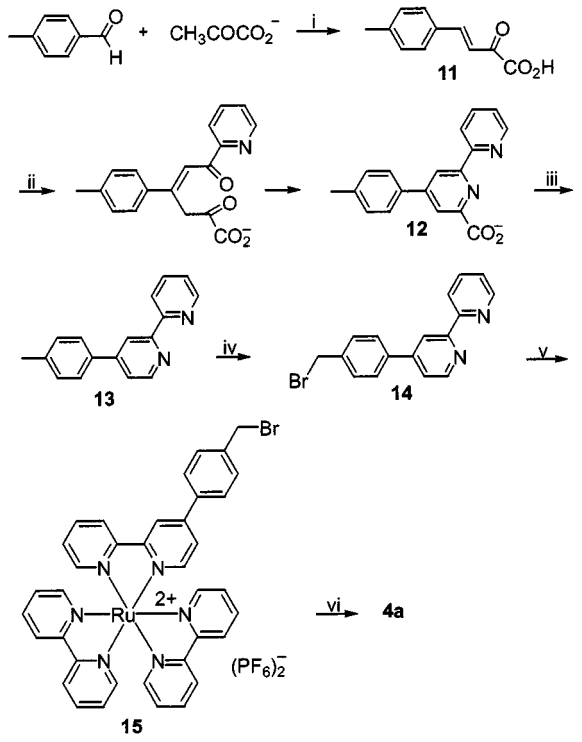

(i) 1) EtOH, NaOH(10%), 2) HCl(2M); (ii) 2-pyridacyl pyridinium iodide, NH_4OAc, H_2O; (iii) Δ; (iv) NBS, AIBN, CCl_4; (v) $Ru(bpy)_2Cl_2$, CF_3SO_3Ag, acetone; (vi) dipicolylamine, Et_3N, MeCN

Scheme 3

ESI-MS

In the ESI-MS spectra of complexes **3a**, **4a**, **5a**, **6a**, and **7a**, the singly-, doubly-, and/or triply charged species of the molecular ion were identified as the primary peaks of the spectra and are listed in the Experimental Section. Complexes **3b**, **4b**, **6b**, and **7b** gave rise to Mn-containing peaks, whereas **5b** gave a complicated pattern that could not be interpreted. The ESI-MS spectra of complexes **3b**, **4b**, **6b**, and **7b** in which Mn^{II} ions are incorporated into the ligands, contain numerous peaks from several species, differing by either the number of chlorides coordinated to manganese or by the presence of salt and/or solvent molecules held in the cavities. This apparent complexity clearly shows that manganese has been incorporated in the ligands.

EPR

The EPR spectra of solutions of the Ru−Mn complexes in MeOH/water (9:1) were recorded at 100 K. The very similar, jagged six-line spectra indicate that the coordination is very similar in the complexes **3b**, **4b**, **5b**, and **7b**. (Figure 1) The spectrum of **5b** is particularly interesting. Control experiments were conducted to exclude the possibility of Mn^{II} monomers or dimers bound to e.g. dissolved carbonate (CO_2 from the air). None of these control experiments showed spectra similar to those of the Ru−Mn complexes. In fact, when carbonate was added to a solution of $Mn^{II}Cl_2$, carbonate-bridging Mn^{II}−Mn^{II} dimers were

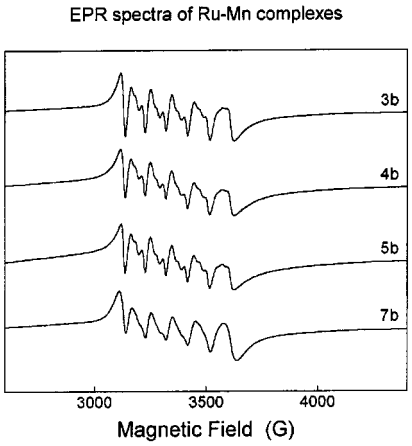

Figure 1. EPR spectrum showing the characteristic jagged 6-line trace for $Ru^{II}-Mn^{II}$ complexes (**3b**, **4b**, **5b**, and **7b**) in MeOH at 100 K

formed, yielding a broad spectrum with no hyperfine structure at 100 K.

Incorporation of manganese is rapid with bipyridyl and bispicen ligands,[6] and slow with the tpa, dpa, and ada ligands. It could be shown that this was partly due to complexation of CO_2 by the free ligands. When the solution was bubbled with nitrogen before the introduction of manganese, the rate of its incorporation was greatly increased. When excess $MnCl_2$ was added, and the solution was allowed to equilibrate for several days, the coordination of manganese into the ligands approached 100% in complexes **3b**, **4b**, **5b**, and **7b**.

UV/Vis Spectroscopy

The UV/Vis absorption spectra of all the ruthenium tris-bipyridyl complexes were similar to those of the parent $Ru(bpy)_3^{2+}$ complex (**9a**). Complexes **3a**, **4a**, **5a**, **6a**, and **7a** had the same absorption maxima (λ in nm): 245 (s), 253 (s), 287 (vs), and 453 (m) [for **9a**: 238, 259, 285, and 452 nm; for the dpa-ligand: 259 nm and a shoulder at 287 nm]. When manganese was coordinated into the ligand cavities of these complexes, thereby giving **3b**, **4b**, **5b**, **6b**, and **7b**, the absorption spectra were unchanged.

Emission Lifetimes and Quenching

The emission spectra of all complexes were typical of emission from the ^{3}MLCT state of $Ru(bpy)_3^{2+}$ complexes, with corrected emission maxima for the compounds without Mn listed in Table 1. Upon binding of Mn, emission was quenched, the curves were somewhat broadened, and the maxima underwent a red-shift. Since much emission comes from the unquenched, manganese-free complexes, the values for the Ru−Mn complexes are uncertain in some cases. All complexes without manganese had excited-state lifetimes of approximately 1000 ns (1300 for **4a**). The emission lifetimes of the complexes with coordinated manganese were very short for complexes **3b** and **7b** (2.2 and 0.8 ns, respectively). The bispicene complex **2b**, which has a similar Ru−Mn distance, also has a short lifetime.[6] The lifetime

Table 1. Photophysical data for complexes **1a**−**7a** and **10a**

Complex	Room temp. emission lifetime (fraction) τ [ns]	Room temp. corrected emission maximum λ [nm]	77 K corrected corrected emission maximum λ [nm]
1a	919	626	
2a	1050		
3a	880	640	585, 635, 697
4a	1300	629	588, 638, 699
5a	900	637	
6a		630	
7a	1090 (96%), 110 (4%)[a]	634	
10a	990		

[a] From reference [6]

of the ada complex **5b** was somewhat longer but because of poor coordination of manganese, the value is uncertain. For complexes **4b** and **6b**, which have approximately the same Ru−Mn distances as **1b**, it is interesting to note that the lifetime of **6b** was 120 ns, similar to that of **1b** (280 ns), but that of complex **4b** was only 23 ns (see Table 2).

The emission intensity of a 10 μM sample of **4b** in acetonitrile that was in a sealed, evacuated sample, remained constant over a period of 20 h. However, the emission of a second sample that was in a closed cuvette, but in acetonitrile saturated with air, increased to the level of the Mn-free complex **4a** with a half-life of 4 hours. Because the emission intensity is determined by the amount of bound manganese, this experiment demonstrated that atmospheric conditions promote manganese dissociation in this compound.

Flash Photolysis Studies

Electron-transfer reactions were studied by monitoring the transient absorptions of Ru^{II} species and the methylviologen radical ($MV^{+\cdot}$). The Ru^{III} species and $MV^{+\cdot}$ were generated by a laser flash which resulted in excitation of Ru^{II} followed by electron transfer to MV^{2+}, i.e. Equation (1).[5a,6]

$$Ru^{II}* + MV^{2+} \rightarrow Ru^{III} + MV^{+} \quad (1)$$

Since the formation of Ru^{III} occurred by means of a diffusion encounter of $Ru^{II}*$ with methylviologen, very high concentrations of MV^{2+} were necessary for compounds that have rapid intramolecular quenching of $Ru^{II}*$ by manganese (details in Experimental Section). This reaction was monitored by using the $MV^{+\cdot}$ absorption at approximately 600 nm, and the Ru^{II} ground-state bleaching at approximately 450 nm. In a subsequent reaction, the 450-nm absorption returned with a lifetime of the order of 1−10 μs, which we attributed to intramolecular electron transfer from the manganese [Equation (2)].

$$Ru^{III}-Mn^{II} \rightarrow Ru^{II}-Mn^{III} \quad (2)$$

In contrast, the $MV^{+\cdot}$ absorption at 600 nm remained for more than 100 μs. It decayed in a second-order reaction

Table 2. Emission and electron-transfer data for Ru−Mn complexes and calculated Ru−Mn distances

Complex	Emission lifetime (fraction) τ [ns]	Ru−Mn complex[a] [%]	Electron transfer rate[b] [s^{-1}]	Calculated Ru−Mn distance[c] [A]
1b[d]	260	80	$1.8\cdot10^5$	13
2b[e]	7	93	−	9
3b	2.2	65	$1.3\cdot10^6$	9
4b	23	68	$1.6\cdot10^6$	14
5b	19[f]	8	[g]	9
6b	120	97	$1.3\cdot10^5$	14
7b	0.8 (76%), 2.9 (24%)[h]	94	[g]	9
10b	−	0	[g]	9

[a] These percentages are from the fitting of the fluorescence decay curves of the Ru−Mn complexes. Each curve was fitted by a sum of two exponentials (three for **7b**), one exponential corresponding to the bound complex, and the other to the dissociated complex. Approximately 30 μM solutions of the 1:1 Ru−Mn complexes in acetonitrile were used. The percentages of bound complex are probably all concentration dependent. − [b] This is the half-life of the fastest component of the 450 nm Ru^{II} recovery. − [c] These are maximum Ru−Mn distances estimated by molecular mechanics starting from the most extended conformations using constrained metal−ligand distances. − [d] **1b** in acetonitrile (39μM). From reference [6a]. − [e] **2b** in acetonitrile (67 μM). From reference [6a]. − [f] Determined with a twofold excess of $MnCl_2$ in acetonitrile, in order to obtain a larger fraction of attached Mn and thus a more reliable value. − [g] Not measured due to a low degree of Mn association or inability to quench the very short-lived excited state with methylviologen (see text). − [h] The fluorescence decay curve was fitted by a sum of two exponentials. This may be due to the presence of an impurity.

with $k_{ET} = 5\cdot10^9$ $M^{-1}s^{-1}$, which we attributed to a diffusion-controlled recombination with the Mn^{III} species and some recombination with Ru^{III}.

When manganese was not present e.g. in **4a**, the 450 nm absorption and the 600 nm decay were mirror images, showing that the oxidized Ru^{III} regained an electron from the $MV^{+\cdot}$ in a recombination reaction that reformed the ground-state reactants [Equation (3)].

$$Ru^{III} + MV^{+\cdot} \rightarrow Ru^{II} + MV^{2+} \quad (3)$$

For **3a**, the Ru^{II} recovery at 450 nm was somewhat faster (first-order rate constant $k_{ET} \approx 1\cdot10^5$ s^{-1}) owing to irreversible electron transfer from the dpa ligand, which leads to a build-up of $MV^{+\cdot}$. For **6a**, an even faster recovery was observed, $k_{ET} \geq 1\cdot10^7$ s^{-1}, accompanied again by a build-up of $MV^{+\cdot}$. However, the ligands were stabilized against oxidation when Mn^{II} was coordinated. Thus, in **3b**, **4b**, and **6b** it was the Mn^{II} that was oxidized, and the $MV^{+\cdot}$ did not accumulate, presumably because it recombined with the Mn^{III} species (Figure 2). Complexes **3b** and **4b** displayed much faster Ru^{II} recovery then their Mn-free counterparts. In contrast, the recovery was much slower for **6b** (Figure 1) than for the manganese-free complex **6a**. The electron-transfer rate constants are summarized in Table 2.

Owing to partial dissociation of the Mn, the Ru^{II} recovery traces for **3b** and **4b** were fitted to a sum of two exponential processes, with a dominating fast recovery followed by a much slower one with smaller amplitude. The slower recovery rates agreed with measurements made with the Mn-free complexes. Only a small part of the slow recovery phase was seen on the timescale of the fast ET process [Equation (1)]. Therefore it could be represented by an exponential function in the fit, even though it was a second- or mixed first/second-order process.

For complex **6b**, a clean single-exponential first-order recovery of Ru^{II} was observed upon flash excitation in the presence of MV^{2+}. The rate constant ($1\cdot10^5$ s^{-1}) was much lower than for complexes **3b** ($1.3\cdot10^6$ s^{-1}) and **4b** ($1.6\cdot10^6$ s^{-1}).

Cyclic Voltammetry

The half-wave potential ($E_{1/2}$) of the complexes **3a**, **3b**, **4a**, **4b**, **6a**, **6b**, and **9a** were determined by cyclic voltammetry (Table 3). For all the measured complexes, the peak split, ΔE_p, between the anodic (E_{pa}) and the cathodic (E_{pc}) peak potentials is less than 134 mV for the $Mn^{III/II}$ peak and less than 84 mV for the $Ru^{III/II}$ and the first reduction peak. The cyclic voltammograms of **4a** and **4b** are shown in Figure 3.

The reversible oxidation peak at approximately 1.30 V vs. SCE and the three reversible reduction peaks are typical of $Ru^{III/II}$ oxidation and ligand reduction in $Ru(bpy)_3^{2+}$ complexes. The irreversible oxidative peak for **4a** at approximately +1.1 V vs. SCE, also present for **3a**, was assigned to oxidation of the dpa ligand. When Mn^{II} was coordinated (**4b**), a reversible peak, which was assigned to the $Mn^{III/II}$ couple, appeared at +0.90 V vs. SCE. Complexes **6a** and **6b** gave similar values for the corresponding peaks. Thus, the free energy changes ($\Delta G°$) of electron transfer from Mn^{II} to Ru^{III} were −0.39 eV and −0.49 eV (ignoring work term corrections) for **4b** and **6b**, respectively. The $Ru^{III/II}$ and the first ligand reduction potentials were very similar for **4a** and **4b**, and for **6a** and **6b**, showing that insertion of the neutral Mn^{II} complex only has a small coulombic effect on the ruthenium complex.

Discussion

Synthesis and Characterization

In the synthesis of complex **1b**, the bridging bipyridyl ligand was treated with *cis*-$Ru(bpy)_2Cl_2$ to give a mixture of mono- and diruthenium complexes, from which the mono-

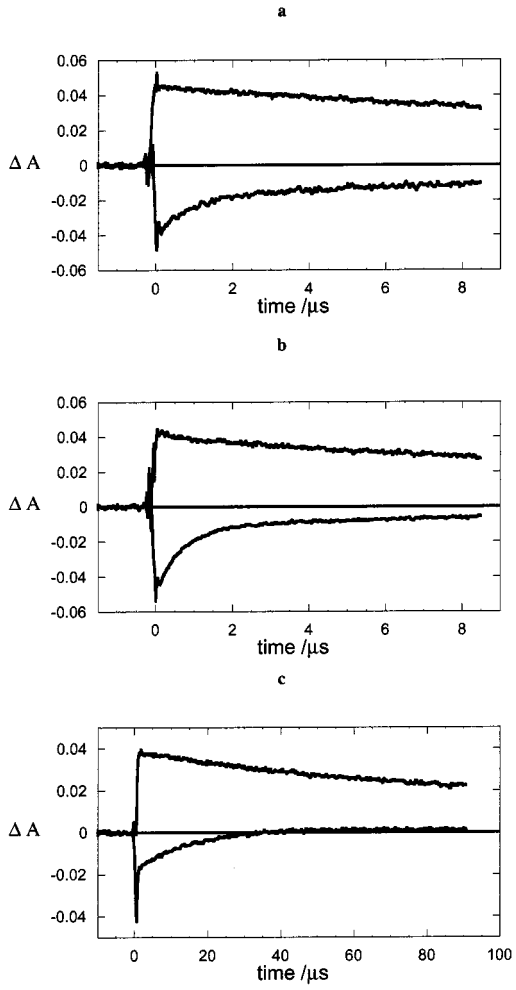

Figure 2. Transient absorption curves of Ru−Mn complexes (ca. $4\cdot10^{-5}$ M) with $MV(PF_6)_2$ in deoxygenated acetonitrile at room temperature: (a) **3b** with 0.30 M $MV(PF_6)_2$, (b) **4b** with 0.11 M $MV(PF_6)_2$, and (c) **6b** with 10 mM $MV(PF_6)_2$. It is worth noting that the relative contribution from the manganese-free fraction decreases regularly when going from (a) to (c). This is both due to an increasing degree in manganese binding, and to an increase in the excited-state lifetime for the Ru−Mn complex. Even with 0.30 M methyl viologen in (a), only a small part of the short-lived excited state of **3b** reacts, while the long-lived fraction of manganese-free complex present reacts quantitatively.

Table 3. Redox potentials determined by cyclic voltammetry in 0.1 M $TBA\cdot BF_4/CH_3CN$ at a glassy-carbon electrode (scan rate 100 mV/s). $E_{1/2}$ = redox half-way potential, $(E_{pa} + E_{pc})/2$

Complex	$E_{1/2}$ ($Mn^{III/II}$) V vs. SCE	$E_{1/2}$ ($Ru^{III/II}$) V vs. SCE	$E_{1/2}$ (ligand) V vs. SCE
3a	–	1.30	−1.32
3b	[a]	1.28	−1.31
4a	–	1.30	−1.27
4b	0.90	1.29	−1.28
6a	–	1.28	−1.32
6b	0.79	1.28	−1.31
$Ru(bpy)_3^{2+}$	–	1.32	−1.29

[a] The $Mn^{III/II}$-couple was not seen (see text).

complex could be isolated by chromatography. However, the substituted bipyridyl ligand in **2b** is unsymmetrical, and this strategy was therefore less attractive for the preparation

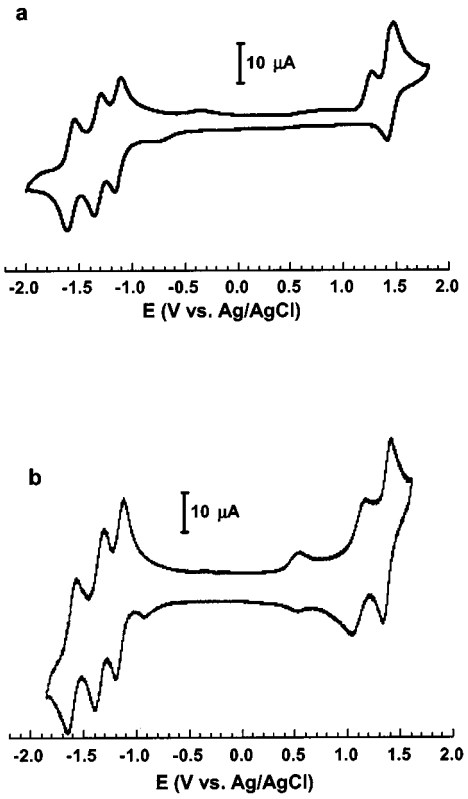

Figure 3. Cyclic voltammogram of (a) **4a** (0.92 mM) (b) **4b** (1.02 mM) in 0.1 M $TBA\cdot BF_4$/MeCN at a glassy-carbon electrode. The small peak at ≈0.5 V vs. Ag/AgCl is due to an impurity present in the electrolyte which is adsorbed onto the electrode. The scan rate used is 100 mV/s

of this complex. Instead, the Ru^{II} trisbipyridyl moiety was prepared before introducing the ligand for manganese.[6] Both strategies have been applied for the preparation of the complexes reported here. In the synthesis of **5b**, the ligand **8e** was first prepared and ruthenium could then be introduced selectively. Manganese could then be added after hydrolysis of the ester groups. In the synthetic routes to complexes **3b**, **4b**, **6b**, and **7b**, in which the final ligand could coordinate both ruthenium and manganese quite strongly, the intermediate ruthenium complexes **9b**, **9c**, and **15** were prepared first. As in the synthesis of **2b**, the ligand for manganese was then introduced, followed by manganese(II), to give the dinuclear complexes **3b**, **4b**, **6b**, and **7b**.

The EPR spectra of the Ru−Mn complexes all show essentially the same pattern (Figure 1). It can be concluded that the coordination geometry around manganese in the complexes is similar. Furthermore, the EPR spectra are identical whether the Mn^{II} is coordinated to an N- or to an O-donor; the patterns of the EPR spectra are mainly dependent on the coordination geometry around manganese.

With the exception of **5b**, the bipyridine ligand in **1b** is the weakest chelator for manganese of all the complexes described in this paper. The lifetime measurements show that in a dilute acetonitrile solution (ca. 30 μM), approximately 30% of the manganese is dissociated in complexes **3b**, **4b**, and **7b**. This indicates stability similar to that of com-

plex **2b**. In contrast, only ca. 3% dissociation was observed with the tpa-complex **6b**. In aqueous solution, however, the coordinated manganese is rapidly lost from all the complexes **3b**−**7b**.

The bis-manganese complex **7b** gave a similar EPR spectrum as complex **3b**, suggesting the presence in **7b** of two nonbridging manganese(II) ions which do not interact. The molecular model of complex **7b** suggests that the two dpa moieties stretch away from each other in space owing to steric restriction, thus minimizing the likelihood of bridge formation between the two dpa units. An increase in the spacer length between the bipyridine and the dpa unit, or an uncoordinated bipyridine with free rotation about the bond between the pyridine rings would most probably allow for the formation of a Mn-oxo or Mn-acetato bridge.

The low rate of incorporation of manganese into the dpa cavity, as observed by EPR, could be due to the need to displace a molecule of CO_2, solvent, or ions already coordinated in the cavity. However, the introduction of a phenyl group to act as a rigid spacer between the Mn-coordinating ligand and the ruthenium entity did not change the coordination affinity for manganese: **3b** and **4b** have approximately the same amount of Mn dissociation (Table 2). Furthermore, the redox potential of Ru^{II} is the same in **4a**, in which manganese is absent, and in **4b**. This indicates that the weak coordination of manganese is mainly due to the nature of the ligand. The steady-state emission yield experiments (see Results section) demonstrated that Mn^{II} dissociated completely within hours in air-equilibrated solution, but that it remained bound in evacuated samples. This suggests that manganese is displaced either directly, for example by CO_2 in air, or indirectly as a result of oxidation of the dpa ligand.

Quenching of the Ru^{II}-Excited State by Manganese

Before coordination of manganese, the ruthenium complexes **1a**−**7a** have lifetimes of approximately 1000 ns, very similar to the lifetime of the parent bipyridine complex **9a**. On coordination of manganese, the lifetime is decreased, probably due to energy transfer by an exchange mechanism[6b] involving the low-lying d−d states of the Mn^{II}. It would be expected that a short intermetallic distance would lead to more rapid quenching of the ruthenium excited state. The Ru−Mn distances determined by Chem 3D are summarized in Table 2. In general, complexes with shorter Ru−Mn distances (**3b**, **5b**, and **7b**) indeed have shorter emission lifetimes (Table 2). An exception is complex **4b**, which has an estimated Ru−Mn distance of ca. 14 Å but a lifetime of only 23 ns. This may be due to significant electron delocalization over the phenyl group.[9] This would lead to a MLCT state that would be located more on the phenyl-substituted bipyridine. In contrast, complexes **1b** and **6b**, which have comparable Ru−Mn distances (13−14 Å), have much longer lifetimes: 260 ns and 120 ns, respectively.

The Ru^{II}* quenching rate constant in **7b** is almost double that of **3b**, which supports the suggestion that the two manganese units in **7b** act as independent moieties. The fact that an additional exponent with a lifetime of 2.9 ns is needed to describe the decay in **7b** indicates that there may be a small fraction present where only one manganese atom is coordinated. The Mn-free complex **7a** also exhibits emission decay with a major ($\tau \approx 1000$ ns) and a very minor component (4% with $\tau \approx 100$ ns). Complex **6b** displays a distinct mono-exponential decay, in sharp contrast to the results obtained with complexes **3b**−**5b**.

Electron Transfer

The regeneration of the Ru^{II} sensitizer after photo-oxidation by methylviologen was very fast for **3b** and **4b** (Table 2). The reduction potentials show that electron transfer from Mn^{II} to Ru^{III} is energetically favorable, e.g. for **4b** $\Delta G^\circ = -0.39$ eV. Furthermore, the Ru^{II} recovery rates for **3b** and **4b** are much higher than those for the Mn-free complexes **3a** and **4a**. The measured Ru^{II} recovery rates are too high to be explained by a bimolecular reaction between Ru^{III} and Mn^{II} at the low concentrations (0.04 mM) employed. In addition, it could be shown that the rate constant for electron transfer was independent of the concentration for **4b**. We therefore attributed the Ru^{II} recovery in **3b** and **4b** to an intramolecular electron transfer from the Mn^{II} to the photogenerated Ru^{III}, in agreement with our previous reports on Ru−Mn complexes.[6]

Similarly, intramolecular electron transfer is observed for complex **6b**. In this case, the rate constant is lower than for the manganese-free complex **6a**. However, in **6a** the ligand is the electron donor, but in **6b** it is the manganese ion, because the ligand is stabilized against oxidation after binding the metal. As a consequence, the electron transfer in **6b** is reversible, and the methylviologen radical is not accumulated. A possible reason for the rapid reaction of the amine in **6a** relative to **3a** could be that the longer link in the former could fold back towards the ruthenium. When the manganese atom is coordinated, the ligand is probably less flexible.

The electron-transfer rates for **3b** and **4b** are both nearly an order of magnitude faster than those observed for complexes **1b**[6] and **6b**. The faster rate in **3b** is not surprising considering its shorter Ru−Mn distance. The rapid Mn^{II} to Ru^{III} electron transfer rate in **4b** however, was unexpected. Although the rate constant for electron transfer through phenylene spacers may decrease relatively slowly with distance,[10] the fact that the Ru−Mn distance is 5 Å longer was expected to result in a much lower rate for **4b**. The high rate observed could be due to either a folding of the dpa unit or to conjugation through the phenylene spacer. The latter effect is perhaps the most probable since the spacer in **4a**, which has no manganese, has an influence both on the wavelength of the emission from the excited state of ruthenium (red shift of ca. 5 nm relative to **3a**) and on the lifetime of this state (1300 ns vs. 950 ns for **3a**).

Conclusions

A series of supramolecular complexes with a $Ru(bpy)_3^{2+}$ core covalently linked to Mn-binding ligands have been pre-

pared and characterized. The coordinated manganese(II) was found to act as a strong quencher for the excited state of ruthenium, probably by energy transfer. In the absence of manganese, the excited-state lifetime of the $Ru(bpy)_3^{2+}$-type complexes was typically approximately 1000 ns. When the manganese ions were coordinated, the lifetimes were much shorter and there appeared to be a close relationship between the Ru−Mn distance and the emission lifetime. Thus the lifetimes of complexes **1b** and **6b**, in which the Ru−Mn distances were estimated to be 13−14 Å (by Chem 3D), were decreased to 255 and 120 ns, respectively. As the Ru−Mn distances were further shortened to ca. 9 Å, as in complexes **2b**, **3b**, and **7b**, the lifetimes became dramatically short: 7, 1.6, and 0.8 ns, respectively. The short lifetime of **4b**, (23 ns) in which the Ru−Mn distance is ca. 14 Å, is an exception which can be rationalized by delocalization of the excited state over the conjugated phenyl spacer.

Although we still have a fairly limited number of examples, the results so far seem to indicate that the rates of intramolecular electron transfer from manganese(II) to photo-generated ruthenium(III) also show some correlation with the Ru−Mn distances, increasing from ca. $1\cdot10^5$ s^{-1} for complexes **1b** and **6b** to $1.3\cdot10^6$ s^{-1} for complex **3b**.

In an artificial system, the electron transfer from manganese to the photo-generated ruthenium(III) must probably be fast in order to compete efficiently with back electron transfer from the acceptor. Our results suggest that this will be difficult with systems in which the manganese and ruthenium atoms are sufficiently close for rapid electron transfer because of the efficient quenching caused by the manganese atom. This problem presumably also exists in the natural PS II, where it has been solved by the insertion of a tyrosine unit (TyrosineZ) between the photosensitizer, chlorophyll P_{680} and the manganese cluster. This tyrosine unit then acts as an electron transfer relay. We have recently shown that a tyrosine group does not quench the excited state of Ru^{II} [11] and also that it can transfer an electron to the photo-oxidized ruthenium and recover it in an intramolecular reaction with a manganese(II)/(II) dimer.[12] In our future work we will therefore try to prepare supramolecular complexes in which a ruthenium(II) and a manganese(II) ion are linked by a tyrosine type unit.

Experimental Section

NMR, MS, and EPR: The ^1H NMR spectra were recorded on a Bruker AM400 MHz spectrometer or on a Bruker DMX500 MHz spectrometer, using TMS as internal standard. The electrospray ionization mass spectrometry (ESI-MS) experiments were performed on a TSQ700 (nanoES ion source) with acetonitrile or acetone as solvent. The EPR spectra were measured on a Bruker EMX spectrophotometer at 100 K using a 9:1 mixture of MeOH/H_2O as solvent.

Absorption and Emission Measurements: Spectroscopic grade acetonitrile was used for all measurements. The UV spectra were measured on a Varian Cary 5E UV/Vis-NIR spectrophotometer. Emission spectra were recorded using a SPEX fluorolog II system. Emission lifetimes were determined by using time-correlated single photon counting. The samples were purged with nitrogen gas and excited either at 327 nm by the frequency-doubled output from a YAG-pumped DCM dye laser, or at 400 nm by the frequency-doubled fundamental from a Ti-sapphire laser. A monochromator or interference filter centered at 610 nm was used to select the emission wavelength, which was detected with a microchannel plate. The two systems gave identical lifetimes within experimental error. The instrumental responses corresponded to four points or less out of 512 of the experimental decay curves and were not considered in the curve fitting.

Transient absorption studies were done by using an excimer laser pumping a Coumarin 47-dye laser to produce excitation pulses at 460 nm with a 15 ns width and an energy of 1 mJ/pulse at the sample. A pulsed Xe lamp provided analyzing light and the detection wavelengths were selected with a monochromator. All solutions were bubbled with nitrogen gas. The concentrations of the complexes were approximately 30 μM and that of methylviologen bis(hexafluorophosphate), $(MV(PF_6)_2$, was 0.15−0.30 M in the studies of complexes **3b** and **4b**, and 10−20 mM for all other samples. The transient absorption curves were fitted to single- or double-exponential functions.

Cyclic Voltammetry: The electrolyte was a 0.1 M solution of tetrabutylammonium tetrafluoroborate (TBA·BF_4, Aldrich) in acetonitrile. The TBA·BF_4 was vacuum dried at 140 °C for 48 hours before use, and acetonitrile (Aldrich, 99.8%) was used as received. The glassware was cleaned, oven-dried, and transferred while hot to an argon filled glove box in which the experiments were performed.

A three-electrode system connected to an Eco Chemie model Autolab/GPES electrochemical interface was used. The working electrode was a freshly polished glassy-carbon disc (diameter 3 mm) and the counter electrode consisted of glassy carbon. The reference electrode was Ag/AgCl in LiCl saturated acetonitrile. Both the reference and the counter electrodes were separated from the solution by a salt bridge in contact with the working electrode.

The $E_{1/2}$ for **3a**, **3b**, **4a**, **4b**, **6b**, and $Ru(bpy)_3(Cl)_2$ (**9a**) were measured relative to a ferrocenium/ferrocene internal reference. The $E_{1/2}$ values are reported relative to SCE. The conversion was made by setting the $Ru^{III/II}$ value obtained for $Ru(bpy)_3(Cl)_2$ equal to 1.324 V relative to SCE.[13]

Materials: Azobis(isobutyronitrile) was recrystallized from EtOH. All other commercial reagents were used as obtained without further purification. Carbon tetrachloride was distilled from P_2O_5 prior to use. All other solvents were of HPLC grade (>99.7%) for synthesis or spectroscopic grade for optical measurements and were used as received. Silica gel 60 (230−400 mesh, Merck, Darmstadt, Germany) and neutral aluminum oxide gel (Aldrich) were used for column chromatography. The $MV(PF_6)_2$ was prepared by reacting 4,4′-bipyridine with MeI, then adding aqueous NH_4PF_6 to precipitate the PF_6 salt. The product was purified by recrystallization from EtOH.

4-Hydroxymethyl-4′-methyl-2,2′-bipyridine (8a): To a stirred suspension of 4,4′-dimethyl-2,2′-bipyridine (2.0 g, 11 mmol) in 1,4-dioxane (100 mL) was added SeO_2 (2.0 g, 18 mmol). The mixture was heated at reflux for 24 h. After cooling to room temperature, the mixture was filtered, and the solvent was removed under reduced pressure. The resulting pink solid was redissolved in chloroform, and the suspension was filtered to remove selenium by-products. After three successive dissolution and filtration treatments, crude product (1.4 g) was obtained. The resulting solid was suspended in methanol (15 mL), and sodium borohydride (0.3 g) in NaOH (0.2

M, 2.5 mL) was added dropwise to the stirred mixture cooled on ice. The mixture was stirred at room temperature for an additional hour and the methanol was then removed under reduced pressure. The remaining aqueous suspension was diluted with saturated Na_2CO_3 solution (6 mL) and extracted with chloroform. The organic phase was dried and the solvent evaporated. The crude product was purified by column chromatography (MPLC)[14] to give 4-hydroxymetyl-4′-methyl-2,2′-bipyridine (1.2 g, 83%). All analytical data were in agreement with those reported by Geren et al.[15]

4-Bromomethyl-4′-methyl-2,2′-bipyridine (8b): 8a (1.0 g, 5.0 mmol) was dissolved in HBr (48%, 50 mL), and H_2SO_4 (conc., 2 mL) was added to the solution. The red solution was heated at reflux until all the starting material had been consumed as monitored by TLC (Al_2O_3, hexane/EtOAc, 10:90). After the reaction had gone to completion (5−6 h), H_2O (13 mL) and CH_2Cl_2 (13 mL) were added. The aqueous layer was brought to pH 8 by adding saturated sodium carbonate solution and extracted with 10 mL portions of CH_2Cl_2 until the organic layer was colorless. The combined organic layers were dried with $MgSO_4$ and the CH_2Cl_2 removed in vacuo to yield 4-bromomethyl-4′-methyl-2,2′-bipyridine (**8b**) (1.3 g, 98% yield). All analytical data were in agreement with those previously reported.[6]

Ru(bpy)$_2$(4-bromomethyl-4′-methylbipyridine)(PF$_6$)$_2$ (9b): Complex **9b** was isolated and characterized as reported earlier by Sun et al.[6]

Ru(bpy)$_2$[4-(dpa-CH$_2$)-4′-methylbipyridine](PF$_6$)$_2$ (3a): Dipicolylamine[16] (0.015 g, 0.073 mmol) and Et_3N (1 equiv.) were dissolved in acetonitrile and added dropwise to a solution of Ru(bpy)$_2$(4-bromomethyl-4′-methylbipyridine)(PF$_6$)$_2$ (**9b**) (0.071 g, 0.073 mmol) in acetonitrile. The reaction mixture was heated at reflux under argon for 3 h, then cooled and filtered. The filtrate was evaporated in vacuo and the product was purified by chromatography (MPLC)[14] (silica gel, MeCN/water/KNO_3(sat.), 28:1:2). The desired product eluted as the second band and excess KNO_3 was removed by filtration after dissolving the product in acetone. Water and NH_4PF_6 were added to a MeOH solution of the product to afford a red−orange product which was collected by filtration, washed and dried to yield Ru(bpy)$_2$[4-(dpa-CH$_2$)-4′-methylbipyridine](PF$_6$)$_2$ (**3a**) (0.042 g, 53%). − ^{1}H NMR ([D$_6$]acetone): δ = 2.58 (s, 3 H, MebpyCH_3), 4.37 (s, 2 H, MebpyCH_2N−), 4.49 (s, 4 H, dpaCH_2N−), 7.37−7.42 (m, ^1J = 6 Hz, 1 H, MebpyPy′−*H*), 7.50−7.55 (m, 3 H, bpyPy−*H*), 7.52−7.58 (m, ^1J = 6 Hz, 1 H, MebpyPy−*H*), 7.64−7.68 (m, 1 H, bpyPy−*H*), 7.67−7.72 (m, 4 H, dpaPy−*H*), 7.77 (d, ^1J = 6 Hz, 1 H, MebpyPy−*H*), 7.83 (d, ^1J = 6 Hz, 1 H, MebpyPy′−*H*), 7.85 (ddd, 1 H, bpyPy−*H*), 7.99 (d, ^1J = 5 Hz, 2 H, bpyPy−*H*), 8.02 (ddd, 1 H, bpyPy−*H*), 8.14 (dd, 2 H, dpaPy−*H*), 8.18 (ddd, 1 H, bpyPy−*H*), 8.19 (ddd, 2 H, bpyPy−*H*), 8.26 (ddd, 1 H, bpyPy−*H*), 8.58 (s, 1 H, MebpyPy′−*H*), 8.75 (s, 1 H, MebpyPy−*H*), 8.79 (d, ^1J = 8 Hz, 3 H, bpyPy−*H*), 8.83 (d, ^1J = 8 Hz, 1 H, bpyPy−*H*), 9.02 (d, ^1J = 5 Hz, 2 H, dpaPy−*H*). − ESI-MS (*m/z*): 1086.2 [M + H$^+$], 940.2 [M − PF$_6^-$], 398.0 [M − 2 PF$_6^-$].

2-Oxo-4-(tolyl)but-3-enoic Acid (11): This compound was prepared by a method described by Baba et al.[17] To a solution of sodium pyruvate (8.3 g, 0.075 mol) in water (15 mL) cooled in an ice bath, was added tolualdehyde (6.0 g, 0.050 mol) dissolved in EtOH (85 mL). To this rapidly stirred mixture was added NaOH (10% w/w, 30 mL). After stirring for an additional 15 min, the mixture was acidified with HCl (2 M), and stirred for 5 min. The yellow precipitate was filtered and washed with water and EtOH, and dried to give the acid **11** (4.9 g, 52%). − ^{1}H NMR ([D$_6$]DMSO): δ = 2.33 (s, 3 H, −phenylCH_3), 6.70 (d, 1 H, −HC=C*H*CO−), 7.23 (d, 2 H, phenyl−*H*), 7.40 (d, 1 H, −*H*C=CHCO−), 7.53 (d, 2 H, phenyl−*H*).

4-(*p*-Tolyl)-2,2′-bipyridine (13): This compound was prepared by a modification of the method described by Baba et al.[17] A suspension of the acid **11** (4.0 g, 0.021 mol), 2-pyridacylpyridinium iodide[18] (9.7 g, 0.030 mol) and ammonium acetate (16 g, 0.21 mol) in water (150 mL) was heated at reflux for 3 h. The resulting precipitate was filtered from the hot solution and washed with water and dried to yield the ammonium salt of -4-(*p*-tolyl)-2,2′-bipyridine-6-carboxylic acid (**12**) (3.5 g, 53%). Mp: 181 °C (uncorr.). − ^{1}H NMR ([D$_6$]DMSO): δ = 2.39 (s, 3 H, −phenylCH_3), 7.37 (d, ^1J = 8 Hz, 2 H, phenyl−*H*), 7.48 (dd, ^1J = 8 Hz, 5 Hz, 1 H, Py′−*H*), 7.76 (d, ^1J = 8 Hz, 2 H, phenyl−*H*), 7.98 (t, ^1J = 8 Hz, 1 H, Py′−*H*), 8.14 (s, 1 H, Py−*H*), 8.50 (d, ^1J = 8 Hz, 1 H, Py′−*H*), 8.58 (s, 1 H, Py−*H*), 8.72 (d, ^1J = 5 Hz, 1 H, Py′−*H*).

The ammonium salt **12** (2.0 g, 6.5 mmol) was gently heated over a Bunsen flame until evolution of CO_2 had ceased. The solution was cooled, suspended in Et_2O, and stirred in the presence of activated charcoal for 15 min. Filtration and evaporation of the solvent gave a brown solid (1.2 g). Column chromatography (Al_2O_3, CH_2Cl_2/EtOH, 9:1) gave 4-(*p*-tolyl)-2,2′-bipyridine (tolbpy) (1.0 g, 38%) as a pale yellow powder. Mp: 112 °C (uncorr.). − ^{1}H NMR ([D$_6$]DMSO): δ = 2.39 (s, 3 H, −phenylCH_3), 7.38 (d, 2 H, phenyl−*H*, *J* = 8 Hz), 7.49 (dd, 1 H, Py′−*H*, *J* = 8 Hz, 5 Hz), 7.75 (d, 1 H, Py′−*H*, *J* = 5 Hz), 7.78 (d, 2 H, phenyl−*H*, *J* = 8 Hz), 7.98 (t, 1 H, Py′−*H*, *J* = 8 Hz), 8.45 (d, 1 H, Py′−*H*, *J* = 8 Hz), 8.66 (s, 1 H, Py−*H*), 8.73 (d, 2 H, Py−*H* and Py′−*H*, *J* = 5 Hz). MS (EI) (*m/z*): 246.2 [M$^+$].

{4-[*p*-(Bromomethyl)phenyl]}-2,2′-bipyridine (14): A solution of *p*-tolbpy (**13**) (0.5 g, 2.0 mmol), *N*-bromosuccinimide (0.4 g, 2.0 mmol), and azobis(isobutyronitrile) (0.010 g, 0.065 mmol) in dry CCl_4 (20 mL) was heated at reflux for 19 h under argon. The cooled reaction mixture was filtered. On removal of the solvent, a yellow oil was obtained which soon crystallized to give a yellow solid (0.58 g, 88% yield). This crude product was used in the next reaction without further purification. A peak at δ = 4.6 ($CDCl_3$) in the NMR spectrum was identified as the methylene protons between the bromine and the phenyl group.

Ru(bpy)$_2${[4-(*p*-bromomethyl)phenyl]-2,2′-bipyridine}(PF$_6$)$_2$ (15): A solution of *cis*-Ru(bpy)$_2$Cl$_2$ · 2 H$_2$O[19] (0.89 g, 1.7 mmol) and silver triflate (0.89 g, 3.5 mmol) in anhydrous acetone (65 mL) was stirred for 15 h at room temperature under argon and protected from light. The precipitated AgCl was removed by filtration, and compound **14** (0.55 g, 1.7 mmol) was added to the red filtrate. This reaction mixture was stirred in the dark at room temperature for 6 h under an argon atmosphere. The acetone was evaporated and the red residue was dissolved in a mixture of MeOH (15 mL) and water (25 mL). The ruthenium complex was precipitated from the solution by addition of concentrated NH_4PF_6. The red−brown precipitate was collected by suction filtration and washed with water. Purification by column chromatography (MPLC)[14] (Al_2O_3, CH_2Cl_2/EtOH, 95:5) afforded the red complex (0.50 g, 29% yield). − ^{1}H NMR ([D$_6$]acetone): δ = 4.76 (s, 2 H, −phenylCH_2Br), 7.59−7.64 (m, 5 H, Py′−*H* and Py′′−*H*), 7.71 (d, ^1J = 8 Hz, 2 H, phenyl−*H*), 7.91 (dd, ^1J = 7 Hz, 2 Hz, 1 H, Py−*H*), 7.99 (d, ^1J = 8 Hz, 2 H, phenyl−*H*), 8.10−8.12 (m, 5 H, Py−*H* and Py′′−*H*), 8.19 (d, ^1J = 5 Hz, 1 H, Py′−*H*), 8.24−8.28 (m, 5 H, Py′−*H* and Py′′−*H*), 8.88 (d, ^1J = 6 Hz, 4 H, Py′′−*H*), 9.13 (d, ^1J = 8 Hz, 1 H, Py′−*H*), 9.18 (d, ^1J = 2 Hz, 1 H, Py−*H*).

Ru(bpy)$_2$[{4′-[4-bis(2-methylpyridine)aminomethyl]phenyl}bipyridine](PF$_6$)$_2$ (4a): Compound **15** (0.084 g, 0.082 mmol) and dipicolylamine[16] (0.021 g, 0.11 mmol) were dissolved in acetonitrile (2 mL). After the addition of 3 drops of Et_3N, the solution was

heated at reflux for 7 h. The solvent was evaporated and the resulting residue was purified by column chromatography on silica gel using MeCN/water/KNO_3(sat.) (28:1:2) as eluent to afford the pure product (0.019 g, 20%). − ^{1}H NMR ([D$_6$]acetone): δ = 3.89 (s, 2 H, phenylCH_2N−), 3.91 (s, 4 H, dpaCH_2N−), 7.30 (dd, ^1J = 5 Hz, 2 H, dpaPy−*H*), 7.56−7.62 (m, 5 H, bpyPy−*H* (4 H) and tolbpyPy′−*H* (1 H)), 7.68 (d, ^1J = 7 Hz, 2 H, dpaPy−*H*), 7.71 (d, ^1J = 9 Hz, 2 H, phenyl−*H*), 7.82 (dt, ^1J = 7 Hz, 2 Hz, 2 H, dpaPy−*H*), 7.87 (dd, ^1J = 6 Hz, 2 Hz, 1 H, tolbpyPy−*H*), 7.96 (d, ^1J = 9 Hz, 2 H, phenyl−*H*), 8.06 (d, ^1J = 6 Hz, 1 H, tolbpyPy−*H*), 8.07−8.11 (m, 4 H, bpyPy−*H*), 8.15 (d, ^1J = 6 Hz, 1 H, tolbpyPy′−*H*), 8.19−8.25 (m, 5H; bpyPy−*H* (4 H) and tolbpyPy′−*H* (1 H)), 8.57 (d, ^1J = 5 Hz, 2 H, dpaPy−*H*), 8.85 (d, ^1J = 8 Hz, 4 H, bpyPy−*H*), 9.12 (d, ^1J = 9 Hz, 1 H, tolbpyPy′−*H*), 9.13 (s, 1 H, tolbpyPy−*H*). − ESI-MS (*m*/*z*): 1002.3 [M − PF_6^-], 501.3 [M − PF_6^- + H^+], 428.3 [M − 2 PF_6^-].

4-[Bis(methyl acet-2-yl)aminomethyl]-4′-methyl-2,2′-bipyridine (8e): The hydrochloride salt of iminodiacetic acid dimethyl ester (0.44 g, 2.4 mmol) and anhydrous sodium carbonate (1.0 g) were dissolved in acetonitrile (150 mL). 4-Bromomethyl-4′-methyl-2,2′-bipyridine (**8b**) (0.63 g, 2.4 mmol) was added and the reaction was stirred for 10 h at 4 °C. After heating at reflux overnight, the reaction mixture was cooled and filtered. The solid was washed with ethyl acetate and the solvent evaporated under reduced pressure. The crude dark red product was purified on silica gel using ethyl acetate as eluent. The desired product was obtained as an uncolored oil (0.57 g, 76%). − ^{1}H NMR ($CDCl_3$): δ = 2.43 (s, 3 H, bpyCH_3), 3.59 (s, 4 H, CH_2COO), 3.70 (s, 6 H, ester OCH_3), 4.04 (s, 2 H, bpyCH_2), 7.12 (d, 1 H, bpyPy−*H*), 7.48 (d, 1 H, bpyPy−*H*), 8.22 (s, 1 H, bpyPy−*H*), 8.33 (s, 1 H, bpyPy−*H*), 8.54 (d, ^1J = 5 Hz, 1 H, bpyPy−*H*), 8.64 (d, ^1J = 5 Hz, 1 H, bpyPy−*H*).

Ru(bpy)$_2${4-[CH$_2$N(CH$_2$COOH)$_2$]-4′-methylbipyridine}(PF$_6$)$_2$ (5a): Hydrolysis of ester **10a** in a NaOH/H_2O solution overnight gave the desired diacid **5a** in quantitative yield. − ^{1}H NMR (D_2O): δ = 2.50 (s, 3 H, MebpyCH_3), 3.21 (s, 4 H, −NCH_2COOH), 3.90 (s, 2 H, MebpyCH_2N−), 7.24 (d, 1 H, MebpyPy′−*H*), 7.32−7.43 (m, 4 H, bpyPy−*H*), 7.46 (d, 1 H, MebpyPy−*H*), 7.63 (d, 1 H, MebpyPy′−*H*), 8.00−8.06 (m, 4 H, bpyPy−*H*), 8.43 (s, 1 H, MebpyPy′−*H*), 8.51 (d, 4 H, bpyPy−*H*), 8.60 (s, 1 H, MebpyPy−*H*). − ESI-MS (*m*/*z*): 874.3 [M − PF_6^-], 364.2 [M − 2 PF_6^-].

{2-[(Dipicolyl)aminomethyl]}-3-hydroxypyridine (16): 2-Bromomethyl-3-hydroxypyridine hydrobromide (3.8 g, 0.014 mol), obtained according to a literature procedure[20] was added over a period of 3 h, to a refluxing solution of dipicolylamine[16] (2.8 g, 0.014 mol) in MeCN (400 mL), containing sodium carbonate (10 g). The mixture was heated at reflux overnight, cooled, and purified by column chromatography on silica gel, using CH_2Cl_2/MeOH (94:6) as eluent, to give compound **16** (HO-tpa) in 78% yield. ^{1}H NMR ($CDCl_3$): δ = 7.16 (d, ^1J = 2.6 Hz, 2 H), 7.25 (m, 2 H), 7.37 (d, ^1J = 8.6 Hz, 2 H), 7.72 (td, ^1J = 8.6 Hz, 1.2 Hz, 2 H), 7.92 (m, 1 H), 8.47 (d, ^1J = 4.8 Hz, 2 H). − ^{13}C NMR ($CDCl_3$): δ = 123.0, 123.3, 123.5, 124.4, 137.5, 139.7, 144.6, 149.0, 153.6, 158.3. − ESI-MS (*m*/*z*): 306 [M^+].

Ru(bpy)$_2$[4-(CH$_2$O-tpa)-4′-methylbipyridine](PF$_6$)$_2$ (6a): Metallic sodium (3.1 mg) was dissolved in dry MeOH (5 mL), and **16** (HO-tpa) (0.041 g, 1.35 mmol) was added followed by DMSO (4 mL). MeOH was evaporated under reduced pressure. Ru(bpy)$_2$(4-bromomethyl-4′-methylbipyridine)(PF$_6$)$_2$ (**9b**, 0.13 mg) was added and the mixture was heated at 80 °C for 4 d in the dark. DMSO was removed under vacuum and the resulting product was purified by chromatography (silica gel, MeCN/water/KNO_3(sat.), 7:1:1). The compound was precipitated by the addition of saturated NH_4PF_6 (aq.) and purified further by MPLC[14] on aluminum oxide using CH_2Cl_2/MeOH (95:5) to give compound **6a** in 46% yield. − ^{1}H NMR ([D$_6$]acetone): δ = 2.53 (s, 3 H, bpyCH_3), 3.96 (s, 4 H, pyCH_2N−), 4.07 (s, 2 H, pyCH_2N−), 5.42 (s, 2 H, bpyOCH_2−), 7.06 (m, 2 H, py−*H*), 7.24 (m, 1 H, py−*H*), 7.43 (m, 2 H, py−*H*), 7.56−7.65 (m, 9 H, py−*H*), 7.87 (d, ^1J = 5.8 Hz, 1 H, Mebpy−*H*), 7.98−8.10 (m, 6 H, py−*H*), 8.18−8.24 (m, 5 H, py−*H*), 8.33 (d, ^1J = 6.0 Hz, 1 H, Mebpy−*H*), 8.69 (s, 1 H, Mebpy−*H*), 8.82 (m, 4 H, bpy−*H*), 8.94 (s, 1 H, Mebpy−*H*). − ESI-MS (*m*/*z*): 1046 [M − PF_6^-], 450 [M − 2 PF_6^-].

[4,4′-Bis(bromomethyl)]-2,2′-bipyridine (8d): Compound **8d** was prepared via the diol **8c** in the same manner as **8b**, but with a large excess of SeO_2 to oxidize the dimethylbipyridine and 2 mol equivalents of $NaBH_4$ to reduce the dialdehyde. Due to problems with hydrolysis during attempted purification of this ligand, the crude product was used directly in the following step.

Ru(bpy)$_2$[4,4′-bis(CH$_2$Br)bpy](PF$_6$)$_2$ (9c): *cis*-Ru(bpy)$_2$Cl$_2$·2 H_2O[19] (0.10 g, 0.20 mmol) and silver triflate (2 equiv.) were dissolved in anhydrous acetone. The mixture was stirred for 7 h at room temperature under argon. The AgCl that formed during the reaction was removed by filtration. [4,4′-Bis(bromomethyl)]-2,2′-bipyridine (**8d**) (0.068 g, 0.20 mmol) was added to the filtrate and the reaction mixture was allowed to stir at room temperature under argon. After 1.5 h, the solvent was evaporated under reduced pressure and the red product was redissolved in MeOH. The product was precipitated by the addition of concentrated aqueous NH_4PF_6. The resulting product was purified by column chromatography (MPLC)[14] on neutral Al_2O_3, gradient elution, EtOH/CH_2Cl_2, 0:100 to 10:90, to afford Ru(bpy)$_2$[4,4′-bis(CH_2Br)-bpy](PF$_6$)$_2$ (**9c**) (0.072 g, 35% yield).

Ru(bpy)$_2$[4,4′-bis(CH$_2$-dpa)bpy](PF$_6$)$_2$ (7a): A solution of dipicolylamine[16] (0.028 g, 0.14 mmol) and Et_3N (slight excess) was added dropwise to a solution of **9c** (0.072 g, 0.069 mmol) in MeCN. The reaction was allowed to stir for 7 h under argon. The solvent was removed under reduced pressure and the product was purified by column chromatography (silica gel, MeCN/water/KNO_3(sat.), 28:1:2). The desired product was eluted as the second band and excess KNO_3 was removed by filtration after dissolving the product in acetone. The product was then precipitated from a MeOH/water solution by adding concentrated aqueous NH_4PF_6 to yield **7a** (0.070 g, 79%). − ^{1}H NMR ($CDCl_3$): δ = 3.94 (s, 8 H, dpaCH_2N−), 4.08 (s, 4 H, bpyCH_2N−), 7.19−7.22 (ddd, 4 H, dpaPy−*H*), 7.50 (dd, 4 H, dpaPy−*H*), 7.52−7.55 (m, 4 H, bpyPy−*H*), 7.65 (d, 2 H, bpyPy′−*H*), 7.66 (d, 2 H, bpyPy′−*H*), 7.66−7.71 (ddd, 4 H, dpaPy−*H*), 7.74−7.76 (dd, 4 H, bpyPy−*H*), 8.14−8.17 (m, 4 H, bpyPy−*H*), 8.58 (dd, 4 H, dpaPy−*H*), 8.91 (s, 2 H, bpyPy′−*H*), 9.11−9.14 (dd, 4 H, bpyPy−*H*). − ESI-MS (*m*/*z*): 495.8 [M − 2 PF_6^-], 331.1 [M − 2 PF_6^- + H^+].

Ru(bpy)$_2${4-[CH$_2$N(CH$_2$CO$_2$CH$_3$)$_2$]-4′-methylbipyridine}(PF$_6$)$_2$ (10a): *cis*-Ru(bpy)$_2$Cl$_2$ · 2 H_2O[19] (0.89 g, 1.8 mmol) and **8e** (0.60 mg, 1.8 mmol) were dissolved in MeOH (200 mL) and heated at reflux overnight. The solvent was removed and water (80 mL) was added. After filtration of the red solution, a large excess of NH_4PF_6 (1.0 g) was added to the filtrate and the orange precipitate was collected by filtration, washed with water and dried to yield **10a**. The product was purified by column chromatography (MPLC)[14] (Al_2O_3, CH_2Cl_2/EtOH, 97:3) and obtained in 65% yield. − ^{1}H NMR ([D$_6$]-acetone): δ = 2.64 (s, 3 H, MebpyCH_3), 3.67 (s, 6 H, −COOCH_3), 3.72 (s, 4 H, −NCH_2COOCH$_3$), 4.25 (s, 2 H, MebpyCH_2), 7.48 (d, 1 H, MebpyPy′−*H*), 7.61−7.67 (m, 4 H, bpyPy−*H*), 7.71 (d, 1 H,

MebpyPy−*H*), 7.92 (d, 1 H, MebpyPy′−*H*), 8.00 (d, 1 H, MebpyPy−*H*), 8.06−8.15 (m, 4 H, bpyPy−*H*), 8.23−8.29 (m, 4 H, bpyPy−*H*), 8.46 (s, 1 H, MebpyPy′−*H*), 8.88 (d, 4 H, bpyPy−*H*), 8.92 (s, 1 H, MebpyPy−*H*). − ESI-MS (*m/z*): 902.3 [M − PF_6^-], 378.1 [M − 2 PF_6^-].

Ru(bpy)$_2$[4-(CH$_2$-O-tpa-Mn)-4′-methylbipyridine](PF$_6$)$_2$ (6b): $MnCl_2 \cdot 4\,H_2O$ (0.030 g, 0.15 mmol) was added to compound **6a** (0.12 g, 0.10 mmol) dissolved in MeOH (10 mL). After 10 min, a concentrated aqueous solution of NH_4PF_6 was added and a red precipitate was formed after 5 min of stirring at room temperature. Filtration and washing with cold MeOH and Et_2O, followed by drying gave **6b** as a red solid (0.11 g, 83% yield). − ^{1}H NMR ([D$_6$]acetone): proton signals from the ligands in the ruthenium moiety were broadened, and proton signals for the manganese ligands were not seen when using a spectral width of 15 ppm. − ESI-MS (*m/z*): 1175 [M − PF_6^-], 567 [M − PF_6^- − Cl^-], 514 [M − 2 PF_6^-], 331 [M − 2 PF_6^- − Cl^-].

The Mn complexes **3b**, **4b**, **5b**, and **7b** were prepared in a similar way as **6b**, except that the reaction times with $MnCl_2$ varied from a few hours to two days. After the addition of NH_4PF_6, filtration and drying, the complexes **3b**, **4b**, **5b**, and **7b** were obtained as fine powders. Complex **5b** was only obtained in an impure state and was not fully characterized.

Ru(bpy)$_2$(bpy-dpaMn)(PF$_6$)$_2$Cl$_2$ (3b): ESI-MS (*m/z*): 569.8 [M − 2 Cl^-], 533.3 [M − PF_6^- + H^+], 514.5 [M − PF_6^- − Cl^-], 460.3 [M − 2 PF_6^-].

Ru(bpy)$_2$(bpy-tolyl-dpaMn)(PF$_6$)$_2$Cl$_2$ (4b): ESI-MS (*m/z*): 1127.2 [M − PF_6^-], 600.7 [M − 2 Cl^-], 545.7 [M − PF_6^- − Cl^-], 315.5 [M − 2 PF_6^- − Cl^-].

Ru(bpy)$_2$(bpy-bisdpaMn$_2$)(PF$_6$)$_2$Cl$_4$ (7b): ESI-MS (*m/z*): 749.3 [M − Cl^- + H^+], 731.2 [M − 2 Cl^-], 676.9 [M − PF_6^- − Cl^-].

Acknowledgments

The financial support for this work was provided by the Nordic Energy Research Council, the Knut and Alice Wallenberg Foundation, the Swedish Research Council for Engineering Sciences, the Swedish Natural Science Research Council, and the European TMR Program (TMR Network CT 96-0031). We are also very thankful to Jens Z. Pedersen for recording the EPR spectra, Tina Esbech for measuring the ESI-MS spectra, and Daniel Czermac for contributions to the synthesis.

[1] For recent general reviews, see e. g.: [1a] A. J. Bard, M. A. Fox, *Acc. Chem. Res.* **1995**, *28*, 141. − [1b] E. Amouyal, *Sol. Energy Mater. Sol. Cells* **1995**, *38*, 249.

[2] [2a] R. D. Britt, *In Oxygenic Photosynthesis: The Light Reactions* (Eds. D. R. Ort, C. F. Yocum), Kluwer Academic, Dordrecht, Netherlands, **1996**, p. 137. − [2b] V. K. Yachandra, M. P. Sauer, M. P. Klein, *Chem. Rev.* **1996**, *96*, 2927. − [2c] R. J. Debus, *Biochim. Biophys. Acta* **1992**, *269*, 1102. − [2d] G. W. Brudvig, *Mechanistic Bioinorganic Chemistry: Advances in Chemistry Ser. 246* (Eds. H. H. Thorp, V. L. Pecoraro), ACS Washington DC, **1995**, p. 249.

[3] [3a] J. Limburg, V. A. Szalai, G. W. Brudvig, *J. Chem. Soc., Dalton Trans.* **1999**, 1353. − [3b] P. E. M. Siegbahn, R. H. Crabtree, *J. Am. Chem. Soc.* **1999**, *121*, 117. − [3c] G. Blondin, R. Davydov, C. Philouze, M.-F. Charlot, S. Styring, B. Åkermark, J.-J. Girerd, A. Boussac, *J. Chem. Soc., Dalton Trans.* **1997**, 4069. − [3d] V. K. Yachandra, V. J. DeRose, M. J. Latimer, I. Mukerji, K. Sauer, M. P. Klein, *Science* **1993**, *260*, 675.

[4] [4a] W. Rüttinger, C. G. Dismukes, *Chem. Rev.* **1997**, *97*, 1. − [4b] S. Pal, M. K. Chan, W. H. Armstrong, *J. Am. Chem. Soc.* **1992**, *114*, 6398. − [4c] R. Manchanda, G. W. Brudvig, R. H. Crabtree, *Coord. Chem. Rev.* **1995**, *144*, 1. − [4d] V. L. Pecoraro, J. M. Baldwin, A. Gelasco, *Chem. Rev.* **1994**, *94*, 807. − [4e] R. Hage, *Recl. Trav. Chim. Pays-Bas* **1996**, *115*, 385. − [4f] K. Wieghardt, *Angew. Chem. Int. Ed. Engl.* **1989**, *28*, 1153; *Angew. Chem.* **1989**, *28*, 1153.

[5] [5a] K. Kalyanasundaram, *Photochemistry of Polypyridine and Porphyrin Complexes*, Academic Press, London, **1992**. − [5b] V. Balzani, F. Scandola, *Supramolecular Photochemistry*, Ellis Horwood, Chichester, UK, **1991**. − [5c] H. Kurreck, M. Huber, *Angew. Chem. Int. Ed. Engl.* **1995**, *34*, 849. − [5d] M. R. Wasielewski, *Chem. Rev.* **1992**, *92*, 435. − [5e] V. Balzani, A. Juris, M. Venturi, S. Campagna, S. Serroni, *Chem. Rev.* **1996**, *96*, 759. − [5f] A. Osuka, S. Nakajima, T. Okada, S. Taniguchi, K. Nozaki, T. Ohno, I. Yamazaki, Y. Nishimura, N. Mataga, *Angew. Chem. Int. Ed. Engl.* **1996**, *35*, 92. − [5g] A. Harriman, J.-P. Sauvage, *Chem. Soc. Rev.* **1996**, 41. − [5h] G. Steinberg-Yfrach, J.-L. Rigaud, E. N. Durantini, A. L. Moore, D. Gust, T. A. Moore, *Nature* **1998**, *385*, 239. − [5i] C. A. Slate, D. R. Striplin, J. A. Moss, P. Chen, B. W. Erickson, T. J. Meyer, *J. Am. Chem. Soc.* **1998**, *120*, 4885.

[6] [6a] L. Sun, H. Berglund, R. Davydov, T. Norrby, L. Hammarström, P. Korall, A. Börje, C. Philouze, K. Berg, A. Tran, M. Andersson, G. Stenhagen, J. Mårtensson, M. Almgren, S. Styring, B. Åkermark, *J. Am. Chem. Soc.* **1997**, *119*, 6996. − [6b] L. Sun, L. Hammarström, T. Norrby, H. Berglund, R. Davydov, M. Andersson, A. Börje, P. Korall, C. Philouze, M. Almgren, S. Styring, B. Åkermark, *Chem. Commun.* **1997**, 607. − [6c] H. Berglund-Baudin, L. Sun, R. Davydov, M. Sundahl, S. Styring, B. Åkermark, M. Almgren, L. Hammarström, *J. Phys. Chem. A* **1997**, *102*, 2512.

[7] G. Anderegg, E. Hubmann, N. G. Podder, F. Wenk, *Helv. Chim. Acta* **1977**, *60*, 123.

[8] [8a] D. K. Towle, C. A. Botsford, D. J. Hodgson, *Inorg. Chim. Acta* **1988**, *141*, 167. − [8b] A. R. Oki, J. Glerup, D. J. Hodgson, *Inorg. Chem.* **1990**, *29*, 2435. − [8c] P. A. Goodson, A. R. Oki, J. Glerup, D. J. Hodgson, *J. Am. Chem. Soc.* **1990**, *112*, 6248.

[9] [9a] J. A. Treadway, B. Loeb, R. Lopez, P. A. Anderson, F. R. Keene, T. J. Meyer, *Inorg. Chem.* **1996**, *35*, 2242. − [9b] L. Hammarström, F. Barigelletti, L. Flamigni, M. T. Indelli, N. Armaroli, G. Calogero, M. Guardigli, A. Sour, J.-P. Collin, J.-P. Sauvage, *J. Phys. Chem. A* **1997**, *101*, 9061. − [9c] N. H. Damrauer, T. R. Boussie, M. Devenney, J. K. McCusker, *J. Am. Chem. Soc.* **1997**, *119*, 8253.

[10] [10a] P. Finckh, H. Heitele, M. E. Michel-Beyerle, *J. Phys. Chem.* **1988**, *92*, 6584 and references therein. − [10b] A. Helms, D. Heiler, G. McLendon, *J. Am. Chem. Soc.* **1992**, *114*, 6227.

[11] A. Magnuson, H. Berglund, P. Korall, L. Hammarström, B. Åkermark, S. Styring, L. Sun, *J. Am. Chem. Soc.* **1997**, *119*, 10720.

[12] [12a] D. Burdinski, K. Wieghardt, S. Steenken, *J. Am. Chem. Soc.* **1999**, *121*, 10781. − [12b] D. Burdinski, E. Bothe, K. Wieghardt, *Inorg. Chem.* **2000**, *39*, 105. − [12c] L. Sun, M. K. Raymond, A. Magnuson, D. LeGourierrec, M. Tamm, M. Abrahamsson, P. Huang-Kenéz, J. Mårtensson, G. Stenhagen, L. Hammarström, S. Styring, B. Åkermark, *J. Inorg. Biochem.* **2000**, *78*, 15.

[13] N. E. Tokel-Takvoryan, R. E. Hemingway, A. J. Bard, *J. Am. Chem. Soc.* **1973**, *95*, 6582.

[14] P. Baeckström, K. Stridh, L. Li, T. Norin, *Acta Chem. Scand.* **1987**, *B41*, 442.

[15] L. Geren, H. Seung, B. Durham, F. Millett, *Biochemistry* **1991**, *30*, 9450.

[16] S. Larsen, K. Michelsen, E. Pedersen, *Acta Chem. Scand.* **1986**, *A40*, 63.

[17] A. Baba, W. Wang, K. W. Yong, L. Strong, R. H. Schmehl, *Synth. Comm.* **1994**, *24*, 1029−1036.

[18] F. Krohnke, K. F. Gross, *Chem. Ber.* **1959**, *92*, 22.

[19] T. J. Meyer, D. J. Salmon, B. P. Sullivan, *Inorg. Chem.* **1978**, *17*, 3334.

[20] T. Urbanski, *J. Chem. Soc.* **1946**, 110.

Received April 17, 2000
[I00151]

Chlorination of Platinum-Bound Salicylaldoxime. The First Example of a Structurally Characterized Monodentate Salicylaldoxime-Type Ligand

Savelii F. Kaplan,[a] Vadim Yu. Kukushkin,*[a] Sergiu Shova,[b] Kinga Suwinska,[c] Gabriele Wagner,[d] and Armando J. L. Pombeiro*[d]

Keywords: Salicylaldoxime complexes / Platinum / Ligand reactivity / Metal-mediated synthesis / Chlorination

The reaction of $K_2[PtCl_4]$ and salicylaldoxime in an approximate 1:2 molar ratio in water resulted in the isolation of a mixture of four compounds from which [Pt(*o*-OC_6H_4CH=NOH)$_2$] (**1**) and [PtCl(OC_6H_4CH=NOH)(HOC_6H_4CH=NOH)] (**2**) were isolated, whereas the other two were shown to be unstable and decomposed both in solution and on SiO_2 during chromatography. Chlorination of **1** and **2** with Cl_2 resulted in the oxidative addition of chlorine to the platinum(II) center and in the chlorination of the benzene ring, giving the platinum(IV) complexes [$PtCl_2$(3,5,2-Cl,Cl,OC_6H_2CH=NOH)$_2$] (**3**) and [$PtCl_3$(3,5,2-Cl,Cl,OC_6H_2CH=NOH)(3,5,2-Cl,Cl,HOC_6H_2CH=NOH)] (**5**), respectively, containing commercially unavailable 3,5-dichloro-2-hydroxybenzaldehye oxime. Alternatively, treatment of **1** with NOCl resulted only in the oxidation of the platinum(II) center to furnish [$PtCl_2$(*o*-OC_6H_4CH=NOH)$_2$] (**4**), whereas the benzene rings of salicylaldoximato ligands remained intact. All complexes were characterized by C, H, N, Cl and Pt elemental analyses, FAB^+ mass spectrometry, IR and ^1H, $^{13}C\{^1H\}$ and ^{195}Pt NMR spectroscopy. Compounds **1**, **3** and **5** were analyzed by X-ray crystallography. In **1**, the salicylaldoximato ligands adopt a *trans* configuration and the hydrogen atoms of the OH groups are involved in intramolecular hydrogen bonding, forming five-membered rings. In **3**, every molecule of the complex forms the repeating unit for a self-assembly that produces infinite one-dimensional polymeric chains directed along the z axis held by hydrogen bonds. The complex **5** represents the first example of a structurally characterized metal complex with a monodentate salicylaldoxime-type ligand, although the conventional bidentate *N,O*-coordination mode is a classical topic in coordination chemistry.

Introduction

Although oximes (RR′C=NOH) display one of the most versatile modes of reactivity in metal-mediated processes, their conversions at a metal center have attracted attention only in the last decade.[1,2] Being involved in these studies for the last five years, we have been investigating some aspects of oxime ligand reactivity, in particular with respect to (*i*) the OH group, e.g. their facile deprotonation and the self-assembly of the oxime-oximato species formed,[3] addition to nitriles bound to Pt^{IV},[4,5] Re^{IV} [6] and Rh^{III} [7] ions, addition to ketones in a Pt^{IV} complex,[8] formation of metallacycles accompanied by the OH addition;[9] (*ii*) the N−OH group, e.g. its oxidative addition to an electron-rich rhenium(I) center,[10] (*iii*) the oxime N atom, e.g. its oxidation to give (nitrosoalkane)Pt complexes[11,12] or its reduction in a strongly acidic solution,[13] (*iv*) the C=N group, e.g. its metal-mediated hydrolysis[14] and the conversion into the nitrile group upon Ru-assisted dehydration of aldoximes.[15] Following these studies, we turned our attention to the reactions of *peripheral* R/R′ groups and have recently reported the chlorination, by molecular chlorine, of the platinum(II) salicylaldoxime, *trans*-(*S,N*)-[$PtCl_2$(*o*-HOC_6H_4-CH=NOH)(Me_2SO)]·H_2O, and the salicylaldoximato(1$^-$), *trans*-(*S,N*)-[PtCl(*o*-OC_6H_4CH=NOH)(Me_2SO)], complexes.[16] Instead of the Piloty reaction, which in the case of aldoximes leads to chloro oximes, RC(Cl)=NOH (*via* RCH(Cl)−N=O),[17] or to the formation of platinum(III) derivatives previously detected upon the chlorination of (*vic*-dioximato)platinum(II) compounds,[18] we observed both the chlorination of the salicylaldoxime benzene ring and the oxidative addition of Cl_2 to the platinum(II) center. Conclusions that can be derived from the latter work indicate that platinum acts as a protecting center for the oxime functionality and this allows for the formation of the chlorinated species, which cannot be synthesized by direct chlorination of the corresponding salicylaldoxime.

Our interest in the continuation of the chlorination experiments lied in at least three areas. Firstly, we wondered if the protection of the NOH group and the concomitant chlorination of the benzene ring was peculiar for the complexes being investigated or if the reaction could be extended to other salicylaldoxime platinum compounds. Secondly, it was expected to contribute to the almost unexplored chemistry of salicylaldoxime coordinated to plat-

[a] Department of Chemistry, St. Petersburg State University, Universitetsky Pr. 2, 198904 Stary Petergof, Russian Federation
E-mail: kukushkin@VK2100.spb.edu
[b] Department of Chemistry, State University of Moldova, MD 2009, Chisinau, Republic of Moldova
[c] Institute of Physical Chemistry, Polish Academy of Sciences, Warsaw, Poland
[d] Centro de Química Estrutural, Complexo I, Instituto Superior Técnico, Av. Rovisco Pais, 1049−001 Lisboa, Portugal
E-mail: pombeiro@ist.utl.pt

 © WILEY-VCH Verlag GmbH, 69451 Weinheim, 2001 1434−1948/01/0404−1031 $ 17.50+.50/0

inum. Thirdly, our own observations[16] and also some earlier studies[19] indicated the possibility of *N-monodentate* coordination of classical *bidentate chelating* ligands such as salicylaldoxime and its derivatives. We therefore focused our efforts on the structural determination of previously uncharacterized monodentate species. In this paper we present the revisited synthesis (previously reported by Cox et al.[19]) of two salicylaldoxime complexes of platinum(II). We report the X-ray structure of one of the compounds, as well as the isolation of a new product, chlorination studies of the two platinum(II) compounds with Cl_2 and NOCl giving, in one case, a Pt^{IV}-based *monodentate* chlorinated salicylaldoxime that was successfully characterized by X-ray single-crystal diffraction. Furthermore, an unusual intermolecular hydrogen bonding was shown by an X-ray study of one of the Pt^{IV} products. This hydrogen bonding results in a self-assembly, forming infinite one-dimensional polymeric chains, and is significant in the developing field of self-assembly of metal complexes by hydrogen bonding, which has applications in crystal engineering and materials science.[3]

Results and Discussion

Synthesis of Platinum(II) Compounds with Salicylaldoxime(ato) Ligands

Cox and co-authors[19] reported the reaction of $K_2[PtCl_4]$ and salicylaldoxime in a molar ratio of approximately 1:2 in water, resulting in the isolation of a mixture of the *bis*-chelate [Pt(*o*-$OC_6H_4CH{=}NOH)_2$] and the complex [$PtCl_2$(*o*-$HOC_6H_4CH{=}NOH)_2$] that contains, as had been suggested,[19] monodentate salicylaldoxime ligands. It was pointed out[19] that the latter complex is unstable in solutions and decomposes on standing.

The ^{195}Pt NMR spectrum of the crude mixture, prepared according to a known procedure,[19] showed four signals of similar intensities, and TLC showed four well-defined spots. The signal at $\delta = -1611$ (480 Hz) in the spectrum was assigned to [Pt(*o*-$OC_6H_4CH{=}NOH)_2$] (**1**) and the peak at $\delta = -1842$ (360 Hz) was ascribed to [$PtCl(OC_6H_4CH{=}NOH)(HOC_6H_4CH{=}NOH)$] (**2**) (both are depicted in Scheme 1). The former was isolated by following the method of Cox,[19] and the latter was separated from the mixture by chromatography, and both were characterized by C, H, N, Cl and Pt elemental analyses, FAB^+ mass spectrometry, IR and ^1H, $^{13}C\{^1H\}$ and ^{195}Pt NMR spectroscopy. Compound **1** was analyzed by X-ray crystallography. Our attempts to isolate two other compounds [^{195}Pt NMR: $\delta = -1999$ (500 Hz) and $\delta = -2064$ (250 Hz)] failed because of their decomposition both in solution and on SiO_2 during chromatography. Although the values of the chemical shifts for these yet unidentified species seem to be reasonable for *cis* and *trans* isomers of **1**, no further evidence in favor of these complexes was obtained.

Complex **1** was characterized by X-ray single-crystal diffractometry. The coordination polyhedron of the centrosymmetric compound is a slightly distorted square plane (Figure 1).

The salicylaldoximato ligands in the structure adopt a *trans* configuration and the hydrogen atoms of the OH groups are involved in intramolecular hydrogen bonding, forming a five-membered ring. Interestingly, these H atoms, found from the difference synthesis, are disordered by two positions with a 50% population at each one, i.e. at the oxime =NOH group and at the phenol OH group, thus indicating the existence of two solid tautomers. However, careful comparison of bond lengths in the chelated ring of **1** with (*i*) typical bond lengths in oxime/oximato compounds; (*ii*)

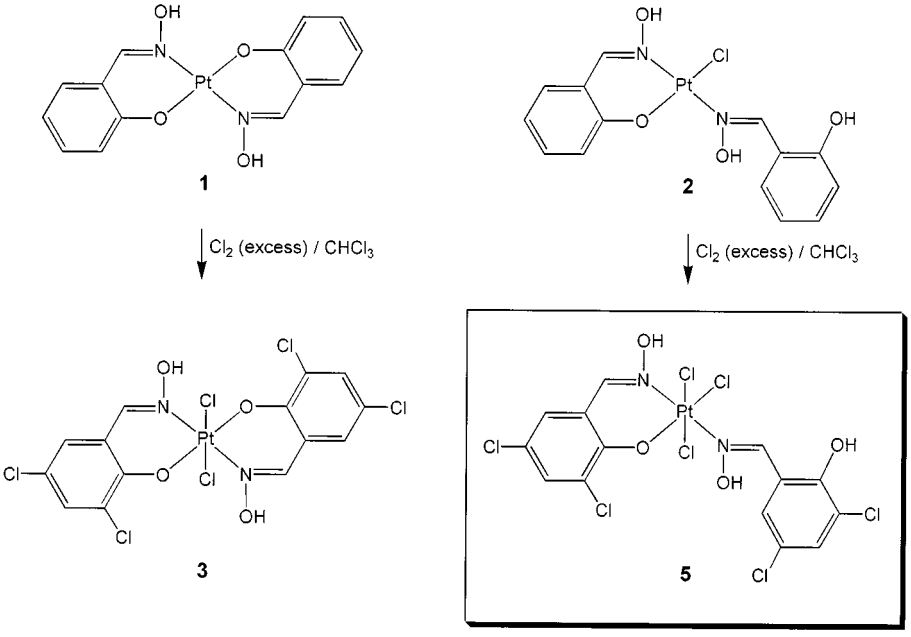

Scheme 1

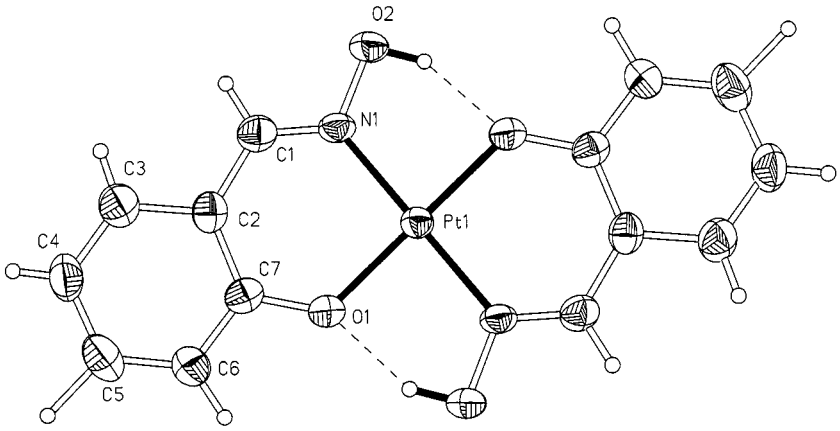

Figure 1. View of *trans-(N,N)*-[Pt(*o*-$OC_6H_2CH{=}NOH)_2$] (**1**) with atomic numbering

Table 1. Selected bond lengths for the (salicylaldoximato)Pt^{II} complexes and literature data

Complexes/bond lengths, Å	=N−O	C=N	C−C(H)=	C=C	C−O
[Pt(*o*-$OC_6H_4CH{=}NOH)_2$] (**1**)	1.385(8)	1.268(9)	1.434(11)	1.415(11)	1.327(9)
[$PtCl_2$(3,5,2-Cl,Cl,$OC_6H_2CH{=}NOH)_2$] (**3**)	1.367(7)	1.292(9)	1.452(10)	1.409(10)	1.331(8)
[$PtCl_3$(3,5,2-Cl,Cl,$OC_6H_2CH{=}NOH$)-(3,5,2-Cl,Cl,$HOC_6H_2CH{=}NOH$)] (**5**)					
monodentate ligand	1.390(16)	1.299(17)	1.44(2)	1.40(2)	1.36(2)
bidentate ligand	1.390(17)	1.270(19)	1.43(2)	1.41(2)	1.340(16)
ref. average[31,32]	1.402[a]	1.281[c]	1.455[d]	1.397[e]	1.321[f]
	1.367−1.393[b]				

[a] N−O in (C=)(CC_{sp^3})−C=N−OH oximes. − [b] N−O in oxime and oximato Pt^{II} complexes.[3] − [c] C=N in oximes. − [d] C_{sp^3}−CC_{sp^2} conjugated. − [e] In substituted phenyl ring. − [f] Aryloxy complexes.

distances within both the chelated salicylaldoximato ring and the monodentate salicylaldoxime ligand in the two platinum(IV) complexes from both the current (see Table 1) and previous work;[16] and (*iii*) bond lengths in some other salicylaldoximato complexes,[20] does not give any further evidence in favor of the phenol tautomeric structure.

Chlorination of [Pt(*o*-$OC_6H_4CH{=}NOH)_2$] (1)

Passage of excess Cl_2 through a chloroform solution of **1** for 20 min at room temperature resulted in the oxidative addition of chlorine to the platinum(II) center and in the chlorination of the benzene ring (Scheme 1). As a result of the overall process, the platinum(IV) complex [$PtCl_2$(3,5,2-Cl,Cl,$OC_6H_2CH{=}NOH)_2$] (**3**) (Scheme 1), containing commercially unavailable 2-hydroxy-3,5-dichlorobenzaldehyde oxime was isolated in 85% yield. The oxime 3,5,2-Cl,Cl,$HOC_6H_2CH{=}NOH$ was prepared earlier by the chlorination of salicylaldehyde to give 3,5,2-Cl,Cl,$HOC_6H_3CH{=}O$ and its subsequent condensation with hydroxylamine.[21] We have also observed that when nitrosyl chloride is used instead of molecular chlorine, only oxidation of the central ion is observed, to give [$PtCl_2$(*o*-$OC_6H_4CH{=}NOH)_2$] (**4**), and the benzene rings remain intact.

As already indicated,[16] chlorination of *free* salicylaldoxime under the same conditions as for the platinum(II) complexes gave a variety of products due to oxidative deoximation[1,2] and chlorination, with no dominant compound. The latter fact suggests that coordination affects the reaction by blocking and thus protecting the oxime N atom from oxidation, thus also making the chlorination selective.

The structure of **3** was determined by X-ray crystallography. In the centrosymmetric complex, the coordination polyhedron of platinum is a slightly distorted octahedron with the ligands in a *trans* configuration (Figure 2). All bonds around the Pt center have normal values. The chelate ring is in the envelope-like conformation where the Pt atom deviates from the organic unit by 0.256 Å.

The oxime group is involved in an unusual hydrogen bonding (Figure 3), e.g. the *intermolecular* − rather than *intramolecular* as in the case of [Pt(*o*-$OC_6H_4CH{=}NOH)_2$] (**1**) − O(2)−H···Cl(3) hydrogen bond [O(2)···Cl(3)(*x,y,z* − 1) = 3.155, H···Cl(3) 2.34 Å, angle O(2)−H···Cl(3) 161°]. According to Wells,[22] O···Cl^- distances in the range 2.95−3.4 Å are found for O−H···Cl^- hydrogen bonds (for Cl^-···H_3O^+ the distance is 2.95[22]). Every molecule of the complex forms the repeating unit for a self-assembly that produces infinite one-dimensional polymeric chains directed along the *z* axis held by H-bonds. It is worth noting that the study of self-assembly of metal complexes, in particular by hydrogen bonding, is a rapidly developing field

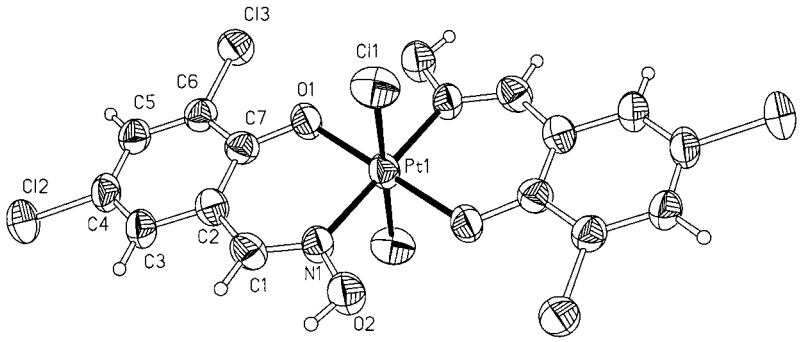

Figure 2. View of *trans-(N,N)*-[$PtCl_2$(3,5,2-Cl,Cl,$OC_6H_2CH{=}NOH)_2$] (**3**) with atomic numbering

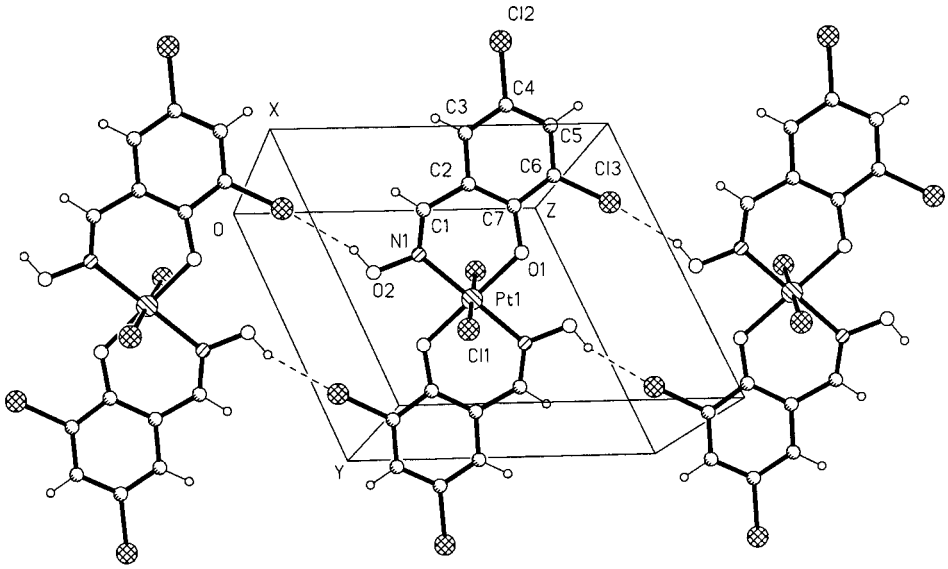

Figure 3. Packing diagram for *trans-(N,N)*-[$PtCl_2$(3,5,2-Cl,Cl,$OC_6H_2CH{=}NOH)_2$] (**3**) showing the hydrogen-bonding scheme

that is intrinsic for crystal engineering and materials science,[3] and from that point of view, it is likely that the observation of hydrogen bonding in the (salicylaldoximato)-Pt^{IV} compound deserves further investigation.

Chlorination of [PtCl($OC_6H_4CH{=}NOH$)($HOC_6H_4CH{=}NOH$)] (2) and Crystal Structure of *trans-(N,N)*-[$PtCl_3$(3,5,2-Cl,Cl,$OC_6H_2CH{=}NOH$)(3,5,2-Cl,Cl,$HOC_6H_2CH{=}NOH$)] (5)

The chlorination of **2** with molecular chlorine proceeded similarly to that described above for **1** (Scheme 1), but the reaction with NOCl gave a variety of products, which were not separated. In the former case, both monodentate and chelating ligands are chlorinated selectively at the 3- and 5-positions of the aromatic ring rather than at the oxime CH=N group, indicating that coordination of the phenolic oxygen has no influence on the course of the chlorination. However, the most interesting result from this part of the work is that the salicylaldoxime ligand maintains its monodentate coordination, which was unambiguously confirmed by X-ray study. In *trans-(N,N)*-[$PtCl_3$(3,5,2-Cl,Cl,$OC_6H_2CH{=}NOH$)(3,5,2-Cl,Cl,$HOC_6H_2CH{=}NOH$)] (**5**), the platinum exhibits a slightly distorted octahedral geometry with three meridian Cl ligands (Figure 4).

The values of the Pt−Cl bond lengths (Table 2) agree well with those of previously characterized platinum(IV) chloride compounds,[4,5] although the Pt−Cl(2) bond [2.316(4) Å] is slightly shorter that the other two [2.338(4) and 2.336(4) Å]. The most interesting feature of the structure is the presence of two different salicylaldoxime species, i.e. one is an unusual monodentate ligand and the other is the conventional *N,O*-salicylaldoximato chelate. Surprisingly, the corresponding bond lengths in the two types of salicylaldoximato ligands are the same within 3σ. Although the hydrogen atoms at the =NOH moieties were not found, the bond lengths indicated in Table 1 favor the oxime tautomeric structure in both cases.

IR and NMR Spectroscopic Characterization of 5

In IR spectra, only one band of ν(C=N) stretching vibrations appears for the *bis*-chelated species **1** and **3**, whereas complexes **2** and **5**, containing both chelating and monodentate ligands, display two ν(C=N) bands. ^1H and $^{13}C\{^1H\}$ NMR spectra of **1** and **3** show only one set of signals for

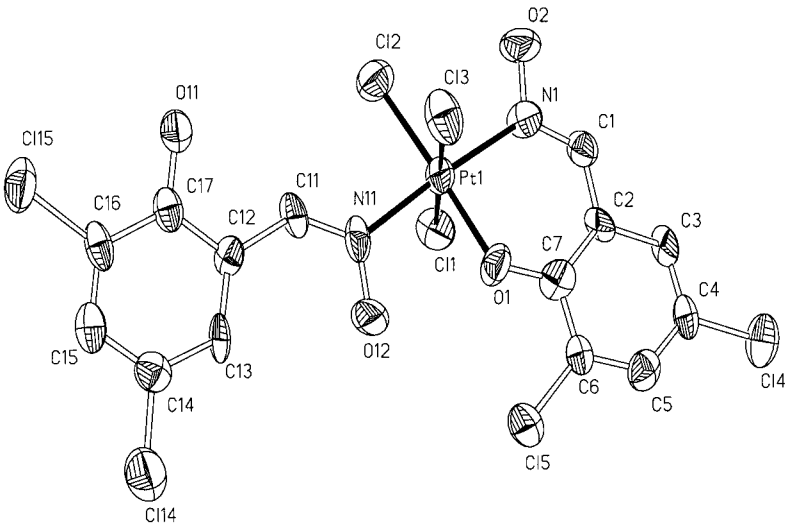

Figure 4. View of *trans-(N,N)*-[$PtCl_3$(3,5,2-Cl,Cl,$OC_6H_2CH{=}NOH$)(3,5,2-Cl,Cl,$HOC_6H_2CH{=}NOH$)] (**5**) with atomic numbering

Table 2. Bond lengths (Å) and bond angles (°) for **1**, **3** and **5**

Bond	Complex **1**	**3**	**5**
Pt(1)−O(1)	1.978(5)	1.980(5)	2.023(10)
Pt(1)−N(1)	1.974(6)	1.997(5)	2.032(13)
Pt(1)−Cl(1)		2.316(2)	2.338(4)
Pt(1)−Cl(2)			2.316(4)
Pt(1)−Cl(3)			2.336(4)
Pt(1)−N(11)			2.030(12)
Cl(1)−Pt(1)−Cl(2)			90.54(15)
Cl(1)−Pt(1)−Cl(3)			178.77(15)
Cl(1)−Pt(1)−O(1)		89.9(2)	89.5(3)
Cl(1)−Pt(1)−O(1)*		90.1(2)	
Cl(1)−Pt(1)−N(1)		90.6(2)	91.5(4)
Cl(1)*−Pt(1)−N(1)		89.5(2)	
Cl(1)−Pt(1)−N(11)			89.6(3)
Cl(2)−Pt(1)−Cl(3)			90.07(15)
Cl(2)−Pt(1)−O(1)			177.8(3)
Cl(2)−Pt(1)−N(1)			90.2(4)
Cl(2)−Pt(1)−N(11)			94.3(3)
Cl(3)−Pt(1)−O(1)			89.9(3)
Cl(3)−Pt(1)−N(1)			89.6(4)
Cl(3)−Pt(1)−N(11)			89.3(3)
O(1)−Pt(1)−N(1)		93.6(2)	92.0(5)
O(1)−Pt(1)−N(1)*		86.4(2)	
O(1)−Pt(1)−N(11)			83.5(4)
N(1)−Pt(1)−N(11)			175.4(5)

the salicylaldoximato-type ligands, while two sets are observed for **2** and **5**. Full assignment of the ^{1}H NMR peaks for **1**−**3** and **5** was made by means of one-dimensional homodecoupling and NOE experiments. By measuring NOE interactions between the oxime CH=N proton and the proton at the 6-position of the aromatic ring, one might distinguish between signals arising from the chelating and the monodentate ligands. In the chelate, in which the conformation of the ligand is fixed, the CH=N and 6-H protons are held at a distance of approximately 2.47 Å, as confirmed by the X-ray analysis of **5** (see above). This distance is sufficiently short to give rise to a NOE signal, and indeed this peak was observed for the *bis*-chelated complex [Pt(*o*-$OC_6H_4CH{=}NOH)_2$] (**1**) (δ = 8.51 to 7.50). The monodentate ligand, however, has more conformational freedom and, consequently, the average distance between the corresponding protons is much larger than in the chelated ligand. Therefore, one would expect a much weaker or even no observable NOE signal for the monodentate ligand. In agreement with this hypothesis, in both compounds **2** and **5**, only one CH=N proton revealed a strong NOE interaction with the 6-H proton (δ = 8.44 to 7.53 for **2**, δ = 8.64 to 7.76 for **5**), whereas irradiation of the second CH=N proton (δ = 8.84 for **2** and δ = 9.03 for **5**) did not show any NOE interaction. Furthermore, a comparison of the chemical shift and the coupling constants $^3J_{PtH}$ of the CH=N protons of the two ligands shows that, for the monodentate ligand, the δ value is higher (δ = 8.84−9.03 vs. δ = 8.44−8.77 for the chelate), while the $^3J_{PtH}$ value is smaller (23−30 Hz vs. 35−45 Hz for the chelate).

^{1}H NMR spectroscopic experiments with **2** or **5** also showed that the monodentate ligands do not interconvert into chelating ligands. For **2**, slow decomposition occurs upon prolonged storage (3 weeks at 20−25 °C) or on heating (3 d at 56 °C) to give a mixture of unidentified products. In contrast, **5** is stable and even after storage at room temperature for two months or on heating at 56 °C for 4 d in the presence of pyridine, neither transformation into the corresponding *bis*-chelated complex **3**, substitution of the monodentate ligand for pyridine, or decomposition were observed.

It is also worth mentioning that chlorination of the mixture of (salicylaldoxime)Pt^{II} complexes, prepared according to the method of Cox and co-authors,[19] gave, besides [$PtCl_2$(3,5,2-Cl,Cl,$OC_6H_2CH{=}NOH)_2$] (**3**) and [$PtCl_3$-(3,5,2-Cl,Cl,$OC_6H_2CH{=}NOH$)(3,5,2-Cl,Cl,HOC_6H_2-$CH{=}NOH$)] (**5**), a purely organic material, i.e. 3,5,2-Cl,Cl,$HOC_6H_2C(Cl){=}NOH$. The latter is, at least formally, derived from both the Piloty reaction and the chlorination of the benzene ring. Since this compound was not observed in the course of the chlorination of salicylaldoxime itself,[16] and furthermore, chlorination of the individual platinum(II) complexes does not give 3,5,2-

Cl,Cl,$HOC_6H_2C(Cl)$=NOH, we anticipate that the chlorination occurs in the benzene ring of coordinated ligand followed by liberation of the chlorinated species. An investigation of this reaction is underway in our group.

Experimental Section

Materials and Apparatus: Salicylaldoxime (Aldrich) and solvents were obtained from commercial sources and used as received. Cl_2 for chlorination was obtained from the reaction of $KMnO_4$ and HCl by a standard procedure.[23] Traces of HCl were removed by bubbling through water and dried over H_2SO_4. Nitrosyl chloride was obtained by the reaction of an aqueous solution of $NaNO_2$ with concentrated HCl. Residues of HCl were removed over $NaNO_2$, and NO_2 was removed by treatment with moist KCl. The nitrosyl chloride was finally dried over $CaCl_2$.[24] − Melting points were determined on a Kofler table. For TLC, Silufol UV 254 SiO_2-plates were used. − Positive-ion FAB mass spectra were obtained on a Trio 2000 instrument by bombarding 3-nitrobenzyl alcohol (NBA) matrices of the samples with 8 keV (ca. 1.28×10^{15} J) Xe atoms. Mass calibration for the data-system acquisition was achieved using CsI. EI-MS of 3,5,2-Cl,Cl,$HOC_6H_2C(Cl)$=NOH was measured on the same mass spectrometer. − Infrared spectra (4000−400 cm^{-1}) were recorded on a BIO-RAD FTS 3000MX instrument in KBr pellets, while spectra in the range 400−140 cm^{-1} were measured on a Hitachi FYS-3 spectrometer in polyethylene pellets. − ^1H, $^{13}C\{^1H\}$ and ^{195}Pt NMR spectra were obtained on a Varian UNITY 300 spectrometer at ambient temperature. ^{195}Pt chemical shifts are reported relative to aqueous $K_2[PtCl_4]$ = −1630 ppm, half-height line widths are given in parenthesis.

Synthetic Work and Characterization

Preparation of (Salicylaldoximato)Pt^{II} Complexes: The complexes were prepared by treatment of $K_2[PtCl_4]$ with salicylaldoxime as described by Cox et al.[19] Complex [PtCl(OC_6H_4CH=NOH)(HOC_6H_4CH=NOH)] (**2**) was separated from the other species by TLC on SiO_2 (Silica gel L 5/40 μ, CHEMAPOL) with $CHCl_3$ as eluent (R_f [Pt(*o*-OC_6H_4CH=NOH)$_2$] (**1**) = 0.62, R_f [PtCl(OC_6H_4CH=NOH)(HOC_6H_4CH=NOH)] (**2**) = 0.29, while other species remain on the baseline). [PtCl(OC_6H_4CH=NOH)(HOC_6H_4CH=NOH)] (**2**) was then desorbed with acetone, and the solvent was removed in vacuo at room temperature. The residue was crystallized over a layer of cold water (5−10 °C). The *bis*-chelate [Pt(*o*-OC_6H_4CH=NOH)$_2$] (**1**) was obtained in according to a published method[19] and recrystallized from acetone.

[PtCl(OC_6H_4CH=NOH)(HOC_6H_4CH=NOH)] (2): − $C_{14}H_{13}N_2ClO_4Pt$: calcd. C 33.38, H 2.60, N 5.56, Cl 7.04, Pt 38.72; found C 33.78, H 2.91, N 5.71, Cl, 6.60, Pt 38.94. − FAB^+ MS; *m/z*: 504 $[M]^+$. − M.p. 197−198 °C (dec.). − TLC, R_f = 0.58 (eluent $Me_2CO/CHCl_3$, 1:8, v/v). − IR (KBr, selected bands): $\tilde{\nu}$ = 3488 m, br ν(OH), 1627 mw and 1601 vs ν(C=N) +ν(C=C), 1458 vs and 1475 vs br. δ(O−H), 1198 ms ν(C−O), 912 ms ν(N−O), 742 s δ(C−H) cm^{-1}. − ^1H NMR ([D_6]acetone): δ = 6.99 (t, J_{HH} = 7.5 Hz, 1 *H*), 7.05 (d, J_{HH} = 8.1 Hz, 1 *H*), 7.44 (t, J_{HH} = 7.5 Hz, 1 *H*), 8.44 (d, J_{HH} = 8.0 Hz, 1 *H*) (phenyl H), 8.84 (s + d, $^3J_{PtH}$ = 30.0 Hz, 1 *H*, =C(H)−, monodentate ligand), 6.83 (t, J_{HH} = 7.5 Hz, 1 *H*), 7.18 (d J_{HH} = 8.7 Hz, 1 *H*), 7.44 (t, J_{HH} = 7.5 Hz, 1 *H*), 7.53 (d, J_{HH} = 8.5 Hz, 1 *H*, phenyl H), 8.44 (s + d, $^3J_{PtH}$ = 40.0 Hz, 1 *H*, strong NOE to the signal at δ = 7.53, =C(H)−, bidentate ligand), 9.67 (br, OH), 10.12 (s, OH), 12.16 (br., OH). − $^{13}C\{^1H\}$ NMR ([D_6]acetone): δ = 116.8, 119.0, 119.4, 120.6, 133.1, 133.9, 134.9, 135.4 (aromatic CH's), 146.1 (J_{PtC} not observed) and 148.1 (J_{PtC} not observed, N=CH), 158.3 and 158.9 (quaternary C's, two signals were not detected). − ^{195}Pt NMR ([D_6]acetone): δ = −1842 (360 Hz).

[Pt(*o*-OC_6H_4CH=NOH)$_2$] (1): − $C_{14}H_{12}N_2O_4Pt$: calcd. C 35.98, H 2.59, N 5.99, Pt, 41.74; found C 35.96, H 2.61, N 5.95, Pt, 41.97. − FAB^+-MS, *m/z*: 467 $[M]^+$. − M.p. 255 °C (melting with concomitant sublimation), 276 °C (melting of the sublimed compound). − TLC, R_f = 0.57 (eluent $CHCl_3/CCl_4$ 1:1, v/v). − IR spectrum in KBr (selected bands) cm^{-1}: $\tilde{\nu}$ = 1645 m-w ν(C=N), 1599 m-s ν(C=C), 1188 m ν(C−O), 741 δ(C−H). − ^1H NMR ([D_6]acetone): δ = 6.76 (ddd, J_{HH} = 8.1 Hz, 7.2 Hz, 1.2 Hz, 1 *H*), 7.16 (d, 8.4 Hz, 1 *H*), 7.39 (ddd, J_{HH} = 8.7 Hz, 6.9 Hz, 1.8 Hz, 1 *H*), 7.50 (dd, J_{HH} = 7.8 Hz, 1.8 Hz, 1 *H*, phenyl H), 8.51 [s + d, $^3J_{PtH}$ = 45.5 Hz, 1 *H*, strong NOE to the signal at δ = 7.50, =C(H)−], 10.91 (s, $^3J_{PtH}$ = 23.6 Hz, 1 H, OH). − $^{13}C\{^1H\}$ NMR ([D_6]acetone): δ = 118.3, 120.4, 134.0, 134.3 (aromatic CH's), 144.8 (broad, N=CH), quaternary C's not observed. − ^{195}Pt NMR ([D_6]acetone): δ = −1611 (480 Hz).

Chlorination of [Pt(*o*-OC_6H_4CH=NOH)$_2$] (1) by Cl_2: Molecular chlorine was passed through a lemon-yellow solution of **1** (0.136 g, 0.29 mmol) in $CHCl_3$ (80 mL) for 20 min at 20−25 °C. A cherry-brown solution formed, and was left to evaporate at 14−18 °C in an open 100-mL beaker to ca. 10 mL. Transparent, glittering rhombic-like brownish crystals of *trans-(N,N)*-[$PtCl_2$(3,5,2-Cl,Cl,OC_6H_2CH=NOH)$_2$] (**3**) were separated by filtration, washed with a Me_2CO/CCl_4 mixture (1:2, v/v, 3 × 3 mL), diethyl ether (3 × 3 mL) and dried in a vacuum-desiccator at room temperature over $CaCl_2$. Yield: 0.167 g, 85%.

***trans-(N,N)*-[$PtCl_2$(3,5,2-Cl,Cl,OC_6H_2CH=NOH)$_2$] (3):** − $C_{14}H_8N_2Cl_6O_4Pt$: calcd. C 24.85, H 1.18, N 4.14, Cl 31.46, Pt 28.85; found C 24.60, H 1.26, N 3.94, Cl 32.00, Pt 28.52. − FAB^+-MS, *m/z*: 606 $[M - 2Cl]^+$, 588 $[M - 2Cl - OH]^+$, 571 $[M - 2HCl - 2OH]^+$. − M.p. 238 °C. − TLC, R_f = 0.48 (eluent $CHCl_3$). − IR (KBr, selected bands): $\tilde{\nu}$ = 1645 mw ν(C=N), 1596 s ν(C=C), 1422 s, br. δ(O−H), 1189 ms ν(C−O), 912 s ν(N−O), 358 ms ν(Pt−Cl) cm^{-1}. − ^1H NMR ([D_6]acetone): δ = 7.82 and 7.84 (two d, 2.2 Hz, 1*H* each, phenyl H), 8.91 [s + d, $^3J_{PtH}$ = 37.9 Hz, 1 *H*, =C(H)−], 11.00 (s, 1 *H*, NOH). − $^{13}C\{^1H\}$ and ^{195}Pt NMR spectra were not measured even at high acquisition time owing to the low solubility of the complex in common deuterated solvents.

Chlorination of [PtCl(OC_6H_4CH=NOH)(HOC_6H_4CH=NOH)] (2) by Cl_2: Complex **2** (0.034 g, 0.068 mmol) was dissolved in $CHCl_3$ (10 mL) and molecular chlorine was passed through this solution for 20 min at 18−20 °C. The color of the reaction mixture turned from lemon-yellow to dark red during the chlorination. The reaction mixture was transferred to a long narrow tube, the solvent was evaporated at room temperature and cherry-red crystals of *trans-(N,N)*-[$PtCl_3$(3,5,2-Cl,Cl,OC_6H_2CH=NOH)(3,5,2-Cl,Cl,HOC_6H_2CH=NOH)] (**5**) were collected from the bottom part of the tube (0.015 g, 29%). A brownish material was collected from the upper part of the tube. Stirring this brownish material in heptane gave an additional amount of less pure **5** (0.021 g, 41%).

***trans-(N,N)*-[$PtCl_3$(3,5,2-Cl,Cl,OC_6H_2CH=NOH)(3,5,2-Cl,Cl,HO-C_6H_2CH=NOH)] (5):** − $C_{14}H_9N_2Cl_7O_4Pt$: calcd. C 23.58, H 1.26, N 3.93, Cl 34.83, Pt 27.38; found C 23.85, H 1.28, N 3.87, Cl 35.00, Pt 27.52. − FAB^+-MS, *m/z*: 643 $[M - 2Cl + H]^+$, 603 $[M - 3HCl]^+$. − M.p. 211 °C (dec.). − TLC, R_f = 0.62 (eluent acetone/ chloroform 1:2, v/v). − IR spectrum (KBr, selected bands): $\tilde{\nu}$ = 1655 w and 1635 w ν(C=N) and ν(C=C), 1187 m

ν(C−O), 357 m and 347 m ν(Pt−Cl) cm^{-1}. − ^1H NMR ([D$_6$]acetone): δ = 7.83 (d, J_{HH} = 2.7 Hz, 1 *H*, phenyl H), 8.47(d, J_{HH} = 2.7 Hz, 1 *H*, phenyl H), 9.03 [s + d, $^3J_{PtH}$ = 23.4 Hz, 1 *H*, = C(H)−, monodentate ligand], 7.76 (d, J_{HH} = 2.7 Hz, 1 *H*, phenyl H), 7.79 (d, J_{HH} = 2.7 Hz, 1 *H*, phenyl H), 8.64 [s + d, $^3J_{PtH}$ = 35.7 Hz, 1 H strong NOE to the signal at δ = 7.76, =C(H)−, bidentate ligand], 10.94 (br., OH). − $^{13}C\{^1H\}$ NMR ([D$_6$]acetone): δ = 131.0, 132.7, 135.8 and 136.0 (aromatic CH's), 149.1 (J_{PtC} = 28 Hz) and 151.4 (J_{PtC} not observed)(N=CH), 118.7 (J_{PtC} = 22 Hz), 119.8 (J_{PtC} = 25 Hz), 122.0, 123.5, 124.8, 125.6, 132.0 and 136.7 (quaternary C's). − ^{195}Pt NMR ([D$_6$]acetone): δ = +252 (440 Hz).

3,5,2-Cl,Cl,HOC$_6$H$_2$C(Cl)=NOH: This purely organic material was formed by the chlorination of a mixture of salicylaldoxime complexes, prepared in agreement with Cox et al.,[19] and was separated mechanically upon fractional crystallization of the products of the reaction from an acetone/toluene (3:1, v/v) mixture. Colorless needles. − $C_7H_4NCl_3O_2$: calcd. C 34.94, H 1.66, N 5.83, Cl 44.29; found C 34.45, H 2.10, N 5.65, Cl 45.10. − EI-MS, *m/z:* 241 $[M]^+$, 203 $[M - HCl]^+$. − M.p. 141 °C [vs. *ref.* m.p. 194−195 °C for 3,5-Cl,Cl-C$_6$H$_3$CH=NOH[21]). − TLC, R_f = 0.67 (eluent: chloroform). − IR (KBr, selected bands): $\tilde{\nu}$ = 3423 vs ν(O−H), 1651 mw and 1605 mw ν(C=N) and ν(C=C), 1180 m ν(C−O) cm^{-1}. − ^1H NMR ($CDCl_3$): δ = 7.48 (d, 1 *H*, J_{HH} = 2.2 Hz), 7.76 (d, 1 *H*, J_{HH} = 2.6 Hz), 9.02 (s, 1 *H*, C−OH), 10.64 (s, 1 *H*, oximic OH). − $^{13}C\{^1H\}$ NMR ($CDCl_3$): δ = 132.01 (CH), 127.34 (CH) quaternary carbons were not observed owing to the low solubility of the compound.

Chlorination of [Pt(*o*-OC$_6$H$_4$CH=NOH)$_2$] (1) by NOCl: Nitrosyl chloride was passed through a lemon-yellow solution of **1** (0.13 g, 0.28 mmol) in a mixture of CCl_4 (10 mL) and $CHCl_3$ (50 mL) for 20 min at 5 °C. A cherry-brown solution was formed and left to evaporate at 14−18 °C in an open 100-mL beaker to ca. 10 mL. Transparent, glittering rhombic-like brownish crystals of **4** were separated by filtration, washed with a Me_2CO/CCl_4 mixture (1:2, v/v, 3 × 3 mL), diethyl ether (3 × 3 mL), and dried at room temperature in a vacuum-desiccator over $CaCl_2$. Yield: 0.11 g, 73%.

***trans-(N,N)*-[PtCl$_2$(*o*-OC$_6$H$_4$CH=NOH)$_2$] (4):** − $C_{14}H_{12}N_2Cl_2O_4Pt$: calcd. C 31.24, H 2.25, N 5.20, Cl 13.17, Pt 36.24; found C 30.99, H 2.30, N 5.11, Cl 13.69, Pt 35.8. − FAB$^+$-MS, *m/z*: 538 $[M]^+$. − M.p. 149−152 °C (dec.). − IR (KBr, selected bands): $\tilde{\nu}$ = 1652 m ν(C=N), 1597 s ν(C=C), 912 s ν(N−O) cm^{-1}. − ^1H NMR ([D$_6$]DMSO): δ = 6.82 (t, J_{HH} = 7.7 Hz, 1 *H*), 7.29 (d, J_{HH} = 9.2 Hz, 1 *H*), 7.45 (t, J_{HH} = 7.2 Hz, 1 *H*), 7.56 (d, J_{HH} = 7.2 Hz, 1 *H* each *o*-phenyl H), 8.77 [s + d, $^3J_{PtH}$ = 34.8 Hz, 1 *H*, =C(H)−], 11.78 (s, br, 1 *H*, NOH). Solubility of the complex in [D$_6$]DMSO was insufficient to allow for the accumulation of either $^{13}C\{^1H\}$ or ^{195}Pt NMR spectra, even with long acquisition times.

X-ray Crystal Structure Determinations

(*i*) Dark yellow prismatic crystals of **1** were grown by the slow evaporation of a solution in CCl_4 at room temperature. Diffraction data were collected on an Enraf−Nonius CAD 4 diffractometer. Diffractometer data were processed by the program PROFIT,[25] with profile analysis of reflections. The structures were solved by means of Fourier synthesis based on the Pt-atom coordinates obtained from the Patterson synthesis using SHELXTL package.[26] All non-hydrogen atoms were treated anisotropically. H atoms were located in a difference Fourier map and refined isotropically. An extinction correction was applied. Lorentz, polarization and absorption corrections were made.[27]

(*ii*) Transparent, glittering rhombic-like brownish crystals of **3** were obtained directly from the reaction mixture. The crystallographic measurements were performed on an Enraf−Nonius CAD-4 CCD diffractometer using the technique described in ref.[28] The structure was solved by direct methods and refined anisotropically for non-hydrogen atoms and isotropically for H atoms using SHELXL-97.[29] Positions of hydrogen atoms bonded to carbons were calculated based on known atom geometry. These hydrogen atoms were allowed to ride on their neighboring carbons during the refinement.

Table 3. Crystal data and structure refinement for **1**, **3** and **5**

Empirical formula	$C_{14}H_{12}N_2O_4Pt$	$C_{14}H_8N_2Cl_6O_4Pt$	$C_{14}H_9N_2Cl_7O_4Pt$
Formula weight	467.34	676.0	712.5
Space group	monoclinic	triclinic	triclinic
Crystal system	$P2_1/n$ (No 14)	$P\bar{1}$	$P\bar{1}$
a [Å]	4.5410(10)	6.9940(8)	9.559(4)
b [Å]	25.007(5)	8.2560(7)	10.266(5)
c [Å]	5.847(10)	9.1310(11)	10.565(3)
α [°]	90	66.026(6)	93.64(3)
β[°]	97.65(3)	77.142(5)	93.45(3)
γ [°]	90	89.253(7)	97.82(4)
V [Å^3]	658.1(2)	467.91(9)	1023(3)
Z	2	1	2
D_c [Mg/m^3]	2.358	2.399	2.314(3)
F(000)	440	318	672
μ(Mo−K_α) [mm^{-1}]	10.679	8.378	8.148
$2\theta_{max}$ [°] and sinθ/λ for data collection	51.9	52.0	59.94 and 0.703
Refinement method	full-matrix (anisotropic for all non-H atoms) least squares on F^2 for **1** and **3**, and based on *F* for **5**		
Crystal size, mm	0.18 × 0.42 × 0.52	0.30 × 0.10 × 0.10	0.3 × 0.2 × 0.1
Index ranges	−5<*h*<5 −0<*k*<30 0<*l*<7	0<*h*<8 −10<*k*<10 −10<*l*<11	0<*h*<12, −7<*k*<7 −7<*l*<7
Collected reflections	1365	1834	2024
Unique reflections	802 [$I \leqslant 2\sigma(I)$]	1834 [$I \leqslant 2\sigma(I)$]	1800 [$F(hkl) \geq 4\sigma(F)$]
Refinement parameters	118	125	327
Extinction coefficient	0.003(6)	0.032(3)	−
Goodness-of-fit on *F*	1.093	1.014	1.101
R	0.0227	0.0389	0.0373
wR	0.0590	0.0411	0.0353

Their thermal parameters were assigned the value of 1.2 times the initial equivalent isotropic thermal parameters of their neighboring carbons and were not refined. The oxime H atom was located by difference Fourier synthesis and refined with restraints to maintain the geometry derived from the difference map. Its thermal parameter was assigned the value of 1.5 times the initial equivalent isotropic thermal parameter of its neighboring oxygen and was not refined. The final *R*-value was 0.0389 for 1779 reflections with $I = 2\sigma(I)$.

(*iii*) Dark cherry-red prismatic crystals of **5** were obtained after the slow evaporation of a solution in acetone/toluene (3:1, v/v) in a long (150 mm) narrow (5 mm) tube. Diffraction data were collected on a Syntex $P2_1$ diffractometer. An extinction correction was not made. Before anisotropic refinement, an absorption correction was made using DIFABS[30] program. The contributions of hydrogen atoms were included at fixed calculated positions, based on geometrical requirements. All experimental data processing, solving and refinement were performed using the CSD[27] program. Crystal data for **1**, **3** and **5** are given in Table 3.

Crystallographic data (excluding structure factors) for the structure(s) reported in this paper have been deposited with the Cambridge Crystallographic Data Centre as supplementary publication no. CCDC-144573 (**1**), CCDC-144575 (**3**) and CCDC-144574 (**5**). Copies of the data can be obtained free of charge on application to CCDC, 12 Union Road, Cambridge CB2 1EZ, UK [Fax: (internat.) + 44-1223/336-033; E-mail: deposit@ccdc.cam.ac.uk].

Acknowledgments

V. Yu. K., S. K. and S. S. thank INTAS for the grant (97−0166). V. Yu. K. is very grateful for financial support of this study by the PRAXIS XXI program (grant BCC16428/98). G. W. is grateful to the PRAXIS XXI program for a fellowship (BPD11779/97). A. J. L. P. thanks the FCT (Foundation for Science and Technology) and the PRAXIS XXI program for financial support.

[1] V. Yu. Kukushkin, D. Tudela, A. J. L. Pombeiro, *Coord. Chem. Rev.* **1996**, *156*, 333.
[2] V. Yu. Kukushkin, A. J. L. Pombeiro, *Coord. Chem. Rev.* **1999**, *181*, 147.
[3] V. Yu. Kukushkin, T. Nishioka, D. Tudela, K. Isobe, I. Kinoshita, *Inorg. Chem.* **1997**, *36*, 6157 and references therein.
[4] V. Yu. Kukushkin, T. B. Pakhomova, Yu. N. Kukushkin, R. Herrmann, G. Wagner, A. J. L. Pombeiro, *Inorg. Chem.* **1998**, *37*, 6511.
[5] V. Yu. Kukushkin, T. B. Pakhomova, N. A. Bokach, G. Wagner, M. L. Kuznetsov, M. Galanski, A. J. L. Pombeiro, *Inorg. Chem.* **2000**, *39*, 216.
[6] G. Wagner, A. J. L. Pombeiro, N. A. Bokach, V. Yu. Kukushkin, *J. Chem. Soc., Dalton Trans.* **1999**, 4083.
[7] V. Yu. Kukushkin, I. V. Ilichev, G. Wagner, J. J. R. Fraústo da Silva, A. J. L. Pombeiro, *J. Chem. Soc., Dalton Trans.* **1999**, 3047.
[8] V. Yu. Kukushkin, V. K. Belsky, D. Tudela, *Inorg. Chem.* **1996**, *35*, 510.
[9] M. F. C. Guedes da Silva, C. M. P. Ferreira, E. M. P. R. P. Branco, J. J. R. Fraústo da Silva, A. J. L. Pombeiro, R. A. Michelin, U. Belluco, R. Bertani, M. Mozzon, G. Bombieri, F. Benetollo, V. Yu. Kukushkin, *Inorg. Chim. Acta (Topical Volume on Platinum Chemistry)* **1997**, *265*, 267.
[10] C. M. P. Ferreira, M. F. C. Guedes da Silva, V. Yu. Kukushkin, J. J. R. Fraústo da Silva, A. J. L. Pombeiro, *J. Chem. Soc., Dalton Trans.* **1998**, 325.
[11] V. Yu. Kukushkin, D. Tudela, Yu. A. Izotova, V. K. Belsky, A. I. Stash, *Inorg. Chem.* **1996**, *35*, 4926.
[12] V. Yu. Kukushkin, V. K. Belsky, E. A. Aleksandrova, V. E. Konovalov, G. A. Kirakosyan, *Inorg. Chem.* **1992**, *31*, 3836.
[13] M. F. C. Guedes da Silva, Yu. A. Izotova, A. J. L. Pombeiro, V. Yu. Kukushkin, *Inorg. Chim. Acta* **1998**, *277*, 83.
[14] V. Yu. Kukushkin, I. V. Ilichev, M. A. Zhdanova, G. Wagner, A. J. L. Pombeiro, *J. Chem. Soc., Dalton Trans.* **2000**, 1567.
[15] Yu. N. Kukushkin, M. V. Bavina, A. V. Zinchenko, V. K. Belsky, V. Yu. Kukushkin, *Polyhedron* **1997**, *16*, 2429.
[16] Yu. N. Kukushkin, V. K. Krylov, S. F. Kaplan, M. Calligaris, E. Zangrando, A. J. L. Pombeiro, V. Yu. Kukushkin, *Inorg. Chim. Acta* **1999**, *285*, 116.
[17] [17a] O. Piloty, *Ber. Dtsch. Chem. Ges.* **1898**, *31*, 452. – [17b] O. Piloty, A. Stock, *Ber. Dtsch. Chem. Ges.* **1902**, *35*, 3093. – [17c] J. G. Aston, D. F. Menard, *J. Am. Chem. Soc.* **1935**, *57*, 1920. For reviews on the Piloty reaction see: N. Boyer, in *The Chemistry of the Nitro and Nitroso Groups*, (Ed.: H. Feuer), Interscience, New York, Part 1, **1969**, p. 235; H. Metzger, in *Houben−Weyl. Methoden der Organischen Chemie*, vol. X, Part 4, Georg Theime Verlag, Stuttgart, **1968**, p. 98 and 239.
[18] L. A. M. Baxter, G. A. Heath, R. G. Raptis, A. C. Willis, *J. Am. Chem. Soc.* **1992**, *114*, 6944.
[19] E. G. Cox, F. W. Pinkard, W. Wardlaw, K. C. Webster, *J. Chem. Soc.* **1935**, 459.
[20] [20a] R. C. Srivastava, E. C. Lingafelter, P. C. Jain, *Acta Crystallogr.* **1967**, *22*, 922. – [20b] M. Lalia-Kantouri, M. Hartophylles, P. D. Jannakoudakis, G. P. Voutsas, *Z. Anorg. Allg. Chem.* **1995**, *621*, 645. – [20c] G. P. Voutsas, K. G. Keramidas, M. Lalia-Kantouri, *Polyhedron* **1996**, *15*, 147. – [20d] C. E. Pfluger, R. L. Harlow, S. H. Simonsen, *Acta Crystallogr., Sect. B* **1970**, *26*, 1631. [20e] P. L. Orioli, E. C. Lingafelter, B. W. Brown, *Acta Crystallogr.* **1964**, *17*, 1113. – [20f] M. A. Jarski, E. C. Lingafelter, *Acta Crystallogr.* **1964**, *17*, 1109.
[21] H. Biltz, K. Stepf, *Ber. Dtsch. Chem. Ges.* **1904**, *37*, 4022.
[22] A. F. Wells, *Structural Inorganic Chemistry*, 5th ed.; Oxford University Press: Oxford, **1986**, pp. 357, 692.
[23] [23a] G. Graebe, *Ber. Dtsch. Chem. Ges.* **1901**, *34*, 645.[23b] G. Graebe, *Ber. Dtsch. Chem. Ges.* **1902**, *35*, 43.
[24] J. R. Morton, H. W. Wilcox, *Inorg. Synth.* **1953**, *4*, 48.
[25] V. A. Strel′tsov, V. E. Zavodnik, *Kristallografia* **1989**, *34*, 1369.
[26] G. M. Sheldrick, *SHELXTL* User Manual, Revision 3; Nicolet XRD Corp.: Cupertino, CA, **1981**.
[27] L. G. Axelrud, Yu. N. Grin, P. Yu. Zavalii, V. K. Pecharsky, V. S. Fundamensky, CSD-universal program package for single crystal and/or powder structure data treatment. Collected Abstracts, *XII-th European Crystallographic Meeting*, Moscow, August **1989**; USSR Academy of Sciences, Moscow, **1989**, p 155.
[28] Z. Otwinowski, Denzo-SMN − Programs Denzo and Scalepack developed Z. Otwinowski. Copyright **1994−1997** by Texas Southwestern Medical Center at Dallas.
[29] G. M. Sheldrick: *SHELXL97. Program for crystal structure refinement*, University of Göttingen, Germany.
[30] N. Walker, D. Stuart, *Acta Crystallogr., Series A* **1983**, *39*, 158.
[31] F. H. Allen, O. Kennard, D. G. Watson, L. Brammer, A. G. Orpen, R. Taylor, *J. Chem. Soc., Perkin Trans. 2* **1987**, *S1*.
[32] A. G. Orpen, L. Brammer, F. H. Allen, O. Kennard, D. G. Watson, R. Taylor, *J. Chem. Soc., Dalton Trans.* **1989**, *S1*.

Received May 18, 2000
[I00207]

Europium "Second Generation" Precursors for Metal-Organic Chemical Vapor Deposition: Characterization and Optical Spectroscopy

Graziella Malandrino,*[a] Marco Bettinelli,*[b] Adolfo Speghini,[b] and Ignazio Luciano Fragalà[a]

Keywords: Luminescence / Chemical vapor deposition / Europium / Polyether adducts

The novel complex precursor $Eu(hfa)_3$·monoglyme and the analogous $Eu(hfa)_3$·diglyme [Hhfa = 1,1,1,5,5,5-hexafluoroacetylacetone, monoglyme = $CH_3OCH_2CH_2OCH_3$, diglyme = $CH_3O(CH_2CH_2O)_2CH_3$] have been synthesized in a single step reaction and characterized by elemental analysis, mass spectrometry, and IR and Raman spectroscopy. Thermogravimetric data and the linear evaporation behavior have shown that both complexes are thermally stable and can be evaporated to leave less than 4% residue. Luminescence spectra in the visible region provided evidence of a remarkable covalent character of the metal-ligand bonding in both complexes with the distortion of the coordination sphere around the europium(III) ion in $Eu(hfa)_3$·monoglyme greater than that in $Eu(hfa)_3$·diglyme. DSC measurements and variable temperature luminescence spectra have shown the presence of a structural transition at 71.4 °C from a solid to a plastic phase for $Eu(hfa)_3$·diglyme.

Introduction

Several efforts have recently been devoted to the design of novel lanthanide complexes with suitable mass transport properties for metal-organic chemical vapor deposition (MOCVD) applications.[1−4] This is due to the severe drawbacks of first generation MOCVD precursor complexes, i.e. their thermal instability, reactivity with oxygen, low volatility, and high residues left upon sublimation. In addition, their use as precursors for MOCVD deposition of LnF_3 and LnOF requires the use of an additional fluorine source.[5]

Conversely, the polyether adducts of lanthanide fluorinated β-diketonates[6−14] exhibit improved properties in terms of thermal stability and volatility, thus representing a class of novel second-generation precursors that has been successfully applied to the MOCVD fabrication of various materials.[7,8,14−17] These adducts represent single-source precursors for the MOCVD fabrication of LnF_3 and LnOF (Ln = La, Gd) phases[7,8,17] which are challenging host matrices for different applications such as X-ray storage phosphors, laser materials, and optical waveguides.

In this context, MOCVD techniques offer several advantages[18] over classical physical techniques and are well suited for depositing good quality films even for those applications where high performances are required as, for example, the deposition of epitaxial Pr-doped BaF_2 on a CaF_2 substrate for optical waveguide applications.[19]

Herein, we report the synthesis, physicochemical characterization, and mass transport properties of the novel europium MOCVD precursor $Eu(hfa)_3$·monoglyme [Hhfa = 1,1,1,5,5,5-hexafluoroacetylacetone, monoglyme = $CH_3OCH_2CH_2OCH_3$]. We also report a viable and safer route (than that already proposed[20]) to the analogue $Eu(hfa)_3$·diglyme [diglyme = $CH_3O(CH_2CH_2O)_2CH_3$]. The europium(III) ion has been chosen among the trivalent lanthanide ions due to its intense luminescence in the visible region that opens up several opportunities for technological applications and represents an important tool to study both the coordination geometry and the coupling with the surrounding vibrations.[21] In addition, the laser-excited and vibrational Raman spectroscopy of these adducts are discussed and compared with the Gd analogues.[7]

Results and Discussion

Synthesis

The $Eu(hfa)_3$·L adducts have been prepared through a one-pot reaction from europium oxide, hexafluoroacetylacetone and the polyether in hexane [Equation (1)]:

$$1/2Eu_2O_3 + 3Hhfa + L \rightarrow Eu(hfa)_3\cdot L + 3/2H_2O \quad (1)$$

The slight excess of europium oxide favors the isolation of the product since the insoluble unreacted Eu_2O_3 may be easily filtered off. In contrast with the previously reported procedures for the analogous lanthanum precursors[6] as well as for $Eu(hfa)_3$·diglyme,[20] the present methodology avoids the use of carcinogenic benzene. It is worth noting that the present $Eu(hfa)_3$·monoglyme adduct, at variance with the $La(hfa)_3$·monoglyme·H_2O homologue, is water-free. This is clearly due to the smaller ionic radius of the europium(III) ion, which enables the monoglyme ligand to saturate the coordination sphere, thus preventing any water coordination.

[a] Dipartimento di Scienze Chimiche, Università di Catania, Viale A. Doria 6, 95125 Catania, Italy
[b] Dipartimento Scientifico e Tecnologico, Università di Verona, Ca' Vignal, Strada Le Grazie 15, 37134 Verona, Italy

 © WILEY-VCH Verlag GmbH, 69451 Weinheim, 2001 1434−1948/01/0404−1039 $ 17.50+.50/0

The present adducts are very soluble in common organic solvents such as ethanol, chloroform, acetone, pentane, toluene and slightly soluble in cyclohexane. Both adducts have low melting points and sublime quantitatively at low temperature under vacuum. They are nonhygroscopic and can be handled in air.

Infrared Spectra

The IR spectra of the crude and sublimed $Eu(hfa)_3$·polyether adducts show identical features. The absence of any bands around 3600 cm^{-1} in the spectra of **1** and **2** is indicative of H_2O-free species. All the spectra show singular absorption bands around 1650 cm^{-1}, due to C=O stretching vibrations, and at 1520 cm^{-1}, due to the C=C stretching vibrations. The other bands, observed at 1100−1300 cm^{-1}, represent C−O bending and/or stretching of the polyether ligand overlapping with the C−F stretching frequencies. Peaks around 860 and 1050 cm^{-1} are indicative of glyme coordination to the europium hexafluoroacetylacetonate moiety.[8]

Raman Spectra

The room temperature vibrational Raman spectra of pelletized powders of **1** and **2** and of the corresponding gadolinium analogues are virtually identical for wavenumbers lower than 1500 cm^{-1}. As a representative example, we show in Figure 1 the Raman spectrum of **2**.

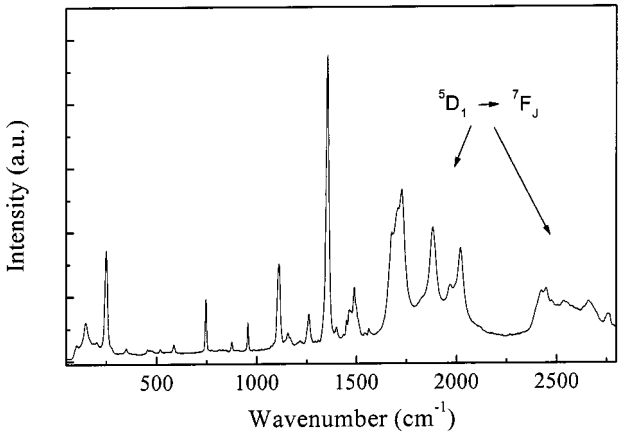

Figure 1. Room temperature Raman spectrum of **2** (λ_{EXC} = 488.0 nm)

The prominent peak at about 1350 cm^{-1} is assigned to vibrations involving the -CF_3 grouping, whilst the bands close to 1500 cm^{-1} are assigned to modes involving -CH_2- deformations.[22] The sharp peak at 250 cm^{-1} is due to a metal-oxygen vibration.[23] In the case of the spectra of the europium(III) compounds **1** and **2**, additional peaks are present in the 1500−3000 cm^{-1} spectral region which are missing in the corresponding spectra of the gadolinium analogues. These features are assigned to electronic emission transitions from the $^5D_1$ excited state to the ^7F_J ground multiplet of europium(III), as they are not observed in the Raman spectrum of the isostructural gadolinium complex, and on the basis of the energy level structure of europium(III) ion, as already observed for different hosts.[24]

Thermogravimetric and Calorimetric Data

The thermal behavior of the raw adducts **1** and **2** has been studied by thermal gravimetric analysis (TG), and differential scanning calorimetry (DSC) under N_2. The TG curves of **1** and **2** show singular sublimation steps (Figure 2) in the 100−246 °C (residue = 3% to 290 °C) and 113−255 °C (residue = 2% to 260 °C) temperature ranges, respectively.

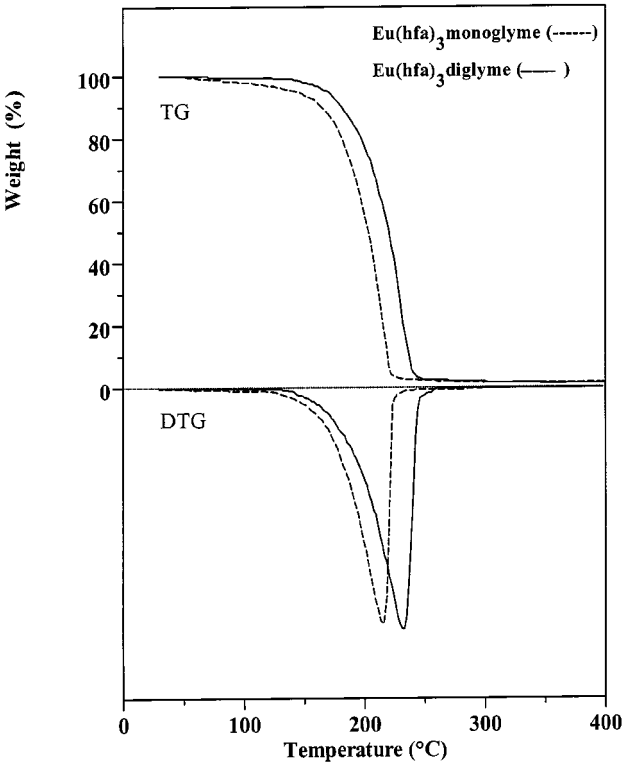

Figure 2. TG-DTG curves of adducts **1** and **2**

The linear behavior of the TG atmospheric pressure vaporization rates (Figure 3) of adducts **1** and **2** indicate that both adducts are thermally stable and, therefore, represent interesting precursors for MOCVD applications.

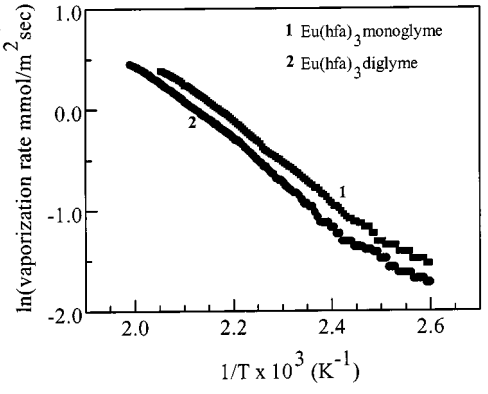

Figure 3. DSC curves of adducts **1** and **2**

The DSC curves of $Eu(hfa)_3$·L adducts are reported in Figure 4. Adduct **1** shows a sharp melting point at 81.2 °C (9.14 cal/g), in good agreement with that observed with a Koffler Microscope (80−82 °C). Evaporation from the melt occurs afterwards. The DSC curve of the diglyme adduct **2** shows some interesting features. Two sharp endothermic peaks are observed at 71.4 °C (9.26 cal/g) and 122.0 °C (1.04 cal/g). Several consecutive heating and cooling DSC experiments in the 30−150 °C temperature range have shown the disappearance of the first peak after the first cycle. The second peak, in contrast, remains unchanged in terms of both the temperature and the ΔH associated with the process. The peak at 71.4 °C again becomes evident after standing for several hours at room temperature. This endothermic process represents a "thermal anomaly"[25] and may be associated with a transition from the solid to a plastic phase.[9] The second peak is associated with the complete melting. This conclusion agrees well with the optical microscopy observations upon heating, which show the disappearance of the crystal color at 73−76 °C and complete melting at 123−126 °C.

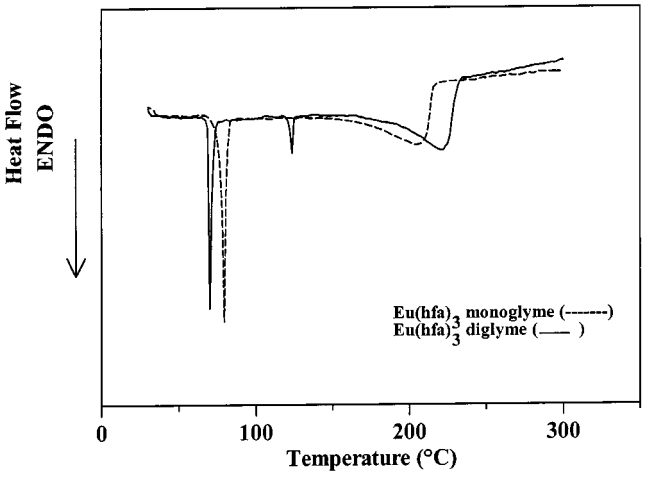

Figure 4. Atmospheric pressure TG vaporization rate data of adducts **1** and **2** as a function of the temperature

Finally, it is interesting to remark that the DSC features of **1** and **2** are almost identical to those of the Gd homologues. Note that both the Eu[20] and Gd[7] diglyme adducts, in fact, have identical crystal structures within the same space group and almost identical unit-cell dimensions (0.01 Å difference between corresponding cell parameters).

Mass Spectra

The FAB spectra of adducts **1** and **2** show peaks due to the loss of both the hfa ligand and the polyether (see Table 1).

Peaks arising from the characteristic fluorine transfer process, already found in the spectra of the alkaline earth[26] and analogous lanthanide[7,8] β-diketonate polyether adducts, are also observed. The observed MS peaks are associated with $[Eu(hfa)_2$·polyether$]^+$, $[Eu(hfa)$·polyether + $F]^+$, $[Eu(hfa)_2]^+$, $[Eu(hfa) + F]^+$, $[Eu$·polyether + $2F]^+$ and $[EuF_2]^+$ fragments. No molecular ion peaks or peaks at higher mass have been observed, in agreement with the monomeric nature of the complexes.

Table 1. Major peaks in the mass spectra of adducts **1** and **2**; the given *m*/*z* ratios are related to the isotope ^{153}Eu

Assignment	$Eu(hfa)_3$·monoglyme	$Eu(hfa)_3$·diglyme
$[Eu(hfa)_2$·L$]^+$	657 (100%)	701 (100%)
$[Eu(hfa)$·L + F$]^+$	469 (28%)	513 (19%)
$[Eu(hfa)$·L$]^+$	450 (15%)	494 (36%)
$[Eu(hfa)$ + F$]^+$	379 (11%)	379 (<5%)
$[Eu(hfa)]^+$	360 (75%)	360 (21%)
$[Eu$·L + 2F$]^+$	281 (12%)	325 (11%)
$[Eu$·L + F$]^+$	262 (<5%)	306 (9%)

Luminescence Spectra

The room-temperature, laser-excited luminescence spectra of powders of **1** and **2**, measured with an excitation wavelength of 488.0 nm, consist of $f \rightarrow f$ emission transitions from the $^5D_0$ excited state to the ^7F_J multiplet of the europium(III) ion. The $^5D_0 \rightarrow {}^7F_0$ transition cannot be split by the crystal field and its profile gives information on the number of different coordination sites accommodating the europium(III) ion. The presence of a single band in the high resolution luminescence spectra of both **1** and **2** indicates that the europium(III) ion occupies a single site in both compounds. In the case of **2**, this observation agrees well with the X-ray single-crystal structure reported by Kang et al.,[20] in which only one europium(III) site is present, as well as with the crystal structure of the isostructural gadolinium(III) compound.[7]

The peak position of the $^5D_0 \rightarrow {}^7F_0$ transition is related to the nephelauxetic effect and to the covalency of the europium(III)−ligand bond.[27] In both **1** and **2** the $^5D_0 \rightarrow {}^7F_0$ maxima are located in the "covalent" region of the nephelauxetic scale,[27,28] but in the case of **1** the $^5D_0 \rightarrow {}^7F_0$ peak occurs at a longer wavelength than in **2** (see Table 2). This is indicative of a greater europium(III)-ligand covalency in the former.

The ratio of the integrated intensities of the $^5D_0 \rightarrow {}^7F_2$ and $^5D_0 \rightarrow {}^7F_1$ transitions [Equation (2)] can be considered indicative of the asymmetry of the coordination polyhedron of the europium(III) ion[29] and can thus be used to compare the degree of distortion in complexes having similar ligand arrays. The rather high R value (6.6) of **2** points to a distorted first coordination sphere around the europium(III) ion (point symmetry C_1), as found in the crystal structure determination.[20] In the case of **1**, whose crystal structure is not known, the even higher R value (11.0) is indication of a very asymmetric europium(III) site.

$$R = \frac{I(^5D_0 \rightarrow {}^7F_2)}{I(^5D_0 \rightarrow {}^7F_1)}$$

The overall crystal field (CF) splitting values associated with the $^7F_1$ state are reported in Table 2. The smaller crystal field splitting observed in **1** can be correlated to a smaller (than in **2**) europium(III) coordination number. In fact, the crystal data of $Eu(hfa)_3$·diglyme[20] point to a coor-

Table 2. Measured intensity ratios R, peak luminescence wavelengths λ_{max} of the $^5D_0 \rightarrow {}^7F_0$ transition, crystal field splittings of the $^7F_1$ state and lifetimes τ of the $^5D_0$ excited state of europium(III) for the two compounds under investigation

Compound	R	$\lambda_{max}(^5D_0 \rightarrow {}^7F_0)$/nm	CF splitting ($^7F_1$)/cm^{-1}	$\tau(^5D_0)$/ms
Eu(hfa)$_3$·monoglyme	11.0	579.9	251	0.93
Eu(hfa)$_3$·diglyme	6.6	579.4	292	0.96

dination number of nine for the europium(III) ion, while an eight-coordinate environment can be assumed for **1**, with both hfa and monoglyme acting as bidentate ligands, since no water molecules are coordinated to the metal ion.

The luminescence excitation spectra of both **1** and **2**, associated with the $^5D_0 \rightarrow {}^7F_2$ transition, consist of sharp $f \rightarrow f$ transitions for wavelengths higher than 450 nm, and of a broad band peaking at about 400 nm (Figure 5). The latter feature is assigned to an Eu−O ligand-to-metal charge transfer transition[30] since both polyether and hfa ligands do not show absorption bands in this spectral region.

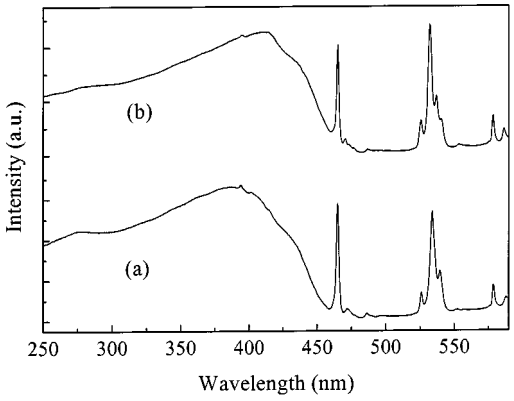

Figure 5. Room temperature excitation spectra of adducts **1** (a) and **2** (b)

Inspection of the high resolution, room-temperature luminescence spectrum (Figure 6) shows that a weak structure is located in both the high- and low-energy sides of the $^5D_0 \rightarrow {}^7F_0$ pure electronic transition. These features are assigned to vibronic sidebands due to coupling between the $^5D_0 \rightarrow {}^7F_0$ electronic transition and the vibrational modes involving the europium(III) ion.[31,32] Vibronic sidebands have often been observed in the luminescence and excitation spectra of europium(III)-doped crystalline and noncrystalline solids.[33,34] Less frequently they have also been observed in the spectra of europium(III) coordination compounds.[35] In general, vibronic sidebands mainly relative to the $^5D_0 \rightleftarrows {}^7F_2$ transition have usually been studied.[36]

The maxima in the vibronic sideband at lower energy are located about 80, 150 and 250 cm^{-1} from the pure electronic line in the case of **1,** and 80, 140, 185 and 250 cm^{-1} in the case of **2**. These differences are assigned to the wavenumbers of vibrational modes coupled to the europium(III) electronic transitions and, therefore, localized close to the metal ion. The vibrations are assigned to Eu−O modes, due to their small wavenumber values. In particular, the maximum at 250 cm^{-1} agrees with the presently proposed assignment of the Raman band at the same frequency to the

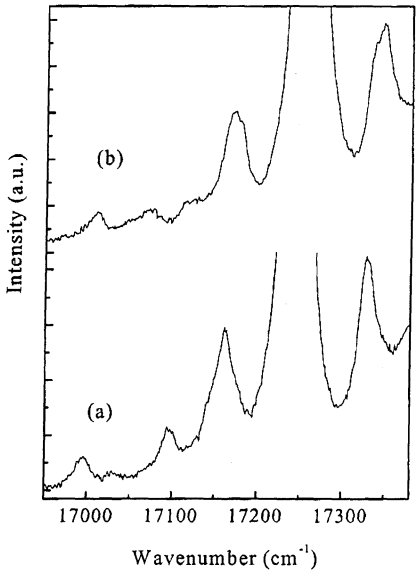

Figure 6. Room temperature luminescence spectra of adducts **1** (a) and **2** (b)

Eu−O stretching mode (vide supra). The other modes observed in the vibronic sideband probably represent other stretching and bending modes at the europium(III) center.

The luminescence decay curves from the europium(III) $^5D_0$ state in **1** and **2**, measured at room temperature, with excitation and observation wavelengths of 395.0 and 613.0 nm, respectively, are perfectly exponential for about three decades. The associated lifetimes of the $^5D_0$ state [$\tau(^5D_0)$, Table 2] are relatively short for europium(III) compounds (<1 ms), but compatible with both the high intensity of the hypersensitive $^5D_0 \rightarrow {}^7F_2$ emission transition and the presence of high frequency vibrations in the complexes. The exponential decays, in addition, are indicative that energy transfer and migration processes are probably inefficient in these compounds due to the rather long distance [8.047 Å in the gadolinium(III) homologue of **2**][37] between neighboring metal centers in the crystals.

The nature of the "thermal anomaly" observed at 71.4 °C in the DSC curves of **2** has been also investigated by low resolution luminescence spectra in the temperature range 20−90 °C. The experimental data show that the spectra do not change significantly for temperatures up to about 80 °C. Beyond this temperature, the intensities of the $^5D_0 \rightarrow {}^7F_2$ and $^5D_0 \rightarrow {}^7F_0$ emission transitions increase abruptly, compared to the magnetic dipole $^5D_0 \rightarrow {}^7F_1$ transition, so that the asymmetry ratio *R* approaches the value of 12 at 90° C. This clearly indicates that beyond 80 °C the first coordination sphere of the europium(III) ion undergoes a marked distortion, possibly due to the transition to a plastic phase.

We note that the *R* value associated with **2** in the plastic phase lies close to that found for **1** in the solid phase. Therefore, it is possible that packing constraints force the coordination geometry of europium(III) in the solid phase of **2** to be more symmetrical than in the plastic phase.

MOCVD Depositions

Preliminary MOCVD experiments indicate that both adducts are well suited for the deposition of europium-containing films. In particular, the diglyme adduct has been successfully applied to Eu−O−F film deposition. A typical X-ray glancing incidence diffraction (GID) pattern of an Eu−O−F film deposited at 700 °C on quartz substrate is shown in Figure 7. Reflections point to the formation of two different polycrystalline oxyfluoride phases, the orthorhombic $Eu_6O_5F_8$ [38] and the rhombohedral EuOF.[39] The observed intensities are different from those reported for a polycrystalline powder, thus suggesting that some texturing occurs upon growth. An SEM micrograph of an Eu−O−F film deposited at 700 °C is reported in Figure 8. The image shows a very homogeneous surface with ≈1 μm diameter grains uniformly distributed.

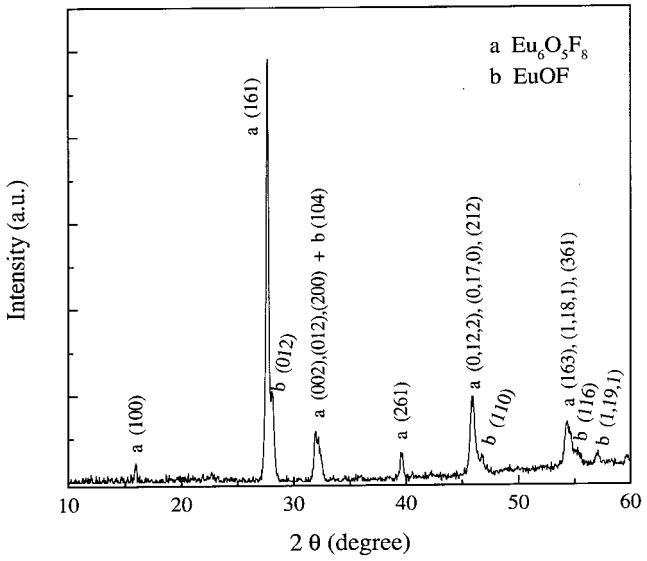

Figure 7. X-ray GID pattern of an MOCVD grown Eu−O−F film on a quartz substrate using the $Eu(hfa)_3$·diglyme precursor

Conclusions

The optical spectroscopy of the two $Eu(hfa)_3$·monoglyme and $Eu(hfa)_3$·diglyme adducts has been studied. The experimental results have provided information on the distortion of the coordination sphere around the lanthanide ion, on the covalence of the metal-ligand bond and on the coupling between electronic transitions and vibrational modes involving the europium(III) ion. Luminescence spectroscopy data have also been used to complement the DSC data of $Eu(hfa)_3$·diglyme in order to understand the nature of the phase transition at 71.4 °C.

There is evidence that the present $Eu(hfa)_3$·monoglyme and $Eu(hfa)_3$·diglyme adducts are thermally stable, highly volatile compounds that can be used even in atmospheric-pressure MOCVD deposition at temperatures lower than 200 °C. Low melting points allow their use as thermally stable precursors in the liquid phase, hence under constant vaporization and mass transport rates. Finally, both adducts **1** and **2**, analogously to the $La(hfa)_3$·diglyme precursor,[16] could act as liquid solvents for a large variety of metal precursors of relevance for MOCVD applicability, thus providing liquid multi-element single-sources for simultaneous delivery of different metal components in the required stoichiometries.

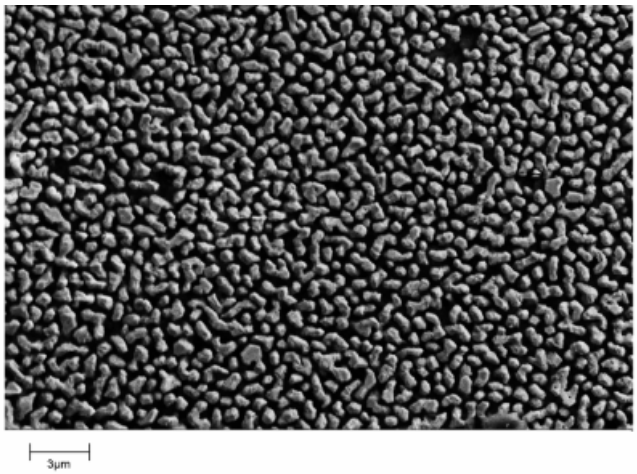

Figure 8. SEM micrograph of an MOCVD grown Eu−O−F film on a quartz substrate using the $Eu(hfa)_3$·diglyme precursor

Their vapor-phase transport characteristics at low- and atmospheric pressure make them attractive candidates not only for laboratory MOCVD processes but also for industrial applications.

Experimental Section

Reagents: Commercial Eu_2O_3, Hhfa, monoglyme, and diglyme (Aldrich) were used without any further purification.

General Procedures: Elemental microanalyses were performed in the Analytical Laboratories of the University of Catania. Infrared data were collected on a 684 Perkin−Elmer spectrometer either as nujol or hexachlorobutadiene mulls between KBr plates. Thermal measurements were made using a Mettler 3000 system equipped with a TG 50 thermobalance, a TC 10 processor and DSC 30 calorimeter. Weights of the samples were between 15−20 mg (TGA) and 4−10 mg (DSC). Analyses were made under prepurified nitrogen using a 5 °C/min heating rate. FAB mass spectra were obtained with a Kratos MS 50 spectrometer. The 488.0 nm line of a Spectra-Physics 2017 Argon laser was used to excite room temperature luminescence and Raman spectra. A fiber optic probe coupled to a Dilor Superhead, equipped with a suitable notch filter, was employed. The scattered signal was analyzed by a Jobin-Yvon HR460 monochromator and a Spectrum One CCD detector. A 1200 lines/mm grating was used to collect Raman and high resolution (≈2 cm^{-1}) luminescence spectra in the region of the $^5D_0 \rightarrow {}^7F_0$ transition of europium(III), whilst the other laser-excited luminescence spectra were measured using a 150 lines/mm grating. Low resolution emission and excitation spectra in the visible and UV regions were measured in the temperature range 20−90 °C using a JASCO FP-

777 spectrofluorimeter (bandwidths of 1.5 nm for both excitation and emission) and a conventional circulation thermostat. The decay curves of the luminescence were measured at room temperature using a Perkin−Elmer LS50 pulsed lamp spectrofluorimeter.

Synthesis of $Eu(hfa)_3$·monoglyme (1): The adduct was synthesized adopting a synthetic strategy analogous to that previously reported for the Gd analogue.[7] Eu_2O_3 (2.035 g, 5.78 mmol) was first suspended in hexane (200 mL) and then monoglyme (1.040 g, 11.56 mmol) was added to the suspension. Hhfa (7.217 g, 34.69 mmol) was added under vigorous stirring after 10 min. and the mixture was refluxed under stirring for 1 hour. The excess of europium oxide was then filtered off. Pale yellow crystals precipitated after partial evaporation of the solvent. The crystals were collected by filtration and dried under vacuum. The yield was 8.589 g (86%). The melting point of the crude product was 80−84 °C. − $C_{19}H_{13}EuF_{18}O_8$ (863.23): calcd. C 26.41, H 1.52; found C 26.52, H 1.47. The adduct quantitatively sublimes at 75−80 °C/10^{-3} Torr. − IR (nujol or hexachlorobutadiene): $\tilde{\nu}$ = 3620 (w), 3540 (w), 2930 (vs), 1660 (vs), 1610 (w), 1570 (m), 1540 (m), 1495 (s), 1455 (s), 1380 (m), 1350 (vw), 1260 (s), 1200 (s), 1150 (s), 1100 (m), 1060 (s), 1030 (w), 1010 (vw), 950 (w), 860 (m), 805 (m), 770 (w), 740 (w), 660 (s) cm^{-1}. The MS and IR data of the raw[40] and sublimed adduct are identical.

Synthesis of $Eu(hfa)_3$·diglyme (2): Prepared as described for the monoglyme adduct from Eu_2O_3 (1.956 g, 5.56 mmol), Hhfa (6.939 g, 33.36 mmol) and diglyme (1.489 g, 11.11 mmol). Yield 9.180 g (91%). The "apparent" melting point of the crude product was 72−74 °C (vide infra the DSC data). − $C_{21}H_{17}EuF_{18}O_9$ (907.28): calcd. C 27.77, H 1.89; found C 27.94, H 1.92. The adduct quantitatively sublimes at 85−90 °C/10^{-3} Torr. − IR (nujol or hexachlorobutadiene): $\tilde{\nu}$ = 2930 (s), 1650 (vs), 1605 (w), 1555 (m), 1530 (m), 1495 (s), 1460 (s), 1380 (m), 1350 (w), 1260 (s), 1205 (s), 1140 (s), 1090 (s), 1065 (m), 1045 (s), 1010 (m), 945 (m), 870 (m), 835 (vw), 800 (m), 770 (w), 740 (m), 650 (s) cm^{-1}. The MS and IR data of the raw and sublimed adduct are identical.

MOCVD Experiments: Low-pressure MOCVD depositions of Eu−O−F films were carried out under O_2 (500 sccm) flow as carrier and reaction gas, using a horizontal hot-wall reactor. The $Eu(hfa)_3$·diglyme source temperature was maintained at 120 °C. Quartz slides were used as substrates in the 600−700 °C temperature range. Scanning Electron Microscopy (SEM) micrographs were recorded using a LEO IRIDIUM 1450 Electron Microscope. X-ray glancing incidence diffraction (GID) patterns were recorded on a Bruker-AXS D5005 θ-θ X-ray diffractometer equipped with a Goebel mirror and a thin film attachment using Cu-K_α radiation operating at 40KV/ 30 mA.

Acknowledgments

The authors gratefully thank Erica Viviani (Università di Verona) for expert technical assistance. The Ministero dell'Università e della Ricerca Scientifica e Tecnologica (MURST, Rome) is also gratefully acknowledged for financial support within P.R.I.N. programs.

[1] S. R. Drake, A. Lyons, D. J. Otway, A. M. Z. Slawin, D. J. Williams, *J. Chem. Soc., Dalton Trans.* **1993**, 2379−2386.
[2] S. R. Drake, M. B. Hursthouse, K. M. A. Malik, S. A. S. Miller, D. J. Otway, *Inorg. Chem.* **1993**, *32*, 4464−4471.
[3] D. C. Bradley, H. Chudzynska, M. B. Hursthouse, M. Motevalli, *Polyhedron* **1994**, *13*, 7−14.
[4] I. Baxter, S. R. Drake, M. B. Hursthouse, K. M. A. Malik, J. MacAleese, D. J. Otway, J. C. Plakatouras, *Inorg. Chem.* **1995**, *34*, 1384−1394.
[5] R. Amano, Y. Shiokawa, N. Sato, Y. Suzuki, *J. Radioanal. Nucl. Chem.* **1993**, *172*, 81−86.
[6] G. Malandrino, R. Licata, F. Castelli, I. L. Fragalà,, C. Benelli, *Inorg. Chem.* **1995**, *34*, 6233−6234.
[7] G. Malandrino, O. Incontro, F. Castelli, I. L. Fragalà, C. Benelli, *Chem. Mater.* **1996**, *8*, 1292−1297.
[8] G. Malandrino, C. Benelli, F. Castelli, I. L. Fragalà, *Chem. Mater.* **1998**, *10*, 3434−3444.
[9] G. Malandrino, I. L. Fragalà, S. Aime, W. Dastrù, R. Gobetto, C. Benelli, *J. Chem. Soc., Dalton Trans.* **1998**, 1509−1512.
[10] K. D. Pollard, J. J. Vittal, G. P. A. Yap, R. J. Puddephatt, *J. Chem. Soc., Dalton Trans.* **1998**, 1265−1267.
[11] J. H. Lee, Y. S. Jung, Y. S. Sohn, S. J. Kang, *Bull. Kor. Chem. Soc.* **1998**, *19*, 231−235.
[12] S. J. Kang, Y. S. Jung, I. H. Suh, *Bull. Kor. Chem. Soc.* **1999**, *20*, 95−98.
[13] K. D. Pollard, H. A. Jenkins,, R. J. Puddephatt, *Chem. Mater.* **2000**, *12*, 701−710.
[14] G. Malandrino, R. Lo Nigro, C. Benelli, F. Castelli, I. L. Fragalà, *Chem. Vap. Depos.* **2000**, *6*, 233−238.
[15] G. Malandrino, A. Frassica, I. L. Fragalà, *Chem. Vap. Depos.* **1997**, *3*, 306−309.
[16] G. Malandrino, I. L. Fragalà, P. Scardi, *Chem. Mater.* **1998**, *10*, 3765−3768.
[17] G. Malandrino, I. L. Fragalà, *Electrochemical Society Proceedings*, **1997**, Vol. *97−25*, 844−851
[18] *Chemical Vapor Deposition: Principles and Applications* (Eds.: M. L. Hitchman, K. F. Jensen , Academic Press, London, **1993**.
[19] H. Sato, *Jpn. J. Appl. Phys.* **1994**, *33*, L371−L373.
[20] S. J. Kang, Y. S. Jung, Y. S. Sohn, *Bull. Kor. Chem. Soc.* **1997**, *18*, 75−80.
[21] G. Blasse, B. C. Grabmaier, *Luminescent Materials*, Springer Verlag, Berlin, **1994**.
[22] D. Lin-Vien, N. B. Colthup, W. G. Fateley, J. G. Grasselli, *The Handbook of Infrared and Raman Characteristic Frequencies of Organic Molecules*, Academic Press, San Diego, CA, **1991**.
[23] I. K. Igumenov, P. P. Semyannikov, S. V. Belaya, A. S. Zanina, S. I. Shergina, I. E. Sokolov, *Polyhedron* **1996**, *15*, 4521−4530.
[24] M. Wachtler, A. Speghini, K. Gatterer, H. P. Fritzer, D. Ajò, M. Bettinelli, *J. Amer. Ceram. Soc.* **1998**, *81*, 2045−2052.
[25] D. Braga, *Chem. Rev.* **1992**, *92*, 633−665.
[26] G. Malandrino, F. Castelli, I. L. Fragalà, *Inorg. Chim. Acta* **1994**, *224*, 203−207.
[27] J. A. Capobianco, P. P. Proulx, N. Raspa, *Chem. Phys. Lett.* **1989**, *161*, 151−157.
[28] P. Caro, O. Beaury, E. Antic, *J. Phys.* **1976**, *37*, 671−676.
[29] E. W. J. L. Oomen, A. M. A. van Dongen, *J. Non-Cryst. Solids* **1989**, *111*, 205−213.
[30] G. Blasse, *Structure and Bonding (Berlin)* **1976**, *26*, 43−79.
[31] *Vibronic Processes in Inorganic Chemistry* (Ed.: C. D. Flint), Kluwer, Dordrecht, **1989**.
[32] G. Blasse, *Int. Rev. Phys. Chem.* **1992**, *11*, 71−100.
[33] G. Blasse, *Inorg. Chim. Acta* **1990**, *167*, 33−37.
[34] M. Wachtler, A. Speghini, S. Pigorini, R. Rolli, M. Bettinelli, *J. Non-Cryst. Solids* **1997**, *217*, 111−114.
[35] *Lanthanide Probes in Life, Chemical and Earth Sciences, Theory and Practice* (Eds.: J.-C. G. Bünzli, G. R. Choppin), Elsevier, Amsterdam, **1989**, p. 219−293.
[36] S. Todoroki, K. Hirao, N. Soga, *J. Alloys Compd.* **1993**, *193*, 207−209.
[37] Although the X-ray crystal structure of **2** has been reported,[20] this value is not available and, therefore, the M−M distance in the Gd isostructural compound has been considered.
[38] ICDD No. 26−637.
[39] ICDD No. 26−636.
[40] Used without any further purification.

Received August 12, 2000
[I00304]

Synthesis and Magnetic Properties of a Polymeric Nitridochromium(V) Complex with a Tetradentate Schiff Base Ligand

Masanobu Tsuchimoto,*[a] Naoki Yoshioka,*[b] and Shigeru Ohba[a]

Keywords: Nitrides / Chromium / Polymers / Schiff bases / Magnetic properties

A novel polymeric nitridochromium(V) complex with a Schiff base ligand [CrN(salpn)] [H_2(salpn) = *N,N′*-disalicylidene-1,3-propanediamine] was prepared by photolysis of an azidochromium(III) complex in acetonitrile. X-ray crystal structure analyses of the starting material $\{(CH_3)_2NH_2\}_2[CrCl_2(salpn)]Cl$ (**1**) and the polymeric complex [CrN(salpn)] (**3**) were carried out. The orange complex **3** has a linear ···Cr≡N···Cr≡N··· chain structure with the N···Cr distance being 2.508(2) Å. Magnetic data show that **3** has a ferromagnetic intermolecular interaction in the chains (J = +8.4 cm^{-1}).

Introduction

The synthesis of new linear-chain polynuclear metal complexes is important because of their physical properties (e.g. magnetism and electric conductivity) and structural characteristics. Several oxovanadium(IV) complexes with tetradentate Schiff base ligands, such as [VO(salpn)] (H_2salpn = *N,N′*-disalicylidene-1,3-propanediamine), have linear-chain structures (···V=O···V=O···) in the solid state.[1] It has been reported that these polymeric oxovanadium(IV) complexes with a $(d_{xy})^1$ electron configuration (z axis oriented along the V=O bond) have an intermolecular ferromagnetic interaction in the chains with an exchange coupling parameter, $J \approx +5$ cm^{-1}.[2,3] The occurrence of a ferromagnetic interaction for these complexes has been explained in terms of McConnell's spin polarization theorem.[2]

Recently, the preparation of a polymeric nitridomanganese(V) complex [MnN(salpn)], by photoirradiation of an azidomanganese(III) complex has been reported.[4] The diamagnetic polymeric nitridomanganese(V) complex with a $(d_{xy})^2$ electron configuration has ···Mn≡N···Mn≡N··· chains in the crystal. This result led us to prepare a polymeric nitridochromium(V) complex with a $(d_{xy})^1$ electron configuration. All the polymeric nitridometal complexes (···M≡N···M≡N···) reported so far are diamagnetic with a d^0 (V^V,[5,6] Mo^{VI},[7] W^{VI},[8] Re^{VII} [9]) or a d^2 (Mn^V [4]) electron configuration. This paper reports the first preparation and crystal structure of a polymeric nitridochromium(V) complex [CrN(salpn)]. The temperature dependence of magnetic susceptibilities and low-temperature magnetization experiments are also reported.

[a] Department of Chemistry, Faculty of Science and Technology, Keio University,
Hiyoshi 3−14−1, Kohoku-ku, Yokohama 223−8522, Japan
Fax: (internat.) +81-45/566-1697
E-mail: tmoto@chem.keio.ac.jp; ohba@chem.keio.ac.jp
[b] Department of Applied Chemistry, Faculty of Science and Technology, Keio University,
Hiyoshi 3−14−1, Kohoku-ku, Yokohama 223−8522, Japan
Fax: (internat.) +81-45/566-1551
E-mail: yoshioka@applc.keio.ac.jp

Results and Discussion

Synthesis

The starting chromium(III) complex $\{(CH_3)_2NH_2\}_2$-$[CrCl_2(salpn)]Cl$ (**1**) was prepared by the reaction of the Schiff base ligand with anhydrous chromium(III) chloride in DMF.[10] The dimethylammonium cation in **1** originates from the decomposition of DMF. The azidochromium(III) complex $(CH_3)_2NH_2[Cr(N_3)_2(salpn)]$ (**2**) was prepared by the reaction of **1** with sodium azide in acetone. The nitridochromium(V) complex [CrN(salpn)] (**3**) was prepared by photoirradiation of **2** in acetonitrile. The orange complex **3** is stable in air at ambient temperature. The IR spectrum of **3** shows the Cr≡N stretching bands at 956 and 961 cm^{-1}, which are significantly shifted to lower energy than that of monomeric [CrN(salen)] (1012 cm^{-1}).[11] The electronic spectrum of **3** in acetonitrile shows a d−d transition band around 569 nm as a shoulder. This d−d band is assigned to the $3d_{yz,zx} \leftarrow 3d_{xy}$ transition, which is observed at 535 nm in the spectrum of [CrN(salen)].[12]

X-ray Crystal Structures

X-ray structure analyses of **1** and **3** were carried out. The molecular structures of **1** and **3** are shown in Figure 1 and 2, respectively. Selected bond lengths and angles are listed in Table 1 and 2, respectively.

Complex **1** has an octahedral structure with the chloro ligands in the *trans* position. The dimethylammonium cations are hydrogen bonded to the oxygen atoms of the ligand and the chloride ion [Figure 1(b)]. The distances N26···O4, N26···O5, N27···O4, N27···O5 are in the range 2.972(2)−3.151(2) Å, and the distances N26···Cl25 and N27···Cl25 are 3.140(2) Å and 3.151(2) Å, respectively. Prismatic crystals of **1** show dichroism; the (1 −1 0), (−1 1 0),

 © WILEY-VCH Verlag GmbH, 69451 Weinheim, 2001 1434−1948/01/0404−1045 $ 17.50+.50/0

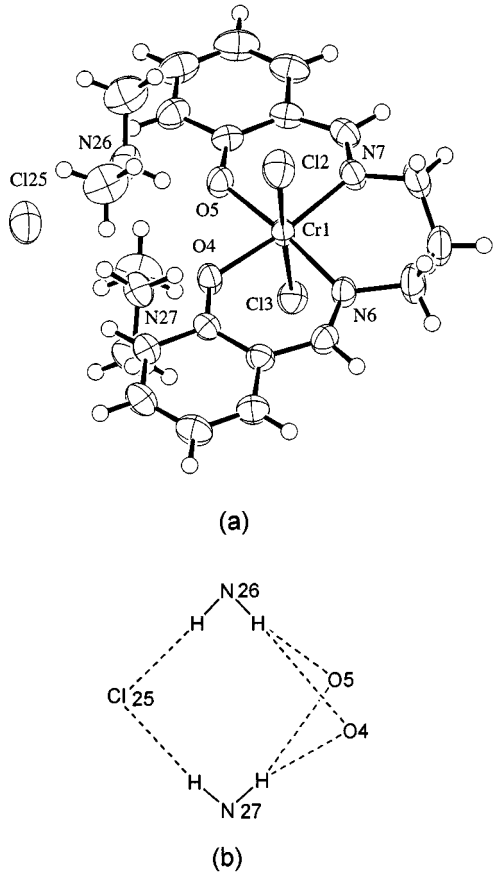

Figure 1. (a) ORTEP drawing of **1** with 50% probability ellipsoids; (b) schematic drawing of the hydrogen bonding in **1**

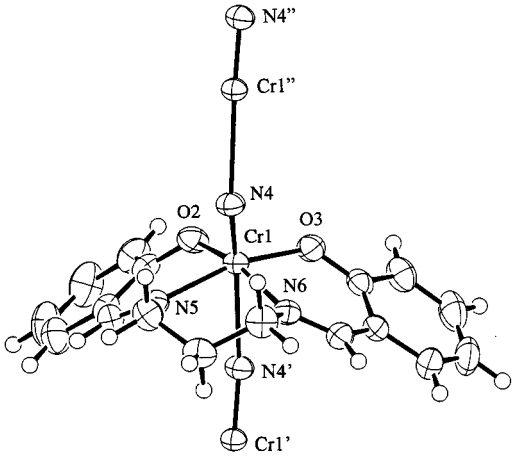

Figure 2. ORTEP drawing of **3** with 50% probability ellipsoids

(−1 0 1), (1 0 −1) planes are green, and the (1 1 0), (−1 −1 0) planes are brown.

Complex **3** has a polymeric structure with a distorted octahedral coordination geometry. The linear ···Cr≡N···Cr≡N··· chains run along the 2_1 screw axes parallel to the *c* axis. The Cr≡N and Cr···N distances are 1.559(2) Å and 2.508(2) Å, respectively. The Cr≡N···Cr angle is 153.7(1)°. The Cr1 atom is displaced by 0.321(1) Å from the N_2O_2 coordination plane. The six-membered N−N chelate ring shows a chair conformation. The crystal

Table 1. Selected bond lengths (Å) and angles (deg) of **1**

Cr1−Cl2	2.3615(6)	Cr1−Cl3	2.3522(6)
Cr1−O4	1.948(1)	Cr1−O5	1.946(1)
Cr1−N6	2.068(1)	Cr1−N7	2.052(2)
Cl2−Cr1−Cl3	176.66(2)	Cl2−Cr1−O4	89.88(4)
Cl2−Cr1−O5	92.73(4)	Cl2−Cr1−N6	89.46(4)
Cl2−Cr1−N7	89.16(4)	Cl3−Cr1−O4	90.81(4)
Cl3−Cr1−O5	90.59(4)	Cl3−Cr1−N6	87.25(4)
Cl3−Cr1−N7	90.54(4)	O4−Cr1−O5	83.26(5)
O4−Cr1−N6	91.74(6)	O4−Cr1−N7	173.09(6)
O5−Cr1−N6	174.53(6)	O5−Cr1−N7	89.96(6)
N6−Cr1−N7	95.09(6)		

Table 2. Selected bond lengths (Å) and angles (deg) of **3**[a]

Cr1−O2	1.934(2)	Cr1−O3	1.932(2)
Cr1−N4	1.559(2)	Cr1−N5	2.048(2)
Cr1−N6	2.039(2)	Cr1−N4′	2.508(2)
O2−Cr1−O3	85.85(9)	O2−Cr1−N4	102.7(1)
O2−Cr1−N5	88.49(9)	O2−Cr1−N6	161.11(9)
O3−Cr1−N4	102.7(1)	O3−Cr1−N5	161.27(9)
O3−Cr1−N6	88.43(9)	N4−Cr1−N5	96.0(1)
N4−Cr1−N6	96.1(1)	N5−Cr1−N6	91.23(9)
N4−Cr1−N4′	169.87(5)	Cr1−N4′−Cr1′	153.7(1)

[a] Primed atoms are generated by 1/2 − x, −y, 1/2 + z.

structure of **3** is isostructural with that of polymeric [MnN(salpn)], whose Mn≡N and Mn···N distances are 1.520(3) Å and 2.528(3) Å, respectively.[4] On the other hand, the V···O distance in polymeric [VO(salpn)] [2.213(9) Å][1] is shorter than the Cr···N distance in **3**. The V=O units in [VO(salpn)] are more strongly bonded to each other than the Cr≡N units in **3**.

Magnetic Properties

The ESR spectrum of **3** in benzene at room temperature is shown in Figure 3. The spectrum shows a strong isotropic ESR signal due to the chromium isotope with $I = 0$ at $g_{iso} = 1.978$, with a satellite quartet pattern ascribed to the less-abundant (9.5%) ^{53}Cr isotope with $I = 3/2$. The central strong signal and low-field satellite signals show a well-resolved septet superhyperfine structure [$A(N) = 0.26$ mT] with an intensity ratio of 1:3:6:7:6:3:1 due to three equivalent nitrogen nuclei, two from the salpn ligand and one

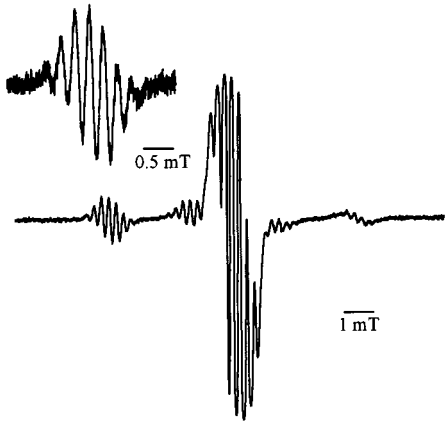

Figure 3. ESR spectrum of **3** in benzene at room temperature

from the apical nitrido atom. A similar extent of the Fermi-contact interaction occurs for the three nitrogen nuclei, despite their chemical nonequivalence. The equivalent isotropic superhyperfine coupling constants for the apical nitrido atom and the basal nitrogen atom are observed for [CrN(salen)][12] and other nitridochromium(V) complexes with tetradentate ligands.[13–15] The superhyperfine coupling constant (0.26 mT) in the spectrum of [CrN(salpn)] corresponds to a spin density of 0.005 on each nitrogen, based on the value of an isolated nitrogen atom (55.7 mT).[16]

The magnetic susceptibility data for **3**, plotted as the thermal variation of reciprocal molar susceptibility χ_m^{-1}, and $\chi_m T$, are shown in Figure 4 and 5, respectively. The behavior of the χ_m^{-1} vs. T plots in Figure 4 is well described by the Curie-Weiss law, $\chi_m = C/(T - \theta)$, with $C = 0.367$ emu K/mol and $\theta = +5.9$ K above 14 K. The positive θ value indicates the ferromagnetic interaction between the nitridochromium(V) spin centers. The overall appearance of the $\chi_m T$ vs. T plots in Figure 5 also indicates a ferromagnetic interaction. Although the $\chi_m T$ plots at 5000 G (represented as circles) show saturation below 5 K, the $\chi_m T$ value at 200 G (represented as triangles) increases even near $T =$ 1.8 K. The magnetic susceptibility data can be analyzed using the Heisenberg model with the exchange interaction between the nitridochromium(V) ion on a chain [Equation (1)].

$$H = -J\sum_{i=1}^{n-1} S_i \cdot S_{i+1} \tag{1}$$

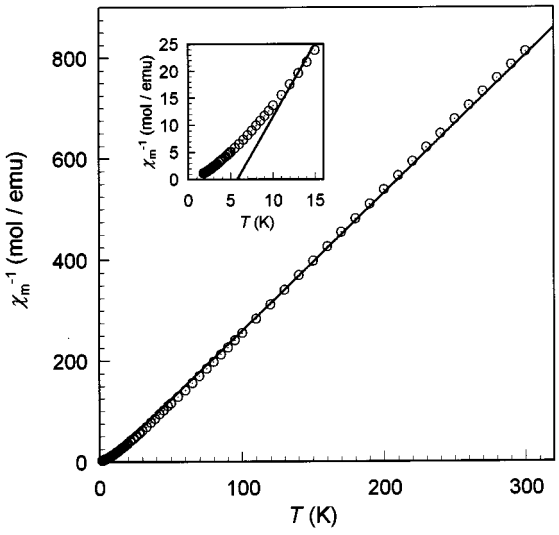

Figure 4. χ_m^{-1} vs. T (○) plot of **3**; the inset shows the χ_m^{-1} vs. T plot in the low-temperature region; the solid lines were calculated from the Curie-Weiss law

The thermal variation of magnetic susceptibility of a magnetic chain can be described by the empirical function introduced by Baker et al. [Equation (2)].[17]

$$\chi_m = \frac{N_A g^2 \beta^2}{kT} F(J,T)$$

with

$$F(J,T) = \frac{1}{4}[(1 + 5.7979916x + 16.902653x^2 + 29.376885x^3 + 29.832959x^4 + 14.036918x^5)/(1 + 2.7979916x + 7.0086780x^2 + 8.6538644x^3 + 4.5743114x^4)]^{2/3} \tag{2}$$

and

$$x = \frac{J}{2kT}$$

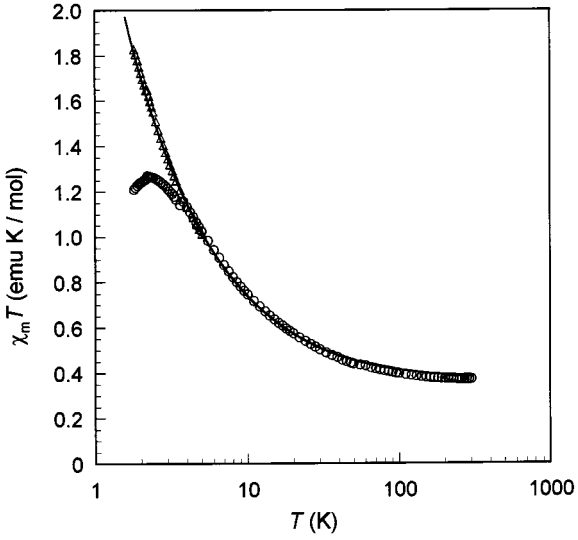

Figure 5. $\chi_m T$ vs. T plots of **3** under an applied field of 0.02 T (△) and 0.50 T (○)

The best-fit curve using Equation (2) is shown as a solid line in Figure 5, corresponding to $J = +8.4$ cm^{-1}. To clarify the intermolecular coupling, the magnetization of **3** was measured at 1.8 K (Figure 6). The magnetization curve of **3** exceeds the Brillouin function with $S = 1/2$ and nearly coincides with that of $S = 12/2$ at 1.8 K, indicating the formation of a high-spin cluster with $S = 12/2$ on average.

According to the McConnell theorem,[18] the exchange interaction between two aromatic radicals A and B can be described by the sum of the two-center exchange integrals in the form

$$H^{AB} = -S^A \cdot S^B \sum_{ij} J_{ij}^{AB} \rho_i^A \rho_j^B \tag{3}$$

where S^A and S^B are the total spin operators for molecules A and B, respectively, and ρ_i^A and ρ_j^B are the π-spin densities on atoms i and j of A and B, respectively. If we apply Equation (3) to a dimer of nitridochromium(V) units (each is denoted as A and B) in **3**, and consider that i and j correspond to the chromium(V) ion and the nitrido ion, respectively, Equation (3) can be written in the form

$$H^{AB} = -S^A \cdot S^B J_{Cr\cdots N}^{AB} \rho_{Cr}^A \rho_N^B \tag{4}$$

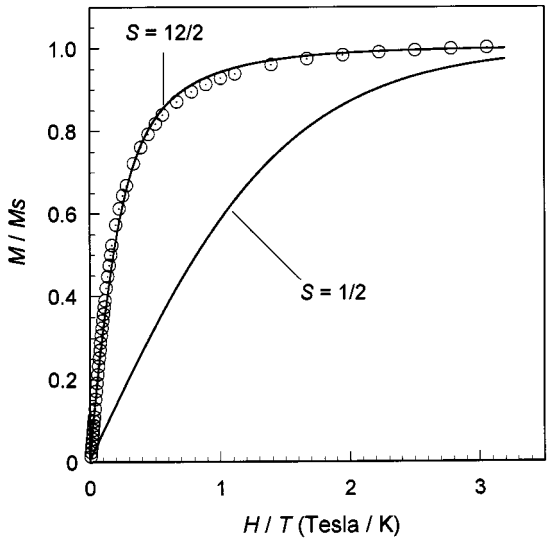

Figure 6. Magnetization isotherm of **3** at 1.8 K; the solid lines were calculated with the Brillouin function

When a ferromagnetic intermolecular coupling is observed between molecules A and B, $J^{AB}_{Cr\cdots N}$ is negative and ρ^{A}_{Cr} and ρ^{B}_{N} are positive and negative, respectively. Spin polarization on the nitrido ion was observed in the ESR spectrum of **3**, although the sign of the polarized spin is uncertain. A negative spin density is expected for the polarized spin on the nitrido ion.

In the present study, a ferromagnetic intermolecular interaction between the nitridochromium(V) spin centers is observed for **3**. A similar ferromagnetic intermolecular interaction is observed for polymeric [VO(salpn)] with the same $(d_{xy})^1$ electronic configuration. However, the magnetic interaction in **3** ($J = +8.4$ cm^{-1}) is larger than that in [VO(salpn)] ($J = +5.2$ cm^{-1}),[2] while the distance between the Cr≡N units in **3** is longer than that between the V=O units in [VO(salpn)] (vide supra). Further investigations are necessary to elucidate the intermolecular ferromagnetic coupling in the Cr≡N and V=O polymeric systems.

Experimental Section

{(CH$_3$)$_2$NH$_2$}$_2$[CrCl$_2$(salpn)]Cl (1): The ligand H$_2$salpn was prepared by the reaction of 1,3-propanediamine with two equivalent amounts of salicylaldehyde in ethanol. The solvent was evaporated from the reaction mixture to yield an oily product, which was used for the following reaction without purification. To a DMF solution (300 mL) of the ligand (50 mmol), was added anhydrous chromium(III) chloride (7.92 g, 50 mmol). The reaction mixture was refluxed for 4 h. After cooling, unreacted chromium(III) chloride was removed by filtration, and the filtrate was evaporated to dryness. The residue was suspended in ethanol, and the precipitate was collected by filtration. The light green powder was washed with ethanol and ether, and dried. Yield: 18.1 g (68%). − $C_{21}H_{32}Cl_3Cr_1N_4O_2$ (530.86): calcd. C 47.51, H 6.08, N 10.55; found C 47.56, H 6.10, N 10.54.

(CH$_3$)$_2$NH$_2$[Cr(N$_3$)$_2$(salpn)] (2): To a suspension of {(CH$_3$)$_2$NH$_2$}$_2$[CrCl$_2$(salpn)]Cl (8.0 g, 15 mmol) in acetone (1 L), was added sodium azide (2.6 g, 40 mmol). The mixture was refluxed for 3 h, and filtered. The green precipitate was dissolved in hot acetone (2 L), and insoluble salts were removed by filtration. The combined filtrate was evaporated to dryness, and the residue was suspended in diethyl ether. A green crude product was collected by filtration and dried. Yield: 6.6 g (96%). IR (KBr): $\tilde{\nu}$ = 2058 cm^{-1} ν(N$_3$). The complex was used for the following reaction without purification.

[CrN(salpn)] (3): Although no problems were encountered in this study, azide complexes are explosive and photolysis of the complex was carried out with caution. (CH$_3$)$_2$NH$_2$ [Cr(N$_3$)$_2$(salpn)] (1.39 g, 3 mmol) was suspended in acetonitrile (1 L), and the mixture was irradiated with a 400 W high-pressure mercury lamp below 20 °C under an argon atmosphere, with stirring. After 2 h, another 3 mmol of the azido complex was added to the reaction mixture, and the mixture was irradiated for 24 h. The color of the mixture gradually turned to red during the irradiation. After irradiation, the mixture was filtered, and the filtrate was evaporated to ca. 5 mL. The resulting orange precipitate was collected by filtration, and dried. This crude product was dissolved in dichloromethane, and applied to a silica gel column (∅ 3.5 cm × 20 cm). The product was eluted with dichloromethane/ethyl acetate (10:1 v/v). A main orange band was collected and evaporated to dryness to yield orange needle crystals. Yield: 1.12 g (54%). − $C_{17}H_{16}Cr_1N_3O_2$ (346.33): calcd. C 58.96, H 4.66, N 12.13; found C 58.83, H 4.66, N 12.09. − IR (KBr): $\tilde{\nu}$ = 956 cm^{-1}, 961 ν(Cr≡N). − UV/Vis {CH$_3$CN, $\sigma/10^3$ cm^{-1} (log ε/M^{-1}cm^{-1})}: λ = 17.6 (1.70, sh), 21.7 (sh), 27.0(3.87), 36.0 (4.37), 41.2 (4.69).

X-ray Crystallographic Study: Dichroic (green and brown) prismatic crystals of {(CH$_3$)$_2$NH$_2$}$_2$[CrCl$_2$(salpn)]Cl (**1**) were obtained by slow diffusion of diethyl ether vapor into a DMF solution of the complex. Orange needle crystals of [CrN(salpn)] (**3**) were grown from a dichloromethane solution. The intensity data were collected at 25 °C on a Rigaku four-circle AFC-7R diffractometer with graphite-monochromatized Mo-K_α radiation (λ = 0.71073 Å) up to 2θ = 55° by $\theta-2\theta$ scans. Three standard reflections were measured at every 150 reflections. Absorption corrections were made by the numerical integration method for **1**,[19] and the Ψ scans method for **3**.[20] The structures were solved by direct methods on a Silicon Graphics O^2 workstation with the program system TEXSAN.[21] Non-hydrogen atoms were treated anisotropically, and hydrogen atoms were introduced at ideal positions. Refinement was based on F^2 against all the 5837 reflections for **1**, and against 2062 reflections for **3**. The R value was 0.031 for the 4912 reflections with $I > 2\sigma(I)$ for **1**, and 0.029 for 1780 reflections with $I > 2\sigma(I)$ for **3**. The absolute structure of **3** was determined with the Flack parameter $x = -0.05(3)$.[22] The crystal data and experimental details are listed in Table 3.

Crystallographic data (excluding structure factors) for the structures reported in this paper have been deposited with the Cambridge Crystallographic Data Centre as supplementary publication no. CCDC-148481 (**1**) and -148482 (**3**). Copies of the data can be obtained free of charge on application to CCDC, 12 Union Road, Cambridge CB2 1EZ, UK [Fax: (internat.) +44-1223/336-033; E-mail: deposit@ccdc.cam.ac.uk].

Magnetic Measurements: The magnetic susceptibility measurements were carried out with a SQUID magnetometer (Quantum Design MPMS-5) in the temperature range 1.8−300 K using a magnetic field of 0.5 and 0.02 T. The susceptibilities of **3** have been corrected for the diamagnetic contribution of $\chi_{dia} = -166 \times 10^{-6}$ emu mol^{-1}, calculated by Pascal's method. Magnetization experiments up to 5.5 T were carried out at 1.8 K.

Table 3. Crystallographic Data for **1** and **3**

	1	**3**
Formula	$C_{21}H_{32}Cl_3Cr_1N_4O_2$	$C_{17}H_{16}Cr_1N_3O_2$
Fw	530.9	346.3
Crystal size, mm	0.50 × 0.40 × 0.15	0.55 × 0.10 × 0.10
Space group	$P\bar{1}$	$P2_12_12_1$
a, Å	10.810(2)	11.670(3)
b, Å	11.362(1)	16.785(2)
c, Å	10.736(2)	7.928(3)
α, °	92.90(1)	90
β, °	103.56(2)	90
γ, °	94.95(1)	90
V, Å^3	1273.7(3)	1553.0(6)
Z	2	4
ρ_{calc}, g/cm^3	1.384	1.481
μ, mm^{-1}	0.788	0.750
λ, Å	0.71073	0.71073
T, °C	25	25
R[a]	0.031	0.029
R_w[b]	0.090	0.080

[a] $[\Sigma(F_o^2 - F_c^2)^2/\Sigma w(F_o)^2]^{1/2}$. — [b] $R_w = [\Sigma w(F_o^2 - F_c^2)^2/\Sigma w(F_o^2)^2]^{1/2}$, $w^{-1} = \sigma^2(F_o^2) + (0.0445P)^2 + 0.4789P$ for **1** and $R_w = [\Sigma w (F_o^2 - F_c^2)^2/\Sigma w(F_o^2)^2]^{1/2}$, $w^{-1} = \sigma^2(F_o^2) + (0.0446P)^2 + 0.2606P$ for **3**, where $P = (F_o^2 + 2F_c^2)/3$.

Other Measurements: IR spectra were recorded on a JASCO A-202 spectrophotometer. The electronic spectrum was recorded on a JASCO V-570 spectrophotometer. The ESR spectrum in benzene at room temperature was recorded on a JEOL JES-RE3X spectrometer with a 100 kHz field modulation.

[1] M. Mathew, A. J. Carty, G. J. Palenik, *J. Am. Chem. Soc.* **1970**, *92*, 3197−3198.
[2] M. Tsuchimoto, N. Yoshioka, *Chem. Phys. Lett.* **1998**, *297*, 115−120.
[3] R. F. Drake, V. H. Crawford, W. E. Hatfield, G. D. Simpson, G. O. Carlisle, *J. Inorg. Nucl. Chem.* **1975**, *37*, 291−293.
[4] M. Tsuchimoto, H. Iwamoto, M. Kojima, S. Ohba, *Chem. Lett.* **2000**, 1156 −1157.
[5] W. Willing, R. Christophersen, U. Müller, K. Dehnicke, *Z. Anorg. Allg. Chem.* **1987**, *555*, 16−22.
[6] S. C. Critchlow, M. E. Lerchen, R. C. Smith, N. M. Doherty, *J. Am. Chem. Soc.* **1988**, *110*, 8071−8075.
[7] D. M. -T. Chan, M. H. Chisholm, K. Folting, J. C. Huffman, N. S. Marchant, *Inorg. Chem.* **1986**, *25*, 4170−4174.
[8] M. H. Chisholm, D. M. Hoffman, J. C. Huffman, *Inorg. Chem.* **1983**, *22*, 2903−2906.
[9] W. Liese, K. Dehnicke, I. Walker, J. Strähle, *Z. Naturforsch* **1979**, *34B*, 693−696.
[10] C. M. Che, J. X. Ma, W. T. Wong, T. F. Lai, C. K. Poon, *Inorg. Chem.* **1988**, *27*, 2547−2548.
[11] S. I. Arshankow, A. L. Poznjak, *Z. Anorg. Allg. Chem.* **1981**, *481*, 201−206.
[12] N. Azuma, Y. Imori, H. Yoshida, K. Tajima, Y. Li, J. Yamauchi, *Inorg. Chim. Acta* **1997**, *266*, 29−36.
[13] J. W. Buchler, C. Dreher, K.-L. Lay, A. Raap, K. Gersonde, *Inorg. Chem.* **1983**, *22*, 879−884.
[14] J. T. Groves, T. Takahashi, W. M. Butler, *Inorg. Chem.* **1983**, *22*, 884−887.
[15] N. Azuma, T. Ozawa, S. Tsuboyama, *J. Chem. Soc., Dalton Trans.* **1994**, 2609−2613.
[16] B. A. Goodman, J. B. Raynor, *Adv. Inorg. Chem. Radiochem.* **1970**, *13*, 135−362.
[17] G. H. Baker, Jr., G. S. Rushbrooke, H. E. Gilbert, *Phys. Rev. A* **1964**, *135*, 1272−1277.
[18] H. M. McConnell, *J. Chem. Phys.* **1963**, *39*, 1910.
[19] P. Coppens, L. Leiserowitz, D. Rabinovich, *Acta Cryst.* **1965**, *18*, 1035−1038.
[20] A. C. T. North, D. C. Phillips, F. S. Mathews, *Acta Cryst.* **1968**, *A24*, 351−359.
[21] TEXSAN, Version 1.9, Single crystal structure analysis software, MSC, 3200 Research Forest Drive, The Woodlands, TX 77381, U.S.A and Rigaku, 3-9-12 Akishima, Tokyo, Japan.
[22] H. D. Flack, *Acta Cryst.* **1983**, *A39*, 876−881.

Received August 25, 2000
[I00328]

Chiral Chloro-Bridged η^6-Phenylglycine Ruthenium(II) Complexes Formed by Dehydrogenation of (*R*)-2,5-Dihydrophenylglycine[‡]

Harald Dialer,[a] Peter Mayer,[a][‡‡] Kurt Polborn,[a][‡‡] and Wolfgang Beck*[a]

Dedicated to Professor Kurt Dialer on the occasion of his 80th birthday

Keywords: Ruthenium / Iridium / Palladium / Amino acids

The reaction of N- or C-terminal protected (*R*)-2,5-dihydrophenylglycines with ruthenium(III) chloride gives the chloro-bridged η^6-phenylglycine complexes **1**–**3** without racemization. Dehydrogenation also occurs with (*R*)-2,5-dihydrophenylglycine and $[(n\mathrm{Bu}_3\mathrm{P})\mathrm{PdCl}_2]_2$ on exposure to air to yield the phenylglycinate chelate complex **6**. The structures of a pyridine complex from **2** $[\mathrm{Cl}_2(\mathrm{pyridine})\mathrm{Ru}\{\eta^6\text{-}\mathrm{C}_6\mathrm{H}_5\mathrm{CH}(\mathrm{CO}_2\mathrm{Et})\mathrm{NHCOCF}_3\}]$ **(4)** and of $[\mathrm{Cp}^*(\mathrm{Cl})\mathrm{Ir}(N,O\text{-dihydrophenylglycinate})]$ (**5**) were determined by X-ray diffraction.

Introduction

The broad scope of the chemistry and application of organometallic complexes of transition metals with α-amino acids and peptides was recently reviewed.[2] Various η^6-arene complexes of aromatic amino acids formed with CpRu and (*p*-cymene)Ru fragments may be useful for the labelling of peptides and proteins.[3−11] Recently, much attention has focused on the development of chiral (arene)ruthenium complexes for the catalytic transfer hydrogenation of ketones[12−19] and for asymmetric Diels−Alder reactions.[20] In addition, there is great interest in the coordination behaviour of ruthenium(II) complexes with ligands tethered to the η^6-arene donor.[21,22] (Arene)ruthenium complexes with functional substituents at the η^6-arene moiety could give rise to homogeneous catalysts which display special solubility properties or can be immobilized on resins.

Our synthetic approach is based on the dehydrogenation of functional cyclohexadienes with ruthenium(III) trichloride in ethanol, a method established by Bennett et al.[23,24] Here we report the synthesis of novel chloro-bridged η^6-phenylglycine ruthenium(II) complexes starting from the synthetic amino acid (*R*)-2,5-dihydrophenylglycine,[25] which is easily accessible by Birch reduction from D-phenylglycine[26] and which is applied as a β-lactam antibiotic side chain.

Results and Discussion

In order to avoid side reactions N- and C-terminal protection of the substrate (*R*)-2,5-dihydrophenylglycine is necessary. Due to the strongly acidic conditions during the dehydrogenation reaction, acid-stable protecting groups (acetyl and trifluoroacetyl) are favourable for the amino terminus. Subsequent reaction of these protected cyclohexadienyl amino acids with ruthenium(III) chloride hydrate in refluxing ethanol produces the novel chloro-bridged η^6-phenylglycine ruthenium(II) complexes **1** and **2** which can be isolated in good yields as orange powders (Scheme 1).

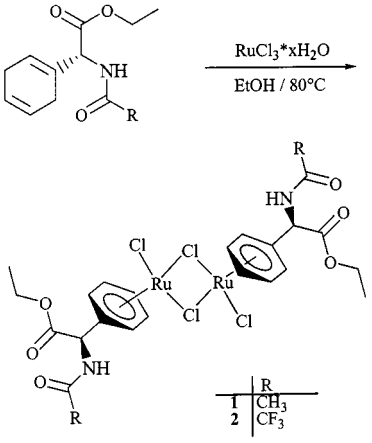

Scheme 1

Protection of the cyclohexadienyl amino acid can also be achieved by protonation with HCl/ethyl acetate to yield the amino acid hydrochloride as an intermediate. During the dehydrogenation reaction, esterification of the carboxylate moiety is observed giving rise to the chloro-bridged η^6-phenylglycine ruthenium(II) complex **3** (Scheme 2).

In the IR spectra of the η^6-phenylglycine ruthenium(II) complexes **1**−**3** the absorptions of the ester function can be observed at about 1740 cm^{-1}. For the amide-protected derivatives **1** and **2** the amide absorptions appear in the typical range. There is no evidence for racemization under the

[‡] Metal Complexes of Biologically Important Ligands, 130. − Part 129: Ref.[1]
[‡‡] X-ray structure determination.
[a] Department Chemie der Ludwig-Maximilians-Universität München,
Butenandtstraße 5−13, Haus D, 81377 München, Germany
E-mail: wbe@cup.uni-muenchen.de

 © WILEY-VCH Verlag GmbH, 69451 Weinheim, 2001 1434−1948/01/0404−1051 $ 17.50+.50/0

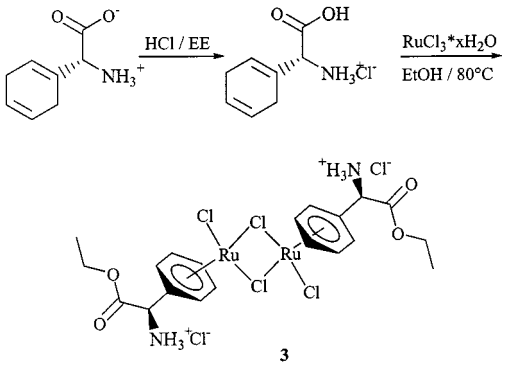

Scheme 2

acidic reaction conditions; this is confirmed by NMR spectroscopy. The ^{1}H NMR spectra of the complexes **1**−**3** display only a single set of signals appearing in the region δ = 5.5−6.1 for the aromatic protons. In the ^{13}C NMR spectra of the compounds **1**−**3** the signals of the aromatic carbon atoms can be observed in the area δ = 80−90 thus confirming an η^6-coordination of phenylglycine to the ruthenium centre.

Compared to the known chloro-bridged arene ruthenium complexes (e.g. arene = benzene, cymene)[23,24] the complexes **1**−**3** exhibit strongly enhanced solubility in polar solvents and even in water, which could make them useful for the labelling of peptides or proteins. Unfortunately, all η^6-phenylglycine ruthenium(II) complexes are sensitive to light in the solid state and in solution leading to greenish decomposition products. This could be due to coordination of the side chain and to a change of the arene coordination mode.

Saponification of the ester group in **3** should lead to deprotection which could allow coordination of the amino acid side chain.

Cleavage of the chloro bridges in complex **2** with pyridine produces the monomeric pyridine adduct **4** (Scheme 3) which was characterized by X-ray diffraction.

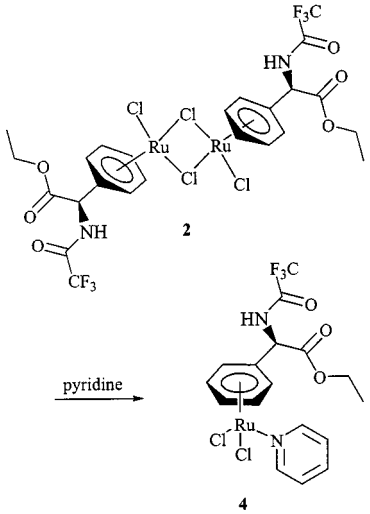

Scheme 3

The structure of complex **4** is shown in Figure 1. Relevant bond lengths and angles for complex **4** are collected in Table 1 and the crystallographic data in Table 2.

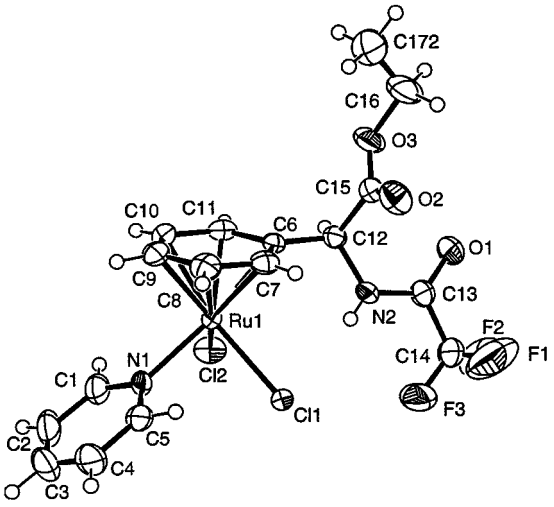

Figure 1. ORTEP projection of the ruthenium complex **4** with the atom numbering scheme

X-ray crystallography confirms the η^6-coordination of phenylglycine, but reveals racemisation at the α-carbon leading to a 1:1 mixture of enantiomers in the crystal. This racemisation occurs due to the basicity of pyridine which is also a typical feature of free phenylglycine.[27]

(*R*)-2,5-dihydrophenylglycine reacts with base and the chloro-bridged complex [Cp*IrCl$_2$]$_2$ to give the *N*,*O*-chelate **5** (Scheme 4).

As confirmed by NMR spectroscopy, complex **5** is produced as a 1:1 mixture of the diastereomers R_CR_{Ir} and R_CS_{Ir}. Two sets of signals in the ^{1}H NMR spectrum of **5** reveal the typical pattern of a monosubstituted cyclohexadiene moiety with a multiplet in the area δ = 2.61−2.79 for the aliphatic protons and a multiplet in the range δ = 5.62−5.84 for the olefinic protons.

Only one diastereomer crystallises from dichloromethane (confirmed by NMR spectroscopy) which was assigned to the R_CS_{Ir} configuration by X-ray diffraction. The structure of complex **5** (shown in Figure 2) is analogous to that of half-sandwich complexes (arene)(Cl)M(α-aminocarboxylate) with other α-amino acids.[2,28,29] Due to the rather high standard deviations a closer discussion of the bonding parameters is not appropriate.[40]

The cyclohexadiene moiety in 2,5-dihydrophenylglycine shows a strong tendency towards rearomatisation to a phenyl group when exposed to air. This was demonstrated by the synthesis of complex **6** from (*R*)-2,5-dihydrophenylglycine and [(*n*Bu$_3$P)PdCl$_2$]$_2$ in nondegassed methanol (Scheme 5).

The ^{1}H NMR spectrum of complex **6** does not show any signals of a cyclohexadiene moiety. In contrast the typical pattern of a monosubstituted benzene is observed in the area δ = 7.33−7.69. As confirmed by an ^{31}P NMR experi-

Table 1. Selected bond lengths [Å], angles [°] and torsion angles [°] of complex **4**

Ru1−N1	2.130(3)	N1−Ru1−Cl2	86.76(10)	C7−C6−C12−N2	32.9(5)
Ru1−C11	2.156(4)	C7−C6−C12	122.6(4)	C11−C6−C12−C15	119.0(4)
Ru1−C6	2.182(3)	N2−Cl2−C6	111.7(3)	C11−C6−C12−N2	121.1(4)
C6−C12	1.507(5)	C6−C12−C15	108.4(3)	C6−C7−C8−C9	2.39(4)
Ru1−Cl2	2.3908(11)	C1−N1−Ru1	122.1(3)	C8−C9−C10−C11	0.19(4)
Ru1−Cl1	2.4167(10)	N1−Ru1−C7	130.67(14)		
C6−C7	1.418(5)	C6−C7−C8	122.2(4)		

Table 2. Selected crystallographic data of complex **4**[40]

Empirical formula	$C_{17}H_{17}N_2O_3F_3Cl_2Ru$
Formula mass	565.85
Temperature	200(3) K
Wavelength	0.71073 Å
Crystal system	monoclinic
Space group	$P2_1/c$
Unit cell dimensions	a = 23.6573(15) Å, α = 90° b = 11.5507(5) Å, β = 102.930(8)° c = 14.9545(10) Å, γ = 90°
Volume	3982.8(4) Å^3
Z	4
Absorption coefficient	1.103 mm^{-1}
F(000)	1336
Crystal size	0.30 × 0.18 × 0.12 mm
Theta range for data collection	1.77 to 25.85°
Index ranges	$-29 \le h \le 28$, $-11 \le k \le 14$, $-1 \le l \le 14$
Reflections collected	7380
Independent reflections	5102 [R(int) = 0.0308]
Absorption correction	Semi-empirical from psi-scans
Max. and min. transmission	0.8900 and 0.8179
Refinement method	Full-matrix least-squares on F^2
Data/restraints/parameters	7380/0/578
Goodness-of-fit on F^2	0.953
Final R indices [$I>2\sigma(I)$]	$R1$ = 0.0359, $wR2$ = 0.0867
R indices (all data)	$R1$ = 0.0586, $wR2$ = 0.0927
Largest diff. peak and hole	1.107 and −0.626 e Å^{-3}

ment, complex **6** is produced as a mixture of the *cis* and *trans* isomers **6a** and **6b** in the ratio 2:3. For several other Pd and Pt complexes with P and N donors[30−36] the *trans* P−M−N configuration is favoured.

Conclusion

The chiral chloro-bridged η^6-phenylglycine ruthenium complexes **1**−**3** can be synthesized by a dehydrogenation reaction of derivatives of (*R*)-2,5-dihydrophenylglycine without racemization. The reaction provides an easy access to organometallic complexes with π-coordinated optically active amino acids, and further ligands can be introduced into the chloro-bridged compounds. Cleavage of the chloro bridges in **2** with pyridine to form the monomeric complex **4** leads to a 1:1 mixture of enantiomers. In the reaction of (*R*)-2,5-dihydrophenylglycine with the complex $[Cp^*IrCl_2]_2$ the *N,O*-chelate **5** is produced. The strong tendency of 2,5-dihydrophenylglycine towards rearomatisation in air was demonstrated with the synthesis of complex **6** from (*R*)-2,5-dihydrophenylglycine and $[(nBu_3P)PdCl_2]_2$ in nondegassed methanol.

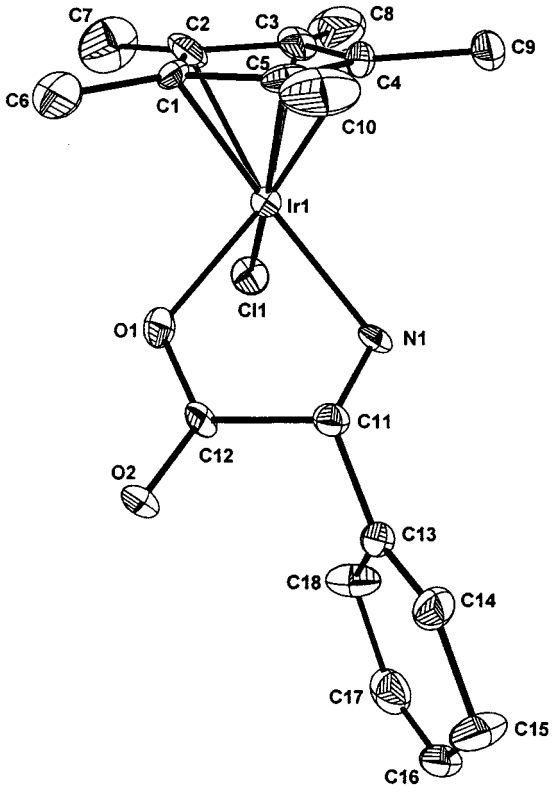

Figure 2. ORTEP projection of the iridium complex **5** with the atom numbering scheme

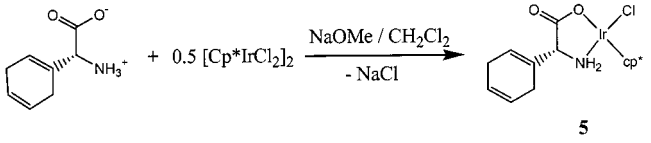

Scheme 4

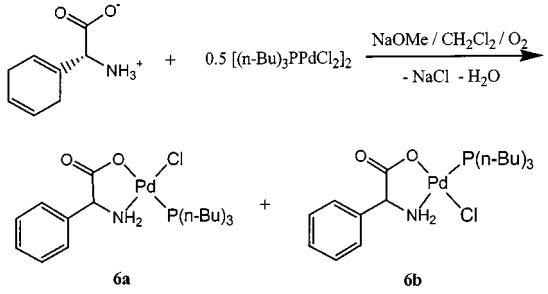

Scheme 5

Experimental Section

General Remarks: All reactions were performed under an atmosphere of argon in Schlenk tubes. Ethanol was degassed prior to use. NMR measurements were recorded on Jeol GSX 270 and Jeol EX 400 spectrometers. IR analyses were obtained on a Nicolet 520 FT-IR spectrometer. Derivatives of (*R*)-2,5-dihydrophenylglycine were prepared according to literature procedures .[25,37]

1: $RuCl_3 \cdot 3H_2O$ (347 mg, 1.32 mmol) was added to *N*-acetyl-(*R*)-2,5-dihydrophenylglycine ethyl ester[25] (1.221 g, 5.47 mmol) in 100 mL of ethanol and the mixture heated under reflux. The dark solution turned green after approximately 1 h. After an additional 4 h the reaction was complete, resulting in a clear red solution which was reduced in vacuo to half of the volume. Upon cooling to −30 °C for 16 h orange microcrystals of **1** precipitated which were filtered off, washed with cold ethanol and dried in vacuo. Yield: 851 mg (82%). − IR (KBr): $\tilde{\nu}$ = 3304 m, 3077 w, 2960 w, 1740 vs (CO_2), 1664 vs, 1531 s (NCO), 1447 m, 1371 m, 1296 m, 1209 m, 1023 m, 857 m cm^{-1}. − ^1H NMR (270 MHz, CD_2Cl_2): δ = 1.23 (t, ^3J = 7.1 Hz, 6 H, CH_2CH_3), 2.13 (s, 6 H, CH_3), 4.17 (q, ^3J = 7.1 Hz, 2 H, OCH_2), 4.18 (q, ^3J = 7.1 Hz, 2 H, OCH'_2), 5.14 (d, ^3J = 6.5 Hz, 2 H, α-H), 5.52−5.83 (m, 10 H, H_{arom}), 7.90 (d, *J* = 6.4 Hz, 2 H, NH). − ^{13}C NMR (100.5 MHz, CD_2Cl_2): δ = 13.88 (CH_2CH_3), 22.57 (CH_3), 54.82 (α-C), 62.34 (CH_2CH_3), 80.20, 80.29, 81.58, 83.13, 92.89 (C_{arom}), 167.76 (CO_2), 170.81 (CON). − $C_{24}H_{30}Cl_4N_2O_6Ru_2$ (786.46): calcd. C 36.65, H 3.84, N 3.56; found C 36.22, H 3.93, N 3.42.

2: $RuCl_3 \cdot 3H_2O$ (347 mg, 1.32 mmol) was added to 825 mg (2.98 mmol) of *N*-trifluoroacetyl-(*R*)-2,5-dihydrophenylglycine ethyl ester (prepared according to references [37] and [25]) in 20 mL of ethanol and the mixture heated under reflux. The dark solution turned greenish-brown after approximately 1 h. After an additional 4 hours the reaction was complete, resulting in a clear red solution which was reduced in vacuo to half of the volume. Upon cooling to −30 °C orange microcrystals of **2** precipitated which were filtered off, washed with cold ethanol and dried in vacuo. Yield 351 mg (71%). − IR (KBr): $\tilde{\nu}$ = 3077 m, 2989 m, 2601 w, 1744 vs (CO_2), 1635 w, 1544 m, 1467 w, 1371 w, 1285 m, 1236 s, 1182 m, 1021 m, 860 w cm^{-1}. − ^1H NMR (270 MHz, CD_2Cl_2): δ = 1.25 (t, ^3J = 7.1 Hz, 6 H, CH_2CH_3), 4.21 (q, ^3J = 7.0 Hz, 2 H, OCH_2), 4.24 (q, ^3J = 7.0 Hz, 2 H, OCH'_2), 5.37 (d, ^3J = 7.0 Hz, 2 H, α-H), 5.53 (q, *J* = 5.4 Hz, 2 H, H_{arom}), 5.60 (q, *J* = 5.9 Hz, 2 H, H_{arom}), 5.69 (d, *J* = 5.8 Hz, 4 H, H_{arom}), 5.98 (t, *J* = 5.4 Hz, 2 H, H_{arom}), 9.03 (s, br, NH). − ^{13}C NMR (100.5 MHz, CD_2Cl_2): δ = 13.54 (CH_2CH_3), 54.87 (α-C), 63.02 (CH_2CH_3), 78.55, 79.03, 82.55, 84.97, 87.51, 89.43 (C_{arom}), n.o. (CF_3), 156.98 (CON), 166.23 (CO_2). − $C_{24}H_{24}Cl_4F_6N_2O_6Ru_2 \cdot 2EtOH$ (986.54): calcd. C 34.09, H 3.67, N 2.84; found C 34.45, H 3.37, N 2.95.

3: (*R*)-2,5-dihydrophenylglycine (600 mg, 3.92 mmol) was stirred with 10 mL of a solution of HCl in ethyl acetate (approx. 2 M) for 1 h. To this suspension $RuCl_3 \cdot 3H_2O$ (205 mg, 0.78 mmol) and 35 mL of ethanol were added and the resulting mixture heated under reflux for 16 h. The orange precipitate was filtered off, washed with cold ethanol and dried in vacuo. Yield 472 mg (78%). − IR (KBr): $\tilde{\nu}$ = 3063 m, 2990 w, 2601 w, 1746 vs (CO_2), 1637 w, 1472 s, 1374 m, 1294 m, 1240 s, 1185 m, 1098 m, 1008 m, 857 m cm^{-1}. − ^1H NMR (270 MHz, CD_3OD): δ = 1.25 (t, ^3J = 7.2 Hz, 6 H, CH_2CH_3), 4.29 (q, ^3J = 7.2 Hz, 2 H, OCH_2), 4.31 (q, ^3J = 7.2 Hz, 2 H, OCH'_2), 5.17 (s, 2 H, α-H), 5.85−6.14 (m, 10 H, H_{arom}), 7.48 (s, NH_3). − ^{13}C NMR (67.9 MHz, CD_3OD): δ = 13.24 (CH_2CH_3), 55.48 (α-C), 63.96 (CH_2CH_3), 83.12, 83.27, 85.03 (C_{arom}), 165.94 (CO_2). − $C_{20}H_{28}Cl_6N_2O_4Ru_2$ (775.31): calcd. C 30.98, H 3.64, N 3.61; found C 30.09, H 3.77, N 3.27.

4: A solution of the ruthenium complex **2** (99 mg, 0.12 mmol) in 10 mL of pyridine was stirred for 12 h. The solvent was then removed under reduced pressure and the residue dried in vacuo. Recrystallisation from dichloromethane/hexane afforded orange crystals suitable for X-ray diffraction. Yield 128 mg (91%). − IR (KBr): $\tilde{\nu}$ = 3201 m, 3062 m, 2981 w, 1748 vs (C=O), 1725 vs, 1636 m, 1604 m, 1545 s, 1447 s, 1216 s, 1181 s, 1164 s, 1069 m, 1017 m, 860 w, 761 s, 695 s cm^{-1}. − ^1H NMR (270 MHz, CD_2Cl_2): δ = 1.27 (t, ^3J = 7.0 Hz, 3 H, CH_2CH_3), 4.28 (pt, ^3J = 7.1 Hz, 2 H, OCH_2), 5.44 (d, ^3J = 6.9 Hz, 1 H, α-H), 5.53−5.72 (m, 3 H, H_{arom}), 5.95 (m, 1 H, H_{arom}), 6.09 (m, 1 H, H_{arom}), 7.48 (m, 3 H, H_{py}), 8.98 (m, 2 H, H_{py}), 9.01(s, br, NH). − ^{13}C NMR (100.5 MHz, CD_2Cl_2): δ = 13.84 (CH_2CH_3), 55.73 (α-C), 63.01 (CH_2CH_3), 81.48, 81.65, 86.47, 87.11, 88.67, 88.93 (C_{arom}), 125.11, 129.16, 138.48 (py), 155.12 (CON), 166.80 (CO_2). − $C_{17}H_{17}Cl_2F_3N_2O_3Ru \cdot 1/2py$ (565.85): calcd. C 41.39, H 3.48, N 6.19; found C 41.43, H 3.66, N 6.34.

5: A suspension of (*R*)-2,5-dihydrophenylglycine (58 mg, 0.38 mmol) in 10 mL of methanol was stirred with a 1.3 M solution of NaOMe in methanol (290 μL, 0.38 mmol). After 30 min. $[Cp^*IrCl_2]_2$ [38] (150 mg, 0.19 mmol) was added and the mixture stirred for an additional 2 h. The solvent was then removed at reduced pressure and the residue dissolved in 5 mL of dichloromethane. After filtration through Celite the clear yellow solution was set aside. Within 12 h yellow crystals of **5** precipitated. Yield 181 mg (86%). − IR (KBr): $\tilde{\nu}$ = 3223 m, 3223 m (NH), 2917 w, 1637 vs (C=O), 1455 m, 1361 s, 1256 m, 1163 m, 1034 m, 960 m cm^{-1}. − ^1H NMR (270 MHz, CD_3OD): δ = 1.70 (s, 15 H, CH_3), 2.61−2.79 (m, 4 H, CH_2), 3.87 (d, *J* = 14.9 Hz, 1 H, α-H), 5.62−5.84 (m, 3 H, CH). − ^{13}C NMR (100.5 MHz, CD_2Cl_2): δ = 8.70 ($C_5(CH_3)_5$), 24.75, 26.63 (CH_2), 59.90 (α-C), 84.24 ($C_5(CH_3)_5$), 123.60, 124.87, 126.22, 126.48 (CH), 177.98 (CO_2). − $C_{18}H_{25}ClIrNO_2 \cdot 1/2CH_2Cl_2$ (557.54): calcd. C 39.86, H 4.88, N 2.51; found C 40.10, H 5.13, N 2.40.

6: A suspension of (*R*)-2,5-dihydrophenylglycine (61 mg, 0.40 mmol) in 7 mL of nondegassed methanol was stirred with a 1.3 M solution of NaOMe in methanol (304 μL, 0.40 mmol). After 30 min. $[(nBu_3P)PdCl_2]_2$ [39] (150 mg, 0.20 mmol) was added and the mixture stirred for an additional 12 h. The yellow precipitate was then removed by centrifugation, dried in vacuo and redissolved in dichloromethane. After filtration through Celite the solvent was removed under reduced pressure. The residue was recrystallized from dichloromethane/*n*-hexane. Yield 169 mg (83%). − IR (KBr): $\tilde{\nu}$ = 3216 s (NH), 3121 m, 2930 vs, 2872 s, 1634 vs (C=O), 1597 m, 1465 m, 1455 m, 1377 s, 1210 m, 1093 m, 907 m, 804 w, 787 w, 762 m, 725 m, 699 s cm^{-1}. − ^1H NMR (270 MHz, CD_2Cl_2): δ = 0.86−0.98 (m, 9 H, CH_3, *n*Bu), 1.39−1.84 (m, 18 H, CH_2, *n*Bu), 3.59 (m, br, NH_2), 4.61 (m, 1 H, α-H), 7.33−7.45 (m, 3 H- and *p*-C_6H_5), 7.61−7.69 (m, 2 H, *o*-C_6H_5). − ^{13}C NMR (100.5 MHz, CD_2Cl_2): δ = 13.54 ($PCH_2CH_2CH_2CH_3$, A+B), 25.92 ($PCH_2CH_2CH_2CH_3$, A), 25.94 ($PCH_2CH_2CH_2CH_3$, B), 24.15 (d, *J* = 14.5 Hz, $PCH_2CH_2CH_2CH_3$, A), 24.24 (d, *J* = 14.0 Hz, $PCH_2CH_2CH_2CH_3$, B), 21.78 (d, *J* = 30.0 Hz, $PCH_2CH_2CH_2CH_3$, A), 22.82 (d, *J* = 31.0 Hz, $PCH_2CH_2CH_2CH_3$, B), 61.41 (α-C, A), 64.12 (α-C, B), 127.20, 128.28, 128.66, 129.09 (Ph, A+B), 181.29 (CO_2, A+B). − 31P NMR (109.4 MHz, CD_2Cl_2): δ = 27.55 (s, A), 28.80 (s, B); (1.5:1). − $C_{20}H_{35}ClNO_2PPd \cdot H_2O$ (512.34): calcd. C 46.88, H 7.28, N 2.73; found C 46.83, H 7.50, N 2.64.

Acknowledgments

Generous support by Deutsche Forschungsgemeinschaft and Fonds der chemischen Industrie is gratefully acknowledged. We thank Degussa AG, Hanau for chemicals.

[1] W. Bauer, P. Ponikwar, W. Beck, *Z. Naturforsch.* **2000**, *556*, 946.
[2] K. Severin, R. Bergs, W. Beck, *Angew. Chem.* **1998**, *110*, 1722; *Angew. Chem. Int. Ed.* **1998**, *37*, 1634.
[3] D. B. Grotjahn, *Coord. Chem. Rev.* **1999**, *190−192*, 1125.
[4] R. M. Moriarty, Y.-Y. Ku, U. S. Gill, *J. Chem. Soc., Chem. Commun.* **1987**, 1493.
[5] R. M. Moriarty, Y.-Y. Ku, U. S. Gill, *J. Chem. Soc., Chem. Commun.* **1987**, 1837.
[6] R. M. Moriarty, Y.-Y. Ku, U. S. Gill, *J. Organomet. Chem.* **1989**, *362*, 187.
[7] W. S. Sheldrick, A. J. Gleichmann, *J. Organomet. Chem.* **1994**, *470*, 183.
[8] A. J. Gleichmann, J. M. Wolff, W. S. Sheldrick, *J. Chem. Soc., Dalton Trans.* **1995**, 1549.
[9] J. M. Wolff, W. S. Sheldrick, *Chem. Ber./Recueil* **1997**, *130*, 981.
[10] J. M. Wolff, W. S. Sheldrick, *J. Organomet. Chem.* **1997**, *531*, 141.
[11] D. Agaid Herebian, C. S. Schmidt, W. S. Sheldrick, C. van Wüllen, *Eur. J. Inorg. Chem.* **1998**, 1991.
[12] R. Noyori, S. Hashiguchi, *Acc. Chem. Res.* **1997**, *30*, 97.
[13] T. Ohta, S.-I. Nakahara, Y. Shigemura, K. Hattori, I. Furukawa, *Chem. Lett.* **1998**, 491.
[14] D. A. Alonso, P. Brandt, S. J. M. Nordin, P. G. Andersson, *J. Am. Chem. Soc.* **1999**, *121*, 9580.
[15] D. G. I. Petra, J. N. H. Reek, J.-W. Handgraaf, E. J. Meijer, P. Dierkes, P. C. J. Kamer, J. Brussee, H. E. Schoemaker, P. W. N. M. van Leeuwen, *Chem. Eur. J.* **2000**, *6*, 2818.
[16] D. G. I. Petra, P. C. J. Kamer, P. W. N. M. van Leeuwen, K. Goubitz, A. M. Van Loon, J. G. de Vries, H. E. Schoemaker, *Eur. J. Inorg. Chem.* **1999**, 2335.
[17] K. Severin, K. Polborn, *Chem. Commun.* **1999**, 2481.
[18] M. Yamakawa, H. Ito, R. Noyori, *J. Am. Chem. Soc.* **2000**, *122*, 1466.
[19] A. Kathó, D. Carmona, F. Viguri, C. D. Remacha, J. Kovács, F. Joó, L. A. Oro, *J. Organomet. Chem.* **2000**, *593−594*, 299.
[20] D. L. Davies, J. Fawcett, S. A. Garratt, D. R. Russell, *Chem. Commun.* **1997**, 1351.
[21] B. Therrien, A. König, T. R. Ward, *Organometallics* **1999**, *18*, 1565.
[22] T. Ohnishi, Y. Miyaki, H. Asano, H. Kurosawa, *Chem. Lett.* **1999**, 809.
[23] M. A. Bennett, A. K. Smith, *J. Chem. Soc., Dalton Trans.* **1974**, 233.
[24] P. Pertici, P. Salvadori, A. Biasci, G. Vitulli, M. A. Bennet, L. A. P. Kane-Maguire, *J. Chem. Soc., Dalton Trans.* **1988**, 315.
[25] G. Zvilichovsky, V. Gurvich, *Tetrahedron* **1995**, *51*, 5479.
[26] J. E. Dolfini, H. E. Applegate, G. Bach, H. Basch, J. Bernstein, J. Schwartz, F. Weisenborn, *J. Med. Chem.* **1971**, *14*, 117.
[27] M. Bodanszky, A. Bodanszky, *J. Chem. Soc., Chem. Commun.* **1967**, 591.
[28] R. Krämer, K. Polborn, H. Wanjek, I. Zahn, W. Beck, *Chem. Ber.* **1990**, *123*, 767.
[29] D. Carmona, A. Mendoza, F. J. Lahoz, L. A. Oro, M. P. Lamata, E. San Jose, *J. Organomet. Chem.* **1990**, *396*, C17.
[30] E. Ambach, U. Nagel, W. Beck, *Chem. Ber.* **1983**, *116*, 659.
[31] Y. Zhou, B. Wagner, K. Polborn, K. Sünkel, W. Beck, *Z. Naturforsch.* **1994**, *49b*, 1193.
[32] W. Hoffmüller, K. Polborn, J. Knizek, H. Nöth, W. Beck, *Z. Allg. Anorg. Chem.* **1997**, *623*, 1903.
[33] M. Gómez-Simón, S. Jansat, G. Muller, D. Panyella, M. Font-Bardía, X. Solans, *J. Chem. Soc., Dalton Trans.* **1997**, 3755.
[34] O. Briel, A. Fehn, K. Polborn, W. Beck, *Polyhedron* **1999**, *18*, 225.
[35] A. Böhm, K. Polborn, W. Beck, *Z. Naturforsch.* **1999**, *54b*, 300.
[36] A. Lombardi, O. Maglio, V. Pavone, B. Di Blasio, M. Saviano, F. Nastri, C. Pedone, E. Benedetti, *Inorg. Chim. Acta* **1993**, *204*, 87.
[37] D. L. Boger, D. Yohannes, *J. Org. Chem.* **1989**, *54*, 2498.
[38] C. White, A. Yates, P. M. Maitlis, *Inorg. Synth.* **1992**, *29*, 228.
[39] F. R. Hartley, *Organomet. Chem. Rev. A* **1970**, *6*, 119.
[40] Crystallographic data for the structures reported in this paper have been deposited with the Cambridge Crystallographic Data Centre as supplementary publication no CCDC-151248 (**4**). Copies of this data can be obtained free of charge on application to the Director, CCDC, 12 Union Road, Cambridge CB2 1EZ [Fax: (internat.) +44-1223/336-033; E-mail: deposit@ccdc.cam.ac.uk].

Received September 1, 2000
[I00331]

Synthesis, Structure and Characterization of the New Complex $[L_1(H_2O)Fe(\mu\text{-}O)Fe(OH_2)L_1]^{4+}$ [L_1 = *N,N′*-Bis(1-methylimidazolyl-2-methyl)-*N,N′*-Bismethyl-1,2-ethanediamine] − Formation of the $(\mu\text{-}O)(\mu\text{-}H_3O_2)$ Complex upon Deprotonation

Sandrine Poussereau,[a] Geneviève Blondin,*[a] Geneviève Chottard,[b] Jean Guilhem,[c] Luba Tchertanov,[c] Eric Rivière,[a] and Jean-Jacques Girerd[a]

Keywords: Iron / Oxo complexes / Methane monooxygenase / UV/Vis spectroscopy / Raman spectroscopy

The compound $[L_1(H_2O)Fe(\mu\text{-}O)Fe(OH_2)L_1](ClO_4)_4\cdot 2H_2O$ [**1**$(ClO_4)_4\cdot 2H_2O$] [L_1 = *N,N′*-bis(1-methylimidazolyl-2-methyl)-*N,N′*-bismethyl-1,2-ethanediamine] was synthesized. It is characterized by a linear Fe–(μ-O)–Fe motif with an Fe···Fe distance of 3.584(1) Å. The measurement of the magnetic susceptibility as a function of temperature indicated a strong antiferromagnetic coupling between the two high-spin Fe^{III} ions ($J = -223\ cm^{-1}$ with $H = -J\cdot S_1\cdot S_2$). In the solid state, the symmetric stretching vibration mode of the Fe–(μ-O)–Fe core unit was detected at 347 cm^{-1}, in agreement with a straight Fe–(μ-O)–Fe angle. Upon addition of up to one equivalent of triethylamine to an acetonitrile solution of **1**, conversion to the $[L_1(H_2O)Fe(\mu\text{-}O)Fe(OH)L_1]^{3+}$ complex **2** was observed. This last species was isolated as a perchlorate salt [**2**$(ClO_4)_3\cdot H_2O$]. Susceptibility measurements and Raman and UV/Vis investigations on the powder and/or an acetonitrile solution confirmed the presence of an intramolecular hydrogen bond between the coordinated water molecule and the hydroxide group leading to a bent $[Fe(\mu\text{-}O)Fe]^{4+}$ core structure.

Introduction

The oxidation of methane to methanol with dioxygen catalyzed by soluble methane monooxygenase (MMO) has elicited much interest during recent years. This reaction takes place in the hydroxylase component of MMO (MMOH),[1,2] the structure of which has been determined by X-ray diffraction studies in the native ($MMOH_{ox}$) and reduced ($MMOH_{red}$) forms for *Methylococcus capsulatus*,[3,4] and in the native form only for *Methylosinus trichosporium*.[5] The catalytic site determined in the two forms is constituted by two iron atoms bridged by the carboxylato group of a glutamate residue (E144). Both iron sites are in the +III oxidation state in $MMOH_{ox}$ and connected by two extra bridges: one water molecule and one hydroxide group.[4,5] In the reduced state, both metallic centers have the +II oxidation degree, a single oxygen atom of the carboxylate side function of the glutamate residue E243 being present as a second bridge.[4] The only exogeneous ligand is a water molecule that is coordinated to one Fe^{II} site and that recent investigations in the catalytic cycle of the enzyme have brought to the fore. It has been suggested that one of its protons is transferred to one oxygen atom of the O−O bridge in the peroxo form of MMOH (compound P)[6,7] formed by reaction of $MMOH_{red}$ with dioxygen.[8−11] This would leave a hydroxo group ligated to one Fe^{III} site or bridging the two metallic centers.[6,7] Compound P spontaneously converts to compound Q, which has been shown by Mössbauer and X-ray absorption studies to present a di-Fe^{III}-di-μ-oxo core unit.[12] It has been proposed that upon this evolution, a second proton is transferred from the hydroxide molecule to the hydrogenated peroxo bridge, allowing the release of a water molecule.[6,7] The two bridging oxygen atoms of the $[Fe_2(\mu\text{-}O)_2]^{4+}$ unit would thus have different origins, one coming from the dioxygen molecule and the other one being the doubly deprotonated coordinated water molecule present in $MMOH_{red}$. Compound Q is the active catalytic species that interacts with the alkane substrate.[6,8,9,13]

Many efforts have been made to synthesize dinuclear iron complexes presenting the diamond core structure. For this purpose, tetradentate ligands are used.[14−18] Starting with a $[(H_2O)Fe(\mu\text{-}O)Fe(OH)]^{3+}$ core unit, we have shown recently the possibility to obtain the double-bridged structure $[Fe(\mu\text{-}O)(\mu\text{-}OH)Fe]^{3+}$.[14] The protonated form of the diamond core structure is thus formed in the same way as would be the di-iron-di-μ-oxo unit of compound Q, an oxygenated group converting from a η^1- to a μ-type coordination. This behavior seems to be common to several systems.[14,16,19] In our effort to model the active site of MMOH, the synthesis of two new iron-oxo complexes with

[a] Laboratoire de Chimie Inorganique, UMR CNRS 8613, Institut de Chimie Moléculaire d′Orsay, Université Paris-Sud, 91405 Orsay Cedex, France
Fax: (internat.) +33-1/6915-4754
E-mail: gblondin@icmo.u-psud.fr
[b] Laboratoire de Chimie Inorganique et Matériaux Moléculaires, ESA CNRS 7071, Université Pierre et Marie Curie, 75250 Paris Cedex 05, France
[c] Institut de Chimie des Substances Naturelles, UPR CNRS 2301, 91198 Gif-sur-Yvette, France

 © WILEY-VCH Verlag GmbH, 69451 Weinheim, 2001 1434−1948/01/0404−1057 $ 17.50+.50/0

the tetradentate ligand containing imidazole groups *N,N′*-bis(1-methylimidazolyl-2-methyl)-*N,N′*-bismethyl-1,2-ethanediamine (L_1, see Scheme 1) are presented. Complex **1**$(ClO_4)_4{\cdot}2H_2O$ has a $[(H_2O)Fe(\mu\text{-}O)Fe(OH_2)]^{4+}$ core unit and we show here the possibility to abstract one proton from one water molecule and to isolate the $[(H_2O)Fe(\mu\text{-}O)Fe(OH)]^{3+}$ system (**2**). This second complex is shown to be stable in solution and insensitive to further deprotonation.

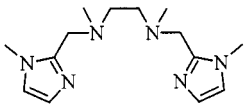

L_1

Scheme 1

Results and Discussion

X-ray Crystal Structure of $[L_1(H_2O)Fe(\mu\text{-}O)Fe(OH_2)L_1](ClO_4)_4{\cdot}2H_2O$

The structure consists of one $[L_1(H_2O)Fe(\mu\text{-}O)Fe(OH_2)L_1]^{4+}$ complex cation, four perchlorate anions and two water molecules. An ORTEP view of the cation is presented in Figure 1, and selected bond lengths and angles are listed in Table 1.

The cation possesses a crystallographicaly imposed symmetry, with the two iron atoms bridged by an oxygen atom which lies on an inversion center. The iron atom shows a pseudo-octahedral coordination with the two nonmethylated nitrogen atoms of the imidazole rings in axial positions and the two nitrogen amine atoms in equatorial positions

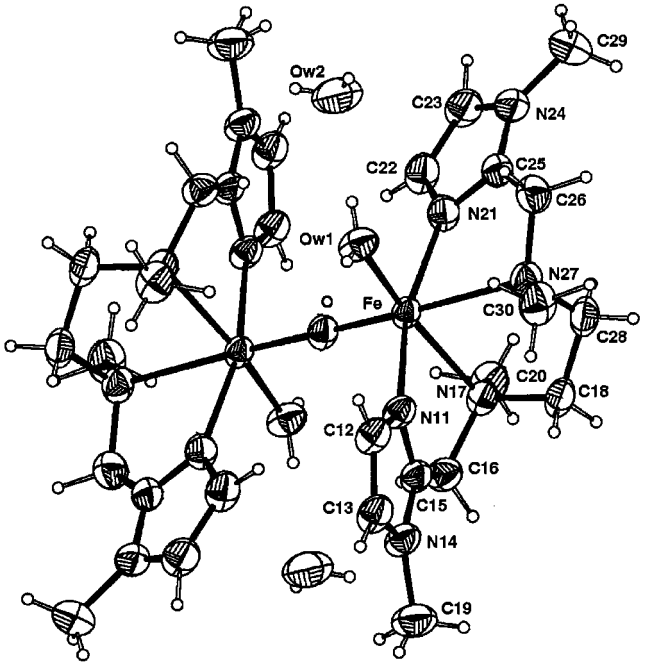

Figure 1. ORTEP view of the $[L_1(H_2O)Fe(\mu\text{-}O)Fe(OH_2)L_1]^{4+}$ cation in the crystal of compound **1**$(ClO_4)_4{\cdot}2H_2O$, showing the 50% probability thermal ellipsoids

Table 1. Selected bond lengths (Å) and angles (deg) for $[L_1(H_2O)Fe(\mu\text{-}O)Fe(OH_2)L_1]^{4+}$

Fe−O	1.7918(5)	Fe−N(21)	2.084(2)
Fe−Ow1	2.052(2)	Fe−N(17)	2.210(2)
Fe−N(11)	2.125(2)	Fe−N(27)	2.337(2)
O−Fe−Ow1	100.54(7)	N(21)−Fe−N(17)	97.94(9)
O−Fe−N(21)	97.34(7)	N(11)−Fe−N(17)	76.77(8)
Ow1−Fe−N(21)	90.3(1)	Ow1−Fe−N(27)	86.4(1)
O−Fe−N(11)	98.29(7)	N(21)−Fe−N(27)	74.04(9)
Ow1−Fe−N(11)	90.5(1)	N(11)−Fe−N(27)	90.01(9)
N(21)−Fe−N(11)	163.95(9)	N(17)−Fe−N(27)	78.89(9)
O−Fe−N(17)	96.03(7)	Fe#−O−Fe[a]	180.0
Ow1−Fe−N(17)	160.42(9)	O−Fe−N(27)	169.08(6)

[a] Symmetry transformations used to generate equivalent atoms: #1−x,−y,−z+1.

providing the *cis*-α conformation. This conformation is also adopted by tetradentate ligands derived from the *N,N′*-bis(2-pyridylmethyl)ethane-1,2-diamine (bispicen)[14,16−20] or the very similar ligand to L_1 *N,N′*-bis(imidazol-4-ylmethyl)ethane-1,2-diamine in a di-Mn-di-μ-oxo complex.[21] A water molecule occupies the sixth coordination site of each iron. The two coordinated water molecules are in *trans* positions with respect to one another due to the inversion center at the bridging oxygen atom.

The coordination at the Fe atom indicates an important deviation from octahedral geometry. The Fe atom and the four equatorial atoms form an approximate plane with a mean deviation from the respective least-squares planes of 0.2 Å. The axial nitrogen atoms N17 and N27 lie above and below the equatorial plane by 2.082(2) and −2.054(2) Å, respectively. The imidazole moieties are oriented nearly perpendicularly relative to the equatorial plane with dihedral angles 87.91(9)° and 84.7(1)°. The dihedral angle between the imidazole ring planes of 62.8(1)° indicates a significant rotation of the five-membered rings around the coordination bonds.

The two $Fe-N_{amine}$ distances as well as the two $Fe-N_{imidazole}$ distances in the $[L_1(H_2O)Fe(\mu\text{-}O)Fe(OH_2)L_1]^{4+}$ cation are not identical. Thus, Fe−N11 [2.125(2) Å] is longer than Fe−N21 [2.084(2) Å] and Fe−N27 [2.337(2) Å] is longer than Fe−N17 [2.210(2) Å]. Such an important difference between the chemically identical bonds, especially for the pair of $Fe-N_{amine}$ bond lengths (δ = 0.23 Å) can be attributed to a *trans* effect. Indeed, the disposition of the atoms N27, the metallic centre and bridging oxygen is nearly linear with a bond angle of 169.08(6)°.

The $[(H_2O)Fe(\mu\text{-}O)Fe(OH_2)]^{4+}$ core structure has been previously obtained using the bidentate 1,10-phenanthroline (phen) ligand[22] or tetradentate ones like 2,2′:6′,2′′:6′′,2′′′-quaterpyridine (qpy),[23] tris(2-pyridylmethyl)amine (tpa),[24,25] tris[(1-methylimidazol-2-yl)methyl]amine (tmima),[26] 3-[bis(2-pyridylmethyl)amino]propionate (bpp^-),[27] or nitrilotriacetate (nta^{3-}).[28] The Fe−(μ-O) distance [1.7918(5) Å] observed here is very similar to the ones observed in the other complexes [from 1.771(5) to 1.83(1) Å]. The complex with the ligand qpy has a linear Fe−(μ-O)−Fe core structure as observed in **1**, the other

cores having a bent geometry with bridging angles ranging from 153.2(6) to 177.5(5)°. The Fe···Fe separation [3.584(1) Å] in **1** is the longest among the seven complexes mentioned here.

The bond length Fe−Ow of 2.052(2) Å is in the range of those previously reported value for Fe^{III} complexes coordinated by water [2.021(5)−2.19(1) Å]. The main difference lies in the torsion angle Ow−Fe···Fe−Ow which is equal, in increasing order, to 7.7° in $[(nta)(H_2O)Fe(\mu\text{-}O)Fe(H_2O)(nta)]^{2-}$, 8.8° in $[(bpp)(H_2O)Fe(\mu\text{-}O)Fe(H_2O)(bpp)]^{2+}$, 81.9° in $[(phen)_2(H_2O)Fe(\mu\text{-}O)Fe(OH_2)(phen)_2]^{4+}$, 123.0° in $[(tpa)(H_2O)Fe(\mu\text{-}O)Fe(OH_2)(tpa)]^{4+}$, 131.7° in $[(tmima)(H_2O)Fe(\mu\text{-}O)Fe(OH_2)(tmima)]^{4+}$ and 180° in **1** (not defined for $[(qpy)(H_2O)Fe(\mu\text{-}O)Fe(OH_2)(qpy)]^{4+}$ since the four atoms are aligned). The intramolecular π-π stacking of the phenanthroline rings in $[(phen)_2(H_2O)Fe(\mu\text{-}O)Fe(OH_2)(phen)_2]^{4+}$ may impose such a disposition. In the mentioned complexes, the coordinated water molecules are involved in the hydrogen bond network that may be at the origin of the variety of torsion angles observed.

As mentioned above, the studied complex crystallizes as a hydrate salt. The water molecule coordinated to the iron is involved in a strong hydrogen bond Ow1−H2w1···Ow2 with one solvent molecule [the distances Ow1···Ow2 and H2w1···Ow2 are 2.594(4) and 1.81(2) Å, respectively, and the angle at H is 174(4)°]. The other hydrogen atoms of both water molecules participate in hydrogen bonding with the perchlorate anions.

Magnetic Susceptibility Measurements

The molar magnetic susceptibilities χ_M of a powder sample of $\mathbf{1}(ClO_4)_4\cdot 2H_2O$ and $\mathbf{2}(ClO_4)_3\cdot H_2O$ were measured as functions of the temperature. For **1**, $\chi_M T$ decreases from 0.74 $cm^3\cdot mol^{-1}\cdot K$ at 300 K to a plateau at 0 below 55 K, indicating a strong antiferromagnetic coupling interaction between the two high spin Fe^{III} ions ($S_1 = S_2 = 5/2$).

The same behavior was detected for **2**: at 300 K, $\chi_M T$ equals 1.40 $cm^3\cdot mol^{-1}\cdot K$ and diminishes to reach a plateau at 0 below 35 K. The decrease of $\chi_M T$ is again characteristic of an antiferromagnetic exchange interaction between the two high spin Fe^{III} sites, but the higher value of $\chi_M T$ detected at 300 K for **2** reveals a weaker coupling than in **1**.

The best fits were obtained by setting the *g* factor to 2: $J = -223$ cm^{-1} for **1** and $J = -133$ cm^{-1} for **2**. The *J* value calculated for **1** is of the same magnitude as the one measured for the other di-aquo-di-iron-μ-oxo complexes: −210 cm^{-1} in $[(tpa)(H_2O)Fe(\mu\text{-}O)Fe(H_2O)(tpa)]^{4+}$,[24] −220 cm^{-1} in $[(phen)_2(H_2O)Fe(\mu\text{-}O)Fe(OH_2)(phen)_2]^{4+}$ [22] and −228 cm^{-1} in $[(bpp)(H_2O)Fe(\mu\text{-}O)Fe(OH_2)(bpp)]^{2+}$.[27]

However, the value determined for **2** is significantly less negative than the ones measured for $[(H_2O)Fe(\mu\text{-}O)Fe(OH)]^{3+}$ core complexes: −194 cm^{-1} with TPA,[24] −196 cm^{-1} with 5-Et_3-TPA[15] and −184 cm^{-1} with bispicMe_2en.[14] This weaker coupling interaction reveals a less efficient superexchange pathway. As previously mentioned in the literature, the latter is essentially governed by the Fe−(μ-O) distances for bridging angles ranging from 120 to 180°.[29,30] It has been established that the coupling constant *J* is correlated to half of the shortest superexchange pathway between the two Fe^{III} ions, designated as P according to Equation (1):

$$J = A\cdot\exp[B(P - 2)] \quad (1)$$

with $A = -17.52$ cm^{-1} and $B = -12.663$ $Å^{-1}$ if *P* is expressed in Å and *J* in cm^{-1}.[29,31,32] For **1**, *P* equals 1.791 Å, which gives a coupling constant of −247 cm^{-1}, in agreement with the value of −223 cm^{-1} observed experimentally. For compound **2** it is possible to evaluate from the *J* value an average Fe−(μ-O) distance of 1.84 Å, a value slightly greater than the ones measured by X-ray diffraction studies on the three $[(H_2O)Fe(\mu\text{-}O)Fe(OH)]^{3+}$ core structures for which the *P* parameter ranges from 1.80 to 1.82 Å.[14,15,24]

One can argue that the exchange coupling constant calculated here for compound **2** is closer to the values determined for the double-bridged $[LFe(\mu\text{-}O)(\mu\text{-}OH)FeL]^{3+}$ systems {−113 cm^{-1} for L = 6-Me_3-TPA,[19] −106 cm^{-1} for L = bispicEt_2en,[19] −84 cm^{-1} for L = bispicMe_2en[16] (see also remark 42 in ref. [19])}, a formulation that cannot be rejected on the basis of the elementary analysis alone. Nevertheless, as will be shown in the next section, the Raman studies support the hypothesis of a single μ-oxo bridge.

Raman Spectra

We will focus on the frequency domain (330 to 650 cm^{-1}) where the symmetric stretching vibration mode of the Fe−(μ-O)−Fe core unit is expected to be detected. This vibration mode has been shown to be strongly dependent on the bridging angle,[33] and is thus indicative of the core unit geometry. In the solid state, the Raman spectrum of compound $\mathbf{1}(ClO_4)_4\cdot 2H_2O$ exhibits a band centered at 347 cm^{-1}, while it is detected at 455 cm^{-1} for complex $\mathbf{2}(ClO_4)_3\cdot H_2O$. Only the acetonitrile solution of **2** was investigated and the recorded spectrum is very similar to that obtained in the solid state. The band detected at 455 cm^{-1} in the solid state is shifted to 458 cm^{-1} in solution. From the published correlation of the ν_s frequency as a function of the Fe−(μ-O)−Fe angle, 347 cm^{-1} would correspond to a straight angle and is in good agreement with the X-ray diffraction results.

The higher frequency observed for **2** indicates a bent core structure. The double-bridged $[Fe(\mu\text{-}O)(\mu\text{-}OH)Fe]^{3+}$ cores are characterized by an even higher frequency for the symmetric vibration, around 600 cm^{-1}.[14,16,19] The μ-oxo-μ-hydroxo core can thus be dismissed since no signature is detected at such a high frequency. The approximate 150° bridging angle value deduced from the correlation mentioned above is slightly too high to be compatible with the presence of $H_3O_2^-$ as a second bridge, since the X-ray diffraction studies performed on such complexes lead to the determination of Fe−(μ-O)−Fe angles in the range 136−139°.[14,15,24] The likelihood of the presence of a $H_3O_2^-$ bridge is enforced, however, by the fact that the correlation we are referring to has been established for clusters presenting shorter Fe−(μ-O) distances than the one ex-

pected from the magnetic measurements. As the separation between the iron and the oxygen atoms increases, one can expect the ν_s frequency to decrease.[34] The bridging angle value of 150° may hence be an overestimation.

Both the magnetic and the Raman studies performed in the solid state support the existence in **2** of an intramolecular hydrogen bond between the coordinated water and hydroxide molecules, this interaction persisting in solution (Scheme 2).

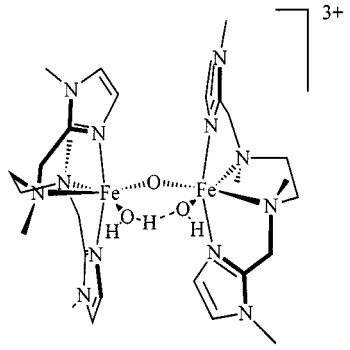

2

Scheme 2

UV/Vis Absorption Spectra

The spectra of **1** [spectrum (a)] and **2** [spectrum (e)] recorded on acetonitrile solutions are shown in Figure 2.

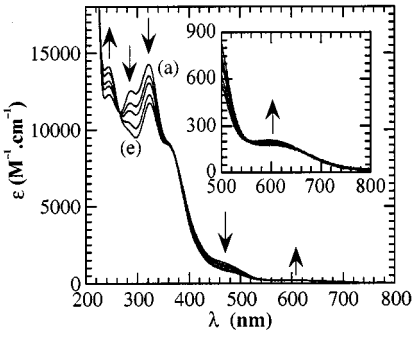

Figure 2. UV/Vis spectra of complexes $\mathbf{1}(ClO_4)_4{\cdot}2H_2O$ [spectrum (a)] and $\mathbf{2}(ClO_4)_3{\cdot}H_2O$ [spectrum (e)] dissolved in dry acetonitrile; spectra (b) to (e) correspond respectively to the addition of 0.3, 0.5, 0.8 and 1 equivalent of Et_3N to a solution of **1**; the inset shows an amplification of the 500 to 800 nm region

Similar features between those two spectra may be noted. The bands at 245 nm (ε = 12300 $M^{-1}{\cdot}cm^{-1}$ for **1** and ε = 14100 $M^{-1}{\cdot}cm^{-1}$ for **2**) can be assigned to $\pi\rightarrow\pi^*$ transitions in the aromatic groups of the ligand. Other bands are observed at 287 nm (ε = 12500 $M^{-1}{\cdot}cm^{-1}$ for **1**, ε = 9800 $M^{-1}{\cdot}cm^{-1}$ sh for **2**), 323 nm (ε = 14250 $M^{-1}{\cdot}cm^{-1}$ for **1** and ε = 11750 $M^{-1}{\cdot}cm^{-1}$ for **2**), 365 nm (ε = 8900 $M^{-1}{\cdot}cm^{-1}$ for **1** and **2**) and 472 nm (ε = 1300 $M^{-1}{\cdot}cm^{-1}$ for **1** and ε = 830 $M^{-1}{\cdot}cm^{-1}$ for **2**). The last two originate from weak oxo-to-iron LMCT transitions and, more specifically, the transition at 472 nm is assigned to the $^6A_1 \rightarrow (^4A_1, {}^4E)$ transition and is the signature of the Fe−(μ-O)−Fe motif, independent of the bridging angle value.[16,35] Another important characteristic of the μ-oxo core is expected in the 550−700 nm region, the response being strongly dependent on the Fe−(μ-O)−Fe angle: the more bent, the less energetic and/or the more intense.[36] Magnifying the 550−800 nm region reveals the existence of a low-intensity band centered around 600 nm with a molar extinction coefficient larger for **2** (ε = 205 $M^{-1}{\cdot}cm^{-1}$) than for **1** (ε = 175 $M^{-1}{\cdot}cm^{-1}$). A similar increase in the intensity of the absorption has been observed for the tpa complexes[16]: the band at 572 nm (ε = 125 $M^{-1}{\cdot}cm^{-1}$) for $[tpa(H_2O)Fe(\mu\text{-}O)Fe(OH_2)tpa]^{4+}$ is shifted to 608 nm (ε = 165 $M^{-1}{\cdot}cm^{-1}$) in $[tpa(H_2O)Fe(\mu\text{-}O)Fe(OH)tpa]^{3+}$. Such a behavior indicates that **2** presents a bent structure in contrast to the linear arrangement in **1**. The molar extinction coefficient value measured for **2** is in agreement with a mono-μ-oxo core unit, the protonated diamond core $[Fe(\mu\text{-}O)(\mu\text{-}OH)Fe]^{3+}$ being characterized by an epsilon value greater by at least a factor of three. Results from UV/Vis absorption spectroscopy thus corroborate the conclusion formulated from Raman analysis, i.e. the persistence in solution of the internal hydrogen bond in **2**.

The conversion between **1** and **2** may be achieved in solution by addition of one equivalent of triethylamine to a solution of **1**, or by addition of one equivalent of perchloric acid to a solution of **2**. Figure 2 reproduces the changes in the UV/Vis spectrum of **1** upon the addition of Et_3N. Three isosbestic points are detected at 260, 555 and 680 nm, supporting the existence in solution of two chromophores. Spectra (b) to (d) can indeed be reproduced by assuming a linear combination of spectra (a) and (e), the coefficient for (e) being the number x of equivalents of base added and the one for (a) being $(1 - x)$. This indicates that the reaction is quantitative. The same holds if $HClO_4$ is added to **2** (see Scheme 3). A parallel control of the acido-basic conversions have been performed by X-band EPR and no signal has been detected, supporting the persistence in solution of dinuclear complexes.

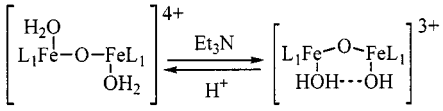

Scheme 3

It was not possible to further deprotonate compound **1** with Et_3N contrary to what has been reported for the analogous phenanthroline complex.[37] This suggests that even in acetonitrile solution, the coordinated water molecule in **2** is engaged in a hydrogen bond interaction, which is in agreement with the postulated $H_3O_2^-$ bridge.

Conclusion

We have studied here the $[L_1(H_2O)Fe(\mu\text{-}O)Fe(OH_2)L_1](ClO_4)_4{\cdot}2H_2O$ [$\mathbf{1}(ClO_4)_4{\cdot}2H_2O$] species and the

associated monodeprotonated form $[L_1(H_2O)Fe(\mu\text{-}O)Fe(OH)L_1](ClO_4)_3\cdot H_2O$ [**2**$(ClO_4)_3\cdot H_2O$]. The two complexes have been characterized by different spectroscopic techniques such as UV/Vis and Raman. Compound **1**$(ClO_4)_4\cdot 2H_2O$ has, moreover, been characterized by an X-ray diffraction study. The interconversion between **1** and **2** by addition of one equivalent of base or acid has been followed by UV/Vis absorption spectroscopy. No evolution towards a di-bridged system in a dry acetonitrile solution has been noted for **2** contrary to what has been observed for other $[(H_2O)Fe(\mu\text{-}O)Fe(OH)]^{3+}$ systems containing coordinated pyridine groups.[14,15] The generation of the diamond core structure seems to be related to the lability of the coordinated water molecule and the nature of the polydentate ligand. Imidazole is a stronger σ-donor and weaker π-acceptor ligand than pyridine. This could be the origin of the elongation of the Fe−(μ-O) bond that is suggested from magnetic susceptibility and Raman data. The Fe^{III} ions could thus be less electrophilic when coordinated to imidazoles instead of pyridines, and less sensitive to a nucleophilic attack of the coordinated hydroxide ion, preventing the formation of the protonated diamond core structure.

Experimental Section

General Remarks: Reagents and solvents were purchased commercially and used as received. Acetonitrile used for solution studies was distilled before use and dried on an alumina column. The synthesis of *N,N′*-dimethyl-*N,N′*-bis(1-methylimidazol-2-ylmethyl)-ethane-1,2-diamine (L_1) has been described previously.[38]

Caution! *Perchlorate salts of metal complexes with organic ligands are potentially explosive. Only small quantities of these compounds should be prepared and handle behind suitable protective shields.*

$[L_1(H_2O)Fe(\mu\text{-}O)Fe(OH_2)L_1](ClO_4)_4\cdot X$ [X = $2H_2O$, **1$(ClO_4)_4\cdot 2H_2O$; X = C_2H_5OH, **3**$(ClO_4)_4\cdot C_2H_5OH\cdot H_2O$]:** An ethanol/water solution (1:1, 5 mL) containing L_1 (138 mg, 0.5 mmol) was mixed with one equivalent of sodium hydroxide (0.1 mL of a 5 M solution). $Fe(ClO_4)_3\cdot 6H_2O$ (232 mg, 0.5 mmol) dissolved in 2 mL of water was then added. An orange precipitate appeared that was then filtered and washed with water to give138 mg of product (48% yield versus Fe). When $Fe(ClO_4)_3\cdot 6H_2O$ was added as an ethanolic solution, an orange precipitate was also formed. In both cases orange crystals were obtained by slow evaporation of an acetonitrile solution differing only in the nature of the solvation molecules. − $[L_1(H_2O)Fe(\mu\text{-}O)Fe(OH_2)L_1](ClO_4)_4\cdot C_2H_5OH\cdot H_2O$ ($C_{30}H_{60}Cl_4Fe_2N_{12}O_{21}$, 1178.38): calcd. C 30.58, H 5.13, N 14.26, Cl 12.03; found C 30.47, H 5.05, N 14.06, Cl 12.00.

$[L_1(H_2O)Fe(\mu\text{-}O)Fe(OH)L_1](ClO_4)_3\cdot H_2O$ (2**$(ClO_4)_3\cdot H_2O$):** To 10 mL of a methanolic degassed solution containing L_1 (138 mg, 0.5 mmol) and triethylamine (0.139 mL, 1.0 mmol) was added, under an argon atmosphere, 5 mL of a degassed methanolic solution of $Fe(ClO_4)_3\cdot 6H_2O$ (232 mg, 0.5 mmol). A small argon gas current was maintained overnight and tiny brownish green crystals were obtained (95 mg, 37% yield versus Fe). They were too small to allow an X-ray diffraction measurement. − $[L_1(H_2O)Fe(\mu\text{-}O)Fe(OH)L_1](ClO_4)_3\cdot H_2O$ ($C_{28}H_{53}Cl_3Fe_2N_{12}O_{16}$, 1031.85): calcd. C 32.59, H 5.17, N 16.29; Cl, 10.31; found C 32.64, H 5.11, N 16.01; Cl, 10.62.

Raman Spectroscopy: Raman spectra were recorded on a Jobin-Yvon double monochromator U_{1000} equipped with an As/Ga photomultiplier and photocounting detection. The excitation wavelength line was the 413.1 nm line of a Kr^+ laser at 10−15 mW incident power level. Solid samples of compounds **1**$(ClO_4)_4\cdot 2H_2O$ and **2**$(ClO_4)_3\cdot H_2O$ were mounted on a disk rotating at about 1000 rpm. The spectral width was 4 cm^{-1}. The solution sample of **2** was transferred in a degassed rotating cell. The spectral resolution was 6 cm^{-1}.

Magnetic Susceptibility Measurements: Magnetic susceptibility data were recorded on a MPMS5 magnetometer (Quantum Design Inc.). The calibration was made at 298 K using a palladium reference sample furnished by Quantum Design Inc. The data were collected over a temperature range of 10−300 K at a magnetic field of 1.0 T and were corrected for diamagnetism. The $\chi_M T$ vs. T curves were fitted using the van Vleck formula where the same g factor was assumed for each spin state S. The energies appearing in the exponential arguments are derived from the Heisenberg-van Vleck-Dirac Hamiltonian $-J\boldsymbol{S_1}\cdot\boldsymbol{S_2}$. The total spin S runs from $|S_1 - S_2|$ to $S_1 + S_2$ by unit steps.

EPR Spectroscopy: EPR spectra were recorded on Bruker ER 200 D and 300 spectrometers at X-band. For low temperature studies, an Oxford Instrument continuous-flow liquid helium cryostat and a temperature control system were used.

UV/Vis Spectroscopy: UV/Vis spectra were recorded on a Varian Cary 5E spectrophotometer.

X-ray Crystallographic Study: **1**$(ClO_4)_4\cdot 2H_2O$ ($C_{28}H_{56}Cl_4Fe_2N_{12}O_{21}$; M = 1150.33 g·mol^{-1}) crystallizes in the orthorhombic space group P_{bca} with a = 17.101(2) Å, b = 13.824(3) Å, c = 20.922(6) Å and α = β = γ = 90°, Z = 8, d = 1.545 g·cm^{-3}. The unit-cell and intensity data were measured with an Enraf−Nonius CAD-4 diffractometer with graphite monochromated Mo-K_α radiation (λ = 0.71073 Å). A prismatic orange crystal of $[L_1(H_2O)Fe(\mu\text{-}O)Fe(OH_2)L_1](ClO_4)_4\cdot 2H_2O$ with the dimensions 0.53 × 0.33 × 0.25 mm was chosen for the X-ray diffraction measurement. The cell constants were obtained by least-squares procedures based upon the 2Θ values of 25 reflections measured in the range 22.0 < 2Θ < 23.7° at ambient temperature. During data collection, three control reflections were measured every three hours. The crystal was stable and the check reflections showed a negligible decay in intensity of 0.45% during all the X-ray data collection. A total of 8682 reflections were collected in the range 4.26 < 2Θ < 50.0° within [−20 ≤ h ≤20, 0 ≤ k ≤ 16, 0 ≤ l ≤ 24]. From 4348 independent reflections, 2867 were considered as observed [$I > 2\sigma(I)$]. The structure was solved by direct methods with the program SHELXS-86[39] and refined by using the SHELXL-93[40] program. The molecular cation was located in a special crystallographic position with the oxygen atom at an inversion center (0,0,0.5). The perchlorate anions were located in a general crystallographic position. The observed disorder in the structure involved the anions; both perchlorates were disordered over two sites with nonidentical occupations (0.74 and 0.26; 0.70 and 0.30). The structure was refined anisotropically (non-hydrogen atoms) by full-matrix least-squares approximation based on F^2. The hydrogen atoms at the oxygen atoms of water molecules were localized in a difference Fourier synthesis and refined isotropically. Other hydrogen atom positions were calculated by assuming geometrical positions and were included in the structural model. The final weighting scheme was $w = 1/[\sigma^2(F_o^2) + (0.0568\ P)^2 + 0.001\ P]$, where $P = (F_o^2 + 2F_c^2)/3$. The final refinement of this model was continued until convergence when $R1$ = 0.0360 for $F^2 > 2\sigma(F^2)$ and R_w =

0.0840 were reached. The final difference map showed the largest residual peaks of 0.398 and −0.169 e·Å^{-3}. The two largest peaks were found at the Fe atoms.

Crystallographic data (excluding structure factors) for the structure(s) included in this paper have been deposited with the Cambridge Crystallographic Data Centre as supplementary publication no. CCDC-143394. Copies of the data can be obtained free of charge on application to CCDC, 12 Union Road, Cambridge CB2 1EZ, UK [Fax: (internat.) + 44-1223/336-033; E-mail: deposit@ccdc.cam.ac.uk].

Acknowledgments

We are grateful to Prof. Jean-Baptiste Verlhac for providing us with the precursors of the ligand L_1.

[1] B. J. Wallar, J. D. Lipscomb, *Chem. Rev.* **1996**, *96*, 2625−2657.
[2] E. I. Solomon, T. C. Brunold, M. I. David, J. N. Kemsley, S.-K. Lee, N. Lehnert, F. Neese, A. J. Skulan, Y.-S. Yang, J. Zhou, *Chem. Rev.* **2000**, *100*, 235−349.
[3] A. C. Rosenzweig, C. A. Frederick, S. J. Lippard, P. Nordlund, *Nature* **1993**, *366*, 537−543.
[4] A. C. Rosenzweig, P. Nordlund, P. M. Takahara, C. A. Frederick, S. J. Lippard, *Chem. Biol.* **1995**, *2*, 409−418.
[5] N. Elango, R. Radhakrishnan, W. A. Froland, B. J. Wallar, C. A. Earhart, J. D. Lipscomb, D. H. Ohlendorf, *Protein Sci.* **1997**, *6*, 556−568.
[6] S. K. Lee, J. D. Lipscomb, *Biochemistry* **1999**, *38*, 4423−4432.
[7] T. C. Brunold, N. Tamura, N. Kitajima, Y. Moro-oka, E. I. Solomon, *J. Am. Chem. Soc.* **1998**, *120*, 5674−5690.
[8] S. K. Lee, J. C. Nesheim, J. D. Lipscomb, *J. Biol. Chem.* **1993**, *268*, 21569−21577.
[9] Y. Liu, J. C. Nesheim, S. K. Lee, J. D. Lipscomb, *J. Biol. Chem.* **1995**, *270*, 24662−24665.
[10] K. E. Liu, A. M. Valentine, D. Qiu, D. E. Edmonson, E. H. Appelman, T. G. Spiro, S. J. Lippard, *J. Am. Chem. Soc.* **1995**, *117*, 4997−4998.
[11] K. E. Liu, D. Wang, B. H. Huynh, D. E. Edmonson, A. Salifoglou, S. J. Lippard, *J. Am. Chem. Soc.* **1994**, *116*, 7465−7466.
[12] L. Shu, J. C. Nesheim, K. Kauffmann, E. Münck, J. D. Lipscomb, L. Que, Jr., *Science* **1997**, *275*, 515−518.
[13] J. C. Nesheim, J. D. Lipscomb, *Biochemistry* **1996**, *35*, 10240−10247.
[14] S. Poussereau, G. Blondin, M. Cesario, J. Guilhem, G. Chottard, F. Gonnet, J.-J. Girerd, *Inorg. Chem.* **1998**, *37*, 3128−3132.
[15] Y. Dong, H. Fujii, M. P. Hendrich, R. A. Leising, G. Pan, C. R. Randall, E. C. Wilkinson, Y. Zang, L. Que, Jr., B. G. Fox, K. Kauffmann, E. Münck, *J. Am. Chem. Soc.* **1995**, *117*, 2778−2792.
[16] R. Hazell, K. B. Jensen, C. J. McKenzie, H. Toftlund, *J. Chem. Soc., Dalton Trans.* **1995**, 707−717.
[17] N. Arsulamy, P. A. Goodson, D. J. Hodgson, J. Glerup, K. Michelsen, *Inorg. Chim. Acta* **1994**, *216*, 21−29.
[18] T. Okuno, S. Ito, S. Ohba, Y. Nishida, *J. Chem. Soc., Dalton Trans.* **1997**, 3547−3551.
[19] H. Zheng, Y. Zang, Y. Dong, V. G. Young, Jr., L. Que, Jr., *J. Am. Chem. Soc.* **1999**, *121*, 2226−2235.
[20] J. Simaan, S. Poussereau, G. Blondin, J.-J. Girerd, D. Defaye, C. Philouze, J. Guilhem, L. Tchertanov, *Inorg. Chim. Acta* **2000**, *299*, 221−230.
[21] Y.-M. Frapart, A. Boussac, R. Albach, E. Anxolabéhère-Mallart, M. Delroisse, J.-B. Verlhac, G. Blondin, J.-J. Girerd, J. Guilhem, M. Césario, A. W. Rutherford, D. Lexa, *J. Am. Chem. Soc.* **1996**, *118*, 2669−2678.
[22] J. E. Plowman, T. M. Loehr, C. K. Schauer, O. P. Anderson, *Inorg. Chem.* **1984**, *23*, 3553−3559.
[23] F. Calderazzo, L. Labella, F. Marchetti, *J. Chem. Soc., Dalton Trans.* **1998**, 1485−1489.
[24] A. Hazell, K. B. Jensen, C. J. McKenzie, H. Toftlund, *Inorg. Chem.* **1994**, *33*, 3127−3134.
[25] B. R. Whittlesey, Z. Pang, R. A. Holwerda, *Inorg. Chim. Acta* **1999**, 124−126.
[26] R. M. Buchanan, S. Chen, J. F. Richardson, M. Bressan, L. Forti, A. Morvillo, R. H. Fish, *Inorg. Chem.* **1994**, *33*, 3208−3209.
[27] A. Hazell, K. B. Jensen, C. J. McKenzie, H. Toftlund, *J. Chem. Soc., Dalton Trans.* **1993**, 3249−3257.
[28] S. L. Heath, A. K. Powell, H. L. Utting, M. Helliwell, *J. Chem. Soc., Dalton Trans.* **1992**, 305−307.
[29] S. M. Gorun, S. J. Lippard, *Inorg. Chem.* **1991**, *30*, 1625−1630.
[30] R. Hotzelmann, K. Wieghardt, U. Flörke, H.-J. Haupt, D. C. Weatherburn, J. Bonvoisin, G. Blondin, J.-J. Girerd, *J. Am. Chem. Soc.* **1992**, *114*, 1681−1696.
[31] The equation given in ref 19 in erroneous in the exponential argument.
[32] H. Weihe, H. U. Güdel, *J. Am. Chem. Soc.* **1997**, *119*, 6539−6543.
[33] J. Sanders-Loehr, W. D. Wheeler, A. K. Shiemke, B. A. Averill, T. M. Loehr, *J. Am. Chem. Soc.* **1989**, *111*, 8084−8093.
[34] R. M. Wing, K. P. Callahan, *Inorg. Chem.* **1969**, *8*, 871−874.
[35] R. C. Reem, J. M. McCormick, D. E. Richardson, F. J. Devlin, P. J. Stephens, R. L. Musselman, E. I. Solomon, *J. Am. Chem. Soc.* **1989**, *111*, 4688−4704.
[36] R. E. Norman, R. C. Holz, S. Ménage, C. J. O′Connor, J. H. Zhang, L. Que, Jr., *Inorg. Chem.* **1990**, *29*, 4629−4637.
[37] C. Duboc-Toia, S. Ménage, J.-M. Vincent, M. T. Averbuch-Pouchot, M. Fontecave, *Inorg. Chem.* **1997**, *36*, 6148−6149.
[38] D. Tétard, J.-B. Verlhac, *Journal of Molecular Catalysis A: Chemical* **1996**, *113*, 223−230.
[39] G. M. Sheldrick, *Acta Crystallogr., Sect. A* **1990**, *46*, 467.
[40] G. M. Sheldrick, Program for the refinement of crystal structures, University of Göttingen, Germany.

Received September 8, 2000
[I00338]

The Syntheses and Luminescent Properties of Eu^{III} and Tb^{III} Cryptates in Solution

Qiu-Yun Chen,[a] Chang-Jian Feng,[a] Qin-Hui Luo,*[a] Chun-Ying Duan,[a] Xin-Sheng Yu,[a] and De-Jun Liu[a]

Keywords: Europium / Lanthanides / Cryptands / Luminescence / Mass spectrometry

The syntheses, characterization and luminescent properties of europium(III) and terbium(III) cryptates synthesized by [2+3] condensation of tris(2-aminoethyl)amine with 2,6-diformyl-4-R-phenol (R = Cl, F, *t*Bu) in the presence of Eu^{3+} or Tb^{3+} have been reported. The crystal structure of the europium cryptate (R = Cl) shows that the coordination number of the Eu^{III} ion is nine and that a guest water molecule is encapsulated in the cavity. The cryptates have a high stability which confers good fluorescence properties in solution.

Introduction

Studies on the syntheses and properties of lanthanide macrocyclic complexes are a fascinating area.[1,2] Their novel structures and interesting properties make macrocyclic lanthanide complexes valuable for technological applications.[3−5] Europium(III) complexes, for instance, can be used as luminescence probes in biology,[6−9] as luminescence labels in medical diagnostics,[10,11] and as contrast agents for magnetic resonance imaging.[12,13] Recent research has demonstrated that cryptands are useful as potential ligands for encapsulating lanthanide(III) ions and are able to shield metal ions from interaction with solvents to avoid radiationless deactivation processes in luminescence emission. Cryptates have high thermodynamic and kinetic stability and metal ion dissociation is negligible at high dilution.

Lanthanide cryptates with valuable luminescence properties can be obtained by a suitable choice of ligands with antenna chromophores.[1] Recently, the syntheses and metal luminescence properties of some cryptates have been reported, such as the cryptates based on oxamacrocycles,[14,15] azamacrocycles,[16,17] macrocycles with bipyridyl[18,19] and phenanthroline groups,[20] and macrocycles with functionalized calixarenes.[21,22] However, the number and type of cryptates are still quite limited.[23] A new kind of lanthanide cryptate (Gd^{III}, Tb^{III}, Eu^{III} and Dy^{III} etc.) derived from tris(2-aminoethyl)amine (tren) and 2,6-diformylphenol (dfp) was reported previously by Nelson,[24] Fenton[25] and our group,[26] although their luminescence properties were hardly mentioned. Recently, Plates et al.[27] made a detailed study on the solid fluorescence of phenolic cryptates of Eu, Dy, Yb; in solution; their fluorescence, however, is quenched completely by nonradiative deactivation. Herein we report some europium(III) and terbium(III) cryptates derived from the reaction of tren with 2,6-diformyl-4-R-phenol [R = Cl (dcp), F (dfp), *t*Bu (dbp)] (Figure 1). Their compositions and structures are slightly different from those previously reported[24,25] due to different reaction conditions. They possess a high coordination number (nine), a water molecule encapsulated in the inner sphere of the complex as a guest (not coordinated to the metal ion), and a high stability. These features result in their good fluorescence properties in solutions.

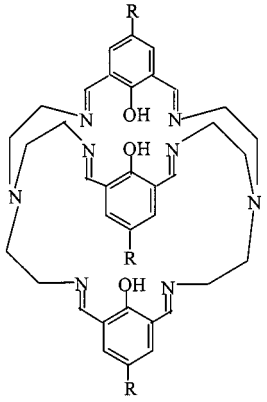

Figure 1. The chemical formula of H_3L [L^1, R = Cl; L^2, R = F; L^3, R = $C(CH_3)_3$]

Results and Discussion

Characterization of the Cryptates

According to the elemental analyses and molar conductivities (Table 1), the cryptates can be divided into three kinds: (a) 1:1 electrolytes $[Ln(H_2L^1)(NO_3)(H_2O)]NO_3$ [Ln = Eu^{III} **2**; Tb^{III} **3**]; (b) 2:1 electrolytes $[Eu(H_3L^1)(NO_3)(H_2O)](NO_3)_2$ **1**; (c) double salts (1:1 electrolytes) $[Ln(H_2L^{2,3})(NO_3)(H_2O)][Ln(NO_3)_4]$ (Ln = Eu^{III}, Tb^{III}, **4**−**7**]. The type of complex obtained was determined chiefly by the reaction conditions. For example, when using excess tren (i.e. a molar ratio tren:dfp (or dcp):Ln^{III} of 2:2:1), the phenolic protons were neutralized because of the slight basicity of the solution and the 1:1 electrolytes were obtained; when the molar ratio of the three materials is 2:3:1, the

[a] Coordination Chemistry Institute and State Key Laboratory of Coordination Chemistry, Nanjing University, Nanjing 210093, P. R. China

 © WILEY-VCH Verlag GmbH, 69451 Weinheim, 2001 1434−1948/01/0404−1063 $ 17.50+.50/0

Table 1. Elemental analysis and molar conductance data for the cryptates

No.	Cryptate (Formula)[a]	Yield (%)	Analysis(%) C, H, N[b]	Λ_m (298 K) scm^2mol (DMF)
1	$[Eu(H_3L^1)(NO_3)(H_2O)](NO_3)_2$ $(C_{36}H_{41}Cl_3EuN_{11}O_{13})$	65	39.30, 4.01, 13.45 (39.90), (3.87), (13.86)	125
2	$[Eu(H_2L^1)(NO_3)(H_2O)](NO_3)\cdot 4H_2O$ $(C_{36}H_{48}Cl_3EuN_{10}O_{14})$	73	38.78, 4.35, 12.34 (39.18), (4.35), (12.70)	88
3	$[Tb(H_2L^1)(NO_3)(H_2O)](NO_3)\cdot 9H_2O$ $(C_{36}H_{58}Cl_3N_{10}O_{19}Tb)$	68	35.80, 4.79, 11.77 (36.03), (4.87), (11.67)	81
4	$[Eu(H_2L^2)(NO_3)(H_2O)][Eu(NO_3)_4]\cdot 2H_2O$ $(C_{36}H_{44}Eu_2F_3N_{13}O_{21})$	58	31.72, 3.62, 13.30 (31.86), (3.30), (13.40)	65
5	$[Tb(H_2L^2)(NO_3)(H_2O)][Eu(NO_3)_4]\cdot 3H_2O$ $(C_{36}H_{46}F_3N_{13}O_{22}Tb_2)$	52	30.72, 3.32, 13.51 (31.14), (3.34), (13.12)	84
6	$[Eu(H_2L^3)(NO_3)(H_2O)][Eu(NO_3)_4]\cdot 3H_2O$ $(C_{48}H_{73}Eu_2N_{13}O_{21})$	48	38.84, 4.77, 12.68 (39.16), (4.94), (12.37)	84
7	$[Tb(H_2L^3)(NO_3)(H_2O)][Tb(NO_3)_4]\cdot 4H_2O$ $(C_{48}H_{75}N_{13}O_{22}Tb_2)$	47	38.40, 5.32, 12.46 (38.37), (5.02), (12.13)	81

[a] H_3L^1, H_2L^2, H_2L^3 denote the cryptand; the subscripts of H denote the number of protons on the phenoxy group in the cryptand. – [b] Calculated values for the formula of cryptates are given in parentheses.

2:1 electrolyte was produced; when excessive lanthanide(III) nitrate was added the double salts were obtained. Our one-step synthesis is quite different from the two-step procedure which includes the preparation of sodium complexes and a subsequent transmetallation reaction. In our cryptates, the coordination entities are also quite different from those of other authors[24,25,38] (see below).

The IR spectra of the cryptates (Table 2) show a band at ca. 1650 cm^{-1} attributable to ν(C=N). The bands at 1478 cm^{-1} and 1296 cm^{-1} are due to ν(N=O) (ν_1) and $\nu_{aym}(NO_2)$ (ν_5), respectively, of the coordinated nitrate. The $\nu_{sym}(NO_2)$ vibration (ν_2) at 1051 cm^{-1} is characteristic of a bidentate nitrate group. The strong sharp band at 1384 cm^{-1} is characteristic of an ionic nitrate.[36] The IR spectra show that there are both coordinated and ionic nitrates in the complexes.

The electronic spectra of the cryptates display three strong absorption bands. The band centered around 400 nm is assigned to the C=N chromophores, whereas the other two bands at ca. 270 nm and 230 nm are assigned to the π–π* transition of the K band of the benzene rings.

Thermogravimetric analysis of $[Eu(H_3L^1)(NO_3)(H_2O)](NO_3)_2$ shows that there are three weight-loss processes. The cryptate begins to lose 1.55% of its weight below 120 °C, corresponding to the loss of one water molecule (calcd. 1.65%), indicating that the water molecule in the cavity is only weakly bound. The second step occurs at 210–310 °C, where 11.1% of the total weight was lost, corresponding to the loss of the two nitrate ions in the outer sphere (calcd. 11.34%). In the range 311–340 °C, a weight loss of 5.8% is observed due to loss of the coordinated nitrate ion (calcd. 5.67%).

Electrospray Mass Spectrum

The positive-ion ES mass spectrum of $[Eu(H_2L^1)(NO_3)(H_2O)]^+$ is shown in Figure 2. The base peak at m/z = 887.5 corresponds to $[Eu(HL^1)]^+$ ($C_{36}H_{37}Cl_3EuN_8O_3$) whose isotopic distribution is shown in Figure 3a. From the numbers and natural isotopic abundances of the atoms in $[Eu(HL^1)]^+$, a revised program[37] was used to calculate the isotopic distribution at m/z = 887.5. The calculated pattern (Figure 3b) agrees well with the experimental one. The other peaks in Figure 2 can be assigned to the species formed by solvation, loss of protons and loss of the chlorine atoms from the benzene ring of the cryptate. The ES-MS peaks of the representative cryptates are shown

Table 2. IR and UV spectroscopic data for the cryptates **1**–**7**

Cryptate	IR ν_{max} (cm^{-1})						UV(MeCN) λ_{max} (nm) ($\varepsilon/dm^3mol^{-1}cm^{-1}$)		
	O–H	C=N	N=O	NO_3^-	NO_2 (asymm)	NO_2 (sym)			
1	3380	1650s 1640s	1478s	1384s	1296s	1051s	230 (83000)	264 (30000)	406 (16000)
2	3381	1653s	1478s	1384s	1297s	1050s	226 (86000)	269 (31000)	412 (13000)
3	3400	1645s	1475s	1384s	1292s	1060s	228 (96000)	268 (37000)	412 (18000)
4	3380	1655s	1478s	1384s	1290s	1040s	229 (79000)	272 (39000)	408 (25000)
5	3384	1645s	1475s	1384s	1292s	1040s	225 (58000)	272 (45000)	412 (33000)
6	3410	1642s	1478s	1384s	1296s	1042s	228 (73000)	267 (42000)	410 (10000)
7	3402	1640s	1478s	1384s	1296s	1041s	228 (94000)	251 (33000)	410 (12000)

in Table 3. The base peaks of the three cryptates formed by losing the encapsulated water molecule and the coordinated nitrate anion, namely $[Ln(H_nL)]^{n+}$, are different from those of the Nd^{III} cryptates,[26] with a base peak corresponding to $[Nd(HL^1)(NO_3)(H_3O)]^+$, indicating that under similar ES-MS conditions, the encapsulated water molecule and the coordinated nitrate anion in $[Eu(H_3L^1)(NO_3)(H_2O)]^{2+}$ can be lost easier than those in $[Nd(HL^1)(NO_3)(H_3O)]^+$. This may be due to the different distances between the water molecule and the metal atom in the cavity. In the cryptate **1** the distance for Eu−O(1w) is 3.070 Å, which is longer than the Nd−O(oxonium) bond (3.027 Å), as shown by X-ray structural analysis.

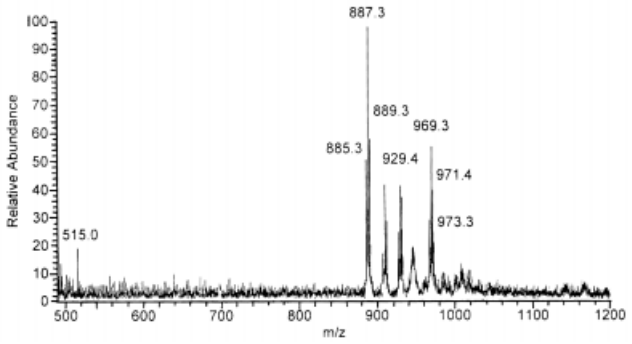

Figure 2. The ES-MS spectrum of the $[Eu(H_2L^1)(NO_3)(H_2O)]^+$ in MeOH

Crystal Structure

The structure of the cryptate cation $[Eu(H_3L^1)(NO_3)(H_2O)]^{2+}$ is shown in Figure 4. The crystal structure data are listed in Table 4 and 5. In the complex, Eu^{III} is located asymmetrically at one end of the cavity and is nine-coordinated, by three imino nitrogen atoms N(3), N(6), N(8), three phenolic oxygens O(1), O(2), O(3), two oxygens of the bidentate nitrate O(4), O(5) and one of the bridgehead nitrogen atoms, and forms a distorted monocapped square antiprism. The coordination distances are 2.491 and 2.532 Å, respectively, for two oxygens of the bidentate nitrate, in the range 2.288−2.416 Å for the phenolic oxygens, 2.492−2.562 Å for the imino nitrogens, and the Eu^{III}−N(4) distance is 2.761 Å, showing a weak interaction between Eu^{III} and the bridgehead nitrogen atom. Except for the coordination distance of Eu^{III}−N(4), the other bond distances are shorter than those of the Nd^{III} cryptate containing the same ligand.[26] This may be because the Eu^{3+} ion has a smaller radius than Nd^{3+}. In the distorted, capped, square antiprism, N(4) is the capped atom and the four oxygen atoms O(1), O(2), O(3), O(4) form the distorted basal plane (mean deviation 0.1862 Å); the distance between Eu^{III} and the basal plane is 1.3602 Å. The upper plane is composed of N(3), N(6), N(8) and O(5) (mean deviation 0.0776 Å), and the distance between the upper plane and Eu^{III} is 0.9551 Å. The biplanar angle between the two planes is 5.2°. The distance between the two bridgehead nitrogens N(1) and N(4) is 8.407 Å.

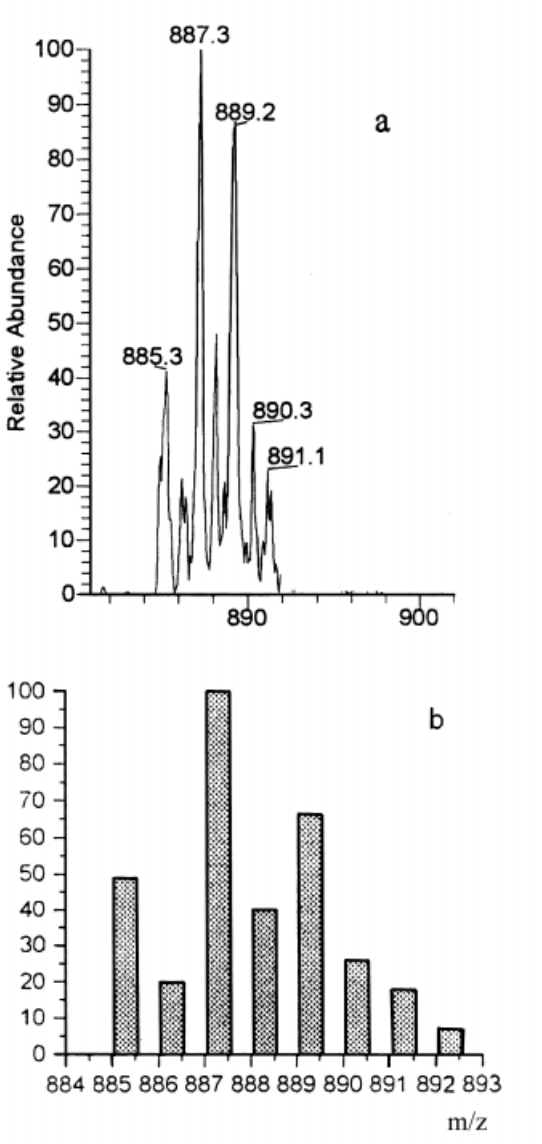

Figure 3. The isotopic distribution of the peak cluster at m/z = 887.5 for $[Eu(H_2L^1)(NO_3)(H_2O)]^+$: (a) experimental pattern, (b) calculated pattern

At one end of the cavity, a water molecule is encapsulated in the host macrocycle as a guest; the distance between O(1w) of the water molecule and Eu^{III} is 3.070 Å, and is longer than that of reported analogous cryptates whose distances are in the range 2.304−2.437 Å.[24,38] This confirms that the water molecule in our cryptate is not coordinated to the Eu^{III} atom.

Luminescence Properties of the Cryptates

Excitation of the Eu^{III} cryptates in MeCN solution with light at 400 nm gives rise to the characteristic emission of the Eu^{3+} ion and all four cryptates have similar emission spectra. Comparing the excitation band with the absorption band of the cryptate **2** at ca. 400 nm, the similarity between the absorption and excitation spectra indicates energy transfers from the excited state of the ligand to the Eu^{III} vibration level.[6] The emission spectrum of the cryptate **2**

Table 3. ES-MS spectroscopic data for the cryptates **2**, **6** and **7** in methanol solution

	Cryptate	Peak (*m*/*z*)	Assignment
2	$[Eu(H_2L^1)(NO_3)(H_2O)]^+$	969.5 (60)	$[Eu(H_2L^1)(NO_3)(H_2O)]^+$
		947.5 (25)	$[Eu(H_2L^1-2Cl)(NO_3)(H_2O)_2+MeOH]^+$
		929.5 (55)	$[Eu(H_2L^1-2Cl)(NO_3)(H_2O)+MeOH]^+$
		887.5 (100)	$[Eu(HL^1)]^+$
		515.0 (20)	$[Eu(H_3L^1\text{-}Cl)(NO_3)(H_2O)+3MeOH]^{2+}$
6	$[Eu(H_2L^3)(NO_3)(H_2O)]^+$	975.4 (45)	$[Eu(HL^3\text{-}C(CH_3)_3](NO_3)(H_2O)]^+$
		952.5 (100)	$[Eu(HL^3)]^+$
		476.8 (30)	$[Eu(H_2L^3)]^{2+}$
7	$[Tb(H_2L^3)(NO_3)(H_2O)]^+$	1022.2 (24)	$[Tb(H_2L^3)(NO_3)]^+$
		959.4 (48)	$[Tb(HL^3)]^+$
		511.7 (14)	$[Tb(H_3L^3)(NO_3)]^{2+}$
		480.2 (100)	$[Tb(H_2L^3)]^{2+}$

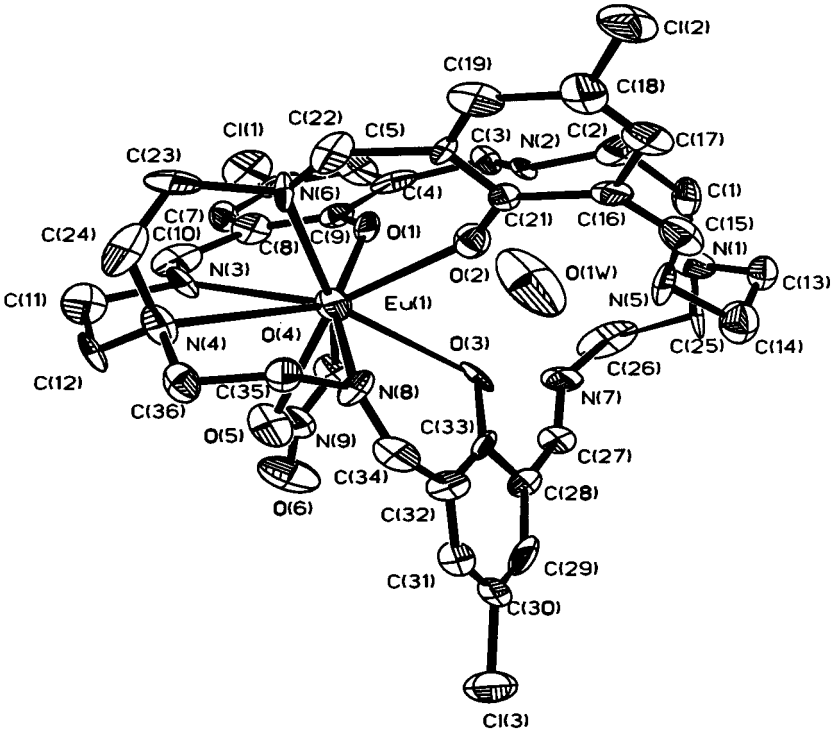

Figure 4. Crystal structure of $[Eu(H_3L)(NO_3)(H_2O)]^{2+}$ ion

is shown in Figure 5. All emissions arise from the $^5D_0$ level corresponding to the $^5D_0 \rightarrow {}^7F_1$ ($\Delta J = 0, 1-4$) transition. The weak band at 580 nm arises from the $^5D_0 \rightarrow {}^7F_0$ transition. The band around 593 nm for $^5D_0 \rightarrow {}^7F_1$, which is magnetic-dipole allowed, is hardly affected by a change of the coordination environment. The intense band around 613 nm for $^5D_0 \rightarrow {}^7F_2$ is an electric-dipole allowed transition and its emission intensity is sensitive to the coordination environment of Eu^{III}. The intensity for the $^5D_0 \rightarrow {}^7F_2$ transition is much higher than that for $^5D_0 \rightarrow {}^7F_1$, showing that the complex has no inversion center. All the ratios of the intensities of the $^5D_0 \rightarrow {}^7F_2$ to the $^5D_0 \rightarrow {}^7F_1$ transition are about 4.5:1 for the three cryptates (**2**, **4** and **6**) with different substituents, implying a similar symmetry.[23] The bands around 655 nm and the bands around 700 nm are produced from the transitions $^5D_0 \rightarrow {}^7F_3$ and $^5D_0 \rightarrow {}^7F_4$, respectively. A wide band around 480 nm is observed corresponding to the ligand emission whose quantum yield is 8.8×10^{-2} (MeCN).

Under the same experimental conditions, the Tb^{III} cryptate **7** displays a weak band at 542 nm, due to the $^5D_4 \rightarrow {}^7F_5$ transition, which is overlapped partly by a strong emission band of the ligand. For cryptates **3** and **5**, only a ligand-centered band is observed, implying a poor energy transfer between the ligand triplet state and the $^5D_4$ state of Tb^{III}.

The luminescent quantum yields and the life times at 613 nm of some Eu^{III} cryptates in MeCN are shown in Table 6. From this table it can be seen that the quantum yield and lifetime of the cryptate **2** with a chlorine substituent are higher than those of **3** and **6**. The reason for this is not clear yet as there are very few of these cryptates with which to make a good comparison.

Table 4. Crystal data and structure refinement

Formula	$C_{36}H_{41}Cl_3EuN_{11}O_{13}$
M_r	1091.11
Color/habit	Orange, block
Crystal system	Orthorhombic
Space group	*Pbca*
a (Å)	16.987(7)
b (Å)	20.688(5)
c (Å)	24.641(6)
V (Å^3)	8659.3(47)
Z	8
$D_{calcd.}$ (Mg m^{-3})	1.678
F(000)	4416
Crystal dimensions	0.4 × 0.3 × 0.3
Mo-K_α radiation (Å)	0.71073
2θ range (°)	1.76 to 22.50
Absorption coefficient (mm^{-1})	1.710
Index ranges	$-1 \le h \le 18$ $-1 \le k \le 22$ $-1 \le l \le 26$
Reflection collected	6866
Independent reflections	5663
Observed reflections	2115
R, *wR* (observed data)	0.0768, 0.1303
w^{-1}	$\sigma^2(F_0)^2 + (0.0000P)^2 + 0.0000P$ $P = [(F_0)^2 + 2(F_c)^2]/3$
Goodness of fit	1.004
Largest difference peak (eÅ^{-3})	0.956
Largest difference hole (eÅ^{-3})	−0.740

Table 5. Selected bond lengths (Å) and angles (°) for cryptate **1**

Eu(1)−O(1)	2.288(6)	Eu(1)−O(2)	2.374(6)
Eu(1)−O(3)	2.418(6)	Eu(1)−N(8)	2.492(7)
Eu(1)−O(5)	2.491(7)	Eu(1)−N(3)	2.532(7)
Eu(1)−N(6)	2.562(7)	Eu(1)−O(4)	2.649(7)
Eu(1)−N(4)	2.761(7)		
C(15)−N(5)	1.334(12)	C(22)−N(6)	1.260(11)
C(3)−N(2)	1.242(12)	C(34)−N(8)	1.289(12)
C(27)−N(7)	1.185(12)	C(10)−N(3)	1.281(12)
O(1)−Eu(1)−O(2)	78.5(2)	O(1)−Eu(1)−O(3)	97.9(2)
O(2)−Eu(1)−O(3)	70.8(2)	O(1)−Eu(1)−N(8)	160.7(2)
O(2)−Eu(1)−N(8)	83.8(2)	O(3)−Eu(1)−N(8)	68.7(2)
O(1)−Eu(1)−O(5)	118.9(2)	O(2)−Eu(1)−O(5)	144.2(2)
O(3)−Eu(1)−O(5)	75.7(2)	N(8)−Eu(1)−O(5)	72.5(2)
O(1)−Eu(1)−N(3)	71.3(2)	O(2)−Eu(1)−N(3)	140.4(2)
O(3)−Eu(1)−N(3)	137.4(2)	N(8)−Eu(1)−N(3)	127.9(2)
N(8)−Eu(1)−N(3)	128.1(2)	O(5)−Eu(1)−N(3)	74.6(2)
O(1)−Eu(1)−N(6)	87.1(2)	O(2)−Eu(1)−N(6)	66.9(2)
O(3)−Eu(1)−N(6)	135.4(2)	N(8)−Eu(1)−N(6)	93.1(2)
O(5)−Eu(1)−N(6)	139.0(2)	N(3)−Eu(1)−N(6)	86.2(2)
O(1)−Eu(1)−O(4)	71.0(2)	O(2)−Eu(1)−O(4)	124.2(2)
O(3)−Eu(1)−O(4)	68.7(2)	N(8)−Eu(1)−O(4)	114.1(2)
O(5)−Eu(1)−O(4)	49.7(2)	N(3)−Eu(1)−O(4)	68.8(2)
N(6)−Eu(1)−O(4)	150.7(2)	O(1)−Eu(1)−N(4)	130.4(2)
N(8)−Eu(1)−N(4)	66.0(2)	O(5)−Eu(1)−N(4)	73.9(2)
N(3)−Eu(1)−N(4)	66.8(2)	N(6)−Eu(1)−N(4)	65.2(2)
O(4)−Eu(1)−N(4)	114.8(2)	O(3)−Eu(1)−N(4)	130.9(2)
O(2)−Eu(1)−N(4)	120.5(2)		

The fluorescence properties of the europium(III) cryptates derived from 2,6-diformylphenol have attracted much attention. These studies have focused on the cryptates with CH_3, OCH_3 and phenyl substituents,[27,38] although they do not display fluorescent emission in solution. The luminescence difference between our cryptates and other authors' ones results from the different structures. As shown by the crystal structure, the coordination number of Eu^{III} in cryptate **1** is nine, and in **2**−**7** it is also nine. Coordinative saturation of Eu^{III} blocks the coordination of solvent molecules to the metal centre. It is of interest to note that, for **1**, the water molecule does not coordinate to Eu^{III} even though it is located within the cryptate cavity. This is not the case for the Eu^{III} phenolic cryptates reported by other authors,[24,25,38] in which coordination numbers of seven or eight, and a water molecule or monodentate ligand, which can dissociate easily (SCN^-,NO_3^-, etc.), are found coordinated to the metal ion. In these cases, in solution, the interaction between the Eu^{III} and water or solvent molecules results in nonradiative deactivation which quenches the fluorescence.

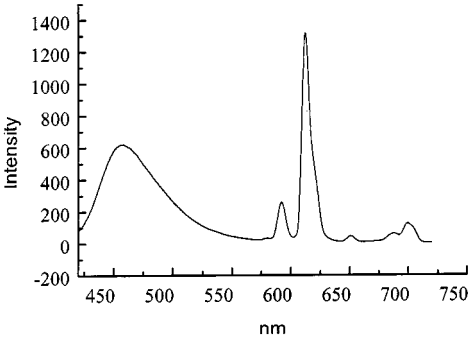

Figure 5. Emission spectra for the cryptate **2** in MeCN at an excitation wavelength of 400 nm

Table 6. Luminescent quantum yield(Φ) and lifetime (τ) of the mononuclear Eu^{III} complexes in MeCN solution at 293 K

Complex	$\Phi_{Eu^{III}} \times 10^{2}$[a], [b]	τ (ms)
2	4.3	0.88
3	0.20	0.51
6	0.24	−

[a] Excitation at 400 nm; concentration of Eu^{III}complexes is 2 × 10^{-6} M. − [b] Experimental errors ± 20%.

Experimental Section

Materials: $Ln(NO_3)_3 6H_2O$ (Ln = Eu, Tb) was prepared by dissolving Ln_2O_3 (99.99%) in an excess of nitric acid; 2,6-diformyl-4-R-phenol (R = Cl, F, *t*Bu)[28] and tris(2-aminoethyl)amine (tren) were prepared by literature methods.[29] Their physical constants and spectroscopic data are in agreement with literature values. The acetonitrile for the fluorescence study was dried by treatment with CaH_2 and distillation over P_2O_5. The $[Ru(bipy)_3]Cl_2$ used as a standard material in the quantum yield measurement was synthesized according to a literature procedure[30] and recrystallized twice from doubly distilled water. Its spectroscopic data were in agreement with literature values; its quantum yield value was checked against rhodamine B[31] and was also in accordance with the literature value.

Physical Measurements: Elemental analysis was performed on a Perkin−Elmer 240c analytical instrument. The molar electrical conductivitives in DMF solution containing ≈10^{-4} mol dm^{-3} com-

plexes were measured at 25 °C ± 0.1 °C using a BSD-A conductometer. The IR spectra were measured as a KBr disc using a Nicolet 5 DX FT-IR spectrophotometer. Electronic spectra were recorded on a UV-3100 spectrophotometer. Thermoanalysis of the complexes was performed on a SDT 2960C TA thermoanalyser under an argon atmosphere at a rate of 10 °C min^{-1}. The electrospray mass spectra (ES-MS) were determined on a Finnigan LCQ mass spectrometer; the concentrations of the samples were about 1.0 μmol dm^{-3}. The diluted solutions were electrosprayed at a flow rate of 5×10^{-6} dm^{-3} min^{-1} with a needle voltage of +4.5 kV. The mobile phase was an aqueous solution of methanol (v/v, 1:1). The samples were run in the positive-ion mode.

Luminescence Measurement: The luminescence spectra were measured with a Hiachi Model F4500 spectrofluorometer. In measurements of emission and excitation spectra the bandpass was 5.0 nm. The quantum yield of the Eu^{III} complexes was measured using a relative method with $[Ru(bipy)_3]Cl_2$ as the standard. Its quantum yield is 0.042 in aqueous solution at 20 °C.[35] The quantum yields of the Eu^{III} complexes were calculated from Equation (1):

$$\Phi_x/\Phi_s = [A_s/A_x]\,[n_x^2/n_s^2][D_x/D_s] \quad (1)$$

where Φ is the quantum yield, subscript s stands for the reference and x for the sample, A is the absorbance at the excitation wavelength, n is the refractive index (1.343 for MeCN solution and 1.344 for aqueous solution),[31] and D is the emission integrated area. The sample absorbances at excitation wavelength were kept as low as possible to avoid fluorescence errors (A_{exc} = 0.09−0.11). Solutions containing complexes of about 1.0×10^{-6} mol dm^{-3} were deoxygenated with a stream of super-pure nitrogen for 15 minutes.

The fluorescence lifetimes of the complexes were measured on a SPEX-FL2T2 spectrofluorimeter equipped with a flash lamp. The signals were recorded by photomultiplier using single-photon counting. Because in each solution only a single light-emitting species is present and there is no quenching of the emissive state by other excited state molecules, the fluorescence intensities decay exponentially over time t, obeying Equation (2):[34]

$$I_t = I_0 \exp(-t/\tau) \quad (2)$$

where I_0 and I_t are the fluorescence intensities at the time t = 0 and time t, respectively. The emission lifetime of fluorescence, τ, was obtained by fitting the fluorescence-decay curve into Equation (2).

Crystal Structure Determination: A summary of the crystal data, intensity collection and structure refinement is given in Table 4. Intensity data were measured on a Siemens P4 four-circle diffractometer with monochromatic Mo-K_α (λ = 0.71073) radiation in the ω-scan mode with a variable scan speed of 4.0−60.0° $min.^{-1}$ in ω. All data were corrected for Lorentz and polarization effects during data reduction using XSCANS.[32]

The structure was solved by direct methods. All non-hydrogen atoms were refined anisotropically by full-matrix least-squares. The hydrogen atoms of the ligands were placed in their calculated positions with C−H = 0.93 Å. The hydrogen atoms of the water molecules in the cryptate **1** were found in the difference Fourier map. All the hydrogen atoms were assigned fixed isotropic thermal parameters (1.2 times that of the atoms to which they are attached) and allowed to ride on their respective parent atoms. The contributions of these hydrogen atoms were included in the structure-factor calculations. One of the two nitrate anions was found to be disordered. The s.o.f.′s were 0.54 and 0.46 for the disordered parts containing nitrogen atoms N(11) and N(11′), respectively. All computations were carried out using the SHELXTL-PC program package.[33]

Syntheses of the Cryptates

$[Eu(H_3L^1)(NO_3)(H_2O)](NO_3)_2$ (1): A methanol solution (10 cm^3) containing tren (0.058 g, 0.40 mmol) was added dropwise to a stirred methanol solution (15 cm^3) containing dcp (0.111 g, 0.6 mmol) and $Eu(NO_3)_3{\cdot}6H_2O$ (0.112 g, 0.25 mmol). The reaction mixture was refluxed for 4 hours. Concentration of the solution resulted in the yellowish product $[Eu(H_3L^1)(NO_3)(H_2O)](NO_3)_2$ which was filtered off, washed with methanol and diethyl ether, and dried in a vacuum desiccator.

The cryptates **2**−**7** were prepared by a similar procedure except that the molar ratios were changed. For **2** and **3**: tren:dcp:Eu^{3+} = 1:1.2:0.5; for **4**−**7**: tren:dfp (or dbp):Eu^{3+} = 1:1.2:1.

Acknowledgments

The work was supported by the National Natural Science Foundation and the 211 project of China.

[1] V. Alexander, *Chem. Rev.* **1995**, *95*, 237−342.
[2] J.-M. Lehn, *Angew. Chem. Int. Ed. Engl.* **1990**, *29*, 1304−1319.
[3] N. Sabbatini, M. Guardigi, *Coord. Chem. Rev.* **1993**, *123*, 201−228.
[4] G. R. Choppin, D. R. Peterman, *Coord. Chem. Rev.* **1998**, *174*, 283.
[5] P. Ghosh, P. K. Bharadwaj, J. Roy. S. Ghosh, *J. Am. Chem. Soc.* **1997**, *119*, 11903−11909.
[6] D. Parker, J. A. G. Williams, *J. Chem. Soc., Dalton Trans.* **1996**, 3613−3628.
[7] F. Richardson, *Chem. Rev.* **1982**, *82*, 541−552.
[8] G. Mathis, *Clin. Chem. (Washington, D.C.)* **1993**, *39*, 1953−1959.
[9] E. Soini, I. Hemmila, *Clin. Chem.* **1979**, *25*, 353−358.
[10] J. L. Toner, in *Inclusion Phenomena and Molecular Recognition* (Ed.: J. Atwood), Plenum Press, New York, **1990**, p 185.
[11] C. H. Evans, *Biochemistry of the Elements*, vol. 8 ("Biochemistry of the Lanthanides"), Plenum, New York, N.Y., **1990**.
[12] P. Caravan, J. J. Ellison, T. J. McMurry, R. B. Lauffer, *Chem. Rev.* **1999**, *99*, 2293−2353.
[13] [13a]P. R. Selvin, T. M. Rana, J. E. Hearst, *J. Am. Chem. Soc.* **1994**, *116*, 6029−6030. − [13b] R. Edelman, S. Warach, *New Eng. J. Med.* **1993**, *328*, 708−714.
[14] B. Alpha, E. Anklam, R. Deschenaux, J.-M. Lehn, M. Pietraszkiewicz, *Helv. Chim. Acta.* **1988**, *71*, 1042−1052.
[15] J.-M. Lehn, M. Pietraszkiewicz, J. karpiuk, *Helv. Chim. Acta.* **1990**, *73*, 106−111.
[16] L. Prodi, M. Maestri, R. Ziessei, V. Balzani, *Inorg. Chem.* **1991**, *30*, 3798−3802.
[17] F. Bodar−Houillon, A. Marsura, *New. J. Chem.* **1996**, *20*, 1041−1045.
[18] N. Sabbatini, M. Guardigilli, I. Manet, F. Bolletta, *Inorg. Chem.* **1994**, *33*, 955−959.
[19] V. Balzani, J.-M. Lehn, J. Van De Loosdrecht, A. Mecati, N. Sabbatini, R. Ziessel, *Angew. Chem. Int. Ed. Engl.* **1991**, *30*, 190−191.
[20] K. Sasamoto, *European Patent*, EP. 0,493,745 AI. **1991**.
[21] H. Matsumoto, S. Shinkai, *Chem. Lett.* **1994**, 901−904.
[22] F. J. Steemer, W. Verboom, D. N. Reinhoudt, E. B. Van Der Tol, J. W. Verhoeven, *J. Am. Chem. Soc.* **1995**, *117*, 9408−9414.
[23] C. Galaup, C. Picard, B. Cathala, L. Cazaux, P. Tisnes, H. Autiero, D. Aspe, *Helv. Chim. Acta* **1999**, *82*, 543−560.
[24] M. G. B. Drew, O. W. Howarth, C. J. Harding, N. Martin, J. Nelson, *J. Chem. Soc., Chem. Commun.* **1995**, 903−905.
[25] F. Avecilla, R. Bastida, A. de Blas, D. E. Fenton, A. Macias, A. Rodriguez, T. Rodriguez-Blas, S. Garcia-Granda, R. Corza-Suarez, *J. Chem. Soc., Dalton Trans.* **1997**, 409−415.
[26] [26a] C.-J. Feng, Q.-H. Luo, C.-Y. Duan, M.-C. Shen, Y.-J. Liu, *J. Chem. Soc., Dalton Trans* **1998**, 1377−1380. − [26b] J.-J.

Zhang, W. Zhang, Q.-H. Luo, Y.-H. Mei, *Polyhedron* **1999**, *18*, 3637−3642.
[27] C. Platas, F. Avecilla, A. de Blas, T.Rodrigues−Blas, C. F. G. C. Geraldes, E. Toth, A. E. Merbach, J.-C. G. Bunzli, *J. Chem. Soc., Dalton Trans.* **2000**, 611−618.
[28] E. Kimura, S. Young, J. P. Collman, *Inorg, Chem.* **1970**, *9*, 118−124.
[29] S. Taniguchi, *Bull. Chem. Soc. Jpn.* **1984**, *57*, 2683−2684.
[30] F. H. Burstall, *J. Chem. Soc.* **1936**, *1*, 173−175.
[31] K.Nakamaru, *Bull. Chem. Soc. Jpn.* **1982**, 2697−2705.
[32] XSCANS (Version 2.1), Siemens Analytical X-ray Instruments, Inc., Madison, WI, **1994**.
[33] SHELXTL (Version 5.0), Siemens Industrial Automation, Inc., Analytical Instrumentation, Madison, WI. **1995**.
[34] D. E. Eaton, *Pure Appl. Chem.* **1988**, *60*, 1107−1114.
[35] J. V. Houten, R. J. Watts, *J. Am. Chem. Soc.* **1976**, *98*, 4853−4858.
[36] K. Nakampto, *Infrared and Raman Spectra of Inorganic and Coordination Compounds* 3rd ed., Wiley−Interscience, New York, **1978**.
[37] J. D. Tee, *Talanta* **1973**, *20*, 1029−1038.
[38] S.-Y. Yu, Q. Huang, B. Wu, W.-J. Zheng, X.-T. Wu, *J. Chem. Soc., Dalton Trans.* **1996**, 3883−3888.

Received September 12, 2000
[I00343]

First Dioxomolybdenum(VI) Complexes Containing Chiral Oxazoline Ligands: Synthesis, Characterization and Catalytic Activity

Montserrat Gómez,*[a] Susanna Jansat,[a] Guillermo Muller,[a] Gladys Noguera,[b] Helena Teruel,*[b] Vicent Moliner,[c] Elena Cerrada,[d,e] and Michael Hursthouse[e]

Keywords: Molybdenum / Oxo ligands / Oxidation / Catalysis / N ligands / Density functional calculations

The *cis*-[$MoO_2(N,O)_2$] complexes containing chiral oxazoline ligands (*N,O*) [**1**: *N,O* = **A**, (4′*R*)-2-(4′-ethyl-3′,4′-dihydroxazol-2′-yl)phenolato; **2**: *N,O* = **B**, (4′*S*)-2-(4′-isopropyl-3′,4′-dihydroxazol-2′-yl)phenolato] were synthesised and characterised, both in solution and in the solid state. These pseudo-octahedral neutral complexes were obtained as mixtures of diastereomers due to the chirality of the ligand and at the metal centre (Δ or Λ). Theoretical DFT calculations corroborate the isomer distribution. For complex **1**, the two major diastereomers, **Δ-*N*-*cis*-1** and **Λ-*N*-*trans*-1**, crystallised independently and the molecular structures were determined by single-crystal X-ray diffraction. NMR experiments at 800 MHz for **2** allowed the determination of the isomeric composition in solution. The product distribution depends on the coordinating nature of the solvent. Complexes **1** and **2** catalyse the oxidation of triphenylphosphane and styrene.

Introduction

Transition metal oxo compounds are involved in oxygen transfer chemistry in both biological[1] and industrial processes.[2] Molybdenum complexes have been extensively studied, especially as models for heterogeneous oxidation catalysts and as the active site of oxo-transfer, molybdenum-containing enzymes.[3] Until recently, most oxo compounds used as oxidation catalysts contained sterically demanding sulfur ligands, since they were believed to be suitable models.[4] Indeed, the nature of the ligands around the molybdenum centre is critical for the success of the catalytic reaction.[5]

To understand oxo-transfer properties, numerous dioxomolybdenum complexes involving a wide range of ligands have been prepared and characterized.[6] Bidentate *S,S*-, *N,N*-, *O,O*- or *N,O*-donor ligands are common in monometallic complexes with the $[MoO_2]^{2+}$ core.[7] Among them, *N*-donor ligands[8] are of interest because they are robust in oxygen transfer reactions. In particular, chiral oxazoline ligands are especially useful in many organic transformations.[9] However, to the best of our knowledge, this kind of ligand has not been studied with molybdenum systems.

Therefore, we decided to synthesise neutral, monometallic complexes containing anionic ligands with oxazoline moieties. Here we describe the synthesis and characterization, both in solution and in the solid state, of new chiral oxomolybdenum complexes containing phenolatooxazoline ligands of the general formula *cis*-[$MoO_2(N,O)_2$] (where *N,O* = **A** or **B**). Moreover, we report on the ability of these complexes to act as oxo transfer reagents in oxidation processes.

Results and Discussion

A one-pot reaction of [$MoO_2(acac)_2$] and the optically pure oxazoline ligands [(*R*)-**AH**, (*S*)-**BH**] in methanol afforded the neutral dioxomolybdenum (VI) complexes **1** and **2**, respectively (Scheme 1), in a similar manner to that reported for Mo[10] and other metals (Ni, Pd, Mn).[11] All the compounds were obtained in high yields and are stable both in the solid state and in solution, although after several days in chloroform some oxazoline decoordination was detected by ^{1}H NMR spectroscopy.

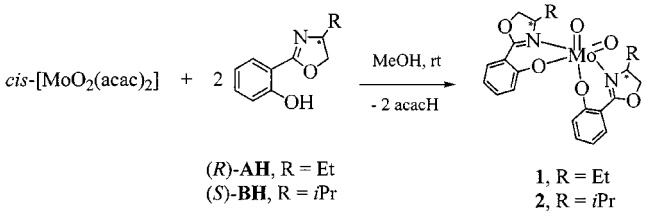

Scheme 1

A relevant feature of these hexacoordinate complexes is the relative position of the bidentate anionic *N,O* oxazoline ligands, which leads to the formation of several geometrical isomers. According to the relative position of the iminic nitrogen atoms and the oxo groups, three arrangements are expected: a) the two oxazoline nitrogen atoms *cis* to both oxo groups (*N-cis*); b) each nitrogen atom *trans* to one oxo group (*N-trans*) and c) one nitrogen atom *cis* to the oxo groups and one *trans* to one oxo group (*N-cis,trans*) (Scheme 2). Owing to the asymmetrical environment

[a] Departament de Química Inorgànica, Universitat de Barcelona, Martí i Franquès 1−11, 08028 Barcelona, Spain
[b] Departamento de Química, Universidad Simón Bolívar, Baruta 89000, Caracas 1081, Venezuela
[c] Departament de Ciències Experimentals, Universitat Jaume I, P. O. Box 224, 12080 Castelló, Spain
[d] Departamento de Química Inorgánica, Instituto de Ciencias de los Materiales de Aragón, Universidad de Zaragoza-CSIC, 50009 Zaragoza, Spain
[e] Department of Chemistry, University of Wales, P. O. Box 912, Cardiff CF13TB, United Kingdom

 © WILEY-VCH Verlag GmbH, 69451 Weinheim, 2001 1434−1948/01/0404−1071 $ 17.50+.50/0

around the metal atom, each of these possibilities has a pair of isomers, Δ and Λ. Therefore, for each complex, six diastereomers are possible.

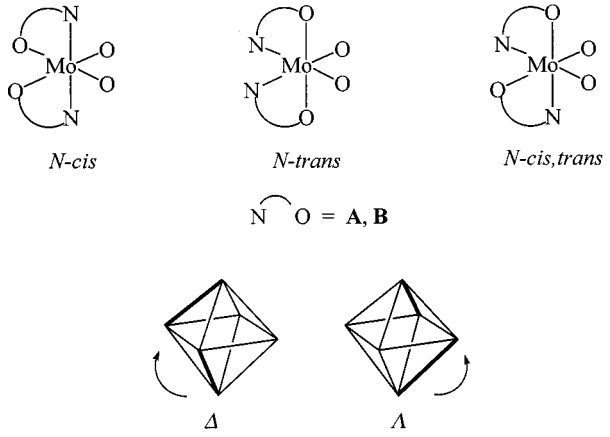

Scheme 2

Solid State Structures

The IR spectra for these Mo complexes exhibit two very strong absorption bands at ca. 920 and 890 cm^{-1}, which were assigned to the *cis*-[MoO_2] fragment. In addition, a strong signal at ca. 1620 cm^{-1} corresponds to the stretching of the C=N imine bond.

For complex **1**, monocrystals corresponding to two isomers were isolated from a dichloromethane/diethyl ether solution upon recrystallization. The crystal structures of complexes **Δ-*N-cis*-1** and **Λ-*N-trans*-1** determined by single-crystal X-ray diffraction analysis are shown in Figure 1 and 2, respectively.

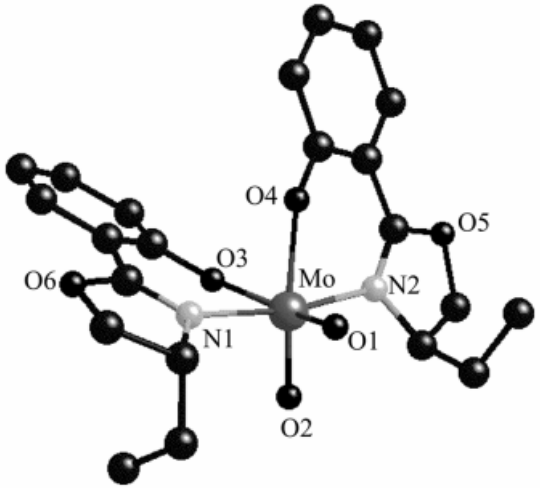

Figure 1. View of the molecular structure of complex **Δ-*N-cis*-1**; hydrogen atoms have been omitted for clarity

In both structures, the molecules show a distorted octahedral geometry around the molybdenum atom (Table 1). An expansion of the dioxo fragment O(1)−Mo−O(2) from 90° to 100.7° and 105.4° was observed for **Δ-*N-cis*-1** and **Λ-*N-trans*-1**, respectively, as reported for similar complexes.[10b,12] Furthermore, the N(1)−Mo−N(2) angle showed a contraction from 180° to 168.8° for **Δ-*N-cis*-1**, and from 90° to 75.4° for **Λ-*N-trans*-1**. A similar trend was observed for the O(3)−Mo−O(4) angle, from 90° to 80.5° and from 180° to 158.8° for **Δ-*N-cis*-1** and **Λ-*N-trans*-1**, respectively. The bite angles O(3)−Mo−N(1) and O(4)−Mo−N(2) were ca. 79° in both cases, an observation which is consistent with other dioxomolybdenum six-membered *N,O*-coordinated complexes.[10a,13]

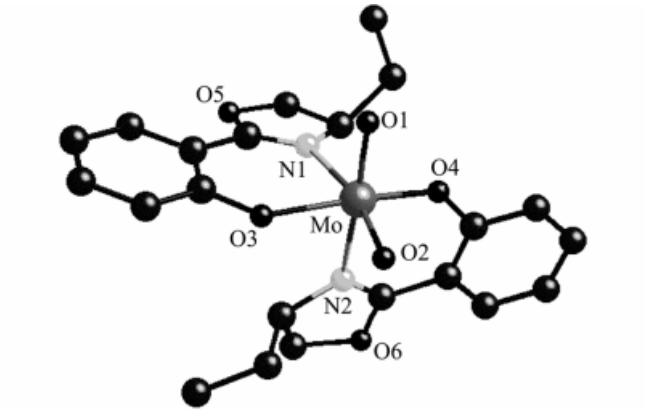

Figure 2. View of the molecular structure of complex **Λ-*N-trans*-1**; hydrogen atoms have been omitted for clarity

Table 1. Selected bond lengths (Å) and bond angles (°) for **Δ-*N-cis*-1** and **Λ-*N-trans*-1** (with esd's in parentheses)

	Δ-*N-cis*-1	**Λ-*N-trans*-1**
Mo−O(1)	1.700(2)	1.6991(14)
Mo−O(2)	1.708(2)	1.704(2)
Mo−O(3)	2.056(2)	1.964(2)
Mo−O(4)	2.045(2)	1.9541(14)
Mo−N(1)	2.149(3)	2.334(2)
Mo−N(2)	2.151(3)	2.312(2)
O(1)−Mo−O(2)	100.73(13)	105.37(8)
O(3)−Mo−N(1)	79.18(9)	78.91(6)
O(4)−Mo−N(2)	79.39(9)	78.15(6)
O(3)−Mo−O(4)	80.49(9)	158.81(7)
N(1)−Mo−N(2)	168.80(10)	75.37(6)

The Mo−O bond lengths for the dioxo group were ca. 1.7 Å in both structures, as reported previously.[14] The distances Mo−N for **Λ-*N-trans*-1** [Mo−N(1) = 2.31 Å and Mo−N(2) = 2.33 Å] were longer than for **Δ-*N-cis*-1** (Mo−N ≈ 2.15 Å) due to the oxo *trans* influence. However, the molybdenum phenolic oxygen lengths either in **Δ-*N-cis*-1** or **Λ-*N-trans*-1** showed a negligible influence of the geometrical arrangement.

To date, no *N-cis* dioxo bis(bidentate-*N,O*) molybdenum complexes have been described in the solid state in the literature. As this arrangement is only observed for complexes containing polydentate ligands, and is constrained by coordination requirements,[15] we carried out theoretical studies. DFT calculations for complex **1** showed that **Δ-*N-cis*-1** was the most stable conformer and that **Λ-*N-trans*-1** and **Λ-*N-**

***cis,trans*-1** were higher in energy by 2.6 and 10.9 kcal·mol^{-1}, respectively. Removal of the substituent at the stereocentre showed the same energy trend, but values were similar for Λ-*N-trans* and Λ-*N-cis,trans* (1.85 and 2.32 kcal·mol^{-1}, respectively). Therefore, the relative stability of Δ-*N-cis* and Λ-*N-trans* was independent of the substituent, while Λ-*N-cis,trans* was not.

NMR Spectroscopic Studies

NMR spectroscopy allowed us to detect the presence of several species for these molybdenum complexes in solution. To assign accurately the signals, the monocrystals obtained for complex **1**, ***N-cis*-1** and ***N-trans*-1**, were independently dissolved in deuterated chloroform at 233 K. Under these conditions, the spectra showed mainly the presence of the isomer found in the crystal. Remarkable differences in the chemical shifts for H_b were observed. Compared to the free oxazoline [$\delta(H_b) = 4.10$], for ***N-cis*-1**, the signal shifted downfield ($\delta = 4.68$), but upfield for ***N-trans*-1** ($\delta = 3.72$; Table 2). This behaviour can be attributed to interactions with the oxo groups, as shown by the average interatomic distances H···O=Mo from the crystallographic data (for ***N-cis*-1**, ca. 3.2 Å and for ***N-trans*-1**, ca. 4.6 Å).

For complex **2**, we distinguished four compounds in deuterated chloroform solution, with a ratio of 42:11:5:1. For complex **1**, the signals of the different species were less split, but in addition to the signals corresponding to the two major isomers (in a relative ratio of 17:8), other less-intense signals were also observed. No isomeric composition change was observed in either compound in the temperature range studied (from 233 K to 323 K).

The ^{1}H NMR spectra (monodimensional and 2D NOESY experiments) revealed that the two anionic *N,O* ligands (**A** and **B** fragments) are equivalent for the two major isomers, *N-cis* and *N-trans* (Table 2), for both complexes **1** and **2**. This observation suggests that, in solution, the pseudo-octahedral environment around the metal atom is more symmetric than in the solid state, where the two oxazoline ligands are inequivalent. However, the anionic ligands in the *N-cis,trans* isomer are not equivalent, as observed in the 800 MHz ^{1}H NMR spectrum for complex **2**

Table 2. Selected ^{1}H NMR spectroscopic data[a] (δ) for **1** ($CDCl_3$, 500 MHz, 298 K), **2** ($CDCl_3$, 800 MHz, 298 K) and **I** (CD_3COCD_3, 250 MHz, 200 K)

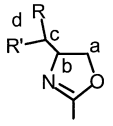

1, R = H, R' = CH_3
2, R = R' = CH_3

Complex	H_a[b]	H_b	H_c	H_d	$H_{aromatic}$
***N-cis*-1**	4.74 (dd, 2 H, 10.0, 8.0) 4.39 (dd, 2 H, 8.0, 6.0)	4.68 (m, 2 H)	2.24 (m, 2 H) 1.97 (m, 2 H)	0.93 (t, 6 H, 7.5)	7.62 (dd, 2 H, 7.75, 1.5) 7.03 (td, 2 H, 7.75, 1.5) 6.61 (td, 2 H, 7.5, 0.75) 6.04 (d, 2 H, 8.0)
***N-trans*-1**	4.23 (pd, 4 H, 7.0)	3.72 (m, 2 H)	2.17 (m, 2 H) 1.83 (m, 2 H)	0.80 (t, 6 H, 7.5)	7.71 (dd, 2 H, 8.0, 2.0) 7.44 (td, 2 H, 7.75, 1.5) 7.00 (dd, 2 H, 8.2, 1.5) 6.91 (td, 2 H, 7.5, 1.0)
***N-cis*-2**	4.66 (pt, 2 H, 8.4) 4.54 (pdd, 2 H, 8.4, 6.0)	4.73 (m, 2 H)	2.94 (m, 2 H)	1.04 (d, 6 H, 7.2) 0.83 (d, 6 H, 7.2)	7.67 (dd, 2 H, 8.0, 1.6) 7.07 (td, 2 H, 8.0, 1.6) 6.66 (pt, 2 H, 7.2) 6.09 (d, 2 H, 8.8)
***N-trans*-2**	4.38 (dd, 2 H, 8.8, 4.8) 4.12 (t, 2 H, 9.6)	3.80 (m, 2 H)	2.82 (m)[c]	0.91 (d, 6 H, 6.4) 0.75 (d, 6 H, 7.2)	7.76 (pdd, 2 H, 7.6, 2.0) 7.50 (td, 2 H, 8.0, 1.6) 7.04 (m, 2 H) 6.95 (m, 2 H)
***N-cis,trans*-2**	4.86 (pdd, 1 H, 10.4, 8.8) 4.78 (pdd, 1 H, 10.0, 8.4) 4.67 (pdd, 1 H, 8.4, 6.0)[d]	5.75 (m, 1 H) 5.13 (m, 1 H)	3.25 (m, 1 H)[c]	1.18 (d, 3 H, 6.4) 1.09 (d, 3 H, 7.2) 1.07 (d, 3 H, 7.2) 0.94 (d, 3 H, 7.2)	7.73 (dd, 1 H, 8.0, 1.6) 7.58 (pdd, 1 H, 7.6, 2.0) 7.46 (m, 1 H) 7.43 (m, 1 H) 6.62 (m, 1 H) 6.61 (m, 1 H) 6.11 (d, 1 H, 8.8) 5.83 (d, 1 H, 8.8)
I	4.55 (m, 2 H) 4.28 (bt, 2 H, 9.3)	3.81 (m, 2 H)	2.67 (m, 2 H)	0.79 (d, 3 H, 6.7) 0.68 (d, 3 H, 6.7)	7.77 (bd, 2 H,7.9) 7.59 (bt, 2 H,7.9) 7.03 (m, 4 H)

[a] Multiplicity (d, doublet; dd, doublet of doublets; m, multiplet; p, pseudo; t, triplet; td, triplet of doublets), relative integration, and coupling constants (in Hz) in parentheses. – [b] For atom labelling, see figure above table. – [c] Two overlapped multiplets for the ***N-trans*-2** and ***N-cis,trans*-2** isomers. – [d] One proton under $\delta = 4.66$ signal of ***N-cis*-2** isomer.

(Table 2). For this compound, the 2D NOESY spectra did not show exchange signals (at various mixing times: 250, 500 and 600 ms at 800 MHz) among the three isomers (***N-cis*-2**, ***N-trans*-2** and ***N-cis,trans*-2**). In addition, a fourth species (**I**) was observed, which showed broader signals and exchange signals with ***N-cis*-2** and ***N-trans*-2**.

Nevertheless, in deuterated acetone at 200 K, a mixture of two compounds (6:1) was observed, where **I** can be assigned to the more abundant species and the minor species seems to be ***N-cis*-2**. At higher temperatures, other signals associated with ***N-cis,trans*-2** appear and those belonging to **I** became less intense. A similar behaviour was observed for a solution of complex **2** in $CDCl_3/CD_3CN$ (1:1). These data indicate that acetone or acetonitrile compete with the oxazoline nitrogen for coordination to the metal. Therefore, the observed exchange process described above could be associated to the rupture of one Mo−N bond of one of the two major isomers (*N-cis* or *N-trans*) and subsequent nitrogen coordination to the metal, giving the other isomer (*N-trans* or *N-cis*).

Oxo-Transfer Reactions

The stoichiometric oxidation of PPh_3 by **1** or **2** was carried out in $CDCl_3$ at room temperature, and the solution was analysed by ^{31}P NMR spectroscopy. Total conversion of PPh_3 to $OPPh_3$ occurred in less than an hour and in 80 minutes with complex **2** and **1**, respectively, as shown in Figure 3.

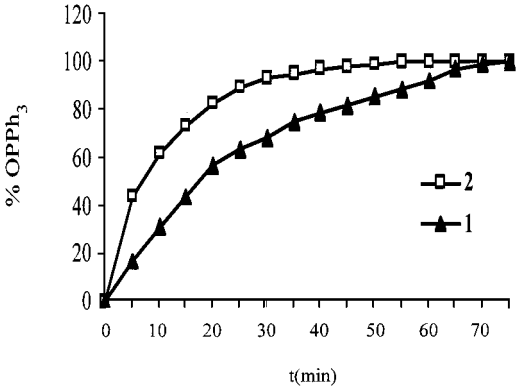

Figure 3. Plot of percent of triphenylphosphane formed against time for **1** or **2**

When complexes **1** and **2** reacted with an excess of PR_3 and DMSO, a fast reaction was observed, transforming the substrate into the corresponding oxide in a catalytic manner [Equation (1)].

$$PPh_3 + (CH_3)_2SO \xrightarrow{[Mo]} OPPh_3 + (CH_3)_2S \quad (1)$$

[Mo] = **1**, **2**

After three days, no phosphane was detected in either case. The colour of the reaction mixtures changed from yellow to yellow-green for complex **2**, and from yellow to yellow-orange for **1**. These reactions contrast with other disubstituted dioxomolybdenum compounds such as $[MoO_2(S_2CNR_2)_2]$,[16] which immediately turns purple (Mo^V), thus our results indicate that the oxo transfer process with complex **1** or **2** does not involve a Mo^V-oxo intermediate.

Styrene Epoxidation

Complexes **1** and **2** were also tested as catalytic precursors in styrene epoxidation, using several oxidants: DMSO, hydrogen peroxide and *t*BuOOH. Conversion of the substrate was only observed with the organic peroxide. No epoxide was obtained in the absence of the molybdenum complex.

The activity obtained with complexes **1** and **2** (25−29% conversion of the olefin) was relatively low when compared, under identical experimental conditions, with other dioxomolybdenum systems such as $[MoO_2(S_2CNEt_2)_2]$ and $[MoO_2(NCS)_2(bipy)]$, but was similar to $[MoO_2(acac)_2]$ (Table 3). However, **1** and **2** showed a better selectivity towards styrene oxide and its diol than the other complexes tested, while benzaldehyde, the cleavage product, was produced in a small amount (10.4−11.5%). The asymmetric induction for **1** and **2** was practically negligible (ca. 2% *ee*).

Table 3. Mo-catalyzed styrene epoxidation[a] with *t*BuOOH as oxidant

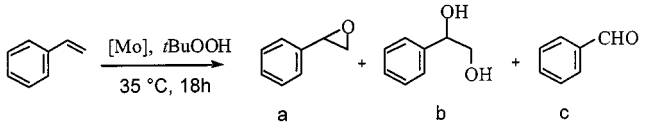

[Mo]	Conv. (%)[b]	**a** (%)[c]	**b** (%)[c]	**c** (%)[c]
1	29.0	12.8	5.8	10.4
2	25.0	8.8	4.7	11.5
$[MoO_2(acac)_2]$	26.0	2.8	6.4	17.0
$[MoO_2(S_2CNEt)_2]$	42.0	6.1	10.6	25.4
$[MoO_2(NCS)_2(bipy)]$	66.5	13.0	4.6	48.8

[a] Reaction conditions: 0.05 mmol of catalyst, 2 mmol of olefin, 3 mmol of *t*BuOOH and 2 cm^3 of toluene at 35 °C for 18 h. − [b] Yield based on amount of oxygenated products as determined by GC chromatography. − [c] Yield based on reacted styrene determined by GC chromatography.

Conclusions

We conclude that the oxazoline ligands [(*R*)-**AH** and (*S*)-**BH**] allow the stabilisation of molybdenum(VI) complexes of general formula *cis*-$[MoO_2(N,O)_2]$ (**1** and **2**), which are obtained as mixtures of three diastereomers due to the ligand and metal chirality. The structural elucidation of these mixtures was performed by means of NMR spectroscopy and X ray diffraction. Theoretical studies (DFT) have allowed us to corroborate that the Δ-*N-cis* coordination is the most stable arrangement. Moreover, a fourth species, **I**, is present in solution. In chloroform, the major compound is Δ-*N-cis*, an arrangement which until now has only been observed for polydentate ligands. In contrast, in coordinating solvents (acetone and acetonitrile), **I** becomes the major

species. Although the catalytic activity of complexes **1** and **2** in styrene oxidation is relatively low, the selectivity towards styrene oxide and its diol is important under the mild experimental conditions tested.

Experimental Section

General: All compounds were prepared under a purified nitrogen atmosphere using standard Schlenk and vacuum line techniques. The solvents were purified by standard procedures and distilled under nitrogen.[17] *cis*-$[MoO_2(acac)_2]$[18] and the ligands (*R*)-**AH** and (*S*)-**BH**[19] were prepared as described previously. NMR spectra were recorded on Bruker Avance 600, Bruker Avance 800, Varian XL-500, Varian Gemini or Bruker DRX 250 spectrometers. Chemical shifts are reported downfield from standards (TMS for ^1H NMR spectra and H_3PO_4 for ^3P NMR spectra). IR spectra were recorded on a Nicolet 520 FT-IR and Bruker IFS 55 FTIR spectrometer. FAB mass spectra were obtained on a Fisons V6-Quattro instrument. The GC-MS analyses were performed on a Hewlett-Packard 5890 Series II gas chromatograph (50 m Ultra 2 capillary column) interfaced to a Hewlett-Packard 5971 mass selective detector. Enantiomeric excesses were determined by GC on a FS-cyclodex-β-I/P column. Elemental analyses were carried out by the Serveis Cientifico-Tècnics de la Universitat de Barcelona in an Eager 1108 microanalyzer.

Dioxo-bis[(4′*R*)-2-(4′-ethyl-3′,4′-dihydroxazol-2′-yl)phenolato-*N,O*]molybdenum(VI) (1): A solution of (+)-(4′*R*)-2-(4′-ethyl-3′,4′-dihydrooxazol-2′-yl)phenol (0.258 g, 1.350 mmol) in CH_3OH (5 cm^3) at room temperature was added to a solution of $[MoO_2(acac)_2]$ (0.200 g, 0.617 mmol) in CH_3OH (20 cm^3). The reaction mixture was stirred for 4 h and the light orange precipitate was filtered and recrystallised from CH_2Cl_2/diethyl ether (2:1). Yield: 0.251 g (80%). − $C_{22}H_{24}MoN_2O_6$ (508.38): calcd. C 51.98, H 4.76, N 5.51; found C 50.90, H 4.86, N 5.40. − MS (FAB positive): *m*/*z* = 508 [M^+]. − IR(KBr): $\tilde{\nu}$ = 1648 (st, C=N), 910, 882 (Mo=O) cm^{-1}.

Dioxo-bis[(4′*S*)-2-(4′-isopropyl-3′,4′-dihydroxazol-2′-yl)phenolato-*N,O*]molybdenum(VI) (2): A solution of (−)-(4′*S*)-2-(4′-isopropyl-3′,4′-dihydrooxazol-2′-yl)phenol (0.277 g, 1.350 mmol) in CH_3OH (5 cm^3) at room temperature was added to a solution of $[MoO_2(acac)_2]$ (0.200 g, 0.617 mmol) in CH_3OH (20 cm^3). The reaction mixture was stirred for 4 h and the yellow precipitate was filtered and recrystallised from CH_2Cl_2/diethyl ether (2:1). Yield: 0.288 g (87%). − $C_{24}H_{28}MoN_2O_6$ (536.43): calcd. C 53.74, H 5.26, N 5.22; found C 53.50, H 5.29, N 5.25. − MS (FAB positive): *m*/*z* = 537 [M^+]. − IR (KBr): $\tilde{\nu}$ = 1650 (st, C=N), 919, 885 (Mo=O) cm^{-1}.

Oxidation of PPh_3 by Complex 1 or 2: A solution of PPh_3 (30 mg, 0.115 mmol) in $CDCl_3$ (0.6 cm^3) was added to **1** (20 mg, 0.039 mmol) or **2** (20 mg, 0.037 mmol) in an NMR tube and the solution was monitored immediately by $^{31}P\{^1H\}$ NMR spectroscopy at 25 °C. The first kinetic point was taken at *t* = 5 min. The reaction was followed by integrating the signals corresponding to triphenylphosphane and triphenylphosphane oxide.

Oxidation of PPh_3 by DMSO in the Presence of Complex 1 or 2: DMSO (0.5 cm^3) was added to a mixture of **1** (20 mg, 0.039 mmol) or **2** (20 mg, 0.037 mmol) and an excess of PPh_3 (30 mg, 0.115 mmol) in $CDCl_3$ (0.6 cm^3). An aliquot of this solution was transferred to an NMR tube and the solution was monitored immediately by $^{31}P\{^1H\}$ NMR at 25 °C. The first kinetic point was taken at *t* = 5 min. The reaction was followed by integrating the signals corresponding to triphenylphosphane and triphenylphosphane oxide.

Molybdenum-Catalysed Styrene Epoxidation: The precursor (0.05 mmol of complex: 25.7 mg for **1**; 27.1 mg for **2**) was dissolved in

Table 4. Crystal data for complexes **Δ-*N-cis*-1** and **Λ-*N-trans*-1**

	Δ-*N-cis*-1	**Λ-*N-trans*-1**
Empirical formula	$C_{22}H_{24}MoN_2O_6$	$C_{22}H_{24}MoN_2O_6$
Molecular weight	508.37	508.37
Crystal size, mm	0.2 × 0.15 × 0.08	0.3 × 0.25 × 0.2
Temperature, K	293(2)	150(2)
Crystal system	Monoclinic	Orthorhombic
Space group	$P2_1$	$P2_12_12_1$
a, Å	10.007 (2)	9.239 (2)
b, Å	10.857 (2)	9.408 (2)
c, Å	10.075 (2)	24.300 (5)
α, deg	90	90
β, deg	90.70 (3)	90
γ, deg	90	90
V, $Å^3$	1094.5 (4)	2112.2 (8)
Z	2	4
Density (calcd.), g·cm^{-3}	1.543	1.599
Absorption coefficient, mm^{-1}	0.640	0.663
F(000)	520	1040
θ range for data collection	2.04 to 27.53°	1.68 to 27.49°
Reflections collected	28888	23583
Data/restraints/parameters	5027/1/282	4775/0/282
Independent reflections	5027 [*R*(int) = 0.0435]	4779 [*R*(int) = 0.0374]
Final *R* indices [$I > 2\sigma(I)$]	$R1^{[a]}$ = 0.0305	$R1^{[a]}$ = 0.0252
	$wR2^{[b]}$ = 0.0760	$wR2^{[b]}$ = 0.0753
R indices (all data)	*R*1 = 0.0369	*R*1 = 0.0271
	*wR*2 = 0.0808	*wR*2 = 0.0831
GOF on F^2	0.899	0.693
Absolute structure parameter	0.02 (3)	−0.03 (2)
Largest diff. peak and hole, e·$Å^{-3}$	0.340 and −0.581	0.499 and −0.584

[a] $R1 = \Sigma||F_o| - |F_c||/\Sigma|F_o|$. − [b] $wR2 = \{\Sigma[w(F^2_o - F^2_c)]/\Sigma[w(F^2_o)^2]\}^{1/2}$.

2 cm^3 of toluene. Styrene (208 mg, 2 mmol) was added, followed by an aqueous solution of *tert*-butyl hydroperoxide (*t*BuOOH/H_2O: 3:2; 0.19 cm^3, 3 mmol). The mixture was stirred for 18 h at 35 °C, until no conversion of styrene was observed (monitored by gas chromatography). After removing the solvent under reduced pressure, the oil was purified by column chromatography (SiO_2; ethyl acetate). The conversion of styrene was determined by gas chromatography. The enantiomeric excesses were determined by gas chromatography.

Crystallography: The crystallographic data for **Δ-*N-cis*-1** and **Λ-*N-trans*-1** are summarized in Table 4. Single crystals were grown by diffusing diethyl ether into a dichloromethane solution of the isomer mixture, thereby obtaining orange (**Δ-*N-cis*-1**) and yellow (**Λ-*N-trans*-1**) crystals.

The crystal data for both isomers were collected using a Delf Instrument FAST TV area-detector diffractometer positioned at the window of a rotating-anode. Intensities were collected with graphite monochromated Mo-K_α radiation (λ = 0.71069 Å), using the $\omega/2\theta$ scan technique. Structures were solved by direct methods using the SHELXS-97 program and refined by full-matrix least-squares on F_o^2 using SHELXL-97.[20] Data were corrected using the SORTAV program.[21] All hydrogen atoms were included in idealised positions.

Crystallographic data (excluding structure factors) for the structures reported in this paper have been deposited with the Cambridge Crystallographic Data Centre as supplementary publication nos. CCDC-153158 (**Λ-*N-trans*-1**) and -153159 (**Δ-*N-cis*-1**). Copies of the data can be obtained free of charge on application to CCDC, 12 Union Road, Cambridge CB2 1EZ, UK [Fax: (internat.) +44-1223/336-033; E-mail: deposit@ccdc.cam.ac.uk].

Theoretical Calculations: The geometry of the isomers ***N-cis***, ***N-trans*** and ***N-cis,trans*** was optimized[22] in vacuo by means of the GAUSSIAN98 package of programs.[23] Ab initio molecular orbital calculations were carried out at the Hartree−Fock (HF) level with methods based on Density Functional Theory (DFT), and using the standard 3−21G basis set. We used Becke′s three-parameter functional (B3)[24] which includes the Slater exchange along with corrections involving the gradient of electron density, and the correlation functional of Lee, Yang and Parr, which includes both local and nonlocal terms (LYP).[25,26] The parameters are those determined by Becke by fitting to the G1 molecule set.[24b,27]

Acknowledgments

We would like to thank the Spanish Ministerio de Educación y Cultura (PB97-0407-C05-04) and the Decanato de Investigación y Desarrollo (Universidad Simón Bolívar) for financial support. E. Cerrada thanks The Royal Society of Chemistry for a grant.

[1] R. H. Holm, *Coord. Chem. Rev.* **1990**, *100*, 183 and references therein.
[2] R. C. Maurya, D. D. Mishra, S. N. Rao, R. Verma, N. N Rao, *Ind. J. Chem.* **1997**, *36A*, 599.
[3] J. B. Howard, D. C. Rees, *Chem. Rev.* **1996**, *96*, 2965.
[4] J. Topich, J. T Lyon, *Inorg. Chem.* **1984**, *23*, 3202.
[5] H. Teruel, A. Sierraalta, *J. Mol. Cat. A: Chemical* **1996**, *107*, 379.
[6] [6a] R. Hille, *Chem. Rev.* **1996**, *96*, 2757. − [6b] M. K. Johnson, D. C. Rees, M. W. W. Adams, *Chem. Rev.* **1996**, *96*, 2817.
[7] E. I. Stiefel, in *Comprehensive Coordination Chemistry* (Ed.: G. Wilkinson), Pergamon Press, New York, **1987**, p. 1375−1420.
[8] A. Togni, L. M. Venanzi, *Angew. Chem. Int. Ed. Engl* **1994**, *33*, 497.
[9] A. Pfaltz, *Adv. Catal. Processes* **1995**, *1*, 61 and references therein.
[10] [10a]S. N. Rao, K. N. Munshi, N. Nageswara Rao, M. M. Bhadbhade, E. Suresh, *Polyhedron* **1999**, *18*, 2491. − [10b] S. Bellemin-Laponnaz, K. S. Coleman, J. A. Osborn, *Polyhedron* **1999**, *18*, 2533.
[11] M. Gómez, S. Jansat, G. Muller, D. Panyella, M. Font-Bardía, X. Solans, *J. Chem. Soc., Dalton Trans.* **1997**, 3755.
[12] B. E. Schultz, S. F. Gheller, M. C. Muetterties, M. J. Scott, R. H. Holm, *J. Am. Chem. Soc.* **1993**, *115*, 2714 and references therein.
[13] [13a] B. V. Merinov, A. S. Kuzharov, N. G. Furmanova, *Krystallografya* **1986**, *31*, 93. − [13b] T. N. Sorrell, D. J. Ellis, E. H. Cheesman, *Inorg. Chim. Acta* **1986**, *113*, 1. − [13c] C. J. Hinshaw, G. Peng, P. Singh, J. T. Spence, J. H. Enemark, M. Bruck, J. Kristofzski, S. L. Merbe, R. E. Ortega, P. A. Mexler, *Inorg. Chem.* **1989**, *28*, 4483.
[14] K. Wieghardt, M. Hahn, J. Weiss, W. Swiridoff, *Z. Anorg. Allg. Chem.* **1982**, *492*, 164.
[15] F. H. Allen, O. Kennard, *Chem. Des. Autom. News* **1993**, *8*, 31. Cambridge Strucural Data, Version 5.19.
[16] F. W. Moore, M. L. Larson, *Inorg. Chem.* **1967**, *6*, 998.
[17] D. D. Perrin, W. L. F. Armarego, D. R. Perrin, *Purification of Laboratory Chemicals, 3rd ed.*, Pergamon Press, Oxford, U.K., **1988**.
[18] R. N. Grimes, *Inorg. Synth.* **1992**, *29*, 130.
[19] C. Bolm, K. Weickhardt, M. Zehnder, T. Ranff, *Chem. Ber.* **1991**, *124*, 1173.
[20] G. M. Sheldrich, **1997**, University of Göttingen, Germany.
[21] [21a]R. H. Blessing, *Acta Cryst.* **1995**, *A51*, 33. − [21b] R. H. Blessing, *J. Appl. Cryst.* **1997**, *30*, 421.
[22] The requested convergence on the density matrix was 10^{-9} atomic units and the threshold value of maximum displacement was 0.0018 Å and that of maximum force was 0.00045 hartree/bohr using the Berny analytical gradient optimization routine.
[23] M. J. Frisch, G. W. Trucks, H. B. Schlegel, G. E. Scuseria, M. A. Robb, J. R. Cheeseman, V. G. Zakrzewski, J. A. Montgomery Jr., R. E. Stratmann, J. C. Burant, S. Dapprich, J. M. Millam, A. D. Daniels, K. N. Kudin, M. C. Strain, O. Farkas, J. Tomasi, V. Barone, M. Cossi, R. Cammi, B. Mennucci, C. Pomelli, C. Adamo, S. Clifford, J. Ochterski, G. A. Petersson, P. Y. Ayala, Q. Cui, K. Morokuma, D. K. Malick, A. D. Rabuck, K. Raghavachari, J. B. Foresman, J. Cioslowski, J. V. Ortiz, A. G. Baboul, B. B. Stefanov, G. Liu, A. Liashenko, P. Piskorz, I. Komaromi, R. Gomperts, R. L. Martin, D. J. Fox, T. Keith, M. A. Al-Laham, C. Y. Peng, A. Nanayakkara, C. Gonzalez, M. Challacombe, P. M. W. Gill, B. Johnson, W. Chen, M. W. Wong, J. L. Andres, C. Gonzalez, M. Head-Gordon, E. S. Replogle, J. A. Pople, Gaussian, Inc., Pittsburgh P. A., **1998**.
[24] [24a] A. D. Becke, *Phys. Rev. A* **1988**, *38*, 3098. − [24b] A. D. Becke, *J. Chem. Phys.* **1993**, *98*, 5648.
[25] C. Lee, W. Yang, R. G. Parr, *Phys. Rev. B* **1988**, *37*, 785.
[26] B. Miehlich, A. Savin, H. Stoll, H. Preuss, *Chem. Phys. Lett.* **1989**, *157*, 200.
[27] [27a] J. A. Pople, M. Head-Gordon, D. J. Fox, K. Raghavachari, L. A. Curtis, *J. Chem. Phys.* **1989**, *90*, 5622. − [27b] L. A. Curtis, C. Jones, G. W. Trucks, K. Raghavachari, J. A. Pople, *J. Chem. Phys.* **1990**, *93*, 2537.

Received October 11, 2000
[I00384]

First Direct Synthesis of a *trans*-III Complex of Tetramethylcyclam − Physicochemical Characterization, Electrochemistry and X-ray Crystal Structure of 1,4,8,11-Tetramethyl-1,4,8,11-tetraazacyclotetradecane Copper(II) Bistetrafluoroborate

Christophe Bucher,[a] Emmanuelle Duval,[b] Enrique Espinosa,[a] Jean-Michel Barbe,[a] Jean-Noël Verpeaux,[b] Christian Amatore,*[b] and Roger Guilard*[a]

Keywords: Macrocycles / N ligands / Copper / Structure elucidation / Electrochemistry

We report the first direct synthesis of a *trans*-III copper(II) complex of tetramethylcyclam. This new derivative is hexacoordinate in the solid state and square planar in solution. Reduction of this latter leads to a complex voltammetry pattern which could be explained considering an isomerization process.

Introduction

N-substituted polyazamacrocycles have several potential applications: *N*-substituted cyclams, which represent the most widely studied series of tertiary amine macrocycles can be used for medical purposes,[1,2] treatment of water wastes containing heavy metals,[3] or catalysis.[4] Therefore the understanding of the influence of *N*-substitution of the ligand on the coordination mode still remains an important field of interest.

The *N,N′,N″,N‴*-tetramethylcyclam derivative (tmc) was first obtained by Barefield and co-workers in the early 70′s.[5,6] A recently described alternative to this seminal synthesis involves the reduction of a bisammonium salt of the bisaminal 1,4,8,11-tetraazatricyclo[9,3,1,1^{4,8}]hexadecane and allows the preparation of tmc without further purification with an overall yield of ca. 80% starting from cyclam.[7]

Metallation of tmc by transition metal ions systematically led to five-coordinate type-I isomers[8] with all substituents (methyl groups and metal axial ligand) pointing in the same direction. This geometry, first suggested by UV/Vis spectroscopy, has since been confirmed by X-ray diffraction studies of numerous tmc complexes of Ni^{II},[9,10] Cu^{II},[11] Fe^{II},[12] Zn^{II},[13] and Co^{II}.[14] Although different conformations were reported for the macrocycle, the isomers were all characterized by the pentacoordination of a metal ion located above the macrocyclic cavity, and bearing one axial ligand, either an anion or a neutral coordinating solvent molecule. Type-III isomers could, until now, only be obtained by tetramethylation of the easily available cyclam type-III homologues;[15,16] clean isomerisation of type-I to type-III isomers could not be achieved, although an interconversion process restricted to nickel species in strongly coordinating solvent has been reported.[9,10,17,18]

[a] Laboratoire d'Ingénierie Moléculaire pour la Séparation et les Applications des Gaz (L.I.M.S.A.G.), U.M.R. 5633, Faculté des Sciences "Gabriel",
6, Boulevard Gabriel, 21000 Dijon, France
Fax: (internat.) + 33-3/80396117
E-mail: rguilard@u-bourgogne.fr
[b] Ecole Normale Supérieure, Département de Chimie (UMR 8640),
24, Rue Lhomond, 75231 Paris, Cedex 05, France

Results and Discussion

We report here the first direct synthesis of a type-III [tmcCu]$^{2+}$ starting from the free ligand and the metallic salt: indeed, when tmc was dissolved in a refluxing solution of sodium hydroxide in water followed by addition of copper bis(tetrafluoroborate), only the type-III [(tmc)Cu](BF$_4$)$_2$ isomer was isolated (See Experimental Section). UV/Vis spectroscopic data correspond to a type-III square-planar (N$_4$) structure in solution, whereas a *trans*-III configuration with two BF_4^- counterions coordinated to the copper ion could be established in the solid state by X-ray crystallography (see below). Since complexation in water at room temperature affords the pentacoordinated I isomer, it appears that the temperature and basicity of the reaction medium are the key parameters responsible for the stereochemistry of the complexation; a very similar observation has been reported in the case of *N,N′*-difunctionalised derivatives.[19]

The visible spectrum of (tmc)Cu^{2+} is rather insensitive to the nature of the solvent; shifting from coordinating (water) to noncoordinating (nitromethane) solvents led to a shift of λ_{max} from 558 to 530 nm and ε from 193 to 142. This fact suggests that the solvent does not take place in the first coordination sphere and leads us to propose a square-planar (N$_4$) coordination scheme for [(tmc)Cu](BF$_4$)$_2$ in solution. These data are close to those observed for related copper complexes known for their square-planar geometry. For example, Elias et al. and Delgado et al. reported absorption maxima (epsilon values) of 520−600 nm (131−139), and 580 nm (192), respectively.[20−22] Moreover, these values differ significantly from those obtained for pen-

 © WILEY-VCH Verlag GmbH, 69451 Weinheim, 2001 1434−1948/01/0404−1077 $ 17.50+.50/0

tacoordinate tmc copper complexes ($\lambda_{max} \approx 690$ nm, $\varepsilon \approx 260$)[23] and hexacoordinate cyclam copper complexes ($\lambda_{max} = 586-620$ nm, $\varepsilon \approx 50$).[19]

Conversely, in the solid state, the complex exhibits a hexacoordinate *trans*-III geometry. The asymmetric unit (see ORTEP[24] view in Figure 1) is composed of one half of the complex (with the Cu^{2+} cation lying on an inversion centre) and a BF_4^- anion. The complex presents a distorted octahedral geometry with the copper atom located in the N_4 plane and a fluorine atom coordinating the latter in an axial position on both sides of the macrocycle.

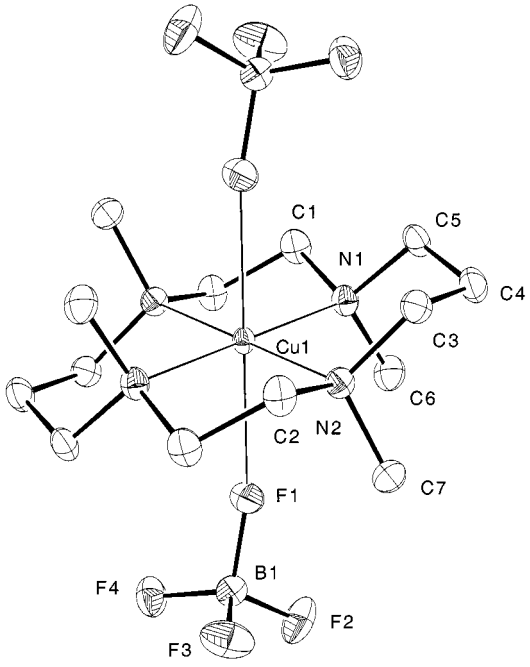

Figure 1. ORTEP drawing of *trans*-III $[(tmc)Cu](BF_4)_2$; the thermal ellipsoids are at the 50% probability level

The anion coordination is evidenced by the distance F1−Cu (2.529 Å), the almost four right angles F1−Cu−N ($89.30 < \alpha < 90.70°$) and the longer distance B−F1 (1.421 Å) when compared to the other three B−F bond lengths (1.376−1.386 Å). The equatorial Cu−N distances are almost equivalent [2.074(1) and 2.077(1) Å] and the N−Cu−N angles are close to right angle values [86.89(5) and 93.11(5)°]. The N−C and C−C distances range from 1.489 to 1.497 Å and from 1.513 to 1.526 Å, respectively, indicating a very small dispersion around their respective mean values 1.493(5) and 1.519(5) Å. All bond lengths and angles are comparable to typical values found in the literature for this kind of complex.[25] The six- and five-membered rings building the complex have chair and envelope conformations, respectively.

Electrochemical reduction of this type-III $[(tmc)Cu](BF_4)_2$ dissolved in acetonitrile leads to a complex voltammetry pattern. The reduction happens at a rather high potential (−0.41 V vs. SCE, 2 V/s), in agreement with the general trend of tmc ligands stabilising lower oxidation states than unsubstituted cyclam; however, the reduction wave remains chemically irreversible even at potential scan rates as high as 2000 V s^{-1} and a new redox couple appears at $E^0 = -0.28$ V as shown in Figure 2. This clearly establishes that the initially formed type III $[(tmc)Cu]^+$ has a lifetime shorter than 50 μs and very rapidly evolves to another copper(I) species that is fairly stable on the cyclic voltammetry time scale, as evidenced by its chemically reversible oxidation wave (Figure 2A). At longer time scales, corresponding to slow cyclic voltammetry, this new Cu^I species also undergoes a rearrangement to yield a third form of $[(tmc)Cu]^+$, the reversible oxidation of which now takes place around $E^0 = +0.07$ V (Figure 2B).

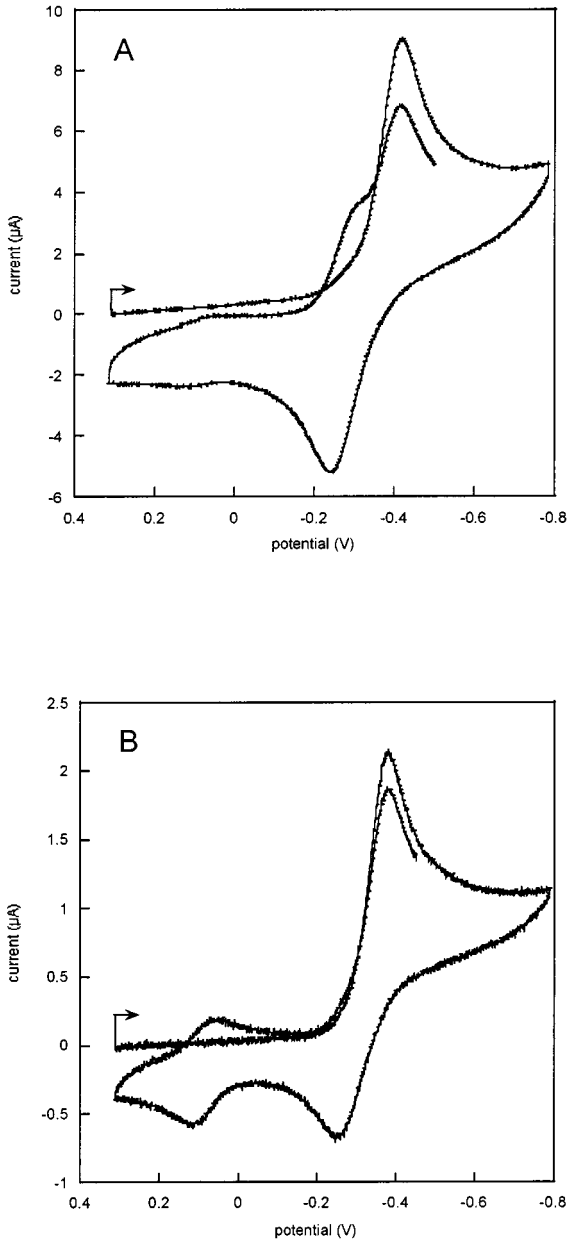

Figure 2. Cyclic voltammograms of a 2 mm solution of type-III $[(tmc)Cu](BF_4)_2$ in acetonitrile 0.1 M $nBu_4N(BF_4)$ recorded at a platinum disc electrode (0.5 mm diameter) at room temperature; potential scan rate 10 V/s (A) and 0.5 V/s (B)

This general pattern is reminiscent of what has been observed and described for a related *trans*-III derivative of copper(II) coordinated to a hexadentate tetra-*N*-substituted

cyclam derivative.[19] In the latter case, the observation of two subsequent isomerisations of the initial copper(I) complex has been attributed to partial decoordination associated with a modification from a type-III to a type-I configuration. Further investigations concerning the assignment of the structure of the electrogenerated (tmc)Cu^+ derivatives are required to confirm the analogy and establish the occurrence of a related type-III to type-I transformation process taking place at the level of the tmc copper(I) derivative.

Work is in progress to clearly establish the influence of the experimental conditions (pH, temperature, ...) on the stereochemistry of tetra-*N*-substituted cyclam complexes.

Experimental Section

General: UV/Vis spectroscopic data were collected on a Varian Cary 5 spectrophotometer. Mass spectra were recorded on a Bruker ProFlex III MALDI/TOF mass spectrometer using dithranol as matrix. X-ray diffraction data were collected on an Enraf−Nonius Kappa-CCD diffractometer equipped with an Oxford Cryostream low temperature device.

All the electrochemical experiments were run under argon. $n$$Bu_4NBF_4$ was used as the supporting electrolyte; it was obtained from $n$$Bu_4N(HSO_4)$ and $NaBF_4$, recrystallized from ethyl acetate/hexane and dried at 60 °C under vacuum.

Cyclic voltammetry experiments were performed in an air-tight, three-electrode cell connected to a vacuum line. The reference electrode was SCE (Tacussel) separated from the solution by a bridge compartment filled with the same solvent supporting electrolyte solution as that used in the cell. The counter electrode was a platinum spiral wire with ca. 1 cm^2 apparent surface area. The working electrodes were disks obtained from cross sections of gold wires (diameters 25 to 500 μm). An EG & G PAR-175 signal generator was used; the potentiostat was home-made, with a positive feedback loop for ohmic drop compensation. The currents and potentials were recorded on a Nicolet 310 oscilloscope.

[(tmc)Cu](BF$_4$)$_2$: Tetramethylcyclam (0.64 g, 2.5 mmol) and NaOH (0.3 g, 7.5 mmol) in 20 mL of water were heated under stirring at 90 °C. $Cu(BF_4)_2{\cdot}H_2O$ (0.64 g, 2.5 mmol) was then added. The mixture was stirred at 90 °C for one hour. After filtration and slow evaporation of the solvent, purple crystals of *trans*-III [(tmc)Cu]$(BF_4)_2$ suitable for an X-ray study were collected (0.62 g, 50%). − MS (MALDI/TOF): m/z = 319 [(tmc)Cu]$^+$. − $C_{14}H_{32}B_2CuF_8N_4$ (493.58): calcd. C 34.07, H 6.53, N 11.35; found C 34.48, H 6.22, N 11.33.

X-ray Crystallographic Study: Crystal data for $[C_{14}H_{32}N_4Cu][2(BF_4)]$, dark blue prismatic crystal of dimension 0.42 × 0.20 × 0.14 mm, M = 493.60, monoclinic, space group $P2_1/n$, Z = 2, a = 8.9279(3) Å, b = 9.2302(2) Å, c = 12.6028(4) Å, β = 91.55(1)°, U = 1038.17(5) Å^3, D_c = 1.579 g cm^{-3}, T = 130(2) K, F(000) = 510, Mo-K_α radiation (λ = 0.71073 Å), μ = 1.130 mm^{-1}, 16925 reflections measured in the range 2.74° ≤ θ ≤ 30.02°, with 3016 being unique (R_{int} = 0.0752) which were used in all calculations. The structure was solved by direct methods and refined using full-matrix least-squares on F^2 to $R1$ = 0.0330, S = 1.009, for 2548 reflections with $I > 2\sigma(I)$ and 133 refined parameters, $wR2$ (all data) = 0.0805. Programs used: SHELXS-97 for structure determination and SHELXL-97 for refinement (G. M. Sheldrick, University of Göttingen).

Crystallographic data (excluding structure factors) for the structure reported in this paper have been deposited with the Cambridge Crystallographic Data Centre as supplementary publication no. CCDC-150973. Copies of the data can be obtained free of charge on application to CCDC, 12 Union Road, Cambridge CB2 1EZ [Fax: (internat.) +44-1223/336-033; E-mail: deposit@ccdc.cam.ac.uk].

Acknowledgments

This work was supported by grants from the French Ministry of Research (MENRT) and CNRS (UMR 5633, UMR 8640). The authors are also grateful to M. Soustelle for assistance in the synthesis of the tmc precursor.

[1] M. F. Tweedle, *Lanthanide Probes in Life, Chemical and Earth Sciences*, Amsterdam, **1989**, pp. 127−179.
[2] D. Parker, *Chem. Soc. Rev.* **1990**, *19*, 271−291.
[3] R. Guilard, H. Chollet, P. Guiberteau, P. Cocolios, *PCT Int. Appl.* 1996.
[4] E. Kimura, *Tetrahedron* **1992**, *48*, 6175−6217.
[5] E. K. Barefield, F. Wagner, *Inorg. Chem.* **1973**, *12*, 2435−2439.
[6] E. K. Barefield, M. T. Mocella, *J. Am. Chem. Soc.* **1975**, *97*, 4238−4246.
[7] G. Royal, V. Dahaoui-Gindrey, S. Dahaoui, A. Tabard, R. Guilard, P. Pullumbi, C. Lecomte, *Eur. J. Org. Chem.* **1998**, 1971−1975.
[8] B. Bosnich, C. K. Poon, M. L. Tobe, *Inorg. Chem.* **1965**, *4*, 1102−1108.
[9] T. W. Hambley, *J. Chem. Soc., Dalton Trans.* **1986**, 565−569.
[10] S. F. Lincoln, T. W. Hambley, D. L. Pisaniello, J. H. Coates, *Aust. J. Chem.* **1984**, *37*, 713−723.
[11] T. J. Lee, T. Y. Lee, C. Y. Hong, D. T. Wu, C. S. Chung, *Acta Crystallogr. C* **1986**, 999−1001.
[12] K. D. Hodges, R. G. Wollmann, S. L. Kessel, D. N. Hendrickson, D. G. Van Derveer, E. K. Barefield, *J. Am. Chem. Soc.* **1979**, *101*, 906−917.
[13] K. Panneerselvam, T. H. Lu, T. Y. Chi, S. F. Tung, C. S. Chung, *Anal. Sci.* **1999**, *15*, 205−206.
[14] S. Reimer, M. Wicholas, B. Scott, R. D. Willet, *Acta Crystallogr. C* **1989**, 1694−1697.
[15] F. Wagner, M. T. Mocella, M. J. D′Aniello, A. H. J. Wang, E. K. Barefield, *J. Am. Chem. Soc.* **1974**, *96*, 2625−2627.
[16] E. K. Barefield, G. M. Freeman, D. G. Van Derveer, *Inorg. Chem.* **1986**, *25*, 552−558.
[17] P. Moore, J. Sachinidis, G. R. Willey, *J. Chem. Soc., Chem. Commun.* **1983**, 522−523.
[18] S. F. Lincoln, J. H. Coates, D. A. Hadi, *Inorg. Chim. Acta* **1984**, *81*, L9−L10.
[19] C. Bucher, E. Duval, J. M. Barbe, J. N. Verpeaux, C. Amatore, R. Guilard, *C R Acad Sci Ser Ii C* **2000**, *3*, 211−222.
[20] J. R. Roeper, H. Elias, *Inorg. Chem.* **1992**, *31*, 1210−1214.
[21] J. Costa, R. Delgado, *Inorg. Chem.* **1993**, *32*, 5257−5265.
[22] V. Felix, M. J. Calhorda, J. Costa, R. Delgado, C. Brito, M. T. Duarte, T. Arcos, M. G. B. Drew, *J. Chem. Soc., Dalton Trans.* **1996**, 4543−4553.
[23] M. R. Oberholzer, M. Neuburger, M. Zehnder, T. A. Kaden, *Helv. Chim. Acta* **1995**, *78*, 505−513.
[24] L. J. Farrugia, *J. Appl. Crystallogr.* **1997**, *30*, 565.
[25] M. Meyer, V. Dahaoui-Gindrey, C. Lecomte, R. Guilard, *Coord. Chem. Rev.* **1998**, *180*, 1313−1405.

Received October 30, 2000
[I00413]

New Alkyl−Cobalt(III) Complexes with Tridentate Amino−Oxime Ligands: Synthesis, Structure, and Reactivity

Renata Dreos, Alessandro Felluga, Giorgio Nardin, Lucio Randaccio,* Patrizia Siega, and Giovanni Tauzher*

Eur. J. Inorg. Chem. **2001**, 267−276

In Figure 1 on page 269 a wrong ORTEP diagram of ***2a*** *is shown; the correct ORTEP representation for* ***2a*** *is given below.*

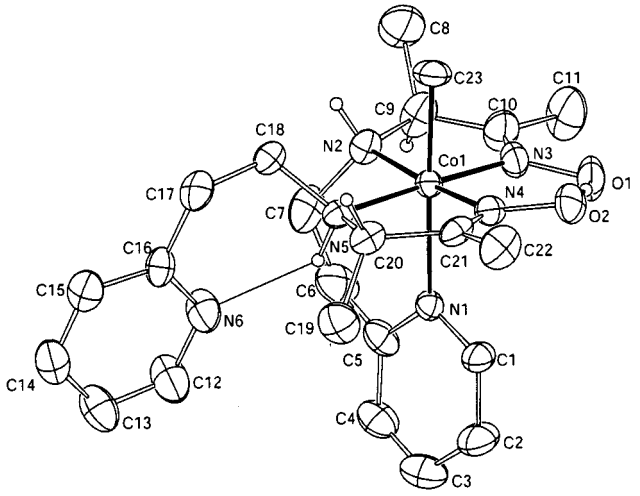

2a

The Editors
[C I00238]

 © WILEY-VCH Verlag GmbH, 69451 Weinheim, 2001 1434−1948/01/0404−1081 $ 17.50+.50/0

Electrochemical Strategies for the Strengthening of Polymer−Metal Interfaces

Noëlle Baute,[a] Christine Jérôme,[a] Lucien Martinot,[b] Marc Mertens,[a] Viktor M. Geskin,[c] Roberto Lazzaroni,[c] Jean-Luc Brédas,[c] and Robert Jérôme*[a]

Keywords: Electrochemistry / Polymers / Surface chemistry

Polymers have been widely used for the protection of metals against corrosion and for improving the performance of structural adhesive joints. In this contribution, the weakness and short-term durability of these polymer–metal interactions and some common approaches for alleviating this problem are briefly reviewed. Among the existing techniques, electrochemical processes offer the advantage of controlled interfacial reactions. Promising results have been reported by Stratmann et al. and Lécayon et al., who have emphasized the interest and opportunity to create strong chemical bonds between the organic coating and the metallic substrate. Their work is discussed in this review, along with results recently obtained in our group.

1. Polymer−Metal Associations

Suitable combinations of metals and organic polymers play an increasingly important role in modern technology. One of the most direct examples is the use of polymers as glue for metal objects. The adhesive bonding for structural joint formation has several distinct advantages over more conventional joining techniques: (i) the lack of local stress concentration, in contrast to riveted joints; (ii) the limitation of electrolytic corrosion when different metals are joined; and (iii) easy design and construction techniques.[1] Furthermore, polymer coatings have the potential to protect metals from chemical corrosion by acting as barriers.[2,3] Generally, only permanent polymer−metal interactions can delay delamination when the environment contains very aggressive species (e.g. ions, oxygen, water), prone to electrochemical and chemical attack.[4−8] As a rule, as long as the coating adheres strongly to its substrate, the metal is efficiently protected from any corrosion processes. Conversely, any defect or discontinuity in the coating (e.g., as a consequence of mechanical stress), makes the metal accessible to the electrolyte, thereby forming an aqueous corrosion cell between this defect and the delamination front. It is generally accepted that corrosion does not play a decisive role in the loss of adhesion in metal−polymer joints, but that this problem is rather a post-failure phenomenon.[9−11]

[a] Center for education and research on Macromolecules (CERM), University of Liège,
Sart-Tilman B6, 4000 Liège, Belgium
[b] Radiochemistry, University of Liège,
Sart-Tilman B16, 4000 Liège, Belgium
[c] Service de Chimie des Matériaux Nouveaux, Centre de Recherche en Electronique et Photonique Moléculaires, Université de Mons-Hainaut,
Place du Parc 20, 7000 Mons, Belgium

Noëlle Baute was born in Verviers (Belgium) in 1972, and studied chemistry at the University of Liège where she obtained her degree in 1994. In 1995, she joined the group of Professor R. Jérôme at the "Center for Education and Research on Macromolecules", where she studied the electrochemical grafting of polymers onto metals and contributed to the extension of this process to various acrylic and methacrylic monomers. She received a PhD for this research work in 1999. She is currently working at AEROFLEET (Liège, Belgium), in the section for high technology composite materials.

Christine Jérôme was born in Belgium in 1971, and studied chemistry at the University of Liège. In 1995 she joined the group of Professor R. Jérôme at the "Center for Education and Research on Macromolecules" where she studied conducting polymers as ion-exchange resins for radioactive waste treatment. She received a PhD for this research work in 1999. She currently holds a Postdoctoral Researcher Position from the "National Foundation for Scientific Research" (FNRS) and is working in the field of electropolymerization.

MICROREVIEWS: This feature introduces the readers to the authors' research through a concise overview of the selected topic. Reference to important work from others in the field is included.

 © WILEY-VCH Verlag GmbH, 69451 Weinheim, 2001 1434−1948/01/0505−1097 $ 17.50+.50/0

Figure 1 schematically shows the primary corrosion reactions that occur in the case of delamination of an epoxy coating from a steel substrate. The anodic reaction is the dissolution of iron, which is expected to occur in any location where an aqueous medium is available to accept ferrous ions, for example, within a defect of the polymer coating. The primary cathodic reaction is the formation of hydroxide ions by the reduction of oxygen at the metal−polymer interface. Five components are required for this reaction to occur: water, oxygen, electrons flowing from the local anode to the local cathode, positive counterions (e.g., Na^+) for the generated OH^- anions, and metal oxide, which is an active catalyst in the reduction reaction. All these components are commonly present beneath the coating at the boundary of the defect. In the case of weak metal−coating interactions (hydrogen bonding between an hydrated metal oxide and the epoxy resin in Figure 1), the cathodic reaction is responsible for the detachment of the polymer from the metal. As delamination proceeds, the cathodic site moves, remaining just in front of the debonding region.

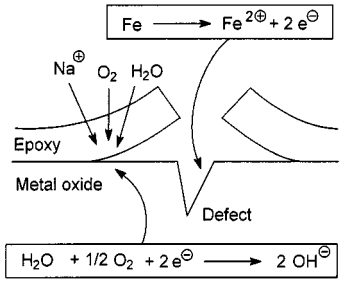

Figure 1. Schematic diagram of the delamination mechanism initiated by corrosion in a steel/epoxy coating system[11]

Numerous methods have been proposed to limit the extent of this loss of adhesion initiated by corrosion,[11] the general principle being to prevent at least one of the required components from being present at the metal−polymer interface. Although the fundamentals that govern the corrosion processes under protective coatings are generally well understood, little progress has been made to successfully prevent their occurrence. Nevertheless, these methods rely upon simple chemical and physical concepts that are easily implemented by adding at most one step in the coating process. As representative examples of these techniques, let us mention (i) the use of fluorinated polymers that limit the extent of water permeation usually occurring through most organic coatings;[3−11] (ii) the addition of fillers in order to reduce both the oxygen permeation rate[12] and internal stresses through the polymer layer; or (iii) metal pre-treatments by corrosion inhibitors, which is the most commonly used method. A thorough review of inhibitors, together with their corrosion-retarding mechanism, has been published by Trabanelli and Carasitti.[13]

Although corrosion of the metal substrate plays an important role in the delamination process, it must be stressed that joint delamination is essentially initiated by weak polymer−metal interactions.[11,14] To solve this problem in many technological applications, stable and porous oxide layers are prepared on top of the metal by adequate pre-treatment (chromic acid etching, phosphoric acid anodizing, etc.)[11,15] before coating with the polymer. This technique can impart a reasonable durability upon exposure to environmental attacks. The origin of the good adhesion between this inorganic conversion coating and the polymer is not well understood. It is probably due to mechanical interlocking between the polymer and the porous surface oxide of the substrate. However, the formation of strong chemical bonds between the substrate and the polymer, instead of weak secondary interaction forces, is expected to be more efficient in inhibiting any electrochemical reaction at the interface. Although physical treatments, such as plasma polymerization,[16,17] are of great interest, this review will mainly focus on electrochemical techniques. Their advantage over surface plasma modification is essentially that controllable reactions are involved. Furthermore, electrochemistry is a valuable technique for the polymerization of various monomers at metal surfaces, which allows for the broadening of the search for improved polymer−metal interactions. In this respect, two main electrochemical strategies have been proposed to create strong chemical bonds between organic polymers and metals.

The first strategy devised by Stratmann[18] consists of three main steps (Figure 2). The metal surface is first cleaned carefully (step 1) in order to make reactive centers (A) available. A monolayer of specially designed (A−B) molecules is then chemisorbed onto this surface (step 2), and finally a polymer is covalently bonded to these immobilized molecules (step 3).

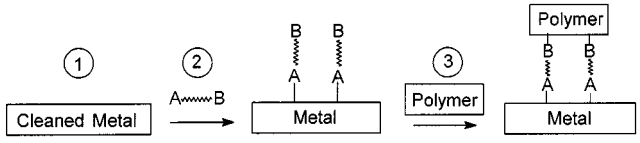

Figure 2. Reaction scheme proposed by Stratmann,[18] in which "cleaned metal" refers to the surface covered by a monolayer of sites A after electrochemical reduction

The second strategy is based on the pioneering work by Lécayon et al.,[19] who proposed that direct "grafting" of a polymer onto a metal can be achieved by controlled cathodic electropolymerization of the parent monomer (Figure 3).

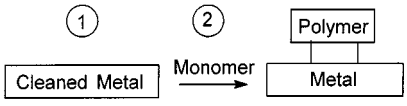

Figure 3. Reaction scheme proposed by Lécayon et al.[19]

2. Organic Molecules as Anchors for Further Polymerization

2.1. Chemical Approach

During the last decades, chemical modification of the surface of metals and carbon has been widely investigated.[20−22] It is well known that metal surfaces can be pre-treated, for example, by chromic acid etching, in order to remove old oxide layers and to generate new ones

that exhibit well-defined microdepressions acting as efficient mechanical interlocking sites.[11,15] This renewed surface is favorable not only to physisorption, but also to chemisorption as a result of secondary interactions (e.g. hydrogen bonding) between polar groups on the polymer and hydroxy groups on the metal oxide surface. These hydroxy groups have been widely exploited in order to anchor "chemical coupling agents," which are most often low molecular weight multifunctional molecules (organosilanes) able to anchor the polymer coating to the metal substrate through water-resistant covalent bonds.[11,23] It is, however, a delicate task to generate a perfect monolayer of the coupling agent attached to the substrate surface. Usually, several layers of physisorbed coupling agents are deposited on the surface from the cast solution. Since these layers are cohesively weak, fracture is generally observed in this region, as confirmed by Auger and X-ray photoelectron spectroscopy (XPS).[24]

2.2. Electrochemical Approach

The approach proposed by Stratmann[18] is an improvement of the aforementioned concept. As a model system, this author used polycrystalline iron (cleaned of any organic impurities) as substrate and thiols (e.g., *n*-decanethiol: *n*-$C_{10}H_{21}SH$) as model coupling agents. Thiols are indeed reported to strongly chemisorb onto the clean iron surface by formation of Fe−S bonds as result of S−H bond cleavage. It has been shown that OH groups present on the metal oxide surface cannot be displaced by the thiol groups, whereas stable bonds are formed between clean metals and thiols, as confirmed by X-ray photoelectron spectroscopy.[18,25−26] The first step of the process is thus the careful removal of the metal oxide layer from the surface under electrochemically controlled conditions. Figure 4 shows the cell used for the preparation of the iron surface and the binding of the thiol onto this surface. The iron surface, free from any oxide layer, is prepared by polarization in perchloric acid (1 M, $HClO_4$) at a potential of −0.72V vs. the standard hydrogen electrode (SHE). Under these conditions, the metallic state of the iron surface is thermodynamically stable.[25] In the next step, the thiol is poured onto the surface of the aqueous electrolyte and the iron electrode is slowly pulled out of the electrolyte through this organic layer, under controlled potential (Figure 4). The hydrophilic thiol groups (SH), which are preferentially oriented towards the polar electrolyte, are transferred to the new iron/thiol phase boundary.

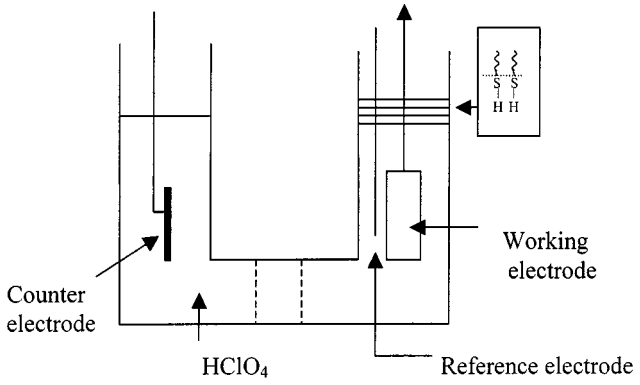

Figure 4. Electrochemical cell used by Stratmann[18]

As result of the formation of a well-ordered thiol monolayer, water does not wet this surface anymore. It has been also observed by Auger Electron Spectroscopy (AES) that an appropriate electrochemical post-treatment of the samples in neutral aqueous electrolytes significantly increases the packing density of the thiol on the iron substrate, while keeping the bond between the thiol and the metal surface intact.[26]

In view of the high reactivity of the clean iron surface either in air or in aqueous electrolytes, the high stability of this surface after modification by thiols is quite remarkable. Since this organic layer is very thin, this stability does not result from a barrier effect blocking the diffusion of oxygen and/or water. Rather, the change in the chemical and electrochemical reactivity of iron is the direct consequence of the chemisorption that saturates the clean metal surface.[27] All these results are very promising and point to the key importance of creating stable bonds between the metal and the coupling agents. These studies were, however, conducted with monofunctional molecules in order to avoid any competitive reactions of two different reactive groups of the organic molecules with the metal surface. The structure of bifunctional organic molecules now has to be optimized in order to strongly bridge metals and polymers. In this respect, the work by Itoh et al.[28] dealing with the modification of copper surfaces by bifunctional thiols is worth mentioning.

3. Electropolymerization

3.1. Brief Overview

Among the techniques suitable for the coating of metals by polymer films, electropolymerization has the advantage of proceeding through controlled reactions initiated by electron transfer to/from the monomer dissolved in the electrolytic medium. The combination of electrochemistry and polymer chemistry is far from being new and has been extensively reviewed in the last decades.[29−32] This paper does not aim at duplicating the survey of earlier works on electropolymerization, but rather at emphasizing the possible contribution of electropolymerization to the coating of metal surfaces by polymers formed in situ. Before focusing on the most relevant results obtained by Lécayon et al.[19] and our group, we will rapidly review the other contributions reported in the literature.

Wilson et al. were the first to report the electrochemical initiation of the polymerization of vinyl monomers.[33] Early works[29−33] dealt with electropolymerization occurring in solution. The formation of the initiating species results from indirect electron transfer at the electrode, i.e., by reaction of the electrolyte, followed by interaction with the monomer. These reactions are either cathodic or anodic. While free radicals are generated by the discharge of protons, per-

oxides or easily reducible compounds at the cathode,[33] Kolbe's reaction is the process at the anode reported most often[34] (Figure 5).

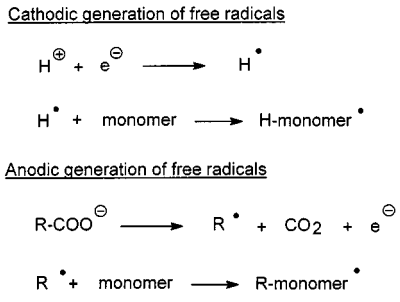

Figure 5. Polymerization initiated by free radicals[30]

Direct electron transfer from the cathode to the monomer was first suggested by Yang et al.[35] in 1957 and supported later by Funt et al.[36] Radical anions can, however, be formed by both direct and indirect processes (Figure 6).

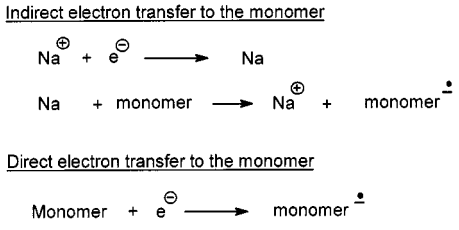

Figure 6. Polymerization initiated by radical anions[30]

According to Yamazaki et al.,[37] indirect initiation better accounts for the results reported by Funt et al. These authors proposed that direct initiation is only possible when the electrolysis is conducted under specific conditions: (i) the reduction potential of the conducting salt has to be more negative than that of the monomer, in order to avoid any indirect transfer, (ii) the electrical conductivity of the electrolytic solution must be high, and (iii) aprotic solvents have to be used in order to avoid indirect initiation by free radicals.

The deposition of polymer on the metal has been long considered as an unexpected and undesirable side-reaction, because the rapid formation of an insulating film makes the control of the process or the study of the reaction mechanism very difficult. Attempts to overcome this problem include the use of a solvent for the polymer formed, more efficient stirring and reduced electrode surface area. Lately, nevertheless, increasing attention has been paid to polymer deposition as an interesting method to protect metals against corrosion.[38−42] This coating approach is significantly different from conventional electrocoating methods that require the electrophoretic deposition of a preformed ionizable polymer from solution or suspension onto the substrate.[43−45]

Because of the high cost and potential environmental drawbacks of organic solvents, aqueous media have been extensively studied.[39] Nevertheless, Mengoli and Tidswell have investigated the cathodic electropolymerization on steel of several acrylic and methacrylic monomers in dimethylformamide and dimethyl sulfoxide.[46] The use of an organic solvent has the advantage of dissolving most organic conducting salts and of swelling most polymers of interest. Obviously, the monomer/solvent pair has to be selected in terms of poor solubility of the polymer, thus leading to film formation either by polymer precipitation or by polymer cross-linking.[47−49] The main difficulties and drawbacks met in these studies are the partial covering of the electrode, poor adhesion and poor chemical stability.

Since 1980, an increasing number of interesting papers have been published on this topic,[50] particularly on the synthesis of polymer composites containing carbon fibers[51] and on the coating of metal surfaces for aerospatial or electronic applications.[52] Undoubtedly as soon as new techniques dedicated to the design of stable polymer−metal associations are available, new application fields will develop rapidly. In this respect, the contribution of Lécayon et al., reviewed in ref.[19], is of major importance.

3.2. Electrografting of Organic Polymers onto Common Metals

Lécayon et al. have demonstrated that electrochemistry is well suited to the building up of an adherent insulating polyacrylonitrile (PAN) film onto the surface of common metals.[19,53,54] They have studied the cathodic electropolymerization of acrylonitrile (AN) in rigorously anhydrous acetonitrile (ACN), containing tetraethylammonium perchlorate (TEAP) as a conducting salt. In the case of the acrylonitrile (AN)/nickel system, the mechanism proposed for the surface modification is sketched in Figure 7. The negative polarization of the nickel electrode has three major effects: (i) the formation of the cathode double layer, (ii) the reduction of the metal oxide layer, and (iii) the formation of an electron-rich metal surface, which can act as a base. As a result of the electric field at the cathode and the strong dipole moment of AN (3.9 D[55]), the acidic vinyl β-carbon atom of acrylonitrile is orientated towards the metal. A Lewis acid−base reaction can then occur, leading to strong bonding between AN and Ni (chemisorption). According to the authors, the π electron doublet referring to the original vinyl bond of AN is transferred to the substituted carbon atom (CH), so that the basic character originally located at the surface of the electrode is displaced to the end of the first attached AN molecule. Monomer addition can then be repeated many times, which leads to the formation of a strongly bonded PAN film. The PAN film and the PAN/metal interface have been investigated by a number of spectroscopic techniques:[56−60] XPS, IR, ellipsometry, ultraviolet photoemission spectroscopy (UPS), electron-induced X-ray emission spectroscopy (EXES). Electrochemical impedance data[60] show that the metal surface is more efficiently blocked by electrodeposited PAN than by PAN merely cast from solution. The direct observation of C−Ni bonds formed at the interface has also been reported.[59]

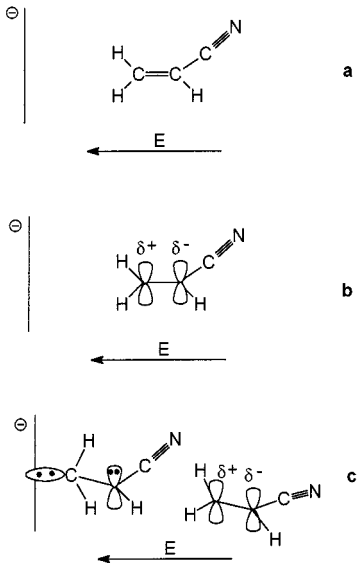

Figure 7. Molecular model for the acrylonitrile/metal interaction in the cathode double layer according to Lécayon et al.:[54] a) the molecule is oriented; b) the molecule is polarized; c) a chemisorbed radical anion is formed, which can interact with another molecule; polymerization then propagates by means of an anionic mechanism

The "grafting" reaction reported by Lécayon et al. differs from previous studies [61−63] that showed the formation of AN radical anions, followed by rapid dimerization and anionic polymerization initiated in solution by both anionic ends of the species. It is worth noting that the two peaks in the voltammogram recorded during AN reduction (Figure 8) were never observed before. According to Viel,[64] the two reduction peaks stem from surface passivation (less cathodic peak, referred to as peak I) and from a diffusion-controlled process (peak II), respectively.

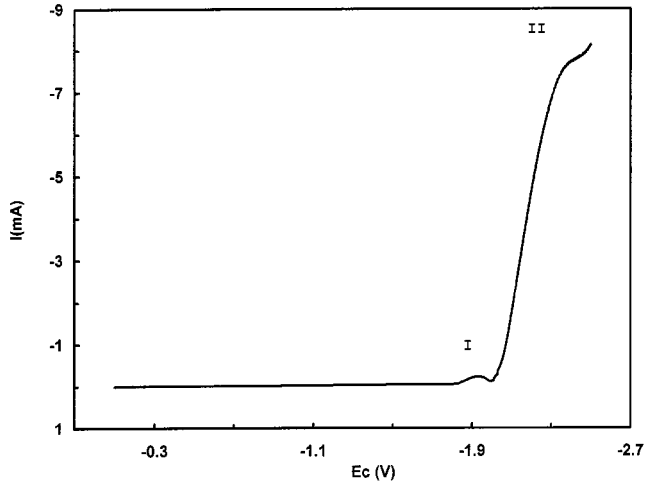

Figure 8. Cathodic response of a 0.1 M AN solution in acetonitrile; [TEAP] = $5\cdot10^{-2}$ M, v = 20 mV·s^{-1}

In addition to the so-called grafted polymer, this author also mentions the formation of non-grafted chains[64] which are easily removed by rinsing the electrode with a solvent for PAN, such as dimethylformamide (DMF). It is also proposed that the "grafting reaction" is likely to occur at potentials less cathodic than peak II, but no clear experimental information is provided about the formation of non-grafted chains. Originally, the grafting reaction, i.e., the chemisorption of AN radical anions, was described as a "secondary electrode reaction",[65] when compared to dimerization and polymerization occurring in solution.[63] In fact, the grafting reaction has been observed thanks to the rigorous experimental conditions used by Lécayon et al.[66]

3.2.1. Experimental Requirements

Contamination of the metal surface by oxide and any organic impurities is detrimental to strong monomer chemisorption. Thus, careful cleaning of the electrode substrate is a prerequisite to impart stability to the interface between the metal and the organic molecule, as confirmed by Stratmann et al.[18] The whole grafting reaction must thus be conducted in a glove box under dry and inert conditions. The nickel oxide is reduced in the electrochemical cell filled with a solution of the monomer and the conducting salt at potentials less cathodic than the potential required for the AN reduction (Figure 9).

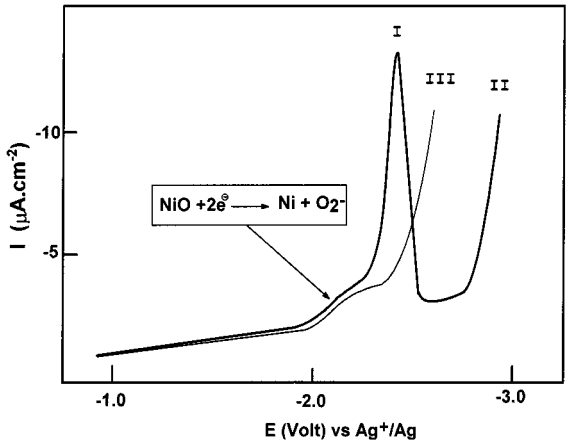

Figure 9. Voltammograms in ACN/TEAP solutions: I and II are the inhibition peak and the diffusion peak, respectively, when the solution contains AN; III in absence of AN[54]

Ellipsometric measurements have been carried out in situ during the first step of the cathodic electropolymerization of acrylonitrile on nickel, and they have confirmed that the grafting reaction is initiated at the electrode sites released by the reduction of the native oxide.[58] This observation explains why grafting is usually observed on metals such as Ni, Fe, or Cu, whereas it does not occur on metals for which the oxide cannot be reduced electrochemically (e.g. Al, Zn).[67−69]

The use of a conducting salt which is inert in the potential range in which the electrochemical signature of the AN electroreduction is observed has to be pointed out. Indeed, according to Yamazaki et al.,[37] inorganic conducting salts such as $NaNO_3$, are commonly reduced at potentials less cathodic than the monomer, leading to the indirect initiation of the polymerization in solution (Figure 6). In a patent,[66] Lécayon et al. recommend the use of tetraethyl-

ammonium perchlorate (TEAP), which is known for its electrochemical stability up to high cathodic potentials.[70]

The purity of solvents and monomer has also a critical importance for the grafting reaction to be successfully achieved. According to Lécayon et al.,[67] impurities, such as H_2O and O_2, can slow down or inhibit the polymer deposition. Their content in the electrochemical solution has to be lower than 5−10 ppm. These features have been confirmed by Mertens[68] who deliberately contaminated the electrochemical solution by increasing amounts of water or oxygen. The main effect of small quantities of water added to the ACN/TEAP solution is to shift the upper limit of the cathodic window (current rise attributed to the solvent reduction) towards less cathodic values and to increase the intensity of peak I (Ip_1, Table 1).[68]

Table 1. Peak *I* intensity [μA] with increasing water amount, [AN] = 1 M; ACN/TEAP; $v = 20\ mV \cdot s^{-1}$

Water content [ppm]	Ip_1 on Ni [μA]	Ip_1 on steel [μA]
10	30	30
100	125	80
400	200	−

According to Viel,[64] the intensity of peak I is strongly dependent on the polymerization kinetics, the inhibition time being controlled by the rate of formation of the insulating polymer film.

The increase in the intensity of peak I thus indicates a slower inhibition of the cathode. An explanation might be the earlier termination of the grafted chains by water, consistent with formation of thinner films as measured by ellipsometry (ex situ measurements).[71] When the water content is increased further, non-bonded chains are predominantly formed as a result of indirect initiation by hydrogen radicals (Figure 5). The film adhesion is rapidly lost, since it is composed mainly of non-bonded polymer chains embedded in a few grafted ones.

In contrast to water, the reduction of oxygen ($O_2 + e^- \rightarrow O_2^-$) dissolved in the electrochemical medium gives rise to a well-defined voltammetric wave at potentials less cathodic than the AN reduction. In that case, according to Mertens, the indirect initiation of the AN polymerization by the reduction by-product is the predominant process, at the expense of the grafting reaction.[68]

3.2.2. Recent Advances

Owing to the interest and potential of this unusual electrografting reaction, Mertens et al. recently reinvestigated[68,72−73] the cathodic reduction of acrylonitrile (AN). In the opinion of those authors, the intimate mechanism of the AN electropolymerization was still unclear. This is the reason why they studied this electrochemical reaction in acetonitrile (ACN), a poor solvent for PAN commonly used by Lécayon et al., as well as in dimethylformamide (DMF), a good solvent for the polymer.

Mertens et al. used mechanically polished metal plates as working electrodes, instead of polycrystalline substrates prepared by sputtering a thin layer of pure Ni onto polished metal plates under high vacuum.[67] The surface oxide of the electrode was electrochemically reduced in an ACN/TEAP solution in a glove box just prior to polymer deposition from a fresh solution of monomer. This two-step process prevents O_2^- species from being formed in the monomer solution, thus avoiding possible cross-linking of PAN.[68]

Mertens et al.[72][73] pointed out the critical role of the applied potential, showing that PAN is strongly bonded to the nickel cathode only at the potential of peak I (Figure 8). In this potential range, a thin homogeneous and colorless polymer film is formed, even when the reaction is conducted in a good solvent for PAN, such as dry DMF. This observation confirms the strong adhesion of the PAN film onto the cathode, consistently with the grafting claimed by Lécayon et al.[53] In sharp contrast, a PAN film spin-coated onto nickel is rapidly dissolved in this solvent. When the potential is further increased (Figure 8, peak II), no grafting is observed anymore; the polymerization then proceeds in solution. These non-grafted chains are rapidly dissolved in DMF, while they are merely precipitated on the cathode as a thick yellowish non-adherent film in ACN. Although PAN films formed at the potential of peak I are generally too thin and too smooth to be visible by scanning electron microscopy (SEM), Figure 10 shows the nucleation of the PAN chains formed at the potential of peak II in ACN, leading to a cauliflower-like morphology.

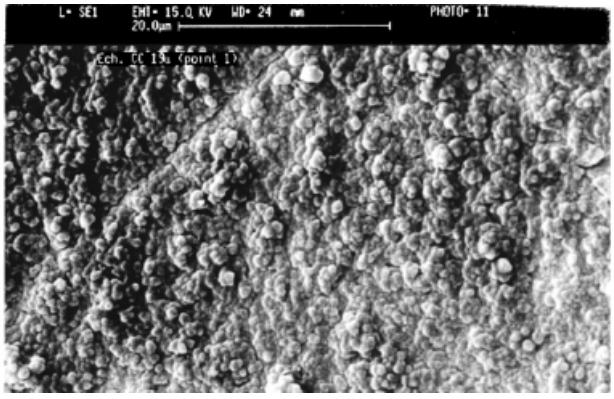

Figure 10. Scanning electron micrograph of PAN film deposited on Ni in a 0.05 M TEAP solution in ACN at the potential of peak II[68]

Mertens et al.[74] investigated the identification of the species responsible for the polymer propagation and tentatively proposed two different mechanisms for the AN electropolymerization in relation to the applied potential. The reaction that occurs at the potential of peak I does not fit classical electrochemical models since the intensity of peak I decreases when the monomer concentration increases; the process seems to be neither fully faradaic nor fully capacitive in nature. In order to identify the species active at the two reduction potentials, agents able to react selectively with radicals or anions and inert in the potential range of interest were added to the electrolyte solution. The addition of either diphenylpicrylhydrazyl (DPPH), radical scavenger

or ε-caprolactone (probe for anionic polymerization) led to evidence for the formation of a radical species that initiates and propagates the PAN firmly attached to the Ni cathode (Figure 11).

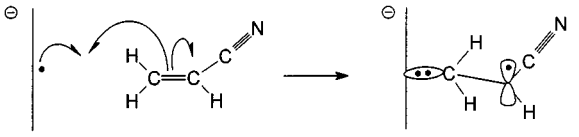

Figure 11. Mechanism proposed by Mertens et al. for the AN grafting reaction at peak I[74]

At the more cathodic potential (peak II), reduction of AN is a faradic process based on the transfer of one electron to the monomer, and on the formation of a radical-anion that rapidly dimerizes and initiates the AN polymerization in solution, in agreement with previous work by Bhadani et al.[63] In addition to this dual mechanism, a possible bond-breaking of the originally "grafted" PAN chains has to be considered when the potential becomes more cathodic than that of peak I.[74] In ACN, an increasingly more cathodic potential is also responsible for the strain of the originally grafted film, so that the conductivity of the cathode is restored locally, allowing the anionic polymerization of AN to occur and to lead to PAN films with a cauliflower aspect (Figure 10).

The model proposed by Mertens et al. (Figure 11) differs markedly from that of Lécayon et al. (Figure 7), who proposed an anionic mechanism for the grafted growing chains. Nowadays, the electrografting mechanism is still a matter of controversy.[75] Whatever the structure of the propagating species, the most important result is the clear identification of the potential range in which the formation of an adherent polymer film can be controlled. In this respect, dynamic mechanical thermal (DMTA) and infrared spectroscopic analyses[76] have recently shown that the structure of the PAN film depends on the potential at which it is formed. Indeed PAN "grafted" at the potential of peak I is mainly isotactic and the film is amorphous, in contrast to ungrafted PAN formed at more cathodic potentials, which is mainly atactic and forms a paracrystalline film in ACN.

In order to control the film thickness and roughness, these features have been studied in relation to the solvent used and the monomer concentration. The thickness of dried films prepared in the potential range of peak I was measured by ellipsometry; it clearly depends on these experimental parameters[72] (Figure 12). The film was thicker in DMF than in ACN and this can be rationalized on the basis of the precipitation of the growing PAN chains in the latter case and the solvation of the chains in the former case. Indeed, as soon as the PAN chains reach some critical length in ACN, they precipitate on the electrode, which is detrimental to their propagation. The situation is completely different in DMF, since the growing chains are solvated during the whole polymerization.

This qualitative explanation is supported by Atomic Force Microscopy (AFM) data which show that PAN films deposited in DMF at high monomer concentration are thick enough to mask the morphological features of the

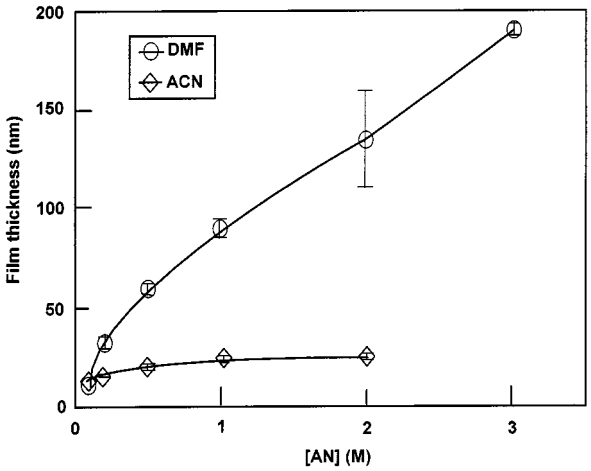

Figure 12. Dependence of the PAN film thickness on the monomer concentration in ACN and DMF[72]

substrate. Figure 13 is a typical image of the bare nickel surface which is used as a reference for the observation of the coated electrodes. Generally, the morphology of thin PAN films, grafted in ACN or DMF at low AN concentration (0.1−0.2 M), appears to consist of small polymer grains deposited on the electrode (Figure 14, A and 14, B). The average size of the grains is in the 40−60 nm range over the whole surface. The polymer deposit is not thick enough to mask the largest defects of the nickel surface (as ridges present on Figure 13 are still visible on Figure 14, A and B). At higher AN concentrations (1−2 M), clear morphological differences are observed depending on the solvent used (Figure 15, A and B). Films prepared in ACN show the same granular morphology as in dilute solution, with characteristic sizes of approximately 50 nm (Figure 15, A). However, the ridges of the original metal surface are less visible, in agreement with the formation of thicker films. Details reminiscent of the metal surface are no longer ob-

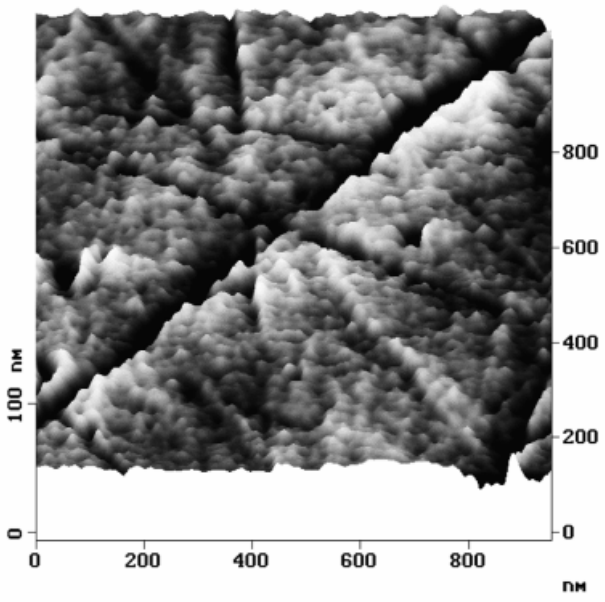

Figure 13. Atomic force micrograph of bare nickel

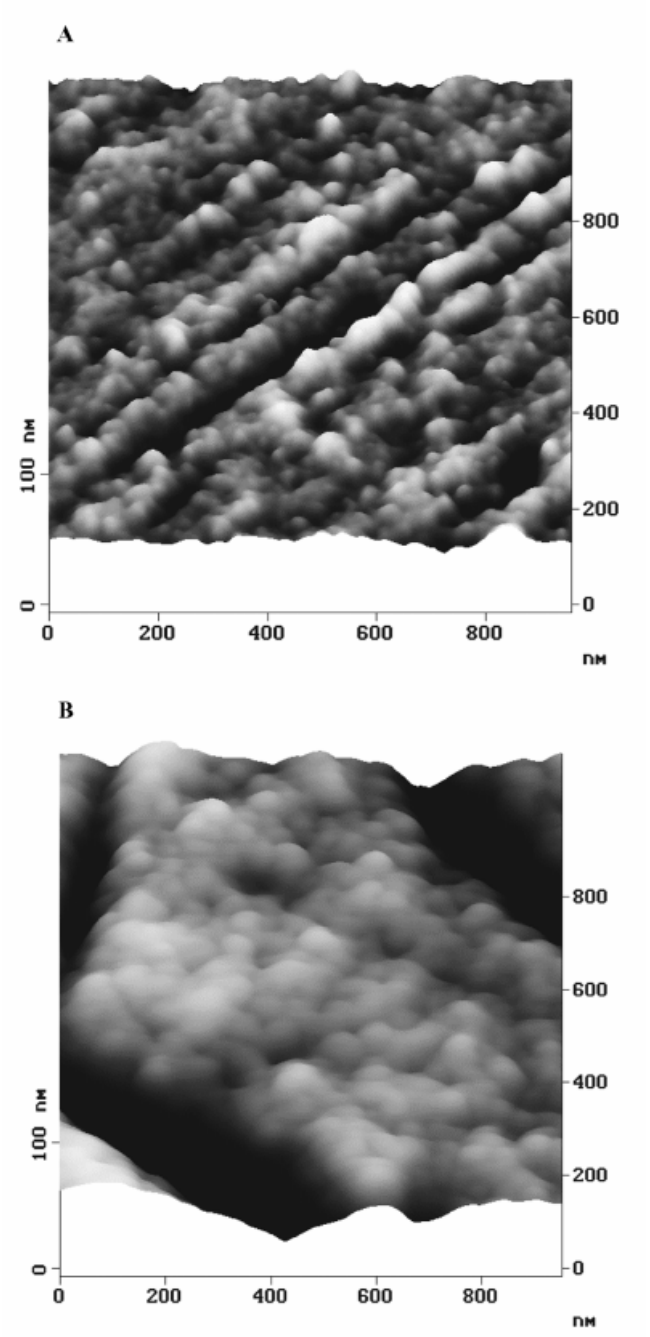

Figure 14. Atomic force micrographs of PAN films deposited on Ni in the potential range of peak I: A) AN 0.1 M in ACN; B) AN 0.2 M in DMF

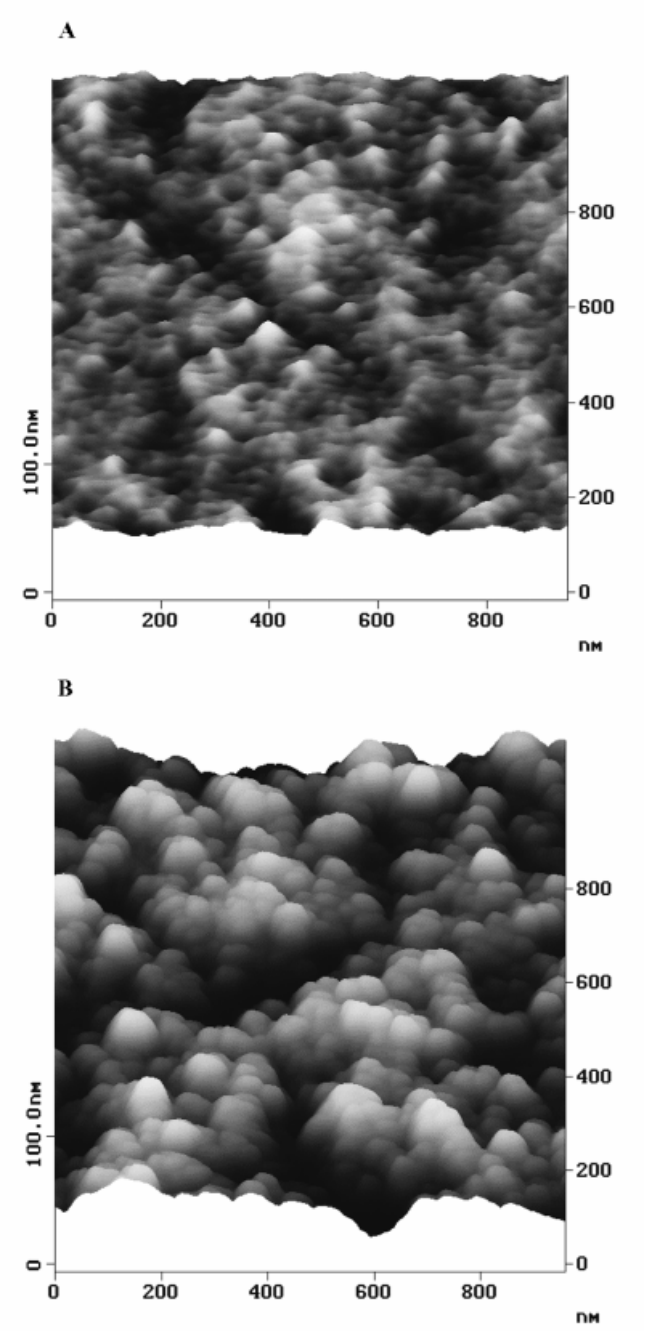

Figure 15. Atomic force micrographs of PAN films deposited on Ni in the potential range of peak I: A) AN 1 M in ACN; B) AN 2 M in DMF

served in films grafted in DMF (Figure 15, B). In this case, the PAN deposit is clearly thicker and the film consists of nodules much larger in size (100 to 150 nm) than the grains observed in ACN.

As direct applications of the fine control of the AN electrografting, specific achievements have been reported, for example, preparation of thin α-emitting sources by simultaneous electroreduction of AN and uranium salts,[77] preparation of electrical connectors by an adequate thermal post-treatment of electrografted PAN thin films[78] and protection of art pieces.[68,79]

Very recently, efforts have been devoted to improve the understanding of the electrografting reaction and to functionalize the very adherent thin films formed. The unusual electrografting reaction has been shown to strongly depend on the ability of the monomer to be adsorbed onto the clean cathode. Therefore, the monomer has to compete efficiently with the solvent and with the conducting salt[80] to be adsorbed and react at the cathode surface rather than in solution. ^{13}C NMR spectroscopic data and theoretical calculations[81] have shown that AN is particularly prone to interact strongly with the cathode. Nevertheless, paying

special attention to the competitive adsorption of monomer and solvent (or conducting salt), (meth)acrylic monomers have been successfully grafted.[80,82]

Furthermore, the use of coupled quartz crystal microbalance and cyclic voltammetry has confirmed that the inhibition peak is the actual signature of the strong monomer chemisorption and growth of grafted chains.[82] At more cathodic potentials, polymerization occurs in solution, while previously bonded chains are detached from the electrode. In this respect, a major difference has been pointed out in the behavior of acrylic and methacrylic monomers. Indeed, in the latter case, bonded and non-bonded chains are simultaneously formed in the potential range of peak I. Acrylic polymers are thus better candidates for the efficient coating and long-term protection of metals.

The possibility of electrografting acrylonitrile-containing copolymers has also been investigated.[83] As a rule, the composition of the grafted chains depends on the local concentration of the comonomer. If the comonomer has no tendency to accumulate in the close vicinity of the cathode (e.g. vinyl acetate), then only homopolyacrylonitrile is grafted. In the reverse case (e.g. ethyl acrylate), copolymer chains are grafted, and the composition of the film depends mainly on the capability of each comonomer to compete with the solvent for adsorption. However, the capacity of the films to cover the electrode seems limited, possibly as consequence of the extra competition of the two monomers to adsorb onto the cathode. In order to alleviate this disappointing situation, the sequential electrografting of each monomer in two different cells has been proposed.[84] Mixed films, combining the properties of two polymers, are formed when the monomer less prone to compete with the solvent molecules is electrografted first at a more cathodic potential than the second monomer. Since the grafting density is expected to depend on the adsorption of the monomer, this result supports the general idea of the competitive monomer/solvent adsorption onto the cathode in the very first step of the grafting process. In the same way, the full electrochemical synthesis of insulating/conducting composites has also been investigated.[85] An unexpected application has also been found by using electrografted substrates as templates for the synthesis of conducting polymers leading to formation of polypyrrole wires.[86]

The electrografting technique thus allows for the control not only of the adherence of organic coatings on metals, but also of their nature and composition. For example, it is now possible to prepare electrografted films containing epoxy groups in one step, and films containing hydroxy groups in two steps (Scheme 1).[87] In this respect, it is worth noting that the electrografting of 2-hydroxyethyl methacrylate (Scheme 1) could pave the way for biomedical applications (e.g., catheters).

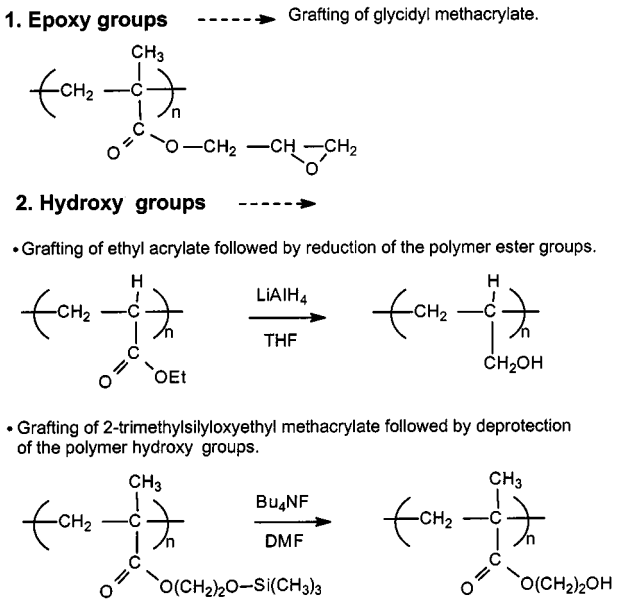

Scheme 1. Functionalization of electrografted films

4. Conclusions and Challenges

The electrochemical strategies proposed by Stratmann et al.[18] and Lécayon et al.[19] have brought valuable answers to the problems caused by the weakness and short lifetimes of polymer−metal associations. From an economic point of view, the approach by Stratmann et al. is more advantageous, since it can be carried out under mild conditions in water, in contrast to the electrografting proposed by Lécayon et al. Extension of the model systems studied by Stratmann et al. to real systems consisting of the adsorption of bifunctional organic molecules and the reaction of the modified surface with film-forming monomers in the next turning point to pass.

Despite some stringent experimental conditions, electrografting appears to have a promising future for the preparation and protection of small-size and high-value devices.[77−79] One pending problem is the small thickness of the grafted films. Indeed, a polymer coating usually imparts corrosion resistance to a substrate when the thickness is greater than 50μm.[88] At present, the electrografted films do not provide this beneficial effect since the number of deposition cycles and the deposition techniques (voltamperometry, chronoamperometry, chronopotentiometry) do not allow for an increase in the final thickness of the film.[72]

The use of the grafted coating as a primer also becomes more promising with the ability to graft a larger number of monomers.[80−82,87,89−92] In this field, the controlled chemical modification of grafted films remains a challenging issue. The copolymerization of AN with "functional" monomers such as acrylate, and the electrografting of blends could be an interesting way to combine various interesting properties at the surface. Recent developments resulting in the diversification of the grafted substrate allow for the preparation of primers able to interact strongly with a top-coat.

The search for new monomers prone to electrografting remains the best way to simultaneously overcome the two main drawbacks of the polymer−metal association; i.e., the

weakness of both the substrate/polymer and polymer/surrounding medium interfaces.

Acknowledgments

The authors are indebted to the "Services Fédéraux des Affaires Scientifiques, Techniques et Culturelles" for general support under the auspices of the "Pôles d'attraction Interuniversitaires: Supramolecular Chemistry and Supramolecular Catalysis". R. L. is Maître de Recherches and C. J. is Chargé de Recherches du Fonds National de la Recherche Scientifique (FNRS Belgium)

[1] A. J. Kinloch, *Adhesion and adhesives, Science and Technology*, Chapman & Hall, London, **1987**.
[2] H. L. Gerhart, *Ind. Eng. Chem. Prod. Res. Dev.* **1978**, *17*, 1.
[3] F. Deflorian, L. Fedrizzi, A. Locaspi, P. L. Bonora, *Electrochim. Acta* **1993**, *38*, 1945.
[4] S. Maeda, T. Asai, S. Fujii, Y. Nomura, A. Nomoto, *J. Adhes. Sci. Technol.* **1988**, *2*, 271.
[5] A. J. Kinloch, in: *Polymer Surfaces and Interfaces* (Eds.: W. J. Feast, H. S. Munro), New York, **1987**, p. 75.
[6] R. A. Dickie, in: *Polymeric Materials for Corrosion Control* (Eds.: R. A. Dickie, F. Floyd), ACS, Washington, **1986**, p. 136.
[7] J. W. Holubka, W. Chun, A. R. Krause, J. Shyu, in: *Polymeric Materials for Corrosion Control* (Eds.: R. A. Dickie, F. Floyd), ACS, Washington, **1986**, p. 194.
[8] E. L. Koehler, *Corrosion, NACE* **1977**, *33*, 209.
[9] H. Leidheiser, Jr, W. Wang, L. Igetoft, *Prog. Org. Coat.* **1983**, *11*, 19.
[10] H. Leidheiser, Jr, in: *Polymeric Materials for Corrosion Control* (Eds.: R. A. Dickie, F. Floyd), ACS, Washington, **1986**, p. 124.
[11] R. G. Schmidt, J. P. Bell, *Adv. Polym. Sci.* **1986**, *75*, 33−72.
[12] A. G. Smith, R. A. Dickie, *Ind. Eng. Chem. Prod. Res. Dev.* **1978**, *17*, 42.
[13] G. Trabanelli, V. Carassiti, *Adv. Corros. Sci. Technol.* **1970**, *1*, 147.
[14] M. Stratmann, R. Feser, A. Leng, *Electrochim. Acta* **1994**, *39*, 1207−1214.
[15] F. Nitschke, *J. Adhesion Technol.* **1990**, *4*, 41.
[16] P. Benoist, G. Legeay, R. Morello, F. Poncin-Epaillard, *Eur. Polym. J.* **1992**, *28*, 1383.
[17] K. Doblofer, *Bull. Electrochem.* **1992**, *8*, 73.
[18] M. Stratmann, *Adv. Mater.* **1990**, *2*, 191.
[19] C. Boiziau, G. Lécayon, *La Recherche* **1988**, *19*, 888.
[20] R. W. Murray, *Acc. Chem. Res.* **1980**, *13*, 135.
[21] E. Katz, H. L. Shmidt, *J. Electroanal. Chem.* **1993**, *360*, 337.
[22] M. S. Wrighton, *Science* **1986**, *231*, 32.
[23] E. P. Pluedemann, in *Encyclopedia of Polymer Sciences and Engineering*, 2nd ed., Wiley Interscience, **1986**, vol. 4, p. 284.
[24] M. Gettings, F. S. Baker, A. J. Kinloch, *J. Appl. Polym. Sci.* **1977**, *21*, 2375.
[25] M. Volmer, M. Stratmann, H. Viefhaus, *Surf. Interf. Anal.* **1990**, *16*, 278.
[26] M. Volmer-Uebing, M. Stratmann, *Appl. Surf. Sci.* **1992**, *55*, 19.
[27] R. Losch, M. Stratmann, H. Viefhaus, *Electrochim. Acta* **1994**, *39*, 1215.
[28] M. Itoh, H. Nishihara, K. Aramaki, *J. Electrochem. Soc.* **1994**, *141*, 2018.
[29] J. W. Breitenbach, C. Srna, *Pure Appl. Chem.* **1962**, *4*, 245.
[30] Yamazaki, *Adv. Polym. Sci.* **1969**, *6*, 377.
[31] G. Parravano, *Organic Electrochemistry*, Marcel Dekker New York, **1973**, p. 947−974.
[32] B. L. Funt, J. Tanner, *Tech. Electroorg. Synth.* **1975**, *5*, 559.
[33] E. Dineen, T. C. Schwan, L. C. Wilson, *Trans. Electrochem. Soc* **1949**, *96*, 226.
[34] W. B. Smith, H. G. Gilde, *J. Am. Chem. Soc.* **1960**, *82*, 659.
[35] J. Y Yang, W. E. McEwen, J. Kleinberg, *J. Am. Chem. Soc.* **1957**, *79*, 5833.
[36] B. L. Funt, K. C. Yu, *J. Polym. Sci.* **1962**, *62*, 359.
[37] Yamazaki, I. Tanaka, S. Nakahama, *J. Macromol. Sci. Chem* **1968**, *A2*, 1121.
[38] F. S. Teng, R. Mahaligan, R. V. Subramanian, R. A. V. Raff, *J. Electrochem. Soc.* **1977**, *124*, 995.
[39] G. Mengoli, *Adv. Polym. Sci.* **1979**, *33*, 1.
[40] G. Mengoli, S. Daolio, U. Giulio, C. Polonari, *J. Appl. Polym. Sci.* **1979**, *23*, 2117.
[41] B. K. Garg, R. A. V. Raff, R. V. Subramanian, *J. Appl. Polym. Sci.* **1978**, *22(1)*, 65.
[42] R. V. Subramanian, *Adv. Polym. Sci.* **1979**, *33*, 34.
[43] R. Dobreva, J. Sledj, F. Schue, J. A. Alary, *L'actualité Chimique*, Janvier/Fevrier **1993**, p. 60.
[44] C. P. Yang, C. Y. Ting, *J. Appl. Polym. Sci.* **1993**, *49*, 1019.
[45] K. Arlt, *Electrochim. Acta* **1994**, *39*, 1189.
[46] G. Mengoli, B. M. Tidswell, *Polymer* **1975**, *16*, 881.
[47] T. Asahara, M. Seno, M. Tsuchiya, *Kinzunku Hyomen Gijutsu* **1969**, *20*, 617.
[48] L. A Korschikov, L. I. Kravtsova, V. D. Bezugly, *Electrokhimiya* **1974**, *10*, 990.
[49] F. Bruno, M. C. Phan, J. E. Dubois, *J. Chim. Phys.* **1975**, *72*, 490.
[50] W. Yuan, J. O. Iroh, *Trends Polymer Sci.* **1993**, *1*, 388.
[51] R. V. Subramanian, J. J Jakubowski, *Polym. Eng. Sci.* **1978**, *18*, 590.
[52] L. E. A Berlouis, D. J. Schriffrin, *Trans. Inst. Met. Finish* **1986**, *64*, 42.
[53] G. Lécayon, Y. Bouizem, C. Le Gressus, C. Reynaud, C. Boiziau, C. Juret, *Chem. Phys. Lett.* **1982**, *91*, 506.
[54] C. Boiziau, S. Leroy, C. Reynaud, G. Lécayon, C. Le Gressus, P. Viel, *J. Adhesion* **1987**, *23*, 21.
[55] A. L. Mc Clellan, *Tables of Experimental Dipole Moments*, W. H. Freeman and Co., San Francisco, **1963**.
[56] P. Viel, S. de Cayeux, G. Lécayon, *Surf. Interf. Anal.* **1993**, *20*, 468.
[57] D. Mathieu, M. Defranceschy, P. Viel, G. Lécayon, J. Delhalle, *Polym. Solid Interf., Proc. Int. Conf., 1st*, Institute of Physics, Bristol, **1992**, p. 379.
[58] Y. Bouizem, F. Chao, M. Costa, A. Tadjedinne, G. Lécayon, *J. Electroanal. Chem.* **1984**, *172*, 101.
[59] P. Jonnard, F. Vergand, P. F. Staub, C. Bonnelle, G. Deniau, C. Bureau, G. Lécayon, *Surf. Interface Anal.* **1996**, *24*, 339.
[60] J. Tanguy, P. Viel, G. Deniau, G. Lécayon, *Electrochim. Acta* **1993**, *38*, 1501.
[61] B. L. Funt, F. D. Williams, *J. Polym. Sci.* **1964**, *A2*, 865.
[62] B. Yurttas, L. Toppare, U. Akbulut, *J. Macromol. Sci.* **1988**, *A25*, 219.
[63] S. N. Bhadani, Q. Ansari, S. K. S Gupta, *J. Appl. Polym. Sci.* **1992**, *44*, 121.
[64] P. Viel, Ph. D. Thesis, Université de Paris VI, France, **1990**.
[65] G. Hennico, J. Delhalle, E. Younang, M. Defranceschi, G. Lécayon, C. Boiziau, *Int. J. Quantum Chem., Quantum Chem. Symp.* **1991**, *25*, 507.
[66] G. Lécayon, C. Le Gressus, A. Le Moël, *Eur. Patent* no. 0038244, **1981**.
[67] G. Lécayon, A. Le Moël, C. Le Gressus; *Vide, les couches minces*, **1980**, vol. *201*, p. 638.
[68] M. Mertens, Ph. D. Thesis, University of Liège, Belgium, **1995**.
[69] C. Fredrikson, R. Lazzaroni, J. L. Brédas, M. Mertens, R. Jérôme, *Chem. Phys. Lett.* **1996**, *258*, 356.
[70] J. D. B. Smith, D. C. Phillips, D. H. Davies, *J. Polym. Sci., Chem. Ed.* **1977**, *15*, 1555.
[71] C. Calberg, M. Mertens, R. Jérôme, X. Arys, A. M. Jonas, R. Legras, *Thin Solid Films* **1997**, *310*, 148−155.
[72] R. Jérôme, M. Mertens, L. Martinot, *Adv. Mater.* **1995**, *7*, 807.
[73] M. Mertens, C. Calberg, L. Martinot, R. Jérôme, *Macromolecules* **1996**, *29*, 4910−4918.
[74] V. Geskin, R. Lazzaroni, M. Mertens, R. Jérôme, J. L. Brédas, *J .Chem. Phys.* **1996**, *105*, 3278.
[75] C. Bureau, G. Deniau, P. Viel, G. Lécayon, *Macromolecules* **1997**, *30*, 333.
[76] C. Calberg, M. Mertens, N. Baute, R. Jérôme, V. Carlier, M. Sclavons, R. Legras, *J. Polym. Sci., Part B: Polym. Phys* **1998**, *36*, 543−553.
[77] L. Martinot, M. Mertens, L. Lopes, P. Faack, M. Krausch, J. Guillaume, G. Ghitti, J. Marien, J. Riga, R. Jérôme, J. Schrijnemackers, *Radiochim. Acta* **1996**, *75*, 111−119.

[78] F. Houzé, L. Boyer, S. Noël, P. Viel, G. Lécayon, J-M. Bourin, *Synth. Met.* **1994**, *62*, 207.
[79] M. Mertens, C. Calberg, R. Jérôme, L. Martinot, J. Schrijnemackers, J. Guillaume, *Revue des Historiens de l'Art, des Archéologues, des Musicologues et des Orientalistes de l'Université de Liège*, **1997**, p. 16.
[80] N. Baute, P. Teyssié, L. Martinot, M. Mertens, P. Dubois, R. Jérôme, *Eur. J. Inorg. Chem.* **1998**, 1711.
[81] X. Crispin, R. Lazzaroni, V. Geskin, N. Baute, P. Dubois, R. Jérôme, J. L. Brédas, *J. Am. Chem. Soc.* **1999**, *121*, 176.
[82] N. Baute, L. Martinot, R. Jérôme, *J. Electroanal. Chem.* **1999**, *472*, 83.
[83] N. Baute, Ph. D. Thesis, University of Liege, **1999**.
[84] N. Baute, V. Geskin, R. Lazzaroni, J. L. Brédas, X. Arys, A. Jonas, R. Legras, C. Poleunis, P. Bertrand, R. Jérôme, *Thin Solid Films*, submitted.
[85] C. Jérôme, V. M. Geskin, R. Lazzaroni, J. L. Brédas, A. Thibaut, C. Calberg, I. Bodart, M. Mertens, L. Martinot, D. Rodrigue, J. Riga, R. Jérôme, *Chem. Mater.*, submitted.
[86] C. Jérôme, R. Jérôme, *Angew. Chem. Int. Ed.* **1998**, *37*, 2488.
[87] D. E. Labaye, Ph. D. Thesis, University of Liege, in preparation.
[88] G. Deniau, G. Lécayon, C. Bureau, J. Tanguy, in: *Protective Coatings and Thin Films* (Eds.: Y. Pauleau, P. B. Barna), Kluwer, Dordrecht (Proceedings of the Nato Advanced Research Workshop held in Portimao, Portugal, **1996**), **1997**, p. 265.
[89] G. Deniau, G. Lécayon, P. Viel, G. Zalczer, C. Boiziau, G. Hennico, J. Delhalle, *J. Chem. Soc., Perkin Trans. 2* **1990**, 1433.
[90] J. Tanguy, G. Deniau, C. Auge, G. Zalczer, G. Lécayon, *J. Electroanal. Chem.* **1994**, *337*, 114.
[91] J. Tanguy, G. Deniau, G. Zalczer, G. Lécayon, *J. Electroanal. Chem.* **1996**, *417*, 175.
[92] G. Deniau, P. Viel, G. Lécayon, *Surf. Interf. Anal.* **1992**, *18*, 443.

Received April 17, 2000
[I00154]

The Control of Nanostructured Solids: A Challenge for Molecular Chemistry

Robert J. P. Corriu[a]

Keywords: Silicates / Organic-inorganic hybrid composites / Materials science / Sol-gel processes / Nanostructures

Nanostructured hybrid organic-inorganic solids are a class of materials of growing interest because of their great potential in synthesis and possible applications. All organic molecules containing at least two $-Si(OR)_3$ groups can be transformed by hydrolytic polycondensation at silicon into materials in which the $-Si(OR)_3$ groups are changed into $-SiO_{1.5}$. Moreover, the physical properties of the organic units included in the silica matrix are maintained in the solid. This sol-gel-type transformation leads initially to a viscous sol that allows devices to be made (films, matrices and even fibres in some cases). Finally, these materials exhibit both short-range and long-range organisation in the solid when the organic units have a rigid geometry.

I. Introduction

The concept of "Chimie Douce" has been introduced recently in the field of Materials Science.[1,2] This method of obtaining solids represents a breaking down of the preparation of materials and this concept, which is based on inorganic polymerisation, has opened the field of Materials Science to molecular chemistry.

The methodology used in classical solid state chemistry is based on the thermodynamic evolution of the reaction. Whatever the experimental conditions, success is based on the self arrangement of the system leading to stable (or metastable) materials. This approach to the elaboration of materials includes the high temperature methodologies leading to crystals, glasses or ceramics, as well as to other techniques that require lower temperatures such as the synthesis of crystalline aggregates, the preparation of polyanions from solutions, or the hydrothermal synthesis of zeolites.

[a] Laboratoire de Chimie Moléculaire et Organisation du Solide, UMR 5637, Université Montpellier II,
Place E. Bataillon, 34095 Montpellier Cedex 5, France

The properties of the solid materials obtained by these methods are always governed by the general thermodynamic laws represented by the phase diagram.

In contrast, the methodologies encompassed by the phrase "Chimie Douce" are based on kinetic control of the solid synthesis. The solids obtained are not the most thermodynamically stable, but they are the result of a multiparametric chemistry based on mechanistic control of the chemical reactions. One commonly used approach of "Chimie Douce" chemistry is the sol-gel methodology,[3,4] which corresponds to an inorganic polymerisation (Scheme 1). Scheme 2 illustrates the complexity of the hydrolytic polycondensation of $Si(OR)_4$ by showing the possible competitive reactions occurring at the same time.

The preparation of SiO_2 by this route is controlled by the kinetics of the hydrolytic polycondensation that occurs around the silicon atom through nucleophilic substitution at silicon. In this process H_2O acts as a nucleophile and displaces ROH in the first step. The condensation leading to Si−O−Si bonds occurs by hetero or homo condensation (see Scheme 2). This mechanism is a highly complex one because of the four functionalities, the possibility of redistribution, and the formation of chains or rings leading to a

Robert Corriu, born in 1934 in Port-Vendres, France, obtained his Docteur des Sciences Physiques in 1961 from the Université de Montpellier. He became Assistant Professor at the Université de Perpignan in 1963, Associate Professor at the Université de Poitiers in 1964, and Professor at the Université de Montpellier in 1969. His research interests in organometallic chemistry have been focused on organosilicon, organogermanium, and organophosphorus compounds, transition metal complexes, and hypercoordinated silicon and phosphorus compounds. More recently, he has concentrated his research efforts on the elaboration of solids from molecular precursors. His main interest is now connected with hybrid organic-inorganic materials and molecular chemistry permitting solid organisation. He has obtained awards from the French Chemical Society (Prix Sue in 1969 and Prix Lebel in 1985), from the CNRS (silver medal in 1982), and from the American Chemical Society (Kipping Award in 1984). He was elected to the French Academy of Sciences in 1991 and Polish Academy in 1997. He obtained the Alexander Von Humboldt Research Award in 1992, the Max Planck Research Award in 1993, and the Wacker Silicon Award in 1998.

MICROREVIEWS: This feature introduces the readers to the authors' research through a concise overview of the selected topic. Reference to important work from others in the field is included.

 © WILEY-VCH Verlag GmbH, 69451 Weinheim, 2001 1434−1948/01/0505−1109 $ 17.50+.50/0

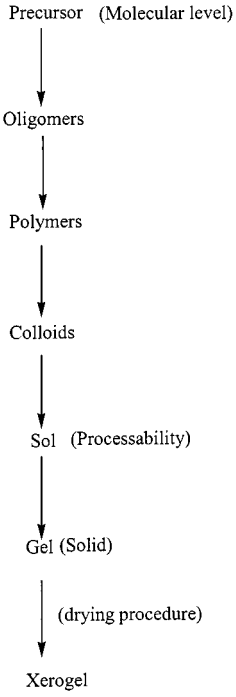

Scheme 1. A general scheme for inorganic polymerisation

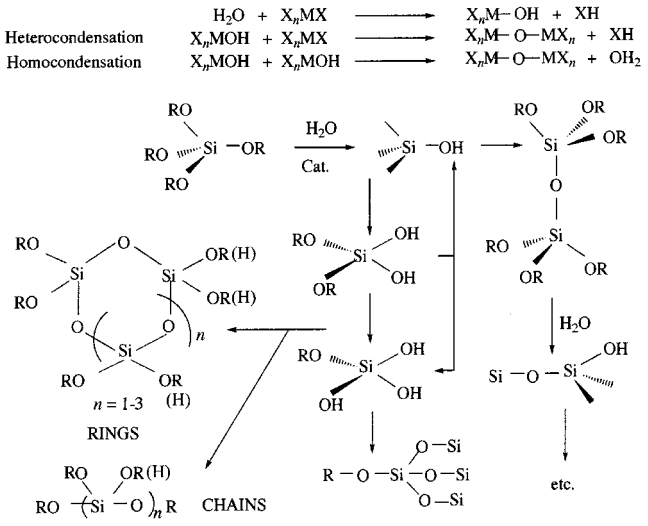

Scheme 2. Sol-gel hydrolytic polycondensation of metal alkoxides

highly crosslinked solid. The detailed mechanism for this process is unknown. However, several attempts to elucidate this aspect of the reaction have been made, leading to isolated but interesting results.[5−7]

The use of this chemistry for solid preparation is nowadays strongly connected to polymer science. The physical properties of the highly crosslinked polymers obtained are controlled by the mechanism of the reaction used to build the chains of the resulting macromolecules.[8] In the same manner, the synthesis of the inorganic materials performed by sol-gel corresponds to a kinetically controlled process. The texture of the solid obtained, described in terms of macroscopic properties (specific surface area, porosity, density etc.), is highly dependent on the experimental conditions, a fact that strongly suggests kinetic control of the solid.[9−12] Thus, although it is not possible to predict the texture of the solid, the method is highly flexible because of the great number of parameters that can be manipulated (temperature, concentrations, solvent, catalyst, nature of leaving group etc.) to give experimental control over the texture obtained. It is also important to point out the flexible processability inherent in the formation of the sol. The sol is a viscous liquid that allows devices to be obtained: e.g. films by coating and fibres by spinning, as well as matrices with the possibility of inclusions.

In materials science the gels are described as unstable solids.[4] They cannot be classified as metastable since their stability can be dependent on experimental conditions. This fact has led to difficulties as far as reproducibility is concerned. However, after extensive studies performed on silsesquioxanes and nanostructured hybrid organic-inorganic materials, we have shown that *reproducibility is attained when the experiments are carefully performed with the precision that is necessary for physical chemistry experiments or analytical measurements.*[8−11] Moreover, the stability of these solids is very good when they are stored under very strictly controlled conditions that exclude the presence of reagents such as air humidity.[13]

The sol-gel methodology is an alternative to the classical thermodynamic routes for the synthesis of solids. It allows materials to be obtained by "step-by-step" chemistry starting from molecular precursors at low temperatures. The preparation of the solids through "Chimie Douce" processes is the natural bridge between molecular and solid state chemistry. There is a wonderful way to obtain, in one step, new materials in which organic, inorganic, organometallic molecules or polymers can been included or chemically bound to inorganic matrices. A wide field of research is now open to chemists, including the possibility of designing the organisation of the porosity of the inorganic matrix using templates or micellar media.[14−27]

This paper focuses on the organic-inorganic hybrid materials obtained from molecular precursors. However, it is important to make the distinction between nanocomposites and the nanostructured hybrid materials[28−40] that are the topic of this paper.

The polycomponent solids corresponding to nanocomposites are obtained by hydrolytic polymerisation of a metal alkoxide previously mixed with organic molecules (or polymers). These solids can be separated into two phases by washing with an organic solvent. However, it is important to point out that this approach to the synthesis of materials is the simplest and most efficient. The method allows interesting devices to be obtained very quickly in order that their properties can be studied. The method also provides a very flexible way to obtain new materials and to include organic units, with desirable physical properties, within inorganic matrices. Silica is currently the most useful oxide matrix because of its physical and chemical properties and also due to its ease of preparation and processability by the sol-gel methodology. The number of possibilities open is vast and includes, amongst others, the preparation of controlled me-

soporous materials, molecular imprinting and foot printing, and optical devices. etc. Indeed, in this area a large number of papers[21−31] have been published that describe numerous very interesting materials.

In contrast, the nanostructured hybrid materials that form the topic of this paper are obtained by hydrolytic polycondensation of a molecular precursor in which trifunctional silicon atoms SiX_3 are covalently bound to the organic moiety (Scheme 3).

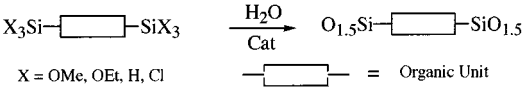

Scheme 3. Elaboration of organic-inorganic hybrid solids from bis-silylated precursors

The hydrolytic polycondensation allows the $SiO_{1.5}$ groups to be crosslinked around the organic unit to give to monophasic solids. These solids correspond to nanostructured materials. This aspect will be developed in more detail later in the paper.

II. Monophasic Hybrid Organic-Inorganic Materials: Scope and Limitations

Scheme 3 outlines the principle used in the synthesis of these materials. It is important to summarise the main results obtained in this field to date and to point out the main features of this class of materials.

The main prerequisite is the presence of non-hydrolysable and non-oxidisable bonds between the organic unit and the oxide matrix. The second requirement is the presence of groups that permit the formation of the oxide matrix by a hydrolytic polycondensation (''Chimie Douce'' process). Trifunctional silicon groups (SiX_3) are very convenient for this purpose and trialkoxysilyl groups [$-Si(OR)_3$ (R = Me, Et, *i*Pr)] are commonly used.[32−40] However, $-SiCl_3$ [41] and $-SiH_3$ [42] groups can also lead to silica matrices. Moreover, Si−C bonds are highly stable towards hydrolysis and oxidation and many routes have been found for the introduction of a silicon group into an organic molecule.

II.a. Materials Obtained from Mono-silylated Precursors

The focus of this paper is on nanostructured materials obtained from precursors containing at least two Si−C bonds.[34−40] The case of monocomponent hybrids with only one Si−C bond has been reviewed recently.[32,33] Monocomponent systems are particularly interesting since they open the way to functionalised surfaces. It has been demonstrated that the hydrolytic polycondensation of $R-SiX_3$ leads to solids in which the organic part is mainly located at the surface of the material, as evidenced by TOF-SIMS (Time of Flight Secondary Ion Mass Spectrometry),[43] by the hydrophobicity of the material obtained, and by the reactivity of the functionalities attached to the organic group R[44,45] (Scheme 4).

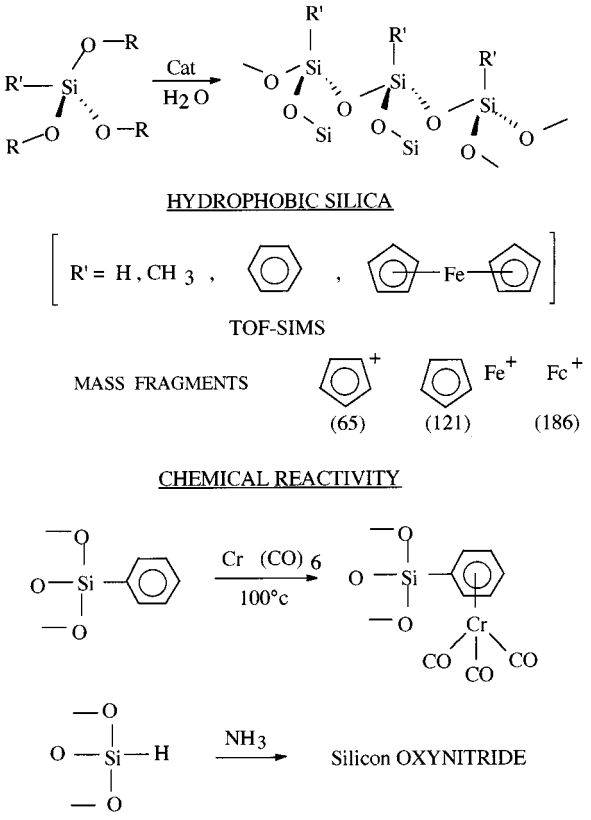

Scheme 4. Hybrid materials obtained from mono-silylated precursors

The characteristics of the materials obtained for catalysis, separation, its physical properties or other purposes are related to the accessibility of the functional groups in the solid.

The location of the functionalities at the surface is a very important feature and two routes are used for the preparation of these materials: grafting of an oxide surface (generally SiO_2) (route A) or preparation by the sol-gel methodology (route B) (Scheme 5).

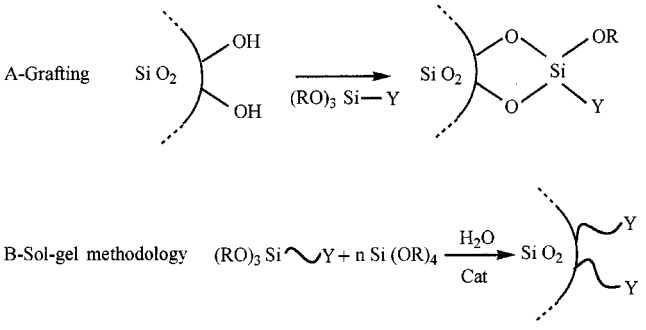

Scheme 5. Functionalisation in hybrid solids

Although grafted silica with interesting applications has been prepared by route A, route B is generally a more efficient way to obtain materials than route A. A similar trend is observed in the case of the mesoporous materials prepared using a micellar medium.[46,47] The sol-gel polycond-

ensation of $Si(OR)_4$ in the presence of a surfactant solution in H_2O leads to a hybrid material with a regular hexagonal distribution of the surfactant. After elimination of the surfactant it is possible to obtain a mesoporous SiO_2 in which the pores are regularly distributed within the material.[22]

Functionalisation of mesopores can be achieved by grafting (route A) using the reactive groups located inside the mesopores.[21,48−52] However, it is possible to obtain directly a mesoporous silica that has a narrow and organised porosity and contains chemical functionalities located inside the pores. The methodology used is similar to that shown in route B, but is performed in presence of surfactant. The lipophilicity of the precursor permits its inclusion in the surfactant. Thus, during the formation of SiO_2, the polar Si−OH head is at the surface and the lipophilic and functional tail is included in the micelle.[21,47,53−56]

Scheme 6 illustrates the synthesis of thiophosphane-containing materials either by direct preparation using method B in presence of a micellar medium, or by reaction of S_8 on the phosphane-containing material prepared by the same method.[53] The materials obtained by the two methods exhibit the same characteristic features in terms of ^{31}P, ^{13}C, ^{29}Si NMR, porosity etc.

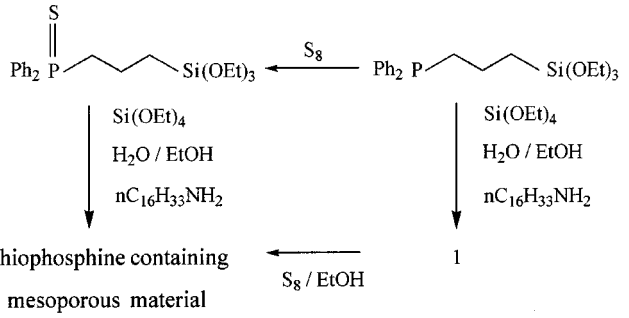

Scheme 6. A phosphane-containing material elaborated in micellar media

II.b. Bis-Silylated Precursors

The main features of these systems are summarised by four key points, which will be discussed in greater depth in the following sections.

(1) Processability. (2) Wide range of synthetic possibilities. (3) Inclusion in the oxide matrix of the desired physical properties using appropriate organic moieties. (4) Inclusion of the desired chemical properties.

II.b.1. Processability

In all cases the sol-gel methodology allows processable materials to be obtained since the inorganic polymerisation occurs with formation of a highly viscous sol. Thus, it is always possible to obtain films (by coating), matrices, and also fibres (by spinning).

II.b.2. Wide Range of Possibilities

The wide range of possibilities for the synthesis of materials is exemplified by the fact that, in all cases studied to date, the organic unit is included within the silica matrix without any transformations. The hydrolytic polycondensation occurs under mild conditions and it does not induce any rearrangement or bond breaking in the organic compound: the ^{13}C NMR spectra of the organic units are almost identical in solution and in the oxide matrix. ^{29}Si NMR spectroscopy, which is sensitive to the first and second nearest neighbours, allows easy discrimination between the T ($C-SiO_3$) and the Q (SiO_4) units.[57][58] The cleavage of the Si−C bonds corresponds to the formation of Q units whose signals are located in the range $\delta = -90$ to -110, and are shifted to higher field in comparison to the T units ($\delta = -40$ to -80) depending on the nature of the organic group. The only exception is the case of the Si−C≡C bond, which can be cleaved by H_2O when fluoride ions are used as the catalyst.[17−20,59−73] Scheme 7 shows, as an example, the ^{29}Si NMR and IR spectra observed before and after cleavage of Si−C bonds in the case of the tetraethynylbenzene hybrid material.[61] The solid (I) is obtained from the corresponding precursor by hydrolysis. Treatment with NH_4F/H_2O in MeOH leads to Si−C≡C cleavage. However, the tetraethynylbenzene formed (II) cannot be separated from SiO_2. It is possible to show by spectroscopic analysis that the reaction is complete, as illustrated in Scheme 7.

Any organic molecule containing at least two SiX_3 units can be transformed into a nanostructured hybrid material by hydrolytic polycondensation (Scheme 8). Thus, this very flexible synthetic route does not suffer from any limitation in terms of access to materials. In this way chemists have the opportunity to include in a solid material any organic molecule that has a desirable physical property in solution. It also offers an alternative to the thermodynamic approach to the preparation of materials since is allows all the possibilities available by molecular chemistry to be combined in the design of new kinds of materials (Scheme 8).

II.b.3. Physical Properties in the Hybrid Materials

Generally speaking the physical properties of the organic part are maintained in the hybrid solid. However, these properties can be different depending on whether the location of the organic part is at the surface or in the core of the material. Moreover, possible strains induced by the rigidity of the solid can lead to some distortion of the physical properties of the organic compound. A few examples are given below.

(i) Electrochemistry

Ferrocene is a good example because of its high stability and precise electrochemical behaviour.[74] The electrochemistry observed is very different in the cases of mono- and bis-silylated ferrocene.[75]

Gels III and IV, respectively formed from trimethoxysilylferrocene and 1,1′-bis(trimethoxysilyl)ferrocene copolymerized with tetramethoxysilane and deposited onto platinum, allow modified electrodes to be built and these systems have interesting electrochemical properties (Scheme 9).[75]

Solid IV, obtained from the bis-silylated ferrocene, displays a Cottrelian diffusion of charge transfer and exhibits

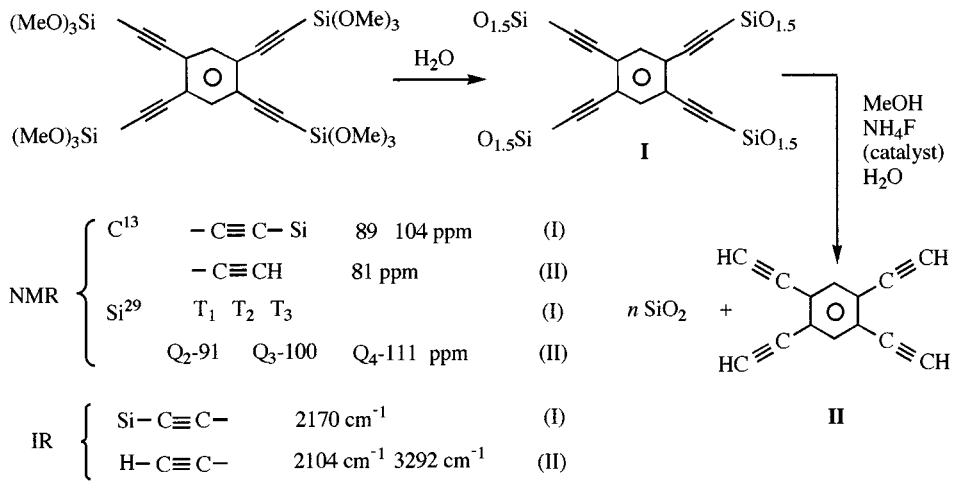

Scheme 7. Cleavage of the Si−C≡C bond catalysed by fluoride ions; spectroscopic characterisation

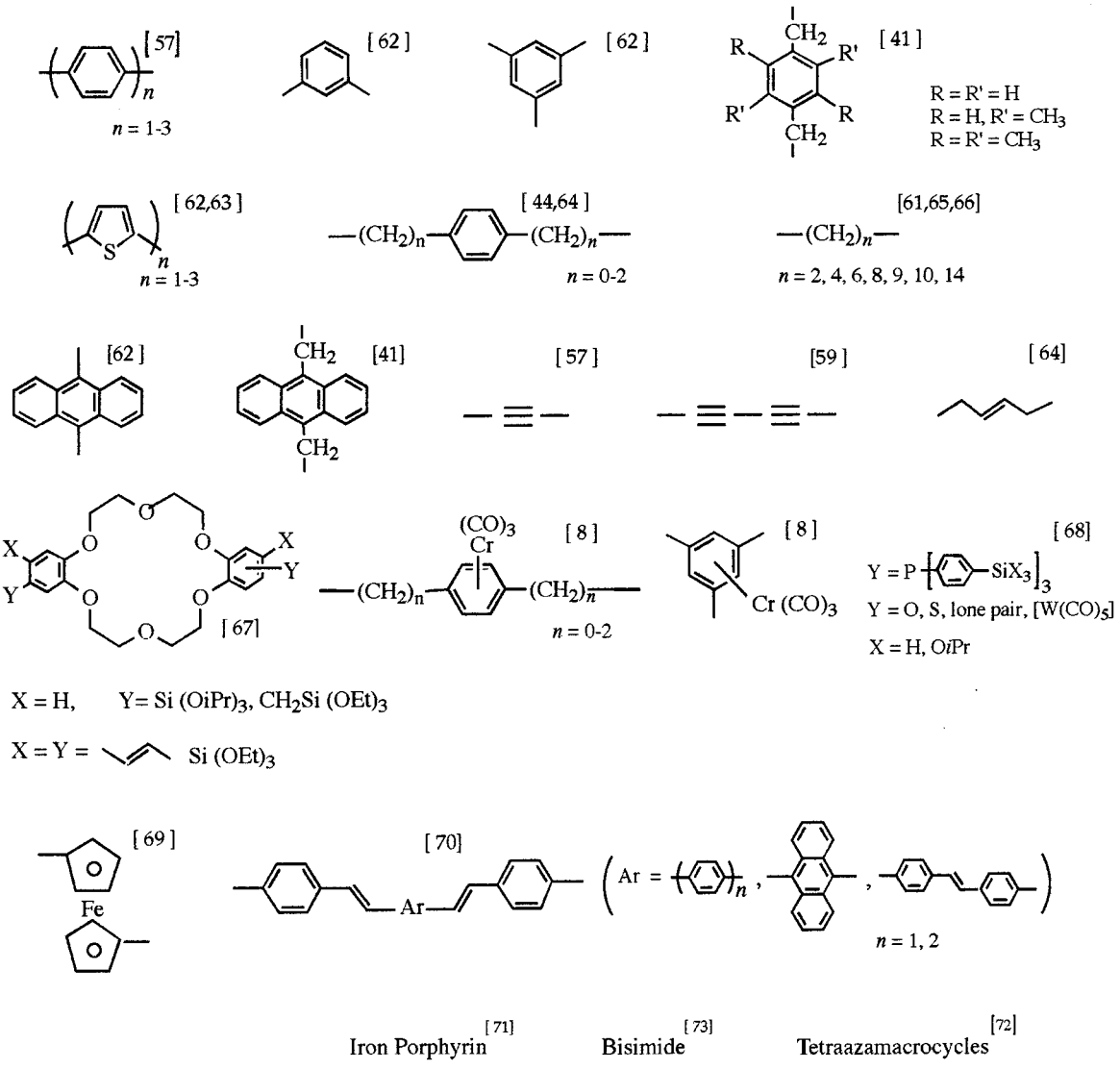

Scheme 8. Examples of organic units included in nanostructured materials

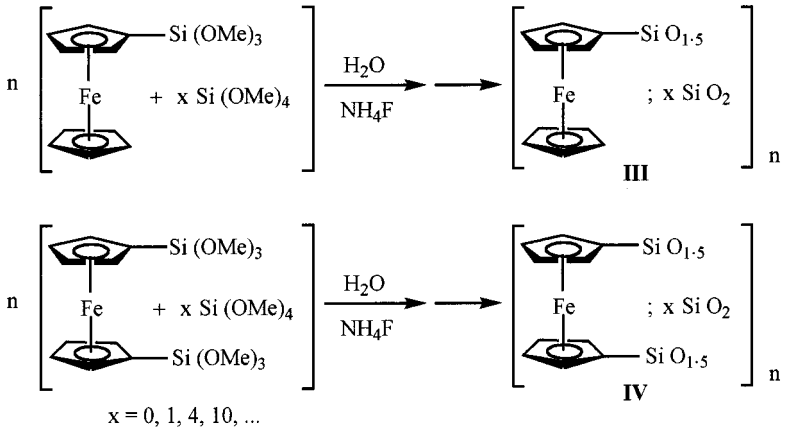

Scheme 9. Gels obtained from mono and bis-silylated ferrocene

classical reversible cyclic voltammograms: the peak current scales in a linear way with the square root of the scan rate (Figure 1).

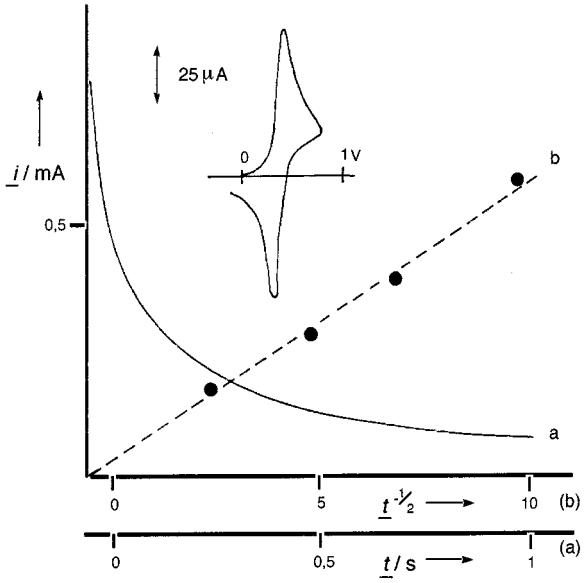

Figure 1. Typical chronoamperometric and linear Cottrell curves of a gel prepared from a bis-silylated ferrocene precursor: (a) plot of current i versus time t, (b) plot of current i versus $t^{-1/2}$

Furthermore, it proved impossible to perform complete oxidation of Fe^{II} into Fe^{III} in a macroelectrolysis carried out on a suspension of IV.[76] The process is, however, reversible (Figure 2). Such behaviour is due to the fact that some ferrocenyl units are embedded in the core of the solid and do not participate to the electrochemical process.

In the gels III (Scheme 9), derived from the mono-silylated ferrocene, the charge transfer follows a law with a fractional exponent. This unique behaviour is indicative of a particular substructure in the gels. Moreover in this case, complete and reversible oxidation of Fe^{II} into Fe^{III} is observed in macroelectrolysis, as evidenced by Mössbauer spectroscopy[76] (Figure 2).

(ii) Optical Properties

Molecular precursors containing 1−4 phenylene vinylene units have been prepared.[70] These organic units are known for their photoluminescence properties.[77]

Solid materials containing these organic fragments have been easily prepared by sol-gel from the appropriate precursors. These materials provide examples of the inclusion of chromophores into silica frameworks (Scheme 10).

The absorption and fluorescence spectra of the gels exhibit maxima at 495−496 nm, which are similar to the values observed with the corresponding precursors in the solid state. However, the high energy emission of the precursor at 466 nm is absent (Figure 3). The optical properties of the chromophores are retained in the solid and they lead to materials with potential optical and electro-optical applications. Moreover, it was observed that upon formation of the solid the position and form of the photoluminescence spectra changes. The modifications observed are different depending on the nature of the aromatic fragment Y.

II.b.4. Chemical Properties of the Hybrid Materials

The chemistry in the solid state is essentially the same as the chemistry occurring in homogeneous phases (liquid or gas). However, working with the solid does cause some very important changes, the first one being due to the highly restricted mobility of the compound in question. At room or moderate temperatures the motions of the atoms are limited to vibration and to a very low conformational flexibility. This restricted mobility is connected with a large decrease of the entropy. The second change in the chemistry involves the location of the organic part either at the surface or in the core of the solid. Thus, the accessibility of the reactive sites towards a particular reagent will be different depending on the texture (mainly specific surface area and porosity) and the structure of the solid: the structure corresponds to the relative arrangements of the organic units within the material.

A few examples are given in order to illustrate the chemical reactivity of such solids.

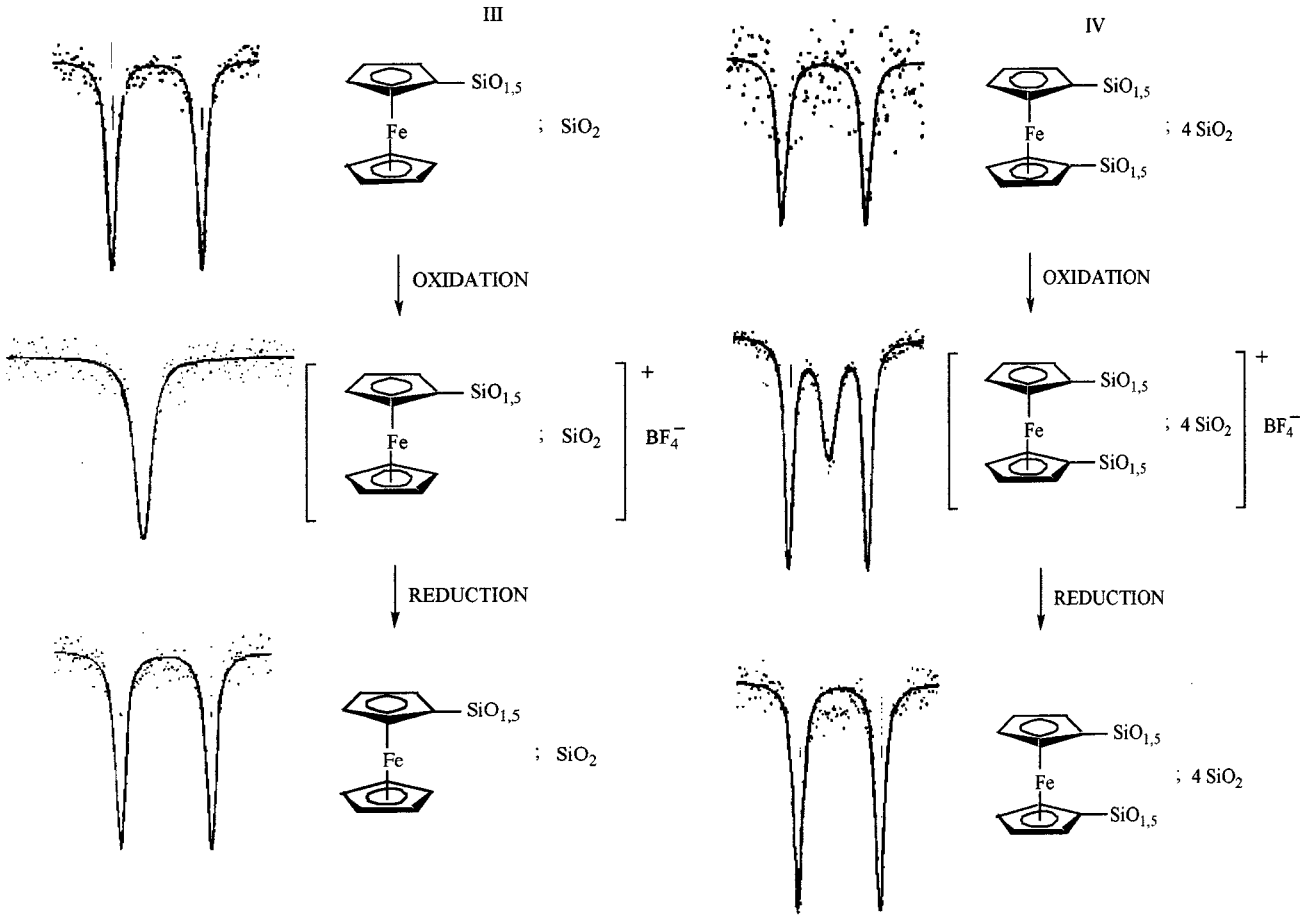

Figure 2. Mössbauer spectra of hybrid solids with ferrocenyl units

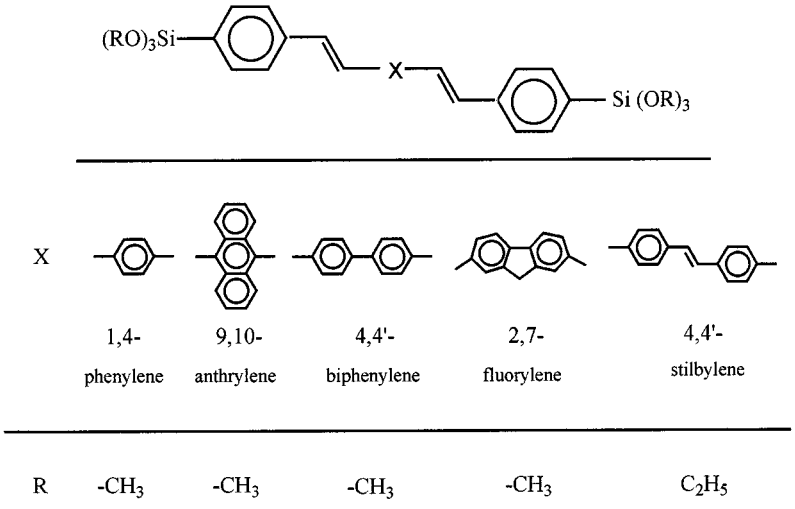

Scheme 10. Precursors with oligo-1,4-phenylene vinylene precursors

(i) Chemical Accessibility at Phosphorus and Crosslinking Ratio

The phosphorus atom is a good probe for the study of the chemical accessibility due to the fact that it has a wide range of reactivity towards both uncrowded (O_2, S_8, CH_3I etc.) and more crowded reagents (alkyl halides or transition metals). Moreover, its very high NMR sensitivity (^{31}P) permits a very reliable measurement of chemical changes at phosphorus.[78]

We have considered the reactivity on the solids V to VII, which were obtained by hydrolytic polycondensation from the corresponding $Si(OiPr)_3$ precursors. The reagents H_2O_2, S_8, CH_3I, φCH_2Br, $THF/W(CO)_5$, and BH_3 were used (Scheme 11).[79]

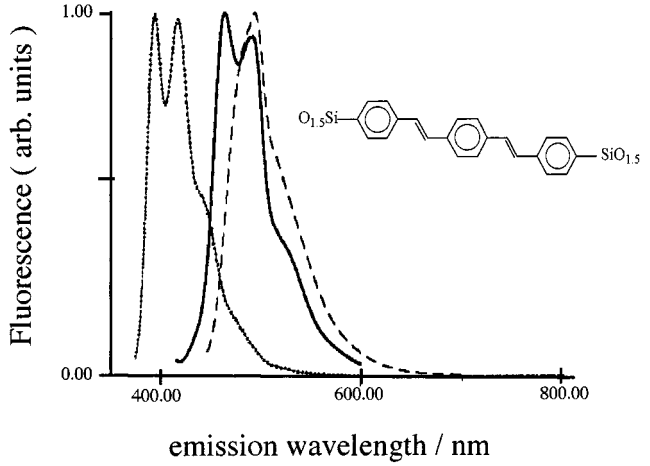

Figure 3. Photoluminescence spectra of gels with 1,4-phenylene vinylene units (precursor in THF (····) and KBr (−−) and the corresponding gel (---)

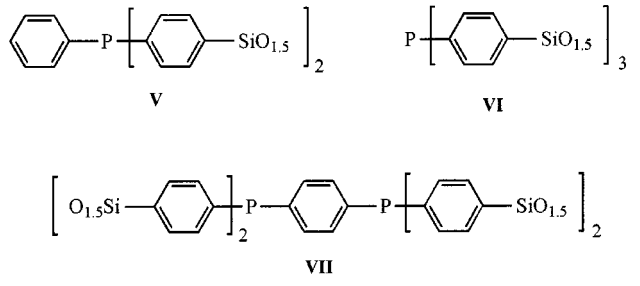

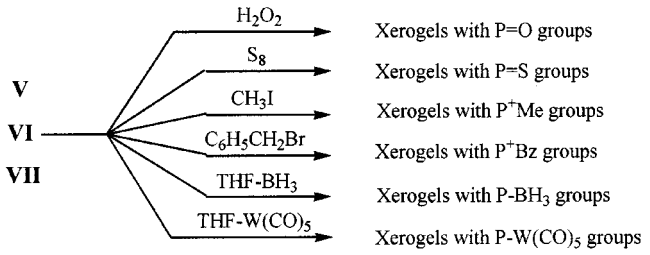

Scheme 11. Chemical accessibility of phosphorus atoms in hybrid solids incorporating phosphane units

Table 1 shows that all the phosphorus atoms are accessible to uncrowded reagents (H_2O_2, S_8, CH_3I), regardless of the specific surface area and the degree of crosslinking of the solid measured by the number of functionalities. (The degree of polycondensation at silicon has a similar magnitude for all the solids prepared.)

Table 1

Solid	S[a]	f	H_2O_2 or S_8[b]	CH_3I[b]	THF/$W(CO)_5$ [b]
V	<10	6	100	100	100
VI[c]	30	9	100	95	5
VI[d]	400	9	100	100	80
VII	460	12	100	100	20

[a] Specific surface area (BET) [$m^2\ g^{-1}$]. − [b] Reaction yield obtained from NMR spectroscopy on solids; f = number of functionalities at silicon. − [c] Solids obtained with *p*-toluene sulfonic acid (1%) as catalyst. − [d] Solids obtained with HCl (10%) as catalyst.

In contrast, the reactivity of the crowded reagent THF/$W(CO)_5$ is highly dependent on the crosslinking of the solid, which appears to be the dominant parameter. The specific surface area also plays a role, but to a lesser extent.

The steric hindrance of the reagent involves drastic requirements and the most rigid materials are not mobile enough to allow access to phosphorus. Thus, solid VII, which has twelve condensation directions, exhibits poor reactivity.[79]

(ii) Influence of the Solid on Crown-Ether Properties

Hybrid materials incorporating crown ethers have been prepared as shown in Scheme 12.[67]

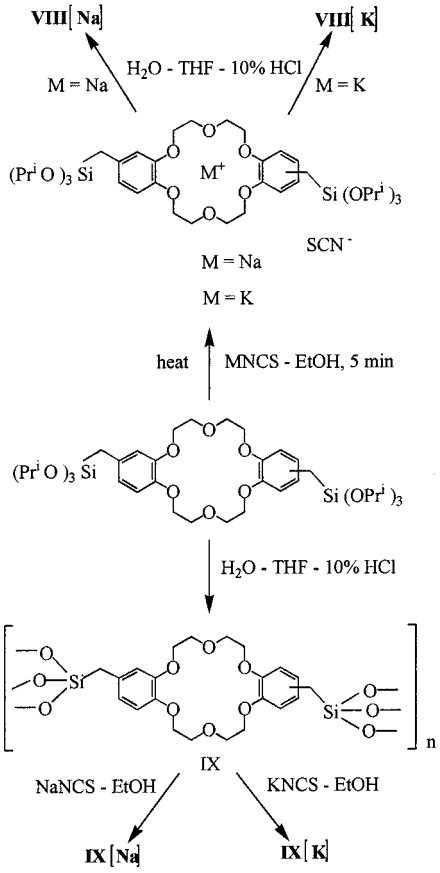

Scheme 12. Hybrid materials incorporating crown ether units from bis-silylated precursors

We prepared the gels VIII [Na] and VIII [K] by hydrolysis of the complexes of crown ethers with Na^+ and K^+. These solids were compared to the materials obtained by treatment of the solids IX with Na^+ and K^+, which gave IX [Na] and IX [K]. The degree of complexation of VIII [Na] and VIII [K] is high (95%), suggesting that the polycondensation at silicon does not induce a strong distortion of the geometry of the crown ether, a situation that could lead to the elimination of complexed salts. In contrast, IX [Na] and IX [K], obtained by direct complexation of the solids, are totally different: only 45% of the sites are complexed by Na^+ (IX [Na]) and 73% by K^+ (IX [K]). These observations

suggest that during the polycondensation of the non-complexed precursor, a distortion occurs that restricts the conformational aptitude of the crown ether ring for complexation of Na^+ and K^+. In this case, the use of complexed and non-complexed crown ethers as precursors leads to different materials. In order to verify this hypothesis we prepared the precursor X, which can lead to more crosslinked solids by increasing the number of functionalities.

In this case the possibility of direct complexation of the solid X′, obtained after hydrolytic polycondensation, is very low: 12% for Na^+ and 37% for K^+ (Scheme 13) and, in addition, ≈ 40% of the crown ether units do not exhibit the appropriate geometry for complexation with Na^+ or K^+. The rigidity of the crown ether in the solid prevents the conformational mobility necessary for complexation.

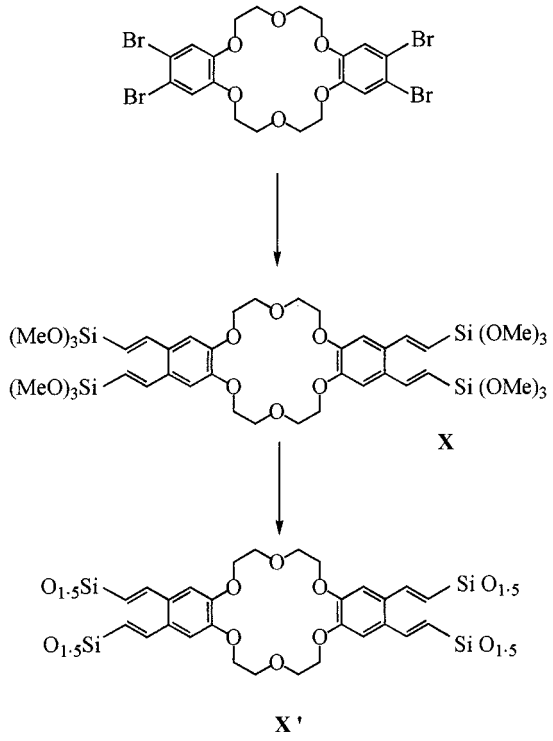

Scheme 13. Hybrid material incorporating crown ether units from tetra-silylated precursors

(iii) Chemical Reactivity Connected with Solid Organisation

A number of previous observations have shown that the molecular geometry is a very important parameter in controlling solid organisation. The example presented here illustrates the drastically different behaviours observed between the solids obtained from two similar precursors.[8,44]

Despite the fact that the two precursors are very similar, materials XI and XII, obtained using the same experimental conditions, exhibit completely different chemical and physical properties (Scheme 14).

XI is a hydrophilic solid with a high specific surface area (550 $m^2\ g^{-1}$) for which the TOF-SIMS does not exhibit any fragment arising from C_6H_4. Indeed, only Si−OH fragments can be detected. Interestingly, XI does not react with

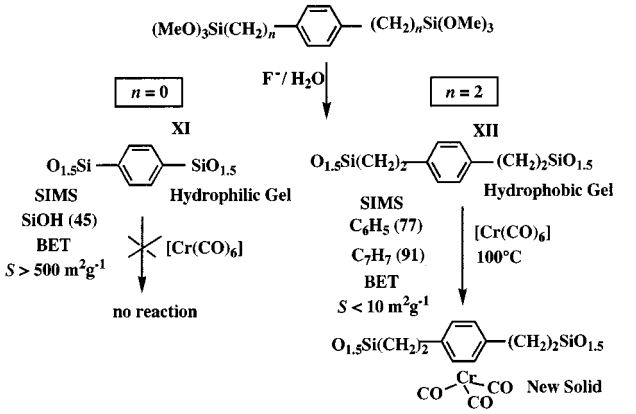

Scheme 14. Influence of the molecular geometry of the precursor on chemical and physical properties of the solid

$Cr(CO)_6$, which is consistent with the fact that the organic groups are embedded in the core of the solid.

In contrast, XII is a hydrophobic resin that has a very low specific surface area and the TOF-SIMS mass fragments exhibit phenyl (m/z = 77) and tropylium (m/z = 91) units. Moreover, Si−OH fragments cannot be detected.[43] These results suggest strongly that the organic groups are located at the surface of the solid. This fact is evidenced by the good yield observed in the reaction with $Cr(CO)_6$ (about 80%).

These two examples illustrate very well the significance of the organic unit in controlling the solid arrangement under identical experimental conditions. The rigid precursor leads to a solid with a completely different chemical reactivity to that of the solid obtained by polycondensation of a more flexible precursor.

III. Organisation of Hybrid Materials

All the hybrid materials reported in the literature to date are described as amorphous materials. Their XRD patterns are generally similar to those of amorphous silica. However, it is known that the XRD patterns can only be observed in solids with a long-range organisation. Moreover, at the moment a physical method that permits the study of short-range organisation in the solids is not available, with the exception of SAXS (Small Angle XR Scattering).[77]

(i) Preliminary Reports: Local Order in the Solid

The possibility and the nature of organisation were chemically assessed chemically. In section II.b.4(iii), we discussed the results obtained with XI and XII, which suggest that the arrangements of their organic units in the solid are completely different.[9,44] The hydrophobic material XII, in which the aromatic groups are at least partly located at the surface (detection by SIMS) and are also chemically accessible with good yield, can be more or less described as a solid in which molecular chains are crosslinked. Thus, $Cr(CO)_6$ dissolved in an organic solvent is able to pass through the material and react with the aromatic groups (Schemes 15 and 16).

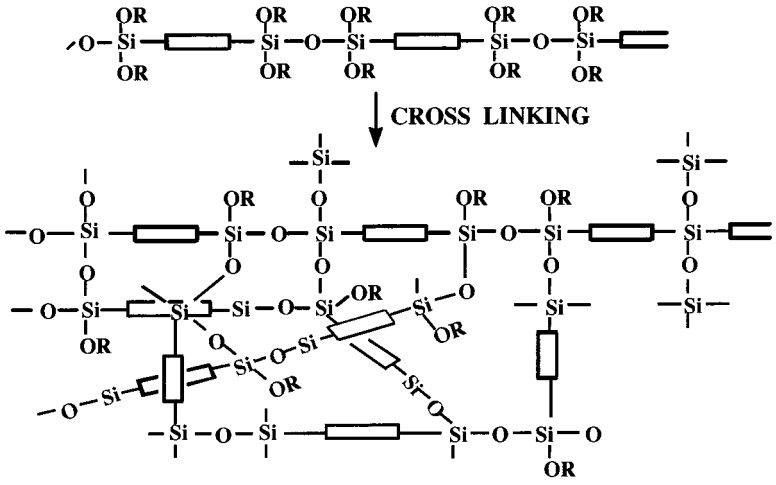

Scheme 15. Short-range organisation in the solid

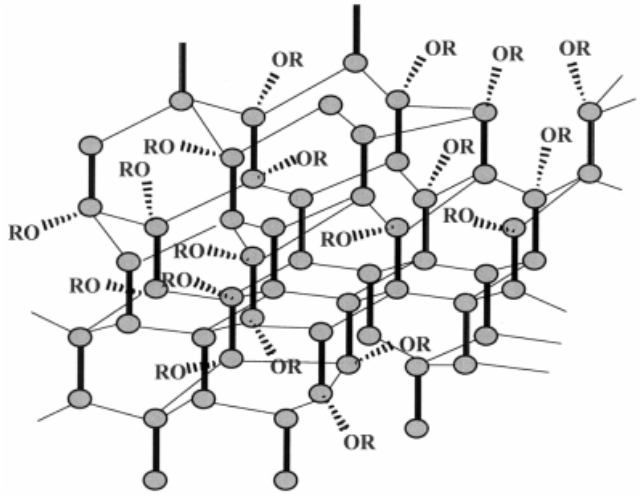

Scheme 16. Short-range organisation in the solid

In the hydrophilic material, XII, the aromatic groups are not detected by TOF-SIMS and they are not chemically accessible.

Moreover, a local order in the material is evidenced by the presence of a broad XR diffraction signal in SAXS.[80] Besides XII, this kind of XR diffraction signal has been observed in the case of three hybrids (XIII, XIV, XV), which were synthesized from precursors that also have a rigid geometry[81] (Scheme 17).

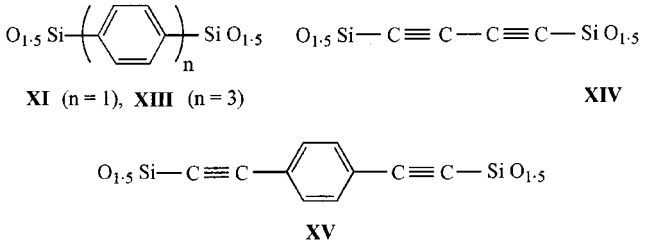

XI (n = 1), **XIII** (n = 3) **XIV** **XV**

Scheme 17. Hybrid solids from precursors with a rigid geometry

We propose the formation of local order (Scheme 16) in which the organic units are regularly alternated. The representation proposed here allows us to explain the presence of OCH_3 and OH fragments in TOF-SIMS and the absence of aromatic units since only one Si−C bond is located at the surface. This model also explains the hydrophilicity. The lack of flexibility accounts for the very poor reactivity towards $Cr(CO)_6$ and the regularity of the arrangements is in agreement with the SAXS results, which show a diffraction peak for a distance close to the size of the organic spacer.

In the case of XIII, a diffraction signal was observed at 15 Å.[82]

These values are estimated from the q values using the Bragg law as a first approximation. They provide evidence for the existence of a short-range order in the solid. However, the distance is only indicative, since the Bragg law is valid only for narrow diffraction signals. In the case of the two other materials, we reported the scattering peaks at 8.1 Å for XIV[59] and two signals at 11.4 Å and 5.5 Å for XV.[81] In this case, it was observed that the order demonstrated by the XR diffraction signal is independent of experimental parameters like the solvent, concentration, or catalyst. Moreover, the study of the copolymerisation between the precursor XV and TMOS shows a unidimensional swelling. The q values vary in a linear manner with the volumic fraction of added silica:

$q_{1,n} = q_{1,0}\ (1 - 0.48\ \ SiO_2)$ (n = mol number of TMOS, = volumic fraction), indicating the unidimensional swelling of a short-range organised solid.[83]

All these facts are in agreement with a local order in the solid that arises during its formation.

(ii) Physical Evidence of Long Range Organisation

We have obtained some physical evidence of long-range organisation in the solid by birefringence experiments performed with the solid derived from the precursor XV.[83]

A homogeneous solution of XV in THF with an equimolecular amount of H_2O was introduced into a confined cell made of glass plates treated with oriented Teflon. In the sealed cell the isotropic solution always appeared dark regardless of the angle of the crossed polarizers. After a few minutes bright domains appeared in different places due to

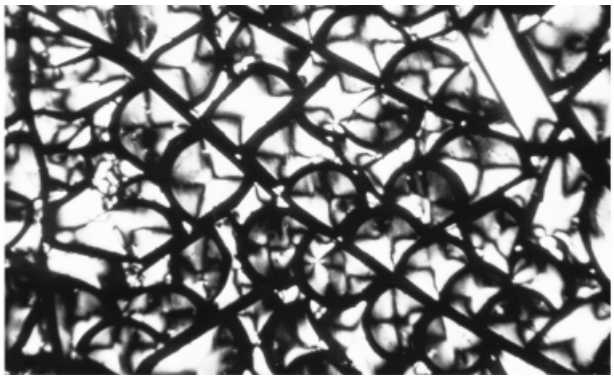

Figure 4. Physical evidence for long-range organisation by birefringence experiments

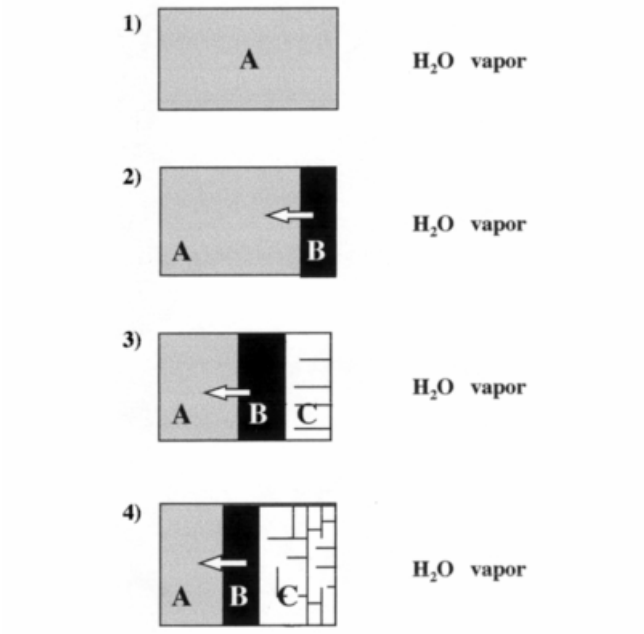

Scheme 18. Birefringence experiments: evolution of a part of a cell during the polycondensation process: A = precursor; B = liquid-to-gel isotropic medium; C = anisotropic gel and xerogel (dark lines: cracks)

birefringence. A few hours later the whole field of view the cell was birefringent and some cracks appeared (Figure 4).

Another set of experiments was performed with a controlled partial pressure of water using open cells containing the pure crystalline precursor. The results are represented in Scheme 18.

The microcrystalline precursor XV is birefringent and was converted into an isotropic liquid from which a birefringent solid formed. The birefringence subsequently increases upon ageing the gel and birefringent cracks were observed. This experimental procedure allows the history of the xerogel formation to be traced through the successive states: precursor, oligomers, polymers, sol, gel and cracks.

Thus, birefringence that corresponds to a micrometric scale organisation is observed when the polycondensation at silicon occurs to give crosslinked solids. Interestingly, the driving force for the organisation in the material during the polycondensation appears to be the rigidity of the organic unit included in the silica matrix.

IV. Conclusion

This short review has briefly covered only a few aspects of the wide possibilities opened up by the combination of Molecular Chemistry and "Chimie Douce" for the preparation of new kinds of materials.

Both approaches are based on kinetic control of the synthesis and their wedding has opened the way to materials that combine organic, inorganic and also macromolecular chemistry with inorganic polymerisation.

These new avenues are made accesible by the flexibility of "Chimie Douce", which permits the elaboration of oxides by a hydrolytic polycondensation mechanism. This low temperature polymerisation is compatible with the existence of covalent bonds between the oxide and organic, inorganic or macromolecular units. These hybrid materials combine the properties of the oxide matrix and the physical and chemical properties of the units included in the solid material. In the case of silica, the physical properties are restricted. However, this matrix has the great advantage of having a very wide chemical flexibility, good stability and excellent processability in the viscous sol state. The matrix allows the organic or organometallic partner to jump from its molecular state to the solid material. In this state the molecule becomes a part of the whole and the properties cannot be described in terms of isolated systems but as the properties of the material. For instance, the possible organisation of the organic or organometallic groups may enhance the physical properties in comparison to the isolated units. It is also possible to modify the chemical properties. A good example is the case of mesoporous materials obtained by the MCM-type route. These materials, called catalytic materials, have interesting possibilities in polyfunctional catalysis as well as for selective separation and purification.

The new horizons provided by hybrid organic-inorganic materials appear very wide and the future offers the prospect of many developments as chemists explore new routes to other oxides and to other kinds of matrices.

Acknowledgments

The author wishes to thank his co-workers who were involved in this research area − Professors G. Cerveau and C. Reyé, Doctors J. P. Bezombes, B. Boury, C. Chuit, G. Dubois, E. Framery, C. Lepeytre, V. Le Strat, A. Mehdi − for their cooperation, fruitful discussions and great efficiency. Professor Delord and Doctors Combarieu and Nobili are also acknowledged for their cooperation.

[1] J. Rouxel, *Chem. Scr.* **1988**, *28*, 33.
[2] L. Livage, *Chem. Scr.* **1988**, *28*, 9.
[3] S. Sakka, K. Kamiya, *J. Non-Cryst. Solids* **1980**, *42*, 403.
[4] C. J. Brinker, G. W. Scherer, *Sol-Gel Science: The Physics and Chemistry of Sol-Gel Processing*, Academic Press, San Diego, **1990**.

[5] R. Corriu, D. Leclercq, A. Vioux, M. Pauthe, J. Phalippou, in *Ultrastructure Processing of Advanced Ceramics* (Eds.: J. D. Mackenzie, D. R. Ulrich), Wiley, Chichester, **1988**, p. 113.
[6] R. K. Iler, *Chemistry of Silica*, Wiley, New York, **1979.**
[7] [7a] J. Chojnowski, M. Cypryk, K. Kazmierski, K. Rozga, *J. Non-Cryst. Solids* **1990**, *125*, 40. – [7b] J. Sefcik, A. V. Cormick, *Catalysis Today* **1997**, *35*, 205.
[8] *Recent Advances in Mechanistic and Synthetic Aspects of Polymerization* (Eds.: M. Fontanille, A. Guyot), *Nato Asi Series* Serie C vol. 215, D. Reidel, Dordrecht, **1987.**
[9] G. Cerveau, R. Corriu, C. Lepeytre, *Chem. Mater.* **1997**, *9*, 2561.
[10] G. Cerveau, R. Corriu, C. Fischmeister-Lepeytre, *J. Mater. Chem.* **1999**, *9*, 1149.
[11] G. Cerveau, R. Corriu, C. Fischmeister-Lepeytre, H. Mutin, *J. Mater. Chem.* **1998**, *8*, 2707.
[12] G. Cerveau, R. Corriu, E. Framery, *Chem. Commun.* **1999**, 2081.
[13] G. Cerveau, R. Corriu, B. Dabiens, *J. Mater. Chem.* **2000**, in press.
[14] N. K Raman, M. T. Anderson, C. J. Brinker, *Chem. Mater.* **1996**, *8*, 1682 and references therein.
[15] M. Hunnius, A. Rufinska, W. F. Maier, *Micropor. Mesopor. Mater.* **1999**, *29*, 389 and references therein
[16] C. J. Brinker, R. Sehgal, S. L. Hietal, R. Despande, D. M. Smith, D. Loy, C. S. Ashley, *J. Membrane Sci.* **1994**, *94*, 85.
[17] P. Chevalier, R. Corriu, P. Delord, J. Moreau, M. Wong Chi Man, *New J. Chem.* **1998**, 423.
[18] B. Boury, P. Chevalier, R. Corriu, P. Delord, J. Moreau, M. Wong Chi Man, *Chem. Mater.* **1999**, *11*, 281.
[19] B. Boury, R. Corriu, V. Le Strat, P. Delord, *New J. Chem.* **1999**, *23*, 531.
[20] B. Boury, R. Corriu, V. Le Strat, *Chem. Mater.* **1999**, *11*, 2796.
[21] A. Corma, *Chem. Rev.* **1997**, *6*, 2373 and references therein.
[22] [22a] J. S. Beck, J. C. Vartuli, W. J. Roth, M. E. Leonowicz, C. T. Kresge, K. D. Schmitt, C. T.-W. Chu, D. H. Olson, E. W. Sheppard, S. B. McCullen, J. B. Higgins, J. L. Schenker, *J. Am. Chem. Soc.* **1992**, *114*, 10834. – [22b] C. T. Kresge, M. E. Leonowicz, W. J. Roth, J. C. Vartuli, J. S. Beck, *Nature* **1992**, *359*, 710.
[23] F. Di Renzo, H. Cambon, R. Dutartre, *Micropor. Mesopor. Mater.* **1997**, *10*, 283.
[24] P. T. Tanev, T. J. Pinnavaia, *Science* **1995**, *267*, 865.
[25] S. A. Bagshaw, E. Prouzet, T. J. Pinnavaia, *Science* **1995**, *269*, 1242.
[26] G. S. Attard, J. C. Glyde, C. G. Goltner, *Nature* **1995**, *378*, 366.
[27] S. Inagaki, Y. Fukushima, K. Kuroda, *J. Chem. Soc., Chem. Commun.* **1993**, 680.
[28] C. Sanchez, F. Ribot, *New J. Chem. Special Issue* **1994**, *18*, 1007; C. Sanchez, F. Ribot, *Comment. Inorg. Chem.* **1999**, *20*, 327.
[29] J. P. Boilot, F. Chaput, T. Gacoin, L. Malier, M. Canva, A. Brun, Y. Levy, J. P. Galaup, *C. R. Acad. Sci. Paris, t. 322 Série IIb* **1996**, 27.
[30] P. Judenstein, C. Sanchez, *J. Mater. Chem.* **1996**, *6*, 54.
[31] H. K. Schmidt, *J. Sol-Gel Sci. Technol.* **1994**, *1*, 217.
[32] U. Schubert, N. Husing, A. Lorenz, *Chem. Mater.* **1995**, *7*, 2010.
[33] N. Husing, S. Schubert, *Angew. Chem. Int. Ed.* **1998**, *37*, 22.
[34] D. A. Loy, K. J. Shea, *Chem. Rev.* **1995**, *95*, 1431.
[35] E. Lindner, T. Schneller, F. Auer, H. A. Mayer, *Angew. Chem. Int. Ed.* **1999**, *38*, 2154.
[36] For a general survey, see: [36a] Hybrid organic-inorganic composites, *ACS Symp. Ser. n°585* (Eds.: J. J. E. Mark, C. Y. Lee, P. A. Bianconi), San Diego, **1995**. – [36b] *New J. Chem. Special Issue* **1994**, 18. – [36c] *Tailor-made Silicon Oxygen Compounds, From Molecules to Materials* (Eds.: R. Corriu, P. Jutzi), Vieweg, Braunschweig, **1996**.
[37] R. Corriu, D. Leclercq, *Angew. Chem. Int. Ed. Engl.* **1996**, *35*, 1420.
[38] R. Corriu, *Polyhedron* **1998**, *17*, 925; R. Corriu, *C. R. Acad. Sci. Paris t 1, série II C*, **1998**, 83.
[39] R. Corriu, G. Cerveau, *Coord. Chem. Rev.* **1998**, *180*, 1047.
[40] R. Corriu, *Angew. Chem. Int. Ed.* **2000**, *39*, 1377.
[41] [41a] P. J. Barri, S. W. Carr, D. Li Ou, A. C. Sullivan, *Chem. Mater.* **1995**, *7*, 265. – [41b] S. W. Carr, M. Motavelli, D. Li Ou, A. C. Sullivan, *J. Mater. Chem.* **1997**, *7*, 865.
[42] [42a] R. Corriu, J. Moreau, M. Wong Chi Man, *J. Sol-Gel Sci. Technol.* **1994**, *2*, 87. – [42b] G. Cerveau, R. Corriu, C. Lepeytre, *J. Organomet. Chem.* **1997**, *548*, 99.
[43] [43a] G. Cerveau, J. Dabosi, R. Corriu, J. L. Aubagnac, R. Combarieu, Y. De Puydt, *J. Mater. Chem.* **1998**, *8*, 1761. – [43b] G. Cerveau, R. Corriu, J. Dabosi, C. Fischmeister-Lepeytre, R. Combarieu, *Rapid Commun. Mass Spectrom.* **1999**, *13*, 2183.
[44] G. Cerveau, R. Corriu, C. Lepeytre, *J. Mater. Chem.* **1995**, *5*, 793.
[45] V. Belot, R. Corriu, D. Leclercq, A. Vioux, M. Pauthe, J. Phalippou, *J. Non-Cryst. Solids* **1990**, *125*, 187.
[46] [46a] A. Sayari, *Chem. Mater.* **1996**, *8*, 1840. – [46b] L. Mercier, T. J. Pinnavaia, *Chem. Mater.* **2000**, *12*, 188.
[47] D. J. Macquarrie, D. B. Jackson, J. E. G. Mdoe, J. H. Clark, *New. J. Chem.* **1999**, *23*, 539.
[48] D. Brunel, A. Cauvel, F. Fajula, F. Di Renzo, *Stud. Surf. Sci. Catal.* **1995**, *97*, 173.
[49] A. Cauvel, D. Brunel, F. Di Renzo, F. Fajula, *Am. Inst. Phys.* **1996**, *354*, 477.
[50] D. Brunel, N. Bellocq, P. Sutra, A. Cauvel, M. Lasperas, P. Moreau, F. Di Renzo, A. Galarneau, F. Fajula, *Coord. Chem. Rev.* **1998**, *178–180*, 1085.
[51] D. Brunel, *Micropor. Mesopor. Mater.* **1999**, *27*, 329.
[52] [52a] S. O'Brien, J. Tudor, S. Barlow, M. J. Drewitt, S. Heyes, *Chem. Commun.* **1997**, 641. – [52b] T. Maschmeyer, F. Frey, G. Sankar, J. M. Thomas, *Nature* **1995**, *378*, 159.
[53] R. Corriu, A. Mehdi, C. Reyé, *C. R. Acad. Sci. Paris, t 2, Série II c* **1999**, 35.
[54] R. Richer, L. Mercier, *J. Chem. Soc., Chem. Commun.* **1998**, 1775.
[55] M. H. Lim, A. Stein, *Chem. Mater.* **1999**, *11*, 3285.
[56] [56a] C. E. Fowler, S. L. Burkett, S. Mann, *Chem. Commun.* **1997**, 1769. – [56b] S. L. Burkett, S. D. Sims, S. Mann, *Chem. Commun.* **1996**, 1367.
[57] K. J. Shea, D. A. Loy, O. W. Webster, *J. Am. Chem. Soc.* **1992**, *114*, 6700.
[58] [58a] E. A. Williams, in *The Chemistry of Organic Silicon Compounds.* (Eds.: S. Patai, Z. Rappoport), Wiley, New York, **1989**, Vol. 1, Ch. 8, p. 511. – [58b] H. C. Marsmann, *Silicon ^{29}NMR*, and G. Engelhardt, *Silicon ^{29}NMR of Solid, Silicates*, in *Encyclopedia of Nuclear Magnetic Resonance*, Wiley, New York, **1996**. – [58c] H. C. Marsmann, in *NMR Basic Principles and Progress* (Eds.: P. Diehl, E. Fluck, R. Kasfeld), Springer, Berlin, **1981**, *17*, 235.
[59] [59a] R. Corriu, J. Moreau, P. Thépot, M. Wong Chi Man, *Chem. Mater.* **1992**, *4*, 1217. – [59b] R. Corriu, J. Moreau, P. Thépot, M. Wong Chi Man, *Chem. Mater.* **1996**, *8*, 100.
[60] P. Chevalier, R. Corriu, J. Moreau, M. Wong Chi Man, *J. Sol-Gel Sci. Technol.* **1997**, *8*, 603.
[61] P. Chevalier, Doctoral Thesis, Université Montpellier II, **1995**.
[62] J. H. Small, K. J. Shea, D. A. Loy, *J. Non-Cryst. Solids* **1993**, *160*, 234.
[63] [63a] P. Chicart, R. Corriu, J. Moreau, *Chem. Mater.* **1991**, *3*, 8. – [63b] R. Corriu, J. Moreau, P. Thépot, M. Wong Chi Man, C. Chorro, J. P. Lère Porte, J. L. Sauvajol, *Chem. Mater.* **1994**, *6*, 640.
[64] R. Corriu, J. Moreau, P. Thépot, M. Wong Chi Man, *J. Mater. Chem.* **1994**, *4*, 987.
[65] D. A. Loy, G. M. Jamison, B. M. Baugher, E. M. Russik, R. A. Assink, S. Prabakar, K. L. Shea, *J. Non-Cryst. Solids* **1995**, *186*, 44.
[66] H. W. Oviatt Jr., K. J. Shea, J. H. Small, *Chem. Mater.* **1993**, *5*, 943.
[67] [67a] C. Chuit, R. Corriu, G. Dubois, C. Reyé, *Chem. Commun.* **1999**, 723. – [67b] G. Dubois, Doctoral Thesis, Université Montpellier II, **1998**.
[68] J. P. Bezombes, C. Chuit, R. Corriu, C. Reyé, *J. Mater. Chem.* **1998**, *8*, 1749.
[69] R. Corriu, N. Costa, *J. Non-Cryst. Solids* **1993**, *163*, 226.
[70] R. Corriu, P. Hesemann, G. Lanneau, *Chem. Commun.* **1996**, 1845.
[71] P. Battioni, E. Cardin, M. Louloudi, B. Schölhorn, G. A. Spyroulias, D. Mansuy,T. G. Traylor, *Chem. Commun.* **1996**, 2037.

[72] G. Dubois, R. Corriu, C. Reyé, S. Brandes, F. Denat, R. Guilard, *Chem. Commun.* **1999**, 2283.
[73] S. T. Hobson, K. J. Shea, *Chem. Mater.* **1977**, *9*, 616.
[74] [74a] M. Rosenblum, *Chemistry of Iron group Metallocenes*, Wiley, New York, **1965**. – [74b] W. E. Watts, *Organomet. Chem. Rev.* **1967**, *2*, 231.
[75] P. Audebert, P. Calas, G. Cerveau, R. Corriu, N. Costa, *J. Electroanal. Chem.* **1994**, *372*, 275; P. Audebert, P. Calas, G. Cerveau, R. Corriu, N. Costa, *J. Electroanal. Chem.* **1996**, *413*, 89.
[76] N. Costa, Doctoral Thesis, Université Montpellier II, **1996**; G. Cerveau, R. Corriu, N. Costa, to be published.
[77] J. H. Burroughes, D. D. C. Bradley, A. R. Brown, R. N. Marks, K. Mackag, R. H. Friend, P. L. Burn, A. B. Holmes, *Nature* **1990**, *347*, 539.
[78] R. A. Komoroski, A. J. Magistro, P. P. Nicholas, *Inorg. Chem.* **1986**, *25*, 3917.
[79] [79a] J. P. Bezombes, C. Chuit, R. Corriu, C. Reyé, *J. Mater. Chem.* **1998**, *8*, 1749. – [79b] J. P. Bezombes, C. Chuit, R. Corriu, C. Reyé, *J. Mater. Chem.* **1999**, *9*, 1727. – [79c] J. P. Bezombes, C. Chuit, R. Corriu, C. Reyé, *Can. J. Chem.* **2000**, in press.
[80] [80a] A. Guinier, G. Fournet, Small Angle Scatttering of X-rays, John Wiley, New York **1955**. – [80b] O. Glatter, O. Kratky, *Small Angle X-ray Scattering*, Academic, London, **1982.**
[81] B. Boury, R. Corriu, P. Delord, V. Le Strat, *J. Non-Cryst. Solids* **2000**, *265*, 41.
[82] D. W. Schaefer, G. B. Beaucage, D. A. Loy, T. A. Ulibarri, E. Black, K. J. Shea, R. J. Buss, in *Better Ceramics through Chemistry VII* (Eds.: B. K. Coltrain, C. Sanchez, D. W. Schaeffer, G. L. Wilkes), *Mat. Res. Soc. Symp. Proc.*, Pittsburgh, **1996**, *435*, 301.
[83] B. Boury, R. Corriu, P. Delord, V. Le Strat, M. Nobili, *Angew. Chem. Int. Ed.* **1999**, *383*, 172.

Received July 3, 2000
[I00261]

On the Crystal Engineering of Organogallium Alkoxides Derived from Primary-Amine Alcohols − Relationships between Hydrogen Bonding and Donor−Acceptor Bonds

Janusz Lewiński,*[a] Janusz Zachara,[a] Tomasz Kopeć,[a] Kazimierz B. Starowieyski,[a] Janusz Lipkowski,[b] Iwona Justyniak,[a,b] and Edyta Kołodziejczyk[b]

Keywords: Gallium / Alkoxides / Crystal engineering / Donor-acceptor systems / Hydrogen bonds

The crystal structure analysis of model organogallium amine-alkoxides $Me_2Ga(OCH_2CH_2CH_2NH_2)$ (**2**) and $[Me_2Ga\{\mu\text{-}OCH_2CH(CH_3)NH_2\}]_2$ (**3**), demonstrate how hydrogen bonding can effectively compete with metal–ligand coordination preferences in determining the molecular and crystal structure and how conformational changes in a ligand and increased steric bulk on the carbon atom adjacent to the amine group can impart on a network morphology and molecular aggregations.

Introduction

In the last two decades, a detailed analysis of intermolecular interactions in crystals and the design of supramolecular architecture have become a rapidly expanding area.[1] Investigations of the self-assembly of organic molecules through intermolecular interactions have lead to the identification of a number of useful tools for supramolecular design, the most efficient being hydrogen bonding.[2] In spite of the large number of contributions and advances in the self-assembly of organic molecules based on noncovalent interactions, the area of organometallic compounds in this context remains largely unexplored.[3] Here we report preliminary results in aiding our understanding of relationships between intra- and intermolecular forces resulting from donor-acceptor and hydrogen bonding interactions using gallium alkoxides with primary-amine termini as model complexes.

Starting with pioneering work on the ligative possibilities of gallium alkoxides derived from amine alcohols,[4] considerable research has been devoted to the determination and understanding of the structure of this class of compounds.[5−15] Over twenty years ago Chong et al. reported the structural characterization of the dimethylgallium derivative of amine ethanol, $Me_2Ga(OCH_2CH_2NH_2)$ (**1**), and demonstrated that the latter compound exists as discrete four-coordinate monomers linked by an extensive network of N−H···O hydrogen bonds in the solid state.[6] Although the authors have not discussed in detail the hydrogen bond network, our analysis revealed a symmetrical three-dimensional architecture (structure **I**, Scheme 1). Surprisingly, to the best of our knowledge, competition between the four-coordinate complexes with an extended hydrogen bond network and the metal-ligand coordination preferences, for example the formation of the five-coordinate $[R_2Ga(O,N)]_2$-type adduct **II**, have not been studied. In order to test how the molecularity and network architecture of gallium alkoxides may be controlled by an appropriate choice of primary-amine-terminated alcohols, dimethylgallium derivatives of 3-amino-1-propanol, $Me_2Ga(\mu\text{-}OCH_2CH_2CH_2NH_2)$ (**2**), and 2-amino-1-propanol, $\{Me_2Ga[\mu\text{-}OCH_2CH(CH_3)NH_2]\}_2$ (**3**), were synthesized and structurally characterized, and the structural features were compared with those of the previously reported 2-amino-1-ethanol analogue.

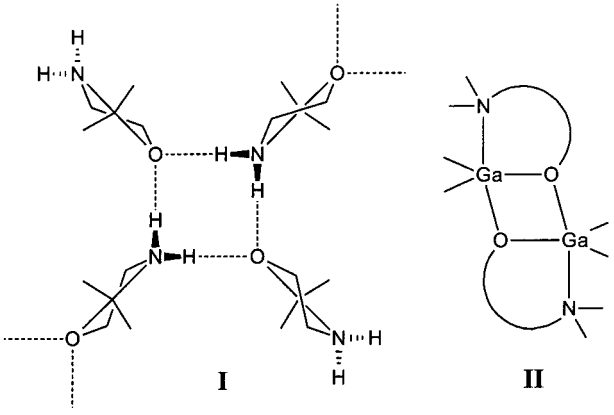

Scheme 1

Results and Discussion

The interaction of Me_3Ga with an equimolar amount of the corresponding amino alcohol in CH_2Cl_2 at −78 °C results in methane evolution and the quantitative formation of the dialkylgallium *O,N*-chelate complexes **2** and **3**. Single crystals suitable for an X-ray analysis were obtained from the concentrated solution at −20 °C.

[a] Department of Chemistry, Warsaw University of Technology, Noakowskiego 3, 00−664 Warsaw, Poland
Fax: (internat.) +48-22/660-7279
E-mail: lewin@ch.pw.edu.pl
[b] Institute of Physical Chemistry, Polish Academy of Sciences, Kasprzaka 44/52, 01-224 Warsaw, Poland

 © WILEY-VCH Verlag GmbH, 69451 Weinheim, 2001 1434−1948/01/0505−1123 $ 17.50+.50/0

The crystal structure of **2** contains four crystallographically independent monomeric molecules with essentially the same geometry, in which each Me_2Ga moiety is chelated in a tetrahedral geometry by the amine alkoxide ligand (average Ga−O and Ga−N distances are 1.879 Å and 2.037 Å, respectively) (Figure1). The alkoxide oxygen and amine nitrogen atoms act as complementary hydrogen donors and acceptors leading to a fully hydrogen-bonded network. The molecules in the ribbon assemble with pairs of strongly hydrogen-bonded chains (average NH···O distance is 1.90 Å; the N−H···O angles range from 170 to 176°). The chains are then cross-linked by very weak N−H···O interactions (average H···O distance is 2.45 Å and mean N−H···O angle 170°), forming the hydrogen bond network shielded by hydrophobic groups.

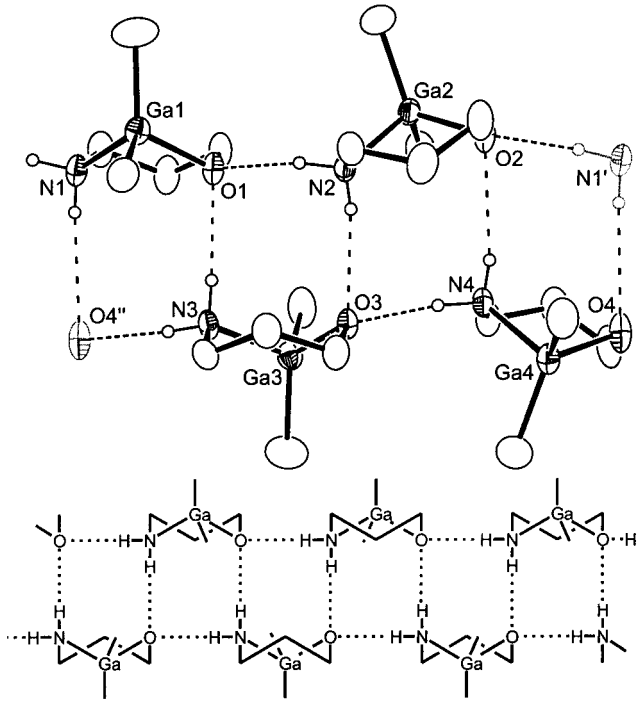

Figure 1. The hydrogen bonding observed in crystalline $Me_2Ga(OCH_2CH_2CH_2NH_2)$ (**2**) showing molecular chains parallel to [010], linked together by hydrogen bonds formed by the axial amine hydrogens and alkoxide oxygens; top: the arrangement of four independent molecules; bottom: schematic representation of the hydrogen bonding network; selected bond lengths (Å) and angles (°): Ga(2)−O(2) 1.874(3), Ga(3)−O(3) 1.885(3), Ga(4)−O(4) 1.870(3), Ga(1)−N(1) 2.043(4), Ga(2)−N(2) 2.039(4), Ga(3)−N(3) 2.026(4), Ga(4)−N(4) 2.041(4), Ga(1)−O(1) 1.887(3); O(1)−Ga(1)−N(1) 91.48(15), O(2)−Ga(2)−N(2) 92.94(15), O(3)−Ga(3)−N(3) 91.65(14), O(4)−Ga(4)−N(4) 92.26(15)

The monomeric moieties in the idealized chains are related by the glide plane passing through the oxygen and nitrogen atoms. Thus, the elongation of the backbone in 3-amino-1-propanol relative to 2-amino-1-ethanol enforces the crystal structure of gallium alkoxides. An explanation of this different supramolecular behavior of **1** and **2** in the crystal is provided by an analysis of the heterocycle conformation in both compounds. The six-membered GaOCCCN rings in **2** adopt a chair-like conformation. As a consequence of this geometry both the amine hydrogens and oxygen lone-pairs become nonequivalent and situated in axial and equatorial positions. Inspection of the space-filling representation of the crystal structure of **2** undoubtedly shows that steric requirements favor interactions between the equatorial hydrogen and equatorial lone-pair. However, in the crystal structure involving the gallium alkoxide derived from 2-amino-1-ethanol, the five- membered GaOCCN chelate rings are slightly twisted around the C−C bond giving rise to spatial equivalency of the amine hydrogens and oxygen lone-pairs. The bisectionally positioned hydrogens and lone pairs form a symmetrical, three-dimensional, hydrogen bond network (**I**, Scheme 1).

In contrast to the four-coordinate hydrogen bonded polymeric structures of **1** and **2**, compound **3** is dimeric, being bridged by the oxygens of the chelating alkoxide ligand (Figure 2). The crystal structure of **3** comprises individual five-coordinate dimeric molecules with no unusually short intermolecular contacts. The general structural features of the molecules are consistent with those observed for related gallium alkoxides (average $Ga-O_{equatorial}$, $Ga-O_{axial}$ and Ga−N distances are 1.923 Å, 2.113 Å and 2.348 Å, respectively).[5,13] It is worth noting that the crystal structure exhibits disorder indicating the presence of the (*R**,*R**)-$[Me_2Ga(O,N)]_2$ and (*R*,*S*)-$[Me_2Ga(O,N)]_2$ diastereomers (Figure 2). These diastereomers result from the association of monomeric moieties of the same or opposite configuration as the chiral center in the *O*,*N*-chelating ligand. Thus, the formation of the dialkylgallium alkoxide adducts derived from chiral amine-functionalized alcohols is not a stereoselective reaction, contrary to the highly stereoselective association of dialkylaluminum alkoxides derived from chiral carbonyl-functionalized alcohols recently reported by our group.[16]

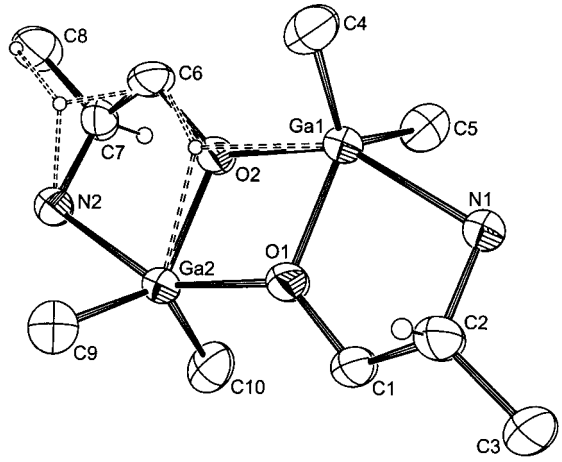

Figure 2. ORTEP view of the molecular structure of $\{Me_2Ga[\mu\text{-}OCH_2CH(CH_3)NH_2]\}_2$ (**3**) showing the disordered 2-amino-1-propanolato ligands of opposite configuration as the chiral center; thermal ellipsoids are drawn at 30% probability level; selected bond lengths (Å) and angles (°): Ga(1)−O(1) 1.916(3), Ga(1)−O(2) 2.127(15), Ga(1)−N(1) 2.349(4), Ga(2)−O(2) 1.929(14), Ga(2)−O(1) 2.106(4), Ga(2)−N(2) 2.347(4); O(1)−Ga(1)−N(1) 76.57(14), O(2)−Ga(1)−N(1) 149.8(4), O(2)−Ga(2)−N(2) 75.9(4), O(1)−Ga(2)−N(2) 150.14(14)

A question arises why compounds **1** and **2** crystallize as discrete four-coordinate monomers linked by an extensive network of N−H···O hydrogen bonds and **3** occurs as a five-coordinate dimer in the solid state. It is apparent that the relative stability of the five-coordinate dimer vs. the four-coordinate, hydrogen-bonded polymer depends on the balance between the energy of coordinate bonds and hydrogen bonds; however, energy-related questions are difficult to answer at present. The reported results show that for **1** and **2** cooperative hydrogen bond interactions effectively compete with the metal ligand coordination preferences in determining the molecular and crystal structure. On the other hand, the substitution of a hydrogen by a methyl group on the carbon atom adjacent to the hydrogen donor presumably results in a weakening of the intermolecular hydrogen bond interactions and enforces the structural changes.

Conclusion

In conclusion, metal alkoxides with a primary-amine functionalized side chain provide the means to study intra- and intermolecular forces resulting from donor-acceptor and hydrogen bonding interactions. Further studies on the effects of conformational and steric changes in a subunit structure on the molecular and crystal structure of metal alkoxides are in progress.

Experimental Section

General Remarks: All reactions were carried out under dry nitrogen using standard Schlenk techniques. Solvents were dried and distilled prior to use. NMR spectra were recorded on a Varian 300 VXL spectrometer.

(3-Aminopropanolato)dimethylgallium (2): A solution of 3-amino-1-propanol (0.60 g, 8.0 mmol) in CH_2Cl_2 (10 cm^3) was cooled to −78 °C and Me_3Ga (0.92 g, 8.0 mmol) was added dropwise. After the addition was completed, the reaction mixture was warmed to room temperature and stirred for 0.5 h. Concentration of the mother solution followed by crystallization at −20 °C gave a colorless solid. Yield: 80%. − ^{1}H NMR (C_6D_6, 300 MHz): δ = −0.14 (s, 6 H, Ga−CH_3), 0.82−1.35 (2 H, NH_2), (br. m, 2 H, CH_2), 2.27 (br. t, 2 H, CH_2), 3.81 (br. t, 2 H, OCH_2). − $C_5H_{14}GaNO$ (173.89): calcd. C 34.53, H 8.11, N 8.05; found C 34.46, H 8.18, N 8.06.

Bis(μ-2-aminopropanolato-*N*,*O*)tetramethyldigallium (3): A solution of 2-amino-1-propanol (0.60 g, 8.0 mmol) in CH_2Cl_2 (10 cm^3) was cooled to −78 °C and Me_3Ga (0.92 g, 8.0 mmol) was added dropwise. After the addition was completed, the reaction mixture was warmed to room temperature and stirred for 0.5 h. Complex **3** was isolated at −20 °C as colorless crystals. Yield: 90%. − ^{1}H NMR (C_6D_6, 300 MHz): δ = −0.07 (s, 12 H, Ga−CH_3), 0.42 (br, 4 H, NH_2), 0.50 (d, 6 H, CH_3), 2.38 (br. m, 2 H, CH) 2.97 and 3.51 (dd, 4 H, OCH_2). − $C_{10}H_{28}Ga_2N_2O_2$ (347.78): calcd. C 34.53, H 8.11, N 8.05; found C 34.48, H 8.15, N 8.03.

X-ray Crystal Structure Analysis: Single crystals of **2** and **3** suitable for X-ray diffraction studies were placed in a thin-walled capillary tube (Lindemann glass 0.5 mm) in an inert atmosphere. The tube was plugged with grease, then flame-sealed and mounted on a goniometer head. Selected crystallographic data, the parameters for data collection and refinement procedures are presented in Table 1.

Compound 2: Unit cell parameters and intensity data for compound **2** were collected with a P3 Siemens diffractometer employing graphite monochromated Mo-K_α radiation. The crystal classes and the orientation matrices were obtained by the least-squares refinement of 30 well-centered reflections randomly selected in the 2θ range 16−29°. The intensities were collected in the ω−2θ mode

Table 1. Crystal data and data collection parameters for **2** and **3**

Compound	**2**	**3**
Empirical formula	$C_5H_{14}GaNO$	$C_{10}H_{28}Ga_2N_2O_2$
Molecular weight	173.89	347.78
Temperature [K]	293(2)	293(2)
Wavelength [Å]	0.71073 (Mo-K_α)	0.71073 (Mo-K_α)
Crystal system	Monoclinic	Monoclinic
Space group	$P2_1/c$	$P2_1/a$
Unit cell dimensions	a = 16.171(2) Å	a = 8.663(2) Å
	b = 10.9828(14) Å	b = 11.738(2) Å
	c = 20.146(3) Å	c = 16.293(3) Å
	β = 111.411(12)°	β = 94.17(3)°
Volume [$Å^3$]	3331.1(8)	1652.4(6)
Z	16	4
Density [Mg/m^3]	1.387	1.398
Absorption coefficient [mm^{-1}]	3.227	3.253
F(000)	1440	720
Crystal size [mm^3]	0.64 × 0.19× 0.15	0.30 × 0.26× 0.14
θ range for data collection	2.1 to 25.0°	3.0 to 27.4°
Index ranges	$0 \le h \le 19$, $0 \le k \le 13$, $-24 \le l \le 22$	$0 \le h \le 11$, $0 \le k \le 15$, $-21 \le l \le 21$
Independent reflections	5863 (R_{int} = 0.0142)	3752
Absorption correction type	Gaussian	Semi-empirical
Data/restraints/parameters	5863/0/364	3752/20/190
Final R indices [$I > 2\sigma(I)$][a]	$R1$ = 0.0381, $wR2$ = 0.0681	$R1$ = 0.0549, $wR2$ = 0.1098
Goodness-of-fit on F^2[b]	0.920	1.089
R indices (all data) [a]	$R1$ = 0.0863, $wR2$ = 0.0789	$R1$ = 0.0844, $wR2$ = 0.1271
Extinction coefficient	0.00029(5)	0.0035(6)
Largest diff. peak and hole	0.37 and −0.29 e·$Å^{-3}$	0.91 and −0.81 e·$Å^{-3}$

[a] $R1 = \Sigma|F_o - F_c|/\Sigma|F_o|$; $wR2 = [\Sigma w(F_o^2 - F_c^2)^2/\Sigma wF_o^4]^2$. − [b] Goodness of fit $S = [\Sigma w(F_o^2 - F_c^2)^2/\Sigma(n-p)]^{1/2}$.

and corrected for Lorentz-polarization effects and crystal decomposition (3.8%). A Gaussian absorption correction based on the crystal shape was applied, which resulted in transmission factors ranging from 0.531 to 0.634. The structure was solved by direct methods using the SHELXS-86 program.[17] The distribution of the peaks showed that compound **2** crystallizes with four independent molecules in the asymmetric unit. The structure of **2** was refined by full-matrix least-squares on F^2 using the program SHELXL-97.[18] All non-hydrogen atoms were refined with anisotropic thermal parameters. The hydrogen atoms of the methyl groups C(25) and C(35) were refined as disordered groups with two positions rotated by 60° about the C−C bond. The remaining hydrogen atoms were located from the Fourier-difference map and isotropically refined.

Compound 3: Diffraction data were collected at room temperature on a Nonius Kappa diffractometer equipped with a CCD area detector. The structure was solved by direct methods (SHELXS-86 program[17]). Compound **3** crystallizes with one independent dimeric molecule in the asymmetric unit. Full-matrix least-squares refinement was carried out on F^2 (SHELXL-97[18]). All non-hydrogen atoms were refined anisotropically. The O(2)C(6)C(7)C(8)N(2) ligand revealed substantial disorder, which was modeled in terms of two sets of $OCH_2CH(CH_3)NH_2$ atoms (two moieties of opposite configuration as the chiral center) with adjusted occupancy factors of 0.61(1) and 0.39(1), respectively. Both disordered moieties were refined anisotropically using similarity restraints for the chemically equivalent C−C, C−O and C−N distances. Hydrogen atoms were added to the structure model at geometrically idealized coordinates with fixed isotropic temperature factors.

Crystallographic data (excluding structure factors) for the structures reported in this paper have been deposited with the Cambridge Crystallographic Data Centre as supplementary publication nos. CCDC-151158 (**2**) and CCDC-151159 (**3**). Copies of the data can be obtained free of charge on application to CCDC, 12 Union Road, Cambridge CB2 1EZ, UK [Fax: (internat.) +44-1223/336-033; E-mail: deposit@ccdc.cam.ac.uk].

Acknowledgments

Financial support for this work was provided by the State Committee for Scientific Research, Grant No. 3 T09A 016 15.

[1] J.-M. Lehn, *Angew. Chem. Int. Ed. Engl.* **1988**, *27*, 89; G. R. Desiraju, *Crystal Engineering: The Design of Organic Solids*, Elsevier, Amsterdam, **1989**; J.-M. Lehn, *Supramolecular Chemistry, Concepts and Perspectives*, VCH, Weinheim, **1995**; C. V. K. Sharma, G. R. Desiraju, *Perspectives in Supramolecular Chemistry. The Crystal as a Supramolecular Entity*, Wiley, Chichester, **1996**.

[2] G. A. Jeffrey, *An Introduction to Hydrogen Bonding*, Oxford University Press, **1997**; C. B. Aakeröy, K. R. Seddon, *Chem. Soc. Rev.* **1993**, 397−407; J. C. MacDonald, G. M. Whitesides, *Chem. Rev.* **1994**, *94*, 2383−2420.

[3] D. Braga. F. Grepioni, G. R. Desiraju, *Chem. Rev.* **1998**, *98*, 1375−1405; D. Braga. F. Grepioni, *Coord. Chem. Rev.* **1999**, *183*, 19−41.

[4] G. E. Coates, R. G. Hayter, *J. Chem. Soc.* **1953**, 2519−2524.

[5] S. J. Rettig, A. Storr, J. Trotter, *Can. J. Chem.* **1975**, *53*, 58−66.

[6] K. S. Chong, S. J. Rettig, A. Storr, J. Trotter, *Can. J. Chem.* **1979**, *57*, 586−590.

[7] S. J. Rettig, A. Storr, J. Trotter, K. Uhrich, *Can. J. Chem.* **1984**, *62*, 2783−2792.

[8] E. C. Onyiriuka, S. J. Rettig, A. Storr, J. Trotter, *Can. J. Chem.* **1987**, *65*, 782−788.

[9] G. D. Gracey, S. J. Rettig, A. Storr, J. Trotter, *Can. J. Chem.* **1987**, *65*, 2469−2477.

[10] W. T. Tao, Y. Han, Y. Z. Huang, X. L. Jin, J. Sun, *J. Chem. Soc., Dalton Trans.* **1993**, 807−809.

[11] H. Schumann, S. Wernik, F. Girgsdies, R. Weimann, *Main Group Metal Chemistry* **1996**, *19*, 331−338.

[12] K.-H. Thiele, E. Hecht, T. Gelbrich, U. Dümichen, *J. Organomet. Chem.* **1997**, *540*, 89−94.

[13] E. Hecht, T. Gelbrich, S. Wernik, R. Weiman, K.-H. Thiele, J. Sieler, H. Schumann, *Z. Anorg. Allg. Chem.* **1998**, *624*, 1061−1066.

[14] H. S. Sun, Q. Zhao, Y. J. Liu, H. M. Hu, X. Z. You, Z. Y. Zhou, *J. Coord. Chem.* **1999**, *47*, 459−465.

[15] J. Z. Tian, J. Q. Zhang, X. Shen, H. X. Zou, *J. Organomet. Chem.* **1999**, *584*, 240−245.

[16] J. Lewiński, J. Zachara, I. Justyniak, *Chem. Commun.* **1997**, 1519−1520; J. Lewiński, J. Zachara, I. Justyniak, *Organometallics* **1997**, *16*, 3859−3862; J. Lewiński, I. Justyniak, Z. Ochal, J. Zachara, *J. Chem. Soc., Dalton Trans.* **1999**, 2909−2911.

[17] G. M. Sheldrick, *Acta Crystallogr., Sect. A* **1990**, *46*, 467−473.

[18] G. M. Sheldrick, *SHELXL 97*, *Program for Refinement of Crystal Structures*, University of Göttingen, **1993**.

Received October 25, 2000
[I00406]

Preparation and Structural Characterization of the First Germylaluminate

Tassilo Habereder,[a] Klaus Knabel,[a] and Heinrich Nöth*[a]

Keywords: Lithium / Germanium / Aluminum / Anions / Structure elucidation

The reaction of $LiGePh_3$ with Me_2AlCl in ether yields the trisgermylaluminate $Li(OEt_2)_n[(Ph_3Ge)_3AlMe]$. The Ge–Al bond length is 2.520 Å and the geometry around the Al center almost tetrahedral.

Introduction

The chemistry of compounds with direct bonds between boron atoms and group 14 elements has found increased interest in recent years. Silylboranes and stannylboranes have proved to be versatile reagents in organic synthesis[1] and they are particularly useful for transition metal-catalyzed addition reactions to unsaturated organic compounds.[2] More recently, compounds containing Si–Al[3] or Si–Ga[4] bonds moved into focus because the $(Me_3Si)_3Si$ or $(Me_3C)_3Si$ groups stabilize polyhedral aluminum, gallium and indium clusters;[5] silylalanes and silylaluminates are also known. The molecular structures of the adducts $(Me_3Si)_3Al{\cdot}L$[6] [L = THF, NMe_3, $P(SiMe_3)_3$] and $Ph_2Al-Si(SiMe_3)_3{\cdot}THF$[7] have been described, as well as those of $(Me_3Si)_3Si-Al(tmp)_2$ (tmp = 2,2,6,6-tetramethylpiperidino),[8] $(t\mathrm{Bu}_3Si)_2Al-Al(Si t\mathrm{Bu}_3)_2$,[9] $Si(AlCl_2{\cdot}OEt_2)_4$,[10] $[Ph_2PAl(SiMe_3)_2]_2$ [11] and silylaluminates such as $Li(THF)_4[Cl_3AlSi(SiMe_3)_3]$ and $Na(THF)_2[Al(SiMe_3)_4]$.[12] As far as we are aware no molecular compound containing an Al–Ge bond has been structurally characterized. Dufaut et al.[13] reported that the reduction of digermanes with $LiAlH_4$ yields various germylaluminates amongst which only $Li(Ph_3GeAlH_3){\cdot}THF$ was identified by microanalysis; all other compounds were identified from the products of their controlled hydrolysis. Rösch et al.[14] succeeded in the preparation of $Al(GeMe_3)_3{\cdot}THF$ by reacting $Hg(GeMe_3)_2$ with elemental aluminum. A structural characterization by X-ray methods was, at the time, not standard. Here we report the synthesis and molecular structure of a novel germylaluminate.

Because salt elimination is the most straightforward pathway to synthesize B–Ge bonds[15] we also utilized this method for the synthesis of new molecules with Al–Ge bonds. To this end a solution of triphenylgermyllithium[16] in Et_2O was allowed to react with an equimolar amount of dimethylaluminum chloride [Equation (1)]. The reaction mixture was monitored by ^{27}Al NMR spectroscopy. The spectrum showed two signals at δ = 189 and 62.

These data indicate the formation of methylalanes as well as possibly a pentacoordinated aluminum species.[17] On layering a concentrated toluene solution with hexane single

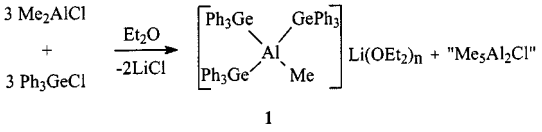

1 (1)

crystals separated which were suitable for an X-ray structure analysis. The crystalline product was unambiguously identified as lithium{methyltris(triphenylgermyl)aluminate} (**1**). Its elemental analysis indicated that five molecules of ether are coordinated but the crystal structure analysis showed only three ether molecules. Compound **1** is responsible for the high field Al NMR signal and is similar to the ^{27}Al NMR signal for $Li[Al(SiMe_3)_4]$.[17] The filtrate contained no other germanium compound, although its ^{27}Al NMR spectrum showed the presence of an aluminum species with $\delta^{27}Al$ = 189. We assigned this broad signal to Me_5Al_2Cl as we found a ^{27}Al NMR signal for Me_2AlCl at δ = 165 in ether solution, and at δ = 179 in hexane solution. That only a single signal is observed for "Me_5Al_2Cl" can be explained by substituent exchange, which is common in the chemistry of aluminum alkyls.[18] Compound **1** crystallizes in the space group $P2_1/c$ with four formula units in the unit cell. The unit cell contains methyltris(triphenylgermyl)aluminate anions and ether-solvated lithium cations. The ether molecules are highly disordered. No accurate coordination geometry was found. Much more interesting is the anionic part of compound **1** (see Figure 1). It shows three Al–Ge bonds of almost equal lengths with an average of 2.520(2) Å. This value is slightly longer than the sum of the covalent radii of these two atoms [Al = 1.25, Ge = 1.22; Σ = 2.47 Å].[10] This complies with the presence of a tetracoordinated Al center. As far as we are aware this is the first Al–Ge bond length determined in a molecular unit. The Al atom in **1** shows only a minor distortion from a tetrahedral environment. The Ge–Al–Ge angles were determined to be on average 110.2(3)°, whereas the average Ge–Al–C bond angle is 108.6(2)°. This indicates that the methyl group almost demands as much space as a Ph_3Ge group.

The unexpected formation of **1** described in Equation (1) can be explained on the basis that Me_2AlCl was added to Ph_3GeLi. Thus at the beginning of the reaction there is a

[a] Department of Chemistry, University of Munich, Butenandtstraße 5–13, 81377 München, Germany

 © WILEY-VCH Verlag GmbH, 69451 Weinheim, 2001 1434–1948/01/0505–1127 $ 17.50+.50/0

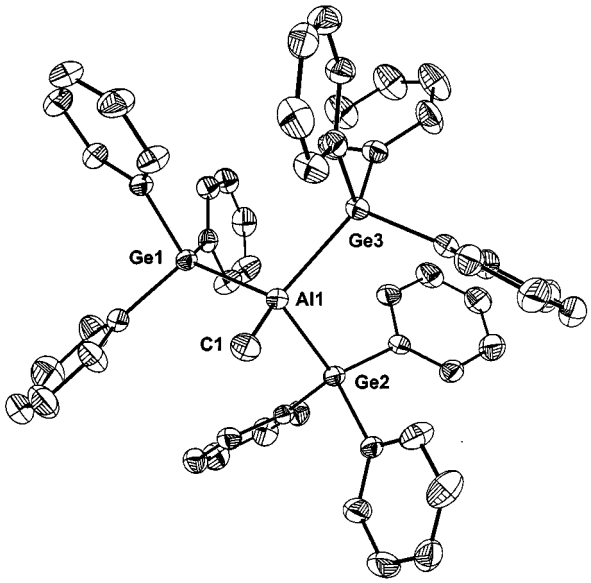

Figure 1. View of the anionic part of the molecular structure of **1**; thermal ellipsoids are shown at a 25% probability level and hydrogen atoms are omitted for clarity; selected interatomic distances [Å] and angles [°]: Ge1−Al1 2.526(2), Ge2−Al1 2.511(2), Ge3−Al1 2.523(2), C1−Al1 1.982(6); C1−Al1−Ge1 110.1(2), C1−Al1−Ge2 107.0(2), C1−Al1−Ge3 108.9(2), Ge1−Al1−Ge2 109.8(1), Ge1−Al1−Ge3 113.3(1), Ge2−Al1−Ge3 107.5(1)

large excess of the germyllithium compound. In the first step an aluminate $[(Ph_3Ge)AlMe_2Cl]^-$ is expected to be formed. This anion will lose a chloride, with formation of insoluble LiCl, producing $Ph_3GeAlMe_2$. This latter, on reaction with a second equivalent of Ph_3GeLi, will generate $Li[(Ph_3Ge)_2AlMe_2]$ as an intermediate which may either directly react with Me_2AlCl to form $(Ph_3Ge)_2AlMe$ and LiCl or methylate Me_2AlCl with formation of $AlMe_3$. This and Me_2AlCl will produce "Me_5Al_2Cl". Substituent exchange reactions are well-known in alkyl aluminum chemistry.[18] Further investigations of the chemistry of Al−Ge compounds are in progress.

Experimental Section

The experiments were performed under anhydrous conditions under an argon atmosphere using Schlenk techniques. $LiGePh_3$ was prepared according to a literature procedure.[16] NMR spectra were recorded with a JEOL 400 instrument. For X-ray work a Siemens P4 diffractometer (graphite monochromator, Mo-K_α radiation) equipped with an area detector and a low temperature device LT2 was employed. Data collection was performed with the program SMART,[20] data reduction with the program SAINT,[20] and absorption correction with the program SADABS.[21] For all other calculations the program package SHELXTL was used.[22] The Li atom and the non-hydrogen atoms of the anion were refined anisotropically. The hydrogen atoms of the Ph and Me groups were placed in calculated positions and included in the final refinement isotropically. The O and C atoms of the ether molecules were included isotropically with free SOF values.

Lithium{methyltris(triphenylgermyl)aluminate}·$(Et_2O)_5$ (1): A solution of Ph_3GeLi (1.5 mmol) in approximately 40 mL of Et_2O was cooled to −78 °C and slowly treated with a hexane solution containing of Me_2AlCl (1.45 mmol). After stirring for 1 h at ambient temperature all volatile components were removed in vacuo. The solid residue was dissolved in 50 mL of toluene, the solution filtered and layered with 20 mL of hexane. This afforded 0.60 g of **1** (yield 90% based on Ph_3GeLi), as colorless prisms; m.p. 152 °C. − ^{1}H NMR (270 MHz, C_7D_8): δ = 0.49 (s, 3 H $AlCH_3$), 1.30 (t, $^3J_{HH}$ = 8.2 Hz, 16 H, OCH_2CH_2), 1.65 (br. s, 14 H, OCH_2CH_2), 3.46 (q, $^3J_{HH}$ = 8.2 Hz, 11 H, OCH_2), 3.77 (br. m, 9 H, OCH_2), 7.35 (m, 27 H, *p*-Ph-*H* and *m*-Ph-*H*), 7.76 (m, 18 H, *o*-Ph-*H*). − ^{27}Al NMR (104 MHz, C_7D_8): δ = 62 ($h_{1/2}$ = 5850 Hz).

X-ray Structure Determination: $C_{67}H_{48}Ge_3LiO_3$, mol. wt. 1152.74, colorless prism, cryst. size: 0.10 × 0.20 × 0.20 mm, a = 14.2369(8), b = 19.5112(1), c = 22.766(2) Å, β = 92.523(1)°, V = 6317.9(7) Å^3, monoclinic, space group $P2_1/c$, Z = 4, $d_{calcd.}$ = 1.212 Mg/m^3, F(000) = 2344, index ranges: $-15 < h < 12$, $-21 < k < 21$, $-25 < l < 24$; 2θ range 2−46.52°, T = −80 °C; refl. collected: 27052; refl. unique: 5808; R_{int} = 0.0754, no. variables: 607, GOOF 1.1015, $R_1(4\sigma)$ = 0.628, wR_2 = 0.1605. larg. res. peak: 1.62 e/Å^3. Crystallographic data (excluding structure factors) for the structure(s) included in this paper have been deposited with the Cambridge Crystallographic Data Centre as supplementary publication no. CCDC-152468. Copies of the data can be obtained free of charge on application to CCDC, 12 Union Road, Cambridge CB2 1EZ, UK [Fax: (internat.) + 44-1223/336-033; E-mail: deposit@ccdc.cam.ac.uk].

Acknowledgments

We thank Fonds der Chemischen Industrie and Chemetall mbH for support of this study.

[1] [1a] T. Ishiyama, N. Matsuda, N. Miaura, A. Suzuki, *J. Am. Chem. Soc.* **1993**, *115*, 11018−11019. − [1b] C. N. Iverson, M. R. Smith, *J. Am. Chem. Soc.* **1995**, *117*, 4403−4404. − [1c] T. Ishiyama, N. Matsuda, M. Murata, F. Ozawa, A. Suzuki, N. Miyaura, *Organometallics* **1996**, *15*, 713−720. − [1d] M. Bluhm, A. Maderna, H. Pritzkow, S. Bethke, R. Gleiter, W. Siebert, *Eur. J. Inorg. Chem.* **1999**, 1693−1700. − [1e] M. Suginome, H. Nakamura, Y. Ito, *Chem. Commun.* **1996**, 2777−2778. − [1f] M. Suginome, H. Nakamura, Y. Ito, *Angew Chem.* **1997**, *109*, 2626−2628; *Angew. Chem. Int. Ed. Engl.* **1997**, *36*, 2516−2518. − [1g] M. Y. Ohmori, Y. Ito, *Synlett.* **1999**, *10*, 1567−1568. − [1h] S. Onzawa, Y. Hatanaka; M. Tanaka, *Chem. Commun.* **1999**, 1863−1864. − [1i] L. B. Han, M. Tanaka, *Chem. Commun.* **1999**, 395−402.

[2] S. Onozawa,Y. Hatanaka, T. Sakakua, T. Hayashi, M. Tanaka, *Organometallics* **1996**, *15*, 5450−5452.

[3] A. Purath,.H. G. Schnöckel, *J. Organomet. Chem.* **1999**, *579*, 373−379.

[4] G. Linti, W. Köstler, A. Rödig, *Eur. J. Inorg. Chem.* **1998**, 745−749; G. Linti, W. Köstler, *Angew. Chem.* **1997**, *109*, 2758−2760; *Angew. Chem. Int. Ed. Engl.* **1997**, *36*, 2644−2645; G. Linti, *J. Organomet. Chem.* **1995**, *520*, 107−113.

[5] N. Wiberg, T. Blank, W. Ponikwar, H. Nöth, *Angew. Chem.* **1999**, *111*, 887−890; *Angew. Chem. Int. Ed.* **1999**, *38*, 846−848.

[6] L. Rösch, W. Erb, *Angew Chem.* **1977**, *89*, 497; *Angew. Chem. Int. Ed. Engl.* **1977**, *16*, 480; J. F. Janik, E. N. Duesler, R. T. Paine, *J. Organomet. Chem.***1997**, *539*, 19−25; M. Stenda, E. Hey-Hawkins, *Z. Anorg. Allg. Chem.* **1999**, *625*, 2081−2084.

[7] M. Sierra, V. S. J. de Mel, J. P. Oliver, *Organometallics* **1989**, *8*, 2312−2316.

[8] K. Knabel, I. Krossing, H. Nöth, H. Schwenk-Kircher, M. Schmidt-Amelunxen, T. Seifert, *Eur. J. Inorg. Chem.* **1998**, 1095−1114.

[9] N. Wiberg, K. Amelunxen, T. Blank, H. Nöth, J. Knizek, *Organometallics* **1978**, *17*, 5431−5433.

[10] A. Purath, C. Dohmeier, E. Baum, R. Koppe, H. G. Schnöckel, *Z. Anorg. Allg. Chem.* **1999**, *625*, 2144−2148.
[11] J. F. K. Janik, E. N. Duesler, W. F. McNamara, M. Westerhausen, R. T. Paine, *Organometallics* **1989**, *8*, 506−514.
[12] A. Heine, D. Stalke, *Angew. Chem.* **1993**, *105*, 90−92; *Angew. Chem. Int. Ed. Engl.* **1993**, *32*, 121−123; L. Rösch, G. Altnau, C. Krüger, Y.-H. Tsay, *Z. Naturforsch.* **1983**, *38B*, 34−41.
[13] N. Duffaut, J. Dunogues, R. Calas, J. Gerval, P. Riviere, J. Satge, A. Cazes, *J. Organomet. Chem.* **1978**, *149*, 57−63.
[14] L. Rösch, W. Erb, *Angew. Chem.* **1978**, *90*, 631−632; *Angew. Chem. Int. Ed. Engl.* **1978**, *17*, 604.
[15] T. Habereder, *PhD Thesis*, University of Munich, **2000**, and literature cited therein.
[16] C. Tamborski, F. Ford, E. Soloski, *J. Org. Chem.* **1963**, *28*, 237−239.
[17] J. Mason, *Multinuclear NMR*, Plenum Press, Nedw York, London, **1987**, 259−278.
[18] Ch. Elschenbroich, A. Salzer, *Organometallics* VCH, Weinhein, New York, **1992**.
[19] A. F. Holleman, E. Wiberg, N. Wiberg, *Lehrbuch der anorganischen Chemie*, Edition 101, **1995**, Walter de Gruyter, Berlin, New York.
[20] SMART and SAINT, Siemens Analytical Instruments, Madison, Version 5.01.
[21] SADABS, G. W. Sheldrick, Absorption correction for data collection with SAINT.
[22] SHELXTL, Siemens Analytical Instgruments, Madison Version 4.02.

Received November 14, 2000
[I00432]

Metallic Palladium in the Heck Reaction: Active Catalyst or Convenient Precursor?

Andrea Biffis,*[a] Marco Zecca,[a] and Marino Basato[a]

Keywords: Palladium / Heterogeneous catalysis / Heck reaction

Novel experimental evidence is presented pointing out that "heterogeneous" palladium metal catalysts employed in Heck-type reactions mainly act as sources of soluble palladium(II) complexes, which are the true catalytically active species.

The Heck reaction has been the subject of thorough investigation for several years. This reaction is usually homogeneously catalyzed by palladium(II) complexes with ligands such as phosphanes, amines or heterocyclic carbenes.[1] However, Heck-type reactions can also be efficiently catalyzed by palladium metal dispersed onto a number of supports including carbon, silica, magnesium oxide or zeolites;[2−15] for example, palladium on carbon is reported to be currently employed in some small-scale industrial processes.[16,17] Palladium metal colloids appear to be active catalysts as well,[18−23] and there is speculation that metal colloids formed in situ are involved also in ligandless homogeneous Heck reactions with simple palladium salts.[22]

In spite of many claims that with all these catalysts the reaction takes place on the metal surface, more sound evidence that the catalysis is truly heterogeneous would be desirable. In fact, whereas some authors reported that the reaction stops after separating the catalyst,[8,12] this did not occur in other cases.[10,15] Indeed, a significant palladium leaching into the solution after just one catalytic cycle was often observed.[12,13]

In this communication, we wish to report that: (i) under Heck conditions heterogeneous palladium metal catalysts undergo significant metal leaching, caused primarily by the presence of aryl halides (bromides and even chlorides); (ii) the presence of a coordinating base such as sodium acetate promotes metal leaching with relatively less reactive aryl halides; (iii) the released soluble metal species are active catalysts for the Heck reaction.

We have tested a 1% w/w Pd/Al_2O_3 catalyst (from Alfa, serial 89112, lot 1969000), hereafter coded AO-Pd, and a 1% w/w Pd catalyst supported on a tailor-made ion-exchange resin (0.38 meq./g sulfonate groups, sodium form), hereafter coded PS-Pd (see Experimental Section). The catalysts were first employed in the Heck reaction of 4-bromo- and 4-chloroacetophenone (BA and CA, respectively) with *n*-butylacrylate (NBA) in *N*,*N*-dimethylacetamide (DMA) (Table 1). Both catalysts were active with BA, AO-Pd being slightly superior. In contrast, the yields with CA were low and did not increase even after 24 h. Remarkably, the catalysts invariably lost palladium: leaching from PS-Pd was virtually complete after the reaction with BA!

Table 1. Heck reactions[a] with supported Pd metal

Catalyst	Aryl halide	Yield (%)	Pd leached (%)
AO-Pd	BA	97	79
PS-Pd	BA	82	100
AO-Pd	CA	5	22
PS-Pd	CA	6	92

[a] Reaction conditions: 10 mmol aryl halide, 10 mmol NaOAc, 17 mmol NBA, 0.1 g catalyst (0.1% mol/mol), 25 mL DMA; inert atmosphere (N_2), 120 °C, 3 h. Selectivity for the Heck product was 100% in all cases.

In order to ascertain which agent caused the metal leaching, both catalysts were allowed to react separately with different components of the reaction mixture under the same conditions of the previous tests. The results are summarized in Table 2. No metal leaching occurred upon treatment with DMA alone or after addition of NaOAc and/or the acrylate. PS-Pd underwent extensive metal leaching when treated with a solution of BA in DMA. The combination of the aryl bromide with NaOAc caused an even higher leaching from PS-Pd and a noticeable leaching from AO-Pd. CA alone was ineffective; significant palladium dissolution took place only when it was combined with NaOAc. We did not observe palladium leaching with chlorobenzene, either alone or in combination with NaOAc (entries 8−9, Table 2).

After the leaching tests, we checked for the presence of active species in solution. The suspensions were filtered hot under an inert gas atmosphere, then NaOAc and NBA were added to the filtrate, which already contained the aryl halide. The resulting mixture was stirred for 3 h at 120 °C and then analyzed for the reaction products (Table 3). Yields were fully comparable to those reported in Table 1. This findings suggest that released palladium is actually also responsible for catalysis in the presence of the "heterogen-

[a] Dipartimento di Chimica Inorganica Metallorganica ed Analitica, Università di Padova, and Centro di Studio sulla Stabilità e Reattività dei Composti di Coordinazione, C.N.R., Via Marzolo 1, 35131 Padova, Italy
Fax: (internat.) +39-049/827-5223
E-mail: biffis@chin.unipd.it

 © WILEY-VCH Verlag GmbH, 69451 Weinheim, 2001 1434−1948/01/0505−1131 $ 17.50+.50/0

Table 2. Metal leaching from catalysts PS-Pd and AO-Pd in the presence of different components of the reaction mixture

Entry	Component(s)[a]	PS-Pd[b]	AO-Pd[b]
1	DMA	0	0
2	DMA + NaOAc	0	0
3	DMA + NaOAc + NBA	0	0
4	DMA + BA	85	nd
5	DMA + BA + NaOAc	88	11
6	DMA + CA	0	0
7	DMA + CA + NaOAc	92	10
8	DMA + CB	0	nd
9	DMA + CB + NaOAc	0	nd

[a] CB = chlorobenzene. – [b] Pd leaching (% w/w) after 18 h at 120 °C.

eous'' catalyst. The Pd species released by CA (entry 7, Table 2) are almost as active as the species released by BA (entry 5, Table 3). The observed reactivity was quite comparable to that of $Pd(OAc)_2$ (last entry in Table 3). After the coupling, the solutions usually exhibited the typical orange color of palladium(II) species; tiny amounts of Pd black were observed only occasionally. It was even possible to perform a second reaction cycle by adding fresh reagents to the solution, although the residual catalytic activity was slightly lower. In one of the filtrates from AO-Pd (entry 4, Table 2) the second Heck coupling of BA occurred with 96% yield after 24 h.

Table 3. Homogeneous Heck reactions promoted by leached palladium species

Entry	Palladium source	Dissolved Pd (mmol)	Coupled aryl halide	Yield (%)[a]
1	PS-Pd (entry 5, Table 2)	0.088	BA[b]	100
2	PS-Pd (entry 4, Table 2)	0.085	BA[b]	100
3	AO-Pd (entry 5, Table 2)	0.011	BA[b]	83
4	AO-Pd (entry 7, Table 2)	0.020	CA[b]	8
5	PS-Pd (entry 7, Table 2)	0.092	CA[b] + BA[c]	95[d]
6	$Pd(OAc)_2$	0.050	BA	80

[a] Reaction conditions: 10 mmol aryl halide, 10 mmol NaOAc, 17 mmol NBA, 25 mL DMA; inert atmosphere (N_2), 120 °C, 3 h. – [b] Residue from leaching tests. – [c] Added to the filtrate. – [d] The yield is referred to BA.

As palladium leaching occurs only in the presence of an aryl halide, it should be the direct consequence of the oxidative addition of the halide to surface atoms of the metal particles. Hence, the palladium should be released in the +II oxidation state, and good coordinating agents towards palladium(II) should enhance the extent of metal leaching. The data of Table 2 show that NaOAc helps the solubilization of palladium in particular when the supposed oxidant is CA, which is less prone to oxidative addition than the analogous bromide. As acetate ions are much better ligands for palladium(II) than for palladium(0), this observation supports our hypothesis that the metal is released into solution in an oxidized form. Accordingly, we argue that the soluble palladium(II) species directly enter the catalytic cycle just after being generated from the supported metal (Scheme 1). Virtually the same cycle was originally proposed by Heck to account for the observed catalytic action of palladium black.[3]

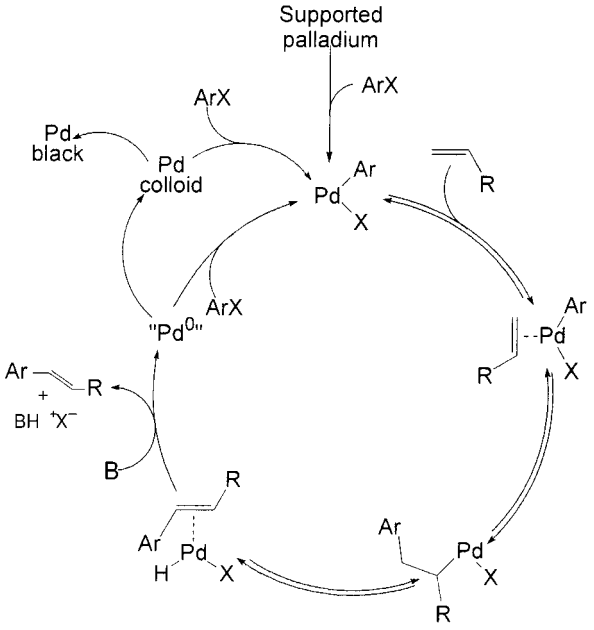

Scheme 1. A possible catalytic cycle for the Heck reaction with Pd metal catalysts

It may be argued that the released palladium(II) species can in principle be reduced just after leaching to form soluble palladium colloids. This was proposed in order to explain "ligandless'' catalysis of the Heck reaction by simple palladium(II) salts. Indeed, very recently Reetz has shown that the formation of Pd colloids parallels the onset of the Heck reaction catalyzed by bis(benzonitrile)dichloropalladium(II).[22] However, he also gave experimental evidence that Pd colloids are readily and quantitatively oxidized to palladium(II) species by a *stoichiometric* quantity of an activated aryl halide (iodobenzene). As we employed a 1000:1 excess of aryl halide to the metal, the presence of colloidal palladium under our conditions is very unlikely.

We did not measure the leaching rate in our experiments, but qualitative observations suggest that the accumulation of active palladium(II) species in the solution is a relatively slow process under the conditions employed in this work. This could explain why some authors did not observe significant catalytic activity in the filtrate after removal of the "heterogeneous'' catalyst shortly after the onset of the reaction. Furthermore, this hypothesis can also explain the observations of other authors on the influence of the support[15] and of the structure of the Pd particles[21] on catalyst activity. Indeed, if the leaching process is slow, the overall reaction rate can become limited by the leaching process. Since leaching is truly a surface reaction, structure-activity relationships may be expected.

We believe that our results represent strong evidence that "heterogeneous'' palladium metal catalysts employed for the Heck reaction are mainly sources of soluble palladium(II) complexes, which are the actual catalytic species (Scheme 1). We have investigated for the first time the mechanism of metal leaching and we have demonstrated

that leaching is critically dependent on the presence of the aryl halide; the presence of a coordinating base may have a promoting effect. We have shown that metal leaching takes place not only with the more activated aryl halides such as iodobenzene, but also with bromo- and even chloroarenes, and that the leached species are active catalysts for the Heck reaction.

In conclusion, it seems that the only way to have a catalytic system for this reaction which could be properly defined "heterogeneous" is to devise a support able to coordinate and therefore to heterogenize the palladium(II) and palladium(0) species which occur in the different stages of the reaction cycle. In this area, Arai and co-workers recently reported that some inorganic supports are able to rebind leached Pd species after the end of the reaction.[13] We are currently engaged in the development of novel resin supports for this purpose.

Experimental Section

Preparation of Catalyst PS-Pd: Styrene (8.63 g) and technical grade divinylbenzene (0.65 g) (55% of crosslinking monomers) were dissolved in dimethyl sulfoxide (4 g). After addition of sulfoethyl methacrylate (0.76 g) the solution was exposed to γ-rays (^{60}Co) at 0.5 Gy s^{-1} and at a distance of 21 cm for 72 h at room temp. The obtained resin rod was crushed, extensively washed with methanol, acetone and diethyl ether, vacuum dried and sieved to a particle size of <0.18 mm. Palladium was incorporated by treating 2 g of the resin overnight with a solution of $Pd(OAc)_2$ (43.7 mg) in 40 mL THF, followed by reduction with 10 equivalents $NaBH_4$ in ethanol/THF (4:1). Pd was quantitatively incorporated into the resin as metal nanoparticles with an average size of 3−4 nm (TEM).

General Procedure for the Catalytic Tests: Aryl halide (10 mmol), NaOAc (0.84 g, 10 mmol), catalyst (0.1 g, 0.01 mmol Pd) and *N*,*N*-dimethylacrylamide (25 mL) were mixed at room temperature in a three-necked, round-bottomed flask equipped with a reflux condenser. The resulting mixture was degassed and put under an inert atmosphere (N_2). *n*-Butylacrylate (17 mmol) was added and the flask was put into an oil bath at 120 °C and stirred for 3 h. Yields were determined by GC.

General Procedure for the Leaching Tests: The catalyst (0.1 g) was suspended in *N*,*N*-dimethylacrylamide (25 mL) in a three-necked, round-bottomed flask equipped with a reflux condenser. One or more of the other reaction components was then added (Table 2); the quantity of each component was the same as in the catalytic experiments described above. The resulting mixture was degassed, put under an inert atmosphere (N_2) in an oil bath at 120 °C and stirred for 18 h. The resulting mixture was filtered hot under an inert atmosphere; the missing reaction components were immediately added to the liquid phase, after which the reaction mixture was put again in the oil bath at 120 °C and stirred for the desired reaction time. Yields were determined by GC. The filtered solids were extensively washed with water and acetone and dried under vacuum. The Pd content in the residual solid catalyst was determined, after mineralization, by ICP-AES spectroscopy.

Acknowledgments

We are grateful to MURST (PRIN 1999) for financial support.

[1] I. P. Beletskaya, A.V. Cheprakov, *Chem. Rev.* **2000**, *100*, 3009−3066.
[2] T. Mizoroki, K. Mori, A. Ozaki, *Bull. Chem. Soc. Jpn.* **1971**, *44*, 581.
[3] R. F. Heck, J. P. Nolley, Jr., *J. Org. Chem.* **1972**, *37*, 2320−2322.
[4] M. Julia, M. Duteil, *Bull. Soc. Chim. Fr.* **1973**, 2790.
[5] D. Savoia, C. Trombini, A. Umani-Ronchi, G. Verardo, *Chem. Commun.* **1981**, 541−542.
[6] K. Kaneda, M. Higuchi, T. Imanaka, *J. Mol. Catal.* **1990**, *63*, L33−L36.
[7] Z. Zhuangyu, P. Yi, H. Honwen, K. Tsi-yu, *Synthesis* **1991**, 539−542.
[8] R. L. Augustine, S. T. O'Leary, *J. Mol. Catal.* **1992**, *72*, 229−242.
[9] A. Wali, S. M. Pillai, V. K. Kaushik, S. Satish, *Appl. Catal.* **1996**, *135*, 83−93.
[10] A. F. Shmidt, L. V. Mametova, *Kinet. Catal.* **1996**, *37*, 406−408.
[11] J. Li, A. W.-H. Mau, C. R. Strauss, *Chem. Commun.* **1997**, 1275−1276.
[12] P. Mehnert, D. W. Weaver, J. Y. Ying, *J. Am. Chem. Soc.* **1998**, *120*, 12289−12296.
[13] F. Zhao, B. M. Bhanage, M. Shirai, M. Arai, *Chem. Eur. J.* **2000**, *6*, 843−848.
[14] J. H. Ding, D. L. Gin, *Chem. Mater.* **2000**, *12*, 22−24.
[15] M. Wagner, K. Köhler, L. Djakovitch, S. Weinkauf, V. Hagen, M. Muhler, *Top. Catal.* **2000**, *13*, 319−326.
[16] A. Eisenstadt, *Chem. Ind. (Dekker)* **1998**, *75*, 415−427.
[17] V. M. Wall, A. Eisenstadt, D. J. Ager, S. A. Laneman, *Platinum Metals Rev.* **1999**, *43*, 138−145.
[18] M. Beller, H. Fischer, K. Kühlein, C.-P. Reisiger, W. A. Herrmann, *J. Organomet. Chem.* **1996**, *520*, 257−259.
[19] M. T. Reetz, G. Lohmer, *Chem. Commun.* **1996**, 1921−1922.
[20] S. Klingelhöfer, W. Heitz, A. Greiner, S. Oestereich, S. Förster, M. Antonietti, *J. Am. Chem. Soc.* **1997**, *119*, 10116−10120.
[21] J. Le Bars, U. Specht, J. S. Bradley, D. G. Blackmond, *Langmuir* **1999**, *15*, 7621−7625.
[22] M. T. Reetz, E. Westermann, *Angew. Chem. Int. Ed.* **2000**, *39*, 165−168.
[23] A. Biffis, *J. Mol. Catal. A*, in press.

Received November 8, 2000
[I00421]

Hydrothermal Synthesis of a Two-Dimensional Coordination Polymer $[Fe(phen)(\mu_6\text{-bta})_{1/2}]_n$ (bta = Benzene-1,2,4,5-tetracarboxylate, phen = 1,10-Phenanthroline)

De-Qing Chu,[a] Ji-Qing Xu,*[a] Li-Mei Duan,[c] Tie-Gang Wang,[a] Ao-Qing Tang,[b] and Ling Ye[d]

Keywords: Carboxylate ligands / Crystal engineering / Iron / N ligands / X-ray diffraction / Polymers

A metal-ligand complex $[Fe(phen)(\mu_6\text{-bta})_{1/2}]_n$ (phen = 1,10-phelanthroline; bta = benzene-1,2,4,5-tetracarboxylate ligand) has been hydrothermally synthesized and structurally characterized by single crystal X-ray crystallography, showing that it possesses a novel, two-dimensional polymeric structure.

Introduction

The recent interest in the crystal engineering of special geometrical and topological coordination polymers arises from their potential application in catalysis, chemical absorption, magnetism and electrical conductivity.[1] Due to their widespread utility, the ability to modify the structures of such materials or design of new materials is of the utmost importance. A synthetic strategy widely used in this area is by coordination of metal ions to polydentate ligands that function as connectors. In this context, multi-connecting ligands which provide two or more bidentate metal-binding sites are appealing as building blocks for coordination polymers because they promise robust networks with good electronic communication between the metal centers.[2] They also offer new network architectures, many of which do not exist in natural solids. "Clay mimics" or "zeolite mimics" have the gross analogues but are based upon very different chemical components, and, most importantly, they are inherently modular and therefore fine-tunable.[3] Presently, there are considerable efforts devoted to the formation of metal-polycarboxylate assemblies.[4] A particular case in this area is the assembly of benzenetricarboxylate-based supramolecules. Interesting two-dimensional structures such as $[Cu_3(tma)_2(H_2O)]_n$,[4a] $[Ni(C_{12}H_3ON_6O_2)]_3(tma)_2\cdot 18H_2O$,[4e] and $[M_3(tma)_2]\cdot 12H_2O$[4b] (M = Co, Ni, Zn, tma = benzenetricarboxylate) etc., are all reported to be based on this bridging ligand and transition metal ions.

The benzene-1,2,4,5-teracarboxylate ligand (= bta) as a multi-connecting ligand is also an excellent candidate for the planning of coordination polymers; comparatively few examples have been reported to date in relation to applying it to the building of coordination polymers. The use of a system of one kind of metal ion and two kinds of organic ligands that contain such a ligand for the assembly of coordination polymers has also never been described. We have therefore conducted an investigation of such a system $FeCl_2$-Na_4bta-phen-H_2O by a hydrothermal method. The obtained compound $[Fe(\mu_6\text{-bta})(phen)]_n$ (**1**) is unprecedented, exhibiting a two-dimensional polymeric structure, linking the metal ions with bta bridging units. We report here the synthesis and structural characterization of this novel compound.

[a] Department of Chemistry, Jilin University, Changchun 130023, P. R. China
Fax: (internat.) +86-431/892-3907
E-mail: xjq@mail.jlu.edu.cn
[b] Institute of Theoretical Chemistry, Jilin University, P. R. China
[c] Department of Chemistry, Inner Mongolia Teachers' College of Nationalities, P. R. China
[d] Key Laboratory for Supramolecular Structure and Spectroscopy, Jilin University, P. R. China

Results and Discussion

Crystal analysis reveals the details for the structure of compound **1**. It consists of two-dimensional polymeric layers $[Fe(phen)(\mu_6\text{-bta})_{1/2}]_n$ formed by bta units bridging [Fe(phen)] groups. As illustrated in Figure 1, each Fe^{II} ion is six coordinated by one phen and three bta ligands. Eight oxygen atoms from four deprotonated carboxyl groups of each bta unit are all used as coordinating atoms, and bind to six metal ions. Four oxygen atoms from two neighboring carboxyl groups of one bta unit coordinate to three metal atoms, two of which bind to one Fe^{II} ion with the other two binding to two Fe^{II} ions; the remaining four oxygen atoms of the bta unit coordinate to a further three metal atoms with the same mode. The layer grids consist of two kinds of holes, one is an eight-membered-ring hole consisting of two carboxyl groups and two metal atoms, and the other is a 14-membered-ring hole, around which are two bta units and two Fe^{II} ions. The local geometry around each Fe^{II} center can be described as a slightly distorted octahedron. The Fe^{II} center coordinates to six ligating atoms with four Fe−O distances of 2.083(2), 2.091(2), 2.166(2), 2.199(2) Å and two Fe−N distances of 2.232(3) and 2.182(3) Å.

 © WILEY-VCH Verlag GmbH, 69451 Weinheim, 2001 1434−1948/01/0505−1135 $ 17.50+.50/0

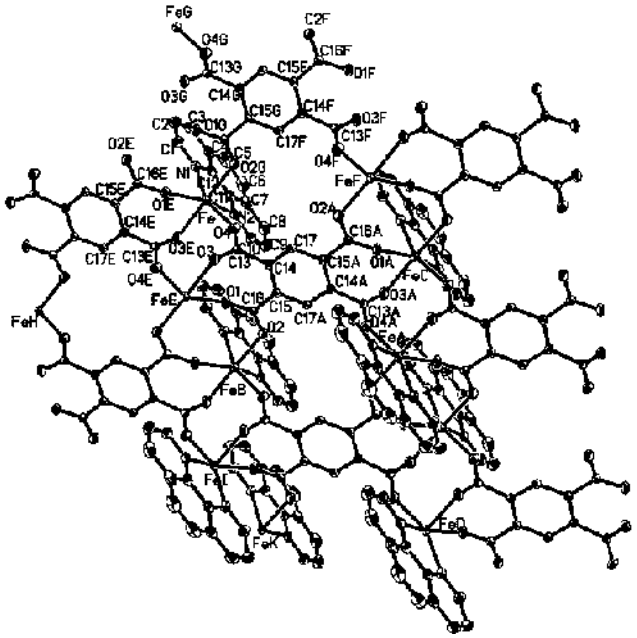

Figure 1. A view of the polymeric layer for compound [Fe(phen)-(μ_6-bta)$_{1/2}$]$_n$; selected bond lengths and angles: Fe−O_{1E} 2.083(2), Fe−O_4 2.091(2), Fe−O_{2G} 2.166(2), Fe−N_2 2.182(3), Fe−O_{3E} 2.199(2), Fe−N_1 2.232(3); O_{1E}−Fe−O_4 105.80(10), O_{1E} −Fe−O_{2G} 98.48(9), O_4−Fe−O_{2G} 81.08(9), O_{1E}−Fe−N_2 158.31(9), O_4−Fe−N_2 86.56(10), O_{2G}−Fe−N_2 101.05(9), O_{1E}−Fe−O_{3E} 80.64(9), O_4−Fe−O_{3E} 96.79(9), O_{2G}−Fe−O_{3E} 177.40(9), N_2−Fe−O_{3E} 80.24(9), O_{1E}−Fe−N_1 96.97(10), O_4−Fe−N_1 155.02(10), O_{2G}−Fe−N_1 85.60(10), N_2−Fe−N_1 75.34(10), O_{3E}−Fe−N_1 96.93(9)

Figure 2 is a view of the packing diagram for compound **1**. It shows that along the crystallographic *b* axis, all the two-dimensional polymeric layers are arranged in an ABAB fashion. Between two neighboring layers, the phen rings from different layers interdigitate. The alternate A···A or B···B interlayer distance is 18.504 Å, and the average interlayer distance is 9.252 Å.

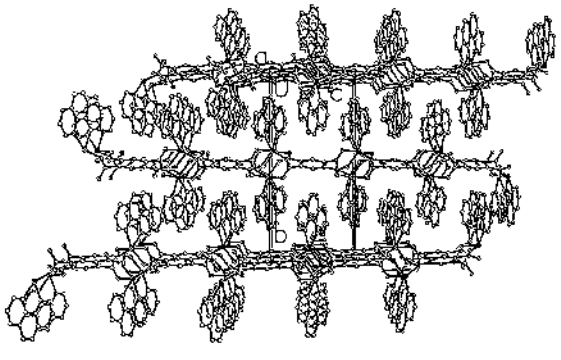

Figure 2. Crystal packing of the compound [Fe(phen) (μ_6-bta)$_{1/2}$]$_n$

Figure 3 shows that between two neighboring layers the interdigitated phen rings are parallel groups such as CQA/CQQ, CFF/CFA, CJJ/CJA, or CHH/CHA (here, the eight groups of three letters such as CQA represent 1,10-phenanthroline planes). The average distance between two adjacent parallel phen planes is small (3.2 Å), indicating that there are weak spatial π-π interactions between these phen rings. This type of π-π packing may be of high interest for the design of advanced materials.

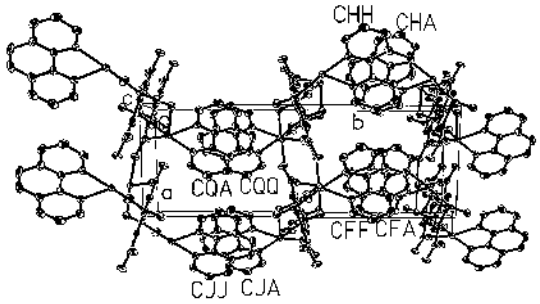

Figure 3. The parallel π-π packing of 1,10-phenanthroline plane between neighbouring polymeric layers in the crystal; the 1,10-phenanthroline planes CQA/CQQ, CFF/CFA, CJJ/CJA and CHH/CHA are parallel groups, but they are each bonded to different polymeric layers

In the chemical realization of multi-dimensional metal and polycarboxylate solids, a major challenge may come from the control of dimensionality. There are at least four problems in this respect. Firstly, since H_2O molecules are also excellent ligands for hard metal ions such as Fe^{II}, ancillary ligation of metal ions by water may result in low dimensionality such as discrete $Co(H_2bta)$[5] or $\{[Mn(H_2O)_5]_2(bta)\}\cdot H_2O$ units.[6] Secondly, in a system with a metal ion and two kinds of organic ligands, low dimensionality may come from the coordinating competition between the two kinds of organic ligands, such as full occupation of six sites per metal ion by three phen ligands, forming discrete metal complex cations $[Fe(phen)_3]^{2+}$. Thirdly, the low dimensionality may be caused by competition from polycarboxylate itself, due to its facile formation of hydrogen-bonded dimers or polymers.[7] Finally, in basic and even neutral aqueous solutions, the formation of Fe^{II}−ligand complexes will compete with the process of forming hydroxo- and oxo-bridged metal networks,[8] and result in much lower yields of the target coordination polymer.

During our exploration of the above-mentioned system, we maintained the molar ratio of phen:Fe^{II} at less than 0.7:1, thus favoring the formation of compound **1**. As the ratio gets larger, $Fe(phen)_3^{2+}$ cations form more easily, resulting in the formation of low dimensional products. The pH value of the reaction system is also an important factor: it must be maintained higher than 9.5 in order to obtain the target complex.

For entropic reasons, synthesis at higher temperature can promote the formation of polymer frameworks of higher dimensionality through the loss of terminal ancillary ligands. This may be justified by the following analysis. From the viewpoint of thermodynamics, self-assembled structures represent thermodynamic minima. For compound **1**, a possible formatting reaction may be described as follows:

$$\tfrac{1}{2}n\ [bta]^{4-} + n\ [Fe(H_2O)_6]^{2+} + n\ Phen \rightarrow [Fe(phen)](bta)_{1/2}]_n + 6n\ H_2O$$

$$\tfrac{1}{2}n \qquad n \qquad n \qquad 1 \qquad 6n$$

The variation of molecular number in this reaction is $1/2n + n + n \rightarrow 1 + 6n$ (mol) and the entropy of the system increases ($\Delta S > 0$). The replacement of six water molecules with the stronger ligand phen and with carboxyl O-atoms may favor lowering the enthalpy of the system ($\Delta H < 0$). Thus giving $\Delta G = \Delta H - T\Delta S$ to be less than 0. Synthesis at higher temperature can make $T\Delta S$ greater, and thus contribute more to the variation of the free energy, facilitating the production of the target complex. This kind of consideration is easy to confirm in the crystal engineering of target complexes by self-assembly methods.[9]

This compound appears to provide a matrix for the generation of a particular metal-benzene-tetracarboxylate sheet. As a natural extension of the structural chemistry of such a network, the replacement of phen with other similar ligands, such as bipyridine, is possible, and this work is currently under way. The experimental verification of compound **1** may help us to understand more about polycarboxylate ligands, and to engineer new supramolecular architectures.

Experimental Section

Synthesis: We prepared the compound with a mixture of $FeCl_2{\cdot}4H_2O$ (1.00 g), 1,10-phenanthroline (0.33 g), sodium benzenetetracarboxylate [Na_4(bta), 1.70 g] and H_2O (24 mL) in a 30cm^3 Teflon-lined reactor (pH = 10). The reactor was sealed and heated to 160 °C for 72 hours under autogenous pressure. The obtained deep red crystals were isolated by filtration and washed with distilled water (yield 36% based on phen). IR spectra were recorded on a Perkin−Elmer 783 spectrometer as KBr pellets: $\tilde{\nu}$ = 2358(s). 1602(vs), 1510(s), 1478(s), 1423(s), 1410(s), 1370(vs), 1285(m), 1140(s),1103(s), 918(s), 852(vs), 814(s), 780(s), 740(s), 732(s), 662(m), 640(m), 600(s), 510(s), 420(m) cm^{-1}. − $C_{17}H_9FeN_2O_5$ (377.11): calcd. C 56.54, H 2.51, N 7.76, Fe 15.47; found C 56.50, H 2.55, N 7.550, Fe 15.40.

X-ray Crystal Structure Determination: Crystal data and structure refinement for the title compound are listed in the Table 1. A single crystal of compound **1** was studied on a Siemens P4 four-circle diffractometer using graphite-monochromated Mo-K_α radiation (λ = 0.71073Å) and ω-2θ scans. The structure was solved by the heavy-atom method and successive Fourier syntheses [SHELXS and SHELXL (Version 5.03, 1993)]. The refinement was performed by full-matrix least-squares refinement.

Crystallographic data (excluding structure factors) for the structure(s) included in this paper have been deposited with the Cambridge Crystallographic Data Centre as supplementary publication no. CCDC-151718. Copies of the data can be obtained free of charge on application to CCDC, 12 Union Road, Cambridge CB2 1EZ, UK [Fax: (internat.) + 44-1223/336-033; Email: deposit@ccdc.cam.ac.uk].

Table 1. Crystal data for compound [Fe(phen)(μ_6-bta)$_{1/2}$]$_n$

Empirical formula	$C_{17}H_9FeN_2O_4$
M	361.11
Crystal system	Monoclinic
Space group	$P2_1/c$
a, Å	7.482(2)
b, Å	19.701(2)
c, Å	9.574(3)
β, deg	111.78(2)
Z	3
V, Å^3	1310.5(5),
D_{calc}, g/cm^3	1.373
μ	0.884 mm^{-1}
Final R indices [$I > 2\sigma(I)$][a]	R_1 = 0.0387, wR_2 = 0.0857

[a] $R_1 = \Sigma(||F_o| - |F_c||)/\Sigma|F_o|$; $wR_2 = [\Sigma w(F_o^2 - F_c^2)^2/\Sigma w(F_o^2)^2]^{1/2}$.

Acknowledgments

This work was supported by the National Natural Science Foundation of China under grant No.29733090 and the Research Founds for the Doctoral Program of Higher Education and The state Key Laboratory of Coordination Chemistry, Najing University, 210093.

[1] [1a] C. N. R. Rao, A. Rangnathan, V. R. Pedireddi, A. R. Raju, *Chem. Commun.* **2000**, 39−40. − [1b] P. J. Hagrman, D. Hagrman, J. Zubieta, *Angew. Chem. Int. Ed.* **1999**, *38*, 2639−2683.

[2] [2a] B. F. Adrahamas, S. R. Batten, M. J. Grannas, H. Hamit, B. F. Hoskins, R. Robson, *Angew. Chem. Int. Ed.* **1999**, *38*, 1475−1476. − [2b] M. J. Zaworotko, *Angew. Chem. Int. Ed.* **1998**, *37*, 1211−1213.

[3] H.Gudbjartson, K. Biradha, K. M. Poirier, M. J. Zaworotko, *J. Am. Chem. Soc.* **1999**, *121* 2599−2600.

[4] [4a] S. S.-Y. Chui, S. M.-F. Lo, J. P. H. Charmant, A. G. Orpen, I. D. Williams, *Science* **1999**, *283*, 1148−1150. − [4b] O. M. Yaghi, H. Li, T. L. Groy, *J. Am. Chem. Soc.* **1996**, *118*, 9096−9101. − [4c] S. Decurtins, M. Gross, H. W. Schmalle, S. Ferlay, *Inorg. Chem.* **1998**, *37*, 2443−2449. − [4d] O. M. Yaghi, C. E. Davis, G. Li, H. Li, *J. Am. Chem. Soc.* **1997**, *119*, 2861−2868. − [4e] H. J. Choi, M. P. Suh, *J. Am. Chem. Soc.* **1999**, *120*, 10622−10628. − [4f] O. M. Yaghi, G. Li, H. Li, C. Davis, D. Richardson, T. L. Groy, *Acc. Chem. Res.* **1998**, *31*, 474−484.

[5] D. L. Ward, D. C. Luehrs, *Acta Cryst.* **1983**, *C39*, 1370.

[6] D. Cheng, Y.Zheng, J. Lin, D. Xu, Y. Xu, *Acta Cryst.* **2000**, *C56*, 523−524.

[7] D. Braga, F. Grepioni, G. R. Desiraju, *Chem. Rev.* **1998**, *98*, 1375−1405.

[8] J. Burger, C. Gack, P. Klüfers, *Angew. Chem. Int. Ed. Engl.* **1995**, *23/24*, 2647−2649.

[9] G. M. Whitesides, J. P. Mathias, C. T. Seto, *Science* **1994**, *254*, 1313−1318.

Received November 17, 2000
[I00449]

Lithium Insertion and XPS Study in $La_{0.5+x+y}Li_{0.5-3x}Ti_{1-3y}Cr_{3y}O_3$

María-Luisa Martínez-Sarrión,*[a] Lourdes Mestres,[a] Rosa Palacín,[b] and Marta Herráiz[a]

Keywords: Lithium / Insertions / Electrochemistry / Photoelectron spectroscopy

The stoichiometry and lithium insertion reactions with *n*BuLi and by electrochemical techniques of solid solutions $La_{0.5+x+y}Li_{0.5-3x}Ti_{1-3y}Cr_{3y}O_3$ with a perovskite-type structure have been studied. Stoichiometry data are given in the form of a solid solution triangle. In general, the amount of lithium inserted is consistent with the number of vacancies. The results of the chemical and electrochemical lithium insertion are similar: upon lithium insertion Cr^{VI} is reduced to Cr^{III}.

Introduction

Materials with structures derived from the high temperature phase γ-Li_3PO_4 comprise an extensive family of lithium-ion-conducting solid electrolytes known as LISICONS or γ-structures. Recently, a new group of lithium-ion conductors and mixed conductors in the LISICON family have been found that contain $Cr^{[5+]}$ as a framework cation.[1,2] The electrochemical intercalation of lithium into chromium(V)-containing oxides isostructural with β- and γ-Li_3PO_4 has been studied. β-Li_3CrO_4 can reversibly intercalate around one mol of Li per formula unit to give $Li_{3+x}CrO_4$ ($0 < x < 1$) with a discharge capacity of 196 $mAhg^{-1}$. Electrochemical data indicate that there may be a region with two phases in the approximate range $0.3 < x < 0.8$. Essentially, these materials are dimensionally stable to intercalation and de-intercalation.[3]

The X-ray photoelectron spectra of the different compounds of Cr^{III} were measured and from these data the chemical shifts of the core electrons were determined and related to a calculated charge based on Pauling's electronegativities.[4] A few years ago the binding energies of the chromium(III) 2p electrons was proposed to be dependent primarily on the oxidation number, although perturbations result from changes in the structure and in the Madelung potential. Multiplet splitting in chromium(III) compounds contributes to peak widths and the chemisorption of water and oxygen has a marked effect on the peak profiles and the accuracy of binding energy measurements.[5]

The electronic structures of the perovskite system $La_{1-x}(M^{2+})_xCrO_3$ (M = Mg, Sr) has been more widely studied than Cr_2O_3 and La_2O_3 by X-ray photoelectron spectroscopy. The main peaks and satellites of inner and outer electrons were properly assigned.[6]

Spinel solid solutions of general formula $ZnCr_xGa_{2-x}O_4$ have been studied by X-ray photoelectron spectroscopy. These XPS spectra indicated that in the spinel solid solutions no significant change in the electronic structure of Cr^{3+} ions occur, and a similar covalency in all the $ZnCr_xGa_{2-x}O_4$ solid solutions, irrespective of their composition, has been reported.[7]

In a previous paper[8] we studied the $La_{0.5+x+y}Li_{0.5-3x}Ti_{1-3y}Mn_{3y}O_3$ system, and the bulk conductivity data from the impedance complex plane plots were plotted in an Arrhenius format. The plots are linear and the conductivity decreases as the amount of lithium decreases. The variation in ionic conductivity with the lithium composition is quite large, although the ionic and electronic conductivity remain similar for $y = 0.01$.

The $Pr_{0.5+x+y}Li_{0.5-3x}Ti_{1-3y}Cr_{3y}O_3$ system showed similar behavior.[9] AC/DC measurements indicated that these compounds are mixed conductors. The Li^+ conductivity decreases as the amount of lithium decreases, while electronic conductivity increases with the amount of chromium. Similar measurements indicate that $La_{0.5+x+y}Li_{0.5-3x}Ti_{1-3y}Cr_{3y}O_3$ compounds are mixed conductors. The lithium ion conductivity decreases as the amount of lithium decreases, meanwhile electronic conductivity increases with the amount of chromium.[10]

Here we examine the chemical and electrochemical insertion and de-insertion of lithium in $La_{0.5+x+y}Li_{0.5-3x}Ti_{1-3y}Cr_{3y}O_3$ mixed conductors.

Results and Discussion

Chemical lithium intercalation was carried out on different compositions of the region of perovskite-like solid solutions on the phase diagram.[10] Along join 1 ($La_{0.583}Li_{0.25}TiO_3-LaCrO_3$), the lithium and lanthanum composition and the number of vacancies changes, along join 2 ($La_{0.60}Li_{0.20}TiO_3-La_{0.80}Li_{0.20}Ti_{0.40}Cr_{0.60}O_3$) the amount of lithium was constant, along join 3 ($La_{0.567}Li_{0.30}TiO_3-La_{0.86}Ti_{0.40}Cr_{0.60}O_3$), the number of vacancies was constant, along join 4 ($La_{0.583}Li_{0.25}TiO_3-La_{0.75}Li_{0.25}Ti_{0.50}Cr_{0.50}O_3$), the amount of lithium was constant, and along join 5

[a] Departament de Química Inorgànica, Universitat de Barcelona, Diagonal 647, 08028 Barcelona, Spain,
Fax: (internat.) +34-93/490-7725
E-mail: marialuisa.martinez@qi.ub.es
[b] Institut de Ciència de Materials de Barcelona (C.S.I.C.), Campus U.A.B., 08193 Bellaterra, Spain

 © WILEY-VCH Verlag GmbH, 69451 Weinheim, 2001 1434−1948/01/0505−1139 $ 17.50+.50/0

($La_{0.86}Ti_{0.40}Cr_{0.60}O_3-La_{0.80}Li_{0.20}Ti_{0.40}Cr_{0.60}O_3$) the chromium amount was constant (Figure 1).

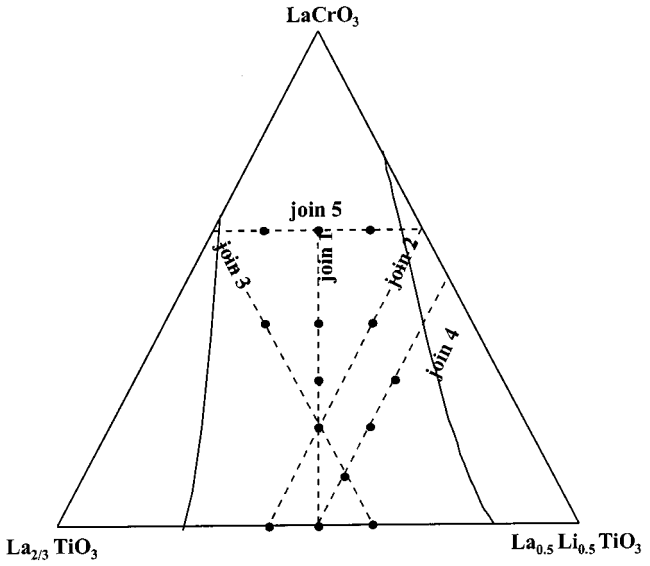

Figure 1. Composition triangle and joins of chemical lithium intercalation

ICP analyses were then carried out and these results are shown in Table 1, with the (Cr + Ti) amount set to unity and the remaining values re-normalised in the formula $La_{0.5+x+y}Li_{0.5-3x}Ti_{1-3y}Cr_{3y}O_3$. In general, the amount of lithium inserted is consistent with the number of vacancies. For all compositions the Li:La:Ti:Cr ratios were in good agreement with the values expected from the starting compositions.

The compositions along join 1 were measured by EPMA. The experimental values of oxygen contents have larger uncertainties than the values for La, Ti and Cr due to the difficulty in separating the O-K_α signal from that emitted by the carbon coating and partial absorption of the O-K_α signal by the carbon. $SrTiO_3$, which was the standard for oxygen, and some samples were coated together to improve the oxygen measurements. The results obtained in join 1,[10] allowed us to establish that the oxygen content varies between 2.95 and 3.01. For this reason we assume that the oxygen content in all the samples is nearly to 3.

Figures 2–5 show the amount of lithium inserted versus amount of lanthanum for joins 1, 3, 4 and 5, respectively. In join 1 (where the lithium and lanthanum composition and the number of vacancies changes), when the lanthanum and chromium amount increases, the number of vacancies decreases, therefore the amount of lithium inserted must also decrease. In Figure 2 we can see this behavior, except for the sample $La_{0.71}Li_{0.19}Ti_{0.69}Cr_{0.31}O_3$ in which 0.16 mol of lithium is inserted. This behaviour can be attributed to the cubic structure of the $La_{0.58}Li_{0.25}TiO_3$ and $La_{0.70}Li_{0.21}Ti_{0.79}Cr_{0.21}O_3$ compounds and the orthorhombic structure of $La_{0.71}Li_{0.19}Ti_{0.69}Cr_{0.31}O_3$, $La_{0.76}Li_{0.17}Ti_{0.59}Cr_{0.41}O_3$, and $La_{0.83}Li_{0.07}Ti_{0.39}Cr_{0.61}O_3$.[10] In join 3 (the number of vacancies was constant), the substitution of chromium for titanium increases the amount of lithium inserted, which decreases with an increase in the amount of lanthanum. In join 4 (the lithium amount was constant), when lanthanum and chromium increase, the number of vacancies decreases, and, consequently, the amount of lithium inserted is reduced. In join 5 (the chromium amount was constant) the lithium insertion increases as the number of vacancies increases.

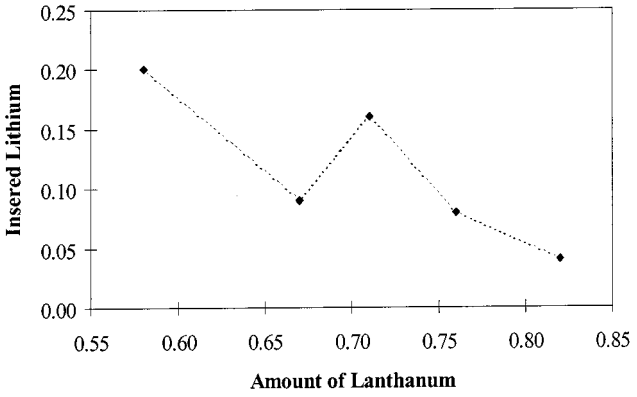

Figure 2. Plot of amount of lithium inserted vs. amount of lanthanum in join 1

Table 1. Samples composition and vacancies before and after the insertion of lithium

Starting composition $La_{0.5+x+y}Li_{0.5-3x}Ti_{1-3y}Cr_{3y}O_3$	Experimental composition	Inserted Lithium $La_{0.5+x+y}Li_{0.5-3x+\delta}Ti_{1-3y}Cr_{3y}O_3$	A-site vacancy[a]	δ
$La_{0.60}Li_{0.20}TiO_3$	$La_{0.62}Li_{0.18}TiO_3$	$La_{0.62}Li_{0.39}TiO_3$	0.20	0.21
$La_{0.58}Li_{0.25}TiO_3$	$La_{0.58}Li_{0.25}TiO_3$	$La_{0.58}Li_{0.45}TiO_3$	0.17	0.20
$La_{0.57}Li_{0.30}TiO_3$	$La_{0.57}Li_{0.27}TiO_3$	$La_{0.57}Li_{0.45}TiO_3$	0.16	0.18
$La_{0.62}Li_{0.25}Ti_{0.90}Cr_{0.10}O_3$	$La_{0.64}Li_{0.22}Ti_{0.89}Cr_{0.11}O_3$	$La_{0.64}Li_{0.34}Ti_{0.90}Cr_{0.10}O_3$	0.14	0.12
$La_{0.67}Li_{0.20}Ti_{0.80}Cr_{0.20}O_3$	$La_{0.70}Li_{0.21}Ti_{0.79}Cr_{0.21}O_3$	$La_{0.70}Li_{0.30}Ti_{0.79}Cr_{0.21}O_3$	0.09	0.09
$La_{0.65}Li_{0.25}Ti_{0.80}Cr_{0.20}O_3$	$La_{0.67}Li_{0.24}Ti_{0.79}Cr_{0.21}O_3$	$La_{0.67}Li_{0.33}Ti_{0.79}Cr_{0.21}O_3$	0.09	0.09
$La_{0.71}Li_{0.175}Ti_{0.70}Cr_{0.30}O_3$	$La_{0.70}Li_{0.17}Ti_{0.69}Cr_{0.31}O_3$	$La_{0.70}Li_{0.33}Ti_{0.69}Cr_{0.31}O_3$	0.10	0.16
$La_{0.68}Li_{0.25}Ti_{0.70}Cr_{0.30}O_3$	$La_{0.69}Li_{0.24}Ti_{0.69}Cr_{0.31}O_3$	$La_{0.69}Li_{0.32}Ti_{0.69}Cr_{0.31}O_3$	0.07	0.08
$La_{0.77}Li_{0.10}Ti_{0.60}Cr_{0.40}O_3$	$La_{0.80}Li_{0.08}Ti_{0.55}Cr_{0.45}O_3$	$La_{0.80}Li_{0.15}Ti_{0.56}Cr_{0.44}O_3$	0.12	0.07
$La_{0.75}Li_{0.15}Ti_{0.60}Cr_{0.40}O_3$	$La_{0.76}Li_{0.17}Ti_{0.59}Cr_{0.41}O_3$	$La_{0.76}Li_{0.25}Ti_{0.59}Cr_{0.41}O_3$	0.07	0.08
$La_{0.73}Li_{0.20}Ti_{0.60}Cr_{0.40}O_3$	$La_{0.71}Li_{0.20}Ti_{0.59}Cr_{0.41}O_3$	$La_{0.71}Li_{0.28}Ti_{0.59}Cr_{0.41}O_3$	0.09	0.08
$La_{0.85}Li_{0.05}Ti_{0.40}Cr_{0.60}O_3$	$La_{0.84}Li_{0.04}Ti_{0.39}Cr_{0.61}O_3$	$La_{0.84}Li_{0.09}Ti_{0.39}Cr_{0.61}O_3$	0.12	0.05
$La_{0.83}Li_{0.10}Ti_{0.40}Cr_{0.60}O_3$	$La_{0.82}Li_{0.07}Ti_{0.39}Cr_{0.61}O_3$	$La_{0.82}Li_{0.11}Ti_{0.39}Cr_{0.61}O_3$	0.11	0.04
$La_{0.82}Li_{0.15}Ti_{0.40}Cr_{0.60}O_3$	$La_{0.80}Li_{0.13}Ti_{0.39}Cr_{0.61}O_3$	$La_{0.80}Li_{0.15}Ti_{0.39}Cr_{0.61}O_3$	0.07	0.02

[a] (calculated A-site vacancy) = 1 − (La content + Li content).

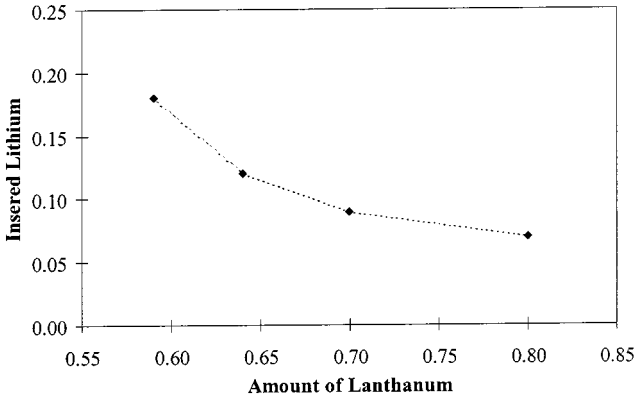

Figure 3. Plot of amount of lithium inserted vs. amount of lanthanum in join 3

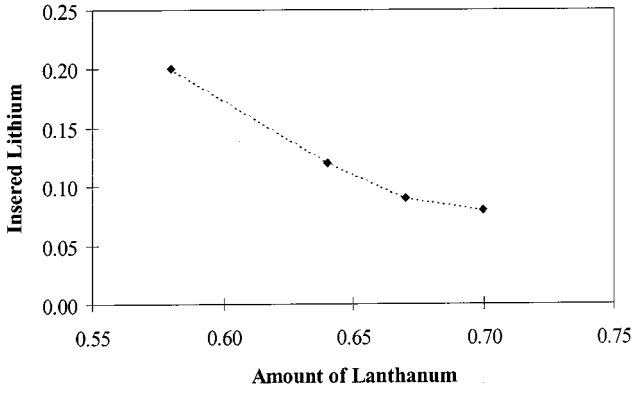

Figure 4. Plot of amount of lithium inserted vs. amount of lanthanum in join 4

The cell parameters of the lithium inserted phases show no differences with the non-lithium inserted phases (Table 2).

De-lithiation reactions were performed by treating some compositions of the lithiated compounds with iodine in dry acetonitrile. The results are shown in Table 3. The process of lithium insertion-delithiation is reversible.

The degrees of lithium uptake observed in electrochemical experiments down to 1.5 V vs. Li^0-Li^+ were approximately consistent with those obtained after chemical lithiation. Some typical composition-voltage profiles are shown in Figure 6, corresponding to samples along join 4 containing both titanium and chromium. Contrary to what has been reported for pure La−Li−Ti−O perovskites,[11,12] the degree of lithium intercalation in chromium-containing samples is never higher, within the experimental errors, than the number of A-type vacancies. On the other hand, the increase in the chromium content seems to be associated with an electrochemical step appearing at about 2.3 V vs. Li^0-Li^+ upon reduction of the samples. The electrochemical de-intercalation (i.e. oxidation) is difficult to achieve and only takes place at ≈4V, (Figure 6) for sample $La_{0.69}Li_{0.24}Ti_{0.69}Cr_{0.31}O_3$.

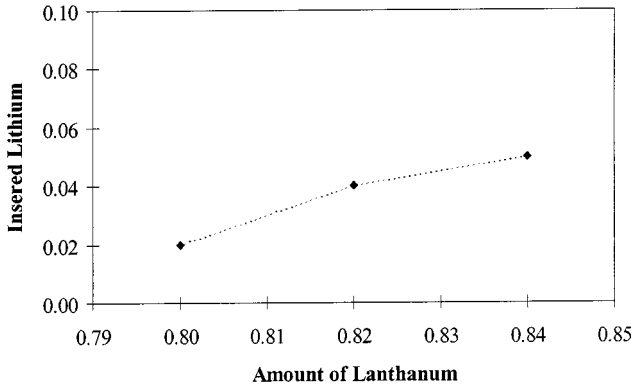

Figure 5. Plot of amount of lithium inserted vs. amount of lanthanum in join 5

The X-ray photoelectron spectroscopy of different compositions were compared with the values from Table 4. Figure 7 shows the Cr (2p) spectrum for the composition $La_{0.92}Li_{0.05}Ti_{0.21}Cr_{0.79}O_3$ (c in Figure 7), and we compared this with the patterns of Cr_2O_3 (a) and CrO_3 (b) from 565 to 605 eV. The main peaks of this sample, located at 576.2 eV ($Cr2p_{3/2}$) and 585.9 eV ($Cr2p_{1/2}$), correspond to Cr^{3+}. The shake-up satellite of $Cr2p_{3/2}$ is seen at ≈582 eV and, for $Cr(2p_{1/2})$, the satellite appears at ≈597 eV. The main peaks of chromium show a shoulder that indicates the presence of chromium in another number state, probably Cr^{6+} (Fig-

Table 2. Cell parameters of the samples before and after the insertion of lithium

Starting sample	Inserted sample	*a* (A)	*b* (A)	*c* (A)	*V* (A^3)
$La_{0.64}Li_{0.22}Ti_{0.89}Cr_{0.11}O_3$		3.8775(6)	3.8775(6)	3.8775(6)	58.298(2)
	$La_{0.64}Li_{0.34}Ti_{0.90}Cr_{0.10}O_3$	3.8775(6)	3.8775(6)	3.8775(6)	58.298(2)
$La_{0.70}Li_{0.21}Ti_{0.79}Cr_{0.21}O_3$		3.8768(6)	3.8768(6)	3.8768(6)	58.266(2)
	$La_{0.70}Li_{0.30}Ti_{0.79}Cr_{0.21}O_3$	3.8767(6)	3.8767(6)	3.8767(6)	58.262(2)
$La_{0.67}Li_{0.24}Ti_{0.79}Cr_{0.21}O_3$		3.8765(7)	3.6765(7)	3.8765(7)	58.25(2)
	$La_{0.67}Li_{0.33}Ti_{0.79}Cr_{0.21}O_3$	3.8767(6)	3.8767(6)	3.8767(6)	58.267(2)
$La_{0.70}Li_{0.17}Ti_{0.69}Cr_{0.31}O_3$		5.491(9)	5.481(3)	7.757(9)	233.46(2)
	$La_{0.70}Li_{0.33}Ti_{0.69}Cr_{0.31}O_3$	5.491(6)	5.479(6)	7.754(7)	233.28(2)
$La_{0.69}Li_{0.24}Ti_{0.69}Cr_{0.31}O_3$		3.8765(7)	3.8765(7)	3.8765(7)	58.25(2)
	$La_{0.69}Li_{0.32}Ti_{0.69}Cr_{0.31}O_3$	3.8767(3)	3.8767(3)	3.8767(3)	58.262(1)
$La_{0.80}Li_{0.08}Ti_{0.55}Cr_{0.45}O_3$		5.497(7)	5.480(5)	7.759(8)	233.73(2)
	$La_{0.80}Li_{0.15}Ti_{0.56}Cr_{0.44}O_3$	5.495(6)	5.479(6)	7.762(9)	233.69(2)
$La_{0.76}Li_{0.17}Ti_{0.59}Cr_{0.41}O_3$		5.493(8)	5.480(4)	7.756(8)	233.47(2)
	$La_{0.76}Li_{0.25}Ti_{0.59}Cr_{0.41}O_3$	5.493(9)	5.480(6)	7.756(9)	233.47(2)
$La_{0.82}Li_{0.07}Ti_{0.39}Cr_{0.61}O_3$		5.499(6)	5.479(6)	7.761(9)	233.83(2)
	$La_{0.82}Li_{0.11}Ti_{0.39}Cr_{0.61}O_3$	5.500(7)	5.480(5)	7.763(8)	233.98(2)

Table 3. Sample compositions after chemical lithium removal

Starting composition	Inserted composition	Deintercalation composition
$La_{0.64}Li_{0.22}Ti_{0.89}Cr_{0.11}O_3$	$La_{0.64}Li_{0.34}Ti_{0.90}Cr_{0.10}O_3$	$La_{0.65}Li_{0.21}Ti_{0.90}Cr_{0.10}O_3$
$La_{0.67}Li_{0.24}Ti_{0.79}Cr_{0.21}O_3$	$La_{0.67}Li_{0.33}Ti_{0.79}Cr_{0.21}O_3$	$La_{0.65}Li_{0.22}Ti_{0.79}Cr_{0.21}O_3$
$La_{0.70}Li_{0.17}Ti_{0.69}Cr_{0.31}O_3$	$La_{0.70}Li_{0.33}Ti_{0.69}Cr_{0.31}O_3$	$La_{0.71}Li_{0.16}Ti_{0.61}Cr_{0.39}O_3$
$La_{0.69}Li_{0.24}Ti_{0.69}Cr_{0.31}O_3$	$La_{0.69}Li_{0.32}Ti_{0.69}Cr_{0.31}O_3$	$La_{0.70}Li_{0.23}Ti_{0.69}Cr_{0.31}O_3$
$La_{0.80}Li_{0.08}Ti_{0.55}Cr_{0.45}O_3$	$La_{0.80}Li_{0.15}Ti_{0.56}Cr_{0.44}O_3$	$La_{0.80}Li_{0.10}Ti_{0.57}Cr_{0.43}O_3$
$La_{0.84}Li_{0.04}Ti_{0.39}Cr_{0.61}O_3$	$La_{0.84}Li_{0.09}Ti_{0.39}Cr_{0.61}O_3$	$La_{0.84}Li_{0.06}Ti_{0.63}Cr_{0.37}O_3$
$La_{0.80}Li_{0.13}Ti_{0.39}Cr_{0.61}O_3$	$La_{0.80}Li_{0.15}Ti_{0.39}Cr_{0.61}O_3$	$La_{0.79}Li_{0.10}Ti_{0.39}Cr_{0.61}O_3$

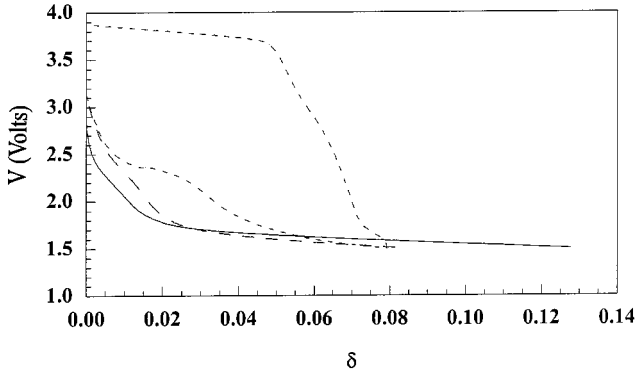

Figure 6. Discharge-charge curves operating in galvanostatic low current mode at 1MLi/200 h

Table 4. Binding energy (eV) observed from the photoelectron spectra for elements in various chromium and titanium compounds

Pattern	Cr 2p 1/2	Cr 2p 3/2	Ti 2p 1/2	Ti 2p 3/2	Ref.
$Cr_2^{III}O_3$	586.67	576.63	–	–	This work
$Cr^{VI}O_3$	588.84	579.54	–	–	This work
$LaCr^{III}O_3$	585.5	575.8	–	–	[6]
$Li_2Cr^{VI}O_4$	587.8	578.6	–	–	[5]
$LiCr^{III}O_2$	585.6	575.8	–	–	[15]
$Mn_2Ti^{IV}O_4$	–	–	462.54	456.60	
+ $MnTi^{III}O_3$	–	–	–	–	This work
			463.98	458.23	

ure 7). These shoulders appear at 578.9 eV and 585.5 eV. The presence of chromium in two different number states is the origin of the electronic conductivity in these compounds.[6]

In an attempt to study the variation in the number state of chromium caused by lithium insertion, the X-ray photoelectron spectrum of $La_{0.71}Li_{0.19}Ti_{0.69}Cr_{0.31}O_3$ before and after lithiation was recorded. In this sample the amount of inserted lithium was highest. Figure 8a shows the Cr2p spectrum of this sample. In the lithium-inserted sample (Figure 8b), the ratio between the peak areas Cr^{6+}/Cr^{3+} decreases as a result of the reduction of Cr^{6+} to Cr^{3+} with the introduction of positive charges (Li^+) in the structure.

The same study was performed for titanium (Figure 9). In both samples the titanium is present mostly as Ti^{4+}, and no change is produced in its number state during the insertion.

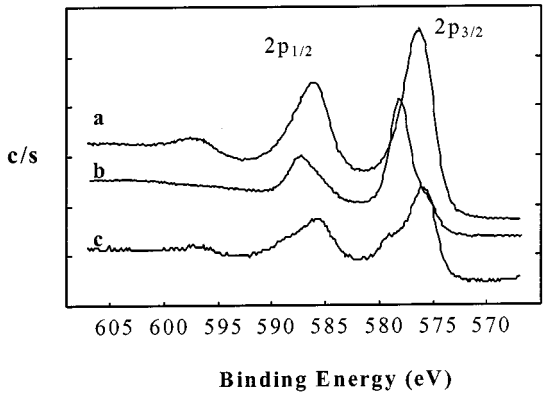

Figure 7. X-ray photoelectron spectra of Cr 2p region of: a) Cr_2O_3, b) CrO_3 and c) $La_{0.92}Li_{0.05}Ti_{0.21}Cr_{0.79}O_3$

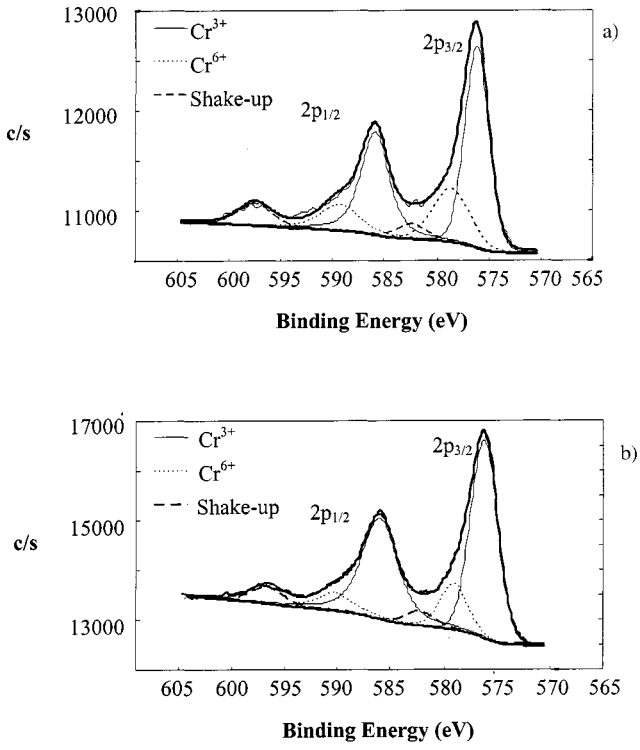

Figure 8. X-ray photoelectron spectra of Cr 2p region of: a) $La_{0.71}Li_{0.19}Ti_{0.69}Cr_{0.31}O_3$ and b) $La_{0.71}Li_{0.35}Ti_{0.69}Cr_{0.31}O_3$

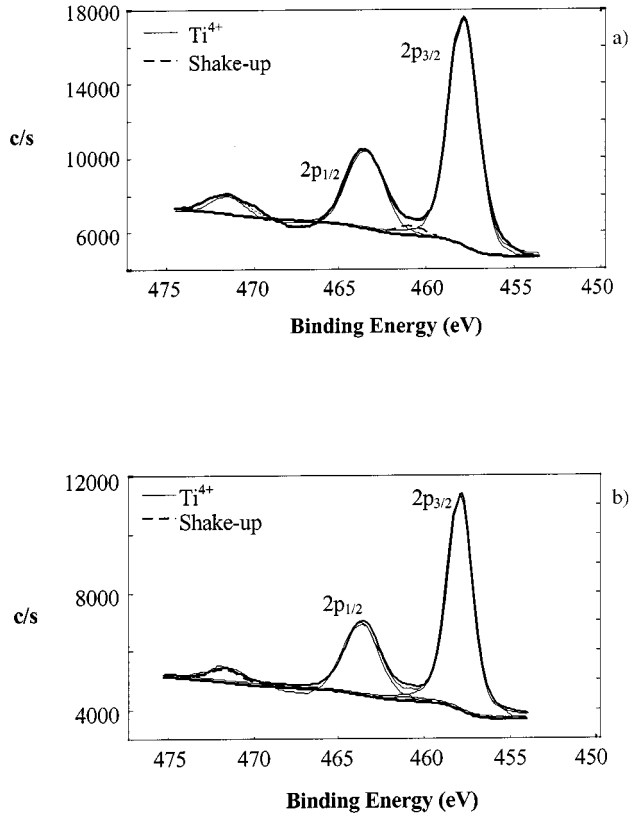

Figure 9. X-ray photoelectron spectra of Ti 2p region of: a)$La_{0.71}Li_{0.19}Ti_{0.69}Cr_{0.31}O_3$ and b) $La_{0.71}Li_{0.35}Ti_{0.69}Cr_{0.31}O_3$

Conclusion

A large range of single-phase solid solutions have been synthesized in the triangle $La_{2/3}TiO_3-LaCrO_3-La_{0.5}Li_{0.5}TiO_3$. The phase diagram in the single-phase region showed two polymorphs with a perovskite-like structure. The polymorph with the lowest chromium content has a cubic perovskite structure, and that with the highest chromium content shows an orthorhombic distortion. The cell parameters of the lithium-inserted phases show no differences with the non-lithium inserted phases. The presence of chromium in two different number states is the origin of the electronic conductivity in $La_{0.5+x+y}Li_{0.5-3x}Ti_{1-3y}Cr_{3y}O_3$.

Experimental Section

Syntheses: La_2O_3 (99.9% Fluka), TiO_2 (Aldrich 99 +%), Cr_2O_3 (>99%, Fluka) and Li_2O_3 (>99% Aldrich) were used as starting materials. La_2O_3, and TiO_2 were dried overnight at 900 °C prior to weighing. These chemicals were weighed, mixed in an agate mortar with acetone, dried and heated at 650 °C for 2 h to drive off CO_2. After grinding, samples were pressed into pellets and covered with powder of the same composition to avoid loss of lithium during the thermal treatment. The pellets were fired at 1100 °C for 8 h giving green products which were reground, repelleted, and fired at 1200 °C and at 1250 °C for 12 h, and again at 1300 °C for 4 h.

X-ray Diffraction: The crystalline phase identification and lattice parameters were obtained by powder X-ray diffraction with a Siemens D-500 diffractometer in reflection mode using Cu-K_α radiation. Lattice parameters were obtained using a silicon internal standard.

Chemical Lithium Intercalation: Chemical lithium intercalation was carried out by reacting the ground sample with *n*BuLi (1.6 M) in a hexane solution in a dried glove box filled with N_2 gas at 50 °C for 3 days with shaking. The X-ray diffraction pattern of the intercalate products was recorded after washing in hexane. After the chemical lithium intercalation, the samples were analysed by ICP, using a Jobin Ybon analyzer.

Electrochemical Lithium Intercalation: Electrochemical intercalation experiments were performed in Swagelok™ cells.[13] The positive electrode consisted of a ground powder mixture of the precursor and SuperP Carbon (kindly supplied by MMM, Belgium). Two sheets of Whattmand GF/D borosilicate glass fiber soaked with 1 M $LiPF_6$ in 1:1 EC/DMC electrolyte (Merck) were used as a separator, and the negative electrode consisted of lithium foil (0.38 mm thick). The cells were monitored with an Arbin BT2042 cycler operating in galvanostatic low current mode at 1Li/200 h.

X-ray Photoelectron Spectra: XPS spectra were recorded on a Perkin Elmer PHI 5500-ESCA SYSTEM with Al-K_α radiation (1486.6 eV). The energy calibration, including sample charging, was made against C(1s) peaks from the usual contamination. With a value of 83.8 eV for Au (4f 7/2), the energy is 284.8 eV. The pressure of the sample chamber was maintained below 10^{-9} Torr. The peaks were fitted by the Multipak computer program.[14]

Electron Probe Microanalysis: Some samples were studied by EPMA, to verify homogeneity, with a CAMECA SX50 EPMA instrument.

Acknowledgments

This study was partially sponsored by 1999GR00044 and PB98−1424−C02−02.

[1] M. A. K. L. Dissanayake, S. García-Martín, R. Saez-Puche, H. H. Sumathipala, A. R. West, *J. Mater. Chem.* **1994**, *4*, 1307−1308.
[2] M. A. K., L. Dissanayake, R. P. Gunawardane, H. H. Sumathipala, A. R. West, *Solid State Ionics* **1995**, *76*, 215−220.
[3] S. García Martín, A. D. Robertson, M. A. K. L. Dissanayake, A. R. West, *Solid State Ionics* **1995**, *76*, 309−314.
[4] J. C. Carver, G. K. Schweitzer, *J. Chem. Phys.* **1972**, *57*, 973−981.
[5] G. C. Allen, M. T. Curtis, A. J. Hooper, P. M. Tucker, *J. Chem. Soc., Dalton Trans* **1973**, 1675−1683.
[6] W. Y. Howng, R. J. Thorn, *J. Phys. Chem. Solids* **1980**, *41*, 75−81.
[7] C. Battistoni, J. L. Dormann, D. Fiorani, E. Paparazzo, S. Viticoli, *Solid State Commun.* **1981**, *39*, 581−585.
[8] I. Moreno, M. Morales, M. L. Martínez Sarrión, *J. Solid State Chem.* **1998**, *140*, 377.
[9] M. Morales, M. L. Martínez Sarrión, *J. Mater. Chem.* **1998**, *8*, 1853.
[10] M. L. Martínez Sarrión, L. Mestres,M. Morales, M. Herráiz, *J. Solid State Chem.* **2000**, 154.
[11] Y. Jin Shan, L. Chen, Y. Inaguma, M. Itoh, T. Nakamura, *J. Power Sources* **1995**, *54*, 397.

[12] F. García-Alvarado, A. Várez, E. Morán, M. A. Alario-Franco, *Phase Transitions* **1996**, *58*, 111.
[13] D. Guyomard, J. M. Tarascon, *J. Electrochem. Soc.* **1992**, *139*, 937.
[14] *Multipak for Windows 95*, Physical Electronics Inc. **1996**.
[15] I. Ikemoto, K, Ishii, S. Kinoshita, H. Kuroda, M. A. A. Franco, J. Thomas, *J. Solid State Chem.* **1976**, *17*, 425.

Received April 25, 2000
[I00158]

The Intramolecular Ligand-Exchange Reaction of (*SP*-4-2)-Dichlorobis-(2-hydroxyethylamine)platinum(II) and (*OC*-6-22)-Tetrachlorobis-(2-hydroxyethylamine)platinum(IV), a ^{1}H and $^{15}N,^{1}H$-HMQC NMR Study

Markus Galanski,[a] Wolfgang Zimmermann,[a] Christian Baumgartner,[a] and Bernhard Klaus Keppler*[a]

Keywords: Platinum / Ligand exchange / X-ray diffraction / NMR spectroscopy / N ligands

The bis(ethanolamine)platinum complexes (*SP*-4-2)-dichlorobis(2-hydroxyethylamine)platinum(II) (**1**) and (*OC*-6-22)-tetrachlororbis(2-hydroxyethylamine)platinum(IV) (**2**) have been synthesized and their chemistry in aqueous solution has been investigated due to the fact that **1** forms very stable monoadducts with 5′-GMP. In water **1** and **2** are converted into (*SP*-4-3)-chloro(2-ethanolatoamine-κ^2N,O)(2-hydroxyethylamine)platinum(II) (**3**) and (*OC*-6-31)-trichloro(2-ethanolatoamine-κ^2N,O)(2-hydroxyethylamine)platinum(IV) (**4**) with a chelating ethanolatoamine ligand by a intramolecular ligand exchange reaction, which was confirmed by ^{1}H and 2D $^{15}N,^{1}H$-HMQC NMR experiments and the crystal structure determination of **4**.

Introduction

Cisplatin,[1,2] *cis*-$[PtCl_2(NH_3)_2]$, is commonly used for the treatment of testicular and ovarian cancer as well as cervical, bladder and head and neck tumors.[3] The application of cisplatin in therapy is limited by the dose-dependent nephrotoxicity, among a variety of other side effects.[4] There are different strategies for the development of new platinum-based anticancer compounds. Great efforts are undertaken to reduce toxicity and side effects of the platinum compounds, to increase their activity spectrum and to circumvent acquired resistance of cells to cisplatin.[5−8]

A key objective of our research in this subject is to achieve a selective accumulation of antitumor platinum complexes in specific tissues of the organism and to investigate the mode of action of tumor-inhibiting platinum compounds. Therefore, the bis(ethanolamine) platinum(II) and (IV) complexes (*SP*-4-2)-dichlorobis(2-hydroxyethylamine)-platinum(II) (**1**, Scheme 1) and (*OC*-6-22)-tetrachlorobis(2-hydroxyethylamine)platinum(IV) (**2**, Scheme 2) have been synthesised. These compounds can, on the one hand, be used for further derivatisation at the OH group with carrier molecules due to the concept of drug targeting,[9] and on the other hand the bis(ethanolamine) complexes themselves are very interesting because their hydroxy groups can act as acceptors or donors for hydrogen bonds, which could play an important role in the binding of platinum complexes to DNA, the major target of platinum-based chemotherapy.[10,11] Furthermore, it has been shown previously that the formation of bisadducts between **1** and 5′-GMP is very slow and that **1** forms extremely stable 5′-GMP monoadducts, which can be detected in solution by capillary electrophoresis over a period of more than 10 days in the presence of 5′-GMP (1:2).[12]

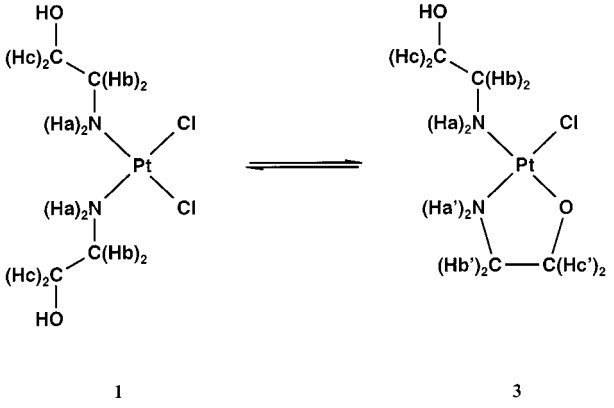

Scheme 1. Equilibrium of complexes **1** and **3** in water

This unexpected observation has led us to focus on the chemistry of **1** and its kinetically more inert tetrachloro analogue **2** in aqueous solution.

Results and Discussion

Whenever (*SP*-4-2)-dichlorobis(2-hydroxyethylamine)-platinum(II) or (*OC*-6-22)-tetrachlorobis(2-hydroxyethylamine)platinum(IV) are dissolved in water intramolecular ligand exchange reactions can be observed: One of the chloro ligands is released and a ethanolatoamine chelate is formed resulting in the complexes (*SP*-4-3)-chloro(2-ethanolatoamine-κ^2N,O)(2-hydroxyethylamine)platinum(II) (**3**) and (*OC*-6-31)-trichloro(2-ethanolatoamine-κ^2N,O)(2-hydroxyethylamine)platinum(IV) (**4**) (Scheme 1 and 2).

[a] Institute of Inorganic Chemistry, Vienna University,
Waehringer Straße 42, 1090 Vienna, Austria
Fax: (internat.) + 43-1/4277-52680
E-mail: Keppler@ap.univie.ac.at

 © WILEY-VCH Verlag GmbH, 69451 Weinheim, 2001 1434−1948/01/0505−1145 $ 17.50+.50/0

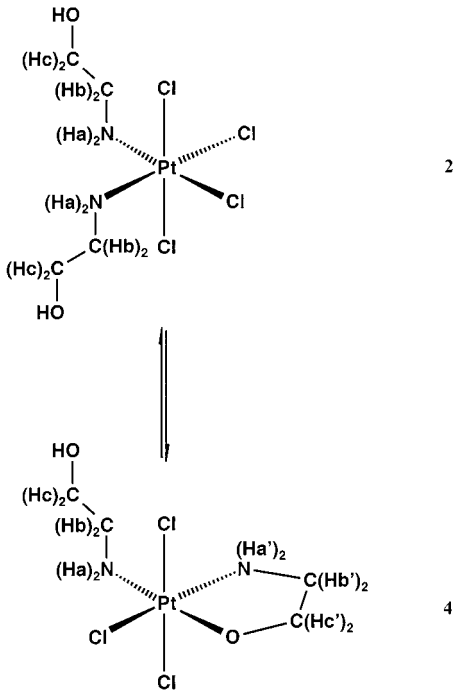

Scheme 2. Equilibrium of complexes **2** and **4** in water

Intramolecular Ligand Exchange Reaction of Compound 1

When dissolving **1** in aqueous solution one should expect three ^{1}H resonances, two multiplets for the CH_2 protons and a broad multiplet for the NH_2 group. However, five minutes after dissolution of **1** in water four additional ^{1}H signals of methylene protons and two additional NH_2 resonances can already be detected; these increase with time (Figure 1). After one day 75% of the bis(ethanolamine) complex **1** and 25% of the ethanolatoamine chelate **3** are present in solution.

The mixture of **1** and **3** shows two sets of three multiplets in the region of the methylene protons, whereas three broad signals for the NH_2 protons can be found. The three methylene protons in the neighborhood of the coordinated amine resonate in the region δ = 2.9 to 2.4. They are broad and not clearly resolved due to coupling with the amine protons and the quadrupolar moment of the ^{14}N nucleus. The before-mentioned signals are separated from the three CH_2 triplets of the methylene protons in the neighborhood of the oxygen atom, which can be found between δ = 3.8 and 3.4.

The amine protons of **1** and **3** are detected between δ = 4.8 and 5.6 and can be assigned to the three different NH_2 groups by 2D ^{15}N,^{1}H-HMQC spectroscopy (Figure 2). The NH_2 protons of complex **1** (trans to Cl) resonate at δ = 4.92 with a ^{15}N chemical shift of δ = −50.02. The cross signal of the coordinated amine ligand of **3** within the chelate ring was found at δ = 5.49/−31.46 whereas the signal of the NH_2 group *trans* to oxygen was detected at δ = 5.11 and −69.98, respectively. With this information the signal assignment of the CH_2 protons to the different ligands [complex **1**: δ = 3.75 (H_c), 2.78 (H_b); complex **2**: δ = 3.71 (H_c), 3.49 ($H_{c'}$), 2.63 (H_b), 2.49 ($H_{b'}$)] was performed by ^{1}H,^{1}H-DQF shift correlation spectroscopy.

As expected, the intramolecular ligand exchange reaction can be suppressed by dissolving complex **1** in DCl solution. Under these conditions only two ^{1}H signals in the CH_2 region at δ = 3.63 (H_c) and 2.95 (H_b) are observed which indicates that the equilibrium is shifted towards complex **1**.

Intramolecular Ligand Exchange Reaction of Compound 2

In case of the kinetically more inert tetrachloroplatinum-(IV) complex **2** the intramolecular ligand exchange reaction can also be observed in water but it is slowed down in com-

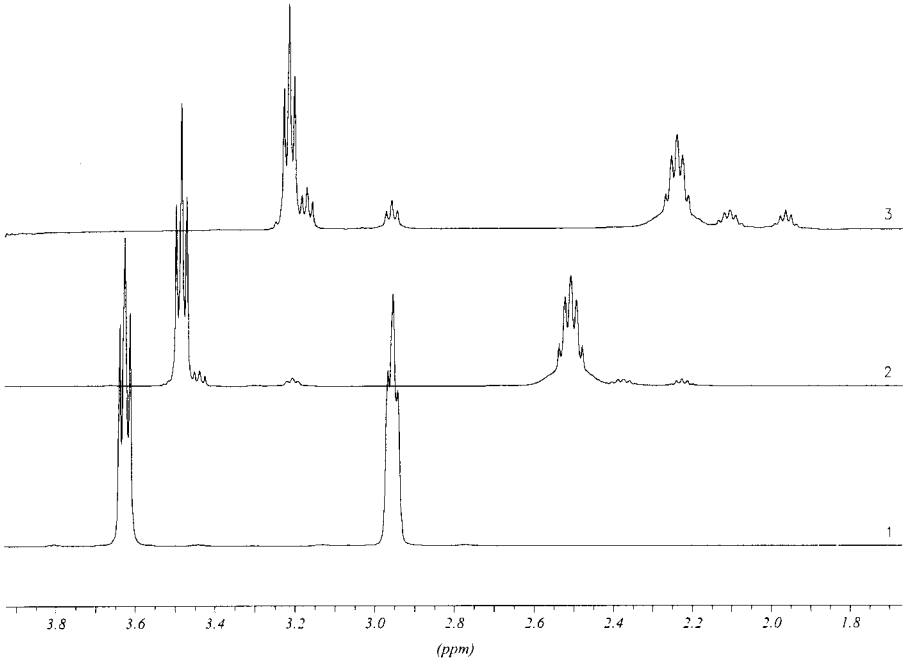

Figure 1. ^{1}H NMR spectra of **1** in DCl solution (1) and after one (2) and 24 hours (3) in H_2O/D_2O (9:1)

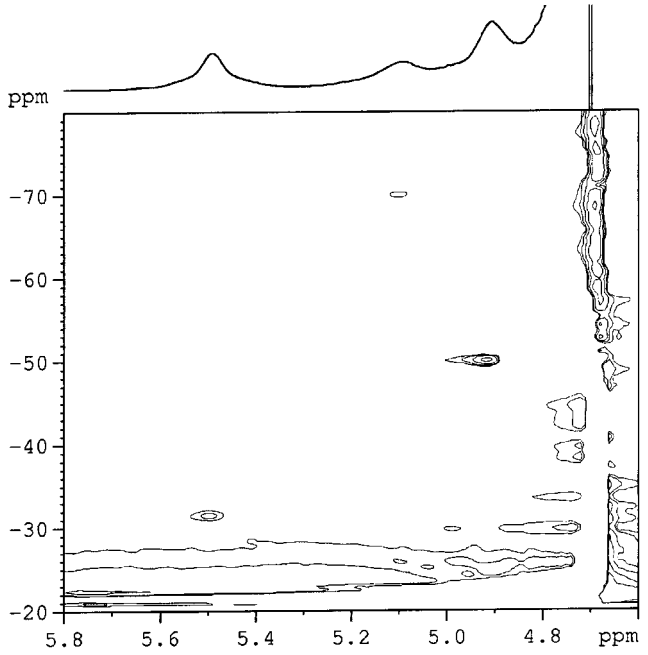

Figure 2. $^{15}N,^{1}H$-HMQC NMR spectrum of **1** after three hours

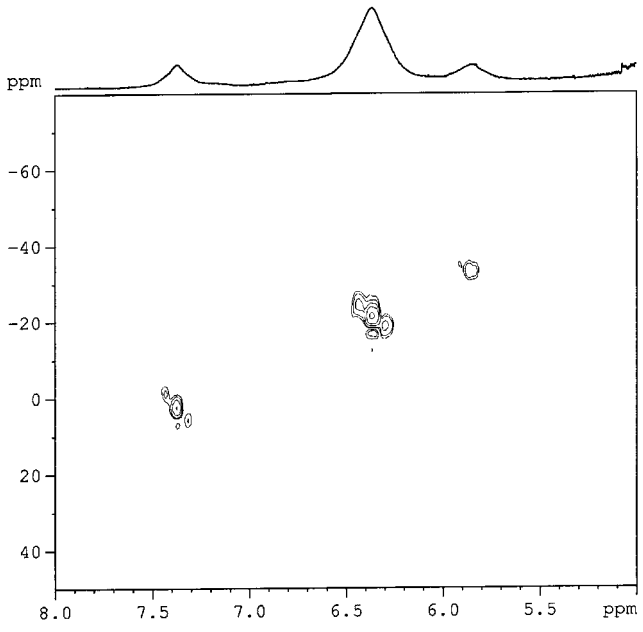

Figure 3. $^{15}N,^{1}H$-HMQC NMR spectrum of **2** after seven days

parison to the platinum(II) analogue **1**. After 12 days a nearly equimolar mixture of **2** and **4** (Scheme 2) is present in solution, whereas after 23 days 20% of **2** and 80% of **4** can be detected. Analogous to the mixture of compounds **1** and **3** there are two sets of CH_2 protons found in the ^{1}H NMR spectrum: three triplets for the methylene protons in the neighborhood of oxygen [**2**: $\delta = 3.70$ (H_c); **4**: 3.65 (H_c), 3.19 ($H_{c'}$)] and two broad multiplets at $\delta = 2.98$ (H_b of **2** and **4**) and 2.60 ($H_{b'}$) for the CH_2 protons in the neighborhood of the coordinated amine.

The NH_2 protons of compound **2** (*trans* to Cl) resonate at $\delta = 6.36$ with a ^{15}N chemical shift of $\delta = -21.78$ (Figure 3). The protons of the coordinated amine of **4** *trans* to the chloro ligand are found at $\delta = 7.31$; the ^{15}N chemical shift is observed at $\delta = 2.52$. The $^{1}H,^{15}N$ cross peak of the amine ligand *trans* to oxygen was detected at $\delta = 5.87$ and -33.02, respectively.

The assignment of the signals was done in this case by 2D $^{15}N,^{1}H$-HMQC, 2D $^{1}H,^{1}H$-COSY and 2D HMQC-TOCSY where the latter experiment combines both the heteronuclear and the homonuclear shift correlation in one experiment.

It was possible to isolate crystals of complex **4** after dissolution of **2** in water for nine days.

The crystal structure of (*OC*-6-31)-trichloro(2-ethanolatoamine-κ^2N,O)(2-hydroxyethylamine)platinum(IV) is shown in Figure 4. The atoms around the platinum center are arranged octahedrally. The two N atoms as well as Cl3 and O1 show a square-planar arrangement around the platinum atom. The angular sum of the equatorial atoms is 360.1° [N1−Pt−N2 = 91.9(2)°, N1−Pt−O1 = 85.3(2)°, N2−Pt−Cl3 = 93.22(17)° and O1−Pt−Cl3 = 89.59(18)°]. The Pt−N [Pt−N1 = 2.059(6) Å, Pt−N2 = 2.066(6) Å] and Pt−Cl [Pt−Cl1 = 2.319(18) Å, Pt−Cl2 = 2.315(19) Å, Pt−Cl3 = 2.331(18) Å] distances are similar to those in (*OC*-6-22)-tetrachlorobis(2-hydroxyethylamine)-platinum(IV).[13] The Cl1 and Cl2 atoms are axial to the equatorial plane and the Cl1−Pt−Cl2 axis is nearly linear [Cl1−Pt−Cl2 = 177.46(7)°]. Four intermolecular hydrogen bonds of each complex are found [N1−H1A···O2 = 2.955 Å (N1−O2); N1−H1B···O1 = 2.895 Å (N1−O1); N2−H2A···O2 2.772 Å (N2−O2); N2−H2B···O1 = 2.791 Å (N2−O1)].

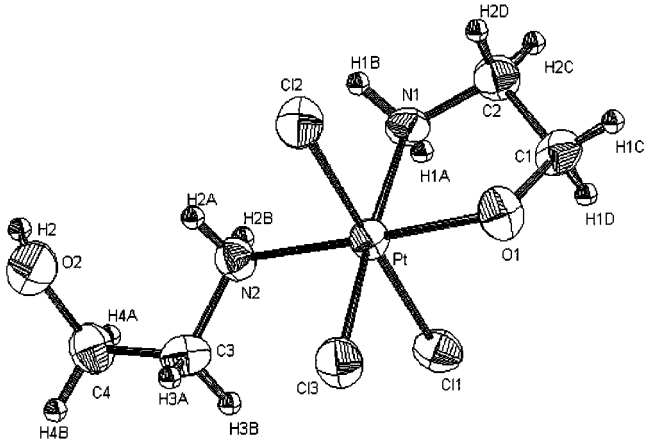

Figure 4. Molecular structure of **4** in the crystal

^{1}H, 2D-$^{1}H,^{1}H$ and 2D $^{15}N,^{1}H$ NMR studies were also carried out with the crystals of compound **4**. In aqueous solution, four ^{1}H signals are observed for the methylene protons at $\delta = 3.66$ (H_c), 3.19 ($H_{c'}$), 2.97 (H_b) and 2.61

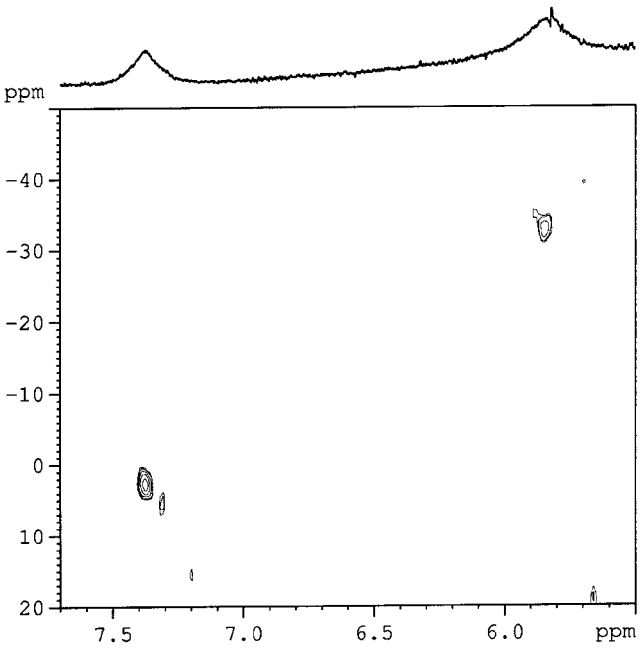

Figure 5. $^{15}N,^{1}H$-HMQC NMR spectrum of the crystals of compound **4**

($H_{b'}$), whereas the protons of the coordinated amine resonate at δ = 7.38 and 5.83. In the $^{15}N,^{1}H$ correlated spectrum of **4** two $^{1}H,^{15}N$ cross peaks (δ = 7.38/2.57 and 5.83/−32.29) are found (Figure 5) in accordance with the signals of compound **2** in solution.

Conclusion

In conclusion, it has been shown that the bis(ethanolamine)platinum complexes **1** and **2** undergo intramolecular ligand exchange reactions in water resulting in platinum compounds **3** and **4** with a chelating ethanolatoamine ligand. This conversion was confirmed by ^{1}H and $^{15}N,^{1}H$-HMQC spectroscopy. The structure of compound **4** in the crystal was also determined. These results clearly indicate that the formation of monoadducts between **1** and 5′-GMP which are very stable over a period of more than 10 days can be explained by the presence of the ethanolatoamine chelate **3** in solution.

Experimental Section

General Remarks: ^{1}H, $^{1}H,^{1}H$-DQF-COSY, $^{15}N,^{1}H$-HMQC and $^{15}N,^{1}H$-HMQC-TOCSY spectra were recorded in H_2O/D_2O (9:1) or DCl at 301 K in a gradient-enhanced mode using a Bruker Avance DPX 400 instrument (UltraShield™ Magnet) and standard pulse programmes at 400.13 (^{1}H) and 40.55 MHz (^{15}N). Chemical shifts were measured relative to the solvent or to external aqueous $^{15}NH_4Cl$ (δ = 0). The X-ray data were collected on a Nonius Kappa CCD diffractometer at room temperature. Elemental analyses were performed by the microanalytical laboratory at the University of Vienna.

(*SP*-4-2)-Dichlorobis(2-hydroxyethylamine)platinum(II) (1) and (*SP*-4-3)-chloro(2-ethanolatoamine-κ²*N,O*)(2-hydroxyethylamine)-platinum(II) (3): The preparation of **1** has been described previously.[13] Compound **1** was dissolved in H_2O/D_2O or D_2O/DCl for NMR spectroscopic studies. Dissolution of **1** in DCl (0.4 mL D_2O and 0.2 mL DCl [20% in D_2O]):
1: ^{1}H NMR (D_2O/DCl): δ = 3.63 [t, ($^{3}J(H_c,H_b)$ = 5.3 Hz), 4 H, H_c], 2.95 [t, ($^{3}J(H_b,H_c)$ = 5.0 Hz), 4 H, H_b].

Upon dissolving **1** in water two products are observed (75% of **1** and 25% of **3** after 24 hours):
1: ^{1}H NMR (H_2O/D_2O, 9:1): δ = 4.92 [m, 4 H, H_a], 3.75 [t, $^{3}J(H_c,H_b)$ = 5.1 Hz, 4 H, H_c], 2.78 [m, $^{3}J(H_b,H_c)$ = 5.1 Hz, 4 H, H_b]. − ^{15}N NMR (H_2O/D_2O, 9:1): δ = −50.02 (N_a).

3: ^{1}H NMR (H_2O/D_2O, 9:1): δ = 5.49 [m, 2 H, $H_{a'}$], 5.11 [m, 2 H, H_a], 3.71 [t, $^{3}J(H_c,H_b)$ = 4.9 Hz, 2 H, H_c], 3.49 [t, $^{3}J(H_{c'},H_{b'})$ = 5.2 Hz, 2 H, $H_{c'}$], 2.63 [m, $^{3}J(H_b,H_c)$ = 4.9 Hz, 2 H, H_b], 2.49 [m, $^{3}J(H_{b'},H_{c'})$ = 5.2 Hz, 2 H, $H_{b'}$]. − ^{15}N NMR (H_2O/D_2O, 9:1): δ = −69.98 (N_a), −31.46 ($N_{a'}$).

(*OC*-6-22)-Tetrachlorobis(2-hydroxyethylamine)platinum(IV) (2) and (*OC*-6−31)-trichloro(2-ethanolatoamine-κ²-*N,O*)(2-hydroxyethylamine)platinum(IV) (4): The preparation of **2** has been described previously.[13] For the preparation of **4** compound **2** (21 mg) was dissolved in 3 mL of water at 50 °C. The solution was stored in an open flask for nine days and orange crystals of **4** were obtained. − $C_4H_{13}Cl_3N_2O_2Pt$ (422.60): calcd. C 11.37, H 3.10, Cl 25.17, N 6.63, Pt 46.16; found C 11.44, H 3.07, Cl 25.03, N 6.44, Pt 45.86. By dissolving **2** in water two products are observed (50% of **2** and **4** after 12 days):
2: ^{1}H NMR (H_2O/D_2O, 9:1): δ = 6.36 (m, 4 H, H_a), 3.70 [t, $^{3}J(H_c,H_b)$ = 5.23 Hz, 4 H, H_c], 2.98 (m, 4 H, H_b). − ^{15}N NMR (H_2O/D_2O, 9:1): δ = −21.78 [^{1}J(N,Pt) = 228 Hz, ^{2}J(H,Pt) = 60 Hz, N_a].

4: ^{1}H NMR (H_2O/D_2O, 9:1): δ = 7.31 (m, 2 H, $H_{a'}$), 5.87 (m, 2 H, H_a), 3.65 [t, $^{3}J(H_c,H_b)$ = 5.2 Hz, 2 H, H_c], 3.19 [t, $^{3}J(H_{c'},H_{b'})$ = 5.5 Hz, 2 H, $H_{c'}$], 2.98 (m, 2 H, H_b), 2.60 (m, 2 H, $H_{b'}$). − ^{15}N NMR (H_2O/D_2O, 9:1): δ = 2.52 [^{1}J(N,Pt) = 282 Hz, ^{2}J(H,Pt) = 48 Hz, $N_{a'}$], −33.02 (N_a).

Upon dissolving **4** in water only one product is observed and the spectrum is equivalent to that of **4** in the mixture of **2** and **4**.

4: ^{1}H NMR (H_2O/D_2O, 9:1): δ = 7.38 (m, 2 H, $H_{a'}$), 5.83 (m, 2 H, H_a), 3.66 [t, $^{3}J(H_c,H_b)$ = 5.3 Hz, 2 H, H_c], 3.19 [t, $^{3}J(H_{c'},H_{b'})$ = 5.5 Hz, 2 H, $H_{c'}$], 2.97 (m, 2 H, H_b), 2.61 (m, 2 H, $H_{b'}$). − ^{15}N NMR (H_2O/D_2O, 9:1): δ = 2.57 [^{1}J(N,Pt) = 251 Hz, ^{2}J(H,Pt) = 52 Hz, $N_{a'}$], −32.29 (N_a).

X-ray Crystallographic Study:[14] The single crystal data were collected on a Nonius Kappa CCD diffractometer at room temperature. The measured intensities were corrected for Lorentz and polarisation effects. The crystal structure was determined by direct methods (SHELXS-97, Sheldrick, 1997a)[15] and subsequent Fourier and difference-Fourier syntheses. Final structure parameters of all three substances were obtained by full-matrix least squares techniques on F^2 (SHELXL-97, Sheldrick, 1997b).[16] Further X-ray structure analysis data are given in Table 1.

Table 1. X-ray crystallographic data of **4**

Molecular formula	$C_4H_{13}Cl_3N_2O_2Pt$
Mol. wt. ($g \cdot mol^{-1}$)	422.6
Space group	*P*4(1)
a (Å)	7.2020(10)
b (Å)	7.2020(10)
c (Å)	20.270(4)
α,β,γ	90
V ($Å^3$)	1051.4(3)
Formula units per cell	4
Density ($g \cdot cm^{-3}$)	2.670
Radiation (Mo-K_α) (Å)	0.71073
$2\theta_{max}$ (°)	56.45
Unique data set	2515
Independent data, [$F_0 > 4\sigma(F_0)$]	2326
Variables	111
Largest difference peak and hole ($eÅ^{-3}$)	2.04/−0.93
*R*1 [for $F_0 > 4\sigma(F_0)$]	0.0294
*wR*2 [for all F_0^2]	0.0691
GOF	1.044
Exposure time/frame (s)	300

Acknowledgments

The support of the FWF (Fonds zur Förderung der wissenschaftlichen Forschung) is gratefully acknowledged. The authors gratefully thank Mrs. R. Strobl for her help in preparing the manuscript.

[1] B. Rosenberg, *Interdiscip. Sci. Rev.* **1978**, *3*, 134.
[2] *Cisplatin: Chemistry and Biochemistry of a Leading Anticancer Drug* (Ed.: B. Lippert), Weinheim, Wiley-VCH, **1999**.
[3] M. C. Christian, *Semin. Oncol.* **1992**, *19*, 720.
[4] D. D. Von Hoff, R. Schilsky, C. M. Reichert, R. L. Reeddick, R. C. Young, F. M. Muggia, *Cancer Treat. Rep.* **1979**, *63* 1527.
[5] R. B. Weiss, M. C. Christian, *Drugs* **1993**, *46*, 360.
[6] L. R. Kelland, S. J. Clarke, M. J. McKeage, *Platinum Metals Rev.* **1992**, *36*, 178.
[7] L. R. Kelland, *Crit. Rev. Oncol. Hematol.* **1993**, *15*, 191.
[8] E. Wong, C. M. Giandomenico, *Chem. Rev.* **1999**, *99*, 2451
[9] W. Zimmermann, M. Galanski, B. K. Keppler, in *Relevance of Tumor Models for Anticancer Drug Development* (Eds.: H. H. Fiebig, A. M. Burger), *Contrib. Oncol. Basel, Karger* **1999**, *54*, 447.
[10] J. Reedijk, *Inorg. Chim. Acta* **1992**, *198/200*, 873.
[11] E. R. Jamieson, S. J. Lippard, *Chem. Rev.* **1999**, *99*, 2467.
[12] A. Zenker, M. Galanski, T. L. Bereuter, B. K. Keppler, W. Lindner, *J. Biol. Inorg. Chem.* in press.
[13] W. Zimmermann, M. Galanski, G. Giesster, B. K. Keppler, *Inorg. Chim. Acta* **1999**, *292*, 127.
[14] Crystallographic data (excluding structure factors) for the structure reported in this paper have been deposited with the Cambridge Crystallographic Data Centre as supplementary publication no. CCDC-132673. Copies of the data can be obtained free of charge on application to CCDC, 12 Union Road, Cambridge CB 1EZ, UK [Fax: (internat.) +44-1223/336-033; E-mail: deposit@ccdc.cam.ac.uk.
[15] G. M. Sheldrick, *SHELXS-97*, University of Göttingen, **1997**.
[16] G. M. Sheldrick, *SHELXL-97*, University of Göttingen, **1997**.

Received July 26, 2000
[I00293]

Synthesis and X-ray Structure of $[\{(Cp'_2Nb)_2WTe_4\}W(CO)_4]\cdot 1.5C_7H_8$, the First Organometallic Derivative of the WTe_4^{2-} Anion, and of $[Cp'_4Nb_2Te_2]$ ($Cp' = \eta^5$-tBuC$_5$H$_4$)

Henri Brunner,[a] Joachim Wachter,*[a] Robert Wanninger,[a] and Manfred Zabel[a]

Keywords: Niobium / Metallocenes / Tungsten / Tellurium / Carbonyl complexes / Anions

Reaction of $[Cp'_2NbTe_2H]$ (**1**) ($Cp' = \eta^5$-tBuC$_5$H$_4$) with $[W(CO)_6]$ in decane at 140 °C gives red $[\{(Cp'_2Nb)_2WTe_4\}W(CO)_4]$ (**2**), whereas in the reaction of **1** with $[Cr(CO)_6]$ green-black $[Cp'_4Nb_2Te_2]$ (**3**) is formed. The crystal structures of **2** and **3** have been determined. The structure of **2** contains a slightly distorted WTe_4 tetrahedron to which two niobocene fragments and one $W(CO)_4$ group are coordinated. The crystal structure determination of **3** reveals the presence of two Cp'_2Nb units bridged by two Te atoms. Complex **2** represents the first example of an organometallic derivative of the unknown WTe_4^{2-} anion.

Introduction

Tetrathiometalates exhibit a rich structural chemistry upon coordination to inorganic and organometallic fragments.[1] The resulting heterometallic complexes possess more or less extended structures and they often show interesting electronic and optical properties.[1,2] Whereas an extension of this chemistry to MSe_4 compounds has been realized only very recently,[1,3] the corresponding tetratellurometalates are still unknown. This fact seems rather surprising if one takes into account the very varied coordination chemistry of Te-derived ligands.[4]

Recently, we have developed a synthetic method for the preparation of bimetallic tetrathio- and tetraselenometalates of the type $[(Cp^*_2Nb)_2ME_4]$ ($Cp^* = C_5Me_5$; M = Cr, Mo; E = S, Se). In these compounds the central "inorganic" core derives from a binary transition metal carbonyl, e.g. $[M(CO)_6]$, whereas the two peripheral niobocene units and the four chalcogen bridges are provided by $[Cp^*_2Nb(\eta^2\text{-}E_2)H]$, a niobocene(V) complex bearing a hydrido and a chalcogenido ligand.[5] In an extension of this work we now wish to report the synthesis of the first organometallic derivative of the still unknown WTe_4^{2-} salt from $[Cp'_2Nb(\eta^2\text{-}Te_2)H]$ (**1**; $Cp' = t$BuC$_5$H$_4$) and $[W(CO)_6]$. Complex **1** has been prepared from Cp'_2NbH_3 and elemental tellurium, and there is sufficient evidence that it bears an η^2-Te_2 ligand along with a hydride atom.[6]

Results and Discussion

The reaction of **1** with one equivalent of $[W(CO)_6]$ in decane (140 °C, 15 h) gives the red complex $[\{(Cp'_2Nb)_2WTe_4\}W(CO)_4]$ (**2**) in 54% yield [Equation (1)]. The composition of complex **2** follows from X-ray crystallography and elemental analyses. As a by-product, a dark green compound of composition $[Cp'_4Nb_2Te_2]$ (**3**) is formed in 6% yield. Compound **3** is formed in much better yield (64%) from the reaction of **1** with $[Cr(CO)_6]$ in boiling toluene along with traces of a red as-yet-unidentified compound [Equation (1)]. Complex **3** has been characterized by means of FD mass spectra and X-ray crystallography; the C value of elemental analyses of **3** differs by 1% for unknown reasons.

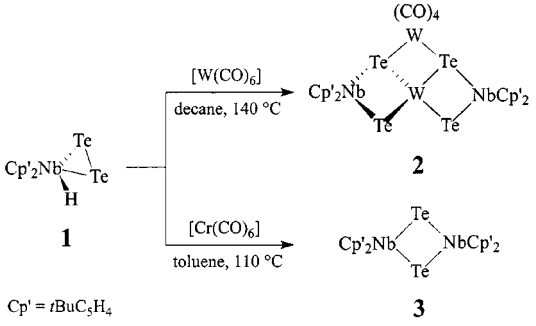

(1)

Complex **2** shows in the IR spectrum (toluene) three strong CO absorptions at 2005, 1972, and 1904 cm^{-1}. This is one less than would be expected from the crystal structure (see below) so we presume that two of the bands are accidentally degenerate. The UV/Vis spectrum reveals one absorption band at $\lambda = 477$ nm. The ^{1}H NMR spectrum contains two singlets for the tBu groups and eight multiplets of equal intensity between $\delta = 3.24$ and 6.05 for the C_5H_4 hydrogen atoms. Thus, the NMR pattern of **2** reflects two orientations of the Cp′ ligands with respect to the $W(CO)_4$ moiety as, due to the solid state structure, both W atoms are lying on a C_2 axis. The ^{1}H NMR spectrum of **3** shows two multiplets at 24 °C for the aromatic hydrogen atoms and one singlet for the tBu groups.

The crystal structure of **2** reveals the presence of four independent molecules in the asymmetric unit, which are practically identical. The central feature of the structure of **2** is a WTe_4 tetrahedron to which two niobocene units are

[a] Institut für Anorganische Chemie der Universität Regensburg, 93040 Regensburg, Germany
E-mail: joachim.wachter@chemie.uni-regensburg.de

 © WILEY-VCH Verlag GmbH, 69451 Weinheim, 2001 1434−1948/01/0505−1151 $ 17.50+.50/0

coordinated (Figure 1), giving rise to a nearly linear Nb−W−Nb arrangement. A $W(CO)_4$ fragment is inserted between two of the Te bridges of the central WTe_4 tetrahedron. The W−Te distances within the WTe_4 unit range from 2.540(2) to 2.604(2) Å, the μ_2-Te−W(1) distances being slightly shorter than those of μ_3-Te−W(1). Similar values have been found in $W(PMe_3)_4(Te)_2$ [2.596(1) Å][7] and in $[WOTe_3]^{2-}$ [2.530(1)−2.544(2) Å],[8] which have been attributed to W−Te double bonds. By contrast, the distances Te(2)−W(2) and Te(3)−W(2) [2.848(2) and 2.845(2) Å, respectively] are much longer, thus reflecting a formally lower oxidation state of the W(2) center.[9] In the central WTe_4 tetrahedron there is a slight distortion of the angle Te(3)−W(1)−Te(2), which is 119.30(6)°. Whereas the distances between opposite Te ligands seem to be far beyond direct bonding interactions, the Nb−W distances (3.333 Å mean) may be a borderline case for direct interactions between both metals.

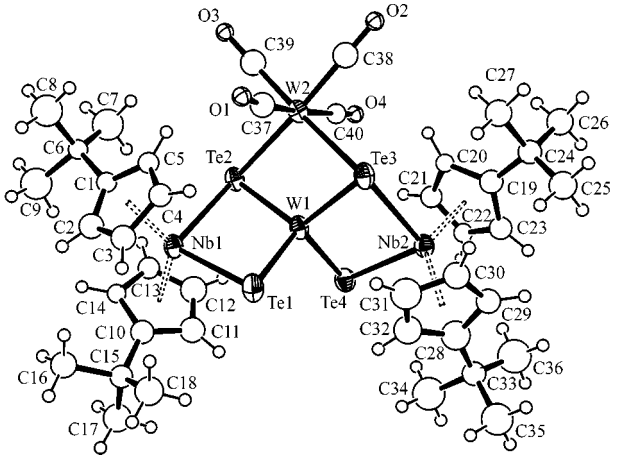

Figure 1. Molecular structure of $[\{(Cp'_2Nb)_2WTe_4\}W(CO)_4]$ (**2**); selected distances [Å] and angles [°]: W(1)−Te(1) 2.539(2), W(1)−Te(2) 2.600(2), W(1)−Te(3) 2.604(2), W(1)−Te(4) 2.553(2), W(2)−Te(2) 2.845(2), W(2)−Te(3) 2.841(2), Nb(1)−Te(1) 2.823(3), Nb(1)−Te(2) 2.827(2), Nb(2)−Te(3) 2.844(3), Nb(2)−Te(4) 2.834(3), Te(1)···Te(2) 4.22(3), Te(3)···Te(4) 4.25(2), Nb(1)···W(1) 3.35(1), Nb(2)···W(1) 3.33(2); Te(1)−W(1)−Te(2) 109.9(1), Te(1)−W(1)−Te(3) 103.5(1), Te(1)−W(1)−Te(4) 108.4(1), Te(2)−W(1)−Te(3) 119.3(1), Te(2)−W(1)−Te(4) 104.8(1), Te(3)−W(1)−Te(4) 110.6(1), Te(2)−W(2)−Te(3) 104.2(1), Nb(1)−Te(1)−W(1) 77.2(1), Nb(1)−Te(2)−W(1) 76.2(1), Nb(2)−Te(3)−W(1) 75.3(1), Nb(2)−Te(4)−W(1) 76.3(1), Te(1)−Nb(1)−Te(2) 96.2(1), Te(3)−Nb(2)−Te(4) 96.6(1), W(1)−Te(2)−W(2) 68.3(1), W(1)−Te(3)−W(2) 68.1(1), Nb(1)−W(1)−Nb(2) 163.8(1)

On the basis of these results a formal description of the bonding system in **2** either includes a W^{II} center, which is chelated by two $[Cp'_2NbTe_2]^-$ anions (structure type **A**), or a derivative of a tetratellurotungstate(VI) with two coordinated niobocene(III) ligands (structure type **B**). Taking into account the relatively short W−Te bonds in the central WTe_4 unit, it seems likely that the canonical forms **B** contribute more to the overall bonding system than **A**. In this sense **2** may be assumed to be the missing link in the series of bis(niobocene)tetrachalcogenido metalates $[(Cp^*_2Nb)_2ME_4]$ (M = Cr, Mo, W; E = S, Se, Te). These compounds are characterized by a delocalized bonding system including the whole metal-ligand system, as has been established by means of spectroscopic and theoretical investigations.[5]

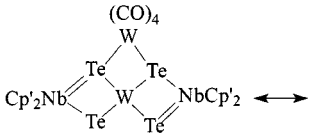

A

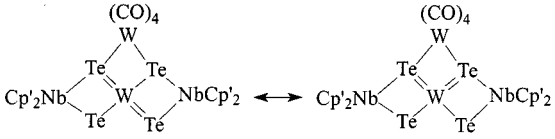

B

The crystal structure of **3** contains a planar rhombohedral Nb_2Te_2 core to which four Cp′ ligands are coordinated. Additionally, the molecule has a crystallographic inversion center and the conformation of the Cp′ ligands corresponds to that of the *meso* diastereomer (Figure 2). A similar conformation has been found in the related compound $[Cp'_4Zr_2(\mu\text{-}Te)_2]$.[10] From the distances (>3.6 Å) one can exclude direct bonding interactions between opposite atoms of the core. The Nb−Te distances (2.80 Å) are only slightly shorter than those in **2** and they are in the range of Nb−Te single bonds.[11] As a consequence, compound **3** should formally contain two Nb^{IV} centers which is in obvious contrast to the observed diamagnetism of the molecule. For these reasons considerable through-space metal−metal coupling must be considered, as has been recently established for $[(C_5H_5)_4Zr_2(\mu\text{-}I)_2$.[12] This point, as well as studies of the chemical behavior, are currently under investigation.

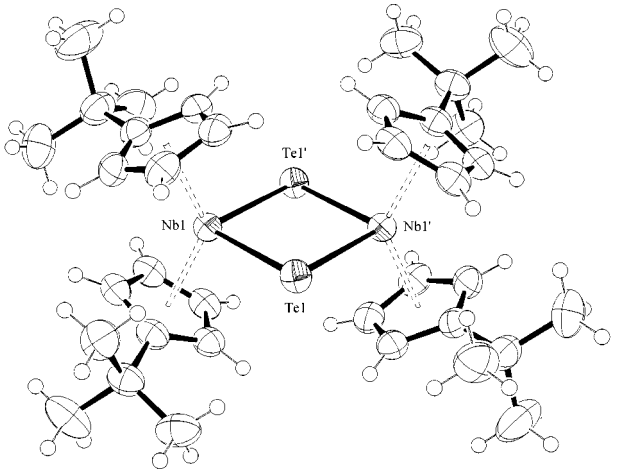

Figure 2. Molecular structure of $[Cp'_4Nb_2Te_2]$ (**3**); selected distances [Å] and angles [°]: Nb(1)−Te(1) 2.7969(4), Nb(1′)−Te(1) 2.8127(4), Nb(1)···Nb(1′) 3.647(1), Te(1)···Te(1′) 4.262(1); Nb(1)−Te(1)−Nb(1′) 81.12(1), Te(1)−Nb(1)−Te(1′) 98.88(1)

In conclusion the reaction of $[Cp'_2NbTe_2H]$ with $[Cr(CO)_6]$ or $[W(CO)_6]$ provides access to new polymetallic telluride complexes. Complex **2** is the first organometallic

derivative of the still unknown WTe_4^{2-} anion, whereas the analogous $CrTe_4$ derivative does not form under comparable conditions. Instead, formation of the dinuclear chromium-free complex **3** has been observed.

Experimental Section

General Methods. Experimental and spectroscopic techniques are reported in ref.[13] [Cp′$_2$Nb(Te$_2$)H] (**1**) was prepared from [Cp′$_2$NbH$_3$] and Te powder in THF.[6]

Synthesis of 2: A solution of [Cp′$_2$NbTe$_2$H] (**1**) (560 mg, 0.946 mmol) and [W(CO)$_6$] (330 mg, 0.938 mmol) in 140 mL of decane was stirred for 12 h at 140 °C in the dark. The color turned from dark orange to red during the reaction. After evaporation of the solvent the residue was dissolved in 12 mL of toluene and transferred to a column containing SiO_2 (15 × 3 cm). A red band was eluted with toluene containing [{(Cp′$_2$Nb)$_2$WTe$_4$}W(CO)$_4$] (**2**) (420 mg, 0.252 mmol, 54%). A following dark green band contained [Cp′$_4$Nb$_2$Te$_2$] (**3**) (25 mg, 0.027 mmol, 6%). Recrystallization of **2** from toluene gave red needles. − IR (toluene): ν(CO) = 2005 (s), 1972 (vs), 1904 (s) cm^{-1}. − ^{1}H NMR (400 MHz, CD_2Cl_2, 24 °C): δ = 6.05 (m, 2 H, C_5H_4), 5.87 (m, 2 H, C_5H_4), 5.59 (m, 2 H, C_5H_4), 5.56 (m, 2 H, C_5H_4), 5.48 (m, 2 H, C_5H_4), 4.78 (m, 2 H, C_5H_4), 4.01 (m, 2 H, C_5H_4), 3.24 (m, 2 H, C_5H_4), 1.53 (s, 18 H, *t*Bu), 1.43 (s, 18 H, *t*Bu). − UV/Vis (THF): λ (ε) (Lmol^{-1}cm^{-1}) = 477 nm (3208). − $C_{40}H_{52}Nb_2O_4Te_4W_2C_7H_8$ (1752.87): calcd. C 32.20, H 3.45; found C 32.38, H 3.49.

Synthesis of 3: Compound **1** (560 mg, 0.946 mmol) and [Cr(CO)$_6$] (200 mg, 0.909 mmol) were dissolved in 140 mL of toluene and stirred for 12 h at 110 °C in the dark. The color turned from dark orange to green-black during the reaction. The mixture was cooled to room temperature and the solvent evaporated. The residue was dissolved in 12 mL of toluene and chromatographed on SiO_2 (column 15 × 3 cm). Elution with toluene first gave a red band containing 20 mg of a still unidentified compound and then a green-black band containing [Cp′$_4$Nb$_2$Te$_2$] (**3**) (280 mg, 0.302 mmol, 64%). Complex **3** was recrystallized from toluene/pentane (1:2). − ^{1}H NMR (400 MHz, CD_2Cl_2, 24 °C): δ = 5.05 (m, 8 H, C_5H_4), 4.46 (m, 8 H, C_5H_4), 1.44 (s, 36 H, *t*Bu). − FD-MS (toluene): *m*/*z* = 925.6 [M$^+$]. − $C_{36}H_{52}Nb_2Te_2$ (925.81): calcd. C 46.70, H 5.66; found C 45.78, H 5.69.

X-ray Structure Determination: For the crystals of both compounds **2** and **3** the shape and the size were determined for numerical absorption correction. The structures of **2** and **3** were solved by direct methods (Table 1). For **3**, subsequent difference Fourier syntheses revealed the position of the non-hydrogen atoms and all these atoms were refined with anisotropic thermal parameters. Hydrogen atoms were included on idealized positions and refined using a riding model.

The structure refinement of **2** was handicapped by two problems: i) For data collection only thin needles were available giving rise to very weak intensities mainly at higher reflection angles. Only one third of the measured reflections were observed with an intensity greater than 2σ(*I*). This causes some peculiarities concerning the results of the refinement. Internal *R* values, especially *R*(σ) = 0.3451, are high and are mainly influenced by the large number of weak reflections. The same is true for the low value of GOF. The unexpectedly high *R*1 for all data can be explained by the fact that too many very weak or even negative intensities are setting a wrong bias, when transformed to *F* values. The "normal" behavior of *R*1 and *wR*2 for the observed data [$I > 2\sigma(I)$] supports this point of view. Also, due to the large number of weak reflections no weighting factor could be refined and so unit weights were applied. Finally, only the heavy atoms could be refined with anisotropic thermal parameters. ii) Five toluene solvent molecules could be located by difference Fourier syntheses but there was still a solvent accessible void present. Since from the remaining difference Fourier peaks no reasonable molecule could be built all these maxima were erased and the size and electron content of this void was determined by the program SQUEEZE.[14] The center of the void was located at (0.5, 0, 0.5), the size and electron content was refined to 766 Å^3 with 65 e$^-$. For one more toluene molecule, the size of the void and the electron number are too high. The possibility that one decane molecule (reaction medium) was still present after chromatography and recrystallisation seemed unlikely. Nevertheless, for the calculation of molecular weight, *F*(000) and density one more toluene molecule was included, because no chance was seen to find the proper molecule from a data set with so many weak reflections at high reflection angles. The final refinement, leading to the given results, was carried out after back-Fourier transformation of all density found in the disordered solvent area.

Table 1. Crystallographic data for compounds **2** and **3**

	2·1.5C$_7$H$_8$	**3**
Formula	$C_{50.5}H_{64}Nb_2O_4Te_4W_2$	$C_{36}H_{52}Nb_2Te_2$
MW	1798.9	925.8
Cryst syst	Triclinic	Monoclinic
Space group	$P\bar{1}$	$P2_1/c$
a, Å	17.927(1)	8.6683(8)
b, Å	23.664(1)	13.336(1)
c, Å	28.799(2)	15.408(1)
α, deg	79.017(8)	
β, deg	76.486(8)	93.691(9)
γ, deg	71.949(8)	
V, Å^3	11202.0(14)	1777.5(3)
Z	8	2
d_{calc}, g/cm^3	2.130	1.730
F(000)	6684	908
Cryst size, mm^3	0.16×0.04×0.04	0.22×0.18×0.14
Diffractometer	STOE-IPDS	STOE-IPDS
Temp, K	173	297
θ, deg	1.82−25.19	2.65−25.95
No. of reflns collected	76102	24820
No. of indep reflns	37186	3418
R_{int}	0.1090	0.0488
No. obsd reflns [$I > 2\sigma(I)$]	12089	2769
μ, mm^{-1}	6.574	2.28
No. of data/restraints/params.	37186/0/1070	3418/0/181
GOF on F^2	0.617	0.988
T_{max}, T_{min}	0.7781, 0.5146	0.7467, 0.6201
*R*1, *wR*2 [$I > 2\sigma(I)$]	0.0527, 0.0792	0.0234, 0.0557
*R*1, *wR*2 (all data)	0.1789, 0.1102	0.0297, 0.0567

The unusual result that four symmetry independent molecules were found in the elementary cell was checked and proved to be right by programs implemented in the PLATON package: a) No different cell choice was suggested by LEPAGE, therefore only an anorthic cell and space group is possible. The highest possible, $P\bar{1}$ was chosen; b) Even if only the heavy atoms were included in the file for calculations, PLATON could not find additional symmetry elements nor did it suggest a higher symmetry than applied. Obviously a denser packing of **2** with higher symmetry of cell and structure is not possible.

Crystallographic data (excluding structure factors) for the structures reported in this paper have been deposited with the Cambridge Crystallographic Data Centre as supplementary publication

nos. CCDC-148287 (**2**) and -148288 (**3**). Copies of the data can be obtained free of charge on application to the CCDC, 12 Union Road, Cambridge CB2 1EZ, U.K. [Fax: (internat.) +44-1223/336-033; E-mail: deposit@ccdc.cam.ac.uk].

Acknowledgments

We gratefully acknowledge financial support from the Deutsche Forschungsgemeinschaft (Wa 485/6−1).

[1] For leading references see: [1a] Q.-F. Zhang, M.-T. Bao, M.-C. Hong, R. Cao, Y.-L. Song, X.-Q. Xin, *J. Chem. Soc., Dalton Trans.* **2000**, 605. − [1b] Q.-F. Zhang, W.-H. Leung, X.-Q. Xin, H.-K. Fun, *Inorg. Chem.* **2000**, *39*, 417.

[2] [2a] K. E. Howard, T. B. Rauchfuss, A. L. Rheingold, *J. Am. Chem. Soc.* **1986**, *108*, 297. − [2b] P. A. Shapley, Z. Gebeyehu, N. Zhang, S. R. Wilson, *Inorg. Chem.* **1993**, *32*, 5646. − [2c] R. Schäfer, W. Kaim, J. Fiedler, *Inorg. Chem.* **1993**, *32*, 3199. − [2d] R. Schäfer, J. Fiedler, M. Moscherosch, W. Kaim, *J. Chem. Soc., Chem. Commun.* **1993**, 896. − [2e] K. E. Howard, T. B. Rauchfuss, S. R. Wilson, *Inorg. Chem.* **1988**, *27*, 3561.

[3] R. J. Salm, A. Misetic, J. A. Ibers, *Inorg. Chim. Acta* **1995**, *240*, 239.

[4] [4a] J. W. Kolis, *Coord. Chem. Rev.* **1990**, *105*, 195. − [4b] L. C. Roof, J. W. Kolis, *Chem. Rev.* **1993**, *93*, 1037.

[5] [5a] H. Brunner, G. Gehart, M. M. Kubicki, E. Lehrl, D. Lucas, W. Meier, Y. Mugnier, B. Nuber, B. Stubenhofer, J. Wachter, *J. Organomet. Chem.* **1996**, *510*, 291. − [5b] O. Blacque, H. Brunner, M. M. Kubicki, D. Lucas, W. Meier, Y. Mugnier, B. Nuber, B. Stubenhofer, J. Wachter, *J. Organomet. Chem.* **1998**, *564*, 71.

[6] R. Wanninger, Ph.D. thesis, Universität Regensburg **2000**.

[7] D. Rabinovich, G. Parkin, *Inorg. Chem.* **1995**, *34*, 6341.

[8] D. R. Gardner, J. C. Fettinger, B. W. Eichhorn, *Angew. Chem. Int. Ed. Engl.* **1994**, *33*, 1859.

[9] [9a] L. C. Roof, W. T. Pennington, J. W. Kolis, *J. Am. Chem. Soc.* **1990**, *112*, 8172. − [9b] W. A. Flomer, S. C. O′ Neal, D. Jeter, A. W. Cordes, J. W. Kolis, *Inorg. Chem.* **1988**, *27*, 969. − [9c] A. W. Flomer, J. W. Kolis, *Inorg. Chem.* **1989**, *28*, 2513.

[10] G. Erker, T. Mühlenbernd, R. Nolte, J. L. Petersen, G. Tainturier, B. Gautheron, *J. Organomet. Chem.* **1986**, *314*, C21.

[11] [11a] W. Tremel, *J. Chem. Soc., Chem. Commun.* **1992**, 126. − [11b] H. Kleinke, W. Tremel, *Chem. Commun.* **1999**, 1175.

[12] [12a] M.-M. Rohmer, M. Bénard, *Organometallics* **1991**, *10*, 157. − [12b] R. L. DeKock, M. A. Peterson, L. E. L. Reynolds, L.-H. Chen, E. J. Baerends, P. Vernoijs, *Organometallics* **1993**, *12*, 2794.

[13] H. Brunner, D. Lucas, T. Monzon, Y. Mugnier, B. Nuber, B. Stubenhofer, A. C. Stückl, J. Wachter, R. Wanninger, M. Zabel, *Chem. Eur. J.* **2000**, *6*, 493.

[14] P. v. d. Sluis, A. L. Spek, *Acta Crystallogr.* **1990**, *A46*, 194.

Received August 15, 2000
[I00315]

New Sterically Encumbered 2,9-Diarylphenanthrolines for the Selective Formation of Heteroleptic Bis(phenanthroline)copper(I) Complexes

Michael Schmittel,*[a] Christoph Michel,[a] Shi-Xia Liu,[a] Daniel Schildbach,[b] and Dieter Fenske[c]

Dedicated to Prof. Dr. Dr. h. c. mult. Siegfried Hünig on the occasion of his 80th birthday

Keywords: Copper / Phenanthroline / Coordination chemistry / Semiempirical calculations / Fluorescence

The synthesis and characterization of several 2,9-diarylphenanthrolines with anthracenyl substituents in the 2-position is described. These compounds were used to prepare a series of homoleptic and heteroleptic bis(phenanthroline)copper(I) complexes, whose cyclic voltammetry, UV/Vis and fluorescence data are investigated. From PM3 semiempirical calculations it becomes clear that two different strategies can be applied to prepare clean heteroleptic complexes.

Introduction

We have recently introduced a new concept to prepare heteroleptic bis(phenanthroline)copper(I)[1] and -silver(I)[2] complexes $[M(\mathbf{L1})(\mathbf{L2})]^+$ in a clean and well-defined manner using a ligand with bulky groups in the 2- and 9-positions. In metallosupramolecular chemistry, control of the clean formation of heteroleptic complexes is extremely valuable for highly selective self-assembly processes with two different ligands **L1** and **L2**, e.g. of linear and macrocyclic oligophenanthrolines,[3] as the number of potential aggregates is markedly reduced. Consequently, we have used this protocol for the synthesis of supramolecular boxes[3] of nanometer dimensions with appropriately spaced internal functional groups.

As bis(phenanthroline)copper(I) complexes are kinetically labile,[4] a thermodynamically controlled setup has to be found that favors the heteroleptic complex over the two alternative homoleptic complexes. In our concept,[1,2] 2,9-diaryl substitution at one phenanthroline (**L2**) plays a critical role. In combination with a second phenanthroline, which does not bear 2,9-aryl substituents (**L1**), the stability sequence of the resulting copper(I) complexes becomes predictable (Scheme 1); the corresponding homoleptic bis-2,9-diarylphenanthroline copper(I) complex $[Cu(\mathbf{L2})_2]^+$ is always the most stable because of the interplay of increased σ-basicity of **L2** and π-π interactions between the 2,9-aryl groups and the second phenanthroline core. The latter stabilization is present in $[Cu(\mathbf{L2})_2]^+$ four times, but only twice in $[Cu(\mathbf{L1})(\mathbf{L2})]^+$ and is absent in $[Cu(\mathbf{L1})_2]^+$.

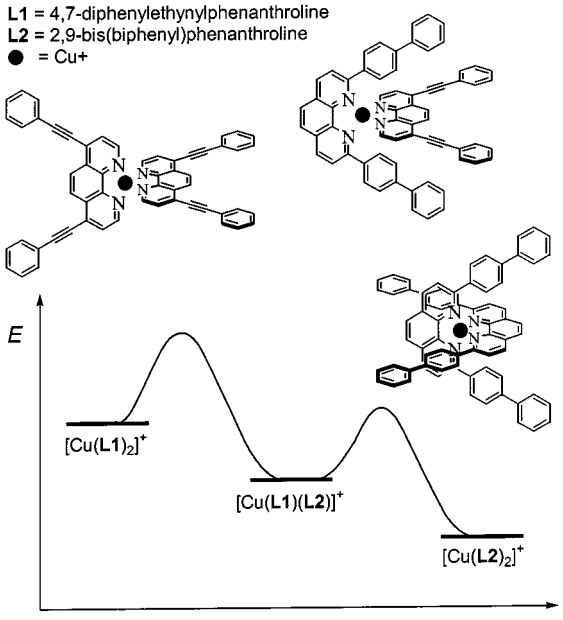

Scheme 1

The straightforward concept to prepare $[Cu(\mathbf{L1})(\mathbf{L2})]^+$ is consequently based on the fact that we have to prevent the formation of the most stable complex $[Cu(\mathbf{L2})_2]^+$ through steric blocking, so that of the remaining complexes it is the heteroleptic $[Cu(\mathbf{L1})(\mathbf{L2})]^+$ that is the thermodynamically favored option. In earlier investigations[1,2] we successfully used **L2** = **1** and would like now to assess whether other aryl substituents, such as naphthyl and anthracenyl, at the phenanthroline would also be suited for the preparation of heteroleptic copper(I) complexes. In the present paper[5] we describe the preparation of ligands **2**–**5** (Scheme 2) and their potential in the selective heteroleptic copper(I) complex formation.

[a] FB 8 – OC1 (Chemie und Biologie), Universität GH Siegen, Adolf-Reichwein-Straße, 57068 Siegen, Germany
Fax: (internat.) + 49–(0)271–3270
E-mail: schmittel@chemie.uni-siegen.de
[b] Institut für Organische Chemie, Universität Würzburg, Am Hubland, 97074 Würzburg, Germany
[c] Institut für Anorganische Chemie, Universität Karlsruhe, Engesserstraße 3045, 76128 Karlsruhe, Germany

 © WILEY-VCH Verlag GmbH, 69451 Weinheim, 2001 1434–1948/01/0505–1155 $ 17.50+.50/0

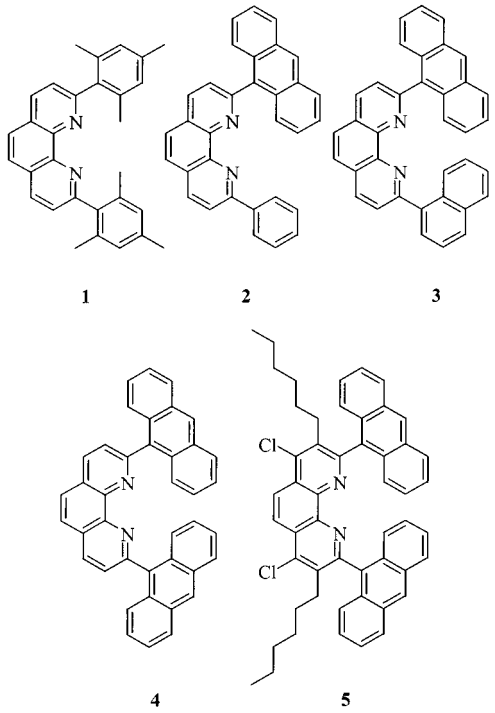

Scheme 2

Moreover, ligands **2**−**5** seemed to be promising candidates because a number of sensing supramolecules contain anthracene as a fluorescent subunit (or fluorophor) given its strong and well-characterized emission and its chemical stability.[6] For example, De Silva has developed many anthracene-based sensors for metal ions.[7] Additionally, compound **5** was prepared because the two hexyl groups at the 3- and 8-positions should increase the solubility of the system.[8]

Results

Phenanthroline Ligands

Synthesis: For the preparation of the 2,9-substituted phenanthrolines, the two-step synthesis shown in Scheme 3 proved to be the method of choice and this is based on a strategy established earlier by Sauvage.[9] Simultaneous arylation of both the 2- and 9-positions of 1,10-phenanthroline either failed completely or proceeded with low yields. In order to overcome this problem, 1,10-phenanthroline was first reacted with a slight excess of the aryllithium reagent at room temperature, followed by hydrolysis and rearomatization of the intermediate with activated MnO_2. Subsequently, the procedure was repeated once again using the monoarylated phenanthrolines **6** and **7** (Scheme 4). The crude product could be purified either by recrystallization or by column chromatography on silica gel and subsequent recrystallization.

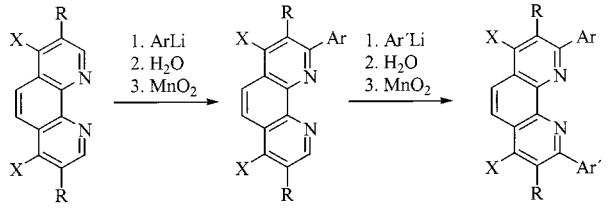

Scheme 3. 2,9-Diaryl-1,10-phenanthrolines from 1,10-phenanthroline by nucleophilic aromatic substitution followed by rearomatization

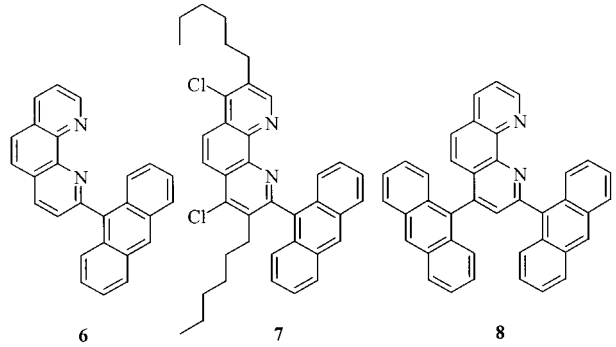

Scheme 4

Yields for the first arylation ranged from 37%−67% (for **7** and **6**, respectively), while the yield of the second step was heavily dependent on the steric bulk of the new substituents [with phenyl: 64%; with naphthyl: 25%, and anthracenyl: 21% (**4**)]. In contrast, the yield for the second arylation **7** → **5** was 59%. The structures of all new phenanthrolines were proved using ^1H and ^{13}C NMR spectroscopy and elemental analysis.

The yields of the nucleophilic aromatic substitution reactions are sometimes lower due to by-product formation. In the reaction of **6** with anthracenyllithium we actually isolated the 2,4-substituted phenanthroline **8** as the main product (39%). It is clear that steric shielding hampers the formation of **4** (21%) and directs arylation to the 4-position, a reaction that is not possible with **5**. An analogous regioselectivity has been reported for nucleophilic substitutions at pyridine, although this is a rare case.[10] However, to the best of our knowledge[11] this is the first time that a nucleophilic arylation has led preferentially to a 2,4-diarylphenanthroline.

Structural Characterization of the Ligands

X-ray Structure of 5: Because of its good solubility and the presence of two large anthracenyl rings, we investigated **5** in greater detail. Ligand **5** could readily be crystallized from dichloromethane and hence was investigated by X-ray crystallography. Figure 1 depicts the structure of **5** in the solid state from a top and a side view.

From Figure 1 one can clearly see the steric demand of the two large anthracenyl groups. To avoid repulsions between the two anthracenyl rings or between the anthracenyl ring and the hexyl groups the two anthracenyl moieties assume an almost orthogonal arrangement with regard to the phenanthroline plane (dihedral angle = 96°). The structure of ligand **5** is well described by the PM3 calculation, as demonstrated by the selected data provided in Table 1.

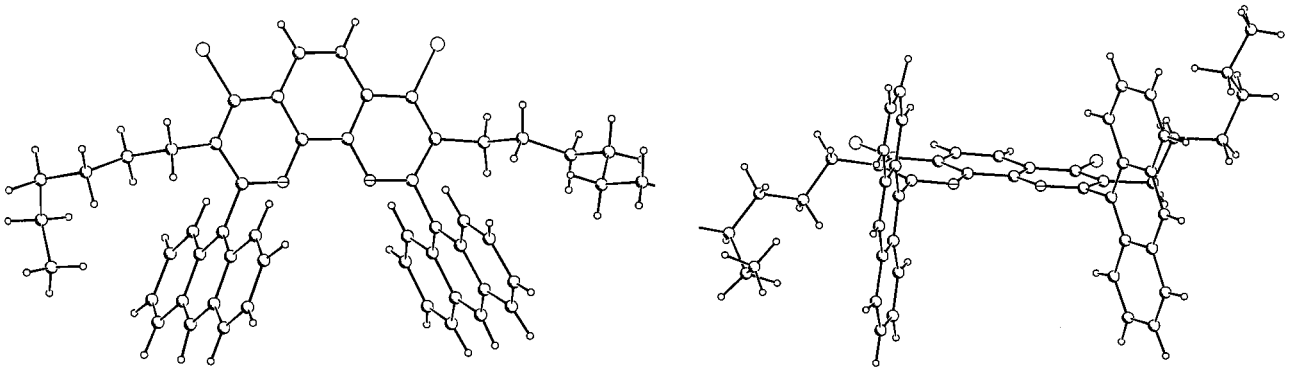

Figure 1. Schakal plot of 2,9-dianthracenyl-4,7-dichloro-3,8-dihexyl-1,10-phenanthroline (**5**)

Table 1. Selected data from X-ray structure analyses and PM3 calculations

Structure Dihedral angle of anthracene at 2-position [°]	**5** (X-ray)	**5** (PM3)	**4** (PM3)	**3** (PM3)	**2** (PM3)
N1−C1−C33−C38	95.83(20)	90.30	−90.49	−90.07	−91.06
N1−C1−C33−C46	−80.47(21)	−88.86	89.92	90.33	89.40
C2−C1−C33−C46	96.74(20)	91.38	−90.12	−89.72	−90.65
C2−C1−C33−C38	−86.96(22)	−89.46	89.47	89.88	88.90
Selected angles [°]					
N1−C1−C33	114.53(15)	116.69	118.49	119.47	118.47
C2−C1−C33	120.94(15)	121.55	119.77	119.78	119.78
C38−C33−C1	120.18(18)	119.87	119.77	119.76	119.73
C46−C33−C1	118.79(15)	119.67	119.74	119.75	119.79
Dihedral angle of second aryl ring [°]					
N2−C10−C19−C20	97.33(19)	90.70	−90.95	−115.50	177.06
N2−C10−C19−C32	−82.75(20)	−88.54	89.46	64.67	−2.91
C11−C10−C19−C32	95.24(20)	91.67	−90.58	−114.05	177.13
C11−C10−C19−C20	−84.69(20)	−89.09	89.01	65.78	−2.90
Selected angles [°]					
N2−C10−C19	115.45(13)	116.74	118.49	118.05	118.46
C11−C10−C19	120.49(14)	121.51	119.77	120.34	120.95
C20−C19−C10	119.40(12)	119.68	119.72	119.187	121.18
C32−C19−C10	119.71(16)	119.85	119.79	120.68	119.76
C−N bond length [Å]					
C1−N1	1.316(2)	1.340	1.340	1.340	1.341
C10−N2	1.318(2)	1.340	1.340	1.341	1.344
C5−N1	1.345(8)	1.374	1.376	1.376	1.376
C9−N2	1.354(20)	1.374	1.376	1.375	1.373

NMR Investigations: As one would anticipate, given the extended aromatic residues, the proton NMR spectra of **5** show a solvent dependence; i.e. the shifts vary with the solvent ($CDCl_3$ or [D_6]benzene). While the 5,6-H phenanthroline signal is not shifted, the signal of the 10-H at the anthracene substituents experiences a high-field shift from $\delta = 8.4$ ($CDCl_3$) to $\delta = 8.1$ ([D_6]benzene). After adding trifluoroacetic acid to the NMR solution in $CDCl_3$ the phenanthroline 5,6-H′s experience the expected down-field shift (by 0.2 ppm), but the doublet for 1-H and 8-H at the anthracene rings is shifted towards high field by about 0.3 ppm.

Luminescence Properties: The emission spectra of the ligands **2**−**7** in dichloromethane were recorded (Figure 2) at room temperature upon excitation at 346 nm. The emission maxima appear between 439−472 nm.

Preparation of the Copper Complexes

Homoleptic Copper Complexes: To assess the feasibility of the various ligands **2**−**7** with regard to our concept (see Introduction) we checked whether they would easily form homoleptic complexes in the presence of copper(I). For ligands **2**, **3**, **6** and **7** the reaction with 0.5 equiv. of [Cu(MeCN)$_4$]BF_4 or [Cu(MeCN)$_4$]PF_6 in dichloromethane

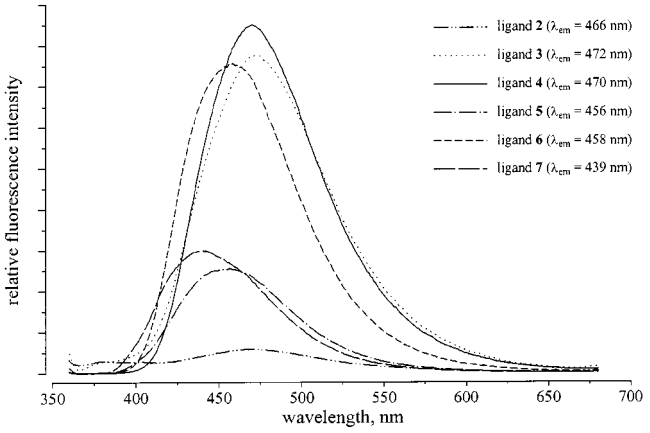

Figure 2. Luminescence spectra of various phenanthrolines at room temperature in CH_2Cl_2 solution (excitation at 346 nm where the absorbance of all the compounds is 1.11)

readily afforded the intensely red-colored homoleptic complexes $[Cu(\mathbf{2})_2]^+$, $[Cu(\mathbf{3})_2]^+$, $[Cu(\mathbf{6})_2]^+$, and $[Cu(\mathbf{7})_2]^+$ in good yields (50−85%) at room temperature.

By using the conditions described above, phenanthrolines **4** and **5** − with bulky anthracenyl groups at the 2- and 9-positions − only afforded yellow complexes, which were assigned as the monophenanthroline complexes $[Cu(\mathbf{4})(MeCN)_2]BF_4$ or $[Cu(\mathbf{5})(MeCN)_2]BF_4$. Additionally, the ^1H NMR spectra of the reaction mixtures showed signals for uncoordinated phenanthroline **4** or **5**. Even when the complexation was performed at 80 °C (in C_6D_6) for three hours the color of the solution did not turn red, indicating that a bis(phenanthroline)copper(I) complex had not been formed. The ESI mass spectrum shows a large ion peak at m/z = 874, which is indicative of the complex $[Cu(\mathbf{5})(MeCN)]^+$, and m/z = 833 for the ion $[Cu(\mathbf{5})]^+$. $[Cu(\mathbf{4})(MeCN)_2]BF_4$ was purified by recrystallization and characterized by elemental analysis.

Heteroleptic Copper Complexes: To test the suitability of the anthracenyl-substituted phenanthrolines **4** and **5** for the clean preparation of heteroleptic complexes, we treated them with 1 equiv. of 4,7-substituted ligands **9** or **10** (Scheme 5) in the presence of 1 equiv. of $[Cu(MeCN)_4]^+$ at room temperature. Evaporation of the solvent led to the precipitation of a red solid, yielding the heteroleptic complexes $[Cu(\mathbf{4})(\mathbf{9})]^+$, $[Cu(\mathbf{5})(\mathbf{9})]^+$, and $[Cu(\mathbf{5})(\mathbf{10})]^+$ in good yields.

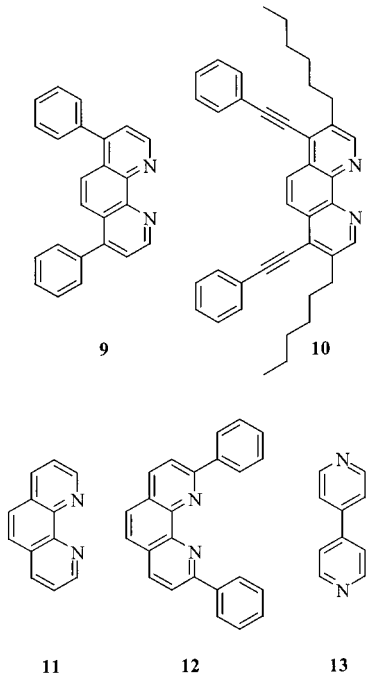

Scheme 5

Characterization of the Copper Complexes

The identities of the copper(I) complexes could be established through elemental analysis, ESI mass spectrometry, IR and NMR spectroscopy.

^1H NMR Spectroscopy: The spectra exhibit well-resolved signals for the homoleptic as well as the heteroleptic complexes in CD_2Cl_2 or $CDCl_3$, which is true even for the sterically loaded complex $[Cu(\mathbf{3})_2]PF_6$. A 2D ROESY ^1H NMR experiment clearly confirms its highly shielded structure. Rotation about the anthracene-phenanthroline axes is no longer possible, as shown by the fact that the inner and the outer ring of the anthracenes can be differentiated. From the literature it is known that aryl substituents with a lower steric demand lead to broadening of the Ar−H signals,[12] and in the absence of *ortho* substituents the aryl rings are free to rotate relative to the phenanthroline on the NMR time scale.[13]

The formation of the heteroleptic complexes is indicated by characteristic ^1H NMR shifts. Coordination of the 2,9-

Table 2. Characteristic ^1H NMR chemical shifts of the 2,9-substituted-1,10-phenanthrolines in heteroleptic complexes

	Phenanthroline core			Arene groups
	δ(4,7-H)	δ(5,6-H)	δ(3,8-H)	δ(aryl-H)
4[a]	8.50	8.07	7.87	8.45, 7.96, 7.83, 7.28−7.41
$[Cu(\mathbf{4})(\mathbf{9})]^+$ [b]	8.97	8.46	8.27	7.41, 7.31, 7.23, 6.92−7.13
5[a]		8.62		8.40, 7.90, 7.17−7.40
$[Cu(\mathbf{5})(\mathbf{9})]^+$ [a]		8.78		7.43, 7.08−7.17, 6.91−6.95
$[Cu(\mathbf{5})(\mathbf{10})]^+$ [a]		8.79		7.10−7.24, 6.98−7.03

[a] In $CDCl_3$. − [b] In CD_2Cl_2.

substituted ligands to the positively charged metal center results in typical downfield shifts for all protons at the phenanthroline core (Table 2). In contrast, the 2,9-H′s at the 4,7-substituted phenanthroline experience a strong high-field shift (Table 3). This is due to the shielding effect of the anthracenyl (and other aryl) groups placed below and above the aromatic plane of the second phenanthroline, i.e. the one with 4,7-substituents, in the tetrahedral copper complex.

Table 3. Characteristic ^{1}H NMR chemical shifts of the 4,7-substituted-1,10-phenanthrolines in heteroleptic complexes

	δ(2,9-H)	δ(5,6-H)	δ(3,8-H)
9[a]	9.22	7.84	7.57
[Cu(**4**)(**9**)]$^+$ [b]	7.14	7.45	6.59
[Cu(**5**)(**9**)]$^+$ [a]	7.03	7.44	6.60
10[a]	9.05	8.43	
[Cu(**5**)(**10**)]$^+$ [a]	7.41	8.08	

[a] In $CDCl_3$. − [b] In CD_2Cl_2.

Electrochemical Data: The oxidation behavior of the homoleptic and heteroleptic copper(I) complexes was studied by cyclic voltammetry. All compounds undergo a reversible one-electron oxidation process, which can be attributed to the $Cu^I \rightarrow Cu^{II}$ couple.[14] The redox potentials (Table 4) range from 0.0−0.3 V for the homoleptic complexes [Cu(**6**)$_2$](BF$_4$), [Cu(**7**)$_2$](PF$_6$), and the heteroleptic complexes [Cu(**4**)(**9**)](PF$_6$), [Cu(**5**)(**9**)](PF$_6$) and [Cu(**5**)(**10**)](PF$_6$). For the complexes whose copper center is shielded efficiently the redox potential is somewhat higher.

Table 4. Electrochemical data of various copper(I) complexes

Compound	$E_{1/2}$ [a]	ΔE_p
[Cu(**6**)$_2$](BF$_4$)	−0.05	107
[Cu(**7**)$_2$](PF$_6$)	0.22	130
[Cu(**2**)$_2$](PF$_6$)	0.50	74
[Cu(**3**)$_2$](PF$_6$)	0.56	68
[Cu(**4**)(CH$_3$CN)$_2$](BF$_4$)	0.53	193
[Cu(**4**)(**9**)](PF$_6$)	0.16	103
[Cu(**5**)(**9**)](PF$_6$)	0.23	156
[Cu(**5**)(**10**)](PF$_6$)	0.28	134

[a] Half-wave potentials $E_{1/2}$ (V vs. ferrocene/ferrocenium) of copper(I) complexes determined by cyclic voltammetry in dichloromethane at $\nu = 100$ mVs^{-1} (electrolyte: 0.1 M Bu_4NPF_6).

Photophysical Data: Absorption data for the homoleptic and heteroleptic complexes in dichlormethane are shown in Table 5. All complexes absorb in a broad region of the UV and visible spectrum. They show very intense ligand-centered (LC) bands in the UV region and much weaker metal-ligand charge-transfer (MLCT) bands in the visible region. The MLCT bands are very broad because the copper(II) complex involved in the electronic transition has an equilibrium geometry very different from that of the ground state copper(I) system.[13]

Table 5. Room temperature absorption data of various copper(I) complexes in dichloromethane at room temperature

Complex	λ_{max} [nm] (ε) [M^{-1}cm^{-1}]
[Cu(**6**)$_2$](BF$_4$)	457 470 (4090)
[Cu(**7**)$_2$](PF$_6$)	470 (6130)
[Cu(**2**)$_2$](PF$_6$)	457 (2640)
[Cu(**3**)$_2$](PF$_6$)	456 (3830)
[Cu(**4**)(**9**)](BF$_4$)	474 (6900)
[Cu(**5**)(**9**)](PF$_6$)	499 (9400)
[Cu(**5**)(**10**)](PF$_6$)	496 (13400)

The homoleptic complexes with the more sterically demanding ligands **2** and **3** exhibit lower absorption wavelengths than the complexes with the 2-substituted phenanthrolines **6** and **7**. This fact is equally clear in the solid state, as the former complexes appear orange whereas the latter complexes are deep red. Moreover, a low-energy shoulder is observed for [Cu(**2**)$_2$]$^+$ and [Cu(**3**)$_2$]$^+$, which can be attributed to distortion of the complexes from D_{2d} symmetry.[15] Such distortion is not possible for complexes [Cu(**2**)$_2$]$^+$ and [Cu(**3**)$_2$]$^+$ because of the steric bulk of the four 2,9-substituents (see also calculated structures).

The room-temperature emission spectrum of [Cu(**3**)$_2$]$^+$ was investigated in dichloromethane. The complex shows an almost complete quenching of fluorescence (at 472 nm).

Quantum Chemical Calculations: To gain a better understanding of the thermodynamics we decided to study the complex equilibria using PM3[16] semi-empirical calculations with parameters for copper (Table 6). Systematic deviations caused by the parametrization should be small due to error cancelation in the calculation of equilibria (or isodesmic reactions).

As the PM3 calculations gave a good prediction about the structure of ligand **5** we also evaluated some of the structural characteristics of the complexes. Of particular interest are the structures of compounds [Cu(**2**)$_2$]$^+$, [Cu(**3**)$_2$]$^+$, [Cu(**4**)$_2$]$^+$, and [Cu(**4**)(**9**)]$^+$ (see Discussion).

*Reaction of **5** with 4,4′-Bipyridine (**13**):* As the large anthracenyl moieties preclude formation of the homoleptic complex [Cu(**5**)$_2$]$^+$, we expected that **5** would also form well-defined Cu^I complexes with ligands binding less strongly than phenanthrolines. The shielded environment about copper in [Cu(**5**)]$^+$ should also bring about some kinetic stabilization. When we treated **5** with 4,4′-bipyridine (**13**) in the presence of copper(I) (molar ratio 2:1:2), only one species was found in solution according to the ^{1}H NMR spectrum, which was indicative of the bisheteroleptic complex [Cu$_2$(**5**)$_2$(**13**)](PF$_6$)$_2$. The protons of the bipyridine moiety exhibit a strong high-field shift ($\Delta\delta = 2.1$ ppm for 2-,2′-H and 1.5 ppm for 3-,3′-H protons), a situation clearly indicative of a heteroleptic complex in which **13** is symmetrically buried in the cavity of two ligands **5**. Unfortunately, crystals of this compound could not be obtained for X-ray analysis, presumably due to the fact that the copper(I) centers weakly bind acetonitrile and dichloromethane, as evidenced by elemental analysis and ES mass spectrometry. For

Table 6. PM3 calculated (see ref.[16]) heats of formation of the ligands and the corresponding homoleptic and heteroleptic complexes

Ligand	ΔH_f [kcal mol^{-1}]	Homoleptic complex	ΔH_f [kcal mol^{-1}]	Heteroleptic complex	ΔH_f [kcal mol^{-1}]
1	73.3	$[Cu(\mathbf{1})_2]^+$	161.2	$[Cu(\mathbf{4})(\mathbf{9})]^+$	327.3
2	164.2	$[Cu(\mathbf{2})_2]^+$	329.8	$[Cu(\mathbf{4})(\mathbf{11})]^+$	275.8
3	183.9	$[Cu(\mathbf{3})_2]^+$	373.0	$[Cu(\mathbf{1})(\mathbf{9})]^+$	193.4
4	207.0	$[Cu(\mathbf{4})_2]^+$	431.8	$[Cu(\mathbf{9})(\mathbf{11})]^+$	195.1
6	139.3	$[Cu(\mathbf{6})_2]^+$	277.2	$[Cu(\mathbf{3})(\mathbf{9})]^+$	304.7
9	124.3	$[Cu(\mathbf{9})_2]^+$	246.4	$[Cu(\mathbf{9})(\mathbf{12})]^+$	245.1
11	71.6	$[Cu(\mathbf{11})_2]^+$	144.0	$[Cu(\mathbf{11})(\mathbf{12})]^+$	193.8
12	122.3	$[Cu(\mathbf{12})_2]^+$	242.4	$[Cu(\mathbf{2})(\mathbf{9})]^+$	286.2

example, mass analysis showed a peak for $[Cu_2(\mathbf{5})_2(\mathbf{13})(CH_3CN)]^{2+}$ at $m/z = 932.0$. In a collisionally activated dissociation (CAD)[17] experiment, complex $[Cu_2(\mathbf{5})_2(\mathbf{13})(CH_3CN)]^{2+}$ readily fragments to form the ion $[Cu(\mathbf{5})]^+$ at $m/z = 833.2$.

Discussion

Formation of the Complexes

The present investigation has disclosed phenanthrolines **4** and **5** as suitable new ligands for controlling the clean preparation of heteroleptic bis(phenanthroline)copper(I) complexes. It is important to state that the heteroleptic complexes $[Cu(\mathbf{4})(\mathbf{9})]^+$, $[Cu(\mathbf{5})(\mathbf{9})]^+$, and $[Cu(\mathbf{5})(\mathbf{10})]^+$ (Scheme 6) were formed without the need for external control from reaction conditions, such as sequence of addition, reaction temperature etc.

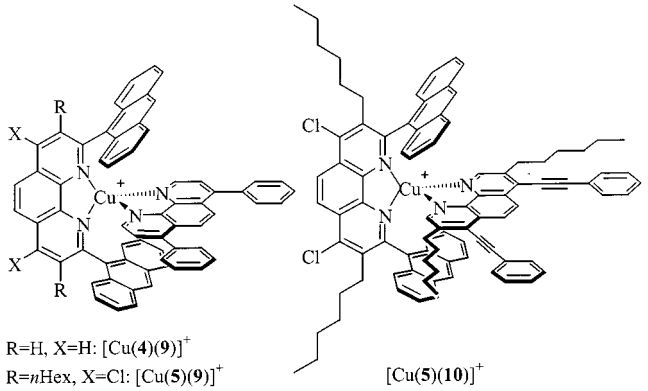

R=H, X=H: $[Cu(\mathbf{4})(\mathbf{9})]^+$
R=*n*Hex, X=Cl: $[Cu(\mathbf{5})(\mathbf{9})]^+$

$[Cu(\mathbf{5})(\mathbf{10})]^+$

Scheme 6

It is well-known that copper(I) phenanthroline complexes with sterically unimpeded ligands are kinetically labile at room temperature (rates $> 6.2 \times 10^4$),[4] and so we have to assume that in the reactions

$$[Cu(CH_3CN)_4]^+ + \mathbf{4} + \mathbf{9} \rightarrow [Cu(\mathbf{4})(\mathbf{9})]^+$$
(no formation of $[Cu(\mathbf{4})_2]^+$ and of $[Cu(\mathbf{9})_2]^+$)

$$[Cu(CH_3CN)_4]^+ + \mathbf{5} + \mathbf{9} \rightarrow [Cu(\mathbf{5})(\mathbf{9})]^+$$
(no formation of $[Cu(\mathbf{5})_2]^+$ and of $[Cu(\mathbf{9})_2]^+$)

the formation of the homoleptic complexes is suppressed by thermodynamic and/or kinetic factors. Indeed, all heteroleptic complexes in Scheme 6 are characterized by a phenanthroline having two large anthracenyl rings in the 2- and 9-positions. In independent experiments we could verify that even under harsh conditions the formation of $[Cu(\mathbf{4})_2]^+$ and $[Cu(\mathbf{5})_2]^+$ does not occur. In contrast, homoleptic complexes were afforded readily with ligands whose 2- and 9-positions were less shielded, e.g. **2**, **3**, **6**, and **7**. However, the question remains as to whether the formation of $[Cu(\mathbf{4})_2]^+$ and $[Cu(\mathbf{5})_2]^+$ is impeded thermodynamically or kinetically.

To answer this question we employed PM3 calculations, although this method does entail a major restriction as, strictly speaking, such calculations are only relevant for the gas phase. Neglecting this constraint, it becomes clear from the calculations that all complexes, even the sterically loaded ones, are thermodynamic minimum structures (for heats of formation, see Table 6). To probe the PM3 calculations we investigated the equilibrium $[Cu(\mathbf{L1})_2]^+ + [Cu(\mathbf{L2})_2]^+ \rightarrow 2\,[Cu(\mathbf{L1})(\mathbf{L2})]^+$ (see Scheme 1). Accordingly, $[Cu(\mathbf{L2})_2]^+$ is favored over $[Cu(\mathbf{L1})(\mathbf{L2})]^+$ by 1.4 kcal mol^{-1}, while experimentally it is favored by roughly 1 kcal mol^{-1}.[18]

Next, we tried to understand the stability of the complexes by evaluating different factors, such as σ-basicity, π-π stacking and steric strain. The critical assessment of the two subsequent equilibria,

$$[Cu(\mathbf{11})_2]^+ + 2 \times \mathbf{12} \rightleftarrows [Cu(\mathbf{12})_2]^+ + 2 \times \mathbf{11} \qquad \Delta H_{rxn} = -3.0 \text{ kcal mol}^{-1},$$

$$[Cu(\mathbf{9})_2]^+ + 2 \times \mathbf{12} \rightleftarrows [Cu(\mathbf{12})_2]^+ + 2 \times \mathbf{9} \qquad \Delta H_{rxn} = 0 \text{ kcal mol}^{-1}$$

indicates that, according to PM3, ligand **12** (with its 2,9-diaryl substituents) forms a more stable homoleptic complex than the parent compound **11**, but this must be due to an increase of the σ-basicity brought about by the 2,9-phenyl groups, and not by π-π stacking. π-π Stacking between the 2,9-aryls and the second phenanthroline is not recognized by PM3 as a stabilizing motif due to the fact that $[Cu(\mathbf{9})_2]^+$ and $[Cu(\mathbf{12})_2]^+$ exhibit the same stability. This is definitely a shortcoming of PM3, since we[18] and others[19] have seen clear structural indications for π-π stacking in phenanthroline copper(I) complexes. Despite this deficiency, PM3 should be useful to evaluate the steric strain encountered in the complex formation with large ligands. To establish a reference point we have defined arbitrarily that the σ-basicity of ligand **12** matches the σ-basicity of 2,9-diaryl-substituted ligands **2**–**4**. As a consequence,

the equilibrium between homoleptic complexes of **12** and **2**−**4** should reflect the steric crowding in the complex.

$$[Cu(\mathbf{12})_2]^+ + 2 \times \mathbf{2} \rightleftarrows [Cu(\mathbf{2})_2]^+ + 2 \times \mathbf{12}$$
$$H_{strain} = \Delta H_{rxn} = +3.6 \text{ kcal mol}^{-1}$$
$$[Cu(\mathbf{12})_2]^+ + 2 \times \mathbf{3} \rightleftarrows [Cu(\mathbf{3})_2]^+ + 2 \times \mathbf{12}$$
$$H_{strain} = \Delta H_{rxn} = +7.4 \text{ kcal mol}^{-1}$$
$$[Cu(\mathbf{12})_2]^+ + 2 \times \mathbf{4} \rightleftarrows [Cu(\mathbf{4})_2]^+ + 2 \times \mathbf{12}$$
$$H_{strain} = \Delta H_{rxn} = +20.0 \text{ kcal mol}^{-1}$$

The strain enthalpy (H_{strain}) in the homoleptic complexes indeed increases with the size of the 2,9-diaryl substituents. In particular, a substantial strain increase is observed when we compare ligand **4** (the same should apply for ligand **5**) with **2** or **3**.

A look at the thermodynamics of the equilibria involving heteroleptic complexes $[Cu(\mathbf{L})(\mathbf{11})]^+$ is also very informative. With ligands **L** = **9** and **12** there is no clear predisposition for the heteroleptic complex. However, the bulky ligands (**L** = **2**−**4**) exhibit an increasing preference for the heteroleptic complex with increasing demand in the series: **4** > **3** > **2** (measured in $[Cu(\mathbf{L})(\mathbf{9})]^+$).

$$[Cu(\mathbf{9})_2]^+ + [Cu(\mathbf{11})_2]^+ \rightleftarrows 2\,[Cu(\mathbf{9})(\mathbf{11})]^+$$
$$\Delta H_{rxn} = -0.2 \text{ kcal mol}^{-1}$$
$$[Cu(\mathbf{11})_2]^+ + [Cu(\mathbf{12})_2]^+ \rightleftarrows 2\,[Cu(\mathbf{11})(\mathbf{12})]^+$$
$$\Delta H_{rxn} = +1.2 \text{ kcal mol}^{-1}$$
$$[Cu(\mathbf{2})_2]^+ + [Cu(\mathbf{9})_2]^+ \rightleftarrows 2\,[Cu(\mathbf{2})(\mathbf{9})]^+$$
$$\Delta H_{rxn} = -3.8 \text{ kcal mol}^{-1}$$
$$[Cu(\mathbf{3})_2]^+ + [Cu(\mathbf{9})_2]^+ \rightleftarrows 2\,[Cu(\mathbf{3})(\mathbf{9})]^+$$
$$\Delta H_{rxn} = -10.0 \text{ kcal mol}^{-1}$$
$$[Cu(\mathbf{4})_2]^+ + [Cu(\mathbf{9})_2]^+ \rightleftarrows 2\,[Cu(\mathbf{4})(\mathbf{9})]^+$$
$$\Delta H_{rxn} = -23.6 \text{ kcal mol}^{-1}$$
$$[Cu(\mathbf{4})_2]^+ + [Cu(\mathbf{11})_2]^+ \rightleftarrows 2\,[Cu(\mathbf{4})(\mathbf{11})]^+$$
$$\Delta H_{rxn} = -24.2 \text{ kcal mol}^{-1}$$

The obvious conclusion from these calculations is that the clean formation of heteroleptic complexes can be brought about by purely thermochemical factors that are controlled by the 2,9-substituents. The thermodynamic preference for heteroleptic complexes with ligands **2**−**4** is apparently due to strain in the homoleptic complexes $[Cu(\mathbf{2}-\mathbf{4})_2]^+$, which is liberated when the heteroleptic complex is formed.

Inspired by our calculations we now wanted to test experimentally whether formation of the heteroleptic complex $[Cu(\mathbf{3})(\mathbf{9})]^+$ is possible despite the fact that a stable complex $[Cu(\mathbf{3})_2]^+$ is known. Indeed, the reaction of ligands **3** and **9** in presence of 1 equiv. of $[Cu(MeCN)_4]BF_4$ at room temperature yielded the heteroleptic complex $[Cu(\mathbf{3})(\mathbf{9})]^+$ in quantitative yield, as evidenced by ^{1}H NMR and ESI mass spectrometry. This is clear evidence for a new way to control heteroleptic bis(phenanthroline)copper(I) complexes just on the basis of their thermodynamic preference. Steric blocking of the formation of the most stable homoleptic complex is no longer needed.

While thermodynamic control of heteroleptic complex formation is certainly the exclusive element to guide the formation of $[Cu(\mathbf{3})(\mathbf{9})]^+$, this is most likely not the case with $[Cu(\mathbf{4})(\mathbf{9})]^+$. While we have not been able to calculate the transition state (TS) for the reaction $[Cu(CH_3CN)_4]^+ + 2 \times \mathbf{4} \rightarrow [Cu(\mathbf{4})_2]^+$, the analysis of structural models clearly indicates that there will be enormous strain in the TS. As such, we suggest that the formation of $[Cu(\mathbf{4})_2]^+$ is precluded by its high TS energy.

Ligands **4** and **5** do not undergo homoleptic complex formation and so they are ideal candidates to react with weaker ligands, such as 4,4′-bipyridine (**13**). This ligand is of particular interest as palladium-4,4′-bipyridine complexes play an important role in molecular triangles and squares.[20] Compound **13** is also often used in the field of *crystal engineering* to prepare coordination polymers.[21,22] In our case, however, only formation of $[Cu_2(\mathbf{5})_2(\mathbf{13})](PF_6)_2$ was observed. The complex carries two additional ligands at copper(I), such as acetonitrile. Because a solid state structure is not available, we present here the PM3 calculated structure that rationalizes the strong NMR shift effects observed in the proton spectrum (Figure 3).

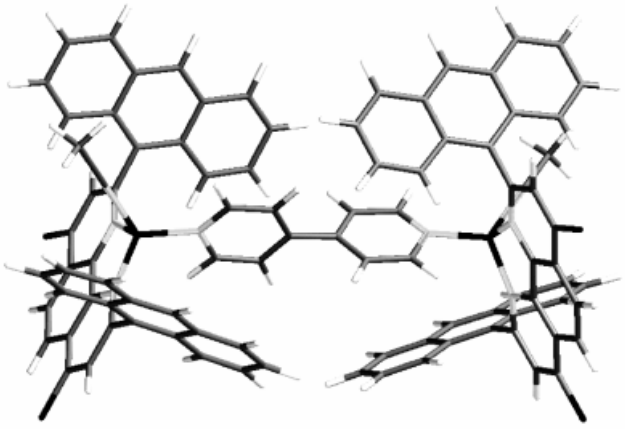

Figure 3. PM3 calculated structure of complex $[Cu_2(\mathbf{5})_2(\mathbf{13})](PF_6)_2$ including two bound acetonitrile ligands

Structure and Properties of the Complexes

Structure: To date there are no crystal structures available for the complexes and for this reason we have used the PM3 calculated structures (Figure 4) to obtain an idea about the arrangement of the phenanthroline and aryl residues. We noted above that the PM3 structure of **5** is in good agreement with the X-ray structure. One has to bear in mind, however, that the PM3 calculations failed to reproduce the weak π-π interaction between the 2,9-aryl groups and the phenanthroline. As this may lead to some distortion in the complex we only want to discuss a few key elements. For example, the angle between the two phenanthrolines is 90° (for $[Cu(\mathbf{4})(\mathbf{9})]^+$) and 87° (for $[Cu(\mathbf{2})]^+$ and $[Cu(\mathbf{3})]^+$), but 80° for $[Cu(\mathbf{4})]^+$. Accordingly, with increased bulk there are deviations from ideal tetrahedral coordination. In complex $[Cu(\mathbf{4})(\mathbf{9})]^+$ the arrangement of the ligands is hardly impeded by strain, but heavy distortions at the metal center and the phenanthroline and the 2,9-aryl substituents do show up in the strained homoleptic complexes. For example, the anthracenyl rings (10° to 14°) and the phenanthroline units (6° to 13°) are severely distorted from

planarity on going from $[Cu(\mathbf{2})]^+$ to $[Cu(\mathbf{4})]^+$, but are planar in the unstrained complex $[Cu(\mathbf{4})(\mathbf{9})]^+$.

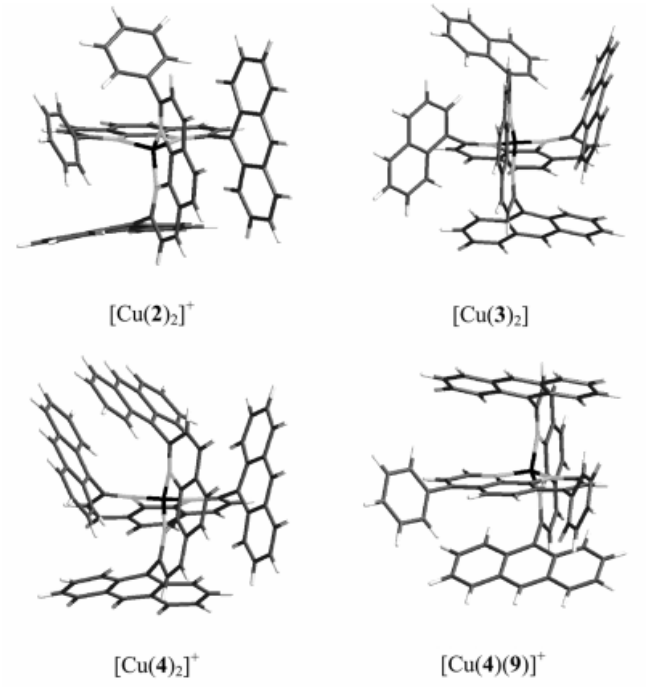

Figure 4. PM3 calculated structures of a few copper complexes

Electrochemical Measurements: The values for the oxidation potential are in the expected range for phenanthroline-type complexes.[23,24] It has been reported that these values depend on the nature of the substituents at the phenanthroline and that the redox potential becomes more positive when the metal ion is subjected to steric constraints that prevent rearrangement in the coordination sphere upon oxidation.[25] Comparison of the homoleptic and heteroleptic complexes shows that the oxidation potentials for the homoleptic complexes are higher than those for the heteroleptic ones because of the rigidity at the metal center. Moreover, the small ΔE_p values for $[Cu(\mathbf{2})_2](PF_6)$ and $[Cu(\mathbf{3})_2](PF_6)$ indicate that their reorganization is rather small on going from Cu^I to Cu^{II}, a situation in contrast to that observed with the other complexes. The results are in agreement with those found in earlier investigations.[12]

On going from $[Cu(\mathbf{4})(\mathbf{9})](PF_6)$ to $[Cu(\mathbf{5})(\mathbf{9})](PF_6)$, phenanthroline **4** is replaced by **5**, a ligand with additional alkyl groups in the 3,8-positions, and thus a small decrease of the oxidation potential is expected as alkyl groups are better σ-donors.[25] However, the reverse is found. Presumably, the back strain effect of the alkyl groups leads to a tighter arrangement at the metal center in $[Cu(\mathbf{5})(\mathbf{9})](PF_6)$.

Luminescence of Ligands and Complexes: Upon excitation at 346 nm all phenanthrolines **2**−**7** exhibit a fluorescence at 439−472 nm that is broadened due to interactions with the solvent. In agreement with textbook knowledge[26] we assign this emission to the $S_1 \rightarrow S_0 + h\nu$ radiative transition of the excited anthracenyl group attached to the 2- (and 9-) position of the phenanthroline core. Apparently, the sp^2-nitrogen donor atoms of the phenanthroline cannot quench the fluorescence, while efficient quenching is usually observed with appended tertiary amines.[27] In the series **2**−**4** (Figure 2), the emission maximum stays roughly the same, but the fluorescence intensity decreases in the order **4** > **3** >> **2**. Such behavior is to be expected from the well-known free rotor effect,[26] as in this series the twisting motion about the phenanthroline and 2,9-diaryl axis is clearly facilitated. When we compare **4** with **5** and **6** with **7** a strong decrease in the fluorescence intensity is registered, which could be due to the presence of 4- and 7-chloro substituents.[28]

Fluorescence at 472 nm is not observed upon complexation of **3** with copper(I). As the absorption maximum of $[Cu(\mathbf{3})_2]^+$ is located at 456 nm, the photoexcited anthracene is quenched by the MLCT process.[29] As a consequence, recognition of the uncomplexed ligand **3** by copper(I) is indicated through fluorescence quenching and, in principle, ligand **3** could be used as a quenchofluorimetric detector[30] towards Cu^I ions.

Conclusion

A series of homoleptic and heteroleptic bis(phenanthroline)copper(I) complexes is presented that is based on ligands carrying sterically bulky groups at the 2- and 9-positions. For the clean preparation of heteroleptic complexes two concepts are elaborated. The first one is based on the fact that steric blocking kinetically prevents the formation of the homoleptic complex having 2,9-diaryl substituents at the phenanthroline. The second one relies on the thermodynamic destabilization of the homoleptic complex having 2,9-diaryl substituents.

Experimental Section

General Remarks: $[Cu(MeCN)_4]BF_4$ [31] and $[Cu(MeCN)_4]PF_6$ [32] were prepared according to literature procedures. All other chemicals were commercially available and used without further purification. The solvents were distilled before use and dried with appropriate desiccants (CH_2Cl_2 from P_2O_5, MeCN from P_2O_5 and NaH, DMSO from calcium sulfate under reduced pressure). − ^1H NMR spectra were recorded on either Bruker AC 200 (200 MHz) or Bruker AC 250 (250 MHz) spectrometers (using the deuterated solvent as the lock and residual solvent as the internal reference). − IR spectra were recorded on a Perkin−Elmer 1605 FT-IR spectrophotometer. − Microanalyses were carried out with a Carlo Erba 1106 Elemental Analyzer. − Electrospray mass spectra (ES-MS) were recorded with a ThermoQuest LCQ Deca Finnigan. − Electrochemical measurements were performed with a Potentiostat Modell 362, Princeton Applied Research.

The solvent used for photophysical studies was CH_2Cl_2 (Merck, Uvasol). UV/Vis spectra were recorded on a J&M TIDAS II absorption spectrometer, while the emission spectra were obtained with a Spex Fluorolog 2 spectrofluorometer. To make comparisons possible in the emission measurements, the absorbance A for all ligands was the same (A = 1.11) at the excitation wavelength λ_{exc} = 346 nm.

The calculations were performed using *Spartan Pro* with the parameter set PM3(tm) for transition metals.[33] The geometries were

optimized using the Merck molecular force field (MMFF) and refined using the semiempirical method PM3(tm).

4,7-Dichloro-3,8-dihexyl-1,10-phenanthroline and 4,7-diethynylphenyl-3,8-dihexyl-1,10-phenanthroline were synthesized as reported previously.[8]

2-(9-Anthracenyl)-1,10-phenanthroline (6): A 1.5 M solution of *n*-butyllithium in pentane (6.60 mL, 9.90 mmol) was slowly added to a solution of 9-bromoanthracene (2.40 g, 9.32 mmol) in 100 mL of diethyl ether at 0 °C. The solution was allowed to stir for 60 min at 0 °C. A suspension of 1,10-phenanthroline (1.00 g, 5.48 mmol) in 40 mL of toluene was added. The solution first became yellow and then turned dark violet. The mixture was stirred for 48 h at room temperature. After the addition of water (60 mL) the layers were separated and the aqueous layer was extracted three times with dichloromethane (3 × 10 mL). The combined organic extracts were stirred with 20 g of activated MnO_2 for 2 h. The mixture was dried with $MgSO_4$ and filtered. After evaporation of the filtrate the resulting solid was separated by column chromatography (SiO_2, trichloromethane, R_f = 0.62). The second fraction contained the pale yellow product (1.30 g, 67% yield). − M.p. > 300 °C. − ^{1}H NMR ($CDCl_3$, 200 MHz): δ = 7.29−7.34 (m, 2 H, 2′-H, 7′-H), 7.40−7.48 (m, 2 H, 3′-H, 6′-H), 7.58 (d, *J* = 8.9 Hz, 2 H, 1′-H, 8′-H), 7.60 (dd, *J* = 8.1 Hz, *J* = 1.7 Hz, 1 H, 8-H), 7.83 (d, *J* = 8.2 Hz, 1 H, 3-H), 7.88 (d, *J* = 8.9 Hz, 1 H, 6-H), 7.95 (d, *J* = 8.9 Hz, 1 H, 5-H), 8.07 (d, *J* = 8.4 Hz, 2 H, 4′-H, 5′-H), 8.28 (dd, *J* = 8.1 Hz, *J* = 1.7 Hz, 1 H, 7-H), 8.44 (d, *J* = 8.2 Hz, 1 H, 4-H), 8.57 (s, 1 H, 10′-H), 9.15 (dd, *J* = 4.4 Hz, *J* = 1.7 Hz, 1 H, 9-H). − ^{13}C NMR ($CDCl_3$, 50 MHz): δ = 122.9 (C-8), 125.0 (C-3), 125.3, 125.6, 126.4, 126.5, 126.8, 127.4, 128.3, 129.0, 130.5, 131.3, 135.8, 135.9, 136.0, 137.8, 146.4 (C-10a), 146.5 (C-1a), 150.5 (C-9), 158.9 (C-2). − IR (KBr): $\tilde{\nu}$ = 3049 cm^{-1}, 1617, 1586, 1504, 1482, 1387, 1192, 844, 731, 668. − $C_{26}H_{16}N_2$: calcd. C 87.62, H 4.52, N 7.86; found C 87.39, H 4.76, N 7.59.

2-(9-Anthracenyl)-4,7-dichloro-3,8-di-*n*-hexyl-1,10-phenanthroline (7): To a solution of 9-bromoanthracene (4.98 g, 19.0 mmol) in dry diethyl ether (150 mL) was added dropwise 1.5 M *n*-butyllithium (13 mL) and the mixture was stirred for 9 h at 0 °C. After the addition of 4,7-dichloro-3,8-hexyl-1,10-phenanthroline (2.43 g, 6.42 mmol) the mixture was stirred for 3 d at room temperature. After hydrolysis with water (50 mL) and separation of the phases, the aqueous layer was extracted with dichloromethane (3 × 20 mL). The combined organic layers were stirred with activated MnO_2 (30.0 g, 343 mmol) for 1 h. The mixture was dried over magnesium sulfate and then filtered. After removing the solvent in vacuo, the residue was purified by column chromatography (SiO_2, trichloromethane, R_f = 0.76) and recrystallized from cyclohexane/*n*-hexane (1:1) to yield a yellow solid (1.40 g, 37%). − M.p. 161 °C. − ^{1}H NMR ($CDCl_3$, 250 MHz): δ = 0.58 (t, *J* = 7.0 Hz, 3 H, CH_3), 0.79−0.90 (m, 2 H, CH_2), 0.87 (t, *J* = 7.0 Hz, 3 H, CH_3), 1.22−1.44 (m, 10 H, CH_2), 1.61−1.70 (m, 4 H, CH_2), 2.54 (t, *J* = 7.8 Hz, 2 H, CH_2), 2.98 (t, *J* = 7.8 Hz, 2 H, CH_2), 7.23−7.47 (m, 6 H, anthracenyl), 8.06 (d, *J* = 8.9 Hz, 2 H), 8.48 (d, *J* = 9.5 Hz, 1 H, 6-H), 8.55 (d, *J* = 9.5 Hz, 1 H, 5-H), 8.57 (s, 1 H, 10′-H), 8.92 (s, 1 H, 9-H). − ^{13}C NMR ($CDCl_3$, 63 MHz): δ = 13.7, 14.0, 21.9, 22.5, 28.4, 28.9, 29.0, 29.6, 30.5, 31.4, 31.5, 31.6, 107.8, 123.5, 123.6, 125.0, 125.8, 125.9, 126.2, 126.5, 127.5, 128.4, 130.5, 131.4, 134.3, 135.4, 137.0, 137.2, 141.0, 142.5, 152.1 (C-9), 159.7 (C-2). − IR (KBr): $\tilde{\nu}$ = 3050 cm^{-1} (m, Ar−H), 2953, 2926, 2855 (s, C−H), 1605 (m), 1570 (s), 1534 (s, arom. C=C), 1464 (s, C−H), 1391 (s), 1347 (m), 1316 (m), 1233 (m), 1040 (m, Ar−Cl). − $C_{38}H_{38}Cl_2N_2$: calcd. C 77.00, H 6.47, N 4.73; found C 76.71, H 6.51, N 4.62.

Synthesis of 2,9-Substituted Phenanthrolines: A typical procedure is shown here for compound **2**.

2-(9-Anthracenyl)-9-phenyl-1,10-phenanthroline (2): Under an inert atmosphere a 1.5 M solution of *tert*-butyllithium in pentane (1.40 mL, 2.10 mmol) was added to bromobenzene (298 mg, 1.86 mmol) in 5 mL of anhydrous diethyl ether at 0 °C. After 1 h stirring at 0 °C the solution was added dropwise to a suspension of **6** (178 mg, 500 μmol) in 10 mL of anhydrous toluene. The resulting deep-red solution was stirred overnight at room temperature. Water (10 mL) was then added. The layers were separated and the aqueous phase was extracted with dichloromethane (3 × 10 mL). The combined extracts were stirred with activated MnO_2 (2.00 g, 23.0 mmol) for 2 h, by which time the intense yellow color had disappeared. The mixture was dried over magnesium sulfate, filtered, and evaporated to give a solid. The crude product was recrystallized from cyclohexane to yield 138 mg (64%) of yellow crystals. − M.p. > 315 °C (decomp.). − ^{1}H NMR ($CDCl_3$, 250 MHz): δ = 7.30−7.70 (m, 9 H), 7.86 (d, *J* = 8.3 Hz, 1 H, 3-H), 7.86−7.90 (m, 3 H, 8-H, 5-H, 6-H), 8.09 (d, 2 H), 8.18−8.22 (m, 2 H, 2′′-H, 6′′-H), 8.34 (d, *J* = 8.6 Hz, 1 H, 7-H), 8.43 (d, *J* = 8.3 Hz, 1 H, 4-H), 8.59 (s, 1 H, 10′-H). − ^{13}C NMR ($CDCl_3$, 63 MHz): δ = 120.4, 123.2, 125.1, 125.7, 125.8, 126.1, 126.6, 126.9, 127.8, 128.4, 128.6, 128.8, 129.1, 129.9, 130.4, 131.4, 135.9, 136.8, 139.6, 140.9, 146.3 (C-10a), 146.6 (C-1a), 157.3 (C-9), 158.3 (C-2). − IR (KBr): $\tilde{\nu}$ = 3042 cm^{-1} (m, C−H), 2923, (s, =C−H), 2845 (m), 1663 (w, C=C), 1587, 1542, 1483 (s, C=C), 1449 (w), 1356 (m), 1314, 1101, 1022, 886, 852 (s), 765, 732, 693 (vs), 615. − $C_{32}H_{20}N_2 \cdot 1H_2O$: calcd. C 85.31, H 4.92, N 6.37; found C 85.49, H 4.43, N 6.37.

Other examples of 2,9-substituted compounds were prepared by following the above procedure.

2-(9-Anthracenyl)-9-(1-naphthyl)-1,10-phenanthroline (3): Yield 25% of a yellow solid. − M.p. > 300 °C. − ^{1}H NMR ($CDCl_3$, 400 MHz): δ = 7.23−7.53 (m, 8 H), 7.64 (d, *J* = 8.6 Hz, 2 H), 7.72 (d, *J* = 7.0 Hz, 1 H), 7.84−7.88 (br. s, 2 H, 5-H, 6-H), 7.86 (d, *J* = 8.3 Hz, 1 H, 3-H), 7.95 (d, *J* = 8.3 Hz, 1 H, 8-H), 8.05 (s, 1 H), 8.09 (d, *J* = 8.4 Hz, 2 H), 8.22 (d, *J* = 8.6 Hz, 1 H), 8.46 (d, *J* = 8.3 Hz, 1 H, 7-H), 8.53 (d, *J* = 8.3 Hz, 1 H, 4-H), 8.59 (s, 1 H, 10′-H). − ^{13}C NMR ($CDCl_3$, 50 MHz): δ = 123.0, 124.8, 124.9, 125.2, 125.6, 125.9, 126.3, 126.4, 126.5, 126.9, 127.3, 127.5, 127.6, 127.7, 127.8, 128.0, 128.1, 128.4, 128.5, 129.3, 130.3, 131.4, 133.9, 135.6, 135.9, 136.4, 138.1, 140.6, 154.5, 158.4. − IR (KBr): $\tilde{\nu}$ = 3048 cm^{-1} (w, =C−H), 1621 (m, C=C), 1577, 1550, 1499, 1442, 1402, 1351, 1136, 1015, 888 (s), 850 (s), 788 (w), 732 (s), 630. − $C_{36}H_{26}N_2 \cdot 0.5H_2O$: calcd. C 87.96, H 4.72, N 5.70; found C 88.41, H 4.82, N 5.69.

2,9-Bis(9-anthracenyl)-1,10-phenanthroline (4): Yield 21% of yellow crystals. − M.p. > 300 °C. − ^{1}H NMR ($CDCl_3$, 250 MHz): δ = 7.28−7.41 (m, 8 H), 7.83 (d, 4 H), 7.87 (d, *J* = 7.9 Hz, 2 H, 3-H, 8-H), 7.96 (d, 4 H), 8.07 (s, 2 H, 5-H, 6-H), 8.45 (s, 2 H, 10′-H), 8.50 (d, *J* = 7.9 Hz, 2 H, 4-H, 7-H). − ^{13}C NMR ($CDCl_3$, 50 MHz): δ = 120.9, 123.5, 124.8, 125.3, 126.1, 126.3, 127.6, 128.1, 128.3, 128.6, 131.3, 138.0, 146.3 (C-1a, C-10a), 158.7 (C-2, C-9). − IR (KBr): $\tilde{\nu}$ = 3046 cm^{-1} (w, =C−H), 1618 (m, C=C), 1578, 1542, 1491, 1442, 1402, 1345, 1187, 1136, 1085, 1014, 886 (s), 845 (s), 788 (w), 732 (s), 628, 613. − $C_{40}H_{24}N_2 \cdot 2H_2O$: calcd. C 84.56, H 4.71, N 5.16; found C 84.48, H 4.96, N 4.93.

2,9-Bis(9-anthracenyl)-4,7-dichloro-3,8-di-*n*-hexyl-1,10-phenanthroline (5): Yield 59% of bright yellow crystals. − M.p. > 269 °C (decomp.). − ^{1}H NMR ($CDCl_3$, 250 MHz): δ = 0.52−0.65 (m, 10 H, CH_3, CH_2), 0.70−0.86 (m, 8 H, CH_2), 1.08−1.30 (m, 4 H, CH_2), 2.50 (t, *J* = 8.0 Hz, 4 H, CH_2), 7.17−7.40 (m, 12 H, anthracenyl),

7.90 (d, J = 8.2 Hz, 4 H, 4′-H, 5′-H), 8.40 (s, 2 H, 10′-H), 8.62 (s, 2 H, 5-H, 6-H). − ^{13}C NMR ($CDCl_3$, 63 MHz): δ = 13.8, 21.9, 28.5, 28.8, 30.6, 31.3, 123.9, 124.8, 125.6, 126.1, 126.3, 127.5, 128.3, 130.3, 131.2, 133.9, 137.2, 142.4, 145.2, 159.3. − IR (KBr): $\tilde{\nu}$ = 3051 cm^{-1} (m, Ar−H), 2955, 2926, 2856 (s, C−H), 1604 (s), 1534 (w, arom. C=C), 1458 (s, C−H), 1140 (w), 1084 (s, Ar−Cl). − $C_{52}H_{46}Cl_2N_2$: calcd. C 81.13, H 6.02, N 3.64; found C 80.90, H 6.24, N 3.56.

2,4-Bis(9-anthracenyl)-1,10-phenanthroline (8): Yield 39% of yellow crystals. − M.p.: > 300 °C. − ^{1}H NMR ($CDCl_3$, 250 MHz): δ = 7.27 (d, J = 8.6 Hz, 1 H, 5-H), 7.35−7.56 (m, 8 H), 7.62 (d, J = 8.6 Hz, 1 H, 6-H), 7.57−7.64 (m, 2 H), 7.64 (dd, J = 7.7 Hz, J = 4.3 Hz, 8-H), 7.87−7.92 (m, 2 H), 7.94 (s, 1 H, 3-H), 8.04−8.16 (m, 4 H), 8.23 (dd, J = 7.7 Hz, J = 1.8 Hz, 1 H, 7-H), 8.56 (s, 1 H, 10′-H), 8.65 (s, 1 H, 10′′-H), 9.23 (dd, J = 4.3 Hz, J = 1.8 Hz, 1 H, 9-H). − ^{13}C NMR ($CDCl_3$, 50 MHz): δ = 124.6, 125.0, 125.4, 125.9, 126.0 (2 ×), 126.4 (2 ×), 127.0, 127.7, 127.9, 128.0, 128.2, 128.5, 128.7, 129.0, 129.5, 130.3, 130.6, 131.5, 135.6, 135.9, 145.9, 146.0, 146.8 (C-10a), 147.1 (C-1a), 150.7 (C-9), 158.6 (C-2). − IR (KBr): $\tilde{\nu}$ = 3045 cm^{-1} (m, =C−H), 1617 (m), 1577 (m), 1541 (s), 1480 (s), 1442 (m), 1375 (w), 1342 (w), 1013 (m), 888 (s), 832 (s), 788 (s), 730 (vs), 652 (m), 614 (m). − $C_{40}H_{24}N_2 \cdot 0.75H_2O$: calcd. C 87.82, H 4.72, N 5.12; found C 87.94, H 4.72, N 4.99.

Data for Homoleptic Complexes. − General Procedure for the Synthesis of the Homoleptic Cu^I Complexes

[Cu(6)$_2$]BF$_4$: $[Cu(MeCN)_4]BF_4$ (42.0 mg, 134 μmol) was dissolved in anhydrous acetonitrile (5 mL) under an inert atmosphere at room temperature. Upon addition of **6** (80.0 mg, 268 μmol) in anhydrous dichloromethane (5 mL) the solution immediately turned to a deep red hue. After 30 min of stirring at room temperature, the solvent was removed in vacuo. The solid was purified by recrystallization from CH_2Cl_2/cyclohexane to yield [Cu(**6**)$_2$]BF_4 as orange needles (84 mg, 84%). − M.p. > 300 °C. − ^{1}H NMR (250 MHz, CD_2Cl_2): δ = 6.81 (d, J = 8.9 Hz, 2 H), 7.02−7.24 (m, 6 H), 7.07 (dd, J = 8.1 Hz, J = 4.6 Hz, 2 H, 8-H), 7.38−7.44 (m, 4 H), 7.57 (d, J = 8.5 Hz, 2 H), 7.65 (dd, J = 4.6 Hz, J = 1.5 Hz, 2 H, 9-H), 7.69 (d, J = 8.0 Hz, 2 H, 3-H), 7.78 (d, J = 8.5 Hz, 2 H), 7.80 (d, J = 9.2 Hz, 2 H, 5-H), 7.83 (s, 2 H), 7.90 (d, J = 9.2 Hz, 2 H, 6-H), 8.25 (dd, J = 8.1 Hz, J = 1.5 Hz, 2 H, 7-H), 8.33 (d, J = 8.0 Hz, 2 H, 4-H). − ^{13}C NMR (50 MHz, CD_2Cl_2): δ = 125.3, 125.7, 125.9, 126.1 (2 ×), 126.3, 127.4, 127.5, 127.6, 128.2, 128.4, 129.1, 129.2, 129.3, 129.7, 130.1, 130.5, 131.0, 131.3, 132.6, 136.4, 137.9, 143.2, 144.2, 147.9 (C-9), 157.5 (C-2). − IR (KBr): $\tilde{\nu}$ = 3049 cm^{-1}, 1705, 1654, 1618, 1560, 1508, 1489, 1444, 1408, 1383, 1357, 1356, 1221, 1198, 1142, 1054, 883, 844, 734, 662. − $C_{52}H_{32}N_4CuBF_4 \cdot 0.5H_2O$: calcd. C 70.88, H 3.89, N 6.36; found C 70.41, H 4.02, N 5.92.

[Cu(2)$_2$]PF$_6$: Reacting $[Cu(MeCN)_4]PF_6$ (23.0 mg, 62.0 μmol) with **2** (54.0 mg, 62.0 μmol) according to the above procedure yielded, after column chromatography with CH_2Cl_2/MeOH (R_f = 0.32), [Cu(**2**)$_2$]PF_6 (33 mg, 50%) as red crystals. − M.p. > 300 °C. − ^{1}H NMR (250 MHz, CD_2Cl_2): δ = 6.48−6.57 (m, 6 H), 6.68−6.84 (m, 6 H), 7.05−7.11 (m, 2 H), 7.19−7.31 (m, 8 H), 7.39 (d, J = 8.3 Hz, 2H, 8-H), 7.63 (d, J = 8.6 Hz, 2 H), 7.67 (d, J = 8.3 Hz, 2 H, 3-H), 7.84 (d, J = 8.6 Hz, 2 H), 7.91 (d, J = 8.9 Hz, 2 H, 6-H), 7.97 (d, J = 8.9 Hz, 2 H, 5-H), 8.05 (s, 2 H, 10′-H), 8.26 (d, J = 8.3 Hz, 2 H, 7-H), 8.42 (d, J = 8.3 Hz, 2 H, 4-H). − ^{13}C NMR (50 MHz, CD_2Cl_2): δ = 124.4, 124.5, 124.6, 125.0, 125.2, 125.3, 126.5, 126.6, 127.0, 127.3 (2 ×), 127.8, 127.9 (2 ×), 128.1, 128.4 (2 ×), 128.6, 128.9, 129.5, 129.7, 130.5, 132.2, 136.9, 137.4, 138.1, 142.6, 144.3, 155.4, 157.1. − IR (KBr): $\tilde{\nu}$ = 3054 cm^{-1}, 2920, 1609, 1525, 1476, 1391, 1350, 1055, 900, 844, 800, 738. 620. − ESI-MS: calcd. for $C_{64}H_{40}N_4Cu^+$: m/z = 927.3, found m/z = 927.4. − $C_{64}H_{40}N_4CuPF_6 \cdot 1H_2O$: calcd. C 70.42, H 3.88, N 5.13; found C 70.11, H 3.92, N 5.04.

[Cu(3)$_2$]PF$_6$: Reacting $[Cu(MeCN)_4]PF_6$ (31.0 mg, 83.0 μmol) with **3** (80.2 mg, 166 μmol) yielded, after recrystallization from dichloromethane/pentane, [Cu(**3**)$_2$]PF_6 (82.0 mg, 85%) as orange crystals. − M.p. > 300 °C. − ^{1}H NMR (600 MHz, CD_2Cl_2): δ = 6.15 (m, 2 H, 3′′-H), 6.64 (d, J = 8.0 Hz, 2 H, 4′′-H), 6.80 (dd, J = 6.3 Hz, J = 6.3 Hz, 2 H, 3′-H), 6.85 (m, 2 H, 4′-H), 6.89 (d, J = 7.6 Hz, 2 H, 5′′-H), 6.93 (m, 2 H, 2′-H), 7.01 (m, 4 H, 8′′-H, 6′-H), 7.13−7.17 (m, 4 H, 7′′-, 6′′-H), 7.27 (d, J = 8.3 Hz, 2 H, 8-H), 7.30 (m, 2 H, 7′-H), 7.38 (d, J = 8.6 Hz, 2 H, 5′-H), 7.45 (d, J = 6.8 Hz, 2 H, 2′′-H), 7.60 (d, J = 8.6 Hz, 2 H, 1′-H), 7.74 (d, J = 8.7 Hz, 2 H, 8′-H), 7.77 (d, J = 8.0 Hz, 2 H, 3-H), 7.87 (d, J = 8.9 Hz, 2 H, 5-H), 7.96 (d, J = 8.9 Hz, 2 H, 6-H), 7.97 (s, 2 H, 10′-H), 8.22 (d, J = 8.3 Hz, 2 H, 7-H), 8.42 (d, J = 8.0 Hz, 2 H, 4-H). − ^{13}C NMR (50 MHz, CD_2Cl_2): δ = 122.6, 123.8, 124.0, 125.0 (2 ×), 125.1, 125.3 (2 ×), 125.8, 126.1, 126.7, 126.8 (2 ×), 127.2, 127.5 (2 ×), 127.9, 128.5 (2 ×), 128.6, 129.0, 129.3, 129.5 (2 ×), 129.7, 130.5, 132.0, 132.2, 134.5, 135.2, 137.6, 137.7, 143.4, 144.5, 154.8, 157.1. − IR (KBr): $\tilde{\nu}$ = 3044 cm^{-1}, 2915, 1623, 1498, 1357, 841, 777, 734, 619, 557. − ESI-MS: calcd. for $C_{72}H_{44}N_4Cu^+$: m/z = 1027.3, found m/z = 1027.2. − $C_{72}H_{44}N_4CuPF_6 \cdot 0.5H_2O$: calcd. C 73.12, H 3.84, N 4.74, found C 72.99, H 3.85, N 4.60.

[Cu(7)$_2$]PF$_6$: $[Cu(MeCN)_4]PF_6$ (34.0 mg, 108 μmol) was allowed to react with **7** (128 mg, 216 μmol) to yield, after filtration and recrystallization from dichloromethane/pentane, [Cu(**7**)$_2$]PF_6 (123 mg, 85%) as dark red crystals. − M.p. 212 °C. − ^{1}H NMR ($CDCl_3$, 200 MHz): δ = 0.46−0.71 (m, 16 H, CH_3, CH_2), 0.72−1.04 (m, 8 H, CH_3, CH_2), 1.04−1.50 (m, 18 H, CH_2), 2.10−2.30 (m, 4 H, CH_2), 2.35−2.52 (m, 2 H, CH_2), 2.85−3.05 (m, 2 H, CH_2), 3.63 (t, J = 6.4 Hz, 2 H, CH_2), 6.63 (d, J = 8.6 Hz, 2 H), 6.91 (m, 2 H), 7.10−7.31 (m, 6 H), 7.36−7.45 (m, 2 H), 7.42 (s, 2 H, 9-H), 7.55 (d, J = 8.7 Hz, 2 H), 7.80 (d, J = 8.7 Hz, 2 H), 7.89 (s, 2 H, 10′-H), 8.28 (d, J = 9.3 Hz, 2 H, 5-H), 8.36 (d, J = 9.3 Hz, 2 H, 6-H). − ^{13}C NMR ($CDCl_3$, 50 MHz): δ = 13.5, 13.9, 14.9, 21.6, 22.4, 28.2, 28.6, 29.0, 30.2, 31.2, 31.3, 32.3, 122.4, 123.4, 124.2, 124.6 (2 ×), 124.8, 125.4, 125.7, 126.5, 126.9, 127.6, 127.7, 128.5, 128.7, 129.1, 129.8, 130.4, 130.5, 137.7, 139.0, 140.7, 141.2, 141.7, 143.4, 147.9, 156.9. − IR (KBr): $\tilde{\nu}$ = 3053 cm^{-1}, 2953, 2926, 2855, 1609, 1545, 1466, 1391, 1348, 1084, 1055, 900, 844, 800, 738. − $C_{76}H_{76}BCl_4CuF_4N_4$: calcd. C 68.34, H 5.74, N 4.20; found C 67.84, H 5.49, N 3.92.

[Cu(4)(CH$_3$CN)$_2$](BF$_4$): Reacting $[Cu(MeCN)_4]PF_6$ (16.6 mg, 53.0 μmol) with **4** (56.0 mg, 105 μmol) yielded, after recrystallization from dichloromethane/pentane, [Cu(**4**)$(CH_3CN)_2$](BF_4) as yellow crystals (56.0 mg, 69%). − M.p. > 300 °C. − ^{1}H NMR ($CDCl_3$, 200 MHz): δ = 7.30−7.49 (m, 12 H), 8.05 (bd, J = 8.1 Hz, 4 H), 8.20 (bd, J = 8.4 Hz, 2 H, 8-H, 3-H), 8.37 (s, 2 H, 5-H, 6-H), 8.59 (s, 2 H, 10′-H), 8.90 (bd, J = 8.4 Hz, 2 H, 4-H, 7-H). − ^{13}C NMR ($CDCl_3$, 50 MHz): δ = 114.6, 125.1, 125.3, 126.5, 127.2, 128.3, 128.5, 128.7, 129.9, 130.9, 132.9, 138.7, 144.6 (C-1a, C-10a), 158.2 (C-2, C-9). − IR (KBr): $\tilde{\nu}$ = 3051 cm^{-1} (w, =C−H), 2926 (w), 1618 (m, C=C arom.), 1578, 1507, 1443, 1406, 1355, 1059 (br. s, B−F), 879 (m), 789 (m), 732 (s), 628. − ESI-MS: calcd. for $C_{40}H_{24}N_2Cu^+$: m/z = 595.3, found m/z = 595.3. − $C_{44}H_{30}BCuF_4N_4 \cdot 1H_2O$: calcd. C 67.58, H 4.12, N 7.15; found C 67.42, H 3.90, N 6.60.

General Procedure for the Synthesis of Heteroleptic Cu^I Complexes: One equivalent of $[Cu(MeCN)_4]PF_6$ or $[Cu(MeCN)_4]BF_4$ was dis-

solved in dry dichloromethane under an inert atmosphere. One equivalent of the sterically hindered 2,9-substituted phenanthroline **4** or **5** was added, resulting in a yellowish solution. After 5 min stirring at room temperature one equivalent of 4,7-substituted phenanthroline was added and a deep red solution formed immediately. The mixture was stirred for another 30 min, and the solvent was removed in vacuo. The red solids were purified by column chromatography (silica gel, dichloromethane/methanol = 10:1) to remove traces of additional ligands and copper salts.

Data for Heteroleptic Cu^{I} Complexes

[Cu(4)(9)]BF$_4$: [Cu(MeCN)$_4$]BF$_4$ (34.5 mg, 110 μmol) was allowed to react with **4** (34.5 mg, 110 μmol) and **9** (58.5 mg, 110 μmol) to yield, after filtration and recrystallization from dichloromethane/cyclohexane, [Cu(**4**)(**9**)]BF$_4$ (99.0 mg, 88%) as orange crystals. − M.p. > 300 °C. − ^{1}H NMR (200 MHz, CD_2Cl_2): δ = 6.59 (d, J = 5.0 Hz, 2 H, 3′′-H, 8′′-H), 6.92−7.13 (m, 8 H, anthracenyl), 7.14 (d, J = 5.0 Hz, 2 H, 2′′-H, 9′′-H), 7.23 (bd, J = 8.4 Hz, 4 H, anthracenyl), 7.31 (bd, J = 7.7 Hz, 4 H, anthracenyl), 7.41 (s, 2 H, 10′-H), 7.45 (s, 2 H, 5′′-H, 6′′-H), 7.57−7.68 (m, 10 H, phenyl), 8.27 (d, J = 8.0 Hz, 2 H, 3-H, 8-H), 8.46 (s, 2 H, 5-H, 6-H), 8.97 (d, J = 8.0 Hz, 2 H, 4-H, 7-H). − ^{13}C NMR (50 MHz, CD_2Cl_2): δ = 125.3, 125.9, 126.6 (2 ×), 127.0, 128.0, 128.7, 129.1, 129.5, 129.8, 130.4, 130.8, 131.0, 131.2, 131.4, 132.0, 136.0, 138.6, 139.0, 143.5, 146.1, 148.0, 148.9, 158.7. − IR (KBr): $\tilde{\nu}$ = 3055 cm^{-1}, 1654, 1618, 1560, 1492, 1421, 1354, 1059, 875, 845, 767, 734, 703, 628. − ESI-MS: calcd. for $C_{64}H_{40}N_4Cu^+$: m/z = 927.3, found m/z = 927.4. − $C_{64}H_{40}N_4CuBF_4 \cdot H_2O$: calcd. C 74.38, H 4.10, N 5.42; found C 74.21, H 4.15, N 5.12.

[Cu$_2$(5)$_2$(13)](BF$_4$)$_2$: [Cu(MeCN)$_4$]BF$_4$ (26.5 mg, 84.4 μmol) was allowed to react with **5** (64.9 mg, 84.8 μmol) and 4,4′-bipyridine (**13**) (6.50 mg, 42.0 μmol) in dichloromethane. After stirring for 2 h the product was precipitated by adding pentane. After filtration and washing with pentane the product was obtained as red crystals (34.1 mg, 49%). − M.p. > 120−135 °C. − ^{1}H NMR (250 MHz, $CDCl_3$): δ = 0.55 (t, J = 7.5 Hz, 12 H, CH_3), 0.65−0.95 (m, 12 H, CH_2), 1.25−1.43 (m, 12 H, CH_2), 2.60−2.75 (m, 8 H, CH_2), 3.65 (m, 8 H, CH_2), 5.96−6.10 (m, 4 H, 3′′-H, 5′′-H), 6.60−6.75 (m, 4 H, 2′′-H, 6′′-H), 7.10−7.20 (m, 12 H, anthracenyl), 7.20−7.35 (m, 12 H, anthracenyl), 7.85−7.95 (m, 8 H, anthracenyl), 8.43 (s, 4 H, 10′-H), 8.77 (s, 4 H, 5-H, 6-H). − ^{13}C NMR (63 MHz, $CDCl_3$): δ = 15.3, 23.7, 30.2, 30.7, 32.4, 33.8, 114.2, 126.7, 126.9, 127.2, 128.6, 129.3, 130.6, 130.7, 131.5, 132.7, 133.9, 142.4, 144.6, 146.6, 159.8, 159.9, 160.7. − IR (KBr): $\tilde{\nu}$ = 3051 cm^{-1} (m, Ar−H), 2955 (s), 2927 (s), 2856 (s, C−H), 1604 (s), 1534 (w, arom. C=C), 1458 (m, C−H), 1410 (w), 1084 (vs, B−F), 819 (m), 800 (m), 738 (s). − ESI-MS: calcd. for $C_{114}H_{100}N_6Cl_4Cu_2 \cdot CH_3CN^{2+}$: m/z = 931.8, found m/z = 932.0. − $C_{114}H_{100}N_6Cl_4Cu_2B_2F_8 \cdot 1CH_3CN \cdot 1CH_2Cl_2$: calcd. C 66.21, H 4.99, N 4.62; found C 66.31, H 5.26, N 4.98.

[Cu(5)(9)]PF$_6$: Reaction of [Cu(MeCN)$_4$]PF$_6$ (18.6 mg, 50.0 μmol) with **5** (38.5 mg, 50.0 μmol) and **9** (16.6 mg, 50.0 μmol) yielded [Cu(**5**)(**9**)]PF$_6$ (58.0 mg, 88%) as a red powder. − M.p. > 170 °C (decomp.). − ^{1}H NMR ($CDCl_3$, 400 MHz): δ = 0.51 (t, J = 6.9 Hz, 6 H, CH_3), 0.73−0.96 (m, 12 H, CH_2), 1.36−1.42 (m, 4 H, CH_2), 2.73−2.77 (m, 4 H, CH_2), 6.60 (d, J = 4.9 Hz, 2 H, 3′-H, 8′-H), 6.91−6.95 (m, 4 H, anthracenyl), 7.03 (d, J = 4.9 Hz, 2 H, 2′-H, 9′-H), 7.08−7.17 (m, 12 H, anthracenyl), 7.43 (s, 2 H, 10′-H), 7.44 (s, 2 H, 5′-H, 6′-H), 7.58−7.66 (m, 10 H, phenyl), 8.78 (s, 2 H, 5-H, 6-H). − ^{13}C NMR ($CDCl_3$, 400 MHz): δ = 13.6, 21.8, 28.7, 28.9, 30.6, 31.2, 123.3, 124.3, 124.5, 124.6, 124.9 (2 ×), 125.7, 126.6 (2 ×), 127.1, 127.5, 129.0, 129.2 (2 ×), 129.9, 133.2, 136.7, 139.8, 141.3, 142.8, 143.0, 146.4, 146.6, 157.5. − IR (KBr): $\tilde{\nu}$ = 3442 cm^{-1}, 2956, 2927, 2866, 2856, 1622, 1560, 1457, 840, 738, 557. − ESI-MS: calcd. for $C_{76}H_{62}N_4Cl_2Cu^+$: m/z = 1165.8, found m/z = 1165.9. − $C_{76}H_{62}N_4Cl_2CuPF_6 \cdot 1.5H_2O$: calcd. C 68.24, H 4.90, N 4.19; found C 68.18, H 4.40, N 4.20.

[Cu(5)(10)]PF$_6$: [Cu(MeCN)$_4$]PF$_6$ (18.6 mg, 50.0 μmol) was allowed to react with **5** (38.5 mg, 50.0 μmol) and 4,7-diethynylphenyl-3,8-di-*n*-hexyl-1,10-phenanthroline (**10**) (27.4 mg, 50.0 μmol) to afford [Cu(**5**)(**10**)]PF$_6$ (37.8 mg, 49%) as a dark red powder. − M.p. 146−148 °C. − ^{1}H NMR ($CDCl_3$, 400 MHz): δ = 0.49 (t, J = 6.9 Hz, 6 H, CH_3), 0.76−0.83 (m, 8 H, CH_2), 0.95 (t, J = 6.9 Hz, 6 H, CH_3), 1.29−1.56 (m, 24 H, CH_2), 2.44 (m, 4 H, CH_2), 2.63 (m, 4 H, CH_2), 6.98−7.03 (m, 4 H, anthracenyl), 7.10−7.24 (m, 12 H, anthracenyl), 7.36 (s, 2 H, 10′-H), 7.41 (s, 2 H, 2′-H, 9′-H), 7.60−7.71 (m, 6 H, phenyl), 7.75 (m, 4 H, phenyl), 8.08 (s, 2 H, 5′-H, 6′-H), 8.79 (s, 2 H, 5-H, 6-H). − ^{13}C NMR ($CDCl_3$, 100 MHz): δ = 13.6, 14.0, 21.7, 22.6, 28.4, 28.7, 29.7, 30.0, 30.4, 31.6, 31.7, 32.8, 83.0, 104.1, 121.8, 124.1, 124.5, 124.6, 124.8, 126.1, 126.3, 127.0, 127.1 (2 ×), 127.8, 128.8 (2 ×), 129.7, 129.9, 131.9, 132.7, 139.2, 139.4, 139.7, 142.7, 143.2, 147.1, 157.4. − IR (KBr): $\tilde{\nu}$ = 3449 cm^{-1}, 2953, 2924, 2854, 2208, 1620, 1558, 1539, 1506, 1457, 840, 756, 737, 557. − ESI-MS: calcd. for $C_{92}H_{86}N_4Cl_2Cu^+$: m/z = 1382.2, found m/z = 1382.0. − $C_{92}H_{86}N_4Cl_2CuPF_6$: calcd. C 72.36, H 5.68, N 3.67; found C 72.08, H 5.80, N 3.75.

X-ray Crystallographic Study: Red squares were grown from a dichloromethane solution of **5**. − Data were collected with a STOE IPDS (Imaging Plate Diffraction System) diffractometer at 203(2) K with graphite-monochromated Mo-K_α radiation (λ = 0.71073 Å). No. of reflns. collected: 18670, No. of unique reflns: 8618, merging factor: R(int) = 0.06671, $2\theta_{max}$ = 28.18°. − Crystal data: empirical formula $C_{52}H_{46}Cl_2N_2$, molecular mass = 769.81, a = 9.314(2) Å, b = 16.469(3) Å, c = 26.486(5) Å, α = 90°, β = 92.31 (3)°, γ = 90°, Z = 4, V = 4059.4(14) Å^3, μ = 0.199 mm^{-1}, F(000) = 1624, $\rho_{calcd.}$ =1.260 mg/m^3, monoclinic, space group $P2_1/n$, final R indices [$I > 2\sigma(I)$]: R1 = 0.0494, wR2 = 0.1536; R indices (all data): R1 = 0.0661, wR2 = 0.1803. − Structure solution and refinement: direct methods, programs Siemens SHELXTL-Ver.5.03. The structure was refined anisotropically against F^2 (full-matrix least squares) for the non-hydrogen atoms. Hydrogens were included at calculated positions using a riding model.

Crystallographic data (excluding structure factors) for the structure reported in this paper have been deposited with the Cambridge Crystallographic Data Centre as supplementary publication no. CCDC-150120. Copies of the data can be obtained free of charge on application to CCDC, 12 Union Road, Cambridge CB2 1EZ, UK [Fax: (internat.) + 44-1223/336-033; E-mail: deposit@ccdc.cam.ac.uk].

Acknowledgments

We would like to thank the Deutsche Forschungsgemeinschaft and the Fonds der Chemischen Industrie for their continued support. Moreover, we are indebted to N. Kemnitzer and Prof. K.-H. Drexhage for help with the luminescence measurements.

[1] M. Schmittel, A. Ganz, *Chem. Commun.* **1997**, 999−1000.
[2] M. Schmittel, A. Ganz, D. Fenske, M. Herderich, *J. Chem. Soc., Dalton Trans.* **2000**, 353−359.
[3] M. Schmittel, C. Michel, A. Ganz, M. Herderich, *J. Prakt. Chem.* **1999**, *341*, 228−236.
[4] [4a] H. L. Hodges, M. A. de Araujo, *Inorg. Chem.* **1982**, *21*, 3236−3239. − [4b] A.-M. Albrecht-Gary, C. Dietrich-Buchecker, Z. Saad, J.-P. Sauvage, *J. Am. Chem. Soc.* **1988**, *110*, 1467−1472.

[5] A preliminary report has been published: M. Schmittel, U. Lüning, M. Meder, A. Ganz, C. Michel, M. Herderich, *Heterocycl. Commun.* **1997**, *3*, 493−498.
[6] L. Fabrizzi, A. Poggi, *Chem. Soc. Rev.* **1995**, 197−202.
[7] [7a] R. A. Bisell, A. P. de Silva, H. Q. N. Gunaratne, P. L. M. Lynch, G. E. M. Maguire, K. R. A. S. Sandanayake, *Chem. Soc. Rev.* **1992**, 187−195. − [7b] S. A. de Silva, A. Zavaleta, D. E. Baron, O. Allam, E. W. Isidor, N. Kashimura, J. M. Percarpio, *Tetrahedron Lett.* **1997**, *38*, 2237−2240.
[8] [8a] M. Schmittel, H. Ammon, *Synlett* **1997**, 1096−1098. − [8b] M. Schmittel, H. Ammon, *Eur. J. Org. Chem.* **1998**, 785−792.
[9] [9a]C. O. Dietrich-Buchecker, P. A. Marnot, J.-P. Sauvage, *Tetrahedron Lett.* **1982**, *23*, 5291−5294. − [9b] C. Dietrich-Buchecker, M. C. Jiménez, J.-P. Sauvage, *Tetrahedron Lett.* **1999**, *40*, 3395−3396.
[10] D. L. Comins, A. H. Abdullah, *J. Org. Chem.* **1982**, *47*, 4315−4319.
[11] Search in Beilstein Crossfire.
[12] M.T. Miller, P. K. Gantzel, T. B. Karpishin, *Inorg. Chem.* **1999**, *38*, 3414−3422.
[13] A. K. Gushurst, D. R. McMillin, C. O. Dietrich-Buchecker, P. A. Marnot, J.-P. Sauvage, *Inorg. Chem.* **1989**, *28*, 4070−4072.
[14] [14a]M. Ruthkosky, F. N. Castellano, G. J. Meyer, *Inorg. Chem.* **1996**, *35*, 6406−6412. − [14b] M. K. Eggleston, D. R. McMillin, K. S. Koenig, A. J. Pallenberg, *Inorg. Chem.* **1997**, *36*, 172−176.
[15] [15a] A. K. Ichinaga, J. R. Kirchhoff, D. R. McMillin, C. O. Dietrich-Buchecker, J.-P. Sauvage, *Inorg. Chem.* **1987**, *28*, 4290−4292. − [15b] F. K. Klemens, C. E. A. Palmer, S. M. Rolland, P. E. Fanwick, D. R. McMillin, J.-P. Sauvage, *New J. Chem.* **1990**, *14*, 129−133.
[16] J. J. P. Stewart, *J. Comput. Chem.* **1989**, *10*, 209−220.
[17] J. Shen, J. Brodbelt, *J. Am. Soc. Mass Spectrom.* **1999**, *10*, 126−135.
[18] Andrea Ganz, Ph.D. thesis, Würzburg, **1999**.
[19] [19a] D. A. Bardwell, A. M. W. Cargill Thompson, J. C. Jeffery, E. E. M. Tilley, M. D. Ward, *J. Chem. Soc., Dalton Trans.* **1995**, 835−841. − [19b] M. Meyer, A.-M. Albrecht-Gary, C. O. Dietrich-Buchecker, J.-P. Sauvage, *Inorg. Chem.* **1999**, *38*, 2279−2287.
[20] [20a] M. J. Fujita, *J. Synth. Org. Chem. Jpn.* **1996**, *54*, 953−963. − [20b] M. J. Fujita, O. Sasaki, T. Mitsuhashi, T. Fujita, J. Yazaki, K. Yamaguchi, K. Ogura, *Chem. Commun.* **1996**, 1535−1536.
[21] [21a] J. Lu, T. Paliwala, S. C. Lim, C. Yu, T. Niu, A. J. Jacobson, *Inorg. Chem.* **1997**, *36*, 923−929. − [21b] M. Julve, M. Verdaguer, J. Faus, F. Tinti, J. Moratal, A. Monge, E. Gutiérrez-Puebla, *Inorg. Chem.* **1987**, *26*, 3520−3527.
[22] S. Subramanian, M. J. Zaworotko, *Angew. Chem.* **1997**, *107*, 2295−2297.
[23] C. O. Buchecker, J.-P. Sauvage, J.-P. Kern, *J. Am. Chem. Soc.* **1984**, *106*, 3043−3045.
[24] [24a] C. O. Dietrich-Buchecker, J.-F. Nierengarten, J.-P. Sauvage, N. Armaroli, V. Balzani, L. De Cola, *J. Am. Chem. Soc.* **1993**, *115*, 11237−11244. − [24b] P. Federlin, J.-M. Kern, A. Rastegar, C. Dietrich-Buchecker, P. A. Marnot, J.-P. Sauvage, *New J. Chem.* **1990**, *14*, 9−12.
[25] J.-M. Kern, J.-P. Sauvage, J.-L. Weidmann, N. Armaroli, L. Flamigni, P. Ceroni, V. Balzani, *Inorg. Chem.* **1997**, *36*, 5329−5338.
[26] N. J. Turro, *Modern Molecular Photochemistry*, Benjamin/Cummings, Menlo Park, **1978.**
[27] G. De Santis, L. Fabbrizzi, M. Licchelli, C. Mangano, D. Sacchi, *Inorg. Chem.* **1995**, *34*, 3581−3582.
[28] E. L. Wehry, in *Practical Fluorescence*, Ed. G. G. Guilbault, chapter 3, Marcel Dekker, New York, **1973**.
[29] C. T. Cunningham, K. L. H. Cunningham, J. F. Michalec, D. R. McMillin, *Inorg. Chem.* **1999**, *38*, 4388−4392.
[30] B. K. Pal, M. S. Rahman, *Microchim. Acta* **1999**, *131*, 139−144.
[31] H. Meerwein, V. Hederich, K. Wunderlich, *Arch. Pharm.* **1958**, *291*, 541−554.
[32] G. J. Kubas, *Inorg. Synth.* **1979**, *19*, 90−92.
[33] *Spartan*, Version *Pro*, Wavefunction, Inc.: 18401 Von Karman Avenue, Suite 370, Irvine, CA 92612.

Received October 2, 2000
[I00371]

Synthesis and Characterization of Epitaxial FAU-on-EMT Zeolite Overgrowth Materials

Ann M. Goossens,[a] Bart H. Wouters,[a] Piet J. Grobet,[a] Veronique Buschmann,[b] Lucien Fiermans,[c] and Johan A. Martens*[a]

Keywords: Crystal engineering / Epitaxial intergrowth / Overgrowth / Faujasite type Zeolites / Two-step synthesis

Epitaxial FAU zeolite films were achieved on micrometer-sized EMT support crystals using a two-step synthetic procedure, in which EMT support crystals with hexagonal-platelet morphology, were added to a synthesis gel for the crystallization of an FAU phase. Identification of the appropriate synthesis parameters made it possible to suppress homogeneous nucleation and initial breeding, and to promote the secondary nucleation of the FAU crystallites on the surface of the EMT support crystals. The presence of both an FAU and an EMT phase was verified with powder X-ray diffraction (XRD). Scanning electron microscopy (SEM) was used to confirm the formation of a layer of FAU crystallites on the EMT support crystals. The growth of the FAU phase was found to start at the corners and edges of the EMT support. An FAU crystallization front progressed from the edges towards the center of the hexagon until the EMT support crystals became completely covered by an FAU zeolite film with a thickness of ca. 300 nm. The compositional difference between the EMT support and the FAU film was investigated with ^{29}Si magic angle spinning (MAS) nuclear magnetic resonance (NMR) spectroscopy, X-ray photoelectron spectroscopy (XPS) and energy-dispersive analysis of X-rays (nano-EDAX). The continuous nature of the film was confirmed by the absence of intracrystalline mesopores, which was evidenced by nitrogen physisorption.

Introduction

The phase-pure zeolite samples used in a diversity of industrial applications are exceptions in the field of zeolite crystallization. Indeed, the majority of zeolite crystallization conditions used result in the formation of physical mixtures of zeolite phases and intergrowth materials. A pure zeolite phase is obtained only when the synthesis parameters are finely tuned. An overview of the different types of intergrowths relevant to zeolites, building on the classification proposed by Rao and Thomas,[1] is provided in Figure 1. Basically, there are two types of intergrowths. Polytypism can be pictured as a regular stacking, without mismatch of bonds, of different structurally uniform domains in each individual zeolite crystal. Epitaxy involves the oriented overgrowth of a zeolite crystal with a compositionally or structurally different zeolite phase. These epitaxial intergrowths, also called overgrowths, can be isotactic. This means that every atom of the interface belongs to both flanking structures constituting that interface.

Polytypical intergrowths of FAU/EMT,[2,3] ERI/OFF,[4,5] MFI/MEL,[6,7] MAZ/MOR,[8,9] and the ABC 6-membered ring structures[10,11] have been described in literature. In these layered materials, the individual domains are all externally accessible. Epitaxial intergrowths are the preferred type of intergrowths for obtaining a controlled microscopic separation, as well as the organization of catalytic, molecular sieving and/or adsorptive functions. Only a few examples of epitaxy have been given in literature so far. Wise et al.[12,13] observed an OFF/LEV overgrowth. De Vos Burchart et al.[14] reported the structural overgrowth of zeolite X onto zeolite A crystals. This was realized by a one-step synthesis in which the gel composition giving rise to zeolite A gradually changed to favor the crystallization of zeolite X. An analogous overgrowth of zeolite P on zeolite A was discussed by Breck[15] in terms of partial conversion of zeolite A into zeolite P. In the proposed molecular model for the oriented growth of zeolite X onto zeolite A, the binding efficiency, defined as the percentage of tetrahedrally coordinated T-atoms, is only 67%,[14] thus classifying this overgrowth amongst the nonisotactic systems.

It is common practice to add seed crystals of the desired zeolite phase to a synthesis batch to ensure product purity and/or to increase the rate of crystallization. The presence of seeds can result in a more rapid crystal growth on the surface of the seed crystals or can provoke secondary nucleation. Several mechanisms of secondary nucleation are known, such as micro-attrition, fluid shear, needle breeding and initial breeding, all resulting in the formation of a new population of crystals which eventually remain attached to the surface of the seed crystals.[16] In this work, we investigated the possibility of synthesizing epitaxial intergrowths of FAU-on-EMT by a two-step synthetic procedure, similar to seeding, in which a zeolite layer is grown over support crystals by a conventional crystallization method. Structural overgrowths of zeolite X onto zeolite A, and vice-versa,

[a] Centrum voor Oppervlaktechemie en Katalyse, Departement Interfasechemie, K. U. Leuven,
Kardinaal Mercierlaan 92, 3001 Heverlee (Leuven), Belgium
Fax: (internat.) + 32-16/321998
E-mail: johan.martens@agr.kuleuven.ac.be
[b] Strukturforschung, FB Materialwissenschaft, T. U. Darmstadt, Petersenstraße 23, 64287 Darmstadt, Germany
[c] Vakgroep Vaste Stofwetenschappen, Universiteit Gent Krijgslaan 281/S1, 9000 Gent, Belgium

 © WILEY-VCH Verlag GmbH, 69451 Weinheim, 2001 1434−1948/01/0505−1167 $ 17.50+.50/0

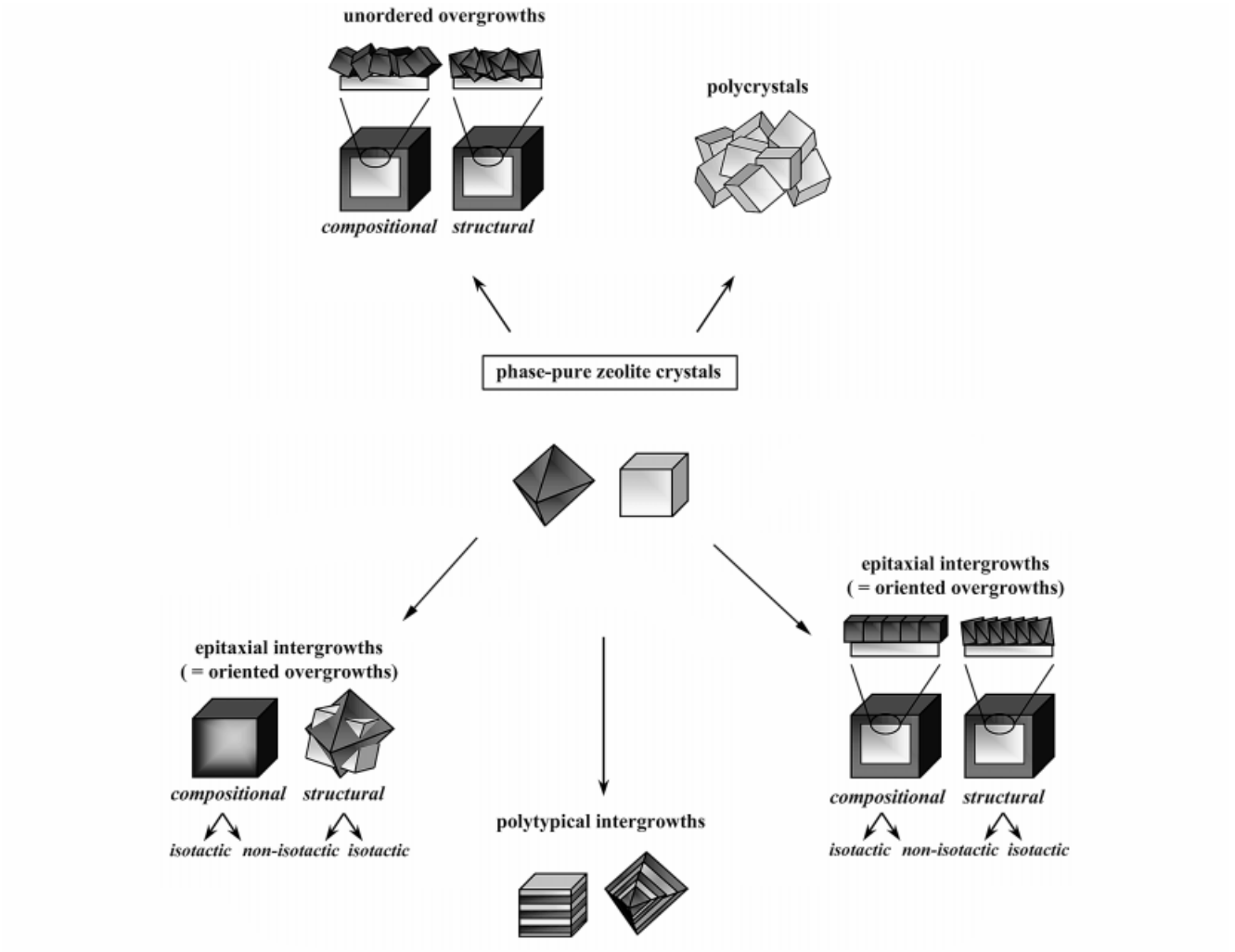

Figure 1. Zeolites and their intergrowths

were previously obtained by using this technique.[14] Compositional overgrowths of ZSM-5 and silicalite were also prepared using such a two-step synthesis.[17–19]

Two structure types with the mnemonic codes FAU and EMT belong to the family of faujasite type zeolites. The FAU and EMT zeolite topologies are structurally related. These zeolite frameworks can be constructed by linking hexagonal prisms into so-called faujasite sheets. Three different relative positions (*a*, *b*, and *c*) exist for these sheets, allowing linkage in the third crystallographic direction. Cubic stacking of faujasite sheets (*abc*) generates the FAU topology, whereas the hexagonal sequence (*ab*) gives rise to the EMT structure. Changes in the stacking sequence from *abc* to *ab* in one crystal produce an FAU/EMT polytypical material. A number of aluminosilicate zeolites have already been identified as polytypical intergrowths of FAU and EMT, ranging from intimately intergrown FAU and EMT layers to segregated FAU and EMT blocks.[3] In previous work, an epitaxial FAU-on-EMT overgrowth material consisting of micrometer-sized hexagonal-platelet EMT support crystals coated with a continuous layer of FAU crystallites was achieved. This was done by introducing the synthesized EMT crystals into a hydrogel for the crystallization of a FAU phase.[20] High-resolution transmission electron microscopy (HRTEM) in combination with selected-area electron diffraction (SAED) revealed the epitaxial relation between the EMT support crystals and the FAU crystallites. The epitaxial relations were: $\{0001\}_{\mathrm{EMTsupport}}$ // $\{111\}_{\mathrm{FAUlayer}}$ and $[11\bar{2}0]_{\mathrm{EMTsupport}}$ // $[\bar{1}10]_{\mathrm{FAUlayer}}$. Furthermore, HREM images of the interface suggested that the overgrowth was isotactic.

The purpose of the present study was to explore the synthesis conditions for the systematic overgrowth of EMT support crystals with an epitaxial and continuous film of FAU crystallites. The synthesis parameters investigated included the molar composition of the synthesis gel, the amount of support crystals added, the pretreatment of the support crystals, the aging and the crystallization time. The

products obtained were identified using X-ray diffraction (XRD) and scanning electron microscopy (SEM). Information about the silicon and aluminum incorporation in the overgrowth materials was obtained from ^{29}Si magic angle spinning (MAS) nuclear magnetic resonance (NMR). The possible presence of compositional heterogeneity in the overgrowing FAU crystallites was investigated using X-ray photoelectron spectroscopy (XPS) and electron nanoprobe analysis of X-rays (nano-EDAX). The crown-ether incorporation was monitored with thermogravimetric-differential thermal analysis (TG-DTA). The continuity of the micropores was verified using nitrogen physisorption.

Results and Discussion

Synthesis of Epitaxial FAU-on-EMT Overgrowth Materials

FAU-on-EMT overgrowth materials were synthesized in two steps. For each experiment, fresh EMT support crystals were prepared using the conventional recipe.[21] According to XRD (Figure 2, a), the EMT support crystals were of excellent crystallinity. The micropore volume of the calcined EMT samples was 0.31 mL/g, confirming the high crystallinity.[21] SEM pictures (Figure 3, a) show the typical hexagonal-platelet morphology. The diagonal dimension of the hexagonal prisms was between 2 and 3 μm, whereas the height varied from 0.5 to 1 μm. The different EMT samples used as supports were not phase-pure, but contained up to 30 wt-% of the FAU structure type. The FAU impurity was detected by XRD as explained in the FAU/EMT quantification section (vide infra). In the SEM pictures, some isolated octahedras were detected next to the abundant hexagonal prisms assigned to the EMT phase. These octahedrally shaped crystals are typical for FAU zeolites. However, their number was too small relative to the amount of FAU estimated by XRD. Most likely, part of the FAU impurity was present as a polytypical intergrowth with EMT. The presence of ca. 10 wt-% of polytypical FAU in EMT samples is not unusual and was also found by other workers.[2,22]

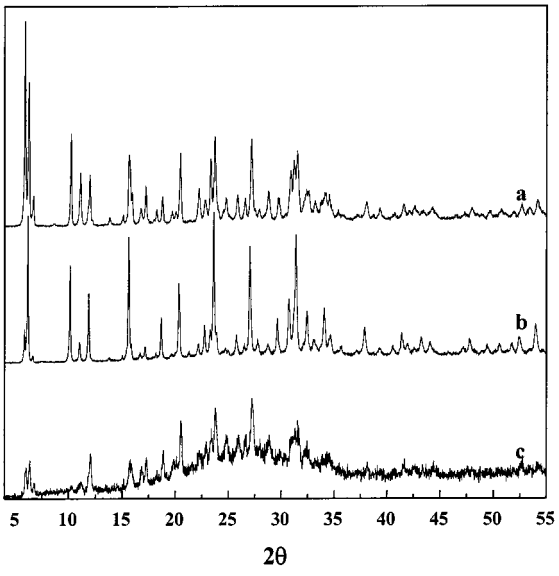

Figure 2. Powder X-ray diffraction patterns of calcined (a) EMT support crystals, (b) sample FauEmt-1a and (c) sample FauEmt-3a

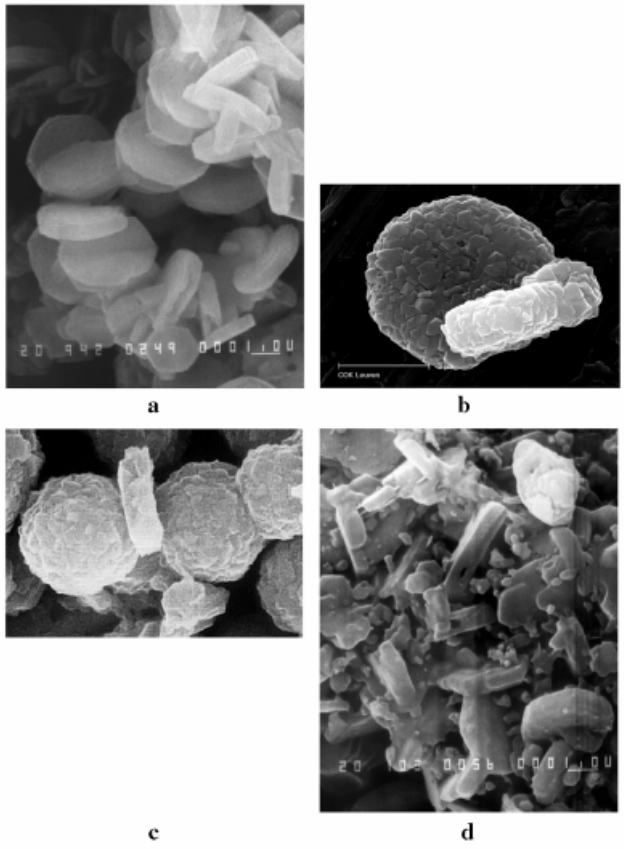

Figure 3. SEM pictures of (a) EMT support crystals, (b, c) sample FauEmt-1a, and (d) sample FauEmt-3a

In the second step, the EMT support crystals were added to a synthesis gel for the crystallization of a FAU phase, which optionally contained crown-ether molecules. Different experiments were conducted in order to explore the influence of the molar composition of the synthesis gel, the amount of EMT support crystals added, the pretreatment of the support crystals, the aging and the crystallization time (Table 1). The products obtained were characterized using powder X-ray diffraction (XRD) and scanning electron microscopy (SEM) (Table 1). The sample notation refers to the crystallographic nature of both phases (Fau for cubic and Emt for hexagonal faujasite). The Arabic number following the hyphen refers to a specific synthesis gel composition, whereas the final letter points to a specific set of synthesis parameters.

Influence of the Molar Composition of the FAU Synthesis Gel

In the first set of experiments (No. 1−5, Table 1), an amount of the synthesized EMT support crystals, typically 0.20 g per g of gel, was added to a freshly prepared FAU synthesis gel which optionally contained crown-ether molecules. The mixtures of gel and support crystals were immediately heated to the crystallization temperature of 373 K. Crystallization took 3 d.

In the literature, several aluminosilicate hydrogel compositions and inorganic bases have been proposed to pro-

Table 1. Molar composition of the FAU synthesis gel, the crystallization conditions and nature of the product obtained

No.	Sample	10 SiO_2; 1 Al_2O_3; x Na_2O; y 15-crown-5; z 18-crown-6; 135 H_2O					g support/g gel		Support pretreatment	t_{293K} + t_{373K}[a] [h]	Product[b]
		x	y	z	Na_2O/SiO_2	OH^-/SiO_2	wet	calcined			
1	FauEmt-1a	3.75	0.00	0.00	0.375	0.75	0.20	0.08	none	0 + 72	FAU-on-EMT
2	FauEmt-2a	3.75	0.00	0.97	0.375	0.75	0.21	0.08	none	0 + 72	FAU-on-EMT
3	FauEmt-3a	2.40	0.97	0.00	0.240	0.48	0.21	0.09	none	0 + 72	EMT + amorphous
4	FauEmt-4a	3.75	0.97	0.00	0.375	0.75	0.20	0.09	none	0 + 72	FAU-on-EMT
5	FauEmt-5a	3.40	0.97	0.00	0.340	0.48	0.21	0.08	none	0 + 72	FAU-on-EMT
6	FauEmt-1b	3.75	0.00	0.00	0.375	0.75	0.41	0.17	none	0 + 72	FAU-on-EMT
7	FauEmt-1c	3.75	0.00	0.00	0.375	0.75	0.59	0.25	none	0 + 72	FAU-on-EMT
8	FauEmt-1d	3.75	0.00	0.00	0.375	0.75	0.10	0.04	none	0 + 72	FAU-on-EMT + FAU
9	FauEmt-2b	3.75	0.00	0.97	0.375	0.75	0.40	0.16	none	0 + 72	FAU-on-EMT
10	FauEmt-2c	3.75	0.00	0.97	0.375	0.75	0.59	0.24	none	0 + 72	FAU-on-EMT
11	FauEmt-2d	3.75	0.00	0.97	0.375	0.75	0.20	0.07	washing	0 + 72	FAU-on-EMT + FAU
12	FauEmt-2e	3.75	0.00	0.97	0.375	0.75	N.D.[c]	0.07	washing, drying and calcining	0 + 72	FAU-on-EMT + FAU
13	FauEmt-2f	3.75	0.00	0.97	0.375	0.75	0.40	0.15	none	0 + 4	EMT + amorphous
14	FauEmt-2g	3.75	0.00	0.97	0.375	0.75	0.40	0.15	none	0 + 8	EMT + amorphous
15	FauEmt-2h	3.75	0.00	0.97	0.375	0.75	0.40	0.15	none	0 + 12	EMT + amorphous
16	FauEmt-2i	3.75	0.00	0.97	0.375	0.75	0.40	0.15	none	0 + 16	EMT + amorphous
17	FauEmt-2j	3.75	0.00	0.97	0.375	0.75	0.40	0.15	none	0 + 20	FAU-on-EMT + amorphous
18	FauEmt-2k	3.75	0.00	0.97	0.375	0.75	0.40	0.15	none	0 + 24	FAU-on-EMT
19	FauEmt-2l	3.75	0.00	0.97	0.375	0.75	0.40	0.15	none	0 + 48	FAU-on-EMT
20	FauEmt-2m	3.75	0.00	0.97	0.375	0.75	0.40	0.15	none	0 + 72	FAU-on-EMT
21	FauEmt-2n	3.75	0.00	0.97	0.375	0.75	0.40	0.15	none	0 + 96	FAU-on-EMT
22	FauEmt-2o	3.75	0.00	0.97	0.375	0.75	0.40	0.15	none	0 + 120	FAU-on-EMT
23	FauEmt-3b	2.40	0.97	0.00	0.240	0.48	0.21	0.09	none	0 + 144	EMT + amorphous
24	FauEmt-3c	2.40	0.97	0.00	0.240	0.48	0.24	0.09	none	3 + 72	FAU-on-EMT + FAU

[a] t_{293K} = aging time; t_{373K} = crystallization time. – [b] According to XRD and SEM. – [c] N.D. = not determined.

duce FAU phases under hydrothermal conditions.[15] It is recognized that the alkalinity of the hydrogel, expressed as the OH^-/SiO_2 ratio, is a crucial parameter. Low alkalinities substantially decrease the nucleation, as well as the crystallization rate, yielding poorly crystalline FAU materials. A very alkaline inorganic gel with a Na_2O/SiO_2 ratio of 0.375 was used in experiment No. 1 (sample FauEmt-1a, Table 1). According to XRD (Figure 2, b), the product contained a considerable amount of FAU, as well as EMT. Since the diffraction lines of the cubic FAU phase coincide with the lines of the hexagonal EMT phase, the detection of FAU was based on the relative intensities of lines belonging to the hexagonal phase alone and of common reflections of the cubic and the hexagonal phase. SEM pictures (Figure 3, b) revealed that a layer consisting of small crystals, some of which had an octahedral shape, covered all faces of the hexagonal platelets. This morphology indicates that the FAU zeolite has nucleated and grown on all faces of the original hexagonal-platelet EMT support crystals, thus yielding a polycrystalline film. As the support crystals were no longer visible, the FAU film was considered to be continuous. The morphology of the overgrowth material further suggests that all FAU crystallites are oriented with one of their {111} planes parallel to the {0001} planes of the EMT support, classifying this FAU-on-EMT overgrowth material as an epitaxial intergrowth. Besides the EMT support crystals being coated with an oriented layer of FAU crystallites, a small number of roughly spherical particles with irregular surfaces were also observed (Figure 3, c). This particular EMT support originally contained 19 wt-% of FAU, part of it being present as isolated FAU crystals with octahedral morphology. Octahedral particles were no longer present in the overgrowth sample, indicating that the octahedral FAU crystals also became overgrown by a layer of FAU crystallites, resulting in these roughly spherical particles. The absence of octahedral crystals also indicated that homogeneous nucleation and initial breeding, both yielding an undesirable population of isolated FAU crystals, were suppressed.

The EMT-type zeolite can be synthesized from aluminosilicate hydrogels doped with 18-crown-6 ether and characterized by an Na_2O/SiO_2 ratio of 0.24.[23] An FAU phase can be obtained from a similar gel provided the sodium content is increased.[21] Inoculation of an 18-crown-6 ether containing FAU synthesis gel characterized by a high Na_2O/SiO_2 ratio of 0.375 with EMT support crystals (sample FauEmt-2a, Table 1), resulted in the formation of an epitaxial FAU-on-EMT overgrowth material.[20]

According to the original synthesis recipe of Delprato et al.,[23] the FAU structure type can crystallize from an aluminosilicate hydrogel containing 15-crown-5-ether, with an Na_2O/SiO_2 ratio of 0.24. The XRD pattern of the crystallization product obtained from such a gel inoculated with the synthesized EMT support crystals (sample FauEmt-3a, Table 1) is characterized by the presence of a broad amorphous background with maximum intensity around a 2θ value of 25° (Figure 2, c). The sharp diffraction lines correspond to those of the EMT support crystals added. SEM pictures (Figure 3, d) show intact support crystals embedded in an amorphous gel matrix. It is concluded that the overgrowth process did not take place in this system. An attempt was made to favor the overgrowth formation by increasing the Na_2O/SiO_2 ratio of the FAU synthesis gel from 0.24 to 0.375 (sample FauEmt-4a, Table 1). The crys-

tallization of FAU during the second step of the synthetic procedure was confirmed by XRD and SEM. Morphologically, sample FauEmt-4a was similar to sample FauEmt-1a and consisted of hexagonal-platelet EMT support crystals coated with a continuous layer of FAU crystallites. However, by increasing the amount of NaOH in the gel, both the sodium content, as well as the alkalinity were increased. In order to find out whether overgrowth formation was dependent on the sodium content or on the alkalinity, another experiment (No. 5) was performed in which the Na^+ content was increased at a constant OH^-/SiO_2 ratio (sample FauEmt-5a, Table 1). This was done by introducing part of the sodium as sodium aluminate. The product crystallized from such a gel was a FAU-on-EMT overgrowth material, similar to sample FauEmt-4a. Therefore, it is concluded that the sodium content of the gel, rather than the alkalinity, is the crucial parameter.

From experiments No. 1−5 (Table 1), it can be concluded that the synthesized EMT support crystals can be overgrown by a continuous, epitaxial layer of FAU crystallites using sodium aluminosilicate hydrogels, which optionally contained crown-ether molecules, provided the Na_2O/SiO_2 ratio of the gel is higher than or equal to 3.40. The crown-ether seemed to have no influence on the overgrowth morphology.

Influence of the Amount of Support Crystals Added

In the next set of experiments (No. 6−10, Table 1) different amounts of EMT support crystals were added in order to obtain samples with different degrees of overgrowth formation. The weight ratio of gel to support crystals was varied between 1.7:1 and 10:1, while keeping the other synthesis parameters constant, i.e. no aging of the synthesis gel and a crystallization time of 3 d.

The use of different amounts of support crystals allowed us to observe discrete stages in the process of overgrowth formation. Figure 4 (a−d) shows SEM pictures of samples for which decreasing quantities of EMT support crystals were used and illustrate the progress of the overgrowth formation. These pictures suggest that the secondary nucleation preference of the FAU phase decreases in the order, corners = edges > faces. This preference for corners and edges, representing the largest concentration of anchoring points, is observed both in the presence (sample FauEmt-2c, Figure 4, a), as well as in the absence of 18-crown-6 ether molecules (sample FauEmt-1c). At intermediate gel/support ratios, it can be seen that a rim of FAU crystallites progresses towards the center of the hexagonal faces (samples FauEmt-1b, Figure 4, b, and FauEmt-2b). When the weight ratio of the synthesized support crystals per gram of FAU synthesis gel is about 0.20, the EMT support crystals become completely covered with FAU crystallites. All of the FAU crystallites were oriented in the same way with respect to the support (samples FauEmt-2a, Figure 4, c, and FauEmt-1a). Further reduction of the amount of EMT support crystals (sample FauEmt-1d, Figure 4, d) resulted in the formation of roughly spherical FAU(18) crystals with an irregular surface, in addition to completely covering the hexagonal prisms. This indicates that, in this instance, the surface offered by the EMT support crystals is not large enough to suppress homogeneous nucleation from the FAU synthesis gel.

Influence of the Pretreatment of the Support Crystals

Thompson and co-workers[24,25] reported that handling seed crystals (washing, drying or calcining) prior to their addition to a synthesis gel always results in so-called initial breeding, hence yielding a new population of isolated crystals. The degree to which initial breeding occurs is dependent on the manner in which the seed crystals are pretreated. Since the two-step synthetic procedure, applied in this work, to produce overgrowth materials is similar to seeding, pretreatment of the support crystals was expected to be detrimental for the process of overgrowth formation.

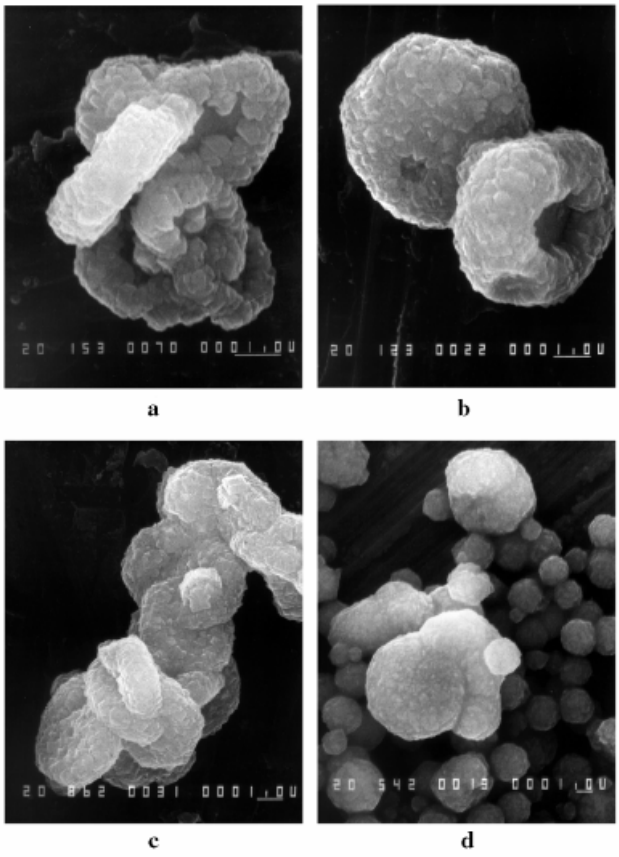

Figure 4. SEM pictures of samples (a) FauEmt-2c, (b) FauEmt-1b, (c) FauEmt-2a, and (d) FauEmt-1d

Two experiments (No. 11 and 12, Table 1) were conducted in which the EMT support crystals were first washed with deionized water until the pH value of the wash water reached 9 (sample FauEmt-2d, Table 1) or washed, dried, and calcined (sample FauEmt-2e, Table 1) before they were added to an FAU gel containing sodium and 18-crown-6 ether. In both cases, there was partial overgrowth with FAU crystallites (Figure 5, a−b). However, overgrowth formation was much less pronounced than in experiments without pretreatment of the support but with the same gel/support

ratio (sample FauEmt-2a, Figure 4, c). An undesirable population of isolated, roughly spherical FAU crystals with diameters of 1 to 2 μm, exhibiting irregular surfaces was also observed. This was most pronounced for sample FauEmt-2e (Figure 5, b). The initial breeding mechanism, favored by the drying and calcination, could have been responsible for the formation of these isolated FAU crystals.

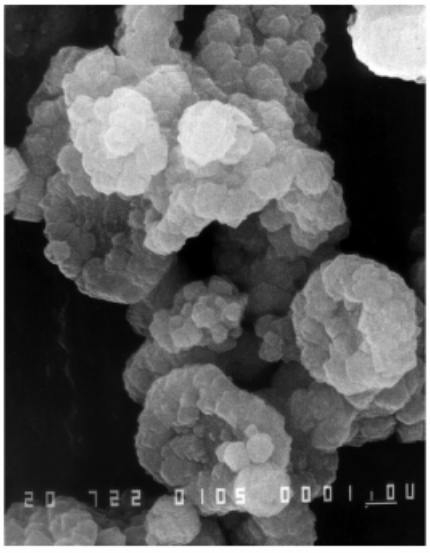

a

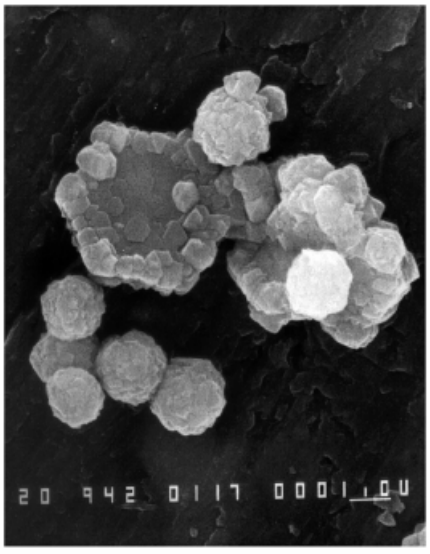

b

Figure 5. SEM pictures of samples (a) FauEmt-2d and (b) FauEmt-2e

Influence of the Aging and Crystallization Time

In all previous experiments the crystallization time was kept constant at 3 d. This length of time was long enough to obtain overgrowth materials from hydrogels with an Na_2O/SiO_2 ratio of 0.34 or 0.375. On the other hand, no crystallization took place from hydrogels with a reduced sodium content. Therefore, a new set of experiments (No. 13−24, Table 1) was conducted in order to investigate the influence of the aging and the crystallization time on the overgrowth process.

Ten overgrowth experiments (No. 13−22, Table 1), in which the synthesized EMT support crystals were added to an FAU synthesis gel containing sodium and 18-crown-6 ether, were performed using crystallization times from 4−120 h (samples FauEmt-2f to FauEmt-2o, Table 1). In the first 16 h of crystallization (samples FauEmt-2f to FauEmt-2i, Table 1), no FAU phase could be observed with XRD (Figure 6, a; sample FauEmt-2i). SEM pictures (Figure 7, a) show EMT support crystals embedded in an amorphous gel matrix. After 20 h of crystallization (sample FauEmt-2j, Table 1), some EMT support crystals were decorated at their edges with small FAU crystallites. A residual amorphous phase was also observed (Figure 7, b). Four hours later (sample FauEmt-2k, Table 1), the amorphous material was no longer present and all EMT support crystals were partially coated with small FAU crystallites (Figure 6, b and Figure 7, c). The use of longer crystallization times did not alter the morphology of the overgrowth product. In this series of experiments (No. 13−22, Table 1), it was clearly shown that the growth of the FAU phase starts at the corners and edges of the hexagonal-platelet EMT support crystals. An FAU crystallization front progresses subsequently from the edges towards the center of the hexagon. The same sequence was encountered in the set of experiments in which the amount of support crystals added was varied, while the crystallization time was kept constant (No. 6−10, Figure 4, a−d).

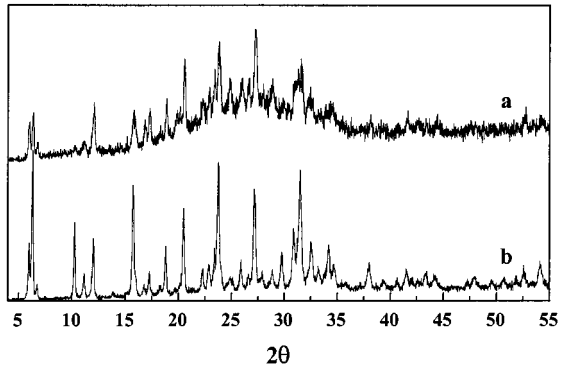

Figure 6. Powder X-ray diffraction patterns of calcined samples (a) FauEmt-2i and (b) FauEmt-2k

In order to evaluate whether a longer crystallization time would be necessary for overgrowth formation in the systems of the present study with a low sodium content, the crystallization time of experiment FauEmt-3a (Table 1) was prolonged from 3 to 6 d (sample FauEmt-3b, Table 1). This did not result in the transformation of the amorphous synthesis gel into a crystalline product, thereby indicating that crystallization of an FAU phase in the presence of support crystals is not possible from freshly prepared synthesis gels characterized by an Na_2O/SiO_2 ratio of 0.24.

Aging the low alkaline FAU synthesis gel containing 15-crown-5 ether for 3 d at room temperature before the EMT support crystals were added to it (sample FauEmt-3c,

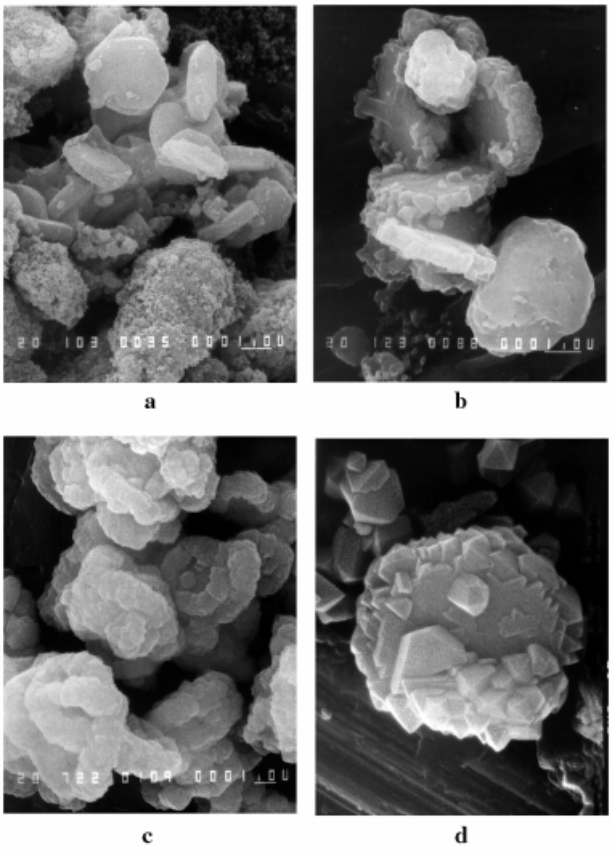

Figure 7. SEM pictures of samples (a) FauEmt-2i, (b) FauEmt-2j, (c) FauEmt-2k, and (d) FauEmt-3c

Table 1), resulted in the formation of an epitaxial FAU-on-EMT overgrowth material. However, the EMT support crystals were not completely covered by FAU crystallites, and a new population of isolated FAU crystals with octahedral morphology was also obtained (Figure 7, d). In this case, the hydrogel was supersaturated, giving rise to homogeneous nucleation of an FAU phase along with secondary nucleation of FAU crystallites on the surface of the EMT support crystals.

FAU/EMT Quantification

The amount of FAU and EMT in the FAU-on-EMT overgrowth materials was estimated with XRD by using a calibration curve. For this purpose, two calcined overgrowth samples were quantified using the Rietveld refinement technique.[26] These reference samples, FauEmt-2a and FauEmt-2c, contained 80 and 51 wt-% of the FAU phase, respectively (Table 2). Most of the FAU-on-EMT overgrowth materials obtained in this study have FAU contents in this range. The reference zeolite powders were physically mixed in five different proportions and the XRD patterns of these mixtures were recorded. The peak intensities of four selected diffraction lines belonging to the EMT phase alone (Table 3) and of five common reflections of the FAU and the EMT phase (Table 3), were obtained by integration and summation. The EMT content (in wt-%) was correlated to the intensity ratio of these sums ($I_{EMT}/I_{EMT+FAU}$). The experimental data points were fitted with the parabolic relation given in Equation (1).

$$\text{EMT (wt-\%)} = 68 \times (I_{EMT}/I_{EMT+FAU})^2 + 108 \times I_{EMT}/I_{EMT+FAU} + 1 \quad (1)$$

The FAU and EMT contents of some selected overgrowth samples and of the EMT support crystals were derived from XRD using Equation (1), and reported as absolute weights in Table 2. It is clear from this table that the weight of EMT in the overgrowth product was systematically lower than the weight of the EMT phase in the support crystals added. This suggests that part of the EMT phase dissolved during the overgrowth process. The dissolution behavior of the EMT crystals was therefore studied in more detail.

Dissolution of the Support Crystals

It is known that in strong mineral bases, siliceous frameworks are more soluble than aluminosilicate frameworks. The reason for this is the more facile base-catalyzed hydrolysis of silyloxy bridges, whereas the tetrahedral aluminum centers in an aluminosilicate lattice are relatively inert to hydroxide attack due to the negative framework charge associated with these centers.[27−29]

In order to obtain some information about the dissolution behavior of the EMT support crystals in basic environments, such as in the gels used for the formation of FAU-on-EMT overgrowth materials, two experiments were conducted. In the first experiment (EMT-A), a FAU synthesis gel containing sodium and 18-crown-6 ether was aged for 3 d at room temperature. The solid phase was separated from the liquid phase by ultra-centrifugation at 17 000 rpm for 2 h. A mass of 5 g of the synthesized EMT crystals was added to 25 mL of this liquid. This particular batch of EMT crystals did not contain any FAU, according to XRD. In the EMT-B experiment, 5 g of the same EMT crystals was suspended in 25 mL of a 2.5 M NaOH solution. The resulting slurries were transferred into PTFE-lined stainless-steel autoclaves, which were kept at 373 K for 3 d. The products were recovered by vacuum filtration, washed with deionized water and dried at 333 K. Calcination was done in a muffle furnace at 823 K for 20 h.

By comparing the weight of the product with that of the EMT crystals added (on a calcined basis), it was found that 52 and 68 wt-% of EMT had dissolved in experiments A and B, respectively. The XRD pattern of EMT-A (Figure 8, a) corresponded to that of EMT. The diffraction lines belonging to the EMT structure type were somewhat less intense than in the original EMT sample (Figure 2, a). In sample EMT-B, XRD confirmed the formation of zeolite P, as well as residual EMT (Figure 8, b). The formation of zeolite P is often observed in Ostwald successive phase transformations of faujasite type zeolites which are left in their mother liquor for some time.[30,31]

The EMT-A and EMT-B samples were examined using SEM (Figure 9, a−b) and HRTEM (Figure 10, a−c). All EMT-A crystals showed dissolution to a similar extent. The dissolution caused the formation of pits over the entire sur-

Table 2. FAU/EMT quantification

Sample	Support EMT [g]	Support FAU[a] [g]	Product EMT [g]	Product FAU [g]	EMT dissolved [g]	FAU dissolved[b] [g]	Support dissolved (%)	Gel [g]	Yield FAU layer [g/g gel]	Support dissolved [g/g gel]
FauEmt-1a	1.93	0.45	1.47	4.20	0.46	0.11	24	28.81	0.13	0.02
FauEmt-2a	1.99	0.44	1.08[c]	4.33[c]	0.91	0.20	46	29.15	0.14	0.04
FauEmt-4ab	2.73	0.00	1.45	4.61	1.28	0.00	47	32.91	0.14	0.04
FauEmt-1b	3.58	0.84	2.83	4.43	0.75	0.18	21	30.82	0.12	0.03
FauEmt-1c	4.66	1.09	4.28	3.50	0.38	0.09	8	23.23	0.11	0.02
FauEmt-2b	3.27	0.72	2.25	3.66	1.02	0.22	31	24.84	0.13	0.05
FauEmt-2c	4.41	0.97	3.11[c]	3.23[c]	1.30	0.29	29	22.41	0.11	0.07
FauEmt-2k	3.50	1.23	3.25	4.68	0.25	0.09	7	32.14	0.11	0.01
FauEmt-2l	2.81	0.99	2.58	3.71	0.23	0.08	8	25.80	0.11	0.01
FauEmt-2m	2.70	0.95	2.51	3.61	0.19	0.07	7	24.82	0.11	0.01
FauEmt-2n	2.73	0.96	2.41	3.62	0.32	0.11	12	25.09	0.11	0.02
FauEmt-2o	2.71	0.95	2.19	3.73	0.52	0.18	19	24.82	0.12	0.03

[a] FAU impurity content of the EMT support samples. – [b] Assuming that the FAU impurity dissolved in the same proportion as the EMT phase. – [c] According to Rietveld refinement.

Table 3. Diffraction angles of the XRD lines used to estimate the amount of FAU and EMT in the FAU-on-EMT overgrowth samples

2θ [°]	Phase	2θ [°]	Phase	2θ [°]	Phase
10.1	FAU+EMT	15.6	FAU+EMT	25.7	FAU+EMT
11.0	EMT	17.2	EMT	28.7	EMT
11.9	FAU+EMT	22.2	EMT	29.5	FAU+EMT

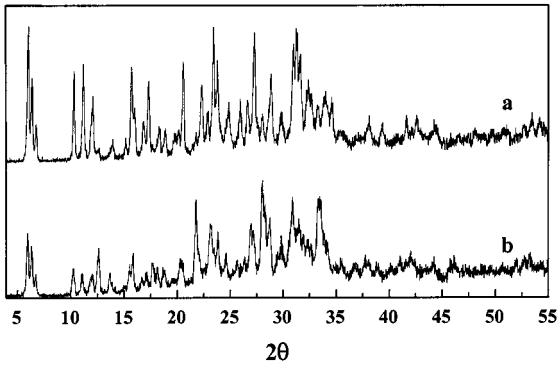

Figure 8. Powder X-ray diffraction patterns of calcined samples (a) EMT-A and (b) EMT-B

face of the crystals (Figure 9, a, and Figure 10, a). The higher degree of dissolution of sample EMT-B relative to that of EMT-A was seen in the SEM and HRTEM pictures (Figure 9, b, and Figure 10, b–c). Many EMT-B crystals had decomposed into smaller fragments. Some particles retained their initial hexagonal-platelet morphology and were more strongly dissolved at the center than at the outer rim. The larger particles with smooth surfaces, which could be observed in sample EMT-B with the SEM (Figure 10, b), are most likely zeolite P crystals. It is known from the literature that the Si and Al positioning in the EMT crystals synthesized with 18-crown-6 ether is not uniform.[32] The 12-MRs circumscribing the hyperchannels running in the direction perpendicular to the hexagonal faces are more siliceous (Si/Al ratio of 5.7) than the 12-MRs delineating the channels running parallel to the hexagonal faces and connecting the hypocages with the hyperchannels. This could explain why the dissolution was more pronounced in the direction of the hyperchannels and why the outer rim, exposing more Al-rich 12-MRs, is more resistant to dissolution by the base.

The Si/Al ratios of the partially dissolved EMT crystals of samples EMT-A and EMT-B, as determined with nano-EDAX, varied between 2.2 and 1.3, depending on the degree of dissolution. These low values indicate that EMT samples recovered after base-treatment are significantly enriched with aluminum, confirming the selective removal of SiO_2 in the alkaline solutions. Phase-pure EMT crystals with such low Si/Al ratios have not been reported previously. The low Si/Al ratios imply that silicon has been substituted by aluminum in the residual EMT framework. Reinsertion of aluminum into faujasite type zeolites is possible provided a concentrated solution of a strong base is present.[33]

The parent EMT sample, and the EMT-A and EMT-B samples were characterized with nitrogen physisorption. The external surface area, the micropore volume and the micropore diameter calculated from the adsorption branch of the isotherms are given in Table 4. All isotherms are of type I revealing the presence of a microporous solid. The micropore volumes of EMT-A and EMT-B were 0.26 and 0.14 mL/g (Table 4), respectively. In both samples, there was very little nitrogen uptake in the P/P_0 range of 0.1 to 0.8, indicating the absence of capillary condensation in small mesopores. The nitrogen uptake at P/P_0 values exceeding 0.8 is indicative of the presence of large mesopores, typically present in the interstitial voids between particles. The generation of 28 and 37 m^2/g of external surface area in EMT-A and EMT-B, respectively, compared with 4 m^2/g in the original EMT sample, can be explained by an increase of the surface roughness (sample EMT-A) and a decrease in the particle size (sample EMT-B). It is concluded that the dissolution process did not generate mesopores in the crystals, suggesting that the dissolution occurred through the removal of framework fragments in a block-wise manner. The micropore diameter determined using the Horvath–Kawazoe approach increased from 0.64 to

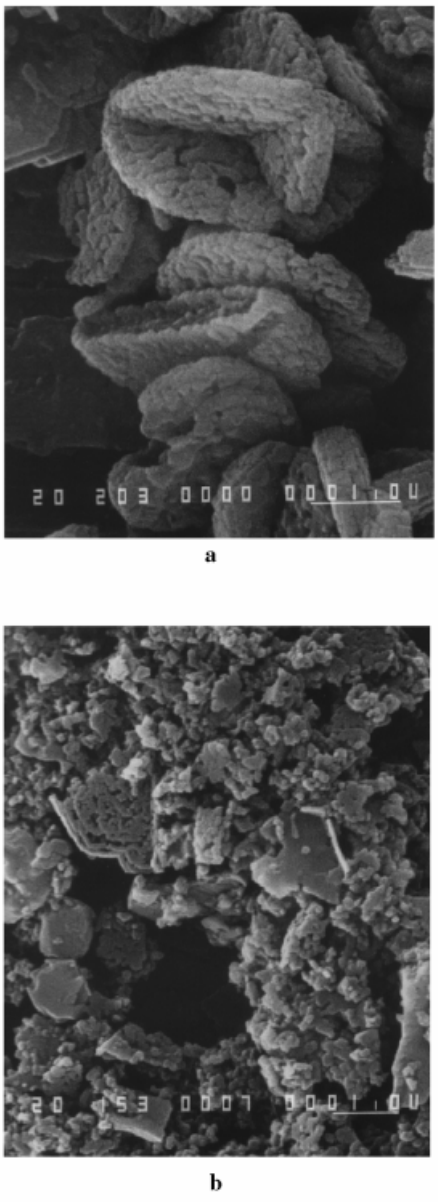

Figure 9. SEM pictures of samples (a) EMT-A and (b) EMT-B

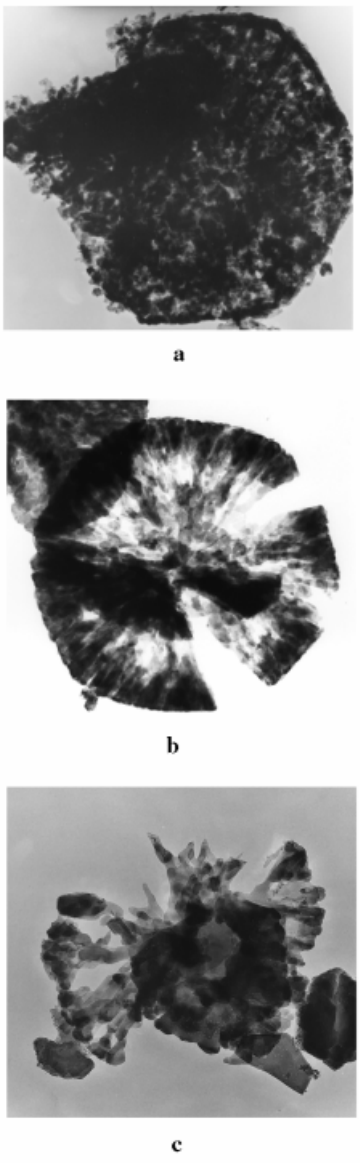

Figure 10. HRTEM pictures of samples (a) EMT-A and (b, c) EMT-B

0.65 nm for sample EMT-A. Such an increase is in agreement with the enrichment of the framework with aluminum.

Characterization of Both the FAU and the EMT Phase

In the previous section, it was shown how EMT crystals partially dissolve in the alkaline conditions of synthesis gels. In the two-step synthetic procedure for overgrowth formation, the material balance suggested that a significant part of the EMT crystals dissolved (Table 2). In this section, the FAU-on-EMT overgrowth materials were characterized in more detail in order to find out the extent to which the EMT support crystals were altered during the overgrowth process.

FAU-on-EMT overgrowth samples synthesized with three types of FAU gels and with different degrees of overgrowth formation were characterized using nitrogen physisorption (Table 5). The adsorption isotherms of the FAU-on-EMT overgrowth materials were similar to those of the EMT support crystals. The absence of nitrogen uptake in the P/P_0 range of 0.1 to 0.8 was indicative of the absence of mesopores inside the particles, and thus for the continuous nature of the FAU film. The micropore volume of all samples was between 0.29 and 0.32 mL/g (Table 5), as is expected for FAU and EMT phases of high quality.[21] The high micropore volume also indicated that the micropores of both the FAU layer, as well as the EMT support were accessible to nitrogen. For all overgrowth samples investigated, the specific external surface area was below 10 m^2/g (Table 5), this value being only a little higher than the specific external surface area of the support crystals (4 m^2/g). The external surface area increased proportionally with the

Table 4. External surface area, micropore volume and micropore diameter of calcined EMT samples, before and after base-treatment, as determined from their N_2 adsorption isotherms

Sample	External surface area [m^2/g]	Micropore volume [mL/g]	Micropore diameter [nm]
EMT	4	0.31	0.64
EMT-A	28	0.26	0.65
EMT-B	37	0.14	–[a]

[a] Determination not reliable.

Table 5. External surface area, micropore volume and micropore diameter of selected overgrowth samples (calcined), as determined from their N_2 adsorption isotherms

Sample	FAU (wt-%)	External surface area [m^2/g]	Micropore volume [mL/g]	Micropore diameter [nm]
FauEmt-1a	74	9	0.29	0.67
FauEmt-2a	80	8	0.30	0.68
FauEmt-4a	76	9	0.29	0.65
FauEmt-1b	61	7	0.29	0.66
FauEmt-1c	45	5	0.30	0.65
FauEmt-2b	51	4	0.32	0.65
FauEmt-2c	62	7	0.31	0.67

FAU content of the overgrowth samples (Table 5). Therefore, the specific external surface area could be attributed to the FAU crystallites exposing more external surface area than the EMT support crystals, owing to their smaller size. The micropore diameters derived from the nitrogen adsorption isotherms using the Horvath–Kawazoe approach were in the range of 0.65 to 0.68 nm, and in agreement with the presence of 12-MRs. The micropore diameters showed a systematic increase with increasing FAU content (Table 5). Nitrogen physisorption showed that the EMT core of the FAU-on-EMT overgrowth materials was rather intact. Furthermore, it showed that the significant alterations, observed in the base-treated EMT-A and EMT-B samples, did not take place in the EMT crystals, which were overgrown by a layer of FAU crystallites. It seems that of all the EMT support crystals added, a fraction became overgrown, whereas the rest dissolved completely. The absence of particles resembling the partially dissolved EMT-A and EMT-B samples in the SEM images of all FAU-on-EMT overgrowth materials supports this hypothesis.

The distribution of Si(*n*Al) environments in the EMT support crystals and in some selected FAU-on-EMT overgrowth samples was determined with ^{29}Si MAS NMR. The ^{29}Si MAS NMR spectrum of the EMT support crystals is shown in Figure 11, a. This spectrum can be simulated by five Gaussian peaks with the maxima positioned at chemical shift values of $\delta = -105.80$, assigned to Si(0Al); at $\delta = -101.21$ and -99.69, both assigned to Si(1Al); at $\delta = -94.06$, assigned to Si(2Al); and at $\delta = -89.13$, assigned to Si(3Al). A signal for Si(4Al) environments expected at $\delta \approx -84$ could not be distinguished from the background. From this simulation, the framework Si/Al ratio of the support crystals was calculated to be 3.4. The ^{29}Si MAS NMR spectra of FAU-on-EMT overgrowth samples with FAU content between 74 and 80 wt-%, and prepared using three types of FAU synthesis gels (samples FauEmt-1a, FauEmt-2a, and FauEmt-4a) are shown in Figure 11 (b–d). The spectra were simulated with Gaussian curves, as explained for the support crystals. An additional small line at $\delta = -84$, representing Si(4Al) environments, was present. The Si(*n*Al) distributions and the framework Si/Al ratios of the support crystals and the overgrowth samples are presented in Table 6. The Si(*n*Al) distributions are similar amongst the selected overgrowth materials, but significantly different from that of the support crystals. The population of silicon in the Si(0Al) and Si(1Al) sites is lower, and that in the Si(2Al) and Si(3Al) sites is higher than in the support (Table 6). The framework Si/Al ratio of the overgrowth sample prepared from an inorganic aluminosilicate hydrogel was 2.7 (sample FauEmt-1a, Table 6). In the presence of crown-ether molecules, a slightly higher Si/Al ratio of 2.9 was obtained (samples FauEmt-2a and FauEmt-4a, Table 6).

In another series of samples, the degree of overgrowth formation was varied between 51 and 80 wt-% by decreasing the amount of support crystals added to an FAU synthesis gel containing sodium and 18-crown-6 ether (samples FauEmt-2c to FauEmt-2a). The Si(*n*Al) distributions of these overgrowth samples are also given in Table 6. It was observed that when the FAU content increased, the concentration of Si(4Al), Si(3Al), and Si(2Al) environments increased, whereas the population of silicon in the Si(1Al) and the Si(0Al) sites decreased. This resulted in a decreasing framework Si/Al ratio with increasing FAU content from 3.1 for an FAU content of 51 wt-% to 2.9 for an FAU content of 80 wt-% (Table 6). The increase in the micropore diameter with increasing FAU content of the FAU-on-EMT overgrowth materials (Table 5) can be explained by the en-

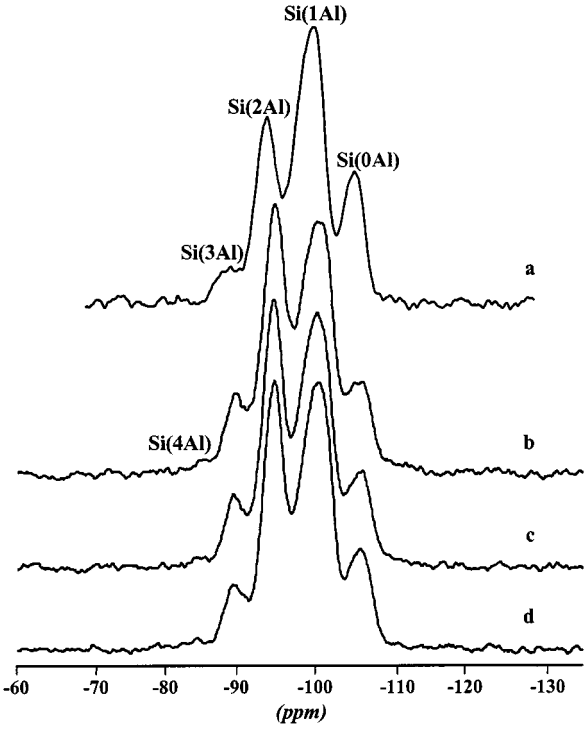

Figure 11. ^{29}Si MAS NMR spectra of: (a) calcined EMT support crystals, and calcined overgrowth samples (b) FauEmt-1a, (c) FauEmt-2a, and (d) FauEmt-4a

represent the weight fractions of support and FAU layer in the FAU-on-EMT overgrowth products, respectively.

$$Si/Al_{FAUlayer} = [Si/Al_{overgrowth} - Si/Al_{support} \times fraction_{support}]/fraction_{FAUlayer} \quad (2)$$

The $Si/Al_{FAUlayer}$ ratios of samples prepared using different FAU gel compositions (samples FauEmt-1a, FauEmt-2a and FauEmt-4a) are listed in Table 6. The FAU layer grown in the presence of crown-ether molecules was characterized by a Si/Al ratio of 2.7 (samples FauEmt-2a and FauEmt-4a). This value is in good agreement with the Si/Al ratio of FAU crystallized homogeneously from such gels in the absence of support crystals.[21] In the absence of crown-ether molecules, a value of 2.3 was obtained (sample FauEmt-1a). This Si/Al ratio is in the expected range for NaY zeolites synthesized from such inorganic gels. The series of samples with different degree of overgrowth formation (samples FauEmt-2c to FauEmt-2a, Table 6) displayed $Si/Al_{FAUlayer}$ ratios from 2.5 for FAU crystallites growing only at the corners and edges of the support crystals (sample FauEmt-2c), to 2.7 for a continuous film of FAU crystallites (sample FauEmt-2a).

In the sample FauEmt-2a, the EMT support crystals were completely covered by FAU crystallites. Therefore, the Si/Al ratio of the FAU layer could also be determined by X-ray photoelectron spectroscopy. The Si/Al ratio according to XPS, and representative of the external surface of the FAU crystallites was 2.8. The agreement with the NMR spectroscopic data which showed a Si/Al ratio of 2.7 was excellent. This provides a strong argument for the validity of the assumptions made in the exploitation of the NMR spectroscopic data with Equation (2), in general, and of the assumed intactness of the EMT support crystals, in particular. According to XPS, the Na/Al stoichiometry was close to unity (Na/Al = 0.97), confirming that the charges originating from the incorporation of Al atoms in the framework were balanced by Na cations.

Table 6. Framework Si/Al ratios and percentage distribution of the different Si(*n*Al) environments as determined by ^{29}Si MAS NMR spectroscopy

Sample	FAU (wt-%)	Si(4Al)	Si(3Al)	Si(2Al)	Si(1Al)	Si(0Al)	Si/Al overgrowth	Si/Al FAU layer
Support	0−19	0	5	25	52	18	3.4	–
FauEmt-1a	74	2	9	34	43	12	2.7	2.4
FauEmt-2a	80	1	9	32	44	14	2.9	2.7
FauEmt-4a	76	1	8	31	47	13	2.9	2.7
FauEmt-2b	62	1	7	31	46	15	3.0	2.6
FauEmt-2c	51	0	7	28	49	16	3.1	2.5

richment of the sample with aluminum through the FAU phase. Indeed, aluminum enrichment is known to give rise to an expansion of the unit cell.

For the calculation of the Si/Al ratio of the FAU layer based on the ^{29}Si MAS NMR spectroscopic data, the following assumptions were made. It was assumed that a number of EMT support crystals added did not become covered with FAU crystallites, but dissolved completely. Furthermore, it was assumed that there was neither dissolution, nor alteration of the Si/Al ratio of the EMT support crystals, which became overgrown by FAU crystallites. An additional complication in the calculation was the presence of FAU in the EMT support. Part of the FAU impurity was present as a polytypical intergrowth with EMT, the rest as isolated crystals with octahedral shapes. It was assumed that the FAU impurity had the same Si/Al ratio as the EMT phase, and that it dissolved or became overgrown in the same proportion as the EMT support crystals. These assumptions led to the expression of Equation (2) for the Si/Al ratio of the FAU layer, in which $fraction_{support}$ and $fraction_{FAUlayer}$

It was possible to determine the Si/Al ratio of individual FAU crystallites of sample FauEmt-2a by using electron nanoprobe analysis (nano-EDAX). It was found that the FAU crystallites grown at the corners and edges of the EMT support crystals had a Si/Al ratio of 2.5, whereas the FAU crystallites grown in the center of the basal $\{0001\}_{EMT}$ planes had an Si/Al ratio of 2.8. There were many more crystallites at faces than at corners and edges, thus explaining why the overall Si/Al ratio of the FAU layer, deter-

mined by NMR spectroscopy and XPS, corresponded to that on the $\{0001\}_{EMT}$ planes. The FAU crystallites start growing at the corners and edges of the EMT support crystals and hence the first FAU crystallites formed are richer in aluminum than the crystallites formed at a later stage. In a sample in which overgrowth formation was limited to the corners and edges of the support by increasing the amount of support crystals added, the Si/Al ratio was indeed 2.5 (sample FauEmt-2c, Table 6). The increase in the Si/Al ratio of the FAU crystallites during the overgrowth process may be explained by the decrease in the pH during the crystallization of the faujasite type zeolite in the presence of crown ethers.[23] Depletion of aluminum in the synthesis gel might be another reason for this behavior.

The EMT support crystals were prepared in the presence of 18-crown-6 ether, whereas the synthesis gel for the FAU layer optionally contained crown-ether molecules. The incorporation of crown-ether molecules in the support crystals and some selected overgrowth materials was studied with thermogravimetric-differential thermal analysis (TG-DTA). Typical TGA/DTA profiles of the EMT support crystals and a representative FAU-on-EMT overgrowth material, recorded under He/O_2 are given in Figure 12. The weight-losses observed during heating can be attributed to the endothermic desorption of water, followed by a multiple-step exothermic decomposition of crown-ether molecules.[34] On the basis of this last weight-loss, the crown-ether content of the support crystals, as well as of some selected overgrowth materials were calculated and expressed as the number of crown-ether molecules per 192 T-atoms, representing 8 large cages in both the FAU and the EMT structure (Table 7). The number of crown-ether molecules in the EMT support crystals corresponded to approximately 9.5 molecules per 8 cages (Table 7). The presence of an excess of crown-ether molecules relative to the number of cages is in agreement with previous data.[21] Assuming that the crown-ether content of the support crystals did not change during the overgrowth process, the amount of crown-ether molecules per 192 T-atoms in the FAU layer ($CE_{FAUlayer}$) could be related to the crown-ether content of the overgrowth ($CE_{overgrowth}$) according to Equation (3).

$$CE_{FAUlayer} = [CE_{overgrowth} - CE_{support} \times fraction_{support}]/fraction_{FAUlayer} \quad (3)$$

These numbers are given in Table 7. The FAU crystallites synthesized in the presence of crown-ether molecules (samples FauEmt-2a to FauEmt-5a) contain approximately one crown-ether molecule per cage, or eight per 192 T-atoms. Even without intentional addition of crown-ether molecules to the FAU synthesis gel, the FAU layer occluded some crown-ether molecules (samples FauEmt-1a to FauEmt-1c, Table 7). Comparison of the amount of crown-ether molecules in the inorganic FAU layer with the amount liberated by partial dissolution of the EMT support crystals showed that the dissolution process alone could not account for all crown-ether molecules incorporated in the FAU layer. Additional crown-ether molecules could be provided by the mother liquor surrounding the support crystals, or as molecules that are physisorbed on the external surface of the support crystals. These phenomena were more pronounced when more support crystals were used, thus resulting in an enhanced incorporation of crown-ether molecules in the FAU layer (Table 7).

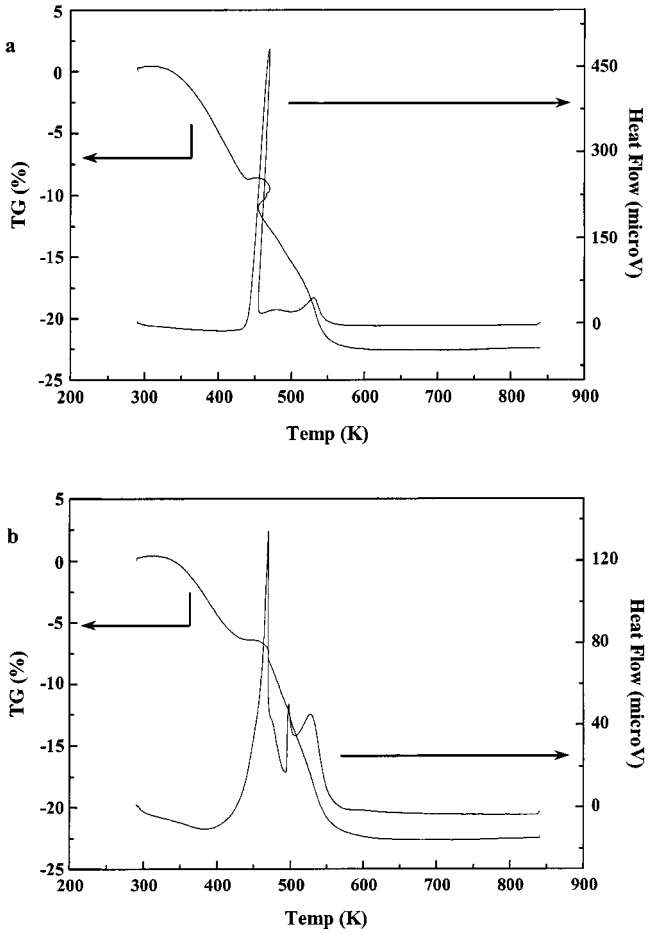

Figure 12. TGA/DTA profiles recorded under He/O_2 of (a) EMT support crystals and (b) sample FauEmt-2a; the oblique nature of the largest heat flow peak and the concomitant bump in the TG curve are due to the higher temperatures caused by the exothermic crown-ether decomposition[34]

Table 7. Crown-ether content of the support crystals, some FAU-on-EMT overgrowth materials and the FAU layer, as determined with TG-DTA

Sample	CE/192 T-atoms		
	support	overgrowth	FAU layer
FauEmt-2a	10.0	8.6	8.2
FauEmt-2b	10.0	8.9	7.9
FauEmt-2c	10.0	9.1	7.9
FauEmt-4a	9.1	8.3[a]–9.9[b]	8.0[a]–10.2[b]
FauEmt-5a	9.5	9.1[a]–10.9[b]	8.9[a]–11.4[b]
FauEmt-1a	9.8	4.9	2.6
FauEmt-1b	9.8	6.5	3.4
FauEmt-1c	9.8	7.9	3.8

[a] Assuming 18-crown-6 is exclusively present. – [b] Assuming 15-crown-5 is exclusively present.

Overgrowth Synthesis Efficiency

In this section, two aspects of synthesis efficiency are discussed, namely the FAU yield with respect to the gel and

the EMT losses due to partial dissolution of the support crystals. Comparison of the weight of EMT in the overgrowth product with the weight of EMT support crystals added, showed that part of the EMT phase dissolved (Table 2). In the calculations in the previous section, it was assumed that the FAU impurity phase of the EMT support crystals dissolved in the same proportion as the EMT phase. This assumption led to reasonable interpretations of the FAU and EMT contents of the FAU-on-EMT overgrowth materials and of the framework Si/Al ratios of the respective phases.

The assumed weights of FAU impurities dissolved during the overgrowth process are given in Table 2. The FAU yield with respect to the gel was obtained by subtracting the weight of the FAU impurity phase which did not dissolve from the weight of FAU in the final product, and dividing this value by the weight of synthesis gel (Table 2). In the experiments with three different FAU gel compositions (samples FauEmt-1a, FauEmt-2a and FauEmt-4a), the amount of FAU crystallites formed per gram of gel was about the same. Approximately 0.14 g (calcined amount) of the FAU structure type crystallized per gram of synthesis gel (Table 2). This value corresponds to a yield of ca. 55 wt-%, in terms of silicon, whereas the yield in terms of aluminum is approximately 100 wt-%, thus suggesting that the maximal possible conversion of the FAU gel was achieved. However, comparison of the EMT yield in the overgrowth product with the weight of EMT support crystals added (Table 2), showed that 24−47% of the support crystals did dissolve. The dissolution was most pronounced in hydrogels containing crown-ether with an OH^-/SiO_2 ratio of 0.75 (samples FauEmt-2a and FauEmt-4a, Table 2). Dissolution of a number of the support crystals enriched the synthesis gel with silicon and aluminum. Assuming that the aluminosilicate species generated through dissolution were consumed during the growth of the FAU phase, the yields of the FAU layer in terms of silicon and aluminum could be recalculated as ca. 45 and 80 wt-%, respectively. Aluminum remains the limiting factor with respect to the yields, as generally encountered with Y type zeolites.

Variation of the crystallization time between 1 and 5 d (samples FauEmt-2k to FauEmt-2o) only had a small effect on the amount of FAU formed per gram of FAU synthesis gel. On the other hand, the amount of support crystals dissolved during the overgrowth process remained constant until a crystallization time of 3 d, after which it increased substantially (Table 2). This observation provides additional evidence for the assumed intactness of the EMT core of the FAU-on-EMT overgrowth materials obtained in the three-day synthetic experiments. As long as there is gel and the overgrowth process is taking place, the EMT support crystals which are covered with FAU crystallites do not dissolve. When the overgrowth process is terminated, the mother liquor becomes depleted and the most siliceous part of the overgrowth, i.e. the EMT core, starts to dissolve. Synthesis time is, therefore, a critical synthesis parameter. Prolongation of the crystallization time might be used for the preparation of hollow particles with a shell composed of Al-rich FAU crystallites, by dissolving the Si-rich EMT core. Hollow crystals are expected to have favorable mass- and heat-transfer properties, and may be advantageous, for example, in rapid-pressure-swing adsorptive separations.

Quantification of the FAU-on-EMT overgrowth materials obtained using different amounts of support crystals (samples FauEmt-1a to FauEmt-1c and FauEmt-2a to FauEmt-2c) showed that the yield of FAU formed per gram of FAU synthesis gel decreased with an increasing amount of EMT crystals added, especially in presence of 18-crown-6 ether molecules (Table 2). A possible explanation for this decrease is that, although the percentage of dissolved support crystals diminishes when more support crystals are used, the absolute amount of support crystals dissolved per gram of FAU synthesis gel increases, thus perturbing the original optimized FAU gel composition to a larger extent.

Conclusions

In this paper, the potential of the two-step synthetic procedure for synthesizing systematic FAU-on-EMT overgrowth materials has been investigated. Inoculation of a FAU synthesis gel with a high sodium content (Na_2O/SiO_2 = 0.34 or 0.375) and which optionally contained crown-ether molecules, with EMT support crystals, resulted in the formation of a continuous film of FAU crystallites on the original micrometer-sized hexagonal-platelet EMT support crystals. The overgrowth was achieved at 373 K within 1 d. On the other hand, no crystallization took place from an FAU synthesis gel containing 15-crown-5 ether and with a low sodium content (Na_2O/SiO_2 = 0.24), unless this gel was aged for 3 d at room temperature prior to the addition of EMT support crystals. However, in this case the support crystals were not completely covered with FAU crystallites and a new population of isolated FAU crystals with octahedral morphology was obtained. Washing or washing, drying and calcining the support crystals before they were added to the FAU synthesis gel was detrimental and resulted in the formation of an undesirable population of isolated FAU crystals. Variation of the amount of support crystals added or the synthesis time showed that the FAU crystallites preferentially nucleate and grow on the corners and edges of the EMT support crystals. Only when the amount of the synthesized EMT support crystals per gram of synthesis gel is approximately 0.20 g, do the support crystals become completely coated with FAU crystallites.

The FAU-on-EMT overgrowth materials obtained were characterized in detail using a variety of physico-chemical characterization techniques. Quantification of the overgrowth materials with XRD revealed that the yield of FAU with respect to the gel was similar for the three types of gel compositions used. After 3 d at 373 K, the overgrowth process was complete and the supply of nutrients from the gel exhausted. The yield of FAU layer in terms of the gel decreased with an increasing amount of support crystals added. Of the EMT support crystals added, a fraction dis-

solved completely, whereas the rest became overgrown. The overgrown support crystals were not damaged and maintained their Si/Al ratio and their original micropore volume.

The dissolution behavior of the synthesized EMT crystals in basic solutions was investigated. The dissolution was found to cause the formation of pits over the entire surface. Extensive dissolution resulted in the formation of particles, which were more strongly dissolved at the center than at the outer rim. The EMT crystals dissolved in a block-wise manner and finally were decomposed into smaller fragments with Si/Al ratios as low as 1.3. Such debris from EMT dissolution were not observed in the overgrowth formation experiments.

The Si/Al ratio of the FAU crystallites was found to be dependent on the gel composition and on the position of the crystallites with respect to the surface of the EMT support. The first crystallites formed, which were positioned at the corners and edges of the EMT support crystals, were richer in aluminum than the crystallites formed at a later stage and present in the center of the basal $\{0001\}_{EMT}$ planes. FAU-on-EMT overgrowth materials synthesized in the presence of crown-ether molecules contain approximately one crown-ether per cage. Even in the absence of crown-ether molecules during the second synthetic step, the FAU phase occluded some crown-ether molecules, which were introduced with the synthesized EMT support crystals. This amount was more pronounced when more EMT support crystals were added to the inorganic FAU synthesis gel. Nitrogen physisorption measurements indicated that all pores were accessible to nitrogen. The low external surface areas of the FAU-on-EMT overgrowth materials were in agreement with the absence of mesopores and a tight fitting of the support and the overgrowing layer.

Experimental Section

Two-Step Synthesis: Hydrogels for the synthesis of FAU type zeolites were obtained following the procedure described by Feijen et al.,[21] and using Ludox HS-40 (DuPont), NaOH pellets (Merck), gibbsite (Fluka), 15-crown-5 ether (1,4,7,10,13-pentaoxacyclopentadecane, Acros) or 18-crown-6 ether (1,4,7,10,13,16-hexaoxacyclooctadecane, Acros) and distilled water. A given amount of the synthesized EMT support crystals was added to these gels, which were optionally aged for 3 d at room temperature. The resulting mixtures were stirred for 15 min and subsequently transferred into PTFE-lined stainless-steel autoclaves. These autoclaves were heated to the crystallization temperature of 373 K under quiescent conditions without aging. After the crystallization time had elapsed, the solid products were recovered by vacuum filtration, washed with deionised water until the pH value of the wash water was below 10 and dried at 333 K. Calcination was done in a muffle furnace at 823 K for 20 h. − EMT support crystals were prepared in a similar way to the hydrogels with the following molar oxide ratios: 10 SiO_2/1 Al_2O_3/2.4 Na_2O/0.97 18-crown-6/135 H_2O. − These gels were aged in PTFE-lined stainless-steel autoclaves for 3 d at room temperature and subsequently heated to the crystallization temperature of 373 K at autogenous pressure without stirring. After 11 d, the autoclaves were cooled in water and a wet cake of the EMT support crystals was recovered by vacuum filtration.

Powder X-ray Diffraction (XRD): XRD patterns were collected with an automated Siemens D-5000matic diffractometer using Cu-K_α radiation. XRD profiles were recorded in the range of 2θ values between 4 and 55°, with steps of 0.02° and counting times of 1.2 s.

Scanning Electron Microscopy (SEM): SEM pictures were taken with a Jeol superprobe 733 and of a Philips XL30 FEG apparatus. A gold film was sputtered onto the samples supported on alumina disks prior to their observation.

High-Resolution Transmission Electron Microscopy (HRTEM): HRTEM investigations were carried out with a 200-kV Philips CM200 Ultra Twin apparatus with a point-to-point resolution of 0.19 nm. The zeolite powder was deposited onto a carbon support and remained stable under the electron beam irradiation for at least several minutes. Nano-EDAX (energy-dispersive analysis of X-rays) was performed with the same apparatus equipped with a Noran EDX-detector having an ultra-thin window. The TEM was operated in the nanoprobe-mode, which implies that the electron beam diameter was reduced to 5 nm or even smaller.

NMR Spectroscopy: ^{29}Si magic angle spinning (MAS) NMR spectroscopy was performed with a Bruker MSL400 (9.4 T) spectrometer at 79.5 MHz, with a pulse length of 4 μs, a repetition time of 5 s, a spinning rate of 4 kHz and 11 000 scans. The ^{29}Si chemical shifts were reported relative to Me_4Si.

X-ray Photoelectron Spectroscopy (XPS): XPS was carried out with a Perkin−Elmer PHI 5500 ESCA system using monochromatic Al-K_α radiation. The binding energies were referred to C(1s) = 286.4 eV. The evaluation of the surface composition was performed using the intensities of the Na(1s), O(1s), Si(2p), and Al(2p) lines.

Nitrogen Physisorption: Nitrogen physisorption isotherms at 77 K were recorded with an Omnisorp-100 analyzer from Coulter, operating in the continuous flow mode. Before recording the isotherms, calcined samples were outgassed at 673 K under high vacuum (10^{-6} kPa) for at least 12 h. Micropore volumes and specific external surface areas were derived from the isotherms using the t-plot method of Lippens and de Boer.[35] The Horvath−Kawazoe method[36] was applied to determine the micropore diameter.

Thermogravimetric and Differential Thermal Analysis (TG-DTA): TG-DT analyses were performed simultaneously with a Setaram TGA92 thermobalance under oxygen/helium (25:75 vol-%) using typically 30 mg of sample and a flow of 35 mL/min. The temperature was increased at a rate of 5 K/min from room temperature to 823 K.

Acknowledgments

A. M. G. and P. J. G. acknowledge the Flemish IWT for a Ph. D. grant and the Flemish FWO for a position as Research Director, respectively. The authors are grateful to F. Pelgrims for the technical assistance with the SEM. The work was sponsored by the Belgian Federal Government in the frame of the IUAP-PAI program.

[1] C. N. R. Rao, J. M. Thomas, *Acc. Chem. Res.* **1985**, *18*, 113−119.
[2] M. W. Anderson, K. S. Pachis, F. Prébin, S. W. Carr, O. Terasaki, T. Ohsuna, V. Alfreddson, *J. Chem. Soc., Chem. Commun.* **1991**, 1660−1664.
[3] M. M. J. Treacy, D. E. W. Vaughan, K. G. Strohmaier, J. M. Newsam, *Proc. R. Soc. Lond. A* **1996**, *452*, 813−840.
[4] K. P. Lillerud, J. H. Raeder, *Zeolites* **1986**, *6*, 474−483.
[5] P. A. Jacobs, J. A. Martens, "Synthesis of High-Silica Alumino-

silicate Zeolites", *Stud. Surf. Sci. Catal.*, vol. 33, Elsevier Science B. V., Amsterdam, **1987**.
[6] J. M. Thomas, G. R. Millward, *J. Chem. Soc., Chem. Commun.* **1982**, 1380−1383.
[7] G. R. Millward, S. Ramdas, J. M. Thomas, M. T. Barlow, *J. Chem. Soc., Faraday Trans. 2* **1983**, *79*, 1075−1082.
[8] M. E. Leonowicz, D. E. W. Vaughan, *Nature* **1987**, *329*, 819−821.
[9] D. E. W. Vaughan, K. G. Strohmaier, in: *Zeolite Synthesis* (Eds.: M. L. Occelli, H. E. Robson), ACS Symp. Ser. No. 398, Washington, DC, **1989**, p. 506.
[10] G. R. Millward, S. Ramdas, J. M. Thomas, *Proc. R. Soc. Lond. A* **1985**, *399*, 57−71.
[11] R. Szostak, K. P. Lillerud, in: "Zeolites and Related Microporous Materials: State of the Art 1994" (Eds.: J. Weitkamp, H. G. Karge, H. Pfeifer, W. Hölderich), *Stud. Surf. Sci. Catal.*, vol. 84, Elsevier Science B. V., Amsterdam, **1994**, p. 535.
[12] W. S. Wise, R. W. Tschernich, *Am. Mineral.* **1976**, *61*, 853−858.
[13] W. S. Wise, D. Pierce, *Scanning Electron Microsc.* **1981**, 633−636.
[14] E. de Vos Burchart, J. C. Jansen, H. van Bekkum, *Zeolites* **1989**, *9*, 432−435.
[15] D. W. Breck, *Zeolite Molecular Sieves: Structure, Chemistry and Use*, John Wiley, New York, **1974**.
[16] A. D. Randolph, M. A. Larson, *Theory of Particulate Processes: Analysis and Techniques of Continuous Crystallization*, Academic Press, New York, **1971**.
[17] L. D. Rollmann, U. S. Patent 4,148,713 **1979**.
[18] S. J. Miller, U. S. Patent 4,394,251 **1983**; US Patent 4,394,362 **1983**.
[19] W. T. Koetsier, Eur. Patent 55,044 **1984**.
[20] A. M. Goossens, B. H. Wouters, V. Buschmann, J. A. Martens, *Adv. Mater.* **1999**, *11*, 561−564.
[21] E. J. P. Feijen, K. De Vadder, M. H. Bosschaerts, J. L. Lievens, J. A. Martens, P. J. Grobet, P. A. Jacobs, *J. Am. Chem. Soc.* **1994**, *116*, 2950−2957.
[22] A. J. Bons, J. L. Lievens, J. P. Verduijn, W. J. Mortier, *Microsc. Res. Technol.* **1993**, *25*, 175−176.
[23] F. Delprato, L. Delmotte, J. L. Guth, L. Huve, *Zeolites* **1990**, *10*, 546−552.
[24] L.-Y. Hou, R. W. Thompson, *Zeolites* **1989**, *9*, 526−530.
[25] E. A. Tsokanis, R. W. Thompson, *Zeolites* **1992**, *12*, 369−373.
[26] V. Buschmann, A. L. Yonkeu, G. Miehe, H. Fuess, A. M. Goossens, J. A. Martens, manuscript in preparation.
[27] R. K. Iler, *The Chemistry of Silica*, John Wiley, New York, **1979**.
[28] R. M. Dessau, E. W. Valyocsik, N. H. Goeke, *Zeolites* **1992**, *12*, 776−779.
[29] A. Cizmek, B. Subotic, I. Smit, A. Tonejc, R. Aiello, F. Crea, A. Nastro, *Microporous Mater.* **1997**, *8*, 159−169.
[30] R. M. Barrer, *Hydrothermal Chemistry of Zeolites*, Academic Press, London, **1982**.
[31] A. Katovic, B. Subotic, I. Smit, Lj. A. Despotovic, M. Curic, in: *Zeolite Synthesis* (Eds.: M. L. Occelli, H. E. Robson), ACS Symp. Ser. No. 398, Washington, DC, **1989**, p. 124.
[32] E. J. P. Feijen, J. L. Lievens, J. A. Martens, P. J. Grobet, P. A. Jacobs, *J. Phys. Chem.* **1996**, *100*, 4970−4975.
[33] J. Klinowski, in: *Stud. Surf. Sci. and Catal.*, vol. 52, Elsevier Science B. V., Amsterdam, **1989**, p. 39.
[34] E. J. P. Feijen, J. A. Martens, P. A. Jacobs, *J. Chem. Soc., Faraday Trans.* **1996**, *92*, 3281−3285.
[35] B. C. Lippens, J. H. de Boer, *J. Catal.* **1965**, *4*, 319−323.
[36] G. Horvath, K. Kawazoe, *J. Chem. Eng. Jpn.* **1983**, *16*, 470−473.

Received October 4, 2000
[I00373]

Sterically Fixed Dithiolate Ligands and Their Zinc Complexes: Derivatives of 1,8-Dimercaptonaphthalene

Markus Tesmer[a] and Heinrich Vahrenkamp*[a]

Keywords: S ligands / Alcohols / Zinc / Structure elucidation / Enzyme models

The synthesis of two new dithiols, 1,8-dimercapto-2,7-di(*tert*-butyl)naphthalene (H_2L^1) and 1,8-dimercaptonaphthoic anhydride (H_2L^2), is described. They react with diethylzinc to yield the polymeric complexes L^1Zn and L^2Zn. L^1Zn dissolves in the presence of pyridine to form $[L^1Zn{\cdot}py]_x$, which is presumed to be dimeric. Both L^1Zn and L^2Zn react with neocuproin. Structure determinations have confirmed the tetrahedral ZnN_2S_2 coordination in the resulting LZn·neo complexes.

Introduction

The chemistry of transition metal thiolates is a world of thiolate-bridged oligomers and polymers.[1,2] This extends into biology with the ubiquitous presence of the $Fe_4S_4(SR)_4$ redox unit and the accumulation of copper, zinc or cadmium in the metallothioneins. Yet Nature is able to prevent thiolate bridging and metal aggregation by isolating the cysteine-thiolate donors and limiting the space available to the metals, thereby making the cysteine sulfur one of the prominent monodentate ligands for metals in biology.

Model studies of sulfur-rich metal environments in metalloenzymes invariably suffer from this problem of complex aggregation.[3,4] As a result, far-reaching advances have often only been made in the exceptional situations where thiolate bridging is not preferred, typical examples being the bioinorganic chemistry of octahedral iron[5] or the ZnN_2S_2 coordination motif of the zinc finger proteins.[6]

In the bioinorganic chemistry of zinc, model studies of the alcohol dehydrogenases have met with this problem.[7,8] The attachment of the metal to the protein by an NS_2 (histidine, cysteine, cysteine) ligation[9] calls for amine bis-thiolates as model ligands. But to date no such thiolate[10,11] has been found to produce mononuclear $(NS_2)Zn-X$ complexes that are free from thiolate bridging and that bear a ligand X as a substitute for the substrate of the enzyme. The best approximation has been achieved by NS_2 ligands in which the sulfur donors are not of the thiolate type.[12]

The standard procedures for reducing the bridging tendency of thiolate ligands (steric hindrance or increased electronegativity) have been applied successfully to zinc complexes: tris(*tert*-butyl)benzene thiolate has been used to produce a tricoordinate $Zn(SR)_2$·pyridine complex,[13] and we have used pentafluorobenzene thiolate to model the $ZnNS_2O$ ligation pattern of the alcohol dehydrogenase enzyme−substrate complexes.[14]

We are not aware that these principles have been applied to chelating bis-thiolate ligands, and our attempts to do so are reported in this paper. We wanted to synthesize a ligand in which the two thiolate donors have fixed positions in space. This should serve the purpose of preorganization (i.e. good chelating properties) while at the same time the lack of conformational freedom would reduce the oligonucleating tendency. We chose the 1,8-dimercaptonaphthalene framework for our purposes. It strictly defines the locations of the two sulfur atoms, while allowing the attachment of bulky substituents at the 2- and 7-positions or the attachment of electron-withdrawing substituents anywhere on the naphthalene skeleton. The target ligands were H_2L^1 and H_2L^2. This paper describes their synthesis and some preliminary chemistry of their zinc complexes.

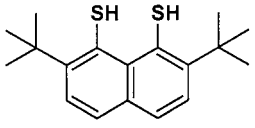

H_2L^1

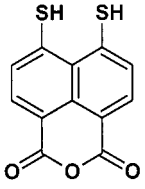

H_2L^2

Results and Discussion

The Ligands

1,8-Dimercaptonaphthalene[15] and 1,8-dimercaptohexachloronaphthalene[16] have been described in the literature, but not investigated extensively as ligands.[16,17] Our approach of generating the 1,8-dithiol functionality in H_2L^1 and H_2L^2 followed the established procedure of introducing sulfur as the naphthalene-1,8-disulfide and then reducing it. Scheme 1 describes this for H_2L^1, using the literature method to prepare naphthalene-1,8-disulfide.[18] The overall yield of H_2L^1 starting from bromonaphthalene was 8%. H_2L^1 is a yellow crystalline solid which is soluble in weakly polar organic solvents. It is easily identified by its simple

[a] Institut für Anorganische und Analytische Chemie der Universität Freiburg,
Albertstraße 21, 79104 Freiburg, Germany
Fax: (internat.) +49-761/203-6001
E-mail: vahrenka@uni-freiburg.de

 © WILEY-VCH Verlag GmbH, 69451 Weinheim, 2001 1434−1948/01/0505−1183 $ 17.50+.50/0

^{1}H NMR spectrum (see Experimental Section). Upon exposure to air, it is oxidized to the disulfide. Upon deprotonation, its colour in solution becomes a deeper yellow.

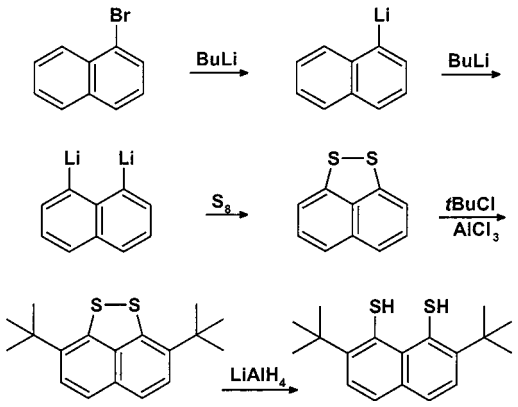

Scheme 1

The synthesis of H_2L^2 was performed according to Scheme 2 starting from acenaphthene, using the literature procedure[19] to generate its 1,8-dibromide. The overall yield of H_2L^2 starting from acenaphthene was again 8%.

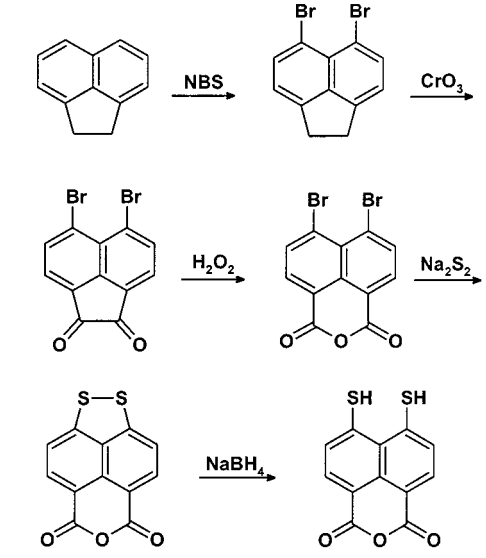

Scheme 2

H_2L^2 is a yellow solid of low solubility which again has a simple ^{1}H NMR spectrum (see Experimental Section). Its air sensitivity is similar to that of H_2L^1. Deprotonation greatly enhances its solubility in polar solvents. Its solutions are deep red, indicating the delocalized nature of the anion according to the following valence structures.

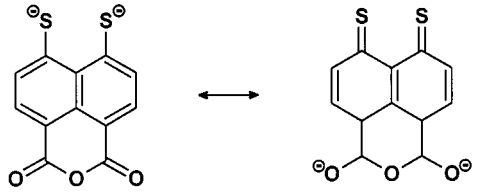

Zinc Complexes

Diethyl zinc was found to be the best reagent to convert H_2L^1 and H_2L^2 into the binary zinc complexes ZnL^1 (**1**) and ZnL^2 (**2**), respectively, by hydrolytic cleavage in aprotic media. The resulting compounds **1** and **2** were obtained in very good yields. They dissolve only in very good donor solvents, in agreement with the assumption that they are oligomeric or polymeric. It is likely that they contain zinc in a ZnS_4 environment, i.e. each thiolate sulfur bridges two zinc ions.

Some attempts were made to isolate adducts of ZnL with monodentate donors. They were successful for the combination ZnL^1/pyridine. Upon addition of equimolar amounts of pyridine to a suspension of ZnL^1 in chloroform, the complex dissolved. However, a new precipitate of composition ZnL^1·pyridine (**3**) formed immediately; again, this complex was of rather low solubility. This reaction did not occur with ZnL^2. Assuming the likely $ZnNS_3$ coordination in this species, it follows that one of the two thiolate functions acts as a bridge. Thus a dimeric structure can be proposed for **3**, in analogy with the one described by Kellogg for the zinc complex of a sterically hindered pyridine-bis(thiolate) ligand.[10]

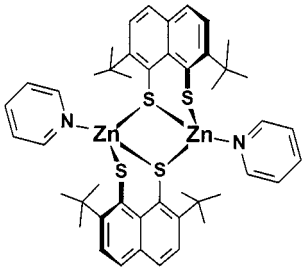

As expected, the highly preferred ZnN_2S_2 coordination with **1** and **2** was readily found in the form of mononuclear complexes. We chose neocuproin (2,9-dimethylphenanthroline, neo) as the bidentate nitrogen co-ligand, as we had previously found it to be most suitable for this purpose.[20] Compounds **1** and **2** dissolve in its presence, and cleanly form the 1:1 complexes (neo)Zn(L^1) (**4**) and (neo)Zn(L^2) (**5**), which are orange crystalline solids suitable for X-ray analysis (see below). In complex **5**, the electron-withdrawing properties of ligand L^2 can be confirmed by the positions of its ν(CO-carboxylate) IR bands: these are shifted by approximately 20 cm^{-1} to lower wavenumbers than those of H_2L^2.

Structures

The structure determinations of **4** and **5** (see Figure 1 and 2) confirmed the identities and compositions of the species described here, and gave some information about the ligating properties of L^1 and L^2. The crystalline structure of compound **4** has an asymmetric unit with two molecules that are quite similar. The overall coordination geometries in **4** and **5** are as expected, with Zn−N and Zn−S distances

in the normal range and with relatively small N−Zn−N and relatively large S−Zn−S angles.

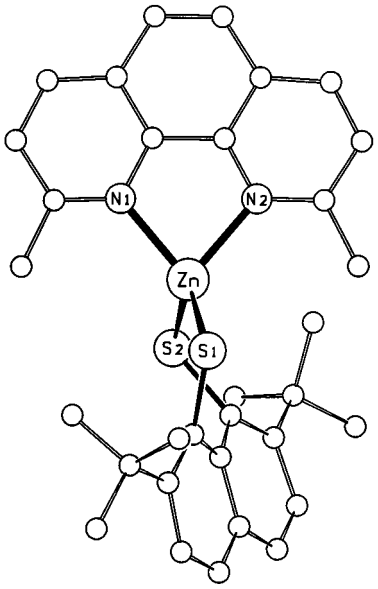

Figure 1. Molecular structure of **4** (one of the two independent molecules); bond lengths [Å]: Zn−S1 2.227(1)/2.222(1), Zn−S2 2.229(1)/2.226(1), Zn−N1 2.086(3)/2.085(3), Zn−N2 2.091(3)/2.092(3); bond angles [°]: S1−Zn−S2 103.06(4)/103.51(4), N1−Zn−N2 80.1(1)/80.5(1), S1−Zn−N1 126.1(1)/126.6(1), S1−Zn−N2 114.5(1)/115.7(1), S2−Zn−N1 113.0(1)/109.0(1), S2−Zn−N2 120.4(1)/122.0(1)

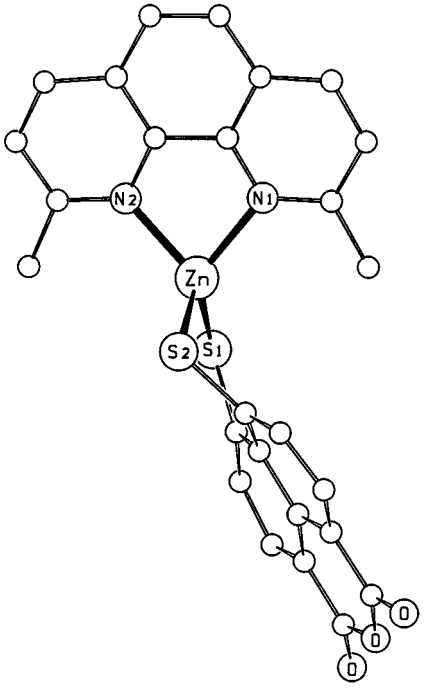

Figure 2. Molecular structure of **5**; bond lengths [Å]: Zn−S1 2.230(2), Zn−S2 2.260(2), Zn−N1 2.058(5),Zn−N2 2.050(4); bond angles [°]: S1−Zn−S2 103.04(7),N1−Zn−N2 81.6(2), S1−Zn−N1 125.1(1), S1−Zn−N2 122.7(1), S2−Zn−N1 111.8(1), S2−Zn−N2 112.0(1)

However, both complexes are severely distorted from their ideal C_{2v} symmetry. The reason for this lies in the conformational requirements of the sulfur atoms which do not allow for the zinc ions to reside together with them in the planes of the naphthalene rings. The necessity for small Zn−S−C angles (101−108°) together with the given Zn−S bond lengths enforces an out-of-plane motion of the zinc ions and/or both sulfur atoms. This geometry is highlighted in Figure 1 and 2. In these figures, the bisector of the S−Zn−S angle is in the plane of the paper with a viewing direction normal to the plane of the neocuproin ligand. The naphthalene rings are bent away from the bisector, and partly rotated with respect to their expected orientation perpendicular to the plane of the paper. This relieves the torsional strain at the sulfur atoms and the intramolecular repulsive forces.

More specifically, in both independent molecules of **4**, the sulfur atoms are bent away in opposite directions from the naphthalene plane by approximately 1.0 and 1.2 Å. The carbon atoms attached to them follow this movement to a lesser degree. The out-of-plane displacement of the sulfur atoms is reversed for the zinc ion which is roughly in the naphthalene plane again. Concomitantly, the naphthalene plane is tilted by only 8° with respect to the bisector of the S−Zn−S angle. In **5**, the sulfur atoms are also bent away from the naphthalene plane in opposite directions, but this time by only 0.75 Å on average. Contrary to the case in compound **4**, both S−Zn bonds in **5** are tilted in the same direction, thereby causing the observed tilt of 30° of the naphthalene ring with respect to the bisector of the S−Zn−S angle. The reason for this difference between **4** and **5** may lie in the *tert*-butyl substituents of **4**, which prevent the pronounced tilting owing to their van der Waals interactions with the methyl groups of the neocuproin ligand. Generally, the observed asymmetry of **4** and **5** seems to effect the necessary relief from the inherent steric strain, thereby making ligand L^1 and L^2 suitable for their intended purpose.

The ZnN_2S_2 ligation in complexes **4** and **5** is also the most common one in zinc finger motifs.[6] The geometric features of the ZnN_2S_2 units in these complexes and in the zinc fingers compare reasonably well but, as was discussed in detail for zinc-neocuproin complexes of bis(cysteinyl)-peptides,[20] the geometric constraints induced by the small bite angle of the neocuproin ligand make the N−Zn−N angles smaller and concomitantly the S−Zn−S angles larger than the situation in the proteins.

Conclusions

The ligands H_2L^1 and H_2L^2 were accessible. They are two new members of a hitherto unexplored group of sterically fixed dithiolate ligands that are geometrically similar to the dithiolene ligands. The ligand H_2L^1 is sterically crowded owing to the favourable positioning of its *tert*-butyl substituents, whereas the Ligand H_2L^2 is electron poor. At the same time, the dianion L^2 should have ligating properties for hard metal ions at its carboxylate oxygen atoms, as in-

dicated by its resonance structures and the IR spectroscopic data of its zinc complex **5**.

The preliminary complexation reactions with zinc have outlined the coordinating potential of both ligands. While the binary ZnL compounds **1** and **2** could be expected to be polymeric, addition of one pyridine ligand to **1** is sufficient to break up its polymeric structure. The excellent coligand neocuproin ensured the formation of the 1:1:1 complexes **4** and **5**, with a ZnN_2S_2 coordination. Their structure determinations have revealed the basic ligation properties of the naphthalene-1,8-dithiolates. The conformational requirements of the sulfur atoms do not allow for a planar arrangement of the naphthalene rings, the sulfur atoms and the zinc ion. However, the two complex geometries that were observed show that a strain-free and strong metal-dithiolate coordination is present.

Experimental Section

For general preparative and measuring procedures, see ref.[21] All reactions were carried out under a nitrogen atmosphere. Starting materials were obtained commercially or prepared according to the references given.

Ligand H_2L^1: a) 2,7-Di(*tert*-butyl)naphthalene-1,8-disulfide: Naphthalene-1,8-disulfide[18] (3.00 g, 15.8 mmol) was dissolved at 50 °C in a mixture of nitromethane (37 mL) and *tert*-butyl chloride (4.38 g, 47.3 mmol). Anhydrous $AlCl_3$ (400 mg, 3.00 mmol) was added and the mixture was stirred at 50 °C for 20 min. After cooling to room temp. the product precipitated. Washing with nitromethane and recrystallization from acetone yielded 2,7-di(*tert*-butyl)-naphthalene-1,8-disulfide (1.82 g, 38%) as orange crystals, m.p. 129 °C. − $C_{18}H_{22}S_2$ (302.5): calcd. C 71.47, H 7.33; found C 71.55, H 7.37. − ^{1}H NMR ($CDCl_3$): δ = 1.50 (s, 18 H, *t*Bu), 7.36 (d, *J* = 8.0 Hz, 2 H, $H^{5,6}$), 7.42 (d, *J* = 8.0 Hz, 2 H, $H^{4,7}$).

b) H_2L^1: A solution of 2,7-di(*tert*-butyl)naphthalene-1,8-disulfide (5.43 g, 28.5 mmol) in THF (50 mL) was treated with $LiAlH_4$ (1.08 g, 28.5 mmol) and heated at reflux for 1 h. After cooling to room temp., water (1 mL) and 10 M HCl (15 mL) were added dropwise to the stirred solution. After extraction with dichloromethane (100 mL), the organic layer was separated, washed with water (3 × 30 mL) and dried over Na_2SO_4. The solvent was removed in vacuo and the residue was recrystallized from cyclohexane/THF (5:1). H_2L^1 was obtained as a yellow powder (8.25 g, 95%), m.p. 137 °C. − $C_{18}H_{24}S_2{\cdot}C_6H_{12}$ (304.5 + 84.2): calcd. C 74.16, H 9.34; found C 75.40, H 9.31. − IR (KBr): $\tilde{\nu}$ = 2544 (SH) cm^{-1}. − ^{1}H NMR ($CDCl_3$): δ = 1.50 (s, 12 H, C_6H_{12}), 1.64 (s, 18 H, *t*Bu), 4.41 (s, 2 H, SH), 7.48 (d, *J* = 8.6 Hz, 2 H, $H^{4,5}$), 7.50 (d, *J* = 8.6 Hz, 2 H, $H^{3,6}$).

Ligand H_2L^2: a) 1,8-Dibromoacenaphthenedione: 1,8-Dibromoacenaphthene[19] (8.51 g, 27.3 mmol) was dissolved in acetic anhydride (1 L) at 110 °C. CrO_3 (21.1 g, 211 mmol) was added carefully to the stirred solution over a period of 2 h. The resulting green suspension was stirred at 160 °C for 30 min., and then poured while hot onto crushed ice (1 kg). Conc. HCl (20 mL) was added and the mixture was filtered. The brownish precipitate was washed with water, dried in vacuo and recrystallized from acetic anhydride (2 L). 1,8-Dibromoacenaphthenedione (6.23 g, 67%) was obtained as a light brown solid, m.p. 239 °C. − $C_{12}H_4Br_2O_2$ (340.0): calcd. C 42.40, H 1.19; found C 42.22, H 1.19. − ^{1}H NMR ($CDCl_3$): δ = 7.93 (d, *J* = 7.6 Hz, 2 H, $H^{4,7}$), 8.27 (d, *J* = 7.6 Hz, 2 H, $H^{3,8}$).

b) 1,8-Dibromonaphthoic Anhydride: 1,8-Dibromoacenaphthenedione (6.23 g, 18.3 mmol) was dissolved in a mixture of 1,4-dioxane (400 mL) and NaOH (2 M, 400 mL) and heated to 100 °C. A solution of H_2O_2 (10%, 400 mL) was added slowly to the stirred solution. After stirring for a further 30 min. at 100 °C, the mixture was cooled to room temp. and filtered. The filtrate was acidified with conc. HCl producing a voluminous precipitate. This was separated by centrifugation, washed twice with water and dried in vacuo. Recrystallization from acetic anhydride (2.5 L) yielded 1,8-dibromonaphthoic anhydride (4.84 g, 74%) as a light brown powder, m.p. 260 °C. − $C_{12}H_4Br_2O_3$ (356.0): calcd. C 40.49, H 1,13; found C 40.45, H 1.11. − ^{1}H NMR ([D_6]acetone): δ = 7.95 (d, *J* = 7.5 Hz, 2 H, $H^{5,8}$), 8.17 (d, *J* = 7.5 Hz, 2 H, $H^{4,9}$).

c) Naphthoic Anhydride-1,8-disulfide: Na (1.56 g, 67.9 mmol) and sulfur (2.18 g, 68.0 mmol) were suspended in DMF (40 mL). The mixture was stirred at 100 °C until the vigorous reaction had produced a voluminous precipitate. A suspension of 1,8-dibromonaphthoic anhydride in DMF (20 mL) was quickly added, upon which the mixture turned deep purple. After heating at 140 °C for 10 min, it was poured while hot into water (300 mL). The resulting orange suspension was acidified with conc. HCl, and the precipitate was isolated by centrifugation, washed twice with water and dried in vacuo. Recrystallization from 1,4-dioxane (1.6 L) in the presence of activated charcoal (1 g) yielded naphthoic anhydride-1,8-disulfide (2.41 g, 68%) as a red solid, m.p. 330 °C (dec.). − $C_{12}H_4O_3S_2$ (356.0): calcd. C 55.37, H 1.55; found C 55.32, H 1.59. − ^{1}H NMR ([D_6]acetone): δ = 7.83 (d, *J* = 8.0 Hz, 2 H, $H^{3,9}$), 8.37 (d, *J* = 8.0 Hz, 2 H, $H^{4,8}$).

d) HL^2: Naphthoic anhydride-1,8-disulfide (0.32 g, 1.20 mmol) was suspended in methanol (10 mL). After the addition of $NaBH_4$ (94 mg, 2.50 mmol) the mixture turned purple. After stirring for 2 h, the mixture was filtered and the filtrate treated with conc. HCl (1 mL) and stirred for 1 h. The resulting yellow precipitate was washed with water and methanol and dried in vacuo to afford H_2L^2 as a yellow powder (0.23 g, 73%), m.p. 280 °C (dec.). − $C_{12}H_6O_3S_2$ (262.3): calcd. C 54.95, H 2.31; found C 54.18, H 2.59. − IR (KBr): $\tilde{\nu}$ = 2537 (SH) cm^{-1}. − ^{1}H NMR ([D_6]acetone): δ = 5.51 (s, 2 H, SH), 7.80 (d, *J* = 8.2 Hz, 2 H, $H^{5,8}$), 8.42 (d, *J* = 8.2 Hz, 2 H, $H^{4,9}$).

Compound 1: A solution of H_2L^1 (0.20 g, 0.66 mmol) in chloroform (10 mL) was treated dropwise with a solution of diethyl zinc (81 mg, 0.66 mmol) in *n*-hexane (2.0 mL). The resulting precipitate was filtered off, washed with chloroform and dried in vacuo, leaving behind compound **1** (0.23 g, 95%) as a yellow powder, m.p. 160 °C (dec.). − $C_{18}H_{22}S_2Zn$ (367.9): calcd. C 58.77, H 6.03, Zn 17.77; found C 57.38, H 5.97, Zn 17.32. − ^{1}H NMR ([D_6]DMSO): δ = 1.68 (s, 18 H, *t*Bu), 7.06 (d, *J* = 8.5 Hz, 2 H, $H^{4,5}$), 7.25 (d, *J* = 8.5 Hz, 2 H, $H^{3,6}$).

Compound 2: Prepared in the same manner as **1** from H_2L^2 (0.10 g, 0.38 mmol) in toluene (15 mL) and diethyl zinc (47 mg, 0.38 mmol). Compound **2** was obtained as a pale orange powder (0.12 g, 97%), m.p. 175 °C (dec.). − $C_{12}H_4O_3S_2Zn$ (325.7): calcd. C 44.26, H 1.24, Zn 20.08; found C 44.07, H 1.16, Zn 19.89. − ^{1}H NMR ([D_6]DMSO): δ = 7.84 (d, *J* = 8.2 Hz, 2 H, $H^{5,8}$), 8.37 (d, *J* = 8.2 Hz, 2 H, $H^{4,9}$).

Compound 3: A suspension of **1** (0.20 g, 0.54 mmol) in chloroform (10 mL) was treated with a solution of pyridine (44 mg, 0.55 mmol) in chloroform (2 mL). A clear solution was formed from which a yellow solid precipitated after a few seconds. The precipitate was

filtered off, washed with chloroform and dried in vacuo, leaving behind compound **3** as a yellow powder (0.21 g, 85%), m.p. 105 °C (dec.). − $C_{23}H_{27}NS_2Zn$ (447.0): calcd. C 61.80, H 6.09, N 3.13, Zn 14.63; found C 59.48, H 5.97, N 3.05, Zn 14.50. − IR (KBr): $\tilde{\nu}$ = 1609 (C=N) cm^{-1}. − ^1H NMR ([D$_6$]DMSO): δ = 1.68 (s, 18 H, *t*Bu), 7.06 (d, *J* = 8.5 Hz, 2 H, H^{4,5}), 7.25 (d, *J* = 8.5 Hz, 2 H, H^{3,6}), 7.41 (m, 2 H, py), 7.82 (m, 1 H, py), 8.58 (m, 2 H, py).

Compound 4: A solution of H_2L^1 (0.20 g, 0.66 mmol) and neocuproin hydrate (0.14 g, 0.67 mmol) in chloroform (10 mL) was treated with diethyl zinc (81 mg, 0.66 mmol) in *n*-hexane (2.0 mL). After stirring for 20 min. the volume was reduced to 2 mL in vacuo. Addition of petroleum ether (4 mL) produced a precipitate which was filtered off and washed with petroleum ether. Recrystallization from dichloromethane/hexane (1:1) yielded **4** as orange crystals (0.36 g, 95%), m.p. 115 °C (dec.). − $C_{32}H_{34}N_2S_2Zn{\cdot}CH_2Cl_2$ (576.2 + 84.9): calcd. C 59.96, H 5.49, N 4.24, Zn 9.89; found C 59.82, H 5.54, N 3.98, Zn 10.03. − IR (KBr): $\tilde{\nu}$ = 1621 and 1591 (C=N) cm^{-1}. − ^1H NMR ($CDCl_3$): δ = 1.77 (s, 18 H, *t*Bu), 3.19 (s, 6 H, CH_3), 5.35 (s, 2 H, CH_2Cl_2), 7.27 (d, *J* = 8.6 Hz, 2 H, H^{4,5}), 7.45 (d, *J* = 8.6 Hz, 2 H, H^{3,6}), 7.74 (d, *J* = 8.4 Hz, 2 H, neo-H^{3,8}), 7.94 (s, 2 H, neo-H^{5,6}), 8.44 (d, *J* = 8.4 Hz, 2 H, neo-H^{4,7}).

Compound 5: A suspension of **2** (0.10 g, 0.31 mmol) in chloroform (3 mL) was treated with neocuproin hydrate (70 mg, 0.31 mmol). The resulting clear solution formed a precipitate upon addition of hexane (6 mL), which was filtered off, washed with hexane and dried in vacuo, leaving behind compound **5** as orange crystals (0.13 g, 77%), m.p. 140 °C (dec.). − $C_{26}H_{16}N_2O_3S_2Zn{\cdot}C_6H_{14}$ (533.9 + 86.2): calcd. C 61.98, H 4.88, N 4.52, Zn 10.54; found C 62.52, H 5.55, N 4.33, Zn 10.11. − IR (KBr): $\tilde{\nu}$ = 1734 and 1700 (C=O), 1617 and 1590 (C=N) cm^{-1}. − ^1H NMR ([D$_6$]acetone): δ = 0.88 (m, 6 H, hexane-CH_3), 1.27 (m, 8 H, hexane-CH_2), 2.76 (s, 6 H, CH_3), 7.99 (d, *J* = 8.2 Hz, 2 H, H^{5,8}), 8.09 (d, *J* = 8.2 Hz, 2 H, H^{4,9}), 8.11 (d, *J* = 8.3 Hz, 2 H, neo-H^{3,8}), 8.27 (s, 2 H, neo-H^{5,6}), 8.90 (d, *J* = 8.3 Hz, 2 H, neo-H^{4,7}).

Table 1. Crystallographic details

	4	**5**
Formula	$C_{32}H_{34}N_2S_2Zn$	$C_{26}H_{16}N_2O_3S_2Zn{\cdot}CHCl_3$
Mol. wt	576.2	533.9 + 119.4
Crystal size [mm]	1.2 × 0.9 × 0.8	0.7 × 0.5 × 0.4
Space group	$P2_1/c$	$P\bar{1}$
Z	8	2
a [Å]	26.231(5)	9.737(2)
b [Å]	10.400(2)	11.834(2)
c [Å]	22.065(4)	13.847(3)
α [°]	90	67.95(3)
β [°]	108.29(3)	84.66(3)
γ [°]	90	66.48(3)
V [Å^3]	5715(2)	1353.9(5)
d (calc.) [g·cm^{-3}]	1.34	1.60
Temp. [K]	273	183
μ (Mo-K_α) [mm^{-1}]	1.03	1.39
hkl range	*h*: −31 to 32	*h*: −10 to 10
	k: 0 to 12	*k*: −13 to 12
	l: −27 to 0	*l*: −15 to 15
Refl. measd.	11909	6312
Indep. refl.	11588	3892
Obs. refl. [$I > 2\sigma(I)$]	6693	2463
Parameters	667	381
Refl. refined	11588	3892
R_1 (obs. refl.)	0.042	0.060
wR_2 (all refl.)	0.127	0.150
Residual el. density [e/Å^{-3}]	+0.6	+0.6
	−0.5	−0.5

Structure Determinations:[22] Crystals of **4** were obtained by layering a dichloromethane solution with hexane, and crystals of **5** were obtained by layering a chloroform solution with hexane. Diffraction data were recorded with the ω/2θ technique on a Nonius CAD4 diffractometer fitted with a molybdenum tube (Mo-K_α, λ = 0.7107 Å) and a graphite monochromator. No absorption corrections were applied. The structures were solved by direct methods and refined anisotropically with the SHELX program suite.[23] Hydrogen atoms were included with fixed distances and isotropic temperature factors which were 1.5 times the value of those of their attached atoms. Parameters were refined against F^2. The *R* values are defined as $R_1 = \Sigma|F_o - F_c|/\Sigma F_o$ and $wR_2 = [\Sigma[w(F_o^2 - F_c^2)^2]\Sigma[w(F_o^2)^2]]^{1/2}$. Drawings were produced with SCHAKAL.[24] Table 1 lists the crystallographic data.

Acknowledgments

This work was supported by the Deutsche Forschungsgemeinschaft and by the Fonds der Chemischen Industrie.

[1] B. Krebs, G. Henkel, *Angew. Chem.* **1991**, *103*, 785−804; *Angew. Chem. Int. Ed. Engl.* **1991**, *30*, 769−788.
[2] J. R. Dilworth, J. Hu, *Adv. Inorg. Chem.* **1993**, *40*, 411−459.
[3] W Kaim, B. Schwederski, *Bioanorganische Chemie*, Teubner, Stuttgart, **1995**.
[4] S. J. Lippard, J. M. Berg, *Principles of Bioinorganic Chemistry*, University Science Books, Mill Valley, **1994**.
[5] D. Sellmann, J. Sutter, *Acc. Chem. Res.* **1997**, *30*, 460−469.
[6] B. A. Krizek, B. T. Amann, V. J. Kilfoil, D. L. Merkle, J. M. Berg, *J. Am. Chem. Soc.* **1991**, *113*, 4518−4523.
[7] *Zinc and its Role in Biology and Nutrition* (Ed.: H. Sigel), Marcel Dekker, New York, **1983**.
[8] *Zinc Enzymes* (Eds.: I. Bertini, C. Luchinat, W. Maret, M. Zeppezauer), Birkhäuser, Basel, **1986**.
[9] C. I. Bränden, H. Eklund, B. Nordström, T. Boiwe, G. Söderlund, E. Zeppezauer, I. Ohlsson, A. Akeson, *Proc. Natl. Acad. Sci. USA* **1973**, *70*, 2439−2442; H. Cho, S. Ramaswamy, B. V. Plapp, *Biochemistry* **1997**, *36*, 382−389.
[10] B. Kaptein, L. Wang-Griffin, G. Barf, R. M. Kellogg, *J. Chem. Soc., Chem. Commun.* **1987**, 1457−1459; B. Kaptein, G. Barf, R. M. Kellogg, F. van Bolhuis, *J. Org. Chem.* **1990**, *55*, 1890−1901.
[11] U. Brand, H. Vahrenkamp, *Z. Anorg. Allg. Chem.* **1996**, *622*, 213−218.
[12] C. Kimblin, T. Hascall, G. Parkin, *Inorg. Chem.* **1997**, *36*, 5680−5681.
[13] M. Bochmann, G. C. Bwembya, R. Grinter, A. K. Powell, K. J. Webb, M. B. Hursthouse, K. M. Abdul Malik, M. A. Mazid, *Inorg. Chem.* **1994**, *33*, 2290−2296.
[14] B. Müller, A. Schneider, M. Tesmer, H. Vahrenkamp, *Inorg. Chem.* **1999**, *38*, 1900−1907.
[15] W. B. Price, S. Smiles, *J. Chem. Soc.* **1928**, 2372−2374; A. Zweig, A. K. Hoffmann, *J. Org. Chem.* **1965**, *30*, 3997−4001.
[16] W. P. Bosman, H. G. M. van der Linden, *J. Chem. Soc., Chem. Commun.* **1977**, 714−715.
[17] W. Baratta, I. Bernal, F. Calderazzo, J. D. Korp, L. S. Magill, F. Marchetti, D. Vitali, *Gazz. Chim. Ital.* **1996**, *126*, 469−474.
[18] S. A. Gamage, R. A. J. Smith, *Tetrahedron* **1990**, *46*, 2111−2128.
[19] Y. Kai, M. Morita, N. Yasuoka, N Kasai, *Bull. Chem. Soc. Jpn.* **1985**, *58*, 1631−1635.
[20] A. Meissner, W. Haehnel, H. Vahrenkamp, *Chem. Eur. J.* **1997**, *3*, 261−267.
[21] M. Förster, R. Burth, A. K. Powell, T. Eiche, H. Vahrenkamp, *Chem. Ber.* **1993**, *126*, 2643−2648.

[22] Crystallographic data for the structures reported in this paper have been deposited with the Cambridge Crystallographic Data Centre as supplementary publication no. CCDC-150527 (for **4**) and -150528 (for **5**). Copies of these data can be obtained free of charge on application to CCDC, 12 Union Road, Cambridge CB2 1EZ [Fax: (internat.) +44-1223/336-033; E-mail: deposit@ccdc.cam.ac.uk].

[23] G. M. Sheldrick, *SHELX-86* and *SHELXL-93*, *Programs for Crystal Structure Determination*, Universität Göttingen, **1986** and **1993**.

[24] E. Keller, *SCHAKAL for Windows*, Universität Freiburg, **1998**.

Received October 9, 2000
[I00380]

Preparation and Crystal Structure of $Na_7Ba_{14}CaN_6$: A New Subnitride in the $Na_xBa_{14}CaN_6$ Series

Grigori V. Vajenine[a] and Arndt Simon*[a]

Dedicated to Professor Kurt Dehnicke on the occasion of his 70th birthday

Keywords: Barium / Calcium / Sodium / Nitrides / Cluster compounds / Subvalent compounds / Structure elucidation

The crystal structure of a new subnitride, $Na_7Ba_{14}CaN_6$, could be solved and refined based on single crystal and powder X-ray diffraction data. The compound contains $Ba_{14}CaN_6$ clusters, which are arranged in a Na matrix as in the other subnitrides of the $Na_xBa_{14}CaN_6$ (x = 8, 14, 17, 21, 22) series. The $Ba_{14}CaN_6$ clusters form a slightly distorted ccp arrangement, with octahedral holes filled by Na_7 units and with tetrahedral holes remaining empty. Details of the crystal structure, such as packing and occurrence of voids, are compared to these in closely related $Na_8Ba_{14}CaN_6$. Preparations of samples composed mostly of $Na_7Ba_{14}CaN_6$ and intergrown crystals of $Na_7Ba_{14}CaN_6$ and $Na_8Ba_{14}CaN_6$ are described.

Introduction

In a recent publication[1] the crystal structure and preparation of a new member of the $Na_xBa_{14}CaN_6$ series with x = 8 was reported. This compound joined the family of the previously known $Na_{14}Ba_{14}CaN_6$,[2,3] $Na_{17}Ba_{14}CaN_6$,[3] $Na_{21}Ba_{14}CaN_6$,[3] and $Na_{22}Ba_{14}CaN_6$.[3,4] All of these compounds feature $Ba_{14}CaN_6$ clusters, which are bonded ionically in their interior and bonded metallically to Na atoms between the clusters.

While probing various synthetic routes leading to $Na_8Ba_{14}CaN_6$, X-ray powder diffraction patterns, presumably belonging to further phases in the $Na_xBa_{14}CaN_6$ series, were observed.[1] One of these phases could be identified as $Na_7Ba_{14}CaN_6$. Below we report the preparation and crystal structure of this new subnitride.

Results and Discussion

The crystal structure of the new phase $Na_7Ba_{14}CaN_6$ is closely related to that of the recently reported $Na_8Ba_{14}CaN_6$.[1] Both structures are built from nearly identical hexagonal layers of $Ba_{14}CaN_6$ clusters separated by sodium atoms, as shown in Figure 1 and 2. This specific type of cluster is a condensate of six face-sharing Ba_5CaN octahedra, as described earlier.[2,3] While in the case of $Na_8Ba_{14}CaN_6$ these clusters stack on top of each other (Figure 2), rhombohedral stacking, a distorted variant of ccp arrangement, is observed in $Na_7Ba_{14}CaN_6$ (Figure 1); because of this, the sodium chains filling the available channels between the clusters in $Na_8Ba_{14}CaN_6$ are interrupted with a formal loss of one sodium atom per cluster. The sodium atoms in $Na_7Ba_{14}CaN_6$ can be viewed as clustered in Na_7 units (Figure 3), although this viewpoint is purely formal. This provides, however, a different approach to describe the structure of the subnitride. If one considers the centers of mass of the Na_7 and $Ba_{14}CaN_6$ blocks in $Na_7Ba_{14}CaN_6$, the trigonally distorted NaCl structure type emerges: while the $Ba_{14}CaN_6$ clusters are arranged in a

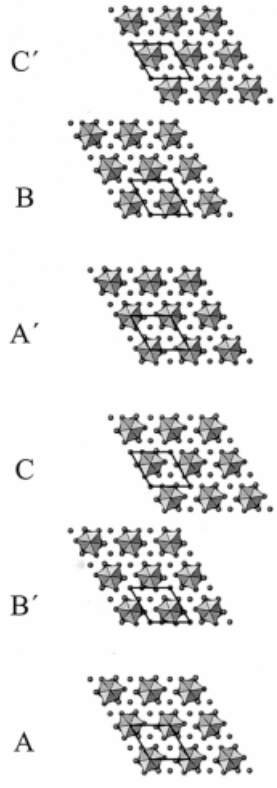

Figure 1. Six layers of $Ba_{14}CaN_6$ clusters with sodium atoms in between comprising a repeat unit of $Na_7Ba_{14}CaN_6$ in the [001] direction viewed along the c-axis; the unit cell is outlined; the nearly ccp arrangement of the clusters is indicated by the AB′CA′BC′ labelling, where the primed and unprimed layers differ in the cluster orientation; this layer representation is purely formal, it does not imply strong anisotropy in bonding

[a] Max-Planck-Institut für Festkörperforschung, Heisenbergstraße 1, 70569 Stuttgart, Germany

 © WILEY-VCH Verlag GmbH, 69451 Weinheim, 2001 1434−1948/01/0505−1189 $ 17.50+.50/0

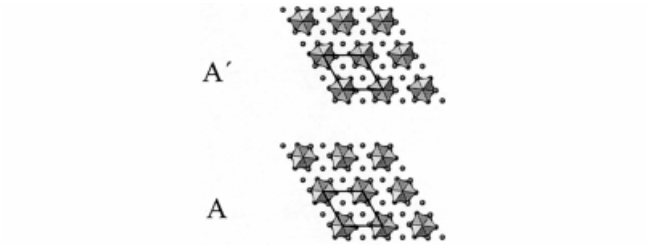

Figure 2. Two layers of $Ba_{14}CaN_6$ clusters with sodium atoms in between comprising a repeat unit of $Na_8Ba_{14}CaN_6$ in the [001] direction viewed along the *c*-axis; the unit cell is outlined; the simple hexagonal packing of the clusters is indicated by the AA′ labelling, where the primed and unprimed layers differ in the cluster orientation (using the same symbols A and A′ in Figures 1 and 2 ignores the slightly different cluster orientation: while the A′ layers are practically identical in both figures, the A layers differ)

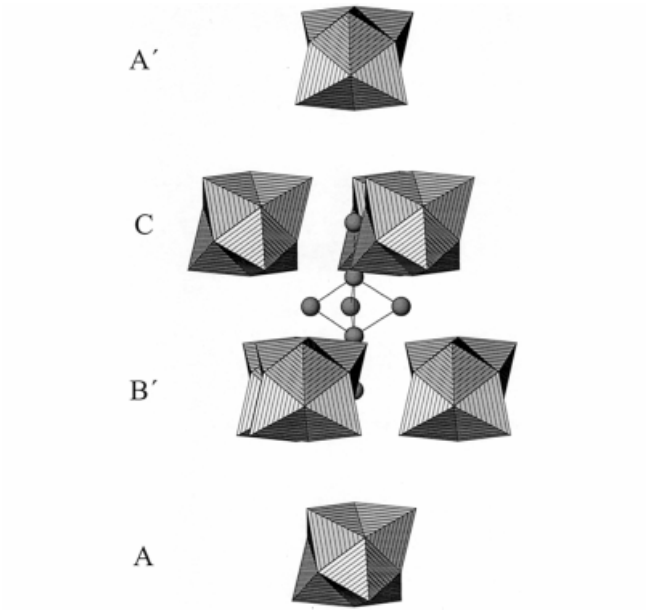

Figure 3. An Na_7 unit in an octahedral hole of the nearly ccp arrangement of $Ba_{14}CaN_6$ clusters in $Na_7Ba_{14}CaN_6$ (the *c*-axis is vertical); the labelling of the cluster layers is the same as in Figure 1

nearly ccp fashion as mentioned above, with the effective *c*/*a* ratio only 13% greater than that of the ideal cubic lattice, the Na_7 units occupy all octahedral holes.

Details of the crystallographic data for $Na_7Ba_{14}CaN_6$ can be found in Table 1. All interatomic distances (see Table 2) in $Na_7Ba_{14}CaN_6$ are similar to these in the other $Na_xBa_{14}CaN_6$ compounds. The intracluster distances are compared to those of $Na_8Ba_{14}CaN_6$ in Table 2; these are characteristic of ionic bonding.[2] The Na−Na (3.44, 3.77, and 3.80 Å) and Na−Ba (4.01−4.51 Å) distances are also in the range of the values observed in the other subnitrides of the series and are indicative of metallic bonding.[2] The intercluster Ba−Ba (4.767 and 4.781 Å) contacts are almost identical to those in $Na_8Ba_{14}CaN_6$.

The displacement factors for the sodium atoms (Table 3 and 4) are relatively large, which also has been linked to the metallic nature of the Na−Na and Na−Ba bonding.[1] In addition, two sodium positions feature strongly elongated thermal ellipsoids (split position refinement was unsuccessful). This, however, could be due to the chemical environment of these sodium atoms: thermal motion along the *c*-direction is much easier, as for the similar positions in $Na_8Ba_{14}CaN_6$, where thermal ellipsoids elongated parallel to the *c*-axis are also observed for the sodium atoms in the channels between $Ba_{14}CaN_6$ clusters.

A strong anisotropy of the Na thermal ellipsoids could also be caused by the presence of voids in the crystal structure of $Na_7Ba_{14}CaN_6$, which are similar to those found in the other compounds of the $Na_xBa_{14}CaN_6$ series. In an earlier investigation[3] it was definitely ruled out that these voids are due to the presence of contaminants, in particular hydrogen. We therefore anticipate that the voids in the structure of $Na_7Ba_{14}CaN_6$ are empty, too, in spite of the presence of hydrogen in the investigated sample as indicated by the contamination by Ba_2NH. The largest void in $Na_7Ba_{14}CaN_6$, located at (0,0,0.1106), is surrounded by a distorted cube of four Na and four Ba atoms (Figure 4). The distances from these atoms to the center of the void are 3.16 Å [Ba(3), 3×], 3.47 Å [Na(1), 1×], 3.66 Å [Ba(1), 1×], and 4.40 Å [Na(3),

Table 1. Details of the single crystal and powder diffraction investigations on $Na_7Ba_{14}CaN_6$

	Single crystal data	Powder data
Radiation, wavelength	Mo-K_α, 0.71073 Å	Cu-$K_{\alpha1}$, 1.54051 Å
Crystal system, space group	Rhombohedral, $R\bar{3}c$ (No. 167), $Z = 6$	
Unit cell dimensions	a = 11.35(1) Å [a]	a = 11.360(1) Å
	c = 62.85(5) Å [a]	c = 63.061(7) Å
Unit cell volume, d_{calc}	7009(11) Å^3 [a]	7048(2) Å^3, 3.121(1) g/cm^3
Refinement method	Full-matrix least-squares	Full profile
2θ and index ranges	3.88°−56.68°	7°−35°
	$-14 \le h,k \le 14$, $-83 \le l \le 83$	$-4 \le h,k \le 4$, $-22 \le l \le 22$
Reflections measured/unique	19286/1931 ($R_{internal}$ = 8.6%)	70
Data/restraints/parameters	1931/0/44	1401/5/18
Final R values	$R1(2\sigma)$ = 13.1%	R(intensity) = 4.8%
	$R1$(all) = 13.5%	R(profile) = 12.8%
	$wR2$(all) = 34.8%	
Largest diff. peak and hole	8.98 and −2.80 Å^{-3}	

[a] The unit cell constants for two investigated crystals differed [a = 11.335(1) Å and c = 62.89(1) Å for one, a = 11.361(1) Å and c = 62.80(1) Å for the other]; the values given in the table are averages of the two data sets. The structure solution and refinement were carried out using the data collected on the first crystal.

Table 2. Bond lengths within the $Ba_{14}CaN_6$ cluster in $Na_7Ba_{14}CaN_6$; the corresponding values for $Na_8Ba_{14}CaN_6$ are given in the rightmost column for comparison; the site symmetry of the cluster is S_6 ($\bar{3}$) in both compounds

Distance (labels of $Na_7Ba_{14}CaN_6$)	Multiplicity (per $Ba_{14}CaN_6$ cluster)	$Na_7Ba_{14}CaN_6$	$Na_8Ba_{14}CaN_6$[1]
Ca(1)−N(1)	6×	2.59(3)	2.560(3)
Ba(1)−N(1)	6×	2.79(3)	2.742(3)
Ba(2)−N(1)	6×	2.71(3)	2.747(3)
	6×	2.77(3)	2.765(4)
	6×	2.84(3)	2.802(4)
Ba(3)−N(1)	6×	2.43(3)	2.463(3)
Ba(1)−Ca(1)	2×	3.318(3)	3.2540(5)
Ba(2)−Ca(1)	6×	3.287(2)	3.2968(3)
Ba(1)−Ba(2)	6×	3.821(3)	3.8091(4)
Ba(2)−Ba(2)	6×	3.788(3)	3.7799(4)
Ba(1)−Ba(3)	6×	4.102(2)	4.0588(4)
Ba(2)−Ba(3)	6×	4.098(3)	4.1262(5)
	6×	4.137(3)	4.1442(6)
	6×	4.158(3)	4.1481(5)

Table 3. Atomic coordinates and equivalent isotropic displacement parameters (Å^2) for $Na_7Ba_{14}CaN_6$; U_{eq} is defined as one third of the trace of the orthogonalized U_{ij} tensor

Atom	Position	x	y	z	U_{eq}
Ba(1)	12c	0	0	0.0526(1)	0.029(1)
Ba(2)	36f	0.2935(2)	0.0471(2)	0.0172(1)	0.032(1)
Ba(3)	36f	0.3213(2)	0.3880(2)	0.0465(1)	0.041(1)
Ca(1)	6b	0	0	0	0.021(2)
Na(1)	12c	0	0	0.1656(7)	0.067(10)
Na(2)	12c	0	0	0.2201(6)	0.060(9)
Na(3)	18e	0.709(2)	0	1/4	0.051(6)
N(1)	36f	0.164(3)	0.203(3)	0.0238(4)	0.031(6)

Table 4. Anisotropic displacement parameters (Å^2) for $Na_7Ba_{14}CaN_6$; the anisotropic displacement factor exponent takes the form: $-2\pi^2[h^2(a^*)^2U_{11} + ... + 2hka^*b^*U_{12}]$

Atom	U_{11}	U_{22}	U_{33}	U_{23}	U_{13}	U_{12}
Ba(1)	0.031(1)	U_{11}	0.027(1)	0	0	$U_{11}/2$
Ba(2)	0.026(1)	0.037(1)	0.033(1)	0.001(1)	−0.004(1)	0.016(1)
Ba(3)	0.035(1)	0.033(1)	0.040(1)	−0.009(1)	−0.006(1)	0.006(1)
Ca(1)	0.020(4)	U_{11}	0.023(6)	0	0	$U_{11}/2$
Na(1)	0.029(8)	U_{11}	0.14(3)	0	0	$U_{11}/2$
Na(2)	0.021(7)	U_{11}	0.14(3)	0	0	$U_{11}/2$
Na(3)	0.063(15)	0.061(11)	0.030(10)	0.008(5)	0.015(10)	0.031(7)
N(1)	0.027(13)	0.035(14)	0.032(13)	−0.006(11)	0.000(10)	0.015(12)

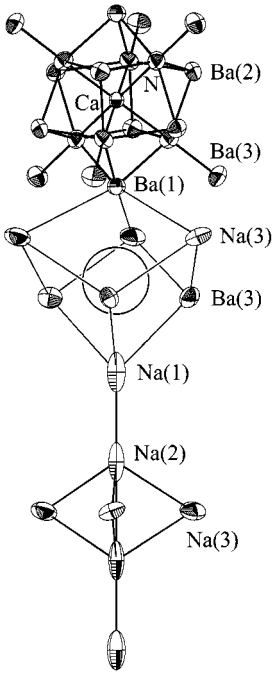

Figure 4. A fragment of the $Na_7Ba_{14}CaN_6$ structure with a $Ba_{14}CaN_6$ cluster (top), a Na_7 fragment (bottom), and the largest void (middle); the rather cube-like surrounding of the void is emphasized; the thermal ellipsoids are drawn for all atoms, the c-axis is vertical

3×]. The strongly anisotropic thermal ellipsoids of the sodium atoms may be considered a consequence of the preferred thermal motion in the direction of the void. We also note that these voids represent the tetrahedral holes in the ccp arrangement of the $Ba_{14}CaN_6$ clusters.

Experimental Section

Preparations: Due to the extreme sensitivity to air and moisture of all substances involved, these were handled either under high vacuum (10^{-6}−10^{-5} mbar) or under purified argon. Preparation of distilled metallic Ba, filtered metallic K, Na−K alloy, and the mixed subnitride $Ba_{1.83}Ca_{0.17}N$ have been described in detail previously. All syntheses mentioned below were carried out, unless stated otherwise, in cleaned Ta containers sealed under argon; these containers were themselves also sealed under argon in Duran glass ampoules. For details of these procedures refer to ref.[1]

$Na_{14}Ba_{14}CaN_6$ was prepared from metallic Ba (291.4 mg, 2.12 mmol), $Ba_{1.83}Ca_{0.17}N$ (1156 mg, 4.24 mmol), and Na-rich Na−K alloy (1300 mg; 31 mmol Na and 15 mmol K). The reagents with the overall stoichiometry $K_{21}Na_{45}Ba_{14}CaN_6$ were mixed and heated to 120 °C, then held at this temperature for a year. During the course of the reaction the ampoule was taken out four times for a short time and gently shaken. The solid reaction product was separated from excess alloy in a press. The product is $Na_{14}Ba_{14}CaN_6$ (the observed reflections matched the expected pattern of the cubic structure with a = 17.895 Å as reported in ref.[2]) with about 10 wt.% of a $NaBa_3N$ impurity (hexagonal with a = 8.4414 Å and c = 6.9817 Å[5]) according to X-ray diffraction. NaBa

was prepared as described in ref.[6] Equimolar amounts of Na and Ba were mixed in a Duran glass container and heated under argon at 140°C for two days. The resulting diffraction pattern matched that of the cubic structure with a = 17.027 Å.[7]

Single crystals of $Na_7Ba_{14}CaN_6$ were obtained in the following way. In sample A, $Ba_{1.83}Ca_{0.17}N$ (687.9 mg, 2.50 mmol), NaBa (203.4 mg, 1.27 mmol), and Na (49.4 mg, 2.2 mmol) with an approximate $Na_8Ba_{14}CaN_6$ overall stoichiometry were mixed, pressed into a pellet, and heated to 192 °C for 10 days, then held at 220 °C for 52 days and at 250 °C for 42 days with intermediate grindings of the pellet. This product (635.4 mg, 0.285 mmol "$Na_8Ba_{14}CaN_6$") was then mixed with K-rich Na−K alloy (206.0 mg; 0.96 mmol Na and 4.7 mmol K), yielding a $K_{17}Na_{11}Ba_{14}CaN_6$ overall stoichiometry. The mixture was heated to 350 °C and held at this temperature for 20 days, then cooled at 0.5°C/hour to 220 °C, held at 220 °C for 24 days, and finally cooled to room temperature by switching off the furnace. Crystals were manually selected from the resulting alloy-solid mixture and sealed under argon in glass capillaries.

A sample composed mostly of $Na_7Ba_{14}CaN_6$ was obtained by extracting sodium from $Na_{14}Ba_{14}CaN_6$ with metallic potassium. In sample B, $Na_{14}Ba_{14}CaN_6$ (217.8 mg, 0.091 mmol) was mixed with potassium (109.2 mg, 2.80 mmol), the resulting molar ratio being K:$Na_{14}Ba_{14}CaN_6$ = 31:1. The mixture was heated to 250 °C for 10 days, cooled at 0.2 °C/hour to 150 °C, and then finally cooled at 0.5 °C/hour to room temperature. Na−K alloy formed in the course of the reaction; the solid residue was separated from the alloy in a press. A portion of the solid product was ground together with glass powder and sealed in a 0.3 mm glass capillary for powder X-ray diffraction analysis.

Crystal Structure Investigations: Crystals obtained from sample A were first tested on a precession camera. Already at this stage it was apparent that most crystals were either pure $Na_8Ba_{14}CaN_6$ (hexagonal with a = 11.419 Å and c = 21.543 Å[1]) or intergrown with crystals of another phase, which is rhombohedral with the a-axis being practically the same as that of the $Na_8Ba_{14}CaN_6$ phase and the c-axis approximately three times that of the $Na_8Ba_{14}CaN_6$ phase, suggesting a structural similarity between the two phases. Two crystals featuring the largest fraction of the new phase (about 50%) were further investigated on a STOE image-plate diffractometer (IPDS). It was possible to separate the reflections belonging to the new phase from those belonging to $Na_8Ba_{14}CaN_6$; the poor quality of the obtained reflection data also introduced some ambiguity in finding the correct space group (see above). The initial measurement of the lattice parameters for the crystals yielded a = 11.35(1) Å and c = 62.85(5) Å (see footnote to Table 1). Using the linear V/Z vs. x correlation in the $Na_xBa_{14}CaN_6$ series,[1] the approximate x value of 6.7 could be obtained, suggesting that the new phase might have the stoichiometry $Na_7Ba_{14}CaN_6$.

Crystal structure solution was attempted based on the data collected at room temperature on one of the two crystals using direct methods (SHELXS-97), followed by full-matrix least-squares structure refinement (SHELXL-97).[8] The structure could be solved in space groups $R\bar{3}$ (No.148), $R32$ (No. 155), and $R3c$ (No. 161); their common subgroup $R3$ (No. 146) could, of course, also be used. A closer inspection of the structures obtained in these space groups revealed their mutual similarity, hence a refinement in the common supergroup $R\bar{3}c$ (No. 167) was attempted. All atoms could be refined anisotropically yielding indeed the stoichiometry $Na_7Ba_{14}CaN_6$ and chemically reasonable distances and displacement factors. The final R value of 13.1% was, however, a cause for concern. Closer inspection of the data set revealed that this relatively high value was mainly due to the inconsistency of equivalent reflections as indicated by the $R_{internal}$ value of 8.6%. This could have been caused by incomplete separation of reflections of $Na_7Ba_{14}CaN_6$ and $Na_8Ba_{14}CaN_6$. The large final R value is also manifested by substantial peaks in the Fourier difference map, the largest of which lie within 1.2 Å of the Ba(3) position.

In order to support the structural solution obtained from the single crystal diffraction data, a Rietveld refinement of the powder diffraction data, which were collected with sample B on a STADI-P STOE diffractometer with Cu-$K_{\alpha 1}$ radiation at room temperature, was attempted using the CSD package.[9] Before the refinement, the impurity reflections belonging to Ba_2NH (≈10 wt.%), $Na_8Ba_{14}CaN_6$ (≈5 wt.%), and $NaBa_3N$ (≈5 wt.%) were removed from the pattern (Figure 5). The refinement was carried out in the 2θ range from 7° to 35°. While the isotropic displacement factors for the barium atoms could be refined, those for all other atoms had to be fixed at the values obtained in the refinement of the single crystal diffraction data. The positions of the atoms obtained in the Rietveld refinement were less accurate than those deduced from the single crystal diffraction data, though both sets were within error bars from each other. The Rietveld refinement resulted in more accurate unit cell parameters: a = 11.360(1) Å and c = 63.061(7) Å. The corresponding unit cell volume leads to the improved x value of 6.9 in $Na_xBa_{14}CaN_6$, if the linear V/Z vs. x correlation[1] is employed.

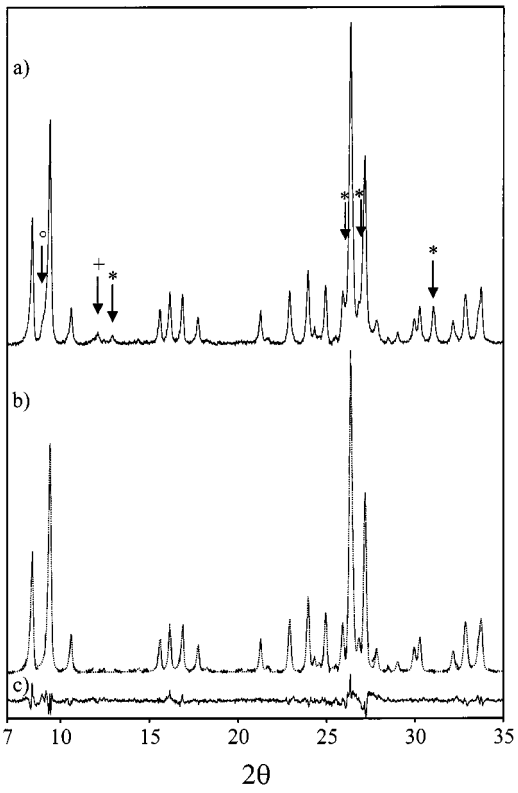

Figure 5. Measured X-ray diffraction pattern of $Na_7Ba_{14}CaN_6$: (a) strong reflections of impurity phases are indicated with arrows: $Na_8Ba_{14}CaN_6$ (°), $NaBa_3N$ (+), and Ba_2NH (*); these impurity reflections were removed from the pattern before Rietveld refinement was carried out; (b) the solid line represents the measured data and the dotted line shows the calculated curve; the difference between the two lines is plotted below (c)

Refinement of Guinier diffraction data (23 reflections) leads to similar lattice constants: a = 11.368(4) Å and c = 63.094(14) Å. In

addition, decomposition of $Na_7Ba_{14}CaN_6$ at ≈272 °C could be observed in a temperature-dependent Guinier measurement. The strongest reflections of the resulting diffraction pattern belong to $Na_8Ba_{14}CaN_6$.

The results of the single crystal and powder diffraction investigations are combined as follows. The unit cell parameters are taken from the Rietveld refinement (see Table 1 for refinement details), but the atomic positions (Table 3) and the anisotropic displacement factors (Table 4) are taken from the refinement of the single crystal diffraction data (see also Table 1 for details).

Further details of the crystal-structure investigation may be obtained from the Fachinformationszentrum Karlsruhe, 76344 Eggenstein-Leopoldshafen, Germany, on quoting the depository number CSD-411488.

Acknowledgments

The authors thank Dr. O. Oeckler for collecting and help with analyzing the single crystal diffraction data, Dr. J. Köhler for providing programs to analyze crystal structures for voids and for help with Rietveld refinement, and W. Röthenbach for temperature-dependent Guinier measurements. Thanks are also due to the Max Planck Society and the Alexander von Humboldt Foundation for providing G.V.V. with financial support during this study.

[1] G. V. Vajenine, U. Steinbrenner, A. Simon, *C. R. Acad. Sci. Paris Ser. IIc* **1999**, 583−589.
[2] U. Steinbrenner, A. Simon, *Angew. Chem.* **1996**, *108*, 595−597; *Angew. Chem. Int. Ed. Engl.* **1996**, *35*, 552−554.
[3] A. Simon, U. Steinbrenner, *J. Chem. Soc., Faraday Trans.* **1996**, *92*, 2117−2123.
[4] U. Steinbrenner, A. Simon, *Z. Kristallogr.* **1997**, *212*, 428−438.
[5] P. E. Rauch, A. Simon, *Angew. Chem.* **1992**, *104*, 1505−1506; *Angew. Chem. Int. Ed. Engl.* **1992**, *31*, 1519−1521.
[6] U. Steinbrenner, *Ph.D. Thesis*, Stuttgart, Germany, **1997**.
[7] G. J. Snyder, A. Simon, *J. Chem. Soc., Dalton Trans.* **1994**, 1159−1160.
[8] SHELXTL Version 5.1, Bruker AXS, 1998.
[9] L. G. Akselrud, Yu. N. Grin, P. Yu. Zavalij, V. K. Pecharsky, V. S. Fundamenskii, CSD − Universal program package for single crystal and/or powder structure data treatment (http://imr.chem.binghamton.edu/zavalij/CSD.html). 12th European crystallographic meeting: Abstract of papers, Moscow, 3, 155, (**1989**).

Received September 27, 2000
[I00369]

Solvates of Lithium Tetrahydridoborates with Various Amines: From Molecular to Extended Structures of Lithium Tetrahydridoborate[‡]

Hans Herrmann Giese,[a] Tassilo Habereder,[a] Jörg Knizek,[a] Heinrich Nöth,*[a] and Marcus Warchhold[a]

Dedicated to Prof. Dr. Dr. h. c. Gerhard Fritz on the occasion of his 80th birthday

Keywords: Lithium / Borates / Coordination chemistry

Several solvates of $LiBH_4$ with amines have been prepared and characterized by X-ray structure determinations. $LiBH_4{\cdot}3H_2NPh$ (**1**) is monomeric with a triply bridging BH_4 group. $LiBH_4{\cdot}2en$ (**3**) is shown to be an ionic compound containing chains of cationic $[Li(en)_2)]^+$ units. In contrast, the BH_4 group of $LiBH_4{\cdot}$triene (**4**) forms triple hydride bridges to the Li centers of a Li(triene) chain, making the Li atoms hexacoordinated by 3 × N and 3 × H atoms. Reaction of $LiBH_4$ with *tert*-butylamine generates the compound $3LiBH_4{\cdot}4H_2NtBu$ (**2**). The structure of **2** consists of an infinite chain of $LiBH_4$ units having three different kinds of Li centers, two of which have an environment of 2 × N and 4 × H atoms, whereas the third type is surrounded by five hydrogen atoms. Pyrrolidine reacts with $LiBH_4$ to give $LiBH_4{\cdot}HNC_4H_8$ (**5**), the structure of which in the solid state shows an infinite chain with heptacoordinated Li centers (N and 6 × H). In contrast, dibenzylamine gives the compound $LiBH_4{\cdot}2HN(CH_2Ph)_2$ (**6**), which is dimeric with hexacoordinated Li centers (2 × N and 4 × H) in the crystal, and a similar structure was found for $LiBH_4{\cdot}(i\text{PrNCH}_2)_3$ (**7**) but with heptacoordinated Li ions (3 × N and 4 × H). Addition of $(MeNCH_2)_3$ to $LiBH_4$ in toluene leads to $4LiBH_4{\cdot}2(MeNCH_2)_3$ (**8**), in which the two amine ligands bind to two Li ions, Li1 being hexacoordinated by (4 + 2) N atoms, Li2 by 2 × N atoms and 4 × H atoms from two different BH_4 groups. Li2 is part of a layer structure composed of $Li_3(BH_4)_4^-$ units. In contrast, a chain structure is evident in $3LiBH_4{\cdot}2(PhCH_2NCH_2)_3$ (**9**), as shown by the presence of separate $Li[(PhCH_2NCH_2)_3]_2$ cations and $Li_2(BH_4)_3$ anionic building blocks.

Introduction

Alkali metal tetrahydridoborates, particularly $NaBH_4$, are commercially produced.[2] Large quantities of $NaBH_4$ are used for the bleaching of pulp[3] and it is also useful for depositing heavy metals in waste water.[4] $LiBH_4$, on the other hand, is a very useful reducing agent of wide applicability.[5] Its reducing power is superior to that of $NaBH_4$ and its solubility is generally greater than that of $NaBH_4$. The solubility of $LiBH_4$ depends on the solvation of this compound by the solvent and a number of ether and amine solvates have been described in the literature.[4,6] However, in most cases, information about their structures in the crystal has not been available until recently.[6]

The structures of solvates of $LiBH_4{\cdot}n$L depend on the type and number (n) of ligand molecules (L). This results in a large variety of structures that range from mononuclear species through a preference for dinuclear molecules to extended chains and double chains to three-dimensional arrays. We report here new information on amine solvates of $LiBH_4$ that adds to the diversity of structures in the crystalline state but also shows that the BH_4 group is a particularly versatile ligand.[7]

Syntheses

It is well known that the alkali metal tetrahydridoborates, particularly $LiBH_4$ and $NaBH_4$, dissolve well in liquid ammonia or primary amines. Extraction of $NaBH_4$ from the solid mixture of $NaOMe/NaBH_4$ by isopropylamine is a known technical process.[8] An even better solvent is liquid ammonia, which dissolves 104 g of $NaBH_4$ in 100 mL,[9] while only 20 g of KBH_4 is soluble in the same amount of solvent.[10] Nevertheless, the composition of the solvates, particularly with primary amines, has yet to be well established in most cases.[11]

In the present work two routes have been used to obtain and isolate amine solvates of $LiBH_4$. The first method involves treatment of $LiBH_4$ with an excess of an amine in the presence of a nonpolar solvent such as toluene. In the second route, $LiBH_4$ is simply dissolved in the amine and the solvate isolated from the resulting solution. The ligand displacement reaction as depicted in Equation (2) was less successful. Reactions according to Equation (1) have been used to prepare compounds **1**–**9**.

$$LiBH_4 + n\text{L} \rightarrow LiBH_4 \cdot n\text{ L} \quad (1)$$

$$LiBH_4 \cdot OEt_2 + n\text{ L} \rightarrow LiBH_4 \cdot n\text{ L} + OEt_2 \quad (2)$$

We report here only on those amine solvates that were obtained in the form of single crystals. Our attempts to pre-

[‡] Metal Hydridoborates and (Hydridoborato)metalates, 27. – Part 26: Ref.[1]

[a] Department of Chemistry, University of Munich, Butenandtstraße 5–13, House D, 81377 Munich, Germany

 © WILEY-VCH Verlag GmbH, 69451 Weinheim, 2001 1434–1948/01/0505–1195 $ 17.50+.50/0

$LiBH_4 \cdot 3\,NH_2Ph$ **1** | $3\,LiBH_4 \cdot 4\,NH_2tBu$ **2** | $LiBH_4 \cdot 2$ en **3**

$LiBH_4 \cdot$ triene **4** | $LiBH_4 \cdot NHC_4H_8$ **5** | $LiBH_4 \cdot 2\,NH(CH_2Ph)_2$ **6**

$LiBH_4 \cdot (i\text{PrNCH}_2)_3$ **7** | $2\,LiBH_4 \cdot (\text{MeNCH}_2)_3$ **8** | $3\,LiBH_4 \cdot 2\,(\text{PhCH}_2\text{NCH}_2)_3$ **9**

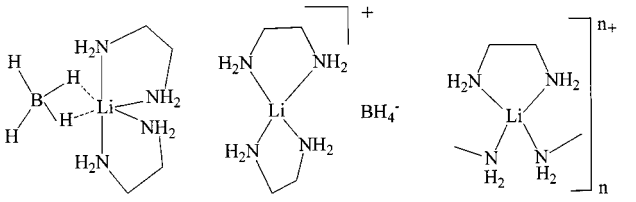

3a 3b 3c

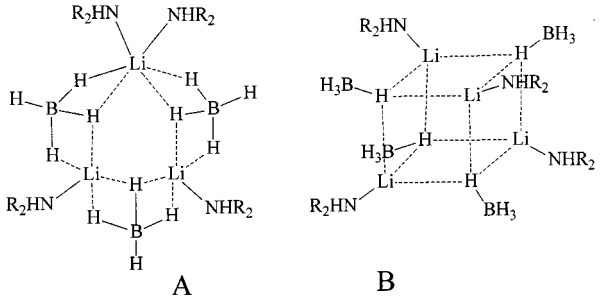

A B

pare single crystals of isopropylamine and ethylamine have so far failed. Even the solid products that we isolated were difficult to analyze due to rapid loss of amine. Therefore, their composition could not be reliably determined.

It should be noted that, according to ^{11}B NMR spectroscopic data, the amine not only solvates $LiBH_4$ but also removes a BH_3 group to form amine−borane adducts $L{\cdot}BH_3$ that are readily identified by the typical 1:3:3:1 quadruplet in the ^{11}B NMR spectra.[12] This kind of behavior is more pronounced for toluene solutions than for hexane solutions. In the case of the formation of **8**, a substantial amount of $(\text{MeNCH}_2)_3{\cdot}BH_3$ was formed; the compound was isolated and subjected to a crystal structure determination.[13]

NMR and IR Spectra

Although the structures of the $LiBH_4$ solvates in the solid state are of special interest, their state in solution is at least of the same importance because reactions, for instance the reduction of functional groups of organic compounds, are performed in solvents. However, knowledge about the structure in the solid state may be helpful in the assignment of IR data.

Table 1 summarizes the ^{11}B and ^{7}Li NMR spectroscopic data. It should be noted that there is only one ^{7}Li signal for each of the compounds investigated. This is, at first glance, a rather surprising observation. If the solid and solution state for the dimeric molecules $[LiBH_4{\cdot}(\text{MeNCH}_2)_3]_2$[6b] and $[LiBH_4{\cdot}(i\text{PrNCH}_2)_3]_2$ (**7**) were the same, one would expect only a single signal. However, the shielding should be different because in the former compound only two of the three ring nitrogen atoms coordinate to Li (in the solid state) while all three nitrogen atoms of the $(i\text{PrNCH}_2)_3$ ligand bind to the Li center. Indeed, the ^{7}Li NMR signal for the latter compound is better shielded. On the other hand, if the solid-state structure of compound **9** was retained in solution then one would expect at least two signals, one of them being highly shielded due to the coordination of one of the three Li centers (vide infra) to six nitrogen atoms. However, only a single signal is observed. Therefore, the ^{7}Li NMR spectrum is not compatible with the structure found in the crystal indicating dynamic behaviour in solution.

Table 1. $\delta^{7}Li$ and $\delta^{11}B$ data and coupling constants $^{1}J(^{11}B^{1}H)$ (1:4:6:4:1 quintuplets) for lithium tetrahydridoborate amine solvates

Compound	$\delta^{7}Li$	$\delta^{11}B$	$^{1}J(^{11}B^{1}H)$ [Hz]	Solvent
1	0.1	−38.0	81	aniline
2	1.07	−38.3	81	C_6D_6
3	2.0	−38.3	81	pyridine
4	1.7	−38.1	81	pyridine
5	1.32	−41.1	87	C_6D_6
6	–	−38.2	81	MeC_6H_{11}
7	0.097	−38.5	81	toluene
8	0.74	−38.6	96	toluene
9	0.347	−39.4	unresolved	C_6D_6

A considerable degree of deshielding occurs for compounds with an $LiBH_4$/N ratio close to 1:1. However, it is unlikely that the chain structure of $3LiBH_4{\cdot}4H_2NtBu$ is retained in solution. The chains are expected to break down into smaller units, possibly into units such as those suggested in formulas **A** (for **2**) or **B** (for **5**). A tetrameric unit is not unfeasible because such a unit has been found for

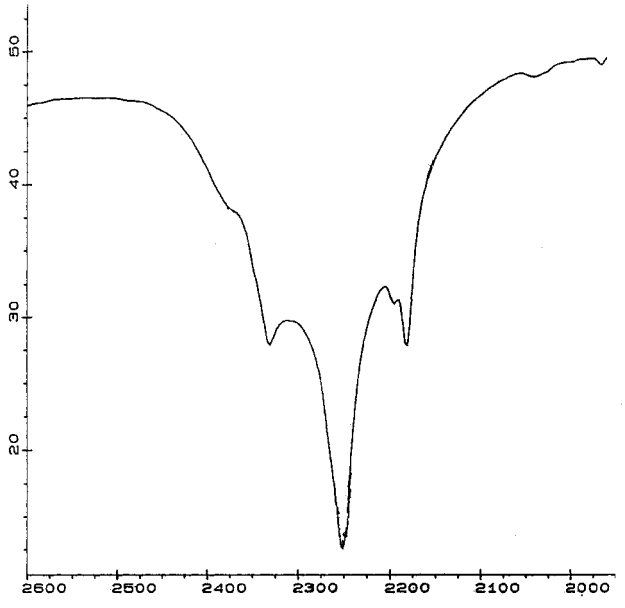

Figure 1. IR spectrum of $LiBH_4{\cdot}3H_2NPh$ (**1**) in Nujol; only the B−H stretching region is depicted

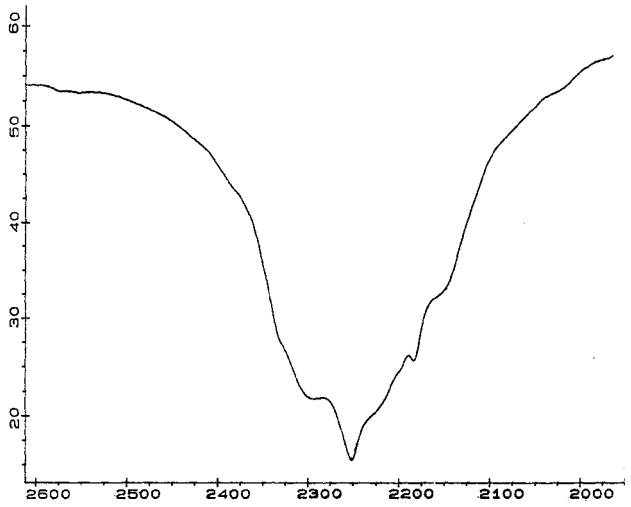

Figure 2. IR spectrum of $LiBH_4 \cdot 2en$ (**3**) in Nujol; only the B−H stretching region is shown

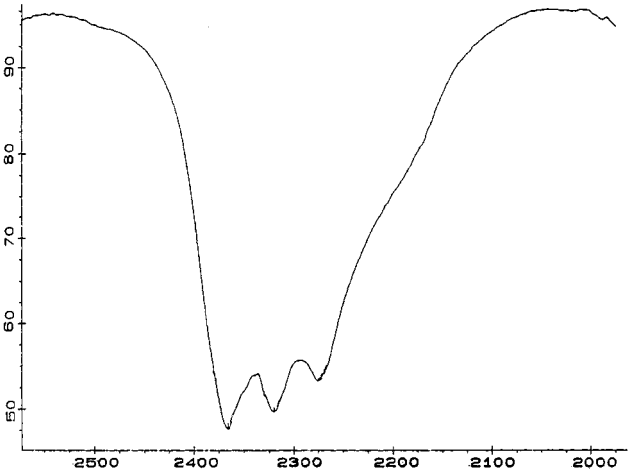

Figure 3. IR spectrum of $3LiBH_4 \cdot 4tBuNH_2$ (**2**) in Nujol showing the B−H stretching region

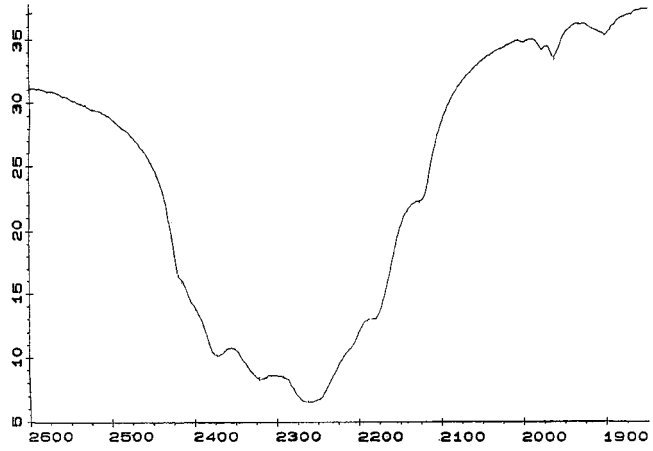

Figure 4. IR spectrum of $\{Li[(PhCH_2NCH_2)_3]_2\}Li_2(BH_4)_3$ (**9**) in Nujol showing the B−H stretching region

$[NaBH_4 \cdot L]_4$ (L = 1,4,7-trimethyl-1,4,7-triazacyclononane).[6b]

All compounds show only one 1:4:6:4:1 quintuplet for the BH_4 anion in the proton-coupled ^{11}B NMR spectrum except for compound **9**, which gave rise to a broad signal without fine structure due to B,H coupling. The $\delta^{11}B$ values span a narrow range from $\delta = -38.3$ to -41.1. Therefore, irrespective of the composition of the compounds, all BH_4 groups are chemically equivalent in solution, as are their H atoms. In addition, $^1J(BH)$ does not allow a structural distinction of the various Li···H−B interactions observed in the crystal structures.

Figure 1 (compound **1**), Figure 2 (**3**), Figure 3 (**2**), and Figure 4 (**9**) show some IR spectra measured from Nujol mulls and the values of the B−H stretching bands observed for compounds **1**−**9** are given in the Exp. Sect.

One might expect that the B−H stretching bands for $[LiBH_4(MeNCH_2)_3]_2$[6b] and **7** should be rather similar because both show the same type of bonding for the BH_4 group (vide infra). Nevertheless, noticeable differences do exist. Even if we neglect the shoulder at 2154 cm^{-1} for $[LiBH_4(MeNCH_2)_3]_2$, the wave numbers are sufficiently different for the two species, as exemplified by the strong bands at 2272 and 2366 cm^{-1} for the former and 2185 and 2378 cm^{-1} for the latter compound. The IR spectrum of compound **9**, with its $Li_2(BH_4)_3$ chain, shows four strong B−H stretching bands with two shoulders, all of which are rather broad. This spectrum is indicative of the presence of different BH_4 groups, and its features are similar to those of the IR spectrum in the B−H stretching region of compound **8** with its sheet-like arrangement of the $Li_3(BH_4)_4$ anionic lattice. In any case, the IR spectra of compounds

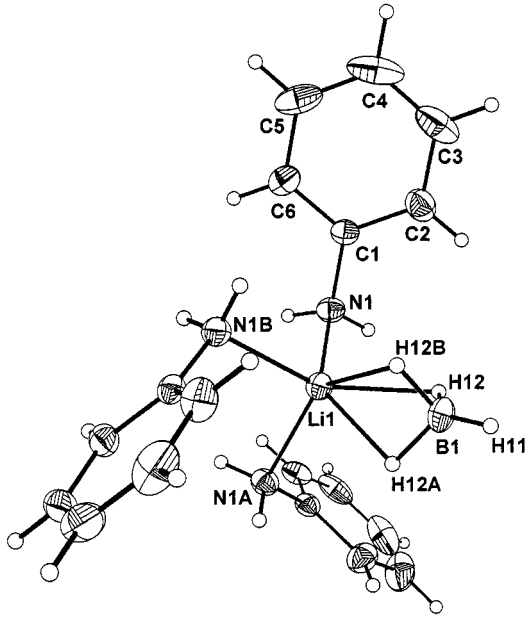

Figure 5. Molecular structure of $LiBH_4 \cdot 3NH_2Ph$ (**1**); only one of the two independent molecules is depicted; thermal ellipsoids represent a 25% probability; selected atom distances (in Å): molecule 1: Li1−N1 2.135(2), Li1···B1 2.279(6), N1−C1 1.416(2), B1−H11(term.) 0.86(5), B1−H12(bridge) 1.10(4); molecule 2: Li2−N2 2.137(2), Li2···B2 2.363(6), N2−C7 1.418(2), B2−H21(bridge) 0.89(5), B2−H22(term.) 0.94(4); selected bond angles (in °): molecule 1; N1−Li1−B1 116.1(1), C1−N1−Li1 113.6(1), N1−Li1−N1A 102.1(1), B1−H12−Li1 92(2), H11−B1−H12 120.9(2); molecule 2: N2−Li2−B2 112.5(1), C7−N2−Li2 113.3 (1), N7−Li2−N(7A) 106.3 (1), B2−H21−Li2 106(2), H21−B2−H22 126(3)

1−**9** do not allow unequivocal assignment to a specific bonding pattern of the BH_4 groups to the Li centers.

Structures of the Amine Solvates of $LiBH_4$

The most simple structure amongst the solvates of primary amines with $LiBH_4$ is the aniline solvate $LiBH_4 \cdot 3H_2NPh$, (**1**, see Figure 5). Compound **1** crystallizes trigonally in the space group $R3$ with $Z = 6$, i.e. there are two independent molecules in the unit cell. Both molecules have C_3 symmetry, with the threefold axis running through the Li and B atoms and the terminal hydrogen atom of a μ_3^1-BH_4 group. The Li−B distances in the two molecules are significantly different [Li1−B1 2.279(6), Li2−B2 2.363(6) Å]. This is due to different N−Li−B bond angles. At atom Li1 the angle is larger [116.1(1)°] than at atom Li2 [112.5(1)°]. However, the bond angles Li−N−C are identical for both molecules.

The crystals that separated from a toluene solution of $LiBH_4$ after addition of tBuNH$_2$ had the (unexpected) composition $3LiBH_4 \cdot 4t$BuNH$_2$ (**2**). This compound crystallizes monoclinically in the space group $C2/c$. Figure 6 represents the contents of the asymmetric unit.

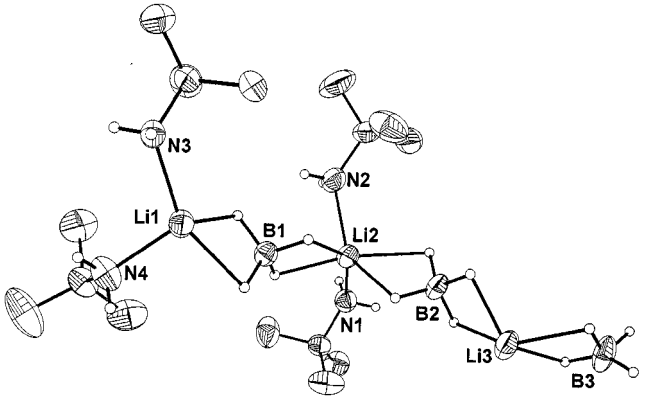

Figure 6. Molecular structure of $3LiBH_4 \cdot 4NH_2t$Bu (**2**) in the asymmetric unit; thermal ellipsoids are presented on a 25% probability scale; selected bond lengths (in Å): Li1−N4 2.076(5), Li1−N3 2.089(5), Li1···B1 2.476(5), B1···Li2 2.609(5), Li2−N1 2.086(5), Li2−N2 2.092(5), Li2···B2 2.500 (5), B2···Li3 2.404(6), Li3···B3 2.382(6); selected bond angles (in °): N3−Li1−N4 108.5(2), N4−Li1−3.1 112.6(2), N3−Li1−B1 127.8(2), B1−Li2−N1 121.9(2), B1−Li2−N2 90.2(2), B2−Li2−B1 116.1(2), N2−Li2−B2 122.1(2), B2−Li3−B3 125.2(2)

It should be noted that there are *three* different Li centers, and it is clear that only atom Li2 is coordinatively saturated (e.g. hexacoordinated) while atoms Li1 and Li3 are not. Only two of the three Li centers bind to two amine molecules each, while atom Li3 does not bear an amine ligand. The N−Li−N bond angles at Li1 and Li2 are close to tetrahedral [N3−Li1−N4, N1−Li2−N2 110.4(2)°]. If we consider the BH_4 group to be a pseudohalide − considering the boron atom as the center of a pseudofluoride − then we can assume that atom Li2 sits in a distorted tetrahedral environment, with bond angles Li−B−Li ranging from 98.1(2) to 122.1(2)°. However, the bridging hydrogen atoms are, of course, closer to the Li center than the boron atoms and are normally taken as the coordination partner. In this case it is clear that the H−Li−H bond angles must be rather sharp as a consequence of the tetrahedral BH_4 group. The typical feature of compound **2** is that, as far as the *asymmetric* unit is concerned, each BH_4 group acts as a $2\mu_2^1$ group. This is shown by the fact that we note two LiH_2B bridges from each BH_4 group to two *different* Li centers (see Figure 6). Inspection of the structure of **2** in the lattice shows that the molecular part of the asymmetric unit is the subunit of an extended chain (see Figure 7). We see that atom Li3 is surrounded by three BH_4 groups that supply, in total, five hydrogen atoms for coordination. For this $Li(BH_4)_3$ unit, two BH_4 groups retain one B−H bond in a terminal position and the other three H atoms form a double hydride bridge and a single bridge to atoms Li3 and Li3A, respectively. The third BH_4 group (B2) interacts with atom Li3 through two hydride bridges. Atom Li1 is hexacoordinated: There are two hydrogen atoms each from two different BH_4 groups (Figure 7). However, the group $B(1)H_4$ is exceptional because all four H atoms coordinate to Li centers (Li1, Li2). The bonding mode in this case is $2\mu_1^2,2\mu_1^1$.[6b] Li2 is also hexacoordinated, but in a different way to Li1 because the two adjacent BH_4 groups supply double hydride bridges. In summary, two Li atoms of **2** are hexacoordinated and one is pentacoordinated.

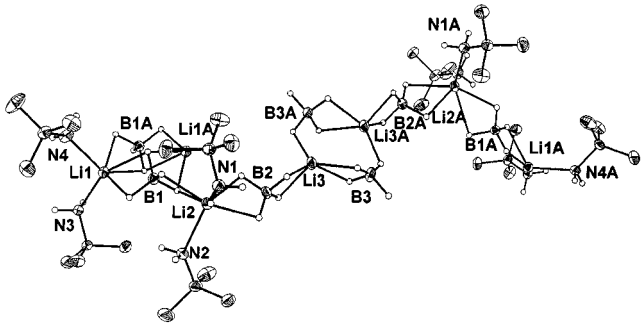

Figure 7. Chain arrangement of $3LiBH_4 \cdot 4NH_2t$Bu (**2**) in the lattice; note the pentacoordination at atom Li3

Ethylenediamine (en) is the simplest primary diamine. It forms the solvate $LiBH_4 \cdot 2$en (**3**) which by X-ray structure determination is shown to be the ionic compound $[Li(en)_2]BH_4$ in the solid state. The cationic part does *not* have the simple structure, as shown by formula **3b**. Rather the $Li(en)_2$ unit forms an extended chain (Figure 8) because every Li center is part of only one LiN_2C_2 five-membered ring. The second en molecule bridges the Li atoms as indicated in formula **3c**. The BH_4 groups do not coordinate with Li atoms. Figure 9 shows a view of the contents of **3** in the unit cell down the b axis.

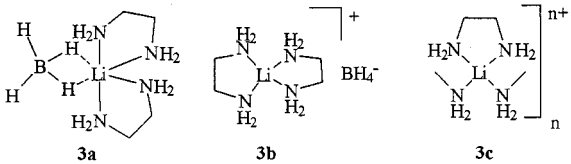

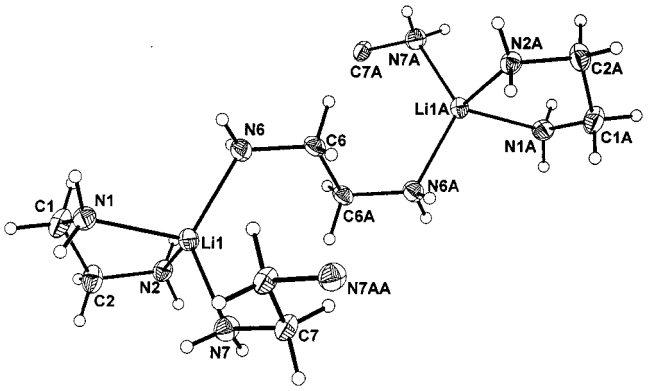

Figure 8. The $Li(en)_2$ chain in the lattice of $LiBH_4$·2en (**3**); only part of one of the two independent chains is presented but data are given for both cations; selected bond lengths (in Å): cation of molecule 1: N1−C1 1.468(3), N2−C2 1.466(2), N1−Li1 2.059(3), N2−Li1 2.052(3), N6−Li1 2.059(4), N7−Li1 2.071(4), B1−H 1.09(6)−1.16(3); cation of molecule 2: N3−C4 1.465(3), N4−Li3 1.464(3), N3−Li2 2.061(3), N4−Li2 2.059(4), N5−Li2 2.060(4), N8−Li2 2.065(4), B2−H 1.05(3)−1.16(3); selected bond angles (in °): C1−N1−Li1 102.5(2), C2−N2−Li1 102.8(1), N7−Li1−N6 123.7(2), N1−Li1−N6 108.8(2), N2−Li1−N7 100.6(2), N1−Li1−N7 113.6(2), N2−Li1−N6 111.0(2), N2−Li1−N1 88.3(1); for molecule 2: N4−Li2−N5 110.2(2), N5−Li2−N3 109.0(2), N5−Li2−N8 124.0(2), N4−Li2−N3 88.2(1), N4−Li3−N8 106.0(2), N3−Li2−N8 113.5(2)

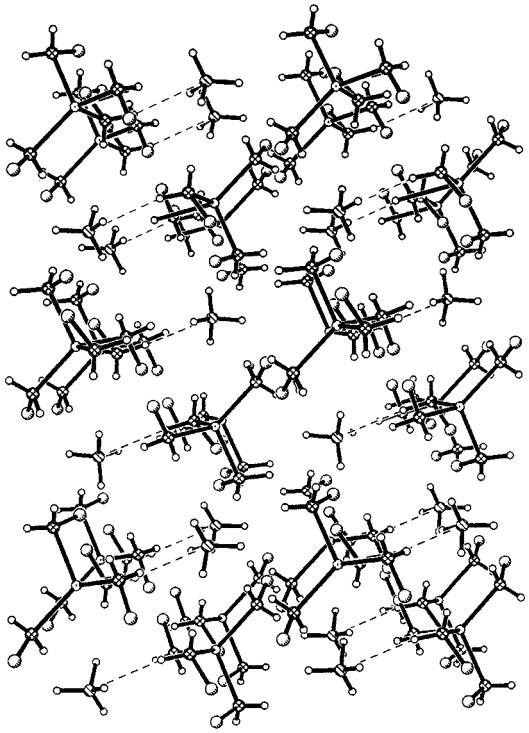

Figure 9. Plot of the structure of compound **3** in the crystal in a view down the *b* axis

The solvate of lithium tetrahydridoborate with diethylenetriamine has the composition $LiBH_4$·$(H_2N-CH_2-CH_2)_2NH$ (**4**). Figure 10 describes the structure of two formula units of **4** in the crystal which form part of an extended chain. Each Li atom is hexacoordinated by three nitrogen and three hydrogen atoms. Each BH_4 group supplies three hydrogen atoms through three Li···H−B bridges (μ_3^1-mode). Consequently, the Li···B atom distance is fairly short at 2.336(4) Å. The Li···N distances range from 2.085(3) to 2.161(3) Å, the longest bond being formed with the secondary nitrogen atom of the triamine. It is interesting that the amine does not act as a tridentate ligand in forming complex **4a**. Rather a chain structure results with a *syn* orientation of the BH_4 groups. Li···H distances span a small range, the shortest distance being 2.13 Å and the longest 2.29 Å, while the B···H distances to the terminal hydrogen atom H [1.17(3) Å] seem to be longer than the three bridge B−H bonds [1.03(3), 1.10(3), and 1.15(3) Å]. Inspection of the geometry of the BH_4 group reveals the presence of a distorted *tetrahedron* whose H−B−H bond angles can be quite narrow (103°) or quite open (122°). As expected, the N2−Li1−N3 bond angle of the LiN_2C_2 five-membered ring is small [85.8(1)°] while the bond angle N(1B)−Li1−N2 is tetrahedral [109.8(1)°]. Astonishingly, the N−C−C bond angles also vary significantly, the smallest one being 109.2(2)° and the largest 116.0(2)°.

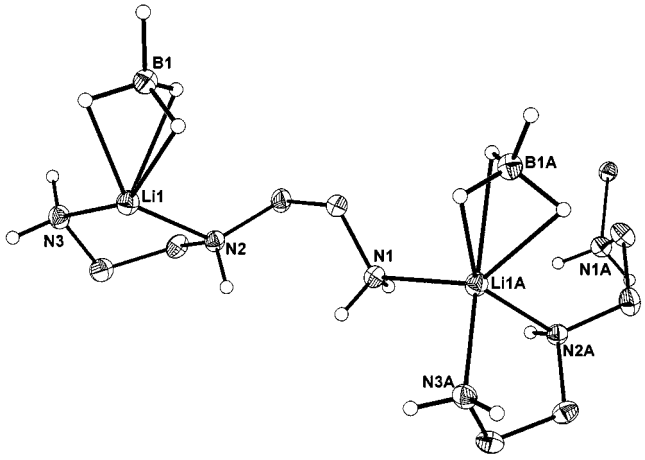

Figure 10. Structure of $LiBH_4$·triene (**4**); two molecular units that are part of a chain are depicted; thermal ellipsoids are drawn on a 25% probability scale; selected atom distances (in Å): Li1−N2 2.161(3), Li1−N3 2.085(3), Li1···B1 2.336(4), N1−Li1A 2.698(3), B−H (term.) 1.17, B−H (bridge) 1.03−1.15; selected bond angles (in °): Li1−N3−C4 101.5(1), Li1−N2−C3 102.8(1), Li1A−N1−C1 117.3(1), H13−B1−Li1 164.2(2), N3−Li1−N2 85.8(1), N1B−Li1−B1 113.3(1), N3−Li1−H13(term.) 151.4(2), N3−Li1−N1B 100.0(1), N2−Li1−N18 109.8(1), N3−Li1−B1 124.4(1), N2−Li1−B1 119.5(1); note that N1B binds to Li1

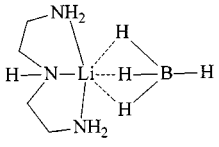

4a

Lithium tetrahydridoborate−pyrrolidine, $LiBH_4$·HNC_4H_8 (**5**), was not expected to have a simple structure because there is only one amine ligand available for coordination to the Li center. Moreover, the crystal contains toluene, its composition being $2LiBH_4$·$2NHC_4H_8$·$C_6H_5CH_3$.

Figure 11 represents the contents of the asymmetric unit of **5** in the triclinic cell. This arrangement is reminiscent of the structure of $[LiBH_4$·tmen$]$[14] because the two BH_4 groups are of the $2\mu_1^1,\mu_1^2$ type, i.e. there are two single Li−H−B bridges to two different Li centers while a third

hydrogen atom bridges two Li atoms. In addition, another BH_4 group supplies two H atoms through LiH_2B bridges. This situation means that the Li centers are heptacoordinated.

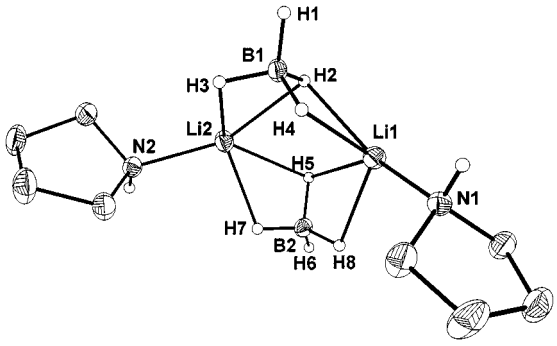

Figure 11. Structure of $LiBH_4 \cdot HNC_4H_8$ (**5**) in the crystal; the contents of the asymmetric unit are depicted; the C atoms of the disordered toluene molecule are not included; thermal ellipsoids are drawn on a 25% probability scale; selected atom distances (in Å): N1−Li1 2.022(6), N2−Li2 2.205(5), Li1−B1 2.561(6), Li1−B2 2.530(6), Li2−B1 2.527(6), Li2−B2 2.569(6), Li1−H 2.08−2.23, Li2−H 2.03−2.09, B1−H 1.08(3)−1.15(3), B2−H 1.05(4)−1.14(4); selected bond angles (in °): N1−Li1−B1 116.5(2), N1−Li1−B2 118.6(2), N2−Li2−B1 118.0(2), N2−Li2−B2 116.7(2), N1−Li1−H8 95(1), N1−Li1−H5 145.0(9), N1−Li1−H2 141.0(9), N1−Li1−H4 93(1), N2−Li2−H7 94(1), N2 − Li2−H5 140.9(9), N2−Li2−H3 92.4(9)

The structure of **5** shows short Li−N bonds [2.024(6) Å] and rather uniform Li···H distances [2.09(3) Å], and this is also true for the B−H bond lengths [1.10(4)−1.15(4) Å]. The H−B−H bond angles are close to tetrahedral, meaning that the asymmetry induced at the BH_4 groups by the different interactions of its hydrogen atoms with the Li centers is not reflected in different bond angles.

Figure 12 shows how the smallest unit forms an infinite chain in the lattice by the action of inversion center. For the sake of clarity several pyrrolidine units are not depicted. The result of this symmetry operation is also depicted in Figure 13, which shows a view down the *b* axis. In the chain each Li center is not only coordinated to an N atom but also to three different BH_4 groups, all of which are of the $2\mu_1^1,\mu_1^2$ type.

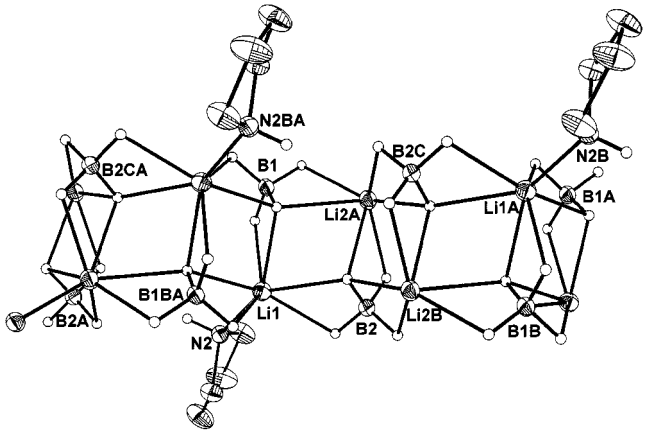

Figure 12. View of the chain of compound **5** in the lattice; only part of the pyrrolidine ligands is depicted in the interest of clarity

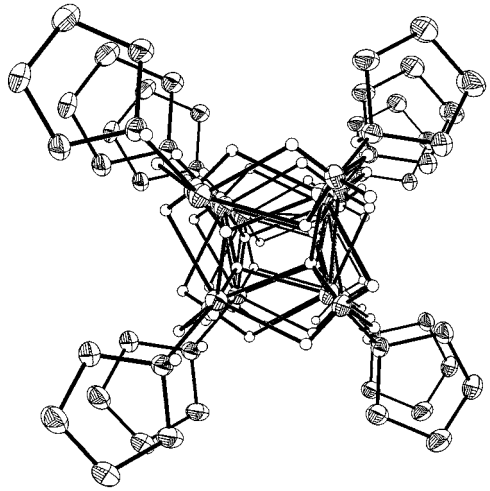

Figure 13. View of the chain down the *b* axis

It is amazing that $LiBH_4$ adds only one pyrrolidine molecule but two dibenzylamines in spite of the fact that the dibenzylamine is sterically more demanding. Compound **6**, $LiBH_4 \cdot 2HN(CH_2Ph)_2$, crystallizes in the monoclinic system and the unit cell contains dimeric units. Figure 14 depicts the molecular structure of this system, which has a center of symmetry.

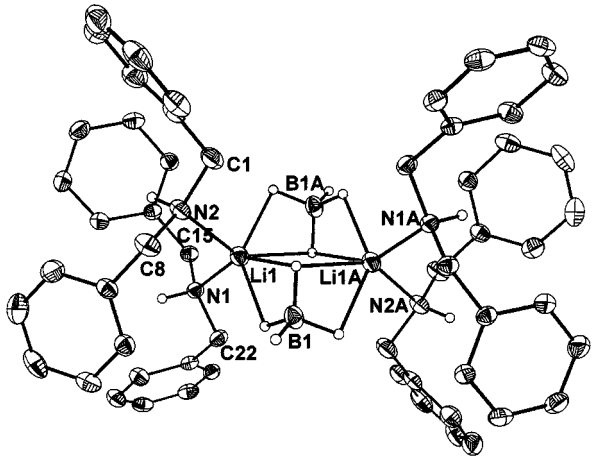

Figure 14. Molecular structure of dimeric $LiBH_4 \cdot 2NH(CH_2Ph)_2$ (**6**); thermal ellipsoids are drawn on a 25% probability scale; selected atom distances (in Å): Li1−N1 2.126(3), Li1−N2 2.131(4), Li1···B1 2.516(4), Li−H 1.9−2.2, B−H 1.1−1.2; selected bond angles (in °): N1−Li1−N2 107.5(1), N1−Li1−B1 122.0(1), N2−Li1−B1 101.9(2), Li1−B1−Li1A 80.3(1), B1−Li1−B1A 99.7(1)

The structure of **6** is analogous to the structure of $(LiBH_4 \cdot tmen)_2$.[14] As expected the N1−Li1−N2 bond angle is wider (107.5°) than for $[LiBH_4 \cdot tmen]_2$ (74.6°) because the nitrogen atoms are not constrained in a five-membered ring. A second consequence is that the Li−N bond lengths are shorter.

We have already reported that $[LiBH_4(MeNCH_2)_3]_2$[6b] has a structure closely related to the structure of $[LiBH_4 \cdot tmen]_2$,[14] because only *two* of the *three* nitrogen atoms of $(MeNCH_2)_3$ coordinate to a Li center.[6b] A structure related but different to $[LiBH_4(MeNCH_2)_3]_2$ is displayed by dimeric $LiBH_4(i\text{PrNCH}_2)_3$ (**7**). As Figure 15 re-

veals, all three nitrogen atoms of the amine ligand are now bonded to the Li ion, and two monomeric units are joined through two $\mu_1^2,2\mu_1^1$-BH_4 units. Nevertheless, the triazacyclohexane ligand is not symmetrically bonded to the Li center; Li−N bond lengths are 2.10(1), 2.20(1), and 2.38(1) Å; Li−H distances range from 1.93 to 2.17 Å.

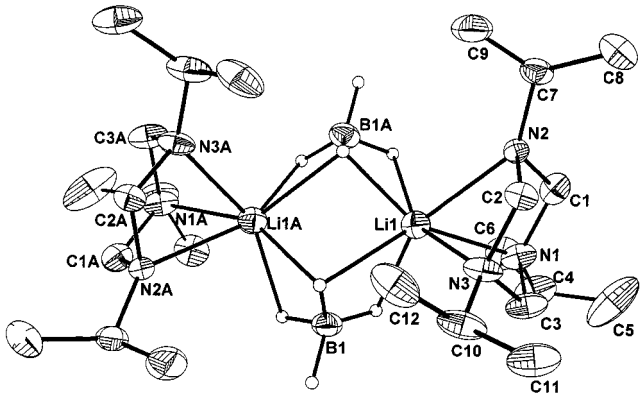

Figure 15. ORTEP plot of dimeric $LiBH_4$·(*i*PrNCH$_2$)$_3$ (**7**); hydrogen atoms bonded to carbon atoms are omitted; thermal ellipsoids represent a 25% probability; selected atom distances (in Å): Li1−N1 2.10(1), Li1−N2 2.38(1), Li1−N3 2.20(1), Li1···B1 2.53(1), Li1−H2 (Li1A) 1.93(6), Li1−H1 2.00(1), B−H (term.) 1.14(6), B−H (bridges) 1.12−1.14(5); selected bond angles (in °): N1−Li1−N3 65.5(4), N1−Li1−N2 62.9(4), N3−Li1−N2 60.8(4), B1−H1−Li1 (μ_1^1) 103.8(9), B1−H2−Li1 (μ_1^2) 100.7(6), B1−H2−Li1A (μ_1^2) 94.4(6), Li1A−H3−B1 (μ_1^1) 94.4(1), Li1−H2−Li1A 97.8(1)

If the reaction of $LiBH_4$ with (MeNCH$_2$)$_3$ is performed in toluene instead of in boiling xylene,[6b] then the product formed does not have a 1:1 composition but is 2$LiBH_4$·(MeNCH$_2$)$_3$ (**8**). The crystals of this compound are orthorhombic with space group *Pcca* but the structure could also be solved in the monoclinic space group $P2_1/c$. Figure 16 shows the contents of the asymmetric unit, which formally consists of a dimeric unit of **8**.

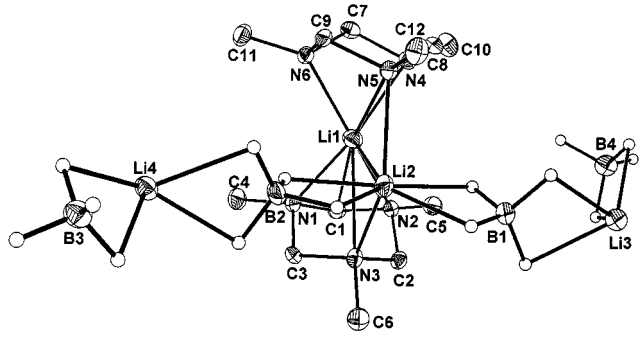

Figure 16. ORTEP plot for the contents in the asymmetric unit of 4$LiBH_4$·2(MeNCH$_2$)$_3$ (**8**); CH hydrogen atoms are omitted; thermal ellipsoids are depicted on a 25% probability scale; selected atom distances (in Å): Li1−N1 2.674(3), Li1−N2 2.141(1), Li1−N3 2.115(2), Li1···Li2 2.770(5), Li2−N1 2.297(2), Li2−B1 2.429(2), Li3···B1 2.376(3), Li3···B2 2.349(3), B3···Li3 2.319(3); selected bond angles (in °): N3−Li1−N1 58.48(6), N2−Li1−N1 57.83(6), N2−Li1−N3 66.28(5), N1−Li−N1A 99.75(1), N2−Li1−N2A 166.8(2), N3−Li1−N3A 157.4(2), N1−Li2−N1A 125.8(2), Li2−B1−Li3 161.2(2), B1−Li3−B2 126.2(1), Li3−B2−Li3B 167.8(2), B3−Li3−B1 126.2(1), B2−Li3−B3 125.4(1)

At first glance the unusual structural feature of compound **8** is that one Li center is "centrally" coordinated to two (MeNCH$_2$)$_3$ molecules while a second Li ion coordinates to two N atoms of the "sandwiched" Li1 atom. A closer look reveals that Li1 is asymmetrically coordinated to the N donor atoms and resides on a crystallographic twofold axis. There are four short Li1−N distances [2.115(2) to 2.142(1) Å] and two long ones [2.674(3) Å]. These latter distances are longer than the Li−C distances of Li1 to atoms C1 and C1A [2.467(2) Å]. The orientation of the two rings with respect to one another represents an "eclipsed" position. Atom Li2 coordinates with atoms N1 and N1A and the Li2−N bond lengths are 2.297(2) Å. One of the reasons for this asymmetry in coordination is the rather short Li1···Li2 distance of 2.770(5) Å.

The second feature is the presence of a layer structure of composition $[Li_3(BH_4)_4]^-$. Each Li center in this layer is hexacoordinated by six hydrogen atoms stemming from three BH_4 groups, each one corresponding to two Li(H$_2$)B units. This kind of $2\mu_2^1$ coordination finally leads to the two-dimensional array of $LiBH_4$ units as depicted in Figure 17. Thus, compound **8** can be given the formula $[Li\{(MeNCH_2)_3\}_2][Li_3(BH_4)_4]$ where the chain atom Li2 "shares" the nitrogen atoms N1 and N1A with Li1.

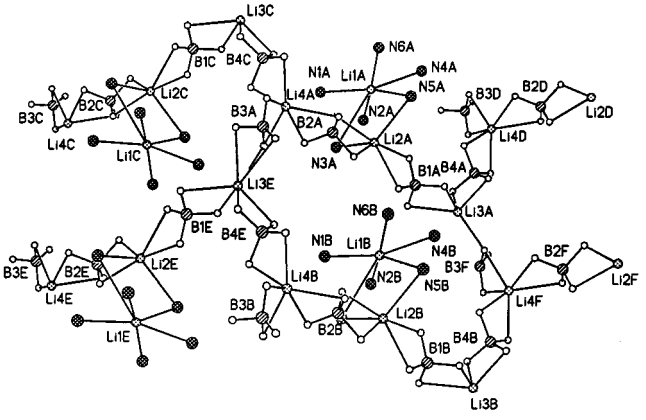

Figure 17. Part of the layer structure of compound **8** in the crystal; extension to the layer is through the B3- and Li3-type atoms; C and H atoms of the amine ligand have been removed for the sake of clarity; here, the structure is shown for the refinement in space group $P2_1/c$; in this space group the atoms on B3 and Li3 could be located and refined. However, it is more likely that the orthorhombic space group *Pcca* is correct; in this case atom B3 resides on a mirror plane and only three hydrogen atoms could be located but not the fourth; the action of the mirror plane leads, of course, to disorder of the H atoms of this BH_4 group

However, when 1,3,5-tribenzyl-1,3,5-triazacyclohexane is employed as a ligand for $LiBH_4$ then compound **9** is formed and this, by X-ray structure determination, can best be described as $\{Li[(PhCH_2NCH_2)_3]_2\}\{Li_2(BH_4)_3]$. The high steric demand of the ligand $(PhCH_2NCH_2)_3$ leads to a separation of one Li cation, out of three $LiBH_4$ units, from its anion with formation of the cation $Li[(PhCH_2NCH_2)_3]_2^+$, as shown in Figure 18. The Li center occupies a special position.

It should be noted that the six Li−N distances of the cations Li1 and Li4 are rather similar, spanning the range from 2.223(2) to 2.293(3) Å. Atoms Li1 and Li4 are located on a crystallographic inversion center and, consequently, three N−Li−N bond angles within each cation are 180°.

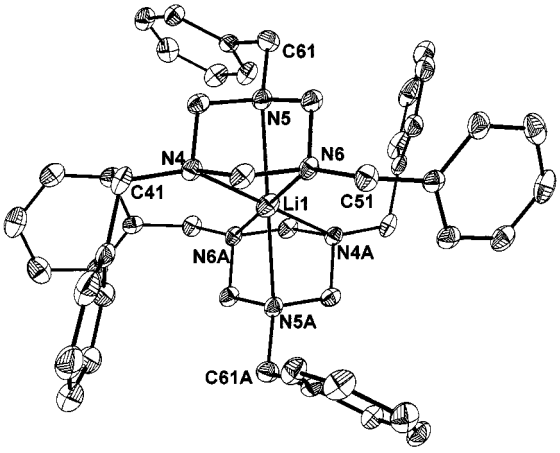

Figure 18. One of the two independent centrosymmetric $[Li(PhCH_2NCH_2)_3]$ cations of compound **9**; hydrogen atoms omitted; selected atom distances (in Å): Li1−N4 2.339(3), Li1−N5 2.285(3), Li1−N6 2.315(3); selected bond angles (in °): N4−Li1−N5 60.9(1), N4−Li1−N6 60.9(1), N5−Li1−N6 61.3(1); N4−Li1−N4A 180

For each heterocycle all N−Li−N bond angles are close to 63°.

The plot shown in Figure 19 demonstrates that the cations $Li[(PhCH_2NCH_2)_3]_2^+$ separate the chain structure of the anionic part of **9**. There are two different kinds of BH_4 units. The BH_4 groups of atoms B1 and B3 are typical $2\mu_1^1,\mu_1^2$ ligands, each having one terminal B−H bond. However, the BH_4 group of atom B3 uses all of its four hydrogen atoms for bridging to three Li atoms in a $3\mu_1^1,\mu_1^2$ function. However, there were non-negligible residuals around atom B2, and particularly at the adjacent Li3 atom. Moreover, the thermal motion of atom B2 was suspect and the tricoordinated H atom shows a somewhat longer Li−H distance [2.17(5) Å] than the dicoordinated H atoms. Indeed, refinement of the H atom positions of this exceptional BH_4 group was best for a disorder involving two sites, one with one Li−H bond (2.1 Å) and an almost planar BH_3 group, and a second site with a distorted BH_4 group. This disorder refined well with SOF = 0.5 (see Figure 20). Indeed, the thermal ellipsoid for B3 is compatible with this kind of disorder. It seems, therefore, that a BH_3 group is stabilized by the lattice. We have noticed this kind of structure in two out of three crystal structure determinations of compound **9**. Consequently, we found an electron density for a hydrogen atom bonded to Li3 (2.1 Å). The plot in Figure 19 demonstrates the packing of the cations and anion in the lattice.

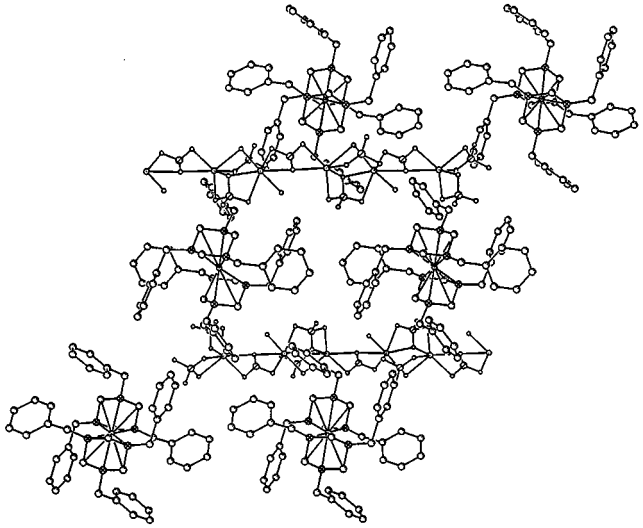

Figure 19. Arrangements of atoms in compound **9** in the crystal separated into $Li[(PhCH_2NCH_2)_3]_2$ cations and anionic $[Li_2(BH_4)_3]$ chains; these are depicted for the BH_3/LiH disorder in the chain

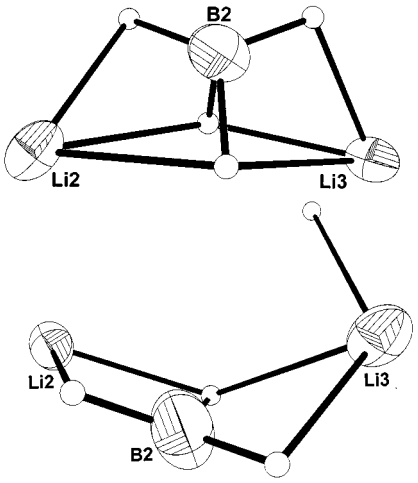

Figure 20. Disordered arrangement of the $B2(H)_4$ group between atoms Li2 and Li3; the tetrahedral BH_4 group (top) and the BH_3 (LiH) group (bottom)

Discussion

It has previously been noted that the bonding mode of the BH_4 group in mononuclear $LiBH_4{\cdot}n$L species depends on the number of ligands L and their steric demand. For $n = 3$ and L = pyridine[6b] or aniline the anion BH_4^- uses three of its hydrogen atoms to form Li−H−B bridges. However, if the ligand is sterically more demanding, e.g. collidine with $n = 2$, only a bidentate μ_2^1-BH_4 group is present.[6b]

On the other hand, if the ratio Li/N is 1:2, as found for $LiBH_4{\cdot}2HN(CH_2Ph)_2$ (**6**), dimers are formed. The structure and bonding of **6** correspond with the prototype of this pattern, $[LiBH_4{\cdot}tmen]_2$,[14] where the BH_4 group functions as a $2\mu_1^1,\mu_1^2$-ligand, i.e. one hydrogen atom binds to two Li centers with the other two forming single Li−H−B bridges. This structural feature is also realized in $[LiBH_4{\cdot}(MeNCH_2)_3]_2$ even if the Li/N ratio is 1:3. However, the effective Li/N ratio is 1:2 because only two out of the three nitrogen atoms of the ligand coordinate strongly to the Li center.[6b] In compound **2**, $3LiBH_4{\cdot}4H_2NtBu$, the Li/N ratio is only 1:1.33. Thus, the Li ions cannot all be coordinated by two nitrogen atoms. The possible structures $(LiBH_4{\cdot}2H_2NtBu){\cdot}2(LiBH_4{\cdot}H_2NtBu)$ or $[Li(H_2NtBu)_4]$-$[Li_2(BH_4)_3]$ are not formed but rather

$2(LiBH_4 \cdot 2H_2NtBu) \cdot (LiBH_4)$. The "$LiBH_4$" part is, of course, coordinatively unsaturated and shares BH_4 groups with the amine carrying $LiBH_4 \cdot 2H_2NtBu$ units, as depicted in Figure 7.

This feature becomes even more apparent for $LiBH_4 \cdot HNC_4H_8$ (**5**) with a ratio Li/N = 1:1. Formation of a chain structure through BH_4 sharing leads to hexacoordinated, coordinatively saturated Li centers. In this case, the BH_4 group joins two Li ions through $2\mu_2^1$ bridges and all four hydrogen atoms are used for coordination through double hydrogen bonds $Li(H)_2B$.

Unexpectedly, $LiBH_4 \cdot (i\text{PrNCH}_2)_3$ (**7**) also forms dimers like $LiBH_4 \cdot$tmen, and $LiBH_4 \cdot (\text{MeNCH}_2)_3$, in spite of the fact that in **7** all three N atoms of the heterocycle coordinate to Li while in the other two compounds the Li centers carry only two N atoms. However, the coordination in **7** is asymmetric: There are two short Li−N distances (2.10, 2.20 Å) and a significantly longer one (2.38 Å). This situation is in contrast to that in $LiBH_4 \cdot$PMDTA,[6b] which is mononuclear in spite of the fact that the three nitrogen atoms of the pentamethyldiethylenetriamine ligand are also asymmetrically bonded. Clearly, PMDTA is sterically more demanding than $(i\text{PrNCH}_2)_3$, and this may be the reason why **7** is dimeric in the crystal.

An Li/N ratio of 1:1.5 is present in the compound $2LiBH_4 \cdot (\text{MeNCH}_2)_3$ (**8**) and a 1:2 ratio in $3LiBH_4 \cdot 2(\text{PhCH}_2\text{NCH}_2)_3$ (**9**). In both cases, extended structures are formed but there are significant differences between the two compounds. Due to the large steric effect of the ligand tribenzyl-1,3,5-triazacyclohexane, one Li center is "sandwiched" between two amine ligands, which surround the cation centrosymmetrically. Thus, compound **9** contains tris(tetrahydridoborato)dilithiate anionic units, which form a chain structure in the crystal. In the case of compound **8** the nitrogen ligand also sandwiches a Li center by four short and two longer Li−N bonds, but two of the six nitrogen atoms bind a second Li atom, which is additionally coordinated to two BH_4 groups. The resulting unit, which finally leads to a layer structure, therefore has the composition $Li_3(BH_4)_4^-$, where one of the three Li centers coordinates with the amine ligand.

Since the BH_4 group can be regarded as a "pseudofluoride" one may expect that amine complexes of lithium halides form similar structures. However, structural analogs of the amine complexes of $LiBH_4$ have not been reported to date. The only compound having an extended chain is LiCl−15-crown-5.[15] All others are either dimeric, trimeric, or tetrameric.[16] In these cases pyridines, tmen, or PMDTA were used as ligands and comparisons are limited. Thus, at the present time, the anion BH_4^- proves to be a most versatile ligand. In addition, it is demonstrated for the first time that certain amine solvates of $LiBH_4$ form polymeric anionic units $[Li_n(BH_4)_{n+1}]^-$. However, the solid-state structures do not seem to be retained in solution because only one type of BH_4 ion is detected by ^{11}B NMR spectroscopy as well as single ^7Li resonances, irrespective of the various kinds of structures found for the solid state.

Experimental Section

All experiments were performed under dry nitrogen with strict exclusion of moisture. Consequently, all solvents were dried and stored under nitrogen. $LiBH_4$ was of commercial grade (Chemetall GmbH), as were the amines, which were dried by treatment with CaH_2 followed by distillation, in the case of liquids, or by recrystallization of the vacuum-dried solids. − NMR: Bruker AC 200 (^{11}B), Jeol 270 (^1H, ^{13}C), Jeol EX400 (^7Li); Standards: $BF_3 \cdot OEt_2$ external; 1 M aq. LiCl solution, external; C_6D_6 and $SiMe_4$ internal. − IR: Nicolet-FT spectrophotometer. − Elemental analyses: Microanalytical Laboratory of the Department of Chemistry, University of Munich.

Lithium Tetrahydridoborate−Aniline(1:3) (1): $LiBH_4$ (231 mg, 10.6 mmol) was suspended in aniline (20 mL). After stirring for 20 min, the turbid solution was filtered and the filtrate stored at 8 °C. Clear needles of **1** suitable for X-ray structure analysis separated within a few days. Yield: 257 mg of **1** (8%), m.p. 58−62 °C (dec.). On removing aniline from the filtrate a larger amount of **1** was isolated (yield not determined). − NMR (in aniline): ^7Li NMR: δ = 0.1(3). − ^{11}B NMR: δ = −38.0 [quint, $^1J(^{11}B^1H)$ = 81 Hz]. − IR (Nujol, B−H stretching region): $\tilde{\nu}$ = 2377 cm^{-1} w, 2331 m, 2252 vst, 2196 m, 2183 m. − $C_{18}H_{25}BLiN_3$ (301.23): calcd. C 71.79, H 8.37, N 13.95; found C 69.77, H 8.52, N 13.53.

Lithium Tetrahydridoborate−*tert*-Butylamine(3:4) (2): $LiBH_4$ powder (250 mg, 11 mmol) was suspended in toluene (10 mL) with stirring and *tert*-butylamine (1.2 mL, 11.3 mmol) was added. The suspension was heated at reflux for 30 min. The insoluble material was removed by filtration (G3 frit) and the solution cooled to −20 °C in a refrigerator. Clear needles separated from the solution within one week. Yield: 190 mg (18%), m.p. ca. 10 °C. A further quantity of compound **2** was isolated from the concentrated filtrate. − NMR (C_6D_6 + TMS): ^7Li NMR: δ = 1.07. − ^{11}B NMR: δ = −38.3 [quint, $^1J(^{11}B^1H)$ = 81 Hz]. − IR (B−H stretching region): $\tilde{\nu}$ = 2366 cm^{-1} st, 2320 st, 2275 st. − $C_{16}H_{56}B_3Li_3N_4$ (357.90): calcd. C 53.69, H 15.77, B 9.06, Li 5.82, N 15.65; found C 51.96, H 15.92, B 8.9, Li 5.9, N 16.62.

Lithium Tetrahydridoborate−Ethylenediamine(1:2) (3): $LiBH_4$ (58.5 mg, 2.69 mmol) was suspended in a mixture of ethylenediamine (171 mg, 2.85 mmol) and pyridine (5 mL). After addition of methylcyclohexane (1 mL) the slightly turbid solution was subjected to filtration and the filtrate kept at 8 °C. Crystals of **3** separated in a few hours. These crystals deteriorated quickly in a stream of nitrogen. Yield: 35 mg of **3** (9%), m.p. 91 °C. From the filtrate a further quantity of **3** could be obtained by reducing the volume of the solution. − NMR (pyridine): ^7Li NMR: δ = 2.0. − ^{11}B NMR: δ = −38.3 [quint, $^1J(^{11}B^1H)$ = 81 Hz]. − IR (Nujol, B−H stretching region): $\tilde{\nu}$ = 2300 cm^{-1} sh, 2252 st, 2220 sh, 2183 m, 2147 m. − A satisfactory elemental analysis could not be obtained.

Lithium Tetrahydridoborate−Diethylenetriamine (4): $LiBH_4$ (190 mg, 8.71 mmol) was dissolved in a mixture of diethylenetriamine (895 mg, 8.67 mmol) and pyridine (10 mL). After stirring for 15 min, toluene (1 mL) was added and insoluble material was removed by filtration. After keeping the solution at 8 °C, colorless prisms separated. Yield: 121 mg (11%), m.p. 110−118 °C (dec.). − NMR (pyridine): ^7Li NMR: δ = 1.7 (s). − ^{11}B NMR: δ = −38.1 [quint, $^1J(^{11}B^1H)$ = 81 Hz]. − IR (Nujol, B−H stretching region): $\tilde{\nu}$ = 2326 cm^{-1} sh, 2251 st br, 2219 sh, 2182 sh. − $C_4H_{17}BLiN_3$ (125.17): calcd. C 38.45, H 13.71, N 33.63; found C 38.68, H 13.39, N 32.14.

Lithium Tetrahydridoborate−Pyrrolidine (5): A suspension of $LiBH_4$ (410 mg, 19 mmol) in toluene (45 mL) and pyrrolidine (1.56 mL, 18.9 mmol) was heated to reflux for 10 min. Most of the solid dissolved and the insoluble material was removed from the hot solution. The filtrate was cooled to −20 °C. Colorless needles separated within 12 h. The needles were isolated by filtration using a cooled frit. Single crystals for X-ray determination were removed directly from the suspension. Yield: 106 mg (54%), m.p. ca. 0 °C. − NMR (C_6D_6 + TMS): ^{7}Li NMR: δ = 1.32. − ^{11}B NMR: δ = −41.1 [quint, $^1J(^{11}B^1H)$ = 87 Hz]. − IR (B−H stretching region): $\tilde{\nu}$ = 2252 cm^{-1} st, 2279 st, 2355 sh. − $C_4H_{13}BLiN$ (92.90): calcd. C 48.05, H 14.87, B 11.64, Li 7.47, N 15.08; found C 48.79, H 14.00, B 11.0, Li 7.4, N 15.47.

Lithium Tetrahydridoborate−Dibenzylamine(1:2) (6): Dibenzylamine (50 mL) was saturated with $LiBH_4$ and excess $LiBH_4$ was removed by filtration. The clear solution was layered with cyclohexane (20 mL). A precipitate formed and was filtered off. ^{11}B NMR of the solution showed the presence of a BH_4 unit and a BH_3 group in a 3:7 ratio. The filtrate was cooled to 8 °C. Crystals of **6** separated as colorless prisms, m.p. 81−83 °C (dec.). − ^{11}B NMR: δ = −38.2 [quint, $^1J(^{11}B^1H)$ = 81 Hz], −14.0 (broad). − ^{1}H NMR (C_6D_6): δ = 0.6 [1:1:1:1 q, $^1J(^{11}B^1H)$ = 81 Hz]. − IR (B−H stretching region): $\tilde{\nu}$ = 2370 cm^{-1} st, 2332 st, 2305 st, 2272 st, 2238 st. − $C_{28}H_{34}BLiN_2$ (416.30): calcd. C 80.78, H 8.23, N 6.73, B 2.60, Li 1.67; found C 76.91, H 7.91, N 6.42, B 2.95, Li 1.97.

Lithium Tetrahydridoborate−1,3,5-Triisopropyl-1,3,5-triazacyclohexane (7): To a stirred suspension of $LiBH_4$ (440 mg, 20 mmol) in toluene (36 mL) was added the ligand (4.84 mL, 20.2 mmol). Most of the $LiBH_4$ dissolved on heating the suspension at reflux for 30 min. Insoluble material had to be rapidly removed from the suspension because crystals settled quite quickly from the solution on cooling to room temperature. Yield: 1.9 g (40%), m.p. 98−102 °C (dec.). − ^{7}Li NMR (toluene): δ = 0.097. − ^{11}B NMR (C_6D_6 + TMS): δ = −15.9 [q, $^1J(^{11}B^1H)$ = 60 Hz], −38.5 [quint, $^1J(^{11}B^1H)$ = 81 Hz], ratio ca. 1:8. − IR (B−H stretching region): $\tilde{\nu}$ = 2185 cm^{-1} st, 2250 m, 2283 m, 2316 w, 2334, w, 2378 st. − $C_{12}H_{31}BLiN_3$ (235.14): calcd. C 61.29, H 13.29, B 4.60, N 17.87; found C 59.92, H 12.96, B 4.30, N 18.52.

Lithium Tetrahydridoborate−(1,3,5-Trimethyl-1,3,5-triazacyclohexane)(4:2) (8): Lithium tetrahydridoborate (1.03 g, 47.4 mmol) was suspended in toluene (40 mL). The amine (6.65 mL, 47.4 mmol) was added to the stirred suspension and stirring was continued for 2 h. The suspension was quickly heated to reflux and kept at this temperature for 10 min. Insoluble materials were removed from the hot solution and the filtrate cooled to −20 °C. Prismatic crystals separated within 12 h. Yield: 2.97 g (73.4%), m.p. 78 °C. − ^{7}Li NMR (toluene): δ = 0.74. − ^{11}B NMR (toluene): δ = −38.6 [quint, $^1J(^{11}B^1H)$ = 86 Hz]. − IR (B−H stretching region): $\tilde{\nu}$ = 2184 cm^{-1} sh, 2253 st, 2319 m, 2328 m, 2373 st. − $C_{12}H_{42}B_4Li_4N_6$ (341.48): calcd. C 42.20, H 12.40, B 12.66, N 24.61; found C 42.10, H 12.05, B 12.10, N 24.62.

Lithium Tetrahydridoborate−(1,3,5-Tribenzyl-1,3,5-triazacyclohexane)(3:2) (9): To a stirred suspension of $LiBH_4$ (220 mg, 10 mmol) in toluene (20 mL) was added the amine ligand (3.57 g, 10.1 mmol). After keeping the mixture at reflux for 1 h, the hot suspension was filtered. Crystals separated within 4 h from the filtrate, which was kept at −20 °C. Yield: 720 mg (28%), m.p. 134−136 °C. A second crop was isolated on reducing the volume of the filtrate under vacuum. The yield of the second crop was not determined. − ^{7}Li NMR (C_6D_6 + TMS): δ = 0.347. − ^{11}B NMR ([D_8]toluene): δ =

Table 2. Crystallographic data and data referring to structure solution and refinement

	1	**2**	**3**	**4**	**5**	**6**	**7**	**8**	**9**
Empirical formula	$C_{36}H_{50}B_2Li_2N_6$	$C_{16}H_{56}B_3Li_3N_4$	$C_8H_{40}B_2Li_2N_8$	$C_4H_{17}BLiN_3$	$C_{10.5}H_{28}BLi_2N_2$	$C_{28}H_{34}BLiN_2$	$C_{12}H_{31}BLiN_3$	$C_6H_2B_2Li_2N_3$	$C_{48}H_{66}B_3Li_3N_6$
Mol. mass	602.32	357.90	283.98	124.96	217.85	416.32	235.15	170.76	780.32
Cryst. size [mm]	0.2×0.2×0.4	0.1×0.2×0.3	0.4×0.4×0.4	0.3×0.4×0.4	0.1×0.1×0.4	0.10×0.1×0.2	0.2×0.2×0.2	0.1×0.2×0.3	0.2×0.2×0.3
Cryst. system	hexagonal	monoclinic	triclinic	orthorhombic	triclinic	monoclinic	monoclinic	orthorhombic	monoclinic
Space group	*R*3	*C*2/*c*	*P*$\bar{1}$	*Pbcn*	*P*$\bar{1}$	*C*2/*c*	*C*2/*c*	*Pcca*	*P*2(1)/*c*
a [Å]	16.089(1)	25.309(1)	8.3580(7)	17.323(2)	7.2034(3)	21.2514(3)	15.818(7)	17.393(1)	20.01(2)
b [Å]	16.089(1)	12.0228(7)	7.8086(7)	10.4162(9)	11.0569(2)	10.4618(2)	17.80(1)	8.1514(6)	18.67(2)
c [Å]	12.659(1)	20.049(1)	15.224(1)	9.7331(8)	11.1010(3)	26.1103(1)	14.51(1)	17.332(1)	13.031(8)
α [°]	90	90	90.021(1)	90	89.052(1)	90	90	90	90
β [°]	90	97.820(1)	94.237(2)	90	80.062(2)	113.72	108.79(2)	90	90.37(2)
γ [°]	120	90	90.005(2)	90	78.593(2)	90	90	90	90
V [Å^3]	2837.7(4)	6044.0(6)	990.9(2)	1756.2(3)	853.55(5)	5314.73(1)	3911(4)	2457.3(3)	4867(6)
Z	3	8	2	8	2	8	8	8	4
ρ(calcd.) [Mg/m^3]	1.057	0.787	0.952	0.945	0.848	1.041	0.799	0.923	1.065
μ [mm^{-1}]	0.061	0.043	0.059	0.057	0.046	0.059	0.046	0.052	0.061
F(000)	972	1632	320	560	242	1792	1056	752	1680
Index range	−18≤*h*≤20	−28≤*h*≤28	−11≤*h*≤8	−21≤*h*≤21	−8 ≤*h*≤4	−26≤*h*≤26	−15≤*h*≤14	−23≤*h*≤21	−25≤*h*≤24
	19≤*k*≤19	−13≤*k*≤13	−9 ≤*k*≤9	−13≤*k*≤13	−12≤*k*≤12	−13≤*k*≤9	−22≤*k*≤22	−10≤*k*≤10	−21≤*k*≤22
	15≤*l*≤15	−21≤*l*≤21	−19≤*l*≤19	−13≤*l*≤8	−13≤*l*≤13	−32≤*l*≤32	−17≤*l*≤17	−21≤*l*≤21	−14≤*l*≤15
2 θ [°]	56.60	47.64	57.84	58.22	49.42	52.74	54.88	58.74	55.18
Temp. [K]	193(2)	163(2)	183(2)	183(2)	163(5)	193(2)	153(2)	187(2)	173(2)
Refl. collected	5510	13237	5760	9257	4064	13893	10260	13752	17190
Refl. unique	2639	4205	3007	1761	2152	4582	3184	2716	7002
Refl. obs. (4σ)	1971	2975	2505	1334	1612	3229	1664	1563	3773
R (int.)	0.0250	0.0691	0.0512	0.1045	0.0287	0.0395	0.0474	0.0437	0.0678
No. variables	157	322	229	92	212	313	176	142	601
Weighting	0.0718/	0..0249/	0.1179/	0.0938/	0.1100/	0.0340/	0.2845/	0.1546/	0.0137/
scheme[a] *x*/*y*	0.000	8.0550	0.3734	0.4630	05769	2.9179	21.2104	0.000	3.3565
GOOF	0.966	1.170	1.040	1.080	1.095	1.084	1.103	1.006	1.180
Final *R* (4σ)	0.0421	0.0808	0.0705	0.0602	0.0794	0.0521	0.1529	0.0645	0.0595
Final *wR*2	0.1023	0.1433	0.1966	0.1524	0.2106	0.1020	0.4378	0.2086	0.1031
Larg. resid. peak [e/Å^3]	0.111	0.228	0.238	0.254	0.304	0.191	0.881	0.466	0.134

$w^{-1} = \sigma^2F_o^2 + (xP)^2 + yP$; $P = (F_o^2 + 2F_c^2)/3$.

−11.9 (br), −39.4 (br), ratio ca. 1:10. − IR (B−H stretching region): $\tilde{\nu}$ = 2415 cm^{-1}, 2372, 2330, 2253, 2189, 2125. − $C_{48}H_{66}B_3Li_3N_6$ (780.32): calcd. C 71.87, H 8.78, N 10.48; found C 71.72, H 7.98, N 10.54.

X-ray Structure Determinations: X-ray structure determinations were performed with a Siemens P4 diffractometer, using Mo-K_α radiation and a graphite monochromator. Data were collected with a CCD area counter at 193 K (Siemens LT2 device). Several drops of a suspension containing the single crystals were transferred to precooled perfluoro polyether oil and kept at −40 °C. The selected single crystal was mounted on a glass fiber. The dimensions of the unit cell were calculated from the reflections of a total of 75 frames recorded for five different settings of the crystal using the program SMART.[17] Data collection was performed in the hemisphere mode by recording 1200 frames with $\Delta = 0.3°$ at two different χ settings. The program SAINT[18] was used for data reduction. Structure solution and refinement was carried out with the programs SHELX93[19] by applying direct methods. Non-hydrogen atoms were refined with anisotropic thermal parameters. Positions of hydrogen atoms attached to boron atoms were taken from the difference Fourier map. Their positions and isotropic thermal parameters were refined. All other H atoms were placed in calculated positions and included in the refinement with a riding model. − Compound **5** was obtained from toluene solution. There were five peaks that we assigned to C atoms of a disordered toluene but the C−C distances were rather irregular. One of these C atoms could not be refined anisotropically. − The structure of compound **8** was solved and refined in two space groups, monoclinic $P2_1/c$ and orthorhombic *Pcca*. The β angle was very close to 90° and, in the first runs, a solution was only obtained for the $P2_1/c$. In this solution all four H atoms could be located at B3. Refinement in *Pcca* led to more favorable *R* values, although the H atoms at B3 refined to give a disordered arrangement at B3 due to its position on a mirror plane. − A disorder was also found for the $B(3)H_4$ group in compound **9**, which indicates a disordered tetrahedral BH_4 group and a BH_3 and LiH group. These were included in the refinement with SOF = 0.5, a value indicated by a previous refinement without constraints. − A summary of crystallographic data and information referring to data collection and refinement is given in Table 2. Additional material (without structure factor tables) are deposited with the Cambridge Crystallographic Data Centre as supplementary publications CCDC-143680 (**1**), -143681 (**2**), -143682 (**3**), -143683 (**4**), -143684 (**5**), -143685 (**6**), -143686 (**7**), -143687 (**8**), -143688 (**9**). Copies of the data can be obtained on application to CCDC, 12 Union Road, Cambridge CB2 1EZ, U.K. [Fax: (internat.) + 44-1223/336-033; E-mail: deposit@ccdc.cam.uk].

Acknowledgments

This work was supported by Fonds der Chemischen Industrie and particularly by Chemetall GmbH. IR spectra were recorded by Mrs. E. Kiesewetter and NMR spectra by P. Meyer and M. Vosteen. We are grateful for this support.

[1] J. Knizek, H. Nöth, *J. Organomet. Chem.*, in press..

[2] A. A. Hinkley, in: Kirk−Othmer, *Encyclopedia of Chemical Technology*, 2nd ed., vol. II, Interscience, New York, London, Sydney, **1966**, p. 210−217.

[3] H. Richtgenhain, B. Abrahamsson, *Svensk Papperstidu.* **1954**, *37*, 538; *Chem. Abstr.* **1956**, *50*, 3755. − W. C. Moyen, C. P. Donofrio, *Pulp. Paper Mag. Canada* **1958**, *59*, 157; *Chem. Abstr.* **1959**, *53*, 9662.

[4] *Gmelin-Handbuch der Anorganischen Chemie*, Ergänzungswerk, Natrium, **1966**, 8. Auflage, Ergänzungsband, Teil 3, p. 1212−1231.

[5] E. Wiberg, E. Amberger, *Hydrides of the Elements of Main Group I−IV*, Elsevier, Amsterdam, London, New York, **1971**.

[6] [6a]A. Heine, D. Stalke, *J. Organomet. Chem.* **1997**, *542*, 25−28. − [6b] H.-H. Giese, T. Habereder, H. Nöth, W. Ponikwar, S. Thomas, M. Warchhold, *Inorg. Chem.* **1999**, *38*, 4188−4196. − [6c] M. Bremer, H. Nöth, M. Thomann, M. Schmidt, *Chem. Ber.* **1995**, *128*, 455−460. − [6d] A. S. Antsyshkina, G. G. Sadikow, V. N. Konoplev, V. D. Makhaev, N. N. Mal'tseva, A. I. Golovanova, N. S. Kendzova, A. S. Sizareva, *Russ. J. Inorg. Chem.* **1996**, *22*, 355−358.

[7] H. Nöth, M. Thomann, M. Bremer, G. Wagner, *Current Topics in the Chemistry of Boron* (Ed.: G. W. Kabalka), Royal Society of Chemistry, Special Publ. No. 143, **1994**, p. 387−398.

[8] W. D. Peterson, American Potash and Chem. Corp. US-Patent 2974015 (**1961**), *Chem. Abstr.* **1961**, 26385; see also ref.[2]

[9] *Gmelin Handbuch der Anorganischen Chemie*, Supplement to the 8th ed., **1976**,vol. 33, part 8, p. 40.

[10] R. M. Adams, A. R. Siedle, in: *Boron, Metallo-Boron Compounds and Boranes* (Ed.: R. M. Adams), J. Wiley Interscience, New York, London, Sydney, **1966**, p. 373−461.

[11] See ref.[9], pp. 40−41, and ref.[10]

[12] See ref.[6b] and: N. N. Mal'tseva, A. S. Antsyshkina, A. I. Golovanova, N. A. Minaeva, *Russ. J. Inorg. Chem.* **1999**, *44*, 24−28; N. N. Mal'tseva, V. N. Konoplev, A. S. Antsyshkina, *Russ. J. Inorg. Chem.* **1995**, *40*, 811−813.

[13] A. Flores-Parra, S. S. Sanchez-Ruiz, C. Gundemann, H. Nöth, *Eur. J. Inorg. Chem.* **1999**, 2069−2074.

[14] D. R. Armstrong, W. Clegg, H. M. Colquhoun, J. A. Daniels, R. E. Mulvey, I. R. Stephenson, K. Wade, *J. Chem. Soc., Chem. Commun.* **1987**, 630−632.

[15] R. Boulatov, B. Du, E. A. Meyers, S. G. Shore, *Inorg. Chem.* **1999**, *38*, 4554−4558.

[16] P. P. Power, *Lithium Chemistry* (Eds.: A. M. Sapse, P. von R. Schleyer), J. Wiley Interscience, New York, London, Sydney, **1996**, chapter 8.

[17] *SMART*: Siemens Analytical Instruments, Version 4.1, **1994**

[18] *SAINT*: Siemens Analytical Instruments, Version 5.1, Version 4.1, **1994**.

[19] *SHELX93/97*: G. W. Sheldrick, University of Göttingen, **1993/1997**.

Received April 14, 2000
[I00144]

Platinum(II) Compounds with Enantiomerically Pure Bis(pinene)-Fused Bipyridine Ligands − Diimine-Dichloro Complexes and Their Substitution Reactions

Brunhilde Kolp,[a] Dirk Abeln,[b] Helen Stoeckli-Evans,[c] and Alexander von Zelewsky*[a]

Keywords: Chirality / Platinum / Substitution reactions / Diastereoselectivity / N ligands

The synthesis of chiral square-planar Pt^{II} complexes using symmetrical and unsymmetrical bis(pinene)-fused 2,2′-bipyridine is described. The neutral diimine dichloro complexes show a strong deviation of the coordination sphere from planarity if the pinene groups are attached at the 5- and 6-positions of the pyridine rings. However, this distortion does not occur in parallel with the chiral configuration at the diimine ligands. The substitution of the two *cis*-chloro ligands with diamines to form five-membered chelate rings shows little diastereoselectivity when racemic mixtures of chiral diamines are used. Also, ligands that are prochiral at the ligating centers show little selectivity upon coordination.

Introduction

Square-planar coordination geometry, the most frequent coordination mode of diamagnetic d^8-metals do not generally exhibit chirality, since genuinely planar structures cannot be chiral in three-dimensional space. Deviations from planarity can, however, lead to chiral configurations. An early example of this type was the platinum(II) complex containing one molecule of *meso*-stilbenediamine and one molecule of isobutylenediamine occuring as a pair of enantiomers.[1] Complexes in which a distortion from planarity occurs in a way that permits chirality have recently been found in the class of bis-cyclometallated compounds. These compounds have a very strong tendency to form *cis*-complexes, leading to helical configurations of ligands that interact strongly, thereby avoiding coplanarity.[2] The advent of nonracemic pyridine and bipyridine ligands derived from naturally occurring terpene compounds[3] has prompted us to investigate the possibility of a stereoselective synthesis of coordination species that show chiral elements within the ligand and around the metal center. It has been shown that metal chirality can be predetermined in "square-planar" complexes (SP-4-complexes) by using this type of ligand in *diastereoselective syntheses.*[4]

Here we present the preparation and characterization of a series of enantiomerically pure Pt^{II} complexes, in which the chirality is located in the "chiralized" bipyridine ligands. The investigations focus on the question whether the ligands **L1**−**L5** induce chiral distortions from planarity in the complex and whether chirality can be transferred in stereoselective reactions to ligands that occupy the coordination sites around the central metal (Scheme 1).

[a] Institute of Inorganic Chemistry, Pérolles, University of Fribourg, 1700 Fribourg, Switzerland
[b] Laboratory for Crystallography, University of Bern, Freiestrasse 3, 3012 Bern, Switzerland
[c] Institute of Chemistry, University of Neuchâtel, Avenue de Bellevaux 51, 2000 Neuchâtel, Switzerland

Results and Discussion

Chiral Bipyridine Ligands

For the synthesis of the substituted bipyridine ligands **L1**−**L5**, the method described by F. Kröhnke[5] was modified. The synthesis of the compounds **L1**, **L2**, and **L5** has already been described.[6,7] The preparation of ligand **L3** was similar to that of **L2** except that for one of the two 'Kröhnke cyclizations', (+)-α-pinene was used as starting material and for the second one (−)-α-pinene was used, which gave the *meso* ligand **L3**.

The preparation of compound **L4** is shown in Scheme 2. Chirality was introduced by using enantiomerically pure (−)-β-pinene (**1**) as starting material. Compound **1** was oxidized to the (+)-nopinone (**2**) following a 'one-pot' method described by Brown.[8] The nopinone was treated with $NaNH_2$ which resulted in the formation of enolate **3**. Treatment of **3** with formaldehyde in a Na_2CO_3 solution gave the α,β-methylene ketone **4**, which was used for the condensation with the 'Kröhnke salt' **5** in the same way as already described by von Zelewsky et al.[7] for **L2**.

Complex Formation and Characterization in Solution

The complexation of **L1**, **L2**, **L3**, **L4**, and **L5** with Pt^{II} was carried out in aqueous hydrochloric acid solution using K_2PtCl_4 as starting material (Scheme 1). The yellow, uncharged dichloro complexes precipitated out of the aqueous solution and were isolated and purified. As expected, the formation of bis-diimine complexes was not observed, since the ligands are sterically bulky.

^1H NMR Spectroscopy

All compounds prepared were fully characterized by ^1H-, ^{13}C-, and ^{195}Pt NMR spectroscopy. Figure 1 shows the

 © WILEY-VCH Verlag GmbH, 69451 Weinheim, 2001 1434−1948/01/0505−1207 $ 17.50+.50/0

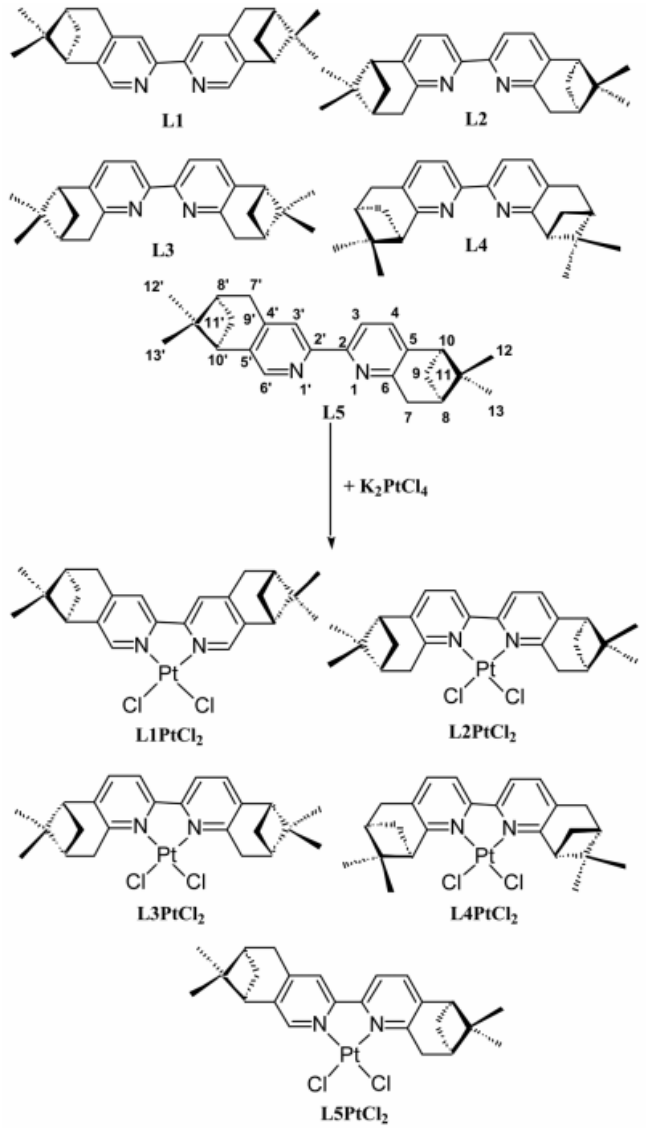

Scheme 1

^{1}H NMR spectra of **L1** and **L2**, and of their Pt-complexes. The pairs of diastereotopic protons H^7 (H^{7endo} and H^{7exo}) are isochronous in free **L1** and **L2**, as well as in **L3**, **L4**, and **L5**. However, a strong downfield shift with a concomitant splitting and a large geminal coupling occurs in the complexes **L2PtCl$_2$**, as well as in **L3PtCl$_2$** and **L5PtCl$_2$**, whereas **L1PtCl$_2$** and **L4PtCl$_2$** still show the same behavior as the free ligand. In **L1PtCl$_2$**, the complex formation strongly influences the aromatic proton H^6, whereas in the case of **L4PtCl$_2$**, the aliphatic proton H^{10} is shifted strongly downfield. The aliphatic protons, except for H^7 in **L2**, **L3**, and **L5**, H^{10} in **L4**, and the aromatic protons H^3 and H^4 are only very slightly influenced by complexation.

Ligands **L1**−**L4** and their Pt complexes all show equivalent halves in the ^{1}H NMR spectra (Figure 1). This equivalence is due to a C_2 axis in **L1**, **L2**, and **L4**, whereas **L3** has a mirror plane. These symmetry elements are no longer present in the solid state, as will be discussed later. In the unsymmetrical ligand **L5**, all the protons of the two halves are nonequivalent, as expected.

^{13}C NMR

In all cases, the ^{13}C NMR spectra show the expected features. Contrary to the ^{1}H NMR spectra, the ^{13}C NMR spectra of the diastereomeric ligands **L2** and **L3** exhibit differences in the chemical shift values of C^5. However the complexes **L2PtCl$_2$** and **L3PtCl$_2$** don't show any differences in the ^{1}H NMR or in the ^{13}C NMR spectra.

^{195}Pt NMR

More information about the isomeric purity of the complexes can be obtained by ^{195}Pt NMR spectroscopy, since chemical shifts are usually very large for this nucleus. All compounds show a single Pt-signal. The values in Table 1 show a small influence ($\Delta\delta$ = 14 ppm) of the pinene groups at the 4- and 5-positions when compared to the complex with unsubstituted 2,2′-bipyiridine. The shift values for the complexes with the 5,6-pinene-bipyridine ligands are much larger, in the order of $\Delta\delta \approx 400$ ppm. The diastereomeric complexes **L2PtCl$_2$** and **L3PtCl$_2$** are not distinguishable.

Electronic and CD Spectra

Neither the UV or the CD spectra are very strongly influenced by complex formation. All free ligands show two absorption maxima in the UV region. Complexation with $PtCl_4^-$ leads to a red shift of these ligand transitions as well as to two additional bands above 300 nm (Table 2). The CD activity, which is very small in the accessible spectral range (250 nm−700 nm) is hardly enhanced through complex formation. This is in marked contrast to complexes where two or three chiral bipyridine ligands coordinate to one metal center.[9]

X-ray Structure Determination

One of the ligands, **L2** gave suitable crystals for structure determination. Tables 3, 6, and 8 contain the relevant crystallographic data. Figure 2 reveals an approximately C_2-symmetric structure with a *transoid* conformation of the two pyridine rings. The values of all the internal coordinates (bond lengths and bond angles) are as expected. A feature that is worth noting is the banana-like deformation of the bpy moiety, which can be expressed in terms of the angle γ, as defined in Scheme 3 and given in Table 6. Although, the ligand changes its conformation from *transoid* to *cisoid*, this type of distortion is preserved and even significantly enhanced (vide infra) upon coordination.

The X-ray structures of the complexes **L2PtCl$_2$**, **L3PtCl$_2$**, and **L4PtCl$_2$** (no suitable crystals of **L1PtCl$_2$** and **L5PTCL$_2$** could be obtained), allow for an investigation of the question as to whether the metal itself assumes a chiral configuration induced by the chiral ligands. Figures 3, 4, and 5 show representations of these molecules in a projection that stresses the out-of-plane position of the ligand atoms. Selected bond lengths and angles are listed in Tables 3, 4, and 5.

L2PtCl$_2$ and **L4PtCl$_2$** crystallize in the triclinic space group *P*1. In the former case, there are two independent complex molecules per asymmetric unit, whereas the latter contains four independent molecules. Compound **L3PtCl$_2$**

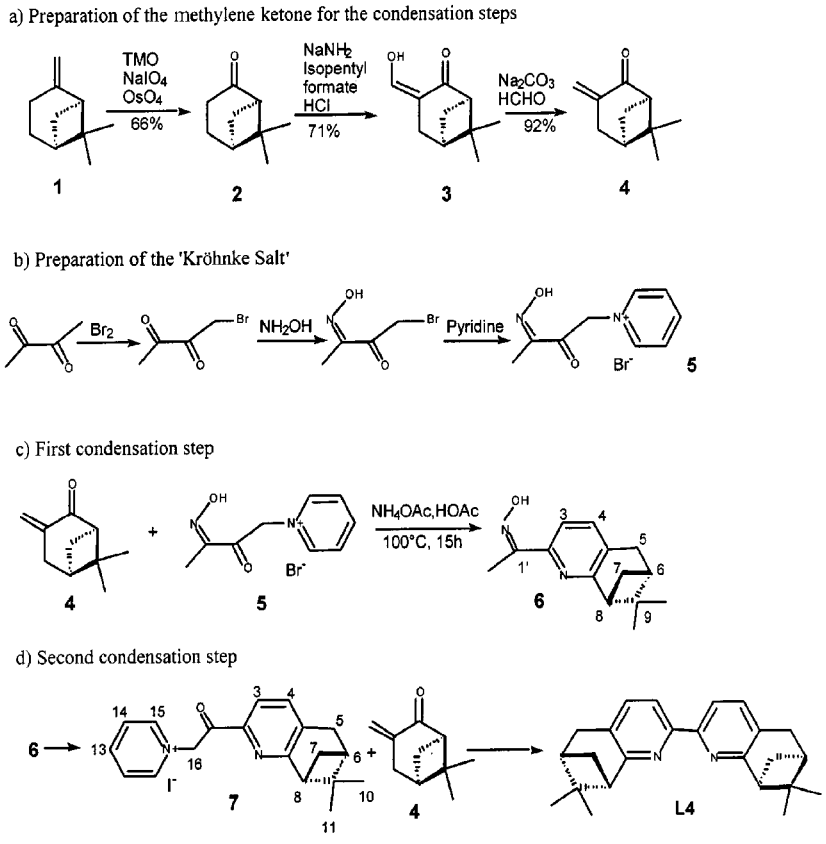

Scheme 2. Synthesis overview for **L4**

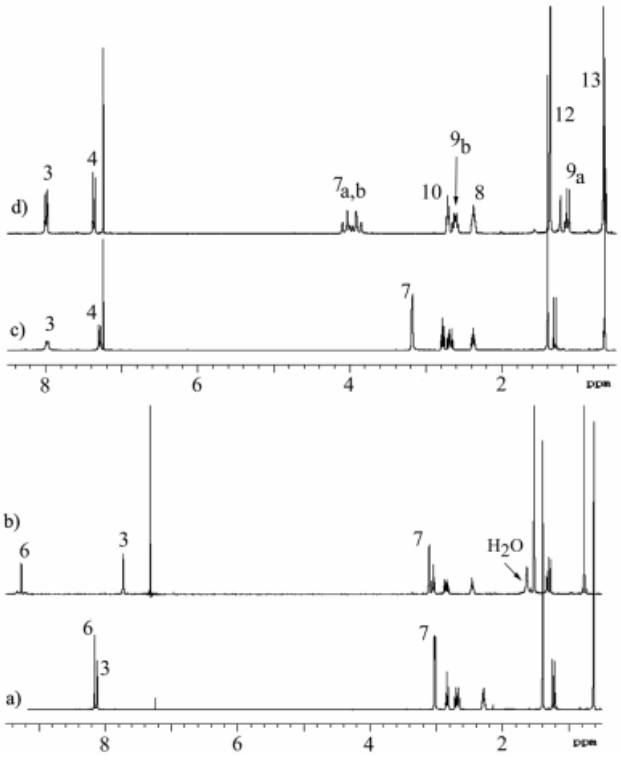

Figure 1. ^{1}H NMR spectra of the ligands **L1** and **L2**, and their platinum complexes: a) free ligand **L1**, b) **$L1PtCl_2$**, c) free ligand **L2**, d) **$L2PtCl_2$**

Table 1. ^{195}Pt NMR spectroscopic data [referenced to $NaPtCl_6$ ($\delta = 0.0$)]

Compound	δ
$[Pt(2,2'\text{-bpy})Cl_2]$	−2315
$L1PtCl_2$	−2329
$L2PtCl_2$	−1884
$L3PtCl_2$	−1887
$L4PtCl_2$	−1939
$L5PtCl_2$	−2066

crystallizes in the triclinic, centrosymmetric space group $P\bar{1}$ with one independent molecule per asymmetric unit.

The independent molecules in the lattice of **$L2PtCl_2$** and **$L4PtCl_2$** do not show strong variations in their structural parameters (Tables 3, 4, and 8). In both cases, the molecules designated as I (Tables 3 and 4), serve as a basis for further discussion.

All three complexes **$L2PtCl_2$**, **$L3PtCl_2$**, and **$L4PtCl_2$** show strong deviation from planarity. Table 6 lists bond angles and distances that characterize these deviations, as given in Scheme 3. In the complex with the *meso*-form ligand **L3**, a strong out-of-plane distortion is observed, whereby both chlorine ligands are displaced to the same side of the coordination plane defined by the five-membered chelate ring. Figure 3 shows how the two chloride ligands are located on the same side as the methyl groups of the pinene moieties of the bent pinene-bpy-ligand. Most surprisingly, exactly the same type of deformation is ad-

Table 2. Absorption data and extinction coefficients from UV/Vis spectra

Ligands	nm	ε	Complexes	nm	ε
L1	256	15200	**L1PtCl$_2$**	289	29400
	295	21200		324	11700
				339	16700
				387	3400
L2	261	12500	**L2PtCl$_2$**	277	21200
	302	22100		291	20100
				341	10800
				356	11300
L3	261	12500	**L3PtCl$_2$**	277	20600
	303	18900		295	21000
				341	11900
				356	13300
L4	258	11500	**L4PtCl$_2$**	291	18700
	304	28200		338	15400
				354	17200
L5	259	14600	**L5PtCl$_2$**	274	24600
	298	20900		287	24100
				334	14900
				348	18800

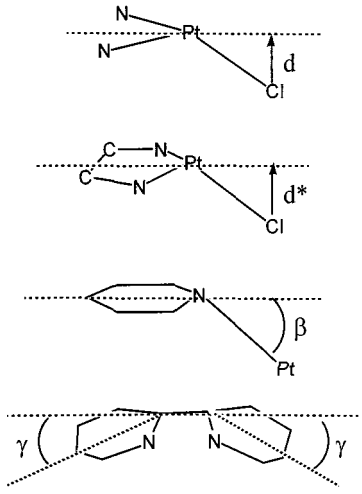

Scheme 3. Definition of parameters from planar coordination geometry for the distortion in the crystal structures for the **L2PtCL$_2$**, **L3PtCl$_2$**, and **L4PtCl$_2$** complexes. **α**, **β**, and **γ** are defined as in ref.[10], **d*** is the distance of a Cl ligand to the best plane defined by the chelate ring

Table 3. Selected bond lengths [Å], angles and dihedral angles [°] of the free ligand **L2** and the complex **L2PtCl$_2$**

L2		**L2PtCl$_2$**: Molecule I		Molecule II	
N1−C6	1.335	Pt1−N1	2.046	Pt2−N3	2.002
N1−C2	1.349	Pt1−N2	2.027	Pt2−N4	2.054
N1′−C6′	1.341	Pt1−Cl1	2.303	Pt2−Cl3	2.306
N1′−C2′	1.354	Pt1−Cl2	2.319	Pt2−Cl4	2.307
C6−N1−C2	118.3	N1−Pt−N2	80.0	N3−Pt2−N4	79.3
C6′−N1′−C2′	117.0	Cl1−Pt1−Cl2	85.2	Cl4−Pt2−Cl4	86.0
N1−C2−C3	121.5	N1−Pt1−Cl1	96.0	N3−Pt2−Cl3	96.2
N1−C2−C2′	115.4	N2−Pt1−Cl2	97.1	N4−Pt2−Cl4	96.6
N1−C2−C2′−N1′	−166.9	C5−N1−Pt1−Cl1	37.8	C29−N3−Pt2−Cl3	−25.5
C3−C2−C2′−C3′	−172.9	C17−N2−Pt1−Cl2	−30.5	C41−N4−Pt2−Cl4	34.2

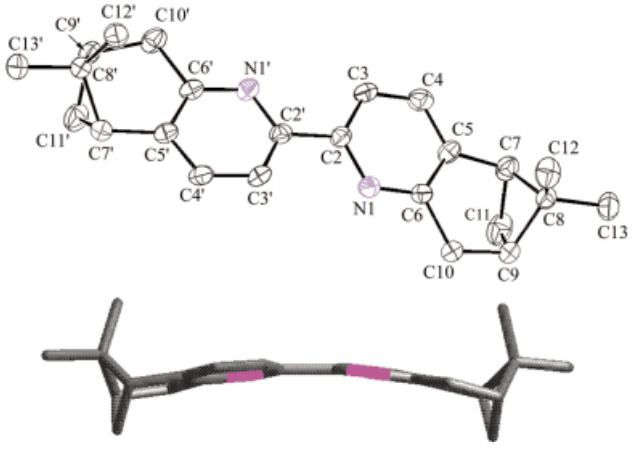

Figure 2. ORTEP[16] plot and Cerius2[17] representation of the crystal structure of the free ligand **L2**

opted by the C_2-symmetric (in the uncoordinated form) ligands in their complexes **L2PtCl$_2$** and **L4PtCl$_2$**. Again, both chlorine ligands are displaced towards the same side of the coordination plane. Even the crystal packing is very similar in all three cases. These three complexes are all strongly distorted from square-planar geometry, yet it seems that the stereogenic centers are not decisive for the type of distortion. In addition, the distortions occur in a counter-intuitive way. We would have expected that both chloride ligands lie on the opposite side of the plane to the methyl groups of the pinene moieties in the *meso*-form complex, and that the complex with the enantiomerically pure ligand would adopt approximately C_2 symmetry.

A similar phenomenon (mismatched symmetry) was observed by Newkome et al.[10] for palladium complexes with bipyridine ligands substituted at the 6- and 6,6′-positions. The parameters **d1** and **d2** in Table 6 are defined in the same way as in literature[10] (Scheme 3). In addition, we introduce the distances **d1*** and **d2***, respectively (Scheme 3), which we consider to be a more reliable measure of the distortion from a square-planar arrangement. It is difficult to know whether these distortions are due to packing effects (e.g.

Table 4. Selected bond lengths [Å], angles and dihedral angles [°] of **L3PtCl$_2$**

Molecule I	
Pt1−N1	2.063
Pt1−N2	2.015
Pt1−Cl1	2.307
Pt1−Cl2	2.305
N1−Pt−N2	80.3
Cl1−Pt1−Cl2	85.9
N1−Pt1−Cl1	96.1
N2−Pt1−Cl2	96.1
C5−N1−Pt1−Cl1	34.3
C17−N2−Pt1−Cl2	−30.3

Table 5. Selected bond lengths [Å], bond angles and dihedral angles [°] of **L4PtCl$_2$**

Molecule I		Molecule II		Molecule III		Molecule IV	
Pt1−N1	2.041	Pt2−N3	2.025	Pt3−N5	2.045	Pt4−N7	2.030
Pt1−N2	2.048	Pt2−N4	2.022	Pt3−N6	2.022	Pt4−N8	2.023
Pt1−Cl1	2.294	Pt2−Cl3	2.305	Pt3−Cl5	2.306	Pt4−Cl7	2.289
Pt1−Cl2	2.306	Pt2−Cl4	2.292	Pt3−Cl6	2.293	Pt4−Cl8	2.311
N1−Pt−N2	97.7	N3−Pt2−N4	80.4	N5−Pt3−N6	80.2	N7−Pt4−N8	80.1
Cl1−Pt1−Cl2	86.0	Cl4−Pt2−Cl4	85.6	Cl5−Pt3−Cl6	85.6	Cl7−Pt4−Cl8	86.6
N1−Pt1−Cl1	95.2	N3−Pt2−Cl3	96.9	N5−Pt3−Cl5	96.4	N7−Pt4−Cl7	94.8
N2−Pt1−Cl2	97.6	N4−Pt2−Cl4	95.7	N6−Pt3−Cl6	96.4	N8−Pt4−Cl8	97.0
C5−N1−Pt1−Cl1	23.5	C29−N3−Pt2−Cl3	31.3	C53−N5−Pt3−Cl5	26.4	C77−N7−Pt4−Cl7	24.4
C17−N2−Pt1−Cl2	−24.7	C41−N4−Pt2−Cl4	−25.3	C65−N6−Pt3−Cl6	−25.1	C89−N8−Pt4−Cl8	−26.8

Table 6. Distortion measurements for the complexes **L2PtCl$_2$**, **L3PtCl$_3$**, and **L4PtCl$_2$**

	L2	L2PtCl$_2$	L3PtCl$_2$	L4PtCl$_2$	Newkome[10]
d1 [Å]	–	0.427	0.380	0.371	0.277
d2 [Å]	–	0.363	0.368	0.345	0.496
d1* [Å]	–	0.814	0.829	0.720	0.699
d2* [Å]	–	0.778	0.831	0.721	0.908
β1 [°]	–	12.3	15.5	16.4	18.8
β2 [°]	–	11.4	13.5	15.9	16.8
γ1 [°]	3.4	17.1	14.4	6.8	7.5
γ2 [°]	7.0	11.1	11.6	7.1	8.5

π-stacking) or whether they are properties of the isolated molecules. In solution, all complexes show the expected symmetrical behavior of the two ligand halves on the NMR time scale.

Substitution Reactions

In order to determine the influence of a chiral ligand on the substitution reactions of the two *cis*-chloride ligands, a series of diamine ligands were treated with the [Pt(pinene-bpy)]Cl$_2$ complexes, as shown in Scheme 4. Table 7 shows the diamines that were treated with the complexes of Scheme 1. The products are numbered according to their position in this 'matrix'. The main point of interest is the stereoselectivity in these cases, where the incoming ligands can adopt a chiral configuration. Coordinated ethylenediamine adopts a chiral conformation.[11] In the complex [Pt(bpy)(en)]$^{2+}$, which was also synthesized for reference purposes[12], the CH$_2$-protons of 'en' appear as a singlet at δ = 2.82. Two satellites due to ^{1}H-^{195}Pt coupling are clearly resolved (Figure 6, a). Here, the λ- and δ- conformers of the five-membered chelate ring of ethylenediamine are enantiomers. The achiral time average between the two conformers has a C_{2v} symmetry, which results in one signal for the four CH$_2$ protons of 'en' (Scheme 5). In the case of the complex **13**, with the *meso*-form of the ligand, two signals for the methylene protons are expected, since the time-averaged symmetry is reduced to C_S, rendering the two protons 'above' and 'below' the coordination plane nonequivalent. With complex **12**, the two conformers are the (*RR*δ)- and (*RR*λ)-diastereomers. Again, two signals for the CH$_2$ protons are expected. Figure 6, b and c, show the relevant parts of the ^{1}H NMR spectra of these compounds. In both cases, the four protons (assigned as '15' in Figure 6) appear as one broad signal. Complexes **11**, **14**, and **15** behave in a very similar way as **12** and **13**, except that the lack of C_2 symmetry in **15** is clearly discernible in its NMR spectrum.

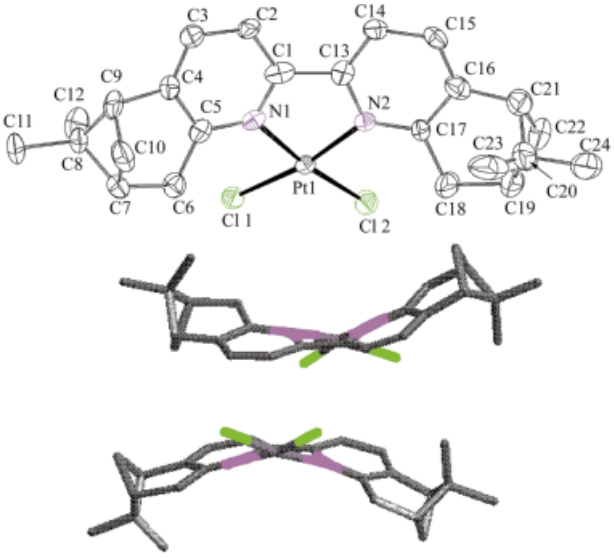

Figure 3. ORTEP[16] plot and Cerius2[17] packing representation of the crystal structure of **L2PtCl$_2$**

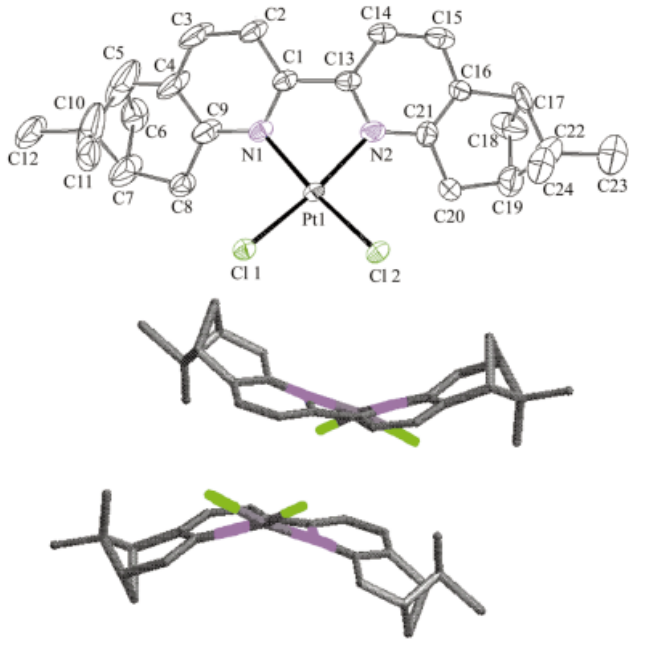

Figure 4. ORTEP[16] plot and Cerius2[17] packing representation of the crystal structure of **L3PtCl$_2$**

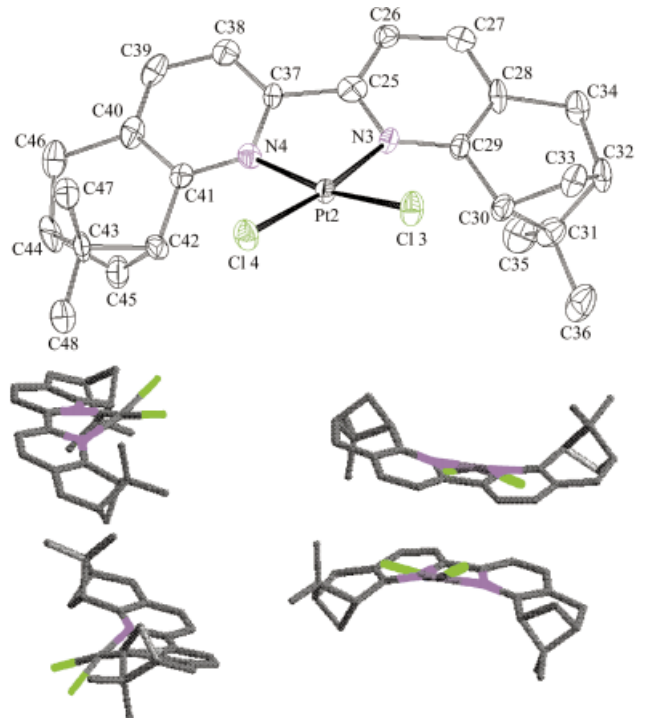

Figure 5. ORTEP[16] plot and Cerius2[17] packing representation of the crystal structure of **L4PtCl$_2$**

The substitution reactions with 'dmen', 'men', piperazine, and homopiperazine were successfully carried out only with **L1PtCl$_2$**. Complexation by replacing the two chlorine atoms with the achiral bidentate ligand 'dmen' with this compound creates stereogenic centers at the nitrogen atoms. The formation of four different diastereomers is possible, as represented in Scheme 6. In addition, the two conformers of the chelate ring, δ and λ, will now probably differ more in energy relative to 'en'. In the NMR spectrum of **51** (Fig-

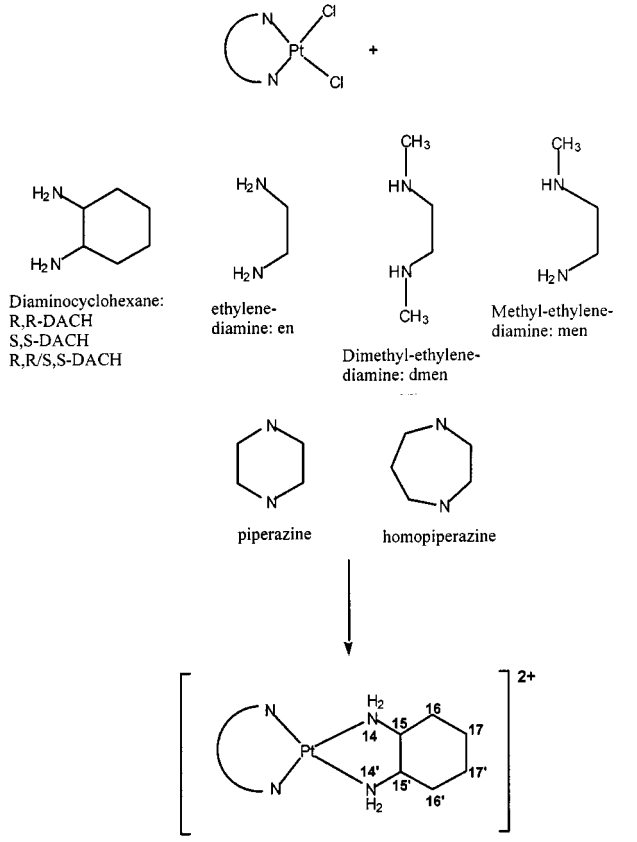

Scheme 4. Bidentate ligands used for the substitution reactions and numbering scheme of the resulting complexes

Table 7. Matrix for the numbering scheme of the substitution reactions (en = ethylenediamine; R,R-DACH = (1*R*,2*R*)-(−)-1,2-diaminocyclohexane; S,S-DACH = (1*S*,2*S*)-(+)-1,2-diaminocyclohexane; dmen = *N*,*N*′-dimethylethylenediamine; men = *N*-methylethylenediamine)

	L1PtCl$_2$	L2PtCl$_2$	L3PtCl$_2$	L4PtCl$_2$	L5PtCl$_2$
en	**11**	**12**	**13**	**14**	**15**
R,R-DACH	**21**	**22**	-	**24**	-
S,S-DACH	**31**	**32**	-	-	**35**
S,S/R,R-DACH	**41**	**42**	-	**44**	**45**
dmen	**51**				
men	**61**				
piperazine	**71**	-	-	-	-
homopiperazine	**81**	-	-	-	-

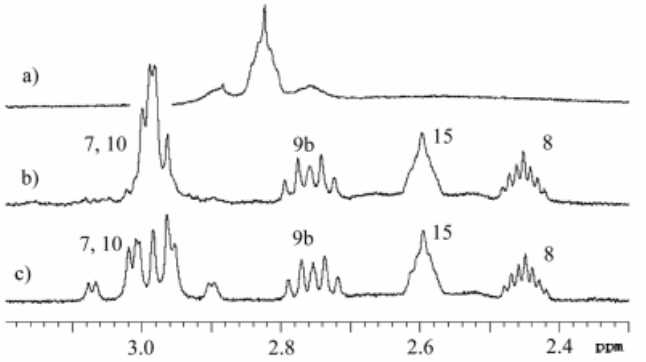

Figure 6. Part of the ^{1}H NMR aliphatic region of a) [Pt(bpy)(en)](PF$_6$)$_2$, b) compound **13**, c) compound **12**

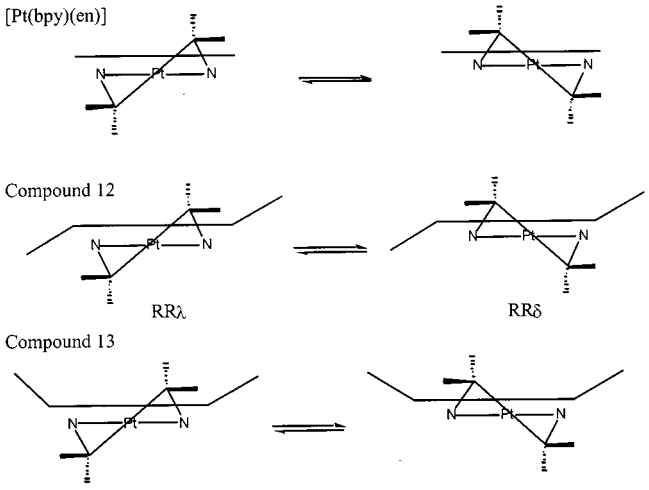

Scheme 5

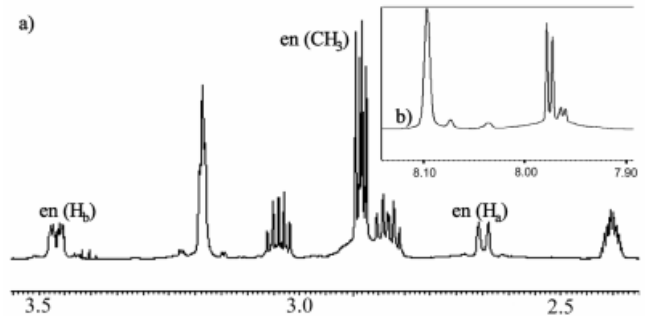

Figure 7. ^{1}H NMR spectrum (500 MHz) of compound **51**; a) aliphatic region, b) aromatic region

ure 7, a and b) most of the signals appear twice, with a ratio of 1:1. Small additional signals are observed in the region of the aromatic protons, as well as for the NH signal and the C(13)-methyl protons in an approximate ratio of 1:0.15. This indicates the formation of two main diastereomers, which are probably the two less constraining (*R,R*)- and (*S,S*)- forms. Furthermore, in this case we observed the expected nonequivalence (as discussed above) of the 'en'-methylene protons, which appear separated by 0.82 ppm as doublets with a coupling constant of 8.8 Hz. The diastereotopicity is much more pronounced owing to the new stereogenic centers located at the neighboring N-atoms.

In the case of 'men', the number of possible diastereomers is reduced to two since only one nitrogen atom becomes stereogenic and in addition a complete loss of symmetry occurs upon complexation with this unsymmetrical ligand. The NMR spectrum of compound **61** shows that both diastereomers, those with (*R*)- and (*S*)- configurations at the methylated N-atom, are formed in an approximate ratio of 1:1. Most of the signals of the ligands are quadrupled. Furthermore, the $H_2-C(15)$ ethylene protons appear as two separate doublets, whereas the $H_2-C(15')$ protons, which are not influenced by a close stereogenic center, gave rise to a singlet (the methyl-bearing nitrogen atom was assigned arbitrarily as N(14)]. The substitution of **L1PtCl$_2$** with piperazine yields only one possible isomer. Compound **71** shows the expected NMR pattern. The diastereotopic protons of the CH_2 groups of the piperazine ring are separated by 0.78 ppm, with a geminal coupling constant of 8.2 Hz.

In the case of homopiperazine, also only one isomer is possible, but the substitution results in a complete loss of symmetry owing to the absence of a C_2 axis of symmetry in the ligand. However, the influence of the unsymmetrical homopiperazine on the proton signals of the pinene group is small. The loss of symmetry could only be observed in the 500 MHz NMR spectra of compound **81**. All the proton signals of the pinene group show the same pattern as in the case of the symmetrical complexes, except that a doubling of the *exo*-oriented CH_3 groups and the *endo*-oriented $H-C(9)$ protons is also evident. Furthermore, two separate signals for the aromatic protons at the 6- and 6′-positions were observed. The signals for the protons of the CH_2 groups 15 and 15′, as well as 16 and 16′ are separated by 0.25 ppm and 0.51 ppm, respectively, in the latter case because of their diastereotopicity. The two protons at the C(17)-position do not show this phenomenon.

The ligand *trans*-1,2-diaminocyclohexane (DACH) is of special interest because of its configurations that are fixed by the six-membered ring. Substitution reactions were carried out with the pure (*S,S*) and (*R,R*)-forms, as well as with the racemic mixture (*S,S*)/(*R,R*) = 1:1. In the case of ligand **L1**, all the spectra of the substitution products **21**,

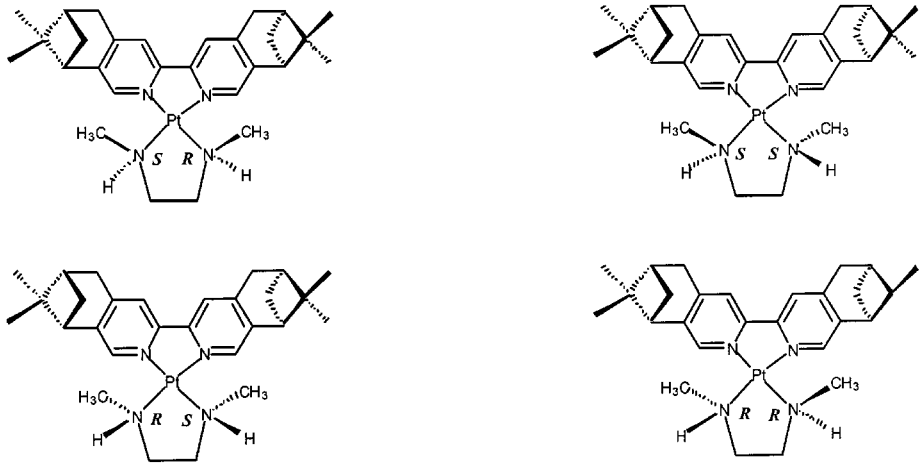

Scheme 6. The four possible diastereoisomers after the substitution reaction of **L1PtCl$_2$** with 'dmen'

31, and **41** are indistinguishable. Although this does not exclude a diastereoselective reaction, it is highly improbable that such selectivity occurs. In the case of the much bulkier ligand **L2**, complexes **22** and **32** can be distinguished by a difference in chemical shifts of one of the methyl groups and of one of the protons of the CH_2-group in the pinene part. From this, a diastereomeric ratio of (*RR*)/(*SS*) = 1:1.3 is calculated. The corresponding analysis for ligand **L4** yields a slightly higher diastereoselectivity for the (*R,R*)-form [(*R,R*)/(*S,S*) = 1.5:1].

Conclusions

Chiral bipyridine ligands induce significant distortions in square-planar platinum complexes if the 'substituents' of the pyridine are at the 6- and 6′-positions. However, C_2-symmetric, homochiral ligands yield molecules of low symmetry if the two other ligand positions are occupied by Cl^-. The distortions are not determined by the chiral nature of these ligands, since an overall achiral *meso*-form behaves in a very similar way. Consequently, substitution of these chlorides by amines proceeds in a nonstereoselective manner.

Experimental Section

Products: Solvents and reagents were purchased from Fluka and Aldrich. Iodine was sublimed before use. Pyridine was dried with KOH and freshly distilled prior to use. Ammonium acetate was dried for 5−6 h before use in a vacuum oven at 40 °C. Diethyl ether was distilled from sodium/benzophenone prior to use. The precursor platinum complex $K_2[PtCl_4]$ was prepared following procedures described by Livingstone.[13]

Measurements: NMR spectra were recorded on a 'Varian Gemini 300' (300.075 MHz) or on a 'Bruker Avance DRX500' (500.13 MHz) spectrometer. Chemical shifts are given in ppm using TMS or the solvent itself as internal standard, and coupling constants *J* are given in Hz. Assignment of the ^1H and ^{13}C NMR signals was performed by COSY, DEPT and HETCOR techniques. Diastereotopic protons are labeled as H_a for the *endo*-oriented protons and H_b for the *exo*-oriented protons. The *exo* methyl groups of the pinene moieties are assigned as 12 and 12′, the *exo*-oriented ones as 13 and 13′. The ^{195}Pt NMR spectra were recorded on the Varian Gemini 300 at 64.376 MHz. The signals were referenced to Na_2PtCl_6[14] (δ = 0.0). − UV/Vis spectra were measured on a Perkin−Elmer Lambda 40 spectrometer. − Mass spectral data were acquired on 'VG Instrument 7070E' equipped with a FAB inlet system. − Elemental analysis were obtained from CIBA Specialties, Marly (Switzerland) and 'Ecole d'ingéneurs de Fribourg' (Switzerland).

General: Compounds **3** and **4** (Scheme 2) were synthesized following a method described by M.Gianini.[7] The preparation of the appropriate Kröhnke salt **5** (Scheme 2) for condensation with **4** was described by Rupprecht.[7] The preparation of ligand **L5** was first described by Philippe Lainé in a private communication.[6]

L3: [2-{(−)-α-Pineno[2,3-*e*]pyridin-2-yl}acetyl]pyridinium iodide (2.27 g, 5.4 mmol, prepared as described in ref.[7]), pinocarvone (0.81 g, 5.40 mmol) prepared from (+)-α-pinene[7], and dry ammonium acetate (3.6 g) were dissolved in glacial acetic acid (7 mL) and stirred at 100 °C for 15 h. After cooling the dark brown reaction mixture to room temperature, water (100 mL) was added, followed by extraction of the water phase with hexane (at least 7 × 50 mL). The collected organic phases were washed with water (100 mL), dried with $MgSO_4$ and filtered. Evaporation of the solvent yielded **L3** (780 mg, 42%). The product was recrystallized from acetone. − ^1H NMR (300 MHz, $CDCl_3$): δ = 8.02 [d, ^3J = 7.9 Hz, 2 H, H−C(3,3′)], 7.30 [d, ^3J = 7.9 Hz, 2 H, H−C(4,4′)], 3.19 [d, ^3J = 2.6 Hz,4 H, H_2−C(7)], 2.78 [dd, ^3J = 5.6, 5.6 Hz, 2 H, H-(10,10′)], 2.68 [ddd, ^2J = 9.6 Hz, ^3J = 5.6, 5.6 Hz, 2 H, H_b−C(9,9′)], 2.37 [m, 2 H, H−C(8,8′)], 1.40 [s, 6 H, H_3−C(12,12′)], 1.28 [d, ^2J = 9.6 Hz, 2 H, H_a−C(9,9′)], 0.65 [s, 6 H, H_3−C(13,13′)]. − ^{13}C NMR (75 MHz, $CDCl_3$): δ = 156.2 [C(2,2′)], 141.8 [C(4,4′)], 133.9 [C(3,3′)], 117.9 [C(2,2′)], 112.8 [C(5,5′)], 46.5 [C(10,10′)], 40.3 [C(8,8′)], 39.5 [C(11,11′)], 36.6 [C(7,7′)], 31.9 [C(9,9′)], 26.1 [C(12,12′)], 21.3 (13,13′)]. − EI-MS: *m/z* (%) = 344 (100) [M^+], 329 (58) [$M^+ - CH_3$], 303 (59), 271 (22), 257 (42), 154 (10). − $C_{24}H_{28}N_2$ (344.5): calcd. C 83.68, H 8.19, N 8.13, found C 82.92, H 8.40, N 7.94.

(6*R*,8*R*)-2-(1′-Ethyloxime)-5,6,7,8-tetrahydro-9,9-dimethyl-6,8-metaquinoline (6): The Kröhnke salt **5** (6.90 g, 26.6 mmol), NH_4 acetate (17.7 g), glacial acetic acid (28 mL), and **4** (4.0 g, 26.6 mmol) were heated at reflux for 15 h. The reaction mixture was cooled to room temperature, diluted with water (100 mL) and extracted with hexane [7 × 50 mL). The combined organic phases were washed with water (100 mL), dried with $MgSO_4$ with active charcoal, and filtered. After evaporating the solvent a brown viscous liquid (3.84 g, 63%) was obtained. − ^1H NMR (300 MHz, $CDCl_3$): δ = 7.51 [d, ^3J = 7.7 Hz, 1 H, H−C(3)], 7.40 [d, ^3J = 7.7 Hz, 1 H, H−C(4)], 3.09 [dd, ^3J = 5.8, 5.8 Hz, 1 H, H−C(8)], 2.93 [d, ^3J = 2.9 Hz, 2 H, H-(5)], 2.72 [ddd, ^2J = 9.8 Hz, ^3J = 5.8, 5.8 Hz, 1 H, H_a−C(7)], 2.35 [s, 3 H, H_3−C(11)], 1.28 [d, ^2J = 9.8 Hz, 1 H, H_b−C(7)], 0.65 [s, 3 H, H_3−C(10)].

1-{2-(Pineno[2,3-*e*]pyridin-2-yl)acetyl}pyridinium Iodide (7): Product **6** (3.80 g, 15 mmol) was reacted with HCl (70 mL, 25%) and heated at reflux for 8 h. After cooling the reaction mixture to room temperature, the black solution was brought to pH = 3 by the addition of NaOH (30%), and then carefully adjusted to pH = 7−8 with Na_2CO_3. This mixture was then extracted with hexane (7 × 50 mL). The organic phases were washed with water (100 mL), dried with $MgSO_4$ and filtered. Evaporation of the solvent gave a brown−yellow, viscous liquid (2.96 g). A portion of this product (2.70 g) was dissolved in pyridine (4 mL) in a 250-mL flask. Iodine (3.20 g, 12.5 mmol) dissolved in pyridine (10 mL) was added, and the mixture was heated at reflux for 3 h. After removing excess pyridine by vacuum distillation, dry diethyl ether (180 mL) was added to the black residue and kept at 4 °C overnight. The brown powder was filtered off, washed twice with diethyl ether and dried under high vacuum for 2 d. In order to obtain a good precipitate, it was essential to carry out this reaction with the exclusion of water, resulting in an hygroscopic product (7.05 g, 90%). The product was a mixture of the desired product **7** and pyridinium iodide. The ratio was determined to be 1:1. − ^1H NMR (300 MHz, [D_6]DMSO): (numbering see Scheme 2) δ = 9.00 [d, ^3J = 6.8 Hz, 2 H, H−C(15)], 8.70 [t, ^3J = 7.8 Hz, 1 H, H−C(13)], 8.25 [dd, ^3J = 7.8, 6.7 Hz, 2 H, H−C(14)], 7.89 [d, ^3J = 7.7 Hz, 1 H, H−C(3)], 7.86 [d, ^3J = 7.7 Hz, 1 H, H−C(4)], 6.48 [s, 2 H, H−C(16)], 3.05 [m, 3 H, H−C(8), H−C(5)], 2.80 [dd, ^2J = 9.8 Hz, ^3J = 5.8 Hz, 1 H, H_a−C(7)], 2.38 [m, 1 H, H−C(6)], 1.44 [s, 3 H, H_3−C(11)], 1.21 [d, ^2J = 9.8 Hz, 1 H, H_b−C(7)], 0.65 [s, 3 H, H_3−C(10)]. −

Pyridinium iodide: δ = 8.91 [d, ^3J = 6.5 Hz, 2 H, H−C(15)], 8.55 [t, ^3J = 7.8 Hz, 1 H, H−C(13)], 8.03 [dd, ^3J = 7.7, 6.6 Hz, 2 H, H−C(14)].

L4: Compound **7** (3.0 g, 4.78 mmol), ammonium acetate (3.1 g) and **4** (0.72 g, 4.78 mmol) were dissolved in glacial acetic acid (6 mL) and stirred at reflux for 15 h. The reaction temperature was gradually raised over a period of 4 h starting at 50 °C. After cooling the reaction mixture to ambient temperature, water (80 mL) was added. The mixture was extracted with hexane [7 × 50 mL). Washing, drying and evaporation of the solvent yielded a yellow powder (0.94 g, 57%). Recrystallization from hexane gave white crystals of **L4**. − ^{1}H NMR (300 MHz, $CDCl_3$): δ = 8.08 [d, ^3J = 7.7 Hz, 2 H, H−C(3,3′)], 7.49 [d, ^3J = 7.7 Hz, 2 H, H−C(4,4′)], 3.09 [dd, ^3J = 5.8, 5.8 Hz, 2 H, H−C(10,10′)], 2.94 [d, ^3J = 2.9 Hz, 4 H, H_2−C(7,7′)], 2.71 [ddd, ^2J = 9.8 Hz, ^3J = 5.8, 5.8 Hz, 2 H, H_b−C(9,9′)], 2.31 [m, 2 H, H−C(8,8′)], 1.40 [s, 6 H, H_3−C(12,12′)], 1.32 [d, ^2J = 9.8 Hz, 2 H, H_a−C(9,9′)], 0.65 [s, 6 H, H_3−C(13,13′)]. − ^{13}C NMR (75 MHz, $CDCl_3$): δ = 165.8 [C(2,2′)], 152.6 [C(6,6′)], 136.0 [C(4,4′)], 130.0 [C(5,5′)], 118.9 [C(3,3′)], 50.5 [C(10,10′)], 40.3 [C(8,8′)], 39.9 [C(11,11′)], 31.2 (C7,7′)], 30.9 [C(9,9′)], 26.0 [C(12,12′)], 21.5 [C(13,13′′)]. − EI-MS: *m*/*z* (%) = 344 (25) [M^+], 329 (10) [$M^+ - CH_3$], 315 (7) [$M^+ - 2\ CH_3$], 301 (100) [$M^+ - 3\ CH_3$]. − $C_{24}H_{28}N_2$ (344.5): calcd. C 83.7, H 8.2, N 8.1; found C 83.6, H 8.2, N 7.9.

L5: [2-{(−)-α-Pineno[2,3-*e*]pyridin-2-yl}acetyl]pyridinium iodide (5.46 g, 13.0 mmol, prepared as described in ref.[7]) was suspended in formamide (50 mL). (1*R*)-(−)-Myrtenal (1.96 g, 13.0 mmol) and dry ammonium acetate (2.51 g) were added to this suspension and the reaction mixture was stirred at reflux for 15 h. After cooling the mixture to 0 °C, water (80 mL) was added and the mixture was stirred for 30 min. The black solution was extracted with diethyl ether (at least 8 × 70 mL). The collected organic phases were washed twice with water (80 mL), dried with $MgSO_4$ and filtered. Evaporation of the solvent yielded a brown powder (3.2 g). Recrystallization from acetone gave pure **L5** (2.50 g, 56%). − ^{1}H NMR (300 MHz, $CDCl_3$): δ = 8.17 [s, 1 H, H−C(6′)], 8.14 [s, 1 H, H−C(3′)], 7.99 [d, ^3J = 7.8 Hz, 1 H, H−C(3)], 7.30 [d, ^3J = 7.8 Hz, 1 H, H−C(4)], 3.18 [d, ^3J = 2.6 Hz, 2 H, H_2−C(7)], 3.03 [d, ^3J = 2.7 Hz, 2 H, H_2−C(7′)], 2.84 [dd, ^3J = 5.5 Hz, 1 H, H−C(10′)], 2.78 [dd, ^3J = 5.7 Hz, 1 H, H−C(10)], 2.68 [m, 2 H, H_b−C(9,9′)], 2.38 [m, 1 H, H−C(8)], 2.28 [m, 1 H, H−C(8′)], 1.40 [s, 6 H, H_3−C(12,12′)], 1.30 [d, ^2J = 9.6 Hz, 1 H, H_a−C(9)], 1.22 [d, ^2J = 9.6 Hz, 1 H, H_a−C(9′)], 0.66 [s, 3 H, H_3−C(13)], 0.62 [s, 3 H, H_3−C(13′)]. − ^{13}C NMR (75 MHz, $CDCl_3$): δ = 156.3 [C(2)], 154.8 [C(4′)], 154.2 [C(6)], 145.5 [C(2′)], 145.2 [C(6′)], 142.6 [C(5′)], 141.4 [C(5)], 133.8 [C(4)], 120.3 [C(3′)], 117.6 [C(3)], 46.4 [C(10)], 44.4 [C(10′)], 40.2 [C(8)], 40.1 [C(8′)], 39.5 [C(11)], 39.3 [C(11′)], 36.7 [C(7)], 32.9 [C(7′)], 31.9 [C(9)], 31.8 [C(9′)], 26.0 [C(12,12′)], 21.3 [C(13,13′)]. − EI-MS: *m*/*z* (%) = 345 (100) [M^+], 330 (44) [$M^+ - CH_3$], 301 (78), 271 (26), 257 (44), 154 (9).

L1PtCl$_2$: Compound **L1** (600 mg, 1.7 mmol) was added to a solution of K_2PtCl_4 (723 mg, 1.7 mmol) dissolved in HCl (0.2 M, 80 mL). After stirring for 3 h at reflux, the yellow precipitate was filtered off and washed with water. The crude product was dried at 50 °C in a vacuum oven. Recrystallization from chloroform/heptane gave bright yellow **L1PtCl$_2$** (1.02 g, 1.6 mmol, 96%). − ^{1}H NMR (300 MHz, $CDCl_3$): δ = 9.20 [s, 2 H, H−C(6,6′)], 7.66 [s, 2 H, H−C(3,3′)]; 3.02 [d, ^3J = 2.5 Hz, 4 H, H_2−C(7,7′)], 2.95 [dd, ^3J = 5.4, 5.4 Hz, 2 H, H−C(10,10′)], 2.77 [m, 2 H, H_b−C(9,9′)], 2.36 [m, 2 H, H−C(8,8′)], 1.42 [s, 6 H, H_3−C(12,12′)], 1.19 [d, ^2J = 10.2 Hz, 2 H, H_a−C(9,9′)], 0.66 [s, 6 H, H_3−C(13,13′)]. − ^{13}C NMR (75 MHz, $CDCl_3$): δ = 181.7 [C(2,2′)], 148.8 [C(4,4′)], 146.4 [C(5,5′)], 145.2 [C(6,6′)], 121.2 [C(3,3′)], 44.8 [C(10,10′)], 39.5 [C(8,8′)], 33.5 [C(11,11′)], 31.3 [C(7,7′)], 29.7 [C(9,9′)], 25.6 [C(12,12′)], 21.5 [C(13,13′)]. − ^{195}Pt NMR (64.376 MHz, $CDCl_3$): see Table 1. − FAB-MS: *m*/*z* (%) = 610 (25) [M^+]; 575 (86) [$M^+ - Cl$]; 537 (18) [$M^+ - 2\ Cl$]; 460 (20), 391 (43), 345 (98) [L1], − $C_{24}H_{28}Cl_2N_2Pt$ (610.5): calcd. C 47.20, H 4.62, N 4.59, found C 47.40, H 4.69, N 5.07.

[{Bis[(−)-pineno]−2,2′-bipyridine}(ethylenediamine)Pt^{II}](PF$_6$)$_3$ (11): To a suspension of **L1PtCl$_2$** (100 mg, 0.16 mmol) in water/acetone (1:1, 25 mL), ethylenediamine (10 μL) was added. After heating the reaction mixture at reflux for 8 h, the solution was cooled to room temperature and unreacted starting material was filtered off. The acetone was evaporated from the filtrate and solid NH_4PF_6 was added to the aqueous solution. The mixture was kept for 1 h at 4 °C. The white precipitate was filtered off, washed with water, and dried in vacuum. Purification by recrystallization from ethanol/diethyl ether gave **11** (90 mg, 62%). − ^{1}H NMR (300 MHz, [D_3]ACN): δ = 8.07 [s, 2 H, H−C(3,3′)], 7.97 [s, $J_{Pt\text{-}H}$ = 29.8 Hz, 2 H, H−C(6,6′)], 5.11 [b, 4 H, H_2−N(14,14′)], 3.17 [d, ^3J = 2.3 Hz, 4 H, H_2−C(7,7′)], 2.96 [dd, ^3J = 5.4, 5.4 Hz, 2 H, H−C(10,10′)], 2.80 [m, 6 H, H_b−C(9,9′), H_2−C(15,15′)], 2.40 [m, 2 H, H−C(8,8′)], 1.45 [s, 6 H, H_3−C(12,12′)], 1.23 [d, ^2J = 9.9 Hz, 2 H, H_a−C(9,9′)], 0.66 [s, 6 H, H_3−C(13,13′)]. − ^{13}C NMR (MHz, [D_3]ACN): δ = 147.0 [C(6,6′)], 124.3 [C(3,3′)], 47.9 (C15,15′)], 45.4 [C(10,10′)], 40.2 [C(8,8′)], 33.9 [C(7,7′)], 31.3 [C(9,9′)], 25.2 [C(12,12′)], 21.3[C(13,13′)], (the quaternary carbon atoms could not be detected). − FAB-MS: *m*/*z* (%) = 744 (12) [$M^+ - PF_6$], 598 (69) [$M^+ - 2\ PF_6$], 537 (13) [M^+ − en], 307 (29), 171 (57), 154 (100).

[{Bis[(−)-pineno]−2,2′-bipyridine}(R,R-DACH)Pt^{II}](PF$_6$)$_2$ (21): Compound **L1PtCl$_2$** (100 mg, 16 mmol) was suspended in water/acetone (1:1, 25 mL). (*R*,*R*)-diaminocyclohexane (30 mg, 26 mmol) was added. After the reaction mixture was heated at reflux for 10 h, unreacted starting materials were filtered off and the acetone was evaporated from the filtrate. To this solution, solid NH_4PF_6 was added and the solution was allowed to stand for 4 h at 4 °C. The white product was filtered off and washed with water. The product (95 mg, 61%), was recrystallized from ethanol/diethyl ether. − ^{1}H NMR (300 MHz, [D_3]acetonitrile): δ = 8.07 [s, 2 H, H−C(3,3′)], 8.00 [s, 2 H, H−C(6,6′)], 5.38 [b, 2 H, H_b−N(14,14′)], 4.77 [b, 2 H, H_a−N(14,14′)], 3.17 [d, ^3J = 3.4 Hz, 4 H, H_2−C(7,7′)], 2.96 [dd, ^3J = 5.3, 5.3 Hz, 2 H, H−C(10,10′)], 2.83 [ddd, ^2J = 10.0 Hz, ^3J = 5.8, 5.8 Hz, 2 H, Hb−C(9,9′)], 2.63 [m, 2 H, H−C(15,15′)], 2.40 [m, 2 H, H−C(8,8′)], 2.15 [d, ^2J = 12.0 Hz, 2 H, H_a−C(16,16′)], 1.65 [d, ^2J = 8.9 Hz, 2 H, H_a−C(17,17′)], 1.45 [s, 8 H, H_3−C(12,12′), H_b−C(16,16′)], 1.25 [d, ^2J = 8.9 Hz, 2 H, H_b−C(17,17′)], 1.24 [d, ^2J = 10.0 Hz, 2 H, H_a−C(9,9′)], 0.67 [s, 6 H, H_3−C(13,13′)]. − ^{13}C NMR (75 MHz, [D_3]acetonitrile): δ = 155.8; 154.5; 153.3; 148.9 [C(4,4′)], 146.9 [C(6,6′)], 124.2 [C(3,3′)], 62.5 [C(15,15′)], 45.3 [C(10,10′)], 40.4 [C(8,8′)], 36.7 [C(11,11′)], 34.2 [C(7,7′)], 33.2 (16,16′)], 31.6 [C(9,9′)], 25.8 [C(12,12′)], 24.8 [C(17,17′)], 21.5 [C(13,13′)]. − FAB-MS: *m*/*z* (%) = 799 (18) [$M^+ - PF_6$], 653 (11) [$M^+ - 2\ PF_6$], 327 (100).

[{Bis[(−)-pineno]−2,2′-bipyridine}(S,S-DACH)Pt^{II}](PF$_6$)$_2$ (31): The synthesis, and purification of compound **31** was carried out as described for compound **21** with **L1PtCl$_2$** (53 mg, 0.086 mmol) in water/acetone (15 mL) and (*S*,*S*)-diaminocyclohexane (22 mg, (0.19 mmol). Yield: 54 mg (66%). − ^{1}H NMR (300 MHz, [D_3]acetonitrile): δ = 8.07 [s, 2 H, H−C(3,3′)], 8.00 [s, 2 H, H−C(6,6′)], 5.38 [b, 2 H, H_b−N(14,14′)], 4.77 [b, 2 H, H_a−N(14,14′)], 3.17 [d, ^3J = 3.4 Hz, 4 H, H_2−C(7,7′)], 2.96 [dd, ^3J = 5.3, 5.3 Hz, 2 H, H−C(10,10′)], 2.83 [ddd, ^2J = 10.0 Hz, ^3J = 5.8, 5.8 Hz, 2 H,

H_b−C(9,9′)], 2.63 [m, 2 H, H−C(15,15′)], 2.40 [m, 2 H, H−C(8,8′)], 2.15 [d, ^2J = 12.0 Hz, 2 H, H_a−C(16,16′)], 1.65 [d, ^2J = 8.9 Hz, 2 H, H_a−C(17,17′)], 1.45 [s, 8 H, H_3−C(12,12′), H_b−C(16,16′)]; 1.25 [d, ^2J = 8.9 Hz, 2 H, H_b−C(17,17′)]; 1.24 [d, ^2J = 10.0 Hz, 2 H, H_a−C(9,9′)]; 0.67 [s, 6 H, H_3−C(13,13′)]. − ^{13}C NMR (75 MHz, [D$_3$]acetonitrile): δ = 155.2; 154.3; 153.1; 149.0 [C(4,4′)], 146.8 [C(6,6′)], 124.6 [C(3,3′)], 62.5 [C(15,15′)], 45.4 [C(10,10′)], 40.8 [C(8,8′)], 36.6 [C(11,11′)], 34.3 [C(7,7′)], 33.4 [C(16,16′)], 31.7 [C(9,9′)], 25.9 [C(12,12′)], 24.6 [C(17,17′)], 21.5 [C(13,13′)], (the aromatic quaternary carbon atoms could not be assigned). − FAB-MS: *m*/*z* (%) = 799 (9) [M^+ − PF_6], 652 (13) [M^+ − 2 PF_6], 631 (14), 327 (100).

[{Bis[(−)-pineno]−2,2′-bipyridine}(S,S/R,R-DACH)Pt^{II}](PF$_6$)$_2$ (41): The synthesis, and purification of compound **41** was carried out as described for compound **21** with **L1PtCl$_2$** (105 mg, 0.17 mmol), (*S,S*)-diaminocyclohexane (23 mg, 0.20 mmol), and (*R,R*)-diaminocyclohexane (23 mg, 0.20 mmol) in water/acetone (25 mL). Yield: 115 mg (71%). − ^{1}H NMR (300 MHz, [D$_3$]acetonitrile): δ = 8.07 [s, 2 H, H−C(3,3′)], 8.00 [s, 2 H, H−C(6,6′)], 5.38 [b, 2 H, H_b−N(14,14′)], 4.77 [b, 2 H, H_a−N(14,14′)], 3.17 [d, ^3J = 3.4 Hz, 4 H, H_2−C(7,7′)], 2.96 [m, 2 H, H−C(10,10′)], 2.83 [ddd, ^2J = 11.2 Hz, ^3J = 5.2, 5.2 Hz, 2 H, H_b−C(9,9′)], 2.63 [m, 2 H, H−C(15,15′)], 2.40 [m, 2 H, H−C(8,8′)], 2.15 [d, ^2J = 12.0 Hz, 2 H, H_a−C(16,16′)], 1.65 [d, ^2J = 8.9 Hz, 2 H, H_a−C(17,17′)], 1.45 [s, 8 H, H_3−C(12,12′), Hb−C(16,16′)], 1.25 [d, ^2J = 8.9 Hz, 2 H, H_b−C(17,17′)], 1.24 [d, ^2J = 11.2 Hz, 2 H, H_a−C(9,9′)], 0.67 [s, 6 H, H_3−C(13,13′)]. − ^{13}C NMR (75 MHz, [D$_3$]acetonitrile): δ = 155.1, 154.4, 153.3, 148.9 [C(4,4′)], 146.7 [C(6,6′)], 124.1 [C(3,3′)], 62.5 [C(15,15′)], 45.2 [C(10,10′)], 40.3 [C(8,8′)], 36.7 [C(11,11′)], 34.2 [C(7,7′)], 33.2 [C(16,16′)], 31.6 [C(9,9′)], 25.8 [C(12,12′)], 24.8 [C(17,17′)], 21.5 [C(13,13′)]. − FAB-MS: *m*/*z* (%) = 798 (25) [M^+ − PF_6], 654 (75) [M^+ − 2 PF_6], 541 (19) [M^+ − DACH], 326 (21), 307 (83), 248 (30), 154 (100).

[{Bis[(−)-pineno]−2,2′-bipyridine}(*N*,*N*′-dimethylethylenediamine)-Pt^{II}](PF$_6$)$_2$ (51): The synthesis, and purification of compound **51** was carried out as described for compound **11** with **L1PtCl$_2$** (60 mg, 0.098 mmol) and dimethylethylenediamine (20 μL, 0.18 mmol) in water/acetone (20 mL). Yield: 55 mg (61%). − ^{1}H NMR (500 MHz, [D$_3$]acetonitrile): δ = 8.09 [s, 4 H, H−C(3,3′), H−C(3,3′)*], 8.06 [s, 0.30 H, H−C(3,3′)*], 8.03 [s, 0.30 H, H−C(3,3′)*], 7.97 [s, 2 H, H−C(6,6′)], 7.96 [s, 2 H, H−C(6,6′)*], 7.95 [s, 0.30 H, H−C(6,6′)*], 7.94 [s, 0.30 H, H−C(6,6′*), 5.78 [b, 0.30 H, H−N(14,14′)*], 5.60 [b, 4 H, H−N(14,14′)], 3.47 [d, ^2J = 8.8 Hz, 4 H, H_a−C(15,15′), H_a−C(15,15′)*], 3.19 [d, ^3J = 2.3 Hz, 8 H, H_2−C(7,7′), H_2−C(7,7′)*], 3.04 [dd, ^3J = 5.4, 5.4 Hz, 4 H, H−C(10,10′), H−C(10,10′)*], 2.89 [d, ^3J = 6.5 Hz, 6 H, H_3−C(N14,14′)], 2.88 [d, ^3J = 6.5 Hz, 6 H, H_3−C(N14,14′)*], 2.83 [dd, ^2J = 9.9 Hz, ^3J = 5.4 Hz, 4 H, H_b−C(9,9′), H_b−C(9,9′)*], 2.65 [d, ^2J = 8.8 Hz, 4 H, H_b−C(15,15′), H_b−C(15,15′)*], 2.40 [m, 4 H, H−C(8,8′), H−C(8,8′)*], 1.46 [s, 6 H, H_3−C(12,12′)], 1.45 [s, 6 H, H_3−C(12,12′)*], [1.25 [d, ^2J = 9.9 Hz, 2 H, H_a−C(9,9′)], 1.23 [d, ^2J = 9.9 Hz, 2 H, H_a−C(9,9′)*], 0.68 [s, 6 H, H_3−C(13,13′), 0.66 [s, 6 H, H_3−C(13,13′)*]. − ^{13}C NMR (125 MHz, [D$_3$]acetonitrile): δ = 155.7 [C(2, 4 or 5)*], 155.6 [C(2, 4 or 5)*], 153.6 [C(2, 4 or 5)], 153.5 [C(2, 4 or 5)*], 149.4 [C(2, 4 or 5)], 149.3 [C(2, 4 or 5)*], 146.1 [C(6,6′), 145.9 [C(6,6′)*], 124.8 [C(3,3′)], 54.1 [C(15,15′)], 45.5 [C(10,10′)], 45.3 [C(10,10′)*], 43.6 [C−N(14,14′)], 43.5 (C−N(14,14′)*], 40.2 [C(8,8′)], 40.1 [C(11,11′)*], 34.1 [C(7,7′)], 34.0 [C(7,7′)*], 31.5 [C(9,9′)], 31.4 [C(9,9′)*], 25.8 [C(12,12′)], 25.7 [C(12,12′)*], 21.5 [C(13,13′)], 21.4 [C(13,13′)*]. − FAB-MS: *m*/*z* (%) = 772 (10) [M^+ − PF_6], 627 (44) [M^+ − 2 PF_6], 598 (13) [M^+ − 2 CH_3], 537 (17), 460 (26), 307 (100). − The asterisk * denotes NMR signals of the other possible diastereomers.

[{Bis[(−)-pineno]−2,2′-bipyridine}(*N*-methylethylenediamine)-Pt^{II}](PF$_6$)$_2$ (61): The synthesis, and purification of compound **61** was carried out as described for compound **11** with **L1PtCl$_2$** (57 mg, 0.093 mmol) and methylethylenediamine (17 μL, 0.19 mmol) in water/acetone (15 mL). Yield: 50 mg (60%) of **61**. − ^{1}H NMR (500 MHz, [D$_3$]acetonitrile): δ = 8.08 [s, 2 H, H−C(3 or 3′), H−C(3 or 3′)*], 8.07 [s, 2 H, H−C(3 or 3′), H−C(3 or 3′)*], 8.00 [s, 1 H, H−C(6 or 6′)], 7.99 [s, 1 H, H−C(6 or 6′)*], 7.91 [s, 2 H, H−C(6 or 6′), H−C(6 or 6′)*], 5.64 [b, 2 H, H−N(14), H−N(14)*], 5.22 [b, 2 H, H_b−N(14′), H_b−N(14′)*], 5.13 [b, 2 H, H_a−N(14′), H_a−N(14′)*], 3.17 [d, ^3J = 2.5 Hz, 10 H, H_2−C(7,7′), H_2−C(7,7′)*, H_b−C(15), H_b−C(15)*], 3.06 [m, 6 H, H_2−C(15′), H_2−C(15′)*, H−C(10 or 10′), H−C(10 or 10′)*], 2.96 [dd, ^3J = 5.5, 5.5 Hz, 2 H, H−C(10 or 10′), H−C(10 or 10′)*], 2.86 [d, ^3J = 6.7 Hz, 3 H, H_3C−N(14)], 2.85 [d, ^3J = 6.7 Hz, 3 H, H_3C−N(14)*], 2.82 [m, 4 H, H_b−C(9), H_b−C(9′), H_b−C(9)*, H_b−C(9′)*], 2.68 [d, ^2J = 9.6 Hz, 2 H, H_a−C(15), H_a−C(15)*], 2.40 [m, 4 H, H−C(8), H−C(8′), H−C(8*), H−C(8′)*], 1.46 [s, 6 H, H_3−C(12 or12′), H_3−C(12 or12′)*], 1.44 [s, 3 H, H_3−C(12 or 12′)*], 1.43 [s, 3 H, H_3−C(12 or 12′)*], 1.24 [m, 4 H, H_a−C(9), H_a−C(9′), H_a−C(9)*, H_a−C(9′)*], 0.69 [s, 3 H, H_3−C(13 or 13′), 0.67 [s, 3 H, H_3−C(13 or 13′)*], 0.66 [s, 3 H, H_3−C(13 or 13′)*], 0.65 [s, 3 H, H_3−C(13 or 13′)*]. − ^{13}C NMR (125 MHz, [D$_3$]acetonitrile): δ = 155.6, 153.5, 149.4, 149.3, 148.8, 146.7, 146.3 [C(6 or 6′), 146.0 [C(6 or 6′)], 124.3 [C(3 or 3′)], 124.2 [C(3 or 3′)], 57.8 [C(15)], 45.5 [C(10 or 10′)], 45.3 [C(10 or 10′)], 43.9 [C-(15′)], 41.7 [C−N(14)], 41.6 [(C−N(14)*], 40.3 [C(8 or 8′)], 40.2 [C(8 or 8′)], 39.7 [C(11 or 11′)*], 39.6 [C(11 or 11′)*], 34.1 [C(7), C(7′)], 31.5 [C(9 or 9′)], 31.4 [C(9 or 9′)], 25.8 [C(12 or 12′)], 25.7 [C(12 or 12′)], 21.5 [C(13 or 13′)], 21.4 [C(13 or 13′)]. − FAB-MS: *m*/*z* (%) = 758 (12) [M^+ − PF_6], 612 (51) [M^+ − 2 PF_6], 598 (11) [M^+ − CH_3], 538 (21) [M^+ − en], 307 (100). − The asterisk * denotes NMR signals of the other possible diastereomers.

[{Bis[(−)-pineno]−2,2′-bipyridine}(piperazine)Pt^{II}](PF$_6$)$_2$ (71): The synthesis, and purification of compound **71** was carried out as described for compound **11** with **L1PtCl$_2$** (56 mg, 0.092 mmol) and piperazine (14 mg, 0.16 mmol) in water/acetone (20 mL). Yield: 30 mg (36%). − ^{1}H NMR (360 MHz, [D$_3$]acetonitrile): δ = 8.37 [s, ^{Pt-H}J = 33.5 Hz, 2 H, H−C(6,6′)], 8.04 [s, 2 H, H−C(3,3′)], 5.73 [b, 2 H, H−N(14,14′)], 3.78 [d, ^2J = 7.0 Hz, 4 H, H_b−C(15,15′), H_b−C(16,16′)], 3.19 [d, ^3J = 2.3 Hz, 4 H, H_2−C(7,7′)], 3.00 [d, ^2J = 7.0 Hz, 4 H, H_a−C(15,15′), H_a−C(16,16′)], 2.95 [dd, ^3J = 5.1, 5.1 Hz, 2 H, H−C(10,10′)], 2.84 [dd, ^2J = 10.0 Hz, ^3J = 5.1 Hz, 2 H, H_b−C(9,9′)], 2.41 [m, 2 H, H−C(8,8′)], 1.47 [s, 6 H, H_3−C(12,12′)], 1.25 [d, ^2J = 10.0 Hz, 2 H, H_a−C(9,9′)], 0.69 [s, 6 H, H_3−C(13,13′)].

[{Bis[(−)-pineno−2,2′-bipyridine}(homopiperazine)Pt^{II}](PF$_6$)$_2$ (81): The synthesis, and purification of compound **81** was carried out as described for compound **11** with **L1PtCl$_2$** (100 mg, 0.16 mmol) and homopiperazine (50 mg, 0.5 mmol) in water/acetone (30 mL). Yield: 110 mg (72%). − ^{1}H NMR (500 MHz, [D$_3$]acetonitrile): δ = 8.28 [s, 1 H, H−C(6 or 6′)], 8.27 [s, 1 H, H−C(6 or 6′)], 8.06 [s, 2 H, H−C(3,3′)], 6.06 (b, 1 H, H−N(14 or 14′)],)], 6.03 [b, 1 H, H−N(14 or 14′)], 3.61 [m, 2 H, H_b−C(16,16′)], 3.49 [m, 2 H, H_b−C(15,15′)], 3.36 [m, 2 H, H_a−C(16,16′)], 3.18 [d, ^3J = 2.4 Hz, 4 H, H_2−C(7,7′)], 2.98 [m, 4 H, H_a−C(15, 15′), H−C(10,10′)], 2.82 [dd, ^2J = 9.9 Hz, ^3J = 5.8 Hz, 2 H, H_b−C(9,9′)], 2.40 [m, 2 H, H−C(8,8′)], 2.14 [m, 2 H, H_2−C-(17)], 1.46 [s, 3 H, H_3−C(12 or 12′)], 1.45 [s, 3 H, H_3−C(12 or 12′)], 1.24 [d, ^2J = 9.9 Hz, 2 H, H_a−C(9,9′)], 0.68 [s, 6 H, H_3−C(13,13′)]. − ^{13}C NMR (125 MHz, [D$_3$]acetonitrile): δ = 153.9 [C(2,2′)], 151.9 [C(5 or 5′)], 151.8 [C(5′ or 5)], 147.4 [C(4 or 4′)], 147.3 [C(4′ or 4)], 146.2 [C(6 or 6′)], 146.1

[C(6′ or 6)], 122.6 [C(3,3′)], 50.9 [C(16, 16′)], 50.0 [C(15,15′)], 43.9 [C(10,10′)], 38.9 [C(8,8′)], 38.3 [C(11,11′)], 32.7 [C(7,7′)], 30.1 [C(9,9′)], 24.5 [C(12 or 12′)], 24.4 [C(12′ or 12)], 20.2 [C(13,13′)], 18.6[C(17)].

L2PtCl$_2$: K_2PtCl_4 (1.20 g, 2.90 mmol) was dissolved in HCl (0.2 M, 100 mL) and **L2** (1.0 g, 2.90 mmol) was added. The synthesis and purification was carried out in the same way as described for **L1PtCl$_2$** above, except that the reaction time was increased to 10 h. Yellow crystals (1.32 g, 75%) of **L2PtCl$_2$** were obtained. − ^{1}H NMR (300 MHz, $CDCl_3$): δ = 7.97 [d, ^3J = 7.7 Hz, 2 H, H−C(3,3′)], 7.39 [d, ^3J = 7.7 Hz, 2 H, H−C(4,4′)], 4.03 [dd, ^2J = 18.1 Hz, ^3J = 2.6 Hz, 2 H, H_b−C(7,7 ′)], 3.91 [dd, ^2J = 18.1 Hz, ^3J = 3.1 Hz, 2 H, H_a−C(7,7 ′)], 2.71 [dd, ^3J = 5.8, 5.8 Hz, 2 H, H−C(10,10,′)], 2.61 [ddd, ^2J = 9.8 Hz, ^3J = 5.8, 5.8 Hz, 2 H, H_b−C(9,9′)], 2.36 [m, 2 H, H−C(8,8′)], 1.35 [s, H_3−C(12,12′)], 1.16 [d, ^2J = 9.8 Hz, H_a−C(9,9′)], 0.62 [s, H_3−C(13,13′)]. − ^{13}C NMR (75 MHz, $CDCl_3$): δ = 163.6 [C(2,2′)], 156.8 [C(6,6′)], 145.9 [C(5,5′)], 135.9 [C(4,4′)], 119.8 [C(3,3′)], 46.8 [C(10,10′)], 40.0 [C(8,8′)], 39.1 [C(7,7′)], 36.4 [C(11,11′)], 30.9 [C(9,9′)], 25.6 [C(12,12′)], 21.9 [C(13,13′)]. − ^{195}Pt NMR (64.376 MHz, $CDCl_3$): see Table 1. − FAB-MS: *m/z* (%) = 1185 (80) [M_2^+ − Cl], 1112* (9), 1075* (4), 1015* (4), 919* (45), 882* (23), 841* (21), 575 (80) [M^+ − Cl], 537 (100) (* further dimer fragments). − $C_{24}H_{28}Cl_2N_2Pt$ (610.5): calcd. C 47.22, H 4.62, N 4.59, found C 49.0, H 4.71, N 4.49. − Crystal structure analysis see Tables 3 and 8, Figure 2.

[{Bis[(−)-pineno]−2,2′-bipyridine}(ethylenediamine)Pt^{II}](PF$_6$)$_2$ (12): The synthesis, and purification of compound **12** was carried out as described for compound **11** with **L2PtCl$_2$** (100 mg, 0.16 mmol) and ethylenediamine (13 μL, 0.19 mmol) in water/acetone (20 mL). Yield: 105 mg (72%). − ^{1}H NMR (300 MHz, [D$_3$]acetonitrile): δ = 7.96 [d, ^3J = 8.1 Hz, 2 H, H−C(3,3′)], 7.80 [d, ^3J = 8.1 Hz, 2 H, H−C(4,4′)], 5.24 [b, 4 H, H_2−N(14,14,′)], 2.98 [d, ^3J = 3.0 Hz, 4 H, H_2−C(7,7′)], 2.97 [dd, ^3J = 5.6, 5.6 Hz, 2 H, H−C(10,10′)], 2.75 [dd, ^2J = 10.1 Hz, ^3J = 5.6 Hz, 2 H, H_b−C(9,9′)], 2.60 [b, 4 H, H_2−C(15,15′)], 2.45 [m, 2 H, H−C(8,8′)], 1.43 [s, 6 H, H_3−C(12,12′)], 1.26 [d, ^2J = 10.1 Hz, 2 H, H_a−C(9,9′)], 0.66 [s, 6 H, H_3−C(13,13′)]. − ^{13}C NMR (75 MHz, [D$_3$]acetonitrile): δ = 161.1 [C(2,2′)], 157.3 [C(6,6′)], 148.0 [C(5,5′)]; 138.9 [C(4,4′)], 121.9 [C(3,3′)], 47.8 [C(15,15′)]; 47.4 [C(10,10′)], 40.6 [C(8,8′)], 39.7 [C(11,11′)], 37.1 [C(7,7′)], 31.0 [C(9,9′)], 25.4 [C(12,12′)], 21.3 [C(13,13′)]. − FAB-MS: *m/z* (%) = 744 (12) [M^+ − PF_6], 598 (70) [M^+ − 2 PF_6], 538 (33) [M^+ − en], 154 (100).

[{Bis[(−)-pineno]−2,2′-bipyridine}(R,R-DACH)Pt^{II}](PF$_6$)$_2$ (22): The synthesis, and purification of compound **22** was carried out as described for compound **21** with **L2PtCl$_2$** (112 mg, 0.18 mmol) and (*R,R*)-diaminocyclohexane (35 mg, 0.30 mmol) in water/acetone (25 mL). Yield: 120 mg (70%) white powder of **22**. − ^{1}H NMR (300 MHz, [D$_3$]acetonitrile): δ = 7.95 [d, ^3J = 8.1 Hz, 2 H, H−C(3,3′)], 7.79 [d,^3J = 8.1 Hz, 2 H, H−C(4,4′)], 5.46 [b, 2 H, H_a−N(14,14′)], 4.80 [b, 2 H, H_b−N(14,14′)], 3.01 [dd, ^2J = 17.1 Hz, ^3J = 2.7 Hz, 4 H, H_a-H_b−C(7,7′)], 2.97 [dd, ^3J = 5.1, 5.1 Hz, 2 H, H−C(10,10′)], 2.74 [dd, ^2J = 10.1 Hz, ^3J = 5.1 Hz, 2 H, H_b−C(9,9′)], 2.46 [m, 4 H, H−C(8,8′), H−C(15,15′)], 2.19 [d, ^2J = 12.4 Hz, 2 H, H_a−C(16,16′)], 1.63 [d, ^2J = 8.8 Hz, 2 H, H_b−C(16,16′)], 1.42 [s, 6 H, H_3−C(12,12′)], 1.38 (b, 2 H, H_a−C17,17′)], 1.24 [d, ^2J = 10.1 Hz, 4 H, H_b−C(17,17′), H_a−C(9,9′)], 0.68 [s, 6 H, H_3−C(13,13′)]. − ^{13}C NMR (75 MHz, [D$_3$]acetonitrile): δ = 139.1, 122.2, 62.7, 47.7, 40.9, 37.4, 32.7, 31.5, 30.5, 25.6, 24.9, 21.7. − FAB-MS: *m/z* (%) = 798 (16) [M^+ − PF_6], 653 (73) [M^+ − 2 PF_6], 539 (51) [M^+ − DACH], 345 (26), 307 (31), 176 (32), 154 (100).

[{Bis[(−)-pineno]−2,2′-bipyridine}(S,S-DACH)Pt^{II}](PF$_6$)$_2$ (32): The synthesis, and purification of compound **32** was carried out as described for compound **21** with **L2PtCl$_2$** (106 mg, 0.17 mmol) and (*S,S*)-diaminocyclohexane (34 mg, 0.30 mmol) in water/acetone (25 mL). Yield: 112 mg (68%) white powder of **32**. − ^{1}H NMR (300 MHz, [D$_3$]acetonitrile): δ = 7.95 [d, ^3J = 8.1 Hz, 2 H, H−C(3,3′)], 7.79 [d,^3J = 8.1 Hz, 2 H, H−C(4,4′)], 5.48 [b, 2 H, H_a−N(14,14′)], 4.83 [b, 2 H, H_b−N(14,14′)], 3.01 [dd, ^2J = 17.1 Hz, ^3J = 2.7 Hz, 4 H, H_a-H_b−C(7,7′)], 2.97 [dd, ^3J = 5.8, 5.8 Hz, 2 H, H−C(10,10′)], 2.74 [dd, ^2J = 10.1 Hz, ^3J = 5.1 Hz, 2 H, H_b−C(9,9′)]; 2.46 [m, 6 H, H−C(8,8′), H_2−C(15,15′)], 2.19 [d, ^2J = 12.4 Hz, 2 H, H_a−C(16,16′)], 1.63 [d, ^2J = 8.8 Hz, 2 H, H_b−C(16,16′)], 1.42 [s, 6 H, H_3−C(12,12′)], 1.38 (b, 2 H, H_a−C17,17′)], 1.30 [d, ^2J = 10.1 Hz, 2 H, H_a−C(9,9′)], 1.22 [d, ^2J = 10.1 Hz, 2 H, H_b−C(17,17′)], 0.64 [s, 6 H, H_3−C(13,13′)]. − ^{13}C NMR (75 MHz, [D$_3$]acetonitrile): δ = 139.1, 122.2, 62.7, 47.7, 40.9, 37.4, 32.7, 31.5, 30.5, 25.6, 24.9, 21.7. − FAB-MS: *m/z* (%) = 798 (11) [M^+ − PF_6], 652 (54) [M^+ − 2 PF_6], 538 (41) [M^+ − DACH], 439 (12), 345 (18), 307 (20), 154 (100).

[{Bis[(−)-pineno]−2,2′-bipyridine}(S,S/R,R-DACH)Pt^{II}](PF$_6$)$_2$ (42): The synthesis, and purification of compound **32** was carried out as described for compound **21** with **L2PtCl$_2$** (92 mg, 0.15 mmol), (*S,S*)-diaminocyclohexane (32 mg, 0.28 mmol) and (*R,R*)-diaminocyclohexane (32 mg, 0.28 mmol) in water/acetone (25 mL). Yield: 108 mg (76%) white powder of **42**. − ^{1}H NMR (300 MHz, [D$_3$]acetonitrile): δ = 7.95 [d, ^3J = 8.1 Hz, 2 H, H−C(3,3′)], 7.79 [d, ^3J = 8.1 Hz, 2 H, H−C(4,4′)], 5.48 [b, 2 H, H_a−N(14,14′)], 4.82 [b, 2 H, H_b−N(14,14′)], 3.01 [dd, ^2J = 17.1 Hz, ^3J = 2.7 Hz, 4 H, H_a-H_b−C(7,7′)], 2.97 [dd, ^3J = 5.8 Hz, 2 H, H−C(10,10′)], 2.74 [dd, ^2J = 10.1 Hz, ^3J = 5.1 Hz, 2 H, H_b−C(9,9′)], 2.46 [m, 4 H, H−C(8,8′), H−C(15,15′)], 2.19 [d, ^2J = 12.4 Hz, 2 H, H_a−C(16,16′)], 1.63 [d, ^2J = 8.8 Hz, 2 H, H_b−C(16,16′)], 1.42 [s, 6 H, H_3−C(12,12′)], 1.38 (b, 2 H, H_a−C17,17′)], 1.30 [d, ^2J = 10.1 Hz, 2 H, H_a−C(9,9′)-(*S,S*-DACH), 1.24 [d, ^2J = 10.1 Hz, 2 H, H_a−C(9,9′)-(*R,R*-DACH)], 1.22 [d, ^2J = 10.1 Hz, 2 H, H_b−C(17,17′)], 0.68 [s, 6 H, H_3−C(13,13′)-(*R,R*-DACH)], 0.64 [s, 6 H, H_3−C(13,13′)-(*S,S*-DACH)]. − ^{13}C NMR (75 MHz, [D$_3$]acetonitrile): δ = 139.1, 122.2, 62.7, 47.7, 40.9, 37.4, 32.7, 31.5, 30.5, 25.6, 24.9, 21.7. − FAB-MS: *m/z* (%) = 798 (12) [M^+ − PF_6], 652 (38) [M^+ − 2 PF_6], 538 (20) [M^+ − DACH], 345 (11), 307 (73), 154 (100).

L3PtCl$_2$: K_2PtCl_4 (240.7 mg, 0.58 mmol) was dissolved in HCl (0.2 M, 33 mL) and **L3** (200 mg, 0.58 mmol) was added. The synthesis and purification was carried the same way as described for **L2PtCl$_2$** above. Yellow crystals (260 mg, 73%) of **L3PtCl$_2$** were obtained. −^{1}H NMR (300 MHz, $CDCl_3$): δ = 7.97 [d, ^3J = 8.1 Hz, 2 H, H−C(3,3′)], 7.37 [d, ^3J = 8.1 Hz, 2 H, H−C(4,4′)], 4.03 [dd, ^2J = 18.7 Hz, ^3J = 2.6 Hz, 2 H, H_b−C(7,7 ′)], 3.91 [dd, ^2J = 18.7 Hz, ^3J = 3.1 Hz, 2 H, H_a−C(7,7 ′)], 2.72 [dd, ^3J = 5.4, 5.4 Hz, 2 H, H−C(10,10,′)], 2.61 [ddd, ^2J = 9.6 Hz, ^3J = 5.6 Hz, 2 H, H_b−C(9,9′)], 2.38 [m, 2 H, H−C(8,8′)], 1.37 [s, H_3−C(12,12′)], 1.13 [d, ^2J = 9.6 Hz, H_a−C(9,9′)], 0.66 [s, H_3−C(13,13′)]. − ^{13}C NMR (75 MHz, $CDCl_3$): δ = 163.6 [C(2,2′)], 156.8 [C(6,6′)], 145.9 (5,5′)], 135.9 [C(4,4′)], 119.8 [C(3,3′)], 46.8 [C(10,10′)], 40.0 [C(8,8′)], 39.1 [C(11,11′)], 36.4 [C(9,9′)], 25.6 [C(12,12′)], 21.9 [C(13,13′)]. − ^{195}Pt NMR (64.376 MHz, $CDCl_3$): see Table 1. − FAB-MS: *m/z* (%) = 609 (13) [M^+], 578 (80) [M^+ − Cl], 539 (48) [M^+ − 2 Cl], 506 (18), 462 (12), 345 (40), 307 (78), 289 (68), 154 (100). − $C_{24}H_{28}Cl_2N_2Pt$ (610.5): calcd. C 47.22, H 4.62, N 4.59, found C 45.77, H 4.74, N 4.70. − Crystal structure analysis see Tables 4 and 8, Figure 3.

[{Bis[(−)-(+)-pineno]−2,2′-bipyridine}(ethylenediamine)Pt^{II}](PF$_6$)$_2$ (13): The synthesis, and purification of compound **13** was carried out as described for compound **11** with **L3PtCl$_2$** (50 mg, 0.081 mmol) and ethylenediamine (10 μL, 0.15 mmol) in water/acetone (15 mL). Yield: 51 mg (70%). − ^{1}H NMR (300 MHz, [D$_3$]acetonitrile): δ = 7.96 [d, ^3J = 8.1 Hz, 2 H, H−C(3,3′)], 7.80 [d, ^3J = 8.1 Hz, 2 H, H−C(4,4′)], 5.26 [b, 4 H, H$_2$−N(14,14′)], 2.98 [d, ^3J = 2.4 Hz, 6 H, H$_2$−C(7,7′), H−C(10,10′)], 2.76 [dd, ^2J = 10.1 Hz, ^3J = 5.2 Hz, 2 H, H$_b$−C(9,9′)]; 2.60 [b, 4 H, H$_2$−C(15,15′)], 2.45 [m, 2 H, H−C(8,8′)], 1.42 [s, 6 H, H$_3$−C(12,12′)], 1.32 [d, ^2J = 10.1 Hz, H$_a$−C(9,9′)], 0.63 [s, 6 H, H$_3$−C(13,13′)]. − ^{13}C NMR (75 MHz, [D$_3$]acetonitrile): δ = 161.3 [C(2,2′)], 157.4 [C(6,6′)], 148.2 [C(5,5′)]; 139.0 [C(4,4′)], 121.9 [C(3,3′)], 47.7 [C(15,15′)]; 47.5 [C(10,10′)], 40.6 [C(8,8′)], 39.7 [C(11,11′)], 37.1 [C(7,7′)]; 31.2 [C(9,9′)], 25.4 [C(12,12′)]; 21.2 [C(13,13′)]. − FAB-MS: *m/z* (%) = 744 (14) [M$^+$ − PF$_6$], 600 (66) [M$^+$ − 2 PF$_6$], 541 (42) [M$^+$ − en], 345 (16), 165 (28), 154 (100).

L4PtCl$_2$: Compound **L4** (700 mg, 2.03 mmol) was added to a solution of K$_2$PtCl$_4$ (843.5 mg, 2.03 mmol) dissolved in HCl (0.2 M, 80 mL). After stirring for 10 h at reflux, the yellow precipitate was filtered off and washed with water. The crude product was dried at 50 °C in the vacuum oven. Recrystallization from chloroform/heptane gave yellow crystals (786 mg, 63%) of **L4PtCl$_2$**. − ^{1}H NMR (300 MHz, [D$_3$]acetonitrile): δ = 8.15 [d, ^3J = 7.7 Hz, 2 H, H−C(3,3′)], 7.50 [d, ^3J = 7.7 Hz, 2 H, H−C(4,4′)], 4.23 [dd, ^3J = 5.8, 5.8 Hz, 2 H, H−C(10,10′)], 2.86 [d, ^3J = 2.6 Hz, 4 H, H$_2$−C(7,7′)], 2.79 [dd, ^3J = 5.8 Hz, ^2J = 9.8 Hz, 2 H, H$_b$−C(9,9′)], 2.25 [m, 2 H, H−C(8,8′)], 1.42 [s, 6 H, H$_3$−C(12,12′)], 1.27 [d, ^2J = 9.8 Hz, 2 H, H$_a$−C(9,9′)], 0.64 [s, 6 H, H$_3$−C(13,13′)]. − ^{13}C NMR (75 MHz, CDCl$_3$): δ = 171.3 [C(2,2′)], 154.2 [C(6,6′)], 137.0 [C(4,4′)], 134.0 [C(5,5′)], 120.5 [C(3,3′)], 51.4 [C(10,10′)], 39.3 [C(11,11′)], 39.1 [C(8,8′)], 31.7 [C(7,7′)], 31.2 [C(9,9′)], 24.8[C(13,13′)], 21.6 [C(12,12′)]. − ^{195}Pt NMR (64.376 MHz, CDCl$_3$): see Table 1. − FAB-MS: *m/z* (%) = 1186 (6) [M$_2^+$ − Cl], 920 (20) and 883 (8) further dimer fragments, 610 (7) [M$^+$], 575 (54) [M$^+$ − Cl], 536 (87) [M$^+$ − 2 Cl], 522 (26), 345 (100). − C$_{24}$H$_{28}$Cl$_2$N$_2$Pt (610.5): calcd. C 47.22, H 4.62, N 4.59; found C 47.00, H 4.62, N 4.44. − Crystal structure analysis see Tables 5 and 8, Figure 4.

[{Bis[(−)-β-pineno]−2,2′-bipyridine}(ethylenediamine)Pt^{II}](PF$_6$)$_2$ (14): The synthesis, and purification of compound **14** was carried out as described for compound **11** with **L4PtCl$_2$** (100 mg, 0.16 mmol) and ethylenediamine (12 μL, 0.18 mmol) in water/acetone (20 mL). Yield: 85 mg (58%) white powder of **14**. − ^{1}H NMR (300 MHz, [D$_3$]acetonitrile): δ = 8.02 [s, 4 H, H−C(3,3′), H−C(4,4′)], 4.61 [b, 4 H, H$_2$−N(14,14′)], 3.10 [m, 6 H, H$_2$−C(7,7′), H−C(10,10′)], 2.87 [dd, ^2J = 10.0 Hz, ^3J = 5.7 Hz, 2 H, H$_b$−C(9,9′)], 2.65 [b, 4 H, H$_2$−C(15,15′)], 2.40 [m, 2 H, H−C(8,8′)], 1.50 [s, 6 H, H$_3$−C(12,12′)], 1.36 [d, ^2J = 10.0 Hz, 2 H, H$_a$−C(9,9′)], 0.70 [s, 6 H, H$_3$−C(13,13′)]. − ^{13}C NMR (75 MHz, [D$_3$]acetonitrile): δ = 141.1, 136.2, 121.6, 51.3, 48.3, 40.6, 40.3, 31.8, 30.8, 25.6, 21.8, (two carbon atoms could not be observed). − FAB-MS: *m/z* (%) = 744 (36) [M$^+$ − PF$_6$], 599 (80) [M$^+$ − 2 PF$_6$], 536 (25) [M$^+$ − en], 345 (100), 307 (81), 154 (100).

[{Bis[(−)-β-pineno]−2,2′-bipyridine}(R,R-DACH)Pt^{II}](PF$_6$)$_2$ (24): The synthesis, and purification of compound **24** was carried out as described for compound **21** with **L4PtCl$_2$** (50 mg, 0.082 mmol) and (*R,R*)-diaminocyclohexane (15 mg, 0.13 mmol) in water/acetone (15 mL). Yield: 43 mg (55%) white powder of **24**. − ^{1}H NMR (300 MHz, [D$_3$]acetonitrile): δ = 8.03 [s, 4 H, H−C(3,3′), H−C(4,4′)], 4.58 [b, 4 H, H$_2$−N(14,14′)], 3.11 [m, 6 H, H$_2$−C(7,7′), H−C(10,10′)], 2.86 [dd, ^2J = 10.4 Hz, ^3J = 5.6 Hz, 2 H, H$_b$−C(9,9′)], 2.44 (b, 2 H, DACH), 2.42 [m, 2 H, H−C(8,8′)], 2.04 (b, 2 H, DACH), 1.61 (b, 2 H, DACH), 1.50 [s, 6 H, H$_3$−C(12,12′)], 1.39 [d, ^2J = 10.4 Hz, 2 H, H$_a$−C(9,9′)], 1.19 (b, 2 H, DACH), 0.68 [s, 6 H, H$_3$−C(13,13′)]. − FAB-MS: *m/z* (%) = 799 (12) [M$^+$ − PF$_6$], 652 (70) [M$^+$ − 2 PF$_6$], 537 (34) [M$^+$ − DACH], 345 (11), 307 (14), 154 (100).

[{Bis[(−)-β-pineno]−2,2′-bipyridine}(R,R/S,S-DACH)Pt^{II}](PF$_6$)$_2$ (44): The synthesis, and purification of compound **44** was carried out as described for compound **21** with **L4PtCl$_2$** (87 mg, 0.14 mmol), (*R,R*)-diaminocyclohexane (20 mg, 0.18 mmol), and (*S,S*)-diaminocyclohexane (20 mg, 0.18 mmol) in water/acetone (15 mL). Yield: 70 mg (52%) white powder of **44**. − ^{1}H NMR (300 MHz, [D$_3$]acetonitrile): δ = 8.02 [s, 4 H, H−C(3,3′), H−C(4,4′)], 4.58 [b, 4 H, H$_2$−N(14,14′)], 3.11 [m, 6 H, H$_2$−C(7,7′), H−C(10,10′)], 2.87 [dd, ^2J = 10.7 Hz, ^3J = 5.7 Hz 2 H, H$_b$−C(9,9′)], 2.44 (b, 2 H, DACH), 2.42 [m, 2 H, H−C(8,8′)], 2.03 (b, 2 H, DACH), 1.60 (b, 2 H, DACH), 1.50 [s, 6 H, H$_3$−C(12,12′)-*R,R*-DACH], 1.49 [s, H$_3$−C(12,12′)-*S,S*-DACH, ratio see discussion], 1.39 [d, ^2J = 10.7 Hz, 2 H, H$_a$−C(9,9′)], 1.37 (b, 2 H, DACH), 1.19 (b, 2 H, DACH), 0.72 [s, 6 H, H$_3$−C(13,13′)-*S,S*-DACH, ratio see discussion], 0.68 [s, 6 H, H$_3$−C(13,13′)-*R,R*-DACH]. − FAB-MS: *m/z* (%) = 798 (16) [M$^+$ − PF$_6$], 653 (63) [M$^+$ − 2 PF$_6$], 539 (34) [M$^+$ − DACH], 307 (28), 154 (100).

L5PtCl$_2$: Compound **L5** (437 mg, 1.26 mmol) was added to a solution of K$_2$PtCl$_4$ (524 mg, 1.26 mmol) dissolved in HCl (0.2 M, 50 mL). After stirring for 10 h at reflux, the yellow precipitate was filtered off and washed with water. The crude product was dried at 50 °C in a vacuum oven. Recrystallization from chloroform/heptane gave a yellow powder (560 mg, 72%) of **L4PtCl$_2$**. − ^{1}H NMR (300 MHz, CDCl$_3$): δ = 9.15 [s, 1 H, H−C(6′)], 7.85 [d, ^3J = 7.9 Hz, 1 H, H−C(3)], 7.75 [s, 1 H, H−C(3′)], 7.50 [d, ^3J = 7.9 Hz, 1 H, H−C(4)], 4.39 [dd, ^2J = 18.8 Hz, ^3J = 3.2 Hz, 1 H, H$_b$−C(7)], 3.60 [dd, ^2J = 18.8 Hz, ^3J = 2.8 Hz, 1 H, H$_a$−C(7)], 3.15 [dd, ^2J = 17.7 Hz, ^3J = 3.3 Hz, 1 H, H$_b$−C(7′)], 2.94 [dd, ^2J = 17.7 Hz, ^3J = 2.6 Hz, 1 H, H$_a$−C(7′)], 2.87 [dd, ^3J = 5.8, 5.8 Hz, 1 H, H−C(10′)], 2.79 [dd, ^3J = 5.8, 5.8 Hz, 1 H, H−C(10)], 2.71 [dd, ^2J = 9.9 Hz, ^3J = 5.8 Hz, 1 H, H$_b$−C(9′)], 2.62 [dd, ^2J = 9.9 Hz, ^3J = 5.8 Hz, 1 H, H$_b$−C(9)], 2.42 [m, 1 H, H−C(8)], 2.34 [m, 1 H, H−C(8′)], 1.39 [s, 3 H, H$_3$−C(12′)], 1.36 [s, 3 H, H$_3$−C(12)], 1.15 [d, ^2J = 9.9 Hz, 2 H, H$_a$−C(9,9′)], 0.59 [s, 3 H, H$_3$−C(13 or 13′)], 0.55 [s, 3 H, H$_3$−C(13′ or 13)]. − ^{13}C NMR (75 MHz, CDCl$_3$): δ = 164.7 [C(2′)], 156.1 [C(2)], 155.9 [C(6)], 149.3 [C(4′)], 147.5 [C(5)], 145.3 [C(5′)], 144.2 (6′)], 135.2 [C(4)], 122.4 (3′)], 120.3 (3)], 47.2 (10)], 44.7 [C(10′)], 39.9 [C(8)], 39.4 [C(8′)], 39.1 [C(11)], 38.9 [C(7)], 38.6 [C(9)], 33.4 [C(11′)], 31.1 [C(7′)], 30.3 [C(9′)], 25.6 [C(12)], 25.2 [C(12′)], 21.3 [C(13)], 21.2 [C(13′)]. − FAB-MS: *m/z* (%) = 1186 (8) [M$_2^+$ − Cl], 920 (9) and 842 (10) [further dimer fragments], 574 (80) [M$^+$ − Cl], 537 (54) [M$^+$ − 2 Cl], 493 (20), 345 (66), 154 (100). − C$_{24}$H$_{28}$Cl$_2$N$_2$Pt (610.5): calcd. C 47.22, H 4.62, N 4.59, found C 47.37, H 4.70, N 4.59.

[{Bis[(−)-pineno]−2,2′-bipyridine}(ethylenediamine)Pt^{II}](PF$_6$)$_2$ (15): The synthesis and purification of compound **15** was carried out as described for compound **11** with **L5PtCl$_2$** (70 mg, 0.11 mmol) and ethylenediamine (10 μL, 0.15 mmol) in water/acetone (20 mL). Yield: 65 mg (63%) white powder of **14**. − ^{1}H NMR (300 MHz, CDCl$_3$): δ = 8.08 [s, 1 H, H−C(6′)], 8.01 [d, ^3J = 7.8 Hz, 1 H, H−C(3)], 7.86 [s, 1 H, H−C(3′)], 7.84 [d, ^3J = 7.9 Hz, 1 H, H−C(4)], 5.30 [b, 2 H, H$_b$−N(14,14′)], 5.18 [b, 2 H, H$_a$−N(14,14′)], 3.16 [d, ^3J = 2.7 Hz, 2 H, H$_2$−C(7′)], 3.03 [dd, ^3J = 5.6, 5.6 Hz, 1 H, H−C(10′)], 2.95 [m, 3 H, H−C(10), H$_2$−C(7)], 2.84−2.61 [m, 6 H, H$_2$−C(15), H$_2$−C(15′), H$_b$−C(9), H$_a$−C(9′)], 2.47 [m, 1 H, H−C(8)], 2.40 [m, 1 H, H−C(8′)], 1.46

[s, 3 H, H_3−C(12′)], 1.44 [s, 3 H, H_3−C(12)], 1.27 [d, ^2J = 9.9 Hz, 1 H, H_a−C(9 or 9′)], 1.22 [d, ^2J = 9.9 Hz, 1 H, H_a−C(9 or 9′)], 0.69 [s, 3 H, H_3−C(13)], 0.67 [s, 3 H, H_3−C(13′)]. − FAB-MS: *m/z* (%) = 744 (21) [$M^+ - PF_6$], 600 (95) [$M^+ - 2\,PF_6$], 543 (58) [M^+ -en], 345 (40), 289 (82), 165 (42), 154 (100).

[{Bis[(−)-pineno]−2,2′-bipyridine}(S,S-DACH)Pt^{II}](PF$_6$)$_2$ (35): The synthesis and purification of compound **35** was carried out as described for compound **31** with **L5PtCl$_2$** (50 mg, 0.082 mmol) and (*S,S*)-diaminocyclohexane (15 mg, 0.13 mmol) in water/acetone (20 mL). Yield: 55 mg (71%) white powder of **35.** − ^{1}H NMR (300 MHz, $CDCl_3$): δ = 8.06 [s, 1 H, H−C(6′)], 8.01 [d, ^3J = 7.9 Hz, 1 H, H−C(3)], 7.86 [s, 1 H, H−C(3′)], 7.85 [d, ^3J = 7.9 Hz, 1 H, H−C(4)], 5.44 [b, 2 H, H_b−N(14,14′)], 4.86 [b, 2 H, H_a−N(14,14′)], 3.16 [d, ^3J = 2.6 Hz, 2 H, H_2−C(7′)], 3.07−2.73 [m, 6 H, H−C(10′), H−C(10′), H_2−C(7), H_b−C(9), H_b−C(9′)], 2.54 (b, 2 H, DACH), 2.48 (b, 2 H, DACH), 2.40 [m, 1 H, H−C(8 or 8′)], 2.21 [m, 1 H, H−C(8 or 8′)], 1.66 (b, 2 H, DACH), 1.46 [s, 3 H, H_3−C(12′)], 1.44 [s, 3 H, H_3−C(12)], 1.43 (b, 2 H, DACH), 1.27−1.23 [m, 4 H, H_a−C(9), H_a−C(9′), DACH], 0.67 [s, 3 H, H_3−C(13)], 0.65 [s, 3 H, H_3−C(13)].

[{Bis[(−)-pineno]−2,2′-bipyridine}(S,S/R,R-DACH)Pt^{II}](PF$_6$)$_2$ (45): The synthesis and purification of compound **45** was carried out as described for compound **41** with **L5PtCl$_2$** (50 mg, 0.082 mmol), (*R,R*)-diaminocyclohexane (15 mg, 0.13 mmol) and (*S,S*)-diaminocyclohexane (15 mg, 0.13 mmol) in water/acetone (20 mL). Yield: 55 mg (70%) white powder of **44**. − ^{1}H NMR (300 MHz, $CDCl_3$): δ = 8.07 [s, 1 H, H−C(6′)], 8.02 [d, ^3J = 8.0 Hz, 1 H, H−C(3)], 7.88 (s, 1 H, H−C(3′)], 7.85 [d, ^3J = 8.0 Hz, 1 H, H−C(4)], 5.45 [b, 2 H, H_b−N(14,14′)], 4.86 [b, 2 H, H_a−N(14,14′)], 3.16 [d, ^3J = 2.8 Hz, 2 H, H_2−C(7′)], 3.07−2.72 [m, 6 H, H−C(10′), H−C(10′), H_2−C(7), H_b−C(9), H_b−C(9′)], 2.54 (b, 2 H, DACH), 2.49 (b, 2 H, DACH), 2.40 (m, 1 H, H−C(8 or 8′)], 2.22 (m, 1 H, H−C(8 or 8′)], 1.66 (b, 2 H, DACH), 1.46 [s, 3 H, H_3−C(12′)], 1.44 [s, 3 H, H_3−C(12)], 1.43 (b, 2 H, DACH), 1.27−1.23 [m, 4 H, H_a−C(9), H_a−C(9′), DACH], 0.67 [s, 3 H, H_3−C(13)], 0.65 [s, 3 H, H_3−C(13)].

Crystallographic Measurements and Structure Solution:[13] Suitable crystals of **L2** were grown from acetone as pale yellow rods. Intensity data were collected at room temperature on a Stoe AED2 4-circle diffractometer using Mo-K_α graphite-monochromated radiation (λ = 0.71073 Å) with ω/2Θ scans in the 2Θ range 5−51°. The structure was solved by direct methods using the program SHELXS-97[14]. The refinement and all further calculations were carried out using SHELXL-97[15]. H-atoms were located from difference Fourier maps and refined isotropically. The non-H atoms were refined anisotropically, using weighted full-matrix least-squares method on F^2. The absolute structure was assigned with reference to the absolute structure of the ligand.

Crystallographic details are given in Table 8 and significant bond lengths and bond angles are listed in Table 3.

Suitable crystals for the platinum complexes were grown by diffusion of heptane into a chloroform solution. The data for **L2PtCl$_2$** and **L4PtCl$_2$** were collected on a 'Siemens SMART CCD′ System, whereas a 'STOE Image Plate Diffraction System′ was used to collect data for **L3PtCl$_2$**. Determinations of the crystal class, orientation matrix, and unit-cell dimensions were performed in a standard fashion. The data were collected using monochromated Mo-K_α

Table 8. Crystallographic data

Compound	L2	**L2PtCl$_2$**	**L3PtCl$_2$**	**L4PtCl$_2$**
Empirical formula	$C_{24}H_{28}N_2$	$C_{24}H_{28}Cl_2N_2Pt{\cdot}2CHCl_3$	$C_{24}H_{28}Cl_2N_2Pt{\cdot}2CHCl_3$	$C_{24}H_{28}Cl_2N_2Pt{\cdot}1.25CHCl_3$
Mol. wt.	344.48	849.21	849.21	759.68
Temperature [K]	293 (2)	133 (2)	223 (2)	133 (2)
Radiation, λ [Å]	Mo-K_α, 0.71073	Mo-K_α, 0.71073	Mo-K_α, 0.71073	Mo-K_α, 0.71073
Crystal system	Monoclinic	Triclinic	Triclinic	Triclinic
Space group	$P2_1$ (No.4)	$P\bar{1}$ (No.1)	$P\bar{1}$ (No.2)	$P\bar{1}$ (No.1)
a [Å]	6.1105 (7)	11.1430 (3)	11.2775 (11)	11.1789 (2)
b [Å]	10.9121 (18)	12.2591 (3)	12.2377 (12)	13.4606 (2)
c [Å]	14.5203 (12)	12.9160 (3)	12.8743 (13)	19.4045 (3)
α [°]	90.0	95.9000 (10)	95.475 (12)	74.6130 (10)
β [°]	94.383 (9)	114.4540 (10)	114.540 (11)	87.3960 (10)
γ [°]	90.0	97.8210 (10)	98.311 (12)	83.63
V [Å^3]	965.4 (2)	1566.19 (7)	1575.3 (3)	2797.47 (8)
Z	2	2	2	4
Density (calculated) [g cm^{-3}]	1.185	1.801	1.790	1.804
Absorption coefficient [mm^{-1}]	0.069	5.182	5.152	5.583
F [000]	372	828	828	1482
Crystal size [mm]	0.46 × 0.23 × 0.11	0.45 × 0.29 × 0.22	0.60 × 0.30 × 0.10	0.34 × 0.28 × 0.11
θ min. and max. [°]	2.34 to 25.47	2.05 to 27.28	2.23 to 25.80	1.58 to 26.70
Reflections collected/unique	3802/1901	13528/10833	12237/5604	23429/18354
Absorpt. correct.	none	ψ-scan	Emp.-DIFABS	ψ-scan
T min/*T* max		0.196/0.308	0.230/0.693	0.197/0.514
Refinement method	Full-matrix least-squares on F^2	Full-matrix least-squares on F^2	Full-matrix least-squares on F^2	Full-matrix least-squares on F^2
Data/restraints/parameters	1901/1/348	10833/3/679	5604/4/339	18354/172/1259
Final *R* indices [$I > 2\sigma(I)$]	*R*1 = 0.0551 *wR*2 = 0.0925	*R*1 = 0.0280 *wR*2 = 0.0703	*R*1 = 0.0670 *wR*2 = 0.1733	*R*1 = 0.0384 *wR*2 = 0.0880
R indices all data	*R*1 = 0.0979 *wR*2 = 0.1067	*R*1 = 0.0303 *wR*2 = 0.0718	*R*1 = 0.0732 *wR*2 = 0.1787	*R*1 = 0.0430 *wR*2 = 0.0909
Absolute structure parameter	−1.00 (6)	0.034 (5)	−	0.000 (5)
Largest diff. peak and hole [e.Å^{-3}]	0.143 and −0.125	0.945 and −0.738	3.056 (near Pt-atom) and −4.470	1.352 and −2.309

graphite-monochromated radiation (λ = 0.71073 Å). Absorption correction for all three compounds were applied. The structures were solved by direct methods using SHELXS-97[14] and refined on F^2 against all reflections with anisotropic thermal parameters by full-matrix least-squares method using SHELXL-97.[15] Crystal data and further details of structure refinement are summarized in Table 8 and significant bond lengths and bond angles are listed in Tables 3, 4, 5, and 6.

The molecular structures and crystallographic numbering schemes for these compounds are illustrated in the PLATON[16] and Cerius2[17] drawings in Figures 2, 3, 4, and 5.

Acknowledgments

The authors wish to thank the Swiss National Science Foundation for financial support. We also thank Felix Fehr for performing the 500 MHz Spectra.

[1] W. H. Mills, T. H. H. Quibell, *J. Chem. Soc.* **1935**, 839.
[2] C. Deuschel-Cornioley, H. Stoeckli-Evans, A. v. Zelewsky, *J. Chem. Soc., Chem. Commun.* **1990**, 121−212. − P. Jolliet, M. Gianini, A. v. Zelewsky, G. Bernardinelli, H. Stoeckli-Evans, *Inorg. Chem.* **1996**, *35*, 4883.
[3] P. Hayoz, A. v. Zelewsky, *Tetrahedron Lett.* **1992**, *33*, 5165−5168. − P. Hayoz, A. v. Zelewsky, H. Stoeckli-Evans, *J. Am. Chem. Soc.* **1993**, *115*, 5111−5114.
[4] M. Gianini, A. v. Zelewsky, H. Stoeckli-Evans, *Inorg. Chem.* **1997**, *36*, 6094. M. Gianini, A. Forster, P. Haag, A. v. Zelewsky, H. Stoeckli-Evans, *Inorg. Chem.* **1996**, 35, 4889.
[5] F. Kröhnke, *Synthesis* **1976**, 1.
[6] [6a]N. C. Fletcher, F. R. Keene, M. Ziegler, H. Stoeckli-Evans, H. Viebrock, A. v. Zelewsky, *Helvet. Chim. Acta.* **1996**, *79*, 1192−1202. − [6b]Philippe Lainé, private communication.
[7] [7a]P. Collomb, S. Rupprecht, A. v. Zelewsky, to be published. − [7b]M. Gianini, A. v. Zelewsky, *Synthesis* **1996**, 702−706
[8] H. C. Brown, S. A. Weissman, P. T. Perumal, U. P. Dhokte, *J. Org. Chem.* **1990**, *55*, 1217.
[9] M. Ziegler, A. v. Zelewsky, *Coordination Chemistry Reviews* **1998**, *177*, 257−300.
[10] G. R. Newkome, F. R. Fronczek, V. K. Gupta, W. E. Puckett, D. C. Pantaleo, G. E. Kiefer, *J. Am. Chem. Soc.* **1982**, *104*, 1782−1783.
[11] E. J. Corey, J. C. Bailar, *J. Am. Chem. Soc.* **1959**, *81*, 2620−2629.
[12] T. G. Morgan, H. F. Burstall, *J. Chem. Soc.* **1934**, 965.
[13] Crystallographic data (excluding structure factors) for the structures reported in this paper have been deposited with the Cambridge Crystallographic Data Centre as supplementary publication no. CCDC-117441 (**L2**), CCDC-115332 (**L2PtCl$_2$**), CCDC-115333 (**L4PtCl$_2$**), and CCDC-115334 (**L3PtCl$_2$**). Copies of the data can be obtained free of charge on application to CCDC, 12 Union Road, Cambridge CB2 1EZ, UK [Fax: (internat.) +44−1223/336-033; E-mail: deposit@ccdc.cam.ac.uk].
[14] G. M. Sheldrick, *Acta Crystallograph.* **1990**, *A46*, 467−273.
[15] G. M. Sheldrick, *SHELXL-97, − Program for Crystal Structure Refinement*, University of Göttingen, Germany, **1997**.
[16] A. L. Spek, *Acta Crystallogr.* **1990**, *A46*, C34.
[17] Reprinted with permission from Cerius^2, Version 3.8, **1998**, Molecular Simulations Inc., San Diego.

Received April 28, 2000
[I00169]

ATP Recognition Through a Fluorescence Change in a Multicomponent Dinuclear System Containing a $Ru(Tpy)_2^{2+}$ Fluorescent Core and a Cyclam−Cu^{2+} Complex

Miguel E. Padilla-Tosta,[a] José Manuel Lloris,[a] Ramón Martínez-Máñez,*[a] Teresa Pardo,[a] Felix Sancenón,[a] Juan Soto,[a] and M. Dolores Marcos[a]

Keywords: Ruthenium / N ligands / Molecular recognition / Fluorescence / Sensors

The Cu^{2+} complex of the ligand L^1 (L^1 = [Ru(tpycyclam)-(mtpy)]$^{2+}$, tpycyclam = 1-[4′-*p*-tolyl-(2,2′:6′,2′′-terpyridyl)]-1,4,8,11-tetraazacyclotetradecane and mtpy = 4′-methyl-2,2′:6′,2′′-terpyridine) is able to display a selective sensing response against anions such as ATP. The L^1–Cu^{2+} system contains a $Ru(tpy)_2^{2+}$ fluorescent core and a cyclam–Cu^{2+} subunit. The fluorescent response of the $Ru(tpy)_2^{2+}$ core in an aqueous environment (acetonitrile/water, 70:30) is governed by the quenching produced by the Cu^{2+} cation. In the presence of anions the L^1–Cu^{2+} system shows a rich emission fluorescent response. Electrochemical studies on the $Cu(cyclam)^{2+}$ complex in propylene carbonate in the presence of certain anions allowed us to conclude that the interaction with the anions sulfate, phosphate, ATP, ADP and GMP is mainly electrostatic whereas chloride and bromide form axial covalent bonds with the copper atom in the $Cu(cyclam)^{2+}$ complex. The addition of anions that coordinate at the axial positions of the square-planar Cu^{2+}–cyclam subunit (such as Cl^-, Br^- and OH^-) produced an enhancement of the emission intensity. This enhancement is attributed to the occupation of the apical positions of copper in the Cu^{2+}–L^1 complex that might reduce the probability of an interaction between the Cu^{2+} ions and the $Ru(tpy)_2^{2+}$ groups reducing the quenching process and, consequently, resulting in an enhancement of the fluorescence. A prediction of the fluorescent behaviour with the anions sulfate, phosphate, ATP, ADP and GMP that give electrostatic interactions with the positively charged cyclam–Cu^{2+} and/or $Ru(tpy)_2^{2+}$ centres is rather difficult. Potentiometric studies on the L^1–Cu^{2+}–H^+–ATP system suggested that the [$Cu(L^1)$(ATP)] complex is responsible for the quenching observed at basic pH in the presence of ATP. It is noticeable that the quenching of the intensity of the fluorescence due to ATP in the pH range 9 to 10 is selective and no other anion studied is able to quench the emission of the $Ru(tpy)_2^{2+}$ core in this pH range.

Introduction

The development of new sensing molecules based on the application of supramolecular chemistry concepts is an area of current interest.[1,2] It involves the functionalisation of suitable coordination sites with appropriate groups that can switch their state upon guest binding. When the switching process is followed by a change in a macroscopically observable parameter such as redox potential, absorption or emission spectrum etc., then it is simple to get information in relation to molecular events (the presence or not of a certain guest).[3−5] In general, some factors can be straightforwardly controlled to procure selectivity against a target guest: (i) the nature of the binding sites; (ii) the nature of the signalling subunit; and (iii) the solvent in which the receptor−guest interaction takes place. Such is the number of combinations that the search for new, selective signalling receptors seems to be wide open.[6]

Although anion recognition and fluorescent sensing methods are both fields of interest there are very few examples dealing with the use of fluorescent receptors for anion sensing.[7−9] The development of such new receptors involves the linkage of fluorescent groups to anion coordination sites. In this sense, we have recently been involved in the study of $Ru(tpy)_2^{2+}$ as a fluorescent signalling subunit.[10] Additionally, several types of anion coordination sites have been tested, among them polyammonium units have been some of the most widely used. In contrast, transition metal ions have been much less studied as potential binding sites in receptors based on the "binding site-signalling subunit" concept.[11] When metal ions are used as centres for metal−ligand interactions it is possible to construct structurally defined complexes with appropriate metal cations that might impose high barriers for anion discrimination.[11] We report here the fluorescent behaviour of a multicomponent dinuclear system containing $Ru(tpy)_2^{2+}$ as the fluorescent signalling subunit and a cyclam−Cu^{2+} complex in the presence of anions such as chloride, sulfate, phosphate, ATP, ADP and GMP.

Results

Quenching Studies

The complex L^1 (see below) contains a ruthenium(II) bisterpyridine core covalently anchored to a polyamine unit. We have recently reported studies on the fluorescence beha-

[a] Departamento de Química, Universidad Politécnica de Valencia,
Camino de Vera s/n, 46071 Valencia, Spain
Fax: (internat.) +34-96/387-7349
E-mail: rmaez@qim.upv.es

 © WILEY-VCH Verlag GmbH, 69451 Weinheim, 2001 1434−1948/01/0505−1221 $ 17.50+.50/0

viour of the $Ru(tpy)_2^{2+}$ centre in L^1 in the presence of transition metal ions in acetonitrile/water solutions. It was found that in the presence of stoichiometric amounts of Cu^{2+}, the fluorescence of the $Ru(tpy)_2^{2+}$ core in L^1 diminished in the pH range of 4−7 (λ_{ex} = 484 nm, λ_{em} = 650 nm). This behaviour is clearly observed in Figure 1, which plots the relative emission intensity for L^1 in the presence of Cu^{2+} at certain pH values ($L^1-Cu^{2+}-H^+$ system). The figure also shows the emission intensity found for L^1 as a function of the pH (L^1-H^+ system). The emission intensity of L^1 is pH-independent: the presence of Cu^{2+} reduces the emission intensity at neutral and acidic pH. Additional solution studies (potentiometric experiments) allowed us to determine that the fall of the fluorescent emission intensity is observed when the complex $[Cu(L^1)]^{4+}$ exists in solution, whereas the protonation of the ligand (to give $[Cu(HL^1)]^{5+}$) at acidic pH, or the formation of hydroxo complexes ($[Cu(L^1)(OH)]^{3+}$ and $[Cu(L^1)(OH)_2]^{2+}$) at basic pH, hinders the quenching mechanism (see below). The $[Cu(L^1)]^{4+}$ complex more likely contains the Cu^{2+} cation coordinated by the cyclam unit in a square-planar environment.[10]

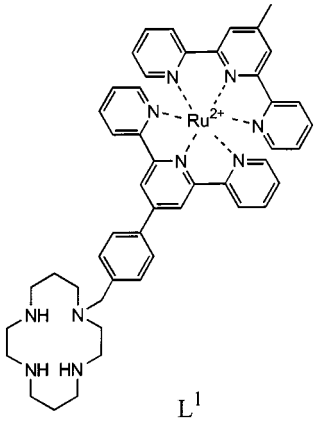

L^1

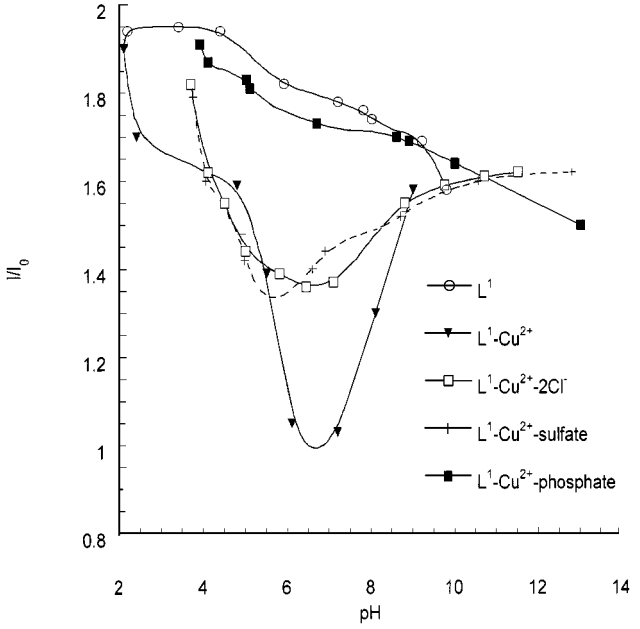

Figure 1. Relative intensity vs. pH for the $L^1-Cu^{2+}-A-H^+$ system, with A = phosphate, sulfate and chloride

We complete now these preliminary fluorescent results with new studies on the effect that the presence of certain anions has on the emission behaviour of the $L^1-Cu^{2+}-H^+$ system. In the first step we studied the fluorescent emission behaviour of the $Ru(tpy)_2^{2+}$ core as a function of the pH when one equivalent of chloride is added to a solution containing L^1 and Cu^{2+}. It was found that the *I* vs. pH profile of this system ($Cu^{2+}-L^1-H^+-Cl^-$) is very close to that found for the $Cu^{2+}-L^1-H^+$ system (without chloride). However, addition of a second equivalent of chloride induces an enhancement of the fluorescence (decrease of quenching) and an additional excess results in an *I* vs. pH profile close to that found for the L^1-H^+ system (deactivation of the quenching process; see Figure 1). A similar effect to that found for chloride (not shown in Figure 1) is observed when Br^- is added to the $Cu^{2+}-L^1$ system.

The fluorescent behaviour of the $Cu^{2+}-L^1-H^+$ system has also been tested against other anions such as sulfate and phosphate (see Figure 1). Whereas sulfate gave a response between that observed for L^1-H^+ and that of the $Cu^{2+}-L^1-H^+$ system, the presence of phosphate resulted in a similar *I* vs. pH profile to that found for the L^1-H^+ system (see Figure 1).

Of special interest is the study of the effect produced by biological anions such as ATP, ADP and GMP on the fluorescence behaviour of the $Cu^{2+}-L^1-H^+$ system (see Figure 2). The AMP anion is insoluble in acetonitrile/water (70:30 v/v) and could not be studied. It was found that the *I* vs. pH curve of the $L^1-Cu^{2+}-H^+-ATP$ system was quite different to that of $Cu^{2+}-L^1-H^+$. This time the quenching effect is still fully effective but it operates for different pH values, from 6 to 11 (see Figure 2) with a minimum for the fluorescent emission intensity at pH 9.2. GMP also modifies the emission intensity vs. pH curve of the $L^1-Cu^{2+}-H^+$ system and shows a minimum at a pH of

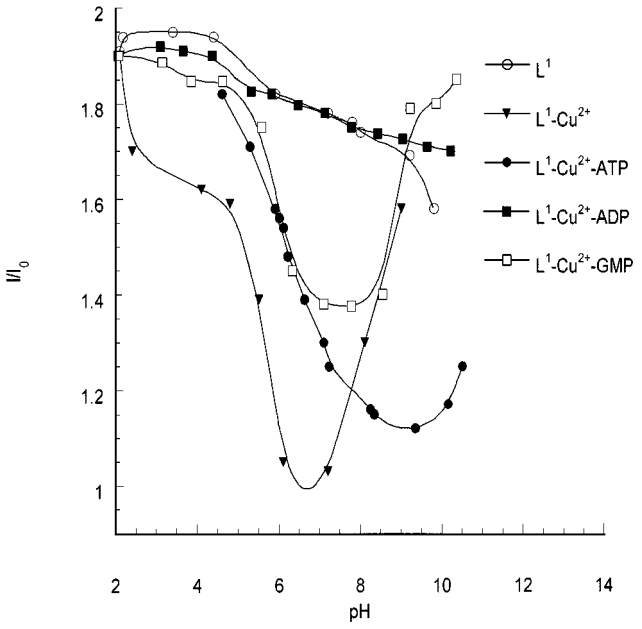

Figure 2. Relative intensity vs. pH for the $L^1-Cu^{2+}-A-H^+$ system, with A = ATP, ADP and GMP

ca. 7.5. In contrast, the ADP anion shows a similar *I* vs. pH profile to that found for the L^1-H^+ system.

In summary, the system containing Cu^{2+} and the ligand L^1 shows a rich fluorescent response in the presence of anions. The most significant feature is that ATP is able to induce quenching of the fluorescent $Ru(tpy)_2^{2+}$ subunit at pH 9.2, a pH at which none of the other anions studied (such as phosphate, sulfate, chloride, bromide, ADP or GMP) are able to produce any significant effect on the fluorescent behaviour of the $Cu^{2+}-L^1$ complex. It is also interesting to note that, in general, L^1 is a poor fluorescent chemosensor for anions, whereas it is the presence of Cu^{2+}, as we show in this work, that induces the mentioned changes in the fluorescence behaviour of the Ru-tpy subunit when anions are also present. In order to rationalise the emission fluorescent behaviour described above we have carried out additional electrochemical and potentiometric studies in an attempt to characterise the nature of the species existing in solution in the presence of certain anions.

Electrochemical Studies

Electrochemical studies on the $Cu(cyclam)^{2+}$ complex in the presence of anions can give information about the kind of interaction between the anion and the Cu^{2+}-cyclam centre. For instance, the axial coordination of anions to Cu^{2+} in a cyclam environment could be studied electrochemically and it is expected that strong axial coordination would reduce significantly the oxidation potential of the process $Cu^{2+} \rightarrow Cu^{3+} + 1e^-$. Electrochemical studies on $Cu(cyclam)^{2+}$ in the presence of phosphate, sulfate, ADP, chloride and bromide in propylene carbonate as solvent (0.1 mol dm^{-3} tetrabutylammonium perchlorate) have been carried out. Other solvents such as acetonitrile/water were discarded because the oxidation potential of Cu^{2+} in $Cu(cyclam)^{2+}$ is poorly defined probably due to the oxidation of water. Attempts to carry out studies in acetonitrile were also unsuccessful as phosphate and sulfate gave insoluble precipitates with the $Cu(cyclam)^{2+}$ complex.

In propylene carbonate, the $Cu(cyclam)^{2+}$ complex gave an irreversible oxidation process at 1.3 V vs. SCE. In the presence of chloride there is a cathodic oxidation potential shift up to 170 mV, whereas in the presence of sulfate and phosphate the electrochemical shift is only of 50 and 90 mV, respectively. The presence of ADP does not induce any significant oxidation potential shift of the Cu^{2+}/Cu^{3+} couple (less than 20 mV). Additionally, the presence of chloride produces a change of colour in the complex $Cu(cyclam)^{2+}$ that is not observed upon addition of sulfate, phosphate, or ADP anions. All these results appear to suggest that the interaction of the anions sulfate, phosphate, ADP and also probably ATP and GMP with the $Cu(cyclam)^{2+}$ unit is mainly electrostatic whereas chloride and also probably bromide and OH^- form covalent bonds with $Cu(cyclam)^{2+}$ in axial positions.

Stability Constants

Taking into account the difficulty of characterising the $L^1-Cu^{2+}-H^+-$anion systems at a molecular level we have accomplished potentiometric studies in an attempt to characterise some of these systems thermodynamically. Bearing in mind the selectivity found for ATP at basic pH (see Figure 2) we have carried out titration experiments in the presence of this biologically important anion in acetonitrile/water (70:30 v/v) solutions. Figure 3 shows the distribution diagram of the $L^1-Cu^{2+}-H^+-$ATP system.

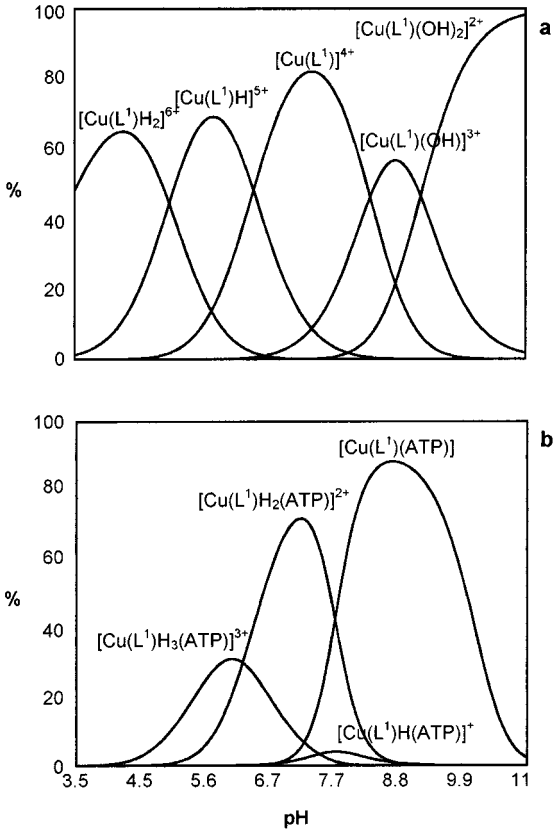

Figure 3. Distribution diagrams for the systems: a) $L^1-Cu^{2+}-H^+$; b) $L^1-Cu^{2+}-ATP-H^+$; in the presence of anions only the ligand−copper−anion species have been plotted

Table 1 shows the formation stability constants for the $L^1-Cu^{2+}-H^+-$ATP system. In the presence of ATP the complexes $[Cu(L^1)H_3(ATP)]^{3+}$, $[Cu(L^1)H_2(ATP)]^{2+}$, $[Cu(L^1)H(ATP)]^+$ and $[Cu(L^1)(ATP)]$ have been detected. Whereas the nature of protonated complexes is not easy to determine bearing in mind that both the ATP anion and the $[Cu(L^1)]^{4+}$ cation can be protonated, we can probably ascribe the formation of the $[Cu(L^1)(ATP)]$ complex to the interaction between the cation $[Cu(L^1)]^{4+}$ and the anion ATP^{4-}. Thus, the logarithm of the stability constant for the equilibrium $[Cu(L^1)]^{4+} + ATP^{4-} \rightleftarrows [Cu(L^1)(ATP)]$ is 6.10. The most interesting feature arises when comparing the distribution diagrams in Figure 3 and the plot of the emission intensity vs. pH for the $L^1-Cu^{2+}-H^+-$ ATP system in Figure 2: the agreement between the pH range where the quenching is observed and the pH range of existence of the $[Cu(L^1)(ATP)]$ complex is noticeable.

Table 1. Logarithms of the stability constants for the $L^1-Cu^{2+}-ATP-H^+$ systems in acetonitrile/water (70:30 v/v, 0.1 mol dm^{-3} tetrabutylammonium perchlorate) at 25 °C

Reaction	log*K*[a][b]
$L^1 + Cu^{2+} + ATP + 3H^+ \rightleftarrows [Cu(L^1)H_3(ATP)]$[c]	41.26(4)[d]
$L^1 + Cu^{2+} + ATP + 2H^+ \rightleftarrows [Cu(L^1)H_2(ATP)]$	35·00(4)
$L^1 + Cu^{2+} + ATP + H^+ \rightleftarrows [Cu(L^1)H(ATP)]$	26.18(4)
$L^1 + Cu^{2+} + ATP \rightleftarrows [Cu(L^1)(ATP)]$	19.40(5)

[a] Stability constants for the $L^1-Cu^{2+}-H^+$ system from ref.[10] are the following: $(L^1)^{2+} + Cu^{2+} + 2H^+ \rightleftarrows [Cu(H_2L^1)]^{6+}$, log*K* = 24.84(5); $(L^1)^{2+} + Cu^{2+} + H^+ \rightleftarrows [Cu(HL^1)]^{5+}$, log*K* = 19.77(8); $(L^1)^{2+} + Cu^{2+} \rightleftarrows [Cu(L^1)]^{4+}$, log*K* = 13.30(7); $(L^1)^{2+} + Cu^{2+} + H_2O \rightleftarrows [Cu(L^1)(OH)]^{3+} + H^+$, log*K* = 4.89(10); $(L^1)^{2+} + Cu^{2+} + 2H_2O \rightleftarrows [Cu(L^1)(OH)_2]^{2+} + 2H^+$, log*K* = −4.36(9). – [b] The formation stability constants for the $L^1-ATP-H^+$ system from ref.[13] are the following: $(L^1)^{2+} + ATP^{4-} + 2H^+ \rightleftarrows [L^1H_2ATP]$, log*K* = 27.82(6); $(L^1)^{2+} + ATP^{4-} + 3H^+ \rightleftarrows [L^1H_3ATP]^+$, log*K* = 36.75(6); $(L^1)^{2+} + ATP^{4-} + 4H^+ \rightleftarrows [L^1H_4ATP]^{2+}$, log*K* = 43.75(6); $(L^1)^{2+} + ATP^{4-} + 5H^+ \rightleftarrows [L^1H_5ATP]^{3+}$, log*K* = 48.02(10); $(L^1)^{2+} + ATP^{4-} + 6H^+ \rightleftarrows [L^1H_6ATP]^{4+}$, log*K* = 52.10(6). – [c] Charges have been omitted for clarity. – [d] Values in parentheses are standard deviations on the last significant figure.

Discussion

Coordinating vs. Noncoordinating Anions

The $[Cu(L^1)]^{4+}$ cation can interact with anions in two different manners: (i) by covalent bonds when anions are able to coordinate the axial positions of the square-planar cyclam−Cu^{2+} unit, or (ii) through electrostatic interactions when anions interact by coulombic forces with the positively charged cyclam−Cu^{2+} and/or $Ru(tpy)_2^{2+}$ centres. As the electrochemical experiments suggest, the anions ATP, ADP, GMP sulfate and phosphate give electrostatic interactions with the $Cu^{2+}-L^1$ species, whereas chloride, bromide and OH^- give axial covalent coordination with the copper centre of the cyclam−Cu^{2+} subunit.

We have recently reported that the quenching of the fluorescence observed for the $[Cu(L^1)]^{4+}$ complex most likely occurs by means of an energy-transfer mechanism.[10] Such a mechanism requires a close proximity between the fluorophore and the copper metal ion, as occurs when copper is in a square planar coordination inside the cyclam polyamine (see Scheme 1a). In the presence of chloride, the occupation of the apical positions might significantly reduce the probability of interaction between Cu^{2+} ions and $Ru(tpy)_2^{2+}$ groups, thus reducing the quenching process (see Scheme 1b) and, consequently, resulting in an enhancement of the fluorescence upon chloride binding. A similar effect is observed when Br^- is added to a $Cu^{2+}-L^1$ system and, in general, the same effect would be expected with anions able to give strong interactions with Cu^{2+} ions through the axial positions (in fact, the OH^- anions also eliminate the Cu^{2+} quenching effect).

Prediction of the fluorescence response of the $L^1-Cu^{2+}-H^+$ system in the presence of anions able to give mainly coulombic interactions (sulfate, phosphate, ATP, ADP and GMP) is rather difficult. The quenching mechanism in Scheme 1 is operative for chloride (and also for bromide and OH^-) but is not valid for sulfate, phosphate, ATP, ADP or GMP. One would expect that the anions able to give mainly coulombic interactions with the $Cu^{2+}-L^1$ complex may impose geometrical constraints that could modulate the distance between the Cu^{2+} and the $Ru(tpy)_2^{2+}$ core and therefore induce changes in the emission behaviour of the $Cu^{2+}-L^1$ system. However, whether the interaction would enhance or reduce the emission intensity is not easy to specify. Nevertheless, the interaction of the $Cu^{2+}-L^1$ complexes with those anions has proved

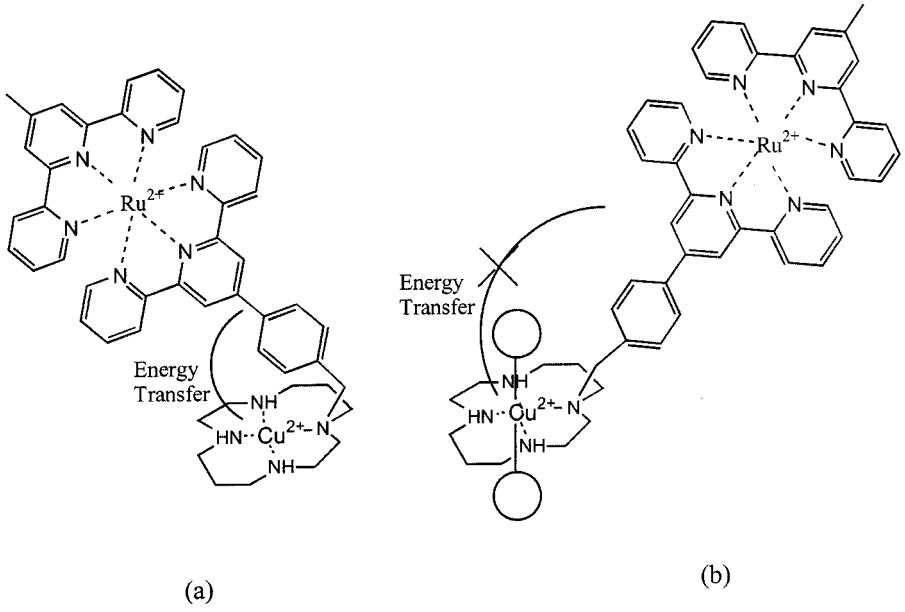

Scheme 1

to produce a rich fluorescent response, as shown in Figure 1 and 2.

Suggested Mechanism for ATP Quenching

For the $L^1-Cu^{2+}-H^+$ and $L^1-Cu^{2+}-H^+-ATP$ systems we have carried out both potentiometric titrations and fluorescent emission studies. Potentiometry allowed us to characterise the nature of the complexes existing in solution (see Figure 3 for the distribution diagrams), whereas fluorescent studies permitted us to determine the emission response as a function of the pH (see Figure 2). By a combination of both techniques it might be possible to determine which species are responsible for a particular change in the emission fluorescence intensity at a certain pH. Thus, for the $L^1-Cu^{2+}-H^+$ system the quenching of the emission behaviour is observed when the $[Cu(L^1)]^{4+}$ complex exists. In fact, there is a close relation between the intensity vs. pH curve for the $L^1-Cu^{2+}-H^+$ system in Figure 1 and the pH range of existence of the $[Cu(L^1)]^{4+}$ complex (see Figure 3). This quenching is related to the existence of Cu^{2+} in a square-planar environment. In a similar manner, the quenching for the $L^1-Cu^{2+}-ATP-H^+$ system in the 6−11 pH range appears to be directly related to the presence in solution of the $[Cu(L^1)(ATP)]$ complex. As stated above this anion-cation complex is probably formed by electrostatic interaction between the species $[Cu(L^1)]^{4+}$ and ATP^{4-}. Additionally, as the presence of ATP probably doesn't induce any change in the coordination mode of the Cu^{2+} inside the cyclam unit, it might be concluded that in the 6−11 pH range the quenching is related to the presence of the "$[Cu(L^1)]^{4+}$" unit (in the $[Cu(L^1)(ATP)]$ complex) which contains Cu^{2+} in a square-planar environment. In this case ATP seems to be able to modulate the pH zone where the $Cu^{2+}-$cyclam square-planar unit responsible for the quenching exists by binding to the $L^1-Cu^{2+}-H^+$ system. In other words, ATP is able to modify the pK_a value for complex protonation and/or formation of hydroxo derivatives. However, it cannot be completely ruled out that the quenching observed could be produced by the nucleotide moiety rather than by the Cu^{2+} cation. It is noticeable that the quenching of the intensity of the fluorescence due to ATP in the pH range 9 to 10 is selective and no other anion studied is able to quench the emission of the $Ru(tpy)_2^{2+}$ core at this pH range. Thus, coordination of ATP with the L^1-Cu^{2+} system results in a selective sensing of the anion through a fluorescent-signalling event.

Conclusions

In conclusion, we have studied a multicomponent system able to display a selective sensing response against target anions such as ATP. The receptor L^1 contains a $Ru(tpy)_2^{2+}$ fluorescent core and a covalently attached cyclam unit. This receptor was reported to show a poor fluorescence response in the presence of anions. In contrast, the formation of the Cu^{2+} complex of L^1 produces a very rich fluorescence response. The $Cu^{2+}-L^1$ fluorescence emission in an aqueous environment is governed by the quenching produced between the $Cu^{2+}-$cyclam subunit and the $Ru(tpy)_2^{2+}$ fluorescent core. The maximum effectiveness for the quenching process takes place when the complex $[Cu(L^1)]^{2+}$ is present. Addition of anions that could coordinate axial positions of the square-planar cyclam$-Cu^{2+}$ unit produces an enhancement of the fluorescence. ATP is selectively recognised through a selective quenching by the $Cu^{2+}-L^1$ system.

Experimental Section

Synthesis: The L^1 complex was prepared following published methods[12] by reaction of $[Ru(mtpy)Cl_3]$ (mtpy = 4′-methyl-2,2′:6′,2′′-terpyridine) and 1-[4′-*p*-tolyl-(2,2′:6′,2′′-terpyridyl)]-1,4,8,11-tetraazacyclotetradecane in the presence of *N*-ethylmorpholine as a mild reductant. The Cu^{2+} complex of L^1 was prepared in situ by addition of stoichiometric amounts of copper(II) perchlorate to an acetonitrile/water (70:30 v/v) solution of L^1. This solution was used for the fluorescent and potentiometric studies in the presence of anions.

Physical Measurement and Instrumentation: Photochemical data were obtained with a FS900CDT steady state T-Geometry Fluorometer, Edinburgh Analytical Instruments. All solutions for photophysical studies were degassed. The concentration of the $Cu^{2+}-L^1$ complex and the concentration of the anions was ca. 1.0×10^{-3} mol dm^{-3}. Potentiometric titrations were carried out in acetonitrile/water (70:30 v/v, 0.1 mol dm^{-3} tetrabutylammonium perchlorate) using a reaction vessel water-thermostatted at 25.0 ± 0.1 °C under nitrogen. The titrant was added with a Crison microburette 2031. Experimental potentiometric details have been published previously.[13] The computer program SUPERQUAD[14] was used to calculate the protonation and stability constants. The titration curves for each system (ca. 250 experimental points corresponding to at least three titration curves, pH range investigated 2.0−10.5, concentration of the ligand and anion was ca. 1.0×10^{-3} mol dm^{-3}) were treated either as a single set or as separate entities without significant variations in the values of the stability constants. Finally the sets of data were merged together and treated simultaneously to give the stability constants.

Acknowledgments

We should like to thank the DGICYT (proyecto PB95−1121−C02−02, 1FD97−0508−C03−01 and AMB99−0504.C02−01) for support.

[1] J.-M. Lehn, *Supramolecular Chemistry: Concept and Perspective*, VCH, Weinheim, **1995.**
[2] E. C. Constable, *Comprehensive Supramolecular Chemistry* (Ed.: J.-M. Lehn) Vol. 9, Pergamon, Oxford, **1996**.
[3] See for example: P. D. Beer, M. G. B. Drew, R. Jagessar, *J. Chem. Soc., Dalton Trans.* **1997**, 881−886; P. D. Beer, *Chem. Soc. Rev.* **1989**, *18*, 409−450; M. E. Padilla-Tosta, R. Martínez-Máñez, T. Pardo, J. Soto, M. J. L. Tendero, *Chem. Commun*, **1997**, 887−888; J. M. Lloris, R. Martínez-Máñez, T. Pardo, J. Soto, M. E. Padilla-Tosta, *Chem. Commun.* **1998**, 837−838.
[4] R. Matínez-Máñez, J. Soto, J. M. Lloris, T. Pardo, *Trends in Inorganic Chemistry* **1998**, *5*, 183−203.
[5] P. D. Beer, P. A. Gale, D. K. Smith, *Supramolecular Chemistry*, Oxford Science Publication, **1999**.
[6] J. C. Lockhart, *Comprehensive Supramolecular Chemistry*, Elsevier Science Ltd., Oxford, **1996**, 605−634.
[7] D. H. Vance, A. W. Czarnik, *J. Am. Chem. Soc.* **1994**, *116*,

9397−9398; M. E. Houston, E. U. Akkaya, A. W. Czarnik, *J. Am. Chem. Soc.* **1989**, *111*, 8735−8737.
[8] P. D. Beer, C. Hazlewood, D. Hasek, J. Hadacova, S. E. Stokes, *J. Chem. Soc., Dalton Trans.* **1993**, 1327−1332.
[9] R. Grigg, J. M. Holmes, S. K. Jones, W. D. J. A. Norbert, *J. Chem. Soc., Chem. Commun.* **1994**, 185−187.
[10] M. E. Padilla-Tosta, J. M. Lloris, R. Martínez-Máñez, A. Benito, J. Soto, T. Pardo, M. A. Miranda, M. D. Marcos, *Eur. J. Inorg. Chem.* **2000**, 741−748.
[11] L. Fabbrizzi, I. Faravelli, G. Francese, M. Licchelli, A. Perotti, A. Taglietti, *Chem. Commun.* **1998**, 971−972.
[12] M. E. Padilla-Tosta, J. M. lloris, R. Martínez-Máñez, T. Pardo, J. Soto, A. Benito, M. D. Marcos, *Inorg. Chem. Commun.* **2000**, *2*, 45−48.
[13] J. M. Lloris, R. Martínez-Máñez, M. E. Padilla-Tosta, T. Pardo, J. Soto, E. Garcia-España, J. A. Ramirez, M. I. Burguete, S. V. Luis, E. Sinn, *J. Chem. Soc., Dalton Trans.* **1999**, 1779−1784.
[14] P. Gans, A. Sabatini, A. Vacca, *J. Chem. Soc., Dalton Trans.* **1985**, 1195−1200.

Received May 23, 2000
[I00213]

Co^{2+} Translocation in a Terpyridine−Cyclam Ditopic Receptor

Miguel E. Padilla-Tosta,[a] José M. Lloris,[a] Ramón Martínez-Máñez,*[a] Teresa Pardo,[a] Felix Sancenón,[a] Juan Soto,[a] and M. Dolores Marcos[b]

Keywords: Translocation / Ditopic receptors / Electrochemistry / Cobalt complexes

The coordination behaviour of the ditopic receptor of 1-[*p*-(2,2′:6′,2′′-terpyrid-4′-yl)tolyl]-1,4,8,11-tetraazacyclotetradecane (L^1) towards Co^{2+} in acetonitrile/water (70:30, v/v) has been investigated. At acidic pH values, the L^1–H^+–Co^{2+} system shows an oxidation wave at 150 mV vs. SCE, characteristic of Co^{2+} in a bis(terpyridine) environment. Upon addition of OH^-, a reduction in the intensity of the wave at 150 mV is observed and a new oxidation wave appears at 1.30 V. This new wave is close to that found for $[Co(cyclam)]^{2+}$ under similar working conditions. The electrochemical data thus suggest that there is a pH-controlled translocation of the Co^{2+} ion from the bis(terpyridine) to the cyclam environment. A similar inference can be made from the results of UV/Vis studies. A thermodynamic characterization of the L^1–H^+–Co^{2+} system has also been carried out. Stability constants have been determined in acetonitrile/water (70:30, v/v, containing 0.1 mol dm^{-3} nBu_4NClO_4 at 25 °C) using potentiometric techniques. The following species were found: $[Co(L^1)_2H_4]^{6+}$, $[Co(L^1)_2H_3]^{5+}$, $[Co(L^1)H]^{3+}$, $[Co(L^1)]^{2+}$, and $[Co(L^1)(OH)]^+$. The 2:1 ligand-to-metal species $[Co(L^1)_2H_4]^{6+}$ and $[Co(L^1)_2H_3]^{5+}$ are assigned to complexes where Co^{2+} is coordinated by two terpyridine units. The $[Co(L^1)H]^{3+}$, $[Co(L^1)]^{2+}$, and $[Co(L^1)(OH)]^+$ species are assigned to complexes where the Co^{2+} cation is in the cyclam binding domain. The pH-induced Co^{2+} jumping between coordination sites is discussed in terms of the different basicities of cyclam and terpyridine. Co^{2+} jumping between coordination sites has also been studied by the sequential acidification of basic mixtures of L^1 and Co^{2+}. Under these conditions, the translocation was observed at a different pH value than when an acid-to-basic path was followed. The effect of anions such as phosphate and chloride on the translocation process has also been studied. In the presence of phosphate, translocation occurs at pH = 11 rather than at pH ≈ 8. The phosphate–L^1 and phosphate–L^1–Co^{2+} systems have been characterized by potentiometry and a remarkably good agreement has been found between the electrochemical and potentiometric data.

Introduction

The appropriate arrangement of suitably predisposed individual molecular elements has recently resulted in the development of systems such as sensors, switches, molecular devices, etc.[1] This has led to the exploration of interesting new effects arising from particular molecular organisations or specific assemblies of individual components with the aim of mimicking the more complex functions observed in biological systems.[2] Among known molecular functions is that of translocation.[3] It has been argued that the translocation process (positional changes of atoms in a molecule) resembles mechanical processes at the macroscopic level but is operative on the molecular scale.[4] Compounds used for such studies generally have in common the property of bi- or multistability. Thus, mechanical microscopically based translocation processes involve interconversion between two structurally different states in bi- or multistable systems. To construct such systems, several suitable components have to be coupled in a specific manner. The prerequisites of the final device are a molecule containing multiple binding sites (a polytopic ligand), a guest (organic or inorganic) capable of being bound by the binding domains, and a suitable switching mechanism to induce jumping of the guest between sites on the polytopic receptor. For instance, several examples have been reported where bound cations shift from one site to another in ditopic receptors as a result of redox triggering.[5] In these systems, the shift arises as a result of the dependence of the binding preference of the metal ion on its oxidation state. Besides redox triggering, ionically controlled translocation is also possible. We describe herein a translocation process found in the interaction of Co^{2+} with the ditopic ligand 1-[*p*-(2,2′:6′,2′′-terpyrid-4′-yl)tolyl]-1,4,8,11-tetraazacyclotetradecane (L^1) possessing 2,2′:6′,2′′-terpyridine and 1,4,8,11-tetraazacyclotetradecane (cyclam) coordination domains. We have found the metal ion jumping between these two coordination sites to be ionically governed by protons. This pH-induced jumping is discussed in terms of the basicities of the cyclam and terpyridine units and the values of the formation stability constants. The effect of certain anions on the translocation process has also been studied.

[a] Departamento de Química, Universidad Politécnica de Valencia,
Camino de Vera s/n, 46071 Valencia, Spain
Fax: (internat.) + 34-96/387-7349
E-mail: rmaez@qim.upv.es
[b] Institut de Ciència dels Materials de la Universitat de València (ICMUV),
P. O. Box 2085, 46071 Valencia, Spain

Results and Discussion

The design of artificial systems for studying translocation processes requires careful choice of each individual component. We have assembled two coordination sites (terpyri-

 © WILEY-VCH Verlag GmbH, 69451 Weinheim, 2001 1434−1948/01/0505−1227 $ 17.50+.50/0

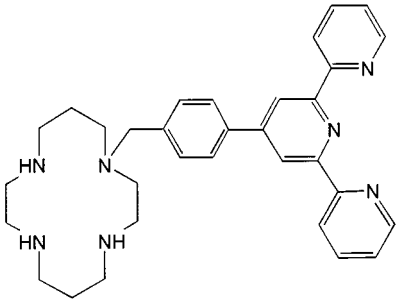

L^1

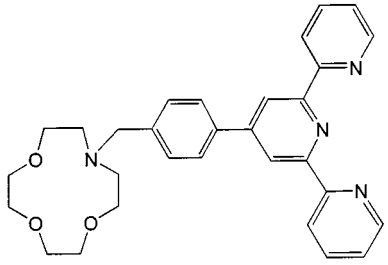

L^2

Scheme 1

dine and cyclam), both of which are capable of coordinating transition metal ions.[6] The use of an appropriate mediator (i.e. protons) makes it possible to control the relative affinity of each binding domain towards a certain metal cation. Terpyridine and cyclam components were chosen in view of the large difference in basicity between their nitrogen atoms. Besides this difference, the terpyridine-cyclam couple also has to meet an important thermodynamic requirement; the stability constants of each binding domain with a certain metal ion must be adequately complemented by the basicities of the binding atoms in order to observe, when the pH value is modulated, jumping between coordination sites (see below).

Terpyridine and cyclam were covalently linked by reaction of 4′-[4-(bromomethyl)phenyl]-2,2′:6′,2′′-terpyridine with an excess of 1,4,8,11-tetraazacyclooctadecane (cyclam) in dichloromethane in the presence of triethylamine as a base, to give the ditopic receptor L^1 (see Scheme 1). Details of the synthesis have been published elsewhere.[7] L^1 is insoluble in water and therefore the coordination studies were carried out in acetonitrile/water (70:30, v/v) mixtures. The use of other solvent mixtures such as dioxane/water or DMSO/water was also precluded by inadequate solubility.

Once the ditopic ligand had been synthesized, the next step was the choice of a suitable metal ion. Co^{2+} was selected in view of the fact that its coordination environment, in both the cyclam and terpyridine moieties, can easily be monitored by electrochemical techniques. Co^{2+} in a bis(terpyridine) coordination environment displays a very characteristic oxidation process at ca. 200 mV vs. SCE, whereas when coordinated by cyclam the oxidation to Co^{3+} becomes much more difficult.

Acidified solutions of Co^{2+} and L^1 (molar ratio L^1/Co^{2+} = 2:1) show a reversible oxidation wave at 150 mV with a ratio between the cathodic and anodic peak intensities, i_{pc}/i_{pa}, of ca. 1. This value is very close to the oxidation potential found for the complex $[Co(MePhtpy)_2]^{2+}$ [MePhtpy = 4′-(4-methylphenyl)-2,2′:6′,2′′-terpyridine] under similar working conditions. However, whereas the oxidation wave of the $[Co(MePhtpy)_2]^{2+}$ complex does not change as a function of the pH value, the addition of OH^- to the $Co^{2+}-L^1$ system leads to a decrease in the intensity of the wave at 150 mV and the appearance of an oxidation process at higher anodic potential (1.35 V). The new wave is similar to that found for the $[Co(cyclam)]^{2+}$ complex in acetonitrile/water. Figure 1 shows the electrochemical behaviour of the $Co^{2+}-L^1$ system at certain pH values. The data suggest that a translocation occurs,[8] which is schematically represented in Scheme 2. Figure 2 shows a plot of the intensity of the oxidation wave of the Co^{2+}−bis(terpyridine) core as a function of the pH value for the L^1-Co^{2+} system.

The large difference in intensity between the 150 mV and 1.35 V waves merits comment. This is not an unexpected behaviour and can be attributed to the low diffusion coefficient of the bis(terpyridine) complex and to adsorption processes observed for the oxidation of the cyclam$-Co^{2+}$ species. Moreover, the oxidation wave at 1.35 V is cathodically shifted when the pH value is very basic, probably due to the formation of hydroxo complexes.

The jumping of Co^{2+} between the terpyridine and cyclam environments can also be observed by UV/Vis spectrophotometry. The visible spectrum of $Co^{2+}-L^1$ is pH-dependent. At acidic pH values, a poorly defined band with a maximum centred at 515 nm is found. When the solution is basified, a dramatic decrease in its intensity is observed. The spectra of the $Co^{2+}-L^1$ system under acidic and basic conditions closely resemble those found for the complexes $[Co(MePhtpy)_2]^{2+}$ and $[Co(cyclam)]^{2+}$, respectively.

The electrochemical and UV/Vis experiments thus suggest that there is a proton-induced jumping of the cobalt cation between the two different sites on the ditopic receptor L^1. In addition, we have completed the study with a thermodynamic characterization of the system. The thermodynamic behaviour of polyamines such as cyclam can be adequately studied by potentiometry. However, this technique is not generally suitable for solution studies on polypyridines. Potentiometry, as a technique for deducing stability constants in polyamines, is based on the competition between the metal ion and protons to bind to the N donor atoms. The nitrogen atoms in polyamines are sufficiently basic to react with protons even in the presence of metal ions to give the protonated free receptors. Thus, a requirement for the deduction of stability constants by means of potentiometry is that both the free receptor and the complex must be observable in the pH range studied (usually 2−10). This is generally the case with polyamines, but not with terpyridines due to their lower basicities. However, although simple titrations of terpyridine in the presence of a metal ion would not lead to accurate determinations of

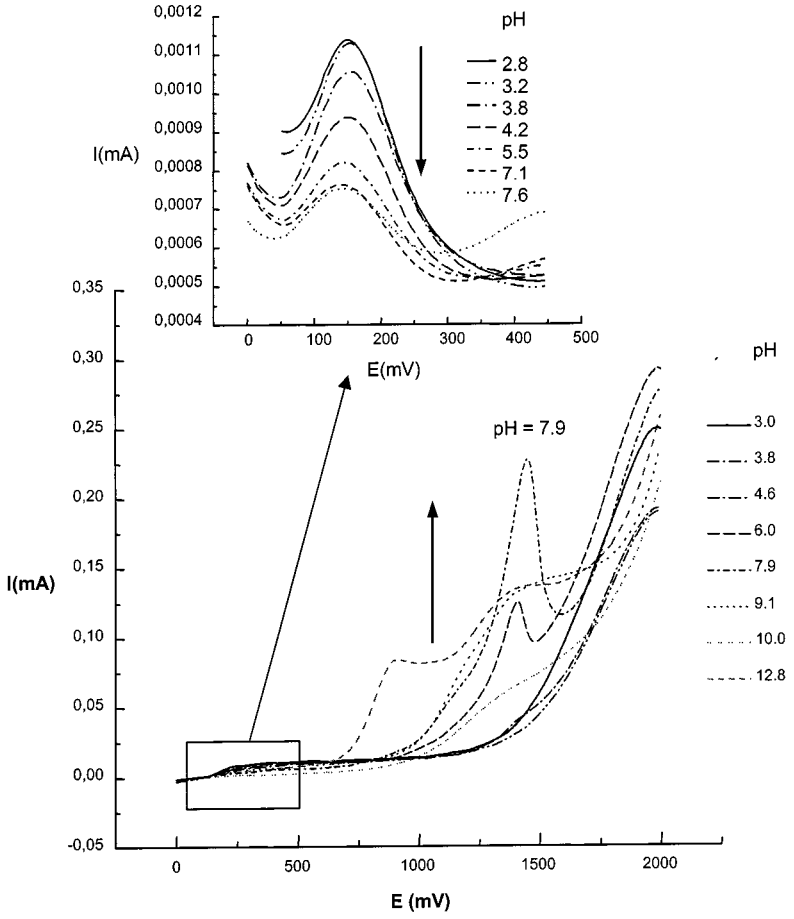

Figure 1. Electrochemical behaviour of the L^1-Co^{2+} system at various pH values using rde and differential pulse voltammetry

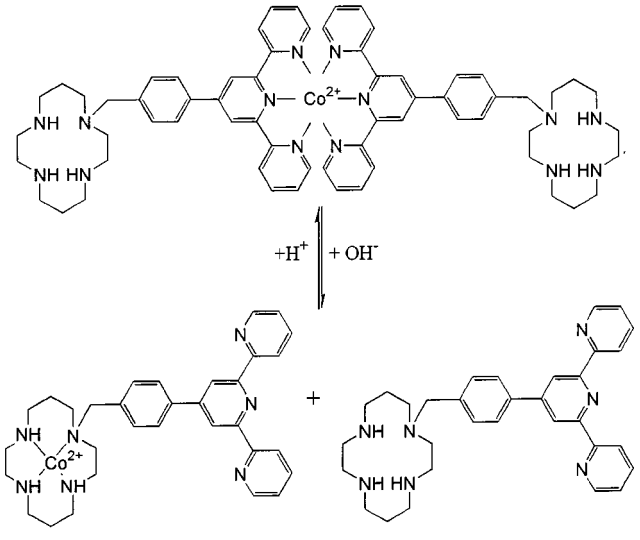

Scheme 2

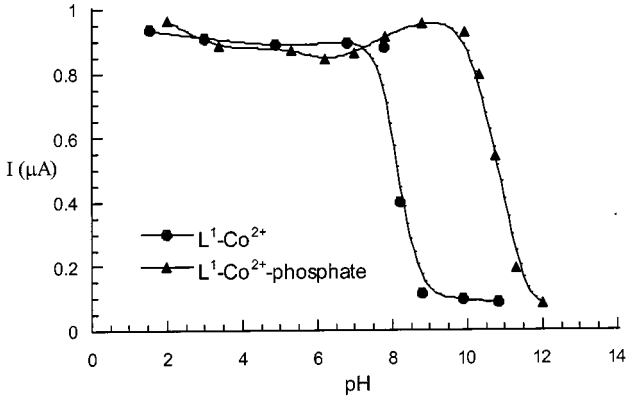

Figure 2. Intensity of the oxidation potential of the Co^{2+}−bis(terpyridine) core at 150 mV vs. SCE as a function of the pH value and in the presence of phosphate for the L^1-Co^{2+} system

the stability constants, more complex experiments can be designed for the thermodynamic characterization of terpyridine−metal mixtures. Thus, a terpyridine−metal solution might be treated with a ligand (appropriate for potentiometric study) that strongly competes with terpyridine in binding the metal cation. At this point, it is important to state that receptor L^1 does indeed meet the requirement outlined above; terpyridine is covalently coupled to a polyamine that, as suggested by the electrochemical experiments, strongly reduces the affinity of the Co^{2+} for the coordination environment of the former. Therefore, one should be able to carry out standard potentiometric experiments to thermodynamically characterize the $L^1-H^+-Co^{2+}$ system.

The first step involved the determination of the protonation constants of L^1 by titrating previously acidified solutions of the ligand in acetonitrile/water (70:30, v/v, 0.1 mol dm^{-3} tetrabutylammonium perchlorate) with KOH.

Although L^1 has seven possible protonation sites, only five constants could be measured, indicating that two protonation processes are too acidic to be determined (see Table 1).

Table 1. Protonation constants (log*K*) of L^1, mftpy, and cyclam [mftpy = 4′-(4-methylphenyl)-2,2′:6′,2′′-terpyridine; cyclam = 1,4,8,11-tetraazacyclooctadecane] in acetonitrile/water (70:30, v/v) containing 0.1 mol dm^{-3} tetrabutylammonium perchlorate at 25 °C

Reaction	L^1 log*K*	mftpy log*K*	cyclam log*K*
$L + H^+ \rightleftarrows (HL)^+$ [a]	9.75(4)[b]	4.35(2)	11.62(2)
$L + 2\,H^+ \rightleftarrows (H_2L)^{2+}$	15.40(4)	6.80(2)	21.85(3)
$L + 3\,H^+ \rightleftarrows (H_3L)^{3+}$	19.71(3)	8.05(1)	23.22(2)
$L + 4\,H^+ \rightleftarrows (H_4L)^{4+}$	23.33(4)		
$L + 5\,H^+ \rightleftarrows (H_5L)^{5+}$	26.21(5)		
$(HL)^+ + H^+ \rightleftarrows (H_2L)^{2+}$	5.65	2.45	10.23
$(H_2L)^{2+} + H^+ \rightleftarrows (H_3L)^{3+}$	4.31	1.25	1.37
$(H_3L)^{3+} + H^+ \rightleftarrows (H_4L)^{4+}$	3.62		
$(H_4L)^{4+} + H^+ \rightleftarrows (H_5L)^{5+}$	2.88		

[a] Charges have been omitted for the sake of clarity. — [b] Values in parentheses are standard deviations in the last significant figure.

In order to compare the protonation behaviour of the ditopic receptor with those of the individual components, the stepwise protonation constants of the cyclam as well as those of 4′-[(4-methyl)phenyl]-2,2′:6′,2′′-terpyridine were also determined in acetonitrile/water (70:30, v/v) mixtures (see Table 1). Three and two protonation processes were observed for the cyclam and terpyridine units, respectively. The protonation constants obtained in acetonitrile/water (70:30, v/v) solutions are in good agreement with the analogous constants reported in water.[9] Cyclam displays two very basic protonation processes in water with log*K* values for the processes cyclam + $H^+ \rightleftarrows$ Hcyclam$^+$ and Hcyclam$^+$ + $H^+ \rightleftarrows$ H_2cyclam^{2+} of 11.5 and 10.5, respectively. In contrast, the third and fourth protonation processes are much less basic with log*K* values of 1.5 and 0.9. Terpyridine shows less basic character in water. Only two protonation constants could be determined, with log*K* values for the processes H^+ + tpy $\rightleftarrows$ Htpy$^+$ and Htpy$^+$ + $H^+ \rightleftarrows$ H_2tpy^{2+} of 4.65 and 3.5. It can be concluded that the difference in basicity found between the terpyridine and the cyclam in water is retained in acetonitrile/water and probably also in the ditopic ligand L^1. Comparison of the basicity constants of L^1 with those of the individual components (see Table 1) suggests that the first two protonation processes occur at the cyclam core, the third and fourth protonations at the terpyridine, whereas the final protonation process relates to the attack of a proton at the cyclic polyamine.

Potentiometric studies aimed at determining the nature of the L^1–Co^{2+} complexes in solution have also been carried out in acetonitrile/water (70:30, v/v) by titrating previously acidified solutions containing the ligand and the metal ion in a 2:1 molar ratio with KOH. The potentiometric data were fitted with a model where the following complexes were found: $[Co(L^1)_2H_4]^{6+}$, $[Co(L^1)_2H_3]^{5+}$, $[Co(L^1)H]^{3+}$, $[Co(L^1)]^{2+}$, and $[Co(L^1)(OH)]^+$. Table 2 shows the formation stability constants for these complexes.

Table 2. Stability constants (log*K*) for the formation of Co^{2+} complexes of L^1 in acetonitrile/water (70:30, v/v) containing 0.1 mol dm^{-3} nBu_4NClO_4 at 25 °C

Reaction	log*K*
$Co^{2+} + 2\,L^1 + 4\,H^+ \rightleftarrows [Co(L^1)_2H_4]^{6+}$	47.20(5)[a]
$Co^{2+} + 2\,L^1 + 3\,H^+ \rightleftarrows [Co(L^1)_2H_3]^{5+}$	42.81(4)
$Co^{2+} + L^1 + H^+ \rightleftarrows [Co(L^1)H]^{3+}$	18.82(4)
$Co^{2+} + L^1 \rightleftarrows [Co(L^1)]^{2+}$	12.76(3)
$Co^{2+} + L^1 + H_2O \rightleftarrows [Co(L^1)(OH)]^+ + H^+$	0.83(5)

[a] Values in parentheses are standard deviations in the last significant figure.

The 2:1 ligand-to-metal species $[Co(L^1)_2H_4]^{6+}$ and $[Co(L^1)_2H_3]^{5+}$ are attributed to complexes where the cobalt(II) is coordinated by two terpyridine units. The additional presence of protons in these complexes indicates that the peripheral cyclam groups are protonated.

The 1:1 ligand-to-metal complexes $[Co(L^1)H]^{3+}$, $[Co(L^1)]^{2+}$, and $[Co(L^1)(OH)]^+$ are attributed to species where the cobalt ion is coordinated by the cyclam binding unit. Scheme 3 shows the assignments of the various com-

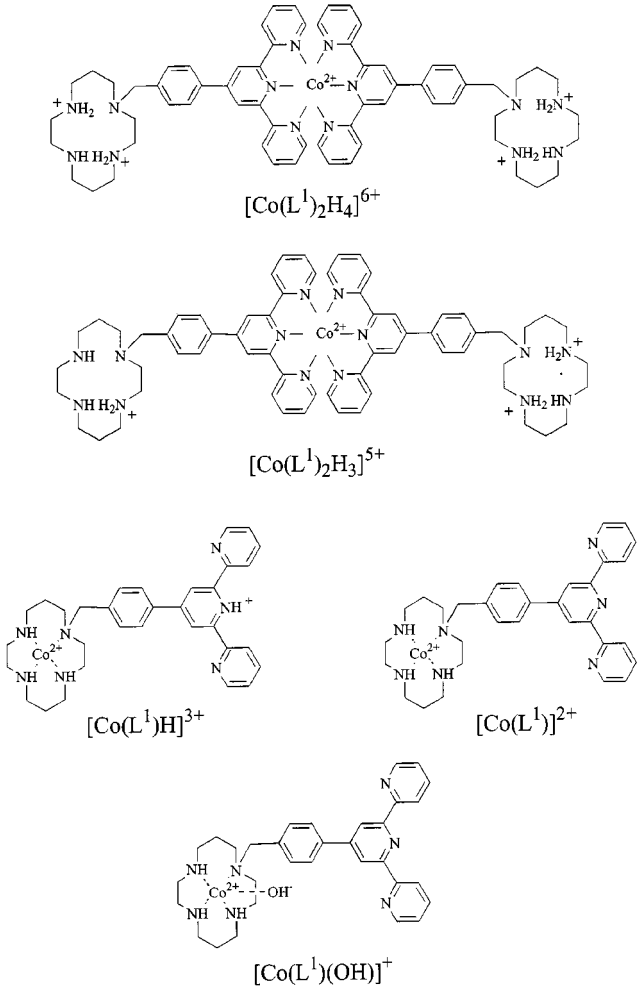

Scheme 3

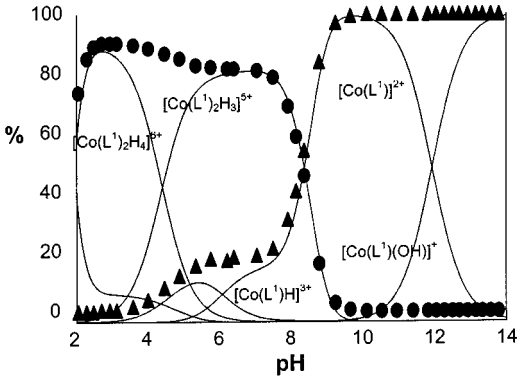

Figure 3. Distribution diagram of the various species derived from the $L^1-H^+-Co^{2+}$ system and a plot of the overall percentages of the Co^{2+}−cyclam (s) and Co^{2+}−bis(terpyridine) complexes (•) as a function of the pH value

plexes existing in solution. Figure 3 shows the distribution diagram for the $L^1-H^+-Co^{2+}$ system. The Co^{2+}−cyclam complexes have formation stability constants very similar to those reported for the Co^{2+}−cyclam−H^+ system. For instance, the stability constant for the formation of the complex $[Co(cyclam)]^{2+}$ is $\log K = 12.71$,[9] which is very close to the value found for the process $Co^{2+} + L^1 \rightleftarrows [Co(L^1)]^{2+}$, i.e. $\log K = 12.76$. This indicates that the presence of a bulky terpyridylphenyl group attached to the cyclam core and the use of acetonitrile/water solutions instead of pure water does not significantly modify the coordination behaviour of the cyclic tetraamine. The $\log K$ value for the formation of the bis(terpyridine)−cobalt(II) complex, $Co^{2+} + 2\,tpy \rightleftarrows [Co(tpy)_2]^{2+}$, is 18.6.[9] The analogous stability constant for $Co^{2+} + 2\,L^1 \rightleftarrows [Co(L^1)_2]^{2+}$ cannot be obtained from the potentiometric titrations of the $Co^{2+}-H^+-L^1$ system. However, it can be approximately deduced from the stability constant for the process $Co^{2+} + 2\,L^1 + 4\,H^+ \rightleftarrows [Co(L^1)_2H_4]^{6+}$, assuming that the process $[Co(L^1)_2]^{2+} + 4\,H^+ \rightleftarrows [Co(L^1)_2H_4]^{4+}$ would have an approximate value of 30.80 [$\log K = 30.80$ is calculated as twice $\log K = 15.40$ corresponding to the $L^1 + 2\,H^+ = (H_2L^1)^{2+}$ process]. This gives a stability constant for the process $Co^{2+} + 2\,L^1 \rightleftarrows [Co(L^1)_2]^{2+}$ of ca. 16.40, which suggests that $\log K$ for the formation of the Co^{2+}−bis(terpyridine) complex of L^1 in acetonitrile/water is of the same order of magnitude as that reported for the formation of the $[Co(tpy)_2]^{2+}$ complex.

Figure 3 also shows a plot of the overall percentages of the Co^{2+}−cyclam and Co^{2+}−bis(terpyridine) species as a function of the pH value. A pH-dependent coordination pattern can be seen, with cyclam complexes as the main species at basic pH values and bis(terpyridine) complexes being present at a level of 80% or more at pH < ca. 8. Remarkably, the translocation process represented in Figure 3 is in good agreement with the electrochemical data presented in Figure 2.

To fully understand how translocation operates one should be aware of the relationship between stability constants and ion jumping. The easiest system one can picture is a receptor containing two coordination sites (A and B), both of which can either be protonated or form a complex with a certain metal ion M. Let us assume that the stability constant for the A + M ⇄ AM process is larger than that for B + M ⇄ BM. Under these circumstances, only when the protonation constant for A + H ⇄ AH is larger than that for B + H ⇄ BH can a complete pH-controlled translocation be observed. Therefore, to observe ionically governed pH-induced jumping of the metal ion between coordination sites, a requirement that has to be fulfilled is a difference in basicity and binding strength towards the metal ion in favour to the more basic binding sites. The translocation process then works as follows: When the proton concentration is low (basic pH values), the metal ion is coordinated by the more basic centre (stronger complex); when the proton concentration is increased, the more basic centre becomes protonated, inducing the jumping of the metal ion to the less basic binding domain. The $Co-L^1-H^+$ system is similar to that described above, the only difference being the presence of 2:1 ligand-to-metal complexes. To observe translocation in this case, the formation stability constant for complexation of the metal ion at the less basic centre (terpyridine) has to be less than twice that for complexation at the more basic coordination environment (cyclam). Bearing in mind that this requirement is fulfilled in the $Co^{2+}-L^1$ system, one would expect pH-induced jumping between coordination sites, as is indeed observed {$Co^{2+} + L^1 \rightleftarrows [Co(L^1)]^{2+}$; $\log K = 12.71$ for Co^{2+} in the cyclam environment, and $Co^{2+} + 2\,L^1 \rightleftarrows [Co(L^1)_2]^{2+}$; $\log K \approx 16.4$ for Co^{2+} in the bis(terpyridine) environment}. At basic pH values, Co^{2+} jumping occurs from the bis(terpyridine) environment to the more basic cyclam binding domain. This process can be represented by the chemical reaction $[Co(L^1)_2H_3]^{5+} \rightleftarrows [Co(L^1)]^{2+} + L^1 + 3\,H^+$; $\log K = -30.05$. As can be seen, the $[Co(L^1)]^{2+}/[Co(L^1)_2H_3]^{2+}$ ratio is controlled by the proton concentration. The more basic the solution, the greater the proportion of Co^{2+} in the cyclam.

We also synthesized the receptor L^2 by reaction of 4′-[(4-bromomethyl)phenyl]-2,2′:6′,2″-terpyridine and 4,7,10-trioxa-1-azacyclododecane. L^2 is similar to L^1 in the sense that it also contains two coordination sites of different basicities. Although we have not carried out potentiometric studies on L^2 in acetonitrile/water, we have found in the literature that cobalt forms 1:1 complexes with the ligand 1,7-dioxa-4,10-diazacyclododecane (L^3) with a stability constant for the process $Co^{2+} + L^3 \rightleftarrows [Co(L^3)]^{2+}$ of $\log K = 6.01$.[10] A similar order of magnitude is presumed for the process $Co^{2+} + L^2 \rightleftarrows [Co(L^2)]^{2+}$. Therefore, as the value of the stability constant of the bis(terpyridine) complex ($\log K \approx 16$) is greater than twice the formation stability constant of Co^{2+} with the oxa-aza ligand, for the $Co^{2+}-L^2-H^+$ system one would expect the bis(terpyridine) species to be predominant over the entire pH range. Indeed, the electrochemical data reveal a unique oxidation process at ca. 150 mV attributable to the presence of Co^{2+} in a bis(terpyridine) coordination environment and the intensity of the electrochemical wave does not change over the pH range studied. There is no evidence for any translocation process. This highlights the importance of a careful

choice of each element in the design of systems displaying pH-modulated translocations.

Ionically controlled metal ion jumping has been demonstrated for the interaction a terpyridine−cyclam ditopic receptor with Co^{2+}. In addition, we have studied some factors that might have an effect on the translocation.

The first effect concerns the fact that demetallation from cyclam is slower than the process of metal incorporation into the macrocycle. This is a well-known effect and is generally operative in cyclic polyamines. The influence of this effect on the Co^{2+} jumping between coordination sites has been studied by monitoring the electrochemical behaviour of basic mixtures of L^1 and Co^{2+} upon their stepwise acidification. Under these conditions, the Co^{2+} ion remains in the cyclam core until pH ≈ 6. Further acidification induces translocation to give bis(terpyridine) species. At neutral pH value, the most stable complex is that involving the bis(terpyridine) and Co^{2+}−cyclam species are transformed to this thermodynamically favoured arrangement. However, this process is very slow; at pH = 7, only after two weeks was a partial translocation of the Co^{2+} from the cyclam to the bis(terpyridine) observed.

The operation of this kinetic process gives a hysteresis loop. Hysteresis phenomena in the solid state are well documented.[11] In contrast, studies of hysteresis loops in solution are, to the best of our knowledge, scarce.[12] This hysteresis phenomenon arises as a consequence of the existence of a bistable system coupled with a large kinetic activation barrier. Although the system is far from comparable with other well-known systems and is far too simple to be of any application, it complies with the very basic requirements for information storage: the existence of two metastable states (Co^{2+} in cyclam and Co^{2+} in terpyridine) for a given environmental condition (neutral solutions) that can be readily interconverted by the variation of an external parameter (pH).

A different approach that might affect the pH value at which translocation occurs involves the addition of anions. If the relative affinities of a certain anionic guest towards Co^{2+}−cyclam and Co^{2+}−terpyridine complexes are different, then a modulation of the translocation might be achieved. To examine this attractive possibility, we studied the Co^{2+} jumping between coordination sites in the presence of phosphate and chloride anions. A plot of the intensity of the Co^{2+}/Co^{3+} oxidation wave in the bis(terpyridine) environment as a function of the pH value in the presence of phosphate is shown in Figure 2. Translocation from the terpyridine to the cyclam environment in the presence of phosphate occurs at pH ≈ 11, quite different from the pH value (8) at which ion jumping is observed in the absence of this anion. In contrast, chloride does not affect the pH value of translocation. It is noteworthy that although some molecular systems have been described where a translocation effect is induced by redox triggering or by the pH value, there have been very few examples reported in the literature where ion jumping is modulated by the presence of anions.[13]

Table 3. Stability constants (log*K*) for the formation of phosphate complexes of L^1 in acetonitrile/water (70:30, v/v) containing 0.1 mol dm^{-3} nBu_4NClO_4 at 25 °C

Reaction	log*K*
$L^1 + PO_4^{3-} + 2\,H^+ \rightleftarrows [L^1H_2PO_4]^-$	26.37(4)[a]
$L^1 + PO_4^{3-} + 3\,H^+ \rightleftarrows [L^1H_3PO_4]$	35.63(3)
$L^1 + PO_4^{3-} + 4\,H^+ \rightleftarrows [L^1H_4PO_4]^+$	43.21(3)
$L^1 + PO_4^{3-} + 5\,H^+ \rightleftarrows [L^1H_5PO_4]^{2+}$	47.25(3)

[a] Values in parentheses are standard deviations in the last significant figure.

We also carried out potentiometric studies to thermodynamically characterize the L^1−phosphate−H^+ and L^1−Co^{2+}−phosphate−H^+ systems. Table 3 shows the stability constants for the formation of the phosphate complexes of L^1 in acetonitrile/water (70:30, v/v). Potentiometric techniques give information about the stoichiometries of the formed complexes, but do not give direct information concerning the nature of the species. Therefore, it is not straightforward to deduce whether the protons in the complexes are bonded to the phosphate or to L^1. Nevertheless, bearing in mind the pH ranges of existence of the various phosphate species and the pH ranges of existence of the protonated $(H_jL^1)^{j+}$ species, we can tentatively assign the complex $[(L^1)H_2(PO_4)]^-$ to the interaction of $(L^1H)^+$ with HPO_4^{2-}, and the complexes $[(L^1)H_3(PO_4)]$, $[(L^1)H_4(PO_4)]^+$, and $[(L^1)H_5(PO_4)]^{2+}$ to the interaction of the anion $H_2PO_4^-$ with $(L^1H)^+$, $(L^1H_2)^{2+}$, and $(L^1H_3)^{3+}$, respectively.

Table 4 shows the stability constants for the formation of the complexes of the L^1−Co^{2+}−phosphate−H^+ system. The following complexes were found: $[Co(L^1)_2H_5(PO_4)]^{4+}$, $[Co(L^1)_2H_4(PO_4)]^{3+}$, $[Co(L^1)_2H_3(PO_4)]^{2+}$, $[Co(L^1)_2H_2(PO_4)]^+$, and $[Co(L^1)(OH)(PO_4)]^{2-}$. Taking into account the pH ranges of existence of the PO_4^{3-}, HPO_4^{2-}, and $H_2PO_4^-$ species and the distribution diagram of the L^1−Co^{2+}−phosphate−H^+ system in Figure 4, we tentat-

Table 4. Stability constants (log*K*) for the formation of complexes of L^1 with Co^{2+} and phosphate in acetonitrile/water (70:30, v/v) containing 0.1 mol dm^{-3} nBu_4NClO_4 at 25 °C

Reaction	log*K*
$2\,L^1 + Co^{2+} + PO_4^{3-} + 5\,H^+ \rightleftarrows [Co(L^1)_2H_5(PO_4)]^{4+}$	68.12(5)[a]
$2\,L^1 + Co^{2+} + PO_4^{3-} + 4\,H^+ \rightleftarrows [Co(L^1)_2H_4(PO_4)]^{3+}$	62.22(4)
$2\,L^1 + Co^{2+} + PO_4^{3-} + 3\,H^+ \rightleftarrows [Co(L^1)_2H_3(PO_4)]^{2+}$	54.65(4)
$2\,L^1 + Co^{2+} + PO_4^{3-} + 2\,H^+ \rightleftarrows [Co(L^1)_2H_2(PO_4)]^+$	46.00(4)
$L^1 + Co^{2+} + PO_4^{3-} + H_2O \rightleftarrows [Co(L^1)(OH)(PO_4)]^{2-} + H^+$	9.30(4)

[a] Values in parentheses are standard deviations in the last significant figure.

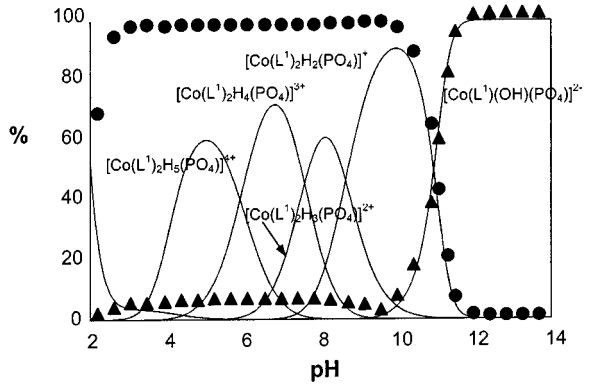

Figure 4. Distribution diagram of the various species derived from the $L^1-H^+-Co^{2+}$−phosphate system and a plot of the overall percentages of the Co^{2+}−cyclam (▲) and Co^{2+}−bis(terpyridine) complexes (•) as a function of the pH value

ively assign the complex $[Co(L^1)_2H_2(PO_4)]^+$ to the interaction of HPO_4^{2-} with $[Co(L^1)_2H]^{3+}$, and the complexes $[Co(L^1)_2H_5(PO_4)]^{4+}$, $[Co(L^1)_2H_4(PO_4)]^{3+}$, and $[Co(L^1)_2H_3(PO_4)]^{2+}$ to the interactions of $H_2PO_4^-$ with $[Co(L^1)_2H_3]^{5+}$, $[Co(L^1)_2H_2]^{4+}$, and $[Co(L^1)_2H]^{3+}$, respectively. On this basis, the stability constant for the process $[Co(L^1)_2H_3]^{5+} + H_2PO_4^- \rightleftarrows [Co(L^1)_2H_5(PO_4)]^{4+}$ is, for instance, $\log K = 3.79$.

The 2:1 ligand-to-metal species $[Co(L^1)_2H_5(PO_4)]^{4+}$, $[Co(L^1)_2H_4(PO_4)]^{3+}$, $[Co(L^1)_2H_3(PO_4)]^{2+}$, and $[Co(L^1)_2H_2(PO_4)]^+$ are attributed to complexes where the cobalt(II) is in a bis(terpyridine) environment, whereas in the complex $[Co(L^1)(OH)(PO_4)]^{2-}$ the Co^{2+} cation is coordinated by the cyclam domain. Figure 4 also shows a plot of the overall percentages of the Co^{2+}−cyclam and Co^{2+}−terpyridine species as a function of the pH value. There is a remarkable agreement between this plot and the electrochemical data presented in Figure 2. The modulation induced in the translocation process by the presence of phosphate suggests that this anion has a greater affinity for Co^{2+}−terpyridine than for Co^{2+}−cyclam complexes. The net result is that translocation occurs at higher pH values than in the absence of phosphate.

Conclusions

In conclusion, we have studied the ionically induced translocation of Co^{2+} in the ditopic receptor L^1, which contains two binding sites, cyclam and terpyridine, of different basicities. The solution mixture L^1-Co^{2+} has been thermodynamically characterized using potentiometric techniques. The pH value at which the translocation takes place can be modified by following a basic-to-acidic path or by the addition of suitable anions. In the latter case, the different affinities of the phosphate anion for the species existing in solution produces a remarkable shift in the pH value at which ion jumping is observed.

Experimental Section

The ditopic ligand L^1 was prepared according to a published method;[7] L^2 was synthesized according to ref.[14]; all other reagents were commercially available and were used as received. − Potentiometric titrations were carried out in acetonitrile/water (70:30, v/v, 0.1 mol dm^{-3} tetrabutylammonium perchlorate) under nitrogen in a water-thermostatted (25.0 ± 0.1 °C) reaction vessel. The titrant was added by means of a Crison 2031 microburette. The potentiometric measurements were made using a Crison 2002 pH meter and a combined glass electrode. The titration system was automatically controlled by a PC using a program that monitors the e.m.f. values and the volume of titrant added. The electrode was calibrated as a hydrogen ion concentration probe by titration of precise amounts of HCl with CO_2-free KOH solution and determining the equivalent point by Gran's method,[15] which gives the standard potential $E'°$ and the ionic product of water ($K'_w = [H^+][OH^-]$). The concentrations of the metal ion solutions were determined using standard methods. The computer program SUPERQUAD[16] was used to calculate the protonation and stability constants. The titration curves for each system (ca. 250 experimental points corresponding to at least three titration curves; $pH = -\log[H^+]$ range investigated 2−10; concentration of the ligand and metal ion ca. $1.2 \cdot 10^{-3}$ mol dm^{-3}) could be treated either as a single set or as separate entities without significant variations in the values of the stability constants. Finally, the data set was merged and treated as one to give the stability constants. Electrochemical experiments were carried out in acetonitrile/water (70:30, v/v, 0.1 mol dm^{-3} tetrabutylammonium perchlorate) using a Tacussel IMT-1 programmable function generator connected to a Tacussel PJT 120-1 potentiostat. The working electrode was platinum with a saturated calomel reference electrode separated from the solution under study by a salt bridge containing the solvent/supporting electrolyte. The auxiliary electrode was a platinum wire.

Acknowledgments

We would like to thank the DGICYT (proyecto PB98-1430-C02-02, 1FD97-0508-C03-01, and AMB99-0504.C02-01) for support.

[1] See, for example: P. L. Boulas, M. Gómez-Kaifer, L. Echegoyen, *Angew. Chem. Int. Ed. Engl.* **1998**, *37*, 216−247. − J.-M. Lehn, *Supramoleular Chemistry*, VCH, Weinheim, **1995**. − M. D. Ward, *Chem. Ind.* **1997**, 640−645. − I. Rubinstein, S. Steinberg, Y. Tor, A. Shanzer, J. Sagir, *Nature* **1988**, *332*, 426−429. − R. A. Bissell, A. Prasanna de Silva, H. Q. N. Gunaratne, P. L. M. Lynch, G. E. M. Maguire, K. R. A. S. Sandanayake, *Chem. Soc. Rev.* **1992**, *21*, 187−195. − P. R. Ashton, R. Ballardini, V. Balzani, I. Baxter, A. Credi, M. C. T. Fyfe, M. T. Gandolfi, M. Gómez-López, M. V. Martínez-Díaz, A. Piersanti, N. Spencer, J. F. Stoddart, M. Venturi, A. J. P. White, D. J. Williams, *J. Am. Chem. Soc.* **1998**, *120*, 11932−11942. − S. Creager, C. J. Yu, C. Bamdad, S. O'Connor, T. MacLean, E. Lam, Y. Chong, G. T. Olsen, J. Luo, M. Gozin, J. F. Kayyem, *J. Am. Chem. Soc.* **1999**, *121*, 1059−1064.

[2] A. E. Doering, D. A. Nicoll, Y. Lu, L. Lu, J. N. Weiss, *J. Biol. Chem.* **1998**, *273*, 778−783. − D. Tortorella, D. Sesardic, C. S. Dawes, E. London, *J. Biol. Chem.* **1995**, *270*, 27446−27452.

[3] G. De Santis, L. Fabbrizzi, D. Iacopino, P. Pallavicini, A. Perotti, A. Poggi, *Inorg. Chem.* **1997**, *36*, 827−832. − P. Isenring, B. Forbush, *J. Biol. Chem.* **1997**, *272*, 24556−24562. − M. Verkhovskaya, M. Verkhovsky, M. Wikstrom, *J. Biol. Chem.* **1992**, *267*, 14559−14562. − V. Amendola, L. Fabbrizzi, C. Mangano, P. Pallavicini, A. Perotti, A. Taglietti, *J. Chem. Soc., Dalton Trans.* **2000**, 185−189.

[4] R. Ballardini, V. Balzani, M. T. Gandolfi, L. Prodi, M. Venturi, D. Philip, H. S. Ricketts, J. F. Stoddart, *Angew. Chem. Int. Ed. Engl.* **1993**, *32*, 1301−1303.

[5] L. Zelikovichi, J. Libman, A. Zhanzer, *Nature* **1995**, *374*, 790−792. − A. Livoreil, C. O. Dietrich-Buchecker, J. P. Sauvage, *J. Am. Chem. Soc.* **1994**, *116*, 9399−9400. − C. Canevet, J. Libman, A. Shanzer, *Angew. Chem. Int. Ed. Engl.* **1996**, *36*, 2657−2660. − C. Belle, J.-L. Pierre, E. Saint-Amar, *New J. Chem.* **1998**, 1399−1402.

[6] J. P. Sauvage, J. P. Collin, J. P. Charnbron, S. Guillerez, C. Coudret, V. Balzani, F. Barigelletti, L. De Cola, L. Flamigni, *Chem. Rev.* **1994**, *94*, 993−1019. − G. W. Gokel (Ed.), in: *Advances in Supramolecular Chemistry*, JAI Press Inc., Greenwich, Connecticut, USA, **1993**. − L. F. Lindoy (Ed.), in: *The Chemistry of Macrocyclic Ligand Complexes*, University Press, Cambridge, U.K., **1989**.

[7] M. E. Padilla-Tosta, J. M. Lloris, R. Martínez-Máñez, A. Benito, J. Soto, T. Pardo, M. A. Miranda, M. D. Marcos, *Eur. J. Inorg. Chem.* **2000**, 741−748. − M. E. Padilla-Tosta, J. M. Lloris, R. Martínez-Máñez, T. Pardo, J. Soto, A. Benito, M. D. Marcos, *Inorg. Chem. Commun.* **2000**, *2*, 45−48.

[8] Due to the ditopic nature of the receptor L^1, the process of Co^{II} displacement is more probably intramolecular (translocation is the term used in this case) although it has to be pointed out that an intermolecular rearrangement cannot be completely ruled out.

[9] R. M. Smith, A. E. Martell (Eds.), *Critical Stability Constants*, Plenum, New York, **1974−1989**; A. E. Martell, R. M. Smith, R. M. Motekaitis, NIST Critical Stability Constants of Metal Complexes Database, Texas A & M University, College Station, **1993**.

[10] E. Luboch, A. Cygan, J. Biernat, *Inorg. Chim. Acta* **1983**, *68*, 201−204. − F. Arnaud-Neu, M. Sanchez, R. Yahya, M. J. Schwing-Weill, *Helv. Chim. Acta* **1985**, *68*, 456−464.

[11] J. F. Létard, P. Guionneau, L. Rabardel, J. A. K. Howard, A. E. Goeta, D. Chasseau, O. Kahn, *Inorg. Chem.* **1998**, *37*, 4432−4441. − J. Kröber, E. Codjovi, O. Kahn, F. Grolière, C. Jay, *J. Am. Chem. Soc.* **1993**, *115*, 9810−9811. − H. Bolvin, O. Kahn, B. Vekhter, *New J. Chem.* **1991**, *15*, 889−895.

[12] M. Sano, H. Taube, *Inorg. Chem.* **1994**, *33*, 705−709. − U. Kölle, *Angew. Chem. Int. Ed. Engl.* **1991**, *30*, 956−958.

[13] M. Montalti, L. Prodi, *Chem. Commun.* **1998**, 1461−1462.

[14] M. E. Padilla-Tosta, J. M. Lloris, R. Martínez-Máñez, M. A. Miranda, J. Soto, M. D. Marcos, *Eur. J. Inorg. Chem.*, submitted.

[15] G. Gran, *Analyst (London)* **1952**, *77*, 661. − F. J. Rossotti, H. J. Rossotti, *J. Chem. Educ.* **1965**, *42*, 375.

[16] P. Gans, A. Sabatini, A. Vacca, *J. Chem. Soc., Dalton Trans.* **1985**, 1195−1200.

Received June 8, 2000
[I00232]

Characterisation and Properties of Amorphous Nonstoichiometric $Ge_{1-x}C_x$:H Compounds Obtained from X-Ray Radiolysis of Germane/Ethylene Mixtures

Paola Benzi,*[a] Mario Castiglioni,[a] and Paolo Volpe[b]

Keywords: Semiconductors / Germanium / Carbides / Radiochemistry / Alloys / Gas-phase reactions

Compounds of amorphous hydrogenated nonstoichiometric germanium carbide were obtained from the radiolysis of GeH_4/C_2H_4 mixtures containing 3–30% ethylene. The composition of the materials varied depending on the ethylene percentage in the irradiated mixture. The bonding and the structure of the compounds so obtained were investigated by infrared spectroscopy, and their optical gap values determined by the Tauc procedure. The variation of optical gap values as a function of carbon content is discussed.

Introduction

In the past two decades, there has been a growth in interest in amorphous alloys (i.e. SiC, SiGe, GeC) due to their possible electronic and photovoltaic applications. A variety of different techniques are used to obtain these materials, some of which involve the decomposition of gaseous reactants.[1−9] Heat or electromagnetic quanta can provide the energy for the decomposition of the reactants. In particular, the use of high-energy quanta (i.e. X or γ) allows one to overcome the problem related with the differential activation of compounds having very different bond energies.

In our laboratory, high-energy radiation has been used to decompose gaseous mixtures with the aim of obtaining amorphous materials, particularly α-GeC:H. In fact, although the properties of germanium carbide are not well known, probably due to a lack of a simple preparation method, the theoretical conversion-yield values obtained from the plot proposed by Prince[10] using the optical gaps calculated from the Davis and Mott equation[11] suggest that the amorphous Ge−C alloys can have good photovoltaic properties depending on the Ge/C ratio.[12]

In previous work, the solids obtained from the radiolysis of mixtures of GeH_4 and saturated hydrocarbons have been studied,[15−18] but the carbon content of the solid is generally low, even when a mixture that is rich in hydrocarbons is used.

The materials prepared from mixtures of GeH_4 and unsaturated hydrocarbons are now under examination, with the aim of increasing the carbon content. In fact, mass spectrometry studies[13,14] have also suggested that the presence of the more reactive unsaturated bond can lead to an increase of carbon content in the solid. In this work we report on the characterisation of materials obtained by radiolysis of GeH_4/C_2H_4 mixtures at room temperature.

Results and Discussion

From the irradiation of germane/ethylene mixtures both volatile and condensed products are obtained, which were analysed using different techniques. The analysis of the residual gas phase (after irradiation) was performed by gas chromatography/mass spectrometry: besides unchanged ethylene and germane, di- and trigermane were revealed; traces of volatile hydrocarbons formed by condensation of two or three ethylene molecules were seldom observed. Several more interesting mixed compounds, containing from one to three germanium atoms and from one to six carbon atoms, were also detected.

In Figure 1 (**a**, **b**) variations in yields of gaseous products as a function of the ethylene percentage in the reaction mixture are shown.

The liquid or solid products obtained from radiolysis were deposited on the bottom of the irradiated vials. The colour, consistency, and physical state of these compounds depend on the ethylene percentage in the mixtures. A brown-orange dusty solid is obtained from the mixture containing 3% ethylene. If the ethylene percentage is increased the solid becomes clearer, and at around 15% ethylene content it becomes waxy. When the ethylene percentage exceeds 15% an orange liquid is formed, but when the ethylene amount reaches 30% the liquid becomes colourless.

In Table 1 the quantity, the average empirical formula and other properties of the condensed phases obtained from irradiation of germane/ethylene mixtures with ethylene ranging from 3 to 30% are reported.

The presence of hydrocarbons in the condensed phase has been excluded by solvent extraction of the products followed by gas chromatography/mass spectrometry analysis. This result is in agreement with the finding of only trace amounts of gaseous hydrocarbons in the residual gas mixture after irradiation. Moreover, the prevailing presence of

[a] Dipartimento di Chimica Generale ed Organica Applicata, Università di Torino,
C.so Massimo D'Azeglio, 48 10125 Torino, Italy
[b] Istituto Nazionale di Fisica della Materia
E-mail address: benzi@silver.ch.unito.it

 © WILEY-VCH Verlag GmbH, 69451 Weinheim, 2001 1434−1948/01/0505−1235 $ 17.50+.50/0

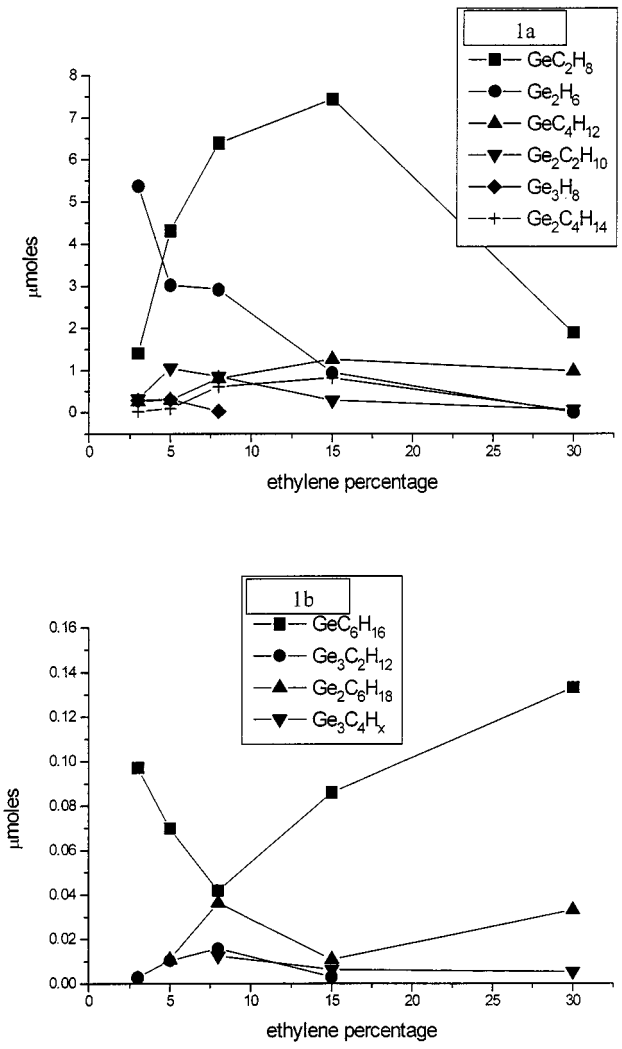

Figure 1. Gaseous products yield obtained after irradiation of germane/ethylene mixtures with different composition as a function of the ethylene percentage in the reaction mixture (the solid lines are to guide the eye); the adsorbed energy is the same for all the mixtures; NB the µmol values are affected by an error of 20%

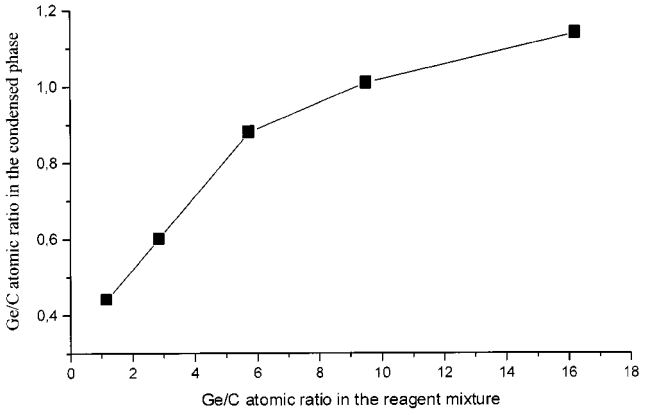

Figure 2. Ge/C atomic ratio in the condensed products obtained from irradiation as a function of Ge/C atomic ratio in the reacting gas mixture (the solid line are to guide the eye)

species containing both germanium and carbon in the gas phase and the results of elemental analysis suggest that the materials obtained from irradiation of GeH_4/C_2H_4 consist of polymeric chains containing Ge−C bonds. The X-ray diffraction spectra of the compounds do not show any crystallinity i.e. the materials are in the amorphous state.

All the species formed from the various mixtures are insoluble in common organic and inorganic solvents, but are rapidly oxidised by strong oxidising agents (such hydrogen peroxide or nitric acid). They are not very stable to the air and when exposed for a few days to the laboratory atmosphere they slowly undergo oxidation and become white. For this reason all the analyses on condensed phases were performed soon after opening the vials.

Figure 2 shows the variation of the Ge/C atomic ratio in the condensed phase obtained from irradiation as a function of the Ge/C ratio in the initial gas mixture.

As the ethylene concentration was increased in the reacting mixture, both the carbon content and the total amount of the condensed phase increased (Table 1). On the contrary, using saturated hydrocarbons,[15−18] the carbon content in the solid products increased, although the total solid yield decreased as the hydrocarbon content in the starting mixture was increased. These findings indicate that in the presence of saturated hydrocarbons, the initiation and propagation process of the polymerisation reaction leading to the solid is due to GeH_x ($n = 1-3$) species, whereas in the present experiment the ethylene molecules start and sustain the polymerisation process.

During irradiation both ionic and radical species may be involved in the formation of volatile and condensed products. From Fourier transform and high pressure mass spectrometric experiments[13] the main ionic reactions are:

$GeH_3^+ + GeH_4 \rightarrow Ge_2H_3^+ + 2H_2$

$GeH_3^+ + GeH_4 \rightarrow Ge_2H_5^+ + H_2$

$GeH_3^+ + C_2H_4 \rightarrow Ge_2H_5^+ + H_2$

Nevertheless, as reported in a previous paper,[19] the radical reactions should give the major contribution to the

Table 1. Composition, weight, and characteristics of the condensed products obtained from irradiation of GeH_4/C_2H_4 mixtures

Ethylene % in the mixture	Condensed products Weight (mg)	characteristics	$Ge_{1-x}C_x$	% carbon[a]	% hydrogen[b]
3%	5.0 ± 0.8	brown-orange dusty solid	$Ge_{0.532}C_{0.468}$	20.6	56.0
5%	7.0 ± 1.4	dark orange dusty solid	$Ge_{0.503}C_{0.497}$	20.9	57.9
8%	10.0 ± 2.0	orange dusty solid	$Ge_{0.469}C_{0.531}$	21.4	59.5
15%	15.0 ± 1.2	orange waxy solid	$Ge_{0.376}C_{0.624}$	23.3	62.6
30%	20.0 ± 2.0	viscous colourless liquid	$Ge_{0.307}C_{0.693}$	24.6	64.5

[a] Percentage of carbon atoms in the condensed phase. − [b] Percentage of hydrogen atoms in the condensed phase.

products formation. In the same paper, from experimental data and ab initio theoretical calculations, we have hypothesised the germane radicals with one or no hydrogen atoms to be the most probable initiators of the polymeric chain:

$GeH_n + C_2H_4 \rightarrow GeC_2H_{n+4}$ $(n = 0, 1)$

$GeH_n + GeH_4 \rightarrow Ge_2H_{n+4}$ $(n = 0, 1)$

The species produced from the above reactions are still reactive and may react further with ethylene or germane molecules, leading to chain propagation up to solid products. Alternatively, they may also react with light radicals (mostly hydrogen) terminating the chain propagation and leading to volatile products.

Figure 3 shows the fraction of decomposed germane as a function of the amount of ethylene in the mixture. It increases from around 0.5 to 2% of germane when the ethylene percentage ranges from 3 to 30%.

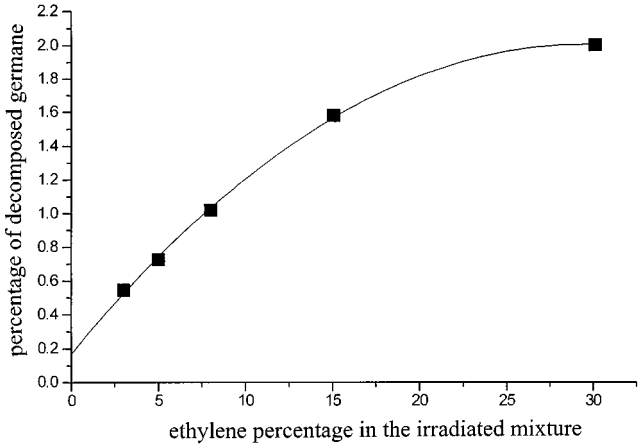

Figure 3. Percentage of decomposed germane (gaseous and condensed products are considered) with respect to the amount initially present in the mixture as a function of ethylene percentage in the irradiated mixture (the solid line is the fit of the experimental data)

This behaviour indicates that the ethylene competes effectively with hydrogen radicals in the reactions with primary and secondary radical species, promoting the chain propagation and inhibiting the radical recombination reactions. This hypothesis is also supported by the decreasing yield of di- and trigermane together with the general increase of Ge−C containing gaseous species observed when the ethylene percentage is increased. Furthermore, the ratio between the yields of condensed and gaseous products is much higher than in the GeH_4/saturated hydrocarbons system (Figure 1 and Table 1).

Bonding and Structure

IR spectroscopy was used to study the bonding configuration and structure of the α-GeC:H materials obtained. In fact the IR spectra can detect the presence and the relative abundance of CH_n, GeH_n, and GeC groups. A typical IR absorption spectrum in the 3200 to 400 cm^{-1} wave-number region, for a sample obtained from the irradiation of a 15:85 mixture of ethylene/germane, is shown in Figure 4a.

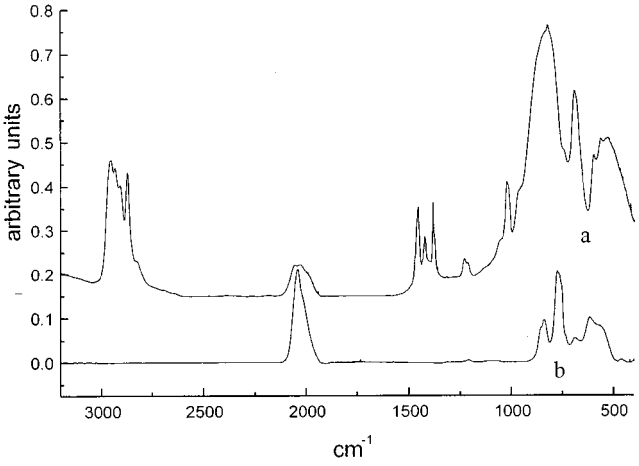

Figure 4. Infrared absorption spectrum in the 3300 to 400 cm^{-1} wave-number region of (a) a sample obtained from irradiation of the mixture with 15% ethylene, and (b) a sample obtained from irradiation of pure monogermane; the former is shifted on the *y* axis

In Figure 4b the spectrum of the solid obtained from irradiation of pure monogermane is shown for comparison.

The IR spectra of samples prepared from gas mixtures containing 3%, 15%, and 30% ethylene have been superimposed and divided into three regions, as depicted in Figure 5.

In the 3050 to 2800 cm^{-1} range (Figure 5a) the absorption of the CH_m ($m = 1-3$) stretching modes take place. Considering the position of the stretching bands of the CH_m ($m = 1-3$) grouping in hydrocarbons and the results reported about analogous bands in α-GeC:H and α-SiC:H,[20−24] we can assign the signals around 2955 and 2872 cm^{-1} to CH_3 groups, the signals around 2934 and 2824 cm^{-1} to CH_2 groups, and the band at 2905 cm^{-1} can be attributed to CH groups. Figure 5a shows that the intensity of the above signals increases with ethylene percentage in the reaction mixture. In particular, the normalised integrated absorption I of deconvoluted signals, defined by[21,25]

$$I = \int \alpha(\omega)\omega / d\omega$$

where α(ω) is the absorption coefficient at wave-number ω], indicates that the peak around 2955 cm^{-1}, attributed to the stretching of CH_3 groups, increases sevenfold, whereas the carbon content of the sample increases only 2.5 times (Table 1). This finding indicates that, as observed for α-SiC:H alloys,[23,24] the increase of carbon content causes the solid to incorporate a larger number of CH_3 groups. The CH_3 bonding configuration leads to a less dense material with inner surfaces or voids,[24] which allows oxygen penetration into the sample if exposed to air. This is in agreement with the above-mentioned oxidation process undergone by our samples, which becomes faster as the carbon content is higher.

Figure 5b shows the IR spectrum between 2125 and 1925 cm^{-1}. The signal is an envelope of bands whose deconvolution exhibits two partially overlapped bands at 2013 and

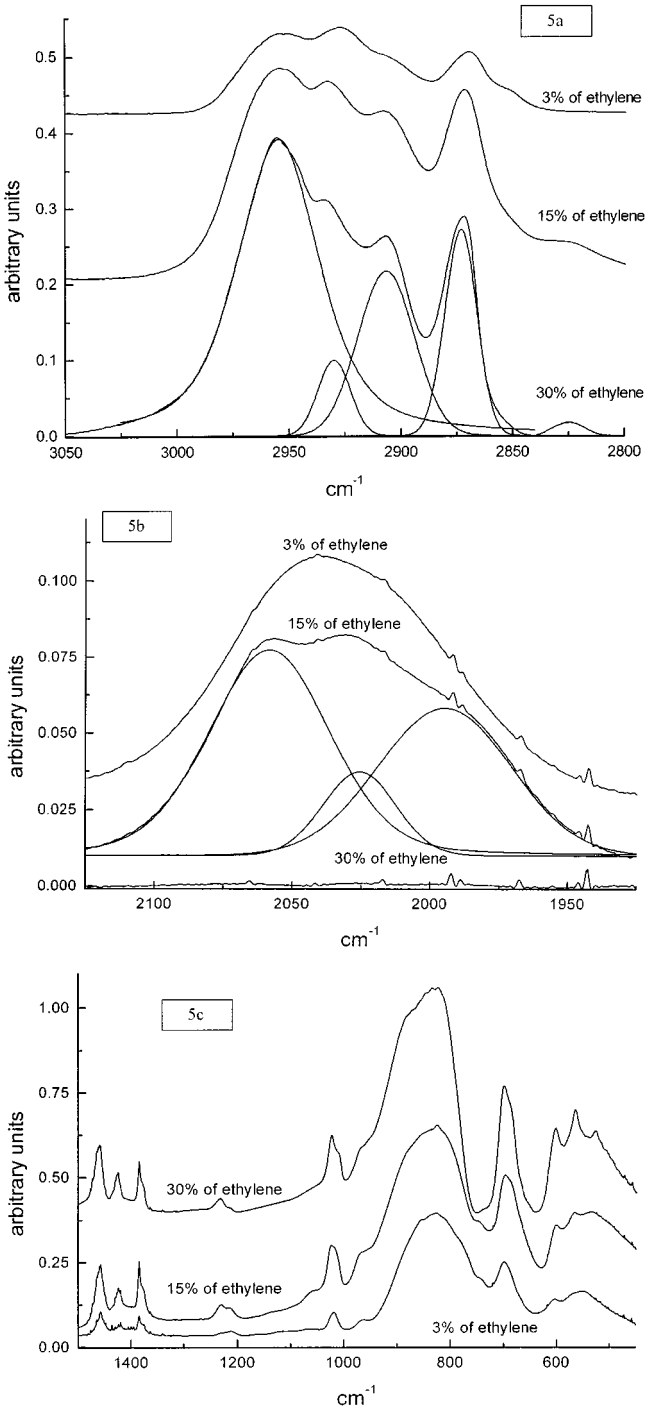

Figure 5. The IR absorption bands of samples obtained from irradiation of mixtures with 3%, 15%, and 30% ethylene: **a**: (3050−2800 cm^{-1}), **b**: (2125−1925 cm^{-1}), **c**: (1500−400 cm^{-1}); in parts **a** and **b** the spectra of the samples obtained from mixtures with 3 and 15% of ethylene are shifted on the *y* axis; in part **c** the spectra of the samples obtained from mixtures with 15 and 30% ethylene are shifted on the *y* axis; the deconvoluted signals for the sample obtained from mixtures with 30 and 15% of ethylene, respectively, are also depicted in parts **a** and **b**

2051 cm^{-1} (the deconvoluted signals are not reported in Figure 5b for clarity) and three bands at 1994, 2025, and 2058 cm^{-1} for the samples obtained from mixtures with 3 and 15% ethylene, respectively. The sample obtained from the mixture containing 30% ethylene does not exhibit any signals in this range. The observed bands can be assigned unambiguously to the Ge−H stretching mode, but the interpretation of the substructure of these bands involves various degrees of uncertainty.[22−28] In α-Ge:H compounds, a band at 1970 cm^{-1} was observed and attributed both to the stretching of GeH groups inside cavities much larger than that corresponding to a monovacancy,[25,26] or to GeH_2 group stretching. Bands at 2000 and 2060 cm^{-1} were attributed to $(GeH_2)_n$ polygermane and GeH_3 groups, respectively. On the other hand, as observed in α-SiC:H for the bands of Si−H bond stretching,[23,26] in α-GeC:H the bands due to Ge−H bond stretching can shift as the environment of the oscillatory species changes due to the presence of carbon atoms bound to germanium atoms.[21] In fact, the stretching bonds are strengthened by attaching carbon atoms to Si or Ge atoms due to the higher electronegativity of carbon with respect to Si or Ge.

In order to estimate the influence of neighbouring atoms on the frequencies of GeH and GeH_2 attached to one, two, or three carbon atoms, we have plotted, as proposed by Lukovsky for SiH and SiH_2,[29] the molecular GeH and GeH_2 vibrational frequencies (obtained from literature data[30−35]) as a function of $\Sigma SR(R_j)$, where $\Sigma SR(R_j)$ is the group-stability-ratio sum for substituting groups. The results are shown in Figures 6a and 6b.

The fits of the points give the following Equations for GeH and GeH_2 frequencies, respectively:

$$\nu(\mathrm{GeH}) = 1740 + 27.0 \sum_{j=1}^{3} SR(Rj) \pm 13$$

$$\nu(\mathrm{GeH_2}) = 1800 + 34.0 \sum_{j=1}^{2} SR(Rj) \pm 11$$

The frequencies for GeH and GeH_2 attached to one, two, or three carbon atoms calculated with Equation (1) and Equation (2), respectively, are summarised in Table 2.

With these indications, the band at 2013 cm^{-1} from the sample obtained in the presence of 3% ethylene could be attributed to GeH or GeH_2 attached to two or one carbon atoms, respectively, whereas the band at 2053 cm^{-1} could be assigned to GeH or GeH_2 bound to three or two carbon atoms, respectively. Considering the Ge/C ratio (see Table 1) we suggest that these bands are more probably due to GeH and GeH_2 modes, respectively.

Analogous considerations suggest that the three bands at 1995, 2025, and 2059 cm^{-1} of the sample with 15% ethylene must be attributed to GeH connected to one carbon atom and to GeH_2 attached to one or two carbon atoms, respectively. However it must be considered that the band position can also be affected by the presence of internal surfaces analogously to α:Ge−H,[25,26] therefore the suggested band attribution suffers from some extent of uncertainty.

It is noteworthy that as the carbon content of the sample increases, the band's intensity in the 1950−2150 cm^{-1} range decreases and no band is present for a sample obtained from a 30% ethylene mixture. This behaviour seems to indicate that hydrogen bound to germanium is substituted by

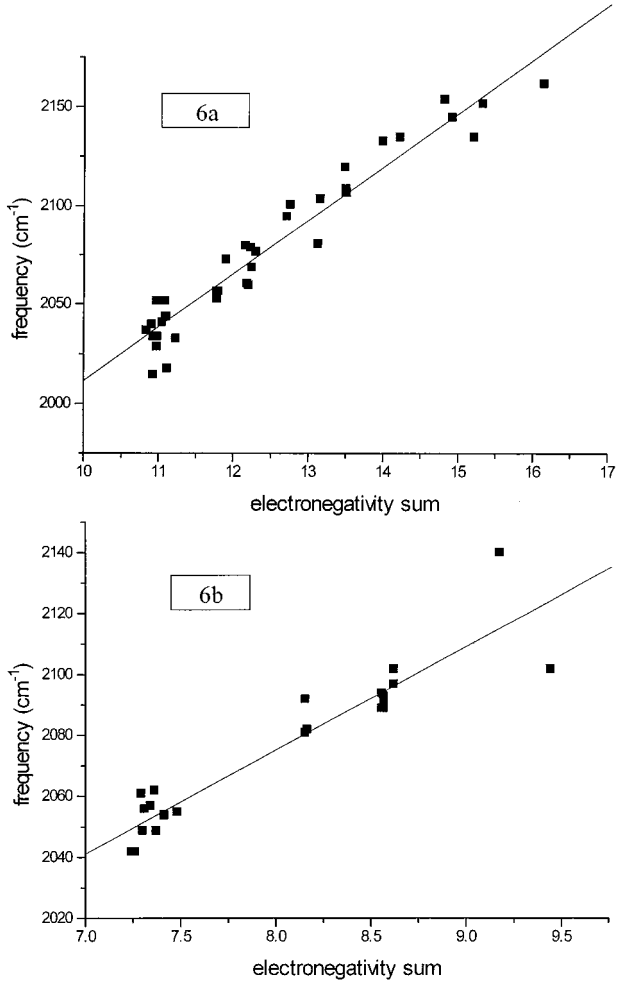

Figure 6. Frequency of GeH (**a**) and GeH_2 (**b**) stretching versus electronegativity for substituted germane molecules; the points are the experimental frequencies and the solid lines are the fits to the molecular data for the di- and trisubstituted molecules

Table 2. Stretching frequencies calculated for GeH and GeH_2 groups

GeH		GeH_2	
Ge_3GeH	1952 cm^{-1}	Ge_2GeH_2	1978 cm^{-1}
Ge_2CGeH	1983 cm^{-1}	$GeCGeH_2$	2018 cm^{-1}
GeC_2GeH	2014 cm^{-1}	C_2GeH_2	2058 cm^{-1}
C_3GeH	2047 cm^{-1}		

carbon even if overall the hydrogen content in the condensed products increases. In fact, it must be considered that $E_{bond}(C-H) > E_{bond}(Ge-H)$[36] and, as observed in the α-SiC:H system,[24] the more probable bonding sites for hydrogen atoms are those having the largest bond energy. This is in agreement with both the above-mentioned increase of the band intensity attributable to CH_3 groups and the observed increase (calculated from the integral of deconvoluted signals) of the CH_3/CH_2 ratio.

Figure 5c shows the spectra in the 1500 and 400 cm^{-1} wavenumber region. In this range many bands are present, and the interpretation is difficult due to the presence of broad bands (which are envelopes of modes) and by the overlapping of Ge−C stretching with Ge−H wagging modes or with $Ge-CH_n$ and GeH_2 bending modes.[21,22,25] Moreover, in this region the deformation modes of $(CH_m)_nC/Ge$ ($m = 1-3$; $n = 1-3$) groups are expected.[21,24]

The signals at 1385 cm^{-1} and 1458 cm^{-1} are attributable to the symmetrical and asymmetrical deformation modes of the $(CH_3)_nC$ groups ($n = 1-3$).[20,24,37] The weak band around 1424 cm^{-1}, whose intensity increases with increasing carbon and hydrogen content in the condensed phase, is probably due to the deformation mode of the CH_3Ge groups.[24,37] Two signals around 1210 and 1225 cm^{-1} are also present. Considering (i) that the intensity of the band at 1225 cm^{-1} increases while that of the band at 1210 cm^{-1} decreases with the carbon and hydrogen content, and (ii) - that Rubel et al.[24] attribute the two bands around 1230 and 1245 cm^{-1} to a bending mode of $(CH_m)_nC/Si$ ($m, n = 1-3$) and to a symmetric deformation mode of the CH_3Si group, respectively, the bands at 1210 and 1225 cm^{-1} have been assigned to analogous vibrational modes of CH_3Ge and $(CH_m)_nC/Ge$ groups. The signal around 1024 cm^{-1} and the shoulder at 965 cm^{-1} are attributable to CH_n rocking and/or wagging modes[38,39] and to C−C stretching modes, respectively. The broad band between 950 and 750 cm^{-1} can be due to both GeH_2 and to GeH_3 bending modes and to $Ge-CH_n$ wagging mode.[21,25] The above attribution of the signal between 2150 and 1950 cm^{-1} and the presence of a strong signal around 850 cm^{-1} for the sample from 30% ethylene (which exhibits no signal attributable to Ge−H stretching modes) support this hypothesis. The peak at 700 cm^{-1}, which exhibits an increasing intensity with ethylene percentage in the gaseous mixture, can be attributed to a rocking vibration of the CH_2 groups in the $-(CH_2)_n-$ chains with $n > 4$.[40] In the 500−650 cm^{-1} region three peaks are observed in the spectra, although other authors refer to one, two, or even four peaks, attributable both to Ge−C stretching and GeH wagging modes.[21,27,36,41] The observation of these signals even for the sample obtained from the mixture with 30% ethylene indicates that the bands between 500 and 650 cm^{-1} can be attributed to a Ge−C bond even if a contribution from the GeH group (if present) cannot be excluded.

To sum up, all the results indicate that the materials obtained from irradiation of GeH_4/C_2H_4 mixtures are amorphous nonstoichiometric $Ge_{1-x}C_x$:H compounds with chains forming a network in which the Ge atoms are less hydrogenated than the C atoms, which present many network-terminating configurations.

Optical Properties

The light absorption measurements of the samples were performed at photon energies between 0.5 and 6.25 eV. The optical gap values (E_{opt}) have been obtained from the intercept with the x axis of the extrapolated linear part of the curves calculated following the usual Tauc procedure.[42] It

consists of plotting $(\alpha h\nu)^{1/2}$ vs. the photon energy, $h\nu$, according to:

$$(\alpha h\nu)^{1/2} = B(h\nu - E_{opt})$$

where α is the absorption coefficient from spectrophotometric measurements, h Planck's constant, ν the photon frequency, B a constant, and E_{opt} the optical band gap.

The values of E_{opt} as a function of carbon molar fraction in the condensed phase are shown in Figure 7a.

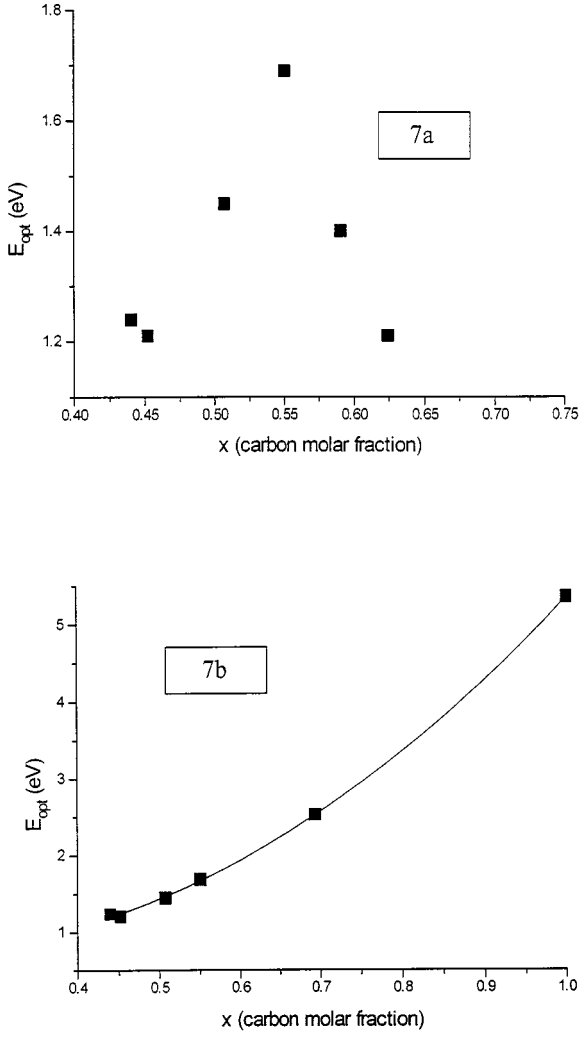

Figure 7. (**a**) Values of E_{opt} as a function of carbon molar fraction in the condensed phase of a few samples with different composition; (**b**) increasing data of part **a** and 2.53 eV are used to extrapolate to $x = 1$

The E_{opt} values are between 1.2 and 1.7 eV, which is in good agreement with previously reported data.[7,17,21,22] In particular, the sample with composition $Ge_{0.49}C_{0.51}$:H shows an E_{opt} of 1.49 eV, which is very close to the value (1.45 eV) reported by Shinar[22] for a sample with a very similar composition. Figure 7a shows that E_{opt} increases with increasing carbon content, reaching a maximum for a sample with composition $Ge_{0.45}C_{0.55}$:H, and then decreases, as reported for α-SiC:H alloys.[7] The variation of optical properties depending on film composition is related to the local bonding. In a binary alloy, such as germanium carbide, Ge−Ge, Ge−C, and C−C bonds are possible, and their relative proportions may change with increasing carbon content. If sp^3-bonded alloys are hypothesised, E_{opt} should continuously increase with the carbon content because Ge−Ge bonds are replaced by stronger Ge−C[36] bonds. When the carbon molar fraction, x, is higher than 0.5, Ge−C bonds are replaced by even stronger C−C bonds.[36,44] Nevertheless, we observe a maximum in the plot of E_{opt} vs. carbon content at around $x = 0.55$. To explain this trend, a C sp^2-bonding configuration must be considered.[7,44,45] It is reasonable to suppose that in our Ge−C alloys with $x > 0.5$ the carbon atoms exceeding the stoichiometric composition show a tendency to form zones in which several carbon atoms are bonded together, forming a threefold coordinated graphite-type local environment, as proposed for Si−C alloys.[7] The occurrence probability of these regions is enhanced if the carbon content increases. The decrease of E_{opt} observed when the carbon content increases over a critical value both in α-GeC:H and α-SiC:H,[7,44,45] is attributed to the presence of this graphit-type carbon. This is in agreement with the approach of conduction and valence band edges shown by Robertson[44] for α-SiC:H alloys when the amount of sp^2-bonded carbon increases. Therefore, we think that the observed trend of E_{opt} for our α-$Ge_{1-x}C_x$:H sample, in which a maximum is present, is related to gap narrowing in carbon rich compounds due to the considerable presence of C sp^2 bonding.

An E_{opt} value of 2.53 eV has also been obtained for a sample with composition $GeC_{2.26}H_{5.92}$ (Figure 7b). This high value, which is in apparent contradiction with the above trend, is attributable to the high hydrogen content of the sample. In fact, hydrogen is found to broaden the band gap both for sp^3- and sp^2-bonded alloys.[44,45] Moreover, hydrogen promotes formation of sp^3-hybridised C atoms over sp^2, terminating any dangling bonds and thus reducing the size of the graphite-type cluster and increasing the gap. This is in agreement with the IR results that indicate that if the carbon and hydrogen content of the samples is increased, the CH_3-groups increase is considerably higher than the relative increase of carbon content. Moreover, it is interesting to note that if only the increasing E_{opt} values of Figure 7a and 2.53 eV are considered, the extrapolation for $x = 1$ of the line in Figure 7b, gives a value close to that of diamond (5.45 eV).[45]

Conclusions

The results obtained above indicate that amorphous non-stoichiometric Ge_{1-x}−C_x:H compounds can be obtained from X-ray radiolysis of germane/ethylene mixtures over a wide range of compositions by varying the ethylene percentage in the mixture. When the ethylene percentage is increased, the carbon and hydrogen content also increases. In the IR spectra, the vibrational modes of CH_n ($n = 1-3$) and GeH_n ($n = 1-2$) groups are evident. Vibrational modes of $GeCH_n$ ($n = 1-3$) groups and Ge−C bonds are also

present. The hydrogen atoms bond preferably to carbon atoms; in fact, when the carbon and hydrogen content increases the carbon hydrogenation degree increases, whereas the hydrogenation of germanium decreases indicating that the Ge−H bonds are substituted by Ge−C bonds.

The optical gaps of the compounds depend on the carbon content: values between 1.2 and 1.7 eV have been found. The E_{opt} increases with increasing carbon molar fraction until it reaches a critical value around 0.55, and then decreases giving a maximum in E_{opt}. This trend is attributed to the presence of sp^2-hybridised C atoms forming π-bonded clusters when the carbon molar fraction exceeds 0.55.

Experimental Section

Monogermane was prepared according to a literature procedure,[46] and purified by bulb-to-bulb distillation. Ethylene was high purity SIAD (Società Italiana Acetilene e Derivati) gas and was used without further purification.

Samples of GeH_4/C_2H_4 mixtures of different composition were irradiated with 250 keV X-rays in 365-mL Pyrex vessels at a total pressure of 700 Torr. During irradiation, performed under static conditions, the irradiated mixture composition did not vary markedly. Moreover, as the condensed products were deposited on the bottom of the vials, out of the main X-ray trajectory, the dose absorbed by the products was negligible.

Standard vacuum techniques were used to handle both reactants and gaseous products.

The X-ray source was a CPXT-320 tube (Gilardoni) with a maximum output of 320 keV. The dose absorbed by each sample was 5.0×10^4 Gy at a rate of 1.0×10^4 Gy/h. During the irradiation the temperature did not exceed 320 K.

Gas phase products were analysed by gas chromatography-mass spectrometry (GC-MS) on a Varian 3400-Finnigan ITD instrument equipped with an Alltech AT-1 chromatographic column (polydimethylsiloxane, length 30 m, I.D. 0.25 mm, film thickness 1.0 μm). The temperature ranged from 243 K to 523 K at 10 K/min. A He carrier head pressure of 10 psi was used. Ionisation in the trap was achieved by 70 eV EI and ion acquisition was recorded in the 20−650 u mass range. Quantitative determination of volatile compounds was accomplished calibrating the gas chromatograph with GeH_4. The values reported are the average of at least four experiments.

The composition of the solids was determined by elemental (C and H) analysis.

The X-ray powder-analyses were performed on a Siemens D 500 diffractometer, using Cu-K_α radiation (graphite monochromator on the secondary beam).

The condensed phases were examined by IR spectroscopy (KBr pellets) with an FTIR Bruker Equinox 55 instrument equipped with a program for the deconvolution of overlapped peaks. The resolution was 2 cm^{-1}. All spectra were gathered at room temperature.

The UV/Vis spectrum was obtained with a Perkin−Elmer Lambda 15 spectrophotometer from the material deposited on the quartz disk, using a clean quartz disk irradiated at the same dose as a reference.

Acknowledgments

The authors thank MURST and the University of Torino for financial support.

[1] T. Drüsedau, A. Panckow, W. Herms, H. Sobotta, V. Riede, R. Böttcher, A. Witzmann, *J. Non-Cryst. Solids* **1993**, *155*, 195.
[2] C. K. Seal, D. Samara, S. K. Banerjee, *Appl. Phys. Lett.* **1997**, *71*, 3564.
[3] T. Drüsedau, B. Schröder, *Appl. Phys. Lett.* **1992**, *61*, 566.
[4] J. Tyczkowski, E. Odrobina, M. Gazicki, F. Olcaytug, *J. Non-Cryst. Solids* **1991**, *137/138*, 875.
[5] Y. Nakayama, S. Akita, M. Nakano, T. Kawamura, *J. Non-Cryst. Solids* **1987**, *97/98*, 1448.
[6] S. Z. Han, H. M. Lee, H-S Kwon, *J. Non-Cryst. Solids* **1994**, *170*, 199.
[7] N. Saito, *J. Non-Cryst. Solids* **1989**, *108*, 211.
[8] D. A. Anderson, W. E. Spear, *Phil. Mag.* **1977**, *35*, 1.
[9] Y. Tawada, K. Tsuge, M. Kondo, H. Okamoto, Y. Hamakawa, *J. Appl. Phys.* **1982**, *53*, 5273.
[10] M. Prince, *J. Appl. Phys.* **1955**, *526*, 534.
[11] E. A Davis, N. F. Mott, *Philos Mag.* **1970**, *22*, 903.
[12] P. Mazerolles, R. Morancho, A. Reynes, *Silicon, Germanium, Tin Lead Compd.* **1986**, *9*, 243.
[13] P. Benzi, P. Operti, G. A. Vaglio, P. Volpe, M. Speranza, R. Gabrielli, *J. Organometal. Chem.* **1989**, *373*, 289.
[14] P. Benzi, L. Operti, G. A. Vaglio, P. Volpe, *Int. J. Mass Spectrom. Ion Proc.* **1990**, *100*, 647.
[15] P. Antoniotti, P. Benzi,M. Castiglioni, L. Operti, P. Volpe, *Chem. Mater.* **1992**, *4*, 717.
[16] P. Benzi, M. Castiglioni, P. Volpe, *J. Mater. Chem.* **1994**, *4*, 1067.
[17] P. Benzi, M. Castiglioni, E. Truffa, P. Volpe, *J. Mater. Chem.* **1996**, *6*, 1507.
[18] P. Antoniotti, P. Benzi, M. Castiglioni, L. Operti, P. Volpe, *Radiat. Phys. Chem.* **1996**, *48*, 457.
[19] P. Antoniotti, P. Benzi, M. Castiglioni, P. Volpe, *Eur. J. Inorg. Chem.* **1999**, 323.
[20] L. J. Bellamy, *The Infrared Spectra of Complex Molecules*, 3rd ed., Chapman and Hall, London, **1975**, p. 13.
[21] T. Drüsedau, A. Andreas, B. Schröder, H. Freisted, *Philos. Mag.* **1994**, *69*, 1.
[22] J. Shinar, H. S. Wu, R. Shinar, H. R. Shanks, *J. Appl. Phys.* **1987**, *62*, 808.
[23] H. Wieder, M. Cardona, C.R. Guarnieri, *Phys. Stat. Sol.* **1979**, *92*, 99.
[24] H. Rübel, B. Schröder, W. Fuhs, J. Krauskopf, T. Rupp, K.Bethge, *Phys. Stat. Sol.* **1987**, *139*, 1351.
[25] M. Cardona, *Phys. Stat. Sol.* **1983**, *118*, 463.
[26] G. Lucovsky, *J. Non-Cryst. Solids* **1985**, *76*, 173.
[27] S. Kumar, S. C. Kashyap, K. L. Chopra, *J. Non-Cryst. Solids* **1988**, *101*, 287.
[28] W. Paul, S. J. Jones, W. A. Turner, P. Wickboldt, *J. Non-Cryst. Solids* **1992**, *141*, 271.
[29] G. Lucovsky, *Solid State Commun.* **1979**, *29*, 571.
[30] R. Mathis, M. Constant, J. Satge, F. Mathis, *Spectrochim. Acta* **1964**, *20*, 515.
[31] R. Mathis, J. Satge, F. Mathis, *Spectrochim. Acta* **1962**, *18*, 1463.
[32] A. N. Egorochkin, E. I. Sevast′yanova, S. Ya. Khorshev, S. Kh. Ratushnaya, J. Satge, P. Riviere, J.Barrau, S. Richelme, *J. Organometal. Chem.* **1978**, *162*, 25.
[33] R. Eujen, R. Mellies, E. Petrauskas, *J. Organometal. Chem.* **1986**, *299*, 27.

[34] A. N. Egorochkin, S. Ya. Khorshev, E. I. Sevastyanova, S. Kh. Ratushnaya, J. Satge, P. Riviere, J. Barrau, S. Richelme, *J. Organometal. Chem.* **1978**, *155*, 175.
[35] R. Mathis, M. Barthelat, F. Mathis, *Spectrochim. Acta* **1993**, *26*, 1993.
[36] *CRC Handbook of Chemistry and Physics*, 78th ed. CRC Press, Boca Raton and New York, **1997−1998**.
[37] G. K. Barker, J. E. Drake, R. T. Hemmings, B. Rapp, *Spectrochim. Acta* **1972**, *28A*, 1113.
[38] F. Demichelis, G. Kaniadakis, A. Tagliaferro, E. Tresso, P. Rava, *Proc. Intern. PVS EC-3* **1987**, 313.
[39] A. Marchand, P. Gerval, P. Riviere, J. Satge, *J. Organometal. Chem.* **1978**, *162*, 365.
[40] B. Schrader, in *Infrared and Raman Spectroscopy*, VCH, Weinheim, **1995**, p. 192.
[41] Y. Chaterine, G. Turban, *Thin Solid Films* **1980**, *70*, 101.
[42] L. Ley, in *The Physics of Hydrogenated Amorphous Silicon II*, Springer-Verlag, Berlin **1984**, p. 142.
[43] G. A. N. Connel, J. R. Pawlik, *Phys. Rev. B* **1976**, *13*, 787.
[44] J. Robertson, *Phil. Mag.* **1992**, *66*, 615.
[45] H. Yuan, R. Williams, *Chem. Mater.* **1993**, *5*, 479.
[46] A. J. Jolly, J. E. Drake, *Inorg. Synth.* **1963**, *7*, 37.

Received June 16, 2000
[I00241]

Cobalt/Mercury Carbide Clusters Based on Trigonal-Prismatic or Octahedral Co_6C Skeletons − X-ray Crystal Structure of $(NEt_4)_2[Co_6C(CO)_{12}\{HgW(CO)_3Cp\}_2]$

Roser Reina,[a] Olga Riba,[a] Oriol Rossell,[a] Miquel Seco,*[a] Dominique de Montauzon,[b] Mercè Font-Bardia,[c] and Xavier Solans[c]

Keywords: Carbonyl complexes / Cluster compounds / Cobalt / Mercury / Rearrangements

The anionic transition metal clusters $(NEt_4)[Co_6C(CO)_x\{HgM\}]$ [M = $W(CO)_3Cp$, $Mo(CO)_3Cp$, $Fe(CO)_2Cp$, $Co(CO)_4$, $Mn(CO)_5$] (x = 13 or 15) have been obtained by reaction of the corresponding octahedral (x = 13) or trigonal-prismatic (x = 15) cobalt carbido carbonyl clusters with the mercury derivatives ClHgM. Metal skeleton rearrangements and some redox processes have been found to be induced by varying both the temperature and the solvent, resulting in new compounds containing tetra- or hexacoordinated mercury atoms.

Introduction

The fact that the mercury units HgM^+ [M = a metal fragment such as $Mo(CO)_3Cp$] can readily be attached to a wide variety of transition metal cluster anions has stimulated their use as general building blocks in the systematic synthesis of heterometallic clusters. In general, *typical* μ_2- and μ_3-HgM modes are found for a large number of polynuclear metal carbonyl clusters, where the mercury fragments bridge metal-metal edges or cap triangular faces of cluster cores.[1] Two-centre two-electron bonding is found only for the simplest bi- and trimetallic compounds.[2]

In comparison with other transition metals, only very few cobalt/mercury systems have been reported to date. This is surprising because cobalt and rhodium, for example, are unique in forming two hexanuclear anions with different metal frameworks, the octahedral $[M_6C(CO)_{13}]^{2-}$ (86 EC) and the trigonal-prismatic $[M_6C(CO)_{15}]^{2-}$ (90 EC), which can be interconverted through the uptake and release of carbon monoxide.[3−5] This process can be rationalized in terms of a trigonal-twist mechanism, which involves the mutual rotation of the two triangles of metal atoms.

These considerations prompted us to explore the possibility of incorporating HgM^+ units into both of the aforementioned hexacobalt frameworks and to identify skeletal isomers. We were also interested in extending our studies to the investigation of potential skeletal rearrangements involving the new mercury/cobalt systems thus synthesized.

[a] Departament de Química Inorgànica, Universitat de Barcelona, Diagonal, 647, 08028 Barcelona, Spain
Fax: (internat.) + 34-93/490-7725
E-mail: miquel.seco@qi.ub
[b] Laboratoire de Chimie de Coordination du CNRS, 205 route de Narbonne, 31077 Toulouse Cedex, France
[c] Departament de Cristallografia, Mineralogia i Dipòsits Minerals, Universitat de Barcelona, Martí i Franqués s/n, 08028 Barcelona, Spain

Results and Discussion

The selected ClHgM species [M = $W(CO)_3Cp$, $Mo(CO)_3Cp$, $Fe(CO)_2Cp$, $Co(CO)_4$, $Mn(CO)_5$] were reacted separately with the NEt_4^+ salts of the anions $[Co_6C(CO)_{15}]^{2-}$ (**1**) and $[Co_6C(CO)_{13}]^{2-}$ (**2**) (see Scheme 1).

Reactions with the Trigonal-Prismatic $[Co_6C(CO)_{15}]^{2-}$ Anion (1)

Treatment of $(NEt_4)_2[Co_6C(CO)_{15}]$ (**1**) with ClHgM in CH_2Cl_2 at −12 °C in the presence of a thallium salt as a halide abstractor gave the brown cluster complexes $(NEt_4)[Co_6C(CO)_{15}\{HgM\}]$ [M = $W(CO)_3Cp$ (**3a**), $Mo(CO)_3Cp$ (**3b**), $Fe(CO)_2Cp$ (**3c**), $Co(CO)_4$ (**3d**), $Mn(CO)_5$ (**3e**)]. Only compound **3a** could be isolated as a crystalline solid; the other mercury derivatives were recovered as oily materials. The ν(CO) patterns in the IR spectra of **3a−e** were found to be almost superimposable if the bands due to the M part were ignored. The ν(CO) bands are shifted to higher wavenumbers (by 30 cm^{-1}), indicating a decrease in electron density at the cobalt atoms. The observation of the ^{13}C NMR signal due to the carbide carbon atom at δ = 357 confirmed that the incorporation of the mercury fragment does not induce a dramatic rearrangement of the metal framework. Mass spectrometry showed that the trigonal-prismatic Co_6C skeleton was preserved following the attachment of the mercury units. Thus, the parent molecular peak $[M^-]$ was observed for all the compounds, except in the case of the mercury/cobalt complex **3d**, where the most intense peak corresponded to [M − 2CO].

In light of these data, we propose a molecular structure for type **3** complexes consisting of a triangular prism of cobalt atoms where one of the triangular faces, corresponding to the most basic sites on the prism surface,[6] is capped by the mercury atom. In fact, this is the structure found for the analogous cluster anion of rhodium

 © WILEY-VCH Verlag GmbH, 69451 Weinheim, 2001 1434−1948/01/0505−1243 $ 17.50+.50/0

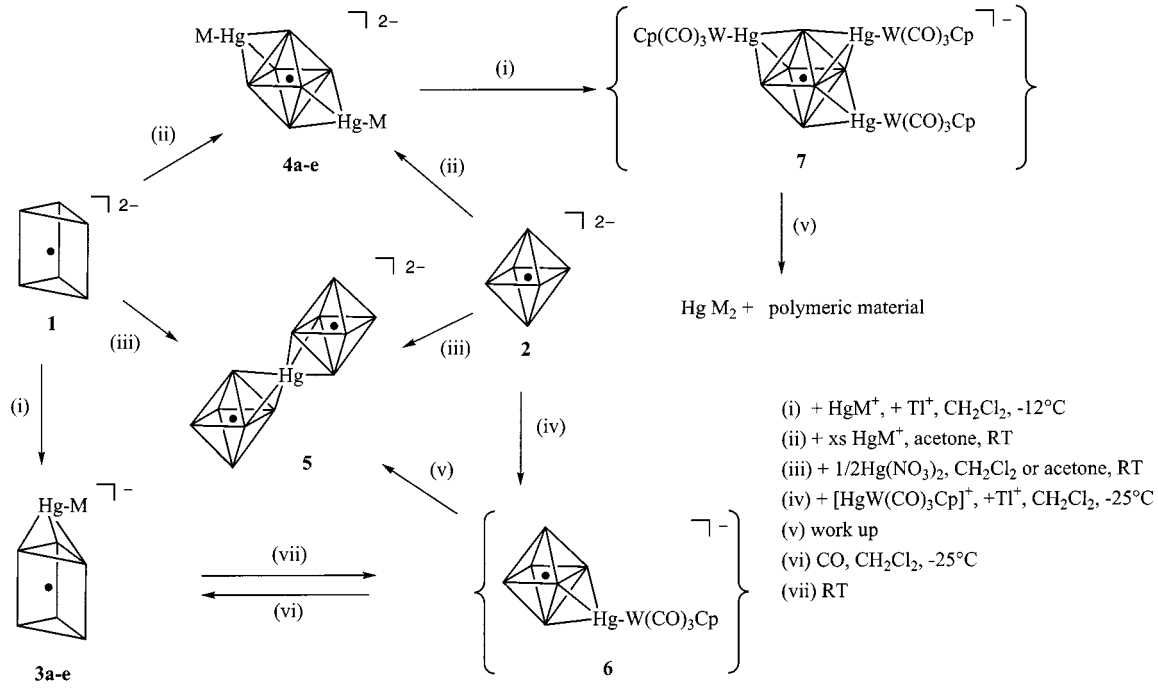

Scheme 1

$[Rh_6C(CO)_{15}\{AuPR_3\}]^-$ (R = Ph, Et),[7,8] which is not surprising in view of the well-known isolobal relationship between the fragments $AuPPh_3$ and HgM.[9] This implies, albeit with some exceptions, that both units occupy the same sites of a given cluster.[10] The remaining negative charge suggested the possibility of introducing another mercury unit into these type **3** complexes. In fact, the reaction of **3** with ClHgM in a 1:1 molar ratio yielded a highly insoluble material that could not be characterized, along with the trimetallic species HgM_2. The formation of these two products can be rationalized in terms of a rapid ligand-redistribution process of the initially formed $[Co_6C(CO)_{15}(HgM)_2]$. This result is in agreement with our predictions that the neutral mercury/transition metal clusters should be unstable with regard to the symmetrization process, while the negatively charged species should be reasonably stable and hence isolable in most cases.[11]

In order to avoid the formation of oily materials and to determine whether the solvent plays an important role in our reactions, we allowed the $[Co_6C(CO)_{15}]^{2-}$ anion (**1**) to react with ClHgM in acetone at room temperature. Surprisingly, under these conditions, we were able to isolate brown crystals of $(NEt_4)_2[Co_6C(CO)_{12}\{HgM\}_2]$ [M = $W(CO)_3Cp$ (**4a**), $Mo(CO)_3Cp$ (**4b**), $Fe(CO)_2Cp$ (**4c**), $Co(CO)_4$ (**4d**), $Mn(CO)_5$ (**4e**)] in moderate yields, accompanied by Co^{II} salts. These complexes were characterized by elemental analyses, spectroscopic data, and mass spectrometry. Their ν(CO) bands were found to be shifted to lower frequencies by around 20 cm^{-1}, which is consistent with an increase in the electron density at the cobalt atoms. Their ^{13}C NMR spectra featured signals corresponding to the CO and Cp ligands, but the carbide signal was not observed. For all the clusters of type **4**, FABMS showed the $[M + H]^-$ peak in accordance with the formula $[Co_6C(CO)_{12}\{HgM\}_2]^{2-}$.

The structure of **4a** was confirmed by X-ray analysis. The geometry of the anion is shown in Figure 1, together with the atom numbering scheme. Selected bond lengths and angles are listed in Table 1.

The structure of this complex is based on that of the parent $[Co_6C(CO)_{13}]^{2-}$ anion and has the two $HgW(CO)_3Cp$ groups capping opposite faces of the distorted Co_6 octahedron. All the other edges are bridged by CO ligands to give a symmetrical structure with the central carbon atom at a crystallographic centre of symmetry. Each cobalt atom bears a terminal carbonyl ligand. As expected, the mercury coordination to the Co_3 faces causes an appreciable lengthening of the distances between these cobalt atoms (average 2.806 Å). The Hg atom resides in a strongly distorted tetrahedral arrangement involving the three Co atoms and the W atom. The $HgW(CO)_3Cp$ moiety shows the usual four-legged piano stool arrangement with a W−Hg distance of 2.781(2) Å.

The coordination of this unit does not lead to any appreciable expansion of the Co_6C octahedron, and the distances between the carbido carbon atom and the cobalt atoms (average 1.873 Å) remain similar to those observed in the $[Co_6C(CO)_{13}]^{2-}$ anion [average 1.87(1) Å].

The Co−Hg distances (average 2.717 Å) are shorter than those observed in other $Co_3(\mu_3\text{-}HgR)$ systems, e.g. $[FeCo_3(CO)_{12}\{\mu_3\text{-}HgMo(CO)_3Cp\}]$ (average 2.816 Å) and $[RuCo_3(CO)_{12}\{\mu_3\text{-}HgCo(CO)_4\}]$ (average 2.756 Å).[12] The Co_6Hg_2 metal framework found for **4a** has no precedent in the chemistry of the Group 9 elements. Its formation re-

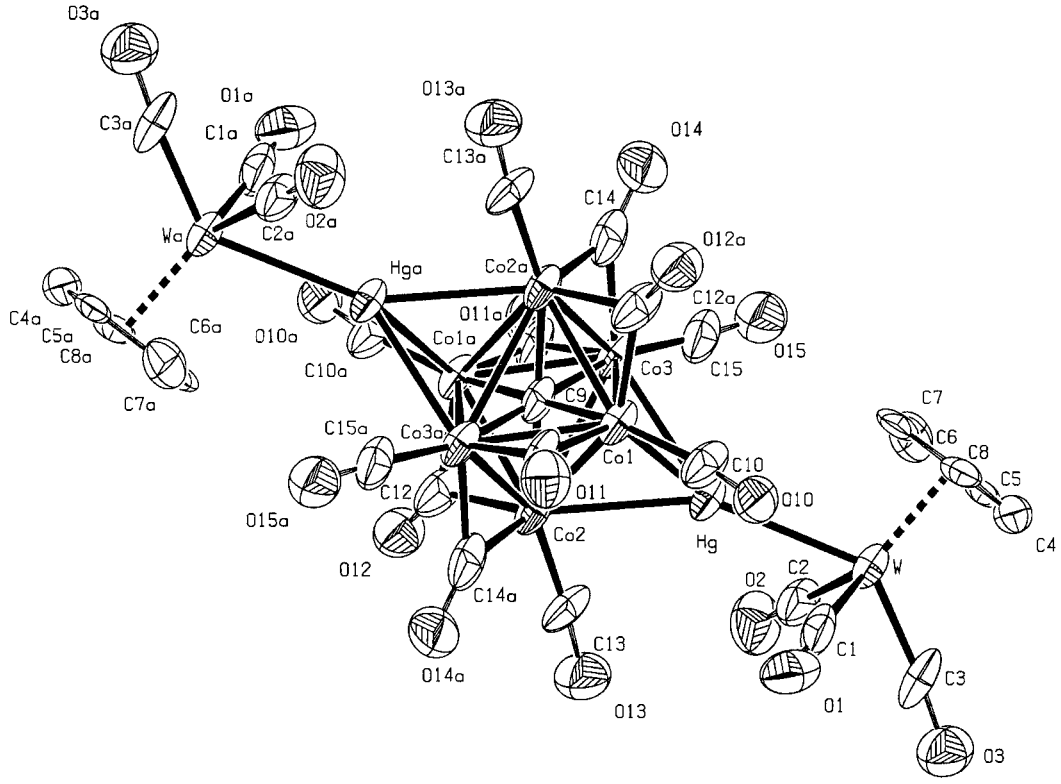

Figure 1. View of the molecular structure of the cluster anion $[Co_6C(CO)_{12}\{\mu_3\text{-}HgW(CO)_3Cp\}_2]^{2-}$ (anion of **4a**) showing the atom numbering scheme

Table 1. Selected bond lengths [Å] and angles [deg] in **4a**

Co(1)−Co(2)	2.799(2)
Co(1)−Co(3)	2.832(2)
Co(2)−Co(3)	2.789(3)
Co(1)−Co(2a)	2.489(2)
Co(1)−Co(3a)	2.470(2)
Hg−Co(3)	2.711(2)
Hg−Co(2)	2.716(2)
Hg−Co(1)	2.7261(19)
Co(1)−C(10)	1.720(9)
Co(1)−C(11)	1.869(11)
Co(1)−C(9)	1.8823(16)
Co(2)−C(13)	1.707(9)
Co(2)−C(9)	1.8633(17)
Co(2)−C(12)	1.905(9)
Co(3)−C(15)	1.682(11)
Co(3)−C(9)	1.8751(19)
Co(3)−C(14)	1.909(10)
Co(3)−Co(1a)	2.470(2)
Co(3)−Co(2a)	2.489(2)
Co(2)−Hg−Co(1)	61.90(6)
Co(3)−Hg−Co(2)	61.86(6)
Co(3)−Hg−Co(1)	62.77(6)
Co(3)−Co(2)−Co(1)	60.89(5)
Co(2)−Co(3)−Co(1)	59.72(6)
Co(2)−Co(1)−Co(3)	59.39(7)
Hg−Co(2)−Co(1)	59.23(4)
Hg−Co(1)−Co(2)	58.87(5)
Co(3)−Hg−Co(2)	61.86(6)
Co(2a)−C(9)−Co(3)	83.49(8)
Co(2)−C(9)−Co(1a)	83.30(7)
Co(3)−C(9)−Co(1a)	82.19(7)
Co(3)−C(9)−Co(1)	97.81(7)
Co(3)−Hg−W	138.95(5)
Co(2)−Hg−W	151.96(4)
Co(1)−Hg−W	138.32(5)

quires the loss of three carbonyl ligands from the starting anion in order to permit both the skeletal rearrangement from the prism to the octahedron and the redox process that gives the double negative charge on the cluster. Considering that each HgM fragment contributes 12 electrons to the polyhedral electron count of the cluster, compound **4** conforms to the number of electrons (110) expected for a bicapped octahedron according to the condensation rules given by polyhedral skeletal electron-pair theory.[13] It is noteworthy that the formation of **4**, possessing a Co_6 octahedral core, proceeds through a skeletal rearrangement of the trigonal prism $[Co_6C(CO)_{15}]^{2-}$ resulting from the incorporation of two mercury units. This structural feature has not previously been observed in the chemistry of rhodium. For example, the reaction of $[Rh_6C(CO)_{15}]^{2-}$ with two equivalents of $ClAuPPh_3$ affords $[Rh_6C(CO)_{15}\{AuPPh_3\}_2]$,[7] which displays a trigonal-prismatic framework of Rh atoms capped on both triangular faces by a gold atom. It is clear that in the present case the driving force for the skeletal rearrangement is the energy involved in the formation of the three new Co−Co bonds as well as three extra Co−Hg bonds and the entropic contribution from the liberation of the three CO ligands required in the transformation of the trigonal prism to the octahedral core. On the other hand, steric interactions between the terminal and in-plane edge-bridging carbonyl ligands and the incoming mercury fragments should not be ruled out as an influence on the skeletal rearrangement process.

In an attempt to obtain other cobalt clusters possessing trigonal-prismatic skeletons, we tried to synthesize $[Hg\{Co_6C(CO)_{15}\}_2]^{2-}$ by reacting the starting cobalt anion $[Co_6C(CO)_{15}]^{2-}$ (**1**) with $Hg(NO_3)_2$ in a 2:1 molar ratio in CH_2Cl_2 or acetone at room temperature (see Scheme 1). However, the spectroscopic data of the brown crystals thus obtained indicated that the new compound was actually $[Hg\{Co_6C(CO)_{13}\}_2]^{2-}$ (**5**). ^{13}C NMR spectroscopy proved to be an excellent tool for determining the geometry of the cobalt core: the carbide carbon atom gives rise to a signal at $\delta \approx 460$ when it is at the centre of the octahedron or at $\delta \approx 350$ when it resides within the trigonal prism. In the case of **5**, the ^{13}C NMR spectrum features a signal at $\delta = 466$, suggesting a metal framework based on a six-coordinate mercury atom capping one triangular face of two octahedra. Consequently, the coordination about mercury can be described as octahedral, which is rather unusual in the organometallic chemistry of this element.[14]

Reactions with the Octahedral $[Co_6C(CO)_{13}]^{2-}$ Anion (2)

When a solution of $(NEt_4)_2[Co_6C(CO)_{13}]$ **(2)** in CH_2Cl_2 was treated with $ClHgW(CO)_3Cp$ (1:1 molar ratio) at −25 °C in the presence of a thallium salt, the IR spectrum of the solution showed a shift of the carbonyl bands to higher wavenumbers (by around 40 cm^{-1}), indicating the attachment of the mercury fragment to the skeleton of the cobalt anion. Efforts to isolate the expected product $(NEt_4)[Co_6C(CO)_{13}\{HgW(CO)_3Cp\}]$ **(6)** were unsuccessful; after workup of the solution we could only separate HgM_2 along with crystals of $(NEt_4)_2[Hg\{Co_6C(CO)_{13}\}_2]$ **(5)**, the identity of which was established by comparison with an authentic sample obtained from the reaction of $[Co_6C(CO)_{13}]^{2-}$ **(2)** with $Hg(NO_3)_2$ (see Scheme 1). In view of the fact that it proved impossible to isolate compound **6**, we submitted a fresh reaction solution in CH_2Cl_2 to mass spectrometric analysis in order to confirm the formation of the desired complex. We thus observed the parent molecular peak, $[M^-]$, corresponding to the formula $[Co_6C(CO)_{13}\{HgW(CO)_3Cp\}]^-$.

The question that arises is the mechanism by which **5** is formed in the above reaction. The simultaneous formation of the symmetrical species in the course of the reaction suggests that **5** is formed from the nonisolated species **6** by slow ligand redistribution. Despite the fact that $[Co_6C(CO)_{13}\{HgW(CO)_3Cp\}]^-$ bears one negative charge and, consequently, is relatively inert to symmetrization processes, with high nuclearity clusters a spontaneous albeit slow symmetrization occasionally takes place.[15,16] The failure to isolate **6** precluded its spectroscopic characterization. However, it was thought that the addition of four electrons to its polyhedral skeleton, by reaction with carbon monoxide, would facilitate skeletal arrangement to the trigonal-prismatic $[Co_6C(CO)_{15}\{HgW(CO)_3Cp\}]^-$ **(3a)**, which has been characterized previously. Indeed, compound **6** was found to react with a smooth stream of CO at −25 °C to give **3a**, thus confirming our expectations. Interestingly, when the reaction mixture was allowed to warm to room temperature, reversion to **6** was noted. Bearing in mind the isolobal relationship between HgM and $AuPPh_3$, and the fact that the crystal structure of the anion $[Co_6C(CO)_{13}\{AuPPh_3\}]^-$ has recently been determined,[17] we propose a similar metal core for **6** consisting of a cobalt octahedron capped at a triangular face by the mercury atom.

The importance of the nature of the solvent as well as the temperature was again evidenced in the reaction of $[Co_6C(CO)_{13}]^{2-}$ (**2**) with HgM^+. When the reaction was carried out in acetone at room temperature, moderate yields of type **4** complexes were obtained. Their formation from the octahedral cobalt anion involves the loss of one carbonyl ligand according to an as-yet-unclear mechanism. Taking into account the dianionic character of type **4** compounds and their relative stability, we decided to test their reactivity further. When **4a** was reacted with another equivalent of $ClHgW(CO)_3Cp$ in CH_2Cl_2 at −12 °C in the presence of a thallium salt, the expected monoanionic $[Co_6C(CO)_{12}\{HgW(CO)_3Cp\}_3]^-$ species **7** could be detected in solution by IR spectroscopy as well as by mass spectrometry (ESMS), where the parent molecular peak was observed. Unfortunately, however, after workup the isolated products were $Hg[W(CO)_3Cp]_2$ and a highly insoluble, intractable material. This behaviour would suggest that the incoming third metal fragment promotes a spontaneous symmetrization reaction.

In conclusion, we have shown that both hexanuclear cobalt clusters react with mercury halide complexes to give mono- and di-capped trigonal prisms or octahedral skeletons. The tendency of the more open trigonal-prismatic cores to rearrange into an octahedral geometry would seem to indicate that the latter metal framework is the most stable for mixed mercury/cobalt clusters.

Electrochemical Studies

The electrochemical properties of these compounds were studied in the electroactivity range of the solvent (CH_2Cl_2) to compare the electrochemical behaviour of the octahedral and prismatic geometry complexes, as well as to allow comparison with related compounds.

The Co_6-based prismatic complex **3a** showed a one-electron irreversible reduction step at $E_{p,c} = -0.80$ V and a one-electron reversible oxidation step at $E^{o\prime} = 0.66$ V (see Table 2), but the instability of the compound did not permit a mechanistic study of its electrochemical processes.

Owing to the rapid decomposition of the cluster **4c** in solution, no electrochemical study could be carried out. The other dianionic octahedral clusters with different mercury fragments showed a reversible reduction at around −1.2 V, except for the cobalt derivative **4d**, for which the reduction step was irreversible. These species were also seen to undergo an irreversible oxidation at around 0.2 V when the scan rate was 0.1 Vs^{-1}, but it became a quasi-reversible process at a scan rate of 0.5 Vs^{-1} (Table 2). The oxidation was a one-electron step, as shown by comparison with the height of the reduction wave (due to passivation phenomena, reliable coulometry could not be performed). When the oxidation was carried out in an EPR tube with $[FeCp_2][PF_6]$

Table 2. Cyclic voltammetry data

[a] compd.	Reduction $E^{o\prime}$ [V]	ΔE [mV]	$i_{p,c}/i_{p,a}$	n	Oxidation $E^{o\prime}$ [V]	ΔE [mV]	$i_{p,a}/i_{p,c}$	n
3a	−0.80[b]			1	0.66	136	0.59	1
4a	−1.30	70	1.03	1	0.18[c]			1
4b	−1.23	73	0.99	1	0.25[c]			1
4d	−1.10[b]			1	0.43[c]			1
4e	−1.24	122	0.74	1	0.32[c]			1
5	−0.55	88	0.80	1	0.26[c]			1
	−0.88	123	1.15	1				

[a] Scan rate: 0.1 Vs^{-1} vs. SCE in 0.1 M Bu_4NBF_4 in CH_2Cl_2 or acetone at −15 °C. − [b] $E_{p,c}$ (irreversible reduction). − [c] $E_{p,a}$ (irreversible oxidation).

in CH_2Cl_2 at −78 °C, the radical species $[Co_6C(CO)_{12}\{HgM\}_2]^{\cdot -}$ was detected. The X-band EPR spectrum consists of a single strong resonance centred at ca. 3373 G (g = 2.0028). The identities of the decomposition products were verified by IR spectroscopy.

Compound **5** shows a one-electron irreversible oxidation step at $E_{p,a}$ = 0.26 V (controlled potential coulometry at 0.3 V). Moreover, this cluster was seen to undergo two well-defined one-electron reversible reductions at $E^{o\prime}$ = −0.55 V and $E^{o\prime}$ = −0.88 V by comparison of the wave heights with that for the oxidation step (Table 2). The instability of this compound in solution and the passivation phenomena at the electrode surface precluded a supplementary electrochemical study.

In summary, we have observed that those compounds which adopt an octahedral geometry exhibit reversible reduction steps, while the prismatic cluster shows an irreversible reduction wave. This behaviour compares well with the irreversible reduction steps found for the prismatic $[Co_6C(CO)_{15}]^{2-}$ starting dianion.[19]

Conclusions

Reaction of the $[Co_6C(CO)_{15}]^{2-}$ and $[Co_6C(CO)_{13}]^{2-}$ anions with one mol of HgM^+ gives the octanuclear species $[Co_6C(CO)_{15}\{HgM\}]^-$ and $[Co_6C(CO)_{13}\{HgM\}]^-$, having spiked Co_6C trigonal-prismatic and spiked octahedral skeletons, respectively. These species can be interconverted through the addition or elimination of CO. On the other hand, the use of an excess of HgM^+ has been found to lead invariably to the cluster $[Co_6C(CO)_{12}\{HgM\}_2]^{2-}$, in which the Co_6C octahedron is doubly-capped by HgM^+ moieties. Finally, electrochemical studies on the dimercury complexes have revealed that their oxidation leads to radical species $[Co_6C(CO)_{12}\{HgM\}_2]^{\bullet -}$, which could be detected by EPR.

Experimental Section

General: All manipulations were performed under an atmosphere of purified N_2 using standard Schlenk techniques. All solvents were distilled from appropriate drying agents. − Infrared spectra were recorded from samples in CH_2Cl_2 or acetone solution on a Nicolet FT-IR 520 spectrophotometer. − ^1H, $^{13}C\{^1H\}$, and $^{31}P\{^1H\}$ NMR spectra were recorded on Bruker DRX 250 and Varian XL-500 spectrometers and were referenced to TMS (δ_H, δ_C = 0.0) and 85% H_3PO_4 (δ_P = 0.0). − FAB and ES mass spectra were recorded on a Fisons VG Quattro spectrometer with samples injected as CH_2Cl_2, methanol, or acetone solutions. − EPR spectra were obtained on a Bruker ESP 300 E spectrometer operating in the X-band mode at 100 K, as maintained by a standard Bruker VT 1000 cryostat. − The compounds ClHgM[20] [M = $Mo(CO)_3Cp$, $W(CO)_3Cp$, $Fe(CO)_2Cp$, $Co(CO)_4$, $Mn(CO)_5$], $(NEt_4)_2[Co_6C(CO)_{15}]$,[6] and $(NEt_4)_2[Co_6C(CO)_{13}]$[3] were synthesized as described previously. The synthetic methodology detailed in this section corresponds to the reactions described in Scheme 1 that afforded better yields and pure final products. The elemental analyses for compounds **3b−e** are not reported because they did not burn properly in the analyser.

Synthesis of $(NEt_4)[Co_6C(CO)_{15}\{\mu\text{-}HgM\}]$ [M = $W(CO)_3Cp$ (3a), $Mo(CO)_3Cp$ (3b), $Fe(CO)_2Cp$ (3c), $Co(CO)_4$ (3d), $Mn(CO)_5$ (3e)]: Details of the synthesis of **3a** also apply to **3b−e**, although the latter were obtained as oily materials. To a precooled solution of $(NEt_4)_2[Co_6C(CO)_{15}]$ (**1**) (0.30 g, 0.28 mmol) in CH_2Cl_2 (15 mL) at −12 °C were added solid $ClHgW(CO)_3Cp$ (0.16 g, 0.28 mmol) and $TlBF_4$ (0.09 g, 0.28 mmol). After stirring for 10 min, the starting material had been consumed and the mixture was filtered to remove the salts. The filtrate was layered with pentane (5 mL). Storage at −30 °C for 8 h resulted in the deposition of **3a** as a brown crystalline solid (0.15 g, 37% yield). − IR (CH_2Cl_2): $\tilde{\nu}$ (ν_{CO} stretch) = 2053 cm^{-1} m, 2011 vs, 1963 s, 1889 m, 1856 m. − ^1H NMR (295 K, CD_2Cl_2): δ = 1.3 (tt, 12 H, CH_3), 3.2 (q, 8 H, CH_2), 5.5 (s, 5 H, C_5H_5). − ^{13}C NMR (295 K, CD_2Cl_2): δ = 7.3 (s, CH_3), 53.0 (s, CH_2), 86.9 (s, C_5H_5), 357.0 (s, C). − FABMS: m/z = 1318 [M^-]. − $C_{32}H_{26}Co_6HgNO_{16}W$ (1449.58): C 26.51, H 1.74, N 0.97; found C 26.59, H 1.72, N 1.00.

3b: IR (CH_2Cl_2): $\tilde{\nu}$ (ν_{CO} stretch) = 2053 cm^{-1} m, 2007 vs, 1963 s, 1882 m, 1852 m. − ^1H NMR (295 K, CD_2Cl_2): δ = 1.3 (tt, 12 H, CH_3), 3.2 (q, 8 H, CH_2), 5.4 (s, 5 H, C_5H_5). − FABMS: m/z = 1233 [M^-].

3c: IR (CH_2Cl_2): $\tilde{\nu}$ (ν_{CO} stretch) = 2069 cm^{-1} w, 2049 m, 2008 vs, 1925 w, 1857 m. − ^1H NMR (295 K, CD_2Cl_2): δ = 1.32 (tt, 12 H, CH_3), 3.2 (q, 8 H, CH_2), 4.7 (s, 5 H, C_5H_5). − FABMS: m/z = 1164 [M^-].

3d: IR (CH_2Cl_2): $\tilde{\nu}$ (ν_{CO} stretch) = 2063 cm^{-1} m, 2049 m, 2011 vs, 1849 m. − FABMS: m/z = 1103 [M^- − 2CO].

3e: IR (CH_2Cl_2): $\tilde{\nu}$ (ν_{CO} stretch) = 2070 cm^{-1} w, 2047 m, 2010 vs, 1860 w. − ESMS: m/z = 1182 [M^-].

Synthesis of $(NEt_4)_2[Co_6C(CO)_{12}\{\mu_3\text{-}HgM\}_2]$ [M = $W(CO)_3Cp$ (4a), $Mo(CO)_3Cp$ (4b), $Fe(CO)_2Cp$ (4c), $Co(CO)_4$ (4d), $Mn(CO)_5$ (4e)]: The general procedure is described for the case of **4a**. To a solution of $(NEt_4)_2[Co_6C(CO)_{15}]$ (**1**) (0.30 g, 0.28 mmol) in acetone (20 mL) at room temperature was added solid $[ClHgW(CO)_3Cp]$ (0.16 g, 0.28 mmol). After the mixture had been stirred for 2 h, addition of a 30% excess of $[ClHgW(CO)_3Cp]$ (0.05 g) was found to be necessary to complete the reaction. The reaction mixture was stirred for a further 2 h and then hexane (20 mL) was added in order to precipitate the salts. After filtration, the slow addition of further hexane (10 mL) under vigorous stirring led to the deposition of red-brown crystals of **4a** (0.18 g, 30% yield). − IR (acetone): $\tilde{\nu}$ (ν_{CO} stretch) = 2001 cm^{-1} w, 1962 vs, 1875 m, 1863 m, 1814 m. − ^1H NMR (295 K, [D_6]acetone): δ = 1.4 (tt, 24 H, CH_3), 3.5 (q, 16 H, CH_2), 5.3 (s, 10 H, C_5H_5). − ^{13}C NMR (295 K, [D_6]acetone): δ = 7.5 (s, CH_3), 52.8 (s, CH_2), 88.6 (s, C_5H_5), 218.0 (m, CO), 237.5 (m, CO). − FABMS: m/z = 1768 [M + H]$^-$. − $C_{45}H_{50}Co_6Hg_2N_2O_{18}W_2$ (2029.37): C 26.61, H 2.48, N 1.37; found C 26.69, H 2.51, N 1.40.

For compounds **4b−e**, the addition of diethyl ether (20 mL) caused the precipitation of the salts. Indeed, all the crystalline solids were obtained with diethyl ether, although varying excesses of ClHgM, different reaction times, and modified final workup conditions were needed.

4b: 40% excess $ClHgMo(CO)_3Cp$; 2 h reaction time; the final precipitation was achieved by the addition of diethyl ether (20 mL) in aliquots of 5 mL. 0.14 g, 27% yield. − IR (acetone): $\tilde{\nu}$ (ν_{CO} stretch) = 2002 cm^{-1} w, 1964 vs, 1882 m, 1868 m, 1814 m. − ^1H NMR (295 K, [D$_6$]acetone): δ = 1.4 (tt, 24 H, CH_3), 3.5 (q, 16 H, CH_2), 5.2 (s, 10 H, C_5H_5). − ^{13}C NMR (295 K, [D$_6$]acetone): δ = 7.5 (s, CH_3), 52.8 (s, CH_2), 89.9 (s, C_5H_5), 235.7−229.7 (m, CO). − FABMS: *m/z* = 1594 $[M + H]^-$. − $C_{45}H_{50}Co_6Hg_2N_2O_{18}Mo_2$ (1853.55): C 29.16, H 2.72, N 1.51; found C 29.19, H 2.75, N 1.52.

4c: 25% excess $ClHgFe(CO)_2Cp$; 6 h reaction time; precipitation occurred after 8 h at −30 °C. 0.12 g, 25% yield. − IR (acetone): $\tilde{\nu}$ (ν_{CO} stretch) = 2053 cm^{-1} m, 1994 m, 1969 vs, 1908 w, 1891 w, 1816 m. − ^1H NMR (295 K, [D$_6$]acetone): δ = 1.4 (tt, 24 H, CH_3), 3.5 (q, 16 H, CH_2), 4.6 (s, 10 H, C_5H_5). − ^{13}C NMR (295 K, [D$_6$]acetone): δ = 7.5 (s, CH_3), 52.8 (s, CH_2), 81.1 (s, C_5H_5), 214.2 (s, CO). − FABMS: *m/z* = 1458 $[M + H]^-$. − $C_{43}H_{50}Co_6Fe_2Hg_2N_2O_{16}$ (1717.34): C 30.07, H 2.93, N 1.63; found C 30.11, H 2.95, N 1.65.

4d: 30% excess $ClHgCo(CO)_4$; 2 h reaction time; the final precipitation was accomplished by the addition of diethyl ether (20 mL) in aliquots of 5 mL. 0.12 g, 25% yield. − IR (acetone): $\tilde{\nu}$ (ν_{CO} stretch) = 2052 cm^{-1} m, 1977 vs, 1963 s, 1890 w, 1825 m. − ^{13}C NMR (295 K, [D$_6$]acetone): δ = 7.5 (s, CH_3), 52.8 (s, CH_2), 209.7 (s, CO), 233.2 (m, CO). − FABMS: *m/z* = 1445 $[M + H]^-$. − $C_{37}H_{40}Co_8Hg_2N_2O_{20}$ (1705.37): C 26.06, H 2.36, N 1.64; found C 26.09, H 2.37, N 1.66.

4e: 25% excess $ClHgMn(CO)_5$; 6 h reaction time; precipitation occurred after 8 h at −30 °C. 0.14 g, 28% yield. − IR (acetone): $\tilde{\nu}$ (ν_{CO} stretch) = 2062 cm^{-1} m, 1981 vs, 1954 s,sh, 1891 w, 1820 m. − ^{13}C NMR (295 K, [D$_6$]acetone): δ = 7.5 (s, CH_3), 52.8 (s, CH_2), 218.1 (m, CO). − FABMS: *m/z* = 1493 $[M + H]^-$. − $C_{39}H_{40}Co_6Hg_2Mn_2N_2O_{22}$ (1753.40): C 26.71, H 2.29, N 1.60; found C 26.73, H 2.32, N 1.62.

$(NEt_4)_2[Hg\{Co_6C(CO)_{13}\}_2]$ (5): Solid $Hg(NO_3)_2$ (0.05 g, 0.15 mmol) was added to a solution of $(NEt_4)_2[Co_6C(CO)_{13}]$ (**2**) (0.30 g, 0.30 mmol) in CH_2Cl_2 (20 mL). The mixture was stirred at room temperature for 5 h and then filtered. The resulting solution was layered with hexane (10 mL) and cooled overnight at −30 °C to give 0.16 g (30% yield) of a dark-brown crystalline solid. − IR (CH_2Cl_2): $\tilde{\nu}$ (ν_{CO} stretch) = 2037 cm^{-1} w, 2007 vs, 1844 w. − ^{13}C NMR (295 K, CD_2Cl_2): δ = 7.8 (s, CH_3), 53.0 (s, CH_2), 219.5 (s, CO), 225.1 (s, CO), 466.0 (s, C). − FABMS: *m/z* = 1633 $[M - CO]^-$. − ESMS: *m/z* = 830 $[M/2]^{2-}$. − $C_{44}H_{40}Co_{12}HgN_2O_{26}$ (1922): C 25.14, H 0.95, N 1.33; found C 25.19, H 0.99, N 1.34.

Reaction of $(NEt_4)_2[Co_6C(CO)_{13}]$ with $ClHgW(CO)_3Cp$ − Formation of $(NEt_4)[Co_6C(CO)_{13}\{\mu_3\text{-}HgW(CO)_3Cp\}]$ (6): To a solution of $(NEt_4)_2[Co_6C(CO)_{13}]$ (**2**) (0.30 g, 0.30 mmol) in CH_2Cl_2 (15 mL) at −25 °C were added solid $ClHgW(CO)_3Cp$ (0.17 g, 0.30 mmol) and $TlBF_4$ (0.09 g, 0.30 mmol). The resulting mixture was stirred for 1 h. Subsequent addition of hexane (5 mL) caused the precipitation of the salts, which were filtered off. The IR and ES mass spectra of the resulting solution confirmed the formation of $[Co_6C(CO)_{13}\{\mu_3\text{-}HgW(CO)_3Cp\}]^-$ (**6**). − IR (CH_2Cl_2): $\tilde{\nu}$ (ν_{CO} stretch) = 2053 cm^{-1} m, 2004 vs, 1870 m, 1845 m. − ESMS: *m/z* = 1263 $[M]^-$.

Reaction of $(NEt_4)_2[Co_6C(CO)_{12}\{\mu\text{-}HgW(CO)_3Cp\}_2]$ with $ClHgW(CO)_3Cp$ − Formation of $(NEt_4)[Co_6C(CO)_{12}\{HgW(CO)_3Cp\}_3]$ (7): To a solution of $(NEt_4)_2[Co_6C(CO)_{12}\{\mu\text{-}HgW(CO)_3Cp\}_2]$ (**4a**) (0.25 g, 0.12 mmol) in CH_2Cl_2 (15 mL) at −12 °C were added solid $[ClHgW(CO)_3Cp]$ (0.07 g, 0.12 mmol) and $TlBF_4$ (0.04 g, 0.12 mmol). The resulting mixture was stirred for 1 h. Subsequent addition of hexane (5 mL) caused the precipitation of the salts, which were filtered off. The IR and ES mass spectra of the resulting solution confirmed the formation of $[Co_6C(CO)_{12}\{\mu\text{-}HgW(CO)_3Cp\}_3]^-$ (**7**). − IR (CH_2Cl_2): $\tilde{\nu}$ (ν_{CO} stretch) = 1993 cm^{-1} vs, 1962 s, 1878 m. − ESMS: *m/z* = 2303 $[M]^-$.

Electrochemical Measurements: Electrochemical measurements were carried out using an Electrokemat potentiostat.[21] Electrochemical experiments were performed at −15 °C with CH_2Cl_2 as a solvent, except in the case of compounds **4a−e**, in an airtight three-electrode cell connected to an argon line. The reference electrode consisted of a saturated calomel electrode (SCE), separated from the nonaqueous solutions by a bridge compartment. The counterelectrode was a spiral of platinum wire 8 cm in length and 0.5 cm in diameter with an apparent surface area of ca. 1 cm^2. The working electrode was an Au wire (0.125 mm diameter). For electrolysis, a gold wire (1 mm in diameter, 10 cm in length) or a platinum foil was used. $E^{o\prime}$ values were determined as the average of the cathodic and anodic peak potentials, i.e. $(E_{p,c} + E_{p,a})/2$. The supporting electrolyte $(n\text{Bu}_4\text{N})[BF_4]$ (Fluka, electrochemical grade) was used as received. Dichloromethane and acetone were freshly distilled prior to use. The solutions used for the electrochemical studies were typically 4×10^{-4} M in the cluster complex and 0.1 M in $(n\text{Bu}_4\text{N})[BF_4]$. Under the same conditions, ferrocene was found to be oxidized at $E^{o\prime}$ = 0.42 V vs. SCE and the peak potential separation ΔE was 60 mV. Cyclic voltammetry experiments were run at a scan rate of 0.1 Vs^{-1}.

X-ray Structure Determination of 4a: A prismatic crystal (0.1 × 0.1 × 0.2 mm) was selected and mounted on an Enraf−Nonius CAD4 four-circle diffractometer. Crystallographic and experimental details are summarized in Table 3. Unit cell parameters were determined from the automatic centring of 25 reflections ($12 < \Theta < 21°$) and refined by least-squares methods. Intensities were collected with graphite-monochromated Mo-K_α radiation using the ω/

Table 3. Crystal data and structure refinement for **4a**

Empirical formula	$C_{45}H_{48}Co_6Hg_2N_2O_{18}W_2$
Formula weight	2027.31
Temperature	293(2) K
Wavelength	0.71069 Å
Crystal system, space group	monoclinic, $P2_1/n$
Unit cell dimensions	a = 13.283(9) Å, α = 90°
	b = 13.544(10) Å, β = 101.75(5)°
	c = 15.409(10) Å, γ = 90°
Volume	2714(3) $Å^3$
Z	2
Calculated density	2.481 Mg/m^3
Absorption coefficient	11.704 mm^{-1}
F(000)	1892
Crystal size	0.1 × 0.1 × 0.2 mm
Θ range for data collection	2.02 to 29.96°
Index ranges	$-18 \le h \le 18$
	$0 \le k \le 19$
	$0 \le l \le 21$
Reflections collected/unique	8354/7845 [R(int) = 0.0220]
Refinement method	Full-matrix least-squares on F^2
Data/parameters	7845/331
Goodness-of-fit on F^2	0.985
Final R indices [$I > 2\sigma(I)$]	$R1$ = 0.0279, $wR2$ = 0.0449
R indices (all data)	$R1$ = 0.1091, $wR2$ = 0.0732
Largest diff. peak and hole	0.616 and −0.597 e.$Å^{-3}$

2Θ scan technique. 8354 reflections were measured in the range $2.02 \leq \Theta \leq 29.96$, 7845 of which were nonequivalent by symmetry [R_{int} (on I) = 0.022]. 6478 reflections were considered as observed, applying the condition $I > 2\sigma(I)$. Three reflections were measured every two hours as an orientation and intensity control; no significant intensity decay was observed. Lorentz polarization but no absorption corrections were made.

The structure was solved by direct methods using SHELXS and refined by full-matrix least-squares methods with SHELX-97,[22] using all 7845 nonequivalent reflections. Very negative intensities were discarded. The function minimized was $\Sigma w||Fo|^2 - |Fc|^2|^2$, where $w = [\sigma^2(I) + (0.0102P)^2]^{-1}$, and $P = (|F_o|^2 + 2|F_c|^2)/3$; f, f', and f'' were taken from the International Tables of X-ray Crystallography.[23]

The cyclopentadiene unit was refined with the C−C bond length and the C−C−C bond angle constrained to 1.420 Å and 108.0°. The final R (on F) factor was 0.027, wR (on $|F|^2$) = 0.044, and goodness of fit = 0.479 for all observed reflections. The number of refined parameters was 331. Max. shift/e.s.d. = 0.00, mean shift/e.s.d. = 0.00. Max. and min. peaks in final difference synthesis: 0.616 and −0.597 eÅ^{-3}, respectively.

Crystallographic data (excluding structure factors) for the structure reported in this paper have been deposited with the Cambridge Crystallographic Data Centre as supplementary publication no. CCDC-145260. Copies of the data can be obtained free of charge on application to the CCDC, 12 Union Road, Cambridge CB2 1EZ, U.K. [Fax: (internat.) +44-1223/336-033; E-mail: deposit@ccdc.cam.ac.uk].

Acknowledgments

This work was supported by the DGICYT (Project PB96−0174) and the CIRIT (Project 1997 SGR 00174).

[1] L. H. Gade, *Angew. Chem. Int. Ed. Engl.* **1993**, *32*, 24−40.
[2] E. Rosenberg, K. I. Hardcastle, *Comprehensive Organometallic Chemistry II*, Pergamon, **1995**, vol. 10, chapter 6, p. 323 and references therein.
[3] V. G. Albano, D. Braga, S. Martinengo, *J. Chem. Soc., Dalton Trans.* **1986**, 981−984.
[4] V. G. Albano, D. Braga, S. Martinengo, *J. Chem. Soc., Dalton Trans.* **1981**, 717−720.
[5] B. T. Heaton, L. Strona, S. Martinengo, *J. Organomet. Chem.* **1981**, *215*, 415−422.
[6] S. Martinengo, D. Strumolo, P. Chini, V. G. Albano, D. Braga, *J. Chem. Soc., Dalton Trans.* **1985**, 35−41.
[7] A. Fumagalli, S. Martinengo, V. G. Albano, D. Braga, *J. Chem. Soc., Dalton Trans.* **1988**, 1237−1247.
[8] B. T. Heaton, L. Strona, S. Martinengo, D. Strumolo, V. G. Albano, D. Braga, *J. Chem. Soc., Dalton Trans.* **1983**, 2175−2182.
[9] See, for example: [9a] P. Braunstein, J. Rosé, A. M. Manotti-Lanfredi, A. Tiripicchio, *J. Chem. Soc., Dalton Trans.* **1984**, 1843−1848. − [9b] C. P. Horwitz, E. M. Holt, C. P. Brock, D. F. Shriver, *J. Am. Chem. Soc.* **1985**, *107*, 8136−8146. − [9c] O. Rossell, M. Seco, R. Reina, *Organometallics* **1994**, *13*, 2127−2130. − [9d] O. Rossell, M. Seco, G. Segalés, S. Alvarez, M. A. Pellinghelli, A. Tiripicchio, *Organometallics* **1994**, *13*, 2205−2212. − [9e] R. Reina, O. Rossell, M. Seco, D. de Montauzon, R. Zquiak, *Organometallics* **1994**, *13*, 4300−4305.
[10] R. Reina, O. Riba, O. Rossell, M. Seco, P. Gómez-Sal, A. Martin, *Organometallics* **1997**, *16*, 5113−5115.
[11] R. Reina, O. Rossell, M. Seco, *J. Organomet. Chem.* **1990**, *398*, 285−291.
[12] P. Braunstein, J. Rosé, A. Tiripicchio, M. Tiripicchio-Camellini, *J. Chem. Soc., Dalton Trans.* **1992**, 911−920.
[13] D. M. P. Mingos, D. J. Wales, *Introduction to Cluster Chemistry*, Prentice Hall International, London, **1990**.
[14] See, for example: [14a] Y. Yamamoto, H. Yamazaki, T. Sakurai, *J. Am. Chem. Soc.* **1982**, *104*, 2329−2330. − [14b] P. Braunstein, J. Rosé, A. Tiripicchio, M. Tiripicchio-Camellini, *Angew. Chem. Int. Ed. Engl.* **1985**, *24*, 767−768. − [14c] Y. Yamamoto, H. Yamazaki, *Inorg. Chim. Acta* **1994**, *217*, 121−127. − [14d] L. H. Gade, B. F. G. Johnson, J. Lewis, M. McPartlin, I. J. Scowen, *J. Chem. Soc., Dalton Trans.* **1996**, 597−601.
[15] O. Rossell, M. Seco, G. Segalés, M. A. Pellinghelli, A. Tiripicchio, D. de Montauzon, *Organometallics* **1997**, *16*, 236−245.
[16] R. Reina, O. Riba, O. Rossell, M. Seco, P. Gómez-Sal, A. Martin, D. de Montauzon, A. Mari, *Organometallics* **1998**, *17*, 4127−4135.
[17] R. Reina, O. Riba, O. Rossell, M. Seco, unpublished results.
[18] P. Lemoine, A. Giraudeau, M. Gross, R. Bender, P. Braunstein, *J. Chem. Soc., Dalton Trans.* **1981**, 2059−2062.
[19] J. Rimmelin, P. Lemoine, M. Gross, R. Mathieu, D. de Montauzon, *J. Organomet. Chem.* **1986**, *309*, 363−367.
[20] M. J. Mays, J. D. Robb, *J. Chem. Soc., A* **1968**, 329−332.
[21] P. Cassoux, R. Dartiguepeyron, D. de Montauzon, J. B. Tommasino, P. L. Fabre, *Actual Chim.* **1994**, *1*, 49−55.
[22] G. M. Sheldrick, *SHELXL-97*, Universität Göttingen, **1997**.
[23] *International Tables of X-ray Crystallography*, Kynoch Press, Birmingham, **1974**, Vol. IV, p. 99−100 and 149.

Received June 15, 2000
[I00243]

Novel Electron-Rich Hydrophilic Phosphanes with Carboxylated Cyclohexyl Substituents[‡]

David J. Brauer,[a] Konstantin W. Kottsieper,[a] Thomas Nickel,[a] Othmar Stelzer,*[a] and William S. Sheldrick[b]

Dedicated to Professor Dr. M. Schmidt on the occasion of his 75th birthday

Keywords: Phosphanes / NMR spectroscopy / Carboxylic acids / Chelates / Palladium

Addition of diphenylphosphane or phenylphosphane to methyl 1-cyclohexenecarboxylate (**1**) under base catalysis, yields the novel tertiary or secondary phosphanes **2a**, **3**, or **4a** containing cyclohexyl backbones with the carboxylic groups in the 2-position. The carboxylated derivative of the borane adduct of tricyclohexylphosphane **5a** is accessible by a related reaction using $Cy_2P(BH_3)Li$ instead of Ph_2PH or $PhPH_2$. The complete analysis of the ^1H NMR spectrum of **2a** using 2D NMR spectroscopy (H,H-, C,H-COSY NMR spectra, ^{13}C-INADEQUATE) reveals the bis(equatorial) position of the Ph_2P and COOMe substituents. This is supported by the results of the X-ray structural analysis of **2b** (space group $P2_1/c$). On addition of $Cy_2P(BH_3)Li$ to **1** and subsequent hydrolysis, **5a**, the first functionalized derivative of tricyclohexylphosphane is obtained. In contrast to **2b**, the COOMe substituent in **5a** occupies the axial position, the bulky phosphanyl group being equatorial as indicated by the X-ray structural analysis (space group $P2_1$). Molybdenum(0) and palladium(II) complexes of **2a** and **2b** have been synthesized. The influence of the carboxylated cyclohexyl substituent on the electronic and steric parameters of **2a** and **2b** is discussed.

Introduction

Phosphanylcarboxylic acids play an important role as bifunctional P,O chelating ligands in important catalytic processes like the Shell higher olefin process (SHOP).[2,3] In catalytic and stoichiometric reactions, the weakly coordinated oxygen donor can be replaced reversibly, thus providing a coordination site for an incoming ligand or a substrate molecule. Some of these "hemilabile" ligands,[4] e.g. **A**−**C**, have been known for a long time[5] and efficient synthetic routes have been developed recently.[2c,6] These employ either nucleophilic phosphanylation reactions or Pd-catalyzed P−C coupling reactions between aromatic bromides or iodides and primary or secondary phosphanes.[7] Using the latter synthetic strategy, multiply functionalized aromatic phosphanylcarboxylic acids, e.g. **D** and **E**, have been obtained.

Phosphanylcarboxylic acids containing a cyclohexane backbone (**F**) have not been reported so far, however. In contrast to aromatic phosphanes, e.g. **A**−**E**, with carboxylated phenyl substituents, the coordination chemistry of ligands of type **F** should show novel aspects connected with the cyclohexane backbone. Due to the substitution pattern at the phosphorus atom, these ligands have a bulky and electron-rich P donor group capable of forming P,O chelates with transition metal ions. The mutual *cis* or *trans* position of the R_2P and carboxylic groups will be determined by the bulkiness of the substituents R, thus controlling the tendency of these ligands to form stable P,O chelates with chirogenic bridging carbon atoms C(1) and C(2).

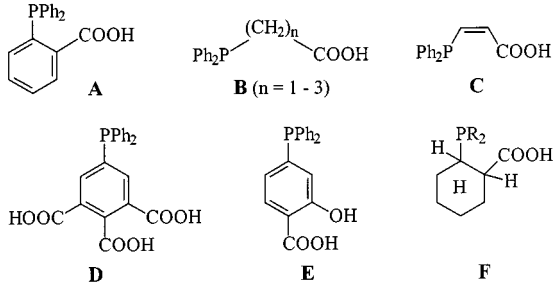

Results

Synthesis of 1-(Diphenylphosphanyl)cyclohexane-2-carboxylic Acid and Derivatives (2a, 2b)

For the syntheses of phosphanylcarboxylic acids and their derivatives containing a 1,2-cyclohexanediyl backbone, methyl 1-cyclohexenecarboxylate (**1**) was used in all cases as a starting material. Base-catalyzed addition of

[‡] Water-Soluble Phosphanes, 16. − Part 15: Ref.[1]

[a] Fachbereich 9, Anorganische Chemie,
Bergische Universität−GH Wuppertal,
Gaußstraße 20, 42097 Wuppertal, Germany
Fax: (internat.) + 49-(0)202/4393053
E-mail: stelzer@uni-wuppertal.de
[b] Lehrstuhl für Analytische Chemie, Ruhr-Universität Bochum,
Universitätsstraße 150, 44780 Bochum, Germany
Fax.: (internat.) + 49-(0)234/7094420
E-mail: shel@anachem.ruhr-uni-bochum.de

 © WILEY-VCH Verlag GmbH, 69451 Weinheim, 2001 1434−1948/01/0505−1251 $ 17.50+.50/0

Ph_2PH to **1** using 0.1 mol-% of KO*t*Bu gave **2a** in 71% yield (Scheme 1). Derivative **2a**, with two centers of chirality (α- and β-C), may be formed as a mixture of two pairs of diastereoisomers (*cis*-**2a**, *trans*-**2a**). The regioselectivity of base-catalyzed addition of secondary phosphanes to activated olefins has been discussed elsewhere,[8] the reactions are assumed to take place by Michael addition, the *anti*-Markownikow products being formed exclusively.

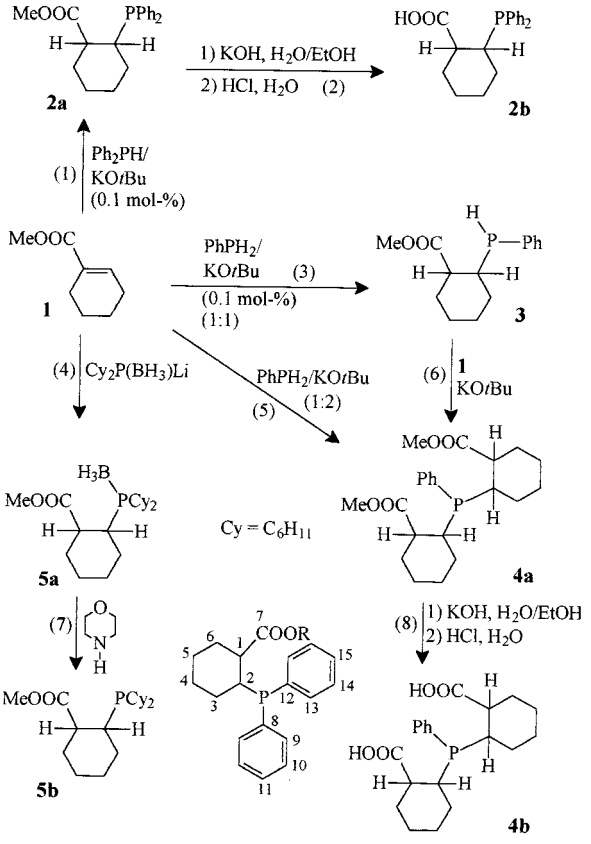

Scheme 1

Immediately after completion of the reaction of Ph_2PH with **1** the $^{31}P\{^1H\}$ NMR spectrum of the reaction mixture shows two resonances at $\delta_P = -1.86$ and -9.47 in a 1:2 intensity ratio. On extending the time of reaction the intensity of the signal at $\delta_P = -1.86$ increases at the expense of that at $\delta_P = -9.47$, which after 24 h had disappeared almost completely. The product **2a** obtained after workup of the reaction mixture shows only one signal in the $^{31}P\{^1H\}$ NMR spectrum at $\delta_P = -1.86$. These observations may be explained by an epimerization process by formation of an enol-type intermediate **G**[9] (Scheme 2).

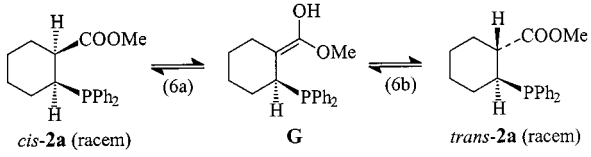

Scheme 2

Initially, the *cis* isomer of **2a** (racemate) is formed preferably under kinetic control of the addition reaction, which is rearranged then to the thermodynamically more stable *trans*-**2a** (racemate).

The solution structure of *trans*-**2a** was obtained by analysis of the 400 MHz ^1H and $^1H\{^{31}P\}$ NMR spectrum (Figure 1a, 1b) in the range between $\delta_H = 0.8-2.95$. The ten nonequivalent protons H(1a)−H(6a) (A, B, C, D, E, F, G, H, M, and N) of the 1,2-disubstituted cyclohexane backbone and the ^{31}P nucleus, give rise to a complicated pattern in the ^1H and $^1H\{^{31}P\}$ NMR spectra by H,H and P,H coupling (Figure 1c). The multiplets in the ^1H NMR spectrum of **2a** at $\delta_H = 2.47$ (N) and 2.81 (M) with the appearance of a doublet of doublets of triplets or a doublet of triplets, respectively, may be assigned to the hydrogen atoms at C(1) ($\delta_C = 46.42$) and C(2) ($\delta_C = 36.18$) by analysis of the C,H-COSY NMR spectrum.[10] In a first approximation they may be considered as the MN part of an MNADEFX spin system [M, N = H(1a), H(2a); A = H(3a); D = H(6a); E = H(3e); F = H(6e); X = ^{31}P] with the P−H coupling being very small (0.64 Hz) for H(2a). Comparison of the ^1H NMR and $^1H\{^{31}P\}$ NMR spectrum reveals $^1H-^{31}P$ coupling fine structure of the resonances at $\delta_H = 1.01$, 1.45, 1.82, 1.92, and 2.47. As indicated by the H,H-COSY-45 NMR spectrum the protons with $\delta_H = 2.81$ (M) and 2.47 (N) are coupled to those with $\delta_H = 2.47$, 1.82, and 1.01 or $\delta_H = 2.81$, 1.92, and 1.74, respectively. The carbon atoms connected with the hydrogen atoms ($\delta_H = 1.82$ and 1.01 or $\delta_H = 1.92$ and 1.74) may be assigned to C(3) and C(6). A value of 9.6 Hz was determined for the coupling constant ^3J(HH) between the protons N and M. The resonances of H(N) and H(M) show a large (ca. 10 Hz) and a small (ca. 3.5−4.0 Hz) additional splitting due to vicinal H,H coupling with the hydrogen atoms of the respective neighbouring CH_2 groups. This pattern of ^3J(HH) is consistent with a bis(axial) position of the hydrogen atoms at C(1) and C(2) and a *trans* arrangement of the COOMe and PPh_2 substituents.

In derivatives of cyclohexane, vicinal H,H coupling constants are typically in the range between 7 and 9 Hz for hydrogen atoms in bis(axial) and 2−5 Hz in axial-equatorial or bis(equatorial) positions.[11] Due to overlapping of correlation peaks in the δ_H range between 0.8 and 2.0, a complete analysis of the H,H-COSY-45 NMR spectrum was not possible. In order to obtain an assignment of the $^{13}C\{^1H\}$ NMR signals for all carbon atoms of the cyclohexane backbone of **2a** an INADEQUATE spectrum[12] in the δ_C range between 12 and 50 was obtained. Making use of these results, the H,H-COSY-45 spectrum of **2a** could further be analyzed, thus allowing us to assign the hydrogen atoms in axial and equatorial positions of the cyclohexane backbone. Employing typical values for the geminal and vicinal H,H coupling constants,[11] the $^1H\{^{31}P\}$ NMR spectrum of **2a** was simulated using the program g NMR.[13] The result is shown in Figure 1b, the values obtained for the various coupling constants ^nJ(HH) ($n = 2-4$) and ^nJ(PH) ($n = 2-5$) are collected in Table 1. In agreement with results reported in the literature for 1,2-substituted derivatives of cyclohexane,[14] geminal H,H coupling constants are in a very narrow range between −13.81 and

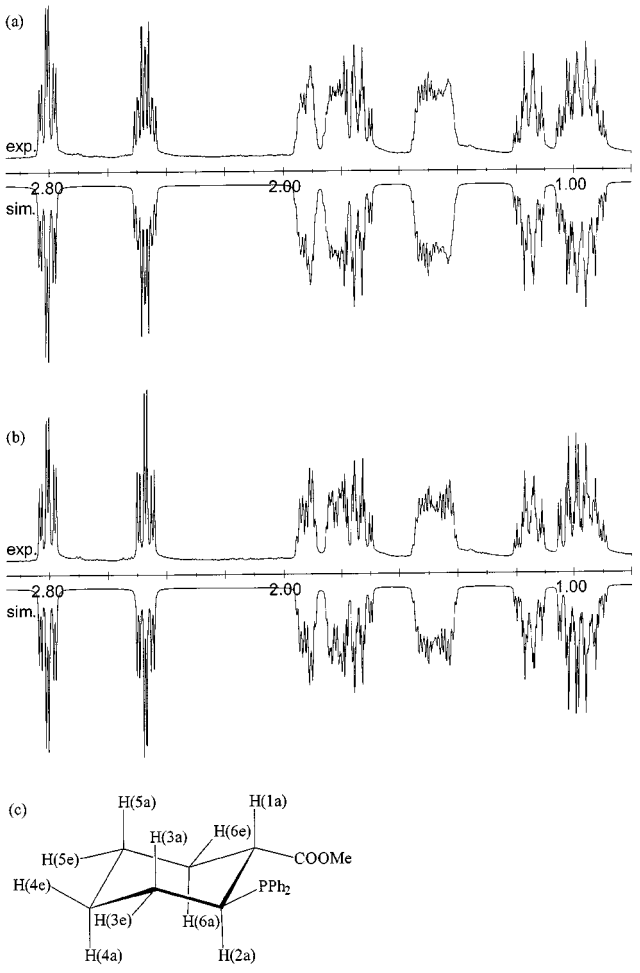

Figure 1. (a) ^{1}H NMR spectrum of **2a** (experimental, simulated); (b) ^{1}H{^{31}P} NMR spectrum of **2a** (experimental, simulated); (c) numbering scheme for the carbon and hydrogen atoms of the cyclohexyl backbones

−13.27 Hz. For axial protons ^3J(HH) is about 10 Hz, with significantly smaller values (ca. 4 or 5 Hz) being observed for protons in axial-equatorial or equatorial-equatorial positions.

The configurational analysis of **2a** was completed by the iterative simulation of the ^{1}H NMR spectrum (Figure 1a). To the best of our knowledge, this is the first complete analysis of a disubstituted derivative of cyclohexane with phosphorus as substituent. Consistent with the results obtained above, the vicinal coupling constants ^3J(PH) (4−7 Hz) obtained are typical for an H−C−C−P arrangement with dihedral angles of about 60°.[15a][15b] The small geminal coupling ^2J(PH) (0.64 Hz) (Table 1) indicates that in the most preferred conformation with respect to the P−C axis the lone pair at the phosphorus atom is in *trans* position to the hydrogen atom.[15c,15d]

Due to the asymmetric substitution at the α- and β-carbon atoms the phenyl groups of the Ph_2P substituent are chemically nonequivalent, as indicated by the doubling of the corresponding resonances in the ^{13}C{^{1}H} NMR spectrum. The assignment of the signals is based on comparison with pertinent data,[16] and ^{13}C{^{1}H}-DEPT NMR spectra.

Ester hydrolysis of **2a** with KOH in an ethanol/water mixture gave the potassium salt of the carboxylic acid **2b**. After concentration of the reaction mixture to dryness, the free acid was precipitated by acidification of the aqueous solution of the residue. The ^{31}P{^{1}H} NMR spectrum of **2b** shows a singlet at $\delta_P = -3.36$. A complete assignment of the 15 signals in the ^{13}C{^{1}H} NMR spectrum of **2b** could be achieved using the ^{13}C{^{1}H}-DEPT NMR spectrum, and by comparison with the results obtained for **2a** (see above). Making use of a C,H-COSY NMR and H,H-COSY-45 NMR spectrum all resonances in the ^{1}H NMR and the ^{1}H{^{31}P} NMR spectrum of **2b** could be assigned to the hydrogen atoms at C(1)−C(6), and their position in axial or equatorial sites of the cyclohexane ring system established. Although the lines are somewhat broadened compared with those of **2a**, the multiplet fine structure of the resonances corresponding to the protons on C(1) and C(2) ($\delta_H = 2.47$ and 2.86) are well resolved. By analysis of this part of the ^{1}H NMR and the ^{1}H{^{31}P} NMR spectrum, the vicinal H,H and H,P coupling constants ^3J(HH) and ^3J(PH) could be obtained. The pattern of the values of these coupling constants compares very well with that in **2a**, indicating a similar stereochemistry in both compounds.

Molecular Structure of 1-(Diphenylphosphanyl)cyclohexane-2-carboxylic Acid (2b)

In order to confirm the stereochemistry of **2b** as derived from the analysis of the NMR spectra, a crystal structure

Table 1. ^{1}H NMR spectroscopic data of **2a**; for the numbering of the hydrogen atoms see Figure 1c

δ_H values [ppm]			
H(1a)	2.47	H(2a)	2.81
H(3a)	1.01	H(3e)	1.82
H(4a)	1.15	H(4e)	1.52
H(5a)	0.94	H(5e)	1.45
H(6a)	1.74	H(6e)	1.92
P−H coupling constants [Hz]			
P−H(1a)	5.70	P−H(2a)	0.64
P−H(3a)	4.25	P−H(3e)	6.39
P−H(5e)	2.39	P−H(6e)	3.03
vicinal $H_{eq}-H_{eq}$ coupling constants [Hz]			
H(3e)−H(4e)	5.47	H(4e)−H(5e)	5.14
H(5e)−H(6e)	5.43		
long-range coupling constants [Hz]			
H(3e)−H(5e)	1.08	H(4e)−H(6e)	1.16
geminal $H_{ax}-H_{eq}$ coupling constants [Hz]			
H(3a)−H(3e)	−13.81	H(4a)−H(4e)	−13.27
H(5a)−H(5e)	−13.49	H(6a)−H(6e)	−13.38
vicinal $H_{ax}-H_{ax}$ coupling constants [Hz]			
H(1a)−H(2a)	9.72	H(2a)−H(3a)	10.19
H(3a)−H(4a)	10.88	H(4a)−H(5a)	10.90
H(5a)−H(6a)	11.09	H(6a)−H(1a)	9.82
vicinal $H_{ax}-H_{eq}$ coupling constants [Hz]			
H(2a)−H(3e)	3.66	H(3a)−H(4e)	3.56
H(5a)−H(4e)	3.76	H(4a)−H(3e)	3.53
H(4a)−H(5e)	3.87	H(1a)−H(6e)	3.92
H(5a)−H(6e)	3.70	H(6a)−H(5e)	3.62

analysis was performed. Recrystallization of **2b** from methanol afforded crystals suitable for X-ray structural analysis. Carboxylic acid **2b** crystallizes in the space group $P2_1/c$ with four molecules in the asymmetric unit showing an (*RS*)

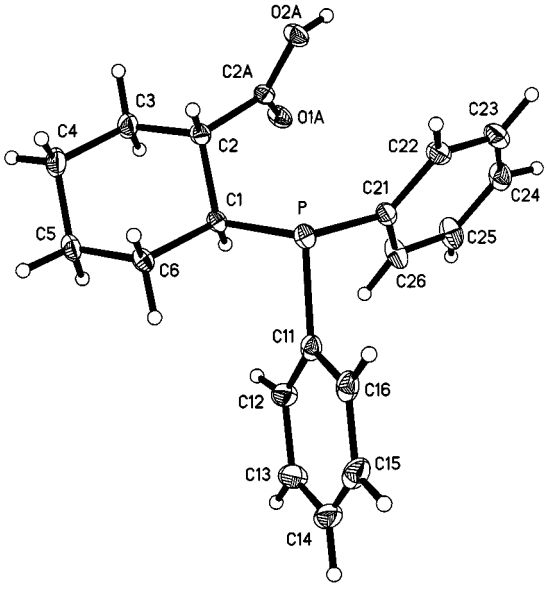

Figure 2. Molecular structure of **2b**; selected bond lengths [Å] and angles [°]: P−C(1) 1.859(3), P−C(11) 1.833(3), P−C(21) 1.832(3), C(1)−C(2) 1.540(3), C(2)−C(3) 1.538(4), C(1)−C(6) 1.533(3), C(5)−C(6) 1.518(4), C(3)−C(4) 1.510(4), C(4)−C(5) 1.504(4), C(2)−C(2A) 1.504(3), C(2A)−O(2A) 1.280(3), C(2A)−O(1A) 1.235(3); C(1)−P−C(11) 101.59(12), C(1)−P−C(21) 103.30(11), C(11)−P−C(21) 99.94(12), P−C(1)−C(2) 111.64(18), C(1)−C(2)−C(2A) 113.45(21), H(1)−C(1)−C(2)−H(2) −178.74, P−C(1)−C(2)−C(2A) 63.96(26)

and (*SR*) configuration. The structure (Figure 2) reveals the bis(equatorial) arrangement of the Ph_2P and COOH substituents with values for the H(1)−C(1)−C(2)−H(2) or P−C(1)−C(2)−C(2A) torsion angles of −178.7 or 63.96(26)°, respectively, in agreement with the solution structure of **2b** obtained by configurational analysis by means of NMR spectroscopy (see above). The carbon−phosphorus distances C(11)−P [1.833(3) Å], C(21)−P [1.832(3) Å], and C(1)−P [1.859(3) Å] (see caption to Figure 2) are in the typical range.[17] Due to the steric effect of the COOH group, the bond angle C(21)−P−C(1) [103.30(11)°] is somewhat enlarged compared with C(11)−P−C(1) [101.59(12)°] and C(21)−P−C(11) [99.94(12)°]. As a result the bond angle C(2A)−C(2)−C(3) [107.56(22)°] is compressed as compared with C(1)−C(2)−C(2A) [113.45(21)°].

Addition of $PhPH_2$ to Methyl 1-Cyclohexenecarboxylate (1)

The base-catalyzed 1:1 addition of $PhPH_2$ to **1** using 0.1 mol-% of KO*t*Bu proceeds stepwise with the secondary phosphane **3** being formed initially. Immediately after the completion of the addition reaction, four signals are observed in the $^{31}P\{^1H\}$ NMR spectrum of the reaction mixture δ_P = −30.02, −36.89, −37.95, and −49.67, of which after 24 h only two signals remain (δ_P = −30.02 and −37.95). As a result of the asymmetric substitution at the phosphorus atom, **3** may exist as four pairs of diastereoisomers [*SSS*/*RRR* (*cis*), *SSR*/*RRS* (*cis*), *RSS*/*SRR* (*trans*), *RSR*/*SRS* (*trans*), the sequence of the stereogenic centers being C,C,P], which have been observed initially in the $^{31}P\{^1H\}$ NMR spectrum. Epimerization processes at the β-carbon and phosphorus atoms yield the thermodynamically most stable two *trans* diastereoisomers (see above). The $^{13}C\{^1H\}$ NMR spectrum of **3** shows 24 signals, 16 of them showing doublet fine structure due to C−P coupling. Assignment of all resonances was achieved by comparison with the corresponding data of **2a** and with the aid of a $^{13}C\{^1H\}$-DEPT NMR spectrum. The resonances at δ_C = 175.1 and 175.2 (CO) or 51.07 and 51.09 (OMe), respectively, may be assigned to the COOMe group. The complex ^1H NMR spectrum of the cyclohexane part of **3** could not be analyzed completely as described for **2a** (see above). The signals in the δ_H range 2.0−2.4 correspond to the hydrogen atoms on C(1) and C(2). For the two diastereoisomers of **3** two doublets at δ_H = 3.98 and 4.18 with a large ^1J(PH) splitting (208 and 210 Hz) are observed. Additional fine structure is due to ^3J(HH) coupling between the hydrogen atoms on P and C(2) (ca. 5.6 and 3.6 Hz, respectively).

If $PhPH_2$ is added to **1** in a 1:2 molar ratio using 0.1 mol-% of KO*t*Bu as catalyst, the tertiary phosphane **4a** is formed in high yield. The four diastereoisomers (*cis* and *trans* isomers) of the secondary phosphane **3** are formed initially. During this time, rearrangement of the *cis*/*trans* isomeric mixture of the intermediate **3** occurred to yield the *trans* isomer only. For a completion of the addition reaction with formation of the tertiary phosphane **4a** the reaction mixture had to be heated under reflux for 8 h.

The tertiary phosphane **4a** has a maximum of five stereogenic centers (four carbon atoms and one phosphorus atom), thus forming six pairs of enantiomers and four *meso* compounds. In all *meso* isomers the phosphorus atom (P) is pseudo-asymmetric,[18] while the molecule as a whole is achiral. The phosphorus atom in two of the racemic pairs [e.g. $S_CS_C(P)S_CS_C$] is achiral. In agreement with these considerations the $^{31}P\{^1H\}$ NMR spectrum of **4a** shows ten signals in a δ_P range typical for tertiary phosphanes,[19] five of them [δ_P = −2.23 (28%), −2.96 (11%), −5.17 (46%), −7.26 (8%), and −10.32 (5%)] having intensities higher than ca. 5%. Due to overlapping of the $^{13}C\{^1H\}$ and ^1H NMR resonances of the numerous diastereoisomers, signal assignments for **4a** were only possible for some groups.

Addition of Cy_2PH to Methyl 1-Cyclohexenecarboxylate (1)

Addition of Cy_2PH to methyl 1-cyclohexenecarboxylate (**1**) under the conditions employed for the synthesis of **2a**, **3**, and **4a** did not succeed due to its lower acidity compared with Ph_2PH and $PhPH_2$.[20] If the lithium phosphanide Cy_2PLi,[21] obtained by metallation of Cy_2PH with methyllithium, was employed in this addition reaction, a mixture of compounds was obtained. The BH_3 adduct of the tertiary phosphane **5a** was formed, however, in high yields if the borane complex $Cy_2P(BH_3)Li$ was used instead of the free phosphide. Phosphane−borane complexes[22] have recently

been used as valuable intermediates in the syntheses of phosphane derivatives not accessible by other methods.[23]

Due to the coupling of the phosphorus with the boron nucleus, the $^{31}P\{^1H\}$ NMR spectrum of **5a** shows a broadened signal at $\delta_P = 32.73$. In the ^{11}B NMR spectrum a doublet [^1J(BP) = 47 Hz] with additional fine structure is observed. In the $^{13}C\{^1H\}$ NMR spectrum of **5a**, 16 of the 20 resonances show $^{31}P-^{13}C$ coupling fine structure. The signal at $\delta_C = 41.0$ corresponds to C(1), while the resonances at 34.9 [^1J(PC) = 28 Hz], 32.09 [^1J(PC) = 9 Hz], and 31.6 [^1J(PC) = 11 Hz] may be assigned to the *ipso*-carbon atoms C(2), C(8), and C(9) using $^{13}C\{^1H\}$-DEPT NMR spectra. The assignments for C(2) and C(6) were proven to be correct by the combination of the results of the C,H-COSY- and H,H-COSY-45 NMR spectra. The ^1H NMR spectrum of **5a** could not be analyzed due to extensive signal overlapping.

Deprotection of **5a** with a large excess of morpholine gave the borane-free tertiary phosphane **5b** in high yield as indicated by $^{31}P\{^1H\}$ NMR spectrum ($\delta_P = 8.52$). This deprotection procedure has been used extensively by Imamoto and others.[24] After evaporation of morpholine and the morpholine−borane complex in vacuo, the free phosphane **5b** was obtained as a colorless oil. The $^{31}P\{^1H\}$ NMR spectrum of **5b** shows a singlet at $\delta_P = 8.52$. In the 100.6 MHz $^{13}C\{^1H\}$ NMR spectra of **5b** eleven of the 20 resonances show a $^{31}P-^{13}C$ coupling fine structure. Due to signal overlapping four resonances in the range of $\delta_C = 28.03-28.19$ could not be assigned. The signal at $\delta_C = 44.02$ [^2J(PC) = 20.3 Hz] corresponds to C(1), while the resonances at 33.35 [^1J(PC) = 22.4 Hz], 33.10 [^1J(PC) = 19.3 Hz], and 32.11 [^1J(PC) = 20.3 Hz] may be assigned to the *ipso*-carbon atoms C(2), C(8), and C(9) as indicated by the $^{13}C\{^1H\}$-DEPT NMR spectrum.

Molecular Structure of 5a

In order to elucidate the structure of **5a**, an X-ray crystallographic study was undertaken. The crystals used in the investigation were grown from a solution in methanol. A view of the molecular structure is given in Figure 3. It shows that the phosphorus atom occupies an equatorial position of each cyclohexyl ring while the COOMe substituent is in an axial position. Since the latter is directed towards the perimeter of the molecule, steric interactions involving this substituent are minimal. In fact, the smallest C−P−B bond angle [108(5)°] involves the cyclohexyl group bearing the ester, the others being on the average 4(1)° larger. The P−B and average P−C bond lengths of 1.920(6) and 1.841(9) Å, respectively, are normal.

The atoms P, B, and C(15) define a pseudo-mirror plane for the molecule which is violated mainly by the methoxycarbonyl group. Since this pseudo-asymmetry element lies perpendicular to the monoclinic axis of the noncentrosymmetric space group $P2_1$, a considerable proportion of the structure is distributed centrosymmetrically in the crystal. This coincidence, along with the large atomic displacements of the cyclohexyl groups are probably responsible for the large variation of the C−C bond lengths, 1.32(1)−1.61(1) Å, which should not be taken seriously.

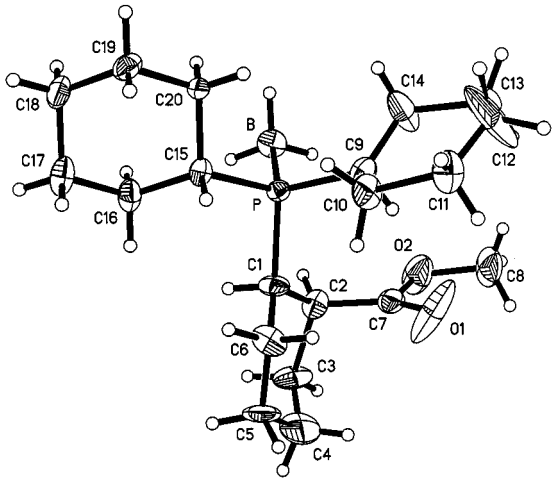

Figure 3. Molecular structure of **5a**; selected bond lengths [Å] and angles [°]: P−C(1) 1.835(6), P−C(9) 1.851(8), P−C(15) 1.837(4), P−B 1.920(6), C(2)−C(7) 1.505(11), C(7)−O(1) 1.267(11), C(7)−O(2) 1.378(9); C(1)−P−C(9) 107.9(3), C(1)−P−C(15) 104.9(4), C(9)−P−C(15) 107.8(3), C(1)−P−B 108.9(5), C(9)−P−B 114.4(5), C(15)−P−B 112.4(3), H(1)−C(1)−C(2)−H(2) 55.3(2)

Transition Metal Complexes of 2a and 2b

In order to obtain some information about the influence of the bulky cyclohexyl substituent on the ligand properties of the phosphanes **2a** and **2b**, molybdenum(0) and palladium(II) complexes were synthesized. Phosphane **2b** reacted with *cis*-$C_7H_8Mo(CO)_4$ in a straightforward manner to give the disubstituted complex **8** (Scheme 3), which is insoluble in most solvents. The corresponding reaction of **2a** proceeded very slowly. Initially, the $^{31}P\{^1H\}$ NMR spectrum of the reaction mixture showed in addition to the signal of **2a** two resonances at $\delta_P = 46.81, 46.24$, which may be assigned to the disubstituted complex **6a** formed as a mixture of diastereoisomers. If the reaction was run for a further couple of hours in order to complete the consumption of **2a** a third resonance at $\delta_P = 47.05$ appeared in the $^{31}P\{^1H\}$ NMR spectrum. This signal increased at the expense of those at $\delta_P = 46.81$ and 46.24 that disappear completely after ca 90 h. The resonance at $\delta_P = 47.05$ could be assigned to the monosubstituted complex **6** being formed by decomposition of **6a** with liberation of **2a**. Compound **6** was isolated from the reaction mixture by thin layer chromatography. Obviously, **2a** is too bulky to form a stable *cis*-disubstituted $Mo(CO)_4$ complex. Decomposition of **8** is not observed since it is precipitated from the reaction mixture during its formation.

The electronic parameter χ_i^{Ni} derived from the $\nu(CO)(A_1)$ stretching frequencies of the complexes $(CO)_3Ni(PR^1R^2R^3)$ may be taken as a measure for the electronic donor−acceptor properties of the phosphane ligands $PR^1R^2R^3$ as proposed by Tolman.[25a] As shown by us and others,[25b,25c] the analogous values χ_i^{Mo} obtained from the *cis*-$(CO)_4Mo(PR^1R^2R^3)_2$ complexes may be used instead of those obtained from the nickel complexes (χ_i^{Ni}). By compar-

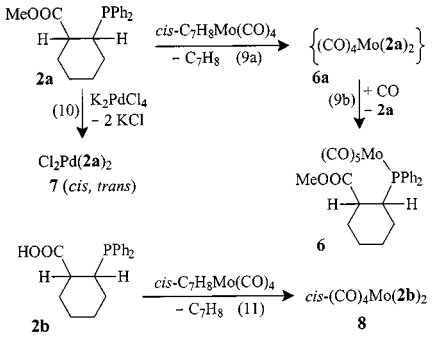

Scheme 3

ison of the χ_i^{Mo} values obtained for **2b** (2020 cm^{-1}) with those of Ph_2PH (2028 cm^{-1}), Ph_3P (2023 cm^{-1}), Me_3P (2016 cm^{-1}), and Cy_3P (2010 cm^{-1}), phosphane **2b** may be placed in between Ph_3P and Me_3P.

On reaction of **2a** with K_2PdCl_4 the palladium(II) complexes of type **7** are formed. The ^{31}P NMR spectrum of the reaction mixture shows two intense signals at $\delta_P = 29.02$ and 28.84, and two weak resonances at $\delta_P = 28.05$ and 27.85. The low-field signals at $\delta_P \approx 29$ may be assigned to the *meso* (*SR*, *RS*) and *rac* forms (*SR*, *SR*) of the *trans* isomer, while the resonances at $\delta_P \approx 28$ correspond to the *cis* isomer. Since the difference in δ_P of the *cis* and *trans* isomers of **7** is much smaller than the typical range (10−15)[26] observed for $Cl_2Pd(PR_3)_2$ complexes it is of no diagnostic value. The assignment of the intense signals at $\delta_P = 29.02$ and 28.84 to the *trans* structure of **7** is based upon the triplet fine structure of some of the resonances in the $^{13}C\{^1H\}$ NMR spectrum of **7** (see Exp. Sect.). The carbon atoms in **7** represent the X part of an ABX spin system (A, B = ^{31}P, X = ^{13}C),[27a] which for a large value of $^2J(PP)$ as in *trans*-$Cl_2Pd(PR_3)_2$ complexes appears as a triplet.[27b][27c]

It has been shown that the ^{31}P NMR chemical shift of *trans*-$(PR_3)_2PdCl_2$ complexes correlates well with the steric parameters θ_{Tol} [28] or θ[29] of the ligands PR_3, derived from X-ray data. For the ligand **2a** a value of ca. 150° may be derived for θ_{Tol}.

Experimental Section

General: For experimental details, see Part 15 of this series.[1] − Phenylphosphane, diphenylphosphane,[30a,30b] dicyclohexylphosphane,[30c] and $C_7H_8Mo(CO)_4$ [31] were synthesized by known methods. Methyl 1-cyclohexenecarboxylate (**1**) was purchased from Aldrich GmbH. ^1H-, ^{31}P-, ^{13}C-, and ^{11}B NMR spectra were recorded with a Bruker AC 400 or AM 250 and a JEOL FX90 Q Fourier transform spectrometer. Mass spectra were obtained with a Varian MAT 311 A.

Synthesis of 2a: Diphenylphosphane (5.21 g, 28 mmol) and KO*t*Bu (0.34 g, 3 mmol) were dissolved in 50 mL of toluene. To this solution methyl 1-cyclohexenecarboxylate (4.21 g, 30 mmol) was added. After stirring for 12 h, 10 mL of water was added and the reaction mixture was neutralized with 6 mL of 0.5 M hydrochloric acid. The organic phase was separated and dried with Na_2SO_4. The product (8.44 g, 92%) obtained after evaporation of the solvent was recrystallized from methanol. Yield 6.49 g (71%). − **2a:** $C_{20}H_{23}O_2P$ (326.4): calcd. C 73.60, H 7.10; found C 73.69, H 6.95. − MS; *m/z:* 326 [M^+]. − $^{13}C\{^1H\}$ NMR (C_6D_6): δ = 46.42 (C1, *J* = 19.3 Hz), 36.18 (C2, *J* = 16.3 Hz), 27.28 (C3, *J* = 4.1 Hz), 25.59 (C4, *J* = 4.1 Hz), 24.94 (C5), 30.05 (C6, *J* = 9.2 Hz), 175.13 (C7, *J* = 3.0 Hz), 137.28, 136.42 (C8, C12, *J* = 14.2, 17.3 Hz), 135.21, 133.03 (C9, C13, *J* = 21.0, 17.2 Hz), 128.60, 128.46 (C10, C14, *J* = 5.7, 7.6 Hz), 129.21, 128.19 (C11, C15), 51.04 (Me, *J* = 2.0 Hz). − $^{31}P\{^1H\}$ NMR (C_6D_6): δ = −1.86.

Synthesis of 3: The synthesis was performed as reported for **2a** using 3.08 g (28 mmol) of $PhPH_2$, 4.21 g (30 mmol) of methyl 1-cyclohexenecarboxylate, and 0.34 g (3 mmol) of KO*t*Bu as the catalyst. The product obtained was purified by distillation in vacuo (113−120 °C, < 0.01 mbar). Yield 4.64 g (66%). − **3:** $C_{14}H_{19}O_2P$ (250.3): calcd. C 67.19, H 7.65; found C 67.05, H 7.51. − MS; *m/z*: 250 [M^+]. − ^1H NMR (C_6D_6): δ = 2.32, 2.37 (H1, m), 2.12, 2.28 (H2, m), 0.78−1.90 (H3, m, H6, m), 1.03, 1.43 (H4, m), 0.94, 1.46 (H5, m), 3.39, 3.40 (Me, s), 7.00−7.60 (arom. H), 3.98, 4.18 [PH, *J*(PH) = 208, *J*(HH) = 5.6, *J*(PH) = 210, *J*(HH) = 3.6 Hz]. − $^{13}C\{^1H\}$ NMR (C_6D_6): δ = 48.4, 47.6 (C1, *J* = 12.2, 12.2 Hz), 36.1, 35.9 (C2, *J* = 14.2, 11.1 Hz), 31.5, 30.8, 30.6, 30.4 (C3, C6, *J* = 2.0, 8.1, 11.2, 8.1 Hz), 26.4, 25.9 (C4, *J* = 6.1, 7.1 Hz), 24.9, 24.8 (C5), 175.2, 175.1 (C7), 134.1, 133.6 (C8, *J* = 13.2, 13.2 Hz), 135.8, 135.0 (C9, *J* = 16.3, 15.3 Hz), 128.53, 128.51 (C10, *J* = 6.1, 5.6 Hz), 128.7, 128.4 (C11), 51.09, 51.07 (Me). − $^{31}P\{^1H\}$ NMR (C_6D_6): δ = −30.02, −37.95 (*J* = 208, 210 Hz).

Synthesis of 4a: The synthesis of **4a** was performed as reported for **3** using 2.20 g (20 mmol) of $PhPH_2$, 7.01 g (50 mmol) of methyl 1-cyclohexenecarboxylate, and 0.22 g (2 mmol) of KO*t*Bu. The oily residue obtained after evaporation of the solvent could not, however, be purified by recrystallization from different solvents. Yield 6.95 g (89%). − **4a:** $^{31}P\{^1H\}$ NMR (C_6D_6): δ = −0.6, −2.23, −2.96, −3.0, −3.12, −4.38, −5.17, −7.26, −7.31, −10.32.

Hydrolysis of 2a and 4a: Compounds **2a** (1.96 g, 6 mmol) or **4a** (6.95 g, 18 mmol) were added to a solution of 0.69 g (11 mmol) or 4.91 g (74 mmol) of KOH (85%) in a water/ethanol mixture (15:50 or 10:30 mL) with gentle warming. The reaction mixtures were heated under reflux for 4 h. Thereafter the solvents were distilled off in vacuo, and the residues were dissolved in 40 mL of water. Insoluble material was removed by filtration and the clear filtrate was acidified with hydrochloric acid (0.5 or 3 M). Colorless precipitates were formed, which were collected by filtration, washed with two aliquots of water (5 mL) and dried in vacuo. Yields 1.51 g (81%) for **2b**, 5.62 g (87%) for **4b**. − **2b**: $C_{19}H_{21}O_2P$ (312.3): calcd. C 73.06, H 6.78; found C 73.18, H 6.97. − ^1H NMR (C_6D_6): δ = 2.47 (H1a, m), 2.86 (H2a, m), 1.02 (H3a, m) 1.80 (H3e, m), 1.14 (H4a, m), 1.55 (H4e, m), 0.98 (H5a, m), 1.44 (H5e, m), 1.72 (H6a, m), 1.95 (H6e, m), 7.00−7.65 (arom. H), 11.9 (COOH, br.). − $^{13}C\{^1H\}$ NMR (C_6D_6): δ = 45.7 (C1, *J* = 19.3 Hz), 35.5 (C2, *J* = 15.3 Hz), 26.7 (C3, *J* = 5.1 Hz), 25.0 (C4, *J* = 4.1 Hz), 24.6 (C5), 29.2 (C6, *J* = 9.2 Hz), 182.4 (C7, *J* = 5.1 Hz), 137.1, 136.3 (C8, C12, *J* = 14.2, 17.3 Hz), 135.2, 133.1 (C9, C13, *J* = 21.4, 18.3 Hz), 128.7, 128.5 (C10, C14, *J* = 6.1, 7.1 Hz), 129.2, 128.4 (C11, C15). − $^{31}P\{^1H\}$ NMR (C_6D_6): δ = −3.36. − **4b:** $C_{20}H_{27}O_4P{\cdot}0.5\ H_2O$ (371.4): calcd. C 64.68, H 7.60; found C 64.05, H 7.19. − MS; *m/z*: 362 [M^+]. − ^1H NMR (C_6D_6): δ = 0.80−3.00 (H1−H6, m), 7.00−7.90 (arom. H), 12.0 (COOH, br.). − $^{13}C\{^1H\}$ NMR (C_6D_6): δ = 45.8−48.6 (C1), 32.2−33.7 (C2), 24.6−30.8 (C3−C6), 133.9, 134.3 (C8, *J* = 21, 16 Hz), 134.8, 135.3, 136.0, 136.4 (C9, *J* = 20, 15, 16, 21 Hz), 127−131 (C10, C11), 181−182 (COOH). − $^{31}P\{^1H\}$ NMR (C_6D_6): δ = 3.10, 2.02, −1.25, −4.45, −6.26.

Synthesis of 5a: To a solution of $Cy_2PH{\cdot}BH_3$ (5.74 g, 27 mmol) in 90 mL of THF was added *n*BuLi (15% in *n*-hexane) (11.79 g, 28 mmol) at −78 °C within a period of 30 min. The reaction mixture was stirred for 10 min at −76 °C and then allowed to warm up to ambient temperature. Thereafter the solution was again cooled down to −45 °C and 3.68 g (26 mmol) of methyl 1-cyclohexenecarboxylate was added. The reaction mixture was warmed to ambient temperature and stirred for 1 h. Water (35 mL) was added, and the reaction mixture was neutralized with 1 M hydrochloric acid. The organic phase was separated and dried with Na_2SO_4. The colorless residue left after removal of the solvent in vacuo was recrystallized from methanol. Yield 6.09 g (66%). − **5a:** $C_{20}H_{38}BO_2P$ (352.3): calcd. C 68.19, H 10.87; found C 67.56, H 10.87. − MS; *m*/*z*: 351 [M^+ − H]. − ^{1}H NMR (C_6D_6): δ = 3.30 (H1, m), 1.86 (H2, m), 1.33, 1.94 (H6, m), 2.19 (H8, m), 1.84 (H9, m), 3.41 (Me, s), 0.6−2.8 (overlapping multiplets). − $^{13}C\{^1H\}$ NMR (C_6D_6): δ = 41.03 (C1), 34.91 (C2, *J* = 27.9 Hz), 32.02 (C6, *J* = 9.4 Hz), 175.35 (C7, *J* = 1.3 Hz), 32.09 (C8, *J* = 9.0 Hz), 31.62 (C9, *J* = 11.2 Hz), 51.94 (Me), 29.94, 29.17 (*J* = 3.9 Hz), 28.80, 28.62 (*J* = 12.2 Hz), 28.23 (*J* = 9.2 Hz), 28.19 (*J* = 8.0 Hz), 27.86 (*J* = 9.8 Hz), 27.77 (*J* = 8.6 Hz), 27.70 (*J* = 4.4 Hz), 27.15 (*J* = 1.3 Hz), 26.98 (*J* = 1.2 Hz), 24.02 (*J* = 4.0 Hz), 22.50 (*J* = 1.1 Hz). − $^{31}P\{^1H\}$ NMR (C_6D_6): δ = 32.73 [$^1J(^{11}B-^{31}P)$ = 47 Hz].

Deprotection of 5a: Compound **5a** (0.27 g, 0.8 mmol) was dissolved in 15 mL of morpholine. The solution was stirred for 2 h at 90 °C. Thereafter the solvent and the morpholine−borane complex were removed in vacuo (100 °C, < 0.01 mbar). The crude **5b** was obtained as a colorless oil. Purification was achieved by recrystallization from methanol. Yield 0.25 g (98%). − **5b:** $C_{20}H_{35}O_2P$ (338.5): calcd. C 70.97, H 10.42; found C 70.14, H 10.35. − MS; *m*/*z*: 338 [M^+ − H]. − ^{1}H NMR (C_6D_6): δ = 2.85 (m, H1), 3.48 (s, Me), 1.00−2.35 (aliph. H). − $^{13}C\{^1H\}$ NMR (C_6D_6): δ = 44.02 (C1, *J* = 20.3 Hz), 33.35 (C2, *J* = 22.4 Hz), 33.10 (C8, *J* = 10.3 Hz), 32.11 (C9, *J* = 20.3 Hz), 50.60 (Me), 174.52 (C7), 32.51 (*J* = 17.3 Hz), 31.75 (*J* = 14.2 Hz), 31.02 (*J* = 9.2 Hz), 30.23 (*J* = 10.2 Hz), 30.22 (*J* = 8.1 Hz), 28.19−28.03 (4 C atoms), 27.43 (*J* = 5.1 Hz), 26.97−26.94 (2 C atoms), 25.16 (*J* = 6.1 Hz), 21.95. − $^{31}P\{^1H\}$ NMR (C_6D_6): δ = 8.52.

Synthesis of 6: $C_7H_8Mo(CO)_4$ (0.15 g, 0.5 mmol) and **2a** (0.33 g, 1 mmol) were dissolved in 10 mL of dichloromethane. The reaction mixture was stirred at ambient temperature for 96 h. Thereafter the solvent was removed in vacuo (20 °C, 0.01 mbar) and the remaining solid was purified by thin layer chromatography (SiO_2 PSC plates, Merck). The yellow zone containing **6** was extracted with CH_2Cl_2 and the solvent removed in vacuo. Yield: 0.11 g (38%). − **6:** $C_{25}H_{23}MoO_7P$ (562.4): calcd. C 53.34, H 4.12; found C 53.25, H 4.40. − MS; *m*/*z*: 533 [M^+ (^{95}Mo) − CO − 4 H]. − ^{1}H NMR (C_6D_6): δ = 2.80 (m, H1), 3.08 (m, H2), 0.8−1.8, 2.2 (m, H3−H6), 2.88 (s, Me), 6.95−7.93 (arom. H). − $^{13}C\{^1H\}$ NMR (C_6D_6): δ = 45.2 (C1), 38.5 (C2, *J* = 14 Hz), 26.0 (C3, *J* = 12 Hz), 28.6 (C4, *J* = 8 Hz), 24.7 (C5), 31.0 (C6, *J* = 6 Hz), 174.8 (C7, *J* = 3 Hz), 137.3, 133.3 (C8, C12, *J* = 32, 30 Hz), 135.4, 132.8 (C9, C13, *J* = 12, 11 Hz), 129.3, 129.1 (C10, C14, *J* = 8, 10 Hz), 131.2, 130.3 (C11, C15, *J* = 2, 2 Hz), 51.5 (Me), 207.2 (CO_{eq}, *J* = 9 Hz), 211.1 (CO_{ax}, *J* = 23 Hz). − $^{31}P\{^1H\}$ NMR (C_6D_6): δ = 47.05. − IR (KBr disc, cm^{-1}): $\tilde{\nu}$ = 2072, 1961, 1930, 1915.

Synthesis of 7: Dichloromethane (30 mL) and methanol (10 mL) were added to a mixture of **2a** (0.65 g, 2 mmol) and potassium tetrachloropalladate (K_2PdCl_4) (0.33 g, 1 mmol). The mixture was stirred at ambient temperature for 5 d and the solid material was removed by filtration through a suction funnel. After removal of all volatiles from the filtrate in vacuo (20 °C, < 0.01 mbar) **7** was obtained as a yellow solid. Yield 0.77 g (93%). − **7:** $C_{40}H_{36}Cl_2O_4P_2Pd$ (830.1): calcd. C 57.88, H 5.59; found C 57.52, H 5.6. − ^{1}H NMR (CD_2Cl_2): δ = 2.40 (m, H1), 3.45 (m, H2), 0.97, 1.62 (m, H5), 3.03, 3.08 (s, Me), 7.96 (m, H9), 7.71 (m, H13), 1.72, 1.59, 2.42, 0.86, 1.64, 1.43 (aliph. H), 7.25−7.65 (arom. H). −

Table 2. Crystal data of **2b** and **5a**

	2b	**5a**
Empirical formula	$C_{19}H_{21}O_2P$	$C_{20}H_{38}BO_2P$
Molecular mass	312.3	352.3
Crystal system	monoclinic	monoclinic
Space group	$P2_1/c$	$P2_1$
a [Å]	8.090(2)	6.859(1)
b [Å]	8.590(2)	11.429(2)
c [Å]	23.910(5)	13.913(2)
β [°]	90.52(3)	100.15(1)
V [Å^3]	1661.5(6)	1073.6(3)
Z	4	2
D(calcd.) [g cm^{-3}]	1.249	1.090
Radiation	Mo-K_α	Mo-K_α
Wavelength [Å]	0.71073	0.71073
Temperature [K]	243	293
Diffractometer	Siemens P4	Siemens P3
Crystal size [mm]	0.30 × 0.36 × 0.60	0.15 × 0.24 × 0.44
μ [mm^{-1}]	0.17	0.14
Transmission	0.642−0.448	0.804−0.923
2 theta (max.) [°]	49.98	50.09
Limiting indices	$0 \le h \le 9$, $0 \le k \le 10$, $-28 \le l \le 28$	$-8 \le h \le 8$, $-13 \le k \le 13$, $-16 \le l \le 16$
Reflections	3123	6018
Unique	2903	3797
R(int)	0.0382	0.0177
Observed ($F > 4\sigma$)	1918	2792
*R*1 (observed)	0.0504	0.1018
*wR*2 (all data)	0.1285	0.2719
Goodness-of-fit	0.881	1.770
Parameters	281	221
Δ*E* [e Å^{-3}]	0.42/−0.34	0.86/−0.74

$^{13}C\{^1H\}$ NMR (CD_2Cl_2): δ = 44.49, 44.37 (C1), 33.93, 33.94 (C2, *N* = 24.0, 22.4 Hz), 24.80, 24.72 (C5), 31.28, 31.22, 28.62, 28.49, 26.00, 25.93 (C3, C4, C6, *N* = 7.6, 7.6, 5.0, 5.0, 14.8, 15.2 Hz), 174.49, 174.39 (C7), 51.28, 51.24 (Me), 128.87, 128.85, 125.45, 125.35 (C8, C12, *N* = 39.2, 39.2, 45.8, 46.2 Hz), 136.74, 136.70 133.69, 133.64 (C9, C13, *N* = 12.8, 12.8, 11.6, 11.2 Hz), 127.98, 127.96, 127.91, 127.88 (C10, C14, *N* = 9.6, 10.2, 10.6, 10.6 Hz), 131.06, 131.06, 130.18, 130.10 (C11, C15). – $^{31}P\{^1H\}$ NMR (CD_2Cl_2): δ = 28.84, 29.01.

Synthesis of 8: To a solution of $C_7H_8Mo(CO)_4$ (0.15 g, 0.5 mmol) in 10 mL of dichloromethane was added **2b** (0.31 g, 1 mmol), and the reaction mixture was stirred at ambient temperature for 12 h. The crystals precipitated were collected by filtration using a suction funnel, washed with three aliquots of 2 mL of dichloromethane and dried in vacuo (20 °C, 0.01 mbar). Yield 0.33 g (78%). – **8:** $C_{42}H_{42}MoO_8P_2$ (832.7): calcd. C 60.58, H 5.08; found C 59.80, H 4.96. – HPLC ESI(–) MS; *m/z*: 749 [M^- – 3 CO – H]. – IR (KBr disc): $\tilde{\nu}$ = 2020, 1915, 1901, 1859 cm^{-1}.

X-ray Structure of 2b: A crystal (0.30 × 0.36 × 0.60 mm) was sealed in a glass capillary. X-ray data were measured with a Siemens P4 diffractometer equipped with a graphite monochromator and employing Mo-K_α radiation. The structure was solved by direct methods using the SHELXTL program package. Selected crystallographic details are listed in the caption to Figure 2. Experimental data are collected in Table 2.

X-ray Structure of 5a: A crystal (0.15 × 0.24 × 0.44 mm) was glued to a glass fiber. X-ray data were collected with a Siemens P3 diffractometer equipped with a graphite monochromator and employing Mo-K_α radiation. A complete set of intensities including Friedel opposites were measured, and they were corrected empirically for absorption. Systematic absences suggested that the space group was either $P2_1$ or $P2_1/m$ and since the latter would impose mirror symmetry on **5a**, the chirality of **5a** suggested that the former would be correct. Direct methods assuming $P2_1$ yield the positions of the P, B, and cyclohexyl-C atoms, but the arrangement of these atoms obeyed the mirror symmetry required by $P2_1/m$. A subsequent difference Fourier synthesis contained a mirror-related pair of COOC fragments, and the pseudo-mirror plane was broken by incorporating only the entity bonded to the C(2) atom. The structure was refined anisotropically with isotropic hydrogen atoms added in idealized positions by various riding models, and the discussion is based on this model. Unfortunately, the Flack absolute structure parameter, 0.4(2), has been determined imprecisely, so the crystal under investigation may have contained molecules exhibiting the (*R*,*R*) configuration shown in Figure 3, the mirror-related (*S*,*S*) configuration or a mixture of both. Because of the poor convergence encountered in the refinement of the structure in the noncentrosymmetric space group, an attempt was made to develop the structure in $P2_1/m$. This effort led to satisfactory coordinates for the cyclohexyl group divided by the mirror plane and the P and B atoms, but other atoms were poorly defined, the C(8) atom residing on the mirror plane, therefore this model was discarded. Experimental data are collected in Table 2.

Crystallographic data (excluding structure factors) for the structures reported in this paper have been deposited with the Cambridge Crystallographic Data Centre as supplementary publication no. CCDC-147247 (**2b**) and -146877 (**5a**). Copies of the data can be obtained free of charge on application to CCDC, 12 Union Road, Cambridge CB2, 1EZ, UK [Fax: (internat.) +44-1223/336-033; E-mail: deposit@ccdc.cam.ac.uk].

Acknowledgments

This work was supported by Ministerium für Bildung, Wissenschaft und Forschung des Landes Nordrhein-Westfalen and the Fonds der Chemischen Industrie. Celanese GmbH and Clariant GmbH are thanked for financial support. We thank Prof. Dr. R. Eujen for his assistance running the INADEQUATE NMR spectra.

[1] D. J. Brauer, M. Hingst, C. Liek, K. W. Kottsieper, M. Tepper, S. Schenk, O. Stelzer, W. S. Sheldrick, *J. Mol. Catal. A: Chemical*, submitted for publication.
[2] [2a] M. Peuckert, W. Keim, *Organometallics* **1982**, *2*, 594. – [2b] S. Mecking, W. Keim, *Organometallics* **1996**, *15*, 2650. – [2c] W. Keim, R. P. Schulz, *J. Mol. Catal.* **1994**, *92*, 21.
[3] J. Bank, P. Steinert, B. Windmüller, W. Wolfsberger, H. Werner, *J. Chem. Soc., Dalton. Trans.* **1996**, 1153.
[4] A. Bader, E. Lindner, *Coord. Chem. Rev.* **1991**, *108*, 27; C. S. Slone, D. A. Weinberger, C. A. Mirkin, *Progr. Inorg. Chem.* **1999**, *48*, 233.
[5] [5a] K. Issleib, H. Zimmermann, *Z. Anorg. Allg. Chem.* **1967**, *353*, 197. – [5b] J. A. van Doorn, N. Meijboom, *Phosphorus, Sulfur, Silicon* **1989**, *42*, 211.
[6] [6a] M. Hingst, M. Tepper, O. Stelzer, *Eur. J. Inorg. Chem.* **1998**, 73. – [6b] C. Liek, P. Machnitzki, T. Nickel, S. Schenk, M. Tepper, O. Stelzer, *Z. Naturforsch.* **1999**, *54b*, 1532.
[7] [7a] O. Herd, A. Heßler, M. Hingst, M. Tepper, O. Stelzer, *J. Organomet. Chem.* **1996**, *522*, 69. – [7b] O. Herd, A. Heßler, M. Hingst, P. Machnitzki, M. Tepper, O. Stelzer, *Catal. Today* **1998**, *42*, 413.
[8] H. R. Hudson, in *The Chemistry of Organophosphorus Compounds*, vol.1 (Ed.: F. R. Hartley) John Wiley & Sons, Chichester, **1990**, p. 385.
[9] P. Braunstein, S. Coco Cea, A. DeCian, J. Fischer, *Inorg. Chem.* **1992**, *31*, 4203; W. Wolfsberger, J. Bank, H. Werner, *Z. Naturforsch.* **1995**, *50b*, 1319.
[10] P. Bigler, *NMR Spectroscopy: Processing Strategies*, VCH Publishers, Weinheim, **1997**.
[11] [11a] H. Friebolin, *Ein- und zweidimensionale NMR-Spektroskopie*, p. 90, VCH Publishers, Weinheim, **1992**. – [11b] J. W. Emsley, J. Feeney, L. H. Suttcliffe, *High Resolution Nuclear Magnetic Resonance Spectroscopy*, vol. 1, Pergamon Press, Oxford, London, New York, Toronto, Sydney, Paris, Braunschweig, **1966**.
[12] [12a] J. Buddrus, H. Bauer, *Angew. Chem.* **1987**, *99*, 642; *Angew. Chem. Int. Ed. Engl.* **1987**, *26*, 625. – [12b] H. Kessler, M. Gehrke, C. Griesinger, *Angew. Chem.* **1988**, *100*, 507; *Angew. Chem. Int. Ed. Engl.* **1988**, *27*, 490.
[13] g NMR program, Ivory Soft, **1995**, P. H. M. Budezelaar, Cherwell Scientific Publishing, Ltd., **1995**.
[14] [14a] H. Günther, *NMR-Spektroskopie*, Georg Thieme Verlag, Stuttgart, **1973**. – [14b] H. Booth, *Progress in Nuclear Magnetic Resonance Spectroscopy*, vol. 5 (Eds.: J. W. Emsley, J. Feeney, L. H. Sutliffe), Pergamon Press, Oxford, **1969**, p. 149.
[15] [15a] W. G. Bentrude, W. N. Setzer, L. D. Quin, *Phosphorus-31 NMR Spectroscopy in Stereochemical Analysis*, vol. 8, VCH Publishers, Deerfield Beach, **1987**, p. 366. – [15b] C. Benzra, *J. Am. Chem. Soc.* **1973**, *95*, 6890. – [15c] J. P. Albrand, D. Gagnaire, J. B. Robert, *J. Chem. Soc., Chem. Commun.* **1968**, 1469; *Bull. Soc. Chim. Fr.* **1969**, 40. – [15d] T. A. Albright, *Org. Magnet. Res.* **1976**, *8*, 489; G. Mavel, *Ann. Report NMR Spectroscopy* **1973**, *5b*, 1.
[16] H. O. Kalinowski, S. Berger, S. Braun, *^{13}C NMR Spektroskopie, Georg Thieme Verlag, Stuttgart,* **1984***, p. 237; J. Schraml, M. Capka, V. Blechta, Magn. Reson. Chem.* **1992**, *30*, 544.
[17] F. H. Allen, O. Kennard, D. G. Watson, L. Brammer, A. G. Orpen, R. Taylor, *J. Chem. Soc., Perkin Trans. 2* **1987**, S1.
[18] E. L. Eliel, S. H. Wilen, *Organische Stereochemie*, Wiley-VCH, Weinheim, **1998**.
[19] S. Berger, S. Braun, H. O. Kalinowski, *NMR-Spektroskopie von Nichtmetallen*, vol. 3 ("^{31}P NMR Spektroskopie"), Georg Thieme Verlag, Stuttgart, **1993**.
[20] K. Issleib, R. Kümmel, *J. Organomet. Chem.* **1965**, *3*, 84.
[21] K. Issleib, A. Tzschach, H. U. Block, *Chem. Ber.* **1968**, *100*, 2931.

[22] H. Schmidbaur, *J. Organomet. Chem.* **1980**, *200*, 287.
[23] [23a] B. Mohr, D. M. Lynn, R. H. Grubbs, *Organometallics* **1996**, *15*, 4317. – [23b] T. Imamoto, T. Oshiki, T. Onozawa, M. Matsuo, T. Hikosaka, M. Yanagawa, *Heteroatom Chem.* **1992**, *3*, 563. – [23c] T. Oshiki, T. Imamoto, *J. Am. Chem. Soc.* **1992**, *114*, 3975.
[24] T. Imamoto, *Pure Appl. Chem.* **1993**, *65*, 655; S. Juge, M. Stephan, J. A. Laffitte, J. P. Genet, *Tetrahedron Lett.* **1990**, *31*, 6357.
[25] [25a] C. A. Tolman, *Chem. Rev* **1977**, *77*, 313. – [25b] T. Bartik, T. Himmler, H. G. Schulte, K. Seevogel, *J. Organomet. Chem.* **1984**, *272*, 29. M. F. Lappert, J. B. Pedley, B. T. Wilkins, O. Stelzer, E. Unger, *J. Chem. Soc., Dalton Trans.* **1975**, 1207. – [25c] C. L. Hyde, D. J. Darensbourg, *Inorg. Chem.* **1973**, *12*, 1286.
[26] S. O. Grim, R. L. Keiter, *Inorg. Chim. Acta* **1970**, *4*, 56; D. A. Redfield, J. H. Nelson, *Inorg. Chem.* **1973**, *12*, 15.
[27] [27a] R. J. Abraham, H. J. Bernstein, *Can. J. Chem.* **1961**, *39*, 216. – [27b] F. B. Ogilvie, J. M. Jenkins, J. G. Verkade, *J. Am. Chem. Soc.* **1970**, *92*, 1916. – [27c] G. Balimann, H. Motschi, P. S. Pregosin, *Inorg. Chim. Acta* **1977**, *23*, 191.
[28] T. Bartik, T. Himmler, *J. Organomet. Chem.* **1985**, *293*, 343; T. Bartik, B. Bartik, B. E. Hanson, I. Guo, I. Toth, *Organometallics* **1993**, *12*, 164.
[29] A. Immirzi, A. Musco, *Inorg. Chim. Acta* **1977**, *25*, L41.
[30] [30a] F. Pass, H. Schindlbaur, *Monatsh. Chem.* **1959**, *90*, 148. – [30b] W. Gee, R. A. Shaw, B. C. Smith, *Inorg. Synth.* **1967**, *9*, 19. – [30c] K. Issleib, A. Tzschach, *Chem. Ber.* **1959**, *92*, 704.
[31] R. B. King, in *Organometallic Synthesis*, vol. 1 ("Transition Metal Compounds") (Eds.: J. Eisch, R. B. King), Academic Press, New York, **1965**, p. 124.

Received July 19, 2000
[I00286]

X-ray Powder Diffraction and Solid-State NMR Investigations in Cadmium−Lead Hydroxyapatites

Béchir Badraoui,[a] Adriana Bigi,*[b] Mongi Debbabi,[a] Massimo Gazzano,[c] Norberto Roveri,[b] and René Thouvenot[d]

Dedicated to Professor Alberto Ripamonti on the occasion of his 70th birthday

Keywords: Hydroxyapatite / Rietveld method / ^{31}P MAS NMR spectroscopy / Ionic substitution / X-ray diffraction

In the proposed experiment, the maximum amount of cadmium substitution in lead hydroxyapatite accounts for about 30 atom-%. The crystal structures of PbHA at different degrees of cadmium substitution for lead (4.9, 10.0, 22.4 and 29.0% Cd atoms) have been investigated by X-ray powder pattern fitting and ^{31}P MAS NMR. The site-occupancy factors of metal atoms clearly indicate a preference of cadmium for site **1** of the apatite structure, which is more selective at low cadmium content. A progressive shift of the OH group towards the center of the triangles formed by the site **2** metals has been observed with increasing cadmium content. The different environments of the phosphate group demonstrated by ^{31}P NMR spectroscopic data are discussed in relation to structural data.

Introduction

Hydroxyapatite (CaHA), $Ca_{10}(PO_4)_6(OH)_2$, is a member of a large family of isomorphous substances, and the study of its physico-chemical properties represents an area of intensive interdisciplinary research activity. CaHA is of great interest in the design of biomaterials, in chromatography, in catalysis and in water treatment.[1,2] The CaHA structure can easily host a variety of substituents, both cationic and anionic, whose presence affects the physico-chemical properties of the compound.[3−7] Ionic substitutions can be involved in several applications: dental and bone pathologies, pollution due to phosphate fertilizers, ion-exchange properties for water treatment, radioactive waste confinement, bioceramics for bone implants, catalysis, luminescence, phosphorescence, etc. The most frequently encountered form of CaHA crystallizes in the hexagonal $P6_3/m$ space group, with lattice constants a = 9.42 Å and c = 6.88 Å.[2] The unit cell contains ten cations arranged in two nonequivalent sites: four at site **1** and six at site **2**, as shown in Figure 1. At site **1**, Ca ions are aligned in columns and surrounded by nine oxygen atoms. Ca ions at site **2** are arranged in equilateral triangles centered on the screw axes and surrounded by seven oxygen atoms, one of which belongs to the OH^- groups and the others to the PO_4^{3-} tetrahedra. The OH^- groups occur in columns parallel to the c axis and pass through the centers of the calcium triangles. Among the divalent cations which can be incorporated into the CaHA structure, cadmium, strontium and lead are known to replace calcium in the whole range of composition, while barium−calcium hydroxyapatite exhibits a zone of immiscibility.[8−12] The lattice parameters of these mixed apatites vary linearly with the composition, with the exception of the c axis of lead−calcium hydroxyapatite that displays a discontinuity at about 50 atom-% of lead. The peculiar variation of the c-axis dimension has been ascribed to an inhomogeneous lead distribution at the two nonequivalent cation sites, on the basis of the results of powder pattern structure refinements of Pb−Ca apatites, which indicate a clear preference of lead for site **2** of the hydroxyapatite structure.[9]

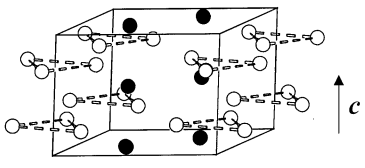

Figure 1. Perspective view of the metal ion in site **1** (black circles) and site **2** (white circles) of HA structure

We now report the results of an X-ray powder pattern fitting study and of a ^{31}P NMR investigation carried out on Cd−Pb mixed hydroxyapatite samples prepared from solutions containing 5 (Cd5), 10 (Cd10), 20 (Cd20) and 30

[a] Laboratoire de Chimie Inorganique et Industrielle, Ecole Nationale d'Ingénieurs de Monastir,
5019 Monastir, Tunisie
[b] Dipartimento di Chimica "G. Ciamician", Università degli Studi,
Via Selmi 2, 40126 Bologna, Italy
Fax: (internat.) + 39-051/209-9456
E-mail: bigi@ciam.unibo.it
[c] Centro di Studio per la Fisica delle Macromolecole, C.N.R.,
Via Selmi 2, 40126 Bologna, Italy
[d] Laboratoire de Chimie Inorganique et Matériaux Moléculaires, Unité CNRS 7071, case courrier 42, Université Pierre et Marie Curie,
75252 Paris Cedex 05, France
Supporting information for this article is available on the WWW under http://www.wiley-vch.de/home/eurjic or from the author.

 © WILEY-VCH Verlag GmbH, 69451 Weinheim, 2001 1434−1948/01/0505−1261 $ 17.50+.50/0

(Cd30) atom-% Cd. The results give important details of the structural modifications induced by cadmium on the lead hydroxyapatite structure.

Results

The results of the structural refinements indicate that the maximum amount of cadmium substitution in lead hydroxyapatite (PbHA; hereafter MHA = metal apatite) accounts for about 30 atom-%. In other words, the upper limit of the solid solutions is $Cd_3Pb_7(PO_4)_6(OH)_2$. In spite of the limited range of Cd incorporation, the decrease in cell parameters is quite regular when the amount of Cd increases, indicating true solid solutions and a behavior according to Vegard's law, where x = Cd × 100/(Cd + Pb) and σ values are the standard deviation:

$a = (9.8765 - 0.0062\ x)$, $\sigma(a) = 1.3 \times 10^{-4}$ Å
$c = (7.4148 - 0.0080\ x)$, $\sigma(c) = 2.4 \times 10^{-4}$ Å

Increasing amounts of CdO are present in the preparations obtained at greater Cd concentrations, up to 60%. At even greater concentrations [i.e. Cd/(Cd + Pb) > 60%], the products display nonapatitic powder X-ray diffraction patterns, characteristic of lead-substituted tricadmium phosphate.

Table 1. Fractional atomic coordinates after Rietveld refinement for the mixed Cd−Pb hydroxyapatites (e.s.d. in parentheses)

Sample	Atom	x	y	z
Cd5[a]	M(1)	0.3333	0.6666	−0.0010(15)
	M(2)	0.2505(4)	1.0038(7)	0.2500
	P	0.394(2)	0.353(2)	0.2500
	O(1)	0.344(3)	0.491(3)	0.2500
	O(2)	0.567(4)	0.482(3)	0.2500
	O(3)	0.323(3)	0.247(2)	0.082(3)
	OH	0.0000	0.0000	0.080(4)
Cd10[b]	M(1)	0.3333	0.6666	0.0021(8)
	M(2)	0.2495(3)	1.0022(6)	0.2500
	P	0.399(1)	0.363(1)	0.2500
	O(1)	0.347(3)	0.482(2)	0.2500
	O(2)	0.577(3)	0.471(3)	0.2500
	O(3)	0.326(2)	0.254(2)	0.083(2)
	OH	0.0000	0.0000	0.120(2)
Cd20[c]	M(1)	0.3333	0.6666	0.0043(2)
	M(2)	0.2480(4)	0.9990(6)	0.2500
	P	0.408(1)	0.380(2)	0.2500
	O(1)	0.349(2)	0.501(3)	0.2500
	O(2)	0.593(3)	0.454(3)	0.2500
	O(3)	0.354(2)	0.285(2)	0.085(2)
	OH	0.0000	0.0000	0.167(5)
Cd30[d]	M(1)	0.3333	0.6666	0.0108(2)
	M(2)	0.2517(5)	1.0005(9)	0.2500
	P	0.413(2)	0.389(3)	0.2500
	O(1)	0.331(4)	0.482(3)	0.2500
	O(2)	0.609(3)	0.473(4)	0.2500
	O(3)	0.346(2)	0.282(3)	0.092(3)
	OH	0.0000	0.0000	0.163(5)

[a] a = 9.861(1) Å, c = 7.3604(1) Å, R_p = 7.8, R_{wp} = 10.1. − [b] a = 9.810(1) Å, c = 7.3315(6) Å, R_p = 5.5, R_{wp} = 7.3. − [c] a = 9.741(1) Å, c = 7.2522(7) Å, R_p = 6.5, R_{wp} = 8.3. − [d] a = 9.692(1) Å, c = 7.174(1) Å, R_p = 10.5, R_{wp} = 13.5.
The pattern R factor R_p is defined as $R_p = 100\{\Sigma|Y_{oi} - Y_{ci}|/\Sigma Y_{oi}\}$. The weighted pattern R factor R_{wp} is defined as $R_{wp} = 100\{\Sigma w_i(Y_{oi} - Y_{ci})^2/\Sigma w_i(Y_{oi})^2\}^{1/2}$.

X-ray Data

The refined structural parameters of the samples Cd5, Cd10, Cd20 and Cd30 are reported in Table 1, and the data about cationic distribution are reported in Table 2. Figure 2 displays the final plot for Cd10 sample as a typical comparison between the observed and calculated profiles. The final agreement indices, R_{wp}, are 10.1, 7.3, 8.3 and 13.5 for Cd5, Cd10, Cd20 and Cd30, respectively. The bond lengths and angles for the two metal environments are reported in Table 3.

The refinement of the four samples of Cd−PbHA indicates that the cadmium content in the crystalline phase of these samples is 8.4, 10.0, 22.4 and 29.0 for Cd5, Cd10, Cd20 and Cd30, respectively. These values are very close to those expected on the basis of the stoichiometry of the reagents and on chemical analysis (4.9, 10.6, 21.0 and 30.6, respectively), with the exception of Cd5, which exhibits an appreciably greater Cd incorporation.

^{31}P NMR Spectroscopic Data

The 162 MHz ^{31}P MAS spectra of Cd5 and Cd30 are presented in Figure 3 and the relevant data are reported on Table 4. Two distinct isotropic signals can be detected for the two low cadmium containing apatites but only a relatively broad band occurs for Cd20 and Cd30.

Discussion

Structural Analysis

Cadmium can replace lead in the hydroxyapatite structure by up to about 30 atom-%, inducing a linear contraction of the lattice constants in agreement with its smaller size. The partial miscibility found for Cd−Pb apatites is in contrast with the behaviour observed for Cd−Ca and Pb−Ca apatites.[6,13] The complete miscibility of Ca and Cd hydroxyapatites is not surprising in view of their similar size, which is not the case for Ca and Pb ions. The miscibility of the Ca−Pb hydroxyapatites can be justified on the basis of the large difference in the polarizabilities of calcium and lead ions: Ca^{2+} is a hard acid, giving mainly ionic interactions with oxygen, whereas Pb^{2+} is a soft acid, displaying a considerable tendency towards polarization and covalent interactions. In the Cd−Pb case, we have two soft acids. Their significant tendency towards covalent interactions and directional bonding, which is most likely the origin of the large distortions of the PO_4 tetrahedra, probably limits the possibility of mutual substitution. In particular, the precipitation of nonapatitic phases at high cadmium concentrations suggests that the presence of lead, even in small amounts, inhibits the formation of CdHA.

The results of the powder fitting structure refinements indicate a clear preference of cadmium for site **1** of the apat-

Table 2. Cadmium substitution (atom-%) in Cd−Pb hydroxyapatites, e.s.d. in parentheses

	Cd1/(Cd1 + Pb1)	Cd1/(Cd1 + Cd2)	Cd2/(Cd1 + Cd2)	Cd2/(Cd2 + Pb2)	Cd/(Cd + Pb)[a]
Cd5	21(1)	99(1)	1(1)	<1	8.4(4)
Cd10	23(1)	92(1)	8(1)	1.3(2)	10.0(5)
Cd20	44(2)	79(1)	21(1)	8.0(4)	22.4(9)
Cd30	49(3)	67(2)	33(2)	16(2)	29(2)

[a] Cd = Cd1 + Cd2, Pb = Pb1 + Pb2.

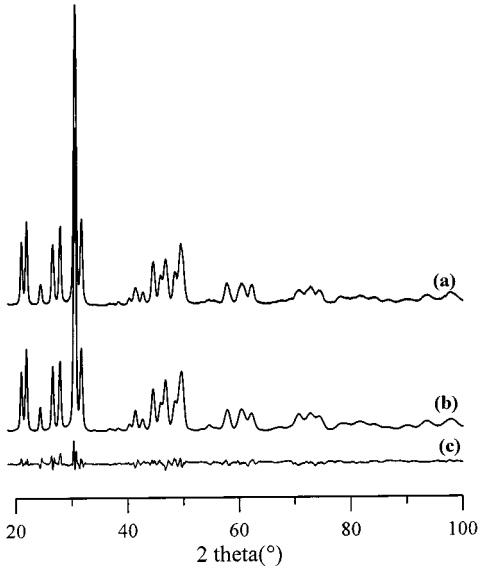

Figure 2. Observed (a) and calculated (b) XRD patterns of the sample Cd10; the curve difference is (c)

Table 3. Environments of metal atoms in Cd−Pb hydroxyapatites, e.s.d. in parentheses

	PbHA[12]	Cd5	Cd10	Cd20	Cd30	CdHA[11]
M(1)−O(1) × 3	2.67(2)	2.57(2)	2.62(2)	2.46(2)	2.47(2)	2.326(7)
M(1)−O(2) × 3	2.54(2)	2.81(4)	2.69(3)	2.48(3)	2.53(3)	2.437(8)
M(1)−O(3) × 3	3.00(2)	3.11(2)	3.09(2)	2.92(2)	2.98(3)	2.826(9)
M(1)−O mean	*2.73*	*2.83*	*2.80*	*2.62*	*2.66*	*2.530*
M(2)−O(1)	2.89(2)	3.05(3)	3.03(2)	3.03(3)	2.85(3)	2.636(9)
M(2)−O(2)	2.54(2)	2.34(2)	2.39(2)	2.51(2)	2.31(3)	2.354(9)
M(2)−O(3) × 2	2.59(1)	2.57(2)	2.51(2)	2.59(2)	2.58(3)	2.487(9)
M(2)−O(3) × 2	2.62(1)	2.45(2)	2.56(2)	2.75(2)	2.66(3)	2.241(7)
M(2)−OH	2.89(2)	2.75(1)	2.616(7)	2.49(2)	2.51(1)	2.351(3)
M(2)−O mean	*2.68*	*2.60*	*2.59*	*2.60*	*2.59*	*2.466*
M(2)−M(2)	4.22(1)	4.422(6)	4.402(5)	4.193(6)	4.221(7)	4.008(1)
M(2)−M(1)	4.19(1)	4.225(6)	4.185(6)	4.128(7)	4.074(8)	3.896(1)
M(1)−M(1)	3.62(2)	3.666(6)	3.697(6)	3.564(6)	3.432(9)	3.288(1)

ite structure. At low concentrations, Cd occupies almost exclusively site **1**, whereas at a higher degree of substitution, the selectivity is smaller, although the preference is maintained. As is clearly shown in Table 2, most of the Cd ions in Cd5 (99%) are at site **1**. The occupancy of site **1** by Cd decreases to 92% in Cd10, to 79% in Cd20 and to 67% in Cd30, in which about 50% of the metal atoms at site **1** are Cd. This result could be expected on the basis of the shorter metal−metal distances at site **1** (M−M = 3.62 Å in PbHA) which is more suitable for the smaller Cd ion, than at site **2** (M−M = 4.22 Å in PbHA). Furthermore, this is in agreement with the preference of Pb for site **2**, where the arrangement of the "staggered" equilateral triangles allows for the optimization of the packing of larger ions, in contrast to site **1** where the strict alignment of the columns causes a stronger repulsion.

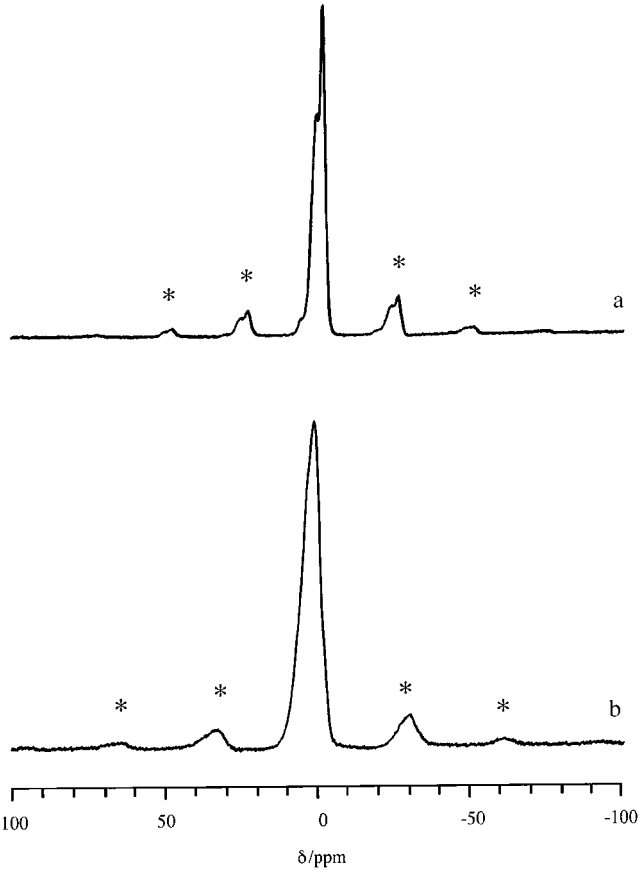

Figure 3. 162 MHz ^{31}P MAS NMR spectra of (a) Cd5 (spinning rate 4 kHz) and (b) Cd30 (spinning rate 5 kHz); asterisks mark spinning side bands

Table 4. ^{31}P MAS solid-state NMR spectroscopic data

Sample	δ_{iso} (ppm)	$\Delta\nu_{1/2}$ [a]	Relative amount[b] (%)
Cd5	−1.1	1.9 (310)[b]	47
	+0.9	3.1 (500)[b]	53
Cd10	−1.0	1.6 (260)[b]	27
	+1.1	4.3 (700)[b]	73
Cd20	+1.8	5.3 (860)	−
Cd30	+1.9	7.0 (1130)	−

[a] In ppm, with the values in Hz in parentheses. − [b] From line-fitting analysis.

For the sample Cd5, the discrepancy between the value of the cadmium content obtained from the Rietveld refinement and the value measured by chemical analysis, can be ascribed to the slight modification of the diffraction pattern induced by cadmium incorporation: 5% of lead substituted by cadmium corresponds to only a 1.5% intensity variation in the region of the most intense peaks (ca. 30° − 2θ). Furthermore, the value of the Cd5 unit-cell volume is an indirect confirmation that cadmium substitution amounts to approximately 5%, since it fits very well with those of the other samples in the plot of volume against Cd%.

The insertion of cadmium into the PbHA lattice appreciably affects the position of the OH group in the channel formed by the metals of site **2**, as can be seen in Figure 3. In CdHA, as well as in CaHA, the OH ion is just a little bit out of the plane of the triangles formed by the site **2** metals; on the other hand, the OH ion in PbHA is approximately halfway between two successive planes of lead triangles, because of the presence of the larger metal ions. The substitution of cadmium for lead causes a shift of the group along the channel toward the center of the plane (see Figure 4) with a behaviour very similar to that previously verified for Pb−Ca hydroxyapatite.[9] The shift is also appreciable when a very small amount of cadmium is inserted at site **2**, as reported in Table 3 for Cd5 and Cd10.

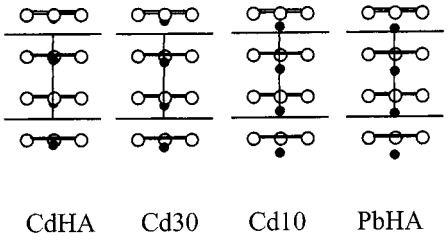

Figure 4. A view of the OH oxygen position (black circles) along the *z* axis in CdHA, PbHA and mixed Cd−Pb hydroxyapatites

The distortion indices of the phosphate group of the solid solutions (data are reported in the Supporting Information) are greater than those of the end members, indicating that the cationic substitution also induces deformations in the phosphate tetrahedra. In any case, the observed distorsions are consistent with the data reviewed by Baur.[14]

Cd−PbHA ^{31}P MAS NMR

The pure phases, $Cd_{10}(PO_4)_6(OH)_2$ and $Pb_{10}(PO_4)_6(OH)_2$, each present a unique isotropic signal at $\delta = +12.2$ and -0.7, respectively, according to the presence of a unique crystallographic site for the phosphate group in the apatitic cell. The chemical shift variation between CdHA and PbHA can be correlated to the increase in the lattice parameters.[15]

It should be noted that the chemical shift difference between these two phases is relatively large ($\Delta\delta \approx 13$), because the signal for CdHA is the most deshielded of the known hydroxyapatites for which δ_{iso} is in the range -0.7 to $+2.9$.[16−18] When considering the partial substitution of Cd for Pb at the metallic sites, one has to consider the cationic environment of the phosphate group. The phosphorous atom displays 9 (O−M) contacts, as shown in Figure 5.

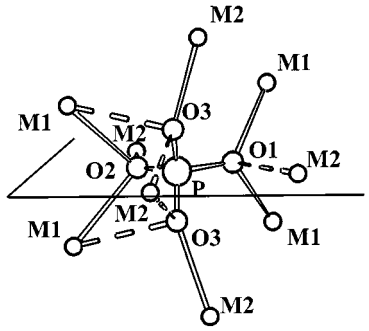

Figure 5. The cationic environment of the phosphate group; the bonds longer than 2.7 Å are dotted; the mirror plane is enhanced

If we assume a statistical distribution of the cadmium atoms over the different sites, one would expect, through progressive replacement of Pb by Cd, various cationic environments, ranging from zero cadmium, nine lead atoms (abbreviated as PPb_9) to nine cadmium, zero lead atoms (abbreviated as PCd_9). In the frame of this assumption, the relative proportion of a $PCd_xPb_{(9-x)}$ environment (x = integer) is given by the statistical formula

$$p_{[PCd_xPb_{9-x}]} = C_9^x\, p_{Cd}^x\, p_{Pb}^{9-x}$$

where C_9^x is the binomial coefficient

$$\left(\frac{9!}{x!(9-x)!}\right)$$

and p_{Cd} and p_{Pb} represent the atomic fractions of Cd and Pb, respectively. Assuming that the first metallic neighbours primarily determine the shielding of the phosphorus nucleus, one therefore expects essentially ten different ^{31}P chemical shifts.

With the oversimplified assumption of regular ^{31}P deshielding by increasing the number x of Cd atoms in the immediate environment of the phosphorus nucleus, the ^{31}P NMR MAS spectrum should present a maximum of ten isotropic signals with an interline separation of approximately (12.2 + 0.7)/9 ppm, i.e. 1.4 ppm (240 Hz at 9.4 T). The relative intensity of each signal is proportional to the probability of each environment. Actually, as shown in Figure 5 where it is evident that P, O1, O2, and three M2 atoms lie in the mirror plane, six types of metal atoms have to be considered and this can affect the shielding of the P nucleus in different ways, that is:

− in the mirror plane, $M_2(O_1)$, $M_2(O_2)$ and $M_2(O_3, O_3)$

− out of the mirror plane, $M_1(O_1)$, $M_1(O_2)$ and $M_2(O_3)$

Furthermore, for a given $[PCd_xPb_{(9-x)}]$ group, the ^{31}P chemical shift is also slightly affected by more remote metallic substituents.

Both these effects, which act as a perturbation of the dominant "nearest-neighbour effect" should, at best, lead to some broadening of the isotropic signal of the $[PCd_xPb_{(9-x)}]$ group with respect to those of the "pure" $[PPb_9]$ and $[PCd_9]$ groups (maximum broadening for the

most disordered cases [PCd_5Pb_4] and [PCd_4Pb_5]). The spectrum of a mixed lead−cadmium hydroxyapatite should therefore appear as a succession of nearly regularly spaced signals between $\delta = -0.7$ and $+12.2$, the most intense signal shifting progressively to higher frequencies by progressive replacement of lead by cadmium. Such types of solid-state MAS spectra were recently observed by ^{207}Pb NMR spectroscopy for solid solutions of lead−strontium nitrates.[19]

If the line width of the individual lines exceeds the chemical shift difference (due to both homogeneous and heterogeneous line broadening), the different signals are no longer resolved and the isotropic resonances should appear as a unique band, eventually with shoulders. The position of this band should shift to higher frequencies when increasing the cadmium content and its width should reach a maximum for an equal content of cadmium and lead. It is what is actually observed with the samples Cd20 and Cd30, for which the isotropic signal ($\Delta\nu_{1/2} \approx 1$ kHz) moves slightly from $\delta = 1.8$ to 1.9, but the spectra for the samples with lower Cd content cannot be explained in the frame of these assumptions.

Actually, the spectra of these mixed phases consist of two isotropic resonances at approximately the same positions [$\delta \approx -1.0$ (narrow) and $\delta \approx +1.0$ (broad)]. The relative intensity of both signals, obtained from line-fitting analysis, amounts to approximately 1:1 for Cd5 and approximately 1:3 for the Cd10 sample (Table 4). Although the overall line width is significantly larger for the latter ($\Delta\nu_{1/2} \approx 800$ Hz) than for the former ($\Delta\nu_{1/2} \approx 600$ Hz), no additional signal could be detected on the high frequency part of the isotropic band for the Cd10 sample. Therefore one must assume that identical $PPb_{(9-x)}Cd_x$ groups are present in both mixed phases, but with different concentrations. Let us return to the results of the Rietveld calculation: it has been demonstrated that cadmium atoms are preferentially located at site **1**. At low cadmium contents, Cd is almost exclusively at site **1**, as confirmed by crystallographic analysis (Table 2).

Furthermore, in manganese-substituted fluorapatites, Suitch et al.[20] showed that one Mn^{2+} ion at site **1** per unit cell distorts the phosphate tetrahedron in such a way that it hinders the fixation of another Mn^{2+} at both sites **1** and **2**, leading to the partial segregation of the Mn^{2+} ions in one of the four channels of the apatitic cell. This situation can also be anticipated in the present case of Pb−Cd apatites.

For an amount of 5% Cd, only one out of eight sites **1** are occupied by a Cd^{2+} ion: That means that only one out of every two unit cells contains a Cd^{2+} ion. Then two different environments for the phosphate group are equally probable, that is PPb_9 and $PCdPb_8$; or when considering only sites **1** in the unit cell (labelled as $_{S1}$): **A** = $[P(Pb_4)_{S1}]$ and **B** = $[P(CdPb_3)_{S1}]$ (see Figure 6), where **A** would give the narrow isotropic signal at $\delta = -1.0$ and **B** the relatively broad signal at $\delta = +1.0$. Distortion of the groups **B** with respect to **A** is apparent from the higher chemical-shift anisotropy of the corresponding NMR signal, leading to a relatively higher intensity of their spinning side bands at either rotor speeds (see Figure 3a).

For the manganese-substituted fluroapatites containing 5 atom-% Mn, Suitch et al.[20] observed two distinct IR stretching $\nu_1(PO_4)$ bands, which they assigned similarly to the two kinds of phosphate, with or without an interaction with a Mn^{2+} cation. For higher manganese content, Suitch et al.[20] observed the progressive disappearance of the IR band assigned to the phosphate group not interacting with an Mn^{2+} cation: they suggested that for the composition [$MnCa_9(PO_4)_6F_2$], there is strictly one Mn atom per unit cell, that is a regular arrangement of Mn^{2+} alternated with Ca^{2+} cations at one site **1** channel or, considering the P environment, there is one unique group $P(Ca_3Mn)_{S1}$.

A similar situation in Cd10 would lead to an NMR spectrum with a unique isotropic resonance at approximately $\delta = +1.0$ (due to group **B**). Actually, the NMR spectrum exhibits two resonances at $\delta = -1.0$ and $+1.0$. In agreement with the results obtained for Cd5, the two resonances could be assigned to a group **A** and to a group **B**. However, taking into account the stoichiometry of the sample, it is necessary to postulate the presence of a third group **C** containing two cadmium atoms at site **1,** with an **A/B/C** ratio of 0.25:0.5:0.25. This hypothesis would also justify the relative amounts of the two NMR signals, provided that the shielding for the **C** group is almost the same as that for the **B** group (that is, the chemical shift increment when substituting the second Cd^{2+} ion is smaller than that due to the first Cd^{2+} cation). The presence of **C** groups, with partial clustering of cadmium atoms in Cd_2 pairs, would explain

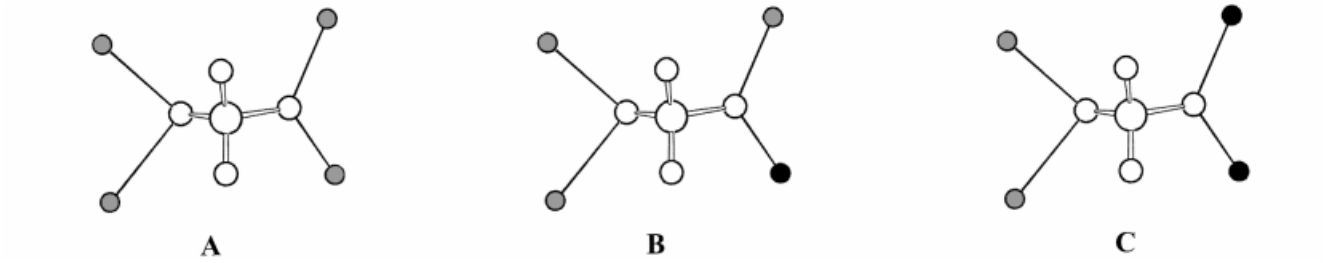

Figure 6. Phosphate group environments displaying three possible distributions of Pb (grey circles) and Cd (black circles) in site **1**

the pronounced phosphate distortion of the samples at low Cd content.

Conclusions

The results of this paper indicate that CdHA and PbHA exhibit only a limited range of solubility: cadmium can substitute lead up to 30 atom-%, whereas lead seems to avoid the incorporation into CdHA. Cadmium ions display a clear preference for site **1** of the apatite structure, in agreement with the shorter metal−metal distances at this site than at site **2**. When the cadmium content is increased, part of the substituent cations begin to fill site **2**, so that at the maximum degree of substitution, two of the four metal ions at site **1** are Cd, whereas only one of the six metal ions in the equilateral triangles characteristic of site **2** is Cd. The preference of cadmium for site **1** is responsible for the observed significant shift of the OH group towards the plane of the site **2** metals, as shown by its increase when the cadmium content at site **1** is increased. Furthermore, the presence of a relatively low amount of cadmium at site **1** induces a limited, but appreciable distortion of the phosphate tetrahedra that might be due to the presence of two different environments for the phosphate group, in agreement with the results of NMR spectroscopic analysis.

Experimental Section

General: Cadmium−lead hydroxyapatites were synthesized in aqueous systems by a double decomposition method,[6,7] starting from solutions containing 5, 10, 20, 30, 40, 50, 60 atom-% Cd, where atom-% = [Cd/Cd + Pb] × 100. The samples obtained are labeled as Cd%, where % is the amount of Cd^{2+} ions in the solution. − Stoichiometric quantities of cadmium nitrate and lead acetate (0.05 M solution A) and disodium hydrogen phosphate (0.03 M, solution B) were prepared separately in distilled water. The (Cd + Pb)/P molar ratio was adjusted to be the stoichiometric one (1.67); each solution was stirred under nitrogen. Solution A was added to solution B, maintained at 100 °C under nitrogen to improve the homogeneity of the precipitate, and to prevent the formation of carbonated apatites. The precipitate was allowed to be in contact with the mother solution for 2 h, then filtered and washed with hot distilled water. An aqueous solution of ammonia was then added in order to maintain the pH value at about 11 during the maturation (3 h) at 100 °C. The precipitate was then filtered and dried at 110 °C for 24 h. − The XRD data were collected with a Philips PW 1710 diffractometer using a graphite monochromator. The step range was from 5 to 95°(2θ), with a counting time of 10 s for each step and a step width of 0.03°. − ^{31}P MAS NMR spectra were obtained at room temperature with a Bruker MSL400 spectrometer (9.4 T) operating at 162 MHz, using a 4-mm MAS Doty probe. − Magic angle spinning (MAS) spectra were obtained with spinning rates up to 5 kHz, using single-pulse excitation. Chemical shifts are reported relative to 85% aqueous orthophosphoric acid H_3PO_4 (δ= 0).

Structural Analysis: The full pattern refinements were carried out by means of the Rietveld method using the DBWS-9411 program.[21,22] − The space group ($P6_3/m$, no. 176) and the atomic positions of the lead hydroxyapatite structure[12] were used as the starting set in the refinement procedure. The X-ray scattering factors for Cd^{2+}, Pb^{2+}, O^- ions and for the P atom were used. A third-order polynomial was employed to assimilate the background while the peaks were fitted by using a pseudo-Voigt function. The halfwidth of the diffraction peaks as a function of 2θ was evaluated by the Caglioti equation.[23] In the first cycles, the scale factor and the background coefficients were refined. Successively, the profile parameters (peak widths and their dependence on 2θ, true 2θ zero, Lorentzian fraction) and the lattice parameters were allowed to vary too. Finally, the occupancy factors (O.F.) were refined and the cation substitution was tested. − No constraint was imposed on the overall cadmium content. The two metal sites were imposed to be fully and complementarily occupied by lead and cadmium. The occupancy factors of O and P were assumed as constant, in agreement with the apatite stoichiometry. The fractional atomic coordinates were refined, starting from the atomic positions of the two metals. No attempt was made to distinguish the position of Pb atoms from that of the substituting Cd atoms. The same thermal factors (t.f.) were used for Cd and Pb atoms; the individual t.f. values were kept constant but an overall thermal parameter was refined. In the last refinement cycles, optimizing 28 variables (structural and nonstructural parameters) simultaneously tested the possible preferred orientations of the 001 reflections. All the nonstructural refined parameters are reported as Supporting Information and are available on the WWW under http://www.wiley-vch.de/home/eurjic or from the author. − Further details of the crystal-structure investigations may be obtained from the Fachinformationszentrum Karlsruhe, 76344 Eggenstein-Leopoldshafen, Germany, on quoting the depository numbers CSD-411418 to -411421.

Acknowledgments

We greatly acknowledge financial support from MURST (Italy), the University of Bologna (Funds for Selected Topics), the Direction Générale de la Recherche Scientifique et Technique (Tunisia) and the Centre National de la Recherche Scientifique (France).

[1] *CRC Handbook of Bioactive Ceramics*, vol. II ("Calcium Phosphates and Hydroxyapatite Ceramics") (Eds.: T. Yamamuro, L. L. Hench, J. Wilson), CRC Press, Boca Raton, **1990.**
[2] J. C. Elliott, *Structure and Chemistry of the Apatites and Other Calcium Orthophosphates*, Elsevier Sci., The Netherlands, **1994.**
[3] A. Bigi, E. Foresti, M. Gandolfi, M. Gazzano, N. Roveri, *J. Inorg. Biochem.* **1995**, *58*, 49−58.
[4] I. Mayer, H. Cohen, J. C. Voegel, F. J. G. Cuisinier, *J. Cryst. Growth* **1997**, *172*, 219−225.
[5] J. Christoffersen, M. R. Christoffersen, N. Kolthoff, O. Bärenholdt, *Bone* **1997**, *20*, 47−54.
[6] A. Bigi, M. Gazzano, A. Ripamonti, E. Foresti, N. Roveri, *J. Chem. Soc., Dalton Trans.* **1986**, 241−244.
[7] A. Bigi, G. Filini, E. Foresti, M. Gazzano, A. Ripamonti, N. Roveri, *J. Inorg. Biochem.* **1993**, *49*, 69−78.
[8] H. Heijiligers, F. C. M. Driessens, R. M. H. Verbeck, *Calcif. Tissue Int.* **1979**, *29*, 127−131.
[9] A. Bigi, A. Ripamonti, S. Brückner, M. Gazzano, N. Roveri, S. A. Thomas, *Acta Crystallogr.* **1989**, *B45*, 247−251.
[10] M. T. Kay, R. A. Young, S. A. Posner, *Nature* **1964**, *204*, 1050−1052.
[11] M. Hata, K. Okada, S. Iwai, M. Akao, H. Aoki, *Acta Crystallogr.* **1978**, *B34*, 3062−3064.
[12] S. Brückner, G. Lusvardi, L. Menabue, M. Saladini, *Inorg. Chim. Acta* **1995**, *236*, 209−212.
[13] A. Bigi, M. Gandolfi, M. Gazzano, A. Ripamonti, N. Roveri, A. Thomas, *J. Chem. Soc., Dalton Trans.* **1991**, 2883−2886.
[14] W. H. Baur, *Acta. Crystallogr.* **1974**, *B30*, 1195−1215.
[15] M. T. Weller, G. Wong, *J. Chem. Soc., Chem. Commun.* **1988**, 1103−1104.

[16] J. P. Yesinowski, *J. Am. Chem. Soc.* **1981**, *103*, 6266−6267.
[17] B. Badraoui, M. Debbabi, R. Thouvenot, *C. R. Hebd. Acad. Sci., Ser. IIC* **2000**, *3*, 107−112.
[18] B. Badraoui, M. Debbabi, R. Thouvenot, unpublished results.
[19] Y.-S. Kye, G. S. Harbison, *Inorg. Chem.* **1998**, *37*, 6030−6031.
[20] P. R. Suitch, J. L. LaCout, A. Hewat, R. A. Young, *Acta Crystallogr.* **1985**, *B41*, 173−179.
[21] M. Rietveld, *J. Appl. Crystallogr.* **1969**, *2*, 65−71.
[22] R. A. Young, A. Sakthivel, T. S. Moss, C. O. Paiva−Santos, *J. Appl. Crystallogr.* **1995**, *28*, 366−367.
[23] G. Caglioti, A. Paoletti, F. P. Ricci, *Nucl. Instrum.* **1958**, *3*, 223−228.

Received August 4, 2000
[I00306]

EXAFS Data Analysis of Vitamin B_{12} Model Compounds − A Methodological Study

Emiliano Fonda,[a,b,c] Alain Michalowicz,[c] Lucio Randaccio,*[a] Giovanni Tauzher,[a] and Gilberto Vlaic[a,b,d]

Keywords: EXAFS spectroscopy / Cobaloxime / Vitamins

In view of several controversial EXAFS results on cobalamins and B_{12} model compounds published in the last ten years, a methodological study is presented to explain the origin of these controversial results and to propose how to improve EXAFS structural-parameter refinement. The advantages and limitations of first-shell filtering, constrained refinement, and the importance of the mapping technique are described in order to suggest and encourage improvement of data-analysis codes. The conclusions can be generalized and applied to the EXAFS analysis of the majority of metal complexes

Introduction

The B_{12}-based enzymes are among the few cofactors known so far that contain a metal−carbon bond. These coenzymes belong to the alkylcobalamin series (RCbl). They consist of a cobalt corrinoid with a pendant nucleotide, which occupies five coordination sites of a pseudo-octahedral Co^{III}, the sixth position being occupied by an R alkyl group or by a CN ligand in vitamin B_{12} itself (Scheme 1).[1,2] All the currently known B_{12} enzymatic reactions involve the making and breaking of the Co−C bond. In order to better understand the structure and reactivity of cobalamins, simple models have been proposed and investigated. The cobaloximes $LCo(DH)_2R$ (L = Lewis base, $(DH)_2$ = bis(dimethylglioximate)] represent the most widely studied class of models.[3] Such model studies have complemented those on cobalamins well,[1,2] thereby providing clues into the elusive mechanisms of B_{12}-dependent enzymatic processes, particularly those involving the homolytic Co−C cleavage.[3] One of the problems was the knowledge of the accurate structure of cobalamins. Up to a few years ago, for reasons previously reported,[4] the available structural determinations, based on conventional X-ray sources, were of poor accuracy, in contrast with the very accurate structures of the simple models.[3] Only recently[4,5,6] have the first accurate determinations based on synchrotron diffraction data appeared.

However, the interest in the structure of these systems has also prompted several Extended X-ray Absorption Fine Structure (EXAFS) studies, principally on cobalamins,[7,8,9] but also on models[10] and more recently on the B_{12} coenzyme bound in methylmalonyl-coenzyme A mutase.[11,12]

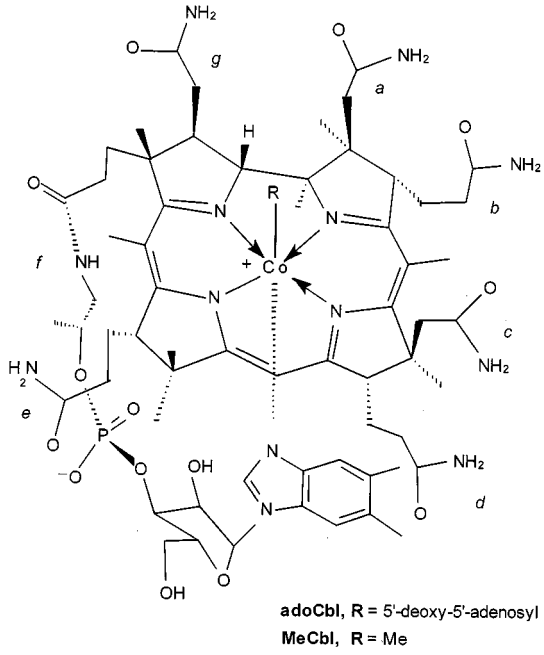

Scheme 1

The main advantage of EXAFS with respect to X-ray Diffraction (XRD) is that it does not require crystalline samples and can be used in solution. Although EXAFS is expected to be an order of magnitude less accurate than XRD for small molecules,[13] EXAFS can be exploited in the structural studies of metallo-proteins when XRD is not available and, more importantly, to follow the variations in the coordination about the metal centres within the active site.[14] In recent years, as the number of EXAFS results on B_{12} derivatives[7,8,9] and related model compounds[10] has increased, the discussion of these results, when compared to crystal structures, has become controversial.

In almost all EXAFS works, the Co−ligand distances have been deduced from fits of the first shell Fourier-filtered spectrum. This method, largely used since the pioneering

[a] Dip. Scienze Chimiche, Università degli Studi di Trieste, Via Licio Giorgieri 1, 34127 Trieste, Italia
[b] Sincrotrone Trieste SCpA, SS14 km 163.5, 34012 Basovizza (Trieste), Italia
[c] Laboratoire GPMD, Univ. Paris XII-Val de Marne, 61, Avenue du Général de Gaulle, 94010 Créteil Cedex, France
[d] INFM, Laboratorio TASC, Padriciano 99, 34012 Trieste, Italia

 © WILEY-VCH Verlag GmbH, 69451 Weinheim, 2001 1434−1948/01/0505−1269 $ 17.50+.50/0

works in EXAFS,[15] has been criticized[16,17] in the case of B_{12} for two reasons: i) Fourier filtering may lose a part of the actual signal. In fact, the contribution of the axial ligands from between the first and second coordination spheres may overlap; ii) The information contained in the first shell Fourier-filtered signal is insufficient to allow for any reliable determinations of the coordination distances of the equatorial Co−N distances and of the two axial ligands. For instance, Chance used this method to determine the local structure of Co in cobalamins and enzyme-bound cobalamins.[7−9] However, in the case of $(H_2OCbl)[ClO_4]$, there were dramatic discrepancies between the accurate XRD structure and that obtained by EXAFS.[8] In fact, the EXAFS value of the Co−N axial distances in H_2OCbl^+ [2.14(3) Å] and in $Co^{II}Cbl$ [1.99(3) Å] appear to be reversed with respect to those determined by XRD [1.925(2) and 2.13(2) Å, respectively]. Furthermore, the *trans* influence of H_2O, CN and SO_3-Cbl appeared to be very similar from EXAFS analysis, the *trans* axial Co−N distances varying in the range 2.14(3)−2.16(4) Å.[9] On the contrary, XRD results indicate a dramatic lengthening of the axial Co−N bond in SO_3^{2-} [2.149(5) Å][5a] and CN^- [2.041(3) Å] derivatives,[5b] with respect to the value of 1.925(2) Å found in the aqua derivative.[6]

Recently, more reliable methods than Fourier filtering of the first shell were employed. Giorgetti et al.[10] worked on a series of Costa-type models $(H_2O)Co(DO)(DOH)R$, in which R = CH_2CF_3, CH_2CO_2Me Me, CH_2Ph, *i*Pr, and (DO)(DOH)=*N*,*N*′-propanediylbis(2,3-butanedione-2-imine-3-oxime). These authors studied the variation of the distances between cobalt and its first neighbours, while the rest of the structure was kept constant. Multiple-scattering (MS) calculations and unfiltered data had been employed. Nevertheless, analogous large discrepancies (0.15−0.2 Å) in the axial coordination bond lengths, also including opposite trends of the R *trans* influence, were detected in a subsequent XRD study.[18] Scheuring et al.[11] employed the so-called "global-mapping technique" to study B_{12} in the glutamate mutase enzyme. Unfiltered data sets and MS calculations were employed. This technique consists of mapping the value of the χ^2 versus the variation of the distances of two ligands, while the rest of the structure is kept fixed. The minima in the map correspond to possible distances. Two possible Co−N axial distances were found. Between the short (2.17 Å) and the long (2.6 Å) distances, they chose the latter, because an XRD structure[19] of the B_{12}-enzyme indicated a long distance. Champloy et al.[12] worked on methylcobalamin bound to the enzymes, glutamate mutase and 2-methylene glutarate mutase. They found identical EXAFS spectra for the free and enzyme-bound MeCbl and two minima at the same distances as those of Scheuring et al.[11] In the free Me-Cbl, the Co−N axial distance is "short" and a recent X-ray structural determination of MeCbl furnished an axial Co−N distance of 2.162(4) Å.[5b] On this basis, they define the long distance found by Scheuring et al.[11] as implausible. However, the reason for the appearance of the other minimum in the EXAFS modelling was not clearly established.

In view of the various approaches adopted so far to examine EXAFS data,[8,10−12,20] it is highly desirable to study and discuss the fundamental aspects of EXAFS data analysis of this kind of compound, in order to find a way to standardize analysis of EXAFS results. In fact, despite the fact that it is becoming a common technique, EXAFS may risk losing its credibility among biochemists and chemists because of the above controversy. Therefore, it is essential to better understand what kind of structural information can actually be obtained by EXAFS. We present here an EXAFS methodological study carried out on several cobaloximes, $RCo(DH)_2py$ with R = Cl, N_3, Me, CH_2Ph, adamantyl (adam)[21] (see Figure 1). These cobaloximes were chosen since their structures have been determined with great accuracy.[22] Furthermore, they are stable under measurement conditions and can be handled without the main problems associated with cobalamins, namely their sensitivity to visible light or X-rays.[23] Finally, their axial fragments exhibit as wide a range of bond lengths as possible. These characteristics are essential to carry out an intensive and reliable methodological study. Using B_{12} compounds would have made this work much more complicated, while leaving much room for ambiguity. However, we plan to carry out a similar analysis on B_{12} complexes in the near future. Such a study would have added significance in view of the recent finding that the lengthening due to the trans influence of R in cobalamins is about twice that in cobaloximes.

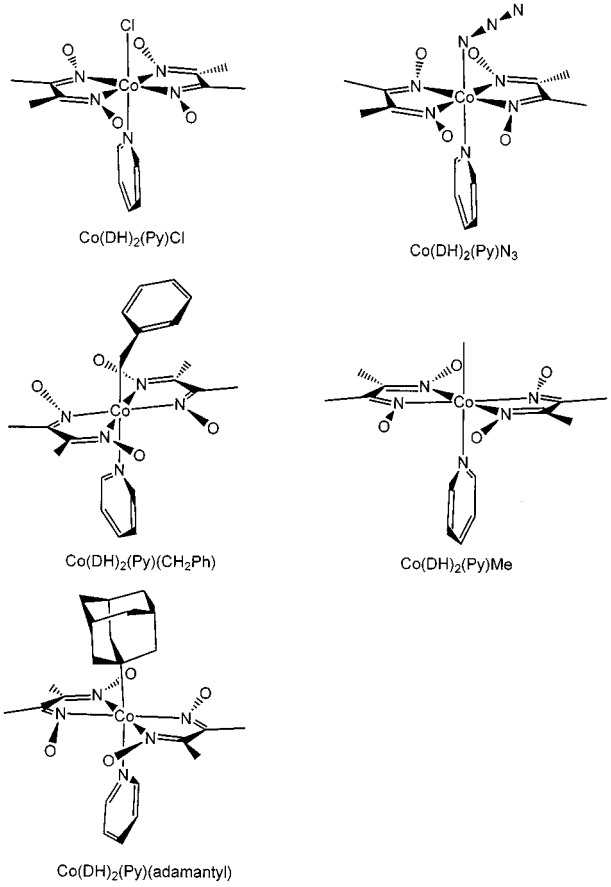

Figure 1. Schemes of the studied complexes, the upper ligand is the only one that changes through the series

Results and Discussion

Limits of the "First-Shell Analysis"

The most common method used to analyze EXAFS data consists of isolating the nearest-neighbours (NN) contributions by Fourier filtering the EXAFS signal. This method has been applied successfully in many cases since the beginning of EXAFS analysis,[24] and its description can be found in a large number of reviews and books.[13,25−27] Although this method is easy to apply because it drastically reduces the complexity of the calculations, it suffers from the limitations discussed in the introduction section. Furthermore, when applying the back-Fourier filtering window, the choice of the limits is not always easy and is always arbitrary. It is a trial and error procedure, while it is often presented as a simple one-way procedure. An example of this and similar problems is given later for R = adam (Figure 2). Finally, if the resolution of EXAFS is expressed as $\Delta r = \pi/(2\Delta k)$, in present case this translates to approximately 0.08−0.10 Å. If the distances do not differ by more than Δr, EXAFS will not resolve them. For the molecules considered in this work, ligands are at distances that differ by approximately 0.1 Å (see Table 2, crystallographic distances) so we are near the limits of the technique.

"First-Shell Analysis" Applied to Cobaloximes

In Table 1, the results of r-space refinements of the first-coordination shell are shown and r-space intervals are shown in Figure 3. When the experimental signal is approximated with a variable number of N atoms at the same distance (Table 1.i), almost 6 neighbours were found only if R = N_3. This should not be surprising: if R = N_3, the Co−R, Co−py, and Co−N(DH)$_2$ distances are quite close (see Table 2, crystal ref.), and this simple model can be used to obtain an acceptable coordination number (CN) and average distance. A lower CN indicates that interference between various contributions reduces the total signal. Therefore, another approach to obtain the actual coordination numbers and distances is to take into account that NN are at two or three different distances. In this case, it has been assumed that 4 N donors are at the same distance (corresponding to the four N donors of (DH)$_2$]. A variable number of N (or Cl or C when indicated in brackets) has been refined as a second contribution to the signal (results are shown in Table 1.ii). In this way, although axial distances are within ±0.05 Å of XRD values (see Table 2, Crystal. ref.), for R = adam, CH_2Ph, and Me, a ligand is apparently missing. For R = Cl, the Cl position is easily determined, but only 4.3 nitrogen atoms are detected in the first shell. Finally, in the case of R = N_3, the coordination number (CN) is correct (5.7 ± 0.4, i.e., 6 NN), but the distance of the first four N donors is 0.05 Å longer, and that of the axial ones is 0.1 Å shorter than the corresponding XRD values. This can be explained in terms of the correlation between the parameters, since the three actual distances are 4 × 1.895, 1 × 1.950, and 1 × 1.973, and it is difficult to resolve them by EXAFS. Finally, a three-distance model, with three free distances and fixed coordination numbers, was employed (the results are reported in Table 1.iii). For R = adam and R = CH_2Ph, the results are acceptable (differences with respect to XRD values are less than ±0.07 Å) and χ^2_v of model ii) and iii) are comparable. On the contrary, for R = Cl, Me, and N_3, errors exceeding 0.1 Å have been found and χ^2_v of model iii) is bigger than that of more

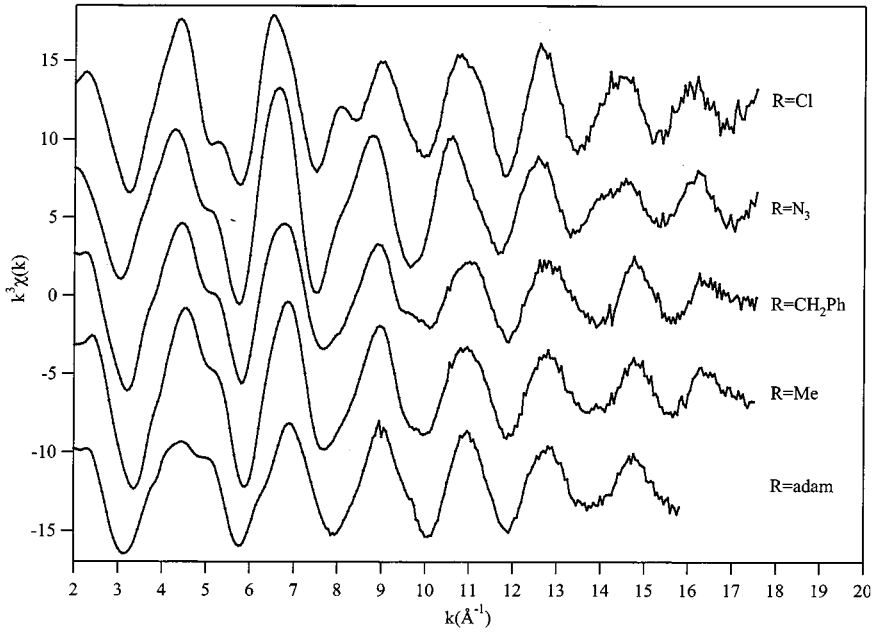

Figure 2. Raw k^3-weighted EXAFS spectra are shown; spectra have been extracted and interpolated on a grid with Δk = 0.02 Å^{-1}; no filtering or smoothing has been applied; spectra are shifted for clarity

Table 1. Results of refinements limited to the first shell; data were obtained with refinements in *r*-space (intervals are shown in Figure 3) assuming i) a model with a variable number of N atoms at the same distance; ii) a model with 4 N at one distance and a variable number of N at another distance (except for R = Cl and Me); iii) a model with 4 N at one distance and the actual atoms of R and Py (N) at a second and third distance, respectively. The refinement degree of freedom is labelled ν

i)	R = adam	R = CH_2Ph	R = Cl	R = Me	R = N_3
N	2.5±0.5	4.0±0.5	/	4.5±0.3	5.6±0.5
σ^2 (Å^2 10^{-3})	2±1	3.8±0.7	/	3.8±0.4	3.7±0.5
R (Å)	1.884±0.009	1.886±0.007	/	1.898±0.004	1.927±0.005
E_0 (eV)	3±3	−4±2	/	3±1	2±2
χ^2_ν	14	3.4		0.93	3
ν	6	3		4	4
ii)	R = adam	R = CH_2Ph	R = Cl	R = Me	R = N_3
N	4	4	4.3±0.6	4	4
σ^2 (Å^2 10^{-3})	3.9±0.5[a]	3.2±0.4[a]	3.3±0.8	3.2±0.3[a]	2±1[a]
R (Å)	1.89±0.01	1.893±0.007	1.918±0.006	1.895±0.006	1.942±0.007
N	1.3±0.5	1.0±0.6	1(Cl)	0.6±0.3(C)	1.7±0.4
σ^2 (Å^2 10^{-3})	3.9±0.5[a]	3.2±0.4[a]	3.2±0.8	3.2±0.3[a]	2±1[a]
R (Å)	2.15±0.03	2.05±0.01	2.247±0.009	2.0±0.04	1.86±0.03
E_0 (eV)	1±4	0±3	3±2	4±2	0±2
χ^2_ν	12.5	2.5	3.9	1.0	3.1
ν	5	2	6	3	3
iii)	R = adam	R = CH_2Ph	R = Cl	R = Me	R = N_3
N	4	4	4	4	4
σ^2 (Å^2 10^{-3})	3.7±0.6[a]	3.4±0.5[a]	2.6±0.8[a]	3.6±0.4[a]	3±1[a]
R (Å)	1.88±0.01	1.89±0.01	1.925±0.007	1.90±0.04	1.94±0.01
N	1	1	1 (Cl)	1	1
σ^2 (Å^2 10^{-3})	3.7±0.6[a]	[a]	3.2±0.7	[a]	[a]
R (Å)	2.12±0.03	2.10±0.03	2.24±0.01	1.9±0.3	1.85±0.05
N	1	1 (C)	1	1 (C)	1
σ^2 (Å^2 10^{-3})	3.7±0.6[a]	[a]	[a]	[a]	[a]
R (Å)	2.23±0.04	2.02±0.05	1.83±0.03	2.07±0.05	1.88±0.07
E_0 (eV)	2±5	1±3	1±2	6±1	0±3
χ^2_ν	15	2.5	4.0	2.0	4
ν	5	2	5	3	3

[a] This symbol indicates that the reported values are the same for a specific model and sample.

simple models. In the case of R = Me the position of Me is undetermined (1.9±0.3 Å). Therefore, unacceptable results are obtained in at least 50% of the cases. The Co−Cl distance and the average distance between cobalt and the four $N(DH)_2$ are accurately determined, because their contributions are dominant.

An Approach to a Complete Simulation

Another way to analyze EXAFS data is to consider the unfiltered spectrum in *k*-space, or an *r*-space interval large enough to cover all relevant peaks (in the studied cobaloximes almost all relevant contributions are below 4 Å). Thus, information from a large number of contributions is included in the analyzed region. On the other hand, the number of independent points is limited (in our case to approximately 25) and is not sufficiently larger than the number of fitted parameters. For this reason, the set of parameters should be carefully chosen before performing a refinement. Care must be taken in choosing the relevant parameters and in linking related quantities, thereby avoiding redundancies. Constraints are based on the knowledge that we have of similar structures. It will be demonstrated that the use of such constraints, whenever possible, is of primary importance. If the system is completely unknown, EXAFS analysis is restricted to a comparison with known systems or first-shell analysis. In most cases, the challenge is to determine which of the several models reproduces the actual structure. In B_{12} model compounds (cobaloximes, in this work) the main problem is to determine the distances of the ligands from cobalt. Schematically a cobaloxime (see Figure 1) may be represented by two coplanar chelate ligands (two DH units referred by a mirror). Thus, the system may be defined by considering ligands as rigid bodies and only specifying the Co−N(DH)$_2$, Co−N(py), and Co−(R) distances and, in the case of R = Ch_2Ph and R = N_3, the angles Co−C_1−C_2 and Co−N_1−N_2 respectively. Actually, such angles are in the range 110°−120° [121.8(1)° for R = N_3[22b] and 116.7(2)° for R = CH_2Ph[22c]]. With regard to the results presented here and in the following discussion, the angles have been fixed at these values. This has been done in order to simplify the calculations and to focus the discussion on the problem of determining distances. However, it has been verified that refinements that include these angles give correct results (within EXAFS accuracy), that is, 127 ± 2° in the case of R = N_3 and 116 ± 3° in the case of R = CH_2Ph. It is worth noting that the use of the structures of rigid bodies directly taken from crystallographic databases suffers from some limitations. Sometimes small

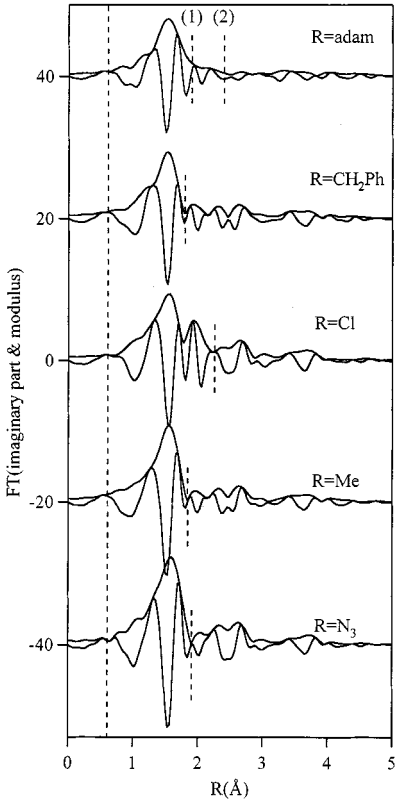

Figure 3. Fourier transform (not phase corrected, imaginary part and modulus plots) of the EXAFS spectra shown in Figure 2; two vertical dashed lines show approximate filtering intervals used to obtain the results in Table 1; for R = adam, two limits (1) and (2) are possible; limit (2) was chosen to obtain the results shown in Table 1; spectra are shifted for clarity

changes (±0.02 Å) to the internal distances can significantly improve the fit of EXAFS data. This happens when two significant contributions interfere, for example, Co−C(DH)$_2$ and Co−O(DH)$_2$ interfere destructively, (see Figures 4 and 5) and their relative distances are critical in determining the signal amplitude. However, it is easy to apply a correction because their contributions are strong and nearly in perfect opposition. Most likely, the best way to do this is a *restrained refinement* as described by Binsted et al.[28] The method used in the present work is a *constrained refinement*,[28] since the former was not possible with the codes in our possession. The remaining relevant parameters are: E_0 to match experiment and theory edge position, S_0^2 (amplitude reduction factor) and a series of Debye−Waller factors (σ_i^2). S_0^2 has been fixed to 1 as suggested by Roy and Gurman[29] (this assumption was tested on $Co(NH_3)_6Cl_3$). The σ_{SS}^2 (single-scattering Debye−Waller factors) values are expected to be very close to each other, and they have been fixed at the same value for similar atoms at similar distances. Only the Co−Cl pair requires its own $\sigma_{Cl,SS}^2$, which is slightly smaller. The MS paths have different σ_i^2, but two relations have been employed to reduce the number of parameters. The σ^2 of triple-scattering paths involving the same couple of atoms in co-linear arrangements is double the single scattering σ_{SS}^2. For example, when the single-scattering (SS) path of Co−N_1−Co has its σ_{SS}^2, the MS path Co−N_1−Co−N_1−Co has $\sigma_{MS}^2 = 2\sigma_{SS}^2$; this was also assumed for paths such as Co−N_1−Co−N_2−Co when N_1 and N_2 are on opposite sides of Co. For triple-scattering paths with angles of approximately 120−160°, instead of using complex relations[20] and due to the homogeneity of the atoms and bonds involved, an average value of three times σ_{SS}^2 has been used. This empirical assumption worked satisfactorily in all five cobaloximes, speeded up calculations while performing contour plots, and did not affect the reliability of the results. Another approach is to calculate Debye−Waller factors using semi-empirical methods.[30] This procedure is flexible and more rigorous, but computationally too heavy for this work. On the other hand, the use of the simple and fast Debye-correlated model is unjustified, even if it was used by other authors for cobalamins.[11] Thanks to the above assumptions the simulation of the entire spectrum required only approximately 6−7 parameters.

Constrained Refinement of Cobaloximes and the Mapping Technique

Numerical results obtained with the assumptions described above are compared with crystallographic distances and listed in Table 2. Distances are determined with some accuracy, but it is evident that discrepancies between XRD and EXAFS are still present. Our EXAFS data were collected at liquid-nitrogen temperature (LNT), while XRD data were collected at room temperature (room temp.). Thus, some small discrepancy is expected, but not as large as 0.05 Å. However, the average accuracy in determining the axial distances with this method can be estimated to be about 0.05 Å. An explanation as to why filtering of the first peak is a risky technique for such molecules can be suggested. The contributions to the EXAFS signal for R = adam (worse simulation) and R = N_3 (better simulation) have been drawn separately in Figure 4 and Figure 5, respectively. In the case of R = adam, the filtering limit used to obtain the results in Table 1 is marked as (2). It is apparent that an important contribution from all NNN (next nearest neighbours) is present well below this limit (see Figure 4). This contribution is not negligible with respect to that of the axial donors. If a narrow filter, as limit (1) in Figure 4, is chosen, almost 50% of the axial contribution is lost (Co−N(Py) and Co−C(adam)]. A different situation is shown in Figure 5 for R = N_3: the first three contributions [Co−N(DH)$_2$, Co−N(Py) and Co−N(N_3)] are in phase and the amplitude of the signal is almost the sum of their amplitudes. This means that the majority of the contributions are included in the filter, and at the same time, the relative importance of the other contributions in the filter is negligible. In fact, for R = N_3, acceptable results have been obtained (see Table 1, a). It is interesting to observe that the Co−C(DH)$_3$ and Co−O(DH)$_2$ contributions (in Figures 4 and 5) have similar amplitudes, and opposite phases giving a very small signal. For this reason, in the region above 2 Å only small features appear, even if several NNN contributions are in that region.

Table 2. Results of fits performed with refinement *c* (see text); crystallographic values are reported for comparison; EXAFS data were recorded at liquid nitrogen temperature, and crystallographic data at room temperature; in the case of R = adam, the crystallographic values are referred to a similar structure where Py is replaced by 4-Me_2N-Py; the refinement degree of freedom is labelled ν

R		Co−N (DH)$_2$		Co−N Py		Co−R		
Adamantyl	EXAFS	1.894	±0.004	2.111	±0.009	2.218	±0.008	Å
	Crystal. ref.	1.876		2.102		2.159		Å
	σ^2_{SS}	3.6	±0.2					10^{-3}Å^2
	χ^2_ν	1.93						
	ν	16						
CH_2Ph	EXAFS	1.887	±0.004	2.07	±0.01	2.00	±0.02	Å
	Crystal. ref.	1.878		2.065		2.056		Å
	σ'^2_{SS}	3.2	±0.3					10^{-3}Å^2
	χ^2_ν	1.26						
	ν	20						
Cl	EXAFS	1.916	±0.005	1.91	±0.02	2.249	±0.004	Å
	Crystal. ref.	1.895		1.959		2.229		Å
	σ^2_{SS}	3.9	±0.2			3.0	±0.3	10^{-3}Å^2
	χ^2_ν	0.79						
	ν	21						
Methyl	EXAFS	1.893	±0.002	2.073	±0.009	1.97	±0.02	Å
	Crystal. ref.	1.896		2.069		1.999		Å
	σ^2_{SS}	3.3	±0.3					10^{-3}Å^2
	χ^2_ν	0.42						
	ν	22						
N_3	EXAFS	1.915	±0.003	1.92	±0.01	1.98	±0.01	Å
	Crystal. ref.	1.895		1.973		1.950		Å
	σ^2_{SS}	3.6	±0.2					10^{-3}Å^2
	χ^2_ν	0.69						
	ν	21						

The finding of multiple solutions, the difference between constrained and unconstrained refinements and the importance of extending the simulation as far as possible should be discussed. For this purpose, χ^2 maps have been calculated. In fact, although constrained refinement dramatically reduces correlation between variables,[28] it does not guarantee that a single solution is found. Some χ^2 maps have been obtained by varying the distances of the axial ligands [Co−N(py), Co−R] and plotting the χ^2, after the other parameters have been refined. Therefore, each point of the grid is the result of an independent refinement. Scattering paths have not been recalculated at each point. Nonetheless, phase and amplitude functions can be regarded as quite accurate in an interval of ±0.2 Å around the contour plot centre. Each minimum of the χ^2 surface is a possible solution to our problem. Contour plots reported in Figures 6, 7, and 8 have been calculated by three different refinement procedures: a) Without constraints; b) With constraints, but limiting the refinement up to 3 Å and thus excluding an isolated large peak between 3 and 4 Å; c) With a constrained refinement up to 4 Å (no contribution is present above 4 Å). Contour plots are presented only for R = adam, CH_2Ph, and Me (Figures 6, 7, and 8, respectively), since they are more representative. Inspection of these plots shows that most contain several minima. For R = adam (Figure 6, a, b, and c), there are always two close minima. They correspond to the interchange of the axial distances (adam at r_1 and py at r_2 or vice versa). The same happens for R = CH_2Ph and Me, as will be discussed later in detail. Looking at Figure 6 (a), two equivalent minima are present. Since C and N are very similar species for EXAFS, swapping the two atoms gives the same solution. If it is important to know at which distance py and adam are, a differentiation between ligands is essential. Constrained refinement is the best tool to differentiate the ligands, but it works only if the interval chosen to make the fit contains significant different contributions from the two ligands. Thus, by refinement b (Figure 6, b) two equivalent minima were found, since the most significant differences between adam and py are above 3 Å. Between 3 and 4 Å, MS is dominant and different geometries can play a significant role. In fact, in plot c, two minima are present, but one is significantly lower than the other. On a statistical basis, it is possible to determine without ambiguity the distance from the metal of each ligand. This means that we can truly distinguish between adam and py. Considering R = CH_2Ph (Figure 7), the maps are more difficult to analyze. At least four minima are present in the centre of map *a*. They can be grouped as follows [Co−C(CH_2Ph); Co−N(py)] ≈ (2.03; 2.08), (2.1; 2.02) and ≈ (1.85; 2.05), (2.05; 1.78). The first two minima correspond approximately to the exchange of the two ligands, as already described for R = adam. The other two

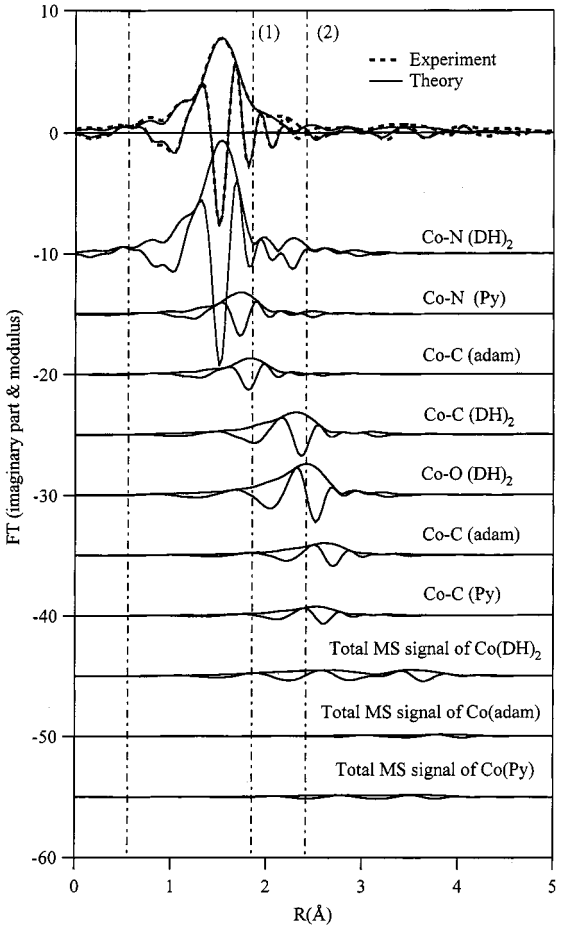

Figure 4. R = adam: comparison of FT (not phase corrected) of experimental and theoretical spectra; all contributions to the total theoretical signal are presented below, ranked for increasing frequency. MS contributions are grouped; spectra are shifted for clarity

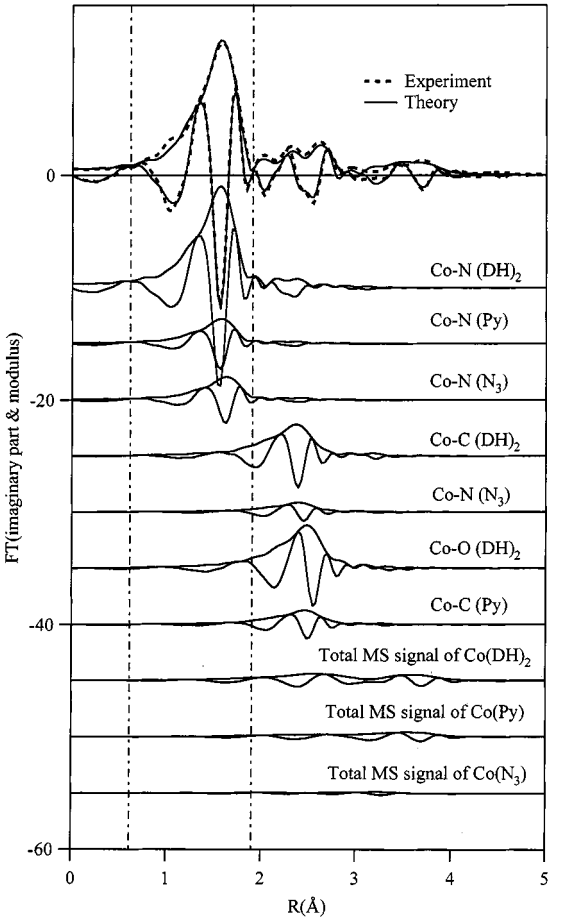

Figure 5. R = N_3: comparison of FT (not phase corrected) of experimental and theoretical spectra; all contributions to the total theoretical signal are presented below, ranked for increasing frequency; MS contributions are grouped; spectra are shifted for clarity

minima correspond to an almost correct position for one of the two axial ligands, while the other is "pushed" into the contribution of the four $N(DH_2)$ donors. Actually, this distance is even shorter than that of $Co-N(DH_2)$. The reasons for the existence of such minima can easily be explained. They are due to the fact that, while fitting the contributions of each atom independently, the $Co-C(CH_2Ph)$ contribution can be masked by the four $Co-N(DH_2)$. A small displacement of the latter and of the Co−N(py) distance then compensates for this error. If the displacement of the atoms in the first shell is linked with that of the bonded atoms and the contributions of the latter are not negligible, this rearrangement is no longer possible. Minima are then better defined, and false minima tend to disappear. For instance, compare plot a with plot b and plot c of Figure 7. Refinement c leads to a marginal improvement, and removes the minimum at $[Co-C(CH_2Ph); Co-N(py)] \approx (1.78; 2.03)$ that can be still obtained by refinement b, but it is possible to discard this solution by the *F*-test. It is worth noting that these "low-distance minima" are also present in Figure 6. These minima are at the lower limits of the map and at a high χ^2 value. In fact, Co−L and Co−R distances for R = adam are longer than for R = CH_2Ph. Thus, they are easier to distinguish and exhibit a poorer correlation with $Co-N(DH_2)$. When R = Me, it is difficult to distinguish py and Me (see minima in Figure 8, a and b) and only with refinement c (when all MS involving the atoms of py are included), can a precise minimum close to XRD results be obtained (see Figure 8, c). Note that in the contour plots for all R (Me, py, CH_2Ph) minima appear at higher distances too. They are always at map upper limits and not perfectly distinguishable, but most likely they correspond to those reported by Champloy et al.[12] The analysis of such far minima is beyond the scope of this paper, since a more complex procedure involving recalculation of scattering paths during refinements should be employed. Work will be carried out in this direction in the future to produce a more flexible and rigorous EXAFS analysis code. However, these far minima appear to be close to the NNN positions. Thus, the explanation is similar to that suggested for the lower distance minima visible in Figure 7 (a).

The approximation of keeping the distance of one axial ligand fixed to an average value obtained from similar structures, while mapping the other, has been reported in

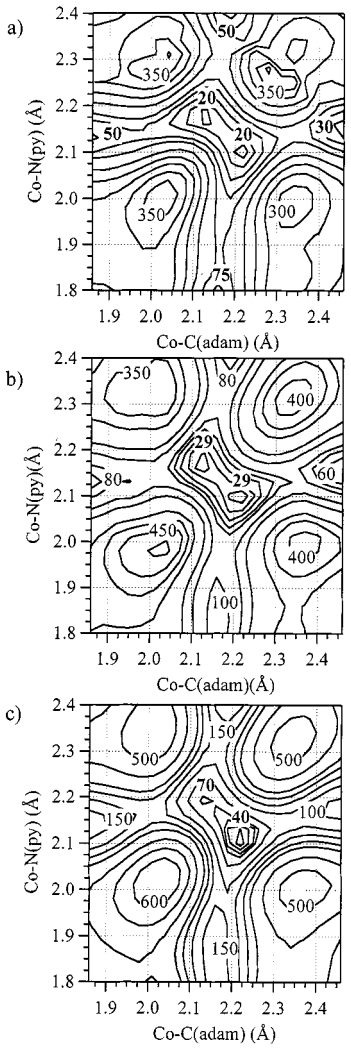

Figure 6. R = adam: contour plots obtained with refinements a, b, and c (see text for details); in case (c) one of the two local minima can be discarded and the axial ligands are distinguishable

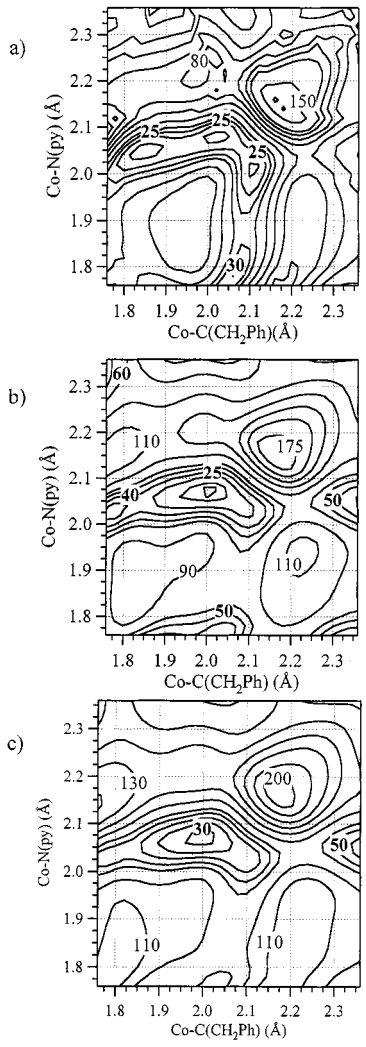

Figure 7. R = CH_2Ph: contour plots obtained with refinements a, b, and c; refinements b and c are almost equivalent (see text for details)

literature.[12] Without questioning the chemical validity of such an assumption, it must be pointed out that in many cases this is risky. In fact, the position of a ligand directly influences the position found for the others. The χ^2 curves obtained by varying the Co−C(Ch_2Ph) distance for different values of the Co−N(py) distance are shown in Figure 9. Co−N(py) values are only 0.02 Å apart, but different χ^2 profiles are obtained. It is apparent that the choice of the "best" minimum for Co−C(Ch_2Ph) distance depends on the value chosen for the Co−N(py) distance (unconstrained refinement).

Finally, with refinement c, answers can be found to such questions as: Is py bonded to Co for R = Cl? Is Me bonded to Co for R = Me? Limiting the analysis to the first shell, the probability of obtaining the presence or absence of the axial ligand (Me, when R = Me; py, when R = Cl) is about 50%. With refinement *c*, the probability that py and Me are bonded (at the correct distance) is at least 75%.

Conclusion

Although the constrained refinement gives an accuracy of about 0.05 Å on the axial distances and an overall correct picture of the actual structure, multiple solutions have been found in some cases. Accordingly to Scheuring et al.,[11] the mapping technique provides a valuable tool to rationalize discrepancies between EXAFS and XRD. It has been shown that multiple minima can be eliminated or discriminated in most cases. The mapping technique plays an essential role in indicating a correct solution and this option should be included in all advanced EXAFS data-analysis codes, together with an advanced constrained/restrained refinement. The principal challenge in fitting EXAFS data of complex systems will be to determine the relevant degrees of freedom of the studied structures and to relate them to as many EXAFS parameters as possible. Thus, the task now is to write codes to integrate ab initio EXAFS calculations,

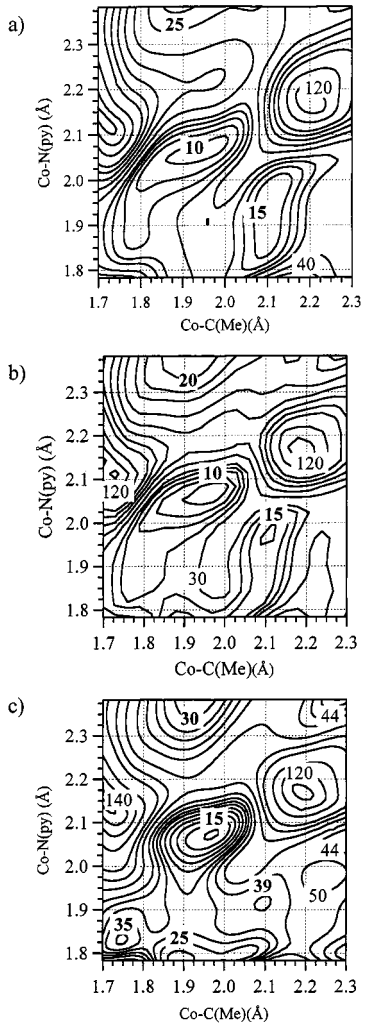

Figure 8. R = Me: contour plots obtained with refinements a, b, and c are shown (see text for details); refinement c is necessary to make the ligands distinguishable

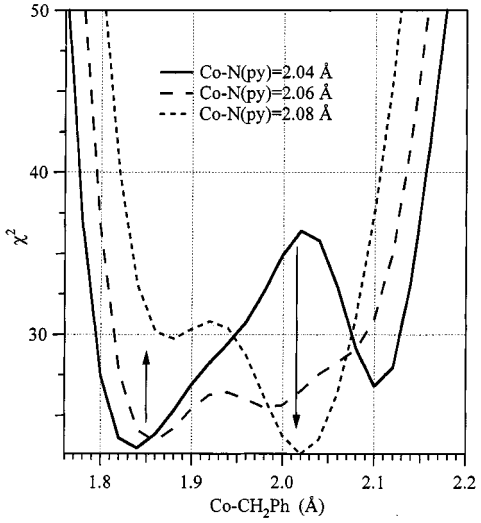

Figure 9. R = CH_2Ph: The χ^2 profile was obtained by varying the Co−CH_2Ph distance for three Co−N(py) values; for very similar values of the latter distance, different values for the Co−CH_2Ph distance were obtained (see position of the minima); arrows indicate minima modifications when the Co−N(py) distance is varied

refinement, and molecular modelling tools, and to make them accessible to the community.

Experimental Section

All reagents and chemicals were commercial products and were used as received. $Co(DH)_2(Py)Cl$,[31] $Co(DH)_2(Py)N_3$,[32] $Co(DH)_2(Py)Me$[32], and $Co(DH)_2(Py)(CH_2Ph)$[33] were synthesized according to reported methods. All these complexes were recrystallized from methanol/H_2O and their purity confirmed by elemental analysis. $Co(DH)_2(Py)$(adamantyl) was obtained by a modification of the synthetic procedure previously reported for the analogous compounds having aniline or 4-dimethylpyridine as axial bases.[22e] Aqueous NaOH solution (2 pellets in 5 mL) was added, with stirring, to dissolve a suspension of $Co(DH)_2(Py)Cl$ (0.8 g, 2 mmol) in methanol (200 mL). While flushing with nitrogen, a suspension of $NaBH_4$ (0.11 g, 3.0 mmol) in water (1 mL) was added, followed by solid 1-iodoadamantane (Aldrich, 1.05 g, 4 mmol). After the solution was vigorously stirred for 40 min, the stream of nitrogen was stopped. The volume of the solution was reduced to ca. 20 mL on a rotary evaporator and the unchanged 1-iodoadamantane was removed by filtration. H_2O (50 mL) was added to the remaining solution, and the red−brown crystals of the desired compound precipitated. The solid was collected by filtration, air dried, and washed with diethyl ether (3 × 10 mL), to remove the residual 1-iodoadamantane. The product was recrystallized by the addition of water to a methanolic solution. Yield 40%. − $C_{23}H_{34}CoN_5O_4$ (503.5): calcd. C 54.9, H 6.81, N 13.9; found C 54.5, H 6.55, N 13.7. − EXAFS data were recorded in the transmission mode at the LURE laboratory (Orsay, France) on beam-line EXAFS-IV in 1999, except for the sample R = adamantyl, which was recorded on EXAFS-1 (now EXAFS-13) in 1994. On beam-line EXAFS-IV, ion chambers were filled with a He/Ne mixture and harmonics were rejected by detuning the two crystals of the Si(331) monochromator. On EXAFS-1, where a Si(331) channel-cut monochromator was the only choice, and no mirrors were available, ion chambers were filled with air to reduce harmonic contamination to a negligible extent. All data were collected at liquid nitrogen temperature. During data analysis, the EXAFS signal $\chi(k)$[34] was multiplied by the cube of the wave-vector modulus $[k^3\chi(k)]$ to balance the decay of the signal due to thermal disorder. Best results were obtained using this weighting, which in some way extends the effective signal range when the signal-to-noise ratio is sufficiently high. Excellent data sets were obtained (see Figure 2). Using a k^0 or k^1 weighting, the signal decayed so quickly that the last part had a small influence on χ^2, and information was partially lost.[16] EXAFS spectra were multiplied by a Hanning window with k_{min} = 3.65 Å^{-1}, k_{max} about 17 Å^{-1} (from 16.5 to 17.5 depending on sample), Δk_{sills} = 2 (except for R = adam: k_{min} = 3.65 Å^{-1}, k_{max} = 14 Å^{-1} Δk_{sills} = 1 Å^{-1}). Fits were performed in *r*-space. We also checked that *k*-space and *r*-space fits did not give results that differed by more than the estimated error bar. Data analysis was carried out on a Red Hat Linux 6.0 powered PC with the UWXAFS suite[35] (Autobk 2.61 and Feffit 2.52 h, version 2.54 for *k*-space fitting) and theoretical standards were obtained using FEFF 7.0.[36] Molecular-modelling structures were obtained from the CSD database, and analyzed with the help of ChemOffice by CambridgeSoft on an iMac. To interface the CSD database and ChemOffice with FEFF 7.0, the Crystalff code was used.[37] The χ^2 maps were obtained using a Perl script to run Feffit on the desired grid points and to archive the results. Contour plots were drawn using Igor Pro 3.0 by WaveMetrics Inc.

Acknowledgments

We thank the Ministero della Ricerca Scientifica e Tecnologica (Roma) (PRIN9803184222) and Consiglio Nazionale delle Ricerche (CNR) for financial support. We are grateful to Dr. K. Provost for code Crystallf, Dr. M. Newville for providing latest improved versions of his Feffit code (2.52 h and 2.54). We acknowledge Dr. F. Champloy for helpful discussions, and the teams of beam-lines EXAFS-13 and EXAFS-IV of LURE for assistance during measurements.

[1] *Vitamin B_{12} and B_{12} Proteins* (Eds.: B. Krautler, D. Arigoni, B. T. Golding); Wiley-VCH, Weinheim, **1998**.
[2] *Chemistry and Biochemistry of vit B12* (Ed.: R. Banerjee),, J. Wiley & sons, N.Y. **1999**
[3] [3a] N. Bresciani-Pahor, M. Forcolin, L. G. Marzilli, L. Randaccio, M. F. Summers, J. P. Toscano, *Coord. Chem. Rev.* **1985**, *63*, 1. – [3b] B. T. Golding, *J. R. Neth. Chem. Soc.* **1987**, *106*, 342. – [3c] L. Randaccio, N. Bresciani-Pahor, E. Zangrando, L. G. Marzilli, *Chem. Soc. Rev.* **1989**, *18*, 225. – [3d] L. Randaccio, *Comm. Inorg. Chem.* **1999**, *21*, 327.
[4] L. Randaccio, S. Geremia, M. Furlan, M. Slouf, *Inorg. Chem.* **1998**, *37*, 5390.
[5] [5a] L. Randaccio, S. Geremia, G. Nardin, M. Slouf, I. Srnova, *Inorg. Chem.* **1999**, *38*, 4087. – [5b] L. Randaccio, M. Furlan, S. Geremia, M. Slouf, I. Srnova, D. Toffoli, *Inorg. Chem.* **2000**, in press.
[6] C. Kratky, G. Färber, K. Gruber, Z. Deuter, H. F. Nolting, R. Konrat, B. Kräutler, *J. Am. Chem. Soc.* **1995**, *117*, 4654.
[7] [7a] I. Sagi, M. D. Wirt, E. Chen, S.M. Frisbie, M. R. Chance, *J. Am. Chem. Soc.* **1990**, *112*, 8639. – [7b] M. D. Wirt, I. Sagi, E. Chen, S. M. Frisbie, R. Lee, M. R. Chance, *J. Am. Chem. Soc.* **1991**, *113*, 5299.
[8] I. Sagi, M. R. Chance, *J. Am. Chem. Soc.* **1992**, *114*, 8061 (cyano and aquo).
[9] E. M. Scheuring, I. Sagi, M. R. Chance, *Biochemistry* **1994**, *33*, 6310 (Co−S).
[10] M. Giorgetti, M. Berrettoni, P. Conti, R. Di Cicco, R. Marassi, I. Ascone, *Organometallics* **1996**, *15*, 3491.
[11] E. Scheuring, R. Padmakumar, R. Banerjee, M. R. Chance, *J. Am. Chem. Soc.* **1997**, *119*, 12192.
[12] F. Champloy, G. Jogl, R. Reitzer, W. Buckel, H. Bothe, B. Beatrix, G. Broeker, A. Michalowicz, W. Meyer-Klaucke, C. Kratky, *J. Am. Chem. Soc.* **1999**, *121*, 11780.
[13] H. Bertagnolli, T. S. Hertel, *Angew. Chem. Int. Ed. Engl.* **1994**, *33*, 45.
[14] P.F. Lidley, in: *X-ray Absorption Fine Structure* (Ed.: S. S. Hasnain), Ellis Horwoord Ldt, Chichester, England, **1999**, 115.
[15] P. A. Lee, H. Citrin, P. Eisenberger, B. M. Kincaid, *Rev. Mod. Phys.* **1981**, *53*, 769
[16] A. Michalowicz, K. Provost, S. Laruelle, A. Mimouni, G. Vlaic, *J. Synchrotron Rad.* **1999**, *6*, 233 (XAFS-X conference proceeding, Chicago)
[17] A. Mimouni, Thesis, University of Paris XII, France, **1997**.
[18] L. Randaccio, S. Geremia, *Organometallics* **1997**, *16*, 4951.
[19] F. Mancia, N. H. Keep, A. Nakagawa, P. F. Leadlay, S. McSweeney, B. Rasmusssen, P. Boesecke, O. Diat, P. R. Evans, *Structure* **1996**, *4*, 339.
[20] Tami E. Westre, A. Di Cicco, A. Filipponi, C. R. Natoli, B. Hedman, E. I. Solomon, K. O. Hodgson, *J. Am. Chem. Soc.* **1995**, *117*, 1566.
[21] In the case of R = adam, the neutral ligand is 4-Me_2N-py.
[22] [22a] S. Geremia, R. Dreos, L. Randaccio, G. Tauzher, L. Antolini, *Inorg. Chim. Acta* **1994**, *216*, 125. – [22b] M. N. Ponnuswamy, J. Trotter, *Acta Crystallogr., Sect. C (Cr. Str. Comm.)* **1983**, *39*, 726. – [22c] N. Bresciani Pahor, L. Randaccio, E. Zangrando, L. Antolini, *Acta Crystallogr., Sect. C(Cr. Str. Comm.)* **1988**, *44*, 2052. – [22d] A. Bigotto, E. Zangrando, L. Randaccio, *J. Chem Soc., Dalton Trans.* **1976**, 96. – [22e] N. Bresciani Pahor, L. Randaccio, E. Zangrando, P. A. Marzilli, *J. Chem. Soc., Dalton Trans.* **1989**, 1941.
[23] F. Champloy, K. Gruber, G. Jodl, C. Kratky, *J. Synchrotron Rad.* **2000**, *7*, 267.
[24] D. E. Sayers, E. A. Stern, F. W. Lytle, *Phys. Rev. Lett.* **1971**, *27*, 1204.
[25] P. A. Lee, H. Citrin, P. Eisenberger, B. M. Kincaid, *Rev. Mod. Phys.* **1981**, *53*, 769
[26] *EXAFS: Basic principles and Data Analysis* (Ed.: Boon K. Teo), Springer Verlag, Berlin, **1986**.
[27] *X-ray Absorption Fine Structure* (Ed.: S. S. Hasnain), Ellis Horwood-Publishers, New York, **1991.**
[28] N. Binsted, R. W. Strange, S. S. Hasnain, *Biochemistry* **1992**, *31*, 12117.
[29] M. Roy, S. J. Gurman, *J. Synchrotron Rad.* **1999**, *6*, 228.
[30] M. Benfatto, C. R. Natoli, A. Filipponi, *Physical Review B* **1989**, *40*, 9626.
[31] N. Dimakis, M.-Ali Al Akhras, G. Bunker, *J. Synchrotron Rad.* **1999**, *6*, 266.
[32] G. N. Schrauzer, *Inorganic Syntheses* **1968**, *11*, 61.
[33] A. Clearfield, R. Gopal, R. J. Kline, M. L. Sipski, L. O. Urban, *J. Coord. Chem.* **1978**, *8*, 5.
[34] G. N. Schrauzer, E. Deutsch, *J. Am. Chem. Soc.* **1970**, *91*, 3341.
[35] The notation could be confusing: $\chi(k)$ is the EXAFS signal, while χ^2 and χ^2_ν are statistical functions.
[36] E. A. Stern, M. Newville, B. Ravel, Y. Yacoby, D. Haskel, *Physica B* **1995**, *208−209*, 117.
[37] J. J. Rehr, C. H. Booth, F. Bridges, S. I. Zabinsky, *Phys. Rev. B* **1994**, *49*, 12347
[38] K. Provost, A. Michalowicz, *J. Synchrotron Rad.* **2000**, manuscript submitted.

Received August 16, 2000
[I00316]

cis-Octahedral Nickel(II) Complexes with Symmetric and Unsymmetric Tripodal Tetraamine Ligands

Christian Ochs,[a] F. Ekkehardt Hahn,*[b] and Thomas Lügger[b]

Keywords: Tripodal ligands / Nickel / Structure elucidation / UV/Vis spectroscopy

Nickel(II) complexes with the aliphatic tripodal tetraamine ligands $N(CH_2CH_2NH_2)_3$ (tren, **1**), $N[(CH_2CH_2CH_2NH_2)(CH_2CH_2NH_2)_2]$ (baep, **2**), $N[(CH_2CH_2CH_2NH_2)_2(CH_2CH_2NH_2)]$ (abap, **3**), and $N(CH_2CH_2CH_2NH_2)_3$ (trpn, **4**) are reported. The tripodal tetradentate N_4 ligands **1**–**4** react with $Ni(NO_3)_2{\cdot}6H_2O$ in acetonitrile or methanol to give the blue nickel(II) complexes $[Ni(\mathbf{1})(\eta^1\text{-}NO_3)_2]$ (**5a**), $[Ni(\mathbf{2})(\eta^1\text{-}NO_3)_2]$ (**5b**), $[Ni(\mathbf{3})(\eta^2\text{-}NO_3)]NO_3{\cdot}CH_3CN$ (**5c**·CH_3CN), and $[Ni(\mathbf{4})(\eta^2\text{-}NO_3)]NO_3{\cdot}CH_3OH$ (**5d**·CH_3OH). With $NiCl_2{\cdot}6H_2O$, the complexes $[Ni(\mathbf{1})Cl(H_2O)]Cl{\cdot}H_2O$ (**6a**), $[Ni(\mathbf{2})(\mu\text{-}Cl)_2Ni(\mathbf{2})]Cl_2{\cdot}2CH_3OH$ (**6b**·$2CH_3OH$), $[Ni(\mathbf{3})Cl(H_2O)]Cl$ (**6c**), and $[Ni(\mathbf{4})(H_2O)_2]Cl_2{\cdot}H_2O$ (**6d**·H_2O) are obtained. The molecular structures of complexes **5a**–**d** and **6b**–**d** have been determined by X-ray diffraction analysis and they are compared with the molecular structure of the previously characterized complex **6a**. Complexes **5a**–**d** and **6b**–**d** exhibit octahedrally coordinated nickel atoms. The tripodal ligands occupy four of the six coordination sites in a *pseudo-facial* manner. Complexes of the unsymmetrical ligands **2** and **3** possess both five- and six-membered chelate rings. The extension of the ligand arms in **1**–**4** leads to a systematic variation in the geometric and UV/Vis spectroscopic properties of the complexes depending on the size of the chelate rings formed by the ligands.

Introduction

The sterically unhindered tripodal tetraamine ligand tren (**1**) is known to form a large number of coordination compounds with different metal ions. Comparatively little is known about the coordination chemistry of the unsymmetric higher tren homologues, e.g. bis(2-aminoethyl)(3-aminopropyl)amine (baep, **2**), (2-aminoethyl)bis(3-aminopropyl)amine (abap, **3**), and the symmetric tris(3-aminopropyl)amine (trpn, **4**) (Figure 1).

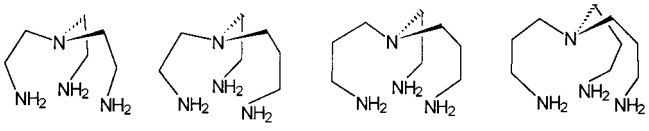

Figure 1. Topology of the tripodal tetraamine ligands studied

Complexes of Ni^{II} with **1** were first described in 1926.[1] Since then, various monomeric octahedral,[2–5] trigonal-bipyramidal,[6–9] and dinuclear coligand-bridged octahedral[10–12] Ni^{II} complexes of **1** or its hexamethylated analogue Me_6tren have been reported. Thermochemical and spectroscopic studies of aqueous solutions of Ni^{II} complexes of **4** have indicated that these complexes are octahedral.[13,14] However, the precise molecular structures of the (trpn)Ni^{II} complexes remain unknown. Nickel complexes of the unsymmetric ligands **2** and **3** have not hitherto been described.

The stepwise insertion of a CH_2 group into each of the ligand arms in **1** leads to the ligands **2**–**4**.[15–17] Compared to **1**, these ligands possess an unchanged set of donor groups with expanded linkers between them. This slight topological variation has profound consequences. Ligands **2**–**4** are more basic than **1**,[17] since the ammonium groups formed upon protonation are further apart in these ligands than they would be in tren. The geometric parameters of the five- and six-membered chelate rings that could be formed by **2**–**4** have been analyzed and it was concluded that for complexes with both macrocyclic and non-macrocyclic ligands, an increase of the chelate ring size from five-membered to six-membered will increase the stability of complexes of smaller relative to larger metal ions.[18]

A systematic study of these contradicting effects was carried out with a complete series of Cu^{II} complexes with the ligands **1**–**4**.[16a,17,19] Depending on the ligand topology, these complexes adopt either a trigonal-bipyramidal or a distorted square-pyramidal geometry.[16,17]

The stability constants of the copper complexes were found to decrease systematically over five orders of magnitude depending on the number of six-membered chelate rings present.[17] Studies on the octahedral Co^{III} complexes with **1**,[20] **2**,[16b] **3**,[15] and **4**[20] revealed differences in the catalytic activities of these complexes in the hydrolysis of phosphate esters. It would appear that the stability and reactivity of complexes with tripodal tetraamine ligands may be controlled and significantly manipulated by the ligand topology if the governing principles are fully understood. This might ultimately prove useful for the modelling of nitrogen-rich active sites in metalloproteins. To study the con-

[a] Institut für Anorganische und Analytische Chemie der Freien Universität Berlin,
Fabeckstraße 34–36, 14195 Berlin, Germany
[b] Anorganisch-Chemisches Institut der Westfälischen Wilhelms-Universität Münster,
Wilhelm Klemm Straße 8, 48149 Münster, Germany

 © WILEY-VCH Verlag GmbH, 69451 Weinheim, 2001 1434–1948/01/0505–1279 $ 17.50+.50/0

sequences of a variation of the ligand topology of tripodal tetraamines with respect to the properties of octahedral metal complexes, we have prepared the Ni^{II} complexes of **1−4**. It was assumed that octahedral complexes with two monodentate coligands in *cis* positions would be formed. Furthermore, we have studied the effects of the counterions by preparing two series of complexes starting from $NiCl_2{\cdot}6H_2O$ and $Ni(NO_3)_2{\cdot}6H_2O$. The molecular structures and spectroscopic properties of the nickel complexes obtained are compared with the data for the previously characterized nickel complex with the ligand tren $[Ni(\mathbf{1})Cl(H_2O)]Cl{\cdot}H_2O$ (**6a**).[2]

Results and Discussion

Seven new octahedral Ni^{II} complexes with the symmetric and unsymmetric tripodal tetraamine ligands **1−4** have been synthesized and structurally characterized. Depending on the ligand topology, complexes of type **5** (Scheme 1) contain either two η^1-coordinated nitrate ions or an η^2-coordinated nitrate ion and a nitrate counterion. A second series of complexes **6** has been synthesized from ligands **1−4** and nickel dichloride in water. In this series, the complex **6a** with the ligand **1** has been described previously.[2] In both series, the ligand topology is systematically varied by the stepwise insertion of methylene groups into the ligand arms. The structural and spectroscopic trends observed in the two series are discussed below.

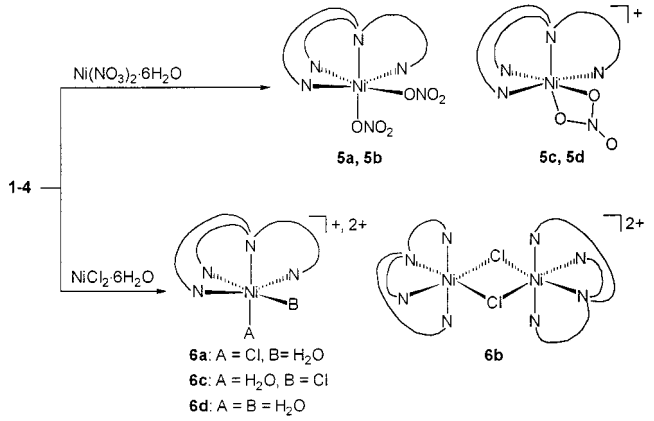

Scheme 1. Preparation of Ni^{II} complexes of ligands **1−4**

Improved Synthesis of Bis(2-aminoethyl)(3-aminopropyl)-amine (2)

The previously described preparation of **2**,[16a] by addition of 1 equiv. of acrylonitrile to ammonia followed by Strecker synthesis, reaction of the resulting dinitrile with glyconitrile ($HOCH_2CN$),[21] and finally reduction of the trinitrile with AlH_3, has not always given satisfactory results. The critical step has proved to be the condensation reaction of the dinitrile with $HOCH_2CN$ for the introduction of the third ligand arm at the central nitrogen atom. Under the conditions described, the reaction often yields polymeric products with the desired trinitrile present only in trace amounts. We assume that this is due to the low basicity of the central nitrogen atom of the dinitrile precursor. It is known that α-cyanomethyl and β-cyanoethyl groups at a nitrogen atom markedly lower its basicity.[22] Under such conditions, decomposition and self-condensation reactions of the glyconitrile are favored over the condensation reaction with the amine. Consequently, the only possible means of enhancing the condensation reaction is through activation of the glyconitrile. This is best achieved by tosylation and tosylated glyconitrile can easily be prepared from glyconitrile and *p*-toluenesulfonyl chloride.[23] The condensation reaction of $TsOCH_2CN$ with $HN(CH_2CN)(CH_2CH_2CN)$ proceeds at 50 °C in DMF within 5 d. The resulting ammonium salt was converted into the free amine with aqueous sodium carbonate. The crude product could be recrystallized from hot chloroform. As reported previously,[16] ligand **2** is obtained from the trinitrile by hydrogenation with AlH_3.

Preparation of Nickel Complexes

Addition of stoichiometric amounts of the tripodal ligands **1−4** to solutions of $Ni(NO_3)_2{\cdot}6H_2O$ in methanol or acetonitrile gives deep-blue solutions, from which the complexes $[Ni(N_4)(\eta^1\text{-}NO_3)_2]$ (**5a**: N_4 = **1**; **5b**: N_4 = **2**) and $[Ni(N_4)(\eta^2\text{-}NO_3)_2]NO_3{\cdot}X$ (**5c**: N_4 = **3**, X = CH_3CN; **5d**: N_4 = **4**, X = CH_3OH) can be crystallized by slow diffusion of gaseous diethyl ether into them. Reactions of **1−4** with

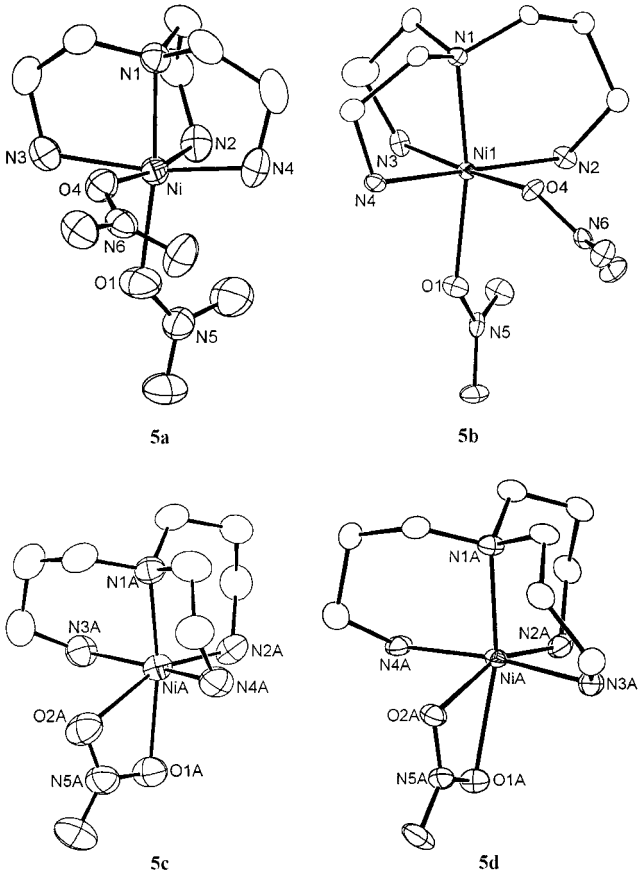

Figure 2. ORTEP plots of complexes **5a** and **5b** and of the cations in complexes **5c** and **5d**; solvent molecules and counterions in **5c** and **5d** have been omitted for clarity

$NiCl_2 \cdot 6H_2O$ in acetonitrile or methanol yield complexes $[Ni(N_4)Cl(H_2O)]Cl$ (**6a**: N_4 = **1**;[2] **6c**: N_4 = **3**), $[Ni(N_4)(\mu\text{-}Cl)_2(N_4)Ni]Cl_2 \cdot 2CH_3OH$ (**6b**: N_4 = **2**), and $[Ni(N_4)(H_2O)_2]Cl_2$ (**6d**: N_4 = **4**). Crystallization of the complexes was achieved in the same manner as described for **5a**−**d**, or by slowly concentrating a methanolic solution. With acetonitrile as the solvent, all the complexes were found to be air-stable and soluble in water. A schematic representation of complexes of types **5** and **6** is presented in Scheme 1.

Molecular Structures of the Nitrate Salts

The molecular structures of complexes **5a**−**d** have been determined by X-ray diffraction methods. In all cases, *cis*-octahedral complexes were formed. As can be seen from Figure 2, the main difference between the complexes lies in the coordination mode of the nitrate anions. In **5a** and **5b**, the *cis*-octahedral coordination is completed by two η^1-coordinated nitrate anions, while in both **5c** and **5d** only one η^2-coordinated nitrate anion is found.

This difference arises from differences in the steric bulk and demand of the coordinated tripodal tetraamines. The relationship between steric demand of the coordinated tetraamine and the coordination mode of the nitrate anions is best reflected in the $N_{tert}-Ni-NH_2$ angles. Complex **5a** contains only five-membered chelate rings and all the $N_{tert}-Ni-NH_2$ angles are smaller than 90° (Table 1). The larger six-membered chelate rings in **5d** lead to $N_{tert}-Ni-NH_2$ angles that are all larger than 90°. Complexes **5b** and **5c**, containing both five- and six-membered chelate rings, are intermediate between these limiting cases with $N_{tert}-Ni-NH_2$ angles larger than 90° for the six-membered rings and smaller than 90° for the five-membered ones. A similar relationship between the $N_{tert}-Cu-NH_2$ angles and the different chelate ring sizes has been described for trigonal-bipyramidal[16a] and tetragonal-pyramidal[17] copper complexes. As a consequence of this geometrical situation, the size of the cavity left for coligands decreases on going from **5a** to **5d**. In **5a** and **5b**, it is still large enough to accommodate two monodentate nitrate anions, while in **5c** and **5d** only one bidentate nitrate anion can fit into the cavity and the second nitrate anion is left uncoordinated as a counterion. Not only the number of coordinated nitrate anions, but also the Ni−O distances are at least partially determined by the topology of the tripodal tetraamine. The shortest Ni−O distance [2.075(3) Å] is observed for **5a** and, as expected, the largest values [2.224(4) Å and 2.195(4) Å] are found in **5d**. It would appear that this is not exclusively due to steric effects. In complexes **5a**, **5b**, and **5c**, the shorter of the two Ni−O distances is found *trans* to the tertiary nitrogen atom of the tripod, while the longer one is found *trans* to a primary amine group [2.075(3) Å vs. 2.280(2) Å for **5a**, 2.087(3) Å vs. 2.171(3) Å for **5b**, 2.139(4) Å vs. 2.280(4) Å and 2.147(4) Å vs. 2.216(4) Å for **5c**; Table 1]. This trend is reversed in **5d**, where the shorter Ni−O distance in each of the two independent molecules in the asymmetric unit lies *trans* to a primary amine group [2.174(4) Å vs. 2.224(4) Å and 2.168(4) Å vs. 2.195(4) Å]. Moreover, the differences in the Ni−O distances (Ni−O *trans* to N_{tert} vs. Ni−O *trans* to NH_2) diminish in the series of complexes on going from **5a** (0.205 Å) to **5c** (0.141 Å and 0.069 Å) and are finally reversed in **5d** (0.05 Å and 0.027 Å). We explain this observation in terms of an increase in the basicity of the central nitrogen atom of the tripodal ligands. The basicity of N_{tert} increases from $pK_a < 2$ for **1** to $pK_a = 5.8$ for **4**, while the basicity of the primary amine groups remains essentially unchanged.[17] The diminishing difference in the basicities of the primary and tertiary amine functions in **1** to **4** leads to a less pronounced difference in the Ni−O distances *trans* to N_{tert} and *trans* to the NH_2 groups. While the Ni−O bond *trans* to the tertiary amine becomes longer on going from **5a** to **5d**, the Ni−O bond length *trans* to a primary amine group changes less and ultimately becomes shorter than the Ni−O bond *trans* to N_{tert} in the case of **5d**. From this, it can be concluded that the ligand topology in complexes **5a**−**d** determines both the steric and, to a lesser extent, the electronic situation at the metal center.

Molecular Structures of the Chloride Salts

The molecular structures of complexes **6b**−**d** are depicted in Figure 3. Again, *cis*-octahedral complexes with chloride or water coligands were formed. It would appear that the distribution of the coligands among the two free coordination sites at the nickel atom is random and seemingly depends on the conditions used for crystallization of the complexes. Complex **6b**, which was obtained by slow concentration of a methanolic solution, crystallizes as a dinuclear species where two bridging chloride atoms complete the octahedral coordination environments at the nickel atoms. On the other hand, **6c** and **6d** were crystallized by diffusion of diethyl ether into acetonitrile solutions and are mononuclear complexes. In complex **6c**, a water molecule occupies the *trans* position and a chloride ion the *cis* position relative to N_{tert}, while in **6d** two coordination sites at nickel are occupied by water molecules. The series is completed by compound $[Ni(\mathbf{1})Cl(H_2O)]Cl \cdot H_2O$ (**6a**).[2] Its molecular structure was first investigated by Jørgensen in 1956.[24] On the basis of its electronic spectra in aqueous solution, it was suggested that **6a** should be formulated as $[Ni(\mathbf{1})(H_2O)_2]Cl_2$. Some years later, it was shown that it is $[Ni(\mathbf{1})Cl(H_2O)]Cl \cdot H_2O$ in the solid state,[2] while $[Ni(\mathbf{1})(H_2O)_2]^{2+}$ cations exist in water. Interestingly, in the solid state, the coordination of the monodentate ligands in **6a** (Cl *trans* to N_{tert}) is exactly opposite to that found in **6c** (Cl *cis* to N_{tert}).

As for the nitrate salts **5**, certain bonding parameters of the tripodal tetraamine in complexes **6** (Table 2) are strongly dependent on the topology of the ligand. The $N_{tert}-Ni-L_{trans}$ axis is essentially linear for all complexes of type **6**. As for the nitrate complexes, the $N_{tert}-Ni-N_{cis}$ angles are smaller than 90° for five-membered chelate rings and larger than 90° for six-membered rings.

In contrast to the nitrate complexes of type **5**, the monodentate ligands in complexes **6** are sterically non-demanding. The distances between the nickel atoms and these ligands allow an evaluation of the dependence of the *trans*

Table 1. Selected bond lengths [Å] and angles [°] for complexes of type **5**

	5a	**5b**	**5c**·CH_3CN		**5d**·CH_3OH	
			molecule A	molecule B	molecule A	molecule B
Ni−N1	2.089(3)	2.109(4)	2.086(4)	2.099(4)	2.109(5)	2.111(5)
Ni−N2	2.055(3)	2.061(4)	2.035(5)	2.054(5)	2.054(5)	2.061(5)
Ni−N3	2.095(3)	2.067(4)	2.061(5)	2.062(4)	2.098(5)	2.068(5)
Ni−N4	2.072(3)	2.095(4)	2.062(5)	2.068(4)	2.065(5)	2.079(5)
Ni−O1	2.075(3)	2.087(3)	2.139(4)	2.147(4)	2.224(4)	2.195(4)
Ni−O2 (O4)	2.280(2)	2.171(3)	2.280(4)	2.216(4)	2.174(4)	2.168(4)
N1−Ni−N2	83.6(1)	94.6(1)	96.6(2)	98.3(2)	100.4(2)	100.9(2)
N1−Ni−N3	83.5(1)	84.4(2)	90.7(2)	91.4(2)	94.6(2)	91.5(2)
N1−Ni−N4	84.4(1)	83.7(2)	84.5(2)	84.0(2)	90.9(2)	92.8(2)
N2−Ni−N3	96.0(1)	94.1(2)	96.3(2)	94.6(2)	90.3(2)	91.8(2)
N2−Ni−N4	94.0(1)	173.0(2)	97.2(2)	96.5(2)	92.6(2)	89.9(2)
N3−Ni−N4	163.4(1)	92.6(2)	166.1(2)	168.5(2)	173.3(2)	175.0(2)
O1−Ni−N1	172.1(1)	166.8(1)	164.1(2)	162.3(2)	159.9(2)	158.8(2)
O2(O4)−Ni−N1	89.3(1)	90.4(2)	106.4(2)	103.8(2)	101.6(2)	99.6(2)
O2(O4)−Ni−O1	84.5(1)	88.1(1)	58.1(1)	58.7(2)	58.5(2)	59.3(2)

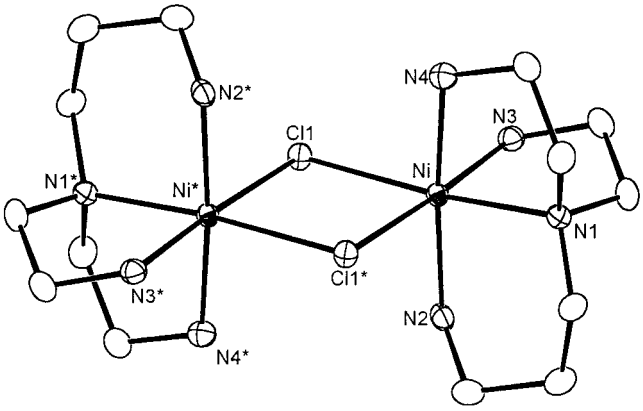

6b

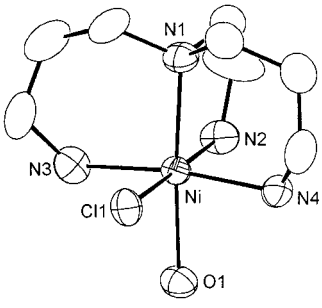

6c

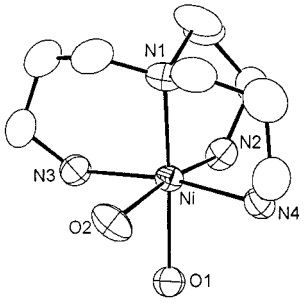

6d

Figure 3. ORTEP plots of the cations in complexes **6b−d**; solvent molecules and chloride counterions have been omitted for clarity

Table 2. Selected bond lengths [Å] and angles [°] for complexes of type **6** ($N_{t\text{-}N1}$ = ligand *trans* to N1, $N_{c\text{-}N1}$ = ligand *cis* to N1; $L_{t\text{-}N1}$ = Cl (**6a**,**b**), H_2O (**6c**,**d**); $L_{c\text{-}N1}$ = H_2O (**6a**,**d**), Cl (**6b**,**c**); see also Figure 2)

	6a[a]	**6b**	**6c**	**6d**
Ni−N1	2.105(3)	2.109(2)	2.144(4)	2.147(3)
N−N2	2.100(2)	2.095(2)	2.093(4)	2.096(3)
Ni−N3	2.095(2)	2.093(2)	2.084(4)	2.114(3)
Ni−N4	2.114(3)	2.106(2)	2.078(4)	2.084(3)
Ni−$L_{t\text{-}N1}$	2.413(3)	2.4449(6)	2.162(3)	2.174(3)
Ni−$L_{c\text{-}N1}$	2.239(2)	2.4840(6)	2.432(1)	2.165(3)
N1−Ni−N2	82.67(8)	90.94(7)	83.1(1)	98.43(13)
N1−Ni−N3	84.0(2)	84.76(7)	94.0(2)	94.45(14)
N1−Ni−N4	82.2(1)	83.23(7)	93.8(1)	94.43(14)
N2−Ni−N3	97.5(2)	91.30(8)	91.7(2)	90.74(13)
N2−Ni−N4	93.7(1)	174.02(8)	91.3(2)	90.92(14)
N3−Ni−N4	161.0(1)	89.50(8)	171.9(1)	170.63(13)
$L_{c\text{-}N1}$−Ni−N1	93.57(9)	96.74(5)	96.22(11)	92.59(13)
$L_{t\text{-}N1}$−Ni−N1	178.61(8)	175.25(5)	174.15(13)	177.09(14)
$L_{t\text{-}N1}$−Ni−$L_{c\text{-}N1}$	87.16(6)	85.59(2)	89.29(9)	84.88(12)

[a] Data from ref.[2]

effect of the different amine groups of the tripodal tetraamine on the ligand topology. For two identical monodentate ligands, as found in **6b** (Cl^-) and **6d** (H_2O), the following trends were found. In **6b**, containing the ligand **2**, the bond to the monodentate ligand *trans* to N_{tert} [Ni−Cl1 2.4449(6) Å] is shorter than that to the ligand *cis* to N_{tert} [Ni−Cl1* 2.4840(6) Å]. This situation is reversed in **6d**, containing ligand **4** with an increased basicity of the central nitrogen atom.[17] In **6d**, the distance to the ligand *cis* to N_{tert} [Ni−O2 2.165(3) Å] is shorter than that to the ligand *trans* to N_{tert} [Ni−O1 2.174(3) Å]. However, even the increase in the basicity of the tertiary nitrogen atom on going from **1** to **4** does not lead to a shortening of the N_{tert}−Ni distance in either series of complexes due to the concomitant increase in the number of sterically less favored six-membered chelate rings.

UV/Vis Spectra

A d^8 ion like Ni^{II} in an octahedral ligand field gives rise to four absorption bands.[25] The three strongest ones are caused by the spin-allowed transitions from the ground state $^3A_{2g}$ to the excited triplet states $^3T_{2g}$, $^3T_{1g(F)}$, and $^3T_{1g(P)}$. A weaker band of low intensity can be attributed to the spin-forbidden transition to the singlet state ^1E_g. In practice, it is seldom observed as a discrete band, but more often as a shoulder of the $^3A_{2g} \rightarrow {}^3T_{2g}$ transition band at about 800 nm.[26,27]

For complexes of types **5** and **6**, three distinct absorption bands are observed. The transitions from $^3A_{2g}$ to the $^3T_{1g(P)}$ and $^3T_{1g(F)}$ excited states appear as sharp bands of high

intensity in the regions 350−380 nm and 560−620 nm, respectively, whereas the absorption band at about 950−1100 nm, due to the $^3A_{2g} \rightarrow {}^3T_{2g}$ transition, is broad and of low intensity. A shoulder at about 800 nm is found for complexes **5a**,**b** and **6a**,**b**, while for the rest of the complexes this feature seems to be superimposed by the long-wavelength $^3A_{2g} \rightarrow {}^3T_{2g}$ transition. The exact values for the absorption maxima and the molar extinction coefficients are listed in Table 3.

Table 3. UV/Vis spectroscopic data (λ [nm], ε [10^3·mol^{-1}·cm^{-1}] for complexes of types **5** and **6**

$^3A_{2g} \rightarrow$	$^3T_{1g(P)}$	$^3T_{1g(F)}$	$^3T_{2g}$
5a	358 (18.6)	565 (13.5)	952 (14.1)
5b	358 (10.7)	572 (8.9)	980 (10.1)
5c	360 (33.9)	570 (22.4)	980 (11.1)
5d	364 (51.0)	577 (28.0)	1070 (8.8)
6a[a]	361	565	952
6a[b]	349 (22.9)	570 (9.3)	962 (11.1)
6b	363 (20.9)	580 (15.6)	984 (20.5)
6c	370 (21.0)	592 (13.0)	1025 (8.5)
6d	380 (33.7)	613 (17.6)	1050 (4.4)

[a] Data from ref.[2] − [b] Complex **6a** synthesized for this study.

One of the most notable results is the observation of a bathochromic shift with increasing number of six-membered chelate rings. This can be ascribed to the weaker ligand field generated by the six-membered chelate rings, which are known to be less stable than five-membered chelate rings.[17,28] Thus, the distance between the energy sublevels is decreased and the transitions are seen to be shifted to longer wavelengths.

Conclusion

With complexes **5a**−**d** and **6b**−**d** we present seven new complexes forming two series of octahedral Ni^{II} complexes with aliphatic tripodal tertraamine ligands. The series **6b**−**d** is completed by compound **6a**, which has previously been characterized by Marzotto et al.[2] The variation of the lengths of the ligand arms leads to complexes with different size chelate rings. This causes a distortion of the octahedral coordination environment, a variation in the space available for binding and in the strengths of the bonds to monodentate coligands, and a slight shift of the absorption maxima in the UV/Vis spectra. These effects will allow, at least in part, control over the binding of monodentate ligands depending on the topology of the tripodal tetraamine without a change in the nature of the donor groups. Ligands **1**−**4** might therefore prove useful for the introduction of minute changes in the modelling of amine-rich reaction centers in metalloproteins.

Experimental Section

Materials and Methods: All manipulations were carried out under air. Solvents were purified by standard methods and freshly distilled prior to use. − Infrared spectra were recorded from samples in KBr with a Perkin−Elmer IR 983 instrument. − Elemental analyses (C, H, N) were performed with a Vario EL Elemental Analyzer. − FAB mass spectra were recorded with Finnigan MAT 112 or Finnigan MAT 711 instruments. − UV/Vis spectra were recorded in methanol with a Perkin−Elmer Lambda 9 UV/Vis NIR spectrophotometer.

Ligand Syntheses: Tris(2-aminoethyl)amine (**1**) was purchased from Aldrich and was used without further purification. Ligands **2**, **3**, and **4** were synthesized according to the method of Dittler-Klingemann and Hahn.[16a] Alternatively, ligand **3** can be prepared by the method of Fanshawe and Blackman.[15] We preferred the preparation outlined in ref.[16] since the free ligand and not the hydrochloride is initially obtained in this preparation. For the present study, the synthesis of **2** was slightly modified compared to the published procedure.[16a]

Modified Preparation of Bis(2-aminoethyl)(3-aminopropyl)amine (2): Ligand **2** has previously been obtained by Michael addition of acrylonitrile to ammonia followed by a Strecker synthesis to yield the dinitrile $HN(CH_2CN)(CH_2CH_2CN)$. The addition of a second $-CH_2CN$ group to the central nitrogen atom using glyconitrile ($HOCH_2CN$) proved more difficult and very often failed due to reasons not yet fully understood. However, reaction of the dinitrile $HN(CH_2CN)(CH_2CH_2CN)$ with $TsOCH_2CN$[23] in DMF at 50 °C over a period of 5 d yielded the salt of the desired trinitrile, $[HN(CH_2CN)_2(CH_2CH_2CN)]OTs$. On addition of an excess of aqueous sodium carbonate and cooling the resulting mixture to 5 °C, colorless crystals of $N(CH_2CN)_2(CH_2CH_2CN)$ separated within a few days. The crude product could be recrystallized from hot chloroform. Reduction of the trinitrile with AlH_3 as described previously[16a] gave bis(2-aminoethyl)(3-aminopropyl)amine (**2**) in 64% yield.

Preparation of Nickel Complexes from $Ni(NO_3)_2$·6H_2O: The preparation of **5a** is described as an example. $Ni(NO_3)_2$·6H_2O (290 mg, 1 mmol) was dissolved in acetonitrile (5 mL) and then ligand **1** (146 mg, 1 mmol) was added dropwise by means of a syringe. The blue solution thus obtained was stirred at room temperature for 30 min, filtered, and concentrated to a volume of 3 mL. Slow diffusion of diethyl ether into the flask led to the deposition of dark-blue crystals of **5a**, which proved to be suitable for X-ray crystallography without the need for recrystallization. The air-stable crystals were collected by filtration, washed with diethyl ether, and carefully dried. This procedure could also be carried out in methanol.

5a: Yield 263 mg [80% based on $Ni(NO_3)_2$·6H_2O]. − $C_6H_{18}N_6NiO_6$ (329.0): calcd. C 21.91, H 5.52, N 25.55; found C 22.18, H 5.40, N 24.93. − MS (FAB, positive ions, DMSO/glycerol): *m*/*z* (%) = 266 (83) $[Ni(\mathbf{1})(NO_3)]^+$, 203 (100) $[Ni(\mathbf{1}) - H]^+$, 58 (6), 44 (53).

5b: Yield 255 mg [74% based on $Ni(NO_3)_2$·6H_2O]. − $C_7H_{20}N_6NiO_6$ (343.0): calcd. C 24.51, H 5.88, N 24.50; found C 24.31, H 5.80, N 24.38. − MS (FAB, positive ions, DMSO/glycerol): *m*/*z* (%) = 280 (100) $[Ni(\mathbf{2})(NO_3)]^+$, 217 (90) $[Ni(\mathbf{2}) - H]^+$, 58 (13), 44 (60).

5c·CH_3CN: Yield 278 mg [78% based on $Ni(NO_3)_2$·6H_2O] of slightly air-sensitive (loss of solvent) crystals. − $C_{10}H_{25}N_7NiO_6$ (398.1): calcd. C 30.18, H 6.33, N 24.63; found C 30.25, H 6.37, N 24.39. − MS (FAB, positive ions, DMSO/glycerol): *m*/*z* (%) = 294 (84) $[Ni(\mathbf{3})(NO_3)]^+$, 232 (100) $[Ni(\mathbf{3}) - H]^+$, 174 (48), 143 (30), 58 (37), 44 (48).

5d·CH_3OH: Yield 269 mg [72% based on $Ni(NO_3)_2$·6H_2O] of slightly air-sensitive (loss of solvent) crystals. − $C_{10}H_{28}N_6NiO_7$ (403.1): calcd. C 29.80, H 7.00, N 20.85; found C 29.77, H 6.94, N

Table 4. Summary of crystallographic data for **5a**, **5b**, **5c**·CH_3CN, **5d**·CH_3OH, **6b**·$2CH_3OH$, **6c**, and **6d**·H_2O

	5a	**5b**	**5c**·CH_3CN	**5d**·CH_3OH	**6b**·$2CH_3OH$	**6c**	**6d**·H_2O
Empirical formula	$C_6H_{18}N_6NiO_6$	$C_7H_{20}N_6NiO_6$	$C_{10}H_{25}N_7NiO_6$	$C_{10}H_{28}N_6NiO_7$	$C_{16}H_{48}Cl_4N_8Ni_2O_2$	$C_8H_{24}Cl_2N_4NiO$	$C_9H_{30}Cl_2N_4NiO_3$
Molecular mass [amu]	328.97	343.00	398.08	403.09	643.84	321.92	371.98
a [Å]	8.284(2)	12.228(5)	8.946(3)	17.436(2)	8.3694(6)	10.283(3)	8.0390(10)
b [Å]	11.800(2)	15.742(4)	9.650(3)	12.605(2)	10.8197(9)	11.125(4)	14.698(2)
c [Å]	12.825(3)	13.730(5)	20.963(8)	18.056(3)	15.9196(9)	12.388(5)	14.574(6)
α [°]	90	90	99.71(3)	90	90	90	90
β [°]	90	90	98.11(3)	118.602(11)	100.135(5)	97.46(3)	94.44(3)
γ [°]	90	90	100.56(2)	90	90	90	90
V [Å^3]	1253.7(5)	2643(2)	1725.7(10)	3484.1(9)	1419.1(2)	1405.2(9)	1716.9(8)
Z	4	8	4	8	2	4	4
Space group	$P2_12_12_1$	$Pbca$	$P\bar{1}$	$P2_1/n$	$P2_1/c$	$P2_1/c$	Cc
$\rho_{calcd.}$ [g/cm^3]	1.743	1.724	1.532	1.537	1.507	1.522	1.439
μ [mm^{-1}]	1.583	1.506	1.167	1.159	1.732	1.749	1.450
Data collection temp. [K]	293(2)	150(2)	293(2)	173(2)	153(2)	293(2)	293(2)
2Θ range [°]	5−45	5−50	4−45	5−50	5−50	4−50	5−52
No. of unique data	1628	2320	4500	6104	2485	2462	1789
No. of obsd. data, $I \geq 2\sigma(I)$	1588	1651	2946	4557	2121	1842	1735
R (%)[a]	3.09	4.16	4.11	6.17	2.71	4.24	3.03
wR (%)[a]	7.67	9.89	9.10	16.42	7.00	10.30	7.34
No. of variables	173	243	434	434	242	144	173

[a] $R = \Sigma||F_o| - |F_c||/\Sigma|F_o|$, $R_w = [\Sigma w||F_o| - |F_c||^2/\Sigma w|F_o|^2]^{1/2}$, all refinement parameters were calculated for observed data only.

20.70. − MS (FAB, positive ions, DMSO/glycerol): *m/z* (%) = 308 (38) [Ni(**4**)(NO_3)]$^+$, 245 (56) [Ni(**4**) − H]$^+$, 143 (26), 58 (75), 44 (38).

Preparation of Nickel Complexes from $NiCl_2$·$6H_2O$: The preparation of the previously synthesized[2] **6a** is described as an example. To a solution of $NiCl_2$·$6H_2O$ (236 mg, 1 mmol) in methanol (5 mL) was added **1** (146 mg, 1 mmol). After stirring for 30 min at room temperature, the mixture was concentrated to a volume of 3 mL. To initiate crystallization, 1 mL of acetonitrile and a few drops of diethyl ether were added to the concentrated mixture and the resulting purple-blue solution was cooled to 5 °C. After a few hours, needle-shaped crystals had formed, which were collected by filtration and washed with diethyl ether. Recrystallization from methanol by slowly concentrating the solution gave blue, plate-shaped crystals suitable for X-ray analysis.

6a: Yield 132 mg (45% based on $NiCl_2$·$6H_2O$). − $C_6H_{20}Cl_2N_4NiO$ (only directly coordinated water was left after drying, 293.9): calcd. C 24.53, H 6.86, N 19.07; found C 24.68, H 6.79, N 18.91. − MS (FAB, positive ions, DMSO/glycerol): *m/z* (%) = 239 (75) [Ni(**1**)Cl]$^+$, 203 (24) [Ni(**1**) − H]$^+$.

6b·2CH_3OH: Yield 309 mg (48% based on $NiCl_2$·$6H_2O$). − $C_{16}H_{48}Cl_4N_8Ni_2O_2$ (643.8): calcd. C 29.85, H 7.51, N 17.40; found C 29.76, H 7.49, N 17.32. − MS (FAB, positive ions, DMSO/glycerol): *m/z* (%) = 253 (70.2) [{Ni(**2**)Cl}$_2$]$^{2+}$, 217 (17.53) [Ni(**2**) − H]$^+$.

6c: Yield 132 mg (41% based on $NiCl_2$·$6H_2O$). − $C_8H_{24}Cl_2N_4NiO$ (321.9): calcd. C 29.85, H 7.51, N 17.40; found C 29.95, H 7.37, N 17.32. − MS (FAB, positive ions, DMSO/glycerol): *m/z* (%) = 267 (89) [Ni(**3**)Cl]$^+$, 232 (47) [Ni(**3**)]$^+$, 174 (36).

6d·H_2O: Yield 176 mg (50% based on $NiCl_2$·$6H_2O$). − $C_9H_{28}Cl_2N_4NiO_2$ (only directly coordinated water was left after drying, 353.9): calcd. C 30.54, H 7.97, N 15.83; found C 30.60, H 7.84, N 15.71. − MS (FAB, positive ions, DMSO/glycerol): *m/z* (%) = 281 (53) [Ni(**4**)$(H_2O)(OH)$]$^+$, 246 (34) [Ni(**4**)]$^+$, 188 (28).

Crystal Structure Analyses: Crystals of **5a−d** and **6b−d** obtained by crystallization from methanol were found to slowly decompose in air, most probably due to loss of solvent of crystallization. However, those obtained by crystallization from acetonitrile proved to be more stable. Complexes **5c**, **5d**, **6b**, and **6d** were crystallized as solvates **5c**·CH_3CN, **5d**·CH_3OH, **6b**·$2CH_3OH$, and **6d**·H_2O. Suitable crystals were mounted on an Enraf−Nonius CAD-4 diffractometer at low temperature (**5b**, **5d**·CH_3OH, **6b**·$2CH_3OH$) or at room temperature. Salient crystal and data collection details are listed in Table 4. Routine search and autoindexing procedures yielded the dimensions of the unit cell for all seven compounds. Diffraction data were collected using ω−2θ scans. Raw data were reduced to structure factors[29] (and their e.s.d. values) by correcting for scan speed, Lorentz and polarization effects. No decay corrections were necessary. Empirical absorption corrections (based on Ψ scans) were applied to the raw data for **5b**, **5d**·CH_3OH, and **6b**·$2CH_3OH$. The structure solutions were found by standard Patterson methods. The positional parameters for all non-hydrogen atoms were refined by using first isotropic and then anisotropic thermal parameters. Difference Fourier maps calculated at this stage showed the positional parameters of the hydrogen atoms. However, hydrogen atoms were added to the structure models in calculated positions and were refined as riding atoms. No hydrogen positions were calculated for non-coordinated solvent molecules. Calculations were carried out with SHELXL-93[30] (refinement on F^2). ORTEP[31] was used for all molecular drawings. The asymmetric unit for **5c**·CH_3CN and **5d**·CH_3OH contains two independent molecules, while **6b**·$2CH_3OH$ possesses a crystallographic inversion center and the asymmetric unit contains 1/2 of the complex. Table 1 and Table 2 list selected bond lengths and angles for complexes **5** and **6**, respectively. Crystallographic data (excluding structure factors) for the structures reported in this paper have been deposited with the Cambridge Crystallographic Data Centre as supplementary publication nos. CCDC-149397 (**5a**), -149398 (**5b**), -149399 (**5c**·CH_3CN), -149400 (**5d**·CH_3OH), -140401 (**6b**·$2CH_3OH$), -149402 (**6c**), and -149403 (**6d**·H_2O). Copies of the data may be obtained free of charge from the CCDC, 12 Union Road, Cambridge CB2 1EZ, U.K. [Fax (internat.) + 44-1223/360-033; E-mail: deposit@ccdc.cam.ac.uk].

UV/Vis Spectra: The UV/Vis spectra of all the complexes were recorded from 250 nm (40000 cm^{-1}) to 1400 nm (7100 cm^{-1}) at room temperature in methanol solution. The

wavelengths of the absorption maxima and the molar extinction coefficients of the absorption bands are listed in Table 3.

Acknowledgments

We thank the Deutsche Forschungsgemeinschaft and the Fonds der Chemischen Industrie for financial support.

[1] F. G. Mann, W. J. Pope, *J. Chem. Soc.* **1926**, 482.
[2] A. Marzotto, D. A. Clemente, G. Valle, *Acta Crystallogr., Sect. C* **1993**, *49*, 1252.
[3] S. E. Rasmussen, *Acta Chem. Scand.* **1959**, *13*, 2009.
[4] P. D. Cradwick, D. Hall, *Acta Crystallogr., Sect. B* **1970**, *26*, 1384.
[5] G. M. Colpas, M. Kumar, R. O. Day, M. J. Maroney, *Inorg. Chem.* **1990**, *29*, 4779.
[6] M. Ciampolini, N. Nardi, *Inorg. Chem.* **1966**, *5*, 41.
[7] I. Bertinti, M. Ciampolini, P. Dapporto, D. Gatteschi, *Inorg. Chem.* **1972**, *11*, 2254.
[8] M. Di Vaira, P. L. Orioli, *Acta Crystallogr., Sect. B* **1968**, *24*, 595.
[9] P. L. Orioli, N. Nardi, *J. Chem. Soc., Chem. Commun.* **1975**, 229.
[10] R. D. Willett, *Acta Crystallogr., Sect. C* **1987**, *43*, 1494.
[11] D. M. Duggan, D. N. Hendrickson, *Inorg. Chem.* **1974**, *13*, 2056.
[12] C. G. Pierpont, D. N. Hendrickson, D. M. Duggan, F. Wagner, E. K. Barefield, *Inorg. Chem.* **1975**, *14*, 604.
[13] A. Vacca, P. Paoletti, *J. Chem. Soc. A* **1968**, 2378.
[14] A. Dei, P. Paoletti, A. Vacca, *Inorg. Chem.* **1968**, *7*, 865.
[15] Ligand **3**: R. L. Fanshawe, A. G. Blackman, *Inorg. Chem.* **1995**, *34*, 421.
[16] [16a] Ligands **2**−**4**: A. M. Dittler-Klingemann, F. E. Hahn, *Inorg. Chem.* **1996**, *35*, 1996. − [16b] Co^{III} complex of ligand **2**: R. J. Geue, A. M. Sargeson, R. Wijesekera, *Aust. J. Chem.* **1993**, *46*, 1021.
[17] A. M. Dittler-Klingemann, C. Orvig, F. E. Hahn, F. Thaler, C. D. Hubbard, R. van Eldik, S. Schindler, I. Fábián, *Inorg. Chem.* **1996**, *35*, 7798.
[18] R. D. Hancock, *Acc. Chem. Res.* **1990**, *23*, 253.
[19] F. Thaler, C. D. Hubbard, F. W. Heinemann, R. van Eldik, S. Schindler, I. Fábián, A. M. Dittler-Klingemann, F. E. Hahn, C. Orvig, *Inorg. Chem.* **1998**, *37*, 4022.
[20] J. Chin, M. Banaszczyk, V. Jubian, X. Zou, *J. Am. Chem. Soc.* **1989**, *111*, 186.
[21] R. Gaudry, *Org. Synth. Coll. Vol.* **1966**, *3*, 436.
[22] [22a] S. Soloway, A. Lipschitz, *J. Org. Chem.* **1958**, *23*, 613. − [22b] G. W. Stevenson, D. Williamson, *J. Am. Chem. Soc.* **1958**, *80*, 5943.
[23] J. Lichtenberger, Ch. Faure, *Bull. Soc. Chim. Fr.* **1948**, 995.
[24] C. K. Jørgensen, *Acta Chem. Scand.* **1956**, *10*, 887.
[25] L. E. Orgel, *J. Chem. Phys.* **1955**, *23*, 1004.
[26] O. Bostrup, C. K. Jørgensen, *Acta Chem. Scand.* **1957**, *11*, 1223.
[27] Y. Ihara, M. Sakura, *Thermochim. Acta* **1988**, *136*, 279.
[28] S. G. Zipp, A. P. Zipp, S. K. Madan, *Coord. Chem. Rev.* **1974**, *14*, 29.
[29] Neutral atomic scattering factors were used. These, as well as terms of anomalous dispersion, were taken from: *International Tables for X-ray Crystallography*, vol. 4, Kynoch Press, Birmingham, U.K., **1974**.
[30] G. M. Sheldrick, *SHELX-93, Program for the Solution of Crystal Structures*, Universität Göttingen, Germany, **1993**.
[31] C. K. Johnson, *ORTEP II*, Report ORNL 5138, Oak Ridge National Laboratory, TN, USA, **1971**.

Received September 7, 2000
[I00335]

Structure, Magnetic Properties and Magnetic Phase Diagram of a Layered, Bimetallic, Cyanide-Bridged Cr^{III}-Ni^{II} Metamagnet

Arnaud Marvilliers,[a] Simon Parsons,[b] Eric Rivière,[a] Jean-Paul Audière,[a] Mohamedally Kurmoo,[c] and Talal Mallah*[a]

To the memory of Olivier Kahn to whom we owe a great deal

Keywords: Chromium / Cyanides / Magnetic properties / Nickel

The reaction of hexacyanochromate(III) with $Ni(tmc)^{2+}$ (tmc = tetramethylcyclam) leads to the formation of the layered compound $[Ni(tmc)]_3[Cr(CN)_6]_2{\cdot}18H_2O$ displaying a corrugated sheet structure. Within each layer, the Ni(tmc) units are surrounded by two $Cr(CN)_6$ complexes in a *trans* fashion while the $Cr(CN)_6$ units are linked to three Ni(tmc) molecules in facial positions. The magnetic studies show ferromagnetic interaction for a $Ni^{II}(d^8, t_{2g}^6e_g^2)$–CN–$Cr^{III}(d^3, t_{2g}^3)$ system within the layers. Below a critical temperature (T_N = 14 K), a bulk antiferromagnetic order is observed due to a small interlayer antiferromagnetic interaction. An antiferromagnetic → ferromagnetic phase transition occurs for an applied field H_C of 1200 Oe expressing the metamagnetic behavior of the compound. The phase diagram of the compound was constructed and the antiferromagnetic interlayer magnetic energy was estimated to be equal to 0.1 cm^{-1}.

Introduction

Over the last ten years, bimetallic, cyanide-bridged systems built from hexacyanometallates have provided new materials possessing three,[1−9] two,[10−16] one[17−21] and zero[22−27] dimensionality.[28] Room temperature molecular-based magnets as well as photoinduced magnets have been synthesized and characterized.[4,29−32] Kahn and coworkers opened new perspectives in the field by preparing a $Mo^{III}-Mn^{II}$ cyanide-bridged, three-dimensional ferromagnet (T_C = 51 K) possessing large magnetic anisotropy.[33,34]

The magnetic properties are intimately related to the dimensionality of the systems. When the cyanide bridges spread in the three directions of space, long-range magnetic ordering occurs. On the other hand, if the cyanide bridges are restricted in zero dimensions, leading to high-spin discrete species,[22,23,26,27] new phenomena like the blocking and the quantum tunneling of the magnetization may be observed.[35,36]

We report here the preparation, crystal structure, magnetic properties and magnetic phase diagram of a new compound $[Cr(CN)_6]_2[Ni(tmc)]_3{\cdot}18H_2O$ obtained from the reaction of $[Ni(tmc)](ClO_4)_2$ (tmc = tetramethylcyclam, a tetradentate ligand) and $K_3[Cr(CN)_6]{\cdot}2H_2O$.

[a] Laboratoire de Chimie Inorganique, UMR 8613, Université Paris-Sud,
91405 Orsay, France
Fax: (internat.) +33-1/6915-4754
E-mail: mallah@icmo.u-psud.fr
[b] Department of Chemistry, The University of Edinburgh, West Mains Road, Edinburgh, EH9 3JJ, United Kingdom
[c] Institut de Physique et Chimie des Matériaux de Strasbourg, UMR 7504,
23, rue du Loess, 67037 Strasbourg, France

Supporting information for this article is available on the WWW under http://www.wiley-vch.de/home/eurjic or from the author.

Results and Discussion

Synthesis and Characterization

The reaction of $[Ni(tmc)](ClO_4)_2$ and $K_3[Cr(CN)_6]{\cdot}2H_2O$ in water leads to the formation of an insoluble pale pink powder. The IR spectrum of the powder shows the presence of all the features expected for the organic tmc ligand in addition to two bands at 2154 and 2129 cm^{-1} assigned to the asymmetric vibrations of bridging and nonbridging cyanides. Elemental analysis is consistent with the following formula $[Cr(CN)_6]_2[Ni(tmc)]_3{\cdot}18H_2O$. In order to estimate accurately the number of water molecules and to study the effect of dehydration, thermogravimetry was carried out in

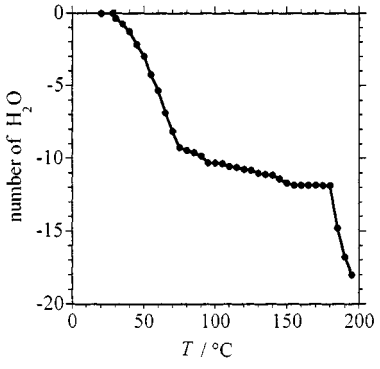

Figure 1. Thermogravimetric analysis in the form of loss of water molecules per unit formula versus temperature

 © WILEY-VCH Verlag GmbH, 69451 Weinheim, 2001 1434−1948/01/0505−1287 $ 17.50+.50/0

the temperature range 20−190 °C. Upon heating, nine water molecules are lost between room temperature and 75°C (Figure 1).

A further three water molecules are lost between 75 and 185 °C, where decomposition occurs. A total loss of 12 water molecules per unit formula is thus observed, although chemical analysis gave a total of 18 water molecules per unit formula. The remaining six water molecules are possibly more strongly bound through hydrogen bonds. The IR spectrum of a powder heated up to 180 °C and that of a nonheated sample are identical. The IR spectrum of the powder heated above 185 °C shows the absence of many bands belonging to the organic ligand.

Single crystals were obtained by a slow diffusion of aqueous solutions of the two precursors in an H tube. The IR spectrum of a few crystals was found to be identical to that of the powder.

Structure

X-ray diffraction studies reveal a layered structure with corrugated sheets as depicted in Figure 2 and 3. Within each layer, each Ni(tmc) unit is surrounded by two hexacyanochromate complexes in a *trans* position, as expected, while the $Cr(CN)_6$ units are linked to three Ni(tmc) disposed in a facial manner. The observed honeycomb-like corrugated layers are the result of: (i) the facial and not the meridional disposition of the three nickel complexes around the chromium anion, and (ii) the presence of an inversion center located on the nickel atoms. The same spatial arrangement has already been found in a related compound reported earlier where the tetradentate ligand cyclam were used instead of tetramethylcyclam.[12]

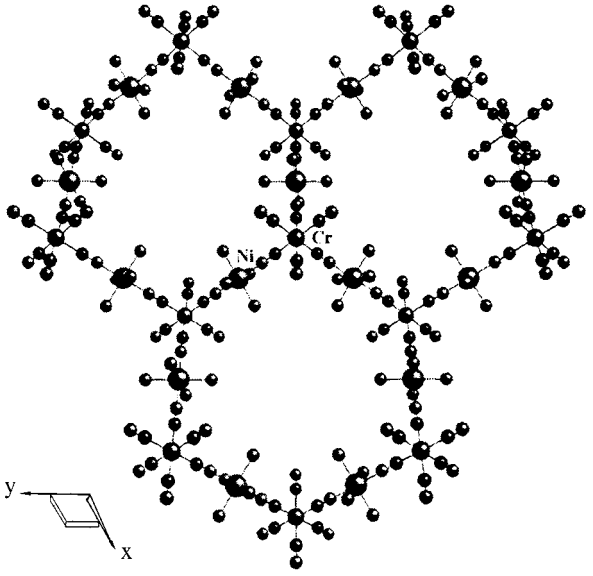

Figure 2. View along the *z* axis showing the honeycomb-like structure of the layers

All chromium atoms are crystallographically equivalent within the structure. The geometry around Cr can be considered as being isotropic. Around the nickel, the shortest distance [Ni(1)−N(10) = 2.089(10)Å] is that with the cyanides′ nitrogen atoms. The Ni−N bonds to the tmc′s nitrogen atoms are 2.185(18) and 2.306(14) Å for Ni(1)−N(1) and Ni(1)−N(4) respectively (Figure 4).

Despite the high *R* factor (14%), there is a clear tendency to have longer Ni−N bonds within the macrocycle than with the apical cyanides′ nitrogen atoms. This lengthening has already been noted for cyclam derivatives.[37] It has been attributed to the nonbonded repulsion between the hydrogen atoms of the alkyl substituents and those of adjacent carbon atoms. This bond lengthening within the macrocycle results in a shortening of the apical Ni−N bond lengths when axial ligands are present. Indeed, the apical Ni−N bond lengths are shorter for *trans*-[Ni(tetrapropylcyclam)$(NCS)_2$] than for *trans*-[Ni(cylam)(NCS).[38,39] The same tendency is observed when comparing the data of the present compound to those of the previously reported cyclam analogue. The shortest Ni−N bond length is found for nitrogen atoms belonging to the organic macrocycle [Ni−N = 2.06(2) Å] for the cyclam analogue, while for the present compound the apical Ni−N bond length is found to be the shortest. Another important difference between the two compounds is the value of the Ni(1)−N(10)−C(10) angle [173.4(1)°] which is closer to linearity in the present compound than when cyclam is used [171.6(1)°].

Magnetic Properties

All the magnetic studies were performed on a powdered sample and it was checked that the properties of a few single crystals were the same as that of the powder. The $\chi_M T = f(T)$ curve (Figure 5, recorded in an applied field of 3000 Oe) shows that $\chi_M T$ increases smoothly between 300 and 50 K upon cooling and then sharply below 50 K. A maximum is observed at $T = 14$ K. The $\chi_M T$ value at $T = 300$ K (8.18 cm^3 K mol^{-1}) is well above what is expected for two noninteracting Cr^{III} and three noninteracting Ni^{II} ions i.e. 7.03 cm^3 K mol^{-1}, obtained by fitting the high temperature part of the $1/\chi_M = f(T)$ curve.[40]

The increase of $\chi_M T$ upon cooling is the signature of a ferromagnetic-exchange coupling between nearest neighbor metal ions through the cyanide bridge. This has already been observed in related systems and has been ascribed to the orthogonality of the Cr^{III} and Ni^{II} magnetic orbitals.[2,22,26] The abrupt increase of $\chi_M T$ below 50 K to a maximum value as large as 156 cm^3 K mol^{-1} indicates the occurrence of a large correlation between the magnetic ions within the layers which is the origin of the magnetic anisotropy within the compound.[41]

In order to investigate the low temperature behavior, the temperature dependence of the magnetization was first measured in the presence of a weak applied field (30 Oe) and then at higher fields ranging from 400 to 1400 Oe.[42] The susceptibility (*M*/*H*) vs. temperature curve performed at $H = 30$ Oe (Figure 6) reveals the presence of a maximum at $T = 14$ K. The presence of such a maximum rules out the possibility of a 3D ferromagnetic order, where a saturation of the susceptibility is expected.

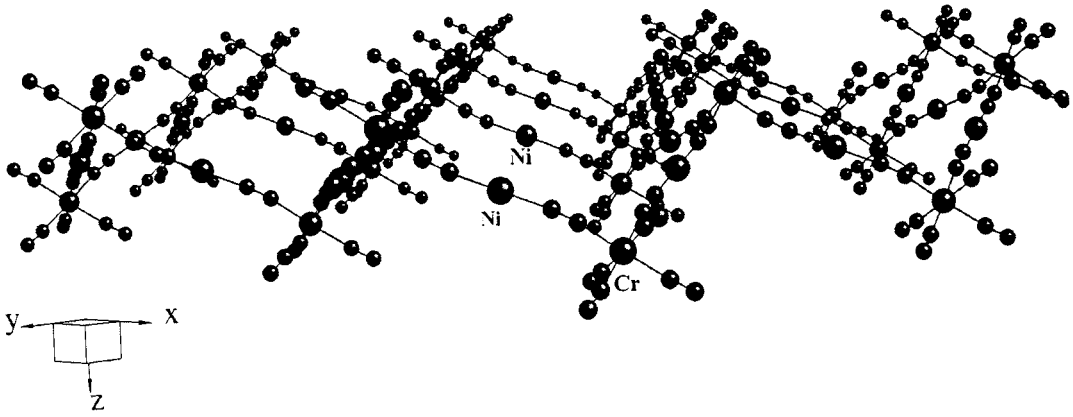

Figure 3. View along the *xy* plane revealing the corrugated sheets (tmc has been removed for clarity)

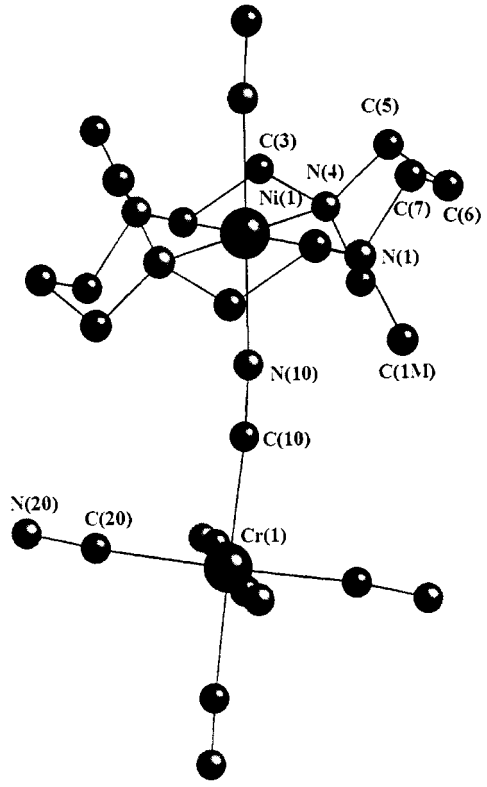

Figure 4. View of a dinuclear unit with atom-numbering scheme (hydrogen atoms are omitted for clarity); selected bond lengths [Å] and angles [°] with standard variations in parentheses: Ni(1)−N(1) 2.185(18), Ni(1)−N(4) 2.306(14), Ni(1)−N(10) 2.089(10), C(10)−N(10) 1.141(14), C(20)−N(20) 1.075(13), Cr(1)−C(10) 2.067(9), Cr(1)−C(20) 2.103(9); C(10)−N(10)−Ni(1) 173.4(10), N(10)−C(10)−Cr(1) 173.6(10), N(10)−C(20)−Cr(1) 174.7(11)

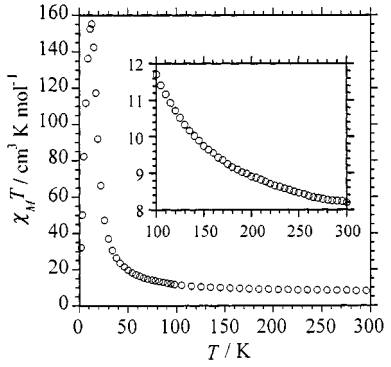

Figure 5. Thermal variation of the product of susceptibility and temperature of $[Cr(CN)_6]_2[Ni(tmc)]_3 \cdot 18H_2O$ ($\chi_M T$ versus T) in an applied field H = 3 kOe; inset: the increase of $\chi_M T$ between 300 and 100 K

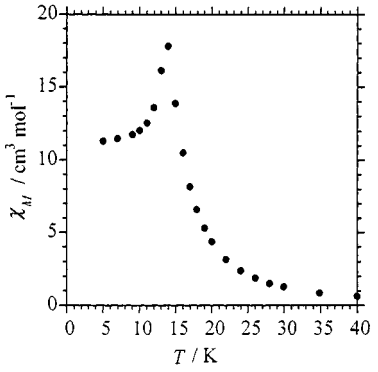

Figure 6. Thermal variation of the susceptibility in a field of 30 Oe

On the other hand, the fact that at low temperature (5 K) the susceptibility value (11.3 cm^3 mol^{-1}) is about two thirds that at the maximum (17.8 cm^3 mol^{-1}) is the signature of the occurrence of antiferromagnetic ordering in a randomly nonoriented sample.[43] For antiferromagnets in noncubic symmetry and within the framework of the mean field approximation, the perpendicular and the parallel components of the susceptibility measured on a single crystal have the same value at the ordering temperature. Below T_N, the perpendicular component remains constant in order to minimize the magnetic energy while the value of the parallel component decreases and vanishes at low temperature. Since the susceptibility of a powder is given by $\chi = (\chi_{\parallel} + 2\chi_{\perp})/3$, its value expected at low temperature corresponds to two thirds that of the maximum, as observed experimentally in the present compound.

Upon increasing the strength of the applied magnetic field, the maximum of the $M = f(H)$ curves (Figure 7) shifts

towards low temperature and disappears beyond $H = 1400$ Oe, showing a saturation of the magnetization.

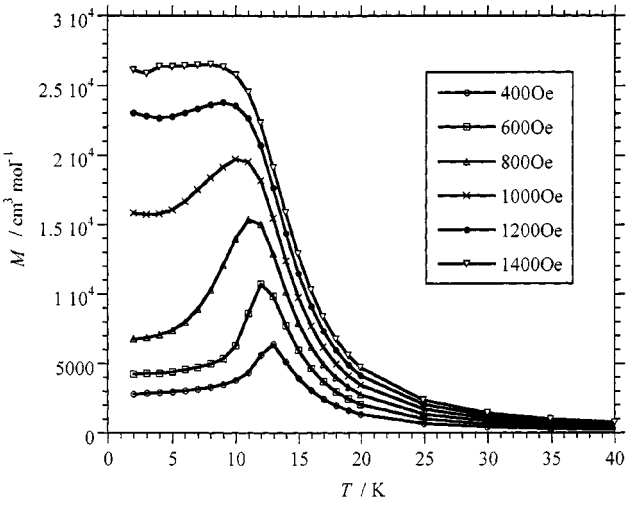

Figure 7. Thermal variation of the magnetization of a polycrystalline sample for different applied magnetic fields

This is the signature of the appearance of a ferromagnetic phase induced by the external applied magnetic field. On the other hand, the magnetization vs. field measurements performed at $T = 2$ K (Figure 8) present a sigmoidal shape. Upon increasing the applied field from zero, the magnetization increases first linearly and then abruptly and reaches saturation around 7 kOe. The sigmoidal shape of the $M = f(H)$ curve is characteristic of a metamagnetic behavior. This is the result of the transition from an antiferromagnetic to a field-induced ferromagnetic phase without going through an intermediate spin-flop phase. Such an abrupt transition is observed only if magnetic anisotropy is of the same order of magnitude or larger than the antiferromagnetic interaction so that the antiparallel magnetic moments remain in the same direction as the increasing applied magnetic field. In the case where the anisotropy energy is weaker than the antiferromagnetic energy, beyond a given magnetic field (which is usually very small) the system goes through an intermediate phase with canted magnetic moments (the spin-flop phase) before reaching the ferromagnetic phase. In such a situation, upon increasing the applied magnetic field a linear increase of the magnetization that extrapolates to zero for $H = 0$ should be observed before saturation is reached.[44,45] Such metamagnetic behavior has been already observed in layered compounds with strong ferromagnetic intralayer interactions and relatively weak interlayer antiferromagnetic interactions so that the magnetic anisotropy energy need not be very strong. The critical field needed to overcome the antiparallel alignment of the magnetic moments is found to be equal to 1170 Oe at $T = 2$K.

In summary, we can conclude that within the layers a ferromagnetic interaction operates leading to a relatively large correlation between the magnetic ions, while between the layers a weak antiferromagnetic interaction occurs leading to an overall antiferromagnetic order at $T_N = 14$ K. This antiferromagnetic order is overcome by an external applied field of 1170 Oe at $T = 2$ K.

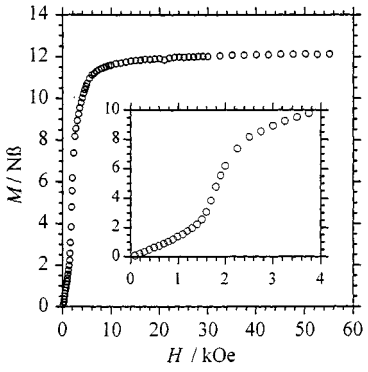

Figure 8. Variation of the magnetization as a function of the applied magnetic field at $T = 2$ K; inset: the sigmoidal shape at low values of the field

Magnetization vs. field isotherms performed at temperatures ranging from 2 to 14 K (not shown here) demonstrate that the critical field value decreases upon increasing the temperature and vanishes at $T = 14$ K. The critical field is estimated at the intersection of two linear slopes before and after the transition. Plotting the critical field H_C(T) as a function of the temperature at which the magnetization isotherms are measured leads to the phase diagram of the metamagnet (Figure 9). This phase diagram (which is partial as explained below) presents two regions delimited by the H_C(T) = f(T) curve. The region below the curve corresponds to the domain of stability of the antiferromagnetic phase while the upper region corresponds to the domains where the field-induced ferromagetic and the paramagnetic phases are stable. These two phases are, of course, well separated but a frontier line is difficult to determine experimentally.

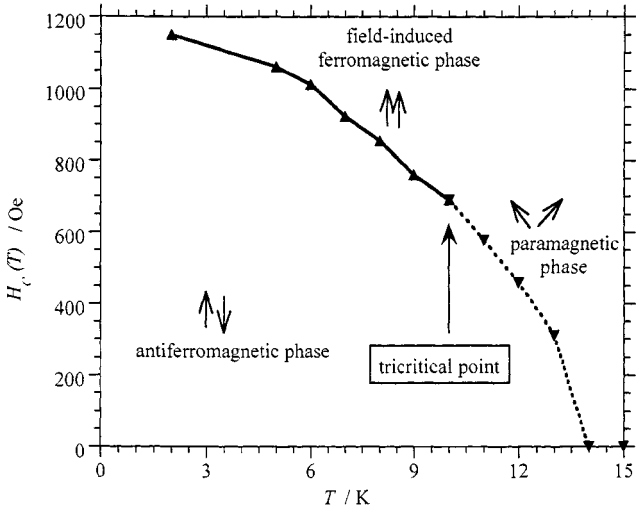

Figure 9. Phase diagram of the metamagnet; the dashed curve represents the range of second order magnetization and the continuous curve represents first order hysteresis magnetization; the tricritical point separates the two regions

However, a metamagnet has a tricritical point (T_{TCP} in the following discussion) where the three phases coexist; this tricritical point belongs to the H_C(T) = f(T) curve.[45] At temperatures below T_{TCP} the antiferromagnetic−ferromagnetic transition is a first order trans-

ition and a hysteresis loop should be observed in the $M = f(H)$ curves, while at temperatures above that of the tricritical point (but below T_N), the antiferromagnetic−paramagnetic phase transition is a second order transition and no hysteresis loop can be present. So, in order to determine the temperature of the tricritical point, we measured the magnetization as a function of the applied field for temperatures ranging from 2 to 12 K. Figure 10 shows the presence of a hysteresis loop in the $M = f(H)$ curve performed at $T = 2$ K.

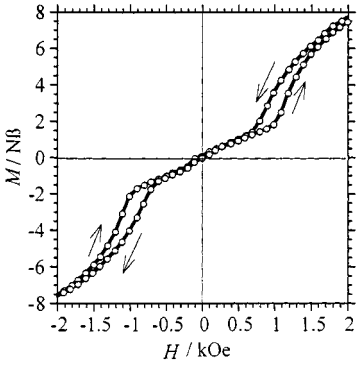

Figure 10. Hysteresis curve recorded between −2 and +2 kOe at $T = 2$ K

The maximum width of the loop is found to be equal to 244 Oe. When the temperature is increased, the width of the hysteresis loop decreases to 70 Oe at $T = 9$ K and almost vanishes at 10 K (Figure 11). Between 10 and 13 K, the $M = f(H)$ curves still have the sigmoidal shape (less pronounced than at lower temperatures) but no hysteresis could be detected anymore. This allows us to place the tricritical point at $T_{TCP} = 10$ K.

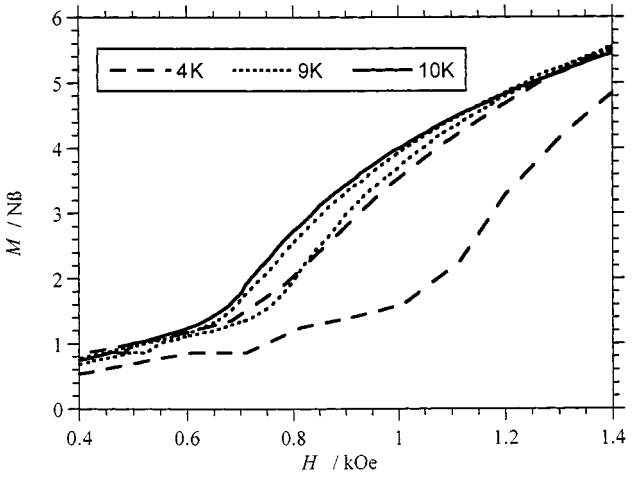

Figure 11. Isothermal magnetization curves measured at $T = 4$ K (-----), 9 K (·····) and 10 K (—); note the hysteresis behavior at 9 and 4 K

The value of the critical field H_C of the metamagnet may be obtained by extrapolating the $H_C(T) = f(T)$ curve to $T = 0$ K; it is found to be equal to 1200 Oe. This corresponds to the magnetic field needed to overcome the antiparallel alignment of the spins. The corresponding magnetic energy is given by $g\beta H_C$ and is found to be equal to 0.1 cm^{-1} when assuming a g value of 2.

Concluding Remarks

The quality of the crystal structure of this compound is not high enough to allow a thorough discussion of the origin of the bulk magnetic properties reported. For instance, the position of the water molecules that occupy the interlayer space (18 per unit formula) could not be refined and there was no possibility of knowing whether a hydrogen-bonded network exists within the compound. However, TGA studies show that six water molecules (per unit formula) cannot be removed before decomposition (which occurs at a rather high temperature). This suggests that these water molecules belong to a hydrogen-bonded network spreading all over the compound and linking the layers together. On the other hand, the magnetic properties of a sample heated at 180 °C under vacuum for 24 hours are the same as those of a nonheated sample. This is in line with the hypothesis of the presence of water molecules linking the layers through hydrogen bonds and thus forming a pathway for the interlayer antiferromagnetic interaction responsible for the antiferromagnetic order. The magnitude of the magnetic energy corresponding to the interlayer antiferromagnetic interaction (0.1 cm^{-1}) is weak but reasonable for a separation of 9.25 Å between the layers. This is still in a distance range where exchange through bonds may be more important than through space (dipolar).

The metamagnetic behavior observed is the result of the presence of a magnetic anisotropy with an energy at least as large as the energy responsible for the antiferromagnetic interaction between the layers. A quantitative determination of the magnetic anisotropy energy may be obtained from single crystal magnetic studies. Unfortunately, such studies could not be carried out because of a lack of crystals of suitable size and shape. However, the large correlation between the magnetic moment evidenced by the rather large value of the susceptibility at the Néel temperature is responsible for the presence of the magnetic anisotropy that leads to the metamagnetic behavior. The large correlation is the result of a relatively large ferromagnetic exchange interaction through the cyanide bridge. The lack of such a correlation in the previously reported cyclam analogue indicates that the magnitude of the $Cr^{III}-Ni^{II}$ ferromagnetic interaction is larger in the present tmc-based compound.[12,46] This may be related to the local structure around the Ni atoms; shorter apical Ni−N bond lengths and Ni−N−C angles (NC being the cyanide bridges) closer to linearity in the present compound may be the origin of the larger ferromagnetic short-range interaction and thus responsible for the bulk magnetic properties observed in the present compound and absent in the cyclam analogue.

Experimental Section

Hazards: Perchlorate salts should be handled with care and used in small quantities.

Syntheses: The $[Ni(tmc)](ClO_4)_2$ salt was prepared as previously reported.[47] The powder samples of the reported compound were obtained as follows: an aqueous solution (50 mL) containing 10^{-3} mol of $[Ni(tmc)](ClO_4)_2$ was added dropwise to 50 mL of an aqueous solution containing an equimolar amount of $K_3[Cr(CN)_6]\cdot 2H_2O$. A pale pink powder immediately formed, which was filtered, thoroughly washed with water and then dried under vacuum. – $C_{54}H_{132}Cr_2N_{24}Ni_3O_{18}$ (1685.9): calcd. C 37.67, H 7.67, N 19.53, Ni 10.24, Cr 6.05; found C 37.61, H 7.70, N 19.49, Ni 10.13, Cr 5.93.

General Remarks: Thermogravimetric studies were carried out in argon atmosphere at a heating rate of 1 °C per minute. The magnetic measurements were performed using a SQUID magnetometer operating in the 300–2 K temperature range and the 0–55 kOe magnetic field range. The drawings were carried out with the CRYSTAL MAKER program.[48]

Crystal Data for 1: $C_{54}H_{132}Cr_2N_{24}Ni_3O_{18}$, M = 1685.97, trigonal, a = 16.055(4), c = 9.248(7) Å, U = 2064.4(17) Å^3, T = 220 K, space group $P\bar{3}m1$, Z = 1, Cu-$K_{\alpha 1}$ = 3.461 mm^{-1}, 3503 reflections measured, of which 1161 were unique (R_{int} = 0.0745). The structure was solved by direct methods (SIR92) and refined with Shelxl-97;[49,50] solvent water was treated in the manner described by van der Sluis and Spek.[51] The final conventional R factor [based on F and 788 data with $F > 4(F)$] was 0.1465. The high R factor reflects complete disorder of the macrocycle about the crystallographic 2/m site occupied by the Ni. Crystallographic data (excluding structure factors) for the structures reported in this paper have been deposited with the Cambridge Crystallographic Data Centre as supplementary publication no. CCDC 147292. Copies of the data can be obtained free of charge on application to CCDC, 12 Union Road, Cambridge CB2 1EZ UK [Fax: (internat.) +44-1223/336-033; E-mail: deposit@ccdc.cam.ac.uk).

Acknowledgments

The authors thank Dr. Jean-Pierre Renard for interesting discussions and the CNRS (Centre National de Recherche Scientifique) for financial support.

[1] D. Babel, *Comments Inorg. Chem.* **1986**, *5*, 285.
[2] V. Gadet, T. Mallah, I. Castro, M. Verdaguer, P. Veillet, *J. Am. Chem. Soc.* **1992**, *114*, 9213–9124.
[3] T. Mallah, S. Thiébaut, M. Verdaguer, P. Veillet, *Science* **1993**, *262*, 1554–1557.
[4] S. Ferlay, T. Mallah, R. Ouahès, M. Verdaguer, P. Veillet, *Nature* **1995**, *378*, 701–703.
[5] W. R. Entley, G. S. Girolami, *Science* **1995**, *268*, 397–400.
[6] M. S. El Fallah, E. Rentshler, A. Caneschi, R. Sessoli, D. Gatteschi, *Angew. Chem. Int. Ed. Engl.* **1996**, *35*, 1947–1949.
[7] W. E. Bushmann, S. C. Paulson, C. M. Wynn, M. A. Girtu, A. J. Epstein, H. S. White, J. S. Miller, *Adv. Mater.* **1997**, *9*, 645–646.
[8] S. Ferlay, T. Mallah, R. Ouahès, P. Veillet, M. Verdaguer, *Inorg. Chem.* **1999**, *38*, 229–234.
[9] M. Ohba, N. Usaki, N. Fukita, H. Okawa, *Angew. Chem. Int. Ed.* **1999**, *38*, 1795–1797.
[10] M. Ohba, H. Okawa, T. Ito, A. Ohto, *J. Chem. Soc., Chem. Commun.* **1995**, 1545–1946.
[11] N. Re, E. Gallo, C. Floriani, H. Miyasaka, N. Matsumoto, *Inorg. Chem.* **1996**, *35*, 6004–6008.
[12] S. Ferlay, T. Mallah, J. Vaissermann, F. Bartolomé, P. Veillet, M. Verdaguer, *Chem. Commun.* **1996**, 2481–2482.
[13] M. Ohba, H. Okawa, N. Fukita, Y. Hashimoto, *J. Am. Chem. Soc.* **1997**, *119*, 1011–1019.
[14] H. Miyasaka, N. Matsumoto, N. Re, E. Gallo, C. Floriani, *Inorg. Chem.* **1997**, *36*, 670–676.
[15] N. Re, R. Crescenzi, C. Floriani, H. Miyasaka, N. Matsumoto, *Inorg. Chem.* **1998**, *37*, 2717–2722.
[16] E. Colacio, J. M. Dominguez-Vera, M. Ghazi, R. Kivekés, F. Lloret, J. M. Moreno and H. Stoeckli-Evans, *Chem. Commun.* **1999**, 987–988.
[17] G. O. Morpugo, V. Mosini, P. Porta, G. Dessy, V. Fares, *J. Chem. Soc., Dalton Trans.* **1981**, 111–117.
[18] M. Ohba, N. Maruono, H. Okawa, T. Enoki, J.-M. Latour, *J. Am. Chem. Soc.* **1994**, *116*, 11566–11577.
[19] M. Ohba, N. Fukita, H. Okawa, *J. Chem. Soc., Dalton Trans.* **1997**, 1733–1737.
[20] M. Ohba, N. Usuki, N. Fukita, H. Okawa, *Inorg. Chem.* **1998**, *37*, 3349–3354.
[21] A. Marvilliers, S. Parsons, E. Rivière, J. -P. Audière, T. Mallah, *Chem. Commun.* **1999**, 2217–2218.
[22] T. Mallah, C. Auberger, M. Verdaguer, P. Veillet, *J. Chem. Soc., Chem. Commun.* **1995**, 61–62.
[23] A. Scuiller, T. Mallah, A. Nivorozkhin, M. Verdaguer, P. Veillet, *New J. Chem.* **1996**, 1–3.
[24] K. Van Langenberg, S. R. Batten, K. J. Berry, D. C. R. Hockless, B. Moubaraki, K. S. Murray, *Inorg. Chem.* **1997**, *36*, 5006–5015.
[25] A. Marvilliers, T. Mallah, E. Rivière, S. Parsons, C. Muñoz, K. E. Vostrikova, *Mol. Cryst. Liq. Cryst.* **1999**, *335*, 1195–1206.
[26] A. Marvilliers, Y. Pei, J. Cano Boquera, K. E. Vostrikova, C. Paulsen, E. Rivière, J.-P. Audière, T. Mallah, *Chem. Commun.* **1999**, 1951–1952.
[27] G. Rogez, A. Marvilliers, E. Rivière, J.-P. Audière, F. Lloret, F. Varret, A. Goujon, N. Mendenez, J.-J. Girerd, T. Mallah, *Angew. Chem. Int. Ed.* **2000**, *39*, 2885–2887.
[28] Here we restrict the word dimensionality to coordination bonds, a two dimensional system is one where coordination bonds (metal–cyanides, for example) spread in the two directions of space.
[29] S. M. Holmes, G. S. Girolami, *J. Am. Chem. Soc.* **1999**, *121*, 5593–5594.
[30] E. Dujardin, S. Ferlay, X. Phan, C. Desplanches, C. Cartier dit Moulin, P. Sainctavit, F. Baudelet, E. Dartyge, P. Veillet, M. Verdaguer, *J. Am. Chem. Soc.* **1998**, *120*, 11347–11352.
[31] O. Sato, T. Iyoda, A. Fujishima, K. Hashimoto, *Science* **1996**, *272*, 704–705.
[32] O. Sato, Y. Einaga, A. Fujishima, K. Hashimoto, *Inorg. Chem.* **1999**, *38*, 4405–4412.
[33] J. Larionova, R. Clérac, J. Sanchiz, O. Kahn, S. Golhen, L. Ouahab, *J. Am. Chem. Soc.* **1998**, *120*, 13088–13095.
[34] J. Larionova, O. Kahn, S. Golhen, L. Ouahab, R. Clérac, *J. Am. Chem. Soc.* **1999**, *121*, 3349–3356.
[35] T. Mallah, S. Ferlay, A. Scuiller, M. Verdaguer, NATO ASI Series C vol. 484, *Magnetism: A Supramolecular Function* **1996**, p.597–614.
[36] N. Vernier, G. Bellessa, T. Mallah, M. Verdaguer, *Phys. Rev. B* **1997**, *56*, 75–76.
[37] A. E. Martell, R. D. Hancock, R. J. Motekaitis, *Coord Chem. Rev.* **1994**, *133*, 39–92.
[38] N. W. Alcock, A. C. Benniston, S. J. Grant, H. A. A. Omar, P. Moore, *J. Chem. Soc., Chem. Commun.* **1991**, 1573–1574.
[39] T. Ito, M. Kato, H. Ito, *Bull. Chem. Soc. Jpn.* **1984**, *57*, 2641–2643.
[40] The $\chi_M T$ value of 7.03 for noninteracting metal ions allows us to compute the g value for Ni^{II} which is found to be equal to 2.10 assuming a g value of 1.99 for Cr^{III}.
[41] The value of $\chi_M T$ has no real meaning because at this temperature the magnetization is field dependent, nevertheless the high value indicates the presence of a large correlation within the layers.
[42] It was checked that ac susceptibility vs. temperature plots performed at 0 and 50 Oe static applied field are identical to those of Figure 6 which indicate that saturation effects are nonexistent at such low fields. On the other hand, such measurements made at different frequencies of the oscillating field and with zero static field confirm the presence of a magnetic ordering at T = 14 K.
[43] A. Herpin, in *Théorie du magnétisme* **1968**, pp. 472–498.
[44] We must be cautious at this stage because our measurements

were carried out on a powder and not on an oriented single crystal with the applied field parallel to the easy axis, but the shape of the $M = f(H)$ curve, which is the sum of the parallel and the perpendicular components of the magnetization, presents a too sharp transition to be that of a spin-flop phase.

[45] L. J. de Jongh, A. R. Miedema, *Adv. Phys.* **1974**, *23*, 1−260.

[46] For the previously reported cyclam-based compound, the largest susceptibility value measured (within the same applied field as for the present compound i.e. 30 Oe) was found to be one order of magnitude smaller than for the present compound.

[47] E. K. Barefield, F. Wagner, *Inorg. Chem.* **1973**, *12*, 2435−2439.

[48] D. Palmer, *CrystalMaker*, Bicester, **1993**.

[49] A. Altomare, G. Cascarano, C. Giacovazzo, A. Guagliardi, *J. Appl. Crystallogr.* **1993**, *26*, 343−350.

[50] G. M. Sheldrick, Institüt für Anorganische Chemie der Universität, Tammanstraße 4, 3400 Göttingen, Germany, **1998**.

[51] H. v. d. Sluis, A. L. Spek, *Acta Crystallogr., Sect A* **1990**, *46*, 194−201.

Received September 7, 2000
[I00337]

Methacrylate-Substituted Mixed-Metal Clusters Derived from Zigzag Chains of $[ZrO_8]/[ZrO_7]$ and $[TiO_6]$ Polyhedra

Bogdan Moraru,[a] Guido Kickelbick,[a] and Ulrich Schubert*[a]

Keywords: Zirconium / Titanium / Alkoxides / Oxo ligands / Cluster compounds / Organic-inorganic hybrid composites

Reaction of titanium butoxide and zirconium butoxide with methacrylic acid in different molar ratios results in the formation of the mixed-metal clusters $Ti_4Zr_4O_6(OBu)_4(OMc)_{16}$, $Ti_2Zr_4O_4(OBu)_2(OMc)_{14}$, $Ti_4Zr_2O_4(OBu)_6(OMc)_{10}$, and $Ti_2Zr_6O_6(OMc)_{20}$ (OMc = methacrylate). The molecular structures of these clusters have been determined by single-crystal X-ray diffraction analysis. They are based on a common structural motif, namely a zigzag chain comprising two terminal $[TiO_6]$ octahedra and two or four central $[ZrO_8]$ dodecahedra or $[ZrO_7]$ pentagonal bipyramids sharing common edges. Two additional $[TiO_6]$ octahedra or $[ZrO_8]$ dodecahedra are condensed at the flank of the main chain.

Introduction

The so-called POSS-reinforced polymers (POSS = polyhedral oligomeric silsesquioxanes) have recently attracted much interest as a new class of inorganic-organic hybrid materials. They are prepared by the copolymerization of organic monomers with oligomeric $(RSiO_{1.5})_x$ species, mainly the cubic $R_8Si_8O_{12}$ clusters, in which one or (less often) more than one of the organic substituents R incorporates a polymerizable group.[1] The POSS-reinforced polymers show interesting improvements in their thermal and mechanical properties relative to those of the parent polymers.

Additional property modifications can be expected upon reinforcement of organic polymers with metal oxide clusters, especially those of transition metals. Thus, changes in the optical properties may result, or polymers with particular magnetic or catalytic properties may be generated.

However, only a few oxometallate clusters substituted with polymerizable organic ligands are available and, to the best of our knowledge, only $Bu_{12}Sn_{12}O_{14}(OH)_6(OMc)_2$ (OMc = methacrylate),[2] $Ti_3O_2(O\mathit{i}Pr)_5(OCMe{=}CH_2)_3(\mathit{i}PrOH)$,[3] and $[SiW_{10}O_{36}(Si_2R_2O)]^{4-}$ or $[SiW_{11}O_{39}(OSi_2R_2)]^{4-}$ (R = unsaturated organic groups)[4] have hitherto been used as co-monomers in polymerization reactions.[5]

We have recently prepared and structurally characterized several acrylate- or methacrylate-substituted oxotitanium and oxozirconium clusters of differing sizes and shapes, such as $Zr_6O_4(OH)_4(OMc)_{12}$,[6] $Zr_4O_2(OMc)_{12}$,[6,7] $[Zr_6O_4(OH)_4(OAcr)_{12}]_2$ (OAcr = acrylate), $Zr_6O_4(OH)_4(OMc)_{12}(PrOH)$,[8] $Ti_6O_4(OEt)_8(OMc)_8$,[9] $Ti_9O_8(OPr)_4(OMc)_{16}$,[10] and $Ti_4O_2(O\mathit{i}Pr)_6(OAcr)_6$.[11] These crystalline clusters are reproducibly obtained in very high yields by treating $Zr(OR)_4$ or $Ti(OR)_4$ with a defined excess of (meth)acrylic acid. In the first step of this reaction, one or more alkoxide ligands are substituted by carboxylate groups. The alcohol thus liberated then undergoes an esterification reaction. The water produced along with the ester serves to hydrolyze the remaining alkoxide groups and acts as the source of the oxide or hydroxide groups in the clusters. The very slow production of water allows a very controlled growth of the carboxylate-substituted oxometallate clusters.

Small amounts of the clusters $Zr_6O_4(OH)_4(OMc)_{12}$, $Zr_4O_2(OMc)_{12}$, $Ti_4O_2(O\mathit{i}Pr)_6(OAcr)_6$, and $Ti_6O_4(OEt)_8(OMc)_8$, which can be considered as structurally well-defined nanosized building blocks, were then used as co-monomers in radical polymerizations with methyl methacrylate and methacrylic acid. Even small proportions of the clusters (typically 0.5−2 mol-%) were found to efficiently crosslink the organic polymer chains. This results, inter alia, in a controllable swelling behavior, a higher thermal stability, and modified dielectric properties of the resulting inorganic-organic hybrid polymers.[7,12,13] Our initial results indicated that not only the proportion of the cluster, but also its size and shape and the number of polymerizable groups around its core, influence the material properties of the hybrid polymers to some extent. For this reason, our aim was to prepare methacrylate-substituted clusters of different sizes and shapes. In this paper, we report the synthesis and structural characterization of four oblong-shaped mixed-metal oxo clusters of Ti and Zr. Surprisingly, the structures of the clusters turned out to be based on a straightforward common construction principle.

Results and Discussion

Reaction of $Ti(OBu)_4$, $Zr(OBu)_4$, and methacrylic acid in a 1:1:8.5 ratio resulted in the formation of crystalline $Ti_4Zr_4O_6(OBu)_4(OMc)_{16}$ (**1**) in almost quantitative yield. The same cluster was obtained when $Ti(OEt)_4$ was employed instead of $Ti(OBu)_4$. The formation of butyl methacrylate could be monitored spectroscopically, which suggested the mass balance given in Equation (1).

[a] Institut für Anorganische Chemie, Technische Universität Wien,
Getreidemarkt 9, 1060 Wien, Austria

 © WILEY-VCH Verlag GmbH, 69451 Weinheim, 2001 1434−1948/01/0505−1295 $ 17.50+.50/0

$$4\,Ti(OBu)_4 + 4\,Zr(OBu)_4 + 22\,CH_2{=}C(Me)COOH \rightarrow Ti_4Zr_4O_6(OBu)_4(OMc)_{16}\,(\mathbf{1}) + 6\,CH_2{=}C(Me)COOBu + 22\,BuOH \quad (1)$$

When the $Ti(OBu)_4/Zr(OBu)_4$ ratio was changed from 1:1 to about 1:2, while keeping the total proportion of methacrylic acid constant (4.2 mol methacrylic acid per mol metal alkoxide), the cluster $Ti_2Zr_4O_4(OBu)_2(OMc)_{14}$ (**2**) was formed. The compositions of **1** and **2** were verified by X-ray structure analyses (see below). The spectroscopic data, elemental analyses, and powder diffractograms confirmed that **1** and **2** were formed as the sole products of the respective reactions. Assignment of the signals in the ^1H and ^{13}C NMR spectra to individual ligands proved difficult because they occupy a number of stereochemically different coordination sites. However, the spectra gave a good "fingerprint" of each particular cluster.

Increasing the $Ti(OBu)_4/Zr(OBu)_4$ ratio to 1:3 resulted in a mixture of clusters. In addition to the previously obtained cluster **2**, the clusters $Ti_4Zr_2O_4(OBu)_6(OMc)_{10}$ (**3**) and $Ti_2Zr_6O_6(OMc)_{20}$ (**4**) were also formed. The composition of the mixture was verified by comparison of the powder diffraction patterns calculated from the individual crystal structure analyses with the powder XRD of the product mixture. Cluster **3** was obtained as the sole product when $Ti(OBu)_4$, $Zr(OPr)_4$ (instead of the butoxide), and methacrylic acid were reacted in a 1:1:8.2 molar ratio.

The latter result is remarkable in that it shows that seemingly minor changes in the reaction conditions may result in different clusters (although they are structurally related − see below): The only difference in the reaction conditions leading to **1** and **3**, respectively, is that zirconium *butoxide* is used in the former case, while zirconium *propoxide* is used in the latter. However, as mentioned above, replacing $Ti(OBu)_4$ by $Ti(OEt)_4$ did not result in a different cluster. These observations show that the relative reaction rates of the two alkoxides play an important role, and that the reactivity of the zirconium alkoxide evidently dominates the formation of the cluster nucleus, eventually leading to a particular cluster geometry. This is consistent with the higher reactivity of zirconium alkoxides relative to titanium alkoxides.

Clusters **1** and **4** have the general composition $M_8O_6X_{20}$ ($M = Ti^{IV}$ or Zr^{IV}; X = singly negatively charged ligand). The $M_6O_4X_{16}$ composition of **2** and **3** corresponds to a higher degree of condensation. Thus, increasing the $Zr(OBu)_4/Ti(OBu)_4$ ratio in the starting mixture from 1:1 to 3:1 not only favors the formation of the clusters with a higher Zr/Ti ratio, but also the formation of more highly condensed clusters ($M_6O_4X_{16}$ as opposed to $M_8O_6X_{20}$). It should be noted at this point that the previously obtained cluster $Zr_6O_4(OH)_4(OMc)_{12}$, obtained by reacting only $Zr(OPr)_4$ with a 3.8-fold excess of methacrylic acid,[6] also has the $M_6O_4X_{16}$ composition.

The molecular structures of clusters **1**−**4** are based on a common structural motif. This can best be visualized by comparing the cluster cores built up from connected polyhedra (Figure 1). In this representation the carbon atoms have been omitted, i.e. the corners of the polyhedra represent the oxygen atoms (from any ligand).

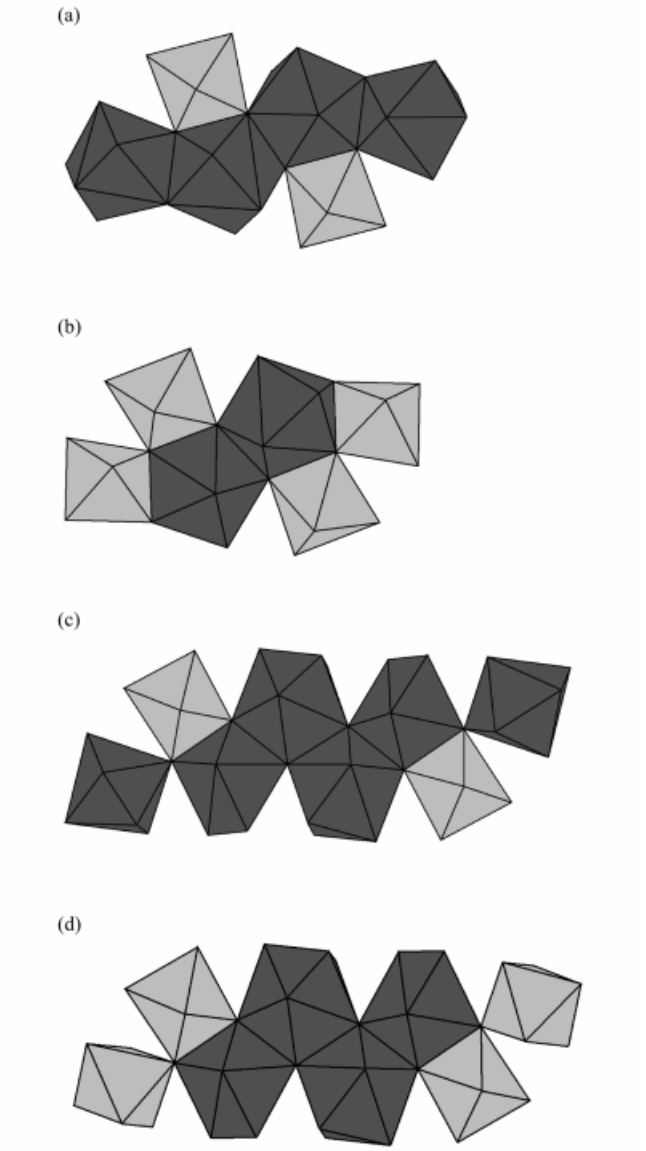

Figure 1. Cores of connected polyhedra present in the clusters **1**−**4**: (a) $Ti_2Zr_4O_4(OBu)_2(OMc)_{14}$ (**2**), (b) $Ti_4Zr_2O_4(OBu)_6(OMc)_{10}$ (**3**), (c) $Ti_2Zr_6O_6(OMc)_{20}$ (**4**), (d) $Ti_4Zr_4O_6(OBu)_4(OMc)_{16}$ (**1**); the central Zr polyhedra in **1** and **4** are 8-coordinate, while the Zr polyhedra bonded to the $[TiO_6]$ octahedra are 7-coordinate

The structural motif common to both six-atom clusters **2** and **3** is a zigzag chain of two $[ZrO_8]$ dodecahedra and two $[TiO_6]$ octahedra, which share common edges. The $[TiO_6]$ octahedra terminate the main chain. The zigzag arrangement is adopted because the central $[ZrO_8]$ dodecahedra share *cis* edges with the neighboring polyhedra (i.e. two $[ZrO_8]$ dodecahedra and one $[TiO_6]$ octahedron are connected by a μ_3-oxygen atom). The main difference between **2** and **3** is the presence of two additional polyhedra condensed onto the $[ZrO_8]$ dodecahedra of the zigzag chain at edges *cis* to the chain-terminating $[TiO_6]$ octahedra. The "extra" polyhedra are $[ZrO_8]$ dodecahedra in **2** and $[TiO_6]$ octahedra in **3**.

In **1** and **4**, the zigzag chain is extended by two oxozirconium polyhedra, but the connectivity is the same. Again, edge-sharing [TiO_6] octahedra terminate the main chain, and there are also additional [ZrO_8] dodecahedra (in **4**) or [TiO_6] octahedra (in **1**) at the flank of the main chain. Contrary to **2** and **3**, the additional polyhedra are condensed onto the main chain through a common corner rather than a common edge. The two polyhedra in **1** and **4** that extend the zigzag chain are distorted [ZrO_7] pentagonal bipyramids, located between the terminal [TiO_6] octahedra and the central [ZrO_8] dodecahedra.

Although both clusters **2** and **3** (composition $M_6O_4X_{16}$) need 16 negatively charged ligands for charge compensation of the M_6O_4 core, the 16 ligands have to occupy a different number of coordination sites due to the different coordination numbers of Ti and Zr. Thus, the $Ti_2Zr_4(\mu_3\text{-}O)_4$ core in **2** has 32 coordination sites (6 per Ti, 8 per Zr, minus the coordination sites occupied by the μ_3-O), while the $Ti_4Zr_2(\mu_3\text{-}O)_4$ core in **3** has only 28. Since each of the methacrylate ligands is bidentate (bridging or chelating), both butoxy groups in **2** need to be bridging (μ_2) (Figure 2). The same calculation shows that two of the butoxy groups in **3** must be bridging, while the remaining four are terminal. The latter are located at the titanium atoms (Figure 3). In both cases, the bridging butoxy groups connect the "extra" polyhedra to the zirconium dodecahedron of the zigzag chain [O(4) bridging Zr(1) and Zr(2) in **2**; O(28) bridging Zr and Ti(2) in **3**]. As previously observed for single-metal oxide clusters of Ti or Zr, methacrylate ligands are invariably coordinated to titanium in a bridging mode, but can either bridge or chelate zirconium atoms.

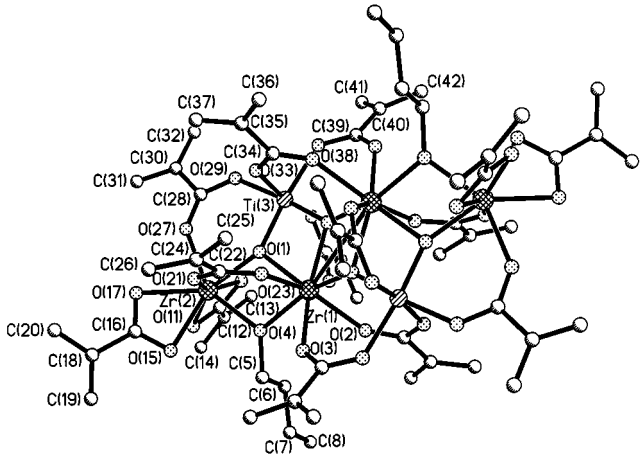

Figure 2. Molecular structure of $Ti_2Zr_4O_4(OBu)_2(OMc)_{14}$ (**2**); hydrogen atoms are omitted for clarity

The 20 ligands of the clusters **1** and **4** (composition $M_8O_6X_{20}$) have to occupy 36 coordination sites in **1** and 40 sites in **4** (in both compounds, two zirconium atoms are only 7-coordinate!). Thus, the four butoxy groups in **1** (Figure 4) must be terminal. They are located at the "extra" titanium atoms. In **4** (Figure 5), the methacrylate ligands occupy all the coordination sites, hence no ligands have to coordinate in a monodentate fashion. This calculation also

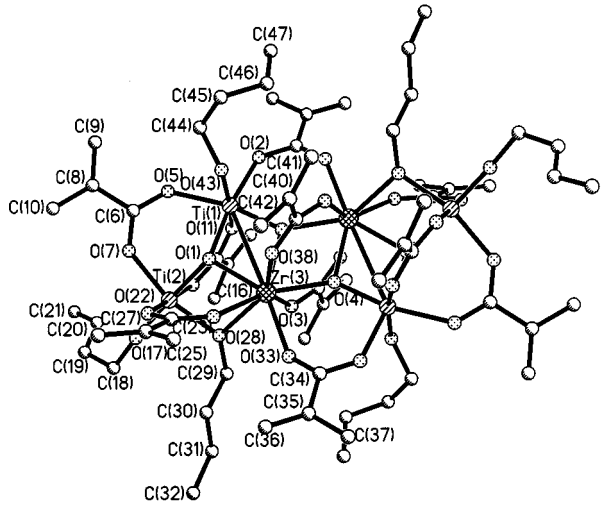

Figure 3. Molecular structure of $Ti_4Zr_2O_4(OBu)_6(OMc)_{10}$ (**3**); hydrogen atoms are omitted for clarity

explains why one of the zirconium atoms in **4** must be 7-coordinate rather than 8-coordinate: the two additional ligands required for 8-coordination could not be compensated by the charge of the cluster core.

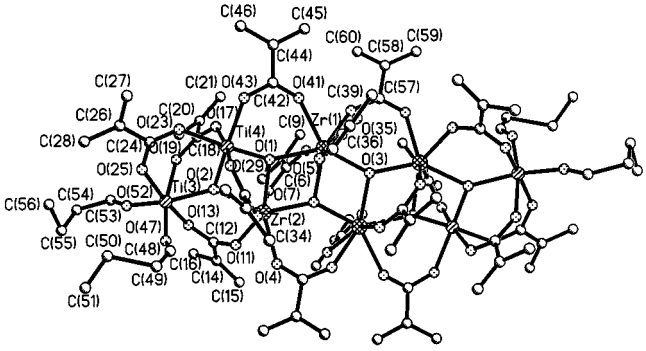

Figure 4. Molecular structure of $Ti_4Zr_4O_6(OBu)_4(OMc)_{16}$ (**1**); hydrogen atoms are omitted for clarity

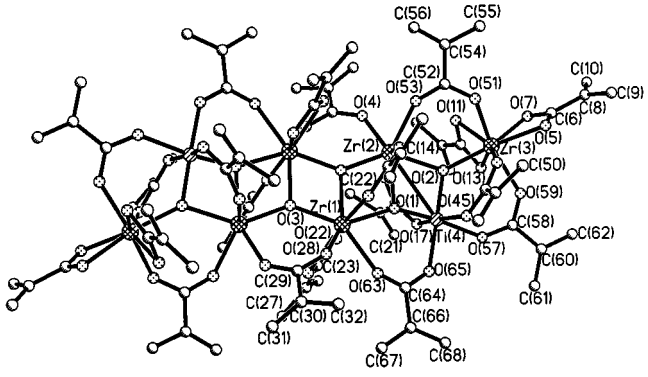

Figure 5. Molecular structure of $Ti_2Zr_6O_6(OMc)_{20}$ (**4**); hydrogen atoms are omitted for clarity

The question arises as to whether it is possible to further extend the zigzag chain observed in the clusters **1** and **4** by the insertion of two additional [ZrO_7] or [ZrO_8] polyhedra. The composition of the resulting clusters would then be $M_{10}O_8X_{24}$ (i.e. $Ti_2Zr_8O_8X_{24}$ or $Ti_4Zr_6O_8X_{24}$). The 24 singly

negatively charged ligands X would then have to occupy 52 coordination sites in a hypothetical $Ti_2Zr_8O_8X_{24}$ species or 48 coordination sites in $Ti_4Zr_6O_8X_{24}$ (for 8-coordinate Zr). Even if some of the zirconium atoms were to be only 7-coordinate and all of the ligands X were bidentate carboxylate ligands, such a $Ti_2Zr_8O_8X_{24}$ cluster would not be possible because the number of ligands X (a consequence of the charge balance) would be insufficient to occupy the existing coordination sites. A zigzag-shaped cluster of the composition $Ti_4Zr_6O_8X_{24}$ would only be possible if some of the carboxylate ligands coordinated to Ti were to be chelating (which is not the case in the known structures). Therefore, clusters with longer zigzag chains based on the same construction principle as that seen in **1**−**4** cannot be expected.

Conclusions

We have shown in this paper that a number of clusters with Ti/Zr ratios ranging from 2:1 to 1:3 can be prepared by reacting the metal alkoxides with methacrylic acid. The clusters **1**−**3** can be obtained in high yields without the need for laborious separation procedures. The formation of the clusters is probably due to the slow generation of water by simultaneous ester formation as outlined in the Introduction. The clusters **1**−**4** fill the gap between the single-metal oxotitanium and oxozirconium clusters that we have isolated previously. Using these new methacrylate-substituted clusters as co-monomers in polymerization reactions, we should be able to tune the properties of the resulting hybrid polymers (e.g., refractive index) by varying the inorganic building blocks. The shape and size of the clusters − as inorganic nanoparticles − may also be important with regard to the modification of the polymer properties. SAXS measurements on poly(methyl methacrylate) crosslinked by the clusters $Zr_6O_4(OH)_4(OMc)_{12}$, $Zr_4O_2(OMc)_{12}$, and $Ti_6O_4(OEt)_8(OMc)_8$ have shown that the scattering objects can be approximated by spheres (Zr_4 clusters) or discs with diameters of about 1 nm,[12] which corresponds to the crystallographically determined cluster sizes. The clusters described herein are rod-shaped, with lengths between 1.2 (**3**) and 1.8 nm (**1**) (distance between the most distant oxygen atoms) and diameters of about 0.65 nm.

The clusters described in this paper also serve to improve the understanding of the structure evolution in multi-component sol-gel systems, especially those modified by carboxylic acids. Although, as discussed above, the kind of cluster obtained to some extent reflects the reactivity differences of the alkoxides, the formation of the mixed-metal clusters also shows that the organic additives may serve to achieve a homogeneous distribution of the two metals through the formation of carboxylate-bridged extended structures. The only Ti/Zr mixed-metal alkoxide derivatives hitherto reported are the pinacolate derivatives $TiZr_2(OCMe_2CMe_2O)_4(OCMe_2CMe_2OH)_2(OiPr)_2$ and $Ti_2Zr_2(OCMe_2CMe_2O)_6(OiPr)_4$.[14]

Experimental Section

All operations were carried out in Schlenk tubes under argon. The alkoxides and methacrylic acid were used as received (Aldrich).

$Ti_4Zr_4O_6(OBu)_4(OMc)_{16}$ (1): A 99% solution of $Ti(OBu)_4$ (1.901 g, 5.53 mmol) in butyl alcohol was mixed with an 80% solution of $Zr(OBu)_4$ (2.681 g, 5.59 mmol) in the same solvent. After the addition of 99% methacrylic acid (4.095 g, 47.1 mmol), the mixture was stored in a closed vessel at room temperature. After 7 d, colorless crystals of **1** had been produced, which were isolated by decanting the mother liquor and drying. Yield 4.23 g (85%); m.p. 124 °C. − ^{1}H NMR ($CDCl_3$): δ = 0.88−0.93 (m, 25 H, $OCH_2CH_2CH_2CH_3$), 1.34−1.39 (m, 16 H, $OCH_2CH_2CH_2CH_3$), 1.51−1.56 (m, 16 H, $OCH_2CH_2CH_2CH_3$), 1.83−1.89 [m, 48 H, $=C(CH_3)COO$], 3.61−3.66 (t, 16 H, $OCH_2CH_2CH_2CH_3$), 5.52−5.56 [m, 16 H, *cis*-$CH_2=C(CH_3)COO$], 6.07−6.17 [m, 16 H, *trans*-$CH_2C(CH_3)COO$]. The higher relative intensity of the OBu group signals in the ^{1}H NMR spectra indicates the presence of four residual butyl alcohol

Table 1. Crystallographic and structural parameters of **1**−**4**

	1	**2**	**3**·methacrylic acid	**4**
Empirical formula	$C_{80}H_{116}O_{42}Ti_4Zr_4$	$C_{64}H_{88}O_{34}Ti_2Zr_4$	$C_{71}H_{104}O_{30}Ti_4Zr_2$	$C_{80}H_{100}O_{46}Ti_2Zr_6$
M_r	2306.2	1862.0	1811.6	2440.7
Crystal system, space group	monoclinic, *C*2/*c*	triclinic, $P\bar{1}$	triclinic, $P\bar{1}$	triclinic, $P\bar{1}$
a [pm]	2776(3)	1174.29(9)	1298.0(2)	1332.67(8)
b [pm]	1583.2(8)	1278.4(1)	1356.4(2)	1335.13(8)
c [pm]	2674(2)	1659.6(1)	1413.4(2)	1692.1(1)
α [°]		73.739(1)	67.787(2)	97.618(1)
β [°]	117.29(5)	73.132(2)	66.829(2)	91.480(1)
γ [°]		69.966(2)	70.926(2)	104.486(1)
Volume [pm^3]	10445(1) × 10^6	2194.3(3) × 10^6	2071.1(4) × 10^6	2883.9(3) × 10^6
Z/calcd. density [gcm^{-3}]	4/1.466	1/1.409	1/1.452	1/1.405
μ [mm^{-1}]	0.754	0.706	0.687	0.729
Crystal size [mm]	0.52 × 0.30 × 0.20	0.40 × 0.32 × 0.12	0.4 × 0.3 × 0.2	0.36 × 0.36 × 0.12
2θ range	1.56−23.28	1.89−26.36	1.97−28.50	1.86−24.71
Reflections coll./unique	24133/7512	13399/8887	14349/10081	15339/9767
Data/parameters	7512/567	8887/470	10081/485	9767/604
GoF	1.063	1.060	1.054	1.061
*R*1 [$I > 2\sigma(I)$]	0.0641	0.0503	0.0477	0.0399
*wR*2	0.1658	0.1420	0.1212	0.1192
Largest diff. peak and hole [eÅ^{-3}]	1.519/−0.827	1.334/−0.585	1.061/−0.742	0.853/−0.724

molecules per cluster. – ^{13}C NMR ($CDCl_3$): δ = 13.8 ($OCH_2CH_2CH_2CH_3$), 18.8 [=C(CH_3)COO], 30.6 ($OCH_2CH_2CH_2CH_3$), 34.7 ($OCH_2CH_2CH_2CH_3$), 62.7 ($OCH_2CH_2CH_2CH_3$), 125.1–126.9 [CH_2=C(CH_3)COO], 136.5–137.8 [CH_2=C(CH_3)COO], 173.7–176.5 (COO). – $C_{80}H_{116}O_{42}Ti_4Zr_4$4 BuOH (2602.8): calcd. C 44.3, H 5.8; found C 43.7, H 5.2. – TiO_2/ZrO_2 from thermogravimetric analysis (TGA): calcd. 35.2%, found 34.3%.

$Ti_2Zr_4O_4(OBu)_2(OMc)_{14}$ (2): A 99% solution of $Ti(OBu)_4$ (1.255 g, 3.65 mmol) in butyl alcohol was mixed with an 80% solution of $Zr(OBu)_4$ (3.856 g, 8.04 mmol) in the same solvent. After the addition of 99% methacrylic acid (4.281 g, 49.2 mmol), the mixture was stored in a closed vessel at room temperature. After 7 d, colorless crystals of **2** had been produced, which were isolated by decanting the mother liquor and drying. Yield 7.00 g (67%); m.p. 129 °C. – ^1H NMR ($CDCl_3$): δ = 0.88–0.94 (m, 35 H, $OCH_2CH_2CH_2CH_3$), 1.34–1.40 (m, 24 H, $OCH_2CH_2CH_2CH_3$), 1.51–1.56 (m, 24 H, $OCH_2CH_2CH_2CH_3$), 1.91 [m, 42 H, $CH_2C(CH_3)COO$], 3.61–3.66 (t, 24 H, $OCH_2CH_2CH_2CH_3$), 5.52–5.59 [m, 14 H, *cis*-CH_2=C(CH_3)COO], 6.07–6.17 [m, 14 H, *trans*-CH_2=C(CH_3)COO]. The higher relative intensity of the OBu group signals in the ^1H NMR spectra indicates the presence of ten residual butyl alcohol molec-

Table 2. Selected bond lengths [pm] and angles [°] in **1** (*: symmetry transformations $-x$, $-y$, $-z + 1$)

Zr(1)–O(1)	218.0(5)	Ti(3)–O(2)	204.1(5)
Zr(1)–O(3)	207.1(4)	Ti(3)–O(13)	207.6(5)
Zr(1)–O(3)*	214.8(4)	Ti(3)–O(19)	211.9(6)
Zr(1)–O(5)	219.2(5)	Ti(3)–O(25)	198.7(6)
Zr(1)–O(35)	234.1(5)	Ti(3)–O(47)	179.7(7)
Zr(1)–O(37)	222.3(5)	Ti(3)–O(52)	187.9(7)
Zr(1)–O(41)	222.7(5)	Ti(4)–O(1)	178.1(4)
Zr(1)–O(56)	220.7(5)	Ti(4)–O(2)	184.9(4)
Zr(2)–O(1)	213.3(4)	Ti(4)–O(17)	199.1(5)
Zr(2)–O(2)	217.8(4)	Ti(4)–O(23)	205.6(5)
Zr(2)–O(3)*	203.4(5)	Ti(4)–O(29)	203.8(5)
Zr(2)–O(4)	213.7(5)	Ti(4)–O(43)	203.4(5)
Zr(2)–O(7)	216.2(5)		
Zr(2)–O(11)	215.8(4)		
Zr(2)–O(31)	217.9(5)		
O(1)–Zr(1)–O(3)*	68.9(2)	O(2)–Ti(3)–O(13)	88.4(2)
O(1)–Zr(1)–O(5)	76.5(2)	O(2)–Ti(3)–O(19)	80.7(2)
O(1)–Zr(1)–O(37)	78.3(2)	O(2)–Ti(3)–O(25)	93.4(2)
O(1)–Zr(1)–O(41)	74.0(2)	O(2)–Ti(3)–O(47)	90.6(3)
O(3)–Zr(1)–O(3)*	72.1(2)	O(13)–Ti(3)–O(19)	80.5(2)
O(3)–Zr(1)–O(5)*	80.6(2)	O(13)–Ti(3)–O(47)	92.0(3)
O(3)–Zr(1)–O(35)	77.7(2)	O(13)–Ti(3)–O(52)	84.5(3)
O(3)–Zr(1)–O(56)	81.4(2)	O(19)–Ti(3)–O(25)	87.1(3)
O(3)–Zr(1)–O(37)*	83.5(2)	O(19)–Ti(3)–O(52)	84.7(3)
O(5)–Zr(1)–O(56)	71.8(2)	O(25)–Ti(3)–O(47)	100.9(4)
O(35)–Zr(1)–O(37)	56.9(2)	O(25)–Ti(3)–O(52)	90.6(3)
O(35)–Zr(1)–O(41)	72.5(2)	O(47)–Ti(3)–O(52)	103.3(4)
O(35)–Zr(1)–O(56)	75.9(2)	O(1)–Ti(4)–O(2)	86.4(2)
O(37)–Zr(1)–O(41)	87.4(2)	O(1)–Ti(4)–O(17)	98.3(2)
O(41)–Zr(1)–O(56)	73.0(2)	O(1)–Ti(4)–O(29)	91.6(2)
O(1)–Zr(2)–O(3)*	71.9(2)	O(1)–Ti(4)–O(43)	90.5(2)
O(1)–Zr(2)–O(2)	70.4(2)	O(2)–Ti(4)–O(17)	90.0(2)
O(1)–Zr(2)–O(7)	79.2(2)	O(2)–Ti(4)–O(29)	91.6(2)
O(1)–Zr(2)–O(31)	80.2(2)	O(2)–Ti(4)–O(23)	99.1(2)
O(2)–Zr(2)–O(31)	79.1(2)	O(17)–Ti(4)–O(43)	85.4(2)
O(2)–Zr(2)–O(7)	91.2(2)	O(17)–Ti(4)–O(23)	88.2(2)
O(2)–Zr(2)–O(11)	81.7(2)	O(23)–Ti(4)–O(29)	81.8(2)
O(3)*–Zr(2)–O(4)	85.6(2)	O(23)–Ti(4)–O(43)	84.6(2)
O(3)*–Zr(2)–O(7)	83.6(2)	O(29)–Ti(4)–O(43)	93.6(2)
O(3)*–Zr(2)–O(31)	92.9(2)	Ti(4)–O(2)–Ti(3)	125.2(2)
O(4)–Zr(2)–O(11)	72.7(2)	Ti(4)–O(2)–Zr(2)	98.8(2)
O(4)–Zr(2)–O(31)	75.1(2)	Ti(3)–O(2)–Zr(2)	135.2(2)
O(11)–Zr(2)–O(7)	75.4(2)	Zr(2)*–O(3)–Zr(1)	140.4(2)
		Zr(2)*–O(3)–Zr(1)*	111.7(2)
		Zr(1)–O(3)–Zr(1)*	107.9(2)

Table 3. Selected bond lengths [pm] and angles [°] in **2** (*: symmetry transformation $-x + 1$, $-y + 1$, $-z + 1$)

Zr(1)–O(1)	217.0(3)	Zr(2)–O(11)	223.3(3)
Zr(1)–O(2)	221.0(3)	Zr(2)–O(15)	227.8(3)
Zr(1)–O(3)	225.2(3)	Zr(2)–O(17)	224.5(3)
Zr(1)–O(4)	218.8(2)	Zr(2)–O(21)	216.7(3)
Zr(1)–O(23)	218.7(3)	Zr(2)–O(27)	218.1(3)
Zr(1)–O(45)	226.8(3)	Ti(3)–O(1)	182.4(3)
Zr(1)–O(49)	214.8(2)	Ti(3)–O(29)	203.0(3)
Zr(1)–O(49)*	214.2(2)	Ti(3)–O(33)	201.3(3)
Zr(2)–O(1)	207.9(2)	Ti(3)–O(38)	201.1(3)
Zr(2)–O(4)	213.5(3)	Ti(3)–O(43)	198.6(3)
Zr(2)–O(9)	228.8(4)	Ti(3)–O(49)	181.5(2)
O(1)–Zr(1)–O(4)	68.3(1)	O(9)–Zr(2)–O(11)	56.5(1)
O(1)–Zr(1)–O(23)	73.9(1)	O(9)–Zr(2)–O(27)	77.1(1)
O(1)–Zr(1)–O(45)	74.6(1)	O(11)–Zr(2)–O(15)	73.7(1)
O(1)–Zr(1)–O(49)	69.4(1)	O(11)–Zr(2)–O(17)	78.6(1)
O(2)–Zr(1)–O(3)	75.0(1)	O(15)–Zr(2)–O(17)	57.4(1)
O(2)–Zr(1)–O(45)	68.9(1)	O(15)–Zr(2)–O(21)	75.1(1)
O(2)–Zr(1)–O(49)*	79.4(1)	O(17)–Zr(2)–O(21)	77.2(1)
O(3)–Zr(1)–O(49)*	77.3(1)	O(17)–Zr(2)–O(27)	73.5(1)
O(3)–Zr(1)–O(23)	71.7(1)	O(1)–Ti(3)–O(29)	90.1(1)
O(3)–Zr(1)–O(4)	76.3(1)	O(1)–Ti(3)–O(33)	97.9(1)
O(4)–Zr(1)–O(45)	81.7(1)	O(1)–Ti(3)–O(49)	85.0(1)
O(23)–Zr(1)–O(49)*	77.5(1)	O(1)–Ti(3)–O(43)	90.4(1)
O(23)–Zr(1)–O(49)	88.5(1)	O(29)–Ti(3)–O(33)	85.9(1)
O(45)–Zr(1)–O(49)	77.7(1)	O(29)–Ti(3)–O(38)	94.0(1)
O(49)–Zr(1)–O(49)*	67.5(1)	O(29)–Ti(3)–O(43)	89.4(1)
O(1)–Zr(2)–O(4)	71.0(1)	O(33)–Ti(3)–O(38)	87.4(1)
O(1)–Zr(2)–O(21)	77.3(1)	O(33)–Ti(3)–O(49)	92.6(1)
O(1)–Zr(2)–O(27)	79.7(1)	O(38)–Ti(3)–O(43)	84.7(1)
O(1)–Zr(2)–O(9)	78.9(1)	O(38)–Ti(3)–O(49)	91.0(1)
O(4)–Zr(2)–O(9)	86.4(1)	O(43)–Ti(3)–O(49)	92.8(1)
O(4)–Zr(2)–O(15)	80.2(1)	Zr(1)–O(4)–Zr(2)	107.5(1)
O(4)–Zr(2)–O(21)	89.4(1)	Zr(1)–O(49)–Zr(1)*	112.6(1)

Table 4. Selected bond lengths [pm] and angles [°] in **3** (* symmetry transformation $-x + 1$, $-y + 2$, $-z + 1$)

Zr(3)–O(1)	212.3(2)	Ti(1)–O(4)*	182.2(2)
Zr(3)–O(3)	219.9(2)	Ti(1)–O(5)	209.3(2)
Zr(3)–O(4)	212.8(2)	Ti(1)–O(11)	208.7(2)
Zr(3)–O(4)*	215.4(2)	Ti(1)–O(43)	181.1(2)
Zr(3)–O(24)	231.7(2)	Ti(2)–O(1)	195.3(2)
Zr(3)–O(28)	225.6(2)	Ti(2)–O(7)	202.4(2)
Zr(3)–O(33)	219.3(2)	Ti(2)–O(13)	204.4(2)
Zr(3)–O(38)	218.6(2)	Ti(2)–O(17)	176.6(2)
Ti(1)–O(1)	187.9(2)	Ti(2)–O(22)	198.0(2)
Ti(1)–O(2)	206.0(2)	Ti(2)–O(28)	194.1(2)
O(1)–Zr(3)–O(4)*	69.52(7)	O(1)–Ti(1)–O(4)*	82.42(8)
O(1)–Zr(3)–O(24)	75.62(7)	O(1)–Ti(1)–O(5)	87.83(8)
O(1)–Zr(3)–O(28)	68.38(7)	O(1)–Ti(1)–O(11)	90.73(8)
O(1)–Zr(3)–O(38)	90.53(7)	O(1)–Ti(1)–O(43)	102.5(1)
O(3)–Zr(3)–O(4)	76.49(7)	O(2)–Ti(1)–O(4)*	91.22(8)
O(3)–Zr(3)–O(4)*	77.73(7)	O(2)–Ti(1)–O(5)	97.05(8)
O(3)–Zr(3)–O(28)	71.88(7)	O(2)–Ti(1)–O(11)	78.23(9)
O(4)–Zr(3)–O(4)*	71.67(8)	O(2)–Ti(1)–O(43)	89.7(1)
O(4)–Zr(3)–O(33)	77.26(7)	O(4)*–Ti(1)–O(11)	92.20(8)
O(4)–Zr(3)–O(38)	75.60(7)	O(4)*–Ti(1)–O(43)	101.5(1)
O(4)*–Zr(3)–O(38)	77.93(7)	O(5)–Ti(1)–O(11)	81.54(9)
O(24)–Zr(3)–O(28)	72.92(7)	O(5)–Ti(1)–O(43)	86.8(1)
O(24)–Zr(3)–O(33)	72.93(7)	O(1)–Ti(2)–O(7)	86.88(8)
O(24)–Zr(3)–O(38)	69.08(7)	O(1)–Ti(2)–O(13)	90.02(8)
O(28)–Zr(3)–O(33)	81.90(7)	O(1)–Ti(2)–O(22)	86.22(8)
Ti(1)–O(1)–Ti(2)	133.2(1)	O(1)–Ti(2)–O(28)	78.48(8)
Ti(1)–O(1)–Zr(3)	103.58(8)	O(7)–Ti(2)–O(13)	86.89(9)
Ti(2)–O(1)–Zr(3)	108.61(8)	O(7)–Ti(2)–O(17)	95.8(1)
Ti(1)*–O(4)–Zr(3)	146.3(1)	O(7)–Ti(2)–O(22)	93.41(9)
Ti(1)*–O(4)–Zr(3)*	104.41(8)	O(13)–Ti(2)–O(17)	90.1(1)
Zr(3)–O(4)–Zr(3)*	108.33(8)	O(13)–Ti(2)–O(28)	88.35(9)
		O(17)–Ti(2)–O(22)	93.6(1)
		O(17)–Ti(2)–O(28)	98.9(1)
		O(22)–Ti(2)–O(28)	90.39(8)

ules per cluster. – ^{13}C NMR ($CDCl_3$): δ = 13.7 ($OCH_2CH_2CH_2CH_3$), 18.4 [$CH_2C(CH_3)COO$], 30.6 ($OCH_2CH_2CH_2CH_3$), 34.8 ($OCH_2CH_2CH_2CH_3$), 62.7 ($OCH_2CH_2CH_2CH_3$), 125.1–127.1 [$CH_2C(CH_3)COO$], 136.5–137.7 [$CH_2C(CH_3)COO$], 173.7–176.5 (COO). – $C_{64}H_{88}O_{34}Ti_2Zr_4$10 BuOH (2603.3): calcd. C 49.2, H 7.1; found C 50.4, H 7.3. – TiO_2/ZrO_2 from TGA: calcd. for **2**·10 BuOH 25.0%, found 23.6%.

$Ti_4Zr_2O_4(OBu)_6(OMc)_{10}$ (3) and $Ti_2Zr_6O_6(OMc)_{20}$ (4): A 99% solution of $Ti(OBu)_4$ (1.303 g, 3.79 mmol) in butyl alcohol was mixed with an 80% solution of $Zr(OBu)_4$ (5.352 g, 11.25 mmol) in the same solvent. After the addition of 99% methacrylic acid (5.259 g, 60.5 mmol), the mixture was stored in a closed vessel at room temperature. After 7 d, a mixture of colorless crystals of **2**–**4** had been produced, which was recovered by decanting the mother liquor and drying. Yield 7.54 g. Crystals of **4** were manually separated from the mixture for a crystal structure determination.

$Ti_4Zr_2O_4(OBu)_6(OMc)_{10}$ (3): A 99% solution of $Ti(OBu)_4$ (1.650 g, 4.80 mmol) in butyl alcohol was mixed with a 70% solution of $Zr(OPr)_4$ (2.144 g, 4.58 mmol) in propanol. After the addition of methacrylic acid (3.363 g, 38.7 mmol), the mixture was stored in a closed vessel at room temperature. After 7 d, colorless crystals of **3** had formed, which were isolated by decanting the mother liquor and drying. Yield 2.361 g (87%); m.p. 133 °C. – ^1H NMR ($CDCl_3$): δ = 0.91 (m, 35 H, $OCH_2CH_2CH_2CH_3$), 1.34–1.40 (m, 12 H, $OCH_2CH_2CH_2CH_3$), 1.54–1.58 (m, 12 H, $OCH_2CH_2CH_2CH_3$), 1.91 [m, 30 H, $CH_2C(CH_3)COO$], 3.59–3.63 (m, 6 H, $OCH_2CH_2CH_2CH_3$), 5.52–5.59 [m, 10 H, *cis*-$CH_2C(CH_3)COO$], 6.07–6.17 [m, 10 H, *trans*-$CH_2C(CH_3)COO$]. – $C_{64}H_{86}O_{30}Ti_4Zr_2$ (1709.4): calcd. C 44.5, H 6.1; found C 42.7, H 5.1. – TiO_2/ZrO_2 from TGA: calcd. 32.8%, found 31.9%.

Table 5. Selected bond lengths [pm] and angles [°] in **4** (*: symmetry transformation $-x + 2, -y + 1, -z$)

Zr(1)–O(1)	220.2(2)	Zr(3)–O(2)	208.6(2)
Zr(1)–O(3)	207.6(2)	Zr(3)–O(7)	225.1(4)
Zr(1)–O(3)*	216.1(2)	Zr(3)–O(5)	226.7(3)
Zr(1)–O(28)	222.0(2)	Zr(3)–O(11)	227.9(3)
Zr(1)–O(22)	222.7(2)	Zr(3)–O(13)	224.1(3)
Zr(1)–O(24)	234.2(2)	Zr(3)–O(47)	225.3(3)
Zr(1)–O(33)	219.8(2)	Zr(3)–O(51)	212.4(3)
Zr(1)–O(63)	224.7(2)	Zr(3)–O(59)	213.1(3)
Zr(2)–O(1)	217.5(2)	Ti(4)–O(1)	178.2(2)
Zr(2)–O(2)	219.1(2)	Ti(4)–O(2)	188.9(2)
Zr(2)–O(3)*	204.7(2)	Ti(4)–O(17)	202.4(2)
Zr(2)–O(4)	214.0(3)	Ti(4)–O(45)	200.2(3)
Zr(2)–O(19)	217.7(2)	Ti(4)–O(57)	209.0(2)
Zr(2)–O(35)	216.8(3)	Ti(4)–O(65)	202.6(3)
Zr(2)–O(53)	217.9(3)		
O(1)–Zr(1)–O(3)*	69.41(8)	O(5)–Zr(3)–O(47)	73.7(1)
O(1)–Zr(1)–O(22)	78.76(9)	O(5)–Zr(3)–O(51)	80.8(1)
O(1)–Zr(1)–O(33)	76.80(9)	O(5)–Zr(3)–O(59)	80.3(1)
O(1)–Zr(1)–O(63)	73.39(9)	O(7)–Zr(3)–O(11)	76.5(1)
O(3)–Zr(1)–O(3)*	71.75(9)	O(7)–Zr(3)–O(13)	76.2(1)
O(3)–Zr(1)–O(24)	77.16(9)	O(11)–Zr(3)–O(13)	57.6(1)
O(3)–Zr(1)–O(28)	81.29(9)	O(11)–Zr(3)–O(51)	76.3(1)
O(3)*–Zr(1)–O(22)	84.12(9)	O(13)–Zr(3)–O(59)	74.0(1)
O(3)*–Zr(1)–O(33)	80.92(9)	O(47)–Zr(3)–O(51)	78.4(1)
O(22)–Zr(1)–O(24)	57.03(9)	O(47)–Zr(3)–O(59)	76.8(1)
O(22)–Zr(1)–O(63)	85.8(1)	O(1)–Ti(4)–O(2)	86.2(1)
O(24)–Zr(1)–O(28)	75.68(9)	O(1)–Ti(4)–O(17)	91.5(1)
O(24)–Zr(1)–O(63)	73.68(9)	O(1)–Ti(4)–O(45)	99.1(1)
O(28)–Zr(1)–O(33)	71.17(9)	O(1)–Ti(4)–O(65)	90.6(1)
O(28)–Zr(1)–O(63)	73.10(9)	O(2)–Ti(4)–O(17)	91.4(1)
O(1)–Zr(2)–O(2)	70.17(8)	O(2)–Ti(4)–O(45)	88.3(1)
O(1)–Zr(2)–O(3)*	72.04(9)	O(2)–Ti(4)–O(57)	99.4(1)
O(1)–Zr(2)–O(19)	78.65(9)	O(17)–Ti(4)–O(57)	83.9(1)
O(1)–Zr(2)–O(35)	79.45(9)	O(17)–Ti(4)–O(65)	94.2(1)
O(2)–Zr(3)–O(13)	82.0(1)	O(45)–Ti(4)–O(57)	85.7(1)
O(2)–Zr(2)–O(19)	78.68(9)	O(45)–Ti(4)–O(65)	86.7(1)
O(2)–Zr(3)–O(51)	91.0(1)	O(57)–Ti(4)–O(65)	84.3(1)
O(2)–Zr(2)–O(53)	83.16(9)	Ti(4)–O(1)–Zr(2)	103.2(1)
O(3)*–Zr(2)–O(4)	85.43(9)	Ti(4)–O(1)–Zr(1)	150.9(1)
O(3)*–Zr(2)–O(35)	83.44(9)	Zr(2)–O(1)–Zr(1)	105.63(9)
O(4)–Zr(2)–O(19)	75.6(1)	Ti(4)–O(2)–Zr(3)	125.0(1)
O(4)–Zr(2)–O(53)	73.1(1)	Ti(4)–O(2)–Zr(2)	99.1(1)
O(35)–Zr(2)–O(53)	74.6(1)	Zr(3)–O(2)–Zr(2)	135.3(1)
O(2)–Zr(3)–O(11)	78.0(1)	Zr(2)*–O(3)–Zr(1)	139.5(1)
O(2)–Zr(3)–O(47)	76.4(1)	Zr(2)*–O(3)–Zr(1)	* 111.9(1)
O(5)–Zr(3)–O(7)	57.2(2)	Zr(1)–O(3)–Zr(1)*	108.25(9)

X-ray Structure Analyses of 1–4: Selected crystals were mounted on a Siemens SMART diffractometer with a CCD area detector. Graphite-monochromated Mo-K_α radiation (λ = 71.073 pm) was used for all measurements. The crystal-to-detector distance was 4.40 cm. A hemisphere of data was collected by a combination of three sets of exposures at 213 K. Each set had a different φ angle for the crystal; each exposure was of duration 20 s and covered 0.3° in ω. The data were corrected for polarization and Lorentz effects and an empirical absorption correction (SADABS) was applied. The cell dimensions were refined using all unique reflections. The structure was solved by direct methods (SHELXS-86). Refinement was carried out by the full-matrix least-squares method based on F^2 (SHELXL-93) with anisotropic thermal parameters for all non-hydrogen atoms. Hydrogen atoms were inserted in calculated positions and refined as riding on the corresponding atom. The asymmetric unit of **3** contains a disordered molecule of methacrylic acid. Only the carbon atoms could be located; they were refined anisotropically without hydrogen atoms attached to them. Crystallographic data (excluding structure factors) for the structures of **1**–**4** have been deposited with the Cambridge Crystallographic Data Centre as supplementary publication nos. CCDC-149355 (**1**), -149356 (**2**), -149357 (**3**), and -149358 (**4**). Copies of the data can be obtained free of charge on application to the CCDC, 12 Union Road, Cambridge CB2 1EZ, U.K. [Fax: (internat.) + 44-1223/336-033; E-mail: deposit@ccdc.cam.ac.uk]. For additional details see (Table 1–5).

[1] See, for example: T. S. Haddad, J. D. Lichtenhan, *Macromolecules* **1996**, *29*, 7302; J. J. Schwab, J. D. Lichtenhan, K. P. Chaffee, P. T. Mather, A. Romo-Uribe, *Mat. Res. Soc. Symp. Proc.* **1998**, *519*, 21; J. D. Lichtenhan, T. S. Haddad, J. J. Schwab, M. J. Karr, K. P. Chaffee, P. T. Mather, *Polym. Prep.* **1998**, *39*, 489; J. Pynn, K. Matyjaszewski, *Macromolecules* **2000**, *33*, 217; A. Sellinger, R. M. Laine, *Macromolecules* **1996**, *29*, 2327; E. K. Lin, C.-R. Snyder, F. I. Mopsik, W. E. Wallace, W. L. Wu, C. X. Zhang, R. M. Laine, *Mat. Res. Soc. Symp. Proc.* **1998**, *519*, 15.

[2] F. Ribot, F. Banse, C. Sanchez, M. Lahcini, B. Jousseaumme, *J. Sol-Gel Sci. Techn.* **1997**, *8*, 529; L. Angiolini, D. Caretti, C. Carlini, R. De Vito, F. T. Niesel, E. Salatelli, F. Ribot, C. Sanchez, *J. Inorg. Organomet. Polym.* **1998**, *7*, 151.

[3] L. G. Hubert-Pfalzgraf, N. Pajot, R. Papiernik, S. Parraud, *Mat. Res. Soc. Symp. Proc.* **1996**, *435*, 137.

[4] P. Judeinstein, *Chem. Mater.* **1992**, *4*, 4. P. Judeinstein, *J. Sol-Gel Sci. Techn.* **1994**, *2*, 147; C. R. Mayer, R. Thouvenot, T. Lalot, *Chem. Mater.* **2000**, *12*, 257. C. R. Mayer, V. Cabuil, T. Lalot, R. Thouvenot, *Angew. Chem. Int. Ed. Engl.* **1999**, *38*, 3672.

[5] Review: G. Kickelbick, U. Schubert, *Monatsh. Chem.*, in press.

[6] G. Kickelbick, U. Schubert, *Chem. Ber.* **1997**, *130*, 473.

[7] G. Trimmel, S. Gross, G. Kickelbick, U. Schubert, *Appl. Organomet. Chem.*, in press.

[8] G. Kickelbick, P. Wiede, U. Schubert, *Inorg. Chim. Acta* **1999**, *284*, 1.

[9] U. Schubert, E. Arpac, W. Glaubitt, A. Helmerich, C. Chau, *Chem. Mater.* **1992**, *4*, 291.

[10] G. Kickelbick, U. Schubert, *Eur. J. Inorg. Chem.* **1998**, 159.
[11] B. Moraru, G. Kickelbick, U. Schubert, unpublished.
[12] G. Trimmel, P. Fratzl, U. Schubert, *Chem. Mater.* **2000**, *12*, 602; U. Schubert, G. Trimmel, B. Moraru, W. Tesch, P. Fratzl, S. Gross, G. Kickelbick, N. Hüsing, *Mat. Res. Soc. Symp. Proc.*, in press.
[13] G. Trimmel, B. Moraru, S. Gross, V. Di Noto, U. Schubert, *Macromol. Symp.*, in press; S. Gross, G. Trimmel, U. Schubert, V. Di Noto, *J. Polym. Adv. Techn.*, in press.
[14] C. A. Zechmann, J. C. Huffman, K. Folting, K. G. Caulton, *Inorg. Chem.* **1998**, *37*, 5856.

Received September 18, 2000
[I00349]

Synthesis, Characterisation and Antiviral Activity of Platinum(II) Complexes with 1,10-Phenanthrolines and the Antiviral Agents Acyclovir and Penciclovir

Nicola Margiotta,[a] Francesco P. Fanizzi,[b,c] Joze Kobe,[d] and Giovanni Natile*[a]

Keywords: Acyclovir / Penciclovir / Platinum / Atropisomerism / Antiviral agents / Drug research

Four novel hybrid drugs $[Pt(acy)_2(Me_2phen)]I_2$ (**1**), $[Pt(pen)_2(Me_2phen)](NO_3)_2$ (**2**), $[Pt(acy)_2(phen)](NO_3)_2$ (**3**), and $[Pt(pen)_2(phen)](NO_3)_2$ (**4**) have been prepared by reaction of the antiviral guanine derivatives acyclovir (acy) and penciclovir (pen) with platinum complexes having 2,9-Me_2-1,10-phenanthroline (Me_2phen) and 1,10-phenanthroline (phen) as carrier ligands. Both the Me_2phen and phen carrier ligands are able to hinder rotation of the guanine bases about the Pt–N(7) bonds rendering the interconversion among rotamers very slow on the NMR time scale. A favourable dipole–dipole interaction between the *cis*-coordinated purine bases stabilises the *HT* rotamers, which are the only species detected in solution. The stability in a physiological medium and the anti-HIV properties in vitro of the complexes have been evaluated. In a 0.1 M solution of NaCl, the compounds with Me_2phen (**1** and **2**) were found to be very stable while the compounds with phen (**3** and **4**) underwent displacement of one purine base by a chloride ion. This rather unexpected result may have some relevance in connection with the stability of major DNA adducts of cisplatin in which two guanines are cross-linked by a $Pt(NH_3)_2$ moiety. Although none of the complexes showed anti-HIV activity, complexes **1** and **2**, bearing methyl substituents in the *ortho* positions of the phenanthroline, were much more cytotoxic than **3** and **4**. This is probably due to a greater stability of the former complexes in biological media caused by the presence of the two methyl groups wrapping the metal centre and inhibiting the nucleophilic attack of an incoming ligand at the platinum centre.

Introduction

The discovery of acyclovir [9-(2-hydroxyethoxymethyl)-guanine, acy] in 1977, the first drug with high selectivity, was the starting point of antiviral chemotherapy.[1] Acyclovir is a synthetic analogue of guanosine with a linear chain in place of the ring sugar, it inhibits selectively the replication of Herpes Simplex Virus (HSV) by interfering with DNA synthesis. After entering into the infected cell, acyclovir is phosphorylated by the virus-induced thymidine kinase (TK) to acyclovir-monophosphate (acyclo-GMP).[2] The rate of phosphorylation by mammalian TK is negligible and this makes acyclovir highly selective towards HSV. The drug is further phosphorylated by cellular enzymes to produce first acyclo-GDP and then acyclo-GTP. The latter is a selective inhibitor of the viral DNA polymerase because it competes with dGTP for incorporation into the growing DNA strand. The inclusion of acyclovir, containing a single hydroxyl group, stops the duplication process.

Acyclovir is the drug of choice for the treatment of HSV and Varicella Zoster Virus (VZV) infections. It is commonly used in the treatment of primary and recurrent genital herpes and mucocutaneous HSV and VZV infections in immunosuppressed patients.

Hundreds of synthetic analogues of acy have been synthesised, among these analogues are ganciclovir and penciclovir (pen). Ganciclovir shows higher activity towards cytomegalovirus (CMV) than acyclovir, while penciclovir shows a similar spectrum of activity as acyclovir, as well as activity against human hepatitis B virus.[3]

The coordination ability of acyclovir and its analogues has attracted the interest of many researchers in view of the fact that DNA polymerases contain Zn^{2+} and/or are activated by metal ions such as Mg^{2+}, Mn^{2+}, and Co^{2+}. Complexes of acyclovir with Cd^{II}, Co^{II}, and Cu^{II} have been synthesised and characterised and,[4] in some instances, their antiviral properties were also investigated.[5,6] The structural analogies of acyclovir with purine nucleotides have inspired the synthesis of complexes with platinum(II).[7–10] Anticancer platinum(II) drugs are known to crosslink DNA at adjacent purine bases, and bifunctional adducts of this type are believed to be responsible for anticancer activity.[11,12]

Amines have usually been used as carrier ligands for platinum drugs;[13] however, polycyclic aromatic amines, such as phenanthroline, in addition to being bidentate N-donor ligands, also have an intercalating ability towards double-helix DNA.[14] The binding to Calf Thymus DNA has been investigated for some phenanthroline complexes.[15]

A special case is that of the *ortho* disubstituted phenanthroline 2,9-Me_2-1,10-phenanthroline (Me_2phen, neocup-

[a] Dipartimento Farmaco-Chimico, Università di Bari, Via E. Orabona 4, 70125 Bari, Italy
E-mail: natile@farmchim.uniba.it
[b] Dipartimento di Biologia, Università di Lecce, Via Monteroni, 73100 Lecce, Italy
[c] Consortium CARSO Cancer Research Center, 70100 Valenzano, Bari, Italy
[d] National Institute of Chemistry, Hajdrihova 19, 1000 Ljubljana, Slovenia
Supporting information for this article is available on the WWW under http://www.wiley-vch.de/home/eurjic or from the author.

 © WILEY-VCH Verlag GmbH, 69451 Weinheim, 2001 1434–1948/01/0505–1303 $ 17.50+.50/0

roine) which has long been investigated for its ability to increase the chemical reactivity of platinum(II) substrates of formula $[PtX_2(Me_2phen)]$ (X = halogen ligand).[16,17] Because of the steric interaction between the *ortho* substituents of the phenanthroline and the *cis* halogen ligands, $[PtX_2(Me_2phen)]$ substrates react readily with an extra ligand (L) to give the corresponding addition product $[PtX_2(L)(Me_2phen)]$. For L = a π-acceptor ligand (such as alkene, alkyne, and carbon monoxide) the addition product has a five-coordinate geometry; in contrast, for L = a σ-donor ligand (such as amine, phosphane, etc.) the platinum remains four-coordinate and the neocuproine acts as a monodentate ligand. With longer reaction times the displacement of one X and back chelation of Me_2phen is also observed.

Pursuing our interest in the synthesis of hybrid drugs combining in one molecule the features of *cis*-amine platinum antitumor drugs and antiviral nucleotide analogues,[7−10] we have carried out the synthesis of platinum complexes containing a bidentate phenanthroline and two antiviral purine bases in the coordination sphere. The stereochemistry of the new compounds, as well as preliminary data on their antiviral activity, are reported in the present work.

Results and Discussion

In a recent paper[8] we investigated the antiviral and anticancer properties of *cis*-$[PtCl(acy)(NH_3)_2](NO_3)$ in comparison to those of acyclovir and cisplatin. The platinum-acyclovir complex maintained the antiviral activity of acyclovir, although it showed a minor efficacy on a molar basis (ID_{50}= 7.85 and 1.02 μM for *cis*-$[PtCl(acy)(NH_3)_2](NO_3)$ and acyclovir, respectively). However, the novel hybrid drug, although less toxic towards tumour cells than cisplatin, showed similar activity when equitoxic doses were administered in vivo to P388 leukaemia-bearing mice (% T/C = 209 and 211 for *cis*-$[PtCl(acy)(NH_3)_2](NO_3)$ and cisplatin, respectively). *cis*-$[PtCl(acy)(NH_3)_2](NO_3)$ was also active against a cisplatin-resistant subline of the P388 leukaemia, thus indicating that the mechanism of action could be different from that of cisplatin.

On this basis we directed our attention to the synthesis of platinum compounds containing antiviral purinic bases and a phenanthroline as ligands (Scheme 1), with the aim of improving the antitumoral and/or the antiviral properties by taking advantage of the intercalating ability of phenanthrolines.

Synthesis of the Compounds

The preparation of the complexes was straightforward. The diiodoplatinum complex $[PtI_2(Me_2phen)]$ is a rather reactive substrate due to the steric clash between the *ortho* methyl substituents of the phenanthroline and the *cis* iodo ligands, which strongly destabilises the square-planar geometry.[16,17] It reacts smoothly with acyclovir (solvent CH_2Cl_2/CH_3OH, 1:1 v/v) to give substitution of the iodo ligands and formation of the cationic species

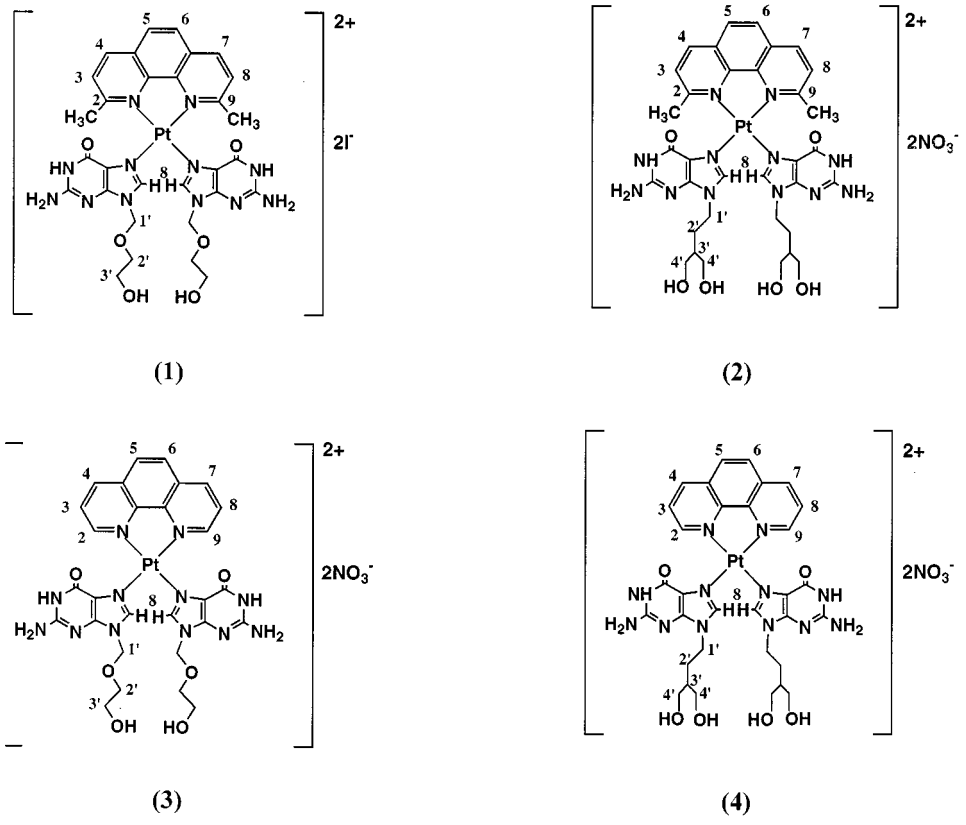

Scheme 1. Schematic drawing of compounds **1**−**4**

$[PtI(acy)(Me_2phen)]^+$ and $[Pt(acy)_2(Me_2phen)]^{2+}$. The separation of the two reaction products was accomplished by taking advantage of their different solubilities in water. The divalent salt $[Pt(acy)_2(Me_2phen)]I_2$ (**1**) is very soluble in water while the monovalent salt $[PtI(acy)(Me_2phen)]I$ (**5**) is sparingly soluble in water but rather soluble in methanol.

The synthesis of $[Pt(pen)_2(Me_2phen)](NO_3)_2$ (**2**) was carried out using DMF as solvent because of the insolubility of penciclovir in more common solvents. The starting $[PtI_2(Me_2phen)]$ substrate was first converted into the solvato species $[Pt(DMF)_2(Me_2phen)]^{2+}$ by reaction with a stoichiometric amount of $AgNO_3$. The solvato species reacts smoothly with a stoichiometric amount of penciclovir (ratio 1:2) to give complex **2**.

The preparation of $[Pt(acy)_2(phen)](NO_3)_2$ (**3**) and $[Pt(pen)_2(phen)](NO_3)_2$ (**4**) was carried out using the same procedure as described for **2**. The use of DMF as solvent was caused by the insolubility of the starting $[PtI_2(phen)]$ complex in common solvents.

Stereochemical Investigations

Complex 1

All complexes were characterised by elemental analysis, IR and NMR spectroscopy. A bathochromic shift of the stretching frequency of the C=O group in position 6 of the purine ring (1697 cm^{-1} in complex **1** and 1717 cm^{-1} in free acyclovir) is indicative of coordination of the guanine base to platinum through N(7).[18,19]

The ^1H NMR spectrum of **1** in D_2O shows a single set of signals (Figure 1, Table 1) which is in agreement with a symmetrical complex. The phenanthroline is symmetrical with chemical shifts at $\delta = 2.35$ for the methyls in positions 2 and 9 and at $\delta = 8.69$ ($J_{H\text{-}H} = 8.4$ Hz), 8.11, and 7.71 ($J_{H\text{-}H} = 8.4$ Hz) for protons 4/7, 5/6, and 3/8, respectively. Also, the two acyclovir ligands give a single set of resonances. The chemical shift of the H(8) protons at $\delta = 8.53$ is also indicative of N(7) coordination of the purine bases to platinum ($\delta = 7.91$ for free acyclovir).[13,20]

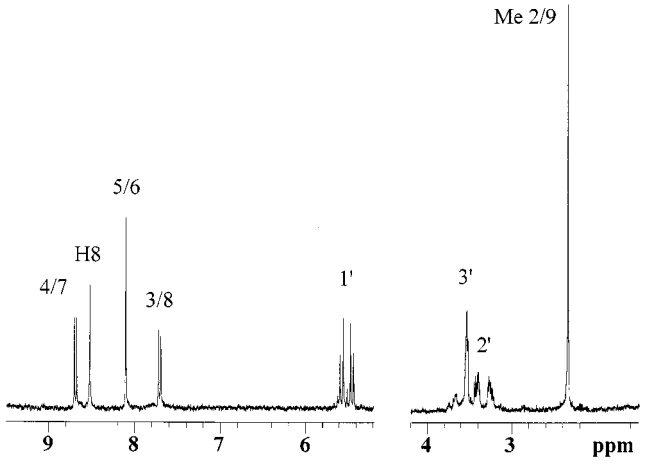

Figure 1. Sections of the ^1H NMR spectrum in D_2O of complex **1**

For $Pt(A)G_2$ complexes (where A is a C_2-symmetrical bidentate ligand and G a guanine derivative) different rotamers are possible: one *HH* conformer (Head-to-Head) with the H(8) of the two G's on the same side of the platinum coordination plane, and two *HT* conformers (Head-to-Tail) with the H(8) on opposite sides of the coordination plane (Scheme 2).[21,22] The two *HT* conformers differ in their chirality (Λ or Δ). The relation between the trace of the helix [a line connecting the O(6) atoms of the two guanines] and the axis of the helix (the perpendicular to the coordination plane passing through the platinum centre) is described by the index and thumb of the left hand in the Λ conformer and of the right hand in the Δ conformer. In the case of nonchiral G ligands all rotamers will be symmetrical (C_s and C_2 symmetry for the *HH* and *HT* rotamers, respectively); moreover the two *HT* rotamers will constitute a couple of enantiomers and will be identical from an NMR point of view.

From previous work[23–27] it is well-known that in $Pt(A)G_2$ complexes the rate of interconversion between rotamers [which requires rotation of the nucleobases around the Pt–N(7) bonds] depends upon the steric bulk of the carrier ligand (A). This interconversion is always fast, with respect to the NMR time scale, for primary amines, but can become very slow (half-lives of hours) for secondary and tertiary amines with a rigid structure. Me_2phen is to be ascribed to this second class of ligands since the steric bulk created by the methyls in positions 2 and 9 of the phenanthroline is expected to hinder the rotation of the two acyclovir molecules about the Pt–N(7) bonds, therefore the observation of only one set of signals was quite surprising. A single set of signals would mean either a free rotation about the Pt–N(7) bonds or slow rotation and a predominance of either the *HH* or the *HT* conformers. To answer this question a similar complex containing guanosine, instead of acyclovir, was prepared.[28] The ribose rings present in the guanosine ligands are chiral and thus render the two *HT* rotamers inequivalent (although they remain C_2-symmetrical) and the *HH* rotamer nonsymmetrical (C_1 symmetry). Assuming a slow interconversion different signals should be observed for the different rotamers. The ^1H NMR spectrum of $[Pt(guo)_2(Me_2phen)]Cl_2$ in D_2O showed, in the region of H(8), two very strong and rather shielded signals (at $\delta = 8.38$ and 8.35), and two very weak and rather deshielded signals (at $\delta = 8.86$ and 8.88). Literature data indicate that the *HT* orientation is stabilised with respect to the *HH* orientation by a better dipole–dipole interaction between the two guanine bases; this must be the case also for the $[Pt(guo)_2(Me_2phen)]Cl_2$ complex. Therefore the two strong signals can be assigned to the H(8) protons of the two *HT* rotamers (ΔHT and ΛHT), while the two very weak signals can be assigned to the single, nonsymmetrical, *HH* conformer. Big changes in the isomer distribution are not expected for substitution of the ribose ring of guanosine by the 2-hydroxyethoxymethyl chain of acyclovir, therefore we can expect that the preferred isomer for **1** has an *HT* conformation. The value of the H(8) chemical shift (at rather high field) supports the above conclusion.

Additional information about the conformational rigidity of complex **1** could be gained from examination of the

Table 1. ^{1}H NMR Shifts (ppm) of the complexes (numbering of the protons as in Scheme 1)[a]

Compound	Solvent	H(4/7)	H(5/6)	H(3/8)	H/Me(2/9)	H(8)	C(1′)H$_2$	C(2′)H$_2$	C(3′)H$_{1/2}$	C(4′)H$_2$
Acyclovir	D_2O	–	–	–	–	7.91 s	5.50 s	3.67 m		–
1	D_2O	8.69 d (8.4)	8.11 s	7.71 d (8.4)	2.35 s	8.53 s	5.52 m	3.36 m	3.55 m	–
	CD_3OD	8.77 d (8.1)	8.18 s	7.78 d (8.1)	2.35 s	8.57 s	5.51 s	3.54 m		–
5	CD_3OD	8.71 d (8.1), 8.62 d (8.1)	8.07 s	7.82 d (8.1), 7.67 d (8.1)	3.34 s, 2.25 s	8.66 s	5.59 s	3.66 m		–
3	D_2O	8.28 dd (8.3, 4.4)	8.23 s	7.91 dd (8.3, 4.4)	8.95 dd (8.3, 4.4)	8.71 s	5.62 dd	3.63 m		–
Penciclovir	D_2O	–	–	–	–	7.85 s	4.18 m	1.88 m	1.68 m	3.62 m
2	D_2O	8.64 d (8.1)	8.04 s	7.69 d (8.1)	2.32 s	8.37 s	4.19 m	1.74 m	1.30 m	3.47 m
4	D_2O	8.27 d (8.2, 5.4)	8.01 s	7.89 dd (8.2, 5.4)	8.79 d (8.2)	8.60 s	4.31 m	1.88 m	1.48 m	3.54 m

[a] $J_{H\text{-}H}$ (Hz) are given in parentheses.

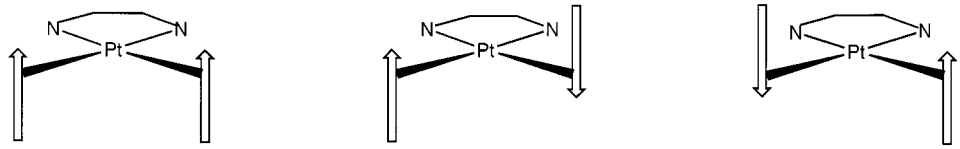

Head-to-*Head* Δ *Head*-to-*Tail* Λ *Head*-to-*Tail*

Scheme 2. Representations of the *HH* (*Head*-to-*Head*) and *HT* (*Head*-to-*Tail)* orientations of the two guanine bases (empty arrows) with respect to the platinum/N4 coordination plane

NMR signals belonging to the 2-hydroxyethoxymethyl chains. The assignment of the multiplet centred at δ = 5.52 to the C(1′)H$_2$ protons was straightforward. Quite more difficult was the assignment of the multiplets at δ = 3.36 and 3.55 to the C(2′)H$_2$ and C(3′)H$_2$ protons, respectively. These two methylenes give coincident signals (δ = 3.67) in free acyclovir. A two dimensional ^{13}C,^{1}H HETCOR experiment was diagnostic for their assignment (an expansion of the aliphatic region of the two dimensional ^{13}C,^{1}H spectrum is shown in Figure 2).

On the basis of characteristic values of ^{13}C chemical shifts for similar organic chains (e.g. diethylene glycol), the cross peak A (at δ = 61 on the ^{13}C axis) is assigned to C(3′)H$_2$ and the two cross peaks B (at δ = 72 on the ^{13}C axis) are assigned to C(2′)H$_2$. It is worth noting that both methylene groups bound to the ether oxygen, C(1′)H$_2$ and C(2′)H$_2$, exhibit a marked diastereotopic splitting of the CH$_2$ protons. Such a splitting is absent in the uncoordinated acyclovir and is indicative of the formation of a chiral centre in the complex. The platinum becomes a chiral centre only in the *HT* rotamers, therefore the observation of such a diastereotopic splitting also lends support to the *HT* conformation being by far the most abundant for compound **1**. Furthermore, the large value of the diastereotopic splitting indicates that the rate of interconversion between *HT* enantiomers is rather slow.

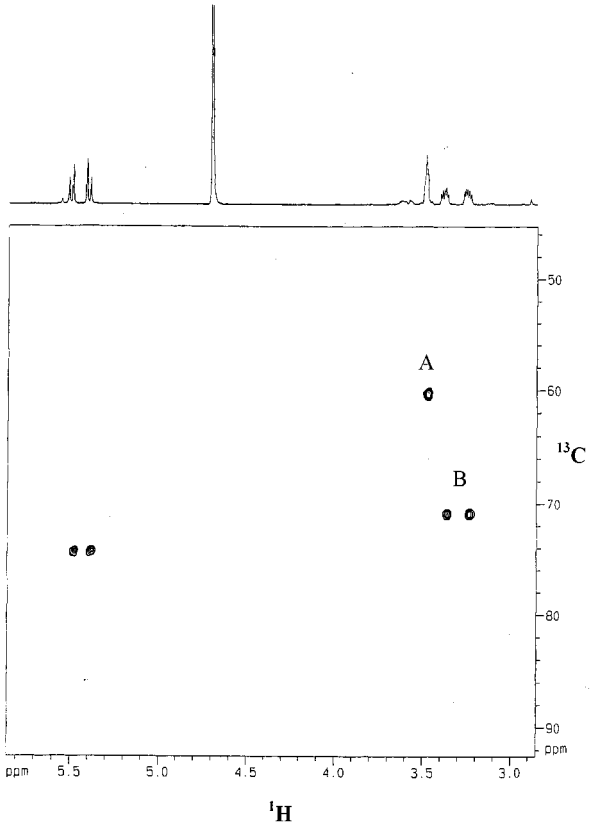

Figure 2. ^{1}H,^{13}C two dimensional (HETCOR) spectrum in D_2O of complex **1** in the region of the aliphatic protons; A = C(3′)H$_2$, B = C(2′)H$_2$

Ligand Exchange in Complex 1

Complex **1** is the only compound of the series which has been isolated with iodide as counterions. In CD_3OD (Figure 3, Table 1) compound **1** is in equilibrium with two new species: one of the new species is easily recognised as free acyclovir, the second species is characterised by having two singlets (at δ = 3.34 and 2.25) in the methyl region of the spectrum indicating that the two methyls of Me_2phen are inequivalent. Furthermore, integration of the signals indicates that the new complex contains only one molecule of

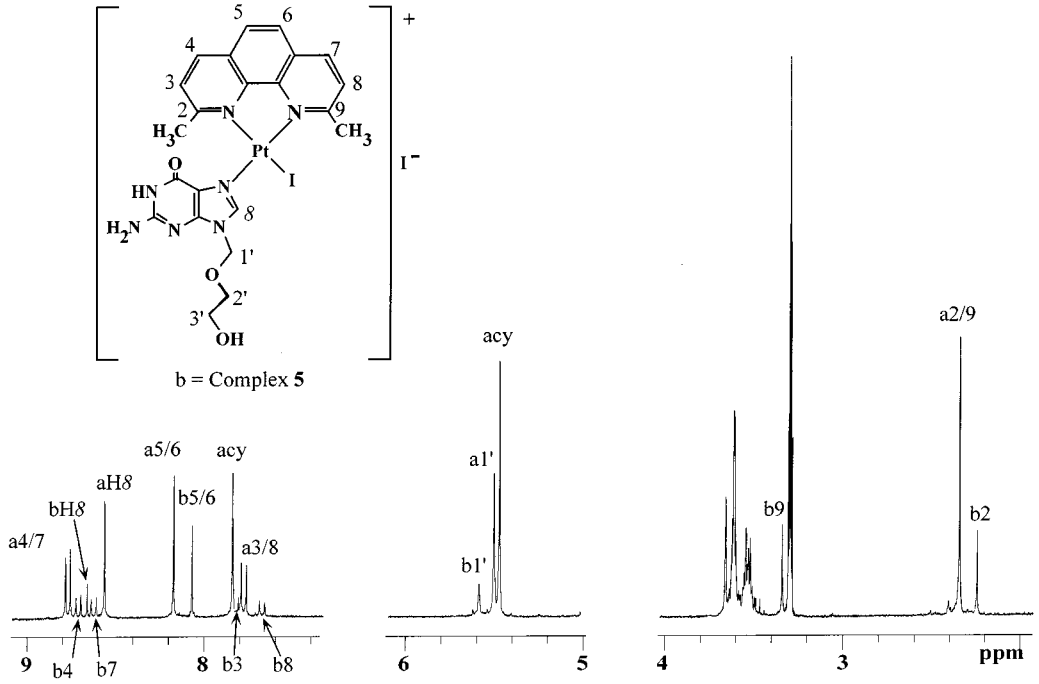

Figure 3. ^{1}H NMR spectrum in CD_3OD of complex **1**; a = complex **1**, b = complex **5**, acy = free acyclovir

acyclovir per phenanthroline and therefore must be formulated as [PtI(acy)(Me_2phen)]I (**5**) with a bidentate Me_2phen, one iodide, and one acyclovir residue in the coordination sphere of platinum.

To check this hypothesis complex **5** was prepared independently by using the same experimental conditions as for the preparation of complex **1** but adding only one equivalent of acyclovir per molecule of platinum substrate. The isolated complex **5**, fully characterised by elemental analysis and IR spectroscopy, exhibits a ^{1}H NMR spectrum in CD_3OD that is identical to that observed for the newly formed complex in the NMR spectrum of **1** in CD_3OD. Therefore we can conclude that in methanol the following equilibrium is established:

$$[Pt(Acy)_2(Me_2phen)]^{2+} + I^- \rightleftharpoons [PtI(Acy)(Me_2Phen)]^+ + Acy$$

The presence of the above equilibrium was also confirmed by addition of KI (five times the stoichiometric amount) to a solution of **1** in CD_3OD. The molar ratio **1**:**5** which was 1.75 before the addition of KI became 0.5 after the addition of KI clearly supporting the involvement of the iodide ion in the equilibrium of displacement of one acyclovir ligand from **1**.

A question to be answered before concluding this section is why the above equilibrium is observed in methanol but not in water. A reasonable explanation for this is that methanol is less efficient than water in solvating charged species and keeping them well separated. A parameter directly related to this property is the dielectric constant, which is far bigger for water (78.5) than for methanol (32.6).

Complex 2

Significant IR data for complex **2** are the C=O stretching vibration at 1691 cm^{-1} and the NO_3^- stretching vibration at 1389 cm^{-1}. A complete assignment of the ^{1}H NMR spectroscopic data is given in Table 1. The discussion given for **1** applies entirely also to **2**.

Complex 3

Significant IR data for complex **3** are the C=O stretching vibration at 1693 cm^{-1} and the NO_3^- stretching vibration at 1384 cm^{-1}.

The ^{1}H NMR spectrum of complex **3** in D_2O is shown in Figure 4 and the chemical shift values are reported in Table 1.

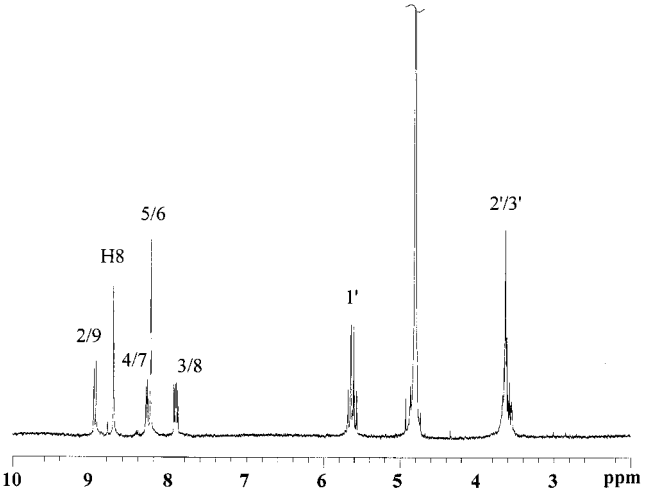

Figure 4. ^{1}H NMR spectrum in D_2O of complex **3**

As with **1**, a single set of signals was also observed for **3**. However, since the phen ligand does not contain bulky substituents in the *ortho* positions, the observation of a single set of resonances could stem from a fast interconversion (on the NMR time scale) of different rotamers (both *HH* and *HT*) and not from the presence of only the enantiomeric *HT* rotamers (as was the case for **1**). To answer this question the analogous compound containing guanosine instead of acyclovir ($[Pt(guo)_2(phen)](NO_3)_2$) was synthesised.[28] The presence of the chiral ribose renders the *HH* rotamer no longer C_s-symmetrical and causes the two *HT* rotamers, although still C_2-symmetrical, to be different from one another. The observation of two major sets of signals (belonging to the two *HT* rotamers) is clearly indicative of slow interconversion among rotamers, therefore we can conclude that the rate of interconversion among the rotamers of **3** is also slow on the NMR time scale and the single set of signals is assignable to the most favoured *HT* enantiomers. Also, the observation of a diastereotopic splitting for the $C(1')H_2$ protons, similar to that seen for complex **1**, supports the idea of a slow interconversion between the *HT* enantiomers of complex **3** in D_2O.

The steric bulk of phen is much smaller than that of Me_2phen (the deviations from the planar geometry caused by the steric interaction between the *cis* ligands is very large in platinum complexes with Me_2phen but is undetectable in platinum complexes with phen); however, the rigidity of the phen ligand does not permit any relief of the steric interaction which builds up when the rotating G comes across the *ortho* hydrogens of the phenanthroline.

Complex 4

Significant IR data for complex **4** are the C=O stretching vibration at 1692 cm^{-1}, and the NO_3^- stretching vibration at 1384 cm^{-1}. The complete assignment of the ^1H NMR spectroscopic data for **4** is given in Table 1. The discussion given for **3** applies also to **4**.

Stability of the Complexes in Physiological Medium

The observation that the iodide counter ion is capable of displacing the coordinated acyclovir from **1** prompted us to investigate the chemical stability of these compounds in physiological medium. Therefore **1**, **2**, **3**, and **4** were each dissolved in D_2O containing 0.1 M NaCl and ^1H NMR spectra were measured over a period of time.

Complexes **1** and **2** were found to be very stable over a period of two weeks. On the other hand, complexes **3** and **4** underwent ligand dissociation equilibria similar to that observed for **1** in methanol (entering of a chloro ligand and displacement of one purine base). After ten days the concentration of **3** and **4** was slightly less than 80% of the initial concentration.

This unexpected result (greater stability of the more sterically hindered compounds **1** and **2**) is probably a consequence of the *ortho* substituents of neocuproine shielding the metal centre and inhibiting the nucleophilic attack of an entering chloride upon the platinum atom.[29]

The displacement of a purine base by a chloride ion in saline solution may have some relevance in relation to the stability of the major DNA adduct of cisplatin in which two purines are cross-linked by a $Pt(NH_3)_2$ moiety.

Biological Activity of Compounds 1−4

While the cytostatic activity of compounds **1**−**4** is still under investigation, preliminary results on their antiviral activity have already been obtained. So far the antiviral activity of the four hybrid drugs has been tested against the Human Immunodeficiency Virus (HIV) and more precisely against HIV-1(IIIB) and HIV-2(ROD) viruses in MT_4 cells. An automated in vitro tetrazolium-based colorimetric assay was used to screen the inhibitory activity of the drugs.[30] The results are reported in Table 2.

Table 2. Anti-HIV-1(IIIB) and HIV-2(ROD) activity and cytotoxicity properties of compounds **1**−**4**, free acyclovir, and penciclovir in MT_4 cells

Compound	HIV Strain	EC_{50} [a]	IC_{50}[b]	SI[c]
1	IIIB	>1.81	1.81	<1
	ROD	>2.47	2.47	<1
2	IIIB	>6.02	6.02	<1
	ROD	>11.8	11.8	<1
3	IIIB	>132	>132	–
	ROD	>132	>132	–
4	IIIB	>124	>124	–
	ROD	>124	>124	–
Acyclovir	IIIB	>555	>555	–
	ROD	>555	>555	–
Penciclovir	IIIB	>493	>493	–
	ROD	>493	>493	–

[a] EC_{50} is defined as the concentration of compound (μM) which inhibits 50% of the viral replication. – [b] IC_{50} is defined as the concentration of compound (μM) which reduces the viability of the treated cells to 50% of that of untreated cells. – [c] SI (Selective Index) = IC_{50}/EC_{50}.

In general, a drug is considered to be active against HIV-1 and HIV-2 viruses if the EC_{50} is ≤1 μM.[3,30,31] None of the tested compounds exhibited anti-HIV activity at subtoxic concentrations. It should be noted, however, that the free acyclovir and penciclovir are also deprived of anti-HIV activity. Therefore a better indication of a synergistic effect, if any, stemming from the coupling of antiviral nucleotides with cisplatin-like substrates will come from anti-HSV and antitumor assays which are in progress.

However, an interesting result stemming from these preliminary experiments is the cytotoxic activity against MT_4 cells, which is far greater for compounds **1** and **2** than for compounds **3** and **4**. The two couples of compounds have a similar charge (+2) and, presumably, similar cell permeability. Therefore, their different behaviour is to be ascribed to a different reactivity in the biological medium determined by the presence in **1** and **2** of two methyl substituents in the *ortho* positions of the phenanthroline.

Conclusions

Platinum(II) complexes containing a bidentate phenanthroline and the antiviral agents acyclovir and penciclovir

have been synthesised and characterised. Both the Me_2phen and the phen carrier ligands are able to hinder rotation of the guanine bases about the Pt−N(7) bond with the consequence that the interconversion between rotamers is very slow on the NMR time scale. This was expected for Me_2phen but was rather unexpected for phen and is a clear demonstration that in addition to the steric bulk the rigidity of the carrier ligand can also deeply influence the rate of interconversion among rotamers in $Pt(A)G_2$ complexes. The rigidity of the phen ligand does not allow any relief of the steric interaction that builds up when the rotating G comes across the *ortho* protons of phen.

The different behaviour in water and methanol of **1** indicates that the solvating ability and the dielectric constant of the solvent play an important role in the stabilisation of cationic platinum species in the presence of coordinating anions such as Cl^- or I^-. In this context, an unexpected result was the greater stability in water solution and in the presence of 0.1 M NaCl of complexes with neocuproine (**1** and **2**) with respect to those with phenanthroline (**3** and **4**). The higher stability of the former complexes is probably favoured by the shielding of the metal centre by the methyl substituents in positions 2 and 9 of the phenanthroline which prevents the chloride ions from entering into the coordination sphere of the metal.

Although complexes **1**−**4** are not active against HIV-1(IIIB) and HIV-2(ROD) viruses; nevertheless there are two important observations: i) the use of neocuproine (a phenanthroline with methyl substituents in positions 2 and 9) instead of unsubstituted phenanthroline can increase the cytotoxicity of the compounds by two order of magnitude, ii) the increase in cytotoxicity appears to be in relation to the greater stability in the biological medium of the neocuproine derivatives.

Experimental Section

Physical Measurements: Elemental analyses were performed on a Elemental Analyzer mod. 1106 Carlo Erba Instrument. IR Spectra were recorded on a spectrophotometer Perkin−Elmer Spectrum One using KBr as solid support for pellets. ^{1}H NMR spectra were recorded on a Bruker AM-WB 300 MHz instrument. Chemical shifts were referred to TMS by using the residual protic solvent peaks as internal references (δ = 4.80 for D_2O and δ = 3.30 for CD_3OD). ^{13}C,^{1}H HETCOR two dimensional experiments were performed on a DRX 500 MHz WB Avance Bruker Instrument with D_2O as solvent and internal CH_3OH as reference for ^{13}C (δ = 50.2).

Starting Materials: Commercial reagent grade chemicals, 2,9-Me_2-1,10-phenanthroline (Me_2phen, neocuproine), 1,10-phenanthroline (phen), guanosine (guo), DMSO and DMF, were used without further purification.

$[PtCl_2(DMSO)_2]$,[32] $[PtX_2(Me_2phen)]$ (X = Cl, I),[33] $[Pt(guo)_2(Me_2phen)]Cl_2$, $[Pt(guo)_2(phen)](NO_3)_2$,[28] acyclovir (acy) and penciclovir (pen)[34] were prepared by previously reported procedures.

Preparation of $[PtI_2(phen)]$: A suspension of $[PtCl_2(DMSO)_2]$ (300 mg, 0.71 mmol) in methanol was treated with a large excess of KI (581 mg, 3.5 mmol). After stirring for one day, the initially yellow suspension became an orange solution containing the dimeric complex $[Pt_2I_4(DMSO)_2]$. This solution was treated with phen (140 mg, 0.71 mmol) and left stirring for one hour during which time a yellow-orange precipitate was formed. The precipitate was collected by filtration of the mother solution, the filtrate was concentrated to half its volume by evaporation of the solvent under reduced pressure and kept at room temperature for a few days during which time another yellow precipitate was formed. The collected solid fractions were washed with methanol and dried under vacuum. Yield 424 mg (95%) based on the starting platinum complex. − $C_{12}H_8I_2N_2Pt$ (629.10): calcd. C 22.9, H 1.3, N 4.5; found C 22.6, H 1.3, N 4.4.

Preparation of $[Pt(acy)_2(Me_2phen)]I_2$ (1): A solution containing $[PtI_2(Me_2phen)]$ (102 mg, 0.155 mmol) dissolved in CH_2Cl_2/CH_3OH (200 mL; 1:1, v/v) was treated with acyclovir (70 mg, 0.31 mmol). After stirring for 2 hours, the initially orange solution became yellow. The solvent was evaporated under vacuum and the yellow residue was suspended in 100 mL of water and stirred overnight. The water solution was then filtered and taken to dryness by evaporation of the solvent under vacuum. The yellow residue proved to be the salt $[Pt(Me_2phen)(acy)_2]I_2$. Yield 178 mg (90%). − $C_{31}H_{36}Cl_2I_2N_{12}O_6Pt$ (**1**·CH_2Cl_2) (1192.5): calcd. C 30.1, H 3.0, N 13.2; found C 30.8, H 2.9, N 13.7.

Preparation of $[PtI(acy)(Me_2phen)]I$ (5): $[PtI_2(Me_2phen)]$ (82 mg, 0.125 mmol) was dissolved in CH_2Cl_2 (70 mL) and treated with a stoichiometric amount of acyclovir (28.4 mg, 0.126 mmol) previously dissolved in 70 mL of CH_3OH. The yellow solution was left stirring for one day and then concentrated to 50 mL by evaporation of the solvent under vacuum. Addition of diethyl ether (300 mL) caused the precipitation of a yellow solid, which was separated by filtration of the solution, carefully washed with ether, and dried under vacuum. Yield 109 mg (90%). − $C_{23}H_{25}Cl_2I_2N_7O_3Pt$ (**5**·CH_2Cl_2) (967.29): calcd. C 28.6, H 2.6, N 10.1; found C 28.1, H 2.4, N 10.2.

Preparation of $[Pt(pen)_2(Me_2phen)](NO_3)_2$ (2): A solution of $[PtCl_2(Me_2phen)]$ (149 mg, 0.31 mmol) in DMF (75 mL) was treated with $AgNO_3$ (109 mg, 0.628 mmol) previously dissolved in a minimum amount of water (1 mL). After stirring in the dark for 12 h at room temperature, the solution was filtered through celite to remove AgCl. The filtered yellow solution was treated with penciclovir (157 mg, 0.62 mmol) and stirred for 4 h. Addition of diethyl ether (300 mL) caused the formation of a creamy precipitate. The precipitate was collected by filtration of the solution, washed with acetone and ether, and dried under vacuum. The crude product was extracted with 100 mL of water, the solution was filtered and taken to dryness by evaporation of the solvent under vacuum. Yield 249 mg (75%). − $C_{34}H_{46}N_{14}O_{14}Pt$ (**2**·$2H_2O$) (1069.9): calcd. C 38.2, H 4.3, N 18.4; found C 38.1, H 4.3, N 18.4.

Preparation of $[Pt(acy)_2(phen)](NO_3)_2$ (3) and $[Pt(pen)_2(phen)](NO_3)_2$ (4): $[PtI_2(phen)]$ (150 mg, 0.24 mmol) was dissolved in DMF (80 mL) at 50 °C and treated with $AgNO_3$ (81.3 mg, 0.48 mmol). The solution was cooled to room temperature and stirred in the dark overnight. The solution was filtered through celite to remove the yellow AgI precipitate and treated with a stoichiometric amount of acyclovir (107 mg, 0.48 mmol) for complex **3** and penciclovir (120 mg, 0.48 mmol) for complex **4**. The solution was left stirring for 4 h and then treated with diethyl ether to induce the precipitation of the platinum complex. The solid was collected by filtration of the solution, washed with acetone and ether, and finally dried under vacuum. The crude product was extracted with

water (40 mL), the solution was filtered and taken to dryness under vacuum to give pure compounds **3** and **4**, respectively. Yields 189 mg (80%) and 200 mg (80%) for complex **3** and **4**, respectively. − $C_{28}H_{36}N_{14}O_{15}Pt$ (**3**·3H_2O) (1003.8): calcd. C 33.5, H 3.6, N 19.5; found C 33.2, H 3.2, N 18.9. − $C_{32}H_{44}N_{14}O_{15}Pt$ (**4**·3H_2O) (1059.3): calcd. C 36.3, H 4.2, N 18.5; found C 35.6, H 3.7, N 18.3.

Biological Tests: The antiviral assays were carried out according to the method reported in ref.[35]

Acknowledgments

Thanks are expressed to Dr. Sandra A. De Pascali for the help in the preparation of the platinum complexes. We are also grateful to Prof. Erik De Clercq and Drs. Christophe Pannecouque and Myriam Witvrouw (Katholieke Universiteit, Rega Instituut, Leuven, Belgium), who carried out the antiviral assays. The authors also thanks the University of Bari (Contribution ex 60%), the Ministero dell'Università e della Ricerca Scientifica e Tecnologica, MURST (Cofin. 1988 no. 9803021072) and the EC (COST Chemistry projects D8/0009/97 and D8/0012/97).

[1] E. De Clercq, *Clinical Microbiology Reviews* **1997**, *10*, 674−693 and references therein.
[2] J. A. Fyfe, P. M. Keller, P. A. Furman, R. L. Miller, G. B. Elion, *J. Biol. Chem.* **1978**, *253*, 8721−8727.
[3] E. De Clercq, *Rev. Med. Virol.* **1995**, *5*, 149−164.
[4] E. Dubler, M. Grüter-Heini, G. Hänggi, M. Knoepfel, H. Schmalle. *EUROBIC II*, Florence (Italy), August 30−September 3, **1994**. Abstract 110.
[5] I. Turel, B. Andersen. E. Sletten, A. J. P. White, D. Williams, *Polyhedron* **1998**, *17*, 4195−4201.
[6] I. Turel, N. Bukovec, M. Goodgame, D. J. Williams, *Polyhedron* **1997**, *16*, 1701−1706.
[7] L. Cavallo, R. Cini, J. Kobe, L. G. Marzilli, G. Natile, *J. Chem. Soc., Dalton Trans.* **1991**, 1867−1873.
[8] M. Coluccia, A. Boccarelli, C. Cernelli, M. Portolani, G. Natile, *Metal-Based Drugs* **1995**, *2*, 249−256.
[9] S. Grabner, J. Plavec, N. Bukovec, D. Di Leo, R. Cini, G. Natile, *J. Chem. Soc., Dalton Trans.* **1998**, 1447−1451.
[10] R. Cini, S. Grabner, N. Bukovec, L. Cerasino, G. Natile, *Eur. J. Inorg. Chem.* **2000**, 1601−1607.
[11] A. Eastman, *Pharmacol. Ther.* **1987**, *34*, 155−166.
[12] A. M. J. Fichtinger-Schepman, J. L. van der Veer, J. H. J. Den Hartog, P. H. M. Lohman, J. Reedijk, *Biochemistry* **1985**, *24*, 707−713.
[13] *Cisplatin. Chemistry and Biochemistry of a Leading Anticancer Drug* (Ed.: B. Lippert), Wiley VCH, Zurich, **1999**.
[14] P. G. Sammes, G. Yahioglu, *Chem. Soc. Rev.* **1994**, *23*, 327−334.
[15] S. Mehadevan, M. Palaniandavar, *Inorg. Chem.* **1998**, *37*, 693−700 and 3927−3934.
[16] R. J. H. Clark, F. P. Fanizzi, G. Natile, C. Pacifico, C. G. van Rooyen, D. A. Tocher, *Inorg. Chim. Acta* **1995**, *235*, 205−213.
[17] F. P. Fanizzi, L. Maresca, G. Natile, M. Lanfranchi, A. Tiripicchio, G. Pacchioni, *J. Chem. Soc., Chem. Commun.* **1992**, 333−335.
[18] N. Hadjiliadis, T. Teophanides, *Inorg. Chim. Acta* **1976**, *16*, 77−88 and references therein.
[19] K. Nakamoto. *Infrared and Raman Spectra of Inorganic and Coordination Compounds.* John Wiley & Sons, inc., New York, **1997**, p. 80.
[20] J. Arpalahti, K. D. Kilka, R. Sillanpä, R. Kivekäs, *J. Chem. Soc., Dalton Trans.* **1998**, 1397−1402.
[21] R. E. Cramer, P. L. Dahlstrom, *J. Am. Chem. Soc.* **1979**, *101*, 3679−3681.
[22] R. E. Cramer, P. L. Dahlstrom, *Inorg. Chem.* **1985**, *24*, 3420−3424.
[23] L. G. Marzilli, S. O. Ano, F. P. Intini, G. Natile, *J. Am. Chem. Soc.* **1999**, *42*, 9133−9142.
[24] K. M. Williams, L. Cerasino, F. P. Intini, G. Natile, L. G. Marzilli, *Inorg. Chem.* **1998**, *37*, 5260−5268.
[25] S. T. Sullivan, A. Ciccarese, F. P. Fanizzi, L. G. Marzilli, *Inorg. Chem.* **2000**, *39*, 836−842.
[26] H. C. Wong, R. Coogan, F. P. Intini, G. Natile, L. G. Marzilli, *Inorg. Chem.* **1999**, *38*, 777−787.
[27] D. Kiser, F. P. Intini, Y. Xu, G. Natile, L. G. Marzilli, *Inorg. Chem.* **1994**, *33*, 4149−4158.
[28] F. P. Fanizzi, N. Margiotta, G. Natile, manuscript in preparation.
[29] Y. Chen, Z. Guo, S. Parsons, P. J. Sadler, *Chem. Eur. J.* **1998**, *4*, 672−676.
[30] F. Rey, F. Barré-Sinoussi, H. Schimdtmayerova, J. C. Chermann, *J. Virol. Methods.* **1987**, *16*, 239.
[31] C. De Michelis, L. Rocheblave, G. Priens, J. C. Chermann, J. L. Krans, *Bioorganic & Medicinal Chem.* **2000**, *8*, 1253−1262.
[32] Yu. N. Kukuskin, Yu. E. Uyazmenskii, L. I. Zorina, Yu. L. Pazukhina, *Russian J. Inorg. Chem. (Engl. Transl.)* **1968**, *13*, 833.
[33] F. P. Fanizzi, F. P. Intini, L. Maresca, G. Natile, M. Lanfranchi, A. Tiripicchio, *J. Chem. Soc., Dalton Trans.* **1991**, 1007.
[34] J. Kobe, J. Gnidovec, P. Zupet. *US Patent* US 4,701,526. **1987**; J. Kobe, J. Gnidovec, P. Zupet. *US Patent* US 4, 826, 981. **1988**.
[35] R. Pauwels, J. Balzarini, M. Baba, R. Snoeck, D. Schols, P. Herdewijn, J. Desmyter, E. De Clercq, *Journal of Virological Methods* **1988**, *20*, 309−321.

Received September 12, 2000
[I00358]

Small Platinum−Thallium Clusters Stabilized by Ethylenediamine, $[(NC)_5Pt-Tl(en)_{n-1}]$ ($n = 1-3$) − Characterization in Solution and in the Solid State

Guibin Ma,[a][‡] Mikael Kritikos,[b] and Julius Glaser*[a]

Keywords: Metal−metal interactions / Platinum / Thallium / N ligands / NMR spectroscopy

Three neutral binuclear platinum–thallium compounds containing a direct and "naked" (unsupported by ligands) metal–metal bond have been prepared in dimethyl sulfoxide (DMSO). The compounds have the formula $[(NC)_5Pt–Tl(en)_{n-1}]$ (n = 1–3, for compounds **1**, **2** and **3**, respectively) and were found to exist in solution by means of multinuclear NMR (^{195}Pt, ^{205}Tl, ^{13}C and ^{1}H) and Raman spectroscopy. The compounds exhibit very large single bond $^{195}Pt–^{205}Tl$ spin-spin coupling constants of 48–66 kHz. In addition, the solid state analogues of **1** and **3**, $[(NC)_5Pt–Tl(DMSO)_4](DMSO)$ and $[(NC)_5Pt–Tl(en)_2](DMSO)_2$, were synthesized and their structures determined by single crystal X-ray diffraction. The metal–metal bond lengths of Pt–Tl are 2.6131(4) Å and 2.6348(5) Å in compounds **1** and **3**, respectively. Crystal data for compound **1:** monoclinic, space group *Cc* (No. 9), $Z = 4$, $a = 17.2367(14)$, $b = 9.5560(11)$, $c = 17.7941(15)$ Å, $\beta = 100.551(10)°$, $V = 2881.4(5)$ Å^3, $T = 110(1)$ K; and for compound **3:** monoclinic, space group $P2_1$ (No. 4), $Z = 2$, $a = 9.3167(14)$, $b = 12.3007(13)$, $c = 11.4586(16)$ Å, $\beta = 112.318(16)°$, $V = 1214.8(3)$ Å^3, $T = 110(1)$ K.

Introduction

A direct metal−metal bond between platinum and thallium atoms in the solid state was first described by Nagle et al.[1] Later, the binuclear compound $[Pt(CN)_2Tl(crown\text{-}P_2)](NO_3)$ {Crown-P_2: 1,10-bis[(diphenylphosphanyl)methyl]-1,10-diaza-4,7,13,16-tetraoxaoctadecane, formula: $C_{38}H_{48}N_2O_4P_2$}[2] and trinuclear Pt−Tl−Pt compounds, e.g. *cis*-$[Tl\{(1\text{-methylthyminato})_2Pt(NH_3)_2\}_2](NO_3)\cdot 7H_2O$[3] and $(NBu_4)_2[Tl\{Pt(C_6F_5)_4\}_2]$,[4] with Pt−Tl metal−metal bonds, have been synthesized. Three compounds containing a slightly larger Pt−Tl cluster unit have also been prepared, namely $[TlPt_3(CO)_3(PCy_3)_3][Rh(\eta\text{-}C_8H_{12})Cl_2]$ (Cy = cyclohexyl),[5] $[TlPt_6(\mu\text{-}CO)_6(\mu\text{-}dppp)_3]^+$ [dppp = $(C_6H_5)_2P(CH_2)_3P(C_6H_5)_2$],[6] and $[Pt_3\{\mu_3\text{-}Tl(acac)\}(ReO_3)(\mu\text{-}dppm)_3]^+$ [dppm = $(C_6H_5)_2PCH_2P(C_6H_5)_2$].[7] Hao et al.[8] have prepared hexaplatinum clusters with carbonyl and diphosphane ligands, e.g. $[Pt_6(\mu\text{-}CO)_6(\mu\text{-}dppp)_2(dppp)_2]$, and were able to trap Hg^0 and Tl^I in $[Pt_6(\mu_6\text{-}Hg)(\mu\text{-}CO)_6(\mu\text{-}dppp)_3]$ and $[Pt_6(\mu_6\text{-}Tl)(\mu\text{-}CO)_6(\mu\text{-}dppp)_3]^+$, respectively. In the latter compound, the Pt−Tl bond lengths are in the range of 2.860(3)−2.992(3) Å.

Recently, a new family of four binuclear platinum-thallium cyano compounds with the formula $[(NC)_5Pt-Tl(CN)_{n-1}]^{(1-n)}$ ($n = 1-4$ for compounds **I**, **II**, **III** and **IV,** respectively), which contain a direct metal−metal bond unsupported by the ligands, have been synthesized from $Tl(ClO_4)_3$, $K_2Pt(CN)_4$ and NaCN in aqueous solution.[9−11] The compounds possess long-term stability but undergo photochemically induced two-electron transfer between the metal ions when exposed to daylight. Thus, possible applications in photovoltaic devices, for example in a "wet" solar cell of the Grätzel type[12] can be envisaged. However, several chemico-physical parameters of the compounds, such as stability, electrochemical properties or light absorption characteristics, have to be tuned in order to fit the demands of the cell. Therefore, we have initiated a study of possible modifications of these compounds, including both preparative efforts and experimental and theoretical characterization in solution and in the solid state.

The binuclear compounds **I**−**IV** can be viewed as consisting of two units, $Pt(CN)_5$ and $Tl(CN)_n$. The platinum unit is stable and relatively inert in all four compounds whereas the geometry of the thallium entity changes depending on the number of cyanide ligands;[9,10] these cyanide ligands have been found to be kinetically labile. Hence, there is a possibility to replace the cyanides by other ligands, for example amines or organic solvent molecules. Here, the bidentate ethylenediamine ligand was deemed suitable for further study due to its "robustness" and to the fact that Tl^{III} can form strong complexes with N-donor ligands.[13−15] Recently, it was found in this laboratory that, although Tl^{III} ethylenediamine complexes are difficult to

[a] Department of Chemistry, The Royal Institute of Technology (KTH),
100 44 Stockholm, Sweden
E-mail: julius@inorg.kth.se
[b] Department of Structural Chemistry, Arrhenius Laboratory, Stockholm University,
106 91 Stockholm, Sweden
[‡] Permanent address: Department of Chemistry,
Shanxi University,
030006, Taiyuan, Shanxi Province, P. R. China
Supporting information for this article is available on the WWW under http://www.wiley-vch.de/home/eurjic or from the author.

 © WILEY-VCH Verlag GmbH, 69451 Weinheim, 2001 1434−1948/01/0505−1311 $ 17.50+.50/0

prepare in aqueous solution, very stable complexes are formed in organic solvents.[16]

In the present paper, complexes of $[(NC)_5Pt-Tl(en)_{n-1}]$ ($n = 1-3$) with a direct Pt−Tl bond have been studied both in DMSO solution and in the solid state.

Results and Discussion

Characterization in Solution by Multinuclear NMR Spectroscopy

The binuclear complexes $[(NC)_5Pt-Tl(DMSO)_4]$ (**1**), $[(NC)_5Pt-Tl(en)(DMSO)_x]$ (**2**) and $[(NC)_5Pt-Tl(en)_2]$ (**3**) were prepared in DMSO solvent according to the following reactions:

$$[Tl(dmso)_6]^{3+} + [Pt(CN)_4]^{2-} + CN^- \rightleftharpoons \underset{\mathbf{1}}{[(NC)_5Pt{-}Tl(dmso)_4]} + 2\ DMSO \quad (1)$$

$$[Tl(dmso)_6]^{3+} + en \rightleftharpoons [Tl(en)(dmso)_x]^{3+} + (6{-}x)\ DMSO \quad (2)$$

$$[Tl(en)(dmso)_x]^{3+} + [Pt(CN)_4]^{2-} + CN^- \rightleftharpoons \underset{\mathbf{2}}{[(NC)_5Pt{-}Tl(en)(dmso)_x]} \quad (3)$$

$$[Tl(en)_3]^{3+} + [Pt(CN)_4]^{2-} + CN^- \rightleftharpoons \underset{\mathbf{3}}{[(NC)_5Pt{-}Tl(en)_2]} + en \quad (4)$$

The compounds **1**, **2** and **3** were prepared, according to the reactions in Equation (1) to (4), in solutions in which the composition was varied in order to achieve different en/Pt−Tl ratios. The content and the concentration of the compounds in each solution were determined by means of ^{205}Tl and ^{195}Pt NMR spectroscopy. Since the chemical shifts of the three compounds fall in different regions (see Table 1), and the spin−spin coupling patterns represent "fingerprints" of each compound, the composition of the solutions could be easily determined.

$[(NC)_5Pt-Tl(en)_2]$ (3)

Reaction of $[Tl(en)_3](ClO_4)_3$, $K_2Pt(CN)_4$ and NaCN [Equation (4)] in DMSO yielded a colorless solution. The ^{195}Pt and ^{205}Tl NMR spectra of this solution showed the existence of only one Pt−Tl bonded complex (Figure 1 a, b). The ^{205}Tl NMR spectrum (Figure 1a) of the resulting solution shows one triplet signal (with the intensity ratio 1:3.9:1) centered at $\delta = 1885$. Two small symmetrical peaks at both sides (with a very large spin-spin coupling constant, ≈48 kHz) arise from spin-spin coupling between the ^{205}Tl and ^{195}Pt nuclei (^{195}Pt: $I = 1/2$, natural abundance 33.8%); together with the central uncoupled peak they give the intensity ratio of 1:3.9:1 as expected for one thallium coupled to one platinum atom. Another peak at $\delta = 2900$ was detected in the ^{205}Tl NMR spectrum of this solution and was assigned to the unreacted $[Tl(en)_3]^{3+}$ complex. The ^{195}Pt NMR spectrum of the Pt−Tl compound (Figure 1b) consists of a 1:1 doublet centered at $\delta = 370$ due to the coupling between ^{195}Pt and ^{205}Tl (^{205}Tl: $I = 1/2$, natural abundance 70.5%) with the same Pt−Tl coupling constant ≈48 kHz to ^{205}Tl as observed in the ^{205}Tl NMR spectrum. In addition, there is another barely resolved doublet due to the coupling of ^{195}Pt to the other thallium isotope, ^{203}Tl, with $I = 1/2$ and natural abundance 29.5%. The huge spin-spin coupling constant of $^1J(^{205}Tl-^{195}Pt)$ ≈48 kHz indicates formation of a direct Pt−Tl bond.

A ^{13}C NMR spectrum of the 99% ^{13}CN enriched complex showed that two types of coordinated cyanides exist in $[(NC^{13})_5Pt-Tl(en)_2]$ (Figure 2). One signal appears at $\delta = 97.3$ with spin-spin coupling constants $^2J(^{13}C^A-^{205}Tl) = 9150$ Hz and $^1J(^{13}C^A-^{195}Pt) = 834$ Hz and is assigned to the axial cyanide, labeled as CN^A. The other signal, at $\delta = 85.9$, with spin-spin coupling constants $^2J(^{13}C^C-^{205}Tl) = 391$ Hz and $^1J(^{13}C^C-^{195}Pt) = 818$ Hz, belongs to the cyanides (CN^C) in the square-planar $Pt(CN)_4$ unit. The ^{13}C NMR signal of the coordinated ethylenediamine ligand overlaps with the signal of deuterated $[D_6]$DMSO at $\delta = 39$. Considering the composition of the solution and the available information on the previously described Pt−Tl complexes **I**−**IV**,[9,10] these findings indicate that the composition of the complex is $[(NC)_5Pt-Tl(en)_2]$.

Table 1. Selected NMR parameters for the complexes $[(NC)_5Pt-Tl(en)_{n-1}]$ ($n = 1-3$) and for some related dimeric (Pt−Tl) and monomeric platinum and thallium species in solution; for the notation of the carbon/cyanide sites in the platinum-thallium cyano complexes, see Figure 6;

	δ_{Tl} [a]	δ_{Pt} [a]	$\delta_C{}^A$	$\delta_C{}^C$	$^1J_{Pt-Tl}$ (Hz)	$^2J_{Tl-C}{}^A$ (Hz)	$^2J_{Tl-C}{}^C$ (Hz)	$^1J_{Pt-C}{}^A$ (Hz)	$^1J_{Pt-C}{}^C$ (Hz)
Tl^{I}[b]	361								
$[Pt^{IV}(CN)_6]^{2-}$[c]		655		100.7					876
$[Tl^{III}(DMSO)_6]^{3+}$ [b]	1889								
$[Tl(en)_3]^{3+}$ in DMSO[b]	2900								
$[(NC)_5Pt-Tl(DMSO)_x]$[b]	887	574	84.7	83.9	65854	12213	605	920	811
$[(NC)_5Pt-Tl(en)(DMSO)_x]$[b]	1448	494	91.3	84.2	55100	9911	480	880	816
$[(NC)_5Pt-Tl(en)_2]$[b]	1885	370	97.3	85.9	47850	9150	391	834	818
$[(NC)_5Pt-Tl]$[c]	786	474	93.4	90.3	71060	12746	592	909	820
$[(NC)_5Pt-Tl(CN)_3]^{3-}$ [c]	2224	68	116.1	97.0	38760	7270	255	742	843
$[Tl^{III}(CN)_2]^+$ [c]	2447								
$[Pt^{II}(CN)_4]^{2-}$ [b]		−189		121.6					1015
$[Pt^{II}(CN)_4]^{2-}$ [c]		−213		130.2					1031

[a] The ^{205}Tl NMR chemical shift is given in ppm toward higher frequency with respect to an aqueous solution of $TlClO_4$ extrapolated to infinite dilution at 25 °C; the ^{195}Pt NMR chemical shift is given in ppm toward higher frequency from $\chi(^{195}Pt) = 21.4$ MHz; $\delta[PtCl_6]^{2-} = 4533$ at 25 °C in aqueous solution. − [b] DMSO solution. − [c] Aqueous solution, ref.[9,10].

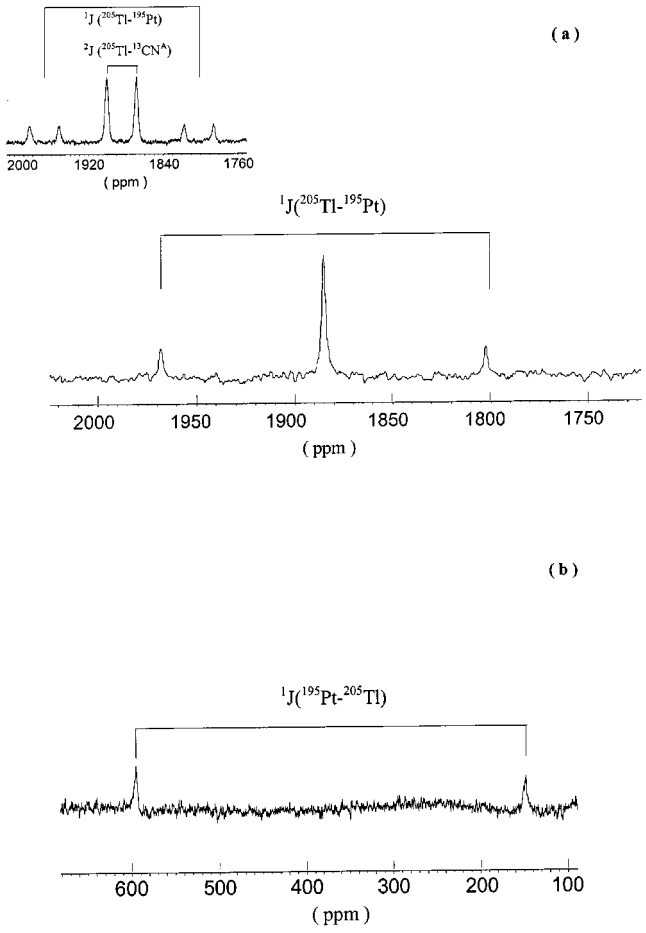

Figure 1. (a) 288.5 MHz ^{205}Tl NMR spectrum of $[(NC)_5Pt-Tl(en)_2]$ in DMSO; the concentrations of $[Tl(en)_3](ClO_4)_3$, $K_2Pt(CN)_4$ and NaCN are all 50 mmol/L (the inset shows the spectrum for a solution of the same compound with all cyanide enriched in ^{13}C, 99%); (b) 107.5 MHz ^{195}Pt NMR spectrum of $[(NC)_5Pt-Tl(en)_2]$ in the same solution, 298 K

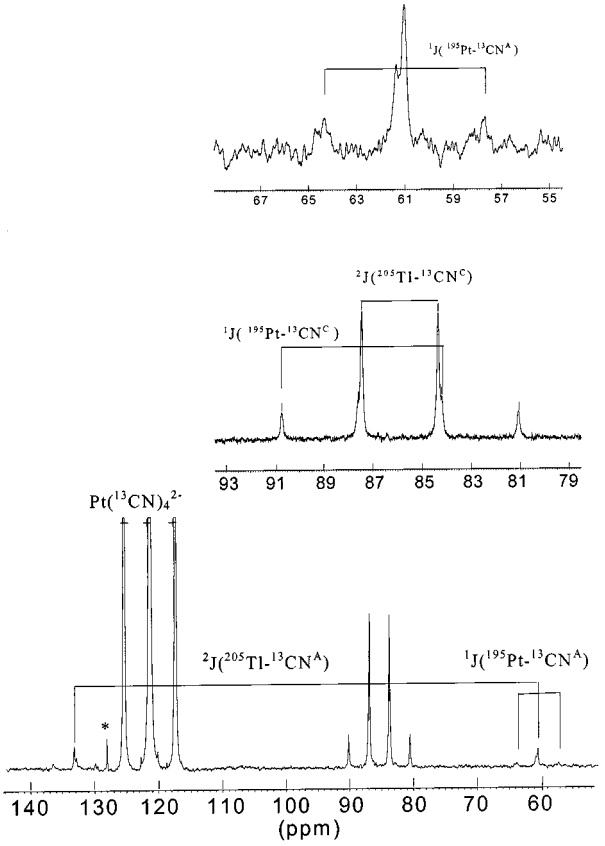

Figure 2. 125.7 MHz ^{13}C NMR of $[(NC^{13})_5Pt-Tl(en)_2]$ in $[D_6]$DMSO solution, 298 K; the composition of the solution is 50 mmol/L $[Tl(en)_3](ClO_4)_3$, 50 mmol/L $NaPt(^{13}CN)_4$ and 50 mmol/L $Na^{13}CN$ (the ^{13}C signal of en at δ = 39 — not shown in the spectrum — overlaps with the ^{13}C signals of the deuterated $[D_6]$DMSO solvent); * impurity; + signals of unreacted $[Pt(^{13}CN)_4]^{2-}$

$[(NC)_5Pt-Tl(DMSO)_4]$ (1) and $[(NC)_5Pt-Tl(en)(DMSO)_x]$ (2)

In a similar way, the two remaining compounds were characterized. The ^{205}Tl NMR spectrum of compound **2** in DMSO solution is a triplet centered at δ = 1448 with the spin-spin coupling constant between ^{205}Tl and ^{195}Pt equal to ≈55 kHz. The ^{195}Pt NMR spectrum of this species is a 1:1 doublet centered at δ = 494 with the same spin-spin coupling constant of about 55 kHz.

For compound **1** in DMSO, the ^{205}Tl NMR chemical shift is δ = 887 and the ^{195}Pt NMR shift is δ = 574 with $^1J(^{205}Tl-^{195}Pt)$ = 65.8 kHz. Selected ^{205}Tl, ^{195}Pt and ^{13}C NMR spectroscopic data of the three compounds are listed in Table 1. (^{205}Tl and ^{195}Pt NMR spectra for compounds **1** and **2** are shown in the Supporting Information).

In the ^{1}H NMR spectra, the signal of the free ethylenediamine CH_2 groups appears at δ = 2.82. For compounds **2** and **3**, signals appear at δ = 3.47 and 3.65, respectively, and are assigned to the protons of the coordinated ethylenediamine ligand.

No metal−metal bonded species were detected when only $[Pt(CN)_4]^{2-}$ and $[Tl(en)_3]^{3+}$ were present in solution. However, with additional cyanide Pt−Tl compounds are formed. This is proved by NMR spectrosocopy (for **1**, **2** and **3)** and X-ray diffraction analysis (for **1** and **3**). Thus, it is apparent that the extra cyanide is necessary for the formation of the Pt−Tl bond.

An important experimental observation should be mentioned in this context: the spin-spin coupling constant $^2J(^{205}Tl-^{13}C)$ for the linear entity ^{A}NC−Pt−Tl (axial cyanide) is more than one order of magnitude larger than that of ^{C}NC−Pt−Tl (equatorial cyanides, i.e. C−N^C is perpendicular to the Pt−Tl bond), cf. Table 1. This indicates that the fifth cyano ligand plays a key role in stabilization of the Pt−Tl bond. It can be explained by an overlap of the Tl s orbital, the Pt d_z^2 orbital and the CN p_z orbital to form a molecular orbital ^{A}NC−Pt−Tl along the *z* axis: thus, the linear ^{A}NC−Pt−Tl- unit is stabilized.

Raman Spectra of 1 and 3 in the Solid State

A characteristic feature of the Raman spectra of the Pt−Tl compounds in aqueous solution is the presence of a strong and sharp band in the low frequency region,[10] which is due to the metal−metal (M−M) bond stretch-

ing.[17] In general, bimetallic compounds with unsupported single metal−metal bonds display M−M stretching bands at wave numbers lower than 200 cm^{-1}, while multiple bonding or ligand bridging in conjunction with an M−M single bond leads to higher wavenumbers.[18] The Raman spectra of the solid compounds **1** and **3** exhibit metal−metal vibrations at 154 cm^{-1} and 156 cm^{-1}, respectively.

The C≡N stretching region of the binuclear species is also informative and can provide an additional support for the structure of the compounds. We assign the two sharp bands at 2174 cm^{-1}, 2161 cm^{-1} for **1** and at 2168 cm^{-1}, 2151 cm^{-1} for **3** to the symmetric (A_{1g}) and antisymmetric (B_{1g}) stretching vibrations of the four equivalent cyanides ($C{\equiv}N^C$) of the $Pt(CN)_4$ unit in D_{4h} symmetry[19] in the compounds $[(^CNC)_4(^ANC)Pt-Tl(en)_{n-1}]$ ($n = 1-3$). These bands shift to high frequency and are very close to the stretching bands at 2153 cm^{-1}(s) and 2137 cm^{-1}(m) for the $[Pt(CN)_4]^{2-}$ complex in the solid state. The higher frequency bands at 2184 cm^{-1} and 2179 cm^{-1} are assigned to the $C{\equiv}N^A$ ligand in compounds **1** and **3**, respectively.

Crystal Structures of $[(NC)_5Pt-Tl(DMSO)_4](DMSO)$ (1) and $[(NC)_5Pt-Tl{\cdot}(en)_2](DMSO)_2$ (3)

The structures of **1** and **3** in the solid state were determined by single crystal X-ray crystallography and are shown in Figure 3 and 4, respectively. Selected bond lengths and angles of **1** and **3** are given in Table 2 and 3, respectively.

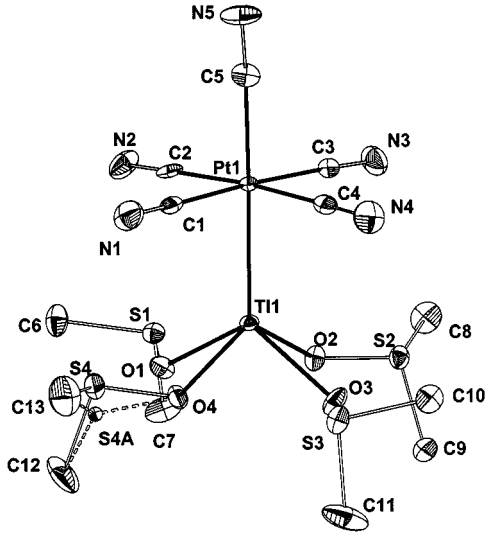

Figure 3. ORTEP view of the binuclear complex $[(NC)_5Pt-Tl(DMSO)_4]$ in the crystal structure of $[(NC)_5Pt-Tl(DMSO)_4](DMSO)$ (ellipsoids at 50% probability level)

In the structure of **1**, a $Pt(CN)_5$ unit is bonded to a $Tl(DMSO)_4$ unit with a Pt−Tl bond length of 2.6131(4) Å. The difference in bond length between the axial and equatorial cyanide groups is less pronounced than in complex **3**. In **1**, the equatorial Pt−C bond lengths are around 2.01(1) Å while the axial Pt−C bond length is 2.037(7) Å. Four crystallographically different DMSO groups are coordinated to thallium with Tl−O bond lengths in the range 2.287(5) to 2.311(4) Å. The Tl atom is coordinated in a square pyramidal fashion, and is located 1.08 (1) Å from the basal plane defined by the four O atoms. In the same way as in **3** (see below), the two en groups and the four cyano ligands are arranged in an eclipsed geometry.

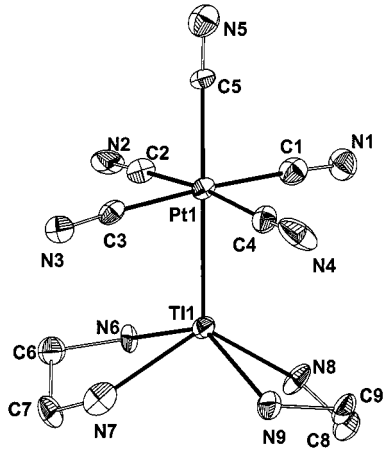

Figure 4. ORTEP view of the binuclear complex $[(NC)_5Pt-Tl(en)_2]$ in the crystal structure of $[(NC)_5Pt-Tl(en)_2](DMSO)_2$ (ellipsoids at 50% probability level)

Table 2. Selected bond lengths (Å) and angles (°) in the crystal structure of $[(NC)_5Pt-Tl(DMSO)_4]{\cdot}(DMSO)$ (**1**)

Tl1−Pt1	2.6131(4)	S1−O1	1.543(6)
Tl1−O1	2.292(5)	S2−O2	1.540(4)
Tl1−O2	2.290(5)	S3−O3	1.543(6)
Tl1−O3	2.287(5)	S4−O4	1.533(5)
Tl1−O4	2.311(4)	S5−O5	1.500(8)
Pt1−C1	2.008(7)	S1−C6	1.779(7)
Pt1−C2	2.018(7)	S1−C7	1.778(9)
Pt1−C3	2.017(8)	S2−C8	1.774(9)
Pt1−C4	2.009(7)	S2−C9	1.768(9)
Pt1−C5	2.037(7)	S3−C10	1.768(7)
N1−C1	1.148(10)	S3−C11	1.779(11)
N2−C2	1.147(10)	S4−C12	1.797(11)
N3−C3	1.147(10)	S4−C13	1.776(12)
N4−C4	1.144(10)	S5−C14	1.760(10)
N5−C5	1.148(10)	S5−C15	1.808(5)
Pt1−C1−N1	177.1(7)	Pt1−Tl1−O3	120.68(1)
Pt1−C2−N2	178.8(6)	Pt1−Tl1−O4	113.97(1)
Pt1−C3−N3	178.5(7)	O1−Tl1−O2	76.30(16)
Pt1−C4−N4	179.4(7)	O1−Tl1−O3	119.73(1)
Pt1−C5−N5	175.5(6)	O1−Tl1−O4	76.93(17)
C1−Pt1−C3	176.8(3)	O2−Tl1−O3	76.29(18)
C1−Pt1−C4	89.1(3)	O2−Tl1−O4	127.24(1)
C1−Pt1−C5	89.2(3)	O3−Tl1−O4	78.96(17)
C1−Pt1−C2	89.3(3)	Tl1−Pt1−C1	89.7(2)
C2−Pt1−C3	92.3(3)	Tl1−Pt1−C2	86.7(2)
C2−Pt1−C4	175.7(3)	Tl1−Pt1−C3	87.6(2)
C2−Pt1−C5	92.3(3)	Tl1−Pt1−C4	89.3(2)
C3−Pt1−C4	89.2(3)	Tl1−Pt1−C5	178.5(2)
C3−Pt1−C5	93.6(3)	Tl1−O1−S1	120.1(2)
C4−Pt1−C5	91.6(3)	Tl1−O2−S2	119.5(3)
Pt1−Tl1−O1	119.58(1)	Tl1−O3−S3	121.8(3)
Pt1−Tl1−O2	118.76(1)	Tl1−O4−S4	115.1(3)

The structure of **3** is closely related to that of **1**. The $Pt(CN)_5$ unit is bonded to the $Tl(en)_2$ group with a Pt−Tl bond length of 2.6348(5) Å. The coordination around Pt consists of two kinds of cyanide groups. The axial cyanide has a Pt−C bond length of 2.082(6) Å, whereas the four cyanide groups located in a square around the metal ion have considerably shorter Pt−C bond lengths of 2.01(1) Å.

Table 3. Selected bond lengths [Å] and angles [°] in the crystal structure of $[(NC)_5Pt-Tl(en)_2](DMSO)_2$ (**3**)

Tl1−Pt1	2.6348(5)	N1−C1	1.140(8)
Tl1−N6	2.376(8)	N2−C2	1.142(8)
Tl1−N7	2.394(10)	N3−C3	1.139(8)
Tl1−N8	2.361(14)	N4−C4	1.142(8)
Tl1−N9	2.373(17)	N5−C5	1.134(7)
Pt1−C1	2.012(7)	N6−C6	1.494(18)
Pt1−C2	2.015(7)	N7−C7	1.50(2)
Pt1−C3	2.007(7)	N8−C8	1.470(10)
Pt1−C4	2.012(7)	N9−C9	1.466(10)
Pt1−C5	2.082(6)	C6−C7	1.497(15)
		C8−C9	1.485(15)
Pt1−Tl1−N6	108.3(3)	C1−Pt1−C2	89.4(6)
Pt1−Tl1−N7	115.2(4)	C1−Pt1−C3	175.4(6)
Pt1−Tl1−N8	123.4(3)	C1−Pt1−C4	91.4(6)
Pt1−Tl1−N9	113.2(3)	C1−Pt1−C5	91.7(9)
Tl1−N6−C6	107.6(9)	C2−Pt1−C3	88.3(6)
Tl1−N7−C7	108.8(9)	C2−Pt1−C4	173.0(6)
Tl1−N8−C8	111.9(9)	C2−Pt1−C5	94.9(8)
Tl1−N9−C9	105.7(9)	C3−Pt1−C4	90.5(6)
N6−Tl1−N7	75.2(5)	C3−Pt1−C5	92.4(9)
N6−Tl1−N8	85.7(5)	C4−Pt1−C5	92.0(8)
N6−Tl1−N9	138.3(5)	Tl1−Pt1−C1	88.9(5)
N7−Tl1−N8	121.4(5)	Tl1−Pt1−C2	85.4(5)
N7−Tl1−N9	84.1(5)	Tl1−Pt1−C3	87.0(5)
N8−Tl1−N9	74.8(5)	Tl1−Pt1−C4	87.6(4)
Pt1−C1−N1	176.1(14)	Tl1−Pt1−C5	179.3(9)
Pt1−C2−N2	177.1(15)	N6−C6−C7	108.9(11)
Pt1−C3−N3	176.8(15)	N7−C7−C6	114.3(10)
Pt1−C4−N4	176.6(14)	N8−C8−C9	113.2(10)
Pt1−C5−N5	176(3)	N9−C9−C8	113.7(11)

Thallium has a distorted square pyramidal coordination geometry and is located 1.00 (1) Å from the basal plane defined by the four N atoms. The two en ligands and the four cyanide groups form an eclipsed conformation to each other.

The Pt−Tl bond lengths in compounds **1** and **3** are significantly shorter than the Pt−Tl bond lengths in $[Tl(crown\text{-}P_2)Pt(CN)_2]^+$ [2.911(2) and 2.958(2) Å] [2] and in $[Pt_6(\mu_6\text{-}Tl)(\mu\text{-}CO)_6(\mu\text{-}dppp)_3]^+$ [2.860(3) − 2.992(3) Å],[8] in which the oxidation states of the metal ions are Pt^{2+} and Tl^+, but very similar to the Pt−Tl bond lengths in $[(NC)_5Pt-Tl(bipy)(DMSO)_3]$ [2.6187(7) Å] and $[(NC)_5Pt-Tl(bipy)_2]$ [2.6117(5) Å] in which the sum of the oxidation states is +5.[20] In the Pt−Tl cyano complexes, $[(NC)_5Pt-Tl(CN)_{n-1}]^{(1-n)}$ (n = 2−4), studied in aqueous solution by the EXAFS technique,[21] the Pt−Tl bond lengths are in the range 2.598−2.638 Å. The Pt−Tl bond length increases with increasing number of cyano ligands attached to the thallium. The X-ray diffraction data show that the Pt−Tl bond lengths in compounds **1** and **3** in the solid state are of the same order of magnitude as those in the Pt−Tl cyano complexes in solution. The Tl−N bond lengths (average 2.376 Å) in **3** are very close to those in $[Tl(en)_3](ClO_4)_3$ (average 2.370 Å),[16] where thallium is hexacoordinated by three en ligands, which is probably due to the lower actual charge on thallium in $[(NC)_5Pt-Tl(en)_2]$ than in $[Tl(en)_3](ClO_4)_3$. The $Tl-O_n$ (n = 1−4) bond lengths in compound **1** (2.287−2.311 Å) are shorter than the Tl−O bond lengths in $[Tl(bipy)_3(DMSO)](ClO_4)_3$ [2.333(10) Å] [20] and in $[TlCl_5(DMSO)]^{2-}$ [2.42(2) Å],[22] but are longer than the Tl−O bond length in $[Tl(DMSO)_6]^{3+}$ [2.224(3) Å].[23]

Discussion

Chemical Shifts

The ^{205}Tl NMR chemical shifts of Tl^{III} complexes are very sensitive to a change in the coordination sphere of the metal ion. In the series of Pt−Tl-en complexes, a linear dependence between δ_{Tl}/δ_{Pt} and the number of coordinated en ligands is observed (Figure 5). A similar behavior was also observed for Tl^{III} ethylenediamine complexes $[Tl(en)_n]^{3+}$ (n = 0−3),[16] where the individual chemical shifts, δ_{Tl}, for the different species were linearly shifted to higher frequency upon an increase of the coordination number.

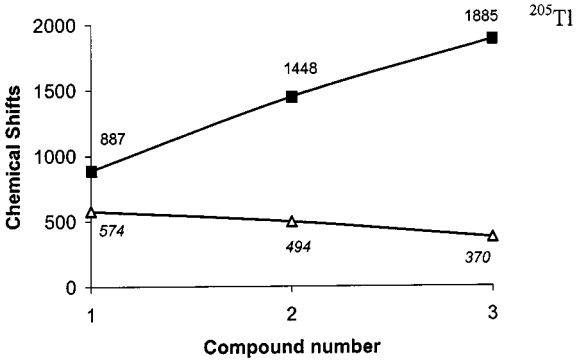

Figure 5. ^{195}Pt and ^{205}Tl NMR chemical shifts for the compounds **1, 2, 3** $[(NC)_5Pt-Tl(en)_{n-1}]$ (n = 1-3, respectively) in DMSO, 298 K; ■ ^{205}Tl NMR; Δ ^{195}Pt NMR

Several earlier studies of Cd^{2+} complexes, which similarly to Tl^{3+} has a d^{10} configuration, indicate the direction and the magnitude of the expected chemical shift change for the complex formation with different ligands, e.g. N-donors to high frequency, O-donors to low frequency.[24−28] A linear correlation between the ^{113}Cd NMR chemical shift and the number of coordinated ligands, very similar to the results of the present work, has also been observed for the Cd-glycine complexes $[Cd(Gly)_n]^{2-n}$ (n = 0−3).[29]

NMR chemical shifts are due to nuclear shielding, which includes the diamagnetic and paramagnetic terms of the Ramsey equation.[30] A theoretical study of metal NMR chemical shifts in metal ion complexes by the ab initio finite perturbation SCF method showed that the paramagnetic term is 10−100 times larger than the diamagnetic contribution.[31] Closed p and d subshells give no contribution to the paramagnetic term, which is caused by the donation of the electrons from the ligands to the metal's outer p orbitals and by the back-donation of electrons from the metal d orbitals to the ligands. Highly electronegative ligands withdraw more σ electrons from the fully occupied d_σ orbitals of the metal. This σ interaction produces holes in the (n − 1)d shell of the metal.[31]

This theoretical description can be used to explain the experimental results observed here for the Tl^{III} complexes.

The coordinated nitrogen (NH_2) is highly electronegative and attracts electrons from Tl d_σ orbitals. The electron cloud density of the thallium atom in its *N*-bonded complexes is lower than without ligands: the higher the ligand coordination number, the lower the electron cloud density around the thallium ion. This effect leads to a deshielding of the thallium nucleus; thus, its chemical shift increases. A similar trend between ^{205}Tl NMR chemical shift and the coordination number was observed in Tl^{III}-cyano complexes, $[Tl(CN)_n]^{3-n}$.[32a]

The ^{195}Pt NMR chemical shift decreases with an increasing number of the Tl-coordinated ethylenediamine ligands in the compounds $[(NC)_5Pt-Tl(en)_{n-1}]$ (n = 1−3). This trend has also been observed in the compounds $[(NC)_5Pt-Tl(CN)_{n-1}]^{(1-n)}$ (n = 1−4)[10] and in $[(NC)_5Pt-Tl(bipy)_{n-1}]$ (n = 2−3).[20] Also for the ^{195}Pt NMR chemical shifts a linear correlation to the number of coordinated ethylenediamine ligands was observed (see Figure 5).

Usually, NMR chemical shifts for heavy metal ions exhibiting a very large chemical shift range are very sensitive to the oxidation state of the metal.[32b,32c] ^{205}Tl NMR chemical shifts of Tl^{I} species are normally in the range from δ = −200 to 200 and those of Tl^{III} species are usually between δ = 2000 and 3000. The ^{195}Pt NMR chemical shifts of $[Pt^{IV}(CN)_6]^{2-}$ and $[Pt^{II}(CN)_4]^{2-}$ are δ = 655 and −213, respectively.[10] In the currently studied compounds, $[(NC)_5Pt-Tl(en)_{n-1}]$ (n = 1−3), the ^{205}Tl NMR chemical shifts fall in the region between Tl^{I} and Tl^{III}, and ^{195}Pt NMR chemical shifts between Pt^{II} and Pt^{IV} (see Table 1). Consequently, the oxidation states of the metal ions in these compounds are close to Pt^{III} and Tl^{II}: this implies that the transfer of two electrons from the substrate $[Pt^{II}(CN)_4]^{2-}$ to Tl^{III} has been partially accomplished. The studied Pt−Tl complexes can thus be treated as intermediates in an overall two-electron transfer process eventually leading to thermodynamically stable products in the stable oxidation states Pt^{IV} and Tl^{I}.[9,10]

Another indication of the changed oxidation states of the metals in these compounds is provided by the bond lengths Tl−O and Tl−N. The bond lengths Tl−O (average 2.295 Å) in **1** and Tl−N (average 2.376 Å) in **3** are somewhat longer than those in $[Tl(DMSO)_6]^{3+}$ [2.227(3) Å][23] and $[Tl(en)_3]^{3+}$ (average 2.370 Å).[16] The slight increase of the bond lengths, despite the lower coordination number in the studied Pt−Tl compounds, is compatible with the change of the oxidation states of the metal ions upon formation of the Pt−Tl bond.

A detailed discussion of the oxidation states of the metal ions is outside the scope of the present work and will be discussed in a forthcoming paper.

Spin-Spin Coupling Constants

The very large values of the spin-spin coupling constants are the most striking feature of the bimetallic Pt−Tl complexes. For the en complexes, they are of the same order as for the Pt−Tl complexes with cyanide (cf. Table 1).[10] It is clear that all the spin-spin coupling constants (except $Pt-C^{C}$) decrease upon coordination of additional ligands L (L = cyanide, bipyridine and ethylenediamine) to the thallium side of the metal−metal entity $[(NC)_5Pt-TlL_n]$. The probable origin for the large coupling constants is the fact that the relativistic contraction of the 6s shell of thallium leads to an increase of 6s electron density on the Tl nucleus. This in turn contributes to the dominant Fermi contact term for the spin-spin coupling which is reflected in large values of $J(^{205}Tl-X)$. A similar situation occurs in the species Hg_3^{2+} where the enormous isotropic spin-spin coupling constant, $^{1}J(^{199}Hg-^{199}Hg)$ = 139600 Hz, is due to the large 6s contribution to the Hg−Hg bond and the large 6s electron density at the mercury nucleus caused by relativistic effects on this heavy atom.[33]

Conclusions

A new series of small Pt−Tl bonded clusters $[(NC)_5Pt-Tl(en)_{n-1}]$ (n = 1−3, for **1**, **2** and **3** respectively) was obtained in DMSO solution from reactions between $[Pt(CN)_4]^{2-}$, $[Tl(en)_n]^{3+}$ (n = 1, 3) and CN^-. The existence of a metal−metal bond in the three complexes was proved in solution by multinuclear NMR spectroscopy [spin-spin coupling constants $^{1}J(^{205}Tl-^{195}Pt)$ in the range 48000−66000 Hz], and in the solid by single crystal X-ray diffraction [Pt−Tl bond length = 2.6131(4) and 2.6348(5) Å, in the solid compounds **1** and **3,** respectively]. Additional support for the Pt−Tl bond was obtained from the metal−metal vibration in the FT Raman spectra of the solids. These solids comprise the shortest Pt−Tl metal−metal bonds among the hitherto structurally known solid compounds[1−8] and constitute the first single crystal structure information of the growing family of "naked" Pt−Tl bond clusters.

The new family of metal−metal bonded, photosensitive compounds synthesized during the last few years, $[(NC)_5Pt-Tl(CN)_{n-1}]^{(1-n)}$ (n = 2−4), has now been enlarged by three new members containing a nitrogen-coordinated thallium (Figure 6). If, as suggested previously,[9,10] these metal−metal bonded compounds are to be used in photovoltaic solar cells,[12] or to serve as a model for such a photovoltaic system, then their structure should be tuned to have properties appropriate for this type of cell, e.g. light absorption in a large part of the visible spectrum, reversible light-induced electron transfer, suitable redox potential and ion diffusion properties in solution. The presently studied Pt−Tl compounds with ethylenediamine can be seen in this

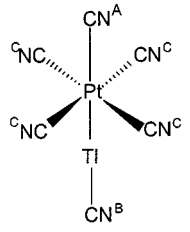

Figure 6. Sketch of the Pt−Tl compound **II** showing the notation for the cyanide sites

context as a first modification showing that tuning of the properties by means of nitrogen coordinating ligands is feasible.

Experimental Section

The solid compounds thallium(III) trifluoroacetate [Aldrich, $Tl(CF_3CO_2)_3$], potassium tetracyanoplatinate(II) [Aldrich, $K_2Pt(CN)_4$], sodium cyanide (Merck, Germany, NaCN), platinum(II) chloride (Aldrich, $PtCl_2$, 98%), sodium cyanide-^{13}C (Cambridge Isotope Laboratories, $Na^{13}CN$, ^{13}C 99%), thallium(I) carbonate (Aldrich, Tl_2CO_3, 99.95%) and liquid ethylenediamine (Merck, 99%) were all analytical grade and were used without further purification. DMSO was dried over molecular sieves (4 Å). During all experimental work the Pt−Tl compounds were protected from light.

$Tl(ClO_4)_3$ Stock Solution: Solid $TlClO_4$ was prepared from Tl_2CO_3 and an equivalent amount of $HClO_4$ and recrystallized from water. An acidic stock solution of $Tl(ClO_4)_3$ (1.2 M) was prepared by anodic oxidation of $TlClO_4$.[34a][34b] The Tl^{III} and acid concentrations were determined by titration with 0.1 M standard NaOH and $KBrO_3$ solutions after adding an excess of solid NaCl to the analyzed solution and using methyl orange as indicator.[34c]

Solid $[Tl(en)_3](ClO_4)_3$: Liquid ethylenediamine (0.08 mL, 1 mmol) was dissolved in 2 mL water. Then, a portion of the acidic aqueous solution of $Tl(ClO_4)_3$ (1.2 M; 0.21 mL 0.25 mmol) was added slowly under stirring. A black precipitate formed instantaneously, but dissolved soon thereafter. After addition of all the thallium (en/Tl ratio 3:1) the solution turned black again. Then, an approximate 10-fold excess of ethylenediamine was added and after half an hour of stirring the solution became colorless. The solution (at pH ≈ 10) was kept in a refrigerator; white round crystals formed at the bottom of the flask. The solution was filtered off and the crystals were dried in vacuum. The thallium content of the crystal compound $[Tl(en)_3](ClO_4)_3$ was determined by ICP (Inductively Coupled Plasma Atomic Emission Spectroscopy): calcd. 29.9%; found 30.1%.

The Raman spectra of $[Tl(en)_3](ClO_4)_3$ were recorded with a Renishaw System 1000 spectrometer equipped with a microscope (Leica DMLM). The band positions and assignment are as follows: 2976s, 2961s, 2897s (NH_2 and CH_2 str.); 1468m, 1278m (CH_2 and NH_2 bend); 1143m, 1021m (CN and CC str.); 936vs, 622s (ClO_4^- str.); 443vs, 302s (TlN str.). Abbreviations: vs: very strong; s: strong; m: medium.

Solid $[Tl(DMSO)_6](ClO_4)_3$: A portion of the acidic aqueous solution of $Tl(ClO_4)_3$ (1.2 M; 80 μL 0.1 mmol) was slowly added to freshly distilled DMSO (1 mL) under stirring. After addition of each drop of the concentrated $Tl(ClO_4)_3$ solution a white precipitate appeared but dissolved quickly. The colorless solution, kept in the dark, was degassed for 10 minutes with a water pump in a vacuum desiccator, and then degassed for 10 minutes again after three days. White cube-shaped crystals were obtained at the bottom of the flask. The composition of $[Tl(DMSO)_6](ClO_4)_3$ was proved by solving the crystal structure by single crystal X-ray diffraction and by Raman and infrared spectroscopic data.[23]

Preparation of Pt−Tl Compounds in Solution: For the synthesis of compound **1** (reaction 1) the solid compounds $[Tl(DMSO)_6](ClO_4)_3$ and $K_2Pt(CN)_4$ (0.05 mmol each) were dissolved in 1 mL DMSO. Then, a DMSO solution containing NaCN (0.05 mmol) was added.

Synthesis of compound **2** (reactions 2 and 3): $[Tl(en)](CF_3COO)_3$ was prepared in 1 mL DMSO by mixing $Tl(CF_3COO)_3$ (0.05 mmol) and liquid en (0.06 mmol). Then, solid $K_2Pt(CN)_4$ (0.05 mmol) was added, followed by addition of a DMSO solution containing NaCN (0.05 mmol).

Compound **3** (reaction 4): Crystalline powder samples of $[Tl(en)_3](ClO_4)_3$ and $K_2Pt(CN)_4$ (0.05 mmol each) were dissolved in 1 mL DMSO. Then, NaCN (0.05 mmol) in DMSO solution was added slowly with stirring. The reaction was slow; after two/three days a high concentration of the product was achieved. For the synthesis of ^{13}C enriched compounds **1, 2** and **3**, totally enriched compounds $Na_2Pt(^{13}CN)_4$ and $Na^{13}CN$(s) were used. $Na_2Pt(^{13}CN)_4$ was prepared in DMSO solution by the reaction between $PtCl_2$(s) and $Na^{13}CN$(s) in 1:4 molar ratio.

Preparation of Crystals: Crystals suitable for Raman and X-ray diffraction experiments were crystallized from solutions used in the NMR measurements. **1·(DMSO)**: 1 mL DMSO solution containing 0.05 mmol $[Tl(DMSO)_6](ClO_4)_3$, $K_2Pt(CN)_4$ and NaCN in a 1:1:1 molar ratio was kept in a vacuum desiccator in the dark. White small round crystals formed at the bottom of the flask after several days. **3·(2DMSO)**: A DMSO solution containing $[(NC)_5Pt-Tl(en)_2]$ (as proved by ^{205}Tl NMRspectroscopy) was degassed for 10 minutes with a water pump in a vacuum desiccator, and after three days degassed again for 10 minutes. After slow evaporation of DMSO under vacuum, rod-shaped white crystals appeared after several days. The crystals used for X-ray structural analysis were collected by filtration and recrystallized from DMSO using the same procedure as described above. Raman spectra of the solid compounds **1** and **3** were recorded with a Renishaw System 1000 spectrometer equipped with a microscope (Leica DMLM). The band positions and assignments are as follows: **1:** 3003m, 2919s (CH_3 str.); 2184s ($C{\equiv}N^A$ str.); 2174m, 2161m ($C{\equiv}N^C$ str.), 1419m, 1318w, 986m, 923m (CH_3 bend), 720s, 684s (CS str.), 453s (TlO str.), 389m, 334m (CSC or OSC bend), 154vs (Pt−Tl str.). **3:** 2950m, 2917s, 2889m (NH_2 and CH_2 str.), 2179s ($C{\equiv}N^A$ str.), 2168m, 2151m ($C{\equiv}N^C$ str.), 1452w, 1416w (CH_2 and NH_2 bend), 1094w, 1012m (CN and CC str.), 430s, 366s (TlN str.), 156vs (Pt−Tl str.). Abbreviations: vs: very strong; s: strong; m: medium; w: weak.

NMR Measurements: All NMR measurements were performed with a Bruker DMX500 spectrometer at a probe temperature of 25 ± 0.5 °C. DMSO was used as solvent for ^{205}Tl and ^{195}Pt NMR measurements and [D$_6$]DMSO for ^{13}C and ^1H NMR spectra.

^{205}Tl NMR spectra were recorded at SF = 288.49 MHz; typical NMR parameters: flip angle ≈30°; spectral window = 86 kHz; pulse repetition time = 0.5 s for Tl^{III} and 1s for Tl^I. The chemical shifts are reported in ppm toward higher frequency with respect to an external aqueous solution of $TlClO_4$ extrapolated to infinite dilution.

^{195}Pt NMR spectra were recorded at SF = 107.49 MHz with typical NMR parameters: flip angle ≈45°; spectral window = 91.4 kHz, pulse repetition time 2.5 s. The chemical shifts are given in ppm toward higher frequency from $\chi(^{195}Pt)$ = 21.4 MHz; $\delta[PtCl_6]^{2-}$ = 4533 at 25 °C in aqueous solution.

^{13}C NMR spectra were recorded at SF = 125.7 MHz with typical NMR parameters: flip angle ≈30°; spectral window = 25.1 kHz; pulse repetition time = 1.5 s; proton decoupled. The chemical shifts are reported in ppm with respect to the DMSO signal at δ = 39.5 from TMS.

^1H NMR spectra were recorded at SF = 500.1 MHz; flip angle ≈ 30°; pulse repetition time = 2 s. Chemical shifts are given in ppm with respect to the DMSO signal δ = 2.49 from TMS.

X-ray Crystal Structure Determination

Data Collection and Refinement: Suitable crystals of **1·(DMSO)** and **3·(2DMSO)** were selected under a polarizing microscope and mounted on a glass fiber. The data were collected on a Stoe image-plate diffractometer and were corrected for Lorentz, polarization and absorption effects using the X-SHAPE program package.[35] The structures were solved by direct methods (SHELXS-97)[36] and refined by full matrix least-squares on F^2 (SHELXL-97).[37] All non-hydrogen atoms were refined anisotropically. Hydrogen atoms were added at their ideal positions and refined using a riding model. Compound **3·(2DMSO)** was refined as a racemic twin [Flack parameter = 0.436(14)] since refinement in the centrosymmetric space group $P2_1/m$ introduced severe disorder in the DMSO molecules and unrealistically short C−C bonds in the en groups. In molecule **1**, the S4 atom of the DMSO ligand was treated as being disordered with occupancy factors of 0.78(1) and 0.22(1) for S4 and S4a, respectively. Selected crystal data for compound **1** and **3** are listed in Table 4.

Table 4. Selected crystal data for $[(NC)_5Pt-Tl(DMSO)_4]$-(DMSO)(**1**) and $[(NC)_5Pt-Tl(en)_2](DMSO)_2$ (**3**)

	1	**3**
Empirical formula	$C_{15}H_{30}N_5O_5PtS_5Tl$	$C_{13}H_{20}N_9O_2PtS_2Tl$
Mw	920.25	797.95
Crystal system	Monoclinic	Monoclinic
Space group	*Cc* (No. 9)	$P2_1$ (No. 4)
a, Å	17.2367(14)	9.3167(14)
b, Å	9.5560(11)	12.3007(13)
c, Å	17.7941(15)	11.4586(16)
β (deg)	100.551(10)°	112.318(16)°
V, Å^3	2881.4(5)	1214.8(3)
Z	4	2
Crystal size (mm^3)	0.14 × 0.28 × 0.30	0.12 × 0.12 × 0.30
ρ_{calc}, g cm^{-3}	2.1214(1)	2.1650(5)
Temperature, K	110(1)	110(1)
μ (Mo-K_α) (mm^{-1})	10.83	12.57
F(000)	1736.0	724.0
N(obs), *N*(par)	4785, 299	3526, 259
R(int)[a]	0.0360	0.0278
Flack parameter	0.000(6)	0.436(14)
S (goodness of fit)	1.140	1.032
*R*1, *wR*2 [$I > 2\sigma(I)$]	0.0197, 0.0485	0.0236, 0.0532
$\Delta\rho_{max}$, $\Delta\rho_{min}$ (e/Å^3)	1.103, −1.331	1.156, −0.944

[a] R values are defined as: $R(\text{int}) = \Sigma|F_o^2 - F_o^2(\text{mean})|/\Sigma[F_o^2]$, $S = [\Sigma[w(F_o^2 - F_c^2)^2]/(n-p)]^{1/2}$
$R1 = \Sigma||F_o| - |F_c||/\Sigma|F_o|$
$wR2 = [\Sigma[w(F_o^2 - F_c^2)^2] / \Sigma[w(F_o^2)^2]]^{1/2}$

Supporting Information Available

^{205}Tl and ^{195}Pt NMR spectra for compounds 1 and 2 are given in the Supporting Information. Ordering information is given on any current masthead page.

Crystallographic data (excluding structure factors) for the structures reported in this paper have been deposited with the Cambridge Crystallographic Data Centre as supplementary publications no. CCDC-145994 (**1**) and -145993 (**3**). Copies of the data can be obtained free of charge on application to CCDC, 12 Union Road, Cambridge CB2 1EZ, UK [Fax: (internat.) +44-1223/336-033; E-mail: deposit@ccdc.cam.ac.uk].

Acknowledgments

The continuous financial support of the Swedish Natural Science Research Council (NFR) is gratefully acknowledged. The authors thank European Commission's INTAS program and the Carl Trygger Foundation for financial support, and the Swedish Institute for the fellowship for G.-B. Ma′s stay in Stockholm.

[1] J. K. Nagle, A. L. Balch, M. M. Olmstead, *J. Am. Chem. Soc.* **1988**, *110*, 319−321.
[2] A. Balch, S. Rowley, *J. Am. Chem. Soc.* **1990**, *112*, 6139.
[3] O. Renn, B. Lippert, *Inorg. Chim. Acta* **1993**, *208*, 219−223.
[4] R. Uson, J. Fornies, M. Tomas, R. Garde, P. Alonso, *J. Am. Chem. Soc.* **1995**, *117*, 1837−38.
[5] O. Ezomo, M. P. Mingos, I. D. Williams, *J. Chem. Soc., Chem. Commun.* **1987**, 924−925.
[6] L.-J. Hao, J. J. Vittal, R. J. Puddephatt, *Inorg. Chem.* **1996**, *35*, 269−270.
[7] L.-J. Hao, J. Xiao, J. J. Vittal, R. J. Puddephatt, L. Manojlovic-Muir, K. W. Muir, A. A. Torabi, *Inorg. Chem.* **1996**, *35*, 658−666.
[8] L.-J. Hao, J. J. Vittal, R. J. Puddephatt, *Organometallics* **1996**, *15*, 3115.
[9] K. E. Berg, J. Glaser, M. C. Read, I. Tóth, *J. Am. Chem. Soc.* **1995**, *117*,7550.
[10] M. Maliarik, K. Berg, J. Glaser, M. Sandström, I. Tóth, *Inorg. Chem.* **1998**, *37*, 2910.
[11] M. Maliarik, J. Glaser, I. Tóth, M. W. da Silva, L. Zekany, *Eur. J. Inorg. Chem.* **1998**, 565.
[12] Md. K. Nazeeruddin, P. Liska, J. Moser, N. Vlachopoulos, M. Grätzel, *Helv. Chim. Acta* **1990**, *73*, 1788.
[13] M. G. B. Drew, O. W. Howarth, N. Martin, G. G. Morgan, J. Nelson, *J. Chem. Soc., Dalton Trans.* **2000**, 1275−1278.
[14] S. Musso, PhD thesis, ETH-Zurich, Switzerland, **1993**.
[15] J. Blixt, J. Glaser, P. Solymosi, I. Tóth, *Inorg. Chem.* **1992**, *31*, 5288−97.
[16] G.-B. Ma, A. Ilyukhin, J. Glaser, I. Tóth, L. Zekany, submitted.
[17] K. Nakamoto, *Infrared and Raman spectra of Inorganic and Coordination Compounds*, 4th ed., John Wiley & Sons, New York, **1986**, p 536.
[18] D. F. Shriver, C. B. Copper, in *Advances in Infrared and Raman spectroscopy* (Eds.: R. J. H. Clark, R. E. Hester), Heyden, London, **1980**, Vol. 6, pp 127−157.
[19] M. N. Memering, L. H. Jones, J. C. Bailar, *Inorg. Chem.* **1973**, *12*, 2793.
[20] G.-B. Ma, M. Kritikos, M. Maliarik, J. Glaser, submitted.
[21] J. Farideh, PhD Thesis. The Royal Institute of Technology (KTH), Stockholm, **2000**, p160.
[22] B. D. James, M. B., Millikan, M. F., Mackay, *Inorg. Chim. Acta* **1983**, *77*, L251.
[23] G.-B. Ma, A. Molla-Abbassi, A. Ilyukhin, V. Kessler, M. Skripkin, M. Kritikos, M. Sandström, J. Glaser, J. Näslund, I. Persson, submitted.
[24] [24a] R. J. Kostelnik, A. A. Bothner-By, *J. Magn. Reson.* **1974**, *14*, 141−151. − [24b] R. A. Haberkorn, L. Que, W. O. Gillum, R. H. Holm, C. S. Liu, R. C. Lord, *Inorg. Chem.* **1976**, *15*, 2408−2414.
[25] L. C. Damude, P. A. W. Dean, *J. Organomet. Chem.* **1979**, *168*, 123−138.
[26] I. M. Armitage, R. T. Pajer, A. J. M. Schoot Uiterkamp, J. F. Chlebouski, J. E. Coleman, *J. Am. Chem. Soc.* **1976**, *98*, 5710−5712.
[27] B. Birgersson, R. E. Carter, T. Drakenberg, *J. Magn. Reson.* **1977**, *28*, 299−302.
[28] A. D. Bain, D. R. Eaton, R. A. Hux, J. P. K. Tong, *Carbohydr. Rev.* **1980**, *84*, 1−12.
[29] H. J. Jakobsen, P. D. Ellis, *J. Phys. Chem.* **1981**, *85*, 3367−3369.
[30] [30a] N. F. Ramsey, *Phys. Rev.* **1950**, *78*, 699. − [30b] J. Mason, *Chem. Rev.* **1987**, *87*, 1299.
[31] H. Nakatsuji, K. Kanda, K. Endo, T. Yonezawa, *J. Am. Chem. Soc.* **1984**, *106*, 4653−4660.
[32] [32a] J. Blixt, B. Györi, J. Glaser, *J. Am. Chem. Soc.* **1989**, *111*, 7784. − [32b] P. Laszlo, *NMR of Newly Accessible Nuclei*, Vol. 2; Academic Press: New York, **1983**. − [32c] J. Mason, *Multinuclear NMR*, Plenum Press: New York, **1987**.
[33] R. J. Gillespie, P. Granger, K. R. Morgan, G. J. Schrobilgen, *Inorg. Chem.* **1984**, *23*, 887−891.
[34] [34a] G. Biedermann, *Arkiv. Kemi* **1953**, *5*, 441. − [34b] J. Glaser,

PhD Thesis. The Royal Institute of Technology (KTH), Stockholm, **1981**, p 15. − [34c] A. A. Noyes, J. L. Hoard, K. S. Pitzer, *J. Am. Chem. Soc.* **1935**, *57*, 1231.
[35] STOE, X-SHAPE revision 1.09, Crystal Optimisation For Numerical Absorption Correction, Darmstadt, Germany, **1997**.
[36] G. M. Sheldrick, *Acta Crystallogr.* **1990**, *A46*, 467−473.
[37] G. M. Sheldrick, SHELXL-97 Program for Refinement of Crystal Structures, University of Göttingen, Germany, **1997**.
Received October 4, 2000
[I00372]

Ruthenium−Cobalt Mixed-Metal Nitrido and Nitrene Carbonyl Clusters: Structure, Reactivity, and ^{15}N NMR Spectroscopy

Emmie Ngai-Man Ho,[a] Zhenyang Lin,[b] and Wing-Tak Wong*[a]

Keywords: Electrochemistry / NMR spectroscopy / Nitrides / Nitrenes / Ruthenium / Cobalt / Cluster compounds

The reaction of $[Ru_3(\mu\text{-}H)_2(CO)_9(\mu_3\text{-}NOMe)]$ (**1**) with $[Cp^*Co(CO)_2]$ ($Cp^* = \eta^5\text{-}C_5Me_5$) in refluxing THF afforded the new clusters $[Ru_3Co(\mu\text{-}H)(CO)_9(\eta^5\text{-}C_5Me_5)(\mu_4\text{-}N)]$ (**2**), $[Ru_2Co(CO)_6(\mu_3\text{-}CO)(\eta^5\text{-}C_5Me_5)(\mu_3\text{-}NH)]$ (**3**), $[Ru_5(\mu\text{-}H)(CO)_9(\mu\text{-}CO)_3(\eta^5\text{-}C_5Me_5)(\mu_4\text{-}NH)]$ (**4**), and $[Ru_6Co(\mu_3\text{-}H)(CO)_8(\mu\text{-}CO)_3(\mu_4\text{-}\eta^2\text{-}CO)(\eta^5\text{-}C_5Me_5)_3(\mu_4\text{-}N)]$ (**5**). Clusters **2** and **3** have typical butterfly nitrido and triangular nitrene structures, whilst compound **4** is a novel square-pyramidal pentaruthenium μ_4-NH carbonyl cluster with a Cp* ligand transferred from the external mononuclear Co complex. Cluster **4** can also be obtained by the reaction of **1** with pentamethylcyclopentadiene in the presence of 1,3-cyclohexadiene, albeit in low yield. Compound **5** consists of a rare Ru_6Co metal framework where a basal Ru–Ru edge of the central Ru_4 tetrahedron is capped by a Cp*Co fragment and another edge is bridged by a diruthenium unit. Complex **2** was found to be converted into **3** upon deprotonation with 1,8-diazabicyclo[5.4.0]undec-7-ene, on refluxing with $[Cp^*Co(CO)_2]$, or on exhaustive electrolysis. Upon thermolysis of **2** with PhC_2Ph in *n*-octane, $[Ru_3Co(CO)_6(\mu\text{-}CO)_2(\eta^5\text{-}C_5Me_5)(\mu_4\text{-}NH)(\mu_4\text{-}\eta^2\text{-}PhC_2Ph)]$ (**6**) and $[Ru_3Co(CO)_5(\mu\text{-}CO)_2(\eta^5\text{-}C_5Me_5)\{\mu_4\text{-}\eta^3\text{-}NC(O)C_2(C_4H_4)CHCH(Ph)\}(\mu_4\text{-}\eta^2\text{-}PhC_2Ph)]$ (**7**) were obtained in moderate yields. The structures of **6** and **7** both consist of a slightly twisted Ru_3Co square base with a quadruply bridging PhC_2Ph ligand. Cluster **6** is capped by a μ_4-NH moiety on the opposite side, while in **7** a CO ligand and an *ortho*-carbon atom of a Ph group from another PhC_2Ph ligand interact with the μ_4-N nitrido atom. Molecular orbital calculations have been carried out in order to gain further insight into the electronic structures of these interesting square-planar Ru_3Co and Ru_4 clusters. The butterfly Ru_2Co_2 nitrido complex $[Ru_2Co_2(CO)_9(\eta^5\text{-}C_5Me_5)(\mu_4\text{-}N)]$ (**8**) was isolated from the reaction of $[Ru_3Co(CO)_{12}(\mu_4\text{-}N)]$ with $[Cp^*Co(CO)_2]$ in refluxing THF as a result of metal exchange of an $Ru(CO)_3$ fragment by a Cp*Co moiety. The redox properties of the compounds described herein have been investigated by means of cyclic voltammetry and controlled potential coulometry. Cluster **6** was shown to be able to tolerate both the addition of two electrons and the removal of one electron without significant structural change. The chemical environments of the nitrogen atoms of these clusters have been investigated by analysis of their ^{15}N NMR chemical shifts.

Introduction

Nitrido and nitrene clusters are members of a potentially vast class of mixed transition metal−main group compounds. Such molecules are currently of structural and chemical interest[1−9] since they offer opportunities to evaluate the validity of current models of bonding for mixed polynuclear systems and to improve on the degradative instability of homonuclear metal compounds. Metal surface-bound nitrido and nitrene species are believed to be central to a number of heterogeneously catalysed chemical processes such as nitrogen oxide reduction, the Haber process, and hydrazine decomposition.[10] In several surface reactions involving NO or N_2, adsorbed nitrogen atoms are known to be key intermediates. In the case of the Haber process, the mechanism is believed to involve formation of the metal nitride followed by successive additions of hydrogen atoms to the nitrogen giving ammonia.[11] In view of the metal cluster−metal surface analogy,[12] chemical reactivity studies of low-valent nitrido and nitrene are of considerable interest.

The chemistry of the triruthenium carbonyl methoxynitrido clusters $[Ru_3(CO)_9(\mu_3\text{-}CO)(\mu_3\text{-}NOMe)]$ and $[Ru_3(\mu\text{-}H)_2(CO)_9(\mu_3\text{-}NOMe)]$ (**1**) has been described in previous papers by ourselves and others.[13−19] These two methoxynitrido clusters were reported to be synthetic precursors for nitrido and nitrene species such as $[Ru_4(CO)_{12}(\mu_4\text{-}N)(\mu\text{-}OMe)]$, $[Ru_6(CO)_{13}(\mu\text{-}CO)(\mu_5\text{-}N)(\mu_3\text{-}NH)(\mu_3\text{-}OMe)\{\mu\text{-}\eta^2\text{-}C(O)OMe\}_2]$, and $[Ru_6(CO)_{16}(\mu\text{-}CO)_2(\mu_4\text{-}NH)(\mu\text{-}OMe)(\mu\text{-}R)]$ (where R = H, OMe, or NCO),[15−17] albeit giving only low yields (≈ 5%). A series of nitrene clusters containing alkyne ligands, $[Ru_4(CO)_9(\mu\text{-}CO)_2(\mu_4\text{-}NR)(\mu_4\text{-}\eta^2\text{-}PhC_2R')]$ [R = H, OMe, or C(O)OMe; R′ = H or Ph], was obtained in more acceptable yields from reactions of $[Ru_3(CO)_9(\mu_3\text{-}CO)(\mu_3\text{-}NOMe)]$ with alkynes.[13,14] It is suspected that the formation of nitrido ligands, and hence of nitrene ligands as well, involves initial N−O bond scission of the methoxynitrido ligand. In the formation of these polynuclear μ_4-nitrido or μ_4-NR species, coupling reactions of the methoxynitrido clusters such as $[Ru_3(CO)_9(\mu_3\text{-}CO)(\mu_3\text{-}NOMe)]$ or **1** with other organometallic moieties (another molecule of a methoxynitrido cluster or some degraded

[a] Department of Chemistry, The University of Hong Kong, Pokfulam Road, Hong Kong, P. R. China
Fax: (internat.) + 852/25472933 or 28571586
E-mail: wtwong@hkucc.hku.hk
[b] Department of Chemistry, The Hong Kong University of Science and Technology, Clear Water Bay, Kowloon, Hong Kong, P. R. China

 © WILEY-VCH Verlag GmbH, 69451 Weinheim, 2001 1434−1948/01/0505−1321 $ 17.50+.50/0

ruthenium carbonyl fragments) is invariably accompanied by N−O bond cleavage. In order to generate some nitrido or nitrene clusters and to study the underlying mechanisms of their formation, methods allowing the incorporation of different external organometallic fragments would be desirable.

Mixed-metal clusters are potential precursors to supported bimetallic catalysts. Moreover, the different metals provide effective labels for ligand fluxionality studies, and varying the metals of the cluster core offers the possibility of metallo- and bond-selectivity and thus of directing reactivity for a range of reagents. Mixed ruthenium−cobalt systems are especially attractive because of the significance of these metals in CO chemistry, e.g. in the catalysis of CO hydrogenation,[20,21] and in the homologation of alcohols[22−24] and esters.[25,26] More recently, Ru/Co mixed-metal clusters have been used as precursors to generate nanoparticles with unusual magnetic properties.[27] The reactions of $[Ru_3(CO)_9(\mu_3\text{-}CO)(\mu_3\text{-}NOMe)]$ with $[(\eta^5\text{-}C_5H_5)Mo(CO)_3H]$/$[\{(\eta^5\text{-}C_5H_5)Mo(CO)_3\}_2Hg]$ have been studied.[28] However, neither the nitrene nor the nitrido species were isolated. In this paper, we report on an initial study of the syntheses, characterization, electrochemical properties, and structures of a series of ruthenium−cobalt mixed-metal nitrido and nitrene carbonyl clusters obtained by addition of Co mononuclear complexes to clusters **1** and $[Ru_3Co(CO)_{12}(\mu_4\text{-}N)]$, as well as on ^{15}N NMR spectroscopic studies of the nitrido/nitrene ligands in these clusters.

Results and Discussion

Synthesis and Characterization

Reaction of $[Ru_3(\mu\text{-}H)_2(CO)_9(\mu_3\text{-}NOMe)]$ (1) with $[Cp^*Co(CO)_2]$

A solution of $[Ru_3(\mu\text{-}H)_2(CO)_9(\mu_3\text{-}NOMe)]$ (**1**) and $[Cp^*Co(CO)_2]$ in THF becomes almost black upon refluxing over a period of 10 h. Subsequent chromatographic separation of the product mixture gives, in order of elution, brown $[Ru_3Co(\mu\text{-}H)(CO)_9(\eta^5\text{-}C_5Me_5)(\mu_4\text{-}N)]$ (**2**, 55%), trace amounts of starting material $[Ru_3(\mu\text{-}H)_2(CO)_9(\mu_3\text{-}NOMe)]$ (**1**) and the known compound $[Ru_3(\mu\text{-}H)(CO)_9(\mu\text{-}NH_2)]$,[15,29] purple $[Ru_2Co(CO)_6(\mu_3\text{-}CO)(\eta^5\text{-}C_5Me_5)(\mu_3\text{-}NH)]$ (**3**, 20%), red $[Ru_5(\mu\text{-}H)(CO)_9(\mu\text{-}CO)_3(\eta^5\text{-}C_5Me_5)(\mu_4\text{-}NH)]$ (**4**, 3%), and green $[Ru_6Co(\mu_3\text{-}H)(CO)_8(\mu\text{-}CO)_3(\mu_4\text{-}\eta^2\text{-}CO)(\eta^5\text{-}C_5Me_5)_3(\mu_4\text{-}N)]$ (**5**, 2%) (Scheme 1). The structures of clusters **2**−**5** were unambiguously established by single-crystal X-ray crystallography and were supported by ^1H and ^{15}N NMR, IR, and UV/vis spectroscopic data, as well as by FAB mass spectrometry (Table 1). These compounds are essentially air-stable in the solid state, have varying degrees of stability in solution, and are all soluble in *n*-hexane.

Cluster **2** readily crystallizes from a rich brown-coloured band over a period of a few days. The presence of the Cp* and metal hydride groups in this compound is apparent from its ^1H NMR spectrum (singlets at δ = 1.98 and −24.40), while the integrals of these resonances reveal a

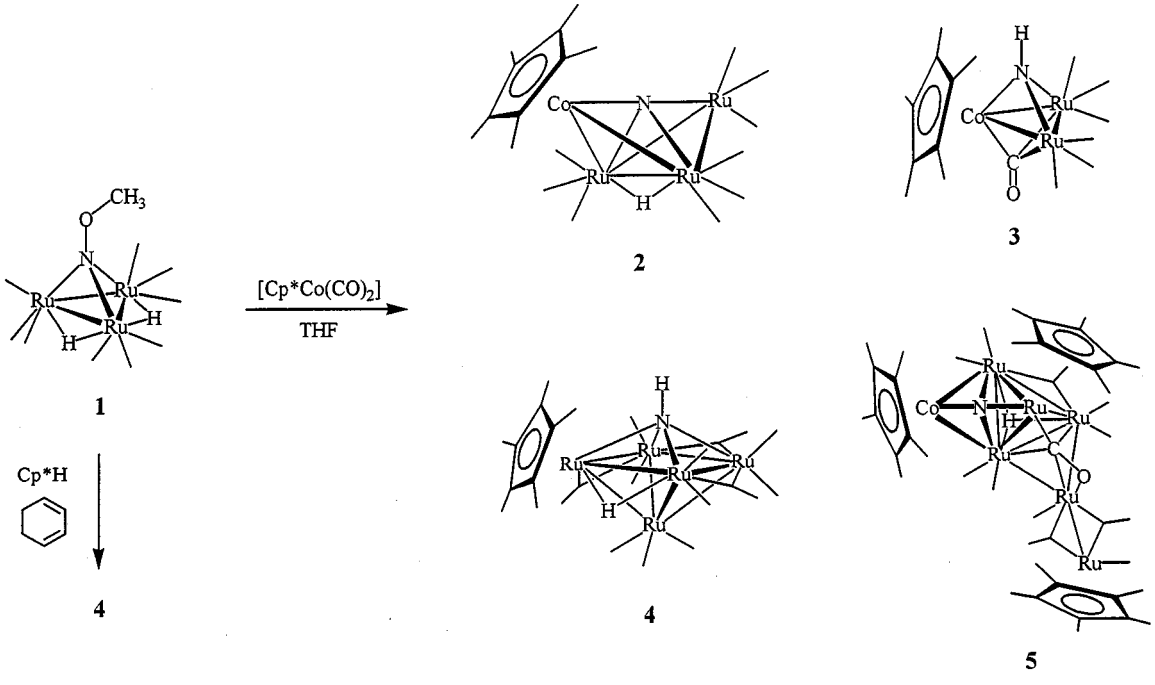

Scheme 1. Treatment of dihydrido cluster **1** with 2 equiv. of $[Cp^*Co(CO)_2]$ led to the formation of the $[Ru_3Co(\mu\text{-}H)(CO)_9(\eta^5\text{-}C_5Me_5)(\mu_4\text{-}N)]$ (**2**), $[Ru_2Co(CO)_6(\mu_3\text{-}CO)(\eta^5\text{-}C_5Me_5)(\mu_3\text{-}NH)]$ (**3**), $[Ru_5(\mu\text{-}H)(CO)_9(\mu\text{-}CO)_3(\eta^5\text{-}C_5Me_5)(\mu_4\text{-}NH)]$ (**4**), and $[Ru_6Co(\mu_3\text{-}H)(CO)_8(\mu\text{-}CO)_3(\mu_4\text{-}\eta^2\text{-}CO)(\eta^5\text{-}C_5Me_5)_3(\mu_4\text{-}N)]$ (**5**) in yields of 55%, 20%, 3%, and 2%, respectively; cluster **4** could be directly synthesized by the reaction of **1** with pentamethylcyclopentadiene and 1,3-cyclohexadiene, albeit in low yield (4%)

Table 1. Spectroscopic data for clusters **1**−**8** with labelling scheme for ^{1}H NMR assignments for clusters **6** and **7**

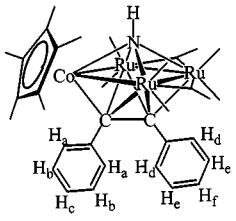

6

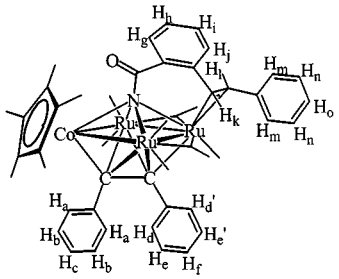

7

Cluster	IR spectra[a] ν(CO) [cm^{-1}]	^{1}H NMR spectra[b] (δ, *J*/Hz)	^{15}N HMR spectra[c] (δ, *J*/Hz)	Mass spectra[d] (*m*/*z*)	λ_{max}[e] (nm) (ε, 8^{-3} dm^3 mol^{-1} cm^{-1})
1	2116m, 2078s, 2057vs, 2048s, 2036sh, 2010vs, 2005s, 1988m	3.46 (s, 3 H, ethoxy) −17.22 (s, 2 H, hydride)	301.0 (s)[f]	602 (602)	295 (9.13) 397 (1.04)[g]
2	2074m, 2047vs, 2033s, 2008vs, 1989m, 1970w	1.98 (s, 15 H, C_5Me_5) −24.40 (s, 1 H, hydride)	481.1 (s)	764 (764)	302 (20.1) 353 (19.6) 430 (5.79) 513 (2.03)
3	2072m, 2045vs, 2024vw, 2005s, 1987m, 1974w	7.46 (t, J_{NH} = 54.80, 1 H, NH) 1.77 (s, 15 H, C_5Me_5)	131.4 [d, J(^{15}NH) = 76.95 Hz]	607 (607)	292 (14.3) 405 (3.26) 542 (1.84)
4	2076m, 2039vs, 2016s, 2006m, 1991w, 1976m, 1958w, 1943vw, 1868m, 1839m	6.28 (t, J_{NH} = 48.82, 1 H, NH) 2.20 (s, 15 H, C_5Me_5) −14.92 (s, 1 H, hydride)	145.4 [d, J(^{15}NH) = 68.26 Hz]	992 (992)	330 (6.32)[g] 345 (5.66)[g] 405 (2.58)[g] 466 (1.83)
5	2084vw, 2070vw, 2033m, 2030m, 2018w, 2005m, 1997vs, 1987m, 1979m, 1974m, 1953w, 1937s, 1763m	2.24 (s, 15 H, C_5Me_5) 2.20 (s, 15 H, C_5Me_5) 1.76 (s, 15 H, C_5Me_5) −26.46 (s, 1 H, hydride)	548.8 (s)	1421(1421)	360 (11.1) 390 (9.86)[g] 579 (2.40)
6	2059m, 2006vs, 2001m, 1954m, 1873w, 1842m	7.00 (m, 2 H, phenyl H_b) 6.85 (tt, J_{HH} = 7.36, 1.84, 1 H, phenyl H_c) 6.70 (m, 2 H, phenyl H_a) 6.60 (m, 2 H, phenyl H_e) 6.51 (tt, J_{HH} = 7.27, 2.23, 1 H, phenyl H_f) 5.65 (m, 2 H, phenyl H_d) 2.76 (t, J_{NH} = 49.08, 1 H, NH) 1.86 (s, 15 H, C_5Me_5)	70.2 [d, J(^{15}NH) = 69.26 Hz]	914 (914)	296 (5.60) 330 (5.60) 420 (1.77) 505 (0.88)
7	2089vw, 2066w, 2030w, 2014vs, 2005m, 1962m, 1879w, 1844m	7.45 (m, 1 H, phenyl H_g) 7.43 (m, 2 H, phenyl H_m) 7.35 (m, 3 H, phenyl H_h, H_n) 7.23 (tt, J_{HH} = 7.18, 1.25, 1 H, phenyl H_o) 7.09 (m, 1 H, phenyl H_i) 7.01 (m, 1 H, phenyl H_j) 6.93 (m, 2 H, phenyl H_b) 6.79 (tt, J_{HH} = 7.33, 1.12, 1 H, phenyl H_c) 6.70 (m, 2 H, phenyl H_a) 6.58 (m, 1 H, phenyl H_e/H_e') 6.50 (m, 1 H, phenyl H_e/H_e') 6.41 (tt, J_{HH} = 7.32, 1.12, 1 H, phenyl H_f) 5.75 (d, 1 H, J_{HH} = 12.26, H_l) 5.60 (m, 1 H, phenyl H_d/H_d') 5.54 (m, 1 H, phenyl H_d/H_d') 2.72 (d, 1 H, J_{HH} = 12.26 Hz H_k) 1.54 (s, 15 H, C_5Me_5)	−	1092 (1092)	−
8	2072s, 2030vs, 2006s, 1983m, 1970w	1.89 (s, 15 H, C_5Me_5)	524.7 (s)	721 (721)	315 (9.13) 360 (7.31) 435 (2.00)[g] 520 (0.88)

[a] In *n*-hexane unless otherwise stated. − [b] In CD_2Cl_2. − [c] In $CDCl_3$, with ^{1}H decoupled except for clusters **3**, **4**, and **6**. − [d] Calculated values in parentheses. − [e] Measured in CH_2Cl_2 at 298 K. − [f] From ref.[29] − [g] Shoulder.

ratio of 15:1. The ^{15}N NMR spectrum features a single resonance at $\delta = 481.1$, which is consistent with the presence of a μ_4-nitrido ligand. Four electronic absorption bands at 302, 353, 430, and 513 nm are seen in the UV/vis spectrum of **2**. The structure of **2** was confirmed by a single-crystal X-ray diffraction analysis; a molecular drawing is shown in Figure 1. Selected bond lengths and angles are given in Table 2.

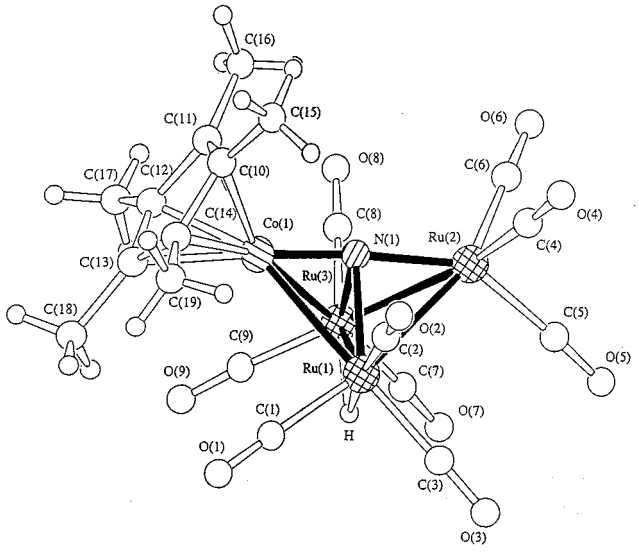

Figure 1. The molecular structure of $[Ru_3Co(\mu\text{-}H)(CO)_9(\eta^5\text{-}C_5Me_5)(\mu_4\text{-}N)]$ (**2**) showing the atom numbering scheme

Table 2. Selected bond lengths [Å] and angles [°] for clusters **2** and **8**

	2	**8**
Ru(1)−Ru(2)	2.7733(5)	2.7333(8)
Ru(1)−Ru(3)	2.7877(5)	–
Ru(1)−Co(1)	2.7192(7)	2.666(1)
Ru(1)−Co(2)	–	2.569(1)
Ru(1)−N(1)	2.105(3)	2.039(5)
Ru(2)−Ru(3)	2.7570(5)	–
Ru(2)−Co(2)	–	2.676(1)
Ru(2)−N(1)	1.935(3)	1.926(5)
Ru(3)−Co(1)	2.6980(7)	–
Ru(3)−N(1)	2.096(3)	–
Co(1)−Co(2)	–	2.545(1)
Co(1)−N(1)	1.714(3)	1.723(5)
Co(2)−N(1)	–	1.950(5)
Co(1)−Cp*(c)[a]	1.66	1.656
Ru(1)−N(1)−Ru(2)	86.6(1)	87.1(2)
Ru(1)−N(1)−Ru(3)	83.1(1)	–
Ru(1)−N(1)−Co(1)	90.2(1)	89.9(2)
Ru(1)−N(1)−Co(2)	–	80.2(2)
Ru(2)−N(1)−Ru(3)	86.2(1)	–
Ru(2)−N(1)−Co(1)	175.0(2)	174.3(2)
Ru(2)−N(1)−Co(2)	–	87.3(2)
Ru(3)−N(1)−Co(1)	89.6(1)	–
Co(1)−N(1)−Co(2)	–	87.5(2)

[a] Cp*(c) denotes the centroid of the C_5Me_5 rings.

Cluster **2**, $[Ru_3Co(\mu\text{-}H)(CO)_9(\eta^5\text{-}C_5Me_5)(\mu_4\text{-}N)]$, consists of a tetranuclear metal core exhibiting a butterfly geometry. The Cp*Co fragment occupies a wing-tip position, and the Ru atoms bear three terminal carbonyl ligands each. The centroid of the η^5-C_5Me_5 ligand is 1.660 Å from the Co(1) atom, which is similar to the typical distance in Cp*Co clusters [Co−$Cp^*_{ave.}$ 1.695 Å].[5,30] The nitrido N(1) is semi-encapsulated within the butterfly and is displaced towards Co(1) at a distance of 1.714(3) Å. The hydride ligand revealed by ^1H NMR spectroscopy was located by Fourier-difference synthesis and was found to bridge the Ru(1)−Ru(3) hinge. Thus, the bond angles Ru(3)−Ru(1)−C(1)/C(3) and Ru(1)−Ru(3)−C(7)/C(9) are larger (average 107.4°) than the corresponding values along the other wings (average 97.1°). The dihedral angle between the butterfly wings in **2** measures 78.6°

The molecular structure of $[Ru_2Co(CO)_6(\mu_3\text{-}CO)(\eta^5\text{-}C_5Me_5)(\mu_3\text{-}NH)]$ (**3**) is depicted in Figure 2, while key bond lengths and angles are listed in Table 3. Cluster **3** contains a heterometallic Ru_2Co triangular metal core, triply-capped in an asymmetric fashion by a μ_3-NH ligand through the coordination of the nitrogen atom [Ru(1)−N(1) 2.017(4) Å, Ru(2)−N(1) 2.019(5) Å, and Co(1)−N(1) 1.862(4) Å] on one side and a μ_3-CO ligand on the other. The nitrene hydrogen and nitrogen atoms give rise to a triplet ($\delta = 7.46$, $J_{NH} = 54.80$ Hz) and a doublet [$\delta = 131.4$, $J(^{15}NH) = 76.95$ Hz] in the ^1H and ^{15}N NMR spectra, respectively. Both signals are downfield shifted compared with those of $[Ru_3(\mu\text{-}H)_2(CO)_9(\mu_3\text{-}NH)]$ {^1H: $\delta = 6.33$ (t, $J_{NH} = 55.0$ Hz); ^{15}N: $\delta = 82.5$ [d, $J(^{15}NH) = 77.5$ Hz]},[18] which suggests that the Cp*Co moiety is more electron-withdrawing than the isolobal $Ru(CO)_3$ group. The μ_3-capping ligand C(7)−O(7) is found to be displaced towards Co(1) at a distance of 1.821(6) Å [Co(1)−C(7)], while the Ru(1)−C(7) and Ru(2)−C(7) distances amount to 2.399(6) and 2.402(6) Å, respectively. The isolation of **3** was unexpected, since one of the ruthenium vertices had to be replaced by an isoelectronic (η^5-C_5Me_5)Co(CO) fragment through a "metal-exchange" reaction.[31] Such metal-exchange reactions are known, but are not common in cluster chemistry.[31−33]

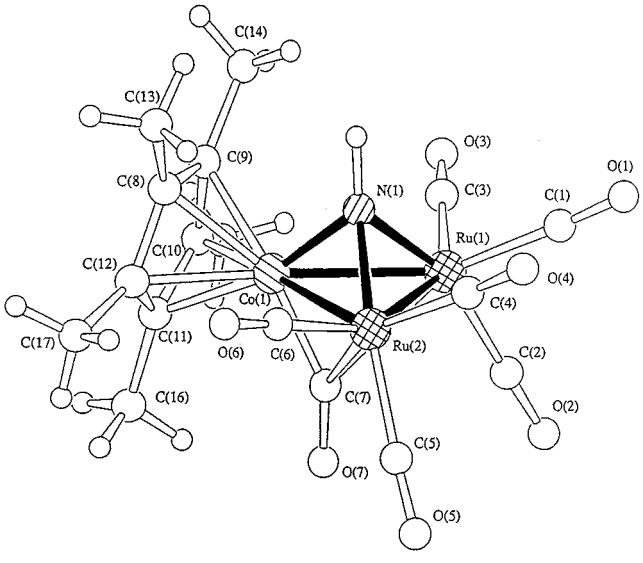

Figure 2. The molecular structure of $[Ru_2Co(CO)_6(\mu_3\text{-}CO)(\eta^5\text{-}C_5Me_5)(\mu_3\text{-}NH)]$ (**3**) showing the atom numbering scheme

Table 3. Selected bond lengths [Å] and angles [°] for cluster **3**

Ru(1)−Ru(2)	2.7093(7)
Ru(1)−Co(1)	2.6009(9)
Ru(1)−N(1)	2.017(4)
Ru(2)−Co(1)	2.6101(8)
Ru(2)−N(1)	2.019(5)
Co(1)−N(1)	1.862(4)
Co(1)−Cp*(c)[a]	1.695
N(1)−H	1.07
Ru(2)−Ru(1)−Co(1)	58.84(2)
Ru(1)−Ru(2)−Co(1)	58.51(2)
Ru(1)−Co(1)−Ru(2)	62.65(2)
Ru(1)−N(1)−Ru(2)	84.3(2)
Ru(1)−N(1)−Co(1)	84.1(1)
Ru(2)−N(1)−Co(1)	84.4(2)

[a] Cp*(c) denotes the centroid of the C_5Me_5 rings.

Besides these heterometallic complexes, a pentaruthenium μ_4-nitrene cluster **4** was also isolated from this reaction. Its IR spectrum features vibrational absorptions due to both the terminal and bridging carbonyl ligands. Its ^{1}H NMR spectrum displays a triplet centred at $\delta = 6.28$ with a coupling constant of 48.82 Hz, which may be attributed to the NH proton. Resonances at $\delta = 2.20$ and -14.92 are assigned to the Cp* and hydride ligands, respectively. The presence of a quadruply-bridging nitrene ligand is evident from the ^{15}N NMR spectrum, which shows a doublet at $\delta = 145.4$ [$J(^{15}NH) = 68.26$ Hz] relative to liquid NH_3. Four absorption bands at 330, 345, 405, and 466 nm are seen in the UV/vis spectrum of **4** (Table 1).

Red crystals of **4**, suitable for X-ray diffraction studies, were grown from a saturated solution in $CHCl_3$/*n*-hexane at −20 °C. The molecular structure of **4** is depicted in Figure 3 and the relevant structural parameters are summarized in Table 4. Cluster **4** consists of a square-pyramidal cluster of five ruthenium atoms, with a quadruply-capping NH ligand spanning the square base. A η^5-coordinated C_5Me_5 ligand, transferred from the external [Cp*Co(CO)$_2$] complex, is coordinated to one basal Ru atom at a distance of 1.856 Å. To the best of our knowledge, [Cp*Co(CO)$_2$] acting as a source of Cp* in an intermolecular ligand-transfer reaction is very rare in cluster chemistry. A ligand-transfer process of Cp in a comparable ruthenium cluster was observed in [$Ru_6(\mu_3$-H)(CO)$_{12}(\mu$-CO)$(\mu_4$-η^2-CO)$_2(\eta^5$-$C_5Me_5)$].[34] Three of the basal Ru−Ru edges are bridged by carbonyl ligands, while the fourth is bridged by a hydride ligand. The bridging carbonyl and hydride ligands involving the Cp*-coordinated Ru(1) are found to be slightly disordered among these sites. These two ligands reside in semi-triply-bridging positions, while the other two cap the equatorial sites of the square base. The nonbonding lengths Ru(5)···C(1) and Ru(5)···H are 2.59 Å and 2.33 Å, respectively [cf. Ru(1)−C(1) 2.00(2), Ru(2)−C(1) 2.15(2), Ru(1)−H 1.95, and Ru(4)−H 2.17 Å]. The μ_4-NH moiety caps the Ru_4 base in a symmetrical fashion, with an average Ru−N distance of 2.145 Å. The mean deviation from the plane defined by Ru(1), Ru(2), Ru(3), and Ru(4) is 0.0067 Å and the nitrene N atom lies 0.91 Å above this mean plane. Cluster **4** might be viewed as an N-protonated product of a ruthenium μ_5-nitrido cluster anion.[3,35] For comparison, in the $[Ru_5(CO)_{14}(\mu_5\text{-N})]^-$ anion, the nitrido atom resides 0.21(2) Å below the basal plane of the ruthenium atoms and acts as a five-electron donor. By Fourier-difference synthesis using low-angle data, the H atom was found to be located 0.88 Å from the nitrene N atom. In **4**, the μ_4-NH moiety is assigned as a four-electron donor, giving a cluster valence electron (CVE) count of 74. This is the same as that for the cluster anion $[Ru_5(CO)_{14}(\mu_5\text{-N})]^-$.[3,35]

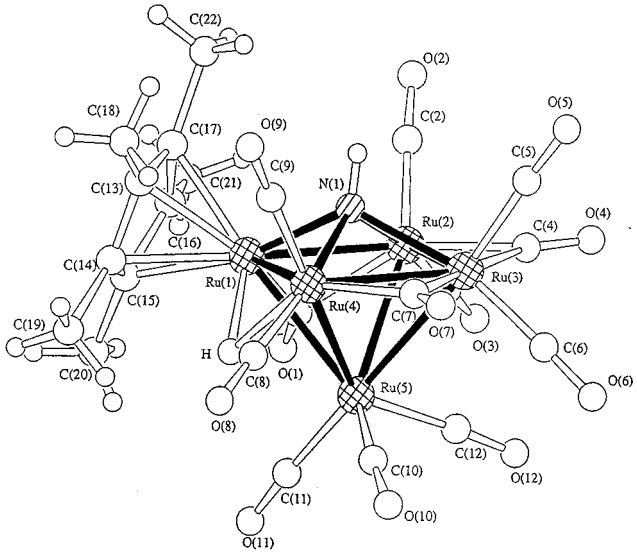

Figure 3. The molecular structure of $[Ru_5(\mu\text{-H})(CO)_9(\mu\text{-CO})_3(\eta^5\text{-}C_5Me_5)(\mu_4\text{-NH})]$ (**4**) showing the atom numbering scheme

Table 4. Selected bond lengths [Å] and angles [°] for cluster **4**

Ru(1)−Ru(2)	2.769(1)
Ru(1)−Ru(4)	2.775(1)
Ru(1)−Ru(5)	2.905(1)
Ru(1)−N(1)	2.098(7)
Ru(2)−Ru(3)	2.726(1)
Ru(2)−Ru(5)	2.868(1)
Ru(2)−N(1)	2.153(8)
Ru(3)−Ru(4)	2.713(1)
Ru(3)−Ru(5)	2.881(1)
Ru(3)−N(1)	2.201(7)
Ru(4)−Ru(5)	2.873(1)
Ru(4)−N(1)	2.128(8)
Ru(1)−Cp*(c)[a]	1.856
N(1)−H	0.88
Ru(1)−N(1)−Ru(2)	81.3(3)
Ru(1)−N(1)−Ru(3)	130.3(3)
Ru(1)−N(1)−Ru(4)	82.1(3)
Ru(2)−N(1)−Ru(3)	77.5(2)
Ru(2)−N(1)−Ru(4)	129.0(3)
Ru(3)−N(1)−Ru(4)	77.6(2)

[a] Cp*(c) denotes the centroid of the C_5Me_5 rings.

In our previous reports,[13−15] all the tetraruthenium μ_4-NH nitrene ligands have been stabilized by bridging $Ru(CO)_4$ or μ_4-η^2-alkyne fragments. However, in the present case, this ligand is stabilized by a quadruply-bridging $Ru(CO)_3$ moiety. This pseudo-octahedral skeletal framework $[Ru_5(\mu_4\text{-ER})]$ (R = alkyl or aryl group, etc.) has been seen with phosphorus,[36−40] sulfur,[41−43] and even carbon.[44] This is the first time that a μ_4-NH fragment has been observed in this type of structure. The square Ru_4 fragment provides a

model for chemical transformations at the (100) face of metallic ruthenium.[45,46] Although ruthenium is a very important catalytic metal, models for the interaction of nitrogen fragments with this (100) array are rare.[13−15]

It is believed that cluster **4** is formed by enlargement of the starting triruthenium cluster, with coordination of a Cp* ligand transferred from the external mononuclear complex. When **1** is heated in THF in the presence of an excess of pentamethylcyclopentadiene and 1,3-cyclohexadiene, **4** is obtained in 4% yield (Scheme 1). In the absence of 1,3-cyclohexadiene, there is no observable reaction under similar conditions, hence the diene must be important is removing a proton from the free Cp*H ligand. In both synthetic methods {involving $[Cp^*Co(CO)_2]$ or Cp*H}, the pentamethylcyclopentadiene is transferred as a Cp^{*-} anion.

The last eluted product is $[Ru_6Co(\mu_3\text{-}H)(CO)_8(\mu\text{-}CO)_3(\mu_4\text{-}\eta^2\text{-}CO)(\eta^5\text{-}C_5Me_5)_3(\mu_4\text{-}N)]$ **5**. Its IR spectrum shows the presence of both terminal and bridging carbonyl ligands (Table 1). The four singlet resonances in its ^1H NMR spectrum, with integrals in the ratio 15:15:15:1, correspond to the three Cp* ligands and one triply-bridging hydride. With reference to clusters **2**−**4**, the relatively upfield signal at $\delta = 1.76$ could be assigned to the Cp* ligand on the Co(1) atom. A downfield singlet at $\delta = 548.8$ is observed in the ^{15}N NMR spectrum. In the electronic absorption spectrum of **5**, three bands are seen at 360, 390 and 579 nm. X-ray quality crystals of cluster **5** were grown from a $CHCl_3$/*n*-hexane solution at −20 °C. A perspective view of the molecular structure is depicted in Figure 4. Selected interatomic distances and angles are listed in Table 5.

The metal framework of **5** consists of a central Ru_4 tetrahedron with an Ru−Ru edge bridged by a Cp*Co fragment and the other edges bridged by a further two Ru atoms. A structurally related Ru_6 cluster, $[Ru_6(\mu_3\text{-}H)(CO)_{12}(\mu\text{-}CO)(\mu_4\text{-}\eta^2\text{-}CO)_2(\eta^5\text{-}C_5Me_5)]$,[34] has been reported. The difference between cluster **5** and this Ru_6 cluster is that one μ_4-η^2-CO of the latter is replaced by a μ_4-nitrido ligand, which is bound to the Cp*Co moiety. Therefore, in **5**, a five-electron μ_4-N and a four-electron μ_4-η^2-CO donor ligand are situated in the two butterfly arrays created by the bridging Co and Ru atoms and the faces of the Ru_4 tetrahedron, respectively. The dihedral angles between the wings of the butterflies are 77.2° and 121.2°. The C−O bond length in the μ_4-η^2-carbonyl ligand is considerably longer than the terminal C−O bonds [1.25(2) vs. ave. 1.17(1) Å], which may be attributed to electron donation from the C−O π-bond and a significant reduction in bond order due to the $d_\pi-p_\pi$ bonding of the three Ru atoms. Besides the η^5-C_5Me_5 ligand on the Co atom, the other two must be transferred from other $[Cp^*Co(CO)_2]$ complexes. One is bound to the apical Ru atom of the central tetrahedron, while the other is coordinated to the spiked-edge Ru(6) atom. The interactions between the Cp^{*-} ligands and Co [Co(1)−Cp*(c) 1.671 Å] are stronger than those involving the Ru atoms [Ru(2)/Ru(6)−Cp*(c) 1.890 and 1.907 Å]. A positive charge is considered to be localized on the Co atom, whereas the charges associated with the Ru atoms are delocalized throughout the cluster. This is also consistent

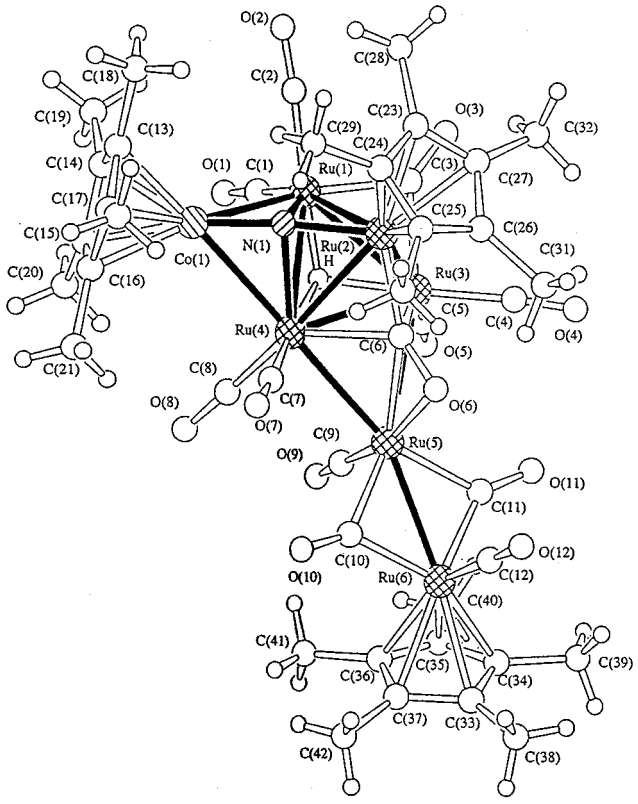

Figure 4. The molecular structure of $[Ru_6Co(\mu_3\text{-}H)(CO)_8(\mu\text{-}CO)_3(\mu_4\text{-}\eta^2\text{-}CO)(\eta^5\text{-}C_5Me_5)_3(\mu_4\text{-}N)]$ (**5**) showing the atom numbering scheme

Table 5. Selected bond lengths [Å] and angles [°] for cluster **5**

Ru(1)−Ru(2)	2.838(2)
Ru(1)−Ru(3)	2.753(2)
Ru(1)−Ru(4)	2.868(2)
Ru(1)−Co(1)	2.709(3)
Ru(1)−N(1)	2.07(1)
Ru(2)−Ru(3)	2.819(2)
Ru(2)−Ru(4)	2.700(3)
Ru(2)−N(1)	1.92(2)
Ru(3)−Ru(4)	2.916(3)
Ru(3)−Ru(5)	2.912(2)
Ru(4)−Ru(5)	2.832(2)
Ru(4)−Co(1)	2.714(3)
Ru(4)−N(1)	2.07(1)
Ru(5)−Ru(6)	2.728(2)
Co(1)−N(1)	1.73(2)
C(6)−O(6)	1.25(2)
Ru(2)−Cp*(c)[a]	1.890
Ru(6)−Cp*(c)[a]	1.907
Co(1)−Cp*(c)[a]	1.671
Ru(2)−Ru(3)−Ru(5)	94.11(6)
Ru(2)−Ru(4)−Ru(5)	98.61(8)
Ru(5)−Ru(4)−Co(1)	170.75(8)
Ru(3)−Ru(5)−Ru(6)	146.94(9)
Ru(4)−Ru(5)−Ru(6)	150.71(8)
Ru(1)−N(1)−Ru(2)	90.7(6)
Ru(1)−N(1)−Ru(4)	87.8(4)
Ru(1)−N(1)−Co(1)	90.5(6)
Ru(2)−N(1)−Ru(4)	85.1(5)
Ru(2)−N(1)−Co(1)	175.5(9)
Ru(4)−N(1)−Co(1)	90.6(7)
Ru(2)−C(6)−O(6)	139(1)

[a] Cp*(c) denotes the centroid of the C_5Me_5 rings.

with the observation of short Ru(2)−Ru(4) and Ru(5)−Ru(6) bond lengths. A further supporting argument provided by the ^{1}H NMR resonances of the relevant Cp* ligands. This Ru_6Co metal skeleton is seldom found in either homo- or heterometallic cluster chemistry. The hydride ligand, which gives rise to a signal at $\delta = -26.46$ in the ^{1}H NMR spectrum, was located by Fourier-difference synthesis and was found to cap beneath the basal plane, Ru(1)−Ru(3)−Ru(4), of the central Ru_4 tetrahedron. The formation of **4** and **5** is clearly a complex transformation involving the scavenging of additional ruthenium atoms and the incorporation of Cp* ligands from the mononuclear complexes. The overall yields of **4** and **5** are accordingly modest and lower than those of clusters **2** and **3**.

Conversion between 2 and 3

(a) Reaction of 2 with DBU

The reaction of cluster **2** with 1 equivalent of DBU (1,8-diazabicyclo[5.4.0]undec-7-ene) was monitored by ^{1}H NMR spectroscopy. The sterically hindered base DBU is commonly used as a deprotonating agent for metal clusters and a mechanism for this type of reaction has been proposed.[47] The hinge-bridged hydride was found to undergo dissociation within a few minutes (Scheme 2). This reaction proved to be irreversible; deprotonated **2** was not converted back to **2** upon addition of a slight excess of CF_3COOH. Instead of re-protonation, the deprotonated cluster **2** underwent degradation to give **3** along with significant decomposition products.

(b) Reaction of 2 with [Cp*Co(CO)$_2$]

Compound **2** was allowed to react with excess [Cp*Co(CO)$_2$] in refluxing THF for 10 h (Scheme 2). After removing the solvent in vacuo, chromatographic separation of the residue gave a moderate yield of cluster **3** as the only isolable product.

(c) Reaction of 3 with [Ru$_3$(CO)$_{12}$]

In an attempt to convert **3** to **2**, compound **3** was allowed to react with a slight excess of [$Ru_3(CO)_{12}$] in a high boiling point solvent such as toluene or *n*-octane. After refluxing for 4 h, the known [$Ru_6(\mu_3\text{-H})(CO)_{12}(\mu\text{-CO})(\mu_4\text{-}\eta^2\text{-CO})_2(\eta^5\text{-}C_5Me_5)$][34] cluster had been produced in 10% yield, accompanied by starting material **3** and decomposition products (see Scheme 2). Cluster **3** was thus largely unreactive under these conditions and no significant change was observed over a period of 12 h. A high energy barrier preventing the desired reaction probably led instead to the degradation of the [$Ru_3(CO)_{12}$] cluster to give mononuclear fragments, thereby accounting for the observed reaction.

Thermolysis of 2 with PhC$_2$Ph

It has been shown previously that protonation of [PPN][$Ru_4(CO)_{12}(\mu_4\text{-N})$] in the presence of diphenylacetylene gives a μ_4-NH containing species, [$Ru_4(CO)_9(\mu\text{-CO})_2(\mu_4\text{-NH})(\mu_4\text{-}\eta^2\text{-}PhC_2Ph)$].[48] Moreover, treatment of

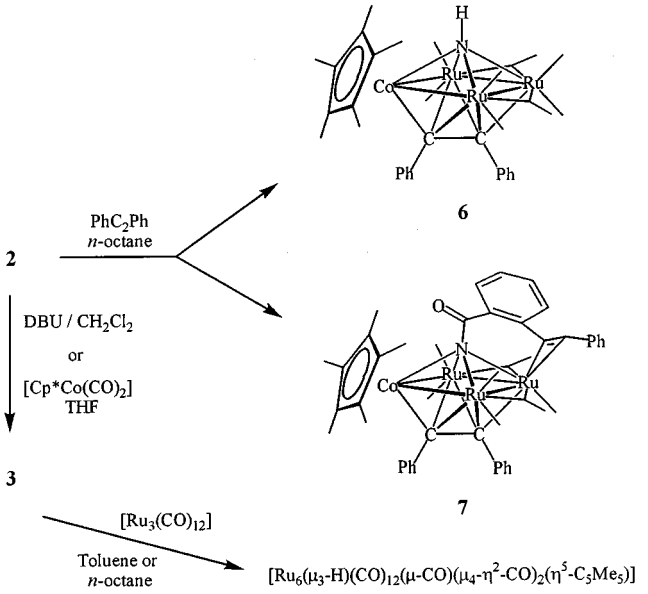

Scheme 2. Deprotonation of cluster **2** in CH_2Cl_2 with DBU afforded only **3**; treatment of **2** with [Cp*Co(CO)$_2$] in refluxing THF also gave **3**; thermolysis of **2** in *n*-octane with a slight excess of PhC_2Ph resulted in the isolation of [$Ru_3Co(CO)_6(\mu\text{-CO})_2(\eta^5\text{-}C_5Me_5)(\mu_4\text{-NH})(\mu_4\text{-}\eta^2\text{-}PhC_2Ph)$] (**6**) and [$Ru_3Co(CO)_5(\mu\text{-CO})_2(\eta^5\text{-}C_5Me_5)\{\mu_4\text{-}\eta^3\text{-NC(O)}C_2(C_4H_4)CHCH(Ph)\}(\mu_4\text{-}\eta^2\text{-}PhC_2Ph)$] (**7**) in yields of 18% and 6%, respectively; attempted preparation of cluster **2** from cluster **3** with [$Ru_3(CO)_{12}$] led only to the known [$Ru_6(\mu_3\text{-H})(CO)_{12}(\mu\text{-CO})(\mu_4\text{-}\eta^2\text{-CO})_2(\eta^5\text{-}C_5Me_5)$][34]

[$Ru_3(\mu\text{-H})_2(CO)_9(\mu_3\text{-NPh})$] with diphenylacetylene was found to afford a μ_4-nitrene cluster [$Ru_4(CO)_9(\mu\text{-CO})_2(\mu_4\text{-NPh})(\mu_4\text{-}\eta^2\text{-}PhC_2Ph)$].[49] Therefore, alkynes are thought to have an important structural stabilizing effect, facilitating the formation and isolation of μ_4-nitrene-containing clusters. Cluster **2**, a molecule with a μ_4-nitrido group coordinated between the wings of an Ru_3Co butterfly, was thus submitted to skeletal expansion reactions with diphenylacetylene in *n*-octane, which led to the incorporation of a two-carbon fragment into the cluster framework (Scheme 2). Separation by preparative TLC gave two major products, [$Ru_3Co(CO)_6(\mu\text{-CO})_2(\eta^5\text{-}C_5Me_5)(\mu_4\text{-NH})(\mu_4\text{-}\eta^2\text{-}PhC_2Ph)$] (**6**) and [$Ru_3Co(CO)_5(\mu\text{-CO})_2(\eta^5\text{-}C_5Me_5)\{\mu_4\text{-}\eta^3\text{-NC(O)}C_2(C_4H_4)CHCH(Ph)\}(\mu_4\text{-}\eta^2\text{-}PhC_2Ph)$] (**7**) in yields of 18% and 6%, respectively. Their spectroscopic data are presented in Table 1. The IR spectra show the presence of both terminal and bridging carbonyl ligands. In the UV/vis spectrum of **6**, absorption bands are seen at 296, 330, 420, and 505 nm. The ^{1}H NMR signals due to the organic moieties of **6** and **7** are fully consistent with the proposed structures. Detailed assignments of the protons of the diphenylacetylene ligands were made with the aid of a 2D HH-COSY experiment (see Table 1). In both **6** and **7**, the protons of the phenyl group on the acetylenic carbon σ-bonded to the Ru atom are seen to have similar chemical shifts as those in [$Ru_4(CO)_9(\mu\text{-CO})_2(\mu_4\text{-NH})(\mu_4\text{-}\eta^2\text{-}PhC_2Ph)$].[48] The signals of the protons of the other phenyl group are subject to a downfield shift due to the effect of the Cp*Co moiety. The resonances of the protons of these two phenyl groups in both **6** and **7** can be easily assigned with the aid of a 2D HH-COSY experiment. The five protons of the phenyl

group on the acetylenic carbon σ-bonded to Ru in **7** have a significantly different environment. This may be due to some extent to the restriction of rotation in this phenyl ring. The ^{15}N NMR spectrum of the ^{15}N-enriched sample of **6** features a doublet at δ = 70.2 [$J(^{15}NH)$ = 69.26 Hz]. The ^{15}N NMR study of **7** was hindered due to the low yield of this cluster. Nevertheless, the structures of both complexes have been established by X-ray crystallographic studies.

Brown crystals of clusters **6** and **7**, suitable for X-ray diffraction studies, were grown from saturated CH_2Cl_2/*n*-hexane solutions at −20 °C. The molecular structures of **6** and **7** are shown in Figure 5 and Figure 6, respectively, and relevant structural parameters are listed in Table 6. The molecular geometries of clusters **6** and **7** are similar in that the three Ru atoms and one Co atom are arranged in a slightly twisted square base. One face of the square is capped by a μ_4-nitrene ligand, while the other is spanned by a quadruply-bridging PhC_2Ph ligand. Species analogous to **6**, with $Ru(CO)_3$ in place of the Cp*Co moiety, have previously been obtained in this laboratory by the reaction of PhC_2R (R = H, Ph) with the triruthenium methoxynitrido cluster $[Ru_3(CO)_9(\mu_3\text{-}CO)(\mu_3\text{-}NOMe)]$.[13,14] The Cp* ligands are coordinated to the Co atoms at distances of 1.687 and 1.722 Å in **6** and **7**, respectively. The quadruply-bridging diphenylacetylene ligands in **6** and **7** are bound to the metal square through C(19)−C(20), with σ interactions to Ru(2) and Co(1) and longer η^2 interactions to Ru(1) and Ru(3). The cluster may also be viewed as a pentagonal bipyramid, the basal plane being defined by Ru(2), C(20), C(19), Co(1), and N(1). The mean deviations from the plane defined by the four metal atoms are 0.200 Å in **6** and 0.198 Å in **7**. In both cases, it is the Co(1) atoms that show the greatest deviations from these mean planes, by 0.365 Å in **6** and 0.380 Å in **7**. To the best of our knowledge, these compounds represent the first examples of the coordination of μ_4-nitrene fragments to a square Ru_3Co metal cluster. The nitrene N atoms asymmetrically cap the square bases, being tilted towards Co(1). The nitrene N atom lies above the basal plane, with a distance to the mean plane of 1.019 Å and 1.102 Å in clusters **6** and **7**, respectively. In cluster **6**, the hydrogen atom was located by Fourier-difference synthesis using low-angle data at 0.75 Å from the μ_4-NH nitrogen atom. A novel coupling reaction is observed in **7**, which involves a carbonyl group, an *ortho*-carbon of a Ph group of the PhC_2Ph ligand, and the μ_4-N atom. The activated acetylenic ligand is also found to be coordinated to Ru(2). The carbonyl group coupled between the Ph group and the μ_4-N ligand has a C−O bond length of 1.22(1) Å, which is typical for a ketone C=O group. The C(39)−C(40) bond length is significantly lengthened to 1.41(1) Å upon coordination to an Ru centre as the alkyne is reduced to a *trans* alkene.

If the μ_4-nitrene and quadruply-bridging diphenylacetylene groups are both assigned as being four-electron donors, the electron count for these metal clusters is 62, which is two electrons less than the expected electron count (64) for a square-planar transition metal cluster.[50] Within the formalism of the 18-electron rule, the 62-electron square

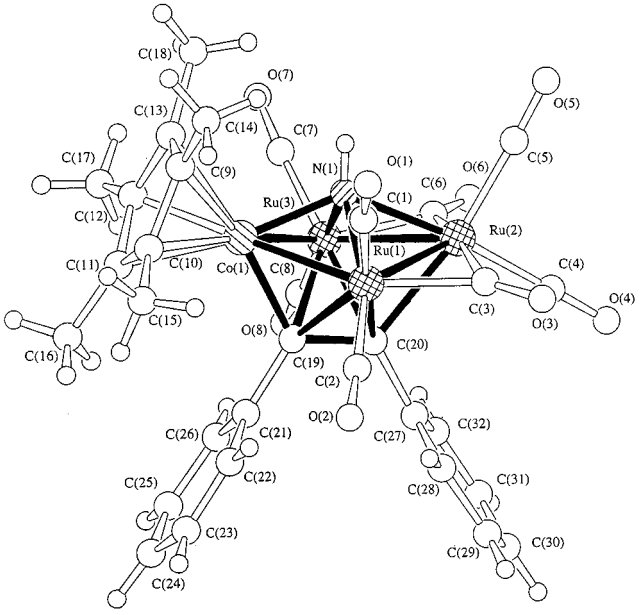

Figure 5. The molecular structure of $[Ru_3Co(CO)_6(\mu\text{-}CO)_2(\eta^5\text{-}C_5Me_5)(\mu_4\text{-}NH)(\mu_4\text{-}\eta^2\text{-}PhC_2Ph)]$ (**6**) showing the atom numbering scheme

clusters **6** and **7** are electronically unsaturated, and a 2 electron-3 centre bond has been proposed as being delocalized between the two 17-electron centres and one 16-electron centre bridged by two μ-CO groups. Clusters **6** and **7** can be described as pentagonal-bipyramidal structures if the N and C atoms in both the μ_4-NH and the PhC_2Ph units are also considered as skeletal atoms. The electron count for the cluster in such a consideration is 70, conforming to the $14n + 4m + 2$ rule,[50] where *n* represents the number of transition metal atoms and *m* denotes the number of main group atoms. To further understand the electronic structure of cluster **6**, we carried out molecular orbital calculations on the model cluster $[Ru_3Co(CO)_6(\mu\text{-}CO)_2(\eta^5\text{-}C_5H_5)(\mu_4\text{-}NH)(\mu_4\text{-}\eta^2\text{-}HC_2H)]$.[51] The NBO analysis[52] shows that the Wiberg bond orders[53] of the metal−metal bonds are all appreciably positive (0.14 for Co−Ru, 0.07 for Ru−Ru), indicating the existence of metal−metal bonding. Lesser bond orders for the Ru−Ru bonds are due to of the bridging carbonyls in these bonds. The bond orders for Ru−N and Ru−C (HC_2H) are 0.20 and 0.30, respectively. Those for Co−N and Co−C (HC_2H) are 0.45 and 0.60, respectively, making them greater than those of the corresponding Ru−N and Ru−C bonds. These results suggest that the interactions between the metal and the bridging main group atoms are crucial with regard to the stabilities of the clusters. Figure 7 shows spatial plots[54] of the highest occupied [Figure 7(a)] and the lowest unoccupied [Figure 7(b)] molecular orbitals. The HOMO is mainly localized on the Ru centres, with a slight Co(d)−Ru(d) antibonding interaction. However, the LUMO is mainly localized on the CpCo fragment, again with a slight Co(d)−Ru(d) antibonding interaction. In the LUMO, the antibonding character between Co and the Cp ligand is also noticeable.

In order to investigate this new class of square-planar μ_4-nitrene clusters in detail, molecular orbital calculations

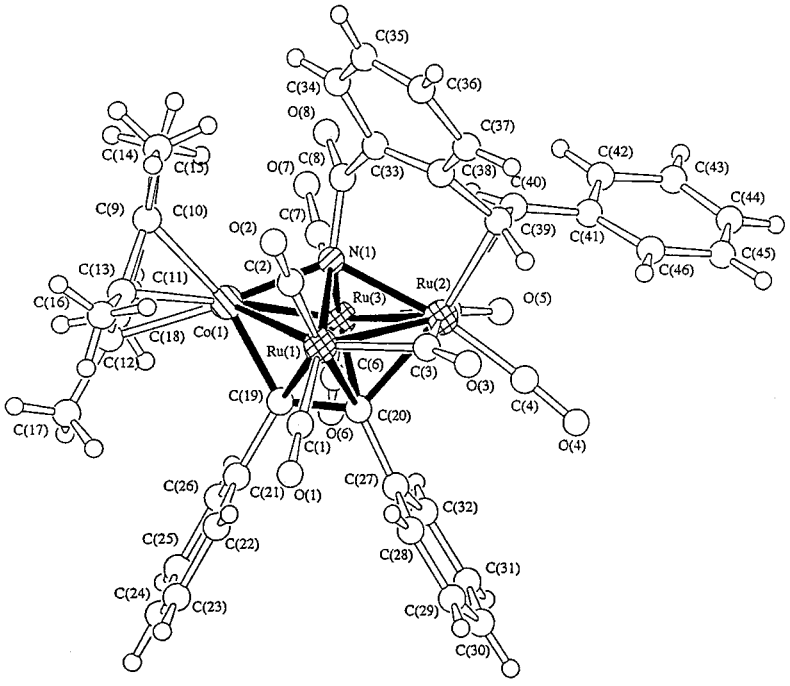

Figure 6. The molecular structure of $[Ru_3Co(CO)_5(\mu\text{-}CO)_2(\eta^5\text{-}C_5Me_5)\{\mu_4\text{-}\eta^3\text{-}NC(O)C_2(C_4H_4)CHCH(Ph)\}(\mu_4\text{-}\eta^2\text{-}PhC_2Ph)]$ (**7**) showing the atom numbering scheme

were also performed on the analogous tetraruthenium $[Ru_4(CO)_9(\mu\text{-}CO)_2(\mu_4\text{-}NOMe)(\mu_4\text{-}\eta^2\text{-}PhC_2Ph)]$ cluster.[13] The electron count of this metal cluster is also thought be 62, which is two electrons less than expected.[50] Therefore, a delocalized picture should better describe the electronic structure of the cluster. If the N and C atoms in both the μ_4-NOMe and PhC_2Ph units are also considered as skeletal atoms, the cluster can actually be described as pentagonal-bipyramidal. In this case, the total electron count is 70, again conforming to the $14n + 4m + 2$ rule.[50] In other words, the cluster obeys Wade's $n + 1$ rule.[55] We have also carried out molecular orbital calculations on the model cluster $[Ru_4(CO)_9(\mu\text{-}CO)_2(\mu_4\text{-}NOH)(\mu_4\text{-}\eta^2\text{-}HC_2H)]$.[56] The NBO analysis[52] shows that the Wiberg bond orders[53] of the four Ru−Ru bonds are all appreciably positive (ca. 0.1), indicating the existence of metal−metal bonding. The corresponding bond orders for Ru−N, Ru−C (HC_2H), and Ru−CO (bridging) range from 0.15 to 0.55. These results suggest that the metal−ligand interactions are crucial with regard to the stability of the cluster. Figure 8 shows spatial plots[54] of the highest occupied molecular orbital (HOMO) [Figure 8(a)] and the lowest unoccupied molecular orbital (LUMO) [Figure 8(b)]. Both the HOMO and LUMO contain the metal(d)−metal(d) antibonding interaction. On careful examination of these orbitals, one can see that the HOMO can be considered as the antibonding combination among the so-called "t_{2g}"-like orbitals derived from the relevant metal fragments. These "t_{2g}"-like orbitals are approximately nonbonding with respect to the coordinated ligands. However, the LUMO can be described as the skeletal antibonding molecular orbital. The corresponding fragment orbitals in the LUMO involve more metal−ligand antibonding character.

The electronic structures of **6** and $[Ru_4(CO)_9(\mu\text{-}CO)_2(\mu_4\text{-}NOMe)(\mu_4\text{-}\eta^2\text{-}PhC_2Ph)]$ show that both are unsaturated square-planar clusters, which may account for the observed NMR anisotropy. Diamagnetic effects had previously been observed in the ^1H and ^{15}N chemical shifts of the μ_4-NH groups in **6** and $[Ru_4(CO)_9(\mu\text{-}CO)_2(\mu_4\text{-}NH)(\mu_4\text{-}\eta^2\text{-}PhC_2Ph)]$.[13,48] In comparison with the electron-precise cluster **4**, the chemical shifts of **6** and the tetraruthenium μ_4-NH clusters appear further upfield. The ^1H chemical shift of the μ_4-NH proton in the saturated compound **4** is $\delta = 6.28$, whereas for the unsaturated compound **6** and the Ru_4 analogue, the corresponding shifts are $\delta = 2.76$ and 1.87, respectively. In fact, the ^1H NMR resonance of the μ_4-NH moiety is a sensitive probe for delineating the bonding type in all these new clusters. The ^{15}N chemical shifts of the μ_4-NH groups follow the same trend; thus, for the unsaturated clusters **6** and $[Ru_4(CO)_9(\mu\text{-}CO)_2(\mu_4\text{-}NH)(\mu_4\text{-}\eta^2\text{-}PhC_2Ph)]$[13,48] the NH signals are seen at $\delta = 70.2$ and 47.6, while for the saturated **4** it is found at $\delta = 145.4$. The nature of the NMR anisotropy leads to a weaker effective magnetic field above the centre of the Ru_3Co/Ru_4 ring in the unsaturated compounds.[57]

Migration of a hydride ligand to the nitrido atom is an essential step in the formation of **6** and **7**. This probably involves a hydride shift to give structure I, as shown below.

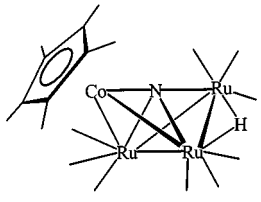

I

Table 6. Selected bond lengths [Å] and angles [°] for clusters **6** and **7**

	6	**7**
Ru(1)−Ru(2)	2.694(1)	2.697(1)
Ru(1)−Co(1)	2.631(2)	2.631(2)
Ru(1)−N(1)	2.176(10)	2.175(8)
Ru(1)−C(19)	2.40(1)	2.366(10)
Ru(1)−C(20)	2.33(1)	2.276(9)
Ru(2)−Ru(3)	2.681(1)	2.703(1)
Ru(2)−N(1)	2.147(10)	2.195(8)
Ru(2)−C(20)	2.23(1)	2.191(10)
Ru(2)−C(39)	–	2.22(1)
Ru(2)−C(40)	–	2.29(1)
Ru(3)−Co(1)	2.634(2)	2.613(2)
Ru(3)−N(1)	2.13(1)	2.180(8)
Ru(3)−C(19)	2.41(1)	2.31(1)
Ru(3)−C(20)	2.328(10)	2.305(9)
Co(1)−N(1)	1.949(10)	2.016(8)
Co(1)−C(19)	1.97(1)	1.970(10)
C(8)−O(8)	1.15(2) [carbonyl]	1.22(1)
N(1)−C(8)	–	1.43(1)
C(8)−C(33)	–	1.50(1)
C(19)−C(20)	1.44(2)	1.43(1)
Co(1)−Cp*(c)[a]	1.687	1.722
N(1)−H	0.75	–
Ru(1)−N(1)−Ru(2)	77.1(3)	76.2(2)
Ru(1)−N(1)−Ru(3)	114.7(4)	110.4(3)
Ru(1)−N(1)−Co(1)	79.1(3)	77.7(3)
Ru(1)−N(1)−C(8)	–	128.6(7)
Ru(2)−N(1)−Ru(3)	77.5(3)	76.3(2)
Ru(2)−N(1)−Co(1)	136.4(5)	132.8(4)
Ru(2)−N(1)−C(8)	–	108.1(7)
Ru(3)−N(1)−Co(1)	80.2(3)	76.9(3)
Ru(3)−N(1)−C(8)	–	120.5(7)
Co(1)−N(1)−C(8)	–	118.9(7)
O(8)−C(8)−N(1)	–	122(1)
O(8)−C(8)−C(33)	–	119(1)
N(1)−C(8)−C(33)	–	118.4(10)
Ru(2)−C(39)−C(40)	–	74.3(6)
C(38)−C(39)−C(40)	–	120.5(9)
Ru(2)−C(40)−C(39)	–	69.3(6)
C(39)−C(40)−C(41)	–	125.6(9)

[a] Cp*(c) denotes the centroid of the C_5Me_5 rings.

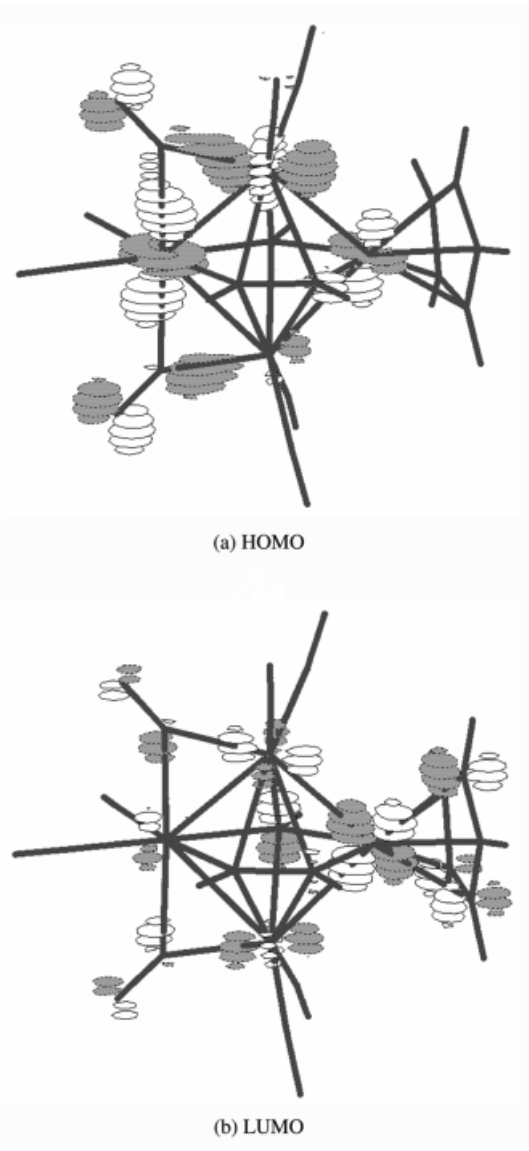

Figure 7. Spatial plots of the highest occupied (a) and the lowest unoccupied (b) molecular orbitals for $[Ru_3Co(CO)_6(\mu\text{-}CO)_2(\eta^5\text{-}C_5H_5)(\mu_4\text{-}NH)(\mu_4\text{-}\eta^2\text{-}HC_2H)]$

This type of skeleton has been structurally established in another system.[58] The hydrogen atom shows a preference for the ruthenium sites as opposed to those involving the Co(1) atom.[59] The hydride ligand eventually migrates to the nitrogen atom to give structure II in the case of **6**.

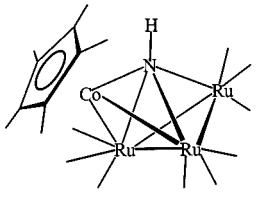

II

Conceptually, the addition of an acetylene group to II can easily be described as an insertion of the C≡C unit into the hinge M−M bond of the cluster. Concomitant unfolding of the wings of the butterfly allows stabilization of the acetylene through direct interaction with all four metal centres. A further coupling of a carbonyl ligand and a PhC_2Ph ligand to the nitrene N atom is observed in cluster **7**. The metal-bonded H atom and the H on the *ortho*-carbon atom are transferred to the acetylenic carbons in a *trans* configuration and give rise to doublet resonances at δ = 5.75 and 2.72 with a mutual coupling of 12.26 Hz. Heating of **6** with PhC_2Ph under similar reaction conditions does not give any observable amount of **7**, indicating that the H atom is not easily detached from the nitrene N atom. The shortcomings of bridging or capping main group atoms as cluster stabilizing entities have long been established.[49,60−70] However, in the present case, the main-group N-atom is shown to be valuable not only for its influence on incoming ligands, but also for its capacity to participate in skeletal rearrangements while maintaining cluster nuclearity.

Reaction of $[Ru_3Co(CO)_{12}(\mu_4\text{-}N)]$ with $[Cp^*Co(CO)_2]$

In order to prepare some Co-rich mixed-metal clusters by a stepwise reaction, the cluster $[Ru_3Co(CO)_{12}(\mu_4\text{-}N)]$[1]

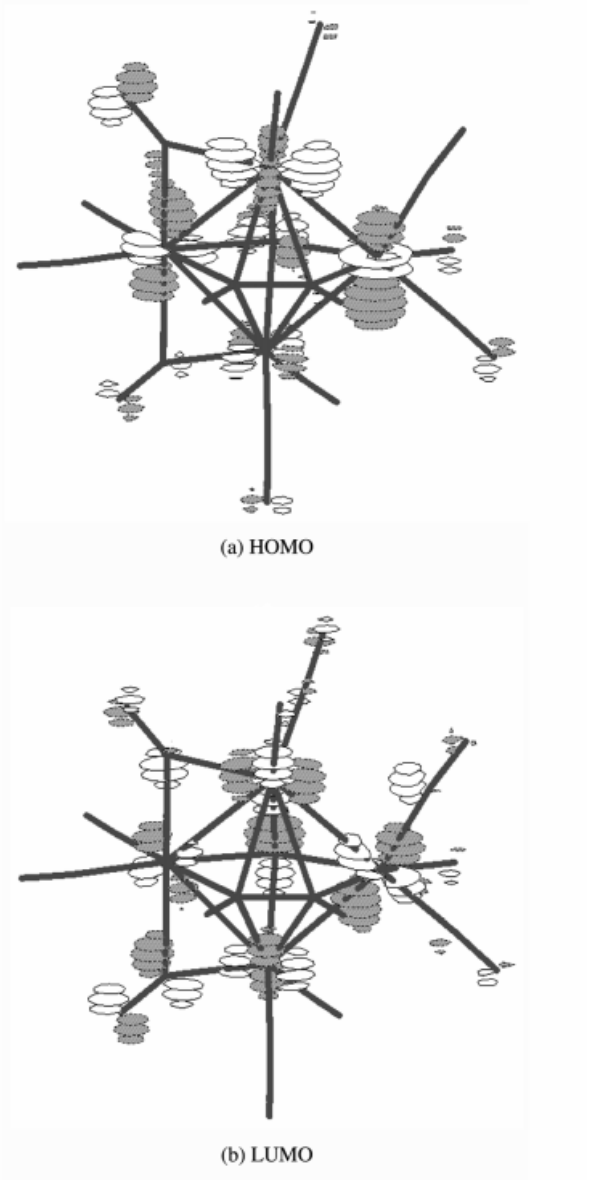

Figure 8. Spatial plots of the highest occupied (a) and the lowest unoccupied (b) molecular orbitals for $[Ru_4(CO)_9(\mu\text{-}CO)_2(\mu_4\text{-}NOH)(\mu_4\text{-}\eta^2\text{-}HC_2H)]$

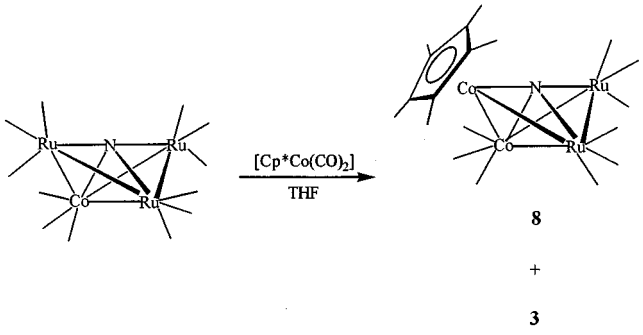

Scheme 3. Treatment of $[Ru_3Co(CO)_{12}(\mu_4\text{-}N)]$ with 2 equiv. of $[Cp^*Co(CO)_2]$ in refluxing THF resulted in the formation of $[Ru_2Co_2(CO)_9(\eta^5\text{-}C_5Me_5)(\mu_4\text{-}N)]$ (**8**) and cluster **3** in yields of 32% and 41%, respectively

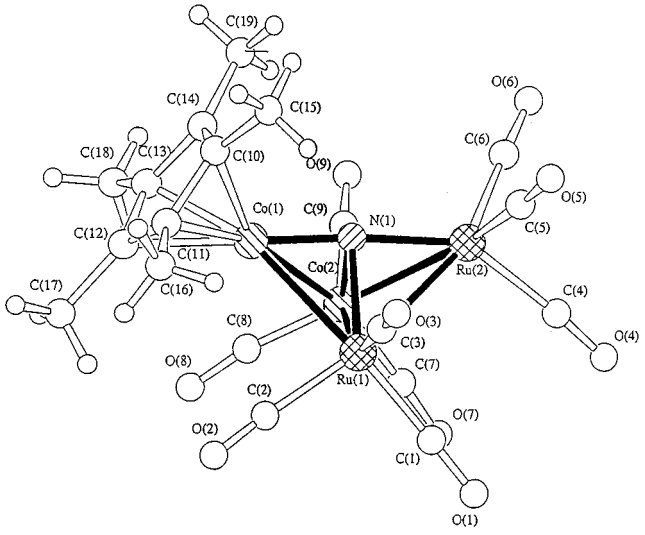

Figure 9. The molecular structure of $[Ru_2Co_2(CO)_9(\eta^5\text{-}C_5Me_5)(\mu_4\text{-}N)]$ (**8**) showing the atom numbering scheme

was allowed to react with $[Cp^*Co(CO)_2]$ in refluxing THF for 4 h (Scheme 3). Dark-brown crystals of $[Ru_2Co_2(CO)_9(\eta^5\text{-}C_5Me_5)(\mu_4\text{-}N)]$ (**8**) were obtained in high yield, accompanied by some **3**. Cluster **8** was fully characterized by conventional spectroscopic techniques and elemental analysis (Table 1). The ^1H and ^{15}N NMR spectra of **8** feature singlet resonances at $\delta = 1.89$ and $\delta = 524.7$, respectively. The electronic absorption spectrum of cluster **8** is virtually identical to that of **2**, consisting of four bands at 315, 360, 435, and 520 nm. A single-crystal X-ray analysis was carried out; the structure of **8** is depicted in Figure 9, while selected bond parameters are collected in Table 2.

The two ruthenium and two cobalt atoms of cluster **8** define a butterfly metal core, with a nitrogen atom bridging the wing-tip positions of the cluster. The Cp* ligand is coordinated to the wing-tip Co atom at a distance of 1.656 Å. The same butterfly core was also observed in cluster **2**. Thus, the structure of **8** is related to that of **2**, with a $Co(CO)_3$ fragment replacing the hinge $HRu(CO)_3$ moiety. Thus, the Cp*Co moiety in molecule **8** occupies a wing-tip position and the other Co atom is placed at a hinge site. The Co(1)−Co(2) bond in **8** [2.545(1) Å] is significantly longer than that in $[Co_3(\mu_3\text{-}CO)(\eta^5\text{-}C_5Me_5)_3(\mu_3\text{-}NH)]$.[5] The M−N bond lengths involving the wing-tip metals [Ru(2)−N(1) 1.926(5) Å and Co(1)−N(1) 1.723(5) Å] are shorter than those involving the hinge metal atoms [Ru(1)−N(1) 2.039(5) Å and Co(2)−N(1) 1.950(5) Å]. The Ru(1)−N(1)−Co(2) and Ru(2)−N(1)−Co(1) angles are 80.2(2)° and 174.3(3)°, respectively. The dihedral angle between the butterfly wings in **8** measures 103.39°, which is very different from that in **2** (78.59°). The formation of cluster **8** is believed to result from a metal-exchange[31,32] reaction, accomplished by an addition−elimination sequence. The first step should be the incorporation of the Cp*Co fragment into the "butterfly" $[Ru_3Co(CO)_{12}(\mu_4\text{-}N)]$ core to give intermediate III.

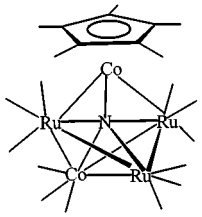

III

Although structure III is an electron-precise species, this kind of wing-tip-bridged butterfly metal skeleton involving a μ_5-nitrido ligand is rarely observed. The only other known example occurs in $[Ru_6(CO)_{13}(\mu\text{-H})(\mu_5\text{-N})(\mu_3\text{-}\eta^2\text{-}PhC_2Ph)_2]$.[13] Thus, an $Ru(CO)_3$ or an $RuCo(CO)_5$ fragment is eliminated to give a more favourable metal framework, i.e. butterfly [**8**] or triangular [**3**] clusters. The source of the nitrene hydrogen in the formation of cluster **3** is uncertain; it may come from the degradation of solvent molecules or from a trace amount of moisture in the solvent.

Electrochemistry

The electrochemistry of clusters **1**−**3**, **6**, and **8** has been examined in CH_2Cl_2 by means of cyclic voltammetry and controlled-potential coulometry, using *n*-tetrabutylammonium hexafluorophosphate (TBAHFP) as the supporting electrolyte. The redox potential values obtained are summarized in Table 7; for comparison, those of compounds $[Ru_4(CO)_9(\mu\text{-CO})_2(\mu_4\text{-NOMe})(\mu_4\text{-}\eta^2\text{-}PhC_2Ph)]$ (**9**), $[Ru_4(CO)_9(\mu\text{-CO})_2(\mu_4\text{-NH})(\mu_4\text{-}\eta^2\text{-}PhC_2Ph)]$ (**10**), and $[Ru_4(CO)_9(\mu\text{-CO})_2\{\mu_4\text{-NC(O)OMe}\}(\mu_4\text{-}\eta^2\text{-}PhC_2Ph)]$ (**11**) are also listed.[13]

Table 7. Electrochemical data for compounds **1**−**3**, **6**, **8**, and $[Ru_4(CO)_9(\mu\text{-CO})_2(\mu_4\text{-NR})(\mu_4\text{-}\eta^2\text{-}PhC_2Ph)]$ [**9**, R = OMe; **10**, R = H, and **11**, R = C(O)OMe][13]

Cluster[a]	Oxidation	Reduction	
	E_{pa1} (V)[b]	E_{pc1} (V)[b]	E_{pc2} (V)[b]
1	0.83	−2.13	–
2	0.56	(−1.26)[c]	–
3	–	−1.68	–
6	(0.79)[c]	(−1.36)[c]	(−1.71)[c]
8	0.55	(−1.13)[c]	–
9	–	−1.31	–
10	–	−1.30	–
11	–	−1.29	–

[a] Ca. 10^{-3} M cluster in 0.1 M TBAHFP in dichloromethane at 298 K, the working electrode was made of glassy carbon, the auxiliary electrode and the reference electrode were a platinum wire and $Ag/AgNO_3$, respectively. Scan rate 100 mVs^{-1}. The potentials are referenced to $Ag/AgNO_3$ (0 V) under the same conditions, calibrated with ferrocene. − [b] E_{pa} and E_{pc} are the anodic and cathodic potentials, respectively. − [c] Values in parentheses are half-wave potential values, $E_{1/2}$.

The cluster $[Ru_3(CO)_9(\mu_3\text{-CO})(\mu_3\text{-NOMe})]$ exhibits an irreversible cathodic wave (E_{pc}) at −1.66 V vs. $Ag/AgNO_3$, along with a weak oxidation wave at −0.63 V. The region where the weak oxidation wave appears was initially empty, with the wave appearing after the cathodic wave was traversed. The ΔE_p values remained virtually unchanged on varying the scan rates from 50 to 1000 mVs^{-1}. For $[Ru_3(CO)_9(\mu_3\text{-CO})(\mu_3\text{-NOMe})]$, an additional irreversible anodic wave is observed at E_{pa} = 1.11 V. Controlled-potential coulometry at the oxidation step (E_w = 1.25 V) indicates that this anodic process consumes 1 faraday/mol of $[Ru_3(CO)_9(\mu_3\text{-CO})(\mu_3\text{-NOMe})]$. On the basis of the relative peak currents of the cathodic and anodic waves, the reduction process could be assigned as a one-electron step. The addition of one electron to the cluster $[Ru_3(CO)_9(\mu_3\text{-CO})(\mu_3\text{-NOMe})]$ is believed to afford the 49e cluster $[Ru_3(CO)_9(\mu_3\text{-CO})(\mu_3\text{-NOMe})]^-$, which is unstable and loses a CO ligand to give the 47e species $[Ru_3(CO)_9(\mu_3\text{-NOMe})]^-$ [71] according to an EC mechanism. Cyclic voltammograms of cluster **1** show the same features as those seen for $[Ru_3(CO)_9(\mu_3\text{-CO})(\mu_3\text{-NOMe})]$, with a pair of cathodic and anodic waves at E_{pc} = −2.13 V and E_{pa} = 0.83 V vs. $Ag/AgNO_3$. A small return oxidation wave at −0.68 V is seen for the transient 47e $[Ru_3(\mu\text{-H})_2(CO)_8(\mu_3\text{-NOMe})]^-$, similar to that seen for $[Ru_3(CO)_9(\mu_3\text{-CO})(\mu_3\text{-NOMe})]$. A salient feature of the electrochemical behaviour of the cluster $[Ru_3(\mu\text{-H})_2(CO)_9(\mu_3\text{-NOMe})]$ (**1**) is that this dihydrido derivative of $[Ru_3(CO)_9(\mu_3\text{-CO})(\mu_3\text{-NOMe})]$ is both harder to reduce and easier to oxidize than the corresponding μ_3-CO-capped cluster $[Ru_3(CO)_9(\mu_3\text{-CO})(\mu_3\text{-NOMe})]$. The greater difficulty in reducing dihydrido cluster **1** in CH_2Cl_2 is shown by the fact that the E_{pc} value for the 0/−1 couple is 470 mV more negative than that for $[Ru_3(CO)_9(\mu_3\text{-CO})(\mu_3\text{-NOMe})]$. Likewise, the +1/0 oxidation couple of **1** is less positive than that for $[Ru_3(CO)_9(\mu_3\text{-CO})(\mu_3\text{-NOMe})]$ by 280 mV. These data are consistent with the premise that the hydrido ligands effectively function as stronger σ-electron donors and as weaker π-acceptors than μ_3-CO ligands.

Although clusters **2** and **8** are obtained from different reactions, they have similar metal architectures and ligand dispositions, with an Ru atom and a hinge μ-H in **2** being replaced by a Co atom in **8**. Both exhibit similar electrochemical behaviour in their cyclic voltammograms. Two electrode processes are evident from their voltammograms: (i) a reversible reduction wave at −1.26 V for **2** and at −1.13 V for **8**, and (ii) an irreversible oxidation wave at around 0.55 V. The species with the higher cobalt-content, cluster **8**, is easier to reduce to the corresponding monoanionic derivative. Controlled-potential electrolyses at E_w = −1.4 V for **2** and −1.3 V for **8** showed that the reduction processes involve one faraday/mol of cluster molecule. Cyclic voltammetric tests run after exhaustive electrolyses showed that the 0/−1 cathodic steps are chemically reversible. On the other hand, controlled-potential coulometry run at 0.7 V for both **2** and **8** showed that two electrons are removed for each molecule. Cluster **8** was found to decompose further, while cluster **2** was stoichiometrically converted into cluster **3**. Analysis of the cyclic voltammetric responses relating to the cathodic peaks of **2** and **8**, with scan rates υ varying from 50 mVs^{-1} to 1000 mVs^{-1}, indicated that: (i) the peak current ratio i_{pa}/i_{pc} remains close to unity, (ii) the current function (proportional to $i_{pc}/\upsilon^{1/2}$) is essentially constant, and (iii) the peak-to-peak separation is between 80 and 100 mV. This trend in peak-to-peak separation parallels that obtained for ferrocene under the same

experimental conditions. Thus, we can assume that the reduction steps of both **2** and **8** proceed by an essentially reversible electron-transfer process. Upon one-electron addition, no gross structural variation should occur in these Ru−Co mixed-metal nitrido complexes. The irreversible two-electron oxidations in **2** and **8** can be assigned as following ECEC or EEC processes. After controlled-potential electrolysis of cluster **2** at 0.7 V for 180 min, the current had decayed to background levels and the experiment was halted. Two faradays of charge were required for each mol of **2**, which was found to be almost completely converted into cluster **3**. In order to verify this oxidation process chemically, attempts were made to react **2** with $Ag[BF_4]$ and $[NO][PF_6]$, since the oxidation of **2** occurred at a potential well within the range of these common oxidizing agents. Although vigorous reactions took place when $Ag[BF_4]$ or $[NO][PF_6]$ was added to the cluster in CH_2Cl_2, no cluster **3** could be detected and only decomposition products were obtained. This may possibly be due to Ag^+ and NO^+ reacting with the cluster rather than merely oxidizing it.[71] A cyclic voltammetric study of compound **3** in CH_2Cl_2 revealed an irreversible one-electron reduction at −1.68 V. With a good π-acceptor μ_3-CO ligand, cluster **3** was found to be reduced at a similar potential as the cluster $[Ru_3(CO)_9(\mu_3\text{-}CO)(\mu_3\text{-}NOMe)]$.

The redox behaviour of $[Ru_3Co(CO)_6(\mu\text{-}CO)_2(\eta^5\text{-}C_5Me_5)(\mu_4\text{-}NH)(\mu_4\text{-}\eta^2\text{-}PhC_2Ph)]$ (**6**) is shown in Figure 10. It displays one oxidation and two separated reduction processes, all of which are reversible. Controlled-potential coulometry corresponding to the first cathodic step ($E_w = -1.5$ V) consumes one electron per molecule. Analyses of the cyclic voltammograms exhibited by $[Ru_3Co(CO)_6(\mu\text{-}CO)_2(\eta^5\text{-}C_5Me_5)(\mu_4\text{-}NH)(\mu_4\text{-}\eta^2\text{-}PhC_2Ph)]^{1+/0}$ and $[Ru_3Co(CO)_6(\mu\text{-}CO)_2(\eta^5\text{-}C_5Me_5)(\mu_4\text{-}NH)(\mu_4\text{-}\eta^2\text{-}PhC_2Ph)]^{1-/2-}$ lead to the same diagnostic results. Thus, the square Cp* $Ru_3Co(\mu_4\text{-}NH)$ core exhibits remarkably flexible redox behaviour and, within the short timescale of cyclic voltammetry, is able to accommodate both the addition of two electrons and the removal of one electron without significant molecular strain. Among the clusters discussed so far, only **2**, **6**, and **8** exhibit reversible one-electron transfers, and one common feature of these clusters should be noted: all three have strongly π-bonding η^5-C_5Me_5 ligands. A correlation of this behaviour may be drawn by comparison with the mononuclear analogues such as ferrocene[72] and dibenzenechromium,[73] which are also reversibly oxidized. Clusters **2**, **6**, and **8** are derived from the chemistry of metallocenes, where the metallic core is "shielded" from destruction by π-ligands. The same conclusion was reached from bonding calculations on cluster **6**. It is expected that reduction of the cluster leads to break-up of the CpCo fragment {in the model cluster $[Ru_3Co(CO)_6(\mu\text{-}CO)_2(\eta^5\text{-}C_5H_5)(\mu_4\text{-}NH)(\mu_4\text{-}\eta^2\text{-}HC_2H)]$} or dissociation of the Cp ligand [see Figure 7(b)]. In view of the weak Co(d)−Ru(d) antibonding character of the LUMO for **6**, one may expect this to be more reversible. While oxidation is predicted to enhance the Ru−Co interaction, it would also significantly weaken the Ru−CO (bridging) interactions because the HOMO contains appreciable Ru(d)→bridging CO(π*) back-donation [see Figure 7(a)]. The square-planar μ_4-nitrene complex **6** is also found to be unsaturated, having 62 CVE's. Electrochemically, it would be expected to take up two electrons to achieve a stable 64-CVE configuration, which is indeed observed; cluster **6** undergoes two sequential, chemically reversible, one-electron additions.

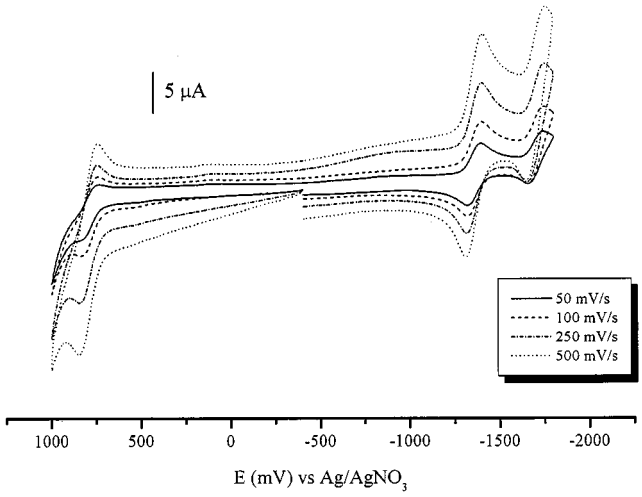

Figure 10. Cyclic voltammogram of **6** in CH_2Cl_2 with 0.1 M TBAHFP as supporting electrolyte using glassy carbon working electrode at 298 K; the increasing current arises from scans at 50, 100, 250, and 500 mV/s, respectively; the voltammograms were recorded against an $Ag/AgNO_3$ reference electrode

We also examined the electrochemical behaviour of the clusters $[Ru_4(CO)_9(\mu\text{-}CO)_2(\mu_4\text{-}NR)(\mu_4\text{-}\eta^2\text{-}PhC_2Ph)]$ [**9**, R = OMe; **10**, R = H, and **11**, R = C(O)OMe]. In view of the close similarities in ligation and structure for these three 62-electron bicapped tetraruthenium clusters containing a diphenylacetylene ligand and a μ_4-capped nitrene moiety, it is not surprising that they show similar redox characteristics. Clusters **9**, **10**, and **11** exhibit only irreversible reductions within the solvent limits. The value of the cathodic peak potential (E_{pc}) is about −1.3 V. Weak oxidation waves are observed at −0.99 V and −0.38 V for **9**, at −0.68 V for **10**, and at −0.78 V for **11** upon scan reversal. Increased scan rates did not lead to any noticeable reversibility of the redox couple. Exhaustive electrolyses on all three clusters **9**, **10**, and **11** at $E_w = -1.45$ V showed that the cathodic step involves the addition of one electron per molecule. The absence of a re-oxidation wave for this 0/−1 redox couple indicates the existence of a fast chemical follow-up step that extricates the mono-reduced clusters from solution before they can be oxidized back to the neutral clusters. In accordance with the electronic structure of **9** outlined above, we expect reduction of the cluster to destabilize the metal−metal interactions and to lead to fragmentation, while oxidation can be expected to enhance the interaction. With respect to the reduction scan, these results are consistent with the electrochemical behaviour of **9**; however, no oxidation wave is observed within the potential range of the solvent, thus the comment regarding the oxidation scan cannot be verified. Cluster **6** has a similar structure to cluster **10**, except that the Cp*Co moiety is replaced by an

$Ru(CO)_3$ moiety. The redox behaviour of **10** has been shown to be different from that of **6**. Apart from enhancing the reversibility of the electrochemical processes, the Cp* Co moiety also makes both reduction and oxidation more feasible within the potential range of CH_2Cl_2 as the solvent. The behaviour of heterometallic carbonyl clusters is still uncertain.

^{15}N NMR Spectroscopy

^{15}N NMR spectroscopy is a sensitive and informative tool in characterizing cluster nitridos and nitrenes. In our previous report,[13] we presented nitrogen-15 magnetic resonance spectroscopic data for a series of μ_4-nitrene [μ_4-NH, NOMe, or NC(O)OMe] clusters. A μ_5-nitrido atom in a bridged-butterfly metal skeleton was found to exhibit an unusually high-frequency signal (δ = 549.8). In order to investigate the environments of the various nitrogen atoms of the homo- or heterometallic compounds in this study, all the clusters except **7** were examined by ^{15}N NMR. Table 1 summarizes the ^{15}N chemical shifts obtained.

The cluster $[Ru_3(CO)_9(\mu_3\text{-}CO)(\mu_3\text{-}NOMe)]$, formed by the reaction of $[PPN][Ru_3(CO)_{10}(\mu\text{-}NO)]$ with $CF_3SO_3CH_3$, shows a resonance at δ = 287.3 (reference: liq. NH_3) in its ^{15}N NMR spectrum when the compound is 90% enriched with ^{15}N. Hydrogenation of $[Ru_3(CO)_9(\mu_3\text{-}CO)(\mu_3\text{-}NOMe)]$ gave cluster $[Ru_3(\mu\text{-}H)_2(CO)_9(\mu_3\text{-}NOMe)]$ (**1**), which showed a ^{15}N chemical shift of δ = 301.0.[29] Clusters **2** and **3** are the major products of the reaction between **1** and $[Cp^*Co(CO)_2]$, and exhibit signals at δ = 481.1 (s) and 131.4 [d, $J(^{15}NH)$ = 76.95 Hz], respectively. The ^{15}N NMR signal of **2** lies in the typical range for butterfly species. The ^{15}N chemical shift of the μ_3-NH N atom of **3** appears 48.9 ppm further downfield compared to that of the corresponding triruthenium μ_3-NH cluster $[Ru_3(\mu\text{-}H)_2(CO)_9(\mu_3\text{-}NH)]$.[29] The ^{15}N NMR spectrum of $[Ru_3(\mu\text{-}H)_2(CO)_9(\mu_3\text{-}NH)]$ features a doublet at δ = 82.5 downfield from liquid NH_3 [$J(^{15}NH)$ = 77.5 Hz], which is characteristic of a direct NH bond. Cluster **4** can be viewed as the *N*-protonated analogue of $[Ru_5(CO)_{14}(\mu_5\text{-}N)]^-$, which gives a ^{15}N resonance at δ = 464.9.[3] Cluster **4** gives a doublet at δ = 145.4 [$J(^{15}NH)$ = 68.26 Hz], which is significantly upfield (319.5 ppm) from the resonance of $[Ru_5(CO)_{14}(\mu_5\text{-}N)]^-$. The ^{15}N resonance of **4** is significantly downfield shifted (by 97.8 ppm) compared to that of $[Ru_4(CO)_9(\mu\text{-}CO)_2(\mu_4\text{-}NH)(\mu_4\text{-}\eta^2\text{-}PhC_2Ph)]$,[13] in which the square-planar Ru_4 skeleton is stabilized by a quadruply-bridging acetylene ligand to give an electron-precise cluster according to the EAN rule. By comparison with the saturated clusters $[Ru_3(CO)_{10}(\mu_2\text{-}NH_2)]$ (δ = −33.5) and $[Ru_3(CO)_9(\mu_3\text{-}CO)(\mu_3\text{-}NH)]$ (δ = 82.5), the resonance of **4** is seen to conform to a smooth trend of increasing magnitude with increasing nuclearity around the hydrogen-bonded nitrogen. Thus, the greater the number of ruthenium atoms bonded to the nitrogen moiety, the more deshielded is the nitrogen resonance. The observed $J(^{15}NH)$ coupling constants are fully consistent with calculated values based on the $J(^{14}NH)$ coupling constants [76.86 Hz for **3** and 68.47 Hz for **4**]. Cluster **5** resembles **2**, but with cluster expansion on the Ru_3 wing face with a triruthenium chain. The further coordination of the triruthenium chain leads to a downfield shift of ca. 68 ppm. $[Ru_3Co(CO)_6(\mu\text{-}CO)_2(\eta^5\text{-}C_5Me_5)(\mu_4\text{-}NH)(\mu_4\text{-}\eta^2\text{-}PhC_2Ph)]$ (**6**) is an analogous complex to $[Ru_4(CO)_9(\mu\text{-}CO)_2(\mu_4\text{-}NH)(\mu_4\text{-}\eta^2\text{-}PhC_2Ph)]$,[13] with an $Ru(CO)_3$ moiety being replaced by a $Co(\eta^5\text{-}C_5Me_5)$ group. This exchange leads to a downfield shift in the nitrogen resonance by 22.6 ppm relative to the corresponding Ru_4 cluster [δ = 47.6, $J(^{15}NH)$ = 70.54 Hz]. The higher field shifts of the unsaturated $[Ru_4(CO)_9(\mu\text{-}CO)_2(\mu_4\text{-}NH)(\mu_4\text{-}\eta^2\text{-}PhC_2Ph)]$ and **6** relative to the saturated cluster **4** can be attributed to diamagnetic anisotropy effects. In the formation of cluster **6** from **2**, migration of a hydride ligand to the nitrido is involved, hence cluster **6** could be viewed as the "protonation" product of **2** to give the μ_4-NH cluster. The large increase in shielding arising from this direct "protonation" of a butterfly interstitial highlights the large contribution to the deshielding of the interstitial by low-energy circulations of quasi-lone-pair electrons. Similar examples of this have been observed in the protonation of $[FeRu_3N(CO)_{10}\{P(OMe)_3\}_2]^-$, both at the hinge and at the nitrogen, to give the μ_4-NH intermediate, where the nitrogen shielding is increased by 231 ppm.[74] Protonation of the hinge-protonated carbide $[HFe_4C(CO)_{12}]^{2-}$ to give the μ_4-η^2-CH compound increases the carbon shielding by a correspondingly large amount, i.e. 129 ppm.[75] The measurements made in this study on cluster **6** are the first to be

Table 8. Coupling constants of selected μ_3-NH and μ_4-NH ligands

μ_3-NH complexes	$J(^{14}NH)$	$J(^{15}NH)$
$[Ru_2Co(CO)_6(\mu_3\text{-}CO)(\eta^5\text{-}C_5Me_5)(\mu_3\text{-}NH)]$ **3**	54.80	76.95
$[Ru_3(\mu\text{-}H)_2(CO)_9(\mu_3\text{-}NH)]$[29]	–	77.5
$[Ru_3(CO)_9(\mu_3\text{-}CO)(\mu_3\text{-}NH)]$[74]	54.0	–
$[FeRu_2(CO)_9(\mu_3\text{-}CO)(\mu_3\text{-}NH)]$[74]	54.0	–
$[Fe_3(CO)_9(\mu_3\text{-}CO)(\mu_3\text{-}NH)]$[77]	57.0	–
μ_4-NH complexes	**$J(^{14}NH)$**	**$J(^{15}NH)$**
$[Ru_5(\mu\text{-}H)(CO)_9(\mu\text{-}CO)_3(\eta^5\text{-}C_5Me_5)(\mu_4\text{-}NH)]$ **4**	48.82	68.26
$[Ru_3Co(CO)_6(\mu\text{-}CO)_2(\eta^5\text{-}C_5Me_5)(\mu_4\text{-}NH)(\mu_4\text{-}\eta^2\text{-}PhC_2Ph)]$ **6**	49.08	69.26
$[Ru_4(CO)_9(\mu\text{-}CO)_2(\mu_4\text{-}NH)(\mu_4\text{-}\eta^2\text{-}PhC_2Ph)]$[13]	50.71	70.54
$[Ru_4(CO)_9(\mu\text{-}CO)_2(\mu_4\text{-}NH)(\mu_4\text{-}\eta^2\text{-}HC_2Tol)]$[13]	49.30	70.64

reported for a square Ru_3Co complex having an exclusively quadruply-bridging nitrene ligand. One interesting aspect worth mentioning is that the coupling constants for direct ^{15}N-^{1}H interaction in the μ_4-NH moieties are smaller than those for the μ_3-NH groups. Table 8 lists coupling constants for the μ_3-NH and μ_4-NH ligands. The ^{15}N-^{1}H coupling constants can be converted into ^{14}N-^{1}H coupling constants by the equation $J(^{14}NH) = -0.713 \times J(^{15}NH)$, where -0.713 comes from γ_{14}/γ_{15}.[76] Thus, these characteristic values provide useful information in ascertaining whether the nitrene is bound to three or four metal centres.

Cluster **8** is another butterfly cluster analogous to **2** with a hinge $HRu(CO)_3$ fragment replaced by an isolobal $Co(CO)_3$ moiety. The ^{15}N resonance signal is seen at δ = 524.7 with a downfield shift of 43.6 ppm. In conjunction with the results in our previous report,[13] the close relationship between cluster structure and the chemical shift of the cluster nitrogen atom in the ^{15}N NMR spectra has turned out to be a useful tool for the analysis of the products in this system.

Conclusion

Triruthenium methoxynitrido carbonyl clusters $[Ru_3(CO)_9(\mu_3\text{-}CO)(\mu_3\text{-}NOMe)]$ and **1** have been extensively studied with regard to deoxygenation to give the coordinated nitrido or nitrene ligands by thermolysis, pyrolysis, or nucleophilic reaction with alkynes. On the basis of various reactivities of the starting clusters, we have demonstrated some new rational high-yielding synthetic routes to the heterometallic tetranuclear nitrido cluster **2**. The formation of this cluster can be simply described as an addition of a mononuclear organometallic complex to the methoxynitrido cluster species with the elimination of two carbonyl ligands and a methanol molecule. The pseudo-octahedral Ru_5N framework arrangement makes cluster **4** a particularly attractive model for surface processes; thus the square Ru_4 fragment generated constitutes an interesting model for a ruthenium (100) surface. The rather unusual Cp* transfer process has also been observed in this study. Decarbonylation of cluster **2** with an alkyne initiates a hydride migration from a hinge to a nitrido nitrogen atom. This leads to a skeletal rearrangement, where the hinge of the butterfly cluster is ruptured through the insertion of the alkyne ligand. This square Ru_3Co face skeleton presents an opportunity to evaluate nitrene chemistry on a mixed transition metal surface. The incorporation of a Cp*Co moiety in a μ_4-nitrene cluster has been shown to enhance the reversibility of electrochemical processes and make both reduction and oxidation more feasible. Thus, the chemistry of this cluster differs significantly from that observed for homometallic analogues. Both the ^{15}N NMR and electrochemistry studies of these clusters have provided valuable information regarding the environment of the nitrene/nitrido nitrogen atoms and their redox properties.

Experimental Section

General Procedures: All reactions and manipulations were carried out under argon using standard Schlenk techniques, except for the chromatographic separations. Solvents were purified by standard procedures and distilled prior to use. Unless otherwise stated, all chemicals were purchased commercially and were used as received. $[Ru_3(\mu\text{-}H)_2(CO)_9(\mu_3\text{-}NOMe)]$,[29] [PPN][$^{15}NO_2$],[78] and [Cp*$Co(CO)_2$][79] were prepared according to literature methods. − Reactions were monitored by analytical thin-layer chromatography (Merck Kieselgel 60 F_{254}) and the products were separated by thin-layer chromatography on plates coated with silica (Merck Kieselgel 60 GF_{254}). − Infrared spectra were recorded on a Bio-Rad FTS-7 IR spectrometer with samples in 0.5 mm calcium fluoride solution cells. − ^{1}H NMR spectra were recorded on a Bruker DPX300 NMR spectrometer with samples in CD_2Cl_2 solution and were referenced to $SiMe_4$ (δ = 0). − ^{15}N NMR spectra were recorded on a Bruker DPX500 NMR spectrometer with samples in $CDCl_3$ solution using liq. NH_3 as a reference. − Positive and negative ionization fast atom bombardment (FAB) mass spectra were recorded on a Finnigan MAT 95 mass spectrometer using *m*-nitrobenzyl alcohol or α-thioglycerol as matrices. − Electronic absorption spectra were measured at room temperature on a Hewlett−Packard 8453 diode-array UV/vis spectrophotometer with samples in quartz cells with 1 cm path length. − Microanalyses were performed by Butterworth Laboratories, U.K.

Reaction of $[Ru_3(\mu\text{-}H)_2(CO)_9(\mu_3\text{-}NOMe)]$ (1) with [Cp*$Co(CO)_2$]: A solution of $[Ru_3(\mu\text{-}H)_2(CO)_9(\mu_3\text{-}NOMe)]$ (**1**, 100 mg, 0.17 mmol) in THF (50 mL) was heated with 2 equivalents of [Cp*$Co(CO)_2$] (83.1 mg, 0.33 mmol) under argon atmosphere. After refluxing for 10 h, the colour of the solution had changed to dark brown. The solvent was then removed under reduced pressure. The residue was redissolved in a small amount of CH_2Cl_2 and separated by preparative TLC eluting with *n*-hexane/dichloromethane (6:1, *v*/*v*). Four new products were isolated, in the following order of elution: brown $[Ru_3Co(\mu\text{-}H)(CO)_9(\eta^5\text{-}C_5Me_5)(\mu_4\text{-}N)]$ (**2**, R_f = 0.80, 69.8 mg, 0.091 mmol, 55%), trace amounts of starting $[Ru_3(\mu\text{-}H)_2(CO)_9(\mu_3\text{-}NOMe)]$ (**1**, R_f = 0.75) and known $[Ru_3(\mu\text{-}H)(CO)_9(\mu\text{-}NH_2)]$[15,29] ($R_f$ = 0.70), purple $[Ru_2Co(CO)_6(\mu_3\text{-}CO)(\eta^5\text{-}C_5Me_5)(\mu_3\text{-}NH)]$ (**3**, R_f = 0.55, 30.3 mg, 0.050 mmol, 20%), red $[Ru_5(\mu\text{-}H)(CO)_9(\mu\text{-}CO)_3(\eta^5\text{-}C_5Me_5)(\mu_4\text{-}NH)]$ (**4**, R_f = 0.10, 3.0 mg, 0.003 mmol, 3%), and green $[Ru_6Co(\mu_3\text{-}H)(CO)_8(\mu\text{-}CO)_3(\mu_4\text{-}\eta^2\text{-}CO)(\eta^5\text{-}C_5Me_5)_3(\mu_4\text{-}N)]$ (**5**, R_f = 0.07, 2.4 mg, 0.0017 mmol, 2%). − $C_{19}H_{16}NO_9CoRu_3$ (**2**, 764.5): calcd. C 29.84, H 2.09, N 1.83; found C 29.7, H 2.3, N 1.9. − $C_{17}H_{16}NO_7CoRu_2$ (**3**, 607.4): calcd. C 33.61, H 2.64, N 2.31; found C 33.7, H 2.4, N 2.4. − $C_{22}H_{17}NO_{12}Ru_5$ (**4**, 992.7): calcd. C 26.61, H 1.71, N 1.41; found C 26.8, H 1.8, N 1.6. − $C_{42}H_{46}NO_{12}CoRu_6$ (**5**, 1422.2): calcd. C 35.47, H 3.24, N 0.99; found C 35.6, H 3.1, N 1.0.

Reaction of Complex 1 with Pentamethylcyclopentadiene and 1,3-Cyclohexadiene: A solution of complex **1** (30 mg, 0.050 mmol) in THF (30 mL) has heated with 1 drop each of pentamethylcyclopentadiene and 1,3-cyclohexadiene under argon atmosphere. The initially yellow solution turned brown upon refluxing. After 10 h, the reaction mixture was concentrated to dryness under reduced pressure. The residue was redissolved in CH_2Cl_2 (2 mL) and separated by preparative TLC eluting with *n*-hexane/CH_2Cl_2 (2:1, *v*/*v*) to afford one red band containing **4** (R_f = 0.40) corresponding to a 4% yield (1.2 mg, 0.0012 mmol). The reaction of complex **1** with a drop of pentamethylcyclopentadiene was also attempted in the absence of 1,3-cyclohexadiene under otherwise similar conditions. The refluxing mixture was monitored by IR and spot TLC, but no reac-

tion was observed. About 80% of the starting material was recovered by TLC work-up on preparative silica plates.

Reaction of Complex 2 with DBU: Compound **2** (20 mg, 0.026 mmol) was stirred in basified dichloromethane (20 mL) [prepared by the addition of DBU (1,8-diazabicyclo[5.4.0]undec-7-ene) (0.2 mL of 0.13 M solution in CH_2Cl_2) to distilled dichloromethane (20 mL)]. The reaction was monitored by spot TLC and ^1H NMR spectroscopy until all the starting material had been consumed (about 10 min). The solvent was then removed under reduced pressure and the residue was chromatographed on silica using *n*-hexane/dichloromethane (6:1, *v*/*v*) as eluent. The only isolable product was cluster **3** (R_f = 0.55; 3.6 mg, 0.0059 mmol, 15%).

Reaction of Complex 2 with [Cp*Co(CO)$_2$]: A solution of cluster **2** (20 mg, 0.026 mmol) and [Cp*Co(CO)$_2$] (9.8 mg, 0.039 mmol) in THF was refluxed for 10 h. The solvent was then removed in vacuo and the residue was subjected to TLC using *n*-hexane/CH_2Cl_2 (6:1, *v*/*v*) as the eluent. Cluster **3** was obtained in 35% yield (R_f = 0.55, 8.4 mg, 0.014 mmol), accompanied by a small amount of unchanged **2** (R_f = 0.80, 1.0 mg, 0.0013 mmol, 5%).

Reaction of Complex 3 with [Ru$_3$(CO)$_{12}$]: Compound **3** (20 mg, 0.033 mmol) and a slight excess of [$Ru_3(CO)_{12}$] (15.4 mg, 0.024 mmol) were dissolved in *n*-octane or toluene (30 mL). The purple solution was heated to reflux for 4 h. The solvent was then removed under reduced pressure and the residue was subjected to TLC using *n*-hexane/CH_2Cl_2 (6:1, *v*/*v*) as eluent. The first band contained [$Ru_3(CO)_{12}$] (R_f = 0.95, 8.9 mg, 0.014 mmol). Two complexes were isolated in the following order of elution: [$Ru_6(\mu_3\text{-}H)(CO)_{12}(\mu\text{-}CO)(\mu_4\text{-}\eta^2\text{-}CO)_2(\eta^5\text{-}C_5Me_5)$][34] ($R_f$ = 0.60, 3.8 mg, 0.0033 mmol, 10%) and cluster **3** (R_f = 0.55, 6 mg, 0.0099 mmol, 30%).

Thermolysis of 2 with PhC$_2$Ph: A solution of compound **2** (20 mg, 0.026 mmol) and diphenylacetylene (9.3 mg, 0.052 mmol) in *n*-octane (30 mL) was refluxed under argon atmosphere for 5 h. The complete consumption of **2** was indicated by spot TLC monitoring. After cooling, the solvent was evaporated in vacuo. Chromatography of the residue on silica eluting with *n*-hexane/dichloromethane (2:1, *v*/*v*) afforded two major bands. Two consecutive bands were then eluted, containing [$Ru_3Co(CO)_6(\mu\text{-}CO)_2(\eta^5\text{-}C_5Me_5)(\mu_4\text{-}NH)(\mu_4\text{-}\eta^2\text{-}PhC_2Ph)$] (**6**, R_f = 0.40, 4.3 mg, 0.0047 mmol, 18%) and [$Ru_3Co(CO)_5(\mu\text{-}CO)_2(\eta^5\text{-}C_5Me_5)\{\mu_4\text{-}\eta^3\text{-}NC(O)C_2(C_4H_4)CHCH(Ph)\}(\mu_4\text{-}\eta^2\text{-}PhC_2Ph)$] (**7**, R_f = 0.15, 1.7 mg, 0.0016 mmol, 6%). − $C_{32}H_{26}NO_8CoRu_3$ (**6**, 914.7): calcd. C 42.01, H 2.84, N 1.53; found C 42.2, H 2.8, N 1.5. − $C_{46}H_{36}NO_8CoRu_3$ (**7**, 1092.9): calcd. C 50.55, H 3.30, N 1.28; found C 50.7, H 3.2, N 1.4.

Reaction of [Ru$_3$Co(CO)$_{12}$(μ$_4$-N)] with [Cp*Co(CO)$_2$]: A suspension of [$Ru_3Co(CO)_{12}(\mu_4\text{-}N)$] (100 mg, 0.14 mmol) and two equivalents of [Cp*Co(CO)$_2$] (70.2 mg, 0.28 mmol) in THF was refluxed. The resulting solution gradually changed from orange to dark-brown. Thermolysis was continued until no starting materials remained (about 4 h, as confirmed by IR spectroscopy). The mixture was then concentrated to dryness in vacuo. The dark-brown residue was redissolved in CH_2Cl_2 (2 mL) and TLC separation (*n*-hexane/dichloromethane, 9:1, *v*/*v*) afforded [$Ru_2Co_2(CO)_9(\eta^5\text{-}C_5Me_5)(\mu_4\text{-}N)$] **8** ($R_f$ = 0.80, 32.4 mg, 0.045 mmol, 32%) and cluster **3** (R_f = 0.48, 35.0 mg, 0.058 mmol, 41%). − $C_{19}H_{15}NO_9Co_2Ru_2$ (**8**, 721.3): calcd. C 31.62, H 2.08, N 1.94; found C 31.8, H 2.2, N 1.8.

Electrochemical Studies

Electrochemical measurements were carried out using an EG & G Princeton Applied Research (PAR) Model 273A potentiostat/galvanostat connected to an interfaced computer employing PAR 270 electrochemical software. Cyclic voltammograms were obtained using a gas (argon) sealed two-compartment cell equipped with a glassy carbon working electrode (Bioanalytical), a platinum wire auxiliary electrode (Aldrich), and an Ag/$AgNO_3$ reference electrode (Bioanalytical) at room temperature; 0.1 mol dm^{-3} *n*-tetrabutylammonium hexafluorophosphate (TBAHFP) in anhydrous deoxygenated CH_2Cl_2 was used as a supporting electrolyte. Ferrocene was added at the end of each experiment as an internal standard.[80] Potential data (vs. Ag/$AgNO_3$) were checked against the ferrocene (0/+1) couple; under the actual experimental conditions the ferrocene/ferrocenium couple is located at +0.18 V. Bulk electrolyses

Table 9. Crystal data and data collection parameters for compounds **2**−**6**

	2	**3**	**4**	**5**	**6**
Empirical formula	$C_{19}H_{16}NO_9CoRu_3$	$C_{17}H_{16}NO_7CoRu_2$	$C_{22}H_{17}NO_{12}Ru_5$	$C_{42}H_{46}NO_{12}CoRu_6$	$C_{32}H_{26}NO_8CoRu_3$
Formula weight	764.48	607.39	992.73	1422.18	914.70
Crystal colour, habit	Brown, block	Purple, block	Red, block	Green, block	Brown, prism
Crystal dimensions/mm	0.23 × 0.24 × 0.26	0.15 × 0.22 × 0.23	0.18 × 0.21 × 0.24	0.13 × 0.15 × 0.20	0.23 × 0.22 × 0.24
Crystal system	Triclinic	Monoclinic	Monoclinic	Monoclinic	Monoclinic
Space group	$P\bar{1}$ (no. 2)	$P2_1/n$ (no. 14)	$C2/c$ (no. 15)	$P2_1/c$ (no. 14)	$P2_1/c$ (no. 14)
a/Å	10.963(1)	8.632(1)	31.589(2)	20.685(2)	10.405(1)
b/Å	9.843(5)	17.702(2)	10.324(1)	11.785(1)	18.875(1)
c/Å	12.027(4)	13.582(1)	19.549(2)	20.782(2)	16.199(1)
α/°	86.72(3)				
β/°	105.06(4)	97.78(2)	114.28(2)	111.01(2)	99.27(1)
γ/°	85.67(7)				
V/Å^3	1245.7(8)	2056.3(4)	5811(1)	4729.3(10)	3139.8(4)
Z	2	4	8	4	4
Density (calcd.)/g cm^{-3}	2.038	1.962	2.269	1.997	1.935
μ(Mo-K_α)/cm^{-1}	24.85	22.85	25.99	22.65	19.87
Diffractometer	Rigaku AFC7R	MAR Research Image Plate	MAR Research Image Plate	MAR Research Image Plate	MAR Research Image Plate
Reflections collected	3463	17185	25154	39075	28865
Unique reflections	3257	3658	5628	5275	5610
Obsd. reflections [$I > 1.5\sigma(I)$]	2946	2857	3970	2950	3943
R	0.023	0.034	0.058	0.062	0.082
R′	0.028	0.047	0.062	0.056	0.090
Goodness of fit, *S*	1.85	1.65	2.21	1.37	1.63

Table 10. Crystal data and data collection parameters for compounds **7−8**

	7·0.5CH_2Cl_2	**8**
Empirical formula	$C_{46.5}H_{37}NO_8ClCoRu_3$	$C_{19}H_{15}NO_9Co_2Ru_2$
Formula mass	1135.40	721.34
Crystal colour, habit	Dark brown, prism	Brown, block
Crystal dimensions/mm	0.21 × 0.22 × 0.26	0.28 × 0.25 × 0.22
Crystal system	Monoclinic	Triclinic
Space group	$P2_1/c$ (no. 14)	$P\bar{1}$ (no. 2)
a/Å	16.205(1)	9.627(1)
b/Å	13.378(1)	10.707(1)
c/Å	20.673(2)	11.974(1)
α/°		75.31(2)
β/°	93.20(2)	88.64(1)
γ/°		92.35(1)
V/Å^3	4474.7(6)	1192.1(2)
Z	4	2
Density (calcd.)/g cm^{-3}	1.685	2.009
μ (Mo-K_α)/cm^{-1}	14.70	26.58
Diffractometer	MAR Research Image Plate	MAR Research Image Plate
Reflections collected	40930	11539
Unique reflections	6558	4003
Obsd. reflections [$I > 1.5\sigma(I)$]	3697	3184
R	0.062	0.044
R'	0.055	0.050
Goodness of fit, S	1.52	1.66

were carried out in a gas-tight cell consisting of three chambers separated at the bottom by fine frits, with a carbon cloth (80 mm^2) working electrode in the middle, and $Ag/AgNO_3$ reference and Pt gauze auxiliary electrodes in the lateral chambers. The working potentials (E_w) for reduction and oxidation processes were ca. 0.15 V more negative and more positive than the corresponding electrode potentials (E_p), respectively; all coulometric experiments were performed in duplicate.

Crystallography

Crystals suitable for X-ray analyses were glued onto glass fibres with epoxy resin or sealed in 0.3 mm glass capillaries. Intensity data were collected at ambient temperature on either a Rigaku-AFC7R diffractometer (complex **2**) or a MAR research image plate scanner (complexes **3−8**) using graphite-monochromated Mo-K_α radiation (λ = 0.71073 Å) in the ω − 2θ and ω scan modes, respectively. Details of the intensity data collection and crystal data are given in Table 9 and Table 10. The diffracted intensities were corrected for Lorentz and polarization effects. The Ψ scan method was employed for semiempirical absorption corrections in the case of **2**,[81] while an approximate absorption correction based on inter-image scaling was applied in the case of **3−8**. Scattering factors were taken from ref.[82] and anomalous dispersion effects[83] were included in F_c. The structures were solved by direct methods (SIR-92[84] for **6−8**; SHELX-86[85] for **2−5**) and expanded by Fourier-difference techniques. Atomic coordinates and thermal parameters were refined by full-matrix least-squares analysis on F, with the ruthenium atoms and non-hydrogen atoms being refined anisotropically whenever possible. The nitrene and metal hydride hydrogens were located by Fourier-difference synthesis, while those of the organic moieties were generated in their ideal positions (C−H 0.95 Å). Calculations were performed on a Silicon Graphics computer, using the program package TEXSAN.[86]

Crystallographic data (excluding structure factors) for the structures reported in this paper have been deposited with the Cambridge Crystallographic Data Centre (CCDC) as supplementary publication nos. CCDC 149061−149067. Copies of the data can be obtained free of charge on application to the CCDC, 12 Union Road, Cambridge CB2 1EZ, U.K. [Fax: (internat.) +44 (0)1223/336033; E-mail: deposit@ccdc.cam.ac.uk].

Acknowledgments

We gratefully acknowledge financial support from the Hong Kong Research Grants Council and the University of Hong Kong. E. N.-M. Ho acknowledges the receipt of a postgraduate studentship, Swire Scholarship 1998−2000, Hung Hing Ying Scholarship 1998−2000, and Epson Foundation Scholarship 2000−2001 administered by the University of Hong Kong and Michael Gale Scholarship 1998−99 awarded by the University of Hong Kong and Hong Kong Telecom Foundation.

[1] D. E. Fjare, D. G. Keyes, W. L. Gladfelter, *J. Organomet. Chem.* **1983**, *250*, 383.
[2] D. E. Fjare, W. L. Gladfelter, *J. Am. Chem. Soc.* **1984**, *106*, 4799.
[3] M. L. Blohm, W. L. Gladfelter, *Organometallics* **1985**, *4*, 45.
[4] A. Gourdon, Y. Jeannin, *J. Organomet. Chem.* **1992**, *440*, 353.
[5] M. L. Bedard, A. D. Rae, L. F. Dahl, *J. Am. Chem. Soc.* **1986**, *108*, 5924.
[6] W. L. Gladfelter, *Adv. Organomet. Chem.* **1985**, *24*, 41.
[7] W. Sun, S. Yang, H. Wang, Y. Yin, *Polyhedron* **1992**, *11*, 1143.
[8] C. E. Anson, J. P. Attard, B. F. G. Johnson, J. Lewis, J. M. Mace, D. B. Powell, *J. Chem. Soc., Chem. Commun.* **1986**, 1715.
[9] A. Gourdon, Y. Jeannin, *Organometallics* **1986**, *5*, 2406.
[10] A. Czaka, K. Aika, *Catal. Sci. Technol.* **1981**, *3*, 87.
[11] P. H. Emmett, *The Physical Basis for Heterogeneous Catalysis* (Eds.: E. Drauglis, R. I. Jaffe), Plenum Press, New York, **1975**, p. 3−34.
[12] E. L. Muetterties, T. N. Rhodin, E. Bard, C. F. Brucker, W. R. Pretzer, *Chem. Rev.* **1979**, *79*, 91.
[13] E. N.-M. Ho, W.-T. Wong, *J. Chem. Soc., Dalton Trans.* **1998**, 4215.
[14] E. N.-M. Ho, W.-T. Wong, *J. Chem. Soc., Dalton Trans.* **1998**, 513.
[15] K. K.-H. Lee, W.-T. Wong, *J. Chem. Soc., Dalton Trans.* **1996**, 1707.
[16] K. K.-H. Lee, W.-T. Wong, *Inorg. Chem.* **1996**, *35*, 5393.
[17] K. K.-H. Lee, W.-T. Wong, *J. Organomet. Chem.* **1995**, *503*, 43.

[18] R. E. Stevens, R. D. Guettler, W. L. Gladfelter, *Inorg. Chem.* **1990**, *29*, 451.
[19] R. E. Stevens, W. L. Gladfelter, *J. Am. Chem. Soc.* **1982**, *104*, 6454.
[20] J. Kiviaho, M. Reinikainen, M. K. Niemelä, K. Kataja, S. Jääskeläinen, *J. Mol. Cat. A: Chem.* **1996**, *106*, 187.
[21] M. Reinikainen, J. Kiviaho, M. Kröger, M. K. Niemelä, S. Jääskeläinen, *J. Mol. Cat. A: Chem.* **1997**, *118*, 137.
[22] T. Matsuzaki, Y. Sugi, H. Arakawa, K. Takeuchi, K.-I. Bando, N. Isogai, *Chem. Ind.* **1985**, 555.
[23] G. Jenner, P. Andrianary, *J. Mol. Cat.* **1990**, *58*, 307.
[24] K.-I. Tominaga, Y. Sasaki, T. Watanabe, M. Saito, *Studies in Surface Science and Catalysis* **1998**, *114*, 495.
[25] M. Hidai, Y. Koyasu, M. Yokota, M. Orisaku, Y. Uchida, *Bull. Chem. Soc. Jpn.* **1982**, *55*, 3951.
[26] G. Jenner, *J. Mol. Cat. A: Chem.* **1995**, *96*, 215.
[27] F. Schweyer, P. Braunstein, C. Estournès, J. Guille, H. Kessler, J.-L. Paillaud, J. Rosè, *Chem. Commun.* **2000**, 1271.
[28] K. K.-H. Lee, W.-T. Wong, *J. Organomet. Chem.* **1999**, *577*, 323.
[29] J. A. Smieja, R. E. Stevens, D. E. Fjare, W. L. Gladfelter, *Inorg. Chem.* **1985**, *24*, 3206.
[30] M. S. Ziebarth, L. F. Dahl, *J. Am. Chem. Soc.* **1990**, *112*, 2411.
[31] S.-H. Han, J.-S. Song, P. D. Macklin, S. T. Nguyen, G. L. Geoffroy, *Organometallics* **1989**, *8*, 2127.
[32] H. Beurich, H. Vahrenkamp, *Angew. Chem.* **1978**, *90*, 915; *Angew. Chem. Int. Ed. Engl.* **1978**, *17*, 863.
[33] Y. Chi, L.-K. Liu, G. Huttner, L. Zsolnai, *J. Organomet. Chem.* **1990**, *390*, 50.
[34] E. Kolehmainen, K. Rissanen, K. Laihia, Z. A. Kerzina, M. I. Rybinskaya, M. Nieger, *J. Organomet. Chem.* **1996**, *524*, 219.
[35] M. L. Blohm, D. E. Fjare, W. L. Gladfelter, *Inorg. Chem.* **1983**, *22*, 1004.
[36] H.-G. Ang, K.-W. Ang, S.-G. Ang, A. L. Rheingold, *J. Chem. Soc., Dalton Trans.* **1996**, 3131.
[37] B. F. G. Johnson, T. M. Layer, J. Lewis, P. R. Raithby, W.-T. Wong, *J. Chem. Soc., Dalton Trans.* **1993**, 973.
[38] C. Z. Tu, R. C. William, J. R. Steven, *Organometallics* **1994**, *13*, 3594.
[39] J. S. Field, R. J. Haines, D. N. Smit, *J. Chem. Soc., Dalton Trans.* **1988**, 1315.
[40] C. A. Tolman, *J. Am. Chem. Soc.* **1970**, *92*, 2956.
[41] B. Ulf, M. Götz, S.-E. Helen, S.-F. Georg, *J. Chem. Soc., Dalton Trans.* **1992**, 2131.
[42] R. D. Adams, J. E. Babin, M. Tasi, T. A. Wolfe, *J. Am. Chem. Soc.* **1988**, *110*, 7093.
[43] R. D. Adams, J. E. Babin, M. Tasi, *Organometallics* **1988**, *7*, 503.
[44] J. R. Galsworthy, C. E. Housecroft, R. L. Ostrander, A. L. Rheingold, *J. Organomet. Chem.* **1995**, *492*, 211.
[45] S. A. R. Knox, B. R. Lloyd, A. G. Orpen, J. M. Vinas, M. Weber, *J. Chem. Soc., Chem. Commun.* **1987**, 1498.
[46] S. A. R. Knox, B. R. Lloyd, D. A. V. Morton, S. M. Nicholls, A. G. Orpen, J. M. Vinas, M. Weber, G. K. Williams, *J. Organomet. Chem.* **1990**, *394*, 385.
[47] B. F. G. Johnson, F. J. Lahoz, J. Lewis, N. D. Prior, P. R. Raithby, W.-T. Wong, *J. Chem. Soc., Dalton Trans.* **1992**, 1701.
[48] M. L. Blohm, W. L. Gladfelter, *Organometallics* **1986**, *5*, 1049.
[49] J.-S. Song, S.-H. Han, S. T. Hguyen, G. L. Geoffroy, A. L. Rheingold, *Organometallics* **1990**, *9*, 2386.
[50] D. M. P. Mingos, D. J. Wales, *Introduction to Cluster Chemistry*, Prentice-Hall, New Jersey, **1990**.
[51] Density functional calculations at the B3LYP level were performed on the model cluster $[Ru_3Co(CO)_6(\mu\text{-}CO)_2(\eta^5\text{-}C_5H_5)(\mu_4\text{-}NH)(\mu_4\text{-}\eta^2\text{-}HC_2H)]$ on the basis of the experimentally determined geometry. The basis set used for C, N, O, and H atoms was 6-31G, while an effective core potential with a LANL2DZ basis set was employed for Ru and Co.
[52] A. Reed, L. A. Curtiss, F. Weinhold, *Chem. Rev.* **1988**, *88*, 899.
[53] K. B. Wiberg, *Tetrahedron* **1968**, *24*, 1083.
[54] G. Schaftenaar, *Molden v3.5*, CAOS/CAMM Centre Nijmegen, Toernooiveld, Nijmegen (Netherlands), **1999**.
[55] K. Wade, *Adv. Inorg. Chem. Radiochem.* **1976**, *18*, 1.
[56] Density functional calculations at the B3LYP level were performed on the model cluster $[Ru_4(CO)_9(\mu\text{-}CO)_2(\mu_4\text{-}NOH)(\mu_4\text{-}\eta^2\text{-}HC_2H)]$ on the basis of the experimentally determined geometry. The basis set used for C, N, O, and H atoms was 6-31G, while an effective core potential with a LANL2DZ basis set was employed for Ru.
[57] T. Jaeger, S. Aime, H. Vahrenkamp, *Organometallics* **1986**, *5*, 245.
[58] M. A. Collins, B. F. G. Johnson, J. Lewis, J. M. Mace, J. Morris, M. McPartlin, W. J. H. Nelson, J. Puga, P. R. Raithby, *J. Chem. Soc., Chem. Commun.* **1983**, 689.
[59] E. Roland, H. Vahrenkamp, *Organometallics* **1983**, *2*, 183.
[60] J. S. Song, G. L. Geoffroy, A. L. Rheingold, *Inorg. Chem.* **1992**, *31*, 1505.
[61] K. Knoll, G. Huttner, T. Fassler, L. Zsolnai, *J. Organomet. Chem.* **1987**, *327*, 255.
[62] K. Knoll, G. Huttner, L. Zsolnai, O. Orama, *Angew. Chem.* **1986**, *98*, 1099; *Angew. Chem. Int. Ed. Engl.* **1986**, *25*, 1119.
[63] K. Knoll, O. Orama, G. Huttner, *Angew. Chem.* **1984**, *96*, 989; *Angew. Chem. Int. Ed. Engl.* **1984**, *23*, 976.
[64] G. Huttner, K. Knoll, *Angew. Chem.* **1987**, *99*, 765; *Angew. Chem. Int. Ed. Engl.* **1987**, *26*, 743.
[65] R. D. Adams, J. A. Belinski, *Organometallics* **1991**, *10*, 2114.
[66] J. S. Haines, R. J. Haines, D. N. Smit, K. Natarajan, O. Scheidsteger, G. Huttner, *J. Organomet. Chem.* **1982**, *240*, C23.
[67] T. Jaeger, H. Vahrenkamp, *Z. Naturforsch.* **1986**, *B41*, 789.
[68] D. Nuel, F. Dahan, R. Mathieu, *Organometallics* **1986**, *5*, 1278.
[69] G. D. Williams, G. L. Geoffroy, R. R. Whittle, A. L. Rheingold, *J. Am. Chem. Soc.* **1985**, *107*, 729.
[70] G. D. Williams, R. R. Whittle, G. L. Geoffroy, A. L. Rheingold, *J. Am. Chem. Soc.* **1987**, *109*, 3936.
[71] S. R. Drake, *Polyhedron* **1990**, *9*, 455.
[72] J. A. Page, G. Wilkinson, *J. Am. Chem. Soc.* **1952**, *74*, 6149.
[73] C. Furlani, E. O. Fischer, *Z. Elektrochem.* **1957**, *61*, 481.
[74] M. L. Blohm, D. E. Fjare, W. L. Gladfelter, *J. Am. Chem. Soc.* **1986**, *108*, 2301.
[75] M. Tachikawa, E. L. Muetterties, *J. Am. Chem. Soc.* **1980**, *102*, 4541.
[76] A. J. Gordon, R. A. Ford, *The Chemists Companion: A Handbook of Practical Data, Techniques, and References*, John Wiley & Sons, **1972**, p. 299.
[77] D. E. Fjare, W. L. Gladfelter, *Inorg. Chem.* **1981**, *20*, 3533.
[78] R. E. Stevens, W. L. Gladfelter, *Inorg. Chem.* **1983**, *22*, 2034.
[79] L. R. Byers, L. F. Dahl, *Inorg. Chem.* **1980**, *19*, 277.
[80] G. Gritzner, J. Kute, *Pure Appl. Chem.* **1984**, *56*, 461.
[81] A. C. T. North, D. C. Phillips, F. S. Mathews, *Acta Crystallogr., Sect. A* **1968**, *24*, 351.
[82] D. T. Cromer, J. T. Waber, *International Tables for X-ray Crystallography*, Kynoch Press, Birmingham, **1974**, Vol. *4*, Table 2.2B,
[83] D. T. Cromer, J. T. Waber, *International Tables for X-ray Crystallography*, Kynoch Press, Birmingham, **1974**, Vol. *4*, Table 2.3.1.
[84] A. Altomare, M. C. Burla, M. Camalli, M. Cascarano, C. Giacovazzo, A. Guagliardi, G. Polidori, *J. Appl. Crystallogr.* **1992**, *25*, 310.
[85] G. M. Sheldrick, *Crystallographic Computing 3* (Eds: G. M. Sheldrick, C. Kruger, R. Goddard), Oxford University Press, **1985**, p. 175.
[86] TEXSAN, Crystal Structure Analysis Package, Molecular Structure Corporation, Houston, TX, **1985** and **1992**.

Received October 13, 2000
[I00389]

Effect of Halide Contaminant Ions in the Hydrothermal Treatment of Amorphous Titania on the Phase Change from Anatase to Rutile During Calcination

James Ovenstone*[a] and Kin-Chau Chan[a]

Keywords: Hydrothermal treatment / Titania / Anatase / Rutile / Phase change

Hydrothermal treatment in salt solutions has been used to crystallise and stabilise the anatase phase of titania. Halide contaminants have been shown to accelerate crystallisation of anatase when compared to reactions in pure water, but as anion size increases, the crystallisation improvement is less. The crystallised anatase has then been calcined to form rutile. The impurity ions appear to adsorb to the titania surface and have been shown to have a strong influence on the anatase/rutile transition, reducing the rutile formation during calcination due to the steric hindrance of the rutile nucleation sites on the titania surface. The adsorption sites for the anions affecting anatase crystallisation and rutile formation are different.

1. Introduction

Many factors which influence the phase change from anatase to rutile in titania have been investigated,[1,2,3] and in particular, the influence of doping ions. It has been proposed that the presence of Co^{2+}, Cu^{2+}, K^+, Na^+, Fe^{3+}, Li^+, and Mn^{4+}, all accelerate the transformation of anatase to rutile by increasing the oxygen ion vacancy concentration, while the presence of W^{6+}, NO_3^-, Cl^-, F^-, SO_4^{2-}, PO_4^{2-}, and Nb^{5+} all hinder the transformation by reducing the oxygen ion vacancy concentration.[4,5,6,7] Most of these studies have only been concerned with the final phase change during calcination, however, and very little work has considered the effects of the synthesis method of the anatase itself.

Previous results have shown that the control over the hydrothermal conditions, as well as over the contaminant ions present after the amorphous titania production are vital to controlling the crystallisation properties of the anatase powder.[8,9] In addition, the preparation route for the amorphous precursor has been shown to be vital for controlling the properties of the hydrothermally crystallised anatase. In recent work we have shown that the presence of a small amount of brookite contaminant in the anatase phase can strongly enhance the phase change to rutile. The preparation route for the amorphous titania, as well as the hydrothermal conditions can be used to control how much brookite is present in the anatase powder.[10]

Criado and Real showed how the presence of the phosphate ion inhibited the formation of rutile during calcination, by adsorption to the titania surface, rather than by lattice ion substitution.[11] In the current work, particular attention has been paid to the hydrothermal systems including the halide ions, since these are common contaminants in titania powders, but also to the influence of the preparation route of the amorphous precursor, as this can also be an important factor.

[a] School of Chemical and Life Sciences, University of Greenwich, London SE18 6PF, UK

2. Results and Discussion

2.1 Crystallisation of the Ethoxide Derived Powder

Hydrothermal reactions in 0.5 M sodium halide salt solutions were studied to see their effect on the phase change to rutile. The hydrothermal products were all anatase, except for the reaction in NaF, which formed a different phase, which has been noted before.[9] This phase could not be identified from the JCPDS database files and will be the subject of further work at a later date. Figure 1 shows the X-ray powder diffraction (XRD) traces for the products after hydrothermal treatment. Anatase has formed in all cases (except for the fluoride reaction).

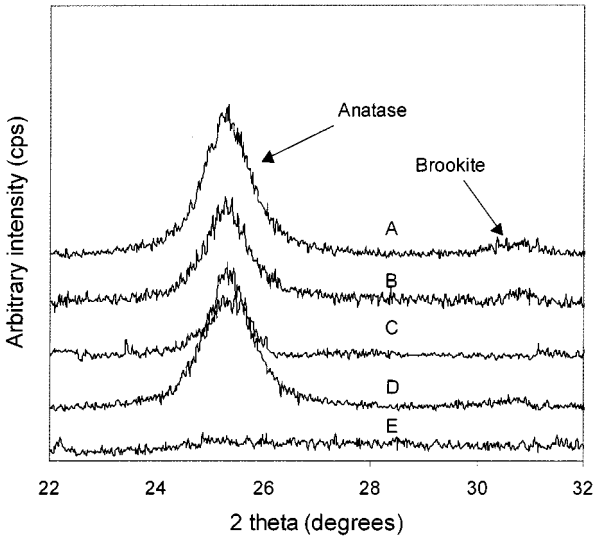

Figure 1. XRD traces of products from hydrothermal treatments in 0.5 M sodium halide salt solutions. A) H_2O, B) NaI, C) NaBr, D) NaCl, E) NaF

 © WILEY-VCH Verlag GmbH, 69451 Weinheim, 2001 1434–1948/01/0505–1339 $ 17.50+.50/0

The extent of crystallisation was estimated from the loss in specific surface area from the original high surface area amorphous material (Figure 2).[8] Ion coupled plasma mass spectrometry (ICPMS) results showed that the concentration of adsorbed contaminant ions after hydrothermal treatment remained constant at around 15 wt% ±5%. Therefore, the number of mol of contaminate ions per mol of titania fell as the molecular weight of the contaminate ion increased. This would suggest that the adsorption of the salts to the surface of the titania powder is controlled by the anion rather than the cation. Clearly, the presence of the halide salts increased the rate of crystallisation (since in all cases the surface area was lower, indicating less amorphous material present). It can also be seen that the rate of crystallisation was enhanced most by the presence of the chloride ion and least by the iodide ion, indicating that the larger ions have the least effect. Furthermore, as the halide ion size increases, so the crystallite size of the anatase formed, decreases. The mechanism by which the ions accelerate the crystallisation is considered to be a surface reaction, where the halide ion can adsorb to the surface, distorting the lattice due to its large size, and thus enabling the rearrangement of the titanium and oxygen ions. Due to the large size difference between the halide contaminant ions and the oxide ions (compare 1.4 Å for O^{2-} with 1.81 Å for Cl^{-}) it would be extremely unlikely that the halides could enter the lattice under the relatively mild conditions of the crystallisation (120 °C). As the anion size increases, its growth accelerating effect decreases, since the ions fluctuate too rapidly between the solvated and surface bound states in the autoclave. This limits the time for anatase crystallite growth, and gives smaller anatase crystallite sizes (Figure 2). As a result, after hydrothermal treatment, the powders treated in salt solutions with larger anions, still have a considerable amount of high surface area amorphous material remaining (measured using the Brunauer, Emmett, and Teller isotherm (BET), Figure 2).[9]

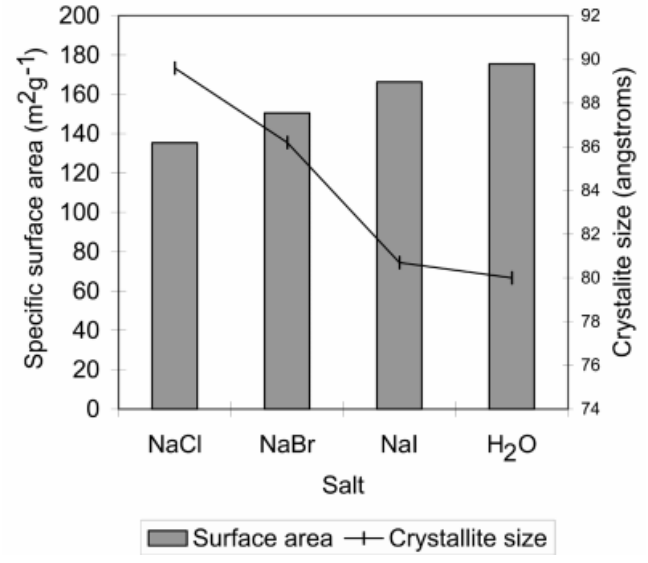

Figure 2. Chart showing the variation in specific surface area (SSA) and crystallite size with salt for hydrothermal reactions carried out at 120 °C for 90 minutes

2.2 Calcination to Form Rutile

The powders treated hydrothermally, produced mostly rutile after calcination, as can be seen from Figure 3, although when sodium fluoride was used, again other phases were formed. Although absolute intensities of peaks in XRD spectra are not quantitatively comparable there is still a very obvious difference in the amount of rutile formed between the samples with different contaminants, with the largest contaminant ions producing the least amount of rutile. Crystallite size data (calculated from the XRD data) showed that the rutile produced from each reaction had a very similar particle size (around 65 nm). This is surprising, since usually, the larger the crystallite size in the anatase product after hydrothermal treatment, then the lower the crystallinity of the rutile after calcination (i.e. the anatase is stabilised). Therefore, the remaining adsorbed salts must have a strong influence over the phase change during calcination.

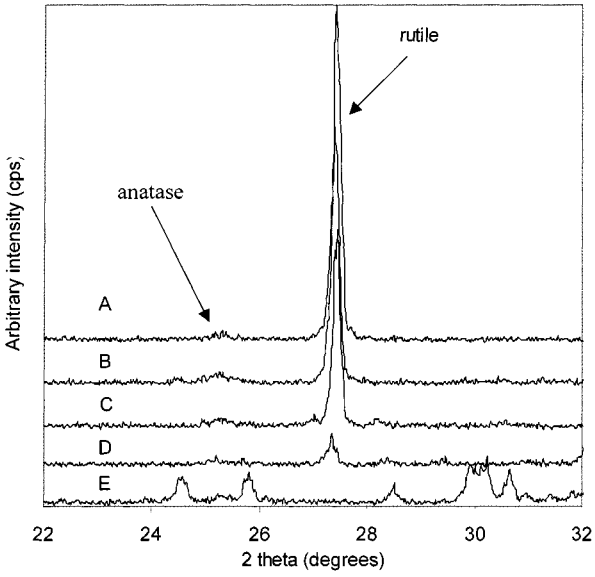

Figure 3. XRD traces for C3 powders hydrothermally treated in 0.5 M sodium halide salt solutions then heated in a DTA apparatus at 20 °C per min to 1000 °C and cooled. A) H_2O, B) NaCl, C) NaBr, D) NaI, E) NaF

This can be explained in terms of the initial reaction in the autoclave, where the anions bind to the surface of the amorphous titania, accelerating the growth of anatase as described previously.[9] The crystallised material has a considerably smaller surface area, and therefore less halide material bound to the surface. The remaining amorphous titania, however, still has a considerable amount of contaminating ions adsorbed to its high surface area material after hydrothermal treatment and these ions (the halide contaminants), reduce the rate of crystallisation by a different mechanism under the dry, ion immobilising, calcination conditions. The literature explanation for the slowing of the phase change of rutile by monovalent anions is the replacement of O^{2-} ions by the cations which would result in the reduction of O^{2-} ion vacancies in the lattice to compensate for the change in charge.[4–7] However, this seems unlikely

due to the difference in size between the monovalent anions used and the oxide ions (ionic radius = 1.4 Å), and particularly doubtful in the case of the large iodide ion (ionic radius = 2.20 Å). In addition, replacement of the small O^{2-} ions in the lattice by the larger halide ions, would doubtless cause a detectable shift in the lattice parameters of the titania, and a noticable shift in the XRD peaks. This is not the case. Therefore, a surface chemistry solution is more likely. Since the halide ions clearly exert a larger stabilising effect than the difference in crystallite size of the hydrothermal anatase product, it would then seem logical that the halide ions in some way block the rutile nucleation site on the titania surface. Since the binding site for the iodide and other halide ions should be the same, and the other halide ions have a far smaller inhibiting effect on the phase change, the binding site may not be the actual rutile nucleation site (which is also on the surface).[1] Instead, a site, which is close to the rutile nucleation site, may be the adsorption point for the halide ions, so that only an ion as large as the iodide ion could sterically inhibit its rearrangement to the rutile phase.

Further evidence for the phase stabilisation as a surface effect rather than an ion exchange is in the products for the reactions carried out in sodium fluoride solutions. Only the hydrothermal treatment in sodium fluoride resulted in phases other than anatase during the hydrothermal stage, and these phases changed to completely new phases during calcination. This implies that only the fluoride ion (1.33 Å) is small enough to either replace the oxide ions in the titania lattice, or enter other sites within the lattice, and that such an incorporation results in the formation of various new phases depending on the reaction conditions. In addition, the incorporation of the cation (sodium) also seems to be controlled by the size of the anion, as only the sodium fluoride formed new phases. If the cation was the controlling agent, the sodium would be expected to enter the lattice in all cases, forming new phases.

2.3 Effect of Changing Amorphous Precursors

As the preparation route to the amorphous titania precursor has been shown to have a strong influence on the anatase product after hydrothermal treatment,[8] and upon the subsequent phase change to rutile,[10] the effect on the phase change of the use of different precursors has been investigated after treatment in different salt solutions. Comparative studies of the effects of the halide ion solutions have been made on two other anatase powders precipitated by different methods. Powder A3 was precipitated from $TiCl_4$ under predominantly acidic conditions, resulting in a powder which retained some adsorbed chloride contamination. This powder was also shown by Raman spectroscopy to have some anatase like short range order, despite being X-ray amorphous. Powder B3 was also precipitated from $TiCl_4$, but under strongly basic conditions, thus eliminating any chloride contamination, but leaving the powder with some ammonium ions adsorbed to the surface. Raman spectroscopy showed this powder to be truly amorphous, as was the C3 powder.[8]

The A3 powder gave products similar to those for the C3 powder after hydrothermal treatment, both in the extent of the reaction when compared to pure water, and in the order of crystallinity of product between the salts. The B3 powder produced much less crystalline powders after hydrothermal treatment, and the relative effects of the different salts on the crystallisation of the anatase was much less clear. After calcination, however, both the A3 and the B3 powders showed a similar trend in rutile formation to the original experiments with the C3 powder.

These results indicate that there may be two types of surface adsorption site on the titania. The first is an acidic site on the amorphous powder and, in the presence of a halide contaminant, allows the rapid growth of the anatase phase after its nucleation by the water. Hence the B3 powder exhibited almost no anatase crystallite growth due to its high surface basicity. The second is probably a less acidic site, on the anatase itself, and so the surface basicity of the B3 powder did not hinder the adsorption of the halide, nor the subsequent effect on the phase change to rutile of the halide ion. The A3 and C3 powders are both effectively neutral, and so would also be expected to exhibit this behaviour during calcination.

To summarise, in terms of contaminant ions, it can be seen that the ion size is crucial in determining its influence on the phase change. Anions can strongly influence the anatase crystallisation, increasing the rate of crystallisation. It has been shown that as their size increases, the strength of surface adsorption decreases in hydrothermal solution, producing less crystalline anatase. The expected surface adsorption site for the halide ions causing this effect is basic in nature. The halide ions also hinder the nucleation of the rutile phase during calcination, however, by means of a steric hindrance effect. The larger halide ions have a larger stabilising effect on the anatase, as they can block the rutile nucleation site more effectively. The ions causing this effect are expected to adsorb to neutral or basic surface sites. The effects of surface adsorbed salts are controlled predominantly by the cations, since the anion (sodium) is capable of entering the lattice (as demonstrated by the NaF reactions), but did not unless the anion was sufficiently small.

Experimental Section

$TiCl_4$ (30 mL, 0.273 mol) was diluted with ice cold water (300 mL). A 1.5 M NH_3 solution was added dropwise to the clear $TiCl_4$ solution until the pH was raised from 0.5 to 3.0 (appox.740 mL). The white precipitate formed was aged for 24 hours before washing with water until the pH reached 7. The amorphous powder (A3) was then dried for 24 hours at room temperature.

$TiCl_4$ (20 mL, 0.182 mol) was diluted with ice cold water (200 mL), and added dropwise to a 7.5 M ammonia solution (1000 mL). The pH fell from 12.5 to 10.9 as the white precipitate formed. Again the amorphous precipitate was aged for 24 hours before washing until the pH reached 9.2. The amorphous powder (B3) was then dried for 24 hours at room temperature.

$Ti(OC_2H_5)_4$ (25 g, 0.108 mol) was added to 550 mL of dry ethanol, and mixed thoroughly before being added to a 0.6 M solution of

water in ethanol [5.94 mL (0.330 mol) of water in 550 mL of ethanol]. After ageing for 25 minutes, the reaction mixture was centrifuged and washed twice with ethanol before drying in a vacuum dessicator.[12]

Hydrothermal crystallisation was carried out by dispersing 60 mg of amorphous titania powder in 10 mL of distilled water in an autoclave (internal volume 20 mL), and then heating the autoclave to 120 °C for 90 minutes. 1 M salt solutions (sodium fluoride, sodium chloride, sodium bromide, and sodium iodide) were sometimes used in place of water.

After treatment in the autoclaves, the powders were washed with water and dried at room temperature under vacuum. Samples of the powders were dissolved, and their halide ion contents and titanium contents measured by ICPMS. The phase was determined by XRD (Rigaku Rotaflex), using a 2θ range of 10−70°, a step size of 0.02°, and a scan speed of 4°/min. A Cu-K_α source with a wavelength of 1.5406 Å, and equipped with a nickel filter to remove the K_β lines. The crystallite size was estimated by Scherrer's method. The formula used for calculation of the particle size was $p_m = k\lambda/\beta_{1/2}\cos\theta°$. In this case, p_m is the mean particle diameter (in nanometres), k is a constant (0.89), λ is the wavelength of the X-ray radiation, and θ is the diffraction angle of the peak. $\beta_{1/2}$ is the pure diffraction breadth at half the maximum value of the peak. This is calculated as $\beta = B - b$, where B is the experimentally observed width, and b is the breadth of a highly crystalline material (particle size >> 1000 Å). In this case silicon powder was used. The XRD step size was reduced to 0.006° at a rate of 0.5°/min. For anatase, the peak with the Miller indices 101 (100%) was used, while for rutile the 110 (100%) peak was used. Although it is not possible to accurately estimate the particle sizes using this method, it is extremely sensitive to the trends in particle size for the same material. In addition, TEM was used to confirm that the particle sizes were in a suitable region. The specific surface area was measured using the 3 point BET method using a Yuasa Ionics NOVA 1000 instrument. Differential thermogravimetric analysis (TG/DTA) was carried out on a Seiko SSC5200H system. The TG/DTA apparatus was used to calcine samples by heating at a ramp of 20 °Cmin^{-1} to 1000 °C before allowing to cool. The phase of these samples was then checked again by XRD, and the anatase/rutile composition estimated by the method outlined by Spurr and Myers.[13] The anatase/rutile proportions using the equation $f = 1/[1+1.26(I_R/I_A)]$. Here f is the weight fraction of anatase, I_R is the intensity of the main rutile XRD peak (Miller indices = 110), and I_A is the intensity of the main anatase XRD peak (Miller indices = 101). They estimated the error in this measurement to be within 1%. Raman spectroscopy was carried out using a Kaiser Optical Systems Holoprobe rpt. System. Salt concentrations in hydrothermal products were obtained using atomic absorption spectroscopy.

Acknowledgments

This project was funded by the EU/JSPS Joint Fellowship Programme. The authors would like to thank Prof. K. Yanagisawa for the use of the hydrothermal apparatus in the Research Laboratory for Hydrothermal Chemistry. Thanks also go to the Daresbury Chemical Database Service.

[1] A.W. Czanderna, C.N.R. Rao, J.M. Honig, *Trans. Farad. Soc.* **1957**, *54*, 1069−1073.
[2] J.C. Jamieson, B. Olinger, *Am. Mineral.* **1969**, *54*, 1477−1481.
[3] F. Dachille, P.Y. Simons, R. Roy, *Am. Mineralol.* **1968**, *53*, 1929−1939.
[4] Y. Ohtsuka, Y. Fujiki, Y. Suzuki, *J. Jap. Assoc. Min.* **1982**, *77*, 117−124.
[5] E.F. Heald, C.W. Weiss, *Am. Mineralol.* **1972**, *57*, 10−23.
[6] F.C. Genari, D.M. Pasquevich, *J. Mater. Sci.* **1998**, *33*, 1571−1578.
[7] S. Hishita, M. Takata, H. Yanagida, *Yogyo-Kyokai-shi* **1978**, *86(12)*, 631−632.
[8] K. Yanagisawa, J. Ovenstone, *J. Phys. Chem. B* **1999**, *103(37)*, 7781−7787.
[9] J. Ovenstone, K. Yanagisawa, submitted to: *J. Am. Ceram. Soc.*, July **1999**.
[10] J. Ovenstone, K. Yanagisawa, *Chem. Mater.* **1999**, *11(10)*, 2770−2774.
[11] J. Criado, C. Real, *J. Chem. Soc., Faraday Trans.* **1983**, *79*, 2765−2771.
[12] E.A. Barringer, H.K. Bowen, *J. Am. Ceram. Soc.* **1981**, *65*, C199−C201.
[13] R.A. Spurr, H. Myers, *Anal. Chem.* **1957**, *29(5)*, 760−762.

Received July 11, 2000
[I00271]

Synthesis, Spectral Characterisation and Crystal Structure of (1,24-Bicyclophthalocyaninato)bismuth(III)

Karim Benihya,[a] Mireille Mossoyan-Déneux,*[a] and Michel Giorgi[b]

Keywords: Bismuth / Phthalocyanines / Bicyclic / Molecular structure / IR spectroscopy / UV/Vis spectroscopy

A new orange bicyclophthalocyanine complex of bismuth(III), [Bi($C_{48}H_{24}N_{13}$)], has been synthesised by means of the template reaction of bismuth(III) acetate with phthalodinitrile. The ligand consists of the phthalocyanine skeleton, which is bridged by two additional isoindole units. The conjugation of the phthalocyanine ring is interrupted by the two bridgehead sp^3-hybridised carbon atoms. The main difference between this new bicyclophthalocyanine and those previously reported in the literature lies in the position of the bridgehead carbon atoms. In order to differentiate between these bicyclophthalocyaninato complexes, we propose a nomenclature: [Bi($C_{48}H_{24}N_{13}$)] is named Bi(1,24-Pcc), and the other bicyclic ligands already reported in the literature are named (1,16-Pcc) and (1,17-Pcc). The molecular structure of Bi(1,24-Pcc) shows the coordination polyhedron around the bismuth atom, made up of the six isoindole nitrogen atoms of the macrocycle, as a strongly distorted trigonal prism. The two Bi–N_{iso} bonds of the bridge and two of the four Bi–N_{iso} bonds of the (Pc) ring have bond lengths between 2.40 and 2.47 Å. One of the remaining bonds is longer (2.55 Å), and the sixth has a very short length of 2.20 Å. This new complex was fully characterised by UV/Vis and IR spectroscopy, also reported here.

Introduction

We recently reported the synthesis and characterisation of a new phase of the triple-decker compound, $Bi_2(Pc)_3$.[1] During the preparation of $Bi_2(Pc)_3$, if reaction mixture was heated to approximately 240 °C and allowed to cool to room temperature, we obtained many bright, orange−red crystals. This compound, **1**, was characterised by X-ray diffraction as a complex containing six units of phthalonitrile organised in three cycles per bismuth atom. The ligand consists of a phthalocyanine skeleton bridged by two additional isoindole moieties (Figure 1). The conjugation of the phthalocyanine ring is interrupted by the two bridgehead pyrrole C_α atoms, which are sp^3 hybridised. Similar phthalocyanine complex precursors were reported by Baumann et al.,[2] and by Perkins and Whelen[3] with cobalt and copper as the central metal atoms, and by Barnhart and Skiles with copper and nickel as the central metal atoms.[4] Although the molecular structure had not yet been elucidated, these authors proposed a structure similar to the one that we obtained. The complete resolution of the molecular structure of a neighbouring yellow−green complex, the bicyclophthalocyaninatochloroniobium(IV), [Nb($C_{48}H_{24}N_{13}$)Cl] (**2**) was reported for the first time by Gingl and Strähle.[5] Janczac and Kubiak obtained other green bicyclophthalocyanine complexes, $M^{III}(C_{48}H_{24}N_{13})$ **3**, with indium(III), gadolinium(III), thallium(III), and cerium(III),[6] and reported the molecular structure of the Gd,[7] In,[6] and Tl[8] complexes. All these complexes contain a ligand with the same overall formula ($C_{48}H_{24}N_{13}$), but these ligands have different structures and point symmetries. The main difference between these macrocyclic ligands lies in the bridgehead carbon atoms.

In **3**, the bridgehead atoms are the pyrrole C_α atoms (C1 and C17 in our numbering scheme, proposed in Figure 1) which belong to the two opposite isoindole rings of the phthalocyanine skeleton, and are on both sides of the metal(III). In **2**, the bridgehead atoms are the pyrrole C_α atoms (C1 and C16) that belong to the two neighbouring isoindole rings of the phthalocyanine skeleton. In **1**, the bridgehead atoms are the pyrrole C_α atoms (C1 and C24) belonging to the two opposite isoindole rings as is the case in **3**, but they are on the same side of the bismuth atom. Thus this bicyclophthalocyanine ligand has an original structure.

Results and Discussion

Proposal for Nomenclature

In the literature, the names of these bicyclophthalocyanines are confusing. The empirical formula of the ligand ($C_{48}H_{24}N_{13}$) does not indicate either the nature of the ligand related to phthalocyanine or the different positions of the bridgehead carbons. The substitutive nomenclature of IUPAC is not easy to use. For example, compound **3** in which the trivalent metal is substituted by three hydrogen atoms, is named 29*H*,31*H*,35*H*-19,5-(nitrilo[1,3]isoindolediylidenenitrilo[1]isoindolyl[3]ylidenenitrilo)phthalocyan-

[a] Université de Provence, Laboratoire de chimie de coordination, Case D 22,
Av. de l'Escadrille Normandie-Niemen, 13397 Marseille Cedex 20, France
Fax: (internat.) + 33-4/91028959
E-mail: mireille.mossoyan-deneux@lcc.u-3mrs.fr
[b] Service de cristallochimie UMR 6517,
Av. de l'Escadrille Normandie-Niemen, 13397 Marseille Cedex 20, France

 © WILEY-VCH Verlag GmbH, 69451 Weinheim, 2001 1434−1948/01/0505−1343 $ 17.50+.50/0

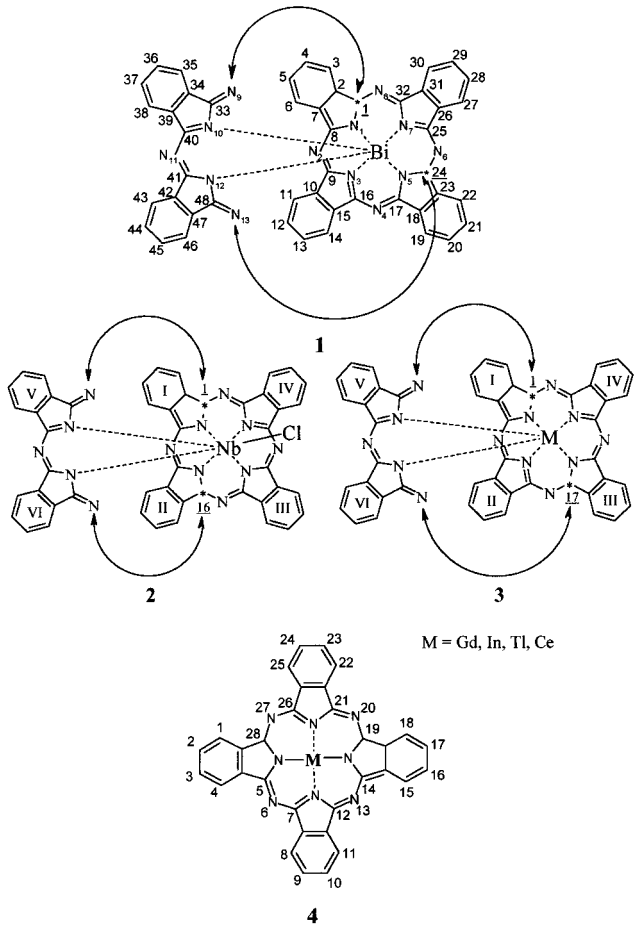

Figure 1. Structure of **1**, Bi(1,24-Pcc), compared to bicyclophthalocyanine complexes **2**, NbCl (1,16-Pcc), and **3**, M(1,17-Pcc) (M = Gd, In, Tl); reported in the literature. Our numbering scheme is used for all structures rather than that adopted for substituted phthalocyanine macrocycles **4**

ine.[9] For simplification, in reference[7] and subsequent papers, Janczak et al. named the bicyclic macrocycle in compound **3** as Pcc, and this name is now an accepted abbreviation of this hexapyrrole ligand.[9] Since three different hexapyrrole ligands of this kind have now been synthesised, we propose to indicate the numbering of the bridgehead carbons as prefixes in the letter code. For phthalocyanine compounds, the numbering scheme generally used in the literature[9,10] is shown in Figures 1−4. It was selected by the authors to indicate the position of the substituted groups at the periphery of the phthalocyanine macrocycle. The IUPAC name mentioned above follows this numbering scheme, but in the clockwise sequence, the numbering prefixes being as small as possible. We think that this numbering scheme is not suitable for that kind of complex. Bicyclophthalocyanines are not substituted phthalocyanines: the colour is different, the visible spectrum does not show the intense Q-band characteristic of phthalocyanine systems, and finally, bicyclophthalocyanines are chemically more reactive than the usual phthalocyanines. All these differences are explained by the interruption of the π-conjugation of the phthalocyanine ring. Furthermore, the differences in the colours of the three different bicyclophthalocyanine ligands reported in the literature are probably due to the different number of benzopyrrole moieties involved in the π-electron delocalisation between the two bridgehead carbon atoms. So it seems to us that the positional indices of the bridgehead atoms have priority over the indices of possible substituents at the periphery of the benzene rings. In the same way as R. Kubiak and J. Janczak,[8,11−13] and some other authors[14−16] did for crystallographic purposes, we started the numbering of the carbons from one pyrrole carbon C_α so that the carbon atoms of the first isoindole ring (I) are numbered from 1 to 8, those of the second (II) from 9 to 16, those of the third (III) from 17 to 24 and those of the fourth (IV) from 25 to 32, nitrogen atoms being numbered separately. In order to have the substitution prefixes as small as possible, we started the numbering of the carbon atoms from a bridgehead carbon. With this numbering scheme, compounds **2** and **3** are named NbCl(1,16-Pcc) and M(1,17-Pcc) (M = Gd, In, Tl), respectively, and **1** is named Bi(1,24-Pcc). There are some advantages in this numbering scheme: a) The indices are independent of the clockwise or anticlockwise sequence and of the bridgehead carbon atom chosen as number one; b) The second index directly indicates the number of benzopyrrole moieties between the two bridgehead carbon atoms, each benzopyrrole moiety being made up of eight carbon atoms.

Synthesis and Properties

It is not surprising that the structure of the bicyclophthalocyanine with niobium(IV), in which the metal is bonded to a chlorine atom, is different to that of bicyclophthalocyanines with trivalent metals, but it is unexpected that **1** has a structure different from those of all the metal(III) bicyclophthalocyanines prepared by Janczak et al. These authors had stated that the chemical composition of the metallophthalocyanines with trivalent metals was strongly dependent on their preparation method.[17] Effectively, **1** and **3** were prepared differently, with a change in the metallation agents, the weight proportions, the pressure and the nature of the atmosphere, the temperature and the reaction time. But we think that the formation of Bi(1,24-Pcc) can also be explained by the properties of the bismuth atom, which are different from those of indium(III), gadolinium(III), and thallium(III) ones. Compound **1** was first obtained using the method employed in the preparation of $Bi_2(Pc)_3$,[1] and the heating was interrupted at approximately 230−240 °C. However, the evolution of the reaction mixture to the triple-decker compound was very fast, and hence, the formation of a larger amount of orange crystals was easier when the ratio of phthalodinitrile/bismuth acetate was reduced to 7.

Compound **1** has been synthesised from the template reaction of phthalodinitrile around the bismuth(III) acetate following the reaction:

$$6\,[C_6H_4(CN)_2] + {}^1/_2\,N_2 + 3\,e^- + Bi^{3+} \rightarrow [C_{48}H_{24}N_{13}]Bi$$

That reaction was performed in air. The phthalodinitrile was involved in an hexamerisation reaction, but was also partly sublimed, and partly involved in secondary polymerisation reactions and in decomposition reactions.[10,18] We believe that the additional nitrogen atom, as well as the three electrons that allow for the formation of the trianionic ligand $[C_{48}H_{24}N_{13}]^{3-}$, arise from these secondary reactions.

Like Tl^{III}(1,17-Pcc), **1** was not soluble in conventional organic solvents: acetone, DMF, DMSO, benzene, toluene, chloronaphthalene. Washing with these solvents allowed us to separate **1** from other by-products of the reaction. A mixture of orange crystals and a light grey powder was retained by the filter. Crystals of **1** are very hydrophobic and, in spite of a very high density (1.48), floated at the interface of a water/acetone/pentane (1/1/1) mixture, while the light grey powder fell to the bottom of the vessel. The crystals were large and very crumbly, and their quality was not good enough for a diffraction study. When dissolved in concentrated acids, the triple-decker compound $Bi_2(Pc)_3$, and **1** decomposed, giving bismuth salts, but the former was converted into free phthalocyanine $H_2(Pc)$ while the latter was converted into phthalimide, the hydrolysis product of phthalonitrile. This experimental result showed that the $(Pcc)^{3-}$ ligand is effectively less stable than the $(Pc)^{2-}$ ligand, as assumed by Gingl and Strähle,[5] because of the interruption of the π-conjugation along the inner 16-membered ring.

Kasuga and Tsutsui reported that the bicyclophthalocyanine complexes have bright colors.[19] Superphthalocyanines are dark blue,[20] metallophthalocyanines with a rigorously planar phthalocyanine ligand, such as Cu(Pc) or Co(Pc), are dark blue−violet and metallophthalocyanines, such as Pb(Pc), in which the ligand is saucer-shaped, are dark green. Janczak and Kubiak assumed that this interruption of the π-conjugation undoubtedly accounts for the specific green colour of metallobicyclophthalocyanines. They suggested that the blue−violet colour was characteristic of all phthalocyanines in which there is full delocalisation of π-electrons along the inner 16-membered ring, and that green was the characteristic colour of bicyclophthalocyanines in which the π-electron delocalisation is interrupted.[7,8] Effectively, all reported bicyclophthalocyanines complexes with the (1,17-Pcc) ligand are green. As proved by X-ray analysis, **1** and **2** are also bicyclophthalocyanines in which the π-electron delocalisation is interrupted: **2** is yellow−green, **1** is not green, but bright orange, closer to red than to yellow. We believe that the color of the complex depends on the length of the π-electron delocalisation and particularly on the number of benzopyrrole moieties involved in the delocalisation. In **2** and **3**, the interruption of the π-conjugation divides the macrocycle (Pc) into two parts, each containing two benzopyrrole moieties, while in **1** there are three benzopyrrole moieties in one part and only one in the other part. Note that boron subphthalocyanines (SubPc)B, which contain only three benzopyrrole moieties, are characterised by their bright color.[21] (SubPc)BPh, which has a phenyl group on the boron atom, is a golden brown solid,[21] and finally, a boron subphthalocyanine substituted with *tert*-butyl groups at the periphery of the macrocycle is magenta-coloured.[22] The bright orange colour of the crystals of Bi(1,24-Pcc) is probably due to the extension of the π-delocalisation along three benzopyrrole moieties.

Crystal Structure of Bi(1,24-Pcc)

Figure 2 shows two ORTEP views of **1**. Part (a) shows a co-crystallised molecule of VII behind the bridging cycle. The molecular structure of **1** was determined unambiguously by the X-ray diffraction study, and a last series of Fourier difference cycles revealed some electronic densities, all lying in the same plane. Among these electronic densities, the most identifiable scheme was a five-membered cycle. They were attributed to a strongly disordered co-crystallised molecule.

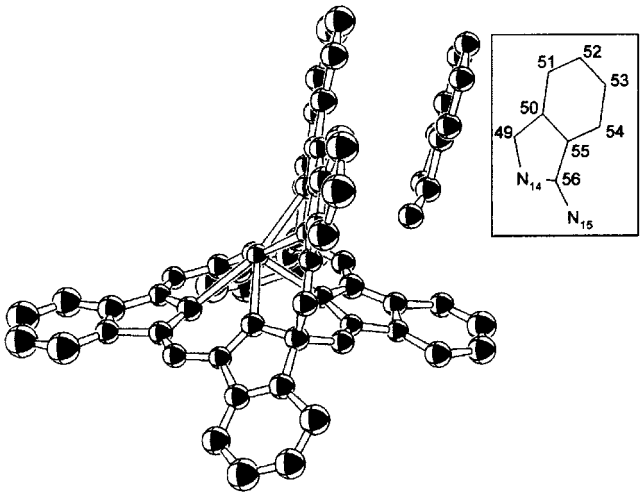

2a

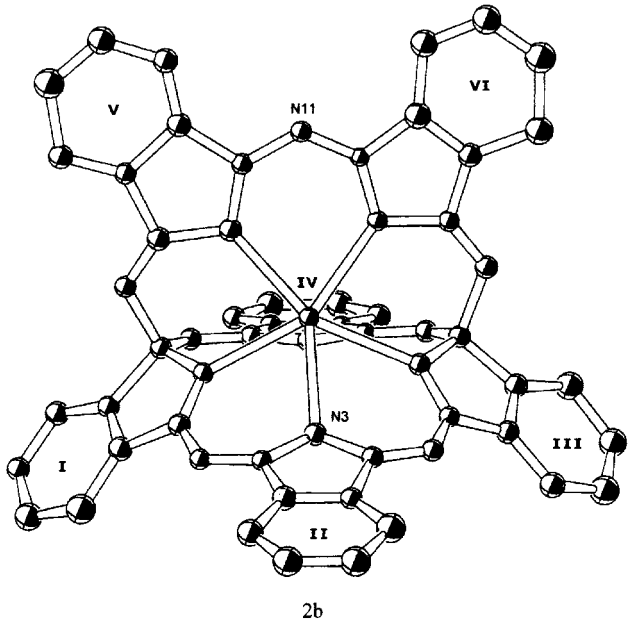

2b

Figure 2. ORTEP drawings of **1** with the co-crystallised molecule (with the atoms numbered in the inset) (2a), and facially viewed with the numbering of all benzopyrrole moieties (2b)

Compound **1** was formed in molten phthalonitrile, and during several attempts to purify it by sublimation, the orange crystals broke up and gave a yellow−orange powder and some sublimed light yellow powder, the IR spectrum of which suggested the presence of a large amount of phthalonitrile. Furthermore, the formation of $Bi_2(Pc)_3$ by heating only washed orange crystals is impossible, but the heating of orange crystals in molten phthalonitrile up to 310 °C always produced the triple-decker compound. On the basis of these experimental observations, we attributed these residual densities to a cyclised phthalonitrile, probably an intermediate in the synthesis of $Bi_2(Pc)_3$, stabilised by the interaction with Bi(1,24-Pcc) in the crystal. This additional benzopyrrole moiety was fixed as $C_8H_4N_2H_2$, numbered as indicated in Figure 2(a) and named VII.

Gingl and Strähle have described their bicyclic complex as two phthalocyaninato anions having a common half. Effectively, in **2**, the macrocycle formed by the benzopyrrole rings I, II, III, and IV on the one hand and that formed by the benzopyrrole rings I, II,VI, and V on the other, make up a ring similar to a phthalocyanine with eight pyrrole α carbons and four N_{aza} bridges, but it is not really a phthalocyanine system owing to the interruption of the π-conjugation. In **3** there is only one phthalocyanine-like ring formed by benzopyrrole rings I, II, III, and IV. The macrocycle formed by I, II,VI, and V rings on the one hand and that formed by the III, IV,VI, and V rings on the other, both have eight pyrrole α carbons but five N_{aza} bridges, and not four. Compound **1** is a molecule that contains a ring similar to a superphthalocyanine formed by the five benzopyrrole moieties I, II, III, V, and VI, and a phthalocyanine-like ring formed by the four benzopyrrole moieties I, II, III, and IV. These two macrocycles have three common isoindole rings (I, II, and III).

While **2** has a twofold axis passing through the Cl and Nb atoms, and through the (N2) N_{aza} atom of the common half (Pc) ring, **1** and **3** have no crystallographic symmetry element. In Figure 2(b) it seems that there is a molecular pseudo symmetry plane passing through N3, N7, and N11, and through the bismuth atom, but the angle values and the bond lengths around the two sp^3 carbons, reported in Table 1, show that some pseudo-symmetrical distances are not equal in the estimated standard deviation limits (e.g., compare C1−N8 and C24−N6 bond lengths). This disymmetry is probably due to the co-crystallised molecule. The observed values are typical for normal sp^3 carbon atoms that are σ-bonded to an sp^2 nitrogen atom or to another sp^2 carbon atom. Furthermore, all bond lengths of the macrocyclic skeleton of **1** are comparable to the corresponding lengths reported for **2**[5] and **3**.[6−8] Because of the interruption of the π-conjugation, the (Pc)-like ring is not planar and it is difficult to find reference planes, as is the case in **3**, in which there are three similar planes, each containing two benzopyrrole units. We choose two reference planes for **1**. The first, P1 is the mean-plane formed by the isoindole nitrogens N1, N3, N5, and N7 and is the reference for the phthalocyanine ring atoms. N1 and N5 are above P1, while N3 and N7 are under P1. The second reference plane P2, formed by C1, N10, N12, and C24, is taken as a reference for the atoms belonging to the bridging cycle. The deviation from P2 of these four atoms is very small (below $2\cdot10^{-3}$ Å). P3 is the mean plane of the co-crystallised molecule. As shown in Figure 3, the dihedral angle between P1 and P2 is 101.70° (±2.96°) and the bismuth atom lies at a distance of 1.259 Å from P1 and 1.212 Å from P2.

Table 1. Characteristic values (bond lengths and angles) around the two sp^3-hybridised carbon atoms

C1 Atom		C24 Atom	
Bond lengths [Å]			
C1−N1	1.513(1)	C24−N5	1.468(1)
C1−N8	1.424(2)	C24−N6	1.476(1)
C1−N9	1.484(2)	C24−N13	1.446(2)
C1−C2	1.492(2)	C24−C23	1.516(2)
Angles [deg.]			
N1−C1−N9	108.1(1)	N5−C24−N13	110.9(1)
N1−C1−C2	104.1(1)	N5−C24−C23	101.7(1)
N1−C1−N8	114.8(1)	N5−C24−N6	117.9(1)
N8−C1−N9	109.2(1)	N6−C24−N13	109.2(1)
N8−C1−C2	110.8(2)	N6−C24−C23	107.6(1)
N9−C1−C2	109.6(1)	N13−C24−C23	109.0(1)

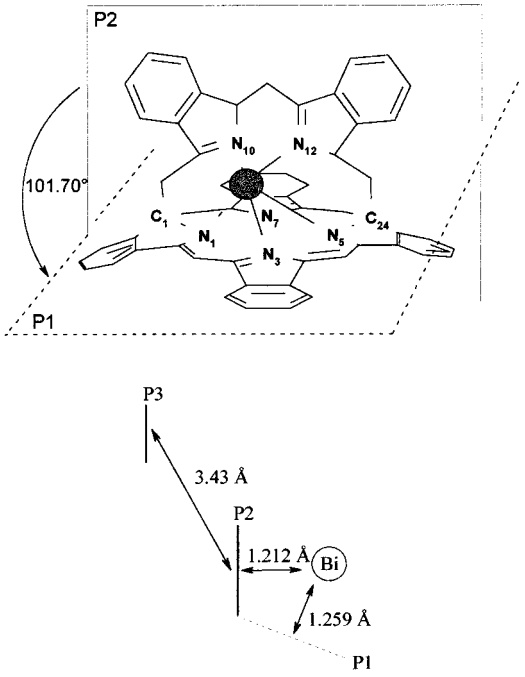

Figure 3. (Above) Dihedral angles [deg.] between mean planes P1 and P2. (Below) Distances [Å] between: 1) the bismuth(III) atom and these planes; 2) mean planes P2 and P3

All benzopyrrole units are planar, and the dihedral angles between the pyrrole and the benzene rings are smaller than the estimated standard deviation. Figure 2 clearly shows that the benzopyrrole II is nearly in P1, but that the other three benzopyrrole groups deviate strongly from P1. The dihedral angles of the benzopyrrole mean planes I, II, III, and IV with P1 are 38.1, 2.9, 38.6, and 22.0° respectively, and the estimated standard deviation is equal to 3.6°. In the bridging moiety, the dihedral angles between mean planes VI and V, and P2 are 7.4° and 170.7°, respectively. P3 was

Table 2. Selected bond lengths [Å] characterising the coordination polyhedron of **1** compared with those of other bicyclophthalocyanine compounds reported in the literature

Compound	(1,16-Pcc)$Nb^{IV}Cl$[5]	(1,17-Pcc)Gd^{III} [7]	(1,17-Pcc)In^{III} [6]	(1,17-Pcc)Tl^{III} [8]	(1,24-Pcc)Bi^{III} (this work)
M−N Bond					
M−N1	2.148(2)	2.235(7)	2.203(4)	2.238(14)	2.4125(9)
M−N3	2.148(2)	2.263(7)	2.221(4)	2.245(17)	2.5538(9)
M−N5	2.257(1)	2.231(6)	2.208(4)	2.266(18)	2.4041(9)
M−N7	2.215(2)	2.241(7)	2.221(5)	2.278(15)	2.2004(8)
M−N10	2.257(1)	2.274(6)	2.262(4)	2.282(13)	2.477(1)
M−N12	2.215(2)	2.282(6)	2.267(4)	2.310(13)	2.460(1)
Ionic radii [pm][26]	82	107.8	94	102.5	117

calculated in order to determine its position relative to the bridging ring, and particularly to unit VI. The dihedral angle between mean plane VI and P3 is 7.9°, with an estimated standard deviation of 4.7° so that the co-crystallised molecule may be considered as nearly parallel to the benzopyrrole VI. The two mean planes are separated by 3.43 Å, but the N15 atom lies only 2.97 Å from mean plane VI: there is some interaction between the co-crystallised molecule and the benzopyrrole VI, and we believe that this interaction allows for the immediate stabilisation of the crystal and a cyclised form of the benzonitrile, an intermediate in the synthesis of the triple-decker compound.

The coordination polyhedron, made up of the six isoindole nitrogen atoms is a strongly distorted trigonal prism. Related distances are reported in Table 2 and compared with other bond lengths for bicyclophthalocyanine compounds reported in the literature. In both phases of $Bi_2(Pc)_3$,[24,1] the bismuth is bonded to the internal (Pc) ring by long $Bi-N_{iso}$ distances (mean value: 2.734 Å) and to the external (Pc) rings by short $Bi-N_{iso}$ distances (mean value: 2.334 Å). In **1** we note that four $Bi-N_{iso}$ bonds (N1, N5, N10, and N12) have bond lengths between 2.40 and 2.47 Å, but that the Bi−N3 bond is longer [2.554(1) Å] and the Bi−N7 bond has a very short length of 2.200(1) Å. The first result is comparable with that found in $Bi(Pc)_2(CH_2Cl_2)$ (2.47 Å) described by Homborg,[23] and slightly larger than that found for $Bi-N_{iso}$ bonds of the external macrocycles in the triple-decker compounds. The second value is intermediate between the two different values obtained in the triple-decker compounds. The Bi−N7 bond length is shorter than the $Bi-N_{iso}$ distances reported by Janczak and Kubiak for $[Bi(Pc)]_4(Bi_4I_{16})$ as the smallest known among the bismuth phthalocyanine complexes[25] [between 2.260(11) and 2.283(10) Å]. The $Bi(Pc)^+$ moiety in $[Bi(Pc)]_4(Bi_4I_{16})$ is the only bismuth monophthalocyanine with an elucidated structure. In the other known phthalocyanine complexes, the metal is sandwiched between two phthalocyanine rings and it is reasonable that the $Bi-N_{iso}$ distances are longer.

We now compare the coordination polyhedron with those of the other bicyclophthalocyanines (Table 2). Except for Bi−N7, all the $Bi-N_{iso}$ bond lengths are longer than those of the $M-N_{iso}$ bonds reported in the literature for bicyclophthalocyanine compounds with M = Gd, Nb, Tl, and In. This is consistent with the fact that the Bi^{3+} cation has the largest ionic radius in the series, as reported by Shannon[26] for a coordination number of six. In **2** and **3**, the shortest $M-N_{iso}$ bond lengths are those in which the pyrrole nitrogen atoms are directly bonded to the sp^3 carbon atoms. Furthermore, in compounds **3** and except for M−N5 in (1,17-Pcc)Tl, the longest $M-N_{iso}$ bonds are those related to the pyrrole nitrogen atom of the bridging cycle. In **1**, the bridge divides the macrocycle (Pc) so that there are three benzopyrrole moieties in the one section and only one in the other section. This disymmetry displaces the bismuth atom on the same side as the lone benzopyrrole so that Bi−N7 is the smallest known $Bi-N_{iso}$ bond among bismuth phthalocyanine complexes and, on the opposite side, Bi−N3 is then the longest $Bi-N_{iso}$ bond in **1**. Among the four remaining $Bi-N_{iso}$ bonds, as observed in the compounds **2** and **3**, the shortest $Bi-N_{iso}$ bond lengths are those in which the nitrogen atoms of the pyrrole moiety are directly bonded to the sp^3 carbon atom and the longest $Bi-N_{iso}$ bonds are those related to the pyrrole nitrogen atoms of the bridge. Compound **1** has six $M^{III}-N_{iso}$ σ-bonds, like compound **3**, but the cation Bi^{3+} has two valence electrons more than thallium or indium. That electron pair is not necessary for the formation of the six bonds and may be located as a non-bonding electron pair on the bis-

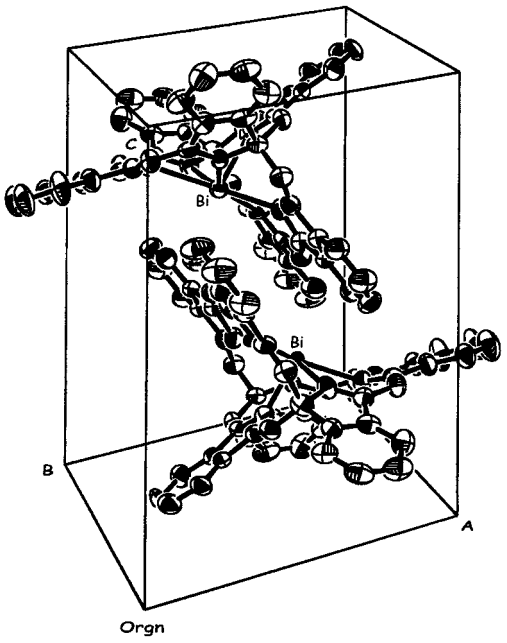

Figure 4. Relative position of two molecules of **1** in the crystal cell

muth atom, inducing the distortion of the coordination polyhedron.

Figure 4 shows the relative position of two molecules of **1** in the crystal cell. Compound **1** is first formed during the synthesis of $Bi_2(Pc)_3$ and its stoichiometry is exactly half that of $Bi_2(Pc)_3$. One can easily deduce that the relative position of these two molecules of **1** in the crystal cell determines the first stage of the dimerisation of **1** to give the triple-decker bismuth phthalocyanine.

The shortest interatomic distances between two successive bicyclophthalocyanine molecules are N3···C29 (3.42 Å) and C28···C8 (3.47 Å). These distances indicate a very weak interaction between the π-electron delocalisation systems of the related benzopyrrole rings. Nevertheless, interactions concerning carbon atoms at the periphery of the phenyl rings cannot participate in the formation of $Bi_2(Pc)_3$. More interesting are the distances between the aza-nitrogen of the first molecule and the α-carbons of the pyrrole ring of the second molecule. These distances can be considered as too long to allow for a dimerisation through these atoms (N9···C48 = 5.66 Å and N13···C33 = 5.64 Å). It is remarkable that two successive bicyclic molecules are closer in **3** than in **1**. These distances are 3.25, 3.36, and 3.36 Å for the indium, gadolinium, and thallium complexes, respectively.

UV/Vis Spectroscopy

Figure 5 shows the UV/Vis spectrum of **1**. We distinguish a very small Q band at λ = 630 nm and a very large and intense B band at 302 nm with two shoulders at 392 nm and at approximately 455 nm. The spectrum of **1** is very different from that of the monophthalocyanine Bi(Pc)Cl reported by Isago and Kagaya.[27] All the bands of **1** are blue-shifted, and the most striking difference is the almost complete disappearance of the Q band.

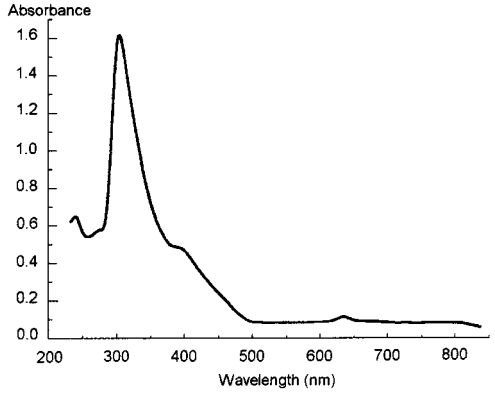

Figure 5. UV/Vis spectrum of **1** recorded using a KBr pellet medium (0.5%)

The appearance of an intense Q band generally characterises the phthalocyanine group and is assigned in the literature to a π → π* transition delocalised over the (Pc) ring.[28] It is then understandable that the interruption of the π-conjugation in the (Pc) ring in **1** involves the important decrease in the Q band. The shoulder between 380 and 480 nm contains at least two bands. Such a shoulder in the visible/near-UV region was reported by Gouterman et al.[28] in the spectrum of Pb(Pc), and was attributed to the presence of an allowed $6p_z$ (metal)→π* (Pc) charge-transfer transition (MLCT: Metal-to-Ligand Charge Transfer), by analogy with the (porphyrinato)lead(II) complex. Following this conclusion, Isago et al.[27] have assigned the extra 415 nm band in the visible spectrum of Bi(Pc)Cl to an hyper MLCT band, an excitation from an $a_{2u}(6p_z)$ orbital of bismuth(III) to an eg(π*) (Pc) orbital. In the same way, Lever et al.[29] and Stillman et al.[30] assigned the transitions at approximately 450 nm to metal-to-ligand (MLCT) or ligand-to-metal (LMCT) charge-transfer transitions, depending on the oxidation state of the transition metal. Other authors have assigned this broad band as evidence for the existence of a free radical (Pc) ring, which is not inconsistent with the proposal of a charge-transfer transition. In the lithium phthalocyanine radical, Li(Pc), a doublet at 427 and 473 nm has been attributed to the free radical monophthalocyanine[31−33] while a similar broad band centred at approximately 450−470 nm has also been attributed to a free-radical phthalocyanine ring in $Ln(Pc)_2$[34−36] and in $In(Pc)_2$.[37] It is difficult to use the interpretation of monophthalocyanine or diphthalocyanine spectra for the interpretation of the spectrum of the compound **1** because Bi(Pc)Cl and other phthalocyanine compounds have a C_{4v} or D_{4h} symmetry, while **1** has no symmetry element, the allowed transitions are different and the molecular orbitals should have different energies and a different electron-density distribution. Nevertheless the shape and the energy of the transition at approximately 390−480 nm is very similar to those reported for Pb(Pc),[28] Bi(Pc)Cl,[27] or $In(Pc)_2$,[37] so we propose to assign that transition to a charge transfer from bismuth to the bicyclophthalocyaninato ligand. The B band, which is mostly an $a_{2u}\rightarrow e_g$ transition, has the same shape as the B band of Bi(Pc)Cl and is very intense, with an ε value of $0.6\cdot10^5$ $M^{-1}cm^{-1}$, close to that measured in porphyrin compounds. In the phthalocyanine compounds, the B band has an ε value much smaller than 10^5 $M^{-1}cm^{-1}$.[28] In addition to the B band, some authors[38−40] described two other bands at lower wavelengths: the N band resulting mainly from a $b_{2u}(\pi) \rightarrow e_g(\pi^*)$ transition, and the L band resulting from a combination of $a_{2u}(\pi)\rightarrow e_g(\pi^*)$ and $b_{2u}(\pi)\rightarrow e_g(\pi^*)$ transitions.[38] The bands appearing in the spectrum of **1** at 275 nm, as a shoulder of the B band, and at 238 nm may be assigned to the N and L transitions, respectively.

Infra-Red Spectroscopy

Figure 6 shows the FTIR spectrum of **1** between 500 and 2000 cm^{-1} (Figure 6a) and between 50 and 650 cm^{-1} (Figure 6b). Our assignments were made based on literature reports[37,41−51] and by comparison with those made for Pb(Pc).[1,27] Some very intense and fairly intense bands characteristic of Pb(Pc) are evident in the spectrum of Bi(1,24-Pcc), with only a slight modification. These are for Pb(Pc)/Bi(1,24-Pcc), respectively: bands at 725/720 cm^{-1} [out-of-plane C−H deformations γ(C−H)[27]], 772/774

cm^{-1} [C−N stretching vibration in pyrrole skeleton, ν(C−N)], 950/953 cm^{-1} and that at 1003/997 cm^{-1}, the band at 1080/1065 cm^{-1} and that at 1161/1162 cm^{-1} both assigned to C−N stretching vibration, and the bands at 1282/1299 and 1479/1482 cm^{-1}, all in the range of the C−C stretching vibration frequencies in the isoindole skeleton, ν(C−C).

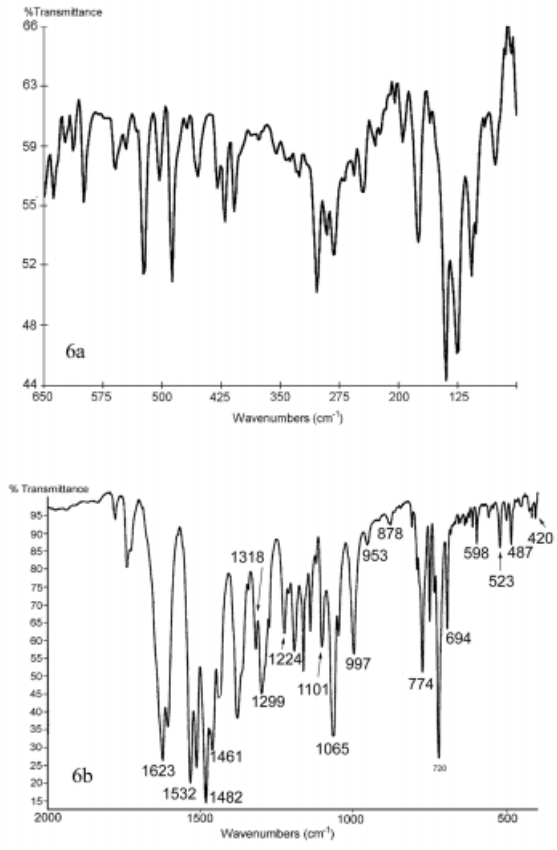

Figure 6. Far (6a) and middle (6b) infra-red spectra of **1**, recorded using 10% polyethylene and 0.5−1% KBr pellets, respectively

Other very intense or fairly intense bands in the spectrum of Pb(Pc) became smaller in the spectrum of Bi(1,24-Pcc): the band at 742/750 cm^{-1}, [out-of-plane C−H deformations γ(C−H)[27]], the bands at 1059/1047 cm^{-1} and 1113/1101 cm^{-1} [both in-plane C−H deformations, β(C−H)], and the band at 1313/1318 cm^{-1} in the range of the C−C stretching vibrations frequencies in the isoindole skeleton, ν(C−C). The band at 882 cm^{-1}, described as a metal-dependent vibration of the macrocycle,[46] is very sharp and intense in Pb(Pc) and becomes very small and broad at 878 cm^{-1} in **1**. That modification is probably due to important differences in the coordination polyhedra of the two complexes. In the range of the ν(C−C) or ν(C−N) stretching vibration frequencies, the bands at 1329 and 1404 cm^{-1} disappear and many new bands appear at 1139, 1192, 1224, 1461, 1512, 1532, and 1623 cm^{-1}. A medium band at 1606 cm^{-1} in the Pb(Pc) spectrum becomes very intense. The complexity of the Bi(1,24-Pcc) spectrum and the large number of new bands in the range of aromatic ν(C−C) or ν(C−N) stretching vibration frequencies is due to the lack of symmetry elements and to the large range of bond lengths observed in the different isoindole rings constituting the Bi(1,24-Pcc) molecule, particularly for the bonds around the sp^3 carbon atoms which are longer than normal $C_\alpha-N_{iso}$ or $C_\alpha-C_\beta$ bonds.

Owing to the presence of a sharp band at 1745 cm^{-1}, we first assumed that the co-crystallised molecule should be a phthalimide, which has an intense C=O vibration at 1746 cm^{-1} and a medium band for the N−H vibration at 3203 cm^{-1}. However, the position and the intensities of the residual electronic densities detected around the identified five-membered cycle in the X-ray diffraction study are not consistent with oxygen atoms. In the IR spectrum, we did not find any band between 2000 and 4000 cm^{-1} which would allow for the unambiguous characterisation of the co-crystallised molecule. This is probably due to the non-stoichiometric ratio of this cyclised phthalonitrile, compared to the six benzopyrrole units in the Bi(1,24-Pcc). Between 3000 and 3200 cm^{-1}, we observed a broad group of small bands that is evident in all phthalocyanine spectra, including that of $Bi_2(Pc)_3$, characteristic of the aromatic C−H vibrations. At approximately 2240 cm^{-1}, a very small band was observed, which we assigned to −CN groups of residual phthalonitrile in the crystal, or to a co-crystallised molecule, intermediate in the synthesis of $Bi_2(Pc)_3$. Janczac and Kubiak studied the formation of the phthalocyaninato (2-) ring from o-dicyanobenzene molecules and observed that, depending on the reaction conditions, only one of the cyano groups of *o*-dicyanobenzene undergoes a transformation, with a change from sp to sp^2 hybridisation.[18]

Below 700 cm^{-1} the spectrum of **1** is not a typical spectrum of phthalocyanine compounds. There is a very sharp and fairly intense band at 694 cm^{-1}, which is not present in usual phthalocyanine spectra. In Pb(Pc) and other common metallophthalocyanines, only four or five bands, characteristic of phthalocyanine ring deformations, are evident between 700 and 360cm^{-1}. For Pb(Pc),[1] they lie at 627, 560, 497, and 436 cm^{-1}. In the spectrum 6b, we observe 13 bands between 360 and 650 cm^{-1}. The ligand of **1** is not a phthalocyanine but, as shown in the structural part, a macrocycle made up of a superphthalocyanine-like ring and a phthalocyanine-like ring having three common isoindole moieties. This fact and the absence of symmetry elements explain the large number of allowed vibrations. The band at 353 cm^{-1} appears with the same shape and intensity in the spectra of Pb(Pc) and $Bi_2(Pc)_3$,[1] at 351 cm^{-1}. It has been described as metal dependant and due to the isoindole ring out-of-plane deformations.[34,44] Between 200 and 350 cm^{-1} in the spectrum of Pb(Pc), only two bands were observed at 231 and 271 cm^{-1}, assigned in the literature to the metal−nitrogen vibrations.[1,37,49] In the same wavenumber range, spectrum 6b shows many bands that we assign to the $Bi-N_{iso}$ stretching vibrations of the different $Bi-N_{iso}$ bonds. Below 200 cm^{-1}, we observe two new bands at 194 and 174 cm^{-1}. The two intense bands at 146 and 125 cm^{-1} in the spectrum of Pb(Pc) are at 140 and 126 cm^{-1} in the spectrum of **1**, in which we note two supplementary new bands at 107 and 101 cm^{-1}. The spectrum of lattice vibra-

tions between 50 and 100 cm^{-1} shows few differences between Pb(Pc) and **1**.

Conclusion

We have prepared a new orange bismuth(III) bicyclophthalocyanine complex. It is a new member of the family of the hexapyrrole ligand complexes in which a $N(C_8H_4N)N(C_8H_4N)N$ bridge is extended between two Cα pyrrole carbon atoms of a phthalocyanine ring, interrupting the π-conjugation of the macrocycle. These hexapyrrole complexes can be now classified into three groups of ligands, differing by the position of the bridgehead carbon atoms. In this paper, we have proposed a numbering scheme in order to differentiate each group of this class of compounds by their names. The positional indices of the bridgehead carbons are indicated as a prefix in front of the letter code (Pcc) of the hexapyrrole ligand. With this numbering scheme indicating the number of benzopyrrole units over which the π-delocalisation is extended, NbCl(1,16-Pcc)[5] is the only reported member of the first group, M(1,17-Pcc) (with M = Gd, In, Tl, and Ce)[6−8] describes the second group, and Bi(1,24-Pcc) is the first member of a new group. This new complex was fully characterised by UV/Vis and IR spectroscopy. The most striking feature of the UV/Vis spectrum is the almost complete disappearance of the Q band, explained by the interruption of the π-conjugation through the (Pc) ring. The IR spectrum from 50 cm^{-1} to 2000 cm^{-1} was reported and compared to usual IR phthalocyanine spectra. The large number of new bands can be explained by the lack of symmetry elements and by the large range of bond lengths observed in the different isoindole rings making up the Bi(1,24-Pcc) molecule, particularly for the bonds around the sp^3 carbon atoms and in the coordination polyhedron. The molecular structure of **1** was established and shows the smallest known $Bi-N_{iso}$ bond among bismuth phthalocyanine complexes. The relative position of the molecules of Bi(1,24-Pcc) in the crystal cell, and the distances between the atoms of two neighbouring molecules indicate a very weak interaction between the two π-electron systems. The distances between the aza-nitrogen atom of the first molecule, and the α-carbons of the pyrrole ring of the second molecule are too long to explain the formation of $Bi_2(Pc)_3$ by a direct dimerisation of two molecules of Bi(1,24-Pcc). This is confirmed by the fact that the isolation of $Bi_2(Pc)_3$ by heating only washed orange crystals is impossible while the heating of orange crystals in molten phthalonitrile up to 310 °C always produced the triple-decker compound. We observed a co-crystallised molecule VII, nearly parallel to one of the two benzopyrrole units of the bridge, and 3.43 Å apart. This strongly disordered molecule was not fully characterised. The IR spectroscopy and X-ray diffraction results suggest that it is a cyclised phthalonitrile molecule. Some experiments are currently underway to identify it, and to understand its importance in the reaction mechanism of the synthesis of $Bi_2(Pc)_3$.

Experimental Section

General Remarks: FT-IR: Nicolet 20 SXB spectrometer with 2 cm^{-1} resolution. Perkin−Elmer Spectrum 1000 with 1 cm^{-1} resolution. KBr pellets (1%) and polyethylene pellets (10%) were used within the range of 4000−400 cm^{-1} and 400−50 cm^{-1}, respectively. Pellets were prepared with some clean crystals, picked out under a microscope. − UV/Vis: Unicam UV 4 spectrometer.

Synthesis and Purification: The synthesis of **1** was performed using the method for the synthesis of $Bi_2(Pc)_3$, in the same vessel and apparatus.[1] Bismuth acetate (1.6 g, 4 mmol), and phthalonitrile (3.64 g, 28 mmol, puriss. 99% Fluka) were ground and placed in an open-reaction vessel which was put in the oven, pre-heated to 180 °C. The temperature probe was placed between the wall of the oven and that of the reaction vessel. The temperature was raised slowly (2°/min) to 230−240° C. The mixture was then slowly cooled to room temperature. The crude product was a mixture of orange crystals with some remaining reactants and by-products. Using a Soxhlet apparatus, the crystals were washed with acetone, DMF, toluene, and then ethanol. The isolated dry powder was a mixture of orange crystals and a light-grey powder, and was shaken in a mixture of acetone/water/pentane (1:1:1). Crystals of **1** were floating at the interface of the phases, (water + acetone/pentane) while the light-grey powder was deposited at the bottom of the vessel. The interface of the solvents was sucked up with a Pasteur pipette connected to a water aspirator pump, and orange crystals were isolated (440 mg, 0.392 mmol, 9.8%). It was impossible to get reliable elemental analytical data: the yield is low (<10%) and the calculations are not precise because of the disordered co-crystallised molecule, in a non-stoichiometric ratio. In spite of these unreliable analyses, the molecular structure of Bi(1,24-Pcc) was determined unambiguously by the X-ray diffraction study.

X-Ray Crystallographic Study: A suitable orange crystal of small size (0.1 × 0.1 × 0.05 mm) was mounted on an Enraf−Nonius Kappa CCD[52] diffractometer. Despite its well-defined shape, the crystal gave a diffraction pattern of medium quality, showing some light rings of diffusion, probably due to the precipitate that could be observed on the surface of the sample. A 180° (through 2°-steps of 240 seconds each) φ scan measurement was performed at room temperature using the Mo-K_α wavelength. The cell parameters were refined (Denzo[53]) with the use of 7053 reflections and are reported in Table 3 with the crystallographic parameters. The data were first corrected for absorption effects with Sortav.[54] The bismuth atom and some cycles of the organic ligand could then easily be located with SIR92.[55] As some remaining undefined fragments could not be assigned in the first steps of the calculations, we performed a series of anisotropic refinements (MaXus[56]), only on the well-defined bicyclophthalocyanine moiety, adding the hydrogen atoms at idealised positions, until the R factor reached a reasonable value. A last Fourier difference gave some peaks of density (all rigorously lying in the same plane) that could be attributed to a cyclised phthalonitrile solvate. The most identifiable scheme among these electron densities was a five-membered cycle. These atoms were finally introduced (with isotropic displacement parameters) in the calculations as $C_8H_4N_2H_2$ and refined as a rigid block fragment to the final R indices: R_1 [$F^2 > 3\sigma(F^2)$] = 0.059, wR_1 [$w = 1/\sigma^2 (F^2) + 0.03F^2$] = 0.093. The residual positive Fourier peak is equal to 1.58 eÅ^3 and is located near the bismuth atom. This density cannot be unambiguously attributed to a free electron pair on the bismuth atom as it can also be due to an absorption problem. This point could not be clarified either by the empirical correction used, or by a numerical one that we also tested. Crystallographic data (ex-

Table 3. Crystallographic data for **1**

Crystal data	
Formula	$C_{56}H_{30}BiN_{15}$
M_w	1121.95
Crystal system	triclinic
Space group	P-1
a [Å]	12.544(2)
b [Å]	13.654(1)
c [Å]	14.868(1)
α [°]	73.83(1)
β [°]	78.75(1)
γ [°]	68.20(1)
V [Å^3]	2258.8(2)
D_{calc} [g cm^{-3}]	1.25
Z	2
μ(Mo-K_α) [cm-1]	78.32
Data collection	
T [K]	298
Scan mode	Φ scan
Scan width	2
$2\theta_{max}$ [°]	48.06
Measured reflections	7113
Unique reflections	7053
R_{int}	0.064
Refinement parameters	
Absorption correction	empirical (Sortav: Blessing, 1997)
Reflections used for refinement	5015
Refined parameters	566
Refinement cut-off	$F^2>3\sigma(F^2)$
H atoms	included, not refined
R_1	0.059
wR_1	0.093
Weighting scheme	$w = 1/(\sigma^2(Fo^2) + 0.03000 \times Fo^2)$
$(Shift/e.s.d.)_{max}$	0.454
Goodness of fit	2.61
$\Delta\rho_{fin}$.(max./min.) [eÅ^3]	1.58; −2.43

cluding structure factors) for the structure(s) reported in this paper have been deposited with the Cambridge Crystallographic Data Centre as supplementary publication no. CCDC-133562. Copies of the data can be obtained free of charge on application to CCDC, 12 Union Road, Cambridge CB2 1EZ, UK [Fax: (internat.) + 44(0)1223/336-033; E-mail: deposit@ccdc.cam.ac.uk].

Acknowledgments

We thank UMR 6516 for financial support.

[1] K. Benihya, M. Mossoyan-Déneux, F. Hahn, N. Boucharat, G. Terzian, *Eur. J. Inorg. Chem.* **2000**, 1771−1779
[2] F. Baumann, B. Bienert, G. Rösch, H. Vollmann, W. Wolf, *Angew. Chem.* **1956**, *68*, 133−150
[3] M. A. Perkins, M. S. Whelen, **1957** *U. S. Pat* 2,782,207
[4] G. Barnhart, B. F. Skiles, *1956 U. S. Pat* 2,772,284, *British Pat.* 745359
[5] F. Gingl, J. Strähle, *Acta Cryst.* **1990**, *C46*, 1841−1843
[6] J. Janczak, R. Kubiak, *J. Chem. Soc., Dalton Trans.* **1994**, 2539−2543.
[7] J. Janczak, R. Kubiak, *Acta Cryst.* **1995**, *C51*, 2039−2042
[8] J. Janczak, R. Kubiak, *Acta Chem. Scand.* **1995**, *49*, 871−877.
[9] *The porphyrin Handbook* (Eds.: K. M. Kadish, K. M. Smith, R. Guilard), vol 3, p. 249, Academic Press, Burlington, MA, USA, **2000**.
[10] C. C. Leznoff, *Phthalocyanines (Properties and Applications)* (Eds.: C. C. Leznoff, A. B. P. Lever), vol 1, VCH Publishers, Weinheim, **1989**.
[11] R. Kubiak, J. Janczak, *J. Alloys Comp.* **1992**, *189*, 107−111.
[12] R. Kubiak, J. Janczak, *J. Alloys Comp.* **1992**, *190*, 117−120.
[13] J. Janczak, R. Kubiak, *J. Alloys Comp.* **1992**, *190*, 121−124.
[14] M. S. Haghighi, C. L. Teske. H. Homborg, *Z. Anorg. Allg. Chem.* **1992**, *608*, 73−80.
[15] C. J. Brown, *J. Chem. Soc. A* **1968**, 2494−2498.
[16] K. J. Wynne, *Inorg. Chem.* **1985**, *24*, 1339−1343.
[17] J. Janczak, R. Kubiak, *J. Chem. Soc., Dalton Trans.* **1993**, 3809−3812.
[18] J. Janczak, R. Kubiak, *J. Mol. Struct.* **2000**, *553*, 157−166.
[19] K. Kasuga, M. Tsutsui, *Coord. Chem. Rev.* **1980**, *32*, 67−95.
[20] T. J. Marks, D. R. Stojakovic, *J. Am. Chem. Soc.* **1978**, *100*, 1695−1705.
[21] J. Rauschnabel, M. Hanack, *Tetrahedron Lett.* **1995**, *36*, 1629−1632.
[22] N. Kobayashi, *J. Chem. Soc., Chem. Commun.* **1991**, 1203−1205.
[23] G. Ostendorp, H. Homborg, *Z. Anorg. Allg. Chem.* **1996**, *662*, 873−880.
[24] J. Janczak, R. Kubiak, *Polyhedron.* **1999**, *18*, 2775−2780.
[25] R. Kubiak, K. Ejsmont, *J. Mol. Struct.* **1999**, *474*, 275−281.
[26] R. D. Shannon, *Acta Cryst.* **1976**, *A32*, 751−767.
[27] H. Isago, Y. Kagaya, *Bull. Chem. Soc. Jpn.* **1994**, *67*, 383−389.
[28] P. Sayer, M. Gouterman, C. R. Connell, *Acc. Chem. Res.* **1982**, *15*, 73−79.
[29] A. B. P. Lever, S. R. Pickens, P. C. Minor, S. Licoccia, B. S. Ramaswamy, K. Magnell, *J. Am. Chem. Soc.* **1981**, *103*, 6800−6806.
[30] M. J. Stillman, A. J. Thomson, *J. Chem. Soc., Faraday Trans. 2* **1974**, *70*, 790−804.
[31] H. Homborg, W. Kalz, *Z. Naturforsch.* **1978**, *33b*, 1067−1071.
[32] H. Sugimoto, T. Higashi, M. Mori, *J. Chem. Soc.,Chem. Commun.* **1983**, 622−623.
[33] P. Turek, J. J. André, J. Giraudeau, J. Simon, *Chem. Phys. Lett.* **1987**, *134*, 471−476.
[34] C. Clarisse, M. T. Riou, *Inorg. Chim. Acta.* **1987**, *130*, 139−144.
[35] D. Markovitsi, T. H. Tran-Thi, R. Even, J. Simon, *Chem. Phys. Lett.* **1987**, *137*, 107−112.
[36] E. Orti, J. L. Bredas, C. Clarisse, *J. Chem Phys.* **1990**, *92*, 1228−1235.
[37] J. Janczak, *Pol. J. Chem.* **1998**, *72*, 1871−1878.
[38] L. K. Lee, N. H. Sabelli, P. R. Lebreton, *J. Phys. Chem.* **1982**, *86*, 3926−3931.
[39] A. Henrikson, B. Roos, M. Sundbom, *Theoret. Chim. Acta* **1972**, *27*, 303−313.
[40] H. Shirai, H. Tsuiki, E. Masuda, T. Koyama, K. Hanabusa, N. Kobayashi, *J. Phys. Chem.* **1991**, *95*, 417−423.
[41] A. N. Sidorov, I. P. Kotlyar, *Opt. Spectr.* **1961**, *11*, 92−96.
[42] H. F. Shurvell, L. Pinzuti, *Can. J. Chem.* **1966**, *44*, 125−136.
[43] T. Kobayashi, F. Kurokawa, N. Uyeda, E. Suito, *Spectrochim. Acta, Ser. A* **1970**, *26*, 1305−1311.
[44] T. Kobayashi, *Spectrochim. Acta, Ser. A* **1970**, *26*, 1313−1322.
[45] F. Cariati, F. Morazzoni, M. Zocchi, *J. Chem. Soc., Dalton Trans.* **1978**, 1018−1024.
[46] F. Morazzoni, F. Cariati, G. Micera, *Spectrochim. Acta* **1980**, *36A*, 867−870.
[47] W. Kalz, H. Homborg, *Z. Naturforsch.* **1983**, *38b*, 470−484.
[48] H. Homborg, W. Kalz, *Z. Naturforsch.* **1984**, *39b*, 1490−1499.
[49] G. Terzian, B. Moubaraki, M. Mossoyan-Déneux, D. Benlian, *Spectrochim. Acta* **1989**, *45*, 675−677.

[50] W. J. Kroenke, M. E. Kenney, *Inorg. Chem.* **1964**, *3*, 696−698.
[51] M .S. Haghighi, H. Homborg, *Z. Anorg. Allg. Chem.* **1994**, *620*, 1278−1284.
[52] Nonius (**1998**). *Kappa CCD Reference Manual.* Nonius B. V., P. O. Box 811, 2600 Av, Delft, The Netherlands.
[53] Z. Otwinowski, W. Minor, *Processing of X-ray Diffraction Data Collected in Oscillation Mode*, Methods in Enzymology, *Volume 276*: Macromolecular Crystallography, part A, pp. 307−326, **1997** (Eds.: C. W. Carter, Jr., R. M. Sweet), Academic Press.
[54] R. H. Blessing, *J. Appl. Cryst.* **1997**, *30*, 421−426.
[55] A. Altamore, G. Cascarano, C. Giacovazzo, A. Guagliardi, M. C. Burla, G. Polidori, M. Camalli, *J. Appl. Cryst.* **1994**, *27*, 435−436.
[56] S. Mackay, C. J. Gilmore, C. Edwards, M. Tremayne, N. Stewart, K. Shankland, *maXus: a computer program for the solution and refinement of crystal structures from diffraction data* University of Glasgow, Scotland, UK, Nonius BV, Delft, The Netherlands and MacScience Co. Ltd., Yokohama, Japan, **1998**.

Received July 26, 2000
[I00296]

A Versatile Approach to the Intramolecular Organization of Two Bipyridine-Like Chelating Units in a Polytopic Ligand

Larissa Kovbasyuk,[a][‡] Markus Hoppe,[a] Hans Pritzkow,[a] and Roland Krämer*[a]

Dedicated to Prof. Dr. Dieter Sellmann on the occasion of his 60th birthday

Keywords: Bioinorganic chemistry / Copper / Enzyme mimics / Ligand design / Catalysis

The synthesis of four novel polypyridyl ligands, in which two 4,6-[bis(2-pyridyl)]pyrimidine units are covalently linked by spacer groups –S– (**1**), –S–S– (**2**), –Se– (**7**), and –Se–Se– (**6**), is reported. A new unsymmetrical dinucleating ligand **4** was isolated as a by-product in the synthesis of **2** and has been characterized by X-ray crystallography. Copper(II) complexes $[(\mathbf{1})Cu](NO_3)_2{\cdot}5H_2O$ and $[(\mathbf{7})Cu](ClO_4)_2{\cdot}6H_2O$ have been isolated, spectroscopic data for which are consistent with tetradentate N_4 coordination by the ligands. In situ prepared polynuclear copper(II) complexes of **1** and **7** show different catalytic activities in the cleavage of the phosphodiester 2-hydroxypropyl *p*-nitrophenyl phosphate. This might be a consequence of the influence of the covalent spacer (S or Se) on the preorganization of two bipyridine-like chelating units in $[LCu]^{2+}$, which bind two catalytic Cu^{2+} ions.

Introduction

In many enzymes, chemical transformations are mediated by the cooperation of two active site metal ions. This functional motif is particularly prominent in phosphoryl transfer enzymes including phosphodiesterases, nucleases, phosphatases, and DNA/RNA-polymerases.[1] During the last 15 years, many dinuclear model complexes have been designed to improve the understanding of metal−metal cooperation in such enzymes.[2] Preorganization, i.e. intermetal distance and relative orientation of coordination polyhedra, is a parameter that is of fundamental importance with regard to reactivity. In practice, it is difficult to design a model system that allows systematic variation of the preorganization while other factors that influence the reactivity are kept constant. Breslow has described dinuclear zinc(II) complexes in which two (chelator) Zn subunits are covalently linked by spacer groups of varying size. This approach requires laborious synthesis of a set of appropriate ligands and allows only rough tuning of metal−metal separation.[3] We have recently described trinuclear complexes $(L)M_sCu_2$, in which a "structural" metal ion M_s is coordinated to the tetradentate site and two "functional" Cu^{2+} ions bind to the bipyridine-like chelating groups of the ligand[4] (Scheme 1). The catalytic activity of this complex in the cleavage of a phosphodiester was shown to be strongly dependent on the nature of the structural metal ion M_s.

This was interpreted in terms of different catalyst conformations, i.e. fine-tuning of the preorganization of the two functional Cu^{2+} ions, depending on the ionic radius of M_s and on its tendency to distort the N_4-M_s coordination plane.

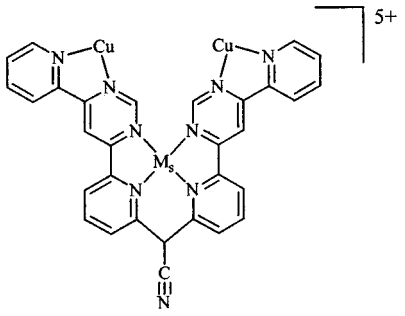

Scheme 1. Trinuclear complex $(\mathbf{L})M_sCu_2$

$(L)M_sCu_2$ constituted the first example of an abiotic allosteric catalyst; M_s is a noncovalent modifier of the reactivity, but is not directly involved in the reaction. In this context, we report herein on the synthesis of related polypyridyl ligands and their metal complexes.

Variation of the spacer group that covalently links the dipyridylpyrimidine subunits (Scheme 2) is tested as an additional possible means of controlling organization of the bipyridine-like chelating groups and of tuning the reactivity of the polynuclear complexes.

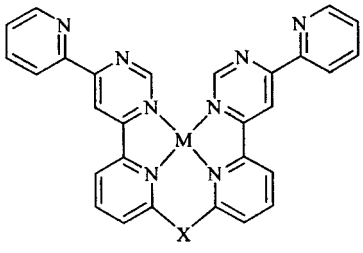

Scheme 2

[a] Anorganisch-Chemisches Institut der Universität Heidelberg, Im Neuenheimer Feld 270, 69120 Heidelberg, Germany
Fax: (internat.) + 49(0)6221/548439
E-mail: roland.kraemer@urz.uni-heidelberg.de
[‡] On leave from: Department of Chemistry, Shevchenko University, 01033 Kiev, Ukraine

 © WILEY-VCH Verlag GmbH, 69451 Weinheim, 2001 1434−1948/01/0505−1353 $ 17.50+.50/0

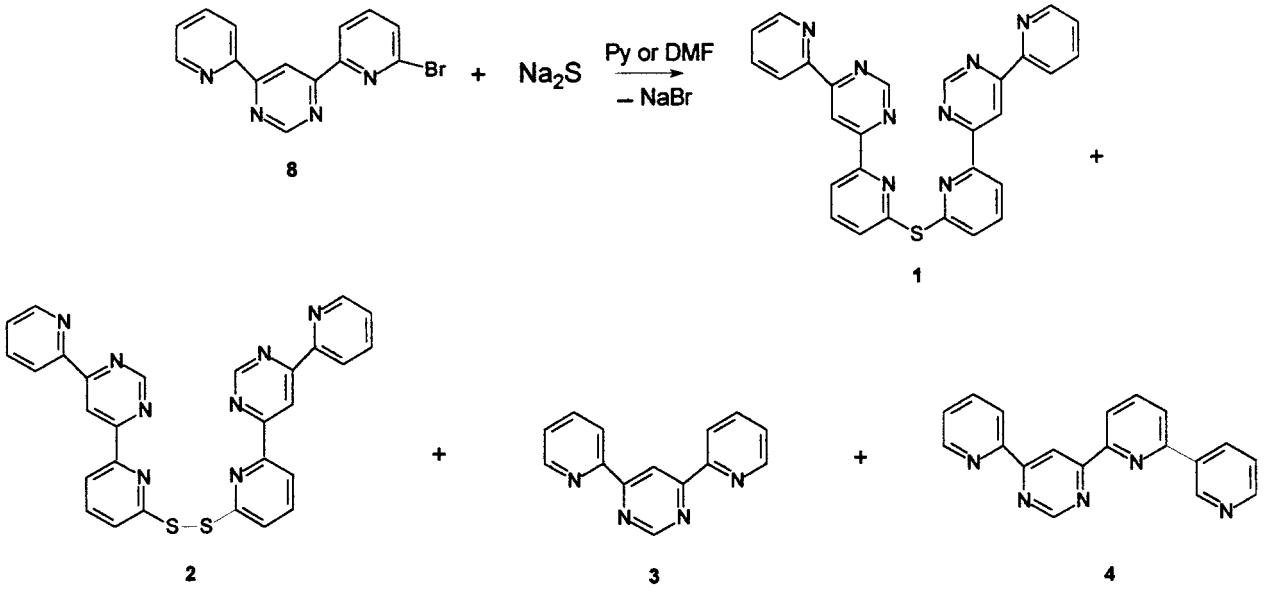

Scheme 3. Synthesis of **1**, **2**, and **4**

Results and Discussion

Preparation of the novel polypyridyl ligands **1**, **2**, **6**, and **7** is outlined in Scheme 3, Scheme 4, and Scheme 5. The synthesis of the precursor 4-(6-bromo-2-pyridyl)-6-(2-pyridyl)pyrimidine (**8**) is described elsewhere.[5]

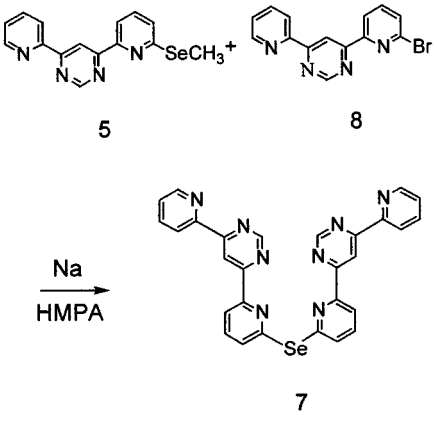

Scheme 4. Synthesis of **7**

The synthesis of compounds with a py−S−py moiety by reaction of pyridyl bromides and thiols has been described previously. In particular, bis(2-pyridyl) sulfide has been isolated following reaction of 2-mercaptopyridine with 2-bromopyridine and K_2CO_3 in DMF.[6] In the present case, the thiol was not isolated but is involved as an intermediate in the formation of **1** from the bromo compound and Na_2S. Oxidation of the thiol intermediate by oxygen during workup gives the disulfide compound **2**. The yields of compounds **1** and **2** were found to be dependent on the ratio of **8** to Na_2S. For optimal yields of **1** and **2**, the requisite **8**/Na_2S ratios proved to be 1:1.5 and 1:5, respectively.

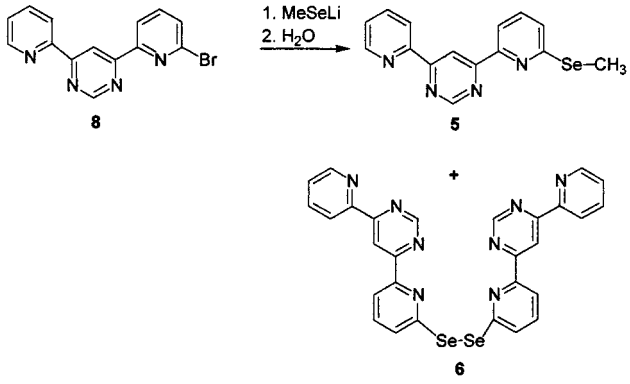

Scheme 5. Synthesis of **5** and **6**

As a side product, 4-[6-(2-pyridyl)-2-pyridyl]-6-(2-pyridyl)pyrimidine (**4**) was isolated when the reaction described in Scheme 3 was conducted in pyridine. The mechanism of its formation is unclear. Ligand **7** was obtained in analogy to a reported method for the synthesis of bis(2-pyridyl) selenide[12] from halopyridines and $LiSeCH_3$. In the first step, methyl 6-[6-(2-pyridyl)-4-pyrimidinyl]-2-pyridyl selenide (**5**) was synthesized by reaction of CH_3Li, selenium, and **8**.

Cleavage of the Se−CH_3 bond was achieved in the second step by treatment with metallic sodium, resulting in the formation of a selenolate intermediate, which displaced the bromine in **8** to give **7** (Scheme 4). **6** was unexpectedly obtained as a side product in the synthesis of **5** (Scheme 5), and its yields could be optimized using a higher ratio of CH_3Li/Se to **8**. Presumably, a selenol(ate) intermediate is involved and the Se−Se bond is formed by air oxidation. Ligands **1** and **2** were obtained as pale-yellow powders, **6** and **7** as yellow powders, and were characterized by mass spectrometry, NMR spectroscopy, and C,H,N analysis. The crystal structure of **4** (white needles) was elucidated by X-ray analysis.

Compound **4** was formed as a by-product when the reaction outlined in Scheme 4 was performed in pyridine, but not when DMF was used as solvent. Thus, the reaction is rationalized in terms of a C−C coupling of **8** with the pyridine solvent. The mechanism of this process is not clear, but activation of pyridine for a C−C coupling reaction at its C-2 position under relatively mild conditions (90−100 °C, 7 h, Na_2S) is, to the best of our knowledge, quite unusual. Thus, for unambiguous determination of the structure of **4**, it was subjected to X-ray crystallographic analysis. Suitable crystals of **4** were obtained by isothermal crystallization from acetone. The molecular structure of **4**, showing the numbering scheme used, is presented in Figure 1. Selected bond lengths and angles are given in Table 1.

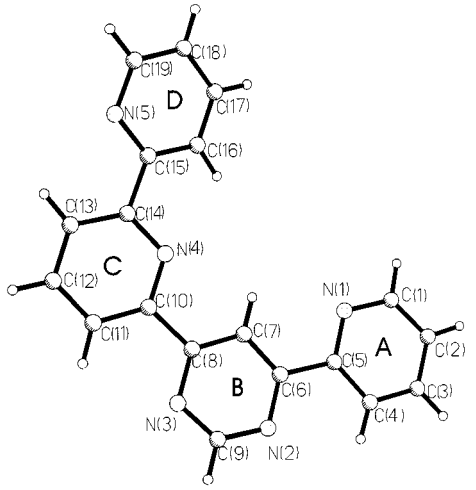

Figure 1. Molecular structure of **4** showing numbering scheme

The unit cell is monoclinic and contains four molecules of **4**. The rings A, B, and C are coplanar, whereas the plane of ring D forms an angle of 30° with the A, B, and C planes. The bond lengths and angles in **4** are typical for pyridine and pyrimidine heterocycles.[7]

Mononuclear copper(II) complexes of **1** and **7** were prepared by mixing the ligands and suitable metal salts in organic solvents and were isolated as green powders. Attempts to crystallize these complexes failed. C,H,N analyses of the solids were consistent with hydrated 1:1 complexes with the formulae [Cu(**1**)]$(NO_3)_2\cdot 5H_2O$ and [Cu(**7**)]$(ClO_4)_2\cdot 6H_2O$. Copper(II) complexes of **2** and **6** could not be isolated, although mass spectrometry indicated the formation of 1:1 complexes. Evidence of the decomposition of the complexes by redox processes was noted. Thus, solutions show the gradual appearance of new bands at around 450 nm in their UV/Vis spectra, similar to $[(bpy)_2Cu^{I}]^+$.

Table 1. Selected bond lengths and angles in **4**

N(1)−C(1)	1.34(2)	C(4)−C(5)	1.38(2)
N(1)−C(5)	1.34(2)	C(6)−C(7)	1.38(2)
N(2)−C(9)	1.33(2)	C(7)−C(8)	1.39(2)
N(2)−C(6)	1.34(2)	C(8)−C(10)	1.49(2)
N(3)−C(9)	1.33(2)	C(10)−C(11)	1.39(2)
N(3)−C(8)	1.34(2)	C(11)−C(12)	1.38(2)
N(4)−C(14)	1.34(2)	C(12)−C(13)	1.37(2)
N(4)−C(10)	1.34(2)	C(13)−C(14)	1.39(2)
N(5)−C(19)	1.34(2)	C(14)−C(15)	1.49(2)
N(5)−C(15)	1.35(2)	C(15)−C(16)	1.39(2)
C(1)−C(2)	1.38(2)	C(16)−C(17)	1.38(2)
C(2)−C(3)	1.37(2)	C(17)−C(18)	1.38(2)
C(3)−C(4)	1.38(2)	C(18)−C(19)	1.38(2)
C(5)−C(6)	1.49(2)		
C(1)−N(1)−C(5)	116.76(13)	C(7)−C(6)−C(5)	121.89(12)
C(9)−N(2)−C(6)	115.44(13)	C(6)−C(7)−C(8)	118.12(13)
C(9)−N(3)−C(8)	115.64(13)	N(3)−C(8)−C(7)	121.14(13)
C(14)−N(4)−C(10)	118.06(12)	N(3)−C(8)−C(10)	117.08(13)
C(19)−N(5)−C(15)	117.06(13)	C(7)−C(8)−C(10)	121.78(13)
N(1)−C(1)−C(2)	124.09(15)	N(3)−C(9)−N(2)	128.18(15)
C(3)−C(2)−C(1)	118.31(15)	N(4)−C(10)−C(11)	122.58(13)
C(2)−C(3)−C(4)	119.09(15)	N(4)−C(10)−C(8)	116.09(12)
C(3)−C(4)−C(5)	118.82(14)	C(11)−C(10)−C(8)	121.32(13)
N(1)−C(5)−C(4)	122.92(13)	C(12)−C(11)−C(10)	118.49(15)
N(1)−C(5)−C(6)	116.07(12)	C(13)−C(12)−C(11)	119.42(15)
C(4)−C(5)−C(6)	121.01(12)	C(12)−C(13)−C(14)	118.95(15)
N(2)−C(6)−C(7)	121.46(13)	N(4)−C(14)−C(13)	122.40(14)
N(2)−C(6)−C(5)	116.65(12)	N(4)−C(14)−C(15)	116.49(13)
C(13)−C(14)−C(15)	121.09(13)	C(17)−C(16)−C(15)	119.16(15)
N(5)−C(15)−C(16)	122.30(13)	C(16)−C(17)−C(18)	119.10(15)
N(5)−C(15)−C(14)	116.34(13)	C(19)−C(18)−C(17)	118.12(15)
C(16)−C(15)−C(14)	121.35(13)	N(5)−C(19)−C(18)	124.26(15)

The MALDI-TOF mass spectra of solutions of the complexes feature major peaks corresponding to $[Cu(\mathbf{1})]^+$, $[Zn(\mathbf{6})]^+$, and $[Cu(\mathbf{7})]^+$ patterns with characteristic isotopic distributions for the relevant metal ions. Attempts to isolate zinc(II) complexes of the prepared ligands were successful only in the case of **6**, for which [Zn(**6**)]$(CH_3COO)_2$ was obtained.

The NMR data of the mononuclear zinc complex of **6** are consistent with tetradentate metal coordination. The ^1H NMR spectrum (solution in $CDCl_3$) is consistent with C_2 symmetry of the complex. In the NOESY spectrum, the signal due to the Pym-5 proton shows an intense cross-peak with the signal due to the Py′-3/Py-3 protons. This indicates that the pyrimidine ring is *cis*-oriented with respect to the internal pyridine ring, as expected for tetradentate coordination of the ligand.

Information about the copper coordination sphere in solution was obtained from EPR spectroscopic data. The EPR spectra of [Cu(**1**)]$(NO_3)_2\cdot 5H_2O$ and [Cu(**7**)]$(NO_3)_2\cdot 6H_2O$ in DMSO glass were recorded at liquid nitrogen temperature. In the spectrum of [Cu(**1**)]$(NO_3)_2\cdot 5H_2O$, specifically the part of perpendicular orientation, *N*-superhyperfine coupling with the nitrogen donor atoms is observed, but is poorly resolved. The spin Hamiltonian parameters obtained are $g_\perp = 2.06$, $g_\parallel = 2.26$, $A_\parallel = 166$ G, and $g_\perp = 2.07$, $g_\parallel = 2.32$, $A_\parallel = 151$ G for

[Cu(**1**)](NO$_3$)$_2$·5H$_2$O and [Cu(**7**)](NO$_3$)$_2$·6H$_2$O, respectively. These parameters are consistent with the presence in both complexes of a tetrahedrally distorted square-planar copper environment with a $d_{x^2-y^2}$ ground state ($g_{\|} > g_{\perp}$).[8] The values of the spin Hamiltonian parameters of these complexes agree well with those reported for flattened N_4 tetrahedral complexes of Cu^{2+} [8,9] and are distinctly different from those of square-planar tetradentate Cu^{2+} in the previously described LCu (L = ligand shown in Scheme 1), $g_{\|}$ = 2.207, $A_{\|}$ = 196 G.[10]

The EPR parameters indicate the degree of distortion of the CuN_4 moiety from planarity, which determines the preorganization of the bidentate, bipyridine-like chelating units in the mononuclear complexes. A near-planar N_4 coordination in LCu (L = ligand shown in Scheme 1), as suggested by the $g_{\|}$ and $A_{\|}$ values, was confirmed by a crystal structure determination of [LCu(MeOH)]ClO_4.[10] In this complex, two pyrimidine 2-H protons approach their van der Waals contact distance. Any decrease in the C−X−C bond angle at spacer atom X (Scheme 2), or any increase in the X−C bond length, should give rise to an increased helical twist of the mononuclear complex with tetrahedral distortion of the CuN_4 plane in order to minimize steric repulsion between the pyrimidine 2-H protons. Thus, the apparent increase in the degree of tetrahedral distortion in the order X = C, S, Se becomes understandable in terms of specific bonding parameters of these spacing atoms.

In our previous study on complexes of ligand L (Scheme 1), spectrophotometric titrations gave evidence concerning the metal complex species present in solution. Attempts to characterize the solution chemistry of the Cu complexes of **1** and **7** under the same conditions (water/DMSO, 3:1) were complicated by insufficient solubility of the ligands in the absence of the metal ion and by slow complex formation.

Fast complexation was observed in a 1:1 dichloromethane/acetonitrile medium, and UV titrations were indicative of the formation of both mononuclear and trinuclear complexes. Sharp isosbestic points were obtained for 0−1 equiv. of Cu when 5% DMSO was added to the solvent mixture (Figure 2 and Figure 3).

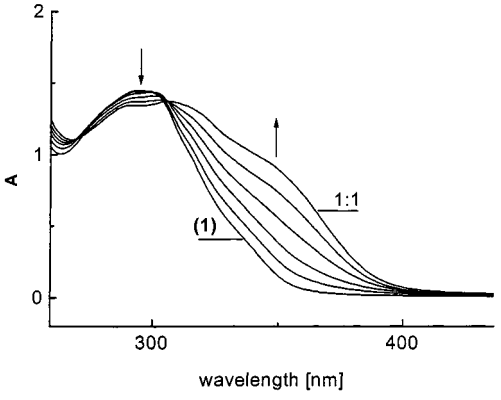

Figure 2. Spectrophotometric titration of **1** with copper(II) perchlorate in a CH_3CN/CH_2Cl_2 (1:1) solution containing 5% DMSO at 20 °C from 0−1 equiv. (spectra correspond to addition of Cu in 0.2-equiv. steps)

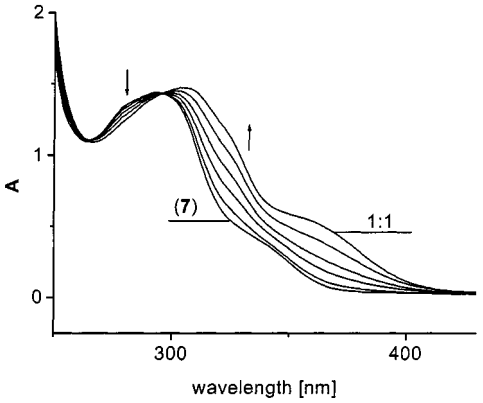

Figure 3. Spectrophotometric titration of **7** with copper(II) perchlorate in a CH_3CN/CH_2Cl_2 (1:1) solution containing 5% DMSO at 20 °C from 0−1 equiv. (spectra correspond to addition of Cu in 0.2-equiv. steps)

The absorbance maxima of the complexes (about 310 nm) are shifted toward higher wavelengths relative to the free ligands (about 290 nm). Interestingly, the competitive solvent DMSO inhibits the formation of polynuclear complexes; no significant spectral changes are observed on addition of > 1 equiv. of Cu (see also the absorbance diagrams, Figure 4 and Figure 5).

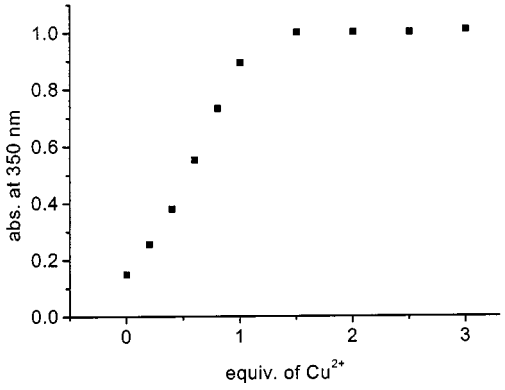

Figure 4. Increase of 350 nm absorbance on photometric titration of **1** ($5\cdot10^{-5}$ M) with copper(II) perchlorate solution; for conditions, refer to Figure 2

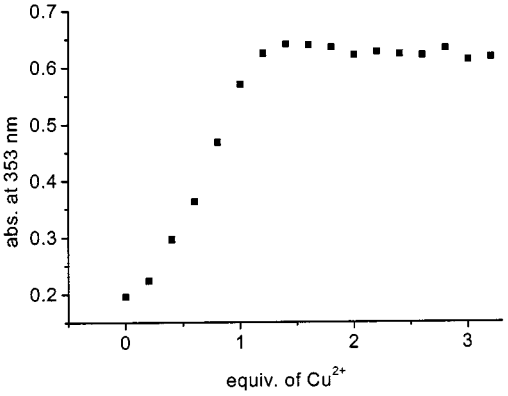

Figure 5. Increase of 353 nm absorbance on photometric titration of **7** ($5\cdot10^{-5}$ M) with copper(II) perchlorate solution; for conditions, refer to Figure 3

In a dichloromethane/acetonitrile (1:1) solution in the absence of DMSO, the lack of an isosbestic point for the titration 0 → 1 equiv. of Cu suggests the formation of an intermediate species when the ligand is present in excess {possibly formed by coordination of free ligand pyridyl groups to axial sites in [Cu(**1**,**7**)]; such species may not be stable in competitive solvents such as DMSO}. In clear contrast to the titrations shown in Figure 2 and Figure 3, the spectrum changes significantly when > 1 equiv. of Cu^{2+} is added and a rather sharp end point is seen after the addition of 3 equiv. of Cu (no further changes beyond 3 equiv. of Cu). For simplicity, Figure 6 shows selected spectra of free ligand **1** and at 1:1, 2:1, 3:1, and 4:1 Cu/**1** ratios.

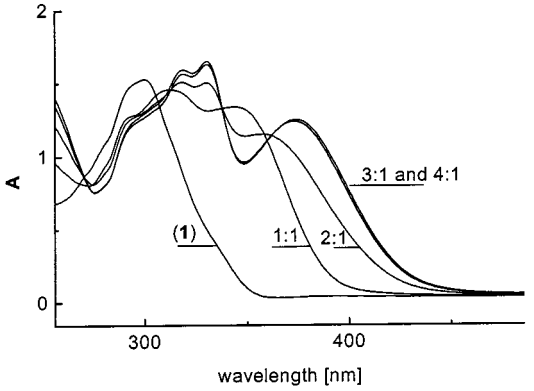

Figure 6. Spectrophotometric titration of **1** with copper(II) perchlorate in CH_3CN/CH_2Cl_2 (1:1) at 20 °C from 0−4 equiv. (spectra correspond to addition of Cu in 1-equiv. steps)

Very similar behaviour is observed for the Cu complexes of **7**, with the trinuclear complex showing nearly identical absorbance maxima.

Since catalytic studies (see below) are performed in buffered water/DMSO (3:1) mixtures, we tried to explore the formation of [(**1**)Cu] complexes under these conditions. The spectrum of [(**1**)Cu]$(ClO_4)_2$ is very similar to that observed in CH_2Cl_2/MeCN (1:1). On addition of Cu^{2+}, only subtle spectral changes are observed, polynuclear complexes apparently being much less stable than in the CH_2Cl_2/MeCN medium.

Interestingly, the spectral changes are qualitatively the same as those seen in CH_2Cl_2/CH_3CN (Figure 6), i.e. an increase in the absorbance maximum at 320 nm (Figure 6: 320 and 340 nm), an isosbestic point at 340 nm (Figure 6: 340 nm), a decrease in the absorbance at 350 nm, an isosbestic point at 370 nm (Figure 6: 360 nm, not sharp), and an increase in the absorbance at 390 nm (Figure 6: maximum at 375 nm).

By comparison with the spectra in Figure 6, we estimated that a maximum of 5% of the polynuclear complex was present after addition of 5 equiv. of Cu^{2+} under the conditions of Figure 7 (HPNP was replaced by the less reactive dimethyl phosphate).

We have examined the reactivity of in situ prepared polynuclear copper(II) complexes of **1** and **7** toward the phosphodiester 2-hydroxypropyl *p*-nitrophenyl phosphate (HPNP), an RNA analogue which is widely used to examine phosphoesterase activity of metal complexes. Intramolecular cyclization of this phosphodiester is easily followed photometrically by monitoring the 400 nm absorbance of the released nitrophenolate (Scheme 6).

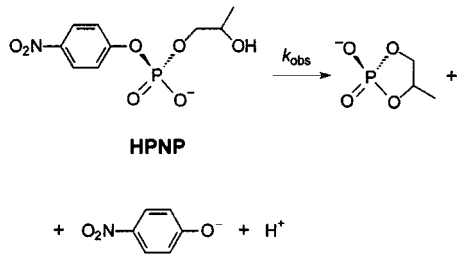

Scheme 6. Intramolecular cleavage of the phosphodiester 2-hydroxypropyl *p*-nitrophenyl phosphate (HPNP)

Kinetic studies were performed at varying Cu^{2+} concentrations in a buffered water/DMSO (3:1) mixture at pH = 7.0, with 10^{-4} M ligand **1** or **7** and $5\cdot10^{-4}$ M HPNP (these conditions were used to allow direct comparison with previously reported kinetic studies on the complexes shown in Scheme 1).

As expected, the 1:1 complexes were found to be practically ineffective in HPNP cleavage. However, the rate increases dramatically when polynuclear complexes are formed upon addition of Cu^{2+}. The profiles in Figure 7 are consistent with our spectrophotometric observations. The concentration of the reactive polynuclear species would seem to increase linearly with Cu^{2+} concentration. This indicates that the bidentate sites of [(**1**)Cu]$^{2+}$ are far from being saturated with metal ions and that the polynuclear complex must be present in low concentration.

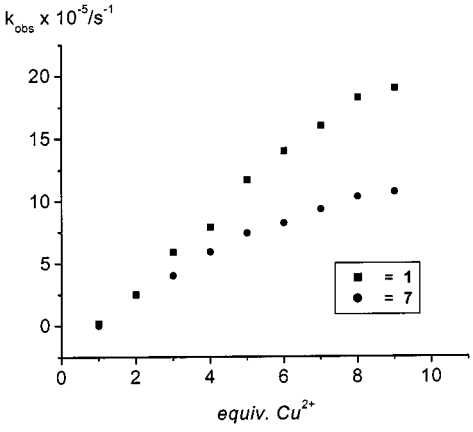

Figure 7. k_{obs} for cleavage of HPNP ($5\cdot10^{-4}$ M) in solutions containing **1** (10^{-4} M) and **7** (10^{-4} M) and varying copper(II) nitrate concentrations; water/DMSO (3:1), pH = 7.0, buffer 5 mM 3-morpholinopropanesulfonic acid (MOPS), T = 20 °C; cleavage by free Cu^{2+} is negligible

This is consistent with our results obtained by photometric titration of [(**1**)Cu]$^{2+}$ with Cu^{2+} in water/DMSO (3:1). In analogy with our previous work on LCu complexes (L = ligand shown in Scheme 1), we suggest that the reactive spe-

cies is a trinuclear complex. Under the conditions of Figure 7, a trinuclear Cu complex of L (Scheme 1) forms quantitatively with a slight excess of Cu and cleaves HPNP with $k_{obs} = 27 \cdot 10^{-5}$ s^{-1}.[4] Given that complexes $[(\mathbf{1})Cu_3]^{6+}$ and $[(\mathbf{7})Cu_3]^{6+}$ are the reactive species and are present only in low concentration, they must be even more reactive than $[LCu_3]^{5+}$ (L = ligand shown in Scheme 1). It is unlikely that a dinuclear complex $[(\mathbf{1}, \mathbf{7})Cu_2]^{4+}$ is the reactive species since the in situ prepared dinuclear Cu^{2+} complex of 4,6-di(2-pyridyl)pyrimidine (which compares to the aforementioned dinuclear complex with bridging pyrimidine) cleaves HPNP only with $k_{obs} = 8 \cdot 10^{-6}$ s^{-1} under the conditions of Figure 7.

The higher tendency of complex LCu (Scheme 1) to bind additional Cu^{2+} ions might, in part, be a result of the negative charge of the ligand, which, to some extent, compensates the electrostatic repulsion between the metal ions in the polynuclear complexes. It is evident from Figure 7 that the reactive Cu^{2+} species of **1** and **7**, presumably the trinuclear complexes, show different reactivity towards HPNP. In the presence of nine equivalents of Cu^{2+}, the complex of **1** is more efficient by a factor of 1.7. Thus, the spacer group (S or Se) clearly influences the catalytic activity of the complexes. In principle, variation of both the spacer groups X and the metal ion M (Scheme 2) promises to offer a versatile approach for fine-tuning the preorganization of two bipyridine-like chelating units and of their coordinated metal ions. Unfortunately, in preliminary attempts to prepare heteronuclear Ni^{II}/Cu^{II} and Pd^{II}/Cu^{II} complexes, it became evident that Ni and Pd are displaced from the tetradentate site by Cu. This is in contrast to the previously reported complexes of L (L = ligand shown in Scheme 1), which are not susceptible to metal exchange.[4]

Experimental Section

General Remarks: Reagents were obtained from either Aldrich or Fluka and were used as received. 4-(6-Bromo-2-pyridyl)-6-(2-pyridyl)pyrimidine was synthesized as described previously.[5] The barium(II) salt of 2-hydroxypropyl *p*-nitrophenyl phosphate was prepared by a reported method.[11] All reactions were carried out in dry solvents (HPLC grade) under nitrogen using Schlenk techniques. Workup was performed using technical grade solvents without protection from air. − Preparative column chromatography was carried out on Merck silica gel 60 (0.040−0.063 mm). Retention factors (R_f) were determined using Macherey−Nagel alumina TLC plates. − ^{1}H,^{13}C COSY and NOESY NMR spectra were recorded with Bruker AC-300 (300.13 MHz) and Bruker AC-400 (400.13 MHz) spectrometers; chemical shifts are reported in ppm. Tetramethylsilane was used as an internal standard. − IR spectra were obtained with a Perkin−Elmer 983 G spectrometer (samples in KBr pellets). − FD and EI mass spectra were recorded with a Finnigan MAT 8230 instrument. MALDI-TOF mass spectra were recorded with a Bruker Biflex TOF-MS spectrometer in negative or positive linear mode. − Elemental analyses were performed by the Microanalytisches Laboratorium des Organisch-Chemischen Instituts der Universität Heidelberg and by the Microanalytisches Laboratorium des Instituts für Anorganische und Analytische Chemie der Universität Mainz.

Ligand Syntheses

Bis{6-[6-(2-pyridyl)-4-pyrimidinyl]-2-pyridyl} Sulfide (1): This ligand was prepared as outlined in Scheme 3. A solution of $Na_2S \cdot 10H_2O$ (2.1 g, 8.1 mmol) in DMF (10 mL) was added to a stirred solution of 4-(6-bromo-2-pyridyl)-6-(2-pyridyl)pyrimidine (1.7 g, 5.4 mmol) in DMF (20 mL). The reaction mixture was stirred for 7 h at 90−100 °C, then allowed to cool, and kept at room temperature for 12 h. The white-yellow precipitate was collected by filtration, washed with DMF (15 mL), and dried in vacuo for 24 h (0.01 mbar). Water (100 mL) was added to the residue, and the product was extracted with chloroform (3 × 100 mL). The combined chloroform extracts were dried with $MgSO_4$, filtered, and concentrated to dryness, and the residue was dried in vacuo for 6 h. Yield: 0.8 g (30%), $R_f = 0.56$ (acetone/hexane, 3:7). − $C_{28}H_{18}N_8S$ (498.56): calcd. C 67.46, H 3.64, N 22.48, S 6.43; found C 67.21, H 3.61, N 22.32, S 5.99. − IR (KBr): $\tilde{\nu}$ [ν(S−R)] = 1100 cm^{-1} s. − ^{1}H NMR ($CDCl_3$): δ = 7.41 (ddd, 1 H, $J_{5,4}$ = 7.6 Hz, $J_{5,6}$ = 4.8 Hz, $J_{5,3}$ = 1.4 Hz, Py-5), 7.74 (dd, 1 H, $J_{5,4}$ = 7.8 Hz, $J_{5,3}$ = 0.9 Hz, Py′-5), 7.85 (td, $J_{4,5}$ = 7.8 Hz, $J_{4,3}$ = 7.8 Hz, Py-4), 7.91 (t, $J_{4,5}$ = 7.8 Hz, $J_{4,3}$ = 7.8 Hz, 1 H, Py′-4), 8.42 (dt, $J_{3,4}$ = 7.8 Hz, $J_{3,5}$ = 1.0 Hz, 1 H, Py-3), 8.46 (dd, $J_{3,4}$ = 7.8 Hz, $J_{3,5}$ = 1.0 Hz, 1 H, Py′-3), 8.75 (dq, $J_{6,5}$ = 4.8 Hz, $J_{6,4}$ = 0.9 Hz, 1 H, Py-6), 9.21 (d, $J_{2,5}$ = 1.4 Hz, 1 H, Pym-5), 9.314 (d, $J_{2,5}$ = 1.3 Hz, 1 H, Pym-2). − MS (FD); *m*/*z* (%): 498.2 (100) [M$^+$].

1,2-Bis{6-[6-(2-pyridyl)-4-pyrimidinyl]-2-pyridyl} Disulfide (2): A solution of $Na_2S \cdot 10H_2O$ (1.6 g, 6.5 mmol) in DMF (10 mL) was added to a stirred solution of 4-(6-bromo-2-pyridyl)-6-(2-pyridyl)pyrimidine (0.39 g, 1.3 mmol) in DMF (30 mL). The reaction mixture was stirred for 12 h at 90−100 °C, then allowed to cool, and kept at room temperature for 12 h. The solvent was evaporated at 50 °C in a rotary evaporator. Water (100 mL) was then added and the by-products **1**, **3**, and **4** were extracted from the resulting suspension with chloroform (3 × 200 mL). The aqueous phase was treated with acetic acid (10 mL) and the solution was stirred for 1 h. The product **2** was then extracted with chloroform (3 × 200 mL). The combined chloroform extracts were dried with $MgSO_4$, filtered, and concentrated to dryness. Yield: 70 mg (10%). − $C_{28}H_{18}N_8S_2$ (530.62): calcd. C 63.38, H 3.42, N 21.12, S 12.08; found C 64.11, H 3.01, N 20.82, S 11.89. − IR (KBr): $\tilde{\nu}$ [ν(R−S)] = 1093 cm^{-1} s. − ^{1}H NMR ([D$_6$]DMSO): δ = 7.02 (t, $J_{4,5}$ = 7.8 Hz, Py-5), 7.98 (dd, $J_{4,5}$ = 7.8 Hz, $J_{3,5}$ = 0.9 Hz, 1 H, Py-4), 8.00 (td, $J_{4,5}$ = 7.8 Hz, $J_{3,5}$ = 7.8 Hz, 1 H, Py′-4), 8.08 (t, $J_{4,5}$ = 7.8 Hz, 1 H, Py′-3), 8.35 (d, $J_{4,5}$ = 1.3 Hz, 1 H, Py′-5), 8.45 (dd, $J_{4,3}$ = 7.8 Hz, $J_{3,5}$ = 1.0 Hz, 1 H, Py-3), 8.70 (dq, $J_{6,5}$ = 4.7 Hz, $J_{4,6}$ = 0.8 Hz, 1 H, Py-6), 9.15 (s, 1 H, Pym-5), 9.35 (s, 1 H, Pym-2). − MS (FD); *m*/*z* (%): 530.4 (100) [M$^+$].

4-[6-(2-Pyridyl)-2-pyridyl]-6-(2-pyridyl)pyrimidine (4): A solution of $Na_2S \cdot 10H_2O$ (0.57 g, 2.3 mmol) in pyridine (10 mL) was added to a stirred solution of 4-(6-bromo-2-pyridyl)-6-(2-pyridyl)pyrimidine (0.7 g, 2.3 mmol) in pyridine (20 mL). The reaction mixture was stirred for 12 h at 90−100 °C, then allowed to cool, and kept at room temperature for 12 h. The solvent was evaporated at 50 °C in a rotary evaporator. Water (100 mL) was then added and **1**, **3**, and **4** were extracted from the resulting suspension with chloroform (3 × 200 mL). The combined chloroform extracts were dried with $MgSO_4$, filtered, and concentrated to dryness. The mixture of products **1**, **3**, and **4** was separated by column chromatography using 10% acetone in hexane as eluent. − 1st fraction: **3**, yield 0.18 g (42%), $R_f = 0.75$ (acetone/hexane, 3:7). − $C_{14}H_{10}N_4$ (234.26): calcd. C 71.78, H 4.30, N 23.92; found C 71.83, H 4.31, N 23.70. − ^{1}H NMR ([D$_6$]DMSO): δ = 7.43 (ddd, 2 H, $J_{3,5}$ = 1.1 Hz, $J_{4,5}$ = 7.8 Hz, $J_{5,6}$ = 4.8 Hz, Py-5), 7.89 (td, 2 H, $J_{3,4}$ = 7.8 Hz, $J_{4,6}$ =

1.2 Hz, Py-4), 8.52 (dt, 2 H, Py-3), 8.80 (ddd, 2 H, Py-6), 9.36 (d, 2 H, $J_{2,5}$ = 1.1 Hz, Pym-5), 9.39 (d, 2 H, Pym-2). − MS (FD); *m/z* (%): 234.3 (100) [M^+]. The data are identical to those reported in the literature.[10] − 2nd fraction: **4**, yield 0.2 g (35%), R_f = 0.68 (acetone/hexane, 3:7). − ^{1}H NMR ([D$_6$]acetone): δ = 7.37 (dd, *J* = 8.3 Hz, *J* = 5.0 Hz, 1 H), 7.45 (dd, *J* = 8.3 Hz, *J* = 5.0 Hz, 1 H), 7.97 (m, 2 H), 8.03 (t, *J* = 8.3 Hz, 1 H), 8.564 (m, 3 H), 8.72 (d, *J* = 1.3 Hz, 1 H), 8.75 (d, *J* = 1.4 Hz, 1 H), 8.84 (d, *J* = 1.3 Hz, 1 H), 9.38 (s, 1 H, Pym-5), 9.51 (s, 1 H, Pym-2). − MS (FD); *m/z* (%): 311.4 (100) [M^+]. − 3rd fraction: **1**, R_f = 0.56 (acetone/hexane, 3:7).

Methyl 6-[6-(2-Pyridyl)-4-pyrimidinyl]-2-pyridyl Selenide (5): A solution of CH_3Li (1.6 M in Et_2O, 2.5 mL, 4 mmol) was added dropwise to a suspension of selenium (316 mg, 4 mmol) in absolute THF (25 mL) and stirring was continued for a further 30 min. The clear solution thus obtained was added dropwise to a solution of 4-(6-bromo-2-pyridyl)-6-(2-pyridyl)pyrimidine (1.25 g, 4 mmol) in absolute DMF (25 mL) and the resulting mixture was stirred for 15 min. The THF was then evaporated under high vacuum (0.01 mbar, 40 °C, 10 min) and the remaining DMF solution was stirred for 2.5 h at 70 °C and then cooled to room temperature. Water (200 mL) was added and the mixture was stirred for a further 12 h. The yellow precipitate formed was collected by filtration, recrystallized from chloroform, and purified by column chromatography eluting with MeOH/CH_2Cl_2 (1:100). Yield: 0.53 g (37%), R_f = 0.58 (hexane/acetone, 6:4). − $C_{15}H_{12}N_4Se$·MeOH (359.29): calcd. C 53.49, H 4.49, N 15.59; found C 52.16, H 4.38, N 14.73. − ^{1}H NMR ($CDCl_3$) δ = 2.64 (3 H, $SeCH_3$, *J* = 11.5 Hz), 7.43 (ddd, 1 H, $J_{4,5}$ = 7.8 Hz, $J_{5,6}$ = 4.8 Hz, $J_{3,5}$ = 0.9 Hz, Py-5), 7.43 [dd, 1 H, $J_{4,5}$ = 7.8 Hz, $J_{3,5}$ = 0.9 Hz, Py′-5 (?)],7.63 (t, 1 H, $J_{3,4}$ = 7.8 Hz, Py′-4), 7.89 (td, 1 H, $J_{3,4}$ = 7.8 Hz, $J_{4,6}$ = 1.9 Hz, Py-4), 8.25 [dd, 1 H, $J_{3,4}$ = 7.8 Hz, $J_{3,5}$ = 0.9 Hz, Py′-3 (?)], 8.50 (dt, 1 H, $J_{3,4}$ = 7.8 Hz, $J_{3,5}$ = 0.9 Hz, Py-3), 8.80 (dq, 1 H, $J_{5,6}$ = 4.6 Hz, $J_{4,6}$ = 0.9 Hz, Py-6), 9.33 (d, 1 H, $J_{2,5}$ = 1.3 Hz, Pym-2), 9.37 (d, 1 H, $J_{2,5}$ = 1.3 Hz, Pym-5). − MS (FAB+); *m/z* (%): 327.1 (40) [M^+ + H] with ^{78}Se, 329.1 (70) [M^+ + H] with ^{80}Se.

1,2-Bis{6-[6-(2-pyridyl)-4-pyrimidinyl]-2-pyridyl} Diselenide (6): The reaction was carried out in a similar fashion as described for **5**, but using a higher CH_3Li/Se to 4-(6-bromo-2-pyridyl)-6-(2-pyridyl)pyrimidine ratio. Thus, a solution of CH_3Li (1.6 M in Et_2O, 5 mL, 8 mmol) was added dropwise to a suspension of selenium (632 mg, 8 mmol) in absolute THF (25 mL) and stirring was continued for a further 30 min. The resulting solution was added dropwise to a solution of 4-(6-bromo-2-pyridyl)-6-(2-pyridyl)pyrimidine (1.25 g, 4 mmol) in absolute DMF (25 mL) and stirring was continued for 15 min. The THF was then evaporated under high vacuum (0.01 mbar, 40 °C, 10 min) and the remaining DMF solution was stirred for 2.5 h at 70 °C and then cooled to room temperature. Water (200 mL) was added and the mixture was stirred for a further 12 h. The yellow precipitate formed was collected by filtration, recrystallized from chloroform, and purified by column chromatography eluting with MeOH/CH_2Cl_2 (1:100). Yield: 0.69 g (27%), R_f = 0.46 (hexane/acetone, 6:4). − $C_{28}H_{18}N_8Se_2$·0.5 MeOH (640.44): calcd. C 53.45, H 3.15, N 17.50; found C 53.52, H 3.20, N 17.40. − ^{1}H NMR ($CDCl_3$): δ = 7.44 (ddd, 1 H, $J_{4,5}$ = 7.8 Hz, $J_{5,6}$ = 3.7 Hz, $J_{3,5}$ = 1.1 Hz, Py-5), 7.76 (t, 1 H, $J_{3,4}$ = 7.7 Hz, Py′-4), 7.90 (td, 1 H, $J_{3,4}$ = 7.7 Hz, $J_{4,6}$ = 1.8 Hz, Py-4), 8.02 [dd, 1 H, $J_{4,5}$ = 7.7 Hz, $J_{3,5}$ = 0.7 Hz, Py′-5 (?)], 8.32 [dd, 1 H, $J_{3,4}$ = 7.8 Hz, $J_{3,5}$ = 1.1 Hz, Py′-3 (?)], 8.50 (dt, 1 H, $J_{3,4}$ = 7.8 Hz, $J_{3,5}$ = 1.4 Hz, Py-3), 8.80 (dq, 1 H, $J_{5,6}$ = 3.7 Hz, $J_{4,6}$ = 0.8 Hz, Py-6), 9.34 (d, 1 H, $J_{2,5}$ = 1.3 Hz, Pym-2), 9.34 (d, 1 H, $J_{2,5}$ = 1.3 Hz, Pym-5). − MS (FAB+); *m/z* (%): 627.1 (40) [M^+ + H] with 2 × ^{80}Se, 625.1 (37) [M^+ + H] with ^{78}Se and ^{80}Se, 623.1 (22) [M^+ + H] with 2 × ^{78}Se. − MS (EI); *m/z*: 546.2 (100) [M^+ − Se] with ^{80}Se remaining, 544.2 (54) [M^+ − Se] with ^{78}Se remaining.

Bis{6-[6-(2-pyridyl)-4-pyrimidinyl]-2-pyridyl)} Selenide (7): According to a procedure for the preparation of bis(2-pyridyl) selenide,[12] a solution of methyl 6-[6-(2-pyridyl)-4-pyrimidinyl]-2-pyridyl selenide (**5**) (300 mg, 0.92 mmol) in hexamethylphosphortriamide (HMPA) (10 mL) was heated with small pieces of sodium (42 mg, 1.83 mmol) at 100 °C for 1.5 h. A solution of 4-(6-bromo-2-pyridyl)-6-(2-pyridyl)pyrimidine (288 mg, 0.92 mmol) in HMPA (10 mL) was then added dropwise. The red mixture was heated for 2.5 h at 120 °C. After cooling to room temperature, it was poured into cold water (100 mL) and the resulting suspension was stirred for 4 h. The brown precipitate formed was collected by filtration, washed with diethyl ether, and purified by column chromatography on SiO_2 eluting first with MeOH/CH_2Cl_2 (1:100) and then with pure $CHCl_3$. Yield 0.11 g (21%), R_f = 0.48 (hexane/acetone, 6:4). − $C_{28}H_{18}N_8Se$·MeOH (577.50): calcd. C 60.31, H 3.84, N 19.40; found C 61.13, H 3.98, N 18.13. − ^{1}H NMR ($CDCl_3$): δ = 7.47 (1 H, Py-5), 7.83 (2 H, Py-4, Py′-5), 7.92 (1 H, Py′-4), 8.44 (2 H, Py-3, Py′-3), 8.80 (1 H, Py-6), 9.25 (1 H, Pym-2), 9.33 (1 H, Pym-5). − MS (FAB$^+$); *m/z* (%): 547.2 (25) [M^+ + H] with ^{80}Se, 545.2 (15) [M^+ + H] with ^{78}Se.

Synthesis of the Complexes

[Cu(1)](NO$_3$)$_2$·5H$_2$O: To a stirred solution of **1** (12 mg, 0.024 mmol) in chloroform/methanol (1:3; 1 mL) was added a solution of $Cu(NO_3)_2$·3H_2O (6 mg, 0.024 mmol) in methanol (3 mL). The clear green solution thus obtained was stirred for 10 min at room temperature. After 1 h, diethyl ether (10 mL) was added, and the green precipitate formed was centrifuged off and dried under high vacuum for 6 h. Yield: 10 mg (54%). − $C_{28}H_{28}CuN_{10}O_{11}S$ (776.20): calcd. C 43.33, H 3.64, N 18.05; found C 42.75, H 3.38, N 18.11. − MS (MALDI); *m/z* (%): 561.5 (100) [^{63}Cu(**1**)]$^+$, 563.5 (54) [^{65}Cu(**1**)]$^+$, 596.5 (7) [^{63}Cu(**1**)(OH)]$^+$, 598.5 (6) [^{65}Cu(**1**)(OH)]$^+$.

[Cu(7)](ClO$_4$)$_2$·6H$_2$O: To a stirred solution of **7** (12 mg, 0.02 mmol) in chloroform (1 mL) was added a solution of $Cu(ClO_4)_2$·6H_2O (7.4 mg, 0.02 mmol) in acetonitrile (2 mL). The resulting mixture was stirred for 3 h at room temperature. The green precipitate formed was centrifuged off, washed with diethyl ether (10 mL), and dried under high vacuum for 4 h. Yield: 6.3 mg (38%). − $C_{28}H_{18}CuCl_2N_8O_8Se$·6$H_2O$ (915.91 g/mol): calcd. C 36.71, H 3.30, N 12.23; found C 35.68, H 2.99, N 10.92. − MS (MALDI); *m/z* (%): 607.2 (55) [^{63}Cu(**7**)]$^+$ with ^{78}Se, 609.2 (100) [^{63}Cu(**7**)]$^+$ with ^{80}Se, [^{65}Cu(**7**)]$^+$ with ^{78}Se, 611.2 (50) [^{65}Cu(**7**)]$^+$ with ^{80}Se.

[Zn(6)](CH$_3$COO)$_2$·CHCl$_3$·CH$_3$CN: A solution of 1,2-bis{6-[6-(2-pyridyl)-4-pyrimidinyl]-2-pyridyl} diselenide (**6**) (12 mg, 0.02 mmol) in chloroform (1.5 mL) was added dropwise to a stirred solution of $Zn(CH_3COO)_2$·2H_2O (4.4 mg, 0.02 mmol) in acetonitrile (2 mL).[13] After stirring for 3 h, a precipitate had formed, which was collected by filtration, washed with diethyl ether (2 × 5 mL), and dried in vacuo. Yield 8.4 mg (44%). − $C_{32}H_{24}N_8O_4Se_2Zn$·$CHCl_3$·CH_3CN (968.32): calcd. C 43.41, H 2.91, N 13.02; found C 42.08, H 3.00, N 12.73. − ^{1}H NMR ($CDCl_3$): δ = 1.90 (3 H, CH_3CN), 2.05 (6 H, CH_3COO), 7.53 (2 H, Py-5), 7.77 (2 H, Py′-4), 7.98 [4 H, Py-4 (?), Py′-5 (?)], 8.35 [4 H, Py-3 (?), Py′-3 (?)], 8.87 (2 H, Py-6), 9.21 (2 H, Pym-5), 9.43 (2 H, Pym-2). − MS (MALDI); *m/z* (%): 684.9 (66) [^{64}Zn(**6**)]$^+$ with 2 × ^{78}Se, 686.9 (91) [^{66}Zn(**6**)]$^+$ with 2 × ^{78}Se, [^{64}Zn(**6**)]$^+$ with 1 ×

^{78}Se and 1 × ^{80}Se, 688.9 (100) [^{66}Zn(**6**)]$^+$ with 1 × ^{78}Se and 1 × ^{80}Se, [^{64}Zn(**6**)]$^+$ with 2 × ^{80}Se, 690.9 (52) [^{66}Zn(**6**)]$^+$ with 2 × ^{80}Se.

Spectrophotometric Titrations: Stock solutions of **1** and **7** (10^{-3} M) were prepared in either DMSO (Figure 2, 3, 4, and 5) or CH_2Cl_2/CH_3CN (1:1) (Figure 6). These stock solutions were diluted with a CH_3CN/CH_2Cl_2 (1:1) mixture, and then the requisite amount of DMSO was added (5% v/v). The final ligand concentration in each case was $5\cdot10^{-5}$ M. Titrations were performed by addition of appropriate amounts of a $Cu(NO_3)_2\cdot3H_2O$ stock solution ($5\cdot10^{-4}$ M in CH_3CN). About 30 s after the addition of the copper salt, UV/Vis spectra were recorded at 25 °C. No further spectral changes with time were detectable on prolonged standing of the solutions.

Kinetics: Reaction solutions were prepared by combining appropriate amounts of the ligands **1** or **7** ($5\cdot10^{-4}$ M stock solutions in DMSO), $Cu(NO_3)_2\cdot3H_2O$ (2 mM stock solution in DMSO), the buffer 3-morpholinopropanesulfonic acid (MOPS) (0.5 M stock solution in H_2O, pH = 7.0), and water or DMSO solvent. Solutions were left to stand for 2 h. The reactions were initiated by addition of the substrate, 2-hydroxypropyl-*p*-nitrophenolphosphate (HPNP, 5 mM stock solution in H_2O). For the experiments summarized in Figure 7, the final concentrations in the reaction mixtures were 0.1 mM **1** or **7**, 0.5 mM HPNP, and 5 mM MOPS buffer in water/DMSO (3:1); the concentration of $Cu(NO_3)_2$ was varied from 0 to 1 mM. Transesterification of HPNP was followed spectrophotometrically by monitoring the release of *p*-nitrophenolate at 400 nm (ε = 18600 μ^{-1} cm^{-1}), considering the equilibrium *p*-nitrophenol/*p*-nitrophenolate at pH = 7.0 (pK_a = 7.15). The pseudo-first-order rate constants k_{obs} were determined from the initial rate of the reaction (< 5% conversion). All reported data are average values of at least three measurements (reproducibility within ± 15%). Measurements were made with a Carl-Zeiss-Technology Specord S 100 spectrophotometer at 20 °C.

Table 2. Crystal data and structure refinement for **4**

Empirical formula	$C_{19}H_{13}N_5$
Molecular mass	311.34
Crystal system	$P2_1/n$
Unit cell	
a [Å]	10.6(9)
b [Å]	7.6(7)
c [Å]	18.5(2)
β [°]	93.2(2)
Volume [Å^3]	1479.5(2)
Z	4
Calcd. density [g cm^{-3}]	1.398
Adsorp. coeff. [mm^{-1}]	0.088
F(000)	648
Crystal size [mm]	0.51 × 0.12 × 0.07
θ range [°]	2.17 ≤ θ ≤ 26.37
No. of reflections	9159
unique	3016
observed [$I > 2\sigma(I)$]	2077
Parameters	269
Final *R* indices	
*R*1 [$I > 2\sigma(I)$]	0.0391
*wR*2	0.1024
Largest diff.peak/hole [e/Å^3]	0.207/−0.180

X-ray Crystallographic Study of 4: Crystal data and details of the structure determination are listed in Table 2. Intensity data were collected at 173 K with a Bruker AXS CCD Smart 1000 diffractometer (Mo-K_α radiation, λ = 0.71073 Å, graphite monochromator, ω scan). The structure was solved by direct methods and refined by least-squares methods based on F^2 with all measured reflections.[14] All non-hydrogen atoms were refined anisotropically; hydrogen atoms were placed in ideal positions and refined isotropically. Crystallographic data (excluding structure factors) for the structure reported in this paper have been deposited with the Cambridge Crystallographic Data Centre as supplementary publication number CCDC-149055. Copies of the data can be obtained free of charge on application to the CCDC, 12 Union Road, Cambridge CB2 1EZ, U.K. [Fax: (internat.) + 44-1223/336-033; E-mail: deposit@ccdc.cam.uk].

Acknowledgments

This work was funded by the Deutsche Forschungsgemeinschaft (Gerhard Hess Programm) and supported by the Fonds der Chemischen Industrie. We thank I. Fritsky for his help with the synthesis of the ligands and R. Ott for her help with the kinetic measurements.

[1] N. Straeter, W. N. Lipscomb, T. Klabunde, B. Krebs, *Angew. Chem. Int. Ed. Engl.* **1996**, *35*, 2024−2055.
[2] [2a] R. Krämer, T. Gajda, in: *Perspectives on Bioinorganic Chemistry*, vol. 4 (Eds.: R. W. Hay, J. R. Dilworth, K. B. Nolan), JAI Press, Greenwich, **1999**, pp. 209−240. − [2b] N. H. Williams, B. Takasaki, J. Chin, *Acc. Chem. Res.* **1999**, *32*, 485−493. − [2c] P. Molenveld, J. F. J. Engbersen, D. N. Reinhoudt, *Chem. Soc. Rev.* **2000**, *29*, 75−87.
[3] W. H. Chapman, Jr., R. Breslow, *J. Am. Chem. Soc.* **1995**, *117*, 5462−5469.
[4] I. O. Fritsky, R. Ott, H. Pritzkow, R. Krämer, *Angew. Chem. Int. Ed.* **2000**, *39*, 3255−3258, *Angew. Chem.* **2000**, *112*, 3403−3406.
[5] R. Krämer, I. O. Fritsky, *Eur. J. Org. Chem.*, in press.
[6] C. Chachaty, G. C. Pappalardo, G. Scarlata, *J. Chem. Soc., Perkin Trans. 2* **1976**, 1234−1238.
[7] I. G. Phillips, P. J. Steel, *Aust. J. Chem.* **1998**, *51*, 371−382.
[8] G. Wilkinson, R. D. Gillard, J. A. McCleverty, *Comprehensive Coordination Chemistry*, vol. 5, Late Transition Elements, Pergamon Press, Oxford, New York, **1987**, pp. 662−673.
[9] S. Siddiqui, R. E. Shepherd, *Inorg. Chem.* **1986**, *25*, 3869−3876.
[10] R. Krämer, I. O. Fritsky, R. Ott, H. Pritzkow, *Chem. Eur. J.*, in press.
[11] D. M. Brown, D. A. Usher, *J. Chem. Soc.* **1965**, 6558−6564.
[12] M. Tiecco, L. Testaferri, M. Tingoli, D. Chianelli, D. Bartoli, R. Balducci, *Tetrahedron* **1988**, *44*, 4883−4894.
[13] C. O. Kienitz, C. Thöne, P. Jones, *Inorg. Chem.* **1996**, *35*, 3990−3997.
[14] G. M. Sheldrick, *SHELXS-V5.1*, Bruker AXS, Madison, Wisconsin USA, **1999**.

Received September 1, 2000
[I00330]

Kinetics and Mechanism of Water Substitution at Half-Sandwich Iridium(III) Aqua Cations $Cp^*Ir(A-B)(H_2O)^{2+/+}$ in Aqueous Solution (Cp^* = η^5-Pentamethylcyclopentadienyl Anion; A−B = Bidentate N,N or N,O Ligand)

Tilo Poth,[a] Helmut Paulus,[c] Horst Elias,*[a] Carlos Dücker-Benfer,[b] and Rudi van Eldik[b]

Keywords: Iridium / Sandwich complexes / Kinetics / N ligands / Reaction mechanisms

The perchlorate complexes of a series of half-sandwich monoaqua cations $Cp^*Ir(A–B)(H_2O)^{2+/+}$ with A–B = prol (D/L-proline anion), picac (picolinic acid anion), *R*,*R*-dach [(−)-(1*R*,2*R*)-1,2-diaminocyclohexane], *R*,*R*-dpen [(+)-(1*R*,2*R*)-1,2-diphenylethylenediamine], phen (*o*-phenanthroline), and bpy (2,2′-bipyridine) (Cp^* = η^5-pentamethylcyclopentadienyl anion) have been prepared and characterized. An X-ray structure analysis of $Cp^*Ir(R,R\text{-dach})(H_2O)(ClO_4)_2{\cdot}H_2O$ has revealed that the cation $Cp^*Ir(R,R\text{-dach})(H_2O)^{2+}$ has a distorted pseudo-octahedral coordination geometry. In the case of A–B = prol, crystallization from water led to the trinuclear complex $[Cp^*Ir(D\text{-prol})]_3(ClO_4)_3$, which has also been characterized by X-ray structure analysis. The experimental data suggest that in aqueous solution the trinuclear proline complex dissociates to form the cation $Cp^*Ir(D\text{-prol})(H_2O)^+$. The proton dissociation constants of the coordinated water in $Cp^*Ir(A–B)(H_2O)^{2+/+}$ have been determined as pK_a = 7.5 (A–B = bpy) and pK_a = 7.1 (A–B = *R*,*R*-dach and picac). Substitution of the water in $Cp^*Ir(A–B)(H_2O)^{2+/+}$ by the monodentate ligands L = py (pyridine), DMS (dimethyl sulfide), TU (thiourea), and monodentate anions according to the Equation $Cp^*Ir(A–B)(H_2O)^{2+/+} + L \rightarrow Cp^*Ir(A–B)L^{2+/+} + H_2O$ has been studied by multi-wavelength stopped-flow spectrophotometry in aqueous solution at I = 0.2 M. This kinetic investigation, carried out at different concentrations, temperatures, and pressures, showed that the process obeys second-order kinetics, where rate = $k_L[Cp^*Ir(A–B)H_2O^{2+/+}][L]$. The magnitude of the second-order rate constant k_L depends on the nature of both A–B and L. The data for k_L have been found to range from 6.4×10^4 $M^{-1}s^{-1}$ (A–B = D-prol; L = TU) to 10.5 $M^{-1}s^{-1}$ (A–B = bpy; L = py) at 298 K. The activation parameters for water substitution at $Cp^*Ir(A–B)(H_2O)^{2+/+}$ (A–B = bpy, *R*,*R*-dach, and picac) by L = TU have been evaluated. The activation volumes of $\Delta V^{\neq}$ = +2.3, +7.4, and +7.3 $cm^3\ mol^{-1}$, respectively, are supportive of an I_d mechanism. The results regarding the kinetic lability of the coordinated water in the monoaqua cations $Cp^*Ir(A–B)(H_2O)^{2+/+}$ are compared to those obtained for the triaqua cation $Cp^*Ir(H_2O)_3^{2+}$.

Introduction

The aqua cations $Cp^*Rh(H_2O)_3^{2+}$ and $Cp^*Ir(H_2O)_3^{2+}$ (**1**) belong to the small group of water-stable organometallic species in which water molecules and carbocyclic ligands, such as π-Cp* (= η^5-pentamethylcyclopentadienyl anion), are bound to the same metal centre.[1] There has been a wide spectrum of studies on the chemistry of these aqua cations, providing insight into the relatively new field of aqueous organometallic chemistry.[2−6]

Our interest in half-sandwich aqua cations lies mainly in their intriguing kinetic properties. The introduction of the Cp* group into the cation $Ir(H_2O)_6^{3+}$ leads to a dramatic increase of 14 orders of magnitude in the rate of water exchange, as described by rate constant k_{ex} in Equation (1), and in the rate of water substitution, as described by rate constant k_f in Equation (2) (L = monodentate ligand).[7−12]

$$Cp^*Ir(H_2O)_3^{2+} + H_2O^* \underset{}{\overset{k_{ex}}{\rightleftharpoons}} Cp^*Ir(H_2O)^*(H_2O)_2^{2+} + H_2O \quad (1)$$

$$Cp^*Ir(H_2O)_3^{2+} + L \underset{k_r}{\overset{k_f}{\rightleftharpoons}} Cp^*Ir(H_2O)_2L^{2+} + H_2O \quad (2)$$

Replacement of two of the coordinated water molecules in the cation **1** by bidentate ligands A−B generates the monoaqua species $Cp^*Ir(A-B)(H_2O)^{2+/+}$. The literature on such iridium compounds is still very limited,[13] but numerous examples of the monochloro analogues $Cp^*Ir(A-B)Cl^{+/0}$ have been described. These species have been found to be particularly effective as catalysts[14−19] and in the coordination of biologically important molecules.[20]

As an extension of our earlier work on the kinetics of Equations (1) and (2),[7,8] we now compare the labilizing effect of the Cp* group, as documented by the rate data available for Equations (1) and (2), with that of bidentate ligands A−B in the monoaqua species $Cp^*Ir(A-B)(H_2O)^{2+/+}$. The kinetics of water substitution according to Equation (3) have been studied in aqueous solution using a series of complexes $Cp^*Ir(A-B)(H_2O)^{2+/+}$

[a] Institut für Anorganische Chemie, Technische Universität Darmstadt,
Petersenstraße 18, 64287 Darmstadt, Germany
E-mail: elias@tu-darmstadt.de
[b] Institut für Anorganische Chemie, Universität Erlangen-Nürnberg,
Egerlandstraße 1, 91058 Erlangen, Germany
[c] Technische Universität Darmstadt, Fachbereich Materialwissenschaft
64287 Darmstadt, Germany
Supporting information for this article is available on the WWW under http://www.wiley-vch.de/home/eurjic or from the author.

 © WILEY-VCH Verlag GmbH, 69451 Weinheim, 2001 1434−1948/01/0505−1361 $ 17.50+.50/0

Table 1. Abbreviations used for the aqua complexes

$Cp^*Ir(H_2O)_3^{2+}$	**1**	$[Cp^*Ir(bpy)(H_2O)](ClO_4)_2$	**5b**
$Cp^*Ir(R,R\text{-dach})(H_2O)^{2+}$	**2**	$Cp^*Ir(picac)(H_2O)^+$	**6**
$[Cp^*Ir(R,R\text{-dach})(H_2O)](ClO_4)_2 \cdot H_2O$	**2b**	$[Cp^*Ir(piac)]_3(ClO_4)_3$	**6b**
$[Cp^*Ir(\text{D-prol})]_3^{3+}$	**3**	$Cp^*Ir(R,R\text{-dpen})(H_2O)^{2+}$	**7**
$[Cp^*Ir(\text{D-prol})]_3(ClO_4)_3$	**3b**	$[Cp^*Ir(R,R\text{-dpen})(H_2O)](ClO_4)_2$	**7b**
$Cp^*Ir(\text{D-prol})(H_2O)^+$	**4**	$Cp^*Ir(phen)(H_2O)^{2+}$	**8**
$Cp^*Ir(bpy)(H_2O)^{2+}$	**5**	$[Cp^*Ir(phen)(H_2O)](ClO_4)_2$	**8b**

(**2**, **4**−**8**) containing neutral or anionic N,N and N,O ligands A−B (see Scheme 1). The incoming ligands L used in the study of the reaction according to Equation (3) have been either neutral species (py, py-nia, DMS, TU)[21] or anions (Br^-, I^-, SCN^-, N_3^-, NO_2^-).

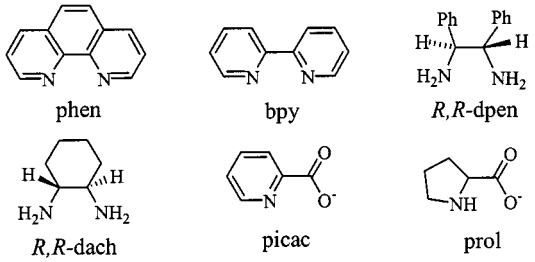

Scheme 1. Bidentate ligands A−B coordinated in monoaqua complexes $Cp^*Ir(A-B)(H_2O)^{2+/+}$ and abbreviations[21]

$$Cp^*Ir(A\text{-}B)(H_2O)^{2+/+} + L \underset{k_{-L}}{\overset{k_L}{\rightleftharpoons}} Cp^*Ir(A\text{-}B)L^{2+/+} + H_2O \quad (3)$$

The present contribution summarizes the kinetic results obtained at various temperatures and pressures. We also present crystallographic data for the perchlorates of the cations $Cp^*Ir(R,R\text{-dach})(H_2O)^{2+}$ (**2**) and $[Cp^*Ir(prol)]_3^{3+}$ (**3**) (*R*,*R*-dach = 1,2-diaminocyclohexane; prol = anion of proline)[21] as well as acidity constants (pK_a) for the coordinated water in some of the mono aqua cations $Cp^*Ir(A-B)(H_2O)^{2+/+}$.

Results and Discussion

Properties of the Monoaqua Species $Cp^*Ir(A-B)(H_2O)^{2+/+}$

The UV spectra of aqueous solutions of the perchlorates of the cations $Cp^*Ir(A-B)(H_2O)^{2+/+}$ led to the absorption data listed in Table 2. The various cations absorb in the range 260−320 nm with absorptivities ε_{max} of the order of 10^3 $M^{-1}cm^{-1}$ in the case of aliphatic ligands A−B (dach, dpen, prol)[21] and 10^4 $M^{-1}cm^{-1}$ in the case of aromatic ligand systems (bpy, phen, picac).[21] In the case of the proline complex, the spectra were recorded using solutions of the trinuclear complex **3b**. However, the spectral data strongly suggest that the trinuclear complex dissociates to form the monoaqua cation $Cp^*Ir(\text{D-prol})(H_2O)^+$ (**4**). This follows from the fact that (i) the data for ε_{max}, when referenced to **4** instead of **3**, are close to those obtained for the other mono aqua species, and (ii) the data obtained for ε_{max} at pH = 2.0, 4.8, and 6.0 are identical.

Table 2. UV absorption {λ_{max} [nm] (ε_{max} [$M^{-1}cm^{-1}$])} of the cations $Cp^*Ir(A-B)(H_2O)^{2+/+}$ in aqueous solution at pH = 2.0 and 293 K

5 (A−B = bpy)	243 (15500), 308 (13500), 317 (13400)
8 (A−B = phen)	298 (4990), 276 (16100), 218 (13200), 201 (16500)
2 (A−B = *R*,*R*-dach)	269 (2070), 302 (1660)
7 (A−B = *R*,*R*-dpen)	265 (1690), 298 (1080)
4 (A−B = D-prol)	282 (1160), 300 (1150)[a][b]
6 (A−B = picac)	311 (4740), 260 (10600)

[a] The data obtained at pH = 6 are identical to those obtained at pH = 2.0. − [b] The values of λ_{max} and ε_{max} refer to 1 mol of **4**, not to 1 mol of **3**.

The spectral changes associated with substitution reaction according to Equation (3) are sufficient to allow reliable spectrophotometric monitoring. As an example, Figure 1 shows a series of spectra describing the reaction of **2** with bromide ions according to Equation (3). The existence of two sharp isosbestic points (at 257 nm and 267 nm) indicates that the reaction does not involve substantial concentrations of intermediates.

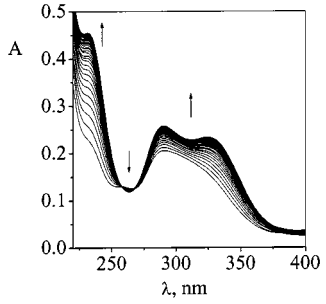

Figure 1. Spectral changes recorded for the reaction of **2** with bromide ions according to Equation (3) within 1.2 s {$[complex]_o$ = 1.0×10^{-4} M, $[Br^-]_o$ = 1.0×10^{-3} M; pH = 2.0 ($HClO_4$), I = 0.2 M ($NaClO_4$), 298 K}

It is well documented that, due to proton dissociation from coordinated water, aqueous solutions of the triaqua iridium species **1** are acidic.[9] For comparison purposes, the acid dissociation of some of the monoaqua species $Cp^*Ir(A-B)(H_2O)^{2+/+}$ according to Equation (4) was therefore investigated by means of spectrophotometric titrations. The pK_a values presented in Table 3 show that (i) the effect of the nature of the bidentate ligand A−B and of the overall charge of the cation on the pK_a is very minor, and (ii) the dissociation constant K_a of the monoaqua species is more than three orders of magnitude smaller than that of the triaqua species **1**. The chelate ligands A−B presumably reduce the electrophilicity of the Ir^{III} centre, such that less electron density is donated by the water oxygen atom. The coordinated water molecule thus becomes a weaker acid.

Table 3. Acidity constants pK_a of the monoaqua species Cp*Ir(A−B)$(H_2O)^{2+/+}$ at 298 K (I = 0.2 M)

Complex	pK_a
5	7.5 ± 0.2[a]
2	7.1 ± 0.5
6	7.1 ± 0.5
1 [= Cp*Ir$(H_2O)_3^{2+}$]	3.86 ± 0.03[b]

[a] Taken from ref.[7] − [b] Taken from ref.[9]

At pH ≤ 5, the formation of monohydroxo species Cp*Ir(A−B)$(OH)^{+/0}$ can be neglected.

$$Cp^*Ir(A\text{-}B)(H_2O)^{2+/+} \overset{K_a}{\rightleftharpoons} Cp^*Ir(A\text{-}B)(HO)^{+/0} + H^+ \quad (4)$$

Structures of the Complexes 2b and 3b

To the best of our knowledge, **2b** represents the first structurally characterized monoaqua half-sandwich iridium Cp* complex of the type Cp*Ir(A−B)$(H_2O)^{2+}$. As shown in Figure 2, the coordination geometry of the cation **2** is of the "three-legged piano stool" type[22] and can be classified as pseudo-octahedral. The perchlorate ions are disordered and the single water molecule of crystallization is far away from the coordination sphere of the iridium centre.

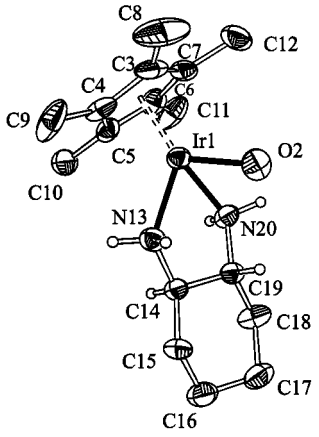

Figure 2. Molecular structure of the cation **2** with thermal ellipsoids drawn at a 30% probability level; most of the hydrogen atoms have been omitted for the sake of clarity

The crystal contains two crystallographically distinct units of **2**. The difference is small and is manifested, for example, in the relative positions of the Cp* and cyclohexane rings. In unit I, the angle between the plane of the Cp* ring and the plane formed by the donor atoms N13, N20, and O2 amounts to 2.7°. In unit II, this angle is found to be just 1.0°.

The bond lengths N13−Ir1 (2.127 Å) and N20−Ir1 (2.130 Å) are very similar (see Table 4), while the bond length O2−Ir1 is slightly longer (2.18 Å). The Ir−OH_2 bond length of 2.18 Å is significantly longer than those reported for other Ir^{III} aqua complexes, which range from 2.057 Å for oxo-bridged trinuclear iridium hexacarboxylate complexes to 2.074 Å for hydroxo-bridged bis(ethylenediamine)iridium complexes.[23,24] This ground-state bond lengthening must be due to the *trans* influence of the Cp* ligand and may account for the high lability of the coordinated water molecule. Ir−O distances in the even more labile cation **1** (longest distance 2.27 Å[6]) are in line with this conclusion. By comparison, the water exchange at $Ir(H_2O)_6^{3+}$ is 10^{14} times slower than that at **1**.[7,10] The bond angles N20−Ir1−N13, N20−Ir1−O2, and N13−Ir1−O2 in **2** are close to 80°, which indicates the deviation from ideal octahedral geometry of 90°. The iridium atom is a centre of asymmetry, but the C_2 symmetry of the ligand *R*,*R*-dach brings about a definite, nonracemic configuration.

Table 4. Selected bond lengths and angles in unit I of the complex **2b**

Atoms	Distance [Å]	Atoms	Angle [°]
Ir(1)−N(20)	2.127(8)	N(20)−Ir(1)−N(13)	79.0(3)
Ir(1)−N(13)	2.130(8)	N(20)−Ir(1)−O(2)	80.9(3)
Ir(1)−O(2)	2.180(7)	N(13)−Ir(1)−O(2)	83.6(3)
Ir(1)−C(3)	2.180(9)	X1a−Ir(1)−O(2)[a]	128.7(3)
Ir(1)−C(4)	2.143(12)	X1a−Ir(1)−N(13)[a]	132.0(4)
Ir(1)−C(5)	2.113(9)	X1a−Ir(1)−N(20)[a]	133.0(4)
Ir(1)−C(6)	2.178(9)	C(19)−N(20)−Ir(1)	110.2(5)
Ir(1)−C(7)	2.170(9)	C(19)−C(14)−N(13)	108.9(6)
Ir(1)−X1a[a]	1.777(2)	C(14)−N(13)−Ir(1)	111.9(5)
N(13)−C(14)	1.502(9)	C(14)−C(19)−N(20)	108.1(6)
C(19)−N(20)	1.510(9)	C(4)−Ir(1)−C(3)	39.6(6)
C(14)−C(19)	1.457(10)	C(5)−Ir(1)−C(4)	41.1(4)
C(3)−C(7)	1.45(2)	C(5)−Ir(1)−C(6)	38.3(4)
		C(7)−Ir(1)−C(6)	36.5(4)
		C(7)−Ir(1)−C(3)	38.9(5)

[a] The position X1a corresponds to the center of the Cp* ring.

While this work was being carried out, a series of complexes containing trinuclear units $[Cp^*M(aa)]_3^{3+}$ (M = Rh, Ir; aa = amino acid anion) was reported.[3,15,25] All of these complexes were obtained by crystallization from methanol. With regard to aqueous solutions, the possibility of trimer dissociation and the formation of mononuclear $Cp^*M(aa)(H_2O)^+$ units has yet to be fully explored.

In the presence of perchlorate ions, crystallization from an acidic aqueous solution of the cation **4** leads to yellow prisms, which are structurally composed of trinuclear units **3** with C_3 symmetry (see Figure 3). The structural backbone of these units is a 12-membered metallacycle, consisting of three iridium atoms and three doubly *O*-bonded carboxylate groups. The pseudo-octahedral coordination sphere about each iridium atom is made up by the η^5-bound Cp* ring, one *N*,*O*-bound proline, and another *O*-bound proline. As shown in Table 5, the Ir1−O18 bond to the *N*,*O*-bound proline (2.138 Å) is slightly longer than the Ir1−O19A bond to the singly coordinated neighbouring proline (2.108 Å).

The trinuclear unit 3 possesses 3 × 3 chiral centres (Ir, N, α-C) and the diastereomer within the crystal has to be described as ($R_CR_CR_C$,$R_NR_NR_N$,$R_{Ir}R_{Ir}R_{Ir}$)-**3b**. The unit is the mirror image of the (all-*S*)-configured analogue reported by Beck and co-workers.[26] The chirality at the metal centre is determined by the configuration of the

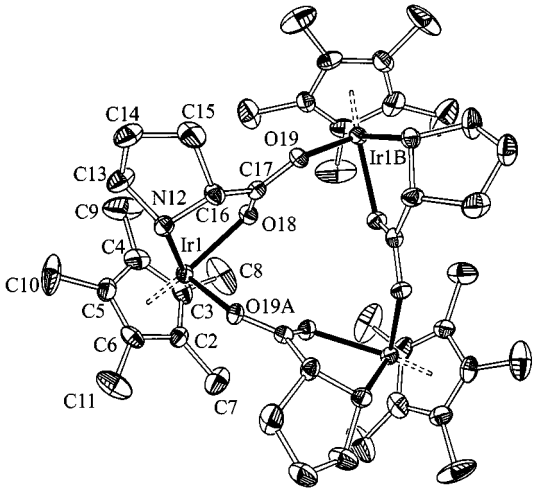

Figure 3. Molecular structure of the trinuclear cation **3** with thermal ellipsoids drawn at a 30% probability level; hydrogen atoms have been omitted for the sake of clarity

Table 5. Selected bond lengths and angles in the complex **3b**

Atoms	Distance [Å]	Atoms	Angle [°]
Ir(1)−O(19A)[a]	2.108(6)	O(19)−Ir(1)−O(18)	81.5(3)
Ir(1)−N(12)	2.136(8)	N(12)−Ir(1)−O(18)	76.8(4)
Ir(1)−O(18)	2.138(5)	O(19)−Ir(1)−N(12)	78.7(3)
Ir(1)−C(6)	2.099(10)	X1a−Ir(1)−N(12)[b]	134.5(5)
Ir(1)−C (4)	2.100(11)	X1a−Ir(1)−O(18)[b]	134.9(5)
Ir(1)−C(5)	2.133(12)	X1a−Ir(1)−O(19)[b]	128.7(5)
Ir(1)−C(2)	2.133(10)	Ir(1)−N(12)−C(16)	112.2(6)
Ir(1)−C(3)	2.140(12)	Ir(1)−O(18)−C(17)	115.0(7)
Ir(1)−X1a[b]	1.754(10)	Ir(1B)−O(19)−C(17)[c]	127.6(5)
N(12)−C(16)	1.484(12)	N(12)−C(16)−C(17)	108.7(8)
C(16)−C(17)	1.503(13)	C(16)−C(17)−O(18)	121.4(8)
C(17)−O(18)	1.249(13)	C(16)−C(17)−O(19)	114.6(7)
C(17)−O(19)	1.284(11)	Ir(1)−N(12)−C(13)	117.1(7)

[a] O(19A): O(19) transformed to $1 - x + y$, $1 - x$, z. − [b] The position X1a corresponds to the center of the Cp* ring. − [c] Ir(1B): Ir(1) transformed to $1 - y$, $x - y$, z.

asymmetric carbon atom, making the complex an example of chiral self-recognition.

Kinetics of Water Substitution

A kinetic investigation of water substitution according to Equation (3) was undertaken to study the reactivity and mechanistic behaviour of the coordinated water in the monoaqua species $Cp^*Ir(A-B)(H_2O)^{2+/+}$ and to compare it with that in the triaqua species **1**. We recently reported that water substitution at the triaqua species follows an I_d mechanism[21] with the rate of substitution being close to the rate of water exchange.[9] For a variety of $Cp^*Ir(A-B)(H_2O)^{2+/+}$/L systems, systematic variation of A−B (with L = constant) and of L (with A−B = constant) was carried out to obtain detailed information on the effect of the bidentate ligands A−B on the kinetics and mechanism of the reaction according to Equation (3).

Water Substitution in Complexes $Cp^*Ir(A-B)(H_2O)^{2+/+}$ by Pyridine

In a series of experiments, water substitution in six monoaqua $Cp^*Ir(A-B)(H_2O)^{2+/+}$ complexes by pyridine was investigated at pH = 2.0 and 4.8. These substitution reactions were expected to be second-order processes. Accordingly, under pseudo-first-order conditions the change of absorbance with time was found to be monophasic and exponential. Fitting of Equation (5) to the (A,t) data led to the observed rate constant k_{obsd} (ΔA = amplitude). As an example, Figure 4a shows the dependence of k_{obsd} on $[py]_{tot}$ for the system **4**/py.

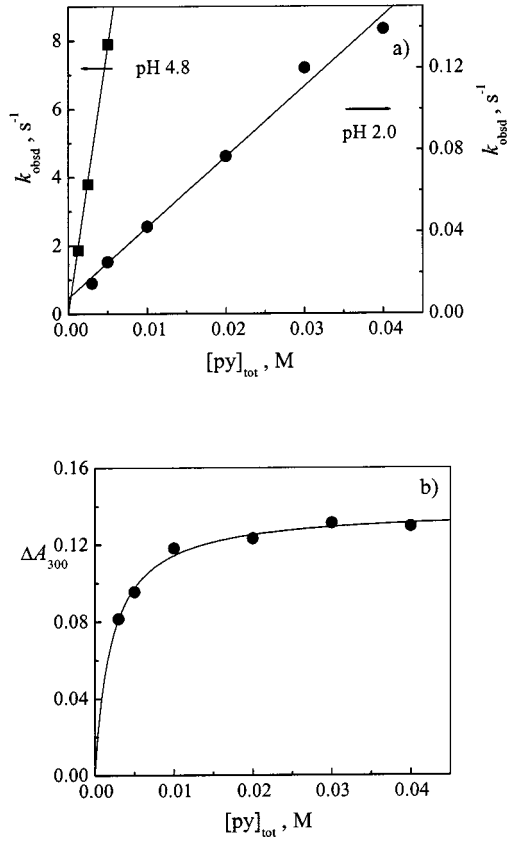

Figure 4. Dependence of the kinetic parameters k_{obsd} (a) and ΔA_{300} (b) on $[py]_{tot}$ for the reaction of the cation **4** with pyridine at pH = 2.0 and 4.8

$$A = \Delta A \exp(-k_{obsd} t) + A_\infty \quad (5)$$

$$k_{obsd} = k_L[py] = m[py]_{tot} \quad (6)$$

$$k_{obsd} = k_L[py] + k_{-L} = m[py]_{tot} + k_{-L} \quad (7)$$

At pH = 4.8, the dependence is linear and conforms to Equation (6) (irreversible pseudo-first-order reaction), whereas at pH = 2.0 the linear dependence has an intercept and conforms to Equation (7) (reversible pseudo-first-order reaction).[27] The slope m of the linear dependencies shown in Figure 4a leads to rate constant k_L and the intercept corresponds to k_{-L}.[28] At pH = 2.0, where most of the pyridine is protonated ($pK_a = 5.26$[29]), the reverse reaction (rate constant k_{-L}) is observed and the equilibrium constant K is obtained from the ratio k_L/k_{-L}. Independently and additionally, K can be derived from the concentration dependence of the amplitude ΔA, as described by Equation (8) and shown in Figure 4b.

Table 6. Rate constants k_L and k_{-L} and equilibrium constants K for water substitution in monoaqua cations Cp*Ir(A−B)$(H_2O)^{2+/+}$ and in the triaqua cation **1** by pyridine at 298 K

Aqua cation	pH	k_L [$M^{-1}s^{-1}$]	k_{-L} [s^{-1}][a]	$K = k_L/k_{-L}$ [M^{-1}]	K [M^{-1}][b]
4	4.8	6270 ± 90	–	–	–
	2.0	6270 ± 330	0.008 ± 0.004	(7.8 ± 4.4) × 10^5	(8.7 ± 0.7) × 10^5
6	2.0	643 ± 15	–[c]	–	–
7	4.8	63 ± 0.8	–[c]	–	–
	2.0[d]	79 ± 1.0	0.0053 ± 0.0004	(0.15 ± 0.01) × 10^5	(0.15 ± 0.01) × 10^5
2	4.8	41.6 ± 0.7	0.0025 ± 0.0009[d]	(0.17 ± 0.07) × 10^5	–
	2.0[d]	44.2 ± 0.5	0.0008 ± 0.0003	(0.5 ± 0.2) × 10^5	(0.41 ± 0.02) × 10^5
8	4.8	16.9 ± 0.6	0.004 ± 0.001	4225 ± 1200	–
5	4.8	10.5 ± 0.3	–[c]	–	–
1	2.0	2610 ± 40[e]	–	–	–

[a] According to Equation (7), rate constant k_{-L} corresponds to the intercept of the plot of k_{obsd} vs. [L]; in most cases, the values of k_{-L} are therefore obtained with high error limits. – [b] As obtained from the amplitude ΔA according to Equation (8). – [c] Error limits too high to accept data for k_{-L} as sufficiently reliable. – [d] Substitution studied with py-nia[21] instead of py. – [e] First substitution step; data taken from ref.[9]

$$\Delta A = A_\infty K[py]_{tot}/(1 + K[py]_{tot}) \quad (8)$$

The values of k_L, k_{-L}, and K obtained are summarized in Table 6.

The data for the system **4**/py demonstrate that the pH value has no effect on k_L, which clearly indicates that in solutions at pH = 2.0 and 4.8 the reacting iridium species is the same. This is in line with the UV absorption data (see Table 2). Within the error limits, equilibrium constant K = 7.8 × 10^5 M^{-1}, as obtained according to $K = k_L/k_{-L}$, is in good agreement with K = 8.7 × 10^5 M^{-1}, as derived from the dependence of ΔA on $[py]_{tot}$ according to the relationship in Equation (8). It is noteworthy that the substitution of water in the proline complex by py is a monophasic process, properly described by a single exponential function. In agreement with the UV absorption data, this finding supports the interpretation that the trinuclear compound **3b** is hydrolyzed to form the monoaqua cation **4** when dissolved in water.[30] If the trinuclear cation **3** were to be present in solution, one should observe biphasic or even triphasic kinetic behaviour.

As described above, the acidity of the coordinated water in the species Cp*Ir(A−B)$(H_2O)^{2+/+}$ is not significantly affected by the nature of A−B (see Table 3). In contrast to this lack of dependence, the magnitude of the rate constant k_L clearly depends on A−B (see Table 6). The proline complex **4** (k_L = 6270 $M^{-1}s^{-1}$) reacts faster than the bipyridine complex **5** (k_L = 10.5 $M^{-1}s^{-1}$) by a factor in excess of 500. As a general rule, it is found that the singly charged complex cations (A−B = prol and picac) react more rapidly than the doubly charged ones (A−B = dpen, dach, phen, and bpy). However, the difference of a factor of 10 between the k_L data for **4** and the picolinic acid complex **6** clearly shows that the charge on the cations is not the only rate-determining parameter.

The reverse reaction is less affected by the nature of A−B. The values obtained for the rate constant k_{-L} only vary between 0.008 s^{-1} and 0.0008 s^{-1}. As a result of the effects of A−B on k_L and k_{-L}, the overall equilibrium constant K ranges from 7.8 × 10^5 M^{-1} (A−B = prol) to 4.2 × 10^3 M^{-1} (A−B = phen).

Due to pH-dependent protonation of the incoming pyridine ligand, rate constant k_{-L} for the reverse reaction was not reliably accessible for some of our complexes under certain conditions (see Table 6). Experiments in which the less basic pyridine derivative py-nia (= nicotinamide; pK_a = 3.47[29]), rather than pyridine (pK_a = 5.26[29]), was treated with Cp*Ir(*R*,*R*-dpen)$(H_2O)^{2+}$ (**7**) and **2** at pH = 2.0 led to reliable data for k_{-L} and K. Further evidence for the reversibility of substitution reaction according to Equation (3) was provided by the results of some pH-jump stopped-flow experiments performed on the system **2**/py-nia.[31] The change in absorbance with time associated with the pH-jump from pH = 2.0 to proton concentrations $[H^+]$ = 0.27, 0.55, and 1.5 M, respectively, proved to be exponential according to Equation (5). The experimental rate constant k_{obsd}, formally described by Equation (7), was found to be independent of $[H^+]$, with a mean value of k_{obsd} = (1.02 ± 0.03) × 10^{-3} s^{-1}.[31] Within the limits of error, this value is in agreement with k_{-L} = (0.8 ± 0.3) × 10^{-3} s^{-1} as determined from the kinetics of the complex formation reaction (see Table 6). This means that the pH-jump from pH = 2 to higher proton concentrations causes aquation of the cation Cp*Ir(*R*,*R*-dach)(py-nia)$^{2+}$ according to Equation (9). Due to pyridine protonation at the high proton concentrations employed, the contribution of the rate term k_L[py] in Equation (7) becomes negligibly small.

$$Cp^*Ir(R,R\text{-dach})(py\text{-nia})^{2+} + H_2O \xrightarrow{k_L} Cp^*Ir(R,R\text{-dach})(H_2O)^{2+} + py\text{-nia} \quad (9)$$

In comparison to other aqueous systems [e.g. $Ni(H_2O)_6^{2+}$/py; K = 81 M^{-1}],[32] the complexes Cp*Ir(A−B)$L^{2+/+}$ prove to be extraordinarily stable. Since the carbon−iridium bonds are resistant to hydrolysis even in very acidic solutions, high proton concentrations can be used to reduce the concentration of the pyridine ligand. It is thus possible to accurately determine large K values.

*Water Substitution in Cp*Ir(A−B)$(H_2O)^{2+/+}$ Complexes by Thiourea, Dimethyl Sulfide, and Monodentate Anions*

The rates of associatively controlled substitution reactions are strongly affected by the nucleophilicity of the in-

coming ligand L. In the case of associative substitutions at Pt^{II} complexes, the nucleophilic discrimination factor *S*, as obtained from n^{o}_{Pt} values according to Equation (10), is used to quantify this effect of the nucleophilicity of L on the rate of the reaction (k = second-order substitution rate constant; n^{o}_{Pt} = empirical measure of the nucleophilicity).[33]

$$\log k = Sn^{o}_{Pt} + c \quad (10)$$

To obtain information on the mechanism of water substitution according to Equation (3), the rate constant k_L was determined for the entry of various ligands L into the monoaqua complexes $Cp^*Ir(A-B)(H_2O)^{2+/+}$. Under pseudo-first-order conditions ($[L]_o \geq 10 \times [complex]_o$), substitution was found to be a practically irreversible process with the (A,t) data conforming to Equation (5). The dependence of k_{obsd} on $[L]_o$ according to Equation (6), led to the k_L data summarized in Table 6. Analysis of these data shows that (i) as found for L = py, water substitution at the various cations $Cp^*Ir(A-B)(H_2O)^{2+/+}$ by TU and DMS is more than two orders of magnitude faster for the singly charged proline and picolinic acid complexes than for the bipyridine complex, (ii) for a given cation $Cp^*Ir(A-B)(H_2O)^{2+/+}$, the magnitude of k_L follows the order TU > DMS > py, and (iii) water substitution at the cations **2** and **5** by the anions Br^-, I^-, SCN^-, N_3^-, and NO_2^- is faster than that by the neutral ligands TU, DMS, and py. The latter result is in line with expectation for charge effects according to the Eigen–Wilkins mechanism.[34]

A plot of log k_L vs. n^{o}_{Pt} for L = py, DMS, and TU is shown in Figure 5. It can be seen that the substitution rate constant k_L increases with increasing nucleophilicity of L, as characterized by the parameter n^{o}_{Pt}. This increase of k_L with n^{o}_{Pt} is found for all of the $Cp^*Ir(A-B)(H_2O)^{2+/+}$ complexes studied. The nucleophilic discrimination factor *S* ranges from 0.25 for the proline complex **4** to 0.41 for the *R*,*R*-dach complex **2**. In line with the second-order rate law obtained for substitution reaction according to Equation (3), this finding excludes a *D* mechanism. However, for typical associative substitutions at Pt^{II} complexes (*A* mechanism) it is found that *S* ranges from 0.6 to 1.4.[33] This im-

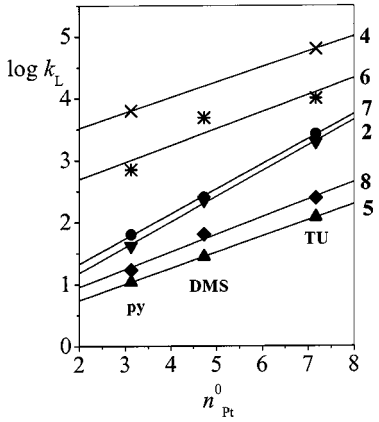

Figure 5. Dependence of rate constant k_L on the nucleophilicity of the neutral ligands py, DMS, and TU (**4**, S = 0.25; **6**, S = 0.27 ± 0.10; **7**, S = 0.40 ± 0.01; **2**, S = 0.41 ± 0.02; **8**, S = 0.28 ± 0.01; **5**, S = 0.26 ± 0.01)

Table 7. Second-order rate constant k_L ($M^{-1}s^{-1}$) for water substitution in monoaqua cations $Cp^*Ir(A-B)(H_2O)^{2+/+}$ and in the triaqua cation **1** by monodentate ligands L according to Equation (3) under pseudo-first-order conditions at 298 K and I = 0.2 M

Cation	pH	Entering ligand L						
		TU[a][21]	DMS[21]	Br^-	I^-	N_3^-	NO_2^-	SCN^-
2	2.0	1960 ± 50	143 ± 5	8830 ± 260	(1.39 ± 0.04) × 10^4	–	3730 ± 110[c]	(1.19 ± 0.04) × 10^4 [c]
7	2.0	2650 ± 60	252 ± 7	–	–	–	–	–
4	2.0	(6.4 ± 0.2) × 10^4 [b]	–	–	–	–	–	–
6	2.0	(1.00 ± 0.04) × 10^4	4880 ± 160	–	–	–	–	–
8	2.0	244 ± 7	63.6 ± 2	–	–	–	–	–
5	2.0	120 ± 4	27.8 ± 1	110 ± 6[c] [d] [e]	285 ± 15[c–e]	181 ± 9[c–e]	–	342 ± 20[c–e]
1[f]	2.0	8660 ± 30	3990 ± 20	(1.34 ± 0.1) × 10^4	(2.5 ± 0.1) × 10^4	–	–	(8.8 ± 0.4) × 10^4

[a] $[L]_o \geq 10 \times [complex]_o$. – [b] As obtained under stoichiometric conditions. – [c] As obtained at pH = 4.8. – [d] Data taken from ref.[7] – [e] Data determined at I = 0.3 M. – [f] First substitution step; data, as taken from ref.[9], refer to the substitution of 1 water molecule in **1**.

Table 8. Rate and activation parameters for water substitution in monoaqua cations $Cp^*Ir(A-B)H_2O^{2+/+}$ and in the triaqua cation **1** according to Equation (3) at I = 0.2 M and pH = 2.0

Aqua cation	Nucleophile L[a]	k_L^{298} [M^{-1} s^{-1}]	$\Delta H^{\neq}$ [kJ mol^{-1}]	$\Delta S^{\neq}$ [J K^{-1} mol^{-1}]	$\Delta V^{\neq}$ [cm^3 mol^{-1}]	Ref.
5	TU	120 ± 4	59 ± 5[b]	+4 ± 9[b]	+2.3 ± 0.5[c]	this work
2	TU	1960 ± 50	63 ± 2	+26 ± 5	+7.4 ± 0.4[d]	this work
6	TU	(10.0 ± 0.4) × 10^3	53 ± 2	+12 ± 4	+7.3 ± 0.4[d]	this work
1	Cl^-	(5.2 ± 0.1) × 10^3	62 ± 2	+35 ± 6	+4.7 ± 0.4[e]	[9]
	Br^-	(13.4 ± 0.3) × 10^3	55 ± 1	+18 ± 4	+3.9 ± 0.3[e]	[9]
	py–CN	(12.3 ± 0.2) × 10^2	–	–	+4.4 ± 0.4[e]	[9]
	py-nia	(17.7 ± 0.2) × 10^2	–	–	+5.4 ± 0.4[e]	[9]

[a] For abbreviations, see ref.[21] – [b] Data taken from ref.[7] – [c] T = 293 K. – [d] T = 288 K. – [e] T = 298 K.

plies that the substitution reactions under study have a rather weak dependence on the nucleophilicity of L.

Activation Parameters

The kinetics of water substitution at three monoaqua $Cp^*Ir(A-B)(H_2O)^{2+/+}$ cations by thiourea were studied at various temperatures and pressures. The corresponding activation parameters, along with related literature data, are listed in Table 8.

The values obtained for $\Delta H^{\neq}$, $\Delta S^{\neq}$, and $\Delta V^{\neq}$ are rather similar in magnitude for all three complexes. When compared to the data obtained for water substitution at the triaqua species **1**[9] and to corresponding data reported in the literature,[35−37] the positive volume of activation, which ranges from $\Delta V^{\neq} = +2.3$ cm^3 mol^{-1} for **5** to $\Delta V^{\neq} = +7.4$ cm^3 mol^{-1} for **2**, suggests the operation of a dissociatively controlled interchange mechanism (I_d). In line with the hypothesis of an I_d mechanism, the activation entropies listed in Table 8 are all positive and small. It is interesting to note that the activation volumes for the complexes **2** and **6** are significantly more positive than that for complex **5**. In the former cases, water substitution by thiourea is considerably faster, which may point to a more dissociative process than in the case of complex **5**. By way of comparison, the activation volumes quoted for water substitution at the triaqua complex **1** by a variety of nucleophiles vary between +3.9 and +5.4 cm^3 mol^{-1}, again typical for an I_d mechanism. All of these reactions are many orders of magnitude faster than water exchange and ligand substitution at hexaaqua iridium(III), which is characterized by a negative volume of activation as befits an I_a mechanism.[10,21] The significant labilization caused by the Cp* ligand is expected to result in a ground-state lengthening of the Ir−OH_2 bond (see earlier discussion). Compared to the case without ground-state labilization, this, in turn, will require a lesser degree of bond breakage (and a smaller volume increase) in going to a dissociative transition state. Therefore, in the absence of structural information on the Ir−O(water) bond lengths in all of the complexes appearing in Table 8, the reported volumes of activation do not rule out the operation of a limiting *D* mechanism.

Conclusions

Comparison of a series of half-sandwich monoaqua complexes $Cp^*Ir(A-B)(H_2O)^{2+/+}$ with the triaqua species **1** has shown that the acidity of the coordinated water in the pseudo-octahedral cations $Cp^*Ir(A-B)(H_2O)^{2+/+}$ is more than three orders of magnitude less than that in **1**. It follows from kinetic investigations of the substitution of water in the monoaqua complexes $Cp^*Ir(A-B)(H_2O)^{2+/+}$ by monodentate ligands L that the formation of the species $Cp^*Ir(A-B)L^{2+/+}$ is a second-order reaction, rate = k_L[complex][L]. The magnitude of the complex formation rate constant k_L is affected by the nature of both the bidentate ligand A−B and ligand L. For a given incoming ligand L, it is found that k_L is smallest for complexes with σ-donor/π-acceptor N,N ligands (bpy and phen), somewhat greater for those with σ-donor N,N ligands (*R*,*R*-dach and *R*,*R*-dpen), and greatest for those with σ-donor N,O$^-$ ligands (picac and prol). The reactivity of complex **6** is lower compared to that of **4**, which is probably due to the π-acceptor properties of the pyridine ring. For a given $Cp^*Ir(A-B)(H_2O)^{2+/+}$ complex, it is found that k_L increases with the nucleophilicity of L, as characterized by the empirical parameter n^o_{Pt}. The effect of L on the second-order rate constant k_L is very similar to the effect of the incoming ligand on the rate of water substitution in the triaqua complex **1**. The overall kinetic data suggest that water substitution in the species $Cp^*Ir(A-B)(H_2O)^{2+/+}$ follows an I_d mechanism.

Ligand substitution is thus mainly governed by the lability of the leaving water molecule. For L = py, the rate of aquation (rate constant k_{-L}) is less affected by the nature of A−B than the rate of water substitution (rate constant k_L). From the values of k_{-L}, it therefore follows that the lability of the coordinated pyridine is roughly of the same order of magnitude for all the $Cp^*Ir(A-B)(py)^{2+/+}$ complexes. The pronounced differences in the lability of the coordinated water are possibly a consequence of its limited polarizability or "hardness". As a general rule, it is found that the iridium centre in the monoaqua species $Cp^*Ir(A-B)(H_2O)^{2+/+}$ as well as in the triaqua cation **1** favours polarizable or "soft" ligands, so as to form kinetically and thermodynamically stable complexes.

Experimental Section

Unless stated otherwise, all manipulations were performed under aerobic conditions using commercial-grade solvents. The metal salts, organic solvents, and ligands (reagent grade) were obtained from commercial sources and were used without further purification. $[Cp^*IrCl_2]_2$ was synthesized according to published procedures.[38] Deionized water was doubly distilled in a quartz apparatus prior to use.

General Procedure for the Preparation of the Complexes: Portions of 0.100 g (0.126 mmol) of $[Cp^*IrCl_2]_2$ were suspended in methanol (5 mL) and 2 equiv. of the bidentate ligand A−B were added at ambient temperature to immediately produce a clear yellow solution. After stirring for 3 h, the solvent was evaporated. The residue was redissolved in water (7 mL) and the resulting solution was heated to ca. 80 °C. A solution of 4 equiv. (0.504 mmol) of $AgClO_4$ in water (5 mL) was added to the acidified solution (pH = 2−3, $HClO_4$) to remove chloride by precipitation of AgCl, which was separated by hot filtration after stirring for 2 h. The solvent was partially evaporated until crystallization occurred. The addition of 1 equiv. of $NaClO_4$ completed the crystallization. − To achieve deprotonation in the case of the ligands picac and prol,[21] following the addition of the ligand A−B, a stoichiometric amount of triethylamine was added to the reaction mixture. − ***Caution:*** Perchlorate salts are potentially explosive; they should be handled with care and in small portions only!

2b: Yellow needles from water (pH = 2−3, $HClO_4$). − Yield 0.118g (69%). − $C_{16}H_{33}Cl_2IrN_2O_{10}$ (676.57): calcd. C 28.40, H 4.92, N 4.14; found C 28.01, H 4.56, N 4.08. − ^{1}H NMR (D_2O): δ = 1.05−1.46 (m, 4 H, cycl.-H), 1.51−1.66 (m, 2 H, cycl.-H), 1.71 (s,

15 H, Cp*), 2.00−2.07 (m, 4 H, cycl.-H). − IR (KBr): $\tilde{\nu}$ = 3288 [m, ν(N−H)], 3254 [m, ν(N−H)], 2943 (m), 2862 (w), 1458 (w), 1386 (w), 1089 (vs), 625 (s) cm^{-1}.

3b: Yellow prisms from water (pH = 2−3, $HClO_4$). − Yield 0.088g (64%). − $(C_{15}H_{23}ClIrNO_6)_3$ (1622.97): calcd. C 33.30, H 4.28, N 2.59; found C 31.32, H 4.02, N 2.48. − ^{1}H NMR (D_2O): δ = 1.78 (s, 15 H, Cp*), 1.86−2.14 (m, 3 H, cycl.-H), 2.41 (m, 1 H, cycl.-H), 3.12 (s, 1 H, cycl.-H), 3.33 (m, 1 H, cycl.-H), 4.05 (t, 1 H, α-H). − IR (KBr): $\tilde{\nu}$ = 3227 [s, ν(N−H)], 2970 (m), 1575 [s, ν(C=O)], 1445 (m), 1385 (m), 1095 (vs), 930 (s), 623 (m) cm^{-1}.

5b: Yellow needles from water (pH = 2−3, $HClO_4$). Yield 0.123 g (72%). − $C_{20}H_{25}Cl_2IrN_2O_9$ (700.55): calcd. C 34.29, H 3.60, N 4.00; found C 33.50, H 3.01, N 3.96. − ^{1}H NMR (D_2O): δ = 1.58 (s, 15 H, Cp*), 7.74 (m, 2 H, Ar-H), 8.17 (m, 2 H, Ar−H), 8.42 (d, 2 H, Ar−H), 8.85 (d, 2 H, Ar−H). − IR (KBr): $\tilde{\nu}$ = 3086 (s), 3121 (s), 2920 (m), 1608 (m), 1466 (m), 1446 (m), 1096 (vs), 772 (s), 625 (s) cm^{-1}.

6b: Yellow prisms from water (pH = 2−3, $HClO_4$). − Yield 0.099g (71%). − $(C_{16}H_{19}ClIrNO_6)_3$ (1647.01): calcd. C 35.00, H 3.49, N 2.55; found C 32.67, H 3.84, N 2.76. − ^{1}H NMR (D_2O): δ = 1.77 (s, 15 H, Cp*), 8.01 (m, 1 H, Ar−H), 8.22 (m, 1 H, Ar−H), 8.38 (m, 1 H, Ar−H), 9.09 (m, 1 H, Ar−H). − IR (KBr): $\tilde{\nu}$ = 1614 (w), 1583 (m), 1547 [s, ν(C=O)], 1475 (m), 1406 (m), 1381 (w), 1335 (w), 1298 (w), 1265 (w), 1093 (vs), 1032 (m), 766 (m), 710 (m), 690 (m), 623 (w) cm^{-1}.

7b: Yellow powder from water (pH = 2−3, $HClO_4$). − Yield 0.136g (70%). − $C_{24}H_{35}Cl_2IrN_2O_{10}$ (774.68): calcd. C 37.21, H 4.55, N 3.62; found C 35.52, H 4.26, N 3.51. − ^{1}H NMR (D_3COD): δ = 1.85 (s, 15 H, Cp*), 3.97 (d, 1 H, ^3J = 12.3 Hz, C−H), 4.56 (d, 1 H, ^3J = 12.3 Hz, C−H), 7.28 (m, 10 H, Ar−H). − ^{1}H NMR (D_2O): δ = 1.77 (s, 15 H, Cp*), 4.17 (s, 2 H, C−H), 7.28 (s, 10 H, Ar−H). − IR (KBr): $\tilde{\nu}$ = 3290 [m, ν(N−H)], 3240 [m, ν(N−H)], 3153 (m), 3066 (m), 3033 (m), 2025 (w), 1884 (w), 1813 (w), 1589 (m), 1498 (m), 1456 (m), 1388 (m), 1093 (vs), 700 (s), 625 (s), 577 (m), 498 (m) cm^{-1}.

8b: Yellow crystals from water (pH = 2−3, $HClO_4$). − Yield 0.137 g (75%). − $C_{22}H_{27}Cl_2IrN_2O_9$ (726.59): calcd. C 36.47, H 3.34, N 3.87; found C 36.58, H 3.35, N 4.18. − ^{1}H NMR ([D_6]DMSO): δ = 1.70 (s, 15 H, Cp*), 8.35 (m, 4 H, Ar−H), 9.14 (d, 2 H, Ar−H), 9.45 (d, 2 H, Ar−H). − IR (KBr): $\tilde{\nu}$ = 3091 (w), 3061 (w), 1430 (m), 1090 (vs), 845 (s), 718 (m), 625 (s) cm^{-1}.

Instrumentation: UV/Vis spectra: diode-array spectrophotometer (Zeiss Specord S10); NMR spectra: FT NMR spectrometer (Bruker AM 200 and WM 300); IR spectra: FT-IR spectrometer (Nicolet Impact 400); pH measurements: glass electrode (Schott) in combination with a potentiometer (Metrohm 691), calibrated at I = 0.1 M ($NaNO_3$) and 25 °C to yield $-\log[H^+]$ = pH − 0.09; kinetics of reaction according to Equation (3): multi-wavelength stopped-flow spectrophotometer (J. & M., TIDAS)[39] and stopped-flow spectrophotometer in combination with a high-pressure cell.[40]

Spectrophotometric Titrations: The dissociation of the monoaqua complexes $Cp^*Ir(A-B)(H_2O)^{2+/+}$ according to Equation (4) was monitored by spectrophotometric titrations of acidic solutions of the complexes with 0.1 M NaOH. Least-squares fitting of Equation (11) to the (absorbance,[H^+]) data led to the acid dissociation constants K_a (A_{H2O} and A_{OH} refer to the absorbances of the aqua and hydroxy complexes, respectively, at the concentration [$complex]_{tot}$).

$$A = (A_{OH} + A_{H2O}[H^+]/K_a)/(1 + [H^+]/K_a) \quad (11)$$

Kinetic Measurements: The reaction according to Equation (3) was monitored in freshly prepared aqueous solutions in the wavelength range 200−500 nm under pseudo-first-order conditions ($[L]_o \geq 10 \times [complex]_o$) at various temperatures (285−318 K) and pressures (10−150 MPa). The ionic strength was fixed at I = 0.2 M ($NaClO_4$ or $NaNO_3$). Measurements were made at either pH = 2 (as adjusted with $HClO_4$) or 4.8 (as adjusted with the noncoordinating buffer 2,6-dimethylpyridine-3-sulfonic acid[41]). Least-squares fitting of the (absorbance,time) data with Equation (5) led to the experimental rate constant k_{obsd}, which is defined by Equations (6) and (7) for irreversible and reversible pseudo-first-order reactions, respectively. Rate constants k_L and k_{-L} were obtained from the dependence $k_{obsd} = f([L]_o)$ according to Equations (6) and (7), respectively. The amplitude ΔA in Equation (5) depends on $[L]_o$ according to Equation (8). Fitting of this Equation to the (ΔA,$[L]_o$) data led to the equilibrium constant $K = k_L/k_{-L}$. − The volume of activation was obtained from the pressure dependence of k_{obsd} according to Equation (12). A correction for the pressure dependence of the activity coefficients (less than 0.6 cm^3 mol^{-1} under the given conditions[42]) was not applied.

$$\Delta V^{\neq}_{exptl} = -RT(\partial \ln k_{obsd}/\partial P)_T \quad (12)$$

Crystallography: The crystals were obtained from aqueous solutions (pH = 2−3, $HClO_4$) as stated above. Measurements were made with a four-circle diffractometer (STOE-STADI-4) using graphite-monochromated Mo-K_α radiation (λ = 0.71069 Å); scan 2θ:ω = 1:1. Cell constants were determined by the least-squares method from the 2θ angles of 58 and 54 reflections for **2b** and **3b**, respectively. The structures were solved by direct methods with SHELXS-86 and refined by least squares to the R values given in Table 9 using the program package SHELXL-93. The non-hydrogen atoms were refined anisotropically. All hydrogen atoms were placed in their calculated positions. Crystal data and data collection parameters are listed in Table 9; selected bond lengths and

Table 9. Crystallographic data for complexes **2b** and **3b**

	2b	**3b**
Empirical formula	$C_{16}H_{33}Cl_2IrN_2O_{10}$	$C_{15}H_{23}ClIrNO_6$
Crystal system	monoclinic	hexagonal
Space group	$P2_1$	$P6_3$
a/Å	12.628(4)	17.766(3)
b/Å	9.462(3)	17.766(3)
c/Å	20.654(6)	11.736(3)
β/°	95.67(1)	90
V/Å^3	2455.8(13)	3208.0(11)
Z	4	6
Molecular mass	676.54	540.99
Measured reflections	9569	4728
Independent reflections	8603	4195
T/K	300(2)	300(2)
λ/Å	0.71069	0.71069
$D_{calcd.}$/gcm^{-3}	1.830	1.680
μ/mm^{-1}	5.705	6.393
$R1$[a] [$I > 2\sigma(I)$]	0.0266	0.0356
$wR2$[b]	0.0661	0.0826
Residual electron density/eÅ^{-3}	0.590/−0.483	1.055/−0.674
Absorption correction	numerical T_{min} = 0.173 T_{max} = 0.391	numerical T_{min} = 0.347 T_{max} = 0.403
Absolute structure parameter	0.071(12)	0.00(2)

[a] $R1 = \Sigma||F_o| - |F_c||/\Sigma|F_o|$. − [b] $wR2 = (\Sigma[w(F_o^2 - F_c^2)^2]/\Sigma[w(F_o^2)^2])^{1/2}$, where $w = 1/[\sigma^2(F_o^2) + qP^2 + jP]$ {q = 0.0496, j = 4.4892 for [Cp*Ir(D-prol)]$_3$(ClO_4) and q = 0.0327, j = 4.3163 for [Cp*Ir(R,R-dach)H_2O](ClO_4)$_2$·H_2O; $P = (F_o^2 + 2F_c^2)/3$}.

angles are given in Table 3 and 4. Crystallographic data (excluding structure factors) for the structures reported in this paper have been deposited with the Cambridge Crystallographic Data Centre as supplementary publication nos. CCDC-146445 (**3b**) and -146446 (**2b**). Copies of the data can be obtained free of charge on application to the CCDC, 12 Union Road, Cambridge CB2 1EZ, U.K. [Fax: (internat.) + 44-1223/336-033; E-mail: deposit@ccdc.cam.ac.uk].

Supporting Information: UV/Vis spectroscopic data (Figures S1−S3, S6), spectrophotometric titration data (Figures S4, S5), observed rate constants at various concentrations, temperatures, and pressures (Tables S1−S26, Figures S7, S8; see also the footnote on the first page of this paper).

Acknowledgments

Sponsorship of this work by the Deutsche Forschungsgemeinschaft and the Verband der Chemischen Industrie e.V. is gratefully acknowledged. A sample of iridium(III) chloride was kindly provided by Degussa−Hüls AG.

[1] U. Koelle, *Coord. Chem. Rev.* **1994**, *135/136*, 623−650.
[2] M. S. Eisen, A. Haskel, H. Chen, M. M. Olmstead, D. P. Smith, M. F. Maestre, R. H. Fish, *Organometallics* **1995**, *14*, 2806−2812.
[3] S. Ogo, H. Chen, M. M. Olmstead, R. H. Fish, *Organometallics* **1996**, *15*, 2009−2013.
[4] S. Ogo, O. Buriez, J. B. Kerr, R. H. Fish, *J. Organomet. Chem.* **1999**, 66−74.
[5] R. H. Fish, *Coord. Chem. Rev.* **1999**, *185−186*, 569.
[6] S. Ogo, N. Makihara, Y. Watanabe, *Organometallics* **1999**, *18*, 5470−5474.
[7] L. Dadci, H. Elias, U. Frey, A. Hörnig, U. Koelle, A. E. Merbach, H. Paulus, J. S. Schneider, *Inorg. Chem.* **1995**, *34*, 306−315.
[8] R. Boca, H. Elias, *Polyhedron* **1996**, *15*, 2425−2431.
[9] S. Cayemittes, T. Poth, M. J. Fernandez, P. G. Lye, M. Becker, H. Elias, A. E. Merbach, *Inorg. Chem.* **1999**, *38*, 4309−4316.
[10] A. Cusanelli, U. Frey, D. T. Richens, A. E. Merbach, *J. Am. Chem. Soc.* **1996**, *118*, 5265−5271.
[11] M. Stebler-Röthlisberger, W. Hummel, P. A. Pittet, H. B. Bürgi, A. Ludi, A. E. Merbach, *Inorg. Chem.* **1988**, *27*, 1358−1363.
[12] A. Cusanelli, L. Nicula-Dadci, U. Frey, A. E. Merbach, *Chimia* **1996**, *50*, 618−620.
[13] The chemistry of the corresponding monoaqua rhodium species Cp*Rh(A−B)$(H_2O)^{2+/+}$ has been dealt with in some detail: [13a] R. P. Hughes, D. C. Lindner, A. L. Rheingold, L. M. Liable-Sands, *J. Am. Chem. Soc.* **1997**, *119*, 11544−11545. − [13b] P. M. Boyer, C. P. Roy, J. M. Bielski, J. S. Merola, *Inorg. Chim. Acta* **1996**, *245*, 7−15. − [13c] D. Carmona, C. Cativiela, R. Garcia-Correas, F. J. Lahoz, M. P. Lamata, J. A. Lopez, M. P. Lopez-Ram de Viu, L. A. Oro, E. Dan Jose, F. Viguri, *Chem. Commun.* **1996**, 1247−1248.
[14] D. Carmona, F. J. Lahoz, S. Elipe, L. A. Oro, M. P. Lamata, F. Viguri, C. Mir, C. Cativiela, M. P. López-Ram de Víu, *Organometallics* **1998**, *17*, 2986−2995.
[15] D. Carmona, F. J. Lahoz, R. Atenico, L. A. Oro, M. P. Lamata, F. Viguri, E. San José, C. Vega, J. Reyes, F. Joó, A. Kathó, *Chem. Eur. J.* **1999**, *5*, 1544−1564.
[16] K. Mashima, T. Abe, K. Tani, *Chem. Lett.* **1998**, 1199−1200.
[17] K. Mashima, T. Abe, K. Tani, *Chem. Lett.* **1998**, 1201−1202.
[18] K. Murata, T. Ikariya, *J. Org. Chem.* **1999**, *64*, 2186−2187.
[19] M. J. Palmer, M. Wells, *Tetrahedron: Asymmetry* **1999**, *10*, 2045−2061.
[20] K. Severin, R. Bergs, W. Beck, *Angew. Chem.* **1998**, *110*, 1722−1743; *Angew. Chem. Int. Ed.* **1998**, *37*, 1634−1654.
[21] Abbreviations used: Cp* = pentamethylcyclopentadienyl anion; phen = 1,10-phenanthroline; bpy = 2,2′-bipyridine; dpen = 1,2-diphenylethylenediamine; dach = 1,2-diaminocyclohexane; picac = anion of picolinic acid; prol = anion of proline; py = pyridine; py-nia = nicotinamide; py-CN = 4-cyanopyridine; DMS = dimethyl sulfide; TU = thiourea; I_d = dissociatively controlled interchange; I_a = associatively controlled interchange.
[22] K. Isobe, B. M. Baily, P. M. Maitlis, *J. Chem. Soc., Dalton Trans.* **1981**, 2003−2008.
[23] O. Almog, A. Bino, D. Garfinkel-Shweky, *Inorg. Chim. Acta* **1993**, *213*, 99−102.
[24] F. Galsbol, S. Larsen, B. Rasmussen, J. Springborg, *Inorg. Chem.* **1986**, *25*, 290−297.
[25] R. Krämer, K. Polborn, Ch. Robl, W. Beck, *Inorg. Chim. Acta* **1992**, *198*, 415−420.
[26] K. Sünkel, W. Hoffmüller, W. Beck, *Z. Naturforsch.* **1998**, *53b*, 1365−1368.
[27] One has to consider that at pH = 2.0 most of the pyridine base is protonated [pK_a(py) = 5.26[29]] and the low concentration of the incoming ligand L = py enables interference of the reverse reaction.
[28] To obtain the rate constant k_L from the slope m of the linear dependencies shown in Figure 4a, one has to correct for partial protonation of the pyridine according to $k_L = m\{1 + [H^+]/K_a[py]_0\}$.
[29] A. E. Martell, R. M. Smith, *Critical Stability Constants*, vol. 2, Plenum Press, New York, **1974**.
[30] The UV spectrum of a solution of **3b** in methanol clearly differs from that in water, which suggests that, in contrast to the situation in water, the trinuclear structure is preserved in methanol. This would be in line with the results reported by Carmona et al.,[15] which showed that in solutions of the complexes [Cp* Ir(aa)$_3$](BF$_4$)$_3$ (aa = α-amino acid anion) in dichloromethane, acetone, or methanol, the complexes remain trinuclear.
[31] The pH-jump stopped-flow experiments were carried out by loading one syringe with the solution of the complex ([**2**] = 0.4×10^{-4} M, [py-nia] = 1×10^{-3} M, [$HClO_4$] = 0.01) and the other with acid ([$HClO_4$] = 0.53 M, 1.1 M, and 3.0 M, respectively). The (A,t) data for the decrease of absorbance at 300 nm were fitted with Equation (5), which led to k_{obsd} = (1.049 ± 0.004) × 10^{-3} s^{-1} ([$HClO_4$] = 0.27 M), k_{obsd} = (0.992 ± 0.003) × 10^{-3} s^{-1} ([$HClO_4$] = 0.55 M), and k_{obsd} = (1.02 ± 0.01) × 10^{-3} s^{-1} ([$HClO_4$] = 1.5 M).
[32] M. S. Sun, D. G. Brewer, *Can. J. Chem.* **1967**, *45*, 2729−2739.
[33] M. L. Tobe, *Inorganic Reaction Mechanisms: Studies in Modern Chemistry*, Nelson, London, **1972**, p. 52.
[34] The Eigen−Wilkins mechanism postulates for ligand substitution reactions such as the reaction according to Equation (3) that $k_L = K_{os}k_i$, where K_{os} is the equilibrium constant for fast formation of an outer-sphere complex between Cp* Ir(A−B)$(H_2O)^{2+/+}$ and L, and k_i is the rate constant for rate-controlling ligand interchange in the outer-sphere complex. For electrostatic reasons, K_{os} is greater for cations interacting with anions than for cations interacting with neutral ligands.
[35] A. Drljaca, C. D. Hubbard, R. van Eldik, T. Asano, M. V. Basilevsky, W. J. le Noble, *Chem. Rev.* **1998**, *98*, 2167−2289.
[36] L. Helm, A. E. Merbach, *Coord. Chem. Rev.* **1999**, *187*, 151−181.
[37] R. van Eldik, C. Dücker-Benfer, F. Thaler, *Adv. Inorg. Chem.* **2000**, *49*, 1−58.
[38] C. White, A. Yates, P. M. Maitlis, *Inorganic Synthesis* (Ed.: R. N. Grimes), John Wiley & Sons, New York, **1992**, vol. 29, pp. 228−234.
[39] H. Elias, F. Sattler, K. J. Wannowius, *GIT Fachz. Lab.* **1985**, *29*, 1138.
[40] R. van Eldik, W. Gaede, S. Wieland, J. Kraft, M. Spitzer, D. A. Palmer, *Rev. Sci. Instrum.* **1993**, *64*, 1355.
[41] U. Bips, H. Elias, M. Hauröder, G. Kleinhans, S. Pfeifer, K. J. Wannowius, *Inorg. Chem.* **1983**, *22*, 3862−3865.
[42] R. van Eldik, Y. Kitamura, C. P. Piriz MacColl, *Inorg. Chem.* **1986**, *25*, 4252.

Received June 27, 2000
[I00256]

A π-Stacked Organometallic Propeller: Experimental and Theoretical Studies on Reactivity and Bonding in the π-Arene-Bridged Nickel Triple-Decker [{(η^5-Me_4EtC_5)Ni}$_2$(μ-η^3:η^3-decacyclene)]

Jörg J. Schneider,*[a][‡] Dirk Spickermann,[a] Dieter Bläser,[a] Roland Boese,[a] Paul Rademacher,[b] Thomas Labahn,[c] Jörg Magull,[c][‡‡] Christoph Janiak,[d][‡‡‡] Naka Seidel,[e] and Klaus Jacob[e]

Dedicated to Prof. H. G. Schnöckel on the occasion of his 60th birthday

Keywords: Sandwich complexes / Nickel / Arenes / EHMO calculations / Cyclopentadienyl ligands

Synthesis, structure, reactivity, and theoretical studies of a new type of Ni triple-decker complexes are reported. A prominent feature of its molecular structure is the (η^3:η^3)-bis-(enyl) coordination of two [(η^5-Me_4EtC_5)Ni] fragments to the central arene ring of the polycondensed π-perimeter decacyclene. The central arene ring of decacyclene displays a distinct chair conformation with significant tilt angles of 25.5 and 26.1°. The three naphthalene units are twisted in a propeller-like fashion with torsion angles of 16°, 16.6°, and 19°, which is twice the twisting observed for the free decacyclene ligand. According to Extended Hückel Molecular Orbital (EHMO) calculations, a qualitative measure for arene lability in the title compound and a number of related arene-bridged metal complexes can be attributed to a subsequent filling of metal–arene antibonding orbitals. The experimentally observed reactivities of π-arene exchange in these complexes are reproduced nicely by the EHMO calculations. The title compound offers access to a number of organonickel chalcogenato complexes under mild conditions by cleavage of the S–S, Se–Se, or Te–Te bonds of diorganyl dichalcogenides R–E–E–R. The title compound is also capable of C_{sp^2}–H activation of azobenzene and [(dimethylamino)methyl]ferrocene resulting in orthometallated complexes containing five-membered metallacycles. PES and semi-empirical ZINDO/S calculations were used to study the product of the orthometallation of the title compound with azobenzene. These studies reveal that the HOMO of the metallacycle (IE = 6.45 eV) has dominant Ni–Cp and Ni–C_{aryl} π-antibonding character.

Introduction

Recently we reported on the first binuclear transition metal complexes of decacyclene containing this large condensed π-perimeter,[1] whose organometallic chemistry is still virtually unexplored, probably owing to its low solubility.[2] During the course of our studies of this π-perimeter we have found that two [(η^5-Me_5C_5)Ni] fragments are able to coordinate in a triple-decker fashion to decacyclene.[1] At that time our findings were based exclusively on the analysis of the characteristic NMR spectroscopic data, which suggest a highly symmetrical coordination mode of the two [(η^5-Me_5C_5)Ni] fragments to decacyclene, and steric arguments were put forward in favor of an antarafacial coordination of the two M−L fragments.[1]

Herein we report on the molecular structure, reactivity, and theoretical studies of the unusual arene-bridged nickel triple-deckers **3** and **4** and their reaction products from reductive cleavage and cyclometallation reactions. A remarkable feature of **3** and **4** are their high capability for controlled release of 15e$^-$-[(C_5R_5)Ni] fragments under mild conditions. Although triple- and multiple-deckers with nickel constitute a most intriguing class of organometallic compounds,[3] such an unusual coordination as in **3** and **4** paired with a high reactivity of a π-coordinated middle deck is a rare case.

Results and Discussion

We found that reaction of [(η^5-Me_4EtC_5)Ni(acac)] (**1**) with the decacyclide dianion produces the title compound **3** in 74% yield as brown to black crystals [Equation (1)].

[a] Institut für Anorganische Chemie, der Universität−GH Essen,
Universitätsstraße 5−7, 45117 Essen, Germany
[b] Institut für Organische Chemie der Universität−GH Essen,
Universitätsstraße 5−7, 45117 Essen, Germany
[c] Institut für Anorganische Chemie der Universität Göttingen,
Tammannstraße 4, 37077 Göttingen, Germany
[d] Institut für Anorganische und Analytische Chemie der Universität Freiburg,
Albertstraße 21, 79104 Freiburg, Germany
[e] Institut für Anorganische Chemie, Martin Luther-Universität Halle-Wittenberg,
06099 Halle/Saale, Germany
[‡] New address: Institut für Chemie, Anorganische Chemie, Universität Graz, Schubertstraße 1, 8010 Graz, Austria,
Fax: (internat.) + 43-316/380-9835,
E-mail: joerg.schneider@uni-graz.at
[‡‡] X-ray crystallography.
[‡‡‡] Theoretical calculations.

 © WILEY-VCH Verlag GmbH, 69451 Weinheim, 2001 1434−1948/01/0505−1371 $ 17.50+.50/0

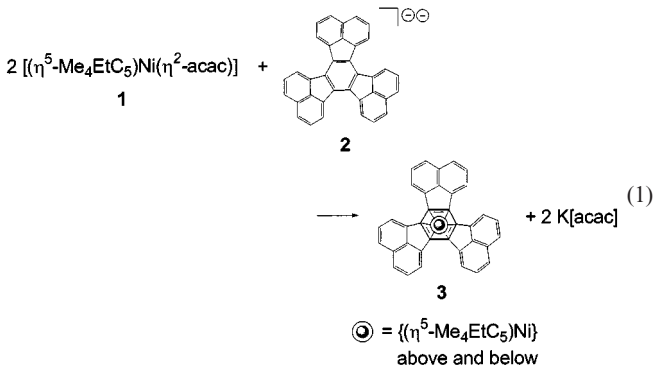

(1)

As for the Me_5C_5 derivative **4**,[1] the NMR spectra of **3** are characteristic for a symmetric coordination of two [(η^5-Me_4EtC_5)Ni] fragments to the decacyclene bridging unit. A high-field coordination shift of the three multiplets (doublet-triplet-doublet) of decacyclene is observed in agreement with a twofold metal coordination to the tris(anullated) center arene ring of decacyclene. However, from NMR experiments on **3** (as for **4**[1]) no distinction between either a symmetric or an asymmetric metal coordination to decacyclene could be made. For supra- and antarafacial complexes containing bridging arenes highly fluxional behavior is well known. However, low-temperature NMR measurements to prove such fluxional behavior for **3** and **4** are precluded by their low solubility. So far, no decision towards the fluxionality and subsequently the hapticity of **3** and **4** in solution could be made. However, we believe **3** and **4** to be highly fluxional in solution.

In contrast to **4**, the Me_4EtC_5 derivative **3** gave suitable crystals for an X-ray structure determination, which allow us to determine its molecular structure in the solid state (Figure 1).[4]

The two [(η^5-Me_4EtC_5)Ni] fragments of **3** display an η^3-enyl bonding in which both metal ligand fragments are bonded in an antarafacial fashion to the central benzene ring of decacyclene (Figure 2). This causes the distortion of the central ring into a chair conformation in which the plane defined by $C^1-C^2-C^3$ is tilted by 25.5°, and the plane defined by C^4, C^5, and C^6 is tilted by 26.1° towards the plane C^3, C^4, C^6, C^1. The η^3:η^3 coordination in **3** has some precedent in the literature when considering polynuclear arenes as bridging ligands (Figure 3).[5–8] However, **3** represents a rare case in which two Ni ligand fragments are coordinated to a single C_6 arene ring.[9]

In **3** both Ni atoms are equally displaced between the bridging η^3-bonded arene part of decacyclene (1.72 Å) and the η^5-Me_4EtC_5 ligands (1.73 Å). As a result of the antarafacial η^3:η^3 coordination, a substantial twist of the mean planes of the crystallographically independent naphthalene moieties of 16°, 16.6°, and 19° results. This exceeds the modest twist disposed on the naphthalene moieties of the free ligand by almost 100% (9.3° and 7.7°) and gives **3** a distinct propeller-like shape when compared to free decacyclene (see Figure 2).[10]

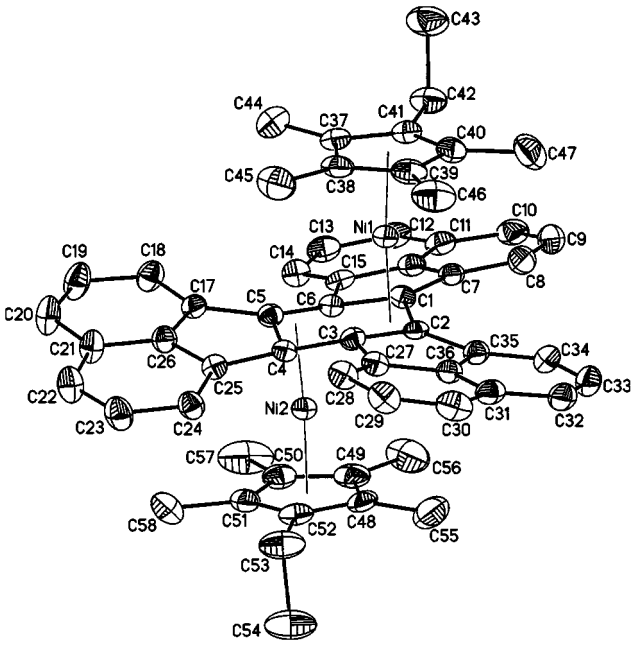

Figure 1. Molecular structure of **3** as determined in the solid state; selected bond lengths [Å] and angles [°]: C^1-C^2 1.445(6), C^1-C^6 1.513(6), C^1-C^7 1.472(6), C^2-C^3 1.453(6), C^2-C^{35} 1.465(6), C^3-C^4 1.484(6), C^3-C^{27} 1.483(6), C^4-C^5 1.482(6), C^4-C^{25} 1.488(6), C^5-C^6 1.415(6), C^5-C^{17} 1.475(6); $C^1-C^6-C^2$ 119.5(4), $C^3-C^4-C^2$ 120.4(4), $C^4-C^5-C^3$ 118.6(4), $C^5-C^6-C^4$ 112.6(4), $C^6-C^5-C^1$ 121.3(4)

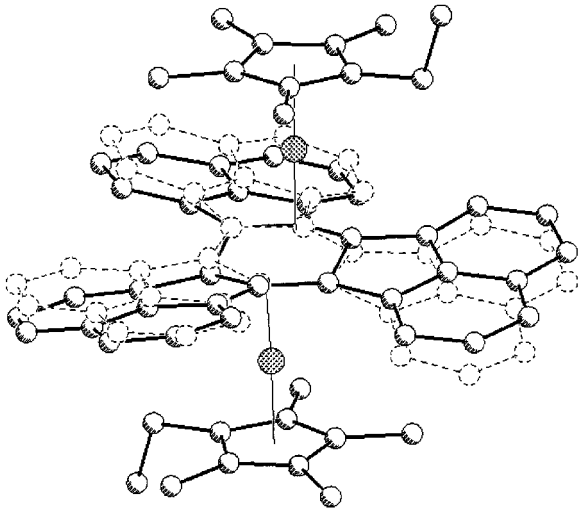

Figure 2. Overlay of the molecular structure of uncomplexed decacyclene **1** and the dinickel triple-decker **3** showing the propeller-like arrangement of the naphthalene units of uncomplexed **1** and the bridging decacyclene ligand of **3**; atom numbering scheme according to Figure 1

Reactivity Studies of 3 and 4

The decacyclene ligand in **3** and **4** can be displaced, resulting in the formation of dinuclear and mononuclear organonickel complexes. Common features of all exchange reactions are the mild reaction conditions (room temperature) and the possibility of the immediate visual progress of the ligand exchange by appearance of a precipitate of highly

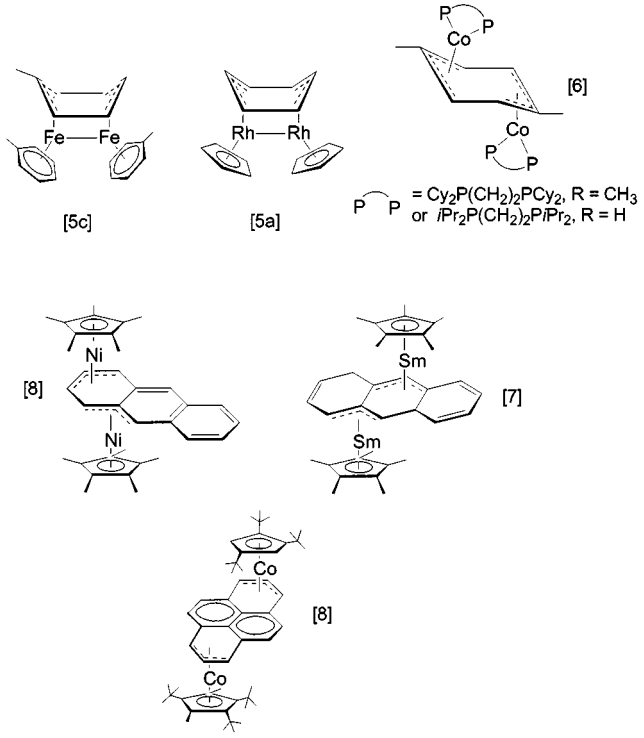

Figure 3. Selection of dinuclear complexes containing polynuclear arenes as bridging ligands

insoluble decacyclene **2**. This lability of the aromatic middle deck make **3** and **4** ideal, and so far rare sources for the mild in situ generation of 15e$^-$-[(η^5-C_5R_5)Ni]$_{solv}$ fragments with a high synthetic potential in organometallic synthesis. To the best of our knowledge, no other comparable sources for [(η^5-C_5R_5)Ni]$_{solv}$ fragments are known so far.

Reactions of 3 with Diphenyl Disulfide (5), Dimesityl Diselenide and Ditelluride (6 and 7), and Dinaphthyl Ditelluride (8) − Formation of (μ-Chalcogenato)dinickel Complexes 9−12

Diorganyl dichalcogenides are prone to homolytic cleavage of the E−E bond by transition metal ligand fragments, which generate reactive R−E fragments. Related oxidative additions of acyclic organic, cyclic organic, and organometallic dichalcogenides are also known.[11] Organonickel thiolate complexes are possible reaction products from cleavage reactions of R−S−S−R compounds. They are often electrochemically active but show a pronounced stability towards one-electron reduction and cleavage of their M−S bond(s).[12]

Our interest in binary and ternary transition metal chalcogen complexes and their electron-transfer properties[13] prompted us to study the reaction of **3** with dichalcogenides **5**−**8** with respect to a transfer of 15e$^-$-[(η^5-Cp^R)Ni] fragments.

Addition of a stoichiometric amount of the appropriate diorganyl dichalcogenide to a solution of **3** in diethyl ether resulted in the precipitation of decacyclene as a tan-colored powder. The chalcogenato complexes **9**−**12** could be isolated in high yields from the filtered solution [Equation (2)]. The formation of **9**−**12** can be understood by reductive cleavage of the E−E bond of the dichalcogenide by reactive [(η^5-Me_4EtC_5)Ni] fragments.

Dinuclear complexes of general type [{(η^5-C_5R_5)Ni(μ-ER)}$_2$] can exist in planar or bent conformations with regard to the Ni_2E_2 core.[14] Varying substituents at the bridging chalcogen atoms S, Se, and Te may cause the Ni_2E_2 core to adopt different orientations, reflecting different hybridization situations at the chalcogen atoms (Figure 4).

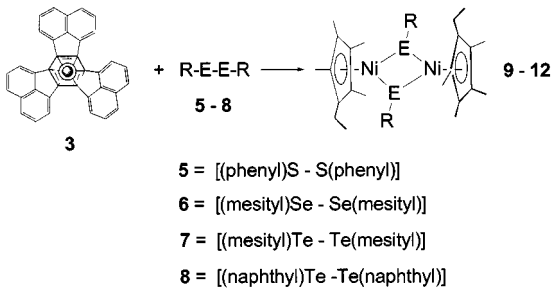

(2)

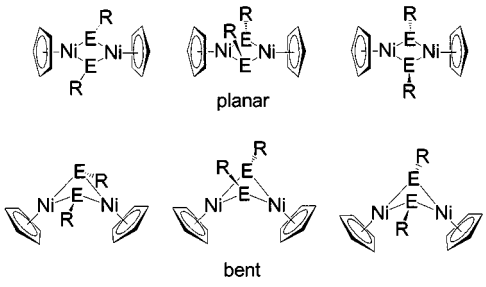

Figure 4. Possible conformations for complexes of the type [{(η^5-Cp^R)Ni(μ-SR)}$_2$]

Despite this possibility, the ^{1}H NMR spectra of the complexes **9**−**12**, show the presence of only one conformer. However, for [{(η^5-Me_4EtC_5)Ni}$_2$(μ-SeMes)$_2$] (**10**), unusually broad signals in the ^{1}H NMR might indeed indicate a dynamic behavior of this compound in solution.

The molecular structure of bis[(μ-benzenethiolato)(η^5-Me_4EtC_5)Ni] (**9**) in the solid state was confirmed by X-ray crystallography and revealed two independent molecules. However, no significant variation in bonding parameters was observed.[4] Each molecule of **9** has a centrosymmetric structure with a nearly square-planar Ni_2S_2 arrangement (Figure 5). The distances between the two nickel atoms are 3.078 Å (Ni^1−Ni$^{1'}$) and 3.109 Å (Ni^2−Ni$^{2'}$; not shown), which is obviously too large to consider Ni−Ni metal bonding when compared to the Ni−Ni distance of 2.4916 Å in metallic Ni.[15] Other bonding parameters for **9** are in close agreement to those in bis[(η^5-C_5H_5)Ni(μ-*S*-phenyl)].[12] Due to the diamagnetic nature of **9**−**12** the two sulfur atoms have either the formal oxidation state +2 or +4 giving the two nickel centers a 16e$^-$ or 18e$^-$ count in these complexes.

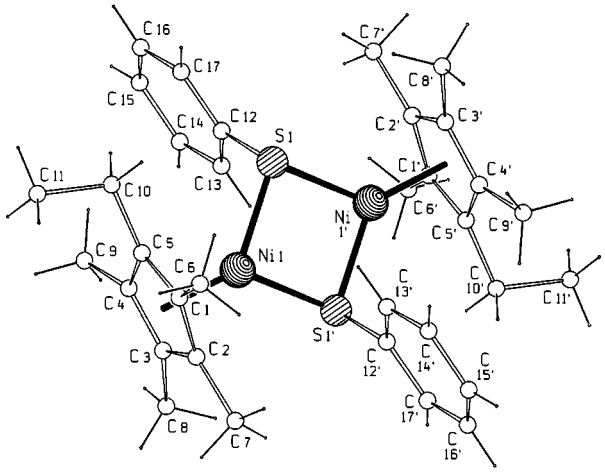

Figure 5. Molecular structure of **9** [only molecule **9**(1) is shown] as determined in the solid state; selected bond lengths [A] and angles [°] of **9**(1): Ni^1-S^1 2.194(2), $Ni^{1'}-S^1$ 2.198(4); $Ni^1-S^1-Ni^{1'}$ 89.00(6), $S^{1'}-Ni^1-S^1$ 91.00(6)

Reactivity Studies

$C_{sp^2}-H$-Activation of Azobenzene and [(Dimethylamino)methyl]ferrocene

Orthometallation reactions involving $C_{sp^2}-H$ bond activation processes represent an important class of reactions with various examples exemplified in the recent literature.[16] From a preparative point of view, transmetallation is a rather attractive preparative route that offers access to orthometallated complexes containing pseudoaromatic rings.[17] During the course of our studies, we have found that **3** and **4** are able to undergo $C_{sp^2}-H$ orthometallations with achiral and prochiral aromatic ring systems under mild conditions by transfer of the [(η^5-Cp^R)Ni] (R = Me_5, $EtMe_4$) moiety.

Reaction of 3 and 4 with Azobenzene

Nickelocene undergoes an orthometallation reaction with azobenzene at high temperatures, leading to a blue crystalline product formulated as [(η^5-Cp){(*o*-phenylazo)phenyl}Ni].[18] In addition, cyclopalladation reactions have been reported for a couple of substituted azobenzenes.[16a,19,20] The palladium−carbon bond is preferentially formed with the benzene ring bearing the electron-donating group, thus pointing towards the electrophilic character of the cyclopalladation reaction.[16a]

Addition of a twofold excess of azobenzene to a solution of **3** or **4** in diethyl ether gives an intense bright blue solution within minutes, accompanied by precipitation of solid decacyclene as tan-colored powder. Deep blue to black, air stable crystals of **13** and **14** could be isolated therefrom [Equation (3)]. The mass spectra of **13** and **14** display the corresponding molecular peaks as base signal, thus establishing a 1:1 ratio azobenzene/[(η^5-C_5R_5)Ni] for both complexes. The ^{1}H NMR spectrum of **13** gives clear evidence of one [(η^5-Me_4EtC_5)Ni] fragment asymmetrically bonded to the azobenzene moiety as a result of an orthometallation reaction. The signal of the α-proton of the metallated phenyl ring is shifted downfield to δ = 7.86 compared to free azobenzene (Δδ = −0.4). Similar ^{1}H NMR coordination shift effects have been observed e.g. for orthometallated pyridine.[21]

The ^{13}C NMR spectrum of **13** shows a characteristic downfield shift for the metallated carbon atom (C^2) compared to free azobenzene (Δδ = −59.2) well in accordance with the ^{1}H NMR spectrum.

The signals of the neighboring carbon atoms C^1 and C^3 are shifted 10 ppm down-field compared to those of free azobenzene. All other carbon resonances do not show significant and characteristic coordination shifts upon Ni coordination. The NMR spectroscopic data of **14** are in agreement with those of **13** (see Exp. Sect.).

Unfortunately, an X-ray crystal-structure analysis of **13** suffers from intense disorder of the $EtMe_4C_5$ ligand. However, the connectivities of all atoms except hydrogen could be unambiguously pinpointed from the crystallographic data set, thus surely confirming the existence and coordination of the orthometallated five-membered nickelabenzpyrazole ring, as it is shown in Equation (3). The (Cp)nickel moiety coordinates to the nitrogen atom of the diazo group via its lone pair, thus allowing the Ni center to attain an $18e^-$ count.

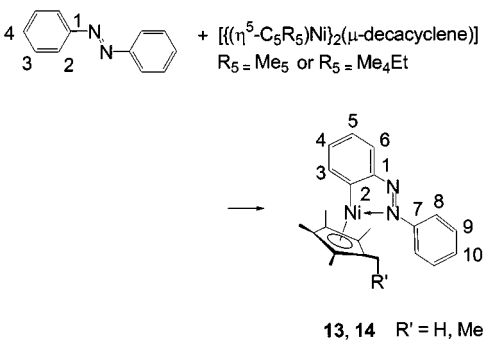

(3)

Corresponding to its elusive bright blue color, the relevant absorption for **13** is found at λ = 609 nm (ε = 6317) (Figure 6). The characteristic absorptions for the azobenzene residue are shifted to higher wavelengths compared to those of free azobenzene. The same effect is observed for the absorptions of the parent corresponding [{*o*-(phenylazo)phenyl}(η^5-Cp)Ni] complex[18] and for [({*o*-(phenylazo)phenyl}$PtCl)_2$],[19] both containing five-membered orthometallated ring systems incorporating the N=N azo group. It is interesting to note that differently alkyl-substituted *o*-hydroxyazobenzene compounds experience a similar bathochromic shift compared to azobenze resulting in a blue to purple color as observed for **13** and **14**.[22] The effect is attributed to hydrogen bonding of an *o*-OH group to the nitrogen atom of the azo group, resulting in formation of six-membered rings and the term *internal halochromism* has been coined for it.[22]

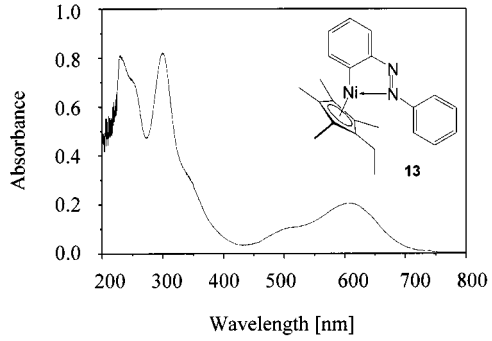

Figure 6. UV/Vis spectrum of **13** in CH_2Cl_2 (27 °C)

In contrast with the reaction of nickelocene with azobenzene, which requires drastic reaction conditions and prolonged reaction times to proceed to completion, the generation of 15e⁻-[(η^5-C_5R_5)Ni] fragments (R = Me_5, $EtMe_4$) from triple-deckers **3** and **4** undergoing the cyclometallation of azobenzene is already achieved at room temperature within minutes. This suggests that [(η^5-C_5R_5)Ni]$_{solv}$ fragments are easily generated by a dissociative pathway from triple-decker complexes **3** and **4**. A dissociative mechanism for ligand exchange has been proven recently for arene-bridged Co triple-deckers [{(η^5-C_5R_5)Co}$_2$(μ-η^4:η^4-arene)] (R = Me_5, 1,2,4 tri-*tert*-butyl) by kinetic and preparative studies.[23]

Photoelectron Spectroscopy (PES) of 13; Experimental and Theoretical Studies

The (He^I) PE spectrum of **13** is shown in Figure 7. Experimental vertical ionization energies are listed in Table 1. The calculated PE spectrum together with relevant MO contributions, obtained from semiempirical ZINDO/S calculations based on the corresponding model compound [(η^5-Cp)Ni(C_6H_4−N=N−C_6H_5-κ*C*,κ*N*)] ***A*** (simplification of alkyl ligand substituents by hydrogen) is depicted in Figure 8. Zerner (Z) et al. have employed an intermediate neglect of differential overlap (INDO) method with spectroscopic parametrization (ZINDO/S) in electronic calculations.[24] Following this work we have used the semi-empirical ZINDO/S method in the calculation of the PE spectrum of **13**.

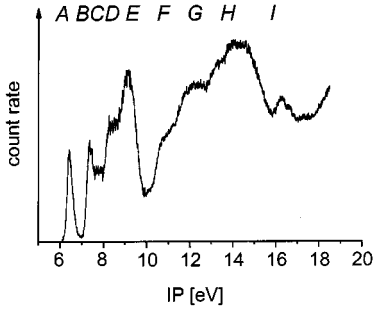

Figure 7. Experimental He^I PE spectrum of **13**; assignment see Figure 8

Table 1. Experimental vertical ionization energies (in eV; ca. 1.60 × 10^{-19} J) for **14**; for a detailed assignment see text and Figure 8

Band	$IE_{vert.}$	Assignment
A	6.45	HOMO: π antibonding
B	7.36	
C	7.50 7.81	HOMO1 − HOMO5:
D	8.43	π ligand
E	9.12	centered
F	10.77	HOMO6 −
I	16.28	HOMO11

The ionization energies of the nickel compound have been evaluated by Koopmans' theorem[25] as the negative of the eigenvalues of the ground state MOs of the neutral molecules. We are aware that Koopmans' approximation is often not valid in the case of organo transition metal complexes. Ferrocene, for example, is a well-known case where the breakdown of Koopmans' theorem was demonstrated.[26] However, the spectroscopic parameterization employed in the INDO/S method resulted in a rather large reduction of relaxation energy and Koopmans' theorem was found to give a correct order of ionization potentials.[24,27] As can be seen from Figure 7, Figure 8, and Table 1 the energies of the molecular orbitals based on a calculation of the model species ***A*** deviate less than 1.0 eV from observed ionization potentials. The low molecular symmetry of ***A*** leads to substantial atomic orbital mixing. This makes an assignment of characteristic molecular orbitals to spectral bands difficult. The band at 6.45 eV is assigned to the HOMO, which is an Ni−Cp and Ni−C_{aryl} π-antibonding orbital. The calculation gives 5 MOs (HOMO-1 to HOMO-5), which are assigned to the region between 7.36 and 9.4 eV. These MOs are dominated by ligand-centered π orbitals. Most prominent are aryl and cyclopentadienyl π sets that contribute significantly to these molecular orbitals (Figure 9). Some nickel d-character is also present, but except for one orbital (HOMO-4/-5) never prominent. There it is part of an Ni−C_{aryl} σ-bonding orbital.

From the HOMO-6 downward, the calculated MOs are assigned to the experimental ionization energy region above 10.7 eV. These not very well resolved bands start with Ni−Cp π-bonding orbitals (HOMO-6, -9) as well as nickel-centered nonbonding d-orbitals (HOMO-7, -8). Some weak Ni−C_{aryl} σ-bonding is also present (HOMO-8, -10). An Ni−N bonding and N-lone-pair combination is calculated around 11.2 eV (HOMO-11).

Reaction of 3 with Bis[2-[(dimethylamino)methyl)]-ferrocenyl]lead(II) (15)

Due to our continued interest in the synthesis of transition metal complexes containing stannylene species :MR_2

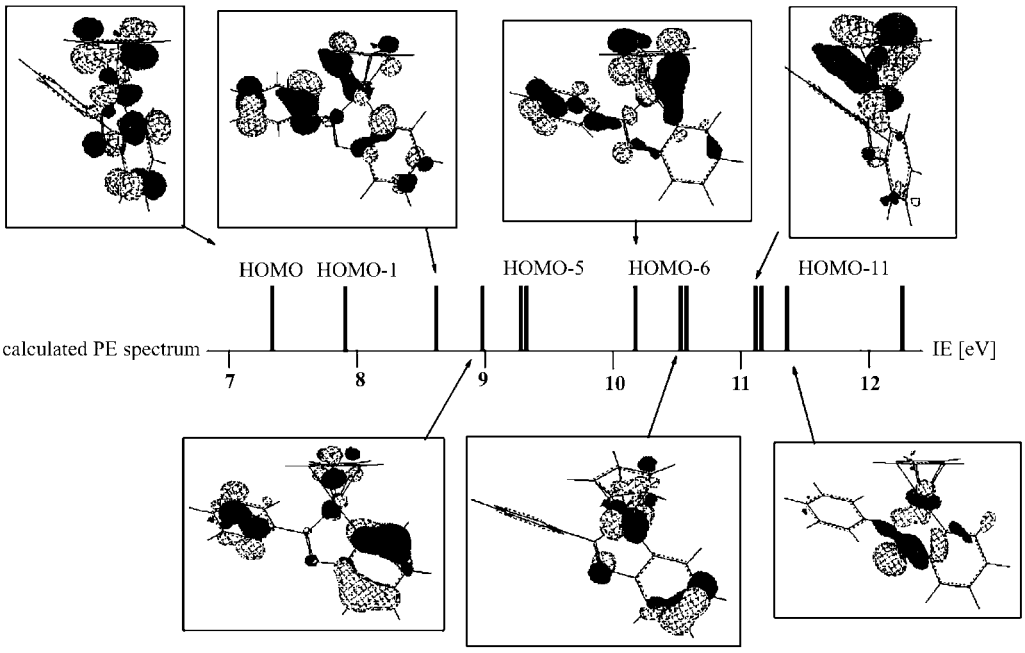

Figure 8. Calculated PE spectrum of **13** together with calculated ZINDO/S MOs assigned to the individual vertical ionization energies

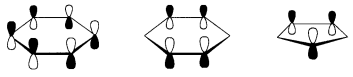

Figure 9. Prominent molecular orbital contributions from aryl and Cp π-sets in the energy window 7.36−9.4 eV

(Sn, Pb)[28] we studied the complexation behavior of **3** towards the unique intramolecular donor-stabilized plumbylene **15**.[29] The obvious ease with which 15e⁻-[(η^5-C_5R_5)Ni] fragments could be generated from **3** spurred our interest in the synthesis of new Ni−plumbylene complexes derived from **15**. Complex **15** is a uniquely chelated Pb^{II} compound, which owes its stability to an intramolecular twofold N-donor stabilization (Figure 10).[33] An intramolecular exchange process is responsible for equivalency of both Fc−N groups in solution, giving rise to temperature- and solvent-dependent equilibrium of *meso*/*rac* diastereoisomers of **15**.[29]

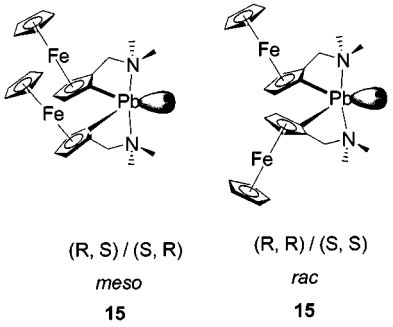

Figure 10. *meso* and *rac* isomer of **15**[29]

Addition of solid **3** to a yellow suspension of **15** in diethyl ether at −78 °C gave a magenta-colored solution, accompanied by immediate elimination of **2** as tan-colored precipitate. However, on warming up to ambient temperature the color changed from magenta to red. From this solution (*R*,*S*)-**16** could be isolated as a racemic mixture, as the only product [Equation (4)]. The cyclometallation of the [(dimethylamino)methyl]ferrocenyl ligand proceeds by a transmetallation reaction of the *meso*/*rac* diastereomer **15**. The intramolecular N→Pb stabilization present in **15** is obviously not sufficient to stabilize a Pb−Ni coordination bond at room temperature. It is obvious that the initially observed magenta color of the reaction mixture is indeed due to formation of a Pb^{II}−Ni species initially formed in the reaction between **3** and **15**. We have found that complexes containing similar Sn^{II}−Co(Fe) bonds do show the same characteristic magenta color; as do initial reaction solutions of **3** and **15**. However, the Sn^{II}−Co(Fe) complexes are fairly stable under ambient conditions.[29] In contrast, the Pb^{II}−Ni species do not prove to be stable and eliminate Pb^0, liberating the ferrocenyl ligands, which undergo subsequent orthometallation to give **16**.

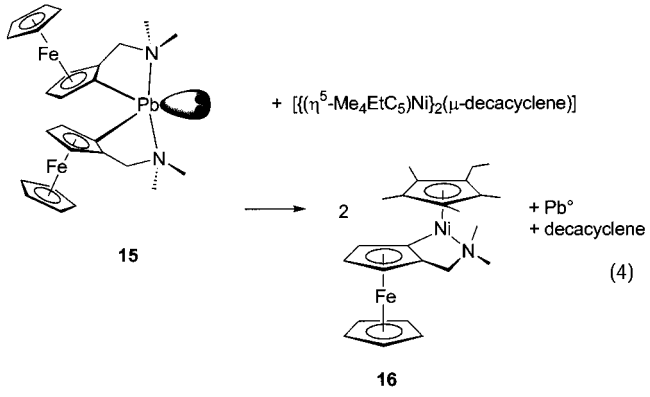

In the ^{13}C NMR spectrum the signal of the metallated carbon atom C^2 ($\delta = 103.8$) is shifted by about 35 ppm to lower field compared with that of the nonmetallated Cp ligand of the ferrocene moiety ($\delta = 69.1$), well in agreement with the observations for the azobenzene complexes **13** and **14**. The ^1H NMR spectroscopic data are in close agreement to the related cationic Co^{III} complex $[(\eta^5\text{-}C_5H_5)Co(\eta^5\text{-}C_5H_5)Fe(\eta^5\text{-}C_5H_3CH_2NMe_2)(PMe_3)]^+PF_6^-$ reported recently.[30]

X-ray Analysis of 16

Figure 11 depicts the molecular structure of **16** as a result of a single-crystal X-ray diffraction study. As concluded from the NMR spectroscopic data, the $[(\eta^5\text{-}Me_4EtC_5)Ni]$ fragment is indeed coordinated to the *o*-carbon atom (C^{10}) and to the nitrogen atom of the [(dimethylamino)methyl]Cp ring of the ferrocene subunit, giving the nickel center a nearly trigonal-planar coordination. The planes of the Me_4EtC_5 ring and the five-membered metallacycle are nearly perpendicular to each other (87.8°) (Figure 12). The Fe distances to the ring centroids of the unsubstituted and the annulated Cp ring of the sandwich unit are equal within experimental error, thus indicating no significant influence of the Ni−chelate ring with respect to bonding in the ferrocene part. The distance $Ni-Cp_{centroid}$ equals that in **16** (1.74 Å). The nickelacycle is slightly puckered as can be seen when viewed along the Ni−N axis (Figure 12). The puckering is related to the torsion angles of the best planes defined by $C^9-C^{22}-Ni$ and $C^9-C^{10}-Ni-N$, which is 11.2°.

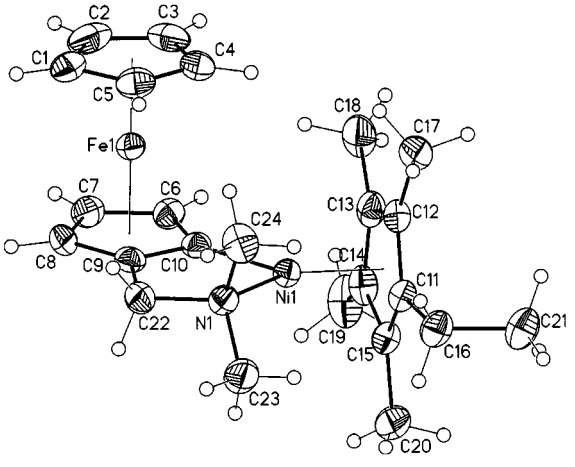

Figure 11. Molecular structure of **16** as determined in the solid state; selected bond lengths [Å] and angles [°]: N^1-C^{10} 1.881(3), Ni^1-N^1 2.001(2), N^1-C^{22} 1.513(3), $C^{10}-Ni^1-N^1$ 86.99(10); $C^9-C^{22}-N^1$ 108.9(2), $C^{22}-N^1-Ni^1$ 111.13(15)

Theoretical Studies on π-Arene Ligand Lability in Arene-Bridged Triple-Deckers of Co and Ni

An intriguing question regarding the reactivity of the (decacyclene)Ni triple-deckers **3** and **4** is the cause of their unusual arene lability under the mild conditions reported herein. Definite notation of arene lability in binuclear complexes has been reported for only a very limited number of cases so far. Thus, we were interested to see whether calculations on the EHMO level could provide, aside from our experimental studies, theoretical insight into this lability for **3** and **4**. Furthermore, we would like to compare our results with other related di- and mononuclear complexes showing related characteristic behavior towards arene exchange.

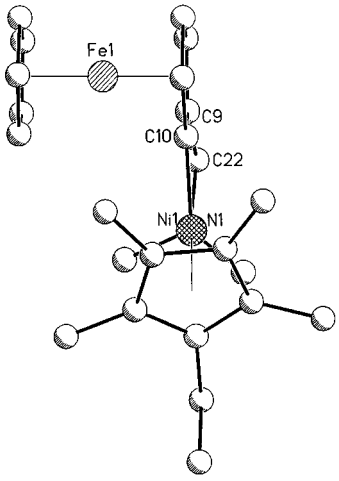

Figure 12. View along the Co−N bond axis of **16**, showing the slight puckering of the metallacycle; atom numbering scheme according to Figure 11

In choosing the EHMO approach we hoped to obtain reliable and still interpretable (at least in well-established chemical paradigms) semiqualitative information on this question.

The arene lability in the triple-decker complexes **3** and **4** can be compared to the following triple-decker compounds: (a) $[(\eta^5\text{-}C_5H_5)V(\mu\text{-}\eta^6\text{:}\eta^6\text{-}C_6H_6)V(\eta^5\text{-}C_5H_5)]$[31] (arene exchange only above 120 °C); (b) $[(\eta^5\text{-}C_5R_5)Co(\mu\text{-}\eta^4\text{:}\eta^4\text{-toluene})Co(\eta^5\text{-}C_5R_5)]$[23] ($R_5$ = 1,2,4-tBu$_3$, Me$_5$) (arene exchange at ambient temperature, compound stable in solution at ambient temperature). In addition the following mononuclear complexes are available for comparison: (c) $[(\eta^6\text{-toluene})Ni(C_6F_5)_2]$[32] (arene extremely labile, arene exchange at ambient temperature); (d) $[(\eta^6\text{-toluene})Co(C_6F_5)_2]$[32] (arene extremely labile, arene exchange at ambient temperature); (e) $[(\eta^6\text{-toluene})Fe(2,2'\text{-bipyridine})]$[33] (arene is not labile); (f) $[(\eta^6\text{-}C_6H_6)Ni(\eta^1\text{-}t\text{Bu}_2PCH_2P\text{-}t\text{Bu}_2)]$[34] (decomposition in solution above −30 °C, probably due to M−arene dissociation, e.g. the compound is not stable in solution at ambient temperature, however, between −80 to −30 °C no arene exchange was found on the NMR time scale).

From these complexes model compounds were constructed through the simplification of alkyl ligand substituents by hydrogen, i.e. in the calculations only C_5H_5 and C_6H_6 were employed. Calculations were performed on the symmetrical triple-decker complexes **A** [(Figure 13)]. The actual η^3:η^3 or η^4:η^4 coordination in the nickel and cobalt triple-deckers was considered by looking at the slipped

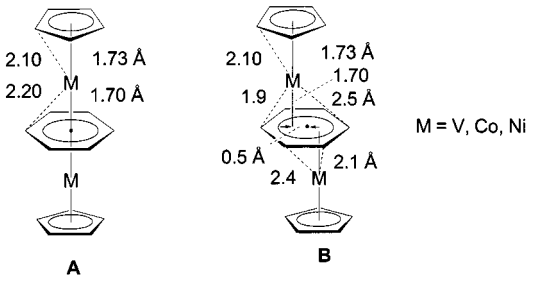

Figure 13. EHMO bonding parameters calculated for the symmetrical (**A**) and the slipped triple deckers (**B**)

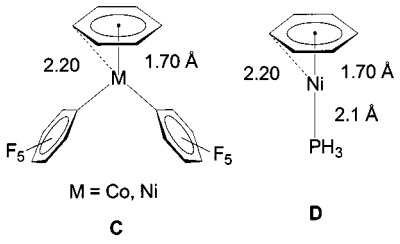

Figure 14. EHMO bonding parameters for the mononuclear complex types **C** and **D**

triple-decker complex **B**. For comparison the mononuclear arene complexes **C** and **D** were included in the calculations (Figure 14).

Triple-decker complexes with middle decks other than arenes have been theoretically analyzed before. Theoretical studies are available for sandwich complexes with middle decks such as C_5H_5,[35] P_5 and As_5, P_6, P_3 and P_4.[36] The orbital interactions of two C_5H_5M fragments with such a middle deck have been well described. In addition, a theoretical study on **C** is available.[37] Furthermore, a photoelectron spectroscopic study, and an MO calculation on **A** with M = V have been carried out.[38]

As a measure of metal−arene bond stability we have used the concept of overlap population. The Mulliken overlap population between two orbitals located on atoms or fragments **X** and **Y** in a molecule is $2c_ic_jS_{ij}$. This corresponds to the amount of electron density transferred to the region between **X** and **Y** on interaction of the two orbitals under consideration. Depending on the signs of the orbital coefficients c_i, c_j, the overlap population, representing the shared electron density of **X** and **Y**, can be positive or negative. A larger positive overlap population correlates with a stronger bond and a larger bond order between atoms **X** and **Y**. However, actual numbers can only be compared within a related series, keeping the atom pair **X**, **Y** constant. For example, the overlap population of a transition-metal−transition-metal bond should not be compared to that of a carbon−carbon bond. The orbital overlap (S_{ij}) term is different for different orbitals or atom pairs. Therefore, it is not so much the single, absolute number that is meaningful, but the trend that is observed upon variation of geometrical or electronic factors.[39,40]

From an Extended Hückel MO study on the model complexes **A**−**D** the following situation emerges: Taking the symmetrical triple-decker **A** we looked at the M−arene overlap population for M = V, Co, Ni in Figure 15. One has to be cautious about comparing the overlap population for different metals. However, this is not necessary by simulating the variation in metal by the electron count and thereby keeping the atom pairs constant. Starting from the neutral complex for M = V (26e$^-$) and Co (34e$^-$) it is obvious that the M−arene overlap drops when adding additional electrons. Conversely, taking electrons away for M = Co (34e$^-$) and Ni (36e$^-$) increases the M−arene overlap. This can be rationalized by the fact that the frontier orbitals are largely metal-centered, but also with metal-to-ligand antibonding combinations.

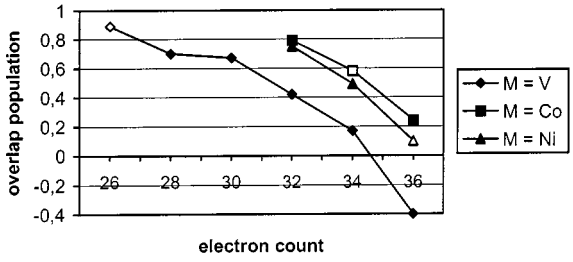

Figure 15. M−arene overlap population in **A** as a function of electron count (open field □, □, Δ is the neutral complex)

Figure 16 compares the M−arene overlap population for the symmetrical and the slipped triple-decker **A** and **B**. Upon slippage, the overlap population is slightly lower for M = V, but increases considerably for M = Co and Ni. This corresponds to the experimental finding of a symmetrical triple-decker for vanadium and η^3:η^3 or η^4:η^4 slipped sandwiches for cobalt and nickel.

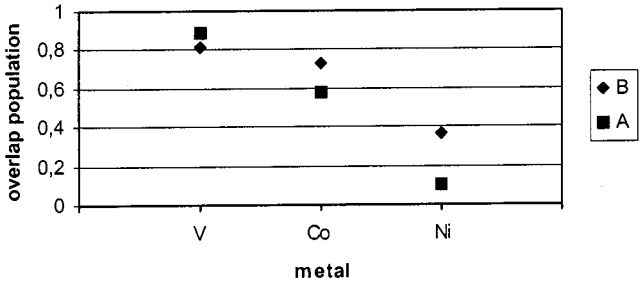

Figure 16. M−arene overlap population in **A** and **B** for M = V, Co, and Ni (neutral complexes)

As a means of calibration we checked the calculated overlap population towards M−arene overlap populations in the mononuclear complexes **C** and **D** with known arene lability. Figure 17 illustrates the results. The overlap population for **C** is lower than for **B** with the same metals. This results corresponds nicely to the experimental finding of a rather low activation energy of 10−11 kcal·mol^{-1} for arene exchange in **C** (M = Ni),[32] thus establishing a slightly higher reactivity for arene exchange for **C** compared to **B**. For **D** the overlap population is the lowest within the nickel series. The low overlap population in **D** compared with **B** or **C** (M = Ni) was surprising, because no arene exchange was reported by NMR techniques for **D**. A closer look re-

vealed, however, that [(η⁶-C_6H_6)Ni(η¹-*t*Bu_2PCH_2P*t*Bu_2)][34] was reported to be stable in solution only up to −30 °C. Above that temperature decomposition took place, probably due to M−arene bond dissociation. Hence, NMR exchange studies were not carried out under ambient conditions as for the other compounds but only at temperatures between −80 and −30 °C, and probably not for an extended period of time.[34] Hence, the instability of [(η⁶-C_6H_6)Ni(η¹-*t*Bu_2PCH_2P*t*Bu_2)] is well reflected in the low M−arene overlap population of **D**.

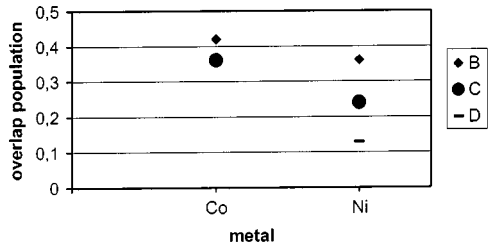

Figure 17. M−arene overlap population in **B**, **C** (M = Co, Ni), and **D**

For useful preparative purposes a labile, yet stable enough character of the M−arene bond is crucial. This results in the combination of two important factors: the ease of handling under ambient conditions, in connection with a still high reactivity for arene exchange under these same conditions. Complexes of type **B** and **C** ideally offer both prerequisites.

Conclusions

Reaction of [(η⁵-$EtMe_4C_5$)Ni(η²-acac)] with the dianion of decacyclene resulted in the formation of the slipped triple-decker **3** with a unique antarafacial bis(η³-enyl)nickel coordination in the solid state as revealed by X-ray crystallography. Complex **3** and its Me_5C_5 derivative **4** display a high reactivity towards ligand loss. This fact has been proven by formation of a number of organonickel chalcogenato complexes of type [(η⁵-Me_4EtC_5)$Ni_2(ER)_2$] (E = S, Se, Te; R = Ph, Mes, Naphth) that are formed by ligand displacement of the polynuclear aromatic middle deck decacyclene. Reaction of **3** and **4** with azobenzene under ligand exchange resulted in C_{sp2}−H activation of the *ortho* ring position giving a remarkable stable five-membered nickelacycle. Complex **3** reacts with the plumbylene **15** in a transmetallation reaction by elimination of Pb^0, giving **16**, which contains a cyclometallated ferrocenyl moiety.

The overlap population from EHMO calculations can be used as a qualitative measure for arene lability in metal−arene complexes. Results obtained from these calculations explain the variation of arene lability in this class of compounds. The increased metal−arene lability observed in cobalt and nickel complexes is due to a filling of metal−arene antibonding orbitals.

Experimental Section

General Information: All reactions were carried out under nitrogen using Schlenk techniques; all solvents were dried properly and distilled under appropriate conditions before use. They were stored under nitrogen prior to use. Products were purified by crystallization. Yields refer to analytically pure samples. Decacyclene (Aldrich) was sublimed in vacuo prior to use. Dichalcogenides R−E−E−R were synthesized according to the literature.[41] − NMR spectra were measured at 25 °C with a Bruker AMX300 or AMX500 and referenced against the deuterated solvents used; coupling constants are given in Hz. NMR samples were prepared by vacuum transfer of dried degassed solvents onto the appropriate amount of solid sample, followed by flame sealing of the NMR tube. − MS spectra were recorded with a MAT 8200 instrument using standard conditions (EI, 70 eV) and the fractional sublimation technique for compound inlet. − UV/Vis spectra were recorded with a Varian Cary 100 spectrometer under air in 10-mm thick cuvettes. − Microanalyses were performed by the microanalytical laboratory of the Chemistry Department of the University−GH Essen.

Photoelectron Spectroscopy Studies (PES): PE spectra were recorded with a Leybold Hereaus UPG200 spectrometer equipped with an He^I radiation source (21.21 eV). Samples were evaporated directly into the target chamber. In order to maintain sufficient vapor pressure of **13** a temperature of 200 °C was used. The energy scale was calibrated with xenon (12.130 and 13.436 eV) and argon (15.759 and 15.937 eV). The accuracy of the measurements was ± 0.03 eV for ionization energies, for broad and overlapping signals ± 0.1 eV.

Theoretical Studies: Qualitative MO computations were performed within the extended Hückel formalism[42] with weighted H_{ij} values[43] with the CACAO program (Version 4.0).[44] Geometrical parameters were taken from X-ray structural studies of the parent compounds[3,23,31,33,35] and averaged. For comparison, the same structural parameters were employed for the different metals in the model compounds [(η⁵-C_5H_5)M(μ-η⁶:η⁶-C_6H_6)M(η⁵-C_5H_5)] (**A**: M = V, Co, Ni), [(η⁵-C_5H_5)M(μ-η³:η³-C_6H_6)M(η⁵-C_5H_5)] (**B**: M = V, Co, Ni), [(η⁶-C_6H_6)M(C_6F_5)₂] (**C**: M = Co, Ni), and [(η⁶-C_6H_6)NiPH_3] (**D**). Keeping the metal−ligand distances constant when changing the metal atom allows for a better comparison on the effect of the metal center. The actual geometric parameters employed in the calculations were as follows (see also the drawings for **A**−**D**): M−C_6H_6(centroid) = 1.70 Å; M−C(η⁶-C_6H_6) = 2.20 Å; M−C_5H_5(centroid) = 1.73 Å; M−C(η⁵-C_5H_5) = 2.10 Å; M−C(σ-C_6F_5) = 1.90 Å; Ni−P = 2.10 Å; C−C(η⁵-C_5H_5) = 1.40 Å; C−C(η⁶-C_6H_6) = 1.39 Å; C−C(C_6F_5, bipy) = 1.40 Å; C−H = 1.05 Å; C−F = 1.35 Å. The distances of M−C(η⁶-arene) found in the X-ray structures lie within 0.15 Å of the 2.20 Å assumed for M−C(η⁶-C_6H_6) with M = V, Co, and Ni. The atomic parameters used were taken from established work and are listed in Table 2.

Horizontal ionization energy calculations were performed with the HyperChem computational package (Version 5.0, Hypercube Inc., Waterloo, Ontario, Canada). Geometry optimizations were carried out on the model complex [(η⁵-Cp)Ni(C_6H_4−N=N−C_6H_5-κ*C*,κ*N*)] ***A*** with the ZINDO/1 method. The Ni−C_{aryl} and Ni−N contacts were refined free to values of $Ni-C^{19}$ = 1.956 Å and $Ni-N^1$ = 1.949 Å. For comparison these values were also restrained to the experimental bond lengths of $Ni-C^{19}$ = 1.864 and Ni−N = 1.816 Å. In addition, the bond angle $C^{12}-N^1-N^2$ was restrained to 113°. No other restrictions were applied. Single-point LCAO−MO−SCF calculations using the ZINDO/S approxi-

Table 2. Parameters used in the Extended Hückel Calculations

	Orbital	Energy H_{ii}/eV	Exponents ζ_1	ζ_2	Coefficients c_1	c_2	Ref.
Ni	3d	−12.99	5.75	2.00	0.5682	0.6292	[33]
	4s	−8.86	2.1				
	4p	−4.90	2.1				
Co	3d	−13.180	5.55	2.10	0.5679	0.6059	[45]
	4s	−9.21	2.0				
	4p	−5.29	2.0				
Fe	3d	−12.700	5.35	1.80	0.5366	0.6678	[45]
	4s	−9.17	1.9				
	4p	−5.37	1.9				
V	3d	−11.000	4.75	1.70	0.4755	0.7052	[46]
	4s	−8.81	1.3				
	4p	−5.52	1.3				
C	2s	−21.4	1.625				[a]
	2p	−11.4	1.625				
F	2s	−40.0	2.425				[a]
	2p	−18.1	2.425				
P	2s	−18.6	1.6				[a]
	2p	−14.0	1.6				
H	1s	−13.6	1.3				[a]

[a] As given in parameter file of the CACAO program; standard EH parameters.

mation with spectroscopic parameterization[24] have been performed on the model complex ***A*** in its respective ZINDO/1 optimized geometry. The restraints did not lead to large changes in orbital composition or energetic order.

Synthesis

[{(η⁵-Me₄EtC₅)Ni}₂(μ-η³:η³decacyclene)] (3): Decacyclene (250 mg, 0.6 mmol) was suspended in 50 mL of THF and transferred into a flask in which a metallic mirror from 60 mg (1.54 mmol) of potassium metal had been prepared. After 3 d, ca. 90% of the metal was dissolved, resulting in a deep red-brown solution. After cooling to −78 °C, [(η⁵-Me₄EtC₅)Ni(η²-acac)][47] (**1**) (370 mg, 1.2 mmol) was added to this solution in one batch under stirring, and the resulting mixture was allowed to warm to room temperature during several hours. After removal of all volatiles, the residue was dissolved in diethyl ether and crystallized from that solvent at −30 °C, resulting in 360 mg (0.42 mmol, 74%) of shimmering black crystals of **3**. − ^{1}H NMR (300 MHz, C_6D_6): δ = 0.52 (t, 6 H), 0.77 (s, 12 H), 0.78 (s, 12 H), 1.27 (q, 4 H), 7.42 (t, ^3J = 7.2 Hz, 6 H), 7.63 (d, ^3J = 7.2 Hz, 6 H), 8.36 (t, ^3J = 7.2 Hz, 6 H). − ^{13}C NMR (75 MHz, C_6D_6): δ = 7.8, 7.9, 14.6, 16.7, 97.5, 98.9, 104.6, 118.9, 123.2, 132.2, 135.9, 142.9. − IR (KBr): ṽ = 3048, 2963, 2925, 2857, 1581, 1482, 1457, 1435, 1378, 1355, 1301, 819, 800, 771, 758 cm^{-1}. − $C_{58}H_{52}Ni_2$ (866.47): calcd. C 80.40, H 6.05; found C 81.00, H 6.38.

The general experimental procedure for reactions of **3** with the dichalcogenides **5**−**8** was as follows: To solution of the dichalcogenide in diethyl ether at 0 °C a diethyl ether solution of **3** was added. Upon warming to ambient temperature precipitation of tan colored decacyclene occurred. The resulting mixture was reduced in volume and filtered through Celite. Crystallization at −30 °C afforded complexes **9**−**12**.

[{(η⁵-Me₄EtC₅)Ni}₂(μ-SPh)₂] (9): Brown crystals; yield: 300 mg (0.4 mmol, 84%). − ^{1}H NMR (300 MHz, C_6D_6): δ = 0.91 (t, 6 H), 1.13 (s, 12 H), 1.20 (s, 12 H), 1.85 (q, 4 H), 7.02 (m, 6 H), 8.36 (m, 4 H). − ^{13}C NMR (75 MHz, C_6D_6): δ = 8.9, 9.0, 14.3, 17.9, 97.6, 99.0, 99.3, 106.9, 125.3, 127.5, 136.1, 138.9. − MS (EI): *m*/*z* (%) = 632 (60) [M$^+$], 316 (100) [M$^+$/2]. − IR (KBr): ṽ = 3059, 2961, 2903, 2854, 1576, 1473, 1450, 1436, 1378, 1347, 1297, 1262, 1153, 1022, 819, 769, 738, 689 cm^{-1}. − $C_{34}H_{44}Ni_2S_2$ (634.266): calcd. C 64.39, H 6.99, S 10.11; found C 67.08, H 6.65, S 7.43.

[{(η⁵-Me₄EtC₅)Ni}₂(μ-SeMes)₂] (10): Brown microcrystals; yield: 360 mg (0.4 mmol, 79%). − ^{1}H NMR (300 MHz, C_6D_6): δ = 0.80 (t, 6 H), 1.23 (s, 24 H), 1.86 (q, 4 H), 2.11 (s, 6 H), 2.55 (s, 6 H) broad, 4.33 (s, 6 H) broad, 6.70 (s, 2 H) broad, 6.99 (s, 2 H) broad. − ^{13}C NMR (75 MHz, C_6D_6): δ = 9.1, 9.2, 14.2, 18.0, 21.0, 98.6, 105.5, 120.1, 135.0. − MS (EI): *m*/*z* (%) = 812 (20) [M$^+$], 406 (100) [M$^+$/2]. − $C_{40}H_{56}Ni_2Se_2$ (812.228): calcd. C 59.15, H 6.95; found C 54.72, H 6.72.

[{(η⁵-Me₄EtC₅)Ni}₂(μ-TeMes)₂] (11): Brown microcrystals; yield: 410 mg (0.4 mmol, 80%). − ^{1}H NMR (300 MHz, C_6D_6): δ = 0.83 (t, 6 H), 1.50 (s, 12 H), 1.52 (s, 6 H), 1.53 (s, 6 H), 2.03 (q, 4 H), 2.10 (s, 6 H), 2.70 (s, 6 H), 3.62 (s, 6 H), 6.68 (s, 2 H), 6.86 (s, 2 H). − ^{13}C NMR (75 MHz, C_6D_6): δ = 9.9, 10.0, 10.1, 10.2, 15.1, 18.9, 21.0, 29.9, 32.1, 98.1, 98.3, 99.4, 99.7, 104.8, 126.4, 127.0, 136.4, 144.6, 146.0. − MS (EI): *m*/*z* (%) = 910 (15) [M$^+$], 791 (17) [M$^+$ − mesitylene], 456 (18) [M$^+$/2], 119 (100) [mesitylene]. − $C_{40}H_{56}Ni_2Te_2$ (909.508): calcd. C 52.82, H 6.21; found C 53.10, H 6.18.

[{(η⁵-Me₄EtC₅)Ni}₂(μ-TeNaphth)₂] (12): Black crystals; yield: 380 mg (0.4 mmol, 73%). − ^{1}H NMR (300 MHz, C_6D_6): δ = 0.75 (t, 6 H), 1.38 (s, 12 H), 1.40 (s, 6 H), 1.41 (s, 6 H), 1.92 (q, 4 H), 7.05 (t, ^3J = 7.7 Hz, 2 H), 7.30 (m, 2 H), 7.45 (m, 2 H), 7.55 (d, ^3J = 8.1 Hz, 2 H), 7.61 (d, ^3J = 7.7 Hz, 2 H), 8.81 (d, ^3J = 7.7 Hz, 2 H), 9.38 (d, ^3J = 8.1 Hz, 2 H). − ^{13}C NMR (75 MHz, C_6D_6): δ = 10.1, 10.2, 10.3, 10.4, 15.3, 19.0, 98.5, 99.0, 99.9, 100.5, 100.7, 105.8, 125.3, 126.0, 126.1, 128.8, 132.8, 133.0, 138.4, 141.9. − MS (EI): *m*/*z* (%) = 926 (15) [M$^+$], 799 (10) [M$^+$ − naphthalene], 464 (15) [M$^+$/2], 253 (100) [binaphthalene]. − $C_{42}H_{48}Ni_2Te_2$ (925.466): calcd. C 54.51, H 5.23; found C 55.05, H 5.36.

[(η⁵-Me₄EtC₅)Ni(C₆H₄−N=N−C₆H₅-κ*C*,κ*N*)] (13): This compound was prepared by adding a stoichiometric amount of azobenzene to a solution of **3** in 500 mL of diethyl ether at room temperature. While stirring for 12 h, the color changed from brown red to deep blue. Crystallization from diethyl ether afforded dark blue crystals; yield: 380 mg (1.0 mmol, 88%). − ^{1}H NMR (300 MHz, CD_2Cl_2): δ = 0.93 (t, 3 H), 1.62 (s, 6 H), 1.73 (s, 6 H), 2.15 (q, 2 H), 7.08 (m, 1 H, C^5−H), 7.13 (m, 1 H, C^4−H), 7.16 (m, 2 H, C$^{8,8'}$-H), 7.37 (m, 1 H, C^{10}−H), 7.47 (m, 2 H, C$^{9,9'}$-H), 7.86 (m, 1 H, C^3−H), 8.11 (m, 1 H, C^6−H). − ^{13}C NMR (75 MHz, CD_2Cl_2): δ = 9.3, 9.5, 15.1, 17.7, 100.4, 101.4, 108.2 [(η⁵-Me₄EtCp)Ni], 123.0 (C$^{8,8'}$), 123.2 (C^4), 123.8 (C^5), 127.5 (C^{10}), 127.6 (C^6), 128.8 (C^9), 138.5 (C^3), 157.4 (C^7), 163.1 (C^1), 181.9 (C^2). − MS (EI): *m*/*z* (%) = 388 (100) [M$^+$]. − IR (KBr): ṽ = 3082, 3055, 3039, 2961, 2912, 2867, 1588, 1567, 1484, 1447, 1296, 1287, 1262, 1032, 1017, 770, 753, 711, 698 cm^{-1}. − UV/Vis (CH_2Cl_2): λ_{max} (ε) = 230 (24923), 250 (21760), 300 (25237), 345 (9203), 510 (3243), 609 nm (6317). − $C_{23}H_{26}N_2Ni$ (389.18): calcd. C 70.98, H 6.73, N 7.20; found C 70.31, H 6.98, N 6.89.

[(η⁵-C₅Me₅)Ni(C₆H₄−N=N−C₆H₅-κ*C*,κ*N*)] (14): As with the synthesis of **13**. Blue, needle-like crystals, prepared from **4**; yield: 350 mg (0.9 mmol, 85%). − ^{1}H NMR (300 MHz, C_6D_6): δ = 1.50 (s, 15 H) 7.0 (m, 1 H, C^{10}−H), 7.06−7.22 (m, 6 H), 7.94 (dd, ^3J =

7.9 Hz, ^4J = 1.1 Hz, 1 H, C^3−H), 8.50 (dd, ^3J = 7.7 Hz, ^4J = 1.5 Hz, 1 H, C^6−H). − ^{13}C NMR (75 MHz, C_6D_6): δ = 9.4, 100.6, 123.2, 123.7, 124.0, 127.1, 138.4, 157.7, 164.1, 182.7. − MS (EI): *m/z* (%) = 374 (100) [M^+]. − IR (KBr): ṽ = 3058, 3039, 2979, 2952, 2898, 2851, 1589, 1484, 1420, 1385, 1297, 1263, 1154, 1068, 1017, 769, 758, 753, 711, 698 cm^{-1}. − $C_{22}H_{24}N_2Ni$ (375.16): calcd. C 70.44, H 6.45, N 7.47; found C 64.17, H 5.99, N 6.95. Although this analysis was repeated several times with recrystallized material, C,H,N values for **15** were repeatedly unsatisfactorily.

[(η^5-C_5H_5)Fe[μ-(η^5-$C_5H_3CH_2NMe_2$-κ*C*,κ*N*)]Ni(η^5-C_5EtMe_4)] (16): Solid **3** (180 mg, 0.2 mmol) was added to a yellow suspension of plumbylene **15** (140 mg, 0.2 mmol) in diethyl ether at −78 °C. Within a few hours precipitation of decacyclene (**2**) occurred and the color of the solution turned to purple, while upon warming to ambient temperature it changed to red-brown. The mixture was reduced in volume and filtered through Celite. Crystallization at −78 °C afforded 60 mg (0.1 mmol, 65%) of complex **16** as red to black crystals. − ^{1}H NMR (300 MHz, C_6D_6): δ = 1.11 (t, 3 H), 1.69 (s, 3 H), 1.70 (s, 3 H), 1.72 (s, 6 H), 1.86 [s, 3 H, $N(CH_3)_2$], 2.24 (q, 2 H), 2.33 [s, 3 H, $N(CH_3)_2$], 2.59 (d, ^2J = 13.6 Hz, 1 H, Fc−CH_2), 2.89 (d, ^2J = 13.6 Hz, 1 H, Fc−CH_2), 3.84 (d, ^3J = 2.1 Hz, 1 H, C_5H_3Fe), 3.98 (d, ^3J = 2.1 Hz, 1 H, C_5H_3Fe), 4.20 (s, 5 H, C_5H_5Fe), 4.24 (t, ^3J = 2.1 Hz, 1 H, C_5H_3Fe). − ^{13}C NMR (75 MHz, C_6D_6): δ = 10.4, 10.5, 15.2, 19.2, 53.2 [$N(CH_3)_2$], 53.4 [$N(CH_3)_2$], 60.8 (C_5H_3Fe), 66.5 (C^4), 68.4 (Fc−CH_2), 69.1 (C_5H_5Fe), 71.7 (C_5H_3Fe), 90.2 (C^1), 92.4 (C^2), 95.5, 96.1, 97.2, 97.4, 103.8. − MS (EI): *m/z* (%) = 449 (100) [M^+], 326 (45) [M^+ − C_5H_5Fe], 242 (20) [M^+ − $C_{11}H_{17}Ni$]. − IR (KBr): ṽ = 3079, 3026, 2961, 2922, 2852, 2769, 1451, 1415, 1383, 1353, 1302, 1227, 1158, 1105, 1043, 1022, 974, 947, 864, 846, 809, 795 cm^{-1}. − $C_{24}H_{33}FeNNi$ (450.09): calcd. C 64.05, H 7.39, N 3.11; found C 57.89, H 6.96, N 3.11. Probably due to excess [(dimethylamino)methyl]ferrocene that could not be removed completely by washing without dissolving most of **16**, the C value is found out of the usually acceptable range.

Acknowledgments

The work of J. J. S. was supported by the DFG (Heisenberg fellowship to J. J. S.), by the Stiftung Volkswagenwerk and the Fonds der Chemischen Industrie which is acknowledged with gratitude. We are grateful to the mass spectrometric department of the MPI für Kohlenforschung, Mülheim, for recording the mass spectra and Mr. K. Kowski, University of Essen, for recording the PE spectrum of **13**. The work of C. J. was supported by the DFG and the Fonds der Chemischen Industrie. A copy of the CACAO program was kindly provided by Dr. D. M. Proserpio.

[1] J. J. Schneider, D. Spickermann, T. Labahn, J. Magull, M. Fontani, F. Laschi, P. Zanello, *Chem. Eur. J.* **2000**, 6, 3686.

[2] [2a] M. Munakata, L. P. Wu, G. L. Ning, T. Kuroda-Sowa, M. Maekawa, Y. Suenaga, N. Maeno, *J. Am. Chem. Soc.* **1999**, *121*, 4968. − [2b] T. Kubo, K. Yamamoto, K. Nakasuji, T. Takui, I. Murata, *Angew. Chem.* **1996**, *108*, 456; *Angew. Chem. Int. Ed. Engl.* **1996**, *35*, 439. − [2c] K. Zimmermann, R. Goddard, C. Krüger, M. W. Haenel, *Tetrahedron Lett.* **1996**, *37*, 8371. − [2d] K. Zimmermann, M. W. Haenel, *Synlett* **1997**, 609.

[3] [3a] J. Edwin, M. Bochmann, M. C. Böhm, D. E. Brennan, W. E. Geiger, C. Krüger, J. Pebler, H. Pritzkow, W. Siebert, W. Swiridoff, H. Wadepohl, J. Weiss, U. Zenneck, *J. Am. Chem. Soc.* **1983**, *105*, 2582. − [3b] W. Siebert, *Angew. Chem.* **1985**, *97*, 924; *Angew. Chem. Int. Ed. Engl.* **1985**, *24*, 943. − [3c] H. Werner, *Angew. Chem.* **1977**, *89*, 1; *Angew. Chem. Int. Ed. Engl.* **1977**, *16*, 1. − [3d] G. E. Herberich, H. Ohst, *Adv. Organomet. Chem.* **1986**, *25*, 199. − [3e] G. E. Herberich in *Comprehensive Organometallic Chemistry* (Eds.: E. W. Abel, F. G. A. Stone, G. Wilkinson), Pergamon Press, Oxford, **1982**, vol. 1, chapter 5, p. 197. − [3f] P. Greiwe, M. Sabat, R. N. Grimes, *Organometallics* **1995**, *14*, 3683. − [3g] R. N. Grimes, *Coord. Chem. Rev.* **1979**, *28*, 47. − [3h] X. Wong, M. Sabat, R. N. Grimes, *J. Am. Chem. Soc.* **1995**, *117*, 12227.

[4] X-ray crystallograpic investigations on **3**, **9**, and **16**. − **3**: Formula $C_{58}H_{52}Ni_2$, *M* = 866.42; crystal dimensions 0.21 × 0.16 × 0.12 mm, black, measured with a Siemens SMART-CCD diffractometer (three-axis platform) with Mo-K_α radiation at 293(2) K. Cell dimensions *a* = 13.6342(10), *b* = 16.8886(12), *c* = 18.6494(13) Å, *V* = 4294.3(5) Å^3; orthorombic crystal system, *Z* = 4, $d_{calcd.}$ = 1.340 gcm^{-3}, μ = 0.917 mm^{-1}, space group *Pca*2$_1$, data collection of 34489 intensities ($2\Theta_{max}$ = 50°, 0.3° ω-scans 120 frames at φ = 0°, four runs 0.3° φ-scans with 600 frames at angles 135, 143, 156 and 169° in ω, more than 97% of the data covered), absorption correction with Siemens SADABS (R_{merg} before/after 0.1414/0.0426, max/min equivalent transmission 1.00/0.59), 10428 independent and 6167 "observed" data [$F_o \geq 4\sigma(F)$], structure solution with direct methods (Siemens SHELXTL-Plus Vers. 5.03) and refined on F^2 (Siemens SHELXL-97) (541 parameters). Hydrogen atom positions were calculated and refined as riding groups with the 1.2-fold (1.5 for methyl groups) isotropic *U* values. *R*1 = 0.0505, *wR*2 = 0.1032, $w^{-1} = \sigma^2(F_o^2) + (0.0592 \cdot P)^2$, where $P = [(\max F_o^2) + (2F_c^2]/3$, GOF = 0.311 eÅ^{-3} close to the heavy atoms. − **9**: Formula $C_{34}H_{44}Ni_2S_2$, *M* = 634.23, *a* = 10.6922(5) Å, *b* = 11.9271(6) Å, *c* = 14.0125(7) Å, α = 84.307(3)°, β = 75.012(3)°, γ = 63.581(2)°, V = 1545.64(13) Å^3, $d_{calcd.}$ = 1.363 g cm^{-3}, μ = 1.375 mm^{-1}, empirical absorption correction with SADABS[a], *Z* = 2, two half-independent molecules in the asymmetric unit (bond parameters identical within esds), triclinic, space group *P*1, λ = 0.71073 Å, *T* = 133(2) K, 15845 reflections collected, 4048 independent and 3695 observed reflections [$I \geq 2\ \sigma(I)$], 353 parameters, *R* = 0.0619, wR_2 = 0.1108, max/min residual electron density: 0.339/−0.694 e Å^{-3}, position of the hydrogen atoms calculated and riding. G. M. Sheldrick, SADABS, **1999**; computer program for correction of diffractometer data, Universität Göttingen. − **16**: Formula $C_{24}H_{33}FeNNi$, *M* = 450.07; crystal dimensions 0.28 × 0.26 × 0.12 mm, dark brown block, measured with a Siemens SMART-CCD diffractometer (three-axis platform) with Mo-K_α radiation at 203(2) K. Cell dimensions *a* = 9.6053(8), *b* = 8.6511(7), *c* = 25.522(2) Å, β = 90.445(2)°, *V* = 2111.2(3) Å^3; monoclinic crystal system, *Z* = 4, $d_{calcd.}$ = 1.416 gcm^{-3}, μ = 0.917 mm^{-1}, space group $P2_1/n$, data collection of 5568 intensities ($2\Theta_{max}$ = 50°, 0.3° ω-scans 120 frames at φ = 0°, four runs 0.3° φ-scans with 636 frames at angles 0.88, 180, 270° in ω, more than 99% of the data covered), absorption correction with Bruker AXS SADABS (R_{merg} before/after 0.0626/0.0485, max/min equivalent transmission 1.00/0.81), 5218 independent and 3610 "observed" data [$F_o \geq 4\sigma(F)$], structure solution with direct methods (Bruker AXS SHELXTL-Plus Vers. 5.10 DOS/WIN95/NT) and refined on F^2 (SHELXL-97) (244 parameters). Hydrogen atom positions were calculated and refined as riding groups with the 1.2-fold (1.5 for methyl groups) isotropic *U* values. *R*1 = 0.0453, *wR*2 = 0.1013, $w^{-1} = \sigma^2(F_o^2) + (0.068 \cdot P)^2$, where $P = [(F_o^2) + (2F_c^2)]/3$, GOF = 0.974, max/min residual electron density 1.522/−0.312 eÅ^{-3} close to the heavy atoms. − Crystallographic data (excluding structure factors) for the structures reported in this paper have been deposited with the Cambridge Crystallographic Data Centre as supplementary publication nos. CCDC-141845 (**3**), -139245 (**9**), and -141844 (**16**). Copies of the data can be obtained free of charge on application to CCDC, 12 Union Road, Cambridge CB2 1EZ, UK [Fax: (internat.) + 44-1223/336-033; E-mail: deposit@ccdc.cam.ac.uk].

[5] [5a] J. Müller, P. Escarpa Gaede, K. Qiao, *Angew. Chem.* **1993**, *105*, 1809; *Angew. Chem. Int. Ed. Engl.* **1993**, *32*, 1697. − [5b] J. Müller, P. Escarpa Gaede, K. Qiao, *J. Organomet. Chem.* **1994**, *480*, 213. − [5c] J. J. Schneider, U. Specht, R. Goddard, C. Krüger, J. Ensling, P. Gütlich, *Chem. Ber.* **1995**, *128*, 941. − [5d] J. J. Schneider, D. Wolf, U. Denninger, R. Goddard, C. Krüger, *J. Organomet. Chem.* **1999**, *579*, 139.

[6] K. Jonas, G. Koepe, L. Schieferstein, R. Mynott, C. Krüger, Y.-H. Tsay, *Angew. Chem.* **1983**, *95*, 637; *Angew. Chem. Int. Ed. Engl.* **1983**, *22*, 620; *Angew. Chem. Suppl.* **1983**, 920.

[7] W. J. Evans, S. L. Gonzales, J. W. Ziller, *J. Am. Chem. Soc.* **1994**, *116*, 2600.

[8] J. J. Schneider, D. Wolf, U. Denninger, R. Goddard, C. Krüger, *J. Organomet. Chem.* **1999**, *579*, 139.

[9] I. Bach, K.-R. Pörschke, R. Goddard, C. Kopiske, C. Krüger, A. Rufinska, K. Seevogel, *Organometallics* **1996**, *15*, 4959 and ref. cited therein.
[10] D. M. Ho, R. A. Pascal, Jr., *Chem. Mater.* **1993**, *5*, 1358.
[11] [11a] N. Tokitoh, Y. Matsuhashi, R. Okazaki, *Organometallics* **1993**, *12*, 2894. – [11b] Y. Matsuhashi, N. Tokitoh, R. Okazaki, *Organometallics* **1994**, *13*, 4387. – [11c] K. Merzweiler, L. Weise, *Z. Naturforsch., Teil B* **1990**, *45*, 971. – [11d] K. Merzweiler, H. Kraus, *Z. Naturforsch., Teil B* **1997**, *52*, 635.[11e] K. Merzweiler, H. Kraus, L. Weise, *Z. Naturforsch., Teil B* **1993**, *48*, 287. –
[12] [12a] N.-F. Ho, T. C. W. Mak, T.-Y. Luh, *J. Chem. Soc., Dalton Trans.* **1990**, 3591–3595. – [12b] R. E. Dessy, R. Kornmann, C. Smith, R. Haytor, *J. Am. Chem. Soc.* **1968**, *80*, 2001. – [12c] R. E. Dessy, L. Wieczorek, *J. Am. Chem. Soc.* **1969**, *91*, 4963.
[13] [13a] J. J. Schneider, N. Czap, D. Bläser, R. Boese, *J. Am. Chem. Soc.* **1999**, *121*, 1409. – [13b] J. J. Schneider, J. Hagen, D. Spickermann, D. Bläser, R. Boese, F. F. de Biani, F. Laschi, P. Zanello, *Chem. Eur. J.* **2000**, *6*, 237.
[14] G. Aullón, G. Ujaque, A. Lledós, S. Alvarez, *Chem. Eur. J.* **1999**, *5*, 1391.
[15] *Handbook of Chemistry and Physics*, 61th ed., CRC Press, Boca Raton, Florida, **1980**, F219.
[16] [16a] A. D. Ryabov, *Chem. Rev.* **1990**, *90*, 403. – [16b] M. Ghedini, D. Pucci, A. Crispini, G. Barberio, *Organometallics* **1999**, *18*, 2116.
[17] [17a] N. L. Cromhout, J. F. Gallagher, A. R. Manning, A. Paul, *Organometallics* **1999**, *18*, 1119. – [17b] N. Gül, J. H. Nelson, *Organometallics* **1999**, *18*, 709. – [17c] S. Attar, J. H. Nelson, J. Fischer, A. de Cian, J. P. Sutter, M. Pfeffer, *Organometallics* **1995**, *14*, 4559. – [17d] Z.-X. Wang, C.-S. Jia, Z.-Y. Zhou, X.-G. Zhou, *J. Organomet. Chem.* **1999**, *580*, 201. – [17e] V. I. Sokolov, L. L. Troitskaya, O. A. Reutov, *J. Organomet. Chem.* **1999**, *580*, 201. – [17f] K. G. Gaw, A. M. Z. Slawin, M. B. Smith, *Organometallics* **1999**, *18*, 3255.
[18] [18a] J. Kleimann, M. Dubbeck, *J. Am. Chem. Soc.* **1963**, *85*, 1544. – [18b] D. Sutton, *Chem. Rev.* **1993**, *93*, 995.
[19] A. C. Cope, R. W. Siekman, *J. Am. Chem. Soc.* **1965**, *87*, 3272.
[20] [20a] H. Takahashi, J. Tsuji, *J. Organomet. Chem.* **1967**, *10*, 511. – [20b] M. I. Bruce, B. C. Godall, F. G. A. Stone, *J. Chem. Soc., Chem. Commun.* **1973**, 558. – [20c] M. I. Bruce, B. C. Godall, F. G. A. Stone, *J. Chem. Soc., Dalton Trans.* **1987**, 687. – [20d] A. K. Yatsimirsky, *Zh. Neorg. Khim.* **1979**, *24*, 2711. – [20e] R. F. Heck, *J. Am. Chem. Soc.* **1968**, *90*, 313.
[21] [21a] P. L. Watson, *J. Chem. Soc., Chem. Commun.* **1983**, 276. – [21b] B. J. Dellman, W. M. Stevels, J. H. Teuben, M. T. Lakin, A. L. Spek, *Organometallics* **1994**, *13*, 3881. – [21c] J. J. Schneider, *Chem. Ber.* **1995**, *128*, 321.
[22] [22a] K. Kokkinos, R. Wizinger, *Helv. Chim. Acta* **1971**, *54*, 330. – [22b] W. I. Cross, K. R. Flower, R. G. Pritchard, *J. Organomet. Chem.* **2000**, *601*, 164.
[23] [23a] J. J. Schneider, U. Denninger, O. Heinemann, C. Krüger, *Angew. Chem.* **1995**, *107*, 631; *Angew. Chem. Int. Ed. Engl.* **1995**, *34*, *592*. – [23b] J. J. Schneider, D. Wolf, C. Janiak, O. Heinemann, J. Rust, C. Krüger, *Chem. Eur. J.* **1998**, *4*, 1982. – [23c] J. J. Schneider, D. Wolf, *Z. Naturforsch., Teil B* **1998**, *53*, 1.
[24] [24a] M. C. Zerner, G H. Loew, R. F. Kirchner, U. T. Mueller-Westerhoff, *J. Am. Chem. Soc.* **1980**, *102*, 589.– [24b] A. D. Bacon, M. C. Zerner, *Theor. Chim. Acta* **1979**, *53*, 21. – [24c] M. C. Zerner in *Reviews in Computational Chemistry II* (Eds.: K. B. Lipkowitz, D. B. Boyd), VCH, Weinheim, **1991**, p. 313.
[25] T. Koopmans, *Physica* **1934**, *104*, 1.
[26] M. C. Böhm, *Z. Naturforsch., Teil A* **1982**, *37*, 1193 and refs. therein.
[27] C. Janiak, N. Kuhn, R. Gleiter, *J. Organomet. Chem.* **1994**, *475*, 223.
[28] [28a] J. J. Schneider, N. Czap, *J. Chem. Soc., Dalton Trans.* **1999**, 595. – [28b] J. J. Schneider, N. Czap, D. Bläser, R. Boese, *J. Am. Chem. Soc.* **1999**, *121*, 1409. – [28c] J. J. Schneider, N. Czap, D. Bläser, R. Boese, *J. Organomet. Chem.* **1999**, *584*, 338. – [28d] J. J. Schneider, J. Hagen, N. Czap, C. Krüger, S. A. Mason, R. Bau, J. Ensling, P. Gütlich, B. Wrackmeyer, *Chem. Eur. J.* **2000**, *6*, 625.[28e] J. J. Schneider, N. Czap, D. Bläser, R. Boese, J. Ensling, P. Gütlich, C. Janiak, *Chem. Eur. J.* **2000**, *6*, 468.
[29] [29a] N. Davidovic, K. Jacob, A. H. van der Zejden, H. Menge, K. Merzweiler, C. Wagner, *Organometallics* **2000**, 19, 1438. – [29b] J. J. Schneider, *Nachr. Chem.* **2000**, *5*, 614.
[30] M. R. Meneghetti, M. Grellier, M. Pfeffer, J. Dupont, J. Fischer, *Organometallics* **1999**, *18*, 5560.
[31] [31a] A. W. Duff, K. Jonas, R. Goddard, H.-J. Kraus, C. Krüger, *J. Am. Chem. Soc.* **1983**, *105*, 5479. – [31b] K. Jonas, *Angew. Chem.* **1985**, *97*, 292; *Angew. Chem. Int. Ed. Engl.* **1985**, *24*, 295.
[32] [32a] L. J. Radonovich, M. W. Eyring, T. J. Groshens, K. J. Klabunde, *J. Am. Chem. Soc.* **1982**, *104*, 2816. – [32b] K. J. Klabunde, B. B. Anderson, M. Bader, L. J. Radonovich, *J. Am. Chem. Soc.* **1978**, *100*, 1313. – [32c] L. J. Radonovich, K. J. Klabunde, C. B. Behrens, D. P. McCollar, B. B. Anderson, *Inorg. Chem.* **1980**, *178*, 197. – [32d] R. G. Gastinger, K. J. Klabunde, *Trans. Met. Chem.* **1979**, *4*, 1.
[33] L. J. Radonovich, F. J. Koch, T. A. Albright, *Inorg. Chem.* **1980**, *19*, 3373.
[34] T. Nickel, R. Goddard, C. Krüger, K.-R. Pörschke, *Angew. Chem.* **1994**, *106*, 908; *Angew. Chem. Int. Ed. Engl.* **1994**, *33*, 879.
[35] J. W. Lauher, M. Elian, R. H. Summerville, R. Hoffmann, *J. Am. Chem. Soc.* **1976**, *98*, 3219.
[36] W. Tremel, R. Hoffmann, M. Kertesz, *J. Am. Chem. Soc.* **1989**, *111*, 2030.
[37] L. J. Radonovich, M. W. Eyring, T. J. Groshens, K. J. Klabunde, *J. Am. Chem. Soc.* **1982**, *104*, 2816.
[38] P. T. Chesky, M. B. Hall, *J. Am. Chem. Soc.* **1984**, *106*, 5186.
[39] T. A. Albright, J. K. Burdett, M.-H. Whangbo, *Orbital Interactions in Chemistry*, Wiley-Interscience, New York, **1985**. R. Hoffmann, *Solids and Surfaces: A Chemists View of Bonding in Extended Structures*, VCH, Weinheim, **1988**.
[40] C. Janiak, R. Hoffmann, *J. Am. Chem. Soc.* **1990**, *112*, 5924.
[41] M. Akiba, M. V. Lakshmikantham, K.-Y. Jen, M. P. Cava, *J. Org. Chem.* **1984**, *49*, 4819.
[42] R. Hoffmann, *J. Chem. Phys.* **1963**, *39*, 1397–1412. R. Hoffmann, W. N. Lipscomb, *J. Chem. Phys.* **1962**, *36*, 2179–2189. R. Hoffmann, W. N. Lipscomb, *J. Chem. Phys.* **1962**, *37*, 2872.
[43] J. H. Ammeter, H.-B. Bürgi, J. C. Thibeault, R. Hoffmann, *J. Am. Chem. Soc.* **1978**, *100*, 3686–3692.
[44] C. Mealli, D. M. Proserpio, *J. Chem. Educ.* **1990**, *67*, 399.
[45] R. H. Summerville, R. Hoffmann, *J. Am. Chem. Soc.* **1976**, *98*, 7240.
[46] P. Kubácek, R. Hoffmann, Z. Havlas, *Organometallics* **1982**, *1*, 180.
[47] E. E. Bunel, L. Valle, J. M. Manriquez, *Organometallics* **1985**, *4*, 1680.

Received June 16, 2000
[I00244]

Formation of Polyesters by Thermally Induced Polymerization Reactions of Molecular Solids

Oliver Herzberg[a] and Matthias Epple*[a]

Dedicated to Prof. Dr. R. D. Fischer on the occasion of his 65th birthday

Keywords: Solid-state polymerization / Halogenocarboxylates / Polymers / Biomaterials / Materials chemistry

The development of solid-state polycondensation reactions, starting in 1857, is reviewed. In many cases, the elimination of metal halides from halogenated carboxylates leads to the formation of polyesters, among them polyglycolide, polylactides, polybutyrates, polymandelide, and poly(hydroxymethyl benzoates). In some cases, a reaction in the solid state is observed, whereas in other cases temporary liquefaction occurs. The resulting polymers usually have a lower degree of polymerization than the products from solution- or melt-polymerization. In some cases, polymers with a distinct micromorphology (high porosity with pores in the sub-μm range) are obtained and may be of interest for special applications, e.g. in medical technology.

Introduction

Polymers constitute one of the major classes of materials. Owing to the tremendous progress made in polymer chemistry since the days of Hermann Staudinger, the properties of polymeric materials can now be fine-tuned within a wide range, so that they have replaced classical materials (metals, wood, ceramics) in many applications (the annual worldwide production of synthetic polymer fibers is approximately 20 Mio t/a). Usually, polymers are prepared in the melt or in solution.

An impressive number of solid-state polymerization reactions occurring in the solid state is known. They may be divided into radiation-induced reactions (photopolymerization reactions) and thermally induced reactions. However, although polymerization reactions in the solid state had been known since the last century,[1,2] they did not find an industrial application, probably due to the inherent difficulties involved in controlling a large-scale exothermic reaction in the solid state. In this article, we review one type of these reactions, i.e. thermally induced reactions that lead to polyesters, accompanied by salt elimination. In some special cases, the resulting materials may be useful for biomedical applications.

[a] Solid State Chemistry, Faculty of Chemistry, University of Bochum,
44780 Bochum, Germany
Fax: (internat.) + 49-(0)234/3214-558
E-mail: matthias.epple@ruhr-uni-bochum.de

Oliver Herzberg was born in 1968 in Flensburg. After studying chemistry at the University of Hamburg from 1989 to 1996, he obtained his PhD in 2000 with M. Epple on the reactivity of molecular solids, including solid-state polymerization reactions of halogenomethylbenzoates.

Matthias Epple was born in Reutlingen in 1966. He finished his studies with a PhD in Physical Chemistry in 1992 (topic: solid-state reactions and solid-state phase transformations) at the Technical University of Braunschweig under the direction of Prof. H. K. Cammenga. In 1993, he worked as a postdoctoral fellow at the University of Washington (Seattle, USA) on colloid and polymer science (Prof. J. C. Berg). From 1994 to 1997 he performed his habilitation at the Institute of Inorganic and Applied Chemistry at the University of Hamburg (Prof. A. Reller), working in the field of molecular solid-state reactivity, including the application of synchrotron radiation techniques. His awards include the Netzsch-GEFTA Young Scientist Award (1995), a DFG Heisenberg stipend (1998) and a DFG Heinz−Maier−Leibnitz Award (1998). Since April 2000, he holds a professorship in Inorganic Chemistry at the Ruhr University of Bochum. He has authored more than 70 publications in reviewed journals. His current research interests include molecular solid-state chemistry, preparation and characterization of biomaterials (polymers, ceramics and metals) and studies on biomineralization (biological and medical).

MICROREVIEWS: This feature introduces the readers to the authors' research through a concise overview of the selected topic. Reference to important work from others in the field is included.

 © WILEY-VCH Verlag GmbH, 69451 Weinheim, 2001 1434−1948/01/0606−1395 $ 17.50+.50/0

Some Background Information on Polyesters

Polyesters, i.e. macromolecules with ester bonds between the repeating units, constitute an important group of materials with a high number of applications. Among the well-known polyesters are poly(ethyleneterephthalic acid) [polyethyleneterephthalate; PET], poly(butyleneterephthalic acid) [polybutyleneterephthalate; PBT], polyglycolide [poly(hydroxyacetic acid); PGA] and polylactide [poly(2-hydroxypropionic acid); PLA]. Note that if the ester groups are placed in side chains in a graft polymer, the polymer is not called a polyester.

Biodegradable polyesters constitute an important subset. The potentially hydrolyzable ester bond is used in a number of poly(hydroxycarboxylic acids) with polyglycolide, polylactide and P-3HB [poly(3-hydroxybutyric acid)] being the most prominent examples. As a contribution to a sustainable development, they may replace nonbiodegradable polymers made from fossil fuels in consumer chemicals.[3] For example, the Cargill−Dow Polymer Corporation has announced that in 2002 it intends to start the production of polylactide from corn starch with an annual capacity of 140,000 t, under the trade name NatureWorks™ PLA. Other examples of commercially available biopolymers are poly[(*R*)-3-hydroxybutyrate] and its copolymer poly[(*R*)-3-hydroxybutyrate-*co*-(*R*)-3-hydroxyvalerate], trade name BIOPOL™, both produced by biofermentation. In 1994, the production of BIOPOL was approximately 1,000 t (ICI−Zeneca).[4] Although these materials from renewable resources have good mechanical and chemical properties, the replacement of fossil fuel based polymers (such as polyethylene and polypropylene) appears to be constrained by the higher price of biodegradable polymers. Another aspect is the existence of operational production facilities and established distribution pathways for conventional polymers, so that a number of companies have again abandoned research on and production of biodegradable polymers.

A more specialized application of biodegradable polymers is in the field of medical technology. As many polyesters and their monomers are nontoxic, they can be used as implants within the body, for example, where a mechanical support of tissue is required. Typical applications are surgical sutures, wound covers (artificial skin), bone-fixation or bone-replacement devices, and carriers for controlled drug release.[5−9] The lifetime in the body depends mainly on the nature of the polymer: While polyglycolide is absorbed within months, polylactide is degraded over years, and the degradation times for poly(3-hydroxybutyrate) are even longer. Fine-tuning of the mechanical properties and of the degradation rate is possible by preparing copolymers, e.g. poly(glycolide-*co*-lactide), PGLA, or poly(3-hydroxybutyrate-*co*-3-valerate), PHBHV. Usually, poly(hydroxycarboxylic acids) are prepared by ring-opening polymerization[10] [Equation (1)] (e.g., polyglycolide, polylactide) or by biotechnological fermentation [(poly(3-hydroxybutyrate)].[4]

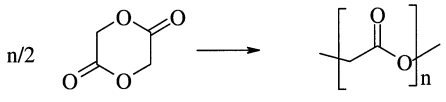

(1)

Solid-State Polymerization Reactions

A considerable number of solid-state polymerization reactions has been reported in the literature. None of them are applied industrially, probably because exothermic solid-state reactions involving potentially flammable compounds (such as organic monomers and polymers) are difficult to scale up, and because of the more heterogeneous nature of the polymeric products. Reactions in the solid state depend on numerous parameters that are not significant in liquid-phase reactions (e.g., crystallinity, polymorphic phase, nucleation, defect structure, particle size). However, solid-state polymerization reactions may give:

- highly crystalline or oriented polymers[11−14]
- special product morphologies[15−18]
- high reaction extents[12,19]
- easily purified products without traces of monomers or catalyst.[11,20]

Table 1 contains a selection of unusual solid-state reactions that are initiated by thermal treatment. Some historical examples of solid-state polymerization reactions date back to the early days of chemistry, even before the concept of a polymer was developed.

The first example (to the best of our knowledge) is the thermally induced polycondensation that occurs in potassium chloroacetate, reported by Hoffmann in 1857.[21] The reaction leads to polyglycolide and potassium chloride as the only products (note that the product was originally postulated to be diglycolide, the cyclic dimer). In Figure 1, the original article from 1857 is shown.

It is interesting that the molecular formulae are different from those used today, because at the time the relative atomic weights of carbon and oxygen were thought to be 6 and 8, respectively. Therefore, potassium chloroacetate was represented as $C_4H_2ClKO_4$ instead of $C_2H_2ClKO_2$. One year later, Kekulé, Hoffmann's mentor, studied the reaction (Figure 2),[22] followed by Heintz in 1862,[23] and Norton and Tcherniak in 1878[24] who studied the reaction of sodium chloroacetate. In 1892, Anschütz studied polyglycolide obtained from such a solid-state reaction.[25,26] By cryoscopic measurements in molten phenol, he determined a molecular weight of approximately 5 to 6 glycolide units ($C_2H_2O_2$) without identifying it as a polymer. Systematic studies were then carried out by Bischoff and Walden in 1894 on sodium chloroacetate and sodium bromoacetate.[27,28] For the first time, a polymer was proposed instead of the dimer that had been suggested before.

In 1906, Emil Fischer observed the reaction of pentaglycylglycine methyl ester after prolonged heating at 100 °C to form an amorphous, water-insoluble, presumably polymeric product.[29,30] Fifty years later, this was corroborated by Sluyterman et al.[31] The product was never clearly identified, but it seems to have been polyglycine. The first oriented polymer from an organic solid-state reaction was prepared by Kohlschütter when he sublimed poly(oxymethylene) and obtained trioxane that contained some highly oriented polymer.[1] Six years later, two different groups independently discovered the solid-state polymerization of acet-

Table 1. A selection of "historical" solid-state polymerization reactions

Reaction	Product	Source (Year)
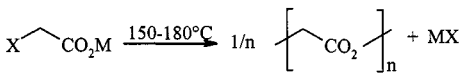	Polyglycolide	Hoffmann (1857[21]), Kekulé (1858[22]), Heintz (1862[23]), Norton and Tcherniak (1878[24]), Anschütz (1892[25,26]), Bischoff and Walden (1893[27,28])
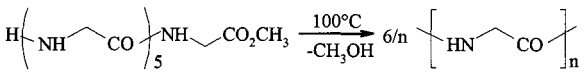	Polyglycine (?)	Fischer (1906[29]) and Sluyterman (1952[31])
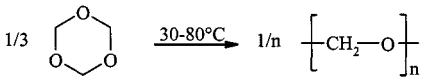	Poly(oxymethylene) (para-formaldehyde)	Kohlschütter (1930[1])
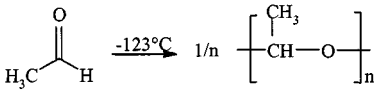	Poly(acetaldehyde)	Travers (1936[32]), Letort (1936[33])
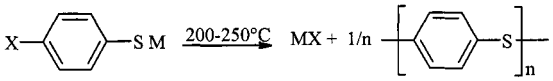 M = Li, Na, K X = F, Cl, Br, I	Poly(p-phenylene Sulfide)	Lenz (1962[11])
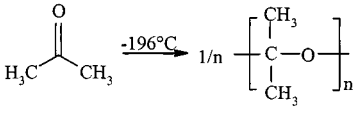	Poly(acetone)	Magat (1962[19])

aldehyde to poly(acetaldehyde), or poly(oxymethylmethylene).[32,33]

In some cases, high-quality polymers can only be obtained by solid-state reactions.[11] An example is the solid-state polymerization of alkali 4-halogenobenzothiolates. If the reaction is carried out in the solid state, a linear polymer results. The polymeric product is poly(4-phenylene sulfide). The eliminated alkali halides can be washed out easily with water. Until 1970, a linear polymer could only be prepared by this route, because the reaction in the melt was accompanied by cross-linking and chain-branching, leading to the formation of an insoluble product. Nowadays, linear poly(4-phenylene sulfide) can also be synthesized by melt polymerization of *p*-dichlorobenzene in the presence of sodium sulfide.[11] Acetone polymerizes only in the solid state due to the low thermal stability of the resulting polymer.[19] The solid-state polymerization of 4-amino-3,5-dihalobenzoyl chlorides to polybenzamides (with concomitant elimination of HCl) was recently shown by Sandor and Foxman. The preparation of this polymer in solution leads only to the formation of low-molecular weight polymers.[34]

Starting in the 1950s and 1960s, attention was mainly focused on radiation-induced solid-state polymerization reactions of unsaturated or cyclic monomers. Prominent examples are diacetylenes, divinyl compounds and acrylic acid derivatives. Details of radiation-induced solid-state polymerization reactions can be found in a number of reviews.[17,19,35−41]

Polyglycolide by Solid-State Reaction

As outlined above, the transformation of solid halogenoacetates to polyglycolide was discovered almost 150 years ago. Since the early studies in the 19th century, only few articles were published on this reaction. Nevertheless, the reaction received industrial interest. The parent compound for ring-opening polymerization, (di)glycolide, can be obtained by the pyrolysis of the (pre)polymer from the solid-state reaction in vacuo. The sublimed dimer is then subjected to ring-opening polymerization according to Equation (1). Little attention was paid to the raw product, and only few papers about this reaction were published until 1996.[42−46] In particular, no mechanistic studies were carried out, and the resulting polymer was not characterized. Essential details of our studies on this system are presented.

Formally, the elimination of metal halide MX from any halogenoacetate $MOOC-CH_2-X$ leads to the formation of polyglycolide (see Table 1). A systematic variation of most combinations of metal and halogen showed that almost all haloacetates undergo the desired reaction. The results are collected in Table 2.[20] Note that fluoroacetates were not included in the study as these compounds (as well as fluoroacetic acid) are highly toxic.

The three lithium salts, sodium iodoacetate and calcium chloroacetate are notable exceptions. The thermoanalytical data for all the compounds are collected in Table 3. It can be seen that the polymerization reaction is associated with a considerable exothermic heat of reaction. The underlying reason is probably the high lattice energy of the formed metal halide. There is a clear trend in the reaction temperatures, which are lowest for the combinations of large metal cations (like Cs^+) and small halogen anions (like Cl^-). Within the rectangle of alkali metals and halogens, the "corner of stability" is in the upper right, and the "corner of reactivity" is in the lower left of Table 3. The lack in

12 *Hoffmann, über Monochloressigsäure.*

Alkali's zu beseitigen, welches etwa erst in einem zweiten Stadium der Zersetzung zur Bildung von Chlormetall hätte Veranlassung geben können, erhielt ich eine wässerige Lösung der neutralen Salze oder auch der Säure selbst während längerer Zeit im Sieden. Die Zersetzung war in allen Fällen dieselbe wie vorher; es bildete sich sogleich Chlormetall und die Lösung wurde sauer, wenn sie vorher neutral gewesen war. Da aber in keinem Fall die Zersetzung vollständig war, erhitzte ich eine Portion des krystallisirten Kaliumsalzes im Luftbad bei allmählig gesteigerter Temperatur. Das Salz blieb unverändert bis etwas über 110°; bei dieser Temperatur verlor es sehr wenig an Gewicht, wurde matt von Ansehen und gelblich und nahm eine saure Reaction an. Durch kaltes Wasser liefs sich Chlorkalium ausziehen und es blieb ein weifses Pulver, welches sauer reagirte und sich in vielem heifsem Wasser auflöste und beim Erkalten wieder herausfiel. — Da ich in keinem der vorher erwähnten Fälle eines von den Producten nachweisen konnte, welche möglicherweise durch Spaltung der Monochloressigsäuren, oder durch eine theilweise Oxydation unter Rückbildung von Essigsäure entstehen könnten, so scheint es mir wahrscheinlich, dafs überhaupt nur Chlormetall austritt und der Rest der organischen Gruppe als ein Ganzes, wahrscheinlich unter Wasseraufnahme, vereinigt bleibt und von neuem eine Säure bildet, welche die Zusammensetzung der Glycocollsäure haben und etwa nach der Formel:

$$C_4H_2ClMO_4 + 2\,HO = C_4H_4O_6 + MCl$$

entstehen könnte. Ich hätte gewünscht, anstatt dieser Hypothese Thatsachen anführen zu können; allein da es mir weder jetzt noch in der nächsten Zeit vergönnt ist, meine Versuche weiter fortzusetzen, so mufs ich es einer späteren Untersuchung überlassen, dieselbe zu bestätigen, oder zu widerlegen.

Figure 1. Facsimile of the original article by R. Hoffmann in *Justus Liebigs Annalen der Chemie*, "Ueber Monochloressigsäure" (On Monochloroacetic Acid) in 1857, the first known example of a solid-state polymerization reaction (see ref.[21])

288 *Kekulé, Bildung von Glycolsäure*

während Wurtz*) bereits gezeigt hat, dafs sie aus dem Glycol durch dieselben Reactionen erhalten werden kann, wie die Essigsäure aus Alkohol.

Monochloressigsaures Kali verhält sich beim Erhitzen genau so, wie es Hoffmann angegeben hat: das weifse lufttrockene Salz wird bei längerem Erhitzen auf 110 bis 120° feucht, färbt sich gelblich und nimmt saure Reaction an. Bei Behandeln mit kaltem Wasser wird viel Chlorkalium und gleichzeitig Glycolsäure ausgezogen, und es bleibt in verhältnifsmäfsig geringer Menge ein weifses Pulver ungelöst, welches in heifsem Wasser etwas löslich ist und beim Erkalten zum Theil wieder ausfällt. Ich habe diefs Pulver immer in relativ geringer Menge und nie von so reinem Aussehen erhalten, dafs ich es der Analyse hätte unterwerfen können; da es indefs bei längerem Kochen mit Wasser zu Glycolsäure wird und beim Kochen mit Kalkwasser glycolsauren Kalk, das am meisten characteristische Salz der Glycolsäure, liefert, so kann kein Zweifel darüber sein, dafs es *Glycolid* ist, dessen Bildung nach dem Schema:

$$C_4H_3ClKO_4 = KCl + C_4H_2O_4$$

erfolgt. Dafs beim Erhitzen des krystallisirten und lufttrockenen monochloressigsauren Kali's nur wenig Glycolid und wesentlich Glycolsäure gebildet wird, erklärt sich daraus, dafs dieses Salz Krystallwasser enthält, welches ihm nicht entzogen werden kann, ohne dafs es selbst Zersetzung erleidet.

Aus der wässerigen Lösung, welche neben Glycolsäure noch viel Chlorkalium enthält, gewinnt man die Säure leicht,

---

*) Diese Annalen CIII, 367; Compt. rend. XLIV, 1306.

Figure 2. Facsimile of the original article by A. Kekulé in *Justus Liebigs Annalen der Chemie* in 1858, "Bildung von Glycolsäure aus Essigsäure" (Formation of Glycolic Acid from Acetic Acid), in which he confirmed Hoffmann's observation (see ref.[22])

reactivity of the lithium salts and sodium iodoacetate corresponds well to this observation: These compounds appear to be have a high thermodynamical stability towards polymerization. After all, this depends on the difference between the free enthalpy of formation of the alkali halide and that of the alkali halogenoacetate, e.g. lithium chloroacetate vs. LiCl. Apparantly, these compounds undergo decomposition before they can polymerize. No thermodynamic data are known, therefore this is merely speculation. We will discuss structural aspects below.

The calcium salt of chloroacetic acid does not show any tendency to form polyglycolide. Hoffmann (1857) also studied barium chloroacetate dihydrate and observed decomposition upon heating.[21] However, no details were given about the decomposition products. Possibly, polymerization did not occur because the divalent cations (Ca and Ba) do not support a topochemical reaction. Note that this cannot be generalized to all solid-state polymerization reactions, as radiation-induced polymerization reactions of salts of acrylic and methacrylic acids were observed for a variety of cations, including alkali metals, alkaline earth metals and zinc (however, this is a different type of reaction).[47–50]

Table 2. Ability of a combination of metal and halogen in different halogenoacetates $MOOC-CH_2-X$ to undergo polymerization; most compounds undergo a thermal elimination of a metal halide to form polyglycolide (see also Table 1); "+" = polymerization, "−" = no polymerization

	Cl	Br	I
Li	−	−	−
Na	+	+	−
K	+	+	+
Rb	+	+	+
Ag	+	+	unstable
Cs	+	+	+
NH_4	(+)	not studied	not studied
$Ca{\cdot}H_2O$	−	not studied	not studied

A molecular solid-state reaction relies on a suitable arrangement of the reactants in the crystal. The peculiarities of such reactions (low temperatures, bulky reactants, small diffusion coefficients) led to the formulation of the "topochemical principle" by Schmidt and co-workers in the 1960s: Solid-state reactions in molecular crystals take place with as little movement of the molecules as possible.[35,51,52] Consequently, knowledge of the crystal structures of all halogenoacetates is a prerequisite to understand the reactivity.

Table 3. Thermochemical data for halogenoacetates that in most cases react to form polyglycolide (values in italics: no polymerization); reaction temperatures are given as onsets and reaction enthalpies in kJ mol^{-1} for the polymerization reaction by DSC with 5 K min^{-1}

	Cl	Br	I
Li	*211 °C/+11.2*[a]	*210 °C/+16.6*[a]	*220 °C/−*[b]
Na	198 °C/−25.2	186 °C/−23.4	*204 °C/−72.0*[b]
K	157 °C/−40.3	171 °C/−36.9	192 °C/−23.5
Rb	120 °C/−42.5	99 °C/−25.4[c]	114 °C/−24.4
Cs	<25 °C/−[d]	35 °C/−26.9[e]	86 °C/−35.7
Ag	134 °C/−64.2	78 °C/−63.9	unstable
NH_4	107 °C/−21.8[e]	not studied	not studied
Ca	*95 °C/+48.3*[g]	not studied	not studied
	198 °C/+15.1[h]		

[a] Endothermic melting of the salt followed by exothermic decomposition. − [b] No melting; exothermic decomposition. − [c] Two peaks at 99 °C and 142 °C. − [d] Polymerization below room temperature. − [e] Partial polymerization below room temperature. − [f] Oligomerization in the melt. − [g] Dehydration of the monohydrate. − [h] Melting of the anhydrous salt.

Unfortunately, the preparation of single crystals suitable for structural analysis is seldom possible for halogenoacetates because they tend to crystallize in the form of thin and disordered platelets or needles. In the literature, only the single-crystal structures of ammonium fluoroacetate[53] and of sodium fluoroacetate[54] are reported. It is unlikely that fluoroacetates undergo a polymerization reaction upon heating, owing to the fact that sodium fluoroacetate decomposes above 200 °C, with concomitant release of HF.

Only the structure of silver chloroacetate could be determined by single-crystal diffraction,[55] whereas the structures of lithium chloroacetate,[56] lithium bromoacetate,[56] lithium iodoacetate,[56] sodium chloroacetate,[57] and sodium bromoacetate[58] had to be solved from powder-diffraction data.

Analysis of the packing in the six known structures shows that the structure is determined by the metal ion rather than by the halide. The three lithium salts are isostructural, and the same is true for sodium chloro- and bromoacetate. Silver chloroacetate crystallizes with a completely different packing. The three structure types are shown in Figure 3.

Silver chloroacetate is discussed first. The structure consists of stacks of silver chloroacetate dimers. There is a short Ag−Cl distance of 2.90 Å that is only slightly longer than in silver chloride, the final reaction product (2.78 Å). We suspect that there is already some kind of interaction in silver chloroacetate. A side-view of the stacks shows that a nucleophilic attack of the carboxy group of a chloroacetate ion at an α-carbon atom is conceivable, a process that would finally lead to the formation of two antiparallel chains of polyglycolide from each stack of silver chloroacetate dimers (see ref.[55] for details). The crystal structure of polyglycolide actually consists of antiparallel chains of polyglycolide (Figure 4).[59] This crystalline phase of polyglycolide was unequivocally identified by X-ray powder diffraction studies.

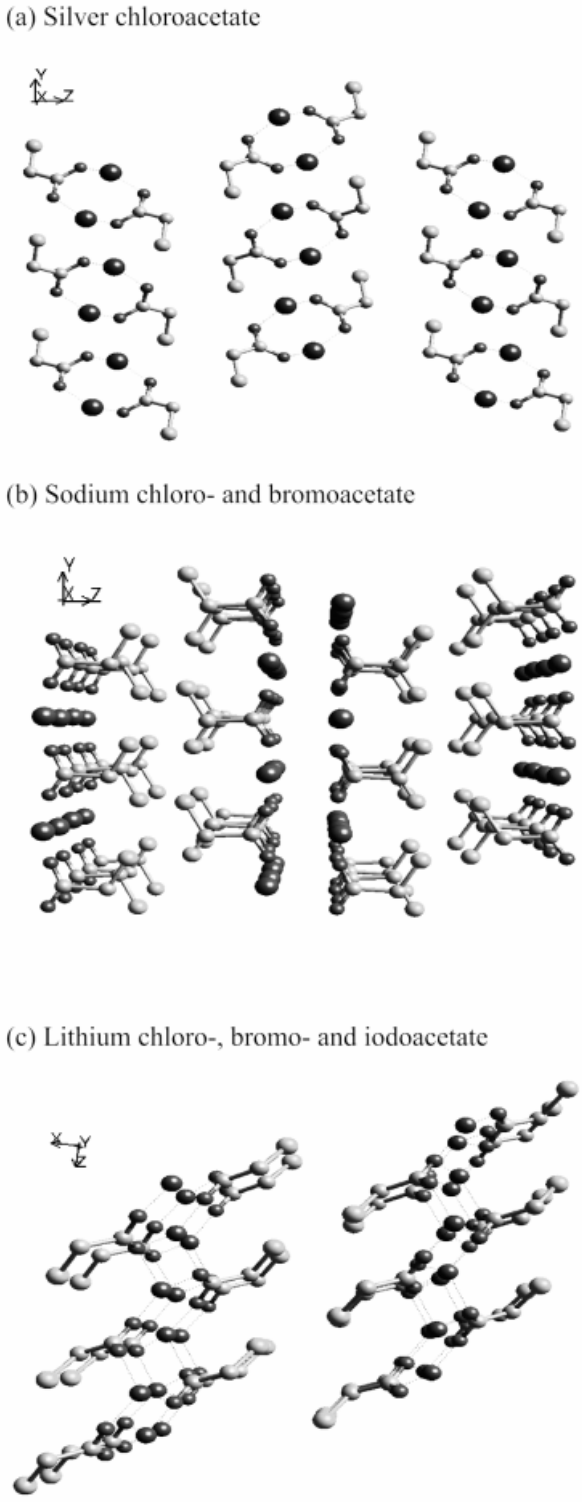

Figure 3. The structure types of silver chloroacetate (a), sodium chloro- and bromoacetate (b), and of lithium chloro-, bromo-, and iodoacetate (c); in cases (a) and (b), solid-state polymerization to form metal halide and polyglycolide is observed, whereas the lithium salts merely decompose

For the sodium salts, the mechanism is less obvious. There is no short distance between the metal and the halogen ions. Layers of metal ions alternate with layers of halogen atoms. However, a polymerization that occurs along

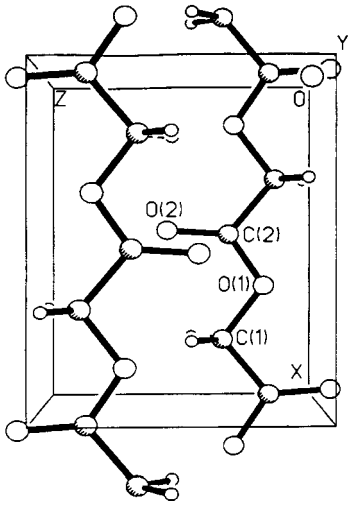

Figure 4. The crystal structure of polyglycolide shows antiparallel chains (see ref.[59])

the crystallographic *b* axis can be postulated (see ref.[57] for details).

The lithium salts do not polymerize. From the crystal structure this can be ascribed to the coordination of lithium by four oxygen atoms from four different carboxy groups. We speculate that the small, strongly polarizing lithium ion keeps the molecules from moving into a suitable orientation for polymerization (see ref.[56] for a detailed discussion).

Even when a topochemical mechanism can be postulated by inspection of the crystal structure, little is actually known about the way the molecules react:

- whether the reaction occurs in a single step,
- whether the crystal structure is preserved, and
- how two solid phases (salt and polyester) are formed from a single phase.

To acquire such information, it is necessary to follow the course of the reaction by suitable in-situ and ex-situ techniques that probe specific sample properties. The in-situ techniques are preferable as they yield more direct information.

The polycondensation reactions of halogenoacetates have been studied with a variety of techniques, each probing different structural features of the reaction. The results are summarized in Table 4. We now have a very detailed insight into this reaction and can therefore formulate a reaction mechanism as depicted in Figure 5.

This reaction can be considered as very well studied. Fortunately, the nature of the reaction makes it susceptible to techniques developed for inorganic solids, organic solids, and polymers and hence most available techniques to obtain structural information in situ have been applied. However, it is still clear that there is a line that we cannot cross, even with the most sophisticated techniques available today.

This is the question of how the actual processes occur on a molecular or on an atomic scale. All techniques probe *integral* sample properties. This does not give information about the changes going on in the actual reaction zone, i.e. the very thin layer between the parent compound and the product. The fraction of molecules that actually react is small at any given time, therefore we see mainly the parent compound and the reaction products, but not necessarily the small amount of transient molecules. We can only try to deduce this microscopic information from the integral parameters that we can measure. The same holds for deductions about the reaction pathway from the crystal structure.

For example, even if the structure of silver chloroacetate supports a topochemical polymerization mechanism, this is no proof but only a hint that the reaction actually follows this pathway. Also, the question as to how metal ions and halogen ions find themselves to form the salt lattice is still completely unresolved. In conclusion, it must be said that there are no experimental techniques available at the moment to answer these questions. Theoretical computations may be the only possible means to tackle such problems.

Finally, it should be mentioned that solvate crystals of halogenoacetates with halogenoacetic acid also undergo a solid-state polymerization. In these cases, an endothermic peak occurs in DSC, followed by an exothermic event. The endothermic event is associated with the release of halogenoacetic acid from the solvate crystal, and its sublimation or boiling. After this, the pure salt recrystallizes and begins to polymerize. This was demonstrated by in-situ EXAFS measurements of rubidium bromoacetate/bromoacetic acid[60] and by time- and temperature-resolved XRD measurements of potassium chloroacetate/chloroacetic acid. Table 5 shows the results collected from the literature.

Poly(hydroxypropionates) by Solid-State Reaction

At least on paper, the polycondensation of haloacetates can be transposed to all salts of halogenocarboxylic acids. The question is whether the actual chemical pathway of such a system lives up to this expectation.

The next higher homologues of halogenoacetates are 2-halogenopropionic acids and 3-halogenopropionic acids. In the first case, we expect poly(2-hydroxypropionic acid), that is, polylactic acid (or polylactide), a polymer with a stereogenic carbon atom. In the second case, the product would be the achiral poly(3-hydroxypropionic acid).

Polylactide was first prepared in 1845 by Pelouze, who heated lactic acid.[61] The known examples of polycondensation reactions of halogenopropionates are collected in Table 6, together with data on similar polycondensation reactions.

In 1894, Bischoff and Walden reported the formation of polyglycolide from sodium chloro- and bromoacetate. They extended their studies to sodium 2-bromopropionate, but obtained no polyester; the only product found was (di)lactide, which sublimed from the reaction mixture. This was probably due to the conditions of the experiments, as the salt was subjected to a temperature of more than 200 °C in vacuo. Under these conditions, pyrolysis of the formed polyester to lactide becomes dominant, and the intermediate product cannot be isolated from the reaction vessel. Furthermore, they did not analyze the solid residue.[62]

Table 4. Collection of facts about the solid-state polycondensation in halogenoacetates; note that side-products were not found with any technique; polyglycolide and the metal halide are the only products

Technique	in-situ?	Property probed	Compound	Results
DSC	yes	enthalpy change	all halogenoacetates	exothermic polymerization reaction (see ref.[18,20,74])
TG-DTA-MS	yes	volatile reaction products	all halogenoacetates	no mass loss during polymerization; at higher temperature, combustion of the formed polyglycolide (see ref.[20,74])
X-ray diffraction (XRD)	yes	crystalline phases	sodium chloroacetate	no detectable crystalline intermediates (see ref.[20])
EXAFS	no	short-range order (Cl) in all phases	sodium chloroacetate	no detectable intermediate containing chlorine (see ref.[74])
EXAFS	yes	short-range order (Br, Rb in all phases	rubidium bromoacetate/ bromoacetic acid	desolvation is followed by polymerization (see ref.[60])
EXAFS-XRD	yes	short-range order (Br) in all phases; crystalline phases	sodium bromoacetate	no detectable intermediates that either contain bromine or are crystalline;coalescence of small NaBr crystals to larger ones during annealing ("Ostwald ripening") (see ref.[79])
EXAFS-DSC	yes	short-range order (Br) in all phases; enthalpy changes	sodium bromoacetate	no detectable intermediates that contain bromine; the reaction enthalpy is proportional to the reaction extent (see ref.[76])
Small- and wide-angle X-ray scattering (SAXS-WAXS)	yes	structural order on different length scales	sodium chloroacetate	no detectable intermediates on all length scales; formation of short-range order in polyglycolide precedes formation of long-range order (long period of amorphous and crystalline domains) (see ref.[80])
Solid-state NMR (^{13}C)	yes	chemical environment of carbon	sodium bromoacetate	no detectable intermediates containing carbon (see ref.[58])
Solid-state NMR (^{23}Na)	yes	chemical environment of sodium	sodium chloroacetate; sodium bromoacetate	no detectable intermediates containing sodium (see ref.[58])
IR	yes	chemical bonds in all phases	sodium chloroacetate	no detectable intermediates (see ref.[75])
Scanning electron microscopy	no	morphologic changes	sodium chloroacetate	phase separation into a polymeric matrix containing microcrystals of NaCl (see ref.[74])
Mercury porosimetry	no	morphologic changes in the formed polyglycolide/NaCl	sodium chloroacetate	the NaCl microcrystals increase in diameter with increasing reaction extent (see ref.[73])
Viscosimetry	no	chain length of polyglycolide	sodium chloroacetate	the degree of polymerization increases with increasing reaction extent (polycondensation) (see ref.[73])
Thermomicroscopy	yes	morphologic changes	sodium chloroacetate; silver chloroacetate	the reaction starts from defects in the crystal or from the surface; the single-crystalline order is not preserved (see ref.[73])

In an explorative study, we showed that sodium 2-chloropropionate indeed gives polylactide if the reaction temperature is 160 °C.[63] Two fractions with degrees of polymerization of 520 and 11, respectively, were detected by GPC. This corroborates the interpretation of the results of Bischoff and Walden that the polylactide formed previously was pyrolyzed during the reaction, leading to volatile lactide.

We found that the corresponding isomer, sodium 3-chloropropionate, gives a mixture of different products upon heating.[63] Oligomers of the desired polymer were formed (weight-average molecular weight of 420 g mol^{-1}), but the main competitive reaction is the intramolecular elimination of NaCl, resulting in the formation of acrylic acid [Equation (2)].

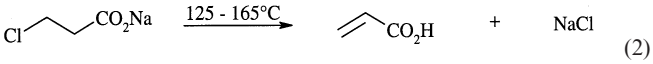

(2)

This unwanted reaction is probably favored at higher temperatures due to the higher gain in entropy relative to polymerization. It also precludes the preparation of the precursor salt by simple neutralization of the acid by NaOH or Na_2CO_3 at room temperature, because elimination occurs readily. Sodium 3-chloropropionate had to be prepared by neutralization at −50 °C, whereas sodium 2-chloropropionate can easily be prepared at room temperature.

Poly(hydroxybutyrates) by Solid-State Reaction

Bischoff and Walden found the cyclic dimer and crotonic acid upon heating sodium 2-bromo-n-butyrate.[62] In contradiction to these results, Naruchi et al. obtained the corresponding polyester and oligomers from the alkaline and alkaline earth metal salts of 2-bromo-*n*-butyric acid.[64] The potassium and sodium salts gave polymeric products with number-average molecular weights between 1000 and 4000, and polydispersities close to 1.4. The alkaline earth and the lithium salts yielded only oligomers. The authors concluded that the crystallinity of the precursors played a decisive role because the salts of Na and K had a good crystallinity, whereas the Li, Mg, Ca, Sr, and Ba salts were of poor crystallinity, or even amorphous. We found oligomers with a degree of polymerization of 4 after heating sodium 2-chlorobutyrate at 160 °C for 30 min.[63]

Sodium 2-bromoisobutyrate starts to decompose at 30 °C, according to Bischoff and Walden. Sodium bromide was eliminated but the main product was methacrylic acid, which partially polymerized to form poly(methacrylic acid). Due to water incorporated in the crystal (they used the

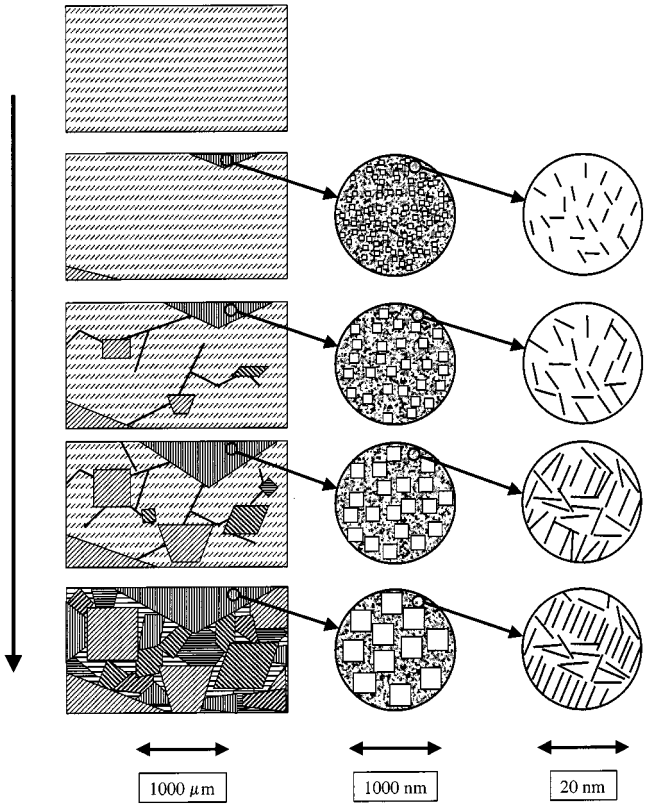

Figure 5. Schematic view of the solid-state polycondensation reaction of sodium chloroacetate to form polyglycolide and NaCl, viewed on different length scales; the following processes occur: 1. nuclei of reaction products form at the surface or at defects (left); 2. the new phase (polyglycolide and NaCl) grows within the halogenoacetate crystal; the local structure is damaged by a change in molar volume, thereby accelerating the reaction (left); 3. together with the phase separation, this leads to complete destruction of the single-crystalline order (left); 4. cubic NaCl crystals keep growing during the reaction within a matrix of polyglycolide (center); 5. after the reaction is complete, Ostwald ripening of the NaCl crystals occurs; larger crystals grow by consuming smaller ones (center); 6. the polyglycolide chains increase in length during the polycondensation reaction (right); 7. after larger amounts of polyglycolide have formed, ordering within the polymer phase into amorphous and crystalline domains occurs (right)

Table 5. Known solvate crystals of halogenoacetates of the type *n* halogenoacetate/*m* halogenoacetic acid; given are the molar ratios *n*:*m*/the temperature of the endothermic decomposition of the solvate/the temperature of the exothermic polymerization of the remaining halogenoacetate

	Cl	Br
K	1:1/142/150[a] 1:1/142/163[c]	2:1/123/130[b]
Rb	1:1/89,131/135[c][d] 1:2/98/135[c]	1:1/119/125[e]
Cs	1:1/108/135[c] 3:5/84/127[c]	

[a] By DSC (5 K min^{-1}, onset temperature). – [b] By DSC (5 K min^{-1}, onset temperature, see also ref.[18] – [c] By DTA (3.2 K min^{-1}, peak maximum temperature, see also ref.[45]). – [d] Two endothermic signals are detected before the exothermic event. – [e] By DSC (5 K min^{-1}, onset temperature, see ref.[60]).

Table 6. Reactivity and resulting polyesters from simple aliphatic carboxylic acids; M = alkali, X = halogen

Precursor	Polymer (T_{fus})	Remarks
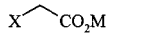 Halogenoacetates	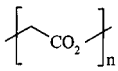 Polyglycolide (220-233°C)	reacts quantitatively in the solid state[20]
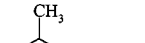 2-Halogenopropionates	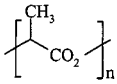 Polylactide (PLA; ~80°C)	dilactide (Na/Br; vacuum at 200°C)[62]; Polylactide (Na/Cl; 160°C)[63];
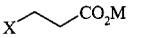 3-Halogenopropionates	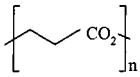 Poly(3-hydroxypropionate) (~90°C)	oligomers, acrylic acid, 3-hydroxypropionic acid (Na/Cl; 120°C)[63]
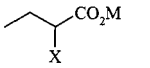 M= alkali ions 2-Halogenobutyrates	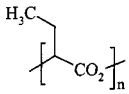 Poly(2-hydroxybutyric acid)	cyclic dimer, crotonic acid (Na/Br; 200-270°C)[62]; oligomers (Na/Cl; 160°)[63]; polymer (Na/Br and K/Br; 110-150°C)[64]; oligomers (Li/Br)[64]
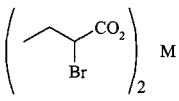 M= alkaline earth ions 2-Halogenobutyrates	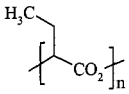 Poly(2-hydroxybutyric acid)	oligomers (Mg, Ca, Sr, Ba/Br; 110-150°C) [64]
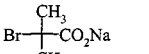 Sodium 2,2,2-bromodimethylacetate	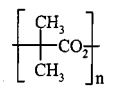 Poly(dimethyl glycolide)	Methacrylic acid, poly(methacrylic acid (Na/Br; 30-130°C)[62]; poly(dimethyl glycolide) (Na/Br; 90-180°C)[66]

hemihydrate), 2-hydroxyisobutyric acid was also formed during the reaction.[62] However, Bezzi reported that he obtained poly(dimethyl glycolide) from sodium 2-bromoisobutyrate by heating the salt up to 90 °C,[65] 160 °C, or 180 °C.[66]

The most important poly(hydroxybutyrate) is P-3HB, as outlined above. Unfortunately, it is very difficult to prepare the corresponding precursor, sodium 3-chlorobutyrate, as elimination prevails even at low temperature. The same is true for sodium 4-chlorobutyrate. Therefore, there is no information available yet as to whether these polyesters can be obtained by solid-state polymerization.

Poly(hydroxymethylbenzoates) by Solid-State Reaction

All previous listed reactions gave aliphatic polyesters. As mentioned in the introduction, linear polyesters with aromatic groups in their backbone are of special interest for industrial applications. The simplest halogenocarboxylic acids containing the benzene ring are halogenobenzoic acids. If the salts of halogenobenzoic acids were to undergo a polymerization reaction in which poly(hydroxybenzoic

acid) were to be formed, a nucleophilic substitution on an aromatic ring system would be necessary (the chlorine atom acts as the leaving group). Therefore, strong nucleophiles or electron-withdrawing groups at the *ortho* or *para* position would be needed. The carboxylate group is an electron-donating substituent and its nucleophilicity is not very strong, thus substitution at the benzene ring appears to be unlikely. However, the polymerization of alkali *p*-halothiophenolates is possible,[11] but admittedly the thiophenoxide ion is a stronger nucleophile than the carboxylate anion. Anyway, the conditions may change in the solid state. For this reason, we prepared the alkali salts of 4-chlorobenzoic acid. No reaction was observed and decomposition took place at temperatures above 400 °C.

Introducing a benzene ring between the carbon−carbon bond in acetates leads to the formation of halogenomethylbenzoates (Table 7). Only the *meta*- and *para*-substituted compounds could be prepared, because the *ortho* compounds tend to form benzolactones by intramolecular substitution. The sodium, potassium and rubidium salts of 3- and 4-chloromethyl- and -bromomethylbenzoic acid undergo the desired polymerization to form poly(hydroxymethylbenzoic acid).[67] The lithium salts of the *para* compounds decompose at temperatures near 300 °C, without the formation of a polymeric product. This can be understood when analyzing the crystal structures of lithium 4-chloro- and 4-bromomethylbenzoate that were solved from powder-diffraction data.[68] They have a strong similarity to the corresponding acetates with the phenyl rings acting as "spacers". Lithium is tetrahedrally coordinated by four different oxygen atoms from four different carboxy groups, a fact that probably prevents polymerization. All attempts to solve the structures of the corresponding sodium or potassium compounds (that polymerize) failed, probably due to the presence of polymorphism, as suggested by solid-state NMR spectroscopy.[68]

For the *para*-halomethylbenzoates, the oxidation of the methylene group in the polyester as a side-reaction was found by IR spectroscopy. This reaction led to the formation of terephthalic acid as side product, via the carboxylic anhydride intermediate, even in the presence of small amounts of oxygen and water.

Table 7. Successful polymerization in other halocarboxylates; M = alkali, X = halogen

Precursor	Polymer (T_{fus})	Remarks
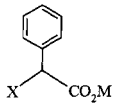 *rac*-2,2-Halogenophenylacetates	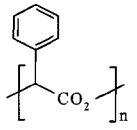 *rac*-Polymandelide (~80°C)	Unidentified solid product (Na/Cl; 117°C)[62]; polymandelide (Me_3Sb/Br; $SnMe_3$/Br; 170°C)[70]; polymandelide (Na, K/Cl, Br; 70-170°C) (this work)
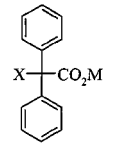 2,2,2-Halogenodiphenylacetates	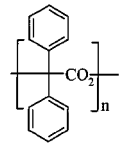 Poly(diphenylglycolide)	(Na/Cl; 90-180°C)[66]; poly(diphenylglycolide) ($SnMe_3$/Br; 25°C)[70]
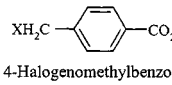 4-Halogenomethylbenzoates	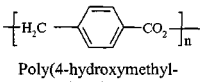 Poly(4-hydroxymethylbenzoic acid) (~250)	reacts in the solid state (Na,K,Rb/Cl,Br; 200-250°C)[68]
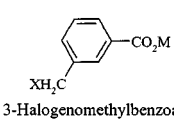 3-Halogenomethylbenzoates	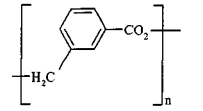 Poly(3-hydroxymethylbenzoic acid) (~150)	reacts in the solid state (Na,K/Cl,Br; 100-160°C)[68]

Table 8. Unsuccessful attempts to induce polymerization in halogenocarboxylates; M = alkali, X = halogen

Precursor	Reaction	Remarks
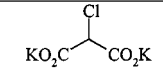 Potassium chloromalonate	no polymerization	decarboxylation at 115°C[71]
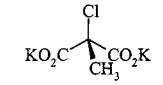 Potassium chloromethylmalonate	no polymerization	decarboxylation at 200°C[71]
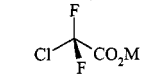 Chlorodifluoroacetates	no polymerization	decomposition above 160°C
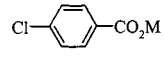 4-Chlorobenzoates	no polymerization	decomposition above 400°C

Other Polyesters by Solid-State Reaction

Besides these major classes of potential precursors to polyesters, other miscellaneous substances were investigated, sometimes with success, and sometimes without. The results can be found in Table 7 and Table 8.

When Bischoff and Walden tried to distill sodium 2,2-chlorophenyl acetate, they obtained a yellowish oil and a solid residue that melted at 117 °C. Further characterization was not carried out. The oil was not identified, and the residue was presumed to be stilbene.[69] Our recent studies on alkali 2,2-halogenophenylacetates showed that poly(mandelide) can be formed by thermal elimination of alkali halides. Similar to the halogenoacetates, the lithium salts do not polymerize, but decompose upon heating. We found a degree of polymerization (obtained by ^{1}H NMR spectroscopic end-group analysis) ranging from 5 to very high numbers for sodium and potassium salts.

The first announcement of a polymeric product from 2,2-bromophenylacetates was in 1973. Okada and Okawara pyrolyzed the trimethyltin salt of the 2,2-bromophenylacetic acid and obtained poly(mandelide).[70] They also reported that the trimethyltin bromodiphenylacetate reacted in the same way. Bezzi reported the synthesis of poly(diphenylglycolide) from sodium chlorodiphenylacetate under the same conditions as for the poly(dimethylglycolide).[65]

Potassium chloromalonate and 2,2-chloromethylmalonate did not give any polymer or oligomer.[71] Instead of a polymeric product from the elimination, carbon dioxide was released in both cases at 115 °C and 200 °C. The mass loss during the reaction of potassium chloromalonate was in good agreement with the value calculated for the loss of one molecule of carbon dioxide per chloromalonate. Potassium chloride and an unidentified organic substance remained. Besides potassium chloride, the organic residue after the elimination reaction of the methylmalonate was identified as potassium acrylate.[71] The synthesis of the alkali salts of 4-bromo-2,2-diphenylbutyric acid was not successful at ambient temperature. It led to the conjugated lactone by intramolecular substitution of the bromo group by the carboxylate group.[72]

No polymerization is possible if further halogen atoms are inserted in the acetates as it is the case in di- and trichloroacetates, or in chlorodifluoroacetates. The additional halogen atoms apparently destabilize the carbon−carbon bond, resulting in bond cleavage if they are heated.

Comparison of Polyesters from Solid-State Reaction and from Conventional Synthesis

If we summarize the preceding paragraphs, we can state that a considerable number of polyesters can be obtained from solid precursors. It remains to be discussed whether or not the obtained polymers are identical to those available from conventional synthesis.

With respect to structural or spectroscopic properties, the polyesters from solid-state reactions are often almost indistinguishable from those obtained in a classical way. The main difference is the degree of polymerization. It seems that polymers from solid-state reactions have a smaller degree of polymerization, i.e. a lower molecular weight. This property was not reported in all examples, but we can demonstrate it for polyglycolide, in which we extensively studied the properties of the polymer.[73]

Polylactide and polyglycolide from ring-opening polymerization with tin catalyst can reach molecular weights of more than 100,000 Da, representing more than 1000 monomeric units in the polymeric chain. As mentioned above, the degree of polymerization reported in the literature for solid-state chemically prepared polyglycolide is not very high. A number-average molecular weight of about 300 Da was determined by Anschütz.[26]

Detailed studies on the solid-state polycondensation reactions of sodium chloroacetate were carried out, with special attention being paid to the polymerization mechanism, and to the development of polymeric properties.[18,56−58,60,73−76] For polyglycolide, we showed that the average chain length (by viscosimetry) passes a maximum of approximately 40 monomeric units before the reaction extent reaches 1.[73] After the maximum, the chain length decreases again. This can be explained by a counterplay between the polycondensation reaction (increasing the chain length) and the thermal degradation of the formed polyglycolide. Degradation plays a minor role, as long as only few and short polymer chains are present. With increasing chain length and with a higher number of ester groups that can be cleaved, the degradation becomes dominant while the chain growth loses importance.

As in most other studies, the conditions were not optimized and in most cases a long reaction time and a high temperature were chosen to ensure that the reaction was complete. Consequently, the polyglycolide from solid-state reaction was obtained with a low molecular weight, due to thermal degradation. It may be inferred that the degree of polymerization for other polyesters from solid-state reactions could also be increased by careful choice of the reaction temperature.

If we take into account the fact that the reaction of haloacetates with polyglycolide occurs in the solid state in a topochemical way, the crystal perfection should have a strong influence on the chain length of the polymer. We speculate that in larger, perfect crystals, the chains could grow longer than in small, disordered crystals in which a defect (such as a dislocation) would lead to chain scission. This statement may be limited by the fact that the single-crystalline order is destroyed during the reaction, probably due to volume change, but nevertheless it remains an interesting assumption.[77] However, this has not been investigated so far for any solid-state polycondensation reaction.

A special feature of polyesters from solid-state reactions is their distinct micromorphology. Generally, a nonvolatile salt is eliminated, and thus the reaction must lead to an intimate mixture of polymer and salt. The geometry of both phases is determined by nucleation and diffusion. In the cases that we have studied (polyglycolide, polylactide, poly(hydroxymethylbenzoic acid)], we have always found micrometer-sized salt crystals within the polymeric matrix. These can be conveniently removed by washing the polymer with water, leaving behind a polymer with micrometer-sized pores.[18,67,78]

The dependence of the pore size on the precursor was studied for polyglycolide. Figure 6 summarizes scanning-electron micrographs of polyglycolide from various halogenoacetates. There are considerable differences in the product morphology. Their origin is not known, but it is clear that the size of the pores (identical to the size of the precipitated salt crystals) depends on the kind of salt that is eliminated. However, it must be noted that different polyglycolides were obtained at different reaction temperatures for each precursor. The highly porous structure of polyglycolide may be advantageous for biomedical applications. Less material has to be absorbed by the body, and a free flow of body fluids is possible through such a highly porous implant. We recently demonstrated the excellent biocompatibility of composite implants of both porous and compact polyglycolide with calcium phosphate.[9]

Do These Reactions Really Occur in the Solid State?

All reactions that yield a polymer are initiated in the solid state, i.e. before the melting of the substance is observed. In

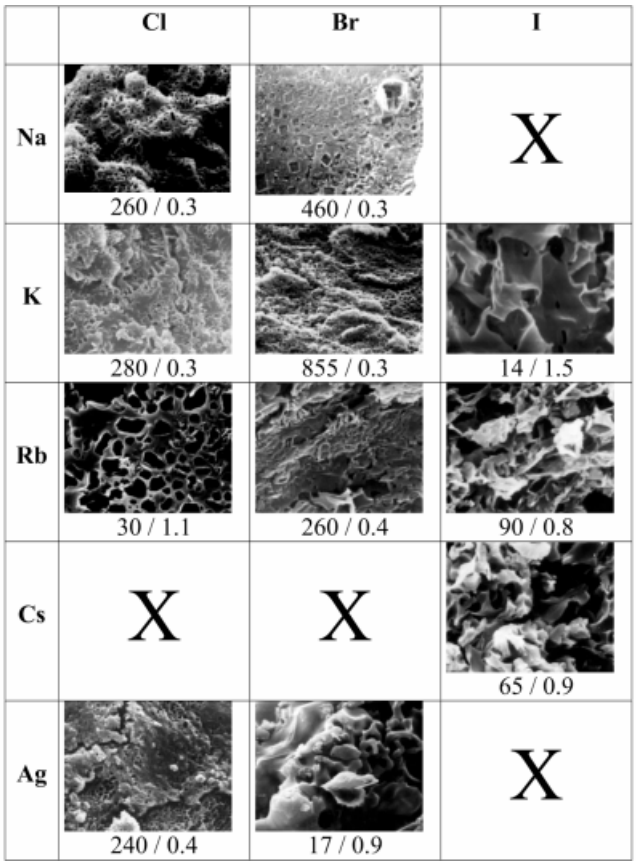

Figure 6. Polyglycolide from the solid-state reaction of various precursors; the polymers were washed out with water (in the case of silver salts, with sodium thiosulfate solution), to obtain the porous polymer; the magnification is 4020× in all cases, and the printed section is approximately 12.5 × 9.5 μm^2; the table illustrates how the different pore-size distribution is dependent on the precursor; X means that the polymer could not obtained in a pure form by solid-state polymerization reaction; the two numbers for each polymer give the number of pores per 100 μm^2, and the average pore size in μm (computed by analysis of larger areas than shown here)

the case of a reaction temperature being higher than the melting point of the corresponding polyester (such as polylactide), the reaction mixture will liquefy with increasing conversion. On the other hand, if the reaction temperature is lower than the melting point of the polyester, a true solid-state reaction is possible (as is the case with polyglycolide). Both cases have been observed. In general, it is rather difficult to unequivocally prove that no liquid intermediates are present. It has been shown for polyglycolide formed from halogenoacetates (see above), but in most other cases there might be temporary liquefaction, followed by recrystallization.

Nevertheless, systems with high-melting polymers can also liquefy locally during the reaction owing to poor heat conduction in powders and subsequent self-heating of the mixture. Polyakov et al. showed that for sodium chloroacetate, a high-temperature gradient appeared inside the reaction vessel between the center of the reactor and the wall. The heat difference reached up to 100 K, depending on the reactor diameter and on the external temperature. This self-heating caused the sample to melt, and in extreme cases the polyester was pyrolyzed.[46] In order to prevent this, it is possible to choose other reactor types with better heat conductance, such as fluid-bed reactors, or to add inert materials such as copper turnings to obtain a better conduction.

Conclusion

Many polyesters can be prepared without solvent. Unfortunately, the reaction pathway theoretically formulated beforehand is not always actually feasible. This is due to the peculiarities of solid-state reactions in which the crystal structure and intracrystalline interactions play a dominant role. This is a major difference from chemistry in solution, where the concept of functional groups is of decisive influence. In addition, thermodynamic data are usually not available and hence proposed reactions have to be tried out, and cannot be predicted.

Side-reactions that lead to different reaction pathways may occur. Possible side-reactions are:

- hydrolysis of the halogen group in the presence of moisture
- elimination of HX leading to the formation of unsaturated carboxylic acids
- decarboxylation
- cyclization to form lactones
- oxidation of the organic residue

However, the new properties of the resulting polymers (such as the porous micromorphology) may lead to applications in special cases. In any case, this is a fascinating field of research where expertise from solid-state chemistry, organic chemistry, physical chemistry and polymer chemistry can be combined to draw conclusions about the underlying processes.

Acknowledgments

We thank the Deutsche Forschungsgemeinschaft and the Fonds der Chemischen Industrie for generous support during the preparation of this work. We also thank our collaborators who performed many of the reported experiments, their names are given in the citations.

[1] H. W. Kohlschütter, *Justus Liebigs Ann. Chem.* **1930**, *482*, 75−104.
[2] W. H. Carothers, G. L. Dorough, F. J. van Natta, *J. Am. Chem. Soc.* **1932**, *54*, 761−772.
[3] E. Chiellini, R. Solaro, *Adv. Mater.* **1996**, *8*, 305−313.
[4] D. Seebach, A. Brunner, B. M. Bachmann, T. Hoffmann, F. N. M. Kühnle, U. D. Lengweiler, *Biopolymers and -oligomers of (R-3-hydroxyalkanoic acids − contributions of synthetic organic chemists*, vol. 28, Ernst Schering Research Foundation, Berlin, **1995**.
[5] A. G. Mikos, A. J. Thorsen, L. A. Czerwonka, Y. Bao, R. Langer, D. N. Winslow, J. P. Vacanti, *Polymer* **1994**, *35*, 1068−1077.
[6] M. Vert, G. Schwarch, J. Coudane, *J. Macromol. Sci. Pure Appl. Chem.* **1995**, *A32*, 787−796.
[7] J. O. Hollinger, K. Leong, *Biomaterials* **1996**, *17*, 187−194.
[8] N. Ashammakhi, P. Rokkanen, *Biomaterials* **1997**, *18*, 3−9.
[9] W. Linhart, F. Peters, W. Lehmann, A. F. Schilling, K. Schwarz, M. Amling, J. M. Rueger, M. Epple, *J. Biomed. Mater. Res.* **2001**, *54*, 162−171.

[10] H. R. Kricheldorf, *Handbook of polymer synthesis*, Marcel Dekker, New York, **1992**.
[11] R. W. Lenz, C. E. Handlovits, H. A. Smith, *J. Polym. Sci.* **1962**, *58*, 351−367.
[12] S. Okamura, K. Hayashi, Y. Kitanishi, *J. Polym. Sci.* **1962**, *58*, 925−953.
[13] G. Wegner, *Z. Naturforsch.* **1969**, *24b*, 824.
[14] R. H. Baugham, *J. Polym. Sci. Polym. Phys. Ed.* **1974**, *12*, 1511−1535.
[15] Y. Tabata, *Adv. Macromol. Chem.* **1968**, *1*, 283−333.
[16] G. Wegner, A. Munoz-Escalona, E. W. Fischer, *Ber. Bunsenges. Phys. Chem.* **1970**, *74*, 909−912.
[17] G. Wegner, *Pure Appl. Chem.* **1977**, *49*, 443−454.
[18] M. Epple, O. Herzberg, *J. Mater. Chem.* **1997**, *7*, 1037−1042.
[19] M. Magat, *Polymer* **1962**, *3*, 449−469.
[20] M. Epple, H. Kirschnick, *Chem. Ber.* **1996**, *129*, 1123−1129.
[21] R. Hoffmann, *Justus Liebigs Ann. Chem.* **1857**, *102*, 1−20.
[22] A. Kekulé, *Justus Liebigs Ann. Chem.* **1858**, *105*, 288−292.
[23] W. Heintz, *Poggendorffs Ann. Chem. Phys.* **1862**, *115*, 452−465.
[24] J. H. Norton, J. Tcherniak, *C. R. Acad. Sci. Paris* **1878**, *86*, 1332−1335.
[25] R. Anschütz, *Ber. Dtsch. Chem. Ges.* **1892**, *25*, 3506−3512.
[26] R. Anschütz, G. Schroeter, *Justus Liebigs Ann. Chem.* **1893**, *273*, 97−101.
[27] C. A. Bischoff, P. Walden, *Ber. Dtsch. Chem. Ges.* **1893**, *26*, 262−265.
[28] C. A. Bischoff, P. Walden, *Justus Liebigs Ann. Chem.* **1894**, *279*, 45−70.
[29] E. Fischer, *Ber. Dtsch. Chem. Ges.* **1906**, *39*, 453−474.
[30] H. Morawetz, "Thermal reactions of organic solids" in *Physics and chemistry of the organic solid state* (Eds.: D. Fox, M. M. Labes, A. Weissberger), vol. 1, Interscience, New York **1963**, p. 287−328.
[31] L. A. A. Sluyterman, M. Kooistra, *Recl. Trav. Chim. Pays-Bas* **1952**, *71*, 277−284.
[32] W. M. Travers, *J. Chem. Soc., Faraday Trans.* **1936**, *32*, 246−250.
[33] M. Letort, *C. R. Acad. Sci. Paris* **1936**, *202*, 767−768.
[34] R. B. Sandor, B. M. Foxman, *Tetrahedron* **2000**, *56*, 6805−6812.
[35] G. M. J. Schmidt, *Pure Appl. Chem.* **1971**, *27*, 647−678.
[36] J. M. Thomas, *Pure Appl. Chem.* **1979**, *51*, 1065−1082.
[37] M. D. Cohen, *Angew. Chem.* **1975**, *87*, 439−447; *Angew. Chem. Int. Ed. Engl.* **1975**, *14*, 386.
[38] A. Gavezzotti, M. Simonetta, *Chem. Rev.* **1982**, *82*, 1−13.
[39] M. Hasegawa, *Chem. Rev.* **1983**, *83*, 507−518.
[40] V. Enkelmann, *Adv. Polym. Sci.* **1984**, *63*, 91−136.
[41] J. D. Jaufmann, C. B. Case, R. B. Sandor, B. M. Foxman, *J. Solid State Chem.* **2000**, *152*, 99−104.
[42] A. Sporzynski, W. Kocay, H. V. A. Briscoe, *Recl. Trav. Chim. Pays-Bas* **1949**, *68*, 613−619.
[43] F. Andreas, R. Sowada, J. Scholz, *J. Prakt. Chemie* **1962**, *18*, 141−149.
[44] J. Pokorny, *Sb. Vys. Sk. Chem.-Technol. Praze, B: Anorg. Chem. Technol.* **1972**, *B14*, 127−152.
[45] J. Pokorny, *Sb. Vys. Sk. Chem.-Technol. Praze, B: Anorg. Chem. Technol.* **1972**, *B14*, 153−166.
[46] D. K. Polyakov, I. A. Tschebotapeva, W. I. Selichova, J. A. Zhubov, *Vysokomol. Soedin., Seriya A* **1998**, *40*, 1925−1931.
[47] H. Morawetz, I. D. Rubin, *J. Polym. Sci.* **1962**, *57*, 669−685.
[48] J. B. Lando, H. Morawetz, *J. Polym. Sci. C* **1966**, *4*, 789−803.
[49] K. Naruchi, S. Tanaka, M. Higuma, M. Yamamoto, K. Yamada, *Polymer* **1982**, *23*, 152−154.
[50] M. Kudoh, F. Akutsu, E. Nakaishi, T. Tobayashi, K. Naruchi, M. Miura, *Macromol. Rapid Commun.* **1994**, *15*, 239−242.
[51] G. M. J. Schmidt, M. D. Cohen, *J. Chem. Soc.* **1964**, 1996−2000.
[52] M. D. Cohen, B. S. Green, *Chem. Br.* **1973**, *9*, 490−497, 517.
[53] K. T. Wei, D. L. Ward, *Acta Crystallogr.* **1976**, *B32*, 2768.
[54] B. M. Vedavathi, K. Vuayan, *Acta Crystallogr.* **1977**, *B33*, 946−948.
[55] M. Epple, H. Kirschnick, *Chem. Ber.* **1997**, *130*, 291−294.
[56] H. Ehrenberg, B. Hasse, K. Schwarz, M. Epple, *Acta Crystallogr. B* **1999**, *55*, 517−524.
[57] L. Elizabé, B. M. Kariuki, K. D. M. Harris, M. Tremayne, M. Epple, J. M. Thomas, *J. Phys. Chem. B* **1997**, *101*, 8827−8831.
[58] A. E. Aliev, L. Elizabé, B. M. Kariuki, H. Kirschnick, J. M. Thomas, M. Epple, K. D. M. Harris, *Chem. Eur. J.* **2000**, *6*, 1120−1126.
[59] K. Chujo, H. Kobayashi, J. Suzuki, S. Tokuhara, *Makromol. Chem.* **1967**, *100*, 267−270.
[60] M. Epple, H. Kirschnick, G. N. Greaves, G. Sankar, J. M. Thomas, *J. Chem. Soc., Faraday Trans.* **1996**, *92*, 5035−5042.
[61] J. Pelouze, *Justus Liebigs Ann. Chemie* **1845**, *13*, 112−124.
[62] C. A. Bischoff, P. Walden, *Justus Liebigs Ann. Chem.* **1894**, *279*, 71−99.
[63] M. Epple, H. Kirschnick, *Liebigs Ann.* **1997**, 81−85.
[64] Y. Takao, Y. Kasashima, M. Inoki, F. Akutsu, K. Naruchi, Y. Yamaguchi, *Polymer J.* **1995**, *27*, 766−771.
[65] S. Bezzi, *Atti Mem. R. Acad. Sci. Lett. Arti Padova* **1939**, *55*, 85−99.
[66] S. Bezzi, *Gazz. Chim. Ital.* **1940**, *70*, 110−118.
[67] O. Herzberg, M. Epple, *Macromol. Chem. Phys.* **1999**, *200*, 2662−2666.
[68] O. Herzberg, H. Ehrenberg, S. J. Kitchin, K. D. M. Harris, M. Epple, *J. Solid State Chem.*, in press.
[69] C. A. Bischoff, P. Walden, *Justus Liebigs Ann. Chemie* **1894**, *279*, 118−129.
[70] T. Okada, R. Okawara, *J. Organomet. Chem.* **1973**, *54*, 149−152.
[71] C. A. Bischoff, *Justus Liebigs Ann. Chemie* **1894**, *279*, 153−187.
[72] C. A. Bischoff, P. Walden, *Justus Liebigs Ann. Chem.* **1894**, *279*, 100−118.
[73] K. Schwarz, M. Epple, *Macromol. Chem. Phys.* **1999**, *200*, 2221−2229.
[74] M. Epple, L. Tröger, *J. Chem. Soc., Dalton Trans.* **1996**, 11−16.
[75] M. Epple, H. Kirschnick, J. M. Thomas, *J. Therm. Anal.* **1996**, *47*, 331−338.
[76] M. Epple, U. Sazama, A. Reller, N. Hilbrandt, M. Martin, L. Tröger, *Chem. Commun.* **1996**, 1755−1756.
[77] O. Herzberg, M. Epple, *J. Therm. Anal. Cal.* **1999**, *57*, 151−156.
[78] M. Epple, O. Herzberg, *J. Biomed. Mater. Res. Appl. Biomat.* **1998**, *43*, 83−88.
[79] M. Epple, G. Sankar, J. M. Thomas, *Chem. Mater.* **1997**, *9*, 3127−3131.
[80] O. Herzberg, R. Gehrke, M. Epple, *Polymer* **1999**, *40*, 507−511.

Received August 29, 2000
[I00329]

A Bis(carboxamido-*N*)diisocyanidobis(sulfenato-*S*)cobalt(III) Complex, Model for the Post-Translational Oxygenation of Nitrile Hydratase Thiolato Ligands

Laurent Heinrich,[a] Yun Li,[a] Jacqueline Vaissermann,[b] and Jean-Claude Chottard*[a]

Keywords: Cobalt / Nitrile hydratase / Isocyanide / Oxygenation / Sulfenato-*S* ligands

A square-planar cobalt(III) complex with an N_2S_2 bis(carboxamido-*N*)dithiolato tetradentate ligand was oxygenated by H_2O_2·urea, after axial coordination of *tert*-butyl isocyanide, to the first bis(carboxamido-*N*)bis(sulfenato-*S*)cobalt(III) complex.

Introduction

Nitrile hydratases (NHases) are non-heme iron or non-corrinoid cobalt-containing enzymes which catalyze the hydration of nitriles to amides.[1a] Recent X-ray studies of NHases indicated that the iron center is bound to two peptide amide nitrogen atoms and three sulfur atoms from cystein-thiolate, cystein-sulfinic and cystein-sulfenic moieties, the latter two resulting from post-translational oxidation.[1a,1b] The two nitrogen atoms and the two sulfur atoms of the modified cystein groups belong to a planar tetradentate eleven-atom ligand from a Cys-Ser-Cys sequence. EXAFS data suggest that the iron and cobalt NHases have similar metal sites.[1c] However, there is no evidence whether post-translational oxidation of cystein-thiolates also occurs in cobalt sites.

A few Co^{III} complexes with both thiolato and carboxamido-*N* ligands have recently been reported as synthetic models of NHases.[2] Two of them have been oxidized by H_2O_2 to give the sulfinato-*S* species,[2b] but no sulfenato-*S* derivative was characterized.

We have recently reported[3] the first example of dioxygen oxidation of a (carboxamido-*N*)(thiolato)Fe^{III} complex $[FeN_2S_3]^{2-}$ into a sulfinato-*O* species $[FeN_2S_2OSO]^{2-}$. The sulfinato-*O* coordination suggested a preferred oxidation of the axial thiolato ligand, compared to that of the thiolates in the equatorial N_2S_2 plane. To address this question in the case of Co NHases, we have synthesized complex **1** ($[Co^{III}L]^-$) from the deprotonated ligand **2** (H_4L)[4] (Scheme 1). The structure of **1** was determined by X-ray diffraction.[5]

The square-planar complex **1** is stable in air, in the solid state and in solution. Its reaction with excess H_2O_2 or H_2O_2·urea leads to decomposition. We have shown by UV/Vis spectroscopy and EXAFS studies, that two CN^- or *t*BuNC ligands are able to bind at the axial positions of **1**, leading to the hexacoordinated diamagnetic complexes $[CoL(CN)_2]^{3-}$ (**3**) and $[CoL(tBuNC)_2]^-$ (**4**), respectively[5]. Here we report the oxygenation of the thiolato ligands in **4**, giving the corresponding bis(sulfenato-*S*) complex **5**.

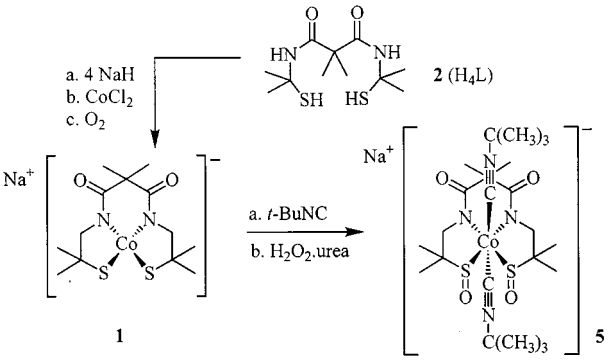

Scheme 1. Synthesis of complexes **1** and **5**

Results and Discussion

At variance with **1**, complexes **3** and **4** undergo fast oxygenation reactions in aerated solution, giving a mixture of presumably sulfinato (-*O* or -*S*) and sulfenato (-*O* or -*S*) species. The addition of H_2O_2·urea to a solution of **1** in the presence of excess *t*BuNC gave the orange complex **5** {$Na[Co^{III}(L\text{-}N_2SOSO)(tBuNC)_2]$·urea·$2H_2O$} which precipitated spontaneously (Scheme 1). The X-ray structure of **5** (Figure 1) reveals the oxygenation of the two thiolato to sulfenato-*S* ligands. It is noteworthy that the urea molecules contribute to the crystal lattice through binding to oxygen atoms of the sulfenato-*S* and carboxamido-*N* ligands and by interaction with the Na^+ ions (Figure 2). Complex **5** contains two axial isocyanide ligands in a distorted octahedron. This suggests that the oxygenation occurred thanks to the formation of **4** {$Na[CoL(tBuNC)_2]$}. The presence of one Na^+ per Co in the unit cell of **5** supports a cobalt(III) state. The Co−N bond lengths are similar to those reported for carboxamido-*N* ligands in hexacoordinated Co^{III} complexes,[2] but are 0.07 Å longer than those in the square-

[a] Laboratoire de Chimie et Biochimie Pharmacologiques et Toxicologiques, Université René Descartes, UMR 8601 CNRS, 45 rue des Saints-Pères, 75270 Paris Cedex 06, France
E-mail: Jean-Claude.Chottard@biomedicale.univ-paris5.fr
[b] Laboratoire de Chimie Inorganique et Matériaux Moléculaires, Université Pierre et Marie Curie, ESA 7071, 75252 Paris Cedex 05, France.

 © WILEY-VCH Verlag GmbH, 69451 Weinheim, 2001 1434−1948/01/0606−1407 $ 17.50+.50/0

planar complex **1**. Very few complexes have been reported with structurally characterized sulfenato-*S*−cobalt(III) bonds; their lengths are in the range 2.198−2.253 Å,[6] in agreement with the 2.223 Å in **5**. The two oxygen atoms of the sulfenato-*S* ligands are on the same side of the N_2S_2 plane, leading to a slight asymmetry of **5**. To our knowledge, only two cyclopentadienyl compounds with isocyanido-*C*−cobalt(III) bonds are known with C−Co^{III} bond lengths of 1.83 and 1.79 Å,[7] comparable to the 1.83 Å in **5**. The isocyanides are linearly coordinated to the metal center, with the following angle values Co(1)−C(14)−N(4) = 175.1°, Co(1)−C(19)−N(3) = 179.5°, C(14)−N(4)−C(15) = 176.5°, C(19)−N(3)−C(20) = 176.6° and a 1.14 Å C−N bond length. This agrees with a C−N triple bond description. The IR spectrum (KBr pellet) of **5** shows the characteristic coordinated carboxamido-*N* ν_{CO} frequency at $\tilde{\nu}$ = 1555 cm^{-1} and a strong absorption at $\tilde{\nu}$ = 965 cm^{-1} corresponding to the ν_{SO} stretching of coordinated sulfenato-*S* ligands.[6b] The weak symmetric and strong asymmetric ν_{CN} stretching frequencies of the isocyanide groups are increased from $\tilde{\nu}$ = 2140 cm^{-1} to 2375 and 2195 cm^{-1} upon coordination, indicating a higher bond order in **5** than in the free ligand, fitting the C−N triple bond description and the σ-donor character of the isocyanide groups which dominates their potential π-acceptor contribution.

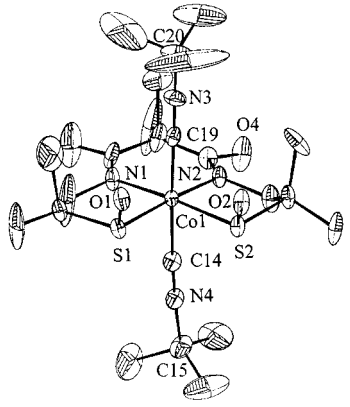

Figure 1. CAMERON representation (ellipsoid at 20% probability level) of **5**; H atoms are omitted for clarity; selected bond lengths [Å] and angles [°]: Co(1)−S(1) 2.223(4), Co(1)−S(2) 2.223(4), Co(1)−N(1) 1.94(1), Co(1)−N(2) 1.95(1), Co(1)−C(14) 1.84(2), Co(1)−C(19) 1.83(2), C(14)−N(4) 1.14(2), C(19)−N(3) 1.14(2); S(1)−Co(1)−S(2) 90.4(1), S(1)−Co(1)−N(1) 87.9(4), N(1)−Co(1)−N(2) 93.5(5), C(14)−Co(1)−C(19) 177.5(6), C(14)−N(4)−C(15) 176.5(17), C(19)−N(3)−C(20) 176.6(20)

The orange solutions of **5** in polar solvents (alcohols, DMSO, DMF, H_2O) are stable in air and the complex appears hexacoordinated with diamagnetic low-spin Co^{III} (Evans method). The electrospray mass spectrum exhibits peaks at *m*/*z* = 559 ([M − Na^+]$^-$) and at *m*/*z* = 476 ([M − Na^+ − *t*BuNC]$^-$), and weaker ones at *m*/*z* = 575 and 492, suggesting partial oxidation of these two species during the mass spectrometry analysis.

Whereas the oxidation of (thiolato)Co^{III} complexes by H_2O_2 is well known,[8] there are only two examples of oxygenation of bis(carboxamido-*N*)(dithiolato)Co^{III} complexes which give the bis(sulfinato-*S*) species.[2b] Sulfenato-*S* complexes are usually difficult to isolate due to their further oxidation to the sulfinato-*S* derivatives. The isolation of **5** was likely due to its precipitation, preventing further oxidation. The oxidation of the thiolato ligands is believed to start by nucleophilic attack on dioxygen or H_2O_2, as in the case of (thiolato)nickel complexes.[8b] The increase of the Co−S bond lengths upon addition of CN^- or *t*BuNC to **1**, to give **3** and **4** (2.13, 2.23 and 2.28 Å for **1**, **3** and **4**, respectively, according to our EXAFS studies)[5] shows that the thiolato ligands become much less tightly bound in the latter two and consequently more nucleophilic.

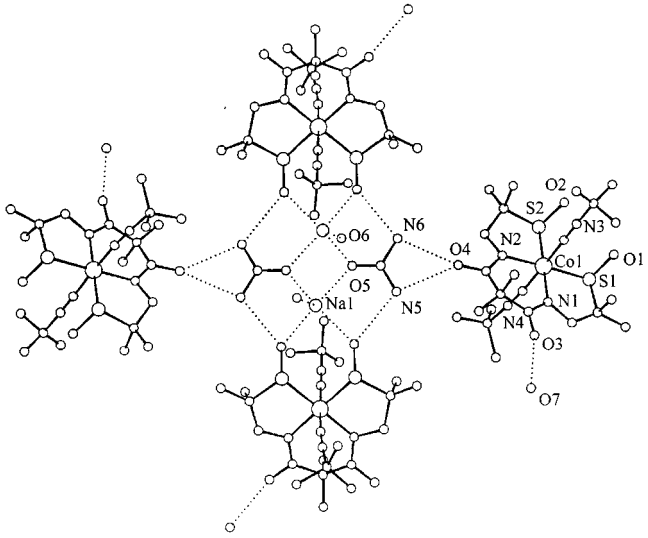

Figure 2. View of the Na^+/O interactions and hydrogen bonds stabilizing the crystal lattice of **5**·urea·$2H_2O$

A preliminary study of the catalytic hydration activity of **5** was conducted without acid or base in a 9:1 acetonitrile/water mixture at room temperature. After 24 h, acetamide was formed (2 turnovers) and **5** remained unchanged (^{1}H NMR criteria). No conversion was observed in the absence of **5**. Although **5** is not an efficient catalyst under these conditions, the hydration mechanism deserves interest. The known[2a] complex $[Co(PyPS)(OH)]^{2-}$ (with one pyridine, two carboxamido-*N* and one thiolato ligands in a plane, and the second thiolato ligand occupying an axial position) converts acetonitrile into acetamide only at 50°C and pH = 9.5 (Tris buffer), most probably via the Co^{III}-bound hydroxide ligand. It is noteworthy that **5** has no free coordination site that would allow either water or acetonitrile binding to Co^{III}. This suggests that the nucleophilicity of the coordinated sulfenato-*S* ligands[9] in **5** might play a crucial role in the hydration reaction of acetonitrile. Further work is in progress to test this hypothesis and its relevance to the case of NHase.

Conclusion

We have shown that H_2O_2·urea allowed the clean oxidation of the dithiolato complex **1** to its bis(sulfenato-*S*)Co^{III} derivative **5** after axial coordination of *tert*-butyl isocyanide.

It is the first example of a cobalt complex with a mixed carboxamido-*N* and sulfenato-*S* coordination sphere. These results suggest that the in-plane thiolates of the metallic site of Co NHases could undergo posttranslational oxidation, as observed for the Fe NHases. Such a reaction would require the presence of σ-donor ligands, a role which could be played by the axial cystein-thiolate and the external hydroxide bound to the metal center at the active site of the enzyme.[1] The coordinated sulfenate-*S* likely plays a key role in the activity of NHases.

Experimental Section

Complex 5: To a solution of **1** (42 mg, 0.1 mmol) and *t*BuNC (36 mg, 0.44 mmol) in degassed DMF (1 mL) cooled to 0°C was added a filtered solution of H_2O_2·urea (200 mg, 2.2 mmol) in degassed acetone (2 mL), leading to the formation of an orange precipitate. After 30 min at 0°C, the precipitate was isolated, dried under vacuum and dissolved in ethanol. Diethyl ether diffusion into this solution afforded **5** {Na[Co^{III}(L-N_2SOSO)(*t*BuN*C*)$_2$]·urea·$2H_2O$} as orange crystals (45 mg, 60%). − $C_{24}H_{48}CoN_6NaS_2O_7$ (678.73): calcd. C 42.47, H 7.13, N 12.38, S 9.45; found C 42.58, H 6.86, N 12.38, S 9.48. − UV/Vis (MeOH): λ_{max} (ε) = 460 (sh), 377 (9050), 297 (9380), 217 nm (12800 M^{-1} cm^{-1}). − IR (KBr) $\tilde{\nu}$ = 2375 (w, ν_{CN}) and 2195 (s, ν_{CN}), 1555 (s, ν_{CO}), 965 cm^{-1} (s, ν_{SO}). − ^{1}H NMR (250 MHz, [D_6]DMSO): δ = 7.65 (s, 4 H, H_2O), 5.44 (s, 4 H, urea), 3.60 (d, 2 H, NCH_AH_B, J = 13.3 Hz), 3.09 (d, 2 H, NCH_AH_B), 1.39 (s, 18 H, isocyanides), 1.28, 1.17 and 1.12 (3 s, 3 × 6 H, methyl groups). − Electrospray MS (MeOH); *m*/*z* (%): 476 (100), 492 (22), 559 (86), 575 (16).

Crystal Data for 5·Urea·2H$_2$O: $C_{24}H_{48}CoN_6NaS_2O_7$, M = 678.73, orange hexagonal block 0.20 × 0.40 × 0.80 mm, monoclinic, space group $P2_{1/m}$, a = 10.488(3), b = 18.789(18), c = 21.474(13) Å, Z = 4, β = 98.14(6)°, V = 4189(5) Å^3, D_c = 1.076 g·cm^{-3}, T = 295 K, Mo-K_α radiation (λ = 0.71069 Å), 8208 reflections were measured, 2227 of which were used in all calculations (R_{int} = 0.04). The structure was solved by SHELXS-86 and refined by least-squares analysis using anisotropic thermal parameters, H atoms were introduced in calculated positions, with $F_o > 3\sigma(F_o)$, the programs CRYSTALS and CAMERON were used. R = 0.0935, R_W = 0.1071. It is noteworthy that the refinement factors R and R_W could not be reduced despite several attempts including measurements at lower temperatures. Crystallographic data (excluding structure factors) for the structure reported in this paper have been deposited with the Cambridge Crystallographic Data Center as supplementary publication no. CCDC-146921. Copies of the data can be obtained free of charge on application to CCDC, 12 Union Road, Cambridge CB2 1EZ, UK [Fax: (internat.) + 44-1223/336-033; E-mail: deposit@ccdc.cam.ac.uk].

Acknowledgments

This work was supported by the European Commission TMR-NOHEMIP research network no. ERB FMRX-CT98-0174.

[1] [1a] S. Nagashima, M. Nakasato, N. Dohmae, M. Tsujimura, K. Takio, M. Odaka, M. Yohda, N. Kamiya, I. Endo, *Nat. Struct. Biol.* **1998**, *5*, 347−351. − [1b] W. Huang, J. Jia, J. Cumming, M. Nelson, G. Schneider, Y. Lindqvist, *Structure* **1997**, *5*, 691−699. − [1c] B. A. Brennan, G. Alms, M. J. Nelson, L. T. Durney, R. C. Scarrow, *J. Am. Chem. Soc.* **1996**, *118*, 9194−9195.

[2] [2a] J. C. Noveron, M. M. Olmstead, P. K. Mascharak, *J. Am. Chem. Soc.* **1999**, *121*, 3553−3554. − [2b] L. A. Tyler, J. C. Noveron, M. M. Olmstead, P. K. Mascharak, *Inorg. Chem.* **2000**, *39*, 357−362.[2c] S. Chatel, M. Rat, S. Dijols, P. Leduc, J. P. Tuchagues, D. Mansuy, I. Artraud, *J. Inorg. Biochem.* **2000**, *80*, 239−246.

[3] L. Heinrich, Y. Li, J. Vaisserman, G. Chottard, J. C. Chottard, *Angew. Chem. Int. Ed.* **1999**, *38*, 3526−3528.

[4] L. Heinrich, Y. Li, J. C. Chottard, *Synth. Commun.*, in press.

[5] The X-ray diffraction structure of **1** will be reported in a forthcoming paper together with the UV/Vis and EXAFS structural determinations of **3** and **4**: L. Heinrich, Y. Li, K. Provost, A. Michalovich, J. Vaisserman, J. C. Chottard, *Inorg. Chim. Acta*, in press.

[6] [6a] K. I. Okamoto, T. Konno, H. Einaga, J. Hidaka, *Bull. Chem. Soc. Jpn.* **1987**, *60*, 393. − [6b] I. K. Adzamli, K. Libson, J. D. Lydon, R. C. Elder, E. Deutsch, *Inorg. Chem.* **1979**, *18*, 303−311.

[7] [7a] J. Doherty, J. Fortune, A. R. Manning, F. S. Stephens, *J. Chem. Soc., Dalton Trans.* **1984**, 1111−1116. − [7b] Y. Wakatsuki, K. Aoki, H. Yamazaki, *J. Chem. Soc., Dalton Trans.* **1986**, 1193−1199.

[8] [8a] K. Yamanari, T. Kawamoto, Y. Kushi, T. Komorita, A. Fuyuhiro, *Bull. Chem. Soc. Jpn.* **1998**, *71*, 2635−2643. − [8b] C. A. Grapperhaus, M. Y. Darensbourg, *Acc. Chem. Res.* **1998**, *31*, 451−459.

[9] J. D. Lydon, E. Deutsch, *Inorg. Chem.* **1982**, *21*, 3180−3185.

Received November 15, 2000
[I00436]

Lithium Alkylselenolates and -tellurolates − A Solid-State and Solution Structural Study

William Clegg,[a] Robert P. Davies,*[b] Ronald Snaith,[c][†] and Andrew E. H. Wheatley[c]

Keywords: Chalcogens / Lithium / Insertion / NMR spectroscopy

Facile insertion of elemental Se or Te into the C–Li bond of *n*BuLi in the presence of TMEDA gives [*n*BuXLi·TMEDA]$_2$ (X = Se **1**; Te **2**). Both **1** and **2** have been fully characterised in the solid and solution states resulting in the first crystal structures of a lithium alkylselenolate and -tellurolate and giving a unique insight into the coordination chemistry of the less sterically demanding chalcogenolate ligands.

Introduction

The desire for new and efficient syntheses for both metal chalcogenolates (primarily used as precursors to semiconducting metal chalcogenolides[1] and as model systems for various biologically active metalloproteins[2]) and also for new reagents for the synthesis of selenium- and tellurium-containing organics[3] has resulted in a growing interest in alkali metal complexes with selenolate (RSe^-) and tellurolate (RTe^-) ligands. However, there still remains a scarcity of both solid-state and solution studies of these species, especially when compared to the multitude of data available on the analogous alkali metal alkoxide (RO^-) and thiolate (RS^-) complexes.[4] Moreover, the majority of studies to date have utilised sterically bulky ligands, such as substituted silyl chalcogenolates (R_3SiX^-; R = Me, $SiMe_3$; X = Se, Te)[5−9] or substituted aromatics (Mes*X^-; Mes* = 2,4,6-*t*Bu$_3$C$_6$H$_2$; X = Se, Te)[10−12] so as to confer extra kinetic stability upon the resulting complex. To the best of our knowledge the only other examples of alkali-metal organochalcogenolates to be structurally characterised are the 2,2′-bipyridine complexes [PhSeLi·bipy]$_2$ and [2-PyrSeLi·bipy]$_2$,[13] the phenylacetyl selenolate PhC≡CSeLi·TMEDA·THF[14] and the heterobimetallic species [CpFe{C$_5$H$_3$(CH$_2$NMe$_2$)TeLi·DME}],[15] [(C$_5$H$_5$)$_2$Lu(μ-SePh)$_2$Li·2THF][16] and [(py)$_2$Yb(SePh)$_2$(μ-SePh)$_2$Li(py)$_2$] (py = pyridine).[17] In order to confront this lack of structural knowledge, particularly of the less sterically demanding ligands, we report here the first solid-state characterisation of both a lithium alkylselenolate (*n*BuSeLi·TMEDA)$_2$ (**1**) and -tellurolate (*n*BuTeLi·TMEDA)$_2$ (**2**) [TMEDA = (Me$_2$NCH$_2$)$_2$].

[a] Dept. of Chemistry, Bedson Building, University of Newcastle upon Tyne,
Newcastle upon Tyne NE1 7RU, UK
[b] Dept. of Chemistry, Imperial College of Science, Technology and Medicine,
Exhibition Road, London SW7 2AY, UK
Email: r.davies@ic.ac.uk
[c] Department of Chemistry, University of Cambridge,
Lensfield Road, Cambridge CB2 1EW, UK
[†] Deceased.

Results and Discussion

Two main synthetic routes have been documented for the preparation of lithium chalcogenolates: metallation of an organic acid (RSeH or RTeH) and insertion of elemental Se or Te into a C−Li or Si−Li bond.[2,3] The second of these procedures was employed in the synthesis of **1** and **2** since it provided a clean, high yield of the desired products and avoided the synthesis of the readily oxidised butylselenol and butyltellurol species. Reaction in toluene of *n*BuLi with elemental Se or Te (1:1 ratio) in the presence of TMEDA (1 equivalent) resulted in the dissolution of the Group 16 element to give a clear pale yellow solution from which it proved possible to grow, at room temperature, crystals of the lithium chalcogenolates **1** and **2** in yields 36 and 52%, respectively. Both **1** and **2** are highly air sensitive and extremely pungent compounds.

A low temperature X-ray structural characterisation of **1** and **2** reveals that they both crystallise in the monoclinic space group *I*2/*a* and that they both contain two isostructural dimeric molecules within the asymmetric unit, each of which exhibits twofold symmetry (Figure 1). These dimeric units are based around a central Li_2X_2 (X = Se, Te) ring with the *n*-butyl groups in a *cis* conformation and each of the lithium ions solvated by one TMEDA molecule. The free ends of the butyl groups are disordered in the solid-state structures of both **1** and **2**. The Se−Li mean average bond length in **1** [2.583 Å; range 2.544(17) to 2.592(15) Å] is comparable to the Se−Li bond lengths of previously studied lithium selenolates [range 2.462(13) to 2.622(8) Å].[5,11−14] However, the Se−C bond lengths in **1** [1.98(1) and 2.02(2) Å] are longer than the Se−C bonds in the previously characterised arylselenolates [range 1.896(4) to 1.942(7) Å][11−13] and also longer than the Se-C bond [1.813(4) Å] in the alkylnylselenolate [PhC≡CSeLi·TMEDA·THF].[14] This can be accounted for by the sp^3 hybridisation of the α-carbon in **1** whose larger, more diffuse orbitals form longer bonds than the α-carbon sp^2 hybrid orbitals in the arylselenolates and the α-carbon sp orbitals in the alkynylselenolate. The C−Se−Li angle [mean 95.8°, range 92.9(5) to 97.4(7)°] is more acute than in any

 © WILEY-VCH Verlag GmbH, 69451 Weinheim, 2001 1434−1948/01/0606−1411 $ 17.50+.50/0

other selenolate previously reported [range 98.2(3) to 104.3(2)°][11−14] presumably by virtue of the low steric demands of the *n*-butyl group. The Li−Se−Li inter-ring angle is also very acute, 69.2(6) and 70.1(6)° in **1** *cf.* 77.0(2) and 75.8(4)° in the only other dimeric lithium selenolates [Li(DME)SeSi(SiMe$_3$)$_3$]$_2$ [5] and [Li(bipy)(SePh)]$_2$,[13] respectively.

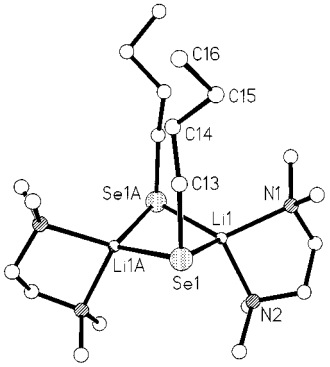

Figure 1. The solid-state structure of [*n*BuSeLi·TMEDA]$_2$ (**1**); only one of the two isostructural dimers in the asymmetric unit is shown; hydrogen atoms and disorder in the *n*-butyl group are omitted for clarity; the molecule lies on a crystallographic twofold rotation axis which relates Li1 and Se1 to Li1A and Se2A

In **2** the Te−Li distances [mean 2.813 Å, range 2.802(6) to 2.824(6) Å] are similar to previously reported Li−Te distances [range 2.70(1) to 2.88(2) Å][6−10,15] and the Te−C (sp^3) distances of 2.259(11) and 2.191(4) Å are larger than the Te−C(sp^2) distances of 2.142(2) Å in [(*o*-C$_6$H$_4$CH$_2$NMe$_2$)TeLi(DME)], 2.184(4) Å in [Mes*TeLi(THF)$_3$][10] and 2.122(2) Å in [CpFe{C$_5$H$_3$(CH$_2$NMe$_2$)TeLi·DME}].[15] The Li−Te−Li bond angles [both of which are 68.2(2) °] are more acute than those observed [75.1(1) °] in the only other dimeric lithium tellurolate [(DME)LiTeSi(SiMe$_3$)$_3$]$_2$,[9] and the mean C−Te−Li bond angle in **2** is 95.0° [range 93.5(2) to 97.2(2)°].

In addition to solid-state X-ray diffraction studies, the solution structures of both **1** and **2** were probed by multinuclear NMR spectroscopy and crysocopic relative molecular mass measurements. Cryoscopic measurements on a 0.030 M solution of **1** in benzene indicated an average association value *n* for [BuSeLi·TMEDA]$_n$ of 3.17 ± 0.08. One possible explanation of this association value is that in nondonor solvents a dimer/tetramer equilibrium is occurring, in which the tetramer is formed from the back-to-back stacking of two of the *cis* dimeric units to give a Li$_4$Se$_4$ cubane structure. A similar result was obtained with a 0.030 M solution of **2** (n = 3.30 ± 0.12). Despite this, ^{7}Li NMR spectroscopic studies at 25 °C on THF solutions of **1** and **2** showed only one peak (δ = −0.04 for a 0.023 M solution of **1**, and δ = 0.25 for a 0.020 M solution of **2**, referenced to PhLi in THF) indicating that any fluxional behaviour between different aggregation states is rapid. This dynamic equilibrium was still observed down to temperatures as low as −80 °C since even at these temperatures only one peak was visible by ^{7}Li NMR spectroscopy. The absence of any observable ^{7}Li coupling to either ^{77}Se or ^{125}Te in these spectra is also indicative of the fluxional behaviour of these species, since any change in aggregation state would involve the breaking and formation of Li−X (X = Se or Te) bonds. As expected, the ^{1}H and ^{13}C NMR spectra of **1** and **2** in [D$_6$]DMSO showed peaks attributable to the TMEDA and *n*-butyl groups, while the main difference between the two ^{13}C NMR spectra was the position of the α-carbon atoms: δ = −1.1 in **1** and δ = −19.4 in **2**. In addition, $^1J_{CTe}$ coupling was observed in the ^{13}C spectrum of **2**, with a coupling constant of 158.0 Hz (this is comparable to previously reported values for dialkyl tellurides).[18] It proved impossible to see Se−C coupling in the ^{13}C NMR spectrum of **1** due to the ready decomposition of this product, hence the poor resolution of its spectra. However, ^{77}Se{^{1}H} NMR spectroscopy of **1** was undertaken and showed a single peak at δ = −660 (referenced to SeMe$_2$ at δ = 0); again no Se−Li coupling was observable.

We now hope to extend this work to look at other sterically undemanding lithium chalcogenolates and also their transmetallation reactions, with particular emphasis placed upon their possible utility in the synthesis of single source precursors to semiconducting materials.[1]

Experimental Section

All reactions and manipulations were carried out under an inert atmosphere of dry nitrogen using standard double manifold and glove-box techniques.

[*n*BuSeLi·TMEDA]$_2$ (1): *n*BuLi (3.2 mL, 1.6 M in hexanes, 5.0 mmol) was added to a suspension of Se (0.40 g, 5 mmol) in toluene (10 mL) and TMEDA (0.75 mL, 5 mmol) under nitrogen at −78 °C. The mixture was then allowed to warm to room temperature with constant stirring to give a pale yellow solution. This solution was filtered under nitrogen and reduced in volume under vacuum to approximately 3 mL. Hexane (6 mL) was then added and the solution left at room temperature for 24 hours to yield a batch of yellow crystalline needles (0.46 g, 36%). − M.p. 128−130 °C. − ^{1}H NMR (400 MHz, C$_6$D$_6$): δ = 2.64 (t, 2 H, -C*H*$_2$Se-), 2.23 (s, 12 H, TMEDA), 2.13 (s, 4 H, TMEDA), 1.95 (m, 2 H, -C*H*$_2$-), 1.64 (m, 2 H, -C*H*$_2$-), 1.11 (t, 3 H, C*H*$_3$CH$_2$-).

[*n*BuTeLi·TMEDA]$_2$ (2): *n*BuLi (3.2 mL, 1.6 M in hexanes, 5.0 mmol) was added to a suspension of Te (0.644 g, 5 mmol) in toluene (15 mL) and TMEDA (0.75 mL, 5 mmol) under nitrogen at −78 °C. The mixture was then allowed to warm to room temperature with constant stirring to give an orange solution. This solution was filtered under nitrogen and left at room temperature for two days to yield a batch of dark-orange, needle-shaped crystals (0.80 g, 52%). − M.p. 144−148 °C. − ^{1}H NMR (400 MHz, C$_6$D$_6$): δ = 2.59 (t, 2 H, -C*H*$_2$Te-), 2.25 (s, 12 H, TMEDA), 2.05 (s, 4 H, TMEDA), 1.92 (m, 2 H, -C*H*$_2$-), 1.59 (m, 2 H, -C*H*$_2$-), 1.03 (t, 3 H, C*H*$_3$CH$_2$-).

X-ray Analysis: Crystals of **1** and **2** were mounted directly into the cold stream of an Oxford Crysotream crystal cooling apparatus, installed on either a Stoe−Siemens four-circle diffractometer (**1**) or a Siemens SMART CCD diffractometer (**2**), using perfluoropolyether oil.

Crystal data for 1: C$_{20}$H$_{50}$Li$_2$N$_4$Se$_2$, M = 518.44, monoclinic, space group *I*2/*a*, a = 16.736(4), b = 19.744(5), c = 17.730(4) Å, β =

91.13(3)°, U = 5857(2) Å^3, Z = 8, D_c = 1.176 g cm^{-3}, μ(Mo-K_α) = 2.535 mm^{-1}, T = 180(2) K. 5916 Reflections (5145 unique, R_{int} = 0.064) measured. Refinement on F^2 values of all data gave final *wR2* = 0.2195, conventional R = 0.0795 on F values of all reflections with $F^2 > 2\sigma(F^2)$, 292 parameters.

Crystal data for 2: $C_{20}H_{50}Li_2N_4Te_2$, M = 615.72, monoclinic, space group *I*2/*a*, a = 17.762(1), b = 19.811(2), c = 17.339(1) Å, β = 90.77(1) °, U = 6101.0(8) Å^3, Z = 8, D_c = 1.341 g cm^{-3}, μ(Mo-K_α) = 1.923 mm^{-1}, T = 160(2) K. 27244 Reflections (7512 unique, R_{int} = 0.036) measured. Refinement on F^2 values of all data gave final *wR2* = 0.1082, conventional R = 0.0375 on F values of all reflections with $F^2 > 2\sigma(F^2)$, 291 parameters.

Crystallographic data for compounds **1** and **2** have been deposited with the Cambridge Crystallographic Data Centre as supplementary publication nos. CCDC-151235 (**1**) and CCDC-152141 (**2**). Copies of the data can be obtained free of charge on application to CCDC, 12 Union Road, Cambridge, CB2 1EZ, UK [Fax (internat.): +44-1223/336-033; Email: deposit@ccdc.cam.ac.uk; www: http://www.ccdc.cam.ac.uk].

Acknowledgments

We would like to thank the EPSRC for funding and St Catharine's (R. P. D.) and Gonville and Caius (A. E. H. W.) Colleges, Cambridge for Research Fellowships.

[1] H. B. Singh, N. Sudha, *Polyhedron* **1996**, *15*, 745; P. O'Brien, *Chemtronics* **1991**, *5*, 61.
[2] J. Arnold, in *Prog. Inorg. Chem.* (Ed.: D. Karlin) Wiley, New York, **1995**, *vol. 43*, p. 353.
[3] H. J. Gysing, in *The Chemistry of Organic Selenium and Tellurium compounds* (Eds.: S. Patai and Z. Rappoport), Wiley, New York, **1986**, *vol. 1*, p. 679.
[4] M. A. Beswick, D. S. Wright, in *Comprehensive Organometallic Chemistry II* (Eds.: E. W. Abel, F. G. A. Stone, G. Wilkinson), Elsevier Science Inc., New York, **1995**, *vol. 1*, vol. ed. C. E. Housecroft, p. 1.
[5] K. E. Flick, *Acta Cryst.* **1994**, *C50*, 674.
[6] P. J. Bonasia, D. E. Gindelberger, B. O. Dabbousi, J. Arnold, *J. Am. Chem. Soc.* **1992**, *114*, 5209.
[7] P. J. Bonasia, V. Christou, J. Arnold, *J. Am. Chem. Soc.* **1993**, *115*, 6777.
[8] G. Becker, K. W. Klinkhammer, W. Massa, *Z. Anorg. Allg. Chem.* **1993**, *619*, 628.
[9] G. Becker, K. W. Klinkhammer, S. Lartiges, O. Bottcher, W. Poll, *Z. Anorg. Allg. Chem.* **1993**, *613*, 7.
[10] P. J. Bonasia, J. Arnold, *J. Organomet. Chem.* **1993**, *449*, 147.
[11] W. −W. du Mont, S. Kuboniok, L. Lange, S. Pohl, W. Saak, I. Wagner, *Chem. Ber.* **1991**, *124*, 1315; K. Ruhlandt-Senge, P. P. Power, *Inorg. Chem.* **1991**, *30*, 3683.
[12] K. Ruhlandt-Senge, P. P. Power, *Inorg. Chem.* **1993**, *32*, 4505.
[13] D. V. Khasnis, M. Buretea, T. J. Emge, J. G. Brennan, *J. Chem. Soc., Dalton Trans* **1995**, 45.
[14] M. A. Beswick, C. N. Harmer, P. R. Raithby, A. Steiner, M. Tombul, D. S. Wright, *J. Organomet. Chem.* **1999**, *573*, 261.
[15] H. Gornitzka, S. Besser, R. Herbst-Irmer, U. Kilimann, F. T. Edermann, *Angew. Chem.* **1992**, *104*, 1252; *Angew. Chem. Int. Ed. Engl.* **1992**, *31*, 1260.
[16] H. Schumann, I. Albrecht, M. Gallagher, E. Hahn, C. Muchmore, J. Pickardt, *J. Organomet. Chem.* **1988**, *349*, 103.
[17] M. Berardini, T. J. Emge, J. G. Brennan, *J. Chem. Soc., Chem. Commun.* **1993**, 1537.
[18] K. Karaghiosoff, T. M. Klapötke, B. Krumm, O.P. Ruscitti, *J. Organomet. Chem.* **1999**, *557*, 69.

Received November 23, 2000
[I00446]

Tris(pyrazolyl)methanesulfonate (Tpms) − A Versatile Alternative to Tris(pyrazolyl)borate in Rhodium(I) Chemistry

Wolfgang Kläui,*[a] Daniel Schramm,[a] Wilfried Peters,[a] Gerd Rheinwald,[b] and Heinrich Lang[b]

Keywords: Rhodium / Tripodal ligands / N ligands / Fluxionality / Carbonyl complexes

Thallium(I) tris(pyrazol-1-yl)methanesulfonate (TlTpms) has been prepared as a new versatile precursor for Tpms complexes. TlTpms readily reacts with the rhodium(I) complexes $[Rh(LL)Cl]_2$ [LL = $(CO)_2$, cod, nbd] to give the corresponding TpmsRh(LL) complexes [LL = $(CO)_2$ (**2a**), cod (**3**), and nbd (**4**)]. In solution, **2a** reversibly forms the binuclear complex TpmsRh(μ-CO)$_3$RhTpms (**2b**). **3** and **4** react with CO to form **2a**. TpmsRh(CO)(PR_3) complexes [PR_3 = PPh_3 (**5a**), PMe_3 (**5b**), PCy_3 (**5d**), $P(Ph)_2(PhSO_3K)$ (**5e**)] have been obtained by reaction of **2a** with the corresponding phosphanes. The solid-state structures of **2a**, **3**, **4**, and **5a** have been determined by X-ray analysis. **2a**, **3**, and **5a** have square-planar geometries with the Tpms ligand coordinating in a κ^2 mode. The non-coordinating pyrazole ring faces either away from (structure **2a**) or towards the rhodium atom (structures **3** and **5a**). **4** has a trigonal-bipyramidal coordination geometry with a genuine κ^3-bonded Tpms ligand. The non-rigid behaviour of the (Tpms)rhodium complexes has been followed by variable-temperature NMR studies. IR studies on **2a** and **5a–e** show that Tpms is a weakly donating ligand, comparable to the $Tp^{CF_3,Me}$ and Tp^{CF_3,CF_3} ligands. Compound **5e** is soluble and stable in dilute acids, showing that Tpms, unlike the Tp ligand, is hydrolytically stable.

Introduction

Since their original synthesis by Trofimenko in 1966,[1] tris(pyrazolyl)borates (Tp′)[2] have proved to be highly useful ligands and are widely used in the synthesis of novel transition metal complexes. Besides their advantages, which make them the most commonly used tripodal nitrogen ligands, tris(pyrazolyl)borates have the disadvantage of being unstable towards hydrolysis. This property can only be attenuated by using substituted pyrazoles in order to protect the labile B−N bonds.[3] Another problem is the low solubility of some (Tp)rhodium compounds. It has been reported several times that $TpRh(CO)_2$ could not be isolated. All attempts to synthesize this compound resulted in the formation of the highly insoluble TpRh(μ-CO)$_3$RhTp.[4]

We have recently reported[5] the synthesis of the novel tris(pyrazolyl)methanesulfonate ligand (Tpms), which was developed in analogy to the Tp ligand (Figure 1).

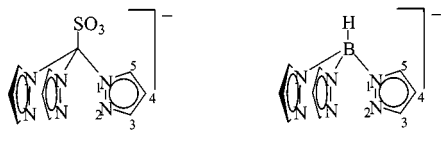

Trispyrazolylmethanesulfonate (Tpms) Trispyrazolylborate (Tp)

Figure 1. Analogy between Tpms and Tp

[a] Institut für Anorganische Chemie und Strukturchemie der Universität Düsseldorf,
Universitätsstraße 1, 40225 Düsseldorf, Germany
E-mail: klaeui@uni-duesseldorf.de
[b] Lehrstuhl für Anorganische Chemie, Technische Universität Chemnitz,
Straße der Nationen 62, 09107 Chemnitz, Germany

Just like Tp, Tpms is a monoanionic, C_{3v}-symmetrical nitrogen-donor ligand. Instead of the boron hydride unit of Tp, Tpms has a methanesulfonate unit, which imparts very good stability towards hydrolysis and an increased solubility in polar solvents.

We describe herein the preparation of the thallium salt of Tpms as a precursor for ligand-exchange reactions and its reactions with $[Rh(LL)Cl]_2$ [LL = cod, nbd, $(CO)_2$]. The solid-state and solution structures of olefin, carbonyl, and phosphane derivatives of (Tpms)rhodium(I) are presented.

Results and Discussion

Synthesis of TlTpms (1)

TlTpms (**1**) was prepared by adding an excess of thallium(I) carbonate to an aqueous solution of LiTpms. After recrystallization from methanol, analytically pure **1** was obtained in 60% yield. The product **1** was found to react readily with transition metal halide complexes.

Although **1** only dissolves freely in water, it has proved to be surprisingly reactive under heterogeneous reaction conditions.

Synthesis of TpmsRh(CO)$_2$ (2a) and TpmsRh(μ-CO)$_3$RhTpms (2b)

Reaction of **1** with $[Rh(CO)_2Cl]_2$ in THF at room temperature gives the corresponding dicarbonyl complex $TpmsRh(CO)_2$ (**2a**) in excellent yield. Solutions of **2a** in THF are unstable and form a pale-yellow deposit. This deposit is highly insoluble in all common organic solvents and has been identified as TpmsRh(μ-CO)$_3$RhTpms (**2b**) by

 © WILEY-VCH Verlag GmbH, 69451 Weinheim, 2001 1434−1948/01/0606−1415 $ 17.50+.50/0

infrared spectroscopy. The characteristic asymmetric μ-CO stretching vibration is found at $\tilde{\nu} = 1860\ cm^{-1}$. The analogous binuclear Tp compound shows a CO stretching vibration at $\tilde{\nu} = 1845\ cm^{-1}$.[4c] This indicates that Tpms is a weaker donor than Tp. Unlike the Tp compound, the Tpms complex **2a** can be kept in solution under a carbon monoxide pressure of about 3 atm. Under these conditions, it is possible to grow yellow crystals of **2a** by diffusion-controlled crystallization from THF/pentane.

Compound **2a** is well soluble in polar organic solvents such as THF and acetone, but only sparingly soluble in less polar solvents such as toluene and dichloromethane. The rate of formation of **2b** appears to be strongly dependent on the concentration of **2a** in solution. At a concentration of 1 g/L under nitrogen, the first traces of **2b** become visible after 30 min. Under 3−4 atm of carbon monoxide pressure, no precipitate is formed within 4 weeks. When the concentration exceeds 2 g/L, the formation of **2b** can only be prevented by higher carbon monoxide pressures. Pressures of 40 atm of carbon monoxide and temperatures up to 80 °C are needed to recover **2a** from **2b** within 24 h.

Just like the tris(pyrazolyl)borates, Tpms is capable of acting as a bidentate or tridentate ligand and thus of forming 16- and 18-electron complexes with the Rh^I d^8-metal centre. NMR studies on **2a** show that all three pyrazoles are equivalent in solution at room temperature. This observation is consistent with either a non-rigid tridentate structure or a bidentate geometry with a dynamic exchange that is fast on the NMR time scale, as is often found in Tp chemistry.[6] In variable-temperature NMR spectra, the signal pattern of the pyrazoles changes from one consistent with C_{3v} symmetry at room temperature to one consistent with C_s symmetry at 203 K. With $\nu_{(CO)}$ stretching bands (sym and asym) of $\tilde{\nu} = 2091$, 2032, and 2023 cm^{-1} in KBr and of $\tilde{\nu} = 2098$, 2090, 2036, and 2024 cm^{-1} in THF, the vibrational frequencies are within the characteristic range for four-coordinate rhodium complexes.[6]

Moreover, the appearance of four bands indicates that there are two different isomers (A and B) in a κ^2-bonding mode (Figure 2).

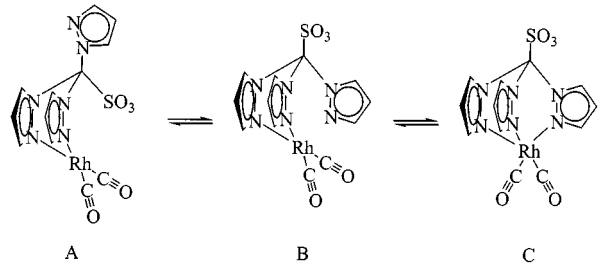

Figure 2. Three possible isomers of $TpmsRh(CO)_2$ (**2a**)

Although evidence for the existence of isomer C could not be observed by IR spectroscopic means, it is probably an intermediate in the dynamic equilibration of the pyrazoles observed by NMR, as ligand exchanges in square-planar d^8 complexes are known to proceed by an associative mechanism involving a five-coordinate intermediate.[7]

The electron-donating capabilities of a ligand can be estimated by comparing the CO stretching vibration bands of a *trans*-CO ligand. Table 1 shows a comparison between **2a** and $Tp'Rh(CO)_2$ compounds. The complexes $Tp^*Rh(CO)_2$,[6] $Tp^{Ph,Me}Rh(CO)_2$[8b] (**2d**), and $Tp^{CF_3,Me}Rh(CO)_2$[8c] (**2e**) show bands that are shifted towards lower energies compared to those of **2a**. Thus, the Tp′ ligands are evidently better donors. Only the highly fluorinated Tp^{CF_3,CF_3} ligand, which has been prepared in order to mimic fluorinated cyclopentadienyl ligands,[9] is a slightly weaker donor than the Tpms ligand. The donor properties of Tpms are intermediate between those of $Tp^{CF_3,Me}$ and Tp^{CF_3,CF_3} in analogous rhodium(I) compounds.

Table 1. CO stretching vibrations (KBr) of **2a** and analogous Tp′ complexes

Complex	ν_{sym}	ν_{asym}
$TpmsRh(CO)_2$ (**2a**)	2091	2023
		2032
$Tp^{Ph,Me}Rh(CO)_2$[8b] (**2d**)	2074	2003
$Tp^{CF_3,Me}Rh(CO)_2$[8c] (**2e**)	2082	2016
		2001
$Tp^{CF_3,CF_3}Rh(CO)_2$[8c]	2096	2038
$Tp^*Rh(CO)_2$[6]	2052	1972

X-ray Structure of 2a

Crystals of **2a** suitable for X-ray analysis were obtained by diffusion-controlled crystallization from THF/pentane. The mother liquor was kept under a carbon monoxide pressure throughout the crystallization in order to avoid the formation of **2b**. **2a** crystallizes in the triclinic space group $P\bar{1}$ with two molecules of **2a** and one molecule of THF per cell unit. The ZORTEP plot given in Figure 3 shows one of the rhodium complexes of **2a**. Selected interatomic distances and angles are presented in Table 2.

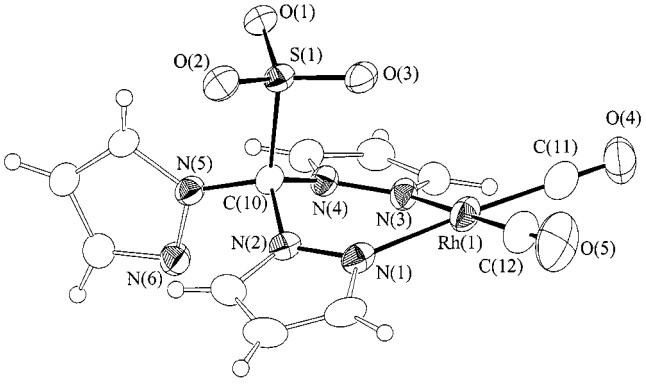

Figure 3. ZORTEP plot of $TpmsRh(CO)_2$ (**2a**) (50% probability)

The rhodium centre is coordinated in a slightly distorted planar geometry. The angle between the planes N(3)−Rh(1)−N(1) and C(11)−Rh(1)−C(12) is 3.0°, shifting the rhodium atom towards the oxygen atom O(3). Tpms acts as a bidentate ligand coordinating with two pyrazole

Table 2. Selected distances [Å] and angles [°] in $TpmsRh(CO)_2$ (**2a**)

Rh(1)−C(12)	1.851(3)	C(12)−Rh(1)−O(3)	105.43(11)
Rh(1)−C(11)	1.852(3)	C(11)−Rh(1)−O(3)	111.83(11)
Rh(1)−N(1)	2.060(2)	N(1)−Rh(1)−O(3)	71.19(7)
Rh(1)−N(3)	2.068(2)	N(3)−Rh(1)−O(3)	75.23(7)
Rh(1)−O(3)	2.8941(18)	O(3)−S(1)−C(10)	102.88(11)
S(1)−C(10)	1.882(3)	S(1)−O(3)−Rh(1)	120.91(10)
O(4)−C(11)	1.137(4)	N(2)−N(1)−Rh(1)	125.11(16)
O(5)−C(12)	1.132(4)	N(1)−N(2)−C(10)	122.5(2)
		N(4)−N(3)−Rh(1)	125.87(15)
C(12)−Rh(1)−C(11)	87.45(14)	N(3)−N(4)−C(10)	123.44(19)
C(12)−Rh(1)−N(1)	94.10(12)	N(6)−N(5)−C(10)	117.98(19)
C(11)−Rh(1)−N(1)	176.13(11)	N(2)−C(10)−N(4)	111.8(2)
C(12)−Rh(1)−N(3)	179.14(11)	N(5)−C(10)−S(1)	111.00(16)
C(11)−Rh(1)−N(3)	91.79(11)	N(2)−C(10)−S(1)	110.08(16)
N(1)−Rh(1)−N(3)	86.63(8)	N(4)−C(10)−S(1)	108.99(17)

Table 3. Selected distances [Å] and angles [°] in **2a**, **2c**, **2d**, and **2e**

Compound	Rh−N	Rh−C	C−O	N−Rh−N
$TpmsRh(CO)_2$ (**2a**)	2.060(2)	1.851(3)	1.137(4)	86.63(8)
	2.068(2)	1.852(3)	1.132(4)	
$[HTp^*Rh(CO)_2]BF_4$[8a] (**2c**)	2.070(4)	1.848(5)	1.127[34]	86.5(1)
	2.093(4)	1.867(6)	1.097[34]	
$Tp^{Ph,Me}Rh(CO)_2$[8b] (**2d**)	2.098(2)	1.851(3)	1.124(4)	86.79(10)
	2.102(2)	1.851(3)	1.134(4)	
$Tp^{CF_3,Me}Rh(CO)_2$[8c] (**2e**)	2.114(5)	1.824(7)	1.147[34]	82.7(2)
	2.116(4)	1.832(9)	1.145[34]	

moieties; one of the sulfonate oxygen atoms points towards the rhodium centre but the Rh(1)−O(3) distance of 2.8941(18) Å exceeds the sum of their van der Waals radii.

From the crystal structures of **2c**, **2d**, **2e**, and **2a** (Table 3), it is evident that the Tpms complex **2a** has the shortest Rh−N bond lengths, which can be attributed to the fact that this complex has the smallest steric demand. The bite angle of **2a** is similar to those found for **2c** and **2d**, but significantly larger than that reported for **2e**.

Synthesis of TpmsRh(cod) (3) and TpmsRh(nbd) (4)

Reactions of **1** with $[Rh(cod)Cl]_2$ and $[Rh(nbd)Cl]_2$ in dichloromethane at room temperature give the corresponding complexes TpmsRh(cod) (**3**) and TpmsRh(nbd) (**4**) in very high yields. Both products were found to be well soluble in most organic solvents. At room temperature, both compounds show ^1H NMR patterns in agreement with C_{3v} symmetry. Again, this is consistent with either a non-rigid κ^3-bonded structure or a κ^2-mode geometry with a dynamic exchange that is fast on the NMR time scale down to 203 K. The methylene protons of the cyclooctadiene allow an assignment of the pyrazole protons by means of NOESY experiments. Complex **3** exhibits peaks at δ = 8.50, 7.68, and 6.55 attributable to the protons attached to C^5, C^3, and C^4, respectively. The corresponding peaks for TpRh(cod) are found at δ = 7.76, 7.58, and 6.21 (not fully assigned).[6]

The prominent downfield shift of the signal of the proton attached to C^5 in Tpms is caused by the deshielding effect of the sulfonate group. The $-I$ effect of the sulfonate group renders the pyrazole groups in the Tpms ligand less electron-rich, whereas the $+I$ effect of the BH group has the opposite effect.

Complexes **3** and **4** readily react with carbon monoxide to give **2a** [Equation (1)]. In the reverse reaction, considerable amounts of **2b** are formed.

$$TpmsRh(LL) \xrightarrow[-\,[LL]]{3 - 4\ atm.\ CO} TpmsRh(CO)_2 \qquad (1)$$

[LL] = 1,5-cyclooctadiene, norbornadiene

X-ray Structure of 3

Crystals of **3** suitable for X-ray analysis were obtained by diffusion-controlled crystallization from dichloromethane/pentane. This complex crystallizes as rods in the monoclinic space group $P2(1)/c$. Figure 4 shows a ZORTEP view of **3**. Selected interatomic distances and angles are given in Table 4.

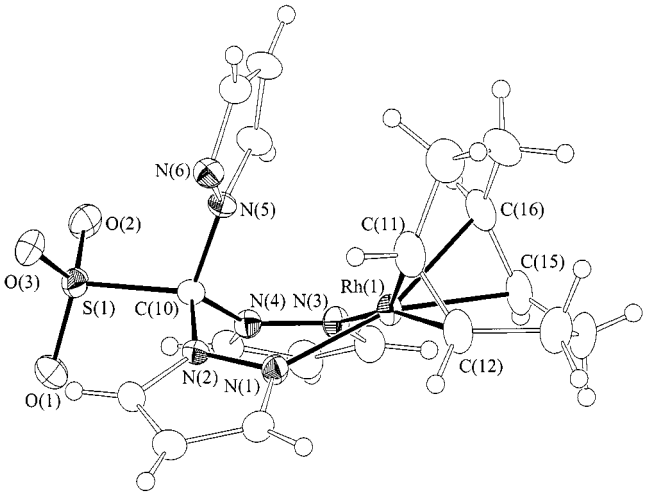

Figure 4. ZORTEP plot of TpmsRh(cod) (**3**) (50% probability)

The rhodium centre adopts a slightly distorted planar geometry with Tpms coordinating as a bidentate ligand. The third pyrazole ring is orientated parallel to the C(11)−Rh(1)−C(16) plane. The distance between the non-coordinating nitrogen atom N(6) and the rhodium centre Rh(1) is 3.535 Å, which exceeds the sum of their van der Waals radii. N(1), N(3), M(1), and M(2) [M(1) and M(2) are the centres of the bond between the olefinic carbon atoms C(11)−C(12) and C(15)−C(16)] deviate from a plane calculated by least-squares fitting by less than 0.05 Å. The rhodium centre is not significantly displaced from this plane. Comparison with the structurally characterized complexes $Tp^{4Bo,3Me}Rh(cod)$,[10] $Tp^{iPr,iPr}Rh(cod)$,[11] $Tp^{Ph}Rh(cod)$,[12] and $B(pz)_4Rh(cod)$[13] shows that the Rh−N and Rh−C bond lengths are equal within experimental errors. Only the bite angles show significant variations. The N−Rh−N angle in **3** [85.46(7)°] resembles the angles in $B(pz)_4Rh(cod)$ [86.6(1)°] and $Tp^{Ph}Rh(cod)$ [84.56(24)°]. The corresponding angles in $Tp^{iPr,iPr}Rh(cod)$

Table 4. Selected distances [Å] and angles [°] in TpmsRh(cod) (**3**)

Rh(1)−N(1)	2.0895(18)	C(16)−Rh(1)−C(12)	90.01(10)
Rh(1)−N(3)	2.1025(18)	C(15)−Rh(1)−C(12)	81.17(10)
Rh(1)−C(11)	2.121(2)	N(2)−N(1)−Rh(1)	122.39(13)
Rh(1)−C(16)	2.125(2)	N(1)−N(2)−C(10)	119.44(16)
Rh(1)−C(15)	2.138(2)	N(4)−N(3)−Rh(1)	121.13(13)
Rh(1)−C(12)	2.140(2)	N(3)−N(4)−C(10)	118.90(16)
S(1)−C(10)	1.891(2)	N(6)−N(5)−C(10)	120.94(17)
N(2)−C(10)	1.450(3)	C(9)−N(5)−C(10)	126.22(18)
N(4)−C(10)	1.465(3)	N(2)−C(10)−N(5)	109.75(16)
N(5)−C(10)	1.454(3)	N(2)−C(10)−N(4)	109.94(16)
C(11)−C(12)	1.386(4)	N(5)−C(10)−N(4)	107.42(16)
C(15)−C(16)	1.386(4)	N(2)−C(10)−S(1)	110.83(14)
		N(5)−C(10)−S(1)	108.75(14)
N(1)−Rh(1)−N(3)	85.46(7)	N(4)−C(10)−S(1)	110.08(13)
N(1)−Rh(1)−C(11)	90.18(9)	C(12)−C(11)−C(18)	125.6(2)
N(3)−Rh(1)−C(11)	157.45(9)	C(12)−C(11)−Rh(1)	71.74(14)
N(1)−Rh(1)−C(16)	160.40(9)	C(18)−C(11)−Rh(1)	110.98(19)
N(3)−Rh(1)−C(16)	95.07(9)	C(11)−C(12)−C(13)	122.5(2)
C(11)−Rh(1)−C(16)	81.82(11)	C(11)−C(12)−Rh(1)	70.30(14)
N(1)−Rh(1)−C(15)	161.64(9)	C(13)−C(12)−Rh(1)	113.73(17)
N(3)−Rh(1)−C(15)	93.86(8)	C(16)−C(15)−C(14)	125.8(2)
C(11)−Rh(1)−C(15)	97.06(10)	C(16)−C(15)−Rh(1)	70.51(14)
C(16)−Rh(1)−C(15)	37.95(11)	C(14)−C(15)−Rh(1)	110.13(18)
N(1)−Rh(1)−C(12)	94.64(8)	C(15)−C(16)−C(17)	124.2(2)
N(3)−Rh(1)−C(12)	164.47(9)	C(15)−C(16)−Rh(1)	71.54(14)
C(11)−Rh(1)−C(12)	37.95(11)	C(17)−C(16)−Rh(1)	112.98(19)

[82.5(1)°] and $Tp^{4Bo,3Me}$Rh(cod) [82.3(2)°] are smaller, probably as a consequence of the levering effect of the bulky substituents in the 5-position of the pyrazoles.[3a]

X-ray Structure of 4

The norbornadiene complex **4** crystallizes in the form of dark-yellow plates in the orthorhombic space group *Pnma*. The ZORTEP plot is shown in Figure 5 and selected interatomic distances and angles are presented in Table 5. Unlike the other structurally characterized Tpms rhodium complexes, **4** has a distorted trigonal-bipyramidal coordination geometry with a genuine κ^3-bonded Tpms ligand. The pyrazole groups of the tripod occupy one axial and two equatorial coordination sites. The atoms N(1), N(1a), Rh(1), C(8), and C(8a) lie in the equatorial plane, while the "axis" N(3)−Rh(1)−M(3) [M(3) is the centre of the bond between the olefinic carbon atoms C(10)−C(10a)] is bent by 10.5°.

The structure resembles those of Tp^{Me}Rh(nbd)[6] (**4a**) and $Tp^{iPr,iPr}$Rh(nbd)[11] (**4b**), where the Tp′ ligands are also bonded in a κ^3-fashion, while in Tp^{Ph}Rh(nbd)[12] and $B(pz)_4$Rh(nbd),[13] the polypyrazolylborates coordinate in a κ^2-mode forming planar complexes. The X-ray analysis shows that all Rh−N separations are significantly shorter in **4** than those in **4a** and **4b** (Table 6), while the Rh−C separations as well as the C=C distances are the same within experimental errors. It is noteworthy that the Rh−N distances to the axially coordinated pyrazole ring in **4**, **4a**, and **4b** are significantly shorter than those to the equatorially coordinated rings. The reason for this is not clear. As a rule, axial bonds are longer than equatorial bonds in trigonal-bipyramidal compounds. However, relatively few trigonal-bipyramidal rhodium(I) complexes are known.[14] A structure correlation analysis of d^8 five-coordinated complexes does not shed any light on the role of trigonal-bipyramidal geometry in favouring the S_N2 pathway in rhodium(I) complexes.[15]

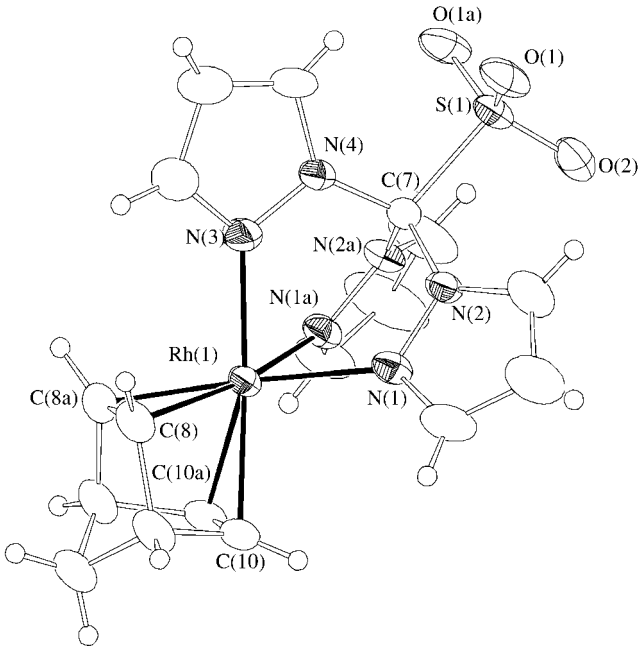

Figure 5. ZORTEP plot of TpmsRh(nbd) (**4**) (50% probability)

Table 5. Selected distances [Å] and angles [°] in TpmsRh(nbd) (**4**)

Rh(1)−N(3)	2.064(3)	C(8)a−Rh(1)−N(1)a	120.79(11)
Rh(1)−C(8)	2.065(3)	C(10)−Rh(1)−N(1)a	117.13(10)
Rh(1)−C(8)a	2.065(3)	C(10)a−Rh(1)−N(1)a	93.09(10)
Rh(1)−C(10)	2.151(3)	N(3)−Rh(1)−N(1)	82.45(9)
Rh(1)−C(10)a	2.151(3)	C(8)−Rh(1)−N(1)	120.79(11)
Rh(1)−N(1)a	2.218(2)	C(8)a−Rh(1)−N(1)	161.15(11)
Rh(1)−N(1)	2.218(2)	C(10)−Rh(1)−N(1)	93.09(10)
S(1)−C(7)	1.895(4)	C(10)a−Rh(1)−N(1)	117.13(10)
N(2)−C(7)	1.464(3)	N(1)a−Rh(1)−N(1)	77.98(11)
N(4)−C(7)	1.455(5)	N(2)−N(1)−Rh(1)	119.95(16)
C(7)−N(2)a	1.464(3)	N(1)−N(2)−C(7)	119.1(2)
C(8)−C(8)a	1.426(7)	N(4)−N(3)−Rh(1)	123.2(2)
C(10)−C(10)a	1.375(6)	N(3)−N(4)−C(7)	119.7(3)
		N(4)−C(7)−N(2)	110.08(19)
N(3)−Rh(1)−C(8)	97.57(12)	N(4)−C(7)−N(2)a	110.08(19)
N(3)−Rh(1)−C(8)a	97.57(12)	N(2)−C(7)−N(2)a	109.6(3)
C(8)−Rh(1)−C(8)a	40.40(19)	N(4)−C(7)−S(1)	109.2(2)
N(3)−Rh(1)−C(10)	158.69(9)	N(2)−C(7)−S(1)	108.94(17)
C(8)−Rh(1)−C(10)	66.80(12)	N(2)a−C(7)−S(1)	108.94(17)
C(8)a−Rh(1)−C(10)	80.02(12)	C(8)a−C(8)−C(9)	105.64(18)
N(3)−Rh(1)−C(10)a	158.69(9)	C(8)a−C(8)−Rh(1)	69.80(9)
C(8)−Rh(1)−C(10)a	80.02(12)	C(9)−C(8)−Rh(1)	99.27(19)
C(8)a−Rh(1)−C(10)a	66.80(12)	C(10)a−C(10)−C(9)	106.67(18)
C(10)−Rh(1)−C(10)a	37.26(17)	C(10)a−C(10)−Rh(1)	71.37(8)
N(3)−Rh(1)−N(1)a	82.45(9)	C(9)−C(10)−Rh(1)	95.80(18)
C(8)−Rh(1)−N(1)a	161.15(11)		

Synthesis of TpmsRh(CO)PPh_3 (5a), TpmsRh(CO)PMe_3 (5b), and TpmsRh(CO)PCy_3 (5c)

All phosphane complexes were synthesized by adding the phosphane to a THF solution of **2a**. The highly basic tri-

Table 6. Selected distances [Å] and angles [°] in **4**, **4a**, and **4b**

Compound	Rh−N	Rh−C	C=C	N−Rh−N
TpmsRh(nbd) (**4**)	2.064(3)	2.065(3)	1.375(6)	77.98(11)
	2.218(2)	2.065(3)	1.426(7)	82.45(9)
	2.218(2)	2.151(3)		82.45(9)
		2.151(3)		
$Tp^{Me}Rh(nbd)$[6] (**4a**)	2.147(7)	2.07(1)	1.37(3)	89.6(4)
	2.247(9)	2.09(1)	1.45(3)	82.2(3)
	2.25(1)	2.154(8)		82.4(4)
		2.16(1)		
$Tp^{iPr,iPr}Rh(nbd)$[11] (**4b**)	2.146(4)	2.069(5)	1.364(6)	90.4(1)
	2.260(4)	2.074(5)	1.448(6)	82.5(1)
	2.273(4)	2.137(5)		81.5(1)
		2.149(4)		

Table 7. $^{31}P\{^1H\}$ NMR and IR data of **5a**−**5c** and selected Tp′ compounds

Compound	$\delta^{31}P$ [ppm]	$^1J_{RhP}$ [Hz]	ν_{CO}[a] [cm^{-1}]
TpmsRh(CO)PPh_3 (**5a**)	44	158	2000
Tp*Rh(CO)PPh_3[17] (**5e**)	42.55	162	1978[b]
$Tp^{Ph,Me}$Rh(CO)PPh_3[8b] (**5f**)	42.39	164	1983
TpRh(CO)PPh_3[19] (**5h**)	44	156	1978
TpmsRh(CO)PMe_3 (**5b**)	2.6	148	1990
Tp*Rh(CO)PMe_3[18] (**5g**)	6.05	146	1961[b]
TpmsRh(CO)PCy_3 (**5c**)	52	153	1978
TpRh(CO)PCy_3[19] (**5i**)			1947

[a] KBr. − [b] CH_2Cl_2.

methylphosphane had to be added slowly in stoichiometric amounts in order to avoid displacement of the second carbon monoxide ligand or the tripod, as was observed in the case of Tp*Rh$(C_2H_4)_2$.[16] The less basic and sterically more crowded tricyclohexyl- and triphenylphosphane could be added in excess. The displacement of carbon monoxide is a fast reaction; it was not necessary to work under carbon monoxide pressure in order to avoid the formation of **2b**. The corresponding TpmsRh(CO)PR_3 complexes were obtained as bright-yellow crystals in excellent yields. They were found to be well soluble in most organic solvents.

At room temperature, all TpmsRh(CO)PR_3 compounds show ^1H NMR patterns in agreement with C_{3v} symmetry, indicating rapid exchange of the pyrazoles on the NMR time scale. ^1H NMR studies on **5a** show that two pyrazole groups become equivalent at 203 K, displaying a 2:1 intensity ratio, which is consistent with a C_s-symmetric complex or a fast exchange of only two pyrazole groups. Similar effects have been observed for the corresponding Tp′ compounds Tp*Rh(CO)PPh_3[17] (**5e**), $Tp^{Ph,Me}$Rh(CO)PPh_3[8b] (**5f**), and Tp*Rh(CO)PMe_3[18] (**5g**). The exchange mechanisms for **5f** and **5g** were suggested to proceed via trigonal-bipyramidal intermediates. The $\Delta G^{\neq}$ values estimated from the coalescence temperatures were 76.5 kJ/mol for the bulky **5f**[8b] and 63 kJ/mol for the less bulky **5g**.[18] As **5a** is even less sterically hindered, it is consistent that its $\Delta G^{\neq}$ value is considerably smaller (46±2 kJ/mol). It can be assumed that the exchange takes place between the free nitrogen atom N(6) and the nitrogen atom N(3) lying *trans* to the CO ligand, because the $\Delta G^{\neq}$ value is similar to those estimated for **2a** (47±2 kJ/mol) and **5b** (47±2 kJ/mol). This is consistent with the fact that CO has a larger *trans* effect than PR_3.[7] The $^{31}P\{^1H\}$ NMR spectrum of **5a** shows a doublet at $\delta = 44$ ($^1J_{RhP} = 158$ Hz), which is comparable with those of **5e**, **5f**, and TpRh(CO)PPh_3[19] (**5h**) (Table 7).

The CO stretching vibration of **5a** is found at considerably higher energy than those of **5e**, **5f**, and **5h**. This indicates that the electronic properties of the tripod have a big influence on the CO stretching vibration. Comparison of the Tp′ compounds **5e**, **5f**, and **5h** shows that the steric properties of the ligands have only small effects on the CO stretching vibration. A similar conclusion is reached on comparing **5b** and **5c** with the corresponding Tp′ compounds **5g** and **5i**.

X-ray Structure of 5a

The Tpms complex **5a** crystallizes as thin rods in the triclinic space group $P\bar{1}$. The asymmetric unit contains one molecule of **5a** and one molecule of THF. Figure 6 shows a ZORTEP plot of **5a**, and a selection of interatomic distances and angles is given in Table 8.

The rhodium atom is coordinated in a slightly distorted planar geometry. The Tpms coordinates as a bidentate ligand and the non-coordinating pyrazole group is located above the coordination plane. The distance between Rh(1) and the non-coordinating N(6) is 3.513 Å, which exceeds the sum of their van der Waals radii. The different *trans* effects of PPh_3 and CO are not manifested in different bond lengths Rh(1)−N(3) [2.100(3) Å] and Rh(1)−N(1) [2.093(3) Å].

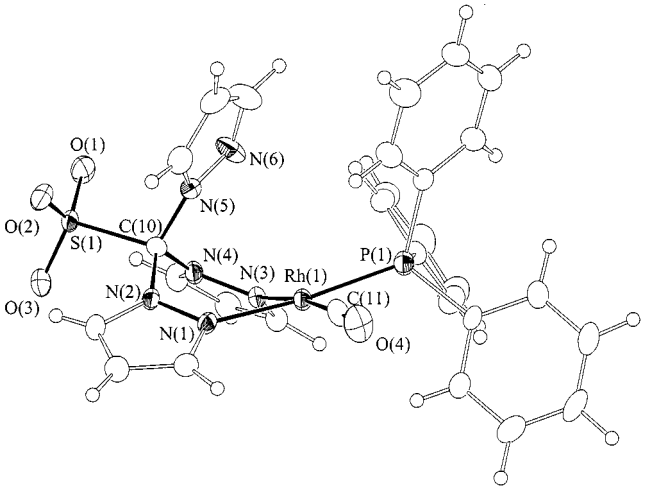

Figure 6. ZORTEP plot of TpmsRh(CO)PPh_3 (**5a**) (50% probability)

Table 8. Selected distances [Å] and angles [°] in $TpmsRh(CO)PPh_3$ (**5a**)

Rh(1)−C(11)	1.816(4)	C(12)−P(1)−C(18)	106.06(17)
Rh(1)−N(1)	2.093(3)	C(12)−P(1)−C(24)	103.28(17)
Rh(1)−N(3)	2.100(3)	C(18)−P(1)−C(24)	102.97(19)
Rh(1)−P(1)	2.2734(13)	C(12)−P(1)−Rh(1)	111.49(14)
P(1)−C(12)	1.825(4)	C(18)−P(1)−Rh(1)	115.07(12)
P(1)−C(18)	1.827(4)	C(24)−P(1)−Rh(1)	116.71(12)
P(1)−C(24)	1.828(4)	N(2)−N(1)−Rh(1)	122.9(2)
S(1)−C(10)	1.893(4)	N(1)−N(2)−C(10)	119.2(3)
O(4)−C(11)	1.148(5)	N(4)−N(3)−Rh(1)	122.7(3)
N(2)−C(10)	1.472(4)	N(3)−N(4)−C(10)	120.2(3)
N(4)−C(10)	1.440(5)	N(6)−N(5)−C(10)	119.8(3)
N(5)−C(10)	1.453(5)	C(9)−N(5)−C(10)	126.9(3)
		N(4)−C(10)−N(5)	109.3(3)
C(11)−Rh(1)−N(1)	92.24(14)	N(4)−C(10)−N(2)	110.5(3)
C(11)−Rh(1)−N(3)	172.68(14)	N(5)−C(10)−N(2)	108.2(3)
N(1)−Rh(1)−N(3)	84.09(12)	N(4)−C(10)−S(1)	111.0(2)
C(11)−Rh(1)−P(1)	87.20(12)	N(5)−C(10)−S(1)	109.1(2)
N(1)−Rh(1)−P(1)	174.21(9)	N(2)−C(10)−S(1)	108.7(2)
N(3)−Rh(1)−P(1)	97.09(9)	O(4)−C(11)−Rh(1)	176.3(3)

Synthesis of $TpmsRh(CO)PPh_2PhSO_3K·H_2O$ (5d)

An excess of $PPh_2PhSO_3K·H_2O$ was added to a THF solution of the dicarbonyl compound **2a**. As this is a slow heterogeneous reaction, it was necessary to keep the mixture under carbon monoxide pressures of about 3 atm in order to avoid formation of the binuclear compound **2b**. The resulting complex **5d** was found to be soluble in wet THF and could be separated from the excess phosphane by filtration. It was then precipitated by overlaying the THF solution with pentane.

Compound **5d** was found to be well soluble in water, but formed colloidal rhodium within a few minutes. This decomposition of the complex was evidently not triggered by decomposition of the ligands, as free Tpms as well as the phosphane could be detected. We suspect that the rhodium centre is attacked by hydroxy ions, which leads to redox reactions and thus to decomposition of the complex. Indeed, it was found that the decomposition could be prevented by dissolving **5d** in very dilute phosphoric or sulfuric acid (pH = 3−4). Tpms is stable under these conditions.[5] At lower pH values, Tpms is protonated and thus loses its coordinative ability towards the rhodium centre. All three pyrazole groups are seen to be equivalent according to the ^1H NMR spectrum. The signals are slightly broadened at room temperature. We could not obtain single crystals of **5d**, but the similarity of its NMR and IR data to those of **5a** is evident.

Conclusion

The thallium salt of the novel ligand Tpms is a convenient starting material for the preparation of rhodium(I) complexes. The sulfonate group of Tpms ensures good solubility in polar solvents. This has allowed the isolation of the planar dicarbonyl complex $TpmsRh(CO)_2$ (**2a**). The corresponding complex of the Trofimenko ligand Tp is not sufficiently stable for a crystal structure analysis. The IR data (ν_{CO}) indicate that Tpms is a remarkably weaker donor than the Tp ligand in carbonylrhodium(I) complexes. Its donor strength is similar to that of the Tp^{CF_3,CF_3} ligand. The lower donor strength of Tpms does not result in longer rhodium−nitrogen bonds. In fact, the X-ray structures of $TpmsRh(CO)_2$ (**2a**) and TpmsRh(nbd) (**4**) show that Tpms forms shorter rhodium−nitrogen bonds than the sterically more demanding Tp ligands (Tp^{Me}, $Tp^{CF_3,Me}$, $Tp^{Ph,Me}$, $Tp^{iPr,iPr}$) in analogous compounds.

It is noteworthy that the Tpms ligand acts as a bis(chelating) ligand in TpmsRh(cod) (**3**) but as a tris(chelating) ligand in TpmsRh(nbd) (**4**). We can see no obvious reason for this behaviour. $TpRh^I$ complexes with a coordination number of five are very rare. To the best of our knowledge, $Tp^{iPr,iPr}$ is the only other Tp ligand that has been shown to act both as a bidentate and as a tridentate ligand in rhodium(I) complexes.[11] Jones et al. have found that the hapticity of Tp ligands correlates with the ^{11}B chemical shift.[20] The corresponding probe for the Tpms ligand would be the ^{13}C chemical shift of the methanesulfonato carbon atom. However, the ^{13}C chemical shifts for the structurally characterized compounds **3**, **4**, and **5a** are not significantly different. Thus, these data do not correlate with the solid-state structures, leaving the denticity of the Tpms ligand in solution ambiguous.

According to our preliminary experiments, all the $TpmsRh^I$ compounds described herein can be used as precursors for catalysts in hydroformylation reactions. We are currently investigating the differences between the ligands Tpms and Tp in rhodium-catalyzed reactions.

Experimental Section

General Remarks: The compounds tris(pyrazolyl)methane,[21] LiTpms,[5] $[\{Rh(CO)_2Cl\}_2]$,[22] $[\{Rh(nbd)Cl\}_2]$,[23] $[\{Rh(cod)Cl\}_2]$,[24] and $P(C_6H_5)_2(p\text{-}C_6H_4\text{-}SO_3K)·H_2O$[25] were synthesized according to literature procedures. All other reagents were commercial samples and were used as received. All reactions were carried out under nitrogen using standard Schlenk techniques unless stated otherwise. Solvents were purified and degassed by standard procedures. Methanol and ethanol used in the work-up of **1** were used without further purification. Filtration was carried out using 1-μm membrane filters (regenerated cellulose, Schleicher & Schuell). Reactions under 3−4 atm pressure were performed in glass tubes equipped with Teflon seals and valves. ***All operations in glass vessels at elevated pressures should be performed using effective body and face protection!*** − One-dimensional ^1H, ^{31}P, and ^{13}C NMR spectra were recorded with Bruker DRX 200 (at 293 K) or Bruker DRX 500 (at 298 K) spectrometers. Two-dimensional NOESY and COSY as well as one-dimensional DEPT spectra were recorded with a Bruker DRX 500 spectrometer. Chemical shifts (δ) are given in ppm referenced to the solvent peak. Spectra recorded using $[D_8]$THF as a solvent were referenced to tetramethylsilane. Spectra recorded using D_2O as a solvent were referenced to sodium

3-(trimethylsilyl)-1-propanesulfonate. The spectrum of **5d** was recorded in dilute D_3PO_4 solution (pH = 3−4), which was prepared from D_2O and P_4O_{10} under inert conditions. Chemical shifts were ±0.01 ppm for δ^1H, ±0.1 ppm for $\delta^{31}P$ and ±0.1 ppm for $\delta^{13}C$. − Infrared spectra were recorded with a Bruker IFS 66 FT spectrometer. − Electron impact (EI) mass spectra were recorded with a Varian MAT 311 A instrument with an ionization energy of 70 eV. FAB mass spectra were recorded with a Finnigan MAT 8200 instrument using an NBA matrix. − Elemental analyses were performed using a Perkin−Elmer CHN-2400/II elemental analyzer.

Thallium(I) Tris(pyrazol-1-yl)methanesulfonate, TlTpms (1): A solution of tris(pyrazolyl)methane (4.9 g, 23 mmol) in THF (100 mL) was cooled to −78 °C and a 1.6 M solution of *n*-butyllithium (16 mL, 26 mmol) was slowly added. The solution was stirred for 1 h while the temperature was allowed to rise to 0 °C. After subsequent cooling to −60 °C, trimethylamine−sulfur trioxide (4.2 g, 30 mmol) was added and the resulting suspension was stirred overnight while the temperature was allowed to rise to 25 °C. The mixture was then filtered through a membrane filter and the solid residue was added to a solution of thallium(I) carbonate (7.1 g, 15 mmol) in water (150 mL). The resulting mixture was stirred at 60−70 °C for 1 h and then the solvent was evaporated under reduced pressure. The residue was extracted for 4 h with wet ethanol to remove less polar by-products. The remaining residue was recrystallized from 1 L of wet methanol to give 6.9 g of colourless crystals (60%). − ^1H NMR (200 MHz, D_2O): δ = 6.56 (dd, $^3J_{HH}$ = 2.7 Hz, $^3J_{HH}$ = 1.8 Hz, 3 H, pyrazolyl 4-H), 7.65 (dd, $^3J_{HH}$ = 2.7 Hz, $^4J_{HH}$ = 0.6 Hz, 3 H, pyrazolyl 3-/5-H), 7.75 (dd, $^3J_{HH}$ = 1.8 Hz, $^4J_{HH}$ = 0.6 Hz, 3 H, pyrazolyl 3-/5-H). − $^{13}C\{^1H\}$ NMR (500 MHz, D_2O): δ = 98.7 (s, C−SO_3), 110.5 (s, pyrazolyl C^4), 135.2 (s, pyrazolyl $C^{3/5}$), 145.4 (s, pyrazolyl $C^{3/5}$). − IR (KBr): $\tilde{\nu}$ = 3150 cm^{-1}, 3137 (w, C−H), 1522 (s, C=C), 1089, 1059, 1052, 1039 (s, S=O). − MS (FAB^+): *m/z* (%) = 499 (1.3) $[M + H]^+$. − $C_{10}H_9N_6O_3STl$ (497.7): calcd. C 24.00, H 1.81, N 16.79; found C 24.04, H 1.80, N 16.87.

Dicarbonyl[tris(pyrazol-1-yl)methanesulfonato]rhodium(I), $TpmsRh(CO)_2$ (2a): A mixture of the carbonylrhodium chloride complex $[\{Rh(CO)_2Cl\}_2]$ (78 mg, 0.20 mmol) and **1** (0.20 g, 0.40 mmol) in THF (200 mL) was pressurized with 3−4 atm of carbon monoxide and stirred for 16 h at room temperature. Thereafter, the precipitated TlCl was allowed to settle and the supernatant solution was siphoned into another vessel by means of a cannula. From the clear yellow solution, 0.19 g (100%) of **2a** was obtained. To obtain yellow crystals of **2a** suitable for X-ray analysis, the solution was overlaid with pentane, pressurized with 3−4 atm of carbon monoxide, and left until crystallization occurred. − ^1H NMR (200 MHz, [D_6]acetone): δ = 6.73 (dd, $^3J_{HH}$ = 3.0 Hz, $^3J_{HH}$ = 2.1 Hz, 3 H, pyrazolyl 4-H), 8.19 (d, $^3J_{HH}$ = 2.1 Hz, 3 H, pyrazolyl 3-/5-H), 8.24 (d, $^3J_{HH}$ = 3.0 Hz, 3 H, pyrazolyl 3-/5-H).[26] − IR (KBr): $\tilde{\nu}$ = 3169 cm^{-1}, 3152 (w, C−H), 1520 (s, C=C), 2091, 2032, 2023 (vs, C=O) 1086, 1073, 1054, 1040 (s, S=O). − MS (FAB^+): *m/z* (%) = 453 (5.6) $[M + H]^+$. − $C_{12}H_9N_6O_5RhS$ (452.2): calcd. C 31.87, H 2.01, N 18.58; found C 32.13, H 2.20, N 18.49.

μ-Tricarbonylbis{[tris(pyrazol-1-yl)methanesulfonato]rhodium(I)}, $TpmsRh(\mu\text{-}CO)_3RhTpms$ (2b): Compound **2b** was formed when a solution of **2a** in THF was left without a positive pressure of carbon monoxide. The solvent was slowly evaporated from a solution of **2a** (45 mg, 0.10 mmol) in THF by passing a gentle stream of nitrogen over it. After 2 d, the residue was dried in vacuo to give 44 mg (100%) of **2b** as an amorphous pale-yellow powder. − IR (KBr): $\tilde{\nu}$ = 3191 cm^{-1}, 3150, 3110 (m, C−H), 1861 (vs, C=O), 1522 (s, C=C), 1081, 1068, 1051 (s, S=O). − $C_{23}H_{18}N_{12}O_9Rh_2S_2$ (876.4): calcd. C 31.52, H 2.07, N 19.18; found C 31.82, H 2.42, N 18.82.

(Cycloocta-1,5-diene)[tris(pyrazol-1-yl)methanesulfonato]rhodium(I), TpmsRh(cod) (3): A mixture of the (cyclooctadiene)rhodium chloride complex $[\{Rh(cod)Cl\}_2]$ (99 mg, 0.20 mmol) and **1** (0.20 g, 0.40 mmol) in dichloromethane (50 mL) was stirred for 16 h at room temperature. The precipitated TlCl was then separated by filtration. Evaporation of the solvent from the filtrate afforded 0.20 g (100%) of **3** as a yellow powder. To obtain yellow crystals of **3** suitable for X-ray analysis, the filtrate was concentrated to 10% of its original volume and then overlaid with pentane. − ^1H NMR (200 MHz, $CDCl_3$): δ = 1.9 (m, 4 H, cod CH_2), 2.3 (m, 4 H, cod CH_2), 4.15 (br. s, 4 H, cod CH), 6.55 (dd, $^3J_{HH}$ = 2.9 Hz, $^3J_{HH}$ = 2.1 Hz, 3 H, pyrazolyl 4-H), 7.68 (d, $^3J_{HH}$ = 2.1 Hz, 3 H, pyrazolyl 3-H), 8.50 (br. s, 3 H, pyrazolyl 5-H). − $^{13}C\{^1H\}$ NMR (500 MHz, CD_2Cl_2): δ = 29.2 (s, cod CH_2), 82.6 (d, $^1J_{RhC}$ = 12.7 Hz, cod = CH), 93.4 (s, C−SO_3), 106.5 (s, pyrazolyl C^4), 135.1 (s, pyrazolyl C^5), 141.2 (s, pyrazolyl C^3). − IR (KBr): $\tilde{\nu}$ = 3165 cm^{-1}, 3148, 3111 (m, C−H), 1521 (s, C=C), 1086, 1081, 1054, 1043 (s, S=O). − MS (EI, 300 °C): *m/z* (%) = 504 (12.7) $[M]^+$, 424 (1.9) $[M - SO_3]^+$, 357 (62.2) $[M - SO_3 - C_3H_3N_2]^+$. − $C_{18}H_{21}N_6O_3RhS$ (504.4): calcd. C 42.86, H 4.20, N 16.66; found C 42.67, H 4.26, N 16.74.

(Bicyclo[2.2.1]hepta-2,5-diene)[tris(pyrazol-1-yl)methanesulfonato]rhodium(I), TpmsRh(nbd) (4): A mixture of the (norbornadiene)rhodium chloride complex $[\{Rh(nbd)Cl\}_2]$ (23 mg, 0.050 mmol) and **1** (50 mg, 0.10 mmol) in dichloromethane (30 mL) was stirred for 16 h at room temperature. The precipitated TlCl was then separated by membrane filtration. Evaporation of the solvent from the filtrate afforded 48 mg (100%) of **4** as a yellow powder. To obtain dark-yellow crystals of **4** suitable for X-ray analysis, the filtrate was concentrated to 10% of its original volume and then overlaid with pentane. − ^1H NMR (200 MHz, CD_2Cl_2): δ = 1.38 (br. s, 2 H, nbd CH_2), 3.89 (br. s, 4 H, nbd =CH), 3.90 (br. s, 2 H, nbd CH), 6.50 (dd, $^3J_{HH}$ = 2.8 Hz, $^3J_{HH}$ = 2.0 Hz, 3 H, pyrazolyl 4-H), 7.55 (d, $^3J_{HH}$ = 2.0 Hz, 3 H, pyrazolyl 3-H), 8.20 (d, 3 H, $^3J_{HH}$ = 2.8 Hz, pyrazolyl 5-H). − $^{13}C\{^1H\}$ NMR (500 MHz, CD_2Cl_2): δ = 49.4 (d, $^2J_{RhC}$ = 2.6 Hz, nbd CH), 52.6 (d, $^1J_{RhC}$ = 11.2 Hz, nbd =CH), 60.4 (d, $^3J_{RhC}$ = 6.9 Hz, nbd CH_2), 93.5 (s, C−SO_3), 106.1 (s, pyrazolyl C^4), 134.6 (s, pyrazolyl C^5), 141.2 (s, pyrazolyl C^3). − IR (KBr): $\tilde{\nu}$ = 3142 cm^{-1}, 3121, 2994, 2898 (m, C−H), 1523 (s, C=C), 1083, 1068, 1053 (s, S=O). − MS (EI, 320 °C): *m/z* (%) = 488 (16.5) $[M]^+$, 408 (7.4) $[M - SO_3]^+$, 341 (100.0) $[M - SO_3 - C_3H_3N_2]^+$. − $C_{17}H_{17}N_6O_3RhS{\cdot}H_2O$ (506.4): calcd. C 40.33, H 3.78, N 16.60; found C 40.65, H 3.57, N 16.31.

Carbonyl(triphenylphosphane)[tris(pyrazol-1-yl)methanesulfonato]rhodium(I), $TpmsRh(CO)PPh_3$ (5a): Triphenylphosphane (0.52 g, 2.0 mmol) was added to solution of **2a** (0.19 g, 0.40 mmol) in THF (200 mL). After 1 h, the solution was concentrated to a volume of 10 mL and overlaid with pentane. Crystallization yielded 0.29 g (100%) of a THF adduct of **5a** as bright-yellow needles. The crystals obtained were suitable for X-ray analysis. − ^1H NMR (200 MHz, CD_2Cl_2): δ = 6.38 (dd, $^3J_{HH}$ = 2.8 Hz, $^3J_{HH}$ = 2.2 Hz, 3 H, pyrazolyl 4-H), 7.29 (d, $^3J_{HH}$ = 2.2 Hz, 3 H, pyrazolyl 3-H), 7.5 [m, 15 H, $P(C_6H_5)_3$], 8.44 (d, $^3J_{HH}$ = 2.8 Hz, 3 H, pyrazolyl 5-H). − $^{31}P\{^1H\}$ NMR (200 MHz, CD_2Cl_2): δ = 45 (d, $^1J_{RhP}$ = 158 Hz). − $^{13}C\{^1H\}$ NMR (500 MHz, CD_2Cl_2): δ = 93.2 (s, C−SO_3), 106.4 (s, pyrazolyl C^4), 127.9 (d, $^2J_{PC}$ = 10 Hz, PPh_3 C^2), 129.9 (br. s, PPh_3 C^4), 130.5 (d, $^1J_{PC}$ = 3 Hz, PPh_3 C^1), 133.7 (d, $^3J_{PC}$ = 12 Hz, PPh_3 C^3), 134.7 (s, pyrazolyl C^5), 143.3 (s, pyrazolyl C^3), 187.3 (dd, $^1J_{RhC}$ = 74 Hz, $^2J_{PC}$ = 23 Hz, CO). − IR (KBr):

$\tilde{\nu}$ = 3168 cm^{-1}, 3154, 3134, 3124 (s, C−H), 1989 (vs, C=O), 1627 (s, C−C C_6H_5), 1520 (s, C=C), 1438 (s, P−C), 1479, 1438, 1405 (s, C−C C_6H_5), 1081, 1070, 1056, 1040 (s, S=O). − MS (FAB$^+$): *m/z* (%) = 686 (0.5) $[M]^+$, 658 (1.3) $[M - CO]^+$. − $(C_{29}H_{24}N_6O_4PRhS)_4(C_4H_8O)_3$ (2962.3): calcd. C 51.90, H 4.08, N 11.35; found C 51.98, H 4.12, N 11.22.

Carbonyl(trimethylphosphane)[tris(pyrazol-1-yl)methanesulfonato]rhodium(I), TpmsRh(CO)PMe$_3$ (5b): A 1 M THF solution of trimethylphosphane (0.1 mL, 0.1 mmol) was slowly added to a solution of **2a** (45 mg, 0.10 mmol) in THF (50 mL). After 1 h, the solution was concentrated to a volume of 4 mL and overlaid with pentane. Crystallization yielded 56 mg (100%) of a THF adduct of **5b** as bright-yellow needles. − ^{1}H NMR (200 MHz, CD_2Cl_2): δ = 1.48 [dd, $^3J_{RhH}$ = 10.3 Hz, $^2J_{PH}$ = 1.5 Hz, 9 H, $P(CH_3)_3$], 6.56 (dd, $^3J_{HH}$ = 2.9 Hz, $^3J_{HH}$ = 0.9 Hz, 3 H, pyrazolyl 4-H), 7.76 (d, $^3J_{HH}$ = 2.9 Hz, 3 H, pyrazolyl 3-H), 8.45 (br. s, 3 H, pyrazolyl 5-H). − ^{31}P{^{1}H} NMR (200 MHz, CD_2Cl_2): δ = 3 (d, $^1J_{RhP}$ = 148 Hz). − ^{13}C{^{1}H} (500 MHz, [D$_8$]THF): δ = 17.4 [d, $^1J_{PC}$ = 36.3 Hz, $P(CH_3)_3$], 107.2 (s, pyrazolyl C^4), 136.6 (s, pyrazolyl C^5), 144.0 (s, pyrazolyl C^3). − IR (KBr): $\tilde{\nu}$ = 3164 cm^{-1}, 3132 (s, C−H), 1990 (vs, C=O), 1519 (s, C=C), 1438 (s, P−C), 1081, 1068, 1057, 1044 (s, S=O). − MS (EI, 200 °C): *m/z* (%) = 500 (21.5) $[M]^+$, 472 (6.5) $[M - CO]^+$, 392 (19.9) $[M - CO - SO_3]^+$. − $(C_{14}H_{18}N_6O_4PRhS)\cdot(C_4H_8O)$ (560.4): calcd. C 37.77, H 4.58, N 14.68; found C 37.39, H 4.80, N 14.49.

Carbonyl(tricyclohexylphosphane)[tris(pyrazol-1-yl)methanesulfonato]rhodium(I), TpmsRh(CO)PCy$_3$ (5c): Tricyclohexylphosphane (0.14 g, 0.5 mmol) was added to solution of **2a** (45 mg, 0.10 mmol) in THF (50 mL). After 1 h, the solution was concentrated to a volume of 5 mL and overlaid with pentane. Crystallization yielded a bright-yellow THF adduct of **5c** (58 mg, 80%). − ^{1}H NMR (200 MHz, CD_2Cl_2): δ = 1−2 [m, 33 H, $P(C_6H_{11})_3$], 6.54 (dd, $^3J_{HH}$ = 2.8 Hz, $^3J_{HH}$ = 0.7 Hz, 3 H, pyrazolyl 4-H), 7.78 (br. s, 3 H, pyrazolyl 3-H), 8.46 (br. s, 3 H, pyrazolyl 5-H). − ^{31}P{^{1}H} NMR (200 MHz, CD_2Cl_2): δ = 52 (d, $^1J_{RhP}$ = 153 Hz).[26] − IR (KBr): $\tilde{\nu}$ = 3168 cm^{-1} (vs, C−H), 2851, 2929 (vs, C−H), 1978 (vs,

Table 9. Crystallographic data for TpmsRh(CO)$_2$ (**2a**), TpmsRh(cod) (**3**), TpmsRh(nbd) (**4**), and TpmsRh(CO)PPh$_3$ (**5a**)

	2a	**3**	**4**	**5a**
Crystal shape	triclinic block	rod	plate	thin rod
Crystal colour	yellow	yellow	yellow	yellow
Crystal size [mm]	0.3 × 0.25 × 0.15	0.8 × 0.3 × 0.2	0.52 × 0.38 × 0.10	0.6 × 0.15 × 0.1
Empirical formula	$(C_{12}H_9N_6O_5RhS)_2\cdot(C_4H_8O)$	$C_{18}H_{21}N_6O_3RhS$	$C_{17}H_{17}N_6O_3RhS$	$(C_{29}H_{24}N_6O_4PRhS)\cdot(C_4H_8O)$
Molecular mass	488.27	504.38	488.34	758.59
Crystal system	triclinic	monoclinic	orthorhombic	triclinic
Space group	$P\bar{1}$	$P2_1/c$	*Pnma*	$P\bar{1}$
a [Å]	7.7753(1)	8.6948(1)	11.8020(9)	8.347(2)
b [Å]	10.7131(1)	14.6997(2)	9.7113(8)	14.353(2)
c [Å]	11.7510(2)	15.3120(1)	15.6993(12)	14.679(3)
α [°]	113.2735(9)	90	90	76.14(3)
β [°]	98.0074(9)	100.980(1)	90	82.12(4)
γ [°]	94.3890(4)	90	90	75.29(4)
V [Å^3]	881.05(2)	1921.21(3)	1799.3(2)	1646.0(6)
Z	2	4	4	2
$\rho_{calcd.}$ [g/cm^3]	1.841	1.744	1.803	1.531
Radiation used (λ [Å])	Mo-K_α (0.71073)	Mo-K_α (0.71073)	Mo-K_α (0.71073)	Mo-K_α (0.71073)
T [K]	173(2)	173(2)	173(2)	173(2)
Scan method	φ scans	φ scans	φ scans	φ scans
μ [mm^{-1}]	1.132	1.032	1.099	0.682
Total reflections	8229	13914	13342	12681
Independent reflections	4694	5218	2815	7173
Unique reflections	3651	4343	2039	5115
Used reflections	4694	5218	2815	7173
R(int)	0.0295	0.0360	0.0459	0.0508
Scan range θ [°]	1.92−30.45	1.94−30.30	2.16−30.91	1.43−30.23
Index ranges	$-10 \le h \le 10$	$-11 \le h \le 12$	$-16 \le h \le 16$	$-11 \le h \le 11$
	$-14 \le k \le 14$	$-20 \le k \le 20$	$-10 \le k \le 13$	$-16 \le k \le 19$
	$-15 \le l \le 16$	$-12 \le l \le 21$	$-21 \le l \le 22$	$-20 \le l \le 18$
Completeness to $\theta_{max.}$ [%]	87.7	90.7	93.9	73.2
F(000)	488	1024	984	776
R,[a] wR^2 [$I > 2\sigma(I)$][b]	0.0335, 0.0729	0.0322, 0.0693	0.0336, 0.0717	0.0509, 0.0935
R indices (all data), *w*R^2	0.0513, 0.0805	0.0449, 0.0726	0.0593, 0.0817	0.0844, 0.1043
Maximum δ/σ	0.740	0.017	0.010	0.008
Max./min. el. density [e·Å^{-3}]	0.444/−0.611	0.677/−0.783	0.518/−0.663	1.043/−0.866
Used reflections	4694	5218	2815	7173
Least-squares restraints	5	0	0	0
Refined parameters	298	346	181	520
Goodness-of-fit on F^2 [c]	0.997	1.044	0.999	0.975
Weighting scheme parameters *a*/*b*[d]	0.0329/0	0.0311/0.4132	0.0321/2.4949	0.0410/0

[a] $R_1 = \Sigma(||F_o| - |F_c||)/\Sigma|F_o|$. − [b] $wR^2 = \{\Sigma[w(F_o^2 - F_c^2)^2]/\Sigma(wF_o^4)\}^{1/2}$. − [c] $S = [\Sigma w(F_o^2 - F_c^2)^2]/(n - p)^{1/2}]$, *n* = number of reflections, *p* = parameters used. − [d] Definition of $w_{calcd.}$: $w = 1/[\sigma^2(F_o^2) + (aP)^2 + bP]$ where $P = (F_o^2 + 2F_c^2)/3$.

C=O), 1520 (s, C=C), 1445 (s, P−C), 1081, 1067, 1054, 1041 (s, S=O). − MS (EI, 220 °C): *m/z* (%) = 704 (12.5) $[M]^+$, 676 (15.8) $[M - CO]^+$, 596 (5.6) $[M - CO - SO_3]^+$. − $(C_{29}H_{42}N_6O_4PRhS)_4 \cdot (C_4H_8O)$ (2890.7): calcd. C 49.86, H 6.14, N 11.63; found C 49.97, H 5.79, N 11.52.

Potassium Carbonyl[diphenyl(4-sulfonatophenyl)phosphane][tris(pyrazol-1-yl)methanesulfonato]rhodate(I), K[TpmsRh(CO)PPh$_2$-PhSO$_3$]·H$_2$O (5d): Potassium diphenyl(4-sulfonatophenyl)phosphane (0.1 g, 0.3 mmol) was added to a solution of **2a** (0.03 g, 0.06 mmol) in THF (10 mL). The vessel was pressurized with 3−4 atm of carbon monoxide and the mixture was stirred for 16 h at room temperature. The suspension obtained was then concentrated to half of its original volume and filtered. The filtrate was overlaid with pentane to yield 0.02 g of a yellow powder (40%). − ^{1}H NMR (200 MHz, D_3PO_4, D_2O): δ = 6.2 (br. s, 3 H, pyrazolyl 4-H), 6.8 (br. s, 3 H, pyrazolyl 3-/5-H), 7.3 [m, 14 H, P(C_6H_5)$_2$($C_6H_4SO_3K$)], 7.7 (br. s, 3 H, pyrazolyl 3-/5-H). − ^{31}P{^{1}H} NMR (200 MHz, D_3PO_4, D_2O): δ = 45 (d, $^1J_{RhP}$ = 159 Hz).[26] − IR (KBr): $\tilde{\nu}$ = 3167 cm^{-1}, 3058 (w, C−H), 1998 (vs, C=O), 1521 (s, C=C), 1436 (s, P−C), 1081, 1058, 1038 (s, S=O). − MS (FAB^+): *m/z* (%) = 805 (100.0) $[M + H]^+$, 776 (23.4) $[M - CO]^+$. − $C_{29}H_{23}KN_6O_7PS_2Rh \cdot H_2O$ (822.7): calcd. C 42.34, H 3.06, N 10.22; found C 42.80, H 3.34, N 9.63.

Crystal Structure Analyses: For all compounds **2a**, **3**, **4**, and **5a**, data were collected with a SMART 1K CCD area detector from Bruker AXS GmbH using graphite-monochromated Mo-K_α radiation (λ = 0.71073 Å). Unless stated otherwise, data were collected at 173 K (Table 9). For protection against oxygen or moisture, single crystals were handled in a perfluoroalkyl ether from ABCR GmbH & Co KG (viscosity 1600 cSt). The unit cell was determined with the program SMART.[27] For data integration and refinement of the unit cell, the program SAINT[27] was used. The space group was determined using the programs XPREP[27] or ABSEN[28] and an empirical absorption correction was made using SADABS.[27] The structures were solved by direct methods using the programs SHELX-97[29] or SIR-97[30] and were refined by least-squares methods based on F^2 using SHELX-97.[29] Graphical representations of the molecular structures were generated using the program ZORTEP.[31] − The positions of disordered or non-refinable solvent molecules were calculated using the PLATON[32]-integrated SQUEEZE[33] procedure and the corresponding electron density was subtracted before the final refinement. − All non-hydrogen atoms were fully refined in the calculated positions; when possible, the hydrogen atoms were located from the electron density difference map and refined freely in both their positions and their thermal parameters. If a localization was not possible, the hydrogen atoms were positioned as a riding model on their neighbouring atoms and were refined depending on the positions of the latter. The figure in parentheses after each calculated value represents the standard deviation in units of the last significant digit. − Crystallographic data (excluding structure factors) for the structures reported in this paper have been deposited with the Cambridge Crystallographic Data Centre as supplementary publication nos. CCDC-151585−151588. Copies of the data can be obtained free of charge on application to the CCDC, 12 Union Road, Cambridge CB2 1EZ, UK [Fax: (internat.) + 44-1223/336-033; E-mail: deposit@ccdc.cam.ac.uk].

Acknowledgments

This work was supported by the Fonds der Chemischen Industrie. W. K. thanks the Degussa AG, Hanau, for a loan of rhodium chloride.

[1] S. Trofimenko, *J. Am. Chem. Soc.* **1966**, *88*, 1842.
[2] The nomenclature for tris(pyrazol-1-yl)borate ligands and their complexes, as proposed by Trofimenko,[3a] is used throughout this publication. Tp′ is used for Tp ligands with varying substituents.
[3] [3a] S. Trofimenko, *Chem. Rev.* **1993**, *93*, 943−980. − [3b] S. Trofimenko, *Scorpionates: The Coordination Chemistry of Polypyrazolylborate Ligands*, Imperial College Press, London, **1999**.
[4] [4a]N. F. Borkett, M. I. Bruce, *J. Organomet. Chem.* **1974**, *65*, C51. − [4b] D. J. O'Sullivan, F. J. Lalor, *J. Organomet. Chem.* **1974**, *65*, C47. − [4c] M. Cocivera, T. J. Desmond, G. Ferguson, B. Kaitner, F. J. Lalor, D. J. O'Sullivan, *Organometallics* **1982**, *1*, 1125−1132.
[5] W. Kläui, M. Berghahn, G. Rheinwald, H. Lang, *Angew. Chem.* **2000**, *112*, 2590−2592; *Angew. Chem. Int. Ed.* **2000**, *39*, 2464−2466.
[6] U. E. Bucher, A. Currao, R. Nesper, H. Rüegger, L. M. Venanzi, E.Younger, *Inorg. Chem.* **1995**, *34*, 66−74.
[7] J. E. Huheey, E. A. Keiter, R. L. Keiter, *Anorganische Chemie*, 2nd ed., Walter de Gruyter, Berlin, **1995**.
[8] [8a] R. G. Ball, C. K. Gosh, J. K. Hoyano, A. D. McMaster, W. A. G. Graham, *J. Chem. Soc., Chem. Commun.* **1989**, 341−342. − [8b] M. Moszner, S. Wolowiec, A. Trösch, H. Vahrenkamp, *J. Organomet. Chem.* **2000**, *595*, 178−185. − [8c] E. Del Ministro, O. Renn, H. Rüegger, L. M. Venanzi, U. Burckhardt, V. Gramlich, *Inorg. Chim. Acta* **1995**, *240*, 631−639.
[9] [9a] H. V. R. Dias, H.-L. Lu, R. E. Ratcliff, S. G. Bott, *Inorg. Chem.* **1995**, *34*, 1975−1976. − [9b] H. V. R. Dias, J. D. Gorden, *Inorg. Chem.* **1996**, *35*, 318−324. − [9c] H. V. R. Dias, W. Jin, H.-J. Kim, H.-L. Lu, *Inorg. Chem.* **1996**, *35*, 2317−2328. − [9d] H. V. R. Dias, H.-J. Kim, H.-L. Lu, K. Rajeshwar, N. R. de Tacconi, A. Derecskei-Kovacs, D. S. Marynick, *Organometallics* **1996**, *15*, 2994−3003.
[10] A. L. Rheingold, B. S. Haggerty, G. P. A. Yap, S. Trofimenko, *Inorg. Chem.* **1997**, *36*, 5097−5103.
[11] M. Akita, K. Ohta, Y. Takahashi, S. Hikichi, Y. Moro-oka, *Organometallics* **1997**, *16*, 4121−4128.
[12] D. Sanz, M. D. Santa María, R. M. Claramunt, M. Cano, J. V. Heras, J. A. Campo, F. A. Ruíz, E. Pinilla, A. Monge, *J. Organomet. Chem.* **1996**, *526*, 341−350.
[13] M. Cocivera, G. Ferguson, B. Kaitner, F. J. Lalor, D. J. O'Sullivan, M. Parvez, B. Ruhl, *Organometallics* **1982**, *1*, 1132−1139.
[14] T. P. E. Auf der Heyde, H.-B. Bürgi, *Inorg. Chem.* **1989**, *28*, 3970−3981.
[15] T. P. E. Auf der Heyde, H.-B. Bürgi, *Inorg. Chem.* **1989**, *28*, 3982−3989.
[16] M. Paneque, S. Sirol, M. Trujillo, E. Gutiérrez-Puebla, M. A. Monge, E. Carmona, *Angew. Chem.* **2000**, *112*, 224−227; *Angew. Chem. Int. Ed.* **2000**, *39*, 218−221.
[17] N. G. Connelly, D. J. H. Emslie, B. Metz, A. G. Orpen, M. J. Quayle, *Chem. Commun.* **1996**, 2289−2290.
[18] V. Chauby, C. S. Le Berre, P. Kalck, J.-C. Daran, G. Commenges, *Inorg. Chem.* **1996**, *35*, 6354−6355.
[19] B. Borak, A. M. Trzeciak, *VIth Regional Seminar of Ph.D. Students on Organometallic and Organophosphorus Chemistry*, Karpacz, Poland, **2000**.
[20] T. O. Northcutt, R. J. Lachicotte, W. D. Jones, *Organometallics* **1998**, *17*, 5148−5152.
[21] S. Juliá, J. M. del Mazo, L. Avila, J. Elguero, *Org. Prep. Proced. Int.* **1984**, *16(5)*, 299−307.
[22] J. A. McCleverty, G. Wilkinson, *Inorg. Synth.* **1967**, *8*, 211−214.
[23] E. W. Abel, M. A. Bennett, G. Wilkinson, *J. Chem. Soc.* **1959**, 3178−3182.
[24] J. Chatt, L. M. Venanzi, *J. Chem. Soc.* **1957**, 4735−4741.
[25] O. Herd, A. Heßler, K. P. Langhans, O. Stelzer, W. S. Sheldrick, N. Weferling, *J. Organomet. Chem.* **1994**, *475*, 99−111.
[26] Due to slow decarbonylation, a satisfactory ^{13}C{^{1}H} NMR spectrum could not be obtained.

[27] Bruker AXS Inc., Madison, WI, USA, **1998**.
[28] P. McArdle, *J. Appl. Crystallogr.* **1996**, *29*, 306.
[29] G. M. Sheldrick, *SHELX-97, Programs for Crystal Structure Analysis*, Release 97-2, University of Göttingen, Germany, **1997**.
[30] A. Altomare, M. C. Burla, M. Camalli, G. L. Cascarano, C. Giacovazzo, A. Guagliardi, A. G. G. Moliterni, G. Polidori, R. Spagna, *J. Appl. Crystallogr.* **1999**, *32*, 115−119.
[31] L. Zsolnai, G. Huttner, University of Heidelberg, Germany, **1994**.
[32] A. L. Spek, *PLATON, A Multipurpose Crystallographic Tool*, Utrecht University, Utrecht, The Netherlands, **1999**.
[33] P. van der Sluis, A. L. Spek, *Acta Crystallogr., Sect. A* **1990**, *46*, 194−201.
[34] These data were taken from the Cambridge Crystallographic Data Centre (CCDC).

Received November 13, 2000
[I00430]

Generating a New Chiral Ligand System for High-Valent Early Transition Metals — Synthesis and Structural Characterization of C_3-Symmetrical Tripodal Alkyl/Silyl Amido Complexes

Patrick Renner,[a] Christian H. Galka,[a] Lutz H. Gade,*[a] Sanja Radojevic,[b] and Mary McPartlin[b]

Dedicated to Professor Max Herberhold on the occasion of his 65th birthday

Keywords: Lithium / Amides / Chirality / Tripodal ligands / Zirconium

The novel C_3-chiral tripodal amine HC{SiMe$_2$NH[(*S*)-3,3-dimethyl-2-butyl]}$_3$ (**1**) and its trilithium triamido derivative [HC{SiMe$_2$N(Li)[(*S*)-3,3-dimethyl-2-butyl]}$_3$] (**2**) have been synthesized and characterized by X-ray diffraction. The lithium reagent was used for the synthesis of a C_3-chiral amidozirconium complex [HC{SiMe$_2$N[(*S*)-3,3-dimethyl-2-butyl]}$_3$ZrCl] (**3**); the preparation of the analogous titanium compound was precluded by the redox activity of the metal. Instead, the lithium amide-lithium chloride adduct [HC{SiMe$_2$N(Li)[(*S*)-3,3-dimethyl-2-butyl]}$_3$LiCl(Et$_2$O)$_3$] (**4**) was isolated from these reactions and structurally characterized by X-ray structure analysis. In this cage compound the chloride ion bridges the three amido lithium atoms and is itself coordinated to an {(Et$_2$O)$_3$Li}$^+$ fragment. Its isolation sheds new light upon the complex reaction sequences leading to halide substitution by a polydentate amido ligand.

Introduction

Ligand design in early transition metal chemistry has, to a large extent, focussed on amides during the past decade.[1−4] It is the realization that the amido donor function R$_2$N$^-$ may be placed into a great variety of structural environments which has driven this development. It may be readily incorporated into complex polydentate ligand systems of podand or macrocyclic topology.[3] The synthesis of the ligands normally proceeds via the (secondary) amines, which can then be deprotonated and coordinated to transition metals.

We have developed a series of tripodal amido ligands which derive from such amine precursors.[5−7] Their synthesis is based either on the derivatization of a primary triamine containing the ligand backbone or the condensation of a suitably activated backbone unit with primary amines. The latter strategy has been applied in the preparation of triamido ligands derived from trisilylmethane (**A**) or trisilylsilane (**B**). An important point in this approach is the great variety of peripheral substituents at the N-functions which may be introduced in what is essentially a one-step synthesis. In this paper we report a novel tripodal ligand containing a trisilylmethane skeleton in which the peripheral substituents are chiral. The tridentate ligand therefore possesses C_3-chirality, and will be applied in the coordination chemistry of the early transition metals.

A **B**

In spite of the burgeoning interest in C_3-chiral reagents and molecules,[8−11] by far the majority of the known systems are late transition metal compounds. The coordination of high-valent early transition metals requires highly charged ligands with strong σ- and π-donor functions such as alkoxides and amides in which chirality may either be introduced in the backbone structure or the peripheral substituents. While the former strategy has been pursued by Nugent, Knochel and Moberg,[12] we report an amido system in which the chiral centre is in the α-position of the peripheral substituent and thus close to a potential reactive site.[13]

Results and Discussion

Synthesis and Crystal Structures of HC{SiMe$_2$NH[(*S*)-3,3-dimethyl-2-butyl]}$_3$ (1) and Its Trilithium Triamido Derivative [HC{SiMe$_2$N(Li)[(*S*)-3,3-dimethyl-2-butyl]}$_3$] (2)

Reaction of the previously characterized trisilylmethane derivative HC(SiMe$_2$Br)$_3$ [6,14] with three molar equivalents

[a] Laboratoire de Chimie Organométallique et de Catalyse (UMR 7513), Institut Le Bel, Université Louis Pasteur,
4, rue Blaise Pascal, 67070 Strasbourg, France
Fax: (internat.) + 33-3/90241531
E-mail: gade@chimie.u-strasbg.fr
[b] School of Applied Chemistry, University of North London, Holloway Road, London N7 8DB, UK

 © WILEY-VCH Verlag GmbH, 69451 Weinheim, 2001 1434−1948/01/0606−1425 $ 17.50+.50/0

of (*S*)-3,3-dimethyl-2-butylamine in the presence of an excess of triethylamine as auxiliary base, after work up, cleanly gave the corresponding triamine HC{$SiMe_2NH$[(*S*)-3,3-dimethyl-2-butyl]}$_3$ (**1**) in good yield (Scheme 1). In a subsequent reaction step, the amine was converted into the corresponding trilithium triamide [HC{$SiMe_2N(Li)$[(*S*)-3,3-dimethyl-2-butyl]}$_3$] (**2**) by reaction with three equivalents of *n*BuLi.

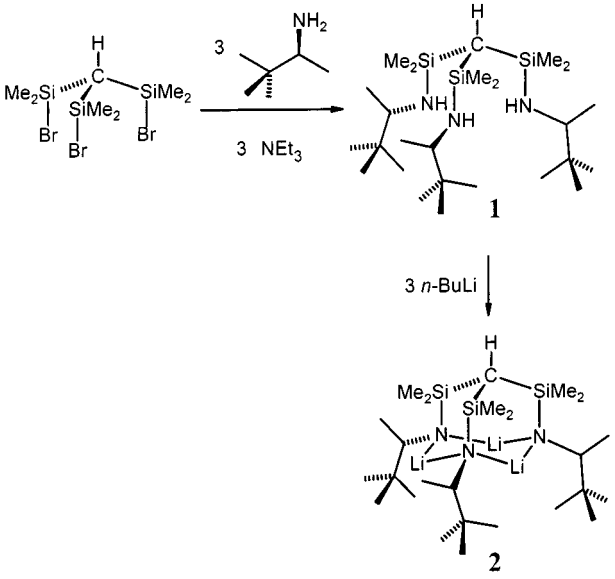

Scheme 2. Synthesis of the triamine **1** and its lithiation giving **2**

The ^1H, ^{13}C and ^{29}Si NMR spectra of both compounds **1** and **2** are consistent with a threefold molecular symmetry on the time scale of the experiment. The ^1H NMR spectroscopic shifts of the apical CH protons in the trisilylmethane backbone are characteristically at high field. They are observed at $\delta = -0.81$ for the amine and at $\delta = -0.75$ in the spectrum of **2** recorded in C_6D_6. As a consequence of the chiral ligand periphery, the methyl groups of the $SiMe_2$ units are diastereotopic and are observed at $\delta = 0.27$ and 0.32 for **1** and slightly shifted to $\delta = 0.34$ and 0.38 for the lithiated derivative. In contrast to alkylamino derivatives of trisilylmethane which we studied previously,[6] the triamine **1** is stable in solution and no dissociation of a molecule of the chiral primary amine is observed even upon heating a sample to 70 °C.

It was possible to obtain single crystals of both compounds and thus establish their detailed molecular structure by an X-ray diffraction study. Both compounds **1** and **2** crystallize in the space group $P2_12_12_1$. The molecular structures of **1** and **2** are depicted in Figure 1 and 2, respectively, along with the principal bond lengths and angles. In both compounds the tripodal ligand adopts a "claw-like" arrangement which is part of an adamantane-related cage structure. In the amine **1** the base of this adamantane-related cage is formed by the three NH groups and, in contrast to the infrared data, the structure shows little evidence of intramolecular hydrogen bonding, with the N−H···N distances being in the range of 2.703−2.883 Å. This orientation of the ligand arms is in stark contrast to the "inverted" structural arrangement found for a range of aryl-substituted triamines of this type,[13a] but similar to the structure of the previously characterized chiral triamine HC{$SiMe_2NH$[(*S*)-1-phenylethyl]}$_3$.[13a] The positions of the NH hydrogen atoms in **1** were determined directly in difference Fourier maps, with the average N−H distance being 0.89 Å.

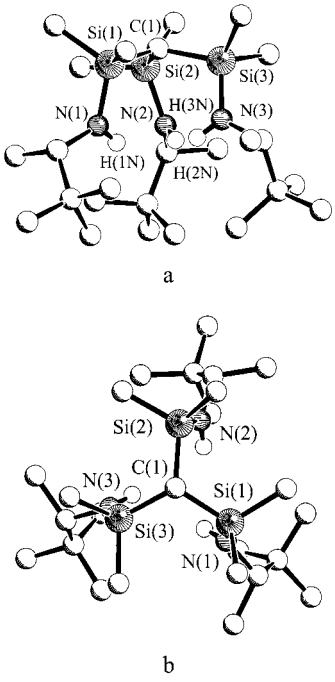

Figure 1. View of the molecular structure of **1** perpendicular (a) and along (b) the molecular axis of the tripod cage; the principal bond lengths (Å) and angles (°): C(1)−Si(1) 1.894(6), C(1)−Si(2) 1.874(6), C(1)−Si(3) 1.891(6), Si(1)−N(1) 1.720(5), Si(1)−C(2) 1.883(6), Si(1)−C(3) 1.884(6), N(1)−C(11) 1.472(7); Si(1)−C(1)−Si(3) 114.4(3), Si(1)−C(1)−Si(2) 114.7(3), Si(2)−C(1)−Si(3) 115.3(3), N(1)−Si(1)−C(1) 107.3(3), C(11)−N(1)−Si(1) 123.8(4), C(12)−C(11)−N(1) 110.0(5), C(13)−C(11)−N(1) 113.1(6)

The structural centrepiece of compound **2** is a heteroadamantane cage consisting of a puckered basal $(LiN)_3$ ring capped by the trisilylmethane unit. The Li−N−Li′−N′ torsion angles in the basal unit lie between 57.3(4) and 59.7(4)°, while the Li−N distances of between 1.890(6) and 1.983(6) Å are similar to those found in other cyclic lithium amides.[15] The lithium atoms are two coordinate [N−Li−N′ angles range between 124.2(3) and 127.8(3)°] although short Li····H−C contacts of between 2.04 and 2.17 Å with the isolated methyl groups of the $CH(CH_3)t$Bu units indicate "internal solvation" by the ligand periphery. Several cases of such interactions of low-coordinate lithium atoms and hydrocarbon units have previously been reported.[16]

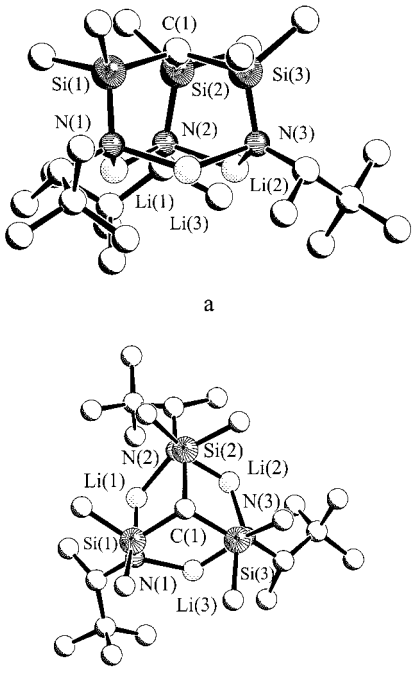

Figure 2. View of the molecular structure of **2** perpendicular (a) and along (b) the molecular axis of the metal-tripod cage; the principal bond lengths (Å) and angles (°): C(1)−Si(1) 1.899(3), C(1)−Si(2) 1.895(3), C(1)−Si(3) 1.904(3), Si(1)−N(1) 1.721(2), N(1)−Li(1) 1.968(6), N(1)−Li(3) 1.890(6), N(1)−C(10) 1.472(4); Si(1)−C(1)−Si(3) 114.36(15), Si(1)−C(1)−Si(2) 114.67(15), Si(2)−C(1)−Si(3) 113.82(14), N(1)−Si(1)−C(1) 107.51(12), N(1)−Li(1)−N(2) 127.8(3), Li(1)−N(1)−Li(3) 93.6(3), Si(1)−N(1)−Li(1) 95.5(2), C(10)−N(1)−Li(1) 107.6(2), Si(1)−N(1)−Li(3) 112.1(2)

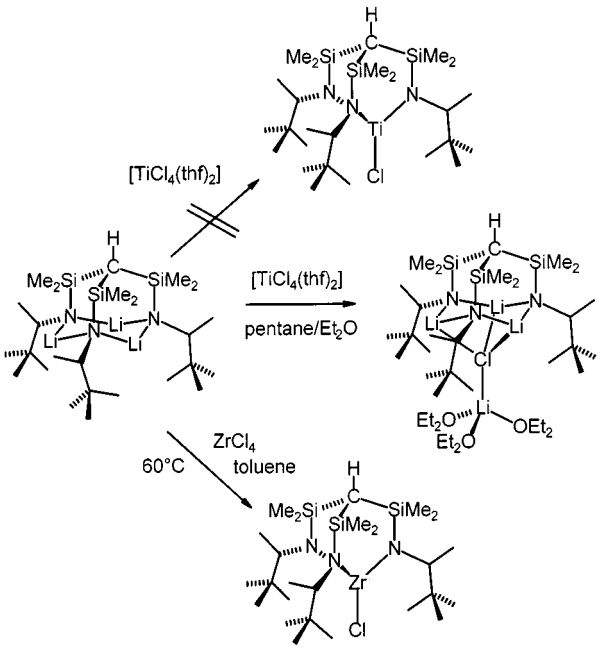

Scheme 2. Reaction of **2** with $[TiCl_4(THF)_2]$ and $ZrCl_4$

Synthesis of a C_3-Chiral Amidozirconium Complex and Isolation and Structural Characterization of the Lithium Amide−Lithium Chloride Adduct $[HC\{SiMe_2N(Li)[(S)\text{-}3,3\text{-dimethyl-2-butyl}]\}_3LiCl(Et_2O)_3]$ (4)

Complexation of the chiral amido tripod was first attempted by reaction of **2** with $[TiCl_4(THF)_2]$ (Scheme 2). However, even after stirring for four days in diethyl ether at ambient temperature, no titanium complex could be identified in the reaction mixture or isolated from it. This is surprising since the related C_3-chiral titanium complexes $[HC\{SiMe_2N[(S)\text{-1-phenylethyl}]\}_3TiCl]$ and $[HC\{SiMe_2N[(S)\text{-1-indanyl}]\}_3TiCl]$ were readily obtained.[17] The lack of reactivity may be due to the sterically crowed peripheral substituents in **2**. Attempts to induce complexation by heating the reaction mixture failed due to the redox activity of the titanium compound under these conditions. Immediate darkening of the solutions and the observation of paramagnetic species in the NMR spectra indicated reduction to Ti^{III}. However, none of these paramagnetic components could be isolated and further characterized.

Analogous to the reaction with $[TiCl_4(THF)_2]$ in diethyl ether, stirring of **2** with $ZrCl_4$ at room temperature did not give the corresponding zirconium complex. However, the synthesis of $[HC\{SiMe_2N[(S)\text{-3,3-dimethyl-2-butyl}]\}_3ZrCl]$ (**3**) was achieved by heating the starting materials in toluene at 60 °C for 1 hour (Scheme 2). The colourless compound was obtained as a microcrystalline solid after work up and its formulation established by elemental analysis. The NMR spectra recorded in solution are consistent with the threefold molecular symmetry of complex **3**. The apical C−H proton of the tripod is observed at $\delta = -0.48$ and the diastereotopic $SiMe_2$ methyl groups resonate at $\delta = 0.28$ and 0.39. A single resonance at $\delta = 1.1$ in the ^{29}Si NMR spectrum confirms the equivalence of all three "claws" in the tripod.

Whereas the titanium complex proved not to be isolable from the reaction mixtures of **2** with $[TiCl_4(THF)_2]$, a colourless highly crystalline solid precipitated from the solutions. While the quantities of this component varied, it was reproducibly obtained from these reactions. While the ^1H, ^{13}C and ^{29}Si NMR spectra were almost identical to those of **2**, the proton NMR spectrum displayed the signals of coordinated diethyl ether and two resonances at $\delta = 0.8$ and −2.9 were observed in the ^7Li NMR spectrum, indicating a second Li environment. Its identity was established by a single crystal X-ray structure analysis. The molecular structure is depicted in Figure 3 along with the principal bond lengths and angles.

The colourless product isolated from the reaction of **2** with $[TiCl_4(THF)_2]$ was found to be the LiCl adduct $[HC\{SiMe_2N(Li)[(S)\text{-3,3-dimethyl-2-butyl}]\}_3LiCl(Et_2O)_3]$ (**4**), the chloride deriving from the Ti complex. Compound **4** crystallizes in the polar trigonal space group *R*3 with two independent molecules in the asymmetric unit, each molecule aligned along a threefold crystallographic axis. The two molecules have virtually identical structures which are illustrated in Figure 3 by the first molecule. Chemically equivalent metric parameters are equal within experimental error

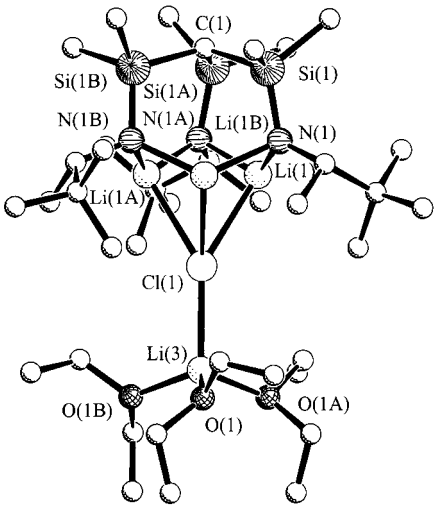

Figure 3. View of the molecular structure of **4** perpendicular to the molecular axis of the metal-tripod cage; the principal bond lengths (Å) and angles (°) (mean values): C(1)−Si(1) 1.887, Si(1)−N(1) 1.708, N(1)−Li(1) 1.990, N(1)−Li(1B) 1.993, Cl(1)−Li(1) 2.586, Cl(1)−Li(3) 2.396, Li(3)−O(1) 1.985; Si(1)−C(1)−Si(1A) 114.1, N(1)−Si(1)−C(1) 109.0, N(1)−Li(1)−N(1A) 122.2, Li(1)−N(1)−Li(1B) 82.0, O(1)−Li(3)−Cl(1) 107.9, Li(3)−Cl(1)−Li(1) 144.3, Cl(1)−Li(1)−N(1) 100.9, Li(1)−Cl(1)−Li(1A) 60.8

for the two molecules, and the mean values of selected bonds lengths and angles are given in the Caption to Figure 3. The chloride ion bridges the three amido lithium atoms and is itself coordinated to a $\{(Et_2O)_3Li\}^+$ fragment. The coordination environment of the anion is trigonally elongated along the molecular axis, probably in part because of the steric repulsion between the 3,3-dimethyl-2-butyl substituents and the Li-coordinated diethyl ether molecules. There are several examples in the literature of compounds in which a chloride ion connects four lithium centres in a fashion similar to that shown in Figure 3. Evans and co-workers reported the crystal structures of the yttrium complexes $[(Me_3SiCH_2)_x(Me_3CO)_{1-x}Y(\mu\text{-}OCMe_3)_4\{Li(THF)\}_4(\mu_4\text{-}Cl)]$ ($x = 0, 1$) in which the lithium atoms and the μ_4-chloride form pyramidal subunits,[18] while Floriani et al. reported $[MnCl(dag)_4Li_4(\mu_4\text{-}Cl)]$ (dag = mono anion of 1,2:5,6-di-*O*-isopropylidene-α-D-glucofuranose) with the same Li_4Cl unit.[19] A Li_4Cl unit, which is highly distorted with respect to the idealized trigonal symmetry, was found by Deacon and White in the structure of $[\{Li(L^1)Li(\mu_4\text{-}Cl)Li(L^1)(THF)_2]$ (HL^1 = *N*,*N*-dimethyl-*N*′-trimethylsilylethane-1,2-diamine).[20]

The isolation of the LiCl adduct of **2** sheds some light upon the possible mechanism of the ligand substitution reactions involving lithium amides. Rather than direct nucleophilic attack by the amide upon a metal centre, the lithium ions play the role of a Lewis-acidic chloride acceptor. This notion of the active alkali metal ion is supported by the well established variations in reactivity upon going from lithium amides to their heavier congeners.

Conclusion

In this paper we have reported the synthesis of a novel C_3-chiral amido ligand, the structural chemistry of its amine precursor and lithiated derivative. While the preparation of a chiral triamidotitanium complex was not achieved due to competing single electron transfer, its zirconium homologue $[HC\{SiMe_2N[(S)\text{-}3,3\text{-dimethyl-2-butyl}]\}_3ZrCl]$ (**3**) was obtained in a straightforward way. This compound probably marks an extreme of steric congestion in the ligand periphery attainable in this class of compounds and current and future studies aim to exploit this structural feature. The isolation of the LiCl adduct of the chiral tripodal lithium amide has shed some light upon the possible primary steps in the mechanism of halide substitution in the synthesis of polydentate amido complexes.

Experimental Section

All manipulations were performed under an inert gas atmosphere of dried argon in standard (Schlenk) glassware which was flame dried with a bunsen burner prior to use. Solvents were dried according to standard procedures and saturated with Ar. The deuterated solvents used for the NMR spectroscopic measurements were degassed by three successive "freeze-pump-thaw" cycles and dried over 4Å molecular sieves.

The ^1H, ^{13}C, ^{29}Si and ^7Li NMR spectra were recorded on a Bruker AC 200 spectrometer equipped with a B-VT-2000 variable temperature unit (at 77.77 MHz) or on a Bruker AMX 400 spectrometer (at 400.13, 100.61 and 79.50 MHz, respectively) with tetramethylsilane or LiI/H_2O (1 M) as reference. The IR spectra were recorded on a Bruker IFS 25 FT-IR spectrometer.

Elemental analyses were carried out in the microanalytical laboratory of the chemistry department at Würzburg. The ligand pre cursor $HC(SiMe_2Br)_3$ was prepared as reported in the literature.[6,14]

Preparation of $HC\{SiMe_2NH[(S)\text{-}3,3\text{-dimethyl-2-butyl}]\}_3$ (1): To a stirred solution of (*S*)-3,3-dimethyl-2-butylamine (3.80 mL, 28.1 mmol) and NEt_3 (4.20 mL, 30.3 mmol) in diethyl ether (30 mL) was added $HC(SiMe_2Br)_3$ (4.00 g, 9.36 mmol) in diethyl ether (20 mL) at 0 °C. After stirring for 14 h at room temperature the ammonium salt formed during the reaction was removed by centrifugation and was washed three times with diethyl ether (ca. 20 mL). The solvent and the unreacted NEt_3 were removed under reduced pressure and the resulting yellow oil was redissolved in diethyl ether (ca. 10 mL) and stored at 4 °C. Compound **1** was obtained as a colourless, highly crystalline solid (yield: 3.87 g, 85%). − M.p.: 110 °C. − ^1H NMR (400.13 MHz, C_6D_6, 295 K): δ = −0.81 [s, 1 H, *H*C(Si...)$_3$], 0.27, 0.32 [2 × s, 2 × 9 H, Si(C*H*$_3$)$_2$], 0.93 [s, 27 H, C(C*H*$_3$)$_3$], 0.99 [d, $^3J_{HCNH}$ = 12.7 Hz, 3 H, N*H*), 1.09 (d, $^3J_{HH}$ = 6.9 Hz, 9 H, HCC*H*$_3$), 2.48 (dq, $^3J_{HCNH}$ = 12.7 Hz, $^3J_{HH}$ = 6.9 Hz, 3 H, *H*CCH$_3$). − $^{13}C\{^1H\}$ NMR (100.61 MHz, C_6D_6, 295 K): δ = 3.9, 4.4 [Si(*C*H$_3$)$_2$], 5.5 [H*C*(Si...)$_3$], 20.6 (HC*C*H$_3$), 27.0 [C(*C*H$_3$)$_3$], 35.4 [*C*(CH$_3$)$_3$], 56.6 (H*C*CH$_3$). − $^{29}Si\{^1H\}$ NMR (79.50 MHz, C_6D_6, 295 K): δ = 0.9. − IR (benzene): $\tilde{\nu}$ = 3355 (s), 2964 (vs), 2903 (s), 2869 (s), 1477 (w), 1412 (m), 1400 (m), 1369 (m), 1362 (w), 1252 (vs), 1122 (vs), 1011 (s), 956 (s), 870 (s), 826 (s), 812 (vs), 668 (m) cm^{-1}. − $C_{25}H_{61}N_3Si_3$ (488.04): calcd. C 61.53, H 12.60, N 8.61; found C 60.65, H 11.88, N 8.40.

Preparation of [HC{SiMe$_2$N(Li)[(*S*)-3,3-dimethyl-2-butyl]}$_3$] (2): To a stirred solution of **1** (3.39 g, 6.95 mmol) in *n*-pentane (30 mL) at −78 °C was added a 2.5 M solution of *n*BuLi in *n*-hexane (8.34 mL, 20.86 mmol). After stirring for 14 h at room temperature the yellow solution was concentrated to ca. 7 mL. Storage of the solution at 4 °C yielded colourless crystals of **2** (yield: 3.32 g, 94%). − M.p.: 172 °C. − ^{1}H NMR (400.13 MHz, C_6D_6, 295 K): δ = −0.75 [s, 1 H, *H*C(Si...)$_3$], 0.34, 0.38 [2 × s, 2 × 9 H, Si(C*H*$_3$)$_2$], 0.76 [s, 27 H, C(C*H*$_3$)$_3$], 0.95 (d, $^3J_{HH}$ = 6.2 Hz, 9 H, HCC*H*$_3$), 2.82 (q, $^3J_{HH}$ = 6.2 Hz, 3 H, *H*CCH$_3$). − ^{13}C{^{1}H} NMR (100.61 MHz, C_6D_6, 295 K): δ = 6.1, 7.1 [Si(*C*H$_3$)$_2$], 12.1 [H*C*(Si...)$_3$], 24.5 (HC*C*H$_3$), 27.7 [C(*C*H$_3$)$_3$], 36.0 [s, *C*(CH$_3$)$_3$], 60.5 (H*C*CH$_3$). − ^{29}Si{^{1}H} NMR (79.50 MHz, C_6D_6, 295 K): δ = −1.8. − ^{7}Li{^{1}H} NMR (77.77 MHz, C_6D_6, 295 K): δ = 0.7. $C_{25}H_{58}Li_3N_3Si_3$ (505.84): calcd. C 59.36, H 11.56, N 8.31; found C 58.82, H 11.16, N 7.94.

Preparation of [HC{SiMe$_2$N[(*S*)-3,3-dimethyl-2-butyl]}$_3$ZrCl] (3): To a stirred solution of **2** (0.35 g, 0.70 mmol) in toluene (5 mL) was added solid $ZrCl_4$ (0.38 mg, 1.60 mmol). After treatment in an ultrasonic bath for 24 h at 60 °C the precipitate of LiCl and unreacted $ZrCl_4$ was separated by centrifugation. Storage of the filtrate at −30 °C yielded the zirconium complex **3** as an off-white microcrystalline solid (yield: 0.14 g, 34%). − ^{1}H NMR (400.13 MHz, [D$_8$]toluene, 295 K): δ = −0.48 [s, 1 H, *H*C(Si...)$_3$], 0.28, 0.39 [2 × s, 2 × 9 H, Si(C*H*$_3$)$_2$], 1.03 [s, 27 H, C(C*H*$_3$)$_3$], 1.45 (d, 9 H, $^3J_{HH}$ = 6.2 Hz, HCC*H*$_3$), 2.88 (m, 3 H, *H*CCH$_3$). − ^{13}C{^{1}H} NMR (100.61 MHz, [D$_8$]toluene, 295 K): δ = 1.5 [H*C*(Si...)$_3$], 5.7, 5.9 [Si(*C*H$_3$)$_2$], 27.5 (HC*C*H$_3$), 27.8 [C(*C*H$_3$)$_3$], 36.4 [s, *C*(CH$_3$)$_3$], 62.5 (H*C*CH$_3$). − ^{29}Si{^{1}H} NMR (79.50 MHz, [D$_8$]toluene, 29: δ = 1.1. − IR (toluene): $\tilde{\nu}$ = 2960 (vs), 2964 (vs), 2871 (s), 1477 (s), 1458 (s), 1254 (vs), 1104 (vs), 1082 (vs), 1011 (m), 951 (vs), 868 (vs), 840 (vs), 815 (vs), 678 (w) cm^{-1}. − $C_{25}H_{58}ClN_3Si_3Zr$ (611.69): calcd. C 49.09, H 9.56, N 6.87; found C 48.66, H 9.45, N 6.99.

Preparation of [HC{SiMe$_2$N(Li)[(*S*)-3,3-dimethyl-2-butyl]}$_3$-LiCl(Et$_2$O)$_3$] (4): To a stirred solution of **2** (0.50 g, 0.99 mmol) in diethyl ether (10 mL) at −20 °C was added [$TiCl_4$(THF)$_2$] (0.33 g, 0.99 mmol). After stirring for four days at room temperature the precipitate was separated by centrifugation. Storage of the dark brown solution at 4 °C yielded colourless crystals of **4** (yield: 0.19 g, 24%). The yield obtained in several runs of this reaction varied between ca. 10% and 30%. Due to facile loss of diethyl ether it was not possible to obtain a correct elemental analysis. − M.p.: 31 °C (dec.). − ^{1}H NMR (400.13 MHz, [D$_8$]toluene, 295 K): δ = −0.75 [s, 1 H, *H*C(Si...)$_3$], 0.32, 0.37 [2 × s, 2 × 9 H, Si(C*H*$_3$)$_2$], 0.77 [s, 27 H, C(C*H*$_3$)$_3$], 0.96 (d, 9 H, $^3J_{HH}$ = 6.2 Hz, HCC*H*$_3$), 1.12 (t, Et$_2$O), 2.82 (q, 3 H, $^3J_{HH}$ = 6.2 Hz, *H*CCH$_3$), 3.28 (q, Et$_2$O). − ^{13}C{^{1}H} NMR (100.61 MHz, [D$_8$]toluene, 295 K): δ = 6.0, 7.0 [Si(*C*H$_3$)$_2$], 12.1 [H*C*(Si...)$_3$], 15.5 (Et$_2$O), 24.5 (HC*C*H$_3$), 27.7 [C(*C*H$_3$)$_3$], 36.0 [s, *C*(CH$_3$)$_3$], 60.6 (H*C*CH$_3$), 65.8 (Et$_2$O). − ^{29}Si{^{1}H} NMR (79.50 MHz, [D$_8$]toluene, 295 K): δ = −1.8. − ^{7}Li{^{1}H} NMR (77.77 MHz, [D$_8$]toluene, 295 K): δ = −2.9, 0.8.

X-ray Crystallographic Study of 1,2 and 4: Data of **1** were collected using a Siemens P4 diffractometer at a temperature of 301(2) K with oil-coated crystals mounted in Lindemann tubes. Data of **2**

Table 1. Crystal data and structure refinement for **1**, **2** and **4**

	1	**2**	**4**
Molecular formula	$C_{25}H_{61}N_3Si_3$	$C_{25}H_{58}Li_3N_3Si_3$	$C_{37}H_{88}ClLi_4N_3O_3Si_3$
M_r	488.04	505.83	770.58
Temperature	301(2) K	193(2) K	193(2) K
Wavelength	0.71073 Å	0.71073 Å	0.71073 Å
Crystal system	Orthorhombic	Orthorhombic	Trigonal
Space group	$P2_12_12_1$ (no. 19)	$P2_12_12_1$ (no. 19)	$R\bar{3}$ (no. 146)
Z	4	4	6
Unit cell dimensions	a = 10.106(4) Å b = 16.461(5) Å c = 20.268(6) Å	a = 9.0263(6) Å b = 17.2032(17) Å c = 21.0887(16) Å	a = 17.0152(8) Å c = 30.264(3) Å
Volume	3372(2) Å^3	3274.7(5) Å^3	7588.1(8) Å^3
$D_{calcd.}$	0.961 g cm^{-3}	1.026 g cm^{-3}	1.012 g cm^{-3}
Absorption coefficient	0.156 mm^{-1}	0.161 mm^{-1}	0.178 mm^{-1}
F(000)	1096	1120	2556
Crystal size	0.38 × 0.38 × 0.38 mm	0.50 × 0.30 × 0.30 mm	0.40 × 0.40 × 0.40 mm
Scan method	$\theta/2\theta$-scan	ω/θ-scan	ω/θ-scan
θ range for data collection	2.01 to 22.00°	2.27 to 24.96°	2.02 to 24.47°
Limiting indices	$-10 \le h \le 10$, $-17 \le k \le 17$, $-21 \le l \le 21$	$-10 \le h \le 1$, $-20 \le k \le 2$, $-25 \le l \le 2$	$-19 \le h \le 1$, $-1 \le k \le 19$, $-35 \le l \le 3$
Reflections collected	4730	4141	3686
Independent reflections ($R_{int.}$)	4138 (0.0472)	3892 (0.0135)	3165 (0.0320)
Refinement method	Full-matrix least-squares on F^2	Full-matrix least-squares on F^2	Full-matrix least-squares on F^2
Data/restraints/parameters	4138/0/280	3892/105/365	3165/25/311
$T_{max/min}$	-/-	0.9994/0.9201	0.9995/0.9701
Goodness-of-fit on F^2	0.910	1.036	1.047
Final R indices	R_1 = 0.0562,	R_1 = 0.0380,	R_1 = 0.0531,
[$I > 2\sigma(I)$]	wR_2 = 0.0996	wR_2 = 0.0883	wR_2 = 0.1303
R indices (all data)	R_1 = 0.1462,	R_1 = 0.0468,	R_1 = 0.0668,
	wR_2 = 0.1293	wR_2 = 0.0948	wR_2 = 0.1391
Absolute structure parameter	0.3(2)	−0.34(13)	−0.02(14)
Largest diff. peak and hole	0.181 and −0.232 e Å^{-3}	0.246 and −0.218 e Å^{-3}	0.299 and −0.236 e Å^{-3}

and **4** were collected using an Enraf−Nonius CAD4 diffractometer at a temperature of 193(2) K with oil-coated shock-cooled crystals[21] mounted on the top of a glass pin under nitrogen. Crystal data and experimental details for the crystals of **1**, **2** and **4** are given in Table 1. All data for the structures **2** and **4** were corrected for absorption using Ψ-scans. No absorption correction was applied for structure **1**. The structures were solved by direct methods (SHELXS-97) and refined on F^2 (SHELXL-97).[22]

In the case of **2** one methyl and one *tert*-butyl group of a ligand arm were found to be 50:50 disordered and refined with anisotropic displacement parameters. In the case of **4**, disorder of all coordinated diethyl ether molecules in a 75:25 ratio was found and refined with isotropic displacement parameters. No hydrogen atoms could be calculated for C5S′ of a disordered Et_2O molecule. In the final cycles of refinement all non-hydrogen atoms of **1**, **2** and **4** were assigned anisotropic displacement parameters. The amino hydrogen atoms of **1** were found in a final difference Fourier transformation analysis, all other hydrogen atoms were included in idealized positions riding on the parent atoms and were assigned isotropic displacement parameters of 1.2 U_{eq} (CH, CH_2) and 1.5 U_{eq} (CH_3) of the parent atom.

Crystallographic data (excluding structure factors) for the structures reported in this paper have been deposited with the Cambridge Crystallographic Data Centre as supplementary publication nos. CCDC-156281 (**1**), -156282 (**2**) and -156283 (**4**). Copies of the data can be obtained free of charge on application to CCDC, 12 Union Road, Cambridge CB2 1EZ, UK [Fax: (internat.) +44-1223/336-033; E-mail: deposit@ccdc.cam.ac.uk].

Acknowledgments

We thank the Deutsche Forschungsgemeinschaft (SFB 347), the European Union (COST D12 Network), the CNRS (France), the EPSRC (UK), the Fonds der Chemischen Industrie, as well as BASF (Ludwigshafen) and Wacker Chemie AG for generous gifts of basic chemicals.

[1] J. G. Verkade, *Acc. Chem. Res.* **1993**, *26*, 483.
[2] R. R. Schrock, *Acc. Chem. Res.* **1997**, *30*, 9.
[3] L. H. Gade, *Chem. Commun.* **2000**, 173.
[4] R. Kempe, *Angew. Chem. Int. Ed.* **2000**, *39*, 469.
[5] [5a] L. H. Gade, N. Mahr, *J. Chem. Soc., Dalton Trans.* **1993**, 489. − [5b] S. Friedrich, H. Memmler, L. H. Gade, W.-S. Li, M. McPartlin, *Angew. Chem.* **1994**, *106*, 705; *Angew. Chem. Int. Ed. Engl.* **1994**, *33*, 676. − [5c] K. W. Hellmann, S. Friedrich, L. H. Gade, W.-S. Li, M. McPartlin, *Chem. Ber.* **1995**, *128*, 29.
[6] L. H. Gade, C. Becker, J. W. Lauher, *Inorg. Chem.* **1993**, *32*, 2308.
[7] [7a] M. Schubart, B. Findeis, L. H. Gade, W.-S. Li, M. McPartlin, *Chem. Ber.* **1995**, *128*, 329. − [7b] B. Findeis, M. Schubart, L. H. Gade, I. Scowen, M. McPartlin, *J. Chem. Soc., Dalton Trans.* **1996**, 125.
[8] For early work, see: [8a] M. Farina, C. Morandi, *Tetrahedron* **1974**, *30*, 1819.[8b] M. Nakazaki, *Top. Stereochem.* **1984**, *15*, 199.
[9] M. C. Keyes, W. B. Tolman, *Adv. Cat. Proc.* **1997**, *2*, 189.
[10] C. Moberg, *Angew. Chem.* **1998**, *110*, 260; *Angew. Chem. Int. Ed.* **1998**, *37*, 248.
[11] [11a] H. Brunner, A. F. M. M. Rahman, *Chem. Ber.* **1984**, *117*, 710. − [11b] M. J. Burk, J. E. Feaster, R. L. Harlow, *Tetrahedron: Asymmetry* **1991**, *2*, 569. − [11c] T. R. Ward, L. M. Venanzi, A. Albinati, F. Lianza, T. Gerfin, V. Gramlich, G. M. R. Tombo, *Helv. Chim. Acta* **1991**, *74*, 983. − [11d] M. J. Baker, P. J. Pringle, *J. Chem. Soc., Chem. Commun.* **1993**, 314.[11e] H. Adolfsson, K. Wärnmark, C. Moberg, *J. Chem. Soc., Chem. Commun.* **1992**, 1054. − [11f] H. Adolfsson, K. Nordström, K. Wärnmark, C. Moberg, *Tetrahedron: Asymmetry* **1996**, *7*, 1967. − [11g] D. D. LeCloux, W. B. Tolman, *J. Am. Chem. Soc.* **1993**, *115*, 1153. − [11h] C. J. Tokar, P. B. Kettler, W. B. Tolman, *Organometallics* **1992**, *11*, 2737. − [11i] D. D. LeCloux, C. J. Tokar, M. Osawa, R. P. Houser, M. C. Keyes, W. B. Tolman, *Organometallics* **1994**, *13*, 2855. − [11j] K. Kawasaki, S. Tsumura, T. Katsuki, *Synlett.* **1995**, 1245.
[12] [12a] W. A. Nugent, R. L. Harlow, *J. Am. Chem. Soc.* **1994**, *116*, 6142. − [12b] F. DiFuria, G. Licini, G. Modena, R. Motterle, W. A. Nugent, *J. Org. Chem.* **1996**, *61*, 5175. − [12c] H. Lütjens, P. Knochel, *Tetrahedron: Asymmetry* **1994**, *5*, 1161. − [12d] H. Lütjens, G. Wahl, F. Möller, F. Knochel, J. Sundermeyer, *Organometallics* **1997**, *16*, 5869. − [12e] M. Cernerud, H. Adolfsson, C. Moberg, *Tetrahedron: Asymmetry* **1997**, *8*, 2655.
[13] [13a] H. Memmler, L. H. Gade, J. W. Lauher, *Inorg. Chem.* **1994**, *33*, 3064. − [13b] H. Memmler, U. Kauper, L. H. Gade, D. Stalke, J. W. Lauher, *Organometallics* **1996**, *15*, 3637. −
[14] C. Eaborn, P. B. Hitchcock, P. D. Lickiss, *J. Organomet. Chem.* **1983**, *252*, 281.
[15] Examples: [15a] M. Rannenberg, H.-D. Hansen, J. Weidlein, *J. Organomet. Chem.* **1989**, *320*, C27. − [15b] D. R. Armstrong, R. E. Mulvey, G. T. Walker, D. Barr, R. Snaith, M. Clegg, D. Reed, *J. Chem. Soc., Dalton Trans.* **1988**, 617.
[16] K. Gregory, P. v. R. Schleyer, R. Snaith, *Adv. Inorg. Chem.* **1991**, *37*, 47 and references cited therein. See also: R. E. Mulvey, *Chem. Soc. Rev.* **1999**, *27*, 339.
[17] P. Renner, H. Memmler, F. Fecher, C. H. Galka, M. Laubender, L. H. Gade, S. Radojevic, M. McPartlin, J. W. Lauher, *Chem. Eur. J.* in press.
[18] W. J. Evans, J. L. Shreeve, R. N. R. Broomhall-Dillard, J. W. Ziller, *J. Organomet. Chem.* **1995**, *501*, 7.
[19] U. Piarulli, A. J. Rogers, C. Floriani, G. Gervasio, D. Viterbo, *Inorg. Chem.* **1997**, *36*, 6127.
[20] [20a] G. B. Deacon, C. M. Forsyth, P. C. Junk, B. W. Skelton, A. H. White, *J. Chem. Soc., Dalton Trans.* **1998**, 1381. − For recent examples of μ_3-capping halides on Li_3 faces see, for example: [20b] R. Fleischer, D. Stalke, *Coord. Chem. Rev.* **1998**, *176*, 431. − [20c] R. Fleischer, S. Freitag, D. Stalke, *J. Chem. Soc., Dalton Trans.* **1998**, 193.
[21] [21a] T. Kottke, D. Stalke, *J. Appl. Crystallogr.* **1993**, *26*, 615. − [21b] T. Kottke, R. J. Lagow, D. Stalke, *J. Appl. Crystallogr.* **1996**, *29*, 465. − [21c] D. Stalke, *Chem. Soc. Rev.* **1998**, *27*, 171.
[22] [22a] G. M. Sheldrick, Acta Crystallogr., *Sect. A* **1990**, *46*, 467. − [22b] G. M. Sheldrick, *SHELXS-97, Program for Crystal Structure Solution*, Universität Göttingen, **1997**. − [22c] G. M. Sheldrick, *SHELXL-97, Program for Crystal Structure Refinement*, Universität Göttingen, **1997**.

Received January 18, 2000
[I01019]

$CsPd_2Cl_5$ – A New Structural Type Containing $^1_\infty[(PdCl_{3/2}Cl)_2^-]$ Chains

Barbara Schüpp[a] and Hans-Lothar Keller*[a]

Keywords: Palladium / Chlorine / Crystal structure / Cesium / MAPLE

$CsPd_2Cl_5$ has been obtained by hydrothermal reaction of cesium chloride and palladium chloride in a 1:2 ratio in quartz glass ampoules at 150 °C. Its crystal structure has been determined by single-crystal X-ray diffraction analysis [*Pnma*, $Z = 4$, $a = 15.725(3)$ Å, $b = 10.526(2)$ Å, $c = 5.275(1)$ Å]. $CsPd_2Cl_5$ represents the first example of a new structural type made up of infinite $^1_\infty[(PdCl_{3/2}Cl)_2^-]$ chains, in which $PdCl_4$ units are connected through their edges as well as their vertices.

Introduction

Halopalladates(II) invariably contain monomeric square-planar $[PdX_4]^{2-}$ groups, although fluoropalladates(II), MPd_2F_5 (M = K, Rb, Cs),[1–2] possess both square-planar and octahedrally coordinated Pd^{II}. Recent experiments have led to the structural characterization of halopalladates(II) with connected groups. Thus, $CsPdCl_3$[3] contains dinuclear $[(PdCl_{2/2}Cl_2)_2]^{2-}$ groups formed by edge connection, whereas $Tl_4Pd_3Cl_{10}$[4] contains corner-sharing tetrameric $[(PdCl_{2/2}Cl_2)_4]^{4-}$ units. The first compound shown to contain edge-to-edge and corner links in a pentameric $[Pd_5Br_{14}]^{4-}$ unit has been the ternary thallium(I) bromopalladate $Tl_8Pd_7Br_{22}$.[5]

The system $CsCl/PdCl_2$ seemed to be sufficiently interesting for further experiments. Safonov and Mireev[6] described the existence of two compounds – Cs_2PdCl_4 and $CsPd_3Cl_7$ – on the basis of phase equilibria studies, although no structural information was given for $CsPd_3Cl_7$. A compound of this formula would be of interest as one would expect it to contain condensed units of the monomeric $PdCl_4$ group. The characterization of the $CsCl/PdCl_2$ system by Safonov and Mireev[6] was incomplete, as was first shown by the detection of Cs_3PdCl_5[7] with a higher proportion of cesium. The first compound to be found with a lower CsCl content, $CsPdCl_3$, involves dinuclear Pd_2Cl_6 units. We expected to observe continuing linkage of these dinuclear units with increasing Pd content. Experiments aimed at preparing $CsPd_3Cl_7$ have not yet been successful, but single crystals of $CsPd_2Cl_5$ have been obtained, the structural characterization of which is reported herein. The compound does not crystallize isotypically to cesium pentafluoropalladate(II), $CsPd_2F_5$, but instead forms a hitherto unknown structural type.

Results and Discussion

Crystal Structure

$CsPd_2Cl_5$ was prepared under hydrothermal conditions. In contrast to the fluoropalladate of the same formula type, it shows exclusively planar coordination at Pd^{II}.

Pd–Cl distances in $CsPd_2Cl_5$ range from 2.260 to 2.326 Å. The average distance of 2.298 Å corresponds to that found in mononuclear $PdCl_4$ groups. The exclusive presence of planar coordinated Pd^{II} necessitates linkage of these units in order to achieve the formula $CsPd_2Cl_5$. In the crystal structures of $CsPdCl_3$ and $PdCl_2$, the linked units are assembled through their edges. In view of the formula type, we expected the formation of tetrameric linear or angular chains $[Pd_4Cl_{10}]^{2-}$, but this could not be confirmed. The $[Pd_2Cl_5]^-$ part stems from $[Pd_2Cl_6]^{2-}$ units, which are connected through opposite vertices forming one-dimensional infinite chains (see Figure 1, a).

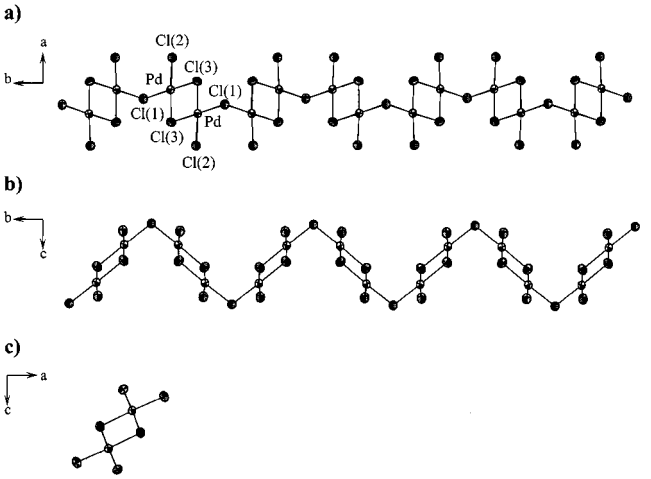

Figure 1. Part of the crystal structure of $CsPd_2Cl_5$; $^1_\infty[(PdCl_{3/2}Cl)_2^-]$ chain; (a) view along [001]; (b) view along [100]; (c) view along [010] (thermal ellipsoids are drawn at a 50% probability level)

The dinuclear Pd_2Cl_6 group is thus the basic unit, just as it is in $CsPdCl_3$. The angle Cl(3)–Pd–Cl(3) at the bridging edge is reduced [86.07(4)°] and is slightly smaller than the corresponding angle in $PdCl_2$.[8] Three crystallographic

[a] Fachbereich Chemie/Anorganische Chemie, Universität Dortmund,
44221 Dortmund, Germany
Fax: (internat.) +49 (0)231/755-5048
E-mail: keller@pop.uni-dortmund.de

 © WILEY-VCH Verlag GmbH, 69451 Weinheim, 2001 1434–1948/01/0606–1431 $ 17.50+.50/0

atom positions for chlorine were found by X-ray analysis: Cl(3) are edge-bridging, Cl(2) are terminal chlorine atoms, and the infinite chains are built by corner-sharing Cl(1). Due to the symmetry, the corner-sharing atoms lie *trans* to one another. The terminal Cl(2) atoms show the shortest Pd−Cl distance and the $^1_\infty[(PdCl_{3/2}Cl)_2^-]$ chains are arranged in such a way that viewed along [100] (Figure 1, b) puckered infinite chains are observed. These are totally eclipsed in the view along [010] (Figure 1, c).

The Pd−Cl structural motif is reminiscent of the connection of Pd units in β-PdI_2,[9] where the dinuclear units build puckered layers. Figure 2 shows a section of the crystal structure of PdI_2. The substructure similar to the Pd−Cl unit in $CsPd_2Cl_5$ is marked. Comparison of these structural units indicates the different puckered sequence of the chains, even though they have almost the same Pd−X−Pd angle (see Figure 3).

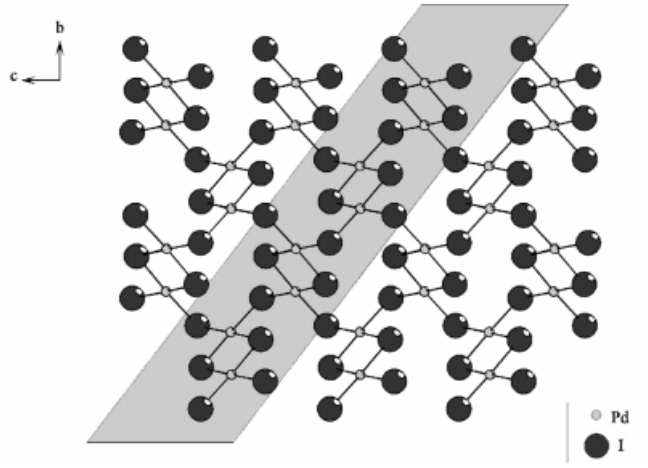

Figure 2. Part of the crystal structure of β-PdI_2

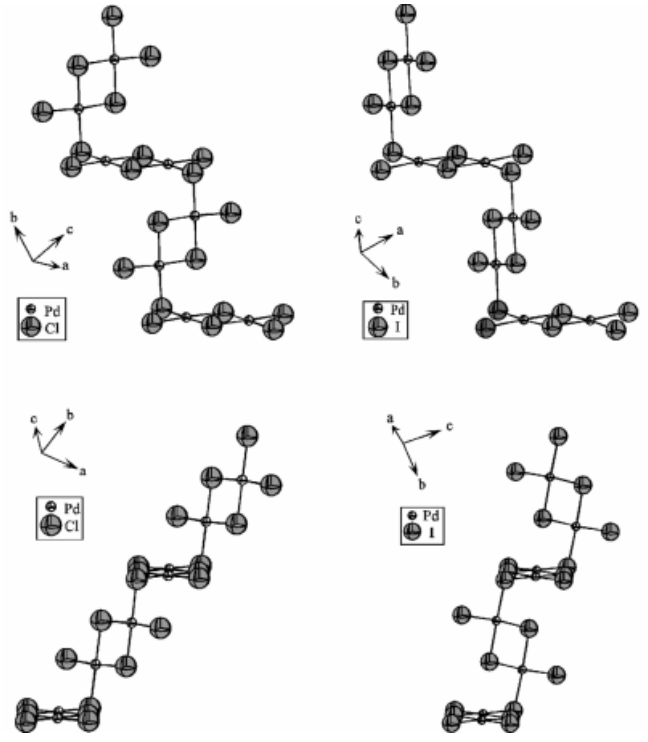

Figure 3. Comparison of a $^1_\infty[(PdCl_{3/2}Cl)_2^-]$ chain to part of the β-PdI_2 layer

The Pd−Cl motif is also reminiscent of the infinite chains in $PdCl_2$.[8] Opening these chains after every second palladium atom and adding a Cl atom leads to the $^1_\infty[(PdCl_{3/2}Cl)_2^-]$ chain found in $CsPd_2Cl_5$, as shown in Figure 1, a.

The arrangement in $CsPd_2Cl_5$ can be rationalized by considering the coordination spheres of the cesium cations. Each Cs is coordinated by nine chlorine atoms belonging to four different $^1_\infty[(PdCl_{3/2}Cl)_2^-]$ chains. We chose a distance of up to 3.85 Å as a first sphere for analysis of the Cs coordination by Cl. Four Cl atoms belong to the first chain, two pairs each come from two further chains, while the ninth Cl comes from the fourth chain. The relevant distances are shown in Table 1.

Table 1. Coordination of Cs by Cl

chain	atom	distance [Å]
1	Cl(2)	3.495(1) (2×)
	Cl(3)	3.722(1) (2×)
2	Cl(2)	3.507(1) (2×)
3	Cl(2)	3.537(1) (2×)
4	Cl(1)	3.818(2) (1×)

The average Cs−Cl distance of 3.593 Å falls within the expected range for Cs−Cl distances with CN 9 (3.519−3.738 Å, from a statistical analysis of ICSD data[10]). The polyhedra around Cs are mainly built-up from terminal chlorine atoms.

The bridging Cl atoms have a coordination number of 3, which is rather unusual. Cl(2) shows a more typical fourfold coordination. Selected distances and angles are collected in Table 2.

Table 2. Selected distances [Å] and angles [°] in $CsPd_2Cl_5$ (ORFFE[19])

Pd−Cl(2)	2.260(1)
Pd−Cl(1)	2.302(1)
Pd−Cl(3)	2.304(1)
Pd−Cl(3)	2.326(1)
Pd−Pd	3.3840(7)
Pd−Pd	3.4961(9)
Pd−Pd	3.6826(8)
Cs−Cl(2)	3.495(1) (2×)
Cs−Cl(2)	3.507(1) (2×)
Cs−Cl(2)	3.537(1) (2×)
Cs−Cl(3)	3.722(1) (2×)
Cs−Cl(1)	3.818(2)
Cl(2)−Pd−Cl(1)	91.70(5)
Cl(1)−Pd−Cl(3)	92.56(5)
Cl(3)−Pd−Cl(3)	86.07(4)
Cl(3)−Pd−Cl(2)	89.68(4)
Pd−Cl(3)−Pd	93.93(4)
Pd−Cl(1)−Pd	98.79(6)
Cl(2)−Cl(3)−Cl(1)	177.83(5)
Cl(2)−Pd−Cl(3)	175.72(4)
Cl(1)−Pd−Cl(3)	178.73(5)
torsion angle Cl(1)−Cl(3)−Cl(3)−Cl(1)	180
torsion angle Cl(2)−Cl(3)−Cl(3)−Cl(2)	180

The $^1_\infty[(PdCl_{3/2}Cl)_2^-]$ chains are aligned along the crystallographic *b* axis. Their arrangement can be described as a distorted hexagonal packing of parallel rods separated only by cesium atoms (Figure 4).

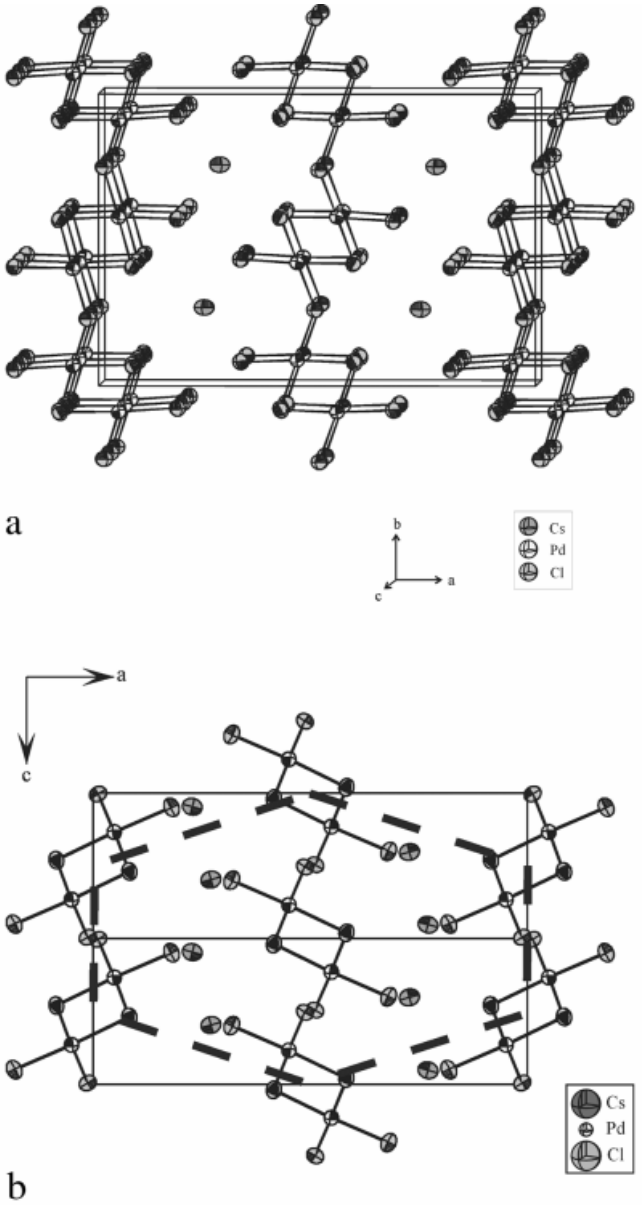

Figure 4. Part of the crystal structure of $CsPd_2Cl_5$; (a) unit cell; (b) hexagonal packing (thermal ellipsoids are drawn at a 50% probability level)

Comparison with Other Compounds of Formula Type AB_2X_5

Few compounds of the formula type AB_2X_5 have appeared in the literature, in which cations B^{2+} show planar coordination. $CsCu_2F_5$ [11] and fluoropalladates(II), MPd_2F_5 (M = K, Rb, Cs),[1,2] are known. $CsPd_2Cl_5$ is not isotypic with any of these.

MPd_2F_5 species, besides containing Pd(1) in square-planar coordination environment, also possess octahedrally coordinated Pd(2). The octahedra are connected through opposite corners forming infinite chains. The remaining fluorine atoms share corners with the planar PdF_4 units of Pd(2), thereby creating Pd–F layers. In contrast, $CsCu_2F_5$ has a complicated structure with CN = 4, 5, and 6 for Cu^{2+}. Consequently, $CsPd_2Cl_5$ represents the first example of a new structural type. Binary palladium halides are the only compounds to which the palladium–chlorine structural motif may be compared.

Calculation of Lattice Energy

The **MA**delung (coulombic) **P**art of **L**attice **E**nergy can be calculated using the program MAPLE.[12–14] Close correspondence between the calculated value and the sum $E_c(CsCl) + 2E_c(PdCl_2)$ lends support to the validity of our structure determination. The calculated Madelung Part of Lattice Energy of $CsPd_2Cl_5$ yields a value of 1358.55 kcal·mol^{-1}, as compared to the sum of 1347.11 kcal·mol^{-1}, a difference of just 0.85%. An analysis of the Madelung Part of Lattice Energy for the different chlorine positions proved interesting (Table 3). The highest MAPLE value was obtained for the corner-sharing Cl, whereas the lowest value was obtained for the terminal Cl. The obtained value was also lower than that for mononuclear $PdCl_4$ units, e.g. in Cs_2PdCl_4 (MAPLE $\approx$ 100–102 kcal·mol^{-1}). The edge-bridging Cl contributes 40% more to the overall lattice energy compared to the terminal ones. The value is also slightly increased compared to that in $PdCl_2$. The difference between the potentials of the corner-sharing and terminal Cl atoms is again increased (57%). The value for the corner-sharing atoms can only be compared with that for the tetrameric group $[(PdCl_{2/2}Cl_2)_4]^{4-}$ in $Tl_4Pd_3Cl_{10}$. The MAPLE value for the bridging atoms in $Tl_4Pd_3Cl_{10}$ amounts to 146 kcal·mol^{-1}, which is 10 kcal·mol^{-1} more than that for these atoms in $CsPd_2Cl_5$. A comparison of values for corner-sharing Cl atoms adjacent to edge-bridging ones is not

Table 3. Results of lattice energy calculations on $CsPd_2Cl_5$ with MAPLE[12–14]

Atom	^{1}MEFIR	^{1}ECoN	distance	potential	PMF	MAPLE[a]	*MAPLE	1MAPLE
Cs	178.48	9.8170	349.56	−0.61497	0.69492	102.0271	102.0271	230.5826
Pd	59.99	3.9841	226.00	−1.05817	2.39148	351.1120	87.7780	198.3795
Cl(1)[b]	173.38	2.6534	230.25	0.82335	0.93039	136.5977	136.5977	308.7127
Cl(2)[b]	173.67	3.8808	226.00	0.52460	0.59280	87.0330	87.0330	196.6957
Cl(3)[b]	175.62	3.1237	230.42	0.73426	0.82972	121.8177	121.8177	275.3098

[a] Madelung constant: 9.2533; Madelung Part of Lattice Energy: 1358.5502 (2) kcal/mol, 5686.8924 (7) kJ/mol. – [b] Cl(1) corner-sharing, Cl(2) terminal, Cl(3) edge-bridging.

possible, because no chloropalladates with such structural characteristics have hitherto been isolated. The importance of the bridging Cl atoms in the adoption of the observed structural type is clearly highlighted by their increased potentials compared to those of the Cl atoms in CsCl, $PdCl_2$, and monomeric $PdCl_4$ units.

Conclusion

$CsPd_2Cl_5$ represents a new compound with a hitherto unknown structural type. Palladium is not coordinated octahedrally as it is in fluoropalladates of the same formula type. Instead, the planar $PdCl_4$ units build polynuclear infinite chains by sharing corners and edges. The bridging motif corresponds to the results of our experiments concerning higher cesium chloropalladates(II). Besides $CsPdCl_3$, we have been able to prepare two further compounds based on dinuclear Pd_2Cl_6 units. We propose following nomenclature for chloropalladates:

Cs_3PdCl_5 [7] = $(Cs^+)_3[PdCl_4]^{2-}Cl^-$
Cs_2PdCl_4 [15] = $(Cs^+)_2[PdCl_4]^{2-}$
$Cs_{12}Pd_9Cl_{30}\cdot 2H_2O$ [15] =
$(Cs^+)_{12}([PdCl_4]^{2-})_3\text{-}\{[(PdCl_{2/2}Cl_2)_2]^{2-}\}_3\cdot 2H_2O$
$Cs_6Pd_5Cl_{16}\cdot 2H_2O$ [15] =
$(Cs^+)_6([PdCl_4]^{2-})\text{-}\{[(PdCl_{2/2}Cl_2)_2]^{2-}\}_2\cdot 2H_2O$
$CsPdCl_3$ [3] = $(Cs^+)_2\{[(PdCl_{2/2}Cl_2)_2]^{2-}\}$
$CsPd_2Cl_5 = (Cs^+)\ {}^1_\infty[(PdCl_{3/2}Cl)_2^-]$

Increasing Pd content leads to additional linkage of the square-planar groups.

Perspective

Further investigations of the system $CsCl/PdCl_2$ can be expected to yield new compounds with several additional connecting patterns, e.g. $CsPd_3Cl_7$, as proposed by Safonov and Mireev.[6]

Experimental Section

Cesium Pentachloropalladate(II), $CsPd_2Cl_5$: The first indication of the existence of a compound containing an increased Pd content in the $CsCl/PdCl_2$ system was obtained in the course of heating experiments. A mixture of CsCl (Merck) and $PdCl_2$ (prepared according to Brauer[20]) in a molar ratio of 1:3 was melted, quenched, and annealed in an evacuated quartz glass ampoule. After heating the ampoule for 6 weeks at 280 °C, the powder diffraction pattern (PW 1050/25, Philips) showed unknown peaks, which did not correspond to those reported for $CsPd_3Cl_7$ in ref.[6]

Preparation under hydrothermal conditions proved more successful. A quartz glass ampoule was charged with 0.5 g of a mixture of

Table 4. Crystal data and details of the data collection for $CsPd_2Cl_5$

Empirical formula	$CsPd_2Cl_5$
Molecular weight	523.01
Diffractometer	CAD4 (Enraf−Nonius)
Radiation, wavelength [Å]	Mo-K_α, 0.71069
Monochromator	graphite
Data collection mode	ω−2θ scan
T [K]	298
Crystal system	orthorhombic
Space group	*Pnma* (no. 62)
a [Å]	15.725(3)
b [Å]	10.526(2)
c [Å]	5.275(1)
$V_{calcd.}/V_{BILTZ}$[18] [Å^3]	873.13/890.2
$\rho_{calcd.}$ [g·cm^{-3}]	3.978
θ range [°]	$4 \le 2\theta \le 70$
Range of indices	$-25 \le h \le 25$
	$-16 \le k \le 16$
	$-8 \le l \le 8$
Data collected	4470
Unique data	2002
$R_{int.}$	0.0376
Refinement method	full-matrix least-squares [SHELXL-93[17]]
Parameters	40
$R1$ [$F_o > 4\sigma(F_o)$]	0.0361 (1208 data)
$R1$ (all data)	0.0850 (2002 data)
$wR2$	0.0758
GooF	1.004
Largest diff. peak/hole [e Å^{-3}]	1.51 (d_{Cs} = 0.70 Å)/−1.26

Table 5. Atomic coordinates, equivalent displacement parameters U_{eq} [Å^2] (U_{eq} = 1/3 $\Sigma_i \Sigma_j$ a_i^* a_j^* $\mathbf{a}_i$ $\mathbf{a}_j$), and anisotropic displacement parameters U_{ij} [Å^2] {exp [$-2\pi^2$ ($U_{11}h^2a^{*2}$ + $U_{22}k^2b^{*2}$ +... + $2U_{12}hka^*b^*$)]} for $CsPd_2Cl_5$

Atom		x	y	z	U_{eq}
Cs	4c	0.22858(3)	1/4	0.09477(9)	0.0411(1)
Pd	8d	0.45086(2)	0.08393(3)	0.76896(6)	0.02635(8)
Cl(1)	4c	0.9882(1)	1/4	0.9924(3)	0.0335(3)
Cl(2)	8d	0.31915(8)	0.0743(1)	0.5986(2)	0.0372(2)
Cl(3)	8d	0.58392(7)	0.0802(1)	0.9613(2)	0.0362(2)

Atom	U_{11}	U_{22}	U_{33}	U_{23}	U_{13}	U_{12}
Cs	0.0530(3)	0.0319(2)	0.0384(2)	0	0.0044(2)	0
Pd	0.0264(1)	0.0240(1)	0.0287(2)	−0.0015(1)	0.0001(1)	0.0008(1)
Cl(1)	0.0383(8)	0.0299(8)	0.0321(7)	0	−0.0061(7)	0
Cl(2)	0.0327(5)	0.0332(5)	0.0456(6)	0.0004(5)	−0.0089(5)	−0.0010(5)
Cl(3)	0.0298(5)	0.0372(6)	0.0417(6)	0.0079(5)	−0.0031(5)	−0.0051(5)

CsCl and $PdCl_2$ (molar ratio 1:2). After the addition of H_2O (0.5 mL), the solvent was frozen and the ampoule (ϕ 6 mm, length 60 mm) was evacuated and sealed. The reaction was carried out at 150 °C. After cooling, the mixture was filtered and the crude product was washed with H_2O, ethanol, and diethyl ether. Dark red-brown single crystals were selected for X-ray investigations.

X-ray Crystallographic Study: The crystal structure was determined by single-crystal X-ray analysis at 298 K. Data were collected on a CAD4 diffractometer (Enraf–Nonius). An empirical absorption correction employing psi-scans was applied to the data set (absorption coefficient = 9.66 mm^{-1}). The crystal structure was determined by direct methods (SHELXS-86[16]) and refined by full-matrix least-squares calculations using the program SHELXL-93.[17] Details of the structural investigations and salient crystallographic data are summarized in Table 4, whereas the final atomic coordinates, equivalent displacement parameters U_{eq}, as well as anisotropic displacement parameters are presented in Table 5. Selected interatomic distances and angles are given in Table 2.

Further details of the crystal structure investigation may be obtained from the Fachinformationszentrum Karlsruhe, D-76344 Eggenstein-Leopoldshafen, Germany, on quoting the depository number CSD-411722.

Acknowledgments

We would like to thank Degussa AG for a donation of palladium and the Fonds der Chemischen Industrie for financial support.

[1] B. Bachmann, B. G. Müller, *Z. Anorg. Allg. Chem.* **1992**, *616*, 7.
[2] B. G. Müller, *Z. Anorg. Allg. Chem.* **1982**, *491*, 245.
[3] B. Schüpp, H.-L. Keller, *Z. Anorg. Allg. Chem.* **1999**, *625*, 1944.
[4] B. Schüpp, H.-L. Keller, *Z. Anorg. Allg. Chem.* **1999**, *625*, 241.
[5] M. Duchâteau, Diplomarbeit, Universität Kiel, **1989**.
[6] V. V. Safonov, V. A. Mireev, *Russ. J. Inorg. Chem.* **1984**, *29*, 1050.
[7] M. Duchâteau, Ph.D. Thesis, Universität Dortmund, **1994**.
[8] A. F. Wells, *Z. Krist.* **1938**, *100*, 189.
[9] G. Thiele, K. Brodersen, E. Kruse, B. Holle, *Chem. Ber.* **1968**, *101*, 2771.
[10] ICSD/RETRIEVE 2.01, Inorganic Crystal Structure Database, M. Berndt, Gmelin Institut, FIZ Karlsruhe, **1997**.
[11] V. Kaiser, D. Babel, *Z. Anorg. Allg. Chem.* **1991**, *595*, 139.
[12] R. Hoppe, *Angew. Chem.* **1966**, *78*, 52; *Angew. Chem. Int. Ed. Engl.* **1966**, *5*, 95.
[13] R. Hoppe, *Angew. Chem.* **1970**, *82*, 7; *Angew. Chem. Int. Ed. Engl.* **1970**, *9*, 25.
[14] R. Hoppe, *Z. Naturforsch., Teil A* **1995**, *50*, 555.
[15] B. Schüpp, Ph.D. Thesis, Universität Dortmund, **1999**.
[16] G. M. Sheldrick, SHELXS-86, *Program for Crystal Structure Determination*, Universität Göttingen, **1986**.
[17] G. M. Sheldrick, SHELXL-93, *Program for Crystal Structure Refinement*, Universität Göttingen, **1993**.
[18] W. Biltz, *Raumchemie der festen Stoffe*, L. Voss Verlag, Leipzig, **1934**.
[19] W. R. Busing, K. O. Martin, H. A. Levy, G. W. Brown, C. K. Johnson, W. E. Thiessen, ORFFE, Crystallographic Function and Error Program, Oak Ridge, **1971**.
[20] G. Brauer, *Handbuch der Präparativen Anorganischen Chemie, 3. Auflage, Band 3*, F. Enke Verlag, Stuttgart, **1981**, p. 1728.

Received August 11, 2000
[I00311]

Synthesis and Complexation of the Metalloligand {(η^5-C_5H_5)[η^5-C_5Me_3-1,2-(PPh_2)$_2$]$TiCl_2$} (TiPHOS): The First Example of a 1,2-Bis(diphenylphosphanyl)titanocene Derivative

Pierre Le Gendre,[a] Emeline Maubrou,[a] Olivier Blacque,[a] Gilles Boni,[a] and Claude Moïse*[a]

Keywords: Phosphanes / Metallocenes / Rhodium / Titanium / Heterobimetallic complexes

The reaction of lithium 1,2-bis(diphenylphosphanyl)trimethylcyclopentadienide (**1**) with $CpTiCl_3$ leads to the formation of the titanocene diphosphane {(η^5-C_5H_5)[η^5-C_5Me_3-1,2-(PPh_2)$_2$]$TiCl_2$} (TiPHOS, **2**). This metalloligand reacts readily with (NBD)$Cr(CO)_4$ and $W(CO)_5$(THF) to give, in both cases, the bimetallic chelate complexes (TiPHOS)$Cr(CO)_4$ (**3**) and (TiPHOS)$W(CO)_4$ (**4**). The structure of **4** has been determined by X-ray diffraction. The synthesis of a new early-late heterobimetallic complex (TiPHOS)Rh(CO)Cl (**5**) is reported.

Introduction

Chelating diphosphanes constitute one of the most versatile ligands in organometallic chemistry.[1] Within this field, diphosphanes built on a bent metallocene skeleton are of particular interest. Indeed, the structural flexibility of such structures allows the chemist to synthesize a wide range of ligands. Furthermore, coordination of the metalloligand to an electron-rich metal leads to early-late heterobimetallic complexes with a high potential for homogeneous catalysis.[2]

Three types of diphosphanes with a bent metallocene framework have already been described (Figure 1).[3−5] Both the phosphorous groups can be linked either to each Cp unit (types I, I′) or directly to the metal (type II), or one to the Cp and one to the metal (type III).

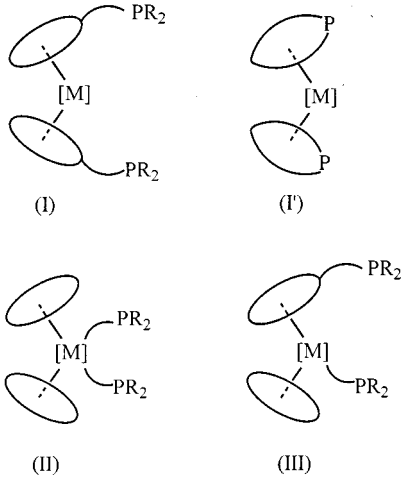

Figure 1. Diphosphanes with a bent metallocene framework

[a] Laboratoire de Synthèse et d′Electrosynthèse Organométalliques, LSEO-UMR 5632,
Université de Bourgogne, Faculté des Sciences Gabriel,
6 bd. Gabriel, 21000 Dijon, France
Fax: (internat.) +33-3/8039-6076
E-mail: claude.moise@u-bourgogne.fr

In this paper we describe the synthesis of a new titanocene dichloride metalloligand with the 1,2-bis(diphenylphosphanyl)trimethylcyclopentadienyl moiety. The 1,2-position of the phosphorus atoms on the cyclopentadienyl ring gives the ligand a rigid chelate structure often required for selective catalytic process. This diphosphane complex could, if necessary, be tuned by replacing the two chloride atoms on the titanium atom with other ligands. The synthesis and the characterisation of three new heterobimetallic complexes Ti−Cr, Ti−W and Ti−Rh are also reported.

Results and Discussion

The ligand **1** was prepared according to an earlier method involving the synthesis of 1,2,3-trimethylcyclopenta-1,3-diene, followed by two repeated sequences of deprotonation-addition to PPh_2Cl and then deprotonation.[6]

The reaction of the lithium salt **1** with $CpTiCl_3$ was carried out in THF at reflux. The reaction is complete after 16 h and leads to the targeted metalloligand **2** (TiPHOS) in good yield (Scheme 1). The ^{31}P NMR spectrum of **2** shows a singlet at $\delta = -21.8$ consistent with a diphosphane not coordinated to a metal atom. The ^1H NMR spectra of **2** displays two singlets at $\delta = 1.7$ and 2.0 for the C_5Me_3-1,2-(PPh_2)$_2$ ligand assignable to the central and to both lateral methyl groups, respectively.

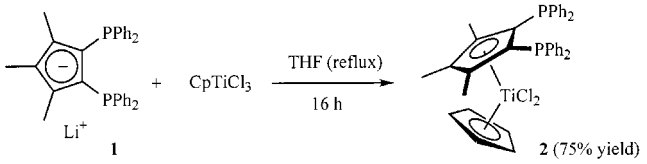

Scheme 1

In order to test the chelating properties of the TiPHOS ligand we coordinated it to the $Cr(CO)_4$ fragment. The metalloligand **2** readily displaces NBD from (NBD)$Cr(CO)_4$ in THF at room temperature to give the

 © WILEY-VCH Verlag GmbH, 69451 Weinheim, 2001 1434−1948/01/0606−1437 $ 17.50+.50/0

bimetallic complex **3** (Scheme 2). This complex may be recrystallized from the same solvent. The infrared spectrum in the CO stretching region exhibits four carbonyl stretching bands at 2008, 1922, 1901 and 1881 cm^{-1} consistent with a *cis*-$L_2Cr(CO)_4$ complex. The ^{31}P NMR spectrum of **3** displays only one singlet at $\delta = 70.70$ corresponding to a downfield shift of about 93 ppm relative to the original bis(diphenylphosphane) **2**. The ^1H NMR spectrum of **3** shows one singlet (intensity six) for both lateral methyl groups bonded to the cyclopentadienyl ring. The above data, closely similar to those obtained by Broussier et al. for a ferrocenic diphosphane,[7] are consistent with the symmetric chelate structure of **3** (Scheme 2).

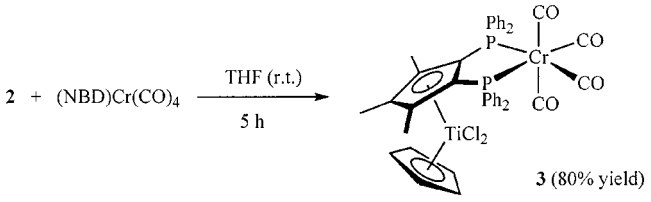

Scheme 2

The easy formation of the bimetallic complex **3** prompted us to check the chelating abilities of TiPHOS with W^0 pentacarbonyl complexes. The reaction of **2** with $W(CO)_5(THF)$ in THF leads to the chelate structure **4** (Scheme 3). The ^{31}P NMR spectrum of **4** shows a singlet at $\delta = 33.60$ with ^{183}W satellites. The ^1H NMR and IR spectra of **4** are similar to those reported for **3** and confirm the structural features. It is worth noting that no trace of the $-W(CO)_5$ mono-coordinated intermediate derived from the chelating diphosphane **2** could be detected.

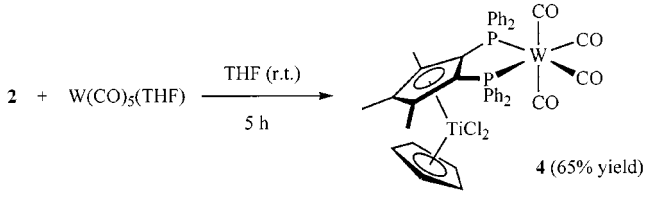

Scheme 3

Suitable crystals of **4** for X-ray measurements were obtained by crystallisation from warm THF. Its molecular structure is shown in Figure 2. The crystallographic study confirms its chelate structure and exhibits the usual tetrahedral (Ti) and distorted octahedral (W) geometries around the metallic fragments. The tungsten−phosphorus distances of 2.528(2) Å are similar to those observed for other tungsten−diphosphane structures (2.52−2.54 Å).[8] The P−W−P bite angle of 80.37(8)° corresponds well to that found in a *cis*-$W(CO)_4$ complex with 1,2-bis(diphenylphosphanyl)ferrocene.[7]

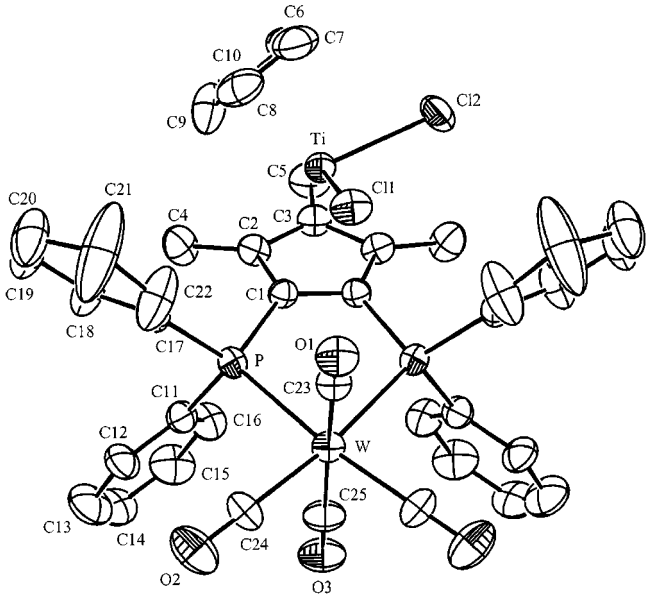

Figure 2. Molecular structure of complex **4**; for clarity the disordered atoms are not represented; selected bond lengths [Å] and angles [°]: Ti−Cp1 2.114, Ti−Cp2 2.072, Ti−Cl1 2.320(4), Ti−Cl2 2.364(9), W−P 2.528(2); P−W−P* 80.37(6), Cl1−Ti−Cl2 94.0(3)

Once the chelating abilities of the metalloligand **2** had been revealed, we investigated its complexation with rhodium. Thus, the reaction with 0.5 molar equiv. of $[(CO)_2RhCl]_2$ gave the 1:1 adduct **5** which was isolated as a brown yellow powder (Scheme 4). The ^{31}P NMR spectrum of **5** reveals a single set of eight signals with an AB pattern split by Rh−P coupling ($^2J_{P-P}$ =36 Hz; $^1J_{P-Rh}$ = 127 Hz and 163 Hz) which is in accordance with the *cis*-coordination of both phosphorus atoms of TiPHOS to rhodium. The ^1H NMR spectrum of **5** differs from that of the precursor phosphane **2** and the other bimetallic systems **3** and **4** in that it displays three methyl resonances instead of two. This anisochrony is indicative of the loss of the plane of symmetry. Finally, the IR spectrum exhibits a single carbonyl stretch at 1984 cm^{-1} which corresponds to the terminal carbonyl band.

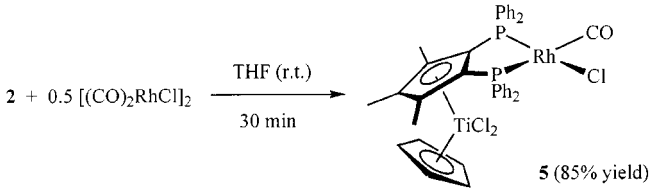

Scheme 4

Conclusion

We have described the preparation of a new class of titanocene diphosphane complexes. This synthesis involves the preparation of the lithium salt $[C_5Me_3$-1,2-$(PPh_2)_2]Li$ (**1**) followed by its treatment with $CpTiCl_3$. The chelating abilities of the metalloligand **2** (TiPHOS) has been revealed by its reaction with $(NBD)Cr(CO)_4$ and $W(CO)_5(THF)$ complexes. In both cases the heterobimetallic chelate complexes

have been obtained in good yields. Finally, the reaction of TiPHOS with the dimer $[(CO)_2RhCl]_2$ has led to the exclusive formation of a new early late Ti−Rh bimetallic complex. Further studies on bimetallic complexes containing the TiPHOS ligand and their catalytic activity are currently in progress.

Experimental Section

All manipulations were carried out under an argon atmosphere using vacuum line techniques. Solvents were dried and distilled under argon before use. $CpTiCl_3$,[9] $(NBD)Cr(CO)_4$,[10] $W(CO)_5(THF)$[11] and $[C_5Me_3$-1,2-$(PPh_2)_2]Li$[6] (**1**) were prepared by literature methods. NMR spectra were recorded on a BRUKER AC200 (200 MHz for ^1H, 81 MHz for ^{31}P, 50 MHz for ^{13}C) spectrometer. IR spectra were obtained on a Bruker IFS 66v; abbreviations: m (medium), s (strong), vs (very strong). Elemental analyses were performed on a FISON EA 1108 within the laboratory.

{(η^5-C_5H_5)[η^5-C_5Me_3-1,2-(PPh_2)$_2$]$TiCl_2$} (TiPHOS) (2): [C_5Me_3-1,2-$(PPh_2)_2$]Li (0.81 g, 1.7 mmol) in 10 mL of THF was added to $CpTiCl_3$ (0.37 g, 1.7 mmol) in 15 mL of THF. After stirring for 16 h at reflux, the solvent was removed in vacuo. The dark red residue was extracted with toluene and filtered through a piece of cotton. The solvent was removed in vacuo, the residue dissolved in CH_2Cl_2 and precipitated by the addition of hexane. The mixture was then placed in a freezer (−20 °C) for 1 h. The precipitate was collected by filtration and dried in vacuo (0.83 g, 75% yield). − ^1H NMR ($CDCl_3$): δ = 1.75 (s, 3 H, CH_3), 1.97 (s, 6 H, CH_3), 6.03 (s, 5 H, C_5H_5), 6.95 (m, 10 H, Ph), 7.26 (m, 4 H, Ph), 7.49 (m, 6 H, Ph). − $^{13}C\{^1H\}$ NMR ($CDCl_3$, partial): δ = 12.9 (s, *C*H_3), 16.2 (s, *C*H_3), 121.6 (s, C_5H_5). − $^{31}P\{^1H\}$ NMR ($CDCl_3$): δ = −21.79 (s, PPh_2). − $C_{37}H_{34}Cl_2P_2Ti$ (659.41): calcd. C 67.39, H 5.20; found C 67.68, H 5.02.

(TiPHOS)Cr(CO)$_4$ (3): A 25 mL flask was charged with **2** (140 mg, 0.2 mmol), $(NBD)Cr(CO)_4$ (54 mg, 0.2 mmol) and 10 mL of THF. The solution was stirred at room temperature for 5 h. The solvent was concentrated in vacuo until an abundant precipitate was formed. The brown precipitate was collected by filtration and dried in vacuo (0.13 g, 80% yield). − IR ($CHCl_3$): ν(CO) = 2008 (m), 1922 (s), 1901 (vs), 1881 cm^{-1} (s). − ^1H NMR ($CDCl_3$): δ = 1.88 (s, 3 H, CH_3), 2.17 (s, 6 H, CH_3), 5.87 (s, 5 H, C_5H_5), 6.97 (m, 4 H, Ph), 7.29 (m, 6 H, Ph), 7.51 (m, 6 H, Ph), 8.14 (m, 4 H, Ph). − $^{13}C\{^1H\}$ NMR ($CDCl_3$, partial): δ = 13.7 (s, *C*H_3), 18.1 (s, *C*H_3), 122.17 (s, C_5H_5), 216.9 (triplet, $^2J_{CP}$ = 10 Hz, *C*O), 223.7 (pseudotriplet, $^2J_{CP}$ = 13 Hz, *C*O), 227.9 (triplet, $^2J_{CP}$ = 8 Hz, *C*O). − $^{31}P\{^1H\}$ NMR ($CDCl_3$): δ = 70.70 (s, PPh_2). − $C_{41}H_{34}Cl_2CrO_4P_2Ti$ (823.45): calcd. C 59.80, H 4.16; found C 59.29, H 3.96.

(TiPHOS)W(CO)$_4$ (4): This compound was obtained following the above procedure but with $W(CO)_5(THF)$ (0.12 g, 65% yield). − IR (KBr): ν(CO) = 2102 (m), 1905 (s), 1893 (vs), 1865 cm^{-1} (s). − ^1H NMR ($CDCl_3$): δ = 1.86 (s, 3 H, CH_3), 2.15 (s, 6 H, CH_3), 5.86 (s, 5 H, C_5H_5), 6.97 (m, 4 H, Ph), 7.28 (m, 6 H, Ph), 7.50 (m, 6 H, Ph), 8.10 (m, 4 H, Ph). − $^{13}C\{^1H\}$ NMR ($CDCl_3$, partial): δ = 14.0 (s, *C*H_3), 18.0 (s, *C*H_3), 122.8 (s, C_5H_5). − $^{31}P\{^1H\}$ NMR ($CDCl_3$): δ = 33.59 (s + d, $^1J_{W-P}$ = 244 Hz, PPh_2). − $C_{41}H_{34}Cl_2O_4P_2TiW$ (955.30): calcd. C 51.55, H 3.59; found C 51.89, H 4.09.

(TiPHOS)Rh(CO)Cl (5): A 25-mL flask was charged with **2** (42 mg, 0.06 mmol), $[RhCl(CO)_2]_2$ (36 mg, 0.03 mmol) and 4 mL of THF. The mixture was stirred at room temperature for 30 min. during which time a brown yellow precipitate formed. The precipitate was collected by filtration and dried in vacuo (42 mg, 85% yield). − IR (KBr): ν(CO) = 1984 cm^{-1} (vs). − ^1H NMR ($CDCl_3$): δ = 1.95 (s, 3 H, CH_3), 2.09 (s, 3 H, CH_3), 2.10 (s, 3 H, CH_3), 5.93 (s, 5 H, C_5H_5), 7.21 (m, 10 H, Ph), 7.48 (m, 6 H, Ph), 8.08 (m, 4 H, Ph). − $^{13}C\{^1H\}$ NMR ($CDCl_3$, partial): δ = 13.7 (s, *C*H_3), 16.8 (s, *C*H_3), 17.1 (s, *C*H_3), 122.0 (s, C_5H_5). − $^{31}P\{^1H\}$ NMR ($CDCl_3$): δ = 36.73 (dd, $^1J_{Rh-P}$ = 127 Hz, $^2J_{P-P}$ = 36 Hz, PPh_2), 56.00 (dd, $^1J_{Rh-P}$ = 163 Hz, $^2J_{P-P}$ = 36 Hz, PPh_2). − $C_{38}H_{34}Cl_3OP_2RhTi$ (825.78): calcd. C 55.27, H 4.15; found C 54.70, H 4.05.

X-ray Crystallographic Study of 4: $C_{41}H_{31}Cl_2O_4P_2TiW{\cdot}4C_4H_8O$, M = 1240.66, orthorhombic, space group $Pn2_1m$ (No. 31), a = 9.2830(2) Å, b = 16.6440(4) Å, c = 19.7850(6) Å, V = 3056.9(1) Å^3, Z = 2, $\rho_{calcd.}$ = 1.348 g·cm^{-3}, $F(000)$ = 1258, μ = 2.198 mm^{-1}, T = 110(2) K, 4720 independent reflections, 4123 observed reflections [$I \geq 2\sigma(I)$], 304 refined parameters, 10 restraints, $R(F)$ = 0.0576, $wR(F^2)$ = 0.1359 for all data and $R(F)$ = 0.0486, $wR(F^2)$ = 0.1276, S = 1.073 for observed reflections. A red crystal of **4** having the approximate dimensions 0.5 × 0.2 × 0.2 mm^3 and suitable for an X-ray analysis was sealed in a glass capillary in an inert oil and mounted on a Nonius KappaCCD diffractometer with graphite-monochromated Mo-K_α radiation (λ = 0.71073 Å). A total of 228 frames of data were collected at 110(2) K with an oscillation range of 1.5°/frame and an exposure time of 40 s/deg.[12] A total of 43869 reflections were indexed, integrated, and corrected for Lorentz and polarization effects using DENZO-SMN and SCALEPACK.[13] Data reduction yielded 4720 unique reflections of which 4123 had $I > 2\sigma(I)$. Refinement of the unit cell parameters gave a = 9.2830(2) Å, b = 16.6440(4) Å, c = 19.7850(6) Å and V = 3056.9(1) Å^3. Systematic absences were consistent with the compound having crystallised in the orthorhombic space group $Pn2_1m$ (No. 31).

The structure was solved by a Patterson search program[14] and refined by full-matrix least-squares on F^2 using SHELXL.[14] All non-hydrogen atoms were refined with anisotropic thermal parameters, except for solvent atoms which were refined with a global isotropic temperature factor (the complex crystallised with four THF solvate molecules). The hydrogen atoms of the complex were included in their calculated positions and refined in a riding model with isotropic displacement coefficients (the hydrogen atoms of solvent molecules were not introduced in the model). The nonsubstitued cyclopentadienyl ring and the two chlorine atoms were found to be disordered. The residual peaks on the final difference Fourier map ranged from −0.82 to 0.88 e·Å^{-3}.

Crystallographic data (excluding structure factors) for the structure reported in this paper have been deposited with the Cambridge Crystallographic Data Centre as supplementary publication no. CCDC-147166. Copies of the data can be obtained free of charge on application to CCDC, 12 union Road, Cambridge CB2 1EZ, UK [Fax: (internat.) + 44-1223/336-033; E-mail: deposit@ccdc.cam.ac.uk].

Acknowledgments

Miss A. Noirot is kindly acknowledged for her assistance with the synthesis of **1**.

[1] G. W. Parschall, S. D. Ittel, *Homogeneous Catalysis*, 2nd ed., John Wiley & Sons, New York, **1992**.

[2] [2a] R. Choukroun, D. Gervais, P. Kalck, F. Senocq, *J. Organomet. Chem.* **1987**, *335*, C9−C12. − [2b] A. M. Trzeciak, J. J. Ziolkowski, R. Choukroun, *J. Mol. Catal.* **1996**, *110*, 135−139. − [2c] B. E. Bosch, I. Brümmer, K. Kunz, G. Erker, R. Fröhlich, S. Kotila, *Organometallics* **2000**, *19*, 1255−1261. − [2d] N. Wheatley, P. Kalck, *Chem. Rev.* **1999**, 3379−3419.

[3] [3a] J. C. Leblanc, C. Moïse, A. Maisonnat, R. Poilblanc, C. Charrier, F. Mathey, *J. Organometal. Chem.* **1982**, *231*, C43−C48. − [3b] D. Morcos, W. Tikkanen, *J. Organometal. Chem.* **1989**, *371*, 15−18. − [3c] X. D. He, A. Maisonnat, F. Dahan, R. Poilblanc, *Organometallics* **1989**, *8*, 2618−2626. − [3d] J. Szymoniak, M. M. Kubicki, J. Besançon, C. Moïse, *Inorg. Chim. Acta* **1991**, *180*, 153−160. − [3e] E. Delgado, J. Fornies, E. Hernandez, E. Lalinde, N. Mansilla, M. T. Moreno, *J. Organomet. Chem.* **1995**, *494*, 261−265. − [3f] T. W. Graham, A. Llamazares, R. McDonald, M. Cowie, *Organometallics* **1999**, *18*, 3490−3501. − [3g] F. Nief, F. Mathey, L. Ricard, *J. Organomet. Chem.* **1990**, *384*, 271−278.

[4] [4a] N. E. Schore, S. J. Young, M. M. Olmstead, P. Hofmann, *Organometallics* **1983**, *2*, 1769−1780. − [4b] R. Choukroun, D. Gervais, J. Jaud, P. Kalck, F. Senocq, *Organometallics* **1986**, *5*, 67−71. − [4c] G. S. White, D. W. Stephan, *Organometallics* **1987**, *6*, 2169−2175. − [4d] R. T. Baker,. C. Fultz, T. B. Marder, I. D. Williams, *Organometallics* **1990**, *9*, 2357−2367. − [4e] D. G. Dick, D. W. Stephan, *Organometallics* **1990**, *9*, 1910−1916. − [4f] G. Boni, M. M. Kubicki, C. Moïse, *Bull. Soc. Chim. Fr.* **1994**, *131*, 895−899.

[5] C. Poulard, G. Boni, P. Richard, C. Moïse, *J. Chem. Soc., Dalton Trans* **1999**, *16*, 2725−2731.

[6] R. Broussier, S. Ninoreille, C. Legrand, B. Gautheron, *J. Organomet. Chem.* **1997**, *532*, 55−60.

[7] R. Broussier, S. Ninoreille, C. Bourdon, O. Blacque, C. Ninoreille, M. M. Kubicki, B. Gautheron, *J. Organomet. Chem.* **1998**, *561*, 85−96.

[8] M. R. Churchill, A. L. Rheingold, R. L. Keiter, *Inorg. Chem.* **1981**, *20*, 2730−2734.

[9] A. F. Reid, P. C. Wailes, *J. Organomet. Chem.* **1964**, *2*, 329−335.

[10] M. A. Bennet, L. Pratt, G. J. Wilkinson, *J. Chem. Soc. (A)* **1961**, 2037−2039.

[11] W. Strohmeier, F. J. Müller, *Chem. Ber.* **1969**, *102*, 3608−3612.

[12] *COLLECT Data Collection Software,* Nonius B. V., Rontgenweg 1, P. O. Box 811, 2600 AV Delft, The Netherlands, **1998**.

[13] Z. Otwinowski, W. Minor, *Methods Enzymol.* **1997**, *276*, 307−326.

[14] G. M. Sheldrick *SHELXS-97* and *SHELXL-97*, University of Göttingen, Germany, **1997.**

Received September 6, 2000
[I00333]

On the Relevance of Mono- and Dinuclear Iron Carbonyl Complexes to the Fixation and Stepwise Hydrogenation of N_2[‡]

Yu Chen,[a] Michael Hartmann,*[a] and Gernot Frenking*[a]

Dedicated to Professor Dieter Sellmann on the occasion of his 60th birthday

Keywords: Ab initio calculations / Density functional theory / Iron / Carbonyl ligands / Nitrogen fixation / Hydrogenation

Density functional theory and high-level ab initio calculations are used to evaluate the influence of mono- and dinuclear iron carbonyl complexes to the fixation and stepwise hydrogenation of dinitrogen via diazene and hydrazine to ammonia. In comparison to the reaction of isolated N_2, only the first step in this reaction sequence (i.e. the reduction of N_2 to N_2H_2) experiences a significant change in its thermochemistry when coordinated to mono- or dinuclear iron tetracarbonyl fragments. The reaction enthalpy ΔH_R^0 (T = 0 K) for the endothermic hydrogenation of $(CO)_4Fe–N_2$ to give $(CO)_4Fe–N_2H_2$ is lower than for the corresponding metal-free process by 16.1 kcal mol^{-1}. The analogous step involving the dinuclear species $(CO)_4Fe–N_2–Fe(CO_4)$ and $(CO)_4Fe–N_2H_2–Fe(CO)_4$ is even less endothermic than the reduction involving only one iron tetracarbonyl complex by 13.1 kcal mol^{-1}. In comparison to that, the second and third step of this reduction sequence, namely the conversion of coordinated diazene to $(CO)_4Fe–N_2H_4$ and the subsequent reduction of coordinated hydrazine to $(CO)_4Fe–NH_3$ show only relatively small thermodynamic changes compared to the analogous reactions of isolated N_2H_2 and N_2H_4. The reduction of $(CO)_4Fe–N_2H_2$ to $(CO)_4Fe–N_2H_4$ is almost as exothermic as the analogue reaction involving isolated N_2H_2, whereas the hydrogenation of $(CO)_4Fe–N_2H_4$ to $(CO)_4Fe–NH_3$ is less exothermic by 4.0 kcal mol^{-1}. Finally, the reduction of $(CO)_4Fe–N_2H_2–Fe(CO)_4$ and $(CO)_4Fe–N_2H_4–Fe(CO)_4$ are both predicted to be less exothermic than their mononuclear analogues by 4.0 and 1.1 kcal mol^{-1}, respectively. Moreover, we find that only N_2 and N_2H_2, which already show a noticeable π-acceptor behavior in their complexes with $Fe(CO)_4$, experience important structural changes in their corresponding dinuclear complexes, i.e. a shortening of the Fe–N bonds and a lengthening of the N–N bonds on going from $(CO)_4Fe–L$ to $(CO)_4Fe–L–Fe(CO)_4$ (L = N_2, N_2H_2). This behavior is in line with a slightly increased π-acceptor ability of these ligands in their respective dinuclear complexes. Such structural changes are absent for N_2H_4, which only exhibits a comparatively weak π-acceptor character in $(CO)_4Fe–N_2H_4$.

Introduction

The stepwise hydrogenation of dinitrogen to ammonia is one of the most important processes in biochemical research[1] and of utmost interest to chemical industry.[2] Besides the well-understood heterogeneously catalyzed reduction following the Haber−Bosch process,[3] deeper insight into the reduction of dinitrogen is necessary, particularly when dealing with biologically relevant systems. An example of this is the enzymatic fixation of N_2 catalyzed by nitrogenases.[4] Although the molecular structure of the Fe−Mo cofactor of a nitrogenase enzyme has been characterized by X-ray structure analysis,[5] details of the catalytically important features involved in the N_2 reduction have still not, however, been unequivocally answered.[6] To this end, the binding site, the binding mode of N_2 and the intermediates involved in the catalytic processes are still the source of much speculation.[4,6]

It is widely accepted that the initial binding of dinitrogen occurs at the iron rather than the molybdenum centers.[4] Theoretical studies based on different model systems of the Fe−Mo cofactor at various levels of theory are available.[7] However, due to the complexity of the overall reduction process and the structure of the Fe−Mo cofactor, a suitable model system for the Fe−Mo nitrogenases that reasonably mimics its catalytic activity may be too large for a quantum chemical treatment at a reasonable level of theory.[7] In addition to that, the nature of the actual intermediates of the enzymatic N_2 fixation process is still unknown.[8] Although there are numerous results indicating that biological N_2 fixation involves diazene and hydrazine species,[4] even the structure of the small four-atom diazene in solution was controversial until recently when Sellmann and Hennige isolated *trans*-N_2H_2 by complexation out of solution.[9] Beside the clarification of the nature of the intermediates involved in the stepwise hydrogenation of N_2 by nitrogenases, another pivotal question regarding the thermochemistry of these reduction steps is of utmost interest: Sellmann and

[‡] Theoretical Studies of Inorganic Compounds, 14. − Part 13: Y. Chen, G. Frenking, *J. Chem. Soc., Dalton Trans.* **2001**, 434−440.

[a] Fachbereich Chemie, Philipps-Universität Marburg, Hans-Meerwein-Strasse, 35032 Marburg, Germany
Fax: (internat.) +49-6421/282-5566
E-mail: frenking@chemie.uni-marburg.de

Supporting information for this article is available on the WWW under http://www.wiley-vch.de/home/eurjic or from the author.

 © WILEY-VCH Verlag GmbH, 69451 Weinheim, 2001 1434−1948/01/0606−1441 $ 17.50+.50/0

co-workers suggested that all of the three reduction steps involved in the hydrogenation sequence should benefit energetically from the coordination of the nitrogen-containing ligands to iron(II) sulfur complexes.[6b]

Due to our interest in the structure and reactivity of iron carbonyl complexes,[10] the present study focuses on the influence and relevance of mono- and dinuclear iron carbonyl complexes of the general type $[\{Fe(CO)_4\}_nL]$ (n = 1 for L = NH_3 and n = 1, 2 for L = N_2, N_2H_2, N_2H_4) to the fixation and stepwise hydrogenation of N_2. We want to emphasize that this approach is not primarily intended to serve as a model study of the Fe−Mo cofactor, but to gain a deeper insight into the reduction steps of N_2 that are most affected by coordination to iron carbonyl fragments.[6] Particular interest is thus drawn to thermodynamic changes between the "metalated" reaction in which the nitrogen-containing ligands are either coordinated by one or two iron tetracarbonyl fragments and the isolated, metal-free hydrogenation of N_2. Moreover, we address the bonding situation of the Fe−L (L = N_2, N_2H_2, N_2H_4 and NH_3) bond in terms of σ-donor/π-acceptor abilities and the preferred coordination site of the ligands.

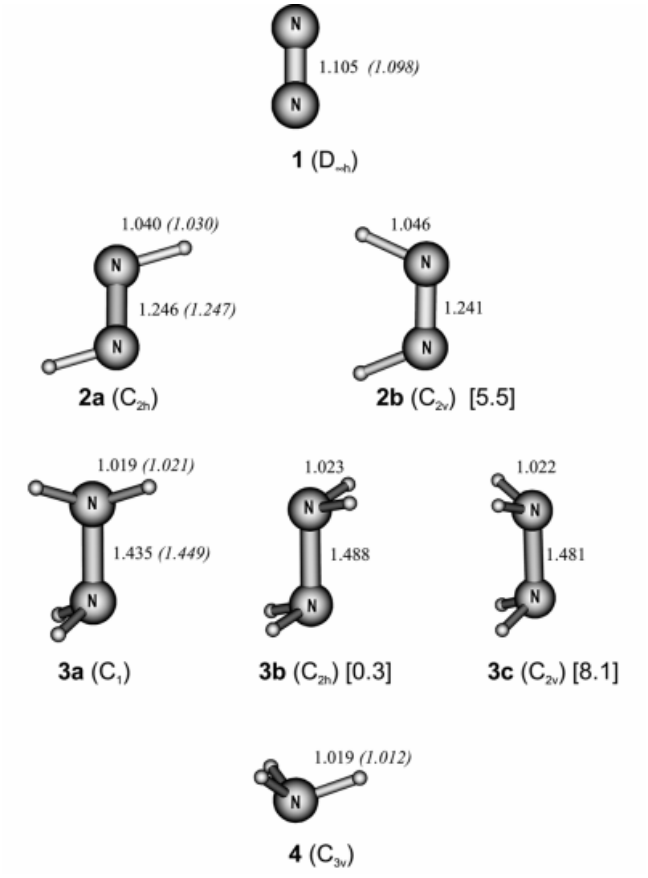

Figure 1. Optimized geometries of N_2 (**1**), N_2H_2 (**2**), N_2H_4 (**3**) and NH_3 (**4**); experimental values are given in italics; all bond lengths are in Å; the symmetry used for the geometry optimization is given in parentheses, while relative energies (kcal mol^{-1}) with respect to the most stable isomers are given in square brackets; angles are omitted for clarity and are provided separately in the Supplementary Information (Figure S1)

Results and Discussion

Stepwise Hydrogenation of Isolated Dinitrogen

The calculated geometries and structural parameters of dinitrogen **1**, diazene **2a** and **2b**, hydrazine **3a**−**3c** and ammonia **4** are shown in Figure 1. The reaction enthalpies obtained using a variety of energy evaluations based on the B3LYP/II geometries are summarized in Table 1. Details of the levels of theory necessary for a reasonable treatment of the stepwise hydrogenation of isolated dinitrogen to ammonia have been reported in a previous paper and the reaction enthalpies provided by this study serve as reference values for our present work.[21] Thus, for the individual hydrogenation steps shown in Equations (1)−(3), the benchmarks for the reaction enthalpies ΔH^0_R are 49.2 kcal mol^{-1} [Equation (1)], −23.1 kcal mol^{-1} [Equation (2)] and −44.7 kcal mol^{-1} [Equation (3)].[21]

$$N_2 + H_2 \rightarrow N_2H_2 \quad (1)$$

$$N_2H_2 + H_2 \rightarrow N_2H_4 \quad (2)$$

$$N_2H_4 + H_2 \rightarrow 2\,NH_3 \quad (3)$$

Table 1. Hydrogenation enthalpies ΔH^0_R (in kcal mol^{-1}) for the stepwise reduction of isolated dinitrogen[a]

	$N_2 + H_2 \rightarrow N_2H_2$ (1)	$N_2H_2 + H_2 \rightarrow N_2H_4$ (2)	$N_2H_4 + H_2 \rightarrow 2\,NH_3$ (3)
B3LYP/			
6−31G(d)	46.9	−18.0	−37.2
6−31G(d,p)	43.2	−19.6	−40.0
6−31+G(d,p)	43.3	−22.0	−43.3
6−31+G(2df,p)	44.1	−22.6	−43.4
6−31++G(2df,p)	44.1	−22.2	−43.1
6−311G(d,p)	47.1	−20.9	−41.6
6−311+G(d,p)	45.3	−22.4	−44.1
6−311+G(2df,p)	46.5	−22.0	−43.7
6−311++G(2df,p)	46.4	−22.0	−43.7
CCSD(T)			
6−31G(d)	55.8	−11.7	−37.3
6−31G(d,p)	49.1	−15.6	−41.6
6−311G(d,p)	44.1	−16.7	−41.7
6−311+G(d,p)	51.9	−18.3	−43.5
6−311+G(2df,p)	51.5	−19.3	−43.2
6−311++G(2df,p)	51.4	−19.3	−43.3
exp.[a]	49.2	−23.1	−44.7

[a] Ref. [21]

The data summarized in Table 1 clearly show that for all three hydrogenation steps convergence of the results is achieved when basis sets of at least 6−311+G(d,p) quality are used. At our highest level of theory, the enthalpies of reaction are 51.4 kcal mol^{-1} for Equation (1), −19.3 kcal mol^{-1} for Equation (2) and −43.3 kcal mol^{-1} for Equa-

tion (3), which is in good agreement with the aforementioned reference data.[21] We note, however, that the predicted ΔH^0_R for the second reduction step [Equation (2)] is 3.8 kcal mol^{-1} too high, while the reaction enthalpies of reactions (1) and (3) are too high by 2.2 and 1.4 kcal mol^{-1}, respectively. A more economic, yet reasonably accurate, alternative is given by CCSD(T) energy evaluations in combination with the 6−311+G(d,p) basis set. The deviations from the reference values are then between 4.8 and 1.2 kcal mol^{-1}, i.e. the ΔH^0_R values are 51.9 kcal mol^{-1} for Equation (1), −18.3 kcal mol^{-1} for Equation (2) and −43.5 kcal mol^{-1} for Equation (3). For larger molecules, for which CCSD(T) is no longer affordable, B3LYP/{II & 6−311+G(d,p)} single-point energies are recommended. This approach leads to deviations from the reference that are particularly small for reactions (2) and (3). The calculated ΔH^0_R values of 45.3 kcal mol^{-1} for Equation (1), −22.4 kcal mol^{-1} for Equation (2) and −44.1 kcal mol^{-1} for Equation (3) thus show that this approach offers a very economic way to reliable hydrogenation enthalpies.

The calculated N−N bond length of **1** is 1.105 Å, whereas the analogous bond lengths of **2a** and **2b** are calculated to be 1.246 and 1.241 Å, respectively. Compared to corresponding experimental data, the differences are quite small and in the range of 0.001 to 0.007 Å.[22,23] The same also holds for the N−H bond length of NH_3 (**4**), that is, a small deviation from the experimental data by 0.007 Å is found.[24] Relatively large deviations from the experimental values are, however, found for the structural parameters of **3a**−**3c**. The experimental N−N bond length of 1.449 Å is larger than the one we calculated for the most stable hydrazine isomer **3a** by 0.014 Å.[24] Our calculated value is, however, in perfect agreement with other high-level ab initio estimates,[21] implying that a re-examination of the experimental N−N bond length might be worthwhile. The calculated bond angles of **2**, **3** and **4** are generally in good agreement with the available literature data and we do not find significant deviations. Further details are given in the Supplementary Information (Figure S1).

At our standard level of theory, *viz*. CCSD(T)/II//B3LYP/II the *trans* isomer of diazene **2a** is predicted to be more stable than the *cis* isomer **2b** by 5.5 kcal mol^{-1}, which is in line with previous results.[21,25] Furthermore, our calculations predict the *gauche* isomer **3a** to be the most stable form of hydrazine, which is consistent with other data.[25] The energy difference to the corresponding *trans* isomer **3b** is, however, very small at only 0.3 kcal mol^{-1}, whereas the analogous *cis* hydrazine **3c** is significantly less stable than **3a** by 8.1 kcal mol^{-1}.

Stepwise Hydrogenation in the Presence of Mononuclear Iron Carbonyl Complexes

The influence of mononuclear iron carbonyl complexes on the stepwise hydrogenation of coordinated N_2 is evaluated by comparing the individual reduction steps shown in Equations (4)−(6) with their metal-free analogues in Equations (1)−(3).

$$(CO)_4Fe{-}N_2 + H_2 \rightarrow (CO)_4Fe{-}N_2H_2 \quad (4)$$

$$(CO)_4Fe{-}N_2H_2 + H_2 \rightarrow (CO)_4Fe{-}N_2H_4 \quad (5)$$

$$(CO)_4Fe{-}N_2H_4 + H_2 \rightarrow (CO)_4Fe{-}NH_3 + NH_3 \quad (6)$$

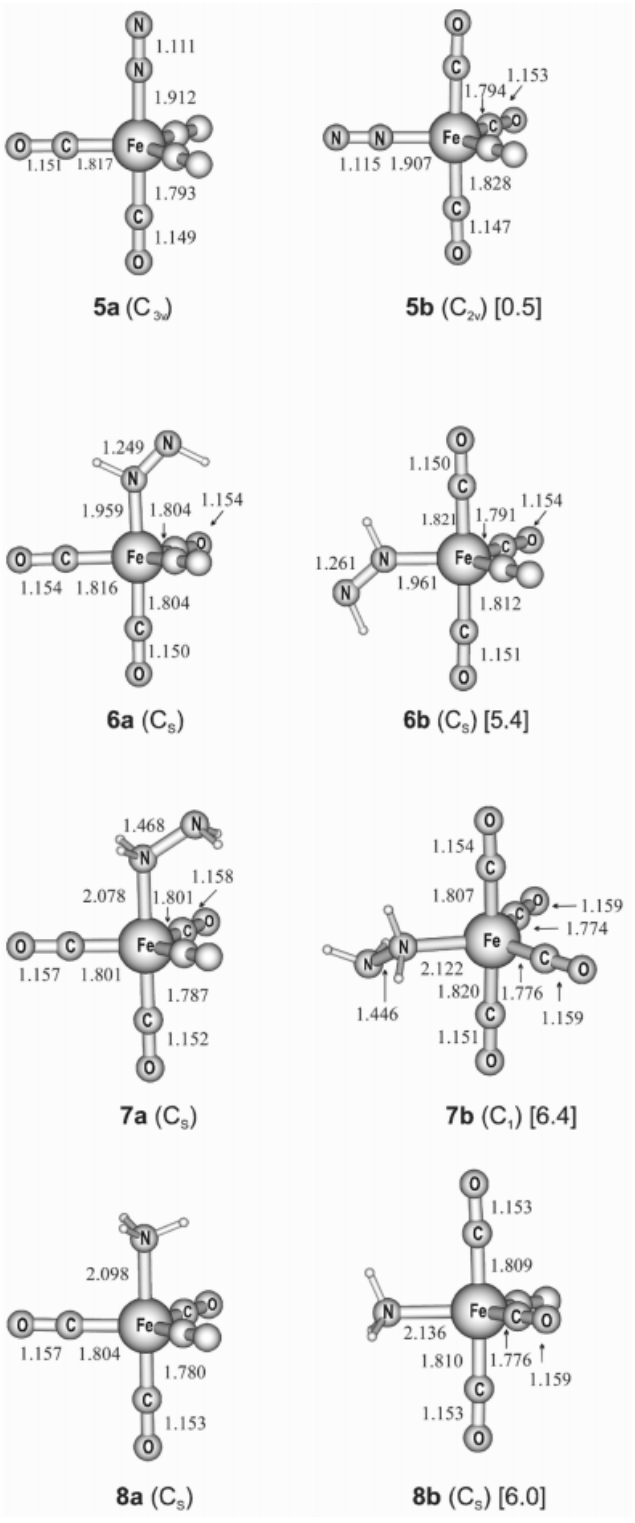

Figure 2. Optimized geometries of the complexes $(CO)_4Fe{-}N_2$ (**5**), $(CO)_4Fe{-}N_2H_2$ (**6**), $(CO)_4Fe{-}N_2H_4$ (**7**), and $(CO)_4Fe{-}NH_3$ (**8**); all bond lengths are in Å and the symmetry used for the geometry optimisation is given in parentheses; relative energies (kcal mol^{-1}) with respect to the most stable isomers are given in square brackets; angles and N−H bond lengths are omitted for clarity and are provided separately in the Supplementary Information (Figure S2)

Table 2. Hydrogenation enthalpies ΔH^0_R (in kcal mol^{-1}) for the stepwise reduction of $(CO)_4Fe-N_2$[a]

	$(CO)_4FeN_2 + H_2 \rightarrow (CO)_4FeN_2H_2$ (4)	$(CO)_4FeN_2H_2 + H_2 \rightarrow (CO)_4FeN_2H_4$ (5)	$(CO)_4FeN_2H_4 + H_2 \rightarrow (CO)_4FeNH_3 + NH_3$ (6)
B3LYP			
6−31G(d)	32.4	−18.6	−35.4
6−31G(d,p)	30.7	−20.2	−38.8
6−311+G(d,p)	31.3	−20.4	−41.6
CCSD(T)			
6−31G(d)	39.2	−15.3	−33.4
6−31G(d,p)	35.9	−18.8	−39.0
6−311+G(d,p)	35.8	−18.5	−39.5

[a] The basis sets given in the table refer to N and H, only. For all other main group elements the 6−31G(d) basis set is used.

The optimized geometries of the iron carbonyl complexes and the relative energies between the respective axial and equatorial isomers are shown in Figure 2. Table 2 summarizes the hydrogenation enthalpies ΔH^0_R for Equations (4)−(6) obtained at various levels of theory. Table 3 lists the calculated bond dissociation energies D_0 between the $Fe(CO)_4$ fragment and the nitrogen-containing ligands together with the NBO and CDA data.

Table 3. Bond dissociation energies D_o (kcal/mol) and NBO/CDA data for mononuclear iron tetracarbonyl complexes $(CO)_4Fe-L$ obtained at the CCSD(T)/II//B3LYP/II level of theory

			NBO[a]			CDA[a]	
Complex	D_o	L	q[$Fe(CO)_4$][b]	q(π)→L	q(σ)→[TM]	*b*	*d*
5a	22.9	N_2	−0.08	0.18	0.26	0.14	0.28
6a	39.3	N_2H_2	−0.18	0.15	0.33	0.10	0.30
7a	42.8	N_2H_4	−0.29	0.10	0.39	0.03	0.36
8a	38.9	NH_3	−0.27	0.13	0.40	−0.01	0.33

[a] [TM] = [$(CO)_4Fe$]; q(σ)→[TM] σ-donation (*d*) and q(π)→L π-back donation (*b*) according to the NBO (*CDA*) analysis. − [b] Total charge of the $Fe(CO)_4$ complex fragment.

The most intriguing effect of the $Fe(CO)_4$ fragment on the stepwise hydrogenation of coordinated N_2 is that the enthalpy of hydrogenation of 35.8 kcal mol^{-1} for the first reduction step [Equation (4)] is significantly lower by $\Delta\Delta H^0_R = -16.1$ kcal mol^{-1} compared to the analogous step of isolated N_2 [Equation (1)]. We do not observe a similarly drastic effect for the second and third reduction steps. To this end, the reduction of $(CO)_4Fe-N_2H_2$ [Equation (5)] is almost as exothermic as the corresponding hydrogenation [Equation (2)] of isolated N_2H_2 ($\Delta\Delta H^0_R = -0.2$ kcal mol^{-1}). For the hydrogenation of $(CO)_4Fe-N_2H_4$ [Equation (6)], we even find a less exothermic behavior than for the metal-free analogue [Equation (3)] and $\Delta\Delta H^0_R$ is calculated to be 4.00 kcal mol^{-1}.

Dinitrogen is both a weak σ-donor and π-acceptor ligand. The small energy difference between the two possible isomers **5a** and **5b** of the complex $(CO)_4Fe-N_2$, in which N_2 is either coordinated axially or equatorially, implies no pronounced coordination site preference.[26] The structures of **5a** and **5b** show $Fe-N_2$ bond lengths of 1.912 Å and 1.907 Å, respectively. This is in contrast to the results of Radius et al.,[27] who predicted the $Fe-N_2$ bond length of axial N_2 to be shorter than that of equatorial N_2. The energy difference of 0.5 kcal mol^{-1} between **5a** and **5b** is in favor of the axial isomer, which is again in contrast to the results of the aforementioned group.[27] Note, however, that the chosen level of theory is surely beyond chemical accuracy (≤ 1.0 kcal mol^{-1}) and therefore our small energy difference is not conclusive. Interestingly, however, the uncertainty of the relative energy between **5a** and **5b** is also found in experimental chemistry. On the one hand, the reaction of $Fe(CO)_5$ with N_2 in polyethylene film implies that N_2 *may* occupy an equatorial rather an axial coordination site,[28] whereas photolysis experiments of $Fe(CO)_5$ in nitrogen-containing matrices[29] show an opposite behavior, that is, a more stable axial than equatorial isomer. The N−N distances of isomers **5a** and **5b** are both slightly longer than in isolated dinitrogen. The bond elongation upon coordination is in the range of 0.006 to 0.010 Å indicating that the N−N triple bond only experiences a weak "activation". In addition, the calculated Fe−N bond energy of 22.9 kcal mol^{-1} also implies a relatively weak interaction between N_2 and the $Fe(CO)_4$ fragment.

The diazene complex formed by the first hydrogenation step [Equation (4)] shows a somewhat different behavior than the analogous dinitrogen complex. First, the energy difference of 5.4 kcal/mol^{-1} between the axial (**6a**) and equatorial (**6b**) isomers is indeed significant and in favor of the axial isomer. Second, this preference towards axial coordination is also mirrored by the σ-donor/π-acceptor abilities of diazene.[26] NBO as well as CDA data both imply that N_2H_2 is at least as poor a π-acceptor as N_2, but at the same time a slightly better σ-donor (Table 3). Finally, the Fe−N bond dissociation energy of **6a** is calculated to be 39.3 kcal mol^{-1}, which is considerably higher than the corresponding value calculated for **5a**. The much stronger bond in $(CO)_4Fe-N_2H_2$ than that in $(CO)_4Fe-N_2$ is the reason why the first hydrogenation step of N_2 becomes energetically more favored upon $Fe(CO)_4$ complexation. Any structural changes of diazene on complexation are again very small and the N−N bond is lengthened by only 0.003 Å.

Further hydrogenation of coordinated N_2H_2 leads to the corresponding hydrazine complex [Equation (5)]. NBO and CDA data suggest that hydrazine is a significantly stronger σ-donor than diazene or dinitrogen (Table 3). Axial coordination of N_2H_4 should therefore be predominant, which is supported by the large energy difference of 6.4 kcal mol^{-1} that favors the axial isomer **7a** over its equatorial analog **7b**. Interestingly, the former, more stable, isomer has hydrazine coordinated as *trans*-N_2H_4, which is not the most stable conformation for the isolated case. At the same time, the less-stable equatorial isomer has N_2H_4 coordinated in its most stable *gauche* conformation. Structural changes of N_2H_4 on coordination are significant as shown by the lengthening of the N−N bond in **7a** by 0.033 Å with respect to isolated N_2H_4. This relatively strong influence on the internal structure of N_2H_4 is also mirrored by the large Fe−N bond dissociation energy of 42.8 kcal mol^{-1}, which is, in fact, the highest D_0 value encountered in this study. Note, that at the same time the calculated Fe−N bond length of **7a** of 2.078 Å is significantly larger than the corresponding bond lengths found in complexes **5** and **6**, which exhibit weaker bonds between iron and the nitrogen-containing ligands.

In the final step [Equation (6)] of the overall reduction process, coordinated hydrazine is reduced to ammonia. The NH_3 ligand is found by CDA and NBO to be an equally strong σ-donor as N_2H_4, whereas its π-acceptor capability is close to zero (Table 3). Again we find a dominant preference of the axial $(CO)_4Fe-N_2$ isomer **8a** over the equatorial isomer by 6.0 kcal mol^{-1}, which is in line with crystallographic data and IR spectra.[30] Our estimate for the Fe−N bond dissociation energy is 38.9 kcal mol^{-1} and the calculated Fe−N bond length is 2.098 Å. Both values show slight deviations from those found for the analogous hydrazine complex **7a**. These differences are, however, small, thus indicating a close resemblance of these two complexes.

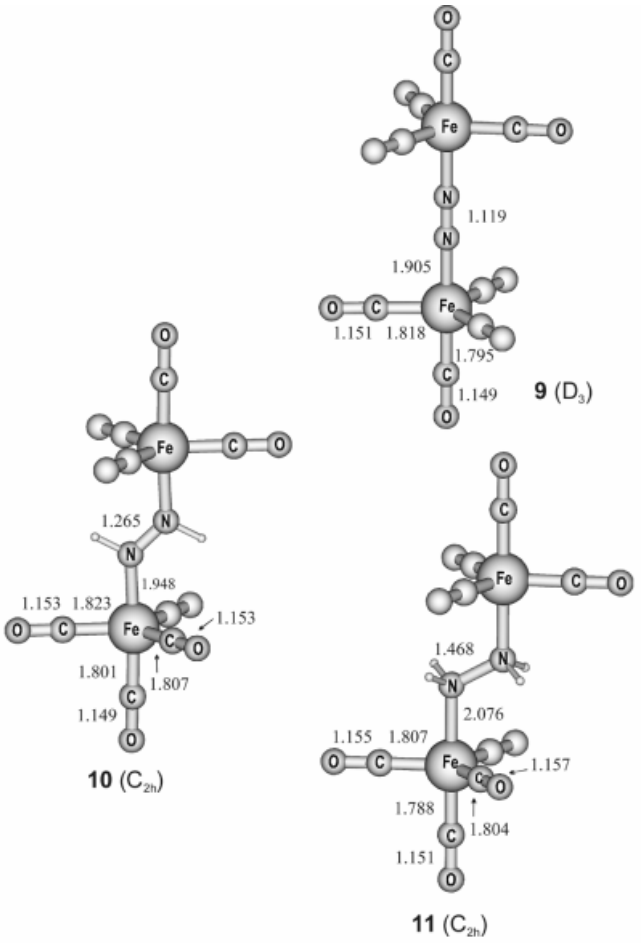

Figure 3. Optimized geometries of the dinuclear iron tetracarbonyl complexes $(CO)_4Fe-N_2-Fe(CO)_4$ (**9**), $(CO)_4Fe-N_2H_2-Fe(CO)_4$ (**10**), and $(CO)_4Fe-N_2H_4-Fe(CO)_4$ (**11**); all bond lengths are in Å; the symmetry used for the geometry optimization is given in parentheses; for more details regarding structural parameters see the Supporting Information (Figure S3)

Stepwise Hydrogenation in the Presence of Dinuclear Iron Carbonyl Complexes

Figure 3 shows the optimized geometries of the dinuclear complexes $(CO)_4Fe-N_2-Fe(CO)_4$ (**9**), $(CO)_4Fe-N_2H_2-Fe(CO)_4$ (**10**) and $(CO)_4Fe-N_2H_4-Fe(CO)_4$ (**11**), considered in the hydrogenation steps according to Equations (7)−(9). Table 4 and 5 summarize the hydrogenation enthalpies for the individual steps and the bond dissociation energies, as well as the NBO/CDA data, respectively.

$$(CO)_4Fe-N_2-Fe(CO)_4 + H_2 \rightarrow (CO)_4Fe-N_2H_2-Fe(CO)_4 \quad (7)$$

$$(CO)_4Fe-N_2H_2-Fe(CO)_4 + H_2 \rightarrow (CO)_4Fe-N_2H_4-Fe(CO)_4 \quad (8)$$

$$(CO)_4Fe-N_2H_4-Fe(CO)_4 + H_2 \rightarrow 2\,(CO)_4Fe-NH_3 \quad (9)$$

The coordination of dinitrogen by two iron tetracarbonyl fragments results in a further significant decrease of the hydrogenation enthalpy of the first reduction step [Equation (7)] by $\Delta\Delta H^0_R = -13.1$ kcal mol^{-1} compared to the analogous step [Equation (4)] involving only one $Fe(CO)_4$ fragment.[31] The overall decrease of the hydrogenation enthalpy with respect to the metal free reaction [Equation (1)] thus becomes 27.1 kcal mol^{-1}.[31] This considerable change of the thermochemistry is so much more interesting as it only affects the first reduction step. To this end, the second [Equation (8)] and third [Equation (9)] hydrogenation steps are even less exothermic than their mononuclear analogues [Equation (5) and (6)]. The $\Delta\Delta H^0_R$ values calculated on going from Equation (5) to (8) and from Equation (6) to (9) are 4.0 and 1.1 kcal mol^{-1}, respectively.

The $Fe(CO)_4$ fragments in **9** are twisted against each other by 8.7°. The rotation barrier is extremely low and we find several different isomers that are energetically not distinguishable from each other. In comparison to the mononuclear analogue **5a** we do not observe further significant alterations of structural parameters. Note that the Fe−N bond length becomes shorter by 0.007 Å, which is paralleled by the lengthening of the N−N bond by 0.008 Å. The CDA and NBO data in Table 5 show that the σ-donor properties of N_2 embraced by two iron tetracarbonyl fragments is hardly changed compared to **5a** — only the π-

Table 4. Hydrogenation enthalpies ΔH^0_R (in kcal mol^{-1}) for the stepwise reduction of $(CO)_4Fe-N_2-Fe(CO)_4$[a]

	$[(CO)_4Fe]_2N_2 + H_2 \rightarrow [(CO)_4Fe]_2N_2H_2$ (7)	$[(CO)_4Fe]_2N_2H_2 + H_2 \rightarrow [(CO)_4Fe]_2N_2H_4$ (8)	$[(CO)_4Fe]_2N_2H_4 + H_2 \rightarrow 2(CO)_4FeNH_3$ (9)
B3LYP			
6−31G(d)	19.9	−16.2	−39.2
6−31G(d,p)	17.6	−17.0	−42.0
6−311+G(d,p)	18.2	−16.4	−40.5

[a] The basis set given in the table refers to N and H, only. All of the other elements use the 6−31G(p) basis set.

Table 5. Bond dissociation energies D_o (kcal/mol) and NBO/CDA data for dinuclear iron tetracarbonyl complexes $(CO)_4Fe-L-Fe(CO)_4$ obtained at the B3LYP/II//B3LYP/II level of theory

Complex	D_o[b]/D_o[c]	L	q[Fe(CO)$_4$][d]	NBO[a] q(π)→L	NBO[a] q(σ)→[TM]$_2$	CDA[a] *b*	CDA[a] *d*
9	16.0/32.5	N_2	−0.05	0.40	0.50	0.28	0.50
10	28.6/59.6	N_2H_2	−0.11	0.38	0.60	0.24	0.57
11	26.1/57.7	N_2H_4	−0.24	0.18	0.66	0.11	0.63

[a] [TM] = [(CO)$_4$Fe]; q(σ)→[TM] σ-donation (*d*) and q(π)→L π-back donation (*b*) according to the NBO (*CDA*) analysis with respect to both Fe(CO)$_4$ fragments. Half of this value equals the charge transferred per Fe(CO)$_4$ unit. − [b] Fe−L bond dissociation energy per Fe(CO)$_4$ fragment according to: $[TM]_2L \rightarrow [TM]L + TM$. − [c] Total Fe−L bond dissociation energy according to: $[TM]_2L \rightarrow TM + TM + L$. − [d] Total charge of the Fe(CO)$_4$ complex fragment.

acceptor characteristics are somewhat enhanced. The overall $Fe-N_2-Fe$ bond dissociation energy is calculated to be 32.5 kcal mol^{-1}, which translates to a Fe−N bond dissociation energy per Fe(CO)$_4$ fragment of 16.0 kcal mol^{-1}. Comparison of these data with the bond dissociation energy obtained for **5a** implies a decreased bond strength between an *individual* Fe(CO)$_4$ subunit and N_2.

Further hydrogenation of **9** results in the formation of the corresponding diazene complex $(CO)_4Fe-N_2H_2-Fe(CO)_4$ (**10**). The Fe−N as well as the N−N bond lengths of **10** are calculated to be 1.948 Å and 1.265 Å, respectively. These values are in good agreement with the structural data of the related [μ-N_2H_2{Fe(PPr$_3$)('S$_4$')}$_2$] ['S$_4$'$^{2-}$ = 1,2-bis(2-mercaptophenylthio) ethane(2-)] complex reported by Sellmann and co-workers.[32] The small deviations of less than 0.052 Å are noteworthy as such Fe^{II}('S$_4$') complexes involving multidentate organosulfur ligands are often used as model compounds for the Fe-Mo, Fe−V and Fe−Fe nitrogenases.[4,6,32] We note a non-negligible shortening of the Fe−N bond by 0.011 Å and a lengthening of the N−N bond by 0.016 Å on going from **6a** to its dinuclear pendant **10**. Interestingly, CDA and NBO data indicate that the ability of diazene to act as σ-donor is almost unaltered. Only a slight increase of the π-acceptor capabilities of N_2H_2 is observed. The Fe−N bond dissociation energy of **10** follows the same trend as shown above for the corresponding dinitrogen complex; that is, the bond strength per Fe(CO)$_4$ fragment is smaller than in the mononuclear case, whereas the overall binding energy obtained by complexation with two Fe(CO)$_4$ fragments is significantly larger.

In the second step of the overall reduction process [Equation (8)], the analogous hydrazine complex $(CO)_4Fe-N_2H_4-Fe(CO)_4$ (**11**) is formed by hydrogenation of coordinated diazene. The comparison with complex **7a** shows hardly any shortening of the Fe−L bond length or lengthening of the N−N bond. We want to point out that the NBO data imply that both the σ-donor as well as the π-acceptor abilities of N_2H_4 decrease slightly on going from the mononuclear complex to **11**. With respect to the σ-donor character this is also supported by the corresponding CDA values. Although the analogue π-acceptor value implies a stronger π back-donation of N_2H_4 in the dinuclear complex **11**, the predicted magnitude is too small to account for a significant π-acceptor character of N_2H_4.

Conclusion

Density functional and ab initio calculations were used to evaluate the influence of iron tetracarbonyl complexes on the stepwise hydrogenation of dinitrogen. In comparison to the metal-free reduction process, we find that complexation by one or two Fe(CO)$_4$ fragments results in a pronounced change of the thermochemistry of the first hydrogenation step, namely the reduction of coordinated N_2 to N_2H_2. The effects on the second and third hydrogenation steps, *viz* the hydrogenation of coordinated N_2H_2 and N_2H_4, are much weaker, and even less-exothermic reduction processes compared with the metal-free hydrogenation are predicted. The decrease of the hydrogenation enthalpy is larger for the reduction of $(CO)_4Fe-N_2-Fe(CO)_4$ than it is for the reduction of $(CO)Fe-N_2$. In conclusion, our calculations thus clearly demonstrate that only one, namely the first, reduction step in the hydrogenation sequence of N_2 is

in fact favored in terms of the reaction enthalpy by complexation with iron tetracarbonyl fragments. Although the systems used in our study are not intended to primarily serve as model complexes for the mode of action of nitrogenase, we suggest that these results should be considered in further discussions of the thermochemistry of N_2 fixation and activation processes.

The binding characteristics of N_2, N_2H_2, N_2H_4 and NH_3 to $Fe(CO)_4$, analyzed in terms of the NBO and CDA partitioning schemes, imply a consistent trend of the σ-donor/π-acceptor behavior of these ligands that correlates with the relative energies between the respective isomers. Thus, ligands with comparatively high σ-donor capabilities like N_2H_4 and NH_3 give iron tetracarbonyl complexes in which the axial isomers are considerably more stable than their equatorial analogues. In addition to that, only ligands like N_2 and N_2H_2 that show noticeable π-acceptor quantities in their respective $Fe(CO)_4$ complexes are affected by the formation of dinuclear complexes. Thus, the Fe−N bond lengths are shorter and the N−N bonds are longer in the dinuclear complexes than in their mononuclear analogues. This behavior is also mirrored by a slight increase of the π-acceptor ability on going from $(CO)_4Fe-X$ to $(CO)_4Fe-X-Fe(CO)_4$ (X = N_2, N_2H_2) complexes. Such structural changes are absent for N_2H_4, and both its σ-donor as well as its π-acceptor behavior are less pronounced in $(CO)_4Fe-N_2H_4-Fe(CO)_4$ than in $(CO)_4Fe-N_2H_4$.

Experimental Section

Computational Details: Geometry optimizations were performed with Becke's three-parameter hybrid functional in combination with the correlation functional according to Lee, Yang and Parr (B3LYP).[11] A small core pseudopotential and a (441/2111/41) split-valence basis set according to Hay and Wadt were used for iron,[12] whereas an all-electron 6−31G(d) basis set was chosen for the main-group elements.[13] It was shown previously that this combination of basis sets (further abbreviated as basis set II) in combination with the aforementioned functional predicts equilibrium geometries of transition metal complexes reasonably well.[14] All structures discussed in this paper were verified to represent local minima on their potential energy surfaces by harmonic frequency calculations at the same level of theory. Refined estimates of relative energies were obtained by single-point calculations of the B3LYP/II geometries using both the B3LYP functional and coupled-cluster theory with singles, doubles and perturbative estimates of triple substitution [CCSD(T)].[15] CCSD(T) and basis set II were used for estimating relative energies between isomeric forms of diazene, hydrazine and all iron carbonyl complexes. Refined reaction enthalpies ΔH^0_R (T = 0 K) for the individual hydrogenation reactions, however, were predicted using basis sets that consisted of the aforementioned basis set for the metal and the elements C and O, but were extended by either the 6−31G(d,p) or the 6−311+G(d,p) basis sets for N and H. These combinations of basis sets are further abbreviated as {II & 6−31G(d,p)} and {II & 6−311+G(d,p)}, respectively.

The ΔH^0_R values obtained for the hydrogenation steps of the metal-free reactions were compared with their analogous steps involving mononuclear iron carbonyl fragments. The resulting $\Delta\Delta H^0_R$ values indicate whether the ΔH^0_R of an individual reduction step decreases ($\Delta\Delta H^0_R < 0$) or increases ($\Delta\Delta H^0_R > 0$) on going from the reactions of the isolated to the coordinated species. The corresponding $\Delta\Delta H^0_R$ values obtained for the individual reduction steps involving mono- and dinuclear iron carbonyl fragments were used likewise. Unless otherwise noted, relative enthalpies obtained at the CCSD(T)/{II & 6−311+G(d,p)}//B3LYP/II level of theory were the basis for the comparison between the metal-free hydrogenation steps of N_2 and the reactions following the reduction of $(CO)_4Fe-N_2$. With respect to the large resources needed for a proper description of the reactions involving dinuclear species, the comparisons between the hydrogenation steps involving mono and dinuclear iron carbonyl complexes were based on the B3LYP/{II & 6−311+G(d,p)}//B3LYP/II energies only. For the evaluation of the reaction enthalpies only the most stable isomers within a reaction sequence were considered.

Reaction enthalpies and relative energies are corrected by zero-point vibrational energy (ZPE) contributions obtained at the B3LYP/II level of theory. The nature of the Fe−N and N−N bonds was examined using the natural bond orbital (NBO)[16] partitioning scheme and the charge decomposition analysis (CDA).[17] All calculations used the program packages Gaussian94/98,[18] MOLPRO96/2000,[19] and CDA2.1.[20]

Acknowledgments

This work was supported by the Deutsche Forschungsgemeinschaft (DFG) and the Fonds der Chemische Industrie. Excellent help by the computer center of Philipps-Universität Marburg is gratefully acknowledged. Additional computer time was provided by the HLRZ Darmstadt, Frankfurt and Giessen and the HLR Stuttgart and is hereby acknowledged.

[1] [1a] J. Kim, D. C. Rees, *Biochemistry* **1994**, *33*, 389. − [1b] P. E. M. Siegbahn, M. R. A. Blomberg, *Chem. Rev.* **2000**, *100*, 421−438.
[2] K. H. Büchel, H.-H. Moretto, P. Woditsch, *Industrielle Anorganische Chemie 3rd edition*, Wiley-VCH, Weinheim, **1999.**
[3] See, for example: [3a] *Catalytic Ammonia Synthesis: Fundamentals and Practice Vol. I* (Ed.: J. R. Jennings), Plenum, New York, **1991**. − [3b] F. A. Cotton, G. Wilkinson, C. A. Murillo, M. Bochmann, *Advanced Inorganic Chemistry 6th edition*, Wiley-Interscience, **1999**, 316−318.
[4] For recent reviews, see: [4a] J. B. Howard, D. C. Rees, *Chem. Rev.* **1996**, *96*, 2965−2982. − [4b] B. K. Burgess, D. J. Lowe, *Chem. Rev.* **1996**, *96*, 2983−3012. − [4c] R. R. Eady, *Chem. Rev.* **1996**, *96*, 3013−3030 [4d] M. D. Fryzuk, S. A. Johnson, *Coord. Chem. Rev.* **2000**, *200−202*, 379−409.
[5] [5a] J. Kim, D. C. Rees, *Science* **1992**, *257*, 1677. − [5b] J. Kim, D. C. Rees, *Nature* **1992**, *360*, 553−560.
[6] [6a] D. Sellmann, J. Sutter, *Acc. Chem. Res.* **1997**, *30*, 460−469. − [6b] D. Sellmann, J. Utz, N. Blum, F. W. Heinemann, *Coord. Chem. Rev.* **1999**, *190−192*, 607−627. − [6c] D. Sellmann, A. Fürsattel, J. Sutter, *Coord. Chem. Rev.* **2000**, *200−202*, 545−561.
[7] [7a] B. C. Machado, E. R. Davidson, *Theor. Chim. Acta* **1995**, *92*, 315326. − [7b] I. Dance, *Chem. Commun.* **1996**, 165−166. − [7c] I. Dance, *Chem. Commun.* **1998**, 523−530.
[8] G. E. Koch, K. C. Schneider, R. H. Burris, *Biochem. Biophys. Acta* **1960**, *37*, 273−279.
[9] D. Sellman, A. Hennige, *Angew. Chem.* **1997**, *109*, 270−271; *Angew Chem. Int. Ed. Engl.* **1997**, *36*, 276.
[10] See, for example: [10a] A.W. Ehlers, G. Frenking, *Organometallics* **1995**, *14*, 423−426. − [10b] M. Torrent, M. Sola, G. Frenking, *Organometallics* **1999**, *18*, 2801−2812.

[11] [11a] A. D. Becke, *J. Chem. Phys.* **1993**, *98*, 5648−5652. − [11b] C. Lee, W. Yang, R. G. Parr, *Phys. Rev.* **1988**, *B37*, 785−789.
[12] P. J. Hay, W. R. Wadt, *J. Chem. Phys.* **1985**, *82*, 299−310.
[13] [13a] J. A. Pople, R. Krishnan, H. B. Schlegel, J. S. Binkley, *Int. J. Quantum Chem.* **1978**, *14*, 545−560. − [13b] R. J. Bartlet, G. D. Purvis, *Int. J. Quantum Chem.* **1978**, *14*, 561−581. − [13c] G. D Purvis, R. J. Bartlett, *J. Chem. Phys.* **1982**, *76*, 1910−1918. − [13d] G. D Purvis, R. J. Bartlett, *J. Chem. Phys.* **1987**, *86*, 7041−7050.
[14] G. Frenking, I. Antes, M. Böhme, S. Dapprich, A. W. Ehlers, V. Jonas, A. Neuhaus, M. Otto, R. Stegmann, A. Veldkamp, S. F. Vyboishchikov, in *Reviews in Computational Chemistry*, *Vol. 8* (Eds.: K. B. Lipkowitz and D. B. Boyd), VCH, New York, **1996**, 63−144.
[15] [15a] J. Cizek, *J. Chem. Phys.* **1966**, *45*, 4256−4266. − [15b] J. Cizek, *Adv. Chem. Phys.* **1969**, *14*, 35−89.
[16] A. E. Reed, L. A. Curtiss, F. Weinhold, *Chem. Rev.* **1988**, *88*, 899−926.
[17] S. Dapprich, G. Frenking, *J. Phys. Chem.* **1995**, *99*, 9352−9362.
[18] [18a] Gaussian 94, Revision D.4, M. J. Frisch, G. W. Trucks, H. B. Schlegel, P. M. W. Gill, B. G. Johnson, M. A. Robb, J. R. Cheeseman, T. Keith, G. A. Petersson, J. A. Montgomery, K. Raghavachari, M. A. Al-Laham, V. G. Zakrzewski, J. V. Ortiz, J. B. Foresman, J. Cioslowski, B. B. Stefanov, A. Nanayakkara, M. Challacombe, C. Y. Peng, P. Y. Ayala, W. Chen, M. W. Wong, J. L. Andres, E. S. Replogle, R. Gomperts, R. L. Martin, D. J. Fox, J. S. Binkley, D. J. Defrees, J. Baker, J. P. Stewart, M. Head-Gordon, C. Gonzalez, and J. A. Pople, Gaussian, Inc., Pittsburgh PA, **1995**. − [18b] Gaussian 98, Revision A.3, M. J. Frisch, G. W. Trucks, H. B. Schlegel, G. E. Scuseria, M. A. Robb, J. R. Cheeseman, V. G. Zakrzewski, J. A. Montgomery, Jr., R. E. Stratmann, J. C. Burant, S. Dapprich, J. M. Millam, A. D. Daniels, K. N. Kudin, M. C. Strain, O. Farkas, J. Tomasi, V. Barone, M. Cossi, R. Cammi, B. Mennucci, C. Pomelli, C. Adamo, S. Clifford, J. Ochterski, G. A. Petersson, P. Y. Ayala, Q. Cui, K. Morokuma, D. K. Malick, A. D. Rabuck, K. Raghavachari, J. B. Foresman, J. Cioslowski, J. V. Ortiz, B. B. Stefanov, G. Liu, A. Liashenko, P. Piskorz, I. Komaromi, R. Gomperts, R. L. Martin, D. J. Fox, T. Keith, M. A. Al-Laham, C. Y. Peng, A. Nanayakkara, C. Gonzalez, M. Challacombe, P. M. W. Gill, B. Johnson, W. Chen, M. W. Wong, J. L. Andres, C. Gonzalez, M. Head-Gordon, E. S. Replogle, and J. A. Pople, Gaussian, Inc., Pittsburgh PA, **1998**.
[19] MOLPRO is a package of ab initio programs written by H.-J. Werner and P. J. Knowles, Universität Stuttgart and University of Birmingham.
[20] CDA 2.1, S. Dapprich, G. Frenking, Marburg, **1994**. The Program is available via anonymous ftp at: ftp://ftp.chemie.uni-marburg.de/pub/cda.
[21] S. Sekusak, G. Frenking, *J. Mol. Struct., Theochem*, in print.
[22] H. Herzberg, *Molecular Spectra and Molecular Structure, Part I − Spectra of Diatomic Molecules 2nd ed.*, Krieger Publishing Co., Malabar, Florida, **1989**
[23] J. Demaison, F. Hegelund, H. Bürger, *J. Mol. Struct.* **1997**, *413−414*, 447−456.
[24] *CRC Handbook of Chemistry and Physics 76th Ed.* (Ed.: D. R. Lide), **1995−1996.**
[25] [25a] J. A. Pople, L. A. Curtiss, *J. Chem. Phys.* **1991**, *95*, 4385−4388. − [25b] M. L. Mckee, D. M. Stanbury, *J. Am. Chem. Soc.* **1992**, *114*, 3214−3219.
[26] Experimental data and qualitative molecular orbital considerations imply that strong π-accepting ligands prefer equatorial coordination sites of trigonal bipyramidal complexes of d^8 metals, whereas σ-donor ligands prefer axial coordination sites. See, for example: [26a]A. R. Rossi, R. Hoffmann, *Inorg. Chem.* **1975**, *14*, 365−374. − [26b] J. K. Burdett, *Inorg. Chem.* **1976**, *15*, 212−219. − [26c] M. C. Favas, D. L. Kepert, *Prog. Inorg. Chem.* **1980**, *27*, 325463.[26d] D. P. Bauer, J. K. Ruff, *Inorg. Chem.* **1983**, *22*, 1686−1689.[26e] D. B. Beach, S. P. Smit, W. L. Jolly, *Organometallics* **1984**, *3*, 556−559. − [26f] T. A. Albright, J. K. Burdett, M. H. Whangbo, *Orbital Interactions in Chemistry*, Wiley: New York, **1985**, pp 324−325.
[27] U. Radius, F. M. Bickelhaupt, A.W. Ehlers, N. Goldberg, R. Hoffmann, *Inorg. Chem.* **1998**, *37*, 1080−1090.
[28] A. I. Cooper, M. Poliakoff, *Chem. Phys. Lett.* **1993**, *212*, 611−616.
[29] [29a] M. Poliakoff, J. J. Turner, *J. Chem. Soc., Dalton Trans.* **1974**, 2276−2285. − [29b] M. Poliakoff, *Chem. Soc. Rev.* **1978**, 527−540.
[30] F. A. Cotton, J. M. Troup, *J. Am. Chem. Soc.* **1974**, *96*, 3438−3443.
[31] Note the levels of theory used for this comparison. Reaction enthalpies of reduction steps following $(CO)_4Fe-N_2-Fe(CO)_4$ use the B3LYP/{II + 6−311+G(d,p)}//B3LYP/II combination of methods.
[32] D. Sellmann, H. Friedrich, F. Knoch, M. Moll, *Z. Naturforsch., Teil B* **1994**, *49*, 76−88.

Received October 12, 2000
[I00388]

Co^{II} Complexes with Mixed Amino-*N* and Thiolato-*S* Donor Sets − Structural Characterization and Electronic Properties of a Stable Bis(μ-thiolato)-Bridged Binuclear Co^{II} Complex

Didier Bonnet,[a] Philippe Leduc,[a] Eckhard Bill,[b] Geneviève Chottard,[c] Daniel Mansuy,[a] and Isabelle Artaud*[a]

Keywords: Cobalt / S ligands / Electrochemistry / Raman spectroscopy / N ligands

Two different ligands [$S_2N_3^{py}$] and [S_2N_2], prepared from 2,6-bis[1-(2-mercaptoanilino)ethyl]pyridine and 2,3-bis(2-mercaptoanilino)butane, respectively, have been used to investigate cobalt coordination with mixed amine nitrogen/sulfur donor sets. The pentadentate [$S_2N_3^{py}$] ligand gave rise to a mononuclear [$Co^{II}(S_2N_3^{py})$] complex, which was found to be stable only at low temperatures under argon, and was characterized as having a high-spin Co^{II} state on the basis of ^1H NMR and EPR measurements. In contrast, the tetradentate [S_2N_2] ligand led to a binuclear bis(μ-thiolato) $[Co^{II}(S_2N_2)]_2$ complex, the structure of which was solved by X-ray crystallography. Each Co^{II} centre was found to reside in an N_2S_3 square-pyramidal environment in the crystal, the two Co atoms being bridged by one of the two thiolates of an [S_2N_2] ligand. On the basis of the temperature dependence of the magnetic susceptibility, the two Co^{II} centres were found to be in a low-spin state and slightly antiferromagnetically coupled with an absolute J value of less than 3 cm^{-1}. In aerated CH_2Cl_2 in the presence of CH_3SO_3H, the binuclear complex proved to be stable in its mixed valence state, [Co^{II}/Co^{III}], which could be converted back to [Co^{II}/Co^{II}] upon addition of NBu_4OH in MeOH. Three different stable oxidation states could be characterized by electro- and spectroelectrochemistry (E [Co^{II}/Co^{II}]/[Co^{II}/Co^{III}] = –0.19 V, E [Co^{II}/Co^{III}]/[Co^{III}/Co^{III}] = 0.2 V vs. SCE). The electronic spectrum of the [Co^{II}/Co^{II}] state features a broad absorption at 630 nm and a sharp band at 565 nm, while that of the [Co^{II}/Co^{III}] state shows two bands at 657 and 800 nm. The Raman spectrum of the [Co^{II}/Co^{II}] state was found to be dominated by a Co_2S_2 core vibration at 223 cm^{-1}, which proved to be strongly resonance-enhanced within the 565 nm absorption band, thus giving a sound basis for its assignment as an S→Co^{II} charge-transfer band. For the [Co^{II}/Co^{III}] state, a significant resonance Raman enhancement was observed within the 657 nm absorption band for a larger number of vibrations involving the Co_2S_2 core as well as the phenyl ring.

Introduction

While mixed nitrogen/sulfur coordination spheres about transition metals are often encountered in the active sites of iron-, copper-, and zinc-containing proteins,[1] only a few enzymes have a cobalt centre with a mixed N/S donor set, such as ATP sulfurylase,[2] nitrile hydratase,[3] and peptide deformylase.[4] The first two of these possess a native cobalt centre, which has been spectroscopically characterized. In contrast, peptide deformylase, which naturally contains iron or nickel as the metal centre for catalytic amide hydrolysis, has been characterized by X-ray crystallography of a cobalt-substituted form. ATP sulfurylase and peptide deformylase contain four-coordinate Co^{II} centres, with NS_3 and N_2SO donor sets, respectively. Co nitrile hydratases have a low-spin Co^{III}, which is thought to be six-coordinate with an N_2S_3 core, by analogy with the more extensively characterized iron-containing enzymes. These newly identified cobalt biological systems have fostered a growing interest in the investigation of new cobalt complexes with mixed nitrogen/sulfur coordination spheres.

In this study, we describe the synthesis and the spectroscopic characterization of two new Co^{II} complexes, a [$Co^{II}(S_2N_3^{py})$] mononuclear species and a $[Co^{II}(S_2N_2)]_2$ dimer derived from 2,6-bis[1-(2-mercaptoanilino)ethyl]pyridine and 2,3-bis(2-mercaptoanilino)butane, respectively. The binuclear complex, for which the structure has been solved, is easily converted in CH_2Cl_2 into the mixed valence state [Co^{II}/Co^{III}] and into the fully oxidized state [Co^{III}/Co^{III}].

Results and Discussion

Synthesis of the Ligands and Complexes

Thiolate-ligated zinc template complexes [S_2N_2Zn] (**1**) and [$S_2N_3^{py}Zn$] (**3**) (Scheme 1) were prepared in three steps according to published procedures:[5−7] (i) condensation of 2-aminobenzenethiol with 2,3-butanedione and 2,6-diacetylpyridine for **1** and **3**, respectively, (ii) opening of the resulting bis(benzothiazolyl) compound with zinc acetate, and (iii) reduction[6] of the zinc complex imine functions with $NaBH_4$.

[a] Laboratoire de Chimie et Biochimie Pharmacologiques et Toxicologiques, CNRS UMR 8601,
45 rue des Saints-Pères, 75270 Paris Cedex 06, France
Fax: (internat.) + 33-1/42868387
E-mail: artaud@biomedicale.univ-paris5.fr
[b] Max-Planck-Institut für Strahlenchemie,
Stiftstrasse 34−36, 45470 Mülheim an der Ruhr, Germany
[c] Laboratoire de Chimie Inorganique et Matériaux Moléculaires, CNRS ESA 7071, Université Pierre et Marie Curie,
75252 Paris Cedex 05, France

Supporting information for this article is available on the WWW under http://www.wiley-vch.de/home/eurjic or from the author.

 © WILEY-VCH Verlag GmbH, 69451 Weinheim, 2001 1434−1948/01/0606−1449 $ 17.50+.50/0

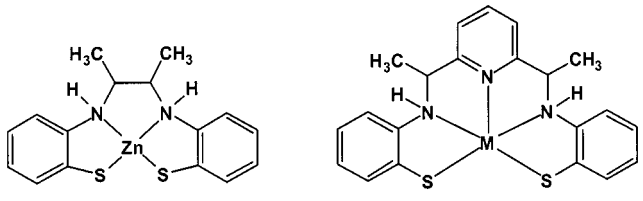

Scheme 1

After demetallation of the zinc derivatives under basic conditions, the free dithiolate ligands were metallated with $CoCl_2 \cdot 6H_2O$ in the presence of a slight excess of base. Complex $[Co^{II}(S_2N_2)]_2$ (**2**) was isolated as a microcrystalline purple powder by precipitation from a solution in dichloromethane by the addition of pentane. In contrast to complex **2**, which was found to be air-stable, complex $[Co^{II}(S_2N_3{}^{py})]$ (**4**), isolated from DMF by precipitation with diethyl ether, proved to be sensitive to trace amounts of dioxygen and consequently had to be handled under argon and at low temperature.

Characterization of Complex 2

Crystal Structure

Single crystals of **2** were grown by vapor diffusion of pentane into a dichloromethane solution of the complex. The ORTEP diagram of the neutral complex **2** is shown in Figure 1. Collection parameters and selected interatomic distances along with bond angles are listed in Table 1 and 2, respectively.

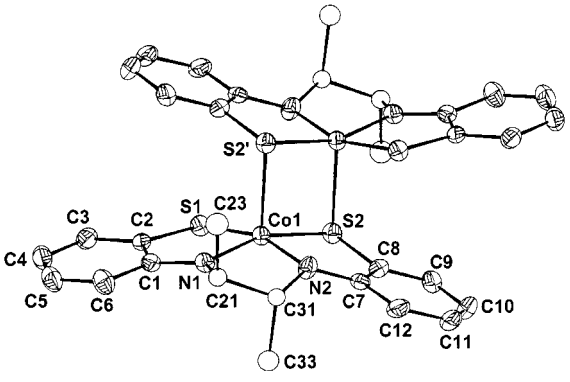

Figure 1. Thermal ellipsoid plot (50% probability level) of the neutral complex $[L_1Co^{II}]_2$ (**2**); carbon atoms C21, C23, C31, C33 are disordered and correspond to two equiprobable *trans* conformations of the methyl groups

The X-ray structure of the binuclear complex **2** reveals a nearly ideal square-pyramidal environment for each cobalt centre, with the four atoms (2 N and 2 S) of an S_2N_2 ligand in the mean equatorial plane and the thiolate of the second $[S_2N_2Co]$ moiety in the axial position. The two cobalt centres are connected through an inversion centre. The average lengths of the Co−S and Co−N bonds in the mean plane are 2.17 Å and 1.85 Å, respectively. These values are in agreement with those previously reported for a binuclear Co^{II} complex derived from thiosalen $[tsalenCo^{II}]_2$.[8] The four atoms (2 N and 2 S) are almost coplanar and deviate by no more than 0.07 Å from the mean plane, while the cobalt cation is displaced by 0.32 Å towards the axial ligand. With a dihedral angle between the (C1−C6, S1, N1) and (C7−C12, S2, N2) planes of only 4°, the two aromatic rings and the S_2N_2 core of the ligand are almost coplanar. The axial Co−S distance (2.37 Å) of the μ-thiolato bridge is 0.2 Å longer than the Co−S bond in the mean plane and is similar to that observed in $[tsalenCo^{II}]_2$ [Co−S(bridging) 2.44 Å].[8] Such a sulfur-bridging bis(μ-thiolato) mode has previously been observed in binuclear Co^{II} [8] and Fe^{II} [9] complexes derived from a tetradentate tsalen (N_2S_2) ligand, as well as in binuclear Co^{III} complexes derived from a

Table 1. Crystallographic data for $[S_2N_2Co^{II}]_2$ (**2**)

Emprical formula	$C_{32}H_{36}N_4S_4Co_2$
Molecular mass	722.8
a [Å]	11.698(4)
b [Å]	8.993(3)
c [Å]	15.064(5)
β [°]	92.38(3)
V [Å^3]	1583.3(9)
Z	2
Crystal system	monoclinic
Space group	$P2_1/n$
μ [cm^{-1}]	13.3
ρ [g·cm^{-3}]	1.52
Diffractometer	CAD4 Enraf−Nonius
T [K]	295
No. of data collected	3132
No. of unique data collected	2782 (R_{int} = 0.06)
No. of unique data used for refinement	1712 $(F_o)^2 > 3\sigma(F_o)^2$
Radiation	Mo-K_α (λ = 0.71069 Å)
$R = \Sigma\|\|F_o\| - \|F_c\|\|/\Sigma\|F_o\|$	0.0529
$Rw = [\Sigma w(\|F_o\| - \|F_c\|)^2/\Sigma w\|F_o\|^2]^{1/2}$	0.0630

Table 2. Selected bond lengths [Å] and angles [°] in **2**

Co(1)−Co(1′)	3.038(1)	Co(1)−S(1)	2.161(2)
Co(1)−S(2)	2.185(2)	Co(1)−S(2′)	2.372(2)
Co(1)−N(1)	1.840(5)	Co(1)−N(2)	1.852(5)
S(1)−C(2)	1.712(6)	S(2)−C(8)	1.739(6)
N(1)−C(1)	1.349(8)	N(1)−C(21)	1.47(2)
N(1)−C(22)	1.49(1)	N(2)−C(7)	1.350(8)
N(2)−C(31)	1.54(1)	N(2)−C(32)	1.46(1)
C(1)−C(2)	1.428(9)	C(7)−C(8)	1.424(9)
C(21)−C(31)	1.50(2)	C(22)−C(32)	1.59(2)
S(1)−Co(1)−S(2)	94.33(7)	S(1)−Co(1)−S(2′)	96.43(6)
S(2)−Co(1)−S(2′)	96.46(6)	S(1)−Co(1)−N(1)	87.8(2)
S(2)−Co(1)−N(1)	160.8(2)	S(2)−Co(1)−N(1)	102.3(2)
S(1)−Co(1)−N(2)	161.5(2)	S(2)−Co(1)−N(2)	87.8(2)
S(2)−Co(1)−N(2)	101.6(2)	N(1)−Co(1)−N(2)	84.3(2)
Co(1)−S(1)−C(2)	98.1(2)	Co(1)−S(2)−Co(1)	83.54(6)
Co(1)−S(2)−C(8)	97.6(2)	Co(1)−S(2′)−C(8′)	107.2(2)
Co(1)−N(1)−C(1)	121.8(4)	Co(1)−N(1)−C(21)	118.7(6)
Co(1)−N(1)−C(22)	113.8(6)	Co(1)−N(2)−C(7)	121.9(4)
Co(1)−N(2)−C(31)	114.3(6)	Co(1)−N(2)−C(32)	116.4(6)

pentadentate N_3S_2 ligand[10] or a bidentate S_2 ligand.[11,12] As for all the other Co(μ-SR)$_2$Co dimers, the two sulfur atoms of the bridge and the two Co atoms are almost planar with a slight tetrahedral distortion, the (Co1−S2−Co′1) angle being close to 90° (97°). The structural parameters of **2** confirm the presence of two amine ligands with C21−N1 and C31−N2 bond lengths of 1.47 Å and 1.54 Å, respectively. If a dehydrogenation had occurred, the C−N distances of the corresponding imines would have been in the range of 1.2−1.3 Å.[13,14] Interestingly, the ESI^+ mass spectrum of **2** displays a 100% peak at $m/z = 718$, which corresponds to the mass of the dimer after the loss of four protons. This could result from the formation of one imine moiety per monomer during the ionization process. Such a dehydrogenation reaction of $[S_2N_2]$ has previously been observed in the one-electron reduction of a dioxomolybdenum complex $[S_2N_2Mo^{VI}O_2]$.[15]

Magnetism, EPR, and ^{1}H NMR

The temperature dependence of the magnetic susceptibility of a solid sample of the binuclear complex **2** was recorded over the range 290−4 K. The effective magnetic moment was found to have a value of 2.92 μB (1.46 μB per Co) at 290 K and dropped to 1.4 μB at 4 K (Supporting Information). This behaviour is consistent with the presence of two low-spin Co^{II} ions, antiferromagnetically coupled with an absolute J value of less than 3 cm^{-1} [$H = -2J\cdot\boldsymbol{S}_1\cdot\boldsymbol{S}_2$] (a tentative fit leading to $J = -\mathbf{1.6}$ cm^{-1} is shown in the Supporting Information). As expected for two antiferromagnetically coupled Co^{II} ions, complex **2** is EPR-silent. However, its ^{1}H NMR spectrum in [D$_6$]DMSO (Supporting Information) at 290 K extends over 270 ppm and is consistent with the two Co^{II} centres being only slightly coupled at this temperature. The ^{1}H NMR spectrum is completely symmetrical featuring only six shifted resonances. This suggests that the interconversion between the two conformations observed in the solid state is rapid in relation to the NMR time scale. Moreover, the S_2N_2 ligand seems to be planar with such a weak interaction between the two cobalt centres that the complex could be regarded as a monomer. The proton resonances of the ligand were assigned on the basis of their chemical shifts, relative integrals, and ^{1}H longitudinal relaxation times (T_1) correlated to the Co···H distances available from the crystal structure, as described in the Exp. Sect. The signals at δ = −18 (12 H) and δ = +166 (4 H) were assigned to the methyl protons and to the equivalent H(21) protons, respectively. The four aromatic rings are equivalent. However, it is difficult to assign the resonances to H(3) and H(6) as well as to H(4) and H(5). The protons H(4) and H(5), being furthest from the cobalt centre, have the largest T_1 values and are believed to be responsible for the signals at δ = +12 and/or δ = +16.5. Finally, the resonances at δ = −107 and δ = −111 were assigned to H(3) and/or H(6).

Electronic Spectra and Stability Towards O_2

In DMF under anaerobic or aerobic conditions, the electronic spectrum of complex **2** exhibits a complex pattern, as is often reported for Co^{II} complexes. It consists of a broad band centred at 630 nm [1000 L mol^{-1} cm^{-1}] with secondary maxima on the high energy side that are roughly spaced by 1300 cm^{-1}, the first maximum appearing at 565 nm [2500 L mol^{-1} cm^{-1}]. The 565-nm band is assigned to a thiolate-to-cobalt S→Co^{II} charge-transfer band on the basis of the resonance Raman experiments described below, whereas the broad band located at 630 nm should correspond to the superimposition of several d-d transitions very close in energy. In CH_2Cl_2 under anaerobic conditions, complex **2** not only exhibits an absorption at 565 nm, as it does in DMF, but also two other bands at 657 nm and 800 nm. Upon exposure to air, the blue-purple CH_2Cl_2 solution turned deep-blue and the spectrum obtained thereafter featured only a sharp absorption at 657 nm (5500 L mol^{-1} cm^{-1}) and a small one at 800 nm (1400 L mol^{-1} cm^{-1}). Thus, the spectrum of the dimer in CH_2Cl_2 under argon is that of a mixture of two species **2** and **2a** characterized by absorptions at 565 nm and 657/800 nm, respectively. In this solvent, complex **2** is obtained exclusively after adding 1 equiv. of NBu_4OH in MeOH, while complex **2a** is formed after adding 1 equiv. of CH_3SO_3H in the presence of dioxygen. The absolute requirement of dioxygen to convert **2** into **2a** under acidic conditions suggests that **2a** is probably an oxidized state of **2**. Finally, we note that under the conditions defined above, the conversion of **2** into **2a** is reversible, both in DMF and in CH_2Cl_2 [Equation (1)].

$$\mathbf{2} \underset{NBu_4OH,\ MeOH}{\overset{MeSO_3H,\ air}{\rightleftharpoons}} \mathbf{2a} \qquad (1)$$

Electro- and Spectroelectrochemistry

The cyclic voltammogram of **2** in DMF at 25 °C displays two quasi-reversible waves of equal intensity located at $E_1 = -0.19$ and $E_2 = +0.05$ V vs. SCE (Supporting Information). This indicates that **2** retains its binuclear [Co^{II}−Co^{II}] structure in DMF solution. On using NBu_4PF_6 instead of NBu_4Cl as the supporting electrolyte, the second oxidation wave was seen to be shifted from +0.05 to +0.2 V and became irreversible, suggesting that chloride anions were required to observe a reversible second oxidation of **2**.

The cyclic voltammogram of **2** obtained at 25 °C in CH_2Cl_2 containing NEt_4Cl as the supporting electrolyte exhibits two quasi-reversible waves as in DMF, located at $E_1 = -0.19$ V and $E_2 = +0.2$ V (Figure 2, A). Nevertheless, in contrast to DMF solution, the zero-current potential in CH_2Cl_2 ($E_0 = -0.19$ V) corresponds to the first potential E_1, indicating that, in agreement with the UV/Vis experiments, both [$Co^{II}Co^{II}$] (**2**) and its first oxidized species [$Co^{II}Co^{III}$]$^+$ (**2a**) are present in solution. As expected for a metal-centred oxidation, the shapes of the cyclic voltammograms of the pure species **2a** and **2**, recorded after the addition of 1 equiv. of $MeSO_3H$ in the presence of dioxygen or of 1 equiv. of NBu_4OH, respectively, remained identical. Only the zero-current potentials were shifted, from $E_0' =$

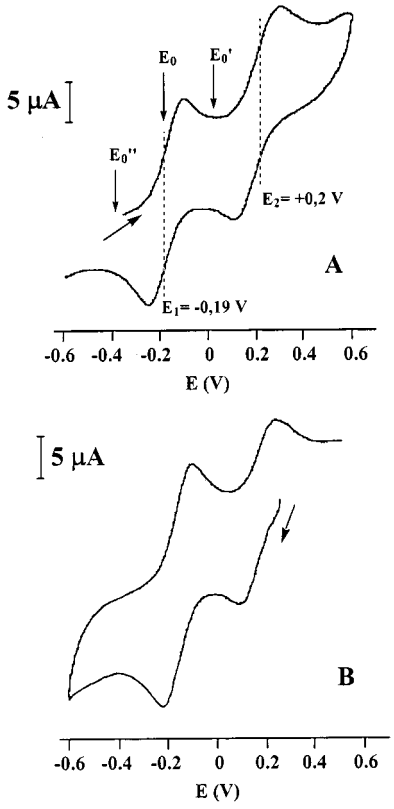

Figure 2. Cyclic voltammograms in CH_2Cl_2 solution at 25 °C (0.1 M Bu_4NCl; glassy carbon working electrode and saturated calomel reference electrode; 50 mV s^{-1}): A: $[Co^{II}Co^{II}]$ compound **2** ($\approx 10^{-3}$ M) obtained after addition of 1 equiv. of Bu_4NOH to a solution of $[S_2N_2Co]_2$ in dichloromethane; E_1 and E_2 correspond to $E_{1/2}$ potentials, E_0, E_0', and E_0'' to the zero-current potentials observed for the initial **2**/**2a** mixture in CH_2Cl_2 and for the unique species **2a** and **2** (obtained after addition of $MeSO_3H$ or Bu_4NOH), respectively; B: **2b** produced by electrolysis of a solution of **2a** at +0.45 V

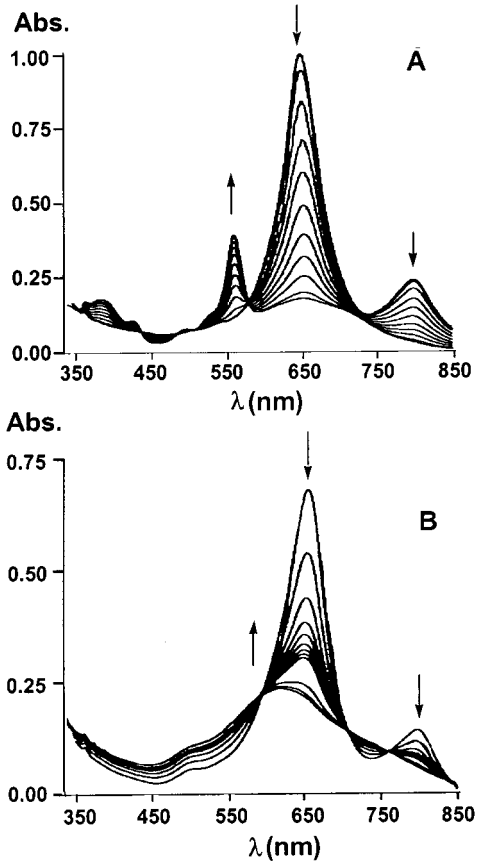

Figure 3. Spectroelectrochemistry of **2a** in CH_2Cl_2 at 25 °C: one-electron reduction (A) (isosbestic points: 435, 490, 585, 730 nm) and one-electron oxidation (B) (isosbestic points: 595, 715, and 795 nm) (conditions: [**2a**] $\approx 10^{-3}$ M with 0.1 M Bu_4NCl); the final spectra correspond to those of **2** and **2b**, respectively

−0.05 V for **2a** to $E_0'' = -0.27$ V for **2** (Figure 2, A). Any ligand-centred oxidation can be excluded since, using the zinc derivative **1**, the ligand is irreversibly oxidized in DMF at 560 mV vs. SCE.

To further investigate the electronic properties of the dimer, spectroelectrochemical reduction (Figure 3, A) and spectroelectrochemical oxidation (Figure 3, B) of **2a** were performed in CH_2Cl_2. Indeed, upon one-electron reduction of **2a** at −0.5 V, the characteristic UV/Vis spectrum of **2** was obtained. The one-electron oxidation of **2a** at 0.6 V led to a new species **2b**, exhibiting a broad absorption at 625 nm. Both reduction and oxidation were found to be reversible. The cyclic voltammogram of **2b** (Figure 2, B) displays the same characteristic binuclear pattern as seen for **2** and **2a**, with the exception of a zero-current potential of +0.45 V. Consequently, compound **2b** is proposed to be the fully oxidized binuclear Co^{III} complex $[LCo^{III}]_2^{2+}$. However, as chloride anions greatly increased its stability, it would be better described as a six-coordinate species $[LCo^{III}Cl]_2$.

Hence, complex **2** represents the first reported example of a bis(μ-thiolato) binuclear Co^{II} complex with a mixed nitrogen/sulfur environment, exhibiting three stable reversible oxidation steps in solution. Ghilardi et al.[16] have previously described a sulfide-bridged binuclear Co^{II}/Co^{III} complex and its corresponding di-Co^{II} and di-Co^{III} complexes, which were obtained by $NaBH_4$ reduction and $NOBF_4$ oxidation, respectively. However, none of the reduced or oxidized states were stable in solution. Both $[Co^{II}/Co^{II}]$ and $[Co^{II}/Co^{III}]$ states of the dimer were easily accessible in solution by treatment with acid or base. A similar reduction of Fe^{III} complexes in the presence of HO^- in MeOH or DMSO has been reported.[17] However, all attempts to crystallize the $[Co^{II}/Co^{III}]$ species failed since it reverted back to the $[Co^{II}/Co^{II}]$ complex in the solid state.

Raman Spectroscopy

The resonance Raman spectra of the $[Co^{II}/Co^{II}]$ and $[Co^{II}/Co^{III}]$ complexes in DMF solution, both recorded using an excitation frequency close to their respective visible absorption maxima, are shown in Figure 4. In the spectrum of **2**, two main bands are seen at 223 and 1295 cm^{-1}, while in that of **2a**, besides the same two bands, which are shifted

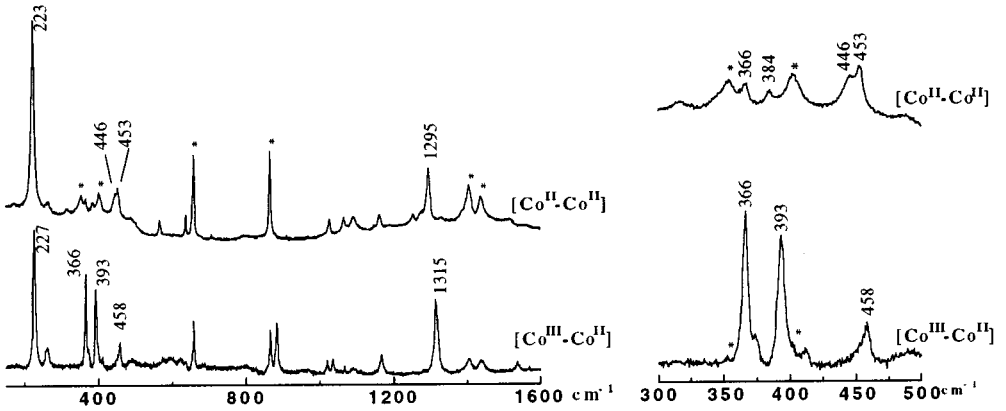

Figure 4. Resonance Raman spectra in DMF solution of the [$Co^{II}Co^{II}$] dimer **2** obtained with 568-nm excitation (upper trace) and of the [$Co^{II}Co^{III}$] complex **2a** obtained with 647-nm excitation (lower trace); * denotes solvent bands

to 227 and 1315 cm^{-1}, three additional bands with comparable intensities are seen at 366, 393, and 1019 cm^{-1}. Weaker bands are seen in the 1000−1150 cm^{-1} region for both complexes and in the 350−650 cm^{-1} region for the [Co^{II}/Co^{II}] complex.

The excitation profiles of these bands were established: They revealed a maximum at a wavelength close to the maximum of the strongest visible absorption band. For the [Co^{II}/Co^{II}] complex (Figure 5, A), an extremely strong enhancement factor was obtained for the 223 cm^{-1} band at 565 nm, at the maximum of the narrow absorption band; the other low-frequency bands were slightly enhanced, as were the high-frequency bands, with the exception of that at 1295 cm^{-1}, which displayed the second highest enhancement factor. We also note the selectivity of the enhancement of the low-frequency bands within the 565 nm band; in contrast, the high-frequency bands show residual intensity on the blue side of the absorption band. This is consistent with the assignment of the latter to phenyl ring vibrations, and of the former to cobalt ligand modes. The very strong and selective enhancement of the 223 cm^{-1} band and the presence of its first harmonic at 446 cm^{-1} suggest an A-term resonance (Franck−Condon mechanism). For the [Co^{II}/Co^{III}] complex (Figure 5, B), the low-frequency bands at 225, 366, and 393 cm^{-1} show the highest enhancement factors, followed by the 458, 1165, and 1315 cm^{-1} bands, the 1019 and 882 cm^{-1} bands being less enhanced.

To the best of our knowledge, no Raman data are available for binuclear bis(μ-thiolato)cobalt complexes, whereas numerous data on Fe−S and Cu−S vibrations have been reported, mainly for Fe−S and Cu−S proteins and some of their model compounds.[18,19] The M−S stretching vibrations have been located in the region 280−430 cm^{-1}. Raman bands in the region 400−280 cm^{-1}, resonance-enhanced within an absorption band at 510 nm, have also been observed for polymeric (thiolato)Co^{III} complexes, the structures of which have not been precisely determined.[20] Therefore, due to its low frequency, the most prominent band of the Co^{II} dimer cannot be assigned to a Co−S stretching vibration; it might correspond to the totally sym-

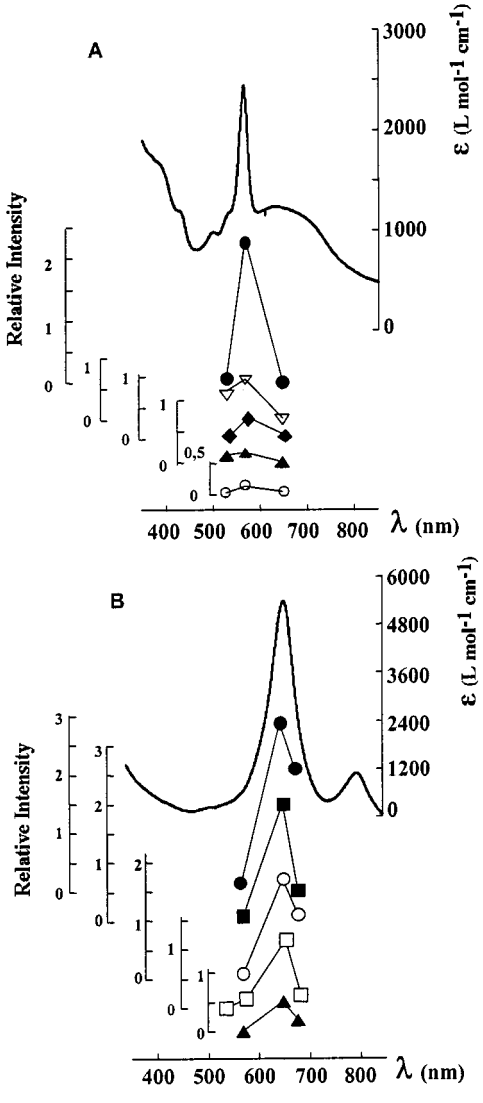

Figure 5. Absorption spectra and excitation profiles of the main Raman bands: A: **2**: ● 222 cm^{-1}, ○384 cm^{-1}, ◆ 453 cm^{-1}, ▲ 1162 cm^{-1}, ▽ 1295 cm^{-1}; B: [$Co^{II}Co^{III}$] dimer **2a**: ● 225 cm^{-1}, ■ 367 cm^{-1}, ▲ 459 cm^{-1}, □ 882 cm^{-1}, ○ 1315 cm^{-1}

metric bending mode of the Co1−S2−Co′1−S′2 core (involving both Co−S−Co and S−Co−S angular deformations): An analogous vibration has been observed at ca. 200 cm^{-1} for the Fe_2S_2 core in the model compound Fe_2S_2(*o*-xylenedithiolate)$_2$ [21] and has been considered as having Fe−Fe stretching character. The two stretching vibrations of the Co_2S_2 core might be located at 453 cm^{-1} (symmetric ring breathing) and 384 cm^{-1}, as these bands show significant enhancement within the 565-nm absorption band. The same three bands are present in the [Co^{II}/Co^{III}]$^+$ complex spectrum at slightly higher frequencies, i.e. 227, 458, and 393 cm^{-1}, respectively. The other strong low-frequency band at 366 cm^{-1} might be the $Co-S_{terminal}$ stretching mode that showed increased intensity in the mixed valence dimer.

Among the high-frequency bands, which correspond to vibrations of the phenylthiolate moiety, the band at ca. 1300 cm^{-1} was seen to be significantly enhanced: It might be analogous to the 1320 cm^{-1} band observed for catecholate complexes of human tyrosine hydroxylase, which has been assigned to a ring deformation of *ortho*-disubstituted benzene and proposed as a marker for bidentate catecholate-type coordination.[22]

Characterization of Complex 4

The electronic spectrum of **4** in DMF features an intense absorption at 420 nm [3000 mol^{-1} L cm^{-1}] and two weak bands at 640 and 350 nm. In the presence of dioxygen, a rapid change in the visible spectrum was observed, associated with complete degradation of the complex. This complex not only proved to be unstable towards dioxygen, but it had to be kept at low temperatures both in solution and in the solid state, otherwise it was very rapidly degraded. For this reason, we were unable to obtain a reliable elemental analysis or crystals suitable for X-ray analysis. Consequently, complex **4** could only be characterized at low temperatures by EPR and ^{1}H NMR spectroscopy. The X-band EPR spectrum in deaerated frozen DMF solution at 10 K (Figure 6) is consistent with a high-spin Co^{II} mononuclear complex. It shows a broad resonance at $g = 4.3$ and a small component at $g = 2$, the second derivative of which exhibits an eight-line hyperfine structure with a spacing of 100 G, a value typical of high-spin Co^{II} complexes. The ^{1}H NMR spectrum of **4** in [D_7]DMF, recorded at −40 °C under argon (Supporting Information), shows the 17 expected sharp signals in the range $\delta = -27$ to +161. The two methyl resonances were assigned to the signals at $\delta = +18$ and +14 on the basis of their integrals, which corresponded to three protons, whereas all the other peaks integrated as one proton.

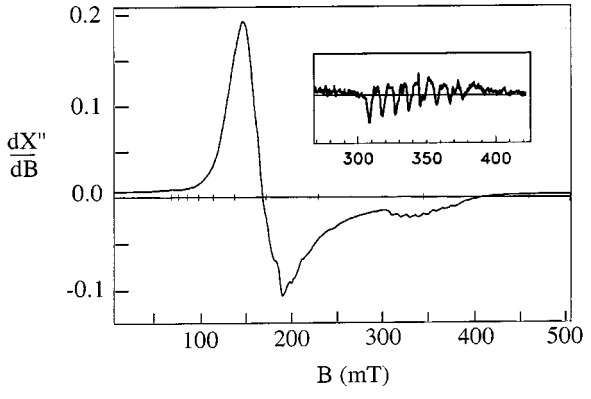

Figure 6. X-band EPR spectrum of **4** (ca. 5×10^{-4} M) in frozen DMF solution recorded at 10 K with a power of 10 mW (33 dB) at a frequency of 9.64 GHz; inset: second derivative signal (amplitude modulation)

Conclusion

Using two different amine/sulfur ligands, S_2N_2 and $S_2N_3^{py}$, we have obtained two new Co^{II} complexes. While the instability of the [$Co^{II}S_2N_3^{py}$] species prevented a complete study, the [$Co^{II}S_2N_2$]$_2$ dimer has been fully characterized both in the solid state and in solution. Its dimeric structure leads to an S_3N_2 coordination sphere for each Co centre, which is probably responsible for its increased stability; this complex can be reversibly oxidized by one and two oxidizing equivalents. A strong resonance Raman band at 220−230 cm^{-1} constitutes the vibrational signature of the Co_2S_2 core in the fully reduced as well as in the mixed valence state of the dimer.

Experimental Section

Caution: Attention is drawn to the highly toxic nature of 2-aminobenzenethiol. − All the syntheses were performed under argon using standard Schlenk techniques. All solvents were dried and distilled prior to use.

Physical Measurements: Electronic spectra were recorded with a Uvikon 820 double-beam spectrophotometer. − ^{1}H NMR spectra were recorded at 300 K with a Bruker ARX-250 spectrometer controlled by UXNMR software run with an Aspect 1 station. Chemical shifts are reported downfield from TMS. Magnetic susceptibilities of powder samples were measured in the range 2−293 K with a SQUID magnetometer (MPMS, Quantum Design) in a 1-T external magnetic field. Diamagnetic corrections were applied by using Pascal's constants. − X-band EPR spectra of samples in frozen solutions in quartz cells ($d = 0.3$ mm) were measured with a Bruker ESP 300E spectrometer operating at 9.5 GHz, equipped with an Oxford Instruments EPR 910 helium-flow cryostat. − Cyclic voltammetry and coulometric experiments were performed with Radiometer equipment using solutions containing 0.1 M tetrabutylammonium chloride (Bu_4NCl) or hexafluorophosphate (Bu_4NPF_6) as supporting electrolytes. The electrode system consisted of an NaCl-saturated calomel electrode (SCE) as the reference, a platinum auxiliary electrode, and a glassy carbon working electrode. The potential sweep rate was 50 mV s^{-1}. Ferrocene was used as an internal standard [$E_{1/2}$ (ferricinium/ferrocene) = +450 mV vs. SCE]. Spectroelectrochemistry was performed using an EG & G PAR-173 apparatus and a Varian spectrophotometer. − Electrospray mass spectra were measured from samples in dichloromethane solution. − Elemental analyses were carried out by the microanalysis service at the Paris VI University. − The crystal structure was solved by the X-ray service at the Paris VI University.

[S_2N_2Zn] {[2,3-Bis(2-mercaptoanilino)butane]zinc(II), 1}: The zinc complex **1** was prepared according to the published procedures of Bayer et al.[5] and Corbin et al.[6]

[$S_2N_2Co^{II}$]$_2$ (2): 2 equiv. of aqueous NaOH (108 μL of a 2 N solution) was added to a solution of [S_2N_2Zn] (40 mg, 0.11 mmol) in DMF (5 mL). After stirring for 10 min, the white precipitate of $Zn(OH)_2$ was removed. A solution of $CoCl_2{\cdot}6H_2O$ (26 mg, 1 equiv.) in DMF was then added dropwise to the free dithiolate ligand. Addition of aqueous NaOH (2 N, 50 μL) resulted in a purple solution of [$S_2N_2Co^{II}$]$_2$. After removal of the DMF in vacuo, the complex was redissolved in CH_2Cl_2 and precipitated by the addition of pentane. The microcrystalline purple precipitate was collected by filtration and washed with methanol (75 mg, 95% yield). Diffusion of pentane into a dichloromethane solution of **2** yielded purple crystals. − $C_{32}H_{36}Co_2N_4S_4{\cdot}0.5CH_2Cl_2$ (706.33): calcd. C 51.01, H 4.87, N 7.32; found C 50.9, H 4.2, N 7.4. − MS (ESI^+): *m*/*z* (%) = 718 (100) {[$S_2N_2Co^{II}$]$_2$ − 4 H; imine formation}. − ^1H NMR (250 MHz, [D_6]DMSO, in the presence of 1 equiv. of 1 M Bu_4NOH in MeOH; the proton resonances were assigned on the basis of their intensity ratios and ^1H longitudinal relaxation times (T_1), which have been correlated to the Co···H distances): CH_3: δ = −18 (s, 12 H), T_1 = 29 ms, Co(1)−C(23) = 3.583(18) Å; H(21): δ = +166 (s, 4 H), T_1 = 30 ms, Co(1)−C(21) = 2.855(15) Å; H(3) and/or H(6): δ = −101 (s, 4 H), T_1 = 32 ms, and δ = −107 (s, 4 H), T_1 = 61 ms, Co(1)−C(3) = 4.336(6) Å and Co(1)−C(6) = 4.167(7) Å; H(4) and/or H(5): δ = +12 (s, 4 H), T_1 = 261 ms and δ = +16.5 (s, 4 H), T_1 = 144 ms, Co(1)−C(4) = 5.263(6) Å and Co(1)−C(5) = 5.170(6) Å.

[$S_2N_3^{py}Zn$] ({2,6-Bis[1-(2-mercaptoanilino)ethyl]pyridine}zinc(II), 3): A solution of $NaBH_4$ (0.717 g, 4.5 mmol) in EtOH/DMF (1:4; 125 mL) was added dropwise to a solution of {2,6-bis[2-(2-mercaptophenyl)-1-methyl-2-azaethenyl]pyridine}zinc(II)[23] (2.0 g, 4.5 mmol) in DMF (120 mL) cooled to 0 °C. The initially red solution became progressively more orange. After stirring at room temperature for 2 h, the DMF and ethanol were removed in vacuo. The residual oil was dissolved in methanol and the product was precipitated by the addition of twice the volume of water. The resulting orange precipitate was isolated in quantitative yield (2.0 g, 100%). − $C_{21}H_{21}N_3S_2Zn$ (444.92): calcd. C 56.69, H 4.76, N 9.44; found C 56.93, H 4.84, N 9.24. − ^1H NMR (250 MHz, [D_6]DMSO): δ = 1.37 (m, 6 H, CH_3), 4.49 (d, 2 H, CH), 5.76 (m, 2 H, NH), 6.87 (m, 4 H, ArH), 7.13 (d, 2 H, ArH), 7.21 (d, 2 H, ArH), 7.68−8.12 (m, 3 H, pyrH). − MS (EI): *m*/*z* (%) = 443 (100) {[$S_2N_3^{py}Zn$] − H}, 428 (60) {[$S_2N_3^{py}Zn$] − CH_3 − H}, 318 (70) {[$S_2N_3^{py}Zn$] − C_6H_5S}.

[$S_2N_3^{py}Co^{II}$] (4): 2 equiv. of aqueous NaOH (2 N, 90 μL) was added to a solution of [$S_2N_3^{py}Zn$] (40 mg, 0.09 mmol) in DMF (5 mL). After removing $Zn(OH)_2$, a solution of $CoCl_2{\cdot}6H_2O$ (21 mg, 1 equiv.) in DMF was added dropwise to the free ligand solution to give a yellow-green solution of **4**. After partial evaporation of the DMF in vacuo, addition of anhydrous diethyl ether (40 mL) led to the deposition of a light-green precipitate, which remained stable only at 0 °C and under argon. The complex was stored at −40 °C and was handled under anaerobic conditions at low temperatures at all times. − ^1H NMR (250 MHz, [D_7]DMF, −40 °C): δ = −27.13 (s, 1 H), −25.47 (s, 1 H), −24.44 (s, 1 H), −20.19 (s, 1 H), −18.53 (s, 1 H), −14.23 (s, 1 H), −9.74 (s, 1 H), −4.31 (s, 1 H), +9.82 (s, 1 H), +11.96 (s, 3 H, CH_3), +14.09 (s, 1 H), +16.31 (s, 1 H), +18.31 (s, 3 H, CH_3), +94.06 (s, 1 H), +101.20 (s, 1 H), +108.83 (s, 1 H), +161.30 (s, 1 H).

X-ray Crystallographic Data and Structure Refinement: Crystals of $C_{32}H_{36}Co_2N_4S_4$ (**2**) suitable for X-ray analysis were obtained by vapour diffusion of pentane into a dichloromethane solution of the complex. A selected crystal of dimensions 0.2 × 0.3 × 0.4 mm was attached to the tip of a glass fibre. Accurate cell dimensions and an orientation matrix were obtained by least-squares refinement of 25 accurately centred reflections with a Nonius-CAD4 diffractometer using graphite-monochromated Mo-K_α radiation. The regular decay (ca. 28%) of two checked reflections data were scaled. Absorption corrections were applied using the DIFABS method with $T_{min.}$ = 0.86 and $T_{max.}$ = 1.[24] Collection parameters and selected crystallographic data for **2** are listed in Table 1 and 2. The data were corrected for Lorentz and polarization effects. Computations were performed using the PC version of CRYSTALS.[25] Scattering factors and corrections for anomalous dispersion were taken from Cromer.[10] The structure was solved by direct methods using SHELXS[27] and refined by full-matrix least squares with anisotropic thermal parameters for all atoms except disordered carbon atoms. The four carbon atoms of the 1,2-dimethylethyl bridge were disordered and were each located in two different sites with occupancies of 0.5, namely (C-21, C-22), (C-23, C-24), (C-31, C-32), (C-33, C-34). The complex is made up of two asymmetric units related through an inversion centre. Hence, all the unlabelled atoms are related to the labelled ones through the inversion centre symmetry operation. Atoms C-22, C-24, C-32, and C-34 are omitted for the sake of clarity. Crystallographic data (excluding structure factors) for the structure reported in this paper have been deposited with the Cambridge Crystallographic Data Centre as supplementary publication no. CCDC-151295. Copies of the data can be obtained free of charge on application to the CCDC, 12 Union Road, Cambridge CB2 1EZ, U.K. [Fax: (internat.) + 44-1223/336-033; E-mail deposit@ccdc.cam.ac.uk]

Resonance Raman Spectroscopy: The resonance Raman spectra were obtained with a J. Y. U1000 double monochromator, equipped with an AsGa photomultiplier and photon-counting electronics. Excitation wavelengths from Ar^+ and Kr^+ lasers (30−50 mW power) were used. The mechanical slit width was set at 400 μm, so that the spectral slit width varied from 2 cm^{-1} at 676.4 nm to 4 cm^{-1} at 528.7 nm. The complexes were studied in CH_2Cl_2 and DMF solutions in a rotating cell (concentration 1 mM). The 657 cm^{-1} band of DMF was used to measure the relative intensities of the bands (based on peak heights) at the various excitation wavelengths.

Supporting Information: Figures S1−S6 show the magnetic susceptibility of **2** as a function of temperature, the cyclic voltammogram of **2** in DMF, the ^1H NMR spectrum of **2**, the ^1H NMR spectrum of **4**, and the resonance Raman frequencies of **2** and **2a** (see footnote on page 1).

Acknowledgments

This work was funded by the European Commission TMR-NOHEMIP research network no. ERBFMRXCT98−0174. We wish to thank J. Vaissermann for performing the X-ray structure determination of the binuclear Co complex. D. B. gratefully acknowledges Rhône−Poulenc for a fellowship.

[1] R. H. Holm, P. Kennepohl, E. I. Solomon, *Chem. Rev.* **1996**, *96*, 2239−2314.
[2] O. Y. Gavel, S. A. Bursakov, J. J. Calvete, G. N. George, J. J. G. Moura, I. Moura, *Biochemistry* **1998**, *37*, 16225−16232.

[3] M. Kobayashi, S. Shimizu, *Eur. J. Biochem.* **1999**, *261*, 1−9.
[4] P. T. Rajagopalan, S. Grimme, D. Pei, *Biochemistry* **2000**, *39*, 779−790.
[5] E. Bayer, E. Breitmayer, *Chem. Ber.* **1968**, *101*, 1579−1593.
[6] J. L. Corbin, D. E. Work, *Can. J. Chem.* **1974**, *52*, 1054−1058.
[7] V. L. Goedken, G. G. Cristoph, *Inorg. Chem.* **1973**, *12*, 2316−2320.
[8] M. F. Corrigan, K. S. Murray, R. M. Sheahan, B. O. West, G. D. Fallon, B. M. Gatehouse, *Inorg. Nucl. Chem. Lett.* **1975**, *11*, 625−628.
[9] K. D. Karlin, D. L. Lewis, H. N. Rabinowitz, S. J. Lippard, *J. Am. Chem. Soc.* **1974**, *96*, 6519−6521.
[10] J. C. Noveron, M. M. Olmstead, P. K. Mascharak, *J. Am. Chem. Soc.* **1999**, *121*, 3553−3554.
[11] M. J. Baker-Hawkes, Z. Dori, R. Eisenberg, H. B. Gray, *J. Am. Chem. Soc.* **1968**, *90*, 4253−4259.
[12] J. H. Enemark, W. N. Lipscomb, *Inorg. Chem.* **1965**, *4*, 1729−1734.
[13] S. C. Shoner, D. Barnhart, J. A. Kovaks, *Inorg. Chem.* **1995**, *34*, 4517−4518.
[14] A. Böttcher, H. Elias, E.-G. Jager, H. Langfelderova, M. Mazur, L. Müller, H. Paulus, P. Pelikan, M. Rudolph, M. Valko, *Inorg. Chem.* **1993**, *32*, 4131−4138.
[15] U. Küsthardt, R. W. Albach, P. Kiprof, *Inorg. Chem.* **1993**, *32*, 1838−1843.
[16] C. A. Ghilardi, C. Mealli, S. Midollini, V. I. Nefedov, A. Orlandini, L. Sacconi, *Inorg. Chem.* **1980**, *19*, 2454−2462.
[17] P. K. S. Tsang, P. Cofre, D. T. Sawyer, *Inorg. Chem.* **1987**, *26*, 3604−3609.
[18] T. G. Spiro, R. S. Czernuszewicz, S. Hans, *Biological Applications of Raman Spectroscopy* (Ed.: T. G. Spiro), Wiley, New York, **1988**, vol. 3, pp. 523−554.
[19] C. R. Andrew, J. Sanders-Loehr, *Acc. Chem. Res.* **1996**, *29*, 365−372.
[20] K. Kanamori, S. Ino, Y. Mizumo, K. Kawai, J. Hidaka, *Bull. Chem. Soc. Jpn.* **1989**, *62*, 2375−2378.
[21] S. Hans, R. S. Czernuszewicz, T. G. Spiro, *J. Am. Chem. Soc.* **1989**, *111*, 3496−3504.
[22] I. Michaud-Soret, K. K. Andersson, L. Que, *Biochemistry* **1995**, *34*, 5504−5510.
[23] L. F. Lindoy, D. H. Busch, *Inorg. Chem.* **1974**, *13*, 2494−2498.
[24] N. Walker, D. Stuart, *Acta Crystallogr.* **1983**, *A39*, 158−166.
[25] D. J. Watkin, C. K. Prout, R. J. Carruthers, P. W. Betteridge, *CRYSTALS*, University of Oxford, U.K., **1996**.
[26] D. T. Cromer, *International Tables for Crystallography*, Kynoch Press, Birmingham, U.K., **1974**, vol. IV.
[27] G. M. Sheldrick, *SHELXS − Program for the Solution of Crystal Structures*, University of Göttingen, Germany, **1986**.

Received October 27, 2000
[I00410]

Dinuclear Zinc(II)−Iron(III) and Iron(II)−Iron(III) Complexes as Models for Purple Acid Phosphatases

Sabine Albedyhl,[c] Marie Therese Averbuch-Pouchot,[a] Catherine Belle,*[a] Bernt Krebs,*[c] Jean Louis Pierre,[a] Eric Saint-Aman,[b] and Stephane Torelli[a]

Keywords: $Zn^{II}Fe^{III}$ complex / $Fe^{II}Fe^{III}$ complex / Purple acid phosphatases / Phosphate ester hydrolysis

The heterodinuclear $Zn^{II}Fe^{III}$ complex **1** and the isostructural $Fe^{II}Fe^{III}$ complex **2** with the dinucleating ligand from 2,6-bis[{bis(2-pyridylmethyl)amino}methyl]-4-methoxyphenol (HBPMOP, **3**) were prepared and characterized by X-ray crystallography. Solution studies (UV/Vis spectroscopy; electrochemistry) are described. A pH-induced change in the coordination spheres of the metal centers is seen. These complexes serve as models for the mixed-valence oxidation state in purple acid phosphatases. The cleavage acceleration of the activated phosphodiester 2-hydroxypropyl *p*-nitrophenyl phosphate (HPNP) was investigated in acetonitrile/water (1:1) in the presence of complexes of the ligand BPMOP and its methyl analogue BPMP with regards to its dependence on the pH value. At the optimum pH value (8.5 ± 0.2), the Zn^{II}-Fe^{III} complex from BPMOP shows a 2-fold higher rate acceleration compared with that of the complex containing BPMP. The diiron complex from BPMOP is 4-fold more reactive than the homologous complex from BPMP. The heterodinuclear $Zn^{II}Fe^{III}$ catalysts are at least 10-fold more reactive than the homonuclear $Fe^{II}Fe^{III}$ catalysts.

Introduction

Purple acid phosphatases (PAPs) catalyse the hydrolysis of activated phosphoric esters like *p*-nitrophenyl phosphate, naphthyl phosphate or ATP, at a pH range from 4 to 7.[1] The active site of red kidney bean purple acid phosphatase (KBPAP) harbours an Fe^{III} and a Zn^{II} ion, while those of the mammalian PAPs, isolated from bovine spleen (BSPAP) or from porcine uterus, contain a diiron site in an $Fe^{II}Fe^{III}$ state for the active form. The inactive purple $Fe^{III}Fe^{III}$ form, involves two high-spin iron ions which are antiferromagnetically coupled ($-J > 150\ cm^{-1}$). In the active Fe^{II}-Fe^{III} pink form, the two iron ions are weakly antiferromagnetically coupled ($-J = 19.8\ cm^{-1}$). The crystal structure of KBPAP, firstly determined at a resolution of 2.9 Å[2] and further at 2.65 Å,[3] reveals a homodimeric 111 kDa enzyme, containing two domains in each subunit. In the active site, located in the carboxyl-terminal domain, the two metal ions are 3.26 Å apart and bridged by Asp164, each one involving octahedral coordination. The iron ion is further coordinated by Tyr167, His325, and Asp135 residues, and the zinc ion by His286, His323, and Asn201 residues. Three exogenous ligands are also included in the X-ray model to complete the coordination sphere: one terminal hydroxo ligand to the iron ion, one terminal water ligand to the zinc ion, and one μ-hydroxo group between the metal ions. The crystal structures of KBPAP complexed with phosphate (the product of the reaction) and with tungstate (a strong inhibitor), have also been determined[3] allowing the proposal of a mechanism for the hydrolysis of phosphomonoesters (Figure 1).

In the proposed mechanism, the phosphate group of the substrate binds to the zinc ion by displacing the presumed water ligand. The terminal Fe^{III}-bound hydroxide ion attacks the phosphorus atom to form a pentacoordinated intermediate, and the P−O bond, opposite from the hydroxide ion attack, breaks to form the leaving group and phosphate which is consistent with the inversion at the phosphorus atom. Another kinetically indistinguishable mechanism has been suggested,[4] involving a nucleophilic attack by a bridging oxide instead of iron-bound hydroxide.

In order to mimic the reactivity of PAPs, two isostructural dinuclear complexes, containing a $Zn^{II}Fe^{III}$ and an Fe^{II}-Fe^{III} center, respectively, have been prepared and studied with the aim of comparing their activity towards phosphate ester cleavage and to allow comparisons between KBPAP and BSPAP. The dinucleating ligand from HBPMOP, which is of the known HBPMP type[5,6] 2,6-bis[{bis(2-pyridylmethyl)amino}methyl]-4-methylphenol has been used. It bears a strong electron-donating methoxy group in the *para* position to the bridging phenoxo group: 2,6-bis[{bis(2-pyridylmethyl)amino}methyl]-4-methoxyphenol (**3**). Heterodinuclear $Zn^{II}Fe^{III}$ complexes have been described as models for the active site of KBPAP. The first heterodinuclear phosphate-bridged model compound, $[FeZn(BPMP)\{(O_2P(OPh)_2\}_2]$, could be obtained by using HBPMP.[5a] The Fe−Zn distance (3.695 Å) in this complex, is significantly larger than in the carboxylate-bridged complex (3.428 Å)[6] compared to the value of 3.33 Å measured on KBPAP in the presence of phosphate. Some other heter-

[a] Laboratoire de Chimie Biomimétique, LEDSS, UMR CNRS 5616, Université J. Fourier,
BP 53, 38041 Grenoble Cedex 9, France
E-mail: Catherine.Belle@ujf-grenoble.fr
[b] Laboratoire d'Electrochimie Organique et de Photochimie Redox, UMR CNRS 5630, Université J. Fourier,
BP 53, 38041 Grenoble Cedex 9, France
[c] Anorganisch-Chemisches Institut der Universität Münster, Wilhelm-Klemm-Strasse 8, 48149 Münster, Germany

 © WILEY-VCH Verlag GmbH, 69451 Weinheim, 2001 1434−1948/01/0606−1457 $ 17.50+.50/0

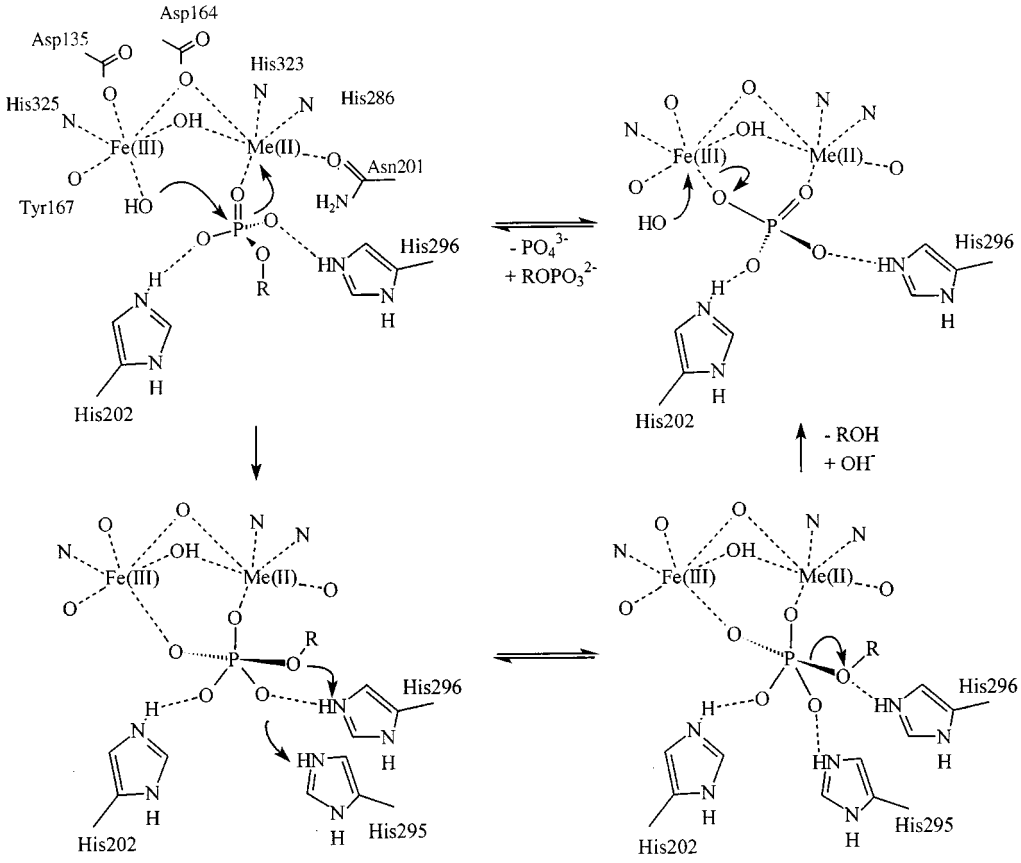

Figure 1. The active site of KBPAP and proposed mechanism of phosphate ester hydrolysis[3]

odinuclear $Zn^{II}Fe^{III}$ complexes have been described,[7−9] all of them containing symmetrical ligands. A Zn−Fe complex involving a constitutionally unsymmetrical ligand, but with identical chemical environments (two N_3O coordination spheres), has also been described in solution.[10] Mixed-valence phenoxo-bridged diiron complexes have also been reported as models for BSPAP by several authors.[5a,6,10−17] A recent review has been published, describing structural and functional model compounds of PAPs.[18]

Results and Discussion

Synthesis of the Complexes

The reaction of equimolecular amounts of $Zn(ClO_4)_2·6H_2O$ and $Fe(ClO_4)_3·H_2O$ with HBPMOP in methanol, yielded blue-green crystals of $[Zn^{II}Fe^{III}BPMOP\{O_2P(OPh)_2\}_2](ClO_4)_2·H_2O$ (**1**) after the addition of diphenyl phosphate. These were suitable for X-ray crystallography. Green crystals of $[Fe^{II}Fe^{III}BPMOP\{O_2P(OPh)_2\}_2](ClO_4)_2·H_2O$ (**2**) were obtained by the analogous reaction with 2 equiv. of $Fe(ClO_4)_3·H_2O$. The only metal species isolated was the mixed-valence diiron complex, indicating the participation of a redox process during complex formation. It is known that the diiron(III) species are strong oxidants, suggesting that the reductant is the methanol solvent.[6]

Crystal Structures of 1 and 2

Compounds **1** and **2** are isostructural complexes and are therefore described in comparison with each other. The triclinic elementary cells of **1** and **2** contain two formulas. The metal centers exhibit octahedral coordination. In the heterodinuclear complex **1** (Figure 2), the metal atoms are linked by a μ-phenoxo group from the ligand and by two μ-diphenylphosphato bridges with a distance of 3.7030(7) Å. The angle over Zn(1)−O(1)−Fe(1) is 122.9(1)°. The two iron centers in the analogous complex **2** (Figure 3) have a distance of 3.6400(6) Å, which is slightly shorter than the corresponding distance in **1**. The angle Fe(1)−O(1)−Fe(2) is 121.44(9)°. The nitrogen donor atoms from BPMOP complete the coordination sphere per facial coordination, resulting in an equivalent N_3O_3 donor set. Selected bond lengths and angles are given in Table 1.

The structure of **2** confirms the mixed valence state. The crystal structure of complex $[Zn^{II}Fe^{III}BPMP\{O_2P(OPh)_2\}_2](ClO_4)_2·1.5CH_3OH·H_2O$ which involves the same coordination sphere as in **1** has been reported.[5a] The Zn−Fe distance of 3.695(1) Å is in the range of the Zn−Fe distance in **1** [3.7030(7) Å]. This distance is significantly shorter in the carboxylate-bridged analogue [3.437(1) Å][6] and larger in the molybdato-bridged complex from 2,6-bis[{bis(2-pyridylmethyl)amino}methyl]-4-*tert*-butylphenol (HBPBP) [3.819(4) Å].[9] This can be due to the different bite distance of the phosphate group and therewith indi-

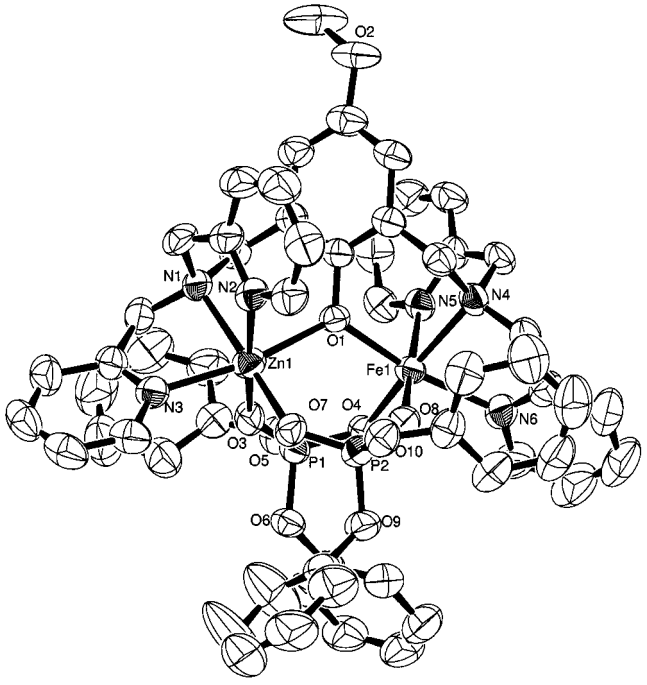

Figure 2. ORTEP molecular representation of complex **1** showing 50% probability displacement ellipsoids; H atoms, water molecule, and perchlorate ions have been omitted for clarity

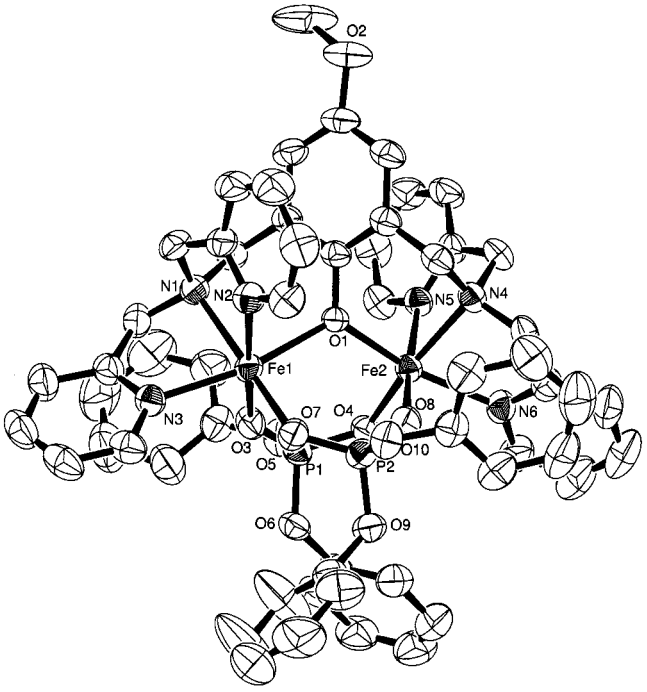

Figure 3. ORTEP molecular representation of complex **2** showing 50% probability displacement ellipsoids; H atoms, water molecule, and perchlorate ions have been omitted for clarity

cates a remarkable structural flexibility of the phenoxo-bridged intermetal(II,III) distance which may be important for the catalytic activity. The Zn−Fe distance in the native KBPAP is 3.33 Å in the presence of phosphate. The $Fe^{II}-Fe^{III}$ distance in **2** [3.6400(6) Å] is also significantly larger than in the carboxylate-bridged $Fe^{II}Fe^{III}$ complex from BPMP [3.365(1) Å][6] and slightly shorter than in the non-bridged $Fe^{II}Fe^{III}$ complex of the ligand BPBP [3.726(2) Å].[9]

Table 1. Selected bond lengths [Å] and angles [°] in **1** and **2**

1		**2**	
Zn(1)−Fe(1)	3.7030(7)	Fe(1)−Fe(2)	3.6400(6)
Zn(1)−O(1)	2.168(2)	Fe(1)−O(1)	2.215(2)
Zn(1)−O(3)	2.042(2)	Fe(1)−O(3)	2.096(2)
Zn(1)−O(7)	2.028(2)	Fe(1)−O(7)	2.060(2)
Zn(1)−N(1)	2.183(3)	Fe(1)−N(1)	2.212(3)
Zn(1)−N(2)	2.122(3)	Fe(1)−N(2)	2.166(3)
Zn(1)−N(3)	2.124(3)	Fe(1)−N(3)	2.160(3)
Fe(1)−O(1)	2.047(2)	Fe(2)−O(1)	1.958(2)
Fe(1)−O(4)	1.974(2)	Fe(2)−O(4)	1.972(2)
Fe(1)−O(8)	1.984(2)	Fe(2)−O(8)	1.956(2)
Fe(1)−N(4)	2.168(3)	Fe(2)−N(4)	2.179(3)
Fe(1)−N(5)	2.128(3)	Fe(2)−N(5)	2.147(3)
Fe(1)−N(6)	2.125(3)	Fe(2)−N(6)	2.131(3)
O(1)−Zn(1)−O(3)	86.52(9)	O(1)−Fe(1)−O(3)	86.13(7)
O(1)−Zn(1)−O(7)	97.33(9)	O(1)−Fe(1)−O(7)	97.77(7)
O(1)−Zn(1)−N(1)	87.0(1)	O(1)−Fe(1)−N(1)	86.17(8)
O(1)−Zn(1)−N(2)	87.3(1)	O(1)−Fe(1)−N(2)	87.33(8)
O(1)−Zn(1)−N(3)	162.4(1)	O(1)−Fe(1)−N(3)	160.29(8)
O(3)−Zn(1)−O(7)	94.5(1)	O(3)−Fe(1)−O(7)	97.40(8)
O(3)−Zn(1)−N(1)	93.5(1)	O(3)−Fe(1)−N(1)	92.88(9)
O(3)−Zn(1)−N(2)	171.8(1)	O(3)−Fe(1)−N(2)	170.37(9)
O(3)−Zn(1)−N(3)	86.5(1)	O(3)−Fe(1)−N(3)	85.03(8)
O(7)−Zn(1)−N(1)	171.2(1)	O(7)−Fe(1)−N(1)	170.13(9)
O(7)−Zn(1)−N(2)	91.7(1)	O(7)−Fe(1)−N(2)	91.48(9)
O(7)−Zn(1)−N(3)	99.3(1)	O(7)−Fe(1)−N(3)	100.70(9)
N(1)−Zn(1)−N(2)	80.8(1)	N(1)−Fe(1)−N(2)	79.62(9)
N(1)−Zn(1)−N(3)	77.3(1)	N(1)−Fe(1)−N(3)	76.72(9)
N(2)−Zn(1)−N(3)	97.9(1)	N(2)−Fe(1)−N(3)	98.97(9)
O(1)−Fe(1)−O(4)	97.17(9)	O(1)−Fe(2)−O(4)	99.41(8)
O(1)−Fe(1)−O(8)	88.3(1)	O(1)−Fe(2)−O(8)	91.24(8)
O(1)−Fe(1)−N(4)	89.7(1)	O(1)−Fe(2)−N(4)	90.44(8)
O(1)−Fe(1)−N(5)	88.6(1)	O(1)−Fe(2)−N(5)	88.36(8)
O(1)−Fe(1)−N(6)	164.7(1)	O(1)−Fe(2)−N(6)	165.42(9)
O(4)−Fe(1)−O(8)	95.2(1)	O(4)−Fe(2)−O(8)	96.41(9)
O(4)−Fe(1)−N(4)	168.0(1)	O(4)−Fe(2)−N(4)	165.30(8)
O(4)−Fe(1)−N(5)	90.9(1)	O(4)−Fe(2)−N(5)	90.30(9)
O(4)−Fe(1)−N(6)	97.5(1)	O(4)−Fe(2)−N(6)	95.08(9)
O(8)−Fe(1)−N(4)	94.8(1)	O(8)−Fe(2)−N(4)	94.25(9)
O(8)−Fe(1)−N(5)	173.4(1)	O(8)−Fe(2)−N(5)	173.26(9)
O(8)−Fe(1)−N(6)	86.1(1)	O(8)−Fe(2)−N(6)	85.54(9)
N(4)−Fe(1)−N(5)	79.4(1)	N(4)−Fe(2)−N(5)	79.03(9)
N(4)−Fe(1)−N(6)	76.6(1)	N(4)−Fe(2)−N(6)	75.66(9)
N(5)−Fe(1)−N(6)	95.5(1)	N(5)−Fe(2)−N(6)	93.17(9)
Zn(1)−O(1)−Fe(1)	122.9(1)	Fe(1)−O(1)−Fe(2)	121.44(9)

Electronic Spectra

The main feature of the electronic spectra of **1** and **2** in acetonitrile is the LMCT transition from phenolate to iron(III) which is observed at λ_{max} = 654 nm ($\varepsilon \approx 900$) in **1** and 673 nm ($\varepsilon \approx 900$) in **2**, respectively. In addition, a shoulder is observed in **2**, at λ_{max} = 385 nm ($\varepsilon \approx 3000$) which can be assigned to a charge-transfer transition from Fe^{II} to pyridine. The analogous complexes from HBPMP[5a] show absorption maxima in methanol at λ_{max} = 569 nm ($\varepsilon \approx 800$) for the $Zn^{II}Fe^{III}$ complex and at λ_{max} = 610 nm ($\varepsilon \approx 950$) for the $Fe^{II}Fe^{III}$ complex. A shoulder in the spec-

trum of the latter is observed at λ_{max} = 365 nm ($\varepsilon \approx$ 3480).[6]

Electrochemistry

Although PAPs catalyse non-redox-active hydrolytic reactions, the catalytic activity is dependent on the oxidation state of the iron active site, the mixed-valence oxidation state being active towards the hydrolysis of the phosphate esters while the oxidized form is inactive. The determination of the electrochemical stability domain of synthetic models thus appears of prime importance. Electrochemical investigations by cyclic voltammetry (CV) of **1** in CH_3CN (Figure 4, A, curve 1) show two reversible one-electron waves at $E_{1/2}$ = 0.13 V and 1.36 V (vs. SCE). This is confirmed by rotating disc electrode (RDE) experiments. The RDE curve recorded under the same experimental conditions (Figure 4, A, curve 2) displays two well-behaved waves of very close intensity, without contamination of the $Fe^{II}Fe^{III}$ complex **2** electrochemical response (see below). The cathodic wave at $E_{1/2}$ = 0.13 V is attributed to the $Fe^{III}Zn^{II}/Fe^{II}Zn^{II}$ redox couple while the anodic wave corresponds to the ligand-based oxidation. The CV curve in CH_3CN of the BPMP analog of **1**, $[Zn^{II}Fe^{III}$ BPMP$\{O_2P(OPh)_2\}_2](ClO_4)_2 \cdot 1.5 \cdot CH_3OH \cdot H_2O$, shows a reversible one-electron transfer at a potential of 143 mV ($Fe^{III}Zn^{II}/Fe^{III}Zn^{II}$ redox couple) and a weak signal at +765 mV, which has been attributed to a slight contamination with Fe^{II}.[5a] The ligand-based oxidation is not observed in the accessible potential range. The electron-donating effect of the methoxy group in *para* position of the bridging phenolic moiety causes a stabilization of the oxidized form of the BPMOP ligand compared to the non-substituted BPMP ligand. In the case of **2**, two reversible one-electron waves are observed on the CV curve (Figure 4, B, curve 1) at $E_{1/2}$ = 0.12 V and 0.74 V (vs. SCE) which are assigned to the redox couples $Fe^{II}Fe^{II}/Fe^{II}Fe^{III}$ and $Fe^{II}Fe^{III}/Fe^{III}Fe^{III}$, respectively. The RDE curve (Figure 4, B, curve 2) is characterized by one cathodic and one anodic wave confirming the mixed-valence character of **2**.

Similar results have been found in the CV behavior of $[Fe^{II}Fe^{III}BPMP\{O_2P(OPh)_2\}_2](ClO_4)_2 \cdot CH_3OH \cdot H_2O$ ($E_{1/2}$ = +135 mV and +755 mV, respectively[5a]). Comparing the electrochemical features of **1** or **2** with those of their BPMP analogs, only a weak cathodic shift, around 20 mV, in the metal-centered electron transfers, are observed, i.e. the substitution by the methoxy group in the *para* position on the bridging phenolic moiety in **1** and **2** did not markedly influence the metal-centered electron transfer potential. From the separation of the redox potentials in **2**, we have determined the stability of the mixed-valence form of **2** by evaluating the comproportionation constant, K_{com}, for the equilibrium according to Equation (1).

$$Fe^{II}Fe^{II} + Fe^{III}Fe^{III} \rightarrow 2\,Fe^{II}Fe^{III},\ \Delta E_{1/2} = (RT/F) \cdot \ln(K_{com}) \qquad (1)$$

Using $\Delta E_{1/2}$ = 0.62 V, a value of $3.0 \cdot 10^{10}$ ($\Delta G = -59$ kJ mol^{-1}) is found, which is close to the value of $3.2 \cdot 10^{10}$ determined for the BPMP analog of **2**. Electron delocalization, electrostatic interaction and steric interaction are the main factors involved in the magnitude of K_{com} although, considering related complexes,[5b] the electron delocalization energy has been found to be too small to contribute significantly to the mixed-valence state stability. Electrostatic interactions may strongly influence the stability domain. Taking into account the close proximity of the two metal ions, the II,II form of the complex will be more readily oxidized than the II,III form leading to an increase in the stability domain of **2**. On the other hand, by comparing other related synthetic models of PAPs,[11,13] it is shown that the replacement of pyridyl groups in phenoxo-bridged diiron complexes by one and two phenolate terminal groups leads to a cathodic shift in the redox potentials by ca. −0.4 V and −1.0 V, respectively, the stability domain ranging between 0.5 and 1.0 V according to the substitution on the phenoxo-bridging ligand and to the exogeneous ligands. It must also be noticed that porcine purple acid phosphatase (uteroferrin) has a reduction potential ($Fe^{III}Fe^{III}/Fe^{II}Fe^{III}$ redox couple) of 367 mV[19] vs. NHE (i.e. 122 mV vs. SCE). This is close to the value of 0.12 V found for **2**.

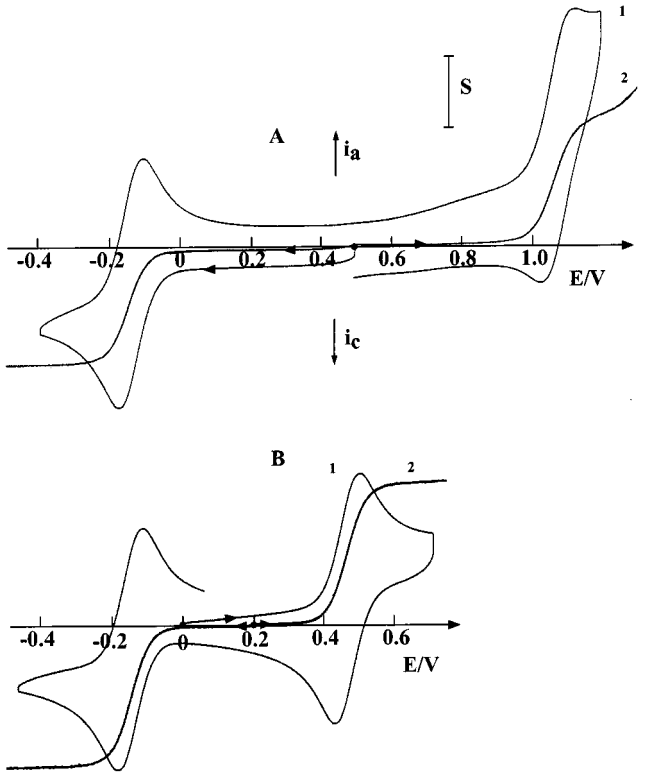

Figure 4. Voltammograms of **1** (A) and **2** (B), 0.9 mM, in CH_3CN + TBAP (0.1 M); *E* vs. $Ag/AgNO_3$ (10 mM) (+339 mV vs. SCE); curve 1: CV at a vitreous carbon disc electrode (5 mm diameter), v = 0.1 Vs^{-1}, *S* (scale) = 20 μA; curve 2: voltammetry at the RDE (3 mm diameter), 600 rpm, S = 10 μA

pH-Induced Changes in the Coordination Sphere

A UV/Vis titration (monitoring of the LMCT band) of a solution of HBPMOP and equimolar amounts of zinc(II) perchlorate and iron(III) perchlorate has been performed in acetonitrile/water (1:9) upon addition of concentrated aqueous solution of NaOH or $HClO_4$ (Figure 5). In the pH range 1.95−3.35, an isosbestic point is observed at 575 nm

indicating the presence of only two absorbing species (Figure 5, A). The spectrophotometric data were fitted and the calculations afforded a pK_1 value of 2.8±0.05. Another equilibrium occurs at higher pH values. At pH ≈ 5, the colour of the solution turns from blue to brown and a new isosbestic point is detected at 525 nm in pH range 4.5−6.1 (Figure 5, B).

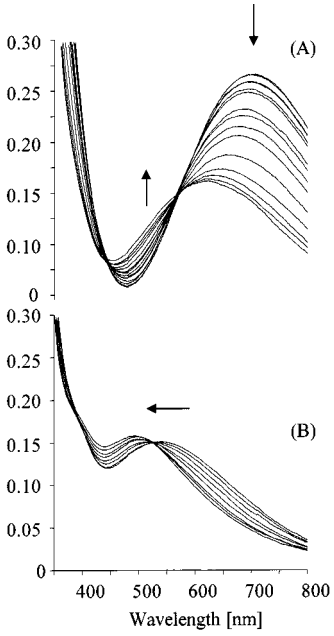

Figure 5. UV/Vis titration curves in acetonitrile/water of **1** as a function of the pH value: (A) in the range of 1.95 < pH < 3.35 and (B) in the range of 4.5 < pH < 6.1; arrows indicate the spectral trends upon increasing the pH value

The fitting of the values of absorbance vs. pH leads to a pK_2 = 4.9±0.26. The species distribution curves are shown in Figure 6, providing evidence for three pH-dependent species. It must be emphasized that the pH-driven conversion between these species is reversible. Same results were obtained by decreasing or increasing the pH value of the solution.

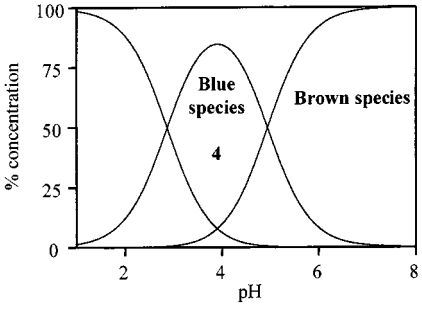

Figure 6. Species distribution curves of **1** as a function of the pH value

Attempts to isolate the pure products involved in this titration have not yet proved successful. Nevertheless by independent preparations, a blue product (**4**) was obtained by addition of equimolecular amounts of $Zn(ClO_4)_2 \cdot 6H_2O$ and $Fe(ClO_4)_3 \cdot H_2O$, dissolved in water, to a solution of HBPMOP in acetone and precipitation as a powder after addition of diethyl ether. The positive ion FAB mass spectrum of **4** exhibits a parent peak corresponding to the respective heterodinuclear core (no peak corresponding to the homodinuclear Zn−Zn or Fe−Fe species was observed). The molecular ion peak is m/z = 681 and corresponds to $[ZnFeBPMOP(OH)]^+$. The electronic spectrum of **4** in acetonitrile shows one absorption maximum at λ_{max} = 661 nm (ε = 2200); this band is shifted to 585 nm (ε = 900) in a solution of acetonitrile/water (1:9). In addition, the UV/Vis spectra of the titration described above, in the intermediate pH range 3−5 (Figure 6), exhibit the same features as the spectrum of the isolated complex **4** for which we propose a μ-OH-bridged heterodinuclear compound. At higher pH values (> 6), the brown species is formed following progressive and reversible deprotonation of **4**. This species will prove to be the active species towards the cleavage of phosphate diesters (vide infra). One possibility is that this complex has at least one pendant hydroxo ligand. Another possibility is that the bridging μ-OH (**4**) was deprotonated to form a μ-oxo ligand between the two metallic ions.[4]

Cleavage of Phosphate Diesters

Model studies have shown that simple dinuclear metal complexes can provide rate accelerations for hydrolyzing phosphate esters, shedding light on how metal ions may promote these reactions.[20−28] A heterodinuclear $Zn^{II}Fe^{III}$ complex has been reported by Komiyama et al. which hydrolyses RNA.[8]

In order to test the activity of complexes towards phosphate ester hydrolysis or cleavage, activated phosphoric acid esters are used. In this work 2-hydroxypropyl *p*-nitrophenyl phosphate (HPNP) was applied. In the absence of the metallocatalysts, HPNP is very stable.[24] The pH dependence of the HPNP cleavage acceleration, in the presence of $Zn^{II}Fe^{III}$ or $Fe^{II}Fe^{III}$ [29] complexes from the ligands BPMOP and BPMP respectively, has been studied. The rate increases corresponding to the pH and optimum values were obtained at pH = 8.5±0.2. The rate constant (k_{uncat}) for background hydrolysis was similarly obtained. Some observed rate constants are listed in Table 2. The rate acceleration was also measured in dependence of the substrate and complexes concentration, showing first order dependence in each case.

Table 2. Observed pseudo-first-order rate constants for transesterification of HPNP hydrolysis in CH_3CN/aqueous buffer CHES (1:1) at pH = 8.5 (± 0.2) and 25 °C with [catalyst] = 0.5 mM and [HPNP] = 0.82 mM

Catalyst	k_{obs} [$10^{-5}s^{-1}$]	k_{obs}/k_{uncat}
$[ZnFe(BPMOP)]^{4+}$	2.39	112
$[ZnFe(BPMP)]^{4+}$	1.14	54
$[Fe_2(BPMOP)]^{4+}$	0.227[a]	11
$[Fe_2(BPMP)]^{4+}$	0.065[a]	3
spontaneous	0.0213	1

[a] 10% of DMSO has been added to avoid precipitate.

The $Zn^{II}Fe^{III}$ complex of the ligand BPMOP shows a 2-fold higher rate acceleration compared with the complex

containing the ligand BPMP. The diiron complex from HBPMOP is 4-fold more reactive than the homologous complex from BPMP. The heterodinuclear $Zn^{II}Fe^{III}$ complexes from BPMOP and BPMP are 10-fold and 18-fold, respectively, more reactive than the corresponding homodinuclear $Fe^{II}Fe^{III}$ complexes. These differences in reactivities may be ascribed to the greater ability of the zinc center compared with the iron center, to coordinate the substrate. The optimum pH value for the hydrolysis of HPNP is notably higher than that for the enzymes. This observation confirms the necessity of a deprotonation process as underlined with the enzymes.[1b] The different activities of the complexes of BPMOP and BPMP can be attributed to the stronger electron donating effect of the methoxy group compared with that of the methyl group in the *para* position to the bridging oxygen atom.

Experimental Section

All chemicals were obtained from commercial sources and used as received. Solvents were purified by standard methods before use. ***Caution:*** Although no problems were encountered during the preparation of perchlorate salts, suitable care should be taken when handling such potentially hazardous compounds.

Spectrometry: Fast-atom bombardment (FAB) mass spectra in the positive mode were recorded with a Nermag R 1010C apparatus equipped with an M scan (Wallis) atom gun (8 kV, 20 mA). − UV/Vis spectra were obtained using a UVIKON 933 spectrometer of Kontron instrument equipped with 1.0-cm matched quartz cells and operating in the range 200−900 nm; ε values are given in $M^{-1}cm^{-1}$. − ^1H NMR and ^{13}C NMR spectra were recorded with a BRUKER AC 200 spectrometer at 25 °C, in $CDCl_3$ or $[D_6]$DMSO as solvent. Chemical shifts (ppm) were referenced to residual solvent peaks.

Electrochemistry: Electrochemical experiments were carried out using a PAR model 273 potentiostat equipped with a Kipp-Zonen *x-y* recorder. All experiments were run at room temperature under argon. A standard three-electrode cell was used. For the experiments performed in acetonitrile as solvent, potentials are referenced to an Ag/10 mM $AgNO_3$ reference electrode with 0.1 M tetra-*n*-butylammonium perchlorate (TBAP) as supporting electrolyte. Vitreous carbon disc electrodes for cyclic voltammetry (CV) (5 mm diameter) and rotating disc electrode (RDE) (3 mm diameter) were polished with 1 μm diamond paste.

X-ray Data Collection and Crystal Structure Determinations: The main details dealing with the diffraction data collections and the strategy used for the structure determinations are gathered in Table 3. The diffraction data were processed through the texSan software[30] for complex **1** and through the Collect Software Nonius BV for complex **2**.[31] Crystallographic data (excluding structure factors) for the two structures reported in this paper have been deposited with the Cambridge Crystallographic Data Centre as supplementary publication nos. CCDC-140082 (**1**) and -140083 (**2**). Copies of the data can be obtained free of charge on application to CCDC, 12 Union Road, Cambridge CB2 1EZ, UK [Fax: (internat.) + 44-1223/336-033; E-mail: deposit@ccdc.cam.ac.uk].

Table 3. Crystallographic data for **1** and **2**

Complexes	**1**	**2**
Formula	$C_{57}H_{53}Fe_1N_6O_{10}P_2Zn_1{\cdot}2ClO_4{\cdot}H_2O$	$C_{57}H_{53}Fe_2N_6O_{10}P_2{\cdot}2ClO_4{\cdot}H_2O$
Molecular mass	1382.18	1372.65
Cell dimensions: *a*, *b*, *c* [Å];	10.237(5), 13.381(7), 23.899(10);	10.269(5), 13.396(5), 23.991(9);
α β γ [°]	106.01(2), 94.08(2), 98.47(2)	105.74(1), 94.26(1), 98.31(1)
Volume [Å^3]	3091(3)	3121(1)
Z	2	2
$d_{calcd.}$	1.483	1.458
System, space group	triclinic/$P\bar{1}$	triclinic/$P\bar{1}$
Diffractometer	Nonius-CAD4	Nonius Kappa CCD
Wavelength [Å]	Mo-K_α = 0.7107	Ag-K_α = 0.5608
Monochromator	graphite plate	graphite plate
Crystal size [mm]	0.27 × 0.31 × 0.32	0.30 × 0.35 × 0.35
Temperature	293 K	293 K
Scan mode	omega	−
Theta range [°]	2−27	2−30
Reflections measured	12107	21780
No of independent rfls.	7625	7713
$I/\sigma(I)$	2.2	3
μ [cm^{-1}]	8.31	3.57
Absorption correction	none	none
Solution	direct methods (SIR92)[32]	direct methods (SIR92)[32]
LS refinements	on *F*/full matrix	on *F*/full matrix
H-atoms location	geometry and Fourier methods	geometry and Fourier methods
Thermal parameters	anisotropic for non-H atoms isotropic for H atoms	anisotropic for non-H atoms isotropic for H atoms
Number of parameters/number of reflections	9.2	9.5
Final R[a] and $R(w)$[b]	0.055/0.062	0.053/0.055
Program used	texSan software[30]	texSan software[30]

[a] $R = \Sigma||F_o| - |F_c||/\Sigma|F_o|$. − [b] $R(w) = [\Sigma(|F_o| - |F_c|)^2/wF_o^2]^{1/2}]$ with $w = 1/[\sigma^2(F_o) + 3.4{\cdot}10^{-4}|F_o|^2]$.

Syntheses

HBPMOP: 2,6-Bis[{bis(2-pyridylmethyl)amino}methyl]-4-methoxyphenol has been synthesized in three steps from *p*-methoxyphenol.

2,6-Bis(hydroxymethyl)-4-methoxyphenol (5): To 4-methoxyphenol (10 g, 80.6 mmol) in 25 mL of methanol was added drop by drop a solution of sodium hydroxide (60 mL, 25%) under nitrogen at 0 °C. After 30 min of stirring, 120 mL of formaldehyde (37% in methanol) was added dropwise. The resulting mixture was refluxed during 12 h. Then the reaction mixture was neutralised at 0 °C to pH = 5 with 15 mL of pure acetic acid in 30 mL of water. Evaporation of the solvent yielded a solid. After addition of 200 mL of water, the product was extracted with ethyl acetate (3 × 200 mL). The combined organic layers were dried with sodium sulfate and concentrated to yield the crude product which was purified by flash chromatography (silica gel, ethyl acetate/cyclohexane, 1:1) and afforded **5** as a white powder (11.2 g, 75% yield); m.p. 114 °C. − ^{1}H NMR (200 MHz, [D$_6$]DMSO): δ = 3.66 (s, 3 H, OC*H*$_3$), 4.51 (s, 4 H, C*H*$_2$), 5.19 (s, 2 H, O*H*), 6.73 (s, 2 H, C*H*). − ^{13}C NMR (50 MHz, [D$_6$]DMSO): δ = 55.8, 59.9, 111.6, 130.4, 145.6, 153.0. − $C_9H_{12}O_4$ (184.19): calcd. C 58.69, H 6.57; found C 58.75, H 6.60. − MS (DCI, NH$_3$, isobutane): *m*/*z* = 202 [M$^+$ + NH$_4^+$], 184 [M$^+$].

2,6-Bis(chloromethyl)-4-methoxyphenol (6): 2,6-Bis(hydroxymethyl)-4-methoxyphenol (2.43 g, 13.2 mmol), suspended in 20 mL of dry dichloromethane under nitrogen atmosphere, was cooled with an ice bath. A solution of freshly distilled thionyl chloride (16 g, 132 mmol) in dry dichloromethane (20 mL) was added dropwise. The reaction was complete after 30 min. The excess thionyl chloride was removed in a rotary evaporator. The remaining solid was washed several times with dry pentane and 2.85 g (12.9 mmol, 98%) of **6** as a white powder was obtained. The product was used without any purification. − ^{1}H NMR (200 MHz, CDCl$_3$): δ = 3.77 (s, 3 H, OC*H*$_3$), 4.66 (s, 4 H, C*H*$_2$), 6.84 (s, 2 H, C*H*). − ^{13}C NMR (50 MHz, CDCl$_3$): δ = 42.4, 55.8, 116.1, 126.0, 146.7, 152.9.

2,6-Bis[bis(2-pyridylmethyl)aminomethyl]-4-methoxyphenol (3): 2,6-Bis(chloromethyl)-4-methoxyphenol (5.0 g, 22.6 mmol) and dry tetrahydrofuran (50 mL) were placed in a two-necked round-bottomed flask under nitrogen and the mixture was cooled with an ice bath. A solution containing dipicolylamine (9.0 g, 45.2 mmol), distilled triethylamine (15 mL, 90.4 mmol) and dry tetrahydrofuran (20 mL) was added dropwise. The reaction was controlled by thin-layer chromatography (ethyl acetate/dichloromethane, 1:1). After 2.5 d of stirring at room temperature, the reaction mixture was filtered, washed with tetrahydrofuran and the filtrate was concentrated to dryness. The resulting oil was dissolved in dichloromethane (150 mL) and water was added (100 mL). The organic phase was separated and the aqueous phase was extracted three times with dichloromethane (100 mL). The organic phases were combined and dried with sodium sulfate. Evaporation of the solvent yielded a yellow oil, which was further purified by flash chromatography (silica gel, acetone). Removal of the solvent afforded 8.9 g (16.3 mmol, 72%) of **3** as a pale yellow powder, m.p. 76 °C. − ^{1}H NMR (300 MHz, CDCl$_3$): δ = 3.75 (s, 3 H, OC*H*$_3$), 3.80 (s, 4 H, C*H*$_2$), 3.88 (s, 8 H, C*H*$_2$), 6.85 (s, 2 H, C*H*), 7.08−7.14 (m, 4 H, Py-*H*), 7.47−7.51 (m, 4 H, Py-*H*), 7.55−7.64 (m, 4 H, Py-*H*), 8.52 (d, *J* = 4.8 Hz, 4 H, Py-*H*), 10.9 (s, 1 H, O*H*). − ^{13}C NMR (75 MHz, CDCl$_3$): δ = 54.6, 55.5, 59.6, 114.1, 121.8, 122.7, 124.7, 136.4, 148.7, 149.5, 151.8, 159.0. − $C_{33}H_{34}N_6O_2$ (546.68): calcd. C 72.50, H 6.27, N 15.37; found C 72.55, H 6.25, N 15.41. − MS (DCI, NH$_3$, isobutane): *m*/*z* = 547 [M$^+$ + H$^+$].

[Zn^{II}Fe^{III}BPMOP{O$_2$P(OPh)$_2$}$_2$](ClO$_4$)$_2$·H$_2$O (1): To a solution of HBPMOP (23.5 mg, 0.043 mmol) in methanol (2 mL), a solution of Zn(ClO$_4$)$_2$·6H$_2$O (16.0 mg, 0.043 mmol) in methanol (1 mL) was added dropwise. Upon the subsequent addition of Fe(ClO$_4$)$_3$·H$_2$O (15.2 mg, 0.043 mmol), dissolved in methanol (1 mL), the solution turned blue-green. Diphenyl phosphate (21.6 mg, 0.086 mmol), dissolved in methanol (1 mL), was added and the solvent was allowed to evaporate slowly at room temperature. Blue-green crystals (13 mg, 0.010 mmol, 23%) suitable for X-ray crystallography were obtained after 2 d. − UV/Vis (acetonitrile): λ$_{max}$ = 654 (ε ≈ 900) nm. − FAB-MS (Matrix NBA): *m*/*z* = 1264 [{Zn^{II}Fe^{III}BPMOP[O$_2$P(OPh)$_2$]$_2$}ClO$_4$]$^+$. − $C_{57}H_{53}FeN_6O_{10}P_2Zn$·2ClO$_4$·H$_2$O (1382.18): calcd. C 48.53, H 4.01, N 6.08; found C 48.59, H 3.98, N 5.85.

[Fe^{II}Fe^{III}BPMOP{O$_2$P(OPh)$_2$}$_2$](ClO$_4$)$_2$·H$_2$O (2): Complex **2** was prepared in a similar manner to complex **1**. To a solution of HBPMOP (23.5 mg, 0.043 mmol) in methanol (2 mL) a solution of Fe(ClO$_4$)$_3$·H$_2$O (32 mg, 0.086 mmol) in methanol (2 mL) was added dropwise. Upon the addition, the solution turned dark green. Diphenyl phosphate (21.6 mg, 0.086 mmol), dissolved in methanol (1 mL), was added and the solvent was allowed to evaporate slowly at room temperature. Green crystals suitable for X-ray crystallography were obtained after 1 d. − UV/Vis (acetonitrile): λ$_{max}$ = 385 (ε ≈ 3000), 673 (ε ≈ 900) nm. − FAB-MS (Matrix NBA): *m*/*z* = 1155 [Fe^{II}Fe^{III}BPMOP{O$_2$P(OPh)$_2$}$_2$]ClO$_4$]$^+$. − $C_{57}H_{53}Fe_2N_6O_{10}P_2$·2ClO$_4$·H$_2$O (1372.65): calcd. C 49.88, H 4.04, N 6.12; found C 49.63, H 3.92, N 6.16.

Blue Powder (4): To a solution of HBPMOP (150 mg, 0.275 mmol) in acetone (2 mL) a solution of Zn(ClO$_4$)$_2$·6H$_2$O (100.5 mg, 0.275 mmol) in water (1 mL) was added dropwise. Upon the addition of Fe(ClO$_4$)$_3$·H$_2$O (95.7 mg, 0.275 mmol), dissolved in water (1 mL), the solution turned blue-green and was stirred for 1 h. The acetone was removed in a rotary evaporator and diethyl ether (100 mL) was added in small portions. The solution was placed in a refrigerator and after a few days a blue powder (134.0 mg, 0.120 mmol, 31%) precipitated which was filtered and washed with diethyl ether. − UV/Vis (acetonitrile): λ$_{max}$ = 661 nm (ε ≈ 2200). − FAB-MS (matrix NBA): *m*/*z* = 681 [Zn^{II}Fe^{III}BPMOP(OH)]$^+$.

The Deprotonation Constants by UV/Vis Spectroscopy: UV/Vis titration (monitoring of the LMCT band) of a solution of the ligand HBPMOP ($2.5 \cdot 10^{-4}$ M^{-1}) and equimolar amounts of zinc(II) perchlorate and iron(III) perchlorate in acetonitrile/water (1:9) with an aqueous solution of sodium hydroxide leads to a formation of new species. The ionic strength was fixed at 0.1 M with sodium perchlorate. The reaction is reversible by addition of an aqueous solution of perchloric acid. The spectrophotometric data were fitted with the LETAGROP-SPEFO program.[33] The program uses a non linear least-squares method and calculates the thermodynamic constants of the absorbing species and their corresponding electronic spectra. The calculations were done from absorbance data of seven wavelengths (between 400 and 800 nm) for 15 solutions in the pH range of 1.95 < pH < 3.35 and for eight solutions in the pH range of 4.5 < pH < 6.1.

HPNP (2-Hydroxypropyl *p*-Nitrophenyl Phosphate) was prepared according to a known procedure.[34]

Kinetic Investigations of the HPNP Cleavage by UV/Vis Spectroscopy: The kinetic investigations were made at 25 °C in buffered solutions of acetonitrile/water (1:1). HEPES {2-[4-(2-hydroxyethyl)-piperazin-1-yl]ethanesulfonic acid} and CHES [2-(cyclohexylamino)ethanesulfonic acid] were used as buffers. The ionic strength was fixed at 0.1 M with sodium perchlorate. The complexes were

synthesized in situ by adding an aqueous solution of $Zn(ClO_4)_2 \cdot 6H_2O$ and $Fe(ClO_4)_3 \cdot H_2O$ to a solution of the ligand in acetonitrile. The spontaneous hydrolysis under these conditions was measured in a buffered acetonitrile/water (1:1) solution containing the substrate and 0.1 M sodium perchlorate. The pH value varied less than 0.1 unit during the experiments. In a typical experiment, an aqueous solution (40 μL, 0.82 mM) of HPNP was injected into a cuvette which contained an aqueous solution of the buffer (400 μL, 0.01 M), an aqueous solution of perchlorate (200 μL, 0.1 M), a solution of the complex in acetonitrile/water (10:2) (120 μL, 8.25 mmol), acetonitrile (990 μL), and water (340 μL). In order to determine the activity towards phosphate ester cleavage, the increase of the concentration of *p*-nitrophenolate (PNPat), was followed by UV/Vis spectroscopy at 400 nm, (ε = 18500 $M^{-1}cm^{-1}$). All kinetic experiments were run twice and the obtained values were merged. In respect to a pH-dependent equilibrium between *p*-nitrophenol (PNP) and *p*-nitrophenolate (PNPat), the increase of the concentration of the reaction product can be calculated (pH = pK_S + log[PNPat]/[PNP]). The k_{obs} values were obtained by Equation (2).

$$k_{obs} \cdot dt = d([PNP]_{total})/[HPNP]_0 \quad (2)$$

Acknowledgments

The authors are grateful to Dr. A. Deronzier for laboratory facilities, to Dr. F. Thomas for help with the p*K* determinations and to Prof. G. Serratrice for fruitful discussions. S. A. and B. K. thank the Deutsche Forschungsgemeinschaft and the Fonds der Chemischen Industrie for support.

[1] [1a] N. Sträter, W. N. Lipscomb, T. Klabunde, B. Krebs, *Angew. Chem. Int. Ed. Engl.* **1996**, *35*, 2024−2055. − [1b] M. B. Twitchett, A. G. Sykes, *Eur. J. Inorg. Chem.* **1999**, 2105−2115.
[2] N. Sträter, T. Klabunde, P. Tucker, H. Witzel, B. Krebs, *Science* **1995**, *268*, 1489−1492.
[3] T. Klabunde, N. Sträter, R. Fröhlich, H. Witzel, B. Krebs, *J. Mol. Biol.* **1996**, *259*, 737−748.
[4] N. H. Williams, A. M. Lebuis, J. Chin, *J. Am. Chem. Soc.* **1999**, *121*, 3341−3348.
[5] [5a] K. Schepers, B. Bremer, B. Krebs, G. Henkel, E. Althaus, B. Mosel, W. Müller-Warmuth, *Angew. Chem. Int. Ed. Engl.* **1990**, *29*, 531−533. − [5b] M. Suzuki, A. Uehara, H. Oshio, K. Endo, M. Yanaga, S. Kida, K. Saito, *Bull. Chem. Soc. Jpn.* **1987**, *60*, 3547−3555.
[6] A. S. Borovik, V. Papaefthymiou, L. F. Taylor, O. P. Anderson, L. Que Jr., *J. Am. Chem. Soc.* **1989**, *111*, 6183−6195.
[7] S. K. Dutta, R. Werner, U. Flörke, S. Mohanta, K. K. Nanda, W. Haase, K. Nag, *Inorg. Chem.* **1996**, *35*, 2292−2300.
[8] J. Kamitani, R. Kawahara, M. Yashiro, M. Komiyama, *Chem. Lett.* **1998**, 1047−1048.
[9] M. Ghiladi, C. J. McKenzie, A. Meier, A. K. Powell, J. Ulstrup, S. Wocadlo, *J. Chem. Soc., Dalton Trans.* **1997**, 4011−4018.
[10] M. Suzuki, S. Fujinami, T. Hibino, H. Hori, Y. Maeda, A. Uehara, M. Suzuki, *Inorg. Chim. Acta* **1998**, *283*, 124−135.
[11] B. Krebs, K. Schepers, B. Bremer, G. Henkel, E. Althaus, W. Müller-Warmuth, K. Griesar, W. Haase, *Inorg. Chem.* **1994**, *33*, 1907−1914.
[12] E. Bernard, W. Moneta, J. Laugier, S. Chardon-Noblat, A. Deronzier, J. P. Tuchagues, J. M. Latour, *Angew. Chem. Int. Ed. Engl.* **1994**, *33*, 887−889.
[13] E. Lambert, B. Chabut, S. Chardon-Noblat, A. Deronzier, G. Chottard, A. Bousseksou, J. P. Tuchagues, J. Laugier, M. Bardet, J. M. Latour, *J. Am. Chem. Soc.* **1997**, *119*, 9424−9437.
[14] B. Bremer, K. Schepers, P. Fleischhauer, W. Haase, G. Henkel, B. Krebs, *J. Chem. Soc., Chem. Commun.* **1991**, 510−512.
[15] B. Eulering, F. Ahlers, F. Zippel, M. Schmidt, H. F. Nolting, B. Krebs, *J. Chem. Soc., Chem. Commun.* **1995**, 1305−1307.
[16] L. Yin, P. Cheng, X. Yao, H. Wang, *J. Chem. Soc., Dalton Trans.* **1997**, 2109−2112.
[17] C. Duboc-Toia, S. Ménage, J. M. Vincent, M. T. Averbuch-Pouchot, M. Fontecave, *Inorg. Chem.* **1997**, *36*, 6148−6149.
[18] R. Than, A. A. Feldmann, B. Krebs, *Coor. Chem. Rev.* **1999**, *182*, 211−241.
[19] [19a] M. A. S. Aquino, A. G. Sykes, *J. Chem. Soc., Dalton Trans.* **1994**, 683−687.[19b] D. L. Wang, R. C. Holz, S. S. David, L. Que Jr., M. T. Stankovich, *Biochemistry* **1991**, *30*, 8187−8194.
[20] M. W. Göbel, *Angew. Chem. Int. Ed. Engl.* **1994**, *33*, 1141−1144.
[21] W. H. Chapman Jr., R. Breslow, *J. Am. Chem. Soc.* **1995**, *117*, 5462−5469.
[22] M. Wall, R. C. Hynes, J. Chin, *Angew. Chem. Int. Ed. Engl.* **1993**, *32*, 1633−1635.
[23] N. H. Williams, W. Cheung, J. Chin, *J. Am. Chem. Soc.* **1998**, *120*, 8079−8087.
[24] P. Molenveld, S. Kapsabelis, J. F. J. Engbersen, D. N. Reinhoudt, *J. Am. Chem. Soc.* **1997**, *119*, 2948−2949.
[25] P. Molenveld, J. F. J. Engbersen, H. Kooijman, A. L. Spek, D. N. Reinhoudt, *J. Am. Chem. Soc.* **1998**, *120*, 6726−6737.
[26] M. Yashiro, A. Ishikubo, M. Komiyama, *J. Chem. Soc., Chem. Commun.* **1995**, 1793−1794.
[27] M. Yashiro, A. Ishikubo, M. Komiyama, *Chem. Commun.* **1997**, 83−84.
[28] T. Koike, M. Inoue, E. Kimura, M. Shiro, *J. Am. Chem. Soc.* **1996**, *118*, 3091−3099.
[29] Electrochemical investigations by RDE voltammetry experiments performed under similar conditions than HPNP cleavage catalysis tests [preparation in situ of the complexes in a mixture acetonitrile/water buffered at pH = 8.5 with CHES (0.1 M)] show that the mixed-valence state for the $Fe^{II}Fe^{III}$ complexes is unambiguously conserved in these conditions.
[30] Molecular Structure Corporation, *texSan, Single Crystal Structure Analysis Software, Version 1.7*, MSC, 3200 Research Forest Drive, The Woodlands, TX 77381, USA, **1995**.
[31] Nonius BV, *Collect software*, Nonius BV, Delft, The Netherlands, **1998**.
[32] A. Altomare, G. Cascarano, C. Giacovazzo, A. Guagliardi, *J. Appl. Crystallogr.* **1993**, *26*, 343−350.
[33] M. Meloun, J. Havel, E. Hogfeldt, *Computation of Solution Equilibria*, Hellis Horwood, Chichester, **1988**.
[34] D. M. Brown, D. A. Usher, *J. Chem. Soc.* **1965**, 6558−6564.

Received October 30, 2000
[I00412]

The First Low-Spin Nickel Complex with Two Coordinated Water Molecules, [Ni(*o*-MeO-dppp)$(H_2O)_2$]$(PF_6)_2$ − Synthesis and Structural Characterization

Ingrid M. Angulo,[a] Elisabeth Bouwman,*[a] Sandra M. Lok,[a] Martin Lutz,[b] Wilhelmus P. Mul,[c] and Anthony L. Spek[b]

Keywords: Homogeneous catalysis / Nickel / Phosphanes / NMR spectroscopy / Structure elucidation

A series of nickel complexes of the didentate ligand 1,3-bis[di(*o*-methoxyphenyl)phosphanyl]propane (*o*-MeO-dppp) has been synthesized and characterized. The first low-spin nickel complex containing two coordinated water molecules, [Ni(*o*-MeO-dppp)$(H_2O)_2$]$(PF_6)_2$ (**1**), and compounds of the general formula [Ni(*o*-MeO-dppp)X_2] [X = Cl, Br, I, or trifluoroacetate (TFA)] are reported. Complex **1** has been characterized by X-ray crystallography. The nickel ion resides in a square-planar coordination environment with two phosphorus donors and two water molecules in a *cis* configuration (Ni–P distance 2.19 Å; Ni–O distance 1.97 Å). The structure of this complex and its behavior in solution are quite different from those of the complexes [Ni(*o*-MeO-dppp)X_2]. The halide complexes [Ni(*o*-MeO-dppp)Cl_2] (**2**) and [Ni(*o*-MeO-dppp)Br_2] (**3**) are seemingly mutually isostructural. In these complexes, the nickel ion also resides in a square-planar geometry, but with a significant tetrahedral distortion. The two different types of mono(*o*-MeO-dppp)nickel(II) complexes, i.e. [Ni(*o*-MeO-dppp)$(H_2O)_2$]$(PF_6)_2$ (**1**) and [Ni(*o*-MeO-dppp)X_2] [X = Cl (**2**), Br (**3**), I, or trifluoroacetate (TFA)] have been analyzed by electronic absorption and NMR spectroscopy. The differences in the crystal structures of **1** and **2** are helpful in rationalizing the fluxional behavior of these complexes, as has been studied by NMR spectroscopy.

Introduction

Recently, it was reported that selected diphosphanenickel(II) complexes are active catalysts in the homogeneous hydrogenation of 1-octene to *n*-octane.[1] In subsequent studies, it was observed that the catalytic hydrogenation activity of the nickel(II) catalyst incorporating the didentate phosphane ligand 1,3-bis[di(*o*-methoxyphenyl)-phosphanyl]propane (*o*-MeO-dppp) is much higher than that of a catalyst incorporating the ligand 1,2-bis[di-(*o*-methoxyphenyl)phosphanyl]ethane (*o*-MeO-dppe) (see Scheme 1).[2,3]

The presence of *ortho*-methoxy groups on the phenyl rings creates so-called hemi-labile ligands.[4] The enhanced enantioselectivities of hydrogenation catalysts bearing such methoxy groups have been attributed to possible metal−oxygen interactions.[5]

A systematic study was undertaken to investigate the nature of species in solution for both the *o*-MeO-dppe and *o*-MeO-dppp ligands, in order to obtain a better insight into the origin of the observed difference in catalytic activity. It appeared that the catalyst formed with the ligand *o*-MeO-dppe is involved in the auto-ionization equilibrium depicted in Scheme 2.[6]

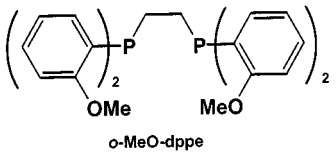

o-MeO-dppe

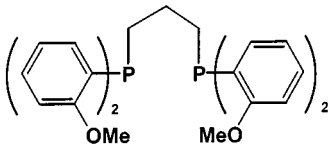

o-MeO-dppp

Scheme 1

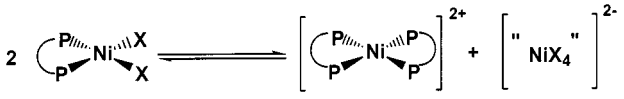

Scheme 2

No bis(chelate) complexes of the unsubstituted ligand 1,3-bis(diphenylphosphanyl)propane (dppp) have hitherto been reported. The presence of the two bulky phenyl groups on each phosphorus atom in the C_3-bridged ligand presumably prevents the formation of the $[Ni(dppp)_2]^{2+}$ complex, which makes the possible auto-ionization reaction of *o*-MeO-dppp-containing nickel complexes doubtful. However, the formation of $[Ni(dppp)_2]^{n+}$ species in electrochemical experiments has been proposed.[7,8] In fact, bis(chelate) complexes have been observed with C_3-bridged ligands bearing smaller methyl groups on the phosphorus atoms[9] or with just one aryl group per phosphorus atom.[10] In the

[a] Leiden Institute of Chemistry, Gorlaeus Laboratories, Leiden University,
P. O. Box 9502, 2300 RA Leiden, The Netherlands
Fax: (internat.) + 31-71/527-4451
E-mail: bouwman@chem.leidenuniv.nl
[b] Department of Crystal and Structural Chemistry, Bijvoet Center for Biomolecular Research, Utrecht University,
Padualaan 8, 3584 CH Utrecht, The Netherlands
[c] Shell Research and Technology Center Amsterdam, Shell International Chemicals B. V.,
P. O. Box 38000, 1030 BN Amsterdam, The Netherlands

 © WILEY-VCH Verlag GmbH, 69451 Weinheim, 2001 1434−1948/01/0606−1465 $ 17.50+.50/0

former case, the bite angle of the C_3-bridged ligand forces the nickel(II) center to adopt a tetrahedral geometry.

In this paper, the synthesis of nickel complexes with the propylene-bridged, sterically crowded ligand *o*-MeO-dppp is described, and the results of NMR investigations are reported.

Results and Discussion

Syntheses

The unique complex [Ni(*o*-MeO-dppp)$(H_2O)_2$]$(PF_6)_2$ (**1**) was obtained in analytically pure form from a mixture of nickel acetate, the ligand *o*-MeO-dppp, and ammonium hexafluorophosphate. This complex represents the first low-spin nickel complex with coordinating water molecules (see below). Complexes of the type [Ni(*o*-MeO-dppp)X_2] [X = Cl (**2**), Br (**3**), I, or trifluoroacetate (TFA)] were readily obtained by reaction of the ligand either with the corresponding nickel(II) salt (X = Cl or Br), or with nickel(II) acetate with subsequent addition of the appropriate acid (X = Cl, I, or TFA).

It would appear that in the case of *o*-MeO-dppp no bis(chelate) complex can be formed. In the presence of the weakly coordinating anion TFA, [Ni(*o*-MeO-dppp)$(TFA)_2$] was obtained, whereas from an aqueous reaction mixture complex **1** crystallized. Therefore, attempts were made to obtain a bis(*o*-MeO-dppp)nickel(II) complex from a dry, apolar solvent. Nickel(II) acetate was heated in vacuo to remove all water molecules and was subsequently mixed with *o*-MeO-dppp in dry dichloromethane. After four months, brick-red crystals had precipitated, which analyzed as [Ni(*o*-MeO-dppp)Cl_2]. The only possible source of the chloride anions in this compound was the chlorinated solvent. The formation of a nickel(II) dichloride species starting from a nickel(0) species in the presence of chloroform has been reported.[11] It appears that such reactions involve oxidative addition of chloroform to the nickel(0) center. It has also been found that in the Kharasch reaction[12] and in atom-transfer radical addition reactions (ATRA),[13] a nickel(II) chloride species can be formed by a radical pathway involving a nickel(III) species. In the present case, a radical pathway might be possible as the chloride compound is formed more rapidly in chloroform than it is in dichloromethane when starting from nickel(II) acetate and the ligand. No further attempts have been undertaken to elucidate the mechanism of the chloride abstraction.

Characterization of the Synthesized Complexes in the Solid Phase

The infrared spectra of all the synthesized nickel(II) complexes are very similar and also resemble that of the free ligand *o*-MeO-dppp. In the infrared spectrum of [Ni(*o*-MeO-dppp)$(H_2O)_2$]$(PF_6)_2$, an additional band is observed at 1616 cm^{-1}, indicating that the complex contains coordinated water molecules. Diffuse reflectance absorption spectra of the halide compounds show only one strong band at around 20,000 cm^{-1}, as seen for the [Ni(dppp)X_2] complexes[14] (X = Cl, Br, or I), which can be ascribed to the $^1A_1 \rightarrow {}^1B_2$ transition for a square-planar geometry. This band shifts to higher energy in the order I (17,800 cm^{-1}) < Br (19,600 cm^{-1}) < Cl (20,600 cm^{-1}), consistent with the established spectrochemical series.[15] The positions of the strong absorption bands found for [Ni(*o*-MeO-dppp)$(TFA)_2$] and [Ni(*o*-MeO-dppp)$(H_2O)_2$]$(PF_6)_2$ at even higher energies (22,100 and 23,400 cm^{-1}, respectively) are also in accordance with the spectrochemical series.[15] The latter two complexes have also been assigned square-planar structures.

Crystal Structure of [Ni(o-MeO-dppp)$(H_2O)_2$]$(PF_6)_2$ (1)

A molecular plot of the structure of the complex cation showing 50% probability ellipsoids is presented in Figure 1. Selected interatomic distances and angles are given in Table 1.

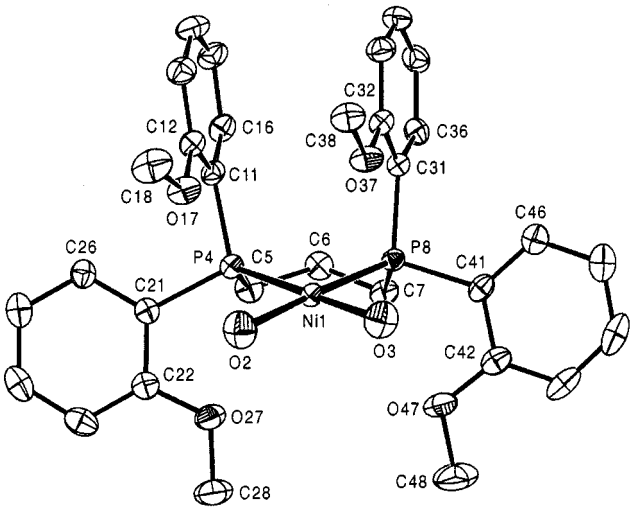

Figure 1. Displacement ellipsoid plot (50% probability) of the cationic unit in [Ni(*o*-MeO-dppp)$(H_2O)_2$]$(PF_6)_2 \cdot 0.6C_2H_5OH \cdot CHCl_3$ showing the atom-labeling scheme; hydrogen atoms are omitted for clarity

In complex **1**, the coordination geometry about the nickel(II) center is essentially square-planar with two phosphane donors and two water molecules in a *cis* configuration. The dihedral angle between the O−Ni−O and P−Ni−P planes does not deviate significantly from zero (2.06°). The water molecules are bound more tightly to the nickel center in a low-spin complex than in a high-spin complex, as indicated by the quite short Ni−O distances of 1.965(2) and 1.966(2) Å as compared to the Ni−O distance of 2.0418(8) Å in the octahedral complex [Ni$(H_2O)_6$](SiF_6).[16] The Ni−P distances are similar to that in the nickel(II) thiosalicylate complex [Ni(dppp)$(SC_6H_4CO_2)$] [2.1697(8) Å].[17] The bite angle of the bidentate phosphane ligand is 89.02(3)° in the present compound, similar to that of the unsubstituted analogue dppp in nickel complexes (87.3°).[18] The short Ni1···O37 distance [2.866(2) Å] indicates the presence of an electrostatic interaction between this

Table 1. Selected interatomic distances, angles, and torsion angles for [Ni(*o*-MeO-dppp)$(H_2O)_2$]$(PF_6)_2$·0.6C_2H_5OH·$CHCl_3$ (**1**), [Ni(*o*-MeO-dppp)Cl_2] (**2**), and [Ni(*o*-MeO-dppp)Br_2] (**3**)

[a]	**1**		**2** (X = Cl)	**3** (X = Br)
Distances [Å]				
Ni1−O2	1.965(2)	Ni1−X1	2.2163(6)	2.3462(4)
Ni1−O3	1.966(2)			
Ni1−P4	2.1875(7)	Ni1−P4	2.1729(5)	2.1751(5)
Ni1−P8	2.1867(7)			
Ni1−O17	3.240(2)	Ni1−O17	3.3827(12)	3.4783(14)
Ni1−O27	3.230(2)			
Ni1−O37	2.866(2)			
Ni1−O47	3.385(2)			
		Ni1−H26	2.8711	2.8435
Angles [°]				
O2−Ni1−O3	85.87(10)	X1−Ni1−X1′	94.50(2)	92.85(2)
O2−Ni1−P4	92.31(8)	X1−Ni1−P4	88.55(2)	89.55(1)
O3−Ni1−P8	92.83(7)			
P4−Ni1−O3	177.80(8)	P4−Ni1−X1′	167.28(2)	166.59(1)
P8−Ni1−O2	177.92(8)			
P4−Ni1−P8	89.02(3)	P4−Ni1−P4′	91.17(2)	91.17(2)
Torsion Angles [°]				
Ni1−P4−C11−C12	−55.4(2)	Ni1−P4−C11−C12	61.50(16)	66.2(2)
Ni1−P8−C31−C32	31.3(2)			
Ni1−P4−C21−C22	−55.3(2)	Ni1−P4−C21−C22	−171.00(15)	−175.30(17)
Ni1−P8−C41−C42	61.0(2)			
P4−C5−C6−C7	55.9(3)	P4−C5−C6−C5′	−35.74(15)	−35.24(18)
C5−C6−C7−P8	−62.4(3)			

[a] Primed atoms at symmetry position: 1 − *x*, *y*, 1.5 − *z*.

ortho-methoxy group and the nickel(II) center. The two axial rings (rings 1 and 3) are stacked, as indicated by the small angle between the planes of these rings of 4.99(14)° and the short interplanar distance of 3.736 Å. The coordinated water molecules in **1** are involved in several hydrogen bonds. Based on the positions of the hydrogen atoms located from the difference Fourier map, these hydrogen bonds are all intermolecular, with the PF_6^- anion and the ethanol solvent as hydrogen-bond acceptors. There are additional short intramolecular O···O contacts (see Figure 2 and Table 2), for which, however, the X-ray experiment provides no evidence for hydrogen-bonding. It must be stated that all observed O···O and O···F distances are relatively long, except for O2···O17, thus an interaction of the coordinated water molecules with the *ortho*-methoxy groups of the ligand cannot be excluded.

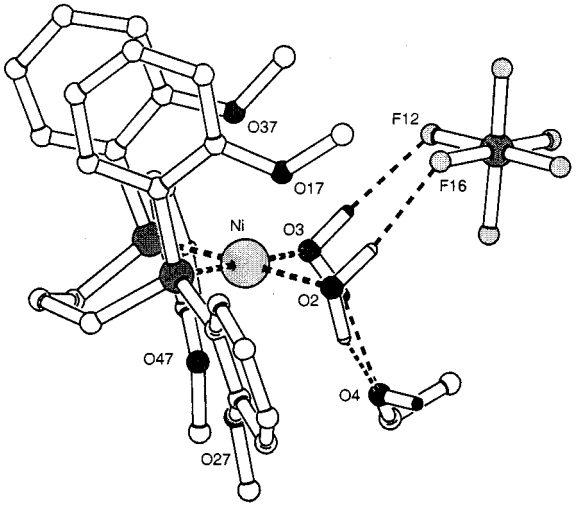

Figure 2. Crystal structure of **1** drawn such that all possible hydrogen-bond acceptors for the coordinated water molecules are visible

Table 2. Selected interatomic distances and angles concerning all possible hydrogen-bond acceptors in the crystal structure of [Ni(*o*-MeO-dppp)$(H_2O)_2$]$(PF_6)_2$·0.6C_2H_5OH·$CHCl_3$ (**1**)

Distances [Å]		Angles [°]	
O2−O4	3.103(5)	Ni1−O2−O4	91.39
O2−F16	3.142(3)	Ni1−O2−F16	105.01
O2−O17[a]	2.873(3)	Ni1−O2−O17	81.77
O2−O27[a]	3.041(3)	Ni1−O2−O27	77.08
O3−O4	3.015(5)	Ni1−O3−O4	93.99
O3−F12	3.139(3)	Ni1−O3−F12	125.49
O3−O37[a]	3.121(3)	Ni1−O3−O37	63.94
O3−O47[a]	3.149(3)	Ni1−O3−O47	79.17

[a] Intramolecular contacts.

No crystal structure of a low-spin nickel complex with coordinated water molecules has hitherto been reported. However, the synthesis of the five-coordinate nickel(II) complex [Ni(dcpe)$(NO_3)_2(H_2O)$] has been reported by Connor and Riley.[19] It remains unclear as to whether this low-spin nickel complex really contains a coordinated water molecule, as this has not been proven unambiguously. The known structures of nickel complexes incorporating coordinated water molecules are all octahedral (high-spin) and do

not contain phosphane ligands.[20] The structures of nickel complexes incorporating phosphane ligands are predominantly square-planar (low-spin) or, due to steric constraints, are sometimes tetrahedral (high-spin). It seems that in complex **1** the electronic factors of the phosphorus atoms, which will favor a low-spin square-planar geometry, predominate over those of the water molecules, which would favor a high-spin octahedral geometry. It seems likely that the ligand *o*-MeO-dppp plays an important role in the formation of the low-spin nickel complex containing coordinated water molecules. The reaction of nickel(II) acetate with the unsubstituted ligand dppp in the presence of ammonium hexafluorophosphate results in a compound that can most probably be formulated as the dimeric hydroxo complex $[\{Ni(dppp)(\mu\text{-}OH)\}_2](PF_6)_2$.[21−23] Whereas the ligand *o*-MeO-dppp is able to stabilize the dicationic nickel atom through an interaction of one methoxy group with the metal center, in the case of dppp the complex is stabilized by the formation of two monocationic metal centers bridged by two hydroxy groups.

Crystal Structures of [Ni(o-MeO-dppp)Cl_2] (2) and [Ni(o-MeO-dppp)Br_2] (3)

A molecular plot of the structure of [Ni(*o*-MeO-dppp)Cl_2] (**2**) showing 50% probability ellipsoids is presented in Figure 3. Selected interatomic distances and angles are given in Table 1.

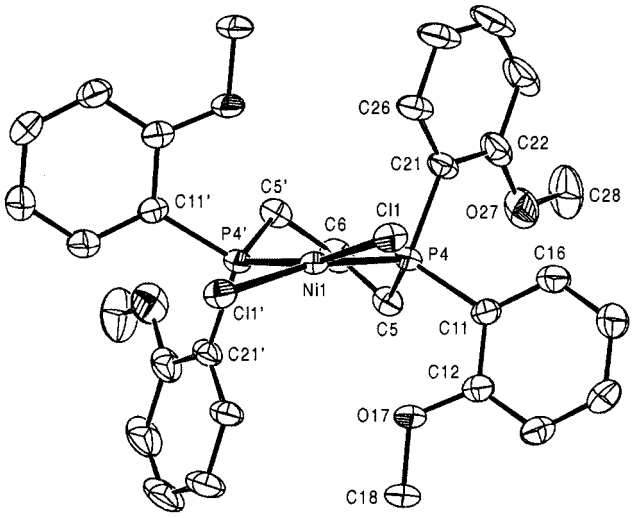

Figure 3. Displacement ellipsoid plot (50% probability) of [Ni(*o*-MeO-dppp)Cl_2] showing the atom-labeling scheme; hydrogen atoms are omitted for clarity; symmetry operation: $1 - x, y, 1.5 - z$

The complex [Ni(*o*-MeO-dppp)Br_2] is isostructural with [Ni(*o*-MeO-dppp)Cl_2], as can be seen from the crystallographic data in Table 3 and from the graphical representation in Figure 4a. Complexes **2** and **3** possess an exact, crystallographic twofold symmetry. In both complexes, the coordination geometry about the nickel(II) center is square-planar, with a significant tetrahedral distortion, as is evident from the dihedral angle between the X−Ni−X and P−Ni−P planes (16.65° for **2** and 19.45° for **3**). To date, no crystal structures of complexes of the parent ligand, [Ni(dppp)X_2] (X = Cl, Br, or I), have been reported. However, the structures of [Ni(*o*-MeO-dppp)X_2] [X = Cl (**2**) or Br (**3**)] resemble that of [Ni(*o*-MeO-dppe)I_2], which has been reported previously.[6] In Figure 4b, [Ni(*o*-MeO-dppe)I_2] and **2** are compared in a graphical representation. The Ni−P distances in **2** and **3** are similar to those in [Ni(*o*-MeO-dppe)I_2]. Due to the extra carbon atom in the bridge, the bite angles in **2** and **3** are larger than that in [Ni(*o*-MeO-dppe)I_2] [86.48(3)°]. The rather long Ni···O17 distances of 3.38 Å in **2** and 3.48 Å in **3** are indicative of an absence of any electrostatic interactions between the nickel ion and the *ortho*-methoxy groups. In Figure 3, it can be seen that the *ortho*-hydrogen atoms (H26, H26′) of the two axial aryl groups are directed towards the nickel atom. The Ni···H distances of 2.87 Å in **2** and 2.84 Å in **3** indicate the presence of either an agostic interaction or an Ni···H−C hydrogen bond, a phenomenon which has been observed previously.[6,24,25]

Comparison of the Structures of [Ni(o-MeO-dppp)-$(H_2O)_2$]$(PF_6)_2$ (1) and [Ni(o-MeO-dppp)X_2] (2 and 3)

In Figure 1 and Figure 3, it can be seen that the orientation of the diphosphane ligand in the two complexes is completely different. In **1**, the six-membered ring is in a chair conformation leading to two axial rings on one side of the coordination plane and two equatorial rings on the other. In **2** and **3**, two axial and two equatorial rings are again observed, but here the twist-boat conformation of the six-membered ring dictates alternating axial and equatorial positions of the aryl groups. The difference in conformation of the six-membered chelate ring in the two complexes may be related to the electrostatic interaction between the dicationic nickel center and the *ortho*-methoxy groups of the ligand. In **1**, all four *ortho*-methoxy groups lie in close proximity to the nickel(II) center, whereas in **2** and **3** only two *ortho*-methoxy groups point towards the nickel center (see torsion angles in Table 2). Complexes **2** and **3** are neutral, whereas **1** is a cationic complex, hence the nickel(II) center in **1** will have more electrophilic character than those in **2** and **3**. This provides a likely explanation for the presence of an electrostatic Ni···O interaction in **1**, while such an interaction is not significant in **2** and **3**. Moreover, the coordinated water molecules in **1** have the ability to form hydrogen bonds, resulting in an orientation of the ligand whereby possible hydrogen-bond acceptors lie in the proximity of these coordinated water molecules.

Characterization of the Synthesized Complexes in Solution

The essential preservation of the geometry seen in the solid-state upon dissolution is confirmed by a comparison of the electronic absorption spectra of **1** and **2** in CH_2Cl_2 solution with the diffuse reflectance electronic spectra of the solids. However, for the closely related nickel(II) species [Ni(dppp)X_2] (where X = Cl, Br, or I), both square-planar and tetrahedral species are observed in dichloromethane solution.[14] Apparently, the presence of the *ortho*-methoxy

Table 3. Crystal data and structure refinement details for [Ni(*o*-MeO-dppp)$(H_2O)_2$]$(PF_6)_2$·0.6C_2H_5OH·$CHCl_3$ (**1**), [Ni(*o*-MeO-dppp)Cl_2] (**2**), and [Ni(*o*-MeO-dppp)Br_2] (**3**)

[a]	**1**	**2**	**3**
Empirical formula	$C_{31}H_{38}NiO_6P_2$·2PF_6 $CHCl_3$·0.6C_2H_6O	$C_{31}H_{34}Cl_2NiO_4P_2$ + solvent	$C_{31}H_{34}Br_2NiO_4P_2$ + solvent
Molecular mass	1064.21	662.13[a]	751.05[a]
Crystal system	orthorhombic	monoclinic	monoclinic
Space group	$P2_12_12_1$ (No. 19)	*C*2/*c* (No. 15)	*C*2/*c* (No. 15)
Crystal size [mm]	0.56 × 0.38 × 0.25	0.30 × 0.12 × 0.06	0.39 × 0.11 × 0.06
Crystal color	red	red	red
a [Å]	12.6547(2)	19.3843(8)	19.8824(8)
b [Å]	16.8230(3)	12.6704(5)	12.2212(5)
c [Å]	21.0013(3)	16.4006(4)	16.7882(6)
β [°]	90	94.186(2)	97.312(2)
V [Å^3]	4470.97(12)	4017.4(2)	4046.1(3)
Z	4	4	4
$D_{calcd.}$ [g cm^{-3}]	1.581	1.095[a]	1.233[a]
μ [mm^{-1}]	0.85	0.72[a]	2.56[a]
refl. meas./unique	27890/10174	24644/4593	29261/4618
param./restraints	554/0	184/0	184/0
*R*1[b] (obs./all refl.)	0.0369/0.0408	0.0350/0.0465	0.0313/0.0356
*wR*2[c] (obs./all refl.)	0.0998/0.1025	0.0875/0.0905	0.0811/0.0827
GoF	1.043	1.058	1.078
Δρ (min./max.) [e Å^{-3}]	−0.37/0.71	−0.26/0.33	−0.87/0.71

[a] Derived values do not contain the contribution of the disordered solvent molecules. − [b] $R1 = \Sigma||F_o| - |F_c||/\Sigma|F_o|$. − [c] $wR2 = [\Sigma w(F_o^2 - F_c^2)^2/\Sigma w(F_o^2)^2]^{1/2}$, $w = 1/[\sigma^2(F_o^2) + (AP)^2 + BP]$, where $P = (F_o^2 + 2F_c^2)/3$, $A = 0.0582$ (**1**), 0.0457 (**2**), 0.0387 (**3**), and $B = 2.2431$ (**1**), 1.2627 (**2**), 3.9813 (**3**).

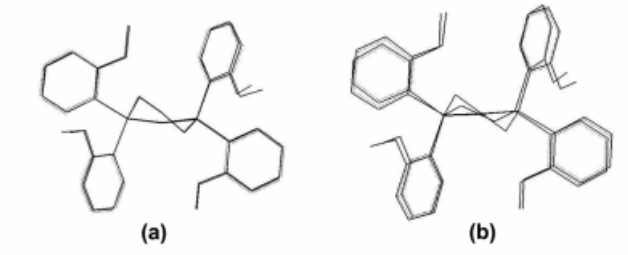

Figure 4. (a) Crystal structures of **2** and of **3** drawn such that the Ni and P atoms of the two structures are coincident; (b) crystal structures of **2** (wire) and of [Ni(*o*-MeO-dppe)I_2] drawn such that the Ni and P atoms of the two structures are coincident; in both representations, the perspective shown is that in which the depicted P atoms point away from the viewer, while the two other, not depicted coordinating atoms point towards the viewer

groups in the *o*-MeO-dppp ligand contributes to the stability of the square-planar geometry. It is difficult to ascertain whether this stabilization is due to the altered electronic or steric features of the diphosphane ligand resulting from the introduction of the *ortho*-methoxy groups. All the new nickel(II) complexes presented in this paper exhibit rather sharp ^{1}H NMR signals, which indicates that they are predominantly diamagnetic (low-spin) in solution. However, some paramagnetism is present, which is mainly manifested in the phosphorus NMR spectra. For [Ni(*o*-MeO-dppp)$(H_2O)_2$](PF_6) (**1**), one sharp resonance is observed in the $^{31}P\{^1H\}$ NMR spectrum at room temperature (δ = −9.8), whereas for [Ni(*o*-MeO-dppp)$(TFA)_2$], a rather broad signal is observed (δ = 4.7). For the complex [Ni(*o*-MeO-dppp)Cl_2] (**2**), a sharp ^{31}P NMR signal can only be observed at −60 °C (δ = 7.2). Apparently, at room temperature, the ^{31}P NMR signal for this complex is very broad, and is not discernible above the spectral noise. This broadening could perhaps be due to a geometric equilibrium (square-planar ⇄ tetrahedral), as at room temperature the ^{1}H NMR signals are also slightly broadened. These differences in line broadening for the various complexes can be related to their solid-state structures. The essentially square-planar geometry about the central nickel atom observed for **1** in the solid phase is retained in solution, whereas the tetrahedral distortion observed for **2** is reflected in the absence of a distinct resonance in the ^{31}P NMR spectrum at room temperature. The difference in the chemical shift (Δδ) of the phosphorus atom between the free and coordinated ligands in these complexes amounts to 30−40 ppm, which is comparable to that seen for other six-membered chelate systems.[26]

Fluxional Behavior of [Ni(*o*-MeO-dppp)Cl_2] and [Ni(*o*-MeO-dppp)$(H_2O)_2$]$(PF_6)_2$

The temperature-dependent ^{1}H NMR spectra of [Ni(*o*-MeO-dppp)Cl_2] (**2**) and [Ni(*o*-MeO-dppp)$(H_2O)_2$](PF_6) (**1**) in CD_2Cl_2 are shown in Figure 5 and Figure 6, respectively.

Both complexes exhibit fluxional behavior. At 25−35 °C, one set of aryl resonances and one methoxy resonance is observed for both complexes, indicating that the four functionalized aryl groups of the *o*-MeO-dppp ligand of both **1** and **2** are spectroscopically equivalent. On lowering the temperature, the ^{1}H NMR resonances of both complexes broaden and ultimately appear as double sets of resonances at −50 °C. The low-temperature spectrum of [Ni(*o*-MeO-dppp)Cl_2] (**2**) is in agreement with the crystal structure, in

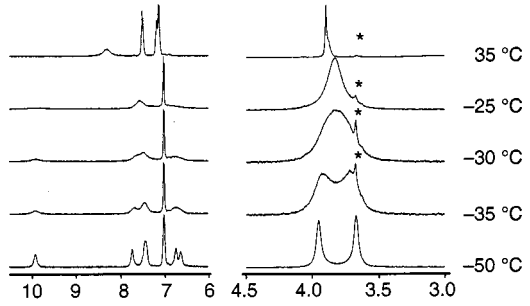

Figure 5. Two sections of the 400-MHz ^{1}H NMR spectra of [Ni(*o*-MeO-dppp)Cl$_2$] in CD_2Cl_2 as a function of temperature; section I: δ = 3−4.5, signals corresponding to the *ortho*-methoxy groups; section II: δ = 6−10.5, signals corresponding to the aryl groups; signals arising from the solvent or impurities are indicated with an asterisk

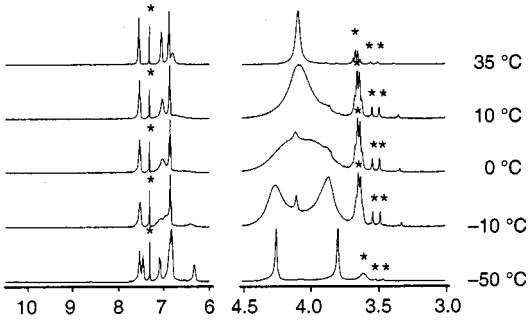

Figure 6. Two sections of the 400-MHz ^{1}H NMR spectra of [Ni(*o*-MeO-dppp)(H$_2$O)$_2$](PF$_6$)$_2$ in CD_2Cl_2 as a function of temperature; section I: δ = 3−4.5, signals corresponding to the *ortho*-methoxy groups; section II: δ = 6−10.5, signals corresponding to the aryl groups; signals arising from the solvent or impurities are indicated with an asterisk

which pairs of the four aryl groups are equivalent: Two are oriented axially with respect to the six-membered chelate ring, while the other two are oriented equatorially. The observed fluxional behavior of **2** is best described as a rapid interchange of the equatorial and axial aryl groups (Scheme 3), which is a slow process on the NMR time scale at low temperature.

Scheme 3

In the low-temperature ^{1}H NMR spectrum of **2**, one of the *ortho*-aryl proton resonances is considerably shifted downfield and is found at δ = 9.9. This anomalous chemical shift can be attributed to the interaction of the two *ortho*-protons of the two spectroscopically identical axial aryl rings with the occupied d_{z^2} orbital of the nickel atom. The downfield shift of these protons in the ^{1}H NMR spectrum, together with the observed Ni···H interaction in the crystal structure of **2**, indicate that this interaction is better described as an Ni···H−C hydrogen bond rather than as an agostic interaction.[25] From the coalescence temperatures of the interconverting *ortho*-methoxy groups, and of two sets of the aryl protons, three estimates were obtained for the $\Delta G^{\ddagger}$ value[27] of the $(aryl)_{eq} \rightleftarrows (aryl)_{ax}$ exchange process: $\Delta G^{\ddagger}_{av}$ (**2**) = 47.6 kJ·mol^{-1}.

The low-temperature ^{1}H NMR spectrum of **1**, in which the fluxional behavior of the complex is in the slow exchange regime, is quite different from that of **2**. The resonances due to the aryl hydrogen atoms are all observed in the δ = 6−8 region, and none is observed further downfield like that seen for **2**, indicating that there is no Ni···H−C$_{aryl}$ interaction in **1**. This is in agreement with the crystal structure, which shows all four aryl rings to be oriented such that the *ortho*-methoxy groups are directed towards the nickel ion. Based on the crystal structure of **1**, four discrete sets of aryl resonances would be expected at low temperature; in fact, only two sets are observed. Apparently, a dynamic process is also operative at low temperatures.

The most likely interpretation of the low-temperature spectrum of **1** is that the $(aryl)_{eq} \rightleftarrows (aryl)_{ax}$ exchange process (see Scheme 4) is slow on the NMR time scale, but that the two slightly differently oriented axial aryl groups observed in the crystal structure are still in rapid exchange by a windshield wiper type of motion, as a result of which each of the *ortho*-methoxy groups of the axial aryl rings points to the metal center for half of the time. One of the two *ortho*-methoxy resonances in the low-temperature spectrum of **1** is shifted considerably downfield (δ = 4.3) with respect to the other (δ = 3.8), as well as to those of the free ligand (δ = 3.64) and those of **2** (δ = 3.67 and 3.95). This downfield resonance is tentatively ascribed to the two rapidly interconverting (axial) *ortho*-methoxy groups interacting with the metal center. From the coalescence temperatures of the *ortho*-methoxy signals, and one of the aryl proton signals, two estimates were obtained for the $\Delta G^{\ddagger}$ value[27] of the $(aryl)_{eq} \rightleftarrows (aryl)_{ax}$ exchange process: $\Delta G^{\ddagger}_{av}$ (**1**) = 51.8 kJ·mol^{-1}.

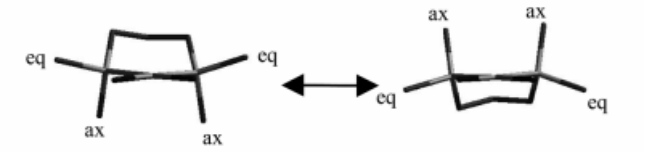

Scheme 4

Auto-Ionization

As discussed above, a complex containing the [Ni(*o*-MeO-dppp)$_2$]$^{2+}$ moiety could not be obtained. However, it has been reported[6] that nickel(II) complexes containing the ligand *o*-MeO-dppe and weakly coordinating anions (such as TFA or OAc) are completely auto-ionized in polar solvents, as observed by ^{1}H NMR spectroscopy. Therefore, the complexes [Ni(*o*-MeO-dppp)(H$_2$O)$_2$](PF$_6$)$_2$ and [Ni(*o*-MeO-dppp)(TFA)$_2$] were dissolved in CD_3OD and ana-

lyzed by ^{1}H NMR. Neither complex is very soluble in methanol, and in the ^{1}H NMR spectra only the monochelate complexes are observed. It seems likely that the *o*-MeO-dppp ligand is too bulky to allow formation of a square-planar bis(chelate) complex. However, this is not solely an effect of the *ortho*-methoxy groups; no complexes containing the $[Ni(dppp)_2]^{2+}$ moiety have hitherto been reported, although the formation of such species in electrochemical experiments has been proposed.[7,8] The presence of the two aryl groups on each phosphorus atom in the C_3-bridged ligand clearly prevents the formation of a bis(chelate)Ni^{II} complex. In fact, bis(chelate) complexes are observed with C_3-bridged ligands bearing smaller methyl groups on the phosphorus atoms[9] or with just one aryl group per phosphorus atom.[10] However, in the former case, the chelate bite angle of the C_3-bridged ligand forces the nickel(II) center to adopt a tetrahedral geometry. Only one structure of a bis(chelate)nickel(II) complex containing C_3-bridged ligands with two aryl groups per phosphorus atom has been reported, namely that of $[Ni\{H_3CC(CH_2PPh_2)_2(CH_2OH)\}_2](BF_4)_2$.[28] In this structure, the nickel(II) center adopts a tetrahedral geometry and the chelate bite angle is somewhat reduced as a result of the substituents on the central carbon atom of the bridge, so that all eight aryl rings can be fitted in the rather limited space around the rather small nickel(II) ion. For the somewhat larger palladium(II) ion, a square-planar bis(*o*-MeO-dppp)palladium(II) complex is easily formed.[29] It seems that the combination of the large bite angle of *o*-MeO-dppp and the rather small nickel(II) ion prevents the formation of the $[Ni(o\text{-MeO-dppp})_2]^{2+}$ moiety. It is for this same reason that nickel(II) complexes containing the ligand *o*-MeO-dppp, unlike their *o*-MeO-dppe counterparts, are not involved in an auto-ionization equilibrium as depicted in Scheme 2.

Conclusion

The first low-spin, square-planar nickel(II) complex with two coordinated water molecules has been synthesized and the presence of the water molecules has been unambiguously proven. The ligand *o*-MeO-dppp appears to be able to stabilize the dicationic nickel atom through interactions of its methoxy groups with the metal center.

It appears that, in contrast to *o*-MeO-dppe-based complexes, nickel(II) complexes containing the ligand *o*-MeO-dppp are not involved in the auto-ionization equilibrium, $2\,[Ni(P{-}P)X_2] \rightleftarrows [Ni(P{-}P)_2]^{2+} + [\text{“}NiX_4\text{”}]^{2-}$. This is not solely an effect of the *ortho*-methoxy groups, as no complexes containing the $[Ni(dppp)_2]^{2+}$ moiety have hitherto been reported. The inability to form a bis(chelate) complex is most likely due to a combination of the large bite angle dictated by the C_3 bridge and the rather small nickel(II) ion. The absence of the bis(chelate) complex might be one of the reasons for the considerably better hydrogenation activity of catalysts based on this ligand, compared to those based on *o*-MeO-dppe. The lower sensitivity to variations in solvents and anions[3] of the catalysts containing *o*-MeO-dppp might also be related to the absence of the auto-ionization equilibrium.

Experimental Section

General Remarks: Elemental analyses were performed with a Perkin−Elmer 2400 Series II analyzer. − Infrared spectra were recorded with a Perkin−Elmer Paragon 1000 IR spectrophotometer equipped with a Golden Gate ATR device, using the reflectance technique (4000−300 cm^{-1}). − Solid-state electronic absorption spectra were obtained with a Perkin−Elmer Lambda 900 spectrophotometer using the diffuse reflectance technique, with MgO as a reference. − Solution electronic absorption spectra were recorded from samples in 1-cm path length cells at ambient temperature, using the neat solvent as the reference. − ^{1}H and ^{31}P{^{1}H} NMR spectra were recorded with a Varian VXR-200 spectrometer at 200.06 MHz and 80.98 MHz, respectively, or with a Bruker WM-300 spectrometer at 300.13 MHz and 121.50 MHz, respectively. The variable-temperature ^{1}H NMR measurements were performed with a Varian INOVA-400 spectrometer equipped with a variable-temperature probe at 399.97 MHz. ^{31}P and ^{1}H chemical shifts are quoted in δ units relative to triphenylphosphane ($\delta_P = -6$) and residual protons in the deuterated solvent (CD_2Cl_2: $\delta_H = 5.24$), respectively.

Syntheses: All chemicals were either reagent grade and were used as received, or were synthesized as described below. Reactions were carried out under dry argon or dry nitrogen, unless stated otherwise, by using standard Schlenk techniques. Tris(*o*-methoxyphenyl)phosphane[30] and 1,3-bis[di(*o*-methoxyphenyl)phosphanyl]-propane (*o*-MeO-dppp)[31] were synthesized according to literature procedures. Generally, the complexes were obtained in yields of 40−80%; no attempts have been undertaken to optimize the yields.

$[Ni(o\text{-MeO-dppp})(H_2O)_2](PF_6)_2$ (1): A solution of $Ni(OAc)_2{\cdot}4H_2O$ (0.12 g, 0.5 mmol) in ethanol (15 mL) was mixed with a solution of *o*-MeO-dppp (0.28 g, 0.55 mmol) in chloroform (15 mL), to give a clear, dark-orange solution. A solution of NH_4PF_6 (0.16 g, 1 mmol) in ethanol (5 mL) was then added, which led to a slight lightening of the orange colour. After several days, orange crystals precipitated from the solution. These crystals proved to be suitable for X-ray diffraction analysis. − $C_{31}H_{38}F_{12}NiO_6P_4{\cdot}CHCl_3$ (1036.58): calcd. C 37.08, H 3.79; found C 37.08, H 3.72. − ^{1}H NMR (CD_2Cl_2, 35 °C): δ = 1.69 (m, 2 H, $CH_2CH_2CH_2$), 2.30 (s, H_2O), 2.51 (m, 4 H, $CH_2CH_2CH_2$), 4.09 (s, 12 H, OCH_3), 6.81 (m, 4 H), 6.91 (t, 4 H, arom. H), 7.05 (d, 4 H, arom. H), 7.55 (t, 4 H, arom. H). − ^{1}H NMR (CD_2Cl_2, −50 °C): δ = 1.67 (m, 2 H, $CH_2CH_2CH_2$), 2.58 (s, H_2O), 2.79 (m, 4 H, $CH_2CH_2CH_2$), 3.79 (s, 6 H, OCH_3), 4.25 (s, 6 H, OCH_3), 6.33 (m, 2 H, arom. H), 6.83 (m, 8 H, arom. H), 7.09 (m, 2 H, arom. H), 7.46 (t, 2 H, arom. H), 7.54 (t, 2 H, arom. H). − ^{31}P{^{1}H} NMR (CD_2Cl_2, 25 °C): δ = −9.8 (s), 104.4 (septet, PF_6). − Diffuse reflectance electronic absorption of the solid: $\tilde{\nu}_{max}$ = 30,300 and 23,400 cm^{-1}. − Electronic absorption in CH_2Cl_2 [molar extinction coefficients (L mol^{-1} cm^{-1})]: $\tilde{\nu}_{max}$ = 30,900 (11,000) and 24,300 cm^{-1} (800).

$[Ni(o\text{-MeO-dppp})Cl_2]$ (2). − Method A: $Ni(OAc)_2{\cdot}4H_2O$ (50 mg, 0.2 mmol) was mixed with an equimolar amount of *o*-MeO-dppp (107 mg, 0.2 mmol) in ethanol (20 mL). The mixture was refluxed for 3.5 h and a clear orange solution was obtained. After the solution had cooled somewhat, HCl (1 M in Et_2O, 0.5 mL, 0.5 mmol) was added. The solution immediately turned red and after several

minutes a brick-red precipitate had formed. The solid was collected by filtration and dried in air. − **Method B:** $NiCl_2·6H_2O$ (0.35 g, 1.5 mmol) was dissolved in ethanol (10 mL) and then mixed with an equimolar amount of *o*-MeO-dppp (0.81 g, 1.5 mmol) dissolved in chloroform (10 mL). After a few seconds, a brick-red solid precipitated. The solid was collected by filtration and dried in air. Yield: 0.55 g (83%). − $C_{31}H_{34}Cl_2NiO_4P_2$ (662.15): calcd. C 56.23, H 5.18; found C 55.96, H 5.50. − ^{1}H NMR (CD_2Cl_2, 35 °C): δ = 1.67 (m, 2 H, $CH_2CH_2CH_2$), 3.07 (m, 4 H, $CH_2CH_2CH_2$), 3.90 (s, 12 H, OCH_3), 7.13 (m, 8 H, arom. H), 7.50 (t, 4 H, arom. H), 8.29 (m, 4 H, arom. H). − ^{1}H NMR (CD_2Cl_2, −50 °C): δ = 1.70 (m, 2 H, $CH_2CH_2CH_2$), 2.16 (m, 4 H, $CH_2CH_2CH_2$), 3.67 (s, 6 H, OCH_3), 3.95 (s, 6 H, OCH_3), 6.62 (m, 2 H, arom. H), 6.73 (m, 2 H, arom. H), 7.00 (m, 4 H, arom. H), 7.42 (m, 4 H, arom. H), 7.72 (m, 2 H, arom. H), 9.91 (m, 2 H, arom. H). − ^{31}P{^{1}H} NMR (H_3PO_4 external standard; $CDCl_3$): 25 °C: no peak; −60 °C: δ = 7.2 (s). − Diffuse reflectance electronic absorption of the solid: $\tilde{\nu}_{max}$ = 30,200 and 20,600 cm^{-1}. − Electronic absorption in CH_2Cl_2 [molar extinction coefficients (L mol^{-1} cm^{-1})]: $\tilde{\nu}_{max}$ = 31,300 (9,000) and 20,700 cm^{-1} (900).

[Ni(*o*-MeO-dppp)Br$_2$] (3): To a suspension of $NiBr_2$ (0.33 g, 1.5 mmol) in ethanol (10 mL) was added a solution of *o*-MeO-dppp (0.53 g, 1 mmol) in chloroform (10 mL) and the mixture immediately turned purple. After several minutes, a purple precipitate had formed. The solid was collected by filtration and dried in vacuo. Yield: 0.66 g (88%). Crystals of [Ni(*o*-MeO-dppp)Br_2] suitable for single-crystal X-ray diffraction analysis were obtained from an autoclave solution containing $NiBr_2$ (0.05 mmol) and *o*-MeO-dppp (0.055 mmol), in methanol (10 mL), dichloromethane (10 mL), toluene (4 mL), and 1-octene (15.6 mL). − $C_{31}H_{34}Br_2NiO_4P_2$ (751.05): calcd. C 49.58, H 4.56; found C 48.47, H 4.00. − Diffuse reflectance electronic absorption of the solid: $\tilde{\nu}_{max}$ = 29,600 and 19,600 cm^{-1}.

[Ni(*o*-MeO-dppp)I$_2$]: $Ni(OAc)_2·4H_2O$ (0.25 g, 1 mmol) was dissolved in ethanol (10 mL) and mixed with an equimolar amount of *o*-MeO-dppp (0.53 g, 1 mmol) in chloroform (10 mL). To the clear orange solution, HI (50% in water, 0.25 mL, 1.8 mmol) was added, and a purple solution was obtained. After several minutes, a dark-purple precipitate had formed. The solid was collected by filtration and dried in air. Yield: 0.61 g (72%). − $C_{31}H_{34}I_2NiO_4P_2·(CHCl_3)_{0.5}$ (904.74): calcd. C 41.82, H 3.84; found C 41.07, H 3.79. − Diffuse reflectance electronic absorption of the solid: $\tilde{\nu}_{max}$ = 24,300 and 17,800 cm^{-1}. − Electronic absorption in CH_2Cl_2 [molar extinction coefficients (L mol^{-1} cm^{-1})]: $\tilde{\nu}_{max}$ = 28,000 (10,000) and 17,800 cm^{-1} (1,600).

[Ni(*o*-MeO-dppp)(TFA)$_2$]: $Ni(OAc)_2·4H_2O$ (0.12 g, 0.5 mmol) was dissolved in methanol (1 mL) and a solution of *o*-MeO-dppp (0.27 g, 0.5 mmol) in dichloromethane (10 mL) was added. When a clear, dark-orange solution had been obtained, trifluoroacetic acid (0.1 mL, 1.3 mmol) was added. The reaction mixture was filtered and layered with diethyl ether, which resulted in the deposition of a dark-orange crystalline precipitate. Yield: 0.18 g (43%). − $C_{35}H_{34}NiF_6O_8P_2$ (817.27): calcd. C 51.44, H 4.19; found C 51.10, H 4.14. − ^{1}H NMR (CD_2Cl_2, 25 °C): δ = 1.82 (m, 2 H, $CH_2CH_2CH_2$), 2.16 (m, 4 H, $CH_2CH_2CH_2$), 3.68 (d, 12 H, OCH_3), 6.95 (m, 8 H, arom. H), 7.49 (m, 4 H, arom. H), 8.36 (m, 2 H, arom. H). − ^{31}P{^{1}H} NMR (CD_2Cl_2, 25 °C): δ = 4.7 (br. s). − Diffuse reflectance electronic absorption of the solid: $\tilde{\nu}_{max}$ = 29,500 and 22,100 cm^{-1}.

Attempted Synthesis of [Ni(*o*-MeO-dppp)$_2$](TFA)$_2$: In an attempt to synthesize this compound, $Ni(OAc)_2·4H_2O$ (0.12 g, 0.5 mmol) was mixed with *o*-MeO-dppp (0.53 g, 1 mmol) in a mixture of dichloromethane (10 mL) and methanol (1 mL). When a clear, dark-orange solution had been obtained, trifluoroacetic acid (0.1 mL, 1.3 mmol) was added. The solvents were partially evaporated in vacuo and diethyl ether was added, which resulted in the deposition of an orange precipitate. The supernatant solution was decanted off and the solid residue was dried in air. − ^{31}P{^{1}H} NMR (CD_2Cl_2): δ = 4.8 (s), −37.2 (s). − When methanol was added to the compound, an orange solution was obtained and a white solid remained that analyzed as the free ligand. After filtration and evaporation of the solvent from the filtrate, an orange compound was obtained. This compound appeared to be the mono-chelate complex [Ni(*o*-MeO-dppp)$(TFA)_2$].

Attempted Synthesis of [Ni(*o*-MeO-dppp)$_2$](OAc)$_2$: In an attempt to synthesize a bis(*o*-MeO-dppp) complex, $Ni(OAc)_24H_2O$ (0.12 g, 0.5 mmol) was first dried in vacuo in order to remove all water molecules. It was then taken-up in dichloromethane to give a green solution. The ligand *o*-MeO-dppp (0.58 g, 1.1 mmol) was dissolved in dichloromethane (20 mL) to give a colorless solution. On mixing the two solutions, a green solution was initially obtained. However, after stirring overnight, a clear orange solution was obtained. After 4 months at 4 °C, brick-red crystals suitable for single-crystal X-ray diffraction analysis had formed. These crystals were characterized as [Ni(*o*-MeO-dppp)Cl_2].

X-ray Crystal Structure Determinations of [Ni(*o*-MeO-dppp)$(H_2O)_2$]$(PF_6)_2·(C_2H_5OH)_{0.6}·CHCl_3$ (1), [Ni(*o*-MeO-dppp)Cl_2] (2), and [Ni(*o*-MeO-dppp)Br_2] (3): Intensities were measured with a Nonius-Kappa CCD diffractometer with a rotating anode (Mo-K_α, λ = 0.71073 Å) at 150 K. The structure was solved by Patterson methods (DIRDIF-97[32]) and refined against F^2 of all reflections up to a resolution of $(\sin\theta/\lambda)_{max}$ = 0.65 $Å^{-1}$ using the program SHELXL-97.[33] Non-hydrogen atoms were refined freely with anisotropic parameters; hydrogen atoms were refined as rigid groups. In the crystal structure of **1**, the hydrogen positions of the water and ethanol molecules were located from the difference Fourier map and were kept fixed during the refinement. The drawings were created and structure calculations and checks for higher symmetry were carried out using the program PLATON.[34] Further experimental details are given in Table 3. The crystal structures of **2** and **3** show large voids (1243 $Å^3$ for **2** and 1273 $Å^3$ for **3**), which are occupied by disordered solvent molecules (dichloromethane). Their contribution to the structure factors was assessed by back-Fourier transformation (program PLATON,[34] CALC SQUEEZE, 484 e^-/unit cell for **2**, 400 e^-/unit cell for **3**). Crystallographic data (excluding structure factors) for the structures reported in this paper have been deposited with the Cambridge Crystallographic Data Centre as supplementary publication nos. CCDC-151615 (**1**), -151616 (**2**), and -151617 (**3**). Copies of the data can be obtained free of charge on application to the CCDC, 12 Union Road, Cambridge CB2 1EZ, U.K. [Fax: (internat.) + 44-1223/336-033; E-mail: deposit@ccdc.cam.ac.uk].

Acknowledgments

This research has been financially supported by the Council for Chemical Sciences of the Netherlands Organization for Scientific Research (CW-NWO). We thank Dr. J. Reedijk and Dr. E. Drent for fruitful discussions. We thank B. van Oort (Shell) for acquiring the low-temperature NMR spectra.

[1] I. M. Angulo, A. M. Kluwer, E. Bouwman, *Chem. Commun.* **1998**, 2689−2690.

[2] Abbreviations: TFA = trifluoroacetate, dppe = 1,2-bis(diphenylphosphanyl)ethane, dppp = 1,3-bis(diphenylphosphanyl)propane, *o*-MeO-dppe = 1,2-bis[di(*o*-methoxyphenyl)phosphanyl]-ethane, *o*-MeO-dppp = 1,3-bis[di(*o*-methoxyphenyl)phosphanyl]-propane.
[3] I. M. Angulo, S. M. Lok, V. F. Quiroga Norambuena, E. Bouwman, in preparation.
[4] A. Bader, E. Lindner, *Coord. Chem. Rev.* **1991**, *108*, 27−110.
[5] W. S. Knowles, *Acc. Chem. Res.* **1983**, *16*, 106−112.
[6] I. M. Angulo, E. Bouwman, M. Lutz, W. P. Mul, A. L. Spek, *Inorg. Chem.*, in press.
[7] A. Miedaner, R. C. Haltiwanger, D. L. Dubois, *Inorg. Chem.* **1991**, *30*, 417−427.
[8] G. Bontempelli, S. Daniele, G. Favero, *Inorg. Chim. Acta* **1984**, *85*, 49−55.
[9] D. E. Berning, B. C. Noll, D. L. Dubois, *J. Am. Chem. Soc.* **1999**, *121*, 11432−11447.
[10] B. W. Arbuckle, W. K. Musker, *Polyhedron* **1991**, *10*, 415−419.
[11] H. Brunner, G. Vitulli, W. Porzio, M. Zocchi, *Inorg. Chim. Acta* **1985**, *96*, 67−75.
[12] R. A. Gossage, L. A. van de Kuil, G. van Koten, *Acc. Chem. Res.* **1998**, *31*, 423−431.
[13] K. Matyjaszewski, *Chem. Eur. J.* **1999**, *5*, 3095−3102.
[14] G. R. van Hecke, W. De Horrocks, Jr., *Inorg. Chem.* **1966**, *5*, 1968−1974.
[15] A. B. P. Lever, *Inorganic Electronic Spectroscopy*, Elsevier, Amsterdam, **1983**, section 6.2.
[16] F. A. Cotton, L. M. Daniels, C. A. Murillo, J. F. Quesada, *Inorg. Chem.* **1993**, *32*, 4861−4867.
[17] L. J. McCaffrey, W. Henderson, B. K. Nicholson, J. E. Mackay, M. B. Dinger, *J. Chem. Soc., Dalton Trans.* **1997**, 2577−2586.
[18] P. C. J. Kamer, J. N. H. Reek, P. W. N. M. van Leeuwen, *Chemtech* **1998**, 27−33.
[19] J. A. Connor, P. I. Riley, *Inorg. Chim. Acta* **1975**, *15*, 197−199.
[20] See, for example: K. Venkatasubramanian, E.Suresh, *J. Coord. Chem.* **1993**, *29*, 225−232.
[21] **[{Ni(dppp)(μ-OH)}$_2$](PF$_6$)$_2$4H$_2$O·0.3CHCl$_3$:** Following the same procedure as for the synthesis of [Ni(*o*-MeO-dppp)(H$_2$O)$_2$](PF$_6$)$_2$ but using dppp, an orange solid was obtained. − $C_{54}H_{54}F_{12}Ni_2O_2P_2$4H$_2$O·0.3CHCl$_3$ (1374.09): calcd. C 47.46, H 4.57; found C 47.51, H 4.63. − Electronic absorption in CH_2Cl_2 [molar extinction coefficients (L mol^{-1} cm^{-1})]: $\tilde{\nu}_{max}$ = 32,200 (15,000) and 22,500 cm^{-1} (1,300). − These data are indicative of a square-planar complex. The IR spectrum shows a sharp band at 3608 cm^{-1} attributable to an O−H stretching vibration. Elucidation of the crystal structure is in progress. Compare refs.[22,23]
[22] C. A. Ghilardi, P. Innocenti, S. Midollini, A. Orlandini, *J. Chem. Soc., Dalton Trans.* **1988**, 1063−1066.
[23] G. Reinhard, R. Solteck, G. Huttner, A. Barth, O. Walter, L. Zsolnai, *Chem. Ber.* **1996**, *129*, 97−108.
[24] E. Bouwman, R. K. Henderson, A. K. Powell, J. Reedijk, W. J. J. Smeets, A. L. Spek, N. Veldman, S. Wocadlo, *J. Chem. Soc., Dalton Trans.* **1998**, 3495−3499.
[25] W. Yao, O. Eisenstein, R. H. Crabtree, *Inorg. Chim. Acta* **1997**, *254*, 105−111.
[26] P. E. Garrou, *Chem. Rev.* **1981**, *81*, 229−266.
[27] $\Delta G^{\ddagger}$ was calculated by using the equation: $\Delta G^{\ddagger} = 19.14T_c(9.97 + \log T_c/\Delta\nu)$ [J mol^{-1}], where T_c is the coalescence temperature [K] and $\Delta\nu$ is the shift difference [Hz] of the two exchange sites in the limiting low-temperature spectra. See: H. Günther, *NMR Spectroscopy, An Introduction*, Wiley, New York, **1973**, p. 243.
[28] A. Muth, G. Reinhard, G. Huttner, T. Seitz, T. Klein, L. Zsolnai, *Z. Naturforsch., Teil B* **1994**, *49*, 889−897.
[29] W. P. Mul, unpublished results. Starting from Pd(OAc)$_2$ the complex [Pd(*o*-MeO-dppp)$_2$]$^{2+}$ can easily be formed.
[30] L. Brandsma, H. D. Verkruijsse, *Synth. Commun.* **1990**, *20*, 2273−2274.
[31] P. H. M. Budzelaar, J. A. van Doorn, N. Meijboom, *Recl. Trav. Chim. Pays-Bas* **1991**, *110*, 420−432.
[32] P. T. Beurskens, G. Admiraal, G. Beurskens, W. P. Bosman, S. García-Granda, R. O. Gould, J. M. M. Smits, C. Smykalla, *The DIRDIF-97 program system*, Technical Report of the Crystallography Laboratory, University of Nijmegen, The Netherlands, **1997**.
[33] G. M. Sheldrick, *SHELXL-97 − A Program for Crystal Structure Refinement*, University of Göttingen, Germany, **1997**.
[34] A. L. Spek, *PLATON − A Multipurpose Crystallographic Tool*, Utrecht University, The Netherlands, **2000**.

Received November 7, 2000
[I00422]

Fluorescent Chemosensors for Heavy Metal Ions Based on Bis(terpyridyl) Ruthenium(II) Complexes Containing Aza-Oxa and Polyaza Macrocycles

Miguel E. Padilla-Tosta,[a] José Manuel Lloris,[a] Ramón Martínez-Máñez,*[a] M. Dolores Marcos,[a] Miguel A. Miranda,[a] Teresa Pardo,[a] Felix Sancenón,[a] and Juan Soto[a]

Keywords: Ruthenium / Terpyridine / Aza-oxa crowns / Fluorescence / Chemosensors

Reactions of 4′-[4-(bromomethyl)phenyl]-2,2′:6′,2′′-terpyridine with 4,10-diaza-15-crown-5 and 1-aza-12-crown-4 in dichloromethane yielded the ligands L^1 and L^3, respectively. Reaction of an excess of 4′-[4-(bromomethyl)phenyl]-2,2′:6′,2′′-terpyridine with 4,10-diaza-15-crown-5 yielded L^2, while treatment of the same terpyridine ligand with 1,4,7,10,13-pentaazacyclopentadecane afforded L^4. Reactions of L^1, L^3, and L^4 with Ru(mtpy)Cl_3 (mtpy = 4′-methyl-2,2′:6′,2′′-terpyridine) in methanol yielded the metallo receptors $[Ru(L^1)(mtpy)][PF_6]_2$, $[Ru(L^3)(mtpy)][PF_6]_2$, and $[Ru(L^4)(mtpy)][PF_6]_2$ after precipitation with ammonium hexafluorophosphate and column chromatography. On treating L^3 with $RuCl_3$, the homoleptic ruthenium complex $[Ru(L^3)_2][PF_6]_2$ was obtained. The synthesized metallo receptors contain oxa-aza crown or polyazacycloalkane moieties as recognition sites and $[Ru(tpy)_2]^{2+}$ cores as the signal-generating centre. The electronic spectra of the complexes are as expected for an $Ru(tpy)_2^{2+}$ chromophore, with the main $Ru[d(\pi)] \rightarrow tpy(\pi^*)$ MLCT transition at ca. 484 nm and intense ligand-centred transitions in the UV region. One of the most interesting aspects of these ruthenium complexes is their multicomponent nature, as they contain both coordination sites and fluorescent $Ru(tpy)_2^{2+}$ cores. The cations $[Ru(L^1)(mtpy)]^{2+}$, $[Ru(L^3)(mtpy)]^{2+}$, and $[Ru(L^3)_2]^{2+}$ display an emission maximum at ca. 650 nm, the intensity of which is pH dependent, showing an enhancement upon protonation. The metallo receptor $[Ru(L^1)(mtpy)]^{2+}$ selectively senses Hg^{2+} in preference to Cu^{2+}, Cd^{2+}, and Pb^{2+}. The emission intensity vs. pH curve for $[Ru(L^2)(mtpy)]^{2+}$ in the presence of Cu^{2+} and Hg^{2+} ions is close to that of the free receptor, but the presence of Cd^{2+} or Pb^{2+} enhances the emission intensity in the range pH 4–6. For the $[Ru(L^3)_2]^{2+}$ complex, Cd^{2+}, Pb^{2+}, and Hg^{2+} induce an enhancement of the fluorescence of the $Ru(tpy)_2^{2+}$ core in the range pH 3.5–7.5. These results are compared with those obtained for the metallo receptor $[Ru(L^4)(mtpy)]^{2+}$ containing a polyazacycloalkane moiety as the binding domain.

Introduction

Ligands with a macrocyclic unit attached to a metal-polypyridyl core are potentially useful in the preparation of luminescent or electrochemical sensors, in which the macroscopic properties of the core are modified by molecular-level interactions between the recognition centre and the substrate.[1−4] The polypyridyl complexes of d^6 metals, with their strong metal-to-ligand charge transfer absorptions and emitting excited states, are good candidates as signalling subunits.[5,6] The metal−polypyridyl complex most widely used as a fluorophore is probably $Ru(bipy)_3^{2+}$.[7,8] In contrast, the ruthenium−terpyridine $Ru(tpy)_2^{2+}$ unit has been less well studied. Although the $Ru(tpy)_2^{2+}$ core is less fluorescent than $Ru(bipy)_3^{2+}$, terpyridine complexes may have some advantages over their bipyridine counterparts. Thus, for instance, it has been reported that the octahedral tpy-type complex has the advantage of being non-chiral (preventing the generation of stereoisomers that may arise with bipy-Ru complexes) and, through functionalization of the ligand at the appropriate position, allows the construction of multicomponent systems with fine control over the geometry of the assembly.[9,10] Additionally, from a practical viewpoint, emission in the visible part of the spectrum (as shown by Ru-tpy complexes) is much more convenient than emission near the UV region, where many other organic fluorophores typically emit.

We have recently reported the functionalization of the $Ru(tpy)_2^{2+}$ unit with cyclam and the use of the resulting compound as a potential sensing receptor for Cu^{2+} ions.[11] Further, we are interested in the development of potential chemosensors for heavy transition metal ions such as Cd^{2+}, Hg^{2+}, and Pb^{2+}. Sensing receptors for toxic heavy metal ions are of interest in areas such as environmental chemistry, where the development of highly selective analytical tools is of importance. In order to direct the sensing ability of $Ru(tpy)_2^{2+}$-based chemosensors towards the selective determination of these metals, we have covalently functionalized the fluorophore core with binding sites that are known to show greater stability constants with large transition metal ions than with smaller ones.[12,13] In fact, it has been established that a combination of O and N donor atoms on such macrocyclic structures promotes the formation of complexes with large-sized transition metal cations as opposed to those with smaller radii.[15] Based on the fact that large stability constants could lead to a high selectiv-

[a] Departamento de Química,
Universidad Politécnica de Valencia,
Camino de Vera s/n, 46071 Valencia, Spain
Fax: (internat.) +34−963877349
E-mail: rmaez@qim.upv.es

 © WILEY-VCH Verlag GmbH, 69451 Weinheim, 2001 1434−1948/01/0606−1475 $ 17.50+.50/0

ity,[17] we report herein on the synthesis of three new oxa-aza functionalized $Ru(tpy)_2^{2+}$ receptors. The main goal of this work has been the quest for new potential chemosensors for toxic heavy metal cations.

Results and Discussion

Synthesis and Characterization

4′-[4-(Bromomethyl)phenyl]-2,2′:6′,2′′-terpyridine (Br-mphtpy) was synthesized according to the procedure of Spahni and Calzaferri.[18] From this derivative, terpyridine-functionalized crowns could be readily prepared by reaction with the appropriate macrocycle in dichloromethane in the presence of Et_3N at 30 °C for 24 h, followed by column chromatography on alumina using a mixture of CH_2Cl_2/MeOH as the eluent. This led to yields of ca. 30% for L^1 and L^2, of 35% for L^3, and of 50% for L^4.

Ligands L^1 and L^2 show very similar ^1H NMR spectra, the main difference being the appearance of the proton signal of the amine group at δ = 2.5 in the spectrum of L^1, which is not observed in the case of L^2. The pyridyl proton signals are seen in the range δ = 7.3−8.8. The spectra are completed by two groups of signals, one in the range δ = 2.7−3.0, corresponding to the protons of CH_2 groups attached to a nitrogen atom in the crown, and the other in the range δ = 3.6−3.9, attributable to benzylic protons and to the protons of CH_2 groups bonded to oxygen atoms. The ^1H NMR spectrum of L^3 shows signals due to the protons of CH_2 groups bonded to an N atom in the crown at δ = 2.8, and signals due to the protons of the CH_2 groups attached to an O atom as well as those of the benzylic protons in the range δ = 3.4−3.8. The ^1H NMR spectrum of L^4 is also in agreement with the proposed formulation.

Reactions of equimolar amounts of L^1, L^3, or L^4 with [Ru(mtpy)Cl_3] in methanol in the presence of *N*-ethylmorpholine as a mild reductant yielded the complexes $[Ru(L^1)(mtpy)][PF_6]_2$, $[Ru(L^3)(mtpy)][PF_6]_2$, and $[Ru(L^4)(mtpy)][PF_6]_2$, respectively, after precipitation with ammonium hexafluorophosphate and column chromatography on silica using acetonitrile/water/satd. aq. KNO_3 (17:1:2, *v*/*v*) as the eluent. The FAB mass spectra showed peaks at *m*/*z* = 1177, 1033, and 887 for $[Ru(L^1)(mtpy)][PF_6]_2$, at *m*/*z* = 1135, 990, and 845 for $[Ru(L^3)(mtpy)][PF_6]_2$, and at *m*/*z* = 1174, 1030, and 885 for $[Ru(L^4)(mtpy)][PF_6]_2$, corresponding to {$[Ru(L)(mtpy)][PF_6]_2$}, {$[Ru(L)(mtpy)][PF_6]^+$}, and {$[Ru(L)(mtpy)]^{2+}$}, respectively. The ^1H NMR spectra of the ruthenium complexes showed the expected signals due to the aromatic protons in the region δ = 7.1−9.1. They were fully assigned with the assistance of ^1H-^1H correlation spectroscopy (COSY). The spectra also featured signals due to the protons of the terminal CH_3 groups, at δ = 2.93 in each case. The signals due to the protons of the CH_2 groups

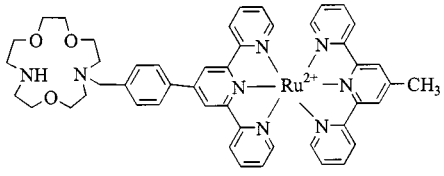

$[Ru(L^1)(mtpy)]^{2+}$

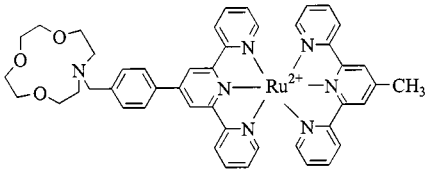

$[Ru(L^3)(mtpy)]^{2+}$

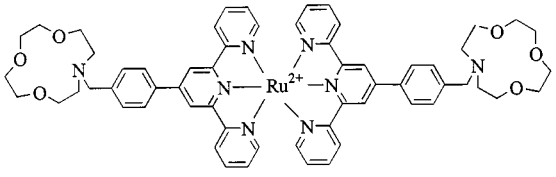

$[Ru(L^3)_2]^{2+}$

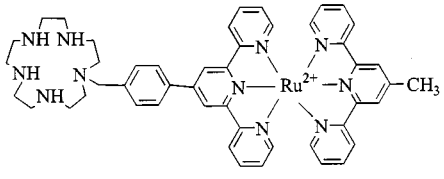

$[Ru(L^4)(mtpy)]^{2+}$

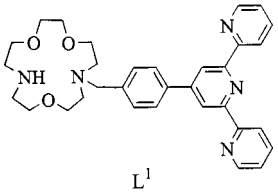

L^1

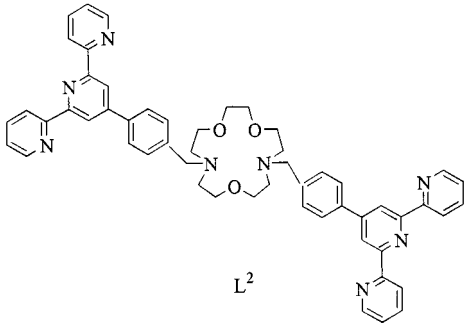

L^2

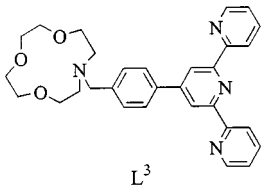

L^3

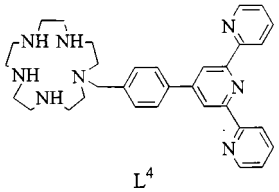

L^4

attached to a nitrogen atom appeared at ca. δ = 3.3, whereas those due to the protons of CH_2 groups bonded to oxygen atoms were seen at δ = 3.6−4.0. The ruthenium complex of L^4 shows signals due to the protons of the polyazacycloalkane ring in the region δ = 2.8−3.2.

The homoleptic complex of L^3 was obtained by treating $RuCl_3$ with two equivalents of L^3 in methanol in the presence of *N*-ethylmorpholine as a mild reductant, followed by precipitation with ammonium hexafluorophosphate and column chromatography. The FAB mass spectrum of $[Ru(L^3)_2][PF_6]_2$ showed peaks at *m*/*z* = 1240, 1094, and 920, corresponding to $\{[Ru(L^3)_2][PF_6]_2\}$, $\{[Ru(L^3)_2][PF_6]^+\}$, and $\{[Ru(L^3)_2]^{2+}\}$, respectively. The ^1H NMR spectrum of the $[Ru(L^3)_2][PF_6]_2$ complex was also in agreement with the proposed formulation.

Photophysical Characterization and pH-Dependence of the Fluorescence

The electronic spectra of the complexes were found to be as expected for an $[Ru(tpy)_2]^{2+}$ chromophore, with the main Ru[d(π)] → tpy(π*) MLCT transition at ca. 484 nm and the usual intense ligand-centred transitions in the UV region.[5,6] It is likely that the absorption band at ca. 484 nm corresponds to a mixture of dπ(Ru) → π(mtpy) and dπ(Ru) → π(L^n) transitions for the heteroleptic $[Ru(L^1)(mtpy)][PF_6]_2$, $[Ru(L^3)(mtpy)][PF_6]_2$, and $[Ru(L^4)(mtpy)][PF_6]_2$ complexes and to the transition dπ(Ru) → π(L^3) in the case of the homoleptic $[Ru(L^3)_2][PF_6]_2$ complex, which would otherwise give a narrower absorption band.[19] The photophysical properties of the complexes $[Ru(L^1)(mtpy)][PF_6]_2$, $[Ru(L^3)(mtpy)][PF_6]_2$, $[Ru(L^4)(mtpy)][PF_6]_2$, and $[Ru(L^3)_2][PF_6]_2$ in acetonitrile/water (70:30, *v*/*v*) at 298 K are summarized in Table 1.

Table 1. Photophysical properties of the complexes $[Ru(L^1)(mtpy)][PF_6]_2$, $[Ru(L^3)(mtpy)][PF_6]_2$, $[Ru(L^4)(mtpy)][PF_6]_2$, and $[Ru(L^3)_2][PF_6]_2$ in acetonitrile/water (70:30, *v*/*v*) at 298 K

	abs. (298 K)		em. (298 K)
	λ [nm]	ε [M^{-1} cm^{-1}]	λ [nm]
$[Ru[L^1](mtpy)][PF_6]_2$	480	17500	652
$[Ru(L^3)(mtpy)][PF_6]_2$	483	17700	650
$[Ru(L^4)(mtpy)][PF_6]_2$	484	17000	650
$[Ru(L^3)_2][PF_6]_2$	482	16800	652

One of the most attractive features of these complexes is their multicomponent nature as they contain sites suitable for coordinating metal ions in the vicinity of a fluorescent $Ru(tpy)_2^{2+}$ group. It is known that, compared to acyclic structures, macrocyclic receptors generally display more selective complexation. Additionally, the introduction of central oxygen donor atoms in macrocycles has been used to achieve selectivity for large metal ions as opposed to small ones.[15] The presence of aza-oxa macrocycles in the metallo receptors $[Ru(L^1)(mtpy)][PF_6]_2$, $[Ru(L^3)(mtpy)][PF_6]_2$, and $[Ru(L^3)_2][PF_6]_2$ thus makes them good candidates as fluorescent signalling systems for toxic heavy metal ions in solution.

The fluorescence behaviour of the complexes $[Ru(L^1)(mtpy)]^{2+}$, $[Ru(L^3)(mtpy)]^{2+}$, $[Ru(L^4)(mtpy)]^{2+}$, and $[Ru(L^3)_2]^{2+}$ was investigated in acetonitrile/water mixtures as a function of the pH, in the absence and presence of transition metal ions M^{2+} (M^{2+} = Cu^{2+}, Cd^{2+}, Hg^{2+}, and Pb^{2+}) {see Figure 1 (a) for $[Ru(L^1)(mtpy)]^{2+}$, Figure 1 (b) for $[Ru(L^3)(mtpy)]^{2+}$, Figure 1 (c) for $[Ru(L^3)_2]^{2+}$, and Figure 1 (d) for $[Ru(L^4)(mtpy)]^{2+}$}.

The complexes $[Ru(L^1)(mtpy)]^{2+}$, $[Ru(L^3)(mtpy)]^{2+}$, and $[Ru(L^3)_2]^{2+}$ display an emission maximum at ca. 650 nm, the intensity of which is seen to be pH-dependent. In the case of $[Ru(L^1)(mtpy)]^{2+}$, an enhancement of the luminescence of ca. 60% is observed upon protonation, which is close to the enhancement seen for the $[Ru(L^3)(mtpy)]^{2+}$ complex. Remarkably, the enhancement in the emission intensity of $[Ru(L^3)_2]^{2+}$ upon protonation is ca. twice that observed for the heteroleptic complexes. In contrast, the emission intensity of the $[Ru(L^4)(mtpy)]^{2+}$ complex is seen to be almost pH-independent, showing only a slight increase at acidic pH. This suggests that the electron- or energy-transfer path from the amine to the $Ru(tpy)_2^{2+}$ fluorophore is more effective in aza-oxa derivatives than in the polyazacycloalkane. In fact, negligible pH-dependence was also found for the ruthenium(II) complex [Ru(cyphtpy)(mtpy)]$^{2+}$ {cyphtpy = 1-[4′-(*p*-tolyl)-2,2′:6′,2′′-terpyridyl]-1,4,8,11-tetraazacyclotetradecane}, which contains a cyclic tetraamine unit anchored to the ruthenium(II) bis(terpyridine) centre.[11]

Typical quantum yields for these complexes are around $5 \cdot 10^{-5}$, comparable to those reported for similar ruthenium bis(terpyridyl) complexes.[19] Unfortunately, these low quantum yields prevent further studies on the lifetimes of the excited states. As stated above, the intensities of the emission maxima (or quantum yields) of the $[Ru(L^1)(mtpy)]^{2+}$, $[Ru(L^3)(mtpy)]^{2+}$, and $[Ru(L^3)_2]^{2+}$ complexes are pH-dependent. In order to gain a better understanding of the pH-dependent fluorescent behaviour seen for the aza-oxa-functionalized bis(terpyridyl) ruthenium(II) complexes, further studies were carried out on the $[Ru(L^1)(mtpy)]^{2+}$ complex. Two possible mechanisms may be invoked to account for the fluorescence quenching of the $Ru(tpy)_2^{2+}$ signalling unit,[19] i.e. electron transfer and energy transfer. The occurrence or otherwise of an electron-transfer mechanism can be assessed on the basis of electrochemical and photophysical data. For instance, the free energy associated with the electron-transfer process $[Ru(tpy)_2^{2+}*-amine] \rightarrow [Ru(tpy)_2^{+}-amine^{+}]$, where an electron from the lone pair of the amine is transferred to an orbital of the fluorophore leading to a quenching process, can be calculated from the equation: $\Delta G = -(hcN_A/\lambda) + F[E^0_{amine+/amine} - E^0_{fl/fl-}]$ (fl = fluorophore), where $E^0_{amine+/amine}$ and $E^0_{fl/fl-}$ are the redox potentials associated with the redox processes 'amine$^+$ + 1 e^- → amine' and 'fl + 1 e^- → fl$^-$', respectively, and λ relates to the so-called spectroscopic energy that can be obtained from the emission fluorescence spectrum. Redox potentials were measured in dry acetonitrile (containing 0.1 mol dm^{-3} tetrabutylammonium perchlorate) at 25 °C. Cyclic voltammograms

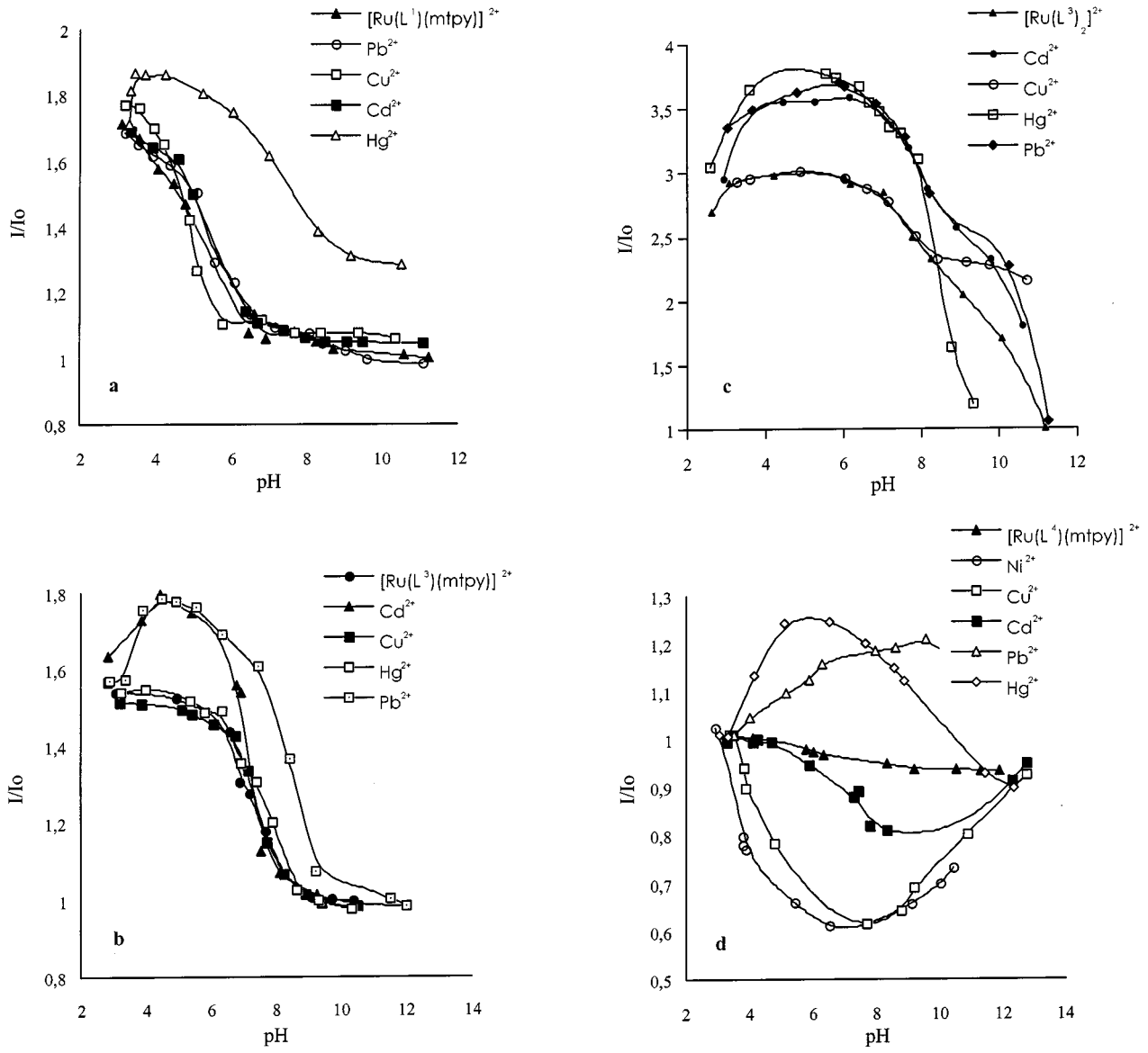

Figure 1. Relative emission intensity versus pH for the L and L−M^{2+} systems: (a) L = $[Ru(L^1)(mtpy)][PF_6]_2$, M^{2+} = Cu^{2+}, Cd^{2+}, Pb^{2+}, Hg^{2+}; (b) L = $[Ru(L^3)(mtpy)][PF_6]_2$, M^{2+} = Cu^{2+}, Cd^{2+}, Pb^{2+}, Hg^{2+}; (c) L = $[Ru(L^3)_2][PF_6]_2$, M^{2+} = Cu^{2+}, Cd^{2+}, Pb^{2+}, Hg^{2+}; (d) L = $[Ru(L^4)(mtpy)][PF_6]_2$, M^{2+} = Ni^{2+}, Cu^{2+}, Cd^{2+}, Pb^{2+}, Hg^{2+}

of the ruthenium complex $[Ru(L^1)(mtpy)]^{2+}$ show two oxidation processes, at 1.05 V and 1.23 V. The first of these is irreversible and can be ascribed to the oxidation of the 4,10-diaza-15-crown-5, whereas the second corresponds to the oxidation of the Ru^{II} centre. The complex $[Ru(L^1)(mtpy)]^{2+}$ also displays two quasi-reversible reduction processes at −1.25 and −1.52 V, attributable to the formal reduction of the $Ru(tpy)_2^{2+}$ core. Taking these data into account, the ΔG value obtained is ca. −6.5 kcal/mol. This negative value suggests that a photoinduced electron-transfer process from the amine to the $Ru(tpy)_2^{2+}$ fluorophore is possible. This is probably the mechanism that is operative under conditions of basic pH (where the amine is not protonated). When the pH is decreased, the amine groups are protonated, and the oxidation of the amine becomes more difficult, thus making ΔG positive. A positive value of the free energy reduces the probability of electron-transfer processes and therefore an increase in the emission intensity would be expected at acidic pH, as is indeed observed (Figure 1).

Sensing Response towards Transition Metal Ions

The I/I_0 vs. pH curve for the free receptor $[Ru(L^1)(mtpy)]^{2+}$ remains essentially unchanged in the presence of the transition metal ions Cu^{2+}, Cd^{2+}, and Pb^{2+} (see Figure 1). In contrast, in the presence of Hg^{2+}, a different I/I_0 vs. pH profile is seen over a wide pH range. The presence of Hg^{2+} led to an enhancement of the emission intensity by as much as 60% at pH 6.5, with some enhancement even being observed at lower pH. This intensity increase may be attributed to the formation of $[Ru(L^1)(mtpy)]^{2+}-Hg^{2+}$ species, in which the lone pair of the nitrogen atom would no longer be available for the photoinduced electron-transfer process owing to its involvement in the coordinative interaction. At this point it is interesting to note that the 4,10-

diaza-15-crown-5 cycle has also been *N*-functionalized with the organic anthrylmethyl fluorophore.[20] Whereas the metal ions Ni^{2+}, Cu^{2+}, Zn^{2+}, Cd^{2+}, and Pb^{2+} had no modifying effect on the fluorescence intensity vs. pH profile of the anthryl derivative, the presence of Hg^{2+} enhanced the emission intensity in the range pH 5−9. This result is similar to that found for the $[Ru(L^1)(mtpy)]^{2+}$ complex in the presence of metal ions, suggesting that both fluorophores, i.e. the $Ru(tpy)_2^{2+}$ and the anthryl signalling subunits, are able to selectively detect the presence of Hg^{2+} through a combination of coordination to an appropriate binding site (the 4,10-diaza-15-crown-5 cycle) and enhancement of the fluorescence.

To gain insight into the interaction of Hg^{2+} with $[Ru(L^1)(mtpy)]^{2+}$, protonation and coordination studies were carried out by means of potentiometric titrations of previously acidified solutions of the ruthenium(II) complex in acetonitrile/water (70:30, *v*/*v*, 0.1 mol dm^{-3} tetrabutylammonium perchlorate) with KOH. Protonation constants are given in Table 2, while stability constants for the formation of Hg^{2+} complexes with $[Ru(L^1)(mtpy)]^{2+}$ are given in Table 3. The $[Ru(L^1)(mtpy)]^{2+}$ complex displays two protonation process with basicity constants of $\log K = 9.47$ and $\log K = 7.67$. These values are close to those found for the analogous ferrocenylmethyl-functionalized derivative 7,13-ferrocenylmethyl-7,13-diaza-15-crown-5 ($\log K = 8.49$ and $\log K = 6.69$ in dioxane/water, 70:30, *v*/*v*).[21]

Table 2. Stepwise protonation constants in acetonitrile/water (70:30, *v*/*v*, 0.1 mol dm^{-3} tetrabutylammonium perchlorate) for $[Ru(L^1)(mtpy)]^{2+}$

Reaction	log *K*[a]
$[Ru(L^1)(mtpy)]^{2+} + H^+ \rightleftarrows [Ru(HL^1)(mtpy)]^{3+}$	9.47(1)
$[Ru(L^1)(mtpy)]^{2+} + 2\ H^+ \rightleftarrows [Ru(H_2L^1)(mtpy)]^{4+}$	17.14(2)

[a] Values in parentheses are standard deviations in the last significant digit.

Table 3. Stability constants (log *K*) for the formation of the Hg^{2+} complexes of $[Ru(L^1)(mtpy)]^{2+}$ in acetonitrile/water (70:30, *v*/*v*, 0.1 mol dm^{-3} tetrabutylammonium perchlorate) at 25 °C

Reaction	log *K*[a]
$Hg^{2+} + [Ru(HL^1)(mtpy)]^{3+} \rightleftarrows \{Hg[Ru(HL^1)(mtpy)]\}^{5+}$	14.24(3)
$Hg^{2+} + [Ru(L^1)(mtpy)]^{2+} \rightleftarrows \{Hg[Ru(L^1)(mtpy)]\}^{4+}$	6.23(3)
$Hg^{2+} + [Ru(L^1)(mtpy)]^{2+} + H_2O \rightleftarrows \{Hg(OH)[Ru(L^1)(mtpy)]\}^{3+} + H^+$	−3.57(4)
$Hg^{2+} + [Ru(L^1)(mtpy)]^{2+} + 2\ H_2O \rightleftarrows \{Hg(OH)_2[Ru(L^1)(mtpy)]\}^{2+} + 2\ H^+$	−13.27(3)

[a] Values in parentheses are standard deviations in the last significant digit.

The coordination behaviour of the receptor $[Ru(L^1)(mtpy)]^{2+}$ towards Hg^{2+} has been studied. Our aim was to explore the coordination ability of the aza-oxa cycle and the effect of the presence of a bulky, charged $Ru(tpy)_2^{2+}$ group on the coordination of metal ions. Hg^{2+} was chosen because of the selective fluorescence response seen in the presence of this cation. An exhaustive and detailed coordination study was beyond the scope of this article, mainly due to the relatively low yields achieved in the synthesis of the complex $[Ru(L^1)(mtpy)][PF_6]_2$ and of the related complexes mentioned in this paper.

From the refinement of the potentiometric data in the range pH 2−10.5 in the presence of Hg^{2+}, the species $\{Hg[Ru(HL^1)(mtpy)]\}^{5+}$, $\{Hg[Ru(L^1)(mtpy)]\}^{4+}$, $\{Hg(OH)[Ru(L^1)(mtpy)]\}^{3+}$, and $\{Hg(OH)_2[Ru(L^1)(mtpy)]\}^{3+}$ were found. The stability constant for the equilibrium $Hg^{2+} + [Ru(L^1)(mtpy)]^{2+} \rightleftarrows \{Hg[Ru(L^1)(mtpy)]\}^{4+}$ was evaluated as $\log K = 6.23$. We have recently studied the interaction of Hg^{2+} with the ferrocene-functionalized ligand 7,13-ferrocenylmethyl-7,13-diaza-15-crown-5. In this case, the logarithm of the formation stability constant of the ligand with Hg^{2+} was measured as $\log K = 8.79$ in dioxane/water (70:30, *v*/*v*).[21] Although a different solvent system has been used for the study of the interaction between Hg^{2+} and the aforementioned $Ru(tpy)_2^{2+}$- and ferrocene-functionalized receptors, it seems that the presence of the positively charged, bulky $Ru(tpy)_2^{2+}$ signalling subunit might impose some constraints on the coordination of Hg^{2+} by the aza-oxa macrocycle and makes the stability constant with $[Ru(L^1)(mtpy)]^{2+}$ lower than that with the analogous ferrocene-functionalized derivative. Figure 2 shows the distribution diagram for the $[Ru(L^1)(mtpy)]^{2+}-Hg^{2+}-H^+$ system.

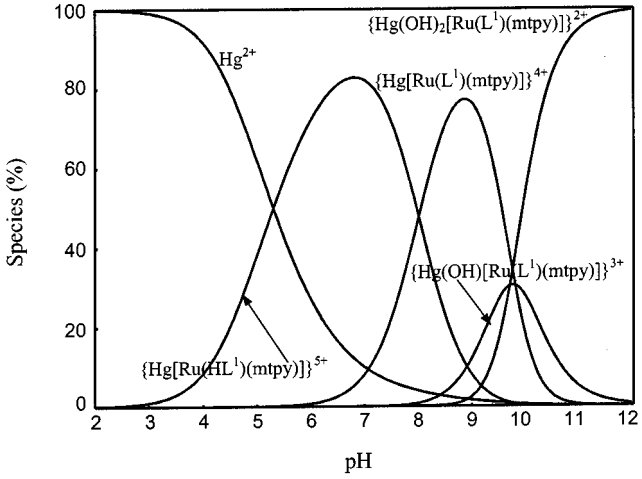

Figure 2. Distribution diagram of the species for the system $[Ru(L^1)(mtpy)]-Hg^{2+}-H^+$

Figure 1b shows the I/I_0 vs. pH curves for the $[Ru(L^3)(mtpy)]^{2+}$ complex in the presence of metal ions. The I/I_0 vs. pH profiles for this complex are similar with Cu^{2+} and Hg^{2+}, but in the presence of Cd^{2+} and Pb^{2+} an enhancement of the emission intensity of the order of 30% is observed in the range pH 4−6. The 1,4,7-trioxa-10-azacyclododecane unit has also been *N*-functionalized with anthryl groups as fluorescent signalling subunits.[20] In contrast to the fluorescent behaviour of the $[Ru(L^3)(mtpy)]^{2+}$ complex, the anthracene-containing derivative does not show any response in the presence of the metal ions Ni^{2+}, Cu^{2+}, Zn^{2+}, Cd^{2+}, Pb^{2+}, or Hg^{2+}. The signalling fluores-

cence behaviour of the ruthenium and anthrylazamacrocycle compounds in the presence of metal ions is quite different, highlighting the active role that the signalling subunit might play in the selectivity of the sensing event.

The fluorescence response of the $[Ru(L^3)_2]^{2+}$ complex has also been studied in acetonitrile/water (70:30, *v*/*v*) as a function of pH in the presence of two equivalents of Cu^{2+}, Cd^{2+}, Hg^{2+}, and Pb^{2+}. This receptor contains two peripheral aza-oxa units, rather than just one as in the analogous $[Ru(L^3)(mtpy)]^{2+}$ complex. The *I* vs. pH curve for $[Ru(L^3)_2]^{2+}$ does not change in the presence of Cu^{2+}, but the presence of Cd^{2+}, Pb^{2+}, or Hg^{2+} induces an enhancement in the luminescence of the $Ru(tpy)_2^{2+}$ core in the range pH 3.5−7.5 (see Figure 1c). The behaviour observed for the $[Ru(L^3)_2]^{2+}$ complex is quite similar to that seen for $[Ru(L^3)(mtpy)]^{2+}$, the only difference being the sensing of Hg^{2+} by the homoleptic complex, which is not observed for the heteroleptic one. This behaviour is not easy to rationalize, but it nevertheless seems to highlight the importance of slight structural modifications of the receptor in determining the final fluorescent behaviour. It is noteworthy that the $[Ru(L^3)(mtpy)]^{2+}$ receptor is able to sense the presence of all three toxic heavy metal ions Cd^{2+}, Pb^{2+}, and Hg^{2+} in an aqueous environment (acetonitrile/water) at the commonly encountered neutral pH in preference to smaller metal ions such as Cu^{2+}.

Finally, the emission properties of the $[Ru(L^4)(mtpy)]^{2+}$ complex in the presence of Ni^{2+}, Cu^{2+}, Cd^{2+}, Hg^{2+}, and Pb^{2+} were monitored as a function of pH. This receptor contains a polyazacycloalkane unit covalently attached to the $Ru(tpy)_2^{2+}$ fluorophore rather than an aza-oxa macrocycle as in $[Ru(L^1)(mtpy)]^{2+}$, $[Ru(L^3)(mtpy)]^{2+}$, and $[Ru(L^3)_2]^{2+}$. This is reflected in the observation of a quite different response towards metal ions. All five metals induce a change in the fluorescence response of the $[Ru(L^4)(mtpy)]^{2+}$ receptor, as shown in Figure 1d. Ni^{2+}, Cu^{2+}, and Cd^{2+} quench the fluorescence intensity of the free receptor over a wide pH range. In contrast, Pb^{2+} and Hg^{2+} enhance the fluorescence of the receptor. The fluorescent response as a function of the pH in the presence of Cu^{2+} resembles that found with the receptor $[Ru(cyphtpy)(mtpy)]^{2+}$, which contains a cyclic tetraamine moiety anchored to the ruthenium(II) bis(terpyridine) centre.[11] It is interesting to note that there seems to be a close relationship between the emission intensity and the radii of the metal cations; large metal ions enhance the fluorescence of the $Ru(tpy)_2^{2+}$ core, whereas smaller ones have a quenching effect. This represents rather unusual behaviour, which, to the best of our knowledge, has not been reported previously. In Figure 3, the relative fluorescence at pH 7.5 found in the presence of Ni^{2+}, Cu^{2+}, Cd^{2+}, Hg^{2+}, and Pb^{2+} ions is plotted as a function of the cationic radius. A linear response between emission intensity and cation size can be seen.

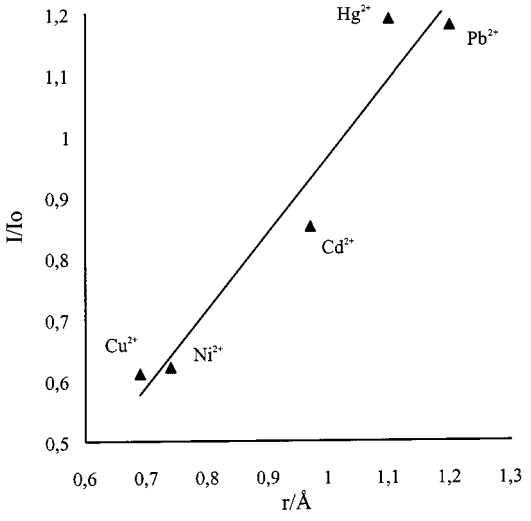

Figure 3. Relative fluorescence at pH 7.5 found for the interaction of Ni^{2+}, Cu^{2+}, Cd^{2+}, Hg^{2+}, and Pb^{2+} ions with $[Ru(L^4)(mtpy)][PF_6]_2$ as a function of the cationic radius

Conclusions

New terpyridine derivatives attached to aza-oxa macrocycles have been synthesized and their homoleptic or heteroleptic ruthenium(II) complexes have been prepared. One of the most interesting features of these metallo receptors is their multicomponent nature, in that they consist of an $Ru(tpy)_2^{2+}$ core capable of acting as a fluorescent signalling subunit and an aza-oxa macrocycle unit that acts as a cation binding site. Studies have been mainly carried out with a view to achieving discrimination between toxic heavy metal ions by means of fluorescence techniques. The receptors $[Ru(L^1)(mtpy)]^{2+}$, $[Ru(L^3)(mtpy)]^{2+}$, and $[Ru(L^3)_2]^{2+}$ are capable of transforming a coordination event occurring at the molecular level into a measurable macroscopic signal, thus allowing the sensing of heavy metal ions such as Cd^{2+}, Pb^{2+}, and especially of Hg^{2+} in water/acetonitrile (70:30, *v*/*v*) mixtures. The $[Ru(L^4)(mtpy)]^{2+}$ receptor, containing a polyazacycloalkane moiety as a binding site, shows a quite different response with the fluorescence of the $Ru(tpy)_2^{2+}$ core being enhanced by large metal ions and quenched by smaller ones. A linear response between emission intensity and cation size was found for this metallo receptor.

Experimental Section

General Remarks: $[Ru(mtpy)Cl_3]$[22] and 4′-[4-(bromomethyl)-phenyl]-2,2′:6′,2′′-terpyridine (Br-mphtpy)[18] were prepared according to the published methods; all other reagents were obtained from commercial sources and were used as received.

Preparations

Synthesis of L^1 and L^3: A solution of 4′-[4-(bromomethyl)phenyl]-2,2′:6′,2′′-terpyridine (Br-mphtpy) (200 mg, 0.5 mmol) in CH_2Cl_2 (20 mL) was added dropwise to a solution of 4,10-diaza-15-crown-5 (545 mg, 2.5 mmol) in order to obtain L^1, or to a solution of 1-aza-12-crown-4 (438 mg, 2.5 mmol) in CH_2Cl_2 (20 mL) in order to afford L^3. The respective solutions were treated with 5 drops of Et_3N and then heated at 30 °C for 24 h. Each reaction mixture was washed with water (3 × 3 mL). The organic phases were dried with $MgSO_4$ and concentrated under reduced pressure. The residues

were purified by column chromatography on alumina using CH_2Cl_2/CH_3OH (99:1, *v*/*v*) as the eluent. A yellow oil was obtained, which solidified on keeping the flask under reduced pressure. Yields: 81 mg, 30% for L^1; 87 mg, 35% for L^3.

L^1: ^{1}H NMR (300 MHz, $CDCl_3$): δ = 2.4 (1 H, NH), 2.70−2.85 (8 H, CH_2N), 3.5−3.7 (12 H, CH_2O and 2 H, CH_2Ph), 7.28−7.32 (2 H, tpy 5-,5′′-H), 7.42−7.48 (2 H, Ph), 7.75−7.85 (2 H, tpy 4-,4′′-H and 2 H, Ph), 8.55−8.60 (2 H, tpy 6-,6′′-H), 8.65−8.70 (2 H, tpy 3-,3′′-H and 2 H, tpy 3′-,5′-H). − ^{13}C NMR ($CDCl_3$): δ = 48.8 (CH_2), 54.3 (CH_2), 60.1 (CH_2), 69.0−71.0 (CH_2), 118.8 (CH, tpy), 121.3 (CH, tpy), 123.8 (CH, tpy), 127.2 (CH, tolyl), 129.4 (CH, tolyl), 149.1 (CH, tpy), 155.9 (C, tpy), 156.1 (C, tpy). − $C_{32}H_{37}N_5O_3{\cdot}CH_2Cl_2$ (624.6): found C 64.0, H 6.0, N 10.8; L^1 requires C 63.5, H 6.2, N 11.2. − FAB MS: *m*/*z* (%) = 540 (60), 461 (35), 401 (30), 327 (65), 281 (50), 221 (55).

L^3: ^{1}H NMR (300 MHz, $CDCl_3$): δ = 2.8 (4 H, CH_2N), 3.65−3.75 (12 H, CH_2O and 2 H, CH_2Ph), 7.33−7.36 (2 H, tpy 5-,5′′-H), 7.52−7.54 (2 H, Ph), 7.85−7.87 (2 H, tpy 4-,4′′-H and 2 H, Ph), 8.69−8.72 (2 H, tpy 6-,6′′-H), 8.72−8.73 (2 H, tpy 3-,3′′-H), 8.74 (s, 2 H, tpy 3′-,5′-H). − ^{13}C NMR ($CDCl_3$): δ = 54.9 (CH_2), 60.6 (CH_2), 70.2 (CH_2), 70.5 (CH_2), 71.3 (CH_2), 119.7 (CH, tpy), 121.3 (CH, tpy), 123.7 (CH, tpy), 127.1 (CH, tolyl), 129.5 (CH, tolyl), 136.8 (CH, tpy), 149.1 (CH, tpy), 150.7 (C, tolyl), 155.8 (C, tpy), 156.1 (C, tpy). − $C_{30}H_{32}N_4O_3{\cdot}CH_2Cl_2$ (581.5): found C 65.0, H 6.0, N 9.8; L^3 requires C 64.0, H 5.8, N 9.6. − FAB MS: *m*/*z* (%) = 497 (100), 322 (45), 193 (15).

Synthesis of L^2: A solution of 4′-[4-(bromomethyl)phenyl]-2,2′:6′,2′′-terpyridine (Br-mphtpy) (200 mg, 0.5 mmol) in CH_2Cl_2 (20 mL) was added dropwise to a solution of 4,10-diaza-15-crown-5 (54.5 mg, 0.25 mmol) in CH_2Cl_2 (20 mL). The resulting mixture was treated with 5 drops of Et_3N and then heated at 30 °C for 24 h. It was subsequently washed with water (3 × 3 mL). The organic phase was dried with $MgSO_4$ and concentrated under reduced pressure. The residue was purified by column chromatography on alumina using CH_2Cl_2/CH_3OH (99:1, *v*/*v*) as the eluent. A yellow oil was obtained, which solidified on keeping the flask under reduced pressure. Yield: 63 mg, 30%.

L^2: ^{1}H NMR (300 MHz, $CDCl_3$): δ = 2.7−2.85 (8 H, CH_2N), 3.40−3.70 (12 H, CH_2O), 4.5 (4 H, CH_2Ph), 7.2−7.3 (4 H, tpy 5-,5′′-H), 7.38−7.44 (4 H, Ph), 7.80−7.90 (4 H, tpy 4-,4′′-H and 4 H, Ph), 8.60−8.62 (2 H, tpy 6-,6′′-H), 8.66−8.72 (4 H, tpy 3-,3′′-H and 4 H, tpy 3′-,5′-H). − ^{13}C NMR ($CDCl_3$): δ = 54.4 (CH_2), 60.1 (CH_2), 69.5 (CH_2), 70.7 (CH_2), 118.1 (CH, tpy), 121.3 (CH, tpy), 123.8 (CH, tpy), 127.1 (CH, tolyl), 129.4 (CH, tolyl), 136.8 (CH, tpy), 149.1 (CH, tpy), 155.9 (C, tpy), 156.1 (C, tpy). − $C_{54}H_{52}N_8O_3{\cdot}CH_2Cl_2$ (946.0): found C 69.0, H 6.0, N 10.8; L^2 requires C 69.8, H 5.7, N 11.8. − FAB MS: *m*/*z* (%) = 861 (40), 322 (90), 281 (45), 207 (60).

Synthesis of L^4: A solution of 4′-[4-(bromomethyl)phenyl]-2,2′:6′,2′′-terpyridine (Br-mphtpy) (200 mg, 0.5 mmol) in CH_2Cl_2 (20 mL) was added dropwise to a solution of 1,4,7,10,13-pentaazacyclopentadecane (500 mg, 2.5 mmol). The resulting mixture was treated with 5 drops of Et_3N and then heated at 30 °C for 24 h. It was subsequently washed with water (3 × 3 mL). The organic phase was dried with $MgSO_4$ and concentrated under reduced pressure. The residue was purified by column chromatography on alumina using CH_2Cl_2/CH_3OH (99:1, *v*/*v*) as the eluent. A yellow oil was obtained, which solidified on keeping the flask under reduced pressure. Yield: 120 mg, 50%.

L^4: ^{1}H NMR (300 MHz, $CDCl_3$): δ = 2.5−2.9 (20 H, CH_2), 3.6 (2 H, CH_2Ph), 7.25−7.28 (2 H, tpy 5-,5′′-H), 7.40−7.42 (2 H, Ph), 7.70−7.80 (2 H, tpy 4-,4′′-H and 2 H, Ph), 8.55−8.60 (2 H, tpy 6-,6′′-H), 8.65−8.70 (2 H, tpy 3-,3′′-H and 2 H, tpy 3′-,5′-H). − ^{13}C NMR ($CDCl_3$): δ = 48.8 (CH_2), 56.3 (CH_2), 60.1 (CH_2), 68.5−71.0 (CH_2), 118.7 (CH, tpy), 121.2 (CH, tpy), 123.8 (CH, tpy), 127.2 (CH, tolyl), 129.4 (CH, tolyl), 148.9 (CH, tpy), 155.8 (C, tpy), 156.3 (C, tpy). − $C_{32}H_{40}N_8$ (536.7): found C 71.2, H 7.8, N 20.8; L^4 requires C 71.6, H 7.5, N 20.9. − FAB MS: *m*/*z* (%) = 537 (100), 323 (100), 281 (35), 237 (35).

Synthesis of $[Ru(L^1)(mtpy)][PF_6]_2$, $[Ru(L^3)(mtpy)][PF_6]_2$, and $[Ru(L^4)(mtpy)][PF_6]_2$: These ruthenium complexes were all prepared in the same way. A mixture of the appropriate ligand (L^1 108 mg, L^3 99.4 mg, L^4 107 mg; 0.2 mmol), $[Ru(mtpy)Cl_3]$ (90 mg, 0.2 mmol), and 3 drops of *N*-ethylmorpholine, as a mild reductant, in MeOH (20 mL) was heated to reflux under stirring for 1 h. The resulting deep-red solution was then filtered through Celite to remove any unchanged $[Ru(mtpy)Cl_3]$. Further purification was accomplished by chromatography on silica using acetonitrile/water/satd. aq. KNO_3 solution (17:2:1) as the eluent. The complexes were isolated as their hexafluorophosphate salts.

$[Ru(L^1)(mtpy)][PF_6]_2$: Yield 48 mg, 20%. − ^{1}H NMR (300 MHz, CD_3CN): δ = 2.98 (s, 3 H, CH_3), 3.3−3.4 (4 H, CH_2N), 3.60−3.65 (4 H, CH_2N), 3.7−3.9 (12 H, CH_2O and 2 H, CH_2Ph), 7.15−7.20 (4 H, tpy 5-,5′′-$H^{1,2}$), 7.40−7.45 (4 H, tpy 6-,6′′-$H^{1,2}$), 7.90−8.00 (2 H, Ph and 2 H, tpy 4-,4′′-$H^{1,2}$), 8.30−8.32 (2 H, Ph), 8.48−8.50 (2 H, tpy 3-,3′′-H^1), 8.68−8.70 (2 H, tpy 3-,3′′-H^2), 8.70 (s, 2 H, tpy 3′-,5′-H^1), 9.08 (s, 2 H, tpy 3′-,5′-H^2); 1 = mtpy; 2 = Phtpy. − $C_{48}H_{50}F_{12}N_8O_3P_2Ru{\cdot}CH_2Cl_2$ (1262.5): found C 45.9, H 3.8, N 9.3; $[Ru(L^1)(mtpy)][PF_6]_2$ requires C 46.4, H 4.1, N 8.8. − FAB MS: *m*/*z* (%) = 1177 (25), 1033 (65), 887 (100), 671 (10).

$[Ru(L^3)(mtpy)][PF_6]_2$: Yield 45 mg, 20%. − ^{1}H NMR (300 MHz, CD_3CN): δ = 2.97 (s, 3 H, CH_3), 3.5 (4 H, CH_2N), 3.7−3.8 (8 H, CH_2O), 3.95−4.0 (4 H, CH_2O), 4.52 (2 H, CH_2Ph), 7.15−7.25 (4 H, tpy 5-,5′′-$H^{1,2}$), 7.40−7.45 (4 H, tpy 6-,6′′-$H^{1,2}$), 7.84 (2 H, Ph), 7.95 (4 H, tpy 4-,4′′-$H^{1,2}$), 8.3 (2 H, Ph), 8.46−8.48 (2 H, tpy 3-,3′′-H^2), 8.66−8.68 (2 H, tpy 3-,3′′-H^1), 8.71 (s, 2 H, tpy 3′-,5′-H^2), 9.01 (s, 2 H, tpy 3′-,5′-H^1); 1 = mtpy; 2 = Phtpy. − $C_{46}H_{45}F_{12}N_7O_3P_2Ru{\cdot}2H_2O$ (1170.9): found C 47.3, H 3.9, N 8.3; $[Ru(L^3)(mtpy)][PF_6]_2$ requires C 47.2, H 4.2, N 8.4. − FAB MS: *m*/*z* (%) = 1135 (20), 990 (55), 845 (100), 671 (10).

$[Ru(L^4)(mtpy)][PF_6]_2$: Yield 52 mg, 20%. − ^{1}H NMR (300 MHz, CD_3CN): δ = 2.8−3.2 (20 H, CH_2), 2.98 (s, 3 H, CH_3), 3.95 (2 H, CH_2Ph), 7.15−7.20 (4 H, tpy 5-,5′′-$H^{1,2}$), 7.40−7.45 (4 H, tpy 6-,6′′-$H^{1,2}$), 7.70−7.72 (2 H, Ph^2), 7.9−7.94 (4 H, tpy 4-,4′′-$H^{1,2}$), 8.25−8.28 (2 H, Ph), 8.50−8.52 (2 H, tpy 3-,3′′-H^1), 8.68−8.70 (2 H, tpy 3-,3′′-H^2), 8.70 (s, 2 H, tpy 3′-,5′-H^1), 9.08 (s, 2 H, tpy 3′-,5′-H^2); 1 = mtpy; 2 = Phtpy. − $C_{48}H_{50}F_{12}N_8O_3P_2Ru{\cdot}2H_2O$ (1214.0): found C 54.5, H 5.5, N 14.8; $[Ru(L^4)(mtpy)][PF_6]_2$ requires C 54.0, H 5.3, N 14.5. − FAB MS: *m*/*z* (%) = 1174 (20), 1030 (30), 885 (40), 670 (65).

Synthesis of $[Ru(L^3)_2][PF_6]_2$: The homoleptic ruthenium complex of L^3 was prepared by reacting L^3 (200 mg, 0.4 mmol) with $RuCl_3 3H_2O$ (52.3 mg, 0.2 mmol), in the presence of 3 drops of *N*-ethylmorpholine as a mild reductant, in MeOH (20 mL). The mixture was heated to reflux under stirring for 2 h. The resulting deep-red solution was filtered through Celite to remove any unchanged $RuCl_3$. Further purification was accomplished by chromatography on silica using acetonitrile/water/satd. aq. KNO_3 solution (17:2:1) as the eluent. The complex was isolated as its hexafluorophosphate salt.

$[Ru(L^3)_2][PF_6]_2$: Yield 28 mg, 19%. − ^{1}H NMR (300 MHz, CD_3CN): δ = 3.5−3.6 (8 H, CH_2N), 3.6−4.1 (12 H, CH_2O), 4.55

(4 H, CH_2Ph), 7.22−7.26 (4 H, tpy 5-,5′′-H), 7.56−7.58 (4 H, tpy 6-,6′′-H), 7.86−7.90 (4 H, Ph), 7.98−8.02 (4 H, tpy 4-,4′′-H), 8.34−8.38 (4 H, Ph), 8.70−8.76 (4 H, tpy 3-,3′′-H), 9.08 (4 H, tpy 3′-,5′-H). − $C_{60}H_{64}F_{12}N_8O_6P_2Ru{\cdot}CH_2Cl_2$ (1468): found C 49.0, H 3.9, N 8.3; $[Ru(L^3)_2][PF_6]_2$ requires C 49.9, H 4.5, N 7.6. − FAB MS: *m*/*z* (%) = 1240 (20), 1094 (25), 920 (35).

Physical Measurements and Instrumentation

Photochemical data were obtained with an FS900CDT steady-state T-Geometry Fluorometer from Edinburgh Analytical Instruments. All solutions for photophysical studies were rigorously degassed. The concentrations of the ligand and of the metal ion were ca. $1.0{\cdot}10^{-4}$ mol dm^{-3}. ^1H NMR spectra were recorded on a Varian Gemini spectrometer. Potentiometric titrations were carried out in acetonitrile/water (70:30, *v*/*v*, 0.1 mol dm^{-3} tetrabutylammonium perchlorate) under nitrogen using a vessel water-thermostatted at 25.0 ± 0.1 °C. The titrant was added by means of a Crison microburette 2031. Further details of the potentiometric experiments have been published previously.[23] The concentrations of the metal ions were determined using standard methods. The computer program SUPERQUAD[24] was used to calculate the protonation and stability constants. The titration curves for each system (ca. 250 experimental points, corresponding to at least three titration curves; pH range investigated 2.5−10.2; ligand and metal ion concentrations ca. $1.0{\cdot}10^{-3}$ mol dm^{-3}) could be treated either as a single set or as separate entities without significant variation in the values of the stability constants. Finally, the sets of data were merged together and treated simultaneously to give the quoted stability constants.

Acknowledgments

We would like to thank the DGICYT (proyecto PB98-1430-C02-02, 1FD97-0508-C03-01, and AMB99-0504-C02-01) for support.

[1] E. C. Constable, in: *Comprehensive Supramolecular Chemistry* (Ed.: J.-M. Lehn), vol. 9, Pergamon, Oxford, **1996**.
[2] E. C. Constable, *Prog. Inorg. Chem.* **1994**, *42*, 67−138.
[3] A. Harriman, J.-P. Sauvage, *Chem. Soc. Rev.* **1996**, *25*, 41−48.
[4] F. Barigelletti, L. Flamigni, J.-P. Collin, J.-P. Sauvage, *Chem. Commun.* **1997**, 333−338.
[5] F. McLoren, P. Moore, A. M. Wynn, *J. Chem. Soc., Chem. Commun.* **1989**, 798−800.
[6] A. M. Josceanu, P. Moore, S. C. Rawle, P. Sheldon, S. M. Smith, *Inorg. Chim. Acta* **1995**, *240*, 159−168.
[7] P. D. Beer, C. Hazlewood, D. Hesek, J. Hodacova, S. E. Stokes, *J. Chem. Soc., Dalton Trans.* **1993**, 1327−1332.
[8] R. Grigg, J. M. Holmes, S. K. Jones, W. D. J. A. Norbert, *J. Chem. Soc., Chem. Commun.* **1994**, 185−187.
[9] A. Harriman, R. Ziessel, *Chem. Commun.* **1996**, 1707−1716.
[10] F. Barigelletti, L. Flamigni, J.-P. Collin, J.-P. Sauvage, A. Sour, E. C. Constable, A. M. Cargill Thompson, *J. Am. Chem. Soc.* **1994**, *116*, 7692−7699.
[11] M. E. Padilla-Tosta, J. M. Lloris, R. Martínez-Máñez, A. Benito, J. Soto, T. Pardo, M. A. Miranda, M. D. Marcos, *Eur. J. Inorg. Chem.* **2000**, 741−748.
[12] A. M. Costero, E. Monrabal, F. Sanjuan, R. Martínez-Máñez, M. Padilla-Tosta, T. Pardo, J. Soto, *Tetrahedron* **1999**, *55*, 15141−15150.
[13] E. Luboch, A. Cygan, J. F. Biernat, *Inorg. Chim. Acta* **1983**, *68*, 201−204.
[14] F. Arnaud Neu, B. Spiess, N. J. Schwing-Weill, *Helv. Chim. Acta* **1977**, *60*, 2633−2643.
[15] K. A. Byriel, K. R. Dunster, L. R. Gahan, C. H. L. Kennard, J. L. Laten, I. A. Swann, P. A. Duckworth, *Inorg. Chim. Acta* **1993**, *205*, 191−198.
[16] V. J. Thom, M. S. Shaikjee, R. D. Hancock, *Inorg. Chem.* **1986**, *25*, 2992−3000.
[17] R. Martínez-Máñez, J. Soto, J. M. Lloris, T. Pardo, *Trends in Inorg. Chem.* **1998**, 183−203.
[18] W. Spahni, G. Calzaferri, *Helv. Chim. Acta* **1984**, *67*, 450−454.
[19] J.-P. Sauvage, J.-P. Collin, J.-C. Chambron, S. Guillerez, C. Coudret, V. Balzani, F. Barigelletti, L. De Cola, L. Flamigni, *Chem. Rev.* **1994**, *94*, 993−1019.
[20] Y. Al Shihadeh, A. Benito, J. M. Lloris, R. Martínez-Máñez, T. Pardo, J. Soto, M. D. Marcos, *J. Chem. Soc., Dalton Trans.* **2000**, 1199−1205.
[21] J. M. Lloris, R. Martínez-Máñez, T. Pardo, J. Soto, M. E. Padilla-Tosta, *Chem. Commun.* **1998**, 837−838.
[22] E. C. Constable, A. Cargill Thompson, D. A. Tocher, A. M. Daniels, *New J. Chem.* **1992**, *16*, 855−867.
[23] For experimental details, see for example: M. J. L. Tendero, A. Benito, R. Martínez-Máñez, J. Soto, J. Paya, A. J. Edwards, P. R. Raithby, *J. Chem. Soc., Dalton Trans.* **1996**, 343−351.
[24] P. Gans, A. Sabatini, A. Vacca, *J. Chem. Soc., Dalton Trans.* **1985**, 1195−1200.

Received November 3, 2000
[I00423]

Ground State Modulation in Nickel(III) Chemistry by Controlling Axial Ligation in Complexes with N_3O_2 Pentadentate Ligands

Dora Pinho,[a] Paula Gomes,[a][‡] Cristina Freire,*[a] and Baltazar de Castro*[a]

Keywords: EPR spectroscopy / Nickel / Redox chemistry / Schiff bases / Voltammetry

The accessibility of the +3 oxidation state for nickel(II) complexes with N_3O_2 pentadentate Schiff base ligands prepared by condensation of naphthaldehyde or 3,5-dichlorosalicylaldehyde with triamines (Scheme 1) has been assessed in several solvents, by combining cyclic voltammetry and EPR spectroscopy of the oxidised metal complexes. The data show that trien/Metrien-based ligands act in pentadentate fashion and allow for the stabilisation of electrochemically and chemically generated nickel(III) complexes in all solvents used. The complexes, formulated as $[Ni^{III}L(solv)]^+$, are low-spin and have a $^2A_1$, [$a\ d_{z^2} + b\ d_{x^2-y^2}$], ground state, with $a \geq b$. For dien-based ligands, steric constraints prevent coordination of the amine nitrogen atom of the pentadentate ligand to the metal centre, thus enforcing a fourfold coordination on the ligand. The resulting complexes can be oxidised to nickel(III) species, but only when using iodine as oxidant, in DMF or $(CH_3)_2SO$. The complexes are formulated as $[Ni^{III}L(solv)_2]^+$, and are low-spin and have a $^2A_1$, [$a\ d_{z^2} + b\ d_{x^2-y^2}$], ground state, with $a >> b$. The binding of pyridine and cyanide ion to Ni^{III} trien/Metrien-based complexes was studied by EPR. The data obtained show that these polydentate ligands provide a flexible coordination sphere, and that by varying the ratio equatorial/axial ligand field it is possible to obtain Ni^{III} in three different ground states. For pyridine adducts, the same ground state as the parent complex was observed with Metrien-based ligands, while for trien-based ligands an inverted ground state ($^2A_1$, [$a\ d_{z^2} + b\ d_{x^2-y^2}$], with $a << b$) was observed, as the latter provides a higher axial ligand field. On the other hand, coordination of cyanide adducts induces a change in the principal molecular axis of the Ni^{III} complexes, in which the cyanide ions occupy equatorial positions, and in which a $^2A_1$, [$a\ d_{z^2} + b\ d_{x^2-y^2}$], ground state, with $a >> b$, is observed.

Introduction

We have become interested in the redox chemistry of nickel(II) complexes with N_2O_2 Schiff ligands, obtained by condensation of salicylaldehyde/naphthaldehyde with diamines, and on the characterisation of the oxidised/reduced species.[1−10] These tetradentate ligands are noninnocent in oxidation and reduction processes, and their solution oxidative behaviour is intricate, as both the metal centre and the ligand can be the final electron donor. It has been found that, although ligands with substantial π delocalisation favour ligand oxidation, the solvent plays a determining role in controlling the final oxidation site,[1−8] since oxidation of square-planar Ni^{II} complexes proceeds with the simultaneous coordination of two solvent molecules. Consequently, complexes are oxidised to Ni^{III} only in strong donor solvents, such as DMF and $(CH_3)_2SO$, whereas in poorly coordinating solvents, ligand oxidation takes place and the products are radical Ni^{II} species[2,3,11] or Ni^{II} conducting polymers.[7,8]

Nickel(III) complexes with these Schiff ligands are six-coordinate, with the polydentate ligand defining the equatorial plane and with the two elongated axial bonds occupied by solvent molecules. The complexes are invariably low-spin, with a $^2A_1$ [$a\ d_{z^2} + b\ d_{x^2-y^2}$] ground state, with $a >> b$.[1−6] Axial bonds are labile, and substitution of solvent molecules by Lewis bases (such as pyridines, imidazole, phosphanes, and CN^-) is easily accomplished.[1−6] All these adducts have the same ground state as the parent Ni^{III} complex, but their decomposition to nickel(II) species is much faster.

In order to reduce solvent influence on the accessibility of the +3 oxidation state in nickel complexes with Schiff bases derived from salicylaldehyde/naphthaldehyde, and thus to increase the range of solvents in which Ni^{III} complexes can be obtained, we have synthesised similar ligands, but ones in which the diamines bear a nitrogen donor atom, thereby constituting potential pentadentate ligands. By changing the donor ability of the inserted nitrogen atom and the length of the carbon imine bridge, it is possible to control the structures of the complexes and the reactivities of the metal centres.

In this work, we report the characterisation, using EPR and electronic spectroscopy, of several electrochemically and chemically generated nickel(III) complexes with N_3O_2 pentadentate Schiff base ligands, prepared by condensation of naphthaldehyde or 3,5-dichlorosalicylaldehyde with a triamine (Scheme 1). The accessibility of the +3 oxidation state to nickel(II) complexes was assessed by cyclic voltammetry in several solvents. EPR was the technique of choice for studying nickel complex oxidation, as this technique allows a clear distinction to be made between metal-based

[a] CEQUP/Departamento de Química, Faculdade de Ciências, Universidade do Porto, 4169-007 Porto, Portugal
[‡] Present address: CIQ(UP), Faculdade de Ciências, Universidade do Porto, 4169-007 Porto, Portugal

 © WILEY-VCH Verlag GmbH, 69451 Weinheim, 2001 1434−1948/01/0606−1483 $ 17.50+.50/0

and ligand-based oxidised species. The characterisation of nickel(III) species has revealed that these pentadentate ligands make the nickel(III) complexes less solvent-dependent, and thus it was possible to observe Ni^{III} oxidised species in methanol, a solvent with moderate coordinating ability. Moreover, by replacing the axially bound atoms with increasingly strong donors, it was possible to demonstrate that the ligands were very flexible and to generate nickel(III) complexes with different ground states, by controlling the ratio of axial to equatorial ligand fields.

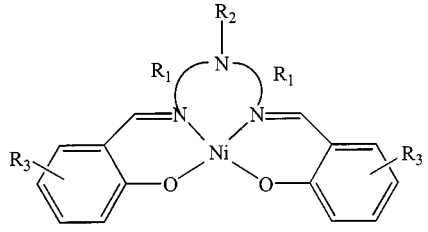

	R_1	R_2	R_3	
1	$-CH_2-CH_2-$	H		[Ni(napdien)]
2	$-CH_2-CH_2-$	H	3,5-Cl_2	[Ni(Cl_4saldien)]

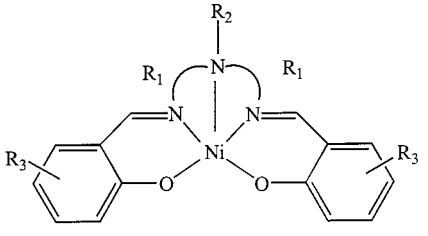

	R_1	R_2	R_3	
3	$-CH_2-CH_2-CH_2-$	H		[Ni(naptrien)]
4	$-CH_2-CH_2-CH_2-$	H	3,5-Cl_2	[Ni(Cl_4saltrien)]
5	$-CH_2-CH_2-CH_2-$	CH_3		[Ni(napMetrien)]
6	$-CH_2-CH_2-CH_2-$	CH_3	3,5-Cl_2	[Ni(Cl_4salMetrien)]

Scheme 1

Results and Discussion

Structural and Electronic Data for Nickel(II) Complexes

Like those of similar Schiff base complexes,[12−15] the electronic spectra of nickel(II) complexes **1**−**6** can be grouped into two sets on the basis of the size of the imine bridge: complexes with dien-based ligands and with trien- and Metrien-based ligands.

Spectra of complexes with dien bridges (**1**, **2**) are very similar and exhibit high intensity bands in the range 380−460 nm, attributed on the basis of their extinction coefficients to CT and intraligand electronic transitions. The lack of any observed d-d bands above $\lambda \approx 500$ nm, since they must be masked by the high intensity bands, implies a four-coordinate environment for the nickel centre.[12,15] Thus, the amine nitrogen atom of the bridge is not bound to the metal centre and the ligand acts in tetradentate fashion in a *cis* conformation.

The crystal structure of [Ni(Cl_4salMetrien)] (**6**) has been determined;[16] the nickel atom was found to be in a distorted octahedral coordination geometry, with the pentadentate ligand acting effectively as an N_3O_2 donor and with a solvent molecule (1,4-dioxane) occupying the remaining coordination site, *trans* to the amine nitrogen atom. Electronic spectra are consistent with this geometry, exhibiting two d-d bands in the near-infrared region, λ_{max} (ε) = 1159 nm (8 $dm^3mol^{-1}cm^{-1}$) and 966 nm (10 $dm^3mol^{-1}cm^{-1}$), one low-intensity d-d band in the visible region, λ_{max} (ε) = 568 nm (36 $dm^3mol^{-1}cm^{-1}$), and high-intensity bands (CT and intraligand) at wavelengths < 500 nm.

The similarity between the electronic spectra of **6** in the solid state and those of the other trien- and Metrien-based complexes, for which no crystal data are available, is taken to imply that the latter complexes may have similar structures. The ligands are thus assumed to act as pentadentate and to bind in a *trans* conformation. Furthermore, the similarity of the electronic data for complexes **1**−**6** in the solid state and in DMF solution additionally suggests that, in solution, the complexes may have structures that resemble those in the solid, with the sixth position occupied by a solvent molecule.

For complexes with the same aldehyde moieties, those with trien bridges have the d-d bands at higher energies than those with Metrien bridges. This hypsochromic shift reflects the relative position of secondary and tertiary amine nitrogen atoms in the spectrochemical series.[17] On the other hand, the d-d bands of complexes derived from naphthaldehyde are red-shifted relative to those of the corresponding chlorosalicylaldehyde derivatives, implying that the latter are stronger ligands in the nickel(II) complexes studied.

Cyclic Voltammetry of Nickel(II) Complexes

Cyclic voltammetric data in MeOH, DMF, and $(CH_3)_2SO$ are presented in Table 1. As with the spectroscopic data, the electrochemical responses can be grouped into two sets: complexes with dien bridges, which are irreversibly oxidised in all solvents, and complexes with trien and Metrien bridges, for which one oxidation process is normally observed in the potential range studied.

For dien-based complexes, scan rates up to 1.0 V s^{-1} were used. For high sweep rates only one incipient anodic wave could be observed for [Ni(napdien)], and this only in DMF and in $(CH_3)_2SO$. Furthermore, when chemically oxidised with iodine, all dien-based complexes exhibit Ni^{III} EPR signals in frozen DMF and $(CH_3)_2SO$ solutions (see below). These observations suggest that a very fast chemical decomposition of the electrogenerated nickel species may occur in these strongly coordinating solvents after charge transfer, as the carbon backbone of the imine bridge is long enough to induce significant tetrahedral distortions in the com-

Table 1. Cyclic voltammetric results for NiL complexes in CH_3OH, DMF and $(CH_3)_2SO$ (0.1 mol·dm^{-3} NEt_4ClO_4) at 25 °C[a]

Complex		CH_3OH					dmf					$(CH_3)_2SO$				
		E_{pa}	E_{pc}	ΔE	$E_{1/2}$	i_{pc}/i_{pa}	E_{pa}	E_{pc}	ΔE	$E_{1/2}$	i_{pc}/i_{pa}	E_{pa}	E_{pc}	ΔE	$E_{1/2}$	i_{pc}/i_{pa}
[Ni(napdien)]	(1)			[b]					[b]					[b]		
[Ni(Cl_4saldien)]	(2)			[b]					[b]					[b]		
[Ni(naptrien)]	(3)			[b]			0.50	0.42	0.08	0.46	0.94	0.45	0.36	0.09	0.40	0.93
[Ni(napMetrien)]	(5)			[b]			0.53	0.46	0.07	0.50	0.99	0.46	0.40	0.06	0.43	1.00
[Ni(Cl_4saltrien)]	(4)	0.71	0.61	0.10	0.66	0.78[c]	0.77	0.70	0.07	0.74	0.76[c]	0.74	0.63	0.11	0.68	0.82[c]
[Ni(Cl_4salMetrien)]	(6)	0.73	0.63	0.10	0.68	0.78[c]	0.90	0.67	0.23	0.78	0.83[c]	0.78	0.67	0.11	0.72	0.77[c]

[a] All potentials in V vs. Ag/AgCl (1 mol·dm^{-3} NaCl). Solute concentration about 10^{-3} mol·dm^{-3}; scan rate: 0.50 V·s^{-1}; $\Delta E = E_{pa} - E_{pc}$; $E_{1/2} = {}^1/_2(E_{pa}+E_{pc})$; E_{pa} and E_{pc} are the anodic and cathodic peak potentials, respectively. Under the conditions used, $E_{1/2}$ (Fc^+/Fc) is 0.45 V in MeOH, 0.47 V in DMF and 0.48 V in Me_2SO. – [b] Irreversible processes. – [c] Values calculated with the Nicholson equation.[18]

plexes and to make it difficult for solvent molecules to coordinate to the metal centre, thus hindering stabilization of the +3 oxidation state.[2,3,11]

On the other hand, the cyclic voltammograms of trien- and Metrien-based complexes (**3**–**6**) show one anodic wave and the corresponding cathodic wave, with the exception of solutions of naphthaldehyde derivatives in MeOH, which are irreversibly oxidised (Figure 1). The $E_{1/2}$ values for complexes with naphthaldehyde derivatives are less positive than those of the corresponding chlorosalicylaldehyde derivatives. The anodic-cathodic peak potential separations in all solvents are similar to, or (in the case of chlorosalicylaldehyde derivatives) somewhat larger than, those observed for the Fc^+/Fc couple. The i_{pc}/i_{pa} ratios in DMF and $(CH_3)_2SO$ are practically constant and equal to 1 for the naphthaldehyde derivatives, whereas for the chlorosalicylaldehyde derivatives the ratios are smaller (ca. 0.80). With increasing scan rates, a linear dependence is observed between i_p and $v^{1/2}$.

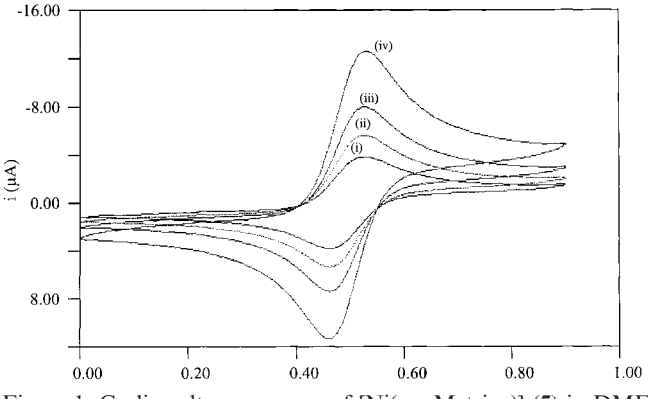

Figure 1. Cyclic voltammograms of [Ni(napMetrien)] (**5**) in DMF at: (i) 0.05; (ii) 0.10; (iii) 0.20, and (iv) 0.50 V·s^{-1}

Electrochemical data for the complexes with trien and Metrien bridges are consistent with one electron diffusion controlled oxidation process $Ni^{II} \rightarrow Ni^{III}$ [18] (see below). For complexes with 3,5-dichlorosalicylaldehyde-based ligands (**4**, **6**), there is direct evidence of a chemical decomposition path for the electrogenerated Ni^{III} species after charge transfer, whereas for naphthaldehyde derivatives, the decomposition path is not evidenced under the experimental conditions used for the cyclic voltammetry. However, during the electrolysis of the complexes (a longer timescale technique), decomposition of the oxidised species was observed for all complexes. Chemical decomposition of electrogenerated Ni^{III} species has also been observed in complexes with N_2O_2 tetradentate Schiff base ligands,[2,3,11] and although no quantitative studies have been performed for the complexes used in this work, we would like to point out that decomposition of the oxidised species are slower for complexes with pentadentate ligands as compared to Ni^{III} species with tetradentate N_2O_2 Schiff bases.

Redox Potentials

Our studies on the electrochemical properties of nickel(II) complexes with N_2O_2 coordination spheres[1–6] have shown that oxidation of the metal centre is markedly dependent on the donor capacity of the solvent, and is restricted to solvents with good donor properties, such as DMF and $(CH_3)_2SO$. When an axial nitrogen donor atom capable of binding to the metal centre is introduced into the ligand (as in trien and Metrien) we observe: (i) a stabilisation of the Ni^{III} species, as inferred from their lower $E_{1/2}$ values and slower decomposition relative to similar N_2O_2 nickel(II) complexes, and (ii) a less marked dependence on the solvent. However, in MeOH, a solvent with lower DN value, a reversible process could only be observed for chlorosalicylaldehyde derivatives (stronger ligands). Our results suggest that, even for these five-coordinate ligands, the oxidation requires a moderately strong solvent, which means that axial interactions with solvent molecules still play an important role in the stabilisation of the +3 oxidation state.

As regards the dependence of redox potential on the ligands for complexes **3**–**6**, those with Metrien bridges exhibit more positive $E_{1/2}$ values than those with trien bridges, contrary to prediction based upon the relative inductive effects of hydrogen atoms and methyl groups. Similar behaviour has been observed in other nickel complexes with similar trien- and Metrien-based ligands and has been attributed to a weakening of the axial bond due to steric constraints between the methyl groups and the propylene backbone of the bridge.[19,20] On the other hand, the complexes with ligands derived from naphthaldehyde exhibit

less positive $E_{1/2}$ values than those derived from chlorosalicylaldehyde, for which the strongly electron-withdrawing substituents (Cl) should reduce electron density on the chelate ring, and thus on the metal ion, making it harder to oxidise the metal centre.

EPR and Electronic Spectra of the Oxidised Species

When nickel(II) complexes **3−6** are oxidised electrochemically in DMF, the solution colour changes from greenish to yellow-brown, implying formation of new species. Frozen-matrix EPR spectra of all electrolysed solutions are similar, and show significant rhombicity and large g tensor anisotropy, with g_{av} [$g_{av} = (g_1 + g_2 + g_3)/3$] in the range 2.13−2.15 ($g_1 \approx 2.24-2.26$, $g_2 \approx 2.13-2.16$ and $g_3 \approx 2.02-2.04$): an indication that the oxidised species must correspond to nickel(III) complexes. Furthermore, all spectra show a well resolved 1:1:1 triplet in the high magnetic field region, with $a \approx 1.80-2.17$ mT. EPR spectra of nickel(III) species with naptrien and napMetrien in DMF are presented in Figure 2 (A) and Figure 3 (A), respectively; EPR data for the electrogenerated nickel(III) species in DMF are summarised in Table 2.

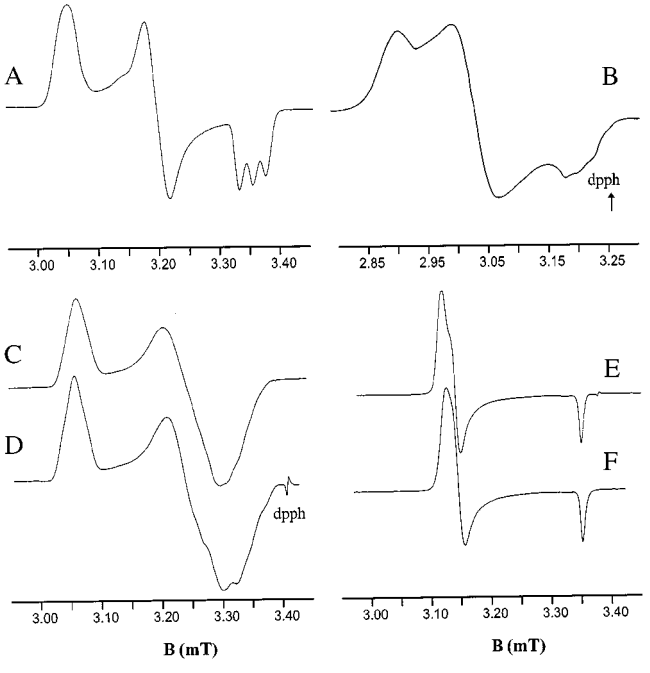

Figure 2. Frozen EPR spectra of $[Ni^{III}(naptrien)]^+$ in: (A) DMF; (B) CH_3CN; (C) pyridine; (D) [^{15}N]pyridine; (E) CN^-, and (F) $^{13}CN^-$

Chemical oxidation of complexes **3−6** with iodine were first performed in DMF. Frozen-matrix EPR spectra of these solutions are identical to those of electrolysed solutions and thus imply the same coordination environment for the nickel(III) species, regardless of the oxidation method used. We also observed that chemically oxidised solutions, owing to the presence in solution of excess oxidant, are more stable at room temperature than those obtained electrochemically.

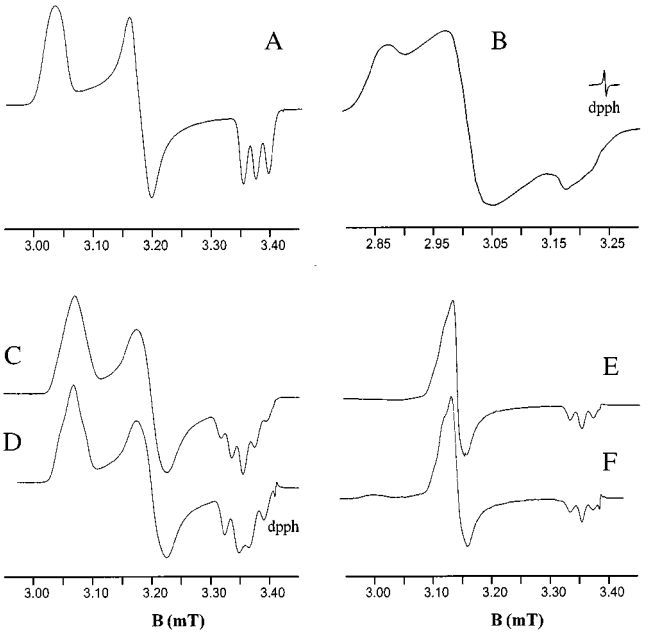

Figure 3. Frozen EPR spectra of $[Ni^{III}(napMetrien)]^+$ in: (A) DMF; (B) CH_3CN; (C) [^{15}N]pyridine; (D) pyridine; (E) CN^-, and (F) $^{13}CN^-$

The similarity of the EPR and the longer half-lives of the chemically oxidised solutions, prompted us to examine chemical oxidation of complexes **1−6** (hence including complexes with dien bridges) in other solvents. The study was extended to two other O-donor solvents, MeOH, and $(CH_3)_2SO$, and to acetonitrile, a N-donor solvent.

Chemically oxidised solutions of complexes **3−6** in MeOH and $(CH_3)_2SO$ exhibit frozen EPR spectra that are very similar to those in DMF, with g values in the same range, and a well resolved triplet (1:1:1) observed in the high magnetic field region, with $a_3 = 2.03-2.30$ mT. Frozen EPR spectra of the chemically oxidised solutions in MeCN exhibit the same g features as those in the O-donor solvents, but with a poorly resolved multiplet, *not a triplet*, in the high magnetic field region. The spectra for nickel(III) species with trien- and Metrien-based ligands in MeCN are presented in Figure 2 (B) and 3 (B), and the EPR parameters are summarised in Table 2.

Solutions of [Ni(napdien)] and [Ni(Cl_4saldien)] (**1**, **2**) were also chemically oxidised in the same solvents, and the oxidised samples were immediately frozen in liquid nitrogen. The oxidised solutions exhibit EPR spectra, but their g features depend on the solvent used. EPR data for **1−2** are presented in Table 2 and spectra of **1** are depicted in Figure 4. In DMF and $(CH_3)_2SO$, the spectra exhibit large g tensor anisotropy, with g_{av} in the range 2.15−2.16, and small rhombicity; however, no hyperfine couplings were detected in any g region (Figure 4, C,D). The EPR spectrum in MeCN shows two superimposed signals with similar intensities: one signal for which the low-field components have a g value similar to those of the chemically oxidised species in DMF and $(CH_3)_2SO$, and one isotropic signal, with $g \approx 2.00$, due to radical species, which masks the high-field component of the other signal (Figure 4, B); in MeOH

Table 2. EPR parameters for nickel(III) species in several solvents

Complex	Solvent	g_x	g_y	g_z	g_{av}[a]	$a(N)_x^1$[b]	$a(N)_y^1$[b]	$a(N)_z^1$[b]	$a(N)_x^2$[b]	$a(N)_y^2$[b]	$a(N)_z^2$[b]
$[Ni(Cl_4saltrien)]^+$ (**4**)	CH_3OH	2.236	2.139	2.038	2.138	1.30	1.60	2.05			
	CH_3CN	2.231	2.140	2.044	2.138	16.00	1.80	2.05	0.80	0.80	1.30
	DMF	2.236	2.132	2.039	2.136	1.30	1.70	2.10			
	$(CH_3)_2SO$	2.236	2.130	2.040	2.135	15.00	1.80	2.05			
$[Ni(Cl_4salMetrien)]^+$ (**6**)	CH_3OH	2.248	2.154	2.034	2.145	1.30	1.50	2.20			
	CH_3CN	2.240	2.153	2.041	2.145	1.40	1.80	2.10	0.80	0.80	1.35
	DMF	2.247	2.154	2.033	2.145	1.30	16.00	2.15			
	$(CH_3)_2SO$	2.248	2.154	2.035	2.146	1.30	16.00	2.20			
$[Ni(naptrien)]^+$ (**3**)	CH_3OH	2.250	2.156	2.032	2.146	1.60	1.80	2.26			
	CH_3CN	2.235	2.145	2.040	2.140	1.60	1.80	2.30	0.80	0.80	1.30
	DMF	2.237	2.143	2.033	2.138	1.60	1.80	2.30			
	$(CH_3)_2SO$	2.237	2.139	2.034	2.137	1.70	19.70	2.35			
$[Ni(napMetrien)]^+$ (**5**)	CH_3OH	2.240	2.144	2.032	2.139	1.90	2.10	2.40			
	CH_3CN	2.250	2.156	2.038	2.148	1.60	1.80	2.20	0.80	0.80	1.30
	DMF	2.255	2.153	2.030	2.146	1.50	1.80	2.20			
	$(CH_3)_2SO$	2.252	2.155	2.032	2.146	1.50	1.95	2.28			
$[Ni(Cl_4saldien)]^+$ (**2**)	CH_3OH	[c]									
	CH_3CN	[d]									
	DMF	2.230	2.200	2.018	2.149						
	$(CH_3)_2SO$	2.220	2.202	2.022	2.148						
$[Ni(napdien)]^+$ (**1**)	CH_3OH	[c])									
	CH_3CN	[d])									
	DMF	2.240	2.210	2.025	2.158						
	$(CH_3)_2SO$	2.230	2.202	2.021	2.151						

[a] The value of g_{av} was calculated as $(g_x + g_y + g_z)/3$. – [b] $a(N)$ values are expressed in mT. – [c] EPR spectrum typical of a radical species with $g = 2.003$. – [d] Two superimposed EPR spectra are observed: typical of Ni^{III} and radical species.

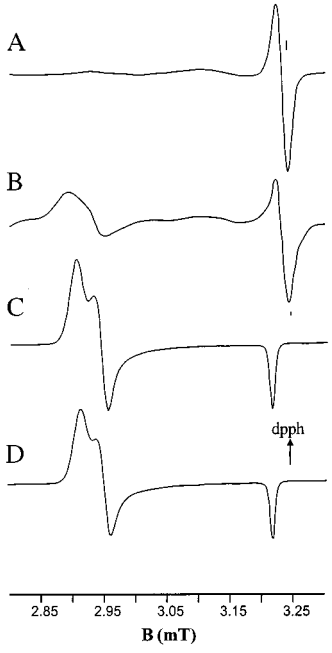

Figure 4. Frozen EPR spectra of $[Ni^{III}(napdien)]^+$ in: (A) CH_3OH; (B) CH_3CN; (C) DMF, and (D) $(CH_3)_2SO$

the spectrum exhibits only the isotropic signal at $g \approx 2.00$ (Figure 4, A).

The similarity between the g values in the spectra of the chemically oxidised [Ni(Cl_4saldien)] and [Ni(napdien)] and in those of low-spin, six-coordinate nickel(III) with N_2O_2-related Schiff ligands may be used as a basis for proposing that complexes **1**–**2** have the same $^2A_1$ ground state, [$a\ d_{z^2} + b\ d_{x^2-y^2}$], with $a >> b$: $C_{2v}(z)$.[1–6,21–25] Thus, the lack of observed hyperfine coupling with any nitrogen atom in the EPR spectra indicates that the amine nitrogen atom remains unbound; hence the ligand behaves as a tetradentate N_2O_2 donor towards Ni^{III}. The transient nickel(III) species are low-spin and six-coordinate, with two solvent molecules (Solv) axially bound, and can be formulated as $[Ni^{III}L(Solv)_2]^+$, with L = napdien or Cl_4saldien (Scheme 2).

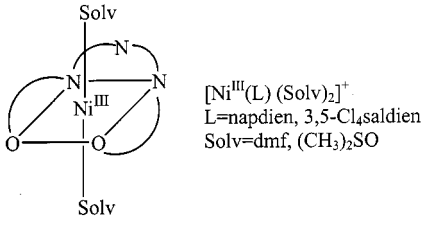

Scheme 2

In MeCN, two EPR signals were observed: one of radical-type and another from one metal-centred oxidised species. The radical species may be short-lived intermediates in the chemical decomposition path of the oxidised Ni^{III} complexes. No analysis of the nickel(III) species can be performed, as the intense signal at $g = 2.00$ masks the high-

field component, but the similarity of the low-field components with those of nickel(III) species in DMF and $(CH_3)_2SO$ implies the formation of $[Ni^{III}L(MeCN)_2]^+$ in solution. In MeOH only the signal assigned to radical species was observed, but this signal cannot be assigned unambiguously, since two possible explanations can be invoked: it may (i) be due to short-lived intermediates in the chemical decomposition of putative Ni^{III} oxidised species, or (ii) be the end result of direct oxidation on the ligand.

In contrast, nickel(II) complexes **3−6** are oxidised to Ni^{III} species in all solvents used, and their EPR spectra show behaviour quite different from that of the related complexes with dien-based bridges (Figure 2, Figure 3, and Figure 4). The EPR spectra are more rhombic, but as the difference $g_1 - g_2$ is still smaller than $g_2 - g_3$, the ground state must also be $^2A_1$, [$a\ d_{z^2} + b\ d_{x^2-y^2}$], although with $a \geq b$, and thus $g_1 = g_x$, $g_2 = g_y$, and $g_3 = g_z$.[21−24] The observation of one well-resolved triplet in the low g region (g_z) in O-donor solvents, changing to a poorly resolved multiplet in MeCN, is indicative that: (i) the polydentate ligands act in pentadentate fashion, with the amine nitrogen atom axially bound as in the parent Ni^{II} complex, and (ii) the sixth coordination site is occupied by a solvent molecule. The Ni^{III} complexes are thus formulated as $[Ni^{III}L(Solv)]^+$, with L denoting pentadentate trien- or Metrien-based ligands (Scheme 3 and Scheme 4).

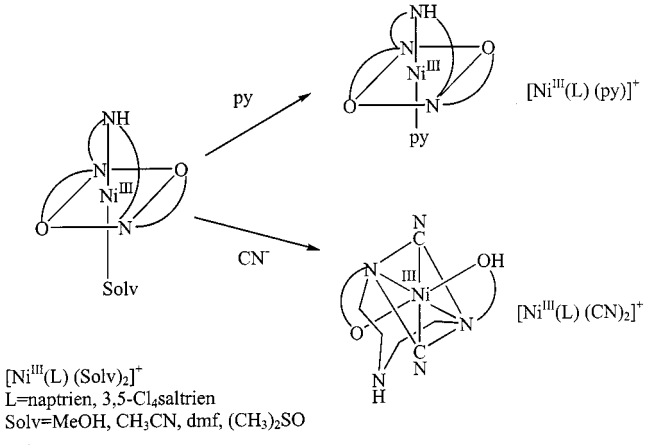

Scheme 3

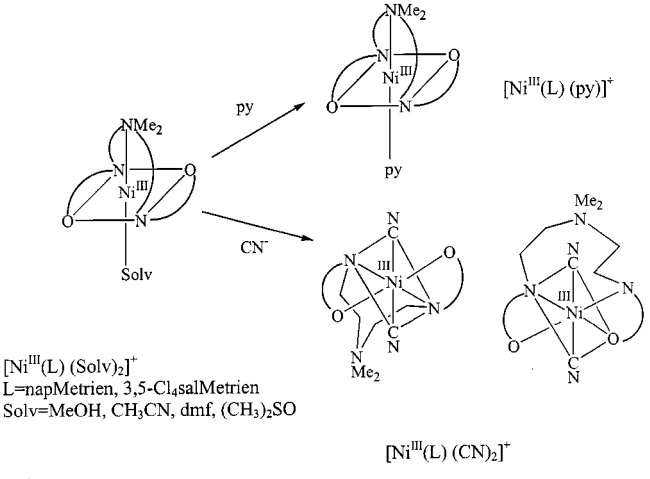

Scheme 4

Electronic spectra of electrochemically and chemically oxidised solutions of complexes **3−6** in DMF are very similar in the NIR region, but the very intense bands due to the iodine/iodide pair in the chemically oxidised solutions prevent comparisons below $\lambda = 600$ nm. No electronic spectra could be obtained for electrochemically or chemically oxidised solutions of complexes **1−2** in DMF, since decomposition of oxidised species is very fast even in cold fluid solutions (just above the melting point).

Electronic spectra of electrochemically oxidised solutions of **3−6** in DMF exhibit a very broad, medium intensity band in the near IR region ($\lambda_{max} = 950-1100$ nm, $\varepsilon = 200-900$ mol^{-1}dm^{3}cm^{-1}) and very intense bands at $\lambda_{max} < 550$ nm ($\varepsilon > 3000$ mol^{-1}dm^{3}cm^{-1}). Spectra recorded sequentially at 5-min intervals reveal (i) a gradual weakening in the NIR band, until it disappears completely, and (ii) a simultaneous blue shift of the high intensity bands. The spectra obtained after the disappearance of the NIR band are typical of nickel(II) complexes and correspond to solutions in which all nickel(III) species have decomposed, as confirmed by their silent EPR spectra. Moreover, since no electronic bands due to nickel(II) precursors could be detected above 400 nm, the medium intensity NIR bands in the spectra of oxidised solutions may thus be unambiguously attributed to d-d transitions of nickel(III) species generated in situ. The high-intensity bands include charge-transfer bands attributed to Ni^{III} species and to Ni^{II} precursor complexes/nickel(II) decomposed species. Electronic spectral data for nickel(III) species are presented in Table 3.

Table 3. Electronic spectral data for Ni^{III} complexes in DMF and in the presence of Lewis bases

Complex	Co-ligand	λ_{max} (nm)/ε (mmol^{-1}dm^{3}cm^{-1})[a]
$[Ni(Cl_4salMetrien)]^+$	DMF	995 br (1.3); < 500
(6)	pyridine	1000 br (0.46); < 500
	CN^-	< 500
$[Ni(napMetrien)]^+$	DMF	1082 br (0.61); < 500
(5)	pyridine	975 br (0.77); < 500
	CN^-	793 br (0.58); < 500
$[Ni(Cl_4saltrien)]^+$	DMF	971 br (0.91); < 500
(4)	pyridine	975 br (0.28); < 500
	CN^-	< 500
$[Ni(naptrien)]^+$	DMF	1043 br (1.2); < 500
(3)	pyridine	980 br (1.1); < 500
	CN^-	700 br (0.37); < 500

[a] ε values were estimated assuming that all complexes had been quantitatively oxidised to Ni^{III} and that no decomposition of the oxidised species had taken place.

Electronic band maxima occur in the range of values observed for six-coordinate nickel(III) complexes with N_2O_2 Schiff base ligands derived from the same aldehyde derivatives and two solvent molecules.[2−6] Analysis of the data in Table 3 reveals that the general trends in band maxima observed for the precursor Ni^{II} complexes also apply to the corresponding nickel(III) species: (i) complexes with dichlo-

rosalicylaldehyde derivatives have electronic bands at shorter wavelengths than those with naphthaldehyde, hence suggesting that the latter ligands also act as weaker ligands for nickel(III), and (ii) given the same aldehyde moiety, complexes with Metrien bridges have band maxima at longer wavelengths than those with trien bridges, indicating that the methyl group, due to steric constraints as outlined for the parent nickel(II) complexes, does not increase the ligand field.

Pyridine Adducts

The solutions obtained by addition of pyridine, and of cyanide ions, to $[Ni^{III}L(Solv)_2]^+$, L = napdien and Cl_4saldien (**1**, **2**) were found to be EPR-silent, which suggests that the decomposition rate of the new species must be fast enough to prevent observation with the experimental set-up used.

Upon addition of pyridine (natural abundance and ^{15}N-enriched) to freshly prepared DMF solutions of $[Ni^{III}L(DMF)]^+$ (L = naptrien, napMetrien, Cl_4saltrien, Cl_4salMetrien), new species were formed, as could be inferred from the rapid colour change to dark brown. The resulting solutions are EPR-active and the frozen solution spectra of complexes with trien and Metrien bridges exhibit different *g* patterns.

Complexes with Metrien Bridge Ligands

The EPR spectra of $[^{14}N]$py adducts with $[Ni^{III}L(DMF)]^+$ (L = napMetrien, Cl_4salMetrien), are similar, with rhombic symmetry and a *g* pattern ($g_1 - g_2 \leq g_2 - g_3$) that resembles that of the nickel(III) precursor complexes. In the high magnetic field region, a well-resolved quintuplet is observed (Figure 3, C), with an apparent 1:2:3:2:1 intensity pattern with $a_3 = 0.19$ mT. The ground state is thus assumed to be $^2A_1$, $[a\ d_{z^2} + b\ d_{x^2-y^2}]$, with $a \geq b$, and $g_1 = g_x$, $g_2 = g_y$, and $g_3 = g_z$.[21−25]

The need to identify the origin of the quintuplet prompted us to perform the same experiments, but using $[^{15}N]$py (^{15}N; $I = {}^1/_2$). The multiplet in the high magnetic field region became a quadruplet (1:2:2:1), arising from the interaction of the unpaired electron with two nitrogen atoms with different *I* values [the amine nitrogen atom (N_{amine}; $I = 1$) and the pyridine nitrogen atom (N_{py}; $I = {}^1/_2$)], but with similar hyperfine couplings [$a_{N(amine)}$ = 1.20; 1.50, and 2.10 mT and $a_{N(py)}$ = 0.80; 0.10, and 2.10 mT]. In this context, the quintuplet observed in the $[^{14}N]$py adducts arises from coupling to two different nitrogen atoms − one from the pentadentate ligand and the other from pyridine − but with similar coupling constants (Table 4). The complexes are thus formulated as low-spin, six-coordinate complexes, $[Ni^{III}(L)(py)]^+$, in which the ligand L (L = napMetrien or Cl_4salMetrien) acts in pentadentate fashion, and one pyridine molecule is bound at the sixth position (Scheme 4).

Complexes with trien Bridge Ligands

The EPR spectra of $[^{14}N]$py adducts with $[Ni^{III}L(DMF)]^+$ when L = naptrien and Cl_4saltrien are different from those with Metrien bridges. They exhibit apparent axial symmetry with large *g* tensor anisotropy, and with a weakly resolved quintuplet ($a_3 \approx 0.17-0.20$ mT) in the high magnetic field region, but with a *g* pattern different to those of the nickel(III) precursor complexes and of the homologous Metrien-based compounds. The *g* pattern is now $g_1 - g_2 > g_2 - g_3$, with $g_1 \approx 2.21$, $g_2 \approx 2.09$ and $g_3 \approx 2.06$ (Table 4). These spectra are consistent with the presence in solution of axially compressed six-coordinate species with a ground state that is essentially $d_{x^2-y^2}$ ($^2A_1$, $[a\ d_{z^2} + b\ ]$, with $a << b$), and in this case $g_1 = g_z$, $g_2 = g_x$, and $g_3 = g_y$.[21−25] Furthermore, the adducts with $[^{15}N]$py exhibit EPR spectra that are identical to those with $[^{14}N]$py, which implies that the hyperfine splittings cannot be due to coordinate pyridine molecules but must arise from the equatorial plane imine nitrogen atoms of the pentadentate ligand, in accordance with the ground state assignment.

Electronic data for the pyridine adducts are summarised in Table 3. The spectra show a broad, medium-intensity band in the NIR region, $\lambda = 975-1000$ nm, and high-intensity bands below 450 nm. On monitoring the spectra at 5-min intervals it was possible to observe a continuous loss of band absorbance for the electronic transition at low energies and a blue shift of the intense bands at high energies, an unambiguous indication that the bands in the NIR are due to d-d transitions in Ni^{III} pyridine adducts. The d-d bands are shifted to higher energies relative to those of the Ni^{III} precursor species, and the shift is related to the increase in ligand field when the sixth axial ligand is changed from DMF to pyridine.

Although no direct information concerning the number of coordinated pyridine molecules could be obtained, we propose that, in the adducts with naptrien and Cl_4saltrien, only one pyridine should be bound (Scheme 3), since in complexes with Metrien base ligands, which impose weaker ligand fields, only one pyridine molecule is bound to the nickel centre.

Cyanide Adducts

Upon addition of potassium cyanide, the solution colour of freshly electrooxidised solutions of $[Ni^{III}L(DMF)]^+$ (with L = naptrien, napMetrien, Cl_4saltrien, Cl_4salMetrien) changes from yellow-brown to green. Frozen solutions of cyanide adducts show EPR spectra that are typical of Ni^{III} species, but with a *g* pattern different to that observed for the parent Ni^{III} complexes and to those of pyridine adducts. These observations provide a clear indication that cyanide binds to the nickel(III) centres.

Frozen-matrix EPR spectra of all cyanide adducts show quasi-axial symmetry and a *g* pattern typical of low-spin, six-coordinate complexes with axial elongation, and with a $^2A_1$ ground state, $[a\ d_{z^2} + b\ d_{x^2-y^2}]$, with $a >> b$; $g_1 = 2.18-2.16$, $g_2 = 2.16-2.15$, $g_3 \approx 2.02$, and $g_1 = g_x$, $g_2 = g_y$, and $g_3 = g_z$ in both cases (Table 4).[1−6,21−25] No hyperfine splittings were detected in the spectra of the adducts with trien-based ligands (Figure 2, E), but those of Metrien-based complexes exhibit a high-field signal split into three lines (not 1:1:1 triplet, $a = 0.19$ mT) (Figure 3, E). In order

Table 4. EPR parameters for nickel(III) species in the presence of pyridine and cyanide ions

Complex	Co-ligand	g_x	g_y	g_z	g_{av}[a]	$a(N)_x^{1}$[b]	$a(N)_y^{1}$[b]	$a(N)_z^{1}$[b]	$a(N)_x^{2}$[b]	$a(N)_y^{2}$[b]	$a(N)_z^{2}$[b]
$[Ni(Cl_4salMetrien)]^+$ (6)	[^{14}N]pyridine	2.223	2.123	2.039	2.128	1.10	1.30	1.89	1.10	1.30	18.90
	CN^-	2.173	2.147	2.022	2.114						
		2.178	2.163	2.022	2.121	1.30	1.30	21.00			
	$^{13}CN^-$	2.177	2.164	2.021	2.121						
		2.183	2.155	2.021	2.120	1.50	1.50	20.00			
$[Ni(napMetrien)]^+$ (5)	[^{14}N]pyridine	2.224	2.132	2.035	2.130	1.00	12.00	19.00	1.00	1.20	1.90
	[^{15}N]pyridine	2.225	2.133	2.034	2.131	1.20	1.50	2.10	0.60	1.00	2.10
	CN^-	2.162	2.150	2.022	2.111						
		2.163	2.161	2.022	2.115	1.30	1.30	2.05			
	$^{13}CN^-$	2.161	2.156	2.022	2.113						
		2.163	2.157	2.022	2.114	1.30	1.30	2.05			
		g_z	g_x	g_y	g_{av} [a]	$a(N)_z$[b]	$a(N)_x$[b]	$a(N)_y$[b]			
$[Ni(Cl_4saltrien)]^+$ (4)	[^{14}N]pyridine	2.205	2.093	2.063	2.120	1.10	2.00	2.00			
	CN^-	2.177	2.142	2.021	2.113						
	$^{13}CN^-$	2.177	2.141	2.021	2.113						
$[Ni(naptrien)]^+$ (3)	[^{14}N]pyridine	2.214	2.096	2.050	2.120	1.10	1.70	1.70			
	[^{15}N]pyridine	2.212	2.094	2.050	2.118	1.05	1.70	1.70			
	CN^-	2.162	2.147	2.019	2.109						
	$^{13}CN^-$	2.165	2.149	2.020	2.111						

[a] The value of g_{av} was calculated as $(g_x + g_y + g_z)/3$. – [b] $a(N)$ values are expressed in mT.

to interpret the spectra, we made use of $^{13}CN^-$ and found that the EPR spectra of the enriched adducts are identical to those with natural abundance CN^- (Figure 2, F, and Figure 3, F): a clear indication that no direct spin interaction of the nickel unpaired electron with the carbon atom of the cyanide ion takes place. Furthermore, we note that the spectrum of $[Ni^{III}(CN)_6]^{3-}$ is completely different from those reported here,[26] which implies that displacement of the pentadentate ligand by cyanide ions had not taken place.

The number of bound cyanide ions could not be determined, and the complexes may thus be formulated as $[Ni^{III}(L)(CN)]$ or, if the cyanide ions replace the solvent molecule and the N(amine) group, as $[Ni^{III}(L)(CN)_2]^{-1}$. However, the latter hypothesis gained some support by the large hypsochromic shift (stronger ligand field) in the d-d transitions, relative to those of the nickel(III) precursor complexes, observed upon cyanide coordination.

Before attempting to interpret the EPR spectra of the cyanide adducts, we must stress that, for all the other Ni^{III} species referred to above, the equatorial plane was defined by the ligand $\{[N_2(imine)O_2]\}$ atoms and the molecular z axis was the $[N(amine)-Ni^{III}-X]$ axis (X = solvent or py) (Scheme 3 and Scheme 4).

Complexes with trien Bridge Ligands

The recognition that the spectra are unambiguously attributable to an axially elongated d_{z^2} ground state and the non-observation of hyperfine splitting in any of the three g regions indicate that neither the cyanide ions ($^{13}CN^-$) nor any nitrogen atom interacts directly with the unpaired electron in the d_{z^2} orbital. Consequently, the oxygen atoms of the pentadentate ligand must occupy the axial positions. The z axis must be the $[O-Ni^{III}-O]$ axis, with the two cyanide ions and the two N(imine) atoms defining the equatorial plane. This arrangement is only possible if the polydentate ligand retains the *trans* configuration of the nickel(II) parent complex (Scheme 3). The ligand field in the $[CN^--Ni^{III}-CN^-]$ direction is very strong and weakens the ligand field in the perpendicular plane, which makes the $[O-Ni^{III}-O]$ bonds longer. A precedent for this proposal is provided by studies on the interaction of cyanide ions with tripeptide complexes of Ni^{III}, for which a change in molecular axis has also been observed upon ligation of cyanide ions.[26–28]

Complexes with Metrien Bridge Ligands

The key difference in the EPR spectra of *Metrien* derivatives is the observation of hyperfine splittings in g_z. As identical spectra were observed for $^{12}CN^-$ and $^{13}CN^-$, the cyanide ions cannot be considered as the origin for the observed splitting. The atoms causing the observed splittings must be the nitrogen atoms of the polydentate ligand, ^{14}N ($I = 1$). The only explanation for the observed multiplet is to assume that the spectra of Metrien derivatives are the superimposition of two spectra: (i) one without any hyperfine splitting and which is similar to those of the trien derivatives, and (ii) the other, which exhibits a 1:1:1 triplet in the g_z region ($a = 2.00-2.10$ mT). The former spectra must correspond to species with the same configuration as those

of $[Ni^{III}(L)(CN)_2]^{-1}$ (with L = naptrien, Cl_4saltrien), with the polydentate ligand in a *trans* conformation. The latter spectra can be accounted for by assuming that the same change in the *z* axis has occurred, but with the *z* axis defined by one imine nitrogen atom and one oxygen atom of the polydentate ligand, which implies a *cis* configuration for the polydentate ligand (Scheme 4).

Conclusions

The accessibility of the +3 oxidation state in the nickel(II) complexes **1−6** is determined primarily by the binding or non-binding of the polydentate ligand amine nitrogen atom to the metal centre, which in turn depends on the number of carbon atoms in the imine bridge. Complexes with dien bridges are irreversibly oxidised in all solvents, under the experimentally used cyclic voltammetric conditions, whereas complexes with trien/Metrien-based ligands show quasi-reversible processes. In the former, steric constraints prevent coordination of the amine nitrogen atom to Ni^{II}, thus enforcing a tetradentate coordination mode for the ligand, but with trien/Metrien bridges the ligand enforces a true N_3O_2 pentadentate coordination sphere.

Formation of nickel(III) complexes takes place with the simultaneous increase of the coordination number to 6, by binding of solvent molecules. Analysis of EPR spectra has permitted unambiguous identification of the oxidised species. Spectra of oxidized trien/Metrien-based complexes are anisotropic, with a $^2A_1$ ground state ($a \geq b$), and provide direct evidence for coordination of the imine bridge nitrogen atom. On the other hand, chemically oxidised dien-based complexes in DMF and $(CH_3)_2SO$ exhibit quasi-axial spectra with a $^2A_1$ ground state ($a >> b$) and no hyperfine couplings, which indicates that the amine nitrogen atom is not coordinated. The difference in stability of dien- and trien/Metrien-based complexes is thus attributable to the binding of the bridging amine nitrogen atom. With one axial coordination position occupied by a strong donor (the ligand amine nitrogen atom), the stabilization of species oxidised at the metal centre is less sensitive to the coordination ability of the solvent molecule bound to the other axial position.

The stability of the Ni^{III} trien/Metrien-based complexes has prompted the study of the interaction of these complexes with pyridine and cyanide ion, ligands of increasing ligand strength. EPR data have made it clear that these polydentate ligands provide a flexible coordination sphere, and that by varying the equatorial/axial ligand field ratio it is possible to obtain Ni^{III} species in three different ground states. Furthermore, it has become evident that the ground state of Ni^{III} species is also dependent on the substituents on the imine bridge nitrogen atom: −H (trien) or $-CH_3$ (Metrien).

For pyridine adducts of Metrien-based complexes, a ground state similar to that of the parent Ni^{III} complex, with $^2A_1$ and $a \geq b$, was obtained, whereas for trien-based complexes an inverted ground state, $^2A_1$, was observed, with $a << b$. The different behaviour was attributed to the stronger axial field induced by the unsubstituted amine nitrogen in the imine bridge, as compared with Metrien, which, when combined with the ligand strength of pyridine, is enough to invert the magnitude of the contribution of the two d orbitals defining the $^2A_1$ ground state.

Upon addition of cyanide ($^{13}CN^-$ and natural abundance CN^-), a more drastic change in the ground state was observed. The rhombic spectra of the parent complexes changed to axial EPR spectra, typical of complexes with a ground state that is formulated as $^2A_1$, with $a >> b$. Combining this result with the non-observation of any hyperfine splitting in trien-based complexes, we propose that the strong ligand field of cyanide ions causes a shortening of the Ni−C bond lengths, so as to change the principal molecular axis of Ni^{III} complexes, but in which the ligand exists in a *trans* conformation. For Metrien-based complexes, similar spectra have been observed, but with hyperfine splittings in the high magnetic field region. The same changes in the principal molecular axis are assumed, but analysis of the hyperfine splitting pattern has prompted us to propose the existence of Ni^{III} complexes in which the ligands exist in *trans* and *cis* conformations, probably a consequence of the steric requirements of the amine nitrogen methyl group.

Experimental Section

Reagents and Solvents: Solvents and reagents for synthesis were obtained from commercial sources and used as received. The solvents used in electrochemistry were from Merck (pro analysi). Pyridine and potassium cyanide were from Merck (p.a.). [^{15}N]Pyridine was purchased from Cambridge Isotope Laboratories and potassium [^{13}C]cyanide from Aldrich. Tetraethylammonium perchlorate (NEt_4ClO_4) was prepared by published procedures[29] from the bromide salt (Aldrich) and perchloric acid (Merck, p.a.).

CAUTION: Perchlorates are hazardous and may explode.

Synthesis of Ligands and Nickel(II) Complexes: The ligands H_2napdien (bis{2-[(2-hydroxynaphthyl)methylimido]ethyl}amine), H_2naptrien (bis{3-[(2-hydroxynaphthyl)methylimido]propyl}amine), H_2napMetrien (bis{3-[(2-hydroxynaphthyl)methylimido]propyl}-(methyl)amine), H_2Cl_4saldien {bis[2-(3,5-dichlorosalicylimido)-ethyl]amine}, H_2Cl_4saltrien {bis[3-(3,5-dichlorosalicylimido)propyl]amine}, and H_2Cl_4salMetrien {bis[3-(3,5-dichlorosalicylimido)propyl](methyl)amine} were prepared by standard methods.[12,17] Typically, the triamine [bis(2-aminoethyl)amine, bis(3-aminopropyl)amine or bis(3-aminopropyl)(methyl)amine] (0.01 mol) was added directly to a warm ethanolic solution of the aldehyde (naphthaldehyde and 3,5-dichlorosalicylaldehyde) (0.02 mol); the reaction mixture was heated to reflux for 30 min and then cooled on ice. The compounds H_2napdien, H_2Cl_4saldien and H_2naptrien precipitated from the solution, yielding yellow solids that were recrystallised from methanol; the other ligands were obtained as brown/yellow oils, after solvent removal.

H_2napdien: Yield: 3.7 g (90%). − $C_{26}H_{25}N_3O_2$ (411.5): calcd. C 75.89, H 6.12, N 10.21; found C 75.80, H 6.12, N 10.19. − ^{1}H NMR ($CDCl_3$, 200 MHz, 297 K): δ = 2.88−3.69 (8 H, *CH*$_2$), 6.68−8.02 (12 H, aromatic H), 9.06 (2 H, *N*=*CH*), 13.91 (2 H, O*H*).

H_2naptrien: Yield: 3.0 g (68%). − $C_{28}H_{29}N_3O_2 \cdot {}^5/_2H_2O$ (484.6): calcd. C 69.40, H 7.07, N 8.67; found C 69.27, H 7.00, N 8.66. − ^{1}H NMR ($CDCl_3$, 200 MHz, 297 K): δ = 1.80−3.70 (12 H, *CH_2*), 6.68−8.02 (12 H, aromatic H), 9.06 (2 H, *N=CH*), 13.95 (2 H, O*H*).

H_2napMetrien: Yield: 3.2 g (70%), obtained as an oil. − ^{1}H NMR ($CDCl_3$, 200 MHz, 297 K): δ = 2.20 (3 H, *CH_3*), 1.85−3.69 (12 H, *CH_2*), 6.69−8.03 (12 H, aromatic H), 9.01 (2 H, *N=CH*), 14.02 (2 H, *OH*).

H_2Cl_4saldien: Yield: 4.2 g (93%). − $C_{18}H_{17}Cl_4N_3O_2$ (449.2): calcd. C 46.03, H 3.86, N 7.67; found C 45.97, H 3.84, N 7.68. − ^{1}H NMR ($CDCl_3$, 200 MHz, 297 K): δ = 2.70−2.82 (8 H, *CH_2*), 7.09−7.38 (4 H, aromatic H), 8.23 (2 H, *N=CH*).

H_2Cl_4saltrien: Yield: 3.5 g (74%), obtained as oil. − ^{1}H NMR ($CDCl_3$, 200 MHz, 297 K): δ = 1.85−2.80 (12 H, *CH_2*), 7.10−7.38 (4 H, aromatic H), 9.86 (2 H, *N=CH*).

H_2Cl_4salMetrien: Yield: 3.4 g (72%), obtained as oil. − ^{1}H NMR ($CDCl_3$, 200 MHz, 297 K): δ = 2.20 (3 H, *CH_3*), 1.86−2.44 (12 H, *CH_2*), 7.08−7.38 (4 H, aromatic H), 8.21 (2 H, *N=CH*)

The nickel(II) complexes were also synthesised by standard procedures;[12,17] typically, ethanolic solutions of the ligands (5 mmol) were added to ethanolic nickel(II) acetate solutions (5 mmol); the resulting solutions were heated to reflux for 60 min. Upon cooling, green solids were collected by filtration, recrystallised from acetonitrile (except for dien-based complexes), and dried under vacuum for several hours.

[Ni(napdien)] (1): Yield: 1.7 g (72%). − $C_{26}H_{23}N_3NiO_2$ (468.2): calcd. C 75.89, H 6.12, N 10.21; found C 75.36, H 6.12, N 10.11. − UV/Vis: λ_{max}/nm (ε/dm^3 mol^{-1} cm^{-1}) = 402 (6600), 420 sh (DMF).

[Ni(naptrien)] (3): Yield: 1.5 g (60%). − $C_{28}H_{27}N_3NiO_2$ (496.3): calcd. C 67.77, H 5.48, N 8.47; found C 67.59, H 5.48, N 8.62. − UV/Vis: λ_{max}/nm (ε/dm^{3}mol^{-1}cm^{-1}) = 1143 (39), 1010 (33), 566 (85), 521 sh, 408 (9700), 389 (11300) (DMF); λ_{max}/nm = 606, 522 sh, 418 (Nujol).

[Ni(napMetrien)] (5): Yield: 1.8 g (68%). − $C_{29}H_{29}N_3NiO_2$ (510.3): calcd. C 68.26, H 5.73, N 8.23; found C 68.79, H 5.72, N 8.17. − UV/Vis: λ_{max}/nm (ε/dm^{3}mol^{-1}cm^{-1}) = 1200 (20), 1013 (10), 570 (63), 521 sh, 408 (10000), 388 (11900) (DMF); λ_{max}/nm = 584, 524 sh, 418 (Nujol).

[Ni(Cl_4saldien)] (2): Yield: 1.9 g (75%). − $C_{18}H_{15}Cl_4N_3NiO_2$ (505.9): calcd. C 48.13, H 3.81, N 9.36; found C 48.97, H 3.82, N 9.39. − UV/Vis: λ_{max}/nm (ε/dm^{3}mol^{-1}cm^{-1}) = 419 (5300), 450 sh (DMF).

[Ni(Cl_4saltrien)] (4): Yield: 1.4 g (53%). − $C_{20}H_{19}Cl_4N_3NiO_2 \cdot 2H_2O$ (533.9): calcd. C 42.15, H 4.07, N 7.37; found C 42.27, H 4.00, N 7.55. − UV/Vis: λ_{max}/nm (ε/dm^{3}mol^{-1}cm^{-1}) = 1088 (10), 935 (11), 564 (30), 384 (8500) (DMF); λ_{max}/nm = 564, 386 (Nujol).

[Ni(Cl_4salMetrien)] (6): Yield: 1.5 g (57%). − $C_{21}H_{21}Cl_4N_3NiO_2$ (547.9): calcd. C 46.03, H 3.86, N 7.67; found C 45.98, H 3.84, N 7.68. − UV/Vis: λ_{max}/nm (ε/dm^{3}mol^{-1}cm^{-1}) = 1159 (8), 966 (10), 568 (36), 381 (10100) (DMF); λ_{max}/nm = 590, 392 (Nujol).

Preparation of the Nickel(III) Complexes and Adduct Formation: Nickel(III) complexes were generated electrochemically by exhaustive electrolysis of DMF solutions 10^{-3} mol·dm^{-3} in nickel(II) precursor and 0.1 mol·dm^{-3} in NEt_4ClO_4 at ca. 4 °C. The time elapsing during the electrolysis was varied from 20 to 45 min; the upper limit was chosen to avoid extensive decomposition of the oxidised species. Chemically oxidised nickel(III) species were obtained by addition of a large excess (ca. 50%) of iodine to solutions of the nickel(II) precursors. Because of the instability of the electrogenerated Ni^{III} species it was not possible to isolate solids, and so these species were generated shortly before measurements and kept frozen in liquid nitrogen. The decay of Ni^{III} species is significantly lessened at low temperatures, and the samples are stable for several days when kept in liquid nitrogen. The adducts were prepared at temperatures just above the softening point of the frozen glass, by addition of freshly electrolysed solution of nickel(III) to frozen solutions or suspensions of the corresponding bases.

Physical Measurements: Elemental analysis (C, H, and N) were performed at the Departmento de Química, Faculdade de Ciências, Universidade do Porto. − Electrochemical measurements were made with a PAR 273 potentiostat, using solutions ca. 10^{-3} mol·dm^{-3} in nickel(II) complex and 0.1 mol·dm^{-3} in NEt_4ClO_4. − Cyclic voltammetry was performed in MeOH, DMF, and Me_2SO, using a platinum microsphere as working electrode, a platinum wire as counter-electrode, and an Ag/AgCl (1 mol·dm^{-3} NaCl) reference electrode. All potentials are reported relative to that of the reference electrode and to $E_{1/2}$ of the ferrocenium/ferrocene couple; under the experimental conditions used, $E_{1/2}$ for the latter couple is 0.48 V in Me_2SO, 0.47 V in DMF and 0.45 V in MeOH. Scan rates from 0.05 to 0.50 V·s^{-1} were used, and the low and high potential limits were 0.00 V and 1.20 V. − Electrolyses in DMF were carried out at controlled potential, at values about 0.10 V higher than the anodic peak potential in a three-electrode cell, using platinum gauze as working and counter-electrodes, and an Ag/AgCl (1 mol·dm^{-3} NaCl) reference electrode (all from Metrohm). − Electronic spectra were recorded with a Shimadzu UV 3101PC spectrophotometer, in the range 1500−300 nm. Conditions used were: room temperature, 10^{-2} and 10^{-4} mol·dm^{-3}, for nickel(II) complexes; and temperature about 4 °C and 10^{-3} mol·dm^{-3} Ni^{II} solutions for chemically and electrolysed Ni^{III} complexes. − EPR spectra were obtained at 77 K with a Bruker ESP 300E X-band spectrometer, using an insert Dewar. The magnetic field was calibrated by using Mn^{2+} in MgO, and diphenylpicrylhydrazyl was used as internal reference (dpph; g = 2.0037). The reported EPR parameters were obtained by spectral simulation using the programme WinEPR Simfonia (Bruker) and assuming rhombic Spin Hamiltonians; line widths were typically in the range 1.5−2.0 (z) to 1.5−3.0 (x, y) mT. The values of $a(N)_{x,y}$ are less accurate, due to the low spectral resolution. Typical experimental conditions used: microwave power 10−15 mW; modulation amplitude 0.5 mT; modulation frequency 100 kHz.

Acknowledgments

This work was partially supported by the "Fundação para a Ciência e Tecnologia" (Lisboa) through project Praxis/2/2.1/QUI/316/94.

[1] I. C. Santos, M. Vilas-Boas, F. Piedade, C. Freire, M. T. Duarte, B. de Castro, *Polyhedron* **2000**, *19*, 655−664.
[2] C. Freire, B. de Castro, *Polyhedron* **1998**, *17*, 4227−4235.
[3] C. Freire, B. de Castro, *J. Chem. Soc., Dalton Trans.* **1998**, 1491−1497.
[4] F. Azevedo, M. A. A. de C. T. Carrondo, B. de Castro, M. Convery, D. Domingues, C. Freire, M. T. Duarte, K. Nielson, I. Santos, *Inorg. Chim. Acta* **1994**, *219*, 43−54.

[5] M. A. A. de C. T. Carrondo, B. de Castro, A. M. Coelho, D. Domingues, C. Freire, J. Morais, *Inorg. Chim. Acta* **1993**, *205*, 157−166.
[6] C. Freire, B. de Castro, *Inorg. Chem* **1990**, *29*, 5113−5119.
[7] M. Vilas-Boas, C. Freire, B. de Castro, P. A. Christensen, A. R. Hillman, *Inorg. Chem.* **1997**, *36*, 4919−4929.
[8] M. Vilas-Boas, C. Freire, B. de Castro, A. R. Hillman, *J. Phys. Chem. B* **1998**, *102*, 8533−8540.
[9] F. Azevedo, C. Freire, B. de Castro, manuscript in preparation.
[10] C. Gosden, J. B. Kerr, D. Pletcher, R. Rosas, *J. Electroanal. Chem. Interfacial Electrochem.* **1981**, *117*, 101−107.
[11] C. Freire, B. de Castro, E. Pereira, *J. Chem. Soc., Dalton Trans.* **1994**, 571−576.
[12] W. M. Coleman, L. T. Taylor, *Inorg. Chem.* **1971**, *10*, 2195−2199.
[13] E. M. Boge, D. P. Freyberg, E. Kokot, G. M. Mockler, E. Sinn, *Inorg. Chem.* **1977**, *16*, 1655−1660.
[14] M. Nemiroff, S. L. Holt, *Inorg. Chem.* **1973**, *12*, 2032−2037.
[15] L. Taylor, W. M. Coleman, *J. Am. Chem. Soc.* **1970**, *92*, 1449−1450.
[16] L. Gomes,D. Pinho, C. Freire, B. de Castro, *Acta Crystallogr.* **1999**, *C55*, 1425−1427.
[17] L. Sacconi, I. Bertini, *J. Am. Chem. Soc.* **1966**, *88*, 5180−5185.
[18] A. J. Bard, L. R. Faulkner, *Electrochemical methods*, Wiley, New York, **1980**.
[19] P. Zanello, R. Cini, A. Cinquanti, *Inorg. Chim. Acta* **1983**, *74*, 89−95.
[20] J. H. Cameron, K. J. Mcullough, *J. Chem. Soc., Dalton Trans.* **1990**, 935−941.
[21] B. R. McGarvey, *Can. J. Chem.* **1975**, *53*, 2498−2511.
[22] A. H. Maki, N. Edelstein, A. Daveson, R. H. Holm, *J. Am. Chem. Soc.* **1964**, *86*, 4580−4587.
[23] C. Daul, C. W. Schlapfer, A. van Zeleewsky, *Struct. Bonding (Berlin)* **1979**, *36*, 129.
[24] P. J. Chmielewski, L. Latos-Graazynski, *Inorg. Chem.* **1997**, *36*, 840−845.
[25] H.-J. Kruger, R. H. Holm, *Inorg. Chem.* **1989**, *28*, 1148−1155.
[26] S. Chandrasekhar, A. McAuley, *Inorg. Chem.* **1992**, *31*, 2234−2240.
[27] T. L. Pappenhagen, D. W. Margerum, *J. Am. Chem. Soc.* **1985**, *197*, 4576−4577.
[28] Y. L. Wang, M. W. Beach, T. L. Pappenhagen, D. W. Margerum, *Inorg. Chem.* **1988**, *27*, 4464−4472.
[29] S. T. Donald, Jr., R. L. Julien, *Experimental Electrochemistry for Chemistry*, John Wiley & Sons, New York, **1988**.

Received October 9, 2000
[I00377]

Synthesis and X-ray Crystal Structure of $[U(\eta\text{-}C_8H_8)(HMPA)_3][BPh_4]$, the First Cationic Monocyclooctatetraenyl Compound of Uranium (III), and its Neodymium Homologue

Sophie M. Cendrowski-Guillaume,*[a][‡] Martine Nierlich,[a] and Michel Ephritikhine*[a]

Keywords: Actinides / Uranium / Neodymium / Lanthanides / Cations / Monocyclooctatetraenyl complexes

The title compound was synthesized in 88% yield by reducing the uranium(IV) dication $[U(COT)(HMPA)_3][BPh_4]_2$ (COT = η-C_8H_8) with sodium amalgam while the neodymium analogue was prepared by substitution of the THF ligands in $[Nd(COT)(THF)_4][BPh_4]$. Comparison of the crystal structures of the complexes $[M(COT)(HMPA)_3][BPh_4]$ (M = U, Nd, Sm) shows that the variations in the M–ligand bond lengths simply reflect the differences in the ionic radii of the metals.

Introduction

Recently we reported the synthesis and structural characterization of the uranium(IV) complex $[U(COT)(HMPA)_3][BPh_4]_2$ (**1**) (COT = η-C_8H_8, HMPA = hexamethylphosphoramide), the first organometallic dication of an f-element, which was obtained by protonolysis of the parent borohydride $U(COT)(BH_4)_2$.[1] Cationic metal compounds are interesting since they are potential precursors in inorganic and organometallic syntheses as well as efficient catalysts in various organic reactions. In the course of our studies on the reactivity of **1**, we found that it could be reduced to the uranium(III) complex $[U(COT)(HMPA)_3][BPh_4]$ (**2**). Such cyclooctatetraenyl uranium compounds in the +3 oxidation state are quite rare, being limited to the anionic bis([8]annulene) complex $[K(diglyme)][U(\eta\text{-}C_8H_7Me)_2]$[2] and the neutral mixed-ring complex $[U(COT)(\eta\text{-}C_5Me_5)(L)]$ (L = THF, 4,4′-dimethyl-2,2′-bipyridine).[3] More generally, very few cationic organometallic complexes of uranium(III) have been described: the bis(pentadienyl) complex $[U(\eta\text{-}2,4\text{-}Me_2\text{-}C_5H_5)_2][BPh_4]$,[4] the metallocene complex $[U(\eta\text{-}C_5Me_5)_2(THF)_2][BPh_4]$,[5] and the trinuclear arene complex $[U_3(\eta\text{-}C_6Me_6)_3(AlCl_4)_3Cl_5][AlCl_4]$;[6] only these latter two have been crystallographically characterized. Here we present the synthesis and X-ray crystal structure of **2**, taking the opportunity to compare this structure with that of the U^{IV} dication of **1**, and also with those of the lanthanide analogues $[M(COT)(HMPA)_3]^+$ [M = Nd (**3**) and Sm (**4**)].

[a] Service de Chimie Moléculaire, DSM, DRECAM, CNRS URA 331, CEA Saclay,
91191 Gif-sur-Yvette, France
Fax: (internat.) +33-1/6908-6640
E-mail: ephri@drecam.cea.fr
[‡] Present address: LCPO, CNRS UMR 5629, ENSCP Bordeaux, B. P. 108, Avenue Pey Berland, 33402 Talence Cedex, France
Fax: (internat.) +33-5/5684-8487
E-mail: guillaume@enscpb.u-bordeaux.fr

Results and Discussion

Synthesis and Characterization

The uranium(III) compound **2** was prepared by treating the orange dication **1** with a slight excess of sodium amalgam in tetrahydrofuran (THF), according to Equation (1).

$$\underset{\mathbf{1}}{[U(COT)(HMPA)_3][BPh_4]_2} + Na(Hg) \xrightarrow{THF} \underset{\mathbf{2}}{[U(COT)(HMPA)_3][BPh_4]} + NaBPh_4 \quad (1)$$

After stirring for 16 h at 20 °C, the green solution was filtered and a green microcrystalline powder of **2** was deposited upon addition of pentane (88% yield). Compound **2** was characterized by elemental analysis (C, H N) and X-ray crystallography (vide infra). The ^1H NMR spectrum exhibits two resonances at δ = 1.7 and −47.4 corresponding to the HMPA and COT ligands, respectively, and shows the presence of only one BPh_4 anion. Oxidation of **2** with $TlBPh_4$ failed to give back the dication **1** and afforded only insoluble unidentified products; this behaviour is not understood.

The synthesis of **2** was not affected by the small excess of sodium amalgam (<3 equivalents), although the monocation reacted further with larger amounts of the reducing agent (>9 equivalents) to give the uranium(IV) compound $U(COT)_2$ as the sole identifiable organometallic product. It is possible that the putative U^{II} species "U(COT)", formed by reduction of **2**, was transformed by disproportionation into uranium metal and uranocene, the latter being inert towards sodium amalgam. While the U^{III} compound $Na[U(\eta\text{-}C_5Me_5)_2Cl_2]$ is known to act as a uranium(II) synthetic equivalent,[7] it is only very recently that the toluene-bridged diuranium complex $[(\mu\text{-}C_7H_8)\{U[N(Ad)Ar]_2\}_2]$ (Ad = adamantyl, Ar = 3,5-C_6H_3-Me_2) was isolated and crystallographically characterized; this complex exhibits a reactivity which is consistent with the formality of divalent uranium.[8]

 © WILEY-VCH Verlag GmbH, 69451 Weinheim, 2001 1434−1948/01/0606−1495 $ 17.50+.50/0

The separation of lanthanide(III) and actinide(III) compounds is an important problem in the context of the reprocessing of nuclear wastes and from a basic point of view. Much attention is thus paid to the structural and chemical differentiation of homologous compounds of 4f and 5f elements.[9] In order to compare the crystal structure of **2** with that of lanthanide counterparts, the neodymium compound $[Nd(COT)(HMPA)_3][BPh_4]$ (**3**) was synthesized by substitution of the THF ligands in $[Nd(COT)(THF)_4][BPh_4]$[10] with HMPA, according to Equation (2).

$$[Nd(COT)(THF)_4][BPh_4] + 3\ HMPA \xrightarrow{\text{pyridine}} [Nd(COT)(HMPA)_3][BPh_4] + 4\ THF \quad (2)$$

3

Pink crystals of the solvate **3**.THF were obtained by crystallization from THF. The analogous samarium complex $[Sm(COT)(HMPA)_3]I$ (**4**) was recently prepared by reaction of samarium metal, cyclooctatetraene, and iodine in the presence of HMPA, and its crystal structure has been determined.[11]

Crystal Structures

The crystals of **2** and **3**·THF are composed of discrete cations and anions. The BPh_4 anions display the expected structural parameters. A view of one of the two independent and almost identical cations of **2** and a view of the cation of **3**·THF are shown in Figure 1 and 2, respectively, together with selected bond lengths and angles; the atom numbering scheme is the same for the uranium and neodymium compounds.

The two structures are very similar, both cations adopting a three-legged piano-stool configuration in which the O−M−O angles vary from 83.3(5) to 88.5(6)° for M = U, and from 83.81(16) to 85.95(16)° for M = Nd; the COT−M−O angles (COT = centroid of the C_8H_8 ring) range between 124.5(8) and 132.3(7)° (M = U), and between 125.6(2) and 131.1(2)° (M = Nd). The U(1) and U(2) atoms are 2.00(1) and 2.03(1) Å from the planar COT ring (within ±0.02 Å) and the mean U(1)−C and U(2)−C bond lengths are 2.71(4) and 2.74(6) Å, respectively. These values are almost identical to those found in the other two crystallographically characterized monocyclooctatetraenyl U^{III} complexes, $[K(diglyme)][U(\eta\text{-}C_8H_7Me)_2]$ [1.999 and 2.707(7) Å][2] and $[U(COT)(\eta\text{-}C_5Me_5)(Me_2bipy)]$ (2.01 and 2.703 Å).[3] The Nd−COT distance of 1.984(5) Å in **3** compares well with those determined in mono(COT) neodymium complexes; for example, 1.906(6) Å in $[Nd(COT)(THF)_4][BPh_4]$[10a] and 2.01(1) Å in $[Nd(COT)I(THF)_3]$.[12]

Not surprisingly, the structure of the cation $[Nd(COT)(HMPA)_3]^+$ is quite similar to that of the samarium analogue **4** (Table 1);[11] the Nd−C and Nd−O distances are systematically slightly longer than the Sm−C and Sm−O distances, in agreement with the 0.03 Å difference between the ionic radii of Nd^{3+} and Sm^{3+}.[13]

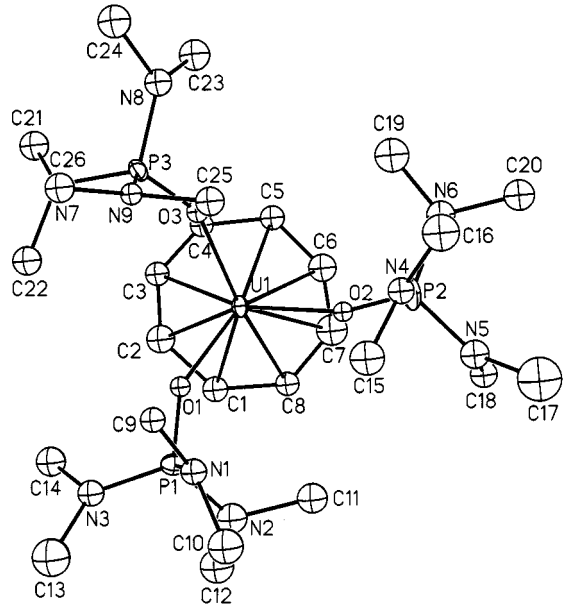

Figure 1. View of the crystal structure of one of the two independent cations $[U(COT)(HMPA)_3]^+$ with thermal ellipsoids drawn at the 30% probability level; selected bond lengths (Å) and angles (°): U(1)−C(1) 2.73(3), U(1)−C(2) 2.65(3), U(1)−C(3) 2.65(3), U(1)−C(4) 2.70(3), U(1)−C(5) 2.75(3), U(1)−C(6) 2.70(3), U(1)−C(7) 2.76(4), U(1)−C(8) 2.72(3), U(1)−O(1) 2.380(16), U(1)−O(2) 2.454(16), U(1)−O(3) 2.401(16), U(1)−COT 2.00(1); O(1)−U(1)−O(2) 84.9(5), O(1)−U(1)−O(3) 85.5(5), O(2)−U(1)−O(3) 83.3(5), COT−U(1)−O(1) 132.3(7), COT−U(1)−O(2) 128.1(8), COT−U(1)−O(3) 126.5(7); COT is the centroid of the C_8H_8 ring

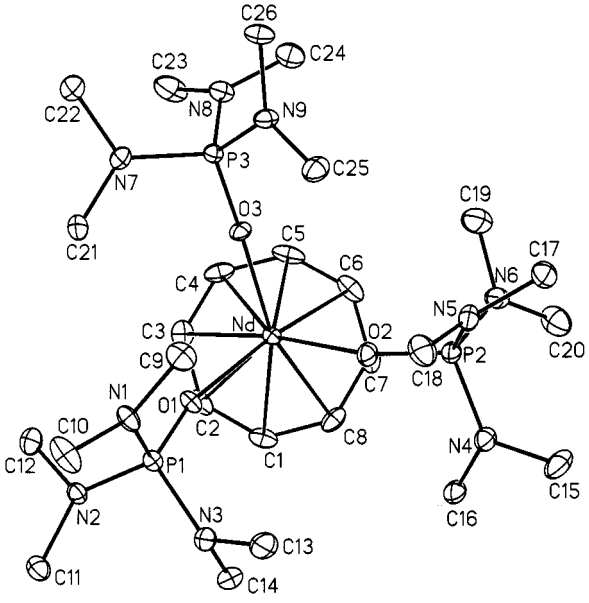

Figure 2. View of the crystal structure of the cation $[Nd(COT)(HMPA)_3]^+$ with thermal ellipsoids drawn at the 30% probability level; selected bond lengths (Å) and angles (°): Nd−C(1) 2.719(7), Nd−C(2) 2.709(7), Nd−C(3) 2.718(7), Nd−C(4) 2.698(7), Nd−C(5) 2.686(7), Nd−C(6) 2.697(7), Nd−C(7) 2.689(8), Nd−C(8) 2.704(7), Nd−O(1) 2.328(5), Nd−O(2) 2.392(5), Nd−O(3) 2.355(4), Nd−COT 1.984(5); O(1)−Nd−O(2) 85.95(16), O(1)−Nd−O(3) 85.76(16), O(2)−Nd−O(3) 83.81(16), COT−Nd−O(1) 125.6(2), COT−Nd−O(2) 131.1(2), COT−Nd−O(3) 129.1(2); COT is the centroid of the C_8H_8 ring

Table 1. Comparison of the geometrical parameters for the cations $[M(COT)L_3]^+$ (M = U, Nd, Sm[10]) and the dication $[U(COT)L_3]^{2+}$ [1] (L = HMPA)

	$[U(COT)L_3]^{+}$[a]	$[Nd(COT)L_3]^+$	$[Sm(COT)L_3]^+$	$[U(COT)L_3]^{2+}$[a]
<M−C> (Å)	2.71(4); 2.74(6)	2.70(1)	2.66	2.65(4); 2.65(3)
M−COT (Å)	2.00(1); 2.03(1)	1.984(5)	1.95	1.92(2); 1.92(2)
<M−O> (Å)	2.41(4); 2.40(6)	2.36(3)	2.31	2.22(2); 2.22(1)
<O−M−O> (deg)	84(1); 87(2)	85(1)	86	86(2); 87(3)

[a] The values for each independent cation are given.

The uranium cation **2** and its neodymium and samarium counterparts **3** and **4** permit a direct comparison of the structural data of homologous uranium(III) and lanthanide(III) compounds. Such comparative examinations have previously been made on only a few pairs of isostructural complexes, with the aim of evaluating and possibly differentiating the nature of the bonds in 4f and 5f element complexes.[14−16] In the cations **2**−**4**, the variations in the metal−ligand bond lengths, listed in Table 1, reflect the differences in the ionic radii of the metals (0.04 Å between U^{3+} and Nd^{3+}, 0.07 Å between U^{3+} and Sm^{3+}).[13] This regular trend agrees with that most generally observed, as for the complexes $[M(\eta\text{-}C_6Me_6)(AlCl_4)_3]$ (M = U, Sm)[14] or $[M(\eta\text{-}C_5Me_5)I_2(THF)_3]$ (M = U, Ce);[15] this was explained by the fact that f orbitals are not substantially involved in ligand bonding. To the best of our knowledge, it is only in the phosphorus complexes $[M(\eta\text{-}C_5H_4Me)_3L]$ (M = U, Ce; L = PMe_3 or $P(OCH_2)_3CEt$) that the U−P bond length was found to be significantly shorter than the Ce−P distance, whereas the U−L and Ce−L distances are the same in the derivatives with oxygen and nitrogen ligands (L = THF, quinuclidine).[16] This difference has been rationalised by postulating uranium-to-phosphorous π bonding which is absent in the lanthanide analogues.

If the structure of the U^{III} cation **2** is now compared with that of the parent U^{IV} dication **1**, it is noteworthy that the difference between the U−O bond lengths, 0.2 Å, is much greater than that observed between the U−C bond lengths, 0.1 Å, which corresponds to the ionic radii variation between U^{4+} and U^{3+}.[13] This feature certainly results from the more positive charge on the dicationic U^{IV} centre, which induces a stronger interaction with the Lewis base.

Experimental Section

General: All preparations were carried out under argon (less than 2 ppm oxygen and water) using standard Schlenk and vacuum line techniques or in a glove box. Solvents were thoroughly dried and deoxygenated by standard methods and distilled immediately before use. $[D_8]$THF was dried over Na-K alloy. The ^{1}H NMR spectra were recorded on a Bruker DPX 200 instrument and were referenced internally using the residual protio solvent resonances relative to tetramethylsilane (δ = 0). Elemental analyses were performed by Analytische Laboratorien at Lindlar (Germany). $[Nd(COT)(THF)_4][BPh_4]$ was synthesized as previously reported.[10]

Synthesis of $[U(\eta\text{-}C_8H_8)(HMPA)_3][BPh_4]_2$ (1): This compound was prepared by a slight modification of the published procedure,[1] resulting in an improved yield. A flask was charged with $[(COT)U(BH_4)_2(THF)]$ (0.488 g, 1.10 mmol) and NEt_3HBPh_4 (1.011 g, 2.40 mmol) in THF (40 mL) and HMPA (1.1 mL, 6.32 mmol) was introduced with a syringe. The reaction mixture was stirred for 5 h at 20 °C during which time evolution of gas was observed and an orange powder was deposited from the dark red solution. After evaporation, the crude solid was dried under dynamic vacuum for 18 h. It was then washed with THF (40 mL) and extracted with pyridine (40 mL). The solution was filtered and the solvent was evaporated in vacuo, leaving **1** as a bright orange powder (1.573 g, 94%).

Synthesis of $[U(\eta\text{-}C_8H_8)(HMPA)_3][BPh_4]$ (2): A flask was charged with **1** (592.9 mg, 0.390 mmol) and 2% Na(Hg) (620.0 mg, 0.539 mmol of Na) in THF (40 mL). The reaction mixture was magnetically stirred for 1 h at room temperature, then immersed in an ultrasound bath (60 W, 40 kHz) for 3 h, and finally magnetically stirred for 12 h at room temperature. The green solution was filtered and its volume reduced to ca 10 mL; a green microcrystalline powder of **2** was deposited upon addition of pentane (20 mL). The powder was filtered off and dried under vacuum (411 mg, 88%). − ^{1}H NMR ($[D_8]$THF): δ = 7.12 (br. t, 8 H, *o*-Ph), 6.72 (t, *J* = 6 Hz, 8 H, *m*-Ph), 6.60 (t, *J* = 6 Hz, 4 H, *p*-Ph), 1.7 (br. s, $w_{1/2}$ = 75 Hz, 54 H, HMPA), −47.4 (br. s, $w_{1/2}$ = 120 Hz, 8 H, COT). − $C_{50}H_{82}BN_9O_3P_3U$ (1199): calcd. C 50.09, H 6.90, N 10.51; found C 50.46, H 6.77, N 10.24.

Reaction of 2 with Na(Hg): An NMR tube was charged with **2** (8.1 mg, 6.76 μmol) and 2% Na(Hg) (72.3 mg, 62.9 μmol of Na) in $[D_8]$THF (0.5 mL). The spectra showed the progressive formation of $U(COT)_2$ as the sole identifiable organometallic product, the reaction being complete after 3 days at 20 °C.

Synthesis of $[Nd(\eta\text{-}C_8H_8)(HMPA)_3][BPh_4]$ (3): A flask was charged with $[Nd(\eta\text{-}C_8H_8)(THF)_4][BPh_4]$ (50.51 mg, 0.059 mmol) in pyridine (10 mL), and HMPA (150 μL, 0.862 mmol) was added with a microsyringe. The colour of the solution turned from green to blue; the volume of the solution was reduced to ca 5 mL by evaporation and upon addition of pentane (10 mL), blue microcrystals of **3**·1/$2C_5H_5N$ were deposited. These were filtered off and dried under vacuum (27.0 mg, 40%). − ^{1}H NMR ($[D_8]$THF): δ = 8.44 (s, 1 H, C_5H_5N), 7.53 (s, 1 H, C_5H_5N), 7.20 (br. t, 8.5 H, *o*-Ph + C_5H_5N), 6.78 (t, *J* = 7 Hz, 8 H, *m*-Ph), 6.63 (t, *J* = 7 Hz, 4 H, *p*-Ph), 2.3 (br. s, $w_{1/2}$ = 70 Hz, 54 H, HMPA), −9.9 (br. s, $w_{1/2}$ = 100 Hz, 8 H, COT). − $C_{52.5}H_{84.5}BN_{9.5}O_3P_3Nd$ (1144): calcd. C 55.08, H 7.44, N 11.62; found C 54.91, H 7.58, N 11.75.

X-ray Crystallography of 2: Single crystals of **2** were obtained by crystallization from THF. A crystal of approximate dimensions 0.25 × 0.20 × 0.10 mm was selected. Diffraction collection was carried out on a Nonius diffractometer equipped with a CCD detector. The lattice parameters were determined from ten images recorded with 2° Φ-scans and later refined on all data. The data were

recorded at 123 K. A 180° Φ-range was scanned with 2° steps with a crystal-to-detector distance fixed at 30 mm. Data were corrected for Lorentz-polarization and absorption[17] effects. The structure was solved by the heavy atom method and refined by full-matrix least-squares on F^2 with anisotropic thermal parameters for the U and P atoms. H atoms were introduced at calculated positions as riding atoms with an isotropic displacement parameter equal to 1.2 (CH) or 1.5 (CH_3) times that of the parent atom. $C_{100}H_{164}B_2N_{18}O_6P_6U_2$ (2397.99), monoclinic, space group $P2_1$, a = 10.419(2), b = 31.018(6), c = 17.601(4) Å, β = 100.46(3)°, V = 5593.7(19) Å^3, Z = 2, D_c = 1.424 g cm^{-1}, Mo-K_α (λ = 0.71073 Å), μ_{Mo} = 3.035 mm^{-1}, F(000) = 2444, total reflections = 18725, independent reflections = 7272 (R_{int} = 0.11), observed reflections [$I > 2\sigma(I)$] = 5613, R_1 = 0.075, wR_2 = 0.143. All calculations were performed on an O2 Silicon Graphics Station with the SHELXTL package.[18]

X-ray crystallography of 3·THF: Pink single crystals of **3**·THF were obtained by crystallization of **3**·1/2C_5H_5N from THF. A crystal of approximate dimensions 0.25 × 0.25 × 0.15 mm was selected. Diffraction collection was carried out on a Nonius diffractometer equipped with a CCD detector. The lattice parameters were determined from ten images recorded with 2° Φ-scans and later refined on all data. The data were recorded at 123 K. A 180° Φ-range was scanned with 2° steps with a crystal-to-detector distance fixed at 35 mm. Data were corrected for Lorentz-polarization and absorption [17] effects. The structure was solved by the heavy atom method and refined by full-matrix least-squares on F^2 with anisotropic thermal parameters for all non-H atoms. H atoms were introduced at calculated positions as riding atoms with an isotropic displacement parameter equal to 1.2 (CH) or 1.5 (CH_3) times that of the parent atom. $C_{54}H_{90}BN_9O_4P_3Nd$ (1177.31), monoclinic, space group $P2_1/c$, a = 10.520(2), b = 21.481(4), c = 27.279(6) Å, β = 101.16(3)°, V = 6048(2) Å^3, Z = 4, D_c = 1.293 g cm^{-1}, Mo-K_α (λ = 0.71073 Å), μ_{Mo} = 0.987 mm^{-1}, F(000) = 2476, total reflections = 29850, independent reflections = 8067 (R_{int} = 0.0842), observed reflections [$I > 2\sigma(I)$] = 5823, R_1 = 0.051, wR_2 = 0.122. All calculations were performed on an O2 Silicon Graphics Station with the SHELXTL package.[18]

Crystallographic data (excluding structure factors) for the structures reported in this paper have been deposited with the Cambridge Crystallographic Data Centre as supplementary publication no. CCDC-151390 (**2**) and -151391 (**3**·THF). Copies of the data can be obtained free of charge on application to CCDC, 12 Union Road, Cambridge CB2 1EZ, UK [Fax: (internat.) +44-1223/336-033; E-mail: deposit@ccdc.cam.ac.uk].

[1] S. M. Cendrowski-Guillaume, M. Lance, M. Nierlich, M. Ephritikhine, *Organometallics* **2000**, *19*, 3257−3259.
[2] T. R. Boussie, D. C. Eisenberg, J. Rigsbee, A. Streitwieser, A. Zalkin, *Organometallics* **1991**, *10*, 1922−1928.
[3] A. R. Schake, L. R. Avens, C. J. Burns, D. L. Clark, A. P. Sattelberger, W. H. Smith, *Organometallics* **1993**, *12*, 1497−1498.
[4] D. Baudry, E. Bulot, M. Ephritikhine, *J. Chem. Soc., Chem. Commun.* **1989**, 1316−1317.
[5] C. Boisson, J. C. Berthet, M. Ephritikhine, M. Lance, M. Nierlich, *J. Organomet. Chem.* **1997**, *533*, 7−11.
[6] F. A. Cotton, W. Schwotzer, C. Q. Simpson, *Angew. Chem. Int. Ed. Engl.* **1986**, *25*, 637−638.
[7] [7a] B. P. Warner, B. L. Scott, C. J. Burns, *Angew. Chem. Int. Ed.* **1998**, *37*, 959−960. − [7b] P. J. Fagan, J. M. Manriquez, T. J. Marks, C. S. Day, S. H. Vollmer, V. W. Day, *Organometallics* **1982**, *1*, 170−180.
[8] P. L. Diaconescu, P. L. Arnold, T. A. Baker, D. J. Mindiola, C. C. Cummins, *J. Am. Chem. Soc.* **2000**, *122*, 6108−6109.
[9] [9a] K. L. Nash, *Solv. Extr. and Ion Exch.* **1993**, *11*, 729−768. − [9b] K. L. Nash, *Separation Chemistry for Lanthanides and Trivalent Actinides*, in *Handbook on the Physics and Chemistry of Rare Earths*, (Eds.: K. A. Gschneidner, L. Eyring, G. R. Choppin, G. H. Lander), North-Holland, Amsterdam, **1994**, vol. 18, 197.
[10] [10a] S. M. Cendrowski-Guillaume, M. Nierlich, M. Lance, M. Ephritikhine, *Organometallics* **1998**, *17*, 786−788. − [10b] S. M. Cendrowski-Guillaume, G. Le Gland, M. Nierlich, M. Ephritikhine, *Organometallics* **2000**, *19*, 5654−5660.
[11] K. Mashima, H. Fukumoto, Y. Nakayama, K. Tani, A. Nakamura, *Polyhedron* **1998**, *17*, 1065−1071.
[12] U. Kilimann, M. Schäfer, R. Herbst-Irmer, F. T. Edelmann, *J. Organomet. Chem.* **1994**, *469*, C10−C14.
[13] R. D. Shannon, *Acta Crystallogr., Sect. A* **1976**, *32*, 751−767.
[14] F. A. Cotton, W. Schwotzer, *Organometallics* **1987**, *6*, 1275−1280.
[15] [15a] L. R. Avens, C. J. Burns, R. J. Butcher, D. L. Clark, J. C. Gordon, A. R. Schake, B. L. Scott, J. G. Watkin, B. D. Zwick, *Organometallics* **2000**, *19*, 451−457. − [15b] P. N. Hazin, J. C. Huffman, J. W. Bruno, *Organometallics* **1987**, *6*, 23−27.
[16] J. G. Brennan, S. D. Stults, R. A. Andersen, A. Zalkin, *Organometallics* **1988**, *7*, 1329−1334.
[17] A. L. Spek, MULABS, *PLATON*, University of Utrecht, The Netherlands, **1997**.
[18] *SHELXTL*: G. Sheldrick **1999**, Bruker-AXS, Madison, WI, USA.

Received October 30, 2000
[I00411]

A Continuous Chirality Analysis of Homoleptic Hexacoordinated Complexes

Santiago Alvarez,*[a] Mark Pinsky,[b,c] and David Avnir*[c]

Keywords: Chirality / Stereochemistry / Coordination chemistry / Molecular symmetry / Quantitative chirality

Hexacoordinated complexes are generally considered to be potentially chiral if they have either at least two bidentate ligands or at least three different monodentate ligands. Here we draw attention to a neglected general possibility, namely that homoleptic hexacoordinated complexes with molecular structures in between octahedral and trigonal prismatic, following the Bailar twisting route, are chiral. A quantitative evaluation of the degree of chirality of such hexakis(monodentate) complexes shows that they reach maximum chirality when the trigonal rotation angle of the prism reaches 23°. Model calculations and analysis of experimental X-ray structures are in good agreement. The most chiral of the complexes with monodentate ligands that have been analyzed is $[Zr(SC_6H_4\text{-}4\text{-}OMe)_6]^{2-}$. The validity of the theoretical prediction is also corroborated by an analysis of the chirality of the coordination sphere in twisted tris(chelate) complexes.

Introduction

The chirality of transition metal complexes is of much current interest mainly because of their potential applications as catalysts for asymmetric synthesis.[1] Following von Zelewsky (and somewhat modifying his list),[2] we note that chirality can be induced in coordination compounds by: (i) the existence of different ligands (as in [Mabcdef]); (ii) a special spatial arrangement of ligands (as in one of the stereoisomers of $[Ma_2b_2c_2]$); (iii) the removal of an improper symmetry element of a bidentate ligand through formation of chelate rings (including the mutual breaking of an improper rotation present in such ligands); (iv) coordination of chiral ligands, of ligands which assume chiral conformations or of prochiral ligands (i.e., ligands which become chiral upon coordination because an improper symmetry is broken); or (v) rotational symmetry wrapping of the ligands around the metal. Within the rotational wrapping option, we distinguish several sub-types, namely helical wrapping,[3] the propeller-type arrangement in bis- and tris(chelate) complexes and, of relevance to this report, the Bailar-type twist,[4] which links octahedricity and trigonal prismacity in hexacoordinated complexes, as shown in **1**.

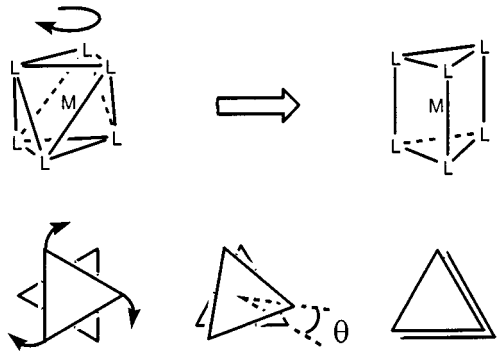

1

Perhaps the most elementary option for obtaining chirality is the Bailar twist, which reduces the achiral point groups O_h and D_{3h} to the chiral D_3 symmetry point group. The simplicity of this option originates from the fact that it allows *homoleptic* $[ML_6]$ complexes to be chiral, with no special requirement for chirality or pro-chirality of the six ligands. Yet, to the best of our knowledge, no enantiomeric crystals of the two D_3 enantiomers have been reported. It is interesting to note that of all the options for obtaining chirality, the one that was highlighted since the dawn of coordination chemistry was option (iii), i.e. the use of bidentate ligands. Starting with the pioneering work of Alfred Werner, who resolved the two enantiomers of the cationic complexes $[CoX(NH_3)(en)_2]^{2+}$ (X = Cl, Br),[5] many other octahedral metal complexes with two or three bidentate ligands have been shown to be chiral.[2,6–12] In fact, option (iii) has overshadowed over the years all the other options for obtaining chirality in hexacoordinated complexes. Thus, it is common to find in textbooks statements such as: "Important examples [of chiral molecules] are bischelate and trischelate octahedral complexes" (ref.[11]); "Chiral complexes occur mainly when chelate rings are formed" (ref.[11] p. 683) "In practice, optical activity is largely confined to octahedral complexes of chelating ligands";[6] **"**The absolute configuration of a chiral complex is described by imagining a view along a threefold rotation axis of a regular octahedron and noting the handedness of the helix formed

[a] Departament de Química Inorgànica and Centre de Recerca en Química Teòrica, Universitat de Barcelona,
Diagonal 647, 08028 Barcelona, Spain
E-mail: santiago@qi.ub.es
[b] Institute of Earth Sciences, The Hebrew University of Jerusalem,
Jerusalem 91904, Israel
[c] Institute of Chemistry and The Lise Meitner Minerva Center for Computational Quantum Chemistry, The Hebrew University of Jerusalem,
Jerusalem 91904, Israel
E-mail: david@chem.ch.huji.ac.il
Supporting information for this article is available on the WWW under http://www.wiley-vch.de/home/eurjic or from the authors.

 © WILEY-VCH Verlag GmbH, 69451 Weinheim, 2001 1434–1948/01/0606–1499 $ 17.50+.50/0

by the ligands'', but again, the figure that accompanies the text shows a complex with bidentate ligands.[8,13]

The main purpose of this paper is to draw attention to the largely neglected possibility of obtaining chiral homoleptic [ML_6] complexes through the Bailar twist. We do so by reporting the results of a quantitative analysis of the chirality of homoleptic hexacoordinated complexes and its variation along the D_3 route, comparing in detail experiment with theory. It was found that *chirality in crystalline hexacoordinated complexes is much more common than previously appreciated*. While it is true that crystalline chirality may not show up in solution if the racemization process has a low energy barrier, one should recall that chiral crystals have been used successfully for product enantiocontrol in many chiral catalytic reactions[28] and that growing interest in crystals as useful materials for optical purposes renders crystal-packing-induced chirality an important issue. Furthermore, even if the handedness flips between the two enantiomers in solution it may be of importance in catalytic processes with chiral substrates since diastereomeric interactions will prefer one of the two enantiomers. We also mention here, computational analysis in progress in our laboratories shows that the energy barriers for racemization of D_3-chiral homoleptic [ML_6] complexes may be surprisingly high (e.g. of the order of 20 kcal/mol for the Zr^{IV} thiolato complex analyzed below).

Results and Discussion

Chirality Changes Along the Bailar-Twist Route

The ML_6 structures can be characterized by the Bailar twist angle θ (**1**) that indicates their deviations from the trigonal prism (θ = 0°) or from the octahedron (θ = 60°). While classically one labels all the intermediate D_3 geometries as simply ''chiral'', the intuitive need arises to express that, for example, a θ value of 0.1° represents much lower chirality than a θ value of 10°. A quantitative evaluation of the degree of chirality is therefore needed here, and such a structural measurement tool will allow one to follow, in a continuous way, how chirality changes with θ. The methodology we use for this purpose is the Continuous Chirality Measures approach,[14] which has already proved useful in numerous applications.[15] In short (readers interested in more details are referred to ref.[14]), the method seeks the minimal distances that the vertices of an object have to undergo to attain achirality. On the scale, which is a function of these distances, an achiral molecule has a chirality value of S = 0 and as the structure is more chiral S increases (up to a maximum value of 100). In most cases — and in all cases reported here — the nearest achiral structure has at least one reflection plane.[16]

The results of computing the S values along a hypothetical Bailar route are shown in Figure 1 (full line) beginning with the ideal, all-equal-edges trigonal prism (TP) at θ = 0° and ending at θ = 60° with the ideal octahedron.[17] Since the end points are achiral while those at intermediate θ values are D_3-chiral, one expects that (at least one) maximum chirality value will appear in between the two achiral ends. This is indeed found for the model at θ = 23° (Figure 1). In a way, this result resembles the chirality analysis of rotating ethane[18] for which an angle of 30° was found to give the maximal chiral rotamer. We proposed therefore to term conformers of maximal chirality *chiramers*, and this term can be used here as well, i.e., the 23° conformer of the hexacoordinated ML_6 group is its chiramer.

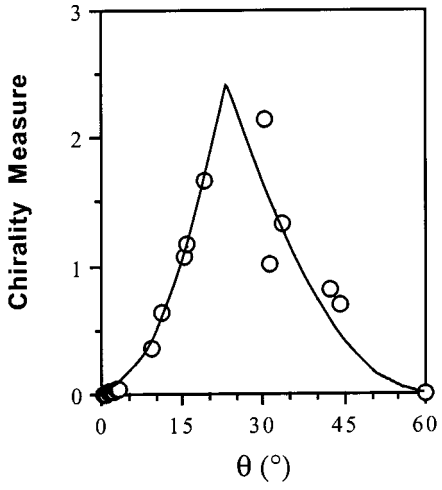

Figure 1. Chirality measure for a model MX_6 molecule (continuous line) along the trigonal twist (see **1**); the experimental chirality measures of heptaatomic MX_6 cores of homoleptic organometallic and thiolato complexes are shown as circles (more information can be found in Table 1)

The fact that the chiramer of the hexacoordinated complexes does not appear halfway (i.e., at 30°) between the two ideal shapes may seem at first sight surprising, but is explained as follows: One of the main features of the CCM approach is that it not only computes the chirality content, but also provides the actual shape of the nearest achiral object. When these objects are observed for the full line in Figure 1, it is seen that from the maximum and to the right (θ = 60°), the nearest achiral structure is a distorted octahedron of C_{2v} symmetry, namely an octahedron that is bent along the z-axis, as shown by **2**. Between the ideal TP on the left of Figure 1 (θ = 0°) and the maximum at θ = 23°, the nearest achiral structure is always a D_{3h}-TP varying in height from point to point (although not very much. Thus, for θ = 0°, 10° and 20°, the edge-to-height ratios are 1.000, 1.028 and 1.049, respectively). The reason why it is that the two branches do not cross at the halfway angle but closer to the achiral distorted octahedron branch is now clear: Unlike the right branch of Figure 1, the left branch represents a more demanding nearest achiral structure in the sense that it does not have two reflection planes but four; therefore, departure from that branch to the less-demanding two-planes branch occurs earlier than 30°. Finally, it should be noted that at the peak (θ = 23°), the chirality measure represents an equal minimum distance to *two* achiral structures: a TP and a bent z-axis octahedron.

Chirality of Homoleptic Complexes

Does the theoretical line of Figure 1 represent a reality for $[ML_6]$ complexes? We have selected for the present study

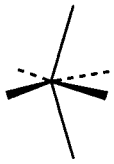

2

the families of organometallic and thiolato homoleptic compounds,[19] and the chirality measures of their MX_6 cores (Table 1) are superimposed in Figure 1 on the Bailar model line. It is seen that all structures fall along that line, suggesting that they indeed represent the Bailar pathway from O_h to TP. It can also be seen that the octahedricity and the trigonal prismacity of such complexes correspond to the Bailar route, as discussed in more detail elsewhere.[20] Analysis of the bonding parameters of the actual structures confirms that these are of D_3-type, as illustrated in Figure 2 for three representative compounds. This observation indicates that chiral hexacoordinated homoleptic complexes have already been synthesized and structurally characterized *but their chirality not recognized and not reported*. Thus, despite the clear chirality of molecules with intermediate rotation angles, the experimental reports of the compounds presented in Figure 1 do not mention such a property and their optical activity has not been investigated. Most of these complexes, however, crystallize in space groups having improper symmetry operations, namely as racemic mixtures.[21] We note that these anionic complexes have been crystallized with achiral cations and propose that obtaining enantiomerically pure compounds may be possible through crystallization with optically pure chiral counter ions. Two complexes, $[NbMe_6]^-$ and $[TaMe_6]^-$, that crystallize[22] in the enantiomorphic space group $P2_12_12_1$ are only slightly-distorted from the octahedron ($\theta \approx 3°$) and have small chirality measures. To the best of our knowledge, only a Zr^{IV} thiolato complex reported recently[23] is expected to be optically active, since it crystallizes in the enantiomorphic *R32* group and has a ZrS_6 core with a high chirality measure ($S = 2.16$ at $\theta = 30.4°$).

Table 1. Chirality measures, twist angle (θ), space group, and references for the hexacoordinate homoleptic metal complexes presented in Figure 1

Compd.[a]	Refcode[b]	θ	S(chir)	Group	ref.
$[Ta(CCSi\mathit{t}Bu_3)_6]^-$	HEQDIQ	18.8	1.67	$P\bar{1}$	[c]
$[Zr(CCSi\mathit{t}Bu_3)_6]^{2-}$	HEQDOW	60.0	0.00	$R\bar{3}$	[c]
$[Hf(CCSi\mathit{t}Bu_3)_6]^{2-}$	HEQDUC	60.0	0.00	$R\bar{3}$	[c]
$[TaPh_6]^-$	REZBAZ	15.1	1.08	$P\bar{1}$	[d]
$[Ta(p\text{-}Tol)_6]^-$	REZBED	15.9	1.18	$P2_1/n$	[d]
$[ZrMe_6]^{2-}$	JAMWOJ	11.2	0.63	$Aba2$	[e]
$[RhMe_6]^{3-}$	KAWVAF	44.0	0.70	$R\bar{3}c$	[f]
$[IrMe_6]^{3-}$	KAWVEJ	42.3	0.82	$R\bar{3}c$	[f]
$*[TaMe_6]^-$	POZHUH	3.2	0.04	$P2_12_12_1$	[g]
$*[NbMe_6]^-$	POZJAP	3.0	0.03	$P2_12_12_1$	[g]
$[WMe_6]$	ZOSXEK01	2.2	0.01	$Pbc2_1$	[g]
		0.6	0.01		
$[ReMe_6]$	ZOSXEL	1.1	0.01	$P2_1/n$	[g]
$[Co(oxazolidyl)_6]^{2+}$	CUXRUI	57.0	0.16	$P2_1/n$	[h]
$[MnMe_6]^{2-}$	GINZEI	60.0	0.00	$Pbca$	[i][j]
$[CrMe_6]^{3-}$	MCRLDX	47.1	0.42	$R\bar{3}c$	[k]
$[MoMe_6]$		1.7	0.02	Cc	[l]
		1.4	0.01		
$[Ti_2(\mu\text{-}SMe)_3(SMe)_6]^{2-}$	POJFOJ	31.1	1.01	$P2_1/a$	[m]
		33.3	1.34		
$[Zr(SC_6H_4\text{-}4\text{-}Me)_6]^{2-}$		9.2	0.35	$P\bar{1}$	[n]
$*[Zr(SC_6H_4\text{-}4\text{-}OMe)_6]^{2-}$		30.4	2.16	$R3_2$	[n]

[a] Compounds marked with an asterisk crystallize in enantiomorphic space groups. – [b] Cambridge Structural Database refcodes. – [c] T. P. Vaid, A. S. Veige, E. B. Lobkovsky, W. V. Glassey, P. T. Wolczanski, L. M. Liable-Sands, A. L. Rheingold, T. R. Cundari, *J. Am. Chem. Soc.* **1998**, *120*, 10067–10079. – [d] S. Kleinhenz, M. Schubert, K. Seppelt, *Chem. Ber.* **1997**, *130*, 903–905. – [e] P. M. Morse, G. S. Girolami, *J. Am. Chem. Soc.* **1989**, *111*, 4114–4116. – [f] R. S. Hay-Motherwell, G. Wilkinson, B. Hussain, M. B. Hursthouse, *J. Chem. Soc., Chem. Commun.* **1989**, 1436–1437. – [g] S. Kleinhenz, V. Pfennig, K. Seppelt, *Chem. Eur. J.* **1998**, *4*, 1687–1691. – [h] U. Plaia, H. Stolzenberg, W. P. Fehlhammer, *J. Am. Chem. Soc.* **1985**, *107*, 2171–2172. – [i] R. J. Morris, G. S. Girolami, *J. Am. Chem. Soc.* **1988**, *110*, 6245–6246. – [j] R. J. Morris, G. S. Girolami, *Organometallics* **1991**, *10*, 792–799. – [k] J. Krausse, G. Marx, *J. Organomet. Chem.* **1974**, *65*, 215–222. – [l] B. Roessler, K. Seppelt, *Angew Chem. Int. Ed.* **2000**, *39*, 1259–1261. – [m] W. Stuer, K. Kirschbaum, D. M. Giolando, *Angew Chem. Int. Ed. Engl.* **1994**, *33*, 1981–1983. – [n] J. C. Friese, A. Krol, C. Puke, K. Kirschbaum, D. M. Giolando, *Inorg. Chem.* **2000**, *39*, 1496–1500.

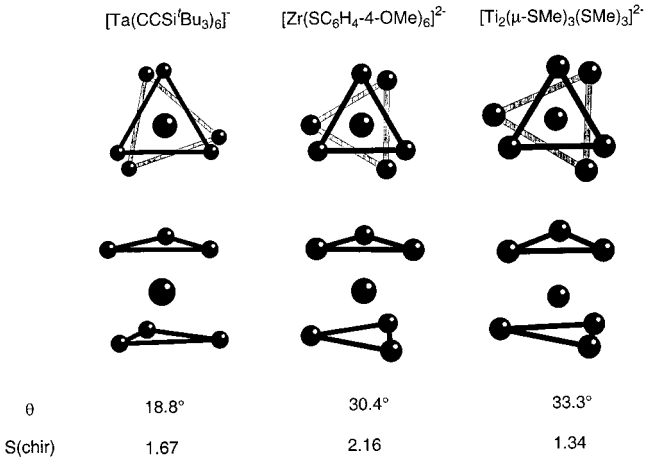

Figure 2. Perspective view and projection about the trigonal axis of the coordination spheres of three chiral homoleptic complexes with monodentate ligands that fall along the Bailar twist pathway **1** (see Table 1 for references)

As a further test of these observations and of the validity of the theoretical chirality line, we also analyzed the chirality of tris(chelate) complexes with twisted octahedra. Since the above analysis focused only on the MX_6 core, a corollary is that in the case of twisted tris(chelate) complexes the chirality is not associated only with the backbone of the bidentate ligands but also with the spatial arrangement of the donor atoms. To check this conclusion we have chosen

the tris(dithiolene), tris(diselenolene), tris(bipyridine) and tris(β-diketonato) metal complexes (structural information, references and symmetry measures are given as Supporting Information),[24] which are known to present structures throughout the whole range of twist angles. The chirality measures of the inner MX_6 core of such complexes, obtained from their crystal structural data (Figure 3 and 4) indeed corroborate the result of Figure 1. Note that the tris(bipyridine) and tris(β-diketonato) complexes appear at the ends of the twist-angle scale: most cluster in the range $45° < \theta \leq 68°$ but two structures are also found at $\theta \approx 2°$. It has been found[20] that the twist angle in nearly octahedral structures of bipyridine and diketonato complexes is associated with the normalized bites (b = L--L/M-L) of these ligands. Since bipyridine has a smaller bite than diketonates [the averages for first row transition metals are b = 1.27(4) and 1.41(5), respectively], the twist angles of the former family are smaller than in the latter. The existence of structures with twist angles larger than 60° corresponds to a rotation towards a trigonal prism (characterized by $\theta = 120°$) in which the bidentate ligand would be placed along the diagonal of a square face rather than along the edges (as happens for $\theta = 0°$). The two nearly trigonal prismatic structures of diketonato complexes correspond to complexes of Y^{III} and Cd^{II} with d^0 and d^{10} electron configurations (b = 1.21 and 1.28, respectively). We will return to these complexes in a separate report on a different issue, namely the relation between the chirality of the inner MX_6 core and the chirality of the ligand sphere.[25]

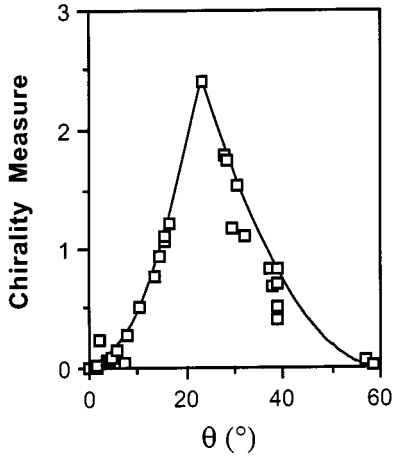

Figure 3. Chirality measures of the MX_6 cores of tris(dithiolene) and tris(diselenolene) complexes (X = S and Se), calculated from the experimental structural data as a function of the twist angle along the trigonal prism to octahedron interconversion path (data provided as Supporting Information); the solid line corresponds to a geometrical model, as in Figure 1

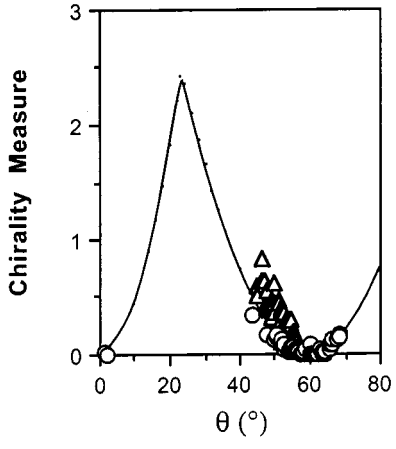

Figure 4. Chirality measures of the MX_6 cores of tris(bipyridine) (X = N, triangles) and tris(β-diketonato) (X = O, circles) complexes, calculated from the experimental structural data as a function of the twist angle along the trigonal prism to octahedron interconversion path (data provided as Supporting Information); the solid line corresponds to a geometrical model, as in Figure 1

In conclusion, we draw attention to $[Zr(SC_6H_4\text{-}4\text{-}OMe)_6]^{2-}$ which is the most chiral homoleptic complex with monodentate ligands among those that have been analyzed, and to the fact that the theoretical maximum at 23° is occupied in Figure 3 by the inner WS_6 core of $(AsPh_4)_2[W(S_2C_6H_4)_3]$,[27] with S = 2.40 making it the most chiral of all MS_6 coordination spheres analyzed in this report. To the best of our knowledge, these pronounced chiralities often go unnoticed. Thus our main message is that *chirality in hexacoordinated complexes with monodentate ligands is a more common phenomenon then currently appreciated*. We hope the stereochemical analysis presented in this report will encourage experimental search for as-yet undetected manifestations of chirality in transition metal complexes.

Acknowledgments

This work has been supported by the Dirección General de Enseñanza Superior (DGES), project PB98-1166-C02-01; Comissió Interdepartamental de Ciència i Tecnologia (CIRIT), grant SGR99-0046 and the US-Israel Binational Science Foundation. D. A. acknowledges continuing useful discussions with Prof. K. Lipkowitz on the issue of continuous chirality. S. A. thanks the Dozor Foundation (Israel) for a Visiting Professorship, J. Granell and J. Bernstein for discussions and P. Román and P. González-Duarte for encouragement.

[1] See, for example: *Catalytic Asymmetric Synthesis* (Ed.: I. Ojima), VCH, New York, **1993**; *Comprehensive Asymmetric Catalysis* (Eds.: E. N. Jacobsen, A. Pfaltz, H. Yamamoto), Springer, Berlin, Vols. 1−3, **1999**; F. Gelman, D. Avnir, H. Schumann, J. Blum, *J. Mol. Catal., A: Chem.* **1999**, *146*, 123−128.
[2] A. von Zelewsky, *Stereochemistry of Coordination Compounds*, J. Wiley, New York **1996**; p 50.
[3] K. P. Meurer, F. Vögtle, *Topics Current Chem.* **1985**, *127*, 1−76.
[4] J. C. Bailar, Jr., *J. Inorg. Nucl. Chem.* **1958**, *8*, 165−175.
[5] A. Werner, *Ber. Dtsch. Chem. Ges.* **1911**, *44*, 1887−1890; V. L. King, *Ber. Dtsch. Chem. Ges.* **1911**, *44*, 1890−1898.
[6] S. F. A. Kettle, *Physical Inorganic Chemistry. A Coordination Chemistry Approach*, Spectrum, Oxford **1996**; p 46.
[7] G. Wilkinson, R. D. Gillard, J. A. McCleverty, *Comprehensive Coordination Chemistry*, Vol. 1, Pergamon, Oxford **1987**, p. 193.
[8] D. F. Shriver, P. W. Atkins, *Inorganic Chemistry*, Oxford University Press, 3rd ed., Oxford **1999**; p 223−226.
[9] J. E. Huheey, E. A. Keiter, R. L. Keiter, *Inorganic Chemistry*, Harper Collins, 4th ed., New York **1993**; p 492−494.
[10] Y. Saito, *Inorganic Molecular Dissymmetry*, Springer Verlag, Heidelberg **1979**; chapters 1 and 4.

[11] F. A. Cotton, G. Wilkinson, C. A. Murillo, M. Bochmann, *Advanced Inorganic Chemistry*, Wiley, 6th ed., New York **1999**; p 1325.

[12] N. N. Greenwood, A. Earnshaw, *Chemistry of the Elements*, 2nd. ed., Butterworth-Heinemann, **1997**.

[13] Other quotes include the following: "The six-coordinated chelate complexes of the type M(bidentate ligand)$_3$....which has D_3 symmetry....are the commonest cases";(ref.[11] p. 639) "...a few cases of optical isomerism are known for planar and tetrahedral complexes involving asymmetric bidentate ligands, but by far the most numerous examples are afforded by octahedral compounds of chelating ligands";(ref.[12] p. 919) "Most of these [optically active inorganic molecules] are six-coordinate complexes with D_3 or closely related symmetry. They will be discussed at greater length in Chapter 12 [all examples given in Chapter 12 correspond to bis- or tris(chelate) complexes]";(ref.[9] p. 64) "Most of the optically active complexes for which experimental and theoretical study has been made involve chelate rings".(ref.[10] p. 53). Other textbooks on Inorganic Chemistry that were consulted also propose as examples of chiral complexes only bis- and tris-chelates.

[14] H. Zabrodsky, D. Avnir, *J. Am. Chem. Soc.* **1995**, *117*, 462−473; Y. Pinto, Y. Salomon, D. Avnir, *J. Math. Chem.* **1998**, *23*, 13−29; Y. Salomon, D. Avnir, *J. Comput. Chem.* **1999**, *20*, 772−780.

[15] D. Gao, S. Schefzick, K.B. Lipkowitz, *J. Am. Chem. Soc.* **1999**, *121*, 9481−9482; K. B. Lipkowitz, D. Gao, O. Katzenelson, *J. Am. Chem. Soc.* **1999**, *121*, 5559−5564; S. Grimme, *Chem. Phys. Lett.* **1998**, *297*, 15−22; S. Alikhanidi, V. Kuz′min, *J. Mol. Model.* **1999**, *5*, 116−124; O. Katzenelson, D. Avnir, *Chem. Eur J.* **2000**, *6*, 1346−1354; O. Katzenelson, H. Zabrodsky, D. Avnir, *Chem. Eur. J*, **1996**, *2*, 174−181; S. Keinan, D. Avnir, *J. Am. Chem. Soc.* **1998**, *120*, 6152−6159.

[16] In other cases, the nearest achiral object may have another improper symmetry element.

[17] The rotation was accompanied by gradually changing the bond angles around the metal in order to fulfill the definition of ideality, namely equal edges within each of the polyhedra. The boundaries for the bond angles are 90° in the octahedron and 81.79° in the trigonal prism, hence the bond-distance-to-edge-length ratio (normalized bite) is 1.414 in the octahedron and 1.309 in the trigonal prism.

[18] H. Zabrodsky, S. Peleg, D. Avnir, *J. Am. Chem. Soc.* **1993**, *115*, 8278−8289. Erratum: **1994**, *116*, 656.

[19] X-ray structural data were retrieved from the Cambridge Structural Database[26] (version 5.18) for the following families of homoleptic hexacoordinated complexes: $[MR_6]^{n-}$, $[M(SR)_6]^{n-}$, $[MCl_6]^{n-}$, $[M(NR_2)_6]^{n-}$, $[M(OR)_6]^{n-}$, $[M(SCN)_6]^{n-}$, $[M(CO)_6]$, $[M(CN)_6]^{n-}$ (where M is any metal belonging to periodic groups 3−12 and, in the case of MR_6, R indicates any group σ-bonded to a metal through a carbon atom). Of these, only the first two families were retained for our chirality analysis, since all structures in the remaining groups were found to be practically octahedral (i.e. $\theta \approx 60°$). Searches were restricted to crystal structures with no disorder and $R < 10\%$. The symmetry measures for the set of metal and six donor atoms were calculated from the experimental structural data with the computer program symm, available free from the authors.

[20] D. Avnir, M. Pinsky, S. Alvarez, manuscript in preparation.

[21] J. P. Glusker, M. Lewis, M. Rossi, *Crystal Structure Analysis for Chemists and Biologists*, VCH, New York **1994**; p. 135 and 600−604.

[22] S. Kleinhenz, V. Pfennig, K. Seppelt, *Chem. Eur. J.* **1998**, *4*, 1687−1691.

[23] J. C. Friese, A. Krol, C. Puke, K. Kirschbaum, D. M. Giolando, *Inorg. Chem.* **2000**, *39*, 1496−1500.

[24] Structural and symmetry data for tris(chelate) complexes are collected as Supporting Information in Tables S1−S3. The criteria applied for the structural database search are reported elsewhere.[25]

[25] S. Alvarez, M. Pinsky, M. Llunell, D. Avnir. *Cryst. Eng.*, in press.

[26] F. H. Allen, O. Kennard, *Chem. Des. Autom. News* **1993**, *8*, 31−37.

[27] F. Knoch, D. Sellmann, W. Kern, *Z. Kristallogr.* **1993**, *205*, 300−302.

[28] H.-U. Blaser, *Tetrahedron: Assymetry* **1991**, *2*, 843−866.

Received November 28, 2000
[I00456]

Rare Earth Complexes of Bulky 2,6-Diphenylphenolates Containing Additional, Potentially Buttressing 3,5-Substituents[‡]

Glen B. Deacon,*[a] Phillip E. Fanwick,[b] Alex Gitlits,[a] Ian P. Rothwell,[b] Brian W. Skelton,[c] and Allan H. White[c]

Keywords: Mercury / Lanthanides / O ligands / Ytterbium

The rare earth aryloxide complexes, $[Yb(OAr^{tBu})_3(THF)]\cdot THF$, $[Sc(OAr^{tBu})_3(THF)]\cdot THF$, $[Yb(OAr^{Me})_3(THF)]$, and $[Sm(OAr^{Ph})_3(THF)_2]$ (OAr^R = 2,6-diphenyl-3,5-di-R-phenolate), have been prepared by redox transmetallation/ligand exchange between the rare earth metal, bis(pentafluorophenyl)mercury, and $HOAr^R$ in tetrahydrofuran. This reaction also provided $[Yb(OAr^{Ph})_3(DME)]\cdot 3/2THF$ by incorporation of adventitious 1,2-dimethoxyethane. A similar reaction between Yb metal, diphenylmercury, and $HOAr^{Me}$ gave $[Yb(OAr^{Me})_2(THF)_3]$. The homoleptic complexes $[Yb(OAr^{Ph})_3]$ and $[Sc(OAr^{H})_3]$ have been prepared by direct reaction of the rare earth element with $HOAr^R$ in a sealed tube in the presence of mercury at elevated temperatures (200–250 °C) and the latter was converted into $[Sc(OAr^{H})_3(THF)]$ by treatment with THF. X-ray crystal structure determinations of $[Yb(OAr^{tBu})_3(THF)]\cdot THF$, $[Sc(OAr^{tBu})_3(THF)]\cdot THF$, and $[Yb(OAr^{Me})_3(THF)]$ show the complexes to be monomeric and four coordinate with a trigonal pyramidal stereochemistry. These structures provide clear evidence that groups *meta* to the phenolate donor can modify the coordination behaviour of the 2,6-diphenylphenolate ligand. In $[Yb(OAr^{Ph})_3(DME)]\cdot 3/2THF$ a distorted square pyramidal stereochemistry is observed. The divalent complex $[Yb(OAr^{Me})_2(THF)_3]$ exhibits a distorted trigonal bipyramidal arrangement of the oxygen donor atoms with apical THF ligands. The homoleptic scandium 2,6-diphenylphenolate has three oxygen atoms in a triangular array with additional π-η^1-Ph···Sc interactions above and below the ScO_3 plane [C–Sc–C = 154.2(8)°], providing a new type of binding of this aryloxide ligand.

Introduction

Amongst rare earth aryloxides and alkoxides,[1] 2,6-di-*tert*-butyl-4-X-phenolates (X = H, Me, *t*Bu) have been seminal in stabilising low coordination numbers,[2] especially in homoleptic complexes.[2a−2c,2h,2i] With the less bulky[3a,3b] 2,6-diphenylphenolate, low coordination number complexes can still be obtained,[4] but the homoleptic lanthanoid(II or III) 2,6-di-phenylphenolates are noteworthy for intramolecular π-Ph···Ln interactions (η^1; η^2; η^3; η^4; η^6)[4a,4c,5] in addition to oxygen coordination, which can be quite irregular.[5a] One way of potentially increasing the bulkiness of 2,6-diphenylphenolate ligands[3b] is to add 3,5-substituents, which should reduce the flexibility of the phenyl groups and cause them to shield the donor atoms more. A range of such ligands is now available (e.g. **1b**−**c**) and exploration of their *d*-block and main group coordination chemistry has commenced.[6]

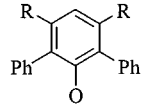

1a OAr^H, R = H
1b OAr^{Me}, R = Me
1c OAr^{tBu}, R = *t*Bu
1d OAr^{Ph}, R = Ph

We now examine the effect of buttressing substituents in rare earth chemistry with the synthesis and structural study of complexes with ligands **1b**−**1d**. In addition the homoleptic scandium complex with the parent ligand **1a** has been prepared and the structure determined. Previous studies of $[Ln(OAr^H)_3]$ complexes[5b] did not extend to the smaller (and much more expensive) Sc. It is of interest to determine the effect of reduced metal size on intramolecular π-Ph···Ln coordination, so far observed in $[Ln(OAr^H)_3]$ complexes as $\eta^6 + \eta^3$ (Ln = La) and $\eta^6 + \eta^1$ (Ln = Ce, Pr, Nd, Y, Yb, Lu).[4a,4c,5b]

Results and Discussion

Syntheses

Reaction of lanthanoid metals with bis(pentafluorophenyl)mercury, and 2,6-diphenyl-3,5-di-R-phenols **1b**−**1d** in tetrahydrofuran yielded the complexes $[Yb(OAr^R)_3THF]$

[‡] Organoamido- and Aryloxo-lanthanoids, 25. − Part 24: G. B. Deacon, A. Gitlits, P. W. Roesky, M. R. Bürgstein, K. C. Lim, B. W. Skelton, A. H. White, *Chem. Eur. J.* **2001**, *7*, 127−138.

[a] Monash University, School of Chemistry, P. O. Box 23, Victoria 3800, Australia
Fax: (internat.) +61-3/9905-4597
E-mail: Glen.Deacon@sci.monash.edu.au
[b] Department of Chemistry, 1393 Brown Building, Purdue University, West Lafayette, IN 47907−1393, USA
Fax: (internat.) +1-765/494-0239
[c] Department of Chemistry, University of Western Australia, Nedlands, WA 6907, Australia
Fax: (internat.) +61-8/9281-1005

 © WILEY-VCH Verlag GmbH, 69451 Weinheim, 2001 1434−1948/01/0606−1505 $ 17.50+.50/0

(R = Me or *t*Bu), [Sm(OAr^{Ph})$_3$(THF)$_2$], and [Sc(OAr^{tBu})$_3$(THF)] [Equation (1)].

$$2\,Ln + 3\,Hg(C_6F_5)_2 + 6\,HOAr^R \longrightarrow 2\,Ln(OAr^R)_3 + 3\,Hg + 6\,C_6F_5H \quad (1)$$

From an analogous reaction with ytterbium metal and HOAr^{Ph}, the product was found to contain fortuitously incorporated DME, even though it was isolated as a THF solvate, [Yb(OAr^{Ph})$_3$(DME)]·1.5THF [Equation (1); R = Ph]. The complex was also obtained as a DME solvate from a similar reaction in DME, but could not be obtained pure (see Experimental Section). When diphenylmercury was used in place of Hg(C$_6$F$_5$)$_2$ in the reaction with HOAr^{Me}, the divalent complex [Yb(OAr^{Me})$_2$(THF)$_3$] was obtained [Equation (2)].

$$Yb + HgPh_2 + 2\,HOAr^{Me} \longrightarrow Yb(OAr^{Me})_2 + Hg + 2\,PhH \quad (2)$$

In previous redox transmetallation/ligand exchange reactions with Hg(C$_6$F$_5$)$_2$, Yb^{III} complexes have been obtained with HOAr^H [4a] whereas Yb^{II} derivatives have been isolated with 2,6-di-*tert*-butylphenolate ligands,[2d−2f] despite the general use of an excess of lanthanoid metal. However, in redox transmetallation/ligand exchange reactions of ytterbium with 3,5-di-*tert*-butylpyrazole, use of Hg(C$_6$F$_5$)$_2$ gave trivalent complexes[7] whereas HgPh$_2$ provided divalent compounds,[8] a relationship now seen with 2,6-diphenyl-3,5-dimethylphenol. Electrochemical studies[9] as well as synthetic behaviour[7,8,10] show that Hg(C$_6$F$_5$)$_2$ is a more powerful oxidant than HgPh$_2$.

The synthesis of homoleptic complexes was also attempted by direct reaction of metals with HOAr^R (R = Ph or *t*Bu) at elevated temperature in the presence of mercury. In general, decomposition products were obtained or the resulting lanthanoid complexes could not be crystallised, viz. from Yb/HOAr^{tBu} at 250 °C, Yb/HOAr^{Ph} at 300 °C and at 200−220 °C, and Nd/HOAr^{Ph} at 200−300 °C. However, reaction of Yb with HOAr^{Ph} strictly at 200 °C (i.e. below the ligand melting point) allowed [Yb(OAr^{Ph})$_3$] to be prepared in good yield [Equation (3), Ln = Yb, R = Ph].

$$Ln + 3\,HOAr^R \xrightarrow{Hg} 3/2\,H_2 + Ln(OAr^R)_3 \quad (3)$$

This contrasts with the corresponding reaction of Yb with HOAr^H, which yields [Yb(OAr^H)$_2$]$_2$ and the mixed oxidation state complex [Yb$^{II}_2$(OAr^H)$_3$][Yb^{III}(OAr^H)$_4$].[5a] In addition, [Sc(OAr^H)$_3$] was obtained by reaction (3) (Ln = Sc, R = H), showing that for the 2,6-diphenylphenolate ligand, the method is applicable to the smallest rare earth metal. Crystallization from THF gave the solvate [Sc(OAr^H)$_3$(THF)].

Properties and Characterisation

Because of the difficulty in obtaining entirely satisfactory microanalyses for Ln(OAr^R)$_3$ (R = Me, *t*Bu, Ph), a feature previously noted for complexes of these buttressed ligands[6] and attributed to carbide formation,[6a] knowledge of the composition of the complexes is particularly dependent on X-ray structure determinations. These have been carried out for [Yb(OAr^{tBu})$_3$(THF)]·THF, [Yb(OAr^{Me})$_3$(THF)], [Sc(OAr^{tBu})$_3$(THF)]·THF, and [Yb(OAr^{Ph})$_3$(DME)]·1.5THF, as well as the analytically satisfactory [Yb(OAr^{Me})$_2$(THF)$_3$] and [Sc(OAr^H)$_3$] (next section). In contrast, complexes of the OAr^H ligand do not normally present analytical difficulties.[4,5] Microanalyses and metal analyses for bulk [Ln(OAr^{tBu})$_3$(THF)]·THF (Ln = Sc, Yb) and [Yb(OAr^{Me})$_3$(THF)] dried for 1−2 h under vacuum at room temperature, though somewhat divergent from calculated C values, suggested that these drying conditions did not remove coordinated THF or THF of solvation. This was supported by NMR integrations in the case of the scandium complex, although meaningful spectra could not be obtained for the paramagnetic Yb^{III} complexes. Both [Ln(OAr^{tBu})$_3$(THF)]·THF complexes have infrared absorptions at ca. 910 and 860 cm^{-1} plausibly attributable[10,11] to ring stretching of free (e.g. solvent of crystallisation) and coordinated THF, respectively. Tris(2,3,5,6-tetraphenylphenolato)samarium(III) was isolated with satisfactory analyses for a bis(THF) species. Since the sample was dried at 80 °C under vacuum, it is plausible that both ether molecules are coordinated, an effect of the larger size of Sm^{3+} than Yb^{3+}.[12] Aryloxide IR absorptions at 910−850 cm^{-1} (see [Yb(OAr^{Ph})$_3$]) rule out the use of IR spectroscopy to ascertain the nature of THF in the Sm complex. Single crystals of [Sc(OAr^H)$_3$(THF)] could not be grown, but it seems uncontentious that THF is coordinated in view of the structure of [Sc(OAr^{tBu})$_3$(THF)]·THF with a bulkier phenolate ligand, and since THF is retained on drying at 150 °C under vacuum. Moreover, the THF resonances are shifted from the "free" values consistent with coordination in solution (see Experimental Section). The analyses of the bulk sample of [Yb(OAr^{Ph})$_3$(DME)] dried at 80 °C are marginally closer for this composition than for [Yb(OAr^{Ph})$_3$(DME)]·1.5THF, which is the composition of the undried single crystals. An IR absorption at 1044 cm^{-1}, not observed for [Yb(OAr^{Ph})$_3$], is indicative of coordinated DME.[4d,13] A sample of the complex prepared in DME and dried at room temperature under vacuum was not obtained analytically pure but the analyses (especially for Yb) favoured the composition [Yb(OAr^{Ph})$_3$(DME)]·DME. The divalent complex [Yb(OAr^{Me})$_2$(THF)$_3$] gave satisfactory analyses and the ^{1}H NMR spectrum in C$_6$D$_6$ is consistent with this composition. However, the detection of two methyl resonances, a single, very broad THF resonance, and underlying broadness in the aromatic region suggests that an equilibrium occurs in C$_6$D$_6$ [Equation (4)] with both complexes detectable by their Me resonances.

$$[Yb(OAr^{Me})_2(THF)_3] \rightleftharpoons [Yb(OAr^{Me})_2(THF)_2] + THF \quad (4)$$

Complexes of both compositions have been observed for the bulky 2,6-di-*tert*-butylphenolate ligands.[2e,2f,2i]

The mass spectra of several representative complexes were recorded. Surprisingly, ions with three OAr^R ligands were detected only for [Yb(OAr^{Me})$_3$(THF)]. In other cases, as well as for [Yb(OAr^{Me})$_2$(THF)$_3$], [Ln(OAr^R)$_2$]$^+$ was the highest structurally significant feature. Near infrared ab-

sorption at 900−1000 nm was observed for the Yb^{III} complexes, as expected,[14] but appropriately was absent for $[Yb(OAr^{Me})_2(THF)_3]$.

Molecular Structures

The Complexes $[Ln(OAr^{tBu})_3(THF)]\cdot THF$ (Ln = Yb or Sc) and $[Yb(OAr^{Me})_3(THF)]$

The structures of these complexes are closely related. Two representative structures in which the metal size and the aryloxide ligand are varied are shown in Figure 1 and 2, with Ln-based distances and angles in Table 1. All three complexes are four-coordinate monomers, displaying a stereochemistry substantially distorted from tetrahedral, similar to that of $[Yb(OC_6H_2tBu_3\text{-}2,4,6)_3(THF)]$.[2g] The striking reduction in coordination number from five in $[Yb(OAr^{H})_3(THF)_2]$,[4a] especially given the further THF present as solvent of crystallisation, indicates that OAr^R (R = *t*Bu, Me and presumably also Ph) ligands can be considered bulkier than the simple 2,6-diphenylphenolate, consistent with buttressing of the 2,6-diphenyl substituents by the 3,5-substituents. There are no unusual features in the packing of the 2,6-diphenyl substituents, which are common to the three compounds, and they do not appear to have any overriding influence on the stereochemistry. Thus the interplanar angles involving the phenyl substituents (Table 2) vary markedly between the three complexes. Some similarity is evident between the two complexes with OAr^{tBu} ligands, but there are still some significant differences (Table 2).

The Ln−OAr^R bond lengths (Table 1) show little variation for each compound and between the two $[Yb(OAr^R)_3(THF)]$ (R = *t*Bu or Me) complexes. Subtraction of an extrapolated radius (from data in ref.[12]) for four coordinate Sc^{3+} or Yb^{3+} (0.62 and 0.75 Å, respectively) from <Ln−OAr^R> gives 1.29−1.30 Å, which is within the usual range for bulky lanthanoid aryloxides, including $[Yb(OC_6H_2tBu_3\text{-}2,4,6)_3(THF)]$ (1.28 Å).[2g] However, the latter compound shows a wider variation in Ln−OAr bond lengths [1.97(1)−2.09(1) Å].[2g] There are similar Yb−O(THF) distances for the two Yb compounds, and subtraction of the four-coordinate ionic radius from Ln−O(THF) values gives 1.49−1.50 Å for the three $[Ln(OAr^R)_3(THF)]$ complexes, at the low end of the range (1.49−1.59 Å) for THF complexes of bulky lanthanoid aryloxides.[2f,2g,4c,4d]

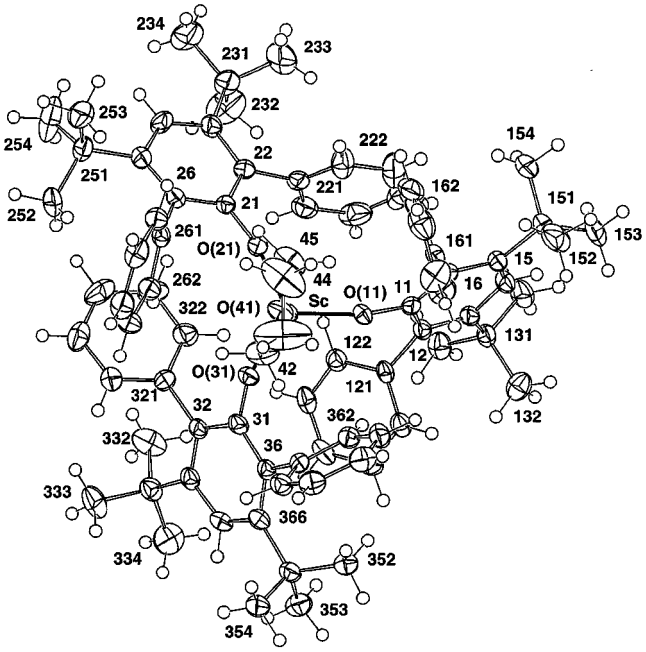

Figure 1. Molecular projection of $[Sc(OAr^{tBu})_3(THF)]$

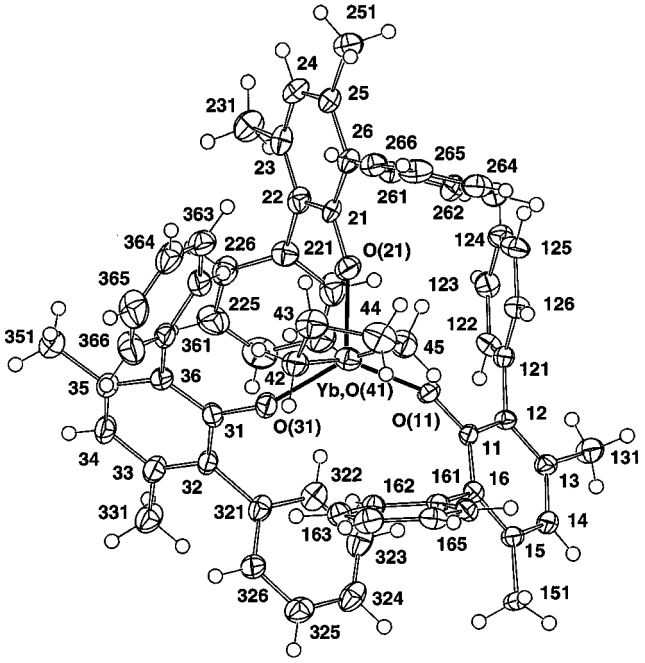

Figure 2. Molecular projection of $[Yb(OAr^{Me})_3(THF)]$

Table 1. Metal atom environments, $[Ln(OAr^R)_3(THF)]$; the three values in each entry are for Ln/R = Sc/*t*Bu, Yb/Me and Yb/*t*Bu, respectively; in this and subsequent tables, *r* is the metal−ligand distance; other entries are the angles subtended at the metal by the relevant atoms at the head of the row and column

Atom	*r*	O(21)	O(31)	O(41)
O(11)	1.913(3)	111.5(1)	116.8(1)	106.4(1)
	2.032(4)	106.4(2)	121.7(1)	106.8(1)
	2.038(3)	111.8(1)	122.39(9)	104.3(1)
O(21)	1.914(3)		117.9(1)	100.6(1)
	2.033(4)		117.6(1)	100.7(2)
	2.029(3)		113.5(1)	99.34(9)
O(31)	1.922(3)			100.7(1)
	2.045(4)			100.7(2)
	2.042(3)			101.6(1)
O(41)	2.118(2)			
(THF)	2.247(4)			
	2.236(2)			

Table 2. Ligand descriptors (Å, degrees) for the complexes $[Ln(OAr^R)_n(L)_m]$; θ values are dihedral angles between the C_6 ring planes [c: central; p2,6: peripheral; O_3: O(n1)$_3$]; δLn_c and δLnO_3 are the deviations of the metal atoms from the central and O_3 planes; R indicates the substituents at the 3- and 5-positions of the central ring; L (co-ligands if present) = THF or DME; Σ(O−Ln−O) is the sum of the angles defined by the phenolate oxygen atoms about the metal[a]

Ln/R Ligand L_m	Sc/*t*Bu THF	Yb/Me THF	Yb/*t*Bu THF	Yb/Ph DME	Yb^{II}/Me $(THF)_3$[a]	Sc/H −
Ligand 1						
O(11)−C(11)	1.357(6)	1.347(6)	1.349(5)	1.35(1)	1.31(1)	1.38(3)
Ln−O(11)−C(11)	162.3(3)	157.0(3)	161.1(2)	170.3(6)	157.9(5)	144(2)
$\theta_{c/p2}$	74.6(2)	57.6(2)	74.5(1)	67.8(5)	56.4(3)	58.2(9)
$\theta_{c/p6}$	78.8(2)	67.7(2)	85.7(2)	71.4(5)	79.2(4)	57.4(10)
$\theta_{p2/p6}$	61.8(2)	82.2(2)	62.4(2)	60.2(6)	69.1(5)	56.6(9)
$\theta_{c/O3}$	66.2(1)	50.2(2)	64.7(1)	68.1(3)	−	83.6(8)
δLn_c	0.803(8)	0.77(1)	0.862(8)	0.40(2)	0.23(2)	0.02(3)
Ligand 2						
O(21)−C(21)	1.354(5)	1.342(6)	1.348(4)	1.34(1)	1.314(9)	1.38(3)
Ln−O(21)−C(21)	167.3(3)	163.0(3)	166.8(3)	161.8(7)	175.8(5)	144(2)
$\theta_{c/p2}$	80.8(2)	58.7(2)	86.6(2)	53.8(4)	47.1(5)	55.5(9)
$\theta_{c/p6}$	70.1(2)	68.9(2)	71.7(2)	54.5(4)	70.8(4)	56.0(9)
$\theta_{p2/p6}$	65.0(2)	49.4(2)	61.6(2)	88.9(4)	49.8(6)	57.1(9)
$\theta_{c/O3}$	45.6(1)	63.7(2)	46.5(1)	45.6(3)	−	79.4(8)
δLn_c	0.434(8)	0.57(1)	0.529(8)	0.06(2)	0.09(2)	0.27(5)
Ligand 3						
O(31)−C(31)	1.349(4)	1.341(6)	1.340(4)	1.35(1)		1.36(2)
Ln−O(31)−C(31)	157.6(3)	153.8(4)	154.5(3)	171.7(7)		178(2)
$\theta_{c/p2}$	70.1(2)	78.0(2)	71.9(2)	54.2(5)		45.0(10)
$\theta_{c/p6}$	74.0(2)	71.5(2)	74.3(1)	50.5(6)		43.7(10)
$\theta_{p2/p6}$	62.3(2)	64.1(2)	64.7(2)	57.7(6)		78.3(9)
$\theta_{c/O3}$	46.7(1)	47.8(2)	47.4(1)	34.0(3)		33.4(7)
δLn_c	0.887(8)	1.15(1)	1.026(7)	0.11(2)		0.12(6)
Σ(O−Ln−O)	$346._2$	$345._7$	$347._7$	$319._6$		$360._0$
δLnO_3	0.416(1)	0.448(1)	0.417(1)	0.772(1)		0.011(9)

[a] Dihedral angles of the second disordered component of substituent ring 6 to its associated central and other peripheral planes are 68.6(6), 49.8(6), and to its first component 2.8(5)°. In $[Yb(OAr^{Ph})_3(DME)]$, 3,5-substituent C_6 planes in the three ligands lie at 55.6(6), 55.3(5); 57.9(5), 52.7(4); 57.1(6), 49.5(5)° to their central C_6 planes.

There are significant variations of the O−Ln−O angles within each of the three structures (Table 1), indicating considerable distortion from tetrahedral stereochemistry. The sum of the OAr^R−Ln−OAr^R angles in all three structures (Table 2) approaches 360°, whereas the sums of the O(THF)−Ln−OAr^R angles are below the 328.5° expected for tetrahedral angles. Thus, the data suggest that four coordination in the three structures can be considered near *triangular pyramidal*. The Ln−O−C angles in the three structures are appreciably nonlinear (Table 2) and are comparable with the average ($156._7$°) found for the more crowded $[Yb(OC_6H_2tBu_3\text{-}2,4,6)_3(THF)]$.[2g] The deviation of the rare earth ions from the LnO_3 (aryloxide) plane (Table 2) is marginally more than 0.392(1) Å for $[Yb(OC_6H_2tBu_2\text{-}2,6\text{-}Me\text{-}4)_3(THF)]$.[2g]

The Complex $[Yb(OAr^{Ph})_3(DME)]\cdot 1.5THF$

This complex has a five-coordinate array of three aryloxide and two DME oxygens (Figure 3). The best fit[15] polyhedron is a square pyramid (though very distorted) with O(11) as the apex, and *cisoid* aryloxides and DME in the base. It is thus very similar to the structures of $[Ln(OAr^H)_3(DME)]$ (Ln = Yb or Nd).[4d] Thus, the 3,5-substituents do not affect the coordination number in contrast to complexation with THF (above). This is because a chelating DME has less steric demand than two THF ligands.[3a]

Since the $Ar^{Ph}O$−Yb−OAr^{Ph} angles (Table 3) lie close to tetrahedral values (*cf.* Σ ArO^R−Yb−OAr^R, Table 2), there is an approximately tetrahedral array of aryloxide oxygens and the centre of the O···O vector of the DME. The *cisoid* aryloxide angle in the square plane [O(21)−Yb−O(31) 109.0(3)°] is surprisingly smaller than the corresponding *cisoid* angles in $[Ln(OAr^H)(DME)]$ [Ln = Nd (120.3(2) and Yb (113.3(2)°].[4d] Although the O(DME)−Yb−O(DME) and the Yb−O(n1)−C(n1) (n = 1 and 2) angles are similar in the two complexes (R = H[4d] or Ph), the Yb−O(31)−C(31) angle in $[Yb(OAr^{Ph})_3(DME)]\cdot 1.5THF$ is $23._4$° greater (Table 3) than in $[Yb(OAr^H)_3(DME)]\cdot 0.5DME$.[4d] Thus, the bond angles present no

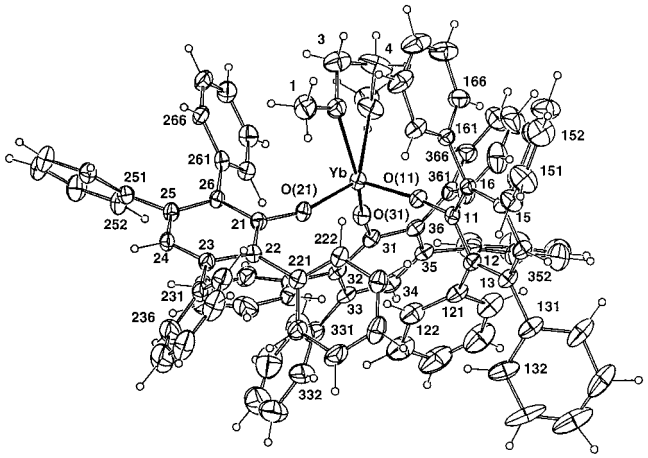

Figure 3. Molecular projection of $[Yb(OAr^{Ph})_3(DME)]$

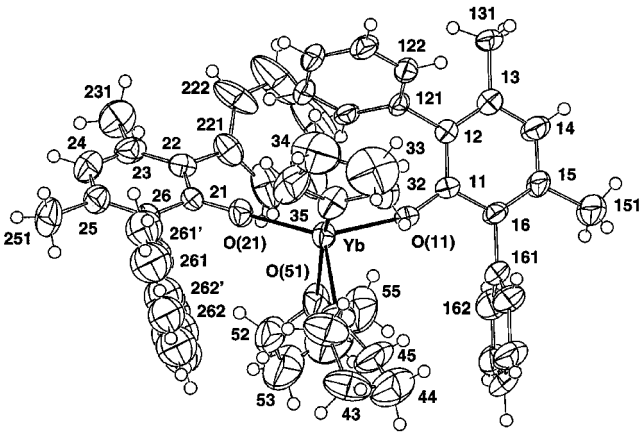

Figure 4. Molecular projection of $[Yb(OAr^{Me})_2(THF)_3]$

Table 3. Ytterbium environment, $[Yb(OAr^{Ph})_3(DME)]$; O(2,5) from DME[a]

Atom	*r*	O(21)	O(31)	O(2)	O(5)
O(11)	2.038(7)	101.8(3)	108.8(3)	97.3(3)	111.2(3)
O(21)	2.048(7)		109.0(3)	84.1(3)	137.4(3)
O(31)	2.043(8)			146.9(3)	85.3(3)
O(2)	2.379(9)				66.1(3)
O(5)	2.349(9)				

[a] Torsions in the DME ring (only bonds specified): Yb−O(2,5) 5.6(9), 22(1); O(2)−C(3) −28(1); O(5)−C(4) −48(2); C(3)−C(4) 48(2); O(5)−Yb−O(2)−C(1) 161(1); O(2)−Yb−O(5)−C(6) −147(1)°.

Table 4. Ytterbium environment, $[Yb(OAr^{Me})_2(THF)_3]$; O(31)−O(51) are derivatives of the THF ligands

Atom	*r*	O(21)	O(31)	O(41)	O(51)
O(11)	2.218(6)	140.9(2)	95.8(2)	100.7(2)	91.1(2)
O(21)	2.202(6)		100.7(2)	117.1(2)	87.6(2)
O(31)	2.397(6)			78.7(2)	156.7(3)
O(41)	2.426(6)				78.1(3)
O(51)	2.436(7)				
C(126)	3.177(9)				

clear picture as to the effect of 3,5-disubstitution on DME complexation. The <Yb−OAr> and <Yb−O(DME)> distances of $[Yb(OAr^{Ph})_3(DME)]\cdot 1.5THF$ correspond closely to those of $[Yb(OAr^{H})_3(DME)]\cdot 0.5DME$ (0.02, 0.03 Å difference).[4d]

The Complex $[Yb(OAr^{Me})_2(THF)_3]$

There is a five coordinate Yb^{II} centre in $[Yb(OAr^{Me})_2(THF)_3]$ (Figure 4), and the best fit polyhedron[15] of the donor atoms is a trigonal bipyramid with the THF oxygens O(31) and O(51) apical and the aryloxide oxygens and O(41) (THF) equatorial. The stereochemistry is severely distorted with a 156.7(3)° angle between the axial donors and considerable variation [100.7(2)−140.9(2)°] (Table 4) in the equatorial angles, though their sum is $358._7$°.

There is also a close approach of a carbon atom [Yb···C(126) = 3.177(9) Å] adjudged just on or outside the limit for meaningful binding. If viewed as six coordinate, subtraction of the appropriate Yb^{2+} ionic radius[12] from the Yb···C distance gives 2.16 Å, which is the upper limit for significant intramolecular π-C(Ph)···Ln interactions,[16] whereas subtraction of the extrapolated five coordinate radius gives 2.22 Å, beyond the range. The calculated position of H(126) is even closer to Yb [2.9(est.) Å] and intrudes into and can explain the large [140.9(2)°] O(11)−Yb−O(21) angle without postulation of an Yb···H interaction. Certainly, the large angle cannot be explained by repulsion between the bulky aryloxide ligands as *cisoid* $Ar^RO-Yb-OAr^R$ angles are well established, for example in $[Yb(OAr^{Ph})_3(DME)]$ (Table 3). Although $[Yb(OAr^{H})_2(THF)_3]$ is also distorted trigonal bipyramidal, the aryloxide ligands are apical [$Ar^HO-Yb-OAr^H$ = 164.6(3)°] with highly distorted angles between the equatorial THF ligands [O−Yb−O = 83.7(4), 138.8(3), 137.5(3)°].[4d] In this case, aryl hydrogens intrude into both of the large O(THF)−Yb−O(THF) angles, though at greater distances [Yb···H = 3.1, 3.2 Å; nearest associated C at 3.45(1) Å] than for $[Yb(OAr^{Me})_2(THF)_3]$.

The average Yb−OAr distance (2.21 Å) is in agreement with those (2.21−2.22 Å) of $[Yb(OAr^{H})_2(THF)_3]$[4d] and square pyramidal $[Yb(OC_6H_2tBu_2\text{-}2,6\text{-}X\text{-}4)_2(THF)_3]$. THF (X = Me, *t*Bu).[2e,2f] Whilst <Yb−O(THF)> (2.42 Å) agrees with that of $[Yb(OAr^{H})_2(THF)_3]$,[4d] it is shorter than those (2.48, 2.46 Å) of the two 2,6-di-*tert*-butylphenolate complexes.[2e,2f] Subtraction of the ionic radius for five coordinate Yb^{2+} gives 1.46 Å, rather lower than the usual range 1.48−1.60 Å for THF in bulky aryloxide complexes of Yb^{II}/Yb^{III}.[2f,2g,4a,4d] (It would be even lower if Yb^{II} were to be taken as six coordinate). Despite the similarity in <Yb−O(THF)> values between $[Yb(OAr^{R})_2(THF)_3]$ (R = H[4d] or Me) derivatives, the present complex shows a much smaller range of lengths (0.03_9 Å) than the earlier complex (0.1_5 Å).[4d] The $Yb-OAr^R-C$ angles are similar in the two

structures (Table 2 and ref.[4d]) despite the different arrangement of ligands.

[Sc(OAr)$_3$]

Single crystals of homoleptic [Yb(OAr^{Ph})$_3$] could not be obtained and hence the effect of 3,5-disubstitution on the structure of homoleptic lanthanoid 2,6-diphenylphenolates could not be determined. However, the complex [Sc(OAr^{H})$_3$] has been shown to be monomeric (Figure 5), with the coordination sphere comprising a triangular array of phenolate oxygens and capping π-η^1-Ph···Sc interactions above and below the ScO_3 plane (see below). Unlike [Ce(OC$_6$H$_3$*t*Bu$_2$-2,6)$_3$][2b] and [Ln(OAr^{H})$_3$] (Ln = Y, La, Ce, Nd, Pr, Yb, Lu)[4a,4c,5b] complexes, in which the LnO_3 units are distorted from triangular planar towards trigonal pyramidal, [Sc(OAr^{H})$_3$] is triangular planar (O−Sc−O deviation from 120°: ≤ 2.3°; Σ O−Sc−O 360°) with minimal deviation of Sc from the O_3 plane (Table 2), much like [Ln(OC$_6$H$_2$*t*Bu$_2$-2,6-Me-4)$_3$] (Ln = Sc, Y).[2a,2c] The <Sc−O> distance is 1.93 Å and is somewhat longer than that of [Sc(OC$_6$H$_2$*t*Bu$_2$-2,6-Me-4)$_3$][2a] (1.87 Å), presumably owing to the higher coordination number of Sc in [Sc(OAr^{H})$_3$] due to the C···Sc interactions.

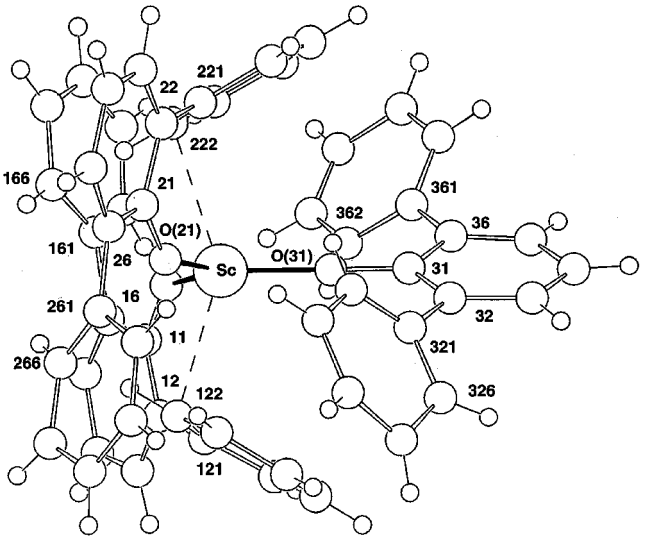

Figure 5. Molecular projection of [Sc(OAr^{H})$_3$]

The phenyl rings 12n and 22n approach the ScO_3 plane from above and below such that C(122) and C(222) are closer to Sc than the next nearest C atoms of the rings by ca. 0.45 Å (Table 5). The Sc···C(122) and Sc···C(222) distances (Table 5) are not greatly lengthened from the π-η^1-Cp−Sc bridging bonds [2.629(4), 2.519(4) Å] of [ScCp$_3$]$_n$,[17] for which the next closest contacts from the η^1-bonded rings are more distant by ca. 0.4−0.6 Å. Subtraction of an extrapolated (from data of ref.[12]) radius (0.68 Å) for five coordinate Sc^{3+} from Sc···C of [Sc(OAr^{H})$_3$] gives 1.94 and 2.00 Å, well within the upper limit (2.16 Å) for significant intramolecular π-Ph···Ln interactions.[16] Accordingly, C(122) and C(222) are considered to be weakly bound to Sc by π-η^1-Ph···Sc interactions. Even subtraction of a three coordinate Sc^{3+} radius from Sc···C(122) gives values within the 2.16 Å limit. With two π-η^1-Ph···Sc interactions, the capping phenyls have a different coordination mode than in [Ln(OAr^{H})$_3$] (Ln = Ce, Pr, Nd, Y, Yb, Lu) (η^6 + η^1)[4a,4c,5b] or [La(OAr^{H})$_3$] (η^6 + η^3),[5b] attributable to the small size of Sc^{3+}.[12] The similar Sc···C binding modes and bond lengths *transoid* to the O_3 plane probably account for the triangular ScO_3 arrangement and minimal deviation [0.011(9) Å] of Sc from the O_3 plane {cf. [Ln(OAr^{H})$_3$]: 0.150(1)−0.353(1) Å (La−Lu)}.[4a,4c,5b] Although the *transoid* C(122)−Sc−C(222) angle [145.2(8)°] deviates considerably from linear, the ring centroids are nearer linear [C(120)−Sc−C(220) = 165.$_7$°]), although still less than the range 173.$_2$−177.$_2$° for the other structurally characterised [Ln(OAr^{H})$_3$] complexes.[4a,4c,5b] The inclinations of the capping phenyl rings 12n and 22n to the ScO_3 plane [30.8(8)°, 28.9(8)° Table 5] are similar to those [28.1(2)−30.1°] of the π-η^1-Ph···Ln bonded rings of [Ln(OAr^{H})$_3$] (Ln = Ce, Pr, Nd, Yb, Lu).[4a,4c,5b] On the other hand, the rings are inclined to each other at 59.2(6)°, quite different from the dihedral angle of the η^6 and η^3 rings of [La(OAr^{H})$_3$] [19.9(3)°] or of the η^6 and η^1 rings of [Lu(OAr^{H})$_3$] [38.8(3)°].[5b]

Table 5. Scandium environment, [Sc(OAr^{H})$_3$]

Atom	*r*	O(21)	O(31)	C(122)	C(222)
O(11)	1.92(2)	122.1(7)	117.7(7)	77.8(8)	86.0(8)
O(21)	1.97(2)		120.2(7)	84.7(8)	78.2(8)
O(31)	1.91(1)			107.2(9)	107.5(9)
C(122)	2.62(3)[a]				145.2(8)
C(222)	2.68(3)[a]				

[a] Next closest Sc···C contacts: Sc···C(121, 123; 221, 223) are 3.12(3), 3.08(3); 3.12(3), 3.19(3) Å. Planes 12n, 22n lie at 30.8(8), 28.9(8) to the O_3 plane and 59.2(6)° to each other; Sc lies 2.56(2) and 2.63(2) Å out of them.

Further examination of the [Sc(OAr^{H})$_3$] structure shows that the Sc−O(11)−C(11) and Sc−O(21)−C(21) angles (ligands 1 and 2) are much smaller than 180° while Sc−O(31)−C(31) is nearly linear (Table 2). Furthermore, the dihedral angles (Table 2) between the C_6 central (phenolate) plane and the O_3 plane ($\theta_{c/}O_3$) are 83.6(8) and 79.4(8)° for ligands 1 and 2 respectively, whilst only 33.4(7)° for ligand 3 (Table 2). Moreover, the angles between the central C_6 ring and the phenyl substituent planes of ligands 1 and 2 average 57.$_8$ and 55.$_8$°, whilst the average value for ligand 3 is 44.4°. The interplanar angles between the 2- and 6-phenyl rings for ligands 1 and 2 also differ from that of ligand 3 (Table 2). These data, in conjunction with the substantial bending of the Sc−O−C angles of ligands 1 and 2, demonstrate the deviation of ligands 1 and 2 towards Sc associated with binding of their phenyl substituents.

Conclusions

The reduction in coordination number from five in [Yb(OAr^{H})$_3$(THF)$_2$][4a] to four in [Yb(OAr^{R})$_3$(THF)] (R =

*t*Bu or Me) (see Figure 2) indicates that the addition of 3,5-substituents to the 2,6-diphenylphenolate ligand is consistent with an increase in ligand bulk, possibly by buttressing the phenyl groups. This reduction in coordination number is foreshadowed by the anomalous "4.5 coordination" in $[Ln(OAr^H)_3(THF)_2]$ (Ln = La and Nd).[4b,4c] In contrast, similar five coordinate structures are observed in $[Yb(OAr^R)_3(DME)]$ [R = H[4d] or Ph (Figure 3)]. In five coordinate $[Yb(OAr^R)_2(THF)_3]$, there is a change from apical aryloxides (R = H)[4d] to (surprisingly) apical THF ligands (R = Me) (Figure 4) in their distorted trigonal bipyramidal stereochemistry. In homoleptic $[Sc(OAr^H)_3]$, the coordination motif, ScO_3 + two π-η^1-Ph···Sc interactions, is new and differs from the ligation in other $[Ln(OAr^H)_3]$ complexes.[4a][4c][5b]

Experimental Section

General: Rare earth aryloxides are extremely air- and water-sensitive hence all operations were carried out under an inert atmosphere (purified Ar or N_2). Handling methods, analytical procedures, and solvent purifications were generally as described previously,[5b,18] with the exception of some infra red spectra and the ^{1}H NMR spectrum of $[Yb(OAr^{Me})_2(THF)_3]$ which were recorded using a Perkin−Elmer Spectrum 2000 FTIR and a Varian Associates Gemini-200 spectrometer, respectively. IR data (4000−650 cm^{-1}) are for compounds as Nujol mulls. ^{1}H chemical shifts are referenced to internal solvent resonances and reported relative to $SiMe_4$. In assignments of ^{1}H NMR spectra involving the OAr^H ligand, primed numbers refer to phenyl protons. In the mass spectra, each listed *m*/*z* value for metal-containing ions (where the metal has more than one isotope) is the most intense peak of a cluster with an isotope pattern in good agreement with the calculated pattern. Those complexes containing OAr^R (R = *t*Bu, Ph) ligands for which data are not reported did not display any metal-containing ions in their mass spectra. Microanalyses were either by the Campbell Microanalytical Service, University of Otago, New Zealand or by Microanalytical services, Department of Chemistry at Purdue University, Indiana, USA. Complexes with THF or DME lose solvent on being heated in sealed capillaries under N_2 hence melting points have little significance (see examples below). 2,6-Diphenylphenol was purchased from Aldrich, while $HOAr^R$ reagents were prepared by previously reported procedures (R = Me,[6b,19] *t*Bu,[20] Ph[21]). Rare earth metals were obtained as powders or chunks from Rhône−Poulenc, Phoenix, USA.

Tris(2,6-diphenyl-3,5-di-*tert*-butylphenolato)tetrahydrofuranytterbium(III)-Tetrahydrofuran (1/1): A 100 mL Schlenk flask was charged with ytterbium powder (0.52 g, 3.01 mmol), bis-(pentafluorophenyl)mercury(II) (1.07 g, 2.00 mmol), 2,6-diphenyl-3,5-di-*tert*-butylphenol (1.43 g, 3.99 mmol) and THF (50 mL). The reaction mixture was stirred for 10 h at 80 °C yielding a dark red-brown solution upon filtration. The volume of the solution was reduced to 15 mL and yellow prismatic *single crystals* formed overnight which were used for X-ray crystal structure determination. More yellow crystals formed on storing the saturated solution at ambient temperature for several days. These were dried under vacuum at room temperature (0.75 g, 40%). − IR: $\tilde{\nu}$ = 1597w, 1576w, 1525w, 1296s, 1239w, 1171w, 1069m, 1027m, 1011m, 998s, 851w, 818w, 780w, 760m, 707s cm^{-1}. − Vis/near IR (THF): λ_{max} (ε) = 395 (52), 758 (25), 912 (3), 979 (10) nm (dm^3 mol^{-1} cm^{-1}). − $C_{82}H_{95}O_4Yb$ [$Yb(OAr^{tBu})_3(THF)$] (1317.62): calcd. C 74.74, H 7.27, Yb 13.13. − $C_{86}H_{103}O_5Yb$ (title compound) (1389.72): calcd. C 74.32, H 7.47, Yb 12.45; found C 73.36, H 7.44, Yb 11.33.

Tris(2,6-diphenyl-3,5-dimethylphenolato)(tetrahydrofuran)ytterbium(III): A mixture of 2,6-diphenyl-3,5-dimethylphenol (0.82 g, 3.00 mmol), bis(pentafluorophenyl)mercury(II) (0.80 g, 1.50 mmol) and ytterbium chips (0.52 g, 3.01 mmol) was stirred in THF (60 mL) at ambient temperature for 21 h. Filtration gave a bright yellow solution, which was partially evaporated and a small volume of hexane (10 mL) added. Large yellow crystals formed which were used for X-ray structure determination. The solution was then further reduced in volume producing more crystalline material which was dried under vacuum at room temperature (combined yield 0.43 g, 40%). − M.p. (sealed tube/N_2): 228−231 °C, prelim. dec. 80−90 °C. − IR: $\tilde{\nu}$ = 1598m, 1572w, 1554m, 1323s, 1169w, 1152w, 1089s, 1067m, 1027m, 1009m, 967m, 912w, 862m, 836m, 785w, 749s, 704s, 664s cm^{-1}. − Vis/near IR (THF): λ_{max} (ε) = 372 (364), 911 (14), 980 (50) nm (dm^3 mol^{-1} cm^{-1}). − MS (70 eV, EI): *m*/*z* (%) = 994 (37) $[Yb(OAr^{Me})_3 + H]^+$, 979 (2) $[Yb(OAr^{Me})_3 - CH_2]^+$, 720 (100) $[Yb(OAr^{Me})_2]^+$, 705 (2) $[Yb(OAr^{Me})_2 - Me]^+$, 447 (18) $[Yb(OAr^{Me})]^+$, 428 (2) $[Yb(OAr^{Me}) - MeH - 3H]^+$, 371 (3) $[Yb(OAr^{Me}) - C_6H_4]^+$, 274 (28) $[ArO^{Me}H]^+$, 273 (35) $[ArO^{Me}]^+$. − $C_{64}H_{59}O_4Yb$ (1065.15): calcd. C 72.16, H 5.58, Yb 16.25; found C 70.08, H 5.67, Yb 15.64.

Tris(2,6-diphenyl-3,5-di-*tert*-butylphenolato)(tetrahydrofuran)-scandium(III) -Tetrahydrofuran (1/1): A mixture of 2,6-diphenyl-3,5-di-*tert*-butylphenol (1.08 g, 3.01 mmol), bis(pentafluorophenyl)mercury(II) (0.80 g, 1.50 mmol), small scandium chunks (0.36 g, 8.01 mmol) and mercury (2 drops) in THF (50 mL) was ultrasonicated at ambient temperature for 227 h. The reaction mixture was filtered through a Celite pad, giving a clear very pale yellow solution which was evaporated to 10 mL. Small colourless crystals appeared in a few hours, and these were used for X-ray crystallography. Bulk crystalline solid deposited from the decanted mother liquor on further standing, and was dried under vacuum at room temperature. More solid crystallised from the filtrate and was similarly treated (combined yield 0.57 g, 45%). − M.p. (sealed tube/N_2): 203−205 °C (dec.), prelim. dec. ca. 150 °C − IR: $\tilde{\nu}$ = 1597m, 1576m, 1522m, 1288s, 1238m, 1200m, 1171m, 1070m, 1027m, 1012s, 998s, 912m, 870m, 819w 780w, 761m, 708s, 658s cm^{-1}. − ^{1}H NMR (C_6D_6): δ = 1.28 (s, 54 H, *t*Bu), 1.41 [br s, 8 H, β-H(THF)], 3.56 [br s, 8 H, α-H(thf)], 6.88−7.58 (m, 33 H, ArH). − MS (70 eV, EI): *m*/*z* (%) = 759 (1) $[Sc(OAr^{tBu})_2]^+$, 743 (3) $[Sc(OAr^{tBu})_2 - MeH]^+$, 727 (1) $[Sc(OAr^{tBu})_2 - 2MeH]^+$, 711 (<1) $[Sc(OAr^{tBu})_2 - 3MeH]^+$, 671 (<1) $[Sc(OAr^{tBu})_2 - MeH - Me - Bu]^+$, 655 (<1) $[Sc(OAr^{tBu})_2 - 2\ MeH - Me - Bu]^+$, 641 (<1) $[Sc(OAr^{tBu})_2 - 3Me - MeH - Bu]^+$, 358 (55) $[Ar^{tBu}OH]^+$, 57 (100) $[Bu]^+$. − $C_{86}H_{103}O_5Sc$, (1262.64): calcd. C 81.87, H 8.23, Sc 3.56; found C 80.89, H 8.26, Sc 4.13.

Tris(2,3,5,6-tetraphenylphenolato)bis(tetrahydrofuran)samarium(III): A mixture of 2,3,5,6-tetraphenylphenol, (1.32 g, 3.31 mmol), bis(pentafluorophenyl)mercury(II) (0.89 g, 1.66 mmol) and samarium powder (1.00 g, 6.65 mmol) was stirred in THF (40 mL) at room temperature for 29 h. Filtration gave a pale yellow solution which was evaporated to 10 mL. Pale yellow crystals formed in a few hours. The solid was dried under vacuum at 80 °C for 1 h giving a colourless-pale yellow powder (0.89 g, 54%). − IR: $\tilde{\nu}$ = 1597m, 1577w, 1531w, 1341s, 1307s, 1274m, 1138s, 1068m, 1025m, 1010m, 946s, 908w, 859w, 792w, 757s, 698s, 668s cm^{-1}. − ^{1}H NMR (C_7D_8): δ = −0.05 [br s, 8 H, β-H(THF)], 0.85 [br s, 8 H, α-H(THF)], 6.26−7.61 (complex m, 63 H, ArH). − $C_{94}H_{71}O_4Sm$ [$Sm(OAr^{Ph})_3(THF)$] (1414.91): C 79.79, H 5.05, Sm 10.63. −

$C_{98}H_{79}O_5Sm$ (1487.01): calcd. C 79.15, H 5.36, Sm 10.11; found C 78.32, H 5.44, Sm 10.02.

Adventitious Synthesis of Tris(2,3,5,6-tetraphenylphenolato)(1,2-dimethoxyethane)ytterbium(III): A mixture of 2,3,5,6-tetraphenylphenol, (1.59 g, 3.99 mmol), bis(pentafluorophenyl)mercury(II) (1.07 g, 2.00 mmol) and ytterbium powder (0.35 g, 2.02 mmol) was stirred in THF (50 mL) at 80 °C for 5 h. Filtration gave a dark red-brown solution which was evaporated to 20 mL and kept at −20 °C for 2 h. A very fine yellow crystalline solid, and later orange-yellow powder formed. This was dissolved in a minimal volume of hot toluene which was contaminated with a substantial amount of 1,2-dimethoxyethane. Meanwhile more crude product was obtained from the original THF solution. This was dissolved in hot toluene and the two toluene solutions were combined and left to stand at room temperature for several days resulting in initial formation of a large yellow crystal, which was cut in three and used for X-ray crystal structure identification as $[Yb(OAr^{Ph})_3(DME)]\cdot 1.5THF$, and then bulk yellow microcrystalline product which was dried under vacuum at 80 °C for 1 h. More microcrystalline yellow product deposited from the filtrate, and was collected and dried as before {combined yield 0.31 g, 16% for $[Yb(OAr^{Ph})_3(DME)]$}. − IR: $\tilde{\nu}$ = 1597m, 1578w, 1530m, 1345s, 1306m, 1275m, 1142s, 1091w, 1071w, 1044m, 1001w, 994w, 952s, 908w, 870w, 846w, 793w, 758s, 698s, 871s cm^{-1}. − Vis/near IR (THF): λ_{max} (ε) = 399 (161), 912 (7), 980 (43) nm ($dm^3\ mol^{-1}\ cm^{-1}$). − $C_{100}H_{85}O_{6.5}Yb$ ($[Yb(OAr^{Ph})_3(DME)]\cdot 1.5THF$] (1563.72): calcd. C 76.80, H 5.48, Yb 11.07. − $C_{94}H_{73}O_5Yb$ (THF-free) (1455.56): calcd. C 77.56, H 5.06, Yb 11.89; found C 78.72, H 5.44, Yb 11.43.

Bis(2,6-diphenyl-3,5-dimethylphenolato)tris(tetrahydrofuran)-ytterbium(II): A mixture of 2,6-diphenyl-3,5-dimethylphenol (1.10 g, 4.01 mmol), diphenylmercury(II) (0.71 g, 2.00 mmol), ytterbium chips (0.69 g, 3.99 mmol) and mercury (2 drops) was stirred in THF at 50 °C for 29 h. Filtration gave a dark red-brown solution, which was evaporated to 5 mL and layered with hexane yielding a dark red crystalline product from which single crystals for X-ray structure determination were derived. The remaining bulk crystalline material was dried under vacuum at ambient temperature (0.83 g, 44%). − IR: $\tilde{\nu}$ = 1598m, 1551m, 1325s, 1296s, 1239w, 1153w, 1089s, 1068s, 966w, 916m, 879w, 788w, 750m, 704s cm^{-1}. − Vis/near IR (THF): no absorptions occurred near 1000 nm. − ^1H NMR (C_6D_6): δ = 0.90 (s, 6 H, CH_3), 1.25 (s, 6 H, CH_3), 2.04 [br s, 24 H, CH_2 (THF)], 6.63−7.08 (m, 22 H, ArH). Integrations are approximate owing to the broadness of the THF peak, the complexity and underlying broadness of the aromatic resonances, and the proximity of strong solvent absorptions to the aromatic resonances. − MS (70 eV, EI): *m/z* (%) = 720 (13) $[Yb(OAr^{Me})_2]^+$, 447 (3) $[Yb(OAr^{Me})]^+$, 274 (100) $[ArO^{Me}H]^+$. Additional clusters centred on *m/z* = 795, 748, and 733 of very low intensity (<1%) did not have a recognizable isotope pattern and could not be assigned. − $C_{52}H_{58}O_5Yb$ (936.02): calcd. C 66.72, H 6.25, Yb 18.49; found C 66.38, H 6.02, Yb 18.70.

Tris(2,3,5,6-tetraphenylphenolato)ytterbium(III): A mixture of ytterbium chips (0.52 g, 3.01 mmol) and 2,3,5,6-tetraphenylphenol (0.60 g, 1.51 mmol) was heated at 200 °C in the presence of mercury (2 drops) in a sealed tube under vacuum for 24 h. The reaction mixture was extracted in hot toluene (70 mL) and filtered giving an orange solution. The volume of the solution was reduced to 2 mL and pentane was layered on top. A microcrystalline yellow solid formed overnight. This was isolated, washed with hexane (2 mL) and dried at 60 °C under vacuum (0.52 g, 76%). − M.p. (sealed tube/N_2): 282−285 °C. − IR: $\tilde{\nu}$ = 1597w, 1581w, 1574w, 1531w, 1513w, 1347s, 1307m, 1276m, 1140m, 1070w, 1027w, 1010w, 949m, 908w, 873, 863, and 855vw, 800w, 775w, 758s, 722m, 698s, 672m cm^{-1}. − Vis/near IR (THF): λ_{max} (ε) = 348 (1634), 913 (8), 980 (40) nm ($dm^3\ mol^{-1}\ cm^{-1}$). − $C_{90}H_{63}O_3Yb$ (1365.44): calcd. C 79.16, H 4.65, Yb 12.67; found C 79.51, H 4.89, Yb 12.12.

Tris(2,6-diphenylphenolato)scandium(III): A mixture of scandium chips (0.36 g, 8.01 mmol) and 2,6-diphenylphenol (0.99 g, 4.02 mmol) was heated in the presence of mercury (2 drops) in a sealed Carius tube at 200−250 °C for 160 h. The reaction mixture was worked up in toluene (70 mL) and filtered while hot giving a colourless solution, which was evaporated to 5 mL. Some colourless single crystals formed overnight which were used for an X-ray crystal structure determination. Further standing gave a colourless microcrystalline solid which was isolated and dried at 80 °C for 1 h (0.44 g, 42%). − M.p. >220 °C. − IR: $\tilde{\nu}$ = 1579m, 1411s, 1307m, 1282s, 1248s, 1172m, 1162w, 1154w, 1112w, 1094w, 1068m, 1026w, 1010w, 990w, 970w, 890s, 867s, 804w, 763s, 702s, 634s, 610s cm^{-1}. − ^1H NMR (C_6D_6): δ = 6.86−6.96 (m, 21 H, H4, H3′, H4′, H5′), 7.19 (d, $^3J_{H\text{-}H}$ = 7.5 Hz, 6 H, H3, H5), 7.31 (dd, $^3J_{H\text{-}H}$ = 7.0 Hz, $^4J_{H\text{-}H}$ = 1.4 Hz, 12 H, H2′, H6′). − MS (70 eV, EI): *m/z* (%) = 535 (21) $[Sc(OAr^H)_2]^+$, 246 (100) $[HOAr^H]^+$. − $C_{54}H_{39}O_3Sc$ (780.81): calcd. C 83.06, H 5.03, Sc 5.76; found C 82.88, H 5.19, Sc 5.65.

Tris(2,6-diphenylphenolato)(tetrahydrofuran)scandium(III): Tris(2,6-diphenylphenolato)scandium was prepared as above and on the same scale, but THF (90 mL) was used rather than toluene to work up the reaction mixture. Filtration gave a colourless solution, which was evaporated to 2 mL, but no solid formed. THF was then removed completely leaving a white solid. Crystallisation from toluene (20 mL) gave a white microcrystalline solid, which was dried under vacuum at 150 °C for 1 h (0.72 g, 63%). − M.p. (sealed tube/N_2): 218−220 °C, prelim. dec. ca. 170 °C. − IR: $\tilde{\nu}$ = 1595m, 1580m, 1410s, 1308m, 1281m, 1258s, 1172w, 1157w, 1085w, 1070m, 1025w, 1004w, 972w, 957w, 884s, 859s, 804w, 769m, 733m, 704s, 635s cm^{-1}. − ^1H NMR (C_6D_6): δ = 0.57 [s, 4 H, β-H(THF)], 2.12 [s, 4 H, α-H(THF)], 6.84−7.04 (m, 21 H, H4, H3′, H4′, H5′), 7.23 (d, $^3J_{H\text{-}H}$ = 7.5 Hz, 6 H, H3, H5), 7.34 (dd, $^3J_{H\text{-}H}$ = 7.5 Hz, $^4J_{H\text{-}H}$ = 1.4 Hz, 12 H, H2′, H6′). − $C_{58}H_{47}O_4Sc$, (852.92): calcd. C 81.67, H 5.55, Sc 5.27; found C 81.57, H 5.84, Sc 5.29.

Attempted Preparation of Tris(2,3,5,6-tetraphenylphenolato)(1,2-dimethoxyethane)ytterbium(III): A mixture of 2,3,5,6-tetraphenylphenol, (2.17 g, 5.45 mmol), bis(pentafluorophenyl)mercury(II) (1.46 g, 2.73 mmol) and ytterbium powder (0.63 g, 3.64 mmol) was stirred in DME (50 mL) at room temperature for 5 h. The reaction mixture turned brown-orange and was stirred for a further 24 h at 70 °C. Filtration gave a dark brown solution which was reduced in volume. Yellow needle-like crystals formed overnight and were dried under vacuum at room temperature (0.65 g, 23% for $[Yb(OAr^{Ph})_3(DME)]\cdot DME$). − IR: $\tilde{\nu}$ = 1597m, 1578w, 1531m, 1346s, 1306s, 1275m, 1143s, 1110m, 1072m, 1043m, 1025m, 952s, 917w, 869w, 840w, 794w, 758s, 699s, 672s cm^{-1}. − Vis/near IR (THF): λ_{max} (ε) = 410 (197), 912 (2), 980 (38) nm ($dm^3\ mol^{-1}\ cm^{-1}$). − $C_{94}H_{73}O_5Yb$ $[Yb(OAr^{Ph})_3(DME)]$ (1299.56): calcd. C 77.56, H 5.06, Yb 11.89; − $C_{98}H_{83}O_7Yb$ $[Yb(OAr^{Ph})_3(DME)_2]$ (1545.68): calcd. C 76.14, H 5.41, Yb 11.19; found C 72.51, H 5.43, Yb 11.20.

Structure Determinations: Full spheres of CCD area-detector data were measured at the specified temperature (Bruker AXS instrument; $2\theta_{max}$ as specified; monochromatic Mo-K_α radiation, λ = 0.7107$_3$ Å) yielding $N_{t(otal)}$ reflections, reducing to N unique (R_{int} quoted) after "empirical"/multiscan absorption correction

(proprietary software), N_o with $F > 4\sigma(F)$ being considered "observed" and used in the full-matrix least-squares refinement (anisotropic thermal parameter forms for the non-hydrogen atoms; (x, y, z, $U_{iso})_H$ constrained at estimated values). Conventional residuals R, R_w (weights: $[\sigma^2(F) + 0.0004\,F^2)^{-1}$] are quoted on $|F|$ at convergence. Neutral atom complex scattering factors were employed within the context of the Xtal 3.4 program system.[22] Pertinent results are given in the figures and tables. In the figures 20% displacement amplitudes are shown for the structures determined at low temperature, 50% for room temperature. Hydrogen atoms have arbitrary radii of 0.1 Å. Individual variations in procedure, idiosyncrasies, difficulties are noted below.

Crystal/Refinement Data

[Yb(OAr^{tBu})$_3$(THF)]·THF: $C_{86}H_{103}O_5Yb$, M = 1389.8. Triclinic, space group $P\bar{1}$ (C_i^1, no. 2), a = 14.930(1), b = 16.601(1), c = 17.281(1) Å, α = 110.491(1)°, β = 99.703(1)°, γ = 104.169(1)°, V = 3735 Å^3. D_c (Z = 2) = 1.23$_6$ g cm^{-3}. μ_{Mo} = 13.0 cm^{-1}; specimen: 0.55 × 0.40 × 0.15 mm; $'T'_{min.,max}$ = 0.61, 0.83. $2\theta_{max}$ = 58°; N_t = 43419, N = 18211 (R_{int} = 0.029), N_o = 12973; R = 0.038, R_w = 0.039. $|\Delta\rho_{max}|$ = 1.37(9) e Å^{-3}. T ca. 300 K. Displacement parameters of the lattice solvent were very large; site occupancy was set at unity after trial refinement.

[Sc(OAr^{tBu})$_3$(THF)]·THF: $C_{86}H_{103}O_5Sc$, M = 1261.7. Triclinic, space group $P\bar{1}$, a = 14.805(2), b = 16.208(2), c = 17.042(2) Å, α = 109.649(2)°, β = 99.719(2)°, γ = 103.981(2)°, V = 3595 Å^3. D_c (Z = 2) = 1.16$_6$ g cm^{-3}. μ_{Mo} = 1.5 cm^{-1}; specimen: 0.25 × 0.20 × 0.04 mm; $'T'_{min.,max}$ = 0.67, 0.82. $2\theta_{max}$ = 58°; N_t = 39461, N = 18825 (R_{int} = 0.079), N_o = 7579; R = 0.062, R_w = 0.055. $|\Delta\rho_{max}|$ = 0.67(6) e Å^{-3}. T ca. 153 K. All hydrogen atoms except those associated with the uncoordinated THF were refined in (x, y, z, U_{iso}).

[Yb(OAr^{Me})$_3$THF]: $C_{64}H_{59}O_4Yb$, M = 1065.2. Triclinic, space group $P\bar{1}$, a = 11.154(1), b = 11.818(1), c = 20.371(2) Å, α = 76.824(2)°, β = 77.809(2)°, γ = 78.415(2)°, V = 2522 Å^3. D_c (Z = 2) = 1.40$_2$ g cm^{-3}. μ_{Mo} = 19.0 cm^{-1}; specimen: 0.35 × 0.17 × 0.10 mm; $'T'_{min.,max}$ = 0.66, 0.83. $2\theta_{max}$ = 58°; N_t = 29447, N = 12359 (R_{int} = 0.028), N_o = 11025; R = 0.046, R_w = 0.065. $|\Delta\rho_{max}|$ = 2.4(1) e Å^{-3}. T ca. 153 K.

[Yb(OAr^{Ph})$_3$DME]·1.5THF: $C_{100}H_{85}O_{6.5}Yb$, M = 1563.8. Monoclinic, space group $P2_1/c$ (C_{2h}^5, no. 14), a = 13.0079(9), b = 32.407(2), c = 24.860(2) Å, β = 91.798(1)°, V = 10474 Å^3. D_c (Z = 4) = 0.99$_2$ g cm^{-3}. μ_{Mo} = 9.4 cm^{-1}; specimen: 0.30 × 0.25 × 0.10 mm; $'T'_{min.,max}$ = 0.62, 0.86. $2\theta_{max}$ = 58°; N_t = 114947, N = 18408 (R_{int} = 0.098), N_o = 11241; R = 0.060, R_w = 0.090. $|\Delta\rho_{max}|$ = 1.54(6) e Å^{-3}. T ca. 300 K. Lattice solvent residues were modelled as 0.5THF at each of three sites, with constrained geometries and isotropic thermal parameter forms.

[Yb(OAr^{Me})$_2$(THF)$_3$]: $C_{52}H_{58}O_5Yb$, M = 936.1. Monoclinic, space group Cc (C_s^4, no. 9), a = 19.945(1), b = 11.8084(5), c = 19.193(1) Å, β = 97.416(3)°, V = 4482 Å^3. D_c (Z = 4) = 1.38$_7$ g cm^{-3}. μ_{Mo} = 21.2 cm^{-1}; specimen: 0.17 × 0.15 × 0.08 mm; $'T'_{min.,max}$ = 0.50, 0.85. $2\theta_{max}$ = 53°; N_t = 23259, N = 7519 (R_{int} = 0.11; 'Friedel pairs' retained distinct), N_o = 6338; R = 0.053, R_w = 0.093. $|\Delta\rho_{max}|$ = 0.9 e Å^{-3}. T *ca* 193 K. Data were measured using a Nonius Kappa CCD instrument. Refinement was carried out using the SHELX-97 system.[23] The phenyl ring pendant at C(26) was modelled as disordered over two sets of sites of equal occupancy, with isotropic thermal parameter refinement for the carbon atoms. The absolute structure was indeterminate.

[Sc(OAr^{H})$_3$]: $C_{54}H_{39}O_3Sc$, M = 780.9. Monoclinic, space group $P2_1/c$, a = 11.261(8), b = 20.10(1), c = 17.81(1) Å, β = 100.02(1)°, V = 3970 Å^3. D_c = 1.30$_6$ g cm^{-3}. μ_{Mo} = 2.3 cm^{-1}; specimen: 0.25 × 0.15 × 0.03 mm; $'T'_{min.,max}$ = 0.59, 0.88. $2\theta_{max}$ = 50°; N_t = 19251, N = 6895 (R_{int} = 0.21), N_o = 1394; R = 0.088, R_w = 0.097. $|\Delta\rho_{max}|$ = 0.86(6) e Å^{-3}. T ca. 153 K. Weak and limited data from a very fragile leaf-like specimen would support meaningful anisotropic thermal parameter form refinement for Sc only, isotropic forms for C, O.

Crystallographic data (excluding structure factors) for the structures reported in this paper have been deposited with the Cambridge Crystallographic Data Centre. The supplementary publication nos. CCDC-153631, -153627, -153628, -153629, -153626, -153630 apply sequentially to the compounds in the Crystal/Refinement Data section. Copies of the data can be obtained free of charge on application to CCDC 12 Union Road, Cambridge CB2 1EZ, UK [Fax: (internat.) +44-1223/336-033; E-mail: deposit@ccdc.cam.ac.uk].

Acknowledgments

We are grateful to the Australian Research Council for support and for an Australian Postgraduate Award and a Monash University travel grant to A. G.; I. P. R. acknowledges the National Science Foundation for financial support of this research.

[1] For reviews [1a] D. C. Bradley, R. C. Mehrotra, D. P. Gaur, *Metal Alkoxides* (Academic Press, London **1978**). – [1b] R. C. Mehrotra, A. Singh, U. M. Tripathi, *Chem. Rev.* **1991**, *91*, 1287–1303. – [1c] W. J. Evans, *New. J. Chem.* **1995**, *19*, 525–533. – [1d] L. G. Hubert-Pfalzgraf, *New. J. Chem.* **1995**, *19*, 727 –750. – [1e] L. G. Hubert-Pfalzgraf, *Coord. Chem. Rev.* **1998**, *178–180*, 967–997. – [1f] M. N. Bochkarev, L. N. Zakharov and G. S. Kalinina, *Organoderivatives of the Rare Earth Elements*, Kluwer Academic, Dordrecht, **1995**. – [1g] D. C. Bradley, R. C. Mehrotra, I. P. Rothwell, A. Singh, *Alkoxo and Aryloxo Derivatives of Metals*, Academic Press, London, **2001**.

[2] [2a] P. B. Hitchcock, M. F. Lappert, A. Singh, *J. Chem. Soc., Chem. Commun.* **1983**, 1499–1501. – [2b] H. A. Stetcher, A. Sen, A. L. Rheingold, *Inorg. Chem.* **1988**, *27*, 1130–1132. – [2c] P. B. Hitchcock, M. F. Lappert, R. G. Smith, *Inorg. Chim. Acta* **1987**, *139*, 183–184. – [2d] G. B. Deacon, C. M. Forsyth, R. H. Newnham, *Polyhedron* **1987**, *6*, 1143–1144. – [2e] G. B. Deacon, P. B. Hitchcock, S. A. Holmes, M. F. Lappert, P. MacKinnon, R. H. Newnham, *J. Chem. Soc., Chem. Commun.* **1989**, 935–937. – [2f] G. B. Deacon, T. Feng, P. MacKinnon, R. H. Newnham, S. Nickel, B. W. Skelton, A. H. White, *Aust. J. Chem.* **1993**, *46*, 387–399. – [2g] G. B. Deacon, T. Feng, S. Nickel, M. I. Ogden, A. H. White, *Aust. J. Chem.* **1992**, *45*, 671–683. – [2h] J. R. van den Hende, P. B. Hitchcock, M. F. Lappert, *J. Chem. Soc., Chem. Commun.* **1994**, 1413–1414. – [2i] J. R. van den Hende, P. B. Hitchcock, S. A. Holmes, M. F. Lappert, *J. Chem. Soc., Dalton Trans.* **1995**, 1435–1439.

[3] [3a] J. Marçalo, A. Pires De Matos, *Polyhedron* **1989**, *8*, 2431–2437. – [3b]J. Marçalo, unpublished results, cited in refs.[4b] and [4c].

[4] [4a] G. B. Deacon, S. Nickel, P. MacKinnon, E. R. T. Tiekink, *Aust. J. Chem.* **1990**, *43*, 1245–1257. – [4b] G. B. Deacon, B. M. Gatehouse, Q. Shen, G. Ward, E. R. T. Tiekink, *Polyhedron* **1993**, *12*, 1289–1294. – [4c] G. B. Deacon, T. Feng, B. W. Skelton, A. H. White, *Aust. J. Chem.* **1995**, *48*, 741–756. – [4d] G. B. Deacon, T. Feng, P. C. Junk, B. W. Skelton, A. H. White, *Chem. Ber./Recueil* **1997**, *130*, 851–857.

[5] [5a] G. B. Deacon, C. M. Forsyth, P. C. Junk, B. W. Skelton, A. H. White, *Chem. Eur. J.* **1998**, *5*, 1452–1459. –[5b] G. B. Deacon, T. Feng, C. M. Forsyth, A. Gitlits, D. C. R. Hockless, Q. Shen, B. W. Skelton, A. H. White, *J. Chem. Soc., Dalton Trans.* **2000**, 961–966.

[6] [6a] R. W. Chestnut, L. D. Durfee, P. E. Fanwick, I. P. Rothwell, K. Folting, J. C. Huffman, *Polyhedron* **1987**, *6*, 2019−2026. − [6b] J. S. Vilardo, M. A. Lockwood, L. G. Hanson, J. R. Clark, B. C. Parkin, P. E. Fanwick, I. P. Rothwell, *J. Chem. Soc., Dalton Trans.* **1997**, 3353−3362. − [6c] J. S. Vilardo, M. G. Thorn, P. E. Fanwick, I. P. Rothwell, *Chem. Commun.* **1998**, 2425−2426. − [6d] J. S. Vilardo, P. E. Fanwick, I. P. Rothwell, *Polyhedron* **1998**, *17*, 769−771. − [6e] P. N. Riley, M. G. Thorn, J. S. Vilardo, M. A. Lockwood, P. E. Fanwick, I. P. Rothwell, *Organometallics* **1999**, *18*, 3016−3024. − [6f] J. S. Vilardo, M. M. Salberg, J. R. Parker, P. E. Fanwick, I. P. Rothwell, *Inorg. Chim. Acta* **2000**, *299*, 135−141.

[7] [7a] J. E. Cosgriff, G. B. Deacon, B. M. Gatehouse, H. Hemling, H. Schumann, *Angew. Chem.* **1993**, *105*, 906−907; *Angew. Chem. Int. Ed. Engl.* **1993**, *32*, 874−875. − [7b] J. E. Cosgriff, G. B. Deacon, B. M. Gatehouse, H. Hemling, H. Schumann, *Aust. J. Chem.* **1994**, *47*, 1223−1235.

[8] [8a] G. B. Deacon, E. E. Delbridge, B. W. Skelton, A. H. White, *Eur. J. Inorg. Chem.* **1998**, 543−545. − [8b] G. B. Deacon, E. E. Delbridge, B. W. Skelton, A. H. White, *Eur. J. Inorg. Chem.* **1999**, 751−761.

[9] [9a] K. P. Butin, A. N. Kashin, I. P. Beletskaya, L. S. German, V. R. Polishchuk, *J. Organomet. Chem.* **1970**, *25*, 11−16. − [9b] K. P. Butin, I. P. Beletskaya, A. N. Kashin, O. A. Reutov, *J. Organomet. Chem.* **1967**, *10*, 197−210.

[10] J. E. Cosgriff, G. B. Deacon, B. M. Gatehouse, H. Hemling, H. Schumann, *Aust. J. Chem.* **1994**, *47*, 1223−1235; and references therein.

[11] [11a] R. J. H. Clark, J. Lewis, D. J. Machin, R. S. Nyholm, *J. Chem. Soc.* **1963**, 379−387. − [11b] J. Lewis, J. R. Miller, R. L. Richards, A. Thompson, *J. Chem. Soc.* **1965**, 5850−5860.

[12] R. D. Shannon, *Acta Crystallogr., Sect. A* **1976**, *32*, 751−767.

[13] J. E. Cosgriff, G. B. Deacon, G. D. Fallon, B. M. Gatehouse, H. Schumann, R. Weimann, *Chem. Ber.* **1996**, *129*, 953−958.

[14] W. T. Carnall, in *The Absorption and Fluorescence Spectra of Rare Earth Ions in Solution*, in *Handbook on the Physics and Chemistry of Rare Earths*, Vol. 3 (Eds.: K. A. Gschneidner, L. Eyring), North-Holland, Amsterdam, **1979**, chapter 24.

[15] M. Johnson, J. C. Taylor, G. W. Cox, *J. Appl. Crystallogr.* **1980**, *13*, 188−189.

[16] G. B. Deacon, Q. Shen, *J. Organomet. Chem.* **1996**, *511*, 1−17.

[17] J. L. Atwood, K. D. Smith, *J. Am. Chem. Soc.* **1973**, *95*, 1488−1491.

[18] G. B. Deacon, C. M. Forsyth, B. M. Gatehouse, A. Philosof, B. W. Skelton, A. H. White, P. A. White, *Aust. J. Chem.* **1997**, *50*, 959−970.

[19] A. Galan, A. J. Sutherland, P. Ballester, J. Rebek, Jr., *Tetrahedron Lett.* **1994**, *35*, 5359−5362.

[20] [20a] D. H. R. Barton, D. M. X. Donnely, P. J. Guiry, J. H. Reibenspies, *J. Chem. Soc., Chem. Commun.* **1990**, 1110−1111. − [20b] D. H. R. Barton, N. Y. Bhatnagar, J.-C. Blazejewski, B. Charpiot, J.-P. Finet, D. J. Lester, W. B. Motherwell, M. T. B. Papoula, S. P. Stanforth, *J. Chem. Soc., Perkin Trans. 1* **1985**, 2657−2665.

[21] [21a] P. Yates, J. R. Hyre, *J. Org. Chem.* **1962**, *27*, 4101−4103. − [21b] A. S. Hay, R. F. Clark, *Macromolecules* **1970**, *3*, 533−535. − [21c] H. Yang, A. S. Hay, *Synthesis* **1992**, 467−472. − [21d] D. E. Dana, A. S. Hay, *Synthesis* **1982**, 164−165.

[22] *The Xtal 3.4 User's Manual* (Eds.: S. R. Hall, G. S. D. King, J. M. Stewart), University of Western Australia, Lamb: Perth, **1995**.

[23] G. M Sheldrick, *SHELXS-97: A Program for Crystal Structure Refinement*, University of Göttingen, **1997**.

Received November 29, 2000
[I00458]

Two-Level Self-Organisation of Arrays of [2×2] Grid-Type Tetranuclear Metal Complexes by Hydrogen Bonding

Esther Breuning,[a] Ulrich Ziener,[a] Jean-Marie Lehn,*[a] Elina Wegelius,[b] and Kari Rissanen[b]

Keywords: Coordination chemistry / Crystal engineering / Grid-type complexes / Hydrogen bonding / Supramolecular chemistry

Here we report on the synthesis and characterisation of four new complexes of the [2×2] M_4^{II} grid-type (M = Co, Fe, Zn) with oligopyridine-derived ligands. The presence of aminopyrazine and aminopyrimidine moieties at the edge of the ligands potentially enables the formation of infinite hydrogen-bonded multi-grid networks. The ligands were synthesised by subsequent stannylations and Stille-type coupling reactions. The complexes were obtained by self-assembly of the ligand with the metal salt. The single-crystal X-ray structure was determined for the Co complex **7** containing aminopyrimidine as the hydrogen-bonding moiety [$P\bar{1}$; a = 15.4976(4), b = 18.2114(6), c = 31.9538(10) Å, α = 86.9809(13), β = 83.4137(18), γ = 67.2828(16)°]. The crystal structure reveals hydrogen bonding in one direction, thus forming infinite chains of grids, whereas in the second direction of a layer, only weak attractive interactions are found. Anions and solvent molecules are situated between the layers, thus inhibiting any direct interaction between them. Cocrystallisation of the complementary complexes should enable the recognition-controlled alternating arrangement of grids incorporating different metal ions in a chessboard-like manner.

Introduction

In the last few years, a vast amount of work has been dedicated to the generation of discrete inorganic architectures in order to establish the principles of inorganic self-assembly processes as well as in view of their possible application in nanotechnology.[1] Of particular interest is the combination of metal coordination with hydrogen bonding in order to achieve the controlled arrangement of such inorganic entities by means of molecular recognition-directed formation of well-defined two- and three-dimensional structures of hydrogen-bonded networks.[2] This amounts to a two-level, sequential self-organisation process in which the initial assembly of coordination architectures from given ligands and metal ions is followed by their organisation into specific arrangements. The use of ligands fitted with complementary hydrogen-bonding subunits provides the possibility of positioning inorganic entities which may contain different metal ions in extended arrays, a feature potentially of great interest to nanotechnology and molecular electronics.

Our laboratory has recently described a new class of polypyridine-derived, tetranuclear metal complexes of the [2×2] M_4^{II} grid-type (M = transition metal)[3,4] formed by self-assembly from ligands containing two tridentate, terpyridine-like, binding subunits and from metal ions of octahedral coordination geometry (Scheme 1). They have been found to present a range of interesting structural[3] and physicochemical (electrochemical,[3a,5] magnetic[6]) properties. In addition, it has been shown that these grid-type compounds self-assemble in monolayers on gold and can be examined and manipulated on a molecular level by means of scanning tunnelling microscopy (STM).[7] Although they assemble in a chessboard-like order, the stability of the monolayer is low and the mobility of the grids on the surface is still high. For possible future applications in the field of information storage devices, a high stability of the monolayer of grids will be required. Furthermore, it would be of great interest to be able to rigorously control the relative positioning of grid structures incorporating different metal ions (and therefore presenting different physicochemical properties) within either two-dimensional layers or three-dimensional lattices. This would for instance lead to "grid-of-grids"-type structures as schematically represented in Figure 1. It would also by-pass the demanding synthetic efforts involved in the generation of grids of higher nuclearity by the replacement of large grids by grids-of-grids, thus making further use of the powerful tool of self-assembly through a two-level sequential process.

In order to increase the stability of layers of grids as well as to allow the introduction of different metal ions into such an assembly, we synthesised the ligands **2** and **3** containing complementary and self-complementary hydrogen-bonding moieties and their corresponding metal complexes **4**–**7**. The complementary interaction of the ligands is schematically shown in Scheme 2. The suitability of aminopyrazine and aminopyrimidine as designed hydrogen-bonding motifs, as used here, has been shown before in mononuclear complexes with terpyridine-derived ligands.[8]

[a] Laboratoire de Chimie Supramoléculaire, ISIS-Université Louis Pasteur,
4, Rue Blaise Pascal, 67000 Strasbourg, France
Fax: (internat.) + 33-3/90241117
E-mail: lehn@chimie.u-strasbg.fr
[b] Department of Chemistry, University of Jyväskylä,
P. O. Box 35, 40351 Jyväskylä, Finland

 © WILEY-VCH Verlag GmbH, 69451 Weinheim, 2001 1434–1948/01/0606–1515 $ 17.50+.50/0

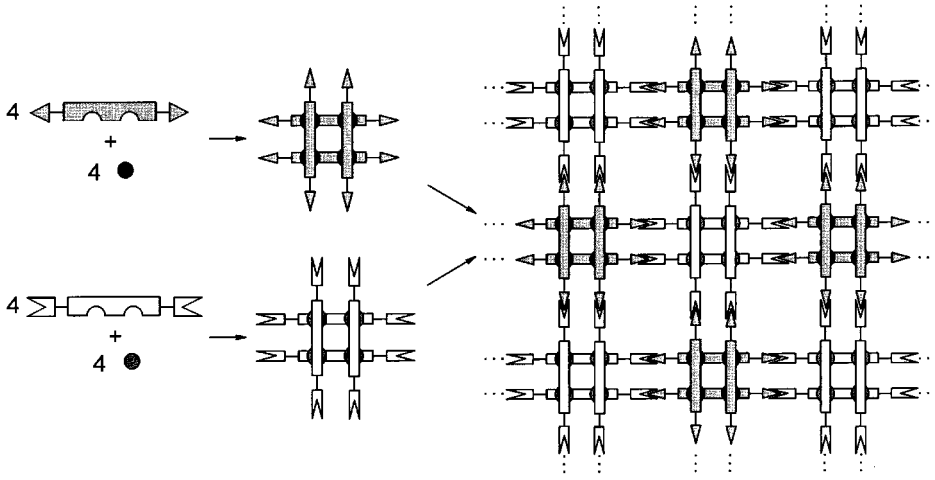

Figure 1. Schematic representation of the generation of the two-level sequential self-assembly of an ordered alternating "grid-of-grids" pattern of two [2×2] M_4^{II} grid-type species (such as **4**−**7**) incorporating different metal ions; the long range organisation is provided by secondary interactions, such as complementary hydrogen bonding (as represented), but also electrostatic interaction or metal ion coordination, between the termini of the ligands from grid to grid

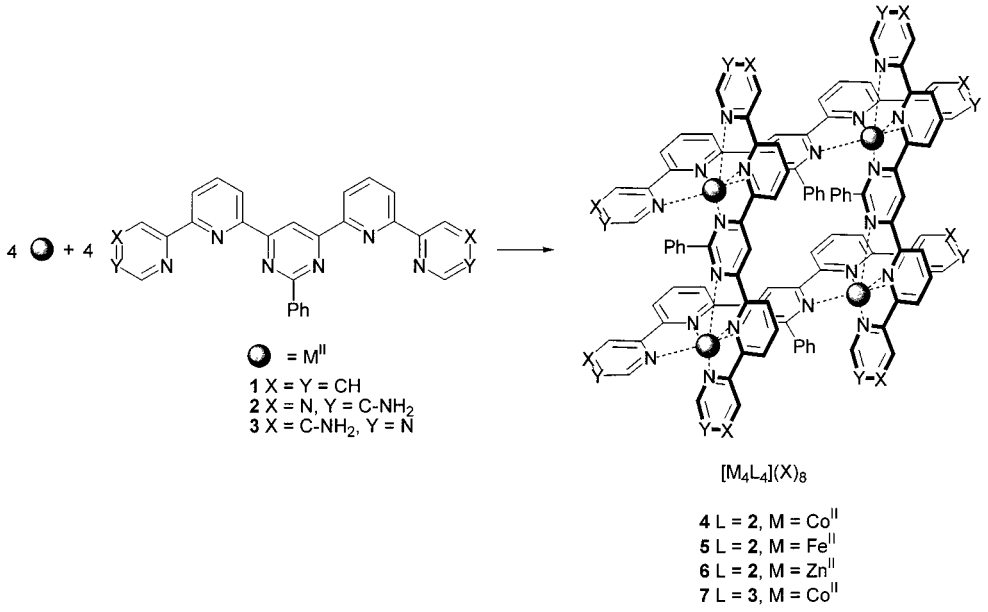

Scheme 1. Self-assembly of the [2×2] M_4^{II} grid-type complexes **4**−**7** from ditopic ligands **2** and **3**

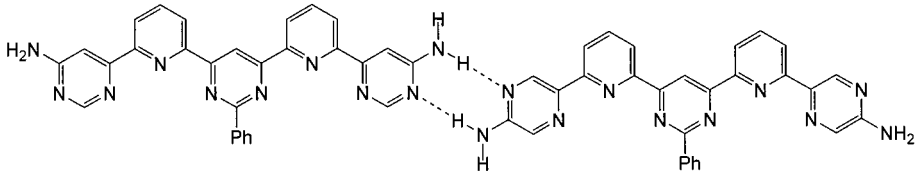

Scheme 2. Representation of the hydrogen-bonding pattern between the complementary subunits of ligand **2** (right) and **3** (left)

Results and Discussion

Synthesis of Ligands 2 and 3

The synthesis of ligand **2** and complexes **4**−**6** is outlined in Scheme 3.

Ligand **2** is produced by palladium-catalysed stannylations followed by coupling reactions of the Stille type. The yields obtained by using a one-pot reaction for the stannylation of **9** and the coupling of **10** with 2,6-dibromopyridine to give **11** were superior to those obtained when purification of the tin compound was performed. This can be explained by the rather low stability of the tin derivative during chromatographic purification. **2** precipitates from the reaction mixture as the analytically pure compound. It is insoluble in most organic solvents and only moderately sol-

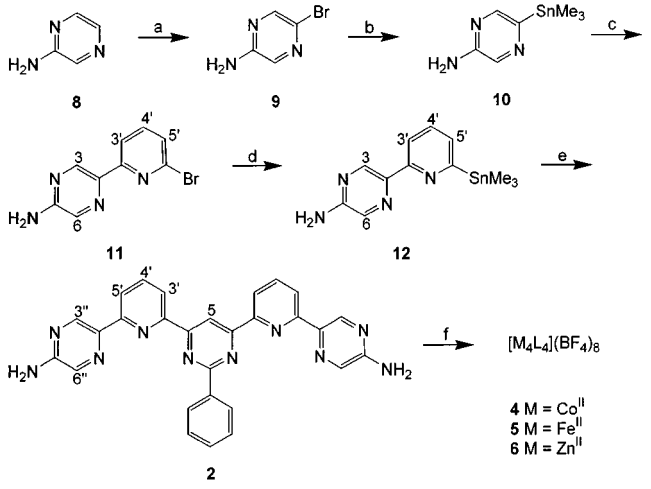

Scheme 3. Synthesis of ligand **2**: a) Br_2, $CHCl_3$ (32%); b) Me_6Sn_2, $Pd(PPh_3)_4$, toluene; c) 2,6-dibromopyridine, $Pd(PPh_3)_4$, toluene (68% over 2 steps); d) Me_6Sn_2, $Pd(PPh_3)_4$, toluene; e) 4,6-dichloro-2-phenylpyrimidine, $PdCl_2(PPh_3)_2$, DMF (69% over 2 steps); f) $M(BF_4)_2{\cdot}xH_2O$ (**4**: M = Co^{II}; **5**: M = Fe^{II}; **6**: M = Zn^{II}), CH_3CN/H_2O

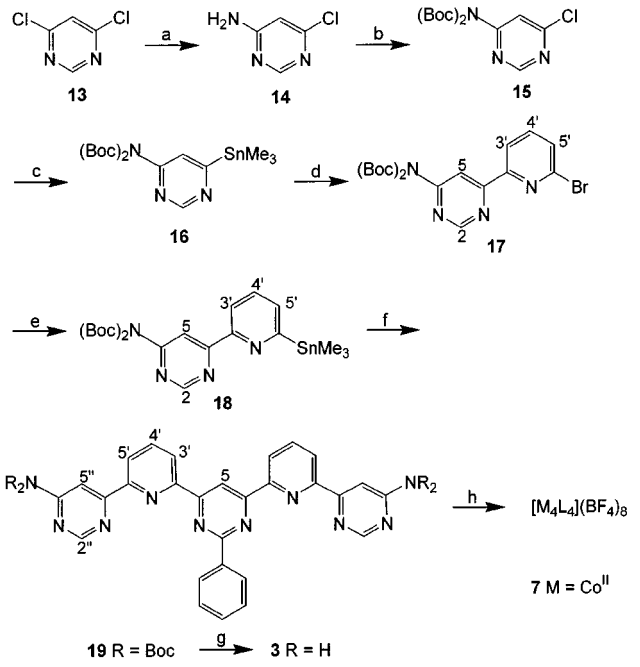

Scheme 4. Synthesis of ligand **3**: a) NH_3, MeOH (44%); b) $(Boc)_2O$, DMAP, CH_3CN (79%); c) Me_6Sn_2, $Pd(PPh_3)_4$, toluene; d) 2,6-dibromopyridine, $Pd(PPh_3)_4$, toluene (41% over 2 steps); e) Me_6Sn_2, $Pd(PPh_3)_4$, toluene; f) 4,6-dichloro-2-phenylpyrimidine, $Pd(PPh_3)_4$, toluene (50% over 2 steps); g) HCl, EtOAc (88%); h) $Co(BF_4)_2{\cdot}6H_2O$, CH_3CN/H_2O

uble in DMSO. This already points to the suitability of this compound for the formation of hydrogen-bonded networks as the low solubility can be explained by strong intermolecular hydrogen bonds between the self-complementary moieties on the edges of the ligand.

The synthesis of ligand **3** and complex **7** is outlined in Scheme 4. Whereas the amino group did not cause any problems in the palladium-catalysed stannylation of **9**, the stannylation of **14** required derivatisation of the amino group due to the low solubility of the starting material under the reaction conditions. We introduced two *tert*-butoxycarbonyl groups to solubilise the compound. The rest of the synthesis follows the same reaction pathway as for **2** and the protection groups were split off by HCl in the last step to give **3** as an extremely insoluble compound. As supported by the results of elemental analysis, **3** is probably formed as HCl salt during the reaction.The deprotonation was not possible even by washing with dilute NaOH, due to the low solubility of the compound which presumably includes the HCl in the solid.

Synthesis and Characterisation of the Complexes 4−7

So far complexes of the grid-type were usually obtained by reaction of the ligand with the metal acetate in methanol or with the metal tetrafluoroborate in acetonitrile or nitromethane;[3] however, these reactions failed for **2** and **3** because of their low solubility. For these ligands, the use of mixtures of acetonitrile and water in variable ratios, specific for each of the ligands, as well as elevated temperatures are required to break the intermolecular hydrogen bonds of the ligand and to solubilise the reaction mixtures. Substitution of the solvents by DMSO solubilised the reaction mixture, but did not result in the assembly of the grids. Even the highly charged complexes themselves are only moderately soluble at room temperature in the solvent mixture. Exchange of the tetrafluoroborate counterions for hexafluorophosphate, triflate or perchlorate did not result in an increased solubility.

The complexes were characterised by ^1H NMR spectroscopy, FAB mass spectrometry, elemental analysis, and in the case of **7** by single-crystal X-ray diffraction. The proton NMR spectrum of the diamagnetic complex **6** shows the signals of a symmetrically coordinated ligand as expected for the grid structure. The protons of the phenyl group on the pyrimidine ring give rise to five distinct signals due to inhibited rotation of the phenyl ring in the complex.[3b] The proton NMR spectra of **4**, **5**, and **7** show strongly shifted signals (Co complexes: δ from −100 to +180 ppm; Fe complex: δ from −30 to +80 ppm) as typical for paramagnetic compounds.[9] Although in all cases sharp signals are obtained, which are typically broader for the Fe complex than for the Co complexes, no coupling patterns can be resolved due to low resolution. However, the number of signals provides information about the symmetry of the complexes indicating that the symmetry of the ligand is maintained during the complexation. Combination of this information with the composition of the complexes obtained from mass spectrometry allows the deduction of the grid-type structure for all complexes described here.

The Fe^{II} cation can exist in the diamagnetic low-spin or in the paramagnetic high-spin state, depending on the ligand field strength. From the NMR spectroscopic data, it may be deduced that the Fe complex **5** is essentially high spin as no signals are found in the region expected for diamagnetic aromatic protons. Preliminary measurements of

the magnetic susceptibility, however, suggest that there remains a low-spin fraction of the complex at room temperature and that it shows thermal spin-crossover behaviour[10] similar to a Fe^{II} grid-type compound of ligand **1** already described.[6b]

Crystal Structure of Complex 7

Crystals of complex **7** were obtained by diffusion of THF into a solution of the complex in acetonitrile/water and its structure was determined by X-ray crystallography (Figure 2). The grid moiety of the complex is comparable to that of the structures of similar compounds.[3b] The four ligands of one entity are aligned in an almost perfect parallel and perpendicular fashion. The shortest distance between the plane of a phenyl ring on one ligand and a perpendicular ligand (3.30 Å) corresponds to a van der Waals contact and indicates that the grid is stabilised by π-stacking of the ligands with the phenyl substituent on the pyrimidine ring. The Co^{II} ions present pseudo-octahedral coordination. The Co−N bond lengths and N−Co−N bond angles are analogous to those found in the parent Co^{II} grid-type complex of ligand **1**.[3b] This may appear surprising as the electron-poor pyrimidine is usually a weaker binding site than pyridine, but in the present ligand this is compensated for by the electron-donating properties of the amino group in *para* position of the binding N atom. The presence of the hydrogen bonds in only one direction (see below) has no influence on the geometry of the grid unit itself.

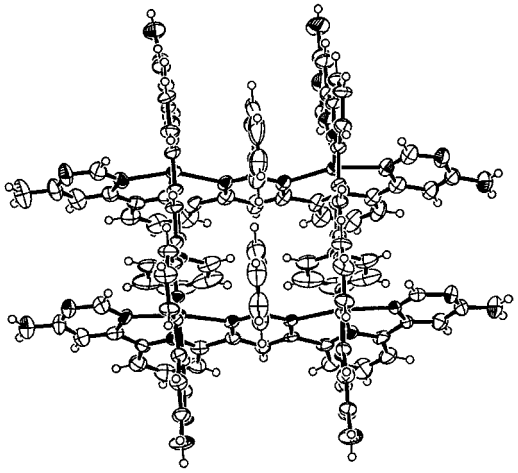

Figure 2. Single-crystal X-ray structure of the grid unit of complex **7** (anions are omitted for clarity); ORTEP representation

The self-complementarity of **2** and **3** enables their metal complexes to form hydrogen-bonded networks of grids. The availability of hydrogen-bonding sites on each edge of the grid might lead to saturation of the hydrogen bonds in two dimensions. The crystal structure of **7**, though, shows that the hydrogen-bonding motif is present in only one dimension, thus forming infinite one-dimensional chains of grids (Figure 3). The hydrogen bond lengths *d*(N−H−N) lie between 3.01(1) and 3.07(1) Å and are thus in the range of strong hydrogen bonds. The hydrogen bonds are almost linear with N−H−N bond angles between 173 and 180°. In the second dimension of the layer, no strong interactions are found between the grids. Neighbouring complexes without hydrogen-bonding contact show only weak π-stacking between their ligands. Although the rows of ligands are parallel with the shortest distance between their planes around 3.25 Å, they are slanted so that there is only a small overlap of the π-systems. A good overlap in the same range of distances can be found between the amino groups and the pyrimidine moieties of neighbouring complexes. It appears that the crystallisation of the complex in this packing is preferred to the saturation of all hydrogen bonds as it helps to avoid unfilled space in the crystal. Comparison with the similar structure of the parent Co_4^{II} [2×2] grid without hydrogen-bonding sites derived from ligand **1** shows that this complex forms layers with a larger overlap of some of the aromatic rings of neighbouring complexes. Although in that case only two out of eight of the edge pyridine rings show π-stacking, the better overlap results in a more efficient stacking.[3b] Thus, the hydrogen bonds in **7** partially break up this packing motif, but they are not strong enough to generate a completely hydrogen-bonded network which would imply the unfavourable formation of large cavities between the grids. The anions and solvent molecules of crystallisation are found between these layers, thus inhibiting any direct interaction between them.

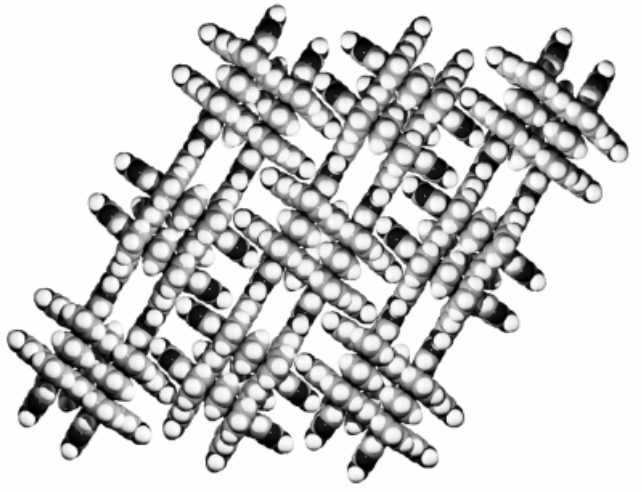

Figure 3. Crystal packing of complex **7** showing the hydrogen bonding in one direction and the formation of infinite chains of grids (anions and solvent molecules from crystallisation are omitted for clarity)

The crystals described here were obtained during an attempt at cocrystallising complexes **5** and **7**. Even though $Co(BF_4)_2{\cdot}6H_2O$ and $Fe(BF_4)_2{\cdot}6H_2O$ were used as metal salts for the complexation, no BF_4^- could be found in the crystal structure. Instead, two chloride anions originating from the last step of the synthesis of **3** and three SiF_6^{2-} units crystallised out. The last one stems probably from the reaction of some free fluoride with the glass vial in which the crystallisation was performed. These rather unexpected results could be further supported by energy-dispersive X-

ray scattering (EDX) of crystals of **5** and **7** which indeed showed significant amounts of Si.

Conclusion

As a further step in the recognition-directed self-organisation of metal complexes, the formation of arrays of four tetranuclear complexes, **4−7**, from the oligopyridine-derived ligands **2** and **3** has been achieved by sequential two-step self-assembly. These ligands were designed to form double self-complementary hydrogen bonds by introduction of aminopyrazine and aminopyrimidine moieties on the edges. Generating arrays of such metal complexes is of special interest in view of the remarkable physicochemical properties (e.g. magnetic,[6b] electrochemical[5]) displayed by [2×2] metallogrids. The single-crystal X-ray structure of Co complex **7** shows saturation of the hydrogen bonds in one direction, thus forming an infinite chain of hydrogen-bonded grids. In the other direction of each layer, weak π-stacking is present whereas no direct interactions are found between the layers of grids. Besides the self-complementarity of the ligands, the aminopyrazine and aminopyrimidine hydrogen-bonding units should also be capable of forming heterocomplementary hydrogen-bonding motifs by two-point interaction, thus allowing the arrangement of grids with different metals in a layered chessboard-like manner (Figure 1). Further experiments for the cocrystallisation of complementary hydrogen bonds between **4−7** with different anions are ongoing to explore these possibilities. In addition, the possibility of deposition of heterometallic arrays of these grids as monolayers on surfaces and their observation by STM (scanning tunnelling microscopy) is currently being investigated. The data described here may also be regarded as a step in the exploration of the ways and means to induce the spontaneous, but controlled generation of even larger organised arrays in view of assembling supramolecular architectures and devices of interest for nanotechnology.

Experimental Section

General: 5-Amino-2-bromopyrazine (**9**),[11] 4-amino-6-chloropyrimidine (**14**),[12] and 4,6-dichloro-2-phenylpyrimidine[13] were prepared according to the literature. Toluene was dried by heating under reflux with sodium under argon, acetonitrile by heating under reflux with CaH_2 for several hours. The other reagents and solvents were used without further purification. − The NMR spectroscopic data were obtained with Bruker AC 200 at 200.1 MHz (^1H) and 50.2 MHz (^{13}C), calibrated against the residue solvent signal ($CDCl_3$: δ = 7.24; [D_6]DMSO: δ = 2.50; CD_3CN: δ = 1.94) and are given in ppm. − IR data were collected with a Perkin−Elmer 1600 series FTIR spectrometer and are reported in cm^{-1}. − Microanalyses of metal complexes sometimes give unsatisfactory results due to incomplete combustion of the complex. It was not possible to obtain a good microanalysis for complex **7** because of this and perhaps also due to an undefined mixture of anions.

5-Amino-2-[6′-bromopyrid-2′-yl]pyrazine (11): 5-Amino-2-bromopyrazine (**9**) (500 mg, 2.87 mmol), hexamethyldistannane (1.04 g, 3.16 mmol), and $Pd(PPh_3)_4$ (183 mg, 0.16 mmol) were combined in toluene (15 mL), flushed with Ar, and heated under reflux for 1 h. After cooling to room temp., 2,6-dibromopyridine (952 mg, 4.02 mmol) and $Pd(PPh_3)_4$ (231 mg, 0.20 mmol) were added and the mixture was heated under reflux for 19 h. The solvent was evaporated and the residue purified by column chromatography on silica with hexane/EtOAc (1:1, v/v) to give **11** as a white powder. Yield 492 mg (68%). − ^1H NMR ($CDCl_3$): δ = 4.84 (s, br, 2 H, NH_2), 7.38 (dd, J = 0.9 Hz and 7.9 Hz, 1 H, $H_{3'\text{ or }5'}$), 7.58 (t, J = 7.9 Hz, 1 H, $H_{4'}$), 7.97 (d, J = 1.2 Hz, 1 H, $H_{3\text{ or }6}$), 8.08 (dd, J = 0.9 Hz and 7.6 Hz, 1 H, $H_{3'\text{ or }5'}$), 9.01 (d, J = 1.5 Hz, 1 H, $H_{3\text{ or }5}$). − ^{13}C NMR ($CDCl_3$): δ =118.3, 126.8, 130.9, 139.1, 139.9, 141.2, 141.6, 154.5, 156.2. − MS (FAB): m/z = 251.0 [M + H^+]. − IR (KBr): $\tilde{\nu}$ = 3436, 3316, 3163, 1641, 1586, 1541, 1432, 1380, 1286, 1154, 1124, 1012, 802, 776, 668, 604, 494, 416. − $C_9H_7BrN_4$ (251.1): calcd. C 43.05, H 2.79, N 22.32; found C 43.14, H 2.40, N 22.04.

5-Amino-2-[6′-(trimethylstannyl)pyrid-2′-yl]pyrazine (12): 5-Amino-2-(6′-bromopyrid-2′-yl)pyrazine (**11**) (550 mg, 2.19 mmol), hexamethyldistannane (789 mg, 2.41 mmol), and $Pd(PPh_3)_4$ (76 mg, 0.066 mmol) were combined in toluene (15 mL), flushed with Ar, and heated under reflux for 20 min. The solvent was evaporated and the residue was taken up in $CHCl_3$. The precipitated Pd was centrifuged off and the residue was used for the next coupling step after evaporation of the solvent without further purification. − ^1H NMR ($CDCl_3$): δ = 0.34 [s, 9 H, Sn(CH_3)$_3$], 4.94 (s, br, 2 H, NH_2), 7.35 (dd, J = 8 Hz and 1.2 Hz, 1 H, $H_{3'\text{ or }5'}$), 7.60 (t, J = 8 Hz, 1 H, $H_{4'}$), 7.95−7.99 (m, 2 H, $H_{3'\text{ or }5'}$ and $H_{3\text{ or }6}$), 9.19 (d, J = 1.4 Hz, 1 H, $H_{3\text{ or }6}$).

4,6-Bis[6′-(5′′-aminopyrazin-2′′-yl)pyrid-2′-yl]-2-phenylpyrimidine (2): 5-Amino-2-[6′-(trimethylstannyl)pyrid-2′-yl]pyrazine (**12**) (660 mg, 1.97 mmol), 4,6-dichloro-2-phenylpyrimidine (222 mg, 0.99 mmol), and $PdCl_2(PPh_3)_2$ (55 mg, 0.079 mmol) were combined in anhydrous DMF (15 mL), degassed, and heated to 100 °C for 21 h. The mixture was cooled to room temp. and the precipitation was centrifuged off, washed 2 × with MeOH/acetone and 1 × with Et_2O to give **2** as a white powder. Yield 373 mg (69% over 2 steps). − ^1H NMR ([D_6]DMSO): δ = 6.96 (s, br, 4 H, NH_2), 7.60−7.65 (m, 3 H, $H_{meta\text{ and }para}$), 8.03 (d, J = 1.2 Hz, 1 H, $H_{3''\text{ or }6''}$), 8.15 (t, J = 7.3, 2 H, $H_{4'}$), 8.31 (d, J = 7.9 Hz, 2 H, $H_{3'\text{ or }5'}$), 8.67 (d, J = 7.3 Hz, 2 H, $H_{3'\text{ or }5'}$), 8.70−8.76 (m, 2 H, H_{ortho}), 9.12 (d, J = 1.2 Hz, 2 H, $H_{3''\text{ or }6''}$), 9.36 (s, 1 H, H_5). − ^{13}C NMR ([D_6]DMSO): δ = 111.4, 121.2, 121.6, 129.0, 129.7, 132.0, 132.3, 138.0, 138.7, 139.5, 141.1, 153.7, 155.9, 157.1, 164.2, 164.8. − MS (FAB): m/z = 497.2 [M + H^+]. − IR (KBr): $\tilde{\nu}$ = 3313, 3159, 1654, 1564, 1534, 1488, 1378, 1298, 1019, 818, 752, 691, 637, 606, 415. − $C_{28}H_{20}N_{10}$ (496.5): calcd. C 67.37, H 4.06, N 28.21; found C 67.75, H 4.26, N 28.03.

Co Complex 4: 4,6-Bis[6′-(5′′-aminopyrazin-2′′-yl)pyrid-2′-yl]-2-phenylpyrimidine (**2**) (1.7 mg, 3.4 μmol) and $Co(BF_4)_2{\cdot}6H_2O$ (1.2 mg, 3.4 μmol) were heated under reflux in CD_3CN (0.4 mL) and D_2O (1 drop) for 3.5 h. The complex was isolated in quantitative yield as a brown powder by evaporation of the solvent. − ^1H NMR (CD_3CN/D_2O): δ = −137.98, −117.95, 12.37, 7.94, 12.70, 24.59, 36.79, 49.11, 80.22, 143.72, 166.16. − MS (FAB): m/z = 2742.5 $[Co_4L_4](BF_4)_6^+$, 2654.5 $[Co_4L_4](BF_4)_5^+$, 2568.4 $[Co_4L_4](BF_4)_4^+$, 2480.6 $[Co_4L_4](BF_4)_3^+$. − $C_{112}H_{80}B_8Co_4F_{32}N_{40}{\cdot}13H_2O$ (3150.5): calcd. C 42.70, H 3.39, N 17.78; found C 42.73, H 3.32, N 17.44.

Fe Complex 5: 4,6-Bis[6′-(5′′-aminopyrazin-2′′-yl)pyrid-2′-yl]-2-phenylpyrimidine (**2**) (10.0 mg, 20.1 μmol) and $Fe(BF_4)_2{\cdot}6H_2O$ (6.8 mg, 20.1 μmol) were heated under reflux in CH_3CN (4 mL)

and H_2O (0.5 mL) for 24 h. The complex was isolated as a dark brown powder by evaporation of the solvent in quantitative yield. − ^{1}H NMR (CD_3CN/D_2O): δ = −13.01, −9.14, −6.06, 40.79, 50.88, 64.64, 75.34. − MS (FAB): *m/z* = 2730.5 $[Fe_4L_4](BF_4)_6^+$, 2643.7 $[Fe_4L_4](BF_4)_5^+$, 2556.3 $[Fe_4L_4](BF_4)_4^+$, 2469.7 $[Fe_4L_4](BF_4)_3^+$. − $C_{112}H_{80}B_8F_{32}Fe_4N_{40}\cdot 7H_2O$ (3030.0): calcd. C 44.40, H 3.13, N 18.49; found C 44.70, H 2.87, N 18.05.

Zn Complex 6: 4,6-Bis[6′-(5′′-aminopyrazin-2′′-yl)pyrid-2′-yl]-2-phenylpyrimidine (**2**) (2.5 mg, 5.0 μmol) and $Zn(BF_4)_2\cdot 8H_2O$ (1.9 mg, 5.0 μmol) were heated under reflux in CD_3CN (0.5 mL) and D_2O (0.05 mL) for 3.5 h. The complex was isolated as an orange powder by evaporation of the solvent in quantitative yield. − ^{1}H NMR (CD_3CN/D_2O): δ = 5.68 (d, *J* = 6.9 Hz, 1 H, H_{ortho}), 5.95 (d, *J* = 7.3 Hz, 1 H, H_{ortho}), 6.08 (d, *J* = 1.5 Hz, 2 H, $H_{3'' \text{ or } 6''}$), 6.38 (t, *J* = 7.7 Hz, 1 H, $H_{meta \text{ or } para}$), 6.81 (t, *J* = 7.3 Hz, 1 H, $H_{meta \text{ or } para}$), 6.91 (t, *J* = 7.3 Hz, 1 H, $H_{meta \text{ or } para}$), 8.38 (t, *J* = 8.2 Hz, 2 H, $H_{4'}$), 8.47 (d, *J* = 8.0 Hz, 2 H, $H_{3' \text{ or } 5'}$), 8.79 (d, *J* = 1.1 Hz, 2 H, $H_{3'' \text{ or } 6''}$), 8.80 (d, *J* = 8.0 Hz, 2 H, $H_{3' \text{ or } 5'}$), 9.41 (s, 1 H, H_5). − MS (FAB): *m/z* = 2680.9 $[Zn_4L_4](BF_4)_5^+$, 2593.6 $[Zn_4L_4](BF_4)_4^+$, 2505.6 $[Zn_4L_4](BF_4)_3^+$, $[Zn_4L_4](BF_4)_2^+$. − $C_{112}H_{80}B_8F_{32}N_{40}Zn_4\cdot 13H_2O$ (3176.3): calcd. C 42.35, H 3.36, N 17.64; found C 42.20, H 3.42, N 17.80.

6-[Bis(*tert*-butoxycarbonyl)amino]-4-chloropyrimidine (15): 6-Amino-4-chloropyrimidine (**14**) (2.05 g, 15.8 mmol) was suspended in anhydrous acetonitrile (8 mL). Dimethylaminopyridine (483 mg, 1.45 mmol) and di-*tert*-butyl carbonate (7.37 g, 39.6 mmol) were added and stirred at room temp. for 23 h. The solvent was evaporated and the residue purified by column chromatography on silica with hexane/EtOAc (1:1, v/v) to give **15** as a white powder. Yield 4.12 g (79%). − ^{1}H NMR ($CDCl_3$): δ = 1.56 [s, 18 H, $C(CH_3)_3$], 7.85 (d, *J* = 0.9 Hz, 1 H, $H_{2 \text{ or } 5}$), 8.66 (d, *J* = 0.9 Hz, 1 H, $H_{2 \text{ or } 5}$). − ^{13}C NMR ($CDCl_3$): δ = 27.5, 84.8, 110.9, 149.4, 157.5, 158.7, 161.4. − MS (FAB): *m/z* = 330.0 $[M^+]$. − IR (KBr): ṽ = 3149, 2980, 1778, 1737, 1567, 1538, 1456, 1365, 1299, 1259, 1234, 1157, 1138, 983, 843, 786. − $C_{14}H_{20}ClN_3O_4$ (329.8): calcd. C 50.99, H 6.11, N 12.74; found C 50.70, H 5.72, N 12.54.

6-[Bis(*tert*-butoxycarbonyl)amino]-4-(trimethylstannyl)pyrimidine (16): 6-[Bis(*tert*-butoxycarbonyl)amino]-4-chloropyrimidine (**15**) (611 mg, 1.85 mmol), hexamethyldistannane (670 mg, 2.04 mmol), and $Pd(PPh_3)_4$ (86 mg, 0.074 mmol) were combined in toluene (10 mL), flushed with Ar, and heated under reflux for 45 min. The solvent was evaporated and the residue used for the following coupling reaction without further purification. − ^{1}H NMR ($CDCl_3$): δ = 0.35 [s, 9 H, $Sn(CH_3)_3$], 1.51 [s, 18 H, $C(CH_3)_3$], 7.77 (d, *J* = 1.5 Hz, 1 H, $H_{2 \text{ or } 5}$), 8.95 (d, *J* = 1.2 Hz, 1 H, $H_{2 \text{ or } 5}$).

4-[6′-Bromopyrid-2′-yl]-6-[bis(*tert*-butoxycarbonyl)amino]-pyrimidine (17): 6-[Bis(*tert*-butoxycarbonyl)amino]-4-(trimethylstannyl)pyrimidine (**16**) (763 mg, 1.76 mmol), 2,6-dibromopyridine (671 mg, 2.83 mmol), and $Pd(PPh_3)_4$ (98 mg, 0.084 mmol) were combined in toluene (10 mL), flushed with Ar, and heated under reflux for 21 h. The solvent was evaporated and the residue purified by column chromatography on silica with hexane/EtOAc (9:1 changing to 4:1, v/v) to give **17** as a white powder. Yield 345 mg (41%). − ^{1}H NMR ($CDCl_3$): δ = 1.53 [s, 9 H, $C(CH_3)_3$], 7.58 (dd, *J* = 0.9 and 7.9 Hz, 1 H, $H_{3' \text{ or } 5'}$), 7.71 (t, *J* = 7.6 Hz, 1 H, $H_{4'}$), 8.41 (dd, *J* = 1.2 and 7.3 Hz, 1 H, $H_{3' \text{ or } 5'}$), 8.53 (d, *J* = 1.2 Hz, 1 H, $H_{2 \text{ or } 5}$), 9.00 (d, *J* = 1.2 Hz, 1 H, $H_{2 \text{ or } 5}$). − ^{13}C NMR ($CDCl_3$): δ = 27.7, 84.3, 110.3, 120.5, 129.8, 139.3, 141.9, 154.8, 157.8, 159.9, 162.4. − MS (FAB): *m/z* = 452.9 $[M + H^+]$. − IR (KBr): ṽ = 2980, 2934, 1777, 1743, 1573, 1534, 1435, 1388, 1370, 1341, 1303, 1279, 1230, 1143, 985, 850, 807, 775, 697, 632. − $C_{19}H_{23}BrN_4O_4$ (451.3): calcd. C 50.57, H 5.41, N 12.41; found C 50.84, H 5.29, N 12.20.

6-[Bis(*tert*-butoxycarbonyl)amino]-4-[6′-(trimethylstannyl)pyrid-2′-yl]pyrimidine (18): 4-[6′-Bromopyrid-2′-yl]-6-[bis(*tert*-butoxycarbonyl)amino]pyrimidine (**17**) (140 mg, 0.32 mmol), hexamethyldistannane (120 mg, 0.36 mmol), and $Pd(PPh_3)_4$ (19 mg, 0.017 mmol) were combined in toluene (2 mL), flushed with Ar, and heated under reflux for 30 min. The solvent was evaporated and the residue used for the next coupling reaction without further purification. − ^{1}H NMR ($CDCl_3$): δ = 0.38 [s, 9 H, $Sn(CH_3)_3$], 1.53 [s, 18 H, $C(CH_3)_3$], 7.53 (dd, *J* = 1.5 and 7.3 Hz, 1 H, $H_{3' \text{ or } 5'}$), 7.68 (t, *J* = 7.3, 1 H, $H_{4'}$), 8.30 (dd, *J* = 1.5 and 7.9 Hz, 1 H, $H_{3' \text{ or } 5'}$), 8.60 (d, *J* = 1.2 Hz, 1 H, $H_{2 \text{ or } 5}$), 9.04 (d, *J* = 1.2 Hz, 1 H, $H_{2 \text{ or } 5}$).

4,6-Bis[6-{6-[bis(*tert*-butoxycarbonyl)amino]pyrimidin-4-yl}pyrid-2-yl]-2-phenylpyrimidine (19): 6-[Bis(*tert*-butoxycarbonyl)amino]-4-[6-(trimethylstannyl)pyrid-2-yl]pyrimidine (**18**) (151 mg, 0.28 mmol), 4,6-dichloro-2-phenylpyrimidine (34 mg, 0.15 mmol), and $Pd(PPh_3)_4$ (17 mg, 0.015 mmol) were combined in toluene (2 mL), flushed with Ar, and heated under reflux for 22 h. The solvent was evaporated and the residue purified by column chromatography on silica with hexane/EtOAc (4:1, changing to 1:1, v/v) to give **19** as a pale yellow powder. Yield 72 mg (50%). − ^{1}H NMR ($CDCl_3$): δ = 1.44 [s, 36 H, $C(CH_3)_3$], 7.52−7.6 (m, 3 H, $H_{meta \text{ and } para}$), 8.09 (t, *J* = 7.9 Hz, 2 H, $H_{4'}$), 8.60 (d, *J* = 7.6 Hz, 2 H, $H_{3' \text{ or } 5'}$), 8.69 (dd, *J* = 0.9 and 7.9 Hz, 2 H, $H_{3' \text{ or } 5'}$), 8.72−8.78 (m, 2 H, H_{ortho}), 8.85 (s, 2 H, $H_{2'' \text{ or } 5''}$), 9.03 (d, *J* = 0.9 Hz, 2 H, $H_{2'' \text{ or } 5''}$), 9.13 (s, 1 H, H_5). − ^{13}C NMR ($CDCl_3$): δ = 27.6, 84.1, 109.5, 112.9, 123.0, 123.9, 128.4, 128.5, 130.8, 137.7, 138.1, 150.2, 153.8, 155.2, 157.7, 159.7, 163.6, 164.3, 164.5. − MS (high-resolution FAB): calcd. for $C_{38}H_{34}N_{10}O_4$: *m/z* = 897.404784, found *m/z* = 897.405728 $[M + H^+]$. − IR (KBr): ṽ = 3059, 2979, 2933, 1777, 1744, 1576, 1537, 1459, 1394, 1370, 1342, 1304, 1282, 1260, 1142, 1109, 988, 847, 824, 759, 692. − $C_{48}H_{52}N_{10}O_8\cdot 3/4EtOAc$: calcd. C 63.65, H 6.00, N 14.56; found C 63.29, H 5.78, N 14.88.

4,6-Bis[6-(6-aminopyrimidin-4-yl)pyrid-2-yl]-2-phenylpyrimidine (3): EtOAc (5 mL) was saturated with HCl gas. This solution was added to 4,6-bis[6-{6′-[bis(*tert*-butoxycarbonyl)amino]pyrimidin-4-yl}pyrid-2-yl]-2-phenylpyrimidine (**19**) (72 mg, 0.080 mmol) and stirred at room temp. for 16 h. The precipitation was centrifuged off and washed with EtOAc, H_2O, NaOH, DMSO and acetone to give **3** as an off-white powder. Yield 35 mg (88%). Because of the low solubility of this compound, no NMR spectrum could be obtained. − MS (high-resolution FAB): calcd. for $C_{28}H_{21}N_{10}$: *m/z* = 497.195066, found *m/z* = 497.195923 $[M + H^+]$. − IR (KBr): ṽ = 3311, 3058, 1658, 1560, 1538, 1369, 1318, 1252, 1169, 1086, 992, 822, 760, 652.

Co Complex 7: 4,6-Bis[6-(6-aminopyrimidin-4-yl)pyrid-2-yl]-2-phenylpyrimidine (**3**) (2 mg, 4.03 μmol) and $Co(BF_4)_2\cdot 6H_2O$ (1.37 mg, 4.03 μmol) were heated under reflux in CD_3CN (0.25 mL) and D_2O (0.25 mL) for 23 h. The complex was isolated as a pale brown powder by evaporation of the solvent in quantitative yield. − ^{1}H NMR (CD_3CN/D_2O): δ = −89.59, −79.40, −42.99, −7.43, −7.18,16.73, 28.99, 49.42, 109.56, 146.53, 177.69. − MS (FAB): *m/z* = 2742.8 $[Co_4L_4](BF_4)_6^+$, 2655.7 $[Co_4L_4](BF_4)_5^+$, 2569.2 $[Co_4L_4](BF_4)_4^+$, 2481.2 $[Co_4L_4](BF_4)_3^+$.

X-ray Structural Analysis for Complex 7: A suitable orange crystal (0.4 × 0.1 × 0.05 mm) of $[C_{112}H_{80}N_{40}Co_4]^{8+} \times 2\ Cl^- \times 3\ SiF_6^{2-} \times 2\ CH_3CN \times 50\ H_2O$ was obtained from acetonitrile/water/THF during the attempt of cocrystallisation with Fe complex **5**; *M* = 3702.0 g mol^{-1}, triclinic $P\bar{1}$, *a* = 15.4976(4), *b* = 18.2114(6), *c* =

31.9538(10) Å, $\alpha = 86.9809(13)$, $\beta = 83.4137(18)$, $\gamma = 67.2828(16)°$, $V = 8263.6(4)$ Å^3, μ(Mo-K_α) = 0.559 mm^{-1}, $Z = 2$, $D_c = 1.447$ g cm^{-3}, $F(000) = 3644$, $T = 173.0(1)$ K. Data were recorded with a Nonius Kappa CCD diffractometer using graphite-monochromatised Mo-K_α ($\lambda = 0.71073$ Å) radiation. $\theta = 2.96-24.97°$ for data collection. 67652 collected reflections, 27325 unique reflections [16258 with $I > 2\sigma(I)$] were used for refinement. The data were processed with DENZO.[14] The absorption correction was made with SORTAV[15] ($T_{min} = 80.74$ and $T_{max} = 97.26°$) and L_p correction was applied. Structure solution was done by direct methods[16] and refinement on F^2.[17] The hydrogen atoms were calculated to their idealised positions with isotropic temp. factors (1.2 or 1.5 times the C temp. factor) and were refined as riding atoms. Four temperature factors were equalised. One Cl^- anion is disordered over two positions (occupancy 0.5). Fluorine atoms of one SiF_6^{2-} anion are disordered between two positions with site occupation values of 0.64 and 0.36. The hydrogen-bonded, complicated water system altogether includes 50 molecules of water (hydrogen atoms could not be located), of which 26 are treated with an occupancy of 1.0, while the others are disordered and refined with a population parameter of 0.5. Final R values were $R = 0.1185$, $wR^2 = 0.2778$ [$I > 2\sigma(I)$], $R = 0.1900$, $wR^2 = 0.3190$ (all data) for 2201 parameters, Goodness-of-fit on $F^2 = 1.057$. A final difference map displayed the highest electron density of 1.07 eÅ^{-3}, which is located near to water molecules. Crystallographic data (excluding structure factors) for the structure reported in this paper have been deposited with the Cambridge Crystallographic Data Centre as supplementary publication no. CCDC-150832. Copies of the data can be obtained free of charge on application to CCDC, 12 Union Road, Cambridge CB2 1EZ, UK [Fax: (internat.) + 44-1223/336-033; E-mail: deposit@ccdc.cam.ac.uk].

Acknowledgments

E. B. thanks the French Government for an undergraduate and the "Ministère de l'Education Nationale, de la Recherche et de la Technologie" for a graduate fellowship. U. Z. thanks the "Deutsche Forschungsgemeinschaft" for a postdoctoral fellowship. Financial support from the "Finnish Ministry of Education" (E. W.) is gratefully acknowledged. We thank Dr. D. Bassani for preliminary work.

[1] [1a] J.-M. Lehn, *Supramolecular Chemistry: Concepts and Perspectives*, VCH, Weinheim, **1995**, chapter 9. – [1b] *Comprehensive Supramolecular Chemistry* (Eds.: J. L. Atwood, J. E. D. Davies, D. D. MacNicol, F. Vögtle, J.-M. Lehn), Pergamon, Oxford, **1996**; P. N. W. Baxter, vol. 9, pp. 165–211. – [1c] *Comprehensive Supramolecular Chemistry* (Eds.: J. L. Atwood, J. E. D. Davies, D. D. MacNicol F. Vögtle, J.-M. Lehn), Pergamon, Oxford, **1996**; M. Fujita, vol. 9, pp. 253–282.

[2] [2a] A. D. Burrows, C.-W. Chan, M. M. Chowdry, J. E. McGrady, D. M. P. Mingos, *Chem. Soc. Rev.* **1995**, 329–339. – [2b] C. B. Aakeröy, A. M. Beatty, *Chem. Commun.* **1998**, 1067–1068. – [2c] C. B. Aakeröy, A. M. Beatty, D. S. Leinen, *Angew. Chem. Int. Ed.* **1999**, *38*, 1815–1819; *Angew. Chem.* **1999**, *111*, 1932–1936. – [2d] Z. Qin, H. A. Jenkins, S. J. Coles, K. W. Muir, R. J. Puddephatt, *Can. J. Chem.* **1999**, *77*, 155–157. – [2e] C. Janiak, S. Deblon, H.-P. Wu, M. J. Kolm, P. Klüfers, H. Piotrowski, P. Mayer, *Eur. J. Inorg. Chem.* **1999**, 1507–1521. – [2f] M. Tadokoro, K. Isobe, H. Uekusa, Y. Ohashi, J. Toyoda, K. Tashiro, K. Nakasuji, *Angew. Chem. Int. Ed.* **1999**, *38*, 95–98; *Angew. Chem.* **1999**, *111*, 102–106.

[3] [3a] G. S. Hanan, D. Volkmer, U. S. Schubert, J.-M. Lehn, G. Baum, D. Fenske, *Angew. Chem. Int. Ed. Engl.* **1997**, *36*, 1842–1844; *Angew. Chem.* **1997**, *109*, 1929–1931. – [3b]J. Rojo, F. J. Romero-Salguero, J.-M. Lehn, G. Baum, D. Fenske, *Eur. J. Inorg. Chem.* **1999**,1421–1428.

[4] For related complexes see: [4a] K. L. V. Mann, E. Psillakis, J. C. Jeffery, L. H. Rees, N. M. Harden, J. A. McCleverty, M. D. Ward, D. Gatteschi, F. Totti, F. E. Mabbs, E. J. L. McInnes, P. C. Riedi, G. M. Smith, *J. Chem. Soc., Dalton Trans.* **1999**, 339–348. – [4b] C. S. Campos-Fernàndez, R. Clérac, K. R. Dunbar, *Angew. Chem. Int. Ed.* **1999**, *38*, 3477–3479; *Angew. Chem.* **1999**, *111*, 3685–3688. – [4c] H. Oshio, O. Tamada, H. Onodera, T. Ito, T. Ikoma, S. Tero-Kubota, *Inorg. Chem.* **1999**, *38*, 5686–5689. – [4d] J. Rojo, J.-M. Lehn, G. Baum, D. Fenske, O. Waldmann, P. Müller, *Eur. J. Inorg. Chem.* **1999**, 517–522.

[5] M. Ruben, E. Breuning, J.-P. Gisselbrecht, J.-M. Lehn, *Angew. Chem. Int. Ed.* **2000**, *39*, 4139–4142; *Angew. Chem.* **2000**, *112*, 4312–4315.

[6] [6a] O. Waldmann, J. Hassmann, P. Müller, G. S. Hanan, D. Volkmer, U. S. Schubert, J.-M. Lehn, *Phys. Rev. Lett.* **1997**, *78*, 3390–3393. – [6b] E. Breuning, M. Ruben, J.-M. Lehn, F. Renz, Y. Garcia, V. Ksenofontov, P. Gütlich, E. Wegelius, K. Rissanen, *Angew. Chem. Int. Ed.* **2000**, *39*, 2504–2507; *Angew. Chem.* **2000**, *112*, 2563–2566.

[7] A. Semenov, J. P. Spatz, M. Möller, J.-M. Lehn, B. Sell, D. Schubert, C. H. Weidl, U. S. Schubert, *Angew. Chem. Int. Ed.* **1999**, *38*, 2547–2550; *Angew. Chem.* **1999**, *111*, 2701–2705.

[8] U. Ziener, E. Breuning, J.-M. Lehn, E. Wegelius, K. Rissanen, G. Baum, D. Fenske, G. Vaughan, *Chem. Eur. J.* **2000**, *6*, 4132–4139.

[9] I. Bertini, C. Luchinat, *NMR of Paramagnetic Molecules in Biological Systems*, Benjamin/Cummings Publishing Company Inc., Sydney, **1986**.

[10] E. Breuning, M. Ruben, J.-M. Lehn, F. Renz, Y. Garcia, V. Ksenofontov, P. Gütlich, work in progress.

[11] L. Crombie, R. C. F. Jones, C. J. Palmer, *J. Chem. Soc., Perkin Trans. 1* **1987**, 317.

[12] D. J. Brown, J. S. Harper, *J. Chem. Soc.* **1961**, 1298.

[13] D. B. Harden, M. J. Mokrosz, L. Strekowski, *J. Org. Chem.* **1988**, *53*, 4137–4140.

[14] Z. Otwinowski, W. Minor, *Methods in Enzymology*, Volume 276: *Macromolecular Crystallography*, part A (Eds.. C. W. Carter Jr., R. M. Sweet), Academic Press, **1997**, pp. 307–326.

[15] R. H. Blessing, *Acta Crystallogr., Sect. A* **1995**, *51*, 33–37.

[16] G. M. Sheldrick, *SHELXS97 – A Program for Automatic Solution of Crystal Structures*, University of Göttingen, Germany, **1997**.

[17] G. M. Sheldrick, *SHELXL97 – A Program for Crystal Structure Refinement*, University of Göttingen, Germany, **1997**.

Received October 20, 2000
[I00399]

Hydrogen-Bonding and Metal-Ion-Mediated Self-Assembly of a Nanoporous Crystal Lattice

Dirk G. Kurth,[a][‡] Katharina M. Fromm,[a][‡‡] and Jean-Marie Lehn*[a]

Keywords: Hydrogen bonds / Self assembly / Mesoporous materials / Crystal engineering / Supramolecular chemistry

Hydrogen-bonding and metal-ion coordination are utilized to assemble a nanoporous crystal lattice. In the initial step of the assembly process, tecton **1** (4b,5,7,7a-tetrahydro-4b,7a-epiminomethanoimino-6*H*-imidazo[4,5-*f*][1,10]phenanthroline-6,13-dione) forms an octahedrally coordinated secondary building block with Fe^{II}, which in the final step assembles through hydrogen-bonding interactions to a nanoporous network. The secondary building blocks hydrogen-bond such that ribbons with two-membered channels are formed. Sheets are generated through hydrogen-bonding of the ribbons, which results in four-membered channels. In the crystal, the sheets are stacked parallel to each other, which results in a three-dimensional porosity.

Introduction

Supramolecular chemistry provides ways and means to design and generate organized equilibrium architectures of nanoscopic dimensions with novel structural and functional properties.[1,2] The final supramolecular entity (or a collection of such) evolves through a sequence of spontaneous but directed recognition, growth, and termination steps of suitably instructed components and specified interaction schemes. Non-covalent interactions, such as hydrogen bonding, metal ion coordnation, electrostatic and hydrophobic forces, permit precise positioning of molecular components in a well-defined supramolecular architecture.[1,2]

The implementation of the underlying principles of non-covalent interactions in molecular based materials allows the generation of spatially confined and macroscopically ordered ensembles. Long-range correlation of positions or orientations of the active constituents will be of paramount importance to fully explore the potential of supramolecular materials and of the derived functional devices. The improvement of existing and the development of novel methods to generate organized supramolecular assemblies represent a central objective and require the availability of structurally reliable, functional synthons to engineer periodic, three-dimensional architectures presenting specific structural characteristics.

Such is the case with nanoporous networks, which are at the focus of materials research due in particular to the commercial interest in chemical separation and heterogeneous catalysis.[3] Zeolites, pillared clays and related microporous materials, which have been studied extensively due to their useful catalytic properties, can now be engineered to some extent.[4−8] The challenges posed by the production of a well-defined porosity i.e. the formation of chiral and chemically functionalizable pores has recently stimulated the application of self-assembly principles originating from supramolecular chemistry based on hydrogen bonding and metal-ion coordination in this area.[1,2,9]

Metal-ion-containing devices are of particular interest as active components in functional materials because they possess a wide range of well-defined geometries and diverse properties that are relevant in electronic, optical, magnetic, and catalytic applications.[10] Self-assembly of the metallosupramolecular architecture is effected through ligands with suitable binding sites in a proper spatial arrangement.[1,2] On the other hand, hydrogen bonding is probably the most widely spread interaction motif in biological systems.[11] It, therefore, appeared of much interest to us to explore both interactions to pursue the goal of constructing well-defined nanoporous architectures containing functional components.[12]

Herein we describe the synthesis and structure of a nanoporous network through sequential self-assembly. Metal ion coordination of 4b,5,7,7a-tetrahydro-4b,7a-epiminomethanoimino-6*H*-imidazo[4,5-*f*][1,10]phenanthroline-6,13-dione (**1**) with Fe^{II} results in the octahedral secondary building block $[Fe^{II}(\mathbf{1})_3]Br_2$. Tecton **1** combines the versatile metal ion receptor phenanthroline[13] with urea[14] as the hy-

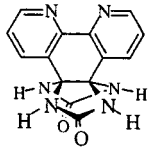

1

[a] Laboratoire de Chimie Supramoléculaire
ISIS − ULP-CNRS ESA-7006
4, Rue Blaise Pascal, 67000 Strasbourg, France
[‡] Present address: Max-Planck-Institute of Colloids and Interfaces,
14424 Potsdam, Germany
[‡‡] Present address: University of Geneva, Sciences II,
30, Quai Ernest-Ansermet, 1211 Geneva 4, Switzerland

 © WILEY-VCH Verlag GmbH, 69451 Weinheim, 2001 1434−1948/01/0606−1523 $ 17.50+.50/0

drogen-bonding component. As a result of the nonplanar topology of the metal ion and hydrogen bond receptors the secondary building block forms a nanoporous, crystal lattice.

Results and Discussion

Ligand **1** was obtained as an insoluble white powder in 61% yield from the condensation of 1,10-phenanthroline-5,6-dione, prepared from 1,10-phenanthroline according to literature procedures,[15] and urea.[16]

When three equivalents of **1** were treated with one equivalent of $FeBr_2$ in degassed water under Ar the reaction mixture turned red (λ = 523 nm, ε = 8825 $cm^{-2}mol^{-1}$), characteristic of tris-phenanthroline Fe^{II} complexes.[17] The complex $[Fe^{II}(\mathbf{1})_3]Br_2$ (**2**) was isolated as red powder. Due to the octahedral symmetry of the complex, the imide protons are diastereotopic and their NMR resonance splits into two signals. Compound **2** is diamagnetic at room temperature in agreement with an octahedral low spin Fe^{II} complex. Compound **2** shows a quantitative loss of ether at 333 K and continuous loss of water between 373 and 564 K, after which it decomposes thermally. The elemental analysis, ^1H NMR spectroscopy, mass spectrometry, and single-crystal X-ray structure analysis are in agreement with the formula mentioned above.

Single crystals of **2** were obtained by crystallization from a water solution layered with *n*-pentane and diethyl ether. The compound crystallizes in the monoclinic space group *P*2/*n* (no. 13) with two cationic building blocks of the composition $[Fe^{II}(\mathbf{1})_3]^{2+}$ and four free bromide ions per unit cell. In addition, there are solvent molecules such as water and diethyl ether in strongly disordered positions. The hydrogen-bonded network made up of the cationic building blocks was identified without ambiguity. The building blocks are composed of an octahedral, monometallic Fe^{II} complex and three ligands of **1** (Figure 1 and 2). Two of the ligands, denoted *A* and *A*′, are equivalent by symmetry; the third nonequivalent ligand is referred to as *B*. The central metal atom and ligand *B* of the cationic building block are located on a C_2 axis [1/4, y, 1/4 (e)]. The coordination sphere of the iron cation can be described as a distorted octahedron of six nitrogen donor atoms, which is flattened along the pseudo-C_3 axis of the complex. A different way of describing the structure is to say that the phenanthroline units of each ligand are coordinated in a helical fashion around the metal center. The Fe−N distances vary between 1.990(8) and 2.066(8) Å. The nitrogen atoms of ligands *A* and *A*′ are denoted as N1 and N2, while those of ligand *B* are denoted as N7 and N7′. The bite angles of the bipyridyl groups are 80.1(3)° for N1−Fe−N2 (*A* and *A*′) and 82.7(4)° for N7−Fe−N7′ (B). The *trans* N−Fe−N angles are 172.3(3)° for N2−Fe−N7 and 175.1(5)° for N1−Fe−N1′. These values are similar to other phenanthroline and bipyridine complexes.[17,18] The pyridine rings in *A* and *A*′ are out of plane from each other by 8.6(5)°, whereas ligand *B* is planar. The central rings of *A* and *A*′ formed by C4, C5, C6, C7, C11 and C12 and the corresponding symmetric equivalents are not planar, with C12 and C12′ being significantly out of plane by 0.27(1) Å. The planes of the urea groups make an angle of 68.8(5)° to each other. The inner-ring angles of the pyridine groups of the phenanthroline entity vary from 114.6 to 119.3° for the C−N−C angles, from 118.8 to 125.5° for the C−C−N angles and from 115.5 to 121.8° for the C−C−C angles. The corresponding angles in the central all-carbon ring range from 114.1 to 124.5°.

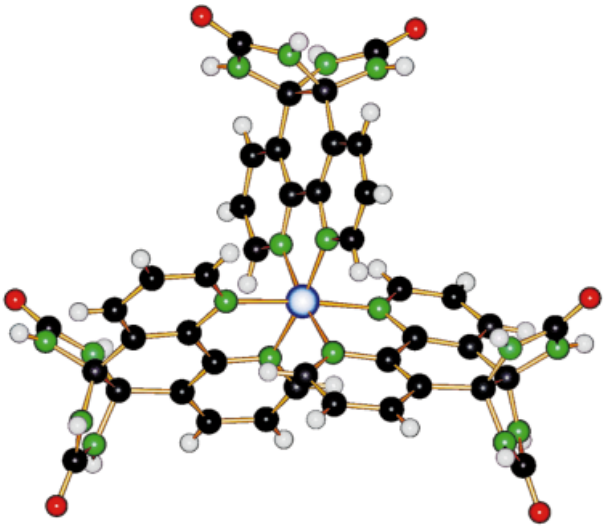

Figure 1. Crystal structure of the $[Fe^{II}(\mathbf{1})_3]$ building block

In the crystal, cationic units $[Fe(\mathbf{1})_3]^{2+}$ of the same helicity are arranged along the C_2 axes within one plane, the Λ-chains being oriented antiparallel to the Δ-chains. These linear strands of Λ- and Δ-building blocks are alternately linked to each other by hydrogen bonds through the urea part of the ligand, leading to a two-dimensional layered network. Thus, ligands *A* and *A*′ each form three (ligand *B* two) hydrogen bonds with two neighboring molecules of the same plane. In one cationic unit, the oxygen O1 of the urea group of *A* is bonded to H5(N5) of ligand *A*′ of the next cationic unit and vice versa: the oxygen O1′ of this neighboring molecule is hydrogen bonded to H5(N5) of the first cation. A crystallographic inversion center is found in the geometric middle of the hydrogen bonding system formed by O1−H5′(N5′) and O1′−H5(N5). The oxygen O2 of the second urea group of *A* is hydrogen bonded to H9(N9) of ligand *B*′ of a second neighboring molecule. The oxygen atom O3 of ligand *B* and its symmetry equivalents do not form hydrogen bonds to neighboring molecules because they point out of the plane in which the other hydrogen bonds are formed. In addition, the distance to the next layer is 11 Å (Fe−Fe distance), which is too far for binding. As a result, a Δ-helical cation only binds to four Λ-cations, and vice versa. Two types of channels are thus formed in the structure, one with an average diameter of about 10 Å, assembled from the formation of two hydrogen bonds between two ligands *B* and two ligands *A* of two neighboring

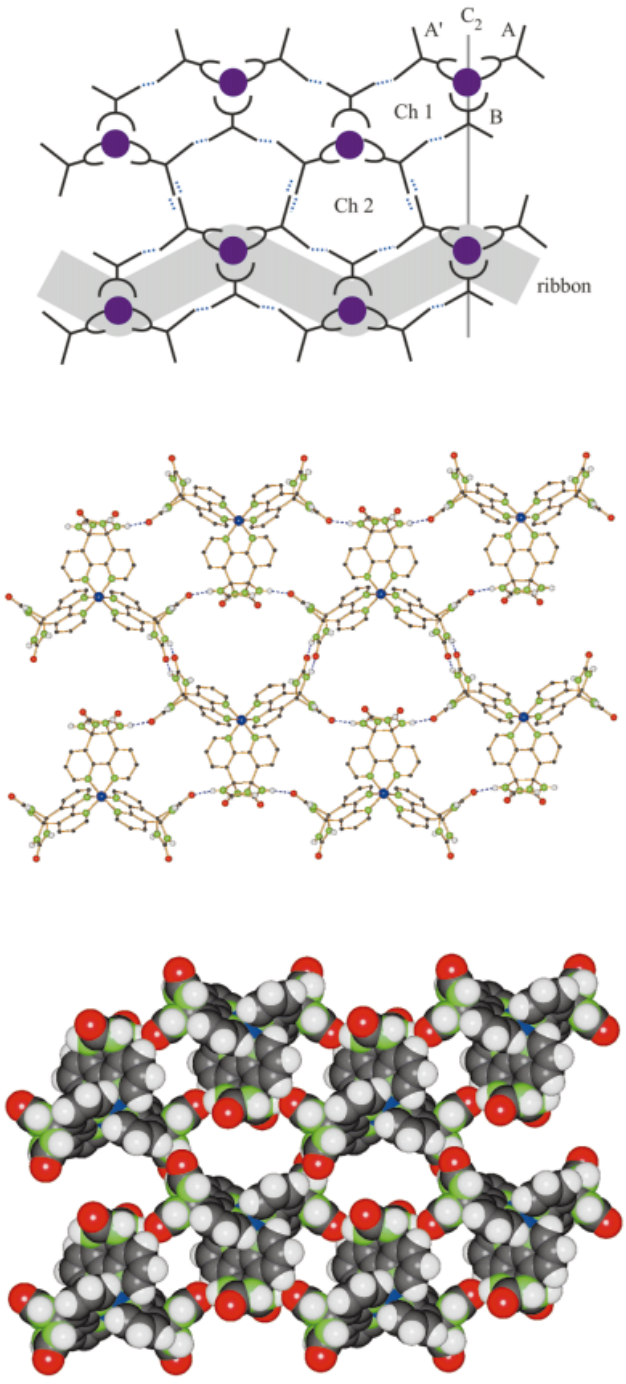

Figure 2. Schematic illustration, X-ray structure, and space-filling representation of a single sheet of the crystal lattice; ligands located on the C_2 axes are denoted *B* (in the plane of the sheet) while the other two ligands are denoted *A*; cationic units $[Fe^{II}(\mathbf{1})_3]$ of opposite chirality are hydrogen-bonded between *A* and *B* ligands, which results in an extended ribbon and a square cavity with a diameter of 1 nm (Ch 1); the ribbons form an extended sheet through the hydrogen bonds of *A* ligands such that homochiral $[Fe^{II}(\mathbf{1})_3]$ building blocks are located along the C_2 axes; four cationic units form a cavity with a diameter of approximately 1.2 nm (Ch 2) (all metal ions are in the plane of the sheet, some hydrogen atoms omitted for clarity)

cationic units, leading to a square two-membered ring system (channel 1). The other channel is due to six hydrogen bonds between ligands *A*, *A'*, and *B* of four cationic units and has the approximate dimensions 8 × 12 Å. It yields a heart-shaped, four-membered cavity (channel 2).

As the cationic units are arranged in a parallel manner, the maximum number of hydrogen bonds is formed with adjacent units in order to stabilize the structure. The bulky urea groups prevent a close approach and consequently a development of pi-stacking interactions of adjacent phenanthroline groups.

The total number of hydrogen bonds for one cationic building block, counting the donors and acceptors, is 18, six H-acceptors (oxygen) and 12 donors (N−H). Considering that the hydrogen bonds are only formed between ligands of different cationic units and that each acceptor reacts with one donor at a time, the maximum number of H-bonds formed is 12, of which only eight (4 donors + 4 acceptors) are used. The remaining donors and acceptors do not participate in bonding interactions due to the two-dimensional structure. Each of the six urea fragments of one cationic building block is thus involved in at least one H-bond. Considering the helical way in which the ligands are arranged around the metal ion, four of the six oxygen atoms come to lie in approximately one plane, whereas the other two are oriented perpendicular to this plane and cannot participate in H-bonding as the next layer is too far away. As for the N−H fragments, four of them are oriented in approximately the same plane as the four coplanar oxygen atoms and participate in the structure formation whereas the other eight point out of the plane of the layer.

The maximum number of strong, linear H-bonds is formed if the cationic units are arranged anti-parallel to each other on C_2 axes. This arrangement results in the formation of a ribbon with two-membered square channels of 1 nm diameter (channel 1). The ribbons are stacked in a plane by formation of six H-bonds to yield a four-membered ring with a heart-shaped cavity of approximately 1.2 nm in diameter (channel 2). Both channels run parallel to the *a* axis of the unit cell [1 0 0]. In the crystal, the layers are stacked parallel to each other in an alternating ABA-type fashion. Due to intercalating solvent molecules the interlayer distance is approx. 9.5 Å, which is too large for direct (short range) interactions.

Conclusion

In conclusion, we describe a potential tecton with a reliable structural paradigm such as is needed for the systematic design of metallosupramolecular crystalline materials with predictable structures and tailorable functions. Complex **2** yields a nanoporous, two-dimensional architecture which is stable up to 564 K. The formation of this material demonstrates self-organization by spontaneous self-assembly involving two types of molecular recognition phenomena, namely metal ion recognition in the first step and hydrogen bonding in the final step to establish the 3D architecture. Finally, it should be pointed out that the connectivity is reminiscent of inorganic architectures such as zeolites and clays. However, the intrinsically chiral metal-

losupramolecular constituents permit, in contrast to many achiral aluminosilicate precursors of other inorganic materials, the formation of chiral porous networks, which would offer attractive possibilities in recognition and catalysis. The nonparticipating H-bonding donors and acceptors may furthermore serve as anchors, for example for suitable amphiphiles, to functionalize the interior. Further studies on creating nano- and microporous architectures based on this compact synthon are in progress.

Experimental Section

Ligand 1: Condensation of 1,10-phenanthroline-5,6-dione (4 g, 119 mmol) and urea (2.5 g, 41.7 mmol) in toluene (100 mL) with trifluoroacetic acid (10.6 g, 93 mmol) yielded 61% (3.4 g, 11.6 mmol) of **1** as an insoluble white powder.[16] 1,10-Phenanthroline-5,6-dione was prepared from 1,10-phenanthroline according to literature procedures in 45% yield.[15] − MS: *m*/*z* = 295.2; calcd. 294.3 [M + H]. − ^{1}H NMR ([D$_6$]DMSO, room temperature): δ = 8.73 (d, J_1 = 4.3 Hz, 2 H), 8.32 (s, 4 H), 8.08 (d, J = 7.8 Hz, 2 H), 7.74 (dd, J_1 = 7.7 Hz, J_2 = 4.6 Hz, 2 H). − $C_{14}H_{10}N_6O_2$ (294.27): calcd. C 57.14, H 3.43, N 28.56; found C 57.29, H 3.51, N 28.52.

[Fe^{II}(1)$_3$]Br$_2$ (2): Three equiv. of **1** (1 g, 3.4 mmol) were treated with 1 equiv. of $FeBr_2$ (237 mg, 1.1 mmol) in degassed water (40 mL) under Ar. The reaction mixture turned red as a result of formation of the tris-phenanthroline Fe^{II} complex.[16] Complex **2** was isolated as red powder in 60% yield (725 mg) after recrystallisation. − MS: *m*/*z* = 724; calcd. 723 [Fe^{II}(**1**)$_2$Br]$^+$. − ^{1}H NMR ([D$_6$]DMSO, room temperature): δ = 7.39 (1 H), 7.71 (1 H), 8.27 (1 H), 8.43 (1 H), 8.70 (1 H). − ^{13}C NMR ([D$_6$]DMSO, 100 MHz, 25 °C): δ = 159.62, 155.39, 151.02, 137.62, 135.14, 129.58, 75.31. − $C_{42}H_{30}Br_2FeN_{18}O_6(H_2O)_{2.5}$ 1143.52): calcd. C 44.12, H 3.09, N 22.05; found C 44.13, H 3.02, N 21.9. − UV/Vis (H_2O): λ (ε [cm^{-2} mol^{-1}]) = 523 nm (8825), 493 (shoulder), 315 (34440).
Compound **2** shows quantitative loss of ether at 333 K and continuous loss of water between 373 and 564 K after which it decomposes thermally.

Crystal Structure Data for 2: $[Fe(C_{14}H_{10}N_6O_2)_3]\cdot 2Br\cdot 2CH_3CN\cdot(CH_3CH_2)_2O\cdot 9H_2O$. Diffractometer and data collection: STOE IPDS (−70 °C), graphite-monochromated Mo-K_α radiation (λ = 0.71073 Å), monoclinic, space group *P*2/*n*, *a* = 11.098(2) Å, *b* = 16.720(3) Å, *c* = 19.760(4) Å, β = 96.79(3)°, *V* = 3640.9(13) Å^3, *Z* = 2, μ = 1.373 mm^{-1}, *F*(000) = 1388, ρ = 1.261 Mg/m^3, $2\Theta_{max}$ = 51.8°. Primary structure solution by direct methods (SHELXS-92).[20] Anisotropic refinement for all non-hydrogen atoms of the cationic complex (SHELXL-93).[21] 6232 Measured reflections, 5961 independent [*R*(int) = 0.1994] of which 5961 reflections were used to refine 437 parameters. The solvent and anionic structure parts show multifold disorder. Therefore atoms of solvent were refined isotropically on split positions. The structure was refined against F^2 (full-matrix least-squares). *R*1 = 0.1395 [for 2994 reflections with $F > 4\sigma(F)$, *R*1 = 0.2717 (all data)] and *wR*2 = 0.2461 [*wR*2 = 0.3288 (all data)]. GooF on F^2 = *S* = 1.117; max./min. residual density +1.045/−0.403 e/Å^3. Crystallographic data (excluding structure factors) for the structure(s) included in this paper have been deposited with the Cambridge Crystallographic Data Centre as supplementary publication no. CCDC-146338. Copies of the data can be obtained free of charge on application to CCDC, 12 Union Road, Cambridge CB2 1EZ, UK [Fax: (internat.)+ 44-1223/336-033; E-mail: deposit@ccdc.cam.ac.uk].

Acknowledgments

D. G. K. acknowledges a stipend by the scientific board of NATO through DAAD and the TMR program of the European Commission for a post-doctoral fellowship. K. M. F. thanks Dr. H. Goesmann, University of Karlsruhe for crystal data collection and the Swiss National Foundation for financial support. We thank Dr. J.-P. Rivera (and H. Lartigue) of the University of Geneva for the magnetic (and DTA) measurements.

[1] J.-M. Lehn, *Supramolecular Chemistry − Concepts and Perspectives*, Wiley-VCH, Weinheim, **1995**.
[2] For reviews see: *Comprehensive Supramolecular Chemistry* (Eds.: J. L. Atwood, J. E. D. Davies, D. D. MacNicol, F. Vögtle, J.-M. Lehn), Pergamon, Oxford, **1996**.
[3] T. J. Barton, L. M. Bull, W. G. Klemperer, D. A. Loy, B. McEnaney, M. Misono, P. A. Monson, G. Pez, G. W. Scherer, J. C. Vartuli, O. M. Yaghi, *Chem. Mater.* **1999**, *11*, 2633−2656.
[4] B. F. Abrahams, B. F. Hoskins, D. M. Michail, R. Robson, *Nature* **1994**, *369*, 727−729.
[5] G. B. Gardner, D. Vankataraman, J. S Moore, S. Lee, *Nature* **1995**, *374*, 792−795.
[6] O. M. Yaghi, G. Li, H. Li, *Nature* **1995**, *378*, 703−706.
[7] S. S.-Y. Chui, S. M.-F. Lo, J. P. H. Charmant, A. G. Orpen, I. D. Williams, *Science* **1999**, *283*, 1148−1150.
[8] V. A. Russel, C. C. Evans, W. Li, M. D. Ward, *Science* **1997**, *276*, 575−579.
[9] See for instance: J. S. Seo, D. Whang, H. Lee, S. I. Jun, J. Oh, Y. Jin, K. Kim, *Nature* **2000**, *404*, 982−986.
[10] V. Balzani, F. Scandola, *Supramolecular Photochemistry*, Ellis Horwood, New York, **1991**.
[11] G. A. J. W. Saenger, *Hydrogen Bonding in Biological Structures*, Springer, Berlin, **1994**.
[12] For combinations of metal-ion coordination and hydrogen-bonding interaction arrays, see: A. D. Burrows, C.-W. Chan, M. M. Chowdhry, J. E. McGrady, D. M. P. Mingos, *Chem. Soc. Rev.* **1995**, 329−337.
[13] P. G. Sammes, G. Yahioglu, *Chem. Soc. Rev.* **1994**, 327−334.
[14] J. C. Macdonald, G. M. Whitesides, *Chem. Rev.* **1994**, *94*, 2383−2420.
[15] C. Hiort, P. Lincoln, B. Nordén, *J. Am. Chem. Soc.* **1993**, *115*, 3448−3454.
[16] A. R. Butler, E. Leitch, *J. Chem. Soc., Perkin Trans. 2* **1980**, 103−105; J. A. A. W. Elemans, R. Degelder, A. E. Rowan, R. J. M. Nolte, *Chem. Commun.* **1998**, 1553−1554.
[17] E. König, *Coord. Chem. Rev.* **1968**, *3*, 471−495.
[18] B. R. Serr, K. A. Anderson, C. M. Elliott, O. P. Anderson, *Inorg. Chem.* **1988**, *27*, 4499−4504.
[19] A. G. Orpen, L. Brammer, F. H. Allen, O. Kennard, D. G. Watson, R. Taylor, *J. Chem. Soc., Dalton Trans.* **1989**, 1−83.
[20] G. M. Sheldrick, *Acta Crystallogr., Sect. A* **1990**, *46*, 467−473.
[21] G. M. Sheldrick, SHELX-93, *Program for Crystal Structure Refinement*, University of Göttingen, **1993**.

Received January 11, 2001
[I01017]

Silver Hydro Sodalite $[Ag_3(H_2O)_4]_2[Al_3Si_3O_{12}]_2$: Synthesis and Structure Determination by Combination of X-ray Rietveld Refinement, Thermogravimetry, FT-IR, and ^{1}H-MAS NMR Spectroscopy

Stefanie Eiden-Aßmann,*[a] Andreas M. Schneider,[b] Peter Behrens,[b] Guenter Engelhardt,[c] Hugo Mändar,[d] and Juergen Felsche[e]

Keywords: Silver / Sodalite / Ion exchange / Rietveld refinement

Sodium hydro sodalite $[Na_3(H_2O)_4]_2[Al_3Si_3O_{12}]_2$ was subjected to ion exchange with aqueous $AgNO_3$ solutions to yield silver hydro sodalite $[Ag_3(H_2O)_4]_2[Al_3Si_3O_{12}]_2$. A Rietveld structure refinement of the silver hydro sodalite structure based on powder X-ray diffraction data recorded at room temperature (cubic, a = 8.950 Å, space group P-43n) led to a model where three silver cations form a triangle nearly parallel to a four-membered ring of the sodalite cage. In combination with the four water molecules, a disorder model $[Ag_3(\mu\text{-}H_2O)_2(H_2O)_2]^{3+}$ is suggested. This structural arrangement is clearly different from that found in sodium hydro sodalite. Whereas the sodium hydro sodalite structure is dominated by cation–water interactions, the silver hydro sodalite structure reflects strong interactions between the cations and the oxygen atoms of the framework, strong interactions between the water molecules, but only weak ones between the cations and water molecules. In addition, weak $Ag^+\cdots Ag^+$ interactions may play a role. ^{1}H MAS NMR spectra show that the hydrogen atoms (which were not found in the Rietveld analysis) of the water molecules are involved in hydrogen bonding of different strengths and dynamics.

Introduction

The framework of 1:1 aluminosilicate sodalites consists of a periodic array of space-filling $[4^66^8]$ polyhedra (β cages) formed by a network of alternating and corner-sharing SiO_4 and AlO_4 tetrahedra with a unit-cell content of $[Al_3Si_3O_{12}]_2^{6-}$.[1] In addition to cations M^+ compensating for the negative charge of the framework, the β cages may contain a large variety of encapsulated salts M^+A^-, hydroxides M^+OH^-, and/or water molecules. The general unit-cell composition of aluminosilicate sodalites can thus be given as $[M_{3+x}A_x(H_2O)_n]_2[Al_3Si_3O_{12}]_2$, where M and A are singly charged cations and anions, respectively. Owing to their structural relationship with the well-known and industrially important A-, X-, and Y-type zeolites, sodalites have been considered as model systems in order to investigate the various kinds of host–guest interactions, static-statistical and/or dynamical guest disorder phenomena, and structural-phase transitions.[2,3]

In addition, sodalites have also attracted considerable attention because of their intracage reaction chemistry and their interesting material properties such as cathodochromism, photochromism, and ion conduction. They are also considered as periodic host matrices for the spatial organization of quantum-sized semiconductor clusters and cluster arrays.[4] Phenomena such as blue shifts in optical absorption edges have been observed for aluminosilicate sodalites that contain silver salts[5] and have been interpreted as quantum-size effects. Stein et. al[6] reported a silver oxalato sodalite $[Ag_8(C_2O_4)][Al_3Si_3O_{12}]$ that can be reversibly marked and erased with a laser beam for many cycles. A large number of different silver sodalites have been synthesized[7] and some of them have been structurally characterized by Rietveld refinements of X-ray diffraction data.[8,9] Notably, the refinement of the structure of the silver hydro sodalite (SHS), i.e. a sodalite containing only Ag^+ ions and water molecules in its cages, did not converge easily and stopped at relatively high R values with the structural model reported.[10] The structure of anhydrous silver sodalite $[Ag_3]_2[Al_3Si_3O_{12}]_2$ was studied in detail at different temperatures and with regard to a phase transition.[11]

As part of our investigation into the synthesis, structure and properties of aluminosilicate sodalites containing heavy metal cations,[11,12] we have studied the ion exchange of the well-characterized sodium hydro sodalite $[Na_3(H_2O)_4]_2[Al_3Si_3O_{12}]_2$ with aqueous $AgNO_3$ solution. This paper reports the characterization of SHS by means of a Rietveld structure refinement based on powder X-ray diffraction, as well as by ^{1}H MAS NMR, ^{29}Si MAS NMR and FT-IR spectroscopy and by thermal analysis.

Results

Treatment of the sodium hydro sodalite $[Na_3(H_2O)_4]_2[Al_3Si_3O_{12}]_2$ with an aqueous solution of $AgNO_3$ (1 M) at

[a] Universität Konstanz, Fachbereich für Physik, 78464 Konstanz, Germany
[b] Universität Hannover, Institut für Anorganische Chemie, 30167 Hannover, Germany
[c] Universität Stuttgart, Institut für Technische Chemie, 70550 Stuttgart, Germany
[d] University of Tartu, Dept. of Physics, 51010 Tartu, Estonia
[e] Universität Konstanz, Fachbereich für Chemie, 78464 Konstanz, Germany

 © WILEY-VCH Verlag GmbH, 69451 Weinheim, 2001 1434–1948/01/0606–1527 $ 17.50+.50/0

383 K affords complete exchange of all sodium cations with silver cations, with retention of the sodalite host structure. The combination of analytical techniques employed by us suggests that the idealized chemical composition $[Ag_3(H_2O)_4]_2[Al_3Si_3O_{12}]_2$ is present in the product phase. Powder X-ray photographs showed that the crystallinity of the reactant sodalite is essentially preserved during ion exchange, and that the product is a single-phase material. No amorphous by-product was visible on scanning electron micrographs, therefore all the analytic data refer to the crystalline compound. The degree of ion exchange, determined by flame photometry and titration according to the method of Volhard, amounts to 95%.

The ^{29}Si MAS NMR spectrum (Figure 1) shows a narrow line at $\delta = -85.4$, indicating that the ordered 1:1 aluminosilicate framework is retained after the ion-exchange reaction.[13]

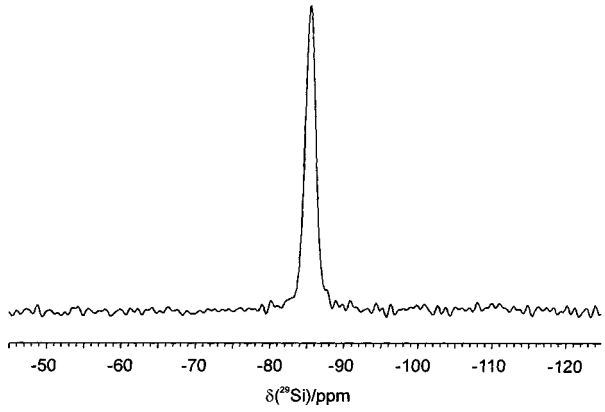

Figure 1. ^{29}Si MAS NMR spectrum of silver hydro sodalite

Thermal analysis (Figure 2) clearly demonstrates the presence of eight water molecules per unit cell. These water molecules are released from the SHS in a two-step reaction, in the temperature range from 400 to 600 K. The IR spectrum exhibits broad bands assigned to H_2O stretching vibrations in the range between 3000 and 3600 cm^{-1}, typical for water molecules involved in hydrogen bonding. In addition, a relatively narrow band appears at 1660 cm^{-1}, assigned to the H_2O deformation mode. The bands below 1200 cm^{-1} originate from framework vibrations.[14]

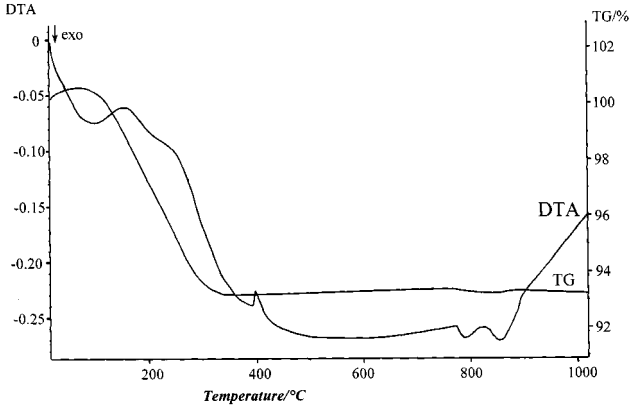

Figure 2. Simultaneous thermal analysis (TG/DTG/DTA) of silver hydro sodalite $[Ag_3(H_2O)_4]_2[Al_3Si_3O_{12}]_2$

Crystal Structure

Atomic coordinates and selected structural data of $[Ag_3(H_2O)_4]_2[Al_3Si_3O_{12}]_2$, as obtained from Rietveld refinement, are summarized in Table 1, Table 2, and Table 3.

Table 1. Fractional atomic coordinates, displacement parameters U and population parameter (PP) for $[Ag_3(H_2O)_4]_2[Al_3Si_3O_{12}]_2$ (data set 1)

Atom	Wyckoff position	x	y	z	U_{iso} [Å^2]	PP
Si	6*c*	1/4	1/2	0	0.0001(6)[a]	1.0
Al	6*d*	1/4	0	1/2	0.0001[a]	1.0
O1	24*i*	0.1390(6)	0.1481(7)	0.4424(5)	0.002(2)	1.0
Ag1	8*e*	0.1723(2)	*x*	*x*	0.032(5)[a]	0.75[b]
Ag2	8e	0.3081(4)	*x*	*x*	0.032[a]	0.25
O2	8*e*	0.3968(7)	*x*	*x*	0.069(7)	0.75

[a] U(Si) and U(Al) were refined as constrained parameters, U(Al) = U(Si). − U(Ag1) and U(Ag2) were refined as constrained parameters, U(Ag1) = U(Ag2). − [b] PP(Ag1), PP(Ag2) and PP(O2) were treated as described in the text during the refinement procedure.

Table 2. Fractional atomic coordinates, displacement parameters U and population parameter (PP) for $[Ag_3(H_2O)_4]_2[Al_3Si_3O_{12}]_2$ (data set 2)

Atom	Wyckoff position	x	Y	z	U	PP
Si	6*c*	1/4	1/2	0	0.0044(6)[a]	1.0
Al	6*d*	1/4	0	1/2	0.0044[a]	1.0
O1	24*i*	0.1392(6)	0.1473(6)	0.4420(3)	0.006(1)	1.0
Ag1	8*e*	0.1729(1)	*x*	*x*	0.0481(4)[a]	0.5[b]
Ag2	8e	0.3103(4)	*x*	*x*	0.0481[a]	0.25[b]
O2	8*e*	0.4000(3)	*x*	*x*	0.054(6)	0.75[b]

[a] U(Si) and U(Al) were refined as dependent parameters, U(Al) = U(Si). − U(Ag1) and U(Ag2) were refined as dependent parameters, U(Ag1) = U(Ag2). − [b] (Ag1), PP(Ag2) and PP(O2) were treated during the refinement procedure as described in the text.

Structural details are shown in Figure 3. The results are practically identical for both data sets, although some small deviations occur. In both refinement procedures, we were able to identify the positions of the silicon, aluminium, and oxygen atoms of the framework, the positions of the six silver cations and the positions of six out of the eight oxygen atoms of the occluded water molecules (Figure 3, **a** and **b**). In both cases it was not possible to determine the positions of the oxygen atoms of the two remaining water molecules. We assume that these are situated on a Wyckoff 8*e* position with a population parameter of 25%, close to the Wyckoff 8*e* position of the silver cation Ag1. The introduction of an oxygen atom O3 at this position during the re-

Table 3. Selected interatomic distances [Å] and angles [°] for $[Ag_3(H_2O)_4]_2[Al_3Si_3O_{12}]_2$

Host Structure					
	data set 1	data set 2		data set 1	data set 2
Al−O1	1.745(6)	1.739(5)	Si−O1	1.635(6)	1.642(6)
O1−Al−O1 (4x)	109.1(2)	109.2(2)	O1−Si−O1 (4x)	108.3(3)	108.5(3)
O1−Al−O1 (2x)	110.1(3)	110.0(3)	O1−Si−O1 (2x)	111.8(3)	111.5(3)
Al−O1−Si	140.5(2)				
Silver and oxygen coordination					
	Data set 1	Data set 2		Data set 1	Data set 2
Ag1−O1	2.459(5)	2.452(3)	Ag2−O1	2.419(7)	2.435(6)
	3.127(6)	3.130(4)		3.349(6)	3.750(6)
Ag1−O2	2.641(7)	2.625(3)	Ag2−O2	3.840(7)	3.774(5)
	3.500(7)	3.540(3)			
Ag1−Ag2	3.287(4)	3.270(4)			

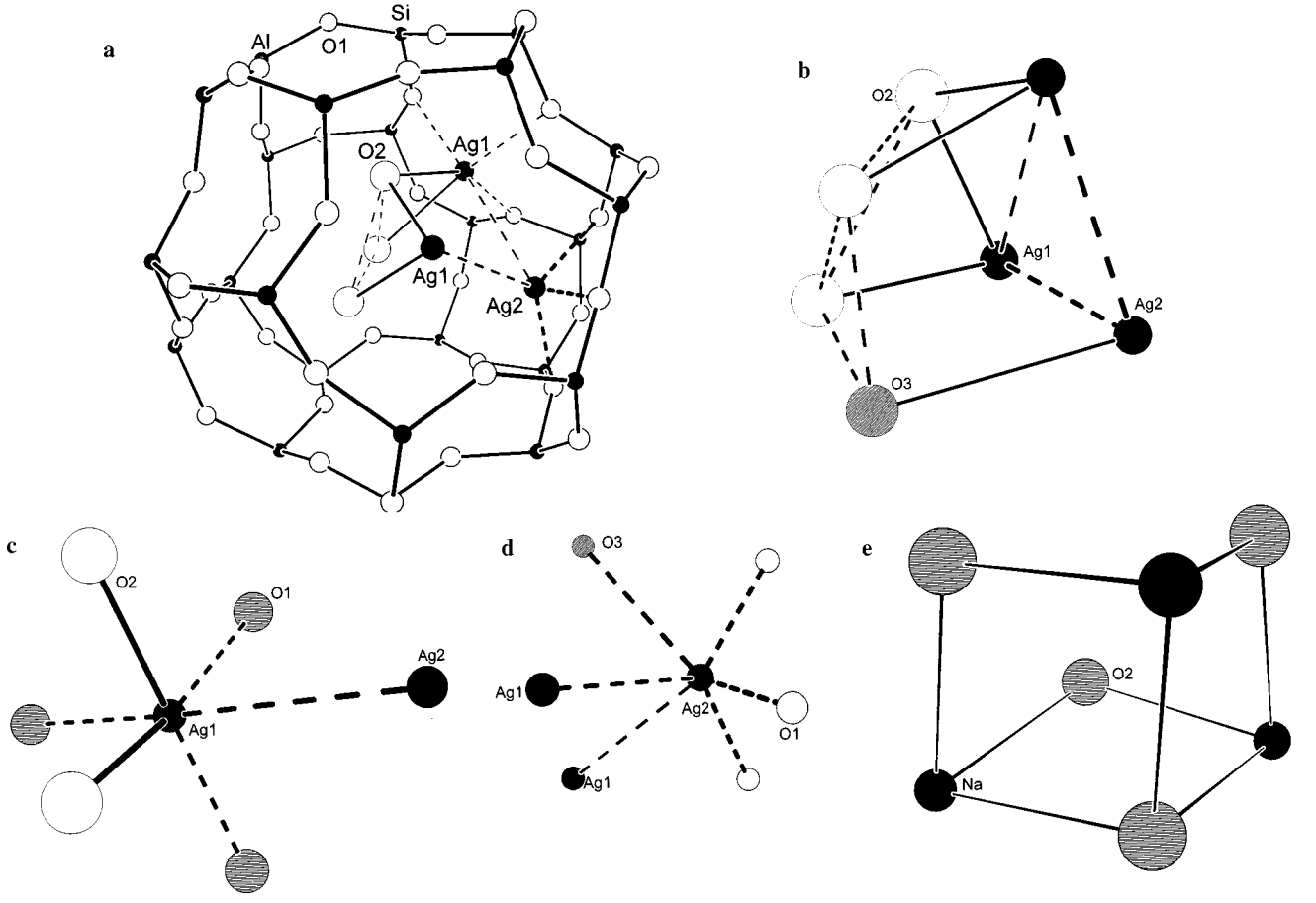

Figure 3. The crystal structure of silver hydro sodalite according to the Rietveld refinement. **a**: The sodalite cage with the positions of the Ag1 and the Ag2 atoms as well as those of O2 atoms. **b**: The arrangement of the intracage atoms (note that the position of O3 could not be refined); full lines indicate Ag−O coordination, dashed lines indicate weak interactions (hydrogen bonding, Ag···Ag interactions); **c**: The (3+2+1) coordination of Ag1; **d**: The (3+1+2) coordination of Ag2; **e**: The arrangement of intracage atoms in sodium hydro sodalite

finement led to unreasonably short distances of d(O2−O3) ≈ 1.85 Å. Therefore the remaining oxygen atoms were neglected. We are conscious of the fact that this omission might lead to results which do not represent the true structure. Nevertheless, there are convincing arguments that the model which we will present is essentially correct.

Owing to the similar results of the two data sets, only the results of the refinement of the second data set will be discussed. Interatomic distances and angles of the framework structure were found mainly in the expected range. Silver cations were found at two 8*e*-Wyckoff positions. The population parameters of 50% for Ag1 and 25% for Ag2 were retained during the refinement procedure, but were relaxed several times to examine their behaviour and to ensure that no large deviations from the fixed values would occur. They were set back to their original values of 50% and 25%, respectively, after such test cycles. The occurrence of two Ag positions and the refined population parameters for the occluded silver cations and oxygen atoms of water molecules may be explained with a disorder model.

This disorder model of the non-framework atoms may be derived from the shortest distances to obtain a reasonable coordination sphere. In general, each sodalite cage contains a $[Ag_3(OH_2)_4]^{3+}$ cluster as a guest species, which is also found in silver-exchanged zeolite A.[15] The same number of metal cations and water molecules are also present as a $[Na_3(H_2O)_4]^{3+}$ cluster in $[Na_3(H_2O)_4]_2[Al_3Si_3O_{12}]_2$. However, there are significant differences between these two compounds and $[Ag_3(H_2O)_4]_2[Al_3Si_3O_{12}]_2$. Whereas in silver zeolite A and in $[Na_3(H_2O)_4]_2[Al_3Si_3O_{12}]_2$ the cations and water molecules are detected at one Wyckoff 8e position each (Figure 3, **e**), leading to coordination of the cations by three framework oxygen atoms and three water molecules, the arrangement is significantly different in SHS.

In SHS, each silver cation Ag1 is surrounded by three oxygen atoms of the framework [d(Ag1−O1) = 2.452(3) Å] and two oxygen atoms of water molecules [d(Ag1−O2) = 2.625(3) Å]. In addition, a relatively short contact between the silver cations Ag1 and Ag2 is found [d(Ag1−Ag2) = 3.270(4) Å], resulting in a sixfold (3+2+1) coordination (Figure 3, **c**). A distance of d(Ag2−O1) = 2.435(6) Å is found for the contacts between the silver cations Ag2 and the framework oxygen atoms. In addition to three framework oxygen atoms, this cation is coordinated to two neighbouring silver cations Ag1, and to one oxygen atom of an occluded water molecule (Figure 3, **d**), although the position of the oxygen atom of this water molecule could not be determined unequivocally. It is likely to be close to the position of the Ag1 silver cation with a population parameter of 25%, as mentioned before. Taken together, this results in a sixfold (3+1+2) coordination. Combining these results, we find an isosceles silver triangle composed of two Ag1 cations and one Ag2 cation, which is surrounded by oxygen atoms of the framework as well as of the occluded water molecules (Figure 3, **b**). The $[Ag_3]$ triangle is a very common motif in silver compounds, e.g. in dehydrated silver zeolite A[15] as well as in many ternary silver oxides.[16] Owing to the population parameters, the triangles show a fourfold orientational disorder with respect to the β-cage. Snapshot pictures of the structural model are given in Figure 3.

Oxygen atoms of the occluded water molecules are found on the corners of a tetrahedron (Wyckoff 8*e* position) with a population of 75%. Within the tetrahedron, the distance between two oxygen atoms was found to be d(O2−O2) = 2.545(4) Å, indicating the prevalence of strong hydrogen bonding between the water molecules at this position (Figure 3, **b**). The distance to the nearest oxygen atom of the host structure is d(O1−O2) = 3.24 Å, which is quite large but might still be indicative of weak hydrogen bonding between the occluded water molecules and the framework oxygen atoms. This is supported by the results of the ^{1}H NMR experiments (Figure 4). Two different types of hydrogen atoms were found. We ascribe these to hydrogen atoms involved in the stronger hydrogen bonding within the cluster of occluded water molecules (type 1, δ = 6), and hydrogen atoms involved in contacts from the water molecules to the framework oxygen atoms (type 2, δ = 5).

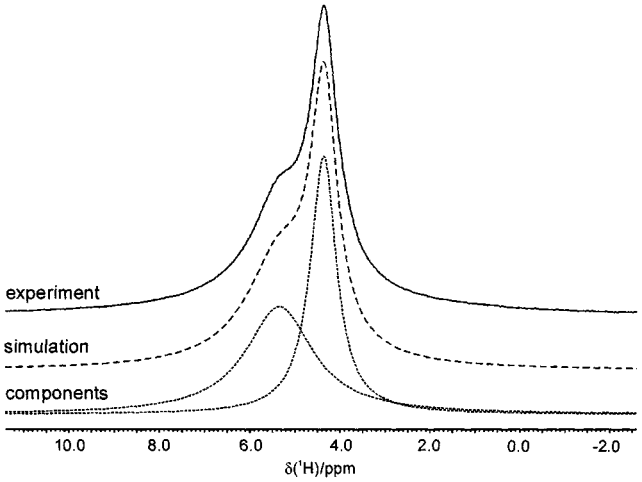

Figure 4. ^{1}H MAS NMR spectrum of silver hydro sodalite

The results of temperature-dependent ^{1}H MAS NMR spectroscopic investigations (Figure 5) indicate that at temperatures above 383 K, the dynamics of the water molecules

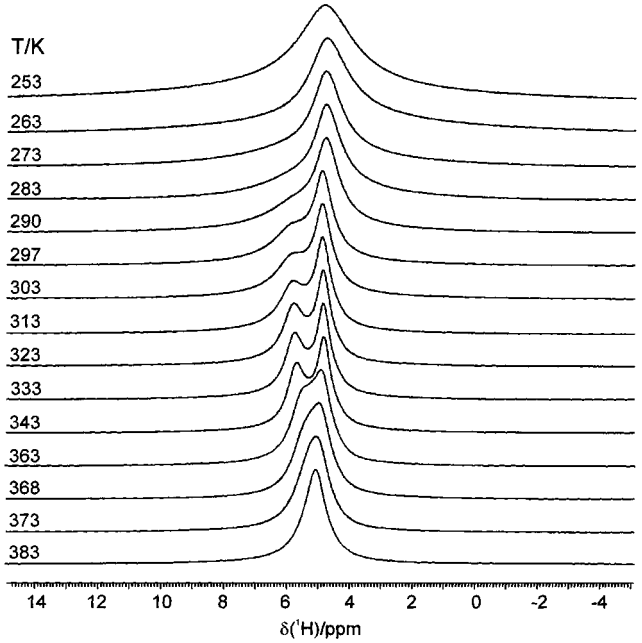

Figure 5. ^{1}H MAS NMR spectra of silver hydro sodalite at different temperatures

inside the sodalite cage is so fast, that the different types of hydrogen atoms become indistinguishable. In the temperature range from 368 K to 290 K, two separate signals were visible. At lower temperatures, one broad, slightly asymmetric peak was observed, and simulation of the spectra clearly shows the presence of two overlapping signals.

Discussion

Our studies demonstrate that the arrangement of the non-framework species in aluminosilicate silver hydro sodalite SHS is considerably different to the corresponding structures in its sodium analogue $[Na_3(H_2O)_4]_2[Al_3Si_3O_{12}]_2$[17] and in the sodalite cages of hydrated silver zeolite A.[15] In all cases, one sodalite cage contains three metal cations and four water molecules. In the sodium hydro sodalite and in the silver zeolite, the metal ions are positioned at the corners of a tetrahedron, with a 75% occupancy and a corresponding disorder between the different cages. The oxygen atoms of the water molecules form another tetrahedron. The principle arrangement of the water molecules is similar in SHS, but the arrangement of the silver cations is different. They are positioned at the corners of a small isosceles triangle.

The distances between the silver ions and the oxygen atoms of the framework, and between the silver ions and the oxygen atoms of the water molecules, d(Ag−O1) = 2.452(3) Å and d(Ag−O2) = 2.625(3) Å, respectively, are similar to the corresponding distances in silver zeolite A [$d(Ag-O_{framework})$ = 2.47 Å, $d(Ag-O_{water})$ = 2.57 Å].[14] However, d(Ag−O1) is considerably larger than the corresponding distance in anhydrous silver sodalite $[Ag_3]_2[Al_3Si_3O_{12}]_2$:[11] $d(Ag-O_{framework})$ = 2.347 Å. This is due to the higher coordination number (*c.n.*) of the Ag^+ ions in the hydrated (*c.n.* = 6) versus the anhydrous (*c.n.* = 3) state. Also, the bonding in the anhydrous silver sodalite is more covalent than in the hydrated form. The silver−oxygen bond lengths in SHS and in hydrated silver zeolite A lie in the range found in ionic silver salts with high coordination numbers of Ag^+, e.g. d(Ag−O) = 2.48 Å in $AgNO_3$.

A comparison between the metal−metal, the metal−oxygen and the oxygen−oxygen distances in SHS and in the sodium analogue gives some indications for the cause of the different structural arrangements in these two compounds:

Coordination of the Metal Atoms

In $[Na_3(H_2O)_4]_2[Al_3Si_3O_{12}]_2$, the metal−oxygen distances to the framework oxygen atoms and to those of the water molecules are very similar [$d(Na-O_{framework})$ = 2.51 Å, $d(Na-O_{water})$ = 2.46 Å].[17] This indicates that the Na^+ ions interact with similar strengths with the framework and with the water molecules. The corresponding values for SHS show that the Ag^+ cations prefer coordination to the framework oxygen atoms. This is in line with the general feature of Ag^+ chemistry that interactions between silver cations and water molecules are rare and weak. Consider, for example, the small number of hydrated silver salts. In SHS, the interactions between the water molecules and the non-framework Ag^+ ions are even weaker than in typical hydrates, e.g. $d(Ag-O_{water})$ = 2.46−2.48 Å in $Ag_2IF{\cdot}2\,H_2O$ or $d(Ag-O_{water})$ = 2.35−2.41 Å in $Ag_7I_2F_5 \cdot 2.5\,H_2O$.[18]

Interactions Between the Water Molecules

As in SHS the water molecules can interact only weakly with the non-framework Ag^+ ions, but undergo stronger hydrogen bonding with each other (Figure 3, **b**). Hence, in SHS, the distance d(O2−O2) between the oxygen atoms of the water molecules is only 2.64 Å, which is shorter than the corresponding value in bulk Ice-I_h (2.75 Å). On the contrary, in sodium hydro sodalite, the corresponding interatomic distance amounts to 3.22 Å, indicating only weak hydrogen bonding interactions between the water molecules (Figure 3, **e**).

Interactions Between Metal Cations

Since the work of Jansen,[19] it is well known that the structural chemistry of Ag^+ ions is often determined by relatively short Ag^+-Ag^+ contacts, and a tendency of the Ag^+ ions to segregate into specified regions of the structure, owing to $d^{10}-d^{10}$ interactions. In SHS, the interatomic Ag−Ag distance d(Ag1−Ag2) = 3.27 Å is at the upper limit of the range of distances in which such interactions can be assumed (the Ag−Ag van der Waals distance is ca. 3.4 Å). In contrast to our interpretation, Seff[20] and Gellens[15] assigned this distance unequivocally to Ag^+-Ag^0 bonding.

Summarizing these arguments, it is the general weakness of Ag^+-H_2O relative to Na^+-H_2O interactions that leads to strong hydrogen bonding between the water molecules in SHS and, in turn, to weak interactions between the water molecules and the framework. This effect is corroborated by weak $d^{10}-d^{10}$ interactions between the Ag^+ cations. Correspondingly, the disorder model shows a clear segregation of the metal ions and the water molecules into different parts of the sodalite cage (Figure 3, **b**).

The structural model derived here is consistent with all available experimental data. We wish to emphasise that our results are significantly different from the findings of Ozin et al.,[10] who on the basis of a Rietveld refinement of SHS suggested a structural model similar to that of sodium hydro sodalite.[18] The authors claimed to have detected only one 8*e* Wyckoff position for the Ag^+ cations (with a population parameter of 75%) and one fully occupied 8*e* Wyckoff position for the oxygen atoms of the water molecules. We were not able to reproduce these results of Ozin et al.[10] A Rietveld refinement taking these results as a starting model did not converge. Huge jumps occurred in the *x* parameter of the O2 atom (Δx = 0.05 corresponding to a distance of 0.8 Å); its population parameter increased to 185%. The attempt was stopped at this stage. We therefore conclude that either the silver hydro sodalite prepared by Ozin et al. was of a different nature to that prepared by us, or that their structure refinement is not correct. The synthesis of

the sodium hydro sodalite carried out by Ozin et al. is different to our synthesis, but the analytical data show that both sodalites are very similar apart from the degree of crystallinity. Ozin et al. work at low temperature and at low pressure; under these conditions the crystallinity of the product sodalites is not as high as when prepared under the high-temperature and high-pressure conditions used by us. The ion-exchange procedures were the same in our work and in that of Ozin et al., so that both SHS should be identical, apart from the degree of crystallinity. High cristallinity is of course very important for a reliable Rietveld refinement. Unfortunately, Ozin et al. did not show a powder pattern of the SHS, but they reported that their data for the silver hydro sodalite sample led to a poor refinement of the framework atoms. We therefore assume that the crystal structure and the structural model presented here give a more reliable picture of SHS than does the work of Ozin et al.[10]

Experimental Section

Synthesis and Methods of Characterization

SHS was prepared in a three-step procedure involving the synthesis of the basic sodium hydro sodalite $[Na_4(OH)(H_2O)]_2[Si_3Al_3O_{12}]_2$ in Teflon-lined steel autoclaves followed by Soxhlet extraction with water at 373 K to give the non-basic hydro sodalite $[Na_3(H_2O)_4]_2[Al_3Si_3O_{12}]_2$.[3] Subsequent ion exchange was performed for one day with a 1 N $AgNO_3$ solution at 383 K in Teflon-lined steel autoclaves filled to 90%. The product was washed with distilled water and dried at 333 K. The degree of exchange was determined indirectly by flame photometry of the exchange solution (Na^+ content of the solution after the exchange reaction) and by titration according to Volhard (Ag^+ content of the solution after exchange). The water content was determined using a Netzsch thermoanalyzer STA 429 (N_2 atmosphere, heating rate 10 K/min) combining thermogravimetry (TG), difference thermogravimetry (DTG) and difference thermal analysis (DTA).

The crystallinity of the product and the purity of the compounds were monitored by powder X-ray diffraction employing a Guinier−Huber camera 600 with Cu-$K_{\alpha 1}$ radiation. Scanning electron micrographs were obtained on a JEOL scanning electron microscope (JSM-840A).

IR absorption analysis (KBr pellets) was performed on a Mattson Polaris TM FT spectrometer in the range of 4000 to 400 cm^{-1}.

^1H MAS NMR spectra were recorded at 400.13 MHz on a Bruker MSL-400 NMR spectrometer using a Bruker double-bearing MAS probe with 4-mm zirconia rotors. Single-pulse excitation was applied with a 4-s pulse width (corresponding to a 45° flip angle) and a 5-s pulse repetition. For each spectrum, 16 scans were accumulated at spinning rates of 10 kHz. Spectra simulations were performed using the PC program WINFIT, part of the Bruker WINNMR software package. ^{29}Si MAS NMR spectra were measured at 79.49 MHz using 7-mm rotors with a spinning speed of 4 kHz. Furthermore, 32 scans were recorded with a 3-s pulse width (corresponding to a 35° flip angle) and a 5-s pulse repetition. ^1H and ^{29}Si chemical shifts were related to tetramethylsilane using adamantane and Q_8M_8, respectively, as secondary standards.

X-ray Diffraction Studies

Powder photographs were taken on a Guinier camera (Huber system G600) with Cu-$K\alpha_1$ radiation (internal standard Si). The unit-cell constant of the cubic cell was obtained by LSQS refinement [8.950(2) Å] employing the software package AXES.[21]

Two different XRD patterns of SHS were recorded. The first was collected at room temperature on a Scintag powder diffractometer (Bragg−Brentano geometry) with Cu-$K\alpha$ radiation. The sample was prepared in a flat platinum sample holder which was spun during the measurement. The step width was set to 0.02 °2Θ in the range of 12 °2Θ to 110 °2Θ, resulting in 4900 data points. Some of the data points had to be removed owing to reflections of the platinum sample holder. Therefore only 3910 data points were considered for the refinement (data set 1). Further experimental details are given in Table 4.

The second data set was recorded on a Huber G642 powder camera with Cu-$K\alpha_1$ radiation (Ge monochromator) employing an X-ray sensitive storage film (Hamamatsu H6780). The sample was prepared between two transparent foils (flat sample), and the sample holder was moved tangentially to the focal circle during the measurement. The film was evaluated using a step width of 0.01 °2Θ in the range of 0 °2Θ to 100 °2Θ, resulting in 10 000 data points. During the Rietveld refinement, only data above 12.00 °2Θ were used (8750 data points, data set 2), because no reflections were detected below this value (Figure 6).

Further experimental details are given in Table 4. Both data sets were analysed in a similar way by the XRS-82 program[23] using the Rietveld method. Prior to refinement, the space group of the compound was determined to be *P*-43*n* (No. 218), the background of the pattern was subtracted manually and the contribution of Cu-$K\alpha_2$ radiation in data set 1 was eliminated by employing the algorithm of Ladell et al.[24] Two profile functions were determined employing Baerlocher's Learned Peak-Shape function,[25] one on the (211) reflection (24.204 °2Θ) and one on the (431) reflection (51.753 °2Θ). Atomic scattering factors were taken from reference 17. The least-squares refinement was started with the coordinates of the atoms Al, Si and O1 of the framework structure of ($[Na_3(H_2O)_4]_2[Al_3Si_3O_{12}]_2$).[17] We did not succeed in using the position and the population parameters of the sodium cations of this compound for the Ag^+ cations in SHS. Therefore the positions of the occluded Ag^+ cations and of the oxygen atoms of the water molecules were determined in subsequent difference Fourier syntheses of the electron density and from structural chemical arguments. All peaks detected in the range from 12.00 °2Θ to 100.00 °2Θ were used in the refinement process.

The first difference Fourier synthesis was carried out after the cautious adjustment of some profile parameters (zero-point and peak-asymmetry correction) and the first cautious relaxation of the position of the framework oxygen atoms. It revealed electron density approximately at positions (0.17, *x*, *x*) and (0.31, *x*, *x*) which were first attributed to the positions of the silver cations [(0.17, *x*, *x*), population parameter 0.75] and of the oxygen atoms of occluded water molecules [(0.31, *x*, *x*), population parameter 1.0]. Further refinement included the relaxation of all profile parameters as well as of the atomic positions and displacement parameters of the different atoms. However, release of the population parameter of the occluded silver cations led to a significant decrease below 0.6, while the refinement of the population parameter of the occluded oxygen atom led to a significant increase above 1.2. The silver cations and oxygen atoms were therefore removed from the system and a new difference Fourier synthesis was performed. The calculation again

Table 4. Details of the measurement of powder X-ray diffraction data and Rietveld refinement for $[Ag_3(H_2O)_4]_2[Al_3Si_3O_{12}]_2$

	Data set 1	Data set 2
Powder X-ray data collection	Bragg−Brentano Scintag diffractometer reflection geometry, graphite monochromator, Cu-$K\alpha$ radiation λ_1 = 1.54051 Å and λ_2 = 1.54051 Å Range of measurement: 12° ≤ 2θ ≤ 110° step width 0.02° 2Θ, 93 contributing reflections, 4900 observations	Huber G642 diffraction asymmetric Guinier transmission geometry Ge monochromator, Cu-$K\alpha_1$ radiation λ = 1.54051 Å Range of measurement: 0° ≤ 2θ ≤ 99.5° step width 0.005° 2Θ, selected range for refinement 12.58° ≤ 2θ ≤ 99.50°, step width 0.01° 2Θ, 80 contributing reflections, 8849 observations
	4642 observations used for refinement	8692 observations used for refinement
Number of parameters refined	Profile parameters: 12 Atomic parameters: 10	Profile parameters: 12 Atomic parameters: 10
Number of refined parameters in final cycle	17 (no simultaneous refinement of parameters of the two profile functions)	18 (no simultaneous refinement of parameters of the two profile functions)
R factors	R_F = 0.097 R_{wp} = 0.133, R_{exp} = 0.099 χ^2 = 1.88, $\Delta/\sigma < 0.03$	R_F = 0.069 R_{wp} = 0.090, R_{exp} = 0.066 χ^2 = 1.86, $\Delta/\sigma < 0.03$
Final difference Fourier synthesis	$\Delta\rho_{max}$= +2.0 eÅ^{-3} (in 0.305, 0.014, 0.307)	$\Delta\rho_{max}$= +1.6 eÅ^{-3} (in 0.263, *x*, *x*)
Computer programs	XRS82 software package[23]	XRS82 software package[23]
Atomic scattering factors	taken from ref.[22]	taken from ref.[22]

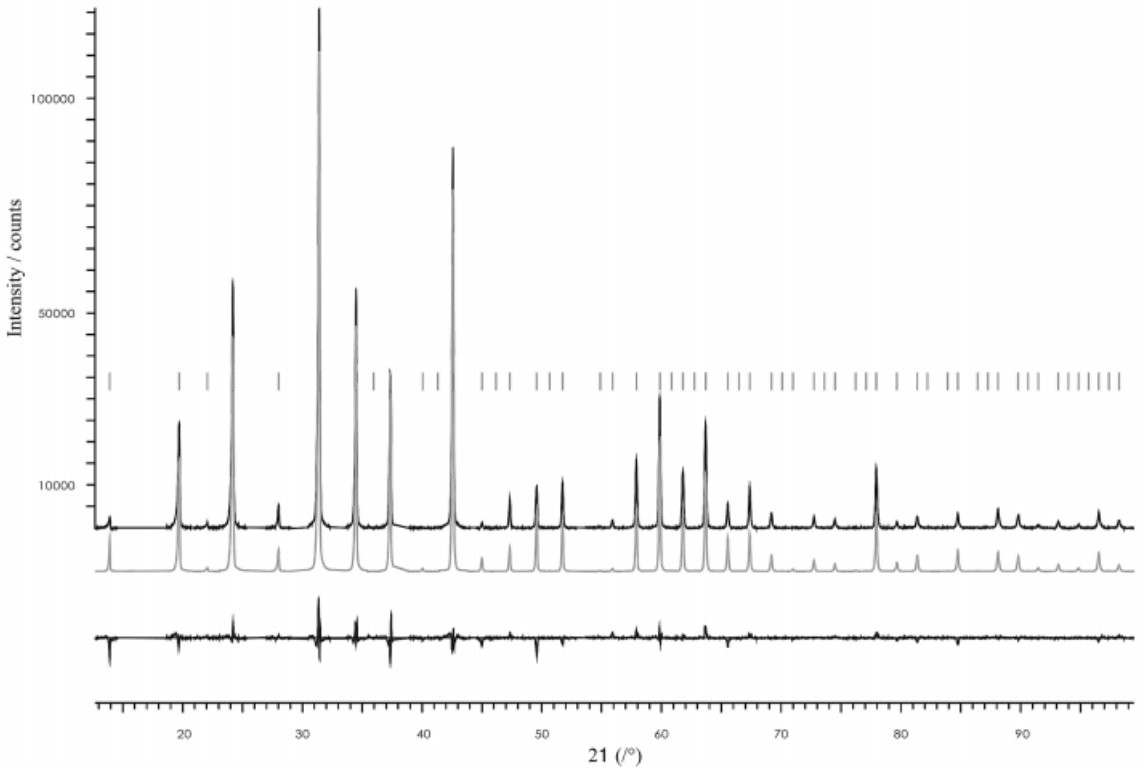

Figure 6. Observed (I_{obs}), calculated (I_{calc}) and difference ($I_{diff} = I_{obs} - I_{calc}$) powder diffraction patterns of $[Ag_3(H_2O)_4]_2[Al_3Si_3O_{12}]_2$ according to the Rietveld refinement

showed electron density at approximately (0.171, *x*, *x*) and at (0.311, *x*, *x*), with an intensity ratio of approximately 2:1. Therefore we concluded, that the silver cations may be located at these two different positions with population parameters of 0.5 for Ag1 and 0.25 for Ag2. After a few refinement cycles, an additional Fourier synthesis revealed remaining electron density at (0.35, *x*, *x*), close to the Ag2 cation. An oxygen atom O2 was placed at position (0.35, *x*, *x*). Taking into account the population parameter of the Ag2 cation (25%), O2 was assigned a population parameter of 75% to avoid very short distances *d*(Ag2−O2). Therefore only six oxygen atoms out of eight could be detected (eight water molecules per formula unit were found by thermal analysis, as shown below). We tested several different structural models in order to find the remaining two oxygen atoms. These models resulted either in very high temperature factors for the additional positions of the oxygen atoms, or unreasonably short distances between the occluded oxy-

gen atoms (shorter than 1.9 A). Therefore, this refinement led to the results given in Table 1−3, with a model containing only one position for the oxygen atoms of the occluded water molecules. In the last refinement cycle of our model, all the position parameters of the occluded atoms as well as all the isotropic displacement parameters were released. Other parameters such as the scaling factor, zero-point shift and peak parameters were released during another cycle. Evaluation of data set 2 followed a similar path and led to similar results. In the two last refinement cycles of the second data set 2, all the parameters were released. (Two refinement cycles were necessary since it is not possible to refine the profile parameters of the two profile functions simultaneously.) All the displacement parameters were treated isotropically. Using anisotropic displacement parameters for the silver cations (which led to a significant improvement in the result of the refinement of ASS[7]) did not lead to any improvement in the present case.

After isotropic refinement of all the atoms, remaining electron densities of approximately $\Delta\rho = 2.0$ $e^{-}Å^{-3}$ at (0.305, 0.014, 0.306) for the first data set and of approximately $\Delta\rho = 1.6$ $e^{-}Å^{-3}$ at (0.26, 0.26, 0.26) for the second set were detected. These positions are close to the centre of the six-membered ring of the framework. However, it was not possible to introduce an atom that could be refined at these positions. Therefore, we regard these electron densities as artefacts (e.g., Hu and Depmeier[26]).

Acknowledgments

We thank Ch. Baerlocher for the measurement of the Bragg−Brentano diffraction pattern. Financial help from the Fonds der Chemischen Industrie is acknowledged.

[1] L. Z. Pauling, *Z. Kristallogr.* **1930**, *74*, 214−216.
[2] J. Felsche, S. Luger, *Thermochim. Acta* **1987**, *118*, 35−55.
[3] G. Engelhardt, P. Sieger, J. Felsche, *J. Am. Chem. Soc.* **1992**, *114*, 1173−1182.
[4] G. A. Ozin, A. Kuperman, A. Stein, *Angew. Chem. Int. Ed. Engl.* **1989**, *28*, 373−390.
[5] A. Stein, G. A. Ozin, G. D. Stucky, *J. Am. Chem. Soc.* **1992**, *112*, 904−905.
[6] A. Stein, G. A. Ozin, G. D. Stucky, *J. Soc. Photogr. Sci. Technol. Japan.* **1990**, *53*, 322−328.
[7] G. A. Ozin, A. Stein, G. D. Stucky, J. Godber, *Inclus. Phenom. Molec. Recogn.* **1990**, 379−393.
[8] A. Stein, P. M. Macdonald, G. A. Ozin, G. D. Stucky, *J. Phys. Chem.* **1990**, *94*, 6943−6948.
[9] A. Stein, G. A. Ozin, P. M. Macdonald, G. D. Stucky, R. Jelinek, *J. Am. Chem. Soc.* **1992**, *114*, 5171−5186.
[10] A. Stein, G. A. Ozin, G. D. Stucky, *J. Am. Chem. Soc.* **1992**, *114*, 8119−8129.
[11] P. Behrens, P. B. Kempa, S. Assmann, M. Wiebcke, J. Felsche, *J. Solid State Chem.* **1995**, *115*, 55−65.
[12] S. Eiden-Assmann, A. M. Schneider, P. Behrens, M. Wiebcke, G. Engelhardt, J. Felsche, *Chem. Eur. J.* **2000**, *6*, 292−297.
[13] G. Engelhardt, D. Michel, *High-Resolution Solid State NMR of Silicates and Zeolites*, Wiley: Chichester, **1987**.
[14] C. M. B. Henderson, D. Taylor, *Spectrochim. Acta* **1979**, *35A*, 929−935.
[15] L. R. Gellens, J. V. Smith, J. J. Pluth, *J. Am. Chem. Soc.* **1983**, *105*, 51−55; L. R. Gellens, W. J. Mortier, R. A. Schoonheydt, J. B. Uytterhoeven, *J. Phys. Chem.* **1981**, *85*, 2783−2788.
[16] M. Jansen, *Angew. Chem. Int. Ed. Engl.* **1986**, *26*, 1098−110.
[17] J. Felsche, S. Luger, Ch. Baerlocher, *Zeolites* **1986**, *6*, 367−372.
[18] M. Molinier, W. Massa, *Z. Anorg. Allg. Chem.* **1994**, *620*, 833−838; K. Persson, B. Holmberg, *J. Solid State Chem.* **1982**, *42*, 1−10.
[19] M. Jansen, *Angew. Chem. Int. Ed. Engl.* **1987**, *26*, 1098; *Angew. Chem.* **1987**, *99*, 1136−1149.
[20] Y. Kim, K. Seff, *J. Phys. Chem.* **1978**, *82*, 1071−1077.
[21] H. Mändar, T. Vajaka, *AXES*, version 1.9A of **1999**.
[22] Th. Hahn, *International Tables for X-ray Crystallography*, Kynoch Press: Birmingham, **1974**; *Vol. IV*, pp. 99, 149.
[23] Ch. Baerlocher, *The X-ray Rietveld System*, version of **1998**.
[24] J. Ladell, A. Zagofsky, S. Pearlman, *J. Appl. Cryst.* **1975**, *8*, 499−506.
[25] A. Hepp, Ch. Baerlocher, *Austral. J. Phys.* **1988**, *41*, 229−236; Ch. Baerlocher, *Proc. 6th Int. Zeolite Conf.*, Reno, USA, 823−829.
[26] X. Hu, W. Depmeier, *Z. Kristallogr.* **1992**, *201*, 99−111.

Received April 28, 2000
[I00168]

Syntheses and Crystal Structures of Coinage Metal Thioether-Thiolato Complexes

Stephan Zeltner,[a] Svea Jelonek,[a] Joachim Sieler,[a] and Ruth-Maria Olk*[a]

Dedicated to Professor Dr. Eberhard Hoyer on the occasion of his 70th birthday

Keywords: Sulfur ligands / Copper / Silver / Gold

Copper(I), silver(I), and two gold(I) complexes of the type $(Ph_3P)_nM(\mathbf{L})$ [n = 1, 2, 3; **L** = 4-(methylthio)-2-thioxo-1,3-dithiole-5-thiolate ($\mathbf{L_a}$), 1,2-dicyano-1-(methylthio)ethene-2-thiolate ($\mathbf{L_b}$)] have been synthesized. The molecular structure of these complexes was determined by X-ray crystallography and shows differences in the coordinated sulfur atoms as well as in the coordination geometry of these $(Ph_3P)_nM(\mathbf{L})$ complexes. In $(Ph_3P)_2Cu(\mathbf{L})$ (**2**), the thioether thiolate ligands act as bidentate ligands, whereas in the silver and gold complexes $(Ph_3P)_3Ag(\mathbf{L})$ (**3**) and $(Ph_3P)_2Au(\mathbf{L})$ (**4**), only the thiolate sulfur is coordinated. Dissociation of one of the phosphane ligands of $(Ph_3P)_2Au(\mathbf{L_a})$ (**4a**) occurs in boiling acetone and a linear two-coordinate gold(I) center is obtained, $(Ph_3P)Au(\mathbf{L_a})$ (**5a**).

Introduction

Metal complexes of 4-(methylthio)-2-thioxo-1,3-dithiole-5-thiolate ($C_3S_5^{2-}$) have been the subjects of numerous studies because some of them have been reported to exhibit conducting or superconducting properties.[1,2] The methylation of one thiolate donor atom of this delocalized dithiolate results in a thioether thiolate compound, 4-(methylthio)-2-thioxo-1,3-dithiole-5-thiolate ($\mathbf{L_a}$). The coordination ability of compounds with such sulfur donors is of interest because of the relevance to biological systems.[3] However, in marked contrast to their extensive studied transition-metal chelates,[4,5] thioether thiolato complexes with d^{10} metals are rare.

The principal difference between thiols and thioethers as ligands is that the former are more highly polarizable, but are not as effective d_π-electron acceptors as the latter.[6] Nevertheless, both kinds of sulfur atoms are soft donors and should be preferably coordinated by the soft coinage metals.[7]

We undertook the complexation of 4-(methylthio)-2-thioxo-1,3-dithiole-5-thiolate ($\mathbf{L_a}$) and 1,2-dicyano-1-(methylthio)ethene-2-thiolate ($\mathbf{L_b}$) with the d^{10} metal ions copper(I), silver(I) and gold(I) in order to examine the complexation behavior of thioether thiolate ligands. Comparison of the structures of these $(Ph_3P)_nM(\mathbf{L})$ chelates highlights differences in the coordinated donor-atom groups as well as in their coordination geometry.

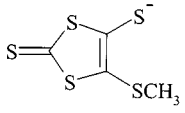

$\mathbf{L_a}$

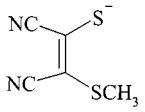

$\mathbf{L_b}$

Results and Discussion

The reaction of cesium 4-(methylthio)-2-thioxo-1,3-dithiole-5-thiolate (**1a**) and cesium 1,2-dicyano-1-(methylthio)-ethene-2-thiolate (**1b**) with the triphenylphosphane-coordinated closed-shell ions copper(I), silver(I), and gold(I) led to the coordination compounds $(Ph_3P)_2Cu(\mathbf{L})$ (**2a**, **2b**), $(Ph_3P)_3Ag(\mathbf{L})$ (**3a**, **3b**), and $(Ph_3P)_2Au(\mathbf{L})$ (**4a**, **4b**), respectively, in good yields.

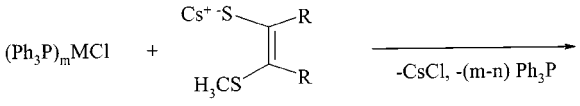

1a : R-R = CS_3
1b : R = CN

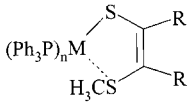

	M	n
2 :	Cu	2
3 :	Ag	3
4 :	Au	2

Complexes **2**–**4** are crystalline, air- and moisture-stable solids. They are soluble in polar organic solvents, and are nonconductors in chloroform solutions, as shown by means

[a] University of Leipzig, Institute of Inorganic Chemistry
Johannisallee 29, 04103 Leipzig, Germany
Fax: (internat.) +49-(0)341/973-6199
E-mail: olk@sonne.tachemie.uni-leipzig.de

 © WILEY-VCH Verlag GmbH, 69451 Weinheim, 2001 1434–1948/01/0606–1535 $ 17.50+.50/0

of conductivity measurements. The cumulative evidence from elemental analyses, IR, and NMR spectra establishes the composition of these compounds. Their ^{31}P NMR spectra measured in $CDCl_3$ at room temperature show only one singlet. However, from the spectrum of $(Ph_3P)_2Au(\mathbf{L_a})$ (**4a**), three nonequivalent phosphorus atoms are detectable after being allowed to stand for several weeks in chloroform. Two additional singlets are observed. These are shifted downfield relative to those of the starting complex **4a** (δ = 20.3); one was assigned to triphenylphosphane oxide (δ = 29.5) and the second at δ = 38.1 is characteristic of linearly coordinated gold(I).[8,9] Therefore it is probable that the gold complex $(Ph_3P)Au(\mathbf{L_a})$ (**5a**) is prepared from $(Ph_3P)_2Au(\mathbf{L_a})$ (**4a**). In fact, the complex **5a** can be isolated in good yields after boiling an acetone solution of the bistriphenylphosphane complex **4a** for few minutes. The trend in going from a trigonal-planar complex to a linear gold complex was not observed for the corresponding bistriphenylphosphane gold complex of 1,2-dicyano-1-(methylthio)ethene-2-thiolate (**4b**).

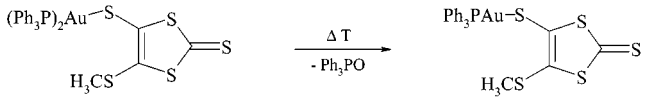

4a **5a**

However, from these results, the exact number of sulfur donors in the coordination sphere of the metal(I) ions remained open to investigation. Consequently, the complexes **2a**, **2b**, **3a**, **3b**, **4b**, and **5a** were further characterized by X-ray structure analysis, providing information about their sulfur-donor set. The complex $(Ph_3P)_2Cu(\mathbf{L})$ (**2**) has a distorted tetrahedral coordination geometry around the copper atom involving the two sulfur donor atoms S(1) and S(2) of $\mathbf{L_a}$ and $\mathbf{L_b}$, and two phosphorus atoms of the phosphanes. This arrangement is depicted in Figures 1 and 2, and selected interatomic distances and angles are given in Table 1.

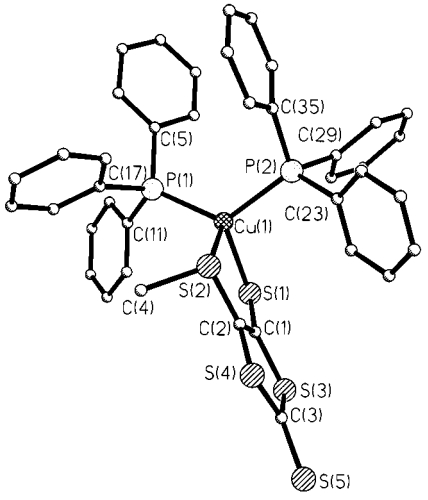

Figure 1. Molecule structure of $(Ph_3P)_2Cu(\mathbf{L_a})$ **2a**, H atoms are omitted

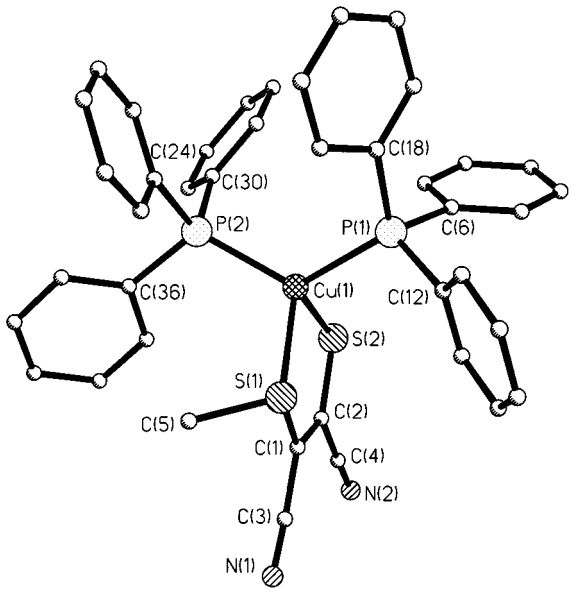

Figure 2. Molecule structure of $(Ph_3P)_2Cu(\mathbf{L_b})$ **2b**, H atoms are omitted

Table 1. Selected bond lengths [Å] and angles [deg] for $(Ph_3P)_2Cu(\mathbf{L})$ **2**

$(Ph_3P)_2Cu(\mathbf{L_a})$ **2a**		$(Ph_3P)_2Cu(\mathbf{L_b})$ **2b**	
Cu(1)−S(1)	2.3223(6)	Cu(1)−S(2)	2.3101(8)
Cu(1)−S(2)	2.4577(6)	Cu(1)−S(1)	2.3973(8)
Cu(1)−P(1)	2.2647(5)	Cu(1)−P(2)	2.2664(8)
Cu(1)−P(2)	2.2977(6)	Cu(1)−P(1)	2.2753(7)
C(1)−C(2)	1.352(3)	C(1)−C(2)	1.367(4)
C(1)−S(1)	1.722(2)	C(2)−S(2)	1.708(3)
C(2)−S(2)	1.754(2)	C(1)−S(1)	1.773(3)
C(4)−S(2)	1.807(3)	C(5)−S(1)	1.817(4)
C(1)−S(3)	1.756(2)	C(1)−C(3)	1.431(4)
C(2)−S(4)	1.807(3)	C(2)−C(4)	1.448(4)
C(3)−S(3)	1.728(2)	C(3)−N(1)	1.134(4)
C(3)−S(4)	1.718(2)	C(4)−N(2)	1.142(4)
C(3)−S(5)	1.655(2)		
P(1)−Cu(1)−P(2)	120.96(2)	P(1)−Cu(1)−P(2)	121.26(3)
S(1)−Cu(1)−S(2)	91.50(2)	S(1)−Cu(1)−S(2)	90.60(3)
P(1)−Cu(1)−S(2)	110.16(2)	P(2)−Cu(1)−S(1)	113.72(3)
P(2)−Cu(1)−S(1)	111.11(2)	P(1)−Cu(1)−S(2)	104.78(3)
P(1)−Cu(1)−S(1)	117.50(2)	P(2)−Cu(1)−S(2)	113.42(3)
P(2)−Cu(1)−S(2)	99.62(2)	P(1)−Cu(1)−S(1)	108.53(3)
Cu(1)−S(1)−C(1)	97.93(7)	Cu(1)−S(2)−C(2)	100.41(10)
Cu(1)−S(2)−C(2)	95.75(7)	Cu(1)−S(1)−C(1)	98.72(9)
Cu(1)−S(2)−C(4)	115.27(12)	Cu(1)−S(1)−C(5)	114.21(15)
C(1)−C(2)−S(2)	124.40(15)	C(2)−C(1)−S(1)	121.6(2)
C(2)−C(1)−S(1)	128.84(16)	C(1)−C(2)−S(2)	127.6(2)
C(1)−C(2)−S(4)	117.35(15)	C(2)−C(1)−C(3)	122.4(3)
C(2)−C(1)−S(3)	113.73(15)	C(1)−C(2)−C(4)	118.0(3)
S(2)−C(2)−S(4)	118.22(12)	S(1)−C(1)−C(3)	115.9(2)
S(1)−C(1)−S(3)	117.43(12)	S(2)−C(2)−C(4)	114.4(2)
C(1)−S(3)−C(3)	98.86(10)	C(2)−C(4)−N(2)	177.3(4)
C(2)−S(4)−C(3)	97.76(10)	C(1)−C(3)−N(1)	177.7(4)
S(3)−C(3)−S(4)	112.27(13)		
S(3)−C(3)−S(5)	124.20(14)		
S(4)−C(3)−S(5)	123.53(14)		

It is notable, perhaps predictably, that the copper−sulfur (thioether) bond lengths are longer [2.4577(6) Å for **2a** and

2.3973(8) for **2b**] than those of the copper-sulfur(thiolate) [2.3223(6) Å and 2.3101(8) Å for **2a** and **2b**, respectively]. But the copper−sulfur (thiolate) bond length in **2a** is longer than the chelating distances [Cu−S: 2.237(2)] found for the complex of the non-methylated ligand with $Cu(Ph_3P)$.[10] An interesting pattern is also observed for the metallaheterocycle [−Cu−S(1)−C(1)−C(2)−S(2)−], which is distorted and folded along the sulfur−sulfur axis (**2a**: 12.7°, **2b**: 8.9°). The copper−phosphorus bond lengths and angles are typical.[11,12]

The silver compounds **3a** and **3b** were prepared by the chloride substitution reaction of chlorotris(triphenylphosphane)silver(I) with the corresponding thioether thiolate ligands. The yellowish orange complex $(Ph_3P)_3Ag(\mathbf{L_a})$ **3a** was found to incorporate solvent of crystallization (acetone). The molecular structures of complexes **3** are illustrated in Figure 3 and Figure 4, and selected bond lengths and angles are given in Table 2.

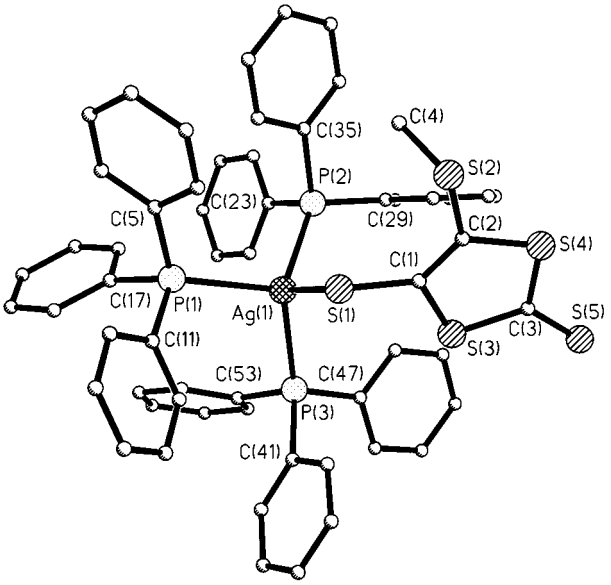

Figure 3. Molecule structure of $(Ph_3P)_3Ag(\mathbf{L_a})$ × acetone **3a**, acetone and H atoms are omitted

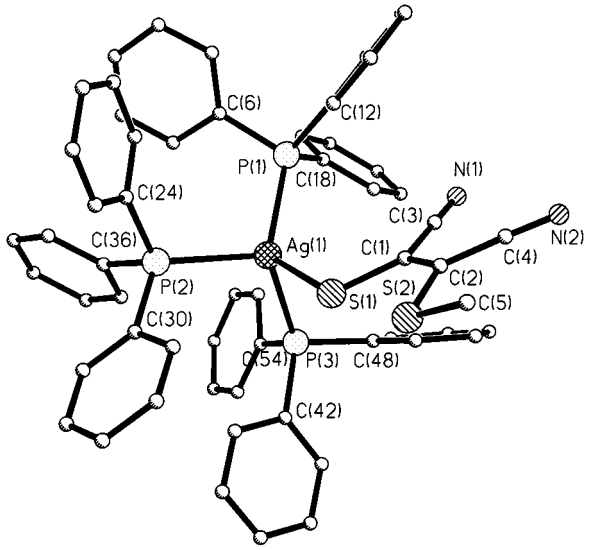

Figure 4. Molecule structure of $(Ph_3P)_3Ag(\mathbf{L_b})$ **3b**, H atoms are omitted

Table 2. Selected bond lengths [Å] and angles [deg] for $(Ph_3P)_3Ag(\mathbf{L})$ **3**

$(Ph_3P)_3Ag(\mathbf{L_a})$ × acetone **3a**		$(Ph_3P)_3Ag(\mathbf{L_b})$ **3b**	
Ag(1)−S(1)	2.5898(9)	Ag(1)−S(1)	2.6406(12)
Ag(1)−P(1)	2.6495(8)	Ag(1)−P(2)	2.6090(11)
Ag(1)−P(2)	2.5825(8)	Ag(1)−P(1)	2.5445(11)
Ag(1)−P(3)	2.5974(8)	Ag(1)−P(3)	2.5947(11)
C(1)−C(2)	1.355(4)	C(1)−C(2)	1.366(6)
C(1)−S(1)	1.719(3)	C(1)−S(1)	1.726(4)
C(2)−S(2)	1.747(4)	C(2)−S(2)	1.755(5)
C(4)−S(2)	1.794(7)	C(5)−S(2)	1.796(7)
C(1)−S(3)	1.749(3)	C(1)−C(3)	1.456(6)
C(2)−S(4)	1.758(4)	C(2)−C(4)	1.435(7)
C(3)−S(3)	1.723(3)	C(3)−N(1)	1.147(6)
C(3)−S(4)	1.710(4)	C(4)−N(2)	1.154(7)
C(3)−S(5)	1.649(4)		
P(1)−Ag(1)−P(2)	113.37(3)	P(1)−Ag(1)−P(2)	111.11(4)
P(1)−Ag(1)−P(3)	111.99(2)	P(1)−Ag(1)−P(3)	113.99(4)
P(1)−Ag(1)−S(1)	92.38(3)	P(1)−Ag(1)−S(1)	121.82(4)
P(2)−Ag(1)−P(3)	113.26(3)	P(2)−Ag(1)−P(3)	114.42(3)
P(2)−Ag(1)−S(1)	112.28(3)	P(2)−Ag(1)−S(1)	98.21(4)
P(3)−Ag(1)−S(1)	111.86(3)	P(3)−Ag(1)−S(1)	95.89(4)
Ag(1)−S(1)−C(1)	109.17(10)	Ag(1)−S(1)−C(1)	119.12(16)
C(1)−C(2)−S(2)	127.1(3)	C(1)−C(2)−S(2)	119.5(3)
C(2)−C(1)−S(1)	128.8(3)	C(2)−C(1)−S(1)	122.7(3)
C(1)−C(2)−S(4)	116.6(3)	C(2)−C(1)−C(3)	117.6(4)
C(2)−C(1)−S(3)	113.4(2)	C(1)−C(2)−C(4)	120.3(4)
S(2)−C(2)−S(4)	116.39(19)	S(1)−C(1)−C(3)	119.6(3)
S(1)−C(1)−S(3)	117.76(17)	S(2)−C(2)−C(4)	120.0(4)
C(1)−S(3)−C(3)	100.06(16)	C(2)−C(4)−N(2)	177.5(6)
C(2)−S(4)−C(3)	98.52(16)	C(1)−C(3)−N(1)	178.7(6)
S(3)−C(3)−S(4)	111.4(2)		
S(3)−C(3)−S(5)	123.8(2)		
S(4)−C(3)−S(5)	123.8(2)		

Three triphenylphosphane groups and a thioether thiolate ligand **L**, which is bonded only through the thiolate sulfur atom to silver, surround the silver ion in **3a** and **3b**. In compounds **3**, the configuration about the silver ion can be described as a distorted tetrahedron. The angles at the metal site range from 92.38(3) to 113.37(3)° and from 95.89(4) to 121.82(4)° for **3a** and **3b**, respectively. The Ag−P distances average 2.6 Å and are longer than the sum of the single-bond covalent radii (2.44 Å),[13] but are comparable with those determined for other triphenylphosphane silver(I) compounds [2.503(5) Å,[14] 2.557(6) Å,[15] and 2.616(3) Å[16]]. The observed silver−sulfur (thiolate) bond lengths of 2.5898(9) Å (**3a**) and 2.6406(12) Å (**3b**) are longer than single covalent bonds, but are appreciably shorter than the van der Waals contact (3.52 Å).[13] Chlorobis(triphenylphosphane) gold(I) reacts with the cesium thiolate salts **1** to $(Ph_3P)_2Au(\mathbf{L})$ (**4**). Figure 5 represents a view of the molecular structure of $(Ph_3P)_2Au(\mathbf{L_b})$ **4b**. Although the angles deviate somewhat from the idealized geometry of 120°, the coordination about the gold ion is essentially trigonal planar. Relevant bond lengths and angles are given in Table 3. The Au−P(2) distance of 2.3806(13) Å is considerably longer than the Au−P(1) distance of 2.3101(13) Å, and

is also longer than the Au−P distances of 2.323(4) Å and 2.339(4) Å in $(Ph_3P)_2AuCl$.[17] It is also interesting to observe that complex **4b** shows longer Au−P and Au−S distances than in the corresponding complexes with the non-methylated dithiolate ligands $[(Ph_3PAu)_2S_2C_2(CN)_2]$[18] and $(Bu_4N)[Ph_3PAu(S_2C_2(CN)_2]$.[19] In boiling acetone, one of the phosphane ligands dissociates from $(Ph_3P)_2Au(\mathbf{L_a})$ (**4a**), whereas $(Ph_3P)_2Au(\mathbf{L_b})$ (**4b**) remains unchanged. The structure of the resulting complex $(Ph_3P)Au(\mathbf{L_a})$ (**5a**) is shown in Figure 6, and selected bond lengths and angles are given in Table 3.

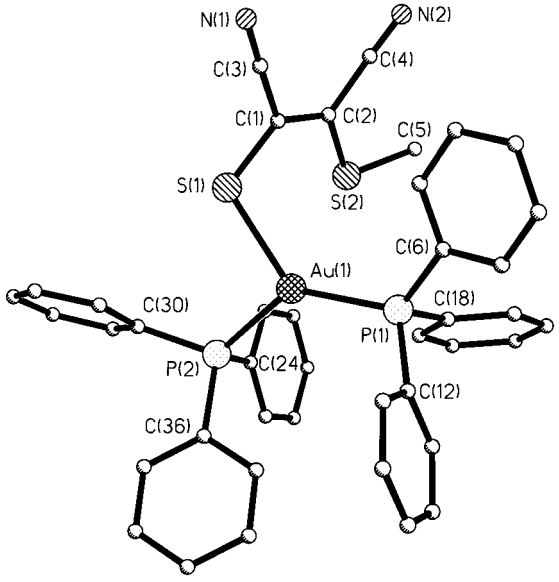

Figure 5. Molecule structure of $(Ph_3P)_2Au(\mathbf{L_b})$ **4b**, H atoms are omitted

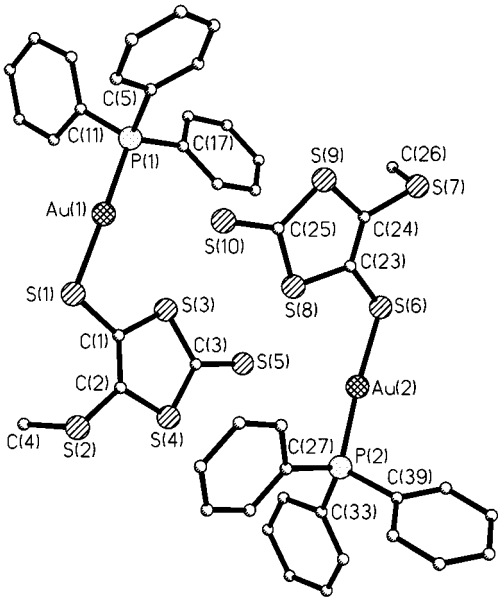

Figure 6. Molecule structure of $(Ph_3P)Au(\mathbf{L_a})$ **5a**, H atoms are omitted

Two crystallographically independent molecules of $(Ph_3P)Au(\mathbf{L_a})$ (**5a**) are present in the asymmetric unit. Each gold atom is bis-coordinated in a linear fashion to the thiolate sulfur of $\mathbf{L_a}$, and the phosphorus atom of the triphenylphosphane. The Au−S distances [2.3078(13) and 2.3144(14) Å] are slightly shorter than those found for triphenylphosphane gold (I) complexes with the non-methylated C_3S_5 ligand, such as $(Ph_3PAu)_2C_3S_5$ [2.3474(11), 2.3435(12) Å] and $(Bu_4N)[Ph_3PAu(C_3S_5)]$ [2.476(3), 2.405(3) and 2.413(3),

Table 3. Selected bond lengths [Å] and angles [deg] for $(Ph_3P)_2Au(\mathbf{L_b})$ (**4b**) and $(Ph_3P)Au(\mathbf{L_a})$ (**5a**)

$(Ph_3P)_2Au(\mathbf{L_b})$ **4b**		$(Ph_3P)Au(\mathbf{L_a})$ **5a**			
Au(1)−S(1)	2.4884(16)	Au(1)−S(1)	2.3078(13)	Au(2)−S(6)	2.3144(14)
Au(1)−P(1)	2.3101(13)	Au(1)−P(1)	2.2592(13)	Au(2)−P(2)	2.2685(13)
Au(1)−P(2)	2.3806(13)	C(1)−C(2)	1.352(7)	C(23)−C(24)	1.347(7)
C(1)−C(2)	1.341(11)	C(1)−S(1)	1.744(5)	C(23)−S(6)	1.739(5)
C(1)−S(1)	1.724(7)	C(2)−S(2)	1.751(5)	C(24)−S(7)	1.758(5)
C(2)−S(2)	1.762(9)	C(4)−S(2)	1.750(7)	C(26)−S(7)	1.766(7)
C(5)−S(2)	1.803(16)	C(1)−S(3)	1.741(5)	C(23)−S(8)	1.752(5)
C(1)−C(3)	1.432(12)	C(2)−S(4)	1.752(5)	C(24)−S(9)	1.754(6)
C(2)−C(4)	1.483(10)	C(3)−S(3)	1.729(5)	C(25)−S(8)	1.743(6)
C(3)−N(1)	1.147(11)	C(3)−S(4)	1.714(5)	C(25)−S(9)	1.715(5)
C(4)−N(2)	1.1081(10)	C(3)−S(5)	1.652(5)	C(25)−S(10)	1.648(6)
P(1)−Au(1)−P(2)	130.71(4)	P(1)−Au(1)−S(1)	177.76(5)	P(2)−Au(2)−S(6)	174.54(57)
P(1)−Au(1)−S(1)	132.40(3)	Au(1)−S(1)−C(1)	101.83(16)	Au(2)−S(6)−C(23)	103.66(17)
P(2)−Au(1)−S(1)	96.63(6)	C(1)−C(2)−S(2)	125.2(4)	C(23)−C(24)−S(7)	126.0(4)
Au(1)−S(1)−C(1)	110.0(2)	C(2)−C(1)−S(1)	126.2(4)	C(24)−C(23)−S(6)	126.0(4)
C(1)−C(2)−S(2)	120.2(5)	C(1)−C(2)−S(4)	116.5(4)	C(23)−C(24)−S(9)	116.7(4)
C(2)−C(1)−S(1)	125.0(6)	C(2)−C(1)−S(3)	114.3(4)	C(24)−C(23)−S(8)	114.6(4)
C(2)−C(1)−C(3)	119.4(7)	S(2)−C(2)−S(4)	118.3(3)	S(7)−C(24)−S(9)	117.2(3)
C(1)−C(2)−C(4)	120.5(8)	S(1)−C(1)−S(3)	119.5(3)	S(6)−C(23)−S(8)	119.4(3)
S(1)−C(1)−C(3)	115.5(6)	C(1)−S(3)−C(3)	99.3(2)	C(23)−S(8)−C(25)	98.6(3)
S(2)−C(2)−C(4)	119.3(7)	C(2)−S(4)−C(3)	98.2(3)	C(24)−S(9)−C(25)	98.2(3)
C(2)−C(4)−N(2)	177.1(9)	S(3)−C(3)−S(4)	111.8(3)	S(8)−C(25)−S(9)	111.9(3)
C(1)−C(3)−N(1)	178.6(10)	S(3)−C(3)−S(5)	122.7(3)	S(8)−C(25)−S(10)	122.6(3)
		S(4)−C(3)−S(5)	125.6(3)	S(9)−C(25)−S(10)	125.5(4)

2.483(3) Å].[20] However, the gold−sulfur (thiolate) bond length in **5a** is very similar to those found for the bis-chelate of the non-methylated C_3S_5 with gold(III) (Bu_4N)-$[Au(C_3S_5)_2]$ [2.311 to 2.327 Å].[21,22]

The Au−P distances [2.2592(13) and 2.2685(13) Å] in **5a** are typical of two-coordinate gold(I) compounds, as are the P−Au−S angles of 177.76(5)° and 174.54(5)°.[8,9,23] This slight deviation from the linearity is common for gold(I) structures.[24]

The present work has shown that the thioether thiolate compounds 4-(methylthio)-2-thioxo-1,3-dithiole-5-thiolate (**L_a**) and 1,2-dicyano-1-(methylthio)ethene-2-thiolate (**L_b**) form stable complexes with closed-shell d^{10} ions. However, the molecular structure of these complexes is not predictable. We believe that the restricted bite angle of the sulfur donor atoms within **L** and their different donor abilities play an important role in determining the final structures of the metal(I) complexes. Additionally, the strong phosphane donors and their size are of relevance in the complexation of coinage metals.[8,12]

Experimental Section

General Remarks: All chemicals and solvents used in the synthesis were of reagent grade and were used without further purification. The metal salts $(Ph_3P)_3CuCl$, $(Ph_3P)_3AgCl$, and $(Ph_3P)_2AuCl$ were prepared by published methods.[17,25,26] − IR: Perkin−Elmer 2000 FT. − UV/Vis: Shimadzu 160A. − NMR: Varian Gemini 300 (300.075 MHz, 75.462 MHz and 121.470 MHz, for ^1H, ^{13}C and ^{31}P, respectively). For ^1H and ^{13}C NMR spectra, $CDCl_3$ was used as solvent with TMS as internal standard. For ^{31}P NMR spectra, $CDCl_3$ was used as solvent with H_3PO_4 (85%) as external standard, δ_P= 82.43. − Melting points: Boetius point apparatus, uncorrected. − Elemental analyses: Heraeus CHN rapid analyzer.

Cesium 4-(Methylthio)-2-thioxo-1,3-dithiole-5-thiolate (1a) and Cesium 1,2-Dicyano-1-(methylthio)ethene-2-thiolate (1b): To a stirred chloroform solution (50 mL) of 4-(benzoylthio)-5-(methylthio)-2-thioxo-1,3-dithiole[27] (10 mmol, 3.16 g) (for **1a**) or 1-(benzoylthio)-1,2-dicyano-2-(methylthio)ethene[28] (2.60 g) (for **1b**) was added cesium hydroxide hydrate (10 mmol, 1.70 g) in methanol (10 mL). After about 1 min, the cesium thiolates started to separate. Diethyl ether (100 mL) was added to precipitate the product completely. This cesium salt was recovered by filtration, washed with diethyl ether and air dried.

1a: Orange crystals (1.85 g, 54%), m.p. > 250 °C. − IR (KBr): $\tilde{\nu}$ = 2978 and 2911 cm^{-1} (CH), 1416 (CH, C=C) 1310 (CH), 1060 and 1030 (C=S). − ^1H NMR (CD_3OD): δ = 2.36 (s, 3 H, $-CH_3$). − ^{13}C NMR (CD_3OD): δ = 18.6 (-CH_3), 121.0 (C-4), 163.6 (C-5), 214.9 (C=S). − $C_4H_3CsS_5 \cdot 0.5\ H_2O$ (353.30): calcd. C 13.60, H 1.14, S 45.38; found C 13.99, H 1.20, S 45.67.

1b: Yellow crystals (2.70 g, 90%), m.p. > 250 °C. − IR (KBr): $\tilde{\nu}$ = 2181 (CN) cm^{-1}, 1457, 1421 (CH, C=C), 1159, 1117, 1050, 969, 858, 520, and 503 (CH). − ^1H NMR (CD_3OD): δ = 2.43 (s, 3 H, $-CH_3$). − ^{13}C NMR (CD_3OD): δ = 16.0 ($-CH_3$), 113.7 (C-1), 117.8 (CN), 119.5 (CN), 138.5 (C-2). − $C_5H_3N_2CsS_2 \cdot 0.5\ H_2O$ (297.14): calcd. C 20.21, H 1.36, N 9.43, S 21.58; found C 20.03, H 1.03, N 9.06, S 21.58.

Complexes $(Ph_3P)_2Cu(L)$, $(Ph_3P)_3Ag(L)$, and $(Ph_3P)_2Au(L)$ (2) − (4): Solid $(Ph_3P)_nMCl$ (0.5 mmol, M = Cu, *n* = 3: 440 mg; M = Ag, *n* = 3: 465 mg; M = Au, *n* = 2: 380 mg) was added to a solution of CsL (0.5 mmol, **1a**: 176 mg; **1b**: 148 mg) in acetone (50 mL). After being stirred for 20 min., the yellow−orange reaction mixture was filtered. The volume of this acetone solution was reduced to 20 mL, and cooled to −5 °C overnight, yielding a crystalline solid, which was filtered off, washed with 2-propanol and air dried.

Cu Complex $(Ph_3P)_2Cu(L_a)$ (2a): Tawny crystals (285 mg, 71%), m.p. 182−184 °C dec. − IR (KBr): $\tilde{\nu}$ = 3050, 3002, 2917, 1184, 1158, 1095, 1005, 961, 881, 741, and 694 cm^{-1} (CH), 1480, 1434, and 1424 (CH, C=C), 1307 (CH), 1054 and 1034 (C=S). − UV/Vis (CH_2Cl_2): λ_{max} (log ε) = 432 nm (3.72), 355 (3.91), 264 (4.43), 232 (4.47). − ^1H NMR ($CDCl_3$): δ = 1.80 (s, 3 H, $-CH_3$), 7.23−7.39 (m, 30 H, -P−C_6H_5). − ^{13}C NMR ($CDCl_3$): δ = 23.8 (-CH_3), 118.6 (C-4), 165.1 (C-5), 214.1 (C=S), 129.4 ($^3J_{C,P}$ = 8.7 Hz), 130.4, 134.0 ($^1J_{C,P}$ = 24.6 Hz), 134.2 ($^2J_{C,P}$ = 15.0 Hz). − ^{31}P NMR ($CDCl_3$): δ = 1.3. − $C_{40}H_{33}CuP_2S_5$ (799.44): calcd. C 60.10, H 4.16, S 20.05; found C 60.21, H 4.05, S 20.98.

Cu Complex $(Ph_3P)_2Cu(L_b)$ (2b): Orange crystals (220 mg, 60%), m.p. 202−205 °C dec. − IR (KBr): $\tilde{\nu}$ = 3470, 3054, 2917, 1183, 1156, 1125, 1095, 1027, 999, 751, 743, 707, 695, 527, 518, 503, and 492 cm^{-1} (CH), 2190 (CN), 1479, 1456, and 1434 (CH, C=C). − UV/Vis (CH_2Cl_2): λ_{max} (log ε) = 397 nm (3.52), 238 (4.32). − ^1H NMR ($CDCl_3$): δ = 1.87 (s, 3 H, $-CH_3$), 7.25−7.41 (m, 30 H, -P−C_6H_5). − ^{13}C NMR ($CDCl_3$): δ = 20.7 (-CH_3), 105.7 (C-1), 116.5 and 116.8 (CN), 147.9 (C-2), 128.8 ($^3J_{C,P}$ = 8.3 Hz), 130.1, 132.6 ($^1J_{C,P}$ = 28.4 Hz), 133.5 ($^2J_{C,P}$ = 13.7 Hz). − ^{31}P NMR ($CDCl_3$): δ = 0.4. − $C_{41}H_{33}CuN_2P_2S_2$ (743.35): calcd. C 66.25, H 4.47, N 3.77, S 8.63; found C 65.86, H 4.48, N 3.65, S 8.24.

Ag Complex $(Ph_3P)_3Ag(L_a)$ × Acetone (3a): Yellowish orange crystals (443 mg, 77%), m.p. 149−151 °C dec. − IR (KBr): $\tilde{\nu}$ = 3052, 3002, 2913, 1184, 1157, 1093, 997, 866, 743, and 694 cm^{-1} (CH), 1478, 1434, and 1414 (CH, C=C), 1307 (CH), 1056 and 1038 (C=S). − UV/Vis (CH_2Cl_2): λ_{max} (log ε) = 416 nm (3.78), 306 (3.92), 257 (4.38), 232 (4.44). − ^1H NMR ($CDCl_3$): δ = 1.91 (s, 3 H, $-CH_3$), 2.18 (s, 6 H, -$(CH_3)_2CO$), 7.30−7.41 (m, 45 H, -P−C_6H_5). − ^{13}C NMR ($CDCl_3$): δ = 21.1 (-CH_3), 31.6 ($CH_3)_2CO$), 118.6 (C-4), 164.3 (C-5), 207.6 ($(CH_3)_2CO$), 212.6 (C=S), 128.8 ($^3J_{C,P}$ = 8.4 Hz), 129.7, 133.7 ($^2J_{C,P}$ = 17.3 Hz), 134.2 ($^1J_{C,P}$ = 11.6 Hz). − ^{31}P NMR ($CDCl_3$): δ = 3.7. − $C_{61}H_{54}AgOP_3S_5$ (1164.12): calcd. C 62.93, H 4.67, S 13.77; found C 63.04, H 4.39, S 14.38.

Ag Complex $(Ph_3P)_3Ag(L_b)$ (3b): Yellow crystals (210 mg, 40%), m.p. 146−149 °C dec. − IR (KBr): $\tilde{\nu}$ = 3469, 3052, 3004, 2922, 1184, 1156, 1115, 1092, 1069, 1047, 1026, 997, 744, 694, 515, 503, and 492 cm^{-1} (CH), 2180 (CN), 1479, 1456, and 1434 (CH, C=C). − UV/Vis (CH_2Cl_2): λ_{max} (log ε) = 367 nm (3.79), 253 (4.50). − ^1H NMR ($CDCl_3$): δ = 1.98 (s, 3 H, $-CH_3$), 7.29−7.34 (m, 45 H, -P−C_6H_5). − ^{13}C NMR ($CDCl_3$): δ = 17.4 (-CH_3), 111.9 (C-1), 115.8 (CN), 117.4 (CN), 139.8 (C-2), 128.9 ($^3J_{C,P}$ = 8.9 Hz), 129.9, 133.6 ($^2J_{C,P}$ = 17.2 Hz), 133.7 ($^2J_{C,P}$ = 17.2 Hz). − ^{31}P NMR ($CDCl_3$): δ = 4.50. − $C_{29}H_{48}AgN_2P_3S_2$ (1049.96): calcd. C 67.49, H 4.61, N 2.67, S 6.11; found C 66.82, H 4.87, N 1.87, S 5.36.

Au Complex $(Ph_3P)_2Au(L_a)$ (4a): Yellowish orange crystals (320 mg, 69%), m.p. 112−113 °C dec. − IR (KBr): $\tilde{\nu}$ = 3050, 2913, 1182, 1158, 1097, 996, 863, 744, and 693 cm^{-1} (CH), 1479, 1434, and 1395 (CH, C=C), 1308 (CH), 1056 and 1037 (C=S). − UV/Vis (CH_2Cl_2): λ_{max} (log ε) = 409 nm (4.02), 300 (4.15), 235 (4.58). − ^1H NMR ($CDCl_3$): δ = 2.28 (s, 3 H, $-CH_3$), 7.38−7.47 (m, 30 H, -P−C_6H_5). − ^{13}C NMR ($CDCl_3$): δ = 19.9 (-CH_3), 125.0 (C-4), 151.0 (C-5), 211.8 (C=S), 129.1 ($^3J_{C,P}$ = 9.9 Hz), 130.6, 133.2 ($^1J_{C,P}$ = 26.7 Hz), 134.1 ($^2J_{C,P}$ = 16.5 Hz). − ^{31}P NMR ($CDCl_3$):

Table 4. Crystallographic Data for $(Ph_3P)_2Cu(\mathbf{L})$ (**2a**, **2b**), $(Ph_3P)_3Ag(\mathbf{L})$ (**3a**, **3b**), $(Ph_3P)_2Au(\mathbf{L_b})$ (**4b**), and $(Ph_3P)Au(\mathbf{L_a})$ (**5a**)

formula	$C_{40}H_{33}P_2S_5Cu$ (**2a**)	$C_{41}H_{33}N_2P_2S_2Cu$ (**2b**)	$C_{61}H_{54}OP_3S_5Ag$ (**3a**)	$C_{59}H_{48}N_2P_3S_2Ag$ (**3b**)	$C_{41}H_{33}N_2P_2S_2Au$ (**4b**)	$C_{22}H_{18}S_5PAu$ (**5a**)
M	799.44	743.29	1164.12	1049.89	876.72	670.60
T [K]	293(2)	293(2)	293(2)	293(2)	293(2)	213(2)
space group	$P2_1/c$	$P2_1/n$	$P\bar{1}$	$P2_1/n$	$P\bar{1}$	$P2_1/c$
a [Å]	10.9131(7)	14.6398(4)	13.950(1)	12.3830(1)	10.066(3)	9.6818(6)
b [Å]	19.955(2)	13.3941(4)	14.226(1)	25.3111(3)	12.968(3)	17.6618(10)
c [Å]	18.1957(12)	19.7794(6)	14.332(1)	16.9067(2)	15.755(6)	27.8585(16)
α [deg]			86.22(1)		98.96(1)	
β [deg]	106.101(5)	104.285(1)	87.02(1)	92.367(1)	105.43(1)	98.8700(10)
γ [deg]			82.22(1)		104.79(1)	
V [Å^3]	3807.0(5)	3758.56(19)	2809.2(3)	5294.5(1)	1860.8(10)	4706.8(5)
Z	4	4	2	4	2	8
d_{calc} [g cm^{-3}]	1.395	1.314	1.376	1.317	1.565	1.893
μ [mm^{-1}]	0.960	0.808	0.670	0.589	4.183	6.771
$F(000)$	1648	1536	1200	2160	868	2592
crystal size [mm^{-3}]	0.5 × 0.4 × 0.3	0.30 × 0.25 × 0.20	0.25 × 0.22 × 0.20	0.25 × 0.25 × 0.20	0.30 × 0.25 × 0.10	0.30 × 0.20 × 0.15
θ range	1.55 to 26.01°	1.56 to 27.95°	1.92 to 26.03°	1.45 to 27.88°	1.67 to 27.03°	1.37 to 27.04°
Index range	$-13 \le h \le 13$	$-19 \le h \le 18$	$-17 \le h \le 17$	$-14 \le h \le 15$	$-12 \le h \le 12$	$-12 \le h \le 12$
	$-18 \le k \le 24$	$-17 \le k \le 15$	$-17 \le k \le 17$	$-32 \le k \le 33$	$-16 \le k \le 16$	$-19 \le k \le 22$
	$-22 \le l \le 22$	$-23 \le l \le 24$	$-10 \le l \le 17$	$-21 \le l \le 19$	$-20 \le l \le 20$	$-33 \le l \le 35$
R (all data)	$R_1 = 0.0497$	$R_1 = 0.0728$	$R_1 = 0.0654$	$R_1 = 0.1006$	$R_1 = 0.0703$	$R_1 = 0.0581$
	$wR_2 = 0.0867$	$wR_2 = 0.1191$	$wR_2 = 0.0963$	$wR_2 = 0.1579$	$wR_2 = 0.0873$	$wR_2 = 0.0917$
R [$I > 2\sigma(I)$]	$R_1 = 0.0305$	$R_1 = 0.0474$	$R_1 = 0.0318$	$R_1 = 0.0526$	$R_1 = 0.0344$	$R_1 = 0.0339$
	$wR_2 = 0.0796$	$wR_2 = 0.1040$	$wR_2 = 0.0852$	$wR_2 = 0.1253$	$wR_2 = 0.0775$	$wR_2 = 0.0829$

δ = 19.9. − $C_{40}H_{33}AuP_2S_5$ (932.94): calcd. C 51.50, H 3.57, S 17.19; found C 51.89, H 3.59, S 17.69.

Au Complex $(Ph_3P)_2Au(L_b)$ (4b): Yellow crystals (500 mg, 63%), m.p. 118−120 °C dec. − IR (KBr): $\tilde{\nu}$ = 3436, 3051, 2918, 1183, 1156, 1096, 998, 747, 694, 533, 520, 508, and 498 cm^{-1} (CH), 2195 (CN), 1468 and 1435 (CH, C=C). − UV/Vis (CH_2Cl_2): λ_{max} (log ε) = 360 nm (4.15), 239 (4.42). − ^{1}H NMR ($CDCl_3$): δ = 2.40 (s, 3 H, −CH_3), 7.39−7.48 (m, 30 H, -P−C$_6H_5$). − ^{13}C NMR ($CDCl_3$): δ = 17.2 (-CH$_3$), 114.2 (C-1), 118.3 (CN), 119.1 (CN), 129.9 (C-2), 128.9 ($^3J_{C,P}$ = 10.0 Hz), 130.6, 132.2 ($^1J_{C,P}$ = 33.1 Hz), 133.9 ($^2J_{C,P}$ = 15.6 Hz). − ^{31}P NMR ($CDCl_3$): δ = 27.8. − $C_{41}H_{33}AuN_2P_2S_2$ (876.77): calcd. C 56.17, H 3.79, N 3.20, S 7.31; found C 56.14, H 3.34, N 3.02, S 8.44.

Au Complex $(Ph_3P)Au(L_a)$ (5a): A mixture of $(Ph_3P)_2Au(L_a)$ **4a** (280 mg, 0.3 mmol) in acetone (20 mL) was heated at reflux for a few minutes and then filtered. 2-Propanol (ca. 5 mL) was added dropwise to the filtrate. The solution was allowed to stand at room temperature. The yellow crystals formed were filtered and air dried to afford yellowish orange crystals (320 mg, 69%), m.p. 153−155 °C dec. − IR (KBr): $\tilde{\nu}$ = 3050, 2913, 1181, 1101, 998, 887, 747, 711, and 692 cm^{-1} (CH), 1479, 1448, 1436, and 1309 (CH, C=C), 1308 (CH), 1060 and 1034 (C=S). − UV/Vis (CH_2Cl_2): λ_{max} (log ε) = 409 nm (4.00), 304 (4.08), 235 (4.46). − ^{1}H NMR ($CDCl_3$): δ = 2.31 (s, 3 H, −CH_3), 7.50−7.58 (m, 15 H, -P−C$_6H_5$). − ^{13}C NMR ($CDCl_3$): δ = 20.0 (−CH$_3$), 125.3 (C-4), 149.3 (C-5), 217.7 (C=S), 128.9, 129.6 ($^3J_{C,P}$ = 11.6 Hz), 132.2 ($^4J_{C,P}$ = 2.9 Hz), 134.3 ($^2J_{C,P}$ = 13.9 Hz). − ^{31}P NMR ($CDCl_3$): δ = 38.1. − $C_{22}H_{18}AuPS_5$ (670.60): calcd. C 39.40, H 2.71, S 23.90; found C 39.67, H 2.98, S 24.17.

X-ray Crystallographic Study: Crystals of $(Ph_3P)_2Cu(\mathbf{L})$ (**2a**, **2b**), $(Ph_3P)_3Ag(\mathbf{L})$ (**3a**, **3b**), $(Ph_3P)_2Au(\mathbf{L_b})$ (**4b**), and $(Ph_3P)Au(\mathbf{L_a})$ (**5a**) were formed by the slow evaporation of their solutions in acetone. Crystal data and crystallographic experimental data for the complexes **2a**, **2b**, **3a**, **3b**, **4b**, and **5a** are listed in Table 4. Data were collected on a Stoe STADI4 diffractometer (**2a**, **3a**, **4b**) and on a Bruker AXS SMART-CCD (**2b**, **3b**, **5a**), using Mo-K_α radiation.

The structures were solved by direct methods and the heavy-atom procedures were used (SHELXS-86[29]). An empirical absorption correction for **2a**, **3a**, **4b** (ψ-scan, 10 reflections) and **2b**, **3b**, and **5a** (SADABS[30]) was applied. Anisotropic displacement parameters for all non-hydrogen atoms were used. For **2a**, **2b**, **3a**, **3b**, and **4b** all hydrogen atoms could be localized unambiguously with a difference Fourier map. These hydrogen atoms were refined isotropically. The hydrogen atoms of the phenyl group of **5a** could not be localized completely, therefore these hydrogen atoms were refined with the "-1.2-option" of the riding modus. Molecular-numbering schemes are shown in Figure 1 [$(Ph_3P)_2Cu(L_a)$ **2a**], Figure 2 [$(Ph_3P)_2Cu(L_b)$ **2b**], Figure 3 [$(Ph_3P)_3Ag(L_a)$ × acetone, **3a**], Figure 4 [$(Ph_3P)_3Ag(L_b)$ **3b**], Figure 5 [$(Ph_3P)_2Au(L_b)$ **4b**], and Figure 6 [$(Ph_3P)Au(L_a)$ **5a**]. Selected bond length and angles are located in Tables 1, 2, and 3.

Crystallographic data (excluding structure factors) for the structures reported in this paper have been deposited with the Cambridge Crystallographic Data Centre as supplementary publication no. CCDC-147226 (**2a**), CCDC-147222 (**2b**), CCDC-147225 (**3a**), CCDC-147223 (**3b**), CCDC-147227 (**4b**), CCDC-147224 (**5a**). Copies of the data can be obtained free of charge on application to CCDC, 12 Union Road, Cambridge CB2 1EZ, UK [Fax: (internat.) + 44(1223)336−033; E-mail: deposit@ccdc.cam.ac.uk].

Acknowledgments

This work was funded by grants from the Deutsche Forschungsgemeinschaft and Fonds der Chemischen Industrie (J. S.).

[1] P. Cassoux, L. Valade, H. Kobayashi, A. Kobayashi, R. A. Clark, A. E. Underhill, *Coord. Chem. Rev.* **1991**, *110*, 115−160.
[2] A. E. Pullen, R.-M. Olk, *Coord. Chem. Rev.* **1999**, *188*, 211−262.
[3] D. Sellmann, *Angew. Chem.* **1993**, *105*, 67−70.
[4] S. E. Livingstone, *J. Chem. Soc.* **1956**, 437−440.
[5] D. Sellmann, D. Häusinger, F. Knoch, M. Moll, *J. Am. Chem. Soc.* **1996**, *118*, 5368−5374.
[6] R. J. P. Williams, *Ann. Repts. Progr. Chem. (Chem. Soc. London)* **1959**, *56*, 87−93.

[7] J. Hagen, *Chem.-Ztg.* **1985**, *109*, 63−75.
[8] B.-K. Teo, J. C. Calabrese, *Inorg. Chem.* **1976**, *15*, 2474−2486.
[9] E. Cerrada, A. Laguna, M. Laguna, P. G. Jones, *J. Chem. Soc., Dalton Trans.* **1994**, 1325−1326.
[10] T. Sheng, H. Li, Q. Huang, X. Wu, *Acta Cryst.* **1995**, *C51*, 2524−2526.
[11] S. J. Lippard, G. Palenik, *J. Inorg. Chem.* **1971**, *10*, 1322−1324.
[12] J. T. Gill, J. J. Mayerle, P.S. Welcker, D. F. Lewis, D. A. Ucko, D. J. Barton, D. Stowens, S. Lippard, *J. Inorg. Chem.* **1976**, *15*, 1155−1168.
[13] L. Pauling, *The Nature of the Chemical Bond*, 3d ed, Cornell University Press, Ithaca, N.Y., **1960**.
[14] D. Coucouvanis, N. C. Baenzinger, S. M. Johnson, *Inorg. Chem.* **1974**, *13*, 1191−1199.
[15] V. Saboonchian, G. Wilkinson, B. Hussain-Bates, M. B. Hursthouse, *Polyhedron* **1991**, *10*, 737−739.
[16] M. Camalli, F. Caruso, *Inorg. Chim. Acta* **1987**, *127*, 209−213.
[17] N. C. Baenziger, K. M. Dittemore, J. R. Doyle, *Inorg. Chem.* **1974**, *13*, 805−810.
[18] R. M. Dávila, A. Elduque, T. Grant, R. J. Staples, J. P. Fackler Jr., *Inorg. Chem.* **1993**, *32*, 1749−1755.
[19] E. Fritsch, K. Polborn, C. Robl, K. Sünkel, W. Beck, *Z. Anorg. Allg. Chem.* **1993**, *619*, 2050−2060.
[20] E.Cerrada, P. G. Jones, A. Laguna, M.Laguna, *Inorg. Chem.* **1996**, *35*, 2995−3000.
[21] E. B. Yakubskii, L. Yu. Ukhin, V. E. Shklover, Yu. T. Struchkov, N. A. Dolgopolova, L. V. Belousova, *Dokl. Akad. Nauk SSR* **1986**, *290*, 115−119.
[22] A. A. Macharashvili, L. V. Belousova, Z. S. Morkovnik, Yu. T. Struchkov, L. Yu. Ukhin, V. E. Shklover, *Zh. Neorg. Khim.* **1987**, *32*, 1897−1900.
[23] E. Colacio, A. Romerosa, J. Ruiz, R. Román, J. M. Gutiérrez-Zorrilla, A. Vegas, M. Martínez-Ripoll, *Inorg. Chem.* **1991**, *30*, 3743−3749.
[24] H. Schmidbaur, *Gold Bull.* **1990**, *23*, 11−21.
[25] S. J. Lippard, D. A. Ucko, *Inorg. Chem.* **1968**, *7*, 1051−1056.
[26] S. J. Lippard, P. S. Welcker, *Inorg. Chem.* **1972**, *11*, 6−7.
[27] S. Zeltner, R.-M. Olk, M. Wagner, B. Olk, *Synthesis* **1994**, 1445−1449.
[28] H. E. Simmons, D. C. Blomstrom, R. D. Vest, *J. Am. Chem. Soc.* **1962**, *84*, 4756−4771.
[29] *SHELXS-86*, program for the solution of crystal structures, G. M. Sheldrick, University of Göttingen, **1985**.
[30] *SADABS*, program for empirical absorption correction, G. M. Sheldrick, University of Göttingen, **1996**.

Received July 26, 2000
[I00295]

Selective Recognition of Copper(II) by a Water-Soluble, Emitter-Receptor Conjugate Containing a Ruthenium Chromophore, a Lysine Bridge, and a Cyclen Unit

Bernd Geißer,[a] Burkhard König,[b] and Ralf Alsfasser*[a]

Dedicated to Prof. Dr. Dieter Sellmann on the occasion of his 60th birthday

Keywords: Bioinorganic chemistry / Amino acids / Luminescence / Macrocyclic ligands / Copper / Ruthenium / Molecular recognition

The amino acid derivative [H-Lys{Ru(bipy)$_2$m}-cyclenH$_2$](PF$_6$)$_5$ (**7**; Lys = lysine, bipy = 2,2′-bipyridyl, m = 4-carbonyl-4′-methyl-2,2′-bipyridyl, cyclen = 1,4,7,10-tetraazacyclododecane) has been synthesized. A modular approach was taken which involves only standard amide-coupling methods well-known from peptide synthesis. Compound **7** is readily soluble in water. It contains a luminescent ruthenium chromophore and a cyclen ligand which serves as a binding site for metal ions. The emission of **7** is pH-independent but efficiently quenched by Cu^{2+} ions in a pH range of 6–7. Copper(II) binding is reversible upon protonation of the ligand at pH values below 6. In contrast, no significant spectral changes are observed with Zn^{2+} and Ni^{2+}, respectively. Thus, **7** selectively recognizes copper(II) in aqueous solution under slightly acidic to neutral conditions. Unfortunately, applications at higher pH values are limited by metal-promoted hydrolysis of **7** under mildly basic conditions.

Introduction

Amino acids with nonnatural functional groups are versatile building blocks for the design of new peptides and synthetic proteins.[1−5] A particularly well-developed field in this research area is the incorporation of organic,[6,7] and inorganic[8−11] chromophores in biologically relevant molecules. However, chromophore-labeled peptides are not only useful as mechanistic probes of the reactivity and physical properties of biomolecules. Interesting applications as chemosensors for zinc(II) ions have been reported by the groups of Berg[12] and Imperiali.[13−15] Sensors generally consist of a signaling unit, a spacer, and a recognition unit.[16] Amino acid building blocks are perfectly suited for such a multicomponent design. They can easily be processed by standard peptide coupling methods and thereby offer excellent perspectives for the combinatorial optimization of each component.

Polypyridyl ruthenium-modified amino acids are well established as useful chromophores in photoredoxactive proteins,[8−11] peptides,[17,18] and chromophore-donor-acceptor triads.[19,20] Long lifetimes, a large Stokes shift of the emission spectra, and solubility in water are the particular benefits of [Ru(bipy)]$_3$ derivatives in luminescence spectroscopic investigations. We have recently studied the pH-dependent luminescence properties of ruthenium-modified amino acids in much detail.[21,22] Our results show that [Ru(bipy)$_2$m]$^{2+}$-substituted lysine (**8**; bipy = 2,2′-bipyridyl; m = 4-carbonyl-4′-methyl-2,2′-bipyridyl) is an ideal chromophore-spacer unit for the synthesis of pH-independent emitter-receptor conjugates. The butylamine side chain is long enough to prevent electronic coupling between the site of protonation and the chromophore. As a consequence, the [Ru(bipy)$_2$m]$^{2+}$-based emission spectrum is independent of the H^+ concentration above pH = 2. On the other hand, luminescence quenching is readily observed upon binding of a [Cu(phen)]$^{2+}$ fragment to the amino acid group.[23]

Several studies have described metal-ion-induced luminescence quenching in [Ru(bipy)$_3$]$^{2+}$ conjugates with a cyclam (cyclam = 1,4,8,11-tetraazacyclotetradecane) receptor.[24−27] However, cyclam traps divalent first row transition metal ions irreversibly. To the best of our knowledge, only one report exists on the use of a [Ru(bipy)$_3$]$^{2+}$ unit in a water soluble emitter-receptor conjugate which reversibly binds to copper(II) and nickel(II) ions.[28] The receptor in this study was dioxo-2,3,2-tet ligand (2,3,2-tet = 1,9-diamino-3,7-diazanonane-4,6-dione). It has also been reported that the binding of metal ions by cyclam derivatives can be tuned to be reversible by the introduction of two weakly coordinating amide functions in the macrocycle.[29] Another possibility should be the appropriate tuning of the ring size. Cyclen (cyclen = 1,4,7,10-tetraazacyclododecane) is too small to accommodate divalent metal ions such as Ni^{2+}, Cu^{2+}, or Zn^{2+} within the ring plane.[30,31] Conjugates of cyclen with naphthyl[32,33] and dansyl[34] chromophores have been synthesized as receptors for divalent metal ions

[a] Institute of Inorganic Chemistry, University of Erlangen, Egerlandstr. 1, 91058 Erlangen, Germany
Fax: (internat.) +49-9131/852-7387
E-mail: Alsfasser@chemie.uni-erlangen.de
[b] Institute of Organic Chemistry, University of Regensburg, 93040 Regensburg, Germany

 © WILEY-VCH Verlag GmbH, 69451 Weinheim, 2001 1434−1948/01/0606−1543 $ 17.50+.50/0

such as Zn^{2+} and Cd^{2+}. Its zinc(II) complexes have also been described as recognition units for nucleobases[35,36] and phenothiazine.[37]

Here we present the synthesis of the copper-selective emitter-receptor conjugate **7**, which consists of a tris(2,2′-bipyridyl)ruthenium(II) chromophore, an amide-substituted cyclen ligand as the metal ion receptor, and a lysine spacer. Compound **7** is water soluble, does not respond to pH changes and selectively binds copper(II) ions at pH 6−7 in the presence of zinc(II) and nickel(II) ions, respectively. The paper discusses advantages such as solubility, selectivity and reversibility, and severe limitations due to the relatively low stability of **7** at higher pH values in the presence of metal ions.

Results

Synthesis of 7 and its Reaction with $Zn(ClO_4)_2 \cdot 6\ H_2O$

Our preparation of **7** involves only well-known, straightforward methods developed for peptide synthesis. Details are shown in Scheme 1. The first step is the dicyclohexylcarbodiimide (DCC)/*N*-hydroxybenzotriazole (HOBt) supported coupling of orthogonally diprotected N_α-*tert*-butoxycarbonyl-N_ε-benzoxycarbonyl-lysine [Boc-Lys(*Z*)-OH, **1**] with 1,4,7-tri-*tert*-butoxycarbonylcyclen (**2**). This reaction produces the tertiary amide Boc-Lys(*Z*)-Boc_3Cyclen (**3**) with yields of over 90% after purification by reversed phase HPLC. Catalytic hydrogenation of **3** results in selective deprotection of its ε-amino function. The resulting free amine **4** is then reacted with the succinimide ester [Ru(bipy)$_2$(m-OSu)]$(PF_6)_2$ (**5**;[17] m = 4-carbonyl-4′-methyl-2,2′-bipyridyl; HOSu = *N*-hydroxysuccinimide). Finally, the coupling product **6** is treated with HCl in dioxane in order to remove the four *tert*-butoxycarbonyl protecting groups. The resulting complex **7** is conveniently purified by cation-exchange chromatography and obtained in its triprotonated form as the pentakis(hexafluorophosphate) salt. Reasonably good overall yields of ca. 50% with respect to Boc-Lys(*Z*)-OH (**1**) are obtained.

Only the first coupling product Boc-Lys(*Z*)-$(Boc)_3$Cyclen (**3**) and the final product [H-Lys{Ru(bipy)$_2$m}-cyclenH_2]$(PF_6)_5$ (**7**) were isolated and purified by HPLC (**3**), and ion-exchange (**7**) column chromatography. All other compounds, including [Ru(bipy)$_2$(m-OSu)]$(PF_6)_2$, were conveniently generated in situ or used as crude products without purification. Characterization was mainly achieved by FD- and FAB-mass spectrometry as well as by ^{1}H NMR spectroscopy.

We have studied the reaction of **7** with $Zn(ClO_4)_2 \cdot 6H_2O$ in methanol solution containing three equivalents of sodium methoxide as a base. However, the tertiary amide connecting the cyclen unit to the amino acid moiety of **7** is not stable under the reaction conditions, as shown in Scheme 2. The bond is cleaved and the ruthenium-modified amino acid [H-Lys{Ru(bipy)$_2$m}(OH)]$(PF_6)_3$ (**8**) can be isolated by ion-exchange chromatography with yields of ca. 70%. This finding has prompted us to study the pH-dependent luminescence properties of **7** alone and in the presence of different metal ions in order to learn more about the stability of the compound in solution.

Luminescence Titrations

Luminescence pH Titrations of 7 and 7-$M(ClO_4)_2$ (M = Mn^{2+}, Fe^{2+}, Co^{2+}, Ni^{2+}, Cu^{2+}, Zn^{2+})

Luminescence spectra as a function of pH were collected for solutions containing **7**, and stoichiometric amounts of **7** and a perchlorate salt $M(ClO_4)_2$ (M = Mn^{2+}, Fe^{2+}, Co^{2+}, Ni^{2+}, Cu^{2+}, Zn^{2+}). Plots of the maximum emission intensities versus pH for **7**, and **7**-$M(ClO_4)_2$ (M = Ni^{2+}, Cu^{2+}), are shown in Figure 1. The emission spectra of the free ligand **7** are almost invariant over the whole pH range. Only a shallow minimum is observed at about pH 9.5 which is insignificant within the experimental error. Interestingly, a more pronounced minimum at the same pH value is observed in the presence of nickel(II). However, the intensity change is still rather small (less than 20%). Manganese(II), iron(II), cobalt(II), and zinc(II) ions did not result in pH-dependent emission quenching. These curves are not shown since they do not differ significantly from that of the free complex **7**.

This is dramatically different for copper(II), which efficiently quenches the ruthenium-based emission at pH 6.8. The pH titration curve shows a distinct minimum at this value. Above pH 7 the emission intensities increase to approach their full maximum at about pH 9. This is due to the rapid cleavage of the tertiary amide bond at higher pH values as is evident from back titration of the basic solution with hydrochloric acid. The luminescence intensity remains at its maximum when the pH is decreased from 12 to 6, as expected for the emission properties of [H-Lys{Ru(bipy)$_2$m}(OH)]$^{3+}$ (**8**).[21] Figure 2 shows the pseudo first order kinetics of the cleavage reaction at pH 6.8 [k_{obs} = (1.96 ± 0.06) × 10^{-4} min^{-1}] and pH 9 [k_{obs} = (1.035 ± 0.009) × 10^{-2} min^{-1}].

Binding of copper(II) by **7** is reversible upon protonation of the macrocycle. This is clearly demonstrated by Figure 3. Starting at pH 2 the emission intensity decreases to reach its minimum at pH 6.8. Back titration from pH 7 to pH 2 results in complete recovery of the original maximum. The cycle is almost reversible as is shown by its repetition. Small deviations are due to the slight decomposition of **7**-Cu-$(ClO_4)_2$ at about pH 7.

Titration of 7 with $M(ClO_4)_2 \cdot 6H_2O$ (M = Ni^{2+}, Cu^{2+}, Zn^{2+}) at Neutral pH

Buffered aqueous solutions (pH 6.8) of the ruthenium(II) complex **7** were titrated with aqueous solutions of nickel(II), copper(II), and zinc(II) perchlorate. The titration curves were followed by emission spectroscopy. Figure 4a contains plots of the maximum intensities as a function of the number of metal diperchlorate equivalents added. The complete spectra obtained at different $Cu(ClO_4)_2$ concentrations are shown in Figure 4b. It is clear from the titration curves that only addition of copper(II) results in a signific-

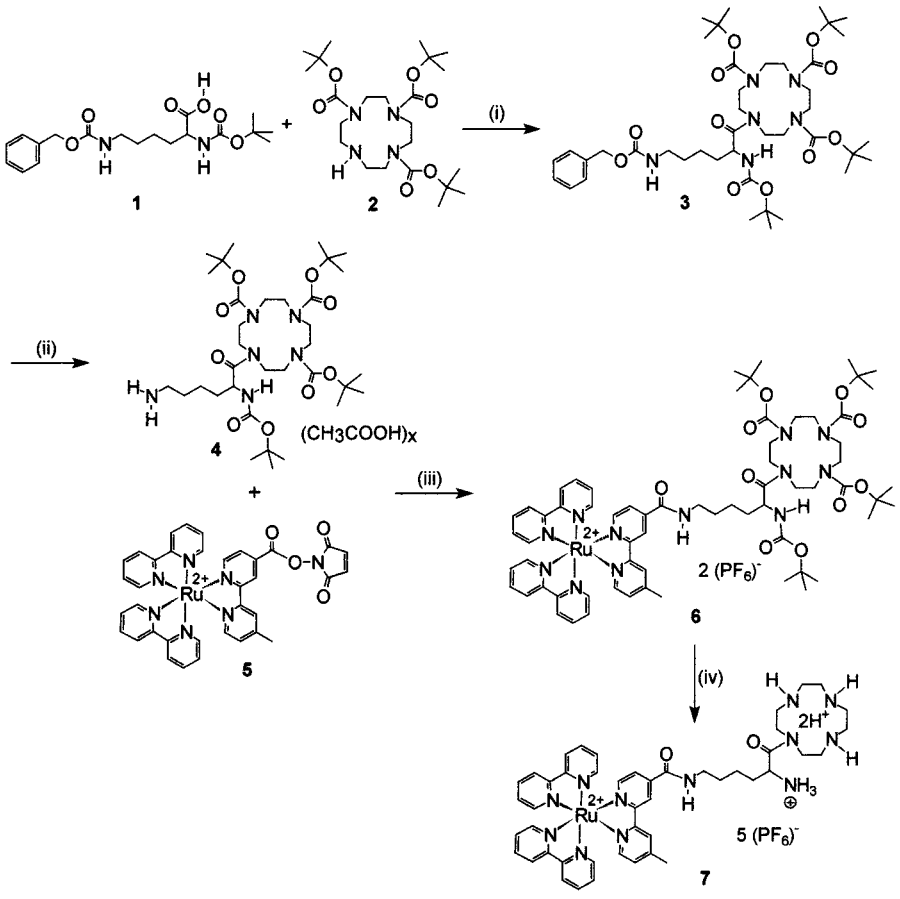

Scheme 1. Synthesis of the $[Ru(bipy)_2m]^{2+}$ labeled cyclen ligand **7**; (i) DCC, HOBt, NEt_3, CH_2Cl_2, 4 °C; (ii) H_2, Pd/C, CH_3COOH, MeOH, 40 °C; (iii) NEt_3, CH_3CN; (iv) HCl, dioxane

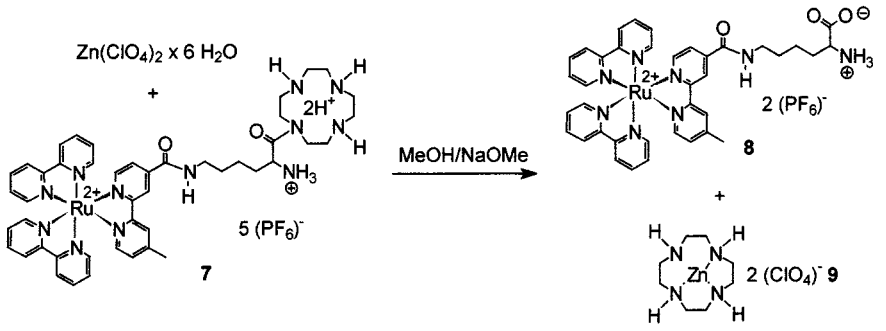

Scheme 2. Reaction of **7** with $Zn(CF_3SO_3)_2$

ant quenching of the ruthenium-based emission. The formation of a 1:1 complex is evident both from the sharp kink in the titration curve, as well as from the Jobs plot shown in Figure 5.[39] The observed deviations from the expected values are mainly due to experimental errors caused by the low metal ion concentrations (10^{-5} M). From several repetitions we estimate the accuracy of our data to be ±0.5 intensity units for the emission spectra, ±0.25 for $x(Cu^{2+})\cdot\Delta I_{Em}$ (Jobs Plot), and ±5% for the equivalents of copper(II) added in the titration experiments. Note that the latter error contains a contribution due to the ruthenium complex concentration. Corresponding error bars are added to both Figure 4b and Figure 5. Addition of nickel(II) results in a slight decrease of the emission intensity which does not reach saturation even in the presence of a more than threefold excess of the perchlorate salt. Finally, zinc(II) does not change the emission properties of the chromophore.

We have investigated the selectivity of metal binding processes involving the cyclen receptor by addition of one equivalent of copper(II) perchlorate to buffered solutions (pH 6.8) containing **7** and a 10-fold excess of zinc(II) and nickel(II) perchlorate. In both cases the emission is quenched equally well as in the absence of competing cations. Copper(II) ions obviously bind much more strongly to the macrocyclic ligand than either nickel(II) or zinc(II) ions.

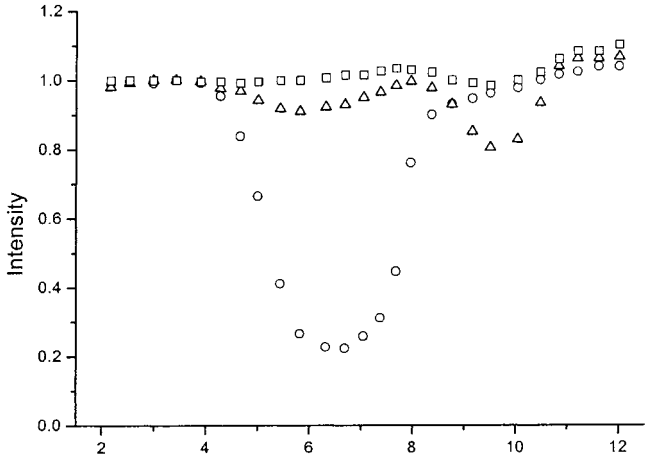

Figure 1. pH-dependent maximum emission intensities of **7** alone (□), and in the presence of one equivalent of nickel (△) and copper (○) perchlorate

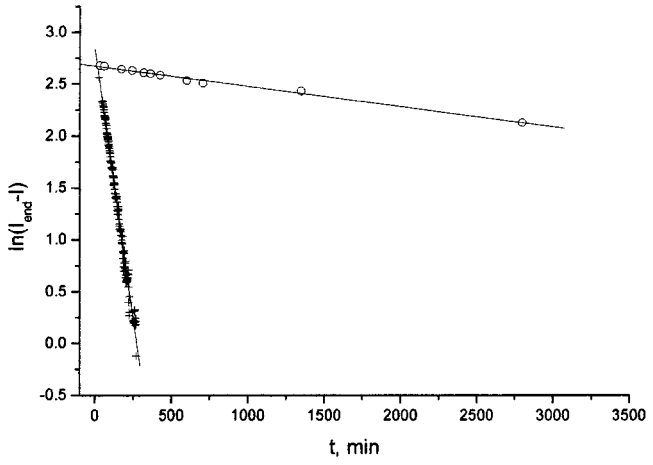

Figure 2. Kinetic plots for the cleavage reaction of **7** in the presence of one equivalent $Cu(ClO_4)$ at pH 6 (O) and pH 9 (+)

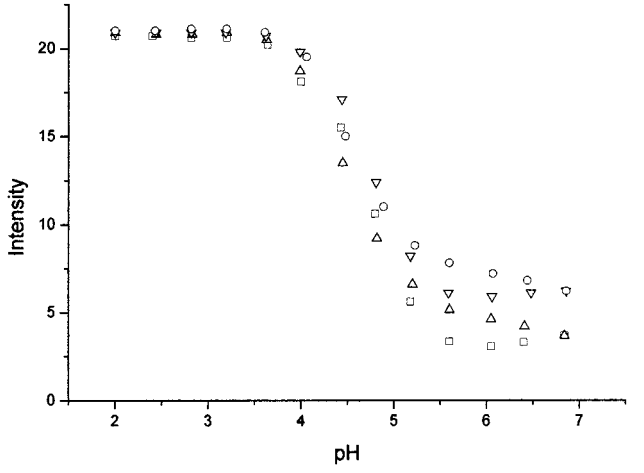

Figure 3. Luminescence pH titration of **7** in the presence of one equivalent of $Cu(ClO_4)_2 \cdot 6H_2O$; 1st cycle from pH 2 to pH 7 (□), then back to pH 2 (Δ); 2nd cycle from pH 2 to pH 7 (▽), then back to pH 2 (O)

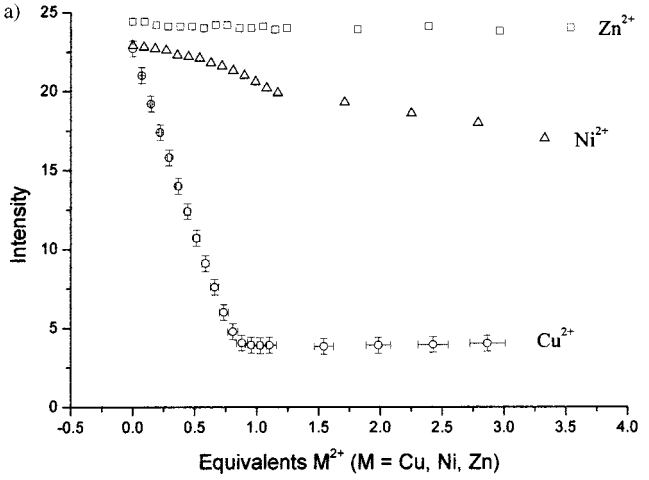

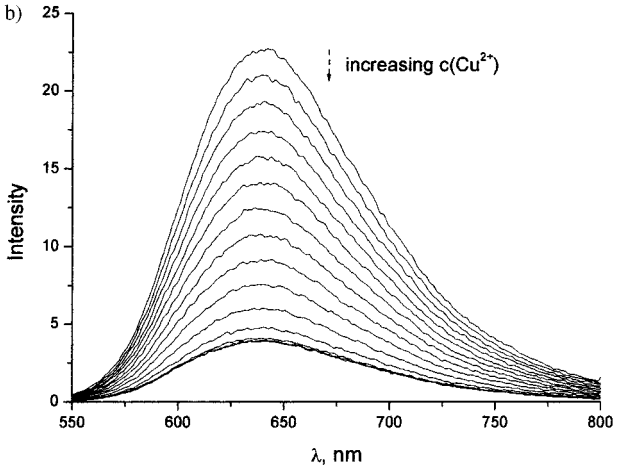

Figure 4. a) Emission titration curves for the reactions of **7** with $M(ClO_4)_2 \cdot 6H_2O$ (M = Ni, Δ; Cu, O; Zn, □) at pH 6.8 (maximum intensities are given with respect to the free ligand at pH 2); b) uncorrected luminescence spectra obtained during the titration of **7** with $Cu(ClO_4)_2 \cdot 6H_2O$

Discussion

The strategy described in Scheme 1 provides a facile route to chromophore-labeled polyamine ligands. Starting from a commercially available amino acid derivative only standard amide coupling methods are involved. We think that this scheme will be generally useful for the synthesis of related compounds with a variety of different chromophores and recognition units. However, a major drawback of the key compound **7** described in this paper is the insufficient stability of its tertiary amide function which couples the amino acid to the cyclen ligand. This amide bond is readily cleaved in the presence of metal ions even at neutral pH. The lability of tertiary amides with respect to transition metal-promoted solvolysis reactions is well-known in the literature. Our rate constant observed at pH 6.8 compares well with that reported by Sayre et al. for the copper-catalyzed hydrolysis of picolinylsarcosine.[40]

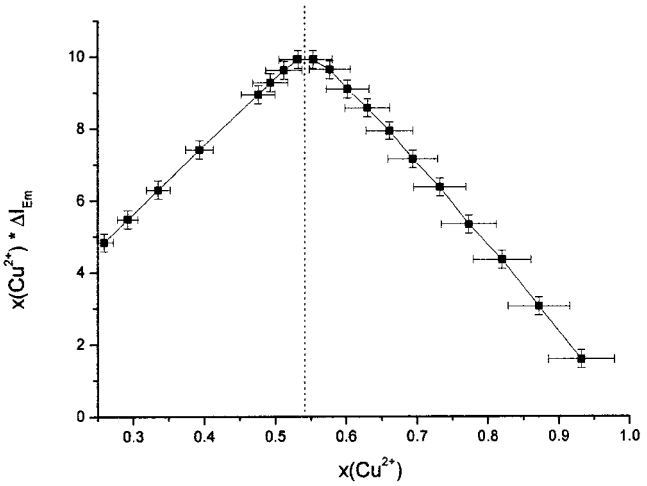

Figure 5. Plot of $x(Cu^{2+})\cdot\Delta I_{Em}$ vs. $x(Cu^{2+})$ [Jobs plot; $x(Cu^{2+})$ = mol fraction of Cu^{2+} in solution; $\Delta I_{Em} = I_{0Em} - I_{xEm}$, with I_{0Em} = emission intensity of **7** without Cu^{2+}, and I_{xEm} = emission intensity after addition of $x(Cu^{2+})$] for the titration of **7** with $Cu(ClO_4)_2\cdot 6H_2O$; a value of x = ca. 0.5 for the intercept of the two straight lines indicates a 1:1 stoichiometry of the complex formed

It is somewhat surprising that amide bond cleavage in **7**-$Cu(ClO_4)_2$ occurs at neutral pH. A similar tertiary amide linkage has been used to connect a zinc cyclen complex to a phenothiazine unit and this compound has been successfully applied in riboflavin recognition studies at pH 7.4.[37] At this time, we cannot offer a proven explanation for the instability of **7**. We suggest that the α-amino group of the lysine spacer may participate in metal ion binding and thereby cause a steric strain at the amide function. In any case, it will certainly be advantageous for our approach to use secondary rather than tertiary amides as coupling functions in future.

On the other hand, the presence of the tertiary amide group is probably beneficial for the metal ion recognition properties of **7**. The poorly electron donating amide is part of the macrocyclic ring and decreases the donor strength of the cyclen unit. Fabbrizzi et al. have demonstrated that neither selectivity nor reversibility can be achieved with a receptor ligand if its binding constants for different metal ions are too high. The lower stability of dioxocyclam complexes compared to cyclam complexes is a prerequisite for the design of copper-selective recognition units.[29] In our case, a second effect reduces the binding constants for metal coordination to the receptor. The cyclen ring is too small to accommodate nickel(II), copper(II), or zinc(II) ions within the ring plane.[30,31] Thus, its stabilizing macrocyclic effect is lower than that of cyclam.

Both features, the reduced electron donor properties and the small ring size, are important for the preference of our cyclen receptor unit for copper(II) over both nickel(II) and zinc(II) ions. As we have mentioned above, the other important prerequisite for an ion-selective recognition unit is the reversibility of the binding process.[29] Compound **7** satisfies both requirements, selectivity and reversibility, as is shown by the complexation-decomplexation cycles shown in Figure 4.

Finally, the properties of the signaling unit are of crucial importance for the performance of a metal-ion-selective emitter-receptor conjugate. Ruthenium chromophores are readily soluble in water which is certainly an advantage over organic compounds.[24] However, their luminescence signals are not as strong as those of, for example, anthracene derivatives.[31−45] Though this may cause some limitations regarding the detection limit, quenching by copper(II) ions is highly efficient in our system providing a sufficiently large effect for measurements at submicromolar concentration levels. Furthermore, the emission spectrum of **7** responds only to the addition of copper(II) ions. Other copper-selective emitter-receptor conjugates exhibit efficient emission quenching also by protons and/or nickel(II) ions in the absence of Cu^{2+}.[24,28,29,46] Most relevant for our study, it has been reported in the literature that the ruthenium-based emission of $[Ru(bipy)_3]^{2+}$-labeled cyclam ligands is readily quenched by nickel(II) ions.[24−28] We observe only a very small effect of Ni^{2+} on the luminescence of **6** at neutral pH. The results of Fabrizzi et al. indicate that Ni^{2+} may bind to the receptor at higher pH values than Cu^{2+}.[29,46] Unfortunately, we cannot access this basic pH range due to the instability of compound **7** in the presence of metal ions. It is therefore not clear whether nickel(II) does not efficiently quench the emission of the signaling unit or if the binding constant is simply not high enough in the accessible pH range. The absence of a signal induced by protonation of the macrocycle is an intended feature of our design. We have shown earlier that the lysine side chain is long enough to efficiently prevent inductive effects of protonated amine functions which modulate the photophysical properties of a ruthenium complex.[21] Consequently, the emission properties of **7** are pH independent in the absence of metal ions.

Conclusions

In our study we have used a commercially available amino acid for the synthesis of the metal ion selective emitter-receptor conjugate **7**. Desirable properties of this compound are its solubility in water, its high selectivity for copper(II) ions at almost neutral pH values between 6 and 7, and the reversibility of the recognition process upon protonation of the cyclen receptor unit. A serious drawback of **7** is its chemical lability in the presence of metal ions under mild basic conditions. This obstacle can most likely be overcome by the use of receptor ligands which bear primary amines as the coupling functions. Current research in our laboratories focuses on this aspect.

Experimental Section

Materials and Methods: The synthesis of $(Boc)_3$cyclen (**2**) has been described elsewhere.[47] $[Ru(bipy)_2(m\text{-}OH)]$ (m-OH = 4-carbonly-4′-methyl-2,2′-bipyridine) was prepared according to a published procedure by Erickson et al.[17] The synthesis of $[Ru(bipy)_2(m\text{-}OSu)](PF_6)_2$ (m-OSu = 4-carboxysuccinimidoester-4′-methyl-2,2′-bipyridine) described in the same report[17] was slightly modified.

$RuCl_3$ was a donation from Degussa. Absolute and reagent grade solvents were obtained from Fluka, NMR solvents from Aldrich and all other chemicals from Fluka. Water for preparations was demineralized. All reactions were carried out under argon.
Spectra were recorded with the following instruments: UV/Vis: Shimadzu UV-2101PC. − IR (KBr pellets): Mattson Polaris FT IR. − ^{1}H NMR: Bruker Avance DPX 300. All chemical shifts are referenced to residual solvent signals as internal standards previously referenced to TMS, with high-frequency shifts recorded as positive. − Elemental analysis: Carlo Erba EA 1106. − FAB: Micromass ZabSpec mass spectrometer. − Luminescence Spectra: Emission titration curves were followed by uncorrected luminescence spectra obtained with a Perkin−Elmer LS 50B spectrophotometer (λ_{exc} = 450 nm; λ_{obs} = 550−800 nm).

Boc-Lys(*Z*)-(Boc)$_3$cyclen (3): Boc-Lys(*Z*)-OH (**1**; 0.45 g, 1.18 mmol), (Boc)$_3$cyclen (**2**; 0.56 g, 1.18 mmol), HOBt (0.17 g, 1.26 mmol), and triethylamine (0.34 mL, 2.40 mmol) were dissolved in 50 mL of dichloromethane. The solution was cooled in an ice/water bath to 4 °C and dicyclohexylcarbodiimide (0.42 g, 2.02 mmol) was added with stirring. A suspension formed which was allowed to warm to room temperature overnight. The solid dicyclohexylurea was removed by filtration and the filtrate subsequently washed with 2 × 20 mL of 0.50 M $NaHCO_3$, 2 × 20 mL 0.05 M of citric acid, 25 mL of saturated NaCl, and 15 mL of water. The organic layer was dried over $MgSO_4$, filtered and evaporated to dryness. Purification was achieved by semipreparative isocratic reversed-phase HPLC (Kontron HPLC Pump 422) on a C18 ODS column (Grom-Sil 80 ODS-2 2FE 5µ, 250 × 20 mm) with acetonitrile as the eluent (7 mL/min.). The product eluted as the second fraction and was obtained as a colorless solid after removal of the solvent and drying under vacuum. Yield: 0.90 g (1.07 mmol, 91%). − FD-MS (CH_2Cl_2): *m*/*z* = 836 [M^+]. − ^{1}H NMR (300 MHz, CD_2Cl_2): δ = 1.65 (m, 6 H, $^{\beta,\gamma,\delta}CH_2$), 2.58 (s, 3 H, m4′-$CH_3$), 3.30 (m, 16 H, 8 × cyclen-CH_2, $^{\varepsilon}CH_2$), 4.12 (m, 2 H, CH_2Ph), 4.39 (m, 1 H, $^{\alpha}CH$) 7.24 (m, 5 H, Ph).

Boc-Lys-(Boc)$_3$cyclen·CH_3COOH (4): Boc-Lys(*Z*)-(Boc$_3$)cyclen (0.90 mg, 1.07 mmol) was dissolved in 20 mL of methanol. Catalytic amounts of Pd/C and a 1.1-fold excess of acetic acid were added. A slow stream of H_2 was passed over the stirred solution for 2 h at 40 °C. The catalyst was then filtered off, all solvent removed by rotary evaporation and the remaining colorless solid dried under vacuum overnight. The crude product was characterized by FD-mass spectrometry and used without further purification. − FD-MS (CH_2Cl_2): *m*/*z* = 702 [HM^+].

[H-Lys{Ru(bipy)$_2$}-cyclenH$_2$](PF$_6$)$_5$ (7): [Ru(bipy)$_2$(m-OH)](PF$_6$)$_2$ (**5**; 0.92 g, 1.00 mmol) and HOSu (0.13 g, 1.10 mmol) were dissolved in 5 mL of absolute CH_3CN. The solution was cooled to 4 °C in an ice/water bath, DCC (0.43 mg, 2.10 mmol) was added and the resulting suspension stirred for 5 h. This mixture was filtered directly into a solution containing triethylamine (0.30 mL, 2.10 mmol) and all of the crude Boc-Lys-(Boc)$_3$cyclen (**4**) obtained as described above in 20 mL of CH_3CN. The resulting red solution was stirred for 1.5 h at 41 °C. After removal of all solvent under vacuum the solid residue was treated with 10 mL of a 4 M HCl/dioxane solution in order to cleave the Boc protecting groups. Deprotection was complete after stirring the mixture for 1 h at 0 °C. The solvent was removed by rotary evaporation and the residual red solid dried overnight under vacuum. The crude product was redissolved in 100 mL of water, neutralized with a 2.0 M NaOH solution, and applied to an ion exchange chromatography column (Sephadex CM-50) using a NaCl gradient in a 0.6 mM phosphate buffer (pH 7.2) solution. The product eluted as the second fraction with 0.25 M NaCl. All solvent was removed by rotary evaporation and the residue dried under vacuum. Most of the excess NaCl was removed by extraction of the orange solid with a minimum of absolute MeOH and subsequent filtration. The filtrate was evaporated to dryness and the product redissolved in 10 mL of water. Slow addition of 1 mL aqueous NH_4PF_6 (1.22 g, 7.50 mmol) resulted in precipitation of the product. The suspension was stirred for 1 h, the orange solid collected on a sintered glass filter funnel, washed with 3 × 5 mL of a cold 10 mM aqueous NH_4PF_6 solution, and dried over silica in a vacuum desiccator. Yield: 1.00 g (0.61 mmol, 61%). − $C_{46}H_{59}F_{30}N_{12}O_2P_5Ru·2H_2O$ (1637.95): calcd. C 32.99, H 3.79, N 10.04; found C 32.87, H 3.93, N 10.25. − FAB-MS (nitrobenzyl alcohol): *m*/*z* = 1347 [M^+ − 2HPF$_6$], 1201 [M^+ − 3HPF$_6$], 1055 [M^+ − 4HPF$_6$]. − ^{1}H NMR (300 MHz, CD_3OD): δ = 1.34 (m, 42 H, $^{\beta,\gamma,\delta}CH_2$, 4 × Boc), 3.23 (br. m, 16 H, 7 × cyclen-CH_2, $^{\varepsilon}CH_2$), 3.93 (m, 1 H, cyclen), 4.20 (m, 1 H, cyclen), 4.35 (m, 1 H, $^{\alpha}CH$), 7.33 (d, 1 H, m5‘), 7.46 (m, 4 H, 4 × b5), 7.60 (d, 1 H, m5), 7.84 (m, 6 H, 4 × b6, m6′, m6), 8.08 (m, 4 H, 4 × b4), 8.64 (m, 5 H, 4 × b3, m3′), 8.94 (s, 1 H, m3). − IR (KBr): $\tilde{\nu}$ = 3110 (m, 3079 (m), 2945 (m), 1637 (m), 1541 (m), 1460 (m), 1445 (m), 1241 (m), 1162 (m), 841 (vs, PF_6^-), 765 (s), 558 (s) cm^{-1}. − UV/Vis (MeOH): λ [nm] (ε, [M^{-1} cm^{-1}]) = 255 (27500), 289 (89500), 456 (15500).

Reaction of [H-Lys{Ru(bipy)$_2$m}-cyclenH$_2$](PF$_6$)$_5$ (7) with Zn(CF$_3$SO$_3$)$_2$: Compound **7** (0.42 g, 0.25 mmol) was dissolved in 20 mL of methanol and 15.5 mL of a 1.5 mM NaOMe/methanol solution. Solid $Zn(CF_3SO_3)_2$ (0.10 g, 0.27 mmol) was added in one portion and the solution stirred for 1 h under reflux conditions. The solvent was removed by rotary evaporation, the red solid residue dried under vacuum and redissolved in a minimum amount of water. A solution of NH_4PF_6 (0.02 g, 0.38 mmol) in 1 mL H_2O was added dropwise resulting in the precipitation of an orange solid. This was collected on a sintered glass filter funnel and dried under vacuum. ^{1}H NMR spectroscopy of the crude product indicated the presence of a complex product mixture. The solid was redissolved in water and applied to an ion exchange chromatography column using the conditions described above. A red band eluted with 50 mM NaCl and the product was isolated following the procedure described for **7**. The compound was identified by ^{1}H NMR spectroscopy and FAB mass spectrometry to be the ruthenium-substituted amino acid [H-Lys{Ru(bipy)$_2$m}-OH](PF$_6$)$_3$ (**8**; yield: 0.21 g, 69%) which has been reported earlier.[21]

Luminescence pH Titrations of 7 and [H-Lys{Ru(bipy)$_2$m}-cyclenM]$^{5+}$ [7-M(ClO$_4$)$_2$; M = Ni^{2+}, Cu^{2+}]: An aquarium pump, a three-neck round bottom flask equipped with a pH electrode, and a luminescence cuvette were connected by Teflon tubes. The flask was charged with an aqueous solution which was 10 µM both in **7** and the respective metal perchlorate salt. This solution was deaerated by bubbling with N_2 for 15 min. and continuously cycled through the apparatus. A slow stream of N_2 was passed through the solution in the flask throughout the measurement. The pH was adjusted with HCl and NaOH solutions. Luminescence spectra were measured after a period of cycling of 5 min. at each pH value.

Kinetics of the Amide Bond Cleavage in the Presence of Cu(ClO$_4$)$_2$·6H$_2$O at pH 6.8 and 9: A 10 µM solution of **7** in an aqueous phosphate buffer (pH 6.8), and a 10 mM solution of copper perchlorate hexahydrate in water were prepared. The ruthenium complex solution was deaerated by bubbling with N_2 for 15 min. through a syringe needle in a fluorescence cuvette which was sealed by a rubber septum. One equivalent of $Cu(ClO_4)_2$ was added and the time-dependent uncorrected luminescence intensity followed at a single emission wavelength of 645 nm (λ_{max}; λ_{exc} = 450 nm). For

the measurement at pH 9, the reaction mixture was also prepared at pH 6.8 and NaOH added to adjust to the new pH after a period of 15 min. This procedure is required to assure complete complex formation. If the reactants are mixed at pH 9, immediate formation of copper hydroxide results in a long induction period which obscures the kinetics.

Luminescence Titration of 7 with $M(ClO_4)_2 \cdot 6H_2O$ ($M = Ni^{2+}$, Cu^{2+}, Zn^{2+}) at pH 6.8: A 10 μM solution of **7** in an aqueous phosphate buffer (pH 6.8), and a 10 mM solution of the respective perchlorate salt in water were prepared. The ruthenium complex solution was deaerated by bubbling with N_2 for 15 min. through a syringe needle in a fluorescence cuvette which was sealed by a rubber septum. This solution was titrated with the respective metal perchlorate salt solution in 0.1 equiv. steps. After addition of 1 equiv. titration was continued in 0.4 equiv. steps. The titration curve was followed by luminescence spectroscopy. The solution was purged with N_2 for 5 min. prior to each measurement.

Detection of Cu^{2+} in the Presence of Ni^{2+} and Zn^{2+}: A 10 μM solution of **7** in an aqueous phosphate buffer (pH 6.8) was prepared. A 10 mM solution of $M(ClO_4)_2 \cdot 6H_2O$ (M = Ni, Zn) was added to adjust the M^{2+} concentration to 10 μM (Ni) or 100 μM (Zn). Luminescence spectra were measured after bubbling the resulting solution with Ar for 15 min. One equivalent of a 0.01 M $Cu(ClO_4)_2 \cdot 6H_2O$ solution was then added and luminescence spectra measured again after 15 min. of bubbling with Ar.

Acknowledgments

The authors gratefully acknowledge financial support from the Deutsche Forschungsgemeinschaft. We also thank Prof. Rudi van Eldik for his generous support.

[1] N. Voyer, J. Lamothe, *Tetrahedron* **1995**, *51*, 9241−9284.
[2] N. Voyer, *Top. Curr. Chem.* **1996**, *184*, 1−37.
[3] M. J. O′Donnell, C. Y. Zhou, W. L. Scott, *J. Am. Chem. Soc.* **1996**, *118*, 6070−6071.
[4] T. Carell, J. Butenandt, *Angew. Chem.* **1997**, *109*, 1590−1593; *Angew. Chem. Int. Ed. Engl.* **1997**, *36*, 1461−1464.
[5] B. Imperiali, R. S. Roy, *J. Am. Chem. Soc.* **1994**, *116*, 12083−12084.
[6] G. Hungerford, M. Martinez-Insua, D. J. S. Birch, B. D. Moore, *Angew. Chem.* **1996**, *108*, 356−359; *Angew. Chem. Int. Ed. Engl.* **1996**, *35*, 326−329.
[7] T. Hohsaka, D. Kajihara, Y. Ashizuka, H. Murakami, M. Sisido, *J. Am. Chem. Soc.* **1999**, *121*, 34−40.
[8] H. B. Gray, J. R. Winkler, *Annu. Rev. Biochem.* **1996**, *65*, 537−561.
[9] I. Hamachi, H. Takashima, S. Tsukiji, S. Shinkai, T. Nagamune, S. Oishi, *Chem. Lett.* **1999**, 551−552.
[10] I. Hamachi, S. Tsukiji, S. Shinkai, S. Oishi, *J. Am. Chem. Soc.* **1999**, *121*, 5500−5506.
[11] A. Polese, S. Mondini, A. Bianco, C. Toniolo, G. Scorrano, D. M. Guldi, M. Maggini, *J. Am. Chem. Soc.* **1999**, *121*, 3446−3452.
[12] H. A. Godwin, J. M. Berg, *J. Am. Chem. Soc.* **1996**, *118*, 6514−6515.
[13] A. Torrado, B. Imperiali, *J. Org. Chem.* **1996**, *61*, 8940−8948.
[14] G. K. Walkup, B. Imperiali, *J. Am. Chem. Soc.* **1996**, *118*, 3053−3054.
[15] G. K. Walkup, B. Imperiali, *J. Am. Chem. Soc.* **1997**, *119*, 3443−3450.
[16] L. Fabbrizzi, A. Poggi, *Chem. Soc. Rev.* **1995**, *24*, 197−202.
[17] B. M. Peek, G. T. Ross, S. W. Edwards, G. J. Meyer, T. J. Meyer, B. W. Erickson, *Int. J. Pept. Protein Res.* **1991**, *38*, 114−123.
[18] D. G. McCafferty, B. M. Bishop, C. G. Wall, S. G. Hughes, S. L. Mecklenburg, T. J. Meyer, B. W. Erickson, *Tetrahedron* **1995**, *51*, 1093−1106.
[19] S. L. Mecklenburg, B. M. Peek, J. R. Schoonover, D. G. McCafferty, C. G. Wall, B. W. Erickson, T. J. Meyer, *J. Am. Chem. Soc.* **1993**, *115*, 5479−5495.
[20] S. L. Mecklenburg, D. G. McCafferty, J. R. Schoonover, B. M. Peek, B. W. Erickson, T. J. Meyer, *Inorg. Chem.* **1994**, *33*, 2974−2983.
[21] B. Geißer, A. Ponce, R. Alsfasser, *Inorg. Chem.* **1999**, *38*, 2030−2037.
[22] B. Geißer, T. Skrivanek, U. Zimmermann, D. J. Stufkens, R. Alsfasser, *Eur. J. Inorg. Chem.* **2001**, 439−448.
[23] B. Geißer, R. Alsfasser, *Eur. J. Inorg. Chem.* **1998**, 957−963.
[24] E. Kimura, X. Bu, M. Shionoya, S. Wada, S. Maruyama, *Inorg. Chem.* **1992**, *31*, 4542−4546.
[25] S. C. Rawle, P. Moore, N. W. Alcock, *J. Chem. Soc., Chem. Commun.* **1992**, 684−687.
[26] E. Fujita, B. S. Brunschwig, T. Ogata, S. Yanagida, *Coord. Chem. Rev.* **1994**, *132*, 195−200.
[27] A. M. Josceanu, P. Moore, S. C. Rawle, P. Sheldon, S. M. Smith, *Inorg. Chim. Acta* **1995**, *240*, 159−168.
[28] F. Bolletta, I. Costa, L. Fabbrizzi, M. Licchelli, M. Montalti, P. Pallavicini, L. Prodi, N. Zaccheroni, *J. Chem. Soc., Dalton Trans.* **1999**, 1381−1385.
[29] L. Fabbrizzi, M. Licchelli, P. Pallavicini, A. Perotti, A. Taglietti, D. Sacchi, *Chem. Eur. J.* **1996**, *2*, 75−82.
[30] R. M. Clay, P. M. Rust, J. M. Rust, *Acta Crystallogr.* **1979**, *35*, 335.
[31] R. Smierciak, J. Passariello, E. L. Blinn, *Inorg. Chem.* **1977**, *16*, 2646.
[32] D. Parker, J. A. G. Williams, J. Chem. Soc., *Perkin Trans. 2* **1995**, 1305−1314.
[33] A. Beeby, D. Parker, J. A. G. Williams, J. Chem. Soc., *Perkin Trans. 2* **1996**, 1565−1579.
[34] T. Koike, T. Watanabe, S. Aoki, E. Kimura, M. Shiro, *J. Am. Chem. Soc.* **1996**, *118*, 12696−12703.
[35] E. Kimura, M. Kikuchi, H. Kitamura, T. Koike, *Chem. Eur. J.* **1999**, *5*, 3113−3123.
[36] E. Kikuta, M. Murata, N. Katsube, T. Koike, E. Kimura, *J. Am. Chem. Soc.* **1999**, *121*, 5426−5436.
[37] B. König, M. Pelka, H. Zieg, T. Ritter, H. Bouaslaurent, R. Bonneau, J. P. Desvergne, *J. Am. Chem. Soc.* **1999**, *121*, 1681−1687.
[38] G. De Santis, L. Fabbrizzi, M. Licchelli, A. Poggi, A. Taglietti, *Angew. Chem. Int. Ed. Engl.* **1996**, *35*, 202−204; *Angew. Chem.* **1996**, *108*, 224−227.
[39] K. A. Connors, *Binding Constants*, Wiley, New York, **1987**.
[40] L. M. Sayre, K. V. Reddy, A. R. Jacobson, W. Tang, *Inorg. Chem.* **1992**, *31*, 935−937.
[41] G. De Santis, L. Fabbrizzi, M. Licchelli, C. Mangano, D. Sacchi, *Inorg. Chem.* **1995**, *34*, 3581−3582.
[42] G. De Santis, L. Fabbrizzi, M. Licchelli, C. Mangano, D. Sacchi, N. Sardone, *Inorg. Chim. Acta* **1997**, *257*, 69−76.
[43] R. Krämer, *Angew. Chem. Int. Ed.* **1998**, *37*, 772−773.
[44] R. Bergonzi, L. Fabbrizzi, M. Licchelli, C. Mangano, *Coord. Chem. Rev.* **1998**, *170*, 31−46.
[45] V. Amendola, L. Fabbrizzi, M. Licchelli, C. Mangano, P. Pallavicini, L. Parodi, A. Poggi, *Coord. Chem. Rev.* **1999**, *192*, 649−669.
[46] L. Fabbrizzi, M. Licchelli, L. Parodi, A. Poggi, A. Taglietti, *Eur. J. Inorg. Chem.* **1999**, 35−39.
[47] S. Brandes, C. D. F. Gros, R. Grilaud, *Bull. Soc. Chim. Fr.* **1996**, *133*, 3068−3076.

Received September 27, 2000
[I00365]

Novel Diazamesocyclic Ligands Functionalized with Pyridyl Donor Group(s) – Synthesis, Crystal Structures, and Properties of Their Copper(II) Complexes

Xian-He Bu,*[a] Miao Du,[a] Zhi-Liang Shang,[a] Lei Zhang,[a] Qi-Hua Zhao,[a] Ruo-Hua Zhang,[b] and Mitsuhiko Shionoya[c]

Keywords: Diazamesocyclic ligands / Copper(II) complexes / Crystal structures / Magnetic properties

Two novel diazamesocyclic ligands based on 1,5-diazacyclooctane (DACO) and functionalized with additional pyridyl donor groups, namely 1,5-bis(2-pyridylmethyl)-1,5-diazacyclooctane (**L¹**) and 1-(2-pyridylmethyl)-1,5-diazacyclooctane (**L²**), have been synthesized and characterized, as have their Cu^{II} complexes. Crystal structure analyses revealed that with $Cu(ClO_4)_2$ **L¹** forms a five-coordinate mononuclear complex $[Cu^{II}L^1Cl]ClO_4$ (**1**), whereas **L²** forms a μ-Cl^--bridged dinuclear complex $[Cu^{II}(L^2)Cl]_2(ClO_4)_2$ (**2**). Furthermore, it has been found that the apical chloride anion of **1** may be easily exchanged by azide anion, forming the mononuclear complex $[Cu^{II}L^1(N_3)]ClO_4$ (**3**). There is a notable difference between **3** and **1** in that **3** forms a quasi-two-dimensional network through intermolecular C–H···O hydrogen bonds and π–π stacking interactions. Each Cu^{II} center in the three complexes is pentacoordinated in a distorted square-pyramidal environment and the DACO ring of each ligand adopts a boat-chair configuration in all the complexes. In the mononuclear complexes **1** and **3**, the Cl^- or N_3^- anions occupy the apical sites, whereas in the dinuclear complex **2** the two bridging Cl^- anions occupy both axial positions as well as one equatorial position, leading to an intramolecular Cu···Cu separation of 3.396 Å. Variable-temperature magnetic susceptibility measurements on **2** in the range 4–300 K indicate a weak intramolecular ferromagnetic coupling between adjacent Cu^{II} centers with $2J = 2.28\ cm^{-1}$; the magneto-structural correlations are discussed in detail. The solution behavior of the complexes has been further studied by UV/vis and ESR techniques.

Introduction

Macrocyclic polyamines bearing functional groups and transition metal complexes thereof have been extensively studied in order to investigate the effects of the functional pendants on the coordination modes and properties of these complexes.[1] Mesocyclic diamines such as 1,5-diazacyclooctane (DACO), functionalized with pendant groups, can form stable metal complexes with unique conformational requirements,[2,3] and the coordinating abilities of such ligands can be adjusted through altering the donor groups on their skeletons.[4] This interesting chemistry prompted our investigation of DACO, in which we introduced functional donor groups on its backbone and examined the coordinating functionality of various pendant donors in relation to the structures and properties of the relevant metal complexes. Furthermore, the study of DACO derivatives and their metal complexes has been an active area of research owing to their use in analytical and biomimetic applications, in the stabilization of high oxidation states of some metal ions, in selective ion recognition, and as a result of their catalytic activities.[5]

[a] Department of Chemistry, Nankai University, Tianjin 300071, P. R. China
Fax: (internat.) + 86-22/2353-0850
E-mail: buxh@nankai.edu.cn
[b] State Key Lab on Coordination Chemistry, Nanjing University, Nanjing 210093, P. R. China
[c] Department of Chemistry, Graduate School of Science, The University of Tokyo, Hongo, Tokyo 113−0033, Japan

Dinuclear Cu^{II} complexes play an important role in the elucidation of spin-coupling or magnetic-exchange phenomena between paramagnetic metal centers. They exemplify the simplest case where two unpaired electrons on two paramagnetic ions are separated by spacer ligands that may intramolecularly mediate the stabilization of a singlet. Several experimental and theoretical investigations have been carried out aimed at elucidating the structures and magnetic properties of bis(μ-chloro)-bridged Cu^{II} dimers, and different magnetic behavior ranging from ferro- to antiferromagnetic interactions has been found in these systems.[6] However, great difficulties remain in establishing a magneto-structural correlation for these complexes since they show pronounced Jahn−Teller distortion. Consequently, further investigations into the magneto-structural correlation of chloro-bridged Cu^{II} dinuclear complexes would seem necessary.

We report herein the synthesis of two new ligands based on DACO bearing one and two pyridine donor groups, respectively, as well as their Cu^{II} complexes (see Scheme 1). These tetra- and tridentate ligands form stable mononuclear and dinuclear complexes with Cu^{II}, the crystal structures of which have been elucidated by X-ray diffraction analysis. The magneto-structural correlations of **2** and the solution behavior of these Cu^{II} complexes have also been studied.

Results and Discussion

Syntheses and General Characterizations

The doubly-substituted ligand **L¹** was prepared by using an excess of 2-chloromethylpyridine hydrochloride, while an

 © WILEY-VCH Verlag GmbH, 69451 Weinheim, 2001 1434−1948/01/0606−1551 $ 17.50+.50/0

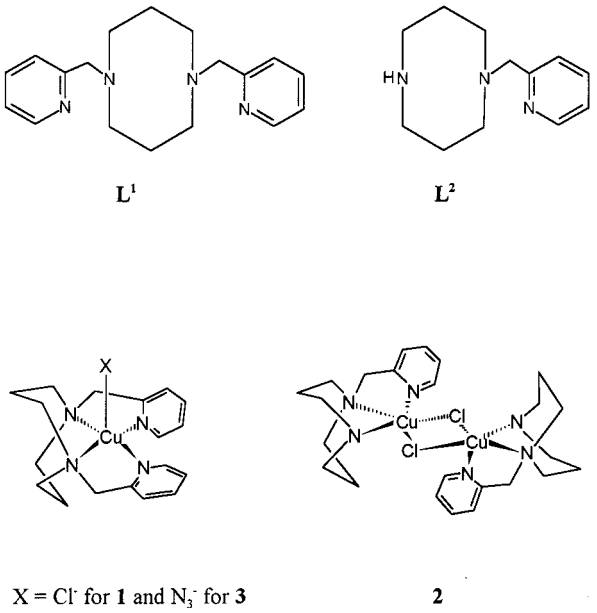

Scheme 1

excess of DACO was used to obtain the monoalkylated product $\mathbf{L^2}$; both ligands were purified by column chromatography on silica gel. Acid-free $\mathbf{L^1}$ and $\mathbf{L^2}$ could only be obtained as oils, hence they were converted into their HCl salts to obtain crystalline solids. The yields of both syntheses were in excess of 65% and all analytical data were in good agreement with the theoretical requirements of the two ligands.

The syntheses of **1** and **2** were accomplished by reacting the respective ligands with $Cu(ClO_4)_2{\cdot}6H_2O$. Since the ligands were handled as their HCl salts, they first had to be neutralized with aqueous NaOH solution prior to complexation. Electrical conductance values in methanol solution indicated that **1** and **3** behave as 1:1 electrolytes, while **2** acts as a 2:1 electrolyte,[7] these findings being consistent with the crystal structural analyses. The IR spectra of the three complexes show absorption bands resulting from the skeletal vibrations of the pyridine rings in the region 1400−1600 cm^{-1}. The absorption bands due to ClO_4^- appear at 1098−1082 and 623−621 cm^{-1} for all three complexes. In addition, **3** exhibits three strong absorption bands at 2125, 2031, and 1098 cm^{-1} due to the ν_{N-N} stretch of the apical azide anion.

X-ray Crystal Structures of Complexes 1−3

The crystal structure of **1** showing the atom numbering scheme is depicted in Figure 1. The structure consists of a discrete $[Cu\mathbf{L^1}Cl]^+$ cation and a perchlorate anion. The Cu^{II} center is coordinated by two pyridine nitrogen atoms and a pair of nitrogen donors of the DACO ring. A chloride anion completes the coordination polyhedron around the central metal ion. The Cu^{II} ion is pentacoordinated (CuN_4Cl) and the coordination polyhedron can best be described as a distorted square-pyramid with the chloride anion occupying the axial position. The Cu^{II} ion lies 0.425 Å above the basal least-squares plane defined by N(1), N(2), N(16), and N(26), in the direction of the apical Cl(1) anion, and the dihedral angle between the two pyridine rings is 36.1°. The ligand adopts a typical boat/chair configuration and with the central Cu^{II} ion forms two five-membered coordination rings N(1)−C(10)−C(11)−N(16)−Cu and N(2)−C(20)−C(21)−N(26)−Cu, resulting in an N(1)−Cu−N(16) angle of 79.8° and an N(1)−Cu−N(16) angle of 84.5°.

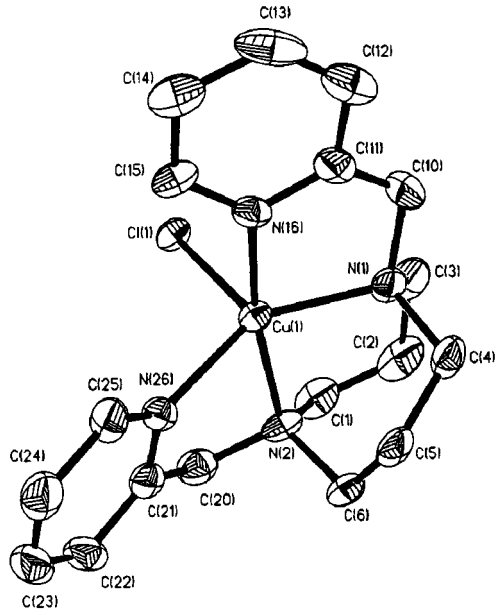

Figure 1. ORTEP view of **1** with thermal ellipsoids drawn at a 35% probability level

The two $Cu-N_{DACO}$ bond lengths are approximately equal (2.032 vs. 2.056 Å), both being normal Cu−N coordination bonds,[8] but the Cu−N(16) (pyridine) bond length is significantly shorter than the Cu−N(26) (pyridine) distance (1.991 vs. 2.113 Å), probably due to the steric interaction of the two pyridine groups.

The apical Cu−Cl(1) coordination bond measures 2.424 Å, which is close to the values reported for some similar complexes.[9,10] The weakly coordinated Cl^- anion may be easily exchanged by other donor molecules or ions, hence the complex may have potential application in homogeneous catalysis or as a functional building block for the construction of larger functional architectures. We have successfully modified this complex by axial ligand exchange of chloride with azide, thereby generating **3**.

The crystal structure of **3** is shown in Figure 2(a); the coordination environment of the central Cu^{II} ion can be seen to be very similar to that in **1**. The Cu^{II} ion lies 0.424 Å above the mean basal plane defined by N(1), N(2), N(3), and N(4), in the direction of the apical N(5) atom. The dihedral angle between the two pendant pyridine rings is 27.7°, which is smaller than that in **1**, probably as a result of the less severe distortion of the coordination geometry about the central Cu^{II} ion. The $Cu-N_{DACO}$ bond lengths (2.041 vs. 2.075 Å) are close to the value found in **1** while, in contrast to **1**, the $Cu-N_{py}$ bond lengths are approximately the same (2.075 vs. 2.114 Å).

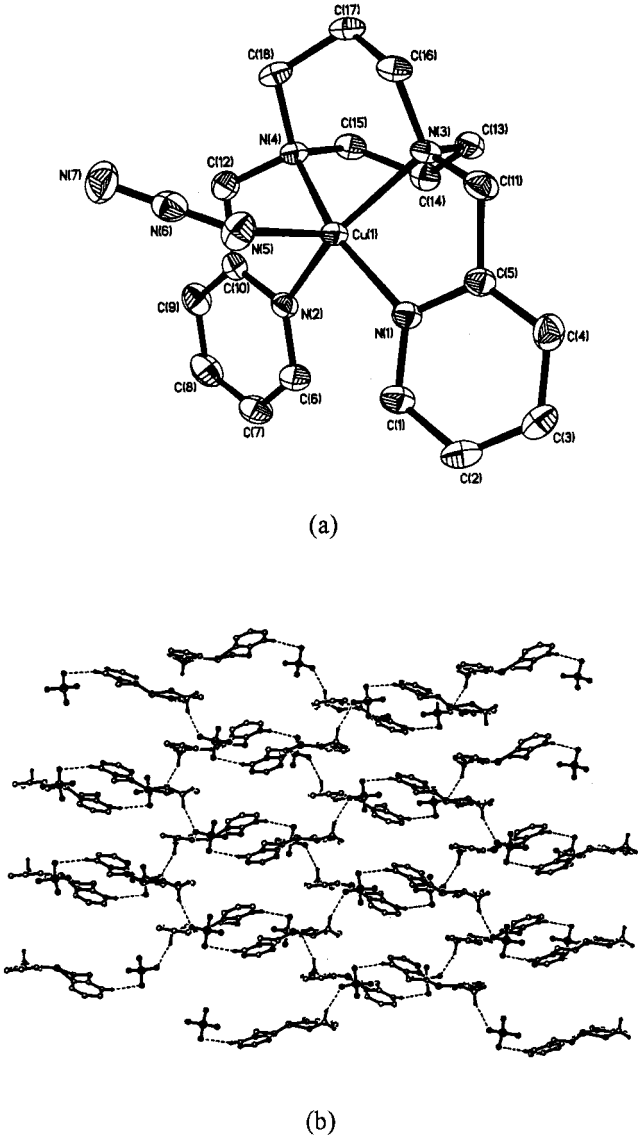

Figure 2. (a) ORTEP view of **3** with thermal ellipsoids drawn at a 30% probability level; (b) view of the two-dimensional network in **3** along the *b* axis; the methylene groups of the DACO ring and irrelevant hydrogen atoms have been omitted for clarity

Selected bond lengths and angles relevant to the Cu^{II} coordination spheres in both **1** and **3** are listed in Table 1. The stereo geometries of both of the five-coordinate (CuN_4X) complexes are distorted square-pyramids, as reflected in their τ values (0.38 and 0.29, respectively) defined by Addison et al. (τ = 0 for an ideal square-pyramid, τ = 1 for an ideal trigonal-bipyramid).[11] In both complexes, $\mathbf{L^1}$ acts as a tetradentate chelating agent. The coordination geometry around Cu^{II} is made up by a pair of nitrogen atoms of the DACO ring and the two nitrogen donors of the pyridine pendants, which occupy *cis* positions in the coordination polyhedron. In both complexes, the DACO ring of the ligand adopts a "boat/chair" configuration and is bent such that the central methylene C−H group of the boat form of the metalladiazacyclohexane ring shields the metal center with a H···Cu distance of 2.565 Å in **1** (2.555 Å in **3**) and a H−Cu−apex angle of 11.9° in **1** (7.9° in **3**). Thus, this methylene hydrogen effectively blocks the sixth coordination position, resulting in the observed five-coordinate metal complexes[4c] (see Scheme 2). The distances between the nitrogen atoms of the DACO ring are restricted to a narrow range with $N_{DACO}-Cu-N'_{DACO}$ angles of 87.2° and 86.7° in the two complexes. The $N_{py}-Cu-N'_{py}$ angles are also restricted within narrow limits (100.8° and 101.8°), due to the steric requirements of the ligand.

Table 1. Selected bond lengths [Å] and angles [°] in **1** and **3** (H* is the hydrogen of the central methylene group nearest to the Cu^{II} center in the boat forms of the metalladiazacyclohexane rings)

Complex **1**			
Cu−Cl(1)	2.424(2)	Cu−N(1)	2.056(7)
Cu−N(2)	2.032(6)	Cu−N(16)	1.991(6)
Cu−N(26)	2.113(6)	Cu···H*	2.565
N(2)−Cu(1)−N(16)	166.5(2)	N(1)−Cu(1)−N(26)	143.7(3)
N(1)−Cu(1)−N(2)	87.2(3)	N(16)−Cu(1)−N(26)	100.8(2)
N(2)−Cu(1)−N(26)	79.8(2)	N(1)−Cu(1)−N(16)	84.5(3)
H−Cu−apex	11.9		
Complex 3			
Cu(1)−N(1)	2.025(2)	Cu(1)−N(4)	2.041(2)
Cu(1)−N(3)	2.075(2)	Cu(1)−N(5)	2.106(3)
Cu(1)−N(2)	2.114(2)	N(6)−N(7)	1.170(3)
N(6)−N(5)	1.174(3)	Cu···H*	2.555
N(1)−Cu(1)−N(3)	83.05(8)	N(4)−Cu(1)−N(2)	80.13(8)
N(4)−Cu(1)−N(3)	86.68(8)	N(1)−Cu(1)−N(2)	101.75(8)
N(3)−Cu(1)−N(2)	146.21(8)	N(1)−Cu(1)−N(4)	163.82(8)
N(7)−N(6)−N(5)	179.5(3)	H−Cu−apex	7.9

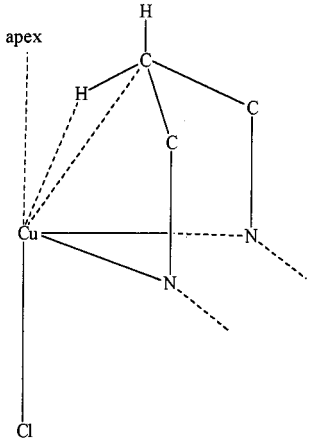

Scheme 2

The most notable difference between **3** and **1** is the ability of **3** to form a quasi-two-dimensional supramolecular network through weak intermolecular C−H···O hydrogen bonds and π−π stacking interactions. This is illustrated in Figure 2(b). The hydrogen atoms of the pyridine ring and of the methylene group connected to the pyridine ring of another adjacent molecule in the cation unit $[Cu\mathbf{L^1}(N_3)]^+$ are activated by the positive charge that arises due to the coordination of the N atoms to the Cu^{II} center. Each perchlorate anion acts as a hydrogen-bond acceptor from two

adjacent $[Cu\mathbf{L^1}(N_3)]^+$ cations, giving a one-dimensional infinite zigzag chain in the lattice. The C···O separations are 3.461 and 3.397 Å, with H···O separations of 2.561 and 2.484 Å. The C···O separations fall within the range of 3.0−4.0 Å suggested by Desiraju et al.,[12] while the bond angles of 161.5 and 163.4° are quite close to 180°. The Cu···Cu intermolecular distance between adjacent chains is 7.54 Å. Furthermore, the H-bonded chains are cross-linked in the unit cell. Two nearest pyridine planes, lying almost parallel to one another between the neighboring chains, show an average interfacial distance of 3.667 Å, indicating significant π-π stacking interactions.[13] As a result of these two types of weak intermolecular interaction, the $[Cu\mathbf{L^1}(N_3)]ClO_4$ molecules are self-assembled into a quasi-two-dimensional network in this complex.

An ORTEP representation of **2**, showing the atom numbering scheme, is depicted in Figure 3, while selected bond lengths and angles are listed in Table 2. The complex consists of a discrete $[Cu\mathbf{L^2}Cl]_2^{2+}$ cation and two perchlorate anions. In the $[Cu\mathbf{L^2}Cl]_2^{2+}$ cation, the two Cu^{II} centers are symmetrically bridged by two chloride anions. Each Cu^{II} ion is bound by $\mathbf{L^1}$ through one nitrogen atom of the pyridyl pendant group and two nitrogen donors of the DACO ring, which again adopts a "boat/chair" configuration. The two bridging chloride anions complete the coordination polyhedron around each Cu^{II} ion. The Cu^{II} ions are pentacoordinated (CuN_3Cl_2) and the coordination polyhedron around Cu^{II} may best be described as a distorted square-pyramid with $\tau = 0.34$.[11] The Cu^{II} ion lies 0.28 Å above the mean basal plane formed by N(1), N(2), N(11), and Cl(1a), in the direction of the apical Cl^- anion, and the axial Cu(1)−Cl(1) distance is ca. 0.29 Å longer than the Cu(1)−Cl(1a) bond length in the basal plane (2.581 vs. 2.291 Å).

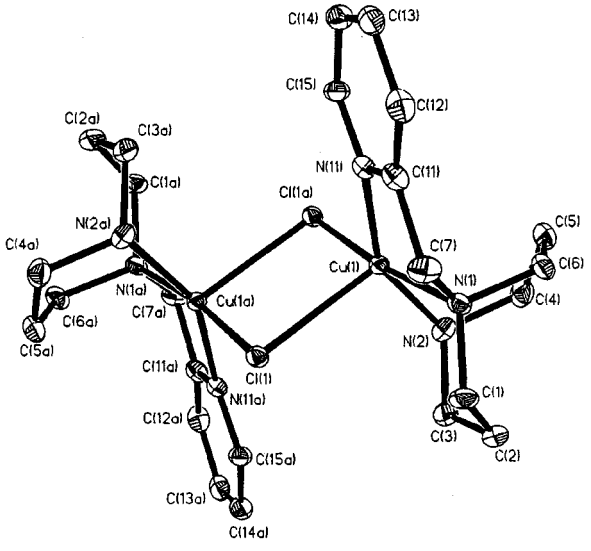

Figure 3. ORTEP representation of **2** with thermal ellipsoids drawn at a 35% probability level

The Cu^{II} centers and chloride anions form a rhombic plane with the angles Cl(1)−Cu(1)−Cl(1a) and Cu(1)−Cl(1)−Cu(1a) measuring 91.8° and 88.2°, respectively. The two intramolecular Cu^{II} centers in **2** have the same coordination configuration and structure. All the Cu−N and Cu−Cl bond lengths fall into the expected ranges for normal coordination bonds,[14] while the shortest Cu···Cu nonbonding length in the dimer is 3.396 Å.

Table 2. Selected bond lengths [Å] and angles [°] in **2**

Bond lengths [Å]			
Cu(1)−Cl(1)	2.581(1)	Cu(1)−N(1)	2.038(4)
Cu(1)−N(2)	2.007(5)	Cu(1)−N(11)	2.020(4)
Cu(1)−Cl(1a)	2.291(1)	Cu···H*	2.507
Bond angles [°]			
Cl(1)−Cu(1)−N(1)	95.2(1)	Cl(1)−Cu(1)−N(2)	105.3(1)
N(1)−Cu(1)−N(2)	86.5(2)	Cl(1)−Cu(1)−N(11)	100.4(1)
N(1)−Cu(1)−N(11)	82.2(2)	N(2)−Cu(1)−N(11)	152.7(2)
Cl(1)−Cu(1)−Cl(1a)	91.8(1)	N(1)−Cu(1)−Cl(1a)	173.0(1)
N(2)−Cu(1)−Cl(1a)	91.4(1)	N(11)−Cu(1)−Cl(1a)	96.8(1)
Cu(1)−Cl(1)−Cu(1a)	88.2(1)	H−Cu−apex	13.45

Electronic and ESR Spectra

The UV/vis spectra of the three complexes in methanol solution show absorption maxima at 621, 622, and 618 nm, respectively, which is in agreement with the absorptions seen for other five-coordinated Cu^{II} complexes with similar coordination geometries. The absorption bands of **1** and **2** display a slightly higher λ_{max} than that of **3**, suggesting that their coordination geometries are more distorted toward trigonal-bipyramid;[15] this is consistent with the degrees of distortion found in the X-ray structural analyses. This spectral feature is typical of pentacoordinated Cu^{II} complexes with distorted square-pyramidal geometry, which generally exhibit a band in the 550−660 nm range (d_{xz}, $d_{yz} \rightarrow d_{x^2-y^2}$).[15,16] In addition, the electronic spectra of all the complexes feature a characteristic absorption at about 260 nm attributable to a ligand $\pi \rightarrow \pi^*$ transition.

The X-band ESR spectra of **1** were measured in the polycrystalline state and in methanol solution, at room temperature and at 110 K. The following ESR parameters were obtained for polycrystalline powdered **1** at room temperature: $g_z = 2.21$, $g_y = 2.10$, and $g_x = 2.04$. The resolution did not improve very much upon cooling to 110 K, with parameters of $g_z = 2.26$, $g_y = 2.15$, and $g_x = 2.09$. Nevertheless, the spectra at 110 K did show some small splitting lines, probably due to the hyperfine splitting of the coordinated nitrogen donors. The g values conform to the relationship: $g_{\|} > g_{\perp} > g_e$, which indicates that the unpaired 3d electron of the Cu^{II} ion should occupy the $d_{x^2-y^2}$ orbital and a predominantly tetragonal component in the solid-state stereochemistry.[17] The different values of g_x and g_y for **1** imply that the Cu^{II} ground-state wavefunction is not pure $d_{x^2-y^2}$, but that it contains some contribution from d_{z^2} as a result of the decreased symmetry of the coordination polyhedron, which is consistent with the crystal structure data. The room-temperature solution spectra show hyperfine splitting lines characteristic of Cu^{II} complexes, as was also observed for a frozen solution of **1**. The approximate

ESR parameters obtained were: $g_{iso} = 2.11$ ($A_{iso} = 74$ G), $g_{\|} = 2.23$ ($A_{\|} = 94$ G), and $g_{\perp} = 2.05$ ($A_{\perp} = 64$ G), where $g_{\perp} = (3g_{iso} - g_{\|})/2$ and $A_{\perp} = (3A_{iso} - A_{\|})/2$.[18] The values again conform to the relationship $g_{\|} > g_{\perp} > g_e$, with a smaller $A_{\|}$ value, indicating some distortion of the coordination geometry about the Cu^{II} center from square-pyramidal in solution,[19] which is similar to the geometry observed in the solid state.

The X-band ESR spectrum of **2** in the solid state at room temperature shows isotropic character with $g_{av} = 2.10$, possibly as a result of exchange narrowing. No absorption is observed at half-field ($\Delta m_s = 2$, $g = 4$), indicating a small ZFS effect.[20] The spectrum of a frozen solution of **2** in methanol likewise exhibits only a quasi-isotropic feature, and the g value (2.10) is essentially the same as that of the polycrystalline sample. This indicates that there is no significant change in the coordination environment under the two sets of conditions.

Magnetic Properties

The magnetic behavior of **2** is shown in Figure 4 as the variation of χ_M (μ_{eff}) versus temperature. The molar magnetic susceptibility of the dinuclear Cu^{II} unit increases with decreasing temperature. However, the effective magnetic moment increases very smoothly on lowering the temperature down to 14 K and finally decreases rapidly at even lower temperatures. This behavior indicates the existence of an intradimer *ferromagnetic exchange interaction*. The experimental data were least-squares fitted to the analytical expression given as Equation (1), according to the modified Bleaney−Bowers model for a Cu^{II} dimer.[21] Here, all the symbols have their usual meanings; ρ is the percentage of non-coupled impurity and $N\alpha$ is the temperature-independent paramagnetism. The following parameters were obtained: $2J = 2.28$ cm^{-1}, $\rho = 0.005$, and $g = 2.12$, which is in good agreement with the average g value deduced from the ESR spectra. The agreement factor R [defined as $\Sigma(\chi_{obs} - \chi_{calc})^2/\Sigma(\chi_{obs})^2$] is equal to 2.0×10^{-5}.

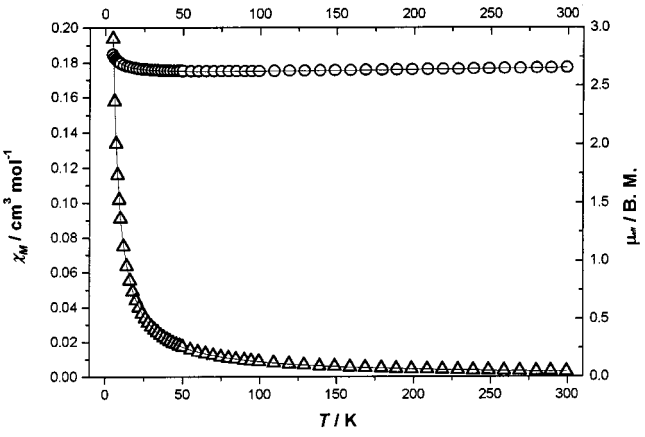

Figure 4. Magnetic coupling diagram of the μ-Cl^--bridged binuclear complex **2**

$$\chi_M = (2Ng^2\beta^2/KT)[3 + \exp(-2J/KT)]^{-1}(1 - \rho) + Ng^2\beta^2\rho/2KT + N\alpha \quad (1)$$

In order to discuss the relationship between the magnitude of the exchange constant and the structural parameters in distorted square-pyramidal coordinated Cu^{II} dimers with bis(μ-chloro) bridges, we have compiled the structural and magnetic parameters of several such Cu^{II} dimers in Table 3.

In **2**, the spin density lies in the parallel planes and the magnetic orbital is almost orthogonal, indicating that the overlap is very small, and this leads to the observed weak magnetic exchange interaction. Hatfield and co-workers[22] have shown that antiferromagnetic interactions are observed when the value of the quotient φ/R (°/Å) is lower than 32.6 or higher than 34.8, whereas ferromagnetic interactions are observed for quotient values falling between these limits. For **2**, the quotient value is 34.17°, falling just within the aforementioned limits, hence the ferromagnetic interaction may be satisfactorily understood. In Cu^{II} complexes, strict orthogonality does not occur,[23] and the ferromagnetic interaction is due to accidental orthogonality of the magnetic orbital involved and/or a polarization effect. In **2**, the π orbitals of the Cl(1) anion interact with the Cu(1) magnetic orbital; electron delocalization from the π orbital into the $d_{x^2-y^2}$ orbital of Cu(1) deposits some unpaired spin density of the same net orientation as that on Cu(1) onto the bridging Cl(1) anion. Therefore, coupling of the unpaired spins in the orthogonal orbitals, π and $d_{x^2-y^2}$ of Cu(2), leads to the triplet ground state.[24] According to the equation $J = J_F + J_{AF}$,[25] where $J_F = 2C$ and $J_{AF} = -2\Delta S$ (C is the two-electron exchange integral, S is the overlap integral, and Δ is the energy separation of the molecular magnetic orbital occupied by the unpaired electrons), J_F is the dominant term for **2**. It is worth noting that the Cu−Cl (equatorial) bond length is a key factor in

Table 3. The structural and magnetic properties of some bis(μ-Cl^-)-bridged Cu^{II} dimeric complexes

Complex	Cu···Cu (Å)	Cu···Cl′ (R/Å)	Cu−Cl−Cu′ (φ/°)	φ/R (°/Å)	$2J$ (cm^{-1})	Ref.
$[Cu(DMGH)Cl_2]_2$	3.445	2.698	88.0	32.62	+6.3	14
$[Cu_2(\mathbf{L^2})_2Cl_2](ClO_4)_2$	3.396	2.581	88.2	34.17	+2.24	this work
$[Cu(Hfsaaep)Cl]_2$	3.825	2.846	95.27	33.47	+0.3	6c
$[Cu(TMSO)Cl_2]_2$	3.737	3.020	88.5	29.30	−17.0	26
$[Cu(TMEN)Cl_2]$	4.089	3.147	96.8	30.76	−5.6	27
$[Cu(2\text{-pic})_2Cl_2]_2$	4.404	3.364	100.63	29.91	−7.4	25, 28

determining the spin-polarization effect, which governs the magnitude of the magnetic exchange interaction.

Conclusion

The described synthetic procedure provides a convenient access to a new family of macrocyclic species and their metal complexes. The effect of substituents and of the apical anion on the five-coordinated Cu^{II} structural geometry is discussed in detail. A study of the magnetic properties has shown that the main structural factor determining the strength of the magnetic interaction is the value of the quotient (φ/R), but that the influence of the Cu−Cl equatorial and axial distances must also be considered.

Experimental Section

Materials and General Methods: The starting compound, DACO·2HBr, was prepared according to a literature method.[29,30] Other commercially available chemical reagents and solvents were of analytical grade and were purified by standard procedures prior to use. − FT-IR spectra were recorded on a Nicolet 170SX spectrometer at room temperature. − ^{1}H NMR spectra were recorded on a Bruker AC-P 200 spectrometer (200 MHz) at 25 °C using tetramethylsilane as an internal reference. − Electronic absorption spectra were recorded on a Hitachi UV-3010 spectrophotometer. − Elemental analyses were carried out on a Perkin−Elmer 240C analyzer. − Solution and polycrystalline EPR spectra (X-band) were recorded on a Bruker ER-200-DSRC10 spectrometer.

Syntheses of Ligands: 1,5-Bis(pyrid-2-ylmethyl)-1,5-diazacyclooctane Tetrahydrochloride Monohydrate (L^1·4HCl·H_2O): A suspension of DACO·2HBr (1.76 g, 6.4 mmol) and potassium hydroxide (0.73 g, 12.9 mmol) in anhydrous ethanol (40 mL) was stirred for 4 h at room temperature. A solution of 2-(chloromethyl)pyridine hydrochloride (2.46 g, 15.0 mmol) and triethylamine (2.09 g, 15.0 mmol) in anhydrous ethanol (20 mL) was then added dropwise to the stirred mixture over a period of 2 h. After the addition was complete, additional triethylamine (5 mL) was added and the resulting mixture was stirred for ca. two days at room temperature. The solvent was then removed under reduced pressure, the residue was redissolved in water (15 mL), and the pH of the resulting solution was adjusted to ca. 10 with anhydrous K_2CO_3. The organic phase that separated from the mixture was concentrated in vacuo and the crude product was purified by column chromatography on silica gel (CH_2Cl_2/MeOH/NH_3·H_2O, 10:10:1). The free ligand was obtained as a colorless oil; it was converted to its HCl salt, which was obtained as a white crystalline material (2.06 g, 70% yield based on DACO). − $C_{18}H_{24}N_4$·4HCl·H_2O (460.3): calcd. C 47.0, H 6.57, N 12.2; found C 46.8, H 6.81, N 11.8. − ^{1}H NMR (D_2O): δ = 1.82−1.88 (m, 4 H, $CH_2CH_2CH_2$), 3.18 (t, J = 5.7 Hz, 8 H, NCH_2CH_2), 4.30 (s, 4 H, CH_2-py), 7.84−8.66 (m, 8 H, py). − IR (KBr pellet): $\tilde{\nu}$ = 2986 cm^{-1} w, 2958 m, 1636 vs, 1617 s, 1541 s, 1468 s, 1443 s, 1390 vs, 930 m, 780 vs.

1-(Pyrid-2-ylmethyl)-1,5-diazacyclooctane Trihydrochloride Dihydrate (L^2·3HCl·2H_2O): A solution of DACO·2HBr (8.68 g, 31.7 mmol) and potassium hydroxide (3.30 g, 58.8 mmol) in anhydrous methanol (50 mL) was stirred for 4 h at room temperature. A solution of 2-(chloromethyl)pyridine hydrochloride (1.23 g, 7.5 mmol) in anhydrous ethanol was then added dropwise. The resulting mixture was refluxed for 1 h and then stirred at room temperature for ca. two days. The solvent was subsequently evaporated under reduced pressure, the residue was redissolved in water (20 mL), the pH of the resulting solution was adjusted to ca. 10 with Na_2CO_3, and then it was extracted with $CHCl_3$ (3 × 100 mL). The combined $CHCl_3$ extracts were dried, the solvent was evaporated, and the residue was purified by column chromatography on silica gel eluting with CH_2Cl_2/MeOH/NH_3·H_2O (5:5:1). The free base, obtained as an oil, was dissolved in anhydrous ethanol; passage of HCl gas into this solution gave the salt as an off-white solid (1.7 g, 65% yield based on 2-(chloromethyl)pyridine hydrochloride used). − $C_{12}H_{19}N_3$·3HCl·2H_2O (350.7): calcd. C 41.1, H 7.47, N 12.0; found C 40.8, H 7.69, N 11.8. − ^{1}H NMR (D_2O): δ = 1.90−1.96 (m, 4 H, $CH_2CH_2CH_2$), 3.02 (t, J = 5.7 Hz, 4 H, NCH_2CH_2), 3.24 (t, J = 5.9 Hz, 4 H, NCH_2CH_2), 4.15 (s, 2 H, CH_2-py), 7.77−8.42 (m, 4 H, py). − IR (KBr pellet): $\tilde{\nu}$ = 2953 cm^{-1} m, 1619 vs, 1546 m, 1466 s, 1406 w, 1327 w, 1230 m, 1073 m, 1038 w, 771 s.

Preparation of the Complexes: The mononuclear complex **1**, [CuL^1Cl]ClO_4, was prepared by mixing $Cu(ClO_4)_2$·6H_2O (147 mg, 0.4 mmol) and L^1·4HCl·H_2O (184 mg, 0.4 mmol) in a 1:1 molar ratio in methanol/water solution. The pH of this solution was adjusted to ca. 6−7 with dilute aqueous NaOH solution. The resulting mixture was filtered and the filtrate was left to stand at room temperature. Blue single crystals suitable for X-ray analysis were obtained upon slow evaporation of the solvent. Yield: 119 mg (60%). − $C_{18}H_{24}Cl_2CuN_4O_4$ (494.9): calcd. C 43.7, H 4.89, N 11.1; found C 43.6, H 4.92, N 11.3. − FT-IR (KBr pellet): $\tilde{\nu}$ = 2952 cm^{-1} w, 2905 m, 1609 s, 1569 m, 1484 s, 1449 s, 1091 vs, 623 s. − Λ_M (methanol): 102 cm^2 Ω^{-1} mol^{-1}. − UV/vis: λ_{max}/nm (ε/dm^3 mol^{-1} cm^{-1}) (methanol): 622 (240), 260 (13300).

The dinuclear complex **2**, [CuL^2Cl]$_2$(ClO_4)$_2$, was obtained in a similar manner as described for the preparation of **1** (52%). − $C_{24}H_{38}Cl_4Cu_2N_6O_8$ (807.5): calcd. C 35.7, H 4.74, N 10.4; found C 35.4, H 4.88, N 10.3. − FT-IR (KBr pellet): $\tilde{\nu}$ = 2940 cm^{-1} w, 1610 s, 1573 m, 1481 m, 1454 s, 1082 vs, 1025 s, 621 s. − Λ_M (methanol): 184 cm^2 Ω^{-1} mol^{-1}. − UV/vis: λ_{max}/nm (ε/dm^3 mol^{-1} cm^{-1}) (methanol): 621 (330), 260 (17900).

[CuL^1(N_3)]ClO_4 (**3**), was synthesized by adding excess NaN_3 to a methanolic solution of **1**. The resulting mixture was filtered and the filtrate was left to stand at room temperature. Green single crystals suitable for X-ray analysis were obtained upon slow evaporation of the solvent (38%). − $C_{18}H_{24}ClCuN_7O_4$ (501.4): calcd. C 43.1, H 4.82, N 19.6; found C 42.9, H 4.98, N 19.3. − FT-IR (KBr pellet): $\tilde{\nu}$ = 2950 cm^{-1} m, 2125 s, 2031 vs, 1609 s, 1570 m, 1483 m, 1447 s, 1309 m, 1098 vs, 623 s. − Λ_M (methanol): 99 cm^2 Ω^{-1} mol^{-1}. − UV/vis: λ_{max}/nm (ε/dm^3 mol^{-1} cm^{-1}) (methanol): 618 (274), 263 (11200).

Magnetic Study: Variable-temperature magnetic susceptibility measurements on **2** were made on a SQUID magnetometer in the 5−300 K temperature range. The susceptibilities were corrected for diamagnetism using Pascal's constants for all the constituent atoms, and magnetic moments were calculated from the equation $\mu_{eff} = 2.828(\chi_M T)^{1/2}$.

Crystallographic Study: The reflection data were collected on an Enraf−Nonius CAD-4 X-ray diffractometer (for **1** and **2**) or a Bruker Smart 1000 CCD diffractometer (for **3**) equipped with a graphite crystal monochromator situated in the incident beam. The determination of unit cell parameters and data collections were performed with Mo-K_α radiation (λ = 0.71073 Å). Reflections in the range 4.5 ≤ θ ≤ 25° (for **1** and **2**) and 1.71 ≤ θ ≤ 25.03° (for **3**)

Table 4. Crystallographic data and structure refinement summary for **1**, **2**, and **3**

Complex	**1**	**2**	**3**
Empirical formula	$C_{18}H_{24}Cl_2CuN_4O_4$	$C_{24}H_{38}Cl_4Cu_2N_6O_8$	$C_{18}H_{24}ClCuN_7O_4$
M_r	494.86	807.50	501.43
Crystal size [mm^3]	0.25 × 0.30 × 0.30	0.20 × 0.30 × 0.55	0.15 × 0.30 × 0.40
Space group	$P2_1/n$	$P2_1/c$	$P2_1/n$
Temp. [K]	299(1)	299(1)	293(2)
a [Å]	7.824(2)	7.124(1)	15.5984(17)
b [Å]	22.562(5)	18.700(4)	7.5357(9)
c [Å]	11.840(2)	12.191(2)	17.799(2)
β [°]	94.50(3)	101.12(3)	91.648(2)
V [Å^3]	2084(1)	1594(1)	2091.3(4)
D [g cm^{-3}]	1.570	1.683	1.593
$F(000)$	1020	828	1036
Z	4	2	4
Unique reflections	2603	2086	3679
Observed reflections	1923	1763	3679
Parameters	262	199	280
R[a]	0.064	0.044	0.0316
R_w[b]	0.068	0.051	0.0827
S[c]	1.28	1.02	0.925
Largest diff. peak [e Å^{-3}]	0.51	0.73	0.294

[a] $R = \Sigma(||F_o| - |F_c||/\Sigma|F_o|)$. – [b] $Rw = [\Sigma w(|F_o| - |F_c|)^2/\Sigma wF_o^2]^{1/2}$, $w^{-1} = \sigma^2(F) + 0.0001F^2$ (for complexes **1** and **2**); $Rw = \{\Sigma[w(F_o^2 - F_c^2)^2]/\Sigma w(F_o^2)^2\}^{1/2}$, $w^{-1} = s^2(F_o^2) + (0.0554P)^2 + 0.7119P$, where $P = (F_o^2 + 2F_c^2)/3$ (for complex **3**). – [c] $S = \{\Sigma[w(F_o^2 - F_c^2)^2]/(n - p)\}^{1/2}$, where n = number of reflections measured and p = number of parameters used.

were collected at room temperature. All the structures were solved by direct methods and empirical absorption corrections were applied. Cu^{II} atoms in each complex were located from *E*-maps. All non-hydrogen atoms were determined by successive Fourier syntheses and were refined isotropically. The final refinement was performed by full-matrix least-squares methods against F (for **1** and **2**) or F^2 (for **3**) with anisotropic thermal parameters for non-hydrogen atoms. The hydrogen atoms were placed in theoretical positions as riding on the relevant atoms and were refined with fixed thermal factors. Crystallographic and refinement data for all three complexes are summarized in Table 4. Crystallographic data (excluding structure factors) for the structures reported in this paper have been deposited with the Cambridge Crystallographic Data Centre and allocated the deposition numbers CCDC-150458 (**1**), -150459 (**2**) and -150460 (**3**). Copies of the data may be obtained free of charge on application to the CCDC, 12 Union Road, Cambridge CB2 1EZ, U.K. [Fax: (internat). +44 (0)1223/336033; E-mail: deposit@ccdc.cam.ac.uk].

Acknowledgments

This work was financially supported by the National Natural Science Foundation of China (Grant Nos. 29771022 and 29971019), the Trans-Century Talents Training Program Foundation from the State Education Ministry of China, and the Natural Science Foundation of Tianjin, China.

[1] [1a] E. Kimura, T. Shiota, T. Koike, M. Shiro, M. Kodama, *J. Am. Chem. Soc.* **1990**, *112*, 5805−5811. – [1b] M. A. Halcrow, G. Christou, *Chem. Rev.* **1994**, *94*, 2421−2481 and references therein. – [1c]E. Kimura, T. Koike, M. Shionoya, *Metal Sites in Proteins and Models* (Eds.: H. A. O. Hill, P. Sadler, A. J. Thompson), *Structure and Bonding*, Vol. 89, Springer-Verlag, Berlin, Heidelberg, New York, **1997**, p 1. – [1d]K. P. Wainwright, *Coord. Chem. Rev.* **1997**, *166*, 35−90.

[2] W. K. Musker, *Coord. Chem. Rev.* **1992**, *117*, 133−157.

[3] [3a] J. I. Legg, D. O. Nielson, D. L. Smith, M. L. Larson, *J. Am. Chem. Soc.* **1968**, *90*, 5030−5031. – [3b] D. O. Nielson, M. L. Larson, R. D. Willett, J. I. Legg, *J. Am. Chem. Soc.* **1971**, *93*, 5079−5082. – [3c] D. K. Mills, J. H. Reibenspies, M. Y. Darensbourg, *Inorg. Chem.* **1990**, *29*, 4364−4366.

[4] [4a] X. H. Bu, Y. Y. Fang, Z. L. Shang, R. H. Zhang, *Acta Crystallogr., Sect. C* **1999**, *55*, 39−41. – [4b] X. H. Bu, Z. L. Shang, W. Weng, R. H. Zhang, H. P. Zhu, Q. T. Liu, *Acta Chem. Scand.* **1999**, *53*, 295−297. – [4c] X. H. Bu, M. Du, Z. L. Shang, R. H. Zhang, D. Z. Liao, M. Shionoya, T. Clifford, *Inorg. Chem.* **2000**, *39*, 4190−4199. – [4d] M. Du, Z. L. Shang, Q. Xu, R. H. Zhang, X. B. Leng, X. H. Bu, *Acta Crystallogr., Sect. C* **2000**, *56*, 769−770. – [4e] M. Du, L. H. Weng, X. B. Leng, X. H. Bu, R. H. Zhang, *Acta Crystallogr., Sect. C* **2000**, *56*, 1090−1091. – [4f] M. Du, X. H. Bu, X. B. Leng, Y. M. Guo, R. H. Zhang, *Acta Crystallogr., Sect. C* **2000**, *56*, 1314−1315.

[5] [5a] P. J. Farmer, T. Solouki, D. K. Mills, T. Soma, D. H. Russell, J. H. Reibenspies, M. Y. Darensbourg, *J. Am. Chem. Soc.* **1992**, *114*, 4601−4605. – [5b] R. M. Buonomo, I. Font, M. J. Maguire, J. H. Reibenspies, T. Tuntulani, M. Y. Darensbourg, *J. Am. Chem. Soc.* **1995**, *117*, 963−973. – [5c] G. Musie, C.-H. Lai, L. W. Sumner, M. Y. Darensbourg, *Inorg. Chem.* **1998**, *37*, 4086−4093.

[6] [6a] R. F. Drake, V. H. Crawford, N. W. Laney, W. E. Hatfield, *Inorg. Chem.* **1974**, *13*, 1246−1250. – [6b] W. E. Marsh, K. C. Patel, W. Hatfield, D. J. Hodgson, *Inorg. Chem.* **1983**, *22*, 511−515. – [6c] F. Tuna, L. Patron, Y. Journaux, M. Andruh, W. Plass, J.-C. Trombe, *J. Chem. Soc., Dalton Trans.* **1999**, 539−545. – [6d] M. Rodriguez, A. Llobet, M. Corbella, A. E. Martell, J. Reibenspies, *Inorg. Chem.* **1999**, *38*, 2328−2334.

[7] W. J. Geary, *Coord. Chem. Rev.* **1971**, *7*, 81−122.

[8] [8a] J. C. Colin, T. Mallah, Y. Journaux, F. Lloret, M. Julve, C. Bois, *Inorg. Chem.* **1996**, *35*, 4170−4176. – [8b] X. H. Bu, D. L. An, X. C. Cao, R. H. Zhang, T. Clifford, E. Kimura, *J. Chem. Soc., Dalton Trans.* **1998**, 2247−2252. – [8c] X. H. Bu, S. L. Lu, R. H. Zhang, D. Z. Liao, S. Aoki, T. Clifford, E. Kimura, *Inorg. Chim. Acta* **2000**, *298*, 50−56.

[9] C. O'Sullivan, G. Murphy, B. Murphy, B. Hathaway, *J. Chem. Soc., Dalton Trans.* **1999**, 1835−1844 and references therein.

[10] M. Brophy, G. Murphy, C. O'Sullivan, B. Hathaway, B. Murphy, *Polyhedron* **1999**, *18*, 611−615 and references therein.

[11] A. W. Addison, T. N. Rao, J. Reedijk, J. V. Rijn, G. C. Verschoor, *J. Chem. Soc., Dalton Trans.* **1984**, 1349−1356.

[12] G. R. Desiraju, *Acc. Chem. Res.* **1991**, *24*, 290−295.
[13] [13a] M. Munakata, L. P. Wu, M. Yamamoto, T. Kuroda-Sowa, M. Maekawa, *J. Am. Chem. Soc.* **1996**, *118*, 3117−3124. − [13b] T. Sugimori, N. Ohata, K. Koiwai, A. Odani, O. Yamauchi, *Inorg. Chem.* **1997**, *36*, 576−583.
[14] R. Haidar, M. Ipek, B. DasGupta, M. Yousaf, L. J. Zompa, *Inorg. Chem.* **1997**, *36*, 3125−3132.
[15] S. J. Brudenell, L. Spiccia, E. R. T. Tiekink, *Inorg. Chem.* **1996**, *35*, 1974−1979.
[16] G. A. McLachlan, G. D. Fallon, R. E. Martin, L. Spiccia, *Inorg. Chem.* **1995**, *34*, 254−261.
[17] [17a] T. Szabo-Planka, A. Rockenbauer, M. Gyor, F. Gaizer, *J. Coord. Chem.* **1988**, *17*, 69−83. − [17b] M. Murali, M. Palaniandavar, T. Pandiyan, *Inorg. Chim. Acta* **1994**, *224*, 19−25.
[18] K. Miyoshi, H. Tanaka, E. Kimura, S. Tsuboyama, S. Murata, H. Shimizu, K. Ishizu, *Inorg. Chim. Acta* **1983**, *78*, 23−30.
[19] I. Bertini, G. Canti, R. Grassi, A. Scazzofola, *Inorg. Chem.* **1980**, *19*, 2198−2200.
[20] R. Lucas, S. Liu, L. K. Thompson, *Inorg. Chem.* **1990**, *29*, 85−88.
[21] Y. Journaux, J. Sletten, O. Kahn, *Inorg. Chem.* **1985**, *24*, 4063−4069.
[22] W. E. Marsh, W. E. Hatfield, D. J. Hodson, *Inorg. Chem.* **1982**, *21*, 2679−2684.
[23] W. E. Marsh, W. E. Hatfield, D. J. Hodson, *Inorg. Chem.* **1988**, *27*, 1819−1822.
[24] [24a] J. F. Villa, W. Hatfield, *Inorg. Chem.* **1971**, *11*, 1331−1334. − [24b] D. M. Duggan, D. N. Hendrickson, *Inorg. Chem.* **1974**, *13*, 2929−2940.
[25] O. Kahn, S. Sikorav, J. Gouteron, S. Jeannin, *Inorg. Chem.* **1983**, *22*, 2877−2883.
[26] D. D. Swank, G. F. Needham, R. D. Willett, *Inorg. Chem.* **1979**, *18*, 761−765.
[27] E. D. Estes, W. E. Estes, W. E. Hatfield, D. J. Hodgson, *Inorg. Chem.* **1975**, *14*, 106−109.
[28] D. Y. Jeter, D. J. Hodgson, W. E. Hatfield, *Inorg. Chim. Acta* **1971**, *5*, 257−259.
[29] E. L. Buhle, A. M. Moore, F. G. Wiseloge, *J. Am. Chem. Soc.* **1943**, *65*, 29−32.
[30] J. H. Billman, L. C. Dorman, *J. Org. Chem.* **1962**, *27*, 2419−2422.

Received October 7, 2000
[I00374]

Reactivity of [1,2-Bis(dimethylphosphanyl)ethane](mesitylidyne)tungsten(IV) Hydride with Group 7 and 8 Transition Metal Carbonyl Complexes

Franck Furno,[a] Thomas Fox,[a] Montserrat Alfonso,[a] and Heinz Berke*[a]

Keywords: Hydride complexes / Formyl complexes / Decarbonylation

The reaction between the tungsten hydride complex *trans*-W(CMes)(dmpe)$_2$H [**1**, dmpe = 1,2-bis(dimethylphosphanylethane)] and a series of electrophilic transition metal carbonyl compounds has been investigated, to explore the generality of W–H reductions of coordinated CO. Hydride transfer to the mononuclear [Fe(CO)$_5$], and to the dinuclear [Re$_2$(CO)$_{10}$], yields the neutral heterobimetallic formyl complexes *trans*-W{(μ-OCH)Fe(CO)$_4$}(CMes)(dmpe)$_2$ (**2**) and *trans*-W{(μ-OCH)Re$_2$(CO)$_9$}(CMes)(dmpe)$_2$ (**3a**), respectively. In the latter case, after one week at room temperature, **3a** is smoothly converted into the stable ionic complex [W(CMes)(CO)(dmpe)$_2$]$^+$[Re$_2$(CO)$_9$H]$^-$ (**3b**). Reaction with the cluster [Ru$_3$(CO)$_{12}$] results in the formation of an unstable formyl complex, which undergoes a direct rearrangement at –20 °C to produce the ionic complex [W(CMes)(CO)(dmpe)$_2$]$^+$-[Ru$_3$(CO)$_{11}$H]$^-$ (**4**) as the final product. The molecular structure of **4** was unambiguously established by single-crystal X-ray diffraction.

Introduction

In recent years our group has investigated the chemistry of activated transition metal hydrides. It has been shown that the carbyne ligand plays a prominent role in the electronic activation of hydride units.[1,2]

The reactivity of **1** towards small unsaturated organic molecules has been studied.[2] These studies, together with density functional calculations,[3] have indicated an enhanced hydricity and a weakness of the W−H bond, due mainly to the mesityl carbyne ligand in the *trans* position, which is known to exert a strong *trans* influence/effect.[4] The use of dmpe ligands, which are strong σ-donors and less effective π-acceptors than (for example) CO, should lead to increased electron density on the metal, and also to enhanced stability of the corresponding metal formyl moieties. Until 1973, when the first isolated anionic formyl complex [(CO)$_4$Fe(CHO)]$^-$ was reported by Collman and Winter,[5] these compounds were conspicuous by their absence from the chemical literature. The first neutral formyl complex, Os(Cl)(CO)$_2$(PPh$_3$)$_2$(CHO), was reported by Collins and Roper in 1976.[6] In the same year, Casey, Gladysz, and Winter[7] reported the first anionic formyl complexes, formed by treatment of suitable hydride sources (in most cases, main group metal "super hydrides") with metal carbonyls. Nelson,[8] however, demonstrated that a transition metal hydride can also be effective as the hydride source. The vast majority of known metal formyl complexes are, however, thermally unstable with respect to decarbonylation.[9] Notable exceptions are the early transition metal complexes,[10] the rhodium porphyrin hydride complex RhOEP(H) (OEP = octaethylporphyrin) described by Wayland and co-workers,[11] and some actinohydrides[12] which produce η^2-formyl products. Transition metal formyl complexes and hydridometal carbonyls are commonly invoked as reactive intermediates in both catalytic and stoichiometric CO reduction reactions.[13] The synthesis and characterization of formyl-metal complexes remains important for fuller investigation of the mechanism of Fischer−Tropsch[14a] reductive hydrogenation of carbon monoxide to hydrocarbons and oxygenates proposed by Olivé and Olivé,[14b] in which the insertion of carbon monoxide into a metal−hydrogen bond to produce a formyl complex is considered to be the initial step. Coordinated CO can be inserted into the M−H bond of metal hydrides,[15] particularly when the reaction is driven by the oxophilic character of early transition metals, allowing formation of η^2-formyl complexes. The generation of η^1-formyl species is generally thermodynamically unfavourable, as demonstrated by several quantum chemical calculations.[16] We therefore examined the reaction between **1** and CO bound in metal carbonyl compounds, in order to explore the generality of W−H addition across the CO bond.

Results and Discussion

Treatment of **1** with one equivalent of [Fe(CO)$_5$] (at room temperature in THF for a few minutes) did indeed quantitatively produce the dinuclear formyl-bridged complex *trans*-W{(μ-OCH)Fe(CO)$_4$}(CMes)(dmpe)$_2$ (**2**, Scheme 1). The mechanism is presumed to involve H$^-$ transfer to a CO ligand, by direct nucleophilic attack on a metal-bound CO. Dedieu and Nakamura have carried out extensive ab initio SCF calculations on the hypothetical gas phase reaction between H$^-$ and [Fe(CO)$_5$], and have concluded that for the [(CO)$_4$FeCHO]$^-$ ion, direct H$^-$ addition to an axial CO is strongly exothermic and occurs without activation.[17] Casey and Neumann have reported a variety of metal formyl compounds, including [Fe(CO)$_4$CHO]$^-$, resulting from the reaction between [Na$^+$][HB(OR)$_3^-$] and M(CO)$_x$.[20]

[a] Anorganisch-chemisches Institut, Universität Zürich, Winterthurerstrasse 190, 8057 Zürich, Switzerland

 © WILEY-VCH Verlag GmbH, 69451 Weinheim, 2001 1434−1948/01/0606−1559 $ 17.50+.50/0

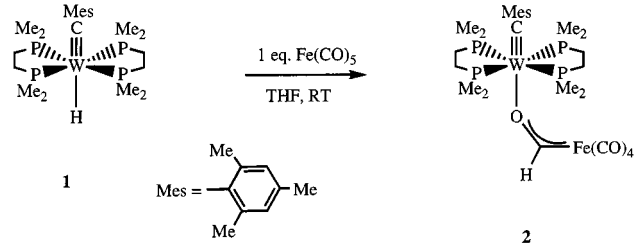

Scheme 1

Compound **2** was isolated, in 84% yield, as an orange, microcrystalline powder after recrystallisation from a saturated diethyl ether solution.

Among other resonances, the ^{1}H NMR spectrum of **2** features a characteristic H_{formyl} nucleus signal at $\delta = 13.67$, in the region reported for $K^+[Fe(CO)_4CHO]^-$ ($\delta = 15.0$)[7d] and *mer*-Mo{(μ-OCH)Fe(CO)$_4$}(CO)(NO)(PMe$_3$)$_3$ ($\delta = 14.09$).[19a] The ^{31}P{^{1}H} NMR spectrum features a singlet at $\delta = 32.2$ for the four equivalent phosphorus nuclei, with satellites from coupling to ^{183}W ($^1J_{PW} = 288$ Hz). The ^{13}C{^{1}H} NMR spectrum includes a quintet at $\delta = 298.6$ for the C_{formyl} atom ($^3J_{CP} = 5$ Hz), shifted by 39 ppm to lower field as compared to $[Fe(CO)_4CHO]^-$,[7b] and another quintet at $\delta = 275.3$ ($^2J_{CP} = 10$ Hz) for the carbyne carbon atom. These chemical shift values can be attributed to more efficient electron withdrawal in the bridging coordination mode. Evidence for the presence of a formyl ligand is most easily found in the IR spectral data. The THF solution infrared spectrum of **2** shows three bands at 2045 (m), 1967 (m) and 1932 (s) cm^{-1} − attributable to the terminal ν(CO) vibrations of the Fe(CO)$_4$ unit − and one other band at 1576 (m) for the iron formyl. This absorption pattern closely resembles that of the reported anion $[Fe(CO)_4CHO]^-$ complex.[18] Compound **2** provided an elemental analysis consistent with the proposed formula.

It was also expected that **2** would react further with excess **1**. Reaction with up to 10 equivalents of **1** at room temperature was therefore attempted, but no further transformations could be observed, indicating that the remaining carbonyls are inert towards further reduction to (for example) a bis(formyl) complex (Scheme 2).

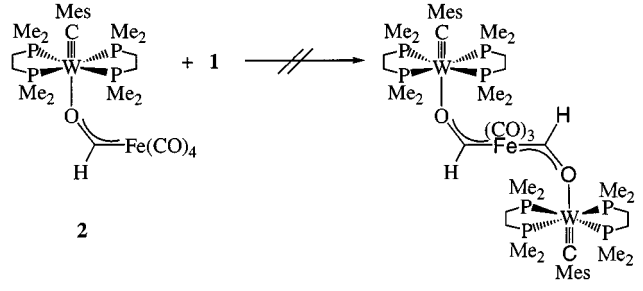

Scheme 2

Steric hindrance probably makes the remaining CO ligands less susceptible to hydridic attack. On heating the reaction mixture at 60 °C for two days, the expected hydride migration to the iron was not detected, and neither was CO ejection. Compound **2** seems to be unusually stable; in the solid state it can be stored at room temperature under inert atmosphere for several weeks without any deterioration.

The reaction between **1** and one equivalent of $[Re_2(CO)_{10}]$ in THF was followed by ^{1}H and ^{31}P{^{1}H} NMR spectroscopy and the primary insertion product (i.e., the formyl-bridged compound *trans*-W{(μ-OCH)Re$_2$(CO)$_9$}(CMes)(dmpe)$_2$ (**3a**)) was detectable almost immediately (Scheme 3).

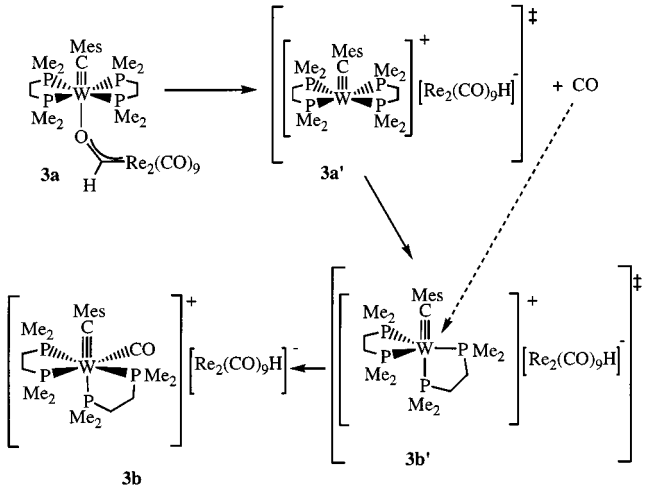

Scheme 3

This reaction proceeds smoothly at room temperature, resulting in the formation of a clear orange/red solution. Here, again, the bridging formyl group of **3a** gives rise to characteristic NMR resonances. The ^{1}H NMR spectrum shows the H_{formyl} resonance at $\delta = 14.98$, close to those observed in $Li^+[Re_2(CO)_9(CHO)]^-$ [15,26] and *mer*-Mo{(μ-OCH)Re$_2$(CO)$_9$}(CO)(NO)(PMe$_3$)$_3$ ($\delta = 15.07$).[19a] ^{31}P{^{1}H} NMR spectroscopy reveals a singlet at $\delta = 29.9$ for the four equivalent phosphorus nuclei, with satellites from coupling to ^{183}W ($^1J_{PW} = 287$ Hz). The ^{13}C{^{1}H} NMR spectrum features a resonance at $\delta = 295.1$ for Re*C*HO. During the course of the reaction, the THF solution infrared spectrum had shown the ReCHO ν(C=O) band at 1535 cm^{-1}. However, unlike the reaction with [Fe(CO)$_5$], an equilibrium − lying to the right hand side, in favour of the product (ratio of **1**/**3a**, 2:3) − seems to have been reached after two days. This was also observed in the case of the similar compound *mer*-Mo{(μ-OCH)Re$_2$(CO)$_9$}(CO)(NO)(PMe$_3$)$_3$.[19a] At the same time, the emergence of a series of large multiplets in the dmpe region of the ^{1}H NMR spectrum was observed. The ^{31}P{^{1}H} NMR spectrum also displayed a number of new resonances. These signals are attributable to the isomeric ionic compound $[W(CMes)(CO)(dmpe)_2]^+[Re_2(CO)_9H]^-$ (**3b**). The colour of the solution mixture was brown at this point, and after one week at room temperature, almost 95% yield of this new salt material **3b** was observed spectroscopically (^{31}P{^{1}H} NMR). The ^{31}P{^{1}H} NMR spectrum features four multiplets of intensity 1:1:1:1 for the four chemically different phosphorus atoms at $\delta = 16.8$ (ddd, $^2J_{P3,P4} = 5$ Hz, $^2J_{P3,P2} = 21$ Hz, $^2J_{P3,P1} = 63$ Hz, $^1J_{P3,W} = 249$ Hz, P3), 14.4 (dd, $^2J_{P1,P3} = 65$ Hz, $^2J_{P1,P4} = 20$ Hz, $^1J_{P1,W} = 294$ Hz,

P1), 8.2 (ddd, $^2J_{P4,P1}$ = 20 Hz, $^2J_{P4,P2}$ = 25 Hz, $^2J_{P4,P3}$ = 5 Hz, $^1J_{P4,W}$ = 202 Hz, P4) and −15.5 (dd, $^2J_{P2,P3}$ = 21 Hz, $^2J_{P2,P4}$ = 23 Hz, $^1J_{P2,W}$ = 35 Hz, P2). The chemically distinct phosphorus atoms P1, P2, P3, and P4 have been assigned as described in Scheme 3. The assignments are in agreement with previously published data[4] and reflect the *trans* influence of the carbyne group on P2. It is therefore weakly bonded to the tungsten centre with a small coupling constant ($^1J_{P,W}$ = 35 Hz). For the same reason, $^2J_{P2,P1}$ is apparently so small as to be undetectable. The ^{1}H NMR spectrum shows a singlet at δ = −17.47 for the Re−H hydride and a series of multiplets in the dmpe region, due to the new arrangement of the dmpe ligands around the tungsten centre. The ^{13}C{^{1}H} NMR spectrum displays a multiplet at δ = 293.7 for the mesitylidyne carbon, due to the coupling with the four different phosphorus atoms, and another multiplet at δ = 230 for the W−CO carbon atom ($^2J_{C,P4}$ = 11 Hz). The THF solution infrared spectrum displays, among other characteristic resonances, one band at 1915 cm^{-1} (s), consistent with a terminal W−CO bond. After isolation, **3b** also gave satisfactory elemental microanalytical data.

An intrinsic chemical property of transition metal formyl complexes is the capability to transfer a hydride ion to several classes of substrate (such as ketones, alkyl halides, or metal carbonyls), thereby acting as hydride donors. The lability of this metal formyl hydrogen was unambiguously demonstrated with isolated formyl complexes about twenty years ago.[7a,20,21] We propose, after initial attack by H$^-$ directly on coordinated CO, an intramolecular hydride migration from the formyl to the Re, presumably with initial loss of CO − i.e., a slow decarbonylation of **3a** at room temperature − to give the unsaturated complex **3a′**, with subsequent rearrangement around the tungsten centre to give **3b** (Scheme 4). The assumed five-coordinate, square-pyramidal cationic intermediate **3a′** is fluxional by the Berry mechanism (pseudorotation) and gives rise to the trigonal-bipyramidal **3b′** intermediate, which is then trapped by the free CO ligand to give **3b**. It is interesting at this stage to note that a CO ligand in a position *trans* to a carbyne unit has never been observed.[22] The rate-determining step in this reaction seems to be the decarbonylation step.

For *mer*-M(H)(CO)(NO)(PMe$_3$)$_3$ (M = Mo, W), it has been calculated that interaction with transition metal carbonyls such as [Fe(CO)$_5$] and [Re$_2$(CO)$_{10}$] is determined by secondary effects such as solvation or steric interactions, since both carbonyl complexes possess comparable hydride affinities.[19a][19b] For the related carbyne complexes, it is anticipated that similar selectivities with a similar physical background apply.

Compound **1** reacts with one equivalent of the triruthenium cluster [Ru$_3$(CO)$_{12}$] under ambient laboratory conditions in THF to afford the compound [W(CMes)(CO)(dmpe)$_2$]$^+$[Ru$_3$(CO)$_{11}$H]$^-$ (**4**) (Scheme 5), presumably formed via a formyl intermediate. In fact, when the reductive reaction is monitored at −50 °C in [D$_8$]THF, the ^{1}H NMR spectrum displays a resonance at δ = 15.6, suggesting that a pendant formyl moiety has been produced. However, upon raising the temperature in the NMR tube to −20 °C, the formyl signal gradually decreases, with concomitant appearance of a new band (s, Ru−H) at δ −12.05, assigned to **4**. It is known that most of the formyl intermediates are likely to decompose more rapidly than they form.[23] These decomposition reactions of formyl complexes, into the corresponding metal hydride with loss of CO, have received a great deal of attention,[9,24] and radical processes have been invoked in many cases. It is still not clear, however, whether this decomposition is determined by thermodynamic factors or is kinetic in origin.[25] The balance between these will depend on the mechanism of CO loss. For the anticipated cluster formyl complex *trans*-W{(μ-OCH)Ru$_3$(CO)$_{11}$}(CMes)(dmpe)$_2$, the decarbonylation step seems to be facilitated relative to that of **3a**. The fact that the stability of cluster formyl complexes is lower than that of the related mononuclear species has already been noted by Thornback et al.[26] These workers suggested that this instability is associated with the availability of an "α-elimination" mechanism in cluster systems, related to the β-elimination observed in mononuclear systems.

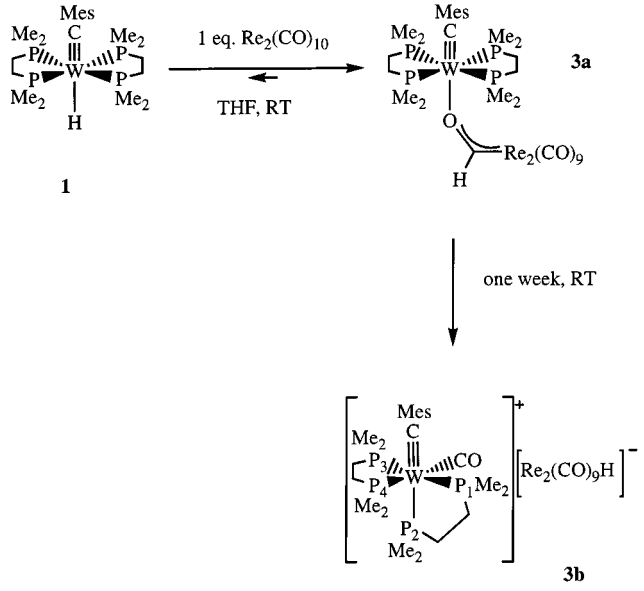

Scheme 4

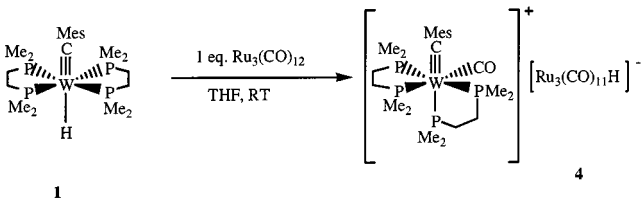

Scheme 5

The reaction proceeds smoothly at room temperature in THF and is complete within a few minutes. Compound **4** can be isolated in 82% yield as a brown, microcrystalline powder after recrystallisation from a saturated diethyl ether solution. The ^{1}H NMR spectrum features a characteristic singlet at δ = −12.05 for the Ru−H hydride moiety in the cluster anion [HRu$_3$(CO)$_{11}$]$^-$,[27] which is consistent with

the value reported in the literature ($\delta = -12.9$).[28] The $^{31}P\{^1H\}$ NMR spectrum shows four different multiplet signals of intensity 1:1:1:1 at $\delta = 15.9$ (ddd, $^2J_{P3,P1} = 66$ Hz, $^2J_{P3,P2} = 20$ Hz, $^2J_{P3,P4} = 6$ Hz, $^1J_{P3,W} = 269$ Hz, P3), 13.9 (dd, $^2J_{P1,P3} = 65$ Hz, $^2J_{P1,P4} = 19$ Hz, $^1J_{P1,W} = 283$ Hz, P1), 7.8 (ddd, $^2J_{P4,P1} = 19$ Hz, $^2J_{P4,P2} = 25$ Hz, $^2J_{P4,P3} = 6$ Hz, $^1J_{P4,W} = 223$ Hz, P4), and -15.6 (dd, $^2J_{P2,P3} = 20$ Hz, $^2J_{P2,P4} = 25$ Hz, $^1J_{P2,W} = 20$ Hz, P2) for the four nonequivalent phosphorus nuclei. The different phosphorus atoms P1, P2, P3, and P4 have been assigned as described on Figure 1. Atom P2 is again, as in **3b**, very weakly bound with the tungsten centre, and therefore the $^1J_{PW}$ is very small: $^1J_{P2,W} = 20$ Hz. This is not surprising, given the assumed strong *trans* influence/effect of the carbyne ligand in the *trans* position. Consequently, the value of the coupling constant $J_{P2,P1}$ is also very small and has been calculated to be around 2 Hz (Table 1). This is also confirmed by the X-ray structure (Figure 2), in which the long W−P2 distance [2.664(4) Å], compared to the other W−P bond lengths, which are around 2.45, can be seen. Here, as for **3b**, the $^{13}C\{^1H\}$ NMR spectrum once more shows a multiplet at $\delta = 292$, which corresponds to the $C_{carbyne}$ carbon; this value is also further downfield than expected (shifted by 31.6 ppm relative to **1**), presumably due to the weakly bound phosphorus atom in the *trans* position. The infrared spectrum in THF solution exhibits, among other characteristic bands, one band at 1900 cm^{-1} (s) for the W-CO terminal carbonyl group. Compound **4** also gave a satisfactory elemental microanalysis. The $^{31}P\{^1H\}$ NMR spectrum of **4** (Figure 1) has been simulated and calculations carried out in order to evaluate the coupling constants between the four different phosphorus nuclei (Table 1).

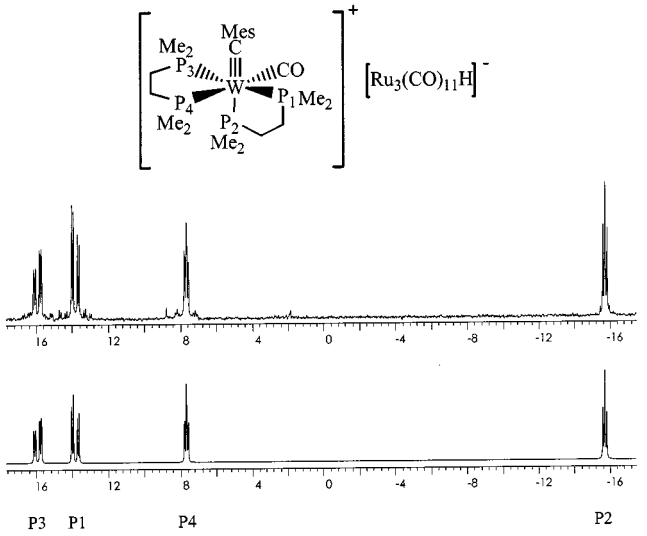

Figure 1. Measured (upper) and simulated (lower) spectra for the dmpe ligands in the $^{31}P\{^1H\}$ NMR spectrum of **4**

Table 1. Calculated shifts and coupling constants between P1, P2, P3, and P4 in compound **4**

Nucleus	Shift (ppm)	Width (Hz)	*J*, P1 (Hz)	*J*, P3 (Hz)	*J*, P4 (Hz)
P1	13.9	4.3		64.6	
P2	−15.7	5.5	2	20.8	23.5
P3	15.9	4.1			
P4	7.7	3.7	19.5	5.8	

Molecular Structure of 4

The structure of the separated ionic complex $[W(CMes)(CO)(dmpe)_2]^+[Ru_3(CO)_{11}H]^-$ (**4**) was finally established unequivocally by single-crystal X-ray diffraction (Figure 2 and Table 2). Suitable crystals were obtained by slow cooling of a saturated diethyl ether solution to −30 °C. Unfortunately, the X-ray structure analysis of **4** was hampered by the poor quality of the crystals, and attempts to achieve suitable crystals of **2** and **3b** were unsuccessful. Therefore, large standard deviations were found for the bond lengths and angles. Selected bond lengths (Å) and angles (°) are listed in Table 3.

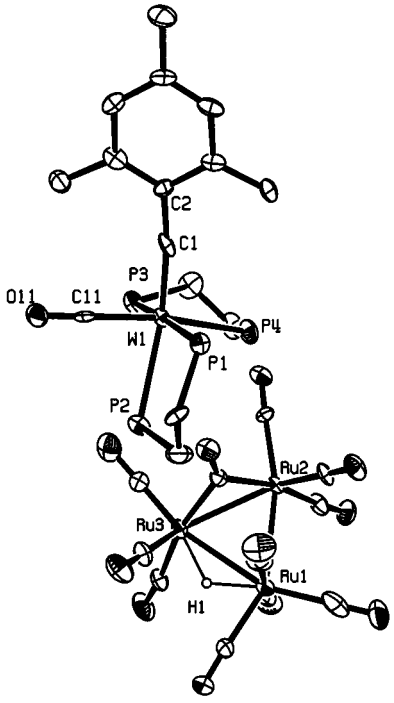

Figure 2. ORTEP plot of compound **4**. Thermal ellipsoids are drawn at the 30% probability level. Hydrogens (except H1) and the Me carbon atoms from the dmpe ligands are omitted for clarity

Compound **4** adopts a pseudo-octahedral geometry, with the carbyne and one phosphorus in axial positions and the equator defined by 3 phosphorus atoms and the carbonyl group.

Conclusions

The results discussed above show that the tungsten hydride complex *trans*-$W(CMes)(dmpe)_2H$ **1** readily reduces group 7 and 8 transition metal carbonyls, acting as a hydride-based nucleophile towards metal-bound CO.

Table 2. X-ray crystal structure, data collection and refinement data for **4**

empirical formula	$C_{34}H_{44}O_{12}P_4Ru_3W$
fw	1255.63
temperature [K]	183(2)
wavelength [Å]	0.71073
cryst habit	dark red block single crystal
cryst size	0.18×0.17×0.14
cryst syst	triclinic
space group	$P\bar{1}$
a [Å]	13.617(1)
b [Å]	13.6388(9)
c [Å]	14.8427(9)
α [deg]	101.211(8)
β [deg]	99.319(8)
γ [deg]	117.923(7)
volume [Å^3]	2285.1(3)
Z	2
density (calcd) [Mg/m^{-3}]	1.825
abs coeff [mm^{-1}]	3.673
F(000)	1220
abs corr	empirical
T_{min}/T_{max}	0.5577/0.6273
θ range [deg]	2.60 to 30.33
index ranges	$-19 < h < 19$
	$-19 < k < 19$
	$-20 < l < 20$
no. of reflns collected	27290
no. of ind reflns	12450 [R(int) = 0.1016]
completeness to θ	30.33°, 90.7%
refinement method	Full-matrix, least-squares on F^2
no. of data/restraints/params	12450/0/483
extinction coefficient	0.0031 (5)
final *R* indices [$I > 2\sigma(I)$]	*R*1 = 0.0827, *wR*2 = 0.2169
R indices (all data)	*R*1 = 0.1455, *wR*2 = 0.2718
Goodness-of-fit on F^2	1.067
largest diff peak and hole [e Å^{-3}]	5.384 and −7.035

Table 3. Selected bond lengths [Å] and angles [°] for **4**

Selected bond lengths [Å][a]	selected angles [°][a]
W(1)−C(1) 1.82(2)	W(1)−C(1)−C(2) 169(1)
C(1)−C(2) 1.48(2)	P(1)−W(1)−P(2) 77.0(1)
W(1)−P(1) 2.458(4)	P(3)−W(1)−P(2) 98.8(1)
W(1)−P(2) 2.664(4)	P(4)−W(1)−P(2) 94.0(1)
W(1)−P(3) 2.474(4)	P(4)−W(1)−P(3) 77.7(1)
W(1)−P(4) 2.566(4)	P(1)−W(1)−P(3) 172.2(1)
W(1)−C(11) 1.97(2)	P(1)−W(1)−P(4) 95.8(1)
C(11)−O(11) 1.17(2)	C(1)−W(1)−P(1) 87.7(5)
Ru(1)−Ru(2) 2.829(2)	C(1)−W(1)−P(4) 102.7(5)
Ru(1)−Ru(3) 2.833(2)	C(1)−W(1)−P(3) 98.0(5)
Ru(2)−Ru(3) 2.816(1)	C(1)−W(1)−P(2) 158.4(4)
	C(1)−W(1)−C(11) 87.4(6)
	C(11)−W(1)−P(1) 93.7(5)
	C(11)−W(1)−P(3) 92.0(5)
	C(11)−W(1)−P(4) 166.4(4)
	C(11)−W(1)−P(2) 78.6(4)
	O(11)−C(11)−W(1) 175(1)
	Ru(2)−Ru(1)−Ru(3) 59.64(5)
	Ru(3)−Ru(2)−Ru(1) 60.26(5)
	Ru(2)−Ru(3)−Ru(1) 60.10(5)

[a] See Figure 2 for atom designations.

This observed high propensity towards carbonyl insertion into the W−H bond resembles that found for metallocene hydride compounds with early transition metal centres.[29]

Experimental Section

General: All manipulations of air-sensitive compounds were carried out either in a Braun Labstar glovebox under nitrogen (dried if appropriate) by conventional Schlenk techniques. Solvents were dried with appropriate drying agents[30] and freshly distilled under nitrogen prior to use. The different transition metal carbonyl compounds $Fe(CO)_5$ (Alfa products), $Re_2(CO)_{10}$ (Fluka), and $Ru_3(CO)_{12}$ (Aldrich) were commercial products and used as received. The deuterated solvents (C_6D_6, [D_8]toluene, and [D_8]THF) were also obtained from commercial suppliers and distilled from appropriate drying agents and vacuum transferred for storage in Schlenk flasks fitted with Teflon stopcocks. The dmpe ligand was synthesized by following modified literature procedures.[31] − ^{1}H, ^{13}C, and ^{31}P NMR spectra were run either on a Varian Gemini 300 spectrometer operating at 300, 75.4, and 121.5 MHz, respectively, or on a Bruker DRX 500 spectrometer at 500.2, 125.8, and 202.5 MHz, respectively. Values of δ(^{1} H), δ(^{13}C), relative to $SiMe_4$, δ(^{31}P) relative to 85% H_3PO_4. − Mass spectra (EI or FAB) were recorded on a Finnigan MAT 8230 mass spectrometer. − IR spectra: Bio-Rad FTS-45 instrument. − Elemental analyses: LECO CHNS-932 machine. − The simulation of the ^{31}P{^{1}H} NMR spectrum was carried out with the aid of the gNMR 4.1 program. The optimal fit was attained by simultaneous iteration of the chemical shifts and coupling constants.

Preparation of *trans*-W(CMes)(dmpe)$_2$(H) (1): The synthesis of **1** has already been published elsewhere.[2] Only the spectroscopic data for **1** are given here. − ^{1}H NMR (C_6D_6, 298 K): δ = 6.72 (s, 2 H, Mes), 2.62 (s, 6 H, 2CH_3-Mes), 2.05 (s, 3 H, CH_3-Mes), 1.67 (s br, 12 H, PMe), 1.52 (m br, 4 H, PCH_2), 1.46 (s br, 12 H, PMe′), 1.42 (m br, 4 H, PCH_2′), −6.58 (quint, $^2J_{HP}$ = 32 Hz, $^1J_{HW}$ = 31 Hz, 1 H, WH). ^{31}P{^{1}H} NMR (C_6D_6, 298 K): δ = 24.4 (s, $^1J_{PW}$ = 281 Hz). ^{13}C {^{1}H} NMR (C_6D_6, 298 K): δ = 260.4 (quint, $^2J_{CP}$ = 10 Hz, CMes), 151.5 (s, *ipso*-Mes), 137.4 (s, *o*-Mes), 135.4 (s, *p*-Mes), 130.8 (s, *m*-Mes), 34.0 (quint, PCH_2), 27.8 (m, PMe), 25.4 (m, PMe′), 22.6 (s, 2CH_3-Mes), 21.5 (s, CH_3-Mes). ^{183}W{^{1}H} NMR ([D_8]toluene, 298 K): δ −1612 (pseudo-q, $^1J_{WP}$ = 281 Hz). MS (FAB, toluene): *m*/*z* = 615 [M$^+$], 310 (M$^+$ − 2dmpe). − $WC_{22}H_{44}P_4$ (615.73): calcd. C 42.87, H 7.15%; found C 42.67, H 7.28%.

Preparation of *trans*-W{(μ-OCH)[Fe(CO)$_4$]}(CMes)(dmpe)$_2$ (2): Compound **1** (30 mg, 0.0487 mmol) was dissolved in THF (5 mL) and $Fe(CO)_5$ (6.6 μL, 0.0487 mmol) added by microsyringe. The mixture was stirred for a few minutes at room temperature. After this period, the solvent was evaporated in vacuo and the precipitate recrystallised from a diethyl ether solution at −30 °C to afford **2** as orange crystals. Yield: 33 mg (84%). − IR (cm^{-1}, THF): 2045, 1967, 1932 [Fe(CO)$_4$], 1576 (formyl), 894 (CMes). − ^{1}H NMR ([D_8]THF, 298 K): δ = 13.67 (s, 1 H, OC*H*), 6.53 (s, 2 H, Mes), 2.25 (s, 6 H, 2CH_3-Mes), 1.94 (s, 3 H, CH_3-Mes), 1.40 (m br, 4 H, PCH_2), 1.34 (s br, 12 H, PMe), 1.28 (m br, 4 H, PCH_2′), 1.20 (s br, 12 H, PMe′). − ^{31}P{^{1}H} NMR ([D_8]THF, 298 K): δ = 32.2 (s, $^1J_{PW}$ = 288 Hz). − ^{13}C{^{1}H} NMR ([D_8]THF, 298 K): δ = 298.6 (q, $^3J_{CP}$ = 5 Hz, O*C*H), 275.3 (quintet, $^2J_{CP}$ = 10 Hz, CMes), 218.5 [s, Fe(CO)$_4$], 151.2 (s, *ipso*-Mes), 135.2 (s, *o*-Mes), 133.1 (s, *p*-Mes), 128.3 (s, *m*-Mes), 33.5 (m, $^1J_{CP}$ = 10 Hz, PCH_2), 22.2 (s, 2CH_3-Mes), 22.1 (m, $^1J_{CP}$ = 7 Hz, PMe), 20.4 (s, CH_3-Mes), 17.4 (m,

$^1J_{CP}$ = 7 Hz, PMe′). − $C_{27}H_{44}P_4O_5FeW$ (811.58): calcd. C 39.92, H 5.42%; found C 40.21, H 4.90%.

Preparations of *trans*-W{(μ-OCH)[$Re_2(CO)_9$]}(CMes)(dmpe)$_2$ (3a) and [W(CMes)(CO)(dmpe)$_2$]$^+$[$Re_2(CO)_9H$]$^-$ (3b): Compound **1** (30 mg, 0.0487 mmol) was dissolved in THF (5 mL), $Re_2(CO)_{10}$ (32 mg, 0.0487 mmol) was added, and the mixture was stirred for a few minutes at room temperature. After this period, NMR examination in [D_8]THF already showed a spectroscopically small amount (36%) of **3a**. After two days at room temperature, the amount of **3a** was about 67%. − IR (cm^{-1}, THF): 1535 (ReCHO). − ^{1}H NMR ([D_8]THF, 298 K): δ = 14.98 (s, 1 H, OC*H*), 6.50 (s, 2 H, Mes), 2.31 (s, 6 H, 2CH_3-Mes), 1.91 (s, 3 H, CH_3-Mes), large multiplets for the dmpe ligands between δ = 1.40 and 1.20. − ^{31}P{^{1}H} NMR ([D_8]THF, 298 K): δ = 29.9 (s, $^1J_{PW}$ = 287 Hz). − ^{13}C{^{1}H} NMR ([D_8]THF, 298 K): selected data: δ = 295.1 (Re-*C*HO), 205.1, 202.5, 195.4, 191.5 (Re-CO).

After one week at room temperature, an almost quantitative yield of **3b** was observed spectroscopically, and recrystallisation from a saturated diethyl ether solution gave a final yield of 72%.

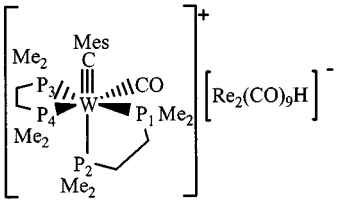

3b

IR (cm^{-1}, THF): 2086, 2028, 1974, 1925, 1895 ($Re_2(CO)_9H^-$), 1915 (W−CO), 891 (CMes). − ^{1}H NMR ([D_8]THF, 298 K): δ = 6.71 (s, 2 H, Mes), 2.51 (s, 6 H, 2CH_3-Mes), 2.01 (s, 3 H, CH_3-Mes), series of large multiplets for the dmpe ligands between δ = 1.87 and 1.34, −17.47 (s, Re-H). − ^{31}P{^{1}H} NMR ([D_8]THF, 298 K): δ = 16.8 (ddd, $^2J_{P3,P4}$ = 5 Hz, $^2J_{P3,P2}$ = 21 Hz, $^2J_{P3,P1}$ = 63 Hz, $^1J_{P3,W}$ = 249 Hz, P3), 14.4 (dd, $^2J_{P1,P3}$ = 65 Hz, $^2J_{P1,P4}$ = 20 Hz, $^1J_{P1,W}$ = 294 Hz, P1), 8.2 (ddd, $^2J_{P4,P1}$ = 20 Hz, $^2J_{P4,P2}$ = 25 Hz, $^2J_{P4,P3}$ = 5 Hz, $^1J_{P4,W}$ = 202 Hz, P4), −15.5 (dd, $^2J_{P2,P3}$ = 21 Hz, $^2J_{P2,P4}$ = 23 Hz, $^1J_{P2,W}$ = 35 Hz, P2). − ^{13}C{^{1}H} NMR ([D_8]THF, 298 K): δ = 293.7 (m, CMes), 230.0 (m, $^2J_{C,P4}$ = 11 Hz, W-CO), 202.2, 201.9, 199.8, 198.7, 190.5 (5s, $Re_2(CO)_9H^-$), 147.0 (s, *ipso*-Mes), 139.2 (s, *o*-Mes), 138.3 (s, *p*-Mes), 129.3 (s, *m*-Mes), 12 multiplets between δ = 32 and 14 for the 12 different carbon atoms in the dmpe ligands, 21.6 (s, 2CH_3-Mes), 20.9 (s, CH_3-Mes). − $C_{32}H_{44}P_4O_{10}Re_2W{\cdot}1/2Et_2O$ (1305.13): calcd. C 30.34, H 3.75%; found C 30.82, H 3.40%.

Preparation of [W(CMes)(CO)(dmpe)$_2$]$^+$ [$Ru_3(CO)_{11}H$]$^-$ (4): A mixture of **1** (30 mg, 0.0487 mmol) and $Ru_3(CO)_{12}$ (31.10 mg, 0.0487 mmol) in THF (5 mL) was stirred for 1 hour at room temperature. After this period, the solvent was evaporated in vacuo and the precipitate recrystallised at −30 °C from a diethyl ether solution to afford **4** as brown microcrystals. Yield: 24.6 mg (82%). − IR (cm^{-1}, THF): 2073, 2014, 1987, 1952 ($Ru_3(CO)_{11}H^-$), 1900 (W−CO), 892 (CMes). − ^{1}H NMR ([D_8]THF, 298 K): δ = 6.49 (s, 2 H, Mes), 2.27 (s, 6 H, 2CH_3-Mes), 1.90 (s, 3 H, CH_3-Mes), series of large multiplets for the dmpe ligands between δ = 1.47 and 1.08, −12.05 (s, Ru-H). − ^{31}P{^{1}H} NMR ([D_8]THF, 298 K): δ = 15.9 (ddd, $^2J_{P3,P1}$ = 66 Hz, $^2J_{P3,P2}$ = 20 Hz, $^2J_{P3,P4}$ = 6 Hz, $^1J_{P3,W}$ = 269 Hz, P3), 13.9 (dd, $^2J_{P1,P3}$ = 65 Hz, $^2J_{P1,P4}$ = 19 Hz, $^1J_{P1,W}$ = 283 Hz, P1), 7.8 (ddd, $^2J_{P4,P1}$ = 19 Hz, $^2J_{P4,P2}$ = 25 Hz, $^2J_{P4,P3}$ = 6 Hz, $^1J_{P4,W}$ = 223 Hz, P4), −15.6 (dd, $^2J_{P2,P3}$ = 20 Hz, $^2J_{P2,P4}$ = 25 Hz, $^1J_{P2,W}$ = 20 Hz, P2). − ^{13}C{^{1}H} NMR ([D_8]THF, 298 K): δ = 292 (m, CMes), 229.1 (m, W-CO), 211 (s), 205 (s), 203 (s), 198 (s) $Ru_3(CO)_{11}H^-$, 146.0 (s, *ipso*-Mes), 138.2 (s, *o*-Mes), 134.1 (s, *p*-Mes), 130.5 (s, *m*-Mes), 12 multiplets between δ = 36 and 15 for the 12 different carbon atoms in the dmpe ligands, 22.6 (s, 2CH_3-Mes), 20.1 (s, CH_3-Mes). − $C_{34}H_{44}P_4O_{12}Ru_3W$ (1254.34): calcd. C 32.51, H 3.51%; found C 32.31, H 3.70%.

Crystallography: Single crystals of **4**, of rather poor quality for X-ray studies, were obtained directly from the preparation as described in the Experimental Section. A dark red crystal of **4** with dimensions 0.18 × 0.17 × 0.14 mm was selected and mounted on the top of a glass fibre covered with a small amount of hydrocarbon oil and immediately placed on the goniometer of a Stoe IPDS diffractometer. The radiation used was Mo-*Kα* (0.71073), monochromatised by a crystal of graphite [the crystal-to-image plate distance was set to 50 mm (θmax = 30.33°)]. Because of the long exposure time, the -oscillation scan mode was selected and a total of 223 images were collected at 183 K. Each exposure required 10 min. and covered 0.9° in . The intensities were integrated after using a dynamic peak profile analysis, and estimated mosaic spread check was performed to prevent overlapping intensities. 7998 reflections were selected out of the whole limiting sphere for the cell parameter refinement. A total of 27290 reflections were collected, of which 12450 reflections were unique (*R*int = 0.1016). A numerical absorption correction based on measured crystal faces was applied without any improvement. Therefore, an empirical absorption correction utilising the program (ABSCOR)[32] was considered (maximum and minimum values of the transmission factor were 0.6273 and 0.5577).

Compound **4** crystallised in the triclinic crystal system. The space group $P\bar{1}$ was assumed and confirmed by the successful solution and refinement of the structure. The structure was solved by a combination of direct methods and difference Fourier synthesis (SHELXS-97)[33] and refined on F^2 by full-matrix, least-squares techniques (SHELXL-97).[33] All non-hydrogen atoms were refined with anisotropic thermal parameters, except C30 which resulted as non-positive definite. All hydrogen atom positions on the ligands were calculated assuming idealised geometries. The position of the hydride was found in a difference Fourier synthesis, but its position could not be refined. It was added as a constant contribution without refinement. At convergence, *R*1 = 0.0827, *wR*2 = 0.2169 and GooF = 1.067 for 483 variables refined using 12450 unique data.

Supplementary Material: Crystallographic data for the structural analysis has been deposited with the Cambridge Crystallographic Data Centre, CCDC No 150504 for compound **4**. Copies of this information may be obtained free of charge from the Director, CCDC, 12 Union Road, Cambridge, CB2 1EZ, UK [Fax: (internat.) +44−1223/336-033; E-mail: deposit@ccdc.cam.ac.uk, or http://www.ccdc.cam.ac.uk].

Acknowledgments

Financial support for this work from the Swiss National Science Foundation and from the University of Zürich is gratefully acknowledged.

[1] E. Bannwart, H. Jacobsen, F. Furno, H. Berke, *Organometallics* **2000**, *19*, 3605.
[2] [2a] F. Furno, T. Fox, H. W. Schmalle, H. Berke, *Organometallics* **2000**, *19*, 3620. − [2b] F. Furno, T. Fox, H. W. Schmalle, H. Berke, *Chimia* **1999**, *53*, 350.
[3] H. Jacobsen, F. Furno, H. Berke, manuscript in preparation.

[4] [4a] F. W. Fee, M. C. W. Chan, K. K. Cheung, C. M. Che, *J. Organomet. Chem.* **1998**, *563*, 191. – [4b] L. Zhang, M. P. Gamasa, J. Gimeno, R. J. Carbajo, F. Lopez Ortis, M. Lanfranchi, A. Tiripicchio, *Organometallics* **1996**, *15*, 4274.
[5] J. P. Collman, S. R. Winter, *J. Am. Chem. Soc.* **1973**, *95*, 4089.
[6] T. J. Collins, W. R. Roper, *J. Chem. Soc., Chem. Commun.* **1976**, 1044.
[7] [7a] C. P. Casey, S. M. Neumann, *J. Am. Chem. Soc.* **1976**, *98*, 5395. – [7b] J. A. Gladysz, J. C. Selover, *Tetrahedron Lett.* **1978**, 319. – [7c] J. C. Selover, M. Marsi, D. W. Parker, J. A. Gladysz, *J. Organomet. Chem.* **1981**, *206*, 317. – [7d] S. R. Winter, G. W. Cornett, E. A. Thompson, *J. Organomet. Chem.* **1977**, *133*, 339.
[8] G. O. Nelson, C. E. Sumner, *Organometallics* **1986**, *5*, 1983.
[9] [9a] J. A. Gladysz, *Adv. Organomet. Chem.* **1982**, *20*, 1 and references therein. – [9b] H. Berke, G. Huttner, O. Scheidsteger, G. Weiler, *Angew. Chem.* **1984**, *96*, 693. [9c] H. Berke, P. Kundel, *Z. Naturforsch., Teil B* **1986**, *41*, 527. – [9d] H. Berke, G. Weiler, G. Huttner, O. Orama, *Chem. Ber.* **1987**, *42*, 203.
[10] D. W. Slocum, W. R. Moser (Eds.), *Catalytic transition metal hydrides, Ann. N. Y. Acad. Sci.* **1983**, 415.
[11] H. D. Kaesz, R. B. Saillant, *Chem. Rev.* **1972**, *72*, 231.
[12] J. R. Norton, in: *Inorganic Reactions and Methods*; Verlag Chemie, Weinheim, **1987**.
[13] [13a] C. Masters, *Adv. Organomet. Chem.* **1979**, *17*, 61. – [13b] G. W. Parshall, *Homogeneous Catalysis. Wiley, New-York* **1981**. – [13c]D. R. Fahey, *J. Am. Chem. Soc.* **1981**, *103*, 136. – [13d] E. L. Muetterties, J. Stein, *Chem. Rev.* **1979**, *79*, 479.
[14] [14a] F. Fischer, H. Tropsch, *Brennst. Chem.* **1926**, *7*, 97. – [14b] G. H. Olivé, S. Olivé, *Angew. Chem. Int. Ed. Engl.* **1976**, *15*, 136.
[15] [15a] W. D. Jones, J. M. Huggins, R. G. Bergman, *J. Am. Chem. Soc.* **1981**, *103*, 4415. – [15b] J. A. Labinger, K. S. Wong, W. R. Scheidt, *J. Am. Chem. Soc.* **1978**, *100*, 3254.
[16] N. Koga, K. Morokuma, in: *Transition Metal Hydrides*, (Ed.: A. Dedieu), VCH Publishers, New York, **1992**, p.185.
[17] [17a] S. Nakamura, A. Dedieu, *Theor. Chim. Acta.* **1982**, *61*, 857. – [17b] A. Dedieu, S. Nakamura, *Nouv. J. Chim.* **1984**, *8*, 317.
[18] [18a] J. P. Collman, S. R. Winter, *J. Am. Chem. Soc.* **1973**, *95*, 4089. – [18b] W. O. Siegl, J. P. Collman, *J. Am. Chem. Soc.* **1972**, *94*, 2516.
[19] [19a] F. Liang, H. Jacobsen, H. W. Schmalle, T. Fox, H. Berke, *Organometallics* **2000**, *19*, 1950. – [19b] J. Höck, H. Jacobsen, H. W. Schmalle, G. R. J. Artus, T. Fox, J. I. Amor, F. Bäth, H. Berke, *Organometallics*, accepted for publication. – [19c] K. R. Lane, R. R. Squires, *Polyhedron* **1988**, *7*, 1609.
[20] C. P. Casey, S. M. Neumann, *J. Am. Chem. Soc.* **1978**, *100*, 2544.
[21] [21a] J. A. Gladysz, J. C. Selover, *Tetrahedron Lett.* **1978**, 319. – [21b] J. A. Gladysz, W. Tam, *J. Am. Chem. Soc.* **1978**, *100*, 2545. – [21c] C. P. Casey, S. M. Neumann, *J. Am. Chem. Soc.* **1976**, *98*, 5395.
[22] A. Mayr, H. Hoffmeister, *Adv. Organomet. Chem.* **1992**, *32*, 227.
[23] K. Inkrott, R. Goetze, S. G. Shore, *J. Organomet. Chem.* **1978**, *154*, 337.
[24] [24a] A. Asdar, C. Lapinte, *J. Organomet. Chem.* **1987**, *327*, C33. – [24b] G. Smith, D. J. Cole-Hamilton, *J. Chem. Soc., Dalton Trans* **1984**, 1023. – [24c] D. S. Barratt, D. J. Cole-Hamilton, *J. Chem. Soc., Dalton Trans* **1987**, 2683. – [24d] D. H. Gibson, K. Owens, S. K. Mandal, W. E. Sattich, J. O. Franco, *Organometallics* **1989**, *8*, 498.
[25] D. F. Brougham, D. A. Brown, N. J. Fitzpatrick, W. K. Glass, *Organometallics* **1995**, *14*, 151.
[26] B. F. G. Johnson, R. L. Kelly, J. Lewis, J. R. Thornback, *J. Organomet. Chem.* **1980**, *190*, C91.
[27] J. Knight, M. J. Mays, *J. Chem. Soc., Dalton Trans.* **1972**, 1022.
[28] R. C. Schoening, J. L. Vidal, R. A. Fiato, *J. Organomet. Chem.* **1981**, *206*, C43.
[29] G. Erker, *Acc. Chem. Res.* **1984**, *17*, 103.
[30] A. J. Gordon, R. A. Ford, *The Chemist's Companion; Wiley: New-York*, **1972**.
[31] [31a] R. J. Burt, J. Chatt, W. Hussain, G. J. Leigh, *J. Organomet. Chem.* **1979**, *182*, 203. – [31b] G. W. Parschall, *J. Inorg. Nucl. Chem.* **1960**, *14*, 291. – [31c] W. Wolfsberger, H. Schmidbaur, *Synth. React. Inorg. Met. Org. Chem.* **1974**, *4*, 149. – [31d] R. A. Zingaro, R. F. McGlothlin, *J. Chem. Eng. Data* **1963**, *8*, 226.
[32] *STOE-IPDS Software package*; Version 2.87 5/1998. STOE & Cie, GmbH, Darmstadt, Germany.
[33] G. M. Sheldrick, *SHELX-97*: Software package for the crystal structure determination, University of Göttingen, Germany; **1997**.

Received October 6, 2000
[I00375]

Defective Double-Cubane, Tetranuclear Manganese(II) and Cobalt(II) Complexes with Simultaneous $\mu_{1,1}$-Azido and μ-O Bridges

Giannis S. Papaefstathiou,[a][‡] Albert Escuer,[b] Catherine P. Raptopoulou,[c] Aris Terzis,*[c] Spyros P. Perlepes,*[a] and Ramon Vicente*[b]

Keywords: Azides / Cobalt / Di-2-pyridyl ketone / Magnetic properties / Manganese

The reactions of $M(O_2CCH_3)_2{\cdot}4H_2O$ (M= Mn, Co) with di-2-pyridyl ketone, $(py)_2CO$, and NaN_3 in CH_3OH or CH_3OH/H_2O allow isolation of the tetranuclear compounds $[Mn_4(\mu_{1,1}\text{-}N_3)_2(N_3)_2\{(py)_2C(OH)O\}_2\{(py)_2C(OCH_3)O\}_2]$ (**1**) and $[Co_4(\mu_{1,1}\text{-}N_3)_2(N_3)_2\{(py)_2C(OH)O\}_2\{(py)_2C(OCH_3)O\}_2]{\cdot}2H_2O$ (**2**). X-ray diffraction analysis reveals defective double-cubane tetrameric entities in which the Mn^{II} or Co^{II} atoms are linked by $\mu_{1,1}\text{-}N_3$ bridges and two kinds of O-bridges. The molar magnetic susceptibility measurements of **1** and **2** in the 2–300 K range indicate weak antiferromagnetic coupling for **1** and clear bulk ferromagnetic coupling for **2**.

Introduction

There is currently a great deal of interest in the synthesis of polynuclear metal complexes exhibiting ground electronic states with a large number of unpaired electrons, since it has been discovered that a fairly large ground-state *S* value is one of the necessary requirements for molecules to be able to exhibit the behaviour of a single-molecule magnet.[1−3] The high-spin ground state results from either ferromagnetic (or ferrimagnetic) exchange interactions between the metal ions in the molecule, or topologically frustrated antiferromagnetic interactions.[4] In the known polynuclear SMM's, magnetic exchange interactions are propagated by bridging OH^-, OR^-, O^{2-}, or RCO_2^- ligands, or a combination of two or more of these groups. These interactions often lead to antiferromagnetic coupling and, thus, it is necessary to arrange the metal ions and bridging ligands in an appropriate manner so that they can give a high-spin ground state for the system. An alternative attractive approach would be the replacement of one or more of the above-mentioned bridging ligands with other groups that are more prone to ferromagnetic coupling.

One of the most well-known ferromagnetic couplers is the azido ligand when it bridges metal ions in the 1,1-fashion. Azides usually bridge through the two terminal nitrogen atoms (μ-1,3-azido) or through only one of the terminal nitrogen atoms (μ-1,1-azido) (Scheme 1). In the latter case, the coupling between the bridged paramagnetic metal ions is ferromagnetic for a wide range of M−N−M angles.[5]

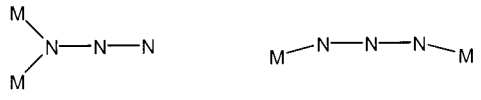

$\mu_{1,1}\text{-}N_3^-$ $\mu_{1,3}\text{-}N_3^-$

Scheme 1

The structural and electronic versatility of the azido ligand has prompted researchers to investigate its coordination chemistry in order to probe deeper into the exchange interactions of azido-bridged complexes and to correlate magnetic behaviour with molecular structure. For example, the work performed on azido-bridged polynuclear manganese(II) complexes has become a fast growing research field, not only due to the large variety of topologies that these compounds adopt, but also because of the interesting magnetic properties that arise from these systems.[6−25] In some of these compounds, the two different bridging coordination modes of the azido ligand (Scheme 1) can be found simultaneously in the same molecule, leading to materials which alternate the ferro- and antiferromagnetic superexchange pathways.

On the other hand, employment of di-2-pyridyl ketone, $(py)_2CO$ (**I**, Scheme 2), as a templating ligand for the synthesis of polynuclear complexes, has resulted, amongst others, in the construction of tetra-,[26−33] hepta-,[34] octa-,[35,36] nona-[32] and dodecanuclear[34] metal cages. The ability of $(py)_2CO$ to undergo metal-mediated nucleophilic addition of small molecules, such as water or alcohols (ROH), to the carbonyl group results in the formation of the hydrate **II** or the hemiacetal **III** (Scheme 2). The structural diversity of the resultant species stems from the ability of the singly and doubly deprotonated anions of the *gem*-diol form **II** to adopt a variety of coordination modes, and sometimes two different modes may also occur in the same complex. The monoanions of **II** and **III** usually bridge three and two metal ions, respectively (Scheme 3), giving rise to high nuclearity metal cages, while the dianion of **II** can bridge as many as five metal ions, resulting in higher nuclearity metal complexes. Since the degree of deprotonation of the *gem*-diol $(py)_2C(OH)_2$ (**II**) has been well established,

[a] Department of Chemistry, University of Patras, 265 00 Patras, Greece
[b] Departament de Química Inorgànica, Universitat de Barcelona, Diagonal 647, 08028 Barcelona, Spain
[c] Institute of Materials Science, NCSR "Demokritos", 153 10 Aghia Paraskevi Attikis, Greece
[‡] ERASMUS student in Barcelona

 © WILEY-VCH Verlag GmbH, 69451 Weinheim, 2001 1434−1948/01/0606−1567 $ 17.50+.50/0

the nuclearity of the resultant species can be considered more or less as "controlled".

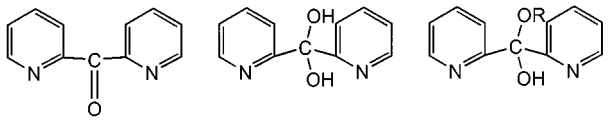

$(py)_2CO$, **I** $(py)_2C(OH)_2$, **II** $(py)_2C(OR)OH$, **III**

Scheme 2

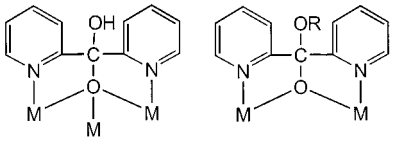

$\eta^1:\eta^3:\eta^1:\mu_3$ $\eta^1:\eta^2:\eta^1:\mu_2$

Scheme 3

The magnetic properties of the metal cages based on the anions of **II** range from noninteracting[28] to antiferromagnetic[29,30,32,34–36] and ferromagnetic-coupled[26,27,31,32] systems. This variety of magnetic properties is a consequence of the metal topology that the cages adopt, which is influenced not only by the coordination mode of the $(py)_2CO$-based anions but also by the other ligands present in the structure. Therefore, an interesting possibility is to combine the azido and $(py)_2CO$-based anionic ligands in the same compound. We report here the synthesis and magneto-structural characterisation of the tetranuclear compound $[Mn_4(\mu_{1,1}\text{-}N_3)_2(N_3)_2\{(py)_2C(OH)O\}_2\{(py)_2C(OCH_3)O\}_2]$ (**1**). In this compound the azido bridging coordination mode is end-on and should furnish a ferromagnetic superexchange pathway. We also report the synthesis and magneto-structural characterisation of the analogous cobalt(II) compound $[Co_4(\mu_{1,1}\text{-}N_3)_2(N_3)_2\{(py)_2C(OH)O\}_2\{(py)_2C(OCH_3)O\}_2]\cdot 2H_2O$ (**2**). The interest in this new compound, apart from the above considerations, is found in the fact that polynuclear Co^{II} compounds with azido bridging ligands are rare.[37–44] Previously, only two mixed azido-$(py)_2CO$ complexes with Ni^{II} as the metal ion have been published.[26,27]

Results and Discussion

Synthesis

The preparation of compounds **1** and **2** can be achieved by the reaction of $M(O_2CH_3)_2 4H_2O$ with $(py)_2CO$ and NaN_3 in CH_3OH (**1**) or CH_3OH/H_2O (**2**) at room temperature. The preparation of both complexes can be summarised by Equation (1).

The metal(II)-mediated solvolysis of $(py)_2CO$ to give the monoanions of the hydrate **II** and the hemiacetal **III** (Scheme 2) involves a nucleophilic attack of ROH molecules (R = Me or H) on the carbonyl group. In such reactions it might not be necessary for the carbonyl atom to be coordinated to the metal centre; the induced polarisation from the pyridyl nitrogen atoms might be sufficient.[45] There are few examples in which the ketone group of $(py)_2CO$ is attacked by alcohols or water in the presence of metal ions, but the presence of the monoanions of both the hydrate and the hemiacetal in the same complex is rare, with the $[Ni_4(\mu_{1,1}\text{-}N_3)_2(N_3)_2\{(py)_2C(OH)O\}_2\{(py)_2C(OCH_3)O\}_2]$[26] complex being the only example until now.

IR Spectra

Complexes **1** and **2** exhibit identical IR spectra and, thus, only the IR spectrum of **1** is discussed. This complex exhibits an intense band centred at 2061 cm^{-1}, assigned to the asymmetric stretching mode of the azide. This band is split (2074 and 2048 cm^{-1}) due to the presence of two coordination modes of the azide in the molecular structure of **1**. The spectrum does not exhibit a band in the region expected for $\nu(C{=}O)$ absorption [1684 cm^{-1} for the free $(py)_2CO$]. The nearest band is at 1600 cm^{-1} and is assigned as a pyridine stretching mode raised from 1582 cm^{-1} on coordination, as observed previously,[30] on complex formation involving the solvolysis of $(py)_2CO$. Additionally, the spectrum reveals the bands corresponding to the skeleton vibrations of the coordinated $(py)_2CO$ which appear at slightly shifted frequencies relative to the free ligand. Thus, bands for coordinated $\{(py)_2C(OR)O\}^-$ [free $(py)_2CO$] are: 1570 [1578/1544] and 1114 [998] cm^{-1} attributed to the pyridyl ring stretching, 774/754 [753/742] for the pyridyl ring C–H out-of-plane bending, and 680 [662] due to the pyridyl ring in-plane vibration.

X-ray Crystal Structures

$[Mn_4(\mu_{1,1}\text{-}N_3)_2(N_3)_2\{(py)_2C(OH)O\}_2\{(py)_2C(OCH_3)O\}_2]$ (1)

A labelled plot of the structure of the tetranuclear compound $[Mn_4(\mu_{1,1}\text{-}N_3)_2(N_3)_2\{(py)_2C(OH)O\}_2\{(py)_2C(OCH_3)\text{-}O\}_2]\cdot 2H_2O$ (**1**) is shown in Figure 1. Selected distances and angles are listed in Table 1. The structure consists of centrosymmetric tetranuclear molecules. The four Mn^{II} atoms are located at four corners of a defective double

$$4M(O_2CCH_3)_2\cdot 4H_2O + 4NaN_3 + 4(py)_2CO + 2CH_3OH + nH_2O \xrightarrow[20\,^\circ C]{S} [M_4(\mu_{1,1}\text{-}N_3)_2(N_3)_2\{(py)_2C(OH)O\}_2\{(py)_2C(OCH_3)O\}_2]\cdot nH_2O + 4CH_3CO_2H + 4CH_3CO_2Na + 14H_2O \quad (1)$$

1: M = Mn^{II}, S = CH_3OH

2: M = Co^{II}, n = 2, S = CH_3OH/H_2O

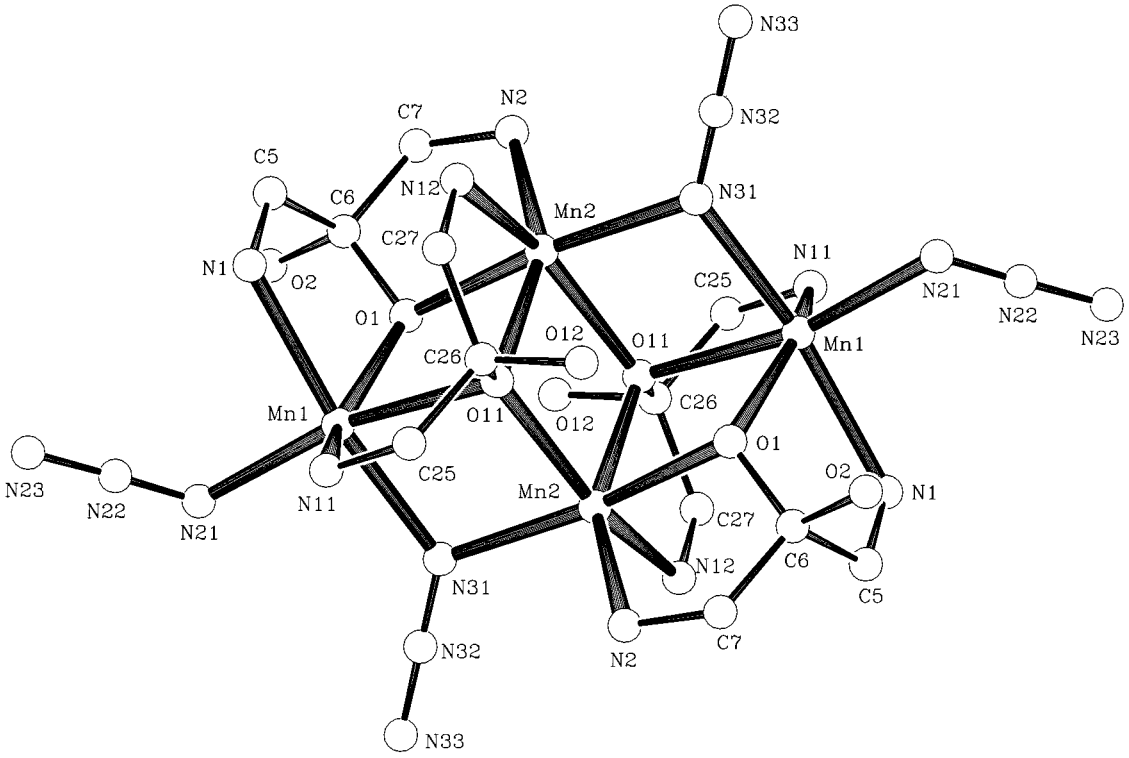

Figure 1. Labelled plot of $[Mn_4(\mu_{1,1}\text{-}N_3)_2(N_3)_2\{(py)_2C(OH)O\}_2\{(py)_2C(OCH_3)\text{-}O\}_2]\cdot 2H_2O$ (**1**); the structure and numbering of the atoms is the same for compound **2**, replacing Mn(1) and Mn(2) with Co(1) and Co(2), respectively

Table 1. Selected distances (Å) and angles (°) for $[Mn_4(\mu_{1,1}\text{-}N_3)_2(N_3)_2\{(py)_2C(OH)O\}_2\{(py)_2C(OCH_3)O\}_2]$ (**1**)[a]

Mn(1)···Mn(2)	3.370(1)	Mn(1)···Mn(2)#1	3.395(3)
Mn(1)···Mn(1)#1	5.892(1)	Mn(2)···Mn(2)#1	3.322(3)
Mn(1)−N(21)	2.111(5)	Mn(1)−O(1)	2.155(3)
Mn(1)−N(31)	2.210(5)	Mn(1)−N(11)	2.287(5)
Mn(1)−N(1)	2.305(5)	Mn(1)−O(11)	2.305(3)
Mn(2)−O(11)	2.137(3)	Mn(2)−N(31)#1	2.167(4)
Mn(2)−O(11)#1	2.186(3)	Mn(2)−N(2)	2.218(4)
Mn(2)−O(1)	2.242(3)	Mn(2)−N(12)	2.279(4)
O(1)−C(6)	1.378(6)	O(11)−C(26)	1.399(6)
N(31)−N(32)	1.195(6)	N(21)−N(22)	1.170(8)
N(22)−N(23)	1.167(9)	N(32)−N(33)	1.152(8)
N(21)−Mn(1)−O(1)	114.7(2)	N(21)−Mn(1)−N(31)	94.0(2)
O(1)−Mn(1)−N(31)	97.2(2)	N(21)−Mn(1)−N(11)	96.9(2)
O(1)−Mn(1)−N(11)	145.8(2)	N(31)−Mn(1)−N(11)	93.2(2)
N(21)−Mn(1)−N(1)	90.8(2)	O(1)−Mn(1)−N(1)	71.7(1)
N(31)−Mn(1)−N(1)	168.8(2)	N(11)−Mn(1)−N(1)	96.2(2)
N(21)−Mn(1)−O(11)	165.3(2)	O(1)−Mn(1)−O(11)	78.7(1)
N(31)−Mn(1)−O(11)	77.5(1)	N(11)−Mn(1)−O(11)	71.8(1)
N(1)−Mn(1)−O(11)	99.7(1)	O(11)−Mn(2)−N(31)#1	107.5(2)
O(11)−Mn(2)−O(11)#1	79.5(1)	N(31)#1−Mn(2)−O(11)#1	81.0(1)
O(11)−Mn(2)−N(2)	152.6(1)	N(31)#1−Mn(2)−N(2)	99.7(2)
O(11)#1−Mn(2)−N(2)	107.7(1)	O(11)−Mn(2)−O(1)	80.5(1)
N(31)#1−Mn(2)−O(1)	164.4(2)	O(11)#1−Mn(2)−O(1)	87.6(1)
N(2)−Mn(2)−O(1)	73.6(1)	O(11)−Mn(2)−N(12)	73.4(1)
N(31)#1−Mn(2)−N(12)	92.5(2)	O(11)#1−Mn(2)−N(12)	148.9(1)
N(2)−Mn(2)−N(12)	103.3(2)	O(1)−Mn(2)−N(12)	102.6(1)
Mn(1)−O(1)−Mn(2)	100.0(1)	Mn(2)−O(11)−Mn(2)#1	100.4(1)
Mn(2)−O(11)−Mn(1)	98.6(1)	Mn(2)#1−O(11)−Mn(1)	98.1(1)
N(22)−N(21)−Mn(1)	125.1(5)	N(32)−N(31)−Mn(2)#1	125.0(4)
N(32)−N(31)−Mn(1)	131.8(4)	Mn(2)#1−N(31)−Mn(1)	101.7(2)
N(23)−N(22)−N(21)	179.4(10)	N(33)−N(32)−N(31)	179.0(8)

[a] Symmetry transformations used to generate equivalent atoms #1: $-x, -y, -z + 1$.

Table 2. Selected distances (Å) and angles (°) for $[Co_4(\mu_{1,1}\text{-}N_3)_2(N_3)_2\{(py)_2C(OH)O\}_2\{(py)_2C(OCH_3)O\}_2]\cdot 2H_2O$ (**2**)[a]

Co(1)···Co(2)	3.184(1)	Co(1)···Co(2)#1	3.286(1)
Co(1)···Co(1)#1	5.640(1)	Co(2)···Co(2)#1	3.172(1)
Co(1)−O(1)	2.063(2)	Co(1)−N(21)	2.083(3)
Co(1)−N(31)	2.099(3)	Co(1)−N(11)	2.115(3)
Co(1)−N(1)	2.170(3)	Co(1)−O(11)	2.227(2)
Co(2)−O(11)	2.030(2)	Co(2)−N(31)#1	2.058(3)
Co(2)−N(2)	2.089(3)	Co(2)−N(12)	2.151(3)
Co(2)−O(1)	2.151(2)	Co(2)−O(11)#1	2.165(2)
O(1)−C(6)	1.378(3)	O(11)−C(26)	1.379(3)
N(31)−N(32)	1.193(4)	N(21)−N(22)	1.141(5)
C(6)−O(2)	1.424(4)	N(22)−N(23)	1.139(6)
N(32)−N(33)	1.141(4)		
O(1)−Co(1)−N(21)	110.8(1)	O(1)−Co(1)−N(31)	94.4(1)
N(21)−Co(1)−N(31)	91.1(1)	O(1)−Co(1)−N(11)	148.2(1)
N(21)−Co(1)−N(11)	97.8(1)	N(31)−Co(1)−N(11)	98.8(1)
O(1)−Co(1)−N(1)	75.4(1)	N(21)−Co(1)−N(1)	89.8(1)
N(31)−Co(1)−N(1)	169.3(1)	N(11)−Co(1)−N(1)	91.6(1)
O(1)−Co(1)−O(11)	80.4(1)	N(21)−Co(1)−O(11)	164.9(1)
N(31)−Co(1)−O(11)	77.6(1)	N(11)−Co(1)−O(11)	74.4(1)
N(1)−Co(1)−O(11)	103.1(1)	O(11)−Co(2)−N(31)#1	103.8(1)
O(11)−Co(2)−N(2)	154.9(1)	N(31)#1−Co(2)−N(2)	99.8(1)
O(11)−Co(2)−N(12)	77.6(1)	N(31)#1−Co(2)−N(12)	91.1(1)
N(2)−Co(2)−N(12)	93.7(1)	O(11)−Co(2)−O(1)	83.0(1)
N(31)#1−Co(2)−O(1)	164.4(1)	N(2)−Co(2)−O(1)	76.3(1)
N(12)−Co(2)−O(1)	104.2(1)	O(11)−Co(2)−O(11)#1	81.8(1)
N(31)#1−Co(2)−O(11)#1	79.9(1)	N(2)−Co(2)−O(11)#1	110.9(1)
N(12)−Co(2)−O(11)#1	154.8(1)	O(1)−Co(2)−O(11)#1	87.3(1)
Co(1)−O(1)−Co(2)	98.1(1)	Co(2)−O(11)−Co(2)#1	98.2(1)
Co(2)−O(11)−Co(1)	96.7(1)	Co(2)#1−O(11)−Co(1)	96.8(1)
N(22)−N(21)−Co(1)	131.7(3)	N(32)−N(31)−Co(2)#1	127.4(2)
N(32)−N(31)−Co(1)	125.5(2)	Co(2)#1−N(31)−Co(1)	104.5(1)
N(23)−N(22)−N(21)	178.2(7)	N(33)−N(32)−N(31)	178.9(4)

[a] Symmetry transformations used to generate equivalent atoms #1: $-x+1, -y, -z+2$.

cubane (two cubanes sharing one face and each missing one vertex) and bridged by means of two end-on azido ligands and O atoms from the $(py)_2C(OH)O^-$ and $(py)_2C(OCH_3)O^-$ anions (Scheme 3). Peripheral ligation is provided by the nitrogen atoms of the two terminal azido ligands and the eight 2-pyridyl rings. The O(11) atoms of the $(py)_2C(OH)O^-$ ligands are triply bridging with distances to the Mn^{II} atoms in the range 2.137(3)−2.305(3) Å. The Mn(1)−O(11)−Mn(2) angles are 98.1(1)° and 98.6(1)°. The O(1) atoms of the $(py)_2C(OCH_3)O^-$ ligands are doubly bridging with distances of 2.155(3) and 2.242(3) Å to Mn(1) and Mn(2), respectively. The Mn(1)−O(1)−Mn(2) angle is 100.0(1)°. One O atom of each $(py)_2C(OH)O^-$ and $(py)_2C(OCH_3)O^-$ ligands remains protonated and unbound to the metal atoms. Mn(1) and Mn(2) are also bridged by the N(31) atom of the $\mu_{1,1}$-azido ligand. The Mn(1)−N(31) and Mn(2)−N(31) distances are 2.210(5) and 2.167(4) Å, respectively. The Mn(1)−N(31)−Mn(2) angle is 101.7(2)°. The Mn(1) octahedral coordination is completed by the N(11) atom of the $(py)_2C(OH)O^-$ ligand, the N(1) atom of the $(py)_2C(OCH_3)O^-$ ligand and the N(21) atom of the terminal azido ligand. The Mn(2) octahedral coordination is completed by the N(2) and the N(12) atoms of the $(py)_2C(OCH_3)O^-$ and $(py)_2C(OH)O^-$ ligands, respectively.

$Co_4(\mu_{1,1}\text{-}N_3)_2(N_3)_2\{(py)_2C(OH)O\}_2\{(py)_2C(OCH_3)O\}_2]\cdot 2H_2O$ (2)

Selected distances and angles are presented in Table 2. The structure of **2** is very similar to the structure of **1**. As expected, distances and angles are slightly different with respect to the analogous parameters in **1**: bond lengths are shorter in **2** and bond angles in the bridging region are ±3°, for details see Table 2.

Magnetic Properties

The $\chi_M T$ vs. T plot of **1** in the 300−2 K range is shown in Figure 2. $\chi_M T$ has a practically constant value of 17.1 cm^3 K mol^{-1} in the 300−115 K range and then decreases to 14.3 cm^3 K mol^{-1} at 2 K. χ_M increases on cooling and does not have any maximum in the studied temperature range. The overall behaviour of **1** indicates a dominant weak antiferromagnetic coupling. The magnetic data of **1**, according to its structure (Scheme 4), should be analysed by an analytical expression based on the Hamiltonian in Equation (2)

$$H = -J_1(S_1S_2 + S_3S_4) - J_2(S_2S_3 + S_4S_1) - J_3(S_2S_4) - J_4(S_1S_3) \quad (2)$$

for local spin values $S = 5/2$. The number of the spins follows the numbering of the atoms in Scheme 4 (J_4 correlates atoms 1 and 3).

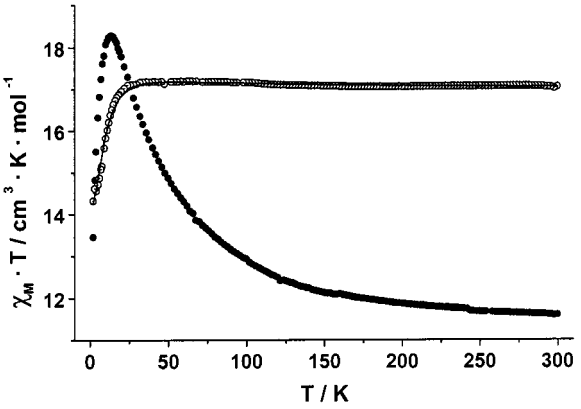

Figure 2. $\chi_M T$ plot versus T for compounds **1** (dot centred circles) and **2** (filled circles); solid lines correspond to the best fit obtained for **1**

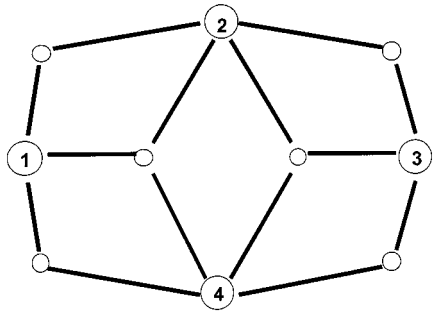

Scheme 4

Although the analytical expression with four different J values does not exist, the eigen values of the spin states can be calculated by means of the full-matrix diagonalisation of Equation (2), by using the CLUMAG program.[47] The best-fit parameters obtained were $J_1 = -1.56$ cm^{-1}, $J_2 = 0.53$ cm^{-1}, $J_3 = -1.49$ cm^{-1}, $J_4 = -0.01$ cm^{-1}, $g = 1.98$, $R = 2.1 \times 10^{-5}$.

The molar magnetisation data at 2 K in the 0−5 T range are shown in Figure 3. On increasing the field, the magnetisation value increases slowly with reference to the expected value for four isolated Mn^{II} atoms with $g = 2.0$, and the final value of 14.91 is far from the expected value of 20, which is in agreement with a dominant antiferromagnetic coupling. The coupling between Mn(2) and Mn(1) through the $\mu_{1,1}$-azido ligand with a Mn−N−Mn angle of 101.7(2)° should be ferromagnetic,[5] but for complexes containing the $\{Mn_2(\mu_2\text{-OR})_2\}^{2+}$ core and an Mn−O−Mn angle in the range of 80−110°, the coupling should be antiferromagnetic,[48] as is the case in **1**. For this reason the superexchange pathway through simultaneous $\mu_{1,1}$-azido and μ-O bridges is indeterminate in sign. From Equation (2), J_1 and J_2 are indistinguishable by symmetry; the values of $J_1 = -1.56$ cm^{-1} and $J_2 = 0.53$ cm^{-1} may be reasonably assigned, by sign, to the $(\mu_2\text{-OR})_2$ and {(μ-OR)($\mu_{1,1}$-Azido)} superexchange pathways, respectively. The value of $J_3 = -1.49$ cm^{-1} is in accordance with a superexchange pathway only through the μ-O bridges. The negligible value of J_4 is, as expected, due to the large distance between the 1 and 3 spin carriers. The EPR spectrum of **1** recorded on a powdered sample at room temperature shows an isotropic signal centred at $g = 2.02$ with a peak-to-peak line width of 1340 G. This signal is temperature dependent and the spectrum at 4 K shows a complicated pattern of signals.

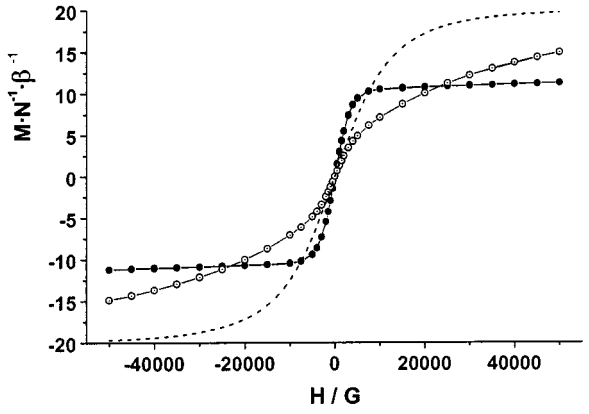

Figure 3. Molar magnetisation isotherms at 2 K for compounds **1** (dot centred circles) and **2** (filled circles); the dashed line corresponds to the generated Brillouin behaviour for four isolated Mn^{II} ions

The plot of $\chi_M T$ vs. T for **2** in the 300−2 K range is also shown in Figure 2 (filled circles). $\chi_M T$ increases quickly on cooling from 11.60 cm^3 K mol^{-1} at 300 K to a maximum of 18.3 cm^3 K mol^{-1} at 13 K, after which it decreases to 13.4 cm^3 K mol^{-1} at 2 K. χ_M increases on cooling and does not have any maximum in the temperature range studied. The overall behaviour of **2** corresponds to a ferromagnetically coupled system. The strong ferromagnetic interaction in **2** is confirmed by the molar magnetisation measurement at 2 K, which shows a quick increase in M by increasing the external field, arriving at a final value of 11.26 (Figure 3). This strong coupling between Co(2) and Co(1) permits us to assume that the interactions through the $\mu_{1,1}$-azido and the μ-OR$^-$ bridge with a Co−O−Co angle of 96.8(1)° are both ferromagnetic, indicating a magnetic behaviour close to the related Ni^{II} derivatives previously reported.[26,27] Analysis of the coupling constants for a high-spin rhombic cobalt(II) tetramer is not possible by means of an effective Hamiltonian based on four $S = 3/2$ spins, due to the large anisotropy of this ion. At low temperature the local spin of the Co^{II} is closer to 1/2, and hence the low-temperature data are better defined as an $S_T = 2$ system with a large g_{eff} value.

The above description is in agreement with the EPR spectrum of **2** recorded on a powdered sample at 4 K (Figure 4), which shows only one absorption at very low field. For an axial integer $S = 2$ spin system, the zero-field interaction (D parameter) splits the m_s levels into two doublets $m_s = |\pm 2>$ and $|\pm 1>$ and one $m_s = |0>$ state. Transitions be-

tween these Kramer doublets are not possible due to the large D value expected for the cobalt(II) ion. For a rhombic distortion, the E parameter splits the $m_s = |\pm 2>$ and $|\pm 1>$ Kramer doublets giving a Δ_2 and Δ_1 gap at zero field. The Δ_1 increase is strongly dependent on E and is usually much greater than the $g\beta H$ energy of an X-band measurement. In contrast, the Δ_2 increase is a function of E^2/D and the ± 2 transition usually lies in the low-field region of the spectra.[49] The expected spectra for an $S = 2$ system then consist of only one signal at very low field, which is in agreement with the experimental spectrum of **2**, and the above assumption to avoid treatment of this system as a simple tetramer of 3/2 spins is correct. This type of EPR spectra is similar to those of manganese(III) and iron(IV) spectra reported in the literature.[50,51]

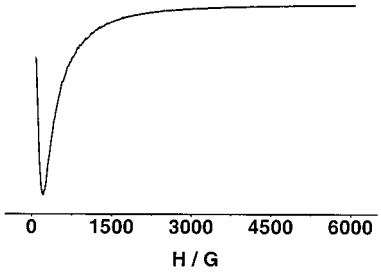

Figure 4. X-band EPR spectrum of a powdered sample of compound **2**, showing the ± 2 transition at low field corresponding to the $S = 2$ anisotropic ground state

Experimental Section

Physical Methods: Magnetic susceptibility measurements were carried out for polycrystalline samples of **1** and **2** with a SQUID susceptometer working in the range 2−300 K under magnetic fields of approximately 0.1 T. Diamagnetic corrections were estimated from Pascal Tables. The infrared spectra (4000−400 cm^{-1}) were recorded from KBr pellets on a Nicolet 520 FTIR spectrometer. EPR spectra were recorded on a Bruker ES200 spectrometer at X-band frequency.

Preparation of $[Mn_4(\mu_{1,1}\text{-}N_3)_2(N_3)_2\{(py)_2C(OH)O\}_2\{(py)_2C(OCH_3)O\}_2]$ (1): Solid $Mn(O_2CCH_3)_2{\cdot}4H_2O$ (0.15 g, 0.61 mmol) was dissolved with stirring in a solution of $(py)_2CO$ (0.22 g, 1.19 mmol) and NaN_3 (0.08 g, 1.23 mmol) in CH_3OH (20 cm^3). The pale brown-yellow solution was allowed to slowly concentrate by evaporation at room temperature for 24 h. The resultant orange well-formed crystals were collected by filtration, washed with small amounts of CH_3OH (5 cm^3) and Et_2O (2 × 5 cm^3), and dried in vacuo. Yield: 95 mg, 50%. − $C_{46}H_{40}Mn_4N_{20}O_8$ (1220.7): calcd. C 45.26, H 3.30, N 22.95; found C 45.12, H 3.28, N 22.97. − Selected IR data (KBr pellet): $\tilde{\nu}$ = 3074 (w), 2964 (w), 2074 (vs), 2048 (vs), 1600 (s), 1570 (m), 1470 (m), 1438 (s), 1334 (m), 1060 (s), 1014 (m), 776 (m), 754 (m), 680 (m) cm^{-1}. Complex **1** can also be isolated by employing $Mn(O_2CCH_3)_2 4H_2O/(py)_2CO/NaN_3$ molar ratios of 1:1:1, 1:3:3, 1:2:4 and 1:4:4.

Preparation of $[Co_4(\mu_{1,1}\text{-}N_3)_2(N_3)_2\{(py)_2C(OH)O\}_2\{(py)_2C(OCH_3)O\}_2]{\cdot}2H_2O$ (2): A solution of NaN_3 (0.04 g, 0.61 mmol) in H_2O (5 cm^3) was added to a stirred solution of $Co(O_2CCH_3)_2{\cdot}4H_2O$ (0.15 g, 0.61 mmol) and $(py)_2CO$ (0.11 g, 0.60 mmol) in CH_3OH (20 cm^3) at ambient temperature. Crystallisation of a pink solid began after ca. 20 min. When precipitation was judged to be complete, the pink microcrystalline solid was collected by filtration, washed with small amounts of CH_3OH (5 cm^3) and Et_2O (2 × 5 cm^3), and dried in vacuo. Yield: 140 mg, 75%. − $C_{46}H_{44}Co_4N_{20}O_{10}$ (1272.7): calcd. C 43.41, H 3.48, N 22.01; found C 43.60, H 3.32, N 22.38. − Selected IR data (KBr pellet): $\tilde{\nu}$ = 3074 (w), 2964 (w), 2074 (vs), 2048 (vs), 1600 (s), 1570 (m), 1470 (m), 1438 (s), 1334 (m), 1060 (s), 1014 (m), 776 (m), 754 (m), 680 (m) cm^{-1}. X-ray quality crystals of **2** were obtained by slow diffusion of a dilute methanolic solution of $(py)_2CO$ into a dilute aqueous solution of $Co(O_2CCH_3)_2 4H_2O$ and NaN_3. Complex **2** can also be isolated by employing $Co(O_2CCH_3)_2 4H_2O/(py)_2CO/NaN_3$ molar ratios of 1:2:2, 1:3:3, 1:2:4 and 1:4:4.

CAUTION: Azide salts are potentially explosive and should be handled in small quantities.

X-ray Structure Determinations: Crystals of **1** and **2** were mounted in air and in a capillary filled with drops of the mother liquor, respectively. Diffraction measurements were made on a Crystal Logic Dual Goniometer diffractometer using graphite-monochromated Mo-K_α radiation. Complete crystal data and parameters for data collection and refinement are listed in Table 3. Unit cell dimensions were determined and refined using the angular settings of 25 automatically centred reflections in the range $11 < 2\theta < 23°$.

Table 3. Crystal data and structure refinement for $[Mn_4(\mu_{1,1}\text{-}N_3)_2(N_3)_2\{(py)_2C(OH)O\}_2\{(py)_2C(OCH_3)O\}_2]$ (**1**) and $[Co_4(\mu_{1,1}\text{-}N_3)_2(N_3)_2\{(py)_2C(OH)O\}_2\{(py)_2C(OCH_3)\text{-}O\}_2]{\cdot}2H_2O$ (**2**)

Parameter	**1**	**2**
Empirical formula	$C_{46}H_{40}Mn_4N_{20}O_8$	$C_{46}H_{44}Co_4N_{20}O_{10}$
Mol. wt.	1220.72	1272.74
Colour and habit	Orange prisms	Pink prisms
Crystal size [mm]	0.10 × 0.20 × 0.30	0.15 × 0.35 × 0.55
Crystal system	Monoclinic	Triclinic
Space group	$P2_1/n$	$P\bar{1}$
a [Å]	13.391(4)	13.593(8)
b [Å]	12.503(4)	10.143(6)
c [Å]	16.007(6)	10.272(6)
α [°]	90.00	82.37(2)
β [°]	107.08(1)	73.83(2)
γ [°]	90.00	88.50(2)
V [Å^3]	2561.5(2)	1348.0(1)
Z	2	1
ρ [Mg m^{-3}]	1.583	1.568
T [°C]	25	25
λ(Mo-K_α) [Å]	0.71073	0.71073
μ [mm^{-1}]	1.037	1.284
F(000)	1240	648
$2\theta_{max}$ [°]	48.9	50.0
Index ranges [°]	$-15 \le h \le 14$	$-16 \le h \le 15$
	$0 \le k \le 14$	$-12 \le k \le 11$
	$0 \le l \le 18$	$-12 \le l \le 0$
No. of reflections collected	4369	5013
No. of indep. refls./R_{int}	4208/0.0506	4730/0.0148
Data with $I > 2\sigma(I)$	4208	4238
Parameters refined	432	433
$[\Delta/\sigma]_{max}$	0.014	0.034
GOF (on F^2)	1.023	1.093
$R1$[a]	0.0554	0.0363
$wR2$[b]	0.1433	0.1120
Residuals [e Å^{-3}]	0.564/-0.630	0.625/−0.447

[a] $R1 = \Sigma(|F_o| - |F_c|)/\Sigma(|F_o|)$. − [b] $wR2 = \{\Sigma[w[(F_o^2 - F_c^2)^2]/\Sigma[w(F_o^2)^2]\}^{1/2}$.

Intensity data were recorded using the θ-2θ scan method. Three standard reflections monitored every 97 reflections showed less than 3% variation and no decay. Lorentz, polarisation and Ψ-scan absorption (only for **2**) corrections were applied with the Crystal Logic software.

The structures were solved by direct methods using SHELXS-86[52] and refined by full-matrix least-squares techniques on F^2 with SHELXL-93.[53] All hydrogen atoms [except those of C(12) in **2** which were introduced at calculated positions as riding on their bonded atom] were located by difference maps and their positions refined isotropically. All non-hydrogen atoms of **1** and **2** were refined anisotropically, with the exception of the oxygen atoms of the solvent H_2O molecules in **2** which were refined isotropically with fixed occupation factors. Further details (excluding structure factors) for the structures reported in this paper have been deposited with the Cambridge Crystallographic Data Centre as supplementary publication nos. CCDC-147441 (**1**) and CCDC-147442 (**2**). Copies of the data can be obtained free of charge on application to CCDC, 12 Union Road, Cambridge CB2 1EZ [Fax: (internat.) +44-1223/336-033; E-mail: deposit@ccdc.cam.ac.uk].

Acknowledgments

This research was partially supported by CICYT (Grant PB96/0163), by the Research Committee of the University of Patras (K. CARATHEODORY Program No 1941 to S.P.P.), and the Greek Secretariat of Athletics, OPAP (to A. T.).

[1] D. Gatteschi, R. Sessoli, A. Cornia, *Chem. Commun.* **2000**, 725.
[2] J. Yoo, E. K. Brechin, A. Yamaguchi, M. Nakano, J. C. Huffman, A. L. Maniero, L. -C. Brunel, K. Awaga, H. Ishimoto, G. Christou, D. N. Hendrickson, *Inorg. Chem.* **2000**, *39*, 3615, and references cited therein.
[3] [3a] R. E. P. Winpenny, *Comments Inorg. Chem.* **1999**, *20*, 233. – [3b] J. M. Clemente-Juan, E. Coronado, *Coord. Chem. Rev.* **1999**, *193–195*, 361, and references cited therein.
[4] G. Aromi, J. -P. Claude, M. J. Knapp, J. C. Huffman, D. N. Hendrickson, G. Christou, *J. Am. Chem. Soc.* **1998**, *120*, 2977.
[5] E. Ruiz, J. Cano, S. Alvarez, P. Alemany, *J. Am. Chem. Soc.* **1998**, *120*, 11122.
[6] M. A. M. Abu-Youssef, A. Escuer, D. Gatteschi, M. A. S. Goher, F. A. Mautner, R. Vicente, *Inorg. Chem.* **1999**, *38*, 5716.
[7] M. A. M. Abu-Youssef, A. Escuer, M. A. S. Goher, F. A. Mautner, G. J. Reis, R. Vicente, *Angew. Chem. Int. Ed.* **2000**, *39*, 1624.
[8] M. A. M. Abu-Youssef, A. Escuer, M. A. S. Goher, F. A. Mautner, R. Vicente, *Eur. J. Inorg. Chem.* **1999**, 687.
[9] R. Cortés, M. Drillon, X. Solans, L. Lezama, T. Rojo, *Inorg. Chem.* **1997**, *36*, 677.
[10] R. Cortés, L. Lezama, J. L. Pizarro, M. I. Arriortua, T. Rojo, *Angew. Chem. Int. Ed. Engl.* **1996**, *35*, 1810.
[11] R. Cortés, L. Lezama, J. L. Pizarro, M. I. Arriortua, X. Solans, T. Rojo, *Angew. Chem. Int. Ed. Engl.* **1994**, *33*, 2488.
[12] R. Cortés, J. L. Pizarro, L. Lezama, M. I. Arriortua, T. Rojo, *Inorg. Chem.* **1994**, *33*, 2697.
[13] A. Escuer, R. Vicente, M. A. S. Goher, F. A. Mautner, *Inorg. Chem.* **1995**, *34*, 5707.
[14] A. Escuer, R. Vicente, M. A. S. Goher, F. A. Mautner, *Inorg. Chem.* **1996**, *35*, 6386.
[15] A. Escuer, R. Vicente, M. A. S. Goher, F. A. Mautner, *Inorg. Chem.* **1997**, *36*, 3440.
[16] A. Escuer, R. Vicente, M. A. S. Goher, F. A. Mautner, *J. Chem. Soc., Dalton Trans.* **1997**, 4431.
[17] A. Escuer, R. Vicente, M. A. S. Goher, F. A. Mautner, *Inorg. Chem.* **1998**, *37*, 782.
[18] M. A. S. Goher, N. A. Al-Salem, F. A. Mautner, *J. Coord. Chem.* **1998**, 119.
[19] M. A. S. Goher and F. A. Mautner, *Croat. Chim. Acta* **1990**, *63*, 559.
[20] J. L. Manson, A. M. Arif, J. S. Miller, *Chem. Commun.* **1999**, 1479.
[21] F. A. Mautner, R. Cortés, L. Lezama, T. Rojo, *Angew. Chem. Int. Ed. Engl.* **1996**, *35*, 78.
[22] F. A. Mautner, S. Hanna, R. Cortés, L. Lezama, M. G. Barandika, T. Rojo, *Inorg. Chem.* **1999**, *38*, 4647.
[23] H. Y. Shen, D. Z. Liao, Z.-H. Jiang, S.-P. Yan, B.-W. Sun, G.-L. Wang, X.-K. Yao, H.-G. Wang., *Chem. Lett.* **1998**, 469.
[24] Z. Shen, J.-L. Zuo, Z. Yu, Y. Zhang, J.-F. Bai, C.-M. Che, H.-K. Fun, J.-J. Vittal, X. -Z. You, *J. Chem. Soc., Dalton Trans.* **1999**, 3393.
[25] M. A. Youssef, A. Escuer, M. A. S. Goher, F. A. Mautner, R. Vicente, *J. Chem. Soc., Dalton Trans.* **2000**, 413.
[26] Z. E. Serna, L Lezama, M. K. Urtiaga, M. I. Arriortua, M. G. Barandika, R. Cortés, T. Rojo, *Angew. Chem. Int. Ed.* **2000**, *39*, 344.
[27] Z. E. Serna, M. G. Barandika, R. Cortés, M. K. Urtiaga, G. A. Barberis, T. Rojo, *J. Chem. Soc., Dalton Trans.* **2000**, 29.
[28] A. C. Deveson, S. L. Heath, C. J. Harding, A. K. Powell, *J. Chem. Soc., Dalton Trans.* **1996**, 3173.
[29] J. Manzur, A. M. García, M. T. Garland, V. Acuña, O. Gonzalez, O. Peña, A. M. Atria, E. Spodine, *Polyhedron* **1996**, *105*, 821.
[30] V. Tangoulis, C. P. Raptopoulou, S. Paschalidou, A. E. Tsohos, E. G. Bakalbassis, A. Terzis, S. P. Perlepes, *Inorg. Chem.* **1997**, *36*, 5270.
[31] S. R. Breeze,S. Wang, J. E. Greedan, N. P. Raju, *Inorg. Chem.* **1996**, *35*, 6944.
[32] A. Tsohos, S. Dionyssopoulou, A. Terzis, E. G. Bakalbassis, S. P. Perlepes, *Angew. Chem. Int. Ed.* **1999**, *38*, 983.
[33] M.-L. Tong, H. K. Lee, S.-L. Zheng, X. -M. Chen, *Chem. Lett.* **1999**, 1087.
[34] V. Tangoulis, C. P. Raptopoulou, S. Paschalidou, E. G. Bakalbassis, S. P. Perlepes, A. Terzis, *Angew. Chem. Int. Ed. Engl.* **1997**, *36*, 1083.
[35] V. Tangoulis, S. Paschalidou, E. G. Bakalbassis, S. P. Perlepes, C. P. Raptopoulou, A. Terzis, *Chem. Commun.* **1996**, 1297.
[36] V. Tangoulis, C. P. Raptopoulou, A. Terzis, S. Paschalidou, S. P. Perlepes, E. G. Bakalbassis, *Inorg. Chem.* **1997**, *36*, 3996.
[37] M. G. B. Drew, F. S. Esho, A. Lavery, S. M. Nelson, *J. Chem. Soc., Dalton Trans.* **1984**, 545.
[38] A. Bencini, C. A. Ghilardi, S. Midollini, A. Orlandini, *Inorg. Chem.* **1989**, *28*, 1958.
[39] G. De Munno, T. Poerio, G. Viau, M. Julve, F. Lloret, Y. Journaux, E. Riviere, *Chem. Commun.* **1996**, 2587.
[40] M. G. B. Drew, C. J. Harding, J. Nelson, *Inorg. Chim. Acta* **1996**, *246*, 73.
[41] A. Escuer, C. J. Harding, Y. Dussart, J. Nelson, V. McKee, R. Vicente, *J. Chem. Soc., Dalton Trans.* **1999**, 223.
[42] G. Viau, M. G. Lombardi, G. De Munno, M. Julve, F. Lloret, J. Faus, A. Caneschi, J. M. Clemente-Juan, *Chem. Commun.* **1997**, 1195.
[43] F. Meyer, K. Heinze, B. Nuber, L. Zsolnai, *J. Chem. Soc., Dalton Trans.* **1998**, 207.
[44] M. A. S. Goher, F. Mautner, *Polyhedron* **1999**, *18*, 2339.
[45] E. W. Constable, *Metals and Ligand Reactivity*, 2nd ed., VCH, Weinheim, Germany, **1996**, pp. 46–48, 57–59.
[46] C. K. Johnson, ORTEP II, Report ORNL-5138, Oak Ridge National Laboratory, Oak Ridge, TN, **1976**.

[47] D. Gatteschi, L. Pardi, *Gazz. Chim. Ital.* **1993**, *123*, 231.
[48] E. Ruiz, S. Alvarez, P. Alemany, *Chem. Commun.* **1998**, 2767.
[49] A. Abragam, B. Bleaney, in *Electron Paramagnetic Resonance of Transition Ions*, Oxford University Press, New York, **1986**, pp. 209−216.
[50] S. L. Dexheimer, J. W. Gohdes, M. K. Chan, K. S. Hagen, W. H. Armstrong, M. P. Klein, *J. Am. Chem. Soc.* **1989**, *111*, 8923.
[51] K. L. Kostka, B. G. Fox, M. P. Hendrich, T. J. Collins, C. E. F. Rickard, L. J. Wright, E. Münch, *J. Am. Chem. Soc.* **1993**, *115*, 6746.
[52] G. M. Sheldrick, *SHELXS-86*, *Program for the Solution of Crystal Structures*, University of Göttingen, Germany, **1986.**
[53] G. M. Sheldrick, *SHELXL-93*, *Program for the Refinement of Crystal Structures*, University of Göttingen, Germany, **1993.**

Received October 9, 2000
[I00378]

X-ray Structure, Magnetic and Catalytic Properties of a Cyclic Trinuclear $Co^{II}/Co^{III}/Co^{III}$ Complex with a μ^3-Hydroxy Anion

Marta Łukasiewicz,[a] Zbigniew Ciunik,[a] Jarosław Mazurek,[a] Jarosław Sobczak,[a] Aldona Staroń,[b] Stanisław Wołowiec,*[b] and Józef J. Ziółkowski*[a]

Keywords: Cobalt / Mixed valent complexes / X-ray structure

The mixed-valent cyclic trinuclear cobalt(II)/cobalt(III)/cobalt(III) complex tris(dibenzoylmethanato-1κ^2O,O';2κ^2O,O';3κ^2O,O')(μ_3-hydroxo-1:2κ^2O;1:3κ^2O;2:3κ^2O)tetrakis(μ-pyrazolato-1:2$\kappa^4N^1N^2$;1:3$\kappa^2N^1N^2$;2:3$\kappa^2N^1N^2$)-1,2-dicobalt(III)-3-cobalt(II) with four bridging pyrazolate anions and a μ^3-hydroxy anion has been synthesized and its molecular structure has been elucidated on the basis of X-ray crystallographic, magnetic, NMR, and EPR studies. The remaining coordination sites of the pentacoordinate cobalt(II) and hexacoordinate cobalt(III) centers are occupied by oxygen donor atoms of dibenzoylmethanate anions, rendering the complex soluble in most organic solvents. The complex has been found to effectively catalyze the decomposition of *tert*-butyl hydroperoxide (TBHP) in chlorobenzene with a short induction period and a half-life of 80 min and to catalyze the oxidation of cyclohexene to 2-cyclohexen-1-one with oxygen and to 2-cyclohexen-1-ol with TBHP.

Introduction

Multinuclear complexes of transition metal ions attract a lot of attention due to their potential catalytic activity. They are constructed using many different polydentate ligands including oxygen donor anionic ligands such as carboxylates[1−8] and other oxy anions.[9,10] Nitrogen-donor bridging ligands, especially pyrazoles, which are well-suited for N,N-bridging, are frequently utilized in the construction of such systems.[11−16] Amongst polynuclear systems, cyclic trinuclear complexes constitute an important class of compounds.[1−10,14−17] Cyclic trinuclear cobalt complexes have been found to show some catalytic activity in the epoxidation of olefins[1,18] and in the autoxidation of hydrocarbons.[19] Therefore, we have focused on the synthesis, isolation, and structural characterization of another, mixed-valent trinuclear cobalt complex soluble in organic solvents. The ligands used in the synthesis were dibenzoylmethanate (DBM) and pyrazolate (pz) anions. Starting from cobalt(II) nitrate, the synthetic procedure led to the isolation of a trinuclear cyclic $Co^{III}/Co^{III}/Co^{II}$ complex, which has been characterized in the solid state by X-ray diffraction analysis. The product has been tested for its catalytic activity in the oxidation of hydrocarbons.

Results and Discussion

Synthetic Procedure and Analytical Data

The optimized synthetic route for obtaining a compound of the analytical formula $Co_3(DBM)_3(pz)_4(OH)\cdot 2THF$ (**1**·2THF) required the use of dibenzoylmethane (DBMH) and pyrazole (pzH) in a 4:3 stoichiometry and excess cobalt(II) salt under basic aerobic conditions. The yield was reasonable considering that a mixture of complexes was formed. The trinuclear complex **1**·2THF could be isolated as a pure compound by extraction into an organic solvent. Special care had to be taken due to the reactivity of **1** towards chlorinated hydrocarbons (vide infra). Brick-red crystals of **1**·2THF, which proved to be stable and analytically pure, were grown by crystallization from THF/hexane.

X-ray Crystallographic Results for the Cyclic Trinuclear Complex $Co_3(DBM)_3(pz)_4(OH)\cdot 2THF$

The molecular structure of **1**·2THF together with bond lengths and angles are presented in Figure 1. The core of the cyclic trinuclear complex **1** consists of three cobalt centers, pentacoordinate Co(1) and hexacoordinate Co(2) and Co(3) (for the numbering, see Figure 2). These are N,N-bridged by four pyrazolate anionic ligands, two of which bridge two cobalt ions, and are further bridged by a μ^3-hydroxide anion. The latter is displaced from the Co(1)-Co(2)Co(3) plane (P) by 0.441(1) Å. Three of the four bridging pyrazolate anions, i.e. pz_{1a}, pz_{1b}, and pz_{2a}, lie at the opposite side of the P plane in relation to μ_3-OH (i.e. in the *exo* position) and the angles between the pyrazolate ring planes and P are 38.5(1)°, 41.4(1)°, and 30.4(1)°, respectively. The fourth bridging pyrazolate, namely pz_{2a}, is *endo* with a pz_{2a} vs. P angle of 67.8(1)°. The three DBM ligands are each involved in O,O-chelation of the cobalt centers. The chelate ring planes of the DBM ligands are twisted in relation to the P plane by about 86.7(1)° (DBM_1 vs. P), 61.5(1)° (DBM_2 vs. P), and 68.4(1)° (DBM_3 vs. P). Consequently, the oxygen donors and phenyl groups of the DBM ligands are non-equivalent, as reflected in the dis-

[a] Department of Chemistry, University of Wroclaw, 14 Joliot-Curie Str., 50-383 Wroclaw, Poland
[b] Faculty of Chemistry, Rzeszów University of Technology, 6 Powstanców Warszawy Ave., 35-959 Rzeszów, Poland

 © WILEY-VCH Verlag GmbH, 69451 Weinheim, 2001 1434−1948/01/0606−1575 $ 17.50+.50/0

tances of the oxygen atom donors from the P plane (see Figure 2). Three of the oxygen donors, i.e. O(2), O(3), and O(6), are *endo*, while O(1), O(4), and O(5) are *exo*. Thus, two sides of the molecule of **1** are different; the *endo* one is occupied by μ_3-OH, pz_{2a}, and mainly by DBM ligands, while the three remaining pyrazolate anions (*exo*) lie at the opposite side of the P plane. The cobalt centers are distinguished not only by their coordination numbers, but also in terms of the cobalt−donor atom distances. The bond lengths between the pentacoordinate Co(1) atom and both the bridging pyrazolate nitrogens and the DBM oxygen atoms are about 2.00 Å, whereas those between Co(2) and Co(3) and the corresponding pyrazolate nitrogen atoms and DBM oxygen atoms are 1.91 Å (Co−N averaged) and 1.89 Å (Co−O averaged), respectively. Furthermore, the bond lengths between the bridging hydroxy oxygen atom and Co(2) and Co(3) (1.91 Å) are shorter as compared to that between Co(1) and O(1B) (2.15 Å), which results in a lower value of Co(2)−O(1B)−Co(3) (108.6°) in comparison with the mean Co(1)−O(1B)−Co(*n*) angle (118.5°). It is also noteworthy that the pyrazolate anion pz_{2a} that bridges the Co(2) and Co(3) centers, i.e. the only *endo* pz, is the most strongly bound to the cobalt ions (1.89 Å) of all the bridging pyrazolate anions; the bond lengths between the pz_{2b} (*exo*) nitrogen atoms and the cobalt ions are longer (1.91 Å), and those between the pz_1 (*exo*) nitrogen atoms and the cobalt centers are longer still (1.92 Å). These structural features clearly demonstrate that the oxidation state of Co(1) is close to Co^{II}, whereas those of Co(2) and Co(3) centers are formally Co^{III}.[20] Analysis of the periphery of **1** revealed different conformations for the three DBM ligands; the phenyl rings at DBM_2 are almost coplanar with its chelate ring, while the *exo*-phenyl rings of the other two DBM ligands are twisted in relation to their chelate rings, presumably due to weak interactions between their *meta*-protons and the face of the *exo*-phenyl of DBM_1 (the contact distance is 2.78 Å, see Figure 1). However, the crystal puckering, including the interaction of **1** with two THF solvate molecules, may also affect the conformations of the DBM ligands.

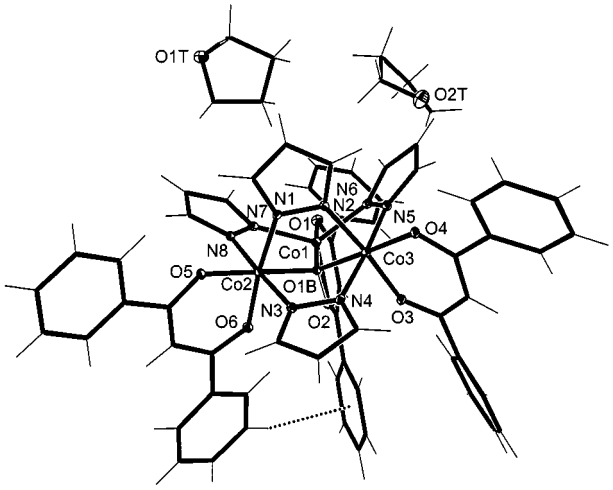

Figure 1. Projection[27] of the trinuclear cobalt complex; thermal ellipsoids are drawn at a 30% probability level; selected bond lengths [Å] and angles [°]: Co(1)−N(7) 1.991(2), Co(1)−N(6) 2.002(2), Co(1)−O(1) 2.014(2), Co(1)−O(2) 1.981(2), Co(1)−O(1B) 2.154(2), Co(2)−N(1) 1.886(2), Co(2)−N(3) 1.900(2), Co(2)−N(8) 1.920(2), Co(2)−O(5) 1.879(2), Co(2)−O(6) 1.881(2), Co(2)−O(1B) 1.912(2), Co(3)−N(2) 1.892(2), Co(3)−N(4) 1.917(2), Co(3)−N(5) 1.926(2), Co(3)−O(3) 1.898(2), Co(3)−O(4) 1.886(2), Co(3)−O(1B) 1.914(2); Co(2)−O(1B)−Co(3) 108.58(8), Co(2)−O(1B)−Co(1) 117.77(8), Co(3)−O(1B)−Co(1) 119.32(8); the ellipsoids at carbon atom positions and most of the atom labels are omitted for clarity; the contact between the *meta*-hydrogen atom of the *endo*-phenyl ring of DBM_2 and the face of the *endo*-phenyl ring of DBM_1 are shown with a dotted line (for acronyms used, see Figure 2)

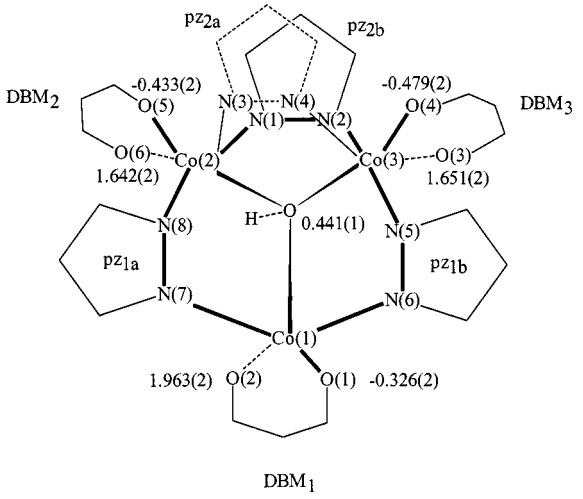

Figure 2. Simplified representation of **1** showing selected donor atoms and acronyms used throughout the discussion; the distances between the oxygen donor atoms of the DBM ligands and the mean Co(1)Co(2)Co(3) plane [Å] are indicated in the scheme; positive values are attributed to the *endo* side; bridging pyrazolates pz_{1a}, pz_{1b}, and pz_{2b} are bound at the *exo* side

Electronic Structure of 1

A rather unusual feature of **1** is that both a well-resolved ^{1}H NMR spectrum and an ESR spectrum (at liquid nitrogen temperature) could be obtained. Therefore, we have measured the magnetic susceptibility of **1**·2THF. The magnetic moment of **1**·2THF is indicative of a total spin of 3/2 and is slightly temperature-dependent (Figure 3, A). At 77 K, **1** gives a rhombic EPR spectrum with $g_1 = 5.35$, $g_2 = 3.34$, and $g_3 = 2.31$ (Figure 3, B). The extent of the delocalization of the unpaired electron could be estimated by ^{1}H NMR spectral studies of the high-spin complex **1**.

The spectrum consists of 22 resonances, which are partially overlapped (Figure 3, C). Although a total assignment could not be made, the two most shifted resonances, appearing at $\delta = 57$ and -59 with relative intensities of 2:1, could be attributed to 3,5-H and 4-H of one of the bridging pyrazolates (pz_2). The large number of resonances seen for **1** indicates that the asymmetry observed in the solid state is retained in solution, leading to a separation of the *o*-, *m*-, and *p*-H phenyl resonances of all three DBM ligands. On the other hand, the rotation of the phenyl groups within each DBM remains fast on the NMR time scale. Consequently, twelve resonances due to the DBM phenyl

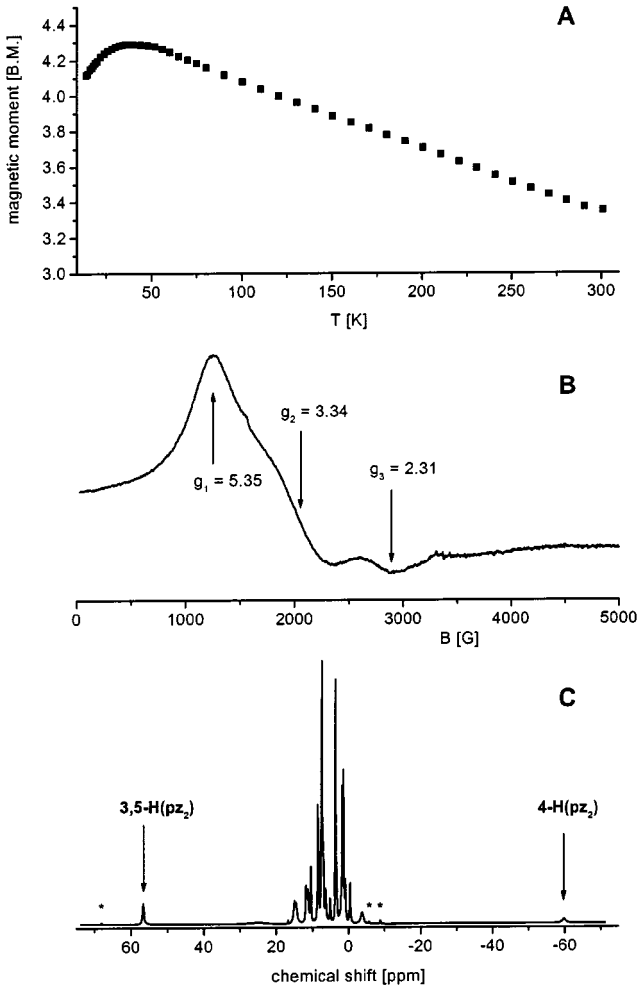

Figure 3. A: temperature dependence of the magnetic moment; B: ESR spectrum measured in toluene glass at 77 K; C: ^{1}H NMR spectrum of **1** in $CDCl_3$ at 293 K; the resonances due to the product of conversion of **1** are labeled with asterisks

groups, two resonances due to the C−H of DBM, the resonance of the central OH, three pz_1 signals, and four pz_2 signals give a total of 22 resonances for **1**. The well-resolved ^{1}H NMR spectrum of **1** is consistent with a high-spin configuration of the Co^{II} center and indicates rather extensive delocalization of the unpaired electron over the formally $Co^{II}/Co^{III}/Co^{III}$ core.

Complex **1** was found to be unstable in chlorinated solvents (chloroform and dichloromethane). Presumably, chloride ions are abstracted from the solvent through formation of a new complex **1′**; the half-life for this conversion was estimated to be ca. 24 h. The spectrum of **1′** is present even in a freshly prepared solution (Figure 3, C). Complex **1′** becomes predominant in a synthetic mixture if removal of CH_2Cl_2 is delayed. In the case of the analogous complex with acetylacetonate (acac) instead of DBM, the instability of the trinuclear OH-bridged complex is even greater and the only product isolated was $Co_3(acac)_3(pz)_4Cl$. We have attempted to replace the DBM in **1** with benzoylacetonate anions; the product thus obtained was found to be a mixture of complexes due to the additional asymmetry introduced by this β-diketonate, resulting in a multiplication of the 3(5)-H and 4-H (pz_2) resonances, although the chemical shift of the latter was very close to that in **1**. This observation confirmed the assignment of the ^{1}H NMR resonances of **1** on the basis of its symmetry and that of its analogues with other β-diketonate anions.

Catalytic Properties

Complex **1** has been found to catalyze the decomposition of *tert*-butyl hydroperoxide (TBHP) in chlorobenzene with a short induction period and a half-life of 80 min. We have tested **1** for its catalytic ability in the oxidation of cyclohexene by TBHP and dioxygen. These two oxidants showed different chemoselectivities; in the former case active oxygen was selectively transferred to the substrate with formation of 2-cyclohexen-1-ol, while in all other cases 2-cyclohexen-1-one was the dominant product (Table 1).

Generation of the active form of the catalyst from **1** in acetonitrile required a long induction period (Entry 3), whereas a short induction period was observed in chlorobenzene. This induction period is consistent with the building-up of an appropriately high concentration of ROOH from R (alkene, alkane) and O_2. Addition of TBHP to the reaction mixtures (Entry 4) obviated the need for such an induction period. The main products clearly showed the involvement of different catalytic forms of **1**, although both are the common products of oxygenated Fenton chemistry.[22−24] Generally, oxidation of organic substrates catalyzed by cobalt complexes can be divided into two categories based on the type of mechanism involved: free-radical autoxidation and catalytic oxygen transfer.[22] In the first type of reaction, the cobalt catalyst induces decomposition of an organic hydroperoxide (ROOH) to form radicals according to a Haber−Weiss mechanism. However, the primary chemistry of ROOH towards metal coordination complexes is nucleophilic addition and ligand substitution with formation of the reactive intermediate for Fenton chemistry and the precursor to the reactive intermediate for oxygenated Fenton chemistry (in the presence of O_2).[23] Catalytic oxygen transfer involves two major active species, namely the peroxometal and oxometal complexes, as the active oxidants.[24] The product derived from **1** in the presence of dioxygen led to the oxidation of cumene in a similar reaction. The products obtained were found to be those derived from attack of the active form of **1** on the secondary carbon atoms (cumene and ethylbenzene, Entries 5 and 7) and not the primary carbon atoms (*p*-xylene, Entry 6) of aliphatic substrates.

Although the catalytic activity and chemoselectivity of **1** are relatively low, we are currently modifying the trinuclear cyclic complexes by replacing DBM with unsymmetrical β-diketonates and by replacing the cobalt ions with other metal ions with a view to improving the catalytic activity of these systems.

Table 1. The results of tests of the catalytic ability of tris(dibenzoylmethanato-1κ^2*O*,*O*′;2κ^2*O*,*O*′;3κ^2*O*,*O*′)(μ$_3$-hydroxo-1:2κ^2*O*;1:3κ^2*O*;2:3κ^2*O*)tetrakis(μ-pyrazolato-1:2κ^4*N*^{1}*N*^{2};1:3κ^2*N*^{1}*N*^{2};2:3κ^2*N*^{1}*N*^{2})-1,2-dicobalt(III)-3-cobalt(II) (**1**)

Test[a]	Substrate (concentration)	Solvent	Oxidant	$\tau_{1/2}$ [min]	Products; yields [%][b]
1	cyclohexene (2.1 M)	chlorobenzene	TBHP (0.276 M)	120	2-cyclohexen-1-ol; 65.4 2-cyclohexen-1-one; 6.4 cyclohexane-1,2-epoxide; 3.2 total yield 75.0 (24 h)
2	cyclohexene (0.97 M)	chlorobenzene	O_2 (1 atm)	120[c]	2-cyclohexen-1-ol; 21.1 2-cyclohexen-1-one; 49.1 cyclohexane-1,2-epoxide; 7.3 total yield 77.4 (18.5 h)
3	cyclohexene (0.97 M)	acetonitrile	O_2 (1 atm)	450[c]	2-cyclohexen-1-ol; 6.4 2-cyclohexen-1-one; 44.8 cyclohexane-1,2-epoxide; 9.9 Total yield 61.4 (20 h)
4	cyclohexene (0.97 M)	acetonitrile	O_2 (1 atm) + TBHP[e]	150	2-cyclohexen-1-ol; 13.1 2-cyclohexen-1-one; 48.8 cyclohexane-1,2-epoxide; 1.0 Total yield 68.1 (18.5 h)
5	cumene (1.0 M)	chlorobenzene	O_2 (1 atm)	600	2-phenylpropan-2-ol; 11.5 acetophenone; 10.8 cumene hydroperoxide; 3.6 Total yield 25.8 (20 h)
6	*p*-xylene (0.98 M)	chlorobenzene	O_2 (1 atm)	[d]	no conversion products were found (20 h)
7	ethylbenzene (0.98 M)	chlorobenzene	O_2 (1 atm)	600	acetophenone; 6.1 (18.5 h)

[a] The concentration of **1** was $5\cdot10^{-4}$ mol/dm^3. – [b] Calculated on the basis of substrate consumed, except for Entry 1, where the yield was calculated on the basis of active oxygen transferred to the organic substrate. – [c] With an induction period of 30 min (Entry 2) and 300 min (Entry 3); $\tau_{1/2}$ calculated starting from the point at which consumption of oxygen commenced. – [d] No consumption of oxygen was noticed. – [e] The initial concentration of TBHP was $1.5\cdot10^{-4}$ M.

Experimental Section

Synthesis: In the optimized procedure, dibenzoylmethane (DBMH, 500 mg, 2.232 mmol) and pyrazole (pzH, 202 mg, 2.976 mmol) were dissolved in tetrahydrofuran (THF, 20 mL) and the resulting solution was added dropwise to a 0.3 mol·dm^{-3} aq. cobalt(II) nitrate solution (75 mL) under vigorous stirring. Then, freshly distilled dichloromethane (150 mL) was added to the mixture to extract the desired, non-electrolyte product into the organic phase. Additionally, 1 M aq. NaOH was added dropwise to the mixture under continuous stirring. After stirring for a further 10 min, the reddish-brown organic phase was collected and the CH_2Cl_2 was removed using a rotary evaporator. The solid residue was redissolved in THF and the crude product was crystallized from a THF/hexane mixture. Recrystallization from this solvent mixture led to the isolation of brick-red crystals of **1**·2THF. The best yield of the product was 14%. – $C_{65}H_{62}Co_3N_8O_9$ (1276.2): calcd. C 61.17, H 4.90, N 9.41; found C 60.49, H 4.88, N 9.60. – IR (KBr and Nujol): $\tilde{\nu}$ = 1591 (s), 1546 (s, br), 1521 (s, br), 1484 (s, br), 1450 (s), 1391 (s, br), 1377 (s), 1319 (m), 1308 (m, sh), 1225 (m), 1194 (w), 1180 (m, br), 1061 (s), 1025 (w), 999 (w), 951 (w), 751 (m, br), 740 (m), 721 (m), 687 (m), 626 (w), 581 (w, br), 543 cm^{-1} (w, br). – UV/Vis: λ (ε) = 537 nm ($3.26\cdot10^2$ mol^{-1}·dm^3·cm^{-1}).

Crystallographic Studies: Crystal data, together with details of the refinement, are given in Table 2. All measurements were made with a Kuma KM4CCD κ-axis diffractometer using graphite-monochromated Mo-K_α radiation. The crystal was positioned 65 mm from the KM4CCD camera; 612 frames were measured at 0.75° intervals with a counting time of 25 s. The data were corrected for Lorentz and polarization effects. No absorption correction was applied. Data reduction and analysis were carried out with the Kuma Diffraction (Wroclaw) programs. The structure was solved by direct methods (program SHELXS-97[25]) and refined by the full-matrix least-squares methods on all F^2 data using the program SHELXL-97.[26] Non-hydrogen atoms were refined with anisotropic thermal parameters; hydrogen atoms were included in geometrical positions and were not refined. The crystallographic data have been deposited with the CCDC, 12 Union Road, Cambridge CB2 1EZ, U.K. and are available on quoting the deposition number CCDC-150406.

Magnetic and Spectral Measurements: The magnetic susceptibility was measured as a function of temperature in the range 14−300 K using a Quantum Design SQUID magnetometer (type MPMS-5). Magnetic moments were calculated for the molecule of **1**·2THF after considering the appropriate diamagnetic corrections. – ^{1}H NMR spectra were recorded with a Bruker AMX 300 MHz instrument, while X-band EPR spectra were measured with a Bruker ESP 300E spectrometer, both for a solid sample and for a solution of **1** in toluene, at 77 K and at ambient temperatures. – UV/Vis spectra in appropriate solvents and IR spectra (Nujol mulls; KBr discs) were recorded with HP 8453 diode-array and Bruker IFS113V FT-IR spectrophotometers, respectively.

Catalytic Tests: The catalytic activity of **1** was tested in oxidations of various organic substrates using *tert*-butyl hydroperoxide (TBHP) and dioxygen as oxidants in chlorobenzene and acetonitrile solution at 348 K. The progress of reactions was monitored by iodometric titration of TBHP and by volumetric measurement of dioxygen consumed. The products were separated and determined

Table 2. Crystal data and structure refinement

Empirical formula	$C_{65}H_{62}N_8O_9Co_3$
Molecular mass	1276.02
T [K]	100(2)
λ [Å]	0.71073
Crystal system	triclinic
Space group	$P\bar{1}$
a [Å]	13.618(3)
b [Å]	14.241(3)
c [Å]	16.069(3)
α [°]	86.69(3)
β [°]	72.47(3)
γ [°]	73.40(3)
V [$Å^3$]	2846.4(10)
Z	2
D_c [$Mg·m^{-3}$]	1.489
μ [mm^{-1}]	0.932
$F(000)$	1322
Crystal size [mm]	0.20 × 0.15 × 0.15
Crystal color and habit	brick-red prisms
Diffractometer	Kuma KM4CCD
θ range for data collection [°]	3.23−28.84
Index ranges	$-18 \le h \le 17$ $-15 \le k \le 18$ $-21 \le l \le 21$
Reflections collected	20661
Independent reflections (R_{int})	12971 (0.0322)
Observed reflections ($I \ge 2\sigma_I$)	7791
Data/parameters	12971/766
Weighting scheme: a, b, c[a]	0.0297, 0, 3
Goodness-of-fit (F^2)	0.851
Final R_1/wR_2 indices (obs. refl.)[a]	0.0380/0.0699
Final R_1/wR_2 indices (indep. refl.)	0.0802/0.0761
Largest diff. peak/hole [$e·Å^{-3}$]	0.881/−0.397

[a] $w = 1/[\sigma^2(F_o^2) + (aP)^2 + bP]$, where $P = [\mathrm{Max}(F_o^2,0) + 2F_c^2]/c$.

by GC-MS using a HP 5890 series II chromatograph coupled to a HP 5971 A mass spectrometer. The decomposition of 0.28 M TBHP in the presence of $5.2·10^{-4}$ M **1** in chlorobenzene at 348 K was monitored by iodometric titration. The half-life for the conversion was found to be 80 min. The products of TBHP decomposition (75% conversion after 180 min) were identified and determined by GC-MS as *tert*-butyl alcohol and a trace amount of bis(*tert*-butyl) peroxide. The results of the oxidation tests are summarized in Table 1.

Acknowledgments

J. S., S. W., and J. J. Z. kindly acknowledge financial support from the State Committee for Scientific Research KBN (Grant PBZ-KBN 15/T09/99/01D).

[1] R. D. Cannon, R. P. White, *Prog. Inorg. Chem.* **1988**, *36*, 195−297.
[2] A. Harton, M. K. Nagi, M. M. Glass, P. C. Junk, J. L. Atwood, J. B. Vincent, *Inorg. Chim. Acta* **1994**, *217*, 171−179.
[3] S. Uemura, A. Spencer, G. Wilkinson, *J. Chem. Soc., Dalton Trans.* **1973**, 2565−2571.
[4] L. Meesuk, R. P. White, B. Templeton, U. A. Jayasooriya, R. D. Cannon, *Inorg. Chem.* **1990**, *29*, 2389−2392.
[5] A. Earnshaw, B. N. Figgis, J. Lewis, *J. Chem. Soc. A* **1966**, 1656−1663.
[6] T. Głowiak, M. Kubiak, T. Szymańska-Buzar, *Acta Crystallogr., Sect. B* **1977**, *33*, 1732−1737.
[7] M. K. Johnson, D. B. Powell, R. D. Cannon, *Spectrochim. Acta* **1981**, *37A*, 995−1006.
[8] J. Catterick, P. Thornton, B. W. Fitzimmons, *J. Chem. Soc., Dalton Trans.* **1977**, 1420−1425.
[9] B. Harrison, N. Logan, *J. Chem. Soc., Dalton Trans.* **1972**, 1587−1589.
[10] W. P. Griffith, *J. Chem. Soc. A* **1969**, 2270−2273.
[11] N. Masciocchi, G. A. Ardizzoia, A. Maspero, G. LaMonica, A. Sironi, *Inorg. Chem.* **1999**, *38*, 3657−3664.
[12] E. Spodine, A. M. Atria, J. Velenzuela, J. Jalocha, J. Manzur, A. M. Garcia, M. T. Garland, O. Pena, J. Y. Saillard, *J. Chem. Soc., Dalton Trans.* **1999**, 3029−3034.
[13] G. A. Ardizzoia, G. LaMonica, A. Maspero, N. Masciocchi, M. Moret, *Eur. J. Inorg. Chem.* **1999**, 1301−1307.
[14] F. B. Hulsbergen, R. W. M. Ten Hoedt, G. C. Verschoor, J. Reedijk, A. L. Spek, *J. Chem. Soc., Dalton Trans.* **1983**, 539−545.
[15] K. Sakai, Y. Yamada, T. Tsubomura, M. Yabuki, M. Yamaguchi, *Inorg. Chem.* **1996**, *35*, 542−544.
[16] A. V. Virovets, I. V. Podbereskaia, L. G. Lavrenova, *Zh. Str. Khim.* **1997**, *38*, 532−538.
[17] J. J. Ziólkowski, F. Pruchnik, T. Szymanska-Buzar, *Inorg. Chim. Acta* **1973**, *7*, 473−476.
[18] T. Szymanska-Buzar, J. J. Ziólkowski, *J. Mol. Catal.* **1981**, *11*, 371−384.
[19] D. E. Babushkin, E. P. Talsi, *J. Mol. Catal. A* **1998**, *130*, 131−137.
[20] A literature search of crystallographic data, performed with the VISTA program as included in the CSD package,[21] showed that oxygen (of β-diketonate)−cobalt bond lengths fall into two well-separated groups with 1.86−1.92 Å and 1.99−2.12 Å for Co^{III} and Co^{II}, respectively. The Co^{II}−N(pyrazole) and Co^{III}−N(pyrazole) bond lengths do not depend on the oxidation state of the metal ion and fall within the range 1.92−2.26 Å.
[21] F. H. Allen, J. E. Davies, J. J. Gelloy, O. Johnson, O. Kennard, C. F. Macrae, E. M. Mitchell, G. F. Mitchell, J. M. Smith, D. G. Watson, *J. Chem. Int. Comp. Sci.* **1991**, *31*, 187−204.
[22] R. A. Sheldon, *CHEMTECH* **1991**, 566−576.
[23] D. T. Sawyer, A. Sobkowiak, T. Matsushita, *Acc. Chem. Res.* **1996**, *29*, 409−416.
[24] G. A. Barf, R. A. Sheldon, *J. Mol. Catal. A* **1995**, *102*, 23−29.
[25] G. M. Sheldrick, *SHELXS-97, Program for Solution of Crystal Structures*, University of Göttingen, **1997**.
[26] G. M. Sheldrick, *SHELXL97, Program for Crystal Structure Refinement*, University of Göttingen, **1997**.
[27] G. M. Sheldrick, *SHELXTL, V5.1*, Bruker AXS, Inc., Madison, Wisconsin, USA, **1999**.

Received October 11, 2000
[I00381]

A New Alternating Ferro- and Antiferromagnetic, One-Dimensional Manganese(II) Azide Complex, $[Mn(dpa)(N_3)_2]$ − Crystal Structure and Spectroscopic and Magnetic Properties

Mónica Villanueva,[a] José L. Mesa,[a] Miren K. Urtiaga,[a] Roberto Cortés,[b] Luis Lezama,[a] María I. Arriortua,[a] and Teófilo Rojo*[a]

Keywords: Coordination chemistry / EPR spectroscopy / Magnetic properties

The synthesis, crystal structure, and spectroscopic and magnetic properties of a new alternating ferro- and antiferromagnetic, one-dimensional manganese(II) azide complex, $[Mn(dpa)(N_3)_2]$ (where dpa is the 2,2′-dipyridylamine ligand), are reported. The compound's crystal structure has been resolved at room temperature. The complex crystallizes in the monoclinic $P2_1/c$ space group, with a = 7.089(2), b = 19.090(4), and c = 9.682(4) Å, β = 104.61(2) °, and Z = 4. The structure consists of neutral chains in which each Mn^{II} cation is alternatively bridged by two end-on and two end-to-end azido bridges. The octahedral coordination of the metallic cation is completed by two dpa ligand nitrogen atoms. Reflectance measurements confirm the hexacoordination of the Mn^{II} ions in the complex. The ESR spectra at room temperature and at 4.2 K are isotropic, with a mean g-value of 2.010(1). Magnetic data were analyzed on the basis of an alternating ferro- and antiferromagnetic Heisenberg chain of Mn^{II} ions. The J-exchange parameters found are 64.3 and –75.7 K. A spin canting phenomenon has been observed in this compound, with a remnant magnetization which vanishes above 15 K. Magnetostructural correlations in manganese(II) systems of alternating magnetic sign are discussed.

Introduction

The synthesis and characterization of new low-dimensional materials (one or two-dimensional) that may show ferromagnetic long-range cooperative phenomena (molecular magnets)[1−6] have in recent years been the main focus of interest in the molecular magnetism area. At present, the field of molecular magnetism is addressing the synthesis and study of discrete polynuclear molecules in an attempt to improve our understanding of the mechanism involved in magnetic coupling[7,8] and the production of new paramagnetic clusters with high spin and strong anisotropy (superparamagnetic molecules).[9,10]

The azide-pseudohalide anion is an excellent ligand for obtaining one-dimensional,[11,12] two-dimensional,[13] or three-dimensional[14] polynuclear systems with divalent metal ions. From the magnetic point of view, the most interesting characteristic of azido-bridged complexes is that the azido ligand can act as a very effective superexchange pathway, due to the different coordination modes. Normally, the end-to-end (EE) bridge produces antiferromagnetic coupling, whereas the end-on (EO) form gives ferromagnetic coupling. Both the EE and EO structural bridges may coexist within the same (one- or two-dimensional) system, owing to different distances and/or angles found in the structure. These systems are globally antiferro- or ferromagnetic, but they belong to the so-called "magnetic systems alternating in sign". In compounds of this kind, two or more exchange coupling parameters (J) are necessary to fit the experimental results, in contrast to the "uniform magnetic systems" in which all azido bridges have both the same coordination mode and the same structural parameters.

Taking the aspects mentioned above into account, this work was focused on the preparation and characterization of a new polynuclear azido complex. With this aim in mind, we used the bidentate ligand 2,2′-dipyridylamine with a metal/bidentate ligand 1:1 ratio, in such a way that the four coordination vacancies around the six-coordinated manganese(II) ion should be completed by the excess of the azido ligands. Following this procedure, we have synthesized a new alternating ferro/antiferromagnetic, one dimensional manganese(II) azide complex, which has been characterized by X-ray diffraction and spectroscopic techniques. Magnetic measurements indicate global antiferromagnetic behavior, with the presence of a weak ferromagnetic component intrinsic to the sample.

Results and Discussion

Description of the Structure

Selected bond lengths and angles of $[Mn(dpa)(N_3)_2]$ are given in Table 1. The structure consists of linear neutral chains extending along the [100] crystallographic direction (Figure 1). The Mn^{II} ions are alternatively linked by two EO (end-on) azido bridges [Mn(1)−N(4),N(4)^{i}; 2.231(2), 2.218(2) Å] and two EE (end-to-end) ones [Mn(1)−N(7),N(9)^{ii};

[a] Departamento de Química Inorgánica and Departamento de Mineralogía-Petrología Facultad de Ciencias, Universidad del País Vasco,
Apdo. 644, 48080 Bilbao, Spain
Fax: (internat.) + 34-94/464-8500
E-mail: qiproapt@lg.ehu.es
[b] Departamento de Química Inorgánica, Facultad de Farmacia, Universidad del País Vasco,
Apdo. 450, 01080 Vitoria, Spain

 © WILEY-VCH Verlag GmbH, 69451 Weinheim, 2001 1434−1948/01/0606−1581 $ 17.50+.50/0

2.275(2), 2.274(2) Å]. The Mn^{II} ions exhibit octahedral coordination, completed by the two N(1) and N(3) nitrogen atoms of the 2,2′-dipyridylamine ligand [Mn(1)−N(1),N(3); 2.253(2), 2.243(2) Å]. The existence of an inversion center induces the Mn(1)−N(4)−Mn(1)^{i}−N(4)^{i} bridging unit to form a plane. The EO bridging azides are quasilinear [N(4)−N(5)−N(6), 178.7(3)°]. The Mn(1)−N(4)−Mn(1)^{i} angle in the EO mode is 102.92(7)°, in good agreement with the results obtained (100−105°) for this kind of bridging ligand.[15−17] For the EE bridges, the Mn(1)−N(7)−N(8) angle is 125.0 (1)° and the Mn(1)^{ii}−N(9)−N(8) angle is 127.74(2)°. The torsion angle τ between the mean plane of Mn(1)−N(7)−N(8)−N(9) and Mn(1)^{ii}−N(9)−N(8)−N(7) for a chair configuration is 64.2(2)°. The dihedral angle δ between the least-squares plane defined by the six nitrogen atoms of the EE bridging azides and the N(7)−Mn(1)−N(9)^{ii} system is 35.10(6)°. The intrachain Mn···Mn distances are 3.479(1) and 5.432(1)Å in the EO and EE bridges, respectively.

Table 1. Selected bond lengths [Å] and angles [°] for $[Mn(C_{10}H_9N_3)(N_3)_2]$, (e.s.d. in parentheses; Symmetry codes: $i = -x,-y,-z$; $ii = -x+1,-y,-z$)

Bond lengths (Å)			
Mn(1)−N(1)	2.253(2)	N(5)−N(6)	1.141(3)
Mn(1)−N(3)	2.243(2)	N(7)−N(8)	1.177(3)
Mn(1)−N(4)	2.231(2)	N(8)−N(9)	1.166(3)
Mn(1)−N(7)	2.275(2)	N(1)−C(1)	1.359(3)
Mn(1)−N(4)^{i}	2.218(2)	N(1)−C(5)	1.333(3)
Mn(1)−N(9)^{ii}	2.274(2)	N(2)−C(5)	1.378(3)
Mn(1)^{i}−N(4)	2.218(2)	N(2)−C(6)	1.378(3)
Mn(1)^{ii}−N(9)	2.274(2)	N(3)−C(6)	1.335(3)
N(4)−N(5)	1.194(3)	N(3)−C(10)	1.356(3)
Bond angles (°)			
N(3)−Mn(1)−N(4)	91.86(7)	N(3)−Mn(1)−N(4)^{i}	168.91(7)
N(3)−Mn(1)−N(7)	99.07(7)	N(4)−Mn(1)−N(7)	168.29(7)
N(3)−Mn(1)−N(1)	82.55(7)	N(8)−N(9)−Mn(1)^{ii}	127.74(2)
N(3)−Mn(1)−N(9)^{ii}	90.3(8)	N(5)−N(4)−Mn(1)^{i}	129.0(1)
N(4)^{i}−Mn(1)−N(1)	99.95(7)	Mn(1)−N(7)−N(8)	125.0(1)
N(4)^{i}−Mn(1)−N(4)	77.08(7)	Mn(1)−N(4)−N(5)	127.3(1)
N(4)^{i}−Mn(1)−N(7)	91.90(7)	Mn(1)−N(4)−Mn(1)^{i}	102.92(7)
N(4)^{i}−Mn(1)−N(9)^{ii}	88.88(8)	N(4)−N(5)−N(6)	178.7(3)
N(1)−Mn(1)−N(4)	99.87(7)	N(7)−N(8)−N(9)	178.6(2)
N(1)−Mn(1)−N(7)	85.77(7)	Mn(1)−N(1)−C(5)	127.7(1)
N(4)−Mn(1)−N(9)^{ii}	90.48(8)	C(5)−N(2)−C(6)	134.4(2)
N(7)−Mn(1)−N(9)^{ii}	85.31(8)	Mn(1)−N(3)−C(6)	127.9(1)
N(1)−Mn(1)−N(9)^{ii}	167.64(7)		

The bond lengths and angles for the 2,2′-dipyridylamine molecule are in the range usually found in this kind of molecule. This ligand may be considered as nonplanar, since the value of the dihedral angle between the pyridine rings is 5.84(8)°.

IR and UV/Visible Spectroscopy

The points of interest in the IR spectrum of the $[Mn(dpa)(N_3)_2]$ complex lie mainly in the bands due to the azido groups. The asymmetrical stretch, $\nu_{asym}(N_3)$, appears split as a strong band at ca. 2095 and 2050 cm^{-1}, in good agreement with the simultaneous existence of EO and EE bridging modes in the complex.[18] The azide symmetric stretch $\nu_{sym}(N_3)$, corresponding to the EO bridging mode, can be observed as a band of medium intensity at about 1330 cm^{-1}. This mode is not active for the symmetrical EE coordination. Finally, the band corresponding to the deformation mode of the azido group, $\delta(N_3)$, is found at ca. 610, 600 cm^{-1}, in good agreement with that observed for all polynuclear azido compounds.[18] Furthermore, the IR spectrum of the title compound features the bands characteristic of the 2,2′-dipyridylamine molecule, seen in the stretching and bending modes of the C−C and C−N bonds in the ranges between ca. 1645−1360 and 1270−750 cm^{-1}.

The diffuse reflectance spectrum of $[Mn(dpa)(N_3)_2]$ exhibits several very weak, spin-forbidden d-d bands, at ca. 17240, 21275, 22990, 25974, and 30770 cm^{-1}, as would correspond to a d^5 high spin cation of ideal octahedral symmetry.[19−21]

ESR and Magnetic Properties

ESR spectra of $[Mn(dpa)(N_3)_2]$, at room temperature and at 4.2 K, were performed on a powdered sample. The spectra are isotropic, with a g-value of 2.010(1). The linewidths are of 116.0 and 304.0 Gauss at 300 and 4.2 K, respectively.

The magnetic susceptibility of $[Mn(dpa)(N_3)_2]$ was measured, using a powdered sample, from 4.2 to 300 K at magnetic fields of 0.1 and 0.01 T. The plots of χ_m and $\chi_m T$ vs. temperature, obtained when the magnetic measurements were recorded at a magnetic field of 0.1 T, are shown in Figure 2. The magnetic susceptibility increases with decreasing temperature down to about 27 K; after that it decreases down to ca. 18 K. An abrupt increase is then observed at about 13.5 K, followed by a decrease down to 4.2 K. A plot of reciprocal molar magnetic susceptibility vs. temperature shows classical Curie-Weiss behavior above 50 K. The calculated Curie and Curie−Weiss constants are $C_m = 4.77\ cm^3$ K/mol and $\theta = -27.5$ K, respectively. The magnetic susceptibility curve obtained using a magnetic field of 0.01 T shows similar features, but the increase observed after the magnetic ordering is more abrupt than that observed at 0.1 T (see inset in Figure 2). The negative Weiss temperature, together with the decrease in the effective magnetic moment observed when the temperature is lowered (5.90 BM at 300 K and 1.46 BM at 4.2 K (see Figure 2), are indicative of the existence of antiferromagnetic exchanges as major interactions for the $[Mn(dpa)(N_3)_2]$ compound. However, the increase in susceptibility at low temperatures indicates the presence of a weak intrinsic ferromagnetic contribution, possibly due to a spin canting effect in the compound.

In order to corroborate this result and to calculate the Neel temperature, magnetization measurements were carried out. Figure 3 shows the zero-field magnetization curve vs. temperature for the compound, previously cooled in a magnetic field of 0.01 T. It can be observed that the remnant magnetization decreases with increasing temperature and vanishes above $T_N = 15$ K. This fact implies the existence of a small amount of ferromagnetic component in the ordered state, which appears to be responsible for the steep

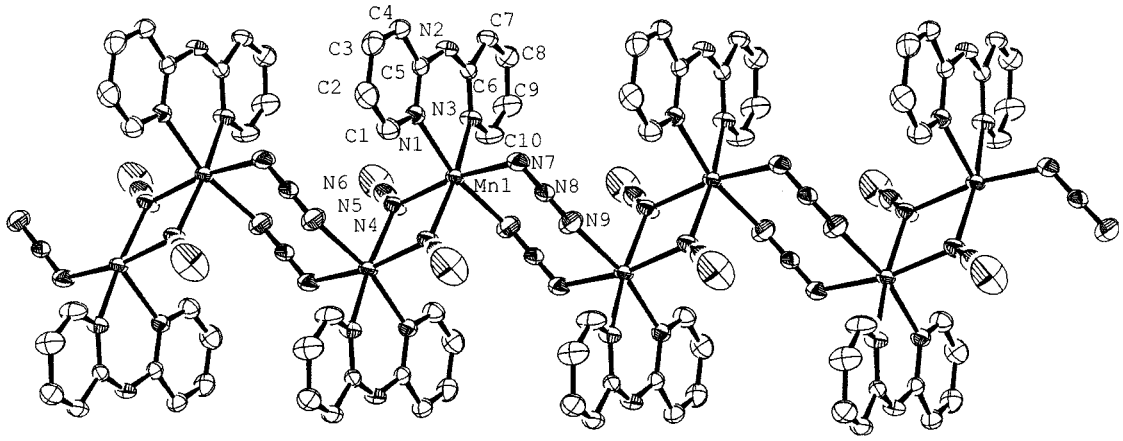

Figure 1. ORTEP drawing (50% thermal ellipsoids) of the $[Mn(dpa)(N_3)_2]$ chain complex showing the alternating end-on and end-to-end coordination of the azido ligands and atom-labeling scheme. The chain runs along the *a*-axis

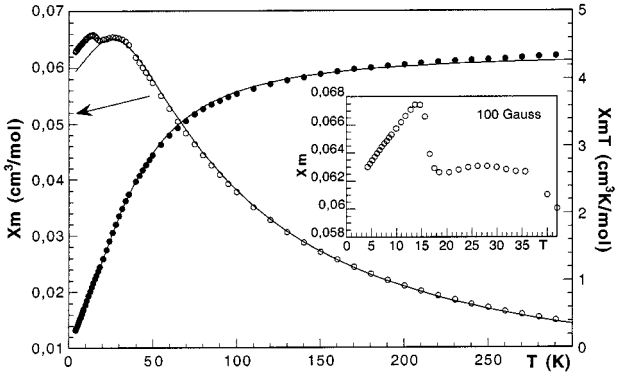

Figure 2. Thermal evolution of χ_m and χ_mT curves of $[Mn(dpa)(N_3)_2]$. The inset shows the χ_m vs. T curve at 100 Gauss. The solid lines show the fit of the χ_m and χ_mT experimental data to the model for alternating ferromagnetic-antiferromagnetic $S = {}^5/_2$ chain

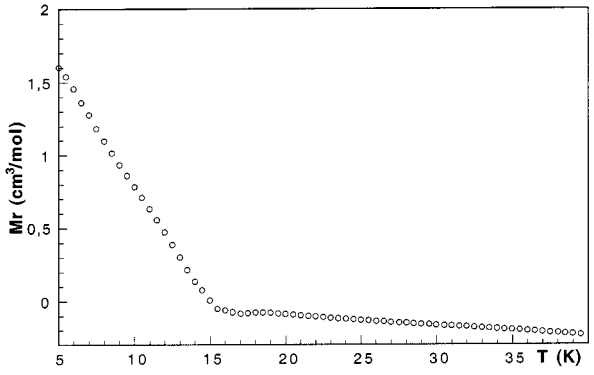

Figure 3. Remnant magnetization vs. temperature of $[Mn(dpa)(N_3)_2]$

increase observed in χ_m at temperatures lower than the ordering temperature.

The magnetic susceptibility data at 0.1 T have been interpreted on the basis of a theoretical model for the alternating ferromagnetic-antiferromagnetic $S = {}^5/_2$ chain, using the following expression for the susceptibility:[18]

$$\chi_m = [Ng^2\beta^2/3kT][1 + u_1 + u_2 + u_1u_2/1 - u_1u_2]$$

where, $u_1 = \coth(J_1/kT) - (kT/J_1)$ and $u_2 = \coth(J_2/kT) - (kT/J_2)$. In order to make a quantitative comparison with the theoretical expression deduced in the classical limit, we used the $J_i \rightarrow J_iS(S+1)$ and $g \rightarrow g[S(S+1)]^{1/2}$ scaling factors. Good agreement between the experimental magnetic data and the theoretical model was obtained when the two interactions, J_1 and J_2, had opposite signs. Fixing "*g*" to the value of 2.01 for manganese(II) ion (from the ESR spectra), the best agreement (solid lines in Figure 2) corresponds to the following parameters: $J_1 = 64.3$ K (45.3 cm^{-1}), and $J_2 = -75.7$ K (-53.3 cm^{-1}). The model used appears to provide a very good description of the susceptibility between 18 and 300 K, as the discrepancy does not exceed the experimental uncertainty. At very low temperature, the agreement is less satisfactory, due probably to the influence of small interchain interactions and the weak ferromagnetic contribution present in this compound.

Magnetostructural Correlations

It is possible to carry out a study concerning magnetostructural correlations in compounds with alternating double EO and EE azido bridges, as several complexes of this kind have recently been reported (Table 2).

The main factor controlling the intensity of the exchange ferromagnetic interactions in the EO bridge appears to be the bridging angle. Here, the larger the bridging angle is, the larger are the ferromagnetic interactions. For EE bridges, however, more structural parameters have recently been studied: namely δ [dihedral angle between the plane defined for the six N-azido atoms and the N(1)−Mn−N(3′) plane] and τ [angle between the mean planes Mn−N(1)−N(2)−N(3) and N(1)−N(2)−N(3)−Mn′]. For the d^5 EE azido-bridged compounds, the most useful parameter is the dihedral angle (δ).

In order to analyze the magnetostructural correlations between δ, τ, and the superexchange *J* parameter, the Hay−Thibeault−Hoffmann[22] relationship between $\Sigma\Delta^2$ and the antiferromagnetic component of *J* is useful. The Δ values (difference in energy between MOs, derived from magnetic orbitals, of the same symmetry) may easily be ob-

Table 2. Magnetostructural Parameters for Several Related Azide 1D-Complexes

Compound	M−N−M (deg)	M...M (Å) EO	M...M (Å) EE	M−N−N (deg)	τ (deg)	δ (deg)	J (cm^{-1}) EE	J (cm^{-1}) EO	α	ref.
$[Mn(bipy)(N_3)_2]_n$	101.0	3.455	5.343	131.1 127.3	41.1	22.7	−11.9	10.0	1.2	18
$[Mn(bpm)(N_3)_2]_n$	102.9	3.496	5.484	129.1 134.2	41.1	20.5	−63.7	15.7	4.2	24
$[Mn(3\text{-}Bzpy)_2(N_3)_2]_n$	100.4	3.416	5.229	126.0 126.1		26.6	−12.3	3.5	3.5	25
$[Mn(dpa)(N_3)_2]_n$	102.9	3.479	5.432	125.0 127.7	64.2	35.1	−53	45	1.2	this work
$[Mn(3\text{-}Et,4\text{-}Mepy)_2(N_3)_2]_n$	99.7	3.402	5.149	124.8 123.2	51.2	31.7	−13.7	2.4	5.7	26
			EE	bridges only						
$[Mn(3\text{-}Etpy)_2(N_3)_2]_n$			5.418	134.7 131.7	13.5	6.9	−11.7	−		27
			5.463	134.8 129.7	23.2	11.6	−13.8	−		
$[Mn(pyOH)_2(N_3)_2]_n$				123.8 122.4	63.1	38.0	−7.0	−		27

tained by means of MO extended Hückel (EHMO) calculations. The CACAO [23] program was used on a modeled fragment possessing double EE bridges − $[(NH_3)_4Mn(NNN)_2-Mn(NH_3)_4]$ (Scheme 1) − varying the δ and τ parameters inside the limits δ = 0°/60° (this range is used because larger angles seem to be sterically hindered) and equivalent τ = 0°/95°. The manganese(II) ions were positioned in a slightly distorted octahedral environment. The N−Mn−N angle was taken as 90°, and the Mn−N(NH_3) and Mn−N(azide) bond lengths were 2.15 and 2.20 Å, respectively, as observed from the structural data. The atomic parameters used for Mn, N, and H were the program standards.

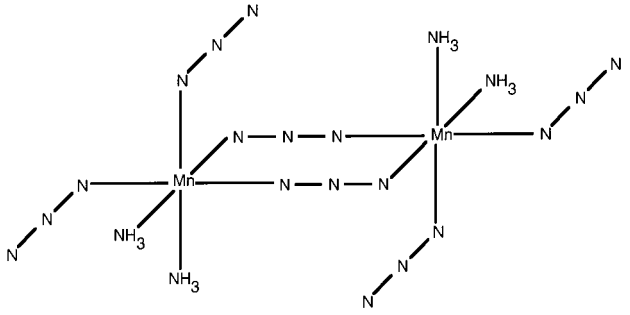

Scheme 1

Ten molecular orbitals are generated from the five magnetic orbitals, with one electron each, corresponding to the two Mn^{II} ions. The antiferromagnetic contribution should be proportional to the sum: $\Sigma\Delta^2 = \Delta^2(d_{x^2-y^2}) + \Delta^2(d_{z^2}) + \Delta^2(d_{xz}) + \Delta^2(d_{xy}) + \Delta^2(d_{yz})$. However, priority was given in each modeled system to the orbitals mainly implicated in the exchange pathway. The results of the calculations were plotted as $\Sigma\Delta^2$ vs. δ or τ (Figure 4). In the light of these data, we can deduce that the antiferromagnetic coupling should decrease for larger δ values, indicating that the loss of overlap due to the increase in the torsion angles becomes the driving parameter controlling the magnitude of the antiferromagnetic coupling.

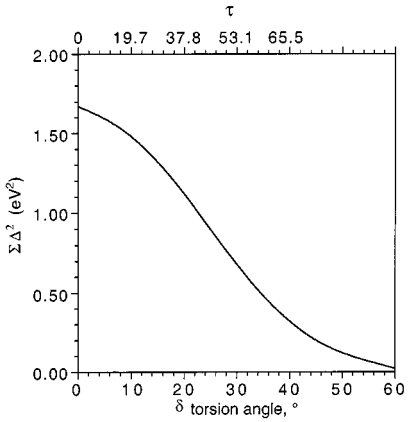

Figure 4. Evolution of the $\Sigma\Delta^2$ parameter vs. δ and τ angles

Several conclusions can be drawn from the magnetostructural parameters of the complexes, shown in Table 2. With respect to the EO bridges, it can be observed that the experimentally determined ferromagnetic J values increase with increasing bridging angle. This demonstrates the general validity of the proposed dependence of the experimental J value on α (the $|J_{EE}/J_{EO}|$ ratio) for this kind of bridging. In the case of the EE bridges, there seems to be a general tendency that the larger the torsion (δ) is, the lower

the antiferromagnetic interactions are. However, the title compound does not follow this general tendency and shows one of the largest antiferromagnetic interactions found experimentally for these alternating chains. For this kind of bridging, other factors may influence the magnitude of the antiferromagnetic exchange component. In fact, low values of Mn−N−N bridging angles have been shown to increase the antiferromagnetic interaction. In this sense, this may be the explanation for the larger J_{AF} value found in the $[Mn(dpa)(N_3)_2]$ compound, as it shows a smaller average bridging angle.

Conclusions

A new alternating ferro/antiferromagnetic, one-dimensional manganese(II) azide complex, $[Mn(dpa)(N_3)_2]$, has been synthesized and the crystal structure solved from single-crystal X-ray diffraction data. The complex exhibits a chain structure, extending along the *a*-axis with the azide anions simultaneously coordinated to the manganese(II) ions in both the end-on and the end-to-end modes. The weak bands observed in the diffuse reflectance spectrum are characteristic of the existence of manganese(II) ions in approximately octahedral environments. Isotropic signals are observed in the ESR spectra, with a mean *g*-value of 2.010(1). The linewidths of the spectra increase with decreasing temperature, probably due to the dipolar homogeneous broadening and a strong spin correlation. Magnetic measurements indicate the existence of a dominant antiferromagnetic coupling. The magnetic data have been analyzed on the basis of a model for alternating ferro- and antiferromagnetic chains of $S = 5.2$, the obtained values for the *J*-exchange parameters being of 64.3 and −75.7 K. Furthermore, the complex displays magnetization at low magnetic fields, probably due to the presence of a weak ferromagnetic component. From the magnetostructural correlations, it was possible to explain the high value obtained for the J_{AF} parameter in the $[Mn(dpa)(N_3)_2]$ complex on the basis of the low observed value of the Mn−N−N bridge angle in this compound.

Experimental Section

Syntheses: $[Mn(dpa)(N_3)_2]$ was synthesized from $Mn(NO_3)_2{\cdot}4H_2O$ (0.110 g, 0.438 mmol), 2,2′-dipyridylamine (0.075 g, 0.438 mmol), and NaN_3 (0.142 g, 2.190 mmol) in a water-methanol solution (1:1). The resulting light yellow solution was filtered off and left to stand at room temperature. After several days, prismatic, light pink, single crystals were obtained. They were separated by filtration, washed with diethyl ether, and dried over P_2O_5 for 1 h. Yield: ca. 80%. The results of CHN elemental analysis and the ICP-AES (inductively coupled plasma atomic emission spectroscopy) technique were: found C 38.4, H 2.7, N 40.3, Mn 17.5; calcd. for $C_{10}H_9MnN_9$ (310.2): C 38.7, H 2.9, N 40.6, Mn 17.7%. The density, measured by the flotation method in a mixture of $CHBr_3/CCl_4$, was 1.63(1) gcm^{-3}.

Crystal Structure Determination: A suitable single crystal of $[Mn(dpa)(N_3)_2]$ was carefully selected under a polarizing microscope and mounted on a glass fiber. Diffraction data were collected at room temperature on an Enraf−Nonius CAD4 automated diffractometer, using graphite-monochromated Mo-K_α radiation. Details of crystal data, intensity collection, and some features of the structure refinement are reported in Table 3. Lattice constants were obtained by a least-squares refinement of the setting angles of 25 reflections in the range $6° < \theta < 11°$. Intensities and angular positions of two standard reflections were measured each hour, and these showed neither decrease nor misalignment during data collection.

Table 3. Crystal data, details of data collection, and structure refinement for $[Mn(C_{10}H_9N_3)(N_3)_2]$

Formula	$C_{10}H_9MnN_9$
Molecular mass [$g{\cdot}mol^{-1}$]	310.2
Formula	$C_{10}H_9MnN_9$
Crystal system	Monoclinic
Space group	$P2_1/c$ (no. 14)
a [Å]	7.089(2)
b [Å]	19.090(4)
c [Å]	9.682(4)
β [°]	104.61(2)
V [$Å^3$]	1267.9(7)
Z	4
$\rho_{calcd.}$ [gcm^{-3}]	1.625
F(000)	628
T [K]	293(2)
μ(Mo-*Kα*) [mm^{-1}]	1.046
Radiation, λ(Mo-*Kα*) [Å]	0.71070
Limiting indices	$0<h<9$, $0<k<26$, $-13<l<13$
R [$I > 2\sigma(I)$]	$R1 = 0.039$, $wR2 = 0.096$[a]
Goodness of fit on F^2	1.065

[a] $R1 = [\Sigma(|F_o| - |F_c|)]/\Sigma|F_o|$; $wR2 = [\Sigma[w(|F_o|^2 - |F_c|^2)^2]/\Sigma[w(|F_o|^2)^2]]^{1/2}$; $w = 1/[\sigma^2|F_o|^2 + (x\,p)^2]$; where $p = [|F_o|^2 + 2|F_c|^2]/3$; $x = 0.0605$.

3944 reflections were measured, in the range $2.1° \le \theta \le 30.0°$. A total of 2664 were independent, applying the criterion $I > 2\sigma(I)$. Correction for Lorentz and polarization effects, and also for absorption with the empirical ψ scan method,[28] was performed by using the XRAYACS program.[29] Direct methods (SHELXS 97)[30] were employed to solve the structure. The metal ion was located first. The nitrogen and carbon atoms were found in difference Fourier maps. The structure was refined by the full-matrix, least-squares method based on F^2, using the SHELXL 97 computer program.[31] The scattering factors were taken from ref.[32] All non-hydrogen atoms were assigned anisotropic thermal parameters. The coordinates of the hydrogen atoms of the 2,2′-dipyridylamine ligand were obtained from difference Fourier maps. The final R factors were $R1 = 0.039$ [$wR2 = 0.096$]. Maximum and minimum peaks in final difference synthesis were 0.488, −0.397 $eÅ^{-3}$. The atomic coordinates and structure factors have been deposited at the Cambridge Crystallographic Data Centre (CCDC 146293). Drawing was made using ORTEP.[33]

Physical Measurements: CHN elemental analysis was carried out with a Perkin−Elmer Model 240 automatic analyzer. ICP-AES analysis was performed with an ARL Fisons 3410 spectrometer. The IR spectrum (KBr pellet) was obtained with a Nicolet FT-IR 740 spectrophotometer in the 400−4000 cm^{-1} range. The diffuse reflectance spectrum was recorded at room temperature on a Cary 2415 spectrometer in the 5000−47500 cm^{-1} range. A Bruker ESP

300 spectrometer was used to record the ESR polycrystalline spectra at room temperature and at 4.2 K. The temperature was stabilized by an Oxford Instrument (ITC 4) regulator. The magnetic field was measured with a Bruker BNM 200 gaussmeter and the frequency inside the cavity was determined using a Hewlett−Packard 5352B microwave frequency counter. Magnetic measurements of powdered sample were performed in the temperature range 4.2−300 K, using a Quantum Design MPMS-7 SQUID magnetometer. The magnetic field was approximately 0.1 T, a value in the range of linear dependence of magnetization vs. magnetic field even at 4.2 K.

Acknowledgments

This work was financially supported by the Universidad del País Vasco/Euskal Herriko Unibertsitatea (Project UPV 130.310-EB201/98), the Gobierno Vasco/Eusko Jaurlaritza (Project PI96/39) and the Ministerio de Educación y Cultura (Project PB97-0637), which we gratefully acknowledge.

[1] D. W. Bruce, D. O'Hare (Eds.), *Inorganic Materials*, Wiley **1992**.
[2] P. Delhaes, M. Drillon (Eds.), *Organic and Inorganic Low-Dimensional Materials*, NATO ASI Series, Vol. 168, Plenum Press, NY **1987**.
[3] D. Gatteschi, O. Kahn, J. S. Miller, F. Palacio (Eds.), *Magnetic Molecular Materials*, NATO ASI Series, Vol. 198. Kluwert, Dordrecht **1993**.
[4] E. Coronado, P. Delhaes, D. Gatteschi, J. S. Miller (Eds.), *Molecular Magnetism: from Molecular Assemblies to Devices*, NATO ASI Series, Vol. 321, Kluwer, Dordrecht **1995**.
[5] C. J. O'Connor (Ed.), *Research Frontiers in Magnetochemistry*, World Scientific, Singapore **1993**.
[6] J. Ribas, A. Escuer, M. Monfort, R. Vicente, R. Cortes, L. Lezama, T. Rojo, *Coord. Chem. Rev.* **1999**, *193−195*, 1027.
[7] R. D. Willet, D. Gatteschi, O. Kahn (Eds.), *Magneto-Structural Correlations in Exchange Coupled Systems*, NATO ASI Series, Reidel, Dordrecht **1985**.
[8] O. Kahn, *Molecular Magnetism*, VCH Publishers, Weinheim **1993**.
[9] M. M. Turnbull, T. Sugimoto, L. K. Thompson (Eds.), *Molecular-Based Magnetic Materials: Theory, Techniques and Applications*, ACS Symposium Series, n. 644, ACS, Washington **1996**.
[10] A. Caneschi, D. Gatteschi, L. Pardi, R. Sessoli, *Clusters, Chains and Layered Molecules: the Chemist's Way to Magnetic Materials*, in: A. F. Williams (Ed.), *Perspectives in Coordination Chemistry*, VCH, Weinheim **1992**.
[11] R. Cortés, L. Lezama, J. L. Pizarro, M. I. Arriortua, X. Solans, T. Rojo, *Angew. Chem. Int. Ed. Engl.* **1994**, *33*, 2488.
[12] G. Viau, M. G. Lombardi, G. D. Munno, M. Julve, F. Floret, J. Faus, A. Caneschi, M. J. Clemente-Juan, *J. Chem. Soc, Chem. Commun.* **1997**, 1195.
[13] F. A. Mautner, R. Cortés, L. Lezama, T. Rojo, *Angew. Chem. Int. Ed. Engl.* **1995**, *35*, 78.
[14] A. Escuer, R. Vicente, M. A. S. Goher, F. A. Mautner, *J. Chem. Soc., Dalton Trans.* **1997**, 4431.
[15] J. Ribas, M. Monfort, C. Diaz, C. Bastos and X. Solans, *Inorg. Chem.* **1994**, *33*, 484.
[16] R. Cortés, J. L. Pizarro, L. Lezama, M. I. Arriortua, T. Rojo, *Inorg. Chem.* **1994**, *33*, 2697.
[17] A. Escuer, R. Vicente, M. A. S. Goher, F. A. Mautner, *Inorg. Chem.* **1997**, *36*, 3440.
[18] R. Cortés, M. Drillon, X. Solans, L. Lezama, T. Rojo, *Inorg. Chem.* **1997**, *36*, 677.
[19] A. B. P. Lever, *Inorganic Electronic Spectroscopy*, Elsevier Science Publishers B.V., Amsterdam, Netherlands **1984**.
[20] J. Escobal, J. L. Mesa, J. L. Pizarro, L. Lezama, R. Olazcuaga, T. Rojo, *J. Mater. Chem.* **1999**, *9*, 2691.
[21] J. Escobal, J. L. Pizarro, J. L. Mesa, L. Lezama, R. Olazcuaga, M. I. Arriortua, T. Rojo, *Chem. Mater.* **2000**, *12*, 376.
[22] J. P. Hay, J. C. Thibeault, R. J. Hoffmann, *J. Am. Chem. Soc.* **1975**, *97*, 4884.
[23] C. Mealli, D. M. Proserpio, *Computer Aided Composition of Atomic Orbitals (CACAO)*. PC version, July **1992**, Kindly supplied by C. Mealli. See also: C. Mealli, D. M. Proserpio, *J. Chem. Edu.* **1990**, *67*, 399.
[24] L. F. Tang, L. Zhang, L. C. Li, P. Cheng, Z. H. Wang, J. T. Wang, *Inorg. Chem.* **1999**, *38*, 6326.
[25] M. A. M. Abu-Youssef, A. Escuer, D. Gatteschi, M. A. S. Goher, F. A. Mautner, R. Vicente, *Inorg. Chem.* **1999**, *38*, 5716.
[26] M. A. M. Abu-Youssef, A. Escuer, M. A. S. Goher, F. A. Mautner, R. Vicente, *Eur. J. Inorg. Chem.* **1999**, 687.
[27] A. Escuer, R. Vicente, M. A. S. Goher, F. Mautner, *Inorg. Chem.* **1998**, *37*, 782.
[28] A. C. T. North, D. C. Philips, F. S. Mathews, *Acta Crystallogr., Sect. A* **1968**, *24*, 351.
[29] A. Chandrasekaran, *XRAYACS*, Program for Single Crystal X-ray Data Corrections, Chemistry Department, University of Massachusetts, Amherst, USA **1998**.
[30] G. M. Sheldrick, *SHELXS 97*, Program for the Solution of Crystal Structures, University of Göttingen, Germany **1997**.
[31] G. M. Sheldrick, *SHELXL 97*, Program for the Refinement of Crystal Structures, University of Göttingen, Germany **1997**.
[32] *International Tables for X-ray Crystallography*, Kynoch Press, Birmingham, England, Vol. IV, p. 99, **1974**.
[33] C. K. Johnson, *ORTEP*, Report ORNL-5138, Oak Ridge National Laboratory, Oak Ridge, TN, **1976**.

Received October 18, 2000
[I00393]

Standard Enthalpies of Formation of Li, Na, K and Tl Cyclopentadienyls

João Paulo Leal,*[a] Vera Cachata,[a] and Adelaide Carvalho[a]

Keywords: Thermochemistry / Alkali metals / Heats of formation / Cyclopentadienyl ligands

The enthalpies of formation of lithium, sodium, potassium and thallium cyclopentadienyls were determined by reaction-solution calorimetry as $\Delta_f H°$ [LiCp] = −76.5 ± 2.9 kJ/mol, $\Delta_f H°$ [NaCp] = −39.7 ± 2.5 kJ/mol, $\Delta_f H°$ [KCp] = −83.2 ± 3.2 kJ/mol, and $\Delta_f H°$ [TlCp] = +117.7 ± 1.9 kJ/mol. Using a previously developed model, the enthalpies of formation of RbCp and CsCp were estimated.

Introduction

Alkali metal compounds have a major importance in synthetic chemistry.[1] The cyclopentadienyl anion ($C_5H_5^-$, Cp^-) can form compounds with almost all metallic elements and is one of the most important ligands in organometallic chemistry.[2−4] The cyclopentadienyl salts of lithium, sodium and potassium have been known for almost a century,[5] and thallium cyclopentadienyl for more than 40 years.[6,7] All of them are basic compounds in organometallic synthesis. Many organometallic compounds whose energetics are known contain one or more Cp ligands and involve MCp (M = Li, Na, K and Tl) reagents in their synthesis.[8−11] However, thermochemical data for these substances are almost absent from literature (a value for TlCp is the exception).[12]

In the present paper the enthalpies of formation of Li, Na, K and Tl cyclopentadienyls were determined by reaction-solution calorimetry, using several different reactions in various environments (water, aqueous hydrochloric acid, ethanol and toluene). These results, together with a previously developed estimation method, allowed us to predict the enthalpies of formation of the Rb and Cs cyclopentadienyls.

Results and Discussion

Enthalpies of formation of metal cyclopentadienyls were calculated by using Scheme 1 (reaction with water, used for Li, Na and K compounds), Scheme 2 (reaction with 0.1 M HCl, used for all the compounds studied in this paper), Scheme 3 (reaction with ethanol, used for NaCp), and Scheme 4 (reaction with ethanol in toluene, used for NaCp). In these schemes, $\Delta_r H°$ represents the reaction enthalpy with all the compounds in their standard state, $\Delta_r H$ the measured reaction enthalpy, $\Delta_{sln}H(2)$ the dissolution enthalpy of stoichiometric amounts of MOH in H_2O, $\Delta_{sln}H(3)$ the dissolution enthalpy of CpH in H_2O + MOH, $\Delta_{sln}H(5)$ the dissolution of MCl in 0.1 M HCl, $\Delta_{sln}H(6)$ the dissolution or mixing of CpH in a 0.1 M HCl + MCl solution, $\Delta_{sln}H(7)$ the dissolution of water in 0.1 M HCl solution, $\Delta_{sln}H(9)$ the dissolution enthalpy of NaOEt in ethanol, $\Delta_{sln}H(10)$ the dissolution enthalpy of CpH in ethanol + NaOEt, $\Delta_{sln}H(11)$ the dissolution enthalpy of EtOH in toluene, $\Delta_{sln}H(12)$ the dissolution enthalpy of NaOEt in toluene + ethanol, and $\Delta_{sln}H(13)$ the dissolution enthalpy of CpH in toluene + ethanol + NaOEt. $\Delta_{sln}H(1)$ (dissolution of water in water), $\Delta_{sln}H(4)$ (dissolution of 0.1 M HCl in 0.1 M HCl), and $\Delta_{sln}H(8)$ (dissolution of ethanol in ethanol) are, obviously, zero.

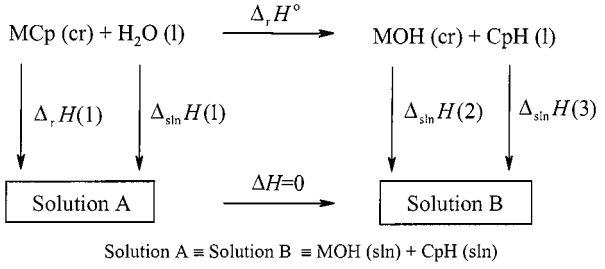

Scheme 1

As the concentrations of MOH in solution were always very small (about 1 mol of MOH in 4×10^5 mol of water), infinite dilution can be assumed and $\Delta_{sln}H(2)$ can be calculated as −23.49 kJ/mol for lithium hydroxide, −44.50 kJ/mol for sodium hydroxide, and −57.61 kJ/mol for the potassium analogue from the data in Table 1.[13] As cyclopentadiene (CpH) is immiscible with water $\Delta_{sln}H(3)$ was taken as zero.

The enthalpies of formation of aqueous 0.1 M HCl and crystalline metal chlorides are known (Table 1).[13] The dissolution of water in the solvent is negligible (smaller than the detection limit of the apparatus) and even when multiplied by 552 [see Scheme 2 and Equation (2) below] yields a minor contribution to the final $\Delta_r H°$ value (smaller than the experimental error). Therefore, $\Delta_{sln}H(7)$ was neglected. All the other dissolution enthalpies needed were measured or calculated from literature data (Table 2).[13−16]

[a] Departamento de Química, Instituto Tecnológico e Nuclear, 2686−953 Sacavém, Portugal
Fax: (internat.) +351-219/941-455
E-mail: jpleal@itn.pt

Supporting information for this article is available on the WWW under http://www.wiley-vch.de/home/eurjic or from the author.

 © WILEY-VCH Verlag GmbH, 69451 Weinheim, 2001 1434−1948/01/0606−1587 $ 17.50+.50/0

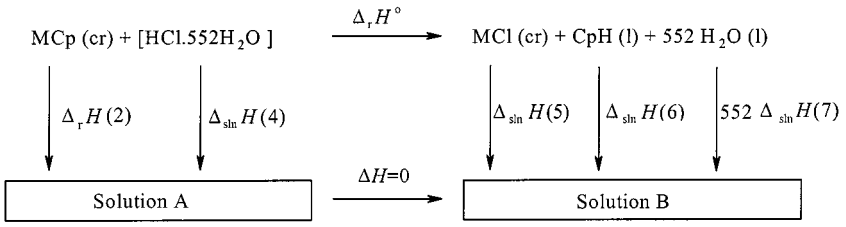

Scheme 2

Solution A ≡ Solution B ≡ MCl (sln) + CpH (sln) + n (HCl .552H_2O)

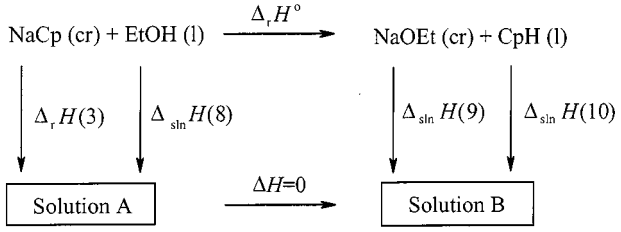

Solution A ≡ Solution B ≡ NaOEt (ethanol) + CpH (ethanol)

Scheme 3

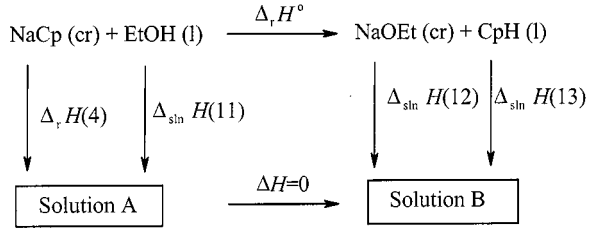

Solution A ≡ Solution B ≡ NaOEt (toluene+ethanol) + CpH (toluene+ethanol)

Scheme 4

Schemes 1−4 lead to Equation (1)−(4), that allow the calculation of the enthalpies of formation of the metal cyclopentadienyls presented in Table 3.

$$\Delta_f H^o(\mathrm{MCp, cr}) = \Delta_f H^o(\mathrm{MOH, cr}) + \Delta_f H^o(\mathrm{CpH, l}) - \Delta_f H^o(\mathrm{H_2O, l}) - \Delta_r H(1) + \Delta_{sln} H(2) \quad (1)$$

$$\Delta_f H^o(\mathrm{MCp, cr}) = \Delta_f H^o(\mathrm{MCl, cr}) + \Delta_f H^o(\mathrm{CpH, 1}) - \Delta_f H^o(\mathrm{HCl{\cdot}552H_2O}) - \Delta_r H(2) + \Delta_{sln} H(5) + \Delta_{sln} H(6) + 552\Delta_{sln} H(7) \quad (2)$$

$$\Delta_f H^o(\mathrm{NaCp, cr}) = \Delta_f H^o(\mathrm{NaOEt, cr}) + \Delta_f H^o(\mathrm{CpH, l}) - \Delta_f H^o(\mathrm{EtOH, l}) - \Delta_r H(3) + \Delta_{sln} H(9) + \Delta_{sln} H(10) \quad (3)$$

$$\Delta_f H^o(\mathrm{NaCp, cr}) = \Delta_f H^o(\mathrm{NaOEt, cr}) + \Delta_f H^o(\mathrm{CpH, l}) - \Delta_f H^o(\mathrm{EtOH, l}) - \Delta_r H(4) - \Delta_{sln} H(11) + \Delta_{sln} H(12) + \Delta_{sln} H(13) \quad (4)$$

For the Li, Na, and K compounds, whose enthalpies of formation were determined from different reactions and thermodynamic cycles, a good agreement between the results is observed (see Table 3, column 3). The recommended values for $\Delta_f H^o$(MCp, cr), shown in Table 4, are weighted averages of the data in Table 3.[17]

Table 1. Auxiliary data (T = 298.15 K)

Compound[a]	$\Delta_f H^o$ (kJ/mol)	Reference
H_2O, l	−285.830	13
LiOH, cr	−484.93	13
LiOH·100000H_2O	−508.423	13
LiOH, ai	−508.48	13
LiCl, cr	−408.61	13
NaOH, cr	−425.609	13
NaOH·∞H_2O	−470.11	13
NaOH, ai	−470.114	13
NaCl, cr	−411.153	13
NaOEt, cr	−411.6 ± 1.9	15
KOH,cr	−424.764	13
KOH·∞H_2O	−482.37	13
KOH, ai	−482.37	13
KCl, cr	−436.747	13
TlOH, cr	−238.9	13
TlOH, ai	−224.64	13
TlCl, cr	−204.14	13
C_5H_6, l	105.9 ± 1.5	14
C_2H_5OH, l	−277.5 ± 0.4	14
C_2H_5OH·∞H_2O	−288.2 ± 0.4	14
HCl·552H_2O	−166.596	13

[a] ai: aqueous solution, ionized substance standard, $m_{\pm}$ = 1 mol/kg; cr: crystalline.

A literature value for the enthalpy of formation of TlCp, $\Delta_f H^o$= 99.8 ± 2.5 kJ/mol, was obtained from measurements of the heat of reaction of aqueous TlOH with gaseous C_5H_6 at 25°C.[12] Recalculation of this value with more recent auxiliary data leading to 101.7 ± 2.6 kJ/mol,[18] only barely improves the discrepancy with the result in Table 4, 117.7 ± 1.2 kJ/mol. According to Hull and Turnbull, the heat of reaction relies on the mass of TlCp collected. If a small fraction of that mass was lost, the true value of the reaction enthalpy of TlOH with CpH would be less negative and the enthalpy of formation higher, in line with the result in Table 4.

The enthalpies of formation in Table 4 together with literature data,[13,19] were used to calculate the lattice energies ($\Delta_{lat} U^o$) of metal cyclopentadienyls, according to Scheme 5. These values are also displayed in Table 4. It is observed that the cyclopentadienyl compounds have a strong ionic character, as their lattice energies are only about 200 kJ/mol lower than the lattice energies for the corresponding hydroxides.[20]

Let us assume a simple ionic model and the Kapustinskii approximation represented by Equation (5).[21]

Table 2. Dissolution enthalpies (T = 298.15 K)

Compound	$\Delta_{sln}H(5)$ (kJ/mol)[a]	$\Delta_{sln}H(6)$ (kJ/mol)[b]	$\Delta_{sln}H(9)$ (kJ/mol)[c]	$\Delta_{sln}H(10)$ (kJ/mol)[d]	$\Delta_{sln}H(11)$ (kJ/mol)[e]	$\Delta_{sln}H(12)$ (kJ/mol)[e]	$\Delta_{sln}H(13)$ (kJ/mol)[f]
LiCl	−37.60 ± 0.52[g]						
NaCl	1.439 ± 0.092[h]						
KCl	19.3 ± 2.8						
TlCl	11.2 ± 1.1						
CpH		5.0 ± 0.3		1.6 ± 0.3			1.5 ± 1.4
NaOEt			−96.3 ± 2.9			−70.4 ± 0.6	
EtOH					17.6 ± 0.8		

[a] Dissolution in 0.1 M HCl. – [b] Dissolution in 0.1 M HCl + NaCl; the same value was considered to be the dissolution in 0.1 M HCl + MCl (M = Li, K, Tl) (see ref.[16]). – [c] Dissolution in ethanol. – [d] Dissolution in ethanol + NaOEt. – [e] Dissolution in toluene. – [f] Dissolution in toluene + NaOEt. – [g] Data from ref.[16]. – [h] Calculated from data in ref.[15], considering that the number of mmols of NaCl formed is 0.619 ± 0.033.

Table 3. Reaction enthalpies, and standard enthalpies of formation of metallic cyclopentadienyl salts (T = 298.15 K)

Metal−Cp	Δ_rH kJ/mol	$\Delta_fH°$(MCp, cr) kJ/mol
LiCp	−40.4 ± 1.7[a]	−76.3 ± 2.3
	−91.5 ± 4.1[b]	−77.2 ± 4.4
NaCp	−38.6 ± 2.5[a],[c]	−39.8 ± 2.9
	−42.4 ± 2.0[a],[d]	−36.0 ± 2.5
	−88.9 ± 1.1[b],[d]	−43.3 ± 1.9
	−82.5 ± 2.8[c],[e]	−40.4 ±4.7
	−72.5 ± 8.5[c],[f]	−42.2 ± 9.0
KCp	−5.8 ± 2.2[a]	−84.8 ± 2.7
	−62.2 ± 3.6[b]	−77.8 ± 4.8
TlCp	−33.1 ± 0.3[b]	+117.7 ± 1.9

[a] Reaction with water. – [b] Reaction with 0.1 M HCl. – [c] Batch 1. – [d] Batch 2. – [e] Reaction with ethanol. – [f] Reaction with ethanol in toluene.

Table 4. Enthalpies of formation and lattice energies of cyclopentadienyls salts

Compound	$\Delta_fH°$(MCp,cr) kJ/mol	$\Delta_{lat}U°$(MCp)[a] kJ/mol
LiCp	−76.5 ± 2.9	823.4 ± 7.5
NaCp	−39.7 ± 2.5	710.2 ± 7.4
KCp	−83.2 ± 3.2	658.6 ± 7.6
TlCp	+117.7 ± 1.9	721.2 ± 7.2

[a] $\Delta_fH°$(Cp, g) = 241 ± 6 kJ/mol,[19] E_{ea}(Cp) = 174.9 ± 3.5 kJ/mol (ref.[19], using only the values from LPES and LPD).

$$\Delta_{lat}U° = \frac{1.079 \times 10^5 . \nu . Z_+ Z_-}{r_+ + r_-} \quad (5)$$

In this expression, ν represents the number of ions in the molecule, Z_+ and Z_- the charges of the cation and the anion, and r_+ and r_- the respective radii in pm. As the ionic radii of Li^+, Na^+, K^+, and Tl^+ are known,[22] the ionic radius of the cyclopentadienide anion can be derived from the lattice energy in each case (Table 5).

The radii calculated through the above procedure are called "thermochemical radii" [they reproduce lattice energies when introduced in Equation (5)] and should not be interpreted as crystallographic radii. However, some correlation seems to exist and this can be confirmed by comparing the sum $r_+ + r_-$ with the crystallographic distances M−Cp (Table 5).[23−26]

When the values of the thermochemical radius for the Cp^- ligand are plotted together with the data for RO^-

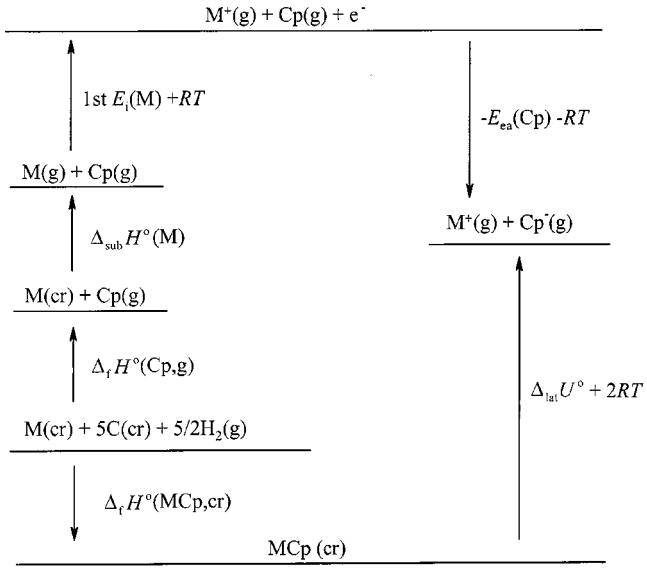

Scheme 5

Table 5. Thermochemical radii calculated or estimated in cyclopentadienyl salts[a] and experimental distances

MCp	$r_+ + r_-$	r_+[b]	r_-	d(M−Cp)
LiCp	262.1 ± 2.4	90±1	172.1±2.6	196.9[c]
NaCp	303.9 ± 3.2	116±1	187.9±3.4	235.7[c]
KCp	327.7 ± 3.8	152±1	175.7±3.9	281.6[c][d]
TlCp	334.2 ± 3.3	164±1	170.2±3.4	319.0[e]
RbCp	(332 ± 5)	166±1	(166±5)	297.4[f][g]296.2[f][h]
CsCp	(347 ± 5)	181±1	(166±5)	312.3[i]

[a] Estimated values in parenthesis. – [b] Data from ref.[22]. – [c] Ref.[23]. – [d] Average value. – [e] Ref.[26]. – [f] Ref.[24]. – [g] Average phase I. – [h] Average phase II. – [i] Ref.[25].

(R = H, Me, Et)[13,15,16,27,28] a similar trend (with a maximum for sodium) is observed (Figure 1), allowing us to estimate the thermochemical radius for Cp^- in RbCp and CsCp as 166 ± 5 pm.[29] From this value, the lattice energy for RbCp and CsCp can be calculated: $\Delta_{lat}U^o$[RbCp] = 650.0 ± 9.8 kJ/mol, and $\Delta_{lat}U^o$[CsCp] = 621.9±9.0 kJ/mol. Finally, the lattice energies and auxiliary data[30] yield (Scheme 5) the enthalpies of formation of the rubidium and caesium compounds: −99 ± 12 kJ/mol and −103 ± 11 kJ/mol, respectively.

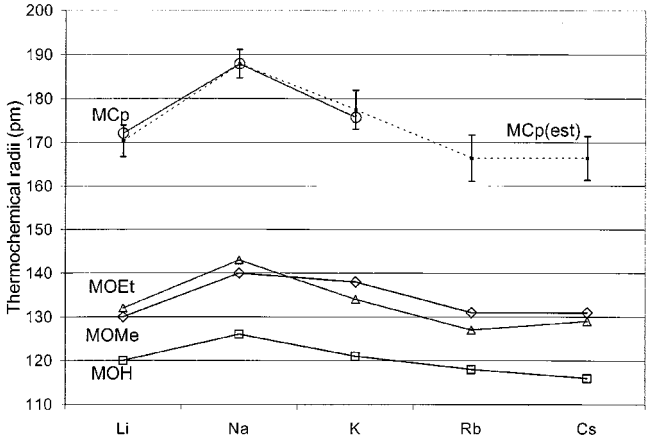

Figure 1. Thermochemical radii of anions (OH^-, OMe^-, OEt^-, and Cp^-); estimated values for Cp^- are presented with error bars (for a detailed calculation of these values see the Supporting Information).

The crystallographic M−C distances for $MgCp_2$, 233.9 pm,[31] 234.8 pm[32] in the gas phase and 230.4 pm[33] by X-ray crystallography are comparable to the Na−C distance in NaCp. There exists in the literature a value of 69.3 ± 4.2 kJ/mol for the enthalpy of formation of $MgCp_2$.[34] From this value and an approach similar to the one used for the compounds studied in this paper a thermochemical radius of 183 ± 8 pm for the Cp^- in $MgCp_2$ [35] is obtained, which is in keeping with the value obtained for Cp^- in NaCp (187.9 ± 3.4 pm).

The above results can be used to understand the stability of TlCp in the presence of water or oxygen when compared to other cyclopentadienyl derivatives of Tl or even with InCp.[36−39] TlCp is quite stable in water and reacts only slowly with oxygen.[40] For example, TlCp was found to be more stable than TlC_5H_4tBu or $TlC_5H_4(SiMe_3)$ (which are of similar stability), and of TlC_5H_4Me which is highly air- and water-sensitive. To explain this behaviour it has been argued that TlCp should have a much higher lattice energy than other cyclopentadienyl salts, such as thallium methylcyclopentadienide, due to different molecular symmetries.[41] We note, however, that the reactivity of thallium hydropentalenide in the presence of water is similar to TlCp.[37]

As noticed by Hull and Turnbull,[12] the enhanced stability of TlCp is mainly due to the low affinity of Tl for oxygen and the solubility of TlOH in water. To check this hypothesis, the enthalpy of the reaction in Equation (6) can be calculated for all four compounds studied, using the enthalpies of formation of MCp measured in this work and auxiliary data from Table 1.

$$MC_5H_5(cr) + H_2O(l) \rightarrow MOH(aq) + C_5H_6(l) \quad (6)$$

The results are −40.2 kJ/mol (Li), −38.7 kJ/mol (Na), −7.4 kJ/mol (K) and 49.4 kJ/mol (Tl). Therefore, only the reaction for TlCp is endothermic. Although the entropy change for this reaction is expected to be positive, the term $T\Delta_rS^o$ at 298.15 K will be much smaller than Δ_rH^o for TlCp, thus implying that $\Delta_rG^o > 0$.

Experimental Section

Materials: Ethanol (Merck, 99.8%) was pre-dried over calcium sulfate, refluxed over activated magnesium and iodine, and finally distilled. Lithium, sodium, potassium and thallium (Sigma) were kept inside an oxygen- and water-free glove-box and used as supplied. Pentane was distilled over P_2O_5 and kept in the glove-box over 4 Å molecular sieves. Tetrahydrofuran was dried over 4 Å molecular sieves, refluxed with sodium and benzophenone, and distilled. Toluene was dried over 4 Å molecular sieves, refluxed with sodium and benzophenone, and distilled. Cyclopentadiene was prepared by cracking the Cp_2 dimer under an inert atmosphere, using a Vigreux column, collected at 0° C and used immediately.

Physical Measurements: Infrared spectra were obtained on a Perkin−Elmer 577 spectrophotometer with samples mounted as Nujol mulls between KBr plates. Elemental analyses were performed on an automatic analyzer Perkin−Elmer 240 C (C, H). Instrumental neutron activation analysis (INAA) was performed on sodium, using sodium acetate as a standard (for experimental procedure and data processing see, for example, ref.[42]).

Cyclopentadienyl Salt Syntheses: The Li, Na, and K compounds are moisture sensitive. Therefore, all syntheses and handling were made inside an oxygen- and water-free (<5 ppm) glove-box or using Schlenk techniques.

The sodium and potassium cyclopentadienyl compounds were synthesised in THF solution according to a literature procedure.[6] The solution was then taken to dryness and the precipitate washed twice with pentane. The resulting compounds were analysed by IR spectroscopy and elemental analysis (C, H). Additionally, the sodium content in NaCp was measured by neutron activation. All analysis found the compounds to be pure.

Lithium cyclopentadienyl was synthesised in THF solution by a similar method to the one used for the sodium and potassium analogues, but instead of metallic lithium we used butylithium in solution. The final solution was then taken to dryness and the precipitate washed twice with pentane. The resulting compound was analysed by IR spectroscopy and elemental analysis (C, H).

Thallium cyclopentadienyl was synthesised from thallium sulfate, sodium hydroxide, and freshly cracked cyclopentadiene in water, according to a literature procedure.[43] After sublimation the yellow product was analysed by IR spectroscopy and elemental analysis (C, H).

Reaction-Solution Calorimetry: The calorimeter used was specially built for the study of oxygen- and water-sensitive compounds, and the experimental procedure was described in a previous paper.[15]

All measurements were made near 298.15 K, and the results are averages of at least four runs. The errors presented are twice the standard deviation of the mean in each case.

Note added in proof (February 1, 2001): During publication a previous value of the enthalpy of formation of NaCp (−14±25 J/mol; E. B. Evstigneeva, H. A. Bartolomeeva, T. H. Hukolskai, A. M. Moosu, *Zh. Fiz. Khim.* **1973**, *47*, 2727−2727) was brougth to our attention. Despite the poor quality of the result, their error bar overlaps the experimental value measured in this paper. The reference gives no details concerning the calculation of that value.

Acknowledgments

The authors thank Dr. Ângela Gouveia (ITN) for performing the instrumental neutron activation analysis (INAA). Financial support from FCT (PRAXIS/2/2.1/QUI/51/94) is gratefully acknowledged.

[1] See, for example: A. Streitwieser, Jr., C. H. Heathcock, *Introduction to Organic Chemistry* (3rd ed.), MacMillan, New York, **1985**.
[2] D. Stalke, *Angew. Chem. Int. Ed. Engl.* **1994**, *33*, 2168−2171.
[3] J. L. Wardell, in *Comprehensive Organometallic Chemistry* (Eds.: G. Wilkinson, F. G. A. Stone) Pergamon Press, Oxford, **1982**.
[4] M. A. Beswick, D. S. Wright, in *Comprehensive Organometallic Chemistry II* (Eds.: E. W. Abel, F. G. A. Stone, G. Wilkinson) Elsevier Science Ltd., Oxford, **1995**.
[5] G. Wilkinson, F. A. Cotton, *Progr. Inorg. Chem.* **1959**, *1*, 1−124.
[6] G. Wilkinson, *Org. Synth.* **1956**, *36*, 31−34.
[7] E. O. Fischer, *Angew. Chem.* **1957**, *69*, 207−209.
[8] See, for example: J. A. Martinho Simões, J. L. Beauchamp, *Chem. Rev.* **1990**, *90*, 629−688, and references cited therein.
[9] See, for example: *Bonding Energetics in Organometallic Compounds* (Ed.: T. J. Marks), ACS Symposium Series, American Chemical Society, Washington, DC, **1990**.
[10] See, for example: *Energetics of Organometallic Species* (Ed.: J. A. Martinho Simões), NATO ASI Series, Kluwer Academic Publishers, Dordrecht, **1992**.
[11] See, for example: *Energetics of Stable Molecules and Reactive Intermediates* (Ed.: M. E. Minas da Piedade), NATO Science Series, Kluwer Academic Publishers, Dordrecht, **1999**.
[12] H. Hull, A. G. Turnbull, *Inorg. Chem.* **1967**, *6*, 2020−2022.
[13] D. D. Wagman, W. H. Evans, V. B. Parker, R. H. Schumm, I. Halow, S. M. Bailey, K. L. Churney, R. L. Nutall, *The NBS Tables of Chemical Thermodynamics Properties, J. Phys. Chem. ref. Data*, **1982**, *11*, Supplement no. 2.
[14] J. B. Pedley, R. D. Naylor, S. P. Kirby, *Thermochemical Data of Organic Compounds* (2nd ed.), Chapman and Hall, New York, **1986**.
[15] J. P. Leal, A. Pires de Matos, J. A. Martinho Simões, *J. Organomet. Chem.* **1991**, *403*, 1−10.
[16] J. P. Leal, J. A. Martinho Simões, *J. Organomet. Chem.* **1993**, *460*, 131−138.
[17] Used formulae (mean, $\bar{x}$, and standard deviation, $\delta\bar{x}$, respectively):

$$\bar{x} = \sqrt{\sum \frac{x_i^2}{\delta_{x_i}^2} \Big/ \sum \frac{1}{\delta_{x_i}^2}}\,,\quad \delta_{\bar{x}} = \sum \frac{1}{\delta_{x_i}} \Big/ \sum \frac{1}{\delta_{x_i}^2}$$

[18] The enthalpy of formation of crystalline TlCp can be recalculated from the enthalpy of the reaction $TlOH{\cdot}2050H_2O + C_5H_6\,(g) \rightarrow TlC_5H_5(cr) + H_2O(l) + 2050\,H_2O(l)$, $\Delta_r H = -91.0 \pm 2.1$ kJ/mol, obtained by Hull and Turnbull,[10] and more recent auxiliary data (kJ/mol): $\Delta_f H^o$ (CpH, g) = 134.3 ± 1.5,[12] $\Delta_f H^o(H_2O, l) = -285.83$,[11] $\Delta_f H^o(TlOH{\cdot}2050H_2O) = -227.95$,[11] enthalpy of dilution due to formed water (−0.43).[11] The obtained value will be 101.7 ± 2.6 kJ/mol.
[19] S. G. Lias, J. E. Bartmess, J. F. Liebman, J. L. Holmes, R. D. Levin, W. G. Mallard, *J. Phys. Chem. ref. Data*, **1988**, *17*, Suppl. 1.
[20] Lattice energies calculated using data from references 11 and 17. $\Delta_{lat}U^o$(LiOH) = 1028 kJ/mol, $\Delta_{lat}U^o$(NaOH) = 886 kJ/mol, $\Delta_{lat}U^o$(KOH) = 790 kJ/mol, $\Delta_{lat}U^o$(TlOH) = 876 kJ/mol.
[21] Kapustinskii noticed that, in the formula for the lattice energy in an ionic model, when dividing the Madelung constants by the number of ions in the molecule the new constant obtained is almost independent of the structure of the lattice. He also assumed that the repulsive part of the energy is 1/9 that of the attractive one and replaced the internuclear equilibrium distance by a sum of two radii (r_+ and r_-). For a detailed discussion see:D. A. Johnson, *Some Thermodynamic Aspects of Inorganic Chemistry*, 2nd ed., Cambridge University Press, Cambridge, **1982**.
[22] R. D. Shannon, *Acta Cryst.* **1976**, *A32*, 751−767.
[23] R. E. Dinnebier, U. Behrens, F. Olbrich, *Organometallics* **1997**, *16*, 3855−3858.
[24] R. E. Dinnebier, F. Olbrich, S. van Smaalen, P. W. Stephens, *Acta Cryst.* **1997**, *B53*, 153−158.
[25] R. E. Dinnebier, F. Olbrich, G. M. Bendele, *Acta Cryst.* **1997**, *C53*, 699−701.
[26] E. Frasson, F. Menegus, C. Panattoni, *Nature* **1963**, *199*, 1087−1089.
[27] P. Nunes, PhD. Thesis, IST − Universidade Técnica de Lisboa, **1999.**
[28] J. P. Leal, M. E. Minas da Piedade, P. Nunes, unpublished results.
[29] For the detailed estimation of the values please see the supporting information.
[30] $\Delta_{sub}H^o$(Rb) = 80.88 kJ/mol, 1st E_i(Rb) = 409.221 kJ/mol, $\Delta_{sub}H^o$(Cs) = 76.065 kJ/mol, 1st E_i(Cs) = 381.899, taken from ref.[11]
[31] A. Haaland, J. Lusztyk, J. Brunvoll, K. B. Starowieyski, *J. Organomet. Chem.* **1975**, *85*, 279−285.
[32] W. Bünder, E. Weiss, *J. Organomet. Chem.* **1975**, *92*, 1−6.
[33] W. Bünder, E. Weiss, Ph.D. Thesis, Universität Hamburg, **1974**.
[34] http://www.webbook.gov/chemistry/
[35] Taking the enthalpy of formation of $MgCp_2$ and using a scheme similar to Scheme 5 a value of 2406 ± 14 kJ/mol for the lattice energy can be derived. From this value and Equation (5) a value of 269.1 ± 7.6 pm for the sum of the radii was calculated, and using a value of 86 ± 1 pm for Mg^{2+} [20] $r_-(Cp^-)$ = 183 ± 8 pm was obtained.
[36] H. Schumann, C. Janiak, J. Pickardt, U. Börner, *Angew. Chem. Int. Ed. Engl.* **1987**, *26*, 789−792.
[37] T. J. Katz, J. J. Mrowca, *J. Am. Chem. Soc.* **1967**, *89*, 1105−1111.
[38] H. Schumann, C. Janiak, H. Khani, *J. Organomet. Chem.* **1987**, *330*, 347−355.
[39] C. Janiak, *Coord. Chem. Rev.* **1997**, *163*, 107−216 (p. 163).
[40] F. A. Cotton, L. T. Reynolds, *J. Am. Chem. Soc.* **1958**, *80*, 269−274.
[41] Ref.[5], p. 10.
[42] F. Dai Kin, M. I. Prudêncio, M. A. Gouveia, E. Magnusson, *Geostandards Newsletter* **1999**, *23*, 47−58.
[43] A. J. Nielson, C. E. F. Richard, J. M. Smith, *Inorg. Synth.* **1986**, *24*, 97−101.

Received October 18, 2000
[I00397]

BF_3-Stabilized Metalated Sulfinylimides and Sulfurdiimides of the Type $Cp(NO)_2CrNSE{\cdot}BF_3$ (E = O, $NSiMe_3$)

Michael Limmert,[a] Ingo-Peter Lorenz,*[a] Jürgen Neubauer,[a] Heinrich Nöth,[a] and Tassilo Habereder[a]

Dedicated to Professor Kurt Dehnicke on the occasion of his 70th birthday

Keywords: Chromium / Metalation / Sulfur / N ligands / Lewis acids / Structure elucidation

The coordination behavior of the imido derivatives of sulfur Me_3SiNSE (E = O, $NSiMe_3$) towards the 16-electron complex $[CpCr(NO)_2]BF_4$ has been studied. In both cases coordination through an η^1-*N* linkage occurs as well as elimination of Me_3SiF to afford the metalated derivatives $Cp(NO)_2CrNSE$, which as N-nucleophiles are additionally bound to the also-formed electrophilic BF_3 molecule (**1**, **2**). Neither the possible addition products $[Cp(NO)_2Cr\{N(SiMe_3)SE\}]BF_4$ as intermediates in the synthesis of **1**, **2** nor the BF_3-free derivatives $Cp(NO)_2CrNSE$ as elimination products of **1**, **2** could be stabilized or generated. The molecular structures of **1**, **2** have been determined by single crystal X-ray analyses. Both compounds contain a distorted tetrahedrally configured chromium center and an almost planar zig-zag conformation of their sulfinyl imido (F_3BNSO) and sulfur diimido ligand ($F_3BNSNSiMe_3$), respectively.

Introduction

In contrast to SO_2 the isoelectronic molecules sulfinylimide HNSO and sulfurdiimide $S(NH)_2$ are not monomeric, are unstable and are difficult to generate and handle.[1] Thus, they more closely resemble the also isoelectronic methylenesulfine CH_2SO. The N-substituted derivatives RNSO and $S(NR)_2$, however, especially with R = aryl are easily accessible, more stable and have proven useful as synthons in organic synthesis.[2] Because of their heterocumulene structure their manifold coordination chemistry has been investigated.[3] They coordinate above all by η^2-*N*=*S*,[4,5] η^1-*S*[4a,6,7] or η^1-*N*[8,9] binding to various electrophilic complex fragments. There are two further ligand functions known. Whereas RNSO additionally undergoes the η^1-*O* linkage,[10] $S(NR)_2$ can also bind as a chelate ligand through both the N atoms (η^2-N_2;[11] see Scheme 1).

Recently we have been able to prepare some new sulfinylimide complexes of the type $CpMn(CO)_2\{S(O)NR\}$ (Cp = C_5H_5, $C_5H_4CH_3$; R = C_6H_5, $SiMe_3$) with η^1-*S* coordination.[12] In the beginning, and with respect to the silyl derivatives, our aim was to generate and stabilize the basic molecule HNSO within the coordination sphere of the transition metal by directed substitution reactions of, for example, Me_3SiX (X = OH, F, Cl). Our attempts, however, were not successful.[12] Hitherto, no HNSO complex has been structurally characterized, although some have been mentioned in the literature.[13–15] Here we report on further attempts at the synthesis of sulfinylimide (RNSO: R = $SiMe_3$, H) and, analogously, sulfurdiimide complexes [$S(NR)_2$: R = $SiMe_3$, H]. We have chosen the cation $[CpCr(NO)_2]^+$ which is isoelectronic with the neutral $CpMn(CO)_2$ used earlier[12] and which seemed to be a suitable complex fragment.

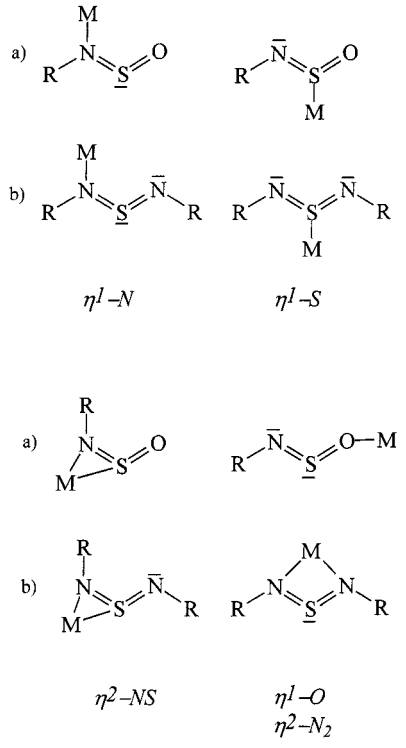

Scheme 1. The most important ligand functions of sulfinylimides (a) and sulfurdiimides (b)

[a] Department Chemie der LMU München,
Butenandtstrasse 5–13 (Haus D), 81377 München, Germany
Fax: (internat.) +49-89/2180-7867
E-mail: ipl@cup.uni-muenchen.de

 © WILEY-VCH Verlag GmbH, 69451 Weinheim, 2001 1434–1948/01/0606–1593 $ 17.50+.50/0

Results and Discussion

The 16-electron species $[CpCr(NO)_2]BF_4$ was generated from the chloride $CpCr(NO)_2Cl$ by dehalogenation with $AgBF_4$ and then reacted with the sulfinylimide Me_3SiNSO in CH_2Cl_2 to afford very surprisingly the neutral BF_3-containing complex $Cp(NO)_2Cr\{N(BF_3)SO\}$ (**1**) [Equation (1)]. The simultaneous elimination of Me_3SiF has been proved by ^1H NMR spectroscopy. Normally, and analogously,[12] we would have expected the formation of the addition compound $[Cp(NO)_2Cr\{N(SiMe_3)SO\}]BF_4$, although with an η^1-*N* linkage because of the strong electrophilicity of $CpCr(NO)_2^+$. The fragment $CpMn(CO)_2$ is amphoteric, has a soft center and forms an Mn−S bond to the same ligand Me_3SiNSO.[12]

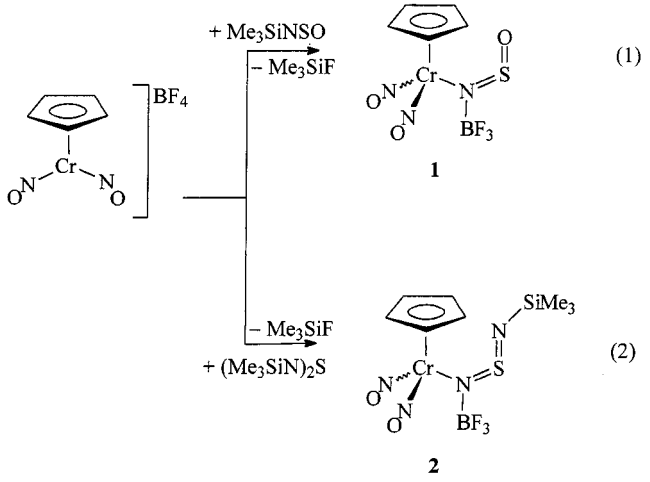

The same reaction occurred when the salt $[CpCr(NO)_2]BF_4$ was reacted with the sulfurdiimide $S(NSiMe_3)_2$, and the neutral BF_3-containing product $Cp(NO)_2Cr\{N(BF_3)SNSiMe_3\}$ (**2**) was obtained [Equation (2)]. Both compounds are dark-green solids which are air stable, but sensitive towards moisture. They dissolve only moderately in $CDCl_3$ and decompose very easily in acetone. In both cases a Cr−N bond has been formed and one $SiMe_3$ group of the sulfinylimide or the sulfurdiimide has been substituted for the isolobal organometallic fragment $CpCr(NO)_2$. The reaction pathway, however, seems to be more complicated.

Despite many efforts, including the use of low reaction temperatures, we could not find any hint of the addition compound mentioned above as a possible intermediate for **1** or **2**. In separate experiments $AgBF_4$ reacts with the molecules Me_3SiNSO and $S(NSiMe_3)_2$ to eliminate Me_3SiF, although no further product could be identified or isolated. Therefore, we assume for the reaction mechanism that, after separation of AgCl, the silyl derivatives are attacked by the BF_4^- anion to give Me_3SiF and the corresponding anions NSO^- and $NSNSiMe_3^-$, respectively. These anions coordinate to the chromium center through the nucleophilic nitrogen, which has been proved previously as their preferred linkage mode.[14,16,17] The resulting metalated sulfinylimide **1** and sulfurdiimide **2** are finally stabilized by the remaining electrophile BF_3 molecule as Lewis acid−base adducts. On the other hand, BF_3 could already bind to the generated anions mentioned above. The presence of BF_4^- and BF_3 is obviously necessary. When $AgCF_3SO_3$ was used for dehalogenation of $CpCr(NO)_2Cl$ to form $[CpCr(NO)_2]CF_3SO_3$, no elimination of Me_3SiX and no coordination of the imides was observed.

The IR, ^1H, ^{11}B, $^{13}C\{^1H\}$, and ^{19}F NMR and mass spectra of compounds **1**, **2** were measured. The IR spectra of **1**, **2** exhibit two ν(NO) bands at about 1815 and 1710 cm^{-1} (in KBr). The frequency range is the same, although the frequency difference of both is less than in the starting material $CpCr(NO)_2Cl$ [IR (KBr): ν(NO) = 1824; 1707/1689 cm^{-1}]. The absorptions for ν(SO) and ν(SN) of **1** are assigned at 1245 and 1123 cm^{-1}, and ν(BF) is found at 1084 cm^{-1} as a broad unresolved absorption. Compound **2** shows two ν(SN) absorptions at 1246 and 1132 cm^{-1} and one broad ν(BF) absorption again at 1096 cm^{-1}.

In the ^1H NMR spectra of **1**, **2** the protons of the Cp ring give singlets at δ = 5.75 and 5.67, respectively. The protons of the $SiMe_3$ group in **2** absorb at δ = 0.30. In the $^{13}C\{^1H\}$ NMR spectrum of **2** singlets are found at δ = 0.9 ($SiMe_3$) and 102 (Cp).

Due to the low solubility of **1** in $CDCl_3$, the expected quadruplet signals in both the ^{11}B and ^{19}F NMR spectra of **1** only appear as unresolved broad signals at δ = 0.98 and 138.7, respectively. Compound **2**, however, dissolves better in $CDCl_3$ and does show, therefore, two quadruplets at δ = 1.0 ($^1J_{BF}$ = 21.2 Hz) and 139.5 ($^1J_{BF}$ = 18.8 Hz). In both the spectra the broadness of the signals and the values of the chemical shifts are similar, indicating that the influence of SO (in **1**) and $NSiMe_3$ (in **2**) on the coordinating N atom seems to be identical.

No mass spectrum of **1** could be recorded; that of **2** does not show the parent signal, but fragments at *m*/*z* = 310, 280, 250 [$M^+ - BF_3 - n$NO] (*n* = 0−2) and 207 [$CpCr(NO)SN_2^+$], confirming the molecular structure.

X-ray Structure Analyses of 1 and 2

Single crystals of **1** and **2** suitable for X-ray diffraction analysis were obtained by covering their CH_2Cl_2 solutions with a layer of *n*-hexane and cooling to −20 °C. The results of the structural determinations are summarized in Table 1 and the molecular structures of **1** and **2** with the most important bonding parameters are given in Figure 1 and 2, respectively.

The analysis of **1** confirms the pseudo-tetrahedral coordination of Cr(1), the trigonal planar environment of N(3) [sum of angles at N(3) = 359.9°], the almost linear NO ligands [Cr(1)−N−O ≈ 172°] and the Cr(1)−N(3) bond length of 2.049(2) Å (η^1-*N*), indicating a typical Cr−N single bond. The bond lengths S(1)−N(3) [1.526(2) Å] and S(1)−O(3) [1.441(2) Å], typical for double bond character, are not very different to free sulfinylimides.[18] The distance N(3)−B(1) [1.662(4) Å] is also typical for borane imino adducts;[19] the B(1)−F_n bonds have an average value of 1.37 Å.

Table 1. Crystallographic data of **1** and **2**

	1	**2**
Empirical formula	$C_5H_5BCrF_3N_3O_3S$	$C_8H_{14}BCrF_3N_4O_2SSi$
Mol. wt.	306.99	378.19
Size	0.10 × 0.10 × 0.10 mm	0.30 × 0.30 × 0.10 mm
Color and habit	Green prism	Colorless prism
Crystal system	Monoclinic	Monoclinic
Space group	$P2_1/n$	$P2_1/c$
Unit cell dimensions		
a [Å]	7.8842(5)	6.5180(4)
b [Å]	10.8873(7)	13.3477(8)
c [Å]	12.1251(8)	17.772(1)
β [°]	102.613(1)	93.079(1)
V [Å]^3	1015.7(1)	1543.97
Z	4	4
$D_{calcd.}$ (g/cm^3)	2.008	1.627
Absorption coefficient [mm^1]	1.374	0.992
F(000)	608	768
Diffractometer	Siemens P4 CCD area detector	Siemens P4 CCD area detector
Radiation	Mo-K_α (λ = 0.71073 Å)	Mo-K_α (λ = 0.71073 Å)
Scan type	Hemisphere	Hemisphere
Temperature [K]	193(2)	193(2)
2θ range	5.08 to 57.62°	3.82 to 57.28°
Index ranges	$-8 \le h \le 10$	$-5 \le h \le 8$
	$-13 \le k \le 14$	$-16 \le k \le 16$
	$-15 \le l \le 15$	$-22 \le l \le 22$
Reflections collected	5722	8592
Independent reflections	1928 (R_{int} = 0.0192)	2757 (R_{int} = 0.0207)
Observed reflections	1747 [$F>4\sigma(F)$]	2455 [$F>4\sigma(F)$]
Absorption correction	SADABS	SADABS
Max./min. transmission	0.962/0.822	0.942/0.706
System	SHELXS−97	SHELXS−97
Solution	Direct methods	Direct methods
Refinement	Full-matrix least squares	Full−matrix least squares
Hydrogen atoms	Riding	Riding
Weighting scheme, x, y	0.05310	0.04220
	1.99650	0.93480
Data/restraints/parameters	1928/0/154	2757/0/193
Data-to-parameter-ratio	12.5:1 {11.3:1 [$F > 4\sigma(F)$]}	14.3:1 {12.7:1 [$F > 4\sigma(F)$]}
R index [$F > 4F(F)$][a]	$R1$ = 0.0361, $wR2$ = 0.0962	$R1$ = 0.0294, $wR2$ = 0.0761
R index (all data)	$R1$ = 0.0401, $wR2$ = 0.1000	$R1$ = 0.0341, $wR2$ = 0.0793
GOOF	1.020	1.057

[a] $w^{-1} = \sigma^2F_o^2 + (xP)^2 + yP$, where $P = (F_o^2 + 2F_c^2)/3$.

The angles at Cr(1) differ significantly. The angle N(1)−Cr(1)−N(2) [90.7(1)°] is the smallest of the three Cr-containing angles, the other two are 100.0(1)° for N(1)−Cr(1)−N(3) and 96.2(1)° for N(2)−Cr(1)−N(3). The same characteristic is found for the angles of N(3). Whereas the angle Cr(1)−N(3)−B(1) is exactly 120.2(2)°, those of Cr(1)−N(3)−S(1) and S(1)−N(3)−B(1) are 123.5(1)° and 116.2(2)°, respectively. The angle N(3)−S(1)−O(3) [115.4(1)°] of **1** is smaller than the analogous angle in $[Cp(CO)_2MnS(O)NSiMe_3]$ [118.8(3)°][12] due to the free electron pair on sulfur demanding more space. The angles N(3)−B(1)−F_n ≈ 108° are almost tetrahedral, the angles F_n−B(1)−F_n average 111°. The dihedral angle defined by O−S−N−B/Cr connectivity is only 1.4° so that the electron delocalization is almost perfect.

Compound **2** possesses structural configurations and parameters very similar to those found for **1**: pseudo-tetrahedral configuration at Cr(1), trigonal planar N(3) (sum of angles at N(3) = 360°), linear NO ligands (≈ 172°) and an almost identical Cr(1)−N(3) bond of 2.043(2) Å. The double-bond containing distances S(1)−N(4) [1.505(2) Å] and S(1)−N(3) [1.546(2) Å] differ due to the different substituents on N(4) and N(3). The distance N(3)−B(1) of 1.593(3) Å is a little bit smaller than that found in **1**.

The angle between both the NO ligands in **2** is, as in **1**, the smallest [N(1)−Cr(1)−N(2) = 95.8(3)°] of the three Cr(1)-containing angles, but it does not differ so much from the others as in **1**. The angles N(1)−Cr(1)−N(3) [98.90(8)°] and N(2)−Cr(1)−N(3) [97.05(8)°] differ only slightly. The angles around N(3) behave as in **1**: the angle Cr(1)−N(3)−S(1) is again 120.5(1)°, whereas the other two are Cr(1)−N(3)−S(1) = 123.0(1)° and S(1)−N(3)−B(1) = 116.5(1)°. The angle 112.0(1)° for N(3)−S(1)−N(4) is comparable to the analogous O(3)−S(1)−N(3) of the metalated

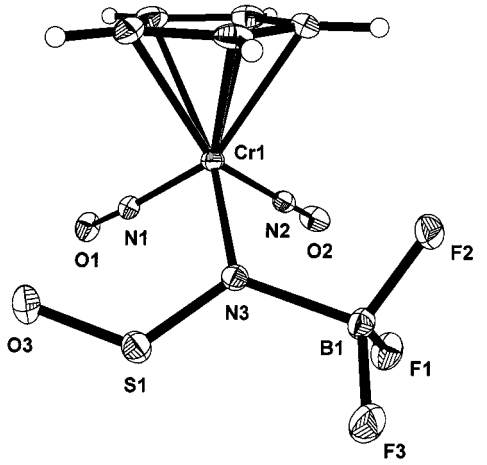

Figure 1. Molecular structure of **1**; selected bond lengths [Å] and angles [°]: Cr(1)−N(1) 1.718(3), Cr(1)−N(2) 1.720(3), Cr(1)−N(3) 2.049(2), N(3)−B(1) 1.622(4), N(3)−S(1) 1.526(2), S(1)−O(3) 1.441(2), B(1)−F_n 1.37; Cr(1)−N−O 172.5, N(1)−Cr(1)−N(2) 90.7(1), N(1)−Cr(1)−N(3) 100.0(1), N(2)−Cr(1)−N(3) 96.2(1), Cr(1)−N(3)−B(1) 120.2(2), Cr(1)−N(3)−S(1) 123.5(1), B(1)−N(3)−S(1) 116.2(2), N(3)−S(1)−O(3) 115.4(1), O(3)−S(1)−N(3)−B(1) 1.4 (dihedral)

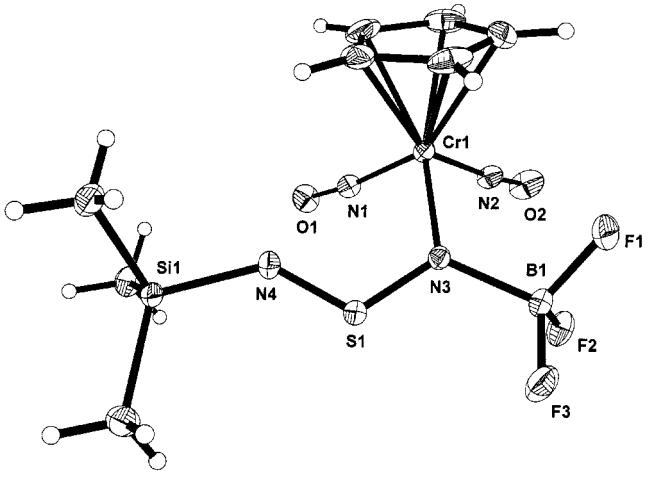

Figure 2. Molecular structure of **2**; selected bond lengths [Å] and angles [°]: Cr(1)−N(1) 1.722(2), Cr(1)−N(2) 1.708(2), Cr(1)−N(3) 2.044(2), N(3)−B(1) 1.593(3), N(3)−S(1) 1.546(2), S(1)−N(4) 1.505(2), N(4)−Si(1) 1.750(2), B(1)−F_n 1.375; Cr(1)−N−O 172.3, N(1)−Cr(1)−N(2) 95.83(8), N(1)−Cr(1)−N(3) 98.90(8), N(2)−Cr(1)−N(3) 97.05(8), Cr(1)−N(3)−B(1) 120.5(1), Cr(1)−N(3)−S(1) 123.0(1), B(1)−N(3)−S(1) 4116.5(1), N(3)−S(1)−N(4) 112.0(1), S(1)−N(4)−Si(1) 130.5(1), Si(1)−N(4)−S(1)−N(3) 2.5 (dihedral)

sulfinylimide **1**, but surprisingly much smaller than that in the free ligand $S(NSiMe_3)_2$ (129.5°) which was measured, however, by electron diffraction in the gas phase.[20] The bond angles with respect to the Lewis acid−base adduct part of **2** are very similar to those in **1** [N(3)−B(1)−F_n ≈ 108°; F_n−B(1)−F_n ≈ 110°].

Experimental Section

All operations were carried out under an argon atmosphere in dry, argon-saturated solvents. $CpCr(NO)_2Cl$,[21] Me_3SiNSO[22] and $S(NSiMe_3)_2$ [23] were prepared according to literature procedures. − IR: Nicolet 520 FT-IR (KBr). − NMR: Jeol EX-400 (^{1}H: 399.784 MHz; ^{11}B: 128.3 MHz; ^{13}C: 100.5 MHz; ^{19}F: 376.1 MHz). − MS: Jeol MS 700 (EI). − X-ray: Siemens P4 CCD area detector.

{*N*-η^5-Cyclopentadienyldinitrosylchromio}sulfinylimide·Trifluoroborane (1): A solution of $CpCr(NO)_2Cl$ (0.1 g, 0.47 mmol) in CH_2Cl_2 (5 mL) was stirred with $AgBF_4$ (0.1 mg, 0.48 mmol) until AgCl precipitated. After 10 min. Me_3SiNSO (0.08 mL, 0.5 mmol) was added to the filtered solution, which was then stirred for at least 20 min. The resulting yellow-green solution was covered with a layer of *n*-hexane and cooled to −20 °C. After one week green crystals of **1** separated, which were filtered off, washed with *n*-hexane and dried in vacuum. Yield: 0.035 g (25%), m.p. 132 °C (dec.). − IR (KBr): $\tilde{\nu}$ = 3143, 3114 (C−H; Cp), 1816, 1705/1696 (N≡O), 1429, 1402 (C=C; Cp), 1298 (S=O), 1245, 1123 (S=N), 1084 (BF) cm^{-1}. − ^{1}H NMR ($CDCl_3$): δ = 5.74 (s, Cp). − ^{11}B NMR ($CDCl_3$): δ = 0.98 (br. m). − ^{19}F NMR ($CDCl_3$): δ = 138.7 (br. m). − Neither a ^{13}C NMR nor an ms spectrum of **1** could be recorded due to its low solubility in $CDCl_3$ and its instability in solution. − $C_5H_5BCrF_3N_3O_3S$ (306.97): calcd. C 19.45, H 1.63, N 13.68; found C 20.10, H 2.03, N 12.78.

{*N*-η^5-Cyclopentadienyldinitrosylchromio}(*N*′-trimethylsilyl)-sulfurdiimide·Trifluoroborane (2): The dehalogenation of $CpCr(NO)_2Cl$ (0.1 g, 0.47 mmol) with $AgBF_4$ (0.1 mg, 0.48 mmol) was carried out as described above for **1**. $S(NSiMe_3)_2$ (0.12 mL, 0.48 mmol) was added to the resulting solution. After stirring for 30 min. a yellow-green solution was formed, which was layered with *n*-hexane and stored at −20 °C for crystallization. After one week green crystals of **2** separated, which were filtered off, washed with *n*-hexane and dried in vacuum. Yield: 0.05 g (40%), m.p. 160 °C (dec.). − IR (KBr): $\tilde{\nu}$ = 3118 (C−H; Cp), 2967, 2902 (C−H), $SiMe_3$), 1818, 1727/1696 (N≡O), 1432, 1417 (C=C; Cp), 1246, 1132 (S=N), 1096 (B−F) cm^{-1}. − ^{1}H NMR ($CDCl_3$): δ = 5.67 (s, Cp), 0.30 (s, $SiMe_3$). − ^{11}B NMR ($CDCl_3$): δ = 1.0 (q, $^1J_{BF}$ = 21.2 Hz, BF_3). − ^{19}F NMR ($CDCl_3$): δ =139.5 (q, $^1J_{BF}$ = 18.8 Hz). − ^{13}C{^{1}H} NMR ($CDCl_3$): δ = 102.2 (s, Cp), 0.9 (s, $SiMe_3$). − EI-MS: *m*/*z* = 310, 280, 250 [M^+ − BF_3 − *n*NO] (*n* = 0−2), 207 [CpCr(NO)NSNF]. Despite repeated attempts no reliable elemental analyses were obtained.

X-ray Crystallography: Single crystals were selected and mounted with perfluoroether oil on the tip of a glass fiber. For all measurements a Siemens P4 diffractometer equipped with a CCD area detector and a low-temperature device LT2 was used with Mo-K_α radiation and a graphite monochromator. Preliminary dimensions of the unit cell were calculated from a strong reflection collected on four different sets of 15 frames. Data collection was performed by the hemisphere method and the data collected on 1360 frames by changing θ by 0.3° increments at two different χ settings. The data were reduced by the program SAINT followed by absorption correction with the program SADABS. The structures were solved by direct methods (SHELXS-97). All non-hydrogen atoms are given in anisotropic description. H atoms were put in calculated positions and included in the final cycles of refinement as riding on the respective C atoms with U_i = 1.2U_c. Relevant crystallographic data are summarized in Table 1.

Crystallographic data (excluding structure factors) for the structure(s) included in this paper have been deposited with the Cam-

bridge Crystallographic Data Centre as supplementary publication nos. CCDC-148949 (**1**) and -148948 (**2**). Copies of the data can be obtained free of charge on application to CCDC, 12 Union Road, Cambridge CB2 1EZ, UK [Fax: (internat.) + 44-1223/336-033; Email: deposit@ccdc.cam.ac.uk].

Acknowledgments

We thank the Fonds der Chemischen Industrie (Frankfurt) for financial support. A doctoral scholarship for M. L. from the Freistaat Bayern is appreciated.

[1] *Gmelin, 5 − Sulfur−Nitrogen Compounds* **1990**, Part 6, 8th Edition, Springer Verlag New York.
[2] R. Beckert, R. Mayer, in Houben−Weyl, *Methoden der Organischen Chemie*, 4. Aufl., p. 558−579, G. Thieme Verlag, Stuttgart.
[3] K. Vrieze, G. von Koten, *Recueil* **1980**, *99*, 145−153.
[4] [4a] D. M. Blake, J. R. Reynolds, *J. Organomet. Chem.* **1976**, *113*, 391−396. − [4b] D. Walther, C. Pfützenreuther, *Z. Chem.* **1977**, *17*, 426−427. − [4c] R. Meij, D. J. Stufkens, K. Vrieze, E. Roosendaal, H. Schenk, *J. Organomet. Chem.* **1978**, *155*, 323−336. − [4d] G. La Monica, M. Pizzotti, S. Cenini, *Gazz. Chim. Ital.* **1978**, *108*, 611−613. − [4e] H. C. Ashton, A. R. Manning, *Inorg. Chem.* **1983**, *22*, 1440−1445. − [4f] M. Herberhold, A. F. Hill, *J. Organomet. Chem.* **1989**, *368*, 111−117.
[5] [5a] R. Meij, D. J. Stufkens, K. Vrieze, *J. Organomet. Chem.* **1978**, *144*, 239−253. − [5b] R. Meij, D. F. Stufkens, K. Vrieze, E. Rosendaal, H. Schenk, *J. Organomet. Chem.* **1978**, *155*, 323−336.
[6] R. Meij, D. J. Stufkens, K. Vrieze, W. van Gerresheim, C. H. Stam, *J. Organomet. Chem.* **1979**, *164*, 353−370.
[7] R. Meij, T. A. M. Kaandorp, D. J. Stufkens, K. Vrieze, *J. Organomet. Chem.* **1977**, *128*, 203−211.
[8] R. Meij, J. Kuyper, D. J. Stufkens, K. Vrieze, *J. Organomet. Chem.* **1976**, *110*, 219−233.
[9] J. Kuyper, K. Vrieze, *J. Organomet. Chem.* **1974**, *74*, 289−305; *J. Organomet. Chem.* **1975**, *86*, 127−138.
[10] A. Brosius, A. Haas, *Chem. Ber.* **1995**, *128*, 651.
[11] R. Meij, K. Olie, *Cryst. Struct. Commun.* **1975**, *4*, 515−520.
[12] I.-P. Lorenz, M. Limmert, K. Polborn, H. Nöth, *Z. Anorg. Allg. Chem.* **2000**, *626*, 2313−2317.
[13] A. A. Bhattacharyya, A. G. Turner, E. M. Holt, N. W. Alcock, *Inorg. Chim. Acta* **1980**, *44*, L185−L186; E. M. Holt, N. W. Alcock, A. A. Bhattacharyya, A. G. Turner, *Inorg. Chim. Acta* **1981**, *47*, 255−259.
[14] R. Short, M. B. Hursthouse, T.G. Purcell, J. D. Woollins, *J. Chem. Soc., Chem. Commun.* **1987**, 407−408.
[15] G. Hartmann, R. Hoppenheit, R. Mews, *Inorg. Chim. Acta* **1983**, *76*, L201−L202.
[16] H. W. Roesky, K. K. Panday, B. Krebs, M. Dartmann, *J. Chem. Soc., Dalton Trans.* **1984**, 2271−2273; H. Plenio, H. W. Roesky, M. Noltemeyer, G. M. Sheldrick, *J. Chem. Soc., Chem. Commun.* **1987**, 1483−1484; H. Plenio, H. W. Roesky, F. T. Edelmann, M. Noltemeyer, *J. Chem. Soc., Dalton Trans.* **1989**, 1815−1818.
[17] M. Herberhold, F. Neumann, G. Süss-Fink, U. Thewalt, *Inorg. Chem.* **1987**, *26*, 3612−3615.
[18] [18a]M. Herberhold, B. Distler, H. Maisel, W. Milius, B. Wrackmeyer, P. Zanello, *Z. Anorg. Allg. Chem.* **1996**, *622*, 1515−1523. − [18b] A. Gieren, B. Dederer, *Angew. Chem. Int. Ed. Engl.* **1977**, *16*, 179.
[19] M. Haddad, J. P. Legros, L. Lopez, M. T. Boisdon, J. Barrans, *Phosphorus, Sulfur, and Silicon* **1992**, *69*, 189−196.
[20] D. G. Anderson, H. E. Robertson, D. W. H. Rankin, J. D. Woollins, *J. Chem. Soc., Dalton Trans.* **1989**, 859−862.
[21] P. Legzdins, J. T. Malito, *Inorg. Chem.* **1975**, *14*, 1875−1878.
[22] O. J. Scherer, G. Wolmershäuser, R. Jotter, *Z. Naturforsch.* **1982**, *37b*, 432−436.
[23] I. Ruppert, V. Bastian, R. Appel, *Chem. Ber.* **1975**, *108*, 2329−2339.

Received October 27, 2000
[I00404]

Heterodicarba-*nido*-hexaboranes from Hydroborations of Exocyclic Unsaturated Heterodiborolanes

Peter Greiwe,[a] Hans Pritzkow,[a] and Walter Siebert*[a]

Dedicated to Prof. Dr. Dieter Sellmann on the occasion of his 60th birthday

Keywords: Boron / Carboranes / Sulfur / Nitrogen / Heterocycles / Hydroboration

The hydroboration of 1-aza-2,5-diduryl-3,4-diisopropylidene- and 2,5-diduryl-1-thia-3,4-diisopropylidene-2,5-diborolanes (**1b**, **2b**) with equimolar amounts of BH_3·thf leads to the corresponding 2-aza-4,5-dicarba- and 4,5-dicarba-2-thia-*nido*-hexaboranes **3c** and **4e**. When an excess of BH_3·thf reacts with the azadiborolane **1b** the azadiborole derivative **5** is obtained as the main product. This surprising result is explained by the addition of three BH_3·thf moieties and the subsequent loss of B_3H_7·thf. The reaction of the sterically less hindered *tert*-butylazadiborolane **1c** with BH_3·thf yields two 2-aza-4,5-dicarba-*nido*-hexaboranes (**3d,e**), both of which carry a *t*Bu group in the apical position. A possible reaction pathway is suggested. The new heterocarboranes **3c,d,e** and **4e** are identified by multinuclear NMR spectroscopy and mass spectrometry. X-ray crystallographic studies of **3c** and **4e** confirm the *nido*-arrangement of the cluster atoms.

Introduction

Recently we described the formation of the 2-aza-4,5-dicarba-*nido*-hexaboranes(6) **3a,b** by substitution/hydroboration reactions of a chlorine-substituted azadiborolane with lithium borates (Scheme 1).[1] The corresponding 4,5-dicarba-2-thia-hexaboranes(5) (**4a**−**d**) have also been prepared by us exploiting the same methodology.[2] This route only gives access to fully BH-substituted derivatives or compounds with one aryl/alkyl group. Since by-products are also formed and the desired compounds are sensitive liquids which are difficult to separate, only the thiacarborane **4d** could be isolated. In order to overcome this problem the aza- and thiadiduryldiborolanes **1b**, **2b** and the didurylox-adiborolane **6** were synthesized[1] as potential starting materials for the preparation of crystalline and more stable heterodicarbahexaboranes. This paper describes how this goal is achieved by using BH_3·thf as the hydroboration agent and presents the first completely refined crystal structure analysis of an azadicarba-*nido*-hexaborane(6) and a thiadicarba-*nido*-hexaborane(5). Ab initio calculations are used to model the reaction sequence and give an explanation for the formation of different products depending on the ratio azadiborolane/BH_3·thf.

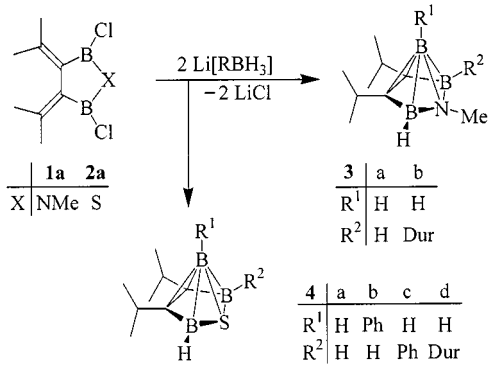

Scheme 1

Results and Discussion

Hydroboration with BH_3·thf

Treatment of the heterodiborolanes **1b** and **2b** with equimolar amounts of BH_3·thf in hexane solution leads to 2-aza-4,5-dicarba-3,6-diduryl-4,5-diisopropyl-2-methyl-*nido*-hexaborane(6) (**3c**) and 4,5-dicarba-3,6-diduryl-4,5-diisopropyl-2-thia-*nido*-hexaborane(5) (**4e**) in good yields (Scheme 2). These colorless, moisture-sensitive compounds are obtained by recrystallization from hexane. The formation of the heterocarboranes is assumed to proceed by bridging hydroboration of the double bonds by one molecule of BH_3. This generates bicyclic heteroorganoboranes (**3e′**, **4e′**) as intermediates which transform into the more stable polyhedral heterocarborane structures.

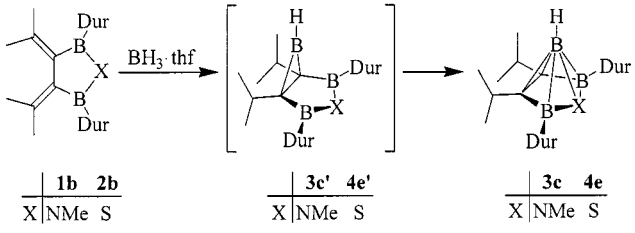

Scheme 2

[a] Anorganisch-Chemisches Institut der Universität Heidelberg
Im Neuenheimer Feld 270, 69120 Heidelberg, Germany
Fax: (internat.) +49-6221/545-609
E-mail: ci5@ix.urz.uni-heidelberg.de

Supporting information for this article is available on the WWW under http://www.wiley-vch.de/home/eurjic or from the author.

 © WILEY-VCH Verlag GmbH, 69451 Weinheim, 2001 1434−1948/01/0606−1599 $ 17.50+.50/0

When an excess of BH_3·thf is employed for the hydroboration of **1b** the azadiborole **5**[3] is the main product instead of the azacarborane **3c**, which is now found in only small amounts. The reaction of **2b** with more than one equivalent of BH_3·thf, on the other hand, does not lead to the corresponding thiadiborole. In this case a partial exchange of substituents obviously takes place since, besides the thiacarborane **4e**, 1,2-diduryldiborane(6) is also found after workup. The formation of **5** formally corresponds to a 1,4-addition of H_2 to the hexadiene part of **1b**. In a related hydroboration reaction an exocyclic doubly unsaturated 1,3-diborolane yielded the expected tricarbahexaborane on treatment with $(EtBH_2)_2$ and, surprisingly, a diborole derivative.[4] Apparently, the excess of BH_3 present during the course of the reaction plays an important role. The addition of two BH_3 molecules to **1b**, one to each double bond, in a *syn* fashion would lead to the BH_2B bridged species **5′′** (via **5′**), which could lose B_2H_4 to give **5**. However, this process seems rather unlikely because of the inherent instability of B_2H_4 unless a suitable Lewis base (e.g. PMe_3) is present. More likely is an attack by a third BH_3·thf on the B_2H_4 moiety in **5′′** followed by the elimination of THF-stabilized B_3H_7 and the simultaneous generation of the azadiborole.

The second hydroboration of **1b** can either be intramolecular, leading to the bicyclic **3c′** (as shown in Scheme 2), or intermolecular involving an additional BH_3 molecule which yields **5′′** (according to Scheme 3). MP2 and DFT computations[5] indicate that the second possibility is favored over the intramolecular reaction by ca. 8 kcal/mol. It thus follows that if an excess of BH_3 is present in solution the BH_2B-bridged **5′′** is more likely to be formed than **3c′/3c**. The *anti* addition of two BH_3 molecules to **1b** is also possible but was not examined since only **5′′** can react to **5**. The transition states for the addition of the third BH_3 and the subsequent liberation of B_3H_7 could not be located. They are assumed to be low in energy. The proposed reaction pathway for the formation of **5** is shown in Scheme 3.

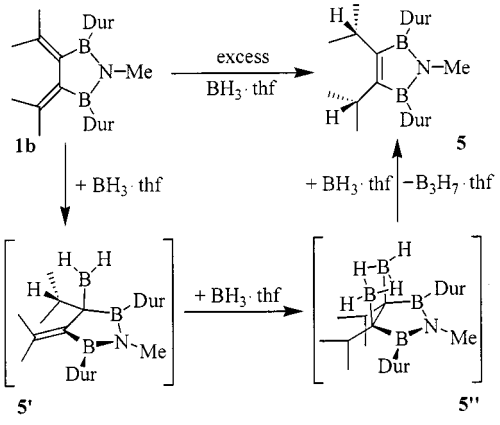

Scheme 3

The reaction of the sterically less constrained di-*tert*-butylazadiborolane **1c** with one equivalent of BH_3·thf yields two azadicarbahexaborane(6) derivatives. Surprisingly, **3e** contains only one *t*Bu substituent, which is located in the apical position. Compound **3d** carries the expected two *t*Bu groups, one in the apical and the other in an equatorial position. At room temperature the ratio **3d:3e** is approximately 2.5:1. After the reaction no BH_3 is found, although $(tBuBH_2)_2$ and **1c** are detected. As ^{11}B NMR spectra reveal, refluxing the solution for some time gives about equal amounts of both azacarboranes and decreases the fraction of $(tBuBH_2)_2$. These findings suggest the following reaction sequence: BH_3 hydroborates **1c** to give a bicyclic intermediate **3d′** in which the BH group can easily exchange its position with one of the *t*BuB groups leading to **3d** (Scheme 4). Alternatively, prior to a hydroboration one of the *t*Bu groups or *t*BuB units in **1c** can be replaced by a hydrogen atom or a BH unit, which in both cases produces **1d** and $tBuBH_2$. After the addition of BH_3 to the double bonds the azaorganoborane **3e′** rearranges to **3e**. Since the ratio **3d:3e** changes at elevated temperatures, i.e. more **3e** is formed although no BH_3 is left in the mixture, additional reactions must occur. Two processes seem rational: **3d** and $(tBuBH_2)_2$ can exchange their H and *t*Bu substituents leading directly to **3e**, or additional BH_3 is generated from $tBuBH_2$. At higher temperatures the BH_3 immediately attacks the remaining **1c** to yield **3d** or **3e**, but now **3e** may be the favored product. Both routes imply the formation of $(tBu)_2BH$, which, however, was not observed in the NMR spectra. Nevertheless, this would explain why more of the azacarborane derivative with only one *t*Bu group is generated and less $tBuBH_2$ is found after heating.

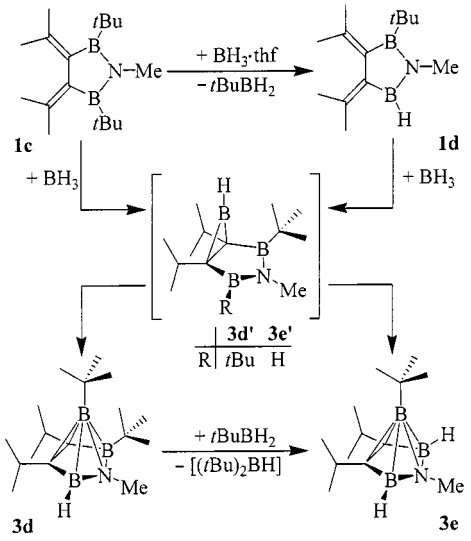

Scheme 4

Hydroboration of the oxadiborolane **6** could in principle lead to an oxacarborane, a heterocarborane family which is as yet unknown. The reaction with BH_3·thf is considerably slower at ambient temperature than the above-mentioned BH_3 additions and produces a mostly insoluble colorless solid. No spectroscopic evidence for an oxacarborane or a bicyclic organoborane is found. In the mass spectrum of the soluble part peaks for the oxadiborole **7** are present (Scheme 5). Ab initio computations show that an oxadicarba-*nido*-hexaborane(5) structure should be more stable

than its bicyclic organoborane structure (of type **3d/e′**) if all substituents are H or only one boron atom carries a methyl group.[6] Accordingly, the reaction of **6** with BH_3 should yield an organoborane which might be highly reactive toward oligomerization and is thus not isolated.

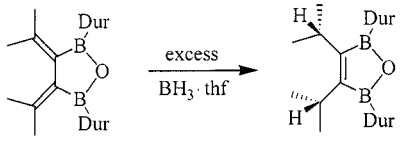

6 **7**

Scheme 5

Hydroboration with Thexylborane

During the reaction of **1c** with BH_3·thf the starting material and $(t\text{BuBH}_2)_2$ are present in solution at the same time and no reaction between these components, i.e. the formation of an azacarborane carrying three *t*Bu groups, is observed. In order to evaluate the hydroboration ability of alkyldihydridoboranes $(\text{RBH}_2)_2$ thexylborane (thexyl = 1,1,2-trimethylpropyl) was allowed to react with the duryl-substituted heterodiborolanes **1b** and **2b** as well as with the *tert*-butyl-substituted **1c**. Compounds **1b** and **2b** do not react with $(\text{thexBH}_2)_2$ in refluxing hexane, probably for steric reasons. At room temperature **1c** also shows no reaction but refluxing the hexane solution for several days causes a slow exchange of substituents and a mixture of equatorially hydrogen-substituted azacarboranes is formed. Organodihydridoboranes are dimers in solution and must separate into monomeric species before they can react. Furthermore, it seems that a hydroboration reaction with RBH_2 is always preceded by an exchange of substituents reducing the steric bulk in the heterocycle and thereby allowing the reaction to take place. No fully alkyl-substituted azacarborane is found which means that a direct hydroboration of **1c** by thexBH_2 does not occur.

Spectroscopic and Structural Characterization

In the ^{1}H and ^{13}C NMR spectra of the heterocarboranes **3c** and **4e** all carbon atoms and methyl groups of the duryl rings and isopropyl substituents can be distinguished indicating a restricted rotation. The isopropyl protons of **4e** give two doublets and a septet, and for **3c** a septet and a pseudo triplet are observed. The signal of a cage carbon atom broadened by coupling to the neighboring boron atoms was observed only in the ^{13}C NMR spectrum of **3c**. The ^{11}B NMR spectra of the heterocarboranes show doublets at high field for the apical BH units at $\delta = -38.2$ ($^1J_{BH} \approx 202$ Hz) (**3c**) and $\delta = -35.2$ ($^1J_{BH} \approx 216$ Hz) (**4e**). The coupling constants have typical values for apical bonding situations. For the basal boron atoms singlets are observed at $\delta = 23.2$ (**3c**) and 28.5 (**4e**). Compounds **3d** and **3e** were obtained as a mixture and only their ^{11}B NMR spectroscopic data can be interpreted. Compound **3e** gives a singlet at $\delta = -34.2$ for the apical boron and a doublet at $\delta = 15.9$ ($^1J_{BH} \approx 160$ Hz) for the equatorial BH units whereas **3d** has a singlet at $\delta = -32.3$ (apical B), a singlet at $\delta = 30.1$ for the equatorial *t*Bu-substituted boron atom and a

Table 1. Crystal data and structure refinements for **3c** and **4e**

	3c	**4e**
Empirical formula	$C_{29}H_{44}B_3N$	$C_{28}H_{41}B_3S$
Mol. wt.	439.08	442.10
Crystal system	Triclinic	Monoclinic
Space group	*P*1(bar)	*C*2/*c*
Unit cell		
a [Å]	10.4398(9)	23.9309(5)
b [Å]	11.5443(10)	7.4024(2)
c [Å]	12.5675(11)	15.7655(4)
α [°]	81.287(2)	90
β [°]	88.893(2)	102.265(2)
γ [°]	67.792(2)	90
V [Å^3]	1384.9(2)	2729.05(12)
Z	2	4
Calcd. density [g/cm^3]	1.053	1.076
Absorp. coeff. [mm^{-1}]	0.058	0.132
F(000)	480	960
Crystal size [mm]	0.42 × 0.40 × 0.20	0.36 × 0.24 × 0.19
Θ_{max} [°]	23.0	26.4
Index ranges	−11/11, −12/12, −13/7	−29/29, 0/9, 0/19
No. of reflections		
Unique	3855	2794
Observed [$I > 2\sigma(I)$]	2545	1925
Transmission	0.928−0.835	0.822−0.894
Parameters	383	193
Final *R* indices		
R1 [$I > 2\sigma(I)$]	0.069	0.055
wR2	0.204	0.166
Res. electron dens. [e/Å^3]	+0.27/−0.27	+0.74/−0.19

doublet at δ = 15.9 ($^1J_{BH} \approx 160$ Hz). These data are in line with polyhedral *nido* structures.

The NMR spectroscopic data of **5** reflect its high symmetry. Two doublets and a septet are found for the isopropyl protons, the methyl groups of the freely rotating duryl rings give only two ^{1}H and ^{13}C NMR signals.

The solid state structures determined by X-ray crystallography (Table 1) confirm that the heterocarboranes **3c** (Figure 1) and **4e** (Figure 2) are *nido*-6<V> clusters as already suggested by their spectroscopic data. The shapes of the molecules are mostly determined by the bulky duryl and isopropyl groups; the apical BH units have only a minor influence. This is the reason for a disordered orientation of the molecules in the crystal, where the apical BH groups may lie above or below the idealized ring plane. The refinements of these disordered structures do not yield very accurate values for the distances and angles, which are in the expected ranges. The gross structural parameters of **3c** and **4e** are very similar. In both structures the substituents adopt almost identical positions: the duryl rings are virtually perpendicular to the B−C−C−B basal planes. The angles of these planes with the three-membered rings C1−B3−C2 in **3c** and C1−B2−C1′ in **4e** differ by 2.8° (58.4° vs. 55.6°) and, because of its smaller covalence radius, which results in shorter bond lengths, the distortion of the nitrogen atom from the B−C−C−B plane (24.8°) toward the apical atom is more pronounced than for the sulfur atom in **4e** (12.0°).

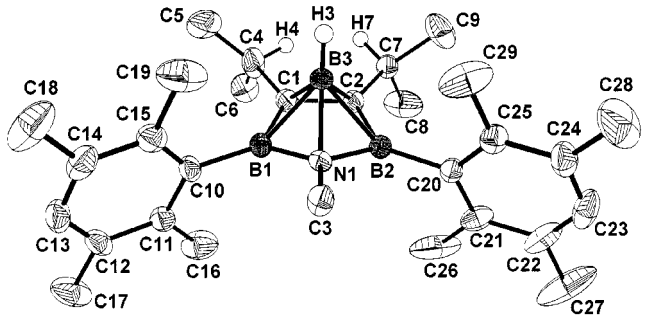

Figure 1. Molecular structure of **3c**; selected bond lengths [Å] and angles [°]: B1−C1 1.501(4), B2−C2 1.502(4), C1−C2 1.499(4), N1−B1/B2 1.491−1.547(8), B3−N1 1.676, 1.693(10), B3−B1/B2 1.901−1.963(8), B3−C1/C2 1.714−1.749(8); [C1−B3−C2]/[B1−C1−C2−B2] 58.4, [B1−C1−C2−B2]/[B1−N1−B2] 24.8

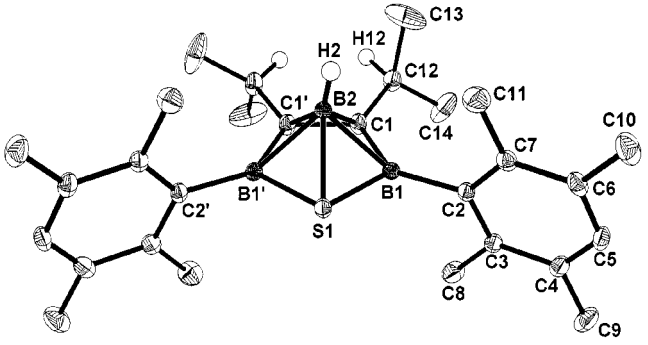

Figure 2. Molecular structure of **4e**; selected bond lengths [Å] and angles [°]: B1−S1 1.881(3), B1′−S1 1.860(4), B2−S1 1.989(4), B1−C1 1.493(4), C1−C1′ 1.508(4), B2−C1 1.606(5), B2−C1′ 1.632(5), B1−B2 1.917(5), B1′−B2 1.892(5), [C1′−B2−C1]/[B1′−C1′−C1−B1] 55.57, [B1−S1−B1′]/[B1−C1−C1′−B1′] 11.96

Conclusion

The above reactions clearly show the influence that the steric shielding of the boron atoms has during hydroborations. Compounds **1b** and **2b** carrying the most bulky groups give only apically BH-substituted heterocarboranes — a B-duryl unit in this location would interfere with the other substituents, especially with the second duryl group. However, under certain conditions, such as a large excess of BH_3·thf, other reactions also occur and $(DurBH_2)_2$ and the azadiborole **5** are obtained. On the other hand, the hydroboration of the double bonds in **1c** leads to **3d**, which surprisingly carries one of the *t*Bu groups in the apical position. In this case the smaller substituents also allow an exchange of *t*Bu for H generating $(tBuBH_2)_2$ and the azacarborane **3e** with only one *t*Bu group bound to the apical boron atom. This indicates that compounds with an apical *t*BuB unit are sterically and/or energetically highly favored over other possible *t*Bu substituted isomers. Compounds having apical BH and equatorial B*t*Bu units were not detected. Furthermore, it can be concluded that neither $tBuBH_2$ nor $thexBH_2$ is an efficient hydroborating agent in the above described cases. Again, steric reasons are the most likely factors inhibiting a reaction.

Experimental Section

General: All reactions and manipulations were performed in dry glassware under argon or nitrogen using standard Schlenk techniques. Solvents were distilled from appropriate drying agents under inert gas before use. − $Et_2O{\cdot}BF_3$ was used as the external standard for ^{11}B NMR. As internal references for ^{1}H and ^{13}C NMR spectra the signals of the deuterated solvents were used and calculated relative to TMS. NMR: Bruker AC 200 and Bruker DRX 200. − MS: Varian MAT CH7 and GCMS HP 5971. − The following starting materials were prepared by literature methods: **1b, 1c**, **2b**, and **6**,[1] 1,2-dithexyldiborane(6).[7] BH_3·thf (1 M) was commercially obtained (Aldrich).

2-Aza-4,5-dicarba-3,6-diduryl-4,5-diisopropyl-2-methyl-*nido*-hexaborane(6) (3c): To a solution of **1b** (330 mg, 0.78 mmol) and 25 mL of hexane was slowly added BH_3·thf (0.78 mL, 0.78 mmol) at −25 °C. The solution was stirred at this temperature for 15 min. and for 15 h at ambient temperature. The solvent was removed, the remaining solid dissolved in hexane and the solution filtered. From the concentrated solution 255 mg (0.58 mmol, 74%) of **3c** was obtained at −30 °C. − ^{1}H NMR (C_6D_6, 200 MHz): δ = 1.22 [pseudo t, $^3J_{HH}$ = 7 Hz, 12 H, $CH(CH_3)_2$], 2.16, 2.18, 2.21, 2.34 (4 s, 4×6 H, C_{aryl}-CH_3), 2.44 [sept, $^3J_{HH}$ = 7 Hz, $CH(CH_3)_2$], 2.53 (N−CH_3), 6.97 (s, 2 H, duryl). − ^{11}B NMR (C_6D_6, 64 MHz): δ = −38.2 (d, B_{apical}, $^1J_{BH}$ = 202 ± 3 Hz), 23.2 ($B_{eq.}$). − ^{13}C NMR (C_6D_6, 50 MHz): δ = 19.8, 20.0, 20.5, 21.4 (4×C_{aryl}-CH_3), 24.5, 24.2 [2×$CH(CH_3)_2$], 25.5 [$CH(CH_3)_2$], 31.8 (N−CH_3), 90.1 [br, BC−$CH(CH_3)_2$], 132.1, 133.3, 133.5, 135.4, 138.0 (5×C_{aryl}). − EI-

MS: *m/z* (%) = 439 [M^+] (98), 427 [M^+ − BH] (81), 396 [M^+ − *i*Pr] (100), 384 (72). − CI-MS (isobutane): *m/z* (%) = 440 [M^+ + H] (100), 428 [M^+ − B] (46), 296 [M^+ + H − BDur] (29). − HR-EIMS ($^{12}C_{29}{}^{1}H_{44}{}^{14}N^{11}B_3$): calcd. 439.3757; found 439.3753 (Δmmu = +0.4).

4,5-Dicarba-3,6-diduryl-4,5-diisopropyl-2-thia-*nido*-hexaborane(5) (4e): The same procedure was used as described for **3c**. Yield: 74 mg (60%) − ^{1}H NMR (C_6D_6, 200 MHz): δ = 1.12, 1.20 [2 d, 2×6 H, $^3J_{HH}$ = 7 Hz, CH(CH_3)$_2$], 2.14, 2.16, 2.33, 2.50 (4 s, 4×6 H, C_{aryl}-CH_3), 2.53 [sept, $^3J_{HH}$ = 7 Hz, CH(CH$_3$)$_2$], 6.95 (s, 2 H, duryl) − ^{11}B NMR (C_6D_6, 64 MHz): δ = −35.2 (d, B_{apical}, $^1J_{BH}$ = 216 ± 3 Hz), 28.5 ($B_{eq.}$) − ^{13}C NMR (C_6D_6, 50 MHz): δ = 20.0, 20.5, 20.7, 21.1 (4×C_{aryl}-CH$_3$), 23.23, 23.28 [2×CH(CH$_3$)$_2$], 28.6 [CH(CH$_3$)$_2$], 132.3, 133.57, 133.62, 134.9, 138.0 (5×C_{aryl}). − EI-MS: *m/z* (%) = 442 [M^+] (100), 399 [M^+ − CH(CH$_3$)$_2$] (21), 266 [M^+ − *i*Pr − Dur] (46), 223 [M^+ − *i*Pr$_2$ − Dur] (30). − HR-EIMS ($^{12}C_{28}{}^{1}H_{41}{}^{11}B_3{}^{32}S$): calcd. 442.32080; found 442.32037 (Δmmu = −0.4).

1-Aza-2,5-diduryl-1,2-dihydro-3,4-diisopropyl-1-methyl-2,5-diborole (5): A sample of **1b** (80 mg 0.19 mmol) was dissolved in 5 mL of hexane and treated with BH_3·thf (0.6 mL, 0.6 mmol, excess) at ambient temperature. The mixture was stirred for 15 h, all volatile components were removed in vacuo and the residue was dissolved in hexane. The filtered and concentrated solution gave, at −30 °C, 42 mg (0.1 mmol, 50%) of crystalline, colorless and air-stable **5**. − ^{1}H NMR (C_6D_6, 200 MHz): δ = 1.07, 1.11 [2 d, 2×6 H, $^3J_{HH}$ = 7 Hz, CH(CH_3)$_2$], 2.14, 2.27 (2 s, 2×12 H, C_{aryl}-CH_3), 2.34 (s, 3 H, N−CH_3), 3.01 [sept, $^3J_{HH}$ = 7 Hz, CH(CH$_3$)$_2$], 6.92 (s, 2 H, duryl). − ^{11}B NMR (C_6D_6, 64 MHz): δ = 54. − ^{13}C NMR (C_6D_6, 50 MHz): δ = 19.3, 19.7 (2×C_{aryl}-CH$_3$), 22.5 [CH(CH$_3$)$_2$], 28.9 [CH(CH$_3$)$_2$], 31.9 (N−CH_3), 131.4, 133.2, 133.5 (3×C_{aryl}), 141.6 [br, BC−C(CH$_3$)$_2$], 142.6 (B-C_{aryl}). − EI-MS: *m/z* (%) = 427 [M^+] (100), 384 [M^+ − *i*Pr] (62), 293 [M^+ − durylH] (30).

2-Aza-1,3-di-*tert*-butyl-4,5-dicarba-4,5-diisopropyl-2-methyl-*nido*-hexaborane(6) (3d) and 2-aza-1-*tert*-butyl-4,5-dicarba-4,5-diisopropyl-2-methyl-*nido*-hexaborane(6) (3e): BH_3·thf (2.1 mL, 2.1 mmol) was slowly added to a solution of **1c** (560 mg, 2.1 mmol) in 25 mL of hexane at −60 °C. The mixture was stirred for 15 h and analyzed by ^{11}B NMR spectroscopy and GC/MS showing a ratio **3e:3d** of 1:2.5. After refluxing the solution for 6 h, samples were again taken and analyzed. The ratio **3e:3d** was now 1:1. All volatile components were removed at about 10 mbar leaving behind a colorless oil (a mixture of **3d**, **3e**) and starting material **1c**. − ^{11}B NMR (C_6D_6, 64 MHz): δ = −34.2 (s, **3e**), −32.3 (s, **3d**), 15.9 (d, $^1J_{BH}$ ≈ 160 Hz, **3e,d**), 30 (s, **3d**). − EI-MS (**3e**): *m/z* (%) = 231 [M^+] (27), 216 [M^+ − Me] (4), 188 [M^+ − *i*Pr] (23), 174 [M^+ − *t*Bu] (13), 41 (100). − EI-MS (**3d**): *m/z* (%) = 287 [M^+] (5), 230 [M^+ − *t*Bu] (4), 41 (100).

X-ray Crystallographic Study: Crystallographic data and details of the structure determinations are presented in Table 1. Data collection: Bruker AXS Smart 1000 area detector (Mo-K_α, ω-scans) at −100 °C. The structures were solved by direct methods and refined by least-squares based on F^2 with all measured reflections[8] and using anisotropic temperature factors for non-hydrogen atoms. Hydrogen atoms were located and refined isotropically or inserted in calculated positions. A refinement of **4e** in the space group *Cc* gave no satisfactory results.

Crystallographic data (excluding structure factors) for the structures reported in this paper have been deposited with the Cambridge Crystallographic Data Centre as supplementary publication nos. CCDC-151546 (**3c**) and -151547 (**4e**). Copies of the data can be obtained free of charge on application to CCDC, 12 Union Road, Cambridge CBV2 1EZ, UK [Fax: (internat.) +44-1223/336-033; E-mail: deposit@ccdc.cam.ac.uk].

Acknowledgments

We thank Dr. Matthias Hofmann for performing ab initio computations and the Deutsche Forschungsgemeinschaft (Schwerpunktprogramm Polyeder) for financial support.

[1] P. Greiwe, V. Beez, H. Pritzkow, W. Siebert, *Eur. J. Inorg. Chem.* **2001**, 381−386.
[2] V. Beez, P. Greiwe, H. Pritzkow, M. Hofmann, P. v. R. Schleyer, W. Siebert, *Eur. J. Inorg. Chem.* **1998**, 1775−1779.
[3] A structure analysis of a single crystal of **5** was carried out. Only a limited data set was obtained which allowed the solution of the structure but not a reliable refinement. Nevertheless, the analysis supports the connectivity and geometry of an azadiborole derivative. All the bond lengths and angles lie in the expected ranges but, due to the great variations, the values are not discussed here. The structure of **5** has approximate C_{2v} symmetry, the five-membered ring and the directly connected atoms define a plane perpendicular to the duryl and isopropyl groups.
[4] W. Siebert, R. Hettrich, H. Pritzkow, *Angew. Chem.* **1994**, *106*, 215−217; *Angew. Chem. Int. Ed. Engl.* **1994**, *33*, 203−204.
[5] Computations for the hydroboration sequences of 1-aza-3,4-dimethylene-2,5-diborolane and its B-phenyl derivative were carried out at the MP2(fc)/6−31G* and B3LYP/6−31G* levels of theory. For details see Supporting Information.
[6] A. Berndt, T. Happel, Y. Sahin, G. Geiseler, W. Massa, M. Hofmann, P. v. R. Schleyer, in *Contemporary Boron Chemistry* (Eds.: M. Davidson, A. K. Hughes, T. B. Marder, K. Wade), The Royal Society of Chemistry **2000**, special publ. no. 253, p. 345.
[7] H. C. Brown, P. Heim, N. M. Yoon, *J. Org. Chem.* **1972**, *37*, 2942−2950.
[8] G. M. Sheldrick, SHELXTL v5.1, Bruker AXS, Madison (Wisconsin, USA), **1998**.

Received October 30, 2000
[I00414]

Interionic Solution Structure of Acetyl Ru^{II} Complexes Bearing Diimine and Diamine Ligands by ^1H-NOESY and $^{19}F\{^1H\}$-HOESY NMR: Still More Specific Anion−Cation Interactions

Gianfranco Bellachioma,[a] Giuseppe Cardaci,[a] Francesca D'Onofrio,[a] Alceo Macchioni,*[a] Stefano Sabatini,[a] and Cristiano Zuccaccia[a]

Keywords: Ruthenium / Acetyl complexes / Ion pairs / ^1H-NOESY / $^{19}F\{^1H\}$-HOESY / NMR

Complexes *trans*-[$Ru(PMe_3)_2(CO)(COMe)(N,N)$]X (N,N = diimine or diamine ligand, $X^- = BF_4^-$ or BPh_4^-) have been synthesized by the reaction of *cis*,*trans*-[$RuI(Me)(CO)_2(PMe_3)_2$] with N,N ligands having different steric and electronic properties. The syntheses were only successful with moderately hindered ligands; in other cases, solvento complexes were formed. Some of these were isolated and characterized. The interionic structures of the aforementioned cationic complexes have been investigated in dichloromethane solution by means of ^1H-NOESY and $^{19}F\{^1H\}$-HOESY NMR experiments. The anion–cation interactions (especially for the diamine complexes) were found to be more specific than those in analogous compounds bearing aromatic N,N ligands. For the first time, we have found that the anion preferentially resides close to the N arm *trans* to the COMe group.

Introduction

Even though the phenomenon of ion-pairing is of great importance in several chemical processes mediated by cationic transition metal complexes,[1] structural studies of such ion pairs in solution are still rare. The principal reason for this is that it is difficult to obtain detailed structural information about ion pairs using classical techniques.

Recently, we showed[2] that direct and detailed structural information about ion pairs containing transition metals can be obtained quite easily using NOE NMR spectroscopy, based on the dependence of the NOE between the interacting nuclei on their distance.[3] In principle, this also makes it possible to investigate the relative structures of non-covalently bonded moieties, such as two charged fragments of an ion pair. In practice, several complications and limitations arise that hamper such investigations to some extent. The first limitation stems from the limit of detection of the NOE, which is ca. 5 Å. Thus, (1) only intimate ion pairs can be investigated. A complication arises if we want to quantify the NOE in order to estimate average interionic distances. Due to the possibility of relative anion−cation motion (2), the rotational correlation times of nuclei belonging to both fragments must be measured in order to check the meaning of the estimated average interionic distances. The first limitation (1) is not so severe because, as might reasonably be assumed, the anion−cation interactions mainly affect the chemical reactivity of the ion-pair under conditions conducive to intimate ion-pair formation (a solvent of moderate dielectric constant, high concentrations, low temperature, etc.). The second complication (2) is more serious,[4] although very often it is not necessary to have explicit knowledge of interionic distances but only of the preferred mutual orientation eventually adopted by the anion and cation. This information can be gleaned in a semi-quantitative manner through observing the NOE contacts (weak, medium, strong, etc.).

Our previous studies were principally carried out on model cationic Ru^{II} compounds bearing bidentate (N,N) or tridentate (N,N,N) ligands,[2a−2e] where the N atoms were incorporated into aromatic rings. These studies were performed in dichloromethane solution, using both symmetrical and unsymmetrical counterions.[2e] In all cases, we observed a remarkable degree of specificity in the NOE interionic contacts. The counterion was found to reside close to the N,N or N,N,N ligands, and, in the case of unsymmetrical counterions, showed a tendency to maximize the lyophilic interactions. With the help of quantum mechanical and molecular mechanics calculations,[2c] we rationalized such specificity in terms of non-centrosymmetric charge distribution and, in particular, an accumulation of positive charge in the aromatic rings containing the N atoms. In order to ascertain whether the presence of N-aromatic ligands is necessary for the delocalization of the positive charge, we decided to synthesize and investigate analogous complexes containing non-aromatic N,N ligands.

In this paper, we report the synthesis and characterization of complexes *trans*-[$Ru(PMe_3)_2(CO)(COMe)(N,N)$]X (N,N = diimine or diamine ligand; see Scheme 1) and the determination of their interionic structure in dichloromethane.

Results and Discussion

Synthesis

The starting material for the synthesis of complexes **2−10** was *cis*,*trans*-[$RuI(Me)(CO)_2(PMe_3)_2$] (**1**).[5] In solvents with

[a] Dipartimento di Chimica, Università di Perugia,
Via Elce di Sotto, 8, 06123 Perugia, Italy
Fax: (internat.) +39 075/5855598
E-mail: alceo@unipg.it

 © WILEY-VCH Verlag GmbH, 69451 Weinheim, 2001 1434−1948/01/0606−1605 $ 17.50+.50/0

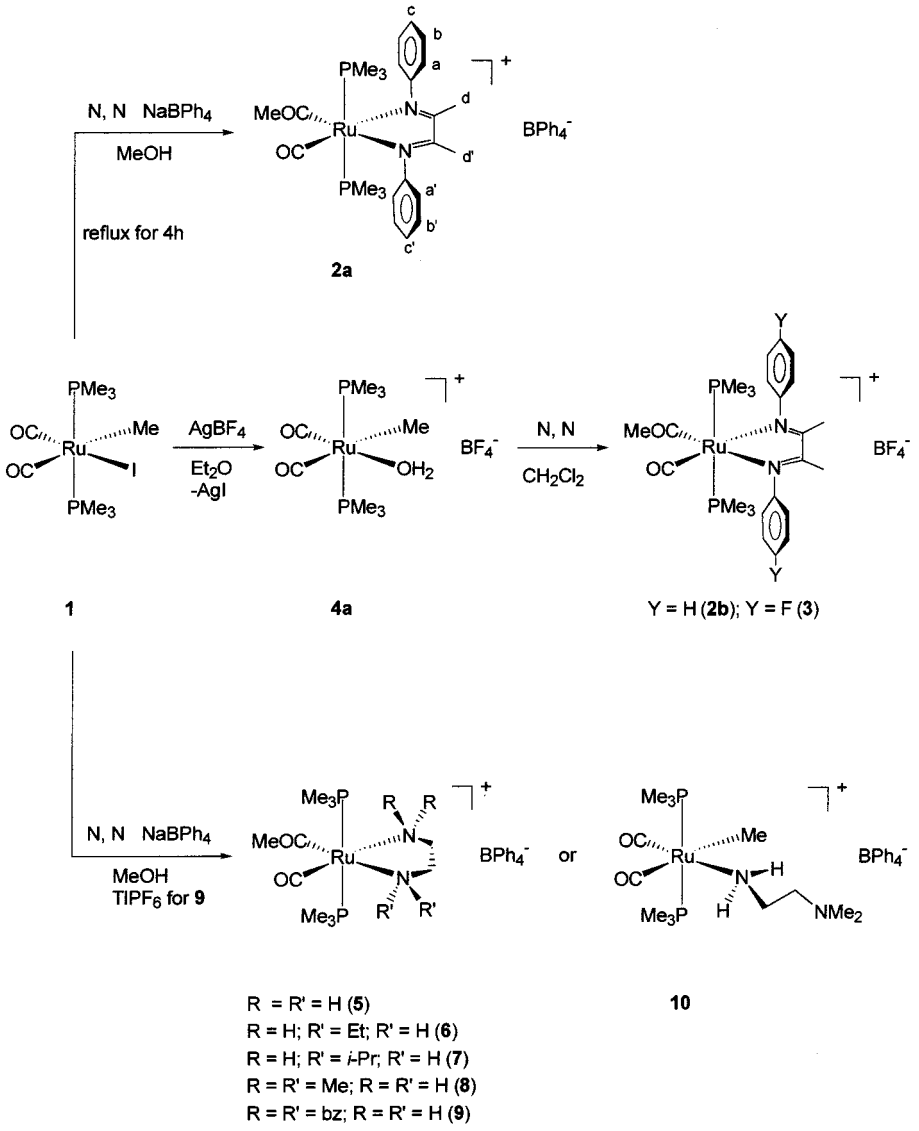

Scheme 1

suitable dielectric constants, complex **1** undergoes dissociation of the Ru−I bond and migration of Me onto a *cis* CO, thereby making two coordination sites available. The reaction of complex **1** with diacetyl bis(phenylimine) ligands in methanol containing excess $NaBPh_4$ at room temperature did not afford the desired acetyl products. Furthermore, it showed that methanol and water may act as competing ligands. The methanolic complex *trans,cis*-[Ru(PMe_3)$_2$(CO)$_2$(Me)(MeOH)]BPh_4 (**4b**) was obtained in good yield by the reaction of complex **1** with $TlPF_6$ in MeOH followed by the addition of a large excess of $NaBPh_4$. By refluxing a methanolic solution of complex **1** for 4 h, complex **2a** was synthesized in low yield (Scheme 1). Complexes **2b**−**3** were synthesized under mild conditions and in acceptable yields by treating **1** with $AgBF_4$ in diethyl ether (see Scheme 1). In each case, the precipitate formed, containing AgI and a solvento complex intermediate, was treated with a solution of the appropriate ligand in dichloromethane. The complexes **2b** or **3** thus obtained were precipitated by adding *n*-hexane. When this synthetic procedure was attempted using diimine ligands bearing substituents in their *ortho* positions (Me, Et, *i*Pr), the reactions were unsuccessful. When the same procedure was carried out in the absence of any ligand, complex **4a** was formed.

The reactions of complex **1** with the diamine ligands were found to proceed quite quickly in methanol at room temperature with *N*-substituted diamines and with *N*,*N*′-disubstituted diamines bearing small substituents (see Scheme 1). In the case of *N*,*N*′-dibenzylethylenediamine, it was found necessary to force the ionization of the Ru−I bond by adding $TlPF_6$ in order to obtain the desired complex in a reasonable time and, consequently, to avoid formation of the methanol complex. The reaction with *N*,*N*-disubstituted ethylenediamine afforded a methyl complex with a η^1-coordinated diamine ligand.

The reactions with both the diimine and diamine ligands indicate that steric factors play a crucial role. In the case of diimine ligands, the interactions of the *ortho* substituents with the acetyl and PMe_3 groups are the limiting factors. In the case of the diamine ligands, the sp^3 nature of the N

atom makes the interaction of the R, R′, and PMe_3 groups the most important. The formation of complex **10** demonstrates that two methyl groups cannot remain on the same coordinated nitrogen.

Intramolecular Characterization

The intramolecular characterization was carried out by IR and ^1H, ^{13}C, ^{31}P, and ^{19}F NMR spectroscopy. The structures of complexes **2−9** could easily be established by considering that: (1) two CO stretching bands were observed, one in the typical region for terminal carbonyls and the other in the region for acyl groups; (2) a deceptive triplet,[6] typical of the *trans* position, was observed for PMe_3 in both the ^1H and $^{13}C\{^1H\}$ NMR spectra of complexes **1−5**, while for the other complexes the observed $^2J_{PP}$ coupling constants were consistent with two mutually *trans* PMe_3 groups, and (3) the protons and carbons of the two N arms are chemically non-equivalent. In the ^1H-NOESY spectra of the *N*-substituted complexes **6** and **7**, no contact between the COMe and the substituents was observed. Consequently, the *N*-substituted arm must lie *trans* to the COMe group. An assignment of all the proton and carbon resonances, a prerequisite for a detailed determination of the interionic structure, proved more difficult. This was especially true for complexes with *N*,*N*′-disubstituted ethylenediamine ligands incorporating two chiral nitrogen atoms. In such cases, a pair of racemic diastereoisomers A (I and II) and B (III and IV) are present in solution (see Scheme 2).[7] For example, two species are discernible in the case of complex **8**. The $^{31}P\{^1H\}$ NMR spectrum features two doublets with relative integrals of 1 and another two with relative integrals of 3 (Figure 1). Even though the aliphatic region of the ^1H NMR spectrum is quite complicated, the four doublets of doublets due to the PMe_3 groups and the four doublets due to the Me groups bonded to N atoms are sufficiently resolved. The ^1H-NOESY spectrum (Figure 2) indicates that: (a) one PMe_3 of the more abundant isomer shows NOE contacts with both Me groups while the other shows none; (b) each PMe_3 group of the less abundant isomer shows an NOE contact with one Me group. The major stereoisomers present in solution are those labelled A in Scheme 2, in which the two substituents are oriented towards the same PMe_3 group. In hindsight, it can be seen that for these isomers the difference in chemical shift of the two P nuclei is greater than for the others, due to the higher extent of octahedral distortion of the ligand sphere. By combining the information provided by ^1H-COSY, ^1H-NOESY, and "normal" and long-range ^1H-^{13}C HMQC experiments, and assuming that N−H and N−Me resonances *cis* to COMe resonate at higher frequencies (due to the previously observed deshielding effect of COMe), it was possible to assign most of the resonances (see Exp. Sect.).

Interionic Structure in Solution by NMR

The relative anion−cation orientation (interionic structure) was investigated in dichloromethane solution by detecting interionic "contacts" in the ^1H-NOESY and $^{19}F\{^1H\}$-HOESY NMR spectra. The most significant results can be summarized as follows.

The ^1H-NOESY spectrum of complex **2a** shows (1) that PMe_3 protons interact quite strongly with all the aromatic protons of BPh_4^-, and (2) that the Me groups of the diimine ligand interact with *o*-H and *m*-H (Figure 3). The interactions between the counterion and the aromatic protons

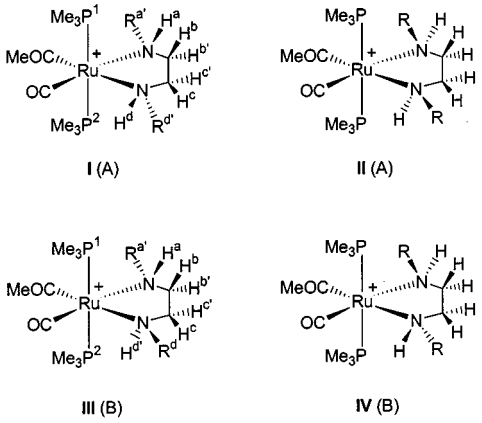

Scheme 2

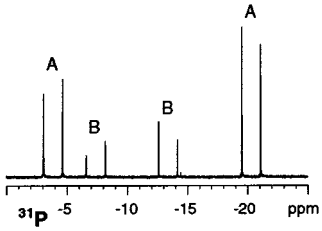

Figure 1. $^{31}P\{^1H\}$ NMR spectrum of complex **8** recorded at 298 K in $[D_2]$dichloromethane showing the presence of two species in a 1:3 ratio

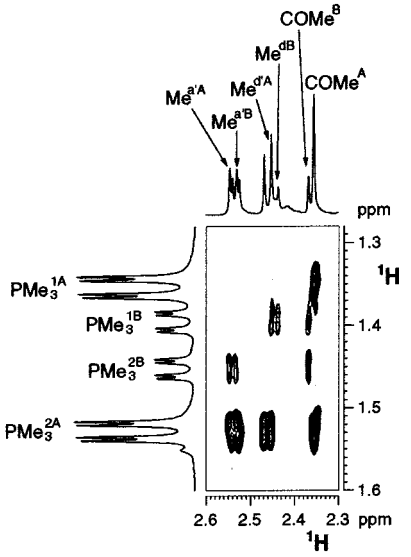

Figure 2. A section of the ^1H-NOESY NMR spectrum of complex **8** recorded at 298 K in $[D_2]$dichloromethane showing the interactions of $PMe_3{}^2$ with both Me groups in the A stereoisomers and the interactions of $PMe_3{}^2$ with $Me^{a'}$ and of $PMe_3{}^1$ with Me^d in the B stereoisomers

of the cation can be detected more readily in the $^{19}F\{^1H\}$-HOESY NMR spectrum of **2b** (Figure 4): BF_4^- shows "contacts" with o^a and $o^{a'}$ and weaker ones with m^b and $m^{b'}$. The same contacts were observed for complex **3**. No contacts were observed between the counterion and the COMe protons or *p*-H or *p*-F in any of the three complexes. The average interionic structure that can be inferred from these observations is one in which the counterion preferentially resides on the side of the N,N ligand above or below the plane defined by the N,N, CO, and COMe ligands.

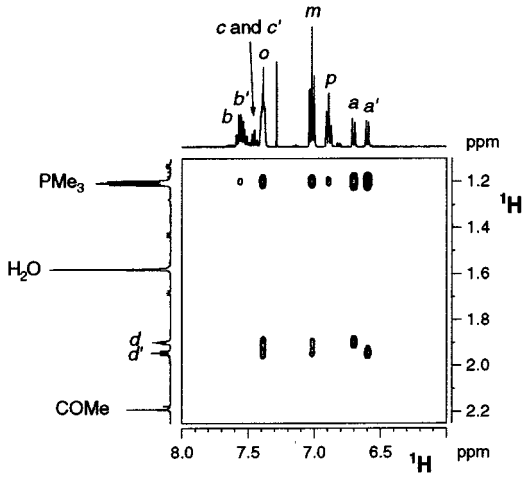

Figure 3. A section of the ^1H-NOESY NMR spectrum of complex **2a** recorded at 298 K in $[D_2]$dichloromethane showing the interionic contacts between the PMe_3 groups and all the aromatic protons of BPh_4^- and between the Me^d protons and *o*-H and *m*-H

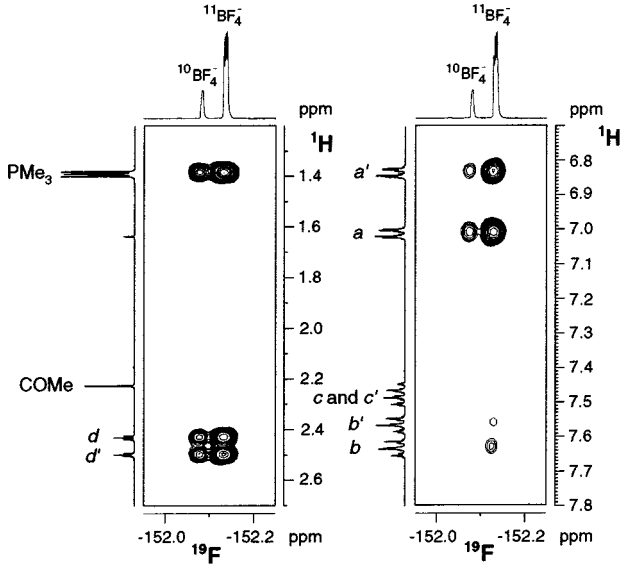

Figure 4. Two sections of the $^{19}F\{^1H\}$-HOESY NMR spectrum of complex **2b** recorded at 298 K in $[D_2]$dichloromethane showing the interionic contacts between BF_4^- and PMe_3 and the *d*, *d'*, *a*, and *a'* protons, as well as weaker contacts with *b* and *b'*

Besides showing strong contacts between PMe_3 and all the aromatic protons of BPh_4^-, the ^1H-NOESY spectrum of complex **5** shows contacts between NH_2^d, CH_2^c, and CH_2^b (very weak) and *o*-H and *m*-H. COMe and NH_2^a do not interact with the counterion (Figure 5). This indicates that the counterion is located close to the N,N ligand and prefers to stay close to the N arm *trans* to the acetyl group.

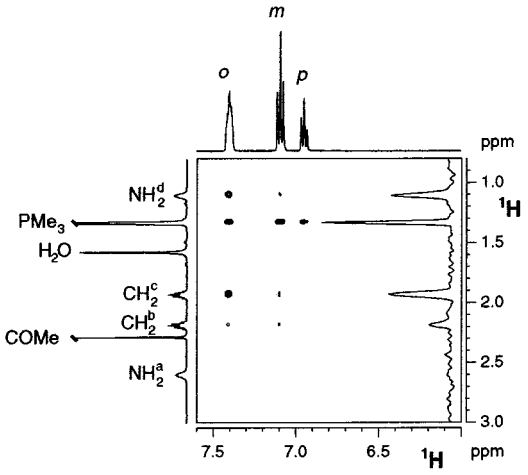

figure 5. A section of the ^1H-NOESY NMR spectrum of complex **5** recorded at 298 K in $[D_2]$dichloromethane showing the gradual decrease of the interionic contact intensity on going from positions *d* to *a*; the 1D trace along the axis corresponding to the *ortho* protons is shown on the right

The ^1H-NOESY spectrum of the two A stereoisomers **8** depicted in Scheme 2 indicates that the counterion shows two preferential interactions, (1) with the protons of the arm *trans* to the COMe group, and (2) with the protons of the less hindered phosphane PMe_3[1]. Once again, there is no interaction with the COMe. The same is true for complex **9**. The position of the counterion is remarkably well defined; it stays on the side of the N,N ligand, shifted towards the arm *trans* to COMe and close to the phosphane that is not hindered by the methyl groups of the N,N ligand.

The interionic structure of the diamine complexes reported here is the most specific that we have never observed in octahedral complexes. The use of non-aromatic N,N ligands does not affect the delocalization of the positive charge that accumulates on the N,N side. In addition, it seems that the positive charge is prevalently delocalized over the N arm *trans* to the COMe group, as indicated by the selective interionic interactions of the protons of this arm with those associated with the counterion.

Conclusions

The use of non-aromatic N,N ligands has unexpectedly led to a higher specificity in the anion−cation interactions, particularly for the diamine complexes. From previous studies,[2c] we know that the stabilization of ion pairs in such complexes is mainly electrostatic, and the fact that the interionic structure is not dependent on the nature of the counterion (BF_4^- or BPh_4^-) further confirms this. The observed specificity can only be attributed to an accumulation of positive charge on the N,N ligands. Not only the lack of unsaturation (as in the diamine ligands) does not affect this accumulation, but it also interrupts the communication be-

tween the two N arms, imparting them with different affinities towards the anion. Steric interactions become important in determining the fine structure, as demonstrated by the interionic structure of the A stereoisomers of complex **9**; here, the electrostatic energy gain directs the counterion to the side of the N,N ligand, while the less hindered P^1-phosphane is favoured by the reduced steric repulsions.

Experimental Section

General Remarks: Complex **1** was prepared according to the literature.[5] Reactions were carried out in dried apparatus under an inert atmosphere of dry nitrogen using standard Schlenk techniques. Solvents were purified by conventional methods prior to use.[8] The diimine ligands were synthesized according to the literature.[9] Diamines were obtained commercially and were used without further purification. − IR spectra were recorded on a Perkin−Elmer 1725 X FTIR spectrophotometer. − One- and two-dimensional ^{1}H, ^{13}C, ^{19}F, and ^{31}P NMR spectra were recorded on Bruker DPX 200 and DRX 400 NMR spectrometers. Spectra were referenced to external TMS (^{1}H and ^{13}C), $CFCl_3$ (^{19}F), and 85% H_3PO_4 (^{31}P). NMR samples were prepared by dissolving about 20 mg of the compound in 0.5 mL of deuterated solvent. Two-dimensional ^{1}H-NOESY and ^{19}F{^{1}H}-HOESY spectra were recorded with a mixing time of 500−800 ms. The assignment of all the resonances was achieved by a combination of ^{1}H-COSY, ^{1}H-NOESY, and "normal" and long-range ^{1}H-^{13}C HMQC experiments.

Synthesis of Complex 2a: Solid diacetyl bis(phenylimine) (131 mg, 0.55 mmol) and $NaBPh_4$ (large excess) were added to a solution of complex **1** (100 mg, 0.22 mmol) in methanol (10 mL). The resulting mixture was stirred and refluxed for 4 h, in the course of which its colour changed from yellow to deep-red. After cooling, the solution was placed in a refrigerator. A white solid precipitated after 15 h, which was filtered off. A red crystalline product precipitated from the remaining solution (10 mg, yield 5%). − $C_{49}H_{57}BN_2O_2P_2Ru$ (879.8): calcd. C 66.90, H 6.53, N 3.18; found C 66.96, H 6.72, N 3.21. − IR (CH_2Cl_2, 298 K): ν_{CO} = 1958 cm^{-1}, ν_{COMe} = 1625 cm^{-1}. − ^{1}H NMR ($CDCl_3$, 298 K, 400.13 MHz): δ = 1.20 (Harris t, $|^2J_{HP} + {}^4J_{HP}|$ = 7.2, PMe_3), 1.90 (t, $^5J_{HP}$ = 2.0, Me^d), 1.94 (t, $^5J_{HP}$ = 2.8, Me$^{d'}$), 2.18 (s, COMe), 6.60 (dd, $^3J_{HH}$ = 6.6, $^4J_{HH}$ = 1.8, $o^{a'}$), 6.69 (dd, $^3J_{HH}$ = 7.3, $^4J_{HH}$ = 1.2, o^a), 6.88 (t, $^3J_{HH}$ = 7.2, *p*), 7.01 (t, $^3J_{HH}$ = 7.3, *m*), 7.41 (br, *o*), 7.45 (m, p^c and $p^{c'}$), 7.53 (m, $m^{b'}$ and m^b). − ^{13}C{^{1}H} NMR (CD_2Cl_2, 298 K, 100.55 MHz): δ = 15.5 (Harris t, $|^1J_{CP} + {}^3J_{CP}|$ = 30.1, PMe_3), 21.7 (s, Me^d), 23.2 (s, Me$^{d'}$), 51.3 (s, CO*Me*), 120.3 (s, $o^{a'}$), 121.5 (s, o^a), 122.1 (s, *p*), 125.9 (q, $^3J_{C11B}$ = 2.6, *m*), 128.5 (s, $p^{c'}$), 128.8 (s, p^c), 129.6 (s, $m^{b'}$), 130.5 (s, m^b), 136.7 (s, *o*), 149.28 (s, C_{ipso}−N), 149.29 (s, C_{ipso}−N), 164.5 (q, $^1J_{C11B}$ = 49.3, C_{ipso}), 173.4 (s, C=N), 176.0 (s, C=N), 204.3 (s, CO), 253.6 (s, *C*OMe). − ^{31}P{^{1}H} NMR (CD_2Cl_2, 298 K, 161.98 MHz): δ = −11.8 (s, PMe_3).

Synthesis of Complex 2b: Complex **1** (100 mg, 0.22 mmol) was dissolved in diethyl ether (5 mL). Solid $AgBF_4$ (41 mg, 0.21 mmol) was then added and the mixture was stirred for 24 h. The precipitate containing AgI and a solvento intermediate complex was collected by filtration, dried, and washed with a solution of diacetyl bis(phenylimine) (78.6 mg, 0.33 mmol) in CH_2Cl_2 (10 mL). The resulting solution was stirred for 4 h; *n*-hexane was then added until precipitation commenced. On placing the solution in a refrigerator at −18 °C, a red solid precipitated, which was collected by filtration, washed with *n*-hexane, and dried in vacuo (30 mg, yield 21%). − $C_{25}H_{37}BF_4N_2O_2P_2Ru$ (647.4): calcd. C 46.39, H 5.76, N 4.33; found C 46.58, H 5.80, N 4.12. − IR (CH_2Cl_2, 298 K): ν_{CO} = 1956 cm^{-1}, ν_{COMe} = 1623 cm^{-1}. − ^{1}H NMR (CD_2Cl_2, 298 K, 400.13 MHz): δ = 1.38 (Harris t, $|^2J_{HP} + {}^4J_{HP}|$ = 7.2, PMe_3), 2.23 (s, COMe), 2.43 (t, $^5J_{HP}$ = 2.7, Me$^{d'}$), 2.49 (t, $^5J_{HP}$ = 1.9, Me^d), 6.84 (dd, $^3J_{HH}$ = 8.4, $^4J_{HH}$ = 1.2, $o^{a'}$), 7.01 (dd, $^3J_{HH}$ = 8.2, $^4J_{HH}$ = 1.1, o^a), 7.46 (tt, $^3J_{HH}$ = 8.6, $^4J_{HH}$ = 1.1, m^c), 7.49 (tt, $^3J_{HH}$ = 7.5, $^4J_{HH}$ = 1.2, $m^{c'}$), 7.56 (t, $^3J_{HH}$ = 7.1, $m^{b'}$), 7.63 (t, $^3J_{HH}$ = 7.5, m^b). − ^{31}P{^{1}H} NMR (CD_2Cl_2, 298 K, 161.98 MHz): δ = −11.7 (s, PMe_3). − ^{19}F NMR (CD_2Cl_2, 298 K, 376.50 MHz): δ = −152.08 (br, $^{10}BF_4^-$), −152.13 (br, $^{11}BF_4^-$).

Synthesis of Complex 3: The procedure was the same as that used for complex **2b**. At the final stage, a mixture of complexes **3** and **4a** was obtained. Characterization of complex **3:** IR (CH_2Cl_2, 298 K): ν_{CO} = 1953 cm^{-1}, ν_{COMe} = 1641 cm^{-1}. − ^{1}H NMR (CD_2Cl_2, 298 K, 400.13 MHz): δ = 1.36 (Harris t, $|^2J_{HP} + {}^4J_{HP}|$ = 7.2, PMe_3), 2.26 (s, COMe), 2.46 (t, $^5J_{HP}$ = 2.8, Me$^{c'}$), 2.53 (t, $^5J_{HP}$ = 1.9, Me^c), 6.84 (dd, $^3J_{HH}$ = 9.0, $^4J_{HF}$ = 4.6, $o^{a'}$), 7.05 (dd, $^3J_{HH}$ = 9.0, $^4J_{HF}$ = 4.6, o^a), 7.27 (t, $^3J_{HH}$ = 9.0, $^3J_{HF}$ = 8.3, $m^{b'}$), 7.33 (t, $^3J_{HH}$ = 9.0, $^3J_{HF}$ = 8.2, m^b). − ^{13}C{^{1}H} NMR (CD_2Cl_2, 298 K, 100.55 MHz): δ = 15.5 (Harris t, $|^1J_{CP} + {}^3J_{CP}|$ = 30.1, PMe_3), 21.8 (s, Me$^{d'}$), 23.3 (s, Me^d), 50.8 (t, $^4J_{CP}$ = 1.6, CO*Me*), 115.9 (d, $^2J_{CF}$ = 28.2, $m^{b'}$), 117.2 (d, $^2J_{CF}$ = 30.6, m^b), 123.2 (d, $^3J_{CF}$ = 9.0, $o^{a'}$), 124.3 (d, $^3J_{CF}$ = 9.6, o^a), 145.4 (s, $p^{d'}$), 145.7 (s, p^d), 161.93 (d, $^1J_{CF}$ = 248.8, C_{ipso}−N), 161.94 (d, $^1J_{CF}$ = 246.6, C_{ipso}−N), 174.6 (s, C=N), 177.6 (s, C=N), 204.8 (t, $^2J_{CP}$ = 14.7, CO), 253.2 (t, $^2J_{CP}$ = 10.5, *C*OMe). − ^{31}P{^{1}H} NMR (CD_2Cl_2, 298 K, 161.98 MHz): δ = −11.6 (s, PMe_3). − ^{19}F NMR (CD_2Cl_2, 298 K, 376.50 MHz): δ = −114.2 (tt, $^3J_{FH}$ = 9.0, $^4J_{FH}$ = 8.0, $p^{d'}$), −115.5 (tt, $^3J_{FH}$ = 9.0, $^4J_{FH}$ = 8.0, p^d), −150.6 (br, $^{10}BF_4^-$), −150.7 (br, $^{11}BF_4^-$).

Synthesis of Complex 4a: The procedure was similar to that used for complex **2b**, but the precipitate was washed with neat dichloromethane free from any ligands (yield 30%). The coordinated water was probably present in the hygroscopic $AgBF_4$ salt. − $C_9H_{23}BF_4O_3P_2Ru$ (429.1): calcd. C 25.20, H 5.40; found C 25.36, H 5.45. − IR (CH_2Cl_2, 298 K): ν_{CO} = 1973, 2042 cm^{-1}. − ^{1}H NMR (CD_2Cl_2, 298 K, 400.13 MHz): δ = 0.08 (t, $^3J_{HP}$ = 7.9, Me), 1.57 (Harris t, $|^2J_{HP} + {}^4J_{HP}|$ = 7.4, PMe_3), 3.93 (s, H_2O). − ^{13}C{^{1}H} NMR (CD_2Cl_2, 298 K, 100.55 MHz): δ = −3.68 (s, Me), 15.0 (Harris t, $|^1J_{CP} + {}^3J_{CP}|$ = 31.7, PMe_3), 189.9 (s, CO), 201.0 (s, CO). − ^{31}P{^{1}H} NMR (CD_2Cl_2, 298 K, 161.98 MHz): δ = −3.21 (s, PMe_3). − ^{19}F NMR (CD_2Cl_2, 298 K, 376.50 MHz): δ = −149.8 (vbr, $^{10}BF_4^-$), −149.9 (br, $^{11}BF_4^-$).

Synthesis of Complex 4b: Solid $TlPF_6$ (73 mg, 0.21 mmol) was added to a solution of complex **1** (100 mg, 0.22 mmol) in methanol (5 mL). Immediately, TlI precipitated from the solution and was filtered off. The filtrate was treated with a large excess of solid $NaBPh_4$. After a few minutes, complex **4b** precipitated; it was collected by filtration, washed with cold methanol, and dried in vacuo (140 mg, yield 94%). − $C_{34}H_{45}BO_3P_2Ru$ (675.6): calcd. C 60.46, H 6.71; found C 60.54, H 6.78. − IR (CH_2Cl_2, 298 K): ν_{CO} = 1975, 2033 cm^{-1}. − ^{1}H NMR (CD_2Cl_2, 298 K, 400.13 MHz): δ = −0.85 (br, *Me*OH), −0.61 (t, $^3J_{HP}$ = 8.0, Me), 1.33 (Harris t, $|^2J_{HP} + {}^4J_{HP}|$ = 7.0, PMe_3), 3.45 (s, MeO*H*), 6.96 (t, $^3J_{HP}$ = 7.2, *p*), 7.10 (t, $^3J_{HP}$ = 7.4, *m*), 7.56 (br, *o*). − ^{13}C{^{1}H} NMR (CD_2Cl_2, 298 K, 100.55 MHz): δ = −6.98 (t, $^2J_{CP}$ = 9.3, Me), 15.6 (Harris t, $|^1J_{CP} + {}^3J_{CP}|$ = 31.7, PMe_3), 30.0 (s, MeOH), 122.8 (s, *p*), 126.6 (s, *m*), 136.1 (s, *o*), 165.0 (q, $^1J_{C11B}$ = 49.5, C_{ipso}), 190.5 (t, $^2J_{CP}$ = 8.6, CO), 199.5 (t, $^2J_{CP}$ = 13.5, CO). − ^{31}P{^{1}H} NMR (CD_2Cl_2, 298 K, 161.98 MHz): δ = −5.57 (s, PMe_3).

Synthesis of Complex 5: Ethylenediamine (22 μL, ca. 0.33 mmol) was added to a solution of complex **1** (100 mg, 0.22 mmol) in methanol (5 mL) and the solution was stirred for 10 min. A large excess of $NaBPh_4$ was then added, which resulted in the precipitation of a white solid. It was collected by filtration, washed with cold methanol, and dried in vacuo (130 mg, yield 85%). − $C_{35}H_{49}BN_2O_2P_2Ru$ (703.6): calcd. C 59.75, H 7.02, N 3.98; found C 59.28, H 6.50, N 3.25. − IR (CH_2Cl_2, 298 K): ν_{CO} = 1944 cm^{-1}, ν_{COMe} = 1614 cm^{-1}. − ^1H NMR (CD_2Cl_2, 298 K, 400.13 MHz): δ = 1.11 (br, NH_2^d), 1.33 (Harris t, $|^2J_{HP} + {}^4J_{HP}|$ = 6.3, PMe_3), 1.93 (m, $^2J_{HH}$ = 11.6, $^3J_{HH}$ = 6.0, CH_2^c), 2.18 (m, $^2J_{HH}$ = 11.7, $^3J_{HH}$ = 5.9, CH_2^b), 2.28 (s, COMe), 2.60 (br, NH_2^a), 6.94 (t, $^3J_{HH}$ = 6.1, *p*), 7.09 (t, $^3J_{HH}$ = 7.4, *m*), 7.41 (br, *o*). − $^{13}C\{^1H\}$ NMR (CD_2Cl_2, 298 K, 100.55 MHz): δ = 15.3 (Harris t, $|^1J_{CP} + {}^3J_{CP}|$ = 29.2, PMe_3), 43.6 (s, CH_2^c), 45.7 (s, CH_2^b), 48.0 (s, CO*Me*), 122.4 (s, *p*), 126.2 (s, *m*), 136.3 (s, *o*), 164.4 (q, $^1J_{C11B}$ = 49.3, C_{ipso}), 202.7 (t, $^2J_{CP}$ = 15.4, CO), 263.6 (t, $^2J_{CP}$ = 10.8, *C*OMe). − $^{31}P\{^1H\}$ NMR (CD_2Cl_2, 298 K, 161.98 MHz): δ = −6.71 (s, PMe_3).

Synthesis of Complex 6: The synthetic procedure was similar to that described for complex **5**. Yield: 60%. − $C_{37}H_{53}BN_2O_2P_2Ru$ (731.7): calcd. C 60.74, H 7.30, N 3.83; found C 59.32, H 7.16, N 3.73. − IR (CH_2Cl_2, 298 K): ν_{CO} = 1945 cm^{-1}, ν_{COMe} = 1603 cm^{-1}. − ^1H NMR (CD_2Cl_2, 298 K, 400.13 MHz): δ = 1.20 (t, $^3J_{HH}$ = 7.2, C*H*$_3$CH$_2$), 1.36 (dd, $^2J_{HP}$ = 7.8, $^4J_{HP}$ = 1.4, PMe_3^1), 1.39 (dd, $^2J_{HP}$ = 7.7, $^4J_{HP}$ = 1.5, PMe_3^2), 1.65 (br, NH^d), 1.71 (br, H^a), 1.77 (m, H^d), 2.34 (s, COMe), 2.43 (br. d, $^2J_{HH}$ = 15.9, H^c), 2.58 (m, H^b), 2.59 (m, NH_2^a and CH_3CH_2), 6.97 (t, $^3J_{HH}$ = 7.2, *p*), 7.10 (t, $^3J_{HH}$ = 7.4, *m*), 7.42 (br, *o*). − $^{13}C\{^1H\}$ NMR (CD_2Cl_2, 298 K, 100.55 MHz): δ = 15.2 (dd, $^1J_{CP}$ = 26.4, $^3J_{CP}$ = 2.9, PMe_3^1), 15.9 (s, *C*H$_3$CH$_2$), 16.9 (dd, $^1J_{CP}$ = 25.8, $^3J_{CP}$ = 3.1, PMe_3^2), 43.7 (s, C^c), 48.1 (s, CO*Me*), 50.4 (s, CH_3CH_2), 54.1 (s, C^b), 122.5 (s, *p*), 126.1 (s, *m*), 136.3 (s, *o*), 164.5 (q, $^1J_{C11B}$ = 49.3, C_{ipso}), 203.7 (t, $^2J_{CP}$ = 15.2, CO), 262.4 (t, $^2J_{CP}$ = 10.8, *C*OMe). − $^{31}P\{^1H\}$ NMR (CD_2Cl_2, 298 K, 161.98 MHz): δ = −10.78 (d, $^2J_{PP}$ = 254.9, $PMe_3^{1\text{ or }2}$), −6.74 (d, $^2J_{PP}$ = 254.9, $PMe_3^{2\text{ or }1}$).

Synthesis of Complex 7: The synthetic procedure was similar to that described for complex **5**. Yield: 95%. − $C_{38}H_{55}BN_2O_2P_2Ru$ (745.7): calcd. C 61.21, H 7.43, N 3.76; found C 61.27, H 7.33, N 3.30. − IR (CH_2Cl_2, 298 K): ν_{CO} = 1944 cm^{-1}, ν_{COMe} = 1599 cm^{-1}. − ^1H NMR (CD_2Cl_2, 298 K, 400.13 MHz): δ = 1.18 (d, $^3J_{HH}$ = 6.2, CH*Me*$_2$), 1.29 (d, $^3J_{HH}$ = 6.5, CH*Me*$_2$), 1.38 (d, $^2J_{HP}$ = 8.3, PMe_3^1), 1.40 (d, $^2J_{HP}$ = 8.0, PMe_3^2), 1.44 (br, NH^d), 1.79 (m, $H^{c\text{ or }c'}$ and $H^{b\text{ or }b'}$), 2.35 (s, COMe), 2.51 (br, $H^{c\text{ or }c'}$ and $NH^{a\text{ and }a'}$), 2.66 (m, CH), 2.75 (br, $H^{b\text{ or }b'}$ and $H^{c\text{ or }c'}$), 6.95 (t, $^3J_{HH}$ = 7.2, *p*), 7.10 (t, $^3J_{HH}$ = 7.4, *m*), 7.42 (br, *o*). − $^{13}C\{^1H\}$ NMR (CD_2Cl_2, 298 K, 100.55 MHz): δ = 15.3 (dd, $^1J_{CP}$ = 25.4, $^3J_{CP}$ = 3.8, PMe_3^1), 16.8 (dd, $^1J_{CP}$ = 25.2, $^3J_{CP}$ = 3.8, PMe_3^2), 22.0 (s, Me), 26.3 (s, Me), 44.2 (s, $CH_2^{b\text{ or }c}$), 47.6 (s, CO*Me*), 51.4 (s, $CH_2^{c\text{ or }b}$), 54.3 (s, CH), 122.3 (s, *p*), 126.3 (s, *m*), 136.2 (s, *o*), 164.3 (q, $^1J_{C11B}$ = 49.3, C_{ipso}), 203.9 (t, $^2J_{CP}$ = 15.2, CO), 260.2 (t, $^2J_{CP}$ = 10.6, *C*OMe). − $^{31}P\{^1H\}$ NMR (CD_2Cl_2, 298 K, 161.98 MHz): δ = −10.4 (d, $^2J_{PP}$ = 254.2, $PMe_3^{1\text{ or }2}$), −7.4 (d, $^2J_{PP}$ = 254.2, $PMe_3^{2\text{ or }1}$).

Synthesis of Complex 8: The procedure used was similar to that described for complex **5**. Yield: 65%. − $C_{37}H_{53}BN_2O_2P_2Ru$ (731.7): calcd. C 60.74, H 7.30, N 3.83; found C 60.22, H 7.11, N 3.70. − IR (CH_2Cl_2, 298 K): ν_{CO} = 1945 cm^{-1}, ν_{COMe} = 1592 cm^{-1}. − ^1H NMR (CD_2Cl_2, 298 K, 400.13 MHz): δ = 1.35 (dd, $^2J_{HP}$ = 8.3, $^4J_{HP}$ = 1.8, PMe_3^{1A}), 1.39 (dd, $^2J_{HP}$ = 8.1, $^4J_{HP}$ = 1.7, PMe_3^{1B}), 1.45 (dd, $^2J_{HP}$ = 7.7, $^4J_{HP}$ = 1.7, PMe_3^{2B}), 1.53 (dd, $^2J_{HP}$ = 7.5, $^4J_{HP}$ = 1.8, PMe_3^{2A}), 1.78 (br, $H^{b\text{ or }b'B}$), 1.80 (br, NH^{dB}), 1.82 (br, $H^{b'\text{ or }bB}$), 1.96 (NH^{dA}), 2.15 (br, $H^{c'A}$), 2.21 (br, H^{bA}), 2.29 (br, $H^{b'A}$), 2.35 (s, $COMe^A$), 2.37 (s, $COMe^B$), 2.39 (br, H^{cB}), 2.41 (br, H^{cA}), 2.44 (d, $^3J_{HH}$ = 6.5, Me^{dB}), 2.46 (d, $^3J_{HH}$ = 6.2, $Me^{d'A}$), 2.53 (d, $^2J_{HH}$ = 6.2, $Me^{a'B}$), 2.54 (d, $^2J_{HH}$ = 6.2, $Me^{a'A}$), 2.67 (m, H^{cB}), 2.93 (br, NH^{aB}), 3.09 (br, NH^{aA}), 6.91 (t, $^3J_{HH}$ = 7.2, *p*), 7.08 (t, $^3J_{HH}$ = 7.4, *m*), 7.39 (br, *o*). − $^{13}C\{^1H\}$ NMR (CD_2Cl_2, 298 K, 100.55 MHz): δ = 14.4 (dd, $^1J_{CP}$ = 28.2, $^3J_{CP}$ = 1.8, PMe_3^{1A}), 16.0 (dd, $^1J_{CP}$ = 29.1, $^3J_{CP}$ = 2.5, PMe_3^{1B}), 17.6 (dd, $^1J_{CP}$ = 26.2, $^3J_{CP}$ = 2.8, PMe_3^{2B}), 18.8 (dd, $^1J_{CP}$ = 25.7, $^3J_{CP}$ = 2.6, PMe_3^{2A}), 42.3 (s, $Me^{d'B}$), 42.7 (br, $Me^{a'A}$, $Me^{d'A}$, and $Me^{a'B}$), 48.9 (s, CO*Me*^{A}), 49.1 (s, CO*Me*^{B}), 52.6 (s, C^{cA}), 54.0 (s, C^{bA}), 54.4 (s, C^{bB}), 54.5 (s, C^{cB}), 122.1 (s, *p*), 126.0 (s, *m*), 136.3 (s, *o*), 164.4 (q, $^1J_{C11B}$ = 49.3, C_{ipso}), 203.3 (s, CO^A), 263.1 (s, *C*OMe^A). − $^{31}P\{^1H\}$ NMR (CD_2Cl_2, 298 K, 161.98 MHz): δ = −3.83 (d, $^2J_{PP}$ = 256.1, $PMe_3^{1\text{ or }2A}$), −7.37 (d, $^2J_{PP}$ = 256.2, $PMe_3^{1\text{ or }2B}$), −13.4 (d, $^2J_{PP}$ = 256.1, $PMe_3^{2\text{ or }1B}$), −20.3 (d, $^2J_{PP}$ = 256.1, $PMe_3^{2\text{ or }1A}$).

Synthesis of Complex 9: (a) The procedure used was similar to that described for complex **5**. The reaction required 2 days and gave a 12% yield of **9**. (b) Solid $TlPF_6$ (73 mg, 0.21 mmol) was added to a solution of complex **1** (100 mg, 0.22 mmol) in methanol (5 mL). Immediately, TlI was precipitated, which was filtered off. The filtrate was treated with liquid *N*,*N*′-dibenzylethylenediamine (0.11 mL, 0.44 mmol) and solid $NaBPh_4$ (large excess). After 2 h, complex **9** precipitated; it was collected by filtration, washed with cold methanol, and dried in vacuo (60 mg, yield 30%). − $C_{49}H_{61}BN_2O_2P_2Ru$ (883.9): calcd. C 66.59, H 6.96, N 3.17; found C 65.21, H 6.72, N 3.10. − IR (CH_2Cl_2, 298 K): ν_{CO} = 1947 cm^{-1}, ν_{COMe} = 1608 cm^{-1}. − ^1H NMR (CD_2Cl_2, 298 K, 400.13 MHz): δ = 1.33 (dd, $^2J_{HP}$ = 7.5, $^4J_{HP}$ = 1.8, PMe^{1A} and PMe^{1B}), 1.47 (dd, $^2J_{HP}$ = 8.1, $^4J_{HP}$ = 1.8, PMe^{2B}), 1.69 (dd, $^2J_{HP}$ = 7.5, $^4J_{HP}$ = 1.8, PMe^{2A}), 1.90 (br, H^{dB}), 1.95 (br, $H^{c'A}$), 2.29 (br, H^{dA}), 2.42 (s, CO*Me*^{B}), 2.46 (s, CO*Me*^{A}), 2.61 (br, $H^{c'B}$), 2.67 (d, $H^{b'B}$), 2.71 (d, H^{bB}), 2.75 (br, $H^{b'A}$), 2.79 (br, $H^{c'A}$), 2.89 (t, $^2J_{HH}$ = 11.6, $H^{bz(I)B}$), 3.2 (br, H^{aB}), 3.35 (t, $^2J_{HH}$ = 12.0, $H^{bz(I)A}$), 3.36 (br, H^{aA}), 3.66 (br, H^{bzA}), 3.70 (H^{bzB} and H^{bzB}), 3.71 (br, H^{cB}), 3.97 (dd, $^1J_{HH}$ = 13.0, $^3J_{HH}$ = 5.1, H^{bzA}), 4.26 (d, $^1J_{HH}$ = 12.1, $H^{bz(I)A}$), 4.50 (br, $H^{bz(I)B}$), 6.90 (tt, $^3J_{HH}$ = 7.2, $^4J_{HH}$ = 1.2, *p*), 7.04 (t, $^3J_{HH}$ = 7.4, *m*), 7.26 (m, o^A), 7.33 (m, o^B), 7.37 (m, *o*), 7.489 (m, m^A), 7.492 (m, $o^{(I)B}$), 7.505 (m, m^B), 7.54 (m, $o^{(I)A}$). − $^{13}C\{^1H\}$ NMR (CD_2Cl_2, 298 K, 100.55 MHz): δ = 14.0 (dd, $^1J_{CP}$ = 28.3, $^3J_{CP}$ = 1.8, PMe_3^{1A}), 15.4 (dd, $^1J_{CP}$ = 27.0, $^3J_{CP}$ = 2.3, PMe_3^{2B}), 17.4 (dd, $^1J_{CP}$ = 26.5, $^3J_{CP}$ = 2.7, PMe_3^{1B}), 19.1 (dd, $^1J_{CP}$ = 26.0, $^3J_{CP}$ = 2.5, PMe_3^{2A}), 47.6 (s, CH_2^{cA}), 48.24, 48.27, and 48.30 (s, CO*Me*^{B}), 48.52 and 48.54 (s, CO*Me*^{A}), 50.0 (s, CH_2^{bA}), 50.8 (s, CH_2^{bB}), 53.8 (s, CH_2^{cB}), 56.9 (dd, $^3J_{CP}$ = 6.8, $^3J_{CP}$ = 2.5, $CH_2^{bz(I)A}$), 59.3 (s, CH_2^{bzB}), 59.7 (s, $CH_2^{bz(I)B}$), 60.0 (s, CH_2^{bzA}), 121.9 (s, *p*), 125.7 (m, *m*), 128.8 (s, o^A), 129.3 (s, $o^{(I)A}$), 129.6 (s, o^B), 129.7 (s, $o^{(I)b}$), 136.1 (m, *o*), 164.4 (q, $^1J_{C11B}$ = 49.0, C_{ipso}), 202.9 (t, $^2J_{CP}$ = 15.8, CO^A), 203.4 (t, $^2J_{CP}$ = 15.8, CO^B), 261.8 (t, $^2J_{CP}$ = 11.6, *C*OMe^B), 262.8 (t, $^2J_{CP}$ = 10.1, *C*OMe^A). − $^{31}P\{^1H\}$ NMR (CD_2Cl_2, 298 K, 161.98 MHz): δ = −4.3 (d, $^2J_{PP}$ = 249, $PMe_3^{2\text{ or }1A}$), −5.7 (d, $^2J_{PP}$ = 256, $PMe_3^{2\text{ or }1B}$), −13.8 (d, $^2J_{PP}$ = 256, $PMe_3^{1\text{ or }2B}$), −20.2 (d, $^2J_{PP}$ = 249, $PMe_3^{1\text{ or }2A}$).

Synthesis of Complex 10: The procedure used was similar to that described for complex **5**. Yield: 27%. − $C_{37}H_{53}BN_2O_2P_2Ru$ (731.7): calcd. C 60.74, H 7.30, N 3.83; found C 60.13, H 7.32, N 3.86. − IR (CH_2Cl_2, 298 K): ν_{CO} = 2039 cm^{-1}, ν_{COMe} = 1950 cm^{-1}. − ^1H NMR (CD_2Cl_2, 298 K, 400.13 MHz): δ = −0.27 (t, $^3J_{HP}$ = 8.0, Me), 1.55 (Harris t, $|^2J_{HP} + {}^4J_{HP}|$ = 6.9, PMe_3), 2.29 (s, Me_2N), 2.32 (br, CH_2^{α}, NH_2), 2.54 (br, CH_2^{β}), 6.93 (t, $^3J_{HH}$ = 7.2, *p*), 7.08 (t, $^3J_{HH}$ = 7.4, *m*), 7.37 (br, *o*). − $^{13}C\{^1H\}$ NMR (CD_2Cl_2, 298 K, 100.55 MHz): δ = −7.13 (t, $^2J_{CP}$ = 9.4, Me), 15.9 (Harris t, $|^1J_{CP} + {}^3J_{CP}|$ = 31.9, PMe_3), 45.5 (s, Me_2N), 48.7 (s, CH_2^{β}), 59.7 (s,

CH_2^{α}), 122.1 (s, *p*), 126.0 (s, *m*), 136.3 (s, *o*), 164.7 (q, $^1J_{C11B}$ = 48.9, C_{ipso}), 191.3 (t, $^2J_{CP}$ = 8.4, CO), 199.3 (s, $^2J_{CP}$ = 13.5, CO). – $^{31}P\{^1H\}$ NMR (CD_2Cl_2, 298 K, 161.98 MHz): δ = 6.87 (s, PMe_3).

Acknowledgments

This work was supported by grants from the Ministero dell' Università e della Ricerca Scientifica e Tecnologica (MURST, Rome, Italy), Programma di Rilevante Interesse Nazionale, Cofinanziamento 2000-1.

[1] See, for example: D. Evans, J. A. Murry, P. von Matt, R. D. Norcross, S. J. Miller, *Angew. Chem. Int. Ed. Engl.* **1995**, *34*, 798. A. Lightfoot, P. Schnider, A. Pfalts, *Angew. Chem. Int. Ed.* **1998**, *37*, 2897. E. Y.-X. Chen, T. J. Marks, *Chem. Rev.* **2000**, *100*, 1391, and references therein.

[2] [2a] G. Bellachioma, G. Cardaci, A. Macchioni, G. Reichenbach, S. Terenzi, *Organometallics* **1996**, *15*, 4349. – [2b] A. Macchioni, G. Bellachioma, G. Cardaci, V. Gramlich, H. Rüegger, S. Terenzi, L. M. Venanzi, *Organometallics* **1997**, *16*, 2139. – [2c] A. Macchioni, G. Bellachioma, G. Cardaci, G. Cruciani, E. Foresti, P. Sabatino, C. Zuccaccia, *Organometallics* **1998**, *17*, 5549. – [2d] G. Bellachioma, G. Cardaci, V. Gramlich, A. Macchioni, M. Valentini, C. Zuccaccia, *Organometallics* **1998**, *17*, 5025. – [2e] C. Zuccaccia, G. Bellachioma, G. Cardaci, A. Macchioni, *Organometallics* **1999**, *18*, 1. – [2f] A. Macchioni, G. Bellachioma, G. Cardaci, M. Travaglia, C. Zuccaccia, B. Milani, G. Corso, E. Zangrando, G. Mestroni, C. Carfagna, M. Formica, *Organometallics* **1999**, *18*, 3061. – [2g] C. Zuccaccia, A. Macchioni, I. Orabona, F. Ruffo, *Organometallics* **1999**, *18*, 4367.

[3] D. Neuhaus, M. Williamson, *The Nuclear Overhauser Effect in Structural and Conformational Analysis*, VCH Publishers, New York, **1989**.

[4] C. Zuccaccia, G. Bellachioma, G. Cardaci, A. Macchioni, paper in preparation.

[5] G. Bellachioma, G. Cardaci, A. Macchioni, A. Madami, *Inorg. Chem.* **1993**, *32*, 554.

[6] R. K. Harris, *Can. J. Chem.* **1964**, *42*, 2275.

[7] The atom labels for compounds **2–3** are shown in the upper part of Scheme 1. The numeration adopted for distinguishing the atoms of the diamine compounds **5–9** is indicated in Scheme 2. For compounds bearing *N,N′*-disubstituted amines, two possibilities exist: (1) structure A: the PMe_3 group that is far away from the R substituents is labelled as PMe_3^1, the other is denoted as PMe_3^2; (2) structure B: the PMe_3 group that "sees" the R group *trans* to COMe is labelled as PMe_3^1. For compounds bearing *N*-substituted amines, we observe that the substituted N arm lies *trans* to COMe (this is deduced from the higher resonance frequency of the NH_2 protons compared to the NHR proton, which is attributed to the deshielding effect of the *cis* COMe group). The numeration is then based on structure I in Scheme 2; the PMe_3 group that interacts with the R substituent is labelled as PMe_3^2.

[8] A. Weissberger, E. S. Proskauer, *Techniques of Organic Chemistry, Interscience*, N.Y., **1955**, Vol. VII.

[9] T. H. Dieck, M. Svoboda, T. Z. Greiser, *Z. Naturforsch., Teil B* **1981**, *36*, 823.

Received November 6, 2000
[I00419]

Synthesis and Structures of Vinamidine Mn^{II}, Zn^{II}, and Cd^{II} Iodine Derivatives

Jörg Prust,[a] Kerstin Most,[a] Ilka Müller,[a] Andreas Stasch,[a] Herbert W. Roesky,*[a] and Isabel Usón[a]

Dedicated to Professor Glen B. Deacon on the occasion of his 65th birthday

Keywords: Cadmium / Manganese / N ligands / Zinc

We have focused on the synthesis of monomeric, functionalized starting materials containing manganese(II), zinc(II), and cadmium(II) by taking advantage of the sterically demanding and chelating property of the substituted vinamidine ligand 2-[(2,6-diisopropylphenyl)amino]-4-[(2,6-diisopropylphenyl)imino]pent-2-ene (NacNacH). Metal iodine derivatives containing vinamidines as the bulky ligand can be regarded as interesting precursors for preparing complexes with low-valent metal centers by reduction as long as they are free of coordinated ether. The vinamidine complexes NacNacM(μ-I)$_2$Li(OEt$_2$)$_2$ [M = Mn (**3**), Zn (**4**), Cd (**5**)] are obtained from the corresponding vinamidine lithium complex and MI_2 (M = Mn, Zn, Cd) in good yields. A crystal structure analysis of **3**, **4**, and **5** shows them to be isostructural. All three structures have the vinamidine backbone in a boat conformation with the tetrahedrally coordinated metal center at the prow and the opposing carbon atom at the stern.

Introduction

Vinamidines were first used in inorganic synthesis by Holm et al. and McGeachin et al. to synthesize moisture-stable Ni^{II}, Co^{II}, and Cu^{II} complexes.[1] In further research the surprising catalytic activity of vinamidine derivatives of various transition and main group metals was analyzed. Feldman et al. synthesized catalytically active aryl-substituted vinamidine complexes of Pd^{II} and Ni^{II}, and Theopold et al. and Gibson et al. tested vinamidine complexes of Ti^{III}, V^{II}, Cr^{III} for olefin polymerization.[2,3]

In the last few years the interest in the synthesis of monomeric and coordinatively unsaturated metal complexes with bulky vinamidine ligands has increased. In this research field several new compounds have been reported.[4] The vinamidine 2-[(2,6-diisopropylphenyl)amino]-4-[(2,6-diisopropylphenyl)imino]pent-2-ene (**1**) (NacNacH) is suitable for the synthesis of derivatives with unusually low coordinate main group elements. Recently we synthesized a monomeric Al^{I} compound using **1** as a stable carbene analogue, and Gibson et al. have prepared a mono-alkylmagnesium complex stabilized by **1**.[5,6] Our research focused on the synthesis of complexes with low coordinate Mn, Zn and Cd atoms.

Preparing the iodine-containing metal complexes of **1** has two functions: the size of the ligand should have a shielding effect on the metal center and therefore the nucleophilic attack should be minimized; these systems should also be interesting precursors for the preparation of complexes with low-valent metal atoms by reduction of the iodine complexes using alkali metals.

[a] Institut für Anorganische Chemie der Universität Göttingen, Tammannstrasse 4, 37077 Göttingen, Germany
Fax: (internat.) +49-551/39-3373
E-mail: hroesky@gwdg.de

We have focused on the synthesis of NacNacMI (M = Mn, Zn, Cd) as monomeric, functionalized starting materials due to the sterically demanding and chelating properties of **1**.

Results and Discussion

The reaction of MeLi with NacNacH (**1**) gives the pale yellow compound NacNacLi·OEt$_2$ (**2**) in good yield (> 95%). This ether-soluble lithium compound is a useful reagent for metathesis reactions with metal halides. Thus, the reaction of **2** with MI_2 affords the iodide complexes NacNacM(μ-I)$_2$Li(OEt$_2$)$_2$ (M = Mn, Zn, Cd) in reasonable yields (77−85%) (Scheme 1).

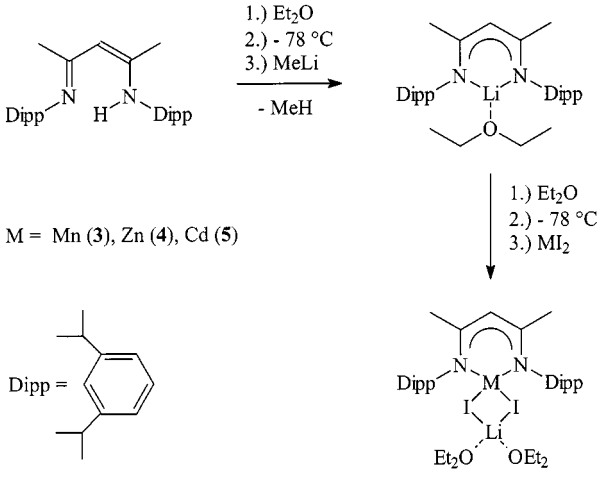

Scheme 1

Unfortunately compounds **3**, **4**, and **5** are moisture sensitive and give **1** as the primary hydrolysis product. ^{1}H NMR

 © WILEY-VCH Verlag GmbH, 69451 Weinheim, 2001 1434−1948/01/0606−1613 $ 17.50+.50/0

spectroscopic data and the elemental analysis of **4** and **5** are consistent with the solid state structures, whereas the mass spectra of **3**, **4**, and **5** show several fragments assignable to the species free of $LiI(Et_2O)_2$.[7]

The X-ray structure analysis of **3**, **4** (shown in Figure 1), and **5** shows that these compounds are isostructural. The crystallographic data are summarized in Table 1. Selected bond lengths and angles for **3**, **4**, and **5** are given in Table 2.

Figure 2 shows a superposition of **3**, **4**, and **5**. The only differences between the three structures are those derived from the different bond lengths in the coordination of the various metals. Therefore, we discuss the overall structure.

The central structural element is a NacNacM(μ-I)$_2$Li unit. The vinamidine ligand NacNac acts as a chelating ligand through its two N atoms, forming a six-membered ring with the metal. The central metal (**3**: Mn, **4**: Zn, **5**: Cd) and the lithium cation are bridged by the two iodine atoms. The N−M−N-angle is about 95° (**3**: 94.2°, **4**: 98.6°, **5**: 91.5°) and the I−M−I-angle is 101° (**3**:101°, **4**:101°, **5**:101°). The tetrahedral coordination of the metal is distorted due to the strain imposed by the six-membered ring of the chelate, and the four-membered ring of the bridging halides.

The M−N−C(CH$_3$)−CH−C(CH$_3$)−N unit is not planar. The six-membered ring displays a boat conformation with the metal at the prow and C(2) at the stern. This deviation from planarity is imposed by the metal, as the planar situation implies more distortion in the tetrahedral environment of the metal. Thus, deviation from planarity increases with the metal radius. The metal is about 0.30 Å (**3**: 0.33 Å, **4**: 0.29 Å, **5**: 0.34 Å) out of the plane defined by

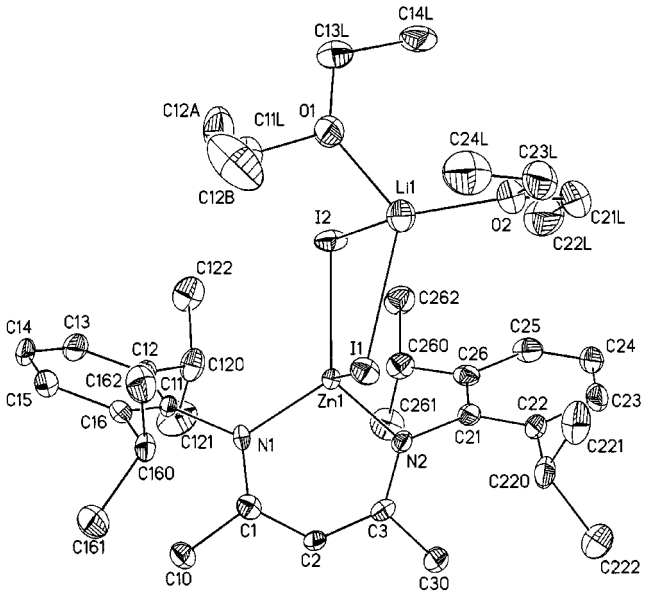

Figure 1. Molecular structure of **4** (hydrogen atoms are omitted for clarity); selected bond lengths [Å] and angles [°] are given in Table 2

Table 1. Crystallographic data for **3**, **4** and **5**

	3	**4**	**5**
Empirical formula	$C_{37}H_{61}I_2LiMnN_2O_2$	$C_{37}H_{61}I_2LiN_2O_2Zn$	$C_{37}H_{61}CdLiI_2N_2O_2$
Molecular weight	881.56	891.99	939.02
Temperature [K]	133(2)	133(2)	133(2)
Wavelength [Å]	0.71073	0.71073	0.71073
Crystal system	triclinic	triclinic	triclinic
Space group	$P\bar{1}$	$P\bar{1}$	$P\bar{1}$
Unit cell dimensions [Å]	a =9.773(2)	a = 9.6715(19)	a = 9.780(2)
	b = 10.413(2)	b = 10.374(2)	b = 10.410(2)
	c = 20.699(4)	c = 20.688(4)	c = 20.658(4)
	α = 86.39(3)°	α = 86.17(3) °	α = 86.70(3)°
	β = 85.01(3)°	β = 84.64(3) °	β = 85.19(3)°
	γ = 78.89(3)°	γ = 78.50(3) °	γ = 79.86(3)°
Volume [Å^3]	2056.9(7)	2022.7(7)	2060.9(7)
Z	2	2	2
Density (calcd.) [Mg/m^3]	1.423	1.465	1.513
Absorption coefficient [mm^{-1}]	1.852	2.164	2.058
F(000)	894	904	940
Crystal size [mm^3]	0.30 × 0.30 × 0.20	0.40 × 0.40 × 0.30	0.40 × 0.30 × 0.20
θ range for data collection	1.98 to 26.34°	2.01 to 23.25°	1.98 to 26.37°
Reflections collected	55863	27007	59137
Independent reflections	8319 [R_{int} =0.0495]	5766 [R_{int} =0.0531]	8429[R_{int} =0.0417]
Data/restraints/parameters	8319/69/429	5766/69/431	8429/69/431
Goodness-of-fit on F^2	1.161	1.144	1.152
Final R indices [$I > 2\sigma(I)$]	$R1$ = 0.0461	$R1$ = 0.0363	$R1$ = 0.0308
	$wR2$ = 0.1180	$wR2$ = 0.0911	$wR2$ = 0.0728
R indices (all data)	$R1$ = 0.0524	$R1$ = 0.0403	$R1$ = 0.0339
	$wR2$ = 0.1217	$wR2$ = 0.0941	$wR2$ = 0.0741
Largest diff. peak and hole [e·Å^{-3}]	1.718 and −1.615	1.175 and −1.013	1.408 and −1.031

Table 2. Comparison of bond length [Å] and angles [°] of **3**, **4**, **5**

	3 (M = Mn)	**4** (M = Zn)	**5** (M = Cd)
M−N(1)	2.067(4)	1.984 (3)	2.188(2)
M−N(2)	2.090(4)	1.991(4)	2.196(2)
M−I(2)	2.7230(9)	2.6142(8)	2.7518(7)
M−I(1)	2.7354(9)	2.6648(8)	2.7920(7)
I(1)Li(1)	2.817(8)	2.784(8)	2.816(6)
I(2)−Li(1)	2.920(9)	2.919(8)	2.975(6)
N(1)−C(1)	1.347(5)	1.318(6)	1.322(4)
N(1)−C(11)	1.447(5)	1.453(6)	1.440(4)
N(2)−C(3)	1.336(5)	1.332(6)	1.332(4)
N(2)−C(21)	1.445(5)	1.436(6)	1.439(3)
C(1)−C(2)	1.411(6)	1.399(6)	1.407(4)
C(1)−C(10)	1.511(6)	1.515(6)	1.519(4)
C(2)−C(3)	1.407(6)	1.398(6)	1.410(4)
C(3)−C(30)	1.523(6)	1.520(6)	1.512(4)
Li(1)−O(1)	1.912(10)	1.930(9)	1.899(6)
Li(1)−O(2)	1.982(10)	1.956(9)	1.962(6)
N(1)−M−N(2)	94.38(14)	98.78(15)	91.46(9)
N(1)−M−I(2)	119.67(10)	118.13(11)	121.77(7)
N(2)−M−I(2)	117.28(10)	116.92(11)	116.92(7)
N(1)−M−I(1)	113.04(10)	111.76(11)	113.31(7)
N(2)−M−I(1)	112.05(11)	110.38(11)	112.92(7)
I(2)−M−I(1)	101.07(4)	101.22(3)	101.13(3)
M−I(1)−Li(1)	82.13(18)	83.38(17)	82.10(12)
M−I(2)−Li(1)	80.45(16)	81.67(16)	79.95(12)
C(1)−N(1)−M	120.3(3)	118.8(3)	120.13(19)
C(3)−N(2)−M	120.3(3)	117.9(3)	120.23(19)
N(1)−C(1)−C(2)	124.5(4)	124.6(4)	125.7(3)
C(3)−C(2)−C(1)	131.1(4)	130.4(4)	132.7(3)
N(2)−C(3)−C(2)	124.4(4)	124.9(4)	124.9(3)
O(1)−Li(1)−O(2)	114.9(5)	114.2(4)	116.2(3)
O(1)−Li(1)−I(1)	118.4(4)	118.3(4)	117.6(2)
O(2)−Li(1)−I(1)	102.9(4)	105.5(3)	102.7(2)
O(1)−Li(1)−I(2)	93.1(3)	93.2(3)	92.1(2)
O(2)−Li(1)−I(2)	133.1(4)	133.8(4)	132.6(3)
I(1)−Li(1)−I(2)	94.5(3)	91.3(2)	95.33(15)

N(1)−C(1)C(10)−C(3)C(30)−N(2) and C(2) is about 0.19 Å (**3**: 0.18 Å, **4**: 0.19 Å, **5**: 0.19 Å) out of this plane.

Nevertheless, the π-electrons of the vinamidine are delocalized since the C(1)−C(2) and the C(2)−C(3) as well as the C(1)−N(1) and the C(3)−N(2) bond lengths are equal within the experimental error and correspond to C−C and C−N distances in aromatic systems. Both N−M bond lengths are equal.

Although the bond lengths of the metal center to I(1) and I(2) are equal within the experimental error (**3**: 2.73/2.72 Å, **4**: 2.66/2.61Å, **5**: 2.79/2.75 Å), the bond lengths of Li to I(1) and I(2) are significantly different (**3**: 2.81/2.92 Å, **4**: 2.78/2.92Å, **5**: 2.82/2.98 Å). We suggest packing effects to be responsible for these differences. The M−I−Li−I ring is not planar (dihedral angle, **3**: 15.5°, **4**: 17.7°, **5**: 14.1°).

The coordination sphere of the Li cation is completed by two diethyl ether molecules.

Conclusion

Unfortunately, the synthesis of low coordinate monomeric metal iodides has so far not been successful as $LiI(Et_2O)_2$ is always found coordinated to the metal centers. Moreover, the reduction of iodides with sodium or potassium was also not successful. Consequently further research is directed toward the synthesis of metal complexes free of $LiI(Et_2O)_2$ using hydrocarbons as solvent.

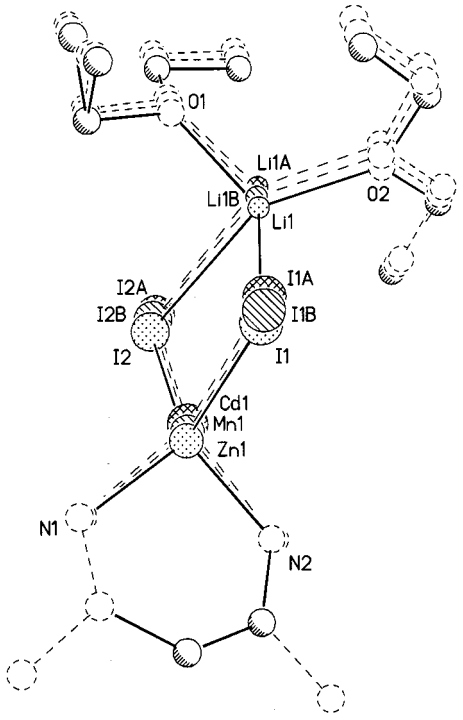

Figure 2. Comparison of the molecular structures of **3**, **4**, and **5**. (organic substituents have been omitted for clarity)

Experimental Section

General: All reactions were performed using standard Schlenk and dry box techniques. Solvents were appropriately dried and distilled under dinitrogen prior to use. All NMR spectra were obtained in 5 mm tubes using dry degassed [D_6]benzene as a solvent, referenced to external $SiMe_4$. Elemental analyses were performed by the Analytisch-Chemisches Laboratorium des Instituts für Anorganische Chemie, Göttingen.

Compound **1** was prepared according to the literature method.[3]

Preparation of 2: MeLi (22.9 mL, 36.6 mmol, 1.6 M in Et_2O) was added dropwise with a syringe over 10 min. to a stirred solution of **1** (15.3 g, 36.6 mmol) in Et_2O (200 mL) at −78 °C. The mixture was stirred at −78 °C for an additional 10 min. and allowed to warm to room temperature, stirred overnight, and reduced in volume to approximately 30 mL. Pale yellow solid **2** was isolated by filtration, washed with pentane (3 × 10 mL), and dried in vacuo. (16.2 g, 89% yield). M.p.: 142−144 °C. − ^{1}H NMR (400 MHz, C_6D_6): δ = 1.03 (t, *J* = 6.8 Hz, 12 H, OCH_2CH_3), 1.19 [d, *J* = 6.8 Hz, 12 H, $CH(CH_3)_2$], 1.22 [d, *J* = 6.8 Hz, 12 H, $CH(CH_3)_2$], 1.93 (s, 6 H, CH_3), 3.33 (q, *J* = 6.8 Hz, 8 H, OCH_2CH_3), 3.40 [sept., *J* = 6.8 Hz, 4 H, $CH(CH_3)_2$], 5.00 (s, 1 H, C*H*), 7.17 (m, 6 H, Ar*H*). − ^{7}Li NMR [155 MHz, C_6D_6, ($LiCl/D_2O$)]: δ = 1.61 (s). − $C_{33}H_{51}LiN_2O$ (498.45): C 79.48, H 10.31, N 5.62; found C 80.26, H 10.21, N 5.63.

Preparation of 3: Compound **2** (2.50 g, 5.01 mmol) in Et_2O (20 mL) was added to a suspension of MnI_2 (1.54 g, 5.01 mmol) in Et_2O (20 mL) at −78 °C. The reaction mixture was stirred at −78 °C for an additional 10 min. and allowed to warm to room temperature. After stirring the pink solution overnight the color changed to yellow. The yellow solution was filtered and the solvent removed under reduced pressure to a volume of 10 mL. Yellow crystals were obtained after 1 day at −24 °C. (3.75 g, 85% yield).[8] − MS (EI): *m/z* (%) = 202 (47) [DippNCCH$_3$], 599 (100) [NacNacMnI]. − IR (Nujol): $\tilde{\nu}$ = 1655 (m), 1625 (m), 1262 (m), 1079 (s), 793 (s), 290 (m) cm^{-1}. − $C_{37}H_{61}I_2LiMnN_2O_2$ (881.58): C 50.41, H 6.97, N 3.18; found C 50.43, H 6.89, N 3.23.[7]

Preparation of 4: Compound **2** (1.26 g, 2.54 mmol) in Et_2O (20 mL) was added to a suspension of ZnI_2 (811 mg, 2.54 mmol) in Et_2O (20 mL) at −78 °C. The reaction mixture was allowed to warm to room temperature and stirred for an additional 24 h. The solution was filtered and the solvent removed under reduced pressure to a volume of 5 mL. Colorless crystals were obtained after 4 days at 2 °C. (1.79 g, 79% yield).[8] − ^{1}H NMR (500 MHz, C_6D_6): δ = 1.05 (t, *J* = 6.8 Hz, 12 H, C*H*$_3$CH$_2$O), 1.14 [d, *J* = 6.8 Hz, 12 H, CH(C*H*$_3$)$_2$], 1.36 [d, *J* = 6.8 Hz, 12 H, CH(C*H*$_3$)$_2$], 1.68 (s, 6 H, C*H*$_3$), 3.20 (t, *J* = 6.8 Hz, 12 H, CH$_3$C*H*$_2$O), 3.51 [sept., *J* = 6.8 Hz, 4 H, C*H*(CH$_3$)$_2$], 4.86 (s, 1 H, C*H*), 7.13 (m, 6 H, Ar*H*). − ^{13}C NMR (125 MHz, C_6D_6): δ = 23.3 (s), 24.3 (s), 24.5 (s), 27.8 (s), 28.9 (s), 97.0 (s), 123.6 (s), 123.7 (s), 124.7 (s), 125.3 (s), 125.9 (s), 126.9 (s), 143.9 (s), 171.2 (s). − MS (EI): *m/z* (%) = 202 (100) [DippNCCH$_3$], 608 (47) [NacNacZnI]. − IR (Nujol): $\tilde{\nu}$ = 1701 (m), 1615 (s), 1465 (m), 1412 (m), 1255 (s), 1054 (s), 763 (m), 243 (m) cm^{-1}. − $C_{37}H_{61}I_2LiN_2O_2Zn$ (892.03): C 49.82, H 6.89, N 3.14; found C 49.60, H 6.61, N 3.59.

Preparation of 5: Compound **2** (1.00 g, 2.01 mmol) in Et_2O (20 mL) was added to a suspension of CdI_2 (733 mg, 2.01 mmol) in Et_2O (20 mL) at −78 °C. The reaction mixture was allowed to warm to room temperature and stirred for an additional 36 h. After filtration from the residue the solvent was removed under reduced pressure to a volume of 10 mL. Colorless crystals were obtained after 6 days at 2 °C. (1.45 g, 77% yield).[8] − ^{1}H NMR (500 MHz, C_6D_6): δ = 1.02 (t, *J* = 6.8 Hz, 12 H, C*H*$_3$CH$_2$O), 1.12 [d, *J* = 6.8 Hz, 12 H, CH(C*H*$_3$)$_2$], 1.33 [d, *J* = 6.8 Hz, 12 H, CH(C*H*$_3$)$_2$], 1.63 (s, 6 H, C*H*$_3$), 3.21 (t, *J* = 6.8 Hz, 12 H, CH$_3$C*H*$_2$O), 3.44 [sept., *J* = 6.8 Hz, 4 H, C*H*(CH$_3$)$_2$], 4.81 (s, 1 H, C*H*), 7.11 (m, 6 H, Ar*H*). − ^{13}C NMR (125 MHz, C_6D_6): δ = 23.4 (s), 24.1 (s), 24.4 (s), 27.9 (s), 28.6 (s), 28.9 (s), 96.8 (s), 123.5 (s), 123.7 (s), 124.8 (s), 125.2 (s), 125.8 (s), 127.1 (s), 145.4 (s), 170.0 (s). − MS (EI): *m/z* (%) = 202 (100) [DippNCCH$_3$], 417 (52) [NacNac], 658 (58) [NacNacCdI]. − IR (Nujol): $\tilde{\nu}$ = 1732 (m), 1440 (m), 1406 (s), 1268 (s), 1021 (m), 759 (s), 435 (m) cm^{-1}. − $C_{37}H_{61}CdI_2LiN_2O_2$ (939.05): C 47.32, H 6.55, N 2.98; found C 46.89, H 6.32, N 2.77.

X-ray Crystallography: Crystals of **3** (mol. wt. 881.58), **4** (892.03), and **5** (939.05) were grown from a concentrated Et_2O solution cooled to −24 °C (**3**) or 2 °C (**4**, **5**). They crystallized in the triclinic crystal system with space group $P\bar{1}$. Relevant details and data statistics are summarized in Table 1. The crystals were mounted on a glass fiber in a rapidly cooled perfluoropolyether.[9] Diffraction data were collected on a Stoe−Siemens−Huber four-circle diffractometer coupled to a Siemens CCD area detector at 133(2) K, with graphite-monochromated Mo-K_α radiation (λ = 0.71073 Å). The structures were solved by direct methods using SHELXS-97[10] and refined against F^2 on all data by full-matrix least-squares with SHELXL-97.[11] All non-hydrogen atoms were refined anisotropically. The hydrogen atoms were included in the model at geometrically calculated positions and refined using a riding model. The hydrogen atoms on C(10) in the structures of **4** and **5**, however, were refined as an idealized disordered methyl group with two half-occupied positions related to one another by a rotation of 60°. These hydrogen atoms were allowed to ride on the carbon atom and rotate about the C(10)−C(1) bond. In all three structures the disordered methyl group of one of the diethyl ether molecules was modeled with the help of similarity restraints for 1−2 and 1−3 distances and displacement parameters. In all three structures there are residual electron density maxima near the iodine atoms and Li(1), presumably due to disorder which could not be modeled. This unmodeled disorder could play a role in the apparently distorted geometry at Li(1).

Crystallographic data (excluding structure factors) for the structures included in this paper have been deposited with the Cambridge Crystallographic Data Centre as supplementary publication nos. CCDC 154416 (**3**), CCDC 154417 (**4**), CCDC 154418 (**5**). Copies of the data can be obtained free of charge on application to CCDC, 12 Union Road, Cambridge CB2 1EZ, UK [Fax: (internat.) + 44-1223/336-033; Email: deposit@ccdc.cam.ac.uk].

Acknowledgments

The financial support of the Deutsche Forschungsgemeinschaft and Göttinger Akademie der Wissenschaften is gratefully acknowledged.

[1] [1a] J. E. Parks, R. H. Holm, *Inorg. Chem.* **1968**, *7*, 1408−1416. − [1b] S. G. McGeachin, *Can. J. Chem.* **1968**, *46*, 903−912.
[2] J. Feldman, S. J. McLain, A. Parthasarathy, W. J. Marshall, J. Calabrese, S. D. Arthur, *Organometallics* **1997**, *16*, 1514−1516.
[3] [3a] W. K. Kim, M. J. Fevola, L. M. Liable-Sands, A. L. Rheingold, K. H. Theopold, *Organometallics* **1998**, *17*, 4541−4543. − [3b] V. C. Gibson, P. J. Maddox, C. Newton, C. Redshaw, G. A. Solan, A. J. P. White, D. J. Williams, *Chem. Commun.* **1998**, 1651−1652.
[4] [4a] N. Kuhn, M. Speis, *Inorg. Chim. Acta* **1988**, *145*, 1. − [4b] B. X. Qian, D. L. Ward, M. R. Smith, III, *Organometallics* **1998**, *17*, 3070−3076. − [4c] N. Kuhn, J. Fahl, S. Fuchs, M. Steinmann, *Z. Anorg. Allg. Chem.* **1999**, *625*, 2108−2114.
[5] C. Cui, H. W. Roesky, H.-G. Schmidt, M. Noltemeyer, H. Hao, F. Cimpoesu, *Angew. Chem.* **2000**, *112*, 4444−4446; *Angew. Chem. Int. Ed.* **2000**, *39*, 4274−4276.
[6] V. C. Gibson, J. A. Segal, A. J. P. White, D. J. Williams, *J. Am. Chem. Soc.* **2000**, *122*, 7120−7121.
[7] NMR spectroscopic data for **4** were not available due to the paramagnetism of Mn^{II}.
[8] According to the elemental analysis of a sample that was treated at 180 °C an appreciable decomposition was already observed at this temperature.
[9] T. Kottke, D. Stalke, *J. Appl. Crystallogr.* **1993**, *26*, 615−619.
[10] G. M. Sheldrick, SHELXS-90/96, Program for Structure Solution, *Acta Crystallogr., Sect. A* **1990**, *46*, 467−473.
[11] G. M. Sheldrick, SHELXL-93/96, *Program for Structure Refinement*, Universität Göttingen, **1993**.

Received December 14, 2000
[I00472]

Bis(cyclopentadienyl) Diimido Complexes of Molybdenum and Tungsten $[Cp_2M(NR)_2]$ at the Limit of Pi-Bond Saturation

Udo Radius,[a] Jörg Sundermeyer,*[b] Karl Peters,[c] and Hans-Georg von Schnering[c]

Dedicated to Professor Max Schmidt on the occasion of his 75th birthday

Keywords: Imides / Molybdenum / Tungsten / Cyclopentadienyl ligands / Rearrangements

The new imido compounds $[(\eta^5\text{-}C_5H_5)M(NR)_2(\eta^1\text{-}C_5H_5)]$ (R = *t*Bu: M = Mo **2a**, W **2b**; R = Mes: M = W **2c**) have been prepared and the crystal structure of **2c** has been determined. Three fluxional processes can be detected by variable temperature proton NMR spectroscopic studies of these cyclopentadienyl complexes, namely: (i) rotation of the $\sigma\text{-}C_5H_5$ ligand about the M–C_{ipso}-bonding axis, (ii) migration of the metal complex fragment between the carbon atoms of the σ-bonded C_5H_5 ligand (metallotropic migration, sigmatropic rearrangement), and (iii) the interconversion of hapticity of σ- and π-bonded C_5H_5 ligands.

Introduction

Molybdenum(VI) and tungsten(VI) bis(organyl) imido complexes of the type $[M(NR)_2R^1R^2]$ (M = Mo, W) have been known for twenty years.[1,2] In the early eighties, the imido-bridged compounds $[M(N\textit{t}Bu)(\mu\text{-}N\textit{t}Bu)(CH_3)_2]_2$ were synthesized and characterized by Nugent and coworkers as the first examples of unsymmetrically bridged dinuclear imido compounds. Mononuclear complexes can be obtained by increasing the steric demand of the organyl ligand of the imido compound. Wilkinson et al.,[3] for example, reported the syntheses of symmetrically substituted bis(aryl) derivatives (R = *t*Bu, $R^1 = R^2$ = mesityl, *o*-tolyl), whereas bis(neopentyl) compounds, like those prepared by the groups of Schrock and Osborn,[4] are attractive starting materials for the synthesis of high valent alkylidene complexes.

Important intermediates for unsymmetrically substituted bis(organyls) ($R^1 \neq R^2$) are monoorganyl complexes of the type $[M(NR)_2R^1Cl]$. During our studies on reactive, N-basic [Mo=NR] and [W=NR] functionalities, we intended to reduce the Lewis acidity of the metal centers of imido complexes $[M(NR)_2Cl_2]$ by introducing excellent σ,π donor ligands. This can be achieved by a formal exchange of a [M−Cl] functionality by $[M(\eta^5\text{-}C_5R'_5)]$ (R′ = H, CH_3).[5] Complexes of the type $[(\eta^5\text{-}C_5H_5)M(N\textit{t}Bu)_2Cl]$ or mixed substituted organyl complexes of the type $[(\eta^5\text{-}C_5H_5)M(N\textit{t}Bu)_2R^2]$ (R^2 = alkyl, aryl)[5] are no longer typical d-metal Lewis acids.[6] Here we wish to report the syntheses, molecular structure and dynamic behavior of the highly π-bond saturated bis(cyclopentadienyl) complexes $[(\eta^5\text{-}C_5H_5)M(NR)_2(\eta^1\text{-}C_5H_5)]$.

[a] Institut für Anorganische Chemie,
Engesserstr., Geb. 30.45, 76128 Karlsruhe, Germany
E-mail: uradius@achibm6.chemie.uni-karlsruhe.de
[b] Fachbereich Chemie der Universität Marburg,
Hans-Meerweinstraße, 35032 Marburg, Germany
E-mail: jsu@chemie.uni-marburg.de
[c] Max-Planck-Institut für Festkörperforschung,
Heisenbergstr. 1, 70506 Stuttgart, Germany

Results and Discussion

Complex Synthesis

The cyclopentadienyl imido complexes $[(\eta^5\text{-}C_5H_5)M(N\textit{t}Bu)_2Cl]$ (M = Mo **1a**; M = W **1b**) were reacted with typical Lewis bases in order to probe the Lewis acidity of these compounds. Reaction of trimethylphosphane with $[(\eta^5\text{-}C_5H_5)W(N\textit{t}Bu)_2Cl]$ (**1b**) led to an ocher colored solid and a brownish oil. One of the products, $[W(N\textit{t}Bu)_2Cl_2(PMe_3)]$ (**3**),[7] was identified by ^{31}P NMR spectroscopy, but no phosphorus resonance was obtained for the second product. The proton NMR spectrum of the oily residue shows one sharp singlet in the *t*Bu imido region at approximately $\delta = 1.2$, and a very broad resonance in the cyclopentadienyl region. The integration of both signals shows a ratio of 9:5. These experimental results are in accordance with a ligand *dismutation* of $[(\eta^5\text{-}C_5H_5)W(N\textit{t}Bu)_2Cl]$ (**1b**) to give $[(C_5H_5)_2W(N\textit{t}Bu)_2]$ (**2b**) and $[W(N\textit{t}Bu)_2Cl_2]$ by a phosphane-induced exchange of a chloride and a cyclopentadienide ligand. The latter Lewis acid is trapped by the phosphane to yield $[W(N\textit{t}Bu)_2Cl_2(PMe_3)]$ (**3**).

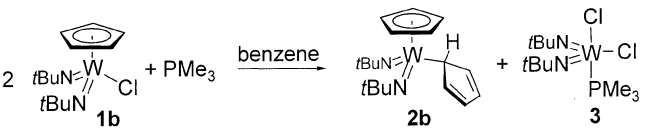

Green and co-workers observed a similar unexpected substitution reaction of a cyclopentadienyl ligand, with stabilization of the resulting Mo^{IV} species, whilst studying the reduction reactions of $[(\eta^5\text{-}C_5H_4Me)Mo(N\textit{t}Bu)Cl_2]$ in the presence of phosphanes.[8]

 © WILEY-VCH Verlag GmbH, 69451 Weinheim, 2001 1434−1948/01/0606−1617 $ 17.50+.50/0

To confirm the results of this rather unusual displacement of an anionic C_5H_5 ligand by a phosphane, we prepared **2b** independently. All experiments to obtain **2b** or its molybdenum analogue $[(C_5H_5)_2Mo(NtBu)_2]$ **2a**, by reaction of the chloro complexes $[(\eta^5\text{-}C_5H_5)M(NtBu)_2Cl]$ **1a,b** with $(C_5H_5)Li$ were unsuccessful. However, refluxing **1a,b** with $(C_5H_5)Na$ in dimethoxyethane for several hours led to the formation of the bis(cyclopentadienyl) compounds $[(C_5H_5)_2M(NtBu)_2]$ **2a,b** isolated as yellow-brown oils. These highly covalent organo imides **2a,b** can be purified by high-vacuum distillation or condensation.

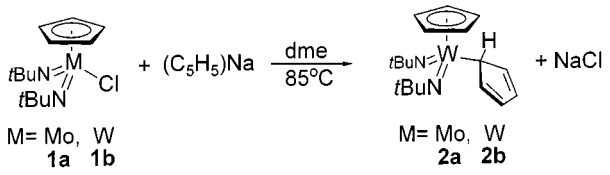

As we were not able to obtain crystalline material of the *tert*-butyl imido complexes **2a,b** by low temperature crystallization techniques, we synthesized the corresponding mesityl imido tungsten complex $[(C_5H_5)_2W(NMes)_2]$ (**2c**) This complex can also be obtained from the reaction of $[(C_5H_5)W(NMes)_2Cl]$ (**1c**) with sodium cyclopentadienide in dimethoxyethane. Single crystals of **2c** were grown by the slow cooling of saturated hexane solutions of **2c** to −60 °C.

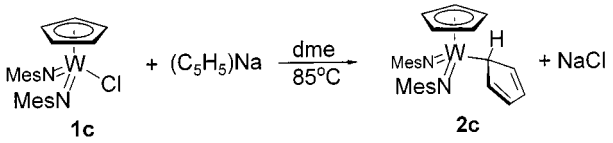

Molecular Structure of 2c

$[(C_5H_5)_2W(NMes)_2]$ (**2c**) crystallizes in the triclinic space group $P\bar{1}$. The molecular structure is shown in Figure 1. Selected bond lengths and angles are given in the caption. Further details of the crystallographic characterization are given in Table 1.

$[(C_5H_5)_2W(NMes)_2]$ (**2c**) is a monomer in the solid state. The tungsten atom is pseudotetrahedrally coordinated by the two imido nitrogen atoms, by the coordinating carbon atom of a σ-bonded cyclopentadienyl ligand, and by the centroid of a π-coordinated cyclopentadienyl unit. The bonding angles N(1)−W−N(2) 107.7(2)°, N(1)−W−C(6) 97.3(2)°, and N(2)−W−C(6) 99.7(2)° reflect some distortion of the coordination polyhedron. The W−N bond lengths of 176.6(4) pm and 175.9(4) pm are consistent, to some degree, with tungsten imido-nitrogen triple bonding, corresponding to a bond order of 2.5[9a] and comparable with that of the π-bond saturated complex $[W(NPh)(NMe_2)_4]$ [W−N(imido) = 175.8(5)].[9b] The W−C(6) distance of 220.0(6) pm is in the range of tungsten(VI)−carbon σ-bonds. The tungsten−carbon bond lengths of the π-coordinated cyclopentadienyl ring show some interesting irregularities: W−C(1) [233.4(6) pm] falls into the range of expected tungsten ring carbon bond

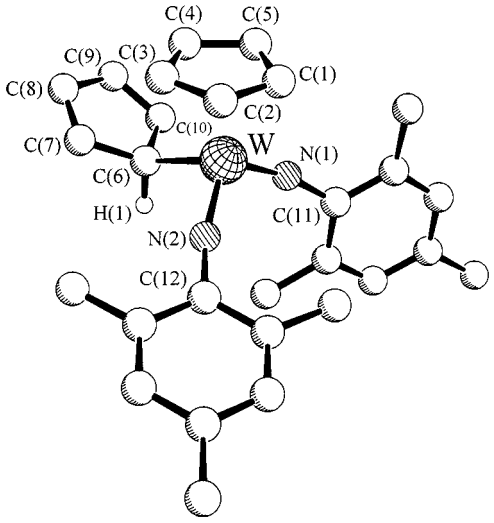

Figure 1. Molecular structure of **2c** in the solid state; SCHAKAL[27] plot; hydrogen atoms are omitted for clarity; selected bond lengths (pm) and angles (°): W−N(1) 176.6(4), W−N(2) 175.9(4), W−C(1) 233.4(6), W−C(2) 244.0(6), W−C(3) 250.2(6), W−C(4) 247.4(6), W−C(5) 241.6(6), W−C(6) 220.0(6), N(1)−C(11) 138.7(7), N(2)−C(12) 139.2(6), C(1)−C(5) 139.9(8), C(1)−C(2) 140.4(10), C(2)−C(3) 139.6(9), C(3)−C(4) 139.9(9), C(4)−C(5) 137.2(11), C(6)−C(7) 149.1(9), C(7)−C(8) 133.5(10), C(8)−C(9) 142.6(11), C(9)−C(10) 136.5(12), C(6)−C(10) 146.5(8); N(1)−W−N(2) 107.7(2), N(1)−W−C(6) 97.3(2), W−N(1)−C(11) 164.4(3), W−N(2)−C(12) 166.8(4), N(2)−W−C(6) 99.7(2)

lengths,[9c] whereas the distances W−C(5) [241.6(6) pm], W−C(2) [244.0(0) pm], W−C(3) [250.2(6) pm], and W−C(4) [247.4(6) pm], are significantly elongated. Comparable elongations of the W−C(ring) bonds trans to strong π-donor ligands have been observed by Bercaw et al. for $[(\eta^5\text{-}C_5Me_5)W(O)_2(O\text{-}C_5Me_5)]$ and $[(\eta^5\text{-}C_5Me_5)W(O)_2(\eta^1\text{-}C_5Me_5)]$, and were attributed to the *trans* influence of the oxo ligands.[10] We have observed similar effects in the structurally characterized half-sandwich imido complex $[(\eta^5\text{-}C_5Me_5)Mo(NtBu)Cl_3]$,[5c] but they are also characteristic for the nitrosyl compounds of the type $[(\eta^5\text{-}C_5H_5)_2Mo(NO)R]$ (R = alkyl)[11] and for the metallocene imido derivatives $[(\eta^5\text{-}C_5H_5)_2V(NoTol)]$[12] and $[(\eta^5\text{-}C_5H_4Me)_2Mo(NtBu)]$.[13] Calculations on the latter 19 and 20 valence electron (VE) complexes show that the HOMO of these compounds is a ligand-centered orbital with significant contributions to the nitrogen atoms of the imido group and to the π-system of the cyclopentadienyl units. In a MO bond description, one of the p orbitals located on the imido nitrogen atoms competes with the two group orbitals of π-symmetry (e_1) of the η^5-coordinated ring for stabilization with one empty d orbital located on the metal center. As a result, a high degree of metal−nitrogen bonding (e.g. M−N triple bond contributions) leads to a decrease in metal−cyclopentadienyl π-bonding, and thus to a ring slippage of the $\eta^5\text{-}C_5R_5$ ring.

Variable Temperature ^{1}H NMR Spectra

The proton NMR spectra of the compounds $[(C_5H_5)_2M(NR)_2]$ **2a−c** are temperature dependant. Three

Table 1. Crystal Structure Analysis of **2c**

Compound	$[Cp_2W(NMes)_2]$
Empirical formula	$C_{28}H_{32}N_2W$
Molecular mass	580.43
a [pm]	1005.7(1)
b [pm]	1606.5(3)
c [pm]	806.7(1)
α [deg]	98.55(1)
ß [deg]	94.43(1)
γ [deg]	105.54(1)
V [pm^3]	$1232.3(3) \times 10^6$
Z	2
d(calcd) [g·cm^{-3}]	1.564
Crystal system	Triclinic
Space group	$P\bar{1}$
Diffractometer	Siemens R3m/V
Radiation	Mo-K_α
Monochromator	graphite
Crystal size [mm]	$0.2 \times 0.45 \times 0.75$
Data collection mode	ω-scan
Theta range [deg]	1.75−27.5
Recip. latt. segment	$h = 0 \rightarrow 13$ $k = -20 \rightarrow 19$ $l = -10 \rightarrow 10$
No. refl. Measd.	5663
No. unique refl.	5663
No. refl. $F > 3\sigma(F)$	4977
Lin. abs. coeff. [mm^{-1}]	4.70
Abs. Correction	ψ-scan
Solution by	Direct phase determination
Method of refinement	Full-matrix LSQ; hydrogen positions of riding model with fixed isotropic *U*
Data-to-parameter ratio	17.71
R, R_w	0.031, 0.030
Weighting scheme	$w = 1/\sigma^2(F)$
Largest difference peak	1.80 eÅ^{-3}
Largest difference hole	1.15 eÅ^{-3}
Program used	Siemens SHELXTL PLUS: G. M. Sheldrick, Program package SHELXTL-PLUS, Release 4.1, Siemens Analytical X-ray Instruments Inc., Madison, WI 53719, USA, **1990**

dynamic processes, which have been observed previously in solutions of other η^1/η^5 bis(cyclopentadienyl) complexes, are responsible for this dynamic behavior (see Scheme 1), namely: (i) hapticity change of σ- and π-coordinated cyclopentadienyl rings, (ii) metallotropic migration of the fragment $[(\eta^5\text{-}C_5H_5)M(NR)_2]$ between the carbon atoms of the monohapto-coordinated cyclopentadienyl ring, and (iii) rotation of the σ-cyclopentadienyl ligand around the $M-C_{ipso}$ bonding axis.

The cyclopentadienyl region between δ = 4.0 and 8.5 in the proton NMR spectra of $[(C_5H_5)_2Mo(NtBu)_2]$ (**2a**), recorded at different temperatures, is shown in Figure 2. At 363 K, the ^{1}H NMR spectrum of **2a** shows one averaged signal at δ = 5.78 assigned to the cyclopentadienyl protons and a resonance at δ = 1.13 assigned to the protons of the imido group (not shown in Figure 2), with a ratio of integration of 5:9. On cooling the signal of the *tert*-butyl imido group remains constant within experimental error, while the cyclopentadienyl resonance broadens and splits into two signals below the coalescence temperature of 308 K. At 283 K, two broad signals of similar width are detectable [$\Delta G^{\neq}$(308 K) = 61.0 kJ/mol]. The signal at δ = 6.26 is assigned to the protons of the η^1-coordinated cyclopentadienyl ring due to its chemical shift[15] and the characteristic splitting at lower temperatures. The resonance at higher field (δ = 5.33) can be assigned to the protons of the η^5-coordinated cyclopentadienyl ligand. A further decrease in the temperature from 308 K (the point of coalescence for the σ/π exchange) to 196 K (the point of coalescence for the metallotropic rearrangement) leads to a broadening of the resonance at δ = 6.26 and to a

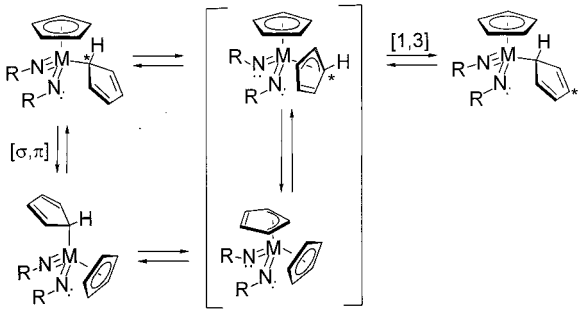

Scheme 1. Hapticity change and mechanistic proposal of a metallotropic rearrangement via allyl intermediates in complexes of the type $[(\eta^5\text{-}C_5H_5)M(NR)_2(\eta^1\text{-}C_5H_5)]$ (M = Mo, W)

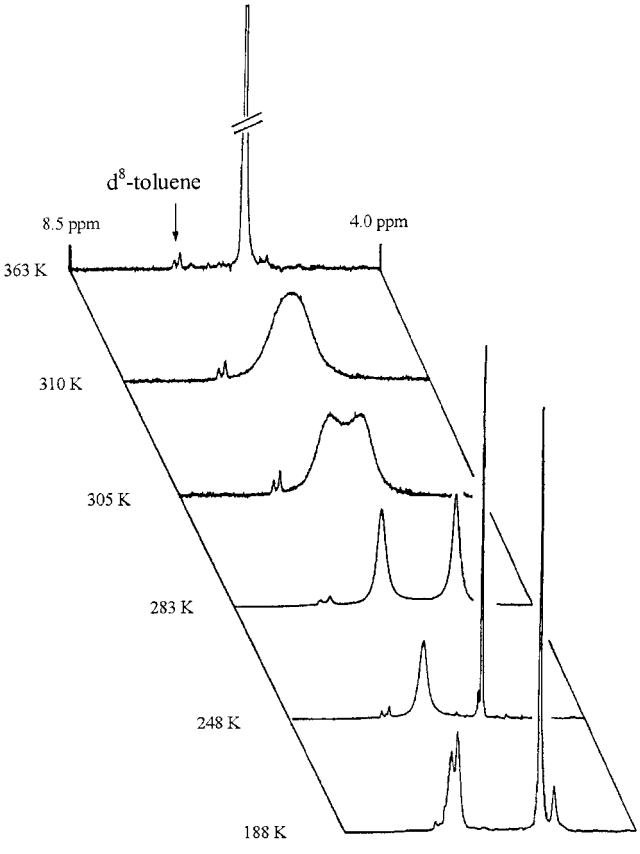

Figure 2. Variable temperature proton NMR spectra of $[(\eta^5\text{-}C_5H_5)Mo(NtBu)_2(\eta^1\text{-}C_5H_5)]$ (**2a**) in [D$_8$]toluene showing the C_5H_5 region from δ = 4.00 to 8.50

sharpening of the η^5-cyclopentadienyl resonance. Below this second coalescence temperature of 196 K, the signal of the η^1-C_5H_5 group splits into two resonances for the olefinic protons at δ = 6.82 and 6.71 (at 188 K), and one signal at δ = 5.05 for the proton of the CH group bound to the metal atom, as expected for a not-yet-resolved AA′BB′X spin-spin system.

Similar spectra can be recorded for the tungsten compound $[(C_5H_5)_2W(N\mathit{t}Bu)_2]$ (**2b**). The coalescence temperature for σ,π exchange is slightly higher for the tungsten complex **2b** [$\Delta G^{\neq}$(310 K) = 64.4 kJ/mol] than for the molybdenum analogue **2a**.

The temperature-dependent ^{1}H NMR spectra of the tungsten compound $[(C_5H_5)_2W(NMes)_2]$ (**2c**) offer some peculiarities. At a relatively high coalescence temperature of 328 K [compared with the *tert*-butyl derivatives **2a** (308 K) and **2b** (310 K)], the resonance for the cyclopentadienyl protons of **2c** splits into two signals at δ = 6.25 and 5.47. By lowering the temperature, the signal at δ = 6.25 further splits into a set of five resonances. They are assigned to the vinylic protons of **2c** $H_{A/A'}$ (δ = 7.01 and 6.90) and $H_{B/B'}$ (δ = 6.57 and 6.55) and to the proton H_X at the *ipso* carbon (δ = 6.57). At 210 K coalescence of the vinylic pairs of protons is observed. In the low temperature limiting spectrum at 193 K, every proton of the η^1-coordinated cyclopentadienyl ligand is chemically inequivalent indicating that at very low temperatures the rotation about the metal *ipso*-carbon bond as a third dynamic process, besides the hapticity change and the metallotropic migration, is slowly resolved on the NMR time scale. The significantly higher coalescence temperature for the mesityl complex **2c** than for **2a,b** may be explained by the higher mass and by the increased steric demand of the migrating group $[(\eta^5\text{-}C_5H_5)W(NMes)_2]$ compared with $[(\eta^5\text{-}C_5H_5)_2M(N\mathit{t}Bu)_2]$ (M = Mo, W). In a similar manner it has been reported by Werner et al.[16] that the rate of the σ/π exchange in $[(\eta^5\text{-}C_5H_5)Pd(\eta^1\text{-}C_5H_5)(PR_3)]$ is dependant on the cone angle[17] of the phosphane ligand PR_3.

Mechanistic Considerations

Hapticity Change

The exchange reaction between σ- and π-bonded cyclopentadienyl ligands has been well investigated, for example, for $[(\eta^5\text{-}C_5H_5)_3Ti(\eta^1\text{-}C_5H_5)]$,[18] $[(\eta^5\text{-}C_5H_5)_2Mo(\eta^1\text{-}C_5H_5)(NO)]$,[11] $[(\eta^5\text{-}C_5H_5)Mo(\eta^1\text{-}C_5H_5)(S_2CNR_2)_2]$ (R = Me, Bu),[19] $[(\eta^5\text{-}C_5H_5)Pd(\eta^1\text{-}C_5H_5)(P\mathit{i}Pr_3)]$,[16] $[(\eta^5\text{-}C_5H_5)V(N\mathit{t}Bu)(\eta^1\text{-}C_5H_5)(O\mathit{t}Bu)]$,[20] and $[(\eta^5\text{-}C_5H_5)_2Nb(N\mathit{t}Bu)(\eta^1\text{-}C_5H_5)]$.[21] Scheme 1 shows a mechanistic proposal for the hapticity change in the imido compounds $[(C_5H_5)_2M(NR)_2]$ (M = Mo, W).

As observed in other molecular compounds with η^1- and η^5-coordinating cyclopentadienyl ligands, for example in $[(\eta^5\text{-}C_5H_5)_2Mo(\eta^1\text{-}C_5H_5)(NO)]$,[11] a stepwise or concerted hapticity change is promoted by additional, electronically flexible ligands. The reduction of the imido ligand bond order (BO) from a six VE donor $[NR]^{2-}$ (BO = 3) to a four VE donor $[NR]^{2-}$ (BO = 2) makes the slippage of an η^1-bonded cyclopentadienyl ligand to η^3-coordination more easy, thus it might initiate the exchange from an η^1- via η^3- to an η^5-coordination. A similar flexibility is characteristic for the NO ligand. A mechanism as proposed in Scheme 1 via intermediates of the type $[(\eta^5\text{-}C_5H_5)(\eta^3\text{-}C_5H_5)M(NR)_2]$ has been observed for $[(C_5H_5)_2W(CO)_2]$, in which one cyclopentadienyl ligand adopts an η^3-, and the other one an η^5-coordination mode.[22]

Metallotropic Migration

Over the last 40 years a large number of η^1-C_5H_5 compounds of main group elements and transition metals have been described.[23] Whilst the migration of the metal substituent between the ring carbon atoms has recently been recognized as an intramolecular process,[24] the exact mechanism of the metallotropic rearrangement has remained an unresolved problem for some time. Conclusions were finally drawn from statistical considerations of the different processes under consideration (1,2 shift vs. 1,3 shift vs. random walk) and the initial broadening of the resonances of the vinyl protons below coalescence temperature. Investigations with prochiral complex fragments finally established the [1,2]-metallotropic migration (see Scheme 2) as the energetically most favorable mechanism.[25] The latter may be regarded as a symmetry-allowed [1,5]-sigmatropic rearrangement.

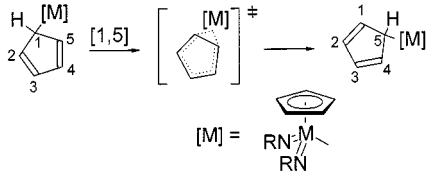

Scheme 2. [1,2]-metallotropic migration as [1,5]-sigmatropic rearrangement

According to Cotton and co-workers,[25] [1,2]-migration can be identified by a preferred broadening of the signals of $H_{A/A'}$ below the coalescence temperature of this process, while a [1,3]-shift can be detected by a preferred broadening of the resonances of $H_{B/B'}$. The proton NMR spectra of **2c** in the relevant temperature range between 220 K and 260 K show a larger broadening for the $H_{A/A'}$ and H_X signals than for $H_{B/B'}$. This is in agreement with a nonrandom mechanism of the metallotropic rearrangement, and the qualitative consideration indicates a [1,2] shift of the molybdenum or tungsten center between the carbon atoms of the σ-(C_5H_5) ligand. It seems that a concerted [1,5]-sigmatropic rearrangement has a lower energy barrier than the formation of an allylic intermediate. However, due to the flexibility in the electron count of the imido ligand it cannot be excluded that, at higher temperatures, both the [1,2]- and the energetically less favorable [1,3]-migration might contribute to the metallotropic migration. We examined the possibility of determining rate constants of the low temperature rearrangements by recording the spectra at higher frequency; how-

ever, the rather complex exchange system turned out to be intractable by the methods available to us.

Conclusions

The new imido complexes $[(\eta^5\text{-}C_5H_5)M(NR)_2(\eta^1\text{-}C_5H_5)]$ (M = Mo, W, R = *t*Bu; M = W, R = Mes) **2a**−**c** have been prepared. Although the metal atoms of the bis(organyl) compounds **2a**−**c** are in their highest formal oxidation state, the Lewis acidity of the d^0 metal centers is well compensated by both types of the excellent σ-,2π- donor ligands $[NR]^{2-}$ and $[C_5H_5]^-$. The compounds **2a**−**c** are π-bond saturated. That means two potential π-bonds of each C_5H_5 ligand (e_1 group orbitals of C_5H_5) and two potential π-bonds of each imido ligand (p orbitals of N atoms) add to a number exceeding the maximum of five π-bonds theoretically possible from orbital symmetry considerations in tetrahedral transition metal complexes.[26] It has been proven that in their competition for π-bonding with the d^0 metal acid, the stronger π-donors $[NR]^{2-}$ are driving the weaker π-donors $[C_5H_5]^-$ out of the π-coordination. Therefore, these complexes may be considered as 18 VE complexes of a d^0 metal center stabilized by four σ-bonds to two C_5H_5 and to two imido ligands, as well as by five π-bonds, two to the $\eta^5\text{-}C_5H_5$ ligand and three π-bonds to both imido ligands, leading to an average bond order of 2.5. This consideration implies that a certain amount of π-electron density remains in ligand-centered nonbonding orbitals. Structural data and the σ,π dynamic behavior of the compounds **2a**−**c** in solution are consistent with this conclusion. The stronger π-donor ability of imido vs. cyclopentadienyl ligands at a d^0 metal center has also been demonstrated by Green et al. for the isolobally related niobium compound $[(\eta^5\text{-}C_5H_5)_2Nb(N\textit{t}Bu)(\eta^1\text{-}C_5H_5)]$.[21] Due to the electronic flexibility of the four vs. six electron imido ligand $[NR]^{2-}$, an allylic species $[(\eta^5\text{-}C_5H_5)(\eta^3\text{-}C_5H_5)M(NR)_2]$ (M = Mo, W) might be considered as an intermediate of the η^5/η^1 exchange process and for the metallotropic [1,3] migration; however, as in the related niobium imido complex, the [1,2]-metallotropic rearrangement is the dominant mechanism in the dynamic behavior at the low temperature limit.

Experimental Section

General: All reactions and subsequent manipulations involving organometallic reagents were performed under argon (4.8) using standard Schlenk techniques. Solvents were dried according to standard procedures, stored over activated 4 Å molecular sieves and degassed prior to use. − Melting and decomposition points were determined in closed capillaries on a Büchi SMP 20 or as DTAs on a duPont 9000 apparatus. − Infrared spectra were recorded as Nujol mulls on KBr windows on a Bruker IFS 25 − NMR spectra were recorded on a Jeol FX90Q, a Bruker AC 200 and a Bruker AMX400 spectrometer. − $[W(NMes)_2Cl_2(dme)]$ (M = Mo, W)[6] and $[(\eta^5\text{-}C_5H_5)M(NR)_2Cl]$[5a] were prepared as described in the literature.

Chloro(cyclopentadienyl)bis(mesitylimido)tungsten(VI) (1c): $[W(NMes)_2Cl_2(dme)]$ (600 mg, 0.96 mmol) was added at −78 °C to a suspension of C_5H_5Li (72.0 mg, 1.00 mmol) in 50 mL diethyl ether. The yellow solution was brought to room temperature within 30 minutes. After 2 h at room temperature, all volatiles were removed and the residue was dried at 50 °C in vacuo and finally extracted into 15 mL toluene. The dark red extract was concentrated to 3 mL. On addition of 15 mL hexane, a red solid precipitated, which was collected and dried in vacuo. − Yield: 333 mg (75%); dec.: 101 °C − IR (nujol): $\tilde{\nu}$ = 3104 w ν(C−H_{ar}), 1600 m ν (C=C), 1348 s, 1320 vs and 1288 vs ν (W=N−C), 1036 w, 1006 w, 988 m, 936 m, 856 m, 812 s ν (C−H_{ar})$_{oop}$, 724 m, 504 w, 460 m, 424 m cm^{-1}. − ^1H NMR (200.1 MHz, $CDCl_3$): δ = 2.32 (s, 18 H, Mes-CH_3), 6.56 (s, 5 H, C_5H_5), 6.84 (s, 4 H, Mes-*H*). − ^{13}C NMR (50.3 MHz, $CDCl_3$): δ = 18.70 (s, *o*-CH_3), 20.69 (s, *p*-CH_3), 109.64 (s, C_5H_5), 127.74 (s, Mes-*C*3), 131.16 (s, Mes-*C*2), 133.46 (s, Mes-*C*4), 152.73 (s, $^2J_{WC}$ = 33.3 Hz, Mes-*C*1). − EI-MS: *m*/*z* (%) = 550 (100) $[M^+]$, 485 (67) $[M^+ - C_5H_5]$. − $C_{23}H_{27}ClN_2W$ (550.8): calcd. C 50.16, H 4.94, N 5.09; found C 49.69, H 5.06, N 5.03.

Bis(*tert*-butylimido)bis(cyclopentadienyl)molybdenum(VI) (2a): Finely powdered **1a** (339 mg, 1.00 mmol) was added to a suspension of $(C_5H_5)Na$ (106 mg, 1.20 mmol) in 20 mL 1,2 dimethoxyethane at −50 °C. The orange colored mixture was brought to room temperature within 30 min. and refluxed for 6 h. All volatiles of the reddish brown suspension were removed in vacuo and the brown, oily residue was extracted with 20 mL hexane. The evaporated hexane extract was distilled at 6×10^{-3} mbar onto a cooled finger (−30 °C). The product separated as an orange-brown solid at the finger, which melted at room temperature to give a brown oil. − Yield: 229 mg (63%). − IR (film): $\tilde{\nu}$ = 3084 m ν(C−H_{ar}), 2968 s, 2920 s, 2892 s, 2860 m, 1696 w, 1660 w, 1588 m ν(C=C), 1440 m, 1356 s, 1248 vs and 1216 vs ν(Mo=N−C), 1116 m, 1080 m, 1020 m, 964 m, 888 w, 840 m, 800 vs and 736 s ν (C−H_{ar})$_{oop}$, 632 w, 584 w, 548 w, 464 w cm^{-1}. −^1H NMR (89.6 MHz, C_7D_8, 188 K): δ = 1.15 (s, 18 H, NCCH_3), 5.05 (br, 1 H, η^1-H_X), 5.30 (s, 5 H, η^5-C_5H_5), 6.71 (br, 2 H, η^1-$H_{B/B'}$), 6.82 (br, 2 H, η^1-$H_{A/A'}$); (89.6 MHz, C_7D_8, 283 K): δ = 1.14 (s, 18 H, NCCH_3), 5.33 (s, 5 H, η^5-C_5H_5), 6.29 (br, 5 H, η^1-C_5H_5); (89.6 MHz, C_7D_8, 363 K): δ = 1.13 (s, 18 H, NCCH_3), 5.78 (s, 10 H, C_5H_5); − ^{13}C NMR (100.6 MHz, C_6D_6): δ = 30.98 (s, NCCH_3), 68.84 (s, N*C*CH_3), 107.95 (br, C_5H_5). − EI-MS: *m*/*z* (%) = 370 (1) $[M^+]$. − $C_{18}H_{28}MoN$ (368.4): calcd. C 58.69, H 7.66, N 7.61; found C 59.01, H 7.98, N 7.74.

Bis(*tert*-butylimido)bis(cyclopentadienyl)tungsten(VI) (2b): Finely powdered **1b** (384 mg, 0.90 mmol) was added to a suspension of $(C_5H_5)Na$ (87.4 mg, 0.99 mmol) in 20 mL 1,2 dimethoxyethane at −50 °C. The temperature of the orange colored mixture was raised to room temperature within 30 min. and refluxed for 6 h. All volatile materials of the brown suspension were removed in vacuo and the brown, oily residue was extracted with 20 mL hexane. The evaporated hexane extract was distilled at 6×10^{-3} mbar onto a cooled finger (−30 °C). The product separated as an orange-brown solid at the finger, which melted at room temperature to give a brown oil. − Yield: 252 mg (61%). − IR (film): $\tilde{\nu}$ = 3084 m ν(C−H_{ar}), 2986 s, 2920 s, 2896 s, 2860 s, 2804 m, 1660 sh, 1612 w ν(C=C), 1448 m, 1356 m, 1288 vs and 1248 vs ν(W=N−C), 1212 s, 1140 w, 1080 m, 1020 m, 960 w, 868 s and 808 vs and 740 vs ν(C−H_{ar})$_{oop}$, 632 w, 576 w, 544 w, 472 w cm^{-1}. − ^1H NMR (89.6 MHz, C_7D_8, 360 K): δ = 1.15 (s, 18 H, NCCH_3), 5.77 (s, 10 H, C_5H_5); (89.6 MHz, C_7D_8, 273 K): δ = 1.16 (s, 18 H, NCCH_3), 5.36 (s, 5 H, η^5-C_5H_5), 6.56 (br, 5 H, η^1-C_5H_5); (89.6 MHz, C_7D_8, 193 K): δ = 1.19 (s, 18 H, NCCH_3), 4.69 (br, 1 H, η^1-H_X), 5.30 (s,

5 H, η^5-C_5H_5), 6.65 (br, 2 H, η^1-$H_{B/B'}$), 6.80 (br, 2 H, η^1-$H_{A/A'}$). – ^{13}C NMR (100.7 MHz, C_7D_8): δ = 31.88 (s, NC*C*H$_3$), 66.69 (s, N*C*CH$_3$), 106.90 (br, *C*$_5$H$_5$). – EI-MS: *m*/*z* (%) = 456 (63) [M$^+$], 441 (59) [M$^+$ – CH$_3$]. – $C_{18}H_{18}N_2W$ (456.3): calcd. C 47.38, H 6.19, N 6.14; found C 47.09, H 6.02, N 6.11.

Bis(cyclopentadienyl)bis(mesitylimido)tungsten(VI) (2c): Finely powdered **1b** (551 mg, 1.00 mmol) was added to a suspension of (C_5H_5)Na (96.1 mg, 1.10 mmol) in 20 mL 1,2 dimethoxyethane at −50 °C. The temperature of the red mixture was raised to room temperature within 30 min. and refluxed for 12 h. All volatile materials of the orange red suspension were removed in vacuo and the oily residue was extracted with 30 mL hexane. The extract was concentrated to approximately 8 mL. Any precipitating product was redissolved by warming the solution. Orange red crystals were isolated after one day at room temperature, and washed with 2 mL cold pentane (−70 °C), and dried in vacuo. – Yield: 429 mg (74%). m.p.: 176 °C. – IR (nujol): $\tilde{\nu}$ = 2986 s, 2920 s, 2896 s, 2860 s, 2804 m, 1604 w ν(C=C), 1448 m, 1356 m, 1311 s and 1281 vs ν(W=N−C), 1153 s, 1056 w, 1024 w, 1010 w, 980 w, 866 s and 810 s and 740 s ν(C−H$_{ar}$)$_{oop}$, 595 w, 582 w, 544 w, 505 w, 440 w cm^{-1}. – ^{1}H NMR (200.1 MHz, C_7D_8, 375 K): δ = 2.07 (s, 6 H, Mes-*p*-C*H*$_3$), 2.19 (s, 12 H, Mes-*o*-C*H*$_3$), 5.88 (s, 10 H, C_5H_5), 6.63 (s, 4 H, Mes-*H*); (200.1 MHz, C_7D_8, 310 K): δ = 2.09 (s, 6 H, Mes-*p*-C*H*$_3$), 2.19 (s, 12 H, Mes-*o*-C*H*$_3$), 5.47 (br, 5 H, C_5H_5), 6.25 (br, 5 H, C_5H_5), 6.60 (s, 4 H, Mes-*H*); (200.1 MHz, C_7D_8, 193 K): δ = 2.15 (s, 6 H, Mes-*p*-C*H*$_3$), 2.24 (s, 12 H, Mes-*o*-C*H*$_3$), 5.15 (s, 1 H, η^1-H_X), 5.26 (s, 5 H, η^5-C_5H_5), 6.55 (s, 2 H, η^1-H_B), 6.57 (s, 1 H, η^1-$H_{B'}$), 6.71 (s, 4 H, Mes-*H*) 6.90 (s, 1 H, η^1-H_A), 7.01 (s, 1 H, η^1-$H_{A'}$). – ^{13}C NMR (50.3 MHz, C_6D_6): δ = 19.47 (s, Mes-*o*-*C*H$_3$), 20.92 (s, Mes-*p*-*C*H$_3$), 108.40 (s, *C*$_5$H$_5$), 128.58 (s, Mes-*C*3), 131.01 (s, Mes-*C*2), 132.76 (s, Mes-*C*4), 153.71 (s, $^2J_{WC}$ = 32.7 Hz, Mes-*C*1). – EI-MS: *m*/*z* (%) = 580 (70) [M$^+$], 515 (100) [M$^+$ – C_5H_5]. – $C_{28}H_{32}N_2W$ (580.4): calcd. C 57.94, H 5.56, N 4.83; found C 57.06, H 5.66, N 4.83.

Bis(*tert*-butylimido)dichloro(trimethylphosphane)tungsten(VI) (3): PMe_3 (100 mg, 1.31 mmol) was added to a solution of **1b** (430 mg, 1.01 mmol) in 15 mL toluene. After 2 h at room temperature, all volatile materials were removed in vacuo, and 15 mL pentane was added to the brown oily residue. Insoluble, ocher colored **3** was filtered off, washed with 5 mL pentane and was dried in vacuo. The mother liquor contained 230 mg (0.50 mmol) of slightly impure **2b**. – Yield: 201 mg (85%). – ^{1}H NMR (400.1 MHz, $CDCl_3$): δ = 1.35 (s, 18 H, NCC*H*$_3$), 1.73 (d, $^2J_{PH}$ = 10.4 Hz, 9 H, PC*H*$_3$); – ^{31}P{^{1}H} NMR (162.0 MHz, $CDCl_3$): δ = 7.55 (s, $^1J_{WP}$ = 363 Hz, *P*CH$_3$); – ^{13}C NMR (100.6 MHz, C_6D_6): δ = 16.63 (d, $^1J_{PC}$ = 34.5 Hz, P-*C*H$_3$), 31.82 (d, $^4J_{PC}$ = 2.0 Hz, NC*C*H$_3$), 69.61 (d, $^3J_{PC}$ = 2.0 Hz, $^2J_{WC}$ = 26.5 Hz, N*C*CH$_3$).

Crystallographic data (excluding structure factors) for the structures reported in this paper have been deposited with the Cambridge Crystallographic Data Centre as supplementary publication no. CCDC-133165. Copies of the data can be obtained free of charge on application to CCDC, 12 Union Road, Cambridge, CB2 1EZ, UK (Fax: (internat.) +44-1223/336-033; E-mail: deposit@ccdc.cam.ac.uk).

Acknowledgments

Support by the *Deutsche Forschungsgemeinschaft* and the *Fonds der Chemischen Industrie* is gratefully acknowledged.

[1] W. A. Nugent, R. L. Harlow, *J. Am. Chem. Soc.* **1980**, *102*, 1759−1760.
[2] [2a] D. L. Thorn, W. A. Nugent, R. L. Harlow, *J. Am. Chem. Soc.* **1981**, *103*, 357−363. – [2b] W. A. Nugent, *Inorg. Chem.* **1983**, *22*, 965−969.
[3] [3a] M. B. Hursthouse, M. Motevalli, A. C. Sullivan, G. Wilkinson, *J. Chem. Soc., Chem. Commun.* **1986**, 1398−1399. – [3b] A. C. Sullivan, G. Wilkinson, M. Motevalli, M. B. Hursthouse, *J. Chem. Soc., Dalton Trans.* **1988**, 53−60.
[4] [4a] R. R. Schrock, R. T. DePue, J. Feldman, K. B. Yap, D. C. Yang, W. M. Davis, L. Park, M. DiMare, M. Schofield, J. Anhaus, E. Walborsky, E. Evitt, C. Krüger, P. Betz, *Organometallics* **1990**, *9*, 2262−2275. – [4b] R. R. Schrock, J. S. Murdzek, G. C. Bazan, J. Robbins, M. DiMare, M. O′Regan, *J. Am. Chem. Soc.* **1990**, *112*, 3875−3886. – [4c] G. Schoettel, J. Kress, J. A. Osborn, J. Chem. Soc., *Chem. Commun.* **1989**, 1062−1063. – [4d] N. Bryson, M.-T. Youinou, J. A. Osborn, *Organometallics* **1991**, *10*, 3389−3392.
[5] [5a] J. Sundermeyer, *Chem. Ber.* **1991**, *124*, 1977−1979. – [5b] U. Radius, J. Sundermeyer, *Chem. Ber.* **1992**, *125*, 2183−2186. – [5c] J. Sundermeyer, U. Radius, C. Burschka, *Chem. Ber.* **1992**, *125*, 2379−2384.
[6] U. Radius, J. Sundermeyer, H. Pritzkow, *Chem. Ber.* **1994**, *127*, 1827−1835.
[7] [7a] B. R. Ashcroft, D. C. Bradley, G. R. Clark, R. J. Errington, A. J. Nielson, C. E. F. Rickard, J. Chem. Soc., *Chem. Commun.* **1987**, 170−171. – [7b] A. J. Nielson, *Polyhedron* **1987**, *6*, 1657−1667.
[8] M. L. H. Green, P. C. Konidaris, P. Mountford, S. J. Simpson, J. Chem. Soc., *Chem. Commun.* **1992**, 256−259.
[9] [9a] W. A. Nugent, J. M. Mayer, *Metal Ligand Multiple Bonds*, Wiley, New York **1988**. – [9b] D. M. Berg, P. R. Sharp, *Inorg. Chem.* **1987**, *26*, 2959−2962. – [9c] R. Poli, *Chem. Rev.* **1991**, *91*, 509−551. – [9d] A. G. Orpen, L. Brammer, F. H. Allen, O. Kennard, D. G. Watson, R. Taylor, J. Chem. Soc., *Dalton Trans.* **1989**, S1−S83.
[10] [10a] G. Parkin, R. E. Marsh, W. P. Schaefer, J. E. Bercaw, *Inorg. Chem.* **1988**, *27*, 3262−3264. – [10b] G. Parkin, J. E. Bercaw, *Polyhedron* **1988**, *7*, 2053−2082.
[11] [11a] F. A. Cotton, A. Musco, G. Yagupski, *J. Am. Chem. Soc.* **1967**, *89*, 6136−6139. – [11b] F. A. Cotton, P. Legzdins, *J. Am. Chem. Soc.* **1968**, *90*, 6232−6233. – [11c] J. L. Calderon, F. A. Cotton, P. Legzdins, *J. Am. Chem. Soc.* **1969**, *91*, 2528−2535. – [11d] F. A. Cotton, G. A. Rusholme, *J. Am. Chem. Soc.* **1972**, *94*, 402−406.
[12] J. H. Osborne, A. L. Rheingold, W. C. Trogler, *J. Am. Chem. Soc.* **1985**, *107*, 7945−7952.
[13] J. C. Green, M. L. H. Green, J. T. James, P. C. Konidaris, G. H. Maunder, P. Mountford, J. Chem. Soc., *Chem. Commun.* **1992**, 1361−1365.
[14] [14a] F. A. Cotton, *Nonrigidity in Organometallic Compounds*, in *Dynamic Nuclear Magnetic Resonance Spectroscopy* (Eds:. L. M. Jackman, F. A. Cotton), Academic Press, New York, **1975**, p. 377−440. – [14b] B. E. Mann, *Nonrigidity in Organometallic Compounds*, in *Comprehensive Organometallic Chemistry I* (Eds:. G. Wilkinson, F. G. A. Stone, E. W. Abel), Vol. 3, Pergamon Press, New York, **1982**, p. 89−171. – [14c] F. A. Cotton, *J. Organomet. Chem.* **1975**, *100*, 29−41.
[15] N. M. Sergeyev, *Progr. Nucl. Magn. Reson. Spectrosc.* **1973**, *9*, 71−144.
[16] [16a] H. Werner, H.-J. Kraus, *Angew. Chem.* **1979**, *91*, 1013−1014; *Angew. Chem. Int. Ed. Engl.* **1979**, *18*, 948−949. – [16b] H. Werner, H.-J. Kraus, U. Schubert, K. Ackermann, P. Hofmann, *J. Organomet. Chem.* **1983**, *250*, 517−536.
[17] C. A. Tolman, *Chem. Rev.* **1977**, *77*, 313−348.
[18] [18a] J. L. Calderon, F. A. Cotton, B. G. DeBoer, J. Takats, *J. Am. Chem. Soc.* **1970**, *92*, 3801−3802. – [18b] J. L. Calderon, F. A. Cotton, J. Takats, *J. Am. Chem. Soc.* **1971**, *93*, 3587−3591.
[19] [19a] W. G. Kita, M. K. Lloyd, J. A. McCleverty, J. Chem. Soc., *Chem. Commun.* **1971**, 420−421. – [19b] M. M. Hunt, W. G. Kita, B. E. Mann, J. A. McCleverty, J. Chem. Soc., *Dalton Trans.* **1978**, 467−479.

[20] F. Preuss, H. Becker, H.-J. Häusler, *Z. Naturforsch.* **1987**, *42B*, 881−888.
[21] M. L. H. Green, D. M. Michaelidou, P. Mountford, A. G. Suárez, L.-L. Wong, J. Chem. Soc., *Dalton Trans.* **1993**, 1593−1597.
[22] [22a] K. L. T. Wong, H. H. Brintzinger, *J. Am. Chem. Soc.* **1975**, *97*, 5143−5146. − [22b] L. G. Bell, H. H. Brintzinger, *J. Organomet. Chem.* **1977**, *135*, 173−176. − [22c] G. Huttner, H. H. Brintzinger, L. G. Bell, P. Friedrich, V. Bejenke, D. Neugebauer, *J. Organomet. Chem.* **1978**, *145*, 329−333.
[23] G. Wilkinson, T. S. Piper, *J. Inorg. Nucl. Chem.* **1956**, *2*, 32−37.
[24] [24a] A. Davison, P. E. Rakita, *Inorg. Chem.* **1970**, *9*, 289−29. − [24b] C. H. Campbell, M. L. H. Green, *J. Chem. Soc. A* **1971**, 3282−3285.
[25] M. J. Bennett, F. A. Cotton, A. Davison, J. W. Faller, S. J. Lippard, S. M. Morehouse, *J. Am. Chem. Soc.* **1966**, *88*, 4371−4376.
[26] Two strong π-bonds are formed by the e set orbitals, three weaker π-bonds by the t_2 set orbitals. For a discussion of the relative π-bond efficiency see: K. F. Miller, R. A. D. Wentworth, *Inorg. Chem.* **1979**, *18*, 984−988.
[27] E. Keller, *Schakal 88B*, Universität Freiburg, **1990**.

Received July 18, 2000
[I00281]

Radical Cation Salts with the Nonplanar $[ReO(dmit)_2]^-$ Complex

Benoît Domercq[a] and Marc Fourmigué*[a]

Keywords: S ligands / Rhenium / Oxo complexes / Magnetic properties / Radical ions

An optimized synthesis of $[PPh_4][ReO(dmit)_2]$ ($dmit^{2-}$ = 2-thioxo-1,3-dithiole-4,5-dithiolato) is reported as well as electrocrystallization experiments of various donor molecules with this electrolyte. Three 1:1 salts have been obtained with $Cp_2Mo(dmit)$, BEDT-TTF [BEDT-TTF = bis(ethylenedithio)tetrathiafulvalene] and BEDO-TTF [BEDO-TTF = bis(ethylenedioxo)tetrathiafulvalene] and their X-ray crystal structures determined. In the three salts, the closed-shell, d^2, $[ReO(dmit)_2]^-$ anions push apart the radical cations, stabilizing structures with noninteracting donors [with $Cp_2Mo(dmit)$] or donor dimers (with BEDT-TTF or BEDO-TTF), as confirmed by conductivity and SQUID magnetic susceptibility measurements.

Introduction

Planar bis(dithiolene) complexes, and particularly with the sulfur-rich $dmit^{2-}$ ligand, have been extensively used for the elaboration of conducting molecular materials,[1,2] as, for example, the mixed-valence salts derived from $Ni(dmit)_2^-$, $[TTF][Ni(dmit)_2]_2$ with the open-shell $TTF^{+\cdot}$ counter cation,[3] or $[NMe_4][Ni(dmit)_2]_2$ with the closed shell NMe_4^+ ammonium cation,[4] both of them reported to become superconductors. On the other hand, their nonplanar tris(dithiolene) analogs such as $[Mo(dmit)_3]^-$ or $[V(dddt)_3]^-$ have been scarcely investigated for the elaboration of conducting salts,[5,6] probably because their more spherical shape hinders a proper overlap interaction network in the solid state. In this respect, heteroleptic complexes with one of the three dithiolene ligands replaced by a smaller one, such as an oxo or a nitrido group, offer an attractive alternative since more compact structures can be anticipated. Several of those heteroleptic complexes have been described with the $dmit^{2-}$ ligand, some of them diamagnetic (d^2), such as $[MoO(dmit)_2]^{2-}$,[7,8] $[ReO(dmit)_2]^-$,[9] $[TcN(dmit)_2]^{2-}$,[10] and $[OsN(dmit)_2]^-$ [11] and some of them paramagnetic (d^1), such as $[VO(dmit)_2]^{2-}$ [12] or $[MoO(dmit)_2]^-$.[7,8] Among these compounds, only $[MoO(dmit)_2]^-$ forms cation radical salts with TTF to afford a 1:1 salt, $[TTF][MoO(dmit)_2]$ which was not structurally characterized.[8] We therefore decided to investigate more closely the cation radical salts derived from those heteroleptic dithiolene oxo complexes, and present here our results with the closed-shell, diamagnetic Re^V $[ReO(dmit)_2]^-$ anion (Scheme 1). Planar donor molecules such as BEDT-TTF or BEDO-TTF were engaged in electrocrystallization experiments with $[ReO(dmit)_2]^-$ as well as the nonplanar Mo^{IV} molybdenum complex, $Cp_2Mo(dmit)$

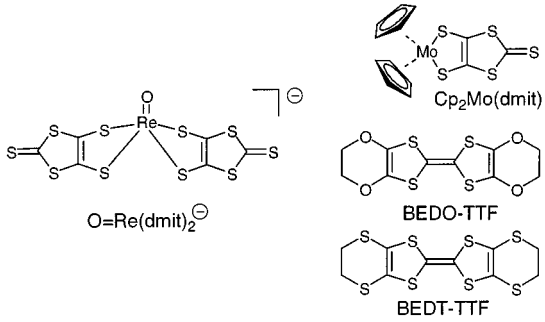

Scheme 1

(Scheme 1),[13] which has been described to be readily oxidized to the corresponding $[Cp_2Mo(dmit)]^{+\cdot}$ radical cation.[14–16]

Results and Discussion

Synthesis

The preparation of $[ReO(dmit)_2]^-$ has been described by Matsubayashi from the reaction of $ReCl_5$ with two equivalents of $dmit^{2-}$ in EtOH.[9] The uncontrolled partial hydrolysis of $ReCl_5$ under those conditions gave the desired anion in only 30% yield, while a similar reaction in anhydrous CH_3CN gave the homoleptic $[Re(dmit)_3]^-$ dithiolene complex. We felt that a higher yield could be obtained by using a preformed $ReOX_4$ moiety, as described for the synthesis[17] of $[ReO(mnt)_2]^-$ or $[ReO(S_2C_2B_{10}H_{10})_2]^-$,[18] and chose accordingly to engage the $ReOBr_4^-$ anion, as its tetraphenylphosphonium salt,[19] in a substitution reaction with two equivalents of $dmit^{2-}$, affording $[PPh_4][ReO(dmit)_2]$ in very good yield (88%) after recrystallization, and identical in every respect to the described compound.[9]

Structure and Electronic Properties of the $ReO(dmit)_2^-$ Cation Radical Salts

The electrocrystallization of $Cp_2Mo(dmit)$, BEDT-TTF and BEDO-TTF in the presence of $[PPh_4][ReO(dmit)_2]$ as electrolyte allowed the isolation of the three corresponding

[a] Sciences Moléculaires aux Interfaces, FRE 2068 CNRS, Institut des Matériaux Jean Rouxel,
2, Rue de la Houssinière, BP32229, 44322 Nantes, France

 © WILEY-VCH Verlag GmbH, 69451 Weinheim, 2001 1434–1948/01/0606–1625 $ 17.50+.50/0

1:1 salts. $[Cp_2Mo(dmit)][ReO(dmit)_2]$ crystallizes in the monoclinic system, space group $P2_1/c$, with both cation and anion in general positions in the unit cell (Figure 1).

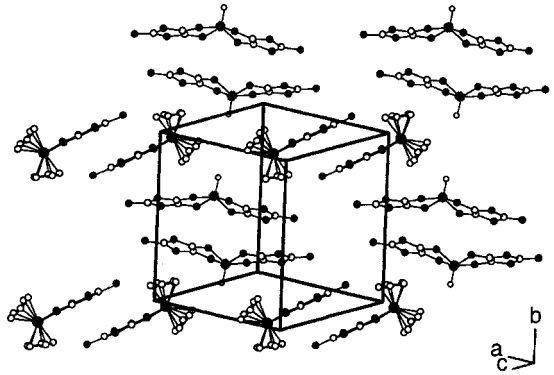

Figure 1. A view of the mixed cation-anion ($a + c$, b) layer in $[Cp_2Mo(dmit)][ReO(dmit)_2]$

The geometry of the $[ReO(dmit)_2]^-$ anion (Figure 2) is very close to that described for its PPh_4^+ salt (Table 1), although the folding angles of the two ReS_2C_2 metallacycles slightly increase from 11−15° to 17°. Bond length evolution within the organometallic cation (Table 2) confirms the oxidized character of the complex, which changes to a more dithioketonic-type structure for the dithiolene ligand (shortening of the C−S bonds and lengthening of the C=C bond). Note also the weak folding angle θ of the MoS_2C_2 metallacycle along the S···S axis in $Cp_2Mo(dmit)^{+\cdot}$ [5.6(5)°] which should be compared to the distortions observed in $[Cp_2Mo(dmit)][TCNQF_4]$ [θ = 10.2(1)°],[14] while a fully planar metallacycle was observed in $[Cp_2Mo(dmit)][AsF_6]$ (θ = 0.0°).[15] The cations are organized into inversion-related dimers with a somewhat large interplanar dmit/dmit distance of 3.58 Å, associated with a lateral offset of 5.51 Å. Those dimers organize into layers in the (a,c) plane, separated from each other by the diamagnetic $ReO(dmit)_2^-$ anions. As a consequence of the weakly interacting radical cations, the closed-shell character of the anion and the full charge-transfer, the salt is insulating with $\sigma_{RT} = 4 \times 10^{-7}$ S cm^{-1}. Its magnetic behavior was deduced from the SQUID susceptibility measurements which show a Curie−Weiss behavior in the whole temperature range with θ = 0.3 K, excluding the possibility of sizeable intermolecular interactions in this salt. $[Cp_2Mo(dmit)][ReO(dmit)_2]$ can therefore be described as paramagnetic $[Cp_2Mo(dmit)]^{+\cdot}$ radical cations, essentially isolated from each other by the closed-shell $[ReO(dmit)_2]^-$ anions. The situation is more complex in the BEDT-TTF and BEDO-TTT salts.

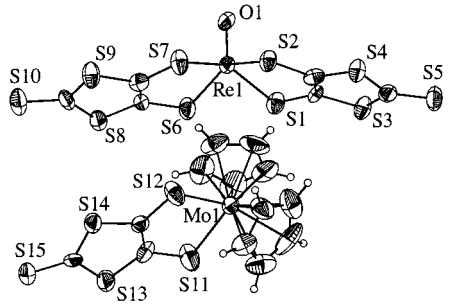

Figure 2. ORTEP view of the $[Cp_2Mo(dmit)]^{+\cdot}$ cation and the $[ReO(dmit)_2]^-$ anion in $[Cp_2Mo(dmit)][ReO(dmit)_2]$; thermal ellipsoids at the 50% probability level

[BEDT-TTF][$ReO(dmit)_2$] crystallizes in the monoclinic system, space group $P2_1/n$, with both anion and cation in general positions in the unit cell (Figure 3). The bond lengths within the $[ReO(dmit)_2]^-$ are similar to those observed above (Table 1). Within the BEDT-TTF moieties, the bond length evolution relative to the neutral molecules con-

Table 1. Geometrical characteristics of the $[ReO(dmit)_2]^-$ with the different counter ions

Counter ion	PPh_4^+ [9]	$[Cp_2Mo(dmit)]^{+\cdot}$	BEDT-TTF$^{+\cdot}$	BEDO-TTF$^{+\cdot}$
Re−O/Å	1.687(10)	1.664(8)	1.681(7)	1.655(11)
Re−S/Å	2.332−2.336(5)	2.297−2.320(3)	2.310−2.331(3)	2.309−2.323(4)
O−Re−S/°	107.2−109.3(4)	106.3−109.4(3)	105.1−110.7(3)	106.6−109.2(4)
$S-Re-S_{intraligand}$	83.4(1), 86.6(1)	85.9(1), 86.4(1)	86.5(1), 86.24(9)	85.95−86.44(5)
$S-Re-S_{interligand}$	81.0(1), 83.4(1)	82.6(1), 82.9(1)	84.3(1), 83.0(1)	81.77−84.03(5)
folding angles	11.4(4), 14.8(4)	17.6(3), 17.7(1)	23.0(3), 20.1(3)	16.5(4), 18.8(3) 19.8(3), 21.2(4)

Table 2. Geometrical characteristics of $[Cp_2Mo(dmit)]^{+\cdot}$ in $[Cp_2Mo(dmit)][ReO(dmit)_2]$ together with data for the reference compounds $Cp_2Mo(dmit)$ and $[Cp_2Mo(dmit)][AsF_6]$

	$Cp_2Mo(dmit)$ neutral[15]	$[Cp_2Mo(dmit)]^{+\cdot}$ as AsF_6^- salt[16]	$[Cp_2Mo(dmit)]^{+\cdot}$ as $[ReO(dmit)_2]^-$ salt
Mo−S (Å)	2.459(3), 2.455(3)	2.441(2)	2.436(3), 2.445(4)
(Mo)S−C (Å)	1.763(9), 1.728(9)	1.691(8)	1.704(11), 1.672(13)
C=C (Å)	1.357(12)	1.41(1)	1.383(16)
S−Mo−S (°)	83.95(8)	83.59(8)	83.42(12)
Folding angle θ (°)	4.2(1)	0.0	5.6(5)

firms the fully oxidized character of the BEDT-$TTF^{+\cdot}$ cation radical (Table 3) when compared with reference compounds,[20,21] hence the formulation [BEDT-$TTF]^{+\cdot}[ReO(dmit)_2]^-$. The organic cation radicals are organized into layers parallel to the (a-c, b) plane (Figure 4), separated from each other by the diamagnetic $[ReO(dmit)_2]^-$ counter anions. Within each organic layer (Figure 5), the $BEDT^{+\cdot}$ cation radicals arrange into inversion-centered dimers with short S···S distances (3.42−3.78 Å) and a short interplanar plane-to-plane distance (2.72−2.74 Å). Those dimers interact only weakly with their neighbors in the plane through S···S overlap (S···S distances at 3.67 Å) with the sulfur atoms of the outer dithioethylene moieties.

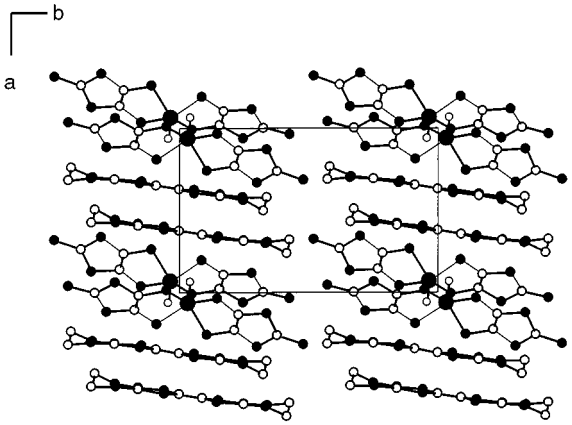

Figure 3. Projection view (along *c*) of the mixed organic-inorganic layers identified in the structure of [BEDT-TTF][$ReO(dmit)_2$]

Table 3. Bond length evolution within the TTF core and charge transfer degree (ρ) in BEDT-TTF and BEDO-TTF, in the neutral donor molecules, the two salts with $[ReO(dmit)]^-$ and reference salts

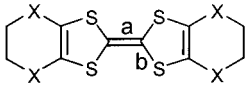

	ρ	C=C bond (a)	C−S bonds (b)	ref.
BEDT-TTF neutral	0	1.343(3)	1.756(3)	20
[BEDT-TTF][ReO(dmit)]	1	1.397(13)	1.716(11)	this work
BEDT-$TTF^{+\cdot}$ in [BEDT-TTF][PF_6]	1	1.394(5)	1.722(4)	21
BEDO-TTF neutral	0	1.357(6)	1.761(5)	22
[BEDO-TTF][ReO(dmit)]	1	1.368(10)	1.719(8)	this work
BEDO-$TTF^{+\cdot}$ in $[BEDO]_2[Pd(dto)]$	1	1.390(14)	1.729(18)	23

[BEDO-TTF][$ReO(dmit)_2$], on the other hand, crystallizes in the monoclinic system, space group $P2_1/c$, with two crystallographically independent anions and cations in the unit cell. This differentiation originates from different orientations of the ethylenedioxo groups of the BEDO-TTF molecules. The bond lengths within the central TTF core also confirm the oxidized character of the donor molecule (Table 3) when compared with reference compounds.[22,23]

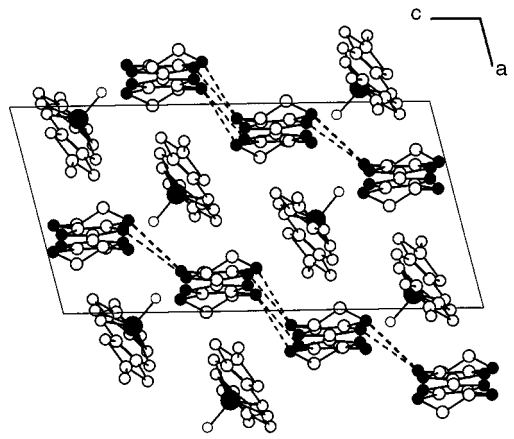

Figure 4. Projection view along *b* in [BEDT-TTF][$ReO(dmit)_2$]; the dotted lines indicate the shortest intermolecular S···S contacts between radical BEDT-$TTF^{+\cdot}$ moieties; the Re atom and the sulfur atoms of the BEDT-$TTF^{+\cdot}$ molecules are shaded

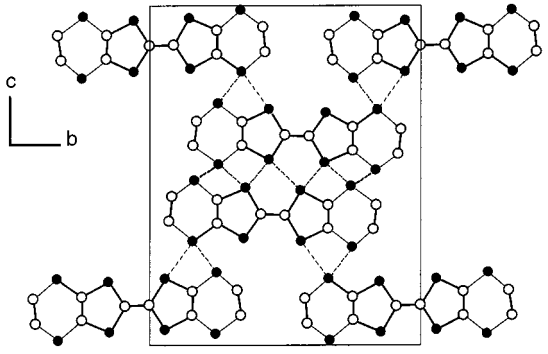

Figure 5. Detail of the intermolecular interaction network between organic BEDT-$TTF^{+\cdot}$ cation radicals in [BEDT-TTF][$ReO(dmit)_2$]

A similar dimer organization of the cation radicals is observed with short S···S (3.56−3.67 Å) and S···O (3.35−3.52 Å) intermolecular contacts (Figure 6), while the dimeric entities are fully isolated from each other by the $[ReO(dmit)_2]^-$ counter ions.

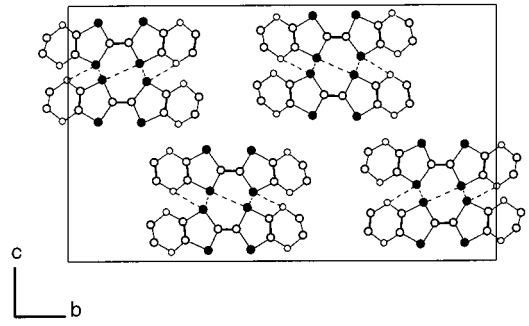

Figure 6. The interaction network identified in the organic layers of BEDO-$TTF^{+\cdot}$ cation radicals in the structure of [BEDO-TTF][$ReO(dmit)_2$]

Conductivity measurements (on compressed pellets) reveal a semi-conducting behavior for both salts with $\sigma_{RT} = 1-3 \times 10^{-6}$ S·cm^{-1}. SQUID measurements of the temperature dependence of the magnetic susceptibility (Figure 7) show, for both salts, an activated behavior in the 100−300 K range together with a Curie tail at low temper-

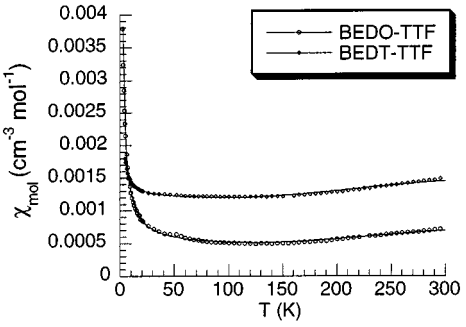

Figure 7. Temperature dependence of the magnetic susceptibility of [BEDT-TTF][ReO(dmit)$_2$] and [BEDO-TTF][ReO(dmit)$_2$]; the solid lines are a fit to the singlet-triplet Bleaney−Bower equation with a low-temperature Curie tail (see text)

ature. The latter represents 0.8 and 2.2% $S = 1/2$ magnetic defects in the BEDT-TTF and BEDO-TTF salts respectively. The structural description of these salts indicates the presence of donor dimers, essentially isolated from each other by the diamagnetic anions. The HOMO−HOMO overlap interaction within those dimers leads therefore to bonding and antibonding combinations which house the two remaining electrons. Accordingly, the conductivity is very low and we expect a singlet-triplet magnetic behavior with a maximum for the susceptibility whose temperature $T(\chi_{max})$ depends upon the HOMO−HOMO interaction energy. The fit of the magnetic susceptibility with the Bleaney−Bower equation,[24] together with the Curie law encompassing the magnetic defects identified at low temperature, affords J/k values of −826(5) and −880(7) K for the BEDT-TFF and BEDO-TTF salts, respectively. The close proximity of those two values is indeed in agreement with the extended-Hückel calculated HOMO−HOMO interaction energies within the dimers, which amount to 0.408 and 0.411 eV in the two salts.

Contrary to the situation encountered in organic conductors based on BEDT-TFF or BEDO-TTF, which is characterized by a two-dimensional segregation of the organic donor molecules and the counter ions, we observed here the formation of mixed cationic/anionic layers with the diamagnetic [ReO(dmit)$_2$]$^-$ units interspersed between the oxidized donor molecules, thus hindering the stabilization of mixed valence, a prerequisite for metallic conductivity. The peculiar alternated structures observed here might be of interest for their magnetic properties, particularly if the diamagnetic [ReO(dmit)$_2$]$^-$ could be replaced by analogous paramagnetic complexes such as the unknown [MoO(dmit)$_2$]$^{-\cdot}$ or [ReN(dmit)]$^{-\cdot}$. Preliminary experiments along those lines showed that ferricinium oxidation of the dianionic [MoO(dmit)$_2$]$^{2-}$ described by Matsubayashi[7,8] afforded a bimetallic [Mo$_2$O$_2$(μ-O)$_2$(dmit)$_2$]$^{2-}$ complex[25] rather than the expected [MoO(dmit)$_2$]$^{-\cdot}$.

Table 4. Electrocrystallization conditions

Donor molecule	$Cp_2Mo(dmit)$	BEDT-TTF	BEDO-TTF
m(donor)	5 mg	10 mg	5 mg
m(electrolyte)	500 mg	50 mg	10 mg
V (CH_2Cl_2)	20 mL	15 mL	15 mL
Current intensity	1 μA	1.4 μA	1 μA
Duration	6 days	10 days	17 days

Table 5. Crystallographic data

	[$Cp_2Mo(dmit)$]·[ReO(dmit)$_2$]	[BEDT-TTF]·[ReO(dmit)$_2$]	[BEDO-TTF]·[ReO(dmit)$_2$]
Formula	$C_{19}H_{10}MoOReS_{15}$	$C_{16}H_8ORES_{18}$	$C_{32}H_{16}O_{10}Re_2S_{28}$
Mol. wt.	1017.31	979.50	1830.53
Crystal system	Monoclinic	Monoclinic	Monoclinic
Space group	$P2_1/c$	$P2_1/n$	$P2_1/c$
a (Å)	14.4017(16)	9.9655(7)	10.6046(10)
b (Å)	14.7254(14)	15.3502(11)	29.3218(18)
c (Å)	13.9482(15)	19.7371(13)	17.8087(14)
β (°)	93.378(13)	104.130(8)	101.488(10)
V (Å^3)	2952.9(5)	2927.9(4)	5426.6(7)
Z	4	4	4
T (K)	293	293	293
d_{calc}, Mg m^{-3}	2.288	2.222	2.241
μ, mm^{-1}	5.6	5.45	5.587
F(000)	1956	1900	3544
Crystal size	0.50×0.04×0.02	0.3×0.1×0.01	0.354×0.04×0.02
θ range	1.98−25.96	1.7−24	1.81−26
Refl. coll.	5732	18364	10575
Refl. ind	5732	4582	10575
R_{int}	0	0.125	0.1740
Abspt. corr.	Numerical	Empirical	Numerical
Max., min. trans.	0.8788, 0.5324	0.6352, 0.4086	0.8641, 0.2888
Data/rest/par.	5732/0/334	4583/0/325	10575/0/649
GOF	0.528	0.753	0.504
$R(F)$, $wR(F^2)$	0.0414, 0.0979	0.0419, 0.0705	0.0464, 0.1177
Res. dens.	1.96, −1.03	1.25, −0.74	1.25, −0.66

Experimental Section

Synthesis: All reactions were performed under nitrogen using vacuum line techniques. Solvents were dried prior to use. $[PPh_4][ReOBr_4]$ was prepared according to Cotton et al.[19] in 44.3% yield. – $C_{24}H_{20}Br_4OPRe$: calcd. C 33.47, H 2.34, Br 37.11, P 3.60; found C 33.72, H 2.39, Br 37.38, P 3.60.

$[PPh_4][ReO(dmit)_2]$: A solution of $dmit(COPh)_2$ (0.5 g, 1.23 mmol) in dry MeOH (5 mL) was treated with a MeOH solution of NaOMe (2.1 equiv.). After stirring for 1 h, the dark red solution was precipitated with Et_2O (20 mL), and the red dithiolene salt decanted, washed with Et_2O and dried. $Na_2(dmit)$ was dissolved in MeOH (40 mL) and added dropwise to a solution of $[PPh_4][ReOBr_4]$ (0.5 g, 0.58 mmol) in MeOH (50 mL). A red solid immediately precipitated. After stirring overnight it was filtered and recrystallized from CH_2Cl_2/EtOH, affording 0.48 g (88%) of the salt as dark red crystals. M.p. 224–225 °C. – $C_{30}H_{20}OPReS_{10}$: calcd. C 38.57, H 2.16, P 3.32, S 34.32; found C 36.18, H 1.98, P 3.71, S 36.15.

Electrocrystallization Experiments: Two-compartment cells with platinum electrodes (l = 2 cm, Ø = 1 mm) were used in the galvanostatic mode at 20 °C. Crystals were harvested on the anode after the indicated time and washed with CH_2Cl_2. Details for each individual compound are given in Table 4.

Data Collection and Structure Determination: Table 5 summarizes the crystallographic data. Data were collected at room temperature on an Imaging Plate Diffraction System (Stoe-IPDS). Structures were solved by direct methods using SHELXS-86 and refined by the full-matrix least-squares method on F^2, using SHELXL-93 (G. M. Sheldrick, University of Göttingen, **1993**) with anisotropic thermal parameters for all non-hydrogen atoms. The hydrogen atoms were introduced at calculated positions (riding model).
Crystallographic data (excluding structure factors) for the structures reported in this paper have been deposited with the Cambridge Crystallographic Data Centre as supplementary publication nos. CCDC-149592–149594 for the $Cp_2Mo(dmit)$, the BEDT-TTF and the BEDO-TTF salts, respectively. Copies of the data can be obtained free of charge on application to CCDC, 12 Union road, Cambridge CB2 1EZ, UK [Fax: (internat.) + 44-1223/336-033; E-mail: deposit@ccdc.cam.ac.uk].

Magnetic Measurements: Magnetic susceptibilities were measured on a Quantum Design MPMS-2 SQUID magnetometer operating in the range 2.5–300 K at 1 T ($[BEDT\text{-}TTF][ReO(dmit)_2]$, 12.32 mg) or 0.5 T ($[BEDO\text{-}TTF][ReO(dmit)_2]$, 6.53 mg). Data were corrected for sample holder contribution and Pascal diamagnetism.

[1] Reviews on $dmit^{2-}$ complexes have appeared: P. Cassoux, L. Valade, H. Kobayashi, A. Kobayashi, R. A. Clark, A.E. Underhill, *Coord. Chem. Rev.* **1991**, *110*, 115–160.
[2] R.-M. Olk, B. Olk, W. Dietzsch, R. Kirmse, E. Hoyer, *Coord. Chem. Rev.* **1992**, *117*, 99–131.
[3] M. Bousseau, L. Valade, J.-P. Legros, P. Cassoux, M. Garbauskas, L. V. Interrante, *J. Am. Chem. Soc.* **1986**, *108*, 1908–1916.
[4] A. Kobayashi, H. Kim, Y. Sasaki, R. Kato, H. Kobayashi, S. Morinaga, Y. Nishino, K. Kajita, T. Tanaka, *Chem. Lett.* **1987**, 1819–1822.
[5] G. Matsubayashi, K. Douki, H. Tamura, M. Nakano, W. Mori, *Inorg. Chem.* **1993**, *32*, 5990–5996.
[6] C. Livage, M. Fourmigué, P. Batail, E. Canadell, C. Coulon, *Bull. Soc. Chim. Fr.* **1993**, *130*, 761–771.
[7] G. Matsubayashi, T. Nojo, T. Tanaka, *Inorg. Chim. Acta* **1988**, *154*, 133–135.
[8] T. Nojo, G. Matsubayashi, T. Tanaka, *Inorg. Chim. Acta* **1989**, *159*, 49–53.
[9] G. Matsubayashi, T. Maikawa, M. Nakano, *J. Chem. Soc., Dalton Trans.* **1993**, 2995–2999.
[10] J. R. Dilworth, R. Hübener, U. Abram, *Z. Anorg. Allg. Chem.* **1997**, *623*, 880–882.
[11] W. A. Reinerth, P. A. Shapley, *Inorg. Chim. Acta* **1998**, *267*, 335–340.
[12] R. Kirmse, W. Dietsch, J. Stach, R.-M. Olk, E. Hoyer, *Z. Anorg. Allg. Chem.* **1987**, *548*, 133–140.
[13] M. Fourmigué, C. Lenoir, C. Coulon, F. Guyon, J. Amaudrut, *Inorg. Chem.* **1995**, *34*, 4979–4985.
[14] M. Fourmigué, B. Domercq, I. V. Jourdain, P. Molinié, F. Guyon, J. Amaudrut, *Chem. Eur. J.* **1998**, *4*, 1714–1723.
[15] R. Clérac, M. Fourmigué, J. Gaultier, Y. Barrans, P.-A. Albouy, C. Coulon, *Eur. Phys. J. B* **1999**, *9*, 431–443.
[16] B. Domercq, C. Coulon, M. Fourmigué, *Inorg. Chem.* **2001**, *40*, 371–378.
[17] A. Davison, C. Orvig, H. S. Trop, M. Sohn, B. V. DePhamphilis, A. G. Jones, *Inorg. Chem.* **1980**, *19*, 1988–1992.
[18] J. D. McKinney, H. Chen, T. A. Hamor, K. Paxton, C. J. Jones, *J. Chem. Soc., Dalton Trans.* **1998**, 2163–2168.
[19] F. A. Cotton, K. J. Lippard, *Inorg. Chem.* **1966**, *5*, 9–16.
[20] P. Guionneau, C. J. Kepert, D. chasseau, M. R. Truter, P. Day, *Synth. Metals* **1997**, *86*, 1973–1974.
[21] H. Kobayashi, R. Kato, T. Mori, A. Kobayashi, Y. Sasaki, G. Saito, T. Enoki, H. Inokuchi, *Chem. Lett.* **1983**, 759–760.
[22] T. Suzuki, H. Yamochi, G. Srdanov, K. Hinkelmann, F. Wudl, *J. Am. Chem. Soc.* **1989**, *111*, 3108–3109.
[23] G. Saito, H. Izukashi, M. Shibata, K. Yoshida, L. A. Kushch, T. Kondo, H. Yamochi, O. O. Drozdova, K. Matsumoto, M. Kusunoki, K. Sakaguchi, N. Kojima, E. B. Yagubskii, *J. Mater. Chem.* **2000**, *10*, 893–910.
[24] O. Kahn, in *Molecular Magnetism*, VCH, Weinheim, **1993**.
[25] B. Domercq, PhD thesis, University of Nantes, France, **1999**.

Received September 13, 2000
[I00346]

Synthesis of Novel Heterotetrametallic (d^6-d^{10}-d^8) Polyalkynyl Complexes Starting from Heterobimetallic Chloride-Bridged (d^6-d^8) Compounds

Irene Ara,[a] Jesús R. Berenguer,[b] Eduardo Eguizábal,[b] Juan Forniés,*[a] Elena Lalinde,*[b] and Antonio Martín[a]

Dedicated to Prof. R. Usón on the occasion of his 75th birthday

Keywords: Iridium / Rhodium / Heteropolymetallics / Chloro-bridged complexes / Alkynide-bridged complexes

The reaction between the half-sandwich cyclopentadienyl complexes [M(η^5-C_5Me_5)Cl_2(PEt_3)] (M = Rh, Ir) and [*cis*-M′(C_6F_5)$_2$(thf)$_2$] (M′ = Pt, Pd; thf = tetrahydrofuran) affords the corresponding chloride-bridged heterobinuclear Rh,Ir/Pt,Pd complexes [(PEt_3)(η^5-C_5Me_5)M(μ-Cl)$_2$M′(C_6F_5)$_2$] (**1**–**4**). In contrast, similar reactions with the chloro-bridged binuclear compounds [{M(η^5-C_5Me_5)Cl(μ-Cl)}$_2$] (M = Rh, Ir) lead instead to the unexpected mixed salt complexes {Cp*M(μ-Cl)$_3$MCp*}$_2$[{(C_6F_5)$_2$M′(μ-Cl)}$_2$] (M = Rh, Ir; M′ = Pt, Pd) (**5**–**8**) as a result of chloride transfer. The structures of [(PEt_3)(η^5-C_5Me_5)Rh(μ-Cl)$_2$Pt(C_6F_5)$_2$] (**1**) and {Cp*Rh(μ-Cl)$_3$RhCp*}$_2$[{(C_6F_5)$_2$Pd(μ-Cl)}$_2$] (**6**) have been determined by X-ray diffraction analyses. The reactivity of the new chloride-bridged heterobinuclear compounds **1**–**4** towards the alkynylating agents [M′′(C≡CR)]$_n$ (M′′ = Cu, Ag) has also been investigated: a new type of tetranuclear product, [(PEt_3)Cp*M(μ-1κC^α:η^2-C≡CPh)$_2$M′′$_2$(μ-4κC^α:η^2-C≡CPh)$_2$Pt(C_6F_5)$_2$] (M = Rh, Ir; M′′ = Cu, Ag) (**9**–**12**), was obtained, and fully characterized in the case of complex [(PEt_3)Cp*Rh(μ-1κC^α:η^2-C≡CPh)$_2$Cu$_2$(μ-4κC^α:η^2-C≡CPh)$_2$Pt(C_6F_5)$_2$] (**9**).

Introduction

The chemistry of bimetallic complexes has aroused much interest and has led to great development in the field of organometallic chemistry.[1] In this area, there have been many reports detailing the preparation and chemistry of symmetrical or asymmetrical dichloro-bridged homobinuclear complexes,[2][3l] mainly because they play a prominent role as starting materials in organometallic chemistry and because of their relevance in catalysis. In marked contrast, the heterobinuclear analogues L_m(μ-Cl)$_2$M′L_n[3a−3e] are very scarce and their chemistry remains essentially undocumented, although efforts to develop this chemistry have recently been reported.[3f−3p]

This paucity of heterobinuclear compounds containing chloride bridging ligands, as well as the potentially rich chemistry that may be expected in these systems, prompted us to prepare binuclear compounds containing Rh^{III} or Ir^{III} fragments together with [*cis*-M′(C_6F_5)$_2$] (M′ = Pt, Pd) units. We were interested in using these systems as precursors for alkynyl-bridged heteropolynuclear complexes.[4] In the course of our ongoing research on alkynyl complexes, we have recently succeeded in synthesizing the first homobridged bis(μ-alkynyl) [(PEt_3)Cp*M(μ-C≡CR)$_2$M′(C_6F_5)$_2$] and hetero-bridged μ-alkynyl,μ-halide [(PEt_3)Cp*M(μ-C≡CR)(μ-X)M′(C_6F_5)$_2$] heterobinuclear Rh,Ir^{III}/Pt,Pd^{II} complexes,[4g] simply by treating mono [MCp*(C≡CR)X(PEt_3)] or bis(alkynyl) [MCp*(C≡CR)$_2$(PEt_3)] compounds with [*cis*-M′(C_6F_5)$_2$(thf)$_2$]. As a continuation of our work in this field, and in order to complete this series with respect to the bridging system, we report herein the synthesis of the dichloro-bridged heterobinuclear complexes [(PEt_3)Cp*M(μ-Cl)$_2$M′(C_6F_5)$_2$] (M = Rh, M′ = Pt: **1**, Pd: **2**; M = Ir, M′ = Pt: **3**, Pd: **4**) and the crystal structure of **1**. Furthermore, in order to explore the potential utility of these new compounds, we have attempted the preparation of alkynyl-bridged complexes by treating them with ethynylating agents such as [CuC≡CR]$_x$ and [Ag(C≡CR)]$_x$. These reactions led to the synthesis of a new type of heteropolynuclear alkynyl-bridged complexes [(PEt_3)Cp*M(μ-1κC^α:η^2-C≡CPh)$_2$M′′$_2$(μ-4κC^α:η^2-C≡CPh)$_2$Pt(C_6F_5)$_2$] (M = Rh, Ir; M′′ = Cu, Ag) (**9**−**12**), in which two widely divergent bis(alkynyl) metal fragments (d^6 and d^8) are connected through d^{10} (Cu or Ag) metal ions. We also describe similar reactions between [{MCp*Cl(μ-Cl)}$_2$] (M = Rh, Ir) and [*cis*-M′(C_6F_5)$_2$(thf)$_2$] (M′ = Pt, Pd) that involve chloride-transfer to yield the mixed salt complexes {Cp*M(μ-Cl)$_3$MCp*}$_2$[{(C_6F_5)$_2$M′(μ-Cl)}$_2$] (M = Rh, Ir; M′ = Pt, Pd) (**5**−**8**), and we present the crystal structure of {Cp*Rh(μ-Cl)$_3$RhCp*}$_2$[{(C_6F_5)$_2$Pd(μ-Cl)}$_2$] (**6**).

[a] Departamento de Química Inorgánica, Instituto de Ciencia de Materiales de Aragón, Universidad de Zaragoza − Consejo Superior de Investigaciones Científica,
50009 Zaragoza, Spain
Fax: (internat.) +34−976/761187
E-mail: forniesj@posta.unizar.es
[b] Departamento de Química − Grupo de Síntesis Química de La Rioja, UA-CSIC, Universidad de La Rioja,
26004 Logroño, Spain
Fax: (internat.) +34−941/299621
E-mail: elena.lalinde@dq.unirioja.es

Results and Discussion

Synthesis of Hetero- and Homobimetallic Chloride-Bridged Complexes

The preparative results are summarized in Scheme 1. The reaction of compounds [*cis*-M′(C_6F_5)$_2$(thf)$_2$] (M′ = Pt, Pd)

 © WILEY-VCH Verlag GmbH, 69451 Weinheim, 2001 1434−1948/01/0606−1631 $ 17.50+.50/0

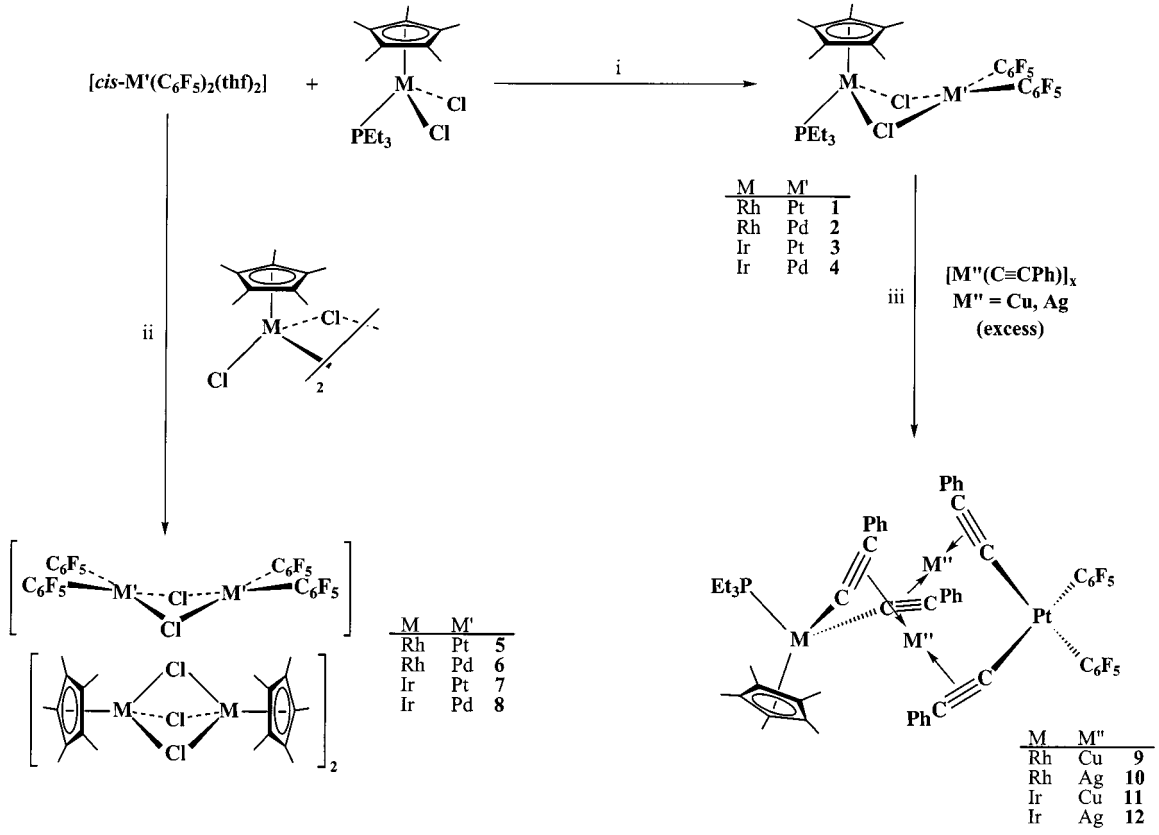

Scheme 1

with metallo species bearing potentially bridging groups in *cis* or even *trans* positions has proved to be an excellent preparative method for the synthesis of bi- and polymetallic complexes.[4a,4g,5] Therefore, we considered it appropriate to use this strategy for the synthesis of the desired doubly chloride-bridged heterobinuclear complexes **1**–**4**. Treatment of a red solution of $[MCp^*Cl_2(PEt_3)]$ (M = Rh, Ir) in acetone with 1 equivalent of the solvated platinum or palladium complex $[cis\text{-}M'(C_6F_5)_2(thf)_2]$ immediately gave an orange solution, from which the corresponding complexes **1**–**4** could be isolated as orange solids in high yields (i, Scheme 1). It should be mentioned that several neutral $[(ppy)_2M(\mu\text{-}Cl)_2M'(PR_3)Cl]$ (M = Rh, Ir; M′ = Pt, Pd; ppy = 2-phenylpyridine anion; R = Bu, Et) or cationic $[(chel)M(\mu\text{-}Cl)_2M'(PEt_3)_2](BF_4)$ (M = Rh, Ir; M′ = Pt, Pd; chel = anion of 2-phenylpyridine, benzo[4]quinoline, $C_6H_5CHRNMe_2$, or η^3-allyl) heterobinuclear (d^6-d^8) chloride-bridged complexes have been very recently prepared by metathesis reactions from the respective chloro-bridged homodimeric compounds.[3l,3o] In addition, related dicationic $[(PMe_3)(\eta^5\text{-}C_5Me_5)M(\mu\text{-}Cl)_2PtL_2]^{2+}(OTf)_2^-$ (M = Rh, Ir; L_2 = dppp, 2 PPh_3) complexes have been prepared by a similar route starting from the bis(triflate) species $[MCp^*(PMe_3)(OTf)_2]$ (M = Rh, Ir) and the corresponding dichloroplatinum derivatives.[3g]

The heterobinuclear platinum complexes **1** and **3** remain stable indefinitely, both in the solid state and in solution, but the mixed palladium compounds are only stable in the solid state. In solution, **2** and **4** slowly decompose with the deposition of metallic palladium. The complexes have been characterized by analytical and spectroscopic techniques. In addition, the structure of complex **1** has been established by an X-ray diffraction study. The IR spectra show two absorptions in the 785–812 cm^{-1} region attributable to the x-sensitive mode of the C_6F_5 groups (A′, A″; C_s), thus indicating the presence of a *cis*-$M(C_6F_5)$ moiety.[6] Furthermore, all the complexes show bands (247–277 cm^{-1}) associated with the ν(M–Cl) stretching vibrations (2A′ + 2 A″; C_s) of the bridges.

The NMR spectroscopic data are consistent with the solid-state structure of complex **1**. This complex crystallizes with a bent $RhCl_2Pt$ central core, and the conformer found (see Figure 1) is that in which the $Pt(C_6F_5)_2$ unit lies *endo* to the Cp* ligand. The room and low-temperature NMR spectroscopic data (^1H, $^{31}P\{^1H\}$, ^{19}F, and $^{13}C\{^1H\}$) reveal no evidence of possible conformers (see Experimental Section for details), although a possible rapid interconversion of conformers (fast inversion of the central $RhCl_2Pt$ core) cannot be excluded. Only the ^{19}F NMR spectra are temperature dependent. Thus, in accordance with the structure depicted in Scheme 1 (see also Figure 1), the room temperature ^{19}F NMR spectra in $[D_6]$acetone show only one type of C_6F_5 ligand, confirming the equivalence of the two C_6F_5 moieties. However, they exhibit the typical AA′MXX′ pattern of three signals of relative intensity 2:1:2, evidencing that the two halves of each C_6F_5 ring appear equivalent at room temperature, and indicating that these complexes are not rigid in solution. As expected, on lowering the temper-

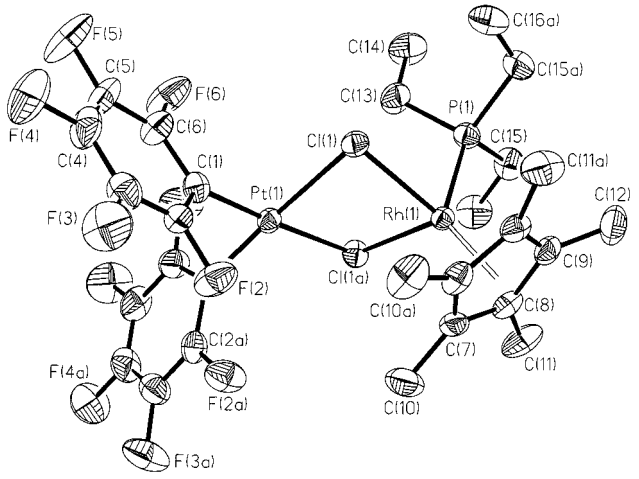

Figure 1. Molecular structure of $[(PEt_3)(\eta^5\text{-}C_5Me_5)Rh(\mu\text{-}Cl)_2Pt(C_6F_5)_2]$ (**1**) showing the atom labelling scheme (ellipsoids are drawn at a 50% probability level; hydrogen atoms have been omitted for clarity)

ature (to −50 °C), five distinct fluorine resonances become clearly resolved for all the complexes. We note that a possible fast inversion of the central MCl_2M' core, which cannot be excluded, would not exchange the two halves of each C_6F_5 moiety. Therefore, the most likely dynamic process that would account for the exchange of the halves of the C_6F_5 rings is their free rotation about the $Pt-C_i(C_6F_5)$ bonds. From the coalescence temperature T_c (258 K) and the difference in chemical shift $\Delta\nu$ of the F_o signals, a $\Delta G^{\#}$ value of 51 kJ·mol^{-1} has been calculated for **4**.[7] For complex **1**, the ^{19}F NMR spectra have also been recorded in $CDCl_3$ and both the room and low-temperature (−50 °C) spectra were found to be almost identical to those obtained in [D$_6$]acetone solution. This fact suggests that dissociative processes, such as the dissociation of an $M'(C_6F_5)_2$ unit or chloride−M′ (M′ = Pt, Pd) bond breaking, which would probably be solvent dependent, are unlikely.

A definitive structural assignment of the heterobimetallic complexes **1**−**4** has been established by an X-ray diffraction study on complex $[(PEt_3)(\eta^5\text{-}C_5Me_5)Rh(\mu\text{-}Cl)_2Pt(C_6F_5)_2]$ (**1**, Figure 1). Suitable dark-orange crystals were obtained by slow diffusion of hexane into a solution of **1** in acetone at low temperature (−30 °C). Selected bond lengths and angles are collected in Table 1. The structure confirms that the complex contains an Rh(III) centre in a pseudo-octahedral environment, formed by the η^5-bonded C_5Me_5 group, which occupies three formal coordination sites, the PEt_3, and the two bridging chlorides, and a Pt atom that completes its usual square-planar coordination with two σ-C_6F_5 groups. The geometries around both metal centres are unexceptional for fragments of this type and are similar to those previously observed in related homo-bridged μ-bis(alkynyl) and hetero-bridged (μ-Cl)(μ-alkynyl) d^6-d^8 systems.[4g] The central $Rh(\mu\text{-}Cl)_2Pt$ core shows a marked deviation from planarity, with a dihedral angle between the ClRhCl plane and the platinum coordination plane of 31.5°. This structural feature contrasts with the planar cores previously found in the corresponding doubly chloride-bridged symmetrical bimetallic species $(NBu_4)_2[(C_6F_5)_2Pt(\mu\text{-}Cl)_2Pt(C_6F_5)_2]$[8] and $[\{Rh(\eta^5\text{-}C_5Me_5)Cl(\mu\text{-}Cl)\}_2]$.[9] A recent theoretical study seems to confirm the observation that asymmetric chloro-bridged complexes tend to have a bent structural arrangement.[3p] Thus, the cationic mixed derivative $[(bzq)_2Rh(\mu\text{-}Cl)_2Pt(PBu_3)_2]^+$ is also considerably bent (29.4°)[3o] and similar nonplanar structures, albeit less severely distorted, have also been found in $[(PMe_3)Cp^*Ir(\mu\text{-}Cl)_2Pt(dppp)]^{2+}$ (ca. 11°)[3g] and $[(ppy)_2Rh(\mu\text{-}Cl)_2PtCl(PBu_3)]$ (13.2°).[3l] However, other theoretical and structural analyses of square-planar d^8 metal complexes of the type $[L_2M(\mu\text{-}Cl)_2ML_2]$ seem to suggest that attractive metal−metal interactions are one of the main factors responsible for the observed bending.[10] In complex **1**, the Pt−Rh distance of 3.407(1) Å suggests that the observed puckering does not lead to any significant metal−metal bonding interaction. However, this distance is markedly shorter than those observed in the respective homobimetallic species $[\{(C_6F_5)_2Pt(\mu\text{-}Cl)\}_2]^{2-}$ [3.528(1) Å][8] and $[\{Rh(\eta^5\text{-}C_5Me_5)Cl(\mu\text{-}Cl)\}_2]$ [3.719(1) Å][9] and in the mixed $Rh^{III}-Pt^{II}$ *ortho*-metallated derivatives $[(ppy)_2Rh(\mu\text{-}Cl)_2PtCl(PBu_3)]$ (3.61 Å)[3l] and $[(bzq)_2Rh(\mu\text{-}Cl)_2Pt(PBu_3)_2]^+$ (3.63 Å).[3o] Clearly, the value mentioned above is more akin to that found in the chloride/alkynide hetero-bridged compound $[(PEt_3)Cp^*Rh(\mu\text{-}Cl)(\mu\text{-}C{\equiv}CPh)Pt(C_6F_5)_2]$ [3.371(1) Å].[4g]

Table 1. Selected bond lengths [Å] and angles [deg.] in complex $[(PEt_3)Cp^*Rh(\mu\text{-}Cl)_2Pt(C_6F_5)_2]$ (**1**) (Cp^*_{cent}: centroid of the Cp* group. Symmetry transformations used to generate equivalent atoms (a): $x, -y + 1/2, z$)

Rh−Cl(1)	2.409(1)	Rh−P	2.313(2)
$Rh-Cp^*_{cent}$	1.799(1)	Pt−C(1)	1.959(4)
Pt−Cl(1)	2.381(1)	Rh···Pt	3.407(1)
P−Rh−Cl(1)	89.27(4)	Cl(1)−Rh−Cl(1a)	84.02(5)
$P-Rh-Cp^*_{cent}$	133.04(5)	$Cl(1)-Rh-Cp^*_{cent}$	123.48(3)
Pt−Cl(1)−Rh	90.65(3)	C(1)−Pt−C(1a)	90.6(2)
C(1)−Pt−Cl(1)	92.07(12)	Cl(1)−Pt−Cl(1a)	85.22(5)

The bridging chloride is slightly asymmetric, with metal−chlorine distances [Rh−Cl(1) 2.409(1) Å; Pt−Cl(2) 2.381(1) Å] rather similar to those found in $[(PEt_3)Cp^*Rh(\mu\text{-}Cl)(\mu\text{-}C{\equiv}CPh)Pt(C_6F_5)_2]$ (≈ 2.43 Å). This structural feature is in marked contrast to the dichloro bridges in the cationic $[(bzq)_2Rh(\mu\text{-}Cl)_2Pt(PBu_3)_2]^+$ and neutral $[(ppy)_2Rh(\mu\text{-}Cl)_2PtCl(PBu_3)]$ complexes, which are highly asymmetric (Rh−Cl ≈ 2.53 Å; Pt−Cl 2.36−2.40 Å). The Cl(1)RhCl(1a) [84.02(5)°] and Cl(1)PtCl(1a) [85.22(5)°] angles are almost identical and are slightly smaller than the angle at the chlorine atom [90.65(3)°].

With the aim of obtaining binuclear derivatives of the general formula $[(S)Cp^*M(\mu\text{-}Cl)_2M'(C_6F_5)_2]$ with one vacant site for bonding, where S could be a solvent molecule such as acetone or thf, we also explored the reactivity of the tetrahydrofuran adducts $[cis\text{-}M'(C_6F_5)_2(thf)_2]$ towards the binuclear derivatives $[\{MCp^*Cl(\mu\text{-}Cl)\}_2]$ in acetone in a 2:1 molar ratio. However, contrary to our expectations,

these reactions did not afford the desired heterobimetallic complexes; instead, low yields of the mixed ionic 2:1 salts $[Cp^*M(\mu\text{-}Cl)_3MCp^*]_2[\{(C_6F_5)_2M'(\mu\text{-}Cl)\}_2]$ (**5**–**8**) (ii, Scheme 1) were obtained. Predictably, better yields were obtained when the reactions were carried out in a 1:1 molar ratio (see Experimental Section). In these reactions, the platinum and palladium fragments "*cis*-$M'(C_6F_5)_2$" act as abstractors of chloride ligands giving $[cis\text{-}(C_6F_5)_2M'Cl]^-$, which dimerizes to $[(C_6F_5)_2M'(\mu\text{-}Cl)_2M'(C_6F_5)_2]^{2-}$, thus leaving the binuclear half-sandwich cationic complexes $[Cp^*M(\mu\text{-}Cl)_3MCp^*]^+$ with the chloro-bridges. Both cationic $[(Cp^*M)_2(\mu\text{-}Cl)_3]BF_4$ (M = Rh, Ir)[11a] species have previously been generated in a more rational manner by treating the binuclear neutral derivatives with $AgClO_4$ or $TlBF_4$ in CH_2Cl_2 and, in the case of $[Cp^*Rh(\mu\text{-}Cl)_3RhCp^*]^+$, also by reaction of $[\{RhCp^*Cl(\mu\text{-}Cl)\}_2]$ with $NaBPh_4$.[11b] We also note that chloride-transfer reactions between the highly charged fragments $[PtCl_6]^{2-}$ and $[RhCp^*(NCMe)_3]^{2+}$,[12] as well as between the neutral half-sandwich complexes $[\{(p\text{-cym})RuCl(\mu\text{-}Cl)\}_2]$ or $[\{MCp^*Cl(\mu\text{-}Cl)\}_2]$ (M = Rh, Ir) and the cationic chloride-bridged palladium(II) substrate,[3o] have been reported previously.

The ionic compounds **5**–**8**, which were obtained as orange (**5**, **6**) or yellow (**7**, **8**) solids, are only slightly soluble in organic solvents, the solubility being especially low in the case of the iridium derivatives. These complexes have been characterized by a combination of microanalysis, mass spectrometry [ES(+) and ES(−)], and spectroscopic methods (IR, ^1H and ^{19}F NMR) (see Experimental Section). Mass spectra in the ES(+) mode feature the expected $[M_2Cp^*_2Cl_3]^+$ (M = Rh, Ir) ion molecular fragment and in the ES(−) or APCI(−) modes they feature the $[M'(C_6F_5)_2Cl]^-$ (M′ = Pt, Pd) ion fragment arising from a fragmentation of the binuclear anion.

The molecular structure of **6** was confirmed by single-crystal X-ray analysis (Figure 2, Table 2). As can be seen, it comprises two $[(Cp^*Rh)_2(\mu\text{-}Cl)_3]^+$ ions and a binuclear dianionic $[(C_6F_5)_2Pd(\mu\text{-}Cl)_2Pd(C_6F_5)_2]^{2-}$ ion. The structural features of the cationic fragment are identical to those reported previously[12,13] hence they are not discussed here.

In contrast, although the crystal structures of the anions $[(C_6F_5)_2Pt(\mu\text{-}Cl)_2Pt(C_6F_5)_2]^{2-}$ [8] and $[(C_6F_5)_2Ni(\mu\text{-}Cl)_2Ni(C_6F_5)_2]^{2-}$ [14] have been published, the structure of the corresponding dipalladium species remains unknown. Therefore, this study completes the series with its final member, $[(C_6F_5)_2Pd(\mu\text{-}Cl)_2Pd(C_6F_5)_2]^{2-}$, providing an opportunity for quantitative structural comparisons. Selected distances and angles are compared in Table 3. It is interesting to note that one of the most remarkable differences can be seen in the M'_2Cl_2 core. Thus, while the nickel and platinum anions exhibit typical[3p,10] $M'_2Cl_2C_4$ planar cores (both have a crystallographic centre of inversion), the anion $[(C_6F_5)_2Pd(\mu\text{-}Cl)_2Pd(C_6F_5)_2]^{2-}$ found in **6** displays a slightly bent chloro-bridge, with the dihedral angle defined by the corresponding palladium coordination planes being 13°. The resulting Pd···Pd distance of 3.464(2) Å is, as expected, longer than that found in the nickel derivative [Ni···Ni 3.28 Å].[14] However, assuming covalent radii for Pd and Pt of

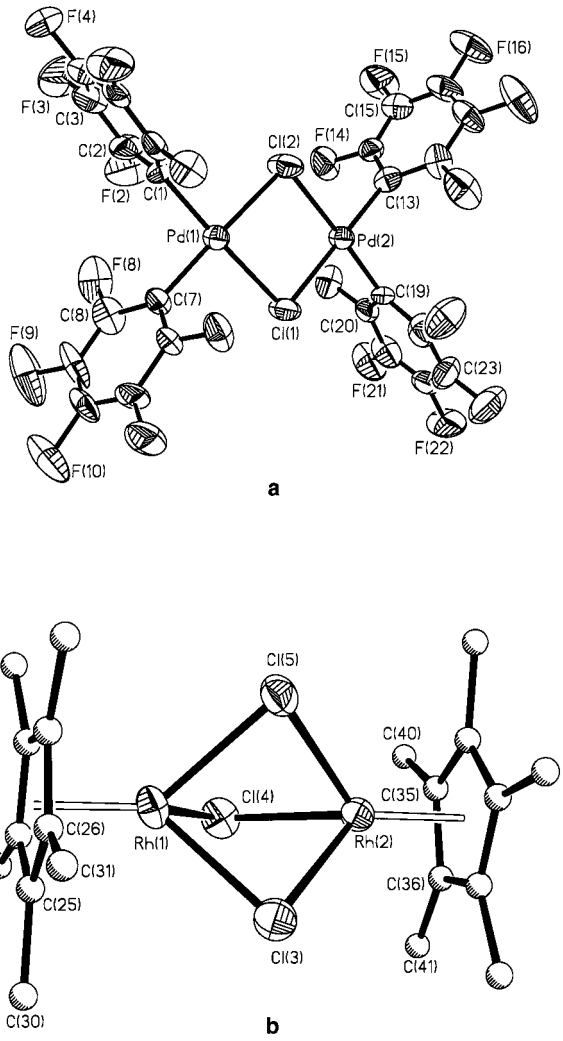

Figure 2. Structure and atom numbering scheme for the anion $[\{(C_6F_5)_2Pd(\mu\text{-}Cl)\}_2]^{2-}$ (a) and one of the cations $[Cp^*Rh(\mu\text{-}Cl)_3RhCp^*]^+$ (b) in complex **6** (ellipsoids are drawn at a 50% probability level; hydrogen atoms have been omitted for clarity)

1.31 and 1.28 Å, respectively,[15] the Pd···Pd distance should be ca. 0.06 Å longer than that found in the diplatinum anion [Pt···Pt 3.528(1) Å],[8] thus suggesting that the experimental value found in the dipalladium anion [3.464(2) Å] might be reduced due to the small degree of bending.

The Pd–C [2.001(13)–2.023(12) Å] and Pd–Cl [2.404(4)–2.421(4) Å] bridging lengths are comparable with those seen in $[(C_6F_5)_2Pd(\mu\text{-}Cl)_2Pt(PEt_3)_2]$ [Pd–C 1.980(7), 1.992(7) Å; Pd–Cl 2.402(2), 2.449(2) Å], which is the only derivative to be crystallographically characterized that also contains the "$(C_6F_5)_2PdCl_2$" fragment.[3f]

Synthesis of Tetranuclear $[(PEt_3)Cp^*M(\mu\text{-}C{\equiv}CPh)_2M''_2(\mu\text{-}C{\equiv}CPh)_2Pt(C_6F_5)_2]$ Complexes (9–12)

We have recently been interested in exploring the reactivity of alkynyl platinate(II) complexes towards suitable electrophilic metal fragments as a useful route to heteropolynuclear complexes containing alkynyl bridging ligands.[4a,4b,4d–4g,4i–4k] As an alternative route, we decided to examine the potential utility of the new chloride-bridged

Table 2. Selected bond lengths (Å) and angles (deg.) in complex $\{Cp^*Rh(\mu\text{-}Cl)_3RhCp^*\}_2[\{(C_6F_5)_2Pd(\mu\text{-}Cl)\}_2]$ (**6**) (C*1, C*2, C*3, C*4: centroids of the Cp* groups)

Pd(1)−C(1)	2.023(12)	Pd(1)−C(7)	2.014(12)
Pd(1)−Cl(1)	2.421(4)	Pd(1)−Cl(2)	2.413(3)
Pd(2)−C(13)	2.008(13)	Pd(2)−C(19)	2.001(13)
Pd(2)−Cl(1)	2.411(3)	Pd(2)−Cl(2)	2.404(4)
Pd(1)··Pd(2)	3.464(2)	Rh(1)−C*1	1.749(1)
Rh(1)−Cl(3)	2.473(4)	Rh(1)−Cl(4)	2.469(4)
Rh(1)−Cl(5)	2.473(3)	Rh(2)−C*2	1.769(1)
Rh(2)−Cl(3)	2.479(4)	Rh(2)−Cl(4)	2.472(3)
Rh(2)−Cl(5)	2.476(4)	Rh(1)··Rh(2)	3.246(2)
Rh(3)−C*3	1.773(1)	Rh(3)−Cl(6)	2.467(4)
Rh(3)−Cl(7)	2.452(4)	Rh(3)−Cl(8)	2.443(4)
Rh(4)−C*4	1.766(1)	Rh(4)−Cl(6)	2.480(4)
Rh(4)−Cl(7)	2.472(4)	Rh(4)−Cl(8)	2.457(4)
Rh(3)··Rh(4)	3.246(2)		
Cl(1)−Pd(1)−Cl(2)	87.23(12)	Cl(1)−Pd(1)−C(7)	91.0(4)
Cl(2)−Pd(1)−C(1)	90.0(4)	C(1)−Pd(1)−C(7)	91.9(5)
Cl(1)−Pd(2)−Cl(2)	87.66(12)	Cl(1)−Pd(2)−C(19)	91.0(4)
Cl(2)−Pd(2)−C(13)	91.0(4)	C(13)−Pd(2)−C(19)	90.4(5)
Pd(1)−Cl(1)−Pd(2)	91.60(11)	Pd(1)−Cl(2)−Pd(2)	91.95(11)
Cl(3)−Rh(1)−Cl(4)	81.49(13)	Cl(3)−Rh(1)−Cl(5)	82.06(12)
Cl(4)−Rh(1)−Cl(5)	81.49(12)	C*1−Rh(1)−Cl(3)	130.07(13)
C*1−Rh(1)−Cl(4)	130.90(10)	C*1−Rh(1)−Cl(5)	131.91(12)
Cl(3)−Rh(2)−Cl(4)	81.31(12)	Cl(3)−Rh(2)−Cl(5)	81.89(13)
Cl(4)−Rh(2)−Cl(5)	81.39(11)	C*2−Rh(2)−Cl(3)	130.07(12)
C*2−Rh(2)−Cl(4)	132.05(11)	C*2−Rh(2)−Cl(5)	130.47(11)
Cl(6)−Rh(3)−Cl(7)	81.7(2)	Cl(6)−Rh(3)−Cl(8)	81.5(2)
Cl(7)−Rh(3)−Cl(8)	82.2(2)	C*3−Rh(3)−Cl(6)	130.39(13)
C*3−Rh(3)−Cl(7)	131.17(11)	C*3−Rh(3)−Cl(8)	131.09(14)
Cl(6)−Rh(4)−Cl(7)	81.0(2)	Cl(6)−Rh(4)−Cl(8)	81.0(2)
Cl(7)−Rh(4)−Cl(8)	81.5(2)	C*4−Rh(4)−Cl(6)	131.59(13)
C*4−Rh(4)−Cl(7)	131.71(12)	C*4−Rh(4)−Cl(8)	130.62(15)
Rh(1)−Cl(3)−Rh(2)	81.94(10)	Rh(1)−Cl(4)−Rh(2)	82.16(10)
Rh(1)−Cl(5)−Rh(2)	81.99(10)	Rh(3)−Cl(6)−Rh(4)	81.72(12)
Rh(3)−Cl(7)−Rh(4)	82.18(13)	Rh(3)−Cl(8)−Rh(4)	82.67(12)

Table 3. Comparison of selected bond lengths [Å] and angles [deg.] in the anions $[(C_6F_5)_2M'(\mu\text{-}Cl)_2M'(C_6F_5)_2]^{2-}$

Parameter	M′ = Ni	M′ = Pd	M′ = Pt
$M'-C_{average}$	1.880(3)	2.012(13)	1.984(10)
$M'-Cl_{average}$	2.253(1)	2.412(4)	2.391(3)
Cl−M′−Cl	86.71(3)	$87.45(12)_{average}$	84.9(1)
M′−Cl−M′	93.29(3)	$91.78(11)_{average}$	95.1(1)
M′····M′	3.28	3.464(2)	3.528(1)

heterobinuclear compounds **1**−**4** as precursors to alkynyl-bridged species by exploring their reactivity towards the well-known ethynylating agents $[M''(C{\equiv}CR)]_x$ (M′′ = Cu, Ag; R = Ph, *t*Bu). The reactions of the polymeric acetylides $[Cu(C{\equiv}CR)]_x$ and $[Ag(C{\equiv}CR)]_x$ with transition metal halide complexes $[ML_nX_m]$ have been extensively investigated. Simple substitution processes giving the corresponding mononuclear complexes $[ML_n(C{\equiv}CR)_m]$, as well as the formation of polynuclear species generated by further interaction of the latter with MX species (X = halide or C≡CR), have been reported.[4g,16]

The results of the reactions of **1**−**4** with $[M''(C{\equiv}CR)]_x$ (M′′ = Cu, Ag; R = Ph, *t*Bu) are shown in Scheme 1 (iii). As can be seen, only the treatment of the platinum mixed species $[(PEt_3)Cp^*M(\mu\text{-}Cl)Pt(C_6F_5)_2]$ (**1**, **3**) with the phenylethynyl substrates (10 equiv. for **9** and 4.5 equiv. for **10**−**12**) produces, after standard work-up, moderate (61−75%) or low yields ($RhAg_2Pt$ **10**, 27%) of yellow products that can be formulated as tetrametallic compounds $[(PEt_3)Cp^*M(\mu\text{-}1\kappa C^{\alpha}{:}\eta^2\text{-}C{\equiv}CPh)_2M''_2(\mu\text{-}4\kappa C^{\alpha}{:}\eta^2\text{-}C{\equiv}CPh)_2Pt(C_6F_5)_2]$ (M = Rh, Ir; M′′ = Cu, Ag) (**9**−**12**). Unfortunately, starting from the mixed palladium complexes **2** and **4**, considerable decomposition takes place and the analogous reactions with the *tert*-butyl alkynyl substrates $[M''C{\equiv}Ct\text{Bu}]_x$ (M = Cu, Ag) yield only complicated mixtures of products, which we have not been able to separate. We also note that the reactions of **1** and **3** with a smaller excess of the polymeric alkynides (2 equivalents) produced mixtures of compounds in which the final tetranuclear species and the heterobinuclear $[(PEt_3)Cp^*M(\mu\text{-}C{\equiv}CPh)(\mu\text{-}Cl)Pt(C_6F_5)_2]$ were easily detectable by $^{31}P\{^1H\}$ NMR spectroscopy.

The new tetranuclear compounds **9**−**12** have been fully characterized by analytical and spectroscopic means and the molecular structure of **9** has been unambiguously confirmed by X-ray diffraction analysis. The presence of bridging alkynyl ligands is evident from the IR spectra, which show two ν(C≡C) absorptions in the expected region (1969−2070 cm^{-1}).[4,16] These bands appear at lower frequencies in the copper derivatives [2009 (s br), 1969 (sh) cm^{-1} **9**; 2006 (s), 1969 (s) cm^{-1} **11**] than in their silver counterparts [2059 (s br) cm^{-1} **10**; 2070 (m), 2036 (m) cm^{-1} **12**] suggesting, in line with previous observations,[16−18] that the η^2-alkyne metal interaction is stronger in copper than in silver complexes. Their NMR spectra (^1H, ^{31}P) confirm the presence of different groups (Cp*, PEt_3, C≡CPh) and, in particular, the room temperature ^{19}F NMR spectra reveal effective mirror planes that render the two C_6F_5 ligands equivalent. Simple AA′MXX′ (2 F_o, F_p, 2 F_m) patterns are seen for all the complexes, presumably because the free rotation of the C_6F_5 rings is relatively fast at room temperature. However, low-temperature spectra could not be obtained due to the low solubilities of the complexes. Furthermore, their relatively low stabilities in solution at room temperature also precluded characterization by $^{13}C\{^1H\}$ NMR spectroscopy. Yellow crystals of $[(PEt_3)Cp^*Rh(\mu\text{-}C{\equiv}CPh)_2Cu_2(\mu\text{-}C{\equiv}CPh)_2Pt(C_6F_5)_2]$ **9** suitable for an X-ray diffraction study were isolated by slow diffusion of hexane into a CH_2Cl_2 solution at low temperature (−30 °C). Figure 3 depicts its molecular structure, while selected bond lengths and angles are summarized in Table 4.

The most remarkable aspect of the structure is that two very different bis(alkynyl) metal fragments "$RhCp^*(C{\equiv}CPh)_2(PEt_3)$" and "*cis*-$Pt(C_6F_5)_2(C{\equiv}CPh)_2$" are connected through two copper centres. As for complex **1**, of the two possible conformers of complex **9**, only that in which the platinum unit lies *endo* to the Cp* ring is observed (Figure 3, b). As expected, the Rh centre is tetrahedrally coordinated, being surrounded by the centroid of the Cp* ring, the PEt_3, and two σ-carbon atoms of the alkynyl groups, which act as bridging ligands between the two copper atoms. The Pt atom is located in a slightly distorted square-planar coordination environment made up of four σ-carbon atoms, two from the mutually *cis* C_6F_5 rings and two from the C≡CPh ligands, the latter also being η^2-bon-

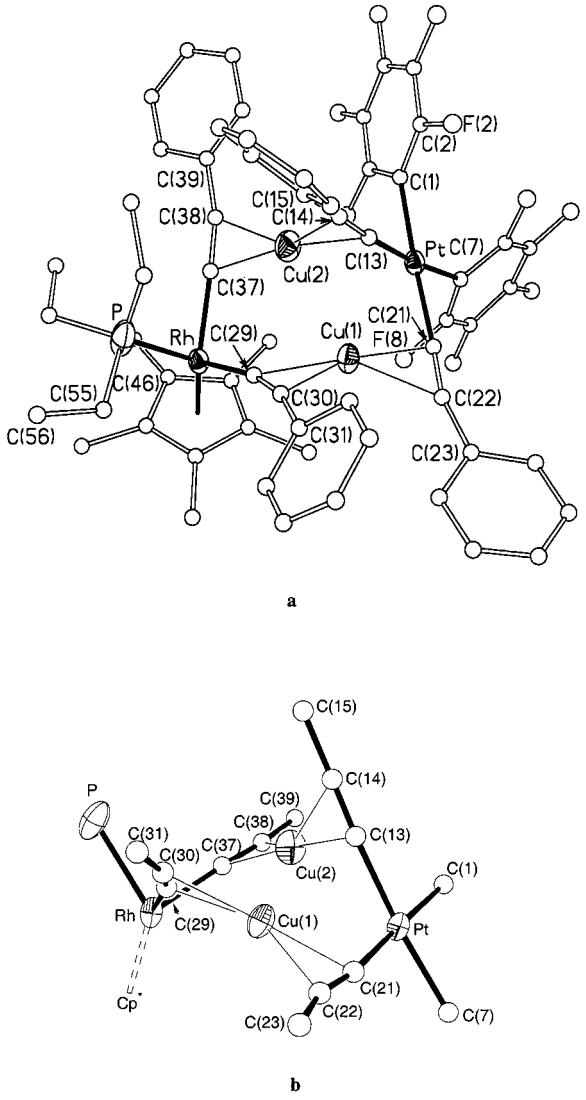

Figure 3. (a) View of the molecular structure of $[(PEt_3)Cp^*Rh(\mu\text{-}1\kappa C^{\alpha}{:}\eta^2\text{-}C{\equiv}CPh)_2Cu_2(\mu\text{-}4\kappa C^{\alpha}{:}\eta^2\text{-}C{\equiv}CPh)_2Pt(C_6F_5)_2]$ (**9**) (ellipsoids are drawn at a 50% probability level; hydrogen atoms have been omitted for clarity; (b) schematic view of the central core of **9**)

ded to the copper centres. The structural parameters for this fragment [Pt−C_α 2.014(8), 2.001(8) Å; C_α−Pt−C_α' 92.1(3)°] are rather similar to those previously observed for the tetranuclear anion $[Pt_2Ag_2(C_6F_5)_4(C{\equiv}CPh)_4]^{2-}$, in which two identical [*cis*-$Pt(C_6F_5)_2(C{\equiv}CPh)_2]^{2-}$ units are connected via two silver centres through η^2-alkyne−silver interactions.[16j]

The most remarkable feature of the rhodium fragment is that the C_α−Rh−C_α' angle (99.3°) is substantially larger compared to related bite angles in doubly alkynyl-bridged complexes $[(PEt_3)Cp^*Ir(\mu\text{-}C{\equiv}CR)_2M'(C_6F_5)_2]$ [M′ = Pt, R = Ph 79.9(8)°; R = $SiMe_3$ 76.9(6)°; M′ = Pd, R = Ph 81.0(7)°], in which the 3-irida-1,4-diyne fragments $[Ir](C{\equiv}CR)_2$ act as chelating bidentate ligands.[4g] This structural feature may be tentatively attributed to the bidentate bridging nature of the $[Rh](C{\equiv}CPh)_2$ unit.

All the alkynyl ligands are η^2-bonded to Cu atoms in such a way that each Cu is stabilized by two alkyne entities (one associated with each metal fragment). The Cu−C_α [1.984(8)−2.098(7) Å] and Cu−C_β [2.080(7)−2.230(8) Å] distances are, as expected, shorter than the corresponding Ag−C distances in $[Pt_2Ag_2(C_6F_5)_4(C{\equiv}CPh)_4]^{2-}$,[16j] but are comparable to those found in related systems such as $[Pt_2Cu_4(C{\equiv}CPh)_8]_3$ [Cu−C_α = 1.981(8)−2.019(8) Å; Cu−C_β = 2.141(9)−2.161(9) Å],[19] $[Ir_2Cu_4(C{\equiv}CPh)_8(PPh_3)_2]$ [Cu−C_α = 1.981(8)−2.019(8) Å; Cu−C_β = 2.141(9)−2.161(9) Å],[16a,16b] $[Mn_2Cu(\mu\text{-}C{\equiv}CtBu)_2(CO)_6(dppe)_2]^+$ [Cu−$C_{average}$ = 2.081(10) Å],[20] and $[\{Re(CO)_5{-}C{\equiv}C{-}Re(CO)_5\}_2Cu]^+$ [Cu−$C_{average}$ = 2.055(10) Å].[17] The parameters for the acetylenic fragments (C−C distances, angles at C_α and C_β) lie within the normal ranges for alkynyl σ,π bonding modes.[4,16−20]

The Cu(1)···Cu(2) distance [2.841(2) Å] is slightly shorter than those found in the cluster $[Pt_2Cu_4(C{\equiv}CPh)_8]_3$ [3.031(2) Å, 3.301(2) Å][19] and is comparable with those observed in the cluster $[Ir_2Cu_4(C{\equiv}CPh)_8(PPh_3)_2]$ [2.665(6) Å, 2.823(5) Å][16a,16b] and in other more common alkynyl polynuclear copper(I) complexes.[21] Nevertheless, it still slightly exceeds the van der Waals limit (2.80 Å),[15] excluding any significant bonding interaction. The Rh···Cu separations of 3.217 and 3.528 Å are considerably longer than the Pt···Cu distances of 2.9226(14) and 2.9384(13) Å, respectively. These latter values are comparable to those seen in $[Pt_2Cu_4(C{\equiv}CPh)_8]_3$ [2.9187(12)−3.0272(10) Å][19] and are considerably shorter than the sum of the van der Waals radii (3.15 Å),[15] probably suggesting the presence of some weak Pt···Cu bonding interactions.[22]

Table 4. Selected bond lengths (Å) and angles (deg.) in complex $[(PEt_3)Cp^*Rh(\mu\text{-}1\kappa C^{\alpha}{:}\eta^2\text{-}C{\equiv}CPh)_2Cu_2(\mu\text{-}4\kappa C^{\alpha}{:}\eta^2\text{-}C{\equiv}CPh)_2Pt(C_6F_5)_2]$ (**9**) (Cp^*_{cent}: centroid of the Cp* group)

Pt−C(21)	2.001(8)	Pt−C(13)	2.014(8)
Pt−C(1)	2.065(7)	Pt−C(7)	2.066(7)
Pt−Cu(1)	2.9226(14)	Pt−Cu(2)	2.9384(13)
Rh−C(37)	2.006(8)	Rh−C(29)	2.027(8)
Rh−P	2.289(2)	Cu(1)−C(21)	2.020(7)
Cu(1)−C(30)	2.080(7)	Cu(1)−C(29)	2.098(7)
Cu(1)−C(22)	2.194(7)	Cu(1)−Cu(2)	2.841(2)
Cu(2)−C(13)	1.984(8)	Cu(2)−C(37)	1.989(7)
Cu(2)−C(38)	2.101(8)	Cu(2)−C(14)	2.230(8)
C(13)−C(14)	1.222(10)	C(21)−C(22)	1.233(10)
C(29)−C(30)	1.213(10)	C(37)−C(38)	1.226(10)
Rh−Cp^*_{cent}	1.871	Rh−Pt	5.247
Rh−Cu(1)	3.528	Rh−Cu(2)	3.217
C(21)−Pt−C(13)	92.1(3)	C(1)−Pt−C(7)	87.8(3)
C(13)−Pt−C(1)	88.2(3)	C(21)−Pt−C(7)	91.7(3)
Cu(1)−Pt−Cu(2)	57.99(3)	C(37)−Rh−C(29)	99.3(3)
C(37)−Rh−P	87.0(2)	C(29)−Rh−P	83.7(2)
C(14)−C(13)−Pt	175.3(7)	C(13)−C(14)−C(15′)	161.7(13)
C(13)−C(14)−C(15)	176(3)	C(22)−C(21)−Pt	171.4(7)
C(21)−C(22)−C(23)	163.4(8)	C(30)−C(29)−Rh	167.7(7)
C(29)−C(30)−C(31)	165.2(8)	C(38)−C(37)−Rh	173.8(7)
C(37)−C(38)−C(39)	165.7(8)	Cp^*_{cent}−Rh−C(29)	122.81
Cp^*_{cent}−Rh−C(37)	122.23	Cp^*_{cent}−Rh−P	131.03
Cu(1)−Rh−Cu(2)	49.56		

Experimental Section

General Remarks: All reactions were carried out under nitrogen atmosphere. Solvents (hexane, alkane mixtures) were dried by

standard procedures and distilled under dry N_2 before use; acetone was treated with $KMnO_4$ and distilled under dry N_2 prior to use. $[MCp^*Cl_2(PEt_3)]$,[4g] $[MCp^*Cl_2]_2$ (M = Rh, Ir),[23] $[MC{\equiv}CPh]_x$ (M = Ag,[24] Cu[25]), and $[cis\text{-}M'(C_6F_5)_2(thf)_2]$ (M′ = Pt, Pd)[26] were prepared by published methods. − ^1H, ^{13}C, ^{19}F, and ^{31}P NMR spectra were recorded on a Bruker ARX-300 spectrometer. Chemical shifts are reported in ppm relative to external standards ($SiMe_4$, $CFCl_3$, and 88% H_3PO_4) and coupling constants are given in Hz. − Infrared spectra were recorded on a Perkin−Elmer 883 spectrometer with samples as Nujol mulls between polyethylene sheets. − C, H, N analyses were carried out with Perkin−Elmer 2400 CHNS/O or Carlo Erba EA1110 CHNS-O microanalyzers. − Mass spectra were obtained on VG Autospec double-focusing (FAB) or HP-5989B (APCI and ES) mass spectrometers. − Conductivities were measured in ca. $5{\cdot}10^{-4}$ M acetone solutions using a Philips 950/01 conductimeter.

Synthesis of $[(PEt_3)Cp^*M(\mu\text{-}Cl)_2M'(C_6F_5)_2]$ (M = Rh, M′ = Pt 1, M′ = Pd 2; M = Ir, M′ = Pt 3, M′ = Pd 4): A red solution of $[RhCp^*Cl_2(PEt_3)]$ (0.10 g, 0.23 mmol) in acetone (10 mL) was treated with $[cis\text{-}Pt(C_6F_5)_2(thf)_2]$ (0.15 g, 0.23 mmol), which immediately afforded an orange solution. The mixture was stirred for 5 min and then concentrated to dryness. Treatment of the solid residue with cold EtOH (ca. 5 mL) furnished complex **1** as an orange solid. Complexes **2**−**4** (also orange solids) were similarly prepared but with omission of the stirring for 5 min in the case of the palladium complexes **2** and **4**. Reagents and quantities used: $[cis\text{-}Pd(C_6F_5)_2(thf)_2]$ (0.14 g, 0.23 mmol) and $[RhCp^*Cl_2(PEt_3)]$ (0.10 g, 0.23 mmol) for **2**; $[cis\text{-}Pt(C_6F_5)_2(thf)_2]$ (0.34 g, 0.51 mmol) and $[IrCp^*Cl_2(PEt_3)]$ (0.26 g, 0.51 mmol) for **3**; $[cis\text{-}Pd(C_6F_5)_2(thf)_2]$ (0.11 g, 0.19 mmol) and $[IrCp^*Cl_2(PEt_3)]$ (0.10 g, 0.19 mmol) for **4**.

1: (0.20 g, 90%). − $C_{28}H_{30}Cl_2F_{10}PPtRh$ (956.42): calcd. C 35.16, H 3.16; found C 34.97, H 2.87. − IR: $\tilde{\nu}$ = 812 (vs), 800 (vs) cm^{-1} $(C_6F_5)_{x\text{-}sens}$; 277 (m), 255 (m), 246 (m) cm^{-1} (M−Cl). − ^1H NMR ($CDCl_3$): at 20 °C: δ = 1.15 (m, 9 H, CH_3, PEt_3), 1.74 (d, $^4J_{P-H}$ = 2.6, 15 H, Cp*), 2.23 (m, 6 H, CH_2, PEt_3); at −50 °C: δ = 1.07 (m, 9 H, CH_3, PEt_3), 1.75 (d, $^4J_{P-H}$ = 2.7, 15 H, Cp*), 2.20 (m, 6 H, CH_2, PEt_3). − ^{13}C NMR ([D$_6$]acetone): at 20 °C: δ = 7.3 (d, $^2J_{P-C}$ = 3.4, CH_3, PEt_3), 9.3 [s, $C_5(CH_3)_5$], 15.4 (d, $^1J_{P-C}$ = 27.8, CH_2, PEt_3), 101.9 (dd, $^1J_{Rh-C}$ = 7.1, $^2J_{P-C}$ = 2.0, C_5Me_5), 135.95 (dm, $^1J_{F-C}$ = 253, C_m, C_6F_5), 136.5 (dm, $^1J_{F-C}$ = 241, C_p, C_6F_5), 148.95 (dm, $^1J_{F-C}$ = 231, C_o, C_6F_5). − ^{19}F NMR ($CDCl_3$): at 20 °C: δ = −163.03 (m, 4 F_m), −163.99 (t, 2 F_p), −119.62 (d, $^3J_{Pt-F}$ = 527.7, 4 F_o); at −50 °C: δ = −165.34 (m, 2 F_m), −164.99 (m, 2 F_m), −163.18 (t, 2 F_p), −119.74 (d, $^3J_{Pt-F} \approx$ 525, 2 F_o), −119.29 (d, $^3J_{Pt-F} \approx$ 510, 2 F_o). − ^{31}P NMR ($CDCl_3$): at 20 °C: δ = 30.27 (d, $^1J_{Rh-P}$ = 138.3); at −50 °C: δ = 31.31 (d, $^1J_{Rh-P}$ = 137.9). − FAB(+) MS: *m/z* (%) = 955 (5) [M^+ − 1], 789 (10) [M^+ − C_6F_5], 391 (100) [$RhCp^*Cl(PEt_3)^+$].

2: (0.16 g, 78%). − $C_{28}H_{30}Cl_2F_{10}PPdRh$ (867.75): calcd. C 38.76, H 3.48; found C 38.43, H 3.41. − IR: $\tilde{\nu}$ = 798 (s), 785 (s) cm^{-1} $(C_6F_5)_{x-sens}$; 268 (m, br) (M−Cl). − ^1H NMR ([D$_6$]acetone): at 20 °C: δ = 1.17 (m, 9 H, CH_3, PEt_3), 1.81 (d, $^4J_{P-H}$ = 3, 15 H, Cp*), 2.38 (m, 6 H, CH_2, PEt_3); at −50 °C: δ = 1.07 (m, 9 H, CH_3, PEt_3), 1.81 (d, $^4J_{P-H}$ = 2.7, 15 H, Cp*), 2.32 (m, 6 H, CH_2, PEt_3). − ^{13}C NMR ([D$_6$]acetone): at −50 °C: δ = 6.1 (d, $^2J_{P-C}$ = 3.5, CH_3, PEt_3), 8.0 [s, $C_5(CH_3)_5$], 14.4 (d, $^1J_{P-C}$ = 27.8, CH_2, PEt_3), 100.7 (dd, $^1J_{Rh-C}$ = 7.1, $^2J_{P-C}$ = 2.3, C_5Me_5), 134.4 (dm, $^1J_{F-C}$ = 257, C_m, C_6F_5), 135.75 (dt, $^1J_{F-C}$ = 241, $^2J_{F-C} \approx$ 14, C_p, C_6F_5), 146.2 (dm, $^1J_{F-C}$ = 226, C_o, C_6F_5). − ^{19}F NMR ([D$_6$]acetone): at 20 °C: δ = −165.63 (m, 4 F_m), −163.27 (t, 2 F_p), −114.54 (d, 4 F_o); at −50 °C: δ = −164.89 (m, 4 F_m), −162.31 (t, 2 F_p), −114.47 (d, 2 F_o), −114.21 (d, 2 F_o). − ^{31}P NMR ([D$_6$]acetone): at 20 °C: δ = 29.66 (d, $^1J_{Rh-P}$ = 139); at −50 °C: δ = 30.75 (d, $^1J_{Rh-P}$ = 138.8). − FAB(+) MS: *m/z* (%) = 832 (6) [M^+ − Cl − 1], 700 (21) [M^+ − C_6F_5], 391 (100) [$RhCp^*Cl(PEt_3)^+$].

3: (0.45 g, 85%). − $C_{28}H_{30}Cl_2F_{10}IrPPt$ (1045.73): calcd. C 32.16, H 2.89; found C 31.94, H 2.89. − IR: $\tilde{\nu}$ = 812 (vs), 800 (vs) cm^{-1} $(C_6F_5)_{x-sens}$; 285 (s), 276 (s), 253 (s) cm^{-1} (M−Cl). − ^1H NMR ([D$_6$]acetone): at 20 °C: δ = 1.14 (m, 9 H, CH_3, PEt_3), 1.81 (d, $^4J_{P-H}$ = 1.6, 15 H, Cp*), 2.44 (m, 6 H, CH_2, PEt_3); at −50 °C: δ = 1.05 (m, 9 H, CH_3, PEt_3), 1.81 (d, $^4J_{P-H}$ = 2.7, 15 H, Cp*), 2.37 (m, 6 H, CH_2, PEt_3). − ^{13}C NMR ([D$_6$]acetone): at −50 °C: δ = 5.4 (d, $^2J_{P-C}$ = 3.3, CH_3, PEt_3), 7.4 [s, $C_5(CH_3)_5$], 13.5 (d, $^1J_{P-C}$ = 35.1, CH_2, PEt_3), 93.4 (d, $^2J_{P-C}$ = 2.3, C_5Me_5), 134.25 (dm, $^1J_{F-C}$ = 260, C_m, C_6F_5), 135.1 (dm, $^1J_{F-C}$ = 240, C_p, C_6F_5), 147.2 (dm, $^1J_{F-C}$ = 238, C_o, C_6F_5). − ^{19}F NMR ([D$_6$]acetone): at 20 °C: δ = −166.74 (m, $^4J_{Pt-F}$ = 124.5, 4 F_m), −164.81 (t, 2 F_p), −118.41 (d, $^3J_{Pt-F}$ = 526.2, 4 F_o); at −50 °C: δ = −165.99 (m, 4 F_m), −163.86 (t, 2 F_p), −118.49 (d, $^3J_{Pt-F} \approx$ 400, 2 F_o), −117.98 (d, $^3J_{Pt-F}$ = 509.9, 2 F_o). − ^{31}P NMR ([D$_6$]acetone): at 20 °C: δ = 4.57 (s); at −50 °C: δ = 5.80 (s). − FAB(+) MS: *m/z* (%) = 1044 (17) [M^+ − 2], 878 (6) [M^+ − C_6F_5], 481 (100) [$IrCp^*Cl(PEt_3)^+$].

4: (0.13 g, 71%) (analyses for a sample recrystallized from $CHCl_3$/hexane, which retained a $^1/_2$ molecule of $CHCl_3$ as observed by ^1H NMR in [D$_6$]acetone). − $C_{28}H_{30}Cl_2F_{10}IrPPd{\cdot}0.5CHCl_3$ requires C 33.67, H 3.02; found C 33.99, H 2.74. − IR: $\tilde{\nu}$ = 798 (s), 785 (s) cm^{-1} $(C_6F_5)_{x-sens}$; 285, 280 (s), 268 (m), 247 (sh) cm^{-1} (M−Cl). − ^1H NMR ([D$_6$]acetone): at 20 °C: δ = 1.16 (m, 9 H, CH_3, PEt_3), 1.81 (d, $^4J_{P-H}$ = 1.3, 15 H, Cp*), 2.43 (m, 6 H, CH_2, PEt_3); at −50 °C: δ = 1.14 (m, 9 H, CH_3, PEt_3), 1.81 (s, 15 H, Cp*), 2.43 (m, 6 H, CH_2, PEt_3). − ^{13}C NMR ([D$_6$]acetone): at −50 °C: δ = 7.1 (d, $^2J_{P-C}$ = 3.5, CH_3, PEt_3), 9.05 [s, $C_5(CH_3)_5$], 13.5 (d, $^1J_{P-C}$ = 35, CH_2, PEt_3), 94.5 (d, $^2J_{P-C}$ = 2.5, C_5Me_5), 135.9 (dm, $^1J_{F-C}$ = 244, C_m, C_6F_5), 137.3 (dm, $^1J_{F-C}$ = 241, C_p, C_6F_5), 147.5 (dm, $^1J_{F-C}$ = 228, C_o, C_6F_5). − ^{19}F NMR ([D$_6$]acetone): at 20 °C: δ = −165.50 (m, 4 F_m), −162.95 (t, 2 F_p), −114.87 (d, 4 F_o); at −50 °C: δ = −164.82 (m, 4 F_m), −162.11 (t, 2 F_p), −114.89 (d, 2 F_o), −114.48 (d, 2 F_o). − ^{31}P NMR ([D$_6$]acetone): at 20 °C: δ = 2.13 (s); at −50 °C: δ = 3.07 (s). − FAB(−) MS: *m/z* (%) = 917 (3) [M^- − Cl − 4], 477 (100) [$Pd(C_6F_5)_2Cl^-$].

Synthesis of $[Cp^*Rh(\mu\text{-}Cl_3)RhCp^*]_2[(C_6F_5)_2Pt(\mu\text{-}Cl_2)Pt(C_6F_5)_2]$ (5): To a red solution of $[RhCp^*Cl_2]_2$ (0.10 g, 0.162 mmol) in acetone (20 mL) was added $[cis\text{-}Pt(C_6F_5)_2(thf)_2]$ (0.11 g, 0.162 mmol) (molar ratio 1:1) and the mixture was stirred for 30 min. Evaporation of the solvent from the orange suspension and treatment of the solid residue with Et_2O (ca. 5 mL) yielded complex **5** (0.13 g, 68%) as an orange solid. − $C_{64}H_{60}Cl_8F_{20}Pt_2Rh_4$ (2294.60): calcd. C 33.50, H 2.63; found C 33.45, H 2.65. − Λ_m (acetone) = 184 $ohm^{-1}{\cdot}cm^2{\cdot}mol^{-1}$. − IR: $\tilde{\nu}$ = 811 (vs), 799 (vs) cm^{-1} $(C_6F_5)_{x-sens}$; 289 (m), 261 (m), 255 (s), 250 (s) cm^{-1} (M−Cl). − ^1H NMR ([D$_6$]acetone): at 20 °C: δ = 1.77 (s, Cp*). − ^{19}F NMR ([D$_6$]acetone): at 20 °C: δ = −167.87 (m, 8 F_m), −166.87 (t, 4 F_p), −117.51 (dd, $^3J_{Pt-F}$ = 526.7, 8 F_o). − APCI(+) MS: *m/z* (%) = 581 (16) [$Rh_2Cp^*_2Cl_3^+$]. − APCI(−) MS: *m/z* (%) = 565 (100) [$Pt(C_6F_5)_2Cl^-$].

Complex **5** could also be obtained, albeit in lower yield (0.09 g, 42% based on Rh), by carrying out the reaction starting from $[RhCp^*Cl_2]_2$ (0.11 g, 0.18 mmol) and $[cis\text{-}Pt(C_6F_5)_2(thf)_2]$ (0.24 g, 0.36 mmol) (molar ratio 1:2) and following the same procedure as above.

Synthesis of $[Cp^*Rh(\mu\text{-}Cl_3)RhCp^*]_2[(C_6F_5)_2Pd(\mu\text{-}Cl_2)Pd(C_6F_5)_2]$ (6): $[cis\text{-}Pd(C_6F_5)_2(thf)_2]$ (0.10 g, 0.16 mmol) was added to a red solution of $[RhCp^*Cl_2]_2$ (0.10 g, 0.16 mmol) in CH_2Cl_2 (20 mL)

(molar ratio 1:1) and the mixture was stirred for 30 min. The resulting solution was then concentrated to a small volume (ca. 5 mL), whereupon **6** (0.14 g, 80%) was precipitated as an orange solid. − $C_{64}H_{60}Cl_8F_{20}Pd_2Rh_4$ (2117.26): calcd. C 36.31, H 2.86; found C 36.16, H 2.58. − Λ_m (acetone) = 167 $ohm^{-1}\cdot cm^2\cdot mol^{-1}$. − IR: $\tilde{\nu}$ = 796 (s), 783 (s) cm^{-1} $(C_6F_5)_{x-sens}$; 288 (m), 278 (m), 249 (s) cm^{-1} (M−Cl). − ^1H NMR ([D$_6$]acetone): at 20 °C: δ = 1.77 (s, Cp*). − ^{19}F NMR ([D$_6$]acetone): at 20 °C: δ = 166.77 (m, 8 F_m), −165.24 (t, 4 F_p), −113.29 (d, 8 F_o). − APCI(+) MS: *m/z* (%) = 581 (100) [$Rh_2Cp^*_2Cl_3^+$]. − APCI(−) MS: *m/z* (%) = 477 (16) [$Pd(C_6F_5)_2Cl^-$].

Complex **6** could also be obtained, albeit in lower yield (0.09 g, 58% based on Rh), by carrying out the reaction starting from [$RhCp^*Cl_2]_2$ (0.09 g, 0.15 mmol) and [*cis*-$Pd(C_6F_5)_2(thf)_2$] (0.17 g, 0.30 mmol) (molar ratio 1:2) and following the same procedure as described for **5**.

Synthesis of [Cp*Ir(μ-Cl$_3$)IrCp*]$_2$[(C$_6$F$_5$)$_2$M′(μ-Cl$_2$)M′(C$_6$F$_5$)$_2$] (M′ = Pt 7, Pd 8): Complexes **7** and **8** were prepared in a manner similar to that described for **5**. Reagents and quantities used: [$IrCp^*Cl_2]_2$ (0.10 g, 0.13 mmol) and [*cis*-$Pt(C_6F_5)_2(thf)_2$] (0.09 g, 0.13 mmol) for **7**; [$IrCp^*Cl_2]_2$ (0.08 g, 0.10 mmol) and [*cis*-$Pd(C_6F_5)_2(thf)_2$] (0.06 g, 0.10 mmol) for **8** (molar ratio 1:1). They were obtained as yellow solids.

7: (0.13 g, 78%). − $C_{64}H_{60}Cl_8F_{20}Ir_4Pt_2$ (2651.86): calcd. C 28.99, H 2.28; found C 28.71, H 2.45. − IR: $\tilde{\nu}$ = 810 (s), 798 (s) cm^{-1} $(C_6F_5)_{x-sens}$; 290 (m), 261 (m) cm^{-1} (M−Cl). − ^1H NMR ([D$_6$]acetone): at 20 °C: δ = 1.77 (s, Cp*). − ^{19}F NMR ([D$_6$]acetone): at 20 °C: δ = −167.89 (m, 8 F_m), −166.91 (t, 4 F_p), −117.47 (d, $^3J_{Pt-F}$ = 526.4, 8 F_o). − ES(+) MS: *m/z* (%) = 761 (100) [$Ir_2Cp^*_2Cl_3^+$]. − ES(−) MS: *m/z* (%) = 565 (42) [$Pt(C_6F_5)_2Cl^-$].

8: (0.1 g, 79%). − $C_{64}H_{60}Cl_8F_{20}Ir_4Pd_2$ (2474.52): calcd. C 31.07, H 2.44; found C 30.86, H 2.08. − IR: $\tilde{\nu}$ = 796 (s), 782 (s) cm^{-1} $(C_6F_5)_{x-sens}$; 287 (m), 261 (m) cm^{-1} (M−Cl). − ^1H NMR ([D$_6$]acetone): at 20 °C: δ = 1.77 (s, Cp*). − ^{19}F NMR ([D$_6$]acetone): at 20 °C: δ = −166.81 (m, 8 F_m), −165.29 (t, 4 F_p), −113.28 (d, 8 F_o). − ES(+) MS: *m/z* (%) = 761 (100) [$Ir_2Cp^*_2Cl_3^+$]. − ES(−) MS: *m/z* (%) = 477 (42) [$Pd(C_6F_5)_2Cl^-$].

Complexes **7** and **8** could also be obtained, albeit in lower yields (0.05 g, 46% for **7**; 0.04 g, 31% for **8**, based on Ir), by carrying out the reactions starting from [$IrCp^*Cl_2]_2$ (0.07 g, 0.09 mmol) and [*cis*-$Pt(C_6F_5)_2(thf)_2$] (0.12 g, 0.18 mmol) for **7** and [$IrCp^*Cl_2]_2$ (0.08 g, 0.10 mmol) and [*cis*-$Pd(C_6F_5)_2(thf)_2$] (0.12 g, 0.20 mmol) for **8** (molar ratio 1:2), following the same procedure as described for **5**.

Synthesis of [(PEt$_3$)Cp*M(μ-1κ*C*^{α}:η^2-C≡CPh)$_2$M′′$_2$(μ-4κ*C*^{α}:η^2-C≡CPh)$_2$Pt(C$_6$F$_5$)$_2$] (M = Rh, M′′ = Cu 9, M′′ = Ag 10; M = Ir, M′′ = Cu 11, M′′ = Ag 12): An orange solution of [$(PEt_3)Cp^*Rh(\mu\text{-}Cl)_2Pt(C_6F_5)_2$] (**1**) (0.15 g, 0.16 mmol) in acetone (10 mL) was treated with $[CuC{\equiv}CPh]_x$ (0.26 g, 1.58 mmol) and the mixture was stirred for 2 h. The resulting yellow suspension was concentrated to dryness, the solid residue was extracted with CH_2Cl_2 (30 mL), and the extract was filtered through Celite to eliminate the excess $[CuC{\equiv}CPh]_x$ and the CuCl formed. The resulting yellow solution was concentrated to dryness and the residue was treated with cold Et_2O (5 mL) to yield complex **9** as a yellow solid. Complexes **10**−**12** were similarly prepared, also as yellow solids. In the case of complex **10**, the pale-brown solid thus obtained was recrystallized from acetone/Et_2O to give **10** as a pure yellow solid; in the case of complex **12**, the solid residue was treated with acetone instead of diethyl ether. Reagents and quantities used: **1** (0.15 g, 0.16 mmol) and $[AgC{\equiv}CPh]_x$ (0.15 g, 0.72 mmol) for **10**; [$(PEt_3)Cp^*Ir(\mu\text{-}Cl)_2Pt(C_6F_5)_2$] (**3**) (0.16 g, 0.15 mmol) and $[CuC{\equiv}CPh]_x$ (0.11 g, 0.69 mmol) for **11**; **3** (0.20 g, 0.19 mmol) and $[AgC{\equiv}CPh]_x$ (0.17 g, 0.81 mmol) for **12**.

9: (0.17 g, 75%). − $C_{60}H_{50}Cu_2F_{10}PPtRh$ (1417.13): calcd. C 50.86, H 3.56; found C 50.44, H 3.38. − IR: $\tilde{\nu}$ = 2009 (s br), 1969 (sh) cm^{-1} (C≡C); 797 (s), 778 (s) cm^{-1} $(C_6F_5)_{x-sens}$. − ^1H NMR ($CDCl_3$): at 20 °C: δ = 0.91 (m, 9 H, CH_3, PEt_3), 1.89 (m, 6 H, CH_2, PEt_3), 2.00 (d, $^4J_{P-H}$ = 1.7, 15 H, Cp*), 7.16 (m, 20 H, Ph). − ^{19}F NMR ($CDCl_3$): at 20 °C: δ = −166.06 (m, 4 F_m), −164.85 (t, 2 F_p), −116.10 (dd, $^3J_{Pt-F}$ = 376.1, 4 F_o). − ^{31}P NMR ($CDCl_3$): at 20 °C: δ = 35.88 (d, $^1J_{Rh-P}$ = 115.7). − FAB(+) MS: *m/z* (%) = 1417 (8) [M^+ + 1], 1148 (20) [M^+ − 2 C_2Ph − Cu − 3], 1047 (12) [M^+ − 3 C_2Ph − Cu − 3], 785 (23) [$(PEt_3)Cp^*Rh(C_2Ph)_3Cu_2^+$], 621 (100) [$(PEt_3)Cp^*Rh(C_2Ph)_2Cu^+$].

10: (0.05 g, 22%). − $C_{60}H_{50}Ag_2F_{10}PPtRh$ (1505.77): calcd. C 47.86, H 3.35; found C 47.33, H 3.35. − IR: $\tilde{\nu}$ = 2053 (s br), 2020 (sh) cm^{-1} (C≡C); 797 (s), 778 (s) cm^{-1} $(C_6F_5)_{x-sens}$. − ^1H NMR ($CDCl_3$): at 20 °C: δ = 0.90 (m, 9 H, CH_3, PEt_3), 1.81 (m, 6 H, CH_2, PEt_3), 1.86 (d, $^4J_{P-H}$ = 1.7, 15 H, Cp*), 7.17, 7.05, 6.92, 6.77 (m, 20 H, Ph). − ^{19}F NMR ($CDCl_3$): at 20 °C: δ = −165.91 (m, 4 F_m), −164.78 (t, 2 F_p), −114.28 (d, $^3J_{Pt-F}$ = 394.9, 4 F_o). − ^{31}P NMR ($CDCl_3$): at 20 °C: δ = 37.18 (d, $^1J_{Rh-P}$ = 119.3). − FAB(−) MS: *m/z* (%) = 1786 (23) [$Pt_2(C_6F_5)_4(C_2Ph)_4Ag_3^-$ − 1], 1604 (4) [M^- + C_2Ph − 3], 630 (24) [$Pt(C_6F_5)_2(C_2Ph)^-$], 441 (100) [$RhCp^*(C_2Ph)_2^-$ + 1].

11: (0.14 g, 61%). − $C_{60}H_{50}Cu_2F_{10}IrPPt$ (1506.44): calcd. C 47.84, H 3.34; found C 47.43, H 3.17. − IR: $\tilde{\nu}$ = 2006 (s), 1969 (s) cm^{-1} (C≡C); 798 (s), 778 (s) cm^{-1} $(C_6F_5)_{x-sens}$. − ^1H NMR ($CDCl_3$): at 20 °C: δ = 0.86 (m, 9 H, CH_3, PEt_3), 1.89 (m, 6 H, CH_2, PEt_3), 2.06 (s, 15 H, Cp*), 7.16−7.08 (m, 20 H, Ph). − ^{19}F NMR ($CDCl_3$): at 20 °C: δ = −165.95 (m, 4 F_m), −164.89 (t, 2 F_p), −115.82 (d, $^3J_{Pt-F}$ = 378.4, 4 F_o). − ^{31}P NMR ($CDCl_3$): at 20 °C: δ = −7.57 (s). − FAB(+) MS: *m/z* (%) = 1507 (4) [M^+ + 1], 1405 (10) [M^+ − C_2Ph], 1337 (6) [M^+ − C_6F_5 − 2], 1238 (18) [M^+ − C_2Ph − C_6F_5], 711 (80) [$Pt(C_6F_5)_2Cu(PEt_3)$], 593 (82) [$Pt(C_6F_5)_2Cu$], 463 (100) [$Pt(C_6F_5)$].

12: (0.20 g, 66%). − $C_{60}H_{50}Ag_2F_{10}IrPPt$ (1595.09): this complex crystallizes with a $^1/_2$ molecule of CH_2Cl_2, as observed by ^1H NMR in $CDCl_3$. $C_{60}H_{50}Ag_2F_{10}IrPPt\cdot 0.5CH_2Cl_2$ requires C 44.38, H 3.14; found C 44.29, H 3.44. − IR: $\tilde{\nu}$ = 2070 (m), 2036 (m) cm^{-1} (C≡C); 797 (m), 777 (m) cm^{-1} $(C_6F_5)_{x-sens}$. − ^1H NMR ($CDCl_3$): at 20 °C: δ = 0.88 (m, 9 H, CH_3, PEt_3), 1.86 (m, 6 H, CH_2, PEt_3), 1.94 (s, 15 H, Cp*), 5.33 (s, CH_2Cl_2), 7.14, 7.04, 6.90, 6.77 (m, 20 H, Ph). − ^{19}F NMR ($CDCl_3$): at 20 °C: δ = −165.87 (m, 4 F_m), −164.76 (t, 2 F_p), −114.34 (d, $^3J_{Pt-F}$ = 387.3, 4 F_o). − ^{31}P NMR ($CDCl_3$): at 20 °C: δ = −5.4 (s). − FAB(+) MS: *m/z* (%) = 1159 (9) [$(PEt_3)Cp^*Ir(C_2Ph)_3Ag_2Pt^+$], 965 (11) [$(PEt_3)Cp^*Ir(C_2Ph)_3Ag_2^+$ − 1], 846 (15) [$Cp^*Ir(C_2Ph)_3Ag_2^+$ − 1], 755 (55) [$(PEt_3)Cp^*Ir(C_2Ph)_2Ag^+$], 637 (100) [$Cp^*Ir(C_2Ph)_2Ag^+$].

X-ray Crystal Structure Determinations: Suitable crystals of **1**·Me_2CO, **6**, and **9**·CH_2Cl_2 were obtained by slow diffusion of hexane into acetone (**1**, **6**) or CH_2Cl_2 (**9**) solutions of these complexes at −30 °C. Relevant crystal data are listed in Table 5. Intensity data for **1**·Me_2CO and **6** were collected on a Siemens P4 four-circle diffractometer and cell constants were calculated from 30 reflections (**1**·Me_2CO) or 52 reflections (**6**) with 2θ angles ranging from 24 to 26°. Intensity data for **9**·CH_2Cl_2 were collected on a Siemens/STOE AED4 four-circle diffractometer and cell constants were refined from 2θ values of 36 reflections ($22.5 < 2\theta < 31.7°$). An absorption correction based on azimuthal data was applied; transmission coefficients were in the range 1.000 to 0.677

Table 5. Crystal data and structure refinement parameters for **1**·Me_2CO, **6**, and **9**·CH_2Cl_2 ($wR2 = [\Sigma w(F_o^2 - F_c^2)^2/\Sigma wF_o^4]^{0.5}$; $R1 = \Sigma|F_o| - |F_c|/\Sigma|F_o|$)

	1·Me_2CO	6	**9**·CH_2Cl_2
Empirical formula	$C_{28}H_{30}Cl_2F_{10}PPtRh{\cdot}Me_2CO$	$C_{64}H_{60}Cl_8F_{20}Pd_2Rh_4$	$C_{60}H_{50}Cu_2F_{10}PPtRh{\cdot}CH_2Cl_2$
Molecular mass	1014.47	2117.16	1501.98
Temperature [K]	200	200	173
Wavelength [Å]	0.71073	0.71073	0.71073
Crystal system	Monoclinic	Orthorhombic	Triclinic
Space group	$P2_1/n$	$Pca2_1$	$P\bar{1}$
a [Å]	10.439(1)	14.820(5)	10.963(3)
b [Å]	14.611(1)	17.993(6)	13.052(4)
c [Å]	11.285(1)	28.296(9)	20.643(6)
α [deg]	90	90	93.44(2)
β [deg]	93.15(1)	90	99.29(2)
γ [deg]	90	90	106.03(2)
Volume [Å^3]	1718.6(3)	7545(4)	2784.7(13)
Z	2	4	2
Density (calcd.) [g/cm^3]	1.960	1.864	1.791
Absorption coeff. [mm^{-1}]	4.827	1.692	3.747
F(000)	984	4128	1476
Crystal dimensions [mm]	0.52 × 0.50 × 0.36	0.48 × 0.44 × 0.24	0.30 × 0.23 × 0.19
θ range [°]	2.28 to 24.00	2.26 to 25.01	2.01 to 25.00
Index ranges	$-1 \le h \le 11$	$-1 \le h \le 17$	$0 \le h \le 13$
	$-1 \le k \le 16$	$-1 \le k \le 21$	$-15 \le k \le 14$
	$-12 \le l \le 12$	$-1 \le l \le 33$	$-24 \le l \le 24$
Reflections collected	3582	8134	10352
Independent reflections	2802 [R(int) = 0.0234]	7058 [R(int) = 0.0423]	9795 [R(int) = 0.0374]
Refinement method		Full-matrix least-squares on F^2	
Data/restraints/parameters	2763/0/226	6587/1/884	9792/2/737
Goodness-of-fit on F^2	1.080	1.025	1.017
Final R indices [$I > 2\sigma(I)$]	$R1$ = 0.0239	$R1$ = 0.0380	$R1$ = 0.0464
	$wR2$ = 0.0585	$wR2$ = 0.0682	$wR2$ = 0.0893
R indices (all data)	$R1$ = 0.0274	$R1$ = 0.0714	$R1$ = 0.0935
	$wR2$ = 0.0643	$wR2$ = 0.1858	$wR2$ = 0.1119
Largest diff. peak and hole [e·Å^{-3}]	0.581 and −1.080	0.562 and −0.749	1.86 and −0.81

(**1**·Me_2CO), 0.974 to 0.704 (**6**), and 1.000 to 0.669 (**9**·CH_2Cl_2). The structures were solved by Patterson (**1**, **9**) or direct (**6**) methods and refined against F^2 using the program SHELXL-93.[27] All non-hydrogen atoms were assigned anisotropic displacement parameters and were refined without positional constraints, except for the disordered carbon atoms of one of the ethyl groups of the PEt_3 ligand in **9**·CH_2Cl_2 (see below), for which the interatomic distances were restrained to be 1.54 Å. A phenyl ring of one phenylacetylide ligand was found to be disordered over two positions, which were refined with partial occupancy factors of 0.5/0.5. One methyl carbon atom of the PEt_3 ligand was found to be disordered over two positions, which were refined with partial occupancy factors of 0.67/0.33. In all three structures, all hydrogen atoms were constrained to idealized geometries and were assigned a refined isotropic displacement parameter equal to 1.2 times that of their parent C atoms (1.5 times for methyl hydrogen atoms). Complex **1**·Me_2CO has a symmetry plane, and so some atoms lying in certain positions were refined at half-occupancy. The crystal of **6** is a racemic twin, with a Flack parameter of 0.49(9).

Crystallographic data (excluding structure factors) for the structures reported in this paper have been deposited with the Cambridge Crystallographic Data Centre as supplementary publication nos. CCDC-151398 (**1**·Me_2CO), -151399 (**6**), and -151400 (**9**·CH_2Cl_2). Copies of the data can be obtained free of charge on application to the CCDC, 12 Union Road, Cambridge CB2 1EZ, U.K. [Fax. (internat.) +44 (0)1223/336033; E-mail: deposit@ccdc.cam.ac.uk].

Acknowledgments

We thank the Dirección General de Enseñanza Superior, Spain (Project PB 98-1595-C02-01,02) and the Universidad de La Rioja (Project API-00/B17) for their financial support.

[1] [1a] N. Wheatley, P. Kalck, *Chem. Rev.* **1999**, *99*, 3379. – [1b] D. W. Stephan, T. T. Nadasdi, *Coord. Chem. Rev.* **1996**, *147*, 147. – [1c] R. M. Bullock, C. P. Casey, *Acc. Chem. Res.* **1987**, *20*, 167. – [1d] D. W. Stephan, *Coord. Chem. Rev.* **1989**, *95*, 41. – [1e] R. D. Adams, in: *Comprehensive Organometallic Chemistry II* (Eds.: G. Wilkinson, F. G. A. Stone, E. W. Abel), Pergamon, Oxford, U. K., **1995**, vol. 10, p. 1.

[2] For several recent examples, see: [2a] N. Feiken, P. Pregosin, G. Trabesinger, *Organometallics* **1998**, *17*, 4510. – [2b] E. Corradi, N. Masciocchi, G. Pályi, R. Ugo, A. Vizi-Orosz, C. Zucchi, A. Sironi, *J. Chem. Soc., Dalton Trans.* **1997**, 4651. – [2c] A. Roucoux, L. Thieffry, J.-F. Carpentier, M. Devocelle, C. Méliet, F. Agbossou, A. Mortreux, A. J. Welch, *Organometallics* **1996**, *15*, 2440. – [2d] J. M. Rosset, M. P. Glenn, J. D. Cotton, A. C. Willis, C. H. L. Kennard, K. A. Byriel, B. H. Riches, W. Kitching, *Organometallics* **1998**, *17*, 1968. – [2e] G. R. Hoel, R. A. Stockland Jr., G. K. Anderson, F. T. Ladipo, J. Braddock-Wilking, N. P. Rath, J. C. Mareque-Rivas, *Organometallics* **1998**, *17*, 1155. – [2f] S. B. Duckett, C. L. Newell, R. Eisenberg, *J. Am. Chem. Soc.* **1994**, *116*, 10548. – [2g] N. M. Boag, M. S. Ravetz, *J. Chem. Soc., Dalton Trans.* **1995**, 3473 and references therein. – [2h] A. Herzog, F.-Q. Liu, H. W. Roesky, A. Demsar, K. Keller, M. Noltemeyer, F. Pauer, *Organometallics* **1994**, *13*, 1251. – [2i] K. C. Shih, A. S. Goldman, *Organometallics* **1993**,

12, 3390. – [2j] M. Martínez, G. Muller, D. Panyella, M. Rocamora, X. Solans, M. Font-Bardía, *Organometallics* **1995**, *14*, 5552.[2k] V. Yu. Kukushkin, V. K. Belsky, V. E. Konovalov, R. R. Shifrina, A. I. Moiseev, R. A. Vlasova, *Inorg. Chim. Acta* **1991**, *183*, 57 and references therein. – [2l] S. A. King, D. Van Engen, H. E. Fischer, J. Schwartz, *Organometallics* **1991**, *10*, 1195. – [2m] F. R. Hartley, S. G. Murray, A. Wilkinson, *Inorg. Chem.* **1989**, *28*, 549. – [2n] R. Usón, J. Forniés, *Adv. Organomet. Chem.* **1988**, *28*, 219. – [2o]See also the tables given in ref.[10]

[3] [3a] R. W. Baker, M. J. Braithwaite, R. S. Nyholm, *J. Chem. Soc., Dalton Trans.* **1972**, 1924. – [3b] C. E. Briant, K. A. Rowland, C. T. Webber, D. M. P. Mingos, *J. Chem. Soc., Dalton Trans.* **1981**, 1515. – [3c] H. C. Clark, G. Ferguson, V. K. Jain, M. Parvez, *Inorg. Chem.* **1985**, *24*, 1477. – [3d] P. D. Smith, J. L. Martin, J. C. Huffman, R. L. Bausemer, K. G. Caulton, *Inorg. Chem.* **1985**, *24*, 2997. – [3e] A. Bencini, A. Caneschi, A. Dei, D. Gatteschi, C. Zanchini, O. Kahn, *Inorg. Chem.* **1986**, *25*, 1374. – [3f] G. López, G. García, G. Sánchez, C. de Haro, M. D. Santana, J. Casabó, M. Caldes, M. Mejías, E. Molins, C. Miratvilles, *J. Chem. Soc., Dalton Trans.* **1991**, 3311. – [3g] P. J. Stang, Y.-H. Huang, A. M. Arif, *Organometallics* **1992**, *11*, 231. – [3h] F. A. Cotton, J. L. Eglin, C. A. James, R. L. Luck, *Inorg. Chem.* **1992**, *31*, 5308. – [3i] J. W. Steed, D. A. Tocher, *Inorg. Chim. Acta* **1995**, *229*, 87. – [3j] K. Severin, K. Polborn, W. Beck, *Inorg. Chim. Acta* **1995**, *240*, 339. – [3k] K. Heinze, G. Huttner, L. Zsolnai, P. Schober, *Inorg. Chem.* **1997**, *36*, 5457. – [3l] K. Polborn, K. Severin, *Eur. J. Inorg. Chem.* **1998**, 1187. – [3m] J. J. Vittal, P. A. W. Dean, *Polyhedron* **1998**, *17*, 1937. – [3n] D. J. Chesnut, R. C. Haushalter, J. Zubieta, *Inorg. Chim. Acta* **1999**, *292*, 41. – [3o] K. Polborn, K. Severin, *J. Chem. Soc., Dalton Trans.* **1999**, 759. – [3p] M. Öhm, A. Schulz, K. Severin, *Eur. J. Inorg. Chem.* **2000**, 2623 and references therein.

[4] [4a] J. Forniés, E. Lalinde, *J. Chem. Soc., Dalton Trans.* **1996**, 2587 and references therein. – [4b] J. R. Berenguer, J. Forniés, E. Lalinde, F. Martínez, *Organometallics* **1996**, *15*, 4537. – [4c] L. R. Falvello, S. Fernández, J. Forniés, E. Lalinde, F. Martínez, M. T. Moreno, *Organometallics* **1997**, *16*, 1326. – [4d] I. Ara, J. R. Berenguer, J. Forniés, E. Lalinde, *Organometallics* **1997**, *16*, 3921. – [4e] I. Ara, J. R. Berenguer, J. Forniés, E. Lalinde, *Inorg. Chim. Acta* **1997**, *264*, 199. – [4f] I. Ara, J. R. Berenguer, J. Forniés, J. Gómez, E. Lalinde, R. I. Merino, *Inorg. Chem.* **1997**, *36*, 6461. – [4g] I. Ara, J. R. Berenguer, E. Eguizábal, J. Forniés, E. Lalinde, A. Martín, F. Martínez, *Organometallics* **1998**, *17*, 4578. – [4h] L. R. Falvello, J. Forniés, A. Martín, J. Gómez, E. Lalinde, M. T. Moreno, J. Sacristán, *Inorg. Chem.* **1999**, *38*, 3116. – [4i] I. Ara, J. R. Berenguer, E. Eguizábal, J. Forniés, E. Lalinde, F. Martínez, *Organometallics* **1999**, *18*, 4344. – [4j] J. P. H. Charmant, L. R. Falvello, J. Forniés, J. Gómez, E. Lalinde, M. T. Moreno, A. G. Orpen, A. Rueda, *Chem. Commun.* **1999**, 2045. – [4k] J. R. Berenguer, E. Eguizábal, L. R. Falvello, J. Forniés, E. Lalinde, A. Martín, *Organometallics* **2000**, *19*, 490.

[5] [5a] I. Ara, L. R. Falvello, J. Forniés, E. Lalinde, A. Martín, F. Martínez, M. T. Moreno, *Organometallics* **1997**, *16*, 5392 and references given therein. – [5b] I. Ara, L. R. Falvello, S. Fernández, J. Forniés, E. Lalinde, A. Martín, M. T. Moreno, *Organometallics* **1997**, *16*, 5923. – [5c] I. Ara, E. Delgado, J. Forniés, E. Hernández, E. Lalinde, N. Mansilla, M. T. Moreno, *J. Chem. Soc., Dalton Trans.* **1998**, 3199. – [5d] J. P. H. Charmant, J. Forniés, J. Gómez, E. Lalinde, M. T. Moreno, A. G. Orpen, S. Solano, *Angew. Chem. Int. Ed.* **1999**, *38*, 3058. – [5e] E. Delgado, B. Donnadieu, E. Hernández, E. Lalinde, N. Mansilla, M. T. Moreno, *J. Organomet. Chem.* **1999**, *592*, 283.

[6] E. Maslowsky Jr., in: *Vibrational Spectra of Organometallic Compounds*, Wiley, New York, **1977**, p. 437.

[7] H. Günther, in: *NMR Spectroscopy*, Wiley, New York, **1992**, p. 344.

[8] R. Usón, J. Forniés, M. Tomás, J. M. Casas, F. A. Cotton, L. R. Falvello, *Inorg. Chem.* **1987**, *26*, 3482.

[9] M. R. Churchill, S. A. Julis, F. J. Rotella, *Inorg. Chem.* **1977**, *16*, 1137.

[10] G. Aullón, G. Ujaque, A. Lledós, S. Alvarez, P. Alemany, *Inorg. Chem.* **1998**, *37*, 804.

[11] [11a] M. Valderrama, M. Scotti, P. Campos, R. Sariego, K. Peters, H. G. von Schnering, H. Werner, *New J. Chem.* **1988**, *12*, 633. – [11b] J. W. Kang, P. M. Maitlis, *J. Organomet. Chem.* **1971**, *30*, 127.

[12] K. Umakoshi, K. Murata, S. Yamashita, K. Isobe, *Inorg. Chim. Acta* **1991**, *190*, 185.

[13] M. N. Vargaftik, Yu. T. Struchkov, A. I. Yanovsky, P. M. Maitlis, *Mendeleev Commun.* **1993**, 247.

[14] M. M. Brezinski, J. Schneider, L. J. Radonovich, K. J. Klabunde, *Inorg. Chem.* **1989**, *28*, 2414.

[15] M. Winter, *Web Elements: The Periodic Table on the WWW* (http://www.webelements.com/), **1993**−**2000**, The University of Sheffield and Web Elements Ltd., U.K.

[16] [16a] O. M. Abu Salah, M. I. Bruce, *J. Chem. Soc., Chem. Commun.* **1972**, 858. – [16b] M. R. Churchill, S. A. Bezman, *Inorg. Chem.* **1974**, *13*, 1418. – [16c] M. R. Churchill, B. G. DeBoer, *Inorg. Chem.* **1975**, *14*, 2630. – [16d] O. M. Abu Salah, M. I. Bruce, *Aust. J. Chem.* **1976**, *29*, 531; **1977**, *30*, 2639. – [16e] O. M. Abu Salah, M. I. Bruce, *J. Chem. Soc., Chem. Commun.* **1974**, 688. – [16f] O. M. Abu Salah, M. I. Bruce, *J. Chem. Soc., Dalton Trans.* **1975**, 2311. – [16g] M. I. Bruce, O. M. Abu Salah, R. E. Davis, N. V. Raghavan, *J. Organomet. Chem.* **1974**, *64*, C48. – [16h] K. Sonogashira, Y. Fujikura, T. Yatake, N. Toyoshima, S. Takahashi, N. Hagigara, *J. Organomet. Chem.* **1978**, *145*, 101. – [16i] P. Espinet, J. Forniés, F. Martínez, M. Tomás, E. Lalinde, M. T. Moreno, A. Ruiz, A. J. Welch, *J. Chem. Soc., Dalton Trans.* **1990**, 791. – [16j] P. Espinet, J. Forniés, F. Martínez, M. Sotés, E. Lalinde, M. T. Moreno, A. Ruiz, A. J. Welch, *J. Organomet. Chem.* **1991**, *403*, 253. – [16k] J. Forniés, M. A. Gómez-Saso, F. Martínez, E. Lalinde, M. T. Moreno, A. J. Welch, *New J. Chem.* **1992**, *16*, 483. – [16l] S. Yamazaki, A. J. Deeming, *J. Chem. Soc., Dalton Trans.* **1993**, 3051. – [16m] K. Osakada, T. Takizawa, T. Yamamoto, *Organometallics* **1995**, *14*, 3531. – [16n] K. Osakada, R. Sakata, T. Yamamoto, *Organometallics* **1997**, *16*, 5354. − see also: [16o] H. Lang, K. Köhler, S. Blau, *Coord. Chem. Rev.* **1995**, *143*, 113. – [16p] A. M. Sladkov, I. R. Gold′ing, *Russ. Chem. Rev. (Engl. Transl.)* **1979**, *48*, 869.

[17] S. Mihan, K. Sünkel, W. Beck, *Chem. Eur. J.* **1999**, *5*, 745.

[18] D. Rais, D. M. P. Mingos, R. Vilar, A. J. P. White, D. J. Williams, *Organometallics* **2000**, *19*, 5209.

[19] J. P. H. Charmant, J. Forniés, J. Gómez, E. Lalinde, R. I. Merino, M. T. Moreno, A. G. Orpen, *Organometallics* **1999**, *18*, 3353.

[20] G. A. Carriedo, D. Miguel, V. Riera, X. Solans, *J. Chem. Soc., Dalton Trans.* **1987**, 2867.

[21] [21a] J. Diez, M. P. Gamasa, J. Gimeno, A. Aguirre, S. García-Granda, *Organometallics* **1991**, *10*, 380. – [21b] J. Diez, M. P. Gamasa, J. Gimeno, E. Lastra, A. Aguirre, S. García-Granda, *Organometallics* **1993**, *12*, 2213. – [21c] V. W.-W. Yam, W.-K. Lee, T.-F. Lai, *Organometallics* **1993**, *12*, 2383.

[22] P. Pyykkö, *Chem. Rev.* **1997**, *97*, 597.

[23] J. W. Kang, K. Moseley, P. M. Maitlis, *J. Am. Chem. Soc.* **1969**, *91*, 5970.

[24] G. van Koten, J. G. Noltes, in: *Comprehensive Organometallic Chemistry* (Eds.: G. Wilkinson, F. G. A. Stone, E. W. Abel), Pergamon Press, Oxford, U. K., **1982**, volume 2, p. 721.

[25] R. D. Stephens, C. E. Castro, *J. Org. Chem.* **1963**, *28*, 3313.

[26] R. Usón, J. Forniés, M. Tomás, B. Menjón, *Organometallics* **1985**, *4*, 1912.

[27] G. M. Sheldrick, *SHELXL-93, A Program for Crystal Structure Determination*, University of Göttingen, Germany, **1993**.

Received October 26, 2000
[I00408]

Substituted Cyclooctatetraenes as Ligands in *f*-Metal Chemistry

Peter W. Roesky[a]

Dedicated to Professor Dr. Dr. h.c. Oskar Glemser on the occasion of his 90th birthday

Keywords: Actinides / Cyclooctatetraenes / Lanthanides / Sandwich complexes

The use of substituted cyclooctatetraenes confers various desired properties on the resulting metal complexes such as a higher thermal and kinetic stability as well as higher solubility relative to the nonsubstituted systems. Furthermore, the formation of polymeric structures is inhibited because intermolecular interactions are reduced. Alkyl- and aryl-substituted cyclooctatetraenes were mainly used as ligands in the 1970s and 1980s. The vast majority of known complexes containing these ligands in the coordination sphere are uranium compounds. Since then the alkyl- and aryl-substituted cyclooctatetraenes have been replaced almost exclusively in synthesis by silyl-substituted ones. Complexes with silyl-substituted cyclooctatetraenes are known for both 4*f* and 5*f* elements.

1. Introduction

The replacement of the classic cyclopentadienyl ligand (C_5H_5 = Cp) with bulkier analogues such as C_5Me_5 (Cp*) and $C_5H_3(SiMe_3)_2$ (Cp′′) in main group and transition metal chemistry has led to complexes with more convenient properties.[1,2] Due to the steric shielding of the metal centers with Cp* and Cp′′ ligands, the resulting compounds are thermally and kinetically more stable. They are more soluble, crystallize more readily, and the formation of polymeric structures is inhibited because intermolecular interactions are reduced. These advantages led to the isolation and structural characterization of a number of main group and transition metal complexes which are difficult to obtain with the unsubstituted Cp ligand.[1,3−7] In particular, in *f*-element chemistry the use of bulky cyclopentadienyl ligands has paved the way for the exploration of their organometallic chemistry.[2,6]

In contrast to the rich chemistry of complexes with substituted cyclopentadienyl ligands, the number of complexes with η^8-coordinated substituted cyclooctatetraenes in the ligand sphere is virtually underdeveloped. Part of the reason for this stems from the fact that the 10-π-aromatic cyclooctatetraene dianion $C_8H_8^{2-}$ can be η^8-coordinated to a limited number of elements only (groups 3 and 4, the lanthanides and the actinides). Furthermore, there is no relevant industrial application for cyclooctatetraene complexes of the *f*-elements.

Since the cyclooctatetraene dianion is one of the most important ligands in organo-f-element chemistry,[8−12] this account presents the conceptual foundations for metal complexes with η^8-coordinated substituted cyclooctatetraenes in the ligand sphere.

[a] Institut für Anorganische Chemie der Universität Karlsruhe, Engesserstraße Geb. 30.45, 76128 Karlsruhe, Germany

2. Discussion

2.1. Alkyl-, Aryl-, Amino-, and Alkoxy-Substituted Cyclooctatetraenes

Most of the alkyl-, aryl-, amino-, and alkoxy-substituted cyclooctatetraenes C_8H_7-R which have been used as ligands in *f*-metal chemistry were first prepared in the 1950s by A. C. Cope et al.[13−17] The synthesis of these compounds

Peter W. Roesky was born in Göttingen, Germany, in 1967. He obtained his diploma in 1992 from the University of Würzburg and his doctoral degree from the Technical University of Munich (with Prof. W. A. Herrmann) in 1994. He was introduced to lanthanide chemistry as a postdoc with Prof. T. J. Marks at Northwestern University (1995–1996). In 1999 he completed his Habilitation at the University of Karlsruhe under the guidance of Prof. D. Fenske. In 1996 he received a Liebig-Stipendium of the Fonds der Chemischen Industrie, in 1999 a Heisenberg-Stipendium, and in 2000 a Karl-Winnacker-Stipendium. His current research interest revolves around the use of coordination compounds of the lanthanides for catalytic applications and for material science.

MICROREVIEWS: This feature introduces the readers to the authors′ research through a concise overview of the selected topic. Reference to important work from others in the field is included.

 © WILEY-VCH Verlag GmbH, 69451 Weinheim, 2001 1434−1948/01/0707−1653 $ 17.50+.50/0

has been reviewed.[18,19] Therefore, only the most common routes leading to C_8H_7-R will be discussed here. Alkyl cyclooctatetraenes can be obtained either by the reaction of C_8H_8 with alkyllithium reagents,[13,14] by the reaction of C_8H_7-Br with the corresponding dialkylcuprates,[20,21] or by a modified Reppe synthesis (the cyclization of ethyne with the corresponding substituted alkyne).[15,16] Many functionalized cyclooctatetraenes such as C_8H_7-$(CH_2)_3NMe_2$ were prepared starting from C_8H_7-$(CH_2)_3OH$, which itself was obtained by copolymerization of ethyne with HC≡C-$(CH_2)_3OH$.[16,17]Alkoxy cyclooctatetraenes, C_8H_7-OR, are obtained by the Williamson reaction of bromocyclooctatetraene, C_8H_7-Br, and the corresponding sodium alkoxides.[22]

Very few lanthanide complexes have been prepared with C_8H_7-R as a ligand. The substituents on the eight-membered ring in these compounds were alkyl groups such as Me, *n*Bu or *t*Bu. Using these ligands the chloride $[(n\text{BuC}_8\text{H}_7)\text{LuCl(THF)}_2]$,[23] the amide $\text{Li}[(n\text{BuC}_8\text{H}_7)\text{Lu}\{\text{NMeCH}_2\text{CH}_2\text{NMe}_2\}_2]$,[23] and the sandwich complex $[\text{K(diglyme)}][\text{Yb}(t\text{BuC}_8\text{H}_7)_2]$[24] were made. The synthesis of these compounds begins with the reaction of C_8H_7-R with potassium which leads to $K_2C_8H_7$-R. The dipotassium salt is then further reacted with the corresponding lanthanide chlorides. Since only $[\text{K(diglyme)}][\text{Yb}(t\text{BuC}_8\text{H}_7)_2]$ has been characterized by X-ray diffraction, the influence of the substituents on the eight-membered ring is hard to judge. The cerocene $[\text{Ce}(\text{MeC}_8\text{H}_7)_2]$ was reported by a two step procedure. In the first step, $K_2(\text{MeC}_8\text{H}_7)$ was reacted with $CeCl_3$ which led to $\text{K}[\text{Ce}(\text{MeC}_8\text{H}_7)_2]$. The anion was then oxidized with AgI to yield $[\text{Ce}(\text{MeC}_8\text{H}_7)_2]$ [Equation (1)].[25] The sandwich complex $[\text{Ce}(\text{C}_8\text{H}_8)_2]$ has conclusively shown to be a Ce^{3+} ($4f^1$) complex by theoretical as well as experimental investigations. Cerocene is best formulated as a sandwich complex containing two coordinated $(C_8H_8)^{1.5-}$ ions. This topic was recently reviewed and therefore will not be discussed further here.[26]

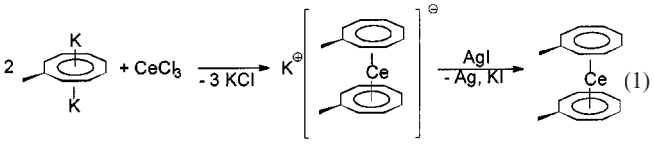

(1)

In contrast to the few reported 4*f*-metal complexes a large number of substituted uranocenes were reported mainly by A. Streitwieser et al. Most of this work was reviewed in 1979[27] and 1985.[28] The majority of the known substituted uranocenes can be prepared by three types of methods: 1) Reaction of $(C_8H_7\text{-R})^{2-}$ with UCl_4;[22,29,30] 2) Reaction of C_8H_7-R with finely divided uranium powder;[28] 3) Functional group reactions of substituted uranocenes.[22] By using these methods 1,1′ substituted uranocenes, $[\text{U}(\text{C}_8\text{H}_7\text{-R})_2]$ were prepared (Table 1).[22,27−37] The first of these methods is also the most common. $K_2C_8H_7$-R, which is obtained from C_8H_7-R and potassium, is reacted with UCl_4 [Equation (2)]. The second method leads more or less to the same products. Functional groups that are not stable in the presence of elemental potassium or uranium can be

Table 1. Monosubstituted actinocenes (IV) $[(C_8H_7\text{-R})_2\text{An}]$

An	R	Ref.
Th	Me	42
	*n*Bu	42
	*t*Bu	42, 43
	C_6H_5	42
	o-tolyl	43
	mesityl	43
U	Me	29, 31
	Et	22, 30, 44
	$CH{=}CH_2$	30
	*c*Pr	30
	*n*Bu	22, 29, 30, 31, 44
	*t*Bu	22, 29, 33
	$(CH_2)_4CH_3$	22
	C_6H_5	29, 35
	o-tolyl	39
	mesityl	38, 39
	C_8H_7	37, 40
	COOEt	36
	COO*t*Bu	36
	$COOCH_2C_6H_5$	36
	OMe	22
	OEt	22, 29
	O*t*Bu	22
	$OCH_2CH{=}CH_2$	22
	NMe_2	22
	CH_2NMe_2	22
	$(CH_2)_3NMe_2$	22
	$N^+Me_3\ I^-$	22, 29
	$CH_2N^+Me_3\ I^-$	22
	PR_2 (R= Et, *t*Bu, Ph)	37
Np	Et	44
	*n*Bu	44
Pu	Et	44
	*n*Bu	44

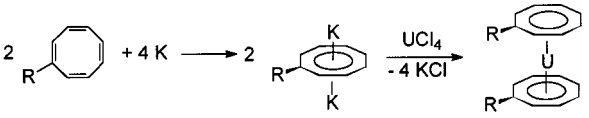

(2)

attached to the eight-membered ring by performing functional group reactions of substituted uranocenes (third method). With this method, amino groups can be transformed into ammonium ions, for example [Equation (3)]. Whereas uranocene itself has low solubility many substituted uranocenes have greater solubility and thus are easier to purify. Strong intramolecular interactions are observed only for very large substituents on the eight membered ring. For R = mesityl, the two groups are markedly bent away from the opposite ring in solution. The ^1H NMR spectrum shows the mesityl groups in a locked position with *exo*- and

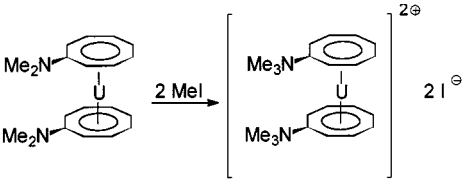

(3)

endo-methyl groups.[27,38,39] A striking example in this series is bis(bicyclooctatetraenyl)diuranium (biuranocenylene) in which two U^{4+} ions are bridged by two $(C_8H_7-C_8H_7)^{4-}$ units (Figure 1).[40,41] Substituted thorocenes,[42,43] plutocenes[44] and neptunocenes[44] are also known, but their number in comparison to uranocenes is more limited. With the exception of the uranocenes, only aryl and alkyl-substituted actinocenes are known (Table 1).

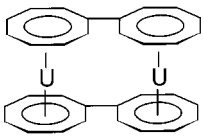

Figure 1. Bis(bicyclooctatetraenyl)diuranium (biuranocenylene)

Similar synthetic routes to those outlined above have been used to prepare di- and multiple ring substituted bis(cyclooctatetraene)actinocenes $[An(C_8H_{8-n}\text{-}R_n)_2]$ (Table 2).[45−51] Most common in this series are the octamethyl compounds $[An(1,3,5,7\text{-}Me_4C_8H_4)_2]$.[27,48,49] The structure of $[U(1,3,5,7\text{-}Me_4C_8H_4)_2]$ was established by single crystal X-ray diffraction (Figure 2).[50] This complex crystallizes as molecules in two rotameric configurations. In one form the methyl groups are essentially eclipsed whereas in the other form the methyl groups are essentially staggered. A truly remarkable species is the highly substituted 1,3,5,7,1′,3′,5′,7′-octaphenyluranocene.[27,51] In contrast to pyrophoric $[U(C_8H_8)_2]$, this material is completely air stable due to the effective shielding of the metal center by eight phenyl groups. Another interesting example in this series is an uranocene in which two (1,6)cyclooctatetraenyl(1,4)cyclophanes were used as ligands (Figure 3).[52]

Table 2. Di- and tetrasubstituted actinocenes(IV) $[(C_8H_{8-n}\text{-}R_n)_2An]$

An	R	Ref.
Th	1,3,5,7-Me_4	48
Pa	1,3,5,7-Me_4	49
U	1,4-tBu$_2$	47
	1,5-tBu$_2$	46
	1,3,5,7-Me_4	27, 50
	1,3,5,7-Ph_4	51
Np	1,3,5,7-Me_4	49
Pu	1,3,5,7-Me_4	49

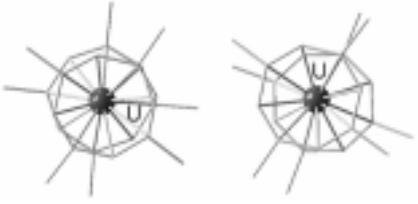

Figure 2. Crystal structure of $[U(1,3,5,7\text{-}Me_4C_8H_4)_2]$

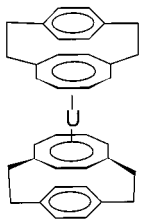

Figure 3. A uranocene containing two (1,6)cyclooctatetraenyl(1,4)-cyclophanes as ligands

Ring fused cyclooctatetraens, which are shown in Table 3, have also been used as ligands for thorocenes and also for uranocenes.[53−56] The structures of dicyclobutenouranocene (Figure 4) and dicyclopentenouranocene were characterized by X-ray diffraction. It was shown that the two annulated four- or five-membered rings are located in *trans* positions. Thus the molecule had approximate C_2 symmetry.[53,54]

Table 3. Ring-fused actinocenes (IV)

Ligand	An	Ref.
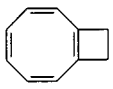	U	53
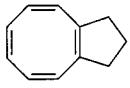	U	54
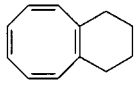	U	56
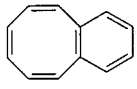	Th, U	56

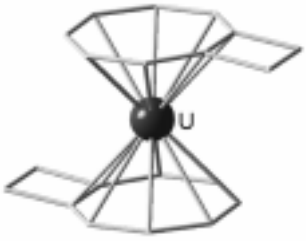

Figure 4. Crystal structure of dicyclobutenouranocene

Besides substituted actinocenes, in which the metal centers are formally in oxidation state +4, there are also some substituted actinocenes(III), $K[An(C_8H_7\text{-}R)_2]$. These compounds can be compared with the lanthanidocenes which are usually found in the same oxidation state. The uranocene(III) [K(diglyme)][U(MeC$_8$H$_7$)$_2$] was obtained by potassium reduction of the corresponding uranocene (Figure 5).[25] The structure shows that the uranium(III) and

potassium ions are bridged by a MeC_8H_7 ligand to give a nearly linear $(MeC_8H_7)U(\mu\text{-}MeC_8H_7)K$ arrangement. The neptunium and plutonium compounds $K[An(tBuC_8H_7)_2]$ (An = Np, Pu) were prepared from the corresponding hexachloride salts, $(Et_4N)_2[AnCl_6]$, and $tBuC_8H_7$. A mixture of $K[An(tBuC_8H_7)_2]$ and $[An(tBuC_8H_7)_2]$ shows rapid electron exchange.[57]

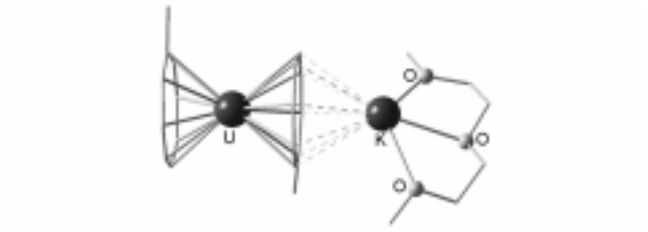

Figure 5. Crystal structure of $[K(diglyme)][U(MeC_8H_7)_2]$

Only a few substituted cyclooctatetraene half-sandwich complexes of the actinides are known. Their synthesis proved to be significantly more difficult than the synthesis of the corresponding sandwich complexes. The thorium complexes $[(C_8H_7\text{-}R)ThCl_2]$ and $[(1,3,5,7\text{-}Me_4C_8H_4)ThCl_2]$ were obtained by a ligand redistribution between the corresponding thorocene and $ThCl_4$.[58] $[(nBuC_8H_7)Th(BH_4)_2]$ can be prepared in a similar reaction of $[(nBuC_8H_7)_2Th]$ and $Th(BH_4)_4$ or by reaction of $[Th(BH_4)_4(THF)_2]$ with $K_2(nBuC_8H_7)$.

2.1. Silyl-Substituted Cyclooctatetraenes

The disadvantage of multiple alkyl-substituted cyclooctatetraenes such as $1,4\text{-}tBu_2C_8H_6$ [47] or $1,3,5,7\text{-}Me_4C_8H_4$ [59] is their lengthy preparation and the resulting low yields. Moreover, C_8H_8 which is used as a starting material for a number of substituted cyclooctatetraenes is getting more and more expensive. This has recently limited the use of alkyl-substituted cyclooctatetraenes as ligands for metal complexes. In 1993, F. G. N. Cloke et al. developed a cheap and convenient one pot synthesis of the silyl-substituted cyclooctatriene $1,4\text{-}(Me_3Si)_2C_8H_8$ which can easily be deprotonated with *n*-butyllithium to yield $[Li_2(THF)_n][1,4\text{-}(Me_3Si)_2C_8H_6]$ (**1a**) (Scheme 1).[60,61] By analogy, the *t*Bu-substituted salt $[Li_2(THF)_n][1,4\text{-}(Me_2tBuSi)_2C_8H_6]$ (**1b**) was also obtained.[62] Further treatment of **1a** with Me_3SiCl and subsequent reaction with KH gave the tris(trimethylsilyl)-substituted compound $[K_2(THF)_3][1,3,6\text{-}(Me_3Si)_3C_8H_5]$ (**2**) (Scheme 1).[63] The easy accessibility of **1a,b** and **2** paved the way to a number of new actinide and lanthanide complexes.

The treatment of various anhydrous lanthanide trichlorides with two equivalents of **1a** gave the ionic sandwich complexes $[Li(THF)_4][Ln\{1,4\text{-}(Me_3Si)_2C_8H_6\}_2]$ (Ln = Y, Ce, Pr, Nd, Sm) [Equation (4)]. Ion exchange of $[Li(THF)_4][Sm\{1,4\text{-}(Me_3Si)_2C_8H_6\}_2]$ with [PPN]Cl afforded $[PPN][Sm\{1,4\text{-}(Me_3Si)_2C_8H_6\}_2]$ (Table 4).[64] The derivatives of **2**, $[K(THF)_3][Ln\{1,3,6\text{-}(Me_3Si)_3C_8H_5\}_2]$ (Ln = Ce, Tb), were obtained in a similar manner (Table 4). Both

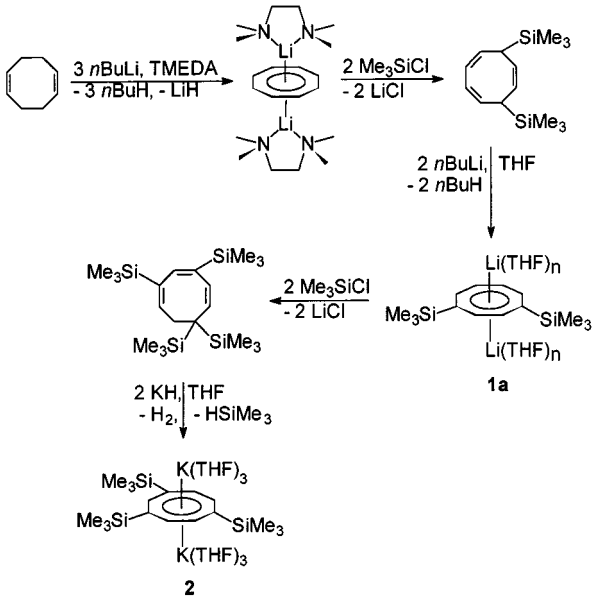

Scheme 1

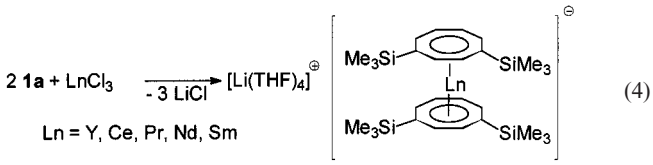

(4)

Table 4. Silyl-substituted lanthanocenes

Ln	Complex	Ref.
Y, Ce, Pr, Nd, Sm	$[Li(THF)_4][Ln\{1,4\text{-}(Me_3Si)_2C_8H_6\}_2]$	64
Sm	$[PPN][Ln\{1,4\text{-}(Me_3Si)_2C_8H_6\}_2]$	64
Ce, Tb	$[K(THF)_3][Ln\{1,3,6\text{-}(Me_3Si)_3C_8H_5\}_2]$	63
Ce	$[Yb(THF)_6][Ln\{1,3,6\text{-}(Me_3Si)_3C_8H_5\}_2]_2$	66
Ce	$[CoCp_2][Ln\{1,3,6\text{-}(Me_3Si)_3C_8H_5\}_2]_2$	63
Ce (**3**)	$[Ln\{1,3,6\text{-}(Me_3Si)_3C_8H_5\}_2]$	63
Ce, Nd, Sm	$[Ln_2\{1,4\text{-}(Me_3Si)_2C_8H_6\}_3]$	67
Nd, Sm	$[Li(diglyme)_2][Ln(1,4\text{-}R_2C_8H_6)_2]$[a]	72

[a] R = *ortho*-(Dimethylsilyl)-*N,N*-dimethylaniline.

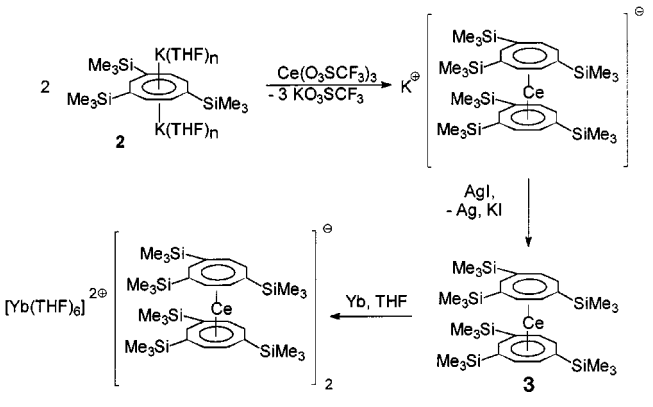

Scheme 2

cerium complexes could be oxidized with AgI to the corresponding neutral sandwich complexes [Ce{1,4-$(Me_3Si)_2C_8H_6$}$_2$] and [Ce{1,3,6-$(Me_3Si)_3C_8H_5$}$_2$] (**3**) (Scheme 2).[63] In contrast to the nonsubstituted complex [Ce$(C_8H_8)_2$] both compounds have good solubility in organic solvents and can be handled in air for a short time. Complex **3** was also characterized by X-ray diffraction (Figure 6). It was shown that the complex crystallizes in a staggered-like conformation.[63] XANES spectra give the assignment of the oxidation state of the cerium ion of **3** as trivalent.[65] In a few investigations **3** was used as an oxidizing reagent. Thus the redox reaction of **3** with ytterbium metal gave the first heterobimetallic organolanthanide complex [Yb$(THF)_6$][Ce{1,3,6-$(Me_3Si)_3C_8H_5$}$_2$]$_2$ (Scheme 2),[66] whereas the redox reaction of **3** and cobaltocene yielded [$CoCp_2$][Ce{1,3,6-$(Me_3Si)_3C_8H_5$}$_2$]$_2$.[63]

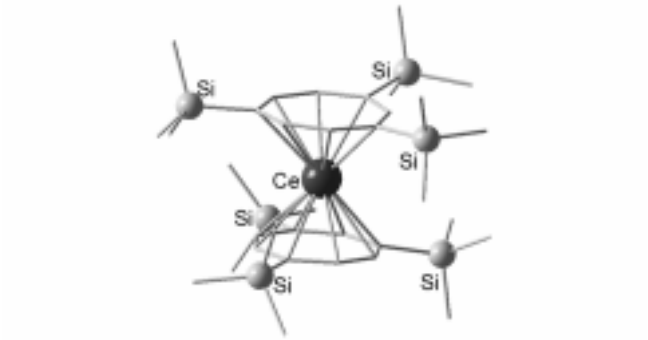

Figure 6. Crystal structure of [Ce{1,3,6-$(Me_3Si)_3C_8H_5$}$_2$] (**3**)

Treatment of anhydrous lanthanide trichlorides with **1a** in a 2:3 molar ratio afforded the first well defined organolanthanide triple-decker sandwich complexes of composition [Ln_2{1,4-$(Me_3Si)_2C_8H_6$}$_3$] (Ln = Ce, Nd, Sm) [Equation (5)].[67] Due to the presence of six trimethylsilyl substituents in the molecules, the intensely colored complexes are readily soluble in most common organic solvents.

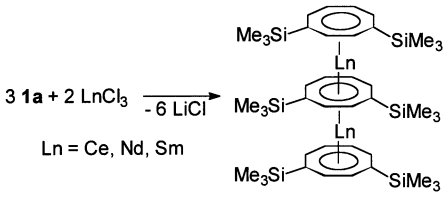

(5)

Cyclooctatetraene half-sandwich complexes of yttrium and scandium were the first complexes with silyl substituents on the eight-membered ring. Reaction of **1a** with [$LnCl_3(THF)_3$] (Ln = Sc, Y) gave the half-sandwich complexes [{{1,4-$(Me_3Si)_2C_8H_6$}Sc(μ-Cl)}$_2$(μ-THF)] and [{1,4-$(Me_3Si)_2C_8H_6$}Y(THF)(μ-Cl)]$_2$, respectively [Equation (6) and (7)].[68] The structure of the scandium compound was determined by single crystal X-ray diffraction (Figure 7). The most interesting feature of the dimeric structure concerns the THF ligand, which is in a bridging position. This structure has no parent C_8H_8 analogue.

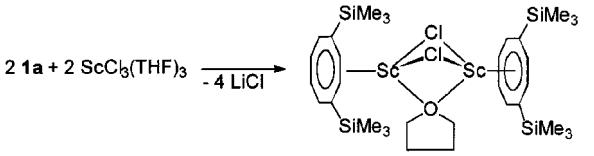

(6)

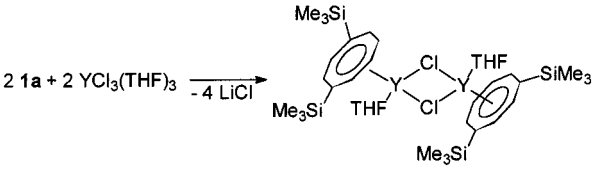

(7)

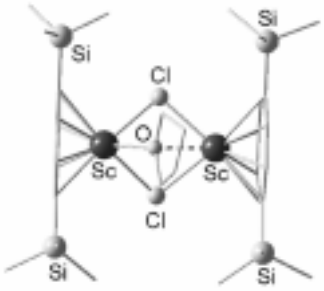

Figure 7. Crystal structure of [{{1,4-$(Me_3Si)_2C_8H_6$}Sc(μ-Cl)}$_2$(μ-THF)]

Derivatives of the cyclooctatetraene half-sandwich halides were usually made in a one-pot reaction starting from $LnCl_3$ and **1a** without isolation of the halogen intermediate (Table 5). Thus, the polysilylated complexes of composition [{1,4-$(Me_3Si)_2C_8H_6$}Ln{1,3-$(Me_3Si)_2C_5H_3$}] (Ln = Pr, Sm, Tb) were prepared by treatment of $LnCl_3$ simultaneously with equivalent amounts of **1a** and Li{1,3-$(Me_3Si)_2C_5H_3$}.[69] The isopropyl-aminotroponimate complexes [{1,4-$(Me_3Si)_2C_8H_6$}Ln{(iPr)$_2$ATI}(THF)] [Ln = Y, Lu; (iPr)$_2$ATI = *N*-isopropyl-2-(isopropylamino)troponiminate] and the enantiomerically pure (*S*)-phenylethyl-aminotroponimate complex [{1,4-$(Me_3Si)_2C_8H_6$}Y{((*S*)-$PhCHCH_3)_2$ATI}(THF)] were obtained by the consecutive treatment of $LnCl_3$ with **1a** and {$(R)_2$ATI}K [Equation (8)].[70] The structure of [{1,4-$(Me_3Si)_2$-C_8H_6}Y{(iPr)$_2$ATI}(THF)] was confirmed by single crystal X-ray diffraction. In contrast, the 1,4-diazadiene (DAD) complexes [{1,4-$(Me_3Si)_2C_8H_6$}Ln(DAD)(THF)] (Ln =

Table 5. Monomeric half-sandwich complexes of the general formula [{1,4-$(Me_3Si)_2C_8H_6$}Ln-R]

Ln	R	Ref.
Pr, Sm, Tb	1,3-$(Me_3Si)_2C_5H_3$	69
Y, Lu	{(iPr)$_2$ATI}(THF)[a]	70
Y	{((*S*)-$PhCHCH_3)_2$ATI}(THF)	70
Sm, Yb	(DAD)(THF)[b]	71

[a] (iPr)$_2$ATI = *N*-isopropyl-2-(isopropylamino)troponiminate. – [b] 1,4-Diazadiene.

Sm, Yb) have been prepared by reacting the cyclooctatriene 1,4-$(Me_3Si)_2C_8H_8$ with the elemental lanthanides and 1,4-diazadienes. As shown by NMR techniques, the interesting feature of these complexes is that by using the same reaction pathway the samarium complex is in the oxidation state +3, whereas the corresponding ytterbium compound is only divalent.[71] The silylated and thus very bulky cyclooctatetraene dianion provides higher solubility and often better crystallinity to organolanthanide derivatives relative to the parent C_8H_8 complexes.

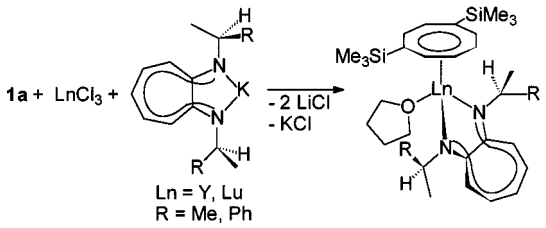

(8)

Recently, by using $[Li_2(THF)_n][1,4\text{-}(o\text{-}Me_2N\text{-}C_6H_4Me_2Si)_2\text{-}C_8H_6]$ (**4**) the first donor-functionalized lanthanide cyclooctatetraene complexes were prepared. Transmetallation of **4** with anhydrous $NdCl_3$ or $SmCl_3$ in a 2:1 stoichiometric ratio gave the sandwich complexes $[Li(diglyme)_2][Ln(1,4\text{-}R_2C_8H_6)_2]$ [Ln = Nd, Sm; R = *ortho*-(dimethylsilyl)-*N,N*-dimethylaniline] (Scheme 3).[72] The single crystal X-ray structures of both complexes show that the dimethylamino group of the aniline ring is turned away from the metal center (Figure 8). Obviously the metal atom is shielded by the two eight-membered rings of the ligand. Thus, neither intra- nor intermolecular coordination is observed in the solid state. The dimeric ionic half-sandwich complex $[Li(diglyme)_2][\{1,4\text{-}R_2C_8H_6\}_2Sm_2(\mu\text{-}Cl)_3]$ was synthesized by the reaction of **4** with $SmCl_3$ in a 1:1 stoichiometric ratio (Scheme 3).[73] The anion of the new complex is a unique example of a dimeric organolanthanide complex that is bridged by three chlorine atoms. In the solid state the donor functionality does not coordinate to the samarium center. As shown by spin lattice relaxation experiments there is a coordination of one amino group to the samarium atom in solution. Density Functional Theory (DFT) calculations show that this coordination might in principle be in an intramolecular fashion.[73]

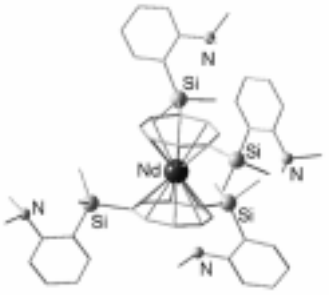

Figure 8. Crystal structure of the anion of $[Li(diglyme)_2][Nd(1,4\text{-}R_2C_8H_6)_2]$ [R = *ortho*-(dimethylsilyl)-*N,N*-dimethylaniline]

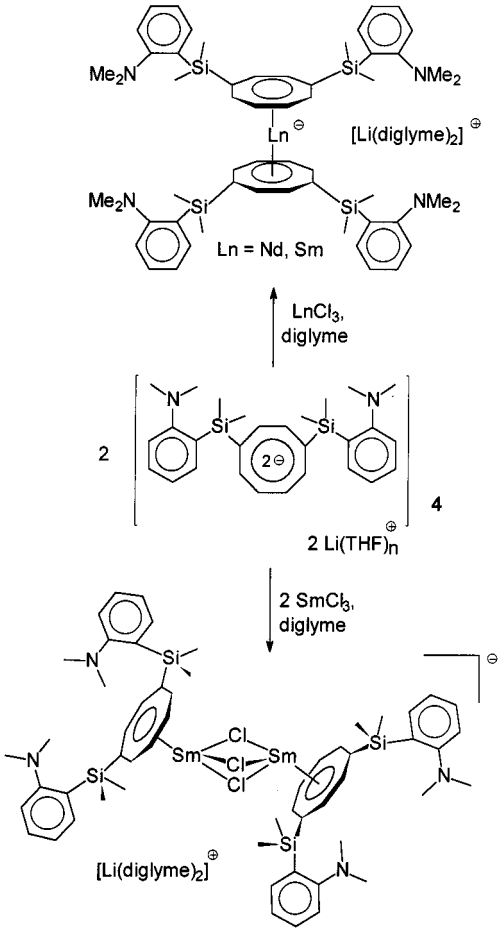

Scheme 3

In contrast to the large number of alkyl-substituted actinocenes only a few silyl-substituted actinocenes are known. Complexes of composition $[An\{1,4\text{-}(Me_3Si)_2C_8H_6\}_2]$ (An = Th, U),[68] $[An\{1,4\text{-}(Me_2tBuSi)_2C_8H_6\}_2]$ (An = Th, U),[62] and $[An\{1,3,6\text{-}(Me_3Si)_3C_8H_5\}_2]_2$ (An = Th, U, Np)[63,74] were obtained by reaction of $AnCl_4$ with **1a,b** and **2**, respectively. Reduction of $[An\{1,4\text{-}(Me_2tBuSi)_2C_8H_6\}_2]$ by potassium in DME yielded the anionic compounds $[K(DME_2)][An\{1,4\text{-}(Me_2tBuSi)_2C_8H_6\}_2]$, which were crystallographically characterized.[62] The thorium complex was the first Th^{III} sandwich to be discovered. EPR spectroscopic studies indicated that the molecule possesses a $6d^1$ ground state.

The first bridged uranocene is also a silyl-substituted complex. The ligand 1,2-bis(cyclooctatetraenyldimethylsilyl)ethane, $C_8H_7\text{-}Si(Me_2)\text{-}CH_2CH_2\text{-}Si(Me_2)\text{-}C_8H_7$, was prepared by the reaction of LiC_8H_7 and 1,2-bis(chlorodimethylsilyl)ethane. Further reaction of the ligand with potassium and UCl_4 gave the corresponding bridged uranocene [Equation (9)].[75] The only known half-sandwich complex of the actinides with silyl-substituted cyclooctatetraenes is $[\{1,4\text{-}(Me_3Si)_2C_8H_6\}U(BH_4)_2]$ which was obtained from **1a** and $[UCl_2(BH_4)_2]$.[68]

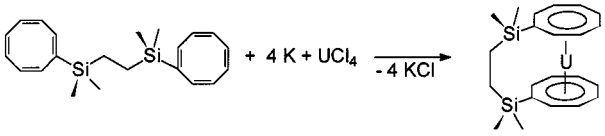

(9)

3. Conclusion

The recent developments in the chemistry of substituted cyclooctatetraenes has shown that silyl-substituted cyclooctatetraenes are becoming more and more popular in *f*-metal chemistry. There are several reasons for this development. In contrast to alkyl-substituted cyclooctatetraenes the silylated ligands are easily accessible from cheap starting materials. As observed for highly substituted alkyl complexes, the silyl groups are bulky enough to shield the highly reactive metal centers. Thus, more stable complexes are available. Furthermore, due to the silyl groups the solubility of the resulting metal complexes is increased. This facilitates the purification of some of the complexes such as half-sandwich lanthanide halides. Additionally, in some cases the steric bulk of the substituents on the eight-membered ring led to new coordination modes on the center metal. Finally, the introduction of the silicon atom facilitates the attachment of functional groups on to the ligand. Due to these advantages all recent publications on substituted cyclooctatetraenes deal exclusively with the silyl-substituted form.

Acknowledgments

This work was supported by the Deutsche Forschungsgemeinschaft (Heisenberg fellowship) and the Fonds der Chemischen Industrie. Additionally, generous support from Prof. Dr. D. Fenske is gratefully acknowledged.

[1] C. Elschenbroich, A. Salzer, *Organometallics: a Concise Introduction*, 2nd Edn., Wiley-VCH, Weinheim, Germany, **1992**.
[2] N. Kaltsoyannis, P. Scott, *The f elements*, Oxford University Press, Oxford, UK, **1999**.
[3] P. Jutzi, *Comments Inorg. Chem.* **1987**, *6*, 123.
[4] P. Jutzi, H. Saleske, U. Meyer, *Phosphorous Sulfur* **1987**, *30*, 161−164.
[5] R. B. King, *Coord. Chem. Rev.* **1976**, *20*, 155−169.
[6] W. J. Evans, *New. J. Chem.* **1995**, *19*, 525−533.
[7] P. J. Fagan, E. A. Maatta, A. M. Afif, T. J. Marks, *Mod. Sci. Technol.* **1982**, *3*, 77−84.
[8] F. T. Edelmann, *New. J. Chem.* **1995**, *19*, 535−550.
[9] F. T. Edelmann, in *Comprehensive Organometallic Chemisty II* (Eds.: E. W. Abel, F. G. A. Stone, G. Wilkinson), Pergamon Press, Oxford, **1995**.
[10] H. Schumann, J. A. Meese-Marktscheffel, L. Esser, *Chem. Rev.* **1995**, *95*, 865−986.
[11] C. J. Schaverien, *Adv. Organomet. Chem.* **1994**, *36*, 283−363.
[12] H. Schumann, *Angew. Chem.* **1984**, *96*, 475−493; *Angew. Chem. Int. Ed. Engl.* **1984**, *23*, 474−493.
[13] A. C. Cope, M. Kinter, *J. Am. Chem. Soc.* **1951**, *73*, 3424−3430.
[14] A. C. Cope, H. O. van Orden, *J. Am. Chem. Soc.* **1952**, *74*, 175−179.
[15] A. C. Cope, R. M. Pike, *J. Am. Chem. Soc.* **1952**, *74*, 179−183.
[16] A. C. Cope, H. C. Campbell, *J. Am. Chem. Soc.* **1953**, *75*, 3220−3223.
[17] A. C. Cope, R. M. Pike, D. F. Rugen, *J. Am. Chem. Soc.* **1954**, *76*, 4945−4950.
[18] H. Röttele, *Methoden der Organischen Chemie*, *Houben-Weyl* (Ed.: E. Müller), G. Thieme, Stuttgart, **1972**, Vol.5/1d, pp. 423−525, and references therein.
[19] G. Schröder, *Cyclooctatetraen*, VCH, Weinheim, Germany, **1965**.
[20] J. Gasteiger, G. Gream, R. Huisgen, W. E. Konz, U. Schnegg, *Chem. Ber.* **1971**, *104*, 2412−2419.
[21] C. A. Harmon, A. Streitwieser, Jr., *J. Org. Chem.* **1973**, *38*, 549−551.
[22] C. A. Harmon, D. P. Bauer, S. R. Berryhill, K. Hagiwara, A. Streitwieser, Jr., *Inorg. Chem.* **1977**, *16*, 2143−2147.
[23] H. Schumann, P. R. Lee, J. Loebel, *Chem. Ber.* **1989**, *122*, 1897−1900.
[24] D. C. Eisenberg, S. A. Kinsley, A. Streitwieser, Jr., *J. Am. Chem. Soc.* **1989**, *111*, 5769−5772.
[25] T. R. Boussie, D. C. Eisenberg, J. Rigsbee, A. Streitwieser, Jr., A. Zalkin, *Organometallics* **1991**, *10*, 1922−1928.
[26] M. Dolg, P. Fulde, *Chem. Eur. J.* **1998**, *4*, 200−204.
[27] A. Streitwieser, Jr., *Organometallics of the f-Elements* (Eds.: T. J. Marks, R. D. Fischer), Nato ASI Series, D. Reidel, Dordrecht, Holland, **1979**, *44*, 149−177.
[28] A. Streitwieser, Jr., *Fundamental and Technological Aspects of Organo f-Element Chemistry* (Eds.: T. J. Marks, I. L. Fragalà), Nato ASI. Series, D. Reidel, Dordrecht, Holland, **1985**, *155*, 77−114.
[29] C. A. Harmon, A. Streitwieser, Jr., *J. Am. Chem. Soc.* **1972**, *94*, 8926−8928.
[30] A. Streitwieser, Jr., C. A. Harmon, *Inorg. Chem.* **1973**, *12*, 1102−1105.
[31] V. A. Il'yushenkov, N. V. Il'yushenkova, M. R. Leonov, I. I. Ginval'd, *Khim. Elementoorg. Soedin* **1980**, *8*, 113−114 [*Chem. Abstr.* **1982**, *97*, 6446z].
[32] V. G. Sevast'yanov, V. G. Slov'ev, V. P. Leonov, V. A. Il'yushenkov, *Radiokhimiya* **1981**, *23*, 78−81 [*Chem. Abstr.* **1981**, *95*, 6288h].
[33] J. T. Miller, C. W. DeKock, *Inorg. Chem.* **1979**, *18*, 1305−1306.
[34] V. G. Sevast'yanov, V. A. Mitin, V. F. Ryurikov, *Zh. Neorg. Khim.* **1986**, *31*, 152−154 [*Chem. Abstr.* **1986**, *105*, 191308a].
[35] R. M. Moore, A. Streitwieser, Jr., H. K. Wang, *Organometallics* **1986**, *5*, 1418−1421.
[36] A. Streitwieser, Jr., H. P. G. Burghard, D. G.; Morrell, W. D. Luke, *Inorg. Chem.* **1980**, *19*, 1863−1866.
[37] A. W. Spiegl, R. D. Fischer, *Chem. Ber.* **1979**, *112*, 116−127.
[38] A. Streitwieser, Jr., M. H. Lyttle, H.-K. Wang, T. Boussie, A. Weinländer, J. P. Solar, *J. Organomet. Chem.* **1995**, *501*, 245−249.
[39] X. Wang, A. Streitwieser, Jr., M. H. Lyttle, J. P. Solar, *Gaodeng Xuexiao Huaxue Xuebao* **1985**, *6*, 412−416 [*Chem. Abstr.* **1986**, *105*, 226856g].
[40] X. Wang, A. Streitwieser, Jr., J. P. Solar, M. H. Lyttle, *Gaodeng Xuexiao Huaxue Xuebao* **1985**, *6*, 699−702 [*Chem. Abstr.* **1986**, *104*, 224985d].
[41] M. J. Miller, A. Streitwieser, Jr., *J. Organomet. Chem.* **1981**, *209*, C52−C54.
[42] C. Le Vanda, A. Streitwieser, Jr., C. A. Harmon, *Inorg. Chem.* **1981**, *20*, 656−659.
[43] X. Wang, A. Streitwieser, Jr., *Gaodeng Xuexiao Huaxue Xuebao* **1985**, *6*, 613−615 [*Chem. Abstr.* **1986**, *105*, 42993f].
[44] D. G. Karraker, *Inorg. Chem.* **1973**, *12*, 1105−1108.
[45] A. Streitwieser, Jr., *Inorg. Chim. Acta.* **1984**, *94*, 171−177.
[46] M. H. Lyttle, A. Streitwieser, Jr., M. J. Miller, *J. Org. Chem.* **1989**, *54*, 2331−2335.
[47] M. J. Miller, M. H. Lyttle, A. Streitwieser, Jr., *J. Org. Chem.* **1981**, *49*, 1977−1984.
[48] C. Levanda, A. Streitwieser, Jr., *Inorg. Chem.* **1981**, *20*, 656−659.
[49] J. P. Solar, H. P. G. Burghard, R. H. Banks, A. Streitwieser, Jr., D. Brown, *Inorg. Chem.* **1980**, *19*, 2186−2188.

[50] K. O. Hodgson, K. N. Raymond, *Inorg. Chem.* **1973**, *12*, 458−466.
[51] A. Streitwieser, Jr., R. Walker, *J. Organomet. Chem.* **1975**, *97*, C41−C42.
[52] J. E. Garbe, V. Boekelheide, *J. Am. Chem. Soc.* **1983**, *105*, 7384−7388.
[53] A. Zalkin, D. H. Templeton, S. R. Berryhill, W. D. Luke, *Inorg. Chem.* **1979**, *18*, 2287−2289.
[54] W. D. Luke, S. R. Berryhill, A. Streitwieser, Jr., *Inorg. Chem.* **1981**, *20*, 3086−3089.
[55] A. Zalkin, D. H. Templton, W. D. Luke, A. Streitwieser, Jr., *Organometallics* **1982**, *1*, 618−622.
[56] A. Streitwieser, Jr., R. Q. Kluttz, K. A. Smith, W. D. Luke, *Organometallics* **1983**, *2*, 1873−1877.
[57] D. C. Eisenberg, A. Streitwieser, Jr., W. K. Kot, *Inorg. Chem.* **1990**, *29*, 10−14.
[58] C. LeVanda, J. P. Solar, A. Streitwieser, Jr., *J. Am. Chem. Soc.* **1980**, *102*, 2128−2129.
[59] T. R. Boussie, A. Streitwieser, Jr., *J. Org. Chem.* **1993**, *58*, 2377−2380.
[60] N. C. Burton, F. G. N. Cloke, S. C. P. Joseph, H. Karamallakis, A. A. Sameh, *J. Organomet. Chem.* **1993**, *462*, 39−43.
[61] P. Poremba, H.-G. Schmidt, M. Noltemeyer, F. T. Edelmann, *Organometallics* **1998**, *17*, 986−988.
[62] J. S. Parry, F. G. N. Cloke, S. J. Coles, M. B. Hursthouse, *J. Am. Chem. Soc.* **1999**, *121*, 6867−6871.
[63] U. Kilimann, R. Herbst-Irmer, D. Stalke, F. T. Edelmann, *Angew. Chem.* **1994**, *106*, 1684−1687; *Angew. Chem. Int. Ed. Engl.* **1994**, *33*, 1618−1621.
[64] P. Poremba, U. Reißmann, M. Noltemeyer, H.-G. Schmidt, W. Brüser, F. T. Edelmann, *J. Organomet. Chem.* **1997**, *544*, 1−6.
[65] N. M. Edelstein, P. G. Allen, J. J. Buchler, D. K. Shuh, C. D. Sofiled, *J. Am. Chem. Soc.* **1996**, *118*, 13115−13116.
[66] U. Reißmann, L. Lameyer, D. Stalke, P. Poremba, F. T. Edelmann, *Chem. Commun.* **1999**, 1865−1866.
[67] P. Poremba, F. T. Edelmann, *J. Organomet. Chem.* **1998**, *553*, 393−395.
[68] N. C. Burton, F. G. N. Cloke, P. B. Hitchcock, H. C. de Lemos, A. A. Sameh, *J. Chem. Soc., Chem. Commun.* **1989**, 1462−1464.
[69] P. Poremba, F. T. Edelmann, *Polyhedron* **1997**, *16*, 2067−2071.
[70] P. W. Roesky, *J. Organomet. Chem.* **2001**, *621*, 277−283.
[71] P. Poremba, F. T. Edelmann, *J. Organomet. Chem.* **1997**, *549*, 101−104.
[72] T. G. Wetzel, P. W. Roesky, *Organometallics* **1998**, *17*, 4009−4013.
[73] T. G. Wetzel, S. Dehnen, P. W. Roesky, *Organometallics* **1999**, *18*, 3835−3842.
[74] C. Apostolides, F. T. Edelmann, B. Kanellakopulos, U. Riessmann, *Z. Naturfosch., B* **1999**, *54*, 960−962.
[75] A. Streitwieser, Jr., M. T. Barros, H.-K. Wang, T. R. Boussie, *Organometallics* **1993**, *12*, 5023−5024.

Received October 11, 2000
[I00382]

Different Transformation Pathways in the Photolysis of [Cp*P{W(CO)$_5$}$_2$]

Michael Schiffer,[a] Eva Leiner,[a] and Manfred Scheer*[a]

Dedicated to Professor Marianne Baudler on the occasion of her 80th birthday

Keywords: Photolysis / Cyclopentadienyl ligands / Tungsten / P ligands

Photolysis of [Cp*P{W(CO)$_5$}$_2$] (**1**) leads to the novel complex [{Cp*(CO)$_6$W$_2$}(μ-H)(μ-η^1:η^1:η^1-P$_2$){W(CO)$_5$}$_2$] (**4**), which was structurally and spectroscopically characterised. The product is formed by a Cp* migration within **1** to give the phosphido complex intermediate [Cp*(CO)$_2$W≡P→W(CO)$_5$], as well as by a Cp* elimination to form an intermediate of the type [P{W(CO)$_5$}$_2$], both of which dimerise to yield product **4**.

The novel class of complexes with a metal−phosphorus triple bond[1] contains two different types of compounds: [L$_n$M≡P] **A**[2] and [L$_n$M≡P→M′(CO)$_5$] **B** (M′ = Cr, W).[3] If in both types of complexes the transition metal is in a high oxidation state, stable compounds are obtained. In the case of a low oxidation state of the transition metal, these complexes exist as highly reactive intermediates.[1] We recently found a synthetic approach to generate complexes **B** directly as highly reactive intermediates.[4] In contrast to the sterically demanding complexes of type **A**, they reveal a high "side-on" reactivity. The principle of their generation is based on the migration of a σ-bound Cp* substituent at the phosphorus atom to an η^5-coordination at the transition metal (Scheme 1). Thus, the thermolysis of [Cp*P{W(CO)$_5$}$_2$] (**1**) leads, via CO elimination, to an intermediate of the formula **D** containing a phosphorus−tungsten triple bond. This intermediate dimerises to form the tetrahedral complex **2** as the major product. As a side-reaction, a C−H activation in a possible precursor intermediate **C** gives the complex **3**. The chemistry of this highly reactive intermediate **D** offers promising synthetic routes to a large variety of unprecedented phosphametallocycles.[5] Herein we report on the photolysis of **1**, which reveals a different transformation pathway in contrast to the transformation involved in the thermolysis reaction of **1**.

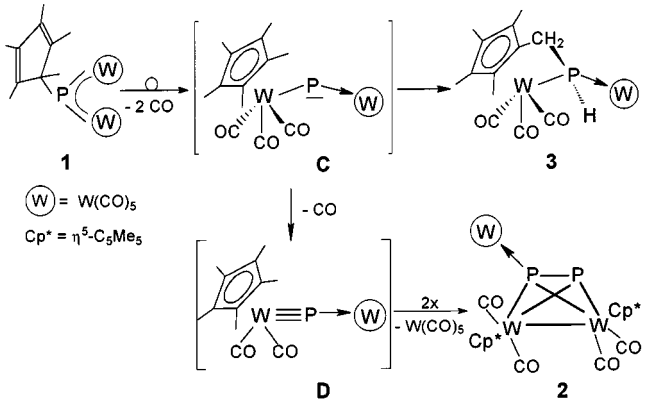

Scheme 1. Proposed reaction pathway of the thermolysis of [Cp*P{W(CO)$_5$}$_2$] (**1**)

The photolysis of **1** in toluene at room temperature results in a colour change from blue to brown after two hours indicating the completeness of the transformation of **1** [Equation (1)]. Column chromatographic workup resulted in a yellow fraction of the minor product **3** as well as an orange fraction from which **4** could be obtained as a red crystalline compound in 60% yield. Complex **4** is sparingly soluble in toluene and readily soluble in THF and CH_2Cl_2. The IR spectrum reveals absorptions for terminal CO ligands. In the mass spectrum of **4**, the highest mass peak found corresponds to the molecular ion peak minus W(CO)$_5$.

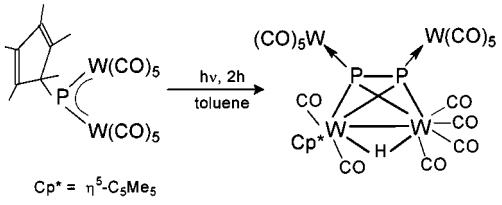

(1)

The $^{31}P\{^1H\}$ NMR spectrum of **4** reveals two doublets at δ = −166.2 and −223.7 with a $^1J_{P,P}$ coupling constant of 447 Hz, indicating magnetically nonequivalent P atoms. This magnetic nonequivalency probably results from the different orientations of the P atoms to the Cp* ligand at one of the W atoms of the stereochemically rigid tetrahedral P_2W_2 framework. While the first doublet shows one $J_{W,P}$ coupling of 233 Hz, the other doublet reveals two $J_{W,P}$ couplings of 69 and 209 Hz, respectively. Since the larger $J_{W,P}$ usually corresponds to the coupling to the terminal W(CO)$_5$ groups, the smaller must reflect the coupling to the W atoms of the W_2P_2 tetrahedral framework, which is probably not resolved in the signal at δ = −166.2

[a] Institut für Anorganische Chemie der Universität Karlsruhe, 76128 Karlsruhe, Germany
Fax: (internat.) +49-721/661-921
E-mail: mascheer@chemie.uni-karlsruhe.de

 © WILEY-VCH Verlag GmbH, 69451 Weinheim, 2001 1434−1948/01/0707−1661 $ 17.50+.50/0

($w_{1/2} > 50$ Hz). For $[\{Cp^*W(CO)_2\}_2(\mu,\eta^2\text{-}P_2)]$[6] and $[\{CpW(CO)_2\}_2(\mu,\eta^2\text{-}P_2)]$,[7] no $^1J_{W,P}$ couplings are observed in the singlets found at $\delta = -154.6$ and -299.0, respectively. In the ^{1}H NMR spectra of **4**, a singlet for the methyl protons of the Cp* ligand is found at $\delta = 2.29$. Furthermore, a singlet at $\delta = -16.7$ for the (μ-H) ligand is observed containing two different $^1J_{W,H}$ couplings of 30 and 38 Hz. The magnitude of the coupling is in good agreement with the data obtained for $[W_2(\mu\text{-}H)(CO)_xL_y]$ (L = NO, RNC, PPh_3; R = Me, *t*Bu, $PhCH_2$, *i*Pr; $x = 6-9$; $y = 1, 2$), where the signal for the μ-hydrido ligand was found between $\delta = -5.21$ and -13.1, with each of them containing two $^1J_{W,H}$ couplings of between 30 and 60 Hz.[8] The origin of the μ-H ligand in **4**, which completes the electronically precise nature of this compound, was confirmed by carrying out the reaction in Equation (1) in $[D_8]$toluene (99% labeled with D) as solvent. Since the obtained compound **4a** contains only traces of the protonated complex **4**, one can speculate that the solvent acts as the source of the proton.

The molecular structure of **4** (Figure 1) shows a slightly distorted W_2P_2 tetrahedron containing a $Cp^*(CO)_2W$ and a $W(CO)_4$ unit. Both of the phosphorus atoms coordinate to $W(CO)_5$ groups. The bond length P(1)−P(2) of 2.166(6) Å is shorter than a single bond length found, for example, in the structure of β-P_4 at −185 °C [2.190−2.212 Å].[9] Since the P−P bond length in **4** is longer than in the non-substituted tetrahedral P_2W_2 complex $[\{CpW(CO)_2\}_2(\mu,\eta^2\text{-}P_2)]$ [2.104(4) Å],[7] and also longer than in the monosubstituted complex $[Cp^*W(CO)_2\}_2(\mu,\eta^2{:}\eta^1\text{-}P_2)\{W(CO)_5\}]$ [2.092(4) Å],[4] one can conclude that the coordination of the phosphorus lone pairs in **4** lengthens the P−P bond. Furthermore, each of the P atoms of **4** is more closely bound to a different W atom of the tetrahedral P_2W_2 moiety. Thus, the bond lengths P(1)−W(1) and P(2)−W(2) are 2.492(4) Å and 2.510(4) Å, respectively, in comparison to the other P(1)−W(2) and P(2)−W(1) bond lengths of 2.540(4) Å and 2.554(4) Å, respectively. The W(1)−W(2) bond length [3.1417(9) Å] in **4** is slightly longer than the W−W bond length in other W_2P_2 tetrahedral complexes: $[\{Cp^*(CO)_2W\}_2\{\mu,\eta^2{:}\eta^1\text{-}P_2W(CO)_5\}]$ [3.0920(7) Å][4] and $[\{Cp(CO)_2W\}_2(\mu,\eta^2\text{-}P_2)]$ [3.0026(11) Å].[7]

The formation of **4** from the photolysis of $[Cp^*P\{W(CO)_5\}_2]$ (**1**) can be regarded as a dimerisation of two reactive intermediates (Scheme 2): the triple bond intermediate **D**, formed by Cp* migration as described in Scheme 1, and a second intermediate **E** created by elimination of the Cp* ligand. Since complex **4** is obtained in high isolated yields, both of the pathways can be regarded as equivalent. Each of these intermediates opens up broad perspectives for trapping reactions to obtain novel main-group−transition-metal cage compounds with unusual coordination polyhedrons.

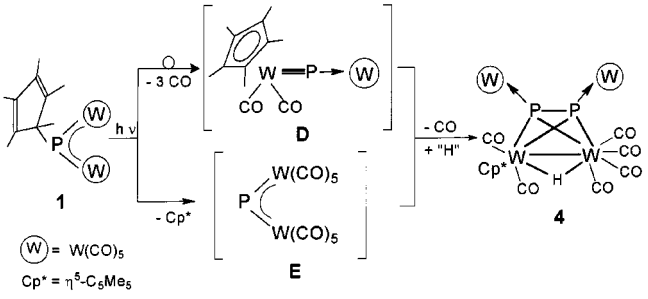

Scheme 2. Proposed reaction pathway of the photolysis of $[Cp^*P\{W(CO)_5\}_2]$ (**1**)

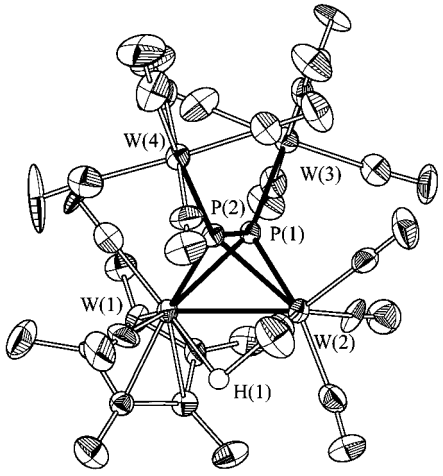

Figure 1. Molecular structure of **4** (showing 50% probability ellipsoids; hydrogen atoms of the Cp* ligand are omitted for clarity); selected bond lengths [Å] and angles [°]: W(1)−P(1) 2.492(4), W(1)−P(2) 2.554(4), W(1)−W(2) 3.1417(9), W(2)−P(2) 2.510(4), W(2)−P(1) 2.540(4), W(3)−P(1) 2.547(4), W(4)−P(2) 2.519(4), P(1)−P(2) 2.116(6); P(1)−W(1)−P)(2) 49.58(13), P(1)−W(1)−W(2) 51.04(8), P(2)−W(1)−W(2) 51.02(9), P(2)−W(2)−P(1) 49.56(13), P(2)−W(2)−W(1) 52.29(8), P(1)−W(2)−W(1) 50.68(6), P(2)−P(1)−W(1) 66.75(15), P(2)−P(1)−W(2) 64.49(14), W(1)−P(1)−W(2) 77.28(10), P(2)−P(1)−W(3) 130.19(18), W(1)−P(1)−W(3) 144.15(15), W(2)−P(1)−W(3) 136.99(15), P(1)−P(2)−W(2) 65.95(15), P(1)−P(2)−W(4) 136.01(19, W(2)−P(2)−W(4) 140.18(16), P(1)−P(2)−W(1) 63.67(14), W(2)−P(2)−W(1) 76.69(11), W(4)−P(2)−W(1) 139.39(17)

Experimental Section

General: All reactions were performed under an atmosphere of dry argon using Schlenk techniques. Solvents were purified and degassed by standard procedures. NMR spectra were recorded on a Bruker AC 250 [^{1}H: 250.13 MHz; ^{31}P: 101.256 MHz; standard Me_4Si (^{1}H), 85% H_3PO_4 (^{31}P)]. The IR spectra were recorded in KBr on a Bruker IFS 28 FT-IR spectrometer, the mass spectrum on a Finnigan MAT 711 at 70 eV and the UV spectra on a Perkin−Elmer Lambda 900 UV/Vis/NIR. Photolysis reactions were carried out with a Hanau type TQ150 mercury lamp.

Synthesis of 4: A solution of **1** (0.39 g, 0.48 mmol)[10] in 50 mL of toluene was photolysed for 2 h until the colour of the solution changed from deep blue to brown. The solvent was completely removed in vacuo, and the resulting brown residue was coated onto 6 g of silica gel and separated by column chromatography (1.5 × 45 cm). Elution with *n*-hexane/toluene (5:1) gave a yellow fraction of **3** (20 mg, 5.6%) followed by an orange fraction (*n*-hexane/toluene 1:1) containing **4**, which was recrystallised to give 0.2 g (60%) of red platelets at −30 °C. − ^{31}P{^{1}H} NMR (C_6D_6): $\delta = -166.2$ (d, $^1J_{PP} = 447$ Hz, $^1J_{WP} = 233$); −223.7 (d, $^1J_{PP} = 447$ Hz, $^1J_{WP} = 69$ Hz, 209 Hz). − ^{1}H NMR ($[D_8]$THF): $\delta = 2.29$ (s, 15 H, Cp*), −16.7 (s, 1 H, $J_{W,H} = 30$ and 38 Hz). − IR (KBr): ν(CO) = 2074 (m), 2063 (w), 1970 (sh), 1930 (s, br) cm^{-1}. − MS (EI): *m*/*z* (%) =

1058 (2) [M − W(CO)$_5$]$^+$, 1002 (1) [M − W(CO)$_7$]$^+$, 890 (3) [M − W(CO)$_{11}$]$^+$. − $C_{26}H_{16}O_{16}P_2W_4$ (1381.75): calcd. C 22.60, H 1.17; found C 22.32, H 1.53

1: UV/Vis (toluene): λ_{max} [nm] (ε) [M^{-1} cm^{-1}] = 572 (13400), 350 (sh, 10300).

4: UV/Vis (toluene): λ_{max} [nm] (ε) [M^{-1} cm^{-1}] = 320 (sh, 6900).

Crystal Structure Determination of 4:[11] A red crystal, obtained from toluene, with the dimensions 0.20 × 0.12 × 0.02 mm was used for data collection at 210(2) K on a STOE IPDS diffractometer with Mo-K_α radiation (λ = 0.71073 Å) with numerical absorption corrections. The structure was solved by direct methods using SHELXS-86,[12a] with full-matrix least-squares refinement on F^2 using SHELXL-97[12b] and anisotropic displacement for non-H atoms (except those of the atoms O6 and C21, due to the insufficient crystal quality). Hydrogen atoms were located in idealised positions and refined isotropically according to a riding model. The bridging H(1) atom was found as residual electron density and was freely refined [U(eq) = 0.06 Å^2]. The flack parameter of the acentric structure of **4** came to a value of −0.07(2). The relatively high residual electron density in the structure of **4** is located close to the atom W(2). Further data of the X-ray structure analysis are given in Table 1.

Table 1. Crystallographic data for **4**

Empirical formula	$C_{26}H_{16}O_{16}P_2W_4$
Molecular weight	1381.73
Space group	Orthorhombic, *Pna*2(1)
a [Å]	21.142(3)
B [Å]	11.706(2)
c [Å]	14.320(2)
V [Å]^3	3544.1(12)
Z	4
ρ(calcd.) [g/cm^3]	2.590
μ [mm^{-1}]	13.098
F(000)	2504
2Θ range [°]	3.86−51.92
Index ranges	$-25 \le h \le 25$
	$-14 \le k \le 13$
	$-17 \le l \le 17$
Reflections collected	23642
Independent reflections	6834 (R_{int} = 0.2167)
Independent reflections [$F_0 > 4\sigma(F_0)$]	6571
Data/restrains/parameters	6834/1/430
Goodness-of-fit on F^2	1.083
$R1$[a] [$I > 2\sigma(I)$]/$wR2$[b]	0.0618, 0.1529
Larg. diff peak/hole [e/Å^3]	4.096, −4.794

[a] $R = \Sigma||F_0| - |F_c||/\Sigma|F_0|$. − [b] $wR_2 = [\Sigma\omega(F_0^2 - F_c^2)^2]/[\Sigma(F_0^2)^2]^{1/2}$.

Acknowledgments

The financial support from the Deutsche Forschungsgemeinschaft and the Fonds der Chemischen Industrie is gratefully acknowledged.

[1] Reviews: [1a] M. Scheer, *Coord. Chem. Rev.* **1997**, *163*, 271−286. − [1b] M. Scheer, *Angew. Chem.* **1995**, *107*, 2151−2153; *Angew. Chem. Int. Ed. Engl.* **1995**, *34*, 1997−1999.

[2] [2a] C. E. Laplaza, W. M. Davis, C. C. Cummins, *Angew. Chem.* **1995**, *107*, 2181−2183; *Angew. Chem. Int. Ed. Engl.* **1995**, *34*, 2042−2043. − [2b] N. C. Zanetti, R. R. Schrock, W. M. Davis, *Angew. Chem.* **1995**, *107*, 2184−2186; *Angew. Chem. Int. Ed.* **1995**, *34*, 2044−2046. − [2c] M. Scheer, J. Müller, M. Häser, *Angew. Chem.* **1996**, *108*, 2637−2641; *Angew. Chem. Int. Ed. Engl.* **1996**, *35*, 2492−2496.

[3] [3a] M. Scheer, P. Kramkowski, K. Schuster, *Organometallics* **1999**, *18*, 2874−2883. − [3b] M. Scheer, K. Schuster, T. A. Budzichowski, M. H. Chisholm, W. E. Streib, *J. Chem. Soc., Chem. Commun.* **1995**, 1671−1672. − [3c] P. Kramkowski, G. Baum, U. Radius, M. Kaupp, M. Scheer, *Chem. Eur. J.* **1999**, *5*, 2890−2898.

[4] M. Scheer, E. Leiner, P. Kramkowski, M. Schiffer, G. Baum, *Chem. Eur. J.* **1998**, *4*, 1917−1923.

[5] M. Schiffer, M. Scheer, *Chem. Eur. J.* **2001**, *7*, 1855−1861.

[6] J. Schwalb, PhD thesis, University of Kaiserslautern, **1988**.

[7] J. E. Davies, M. C. Klunduk, M. J. Mays, P. R. Raithby, G. P. Shields, P. K. Tompkins, *J. Chem. Soc., Dalton Trans.* **1997**, 715−719.

[8] J. T. Lin, C. C. Chen, P. S. Huang, F.-E. Hong, Y. S. Wen, *Organometallics* **1993**, *12*, 4016−4024.

[9] A. Simon, H. Borrmann, J. Horakh, *Chem. Ber./Recueil* **1997**, *130*, 1235−1240.

[10] [10a] R. Kroos, PhD thesis, University of Bielefeld, **1989**. − [10b] P. Jutzi, R. Kroos, *J. Organomet. Chem.* **1990**, *390*, 317−322.

[11] Crystallographic data (excluding structure factors) for the structures reported in this paper have been deposited with the Cambridge Crystallographic Data Centre as supplementary publication no. CCDC-153619. Copies of the data can be obtained free of charge on application to CCDC, 12 Union Road, Cambridge CB2 1EZ, UK [Fax: (internat.) +44-1223/336-033; E-mail: deposit@ccdc.cam.ac.uk].

[12] [12a] G. M. Sheldrick, *SHELXS-86*, University of Göttingen, **1986**. − [12b] G. M. Sheldrick, *SHELXL-97*, University of Göttingen, **1997**.

Received December 6, 2000
[I00462]

Two Isomers of a Tris(dimethylamino)bis(trimethylstannyl) Triborane(5) and the Reaction of $(Me_3Sn)_2B_2(NMe_2)_2$ with $(Ph_3P)_2Pt(\eta^2\text{-}C_2H_4)$[‡]

Tassilo Habereder,[a] Heinrich Nöth,*[a] and Matthias Wagner[a]

Keywords: Boranes / Isomers / Structure elucidation / Platinum

Reactions of $LiSnR_3$ (R = Me, Ph) with $Cl(Me_2N)B–B(NMe_2)Cl$ lead to the corresponding 1,2-(triorganylstannyl)diboranes(4) **1a,b**. Similarly, when the triborane(5) $Cl(Me_2N)B–BNMe_2–B(NMe_2)Cl$ is reacted with Me_3SnLi at low temperature the bis(trimethylstannyl)triborane **2a** is formed. In contrast, when the dibromide $Br(Me_2N)B–BNMe_2–B(NMe_2)Br$ is allowed to react with Me_3SnLi only small amounts of **2a** are formed; the main product being the cyclic isomer **2b**. Compounds **1a** and **2b** were characterized by X-ray crystal structure analysis. Compound **2b** has quite short B–Sn bonds. Oxidative addition of **1a** with ethylenebis(triphenylphosphane)platinum(0) yields *cis*-bis(trimethylstannyl)bis(triphenylphosphane)platinum(II) (**3**) besides trimethylstannyl[trimethylstannylbis(dimethylamino)diboranyl(4)]bis(triphenylphosphane)platinum **4**. These compounds were characterized by NMR spectroscopy.

Transition metal-boryl compounds have come into focus in recent years as they have been proposed as intermediates in a number of catalytic systems. Many well-characterized transition metal-boryl compounds are known today, and the state of the art has been reviewed several times.[2] Many of these complexes were obtained by oxidative addition of diborane(4) compounds to various metal-complex fragments. The oxidative addition of boron−halogen bonds[3] or boron−tin bonds[4] was also successful. So far, no reactivity scale has been developed, although it has recently been shown that the B−B bond of diborane(4) halides is more reactive than the boron−halogen bond. For example the reaction of $B_2Cl_2(NMe_2)_2$ or B_2F_4 with $(C_2H_4)Pt(PPh_3)_2$ leads to $[Pt(PPh_3)_2\{BCl(NMe_2)\}_2]$[5] and $[Pt(PPh_3)_2(BF_2)_2]$,[6] respectively. However, the formation of diborane(4)-1-yl derivatives is also known.[7] In our studies on silyl-, germyl- and stannylboranes, as well as polyboranes,[4,8−10] we became interested in the competition of B−Sn bonds vs. B−B bonds in the oxidative addition of stannyldiboranes(4) and stannyltriboranes(5). In preparing suitable starting materials we detected an interesting pair of isomers derived from a triborane(5) derivative, which we report here together with a new stannyldiborane(4).

Some time ago we described the preparation of $B_2(SnMe_3)_2(NMe_2)_2$ (**1a**) by treatment of $B_2Cl_2(NMe_2)_2$ with Me_3SnLi [Equation (1)].[8a] In analogy to **1a** we have now also obtained $B_2(SnPh_3)_2(NMe_2)_2$ (**1b**).

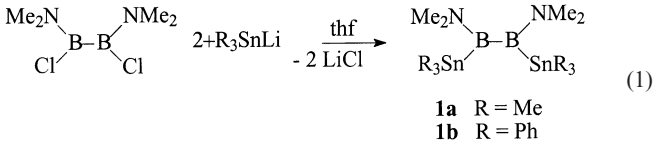

(1)

1a R = Me
1b R = Ph

The ^{11}B NMR spectrum of **1b** shows a broad signal within the expected range at $\delta^{11}B = 61$ ($h_{1/2} = \approx 1500$ Hz). Two different signal sets for the NMe_2 groups were found in the ^1H and ^{13}C NMR spectra consistent with a rotation barrier about the B−N bonds resulting from strong B−N π-bonding. In contrast to **1a**, which is a liquid, **1b** could be obtained as single crystals suitable for an X-ray structure determination (Figure 1). The B−N bond lengths support the view that strong π-bonding is present in **1b** as indicated by an average B−N bond length of 1.384(3) Å. The planes made up of the atoms bonded to the N atoms are almost coplanar with the planes at the boron atoms to which the nitrogen atoms are attached: [B(1)−N(1) = 5.3°,

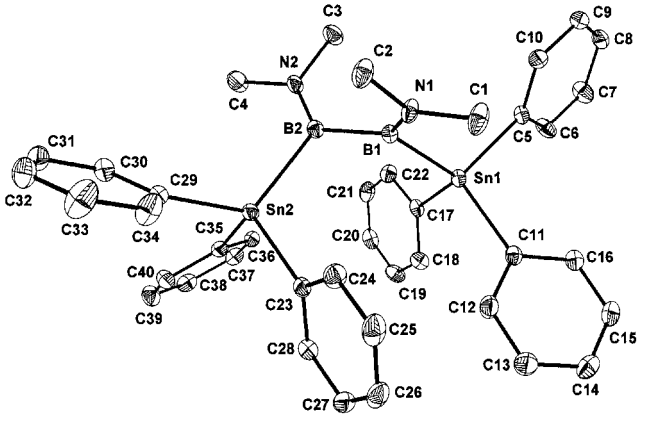

Figure 1. Molecular structure of **1b** in the crystal; hydrogen atoms omitted for clarity; thermal ellipsoids are drawn at a 25% probability level; selected bond lengths [Å] and bond angles [°]: Sn1−B1 2.276(3), Sn2−B2 2.282(3), N1−B1 1.383(3), N2−B2 1.384(3), B1−B2 1.677(4); N1−B1−B2 122.7(2), N1−B1−Sn(1) 118.9(2), B2−B1−Sn(1) 118.4(2), N2−B2−B1 125.7(2), N2−B2−Sn2 119.8(2), B1−B2−Sn2 114.4(2)

[‡] Contributions to the Chemistry of Boron, 248. − Part 247: Ref.[1]

[a] Department of Chemistry, University of Munich, Butenandtstraße 5−13, 81377 München, Germany
E-mail: H.Noeth@lrz.uni-muenchen.de

 © WILEY-VCH Verlag GmbH, 69451 Weinheim, 2001 1434−1948/01/0707−1665 $ 17.50+.50/0

Table 1. NMR spectroscopic data for the isomers **2a** and **2b**

	2a	**2b**
$\delta^{11}B$	61.5 (2B)	49.1 (2B)
	54.7 (1B)	−51.1 (d, $^1J_{BSn}$ = 415 Hz, 1B)
$\delta^{1}H$	0.30 (d, $^2J_{SnH}$ = 40.0 Hz, 18 H) Sn*Me*	0.42 (d, $^2J_{SnH}$ = 39.9 Hz, 18 H) Sn*Me*
	2.66 (s, 6 H) central NMe_2	1.89 (s, 6 H) NMe_2
	2.78 (s, 6 H) NMe_2	2.12 (d, $^5J_{SnH}$ = 7.7 Hz, 6 H) B_2NMe_2
	2.88 (s, 6 H) NMe_2	2.76 (s, 6 H) NMe_2
$\delta^{13}C$	−9.4 ($^1J_{SnC}$ = 196, 205 Hz) Sn*Me*	−5.3 ($^1J_{SnC}$ = 205 Hz, $^3J_{SnC}$ = 19 Hz) Sn*Me*
	45.6 central NMe_2	36.4 ($^4J_{SnC}$ = 30 Hz) NMe_2
	48.3 ($^3J_{SnC}$ = 102 Hz) NMe_2	37.2 ($^4J_{SnC}$ = 102 Hz) NMe_2
	48.9 ($^3J_{SnC}$ = 85 Hz) NMe_2	42.3 (broad) central NMe_2
$\delta^{119}Sn$	−152.0	−8.5 ($^1J_{BSn}$ = 415 Hz)

B(2)−N(2) = 2.9°]. The B−B−N−Sn planes of the two boron atoms are twisted relative to each other by 85.6°. Therefore, there is no electron delocalization across the B−B bond in this molecule although the molecule is isoelectronic and isolobal with a 1,3-butadiene. Rather, the space requirements of the substituents are taken care of by minimizing steric interactions, which results in the observed conformation. The B−B bond is a single bond although the B−B bond length [1.677(4) Å] is on the short side amongst the bond lengths known for diborane(4) molecules.[11] For the B−Sn bonds, atom distances of 2.282(3) Å and 2.276(3) Å were determined. These lengths are consistent with B−Sn bonds in molecules with minor steric hindrance.[1,10a]

The preparation of the corresponding triorganylstannyl triborane(5) compounds was much more complicated. The reaction of $Cl_2B_3(NMe_2)_3$ with two equivalents of Me_3SnLi affords compound **2a** in high yield [Equation (2)]. However, minor changes in the reaction conditions lead to a different product **2b** [Equation (3)] which proved to be an isomer of **2a**. Isomer **2b** is predominantly formed in the reaction of $Br_2B_3(NMe_2)_3$ with Me_3SnLi, whereas compound **2a** was formed only to an extent of about 30%. Compounds **2a** and **2b** can be separated and **2b** purified by fractional crystallization: This allowed an unequivocal assignment of their NMR spectroscopic data (listed in Table 1).

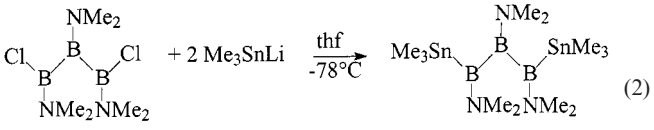

(2)

2a

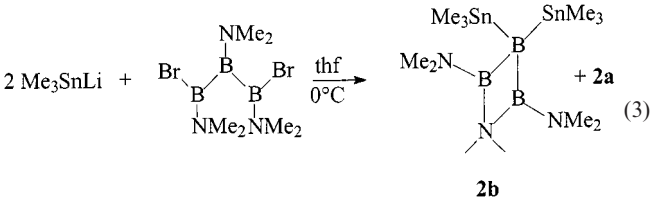

(3)

2b

The acyclic triborane **2a** shows NMR spectra which are typical for symmetric, terminally substituted tris(dimethylamino)triborane(5) compounds. In the ^{11}B NMR spectrum two broad signals in the region for tricoordinate boron atoms are found.[12] The ^1H and ^{13}C NMR signals for the dimethylamino groups (three signal sets each) are consistent with a hindered rotation. The central amino group is represented by a single signal for symmetry reasons. These data point to the presence of strong B−N π-bonding. The ^{119}Sn NMR spectrum shows the expected[12] broad signal at $\delta^{119}Sn$ = −152. In contrast, the NMR spectroscopic data of **2b** seemed, at first sight, not to be compatible with a triborane(5) framework, as a signal for a tetracoordinate boron atom was unexpected, and, as only one signal with double intensity for a tricoordinate boron atom was found, this NMR spectrum could only be explained by the presence of a tetracoordinate boron atom in the center of a chain of three boron atoms. The observed coupling constants: $^1J_{BSn}$ = 415 Hz, $^1J_{CSn}$ = 205 Hz and $^3J_{CSn}$ = 19 Hz confirm that the tetracoordinate boron atom bears the $SnMe_3$ groups. The chemical shift of the central boron atom in **2b** is also unusual with $\delta^{11}{}_B$ = −51.1. As the ^1H and ^{13}C NMR spectra indicate a high symmetry for the molecule the structure depicted for **2b** was deduced. However, the high-field shift of the tetracoordinate boron atom has so far no parallel as no boron atom carrying two boron and two tin atoms is known to date. The closest analogues for high-field shielding are $LiB(SiMe_3)_4$ [13] with $\delta^{11}B$ = −53.4, $LiBH_3SnMe_3$ with $\delta^{11}B$ = −43.7[8a] and $LiB(SnMe_3)_3$-NMePh with $\delta^{11}B$ = −13.1.[1] This indicates that the central boron atom bears a significant negative charge. This assumption is confirmed by a signal at $\delta\delta^{119}Sn$ = −8.5 as this Sn atom is deshielded by about 45 ppm relative to the tin atoms in the two stannyl-borates, and much more so than the tin atoms in isomer **2a.** The low-field singlet in the ^1H and ^{13}C NMR spectra of **2b** confirms the presence of a dimethylammonium group in a planar B_3N four-membered ring. Moreover, the remaining two signals for the dimethylamino groups fit with the suggested structure if they are coplanar with the ring. In this case the two methyl groups at each Me_2N group are nonequivalent, and, moreover, there is hindered rotation about these B−N bonds.

The structure derived from NMR spectroscopic data was fully confirmed by X-ray structure analysis: The molecular structure of **2b** is shown in Figure 2.

The striking key feature of the structure of **2b** is the 1-azonia-2,4-dibora-3-boratacyclobutane ring. The closest

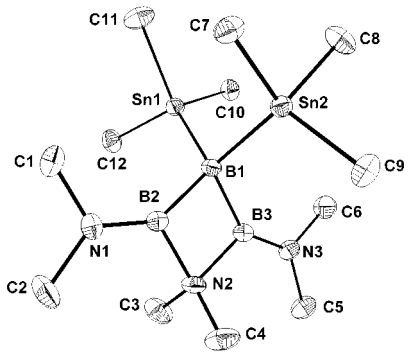

Figure 2. Molecular structure of **2b** in the crystal; hydrogen atoms are not depicted; thermal ellipsoids are drawn at a 25% probability level; selected bond lengths [Å] and bond angles [°]: Sn1−B1 2.223(3), Sn2−B1 2.225(3), N1−B2 1.382(4), N2−B2 1.605(4), N2−B3 1.603(4), N3−B3 1.379(4), B1−B2 1.660(4), B1−B3 1.662(5), N2−C3 1.483(4), N2−C4 1.498(4); Sn1−B1−Sn2 107.7(1), Sn1−B1−B2 116.6(2), Sn1−B1−B3 120.6(2), Sn2−B1−B2 116.7(2), Sn2−B1−B3 112.5(2), B2−B1−B3 81.3(2), B1−B3−N2 96.9(2), B1−B2−N2 96.9(2), B2−N2−B3 84.9(2)

other system for comparison would be an azapolyborane such as hypho-2,3-μ-(*t*BuNH)B_5H_{10} [14] which also has an alkylammonium fragment, although this compound is actually not best suited for a comparison with **2b**. The B_3N four-membered ring is exactly planar (angle sum = 360°). The intra-ring angles at the tetracoordinate atoms B1 and N1 are 81.3(2)° and 84.9(2)°, respectively. The compression at B1 is 12.6° (from tetrahedral symmetry) and for B2 and B3 38.7° (from trigonal-planar symmetry). Therefore, the four-membered ring is highly strained. In spite of this, the B−B bond lengths [av.: 1.661 Å] are almost unaffected as they are the same as in compound **1b**. They are actually only slightly longer than the B−N distances to the coordinated N atom [av.: 1.603 Å]. Thus, the expected increase in the B−B bond lengths that is normally observed upon changing to higher coordination is not found in this case. Therefore, the B−B distances in **2b** can be regarded as rather short. The sums of the bond angles at the nitrogen atoms N1 and N3 are 360° for both atoms and their bonding planes are coplanar with the B_3N ring. The two tricoordinate boron atoms are electronically stabilized by B−N double bonds as confirmed by the short B−N bonds. The two B−N bonds to the tetracoordinate N atom are single bonds. The B−Sn bonds are very short; they are the shortest found to date. Similar results were recently observed for B−Si[8d] and B−Ge[1] compounds. This indicates that for compounds of boron with the higher group 14 elements, a bond shortening with an increasing coordination number at the B atom seems to be a general rule.

Compound **2b** is, to the best of our knowledge, the first example of a tris(amino)triborane(5) in which the central B atom and not just the terminal boron atoms are doubly substituted. The mechanism by which **2b** is formed remains unclear. No equilibrium between the two isomers could be observed by NMR spectroscopy when a pure sample of either **2a** or **2b** was dissolved. The initial formation of **2a**, followed by a subsequent rearrangement to **2b**, can therefore be excluded. With regard to mechanistic speculations it is important to note that two conditions are in any case necessary for the formation of **2b**: The use of $Br_2B_3(NMe_2)_3$ as starting material, and reaction conditions which provide an initial excess of Me_3SnLi. This might indicate that the first step of the formation of **2b** could be a double substitution at one of the terminal boron atoms followed by a rearrangement of the substituents. The final formation of an azonia-bridged cyclic structure is also very likely. Anderson et al.[15] recently reported the favored formation of various 1-azonia-2-borata-5-borol compounds also bearing tri- and tetracoordinate boron and nitrogen atoms.

As we intended to explore whether the B−B or the B−Sn bond is more reactive towards transition metal centers, compound **1a** was reacted with $(C_2H_4)Pt(PPh_3)_2$. However, the product formed was not either of the expected B−B or B−Sn oxidative addition products but rather $(Me_3Sn)_2Pt(PPh_3)_2$ (**3**).[16]

The formation of **3** also requires the formation of a compound like $[B(NMe_2)]_n$, but the only other boron-containing compound which could be isolated was a small quantity of the diborane(4)-1-yl platinum compound **4** [Equation (4)].

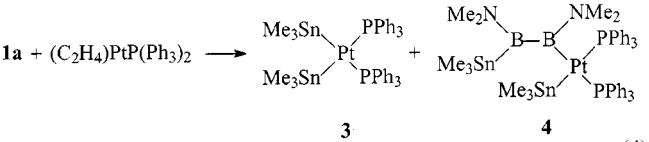

(4)

The structure of **4** was derived from its NMR spectroscopic data. The ^{11}B NMR spectrum of compound **4** shows two signals at $\delta^{11}B = 59.8$ ($h_{1/2} = 480$ Hz) and $\delta^{11}B = 47.0$ ($h_{1/2} = 1840$ Hz). While the latter signal is almost the same as for the starting material, the signal of the boron atom bonded to the platinum atom is found in the range of platinum-boryl complexes.[9b] Apart from this, the B−Pt bond is confirmed by a very large half-width of its ^{11}B NMR signal of 1840 Hz. In the ^{31}P NMR spectrum two signal sets at $\delta^{31}P = 32.9$ [$^1J(^{31}P^{195}Pt) = 2895$ Hz; $^2J_{PP} = 12$ Hz; $^2J(^{31}P^{119}Sn) = 1364$ Hz, $^2J(^{31}P^{117}Sn) = 1304$ Hz] and $\delta^{31}P = 31.2$ [$^1J(^{31}P^{195}Pt) = 1656$ Hz; $^2J(^{31}P^{117}Sn) = 142$ Hz] are found proving the *cis* position of the phosphane groups in **4**. As this compound was obtained only in poor yield, attempts to grow single crystals failed. Nevertheless, the formation of **4** indicates that the B−Sn bonds in **1a** are more reactive than the B−B bonds.

Experimental Section

Experimental conditions, spectrometers and diffractometer are as described in previous contributions.[1]

1,2-Bis(triphenylstannyl)-1,2-bis(dimethylamino)diborane(4) (1b): Ph_3SnLi (2.9 mmol) was added to 50 mL of THF.[17] The solution was cooled to −78 °C and slowly treated with a solution of 1,2-dichloro-1,2-bis(dimethylamino)diborane(4)[18] (0.26 g, 1.44 mmol) in 25 mL of hexane. After stirring for 30 min. at ambient temperature all volatile components were removed in vacuo. The solid

residue was treated with 50 mL of toluene and the resulting suspension filtered. The volume of the filtrate was reduced in vacuo to 30 mL and then layered with 30 mL of hexane. This afforded, after some days standing at room temp., 0.81 g (71%) of **1b** as colorless crystals, m.p.: 119 °C. – ^{1}H NMR (400 MHz, C_6D_6): δ = 2.65 (s, 6 H, CH_3), 2.80 (s, 6 H, CH_3), 7.17–7.22 (m, 18 H, *m*-Ph-*H* and *p*-Ph-*H*), 7.58 (ddd, $^3J_{HH}$ = 5.9 Hz, $^4J_{HH}$ = 2.5 Hz, $^3J_{HSn}$ = 39.4 Hz, 12 H, *o*-Ph-*H*). – ^{11}B NMR (64 MHz, C_6D_6): δ = 60.8 ($h_{1/2}$ = 1500 Hz). – ^{13}C NMR (100 MHz, C_6D_6): δ = 47.6 (NCH_3), 49.3 (NCH_3), 128.5 (t, J_{CSn} = 39.1 Hz, *C*-arom.), 128.9 (t, J_{CSn} = 30.2 Hz, *C*-arom.), 137.6 (t, J_{CSn} = 39.1 Hz, *C*-arom.), 137.8 (t, J_{CSn} = 36.9 Hz, *C*-arom.), 139.2 (*C*-arom.), 142.4 (*C*-arom.). – ^{119}Sn NMR (149 MHz, C_6D_6): no signal observed. – $C_{40}H_{42}B_2N_2Sn_2$ (809.7): calcd. C 59.32, H 5.23, N 3.46; found C 58.71, H 5.23, N 3.32.

1,2,3-Tris(dimethylamino)-1,2-bis(trimethylstannyl)triborane(5) (2a): 1,3-Dichloro-1,2,3-tris(dimethylamino)triborane(5)[12] (2.31 g, 9.8 mmol) was dissolved in 30 mL of hexane. The solution was then cooled to −78 °C and treated dropwise with a THF solution of Me_3SnLi (19.6 mmol).[19] After stirring for 12 h at ambient temperature all volatile components were removed in vacuo. The solid residue was then treated with 30 mL of toluene. After filtration the solution was reduced in volume to 20 mL and then cooled at −78 °C. This afforded 3.18 g (66%) of **2a** as a colorless, polycrystalline solid, m.p.: 51–53 °C. For spectroscopic data see Table 1. – $C_{12}H_{36}B_3N_3Sn_2$ (492.3): calcd. C 29.28, H 7.37, N 8.54; found C 29.64, H 7.55, N 8.75.

1-Azonia-2,4-dibora-3-borata-2,4-bis(dimethylamino)-3-bis(trimethylstannyl)-1-dimethylcyclobutane (2b): A stirred solution of Me_3SnLi[19] (5.2 mmol) in THF was cooled to 0 °C and treated with 1,3-dibromo-1,2,3-tris(dimethylamino)triborane(5)[12] (0.86 g, 2.6 mmol) in 30 mL of toluene. After stirring for 5 h at ambient temperature a suspension had been formed, and the solution showed an ^{11}B NMR spectrum with signals at δ^{11}B = 66.5, 56.9, 50.4, 46.5, 36.2, −33.2 ($h_{1/2}$ = 300 Hz), and −49.8 (d, $^1J_{BSn}$ = 415 Hz). Those at δ = 66.5 and 36.2 are assigned to compound **2a**, and those at δ = 46.5 and −49.8 to **2b**. The signals at δ = 56.9, 50.4 and −33.2 could not be assigned. As the signals were broad and not well separated, integration was not possible, but the ratio of **2a** and **2b** can be roughly estimated as 6:3. All volatile components were removed from the suspension in vacuo. The residue was treated with 50 mL of hexane. Cooling the filtrate to −78 °C afforded 0.8. g (62%) of **2b** as colorless prisms. m.p.: 110 °C. – Spectroscopic data see Table 1. – $C_{12}H_{36}B_3N_3Sn_2$ (492.3): calcd. C 29.28, H 7.37, N 8.54; found C 28.52, H 7.09, N 8.07.

Reaction of 1a with (η^2-Ethene)bis(triphenylphosphane)platinum(0): Compound **1a** (0.41 g, 1.0 mmol) was dissolved in about 40 mL of toluene and treated with (η^2-ethene)bis(triphenylphosphane)platinum(0).[20] After stirring for 12 h at ambient temperature, a brownish precipitate had been formed. The precipitate was filtered, washed with hexane and crystallized from $CHCl_3$/hexane. This afforded colorless crystals, which were identified as **3**.[16] The filtrate was reduced in volume to 20 mL and layered with 20 mL of hexane. Within a few days about 0.03 g of a brown solid separated which was identified as **4** by NMR spectroscopy. Yield: 0.96 g of **3** (92%).
3: ^{31}P (109 MHz, −60 °C, C_6D_6): δ = 32.5 (dd, $^1J_{PPt}$ = 3774 Hz, $^2J_{SnP}$ = 646 Hz). – ^{119}Sn NMR (100 MHz, $CDCl_3$): δ = −13.2 (d, $^2J_{PSn}$ = 646 Hz).
4: ^{1}H (270 MHz, C_6D_6): δ = −0.51 [3 H, Sn(CH_3)$_3$], 0.29 [3 H, Sn(CH_3)$_3$], 0.39 [Sn(CH_3)$_3$], 0.67 [3 H, Sn(CH_3)$_3$], 0.89 [6 H, Sn(CH_3)$_3$], 2.56 (s, 3 H, NCH_3), 2.72 (s, 3 H, NCH_3), 2.76 (s, 3 H, NCH_3), 2.86 (s, 3 H, NCH_3), 6.93 (br. m, 18 H, Ph-*H*), 7.50 (br. m, 12 H, Ph-*H*); – ^{31}P (109 MHz, C_6D_6): δ = 32.9 ($^1J_{PPt}$ = 2895 Hz, $^2J_{PP}$ = 12 Hz, $^2J_P{}^{119}{}_{Sn}$ = 1364 Hz, $^2J_P{}^{117}{}_{Sn}$ = 1304 Hz, P_{cis}B), 31.2 (broad, $^1J_{PPt}$ = 1656 Hz, $^2J_{PSn}$ = 142 Hz, P_{trans}B); – ^{11}B (64 MHz, C_6D_6): δ = 47.0 ($h_{1/2}$ = 1840 Hz, *B*Pt), 59.8 ($h_{1/2}$ = 480 Hz, *B*Sn).

Crystal Structure Determination: A suitable single crystal was covered with perfluoroether oil, mounted on the end of a glass fiber and placed on a goniometer head. The crystal was cooled to −80 °C with a cold stream of dinitrogen using an LT2 device. The unit cell was determined from the reflections of five series of 15 frames each taken at different angles and sweeping φ by 0.3°. A Siemens P4 diffractometer equipped with an area detector and graphite-monochromated Mo-K_α radiation was used. Data collection was performed with the hemisphere mode of the SMART programs.[21] Data were reduced by SAINT[22] and an absorption correction applied with the program SADABS.[23] Structure solution and refinement was carried out with the SHELX-97 program suite. Non-hydrogen atoms were refined anisotropically, and hydrogen atoms were placed in calculated positions and included in the refinement as riding on the respective C atoms. Crystallographic and structure solution data are summarized in Table 2.
Crystallographic data (excluding structure factors) for the structures included in this paper have been deposited with the Cambridge Crystallographic Data Centre as supplementary publication no. CCDC-157308 (**1b**) and -157309 (**2b**). Copies of the data can be obtained free of charge on application to CCDC, 12 Union Road,

Table 2. Crystallographic data for **1b** and **2b**

	1b	**2b**
Chem. formula	$C_{40}H_{42}B_2N_2Sn_2$	$C_{12}H_{36}B_3N_3Sn_2$
Form. wt.	809.76	492.25
Cryst. size [mm]	0.10 × 0.20 × 0.20	0.10 × 0.10 × 0.40
Cryst. system	Monoclinic	Monoclinic
Space group	$P2_1/n$	$P2_1/n$
a, [Å]	11.7751(9)	9.9514(8)
b, [Å]	22.525(2)	14.074(1)
c, [Å]	14.736(1)	15.665(1)
α, [°]	90	90
β, [°]	104.085(1)	90.797(1)
γ, [°]	90	90
V, [Å^3]	3790.8(5)	2193.7(3)
Z	4	4
ρ (calcd.), [Mg/m^3]	1.419	1.490
μ [mm^{-1}]	1.346	2.272
F(000)	1624	976
Index range	$-14 \le h \le 16$ $-28 \le k \le 27$ $-19 \le l \le 18$	$-12 \le h \le 12$ $-18 \le k \le 17$ $-19 \le l \le 18$
2 θ [°]	58.26	58.16
Temp, [K]	183(2)	193(2)
Refl. collected	21768	12423
Refl. unique	7694	4396
Refl. observed (4σ)	6305	3803
R (int.)	0.0240	0.0266
No. variables	419	193
Weighting scheme[a] x/y	0.033/0.237	0.043/0.155
GOOF	1.035	1.055
Final *R* (4s)	0.0242	0.0271
Final *wR*2	0.0561	0.0676
Larg. res. peak [e/Å^3]	0.249	0.492

[a] $w^{-1} = s^2F_o^2 + (xP)^2 + yP$; $P = (F_o^2 + 2F_c^2)/3$.

Cambridge CB2 1EZ, UK [Fax: (internat.) + 44-1223/336-033; E-mail: deposit@ccdc.cam.ac.uk].

[1] T. Habereder, H. Nöth, *Z. Anorg. Allg. Chem.* accepted.

[2] [2a] G. J. Irvine, M. J. G. Lesley, T. B. Marder, N. C. Norman, C. R. Rice, E. G. Robins, W. R. Roper, G. R. Whittell, L. J. Wright, *Chem. Rev.* **1998**, *98*, 2685−2722. − [2b] H. Braunschweig, *Angew. Chem.* **1998**, *110*, 1883−1898; *Angew. Chem. Int. Ed.* **1998**, *37*, 1786−1801. − [2c] H. Wadepohl, *Angew. Chem.* **1997**, *109*, 2547−2550; *Angew. Chem. Int. Ed. Engl.* **1997**, *36*, 2441−2444.

[3] W. Clegg, F. J. Lawlor, G. Lesly, T. B. Marder, N. C. Norman, A. G. Orpen, M. J. Quayle, C. R. Rice, A. J. Scott, F. E. S. Souza, *J. Organomet. Chem.* **1998**, *550*, 183−192.

[4] S. Onozawa, Y. Hatanaka, T. Sakakura, S. Shimada, M. Tanaka, *Organometallics* **1996**, *15*, 5450−5452 and literature cited therein.

[5] D. Curtis, M. J. G. Lesley, N. C. Norman, A. G. Orpen, J. Starbuck, *J. Chem. Soc., Dalton Trans.* **1999**, 1687−1694.

[6] A. Kerr, T. B. Marder, N. C. Norman, A. G. Orpen, M. J. Quayle, C. R. Rice, P. L. Timms, G. R. Whittell, *Chem. Commun.* **1998**, 319−320.

[7] H. Braunschweig, B. Ganter, M. Koster, T. Wagner, *Chem. Ber.* **1996**, *129*, 1099−1101.

[8] [8a] W. Biffar, H. Nöth, H. Pommering, R. Schwerthöffer, W. Storch, B. Wrackmeyer, *Chem. Ber.* **1981**, *114*, 49−60. − [8b] W. Biffar, H.Nöth, *Z. Naturforsch., Teil B* **1981**, *39*, 1509−1515. − [8c] W. Biffar, H. Nöth, R. Schwerthöffer, *Liebigs Ann. Chem.* **1981**, 2067−2080. − [8d] W. Lippert, H. Nöth, W. Ponikwar, T. Seifert, *Eur. J. Inorg. Chem.* **1999**, 817−823.

[9] [9a] T. Habereder, H. Nöth, *Z. Anorg. Allg. Chem.* submitted. − [9b] T. Habereder, *PhD. Thesis*, University of Munich, **2000**.

[10] [10a] P. Frankhauser, H. Pritzkow, W. Siebert, *Z. Naturforsch.* **1994**, *49b*, 250−254. − [10b] H. Nöth, R. Schwerthöffer, *Chem. Ber.* **1981**, *114*, 3056−3062.

[11] A. Moezzi, M. M. Olmstead, P. P. Power, *J. Chem. Soc., Dalton Trans.* **1992**, 2429−2434; W. Clegg, M. R. J. Elsegood, F. J. Lawlor, N. C. Norman, N. J. Pickett, E. G. Robins, A. J. Scott, P. Nguyen, N. J. Taylor, T. B. Marder, *Inorg. Chem.* **1998**, *37*, 5289−5293.

[12] G. Linti, D. Loderer, H. Nöth, K. Polborn, W. Rattay, *Chem. Ber.* **1994**, *127*, 1909−1922.

[13] W. Biffar, H. Nöth, *Chem. Ber.* **1982**, *115*, 934−945.

[14] F. Gaines, R. W. McGaff, D. R. Powell, *Inorg. Chem.* **1993**, *32*, 2612−2613.

[15] M. Anderson, M. J. G. Lesley, N. C. Norman, A. G. Orpen, J. Starbuck, *New. J. Chem.* **1999**, *23*, 1053−1055.

[16] Y. Obora, Y. Tsuij, K. Nishiama, M. Ebihara, T. Kawamura, *J. Am. Chem. Soc.* **1996**, *118*, 10922−10923.

[17] D. Reed, D. Stalke, D. S. Wright, *Angew. Chem.* **1991**, *103*, 1539−1540; *Angew. Chem. Int. Ed. Engl.* **1991**, *30*, 1459−1450.

[18] H. Nöth, W. Meister, *Z. Naturforsch.* **1962**, *17b*, 714−718.

[19] G. Wittig, F. J. Meyer, G. Lange, *Justus Liebigs Ann. Chem.* **1951**, *571*, 167−169.

[20] U. Nagel, *Chem. Ber.* **1982**, *115*, 1998−2001.

[21] SMART, Siemens Analytical Instruments, Madison, Version 4.01.

[22] SAINT, Siemens Analytical Instruments, Madison, Version 5.01.

[23] SADABS, G. W. Sheldrick, Program for absorption correction of data reduced by SAINT

[24] SHELX-97, G. W. Sheldrick, *University of Göttingen*,**1997**.

Received February 7, 2001
[I01044]

Neutral Mononuclear and Binuclear Hexacoordinate Silicon Complexes with SiO_5C Skeletons

Reinhold Tacke,*[a] Christian Burschka,[a] Meike Willeke,[a] and Reiner Willeke[a]

Dedicated to Professor Ernst Mutschler on the occasion of his 70th birthday

Keywords: Chelates / Coordination chemistry / Silicates / Macrocycles / Silicon

Treatment of the silanes $(EtO)_3Si(CH_2)_2SCH_2C(O)OSiMe_3$ and $(EtO)_3Si(CH_2)_3OSiMe_3$ with two molar equivalents of 1-hydroxy-2-pyridone in acetonitrile yielded the neutral hexacoordinate silicon complexes bis[μ-(3-thiapentanoato(2–)-$C^5,O':C^{5'},O$)]tetrakis[1-oxopyridin-2-olato(1–)]disilicon(IV) (**6**) and bis[1-oxopyridin-2-olato(1–)][propanolato(2–)-C^3,O]-silicon(IV) (**8**), respectively. The compounds **6**·$2CH_3CN$ and **8** were characterized by solid-state ^{29}Si VACP/MAS NMR spectroscopy, mass spectrometry (FAB MS), and single-crystal X-ray diffraction.

Introduction

In recent years, significant contributions to the chemistry of pentacoordinate silicon[1] have been made by investigating a new family of compounds, the zwitterionic pentacoordinate silicates.[2] Several hitherto unknown binding situations of pentacoordinate silicon could be realized and studied experimentally by taking advantage of the "zwitterion trick".[3] Compounds **1**,[4] **2**,[5] and **3**[6] with their SiO_2N_2C, $SiONFC_2$, or SiS_4C skeleton are examples of this.[7] To extend this successful concept, we decided to aim for novel zwitterionic pentacoordinate silicate systems with formally positively charged bidentate ligands. For this purpose, we attempted to synthesize compound **4**.

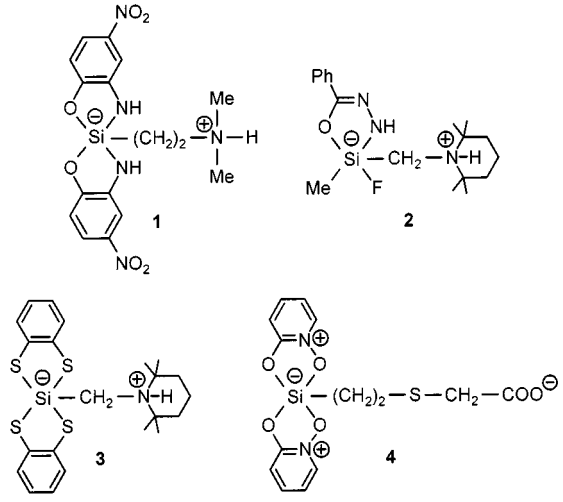

Results and Discussion

To synthesize the pentacoordinate silicon complex **4**, the silane **5** was treated with two molar equivalents of 1-hydroxy-2-pyridone;[8] however, instead of compound **4** the binuclear hexacoordinate silicon complex **6** was obtained (yield 72%; Scheme 1).

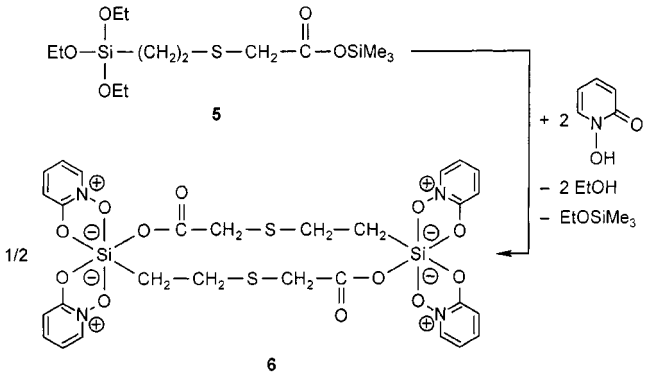

Scheme 1. Synthesis of the binuclear hexacoordinate silicon complex **6**

Formation of **6** can be rationalized (at least from a formal point of view) in terms of a dimerization of **4** through intermolecular Si−O interactions resulting in the generation of two SiO_5C skeletons. Likewise, a related mononuclear hexacoordinate silicon complex with an SiO_5C framework, compound **8**, could be obtained by treatment of the silane **7** with two molar equivalents of 1-hydroxy-2-pyridone (yield 66%; Scheme 2).

Both syntheses were carried out in acetonitrile at room temperature, and the products **6**·$2CH_3CN$ and **8** were isolated as crystalline solids. Their identities were established by elemental analyses (C, H N, S), mass spectrometry (FAB MS), solid-state ^{29}Si VACP/MAS NMR studies,[9] and crystal structure analyses.

[a] Institut für Anorganische Chemie, Universität Würzburg, Am Hubland, 97074 Würzburg, Germany
Fax: (internat.) +49-931/888-4609
E-mail: r.tacke@mail.uni-wuerzburg.de

 © WILEY-VCH Verlag GmbH, 69451 Weinheim, 2001 1434−1948/01/0707−1671 $ 17.50+.50/0

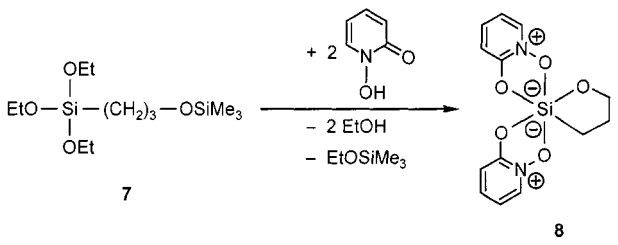

Scheme 2. Synthesis of the mononuclear hexacoordinate silicon complex **8**

The crystal structure of the binuclear complex **6** is characterized by a center of symmetry located in the middle of the macrocyclic 14-membered ring system. The silicon atoms of **6**·2CH_3CN and **8** are octahedrally coordinated (Figure 1 and 2),[10] the maximum deviations from the ideal 90° (180°) angle amounting to 11.9° (11.3°) (**6**·2CH_3CN) and 9.0° (13.9°) (**8**). The Si−O distances are in the ranges 1.7809(18)−1.8644(19) Å (**6**·2CH_3CN) and 1.7096(13)−1.8946(13) Å (**8**). The Si−C distances amount to 1.902(3) Å (**6**·2CH_3CN) and 1.8904(17) Å (**8**). Compounds **6**·2CH_3CN and **8** represent the first hexacoordinate silicon complexes with an *Si*O_5C skeleton that have been characterized by single-crystal X-ray diffraction.[11]

The isotropic chemical shifts of **6**·2CH_3CN ($\delta = -141.8$) and **8** ($\delta = -120.7$) determined by solid-state ^{29}Si VACP/MAS NMR experiments differ significantly from one another ($\Delta\delta = 21.1$). As the geometric data for the *Si*O_5C skeletons of both compounds are quite similar, it is likely that this difference can be attributed to the different nature of the respective O5 oxygen atoms (carboxylate versus alcoholate oxygen atom; see crystal structures). The broadening of the resonance signals in the solid-state ^{29}Si NMR spectra of **6**·2CH_3CN and **8** ($\nu_{1/2} = 80$ Hz) are in accordance with the disorder observed for the oxygen-linked carbon and nitrogen atoms of the 1-oxopyridin-2-olato(1−) ligands.[10]

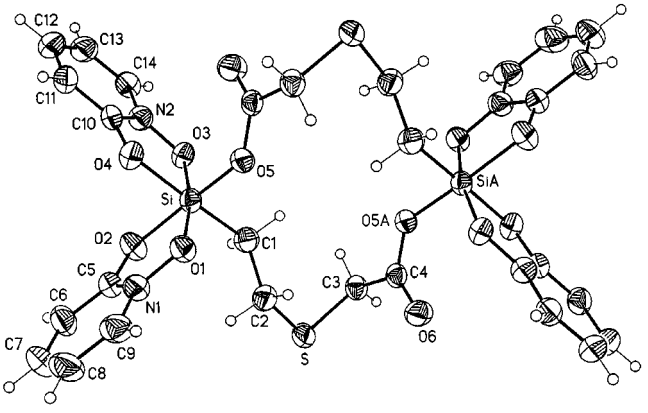

Figure 1. Molecular structure of **6** in the crystal of **6**·2CH_3CN (probability level of displacement ellipsoids 50%), showing the atomic numbering scheme; selected distances [Å] and angles [°]: Si−O1 1.8093(19), Si−O2 1.8644(19), Si−O3 1.7965(19), Si−O4 1.846(2), Si−O5 1.7809(18), Si−C1 1.902(3); O1−Si−O2 84.54(9), O1−Si−O3 168.69(9), O1−Si−O4 86.37(9), O1−Si−O5 84.77(9), O1−Si−C1 100.47(11), O2−Si−O3 88.14(9), O2−Si−O4 87.23(10), O2−Si−O5 168.68(9), O2−Si−C1 91.32(12), O3−Si−O4 84.66(9), O3−Si−O5 101.85(9), O3−Si−C1 88.29(11), O4−Si−O5 88.40(9), O4−Si−C1 172.85(11), O5−Si−C1 94.26(12)

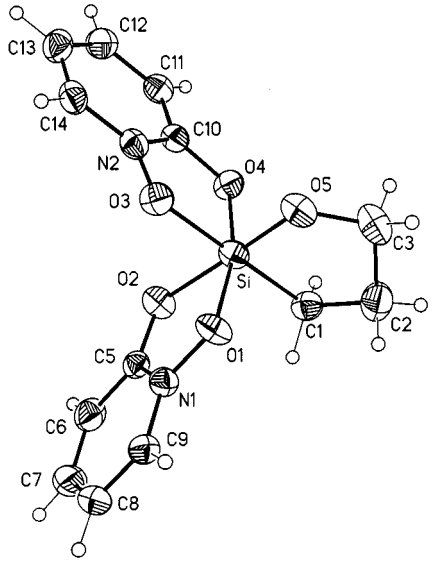

Figure 2. Molecular structure of **8** in the crystal (probability level of displacement ellipsoids 50%), showing the atomic numbering scheme; selected distances [Å] and angles [°]: Si−O1 1.8323(12), Si−O2 1.8946(13), Si−O3 1.8543(12), Si−O4 1.8172(12), Si−O5 1.7096(13), Si−C1 1.8904(17); O1−Si−O2 83.94(5), O1−Si−O3 85.39(6), O1−Si−O4 166.09(6), O1−Si−O5 90.25(6), O1−Si−C1 96.97(7), O2−Si−O3 86.25(6), O2−Si−O4 85.98(6), O2−Si−O5 172.59(6), O2−Si−C1 92.62(7), O3−Si−O4 84.42(6), O3−Si−O5 88.70(6), O3−Si−C1 177.27(6), O4−Si−O5 98.95(6), O4−Si−C1 93.02(7), O5−Si−C1 92.64(7)

In conclusion, we have developed a simple preparative method (EtOH/$EtOSiMe_3$ elimination) for the synthesis of neutral hexacoordinate silicon complexes containing two 1-oxopyridin-2-olato(1−) ligands and one variable ligand of the alkanolato(2−)/alkanoato(2−) type. The hexacoordinate silicon atoms are incorporated in heterocycles with varying ring sizes by one Si−O bond and one Si−C bond. The easy formation of the macrocyclic 14-membered ring system **6** is especially remarkable. It is likely that the preparative method described in this paper will have a great synthetic potential for the preparation of a wide variety of novel neutral heterocycles containing hexacoordinate silicon atoms as integral part of the ring system. Depending on the interplay of thermodynamic and kinetic control, both mononuclear and binuclear hexacoordinate silicon complexes can be formed. In principle, the formation of polymeric species (polynuclear coordination polymers) should also be possible.

Experimental Section

General: All syntheses were carried out under dry nitrogen. The organic solvents used were dried and purified according to standard procedures and stored under nitrogen. Melting points were determined with a DuPont Instruments differential scanning calorimeter, type Thermal-Analyzer 910. Solid-state ^{29}Si VACP/MAS NMR spectra were recorded at 22 °C on a Bruker DSX-400 NMR spectrometer with bottom layer rotors of ZrO_2 (diameter 7 mm)

containing ca. 300 mg of sample [79.5 MHz; TMS as external standard (δ = 0); spinning rate, 5 kHz; contact time, 5 ms; 90° ^{1}H transmitter pulse length, 3.6 μs; repetition time, 4 s]. Mass spectra were obtained with a Finnigan MAT-8430 mass spectrometer (FAB MS; 3-nitrobenzylic alcohol as liquid matrix; xenon as FAB source). The selected *m*/*z* values given refer to the isotopes ^{1}H, ^{12}C, ^{14}N, ^{16}O, ^{28}Si, and ^{32}S.

Synthesis of Bis[μ-{3-thiapentanoato(2−)-*C*^{5},*O*′:*C*$^{5'}$,*O*}]tetrakis[1-oxopyridin-2-olato(1−)]disilicon(IV)−Diacetonitrile (6·2CH$_3$CN): Compound **5**[12] (1.00 g, 2.82 mmol) was added to a solution of 1-hydroxy-2-pyridone (627 mg, 5.64 mmol) in acetonitrile (80 mL) and the mixture left undisturbed at room temperature for 42 h. The resulting crystals were isolated by filtration, washed with acetonitrile (3 × 5 mL), and dried in vacuo (10^{-3} mbar, 20 °C, 12 h); yield 825 mg (1.01 mmol, 72%). M.p. 177 °C (dec.). − ^{29}Si VACP/MAS NMR: δ = −141.8 ($\nu_{1/2}$ = 80 Hz). − FAB MS (positive mode): *m*/*z* (%) = 733 (4) [M + H$^+$], 154 (100) [matrix + H$^+$]. − $C_{32}H_{34}N_6O_{12}S_2Si_2$ (815.0): calcd. C 47.16, H 4.21, N 10.31, S 7.87; found C 47.1, H 4.4, N 10.2, S 7.8.

Synthesis of Bis[1-oxopyridin-2-olato(1−)][propanolato(2−)-*C*^{3},*O*]-silicon(IV) (8): Compound **7**[13] (2.00 g, 6.79 mmol) was added to a solution of 1-hydroxy-2-pyridone (1.51 g, 13.6 mmol) in acetonitrile (80 mL) and the mixture left undisturbed for 4 days at room temperature. The resulting crystals were isolated by filtration, and part of the solvent (50 mL) of the filtrate was removed under reduced pressure (again formation of a precipitate). The precipitate was isolated by filtration, and the combined solids were washed with acetonitrile (2 × 2 mL) and dried in vacuo (10^{-3} mbar, 20 °C, 12 h); yield 1.38 g (4.50 mmol, 66%). M.p. 240 °C (dec.). − ^{29}Si VACP/MAS NMR: δ = −120.7 ($\nu_{1/2}$ = 76 Hz). − FAB MS (positive mode): *m*/*z* (%) = 307 (47) [M + H$^+$], 196 (100) [(M − $C_5H_4NO_2$)$^+$]. − $C_{13}H_{14}N_2O_5Si$ (306.4): calcd. C 50.97, H 4.61, N 9.14; found C 50.8, H 4.7, N 9.2.

Crystal Structure Analyses of 6·2CH$_3$CN and 8: Suitable single crystals were mounted in inert oil (perfluoroalkyl ether, ABCR) on a glass fiber and then transferred to the cold nitrogen-gas stream of the diffractometer (Stoe IPDS; graphite-monochromated Mo-K_α radiation, λ = 0.71073 Å). The structures were solved by direct methods (SHELXS-97) and refined by full-matrix least-squares on F^2 with all unique reflections (SHELXL-97). For the hydrogen atoms, a riding model was employed.

Selected Data for 6·2CH$_3$CN: Single crystal (0.3 × 0.3 × 0.1 mm) obtained from acetonitrile/*n*-pentane at 20 °C, $C_{28}H_{28}N_4O_{12}S_2Si_2$·2CH$_3$CN, M_r = 814.95, analysis at 233(2) K, triclinic, space group $P\bar{1}$, *a* = 8.4667(17), *b* = 9.1712(18), *c* = 12.697(3) Å, α = 105.86(3), β = 92.02(3), γ = 100.07(3)°, *V* = 930.2(3) Å^3, *Z* = 1, $\rho_{calcd.}$ = 1.455 g cm^{-3}, μ = 0.277 mm^{-1}, *F*(000) = 424, $2\theta_{max}$ = 49.42°, 15518 collected reflections, 2975 unique reflections (R_{int} = 0.0441), 241 parameters, R_1 = 0.0393 [$I > 2\sigma(I)$], wR_2 (all data) = 0.1033, *S* = 0.958, largest difference peak and hole 0.200 and −0.270 e·Å^{-3}. The crystal structure contains tubes along [100] which are occupied by the acetonitrile molecules.

Selected Data for 8: Single crystal (0.3 × 0.2 × 0.1 mm) obtained by slow cooling of a boiling solution in acetonitrile to 20 °C, $C_{13}H_{14}N_2O_5Si$, M_r = 306.35, analysis at 173(2) K, monoclinic, space group $P2_1/n$, *a* = 12.351(3), *b* = 8.3092(17), *c* = 13.078(3) Å, β = 98.49(3)°, *V* = 1327.5(5) Å^3, *Z* = 4, $\rho_{calcd.}$ = 1.533 g cm^{-3}, μ = 0.202 mm^{-1}, *F*(000) = 640, $2\theta_{max}$ = 54.12°, 12577 collected reflections, 2863 unique reflections (R_{int} = 0.0261), 192 parameters, R_1 = 0.0371 [$I > 2\sigma(I)$], wR_2 (all data) = 0.1108, *S* = 1.057, largest difference peak and hole 0.479 and −0.259 e·Å^{-3}.

Crystallographic data (excluding structure factors) for the structures reported in this paper have been deposited with the Cambridge Crystallographic Data Centre as supplementary publication nos. CCDC-153448 (**6**·2CH$_3$CN) and CCDC-153449 (**8**). Copies of the data can be obtained free of charge on application to CCDC, 12 Union Road, Cambridge CB2 1EZ, UK [Fax: (internat.) +44-1223/336-033; E-mail: deposit@ccdc.cam.ac.uk].

Acknowledgments

This work was supported by the Deutsche Forschungsgemeinschaft and the Fonds der Chemischen Industrie.

[1] Selected reviews dealing with pentacoordinate silicon compounds: [1a] S. N. Tandura, M. G. Voronkov, N. V. Alekseev, *Top. Curr. Chem.* **1986**, *131*, 99−189. − [1b] W. S. Sheldrick, in *The Chemistry of Organic Silicon Compounds* (Eds.: S. Patai, Z. Rappoport), Wiley, Chichester, UK, **1989**, Part 1, pp. 227−303. − [1c] C. Chuit, R. J. P. Corriu, C. Reyé, J. C. Young, *Chem. Rev.* **1993**, *93*, 1371−1448. − [1d] R. R. Holmes, *Chem. Rev.* **1996**, *96*, 927−950. − [1e] D. Kost, I. Kalikhman, in *The Chemistry of Organic Silicon Compounds* (Eds.: Z. Rappoport, Y. Apeloig), Wiley, Chichester, UK, **1998**, Vol. 2, Part 2, pp. 1339−1445.

[2] Review dealing with zwitterionic pentacoordinate silicates: R. Tacke, M. Pülm, B. Wagner, *Adv. Organomet. Chem.* **1999**, *44*, 221−273.

[3] Generally, these zwitterionic pentacoordinate silicates (which contain a formally negatively charged silicon atom and a formally positively charged nitrogen atom) are characterized by an excellent crystallizability. This particular property is very advantageous for their preparation and isolation and for their structural characterization by single-crystal X-ray diffraction and solid-state NMR spectroscopy. In addition, most of these neutral molecular compounds also exist in solution and can be studied for their structure and dynamic behavior by solution NMR spectroscopy.

[4] B. Pfrommer, R. Tacke, *Eur. J. Inorg. Chem.* **1998**, 415−418.

[5] D. Kost, I. Kalikhman, S. Krivonos, R. Bertermann, C. Burschka, R. E. Neugebauer, M. Pülm, R. Willeke, R. Tacke, *Organometallics* **2000**, *19*, 1083−1095.

[6] R. Tacke, M. Mallack, R. Willeke, *Angew. Chem.* in press.

[7] It is important to note that the indicated positive and negative charges in the formulas are *formal charges* that do not reflect the real charge distribution in the molecules.

[8] In solution a thermodynamic equilibrium between 1-hydroxy-2-pyridone and its tautomer 2-hydroxypyridine *N*-oxide exists, the pyridone species dominating: P. Ballesteros, R. M. Claramunt, T. Cañada, C. Foces-Foces, F. Hernández Cano, J. Elguero, A. Fruchier, *J. Chem. Soc., Perkin Trans. 2* **1990**, 1215−1219.

[9] Due to the poor solubility of **6**·2CH$_3$CN and **8** in organic solvents, solution NMR studies could not be performed.

[10] For both crystal structures, a disorder of the oxygen-linked carbon and nitrogen atoms of the 1-oxopyridin-2-olato(1−) ligands was observed. Refinement of the occupation factors for the respective carbon and nitrogen atoms yielded a congruence with the structures depicted in Figure 1 and 2 of 100% (C10, N2, **6**·2CH$_3$CN), 76% (C5, N1, **6**·2CH$_3$CN), 99% (C5, N1, **8**), and 57% (C10, N2, **8**).

[11] Two hexacoordinate silicon complexes with an SiO_5C skeleton [compounds of the formula type RSi(tropolonato)$_2$OMe (R = Me, Ph)] have been described in the literature; however, these compounds have not been structurally characterized by single-crystal X-ray diffraction: M. Kira, L. C. Zhang, C. Kabuto, H. Sakurai, *Chem. Lett.* **1995**, *8*, 659−660.

[12] Synthesis of **5**: N. S. Fedotov, I. G. Rybalka, V. A. Korolev, V. F. Mironov, *J. Gen. Chem. USSR (Engl. Trans.)* **1978**, *48*, 558−561; *Zh. Obshch. Khim.* **1978**, *48*, 612−615.
[13] Synthesis of **7**: [13a] K. A. Andrianov, V. I. Pakhomov, N. E. Lapteva, *Dokl. Chem. (Engl. Trans.)* **1963**, *151*, 593−596; *Dokl. Akad. Nauk SSSR* **1963**, *151*, 849−852. − [13b] J. Pola, V. Bažant, V. Chvalovský, *Collect. Czech. Chem. Commun.* **1973**, *38*, 1528−1536.

Received March 8, 2001
[I01087]

Dinuclear Pentamethylcyclopentadienyl Rhodium and Iridium Complexes from C=C-Bridged Amino Acid Dimers[‡]

Harald Dialer,[a] Susanne Schumann,[a] Kurt Polborn,[a] Wolfgang Steglich,*[a] and Wolfgang Beck*[a]

Dedicated to Professor Marianne Baudler on the occasion of her 80th birthday

Keywords: Rhodium / Iridium / Amino acids / Amides / N,O ligands

Hippuric acid dimers bridged by a C=C double bond react with the chloro-bridged complexes $(Cp^*)(Cl)M(\mu\text{-}Cl)_2M(Cp^*)(Cl)$ with decarboxylation or loss of a benzoyl group to give the unexpected ligand-bridged dinuclear complexes **2** and **4**, which were characterized by X-ray diffraction. In the iridium complex **2** an oxazolone derivative forms a C,O-N,N′-coordinated bridge, whereas in the rhodium complex **4** a chlorine atom and an amide group bridge the two metal atoms.

Recently, the synthesis and characterization of α-amino acid and peptide dimers bridged by C=C double bonds was reported.[1] These dimers are formed as *Z* and *E* isomers by condensation of α-chloroglycine derivatives with triphenylphosphane and base and are of interest for peptides with a cross-linked backbone. We investigated the coordination behavior of these novel compounds in order to get information on the configuration at the C=C bond of the amino acid dimers. By reaction of chloro-bridged, half-sandwich complexes of rhodium, iridium and ruthenium of the type $(L)ClM(\mu\text{-}Cl)_2M(L)Cl$ with α-amino acids and peptides a series of organometallic N,O- and N,N′-chelate complexes was obtained.[2]

Using this established strategy, the chloro-bridged pentamethylcyclopentadienyl iridium complex $Cp^*(Cl)Ir(\mu\text{-}Cl)_2Ir(Cl)(Cp^*)$ was reacted with the dimeric hippuric acid derivative **1** in the presence of NaOMe or LiOH. Compound **1** was prepared by hydrolysis of the corresponding *Z*-configured dimethyl ester.[1]

The reaction resulted in the formation of the unexpected product **2**, whose structure was solved by X-ray diffraction (Figure 1). Formation of complex **2** occurs by decarboxylation of one carboxylic group of **1** and formation of an oxazolone ring. Decarboxylation is typical for α,β-unsaturated carboxylic acids.[3] Oxazolones are usually formed by dehydration of *N*-acyl-α-amino acids with carbodiimides or carboxylic acid anhydrides.[4] Cyclization to an oxazolone to give **2** is obviously favorable in the coordination sphere of a metal. The X-ray structure determination also reveals metalation at the former C=C bridge of **1**. It is worthwhile to note that the reactions of the dimer $[Cp^*IrCl_2]_2$ with substituted oxazolones afforded either orthometalation [5] or metalation of the oxazolone ring.[6]

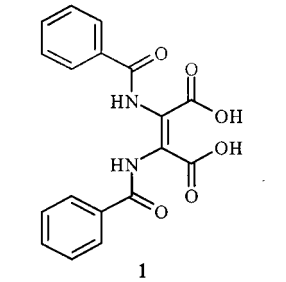

1

1. NaOMe
2. $[Cp^*IrCl_2]_2$

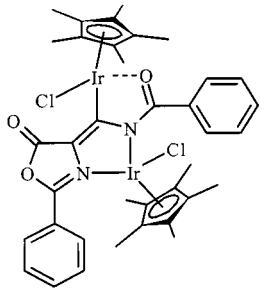

2

Complex **2** contains two different stereogenic centers at the iridium atoms, and the two expected diastereoisomers (as pairs of enantiomers) are observed in the ^1H NMR spectrum. Each diastereoisomer should exhibit two ^1H NMR signals for the nonequivalent Cp* units. In fact four ^1H NMR singlets (δ = 0.97, 1.07, 1.75 and 1.85) are found

[‡] Metal Complexes of Biologically Important Ligands, CXXXIV. − Part CXXXIII: A. Böhm, K. Polborn, W. Beck, *Z. Naturforsch.*, submitted.

[a] Department of Chemistry, University of München, Butenandtstraße 9−13, 81377 München, Germany
Fax: (internat.) +49-089/2180-7866
E-mail: wbe@cup.uni-muenchen.de

 © WILEY-VCH Verlag GmbH, 69451 Weinheim, 2001 1434−1948/01/0707−1675 $ 17.50+.50/0

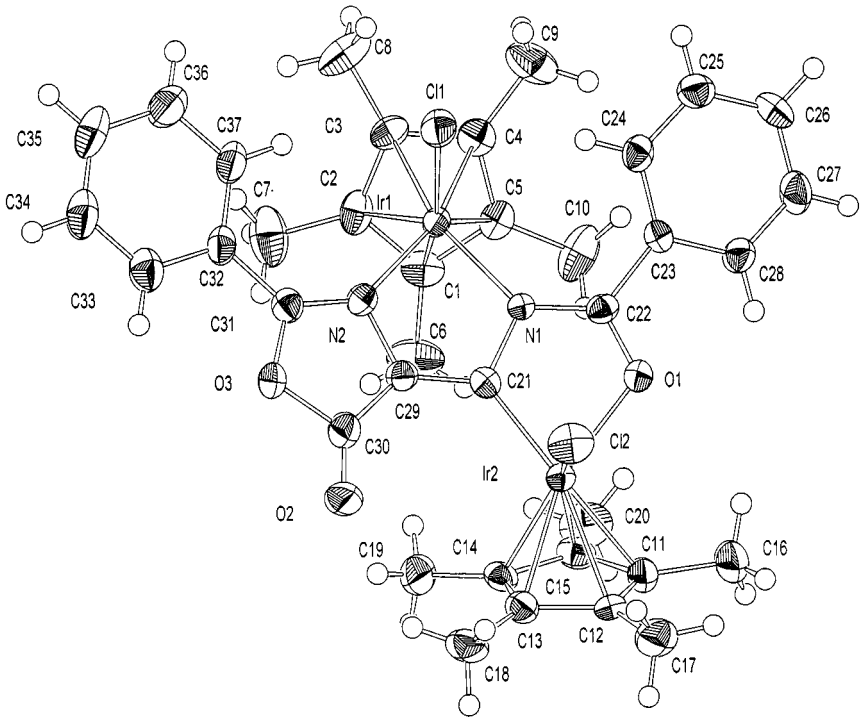

Figure 1. Molecular structure of **2** in the crystal; selected bond lengths (Å), angles (°) and torsion angles (°): Ir1−N2 2.103(5), Ir2−O1 2.083(4), Ir1−Cl1 2.411(2), Ir2−Cl2 2.404(2), N2−C31 1.312(8), C21−C29 1.382(8), C22−O1 1.272(7), Ir1−N1 2.156(5); Cl1−Ir1−N1 92.82(13), N2−C29−C21 120.5(5), N1−C22−O1 120.0(5), Ir2−C21−C29 131.9(5), N2−C29−C21−N1 2.09, Cl2−Ir2−C21 91.0(2), N1−Ir1−N2 76.1(2), Ir2−C21−C29−C30 12.68(6), C21−N1−C22−O1 5.50(5)

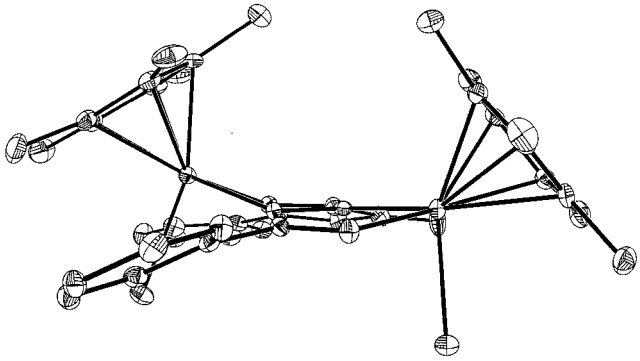

Figure 2. Side view of the molecular structure of **2** in the crystal

in the spectrum of the solution of product **2**. The two diastereoisomers could be separated: from a methanol solution of **2** only one diastereoisomer crystallized, and the crystal of **2** contained only one diastereoisomer as a racemate R_{Ir1}-S_{Ir2} and $S_{Ir1}R_{Ir2}$. In Figure 1 the $S_{Ir1}R_{Ir2}$ isomer is shown. As expected, the solution of the crystal exhibited only two Cp* ^{1}H NMR signals at δ = 1.07 and 1.85. In the ^{13}C NMR spectra the high downfield shift of the NMR signal for the metalated carbon atom at δ = 206 is remarkable, which corresponds to a quite short Ir2−C21 bond length of 1.995(6) Å (Figure 1) in the crystal. For the above-mentioned oxazolones a signal in the area of δ = 70 and 174 was observed.[5,6] On the other hand, the central C=C bond (C21−C29) is, with 1.382(8) Å, longer than the uncomplexed amino acid dimer (1.32−1.33 Å[1,8]). Figure 2 shows a side view of **2** demonstrating the almost planar arrangement of the novel bridging ligand.

A second unexpected product is formed from the reaction of the amino acid dimer **3** with $[Cp^*RhCl_2]_2$ in the presence of NaOMe. It is a chloro- and amido-bridged[7] dinuclear complex **4**, which is formed by cleavage of one benzoyl group from **3** and which was also characterized by X-ray structure determination (Figure 3, Table 1).

The fourth coordination sites of the rhodium atoms are occupied by a carboxylate oxygen donor and a chloro ligand. The formation of **4** involves a $Z \rightarrow E$ isomerization[1] of the amino acid dimer **3**. In the crystal of **4** both enantiomers $R_{Rh1}R_{Rh2}$ and $S_{Rh1}S_{Rh2}$ are present giving rise to two Cp* ^{1}H NMR signals in solution. In Figure 2 the structure of the $R_{Rh1}R_{Rh2}$ isomer with the chiral N1 atom in the *S* configuration is shown. Two hydrogen bonds NH···O−C(O) which fix the amino acid dimer in the *E* configuration can be detected both in solution and in the crystal. The two NH signals appear at rather low field (δ = 10.8 for the bridging amide and δ = 8.21 for the uncoordinated amide group) in the ^{1}H NMR spectra, and relatively short distances N1(H1)···O4 (2.244 Å) and N2(H2)···O2 (2.114 Å) are found in the solid. The crystal data show only a slight elongation of the central C=C bond [C22−C23 1.360(9) Å] in **4**. In both dinuclear complexes **2** and **4** the metal atoms have a distorted tetrahedral environment.

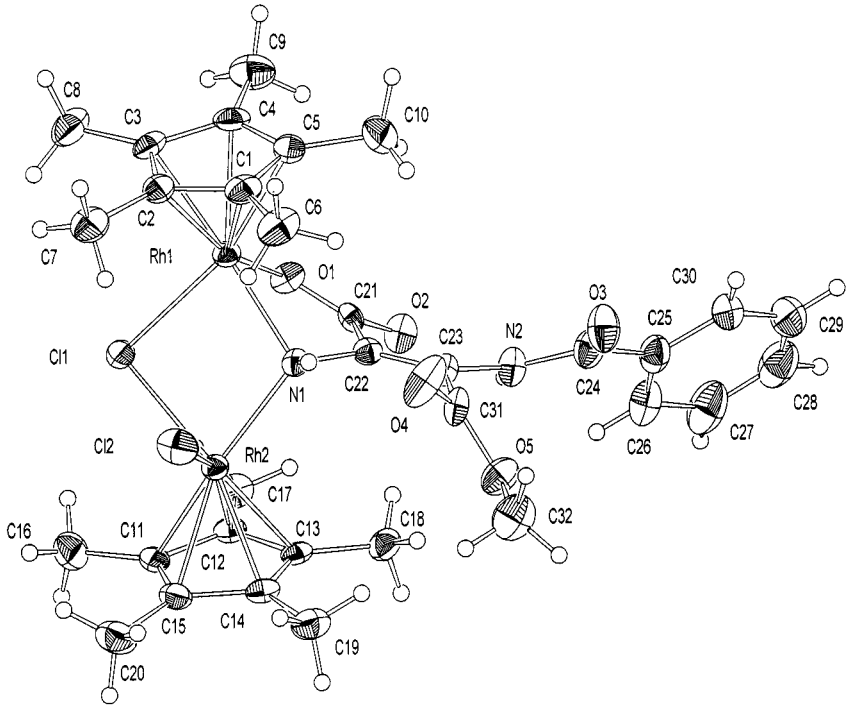

Figure 3. Molecular structure of **4** in the crystal; selected bond lengths (Å), angles (°) and torsion angles (°): Rh1−Cl1 2.441(2), Rh1−N1 2.109(5), Rh1−O1 2.119(5), Rh2−Cl1 2.485(2), Rh2−N1 2.145(5), Rh2−Cl2 2.402(3), N1−C22 1.418(8), C22−C23 1.360(9), C21−C22 1.518(9), C21−O1 1.221(8), C21−O2 1.248(7), H1(N1)−O4 2.244, H2(N2)−O2 2.114, Cl1−Rh1−O1 87.9(2), Cl1−Rh1−N1 84.2(2), N1−Rh1−O1 77.7(2), Cl1−Rh2−N1 82.7(2), N1−C22−C23 124.2(6), N1−C22−C21 112.5(5), O1−C21−O2 125.7(6), O1−C21−C22 115.8(6), N1−C22−C21−O1 25.0(6), N1−C22−C23−C31 2.11(5), N1−Rh2−Cl1−Rh1 2.9(2), Rh1−N1−C22−C21 41.8(6)

Table 1. Crystallographic data of **2** and **4**[10]

Empirical formula	$C_{32}H_{40}Cl_2N_2O_5Rh_2$	$C_{37}H_{40}Cl_2Ir_2N_2O_3$
Molecular weight	809.38	1016.01
Temperature	293(2) K	293(2) K
Wavelength	0.71073 Å	0.71073 Å
Crystal system	Monoclinic	Triclinic
Space group	*P*21/*c*	$P\bar{1}$
Unit cell dimensions	*a* = 12.303(6) Å	*a* = 10.482(2) Å
	α = 90°	α = 91.006(13)°
	b = 14.086(10) Å	*b* = 11.210(2) Å
	β = 91.41(3)°	β = 94.215(13)°
	c = 19.482(7) Å	*c* = 15.785(2) Å
	γ = 90°	γ = 115.10(2)°
Volume	3375(3) Å^3	1672.7(5) Å^3
Z	4	2
Density (calculated)	1.593 Mg/m^3	2.017 Mg/m^3
Absorption coefficient	1.177 mm^{-1}	8.148 mm^{-1}
F(000)	1640	976
Crystal size	0.53 × 0.27 × 0.07 mm	0.27 × 0.13 × 0.07 mm
Theta range for data collection	2.54 to 24.98°	2.15 to 23.97°
Index ranges	$-14 \le h \le 0$	$-11 \le h \le 11$
	$-16 \le k \le 0$	$-12 \le k \le 12$
	$-23 \le l \le 23$	$-18 \le l \le 0$
Reflections collected	6218	5440
Independent reflections	5921 [*R*(int) = 0.0234]	5224 [*R*(int] = 0.0174
Absorption correction	Semi-empirical from ψ-scans	Semi-empirical from ψ-scans
Max. and min. transmission	0.9992 and 0.8716	0.9999 and 0.7075
Refinement method	Full-matrix least-squares on F^2	Full-matrix least-squares on F^2
Data/restraints/parameters	5921/0/399	5224/0/425
Goodness-of-fit on F^2	1.181	1.106
Final *R* indices [$I > 2\sigma(I)$]	*R*1 = 0.0520, *wR*2 = 0.0988	*R*1 = 0.0253, *wR*2 = 0.0468
R indices (all data)	*R*1 = 0.0880, *wR*2 = 0.1125	*R*1 = 0.0406, *wR*2 = 0.0522
Largest diff. peak and hole	0.942 and −0.457 e·Å^{-3}	0.578 and −0.615 e·Å^{-3}

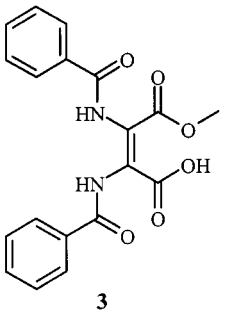

3

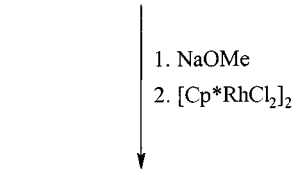

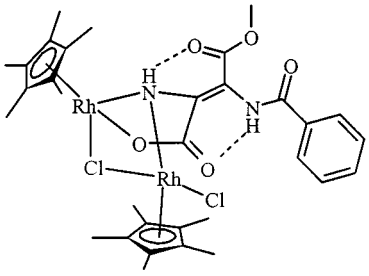

4

Conclusion

Different products were obtained from the reactions of the C=C-bridged amino acid dimers **1** and **3** with chloro-bridged complexes. Protection of one carboxylic group by esterification in **3** prevents decarboxylation and formation of an oxazolone ring as was observed with **1**. One can speculate why the two reactions proceed so differently. An explanation could arise if one considers the first step of these reactions. With **1** formation of an N,N(amide) and an O,O(carboxylate) chelate diiridium complex seems possible, which, after decarboxylation of one carboxylic group followed by metalation at the C=C bond and condensation of the benzoyl and carboxylic groups, gives the product **2**. Coordination of the two former amide nitrogen atoms of the *Z* amino acid dimer is found in the product **2**. In contrast, **3** can coordinate in the first step through the amide and carboxylate group of one half of the *Z*-amino acid dimer to form a chelate, as is present in product **4**. The noncoordinated second half of the amino acid dimer with the carboxylic ester can then undergo the $Z \rightarrow E$ isomerization which is necessary to form product **4**. Base-induced $Z \rightarrow E$ isomerization of C=C-bridged amino acid dimers has already been observed.[8] The fate of the lost benzoyl group remains unclear.

Experimental Section

NMR measurements were recorded on Jeol GSX 270 and Jeol EX 400 spectrometers. IR analyses were obtained on a Nicolet 520 FT-IR spectrometer. FAB MS was performed on a Finnigan MAT 90 instrument. The X-ray structure determination was carried out with a NONIUS CAD4 diffractometer. The dimeric hippuric acid derivatives **1** and **3** were prepared by deprotection of (*Z*)-2,3-bis(*N*,*N*′-benzoylamino)maleic acid dimethyl ester, which was synthesized according to a literature procedure.[9]

To a suspension of the dimethyl ester (382 mg, 1 mmol) in THF (9 mL) and water (3 mL) was added LiOH (72 mg, 3 mmol) at 0 °C and the mixture was stirred overnight. The resulting solution was acidified to pH 2 with a 1.1 M solution of $KHSO_4$ and extracted three times with ethyl acetate (20 mL). The combined organic fractions were washed with 20 mL of water and 20 mL of brine and dried over anhydrous Na_2SO_4. Removal of the solvent under reduced pressure yielded the free acid **1** which was used without further purification. If the deprotection reaction was carried out with a molar ratio dimethyl ester/LiOH of 1:1 the main product was (*Z*)-2,3-bis(*N*,*N*′-benzoylamino)maleic acid mono methyl ester **3**, which was isolated by column chromatography.

2: A solution of (*Z*)-2,3-bis(*N*,*N*′-benzoylamino)maleic acid (**1**; 54 mg, 0.15 mmol) in 5 mL of methanol was stirred with a 1.65 M solution of NaOMe in methanol (185 μL, 0.30 mmol). $[Cp^*IrCl_2]_2$ [10] (121 mg, 0.15 mmol) was added to the resulting yellow solution and the mixture stirred for an additional 15 min. The resulting orange solution was set aside overnight leading to the precipitation of orange crystals suitable for X-ray diffraction. Yield 67 mg (44%). − IR (KBr): $\tilde{\nu}$ = 3063 w, 2918 w, 1776 vs (C=O), 1742 m, 1606 w (C=N), 1590 m, 1469 vs, 1392 s, 1374 s, 1162 m, 1073 m 834 m, 702 cm^{-1} m. − ^1H NMR (270 MHz, CD_2Cl_2): δ = 1.07 [s, 15 H, $C_5(CH_3)_5$], 1.85 [s, 15 H, $C_5(CH_3)_5$], 7.43−7.57 (m, 6 H, *m*- and *p*-C_6H_5), 8.44−8.52 (m, 4 H, *o*-C_6H_5). − ^{13}C NMR (67.9 MHz, CD_2Cl_2): δ = 8.6 [$C_5(CH_3)_5$], 8.9 [$C_5(CH_3)_5$], 86.8 [$C_5(CH_3)_5$], 90.1 [$C_5(CH_3)_5$], 125.7 (*C*=C), 126.6, 127.9, 128.7, 130.3, 131.5, 131.7, 132.3, 134.1 (Ph), 154.7 (C=N), 163.4 (CO_2), 187.0 (CON), 205.9 (C-Ir). − MS(FAB): *m*/*z* = 1016 (17) $[M]^+$. − $C_{37}H_{40}Cl_2Ir_2N_2O_3$ (1016.01): calcd. C 43.74, H 3.97, N 2.76; found C 43.90, H 3.97, N 2.75.

4: A solution of (*Z*)-2,3-bis(*N*,*N*′-benzoylamino)maleic acid monomethyl ester (**3**; 30 mg, 0.08 mmol) in 7 mL of methanol was stirred with a 1.65 M solution of NaOMe in methanol (99 μL, 0.16 mmol). $[Cp^*RhCl_2]_2$ [10] (50 mg, 0.08 mmol) was added to the resulting yellow solution and the mixture stirred overnight. The solvent was removed in vacuo and the residue redissolved in 3 mL of dichloromethane. The red solution was filtered through Celite and concentrated under reduced pressure. Recrystallisation from dichloromethane/*n*-hexane yielded red crystals suitable for X-ray analysis. Yield 22 mg (34%). − IR (KBr): $\tilde{\nu}$ = 3296 w, 2958 w, 2917 m, 2851 m, 1725 w, 1692 w, 1664 s, 1601 vs, 1588 vs, 1540 m, 1478 vs, 1455 vs, 1443 m, 1375 s, 1310 s, 1264 m, 1161 m, 1080 m, 1025 s, 933 w, 801 m, 717 s, 615 cm^{-1} m. − ^1H NMR (400 MHz, CD_2Cl_2): δ = 1.41 [s, 15 H, $C_5(CH_3)_5$], 1.55 [s, 15 H, $C_5(CH_3)_5$], 3.86 (s, 3 H, OCH_3), 7.45−7.57 (m, 3 H, *m*- and *p*-C_6H_5), 7.91−7.94 (m, 2 H, *o*-C_6H_5), 8.21 (d, ^3J = 9.2 Hz, 1 H, NH), 10.81 (s, 1 H, NH−Rh). − ^{13}C NMR (100.5 MHz, CD_2Cl_2): δ = 8.4 [$C_5(CH_3)_5$], 8.5 [$C_5(CH_3)_5$], 52.1 (OCH_3), 92.9 [d, J_{RhC} = 9.3 Hz, $C_5(CH_3)_5$], 93.9 [d, J_{RhC} = 8.4 Hz, $C_5(CH_3)_5$], 117.5 (*C*=C), 127.5, 128.6, 131.8, 133.6 (Ph), 164.9 (CON), 166.1 (CO_2CH_3), 173.7 (CO_2). − MS (FAB): *m*/*z* = 809 (2) $[M]^+$, 774 (23) $[M - Cl]^+$.

Acknowledgments

We thank Deutsche Forschungsgemeinschaft and Fonds der Chemischen Industrie for financial support and Degussa AG, Hanau, for chemicals.

[1] S. Schumann, K. Zeitler, M. Jäger, K. Polborn, W. Steglich, *Tetrahedron* **2000**, *56*, 4187−4195.
[2] K. Severin, R. Bergs, W. Beck, *Angew. Chem.* **1998**, *110*, 1722−1743; *Angew. Chem. Int. Ed.* **1998**, *37*, 1634−1654.
[3] R. T. Arnold, O. C. Elmer, R. M. Dodson, *J. Am. Chem. Soc.* **1950**, *72*, 4359−4361; J. March, *J. Chem. Ed.* **1963**, *40*, 212−213.
[4] W. Steglich, *Fortschr. Chem. Forsch.* **1969**, *12*, 77−118.
[5] W. Bauer, M. Prem, K. Polborn, K. Sünkel, W. Steglich, W. Beck, *Eur. J. Inorg. Chem.* **1998**, 485−493.
[6] W. Bauer, K. Polborn, W. Beck, *J. Organomet. Chem.* **1999**, *579*, 269−279.
[7] Amide-bridged complexes of late transition metals are known: M. D. Fryzuk, C. D. Montgomery, *Coord. Chem. Rev.* **1989**, *95*, 1−40; D. M. Roundhill, *Chem. Rev.* **1992**, *92*, 1−27; A. L. Casalnuovo, J. C. Calabrese, D. Milstein, *J. Am. Chem. Soc.* **1988**, *110*, 6738−6744.
[8] S. Schumann, Dissertation Universität München **1998**.
[9] R. Kober, W. Steglich, *Liebigs Ann. Chem.* **1983**, 599−609.
[10] C. White, A. Yates, P. M. Maitlis, D. M. Heinekey, *Inorg. Synth.* **1992**, *29*, 228−234.
[11] Crystallographic data (excluding structure factors) for the structure(s) included in this paper have been deposited with the Cambridge Crystallographic Data Centre as supplementary publication nos. CCDC-152476 (**2**) and -152477 (**4**). Copies of the data can be obtained free of charge on application to CCDC, 12 Union Road, Cambridge CB2 1EZ, UK [Fax: (internat.) + 44-1223/336-033; Email: deposit@ccdc.cam.ac.uk].

Received January 24, 2001
[I01030]

Varying Topology of Dendrimers − A New Approach toward the Synthesis of Di-Block Dendrimers

Valérie Maraval,[a] Rosa-Maria Sebastian,[a] Frédéric Ben,[a] Régis Laurent,[a] Anne-Marie Caminade,*[a] and Jean-Pierre Majoral*[a]

Keywords: Dendrimers / Phosphorus / Hydrazones / Aldehydes / Azides

A new way to synthesise di-block dendrimers having two types of end groups located in two different areas of their surface is reported. It consists in growing, step-by-step, a second dendritic wedge from the core of a first dendron. This method is mainly applied to the synthesis of di-block dendrimers having phosphanyl groups on one part of the surface.

Introduction

The need for advanced materials has created a tremendous area of research in which dendrimers occupy a growing place.[1−8] Indeed, their very particular, highly branched architectures often exhibit unusual behaviours and properties. It has been largely demonstrated that both the nature of the branches and the nature of the terminal functions influence these properties, but less attention has been paid to the modification of shape or topology. One of the challenges in this area consists of synthesising dendritic molecules having two different properties, due to the location of two types of functional groups in definite areas of the molecular surface. Very few papers have reported the synthesis of this type of di-block dendrimer,[9−18] and all of them to date concern the grafting of two different dendrons by their cores. This type of approach appears to be the most straightforward, but is inapplicable when the surface functions of one dendron may interact with the core function of the other dendron. An alternative route to avoid this problem should consist in a step-by-step, divergent synthesis of a new dendritic wedge starting from the core of a dendron.

In the course of our research on the synthesis[19−29] and applications[30−38] of phosphorus-containing dendrimers, we report here our efforts to find suitable methodologies for obtaining di-block dendrimers by growing a second dendritic wedge from the core of one dendron. The crucial point in the envisaged strategy is the choice of the function that will be located at the core of the first dendron. We decided to use R−P=N−P=S linkages, since we have already demonstrated on one hand that the P=S group can be easily desulfurized to yield a tricoordinated phosphorus atom usable in Staudinger reactions,[24−27,39] and on the other hand that the electronic influence of the P=N−P=S group upon R, when R is a vinyl group, allows us to perform Michael-type additions of amines.[17−18] Depending on the nature of R, other reactions could be envisaged, and chosen in order to be compatible with the nature of the terminal functions. Due to their wide range of uses, particularly in catalysis, phosphanyl groups appear as an interesting function to be linked to one part of the surface of the final dendrimer, the other part of the surface being variously functionalized, for instance with ammonium salts, leading to water-soluble derivatives.

Results and Discussion

Most of the work that will be described here was carried out with low generation of dendrons, in order to be able to detect any defects. In fact, our aim was to validate, on relatively small compounds, methods that could also be used for larger compounds. The desired P=N−P=S linkages are easily obtained using the Staudinger reaction between phosphanes **1a−c** and the azide-dialdehyde **2**,[40] leading to dendrons **3a−c-[G′0]**. The next step in growing these dendrons was the condensation with the phosphorus hydrazide **4**, affording the first generation dendron **3a−c-[G1]** (Scheme 1).

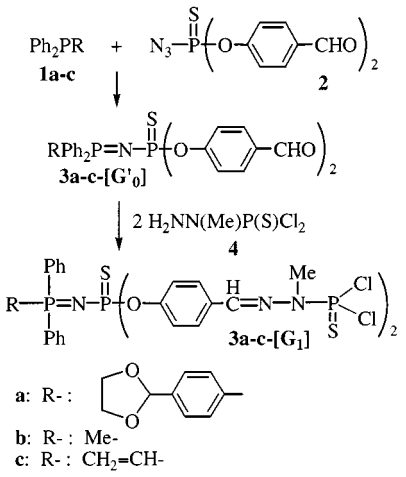

Scheme 1

[a] Laboratoire de Chimie de Coordination CNRS,
205 route de Narbonne, 31077 Toulouse Cedex 4, France
Fax: (internat.) + 33-5/61553003
E-mail: caminade@lcc-toulouse.fr; majoral@lcc-toulouse.fr

 © WILEY-VCH Verlag GmbH, 69451 Weinheim, 2001 1434−1948/01/0707−1681 $ 17.50+.50/0

The continuation of the synthesis depends on the type of reactions envisaged at the core after the growing of the first dendron. For instance, the deprotection of the core of **3a-[G_1]** should regenerate an aldehyde group, whose reactivity with various amines could allow us to grow the second dendritic wedge. Thus, the functions located on the surface of the first dendron must be neither aldehydes, nor any group able to react with primary amines. We decided to graft diphosphanyl groups to the surface, using three steps from **3a-[G_1]**: i) substitution with hydroxybenzaldehyde sodium salt (**5**) leading to **3a-[G'_1]**, ii) condensation with hydrazine leading to **6a-[G'_1]**, iii) condensation with Ph_2PCH_2OH leading finally to **7a-[G_2]** (Scheme 2). The characterisation of compound **7a-[G_2]** shows that none of the preceding steps has damaged the acetal function, with the presence of multiplets at $\delta = 4.0$ for the CH_2CH_2 group and one singlet at $\delta = 5.79$ for the OCHO group in the ^1H NMR spectrum. Furthermore, no aldehyde group is detectable by ^1H or ^{13}C NMR. The next step should be the deprotection of the core. For this purpose, we used the classical method already applied to the deprotection of **1a**,[41] i.e. a catalytic amount (5%) of *p*-toluenesulfonic acid in acetone at 60 °C. However, a side reaction occurs at the level of the external groups of **7a-[G_2]**, which induces the total disappearance of the signal corresponding to the diphosphanyl groups in the ^{31}P NMR spectrum ($\delta = -25$) in favour of the appearance of new signals, in particular a singlet at $\delta = -41$, corresponding to Ph_2PH. The cleavage of the surface end groups precludes any use of **7a-[G_2]** for the growing of a second dendron from its core, consequently we decided to study the reactivity of **3b-[G_1]**, applying another strategy to obtain di-block dendrimers.

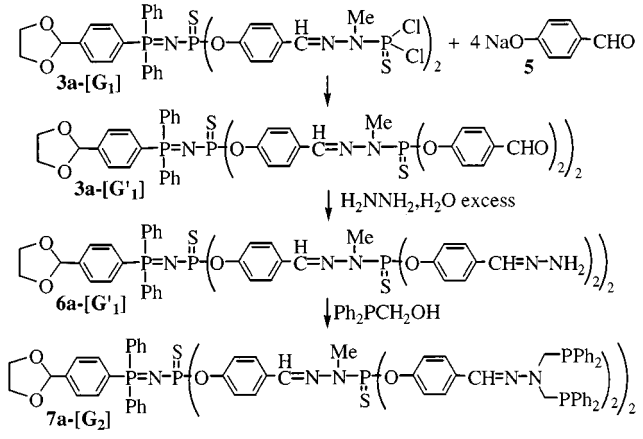

Scheme 2

The only possible reactivity at the core of compound **3b-[G_1]** concerns the alkylation and desulfurization of the P=N−P=S linkage using $MeSO_3CF_3$ and $P(NMe_2)_3$ successively.[24−27,39] The first reagent is incompatible with the presence of phosphane groups on the surface of the first dendron, and the second one is incompatible with the P−Cl groups of **3b-[G_1]**, due to Cl/NMe_2 exchanges. Taking into account these constraints, we decided to graft ammonium groups to the surface of **3b-[G_1]**. Indeed, these functions should render the future di-block dendrimer water-soluble. The reaction of **3b-[G_1]** with 4 equiv. of $H_2NCH_2CH_2NEt_2$ affords compound **8b-[G'_1]** (Scheme 3) as expected.[17−18] This compound is soluble in a variety of solvents, either organic solvents such as chloroform and dichloromethane, or protic solvents such as ethanol, methanol, or water. Remarkably, compound **8b-[G'_1]** is stable for more than three weeks in water, even under acidic conditions at pH = 4.

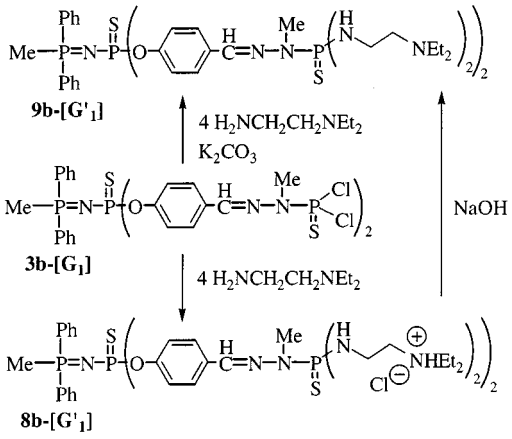

Scheme 3

We tried to apply the first step of the desulfurization process, i.e. the alkylation of the P=S group by $MeSO_3CF_3$ to **8b-[G'_1]** in CH_2Cl_2 solution. Unexpectedly, addition of an excess of $MeSO_3CF_3$ is needed to observe the alkylation, characterised in the ^{31}P NMR spectra by the total disappearance of both doublets corresponding to the PNPS linkage at $\delta = 15.8$ (P=N) and 52.4 (P=S) ($^2J_{PP} = 32$ Hz) and the appearance of a singlet at $\delta = 23.6$. This signal is an AB system, totally degenerated, corresponding to the PNPSMe linkage.[24−27,39] However, other signals are also observed, corresponding to a side reaction presumably inducing the cleavage of the PNP linkage. This side reaction could be due to a reaction with CF_3SO_3H, which could be generated by an H/Me exchange on some ammonium groups. A way of avoiding this problem could be to deprotonate the ammonium groups before using CF_3SO_3Me. The neutral compound **9b-[G'_1]** is easily obtained from **8b-[G'_1]**, using NaOH in water. However, it was extremely difficult to eliminate the last traces of water, which should also generate triflic acid, thus we synthesised **9b-[G'_1]** by another way, the direct reaction of *N*,*N*-diethylethylenediamine with **3b-[G_1]** in the presence of potassium carbonate (Scheme 3); 3 equiv. of CF_3SO_3Me are then added to **9b-[G'_1]**, in order to alkylate both the PNPS and the NEt_2 groups. However, a side and unidentified product appears along with the expected product, thus we decided to avoid the presence of amine in the molecule, and to directly treat **3b-[G_1]** with CF_3SO_3Me.

Addition of methyl triflate to **3b-[G_1]** cleanly affords compound **10b-[G_1]**, characterised in the ^{31}P NMR spectrum by the presence of two doublets (AB system) at $\delta = 23.8$ and 24.1 ($^2J_{PP} = 18.2$ Hz) for the PNPSMe linkage and one

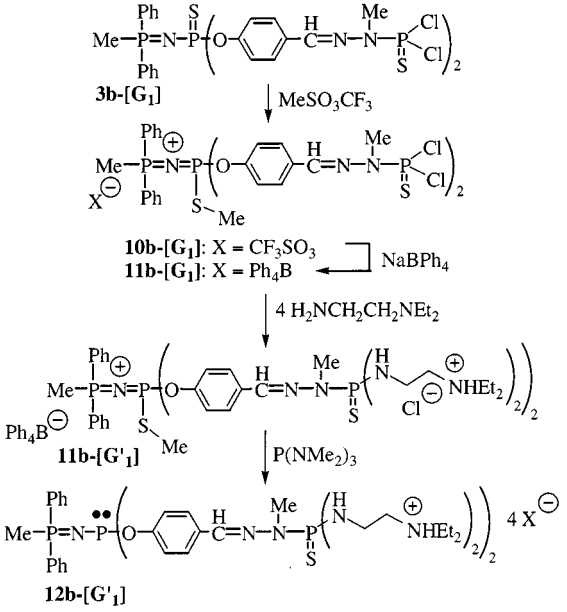

Scheme 4

singlet at δ = 62.8 for the $P(S)Cl_2$ groups (Scheme 4). The second step of the desulfurization process, i.e. the reaction with $P(NMe_2)_3$ cannot be used with **10b-[G$_1$]**. Indeed, exchange reactions can take place, leading to partial or total substitution of the P−Cl bonds, with formation of $P(S)Cl(NMe_2)$ or $P(S)(NMe_2)_2$ end groups; thus, the P−Cl functions must be substituted first. The reaction of **10b-[G$_1$]** with *N*,*N*-diethylethylenediamine did not appear desirable, since it could also generate triflic acid. Thus, we decided first to proceed to an anion exchange with $NaBPh_4$. Elimination of CF_3SO_3Na allowed us to isolate **11b-[G$_1$]**. The anion exchange induces a broadening of the AB system, which gives only a signal having the appearance of a singlet for **11b-[G$_1$]**. No signal is detectable in the ^{19}F NMR spectrum, confirming the total exchange. Compound **11b-[G$_1$]** reacts cleanly with *N*,*N*-diethylenediamine to afford **11b-[G′$_1$]** (Scheme 4). The full substitution of the chlorine atoms is characterised in the ^{31}P NMR spectrum by the deshielding of the signal corresponding to the end groups from δ = 62.7 for **11b-[G$_1$]** to δ = 68.5 for **11b-[G′$_1$]**.

Reaction of **11b-[G′$_1$]** with $P(NMe_2)_3$ induces the expected desulfurization, as shown by the appearance of two doublets for the core at δ = 144.2 (P:) and δ = 10.3 (P=N) ($^2J_{PP}$ = 31.6 Hz) for **12b-[G′$_1$]**. This compound was not fully characterised due to its high sensitivity toward oxidation, but directly treated with the azide **2** (Scheme 5). The formation of the P=N−P=N−P=S linkage of compound **12b-[G′$_1$-G′$_0$]** is characterised by the appearance of two doublets at δ = 18.4 (P=N, $^2J_{PP}$ = 26 Hz) and δ = 47.5 (P=S, $^2J_{PP}$ = 58.4 Hz), and a doublet of doublet at δ = −9.6 (central P=N). The ^1H NMR spectrum shows the remaining end groups are in the cationic form. Indeed, all CH_2 and CH_3N groups form a multiplet for **12b-[G′$_1$-G′$_0$]**, as well as for the other compounds having a cationic form (see data for **8b-[G′$_1$]** and **11b-[G′$_1$]**), whereas the neutral form gives a quadruplet at δ = 3.39 for the NCH_2CH_3 groups, clearly distinguishable and separated from all the other CH_2 and CH_3N groups[32] (see data for **9b-[G′$_1$]**). Concerning the nature of the anionic part of **12b-[G′$_1$-G′$_0$]** (only Cl or a mixture of Cl and BPh_4), one can say that all the signals attributed to BPh_4 in the ^{13}C NMR spectra of **11b-[G$_1$]** and **11b-[G′$_1$]** are also detected for **12b-[G′$_1$-G′$_0$]**, and that the integration of the ^1H NMR spectrum indicates the presence of 1 equiv. of BPh_4. At least 95% of the initial quantity of BPh_4 remains in **12b-[G′$_1$-G′$_0$]**, thus its anionic part is constituted by 3 Cl^- and 1 BPh_4^-.

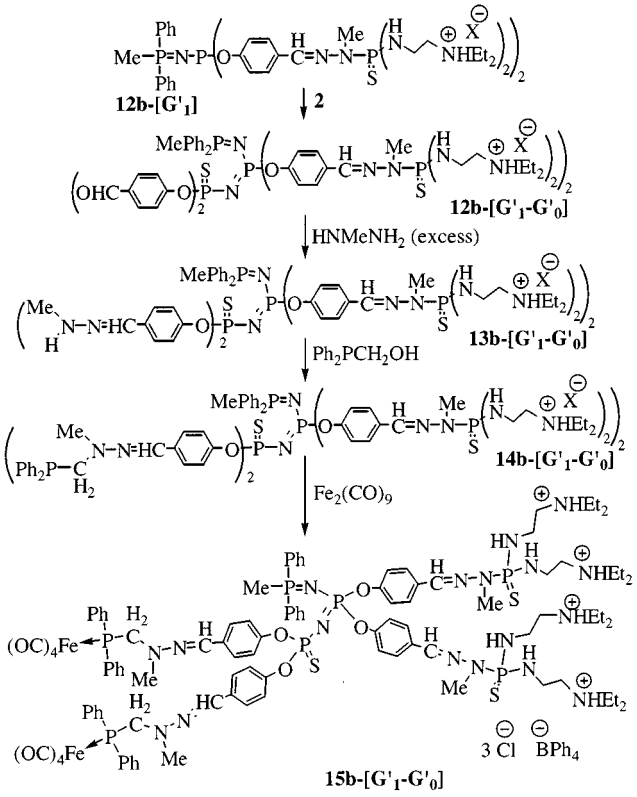

Scheme 5

Compound **12b-[G′$_1$-G′$_0$]** possesses two aldehyde groups that could allow the growing of the second dendritic wedge, using for instance the phosphorus hydrazide **4** followed by hydroxybenzaldehyde sodium salt (**5**). However, we decided to try the grafting of phosphanes. The first step in this process is the condensation of the aldehyde groups with methylhydrazine, leading to **13b-[G′$_1$-G′$_0$]**, characterised by the disappearance of the aldehyde signals in the ^1H and ^{13}C NMR and IR spectra. The grafting of phosphanes is carried out with Ph_2PCH_2OH, affording **14b-[G′$_1$-G′$_0$]**. Then, the phosphanes are readily complexed, in order to avoid any oxidation problem. As an example, the complexation was carried out with $Fe_2(CO)_9$ (Scheme 5). The formation of the complex **15b-[G′$_1$-G′$_0$]** is characterised by the large deshielding of the signal corresponding to the phosphane from δ = −22.9 for **14b-[G′$_1$-G′$_0$]** to δ = 67.5 for **15b-[G′$_1$-G′$_0$]**. The grafting of phosphanes at the previous step is confirmed by the deshielding of the signal of the methyl

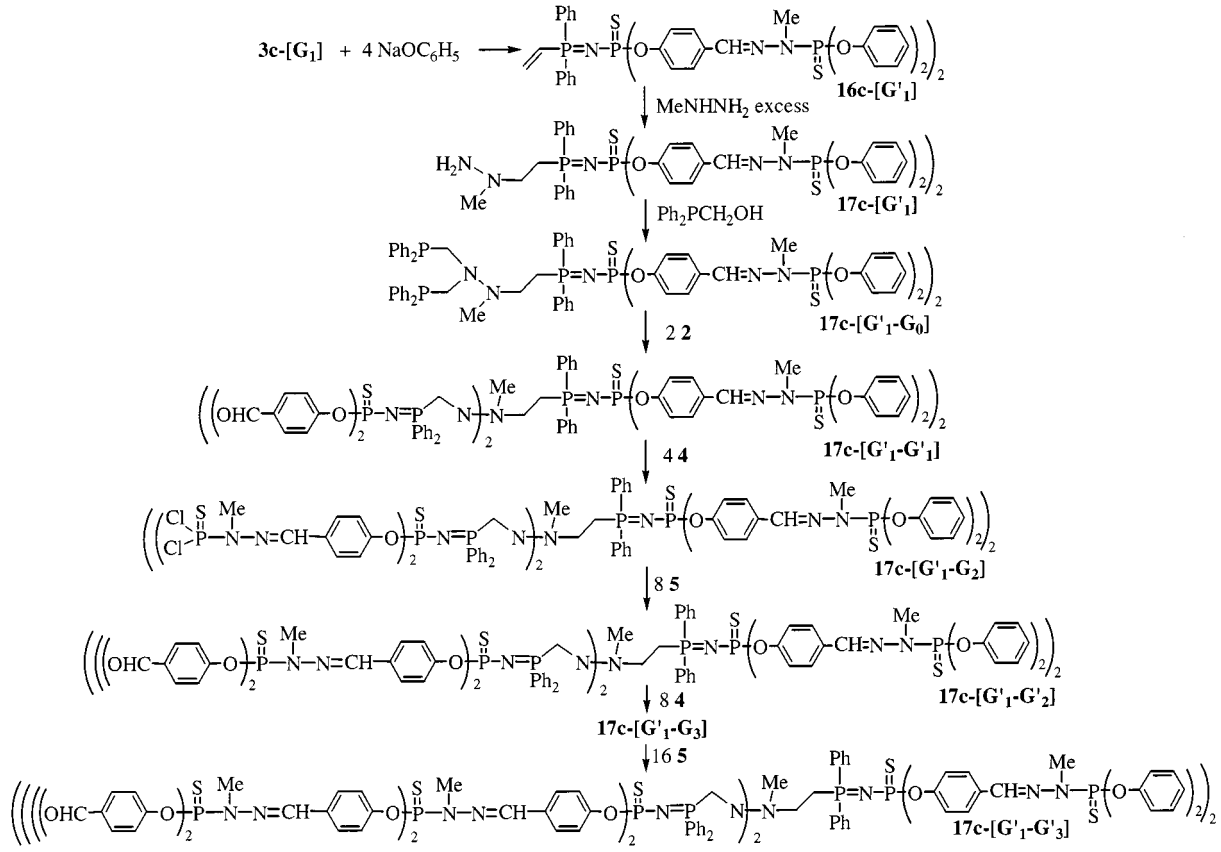

Scheme 6

groups in the ^{13}C NMR spectrum from $\delta = 34.0$ for CH_3NH in **13b-[G′$_1$-G′$_0$]** to $\delta = 39.0$ for CH_3NCH_2 in **15b-[G′$_1$-G′$_0$]**.

Compound **15b-[G′$_1$-G′$_0$]** is a rather small compound, but it possesses all the characteristics of a di-block dendrimer, and the methodology developed here should be applicable to the synthesis of larger compounds. However, the full process is rather lengthy, thus we tried to find a more rapid method. Compound **3c-[G$_1$]** should offer such opportunity, since we have shown that a vinyl group linked to a P=N−P=S moiety reacts with primary and secondary amines under mild conditions.[17−18] However, amines also react with the P−Cl groups, so such reactions are inapplicable to **3c-[G$_1$]**. In order to avoid any problem in the future reactions, we decided to react **3c-[G$_1$]** with sodium phenolate, which gives neutral and poorly reactive end groups (Scheme 6). The reaction of **16c-[G′$_1$]** thus obtained with methylhydrazine leads to compound **17c-[G′$_1$]** by a Michael-type addition of the NHMe moieties on the vinyl group. The phosphanes are then grafted using again Ph_2PCH_2OH, leading to **17c-[G′$_1$-G$_0$]**. This compound is another example of a small di-block dendrimer possessing phosphanes in one part of the molecule.

It would be interesting to complex these phosphanes with transition metal ions, but we decided to use them to grow the second part of the di-block dendrimer by a Staudinger reaction with the azide **2**. The formation of **17c-[G′$_1$-G′$_1$]** is characterised in the ^{31}P NMR spectrum by the presence of two sets of two doublets corresponding to two types of P=N−P=S linkages in a 2:1 ratio at $\delta = 14.0$ and 50.0 ($^2J_{PP}$ = 26.0 Hz) for the NCH_2P=N−P=S groups and at $\delta = 16.7$ and 50.2 ($^2J_{PP}$ = 33.9 Hz) for the CH_2CH_2P=N−P=S group. The growing of the molecule is then carried out without any problem, using alternatively the phosphorus hydrazide **4** and hydroxybenzaldehyde sodium salt (**5**) (Scheme 6). The synthesis was stopped after obtaining dendrimer **17c-[G′$_1$-G′$_3$]** (Figure 1), but it could have been continued to higher generations. The presence of aldehyde groups on part of the surface of **17c-[G′$_1$-G′$_3$]** will open the way to a versatile reactivity, including for instance the grafting of phosphanyl groups, using the method already described in Scheme 2.

Conclusion

We have demonstrated that the growing of a second dendritic wedge from the core of a first dendron is an alternative route for the obtaining di-block dendrimers. This approach is less straightforward than the direct coupling of two dendrons by their cores, but it offers the possibility to have a variety of functional groups located in different areas. Even if several of the molecules presented in this paper are relatively small, we have shown that the methodologies developed here can also be applied to larger com-

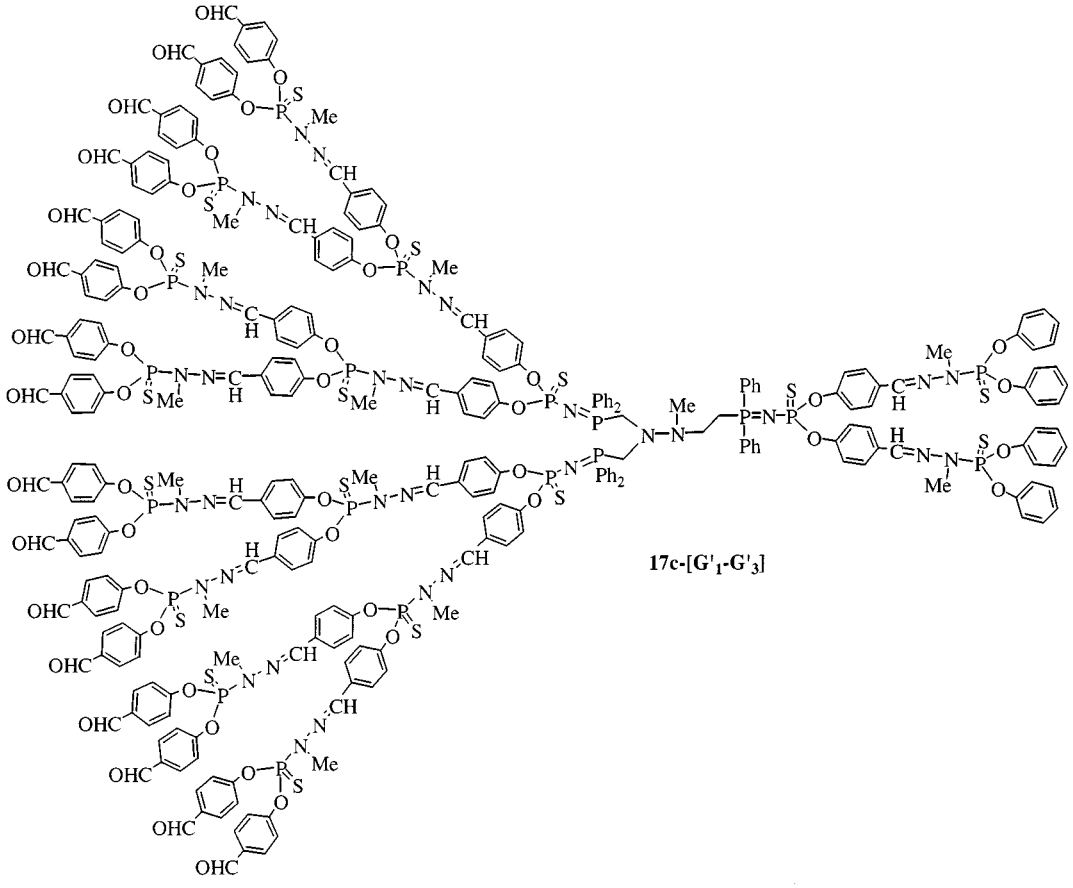

Figure 1. The di-block dendrimer **17c-[G′$_1$-G′$_3$]**

pounds, as indicated by the synthesis of the unsymmetrical third generation dendrimer **17c-[G′$_1$-G′$_3$]**. The presence of two types of end groups should provide new tools for chemistry. The presence of ammonium salts on one side and phosphanes on the other side, i.e. compounds such as **14b-[G′$_1$-G′$_0$]** should lead to biphasic dendritic catalysts. Furthermore, the presence of aldehydes on one side and of other functional groups on the other side of a di-block dendrimer should lead to covalent tailored material surface modifications as already shown with more classical dendrimers.[30−31]

Experimental Section

General Remarks: All reactions except those done in water, were carried out under argon, in the absence of air, using standard Schlenk techniques and vacuum-line manipulations. All solvents were dried and distilled before use. Solvents were also degassed when phosphanes were used. − Perkin−Elmer 1725X was used for FT-IR. − NMR spectra were recorded with Bruker AC80, AC200, or AM250 for ^{1}H, ^{13}C, ^{31}P and ^{19}F NMR, with $SiMe_4$, H_3PO_4, and CF_3CO_2H as references, respectively. The attribution of ^{13}C NMR signals was done using Jmod, two-dimensional HMBC and HMQC, broad-band or CW ^{31}P decoupling experiments when necessary. The numbering scheme used for NMR is depicted Figure 2. − Compounds **1a**,[41] **2**,[40] **3c-[G′$_0$]** and **3c-[G$_1$]**[17] were synthesised according to published procedures.

Synthesis of 3a-[G′$_0$] and 3b-[G′$_0$]: A solution of azide **2** (1.911 g, 5.5 mmol) in THF (20 mL) was added to a solution of phosphane **1a** or **1b** (5 mmol) in THF (10 mL). The reaction induces a strong evolution of N_2. The reaction mixture was stirred for 6 h (**1a**) or 1 h (**1b**) at room temperature, then concentrated to dryness. The residue was dissolved in a minimum amount of CH_2Cl_2 (**1a**) or THF (**1b**) and precipitated with pentane (twice). Compound **3a-[G′$_0$]** was isolated as a white powder (2.482 g, 76% yield), and **3b-[G′$_0$]** was isolated as a pale beige oil (2.031 g, 78% yield).

3a-[G′$_0$]: ^{31}P{^{1}H} NMR ($CDCl_3$): δ = 14.6 (d, $^2J_{PP}$ = 30.6 Hz, P_{00}), 50.2 (d, $^2J_{PP}$ = 30.6 Hz, P_0). − ^{1}H NMR ($CDCl_3$): δ = 4.03 (m, 2 H, CH_2), 4.11 (m, 2 H, CH_2), 5.82 (s, 1 H, OCHO), 7.28 (d, $^3J_{HH}$ = 8.5 Hz, 4 H, $C_0{}^2$H), 7.24−7.69 (m, 14 H, C_6H_5, C_6H_4), 7.77 (d, $^3J_{HH}$ = 8.5 Hz, 4 H, $C_0{}^3$H), 9.92 (s, 2 H, CHO). − ^{13}C{^{1}H} NMR ($CDCl_3$): δ = 65.5 (s, CH_2), 102.7 (s, OCHO), 122.1 (d, $^3J_{CP}$ = 5 Hz, $C_0{}^2$), 126.8 (d, $^3J_{CP}$ = 14 Hz, $C^{3\prime}$), 128.0 (dd, $^1J_{CP}$ = 106 Hz, $^3J_{CP}$ = 4 Hz, $C_0{}^i$), 128. 8 (d, $^3J_{CP}$ = 14 Hz, $C_0{}^m$), 129.2 (br. d, $^1J_{CP}$ = 106 Hz, $C^{1\prime}$), 131.2 (s, $C_0{}^3$), 132.6 (s, $C_0{}^4$), 132.7 (d, $^2J_{CP}$ = 12 Hz, $C_0{}^o$), 132.9 (d, $^2J_{CP}$ = 11 Hz, $C^{2\prime}$), 132.9 (s, $C_0{}^p$), 142.9 (s, $C^{4\prime}$), 156.9 (d, $^2J_{CP}$ = 10 Hz, $C_0{}^1$), 191.1 (s, CHO). − IR (KBr): 1702 cm^{-1} ($\nu_{C=O}$). − $C_{35}H_{29}NO_6P_2S$ (653.63): calcd. C 64.32, H 4.47, N 2.14; found C 64.25, H 4.50, N 2.09.

3b-[G′$_0$]: ^{31}P{^{1}H} NMR ($CDCl_3$): δ = 16.8 (d, $^2J_{PP}$ = 32.2 Hz, P_{00}), 51.0 (m, $^2J_{PP}$ = 32.2 Hz, P_0). − ^{1}H NMR ($CDCl_3$): δ = 2.19 (d, $^2J_{HP}$ = 13.2 Hz, 3 H, CH_3−P), 7.25−7.69 (m, 18 H, C_6H_5,

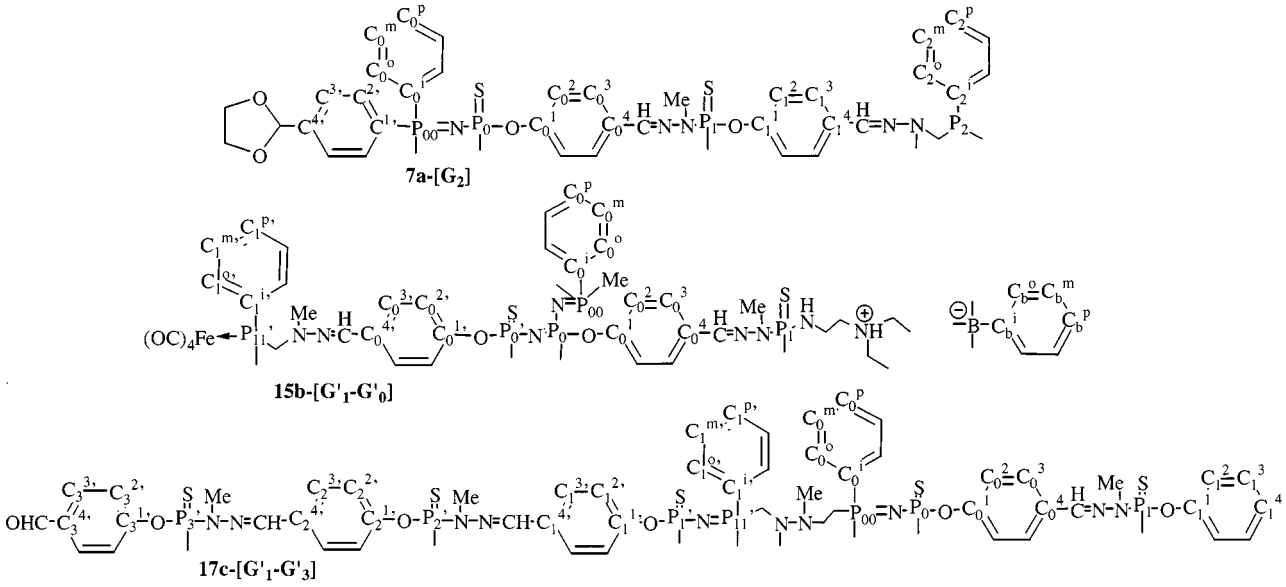

Figure 2. Numbering scheme used for NMR

C_6H_4), 9.77 (s, 2 H, CHO). – $^{13}C\{^1H\}$ NMR ($CDCl_3$): δ = 14.4 (d, $^1J_{CP}$ = 67.4 Hz, CH_3–P), 122.0 (d, $^3J_{CP}$ = 5.9 Hz, C_0^2), 128.8 (s, C_0^3), 128.9 (d, $^3J_{CP}$ = 13.4 Hz, C_0^m), 129.7 (dd, $^1J_{CP}$ = 102.6 Hz, $^3J_{CP}$ = 6.5 Hz, C_0^i), 130.9 (d, $^2J_{CP}$ = 9.7 Hz, C_0^o), 131.2 (s, C_0^p), 132.7 (s, C_0^4), 156.8 (d, $^2J_{CP}$ = 9.9 Hz, C_0^1), 190.9 (s, CHO). – IR (KBr): 1702 cm^{-1} ($\nu_{C=O}$). – $C_{27}H_{23}NO_4P_2S$ (519.50): calcd. C 62.42, H 4.46, N 2.69; found C 62.28, H 4.41, N 2.75.

Synthesis of 3a-[G$_1$] and 3b-[G$_1$]: To a solution of compound **3a-[G′$_0$]** or **3b-[G′$_0$]** (1 mmol) in THF (20 mL) was added a 0.3 M solution of dichloro(1-methylhydrazido)thiophosphane (**4**) (2.2 mmol, slight excess). The reaction mixture was stirred overnight, then concentrated to dryness. Washing the residue twice with CH_2Cl_2/pentane afforded compounds **3a-[G$_1$]** (0.820 g, 84% yield) and **3b-[G$_1$]** (0.724 g, 86% yield) as white powders.

3a-[G$_1$]: $^{31}P\{^1H\}$ NMR ($CDCl_3$): δ = 13.8 (d, $^2J_{PP}$ = 30.2 Hz, P_{00}), 51.4 (d, $^2J_{PP}$ = 30.2 Hz, P_0), 63.5 (s, P_1). – ^1H NMR ($CDCl_3$): δ = 3.45 (d, $^3J_{HP}$ = 14.1 Hz, 6 H, CH_3N), 4.03 (m, 2 H, CH_2), 4.11 (m, 2 H, CH_2), 5.81 (s, 1 H, OCHO), 7.20 (dd, $^3J_{HH}$ = 8.1 Hz, $^3J_{HP}$ = 1 Hz, 4 H, C_0^2H), 7.39–7.69 (m, 16 H, C_6H_5, C_6H_4), 7.62 (d, $^3J_{HH}$ = 8.1 Hz, 4 H, C_0^3H). – $^{13}C\{^1H\}$ NMR ($CDCl_3$): δ = 31.9 (d, $^2J_{CP}$ = 13 Hz, CH_3N), 65.5 (s, CH_2), 102.7 (s, OCHO), 122.1 (d, $^3J_{CP}$ = 6 Hz, C_0^2), 126.7 (d, $^3J_{CP}$ = 14 Hz, C$^{3\prime}$), 128.4 (dd, $^1J_{CP}$ = 106 Hz, $^3J_{CP}$ = 4 Hz, C_0^i), 128.5 (s, C_0^3), 128.8 (d, $^3J_{CP}$ = 12 Hz, C_0^m), 129.5 (br. d, $^1J_{CP}$ = 106 Hz, C$^{1\prime}$), 130.2 (s, C_0^4), 132.8 (d, $^2J_{CP}$ = 11 Hz, C_0^o), 132.8 (s, C_0^p), 132.9 (d, $^2J_{CP}$ = 12 Hz, C$^{2\prime}$), 141.5 (d, $^3J_{CP}$ = 18 Hz, CH=N), 142.6 (s, C$^{4\prime}$), 153.6 (d, $^2J_{CP}$ = 10 Hz, C_0^1). – $C_{37}H_{35}Cl_4N_5O_4P_4S_3$ (975.62): calcd. C 45.55, H 3.62, N 7.18; found C 45.47, H 3.55, N 7.21.

3b-[G$_1$]: $^{31}P\{^1H\}$ NMR ($CHCl_3$): δ = 15.5 (d, $^2J_{PP}$ = 34.6 Hz, P_{00}), 52.4 (d, $^2J_{PP}$ = 34.6 Hz, P_0), 62.1 (s, P_1). – ^1H NMR ($CDCl_3$): δ = 2.28 (d, $^2J_{HP}$ = 13.2 Hz, 3 H, CH_3–P), 3.46 (d, $^2J_{HP}$ = 14.1 Hz, 6 H, CH_3–N–P), 7.24–7.65 (m, 20 H, C_6H_5, C_6H_4, CH=N). – $^{13}C\{^1H\}$ NMR ($CDCl_3$): δ = 14.6 (d, $^1J_{CP}$ = 68 Hz, CH_3–P), 31.8 (d, $^2J_{CP}$ = 14 Hz, CH_3–N–P), 122.0 (d, $^3J_{CP}$ = 4 Hz, C_0^2), 128.4 (s, C_0^3), 128.8 (d, $^3J_{CP}$ = 14 Hz, C_0^m), 130.2 (s, C_0^p), 131.0 (d, $^2J_{CP}$ = 12 Hz, C_0^o), 132.5 (d, $^4J_{CP}$ = 3 Hz, C_0^4), 141.3 (d, $^3J_{CP}$ = 19 Hz, CH=N), 153.5 (d, $^2J_{CP}$ = 8 Hz, C_0^1). – $C_{29}H_{29}Cl_4N_5O_2P_4S_3$ (841.48): calcd. C 41.39, H 3.47, N 8.32; found C 41.27, H 3.42, N 8.25.

Synthesis of 3a-[G′$_1$]: A solution of **3a-[G$_1$]** (0.293 g, 0.3 mmol) in THF (20 mL) was added to hydroxybenzaldehyde sodium salt (**5**) (0.181 g, 1.26 mmol, 5% excess). The resulting mixture was stirred overnight at room temperature, then centrifuged. The solution was concentrated to dryness and the residue was washed with THF/pentane. Compound **3a-[G′$_1$]** was isolated as a white powder (0.308 g, 78% yield).

3a-[G′$_1$]: $^{31}P\{^1H\}$ NMR ($CDCl_3$): δ = 13.8 (d, $^2J_{PP}$ = 30.0 Hz, P_{00}), 51.6 (d, $^2J_{PP}$ = 30.0 Hz, P_0), 60.8 (s, P_1). – ^1H NMR ($CDCl_3$): δ = 3.37 (d, $^3J_{HP}$ = 10.8 Hz, 6 H, CH_3N), 4.01 (m, 2 H, CH_2), 4.04 (m, 2 H, CH_2), 5.79 (s, 1 H, OCHO), 7.19 (d, $^3J_{HH}$ = 7.8 Hz, 4 H, C_0^2H), 7.38 (d, $^3J_{HH}$ = 7.9 Hz, 8 H, C_1^2H), 7.4–7.7 (m, 16 H, CH=N, C_6H_5, C_6H_4), 7.57 (d, $^3J_{HH}$ = 7.8 Hz, 4 H, C_0^3H), 7.85 (d, $^3J_{HH}$ = 7.9 Hz, 8 H, C_1^3H), 9.91 (s, 4 H, CHO). – $^{13}C\{^1H\}$ NMR ($CDCl_3$): δ = 32.5 (d, $^2J_{CP}$ = 13 Hz, CH_3N), 65.5 (s, CH_2), 102.7 (s, OCHO), 122.0 (d, $^3J_{CP}$ = 6 Hz, C_0^2, C_1^2), 126.7 (d, $^3J_{CP}$ = 14 Hz, C$^{3\prime}$), 128.1 (s, C_0^3), 128.4 (dd, $^1J_{CP}$ = 106 Hz, $^3J_{CP}$ = 4 Hz, C_0^i), 128.8 (d, $^3J_{CP}$ = 13 Hz, C_0^m), 129.5 (br. d, $^1J_{CP}$ = 106 Hz, C$^{1\prime}$), 130.5 (s, C_0^4), 131.5 (s, C_1^3), 132.8 (d, $^2J_{CP}$ = 9 Hz, C_0^o), 132.8 (s, C_0^p), 132.9 (d, $^2J_{CP}$ = 12 Hz, C$^{2\prime}$), 133.7 (s, C_1^4), 140.3 (d, $^3J_{CP}$ = 14 Hz, CH=N), 142.7 (s, C$^{4\prime}$), 153.3 (d, $^2J_{CP}$ = 10 Hz, C_0^1), 155.2 (d, $^2J_{CP}$ = 6 Hz, C_1^1), 190.8 (s, CHO). – IR (KBr): 1702 cm^{-1} ($\nu_{C=O}$). – $C_{65}H_{55}N_5O_{12}P_4S_3$ (1318.27): calcd. C 59.22, H 4.21, N 5.31; found C 59.10, H 4.15, N 5.24.

Synthesis of 6a-[G′$_1$]: A solution of **3a-[G′$_1$]** (0.264 g, 0.2 mmol) in CH_2Cl_2 (20 mL) was added dropwise to a strongly stirred solution of hydrazine hydrate (40 mmol, very large excess) in CH_2Cl_2 (30 mL). The resulting mixture was stirred for 2 h at room temperature. The organic phase was separated, dried with Na_2SO_4, filtered, and concentrated to dryness. The residue was washed twice with CH_2Cl_2/pentane to give **6a-[G′$_1$]** as a white powder (0.256 g, 93% yield).

6a-[G′$_1$]: $^{31}P\{^1H\}$ NMR ($CDCl_3$): δ = 13.8 (d, $^2J_{PP}$ = 29.0 Hz, P_{00}), 51.5 (d, $^2J_{PP}$ = 29.0 Hz, P_0), 62.4 (s, P_1). − ^1H NMR ($CDCl_3$): δ = 3.30 (d, $^3J_{HP}$ = 10.7 Hz, 6 H, CH_3N), 3.99 (m, 2 H, CH_2), 4.02 (m, 2 H, CH_2), 5.48 (br. s, 8 H, NH_2), 5.78 (s, 1 H, OCHO), 7.17 (d, $^3J_{HH}$ = 8.5 Hz, 12 H, C_0^2H, C_1^2H), 7.45 (d, $^3J_{HH}$ = 8.5 Hz, 8 H, C_1^3H), 7.4−7.7 (m, 24 H, CH=N, C_6H_5, C_6H_4). − $^{13}C\{^1H\}$ NMR ($CDCl_3$): δ = 32.9 (d, $^2J_{CP}$ = 13 Hz, CH_3N), 65.3 (s, CH_2), 102.5 (s, OCHO), 121.5 (d, $^3J_{CP}$ = 5 Hz, C_1^2), 121.8 (d, $^3J_{CP}$ = 5 Hz, C_0^2), 126.6 (d, $^3J_{CP}$ = 13 Hz, $C^{3\prime}$), 127.0 (s, C_1^3), 127.8 (s, C_0^3), 128.2 (dd, $^1J_{CP}$ = 106 Hz, $^3J_{CP}$ = 3 Hz, C_0^i), 128.5 (d, $^3J_{CP}$ = 13 Hz, C_0^m), 130.0 (dd, $^1J_{CP}$ = 106 Hz, $^3J_{CP}$ = 4 Hz, $C^{1\prime}$), 130.7 (s, C_0^4), 132.4 (s, C_1^4), 132.6 (d, $^2J_{CP}$ = 10 Hz, C_0^o), 132.7 (s, C_0^p), 132.8 (d, $^2J_{CP}$ = 11 Hz, $C^{2\prime}$), 139.2 [d, $^3J_{CP}$ = 13 Hz, $(CH=N)_1$], 141.7 [s, $(CH=N)_2$], 142.4 (s, $C^{4\prime}$), 150.6 (d, $^2J_{CP}$ = 7 Hz, C_1^1), 152.9 (d, $^2J_{CP}$ = 9 Hz, C_0^1). − $C_{65}H_{63}N_{13}O_8P_4S_3$ (1374.4): calcd. C 56.81, H 4.62, N 13.25; found C 56.96, H 4.57, N 13.16.

Synthesis of 7a-[G$_2$]: A mixture of 1.0 mmol of paraformaldehyde and 1.0 mmol of diphenylphosphane was heated without solvent for 2 h at 120 °C in a closed reactor to afford Ph_2PCH_2OH. To this crude product was added a solution of **6a-[G′$_1$]** (0.137 g, 0.1 mmol) in THF (10 mL). The resulting mixture was stirred overnight at 80 °C, then concentrated to dryness. The residue was washed first with CH_2Cl_2/pentane, then with ether/pentane to afford **7a-[G$_2$]** as a white powder (0.219 g, 74% yield).

7a-[G$_2$]: $^{31}P\{^1H\}$ NMR ($CDCl_3$): δ = −25.1 (s, P_2), 13.7 (d, $^2J_{PP}$ = 29.6 Hz, P_{00}), 51.7 (d, $^2J_{PP}$ = 29.6 Hz, P_0), 63.2 (s, P_1). − ^1H NMR ($CDCl_3$): δ = 3.33 (d, $^3J_{HP}$ = 9.3 Hz, 6 H, CH_3N), 3.98 (m, 2 H, CH_2), 4.03 (m, 2 H, CH_2), 4.19 (s, 16 H, CH_2), 5.79 (s, 1 H, OCHO), 7.10−7.80 (m, 124 H, CH=N, C_6H_5, C_6H_4). − $^{13}C\{^1H\}$ NMR ($CDCl_3$): δ = 33.0 (d, $^2J_{CP}$ = 13 Hz, CH_3N), 56.8 (d, $^1J_{CP}$ = 7 Hz, CH_2P), 65.4 (s, CH_2O), 102.6 (s, OCHO), 121.5 (d, $^3J_{CP}$ = 5 Hz, C_1^2), 121.8 (d, $^3J_{CP}$ = 5 Hz, C_0^2), 126.6 (d, $^3J_{CP}$ = 14 Hz, $C^{3\prime}$), 127.2 (s, C_0^3, C_1^3), 128.2 (dd, $^1J_{CP}$ = 106 Hz, $^3J_{CP}$ = 3 Hz, C_0^i), 128.5 (d, $^3J_{CP}$ = 13 Hz, C_0^m), 128.6 (d, $^3J_{CP}$ = 13 Hz, C_2^m), 128.9 (s, C_2^p), 129.9 (dd, $^1J_{CP}$ = 106 Hz, $^3J_{CP}$ = 4 Hz, $C^{1\prime}$), 130.7 (s, C_0^4), 131.3 (s, C_1^4), 132.6 (d, $^2J_{CP}$ = 10 Hz, C_0^o), 132.7 (s, C_0^p), 132.8 (d, $^2J_{CP}$ = 11 Hz, $C^{2\prime}$), 133.1 (d, $^2J_{CP}$ = 20 Hz, C_2^o), 133.1 [s, $(CH=N)_2$], 137.3 (d, $^1J_{CP}$ = 14 Hz, C_2^i), 139.3 [d, $^3J_{CP}$ = 13 Hz, $(CH=N)_1$], 142.5 (s, $C^{4\prime}$), 150.6 (d, $^2J_{CP}$ = 8 Hz, C_1^1), 152.9 (d, $^2J_{CP}$ = 9 Hz, C_0^1).

Synthesis of 8b-[G′$_1$]: To a solution of compound **3b-[G$_1$]** (0.500 g, 0.594 mmol) in THF (20 mL) was added dropwise a solution of *N*,*N*-diethylethylenediamine (334 μL, 2.377 mmol) in THF (20 mL). The reaction mixture was stirred for 12 h at room temperature, and a precipitate of compound **8b-[G′$_1$]** appears. The precipitate was recovered by filtration and washed twice with ether. Compound **8b-[G′$_1$]** was obtained as a white powder (0.528 g, 68% yield).

8b-[G′$_1$]: $^{31}P\{^1H\}$ NMR (THF): δ = 15.8 (d, $^2J_{PP}$ = 32 Hz, P_{00}), 52.4 (d, $^2J_{PP}$ = 32 Hz, P_0), 69.2 (s, P_1). − ^1H NMR ($CDCl_3$): δ = 1.29 (t, $^3J_{HH}$ = 7 Hz, 24 H, CH_2-CH_3), 2.27 (d, $^2J_{HP}$ = 13.2 Hz, 3 H, CH_3-P), 3.16 (m, 6 H, CH_3-N), 3.27 (br. s, 16 H, CH_2-CH_2), 3.44 (q, $^3J_{HH}$ = 7 Hz, 16 H, CH_2-CH_3), 5.31 (d, $^2J_{HP}$ = 5.5 Hz, 4 H, NH), 7.13−7.70 (m, 20 H, C_6H_5, C_6H_4, CH=N), 9.18 (br. s, 4 H, NH^+). − $^{13}C\{^1H\}$ NMR ($CDCl_3$): δ = 8.7 (s, CH_2-CH_3), 14.7 (d, $^2J_{CP}$ = 68 Hz, CH_3-P), 32.2 (d, $^2J_{CP}$ = 11 Hz, CH_3-N), 36.5 (s, CH_2-N^+), 47.4 (s, CH_2-CH_3), 52.9 (s, $NH-CH_2$), 121.7 (s, C_0^2), 127.7 (s, C_0^3), 128.9 (d, $^3J_{CP}$ = 12 Hz, C_0^m), 130.9 (d, $^2J_{CP}$ = 11 Hz, C_0^o), 131.7 (s, C_0^p), 132.5 (s, C_0^4), 137.3 (br. s, CH=N), 152.3 (d, $^2J_{CP}$ = 9 Hz, C_0^1). − $C_{53}H_{93}Cl_4N_{13}O_2P_4S_3$ (1306.3): calcd. C 48.73, H 7.17, N 13.93; found C 48.65, H 7.14, N 13.89.

Synthesis of 9b-[G′$_1$]: To a solution of compound **3b-[G$_1$]** (0.400 g, 0.473 mmol) and potassium carbonate (0.263 g, 1.9 mmol) in CH_2Cl_2 (20 mL), was added *N*,*N*-diethylethylenediamine (267 μL, 1.9 mmol). The reaction mixture was stirred for 6 h at room temperature, then centrifuged (10000 rpm) and filtered. The resulting solution was concentrated to dryness to give compound **9b-[G′$_1$]** as a white powder after two washings with ether (0.423 g, 77% yield).

9b-[G′$_1$]: $^{31}P\{^1H\}$ NMR (CH_2Cl_2): δ = 16.2 (d, $^2J_{PP}$ = 31 Hz, P_{00}), 52.7 (d, $^2J_{PP}$ = 31 Hz, P_0), 68.1 (s, P_1). − ^1H NMR ($CDCl_3$): δ = 1.25 (t, $^3J_{HH}$ = 6.9 Hz, 24 H, CH_2-CH_3), 2.21 (d, $^2J_{HP}$ = 13.2 Hz, 3 H, CH_3-P), 3.08 (m, 6 H, CH_3-N), 3.19 (br. s, 16 H, CH_2-CH_2), 3.39 (q, $^3J_{HH}$ = 6.9 Hz, 16 H, CH_2-CH_3), 5.21 (d, $^2J_{HP}$ = 5.4 Hz, 4 H, NH), 7.10−7.64 (m, 20 H, C_6H_5, C_6H_4, CH=N). − $^{13}C\{^1H\}$ NMR ($CDCl_3$): δ = 8.7 (s, CH_2-CH_3), 14.7 (d, $^1J_{CP}$ = 68 Hz, CH_3-P), 32.1 (d, $^2J_{CP}$ = 11 Hz, CH_3-N-P), 36.6 (s, CH_2-N), 47.4 (s, CH_2-CH_3), 53.1 (d, $^2J_{CP}$ = 6 Hz, $NH-CH_2$), 121.7 (s, C_0^2), 127.7 (s, C_0^3), 128.9 (d, $^3J_{CP}$ = 13 Hz, C_0^m), 130.9 (d, $^2J_{CP}$ = 10 Hz, C_0^o), 131.7 (s, C_0^p), 132.5 (s, C_0^4), 137.3 (d, $^3J_{CP}$ = 13 Hz, CH=N), 152.4 (d, $^2J_{CP}$ = 8 Hz, C_0^1). − $C_{53}H_{89}N_{13}O_2P_4S_3$ (1160.5): calcd. C 54.85, H 7.72, N 15.69; found C 54.86, H 7.59, N 15.58.

Synthesis of 10b-[G$_1$]: To a solution of compound **3b-[G$_1$]** (0.500 g, 0.594 mmol) in CH_2Cl_2 (20 mL), was added methyl triflate (68 μL, 0.601 mmol). The reaction mixture was stirred for 2 h at room temperature, then concentrated to dryness. The residue was washed twice with pentane to afford compound **10b-[G$_1$]** as a white powder (0.561 g, 94% yield).

10b-[G$_1$]: $^{31}P\{^1H\}$ NMR ($CDCl_3$): δ = 23.8 (d, $^2J_{PP}$ = 18.2 Hz, P_{00} or P_0), 24.1 (d, $^2J_{PP}$ = 18.2 Hz, P_{00} or P_0), 62.8 (s, P_1). − ^1H NMR ($CDCl_3$): δ = 2.18 (d, $^2J_{HP}$ = 12.4 Hz, 3 H, CH_3-P), 2.52 (d, $^3J_{HP}$ = 17.7 Hz, 3 H, CH_3-S), 3.48 (d, $^2J_{HP}$ = 13.9 Hz, 6 H, CH_3-N-P), 7.16−7.82 (m, 20 H, C_6H_5, C_6H_4, CH=N). − $^{13}C\{^1H\}$ NMR ($CDCl_3$): δ = 13.6 (s, CH_3-S), 15.1 (d, $^1J_{CP}$ = 73 Hz, CH_3-P), 32.1 (d, $^2J_{CP}$ = 13 Hz, CH_3-N-P), 120.9 (d, $^3J_{CP}$ = 4 Hz, C_0^2), 125.8 (d, $^1J_{CP}$ = 112 Hz, C^i), 129.6 (s, C_0^3), 129.7 (d, $^3J_{CP}$ = 14 Hz, C_0^m), 130.7 (d, $^2J_{CP}$ = 11 Hz, C_0^o), 133.4 (s, C_0^p), 134.2 (s, C_0^4), 140.5 (d, $^3J_{CP}$ = 18 Hz, CH=N), 150.1 (d, $^2J_{CP}$ = 10 Hz, C_0^1). − $^{19}F\{^1H\}$ NMR ($CDCl_3$): δ = −1.9 (s, $CF_3SO_3^-$). − $C_{31}H_{32}Cl_4F_3N_5O_5P_4S_4$ (1005.6): calcd. C 37.02, H 3.20, N 6.96; found C 36.94, H 3.11, N 6.91.

Synthesis of 11b-[G$_1$]: To a solution of compound **10b-[G$_1$]** (0.420 g, 0.417 mmol) in CH_2Cl_2 (30 mL), was added $NaBPh_4$ (0.143 g, 0.417 mmol). The reaction mixture was stirred for 24 h, then filtered. The resulting solution was concentrated to dryness to afford compound **11b-[G$_1$]** as a white powder (0.436 g, 89% yield).

11b-[G$_1$]: $^{31}P\{^1H\}$ NMR ($CDCl_3$): δ = 23.8 (br. s, P_{00} and P_0), 62.7 (s, $P(S)Cl_2$). − ^1H NMR ($CDCl_3$): δ = 1.50 (d, $^2J_{HP}$ = 12.3 Hz, 3 H, CH_3-P), 2.26 (d, $^3J_{HP}$ = 17.9 Hz, 3 H, CH_3-S), 3.30 (d, $^2J_{HP}$ = 13.9 Hz, 6 H, CH_3-N-P), 6.76−7.61 (m, 40 H, C_6H_5, C_6H_4, CH=N). − $^{13}C\{^1H\}$ NMR ($CDCl_3$): δ = 13.4 (d, $^2J_{CP}$ = 6 Hz, CH_3-S-P), 14.6 (d, $^1J_{CP}$ = 73 Hz, CH_3-P), 32.0 (d, $^2J_{CP}$ = 12 Hz, CH_3-N-P), 120.7 (d, $^3J_{CP}$ = 4 Hz, C_0^2), 121.7 (s, C_b^o), 125.5 (s, C_b^m), 125.6 (d, $^1J_{CP}$ = 112 Hz, C^i), 129.5 (s, C_0^3), 129.7 (d, $^3J_{CP}$ = 13 Hz, C_0^m), 130.6 (d, $^2J_{CP}$ = 11 Hz, C_0^o), 133.4 (s, C_0^p), 134.3 (s, C_0^4), 136.3 (s, C_b^p), 139.9 (d, $^3J_{CP}$ = 19 Hz, CH=N), 149.9 (d, $^2J_{CP}$ = 11 Hz, C_0^1), 164.2 (q, $^1J_{CB}$ = 49 Hz, C_b^i). − $C_{54}H_{52}BCl_4N_5O_2P_4S_3$ (1175.7): calcd. C 55.16, H 4.45, N 5.95; found C 55.06, H 4.40, N 5.87.

Synthesis of 11b-[G′$_1$]: A solution of *N*,*N*-diethylethylenediamine (0.180 mL, 1.280 mmol) in CH_2Cl_2 (80 mL) was added to a solu-

tion of compound **11b-[G$_1$]** (0.360 g, 0.306 mmol) in CH_2Cl_2 (80 mL). The resulting mixture was stirred for 2 h, then concentrated to dryness. Compound **11b-[G′$_1$]** was obtained as a white powder after washings with ether (0.361 g, 71% yield).

11b-[G′$_1$]: $^{31}P\{^1H\}$ NMR ($CDCl_3$): δ = 23.7 (br. s, P_{00} and P_0), 68.5 (s, P_1). − ^1H NMR ($CDCl_3$): δ = 1.23 (t, $^3J_{HH}$ = 7.3 Hz, 24 H, CH_2-CH_3), 1.74 (d, $^2J_{HP}$ = 12.2 Hz, 3 H, CH_3-P), 2.34 (d, $^3J_{HP}$ = 17.7 Hz, 3 H, CH_3-S), 2.86−3.23 (m, 38 H, CH_2-CH_2, CH_2-CH_3, CH_3-N), 5.03 (d, $^2J_{HP}$ = 6 Hz, 4 H, NH−P), 6.78−7.77 (m, 40 H, C_6H_5, C_6H_4, CH=N), 10.00 (br. s, 4 H, NH^+). − $^{13}C\{^1H\}$ NMR ($CDCl_3$): δ = 8.6 (s, CH_2-CH_3), 13.5 (d, $^2J_{CP}$ = 11 Hz, CH_3-S-P), 14.7 (d, $^1J_{CP}$ = 64 Hz, CH_3-P), 32.2 (d, $^2J_{CP}$ = 11 Hz, CH_3-N-P), 36.4 (s, CH_2-NH^+), 47.3 (s, CH_2-CH_3), 53.1 (s, $NH-CH_2$), 120.7 (d, $^3J_{CP}$ = 4 Hz, C_0^2), 121.9 (s, C_b^o), 125.6 (s, C_b^m), 125.7 (d, $^1J_{CP}$ = 110 Hz, C_0^i), 128.8 (s, C_0^3), 129.8 (d, $^3J_{CP}$ = 12 Hz, C_0^m), 130.7 (d, $^2J_{CP}$ = 10 Hz, C_0^o), 134.4 (s, C_0^4), 134.8 (d, $^3J_{CP}$ = 10 Hz, CH=N), 136.0 (s, C_b^p), 149.0 (d, $^2J_{CP}$ = 10 Hz, C_0^1), 164.0 (q, $^1J_{CB}$ = 49 Hz, C_b^i). − $C_{78}H_{116}BCl_4N_{13}O_2P_4S_3$ (1640.6): calcd. C 57.10, H 7.12, N 11.09; found C 56.97, H 7.04, N 10.98.

Synthesis of 12b-[G′$_1$]: To a solution of compound **11b-[G′$_1$]** (0.300 g, 0.204 mmol) in CH_2Cl_2 (30 mL), was added $P(NMe_2)_3$ (0.270 mL, 1.428 mmol, excess). The resulting mixture was stirred for 1 h, then concentrated to dryness. Compound **12b-[G′$_1$]** was extracted with toluene; this solution was concentrated to dryness to afford compound **12b-[G′$_1$]**, which was used without further purification.

12b-[G′$_1$]: $^{31}P\{^1H\}$ NMR (CH_2Cl_2): δ = 10.3 (d, $^2J_{PP}$ = 31.6 Hz, P_{00}), 68.5 (s, P_1), 144.2 (d, $^2J_{PP}$ = 31.6 Hz, P_0).

Synthesis of 12b-[G′$_1$-G′$_0$]: To a solution of compound **12b-[G′$_1$]** (0.253 g, 0.200 mmol) in CH_2Cl_2 (10 mL), was added a solution of azide **2** (0.083 g, 0.234 mmol, slight excess) in CH_2Cl_2 (10 mL). The resulting mixture was stirred for 1 h, then concentrated to dryness. The residue was washed three times with pentane to afford compound **12b-[G′$_1$-G′$_0$]** as a white powder (0.315 g, 84% yield).

12b-[G′$_1$-G′$_0$]: $^{31}P\{^1H\}$ NMR (CD_2Cl_2): δ = −9.6 (dd, $^2J_{PP}$ = 26 Hz, $^2J_{PP}$ = 58.4 Hz, P_0), 18.4 (d, $^2J_{PP}$ = 26 Hz, P_{00}), 47.5 (d, $^2J_{PP}$ = 58.4 Hz, P_0'), 70.4 (s, P_1). − ^1H NMR (CD_2Cl_2): δ = 1.26 (t, $^3J_{HH}$ = 6.8 Hz, 24 H, CH_2-CH_3), 2.28 (d, $^2J_{HP}$ = 15.8 Hz, 3 H, CH_3-P), 2.41−3.29 (m, 38 H, CH_2-CH_2, CH_2-CH_3, CH_3-N-P), 5.40 (br. s, 4 H, NH−P), 6.84−7.81 (m, 48 H, C_6H_5, C_6H_4, CH=N), 9.93 (s, 2 H, CHO). − $^{13}C\{^1H\}$ NMR (CD_2Cl_2): δ = 8.7 (s, CH_2-CH_3), 15.6 (d, $^1J_{CP}$ = 69 Hz, CH_3-P), 32.3 (d, $^2J_{CP}$ = 11 Hz, CH_3-N-P), 36.8 (s, CH_2-NH^+), 47.6 (s, CH_2-CH_3), 53.2 (s, $NH-CH_2$), 121.0 (d, $^3J_{CP}$ = 6 Hz, $C_0^{2\prime}$), 121.4 (d, $^3J_{CP}$ = 4 Hz, C_0^2), 122.0 (s, C_b^0), 125.8 (s, C_b^m), 127.9 (s, $C_0^{3\prime}$), 128.1 (s, C_0^3), 129.3 (d, $^3J_{CP}$ = 13 Hz, C_0^m), 131.2 (d, $^2J_{CP}$ = 12 Hz, C_0^o), 132.2 (s, C_0^4), 132.7 (br. s, $C_0^{4\prime}$), 133.1 (s, C_0^p), 136.1 (s, C_b^p), 137.1 (d, $^3J_{CP}$ = 13 Hz, CH=N), 151.9 (d, $^2J_{CP}$ = 10 Hz, C_0^1), 157.1 (d, $^2J_{CP}$ = 8 Hz, $C_0^{1\prime}$), 164.2 (q, $^1J_{CB}$ = 49 Hz, C_b^i), 191.6 (s, CHO). − IR (KBr): 1701 cm^{-1} ($\nu_{C=O}$). − $C_{91}H_{123}BCl_3N_{14}O_6P_5S_3$ (1877.3): calcd. C 58.22, H 6.60, N 10.44; found C 58.14, H 6.54, N 10.38.

Synthesis of 13b-[G′$_1$-G′$_0$]: To a solution of compound **12b-[G′$_1$-G′$_0$]** (0.250 g, 0.158 mmol) in CH_2Cl_2 (15 mL) was added a large excess of methylhydrazine (0.168 mL, 3.15 mmol). The reaction mixture was stirred for 12 h, then concentrated to dryness. The residue was washed several times with ether to afford compound **13b-[G′$_1$-G′$_0$]** as a white powder (0.223 g, 73% yield).

13b-[G′$_1$-G′$_0$]: $^{31}P\{^1H\}$ NMR (CD_2Cl_2): δ = −9.6 (dd, $^2J_{PP}$ = 26.3 Hz, $^2J_{PP}$ = 57 Hz, P_0), 17.9 (d, $^2J_{PP}$ = 26.3 Hz, P_{00}), 48.7 (d, $^2J_{PP}$ = 57 Hz, P_0'), 70.3 (s, P_1). − ^1H NMR (CD_2Cl_2): δ = 1.06 (t, $^3J_{HH}$ = 7.2 Hz, 24 H, CH_2-CH_3), 2.23 (d, $^2J_{HP}$ = 15.6 Hz, 3 H, CH_3-P), 2.58−2.80 (m, 16 H, CH_2-CH_2), 2.92 (s, 6 H, CH_3-NH), 3.05−3.20 (m, 22 H, CH_2-CH_3, CH_3-N-P), 4.43 (s, 2 H, CH_3-N*H*), 5.22 (br. s, 4 H, NH−P), 6.84−7.57 (m, 50 H, C_6H_5, C_6H_4, CH=N). − $^{13}C\{^1H\}$ NMR (CD_2Cl_2): δ = 8.7 (s, CH_2-CH_3), 15.5 (d, $^1J_{CP}$ = 67 Hz, CH_3-P), 32.3 (d, $^2J_{CP}$ = 11 Hz, CH_3-N-P), 34.0 (s, CH_3NH), 36.8 (s, CH_2-NH^+), 47.5 (s, CH_2-CH_3), 53.2 (s, $NH-CH_2$), 121.2 (d, $^3J_{CP}$ = 5 Hz, $C_0^{2\prime}$), 121.5 (d, $^3J_{CP}$ = 4 Hz, C_0^2), 121.9 (s, C_b^0), 125.8 (s, C_b^m), 126.4 (s, $C_0^{3\prime}$), 128.0 (s, C_0^3), 129.2 (d, $^3J_{CP}$ = 13 Hz, C_0^m), 131.2 (d, $^2J_{CP}$ = 12 Hz, C_0^o), 132.0 (s, C_0^4), 132.5 (br. s, $C_0^{4\prime}$), 133.1 (s, C_0^p), 133.8 (s, CH=N-NH), 136.1 (s, C_b^p), 137.2 (d, $^3J_{CP}$ = 13 Hz, CH=N-NP), 151.8 (d, $^2J_{CP}$ = 9 Hz, C_0^1), 153.9 (d, $^2J_{CP}$ = 8 Hz, $C_0^{1\prime}$), 164.2 (q, $^1J_{CB}$ = 49 Hz, C_b^i). − $C_{93}H_{131}BCl_3N_{18}O_4P_5S_3$ (1933.4): calcd. C 57.77, H 6.82, N 13.04; found C 57.64, H 6.75, N 12.94.

Synthesis of 14b-[G′$_1$-G′$_0$]: To a solution of compound **13b-[G′$_1$−G′$_0$]** (0.100 g, 0.062 mmol) in CH_2Cl_2 (5 mL) was added a solution 0.119 M of Ph_2PCH_2OH (1.04 mL, 0.124 mmol) in CH_2Cl_2. The reaction mixture was stirred for 12 h at 40 °C, then was concentrated to dryness. The residue was washed three times with pentane to afford **14b-[G′$_1$-G′$_0$]** as a white powder (0.101 g, 76% yield).

14b-[G′$_1$-G′$_0$]. $^{31}P\{^1H\}$ NMR (CH_2Cl_2): δ = −22.9 (s, P_{11}'), −11.8 (dd, $^2J_{PP}$ = 26.5 Hz, $^2J_{PP}$ = 56.6 Hz, P_0), 15.6 (d, $^2J_{PP}$ = 26.5 Hz, P_{00}), 46.5 (d, $^2J_{PP}$ = 56.6 Hz, P_0'), 68.1 (s, P_1).

Synthesis of 15b-[G′$_1$-G′$_0$]: To a solution of compound **14b-[G′$_1$-G′$_0$]** (0.101 g, 0.049 mmol) in CH_2Cl_2 (10 mL) was added a solution of $Fe_2(CO)_9$ (0.054 g, 0.147 mmol) in CH_2Cl_2 (10 mL). The resulting mixture was stirred for 12 h, then filtered. The solution was concentrated to dryness, and the residue was washed twice with ether to afford compound **15b-[G′$_1$-G′$_0$]** as a brown powder (0.106 g, 81% yield).

15b-[G′$_1$-G′$_0$]: $^{31}P\{^1H\}$ NMR (CD_2Cl_2): δ = −9.3 (m, P_0), 17.4 (d, $^2J_{PP}$ = 26.5 Hz, P_{00}), 48.4 (d, $^2J_{PP}$ = 54.9 Hz, P_0'), 69.5 (s, P_{11}'), 70.9 (s, P_1). − ^1H NMR (CD_2Cl_2): δ = 1.28 (br. s, 24 H, CH_2-CH_3), 2.26 (d, $^2J_{HP}$ = 15.7 Hz, 3 H, CH_3-P), 2.70−2.94 (m, 38 H, CH_3-N-CH_2, CH_2-CH_2, CH_2-CH_3), 3.26 (m, 6 H, CH_3-N-P), 5.05 (br. s, 4 H, CH_2-P-Fe), 6.74−7.89 (m, 70 H, C_6H_5, C_6H_4, CH=N). − $^{13}C\{^1H\}$ NMR (CD_2Cl_2): δ = 8.9 (s, CH_2-CH_3), 15.4 (d, $^1J_{CP}$ = 67 Hz, CH_3-P), 32.1 (br. s, CH_3-N-P), 37.0 (s, CH_2-NH^+), 39.0 (s, CH_2NCH_3), 47.4 (s, CH_2-CH_3), 52.9 (s, $NH-CH_2$), 56.3 (d, $^1J_{CP}$ = 74 Hz, CH_2-P), 121.3 (d, $^3J_{CP}$ = 5 Hz, $C_0^{2\prime}$) 121.6 (d, $^3J_{CP}$ = 4 Hz, C_0^2), 121.9 (s, C_b^o), 125.8 (s, C_b^m), 126.3 (br. s, $C_0^{3\prime}$), 127.9 (br. s, C_0^3), 128.7 (br. s, $C_1^{m\prime}$), 129.1 (d, $^3J_{CP}$ = 13 Hz, C_0^m), 130.5 (s, $C_1^{p\prime}$), 131.2 (d, $^2J_{CP}$ = 12 Hz, C_0^o), 131.2 (s, CH=N-NH), 131.7 (br. s, C_0^4), 132.3 (br. s, $C_0^{4\prime}$), 132.8 (d, $^1J_{CP}$ = 32 Hz, $C_1^{i\prime}$), 132.9 (d, $^2J_{CP}$ = 10 Hz, $C_1^{o\prime}$), 133.2 (s, C_0^p), 136.1 (s, C_b^p), 137.3 (br. s, CH=N), 149.6 (d, $^2J_{CP}$ = 8 Hz, $C_0^{1\prime}$), 151.8 (d, $^2J_{CP}$ = 9 Hz, C_0^1), 164.2 (q, $^1J_{CB}$ = 49 Hz, C_b^i), 213.1 (d, $^2J_{CP}$ = 18 Hz, CO). − IR (KBr): 2043, 1972, 1939 cm^{-1} (ν_{CO}). − $C_{127}H_{153}BCl_3Fe_2N_{18}O_{12}P_7S_3$ (2665.6): calcd. C 57.22, H 5.78, N 9.45; found C 57.13, H 5.69, N 9.39.

Synthesis of 16c-[G′$_1$]: NaOPh (0.487 g, 4.2 mmol) was added to a solution of **3c-[G$_1$]** (0.854 g, 1 mmol) in THF (20 mL). The resulting mixture was stirred overnight at room temperature, then centrifuged. The solution was concentrated to dryness and the residue was washed several times with THF/pentane (1:5). Compound **16c-[G′$_1$]** was isolated as a pale beige powder (1.062 g, 98% yield).

16c-[G′$_1$]: $^{31}P\{^1H\}$ NMR ($CDCl_3$): δ = 9.6 (d, $^2J_{PP}$ = 31.3 Hz, P_{00}), 52.2 (d, $^2J_{PP}$ = 31.3 Hz, P_0), 61.8 (s, P_1). − ^1H NMR ($CDCl_3$): δ = 3.34 (d, $^3J_{HP}$ = 10.6 Hz, 6 H, CH_3N-P), 6.12 (ddd, $^3J_{HP}$ = 24.1 Hz, $^3J_{HH}$ = 18.3 Hz, $^2J_{HH}$ = 1.1 Hz, 1 H, HC=CH_EH_Z*), 6.43 (ddd, $^3J_{HP}$ = 45.9 Hz, $^3J_{HH}$ = 12.4 Hz, $^2J_{HH}$ = 1.1 Hz, 1 H, HC=CH_EH_Z*), 6.82 (dddd, $^2J_{HP}$ = 25.2 Hz, $^3J_{HH}$ = 18.3 Hz, $^3J_{HH}$ = 12.4 Hz, $^4J_{HP}$ = 1.1 Hz, 1 H, HC=CH_EH_Z*), 7.20−7.70 (m, 40 H, C_6H_5, C_6H_4, CH=N) (*: *E* and *Z* refer to the relative position of H versus H through C=C). − $^{13}C\{^1H\}$ NMR ($CDCl_3$): δ = 32.9 (d, $^2J_{CP}$ = 13 Hz, CH_3N-P), 121.3 (d. $^3J_{CP}$ = 4 Hz, C_1^2), 121.8 (d, $^3J_{CP}$ = 5 Hz, C_0^2), 125.2 (s, C_1^4), 127.8 (dd, $^1J_{CP}$ = 100 Hz, $^3J_{CP}$ = 4 Hz, C_0^i), 127.8 (s, C_0^3), 128.6 (d, $^3J_{CP}$ = 13 Hz, C_0^m), 129.3 (s, C_1^3), 130.9 (s, C_0^4), 132.0 (d, $^2J_{CP}$ = 11 Hz, C_0^o), 132.5 (d, $^4J_{CP}$ = 2 Hz, C_0^p), 136.6 (s, CH_2=), 138.9 (d, $^3J_{CP}$ = 13 Hz, C_0^4-*C*H=N), 150.5 (d, $^2J_{CP}$ = 7 Hz, C_0^1), 152.8 (d, $^2J_{CP}$ = 9 Hz, C_1^1). − $C_{54}H_{49}N_5O_6P_4S_3$ (1084.1): calcd. C 59.83, H 4.55, N 6.46; found C 59.76, H 4.48, N 6.40.

Synthesis of 17c-[G′$_1$]: To a solution of compound **16c-[G′$_1$]** (0.542 g, 0.500 mmol) in THF (20 mL) were added 30 equiv. of methylhydrazine (0.800 mL, 15 mmol). The resulting solution was stirred for 3 h at room temperature, then concentrated to dryness. Washing several times with a mixture THF/pentane (1:5) afforded compound **17c-[G′$_1$]** as a white powder (0.537 g, 95% yield).

17c-[G′$_1$]: $^{31}P\{^1H\}$ NMR ($CDCl_3$): δ = 17.9 (d, $^2J_{PP}$ = 32.9 Hz, P_{00}), 52.0 (d, $^2J_{PP}$ = 32.9 Hz, P_0), 62.4 (s, P_1). − ^1H NMR ($CDCl_3$): δ = 2.33 (s, 3 H, CH_3-N-NH_2), 2.65 (m, 2 H, CH_2-CH_2-P), 2.71 (br. s, 2 H, NH_2), 3.02 (m, 2 H, CH_2CH_2-P), 3.34 (d, $^3J_{HP}$ = 10.7 Hz, 6 H, CH_3N-P), 7.20−7.70 (m, 40 H, C_6H_5, C_6H_4, CH=N). − $^{13}C\{^1H\}$ NMR ($CDCl_3$): δ = 25.4 (d, $^1J_{CP}$ = 66 Hz, CH_2CH_2-P), 33.1 (d, $^2J_{CP}$ = 13 Hz, CH_3N-P), 50.6 (s, CH_3-N-NH_2), 54.4 (s, CH_2-CH_2-P), 121.5 (s, C_1^2), 122.1 (d, $^3J_{CP}$ = 3 Hz, C_0^2), 125.4 (s, C_1^4), 127.9 (s, C_0^3), 128.8 (d, $^3J_{CP}$ = 13 Hz, C_0^m), 129.5 (s, C_1^3), 131.1 (s, C_0^4), 131.4 (d, $^2J_{CP}$ = 10 Hz, C_0^o), 132.5 (s, C_0^p), 139.0 (d, $^3J_{CP}$ = 14 Hz, C_0^4-*C*H=N), 150.7 (d, $^2J_{CP}$ = 7 Hz, C_0^1), 153.0 (d, $^2J_{CP}$ = 8 Hz, C_1^1). − $C_{55}H_{55}N_7O_6P_4S_3$ (1130.2): calcd. C 58.45, H 4.90, N 8.67; found C 58.38, H 4.85, N 8.63.

Synthesis of 17c-[G′$_1$-G$_0$]: A solution of compound **17c-[G′$_1$]** (0.150 g, 0.133 mmol) in THF (15 mL) was added to Ph_2PCH_2OH (obtained as described for **7a-[G$_2$]**) and heated at 90 °C under stirring for 12 h, then concentrated to dryness. Washing several times with a mixture THF/pentane (1:5) afforded compound **17c-[G′$_1$-G$_0$]** as a white powder (0.177 g, 87% yield).

17c-[G′$_1$-G$_0$]: $^{31}P\{^1H\}$ NMR ($CDCl_3$): δ = −24.1 (s, P_{11}'), 18.2 (d, $^2J_{PP}$ = 30.3 Hz, P_{00}), 51.6 (d, $^2J_{PP}$ = 30.3 Hz, P_0), 62.9 (s, P_1). − ^1H NMR ($CDCl_3$): δ = 2.12 (s, 3 H, CH_3-N-CH_2), 2.42−2.75 (m, 4 H, CH_2-CH_2-P), 3.34 (d, $^3J_{HP}$ = 10.2 Hz, 6 H, CH_3-N-P), 3.54 (br. s, 4 H, $N-CH_2-P$), 7.20−7.80 (m, 60 H, C_6H_5, C_6H_4, CH=N). − $^{13}C\{^1H\}$ NMR ($CDCl_3$): δ = 26.4 (d, $^1J_{CP}$ = 58 Hz, CH_2CH_2-P), 33.4 (d, $^2J_{CP}$ = 13 Hz, CH_3-N-P), 33.9 (s, CH_3-N-CH_2), 47.3 (s, CH_2-CH_2-P), 53.0 (s, NCH_2-P), 121.9 (d, $^3J_{CP}$ = 5 Hz, C_1^2), 122.4 (d, $^3J_{CP}$ = 5 Hz, C_0^2), 125.8 (s, C_1^4), 128.4 (s, C_0^3), 128.6 (d, $^3J_{CP}$ = 7 Hz, $C_1^{m\prime}$), 129.0 (d, $^3J_{CP}$ = 13 Hz, C_0^m), 129.1 (s, $C_1^{p\prime}$), 129.9 (s, C_1^3), 131.4 (s, C_0^4), 131.7 (d, $^2J_{CP}$ = 9 Hz, C_0^o), 132.6 (s, C_0^p), 133.6 (d, $^2J_{CP}$ = 19 Hz, $C_1^{o\prime}$), 138.1 (d, $^1J_{CP}$ = 14 Hz, $C_1^{i\prime}$), 139.4 (d, $^3J_{CP}$ = 14 Hz, C_0^4-*C*H=N), 151.1 (d, $^2J_{CP}$ = 7 Hz, C_0^1), 153.6 (d, $^2J_{CP}$ = 9 Hz, C_1^1). − $C_{81}H_{77}N_7O_6P_6S_3$ (1526.6): calcd. C 63.73, H 5.08, N 6.42; found C 63.67, H 5.01, N 6.39.

Synthesis of 17c-[G′$_1$-G′$_1$]: A solution of azide **2** (0.073 g, 0.210 mmol) in CH_2Cl_2 (20 mL) was added dropwise to a solution of **17c-[G′$_1$-G$_0$]** (0.135 g, 0.100 mmol) in CH_2Cl_2 (15 mL). The resulting solution was stirred overnight at room temperature, then concentrated to dryness. The residue was washed with THF/pentane (1:5) to give **17c-[G′$_1$-G′$_1$]** as a white powder (0.201 g, 93% yield).

17c-[G′$_1$-G′$_1$]: $^{31}P\{^1H\}$ NMR ($CDCl_3$): δ = 14.0 (d, $^2J_{PP}$ = 26.0 Hz, P_{11}'), 16.7 (d, $^2J_{PP}$ = 33.9 Hz, P_{00}), 50.0 (d, $^2J_{PP}$ = 26.0 Hz, P_1'), 50.2 (d, $^2J_{PP}$ = 33.9 Hz, P_0), 62.5 (s, P_1). − ^1H NMR ($CDCl_3$): δ = 1.83 (s, 3 H, CH_3-N-CH_2), 2.40−2.72 (m, 4 H, CH_2-CH_2-P), 3.34 (d, $^3J_{HP}$ = 10.5 Hz, 6 H, CH_3-N-P), 4.32 (m, 4 H, NCH_2-P), 7.00−7.80 (m, 76 H, C_6H_5, C_6H_4, CH=N), 9.92 (s, 4 H, CHO). − $^{13}C\{^1H\}$ NMR ($CDCl_3$): δ = 24.8 (d, $^1J_{CP}$ = 64 Hz, CH_2CH_2-P), 33.0 (d, $^2J_{CP}$ = 13 Hz, CH_3-N-P), 35.3 (s, CH_3-N-CH_2), 46.4 (s, CH_2-CH_2-P), 50.4 (d, $^1J_{CP}$ = 87 Hz, NCH_2-P), 121.4 (d, $^3J_{CP}$ = 4 Hz, C_1^2), 121.7 (d, $^3J_{CP}$ = 5 Hz, C_0^2, $C_1^{2\prime}$), 125.4 (s, C_1^4), 128.0 (s, C_0^3), 128.8 (d, $^3J_{CP}$ = 11 Hz, C_0^m, $C_1^{m\prime}$), 129.5 (s, C_1^3), 131.2 (s, $C_1^{3\prime}$), 131.4 (s, C_0^4), 132.2 (d, $^2J_{CP}$ = 9 Hz, C_0^o, $C_1^{o\prime}$), 132.6 (s, C_0^p, $C_1^{p\prime}$, $C_1^{4\prime}$), 138.7 (d, $^3J_{CP}$ = 14 Hz, C_0^4-*C*H=N), 150.6 (d, $^2J_{CP}$ = 6 Hz, C_0^1), 152.8 (d, $^2J_{CP}$ = 10 Hz, C_1^1), 156.5 (d, $^2J_{CP}$ = 8 Hz, $C_1^{1\prime}$), 190.0 (s, CHO). − IR (KBr): 1702 cm^{-1} ($\nu_{C=O}$). − $C_{109}H_{97}N_9O_{14}P_8S_5$ (2165.1): calcd. C 60.47, H 4.52, N 5.82; found C 60.45, H 4.48, N 5.75.

Synthesis of 17c-[G′$_1$-G$_n$] (*n* = 2, 3): A slight excess (5%) of phosphorus hydrazide **4** in solution in $CHCl_3$ was added to a solution of **17c-[G′$_1$-G′$_{n-1}$]** in THF. The resulting solution was stirred overnight at room temperature, then concentrated to dryness. The residue was washed several times with THF/pentane (1:5) to afford **17c-[G′$_1$-G$_2$]** (0.404 g, 96% yield) or **17c-[G′$_1$-G$_3$]** (0.510 g, 97% yield) as white powders.

Synthesis of 17c-[G′$_1$-G′$_n$] (*n* = 2, 3): A solution of compound **17c-[G′$_1$-G$_n$]** in solution in THF was added to the sodium salt **5** (5% excess) in THF. The resulting mixture was stirred overnight, then centrifuged and concentrated to dryness. The residue was washed several times with THF/pentane (1:5) to afford **17c-[G′$_1$-G′$_2$]** (0.418 g, 92% yield) or **17c-[G′$_1$-G′$_3$]** (0.448 g, 91% yield) as white powders.

17c-[G′$_1$-G$_2$]: $^{31}P\{^1H\}$ NMR ($CDCl_3$): δ = 13.6 (d, $^2J_{PP}$ = 25.1 Hz, P_{11}'), 16.9 (d, $^2J_{PP}$ = 33.3 Hz, P_{00}), 50.3 (d, $^2J_{PP}$ = 25.1 Hz, P_1'), 51.2 (d, $^2J_{PP}$ = 33.3 Hz, P_0), 62.5 (s, P_1), 62.9 (s, P_2'). − ^1H NMR ($CDCl_3$): δ = 1.82 (s, 3 H, CH_3-N-CH_2), 2.45−2.70 (m, 4 H, CH_2-CH_2-P), 3.34 (d, $^3J_{HP}$ = 10.5 Hz, 6 H, CH_3-N-P_1), 3.43 (d, $^3J_{HP}$ = 14.2 Hz, 12 H, CH_3-N-P_2'), 4.23−4.40 (m, 4 H, NCH_2-P), 7.00−7.70 (m, 80 H, C_6H_5, C_6H_4, CH=N). − $^{13}C\{^1H\}$ NMR ($CDCl_3$): δ = 24.7 (d, $^1J_{CP}$ = 65 Hz, CH_2CH_2-P), 31.9 (d, $^2J_{CP}$ = 13 Hz, CH_3-N-P_2'), 33.1 (d, $^2J_{CP}$ = 13 Hz, CH_3-N-P_1), 35.4 (s, CH_3-N-CH_2), 46.4 (s, CH_2-CH_2-P), 50.5 (d, $^1J_{CP}$ = 87 Hz, NCH_2-P), 121.4 (d, $^3J_{CP}$ = 4 Hz, C_1^2), 121.7 (d, $^3J_{CP}$ = 5 Hz, C_0^2, $C_1^{2\prime}$), 125.4 (s, C_1^4), 128.0 (s, C_0^3), 128.4 (s, $C_1^{3\prime}$), 128.8 (d, $^3J_{CP}$ = 13 Hz, C_0^m, $C_1^{m\prime}$), 129.5 (s, C_1^3), 130.2 (s, $C_1^{4\prime}$), 131.3 (d, $^2J_{CP}$ = 10 Hz, C_0^o, $C_1^{o\prime}$), 132.2 (s, C_0^4), 132.6 (s, C_0^p, $C_1^{p\prime}$), 138.8 (d, $^3J_{CP}$ = 14 Hz, C_0^4-*C*H=N), 141.2 (d, $^3J_{CP}$ = 18 Hz, $C_1^{4\prime}$-*C*H=N), 150.6 (d, $^2J_{CP}$ = 7 Hz, C_1^1), 152.8 (d, $^2J_{CP}$ = 10 Hz, C_0^1), 153.3 (d, $^2J_{CP}$ = 8 Hz, $C_1^{1\prime}$). − $C_{113}H_{109}Cl_8N_{17}O_{10}P_{12}S_9$ (2809.1): calcd. C 48.31, H 3.91, N 8.48; found C 48.24, H 3.87, N 8.40.

17c-[G′$_1$-G′$_2$]: $^{31}P\{^1H\}$ NMR ($CDCl_3$): δ = 14.0 (d, $^2J_{PP}$ = 24.6 Hz, P_{11}'), 17.5 (d, $^2J_{PP}$ = 33.1 Hz, P_{00}), 50.7 (d, $^2J_{PP}$ = 24.6 Hz, P_1'), 51.7 (d, $^2J_{PP}$ = 33.1 Hz, P_0), 60.8 (s, P_2'), 63.0 (s, P_1). − ^1H NMR ($CDCl_3$): δ = 1.82 (s, 3 H, CH_3-N-CH_2), 2.43−2.70 (m, 4 H, CH_2-CH_2-P), 3.34 (m, 18 H, CH_3-N-P), 4.22−4.45 (m, 4 H, NCH_2-P), 7.00−7.80 (m, 112 H, C_6H_5, C_6H_4, CH=N), 9.91 (s, 8 H, CHO). − $^{13}C\{^1H\}$ NMR ($CDCl_3$): δ = 24.7 (d, $^1J_{CP}$ =

64 Hz, CH_2CH_2−P), 33.0 (m, CH_3−N−P), 35.5 (s, CH_3−N−CH_2), 46.2 (s, CH_2−CH_2−P), 50.6 (d, $^1J_{CP}$ = 89 Hz, NCH_2−P), 121.4 (d, $^3J_{CP}$ = 4 Hz, C_1^2), 121.7 (d, $^3J_{CP}$ = 4 Hz, C_0^2, $C_1^{2\prime}$), 122.0 (d, $^3J_{CP}$ = 5 Hz, $C_2^{2\prime}$), 125.4 (s, C_1^4), 128.0 (s, C_0^3), 128.7 (s, $C_1^{3\prime}$), 128.8 (d, $^3J_{CP}$ = 13 Hz, C_0^m, $C_1^{m\prime}$), 129.5 (s, C_1^3), 130.6 (s, $C_1^{4\prime}$), 131.2 (d, $^2J_{CP}$ = 11 Hz, C_0^o, $C_1^{o\prime}$), 131.5 (s, $C_2^{3\prime}$), 132.2 (s, C_0^4), 132.4 (s, C_0^p, $C_1^{p\prime}$), 133.6 (s, $C_2^{4\prime}$), 138.8 (d, $^3J_{CP}$ = 14 Hz, C_0^4-*C*H=N), 140.1 (d, $^3J_{CP}$ = 14 Hz, $C_1^{4\prime}$-*C*H=N), 150.6 (d, $^2J_{CP}$ = 6 Hz, C_0^1), 152.8 (d, $^2J_{CP}$ = 8 Hz, C_1^1), 153.0 (d, $^2J_{CP}$ = 9 Hz, $C_1^{1\prime}$), 155.1 (d, $^2J_{CP}$ = 7 Hz, $C_2^{1\prime}$), 190.8 (s, CHO). − IR (KBr): 1702 cm^{-1} ($\nu_{C=O}$). − $C_{169}H_{149}N_{17}O_{26}P_{12}S_9$ (3494.4): calcd. C 58.08, H 4.29, N 6.81; found C 58.05, H 4.22, N 6.76.

17c-[G′$_1$-G$_3$]: $^{31}P\{^1H\}$ NMR ($CDCl_3$): δ = 13.5 (d, $^2J_{PP}$ = 24.5 Hz, $P_{11}\prime$), 16.9 (d, $^2J_{PP}$ = 33.1 Hz, P_{00}), 50.2 (d, $^2J_{PP}$ = 24.5 Hz, $P_1\prime$), 51.3 (d, $^2J_{PP}$ = 33.1 Hz, P_0), 61.9 (s, $P_2\prime$), 62.5 (s, P_1), 62.9 (s, $P_3\prime$). − ^1H NMR ($CDCl_3$): δ = 1.84 (s, 3 H, C*H*$_3$−N−CH_2), 2.42−2.74 (m, 4 H, CH_2−CH_2−P), 3.32−3.51 (m, 42 H, CH_3−N−P), 4.22−4.45 (m, 4 H, NCH_2−P), 7.00−7.70 (m, 120 H, C_6H_5, C_6H_4, CH=N). − $^{13}C\{^1H\}$ NMR ($CDCl_3$): δ = 24.8 (d, $^1J_{CP}$ = 65 Hz, CH_2CH_2−P), 31.9 (d, $^2J_{CP}$ = 13 Hz, CH_3N−$P_3\prime$), 33.0 (d, $^2J_{CP}$ = 13 Hz, CH_3N−P_1, CH_3N−$P_2\prime$), 35.5 (s, *C*H$_3$−N−CH_2), 46.4 (s, CH_2−CH_2−P), 50.6 (d, $^1J_{CP}$ = 88 Hz, NCH_2−P), 121.4−121.9 (m, C_0^2, C_1^2, $C_1^{2\prime}$, $C_2^{2\prime}$), 125.4 (s, C_1^4), 128.0 (s, C_0^3, $C_1^{3\prime}$), 128.7 (m, C_0^m, $C_1^{m\prime}$, $C_2^{3\prime}$), 129.5 (s, C_1^3), 130.9 (s, $C_1^{4\prime}$), 131.3 (d, $^2J_{CP}$ = 11 Hz, C_0^o, $C_1^{o\prime}$), 131.5 (s, $C_2^{4\prime}$), 132.2 (s, C_0^4), 132.5 (s, C_0^p, $C_1^{p\prime}$), 138.8 (d, $^3J_{CP}$ = 14 Hz, C_0^4-*C*H=N), 139.5 (d, $^3J_{CP}$ = 13 Hz, $C_1^{4\prime}$-*C*H=N), 140.7 (d, $^3J_{CP}$ = 19 Hz, $C_2^{4\prime}$-*C*H=N), 150.7 (d, $^2J_{CP}$ = 7 Hz, C_0^1, C_1^1), 151.9 (d, $^2J_{CP}$ = 7 Hz, $C_2^{1\prime}$), 152.9 (d, $^2J_{CP}$ = 9 Hz, $C_1^{1\prime}$). − $C_{177}H_{173}Cl_{16}N_{33}O_{18}P_{20}S_{17}$ (4782.3): calcd. C 44.45, H 3.64, N 9.66; found C 44.41, H 3.59, N 9.64.

17c-[G′$_1$-G′$_3$]: $^{31}P\{^1H\}$ NMR ($CDCl_3$): δ = 14.0 (d, $^2J_{PP}$ = 24.2 Hz, $P_{11}\prime$), 17.3 (d, $^2J_{PP}$ = 32.5 Hz, P_{00}), 50.5 (d, $^2J_{PP}$ = 24.2 Hz, $P_1\prime$), 51.8 (d, $^2J_{PP}$ = 32.5 Hz, P_0), 60.5 (s, $P_3\prime$), 62.7 (s, $P_2\prime$), 62.8 (s, P_1),. − ^1H NMR ($CDCl_3$): δ = 1.84 (s, 3 H, C*H*$_3$−N−CH_2), 2.42−2.74 (m, 4 H, CH_2−CH_2−P), 3.34 (m, 42 H, CH_3−N−P), 4.20−4.43 (m, 4 H, NCH_2−P), 7.00−7.80 (m, 184 H, C_6H_5, C_6H_4, CH=N), 9.91 (s, 16 H, CHO). − $^{13}C\{^1H\}$ NMR ($CDCl_3$): δ = 24.7 (d, $^1J_{CP}$ = 64 Hz, CH_2CH_2−P), 32.8 (d, $^2J_{CP}$ = 13 Hz, CH_3−N−P), 35.5 (s, *C*H$_3$−N−CH_2), 46.2 (s, CH_2−CH_2−P), 50.5 (d, $^1J_{CP}$ = 88 Hz, NCH_2−P), 121.2−121.8 (m, C_0^2, C_1^2, $C_1^{2\prime}$, $C_2^{2\prime}$, $C_3^{2\prime}$), 125.2 (s, C_1^4), 127.8−128.5 (m, C_0^3, $C_1^{3\prime}$, C_0^m, $C_1^{m\prime}$), 129.4 (s, C_1^3, $C_2^{3\prime}$), 130.7−132.3 (m, C_0^4, C_1^4, $C_1^{4\prime}$, C_0^o, $C_1^{o\prime}$, C_0^p, $C_1^{p\prime}$, $C_3^{3\prime}$), 133.4 (s, $C_3^{4\prime}$), 139.5 (br. d, $^3J_{CP}$ = 14 Hz, CH=N), 150.4 (d, $^2J_{CP}$ = 7 Hz, C_0^1), 151.3 (d, $^2J_{CP}$ = 7 Hz, $C_2^{1\prime}$), 152.7 (d, $^2J_{CP}$ = 9 Hz, $C_1^{1\prime}$, C_1^1), 154.9 (d, $^2J_{CP}$ = 7 Hz, $C_3^{1\prime}$), 190.6 (s, CHO). − IR (KBr): 1702 cm^{-1} ($\nu_{C=O}$). − $C_{289}H_{253}N_{33}O_{50}P_{20}S_{17}$ (6152.9): calcd. C 56.41, H 4.14, N 7.51; found C 56.31, H 4.05, N 7.44.

Acknowledgments

Thanks are due to the CNRS (France) for financial support and to the Fundación Ramon Areces (Spain) for a grant to one of us (R. M. S.).

[1] D. Gudat, *Angew. Chem.* **1997**, *109*, 2039−2043; *Angew. Chem. Int. Ed. Engl.* **1997**, *36*, 1951−1955.
[2] H. F. Chow, T. K. K. Mong, M. F. Nongrum, C. W. Wan, *Tetrahedron* **1998**, *54*, 8543−8660.
[3] O. A. Matthews, A. N. Shipway, J. F. Stoddart, *Prog. Polym. Sci.* **1998**, *23*, 1−56.
[4] C. Gorman, *Adv. Mater.* **1998**, *10*, 295−309.
[5] M. Fischer, F. Vögtle, *Angew. Chem.* **1999**, *111*, 934−955; *Angew. Chem. Int. Ed.* **1999**, *38*, 884−905.
[6] J. P. Majoral, A. M. Caminade, *Chem. Rev.* **1999**, *99*, 845−880.
[7] A. W. Bosman, H. M. Janssen, E. W. Meijer, *Chem. Rev.* **1999**, *99*, 1665−1688.
[8] G. R. Newkome, E. He, C. N. Moorefield, *Chem. Rev.* **1999**, *99*, 1689−1746.
[9] K. L. Wooley, C. J. Hawker, J. M. J. Fréchet, *J. Chem. Soc., Perkin Trans. 1* **1991**, 1059−1070.
[10] K. L. Wooley, C. J. Hawker, J. M. J. Fréchet, *J. Am. Chem. Soc.* **1993**, *115*, 11496−11505.
[11] K. L. Wooley, C. J. Hawker, J. M. Pochan, J. M. J. Fréchet, *Macromolecules* **1993**, *26*, 1514−1519.
[12] C. J. Hawker, K. L. Wooley, J. M. J. Fréchet, *J. Chem. Soc., Perkin Trans. 1* **1993**, 1287−1297.
[13] J. M. J. Fréchet, *Science* **1994**, *263*, 1710−1715.
[14] C. J. Hawker, K. L. Wooley, J. M. J. Fréchet, *Macromol. Symp.* **1994**, *77*, 11−20.
[15] K. Aoi, K. Itoh, M. Okada, *Macromolecules* **1997**, *30*, 8072−8074.
[16] D. J. Pessac, J. S. Moore, *Tetrahedron* **1997**, *53*, 15331−15347.
[17] V. Maraval, R. Laurent, B. Donnadieu, M. Mauzac, A. M. Caminade, J. P. Majoral, *J. Am. Chem. Soc.* **2000**, *122*, 2499−2511.
[18] V. Maraval, R. Laurent, S. Merino, A. M. Caminade, J. P. Majoral, *Eur. J. Org. Chem.* **2000**, 3555−3568.
[19] N. Launay, A. M. Caminade, R. Lahana, J. P. Majoral, *Angew. Chem.* **1994**, *106*, 1682−1684; *Angew. Chem. Int. Ed. Engl.* **1994**, *33*, 1589−1592.
[20] N. Launay, A. M. Caminade, J. P. Majoral, *J. Am. Chem. Soc.* **1995**, *117*, 3282−3283.
[21] C. Galliot, D. Prévôté, A. M. Caminade, J. P. Majoral, *J. Am. Chem. Soc.* **1995**, *117*, 5470−5476.
[22] M. Slany, M. Bardaji, M. J. Casanove, A. M. Caminade, J. P. Majoral, B. Chaudret, *J. Am. Chem. Soc.* **1995**, *117*, 9764−9765.
[23] M. L. Lartigue, B. Donnadieu, C. Galliot, A. M. Caminade, J. P. Majoral, J. P. Fayet, *Macromolecules* **1997**, *30*, 7335−7337.
[24] C. Galliot, C. Larré, A. M. Caminade, J. P. Majoral, *Science* **1997**, *277*, 1981−1984.
[25] C. Larré, A. M. Caminade, J. P. Majoral, *Angew. Chem.* **1997**, *109*, 614−617; *Angew. Chem. Int. Ed. Engl.* **1997**, *36*, 596−599.
[26] C. Larré, B. Donnadieu, A. M. Caminade, J. P. Majoral, *J. Am. Chem. Soc.* **1998**, *120*, 4029−4030.
[27] C. Larré, D. Bressolles, C. Turrin, B. Donnadieu, A. M. Caminade, J. P. Majoral, *J. Am. Chem. Soc.* **1998**, *120*, 13070−13082.
[28] A. M. Caminade, R. Laurent, B. Chaudret, J. P. Majoral, *Coord. Chem. Rev.* **1998**, *178−180*, 793−821.
[29] J. P. Majoral, A. M. Caminade, *Top. Curr. Chem.* **1998**, *197*, 79−124.
[30] B. Miksa, S. Slomkowski, M. M. Chehimi, M. Delamar, J. P. Majoral, A. M. Caminade, *Colloid Polym. Sci.* **1999**, *277*, 58−65.
[31] S. Slomkowski, B. Miksa, M. M. Chehimi, M. Delamar, E. Cabet-Deliry, J. P. Majoral, A. M. Caminade, *React. Funct. Polym.* **1999**, *41*, 45−57.
[32] C. Loup, M. A. Zanta, A. M. Caminade, J. P. Majoral, B. Meunier, *Chem. Eur. J.* **1999**, *5*, 3644−3650.
[33] R. M Sebastian, A. M. Caminade, J. P Majoral, E. Levillain, L. Huchet, J. Roncali, *Chem. Commun.* **2000**, 507−508.
[34] G. Schmid, W. Meyer-Zaika, R. Pugin, T. Savitowski, J. P. Majoral, A. M. Caminade, C. O. Turrin, *Chem. Eur. J.* **2000**, *6*, 1693−1697.
[35] V. Maraval, R. Laurent, A. M. Caminade, J. P. Majoral, *Organometallics* **2000**, *19*, 4025−4029.

[36] R. M. Sebastian, G. Magro, A. M. Caminade, J. P. Majoral, *Tetrahedron* **2000**, *56*, 6269−6977.
[37] M. K Boggiano, G. J. de A. A. Soler-Illia, L. Rozes, C. Sanchez, C. O. Turrin, A. M. Caminade, J. P. Majoral, *Angew. Chem. Int. Ed.* **2000**, *39*, 4249−4254.
[38] F. Le Derf, E. Levillain, A. Gorgue, M. Sallé, R. M Sebastian, A. M. Caminade, J. P. Majoral, *Angew. Chem. Int. Ed.* **2001**, *40*, 224−227.
[39] C. Larré, B. Donnadieu, A. M. Caminade, J. P. Majoral, *Eur. J. Inorg. Chem.* **1999**, 601−611.
[40] J. Mitjaville, A. M. Caminade, R. Mathieu, J. P. Majoral, *J. Am. Chem. Soc.* **1994**, *116*, 5007−5008.
[41] G. P. Schiemenz, H. Kaack, *Justus Liebigs Ann. Chem.* **1973**, 1480−1493.

Received January 3, 2001
[I01001]

Versatile Behavior of β-Heterosubstituted Zirconaindene Complexes: M−Cl Bond Activation (M = Si, P, Au Fragments)

Krzysztof Owsianik,[a] Maria Zablocka,[a] Alain Igau,[b] Jean-Pierre Majoral,*[b] and Aleksandra Skowronska*[a]

Keywords: Addition / Bond activation / Gold / Phosphorus / Zirconium

A new way of M–Cl bond activation (M = Si, P, Au fragments) is reported. It consists on the 1,2-addition of M–Cl containing species on the Zr–N bond of azazirconaindene complexes. Unprecedented imino gold complexes incorporating two electron-deficient metallic centers (Au, Zr) have been prepared.

Introduction

The organic and organometallic chemistry of neutral zirconium derivatives is blossoming probably because of the new perspectives zirconium reagents bring in a number of research areas.[1] Among the zirconium synthons generally used, benzyne zirconocene **1** (prepared in situ by photolysis or thermolysis of diphenylzirconocene) is of particular interest because of its high reactivity towards chalcogens, inorganic unsaturated species, alkenes, alkynes, etc.[2] Reactions generally proceed with insertion of the organic or inorganic fragment into Zr−C bonds of the arynezirconocene complex. It is also known that thermolysis of diphenylzirconocene in the presence of nitriles generates azazirconaindenes **2**−**4**,[2,3] (Scheme 1).

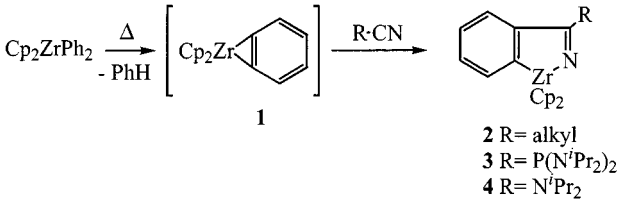

Scheme 1. Insertion of nitriles into a Zr−C bond of benzynezirconocene

These metallacycles are versatile tools allowing the development of new strategies of synthesis of useful linear or heterocyclic reagents and ligands. For example, hydrolysis of azazirconaindenes **2** produces ketones in good to excellent yields[2] [Scheme 2, reaction (a)]. Moreover exchange reactions involving **3** and various dihalogenated species allow the preparation of new heterocycles incorporating

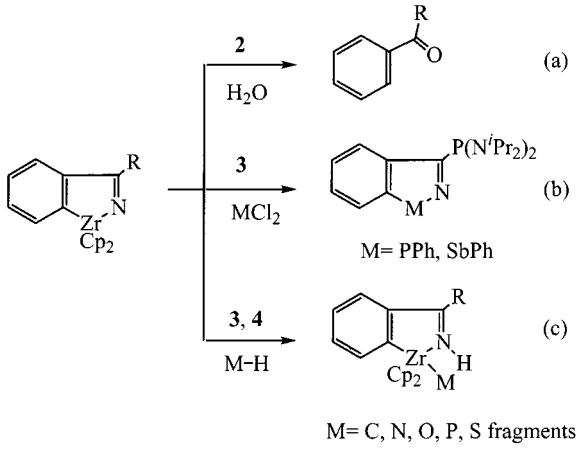

Scheme 2. Reactivity of β-substituted zirconaindenes

phosphorus or antimony, and nitrogen[3] [Scheme 2, reaction (b)]. Furthermore, azazirconaindenes act as unusual bases for the deprotonation of several M−H bonds [Scheme 2, reaction (c)]. However the chemical behavior of these complexes depends on the nature of the C-imino substituent. Indeed stable azazirconacyclopentene-substituted phosphanes **3** or amines **4** {R = -P[N(iPr)2]2, -P[N(Cy)2]2, -N(iPr)2} when reacted with acetylenic systems, malonitrile derivatives, vinyl acetate, diazo compounds, etc., allow sp^2-, and sp^3-C−H bond activations.[4,5] Similarly, activation of N−H, O−H, P−H, S−H bonds easily occurs in very mild conditions when the same complexes **3**−**4** are treated with aromatic amines, alcohols, phenols, phosphonates or thiols[4] [Scheme 2, reaction (c)].

In marked contrast, azazirconaindenes **2** (R = alkyl group) do not react with derivatives incorporating C−H or M−H bonds. Therefore, the basicity of the endocyclic imino nitrogen atom appears to be the driving force in all these M−H bond activations.

The halophilicity of zirconium is also the driving force for many reactions involving zirconium-containing species, but, as illustrated above [Scheme 2, reaction (b)], the reactions generally proceed with Zr−X bond cleavage (X = C, N...) and loss of Cp_2ZrCl_2.

[a] Centre of Molecular and Macromolecular Studies, Polish Academy of Sciences
Sienkiewicza 112, 90−362, Lodz, Poland
[b] Laboratoire de Chimie de Coordination CNRS, 205 route de Narbonne
31077 Toulouse cedex 4, France
Fax: (internat.) +33-5/6155-3003
E-mail: majoral@lcc-toulouse.fr

 © WILEY-VCH Verlag GmbH, 69451 Weinheim, 2001 1434−1948/01/0707−1693 $ 17.50+.50/0

We wish to report here a new facet of the reactivity of azazirconaindene-substituted phosphanes **3** or amines **4**: activation of M−Cl bonds (M = Si, P, Au, H) involving formal 1,2-addition of halogenated compounds to the Zr−N bond of **3** or **4**. These reactions take place without cleavage of the Zr−N and Zr−C bonds, and lead to unprecedented cyclic mono- or bimetallic complexes.

Results and Discussion

Treatment of the azazirconaindene-substituted phosphane **3** with the gold complex $Ph_3P\rightarrow AuCl$ in THF at 0 °C for 30 min. leads to the formation of the zirconium-gold complex **5** in 73% isolated yield (Scheme 3). The reaction can be monitored by ^{31}P NMR spectroscopy which shows the disappearance of the singlets due to **3** (δ = 45.0) and $Ph_3P\rightarrow AuCl$ (δ = 32.5) and the growth of two doublets at δ = 86.0 [$P(N^iPr_2)_2$] and δ = 44.0 (Ph_3P) with $^4J_{PP}$ = 4.5 Hz. If the same reaction is performed with the phospholene gold complex (δ = 40.6), the azazirconaindene gold complex **6** is formed in 89% yield {δ = 86.8 [$P(N^iPr_2)_2$] and 52.9 (Ph−P), $^4J_{PP} < 1$ Hz}. ^1H and ^{13}C NMR and IR spectroscopic data are in agreement with the proposed structures for **5** and **6**, which therefore come from a unique 1,2-addition of the Au−Cl bond to the zirconium−nitrogen bond of the starting zirconaindene **3**.

Such a 1,2-addition can be performed with chlorophosphates $(R'O)_2P(O)Cl$. Insertion of the P−Cl bond of diethoxychlorophosphate or diphenoxychlorophosphate takes place at room temperature, leading to the *N*-aminophosphate, C-phosphanyl-disubstituted azazirconaindenes **7** and **8**, respectively. ^{31}P NMR spectroscopy appears to be the tool of choice to establish the structure of **7** and **8**. Two doublets {**7:** δ = 45.4 [$P(N^iPr_2)_2$], 42.0 [$(O)P(OEt)_2$], J_{PP} = 15.8 Hz; **8:** δ = 45.0 [$P(N^iPr_2)_2$], 50.3 [$(O)P(OPh)_2$], J_{PP} = 17.1 Hz}

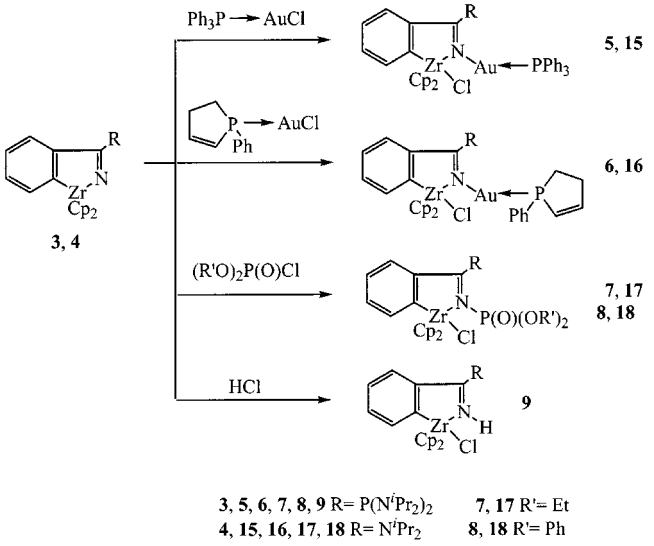

Scheme 3. 1,2-Addition of halogenated compounds to the Zr−N bond of β-heterosubstituted zirconaindenes

were detected strongly suggesting the formation of the $(N^iPr_2)_2P-C=N-P(O)(OEt)_2$ and $(N^iPr_2)_2P-C=N-P(O)(OPh)_2$ imino fragments, respectively.

A similar 1,2-addition can be observed when hydrogen chloride (1 M diethyl ether solution) is added to a toluene solution of **3**. The 18-electron zirconium complex **9** is formed as the unique product of the reaction and was isolated in 92% yield after workup. Monitoring the reaction by ^{31}P and ^1H NMR spectroscopy did not show any intermediate or by-product such as, for example, the zwitterion **10**, which might be generated by protonation of the phosphanyl group. It should be noted that a complex similar to **9** was formed, along with other unidentified products, during an unexpected intramolecular alkylation involving the reaction of the benzyne zirconocene **1** with $Br(CH_2)_3CN$.[2]

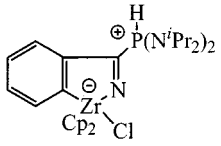

10

Interestingly, complex **9** can be also formed by different strategies: i) cleavage of the N−M bond (M = Au, P fragments) of the 18-electron azazirconaindenes **5** or **7**, or ii) cleavage of the Zr−M bond (M = P, O) of the zirconaindenes **13** and **14**.

The first strategy (Scheme 4) can be illustrated as follows: addition of chlorotrimethylsilane to the gold complex **5** leads to the formation of $Ph_3P\rightarrow AuCl$ and to the unstable azazirconaindene **11** ($\delta^{31}P$ = 61) which, during workup, is transformed into the corresponding NH derivative **9**. It is noteworthy that Si−Cl bond activation is not observed when the 16-electron zirconaindene **3** is reacted directly with chlorotrimethylsilane: no traces of complex **11** (or **9**) are detected in this case.

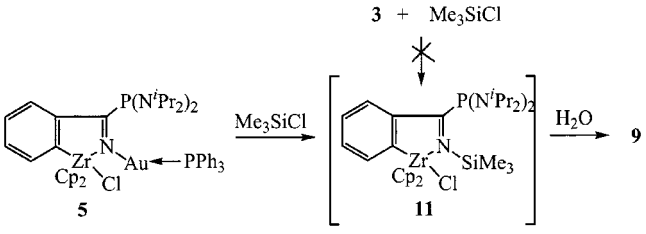

Scheme 4. Reactivity of the β-phosphanyl-substituted zirconaindene **5**

The second strategy implies the direct cleavage of Zr−M bonds with hydrogen chloride or with halogenated phosphane oxide. A phosphoranide-chloride anion exchange with $Zr-P^V$ bond cleavage is observed when the still unique, stable zirconaspirophosphorane **13** (prepared in high yield from the oxidative addition of the P−H spirophosphorane **12** to the azazirconaindene **3**), is treated with hydrogen chloride: the spirophosphorane **12** and the com-

plex **9** (Scheme 5) are the only phosphorus species which can be detected by ^{31}P NMR spectroscopy.

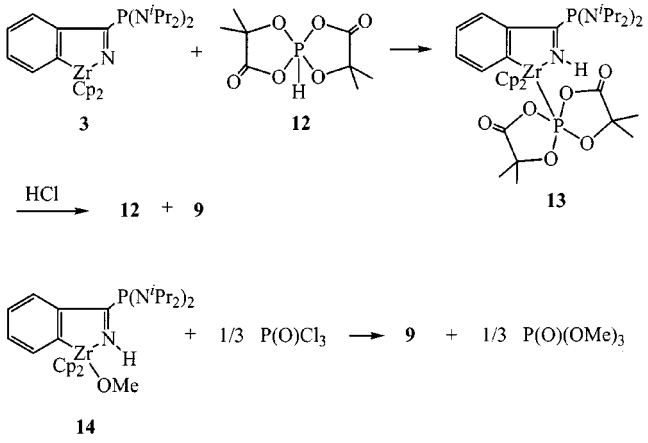

Scheme 5. Synthesis of the β-phosphanyl-substituted zirconaindene **9**

Similarly, the Zr−O bond of the complex **14**,[4] obtained by adding methanol to **3**, can be easily cleaved with trichlorophosphane oxide. The use of 1/3 equiv. of $P(O)Cl_3$ per equivalent of **14** allows us to form **9** and trimethoxyphosphane oxide quantitatively (Scheme 5).

Therefore the 16 electron azazirconaindene-substituted phosphane **3** easily reacts with a variety of halogenated species and is an useful starting reagent for the formation of a number of 18-electron N- and C-disubstituted azazirconaindenes. The corresponding amine **4** presents the same chemical behavior towards gold(I) chloride and chlorophosphates. Thus, complexes **15**−**18** were isolated and fully characterized (Scheme 3).

Conclusion

The versatile behavior of zirconaindene complexes was fully demonstrated. If all the reactions involving these derivatives proceed by a formal 1,2-addition of M−H or M−X reagents to the Zr−N intracyclic bond, the manner of the addition differs dramatically from M−X to M−H species: metallation or phosphorylation at the imino nitrogen atom occurs when halogenated reagents are reacted with zirconaindenes, while protonation takes place with P−H spirophosphorane (Scheme 6). Protonation at nitrogen is also observed with hydrogen chloride. To the best of our knowledge, the gold complexes **5**, **6**, **15**, **16** are the first

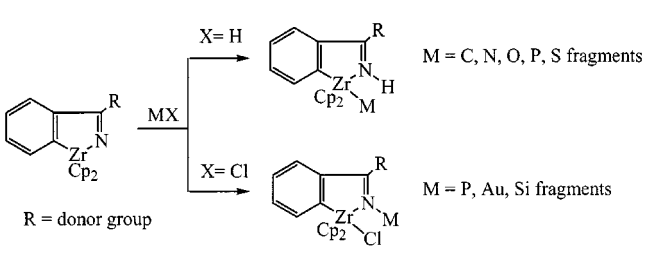

Scheme 6. Versatile behavior of the β-heterosubstituted zirconaindene towards MX (X = Cl, H) derivatives

examples of *N*-imino gold complexes incorporating two electron-deficient metallic centers (Au, Zr). Studies aimed at the generalization of the reactions depicted in Scheme 1 and concerning the use of all these new complexes in organic synthesis is under active investigation.

Experimental Section

General: All reactions were carried out in the absence of air, under argon, using standard Schlenk techniques and vacuum-line manipulations. All solvents were dried, degassed and distilled before use. A Perkin−Elmer 1725X spectrometer was used for FT-IR. NMR spectra were recorded on Bruker AC80, AC200, or AM250 spectrometers for ^{1}H, ^{13}C and ^{31}P NMR spectroscopy, with $SiMe_4$ (^{1}H, ^{13}C) and H_3PO_4 (^{31}P) as references. The assignment of the ^{13}C NMR signals was done using Jmod, two dimensional HMBC and HMQC, broad band or CW ^{31}P decoupling experiments when necessary.

Compound 5: To a solution of **3** (0.232 g, 0.418 mmol) in THF (5 mL) at room temperature was added triphenylphosphanegold(I) chloride (0.207 g, 0.418 mmol solution in 5 mL of THF). The mixture was stirred at room temperature for 15 min. and then evaporated to dryness. The resulting solid residue was extracted with pentane (20 mL) and filtered. The volatiles were removed from the solution to give **5** as a yellow solid in 73% yield (0.321 g). − IR (KBr): $\tilde{\nu}$ = 1579 cm^{-1} ($\nu_{C=N}$). − ^{1}H NMR (CD_2Cl_2): δ = 0.98 (d, J_{HH} = 6.0 Hz, 6 H, CH_3), 1.12 (d, J_{HH} = 6.0 Hz, 6 H, CH_3), 1.22 (d, J_{HH} = 5.9 Hz, 6 H, CH_3), 1.32 (d, J_{HH} = 5.9 Hz, 3 H, CH_3), 1.36 (d, J_{HH} = 6.0 Hz, 3 H, CH_3), 3.35 (sept, J_{HH} = 6.1 Hz, 4 H, NCH), 6.00 (s, 10 H, CH_{Cp}), 7.02−7.66 (m, 19 H, CH_{arom}). − $^{13}C\{^{1}H\}$ NMR (CD_2Cl_2): δ = 24.5 (d, J_{CP} = 5.5 Hz, CH_3), 25.0 (d, J_{CP} = 5.3 Hz, CH_3), 49.1 (d, J_{CP} = 11.4 Hz, NCH), 49.3 (d, J_{CP} = 12.9 Hz, NCH), 49.7 (d, J_{CP} = 11.9 Hz, NCH), 110.9 (s, CH_{Cp}), 124.9 (s, CH_{arom}), 125.8 (d, J_{CP} = 4.4 Hz, CH_{arom}), 126.7 (d, J_{CP} = 5.9 Hz, CH_{arom}), 128.9 (d, J_{CP} = 10.3 Hz, CH_{arom}), 131.0 (s, CH_{arom}), 131.7 (d, J_{CP} = 48.4 Hz, i-Ph), 133.9 (d, J_{CP} = 16.5 Hz, CH_{arom}), 134.4 (d, J_{CP} = 13.8 Hz, CH_{arom}), 139.3 (d, J_{CP} = 7.8 Hz, CH_{arom}), 154.0 (d, J_{CP} = 29.7 Hz, ZrC*C*), 168.8 (d, J_{CP} = 20.0 Hz, ZrC), 198.9 (d, J_{CP} = 3.1 Hz, J_{CP} = 13.2 Hz, PC=N). − $^{31}P\{^{1}H\}$ NMR (CD_2Cl_2): δ = 44.0 (d, J_{PP} = 5.8 Hz, PPh_3), 86.0 [d, J_{PP} = 5.8 Hz, ($iPr_2N)_2P$]. − $C_{47}H_{57}AuClN_3P_2Zr$ (1049.57): calcd. C 53.78, H 5.47; found C 53.89, H 5.54.

Compound 6: To a solution of **3** (0.270 g, 0.486 mmol) in THF (7 mL) at 0 °C was added dihydrophospholegold (I) chloride (0.191 g, 0.486 mmol, solution in 5 mL of THF). The mixture was stirred at room temperature for 0.5 h and then evaporated to dryness. The resulting solid residue was extracted with pentane and filtered. The volatiles were removed from the solution to give **6** as a yellow-brown solid in 89% yield (0.410 g). − IR (KBr): $\tilde{\nu}$ = 1572 cm^{-1} ($\nu_{C=N}$). − ^{1}H NMR (CD_2Cl_2): 0.80−1.52 (m, 24 H, CH_3), 2.34 (m, 1 H, CH_2), 2.92 (m, 2 H, CH_2), 3.28 (m, 4 H, NCH), 3.68 (m, 1 H, CH_2), 5.98 (s, 5 H, CH_{Cp}), 6.00 (s, 5 H, CH_{Cp}), 6.83 (m, 1 H, CH=CH), 7.10 (m, 1 H, CH=CH), 7.11−7.90 (m, 9 H, CH_{arom}),. − $^{13}C\{^{1}H\}$ (CD_2Cl_2): δ = 24.6 (d, J_{CP} = 5.4 Hz, CH_3), 25.1 (d, J_{CP} = 5.7 Hz, CH_3), 27.0 (d, J_{CP} = 32.6 Hz, CH_2), 33.8 (s, PCH_2), 49.7 (d, J_{CP} = 10.8 Hz, NCH), 110.8 (s, CH_{Cp}), 124.5 (s, CH_{arom}), 124.7 (d, J_{CP} = 40.4 Hz, CH_{arom}), 125.8 (s, CH_{arom}), 126.4 (d, J_{CP} = 5.8 Hz, CH_{arom}), 128.8 (d, J_{CP} = 9.9 Hz, CH_{arom}), 131.1 (s, CH_{arom}), 132.9 (d, J_{CP} = 13.9 Hz, CH_{arom}), 139.1 (d, J_{CP} = 8.4 Hz, CH_{arom}), 148.9 (d, J_{CP} = 8.7 Hz, CH_{arom}), 154.4 (d, J_{CP} = 22.8 Hz, ZrCC), 168.8 (d, J_{CP} = 18.0 Hz, ZrC), 198.0 (dd, J_{CP} = 4.1 Hz, J_{CP} = 11.3 Hz, PC=N). − $^{31}P\{^{1}H\}$ (CD_2Cl_2): δ = 52.9 (Au−P),

86.8 [(iPr$_2$N)$_2$P]. − $C_{39}H_{53}AuClN_3P_2Zr$ (949.45): calcd. C 49.34, H 5.63; found C 49.47, H 5.68.

Compound 7: To a solution of **3** (0.262 g, 0.472 mmol) in toluene (5 mL) at room temperature was added chlorodiethylphosphate (0.091 mL, 0.472 mmol). The mixture was stirred at room temperature for 12 h and then evaporated to dryness. The resulting solid residue was extracted with pentane/toluene (5:1, 20 mL) and filtered. The volatiles were removed from the solution to give **7** as a yellow solid in 72% yield (0.342 g). − IR (KBr): $\tilde{\nu}$ = 1579 cm^{-1} ($\nu_{C=N}$), 1247 ($\nu_{P=O}$). − ^{1}H NMR (C_6D_6): δ = 1.09 (t, J_{HH} = 7.1 Hz, 6 H, OCH_2CH_3), 1.20 (d, J_{HH} = 6.6 Hz, 12 H, CH_3), 1.23 (d, J_{HH} = 6.6 Hz, 12 H, CH_3), 3.48 (sept, J_{HH} = 6.6 Hz, 4 H, NCH), 3.94 (dq, J_{HH} = 7.1 Hz, 2 H, OCH_2CH_3), 4.12 (dq, J_{HH} = 7.1 Hz, 2 H, OCH_2CH_3), 6.11 (s, 10 H, CH_{Cp}), 6.89−7.11 (m, 3 H, CH_{arom}), 7.55−8.03 (m, 1 H, CH_{arom}). − ^{13}C{^{1}H} NMR (C_6D_6): δ = 17.2 (d, J_{CP} = 4.7 Hz, OCH_2CH_3), 24.5 (d, J_{CP} = 5.3 Hz, CH_3), 24.7 (d, J_{CP} = 6.0 Hz, CH_3), 48.9 (d, J_{CP} = 11.1 Hz, NCH), 62.8 (d, J_{CP} = 6.1 Hz, OCH_2CH_3), 114.7 (s, CH_{Cp}), 125.4 (dd, J_{CP} = 10.1 Hz, J_{CP} = 17.2 Hz, CH_{arom}), 128.4 (d, J_{CP} = 11.1 Hz, CH_{arom}), 131.4 (d, J_{CP} = 10.5 Hz, CH_{arom}), 132.4 (d, J_{CP} = 2.5 Hz, CH_{arom}), 142.7 (dd, J_{CP} = 36.1 Hz, J_{CP} = 50.7 Hz, ZrC), 192.1 (dd, J_{CP} = 11.3 Hz, J_{CP} = 19.9 Hz, ZrC), 202.4 (d, J_{CP} = 33.9 Hz, PC=N). − ^{31}P{^{1}H} (C_6D_6): δ = 42.0 (d, J_{PP} = 15.8 Hz, P=O), 45.4 [d, J_{PP} = 15.8 Hz, (iPr$_2$N)$_2$P]. − $C_{33}H_{52}ClN_3O_3P_2Zr$ (727.41): calcd. C 54.49, H 7.21; found C 54.60, H 7.28.

Compound 8: To a solution of **3** (0.281 g, 0.506 mmol) in toluene (5 mL) at room temperature was added chlorodiphenylphosphate (0.105 mL, 0.506 mmol). The mixture was stirred at room temperature for 12 h and then evaporated to dryness. The resulting solid residue was extracted with pentane/toluene (5:1, 20 mL) and filtered. The volatiles were removed from the solution to give **8** as a yellow solid in 75% yield (0.313 g). − IR (KBr): $\tilde{\nu}$ = 1188 cm^{-1} (ν_{P-O}), 1259 ($\nu_{P=O}$), 1587 (C=N). − ^{1}H NMR (CD_2Cl_2): δ = 1.22 (d, J_{HH} = 5.7 Hz, 12 H, CH_3); 1.29 (d, J_{HH} = 6.5 Hz, 12 H, CH_3), 3.28 (m, 2 H, NCH), 3.52 (m, 2 H, NCH), 6.37 (s, 5 H, CH_{Cp}), 6.42 (s, 5 H, CH_{Cp}), 6.61−7.25 (m, 12 H, CH_{arom}), 7.80 (m, 1 H, CH_{arom}), 8.04 (m, 1 H, CH_{arom}). − ^{13}C{^{1}H} NMR (CD_2Cl_2): δ = 24.4 (d, J_{CP} = 5.3 Hz, CH_3), 49.1 (d, J_{CP} = 10.4 Hz, NCH), 50.1 (d, J_{CP} = 10.4 Hz, NCH), 114.9 (s, CH_{Cp}), 118.6 (s, CH_{arom}), 120.5 (d, J_{CP} = 4.4 Hz, CH_{arom}), 121.6 (d, J_{CP} = 3.0 Hz, CH_{arom}), 125.9 (d, J_{CP} = 27.8 Hz, CH_{arom}), 128.6 (d, J_{CP} = 10.5 Hz, CH_{arom}), 129.9 (d, J_{CP} = 11.8 Hz, CH_{arom}), 130.4 (s, CH_{arom}), 132.0 (d, J_{CP} = 10.6 Hz, CH_{arom}), 133.4 (s, CH_{arom}), 142.7 (dd, J_{CP} = 33.3 Hz, J_{CP} = 52.3 Hz, ZrC), 150.9 (d, J_{CP} = 8.12 Hz, i-OPh), 165.9 (d, J_{CP} = 14.5 Hz, ZrC), 196.1 (dd, J_{CP} = 11.5 Hz, J_{CP} = 20.5 Hz, PC=N). − ^{31}P{^{1}H} (CD_2Cl_2): δ = 45.0 [d, J_{PP} = 17.0 Hz, (iPr$_2$N)$_2$P], 50.3 [d, J_{PP} = 17.0 Hz, P=O)]. − $C_{41}H_{52}ClN_3O_3P_2Zr$ (823.50): calcd. C 59.80, H 6.36; found C 59.95, H 6.42.

Compound 9: To a solution of **3** (0.201 g, 0.362 mmol) in toluene (5 mL) at −78 °C was added hydrogen chloride (1 M solution in diethyl ether; 0.362 mL). The mixture was stirred for 15 min. at this temperature. The resulting solution was then stirred at room temperature for 15 min. leading to the formation of **9** in quantitative yield as monitored by ^{31}P{^{1}H} NMR spectroscopy. The resulting solid residue was extracted with pentane (15 mL) and filtered to give **9**[5] as a yellow solid in 92% yield (0.197 g). − IR (KBr): $\tilde{\nu}$ = 1576 cm^{-1} ($\nu_{C=N}$), 3305 (ν_{N-H}). − ^{1}H NMR (C_6D_6): δ = 1.11 (d, J_{HH} = 6.6 Hz, 12 H, CH_3), 1.21 (d, J_{HH} = 6.6 Hz, 12 H, CH_3), 3.27 (sept., J_{HH} = 6.6 Hz, 4 H, CH), 5.9 (s, 10 H, CH_{Cp}), 7.20 (m, 2 H, CH_{arom}), 7.88 (m, 1 H, CH_{arom}), 8.25 (m, 1 H, CH_{arom}), 10.12 (d, J_{HP} = 5.02 Hz, 1 H, NH). − ^{13}C{^{1}H} NMR (C_6D_6): δ = 24.4 (d, J_{CP} = 6.8 Hz, CH_3), 25.1 (d, J_{CP} = 5.0 Hz, CH_3), 49.6 (d, J_{CP} = 11.2 Hz, CH), 111.3 (s, C_p), 128.8 (s, CH_{arom}), 129.8 (s, CH_{arom}), 130.1 (d, J_{CP} = 14.3 Hz, CH_{arom}), 141.2 (s, CH_{arom}), 146.1 (d, J_{CP} = 24.1 Hz, C_{arom}), 198.6 (d, J_{CP} = 6.3 Hz, C_{arom}), 202.5 (d, J_{CP} = 40.6 Hz, PC=N). − ^{31}P{^{1}H} NMR (C_6D_6): δ = 58.2. − $C_{29}H_{43}ClN_3PZr$ (823.50): calcd. C 58.90, H 7.33; found C 59.06, H 7.37.

Compound 13: To a solution of **3** (0.212 g, 0.382 mmol) in toluene (5 mL) at room temperature was added tetraoxispirophosphorane (0.071 g, 0.382 mmol). The mixture was stirred at room temperature for 15 min. and then evaporated to dryness. The resulting solid residue was extracted with pentane (15 mL) and filtered. The volatiles were removed from the solution to give **13** as a yellow solid in 88% yield (0.249 g). − IR (KBr): $\tilde{\nu}$ = 1153 cm^{-1} (ν_{C-O}), 1551 ($\nu_{C=N}$), 1657 ($\nu_{C=O}$). − ^{1}H NMR (CD_2Cl_2): δ = 0.98 (d, J_{HH} = 6.6 Hz, 3 H, CH_3), 1.14 (d, J_{HH} = 6.6 Hz, 3 H, CH_3), 1.16 (d, J_{HH} = 6.6 Hz, 3 H, CH_3), 1.21 (d, J_{HH} = 6.7 Hz, 3 H, CH_3), 1.23 (d, J_{HH} = 6.6 Hz, 3 H, CH_3), 1.24 (d, J_{HH} = 6.7 Hz, 3 H, CH_3), 1.30 (d, J_{HH} = 6.7 Hz, 6 H, CH_3), 1.60 [d, J_{HP} = 1.6 Hz, 12 H, $C(CH_3)_2$], 3.42 (m, 4 H, NCH), 5.97 (s, 5 H, CH_{Cp}), 5.98 (s, 5 H, CH_{Cp}), 7.21 (m, 2 H, CH_{arom}), 7.80 (m, 1 H, CH_{arom}), 8.15 (dd, J_{HH} = 6.9 Hz, J_{HP} = 3.25 Hz, 1 H, CH_{arom}), 9.60 (d, J_{HP} = 4.9 Hz, 1 H, C=N−H). − ^{13}C{^{1}H} NMR (CD_2Cl_2): δ = 23.8 (d, J_{CP} = 5.6 Hz, CH_3), 23.9 (d, J_{CP} = 5.6 Hz, CH_3), 24.2 (d, J_{CP} = 5.6 Hz, CH_3), 24.5 (d, J_{CP} = 5.6 Hz, CH_3), 24.6 (d, J_{CP} = 5.1 Hz, CH_3), 26.7 [d, J_{CP} = 4.3 Hz, $C(CH_3)_2$], 28.1 [d, J_{CP} = 4.3 Hz, $C(CH_3)_2$], 48.8 (d, J_{CP} = 11.6 Hz, NCH), 49.0 (d, J_{CP} = 11.6 Hz, NCH), 76.2 [d, J_{CP} = 7.4 Hz, $C(CH_3)_2$], 110.8 (s, CH_{Cp}), 122.5 (s, CH_{arom}), 129.3 (s, CH_{arom}), 129.5 (d, J_{CP} = 14.3 Hz, CH_{arom}), 140.2 (s, CH_{arom}), 145.2 (d, J_{CP} = 26.1 Hz, ZrC), 177.9 (d, J_{CP} = 7.2 Hz, C=O), 197.3 (d, J_{CP} = 6.0 Hz, ZrC), 204.6 (d, J_{CP} = 41.2 Hz, PC=N). − ^{31}P{^{1}H} NMR (CD_2Cl_2): δ = 55.7 {s, P[N(iPr)$_2$]$_2$}, 128.2 (s, ZrP).

Compound 15: To a solution of **4** (0.250 g, 0.558 mmol) in THF (5 mL) at room temperature was added triphenylphosphanegold(I) chloride (0.277 g, 0.558 mmol, solution in 5 mL of THF). The mixture was stirred at room temperature for 12 h and then evaporated to dryness. The resulting solid residue was extracted with CH_2Cl_2/pentane (1:10, 20 mL) and filtered. The volatiles were removed from the solution to give **15** as a yellow solid in 82% yield (0.432 g). − IR (KBr): $\tilde{\nu}$ = 1597 cm^{-1} ($\nu_{C=N}$). − ^{1}H NMR (CD_2Cl_2): δ = 1.10 (d, J_{HH} = 6.7 Hz, 3 H, CH_3), 1.12 (d, J_{HH} = 6.7 Hz, 3 H, CH_3), 1.35 (d, J_{HH} = 6.7 Hz, 3 H, CH_3), 1.41 (d, J_{HH} = 6.7 Hz, 3 H, CH_3), 3.43 (m, 2 H, NCH), 6.32 (s, 10 H, CH_{Cp}), 7.15−7.81 (m, 19 H, CH_{arom}). − ^{13}C NMR (CD_2Cl_2): δ = 18.4 (s, CH_3), 18.8 (s, CH_3), 47.7 (s, NCH), 114.2 (s, CH_{Cp}), 124.6 (s, CH_{arom}), 125.8 (d, J_{CP} = 15.2 Hz, CH_{arom}), 127.4 (s, CH_{arom}), 128.6 (d, J_{CP} = 12.2 Hz, CH_{arom}), 129.1 (d, J_{CP} = 10.2 Hz, CH_{arom}), 131.4 (s, CH_{arom}), 132.0 (d, J_{CP} = 10.1 Hz, CH_{arom}), 134.3 (d, J_{CP} = 14.0 Hz, CH_{arom}), 139.9 (d, J_{CP} = 28.3 Hz, CH_{arom}), 141.2 (s, ZrC), 166.3 (s, ZrC), 194.7 (s, NC=N). − ^{31}P{^{1}H} (CD_2Cl_2): δ = 45.2. − $C_{41}H_{43}AuClN_2PZr$ (918.42): calcd. C 53.62, H 4.72; found C 53.69, H 4.81.

Compound 16: To a solution of **4** (0.248 g, 0.554 mmol) in THF (5 mL) at 0 °C was added dihydrophospholegold (I) chloride (0.230, 0.584 mmol, solution in 5 mL of THF). The mixture was stirred at room temperature for 2 h and then evaporated to dryness. The resulting solid residue was washed with diethyl ether (3 mL) and filtered to give **16** as a white powder in 92% yield (0.440 g.). − IR (KBr): $\tilde{\nu}$ = 1578 cm^{-1} ($\nu_{C=N}$). − ^{1}H NMR (CD_2Cl_2): δ = 0.80−1.72 (m, 12 H, CH_3), 2.22 (m, 1 H, CH_2), 2.62 (m, 2 H, CH_2), 2.95 (m, 2 H, NCH), 3.89 (m, 1 H, CH_2), 6.31 (s, 5 H, CH_{Cp}), 6.33 (s, 5 H, CH_{CP}), 6.87 (m, 1 H, CH=CH), 7.10 (m, 1 H, CH=CH),

7.12−7.92 (m, 9 H, CH_{arom}). − $^{13}C\{^1H\}$ NMR (CD_2Cl_2): δ = 20.1 (s, CH_3), 20.3 (s, CH_3), 26.4 (d, J_{CP} = 34.4 Hz, CH_2), 33.8 (s, PCH_2), 45.4 (s, NCH), 110.8 (s, CH_{Cp}), 124.4 (d, J_{CP} = 29.4 Hz, CH_{arom}), 125.3 (s, CH_{arom}), 127.4 (s, CH_{arom}), 129.1 (d, J_{CP} = 10.4 Hz, CH_{arom}), 131.5 (s, CH_{arom}), 132.9 (d, J_{CP} = 13.7 Hz, CH_{arom}), 139.6 (d, J_{CP} = 19.3 Hz, CH_{arom}), 150.9 (s, ZrC*C*), 167.9 (d, J_{CP} = 13.3 Hz, ZrC), 201.0 (s, NC=N). − $^{31}P\{^1H\}$ (CD_2Cl_2): δ = 57.3. − $C_{33}H_{39}AuClN_2PZr$ (818.30): calcd. C 48.44, H 4.80; found C 48.57, H 4.96.

Compound 17: To a solution of **4** (0.314 g, 0.739 mmol) in toluene (7 mL) at room temperature was added chlorodiethylphosphate (0.097 mL, 0.739 mmol). The mixture was stirred at room temperature for 3 h and then evaporated to dryness. The resulting solid residue was extracted with CH_2Cl_2/pentane (1:8, 15 mL) and filtered. The volatiles were removed from the solution to give **17** as a yellow solid in 75% yield (0.331 g.). − IR (KBr): $\tilde{\nu}$ = 1583 cm^{-1} ($\nu_{C=N}$). 1232 ($\nu_{P=O}$). − ^1H NMR (CD_2Cl_2): δ = 1.07 (d, J_{HH} = 6.8 Hz, 3 H, CH_3), 1.22 (t, J_{HH} = 7.1 Hz, 6 H, OCH_2CH_3), 1.23 (d, J_{HH} = 6.8 Hz, 3 H, CH_3), 1.40 (d, J_{HH} = 6.8 Hz, 3 H, CH_3), 1.61 (d, J_{HH} = 6.8 Hz, 3 H, CH_3), 3.15 (m, 2 H, NCH), 4.07 (dq, J = 7.1 Hz, 4 H, OCH_2CH_3), 6.31 (s, 10 H, CH_{Cp}), 7.18−7.91 (m, 4 H, CH_{arom}). − $^{13}C\{^1H\}$ NMR (CD_2Cl_2): δ = 16.3 (d, J_{CP} = 6.0 Hz, OCH_2CH_3), 20.6 (s, CH_3), 49.3 (s, NCH), 61.6 (d, J_{CP} = 5.9 Hz, OCH_2CH_3), 114.1 (s, CH_{Cp}), 124.1 (s, CH_{arom}), 127.7 (s, CH_{arom}), 131.0 (s, CH_{arom}), 131.5 (s, CH_{arom}), 138.7 (d, J_{CP} = 33.3 Hz, ZrC*C*), 164.3 (d, J_{CP} = 19.6 Hz, ZrC), 193.2 (s, NC=N). − $^{31}P\{^1H\}$ (CD_2Cl_2): δ = 42.1. − $C_{41}H_{52}ClN_3O_3P_2Zr$ (596.26): calcd. C 54.39, H 6.42; found 54.56, H 6.55.

Compound 18: To a solution of **4** (0.290 g, 0.683 mmol) in toluene (8 mL) at room temperature was added chlorodiphenylphosphate (0.141 mL, 0.683 mmol). The mixture was stirred at room temperature for 15 min. and then evaporated to dryness. The resulting solid residue was extracted with pentane/toluene (5: 1, 20 mL) and filtered. The volatiles were removed from the solution to give **18** as a beige solid in 65% yield (0.307 g). − IR (KBr): $\tilde{\nu}$ = 1198 cm^{-1} ($\nu_{P=O}$) 1286 ($\nu_{P\text{-}OPh}$), 1588 ($\nu_{C=N}$). − ^1H NMR ([D_8]toluene): δ = 0.98 (d, J_{HH} = 6.5 Hz, 12 H, CH_3), 2.54 (sept, J_{HH} = 6.5 Hz, 2 H, NCH), 5.92 (s, 5 H, CH_{Cp}), 6.02 (s, 5 H, CH_{Cp}), 6.64−7.52 (m, 14 H, CH_{arom}). − $^{13}C\{^1H\}$ NMR ([D_8]toluene): 21.8 (s, CH_3), 22.3 (s, CH_3), 50.3 (s, NCH), 51.8 (s, NCH), 113.2 (s, CH_{Cp}), 115.4 (s, CH_{Cp}), 119.1, 121.3, 128.2, 129.6, 130.7 (s, CH_{arom}), 166.9 (s, ZrC*C*), 180.6 (s, ZrC), 198.3 (s, NC=N). − $^{31}P\{^1H\}$ ([D_8]toluene): δ = 40.6.

Acknowledgments

This work was completed with support of the European Associated Laboratory financed by CNRS (France) and the Polish Committee for Scientific Research (KBN grant 3TO9A 03619).

[1] [1a] D. W Stephan, *Angew. Chem. Int. Ed.* **2000**, *38*, 314−329. − [1b] J.-P. Majoral, P. Meunier, A. Igau, N. Pirio, M. Zablocka, A. Skowronska, S. Bredeau, *Coord. Chem. Rev.* **1998**, *178−180*, 145−167. − [1c] E. Negishi, J-L. Montchamp, in *Metallocenes, Synthesis, Reactivity, Applications* (Eds.: A. Togni, R. L. Halterman), Wiley-VCH, Weinheim, **1998**, Vol. 1, p. 241. − [1d] P. Wipf, W. Xu, H. Takahashi, H. Jahn, P. D. G. Coish, *Pure Appl. Chem.* **1997**, *69*, 639−644. − [1e] Tetrahedron Symposia in print N° 57 Guest Ed. E. Negishi, *Tetrahedron* **1995**, *51*, 4255−4570. − [1f] U. Annby, S. Karlsson, *Acta Chem. Scand.* **1993**, *47*, 425−433. − [1g] J. A. Labinger, in *Comprehensive Organic Chemistry* (Ed.: I. Fleming), Pergamon Press, **1991**, Vol. 3, Chap. 3, p. 667. − [1h] E. Negishi, in *Comprehensive Organic Chemistry* (Ed.: L. A. Paquette), Pergamon Press, **1991**, Vol. 9, Chap. 5, p. 1163. − [1i] G. Erker, M. Aulbach, M. Mena, R. Pfaff, F. Sosna, *Chemica Scripta* **1989**, *29*, 451−456. − [1j] E. Negishi, *Chemica Scripta* **1989**, *29*, 457−468. − [1k] E. Negishi, *Acc. Chem. Res.* **1987**, *20*, 65−72. − [1l] G. Erker, *Acc. Chem. Res.* **1984**, *17*, 103−109.

[2] [2a] S. L. Buchwald, R. Nielsen, *Chem. Rev.* **1998**, *88*, 1047−1058. − [2b] S. L. Buchwald, A. Sayers, B. T Watson, J. C Dewan, *Tetrahedron Lett.* **1987**, *28*, 3245−3248. − [2c] N. Avarvari, P. Rosa, F. Mathey, P. Le Floch, *J. Organomet. Chem.* **1998**, *567*, 151−155.

[3] V. Cadierno, B. Donnadieu, A. Igau, J.-P. Majoral, *Eur. J. Inorg. Chem.* **2000**, 417−421.

[4] V. Cadierno, M. Zablocka, B. Donnadieu, A. Igau, J.-P. Majoral, A. Skowronska, *Chem. Eur. J.* **2001**, *7*, 221−229.

[5] V. Cadierno, M. Zablocka, B. Donnadieu, A. Igau, J.-P. Majoral, *Angew. Chem. Int. Ed.* **2000**, *39*, 4524−4528.

Received January 3, 2001
[I01002]

Synthesis, Crystal Structure and Solution Behaviour of Palladium(II) Complexes with Tetrazenido or Amido Ligands and Potentially Tridentate Ligands

Laurent Barloy,[a] Régis M. Gauvin,[a] John A. Osborn,*[a][†] Christina Sizun,[b] Roland Graff,[c] and Nathalie Kyritsakas[d]

Keywords: Palladium / Azides / Amides / Tripodal ligands / Fluxionality

$Pd(DBA)_2$ reacts with the azide $C_6F_5N_3$ in the presence of terpy* to form the tetrazenido palladium(II) complex [(η^2-terpy*)Pd{η^2-$N_4(C_6F_5)_2$}] **1**, whereas with TsN_3 the amido complex [(η^3-terpy*)Pd(NHTs)]$^+$ is obtained. Another synthetic route involving abstraction of chloride ions from [(L)PdCl]Cl and transmetallation with KNHTs yields the complexes [(η^3-L)Pd(NHTs)](BF_4) (**4**: L = terpy*; **5**: L = triphos). Compounds **1**, **4** and **5** have been characterized in the solid state by single-crystal X-ray analysis as mononuclear, square-planar complexes. ^{1}H and ^{19}F NMR spectroscopy reveal that **1** is a fluxional molecule. Rotation of both C_6F_5 rings is hindered, with energy barriers of 53.9 kJ·mol^{-1} (293 K) and 60.7 kJ·mol^{-1} (325 K). Additionally, the lateral pyridines and the C_6F_5 rings exchange through an oscillatory process where one terminal pyridine enters the coordination sphere while the other leaves it. The corresponding energy barrier (74.9 kJ·mol^{-1} at 298 K) has been determined from selective inversion NMR experiments.

Introduction

The covalent bond between a late transition metal of the second or third series and nitrogen has received much attention recently. It is frequently involved in important steps of stoichiometric or catalytic reactions; for instance, palladium amido complexes are involved in the formation of C−N bonds.[1] It has long been considered that the high reactivity of the metal−nitrogen bond is a consequence of the mismatch between the soft metal and the hard nitrogen atom, although this interpretation has been put in question.[2]

The synthesis and reactivity of polynuclear palladium(II) complexes with bridging imido ligands has been reported.[2] On the contrary, mononuclear palladium imido complexes have never been fully characterized,[3] although they have frequently been postulated as transient intermediates in reactions such as the palladium-catalyzed carbonylation of nitroaromatics.[4] Thus, it would be desirable to stabilize and isolate such species. In principle, imido complexes could be obtained from azides, or from the deprotonation of an amido complex. Yet the reaction of organic azides with zerovalent group 10 metals leads instead to tetrazenido, amido or azido complexes, or to polymers.[5,6a,6b,7] It has nevertheless been proposed that transient mononuclear imido intermediates should be involved in the formation of the tetrazenido complexes.

We have been interested lately in the use of tridentate ligands in the coordination chemistry of palladium.[8] Such ligands have been found to stabilize reactive organometallic species,[9] and it could be expected that they might stabilize those imido compounds. In addition, a bridged complex should be avoided in favour of a mononuclear complex, provided that only one coordination site remains in a tetracoordinate palladium complex.

We report here the synthesis and characterization of new palladium tetrazenido and amido complexes obtained from the reaction of Pd^0 with organic azides or the reaction of Pd^{II} complexes with potassium tosylamide, in the presence of the potentially tridentate ligands 4,4′,4"-tri(*tert*-butyl)-2,2′:6′,2"-terpyridine (terpy*)[10] or bis(2-diphenylphosphanylethyl)phenylphosphane (triphos).

Results and Discussion

Tetrazenido Palladium Complexes

The reaction of palladium(0) bis(dibenzylideneacetone) $Pd(DBA)_2$ with an excess of terpy* and pentafluorophenyl azide in toluene at room temperature leads to the η^2-terpy* tetrazenido palladium(II) complex **1** (Scheme 1). The yield is moderate (39%), mainly owing to the difficulty of separa-

[†] Deceased 23 April 2000. Please address further correspondence to L. Barloy.
[a] Laboratoire de Chimie des Métaux de Transition et de Catalyse, UMR 7513 CNRS, Institut Le Bel, Université Louis Pasteur, 4 rue Blaise Pascal, 67070 Strasbourg Cedex, France
Fax: (internat.) +33-3/90/241329
E-mail: barloy@chimie.u-strasbg.fr
[b] Laboratoire de RMN, UMR 7510 CNRS, Institut Le Bel, Université Louis Pasteur, 4 rue Blaise Pascal, 67070 Strasbourg Cedex, France
[c] Service commun de RMN, Faculté de Chimie, Université Louis Pasteur, 1 rue Blaise Pascal, 67008 Strasbourg Cedex, France
[d] Service commun des Rayons X, Faculté de Chimie, Institut Le Bel, Université Louis Pasteur, 4 rue Blaise Pascal, 67070 Strasbourg Cedex, France
Supporting information for this article is available on the WWW under http://www.wiley-vch.de/home/eurjic or from the author.

 © WILEY-VCH Verlag GmbH, 69451 Weinheim, 2001 1434−1948/01/0707−1699 $ 17.50+.50/0

tion from other by-products; however, the yield of the synthesis of tetrazenido or tetrazadiene metal complexes from organic azides is usually lower than 50%.[5] If an equimolar amount of terpy* and azide are used in the synthesis, complex **1** is still obtained as the only product, although with a lower yield. To the best of our knowledge, the only other palladium tetrazenido complex reported to date was prepared by another synthetic route.[5a]

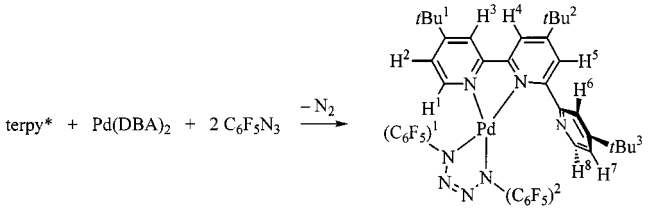

1

Scheme 1. Synthesis of the tetrazenido palladium complex **1**

Compound **1** is soluble in organic solvents like THF, CH_2Cl_2, toluene or even pentane. In general, the complex is not stable in solution, and it slowly decomposes at room temperature in chloroform or methanol, yielding pentafluorophenyl azide and pentafluoroaniline according to ^{19}F NMR analysis. This kind of transformation has been reported for rhodium, iridium or platinum tetrazenido complexes upon treatment with an acid.[11]

The molecular structure of **1** is depicted Figure 1, and selected bond lengths and angles are given in Table 1. Two crystallographically independent, but closely similar, molecules of **1** and two molecules of diisopropyl ether are present within the asymmetric unit; only one molecule of **1** is discussed in the following section. The ORTEP drawing shows a palladium atom coordinated by a bidentate bis(pentafluorophenyl)tetrazenido ligand and a bidentate terpy* ligand. The complex is square planar, but slightly distorted toward a tetrahedral geometry. Pd1, N4, N5, N6, and N7 are nearly coplanar within ±0.03 Å, and their mean plane makes an angle of 19.9(1)° with the N1−Pd1−N2 plane; N1 is located 0.597(3) Å below the mean plane and N2 0.242(3) Å above. The palladium atom deviates from the plane of the coordinating pyridines, as shown by the Pd1−N1−C5−C10 torsion angle of −19(1)°. Those distortions, which arise from steric interactions between terpy* and the tetrazenido ligand, are minimized by the roughly parallel positioning of the uncoordinating pyridine plane and the adjacent pentafluorophenyl plane. Both planes are ca. 3 Å distant one from the other, which is consistent with some π-stacking. The N2−C14−C19−N3 torsion angle is much larger [156.9(9)°] than that found in other η^2-terpy metal complexes;[8a,12,13] the other rotamer, i.e. where this torsion angle would be close to 0°, is not observed in the unit cell. As a consequence of the minimized steric interactions between the two ligands, the difference between the Pd1−N1 and the Pd1−N2 bond lengths (0.02 Å) is small.

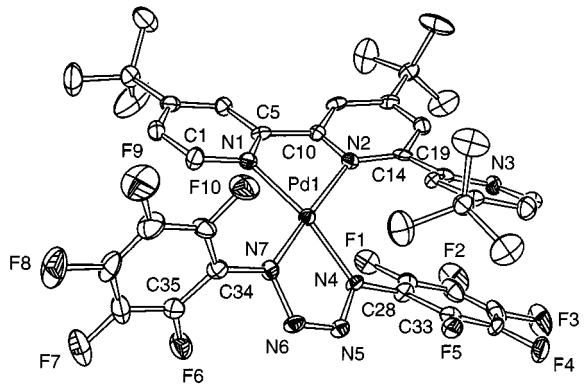

Figure 1. ORTEP drawing of **1** showing 30% probability thermal ellipsoids and the atom-numbering scheme; hydrogen atoms and $i Pr_2O$ are omitted for clarity

Table 1. Selected bond lengths [Å] and bond angles [°] for complex **1**

Pd1−N1	2.052(9)	N4−C28	1.39(1)
Pd1−N2	2.073(9)	N4−N5	1.39(1)
Pd1−N4	1.988(8)	N5−N6	1.25(1)
Pd1−N7	1.986(8)	N6−N7	1.41(1)
		N7−C34	1.39(1)
N1−Pd1−N2	78.9(4)	Pd1−N2−C10	111.2(7)
N1−Pd1−N4	162.9(4)	Pd1−N2−C14	130.4(8)
N1−Pd1−N7	104.0(4)	Pd1−N4−C28	131.7(7)
N2−Pd1−N4	103.4(4)	Pd1−N4−N5	116.6(6)
N2−Pd1−N7	172.7(4)	Pd1−N7−C34	132.7(8)
N4−Pd1−N7	75.9(4)	Pd1−N7−N6	117.2(6)
Pd1−N1−C1	128.4(8)	N4−N5−N6	116.1(9)
Pd1−N1−C5	112.3(7)	N5−N6−N7	114.0(9)

Like the tetrazenido palladium complex $[Pd(PEt_3)_2(N_4Ph_2)]$ described by Trogler et al.,[5a] the N4−N5 and N6−N7 bond lengths [1.39(1) and 1.41(1) Å, respectively] correspond to single bonds, whereas the N5−N6 bond length [1.25(1) Å] is characteristic of a double bond. However, the Pd1−N4 and Pd1−N7 bonds are shorter than in Trogler's complex [1.988(8) and 1.986(8) Å, respectively], which can be related to the lower *trans* influence of pyridines compared to phosphorus ligands. The pentafluorophenyl rings are tilted, as shown by the torsion angles N6−N7−C34−C35 [−54(1)°] and N5−N4−C28−C33 [−43(1)°]. This is another characteristic of the tetrazenido form in contrast to the tetrazadiene form.[5c]

The room-temperature NMR spectrum of **1** is characteristic of an unsymmetrical, bidentate terpy* ligand (Figure 2), and is in agreement with the X-ray structure. The protons of the noncoordinating pyridine are all deshielded in comparison with the equivalent protons of the lateral coordinating pyridine, although the tendency is generally the reverse in η^2-terpy metal complexes.[8,12,14] The latter protons, in particular H^1 and H^2, lie in the anisotropy cone of the pentafluorophenyl ring A, with chemical shifts as low as $\delta = 6.40$ (H^2). In contrast, H^6 is strongly deshielded at $\delta = 10.12$. This may be the effect of a weak agostic CH···Pd

interaction or of the paramagnetic anisotropy of the metal atom;[15] the X-ray structure indicates that H^6 is located ca. 2.7 Å above the palladium atom. The deshielding effect of the nitrogen that is located close to H^5, i.e. N3 on the solid-state structure (vide supra), must also explain the difference between the chemical shifts of H^5 and H^4 ($\Delta\delta$ = 1.14 ppm).[12b]

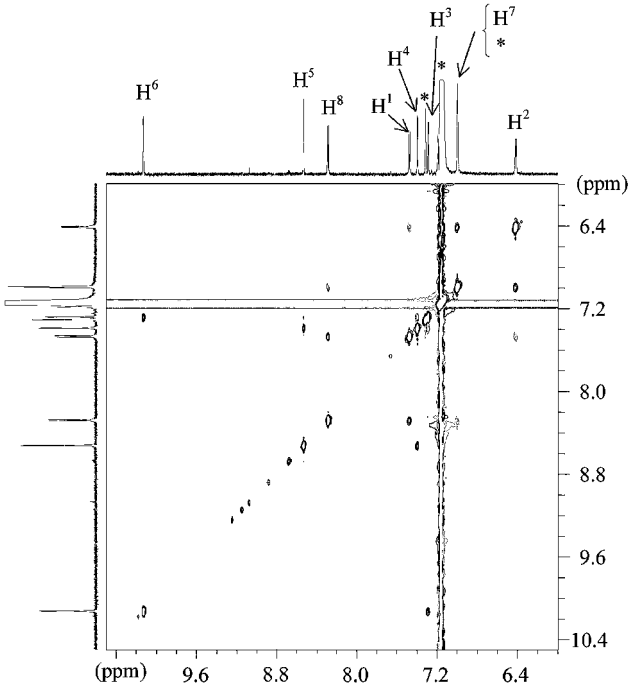

Figure 2. Section of the phase-sensitive $^1H-^1H$ ROESY spectrum of complex **1** (C_6D_6, 298 K, 500 MHz), showing exchange cross-peaks (positive, darker lines) and NOE cross peaks (negative, lighter lines); see Scheme 2 for hydrogen labelling; the asterisks correspond to the solvent

The ^1H-^1H ROESY spectrum shows negative (NOE) cross-peaks that allow us to assign unambiguously the proton signals. In particular, H^3 presents a strong NOE cross-peak with H^4. This was expected since they lie in close proximity, both coordinating pyridines being coplanar. The absence of an NOE interaction between H^5 and H^6 is consistent with the N2−C14−C19−N3 dihedral angle found in the X-ray structure (vide supra).

Exchange (positive) cross-peaks for the H^1/H^8, H^2/H^7, H^3/H^6 and H^4/H^5 pairs (Figure 2), and for the tBu^1/tBu^3 pair are observed in the ROESY spectrum. This fluxionality can be interpreted by the well-known oscillatory mechanism of (η^2-terpy) metal complexes (Scheme 2).[12,14,16] This mechanism is also supported by a ^{19}F-^{19}F NOESY spectrum recorded at room temperature in C_6D_6, which shows that the *para* fluorines of rings A and B exchange with one another. In order to determine the exchange rate of this fluxional mechanism, we ran a selective inversion-recovery NMR experiment.[17] The recovery of the tBu^1 and tBu^3 protons was followed as a function of time after the selective inversion of tBu^1 (Figure 3); the initial decrease in intensity of the tBu^3 signal reflects the chemical exchange. We determined from these NMR spectroscopic data the exchange rate at 298 K as $k = 0.47 \pm 0.05$ s^{-1}, which corresponds to $\Delta G^{\ddagger} = 74.9 \pm 0.3$ kJ·mol^{-1}. The experiment was confirmed by the selective inversion of the tBu^3 protons, leading in turn to an alteration of the intensity of the tBu^1 signal and to the same value of k. This $\Delta G^{\ddagger}_{298}$ value is, to the best of our knowledge, the highest known for an η^2-terpy palladium complex; this is probably linked with the bulkiness of the tetrazenido ligand.

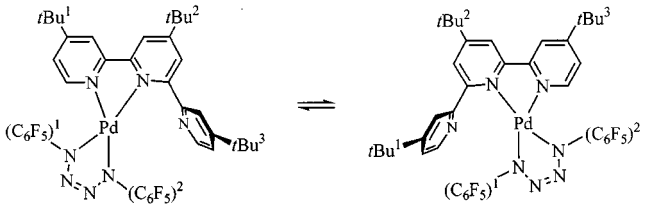

Scheme 2. Fluxional behaviour of complex **1**

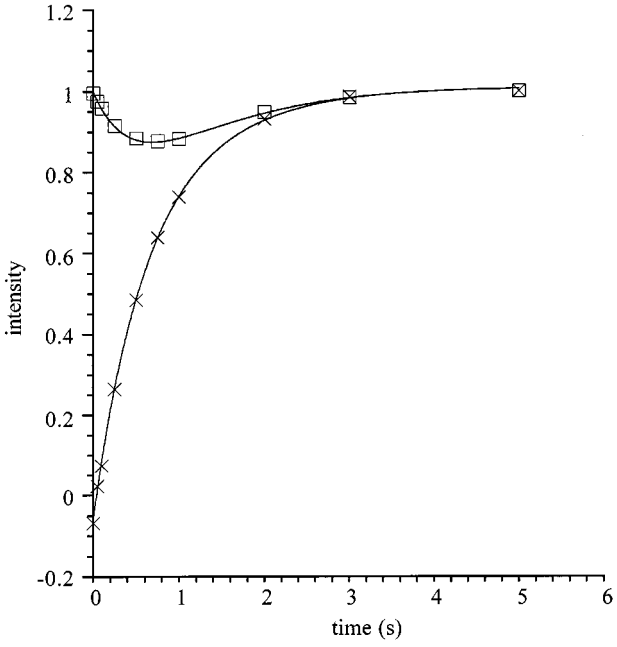

Figure 3. Result of the selective inversion-recovery of the tBu^1 protons of complex **1** at 298 K: evolution vs. time of the intensity of the tBu^1 signal at δ = 0.81 (×) and the tBu^3 signal at δ = 1.46 (square)

The low-temperature ^{19}F NMR spectrum of complex **1** in deuterated chloroform displays ten distinct signals between δ = −170 and −145 (Figure 4). Therefore at this temperature both the oscillatory mechanism and the rotation of the pentafluorophenyl rings around the carbon−nitrogen bonds are frozen; the complex is present as a single conformer, very probably the one which was observed by X-ray crystallography. Upon raising the temperature, we first observe the coalescence of one pair of *meta* signals at δ = −163.52/−162.61 (T_c = 285 K) and one pair of *ortho* signals at δ = −147.62/−145.90 (T_c = 293 K). The same value of $\Delta G^{\ddagger}$ was calculated for both pairs of exchanging signals, i.e. 54.0 kJ·mol^{-1}. Above 272 K, another set

of *ortho* (δ = −151.43/−146.98) and *meta* (δ = −166.06/−164.66) signal pairs starts to coalesce. The complete coalescence into one signal is not reached for any of them at the boiling temperature of the solvent; yet T_c can be estimated for the *meta* signals at 325 K, with a corresponding $\Delta G^{\ddagger} = 60.7\ kJ{\cdot}mol^{-1}$. All those coalescences are obviously the effect of the rotation of the pentafluorophenyl rings. As the rotation of $(C_6F_5)^2$ must be more restricted than the rotation of $(C_6F_5)^1$ because of the proximity of the uncoordinated pyridine, we can assign the values of $53.9\ kJ{\cdot}mol^{-1}$ to ring 1 and of $60.7\ kJ{\cdot}mol^{-1}$ to ring 2. Thus all the signals of the low-temperature ^{19}F NMR spectrum could be assigned. We note that, in general, the fluorines borne by ring 2 are more shielded than the equivalent fluorines of ring 1.

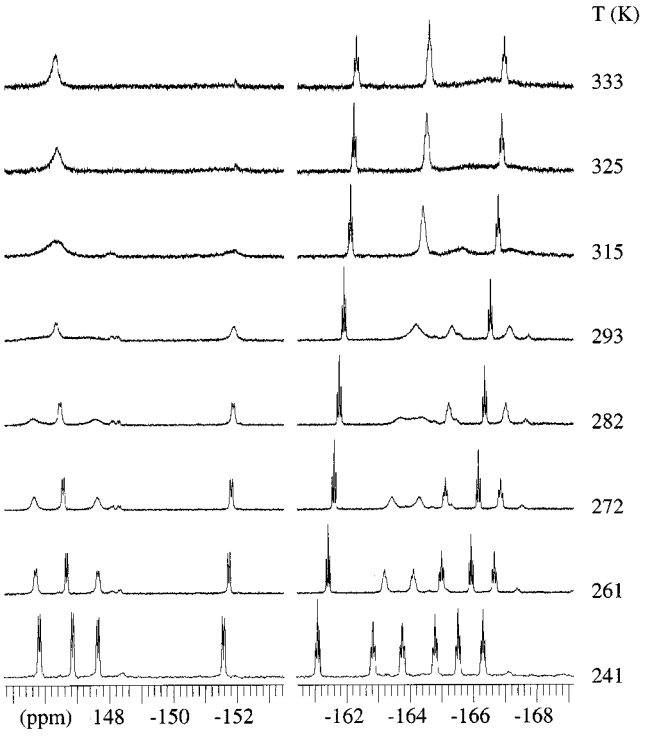

Figure 4. ^{19}F NMR spectra of complex **1** ($CDCl_3$, 376.5 MHz) in the range 241−333 K; see Exp. Section for the complete assignment

the solvent. We therefore had to prepare this cationic amido complex by another synthetic pathway in order to characterize it completely.

The amido complexes **4** and **5** were prepared in very good yield from potassium tosylamide (Scheme 3), since it had been shown that potassium anilide is an efficient reagent for the preparation of palladium amido complexes.[18] The terpy* palladium(II) precursor **3** bearing a labile CH_3CN ligand could be synthesized from terpy* and $[Pd(CH_3CN)_4](BF_4)_2$, following the method described with terpy.[19] An alternative pathway consisted of preparing [(η³-terpy*)PdCl]Cl (**2**) from terpy* and $[Pd(PhCN)_2Cl_2]$, and then removing the chloride anions with silver tetrafluoroborate. The ^1H NMR characteristics of **4** are exactly the same as those of the product obtained from $Pd(DBA)_2$, terpy* and TsN_3. Complex **5** was obtained in a one-pot reaction from [(η³-triphos)PdCl]Cl, removing first the chloride ions with a silver salt at room temperature and then allowing the palladium complex to react at −78° C with the amide anion. Other palladium or platinum sulfonamido complexes have been reported in the literature,[6] but **4** and **5** are, to the best of our knowledge, the first cationic ones reported to date.

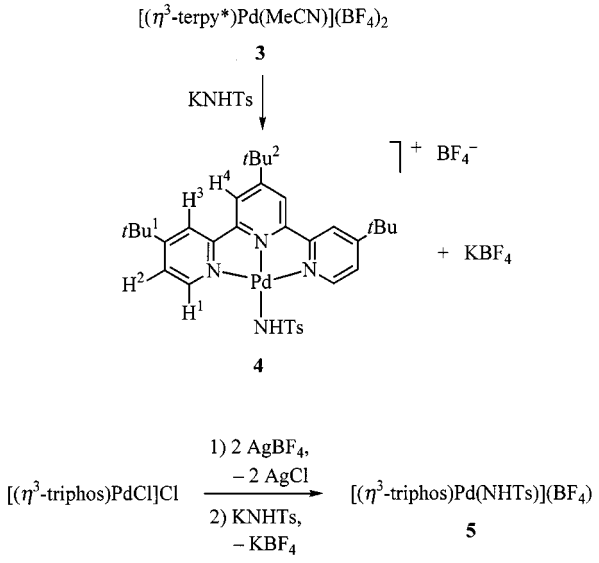

Scheme 3. Synthesis of the amido complexes **4** and **5**

Amido Palladium Complexes

Following the reaction conditions that led to complex **1**, we replaced pentafluorophenyl azide by tosyl azide. It is worth noting that $[Pd(PPh_3)_4]$ reacts with tosyl azide to give, presumably, a polymeric triphenylphosphane derivative of Pd^0.[5b] In spite of our best efforts, the product of the reaction of $Pd(DBA)_2$ with TsN_3 and terpy* could not be completely purified. However, its NMR features reveal one tosylamido moiety and a symmetrical terpy* ligand, suggesting the expected tridentate coordination. In addition, its FAB^+-MS spectrum shows a peak at $m/z = 677.1$ that corresponds to a $[(terpy^*)Pd(NHTs)]^+$ cation. We suppose that the NH proton originates from some residual water in

Complexes **4** and **5** are not air-sensitive, but **5** slowly decomposes in solution at room temperature. Their relative stability is probably connected with the electron-withdrawing tosyl fragment; it has been suggested that amido palladium complexes are stabilized by substituents that can accommodate π-donation from the nitrogen lone pair.[18] The ^1H NMR N*H* signals appear at δ = 3.61 (**4**) and δ = 2.55 (**5**), and are therefore in the same region as for reported palladium or platinum sulfonamido complexes.[6]

The molecular structures of complexes **4** and **5** are depicted in Figure 5 and 6, and selected bond lengths and angles are given Table 2 and 3. Both of them consist of slightly distorted square-planar $[(\eta^3\text{-L})Pd(NHTs)]^+$ cationic

complexes, where L is either terpy* (**4**) or triphos (**5**), and noncoordinating tetrafluoroborate anions. Complex **4** co-crystallizes with two molecules of water each with an occupancy ratio of 50% and 25%. In the case of complex **5**, the asymmetric unit contains two crystallographically independent molecules of **5** and one acetonitrile; those molecules are practically equivalent and only one is discussed.

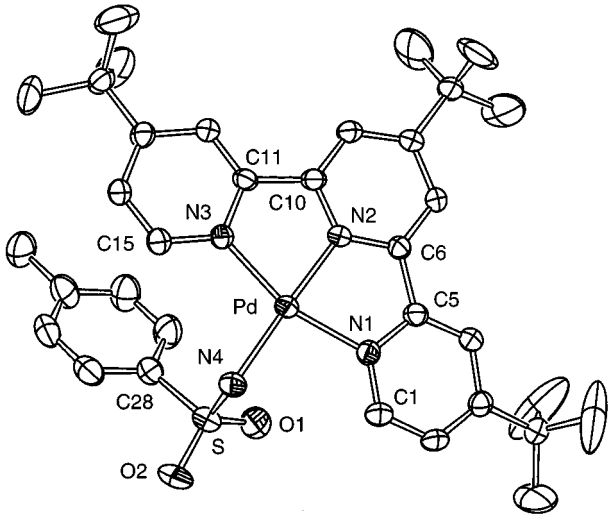

Figure 5. ORTEP drawing of **4** showing 30% probability thermal ellipsoids and the atom-numbering scheme; hydrogen atoms, BF_4^- and H_2O are omitted for clarity

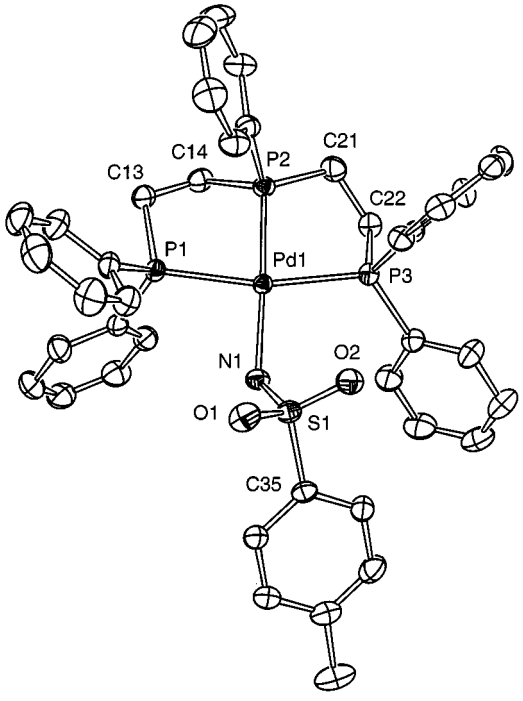

Figure 6. ORTEP drawing of **5** showing 30% probability thermal ellipsoids and the atom-numbering scheme; hydrogen atoms, BF_4^- and CH_3CN are omitted for clarity

For both complexes, the characteristics of the (η^3-L)Pd fragments are very close to those of related terpy[20] or triphos[21] complexes, with the short bond angles N−Pd−N [N1−Pd−N2 = 81.0(3)°, N2−Pd−N3 = 80.5(3)°] or P−Pd−P [P1−Pd1−P2 = 82.64(3)°, P2−Pd1−P3 = 82.07(3)°] expected for five-membered metallacycles. The palladium atom lies out of the N_4 mean plane by only 0.0375(2) Å in complex **4**, and out of the NP_3 mean plane by 0.1178(1) Å in complex **5**.

Table 2. Selected bond lengths [Å] and bond angles [°] for complex **4**

Pd−N1	2.023(7)	Pd−N4	2.027(7)
Pd−N2	1.935(6)	N4−S	1.604(9)
Pd−N3	2.022(7)	S−C28	1.78(1)
N1−Pd−N2	81.0(3)	Pd−N1−C5	113.2(5)
N1−Pd−N3	161.5(3)	Pd−N2−C6	118.4(5)
N1−Pd−N4	96.5(3)	Pd−N2−C10	118.6(6)
N2−Pd−N3	80.5(3)	Pd−N3−C11	114.3(5)
N2−Pd−N4	176.4(3)	Pd−N3−C15	128.3(6)
N3−Pd−N4	101.9(3)	Pd−N4−S	117.1(4)
Pd−N1−C1	128.1(6)	N4−S−C28	107.4(5)

Table 3. Selected bond lengths [Å] and bond angles [°] for complex **5**

Pd1−P1	2.3416(7)	Pd1−N1	2.084(2)
Pd1−P2	2.2293(7)	N1−S1	1.592(2)
Pd1−P3	2.3309(7)	S1−C35	1.778(3)
P1−Pd1−P2	82.64(3)	Pd1−P1−C13	107.12(4)
P1−Pd1−P3	163.32(3)	Pd1−P2−C14	106.15(5)
P1−Pd1−N1	94.96(7)	Pd1−P2−C21	112.06(6)
P2−Pd1−P3	82.07(3)	Pd1−P3−C22	102.29(4)
P2−Pd1−N1	174.84(7)	Pd1−N1−S1	123.50(5)
P3−Pd1−N1	99.72(7)	N1−S1−C35	105.4(1)

Concerning the sulfonamido fragments, the palladium−nitrogen bond length [**4**: 2.027(7) Å; **5**: 2.084(2) Å] is typical of a single bond; it is somewhat longer in **5** than in **4** because of the *trans* influence of the phosphane. In fact, the Pd−N bond in palladium amido complexes is generally a single bond,[6,18] as long as no ligand-to-metal π-donation is possible in d^8 metal complexes.[22] The nitrogen−sulfur bond is rather short [**4**: 1.604(9) Å; **5**: 1.592(2) Å], whereas the N−S bond length measured on a tungsten tosylamido complex is larger [1.641(5) Å].[23] This is indicative of a delocalization of the nitrogen lone pair onto the adjacent electron-withdrawing SO_2 function as in other palladium sulfonamido complexes.[6] We observe a higher value for the Pd1−N1−S1 angle in **5** [123.50(5)°] than for the Pd−N4−S angle in **4** [117.1(4)°]; the phenyl substituents borne by triphos exert a steric influence that may be the origin of this difference.

In complex **4**, the Pd−N−S plane is roughly perpendicular to the coordination plane, with an angle of 87.7(1)° with the N_4 plane, although in complex **5** the angle with the P_3N plane is somewhat smaller [60.39(5)°]. Those large angles can stem from a minimized interaction between the nitrogen lone pair and the filled *d*-orbitals of palladium,[24]

and/or from a reduced steric strain between the tridentate ligand and the tosylamido ligand.

In addition, the tetrafluoroborate anion is disordered in the X-ray structure of **4**. We can, however, observe that some of the fluorine atoms are less than 3 Å distant from N4, suggesting an NH···F hydrogen bond between the complex and BF_4.

Like some other Pd and Rh amido complexes,[2] **4** and **5** could not be deprotonated to imido complexes, despite the electron-withdrawing effect of the tosyl substituent. Most of the reactions with bases like organolithium reagents or LDA led to decomposition and intractable mixtures. The CD_2CN^- anion generated by reaction of butyllithium with CD_3CN substituted the tosylamido ligand in complex **5** according to FAB-MS analysis. Similarly, the reaction of **5** with Cs_2CO_3 in methanol led to a (triphos)Pd(OH)$^+$ cation. We also noted the absence of reactivity of **5** towards CO.

Conclusion

The results described in this paper show that under identical conditions, the reaction of $Pd(DBA)_2$ and terpy* with $C_6F_5N_3$ leads to the tetrazenido complex **1**, whereas with TsN_3 the product is an amido complex. These results contrast with the reported reactions of Pd^0 complexes with azides, which give either bis-azido Pd^{II} complexes[7] or polymeric triphenylphosphane derivatives of Pd^0.[5b] The terpyridine ligand obviously plays a key role in the orientation of the reaction; however, no imido complexes were obtained.

In the product **1**, derived from $C_6F_5N_3$, terpy* binds palladium in a bidentate manner and the complex is fluxional via an oscillatory mechanism. The X-ray structure and NMR properties of **1** also reveal that the rotations of the C_6F_5 rings around the C−N bonds are hindered. In contrast, terpy* is tridentate and the fourth coordination position is occupied by $TsNH^-$ in the product derived from TsN_3. We suspect that steric interactions between the large, tetrahedral sulfonamide function and the pendant pyridine of terpy* would be too important to make a tosyl analogue of **1** stable.

Experimental Section

General: All experiments were carried out at room temperature under a nitrogen or argon atmosphere, using a vacuum line or Vacuum Atmospheres glovebox equipped with Dri-Train HE-493 inert gas purifier, unless otherwise stated. All solvents were dried by standard methods and distilled under nitrogen, except benzonitrile (Fluka) which was used as received. $[Pd(CH_3CN)_4](BF_4)_2$ and $AgBF_4$ were purchased from Strem and used as received. Tosyl azide,[25] pentafluorophenyl azide,[26] potassium tosylamide,[27] 4,4′,4"-tri(*tert*-butyl)-2,2′:6′,2"-terpyridine (terpy*),[10] $Pd(DBA)_2$,[28] $[Pd(PhCN)_2Cl_2]$,[29] [(triphos)PdCl]Cl[30] were prepared following reported procedures.

The NMR spectra were obtained at room temperature (unless otherwise indicated) on Bruker spectrometers. ^1H NMR spectra were recorded at 200.13 MHz (AC-200 instrument), 300.16 MHz (AC-300) or 500.13 MHz (ARX-500) and referenced to $SiMe_4$; the assignments were supported by irradiations and/or 2D analysis. $^{13}C\{^1H\}$ NMR spectra (broadband decoupled) were recorded at 50.32 MHz (AC-200) or 100.62 MHz (AM-400) and referenced to $SiMe_4$; the assignments were supported by DEPT-135° or ^1H-^{13}C HMQC analysis. $^{31}P\{^1H\}$ NMR spectra (broadband decoupled) were recorded at 121.51 MHz (AC-300) and referenced to 85% aqueous H_3PO_4. $^{19}F\{^1H\}$ NMR spectra (broadband decoupled) were recorded at 376.50 MHz (AM-400) and referenced to $CFCl_3$; the assignments were supported by ^{19}F-^{19}F COSY analysis. For variable-temperature spectra, the probe temperature was controlled (±1 K) by a B-VT 2000 unit calibrated with a methanol NMR tube. The $\Delta G^{\ddagger}$ values were calculated with the Eyring equation $\Delta G^{\ddagger} = RT_c\,(22.96 + \ln T_c/\Delta\nu)$ [J·mol^{-1}] where T_c (K) is the temperature of coalescence of two given signals and $\Delta\nu$ (Hz) their difference in chemical shift at low exchange temperature;[31] the error is estimated to be ±1 kJ·mol^{-1}. The phase-sensitive ^1H-^1H ROESY spectrum (mixing time 0.3 s) and the selective inversion-recovery experiments were recorded on the ARX-500 spectrometer, and the phase-sensitive ^{19}F-^{19}F NOESY spectrum on the AM-400 spectrometer (mixing time 0.4 s). The selective inversion-recovery experiments were achieved using a 50 ms Gaussian 180° pulse (5%−truncated waveform) and a 20 s interpulse delay; the curves were fitted either as pairs or all four simultaneously according to Bloch's equations modified for exchange,[32] with a home-written C program using the Powell algorithm from the Numerical Recipes package.[33] The $\Delta G^{\ddagger}$ value was deduced from the equation $\Delta G^{\ddagger} = RT\,(23.76 - \ln k/T)$.[31]

FT-IR spectra were recorded on a Perkin−Elmer 1600 Series spectrometer on KBr pellets.

MS spectra and elemental analyses were carried out by the corresponding facilities at the Centre de Recherche de Chimie, Université Louis Pasteur, Strasbourg.

[(η²-terpy*)Pd{η²-N₄(C₆F₅)₂}] (1): $Pd(DBA)_2$ (1.00 g, 1.74 mmol) was added to a solution of terpy* (1.00 g, 2.49 mmol) in toluene (50 mL) while stirring. A solution of pentafluorophenyl azide (2.00 g, 9.57 mmol) in toluene (10 mL) was added dropwise. After 18 h stirring at room temperature, the colour had turned from reddish-violet to dark-greenish. The solution was filtered and evaporated to dryness, and the residue washed with pentane (4 × 50 mL) and toluene (20 mL). The complex was recrystallized from THF/pentane as an air-stable, dark grey-blue powder (0.61 g, 39%). − $C_{39}H_{35}F_{10}N_7Pd$ (898.14): calcd. C 52.16, H 3.93, N 10.92; found C 51.61, H 3.80, N 10.85. − ^1H NMR (300 MHz, C_6D_6): δ = 0.81 (s, 9 H, *t*Bu^1), 1.04 (s, 9 H, *t*Bu^2), 1.46 (s, 9 H, *t*Bu^3), 6.40 (dd, $^3J_{HH}$ = 6.1 Hz, $^4J_{HH}$ = 1.7 Hz, 1 H, H^2), 6.99 (dd, $^3J_{HH}$ = 5.1 Hz, $^4J_{HH}$ = 1.7 Hz, 1 H, H^7), 7.27 (d, $^4J_{HH}$ = 1.5 Hz, 1 H, H^3), 7.38 (d, $^4J_{HH}$ = 2.0 Hz, 1 H, H^4), 7.47 (d, $^3J_{HH}$ = 6.1 Hz, 1 H, H^1), 8.28 (d, $^3J_{HH}$ = 5.1 Hz, 1 H, H^8), 8.52 (d, $^4J_{HH}$ = 2.0 Hz, 1 H, H^5), 10.12 (d, $^4J_{HH}$ = 1.7 Hz, 1 H, H^6). − $^{19}F\{^1H\}$ NMR (376.5 MHz, $CDCl_3$, 230 K): δ = −166.06, −164.66 (2 dd app. t, $^3J_{FF}$ = 23 Hz, 2 F, F^{2meta}), −165.26 (dd app. t, $^3J_{FF}$ = 22 Hz, 1 F, F^{2para}), −163.52, −162.61 (2 dd app. t, $^3J_{FF}$ = 23 Hz, 2 F, F^{1meta}), −160.86 (dd app. t, $^3J_{FF}$ = 23 Hz, 1 F, F^{1para}), −151.43, −146.98 (2 d, $^3J_{FF}$ = 24 Hz, 2 F, F^{2ortho}), −147.62, −145.90 (2 d, $^3J_{FF}$ = 22 Hz, 2 F, F^{1ortho}).

Reaction of Pd(DBA)₂ with Terpy* and Tosyl Azide: $Pd(DBA)_2$ (0.500 g, 0.870 mmol) was added to a solution of terpy* (0.698 g, 1.74 mmol) in toluene (50 mL) while stirring. A solution of tosyl

azide (1.20 g, 6.08 mmol) in toluene (5 mL) was added dropwise. After 18 h stirring at room temperature, the colour had turned from reddish-violet to dark brown. The suspension was filtered, and the product collected on a frit as a brown-greenish powder was washed with toluene and dried. − MS (FAB^+, NBA matrix): *m*/*z* (%) = 677.1 (79) [(terpy*)Pd(NHTs)$^+$], 507.1 (100) [(terpy*)Pd$^+$]. − ^{1}H NMR (200 MHz, CD_3CN): δ = 1.42 (s, 18 H, *t*Bu^1), 1.52 (s, 9 H, *t*Bu^2), 2.26 (s, 3 H, Me), 3.61 (br s, 1 H, NH), 7.12 (d, $^3J_{HH}$ = 7.8 Hz, 2 H, H$^{arom\ Ts}$), 7.54 (dd, $^3J_{HH}$ = 6.1 Hz, $^4J_{HH}$ = 2.1 Hz, 2 H, H^2), 7.93 (d, $^3J_{HH}$ = 8.2 Hz, 2 H, H$^{arom\ Ts}$), 8.14 (d, $^3J_{HH}$ = 6.0 Hz, 2 H, H^1), 8.28 (m, 4 H, H^3 + H^4). − ^{13}C{^{1}H} NMR (50 MHz, [D$_6$]DMSO): δ = 20.7 (s, 1 C, Me), 29.8 [s, 6 C, *t*Bu^1, C(*C*H$_3$)$_3$], 30.2 [s, 3 C, *t*Bu^2, C(*C*H$_3$)$_3$], 36.0 [s, 2 C, *t*Bu^1, *C*(CH$_3$)$_3$], 37.0 [s, 1 C, *t*Bu^2, *C*(CH$_3$)$_3$], 121.4 (s, 2 C, C−H^4), 122.2 (s, 2 C, C−H^3), 124.1 (s, 2 C, C−H^2), 125.9, 128.7 (2 s, 2 × 2 C, C−H^{Ts}), 140.1, 143.8 (2 s, 2 × 1 C, C−S + C−Me), 151.7 (s, 2 C, C−H^1), 154.1, 157.0 (2 s, 2 × 2 C, C−N), 166.3 (s, 2 C, C−*t*Bu^1), 167.7 (s, 1 C, C−*t*Bu^2).

[(η^3-terpy*)PdCl]Cl (2): Terpy* (1.20 g, 3.00 mmol) was partly dissolved in 250 mL methanol in a round-bottomed flask, and [Pd(PhCN)$_2$Cl$_2$] (1.15 g, 3.00 mmol) was added to the solution. A clear solution was obtained after 3 h reflux, which was cooled and filtered. Evaporation under reduced pressure led to an orange oil, which was recrystallized from a CH_2Cl_2/Et_2O mixture to yield the complex as a pale yellow powder (1.62 g, 94%). − $C_{27}H_{35}Cl_2N_3Pd{\cdot}H_2O$ (596.92): calcd. C 54.33, H 6.25, N 7.04, Cl 11.88; found C 54.56, H 6.28, N 6.93, Cl 11.86. − MS (ES^+): *m*/*z* (%) = 542.3 (100) [M$^+$ − Cl]. − ^{1}H NMR (300 MHz, $CDCl_3$): δ = 1.54 (s, 18 H, *t*Bu^1), 1.70 (s, 9 H, *t*Bu^2), 7.56 (dd, $^3J_{HH}$ = 6.0 Hz, $^4J_{HH}$ = 2.0 Hz, 2 H, H^2), 8.78 (d, $^3J_{HH}$ = 6.0 Hz, 2 H, H^1), 8.98 (d, $^4J_{HH}$ = 1.8 Hz, 2 H, H^3), 9.06 (s, 2 H, H^4).

[(η^3-terpy*)Pd(CH$_3$CN)](BF$_4$)$_2$ (3). Method A: A solution of terpy* (45 mg, 0.112 mmol) dissolved in benzonitrile (2 mL) was added to a yellow solution of [Pd(CH$_3$CN)$_4$](BF$_4$)$_2$ (50 mg, 0.112 mmol) in benzonitrile (5 mL), after which the colour faded slightly. Addition of 60 mL diethyl ether led to an off-white precipitate which was collected on a frit and washed with diethyl ether (79 mg, 98%). The complex could be recrystallized from CH_3CN/Et_2O. − $C_{29}H_{38}B_2F_8N_4Pd$ (722.66): calcd. C 48.20, H 5.30, N 7.75; found C 48.11, H 5.32, N 7.61. − IR: $\nu_{C\equiv N}$ = 2305, 2333 cm^{-1}. − ^{1}H NMR (300 MHz, CD_3CN): δ = 1.47 (s, 18 H, *t*Bu^1), 1.53 (s, 9 H, *t*Bu^2), 7.77 (dd, $^3J_{HH}$ = 6.1 Hz, $^4J_{HH}$ = 2.1 Hz, 2 H, H^2), 8.30 (s, 2 H, H^4), 8.35 (d, $^4J_{HH}$ = 2.0 Hz, 2 H, H^3), 8.42 (d, $^3J_{HH}$ = 6.1 Hz, 2 H, H^1).

Method B: To a solution of **2** (50 mg, 0.0864 mmol) in acetonitrile (5 mL) was added a solution of $AgBF_4$ (67 mg, 0.344 mmol) in acetonitrile (2 mL). The solution was stirred for 18 h in the dark, and the resulting suspension was filtered. The filtrate was evaporated to dryness and the residue recrystallized from a CH_2Cl_2/CH_3CN mixture to yield the complex (51 mg, 82%).

Table 4. Crystal and refinement data for complexes **1**, **4**, and **5**

	1·*i*Pr$_2$O	**4**·0.75 H$_2$O	**5**·0.5 CH$_3$CN
Formula	$C_{39}H_{35}F_{10}N_7Pd{\cdot}C_6H_{14}O$	$C_{34}H_{43}BF_4N_4O_2PdS{\cdot}0.75\ H_2O$	$C_{41}H_{41}BF_4NO_2P_3PdS{\cdot}0.5\ C_2H_3N$
Mol wt	1000.32	778.53	918.51
Colour	Black	Yellow	Red
Cryst system	Orthorhombic	Monoclinic	Triclinic
a (Å)	33.341(5)	11.4382(9)	10.1424(6)
b (Å)	16.4755(3)	17.749(1)	21.419(1)
c (Å)	16.7758(3)	19.427(1)	21.459(1)
α (deg)			66.471(4)
β (deg)		106.437(6)	82.905(5)
γ (deg)			77.310(5)
V (Å^3)	9215(1)	3782.8(4)	4166.4(5)
Z	8	4	4
D_{calc} (g cm^{-3})	1.44	1.37	1.46
*F*000	4096	1606	1876
Wavelength (Å)	0.71073	0.71073	0.71073
μ (mm^{-1})	0.476	0.602	0.654
Space group	*Pna*2$_1$	$P_12_1/n1$	$P\bar{1}$
Diffractometer	Kappa CCD	Enraf Nonius CAD4	Enraf Nonius CAD4
Crystal dimens (mm)	0.23 × 0.19 × 0.12	0.25 × 0.20 × 0.20	0.40 × 0.40 × 0.40
Temperature (K)	173	294	294
Radiation	Mo-K_α graphite monochromated	Mo-K_α graphite monochromated	Mo-K_α graphite monochromated
Scan mode	phi scans	*θ*/*2θ*	*θ*/*2θ*
hkl limits	0,17/0,19/0,37	0,14/0,22/−24,23	0,12/−26,26/−26,26
θ limits (deg)	2.5/24.48	2.5/26.30	2.5/26.29
No. of data measured	42085	8363	17869
No. of data with $I>3\sigma(I)$	5055	3877	12276
Weighting scheme	$4F_0^2/[\sigma^2(F_0^2) + 0.0004\ F_0^4] + 1.0$	$4F_0^2/[\sigma^2(F_0^2) + 0.0064\ F_0^4]$	$4F_0^2/[\sigma^2(F_0^2) + 0.0064\ F_0^4]$
No. of variables	1152	405	983
R	0.045	0.060	0.041
R_w	0.052	0.088	0.064
Largest peak in final difference (e Å^{-3})	0.653	0.993	1.458
GOF	1.065	1.639	1.335

[(η^3-terpy*)Pd(NHTs)](BF$_4$) (4): A suspension of TsNHK (44 mg, 0.210 mmol) in dichloromethane (6 mL) was added to a suspension of **3** (150 mg, 0.208 mmol) in dichloromethane (7 mL) while stirring. The reagents slowly dissolved while the solution turned yellow. After 18 h stirring at room temperature, the resulting suspension was filtered and the solvent was evaporated to dryness. The complex was recrystallized from THF/Et_2O as an air-stable, yellow powder (125 mg, 79%). – $C_{34}H_{43}BF_4N_4O_2PdS$ (765.01): calcd. C 53.38, H 5.67, N 7.32; found C 53.53, H 5.47, N 7.33.

[(η^3-triphos)Pd(NHTs)](BF$_4$) (5): To a solution of [(triphos)PdCl]Cl (136 mg, 0.191 mmol) in dichloromethane (4 mL) was added a suspension of $AgBF_4$ (74 mg, 0.380 mmol) in dichloromethane (2 mL). The mixture was stirred at room temperature for 30 min. and filtered. The filtrate was cooled to −78° C and a suspension of TsNHK (40 mg, 0.191 mmol) in dichloromethane (1 mL) was added. After stirring at −78° C for 30 min., the temperature was raised to 20° C and the suspension filtered. The solvent was evaporated to dryness and the crude product was obtained as an air-stable, orange powder (160 mg, 93%). The complex was recrystallized from acetonitrile/diethyl ether. – $C_{41}H_{41}BF_4NO_2P_3PdS$ (897.98): calcd. C 54.84, H 4.60, N 1.56; found C 54.96, H 4.65, N 1.85. – IR: ν_{NH} = 3303, 3263 cm^{-1}. – ^{1}H NMR (200 MHz, CD_2Cl_2): δ = 2.1−3.4 (m, 8 H, CH_2), 2.31 (s, 3 H, Me), 2.55 (t, $^3J_{HP}$ = 3.1 Hz, 1 H, NH), 6.84, 6.90 (2 d, $^3J_{HH}$ = 8.7 Hz, 4 H, $H^{arom.\ Ts}$), 7.4−8.0 (m, 25 H, H^{Ph}). – $^{13}C\{^1H\}$ NMR (100 MHz, CD_3CN): δ = 21.4 (s, 1 C, Me), 28.3 (d virtual t, $^1J_{CP}$ = 34 Hz, $|^2J_{CP} + {}^4J_{CP'}|$ = 14 Hz, 2 C, C−PPh), 31.3 (d virtual t, $^2J_{CP}$ = 9 Hz, $|^1J_{CP} + {}^3J_{CP'}|$ = 32 Hz, 2 C, C−PPh_2), 126.1, 129.8 (2 s, 2 × 2 C, C−H^{Ts}), 126.6 (d, $^1J_{CP}$ = 52 Hz, 1 C, $C^{ipso\ PPh}$), 128.1, 129.5 (2 virtual t, $|^1J_{CP} + {}^3J_{CP'}|$ = 47 Hz, 2 × 2 C, $C^{ipso\ PPh}{}_2$), 130.3, 130.4 (2 virtual t, $|^3J_{CP} + {}^5J_{CP'}|$ = 11 Hz, 2 × 4 C, $C^{meta\ PPh}{}_2$), 131.0 (d, $^3J_{CP}$ = 11 Hz, 2 C, $C^{meta\ PPh}$), 133.3, 133.4 (2 s, 2 × 2 C, $C^{para\ PPh}{}_2$), 134.4, 134.7 (2 virtual t, $|^2J_{CP} + {}^4J_{CP'}|$ = 14 Hz, 2 × 4 C, $C^{ortho\ PPh}{}_2$), 134.6 (d, $^2J_{CP}$ = 12 Hz, 2 C, $C^{ortho\ PPh}$), 134.8 (d, $^4J_{CP}$ = 2 Hz, 1 C, $C^{para\ PPh}$), 141.4, 145.6 (2 s, 2 C, C−S + C−Me). – $^{31}P\{^1H\}$ NMR (121.5 MHz, CD_3CN): δ = 49.9 (d, $^2J_{PP}$ = 13 Hz, 2 P, PPh_2), 110.9 (t, $^2J_{PP}$ = 13 Hz, 1 P, PPh).

X-ray Crystallographic Study: Single crystals of **1** were obtained from a saturated diisopropyl ether solution cooled to −20° C. Single crystals of **4** and **5** were obtained with the double-layer method: a water layer was stratified with a saturated solution of **4** in an acetone/water mixture, and a saturated solution of **5** in an acetonitrile/toluene/pentane mixture was stratified with a pentane layer. The crystal data were collected at 173 K for complex **1** and at 294 K for complexes **4** and **5** on a Kappa CCD diffractometer for **1** and on a CAD4-MACH3 for **4** and **5**, using monochromated Mo-K_α radiation (λ = 0.71073 Å). Details of data collection parameters and refinements results are listed in Table 4. The structures were solved using direct methods. After refinement of the non-hydrogen atoms, difference-Fourier maps revealed maxima of residual electron density close to positions expected for hydrogen atoms. Hydrogen atoms were introduced as fixed contributors at calculated positions [C−H = 0.95 Å, B(H) = 1.3B_{eq})]. Final difference maps revealed no significant maxima. All calculations were done using the Nonius OpenMoleN package.[34] Neutral atom scattering factor coefficients and anomalous dispersion coefficients were taken from a standard source.[35]

Crystallographic data (excluding structure factors) for the structures reported in this paper have been deposited with the Cambridge Crystallographic Data Centre as supplementary publication no. CCDC-156069 (**1**), CCDC-156070 (**4**) and CCDC-156071 (**5**). Copies of the data can be obtained free of charge on application to CCDC, 12 Union Road, Cambridge CB2 1EZ, UK [Fax: (internat.) + 44-1223/336-033; E-mail: deposit@ccdc.cam.ac.uk].

Acknowledgments

We thank Frederic Paul for helpful discussions at the beginning of this work and Jean Pierre Le Ny for critical reading of the manuscript. Financial support of the Centre National de la Recherche Scientifique is gratefully acknowledged. One of us (RMG) is indebted to the Ministère de l'Enseignement Supérieur for a grant.

[1] J. F. Hartwig, *Angew. Chem. Int. Ed.* **1998**, *37*, 2046−2067.
[2] [2a] P. R. Sharp, *Comments Inorg. Chem.* **1999**, *21*, 85−114 and cited references. – [2b] P. R. Sharp, *J. Chem. Soc., Dalton Trans.* **2000**, 2647−2657.
[3] D. E. Wigley, *Prog. Inorg. Chem.* **1994**, *42*, 239−482.
[4] [4a] F. Ragaini, S. Cenini, *J. Mol. Catal. A: Chem.* **1996**, *109*, 1−25. – [4b] F. Paul, *Coord. Chem. Rev.* **1999**, *203*, 269−323.
[5] [5a] S. W. Lee, G. A. Miller, C. F. Campana, W. C. Trogler, *Inorg. Chem.* **1988**, *27*, 1215−1219. – [5b] S. Cenini, G. La Monica, *Inorg. Chim. Acta* **1976**, *18*, 279−293. – [5c] D. S. Moore, S. D. Robinson, *Adv. Inorg. Chem. Radiochem.* **1986**, *30*, 1−68. – [5d] K. Vrieze, G. van Koten, in *Comprehensive Coordination Chemistry* (Eds.: G. Wilkinson, R. D. Gillard, J. A. McCleverty), Pergamon Press, Oxford, **1987**, vol. 2, chapter 13.5. – [5e] W. C. Trogler, *Acc. Chem. Res.* **1990**, *23*, 426−431.
[6] [6a] W. Beck, M. Bauder, G. La Monica, S. Cenini, R. Ugo, *J. Chem. Soc. (A)* **1971**, 113−118. – [6b] S. Cenini, M. Pizzotti, F. Porta, G. La Monica, *J. Organomet. Chem.* **1975**, *88*, 237−248. – [6c] D. R. Schaad, C. R. Landis, *Organometallics* **1992**, *11*, 2024−2029. – [6d] C. A. Otter, S. M. Couchman, J. C. Jeffery, K. L. V. Mann, E. Psillakis, M. D. Ward, *Inorg. Chim. Acta* **1998**, *278*, 178−184. – [6e] I. Foch, L. Párkányi, G. Besenyei, L. I. Simándi, A. Kálmán, *J. Chem. Soc., Dalton Trans.* **1999**, 293−299.
[7] B. Hessett, J. H. Morris, P. G. Perkins, *Inorg. Nucl. Chem. Letters* **1971**, *7*, 1149−1152.
[8] [8a] S. Ramdeehul, L. Barloy, J. A. Osborn, A. De Cian, J. Fischer, *Organometallics* **1996**, *15*, 5442−5444. – [8b] L. Barloy, S. Ramdeehul, J. A. Osborn, C. Carlotti, F. Taulelle, A. De Cian, J. Fischer, *Eur. J. Inorg. Chem.* **2000**, 2523−2532.
[9] [9a] S.-B. Park, N. Sakata, H. Nishiyama, *Chem. Eur. J.* **1996**, *2*, 303−306. – [9b] M. Ohff, A. Ohff, M. E. van der Boom, D. Milstein, *J. Am. Chem. Soc.* **1997**, *119*, 11687−11688.
[10] T. Ben Hadda, H. Le Bozec, *Inorg. Chim. Acta* **1993**, *204*, 103−107.
[11] G. La Monica, P. Sandrini, F. Zingales, S. Cenini, *J. Organomet. Chem.* **1973**, *50*, 287−296.
[12] [12a] E. R. Civitello, P. S. Dragovitch, T. B. Karpishin, S. G. Novick, G. Bierach, J. F. O'Connell, T. D. Westmoreland, *Inorg. Chem.* **1993**, *32*, 237−241. – [12b] E. W. Abel, V. S. Dimitrov, N. J. Long, K. G. Orrell, A. G. Osborne, V. Sik, M. B. Hursthouse, M. A. Mazid, *J. Chem. Soc., Dalton Trans.* **1993**, 291−298. – [12c] E. W. Abel, V. S. Dimitrov, N. J. Long, K. G. Orrell, A. G. Osborne, H. M. Pain, V. Sik, M. B. Hursthouse, M. A. Mazid, *J. Chem. Soc., Dalton Trans.* **1993**, 597−603. – [12d] E. W. Abel, K. G. Orrell, A. G. Osborne, H. M. Pain, V. Sik, M. B. Hursthouse, K. M. Abdul Malik, *J. Chem. Soc., Dalton Trans.* **1994**, 3441−3449.
[13] [13a] G. B. Deacon, J. M. Patrick, B. W. Skelton, N. C. Thomas, A. H. White, *Aust. J. Chem.* **1984**, *37*, 929−945. – [13b] P. A. Anderson, F. R. Keene, E. Horn, E. R. T. Tiekink, *Appl. Organomet. Chem.* **1990**, *4*, 523−533. – [13c] N. C. Thomas, J. Fischer, *J. Coord. Chem.* **1990**, *21*, 119−128. – [13d] V. Ferretti, P. Gilli, V. Bertolasi, G. Marangoni, B. Pitteri, G. Chessa, *Acta Crystallogr., Sect. C* **1992**, *48*, 814−817. – [13e] E. C. Constable, *Tetrahedron* **1992**, *48*, 10013−10059. – [13f] E. C. Constable, M. J. Hannon, A. M. W. Cargill Thompson, D. A. Tocher, J. V. Walker, *Supramol. Chem.* **1993**, *2*, 243−246.

[14] [14a] E. W. Abel, N. J. Long, K. G. Orrell, A. G. Osborne, H. M. Pain, V. Sik, *J. Chem. Soc., Chem. Commun.* **1992**, 303−304. − [14b] E. W. Abel, K. G. Orrell, A. G. Osborne, H. M. Pain, V. Sik, *J. Chem. Soc., Dalton Trans.* **1994**, 111−116. − [14c] T. Daniel, N. Suzuki, K. Tanaka, A. Nakamura, *J. Organomet. Chem.* **1995**, *505*, 109−117.

[15] [15a] W. Yao, O. Eisenstein, R. H. Crabtree, *Inorg. Chim. Acta* **1997**, *254*, 105−111. − [15b] M.-C. Lagunas, R. A. Gossage, W. J. J. Smeets, A. L. Spek, G. van Koten, *Eur. J. Inorg. Chem.* **1998**, 163−168 and cited references.

[16] [16a] E. Rotondo, G. Giordano, D. Minniti, *J. Chem. Soc., Dalton Trans.* **1996**, 253. − [16b] E. W. Abel, K. G. Orrell, A. G. Osborne, H. M. Pain, V. Sik, M. B. Hursthouse, K. M. Abdul Malik, *J. Chem. Soc., Dalton Trans.* **1996**, 253−254. − [16c] E. W. Abel, A. Gelling, K. G. Orrell, A. G. Osborne, V. Sik, *Chem. Commun.* **1996**, 2329−2330. − [16d] A. Gelling, K. G. Orrell, A. G. Osborne, V. Sik, *J. Chem. Soc., Dalton Trans.* **1998**, 937−945.

[17] See, for example C. Breutel, P. S. Pregosin, R. Salzmann, A. Togni, *J. Am. Chem. Soc.* **1994**, *116*, 4067−4068.

[18] L. A. Villanueva, K. A. Abboud, J. M. Boncella, *Organometallics* **1994**, *13*, 3921−3931.

[19] R. Nesper, P. S. Pregosin, K. Püntener, M. Wörle, *Helv. Chim. Acta* **1993**, *76*, 2239−2249.

[20] W. Zhang, C. Bensimon, R. J. Crutchley, *Inorg. Chem.* **1993**, *32*, 5808−5812.

[21] C. E. Housecroft, B. A. M. Shaykh, A. L. Rheingold, B. S. Haggerty, *Acta Crystallogr., Sect. C* **1990**, *46*, 1549−1551.

[22] [22a] M. H. Chisholm, I. P. Rothwell, in *Comprehensive Coordination Chemistry* (Eds.: G. Wilkinson, R. D. Gillard, J. A. McCleverty), Pergamon Press, Oxford, **1987**, vol. 2, chapter 13.4. − [22b] K. G. Caulton, *New J. Chem.* **1994**, *18*, 25−41.

[23] P. J. Pérez, P. S. White, M. Brookhart, J. L. Templeton, *Inorg. Chem.* **1994**, *33*, 6050−6056.

[24] R. L. Cowan, W. C. Trogler, *J. Am. Chem. Soc.* **1989**, *111*, 4750−4761.

[25] W. von E. Doering, C. H. DePuy, *J. Am. Chem. Soc.* **1953**, *75*, 5955−5957.

[26] K. Kanakarajan, K. Haider, A. W. Czarnik, *Synthesis* **1988**, 566−568.

[27] A. Wolkow, *Z. Chem.* **1870**, *6*, 321−327.

[28] Y. Takahashi, Ts. Ito, S. Sakai, Y. Ishii, *J. Chem. Soc., Chem. Commun.* **1970**, 1065−1066.

[29] G. K. Anderson, M. Lin, *Inorg. Synth.* **1990**, *28*, 60−63.

[30] L. R. Gray, D. J. Gulliver, W. Levason, M. Webster, *J. Chem. Soc., Dalton Trans.* **1983**, 133−141.

[31] H. Günther, *La Spectroscopie de RMN*, Masson, Paris, **1993**.

[32] I. D. Campbell, C. M. Dobson, R. G. Ratcliffe, R. J. P. Williams, *J. Magn. Reson.* **1978**, *29*, 397−417.

[33] W. H. Press, B. P. Flannery, S. A. Teukolsky, W. T. Vetterling, *Numerical Recipes*, Cambridge University Press, Cambridge, **1986**.

[34] *OpenMoleN, Interactive Structure Solution*, Nonius B. V., Delft, The Netherlands, **1997**.

[35] D. T. Cromer, J. T. Waber, *International Tables for X-ray Crystallography*, vol. IV, The Kynoch Press, Birmingham, **1974**. (a) Table 2.2b; (b) Table 2.3.1.

Received January 19, 2001
[I01027]

Cyanide Exchange on $Tl(CN)_4^-$ in Aqueous Solution Studied by ^{205}Tl and ^{13}C NMR Spectroscopy

István Bányai,*[a] Julius Glaser,*[b] and Imre Tóth[c]

Keywords: Ligand exchange / Thallium / Cyanides / Tl NMR

Dynamics of cyanide exchange between $Tl(^{13}CN)_4^-$ and $^{13}CN^-$ was studied by means ^{205}Tl and ^{13}C NMR. The rate law consists of two parts: $w = k_{CN}[Tl(CN)_4^-][CN^-] + k_{OH}[Tl(CN)_4^-][CN^-][OH^-]$ with $k_{CN} = 9.7(\pm0.4) \times 10^6$ $M^{-1}s^{-1}$ and $k_{OH} = 5.4(\pm0.4) \times 10^{10}$ $M^{-2}s^{-1}$. It was shown that the exchange between the two cyano species can be studied, not only by ^{13}C NMR, but also by ^{205}Tl NMR using the heteronuclear carbon–thallium scalar coupling as an indicator, despite the fact that only one Tl site is present in the system. The reaction mechanism is discussed in terms of an associative interchange mechanism, I_A. Penetration of the incoming cyanide ion into the coordination sphere of $Tl(CN)_4^-$ and $Tl(CN)_4(OH)^-$ is suggested to be the rate-determining step for the two parallel reactions paths. Possible reasons for the strong labilizing effect of the cyanide ligand is discussed in the light of thermodynamic and structural data. The possibility of detection of an exceptional exchange reaction, namely cyanide exchange between two $Tl(CN)_4^-$ entities by a direct encounter was theoretically settled, but found to be too slow to be detected.

Introduction

Recently, the formation of strong complexes between Tl^{III} and cyanide, $Tl(CN)_n^{3-n}$, $n = 1-4$, was established, and their stability constants determined.[1] A detailed multimethod study was published on the structure, symmetry, and coordination numbers of chloro, bromo, and cyano Tl^{III} complexes in aqueous solution.[2] In the monocyano complex, Tl^{III} is six-coordinate, $TlCN(OH_2)_5^{2+}$. In the second complex, *trans*-$TlCN_2(OH_2)_4^+$, the thallium ion retains the six-coordination; the Tl−CN bond length is almost the same as in the first complex, 2.11 Å, and Tl−O is 2.42 Å, that is 0.2 Å longer than in the hydrated thallium(3+) ion, $Tl(OH_2)_6^{3+}$. Upon the formation of the third complex, $Tl(CN)_3(OH_2)$, the coordination number decreases to four and the symmetry is C_{3v} with Tl−C 2.15 Å and Tl−O 2.42 Å. The fourth complex is tetrahedral with the Tl−C bond length equal to 2.19 Å.

The dynamics of the ions of group-13 elements in solution has not been well studied, because of the difficulty of monitoring the reactions.[3−8] The dynamic properties of thallium(III) are not well known. The kinetics of complex formation with semixylenol orange and 4-(2-pyridylazo)resorcinol were studied by stopped-flow methods.[9,10] The complex $Tl(OH)^{2+}$ was found to be the active species in complex formation kinetics. Lincoln et al. reported a lower limit of the pseudo-first-order rate constant of the Cl^- ligand substitution on the $TlCl_6^{3-}$ complex.[11] There are only four recent papers dealing in detail with the ligand exchange of hydrated complexed thallium(III) ions in chemical equilibrium. In these papers,[12−14] high-field ^{205}Tl NMR spectroscopy was established as a powerful tool for elucidating exchange paths using line-shape analysis and two-dimensional exchange spectroscopy (2D EXSY).[15] Three types of exchange paths were identified for thallium(III) cyanide complexes.[14] The first path is a ligand "self-exchange" between complexes with no net chemical change, for example according to Equation (1).

$$Tl(*CN)(CN)^+ + Tl(CN)_3 \underset{}{\overset{k_{23}}{\rightleftharpoons}} Tl(*CN)(CN)_2 + Tl(CN)_2^+ \quad (1)$$

The second path is the common anation (or complex formation) reaction of thallium(III) complexes, e.g. according to Equation (2).

$$Tl(CN)_2^+ + CN^- \underset{}{\overset{k'_{23}}{\rightleftharpoons}} Tl(CN)_3 \quad (2)$$

The third path is a ligand substitution according to Equation (3).

$$Tl(*CN)(CN)^+ + HCN \underset{k_{HCN,2}}{\overset{k_{2,HCN}}{\rightleftharpoons}} Tl(CN)_2^+ + H*CN \quad (3)$$

Rate constants for all dominating ligand exchange pathways were determined (see Table 1). The first type of reaction, according to Equation (1), is a very rarely encountered kind of ligand exchange, related to the inner-sphere electron transfer as far as the ligand-bridged transition state is concerned.[16−18] This exchange pattern dominates at low ligand/metal ratios, and the reason why it is observable at all is the very low free-ligand concentration due to the strong complex formation. Taking into account the effect of different ligands and the activation parameters, a dissociatively activated interchange process was suggested to oper-

[a] Department of Physical Chemistry, University of Debrecen (DE),
4010 Debrecen, Hungary
[b] Department of Chemistry, Inorganic Chemistry, Royal Institute of Technology (KTH),
10044 Stockholm, Sweden
E-mail: julius@inorg.kth.se
[c] Department of Inorganic and Analytical Chemistry, University of Debrecen (DE),
4010 Debrecen, Hungary

Supporting information for this article is available on the WWW under http://www.wiley-vch.de/home/eurjic or from the author.

 © WILEY-VCH Verlag GmbH, 69451 Weinheim, 2001 1434−1948/01/0707−1709 $ 17.50+.50/0

Table 1. Kinetic parameters for some exchange reactions of Tl^{III} halide and cyanide complexes in aqueous solution at 298 K; details for the rate-determining step (r.d.s.) are also given

Reaction	Determined rate constant, k_{ij}	Rate constant for r.d.s./s^{-1}, k_{ij}/K_{os}	Leaving/exchanging group	Ref.
$Tl(CN)_3 + Tl(CN)_4^- \rightleftarrows Tl(CN)_4^- + Tl(CN)_3$	444 $M^{-1}s^{-1}$	1500	CN^-	[14]
$Tl(CN)_2^+ + Tl(CN)_4^- \rightleftarrows 2\ Tl(CN)_3$	712 $M^{-1}s^{-1}$	500	CN^-	[14]
$Tl(CN)_2^+ + Tl(CN)_3 \rightleftarrows Tl(CN)_3 + Tl(CN)_2^+$	161 $M^{-1}s^{-1}$	500	CN^-	[14]
$Tl^{3+} + Tl(CN)_2^+ \rightleftarrows 2\ Tl(CN)^{2+}$	4.1 $M^{-1}s^{-1}$	900	CN^-	[14]
$Tl(CN)_2 + CN^- \rightleftarrows Tl(CN)_3$	3.9×10^9 $M^{-1}s^{-1}$	1.1×10^{10}	H_2O	[14]
$Tl(CN)_3 + CN^- \rightleftarrows Tl(CN)_4^-$	4.5×10^8 $M^{-1}s^{-1}$	1.5×10^9	H_2O	[14]
$Tl(*CN)(CN)^+ + CN^- \rightleftarrows Tl(CN)_2^+ + *CN^-$	6×10^9 $M^{-1}s^{-1}$	4×10^9	CN^-	[14]
$Tl(*CN)(CN)_3^- + CN^- \rightleftarrows Tl(CN)_4^- + *CN^-$	9.7×10^6 $M^{-1}s^{-1}$	1.3×10^8	CN^-	this work
$Tl(*CN)(CN)_3^- + CN^- (+OH^-) \rightleftarrows Tl(CN)_4^- + *CN^-$	5.4×10^{10} $M^{-2}s^{-1}$	–	CN^-	this work
$Tl(*Cl)(Cl)_{i-1}^{(3-i)} + Cl^- \rightleftarrows Tl(Cl)_i^{(3-i)} + *Cl^-$		10^6	Cl^-	[11]

ate for bromide and chloride in reactions according to Equation (1), i.e. after the encounter of the two complexes and formation of an outer-sphere complex, the leaving of a water ligand from the first coordination sphere of Tl^{III} is the rate-determining step. However, for the cyano Tl^{III} complexes $Tl(CN)_n(OH_2)_m^{3-n}$, the ligand "self-exchange" was found to be much slower than for the halide systems; hence, breaking of the Tl−CN bond, which is about 0.3 Å shorter than the Tl−halide bond, was suggested to be the rate-determining step.[14]

The anation reactions according to Equation (2) dominate the exchange for higher complexes and the rate of reaction depends on the entering ligand. Therefore, an associatively activated rate-determining step was proposed for both halide and cyanide complexes, where the entering ligand labilizes the coordinated water.

Also, it has been possible to determine the rate constants for the ligand substitution reaction according to Equation (3) on $Tl(CN)_2^+$ by means of ^{13}C NMR.[14] Two parallel reaction paths were identified, one with formal contribution of HCN and the other with CN^-. If the common Eigen−Wilkins-type reaction mechanism is assumed for the reaction path, with contribution of CN^-, then the incoming cyanide ion would have to labilize the bonded cyanide ion with 7 orders of magnitude in first-order rate constant units. This was judged to be less probable, and an alternative mechanism was suggested with the participation of HCN, which proceeded by deprotonation of the transition state.[14] In order to provide more confidence to the mechanism of the ligand substitution process according to Equation (3), additional experimental support was needed.

For the present study, the system $Tl(^{13}CN)_4^-/^{13}CN^-$ in aqueous media was selected. The usual tool for studying the chemical exchange in this system would be ^{13}C NMR, because (i) ^{13}C enrichment provides short measurement time and (ii) there are two exchanging carbon sites. Thus, basic conditions for a dynamic study of such an exchange reaction are fulfilled.[19] The convenient ^{205}Tl NMR [high natural abundance of the NMR active isotope(s), high NMR sensitivity, spin 1/2] can principally not be used in this case because only one chemical environment of Tl^{III} is present.

However, different magnetic thallium sites occur due to the scalar ^{205}Tl-^{13}C coupling, resulting in five signals in the ^{205}Tl NMR spectrum with an intensity ratio of 1:4:6:4:1. In the current paper it is shown that this fact makes the detection of the cyanide exchange possible by means of ^{205}Tl NMR. An additional advantage is provided by the fact that in ^{205}Tl NMR the observed line shape and the transfer of longitudinal magnetization is not affected by other exchange reactions in which the cyanide ion takes part; therefore, evaluation of the rate constants is more facile.

Results and Calculations

Determination of pH

Since knowledge of the pH is vital for the studied system, and the experiments had to be performed in a small volume, the NMR technique was the most straightforward way of measuring the pH. At first, 7 mM phosphate solution was prepared in the same medium as the real experiments. The pH was read using a pH meter with combined glass electrode (its internal solution contained NaCl instead of KCl in order to avoid the precipitation of $KClO_4$), and the chemical shift of the ^{31}P signal was determined. The pH was corrected according to Irving's method,[20] and from the dependence of ^{31}P NMR chemical shift vs. pH the actual pK values (protonation constants) and chemical shift values for the different protonated forms of phosphate were determined. For the actual ionic medium, the following values were obtained: $K_1 = (1.9\pm0.2)\times10^{11}$, $K_2 = (3.4\pm0.4)\times10^6$; $\delta(PO_4^{3-}) = 6.2\pm0.05$, $\delta(HPO_4^{2-}) = 3.47\pm0.06$, $\delta(H_2PO_4^-) = 0.7\pm0.03$. These values were then used for the determination of the actual $\log K_{HCN} = 9.9\pm0.2$ M^{-1}, which is in good agreement with the literature.[21] The latter stability constant was used for calculation of proton exchange rate constants between HCN and CN^-, which affects the ^{13}C NMR dynamics strongly.[22]

1D NMR Line-Shape Analysis

Some representative ^{205}Tl NMR and ^{13}C NMR spectra as a function of pH are shown in Figures 1 and 2, together

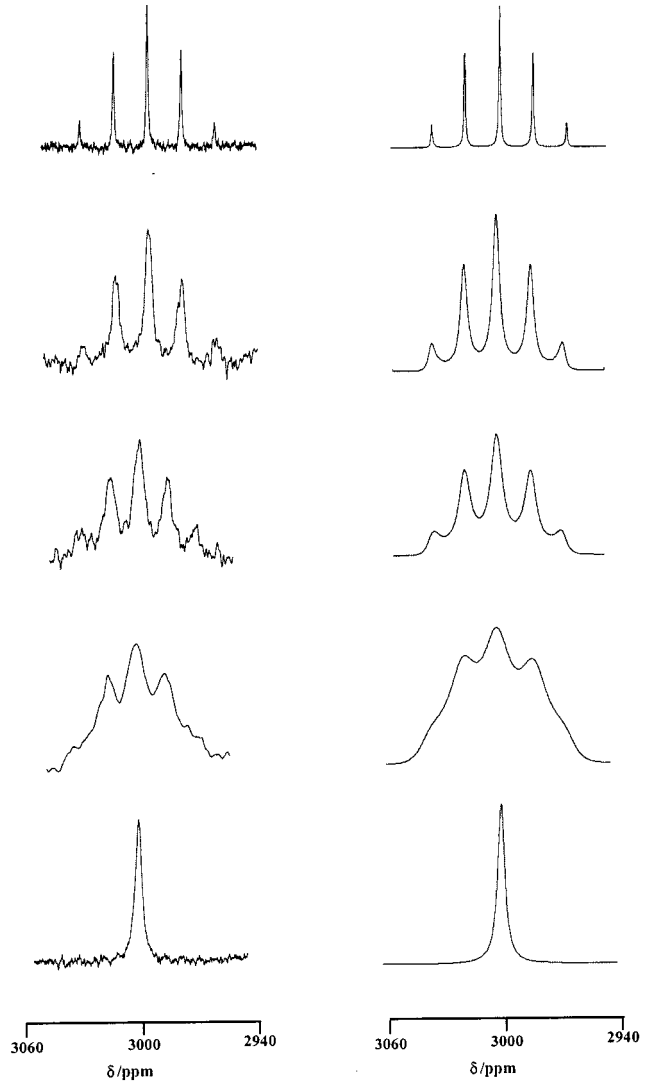

Figure 1. Measured and calculated ^{205}Tl NMR spectra of a solution where $[Tl^{3+}]_{tot}$ = 0.0504 M and $[CN^-]_{tot}$ = 0.135 M as a function of pH; from top to bottom: pH = 6.08 and k_{obs} = 176 s^{-1}, pH = 6.77 and k_{obs} = 861 s^{-1}, pH = 6.98 and k_{obs} = 1400 s^{-1}, pH = 7.16 and k_{obs} = 2120 s^{-1}, pH = 9.15 and k_{obs} = 18400 s^{-1}

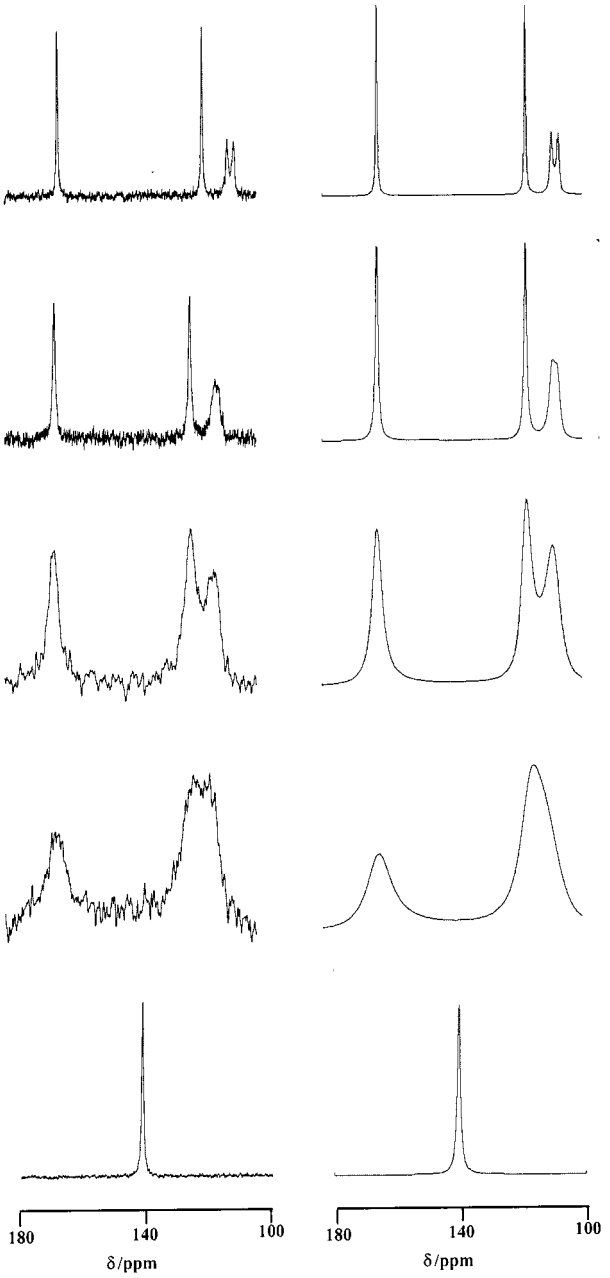

Figure 2. Measured and calculated ^{13}C NMR spectra of a solution in which $[Tl^{3+}]_{tot}$ = 0.0504 M and $[CN^-]_{tot}$ = 0.135 M as a function of pH; from top to bottom pH = 5.53, 6.08, 6.98, 7.16, and 9.82 (see text for details)

with the calculated spectra. It is apparent that complete band-shape analysis had to be used for both ^{205}Tl NMR and ^{13}C NMR.

The simulation of the spectra was made according to Equation (4) given by Reeves and Shaw[23,24] where V is the function of the frequency variable, **P** is the column vector of molar fractions (1/15,4/15,6/15,4/15,1/15 in the thallium pentet), and **C** is a matrix, Equation (5).

$$V = const\,\mathbf{C}^{-1}\,\mathbf{P} \tag{4}$$

$$\mathbf{C} = \mathbf{R_2} + \mathbf{w}\boldsymbol{\varepsilon}\mathbf{w} \tag{5}$$

$\mathbf{R_2}$ is the complete relaxation matrix given as a sum of diagonal matrix of the reciprocal relaxation times $\mathbf{T_{2i}}$ and rate matrix **K**, which contains the pseudo-first-order rate constants. $\boldsymbol{\varepsilon_2} = \mathbf{R_2}^{-1}$, and $\mathbf{w_i}$ is the diagonal matrix of chemical shifts in frequency units. In this case, the creation of the $\mathbf{R_2}$ rate matrix is crucial. It was written in the form for ^{205}Tl NMR [Equation (6)]; k_{obs} is the pseudo-first-order rate constant for all processes that result in exchange of transverse magnetisation between the spin-labelled Tl sites, defined in the usual way from the rate of the exchange reaction $w/[Tl(CN)_4^-]$.[19]

$$\mathbf{K} = \begin{pmatrix} -4k_{obs} & k_{obs} & 0 & 0 & 0 \\ 4k_{obs} & -4k_{obs} & 2k_{obs} & 0 & 0 \\ 0 & 3k_{obs} & -4k_{obs} & 3k_{obs} & 0 \\ 0 & 0 & 2k_{obs} & -4k_{obs} & 4k_{obs} \\ 0 & 0 & 0 & k_{obs} & -4k_{obs} \end{pmatrix} \tag{6}$$

Construction of the rate matrix was made as follows (see Appendix for details). The thallium sites in the ^{205}Tl NMR spectra are observed as five peaks because of the ^{13}C scalar coupling, which can simply be modelled by the spin states α and β of ^{13}C(N) around the thallium ion. The five peaks are Tl(α,α,α,α), Tl(α,α,α,β), Tl(α,α,β,β), Tl(α,β,β,β), and Tl(β,β,β,β) with the intensities according to the probability of existence of each species.[25,26] An exchange reaction, using simplified symbols for the species present, can therefore be written according to Equation (7).

$$\mathrm{Tl}(4\alpha) + \mathrm{CN}(\beta) \underset{}{\overset{k_{4\alpha,3\alpha}}{\rightleftharpoons}} \mathrm{Tl}(3\alpha1\beta) + \mathrm{CN}(\alpha) \qquad (7)$$

Taking into account the ratio of the concentrations of the different forms, and the fact that the rate is the same in both directions, the matrix **K** can be constructed. The principle of microscopic reversibility is fulfilled because the sum of the columns gives 0, while for the off-diagonal elements of the matrix $p_i k_{ij} = p_j k_{ji}$ (where p_i is the ith element of vector **P** and k_{ij} is an element of matrix **K** in ith line and jth column).

In contrast to the apparent simplicity of the rate matrix for ^{205}Tl NMR, the situation for ^{13}C NMR is more complicated both from a kinetic and a spectroscopic point of view. The species H^{13}CN (doublet at δ = 112.7, $^1J_{\mathrm{H\text{-}C}}$ = 270 Hz) exchanges with CN^-, causing line broadening in their signals. The cyanide ions exchange between the free cyanide ion and Tl(^{13}CN)$_4^-$ causing an additional broadening of the signals of the participating sites. Moreover, the species Tl(^{13}CN)$_4^-$ appears in the ^{13}C NMR spectrum as four signals; although the chemical shift is δ = 142.75, the isotopomers containing ^{205}Tl and ^{203}Tl, respectively, have different coupling constants to ^{13}C, resulting in two pairs of doublets.[1] The exchange system therefore requires a 7×7 matrix with rate constants for exchange between Tl(CN)$_4^-$ and CN^-/HCN, and HCN and CN^-. The latter exchange is known from the literature.[22] After a considerable effort the rate matrix could be constructed [see Appendix and Equation (8)]; $k_{\mathrm{HCN}}{}^{\mathrm{H}}$, $k_{\mathrm{CN}}{}^{\mathrm{H}}$ are the rate constants of the proton exchange between HCN and CN^-; k_{HCN} and k_{CN} are the rate constants of cyanide exchange between Tl(CN)$_4^-$ and HCN/CN^-, respectively. Half of the isotopomer ratios of ^{203}Tl and ^{205}Tl, are represented as r_3 (0.295/2) and r_5 (0.705/2), respectively, while the division factors 2 are due to the spin-spin coupling. The diagonal elements (Σ) were set up so that the sum of each column is zero.

Kinetic Analysis

First, the ^{205}Tl NMR spectra were analysed by giving different values for k_{obs} in Equation (6), and comparing the calculated line shapes to the experimental ones. In this way a set of pseudo-first-order rate constants was obtained and analysed as a function of pH (cf. Figure 3). The two models according to Equation (9) could describe the cyanide exchange at constant cyanide concentration.

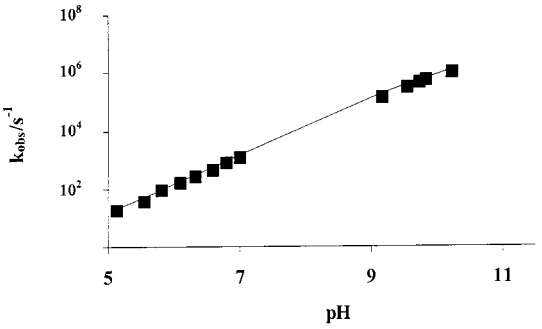

Figure 3. The dependence of the pseudo-first-order rate constants on the [H$^+$] concentration (squares); the line represents the best fit according to Equation (10b) with k_{CN} = (9.7±0.4)×10^6 M^{-1}s^{-1} and k_{OH} = (5.4±0.4)×10^{10} M^{-2}s^{-1}

$$w = k_{\mathrm{CN}}[\mathrm{CN}^-][\mathrm{Tl(CN)_4}^-] + k_{\mathrm{OH}}[\mathrm{OH}^-][\mathrm{Tl(CN)_4}^-] \qquad (9a)$$

or

$$w = k_{\mathrm{CN}}[\mathrm{CN}^-][\mathrm{Tl(CN)_4}^-] + k_{\mathrm{OH}}[\mathrm{OH}^-][\mathrm{CN}^-][\mathrm{Tl(CN)_4}^-] \qquad (9b)$$

Taking into account the facts that w/[Tl(CN)$_4^-$] equals k_{obs} and K_{HCN} = [HCN]/[H$^+$][CN^-], the dependencies on the pH are according to Equation (10), where K_w is the water ion product and T_{CN} is the total concentration of the uncomplexed cyanide.

$$k_{obs} = \frac{k_{OH}K_w + (k_{OH}K_{HCN}K_w + k_{CN}T_{CN})[\mathrm{H}^+]}{(1 + K_{HCN}[\mathrm{H}^+])[\mathrm{H}^+]} \qquad (10a)$$

$$k_{obs} = \frac{k_{OH}T_{CN}K_w + k_{CN}T_{CN}[\mathrm{H}^+]}{(1 + K_{HCN}[\mathrm{H}^+])[\mathrm{H}^+]} \qquad (10b)$$

In order to distinguish between the two possibilities [Equations (9a) and (9b)], the line width was also measured in a solution that had ten times lower free cyanide concentration. At the same pH the line width decreased with a factor of about ten, which shows that the rate Equation (9b) is operative. The results of the least-squares fitting are shown in Figure 3, and the calculated rate constants are:

$$\mathbf{K} = \begin{pmatrix} \Sigma & 0 & \frac{1}{2}k_{HCN}[\mathrm{HCN}] & \frac{1}{2}k_{HCN}[\mathrm{HCN}] & \frac{1}{2}k_{HCN}[\mathrm{HCN}] & \frac{1}{2}k_{HCN}[\mathrm{HCN}] & k_{CN}^H \\ 0 & \Sigma & \frac{1}{2}k_{HCN}[\mathrm{HCN}] & \frac{1}{2}k_{HCN}[\mathrm{HCN}] & \frac{1}{2}k_{HCN}[\mathrm{HCN}] & \frac{1}{2}k_{HCN}[\mathrm{HCN}] & k_{CN}^H \\ k_{HCN}r_5[\mathrm{Tl}] & k_{HCN}r_5[\mathrm{Tl}] & \Sigma & 0 & 0 & 0 & k_{CN}r_5[\mathrm{Tl}] \\ k_{HCN}r_3[\mathrm{Tl}] & k_{HCN}r_3[\mathrm{Tl}] & 0 & \Sigma & 0 & 0 & k_{CN}r_3[\mathrm{Tl}] \\ k_{HCN}r_3[\mathrm{Tl}] & k_{HCN}r_3[\mathrm{Tl}] & 0 & 0 & \Sigma & 0 & k_{CN}r_3[\mathrm{Tl}] \\ k_{HCN}r_5[\mathrm{Tl}] & k_{HCN}r_5[\mathrm{Tl}] & 0 & 0 & 0 & \Sigma & k_{CN}r_5[\mathrm{Tl}] \\ 2\times k_{HCN}^H & 2\times k_{HCN}^H & k_{CN}[\mathrm{CN}] & k_{CN}[\mathrm{CN}] & k_{CN}[\mathrm{CN}] & k_{CN}[\mathrm{CN}] & \Sigma \end{pmatrix} \qquad (8)$$

$k_{CN} = (9.7\pm0.4)\times10^6$ M^{-1}s^{-1} and $k_{OH} = (5.4\pm0.4)\times10^{10}$ M^{-2}s^{-1}.

In order to further verify the rate constants determined by ^{205}Tl NMR these were introduced into the rate matrix of ^{13}C NMR [Equation (8)], and the proton exchange rate constants were taken from the literature.[22] Then, ^{13}C NMR spectra were simulated (Figure 2, right side); good agreement was found considering that the literature values were obtained for a different ionic medium. The largest deviation in the line widths was generally below 10%.

Similarly to the recently established existence of the ligand "self-exchange" between complexes, e.g. $Tl(CN)_3$ and $Tl(CN)_4^-$,[14] it was now considered that cyanide exchange can also occur between two $Tl(CN)_4^-$ species according to Equation (11).

$$Tl(^*CN)_4^- + Tl(CN)_4^- \underset{}{\overset{k_{4,4}}{\rightleftharpoons}} Tl(CN)_4^- + Tl(^*CN)_4^- \qquad (11a)$$

Use of the short notations introduced above, and considering an encounter of two thallium complexes with different spin states of ^{13}C yields Equation (11b).

$$Tl(4\alpha) + Tl(3\alpha\beta) \overset{k_{4,4}}{\rightleftharpoons} Tl(3\alpha\beta) + Tl(4\alpha) \qquad (11b)$$

If this reaction were to occur, then it would be possible to study it by both ^{13}C and ^{205}Tl NMR because of the scalar coupling present in these systems.[25] A solution sample was prepared, suitable for detection of such a reaction, i.e. pH and cyanide concentration was kept as low as possible in order to slow down the exchange paths described by Equations (9a) and (9b). However, pH could not be decreased below a certain value, in order to avoid the exchange between $Tl(CN)_3$ and $Tl(CN)_4^-$. The composition of the sample was: $[Tl^{3+}]_{tot} = 0.0434$ M, $[^{13}CN^-]_{tot} = 0.1816$ (in 3.0 M $NaClO_4$), and the pH was carefully regulated to 6.5 as monitored by ^{31}P NMR. Both ^{205}Tl and ^{13}C NMR spectra were recorded for this sample in order to assure that no significant amount of $Tl(CN)_3$ was present. In order to determine the exchange rate matrix in a facile way, ^{205}Tl NMR 2D-EXSY experiments were run on the sample using mixing times of 4 ms and 8 ms. Cross peaks were detected (cf. Figure 4), indicating chemical exchange between the magnetically labelled spin sites of $Tl(CN)_4^-$. A quantitative analysis resulted in the rate matrices for 4 ms mixing time [Equation (12a)] and for 8 ms mixing time [Equation (12b)].[27]

136.9	45.8	-	-	-
183.5	44.1	64.1	-	-
-	96.1	59.2	84.5	-
-	-	56.3	34.4	172.4
-	-	-	43.1	125.9

(12a)

80.1	26.8	-	-	-
107.2	-6.3	53.6	-	-
-	80.4	-13.0	74.1	-
-	-	49.4	-2.9	119.2
-	-	-	29.8	39.6

(12b)

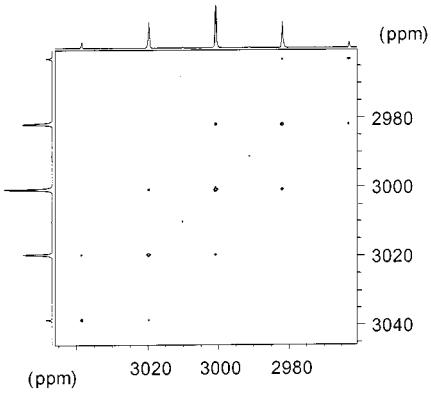

Figure 4. ^{205}Tl 2D EXSY of $Tl(^{13}CN)_4^-$ aqueous solution with mixing time 4 ms; $T = 298$ K; ^{12}C satellites are also visible at $\delta = 2990$ and 3010

The matrix elements denoted by "−" have no real meaning and have been removed. Also, the diagonal elements are not the real ones because we did not use zero mixing time for the calculation.[27] Then, using the rate constants determined above from the 1D NMR spectra, the rate matrix was calculated [Equation (12c)].

-120	30	0	0	0
120	-120	60	0	0
0	90	-120	90	0
0	0	60	-120	120
0	0	0	30	-120

(12c)

Good agreement can be recognized in the off diagonal elements of the matrices [Equation (12)]. Therefore, no further detectable parallel reaction path is needed to describe the system, even at very small cyanide excess. Thus, it can be concluded that NMR makes it possible to detect the otherwise undetectable exchange reactions according to Equation (11), if they match the NMR criteria (lifetime comparable to the NMR relaxation times) and kinetic criteria (high enough exchange rate).

Discussion

For the ligand substitution process according to Equation (13) the rate Equation (14) was found.

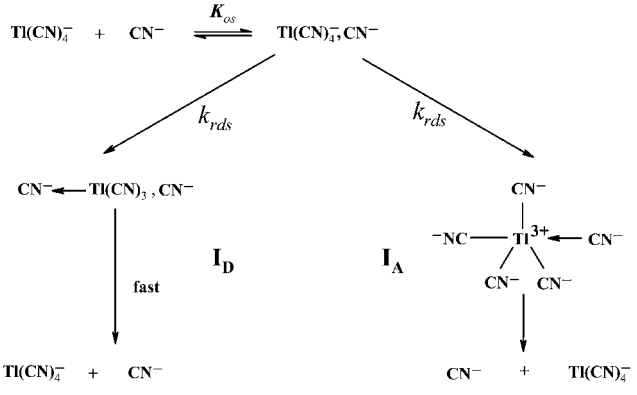

Scheme 1

$$Tl(CN)_4^- + *CN^- \underset{k_{CN,4}}{\overset{k_{4,CN}}{\rightleftharpoons}} Tl(*CN)(CN)_3^- + CN^- \quad (13)$$

$$w = k_{4,CN}[CN^-][Tl(CN)_4^-] + k_{OH}[OH^-][CN^-][Tl(CN)_4^-] \quad (14)$$

In Equations (13) and (14) the notation of the rate constant is $k_{4,CN}$ (instead of k_{CN}), i.e. the same as in our earlier papers on the same or related subject.[12–14]. Usually, the Eigen–Wilkins-type mechanism[28] is used to describe such reactions according to Scheme 1.

During the first, generally fast step an ion pair is formed for which the stability constant can be estimated using the Fuoss equation, by considering only the electrostatic interactions.[28] For the present case this stability constant $K_{os}(-1,-1)$ is 0.074, from which the rate constant of the rate-determining step can be calculated as $k_{rds} = k_{4,CN}/K_{os} = 1.3\ 10^8\ s^{-1}$. There are two parallel paths according to Scheme 1. If the rate of dissociation of a CN^- ligand determines the exchange rate, the path is a dissociative interchange I_D. If the incoming cyano ligand forces out one of the complexed ligands, the process is an associative interchange I_A (or limiting associative A, if a complex with a higher coordination number can be detected).

The hitherto reported rate constants concerning pertinent ligand exchange reactions in chemical equilibrium have been collected (cf. Table 1) and can be helpful for suggesting the mechanism of the presently studied reaction. In the case of a "self-exchange" reaction, when one cyanide ion goes from one metal ion to another (see Table 1, first four lines), it was found that the rupture of a Tl–C bond is a slow process with rate constant of a few hundred s^{-1}.[14] For complex formation reactions (Table 1, lines 6–7) these rate constants are several orders of magnitude larger, because the bottle-neck of these reactions is the rupture of the $Tl-OH_2$ bond activated by the entering ligand, or sometimes the diffusion.[29] These rate constants are equally high for the thallium(III) halide and cyanide complexes, and larger than the estimated water exchange rate.[12] Therefore, it was concluded that an associatively activated process I_A operates. There was some doubt about this, because no pronounced entering ligand effect was found when comparing the chloride, bromide, and cyanide complexes. However, this was attributed to the fact that these complex formation reactions had a rate close to the diffusion control limit; therefore, the differences cannot be observed.[14]

In the case of ligand substitution reactions of $Tl(CN)_2^+$ [Equation (3)] it was difficult to characterise the mechanism: rupture of the Tl–C bond must occur in any case because of the symmetric nature of the reaction according to Equation (3). However, the calculated rate constant of the rate-determining step was also found to be much higher than those found for the ligand exchange between complexes, according to Equation (1).[14] This was surprising, and an alternative mechanism was suggested in the case of $Tl(CN)_2^+$ with participation of HCN (rather than CN^-).[14] In the present work, another rate constant has been determined for ligand substitution, e.g. on $Tl(CN)_4^-$, with an equally fast rate-determining step. A probable explanation is that the incoming cyanide ion coordinates, forming a transition state where the complexes are highly labile. Therefore, an associative interchange or associative mechanism is supposed to be operative.

In order to interpret the details of the reaction mechanism of the ligand substitution reaction paths the data in Table 1 can be utilised. Let us start with ligand exchange reaction between complexes [Equation (1)]. If we suppose that binuclear complexes are temporarily formed so that the attacking "ligand" is complexed as well, it is difficult to assume any labilizing effect of the incoming reactants. Therefore, the most probable rate-determining step is a rupture of the metal–ligand bond in the transition state containing a ligand in a bridging position. The kinetic stability, i.e. inertness, of these intermediates could well be controlled by the lability of the metal–ligand bond. This interpretation is supported by the similarity of the halide ligands in this so called "self exchange", whereas there is a significant difference between the halide ions and the more covalently bonded cyanide ion. For the species $Tl(CN)_n^{3-n}$ this reaction is slower by a few orders of magnitude compared to that for the thallium(III) halide complexes.

If it is accepted that the ligand "self-exchange" [Equation (1)] mirrors the Tl–CN bond breaking with little external influence then the high rate of ligand substitution [Equation (13)] is unexpected. At this point, the physical/chemical properties of the studied species should be considered. The thermodynamic stability of the thallium cyanide complexes[1] is: $\log K_i = 13.21, 13.39, 8.67$, and 7.44, for $i =$ 1 to 4, respectively. The first two Tl^{III} halide complexes are five orders of magnitude stronger, which can serve as an indication for changing of the character of the metal–ligand bond.[31] The first two cyanide complexes show similarity with covalently bonded organometallic Tl^{3+} compounds,[32,33] while $Tl(CN)_3$ and $Tl(CN)_4^-$ show similarity to the usual inorganic ligand coordination mainly by donation of the electrons to the metal ion. This difference can also be discerned in the behaviour of Tl^{III} complexes in organometallic reactions.[33]

The steric arrangement and change of the coordination geometry may play a key role in kinetics and in mechanistic considerations. For the cyano Tl^{III} species, $Tl(CN)_n(OH_2)_{6-n}^{n-3}$ ($n = 1$ and 2) in solution, the coordination number is six with equal and very short Tl–CN bond lengths, 2.10–2.11 Å.[2] For $n = 3$ and 4 this bond is significantly longer, 2.15 and 2.19 Å, respectively, and these complexes are both tetrahedral. However, the bond lengths are still 0.2–0.4 Å shorter than the corresponding bonds of the halides.

Ligand substitution kinetic data for cyanide exchange is known for two species only, $Tl(CN)_2(OH_2)_4^{2+}$ [14] and $Tl(CN)_4^-$ (this work). For $Tl(CN)_2(OH_2)_4^{2+}$, after the attack of the incoming cyanide ligand a new species forms as a transition state in which the Tl–CN bond resembles the one in $Tl(CN)_3$, but still with a number of water molecules (probably four) in the first coordination sphere of the thallium ion. Presumably, this Tl–CN bond is more labile due to the much higher coordination number than the one in the thermodynamically stable third complex, namely

$Tl(CN)_3(OH_2)$.[2] With this argument, the fast ligand substitution can be understood.

For $Tl(CN)_4^-$, a transition state species with five-coordination is expected to be labile. Also in this case, the rate of insertion of the entering ligand determines the rate of leaving of the coordinated ligand; therefore, an associative interchange mechanism is probable.

The hydroxide-dependent parallel path also needs some consideration: (i) Such a path is not often encountered in ligand substitution reactions, but if it exists it proceeds by OH^- catalysis and deprotonation of the coordinated ligands.[28] (ii) Hitherto, formation of ternary hydroxo Tl^{3+} cyanide complexes has not been reported, although binary hydroxo complexes with high stability are well known.[30] However, all earlier investigations were made in acidic solution in order to avoid hydrolysis. In Figure 5, relative contributions of the two reaction paths are presented. It can be seen that the contribution of the hydroxide-assisted reaction path starts to be effective for pH > 9.5.

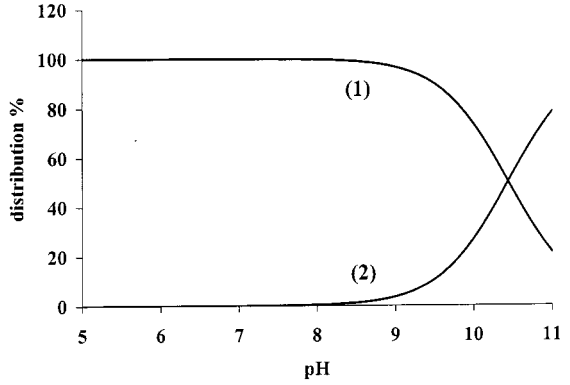

Figure 5. The relative contribution of the two reaction paths, (1) without and (2) with OH contribution, as a function of the pH

A first approximation was to consider both HCN and CN^- as reactive species; however, this was not compatible with the experiments. If $Tl(CN)_3OH^-$ were assumed to be the active species then the rate equation would not have the form of Equation (9b). It is possible that a five-coordinate $Tl(CN)_4OH^{2-}$ acts as kinetically active species which would give a rate equation consistent with the one obtained [Equation (10)]. However, the calculation of the rate-determining step is difficult because the stability constant of the suggested $Tl(CN)_4OH^{2-}$ is not known. In fact, when the pH is increased to > 11 the solution containing Tl^{III} and excess cyanide turns brownish, indicating that in spite of the high stability of the cyanide complexes they can be transferred into (mixed) hydroxo species. In this case, the penetration of the incoming cyanide ion would determine the exchange rate in the same way as discussed above. The limiting associative mechanism, that is the formation of six-coordinate species from $Tl(CN)_4OH^{2-}$, would not be compatible with the experimental findings, namely that a maximum of four cyanide ligands can coordinate to the thallium(III) ion, even at a large cyanide excess.[1] Also, other kinetic data are consistent with the suggested reaction mechanism. Mixed complexes with exceptionally high coordination numbers, for example those between $Tl(edta)^-$ on one side and Cl^-, Br^-, CN^-, and SCN^- on the other side also show high kinetic lability.[34]

In conclusion, two new examples of ligand substitution reactions for cyanothallium(III) complexes were established. The new reactions, similar to the previously described one [Equation (3)], proceed by an associatively activated interchange mechanism.

^{205}Tl NMR was confirmed to be the experimental technique of choice for studies of thallium solution chemistry. In this specific case, due to the magnetic spin labelling it was possible to utilise its power despite the fact that only one thallium-containing species was participating in the chemical process under study.

Experimental Section

Preparation and Analysis of Solutions: A ca. 1.2 M aqueous stock solution of $Tl(ClO_4)_3$ in 3.8 M $HClO_4$ was prepared by anodic oxidation of a $TlClO_4$ solution.[30,31] The concentrations of acid and thallium content in the stock solution were determined as described elsewhere.[35] The samples were prepared from the appropriate volume of the stock solution, solutions of 0.3 M $HClO_4$ and 5 M $NaClO_4$, and a weighted amount of solid $Na^{13}CN$ (Cambridge Isotope Laboratories, > 99% ^{13}C enrichment). In order to keep the activity coefficients of the reacting species approximately constant, the total sodium concentration, $[Na^+]_{tot}$, was kept at 3 M. The composition of the samples was determined by quantitative ^{205}Tl and ^{13}C NMR. Some details of sample preparation and analysis were described in a previous paper.[12] The pH dependence of the ^{205}Tl NMR and ^{13}C NMR spectra was recorded by titration of a 1-mL sample with 0.3 M $HClO_4$ (containing the same ionic medium, i.e. 3 M $NaClO_4$) in an NMR tube using a micro syringe, between pH = 7.4 and pH = 5.12. The change of pH was measured by ^{31}P chemical shifts; this "potentiometer" was calibrated by pH potentiometry in independent experiments.[36] The sample contained 7 mM total PO_4^{3-} in different protonated forms. Another 1 mL of the solution was titrated with NaOH in a similar way. In this case, the $^{13}CN/HCN$ signal was also used for checking the pH.

NMR Measurements: All NMR spectra were recorded at a probe temperature of 25±0.5 °C with a Bruker DMX500 spectrometer. The magnetic field was unlocked; field drift was found to be negligible. ^{205}Tl NMR: spectrometer frequency 289.4 MHz, flip angle 90° (12 μs), pulse repetition time of 5 s was found long enough for complete magnetic relaxation. The chemical shifts are reported in ppm toward higher frequency with respect to an aqueous solution of $TlClO_4$ extrapolated to infinite dilution. ^{13}C NMR: spectrometer frequency 125.8 MHz, flip angle ca. 30° (8 μs), relaxation delay was in the range 4−16 s depending on the relaxation rates of the investigated species. The chemical shifts are reported in ppm toward higher frequency with respect to an external water-soluble sodium derivative of TMS. ^{205}Tl 2D-EXSY NMR spectra were recorded with 512 increment experiments, each consisting of 8 scans and with 5 s relaxation delay. Fourier transformations were performed in a 1K×1K data-point matrix with a window function cosine and an SSB = 2 filter. The Fourier transformation, volume integration and other NMR spectroscopic data treatment was performed using a Bruker program package (2D WinNMR®).

APPENDIX

Construction of Rate Matrices for ^{205}Tl NMR

As was found in a previous paper from this laboratory, in an exchange process between two complexed cyano species only one cyanide ligand changes its position.[15] Therefore, only this type of transition is considered. As an example, we choose the process when one cyanide ion goes from $Tl[CN_4(4\alpha)]^-$ [denoted for the sake of simplicity as Tl(4α)] to $Tl(CN)(3\alpha,1\beta)^-$ [denoted as Tl(3α)]. The labels in brackets give the concentrations of the various carbon-labelled Tl sites. For example: $Tl[CN_4(4\alpha)]^-$ has four α-carbon atoms and the concentration is [4α] while for $Tl(CN)(3\alpha,1\beta)^-$ the notation is [3α]. The rate of exchange from site i to j is written using pseudo-first-order rate constants (or observed rate constants) k_{ij}, as in Equation (15).

$$w_{43} = w_{34} = k_{43}[4\alpha] = k_{34}[3\alpha] \quad (15)$$

From Equation (15) the most important consequence is the relation between the forward and backward observed rate constants [Equation (16)].

$$k_{34}=k_{43}\frac{[4\alpha]}{[3\alpha]}=\frac{1}{4}k_{43} \quad (16)$$

It is easy to generalize Equations (15) and (16) as Equations (17) and (18).

$$w_{ij} = w_{ji} = k_{ij}[j\alpha] = k_{ij}[i\alpha] \quad (17)$$

$$k_{ij} = k_{ij}([i\alpha]/[j\alpha]) = p_j/p_i \quad (18)$$

From these considerations Equation (19) follows.

$$k_{34} = k_{43}\frac{1}{4}; k_{23} = k_{32}\frac{2}{3}; k_{12} = k_{21}\frac{3}{2}; k_{01} = k_{10}\frac{4}{1}; \quad (19)$$

It is obvious that since all exchanges are identical reactions from a chemical point of view (i.e. one cyano ligand is substituted) they cannot be characterized by four different rate constants. Let us consider that if a Tl(3α,1β) meets $CN^-(\alpha)$ the probability of forming Tl(4α) is one, but if this interaction happens between $CN^-(\alpha)$ and Tl(2α,2β) then this probability is twice as high because there are two cyanide ions with β spin state. Following this consideration up to Tl(4α) we can find a series of relations as in Equation (20).

$$k_{10} = k^{obs}; k_{01} = 4k^{obs}; k_{12} = 3k^{obs}; k_{21} = 2k^{obs}; k_{23} = 2k^{obs}; k_{32} = 3k^{obs}; k_{34} = k^{obs}; k_{43} = 4k^{obs} \quad (20)$$

These considerations are a consequent application of microscopic reversibility, therefore the sum of the elements of each column of the rate matrix **K** should be zero provided that the matrix was correctly constructed. It is easy to make mistakes in setting up the rate matrix, especially when the number of elements is large. However, in the test phase of the model, reaching the so called "fast exchange" regime − when only one peak appears − calculation of the chemical shift will be wrong if the matrix setup is not correct, indicating the error. The model calculation was performed so that the k_{obs} values were varied until the band shape of the calculated spectra were identical with the experimental ones. Then, the dependence of the obtained observed rate constant on the pH was analyzed.

Construction of Rate Matrices for ^{13}C NMR

The construction of the ^{13}C rate matrix required somewhat longer, but not more complicated algebra. While for ^{205}Tl NMR we knew that all peaks are determined by one exchange reaction, and as they were side-bands of a main peak they had to behave in exactly the same way, for ^{13}C NMR it is not the case. Still, there are multiplets in the spectrum: Hα and Hβ, Tlα5 and Tlβ5 (for the ^{205}Tl isotope), or Tlα3 and Tlβ3 (for the ^{203}Tl isotope) which behave identically. However, the isotopomers behave as independent species and have different line widths caused by the exchange, because of their different populations. Furthermore, the proton exchange between HCN and CN^- should also be taken into account. First, we denote the seven signals a follows: Hα and Hβ are HCN doublets; Tlα5 and Tlβ5 are the ^{205}Tl-coupled doublets; Tlα3 and Tlβ3 are the ^{203}Tl-coupled doublets; CN is the signal of the cyanide ion. The concentrations according to the previous paragraph are the notations in brackets, e. g. [Hα] is the concentration of the α-spin-state proton-containing HCN. The task is to find the smallest number of observed rate constants from which we can combine the possible 42 elements of the **K** rate matrix. Take a reaction between $Tl(CN)_4^-$ (Tlα5) and H(α)CN. According to Equation (15) the Equations (21) and (22) follow.

$$w_{H\alpha\alpha5} = w_{\alpha5H\alpha} = k_{H\alpha\alpha5}[H\alpha] = k_{\alpha5H\alpha}[Tl\alpha5] \quad (21)$$

$$k_{H\alpha\alpha5} = k_{\alpha5H\alpha}([Tl\alpha5]/[H\alpha]) \quad (22)$$

According to Equations (21) and (22) we can obtain 8 relations between 16 elements of **K**, i. e. exchange between Hα and Tlα5, Tlα3, Tlβ5, Tlβ3; and between Hβ and Tlα5, Tlα3, Tlβ5, Tlβ3. Of course, there is only one chemically determined rate process, namely according to Equation (23).

$$w = k_{HCN}[HCN][Tl(CN)4^-] \quad (23)$$

The rate constant is independent of the spin labelling, therefore Equation (24) follows.

$$w_{H\alpha\alpha5} = w_{\alpha5H\alpha} = k_{HCN}[H\alpha][Tl\alpha5] \quad (24)$$

Considering the relation between the concentration of the chemically identical but magnetically labelled species Equation (25) is given, where 0.705 is the isotopic ratio of the ^{205}Tl isotope.

$$w_{H\alpha\alpha5} = w_{\alpha5H\alpha} = k_{HCN}\frac{1}{2}[HCN]\frac{0.705}{2}[Tl(CN)_4^-] \quad (25)$$

Therefore, the pseudo-first-order rate constants for the forward and backward reaction is given by Equation (26).

$$k_{H\alpha\alpha5} = w/\frac{1}{2}[HCN] = k_{HCN}\frac{0.705}{2}[Tl(CN)_4^-] \quad (26a)$$

$$k_{\alpha5H\alpha} = w/\left(\frac{0.705}{2}[Tl(CN)_4^-]\right) = k_{HCN}\frac{1}{2}[HCN] \quad (26b)$$

Another three pairs of this type of relation is valid for the rest of exchange processes in which H(α)CN is involved [Equation (27) to (29)].

$$k_{H\alpha\alpha3} = w/\frac{1}{2}[HCN] = k_{HCN}\frac{0.295}{2}[Tl(CN)_4^-] \quad (27a)$$

$$k_{\alpha3H\alpha} = w/\left(\frac{0.295}{2}[Tl(CN)_4^-]\right) = k_{HCN}\frac{1}{2}[HCN] \quad (27b)$$

$$k_{H\alpha\beta5} = w/\frac{1}{2}[HCN] = k_{HCN}\frac{0.705}{2}[Tl(CN)_4^-] \quad (28a)$$

$$k_{\beta5H\alpha} = w/\left(\frac{0.705}{2}[Tl(CN)_4^-]\right) = k_{HCN}\frac{1}{2}[HCN] \quad (28b)$$

$$k_{H\alpha\beta3} = w/\frac{1}{2}[HCN] = k_{HCN}\frac{0.295}{2}[Tl(CN)_4^-] \quad (29a)$$

$$k_{\beta3H\alpha} = w/\left(\frac{0.295}{2}[Tl(CN)_4^-]\right) = k_{HCN}\frac{1}{2}[HCN] \quad (29c)$$

Of course, we have four pairs of relations for exchanges where H(β)CN is involved which are exactly the same. Therefore, 16 elements are already determined. Another 8 elements come from the reaction between CN^- and Tlα5, Tlα3, Tlβ5, Tlβ3 [Equations (30) and (31)].

$$w_{CN\alpha5} = w_{\alpha5CN} = k_{CN\alpha5}[CN^-] = k_{\alpha5CN}[\alpha5] \quad (30)$$

$$k_{CN\alpha5} = k_{\alpha5CN}([\alpha5]/[CN^-]) \quad (31)$$

Also here, only one chemical reaction should be taken into account, namely according to Equations (32) and (33).

$$w = k_{CN}[CN^-][Tl(CN)_4^-] \quad (32)$$

$$w_{CN\alpha5} = w_{\alpha5CN} = k_{CN}[CN^-][Tl\alpha5] \quad (33)$$

It is important to note that we consider principally only one reaction path. Of course, there can be many parallel reaction paths, but it principally does not change the final results.

Substitution of the concentrations of the different Tl species into Equation (33) yields Equation (34), which leads to the pseudo-first-order rate constants according to Equations (35) to (38).

$$w_{CN\alpha5} = w_{a5CN} = k_{CN}\left[CN^-\right]\frac{0.705}{2}\left[Tl(CN)_4^-\right] \quad (34)$$

$$w_{CN\alpha5} / \left[CN^-\right] = k_{CN}\frac{0.705}{2}\left[Tl(CN)_4^-\right] \quad (35a)$$

$$w_{\alpha5CN} / \frac{0.705}{2}\left[Tl(CN)_4^-\right] = k_{CN}\left[CN^-\right] \quad (35b)$$

$$w_{CN\alpha3} / \left[CN^-\right] = k_{CN}\frac{0.295}{2}\left[Tl(CN)_4^-\right] \quad (36a)$$

$$w_{\alpha3CN} / \frac{0.295}{2}\left[Tl(CN)_4^-\right] = k_{CN}\left[CN^-\right] \quad (36b)$$

$$w_{CN\beta5} / \left[CN^-\right] = k_{CN}\frac{0.705}{2}\left[Tl(CN)_4^-\right] \quad (37a)$$

$$w_{\beta5CN} / \frac{0.705}{2}\left[Tl(CN)_4^-\right] = k_{CN}\left[CN^-\right] \quad (37b)$$

$$w_{CN\beta3} / \left[CN^-\right] = k_{CN}\frac{0.295}{2}\left[Tl(CN)_4^-\right] \quad (38a)$$

$$w_{\alpha5CN} / \frac{0.295}{2}\left[Tl(CN)_4^-\right] = k_{CN}\left[CN^-\right] \quad (38b)$$

Since it turned out that the reactions between the magnetically labelled Tl species, e.g. Tlα5 and Tlβ5, do not occur, we do not show how they were introduced into the rate matrix.

Acknowledgments

The continuous financial support of the Swedish Natural Science Research Council (NFR) is gratefully acknowledged. The authors thank the Hungarian National Scientific Research Foundation (OTKA T026115), Carl Trygger Foundation for Scientific Research and Wennergren Center Foundation for financial support.

[1] J. Blixt, B. Györi, J. Glaser, *J. Am. Chem. Soc.* **1989**, *111*, 7784.
[2] J. Blixt, J. Glaser, J. Mink, I. Persson, P. Persson, M. Sandström, *J. Am. Chem. Soc.* **1995**, *117*, 5089.
[3] C. Ammann, P. Moore, A. E. Merbach, C. H. McAteer, *Helv. Chim. Acta* **1980**, *63*, 268.
[4] A. E. Merbach, *Pure Appl. Chem.* **1982**, *54*, 1479.
[5] R. van Eldik, *Inorganic High Pressure Chemistry Kinetics and Mechanisms* (Ed.: R. van Eldik), Elsevier, Amsterdam, **1986**.
[6] D. Hugi-Cleary, L. Helm, A. E. Merbach, *Helv. Chim. Acta* **1985**, *68*, 545.
[7] J. Miceli, J. Stuehr, *J. Am. Chem. Soc.* **1968**, *90*, 6967.
[8] A. Bodor, I. Tóth, I. Bányai, Z. Szabó, G. T. Hefter, *Inorg. Chem.* **2000**, *39*, 2530.
[9] Y. Kawai, T. Takahashi, K. Hayashi, T. Imamura, H. Nakayama, M. Fujimoto, *Bull. Chem. Soc. Jpn.* **1972**, *45*, 1417−1423.
[10] R. Funada, T. Imamura, M. Fujimoto, *Bull. Chem. Soc. Jpn.* **1979**, *52*, 1535−1536.
[11] S. F. Lincoln, A. C. Sandercock, D. R. Stranks, *Aust. J. Chem.* **1975**, *28*, 1901−1905.
[12] I. Bányai, J. Glaser, *J. Am. Chem. Soc.* **1989**, *111*, 3186.
[13] I. Bányai, J. Glaser, *J. Am. Chem. Soc.* **1990**, *112*, 4703.
[14] I. Bányai, J. Glaser, J. Losonczy, *Inorg. Chem.* **1997**, *36*, 5900−5908.
[15] G. Batta, I. Bányai, J. Glaser, *J. Am. Chem. Soc.* **1993**, *115*, 6782 and references therein.
[16] H. Taube, H. Myers, R. L. Rich, *J. Am. Chem. Soc.* **1953**, *75*, 4118.
[17] H. Taube, H. Myers, *J. Am. Chem. Soc.* **1954**, *76*, 2103.
[18] H. Taube, E. L. King, *J. Am. Chem. Soc.* **1954**, *76*, 4053.
[19] J. Sandström, *Dynamic NMR Spectroscopy*, Academic Press, London, **1982**.
[20] H. M. Irving, M. G. Miles, L. P. Pettit, *Anal. Chim. Acta* **1967**, *38*, 475.
[21] I. Bányai, J. Blixt, J. Glaser, I. Tóth, *Acta Chem. Scand.* **1992**, *46*, 138.
[22] I. Bányai, J. Blixt, J. Glaser, I. Tóth, *Acta Chem. Scand.* **1992**, *46*, 142.
[23] L. W. Reeves, K. N. Shaw, *Can. J. Chem.* **1970**, *48*, 3641.
[24] S. O. Chan, L. W. Reeves, *J. Am. Chem. Soc.* **1973**, *95*, 670.
[25] Y. Huang, G. Bodenhausen, R. R. Ernst, *J. Am. Chem. Soc.* **1981**, *103*, 6988−6989.
[26] G. Bodenhausen, R. R. Ernst, *Mol. Phys.* **1982**, *47*, 319.
[27] E. R. Johnstone, M. J. Dellwo, J. Hendrix, *J. Magn. Res.* **1985**, *66*, 399.
[28] M. L. Tobe, J. Burgess, *Inorganic Reaction Mechanisms*, Longman, New York, **1999**.
[29] B. H. Robinson, *Proton Transfer Reactions*, Chapman & Hall, London, **1975**.
[30] G. Biedermann, *Arkiv Kemi* **1953**, *5*, 441.
[31] J. Glaser, U. Henriksson, *J. Am. Chem. Soc.* **1981**, *103*, 6642.
[32] M. V. Castano, A. Sánchez, J. S. Casas, J. Sordo, J. L. Brianso, J. F. Piniella, X. Solans, G. Germain, T. Debaerdemaeker, J. Glaser, *Organometallics* **1988**, *7*, 1897, and references therein.
[33] B. Györi, A. Sánchez, J. Glaser, *J. Organomet. Chem.* **1989**, *361*, 1.
[34] J. Blixt, J. Glaser, P. Solymosi, I. Tóth, *Inorg. Chem.* **1992**, *31*, 5288.
[35] A. A. Noyes, K. S. Pitzer, C. L. Dunn, *J. Am. Chem. Soc.* **1935**, *57*, 1223.
[36] P. W. Kuchel, *Biological Application of NMR* (Ed.: P. W. Kuchel), John Wiley & Sons, Chichester, New York, **1989**, pp. 177−182.

Received August 24, 2000
[I00327]

On the Gallanyls $R^*_3Ga_2^{\cdot}$ and $R^*_4Ga_3^{\cdot}$ As Well As Gallanides $R^*_3Ga_2^-$ and $R^*_4Ga_3^-$ (R^* = Si*t*Bu$_3$) − Syntheses, Characterization, Structures[‡]

Nils Wiberg,*[a] Thomas Blank,[a] Kerstin Amelunxen,[a] Heinrich Nöth,[a][‡‡] Jörg Knizek,[a][‡‡] Tassilo Habereder,[a][‡‡] Wolfgang Kaim,[b][‡‡‡] and Matthias Wanner[b][‡‡‡]

Keywords: Anions / EPR spectroscopy / Gallium / Radicals / Silicon / X-ray structural analyses

The reduction of black-blue tris(supersilyl)digallanyl $[R^*_2Ga–GaR^*]^{\cdot}$ (R^* = Si*t*Bu$_3$ = supersilyl) in organic solvents with Na, $NaC_{10}H_8$, or NaR^* leads to deep-red sodium tris(supersilyl)digallanide–THF(1/3) $NaGa_2R^*_3\times3THF$ = $[R^*_2Ga–GaR^*Na(THF)_3]$, which transforms in the presence of 18-crown-6 into deep-blue sodium tetrakis(supersilyl)trigallanide–18-crown-6(1/1)–THF(1/2) $[Na(18\text{-}C\text{-}6)(THF)_2]^+[R^*_2Ga–GaR^*–GaR^*]^-$.The oxidation of the latter anion with R^*Br or TCNE as well as the reaction of the digallanyl $R^*_3Ga_2^{\cdot}$ with R^*Br leads to deep-green tetra(supersilyl)cyclotrigallanyl $[\cdots R^*Ga–GaR^*_2–GaR^*\cdots]^{\cdot}$. The latter radical thermolizes at 100 °C to dark-violet tetrakis(supersilyl)-*tetrahedro*-tetragallane $R^*_4Ga_4$ besides the digallanyl $R^*_3Ga_2^{\cdot}$. This is also prepared from NaR^* and $GaCl_3$ or R^*_2GaCl, as well as by oxidation of $R^*_3Ga_2^-$, and itself thermolizes with formation of the tetrahedrane $R^*_4Ga_4$. According to X-ray structure analyses of the mentioned compounds, the Ga–Ga bond of the digallanide $NaGa_2R^*_3\times3THF$ (NMR spectroscopically observed) is comparably short (2.380 Å), approaching a bond order of 2. In fact, it is distinctly shorter than the Ga–Ga bond (2.420 Å) in the digallanyl $R^*_3Ga_2^{\cdot}$ (EPR spectroscopically observed). The Ga atoms of the trigallanyl $R^*_4Ga_3^{\cdot}$ (EPR spectroscopically observed) are located at the corners of a triangle with two shorter $R^*_2Ga–GaR^*$ sides (2.527 Å) and a comparably longer $R^*Ga–GaR^*$ basis (2.879 Å). The mean value of the two Ga–Ga bonds in the trigallanide $R^*_4Ga_3^-$ (NMR spectroscopically observed) is as long (2.53 Å) as the short Ga–Ga bonds in $R^*_4Ga_3^{\cdot}$. The anion shows an intramolecular $CH_3\cdots Ga$ contact (C–Ga 2.10 Å) between one peripheral methyl group of the R^*_2Ga entity and the anionic Ga atom in $[R^*_2Ga–GaR^*–GaR^*]^-$.

Introduction

As recently reported,[1,2] the reaction of supersilylsodium NaR^* (R^* = Si*t*Bu$_3$ = supersilyl) with aluminium trihalides AlX_3 (X = Cl, Br) in alkanes leads, at room temperature, via isolable bis(supersilyl)aluminium halides R^*_2AlX to tetrakis(supersilyl)dialane $R^*_2Al–AlR^*_2$ (cf. Scheme 1). Thereby, NaR^* reacts with R^*_2AlCl by formation of NaCl as well as of radicals $R^{*\cdot}$ and $R^*_2Al^{\cdot}$. For steric reasons, only dimerization of $R^{*\cdot}$ and $R^*_2Al^{\cdot}$ is possible, but no recombination of both radicals under formation of R^*_3Al. The mentioned dialane $R^*_4Al_2$ thermolizes in heptane at 80 °C in a reversible reaction to bis(supersilyl)alanyl $R^*_2Al^{\cdot}$ in low equillibrium concentration ($R^*_4Al_2 \rightleftarrows 2\ R^*_2Al^{\cdot}$). In an irreversible reaction it thermolizes to tris(supersilyl)dialanyl $R^*_3Al_2^{\cdot}$ as well as to tetrakis(supersilyl)cyclotrialanyl $R^*_4Al_3^{\cdot}$ and to tetrakis(supersilyl)-*tetrahedro*-tetraalane $R^*_4Al_4$ (Scheme 1).[2] Possibly, $R^*_4Al_3^{\cdot}$ forms by a reaction of the monoalanyl $R^*_2Al^{\cdot}$ with the dialanyl $R^*_3Al_2^{\cdot}$. The cyclotrialanyl $R^*_4Al_3^{\cdot}$ itself transforms slowly into $R^*_3Al_2^{\cdot}$ and $R^*_4Al_4$ [1] (cf. Scheme 1).

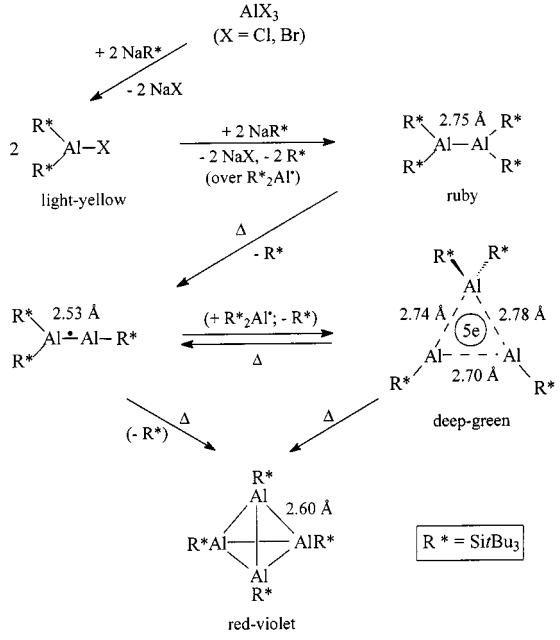

Scheme 1. Syntheses, reactions, colors, Al−Al distances of dialane $R^*_4Al_2$, alanyls $R^*_3Al_2^{\cdot}$ and $R^*_4Al_3^{\cdot}$ as well as tetrahedrane $R^*_4Al_4$ [equations in part not exactly formulated; R^* dimerizes to $(R^*)_2$ or − at higher temperatures − transforms into R^*H)

[‡] Compounds of Silicon and Homologues, 145. − Supersilyl Compounds of Boron and Homologues, 14. − Part 144 and Part 13: A. Donchev, A. Schnepf, G. Stößer, E. Baum, H. Schnöckel, T. Blank, N. Wiberg, *Chem. Eur. J.*, in press.

[a] Department Chemie der Universität München, Butenandtstraße 5−13 (Haus D), 81377 München, Germany
[b] Institut für Anorganische Chemie der Universität Stuttgart, Plattenwaldring 55, 70550 Stuttgart, Germany

[‡‡] X-ray structure analyses.
[‡‡‡] ESR studies.

 © WILEY-VCH Verlag GmbH, 69451 Weinheim, 2001 1434−1948/01/0707−1719 $ 17.50+.50/0

On the other hand, tetrakis(supersilyl)digallane $R^*_2Ga-GaR^*_2$ (**1**) thermolizes at much lower temperature than the dialane. Therefore, the reaction of gallium trichloride with supersilylsodium NaR* in heptane at room temperature leads, via isolable bis(supersilyl)gallium chloride R^*_2GaCl, not at all to the digallane **1**, which is unknown to date, but directly to tris(supersilyl)digallanyl $R^*_3Ga_2^{\cdot}$ (**2**) (Scheme 2).[3] The latter radicals thermolize in heptane at 100 °C exclusively to tetrakis(supersilyl)-*tetrahedro*-tetragallane $R^*_4Ga_4$ (**4**) (cf. preliminary communication[4]). No tetrakis(supersilyl)cyclotrigallanyl $R^*_4Ga_3^{\cdot}$ (**3**) is formed in this case. Therefore, we tried to prepare the cyclotrigallanyl **2** by another route from the digallanyl **2**. These studies are presented here.

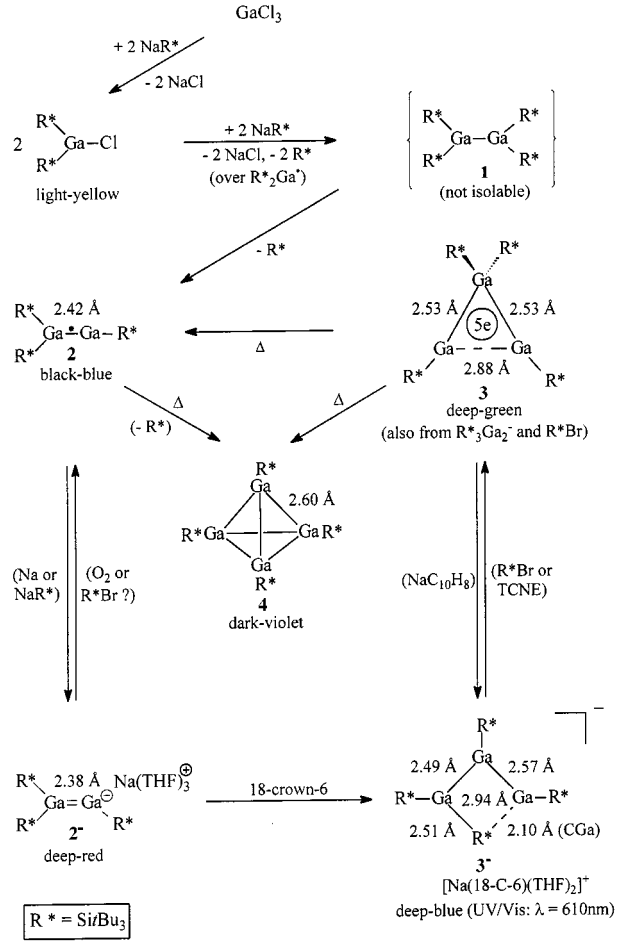

Scheme 2. Syntheses, reactions, colors, and Ga−Ga distances of gallanyls $R^*_3Ga_2^{\cdot}$ (**2**) and $R^*_4Ga_3^{\cdot}$ (**3**), gallanides $R^*_3Ga_2^-$ (**2**$^-$) and $R^*_4Ga_3^-$ (**3**$^-$) as well as tetrahedrane $R^*_4Ga_4$ (**4**) [equations in part not exactly formulated; R* dimerizes to $(R^*)_2$ or − at higher temperatures − transforms into R*H]

Results

Syntheses and Properties of $R^*_3Ga_2^{\cdot}$, $R^*_4Ga_3^{\cdot}$, $R^*_3Ga_2^-$, and $R^*_4Ga_3^-$

According to Scheme 2, the digallanyl $R^*_3Ga_2^{\cdot}$ (**2**) can be reduced in pentane, benzene, or tetrahydrofuran (THF) with sodium in the presence or absence of naphthalene, or with supersilylsodium NaR*×2THF ($NaR^* \rightarrow Na^+ + R^* + e^-$) to sodium tris(supersilyl)digallanide−tetrahydrofuran(1/3) [$NaGa_2R^*_3\times3THF$, **2**$^-$; cation $Na(THF)_3^+$]. In fact, one starts with bis(supersilyl)gallium chloride R^*_2GaCl, which is easily reduced by NaR* or by $NaC_{10}H_8$ in THF. The digallanide **2**$^-$ forms deep-red, air- and moisture-sensitive crystals, which give red solutions in alkanes and benzene, but a blue solution in tetrahydrofuran (THF). The digallanide **2**$^-$ reacts in pentane with Me_3SiCl at low temperature with formation of light-red tris(supersilyl)(trimethylsilyl)digallane [$R^*_2Ga-GaR^*(SiMe_3)$; evidence of the existence of a digallanide; first tetrasilyldigallane to date].

If 18-crown-6 is added to a deep-red solution of **2**$^-$ in benzene, the color of the reaction mixture immediately changes to dark-blue. In fact, **2**$^-$ reacts according to Scheme 2 to give dark-blue, air- and moisture-sensitive sodium tetrakis(supersilyl)trigallanide−18-crown-6(1/1)−tetrahydrofuran(1/2) {$[Na(18\text{-}C\text{-}6)(THF)_2]^+[Ga_3R^*_4]^-$}, which is soluble in benzene and THF, but insoluble in alkanes (for X-ray structure analysis see below). Possibly, a transfer of supersilylgallium R*Ga between two digallanide anions **2**$^-$ takes place as described by $2R^*_3Ga_2^- \rightarrow R^*_2Ga^- + R^*_4Ga_3^-$, whereby the monogallanide $R^*_2Ga^-$ may transfer another supersilylgallium by $R^*_2Ga^- + R^*_3Ga_2^- \rightarrow R^{*-} + R^*_4Ga_3^-$ (R^{*-} is unstable in the presence of 18-C-6 to produce R*H).[5]

The trigallanide $R^*_4Ga_3^-$(**3**$^-$) is oxidized in benzene with supersilyl bromide ($R^*Br + e^- \rightarrow R^* + Br^-$) or tetracyanoethylene ($TCNE + 2e^- \rightarrow TCNE^{2-}$) to deep-green air- and moisture-sensitive, tetrakis(supersilyl)cyclotrigallanyl ($R^*_4Ga_3^{\cdot}$; **3**), soluble in organic media. The latter is itself reduced by sodium naphthalenide to $R^*_4Ga_3^-$ (cf. Scheme 2; for EPR spectrum and X-ray structure analysis see below). Unexpectedly, $R^*_4Ga_3^{\cdot}$ (**3**) besides $(R^*)_2$ is also very simply obtained by reaction of the digallanide $NaGa_2R^*_3\times3THF$ {$Na(THF)_3^+$ **2**$^-$} in pentane with supersilyl bromide R*Br. As the radical **3** is formed faster from $R^*_3Ga_2^-$ (**2**$^-$) and R*Br than from $R^*_4Ga_3^-$ (**3**$^-$) and R*Br, the former reaction obviously does not proceed via anion **3**$^-$, but may involve the radical $R^*_3Ga_2^{\cdot}$ (**2**), which eventually reacts with **3**$^-$ by transfer of R*Ga (cf. production of **3**$^-$ from **2**$^-$).

Radical $R^*_4Ga_3^{\cdot}$ (**3**) thermolizes at 45 °C slowly (within 1 d) with formation of $R^*_3Ga_2^{\cdot}$, besides $R^*_4Ga_4$ (Scheme 2, cf. thermolysis of $R^*_4Al_3^{\cdot}$).[6] The black-blue, air- and moisture-sensitive, in organic media soluble tris(supersilyl)digallanyl $R^*_3Ga_2^{\cdot}$ (**2**) is also synthesized in alkanes from $GaCl_3$ and NaR*, or from R^*_2GaCl and NaR* as well as Na,[3] or from $R^*_3Ga_2^-$ (**2**$^-$) by oxidation. Formally, the radical **3** decomposes with elimination of supersilylgallium R*Ga into the digallanyl **2**, whereby R*Ga tetramerizes. Because the digallanyl **2** itself decomposes at 100 °C in heptane to dark-violet air- and moisture-sensitive, in organic media soluble tetrakis(supersilyl)-*tetrahedro*-tetragallane ($R^*_4Ga_4$; **4**) and $(R^*)_2$,[4] the trigallanyl **3** finally decomposes in pentane at 100 °C exclusively into $(R^*)_2$ and thermostable **4**

(almost no decomposition in solution at 100 °C; decomposition of the solid at the melting point 322 °C).

Characterization of $R^*_3Ga_2^{\cdot}$, $R^*_4Ga_3^{\cdot}$, $R^*_3Ga_2^-$, and $R^*_4Ga_3^-$

The ^{29}Si NMR signals of digallanide $[R^*_2Ga-GaR^*]^-$ [**2**$^-$; the Ga−Na bond in $NaGa_2R^*_3\times3THF$ is according to the formulation $Na(THF)_3^+$ **2**$^-$ undoubtedly ionic[5]] and trigallanide $[R^*_2Ga-GaR^*-GaR^*]^-$ (**3**$^-$) appear at low field [δ = 37.1/54.3 in the first case (area ratio ca. 2:1) and δ = 53.5/42.0/42.3 in the second case (area ratio 2:1:1)]. The ^{29}Si NMR signals of the R* groups in the digallane $R^*_2Ga-GaR^*(SiMe_3)$ show comparable shifts (δ = 48.80/44.80 for 2 Si*t*Bu$_3$/1 Si*t*Bu$_3$). It is worth mentioning in this context that the ^{29}Si NMR signals of alkali metal supersilanides MR* and of supersilyl halides R*Hal appear in the same region at δ = 30−40.[5]

On the other hand, the radicals $R^*_3Ga_2^{\cdot}$ (**2**) and $R^*_4Ga_3^{\cdot}$ (**3**) − not observed in NMR − are characterized by EPR. As the EPR spectrum of **2** has been discussed in detail in a preliminary publication,[3] the following remarks refer only to the EPR spectrum of **3**. Freshly dissolved in cyclohexane, **3** exhibits an unresolved, unsymmetrical EPR signal of $H_T \approx 20$ mT total width at $g = 1.998$. The lack of resolution and the asymmetry point to insufficient averaging of anisotropic contributions to the *g* and *A* (hyperfine) tensors. Similar, but less pronounced effects were observed for the paramagnetic systems $R^*_3Ga_2^{\cdot}$ (**2**)[3] and $R'_4Ga_2^{\cdot-}$with R′ = $CH(SiMe_3)_2$.[6a] In comparison with $R^*_4Al_3$ [1] (g = 2.0053), the gallium analogue exhibits a *g* factor lower than *g*(electron) = 2.0023, which agrees[7] with the presence of low-lying unoccupied orbitals. On the other hand, a glassy frozen solution of **3** at 110 K in cyclohexane produces a broad (H_T = 55 mT), partially resolved EPR spectrum. While the signal could not be unambiguously analyzed due to overlapping *g* components in the X band, the large spectral width confirms the sizeable *g* and *A* anisotropy (^{69}Ga:I = 3:2, 60.1% natural abundance, isotropic hyperfine constant a_0 = 435.68 mT; ^{71}Ga:I = 3:2, 39.9%, a_o = 553.58 mT[8]). The width of the low-temperature spectrum is in agreement with H_T = 15.0 mT for $R^*_4Al_3$ [1] (^{27}Al:I = 5:2, 100%, a_o = 139.55 mT[8]). On prolonged standing or warming, the solution of **3** produces a new EPR signal that could be identified as that of **2**.[3]

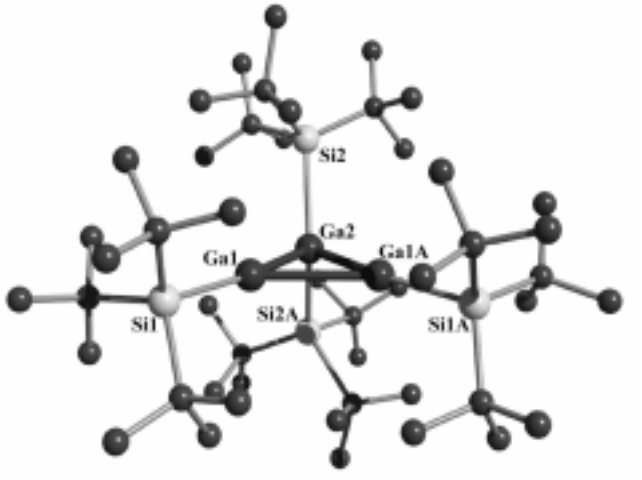

Figure 1. Structure of $R^*_4Ga_3^{\cdot}$ (**3**) in the crystal; atom numbering used (SCHAKAL plot; H atoms omitted for clarity); selected distances [Å] and angles [°] with standard deviations: Ga1−Ga2 2.5267(7), Ga1−Ga1A 2.879(1), Ga1−Si1 2.513(1), Ga2−Si2A 2.536(1), Ga2−Si2 2.536(1), Si−C (mean value) 1.98; Si1−Ga1−Ga2 169.88(4), Si1−Ga1−Ga1A, 134.83(3), Ga2−Ga1−Ga1A 55.27 (2) [angles sum at Ga1/Ga1A 359.98], Ga1−Ga2−Ga1A 69.47(3), Ga1−Ga2−Si2A 106.77(4), Ga1A−Ga2−Si2A 108.85(3), Ga1−Ga2−Si2 108.85(3), Ga1A−Ga2−Si2 106.77(4), Si2A−Ga2−Si2 136.30(7), C−Si−Ga (mean value) 108.62, C−Si−C (mean value) 111.99; Si2−Ga2−Ga1−Si1 81.97, Si1−Ga1−Ga1A−Si1A 1.67

Structures of $R^*_3Ga_2^{\cdot}$, $R^*_4Ga_3^{\cdot}$, $R^*_3Ga_2^-$, and $R^*_4Ga_3^-$

The structures of the trigallanyl $R^*_4Ga_3^{\cdot}$ (**3**), the digallanide $NaGa_2R^*_3\times3THF$ [**2**$^-$; cation $Na(THF)_3^+$], and the trigallanide $[Ga_3R^*_4]^-$ [**3**$^-$; cation $Na(18\text{-}C\text{-}6)(THF)_2^+$] are shown in the Figures 1, 2, and 3, respectively, together with selected bond lengths and angles. The structure of the digallanyl $R^*_3Ga_2^{\cdot}$ (**2**) has already been published.[3]

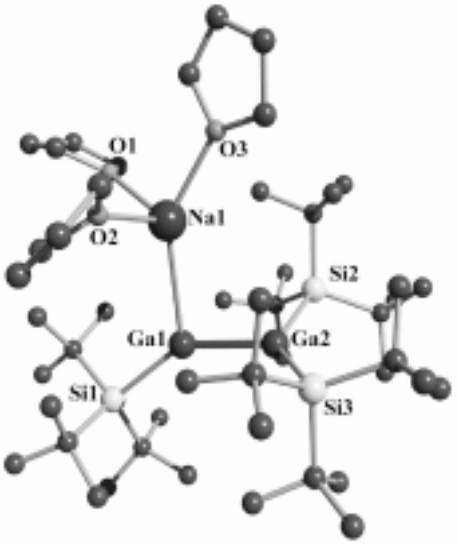

Figure 2. Structure of $NaGa_2R^*_3\times3THF$ [$Na(THF)_3^+\cdot$**2**$^-$] in the crystal; atom numbering used (SCHAKAL plot; H atoms omitted for clarity); selected distances [Å] and angles [°] with standard deviations: Ga1−Ga2 2.3797(6), Ga1−Si1 2.500(1), Ga1−Na1 3.205(2), Ga2−Si2 2.517 (1), Ga2−Si3 2.519(1), Na1−O3 2.316(4), Na1−O1 2.337(5), Na1−O2 2.404(5), Si−C (mean value) 1.96; Ga2−Ga1−Si1 142.41(4), Ga2−Ga1−Na1 91.40(4), Si1−Ga1−Na1 126.14(5) [angles sum at Ga1 359.94], Ga1−Ga2−Si2 112.09(3), Ga1−Ga2−Si3 112.59(3), Si2−Ga2−Si3 133.72(4) [angles sum at Ga2 358.34], O3−Na1−O1 91.3(2), O3−Na1−O2 88.1(2), O1−Na1−O2 97.6(2), O3−Na1−Ga1 112.9 (1), O1−Na1−Ga1 108.2 (1), O2−Na1−Ga1 145.7 (1), C−Si−Ga (mean value) 109.77, C−Si−C (mean value) 109.1; Si1−Ga1−Ga2−Si2/Si3 100.43/−91.99, Na1−Ga1−Ga2−Si2/Si3 82.52/−85.06

As stated elsewhere,[3] the structure of tris(supersilyl)digallanyl ($R^*_3Ga_2^{\cdot}$, **2**) is comparable with the structure of $R^*_3Al_2^{\cdot}$. Both radicals show an almost planar Si_2E-ESi skeleton from which only the Si atom bonded to the biva-

lent E centre deviates by few degrees in line with the E−E vector (E = Al/Ga: 5.1/10°; the E−E−Si plane stands almost orthogonal to the Si−E−Si plane). In both cases, the E−E distance is comparatively short (cf. Schemes 1 and 2). This points to an E−E bonding order greater than one, whereby the shortening of the E−E bond length by going from $R^*_3Al_2^{\cdot}$ to $R^*_3Ga_2^{\cdot}$ may be due to a decrease of the radius by going from Al atoms to Ga atoms. According tothis, and in agreement with EPR studies,[3,9] the radicals $R^*_3E_2^{\cdot}$ contain sp^2- and sp-hybridized E atoms, which are connected via two-electron δ- and one-electron π-bonds. This fact is best described by the formulation $R^*_2E\div ER^*$.

On the other hand, the structure of tetrakis(supersilyl)trigallanyl ($R^*_4Ga_3^{\cdot}$, **3**), shown in Figure 1, is in many respects different from the structure of $R^*_4Al_3^{\cdot}$[1] − except for the Si atoms of the 4 R* groups which occupy in both radicals the corners of a distorted tetrahedron: In $R^*_4Al_3^{\cdot}$ the three Al atoms occupy the corners of a triangle with two longer but unequal $R^*_2AlAlR^*$ sides and a shorter R*AlAlR* basis (cf. Scheme 1), whereas in $R^*_4Ga_3^{\cdot}$ (**3**) the three gallium atoms form a triangle with two shorter and equal long $R^*_2GaGaR^*$ sides and a longer R*GaGaR* basis (cf. Scheme 2). These structural data suggest that the R*Al groups are more weakly bonded to R^*_2Al than to each other, whereas the opposite holds for the R*Ga groups. In addition, the R^*_2Al plane in $R^*_4Al_3^{\cdot}$ stands not orthogonal to the E_3 plane and one R* substituent of the R*AlAlR* group does not lie in the E_3 plane. This is unlike the R^*_2Ga plane in $R^*_4Ga_3^{\cdot}$ (orthogonal to E_3) and the R* substituents of the R*GaGaR* group (both in plane). Intuitively, one might argue that the observed geometry of both radicals looks as if cyclisation of the compounds *catena*-$R^*_2E-ER^*\div ER^*$ (E = Al, Ga), which are homologues of the mentioned radicals *catena*-$R^*_2E\div ER^*$ (see above), stopped half way on the reaction coordinate in the case of $R^*_4Al_3^{\cdot}$, but is finished in the case of $R^*_4Ga_3^{\cdot}$. In the course of this (hypothetic) cyclisation of *catena*-$R^*_2E-ER^*\div ER^*$ the $R^*E\div ER^*$ bond became weaker and the connection between R^*_2E and ER^* − not existing in *catena*-$R^*_4E_3^{\cdot}$ − stronger.

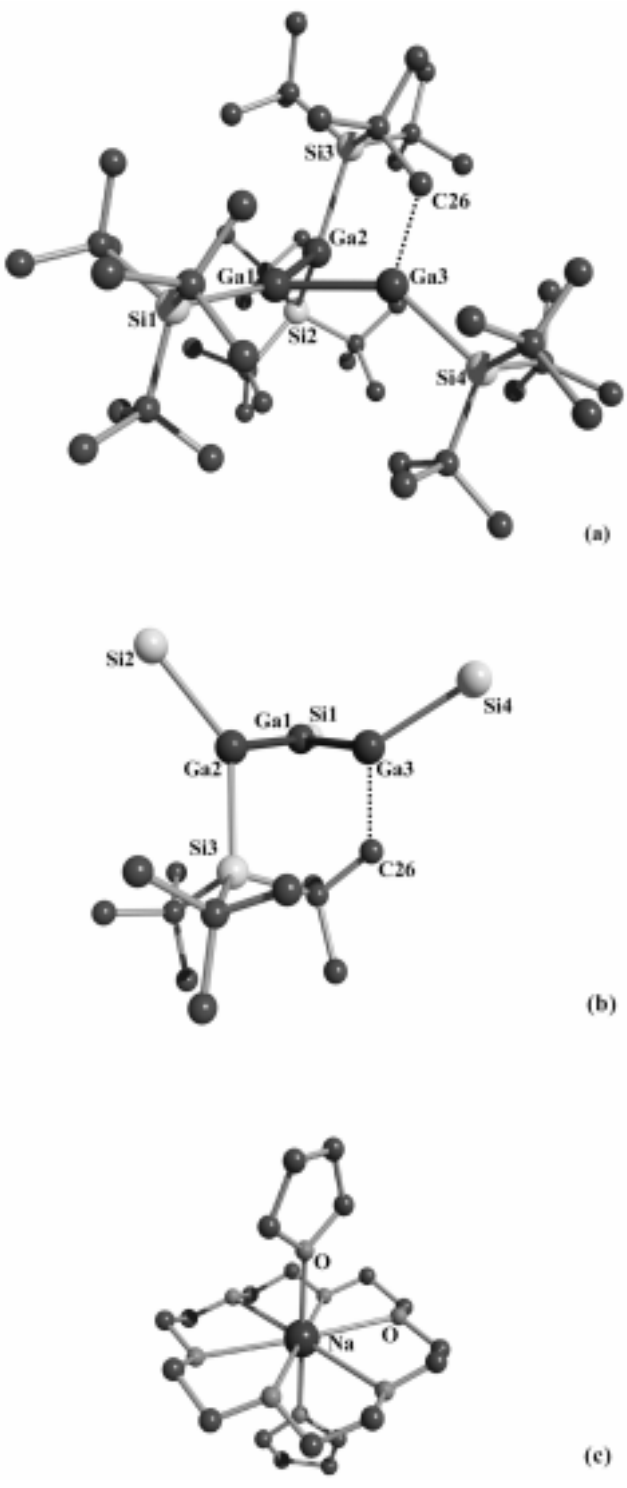

Figure 3. Structure of $R^*_4Ga_3^-$ (**3**$^-$) in the crystal, seen in two directions [(a) and (b)], and of $Na(18\text{-}C\text{-}6)(THF)_2^+$ [(c)]; atom numbering used [SCHAKAL plot; H atoms in (a) and (b), and some *t*Bu groups in (b) omitted for clarity; the dotted line represents the intramolecular $CH_3\cdots Ga$ contact]; selected distances [Å] and angles [°] with standard deviations: anion: Ga1−Ga3 2.494 (1), Ga1−Ga2 2.569 (2), Ga2···Ga3 2.935(2), Ga1−Si1 2.485(3), Ga2−Si3 2.513(3), Ga2−Si2 2.520(3), Ga3−Si4 2.486(3), Ga3···C26 2.10, Si−C (mean value) 1.96; Si1−Ga1−Ga3 137.89(9), Si1−Ga1−Ga2 151.09(8); Ga3−Ga1−Ga2 70.83(5) [angles sum at Ga1 359.81], Si3−Ga2−Si2 133.52(11), Si3−Ga2−Ga1 105.83(8), Si2−Ga2−Ga1 118.76(8) [angles sum at Ga2 358.11], Si4−Ga3−Ga1 136.28(8), Ga1−Ga3−C26 105.6(3), Si4−Ga3−C26 112.7(3) [angles sum at Ga3 354.6], Si4−Ga3−Ga2 140.19(8), Ga1−Ga3−Ga2 55.77(4), Ga1−Ga2−Ga3 53.40(4), C−Si−Ga (mean value) 109.39, C−Si−C (mean value) 109.5; Si2(Si3)−Ga2−Ga1−Si1 67.77/98.65, Si4−Ga3−Ga1−Si1 54.83, C26−Ga3−Ga1−Si1 95.84, Si2(Si3)−Ga2−Ga1−Ga3 117.91/75.67, Si4−Ga3−Ga1−Ga2 129.26, C26−Ga3−Ga1−Ga2 80.77; cation: Na−O(THF) (mean value) 2.31, Na−O(18−C-6) (mean value) 2.76; O−Na−O(THF) 179.24, O−Na−O(18-C-6) (mean value) 60.53, angles sum at O(THF) 359.78, angles sum at O(18-C-6) 343.40; the O_6 ring of 18-C-6 is something corrugated

If the R^*_2E group provides one and each R*E group two electrons for the E_3 framework (Al, Ga), there are 5 electrons available for the E_3 cluster in $R^*_4E_3^{\cdot}$ or $^5/_3 = 1.67$ electron per E−E bond as compared with 3 electrons available for the E_2 group in $R^*_3E_2^{\cdot}$. As a result, the mean value of the E−E distances is evidently larger in $R^*_4E_3^{\cdot}$ (2.74 Å for $R^*_4Al_3^{\cdot}$, 2.65 Å for $R^*_4Ga_3^{\cdot}$) than in $R^*_3E_2^{\cdot}$ (2.53 Å for $R^*_3Al_2^{\cdot}$, 2.42 Å for $R^*_3Ga_2^{\cdot}$). Altogether one might expect that the groups R*Ga in $R^*_4Ga_3^{\cdot}$ are connected with R^*_2Ga by two-electron bonds, and among one another by a one-electron bond.

The structure of sodium tris(supersilyl)digallanide−tetrahydrofuran(1/3) [$NaGa_2R^*_3\times3THF$, **2**$^-$; cation: $Na(THF)_3^+$], shown in Figure 2, resembles that of the radical $R^*_3Ga_2^{\cdot}$ (**2**; see above). Thus, in both molecules the Si_2*Ga*Ga groups are nearly planar (angles sum at *Ga* for **2**$^-$/**2** 358.4/359.7°). The same holds for the Ga*Ga*NaSi group of the anion **2**$^-$ (angles sum at *Ga* 360.0°), whereas the Na center itself is coordinated, distorted tetrahedrally by one Ga and three O atoms (the latter from THF). Moreover, the planes Si−Ga−Si and Ga−Ga−Si are almost orthogonal arranged not only in the anion **2**$^-$ but also in the radical **2**. The Ga−*Ga*−Si group in **2**$^-$ is, however, far away from being linear (angles for **2**$^-$/**2** 142.4°/170.0°). This is obviously a consequence of the Na center, which in addition coordinates the *Ga* atom in **2**$^-$. Certainly, the Ga−Na bond, which runs nearly orthogonal to the Ga−Ga bond (angle Ga−Ga−Na 91.4°) is highly ionic. Therefore, the free electron pair at the anionic Ga atom of **2**$^-$ is available for a π-bond, leading − according to the formulation $[R^*_2Ga-GaR^* \rightleftarrows R^*_2Ga=GaR^*]^-$ − to a comparable short central bond of the anion (Ga−Ga distance for **2**$^-$/**2** 2.38/2.42), approaching a bond order of 2 (Ga=Ga double bond length ca. 2.32 Å; cf. Table 1).

In a way, the tris(supersilyl)digallanide $R^*_3Ga_2^-$ (**2**$^-$) and tetrakis(supersilyl)trigallanide ($R^*_4Ga_3^-$) **3**$^-$, the structure of the latter is now discussed (Figure 3, a), play the role of the second and third member in a homologous row of anions: $R^*_2Ga^-$, $R^*_2Ga-GaR^*{}^-$, $R^*_2Ga-GaR^*-GaR^*{}^-$, $R^*_2Ga-GaR^*-GaR^*-GaR^*{}^-$ {for the structure of $[Na(18\text{-}C\text{-}6)(THF)_2]^+$ cf. Figure 3 (c)}. In fact, the structure of the trigallanide **3**$^-$ differs markedly from the structure of the digallanide **2**$^-$ in showing an intramolecular H contact between one peripheral methyl group of the R^*_2Ga entity and the anionic Ga atom in $[R^*_2Ga-GaR^*-GaR^*]^-$ (cf. Scheme 2). As the contact between the C atom of the mentioned methyl group and gallium atom is also very short (2.10 Å; normal Ga−C single bond lengths 1.99−2.02 Å),[9] it seems not out of question that in addition to H···Ga contacts C···Ga contacts must be taken into account. The latter possibility is in good agreement with a comparable long R^*_2Ga) R*Ga−GaR* distance (2.57 Å), pointing to a Ga−Ga single bond (cf. Ga−Ga bond length of 2.38 Å in $R^*_2Ga-GaR^*{}^-$). Each of the three Ga atoms in $R^*_4Ga_3^-$ (**3**$^-$) are nearly planar coordinated by adjacent atoms [angles sum at *Ga* for Si_2*Ga*Ga/Ga*Ga*SiGa/Ga*Ga*SiC 358.1/359.9/354.8°; the angles between the mentioned planes are 82.89/76.20°; cf. Figure 3 (b)]. The Ga atoms in **3**$^-$ themselves occupy the corners of a triangle with two shorter sides and a much longer basis, which certainly do not represent any chemical bond (cf. Scheme 2). In regard to the central Ga_3 group in $[R^{*(2)}R^{*(3)}Ga-GaR^{*(1)}-GaR^{*(4)}]^-$ the supersilyl groups $R^{*(1)}/R^{*(2)}/R^{*(3)}/R^{*(4)}$ lie − according to Figure 3 (b) − in/below/above/below the Ga_3 plane; thereby the Si atoms of the 4 R* groups form a distorted tetrahedron.

The one-electron reduction of the trigallanyl $R^*_4Ga_3^{\cdot}$ (**3**) to $R^*_4Ga_3^-$ (**3**$^-$) is connected with a structural change (anticyclization process), whereby the bonds $R^*_2Ga-GaR^*$/ according to Figure 3 (b) − in/below/above/below the Ga_3 Scheme 2). Altogether, the mentioned reduction leads to a shortening of the mean Ga−Ga distances [(2.53 + 2.53 + 2.88):3 = 2.65 Å in **3** and (2.49 + 2.57):2 = 2.53 Å in **3**$^-$], but the Ga−Ga distances in **3**$^-$ are distinctly longer than in **2**$^-$. This could be due to the fact that in the former the free electron pair contacts a methyl group [$-CH_3\cdots$:Ga< $\rightleftarrows$ $-CH_2-GaH$<], whereas in the latter the free electron is involved in the Ga−Ga bond [>Ga−Ga$^{\cdot}$− $\rightleftarrows$ >Ga÷Ga−]. On the other hand, the longer Ga−Ga bonds perhaps are simply due to the fact that the extra electron is delocalised over three instead of over two Ga centers such as in **2**$^-$.

Concluding Remarks

The gallium cluster compounds discussed here are further examples of many known compounds with two connected Ga atoms and of some known compounds with three connected Ga atoms.[6,10−25] All these clusters are shown in Table 1, together with their colors and geometries [the bond orders are determined from the single and double Ga−Ga bond lengths (2.52 and 2.32 Å), which themselves are twice the single and double bond radius of Ga[26]].

According to Table 1, the Ga−Ga bond lengths of organyl and certainly also of silyl-substituted digallanes >Ga−Ga< with a two-electron Ga−Ga bond (bond order 1) and tricoordinated Ga atoms span the region 2.48−2.54 Å. Clearly, the Ga−Ga distances of the discussed digallanide $R_3Ga_2^-$ (R = R*) or digallanediide $R_2Ga_2^{2-}$ [R = 2,6-$(Tip)_2C_6H_3$] as well as of the digallanyl $R_3Ga_2^{\cdot}$ (R = R*) or the radical anion $R_4Ga_2^{-\cdot}$ [R = Tip, $(SiMe_3)_2CH$], which formally derive from R_4Ga_2 by removing one or two R^+ cations or one R$^{\cdot}$ radical as well as introducing one electron, are distinctly shorter, due to the presence of more than two electrons per Ga−Ga bond, leading to bond orders of 1.5 to 2, respectively (cf. Table 1). Obviously, substitution of the organyl substituents in R_4Ga_2 by more electronegative groups, shortens the Ga−Ga bonds, as is shown for (2,4,6-$tBu_3C_6H_2)_2Ga_2Cl_2$ (Table 1). The yet unknown monomeric tetrahalides Ga_2Hal_4 should have − due to *electronic effects* of 4 halogen atoms − very short Ga−Ga bond lengths. The comparable long Ga−Ga bond in R_4Ga_2 with four electronegative substituents R = 2,2,4,4-$Me_4C_5H_6N$ probably is due to *steric effects.* On the other hand, addition of two donors to digallanes >Ga−Ga< with formation of tetracoordinated Ga atoms certainly lengthens the Ga−Ga bonds.

Table 1. Compounds with clusters of two and three Ga atoms [R = organyl, silyl, aminyl. X = halogen; D = donor; Fo = formula; CN = coordination number of Ga atoms (including Ga-bonded counter ions); τ = torsion angle R−Ga−Ga−R; BL = Ga−Ga bond length; BO = Ga−Ga bond order, determined from Ga−Ga single bond (2.52 Å) and double bond (2.32 Å); Ref. = references (here = this publication)]

Ga cluster compounds Fo	R/X/D[a]	Color[b]	CN	τ[c]	BL [Å]	BO (ca.)	Ref.
		Two Ga atoms					
R_4Ga_2	Disyl	yellow	3	4.9°	2.54	1	[10]
	Pip	lyellow	3	31°	2.53	1	[11]
	Tip	yellow	3	43.8°	2.51	1	[12]
	Mes_F	?	3	?	2.48	1	[13,14]
	$3R^*/SiMe_3$	red	3	?	?	?	here
	[d]	colorl.	4 ?	?	?	?	[15]
$R_2Ga_2X_2$	Mes*/Cl	colorl.	3	0°	2.42	1.5	[16]
	R′/Cl	colorl.	4	e	2.50	1	[17]
	R′/Br	colorl.	4	e	2.51	1	[17]
$Ga_2X_4D_2$	I/NEt_3	colorl.	4	st	2.50	1	[18]
	I/PEt_3	colorl.	4	st	2.44	1.5	[18]
	Cl/Diox	colorl.	4	st	2.41	1.5	[19]
	Br/Diox	colorl.	4	st	2.40	1.5	[19]
	Cl/Py	colorl.	4	st	2.50	1.5	[20]
	Br/Py	colorl.	4	st	2.48	1.5	[20]
$R_2Ga_2X_4^{2-}$	R′/Br	colorl.	4	st	2.50	1	[17]
	R′/I	yellow	4	st	2.48	1	[17]
$Ga_2X_6^{2-}$	Cl	colorl.	4	st	2.43	1.5	[21]
[f]	Br	colorl.	4	st	to[e]	to	to
	I	yellow	4	st	2.39	1.7	[23]
$R_3Ga_2^{\cdot}$ (**2**)	R*	dblue	3+2	90°	2.42	1.5	here
$R_3Ga_2^-$ (**2**$^-$)	R*	dred	3	90°	2.38	1.7	here
R_2Ga_2	[g]	dred	6	–	2.34	2	[14]
$R_4Ga_2^{\cdot-}$	Tip	dark	3	15.5°	2.34	2	[12]
	Disyl	blue	3	0°	2.40	1.5	[6a]
$R_2Ga_2^{2-}$	[h]	dred	4	180°	2.32	2	[24]
		Three Ga atoms					
$R_4Ga_3^{\cdot}$ (**3**)	R*	dgreen	3+4	–	2.54[i]	1	here
$R_4Ga_3^-$ (**3**$^-$)	R*	dblue	3	–	2.54[i]	1	here
$Ga_3I_5D_3$	PEt_3	yellow	4	–	2.46	1.5	[18]
$R_3Ga_3^{2-}$	[k]	dred	4	–	2.44	1.5	[25]

[a] Disyl = $(SiMe_3)_2CH$; Pip = 2,2,4,4-$Me_4C_5H_6N$; Tip = 2,4,6-$iPr_3C_6H_2$; Mes = 2,4,6-$Me_3C_6H_2$; Mes_F = 2,4,6-$(CF_3)_3C_6H_2$; R* = tBu_3Si; Mes* = 2,4,6-$tBu_3C_6H_2$; R′ = $(SiMe_3)_3Si$; Diox = dioxane; Py = pyridine. – [b] d = deep, dark; l = light. – [c] st = staggered; e = eclipsed. – [d] R = [−*t*BuN−SiMe(N*t*Bu)−N*t*Bu−SiMe(N*t*Bu)−]. – [e] Ga−Ga bond lengths slightly depend on the counter ion. – [f] The gallium(II) chalcogenides GaY also contain Ga−Ga groups with tetracoordinated Ga atoms and Ga−Ga distances of 2.447/2.456/2.437 Å (Y = S/Se/Te). – [g] R = 2,4-bis(trimethylsilyl)-2,4-dicarba-*nido*-hexaboryl. – [h] R = 2,6-$(Tip)_2C_6H_3$. – [i] Mean value of the two shorter Ga−Ga bonds (cf. Scheme 2). – [k] R = 2,6-$(Mes)_2C_6H_3$.

As to Table 1, this "*coordination effect*" is or might be observed by going from $R_2Ga_2Hal_2$ (R = 2,4,6-$tBu_3C_6H_2$) to $[R_2Ga_2Hal_4]^-$ [R = $Si(SiMe_3)_3$] or from Ga_2Hal_4 (unknown) to $[Ga_2Hal_6]^{2-}$.

Unlike triorganylgallium compounds R_3Ga with gallium in oxidation state III, which have been known for a long time,[27] organylgallium compounds R_mGa_n with gallium in oxidation states < III were synthesized and characterized only very recently. This is due to their high tendency of decomposition into R_3Ga and Ga. According to the following equation, the disproportionation of the mentioned gallium cluster compounds R_mGa_n − where R is not only an organic but also an inorganic group [e.g. $(SiMe_3)_2N$] − may proceed over intermediates $R_{m'}Ga_{n'}$ with constantly decreasing m'/n' ratio.

$$R_mGa_n \xrightarrow[(m'/n' < m/n)]{\text{over } R_{m'}Ga_{n'}} R_3Ga/Ga \text{ or } R_2/Ga$$

Substituents R with *greater bulkiness* may inhibit the full scale of this disproportionation at a point which will be specifically determined by the nature of R and the reaction conditions (suitable donors that coordinate with Ga atoms of R_mGa_n may also have a directing effect). This is illustrated by the discussed reaction of gallium trihalides $GaHal_3$ with supersilylsodium NaR*, which according to Scheme 2 leads via R^*_2GaCl to the digallanyl $R^*_3Ga_2^{\cdot}$ (**2**). The latter is metastable at room temperature, but at higher temperatures disproportionates further into R* and the *tetrahedro*-tetragallane $R^*_4Ga_4$ (**4**; cf. Scheme 2). Obviously, the Ga_4 tetrahedrane in $R^*_4Ga_4$ is completely shielded by four supersilyl groups, leading to a high thermal stability of the Ga cluster compound (see above). In accordance with this, the trigallanyl $R^*_4Ga_3^{\cdot}$ (**3**) finally − at elevated temperatures − disproportionates into R* and **4** (cf. Scheme 2).[6] Certainly, **4** reacts further with Na in THF under formation of $Na_2Ga_4R^*_4\times 2THF$.[28]

It is worth mentioning in this context that gallium monohalides GaHal react with supersilylsodium in a different manner to gallium trihalides. Products are the gallanides $R^*_6Ga_{10}^-$ and $R^*_6Ga_{13}^-$ besides $R^*_4Ga_4$ [17] as well as the gallanes $R^*_8Ga_{18}$ and $R^*_8Ga_{22}$.[29] Noticeable, in the course of reactions of NaR* with $GaHal_3$ the products obtained have equal or more supersilyl groups than Ga atoms, whereas reactions of NaR* with GaHal lead to products with equal or less supersilyl groups than Ga atoms. Certainly, this is due to different reaction paths, the nature of which have to be investigated.

Some insights into the mechanisms of the building up of clusters come from the isolated primary and secondary products of the reaction of NaR* with $GaHal_3$. Here, the efficiency of supersilylsodium for acting as reducing agent ($R^*_2GaCl + NaR^* \rightarrow R^*_2Ga^{\cdot} + NaCl + R^*$ and $R^*_3Ga_2^{\cdot} + NaR^* \rightarrow NaGa_2R^*_3 + R^*$) as well as the tendency of the gallium cluster compounds for elimination of R* ($R^*_4Ga_2 \rightarrow R^*_3Ga_2^{\cdot} + R^*$) or transfering group R*Ga ($2\,Ga_2R^*_3^- \rightarrow GaR^*_2^- + Ga_3R^*_4^-$) is important. Certainly, supersilylgallium R*Ga also plays an essential part in the reaction of NaR* and GaHal. The gallylene, which is obviously obtained by supersilylanidation of GaHal, may combine with GaHal, whereby dehalogenations as well as R* eliminations of the formed Ga cluster compounds will produce "naked" Ga atoms in the cluster. These latter clusters may themselves be reduced by NaR* to anions, which may react with GaHal by introducing new "naked" Ga atoms into the Ga cluster framework.

Experimental Section

All experiments were carried out in flame-dried glass apparatus with standard Schlenk techniques under dry argon or nitrogen. During all manipulations, air and moisture were strictly excluded. The solvents (pentane, heptane, THF, C_6D_6, C_6D_{12}) were distilled from sodium/lead or sodium/benzophenone. Available for use were: $GaCl_3$, Na, Me_3SiCl, 18-crown-6, TCNE (tetracyanoethylene). The following compounds were synthesized according to literature procedures: NaR*×2THF,[5] R^*_2GaCl,[30] $NaC_{10}H_8$ (sodium naphthalenide) in THF.[31] − For NMR spectra a Jeol GSX-270 (^1H/^{13}C/^{29}Si: 270.17/67.94/53.67 MHz) and Jeol EX-400 (^1H/^{13}C/^{29}Si: 399.78/100.54/79.43 MHz) were available. The ^{29}Si NMR spectra were recorded with the INEPT or DEPT pulse sequence using empirically optimized parameters for the mentioned groups. − The EPR spectra were recorded with a Bruker System ESP 300.

Syntheses and Reactions of 2. − (i): A solution of NaR*×2THF (0.826 mmol) in heptane (15 mL) was added dropwise to a solution of R^*_2GaCl (0.208 g, 0.413 mmol) in heptane (10 mL) at −78 °C. As the mixture warmed to room temperature, the color of the initially formed yellow solution (R^*_2GaCl, NaR*) changed to green, and finally to intense blue. According to ^1H NMR (exchange of heptane by C_6D_6) and to EPR, the solution contained $(R^*)_2$ and the radical **2**. The former substance is not observed by EPR, the latter not in NMR. After removal of the volatile components (ca. 10^{-3} mbar), the residue was placed in pentane (10 mL), the white precipitate (NaCl) removed by filtration, and the resulting solution reduced in volume to about 5 mL. Within 0.5 d at −23 °C, colorless crystals of $(R^*)_2$ precipitated which were removed by decanting the blue solution. Black-blue crystals of air- and water-sensitive **2** − which at about 80 °C thermolize under formation of the tetrahedrane **4**[4] and react with Na or NaR* in organic solvents under formation of $Na(THF)_3^+\cdot\mathbf{2}^-$ − form from the mother liquor after 5 d at −23 °C (ca. 10%). The identification of products results from comparison with authentic samples of $(R^*)_2$ [5] and **2**.[3] − **(ii):** The radical **2** is also formed from $GaCl_3$ and NaR*×2THF (molar ratio 1:3) in heptane.[3] In addition, the digallanyl **2** seems − according to EPR − to be the first product of the oxidation of $\mathbf{2}^-$ with oxygen. Finally, **2** probably is formed as first product of the reaction of $Na(THF)_2^+\cdot\mathbf{2}^-$ in pentane with R*Br (see below).

Syntheses and Reactions of $Na(THF)_3^+$ $\mathbf{2}^-$. − (i): A solution of NaR*×2THF (3.58 mmol) in THF (6 mL)/pentane (10 mL) was added dropwise to a solution of R^*_2GaCl (0.902 g, 1.79 mmol) in pentane (50 mL). The color of the initially yellow solution (R^*_2-GaCl) changed to green and finally to dark-blue. According to ^1H NMR (exchange of pentane by C_6D_6), the solution contained $(R^*)_2$ [5] and $Na(THF)_3^+$ $\mathbf{2}^-$ [molar ratio ca. 2:1; $2\,R^*_2GaCl + 3\,NaR^* \rightarrow Na^+\cdot\mathbf{2}^0 + 2\,(R^*)_2 + 2\,NaCl$] besides unreacted NaR* ×2THF (all R^*_2GaCl consumed). After removal of the volatile components (ca. 10^{-3} mbar), the residue (now brown-red) was placed in pentane (50 mL), the precipitate (NaCl) removed by filtration, and the resulting dark-red solution reduced in volume to about 15 mL. Within 1 d at −23 °C, deep-red crystals of air- and water-sensitive $Na(THF)_3^+\cdot\mathbf{2}^-$ (0.22 g; 0.26 mmol; 15%) formed from the solution, which reacted with Me_3SiCl and R*Br (see below). − ^1H NMR (C_6D_6, internal TMS): δ = 1.47 (broad; 3 Si*t*Bu$_3$), 1.34/3.42 (m/m; 6-CH_2CH_2O/6-CH_2CH_2O). − $^{13}C\{^1H\}$ NMR (C_6D_6, internal TMS): δ = 24.3/25.3 (6-*C*Me$_3$/6-*C*Me$_3$), 33.2/33.9 (3-C*Me*$_3$/3-C*Me*$_3$), 25.6/67.9 (6-CH_2CH_2O/6-CH_2CH_2O). − $^{29}Si\{^1H\}$ NMR (C_6D_6, external TMS): δ = 37.1 (2 Si*t*Bu$_3$), 54.3 (Si*t*Bu$_3$). − X-ray structure analysis: cf. Figure 2. − It has not yet been possible to obtain a satisfactory elemental analysis. − **(ii):** $NaC_{10}H_8$ (0.272 mmol) in THF (5 mL) was added dropwise to a solution of R^*_2GaCl (0.092 g; 0.181 mmol) in heptane (10 mL) at −78 °C. The color of the initially yellow solution (R^*_2GaCl) changed to violet (**2**) and finally brown-red [$Na(THF)_3^+\cdot\mathbf{2}^-$]. After 6 h, the reaction mixture was warmed to room temperature. According to ^1H NMR (exchange of THF/pentane by C_6D_6) the solution contained $(R^*)_2$ [5] and the digallanide $Na(THF)_3^+\cdot\mathbf{2}^-$ [molar ratio 1:2; $2\,R^*_2GaCl + 3\,Na \rightarrow Na^+\cdot\mathbf{2}^- + 0.5\,(R^*)_2 + 2\,NaCl$]. After removal of the volatile components (ca. 10^{-3} mbar), the residue (brown-red) was placed in heptane (30 mL), the precipitate (NaCl) removed by filtration, and the resulting dark-red solution reduced in volume to 5 mL. Within 1 d at −23 °C, deep-red crystals of $Na(THF)_3^+$ $\mathbf{2}^-$ (0.064 g; 0.066 mmol; 73%) formed from the solution [cf. (i) for characterization]. − **(iii):** In an NMR tube the radical **2** (ca. 0.015 g; 0.02 mmol) and Na (ca. 0.9 mmol) in C_6D_6 (0.6 mL) were heated for 1 d at 60 °C. The color of the initially intensive blue solution changed finally to red. According to ^1H NMR it contained $(R^*)_2$ [5] besides the digallanide Na^+ $\mathbf{2}^-$ (doubtless as the benzene adduct). − ^1H NMR (C_6D_6, internal TMS): δ = 1.421 (s; 2 Si*t*Bu$_3$), 1.434 (s; Si*t*Bu$_3$). − **(iv) Reaction of $Na(THF)_3^+$ $\mathbf{2}^-$ with Me_3SiCl:** A solution of Me_3SiCl (0.220 mmol) in heptane (5 mL) was added dropwise to a solution of $Na(THF)_3^+$ $\mathbf{2}^-$ (0.215 g; 0.220 mmol) in heptane (10 mL). The color of the initially formed dark-blue solution of the starting material changeed to light-red. After removal of the volatile components at −78 °C and ca. 10^{-3} mbar, the residue was warmed to room temperature and dissolved in C_6D_6. According to NMR spectra, $Na(THF)_3^+$ $\mathbf{2}^-$ has exclusively reacted under formation of a new substance, the nature of which is probably the digallane $R^*_2Ga-GaR^*(SiMe_3)$. − ^1H NMR (C_6D_6, internal TMS): δ = 0.173 (s; $SiMe_3$), 1.258 (s; Si*t*Bu$_3$), 2.277 (s; 2 Si*t*Bu$_3$). − $^{13}C\{^1H\}$ NMR (C_6D_6, internal TMS): δ = 1.29 ($SiMe_3$), 25.4/25.6 (6-*C*Me$_3$/3-*C*Me$_3$), 32.4/33.9 (6-C*Me*$_3$/3-C*Me*$_3$). − $^{29}Si\{^1H\}$ NMR (C_6D_6, external TMS): δ = 19.41 ($SiMe_3$), 44.80 (Si*t*Bu$_3$), 48.42 (2Si*t*Bu$_3$).

Syntheses and Reactions of $[Na(18\text{-}C\text{-}6)(THF)_2]^+[\mathbf{3}]^-$. − (i): To a solution of $Na(THF)_3^+$ $\mathbf{2}^0$ (0.147 g; 0.15 mmol) in 0.6 mL of C_6D_6 at room temperature was added 18-crown-6 (0.053 g; 0.20 mmol). The color of the initially red solution immediately changed to dark-blue. According to NMR recorded after 20 h, the trigallanide $[Na(18\text{-}C\text{-}6)(THF)_2]^+[\mathbf{3}]^-$ had formed. From this solution at 5 °C within 2 weeks dark-blue, air- and moisture-sensitive crystals of $[Na(18\text{-}C\text{-}6)(THF)_2]^+[\mathbf{3}]^-$, insoluble in pentane and soluble in benzene or THF, and which may be oxidized by R*Br or TCNE under formation of the radical **3** (see below), were obtained. − ^1H NMR (C_6D_6, internal TMS): δ = 1.532 (broad; 2 Si*t*Bu$_3$), 1.621 (broad; 2 Si*t*Bu$_3$), 1.439/3.545 (m/m; 4-CH_2CH_2O/4-CH_2CH_2O), 3.326 (18-C-6). − $^{13}C\{^1H\}$ NMR (C_6D_6, internal TMS): δ = 22.7/24.9 (6-*C*Me$_3$/6-*C*Me$_3$), 32.2/35.0 (6-C*Me*$_3$/6-C*Me*$_3$), 25.8/67.8 (4-CH_2CH_2O/4-CH_2CH_2O), 70.0 (18-C-6). − $^{29}Si\{^1H\}$ NMR (C_6D_6, external TMS): δ = 42.0/42.3/53.2 (Si*t*Bu$_3$/Si*t*Bu$_3$/2 Si*t*Bu$_3$). − X-ray structure analysis: cf. Figure 3. − It has not yet been possible to obtain a satisfactory elemental analysis. − **(ii):** Deep-blue $[Na(18\text{-}C\text{-}6)(THF)_2]^+[\mathbf{3}]^-$ was formed as an insoluble precipitate by addition of 18-crown-6 (0.010 g; 0.038 mmol) to a red solution of $Na(THF)_3^+$ $\mathbf{2}^-$ (0.033 g; 0.034 mmol) in pentane (3 mL) at room temperature, which dissolved after addition of THF (1 mL). From this solution in 5 d at −23 °C dark-blue crystals of the trigallanide $[Na(18\text{-}C\text{-}6)(THF)_2]^+[\mathbf{3}]^-$ were obtained. − **(iii):** Obviously, the deep-blue trigallanide **3** formed by reduction of the trigallanyl **3** (see below) in THF with $NaC_{10}H_8$ in THF at room temperature.

Syntheses and Reactions of 3. − (i): A solution of R*Br (0.672 g; 2.41 mmol) in pentane (10 mL) was added dropwise to a solution

Table 2. Selected parameters of the X-ray structure analyses of the compounds $R^*_4Ga_3^{\cdot}$ (**3**), $Na(THF)_3^+Ga_2R^*_3^-$ (M^+ $\mathbf{2}^-$) and $[Na(18\text{-}C\text{-}6)(THF)_2]^+[Ga_3R^*_4]^-$ (M^+ $\mathbf{3}^-$)

	3	M^+ $\mathbf{2}^-$	M^+ $\mathbf{3}^-$
Formula	$C_{48}H_{105}Ga_3Si_4$	$C_{48}H_{105}Ga_2NaO_3Si_3$	$C_{68}H_{148}Ga_3NaO_8Si_4$
M_r	1006.92	977.05	1438.45
System	monoclinic	triclinic	monoclinic
Space group	*C*2/*c*	$P\bar{1}$	*P*2(1)/*c*
a [Å]	21.278(2)	12.592(5)	14.9998(2)
b [Å]	12.692(1)	12.6572(5)	20.5701(1)
c [Å]	23.853(2)	19.6557(8)	30.0658(3)
α [Å]	90	80.768(1)	90
β [Å]	90.212(2)	89.154(1)	92.058(1)
γ [Å]	90	68.760(1)	90
V [Å^3]	6442(1)	2879.0(2)	9270.7(2)
Z	4	2	4
D [Mg/m^3]	1.082	1.127	1.108
μ [mm^{-1}]	1.012	1.039	0.967
F(000)	2280	1064	3360
Index range	$-27 \le h \le 27$	$-13 \le h \le 13$	$-16 \le h \le 16$
	$-15 \le k \le 15$	$-13 \le k \le 13$	$-22 \le k \le 22$
	$-24 \le l \le 30$	$-21 \le l \le 21$	$-32 \le l \le 32$
2Θ [°]	3.42−58.42	3.48−46.50	13.62−46.52
Reflections	18377	12733	36480
unique	5554	6645	9921
observed[a]	3821	6288	8007
R(int.)	0.0540	0.0265	0.0427
x/*y*[b]	1/1	0.1067/ 4.7218	0.1209/ 90.4156
GOOF	1.044	1.076	1.034
*R*1[a]	0.0532	0.0379	0.1016
*wR*2	0.1458	0.1256	0.2476
[c]	0.710	0.597	5.696

[a] $F > 4F(F)$. − [b] $w^{-1} = F^2F_o^2 + (xP)^2 + yP$; $P = (F_o^2 + 2F_c^2)/3$. − [c] Max. electron density [e/Å^3].

of $Na(THF)_3^+$ $\mathbf{2}^0$ (2.353 g; 2.41 mmol) in pentane (15 mL) at −100 °C. After 5 h, the mixture was warmed to room temperature. The color of the initially formed deep-blue solution changed finally to deep-green. According to ^{1}H NMR (exchange of heptane by C_6D_6) and EPR, the solution contained $(R^*)_2$ [5] and the radical **3** (the former substance not seen in EPR, the latter not seen in NMR). After removal of the volatile components (ca. 10^{-3} mbar), the residue was placed in pentane (30 mL) and the precipitate (NaBr) removed by filtration. Within 2 months at −23 °C, deep-green, air- and moisture-sensitive crystals of **3** (0.412 g; 0.41 mmol; 36%) were formed. − NMR spectra: Not observable. − EPR spectrum: cf. main section. − X-ray structure analysis: cf. Figure 1. − UV/Vis (heptane): $\lambda_{max.}$ = 610 nm. − **(ii):** The deep-green radical **3** was also formed from $[Na(18\text{-}C\text{-}6)(THF)_2]^+[\mathbf{3}]^-$ (0.086 g; 0.060 mmol) and R*Br (0.027 g; 0.090 mmol) in C_6D_6 (0.8 mL) within a few days as well as from $[Na(18\text{-}C\text{-}6)(THF)_2]^+[\mathbf{3}]^-$ (0.072 g; 0.050 mmol) and TCNE (0.006 g; 0.05 mmol) in C_6D_6 (0.8 mL) at room temperature immediately. In both cases, the color of the initial dark-blue solutions changed to deep green [cf. (i) for characterization]. − **(iii) Thermolysis of 3:** At 25 °C, deep-green **3** in heptane decomposed very slowly into black-blue **2** (observed in EPR) and dark-violet $R^*_4Ga_4$ (observed in NMR).[6] The mentioned decomposition was complete by heating **3** (0.170 g; 0.169 mmol) for 17 h in heptane (2 mL) at 45 °C. After removal of the volatile components (ca. 10^{-3} mbar) and dissolving the residue in pentane (1.5 mL), within 3 d at −23 °C dark-blue crystals of the radical **2** were obtained (for another synthesis cf. above, for characterization cf. ref.[3]). As **2** itself decomposed at higher temperatures under formation of the tetrahedrane **4** besides $(R^*)_2$ (see above), the thermolysis of dark-green **3** (0.151 g; 0.150 mmol) in heptane (5 mL) at 100 °C led within 3 h exclusively to dark-violet **4**. After removal of the volatile components (ca. 10^{-3} mbar) and dissolving the residue in pentane (3 mL), within 3 d at −23 °C dark-violet crystals of **4** (0.075 g; 0.07 mmol; 44%) were obtained (for another synthesis and for characterization see ref.[4]). Compound **4** is itself very thermostable; the tetrahedrane remains almost undecomposed even after heating a solution in C_6D_{12} for 5 d at 100 °C (the NMR spectrum shows only a small amount of R*D formed). As a solid, **4** does not decompose below 322 °C (m.p.).

X-ray Structure Determinations: Siemens SMART Area-detector, Mo-K_α with λ = 0.71073 Å, *T* = 163(2) or 193(2) K ($R^*_4Ga_2^{\cdot}$), graphite monochromator, image plate detector, fixed on glass fibre, crystals mounted in perfluoropolyether oil. − Structure determination: The structures were solved by direct methods, SHELX-93. All non-hydrogen atoms were refined anisotropically and H atoms were included in the refinement at calculated positions with a riding model and fixed isotropic U_i values. There is still a large peak in $[Na(18\text{-}C\text{-}6)(THF)_2]^+[Ga_3R^*_4]^-$ of 5.70 e/Å^3, 1.02 Å from Ga3, that could be due to strong H···Ga and C···Ga contacts between one peripheral methyl group of R^*_2Ga and the anionic Ga atom of the trigallanide $[R^*_2Ga-GaR^*-GaR^*]^-$. The structures of the compounds are shown in Figures 1, 2, and 3, and crystallographic details are summarized in Table 2. Crystallographic data (excluding structure factors) for the structures reported in this paper have been deposited with the Cambridge Crystallographic Data Centre as supplementary publication no. CCDC-152470 (**3**), -152469 $[Na(THF)_3^+$ $\mathbf{2}^-]$, -152583 $\{[Na(18\text{-}C\text{-}6)(THF)_2]^+[\mathbf{3}^-]\}$. Copies of

this data can be obtained free of charge on application to CCDC, 12 Union Road, Cambridge CB2 1EZ, UK [Fax: (internat.) + 44-1223/336-033; E-mail: deposit@ccdc.cam.ac.uk].

Acknowledgments

We are grateful to the Deutsche Forschungsgemeinschaft and the Fonds of Chemische Industrie for their generous financial support.

[1] N. Wiberg, T. Blank, W. Kaim, B. Schwerdeski, G. Linti, *Eur. J. Inorg. Chem.* **2000**, 1475.
[2] N. Wiberg, K. Amelunxen, T. Blank, H. Nöth, J. Knizek, *Organometallics* **1998**, *17*, 5431.
[3] N. Wiberg, K. Amelunxen, H. Nöth, H. Schwenk, W. Kaim, A. Klein, T. Scheiring, *Angew. Chem.* **1997**, *109*, 1258; *Angew. Chem. Int. Ed. Engl.* **1997**, *36*, 1213.
[4] N. Wiberg, K. Amelunxen, H.-W. Lerner, H. Nöth, W. Ponikwar, H. Schwenk, *J. Organomet. Chem.* **1999**, *574*, 246.
[5] N. Wiberg, K. Amelunxen, H.-W. Lerner, H. Schuster, H. Nöth, I. Krossing, M. Schmidt-Amelunxen, T. Seifert, *J. Organomet. Chem.* **1997**, *542*, 1.
[6] In addition, $R^*_6Ga_8$ is formed in low yield (*Z. Naturforsch., B*, in preparation). – [6a] W. Uhl, U. Schütz, W. Kaim, E. Waldhör, *J. Organomet. Chem.* **1995**, *501*, 79.
[7] W. Kaim, *Coord. Chem. Rev.* **1987**, *76*, 187.
[8] J. A. Weil, J. A. Bolton, J. E. Wertz, *Electron Paramagnetic Resonance*, Wiley, New York, **1994**.
[9] W. Uhl, K. W. Klinkhammer, M. Layh, W. Massa, *Chem. Ber.* **1991**, *124*, 279.
[10] W. Uhl, M. Layh, T. Hildenbrand, *J. Organomet. Chem.* **1989**, *364*, 289.
[11] G. Linti, R. Frey, M. Schmidt, *Z. Naturforsch., Teil B* **1994**, *49*, 958.
[12] X. He, R. A. Bartlett, M. M. Olmstead, K. Ruhland-Senge, B. E. Sturegeon, P. P. Power, *Angew. Chem.* **1993**, *105*, 761; *Angew. Chem. Int. Ed. Engl.* **1993**, *32*, 717.
[13] R. D. Schluter, A. H. Cowley, D. A. Atwood, R. A. Jones, M. R. Bernd, C. J. Carrano, *J. Am. Chem. Soc.* **1993**, *115*, 2070.
[14] A. K. Saxena, H. Zhang, J. A. Maguire, N. S. Hosmane, A. H. Cowley, *Angew. Chem.* **1995**, *107*, 378; *Angew. Chem. Int. Ed. Engl.* **1995**, *34*, 332 and ref. cited herein.
[15] M. Veith, F. Gotting, S. Becker, V. Huch, *J. Organomet. Chem.* **1991**, *406*, 105.
[16] A. H. Cowley, A. Decken, C. A. Olazabal, *J. Organomet. Chem.* **1996**, *524*, 271.
[17] M. Kehwald, W. Köstler, A. Rodig, G. Linti, T. Blank, N. Wiberg, *Organometallics*, **2001**, *20*, 860, and ref. cited herein.
[18] A. Schnepf, C. Doriat, E. Möllhausen, H. Schnöckel, *Chem. Commun.* **1997**, *21*, 2111.
[19] J. C. Beamish, R. W. H. Small, I. J. Worrall, *Inorg. Chem.* **1979**, *18*, 220; R. W. H. Small, I. J. Worrall, *Acta Crystallogr. B* **1982**, *38*, 250.
[20] J. C. Beamish, A. Boardman, R. W. H. Small, I. D. Worrall, *Polyhedron* **1985**, *4*, 983; R. W. H. Small, I. J. Warrall, *Acta Crystallogr. B* **1982**, *38*, 86.
[21] R. L. Brown, D. Hall, *J. Chem. Soc., Dalton Trans.* **1974**, 988; M. Khan, C. Oldham, M. J. Taylor, D. G. Tuck, *Inorg. Nucl. Chem. Lett.* **1980**, *16*, 469.
[22] H. J. Cunning, D. Hall, C. E. Wright, *Cryst. Struct. Commun.* **1974**, *3*, 107; W. Hönle, G. Gerlach, W. Weppner, A. Simon, *J. Solid State Chem.* **1986**, *61*, 171; W. Hönle, A. Simon, *Z. Naturforsch. B* **1986**, *41*, 1391.
[23] G. Gerlach, W. Hönle, A. Simon, *Z. Anorg. Allg. Chem.* **1982**, *486*, 7.
[24] J. Su, X.-W. Li, R. C. Crittendon, G. H. Robinson, *Z. Anorg. Allg. Chem.* **1997**, *36*, 5471.
[25] X.-W. Li, W. T. Pennington, G. H. Robinson, *J. Am. Chem. Soc.* **1995**, *117*, 7578; X.-W. Li, Y. Xie, P. R. Schreiner, K. D. Cripper, R. C. Crittendon, C. F. Campena, H. F. Schaeter, G. H. Robinson, *Organometallics* **1996**, *15*, 3798.
[26] Holleman-Wiberg, *Lehrbuch der Anorganischen Chemie*, 101st ed., DeGruyter, Berlin, **1995**, p. 1839.
[27] A. J. Downs (Ed.), *Chemistry of Aluminum, Gallium, Indium and Thallium*, Chapman and Hall, London, **1993**.
[28] N. Wiberg, T. Blank, H. Schnöckel, F. Möllhausen, unpublished results.
[29] A. Donchev, A. Schnepf, G. Stößer, E. Baum, H. Schnöckel, T. Blank, N. Wiberg, *Chem. Eur. J.*, in press.
[30] N. Wiberg, K. Amelunxen, H.-W. Lerner, H. Nöth, J. Knizek, I. Krossing, *Z. Naturforsch., Teil B* **1998**, *53*, 333.
[31] J. L. Wardell, in: *Comprehensive Organometallic Chemistry* (Eds.: G. Wilkinson, F. G. A. Stone), Pergamon, Oxford **1982**, vol. 1, p. 109.

Received November 21, 2000
[I00445]

Solid-state and Solution-state NMR Studies of the Chlorophosphane (2,6-$(CF_3)_2C_6H_3$)(2,4-$(CF_3)_2C_6H_3$)PCl, (ArArPCl), and its Crystal Structure at 150 K

AndreiS. Batsanov,[a] StephanieM. Cornet,[a] LindseyA. Crowe,[a] KeithB. Dillon,[a] RobinK. Harris,*[a] Paul Hazendonk,[a] and MarkD. Roden[a]

Keywords: NMR spectroscopy / Structure elucidation / Phosphanes / Configuration determination

The title compound has been synthesised, and characterised by multinuclear magnetic resonance spectroscopy, both in solution and in the solid state. The bandshapes of variable-temperature solution-state ^{19}F NMR spectra have been iteratively fitted to obtain information on the kinetics of rotation about the PC bond for one of the aryl groups, and values for the enthalpy and entropy of activation of the process have been derived. Magic-angle spinning NMR techniques have been extensively applied to the solid, using ^{19}F, ^{31}P and ^{13}C nuclei. Triple-channel methods and different magnetic field strengths have been employed to yield a range of complementary information. Heteronuclear interactions and intramolecular motions have been investigated. Bandshapes arising from (P, Cl) residual dipolar coupling have been analysed. Satisfactory agreement is found between experimental spectra and those simulated with estimated values of the parameters involved, and it is confirmed that the electric field gradient at chlorine is co-axial with the PCl bond. The sign of the isotropic (PCl) indirect coupling constant is obtained for the first time and is shown to be negative. The crystal structure of the compound at 150K confirms the presence of two different aromatic residues, as deduced from the spectroscopic studies.

Introduction

The novel compound 2,6-bis(trifluoromethyl)phenyl-2,4-bis(trifluoromethyl)phenyl-chlorophosphane (**1**) has been synthesised as part of a continuing study of low-coordinate phosphorus compounds containing bulky electron-withdrawing aromatic groups.[18] The formation of this compound with different bis(trifluoromethyl)phenyl groups arises (Exp. Section) because 1,5-bis(trifluoromethyl) benzene can be lithiated by butyllithium in two different positions: Either *ortho* to both CF_3 groups, giving a 2,6-bis(trifluoromethyl)phenyl-lithio derivative, or *ortho* to one of the CF_3 groups only, yielding the analogous 2,4-substituted compound. These groups are designated Ar and Ar respectively herein. On treatment with PCl_3, both of the dichlorophosphanes are obtained, with the 2,6 derivative (Ar) present in the larger amount. The isomers can be readily distinguished by their ^{31}P and ^{19}F solution-state spectra. The solid disubstituted product isolated from the reaction mixture was shown to be the title compound ArArPCl (Figure1), firstly by solution-state NMR and secondly by extensive (^{31}P, ^{19}F and ^{13}C) solid-state NMR investigations. Its structure was eventually determined by single-crystal X-ray diffraction at 150K. Variable-temperature solution-state ^{19}F NMR spectroscopy was used to determine the enthalpy and entropy of activation for internal rotation about the PC bond of the Ar group. The aims of the solid-state NMR experiments were to gain further structural information, and to investigate the interaction between phosphorus and the quadrupolar chlorine nucleus, as shown by residual dipolar splitting.

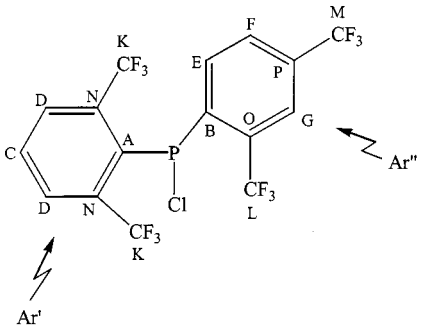

Figure 1. Lettering scheme for carbon atoms in ArArPCl (**1**)

A major feature of interest in the solid-state NMR spectrum of **1** is the bandshape of the ^{31}P resonance. Indirect isotropic (PCl) coupling should split the NMR signal of ^{31}P bonded to a single chlorine into a quadruplet of lines of equal spacing and intensity. In the solid state, dipolar coupling may also come into play; however, such coupling between two spin 1/2 nuclei is generally eliminated by MAS if the spin rate is fast enough. In the case of coupling to a quadrupolar nucleus, however, this may not be true and, although MAS will cause partial averaging, the spin 1/2 spectrum may retain a residual dipolar splitting, with powder bandshapes involved for each of the quadruplet lines mentioned above. Such effects have been fully discussed in many articles and reviews.[9] Most examples refer to $^{13}C^{14}N$

[a] Chemistry Department, University of Durham,South Road, Durham, DH1 3LE, UKFax: (internat.) +44-191/386-1127E-mail: r.k.harris@durham.ac.uk

 © WILEY-VCH Verlag GmbH, 69451 Weinheim, 2001 1434–1948/01/■–■ $ 17.50+.50/0

EurJIC 447/00

interactions, but such effects have been seen[10] for the P/Cl pair in phosphonitrile chloride cyclic trimer. The case of PCl_5 has also been studied, and the effect on the ^{31}P spectrum of such residual dipolar coupling (RDC) to the four and six chlorines of the two counter-ions investigated*((AUTHOR: But PCl_5 doesnt have any counter-ions. Please rephrase this sentence))*.[11] At high temperature, however, both phosphorus environments give rise to sharp singlets because of fast isotropic reorientation and/or short spin-lattice relaxation times of the chlorine nuclei (self decoupling). Isotropic indirect (scalar) effects, when these are present, would only be affected by fast spin-lattice relaxation.

Provided the relevant quadrupole coupling constant, $= e^2qQ/h$, is small compared to the Larmor frequency of the quadrupolar spin, the residual dipolar splitting can be treated by perturbation theory.[9] In such a situation the outer pair of lines in the ^{31}P spectrum influenced by isotropic indirect coupling to a chlorine nucleus will be shifted according to Equation(1):

$$\Delta = -\frac{3}{10}\chi D / \nu_{Cl} \quad (1) \qquad (1)$$

where D is the (PCl) dipolar coupling constant and $_{Cl}$ is the Larmor frequency of the chlorine nuclei. The inner pair of lines move by the same amount but in the opposite direction. In these cases it is often assumed that the electric field gradient tensor, q, is axially symmetric and that q and D (the dipolar tensor) are coaxial, but this is not necessarily true. A further common assumption is that the indirect coupling anisotropy, J, is negligible. Otherwise, D must be replaced by $D = D\ J/3$, though even this assumes that J is axially symmetric and that D and J are coaxial. However, these simple situations are not necessarily the case for the P/Cl nuclear pair, so that use of the full Hamiltonian may be required.

The interactions between phosphorus and chlorine may, in principle, be complicated by the presence of the two different spin 3/2 isotopes for chlorine, ^{35}Cl and ^{37}Cl. However, due to their differing natural abundances and similar nuclear properties, it can be expected that the separate effects will not be resolved, given the observed linewidths. In simulations both isotopes can be accounted for.

Results and Discussion

Solution-State NMR Measurements

The molecular structure of the title compound was first established by solution-state NMR spectroscopy. The ^{31}P spectrum (for a solution in $CH_2Cl_2/CDCl_3$) consists of a complex multiplet at = 67.3. The ^{19}F spectrum (obtained for a $[D_8]$toluene solution) was expected to be composed of two doublets, one having double intensity (from the Ar group), and one singlet (in principle a doublet but with $^6J_{PF}$ negligibly small). At ambient probe temperature, however, a doublet at = 58.9 ($^4J_{PF}$ = 58.3Hz), and two singlets (a broad double-intensity line at = 55 and a sharp peak at = 63.6) were observed. At 98 C, the broad signal was resolved into the expected doublet [= 54.9 ($^4J_{PF}$ = 41.7Hz)], demonstrating that rotation of the Ar group about the PC bond is fast enough on the NMR timescale for the two CF_3 groups to become equivalent. At 90 C, however, two doublets and two singlets were detected (Figure2).

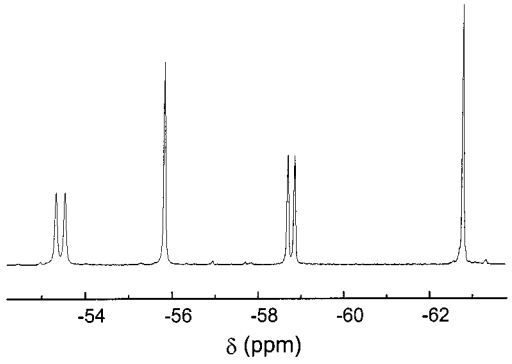

Figure 2. Fluorine-19 spectrum at 376.35MHz and 90 C of a solution of ArAr"PCl in $[D_8]$toluene; the high-frequency doublet and the high-frequency singlet are assigned to the Ar group and are the resonances which broaden and coalesce at higher temperatures; spectrometer operating conditions: pulse angle 34.8, 16 transients, recycle delay 4.0 s

The doublet and singlet assigned to the Ar group were at virtually identical positions to those at room temperature (= 58.8 and 62.8, respectively), suggesting either that rotation about the PAr bond is rapid on the NMR timescale even at low temperature or that there is a single fixed conformation about the PAr bond. For the Ar moiety, a doublet at = 53.4 ($^4J_{PF}$ = 76.7Hz) and a singlet at = 55.8 were found (consistent with the average and J observed at +98 C). We believe that the values of $^4J_{PF}$ in systems involving ArP or ArP linkages may contain a strong contribution from through-space effects. Therefore, this result implies that not only are the two CF_3 groups of Ar inequivalent at 83 C, but also that one of them may be appreciably further away from the phosphorus atom. This was subsequently confirmed by the crystal structure, determined at 123 C (see below). ^{19}F NMR spectroscopic data are summarised in Table1.

The Ar group rotation about the PC bond was investigated in detail by bandshape fitting for 12 temperatures between 15 C and 90 C on the basis of two-site equal-population mutual exchange. The coupling to ^{31}P involves summing the intensity of two such exchange pairs, with equal intensity but slightly different effective chemical shifts for one of the sites. Figure3 shows the Eyring plot for the exchange. The resulting thermodynamic parameters are: H = 51.0 0.6kJ mol^1 and S = 8 3 J K^1 mol^1, the errors quoted representing only the statistics of the linear fit.

The $^{13}C\{^1H\}$ NMR spectrum was also recorded for a toluene/$CDCl_3$ solution at ambient temperature. Probable assignments (see Figure1 for the notation) are shown in Table2, though some of these are necessarily tentative. In particular the signals from the carbons to which the CF_3

EurJIC 447/00

Table 1. Comparison of fluorine chemical shift data in different situations for compound **1**

	Assignment	$_a$/ppmAr	$_b$/ppmAr	$_c$/ppmAr	$_d$/ppmAr (*para*)	Averagelinewidth/Hz
Solution	high temp. 98 C	54.9[a]		58.8[b]	64.0	
ambient temp. 22 C	55[c]		58.9[d]	63.6		
low temp. 83 C	53.4[e]	55.8	58.8[f]	62.8		
Solid	high temp. 50 C	54.1	57.7	59.9	65.3	568
ambient temp.	54.3	58.0	60.3	65.5	597	
low temp. 120 C	55.1	57.9,[g]59.2 [g]	61.4	66.6	680	

[a] Doublet (double intensity). $^4J_{PF}$ = 41.7Hz. [b] Doublet. $^4J_{PF}$ 56.8Hz. [c] Broad, double intensity. [d] Doublet. $^4J_{PF}$ = 58.3Hz. [e] Doublet. $^4J_{PF}$ = 76.7Hz. [f] Doublet. $^4J_{PF}$ = 59.5Hz. [g] Low intensity.

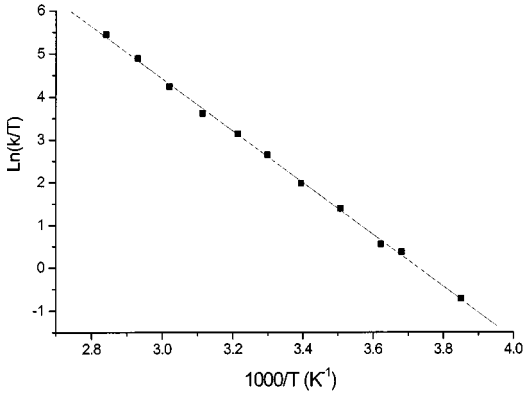

Figure 3. Eyring plot for the exchange of the CF_3 groups of the Ar moiety in ArArPCl by internal rotation about the PC bond in the solution state

groups were attached were of low intensity (presumably because the recycle delay used to secure good S/N for the other peaks was inadequate for relaxation of these carbons), and in a similar region to other signals. The presence of two distinct resonances for carbons *ipso* to phosphorus confirms the asymmetric nature of the title compound, as does the observation of three different *C*F_3 signals, one of double intensity.2

Table 2. Assignments for the solution-state ^{13}C spectrum of **1**

Carbon[a]	/ppm	*J* Hz[b]
A	137.6	d, $^1J_{PC}$ 67.9
B	136.7	d, $^1J_{PC}$ 84.0
C	132.11[c]	s
D	131.1	s (broad, double intensity)
E	134.2	d, $^2J_{PC}$ 8.7
F	128.0	d, $^2J_{PC}$ 3.4
G	123.7	m, $^3J_{FC}$ 5.0
K	123.18[c]	q, $^1J_{FC}$ 275.8 (double intensity)
L	123.24[c]	qd, $^1J_{FC}$ 275.5, $^3J_{PC}$ 3.4
M	123.1	q, $^1J_{FC}$ 272.6
N	132.06[c]	m
O	132.3	m
P	131.8	m

[a] See Figure 1. [b] Only the magnitudes of coupling constants were obtained, not the signs. [c] Although the absolute accuracy of the chemical shifts is only quoted to one decimal place, a further digit is given when two signals are very close but resolved.

Residual Dipolar Coupling Between ^{31}P and $^{35/37}Cl$

A single phosphorus environment for **1** in the solid state is indicated by the ^{31}P CPMAS spectrum, as expected from the fact that the crystallographic asymmetric unit is one molecule (see below). However, the signal was split into four lines at the lowest applied magnetic field used due to the effect of the adjacent chlorine (Figure4, lowest trace). The apparent chemical shifts of these lines were = 75, 72, 66 and 62 for the 200MHz spectrometer, the last two not being completely resolved (though a shoulder was easily observable). The four shifts were obtained by deconvolution using the Spinsight software.[12]

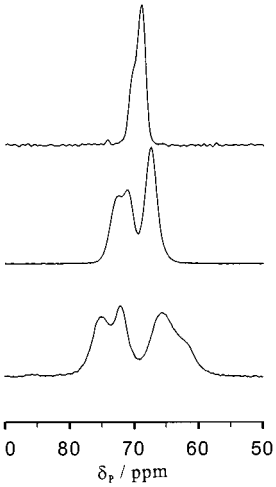

Figure 4. Phosphorus-31 {^1H} spectra of solid ArArPCl; centreband region only; spectral frequencies (top to bottom) 242.95MHz, 121.42MHz, 81.02MHz; cross-polarisation from protons; contact time 9 ms, recycle delay 5 s, number of acquisitions between 150 and 450

The nature of the splitting was identified by running spectra at different field strengths, namely on the 200, 300 and 600MHz (proton) spectrometers (Figure4). The splitting decreased on both a frequency and a ppm scale, confirming that there is a single phosphorus resonance affected by residual dipolar coupling to the adjacent quadrupolar chlorine. Such coupling can be contrasted with the cases of isotropic (indirect) coupling or crystallographic splittings, which decrease in ppm and increase in Hz, respectively, on going to higher magnetic field strength. Where all four lines can be seen (for the CMX 200 spectrometer), the separations of the lines are 228, 602 and 287Hz (from high to low frequency). The first two splittings were still resolved at 121.42MHz and are 188 and 449Hz respectively. At the highest field no splitting was observed within the linewidth

of 650Hz (the separation of a high-frequency shoulder peak from the signal maximum was approximately 350Hz). At each field the individual bandshapes did not show any significant changes over the spinning sideband manifold. The value of the isotropic coupling constant, J_{PCl}, is likely to be around 100130Hz in magnitude,[13] so it is not surprising that no splitting from this cause is resolved at the highest field. At 121.42MHz the appearance of the spectrum approached that of a doublet (i.e. J_{PCl} not significantly effective),[14] whereas at lower field there was further perturbation, producing a more complex multiplet.

From ab initio calculations using Gaussian94,[15] the electric field gradient (EFG) of the quadrupolar chlorine nucleus can be estimated. For this computation the full molecular structure was used, and the calculations to give the NMR parameters also included a structural energy minimisation. Results were converted to an appropriate axis system within a Mathcad worksheet. is calculated by multiplying q (obtained in atomic units as the largest component of the electric field gradient from a HartreeFock approximation using the 631g* basis set) by 2.3495 10^{36} C J^1 s^1. Values of of 55 and 44MHz were calculated for ^{35}Cl and ^{37}Cl respectively, with the major EFG axis approximately along the PCl bond and a low value (but nonzero) for the asymmetry parameter. NQR frequencies of magnitude 25.5, 25.7 and 26.3MHz have been reported for Et_2PCl, Bu_2PCl and $(C_6H_5)_2PCl$, respectively.[16] These represent the magnitude of $1/2e^2Qq/h$ (i.e.1/2) if the asymmetry parameter is zero, and therefore show that the values used in the calculations for the compound studied here are reasonable. The value of D may be obtained for **1** from the known PCl distance of 2.0608(6) Å (this work). For ^{31}P, ^{35}Cl the result is D = 662Hz, whereas for ^{31}P, ^{37}Cl it is 551Hz. Thus values of , the parameter defining the second-order effects under perturbation theory, may be calculated, assuming $D = D$ (i.e. ignoring J). These results are given in Table3. The predicted values are of the correct order of magnitude to account for the observed splittings, but a reasonable fit to the spectra at the different fields cannot be obtained, so a more accurate calculation is required.

tween the PCl interatomic distance and the EFG axis). A nonzero value of the isotropic scalar coupling, J_{PCl}, can also be incorporated. The values of used were: 55MHz for the ^{35}Cl isotope and 44MHz for ^{37}Cl (vide supra). The magnitude of J(^{31}P, ^{35}Cl) was set to a little lower than the literature values for related systems,[13] i.e. to 100Hz (which implies that J(^{31}P, ^{37}Cl) is 83Hz), since this seemed to yield a slight improvement in the fitting, and D was given the value calculated from the crystal structure (therefore assuming a negligible value of the anisotropy in J). As indicated before, a splitting of ca. 100Hz is significantly less than the observed linewidths and so will not be resolved, but it may, however, contribute to the distortion of the multiplet pattern. The relevant parameters were varied in the simulation and fitting by eye attempted. Altering D to include a possible anisotropy in J_{PCl} would lead to a slight change in the total width of the whole pattern, but changing the value of D (D) from 500 to 660Hz does not, in practice, have a significant effect on the simulated spectrum. A larger magnitude of J_{PCl} than 100Hz does lead to an increase in the outer splittings and a smaller value for the largest central splitting. However, changing the sign of J_{PCl} has a much more marked effect. Whereas a positive value led to substantial discrepancies between observed and simulated spectra, a negative value resulted in a good fit (see Figure3 and 4) at both 81.02 and 121.42MHz. Several different angles were used (in the range 0 to 180) and the approximate splittings of the simulated bands compared to the experimental data. The best agreement at 81.02MHz was found with = 0, giving approximate splittings of 200, 670 and 300Hz measured between the centres of gravity of the simulated powder patterns involving ^{35}Cl (experimental values are 228, 602 and 287Hz). If is increased to 20, the splittings move significantly away from the experimental values, giving four bands with more nearly equal separation. At higher values of , of around 90, the lines converge and the difference between the experimental and simulated spectra is obvious. Given that this system consists of a directly bonded spin-pair involving a monovalent quadrupolar nucleus, co-axiality of the EFG and the PCl bond is expected, so this result

Table 3. Theoretical parameters for the reduced P,Cl dipolar splittings observed for compound **1**

^{31}P frequencyMHz	Isotope	DHz[a]	MHz	Hz	2Hz	Observed splittingHz[b]
81.02	^{35}Cl	662	55	557	1114	860
	^{37}Cl	551	44	446	892	
121.42	^{35}Cl	662	55	372	744	560
	^{37}Cl	551	44	297	594	
242.95	^{35}Cl	662	55	186	372	350
	^{37}Cl	551	44	149	298	

[a] Assuming r_{PCl} = 1.93 Å. [b] Doublet splitting at the highest field, and approximate separation of the midpoints of the pairs of doublets at 81.02 and 121.42MHz.

Using a program based on the full Hamiltonian approach,[9,17] the bandshapes at 200 and 300MHz were simulated (Figure5). This calculates the MAS spectrum of a spin 1/2 nucleus under the influence of a quadrupolar (I = 3/2) spin, with the assumption of axial symmetry of the electric field gradient, but with variation allowed for the angle (be-

gives confidence in the methods used. The calculated splittings (for = 0) involving ^{35}Cl at 121.42MHz are 270, 470 and 230Hz (compared with measured values 188 and 449Hz, the third splitting being unresolved in this experimental spectrum). At 242.95MHz, there is not sufficient resolution in the experimental spectrum to make any mean-

ingful comparison with the simulated lineshapes. However, the overall width of the lines shows reasonable agreement with the width of the unresolved doublet.

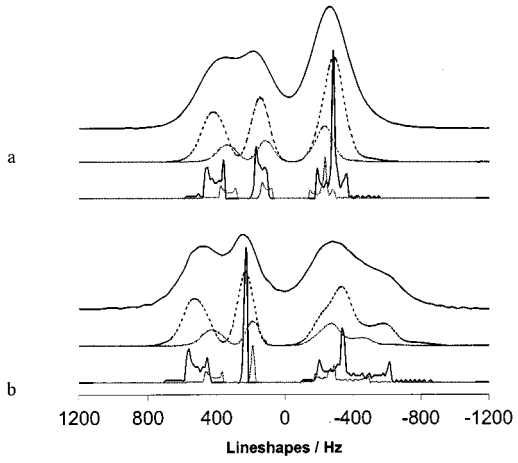

Figure 5. Experimental (upper solid lines) and simulated centreband shapes for the ^{31}P spectra of solid ArArPCl run at 121.42MHz (a) and 81.02MHz (b); the calculated powder bandshapes are shown below for coupling to ^{35}Cl (black lines) and ^{37}Cl (grey lines) in the appropriate proportions, with $J(^{31}P, ^{35}Cl)$ = 100Hz and $J(^{31}P, ^{37}Cl)$ = 83Hz, respectively; the dotted lines represent the two simulated spectra, with a line broadening of 100Hz

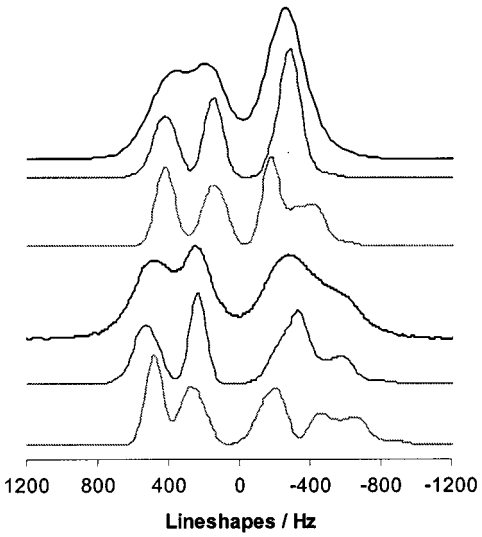

Figure 6. Centreband ^{31}P bandshapes for solid ArArPCl at 121.42MHz (top 3 spectra) and 81.02MHz (bottom 3 spectra); for each trio of spectra the top one is as experimentally observed, the middle one is as simulated for $J(^{35}Cl, ^{31}P)$ = 100Hz and the bottom one as simulated for $J(^{35}Cl, ^{31}P)$ = +100Hz; note that the simulations do not include a contribution from molecules containing the ^{37}Cl isotope

A value of slightly lower in magnitude (around 50MHz) than that calculated by ab initio methods was found to be perhaps more appropriate for the most abundant isotope, ^{35}Cl. In this case the simulated bands are brought slightly more in line with the experimental data. With an even lower value of the intensity differences between calculated and experimental spectra become more significant. Perturbation theory makes it clear that the principal variable is the product *D*.

Figure5 shows a comparison of the experimental and final simulated lineshapes. There is obviously significantly more broadening of the experimental lineshapes, but for ease of distinguishing the individual lines the simulation linewidth was kept low. The contribution from ^{37}Cl gives significantly different lineshapes to that from ^{35}Cl (see Figure5). The simulated spectra were obtained by summing the two contributions in the appropriate proportions. After line broadening has been applied there are only minor discrepancies between observed and simulated spectra, so it is clear that the parameters used for the latter are close to their correct values. In particular, it is proved that isotropic J_{PCl} is negative (Figure6). Because of the quadrupolar nature of the chlorine isotopes, very few values of this coupling constant have been reported, and this is the first determination of the sign.

Of course, there are still assumptions involved in the spectral simulation, especially axial symmetry in the EFG tensor, and there were limitations of not being able to optimise all the parameters by small increments because of the computational time involved in the calculation of each spectrum. This work represents the first time a ^{31}P reduced dipolar coupling pattern has been successfully simulated, including the first use of combined ^{35}Cl and ^{37}Cl effects.

Cross-Polarisation Experiments

Both ^{19}F and ^{1}H nuclei were used for polarisation transfer to phosphorus. All three nuclei are abundant in the sense that their natural isotopic proportion of the element is 99.9%. Therefore cross-polarisation dynamics are more complex than may appear at first sight. For instance, although results from a $^{1}H^{31}P$ variable-contact-time experiment may in general be fitted to only two parameters (a rise time T_{HP}^{eff} and a decay time T_1^{eff}) these cannot be simply related to the specific cross-polarisation time T_{HP} and single-nucleus T_1^H respectively. Instead, both measured parameters depend on T_{CP}, T_1^H and T_1^P. A detailed analysis of this problem may be found in refs.[18,19] On the other hand, for compound **1**, phosphorus is chemically dilute in the sense that there is only one ^{31}P per molecule, which is likely to result in a long T_1^P (motional questions notwithstanding), as for the common case of ^{13}C. When the ratio of spins $_{YX} = N_Y/N_X$ for a system involved in an XY CP experiment is low, deviations from simple behaviour are expected to be small. In the present case $_{PF}$ is 1:12 and $_{PH}$ is 1:6. It is found that for both $^{19}F^{31}P$ and $^{1}H^{31}P$ the rise of magnetisation during a variable contact time is substantially faster than the T_1-dependent decay. For ^{19}F to ^{31}P cross polarisation, both the TORQUE (TOneRhoQUEnching)[20] curve (for which the total constant spin-lock time was 10 ms) and the standard cross-polarisation experiment show an almost horizontal region at long spin-lock times. This implies that T_1^F and T_1^P are both long. The measured cross-polarisation time T_{FP}^{eff} is relatively short (ca. 0.5 ms) and T_1^{eff} is a lot longer than the maximum duration of spin-

lock pulse available from the amplifiers. It is therefore difficult to measure these accurately, but a value for T_1^F of approximately 100 ms was obtained from a $^{19}F^{31}P$ CP experiment, with a variable pre-contact spin-lock time. The effective value of T_{HP} derived from $^1H^{31}P$ cross polarisation is longer, at 3.5 ms, than T_{FP}^{eff}. In the $^1H^{31}P$ experiment the TORQUE curve has a positive slope at long spin-lock time, suggesting[17,18] T_1^H T_1^P, as expected.

Solid-State ^{19}F Spectra

High-resolution ^{19}F spectroscopy of solids containing hydrogen as well as fluorine has been the subject of relatively few investigations to date because the proximity of ^1H and ^{19}F resonance frequencies requires a specialised probe to facilitate proton decoupling with sufficient frequency filtering. The present experiments provide evidence of the value of solid-state ^{19}F NMR spectroscopy for structural characterisation when such problems are overcome. ^{19}F spectra (Figure7) of the solid powdered sample were obtained over the temperature range 120 C to +50 C.

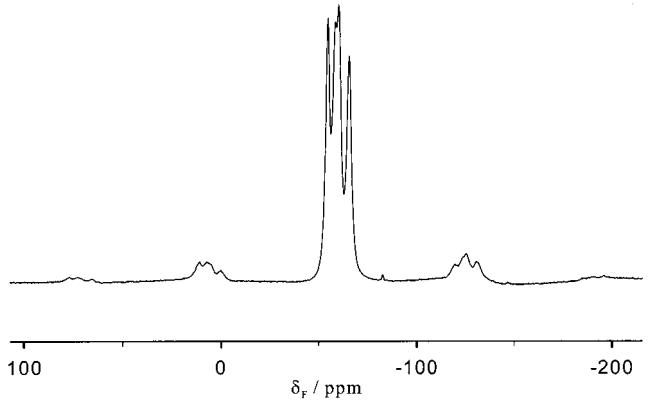

Figure 7. Fluorine-19 direct-polarisation spectrum of solid Ar-ArPCl; spectral frequency 188.3MHz, recycle delay 2 s, number of acquisitions 400, spin rate 12kHz

Throughout this range, the spectra show four peaks of approximately equal intensity within experimental error (considering the overlap of lines), with chemical shifts of = 54, 58, 60, and 65, although no splitting arising from $^4J_{PF}$ was resolved because the linewidths are broader than in solution. These observations indicate that there are different environments for all four CF_3 groups, indicating the lack of molecular symmetry and in conformity to the solution-state spectra. Rapid internal rotation will cause averaging of the positions, and therefore also of the chemical shifts of the three fluorines in each CF_3 group. It is also observed that, in contrast to the solution state differences in splitting due to PF coupling between the four CF_3 bands, there were no obvious variations in linewidths from deconvolution of the four peaks for the solid state, so only average values are quoted in Table1. There was little change in the spectrum as the temperature was lowered, and the value of T_1^F remained relatively constant at around 0.9 0.1 s, within experimental error, from 20 down to 80 C, with a slightly lower value of 0.6 s at ambient temperature (27 C). All four peaks showed small, similar trends in chemical shift to lower values as the temperature decreased, possibly arising from a variation in the referencing.

Solid-State ^{13}C Spectra

The ^{13}C spectrum of the solid (with cross polarisation from protons, using a recycle delay of 5s and a contact time of 8 ms) appears to consist of three peaks with chemical shifts = 134, 133, and 129 (by deconvolution) (Figure8). All these peaks were also observed in a dipolar dephasing experiment[21] in which only quaternary (or methyl) carbons remain. With an echo experiment run with identical conditions apart from the presence of the 50 s dephasing time, a subtraction of the normal and dipolar dephased spectra was made, resulting in a spectrum of protonated carbons only. In this case a broad underlying peak was observed with a maximum intensity at = 134. By taking advantage of the different cross polarisation and decoupling combinations possible in a fluorinated molecule and the triple-channel HFX probe, further conclusions about the carbon spectrum can be made. The low-frequency peak increases significantly in intensity on application of cross polarisation from fluorine, as does that at the highest frequency, indicating proximity of these carbons to the CF_3 groups. The lowest frequency peak also displays narrowing on application of fluorine decoupling. Although all these peaks appear in the aromatic ^{13}C region, no peaks were observed in any other region of this spectrum. It is concluded that the CF_3 resonances are also contained within this region. This result is supported by the solution-state spectrum described earlier, where all the relevant resonances lie between = 138 and 123.

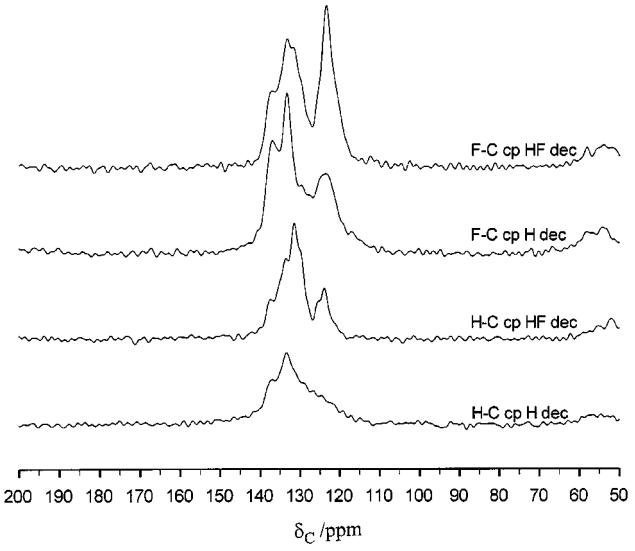

Figure 8. Solid-state ^{13}C spectra at 50.33MHz for compound **1** under various experimental regimes: cross polarisation, with contact time 7 ms, recycle delay 10 s, spin rate 4kHz; $^{19}F^{13}C$ CP and $^1H^{13}C$ CP used 280 and 64 acquisitions, respectively

X-ray Structure of ArArPCl

The crystal structure of the title compound at 150K is shown in Figure9, together with selected bond lengths and angles; according to the October 1999 release of the Cambridge Structural Database (CSD),[22] this is the first Ar_2PCl compound to be structurally characterised. The structure shows some interesting features arising from steric and intramolecular interactions. The three covalent bonds to the P atom have a pyramidal configuration, complemented by two relatively short intramolecular contacts PF(1) at 2.890(1) Å and PF(8) at 2.897(1) Å, approximately in *trans* positions to covalent bonds [angles C(9)PF(1) = 172.45(5); ClPF(8) = 163.08(3)]. These contacts are shorter than the sums of the empirical van der Waals radii[23] of P (1.91 Å) and F (1.40 Å), as well as the theoretical ones (estimated as 2.05 and 1.42 Å respectively).[24] As deduced from the ^{19}F solution-state NMR spectra at low temperatures, there are marked differences in the fluorine-to-phosphorus distances for the two *ortho* CF_3 groups in the Ar moiety. The calculated distances to F(5) and F(6) are 3.68 and 3.25 Å, respectively, compared with 2.89 Å to F(1) or F(2). Rapid rotation of each of these groups about the CCF_3 bonds is expected at higher temperatures, but the average PF distance will still be longer to one CF_3 group than the other. These observations allow the ^{19}F signal at 83 C at $_F$ = 53.4 to be assigned to F(1,2,3), assuming there is a significant through-space contribution to $^4J_{PF}$ (see above). The short PF(8) distance is then consistent with the existence of a moderately large ^4J[P,F(8)]. Such conclusions assume the structure of the molecule in solution is very similar to that in the crystalline solid. There is a possible hydrogen bond between the chlorine and the *ortho* hydrogen of the Ar group, at a calculated distance of 2.52 Å. This H-bond lies in the same plane as that of the aromatic ring of Ar, and may thus play an important role in determining the conformation of the compound. Because of the influence of the bulky CF_3 groups, the two aromatic rings form a dihedral angle of 94.

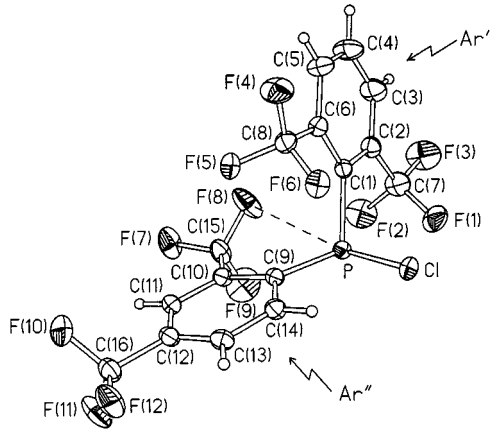

Figure 9. Molecular structure of **1**, showing 50% thermal ellipsoids; selected bond lengths (Å) and angles (): PCl 2.061(1), PC(1) 1.875(1), PC(9) 1.852(1); ClPC(1) 100.23(4), ClPC(9) 102.10(5), C(1)PC(9) 109.23(6)

The PCl bond of 2.061(1) Å is relatively short; in eleven previously reported R_2PCl (where at least one of the R groups is alkyl) structures (CSD) this distance varies from 2.06 to 2.35 Å, with the exception of the four-membered ring compound **II**, where it is reduced to between 2.01 and 2.03 Å.[25] The PCl distance is clearly sensitive to electronic effects from other groups bonded to phosphorus, and its shortening here can be attributed to the electron-withdrawing properties of the CF_3 groups on the aromatic rings.

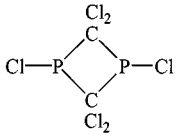

II

Experimental Section

Synthesis of AArPCl: *n*BuLi (57 mL of a 1.6 M solution in hexanes, 91.2mmol) was added dropwise over 10 minutes to a solution of 1,3,5-tris(trifluoromethyl)benzene (ArH) (20.03g, 94mmol) in ether (200 mL) at 78 C. The solution was allowed to warm to room temperature and left stirring for four hours. A dark brown solution containing ArLi and ArLi was formed. It was added dropwise at 78 C to a solution of PCl_3 (16 mL, 25.2g, 162mmol) in ether (100 mL) over 10 minutes. The mixture was allowed to warm to room temperature, and a precipitate of LiCl slowly formed. This was filtered off, and the solvent and excess PCl_3 removed from the filtrate in vacuo, leaving a brown intractable oil. A mixture of $ArPCl_2$ and $ArPCl_2$ (9.46g, 42%) was obtained by distillation at 45 and 0.01 Torr. Further distillation led to ArArPCl at 93 C (0.01 Torr); yield (based on ArH) 7.45g, 26%. The compound was purified by recrystallisation from hexanes. $C_{16}H_6ClF_{12}P$ (492.63): calcd. C 39.01, H 1.23; found C 38.94, H 1.24.

Solution-State NMR Spectroscopy: Solution-state NMR spectra were recorded in 5mm o.d. sample tubes on a Varian VXR 400 Fourier-transform spectrometer, operating at 100.57 (^{13}C), 161.91 (^{31}P) and 376.35 (^{19}F) MHz. Internal reference signals of TMS or $CFCl_3$ were used for ^{13}C and ^{19}F spectra, respectively, while an external reference of 85% H_3PO_4 was employed for all ^{31}P spectra. For the ^{13}C spectrum, 12824 FIDs were accumulated, using pulse angle 48.7 and recycle delay 3 s. The corresponding values for the ^{19}F spectra were 16, 34.8 and 4 s, respectively, whereas those for the ^{31}P spectra were 492, 36 and 3 s, respectively. Fluorine-19 bandshape fitting for the exchange process was carried out using an in-house computer program involving a complete Liouville treatment (including exchange rates, chemical shifts and transverse relaxation rates as variables). This program was developed in the MATLAB environment. Iteration to the bandshape was optimised to ^{2}. Temperatures were calibrated using the chemical shift differences between the CH_3 and OH resonances of methanol (for temperatures below ambient) and between the CH_2 and OH resonances of glycol (for high temperatures). The standard Varian hardware was employed for temperature control.

Solid-state NMR Spectroscopy: Because the sample could be subject to possible decomposition if exposed to moist air, it was sealed in a small plastic insert, which then fitted tightly into the rotors used.

The spectrometers used for solid-state NMR were: Chemagnetics CMX200, Varian Unity Plus 300, and Chemagnetics Infinity 600. Most of the results were obtained on the lowest field spectrometer with which three main probes were used. The diameters of the rotors are: HX and HFX probes, 7.5mm, and HF probe, 4mm. These allow almost any combination of observation, cross polarisation and decoupling to be carried out, with the use of appropriate filters. Recycle delays were initially determined by variable delay-time experiments and checked by measurement of T_1^H where appropriate. A recycle delay of 5 s and a 1 ms contact time were found to be optimum for the ^{31}P spectra. For cross-polarisation experiments, optimum contact times were found by arraying this parameter and choosing that with the greatest signal intensity. Spin rates used were generally 46kHz with the 7.5mm rotors and 1015kHz for the 4mm rotor. However, the small (3.2mm diameter) rotor system used with the Chemagnetics 600 spectrometer meant that a speed of 16.5kHz was easily attained. The frequencies of the individual nuclei on the three spectrometers are: (i) for the Chemagnetics CMX200: ^{31}P, 81.02MHz; ^{13}C, 50.33MHz; ^{19}F, 188.29MHz; ^{1}H 200.13MHz, (ii) for the Varian Unity Plus 300: ^{31}P, 121.42MHz; ^{13}C, 75.43MHz; ^{1}H 299.95MHz, and (iii) for the Chemagnetics Infinity 600: ^{31}P, 242.95MHz; ^{1}H 600.13MHz.

Referencing was done by replacement, setting the chemical shift scales as follows using the compounds named: ^{31}P, $CaHPO_4$ set to = 1.2 (w.r.t. the signal for 85% H_3PO_4 at zero ppm, though this primary standard was used directly as the reference on the 300MHz instrument); ^{19}F, C_6F_6 set to = 166.4 w.r.t. the signal for $CFCl_3$; ^{13}C, high-frequency peak of adamantane set to = 38.4 w.r.t. the signal for $(CH_3)_4Si$. Fluorine shifts are corrected for the BlochSiegert effect[26] at ambient probe temperature by recording the reference ^{19}F resonance with high-power irradiation at the proton frequency applied. The same correction is assumed to apply at low temperatures. In all cases, the standard MAS, direct- or cross-polarisation sequences gave good ^{19}F spectra with sufficient resolution to be able to use deconvolution to extract shift, intensity and linewidth parameters, so that CRAMPS operation was not necessary. Cross polarisation operation has the advantage of removing the small, broad probe background ^{19}F signal (which is observed with direct polarisation), but as direct polarisation for fluorine can lead to a better signal-to-noise ratio, in a comparable time, this may be favoured when the background and desired signals are easily distinguished or where the latter is much greater than the former. Because of the resulting increased averaging of the strong homonuclear interactions, spinning at the higher spin rates (ca.12kHz) was found to give good resolution. Most spectra were recorded at ambient probe temperature, but this may be in excess of room temperature[27,28] by up to 15 degrees for the faster spin rates.

Fluorine-19 and phosphorus-31 spin-lattice relaxation times were measured using the Torchia sequence,[29] i.e. by ^{1}H ^{19}F (or ^{31}P) CP followed by a 90 ^{19}F (or ^{31}P) pulse, a variable delay, and a 90 ^{19}F (or ^{31}P) read pulse. Proton decoupling was applied during acquisition but not during relaxation. In general, coupled spin systems will not yield single-exponential plots for relaxation times. However, the present measurements generally showed reasonably single-exponential curves. For proton spin-lattice relaxation times the pulse sequence used consisted of a 180 pulse on the proton channel followed by a variable delay, then a 90 ^{1}H pulse and contact to observe ^{31}P spectra. The fitting of intensities in relaxation experiments was done within Chemagnetics Spinsight software. That for T_1 used a three-parameter fit, taking into account the efficiency of the inversion. The number of data points recorded at each temperature was 1520 for T_1^F. For all T_1 and T_1 measurements for ^{31}P and ^{1}H 12 data points were recorded, the maximum spin-lock time (an instrumental restriction) for the latter being 20 ms, which obviously limits the accuracy of measurement for long rotating frame relaxation times. Measurements of T_1 and T_1 generally have statistical errors of 28%, with the larger values being for longer relaxation times (where the end of the decay is not observed due to, for instance, limits on spin-lock time).

Spinning sideband analysis was carried out using an in-house program, ssb97,[30] based on the theory of Maricq and Waugh,[31] which includes the error analysis of Olivieri.[17] Between 5 and 11 peaks were fitted for the sideband manifolds analysed. The program anychi-x, used for calculating bandshapes of spin 1/2 spectra involving dipolar coupling to a quadrupolar nucleus, was written in BASIC and provided by Olivieri.[32]

X-ray Diffraction: The X-ray diffraction experiment was performed on a SMART 1K CCD area detector, using graphite-monochromated Mo-K radiation (= 0.71073 Å). The structure was solved by direct methods and refined by full-matrix least-squares against F^2 of all reflections, using SHELXL-97 programs.[33] *Crystal data*: $C_{16}H_6ClF_{12}P$, M = 492.63, T = 150K, triclinic, space group $P\bar{1}$ (No. 2), a = 7.949(1), b = 9.313(1), c = 12.369(1) Å, = 104.25(1), = 90.49(1), = 96.35(1), U = 881.4(2) Å^3, Z = 2, D_c = 1.856g cm^3, = 0.43 mm^1, crystal size 0.36 0.34 0.34mm, 10579 reflections (4735 unique), R = 0.032 [4253 data, I 2(I)], $wR(F^2)$ = 0.086, $_{max}$ = 0.58 eÅ^3.

Crystallographic data (excluding structure factors) for the structure(s) included in this paper have been deposited with the Cambridge Crystallographic Data Centre as supplementary publication no. CCDC-148986. Copies of the data can be obtained free of charge on application to CCDC, 12 Union Road, Cambridge CB2 1EZ, UK [Fax: (internat.) + 44-1223/336-033; Email: deposit@ccdc.cam.ac.uk].

Acknowledgments

Two of us (L.A.C. and S.M.C.) thank the EPSRC for a studentship and another (M.D.R.) is grateful to the Department of Chemistry, University of Durham, for a studentship. We thank the EPSRC also for access both to the Durham-based research service in solid-state NMR (UDIRL) and to the Chemagnetics 600 system at Warwick. We acknowledge the receipt of research grants GR/L02906 and L24250 from the U.K. Engineering and Physical Sciences Research Council in support of this work. We are grateful to A. C. Olivieri for programming details and A. M.Kenwright and C. F. Heffernan for obtaining the solution-state ^{13}C and ^{19}F spectra.

[1] K. B. Dillon, H. P. Goodwin, *J. Organomet. Chem.* **1992**, *429*, 169171.
[2] R. D. Chambers, K. B. Dillon, T. A. Straw, *J. Fluorine Chem.* **1992**, *56*, 385388.
[3] K. B. Dillon, H. P. Goodwin, *J. Organomet. Chem.* **1994**, *469*, 125128.
[4] K. B. Dillon, V. C. Gibson, L. J. Sequeira, *J. Chem. Soc., Chem. Commun.* **1995**, 24292430.
[5] K. B. Dillon, V. C. Gibson, J. A. K. Howard, L. J. Sequeira, J. W. Yao, *Polyhedron* **1996**, *15*, 41734177.
[6] V. C. Gibson, C. Redshaw, L. J. Sequeira, K. B. Dillon, W. Clegg, M. R. J. Elsegood, *Chem. Commun.* **1996**, 21512152.
[7] K. B. Dillon, V. C. Gibson, J. A. K. Howard, C. Redshaw, L. J. Sequeira, J. W. Yao, *J. Organomet. Chem.* **1997**, *528*, 179183.
[8] M. G. Davidson, K. B. Dillon, J. A. K. Howard, S. Lamb, M. D. Roden, *J. Organomet. Chem.* **1998**, *550*, 481484.
[9] R. K. Harris, A. C. Olivieri, *Prog. Nucl. Magn. Reson. Spectrosc.* **1992**, *24*, 435456.

[10] R. C. Crosby, J. F. Haw, *Macromolecules* **1987**, *20*, 23242326.
[11] R. K. Harris, A. Root, *Mol. Phys.* **1989**, *66*, 9931013.
[12] Chemagnetics Spinsight. Version 3.5.2. Otsuka Electronics (U. S. A.) Inc.
[13] V. Mlynárik, *Prog. Nucl. Magn. Reson. Spectrosc.* **1986**, *18*, 277305 and references therein.
[14] S. H. Alarcn, A. C. Olivieri, S. A. Carss, R. K. Harris, M. J. Zuriaga, G. A. Monti, *J. Magn. Reson. A* **1995**, *116*, 244250.
[15] Gaussian 94 (Revison D.1) M. J. Frisch, G. W. Treucks, H. B. Schelegel, P. M. W. Gill, B. G. Johnson, M. A. Robb, J. R. Cheeseman, T. A. Kieth, G. A. Petersson, J. A.Montgomery, K. Raghavachari, M. A. Al-Laham, V. G. Zakrzewski, J. V. Ortiz, J. B. Foresman, J. Cioslowski, B. B. Stefanov, A. Nanayakkara, M. Challacombe, C. Y.Peng, P. Y. Ayalla, W. Chen, M. W. Wong, J. L. Andres, E. S. Replogle, R.Gomperts, R. L. Martin, D. J. Fox, J. S. Binkley, D. J. Defrees, J. Baker, J. P. Stewart, M. Head-Gordon, C. Gonzalez, J. A. Pople, Gaussian, Inc., Pittsburgh PA, **1995**.
[16] G. K. Semin, T. A. Babushkina, G. G. Yakobson, *Applications of NQR in Chemistry*, Khimiya, Leningrad, **1972**.
[17] A. C. Olivieri, *J. Magn. Reson. A* **1996**, *123*, 207210.
[18] S. Ando, R. K. Harris, S. A. Reinsberg, *J. Magn. Reson.* **1999**, *141*, 91103.
[19] S. Ando, R. K. Harris, G. A. Monti, S. A. Reinsberg, *Magn. Reson. Chem.* **1999**, *37*, 709720.
[20] P. Tekely, V. Gerardy, P. Palmas, D. Canet, A. Retournard, *Solid State NMR* **1995**, *4*, 361367.
[21] S. J. Opella, M. H. Frey, *J. Am. Chem. Soc.* **1979**, *101*, 58545856.
[22] F. H. Allen, *Acta Crystallogr., Sect. A* **1998**, *54*, 758771.
[23] Yu. V. Zefirov, P. M. Zorkii, *Russ. Chem. Rev.* **1989**, *58*, 421440.
[24] M. Franck, R. F. Hout Jr., W. J. Hehre, *J. Am. Chem. Soc.* **1984**, *106*, 563570.
[25] A. N. Chernega, G. N. Koidan, A. P. Marchenko, *Zh. Strukt. Khim.* **1992**, *33*, 155.
[26] S. A. Vierktter, *J. Magn. Reson. A* **1996**, *118*, 8493.
[27] T. Bjornholm, H. J. Jakobsen, *J. Magn. Reson.* **1989**, *84*, 204211.
[28] A.-R. Grimmer, A. Kretschmer, V. B. Cajipe, *Magn. Reson. Chem.* **1997**, *35*, 8690.
[29] D. A. Torchia, *J. Magn. Reson.* **1978**, *30*, 613616.
[30] J. R. Ascenso, L. H. Merwin, H.-P. Bai, J. C. Cherryman, unpublished work.
[31] M. M. Maricq, J. S. Waugh, *J. Chem. Phys.* **1979**, *70*, 33003316.
[32] A. C. Olivieri, personal communication.
[33] G. M. Sheldrick, SHELXL-97 programs, University of Gottingen, **1997**.

Received November 23, 2000
[I00447]

Thermodynamics of Hydrogen Bonding between CO and the Supercage Brønsted Acid Sites of the H-Y Zeolite − Studies from Variable Temperature IR Spectrometry

Carlos Otero Areán,*[a] Olga V. Manoilova,[b] Alexey A. Tsyganenko,[b] Gemma Turnes Palomino,[a] Margarita Peñarroya Mentruit,[a] Francesco Geobaldo,[c] and Edoardo Garrone[c]

Keywords: Adsorptions / Thermodynamics / Hydrogen bonds / IR spectroscopy / Zeolites

A procedure was developed for studying the thermodynamics involved in the interaction of carbon monoxide with Brønsted acid sites in zeolites, without the need for microcalorimetric measurements. The observables are the integrated infrared intensity of the C–O stretching mode of the OH···CO adducts, temperature, and equilibrium pressure. These quantities were measured by means of variable-temperature IR spectroscopy, using a home made IR cell equipped with a capacitance pressure gauge. Interaction of CO with Brønsted acid sites at the supercage of the faujasite-type H-Y zeolite involves a standard enthalpy change, $\Delta H°$ of –25.6 kJ mol^{-1}, and a standard entropy change, $\Delta S°$ of –161 J mol^{-1} K^{-1}. These values were compared with the corresponding figures obtained from the calorimetric determination of CO adsorption on a number of metal oxides and zeolites.

Introduction

Carbon monoxide is by far the most extensively used probe molecule for IR spectroscopic studies in surface chemistry, involving both metal oxides[1−5] and zeolites.[5−10] For a detailed characterisation of active solids, which is relevant to the general field of surface chemistry and (in particular) to the more specialised field of heterogeneous catalysis, it is desirable to have a detailed knowledge of the energy involved in the adsorbent-adsorbate interaction, and not only of the spectroscopic changes involving the probe molecule. Relatively strong interactions between CO and strongly adsorbing surface centres, such as coordinatively unsaturated transition metal ions, are readily studied by performing the spectroscopic measurements at room temperature. Interactions with weaker centres, such as alkali metal ions or protons, usually require IR measurements at a lower temperature, typically around the boiling point of nitrogen.[8−12] The same applies to calorimetric studies,[13] although measurements at room temperature are sometimes possible.[14]

Recent infrared spectroscopic[15−18] and quantum chemical[16,19] studies have shown that carbon monoxide can interact with extra-framework alkali[15−17] and alkaline earth[18] metal cations in zeolites forming both, C-bonded and O-bonded adducts; there is strong evidence[16,20] that suggests hydrogen-bonding between CO and Brønsted acid OH groups, however, protonic zeolites have been less studied in this context. The two linkage isomers are characterised by C−O stretching frequencies, which are both higher (C-bonded adduct) and lower (O-bonded adduct) than the 2143 cm^{-1} value corresponding to free CO. Variable temperature FTIR studies[15,17] on Na-ZSM-5 and Na-Y zeolites have shown that the population of the two isomers is a function of temperature, the O-bonded adducts are always a minority, but their relative population grows as the temperature increases.

The only observables needed for the above mentioned studies are the integrated areas of the IR absorption peaks corresponding to the C-bonded and O-bonded CO measured over a large temperature range, and the corresponding temperature values. However, if the equilibrium pressure could be measured simultaneously,[21] a more detailed thermodynamic study of the CO/zeolite system could, in principle, be carried out. The variable temperature IR cell used in our previous studies[15,17] has now been equipped with suitable pressure gauges, and here we report on the results obtained on the CO/H-Y system. It is shown that the whole set of experimental data, which includes temperature, pressure, and integrated IR intensity, allows a full thermodynamic description of the system to be obtained without resorting to microcalorimetric studies. To the best of our knowledge this experimental approach has never been reported before. It opens up a new strategy for the thermodynamic study of weakly interacting adsorbate-adsorbent systems, for which direct calorimetric studies are very cumbersome and very difficult to carry out due to the small energies involved.

[a] Departamento de Química, Universidad de las Islas Baleares, 07071 Palma de Mallorca, Spain
[b] Institute of Physics, St. Petersburg University, 198904 St. Petersburg, Russia
[c] Dipartimento di Scienza dei Materiali ed Ingegneria Chimica, Politecnico di Torino, Corso Duca degli Abruzzi 24, 10125 Torino, Italy

 © WILEY-VCH Verlag GmbH, 69451 Weinheim, 2001 1434−1948/01/0707−1739 $ 17.50+.50/0

Results and Discussion

Data analysed in this paper correspond to two independent sets of measurements. In one of them (series I), 3 Torr of carbon monoxide was admitted into the IR cell which contained a self-supported H-Y zeolite wafer. The cell was then closed and IR spectra were obtained at different temperatures (starting from 77 K), simultaneously recording the equilibrium CO pressure inside the cell (see Experimental Section). After completing this series of measurements, the cell was outgassed and a second run (series II) was started after dosing with 13 Torr of CO.

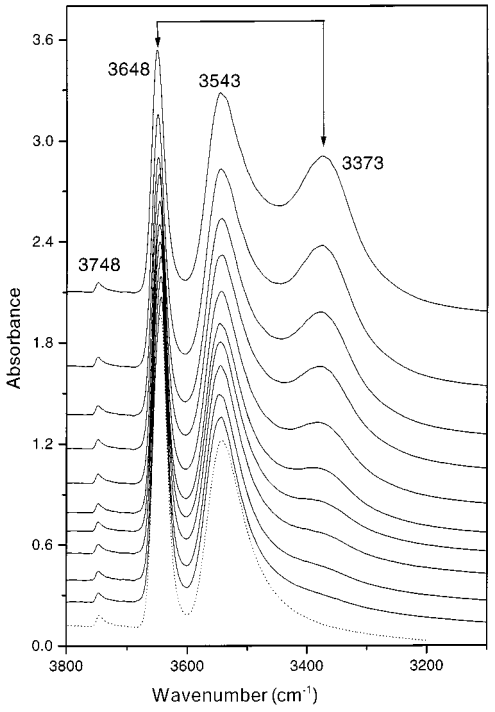

Figure 1. IR spectra, in the O−H stretching region, of CO adsorbed on H-Y. The dotted line is the zeolite blank spectrum at 77 K. Continuous line spectra correspond (from top to bottom) to I1 to I10 in Table 1. For clarity, the spectra have been offset on the vertical scale

Figure 1 reports the IR spectra (in the O−H stretching region) of the blank zeolite sample at 77 K, and at several different temperatures after admitting a dose of CO into the IR cell; corresponding values of temperature and equilibrium pressure are given in Table 1. Note that, although the total amount of CO inside the cell remains fixed, the fraction adsorbed diminishes when the temperature is raised, and this contributes to the increase in pressure. The zeolite blank spectrum shows a sharp band at 3648 cm^{-1}, which corresponds to bridged Si(OH)Al hydroxy groups (Brønsted acid sites) located in the supercage of the faujasite-type structure, and another band at 3543 cm^{-1} which is due to the Si(OH)Al species situated inside sodalite cages.[8] The weak band seen at 3748 cm^{-1} is readily assigned to silanols.[8,9]

Table 1. Numerical data corresponding to two independent runs

Spectra	Temp. (K)	Pressure (Torr)	Absorbance (cm^{-1})	Coverage
Small CO dose				
I1	145	0.14	9.04	0.430
I2	153	0.33	8.39	0.399
I3	159	0.63	7.31	0.348
I4	166	1.03	6.00	0.286
I5	173	1.48	4.54	0.216
I6	179	1.86	3.33	0.158
I7	185	2.20	2.31	0.110
I8	191	2.44	1.61	0.077
I9	197	2.62	1.09	0.052
I10	207	2.82	0.58	0.028
Large CO dose				
II1	155	5.38	18.63	0.887
II2	161	6.04	16.98	0.809
II3	167	6.77	15.00	0.714
II4	173	7.56	12.63	0.601
II5	178	8.36	10.21	0.486
II6	184	9.12	7.94	0.378
II7	190	9.79	5.96	0.284

The band due to the Brønsted acid sites in the supercages decreases upon interaction with the adsorbed CO molecule, and a new broad band (from the hydrogen-bonded OH···CO species[8,22]) develops at 3373 cm^{-1}. This is in accordance with the accessibility of the Brønsted acid sites to the adsorbed CO. In contrast, the band at 3543 cm^{-1} was not affected by the CO. This was expected due to the inaccessibility of the sodalite cages. The shift of the O−H stretching mode (from 3648 down to 3373 cm^{-1}) can be considered to be a measure of the acidity of the Si(OH)Al species available for interaction with the adsorbed (basic) CO molecule.[8,23−25] Although Brønsted acid sites are perhaps not completely homogeneous, the shift observed is quite the same for all coverage values, thus indicating that heterogeneity is in fact very limited. This has implications for the treatment of data given below, where all Si(OH)Al acid centres located in the zeolite supercages are considered to be equivalent and noninteracting, i.e. they constitute an ideal ensemble in the thermodynamic sense.

Figure 2 depicts the same spectra as in Figure 1 in the C−O stretching region. The spectra are dominated by a strong band at 2173 cm^{-1} which corresponds to the fundamental C−O stretching mode of hydrogen-bonded OH···CO adducts.[8,9] A weak band is also observed at 2124 cm^{-1}, which is mainly due to carbon monoxide interacting with the acidic Si(OH)Al species via the oxygen atom of the CO molecule;[15,16] it also contains the ^{13}CO counterpart (natural abundance about 1%) of the band at 2173 cm^{-1}. For the purposes of the present paper the weak band at 2124 cm^{-1} constitutes a minor feature, which shall not be considered any further.

With increasing temperature, the intensity of the 2173 cm^{-1} band decreases, the concomitant increase in pressure notwithstanding. Table 1 reports the integrated intensity

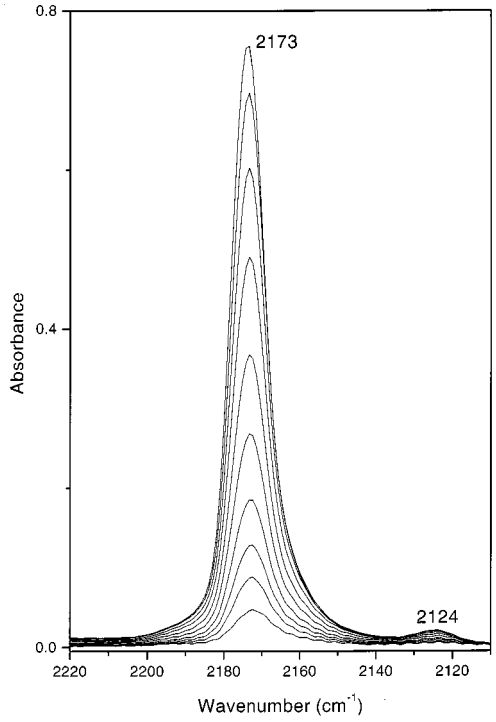

Figure 2. C−O stretching region of the same IR spectra as reported in Figure 1, increasing temperature from top to bottom. The zeolite blank was subtracted from all spectra shown

(A) of the peak at 2173 cm^{-1} (absorbance), and the temperature and pressure for all spectra considered for further treatment. They correspond to the two different CO doses (I and II) in separate experiments. The number of adsorbed molecules should be proportional to the integrated intensity of the 2173 cm^{-1} band, according to the Beer−Lambert law.

At temperatures lower than those reported in Table 1, small shifts (to higher frequency) in the peak position were observed. The corresponding spectra have been consequently discarded from the present treatment, as a small change in the molar absorption coefficient could have taken place and the intensities are not necessarily related to the coverage.

The observables, band intensity (A), temperature (T), and pressure (p), are interrelated by an equation of state. On the basis of the assumption of ideality made above, this equation of state is proposed to be according to Equation (1) which corresponds to the Langmuir isotherm at constant temperature.

$$A/A_M = \theta = K(T)p/[1 + K(T)p] \quad (1)$$

A_M is the highest integrated intensity, corresponding to full coverage, and θ is the fractional coverage. Note that pressure and temperature are not really independent, even for each individual set of measurements, but this is not important in the present context. The equilibrium constant, K, may be written as in Equation (2).

$$K(T) = \exp[\Delta S°(T)/R] \exp[-\Delta H°(T)/RT] \quad (2)$$

As is normally the case, the standard changes in both enthalpy and entropy may be assumed to be constant, in the first instance. This is equivalent to neglecting any role of the standard change in specific heat in the adsorption process. Under this assumption, the equation of state becomes as shown in Equation (3).

$$\theta = \exp(\Delta S°/R) \exp(-\Delta H°/RT)\cdot p/[1 + \exp(\Delta S°/R) \exp(-\Delta H°/RT)\cdot p] \quad (3)$$

It can be linearised as in Equation (4).

$$\ln\{p[(1/\theta) - 1]\} = -\Delta S°/R + \Delta H°/RT \quad (4)$$

For the highest coverage (temperatures close to 77 K in series II), the measured values of the integrated intensity were found to be in the range 20 to 23 cm^{-1}. Transforming the set of intensity data in Table 1 into a corresponding set of θ values, and assuming that $A_M = 21.0$ cm^{-1} for the present set of data (see below), the validity of Equation (4) can be examined as shown in Figure 3, where the left hand side of the equation is plotted against the inverse of the temperature. The two sets of experimental data are seen to line up in a very satisfactory manner, which allowed the determination of $\Delta S°$ and $\Delta H°$. The values obtained are $\Delta S° = -161$ J $mol^{-1}K^{-1}$ and $\Delta H° = -25.6$ kJ mol^{-1}.

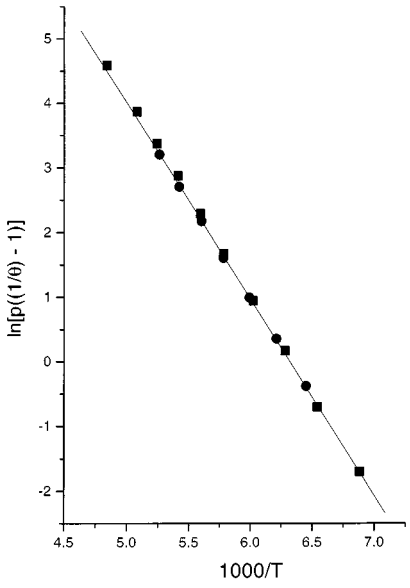

Figure 3. Check of the validity of an ideal model for adsorption; dose I: squares, dose II: circles

Note that the linear plot in Figure 3 was obtained by selecting a value of 21.0 cm^{-1} for the highest intensity, A_M. The selection of an A_M value differing from 21.0 cm^{-1} by as little as ±0.5 cm^{-1}, resulted in a loss of linearity of the plot in Figure 3. Therefore, the accuracy with which A_M can be determined is 0.5 cm^{-1}.

The feasibility of assuming constant $\Delta H°$ and $\Delta S°$ values over a rather wide temperature range (ca. 60 K, i.e. some 30% of the highest temperature used) has been verified as follows. If the opposite assumption is made, i.e. that the

standard change in specific heat, Δc_p°, is not negligible, we can write [Equation (5)].

$$\Delta c_p^\circ = -\gamma R \quad (5)$$

where R is the gas constant and γ is a positive number. Note that Δc_p° is expected to be negative for an adsorption process, since translational degrees of freedom are lost, and rotational degrees of freedom are substituted by intermolecular modes. From Equation (5) the following expressions can be derived [Equation (6) and Equation (7)].

$$\Delta S^\circ(T) = \Delta S^* - \gamma R \ln(T/T^*) \quad (6)$$

$$\Delta H^\circ(T) = \Delta H^* - \gamma R (T - T^*) \quad (7)$$

T^* is a reference temperature, e.g. the ambient one, and ΔH^* and ΔS^* are the standard changes in enthalpy and entropy at that temperature. Accordingly, Equation (4) should be written as Equation (8).

$$\ln \{p[(1/\theta) - 1)]\} - \gamma [\ln(T/T^*) - (1 - T^*/T)] = -\Delta S^*/R + \Delta H^*/RT \quad (8)$$

The choice of different γ values in Equation (8), up to 3/2 (corresponding to complete loss of translational freedom), does not significantly alter the values calculated for the standard enthalpy and entropy changes. As a result the standard enthalpy and entropy changes are considered to be temperature independent.

The values obtained for ΔS° and ΔH° can be directly checked against independent experimental evidence. Concerning the standard enthalpy change, the present value of $\Delta H^\circ = -25.6$ kJ mol^{-1} for the CO/H-Y system compares well with the calorimetrically determined heat of interaction of CO with the protonic form of ZSM-5, which was found to be[13] $\Delta H^\circ = -27$ kJ mol^{-1}. It is well-known[26–28] that the H-Y zeolite is slightly less acidic than H-ZSM-5. Therefore, a slightly smaller value of ΔH° for the CO/H-Y system relative to that of the CO/H-ZSM-5 system was expected.

With respect to the standard change in entropy, the present value of $\Delta S^\circ = -161$ J mol^{-1}K^{-1} can be compared with a set of calorimetrically determined values for the adsorption of CO performed under nearly ideal conditions on different metal oxides and on the zeolite Na-ZSM-5, reported in the literature[14,29,30]. This comparison is made in Figure 4, which shows a linear correlation between log ($-\Delta S^\circ$) and log ($-\Delta H^\circ$) for several CO/adsorbent systems. The discussion of such a linear correlation, usually called the *compensation effect*,[31,32] is outside the scope of this paper. However, it should be noted that the ΔS° value found for the CO/H-Y system satisfactorily fits into the correlation, thereby supporting the overall validity of the thermodynamic treatment developed here. Note that a general criticism can be raised against many correlation diagrams similar to that in Figure 4, because correlation can be an artefact when ΔS° and ΔH° values are simultaneously determined from the variation of an equilibrium constant experimentally measured within a narrow temperature range. However, data in Figure 4 are not biased in this sense, since ΔH° values taken from the cited literature were determined calorimetrically, and the ΔS° and ΔH° values corresponding to the CO/H-Y system were obtained from measurements covering a fairly large temperature range.

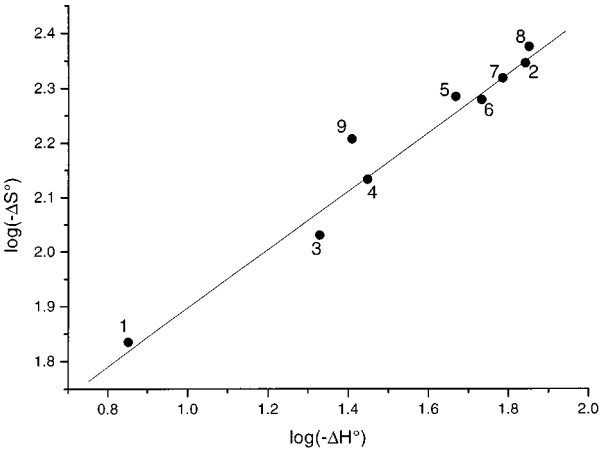

Figure 4. Correlation between ΔS° and ΔH° for CO adsorbed on: 1) alumina (weak Lewis site); 2) alumina (strong Lewis site); 3) silica-supported (reduced) chromia; 4) Na-ZSM-5; 5) zinc oxide; 6) titania (weak Lewis site); 7) titania (intermediate site); 8) titania (strong Lewis site); 9) H-Y. References: metal oxides [29, 30], Na-ZSM-5 [14], H-Y: present work

Conclusions

The integrated intensities observed for the 2173 cm^{-1} band, corresponding to the stretching mode of CO interacting via the carbon atom with Si(OH)Al hydroxy groups inside the supercage of the H-Y zeolite, satisfy a model for ideal adsorption. The derived value of $\Delta H^\circ = -25.6$ kJ mol^{-1} is close to that of $\Delta H^\circ = -27$ kJ mol^{-1} determined calorimetrically for the analogous CO/H-ZSM-5 system. Remarkably also, the value of $\Delta S^\circ = -161$ J mol^{-1}K^{-1} obtained for CO/H-Y fits a correlation diagram applicable to a number of systems involving CO adsorbed on metal oxides and on the zeolite Na-ZSM-5. These facts provide strong evidence that the experimental strategy used in this work yields reliable equilibrium data for thermodynamic studies. Both the experimental and calculation procedures described here should have a general validity for other systems. Furthermore, they can advantageously be used in cases where the weakness of adsorbate-adsorbent interactions precludes the use of calorimetric methods.

Experimental Section

The H-Y zeolite used was synthesized following standard methods;[33] it had a nominal Si/Al ratio of 5.6. Powder X-ray diffraction showed good crystallinity and the absence of any diffraction lines not assignable to the corresponding structure type.

Figure 5 depicts a scheme of the home-made variable temperature IR cell used. It was equipped with a platinum resistance thermo-

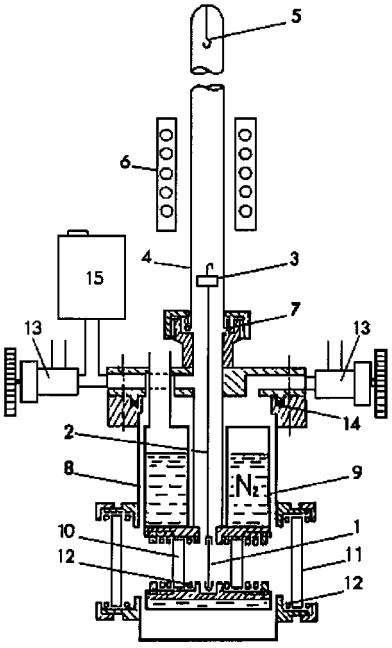

Figure 5. Scheme of the home-made (stainless-steel) variable-temperatur IR cell: 1) sample wafer, 2) sample holder, 3) magnetically driven anchoring piece, 4) quartz tube, 5) hook for fixing the sample wafer inside the furnace, 6) furnace, 7) Viton O-ring, 8) cell body, 9) refrigerated region, 10) BaF_2 windows, 11) NaCl windows, 12) indium gaskets, 13) valve, 14) Teflon gasket, 15) pressure gauge

meter and a capacitance pressure gauge (Edwards, 600). The accuracy of pressure measurements was ± 0.02 Torr. For IR measurements, a thin self-supported wafer of the zeolite was prepared and activated (outgassed) in a dynamic vacuum (residual pressure $<10^{-4}$ Torr) for 2 h at 680 K, inside the IR cell. For variable temperature infrared spectroscopy, liquid nitrogen was used for refrigeration. For better thermal contact between the zeolite wafer and the cooled environment, 0.5 Torr of helium was admitted into the sample compartment before recording the background spectrum at liquid-nitrogen temperature. CO was then dosed to an equilibrium pressure of 3 or 13 Torr (at room temperature), in two different sets of measurements. After dosing with CO, the cell was closed and IR spectra were recorded at 77 K and on gradual warming up of the IR cell following the removal of liquid nitrogen. Transmission IR spectra were recorded, at 2 cm^{-1} resolution, by means of a Bruker IFS66 FTIR spectrometer.

In order to allow for the pressure due to the helium inside the IR cell, a blank experiment was conducted in which a fixed amount of helium was dosed into the cell and the corresponding pressure was measured at different temperatures. These measurements gave a calibration plot from which the pressure correction was deduced.

[1] E. A. Paukshtis, R. I. Soltanov, E. N. Yurchenko, *React. Kinet. Catal. Lett.* **1981**, *16*, 93.
[2] T. A. Rodionova, A. A. Tsyganenko, V. N. Filimonov, *Adsorbtsiya Adsorbenty* **1982**, *10*, 33; *Chem. Abstr.* **1983**, *98*, 1500210.
[3] M. I. Zaki, H. Knözinger, *Mater. Chem. Phys.* **1987**, *17*, 201.
[4] C. Morterra, G. Magnacca, *Catal. Today* **1996**, *27*, 497.
[5] J. C. Lavalley, *Catal. Today* **1996**, *27*, 377.
[6] M. A. Makarova, K. M. Al-Ghefaili, J. Dwyer, *J. Chem. Soc., Faraday Trans.* **1994**, *90*, 383.
[7] J. A. Lercher, C. Gründling, G. Eder-Mirth, *Catal. Today* **1996**, *27*, 353.
[8] A. Zecchina, C. Otero Areán, *Chem. Soc. Rev.* **1996**, *25*, 187.
[9] H. Knözinger, S. Huber, *J. Chem. Soc., Faraday Trans.* **1998**, *94*, 2047.
[10] C. Otero Areán, *Comments Inorg. Chem.* in press.
[11] L. M. Kustov, V. B. Kazansky, S. Beran, L. Kubelkova, P. Jiru, *J. Phys. Chem.* **1987**, *91*, 5247.
[12] M. Jiang, H. G. Karge, *J. Chem. Soc., Faraday Trans.* **1996**, *92*, 2641.
[13] S. Savitz, A. L. Myers, J. R. Gorte, *J. Phys. Chem. B* **1999**, *103*, 3687.
[14] E. Garrone, B. Fubini, B. Bonelli, B. Onida, C. Otero Areán, *Phys. Chem. Chem. Phys.* **1999**, *1*, 513.
[15] C. Otero Areán, A. A. Tsyganenko, E. Escalona Platero, E. Garrone, A. Zecchina, *Angew. Chem. Int. Ed.* **1998**, *37*, 3161.
[16] P. Ugliengo, E. Garrone, A. M. Ferrari, A. Zecchina, C. Otero Areán, *J. Phys. Chem. B.* **1999**, *103*, 4839.
[17] A. A. Tsyganenko, E. Escalona Platero, C. Otero Areán, E. Garrone, A. Zecchina, *Catal. Lett.* **1999**, *61*, 187.
[18] A. A. Tsyganenko, C. Otero Areán, E. Escalona Platero, *Stud. Surf. Sci. Catal.* **2000**, *130*, 3143.
[19] A. M. Ferrari, K. M. Neyman, N. Rösch, *J. Phys. Chem. B* **1997**, *101*, 9292.
[20] C. Otero Areán, B. Bonelli, G. Turnes Palomino, A. M. Canaleta Safont, E. Garrone, *Phys. Chem. Chem. Phys.*, in press.
[21] S. Huber, H. Knözinger, *Appl. Catal. A* **1999**, *181*, 239.
[22] G. C. Pimentel, A. L. McClellan, *The Hydrogen Bond*, W. H. Freeman, San Francisco, **1960**, Chapter 3.
[23] E. A. Paukshtis, E. N. Yurchenko, *React. Kinet. Catal. Lett.* **1981**, *16*, 131.
[24] G. Maes, J. Smets, *J. Phys. Chem.* **1993**, *97*, 1818.
[25] V. Gruver, J. J. Fripiat, *J. Phys. Chem.* **1991**, *95*, 8549.
[26] J. A. Rabo, G. J. Gajda, *Catal. Rev. Sci. Eng.* **1990**, *31*, 385.
[27] M. A. Makarova, V. L. Zholobenko, K. M. Al-Ghefaili, N. E. Thompson, J. Dewing, J. Dwyer, *J. Chem. Soc., Faraday Trans.* **1994**, *90*, 1047.
[28] F. Wakabayashi, J. N. Kondo, K. Domen, C. Hirose, *J. Phys. Chem.* **1996**, *100*, 4154.
[29] E. Garrone, G. Ghiotti, E. Giamello, B. Fubini, *J. Chem. Soc., Faraday Trans. 1* **1981**, *77*, 2613.
[30] V. Bolis, B. Fubini, E. Garrone, C. Morterra, *J. Chem. Soc., Faraday Trans. 1* **1989**, *85*, 1383.
[31] A. K. Galway, *Adv. Catal.* **1977**, *26*, 247.
[32] G. A. Somorjai, *Introduction to Surface Chemistry and Catalysis*, Wiley-Interscience, New York, **1994**, p. 454.
[33] R. Szostak, *Molecular Sieves*, Van Nostrand Reinhold, New York, **1989**, p. 123.

Received December 4, 2000
[I00459]

An Anionic $\{[MnCo(ox)_3]^-\}_n$ Network with Appropriate Cavities for the Enantioselective Recognition and Resolution of the Hexacoordinated Monocation $[Ru(bpy)_2(ppy)]^+$ (bpy = bipyridine, ppy = phenylpyridine)

Muriel Brissard,[a][‡] Michel Gruselle,*[a] Bernard Malézieux,[a] René Thouvenot,[a] Carine Guyard-Duhayon,[a] and Odile Convert[b]

Keywords: Circular dichroism / Chiral resolution / Ruthenium / NMR spectroscopy / Polymers

Partial resolution of the *rac*-$[Ru(bpy)_2(ppy)]^+$ monocation into $[\Delta$-$Ru(bpy)_2(ppy)]PF_6$ (**1Δ**) (*ee* = 44%) and $[\Lambda$-$Ru(bpy)_2(ppy)]PF_6$ (**1Λ**) (*ee* = 50%) enantiomers was achieved by an unprecedented resolving process which involves the diastereoselective preparation of optically active networks of the type $\{[\Lambda$-$Ru(bpy)_2(ppy)][Mn$-Λ-$Co(ox)_3]\}_n$ (**2Λ**) and $\{[\Delta$-$Ru(bpy)_2(ppy)][Mn$-Δ-$Co(ox)_3]\}_n$ (**2Δ**). In these optically active inorganic polymers, the counter-monocation $[Ru(bpy)_2(ppy)]^+$ of appropriate configuration occupies the cavities while the excess $[Ru(bpy)_2(ppy)]^+$, of opposite configuration, remains in solution and is thus recovered. Anion metathesis of the optically active $[Ru(bpy)_2(ppy)]PF_6$ (**1Δ**) (*ee* = 44%) and (**1Λ**) (*ee* = 50%) with [l-cinchonidinium]-[Δ-trisphat] [trisphat = tris(tetrachlorobenzenediolato)-phosphate(V)] provides the related diastereomers $[\Delta$-$Ru(bpy)_2(ppy)][\Delta$-trisphat] (**3Δ**) (*de* = 44%) and $[\Lambda$-$Ru(bpy)_2(ppy)][\Delta$-trisphat] (**3Λ**) (*de* = 50%) in 60% yield. Their diastereomeric excesses were assessed by ^1H NMR analysis. All products were fully characterized and the absolute configuration was determined by circular dichroism techniques in solution or in the solid state. Additionally the X-ray structure of $[Ru(bpy)_2(ppy)]PF_6$ (**1**) was determined.

Introduction

The design and synthesis of networks possessing chiral cavities aimed to resolve optically active molecules represents a big challenge in the area of supramolecular material chemistry.[1] Ruthenium bis-bipyridine complexes $[Ru(bpy)_2L]^{n+}$ (L = bpy, phen...) (bpy = bipyridine; phen = phenanthroline) have been extensively studied for many years for their properties in biology,[2,3] and photo- and electrochemistry.[4−7] Most of these species have already been reported in the literature by several groups, with emphasis on the preparation of pure enantiomers of such propeller-like coordination complexes (Δ and Λ). Various resolution methods have commonly been used such as diastereomeric salt formation[8,9] or chromatographic separation techniques.[8,10] Another route to obtain optically active $[Ru(bpy)_2L]^{n+}$ complexes is based on the use of chiral precursors such as *cis*-$[Ru(bpy)_2(py)_2]^{2+}$ [11,12] (py = pyridine), *cis*-$[Ru(bpy)_2(CO)_2]^{2+}$ [8,13] or *cis*-$[Ru(bpy)_2(DMSO)Cl]^+$;[14−16] subsequent treatment with nucleophiles (phen, bpy...) provides the target complexes with retention of the configuration at the metal center. More recently a stereoselective synthesis has been proposed by Hesek[17] using the chiral ligand *R*-(+)- or *S*-(−)-methyl *p*-tolylsulfoxide that leads to the corresponding ruthenium bis-bipyridine complex with a diastereomeric excess of 50%.

In a pioneering work, Decurtins[18−21] described the synthesis of racemic bimetallic oxalate-bridged networks $\{[M^1(bpy)_3][M^2M^3(ox)_3]\}_n$ (M^1 = Ni^{II}, Fe^{II}; M^2 = Li^I and M^3 = Cr^{III} or M^2 = M^3 = Mn^{II}) starting from racemic materials. We recently reported the synthesis[22,23] of optically active homochiral polymers $\{[M^1(bpy)_3][M^2M^3(ox)_3]\}_n$ (M^1 = Ni^{II}, Ru^{II}; M^2 = Li^I and M^3 = Cr^{III} or M^2 = M^3 = Mn^{II}) and $\{[Ru^{II}(bpy)_2(ppy)][MCr^{III}(ox)_3]\}_n$ (M = Ni^{II}, Mn^{II}, ppy = phenylpyridine) using the tris-chelate complexes $[Cr(ox)_3]^{3-}$, $[M^1(bpy)_3]^{2+}$ and $[Ru^{II}(bpy)_2(ppy)]PF_6$ described by Constable.[24] We have shown that the formation of these polymers is highly diastereoselective and that the chirality control of only one type of building block leads to the selective precipitation of the corresponding homochiral enantiomeric polymer. Furthermore, the $\{[M^{II}M^{III}(ox)_3]^-\}_n$ network presented magnetic properties which can be tuned by modifying the nature of the M^{II}-M^{III} couple. As some of the $[M^{III}(ox)_3]^{3-}$ cannot always be resolved, we have to ensure the control of the chirality of the polymer via an optically active $[Ru(bpy)_2(ppy)]^+$ complex acting as a template. The separation of the latter into its two enantiomeric forms has not been reported so far. All attempts to resolve this $[Ru(bpy)_2(ppy)]^+$ complex by conventional procedures have been unsuccessful. Therefore we explored the possibility of employing the same resolution method that we have applied for $[Ni(bpy)_3]^{2+}$. Previously,[22] we have shown that using resolved $[\Delta$-$Cr(ox)_3]^{3-}$, a twofold excess of racemic $[Ni(bpy)_3]^{2+}$ and Li^+, afforded

[a] Laboratoire de Chimie Inorganique et Matériaux Moléculaires, ESA 7071, case courrier 42, Université Pierre et Marie Curie
4 Place Jussieu, 75252 Paris Cedex 05, France
Fax: (internat.) +33-1/4427-3841
E-mail: gruselle@ccr.jussieu.fr
[b] Laboratoire de Chimie Structurale Organique et Biologique, UMR 7613, case courrier 45, Université Pierre et Marie Curie
4 Place Jussieu, 75252 Paris Cedex 05, France
Fax: (internat.) +33-1/4427-3843
[‡] This work is a part of the Ph. D. thesis of M. Brissard.

 © WILEY-VCH Verlag GmbH, 69451 Weinheim, 2001 1434−1948/01/0707−1745 $ 17.50+.50/0

an optically active insoluble polymer in which all the metal centers possessed the Δ configuration, leaving in solution the unreacted enriched [Λ-Ni(bpy)$_3$]$^{2+}$. Therefore the diastereomeric formation of these polymers could be of general use for the separation of the two enantiomers of tris-chelate complexes.

In this paper, we describe the partial resolution of the racemic [Ru(bpy)$_2$(ppy)]PF$_6$ (**1**) complex into [Δ-Ru(bpy)$_2$(ppy)]PF$_6$ (**1Δ**) (*ee* = 44%) and [Λ-Ru(bpy)$_2$(ppy)]PF$_6$ (**1Λ**) (*ee* = 50%) enantiomers via the formation of the polymers {[Λ-Ru(bpy)$_2$(ppy)][Mn-Λ-Co(ox)$_3$]}$_n$ (**2Λ**) and {[Δ-Ru(bpy)$_2$(ppy)][Mn-Δ-Co(ox)$_3$]}$_n$ (**2Δ**), respectively. Their absolute configuration was determined by circular dichroism. In addition we describe the preparation of the diastereomeric salts [Δ-Ru(bpy)$_2$(ppy)][Δ-trisphat] (**3Δ**) (*de* = 44%) and [Λ-Ru(bpy)$_2$(ppy)][Δ-trisphat] (**3Λ**) (*de* = 50%) from [l-cinchonidinium][Δ-trisphat] and the enriched [Ru(bpy)$_2$(ppy)]PF$_6$ complexes **1Δ** and **1Λ**, respectively. Finally the optical purity of these species was determined by ^{1}H NMR spectroscopy.

Results and Discussion

X-ray Structure of [Ru(bpy)$_2$(ppy)]PF$_6$

Single crystals of [Ru(bpy)$_2$(ppy)]PF$_6$ (**1**) were obtained by diffusion of diethyl ether into a solution of **1** in acetone. The crystallographic data and structure determination parameters obtained by X-ray diffraction studies for [Ru(bpy)$_2$(ppy)]PF$_6$ (**1**) are given in Table 1. [Ru(bpy)$_2$(ppy)]PF$_6$ crystallizes in the space group *C*2/*c* with $Z = 8$. As depicted in Figure 1, we notice that the [Ru(bpy)$_2$(ppy)]$^+$ cation is hexacoordinated and presents a structure similar to that of the dication [Ru(bpy)$_3$]$^{2+}$ [a C atom (C31) replaces an N atom]. The C atom (C31) was arbitrarily placed on the Figure 1 (in fact its distribution is equal on the six atomic sites bonded to the Ru atom). The bond lengths and angles for [Ru(bpy)$_2$(ppy)]PF$_6$ (**1**) and in [Ru(bpy)$_3$]Cl$_2$ [22,25] are quite similar (Table 2). The symmetry of the monocation [Ru(bpy)$_2$ppy]$^+$ is formally C_1. However, as the external shell geometry is very close to that of [Ru(bpy)$_3$]$^{2+}$, one can assume that [Ru(bpy)$_2$ppy]$^+$ has a quasi D_3 symmetry.

Ideally, to differentiate a chiral cationic complex of D_3 symmetry such as [Ru(bpy)$_2$ppy]$^+$, it is essential to choose a chiral shift anionic reagent that also possesses a D_3 symmetry. Therefore we choose the [Δ-trisphat] anion (previously described by Lacour[26–28]) to prepare the related diastereomers of [Ru(bpy)$_2$ppy]$^+$; the results are shown in the next section.

Resolution of the [Ru(bpy)$_2$(ppy)]$^+$ Cation 1Δ and 1Λ by the Synthesis of the Optically Active Polymers 2Λ and 2Δ

Treatment of [l-cinchonidinium][Δ-trisphat] with a stoichiometric amount of *rac*-[Ru(bpy)$_2$(ppy)]PF$_6$ (in acetone, MeOH or acetone/MeOH in ratios 1:1 and 2:3) followed by crystallization provided deep purple powders. Circular

Table 1. Crystal data for [Ru(bpy)$_2$(ppy)]PF$_6$ (**1**)

	[Ru(bpy)$_2$(ppy)]PF$_6$ **1**
Formula	$C_{31}H_{24}N_5Ru{\cdot}PF_6$
Fw (g.mol^{-1})	712.60
Temperature (K)	295
Crystal system	Monoclinic
Space group	*C*2/*c*
a (Å)	23.749 (16)
b (Å)	13.715 (3)
c (Å)	19.334 (6)
α (°)	90
β (°)	114.16 (3)
γ (°)	90
V (Å^3)	5745 (5)
Z	8
Linear abs coef μ (mm^{-1})	0.672
Density ρ (g.cm^{-3})	1.65
Crystal size (mm)	0.4 × 0.4 × 0.3
Color	brown
Shape	parallelepiped
Diffractometer	Enraf−Nonius Cad 4
Radiation	Mo-K_α (λ = 0.71069 Å)
Scan type	2θ/ω
θ limits (°)	1−26
Index range, *h*, *k*, *l*	0, 29; 0, 16; −23, 21
Secondary extinction coeff	505
Percent decay	0.063
Reflections measured	6034
Independent reflections	5626
Reflections used	2486
$R = \Sigma\|\|F_o\| - \|F_c\|\|/\|F_o\|$	0.0668
$Rw^* = [\Sigma w(\|\|F_o\| - \|F_c\|\|)^2/\Sigma wF_o^2]^{1/2}$	0.0738
Weight coefficients[a]	3.11, 0.901, 2.45
Δρmin (e/ Å^3)	−1.06
Δρmax (e/ Å^3)	1.77
σ(I) limit	3.00
Number of parameters	364
Goodness of fit	0.965

[a] $w = w'\{1\text{-}[(\|F_o\| - \|F_c\|)/6.\sigma(F_o)]^2\}^2$ with $w' = 1/\Sigma_r T_r(X)$ with three coefficients for a Chebyshev series for which $X = F_c/F_c(\max)$.

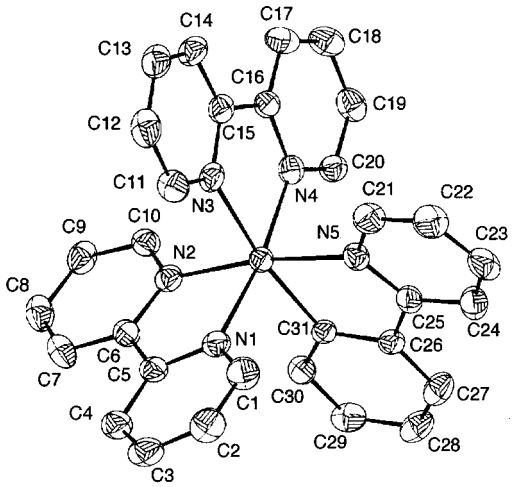

Figure 1. X-ray molecular structure of [Ru(bpy)$_2$(ppy)]PF$_6$ (**1**) with atomic number system

Table 2. Selected bond lengths [Å] and angles [°] for $[Ru(bpy)_2(ppy)]PF_6$ (**1**) and $[Ru(bpy)_3]Cl_2$

	$[Ru(bpy)_2(ppy)]^+$ (**1**)	$[Ru(bpy)_3]^{2+}$ [22]
N1[a]−Ru−N1	95.4 (6)	95.3 (2)
N1−Ru−N2	78.0 (6)	78.9 (2)
N2[a] (C31)−Ru−N2	96.5 (0)	95.6 (2)
N1[b]−Ru−N2	90.6 (0)	90.7 (2)
Ru−N1	2.069 (4)	2.046 (4)
Ru−N2 (C31)	2.044 (1)	2.054 (4)

[a] $-1/2 + y$, $3/2 - z$, $1 - x$. − [b] $1 - z$, $1/2 + x$, $3/2 - y$.

dichroism and ^1H NMR spectroscopy showed that this material is composed only of nonenriched $[Ru(bpy)_2(ppy)][\Delta$-trisphat] (**3**) (equal amounts of the two diastereomers, *de* = 0%). Hence using the [Δ-trisphat] anion, we were unable to resolve the *rac*-$[Ru(bpy)_2(ppy)]^+$ complex by selective crystallization of one diastereomer.

To resolve the *rac*-$[Ru(bpy)_2(ppy)]PF_6$ complex we finally applied the "polymer formation" strategy. To ensure good enantiomeric excess for the unreacted optically active $[Ru(bpy)_2(ppy)]^+$, three conditions were required: i) A full diastereoselectivity in the formation of the polymers. ii) A rapid precipitation relative to the racemization rate of the starting anionic brick $[M^{III}(ox)_3]^{3-}$ to keep a good chiral induction over the synthesized polymer and also on the excess cation left in solution. iii) A good yield for the reaction (almost quantitative). *These conditions are fulfilled in our system*. It should be noted that tris-oxalate cobalt $[Co(ox)_3]^{3-}$ was used instead of $[Cr(ox)_3]^{3-}$ (as previously) because its racemization rate is slower,[29] affording an enhanced enantiomeric excess for the resolved cation (*ee* = 34% versus 44% or 50% according to NMR studies). Thus, the use of resolved $K_3[Co(ox)_3]$ $\{[\alpha]_D = +1667$ (Δ form) or -1892 (Λ form)} (maximum rotation reported in the literature:[30] $[\alpha]_D = +1928$ or -1940), $MnCl_2$ and racemic $[Ru(bpy)_2(ppy)]PF_6$ (**1**) (twofold excess) in a $DMSO/H_2O$ solution results, after five minutes, in the precipitation of the respective polymers either $\{[\Delta\text{-}Ru(bpy)_2(ppy)][Mn\text{-}\Delta\text{-}Co(ox)_3]\}_n$ (**2Δ**) or $\{[\Lambda\text{-}Ru(bpy)_2(ppy)][Mn\text{-}\Lambda\text{-}Co(ox)_3]\}_n$ (**2Λ**) (yield = 90%), depending on the configuration of the $[Co(ox)_3]^{3-}$ building block. As a consequence, the mother liquor phase is now enriched in the opposite enantiomer of $[Ru(bpy)_2(ppy)]PF_6$ (either **1Λ** or **1Δ**) and is thus recovered from the filtrate as a precipitate by addition of diethyl ether (Scheme 1a). Scheme 1b shows a schematic representation[22] of the anionic optically active polymer **2Λ** hosting the $[\Lambda\text{-}Ru(bpy)_2(ppy)]^+$ monocation counter part.

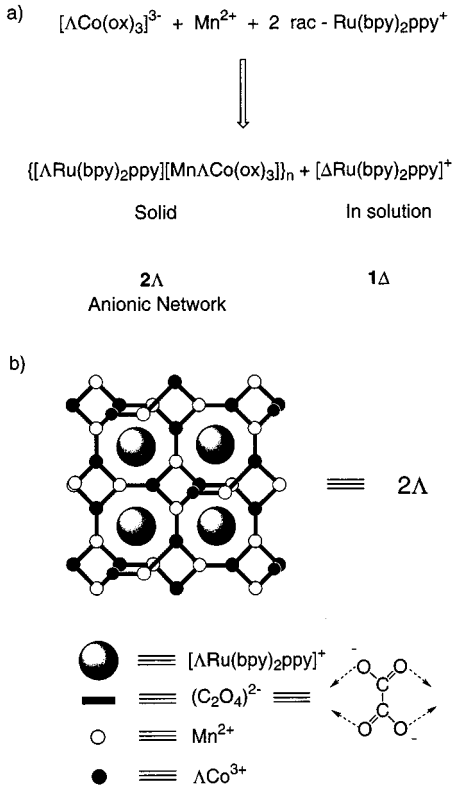

Scheme 1. (a) Preparation of the bimetallic optically active polymer $\{[\Lambda\text{-}Ru(bpy)_2ppy][Mn\text{-}\Lambda\text{-}Co(ox)_3]\}_n$ (**2Λ**) along with the enriched monocation $[\Delta\text{-}Ru(bpy)_2(ppy)]^+$ (**1Δ**); (b) schematic representation[22] of the polymer **2Λ** hosting the $[\Lambda\text{-}Ru(bpy)_2(ppy)]^+$ cation counter part

Assignment of the Metallic Configurations in the Polymers 2Δ and 2Λ and in the Resolved Cations 1Δ and 1Λ by Circular Dichroism

The absolute configuration of the Co and Ru centers in the polymers **2Δ** and **2Λ** and in the enriched cations **1Δ** and **1Λ** was determined by circular dichroism by comparison of their spectra with those of Δ and Λ enantiomers of $[Co(ox)_3]^{3-}$ and $[Ru(bpy)_2L]$. This is based on the principle that two related optically active molecules have the same absolute configuration if they give a Cotton effect of the same sign in the absorption wavelength region of an electronic transition common to both molecules.[31] Due to the extreme insolubility of the polymers, solid state circular dichroism was employed for all compounds. The circular dichroism curves of the polymers **2Δ** and **2Λ** are depicted in Figure 2. They show optical activity and opposite signals typical for two enantiomers. All bands (λ_{max} = 548, 493, 432, 376, 322, 311, 279 nm) are essentially due to intra-ligand or MLCT transitions of $[Ru(bpy)_2ppy]^+$. Indeed, these bands are very strong in comparison with the weak $d \rightarrow d$ bands of $[Co(ox)_3]^{3-}$(in the monomer at λ_{max} = 618, 518, 415, 291 nm) which are totally masked. Therefore the absolute configuration of the Co centers cannot be assigned directly. However, it can be easily predicted from the configuration of the starting optically active $[Co(ox)_3]^{3-}$ salt. The Ru absolute configurations in **2Δ** and **2Λ** are assigned owing to the sign of the band due to the bipyridine ligand at λ_{max} = 322 nm (a positive Cotton effect in the 300−330 nm region is characteristic of the Λ configuration for the metal center[8,9,11,13−17,22]). The Co and Ru centers adopt the same configuration in these polymers, as is the case in the bimetallic polymers templated by $[Ru(bpy)_3]^{2+}$ obtained previously.[22]

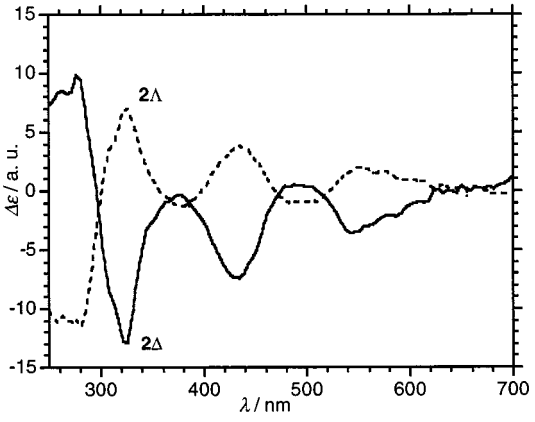

Figure 2. Circular dichroism spectra of **2Δ** and **2Λ** polymers in KBr dispersions

As expected, the circular dichroism curves of the enriched $[Ru(bpy)_2ppy]^+$ (**1Δ** or **1Λ**) (Figure 3) display signals due to the bipyridine ligands (λ_{max} = 598, 494, 390, 307, 259 nm) opposite to that of the respective precipitated polymers **2Λ** or **2Δ**, confirming the partial resolution of the monocation. The typical bipyridine band mentioned above again allows the determination of the Ru absolute configurations. It is worth noting that the dichroism spectra of the compounds **1Δ** and **1Λ** (in CH_2Cl_2 or acetone solutions) remain unchanged after five hours, showing that the racemization of $[Ru(bpy)_2(ppy)]^+$ is very slow in solution.

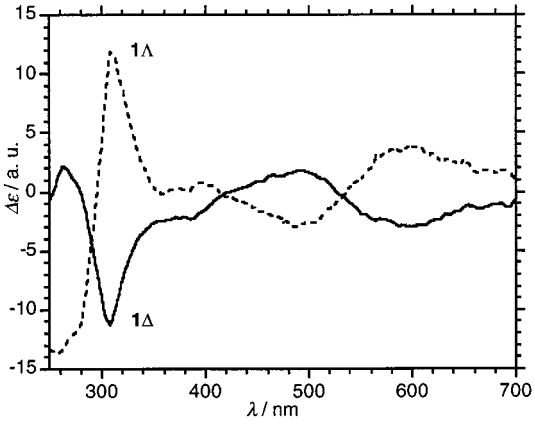

Figure 3. Circular dichroism spectra of **1Δ** and **1Λ** in KBr dispersions

Synthesis and Circular Dichroism of 3Δ and 3Λ

Even if circular dichroism in the solid state allows us to assign the absolute configurations of metal complexes in the optically active compounds, it cannot be used as a device to measure the enantiomeric or diastereomeric excesses.[22] The circular dichroism spectrum of pure $[Ru(bpy)_2(ppy)]^+$ (*ee* = 100%) is still unknown, precluding a useful comparison of the relative intensities. The very deep purple color of the $[Ru(bpy)_2(ppy)]^+$ complex (due to the intraligand bipyridine transitions) also wrecked all attempts to measure the optical rotation. For this purpose the optically active enriched **1Δ** and **1Λ** $[Ru(bpy)_2ppy]^+$ salts were converted into their enriched diastereomeric salts [Δ-$Ru(bpy)_2$-(ppy)][Δ-trisphat] (**3Δ**) and [Λ-$Ru(bpy)_2$(ppy)][Δ-trisphat] (**3Λ**) with [Δ-trisphat] as the counter-anion. The diastereomeric excesses in these two species were determined by ^1H NMR spectroscopy.

Treatment of a solution of **1Δ** (or **1Λ**) with one equivalent of [l-cinchonidinium][Δ-trisphat] for 30 minutes in acetone at room temperature afforded either **3Δ** (or **3Λ**). Subsequent separation of the mixture by column chromatography on an aluminum oxide column (10 cm, CH_2Cl_2) provided **3Δ** (or **3Λ**) as the less-polar purple band while the starting $[Ru(bpy)_2(ppy)]PF_6$ **1Δ** (or **1Λ**) was then eluted as the more polar fraction. We assume in this reaction that the diastereomeric excess in **3Δ** and **3Λ** reflects exactly the enantiomeric excess in **1Δ** and **1Λ** for the following reasons:

– the [l-cinchonidinium][Δ-trisphat] salt is optically pure (*de* = 98%).

– the [l-cinchonidinium][Δ-trisphat] reacts equally (see above and ref.[32]) with both enantiomers of $[Ru(bpy)_2ppy]^+$ even if the transformation of $[Ru(bpy)_2ppy]^+$ into the related diastereomeric salt $[Ru(bpy)_2(ppy)]$[Δ-trisphat] is not quantitative (yield: 60%).

Circular dichroism measurements of **3Δ** and **3Λ** were performed in CH_2Cl_2 (Figure 4). The curves of the two diastereomers exhibited two well-separated regions where the borderline is centered at 270 nm. For the region $\lambda > 270$ nm, the spectra present opposite signals due exclusively to the optically active $[Ru(bpy)_2(ppy)]^+$. Below 270 nm, [Δ-trisphat] bands are predominant exhibiting similar and negative Cotton effects.

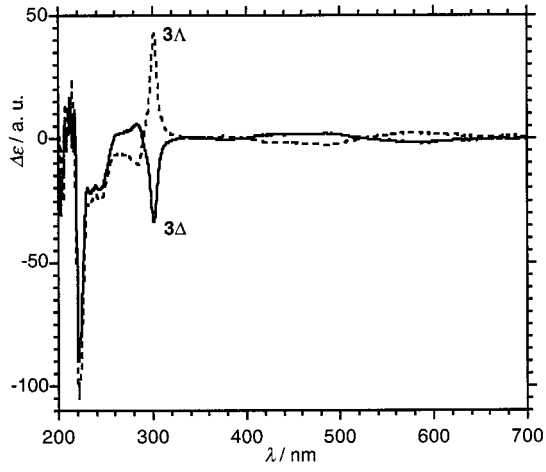

Figure 4. Circular dichroism spectra of **3Δ** and **3Λ** in CH_2Cl_2 solutions ($c = 7.5-9.10^{-5}$ mol·L^{-1})

Determination of the Diastereomeric Excess of [Δ-$Ru(bpy)_2$(ppy)][Δ-trisphat] (3Δ) and [Λ-$Ru(bpy)_2$(ppy)][Δ-trisphat] (3Λ) by ^1H NMR Spectroscopy

The ^1H NMR spectra of *rac*-$[Ru(bpy)_2ppy]PF_6$ (**1**), $[Ru(bpy)_2(ppy)]$[Δ-trisphat] (**3**) (*de* = 0%) and enriched [Δ-$Ru(bpy)_2$(ppy)][Δ-trisphat] (**3Δ**) and [Λ-$Ru(bpy)_2$(ppy)][Δ-

trisphat] (**3Λ**) were recorded in acetone solution (Figure 5a−d). These ^1H NMR studies allowed us to determine the enantiomeric excess of the enriched complex [Δ-$Ru(bpy)_2ppy]PF_6$ (**1Δ**) and [Λ-$Ru(bpy)_2ppy]PF_6$ (**1Λ**) by measurement of the diastereomeric excess in **3Δ** and **3Λ**. As a first approach, we measured the ^1H NMR spectrum of *rac*-$[Ru(bpy)_2ppy]PF_6$. The latter was previously studied by Constable[24] in $[D_6]$DMSO solution. Based on previous studies, and on our own ^1H-^1H NMR homonuclear decoupling and 2D ^1H-^1H experiments, we assigned the multiplet centered at δ = 7.57 to the proton H-10. The spectrum of $[Ru(bpy)_2(ppy)]$[Δ-trisphat] in its nonenriched form **3** appears more intricate than that of the $[Ru(bpy)_2ppy]PF_6$ complex; some resonances split into two components because the two diastereomers exhibit different chemical shifts in their ^1H NMR spectra. The spectra of **3Δ** and **3Λ** clearly show an enrichment in one of the two diastereomers. For quantitative purposes we chose the well-resolved multiplet H-10, which exhibits the most pronounced splitting in the diastereomer formation. The appearance of this multiplet in **1**, **3**, **3Δ**, **3Λ** is shown in Figure 5 (a−d). We were able to assign each peak to each of the two diastereomers by examining and comparing the spectra of **3Δ** and **3Λ**. Thus, the most and the least deshielded doublets of the multiplet are assigned respectively to the [Λ-$Ru(bpy)_2(ppy)$][Δ-trisphat] and [Δ-$Ru(bpy)_2(ppy)$][Δ-trisphat] diastereomers. These signals are sufficiently well separated to afford a precise measurement of the respective ratio of the two diastereomers, and so of the diastereomeric excesses, by integration. As can easily be seen, in the nonenriched product **3** they appear of equal intensity whereas for the enriched compounds **3Δ** and **3Λ** the ratio between the two diastereomers (ΔΔ/ΛΔ) is 72:28 and 25:75, respectively, providing an estimate of the diastereomeric excess in **3Δ** and **3Λ**, and so the enantiomeric excess in **1Δ** and **1Λ**, to be 44% and 50%, respectively.

Conclusion

In this paper we described the preparation of optically active bimetallic networks of the type $\{[\Lambda\text{-}Ru(bpy)_2(ppy)][Mn\text{-}\Lambda\text{-}Co(ox)_3]\}_n$ (**2Λ**) and $\{[\Delta\text{-}Ru(bpy)_2(ppy)][Mn\text{-}\Delta\text{-}Co(ox)_3]\}_n$ (**2Δ**) and showed for the first time that the synthesis of these chiral polymers is a good strategy for resolving the $[Ru(bpy)_2(ppy)]^+$ complex. Furthermore, **2Λ** and **2Δ** can be obtained via either the resolved tris-oxalato $[M^{III}(ox)_3]^{3-}$ anion or $[Ru(bpy)_2(ppy)]^+$ cation building block, whereby each species can play the role of the chiral template-inducer. This implies that an optically active form of either tris-chelated brick (anion or cation) affords the partial resolution of the other one owing to the matrix effect induced by the formation of the optically active polymer. This feature opens new horizons in the resolution of the hexacoordinated quasi-D_3 monocations $[Ru(bpy)_2L]^+$ (L is a bidentate monocharged ligand such as the 8-quinolate). Therefore, separation of enantiomers induced by specific interactions between chiral molecules and optically active molecular frameworks appears to be one of the most promising alternatives to the conventional procedures.

The use of the optically active and configurationally stable $[Ru(bpy)_2(ppy)]^+$ complex will provide an important control over chirality in the building of optically active polymers with various tandems M^{II}-M^{III} displaying interesting magnetic behavior.

Experimental Section

Materials: The following compounds were prepared according to literature methods: $K_3[Co(ox)_3]\cdot 3H_2O$,[33] *rac*-$[Ru(bpy)_2ppy]PF_6$,[24,34] [l-cinchonidinium][Δ-trisphat].[28] The resolution procedure described previously was followed to obtain the Δ and Λ $K_3[Co(ox)_3]\cdot 3H_2O$ enantiomers.[30] The other reagents are commercially available and were used as purchased.

General Procedures: The IR spectra were recorded on a Bio-Rad IRFT spectrophotometer as KBr pellets in the 4000−250 cm^{-1} region. Elemental analyses were performed at the SIARE-UPMC, Paris. Metal analyses were completed at the Service Central d'Analyse-CNRS, Vernaison. The specific rotations of the starting materials were measured at 20 °C, in a 1 dm-tube containing the solutions, using the D-line in an Ameria AA5 polarimeter. The enantiomeric or diastereomeric excess was calculated by comparison with the maximum specific rotation values found in the literature.[28,30] Circular dichroism spectra were measured with a Jasco model J-710 spectropolarimeter. Solid state measurements were made on compounds **1Δ**, **1Λ**, **2Δ** and **2Λ** as dispersions of 0.1−0.5 mg in 100−110 mg of oven-dried KBr. 13 mm-diameter disks were made in a standard disk press. For **3Δ** and **3Λ**, measurements were carried out in CH_2Cl_2 solutions (c = 7.5−9.10^{-5} mol·L^{-1}) in a 1 mm cuvette. The baseline correction was performed with the spectrum of a pure KBr disk or of CH_2Cl_2 prepared under the same conditions. The displayed absorption spectra result from subtraction of the spectrum of the standard KBr disk or of CH_2Cl_2. Spectra were recorded in the wavelength range 700−200 nm for all compounds. The ^1H NMR spectra (300 MHz) were obtained at room temperature in 5 mm o.d. tubes on a Bruker AC 300 spectrometer equipped with a QNP probehead (solutions of $[D_6]$acetone, c = 0.014 mol·L^{-1}). Chemical shifts are given according to the IUPAC convention with respect to $SiMe_4$. The ^{31}P NMR (121.5 MHz) spectra were measured as for ^1H spectra on the same tubes. The chromatography separations were carried out on a 3 cm-diameter column of alumina (10 cm; 0.05−0.15 mm neutral aluminium oxide; eluent: CH_2Cl_2).

X-ray Crystallographic Analysis: Accurate cell dimensions and orientation matrix were obtained by least-squares refinement of 25 accurately centered reflections. The data were corrected for Lorentz and polarization effects. Computations were performed by using Crystals 2000 version. Scattering factors and corrections for anomalous dispersion were taken from reference.[35] The structures were solved by direct methods (SHELXS). All final refinements were carried out by full-matrix least-squares using anisotropic displacement parameters for all phosphorus, fluorine and non-hydrogen atoms. Hydrogen atoms were introduced in calculated positions and only one overall isotropic displacement parameter was refined. All crystallographic data and diffraction parameters are listed in Table 1.

Crystallographic data (excluding structure factors) for the structure reported in this paper have been deposited with the Cambridge

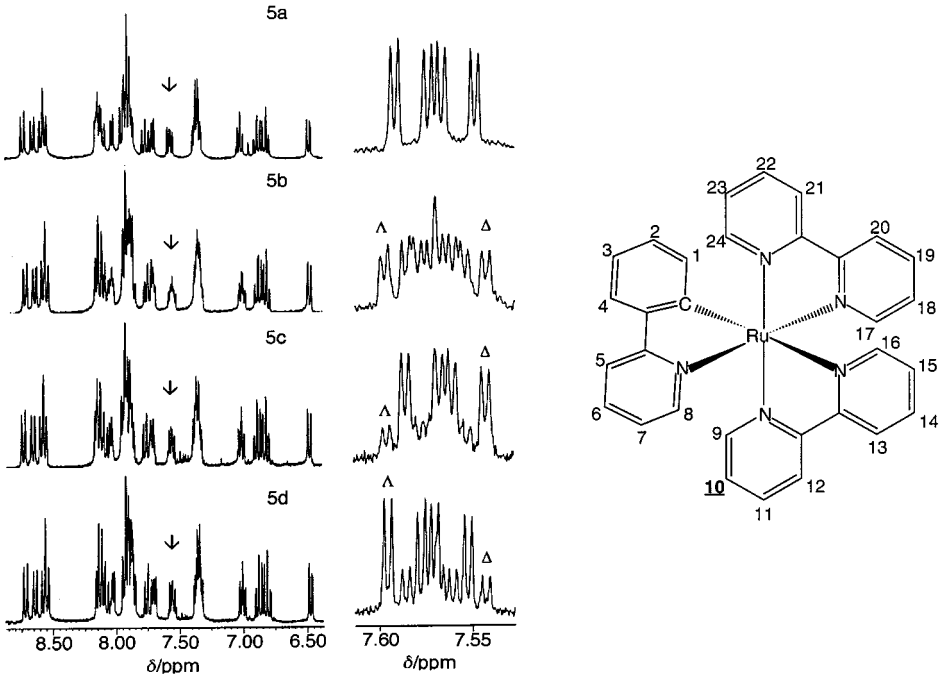

Figure 5. ^{1}H NMR spectra of **1** (5a), **3** (5b), **3Δ** (5c) and **3Λ** (5d) in acetone d^6 solutions (c = 0.014 mol·L^{-1}). Full spectra are shown on the left side and enlargement of the signal H-**10** on the right

Crystallographic Data centre as supplementary publication no. CCDC-151418. Copies of the data can be obtained free of charge on application to CCDC, 12 Union Road, Cambridge CB21EZ, UK [Fax: (internat.) +44-1223/336-033; E-mail: deposit@ccdc.cam.ac.uk].

Preparation of 1Δ, 1Λ, 2Δ and 2Λ: In a hemolysis tube, an aqueous solution (0.2 mL) of optically active $K_3[\Lambda Co(ox)_3]\cdot 3H_2O$ {39.4 mg, 0.08 mmol; $[\alpha]_D = -1892$ (c = 0.02 in H_2O); maximum rotation reported in the literature:[30] $[\alpha]_D = -1940$} and $MnCl_2\cdot 4H_2O$ (15.7 mg, 0.08 mmol) was added quickly to a DMSO solution (0.4 mL) of racemic $[Ru(bpy)_2ppy]PF_6$ (**1**) (100.2 mg, 0.14 mmol; not completely dissolved. To ensure the complete precipitation of the $[\Lambda\text{-}Ru(bpy)_2ppy]^+$ as a polymer we used less than two equivalents of the $[Ru(bpy)_2ppy]PF_6$ complex). During 5 minutes, acetone and H_2O were successively added scratching continuously the walls of the tube with a Pasteur pipette (the additions were made in this order: acetone-H_2O-acetone-H_2O-acetone, 1.2 mL each time). The purple precipitate was filtered off, washed with H_2O (5 mL) and acetone (until the filtrate became colorless) and air-dried leading to the green $\{[\Lambda\text{-}Ru(bpy)_2(ppy)][Mn\text{-}\Lambda\text{-}Co(ox)_3]\}_n$ (**2Λ**) (68.6 mg, 0.0724 mmol; yield: 91%). The purple filtrate was concentrated by rotary evaporator to remove acetone and, after precipitation by addition of diethyl ether (200 mL), the purple enriched [Δ-Ru-(bpy)$_2$ppy]PF$_6$ (**1Δ**) (43.7 mg, 0.0612 mmol) was filtered off and air-dried. The same procedure was employed for the other enantiomers **1Λ** and **2Δ** using $K_3[\Delta Co(ox)_3]\cdot 3H_2O$ {$[\alpha]_D = +1667$ (c = 0.02 in H_2O); maximum rotation reported in the literature:[30] $[\alpha]_D = +1928$}.

2Λ: $C_{37}H_{24}CoMnN_5O_{12}Ru$ (945.56): calcd. C 47.0, H 2.56, N 7.41, Ru 10.69, Mn 5.81, Co 6.23; found C 41.93; H 2.72, N 6.11, Ru 8.15, Mn 5.66, Co 5.87. − IR (KBr): $\tilde{\nu}$ = 1652s, 1629vs, 1600vs (C=O), 1310m, 798m, 780m cm^{-1}.

1Δ: ^{1}H NMR (300.13 MHz, C_3D_6O, 300 K, TMS): δ = 6.48 (d, 1 H), 6.85 (m, 2 H), 7.02 (t, 1 H), 7.36 (m, 3 H), 7.57 (t, 1 H), 7.70 (d, 1 H), 7.76 (t, 1 H), 7.91 (m, 6 H), 8.03 (d, 1 H), 8.12 (m, 3 H), 8.57 (pseudo-t, 2 H), 8.65 (d, 1 H), 8.73 (d,1 H). − ^{31}P NMR (121.5 MHz, C_3D_6O, 300 K, 85% H_3PO_4): δ= −142.72 (sept).

Preparation of 3Δ and 3Λ: [Δ-Ru(bpy)$_2$(ppy)]PF$_6$ (**1Δ**) (128.3 mg, 0.18 mmol) and [l-cinchonidinium][Δ-trisphat] ($[\alpha]_D$=-369 (c = 0.1 in EtOH), *de* = 98%)(1-fold) (191.3 mg, 0.18 mmol) were dissolved in a minimum amount of acetone and stirred for about 30 minutes. The product was first adsorbed on aluminium oxide and then chromatographed on a column of alumina (10 cm, CH_2Cl_2). The less-polar fraction contained exclusively the deep purple diastereomer **3Δ** (or **3Λ**). Enriched [Δ-Ru(bpy)$_2$(ppy)]PF$_6$ **1Δ** (or **1Λ**) appeared afterwards as a second fraction of the same color. [Δ-Ru-(bpy)$_2$(ppy)][Δ-trisphat] (**3Δ**) (150.8 mg, 0.11 mmol; yield: 61%) and [Δ-Ru(bpy)$_2$(ppy)]PF$_6$ (**1Δ**) (46.4 mg, 0.065 mmol) were recuperated after evaporation of the solvent on a rotary evaporator.

$C_{49}H_{24}N_5Cl_{12}O_6PRu$ (%): calcd. C 44.01, H 1.81, N 5.24; found C 44.26; H 2.03, N 5.61;IR (KBr): $\tilde{\nu}$ = 1451vs, 1421s, 1389s, 992vs, 825vs, 757s, 730s, 719m, 672vs, 650s, 620s cm^{-1}. − ^{1}H NMR (300.13 MHz, C_3D_6O, 300 K, TMS): δ = 6.48 (d, 1 H), 6.84 (m, 2 H), 7.00 (m, 1 H), 7.34 (m, 3 H), 7.55 (m, 1 H), 7.73 (m.2 H), 7.90 (m, 6 H), 8.03 (m, 1 H), 8.13 (m, 3 H), 8.55 (pseudo-t, 2 H), 8.63 (d, 1 H), 8.71 (d, 1 H). − ^{31}P NMR (121.5 MHz, C_3D_6O, 300 K, 85 % H_3PO_4): δ = −79.14 (s).

Acknowledgments

We gratefully acknowledge Dr. H. Amouri and Dr. R. Andrès for helpful discussions and Dr. M. Takahashi (Institut Curie, CNRS) for assistance in performing the circular dichroism measurements. We thank CNRS and Université Pierre et Marie Curie for financial support.

[1] J. S. Seo, D. Whang, H. Lee, S. I. Jun, J. Oh, Y. J. Jeon, K. Kim, *Nature* **2000**, *404*, 982−986.
[2] S. A. Tysoe, R. Kopelman, D. Schelzig, *Inorg. Chem.* **1999**, *38*, 5196−5197.

[3] J. G. Collins, A. D. Sleeman, J. R. Aldrich-Wright, I. Greguric, T. W. Hambley, *Inorg. Chem.* **1998**, *37*, 3133−3141.
[4] P. R. Ashton, R. Ballardini, V. Balzani, E. C. Constable, A. Credi, O. Kocian, S. J. Langford, J. A. Preece, L. Prodi, E. R. Schofield, N. Spencer, J. F. Stoddart, S. Wenger, *Chem. Eur. J.* **1998**, *4*, 2413−2422.
[5] V. Balzani, A. Juris, M. Venturi, S. Campagna, S. Serroni, *Chem. Rev.* **1996**, *96*, 759−833.
[6] A. Juris, V. Balzani, F. Barigelletti, S. Campagna, P. Belser, A. von Zelewsky, *Coord. Chem. Rev.* **1988**, *84*, 85−277.
[7] K. Kalyanasundaram, *Coord. Chem. Rev.* **1982**, *46*, 159−244.
[8] T. J. Rutherford, P. A. Pellegrini, J. R. Aldrich-Wright, P. C. Junk, F. R. Keene, *Eur. J. Inorg. Chem.* **1998**, 1677−1688.
[9] J. A. Arce Sagüés, R. D. Gillard, D. H. Smalley, P. A. Williams, *Inorg. Chim. Acta* **1980**, *43*, 211−216.
[10] N. C. Fletcher, P. C. Junk, D. A. Reitsma, F. R. Keene, *J. Chem. Soc., Dalton Trans.* **1998**, 133−138. − N. C. Fletcher, F. R. Keene, *J. Chem. Soc., Dalton Trans.* **1999**, 683−690.
[11] X. Hua, A. von Zelewsky, *Inorg. Chem.* **1995**, *34*, 5791−5797.
[12] X. Hua, A. von Zelewsky, *Inorg. Chem.* **1991**, *30*, 3796−3798.
[13] T. J. Rutherford, M. G. Quagliotto, F. R. Keene, *Inorg. Chem.* **1995**, *34*, 3857−3858.
[14] D. Hesek, Y. Inoue, S. R. L. Everitt, H. Ishida, M. Kunieda, M. G. B. Drew, *J. Chem. Soc., Dalton Trans* **1999**, 3701−3709.
[15] D. Hesek, Y. Inoue, S. R. L. Everitt, H. Ishida, M. Kunieda, M. G. B. Drew, *Chem. Commun.* **1999**, 403−404.
[16] D. Hesek, Y. Inoue, S. R. L. Everitt, M. Kunieda, H. Ishida, M. G. B. Drew, *Tetrahedron: Asymmetry* **1998**, *9*, 4089−4097.
[17] D. Hesek, Y. Inoue, S. R. L. Everitt, H. Ishida, M. Kunieda, M. G. B. Drew, *Inorg. Chem.* **2000**, *39*, 317−324. − F. Pezet, J. C. Daran, I. Sasaki, H. Aït-Haddou, G. Balavoine, *Organometallics* **2000**, *19*, 4008−4015.
[18] S. Decurtins, H. W. Schmalle, R. Pellaux, P. Schneuwly, A. Hauser, *Inorg. Chem.* **1996**, *35*, 1451−1460.
[19] S. Decurtins, H. W. Schmalle, R. Pellaux, R. Huber, P. Fisher, B. Ouladdiaf, *Adv. Mater.* **1996**, *8*, 647−651.
[20] S. Decurtins, H. W. Schmalle, P. Schneuwly, J. Ensling, P. Gütlich, *J. Am. Chem. Soc.* **1994**, *116*, 9521−9528.
[21] S. Decurtins, H. W. Schmalle, P. Schneuwly, H. R. Oswald, *Inorg. Chem.* **1993**, *32*, 1888−1892.
[22] R. Andrés, M. Gruselle, B. Malézieux, M. Verdaguer, J. Vaissermann, *Inorg. Chem.* **1999**, *38*, 4637−4646.
[23] M. Gruselle, R. Andrés, B. Malézieux, M. Brissard, C. Train, M. Verdaguer *The 14th International Symposium on Chirality ISCD 12 Chirality* **2000**, Chamonix (France).
[24] E. C. Constable, J. M. Holmes, *J. Organomet. Chem.* **1986**, *301*, 203−208.
[25] M. Biner, H. B. Burgi, A. Ludi, C. Rohr, *J. Am. Chem. Soc.* **1992**, *114*, 5197−5203.
[26] J. Lacour, S. Torche-Haldimann, J. J. Jodry, C. Ginglinger, F. Favarger, *Chem. Commun.* **1998**, 1733−1734.
[27] J. Lacour, C. Ginglinger, F. Favarger, S. Torche-Haldimann, *Chem. Commun.* **1997**, 2285−2286.
[28] J. Lacour, C. Ginglinger, C. Grivet, G. Bernardinelli, *Angew. Chem. Int. Ed. Engl.* **1997**, *36*, 608−610; *Angew. Chem.* **1997**, *109*, 660−662.
[29] C. H. Johnson, *Trans. Faraday Soc.* **1935**, *31*, 1612−1621.
[30] G. B. Kauffman, L. T. Takahashi, N. Sugisaka, *Inorg. Synth.* **1966**, *8*, 227−232.
[31] A. J. McCaffery, S. F. Mason, R. E. Ballard, *J. Chem. Soc.* **1965**, 2883−2892.
[32] Similar experiments were carried out using the same method of synthesis of the polymers **2Δ** and **2Λ** for the partial resolution of the monocation but starting from the nonenriched $[Ru(bpy)_2(ppy)][\Delta\text{-trisphat}]$ (**3**) instead of *rac*-$[Ru(bpy)_2(ppy)]PF_6$ (**1**). Thus, enriched $[Ru(bpy)_2(ppy)][\Delta\text{-trisphat}]$ **3Δ** and **3Λ** can be directly obtained after filtration of the polymer and precipitated by addition of water. Diastereomeric excesses calculated by ^1H NMR on these compounds leads to the same results that for the experiments with *rac*-$[Ru(bpy)_2(ppy)]PF_6$ (**1**). This fact confirms that the reaction of transformation of $[Ru(bpy)_2ppy]^+$ into diastereomer is no diastereoselective and that the partial resolution of the monocation is exclusively due to the diastereoselective formation of the polymer **2Δ** and **2Λ**.
[33] J. C. Bailar, E. M. Jones, *Inorg. Synth.* **1939**, *1*, 35−38.
[34] B. P. Sullivan, D. J. Salmon, T. J. Mayer, *Inorg. Chem.* **1978**, *17*, 3334−3341.
[35] D. T. Cromer, *International Tables for X-ray Crystallography*, Kynoch Press, Birmingham, UK, **1974**; Vol IV.

Received February 7, 2001
[I01043]

Proton Transfer to CpRuH(CO)(PCy_3) Studied by Low-Temperature IR and NMR Spectroscopy

Natalia V. Belkova,[a] Alexei V. Ionidis,[a] Lina M. Epstein,[a] Elena S. Shubina,*[a] Stephan Gruendemann,[b] Nikolai S. Golubev,[b] and Hans-Heinrich Limbach*[b]

Keywords: Hydrido complexes / Hydrogen bonds / Proton transfer / Kinetics / IR spectroscopy / NMR spectroscopy

The interaction of the ruthenium hydride complex RuH ≡ CpRuH(CO)(PCy_3) (**1**) with various proton donors AH ≡ CF_3CH_2OH (**2a**), $(CF_3)_2CHOH$ (**2b**), $(CF_3)_3COH$ (**2c**), CF_3COOH (**2d**), and HBF_4 (**2e**) has been studied by variable-temperature IR spectroscopy using hexane and CH_2Cl_2 as solvents of different polarity. A low-temperature NMR study of the interaction of **1** with **2c** was performed using [D_8]methylcyclohexane, CD_2Cl_2, and a liquefied mixture of CDF_2Cl/CDF_3 (2:1). The first stage of the proton transfer process was found to be the formation of hydrogen-bonded complexes of the type RuH···HA. The hydrogen bonds in these complexes are of medium strength ($-\Delta H°$ = 5.3–7.6 kcal mol^{-1}). The second stage is the slow conversion of the H-complex to a dihydrogen complex to which a hydrogen-bonded ion-pair structure [Ru(η^2-H_2)]$^+$···A^- was assigned. The kinetics of this unusually slow proton transfer reaction was monitored in the case of **2c** at 200 K in CH_2Cl_2. Fast protonation of **1** by **2d** leads additionally to a species assigned as the free cationic complex [Ru(η^2-H_2)]$^+$, whose formation is driven by the formation of the homoconjugated anionic complex [AHA]$^-$. At temperatures above 220 K both the hydrogen-bonded ion pair and the free cationic complex easily release dihydrogen, producing RuA.

Introduction

The protonation of transition metal hydrides by proton donors constitutes an important pathway for the synthesis of cationic non-classical dihydrogen complexes.[1] The elementary steps of this reaction are, however, still unclear up to date. Usually, proton transfer between a neutral proton donor AH and a neutral base is preceded by the formation of a hydrogen-bonded complex of the type A−H···B, which is converted rapidly into the hydrogen-bonded ion pair A^-···H−B^+, leading finally to the free ions as reaction products. It has therefore been an exciting discovery that proton donors can form "unconventional" intramolecular[2−7] and intermolecular[8−16] hydrogen bonds to the hydride moieties of transition metal complexes MH, taking the role as proton acceptors. For example, intermolecular hydrogen-bonded complexes were observed in the case of rhenium hydrides in the solid state,[8,9] as well as of tungsten and rhenium hydrides in solution.[11−14] The idea that these complexes constitute important intermediates of transition metal hydride protonation was subsequently proposed in a number of papers,[9,11] although evidence for this idea has been obtained only very recently.[17−21] For example, the application of IR and NMR methods in a wide range of temperatures allowed some of us to establish the existence of an unusually slow equilibrium between M−H···H−A and M−H_2^+ A^- in the case of $RuH_2(dppm)_2$,[17] and {$MeC(CH_2PPh_2)_3$}-$Re(CO)_2H$[19]. NMR alone was used similarly in the case of $Cp^*Ru(PCy_3)H_3$.[21] In the latter study where NMR experiments were performed using both toluene and a liquefied freon mixture CDF_2Cl/CDF_3 (2:1) as solvents − where the latter allows measurements down to 100 K − it was realized that protonation takes place if the solvent polarity is large enough. Interestingly, both the above freon mixture as well as CH_2Cl_2 exhibit similar dielectric constants that increase dramatically by lowering the temperature. As a consequence, protonation is a solvent-assisted process occurring at low temperatures. On the other hand, in the case of nonpolar solvents such as hexane or toluene, only the hydrogen-bonded complex M−H···H−A is formed without subsequent protonation.[21]

In order to study the mechanism of a reaction one usually monitors its kinetics. For the systems mentioned above such experiments have not yet been reported. We are aware only of recent papers of Basallote et al.[22−24] that followed the protonation kinetics of two iron and one ruthenium hydrides with strong acids using electrochemical methods. However, this method does not provide information about the structure of reaction intermediates.

In order to identify the various reaction steps and hence the reaction mechanism we decided to study the interaction of a simple transition metal monohydride with proton donors of different strengths, using a combination of IR and NMR spectroscopy. For this purpose we chose the ruthenium hydride CpRuH(CO)(PCy_3) (≡ RuH, **1**), which was first synthesized by Heinekey et al.[25] and is known to

[a] A. N. Nesmeyanov Institute of Organoelement Compounds, RAS,
Vavilov Str. 28, 117813, Moscow, Russia
Fax: (internat.) + 7-095/135-5085
E-mail: shu@ineos.ac.ru
[b] Institute of Chemistry, Freie Universität, Berlin,
Takustraße 3, 14195 Berlin, Germany
Fax: (internat.) + 49-30/83855310
E-mail: limbach@chemie.fu-berlin.de

 © WILEY-VCH Verlag GmbH, 69451 Weinheim, 2001 1434−1948/01/0707−1753 $ 17.50+.50/0

form a stable cationic dihydrogen complex[25,26] under the action of HBF_4. On the other hand this hydride contains a CO group whose stretching band constitutes an excellent IR marker sensitive to hydrogen bond formation and protonation.[11−15,19,27−29]

Thus, in this paper we report the results of variable-temperature IR and NMR studies of interactions of the hydride **1** with CF_3CH_2OH (**2a**), $(CF_3)_2CHOH$ (**2b**), $(CF_3)_3COH$ (**2c**), CF_3COOH (**2d**), and HBF_4 (**2e**) in the nonpolar medium hexane and in the polar media CH_2Cl_2, and CDF_2Cl/CDF_3 (2:1). The results of these experiments will be discussed in terms of the general reaction model depicted in Scheme 1. In addition to free **1**, the hydrogen-bonded complex **3**, and the cationic dihydrogen complex **5**, we have found for the first time, evidence for a further intermediate **4**, a hydrogen-bonded ion pair. We will show that the interconversion between **3** and **4** constitutes the rate-limiting step of the proton transfer. The dissociation of **4** into the free dihydrogen complex **5** is assisted in the case of **2d** by the formation of homoconjugated ions $[AHA]^-$ (**6**). Finally, **5** easily looses a dihydrogen molecule forming the reaction product **7**.

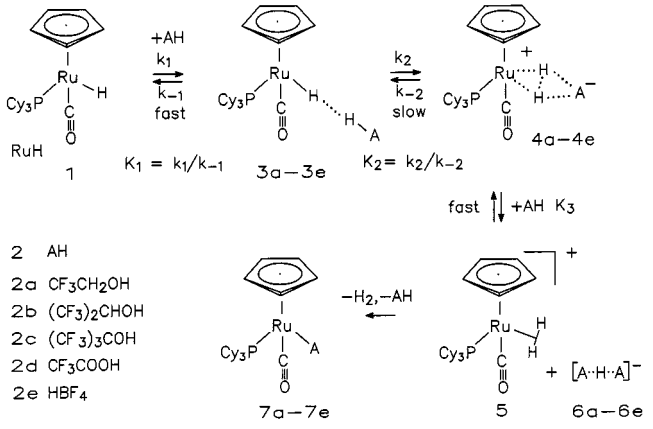

Scheme 1

Results

IR Studies of the Dihydrogen Bonding and Protonation of 1 with Proton Donors

The OH Stretching Region − Dihydrogen Bond of 1 with Weak Proton Donors in Hexane and Dichloromethane

The stretching vibrations ν_{OH} of proton donors at 3600−3000 cm^{-1} are well known to be sensitive to hydrogen bonding. Figure 1 (a) shows the OH stretching region of CF_3CH_2OH (**2a**) at low concentrations in an excess of **1**. We observe a sharp monomer band at 3630 cm^{-1} and a broad bonded band, which is shifted considerably to lower frequencies. Because of the low proton donor concentration and excess of **1**, there are no apparent contributions from complexes $(AH)_n$ or $RuH\cdots(H-A)_n$ involving more than one proton donor molecule. Therefore, the broad band can be assigned to the complex **3a**, and the observed frequency shifts listed in Table 1 are identified as $\Delta\nu_{OH} = \nu_{OH}(AH) - \nu_{OH}(RuH\cdots HA)$, where the position of the broad band corresponds to its center of gravity ($s = \pm 3$ cm^{-1}).

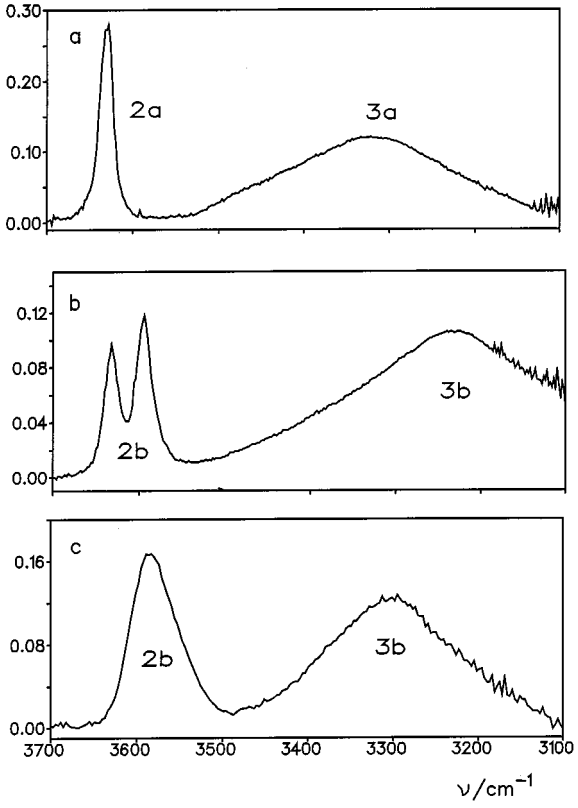

Figure 1. Room-temperature ν_{OH} stretching bands of proton donors (0.02 mol/L) in the presence of a 2.5-fold excess of $CpRu(CO)(PCy_3)H$ (**1**); (a) CF_3CH_2OH (**2a**), hexane; (b) $(CF_3)_2CHOH$ (**2b**), hexane; (c) $(CF_3)_2CHOH$ (**2b**), CH_2Cl_2

When the proton-donating power is increased, $\Delta\nu_{OH}$ increases as illustrated in Figure 1 (b) for the case of complex **2b**. Here, monomeric $(CF_3)_2CHOH$ (**2b**) exhibits two different bands that are due to conformational heterogeneity (two conformers exist) and intermolecular interactions.[30,31] A strong solvent effect is observed in the sense that the hydrogen bond shift $\Delta\nu_{OH}$ is smaller when CH_2Cl_2 is used as solvent (Figure 1, c). In the case of **2c** $\nu_{OH}(RuH\cdots HA)$ was shifted so much that it strongly overlapped with the CH stretching band of the solvent, so that $\Delta\nu_{OH}$ could not be determined properly.

As is known, this region clearly shows the hydrogen bond formation, and is useful for ΔH determination.[11,13,15] It does not, however, give any information on the site of coordination. Therefore, a study of all vibrations should be performed in order to decide whether the hydride atom of **1** is the only hydrogen bond site as assumed in Scheme 1, or whether the oxygen atoms of the CO groups or even the metal center itself acts as proton acceptor site. Unfortunately, the RuH stretching vibration of **1** did not give rise to an observable band, in contrast to the tungsten and rhenium hydrides studied previously.[11,13] Therefore, most of

Table 1. IR data in the ν_{OH} range, formation enthalpies ΔH_1 of the formation of the hydrogen-bonded complex RuH···HA and basicity factors E_j of the hydride hydrogen atom

AH	Solvent	ν_{OH}(**3**) [cm^{-1}]	$\Delta\nu_{OH}$ [cm^{-1}]	$\Delta\nu_{1/2}$ [cm^{-1}]	ΔH_1 [kcal·mol^{-1}]	E_j
2a	hexane	3327	300	220	−5.3[a]	1.04[b]
2b	hexane	3225	385	350	−6.3[a]	1.03[b]
2b	CH_2Cl_2	3302	285	194	−5.1[a]	1.03[b]
2c	hexane	–	–	–	−7.6[c]	1.0[b]

[a] Obtained using Equation (2). – [b] Obtained using Equation (3). – [c] Obtained from the van't Hoff plot of Figure 4.

the information came from a detailed study of the stretching vibrations of the carbonyl ligand (ν_{CO}) of **1**.

The CO Stretching Region – Dihydrogen Bond Formation and Protonation of 1 by Weak Proton Donors in Hexane and Dichloromethane

The changes in the CO stretching region of **1** observed in the presence of proton donors allowed us to show the formation of the dihydrogen-bonded complexes, and to monitor their following transformations. In Figure 2 (a) we have depicted ν_{CO}(**1**) of pure hydride obtained at 200 K using hexane as solvent. This strong band appears at 1905 cm^{-1} and is quite narrow exhibiting a line width of only 7 cm^{-1}. When a proton donor is added, a new band is observed at slightly larger wave numbers, e.g. at 1920 cm^{-1} in the case of **2c** (Figure 2, a). The new band is shifted by $\Delta\nu_{CO}$ = +12 cm^{-1} in the case of **2b** and +15 cm^{-1} in the case of **2c**. These high-frequency shifts show that the oxygen atom of the CO group does not participate in hydrogen bonding.[11–13] Hence, we assign the new band to the ν_{CO} stretching vibrations of the 1:1 complexes RuH···HA (**3**). As the stretching vibration ν_{RuH} could not be observed, the assignment of the structures **3** containing a dihydrogen bond between the proton donor and the hydride site, and not with the metal atom is then tentative. However, further information supporting this assignment comes from the NMR spectroscopy study, as shown below.

The ν_{CO} band of pure **1**, dissolved in CH_2Cl_2, appears at 1890 cm^{-1} as depicted in Figure 2 (b), again using a sample temperature of 200 K. The band is broader than in hexane and exhibits a half width of 22 cm^{-1}, so in the presence of a proton donor we observe only the summary band of **1** and **3c** with a high-frequency shift of +6 cm^{-1} as depicted in Figure 2 (b) for the case of **2c**. These small changes are not unusual; e.g. we observed similar effects for the dihydrogen bonds with {$MeC(CH_2PPh_2)_3$}$Re(CO)_2H$.[19]

We observed an interesting phenomenon, concerning the spectral changes in time. The intensity of ν_{CO}(**1**+**3c**) band decreases after several minutes, and the new high-frequency band at 1960 cm^{-1} appears and grows in intensity (Figure 2, c). After about 30 min, equilibrium is reached, where both bands are present. We assign this new band to an ion pair of the type **4c**. Arguments for this structure arise from the study of the interaction of **1** with stronger proton donors described below. We do not assign this band to the reaction product **7c**, because upon heating to 250 K the band at 1960 cm^{-1} decreases while a new ν_{CO} band at 1944 cm^{-1} appears. This new band we assign to **7c**.

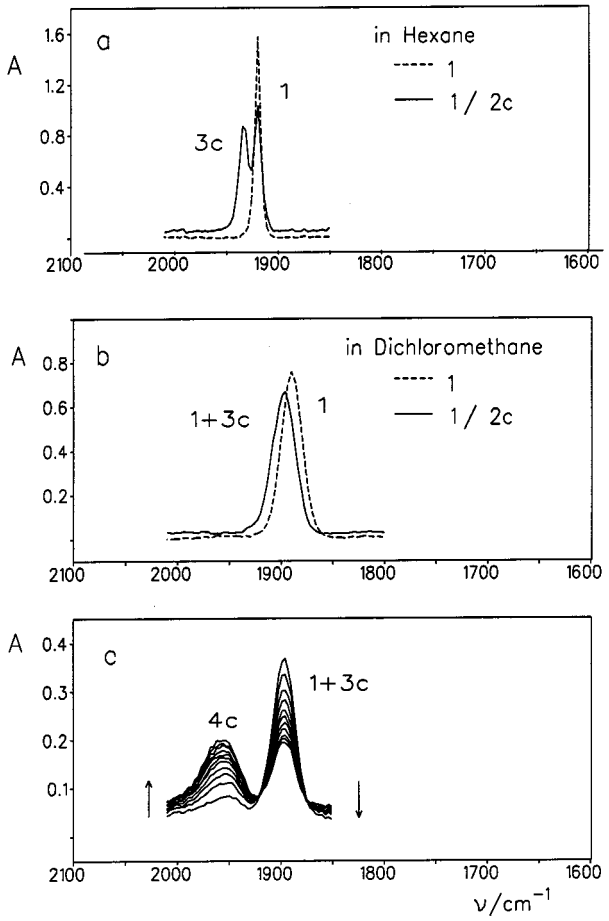

Figure 2. IR spectra in the ν_{CO} range of CpRu(CO)(PCy_3)H (**1**) (0.005 mol/L) at 200 K in hexane (a) and CH_2Cl_2 (b, c) without proton donor (- - - -) and in the presence of 4 equiv. of $(CF_3)_3COH$ (**2c**) (——); (c) time-dependent changes of the sample **1/2c** over a period of 30 min

The CO Stretching Region – Dihydrogen Bond Formation and Protonation of 1 with Strong Proton Donors in Dichloromethane

In principle, the interaction of metal hydrides with strong proton donors will lead to their protonation, constituting a routine procedure for the generation of cationic dihydrogen complexes. However, the choice of acid is crucial for their

stability. There are numerous examples where the labile dihydrogen ligand can be easily displaced by anionic ligands.[13,19,32,33] In the present case, the interaction of hydride **1** with proton donors such as fluorinated alcohols and carboxylic acids also leads to unstable (η^2-H_2) complexes due to the high coordinating ability of the corresponding anions (R^FO^- and CF_3COO^-). The elimination of an H_2 molecule and the addition of an anion upon warming results in the formation of organyloxy derivatives **7**. We succeeded in minimizing and even preventing this unwanted process by carrying out the mixing of the reagents and IR measurements at 200 K.

In order to elucidate the protonation of **1** in more detail, we performed various IR studies of **1** with stronger acids, i.e. CF_3COOH (**2d**) and HBF_4 (**2e**). As mentioned in the introduction, the interaction of hydride **1** with HBF_4 results in the formation of the stable dihydrogen complex [CpRu(CO)(PCy_3)(η^2-H_2)]$^+$ (**5**) with BF_4^- as counter ion, exhibiting a ν_{CO} band at 2020 cm^{-1} in the solid state.[26] Here, upon mixing of the hydride **1** with HBF_4 in CH_2Cl_2 at 200 K we observe a similar value. The position of this band does not change with increasing temperature. These results indicate that the ν_{CO} band at 2020 cm^{-1} indeed belongs to the free protonated complex **5** in CH_2Cl_2, formed upon interaction of **1** with HBF_4.

If **5** is not directly involved in an interaction with the counterion it should be possible to generate **5** also with other acids. For this purpose we chose CF_3COOH (**2d**) and carried out experiments at 200 K using again CH_2Cl_2 as solvent. In addition to ν_{CO} of the CO ligand absorbing in the 2100−1850 cm^{-1} range this system exhibits additional CO stretching vibrations ν_{CO} of the acid and the antisymmetric stretching band ν_{OCO}^{as} of trifluroacetate between 1800 and 1600 cm^{-1}.

The ν_{CO} bands of the separate monomeric **1** and the dimeric CF_3COOH molecules (**2d**) in CH_2Cl_2 are represented by the graphs a and b in Figure 3. The band ν_{CO}(**2d**) appears at 1790 cm^{-1}. However, when both reactants are mixed at low concentrations of **1** (10^{-3} mol/L) in the presence of an excess of **2d**, we obtain spectrum c in Figure 3. Again, at 2020 cm^{-1} we observe a new band that coincides with the ν_{CO} band of **5** with BF_4^- as counter anion. Therefore, we can now safely assign this new band to the free protonated ion **5**. Moreover, another new band arises at 1648 cm^{-1}, which we attribute to ν_{OCO}^{as} of the homoconjugated trifluoroacetate.[34−38] The excess of the acid is demonstrated by the band at 1790 cm^{-1}. We note that there is no band arising from the dihydrogen-bonded complex **3d**.

Interesting spectral changes are observed when the ratio of the hydride to the acid is increased, as indicated by the spectral traces d, e, and f in Figure 3. First, we note again ν_{CO} of **5** at 2020 cm^{-1} whose intensity is gradually reduced, then the typical strong band of ν_{CO}(**1**+**3d**) at 1910 cm^{-1} and for hydrogen-bonded acid in **3d** at 1760 cm^{-1}. These species were already identified before. However, in addition, a new band is observed at 1996 cm^{-1}, which is located closer to the band of **5** than of **3d**. We assign this new band to the ionic hydrogen-bonded complex **4d**. The corresponding ν_{OCO}^{as} vibration of the hydrogen-bonded acetate in this complex is assigned to the new sharp band at 1710 cm^{-1}, which is located between the band of dimeric **2d** and of the homoconjugated anion **6d**. This assignment is in agreement with previous studies of molecular and ionic hydrogen-bonded complexes of trifluoroacetic acid with organic and metal-containing bases.[34−38] Finally, before we discuss the spectral changes between spectra d, f, and g in Figure 3 we have to discuss the origin of the remaining two bands that are assigned to the CO ligand and trifluoroacetate group of **7d**. This assignment was confirmed by the experiment depicted by spectra g and h, where spectrum g is identical with spectrum f. Spectrum h was obtained after heating the sample to 260 K. The bands of **7d** are now increased in intensity after elimination of H_2. The spectral changes are irreversible, i.e. lowering of the temperature does not lead to spectrum g.

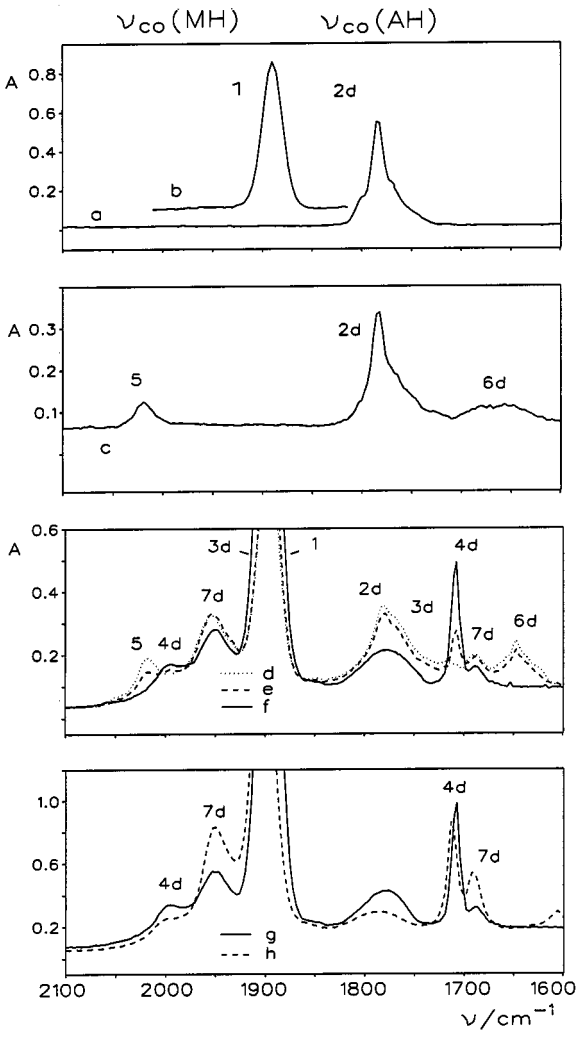

Figure 3. IR spectra of CpRu(CO)(PCy_3)H (**1**) [0.001 mol/L (c), 0.01 mol/L (d−f), 0.03 mol/L (g, h)] in the presence of excess CF_3COOH (**2d**) and a deficiency in CH_2Cl_2; ratio **1/2d** = 1:5 (c), 1:1.5 (d), 1:1 (e), 3:2 (f), 3:1 (g, h); reference spectra of **1** (0.01 mol/L) and of **2d** (0.01 mol/L) are given in b and a, respectively; temperature 200 K (a−g), 260 K (h)

We now consider the series of spectra d, e, and f, where the hydride/acid ratio was increased as indicated by the de-

crease of the band for dimer **2d**, and the relative increase of the acid band of **3d** at 1760 cm^{-1}. We observe in this series that both the bands of **5** and **6d** are reduced in intensity, and these bands have disappeared in spectrum f. On the other hand, **4d** increases in this series. The structure of this species, indicated in Scheme 1, with two hydrogen bonds to the dihydrogen group is speculative.

Finally, the finding of **4d** as a hydrogen bond stabilized ion-pair intermediate between the dihydrogen-bonded complex **3d** and the free protonated ion **5** allows us to confirm the above assignment of the 1960 cm^{-1} band in Figure 2 (c) to the ion pair **4c**. The lower ν_{CO} band position of **4c** as compared to **4d** is probably associated with a higher basicity of the $(CF_3)_3CO^-$ anion as compared to CF_3COO^-. The assignment of this band to ν_{CO} of the product (**7c**) is excluded since this would result in an irreversible appearance of this band, which is in contrast to the experimental findings.

Thermodynamics of Dihydrogen Bonding of 1 with Proton Donors in Hexane and Dichloromethane

The thermodynamics of dihydrogen bond formation of **1** with **2c** as proton donor in hexane was elucidated by analyzing the relative band intensities of **1** and of **3c** in spectra of the type shown in Figure 2 (a), between 250 K and 290 K. Because the ν_{CO} bands of **1** and **3c** in hexane are reasonably well resolved, the equilibrium concentration of free hydride [**1**] can be easily obtained from the spectra. The [**2c**] and [**3c**] concentrations could then be obtained from the total concentrations of **1** and of the proton donor. Thus, we obtained the values of the equilibrium constant defined in Scheme 1 as a function of temperature [Equation (1)].

$$K_1 = [\mathbf{3c}]/([\mathbf{1}][\mathbf{2c}]) = \exp(-\Delta H_1^0/RT + \Delta S_1^0/R) \quad (1)$$

The corresponding van't Hoff plot is depicted in Figure 4, from which we obtain the values of the enthalpy $\Delta H_1^0 = -7.3\pm0.2$ kcal mol^{-1} and $\Delta S_1^0 = -21.6\pm0.6$ cal K^{-1} mol^{-1}. The entropy value decrease is larger here than in the case of rhenium and tungsten hydrides.[11–13]

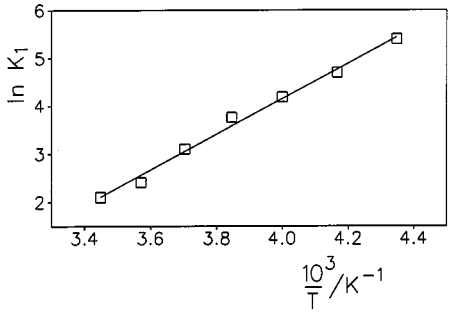

Figure 4. Van't Hoff plot of the hydrogen bonding of CpRu(CO)(P-Cy_3)H (**1**) (0.005 mol/L) in the presence of 4 equiv. of **2c** in hexane

In the case of the other fluorinated alcohols **2a** and **2b** we did not perform extended temperature experiments as we could estimate ΔH_1^0 from the frequency shifts $\Delta\nu_{OH} = \nu_{OH}(\mathbf{2}) - \nu_{OH}(\mathbf{3})$ listed in Table 1 using the correlation proposed for conventional hydrogen bonded complexes[39] according to Equation (2).

$$\Delta H_1^0 = -18\,\Delta\nu_{OH}/(720+\Delta\nu_{OH})\ [\text{kcal mol}^{-1}],\ \Delta\nu_{OH}\ \text{in cm}^{-1} \quad (2)$$

As has been shown, Equation (2) is perfectly applicable to dihydrogen bonding M−H···H−A.[11,12] The values of ΔH^0 obtained in this way for **2a** and **2b** are included in Table 1. Unfortunately, as mentioned above, we could not determine $\Delta\nu_{OH}$ for **2c**. As expected, the dihydrogen bond is stronger in hexane than in CH_2Cl_2. The basicity factors E_j[15,39] of the hydride atom for hydride **1** were calculated using the "rule of factors" equation [Equation (3)].

$$E_j = \Delta H_{ij} / \Delta H_{11} P_i \quad (3)$$

It is noteworthy that the basicity factor E_j[39,40] values of **1** are constant for all proton donors (Table 1) showing good agreement of enthalpy values obtained from empirical correlation [Equation (2)] and from K_1 temperature dependence [Equation (1)].

Thermodynamics and Kinetics of Protonation of 1 by $(CF_3)_3COH$ (2c) in CH_2Cl_2

In this section we quantitatively analyze the experiment that was illustrated in Figure 2 (c), where protonation of the dihydrogen-bonded complex **3c** slowly leads to an equilibrium with the ion pair **4c**. We studied the kinetics of process at 200 K following in time the ν_{CO}(**4c**) and ν_{CO}(**1**+**3c**) intensity changes at different **1**/**2c** ratios (Table 2). The representative kinetic curve (absorbance A vs. time) for **4c** and its first-order logarithmic plot [$\ln(A_\infty - A_t)$ vs. time] are presented in Figure 5.

Table 2. Rate constants k_{obs} for the reaction of hydride **1** with **2c** and conversion ratios α [Equation (5)]

1/**2c** ratio	α [%]	k_{obs} [s^{-1}] (**3**)	k_{obs} [s^{-1}] (**1**+**2**)
1:4	37.5	$1.4\cdot10^{-3}$	$1.6\cdot10^{-3}$
1:6	47.5	$1.7\cdot10^{-3}$	$1.5\cdot10^{-3}$
1:8	55.0	$1.5\cdot10^{-3}$	$1.6\cdot10^{-3}$
1:10	62.5	$1.6\cdot10^{-3}$	$1.4\cdot10^{-3}$

The rate constants k_{obs} obtained from intensity changes of the ν_{CO}(**4c**) band are practically the same as those obtained from ν_{CO}(**1**+**3c**) intensity changes. The k_{obs} values do not depend on the alcohol concentration in the concentration range studied, and the average k_{obs} value is $(1.6\pm0.2)\times10^{-3}$ s^{-1} (Table 2). The process in Scheme 1 is a typical reaction with so-called rapid pre-equilibria:

the diffusion-controlled first stage $\mathbf{1} + \mathbf{2c} \overset{K_1}{\rightleftharpoons} \mathbf{3c}$

and the rate-limiting step $\mathbf{3c} \underset{k_{-2}}{\overset{k_2}{\rightleftharpoons}} \mathbf{4c}$

The observed rate constant of dihydrogen complex **4c** formation (k_{obs}) can be described by Equation (4).

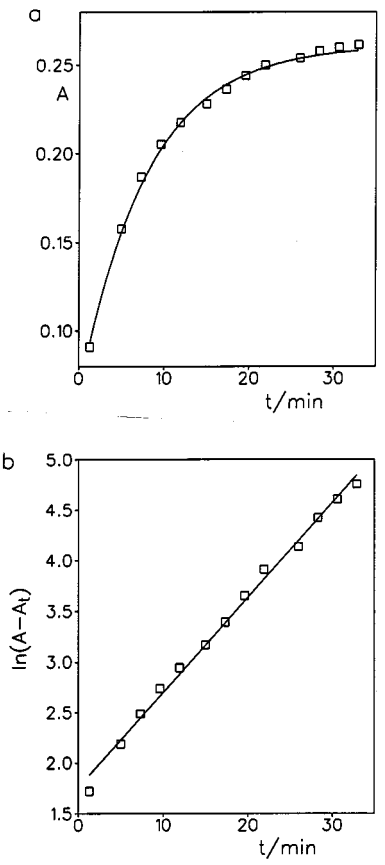

Figure 5. Kinetic curve (a) and its first-order logarithmic plot (b) for the reaction of CpRu(CO)(PCy_3)H (**1**) (0.004 mol/L) with 8 equiv. of $(CF_3)_3COH$ (**2c**) in CH_2Cl_2 at 200 K

$$k_{obs} = k_2\left(\frac{K_1[HA]}{1+K_1[HA]}\right) + k_{-2} \quad (4)$$

In the present case the k_{obs} value does not depend on the alcohol concentration, meaning the value in parentheses is approximately 1. In this case, the product of K_1 by [HA] should be >> 1. Lets suggest it is about 10. So, simple calculation using the **2c** concentrations of the order of 10^{-2} mol/L gives $K_1 \approx 10^3$ L/mol, which looks reasonable because the K_1 value in hexane at 200 K is ca. 2300 L/mol.

We were unable to determine the equilibrium constant K_2 (Scheme 1) due to the overlapping of the ν_{CO}(**1**) and ν_{CO}(**3c**) bands, but we could estimate the conversion ratio α [Equation (5)], where C_1 is the total concentration of hydride **1**, based on the ν_{CO}(**1**+**3c**) intensity fall upon the settlement of the equilibrium.

$$\alpha = [\mathbf{4c}]/C_1 \quad (5)$$

As one can expect, the α value increases as the **2c** concentration increases (Table 2). Although we cannot determine the K_2 equilibrium constant we can estimate its value assuming that at 10-fold alcohol excess and $K_1 \approx 10^3$ L/mol at 200 K, the hydrogen bonding equilibrium should be completely shifted toward **3c**. So, we can determine both **3c** and **4c** concentrations from the corresponding ν_{CO} bands and estimate K_2 = [**4c**]/[**3c**] to be 1.7. The K_2 value estimated seems to be realistic, and the same one has already been observed in other cases.[41] These values correspond to $\Delta G_{200K} \approx -2.7$ kcal/mol for hydrogen bond formation and only −0.2 kcal/mol for proton transfer, showing that the driving force of the proton transfer reaction in the present case is dihydrogen bond formation.

The Study of the Interaction of Hydride 1 with $(CF_3)_3COH$ (2c) by NMR Spectroscopy

The measurements in CD_2Cl_2 and [D_8]methylcyclohexane were carried out at 190−270 K. In the presence of hydride **1**, the proton signal of **2c** shifts to low field from δ = 4.5 to δ = 6. A change of the hydride signal position in the ^{1}H NMR spectra (−12.5 ppm) could not be detected, but a substantial shortening of the relaxation time of the hydride signal was observed. In the presence of **2c** T_1 min. of this signal decreases 1.5−2 times from 753 ms to 389 ms in CD_2Cl_2 and 383 ms in C_7D_8, at 200 K. Such changes of T_1 min. are typical for MH···HA bond formation.[11,19] The ^{1}H-NMR spectra of **1** in the presence of a 5-fold CF_3COOH (**2d**) excess show the signal of the η^2-H_2 ligand of **3** at δ = −7.95, with relaxation time T_1 = 11 ms (200 K, 400 MHz). For comparison, an NMR spectrum of [CpRu(η^2-H_2)(CO)(PCy_3)]BF_4 (**5**) in CD_2Cl_2 was recorded. It shows the signal of the η^2-H_2 ligand at δ = −7.95. The T_1 relaxation time of this signal is 9 ms at 210 K (200 MHz) and matches the value found by Heinekey and coworkers.[25,26]

NMR studies in liquid freons have been shown[14,21] as potential tools in obtaining additional information about hydrogen bonds. Therefore, the interaction of hydride **1** with **2c** was studied in a freon mixture ($CDClF_2$/CDF_3, 2:1) at different ratios hydride/alcohol.

The OH signal of monomeric alcohol molecules is observed at δ = 4.1. This alcohol is not susceptible to self-association and chemical shift of its proton drifts insignificantly with concentration and temperature changes. In the presence of hydride **1** a strong low-field shift (up to δ = 8.5 at 140 K), characteristic for the hydrogen bond formation, is observed.

The resonance of the hydride ligand in **1** is shifted to high field from δ = −12.5 to −12.7 at 170 K when 12 equiv.

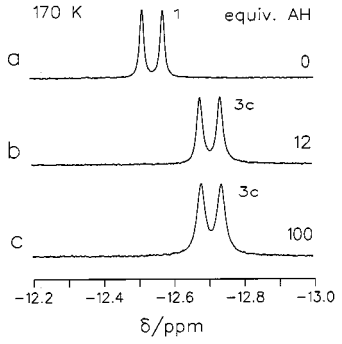

Figure 6. Hydride region of the 500-MHz ^{1}H NMR spectra of CpRu(CO)(PCy_3)H (**1**) at 170 K in $CDClF_2$/CDF_3 (2:1) (a) without proton donor, (b) in the presence of 12 equiv. of **2c**, (c) in the presence of 100 equiv. of **2c**

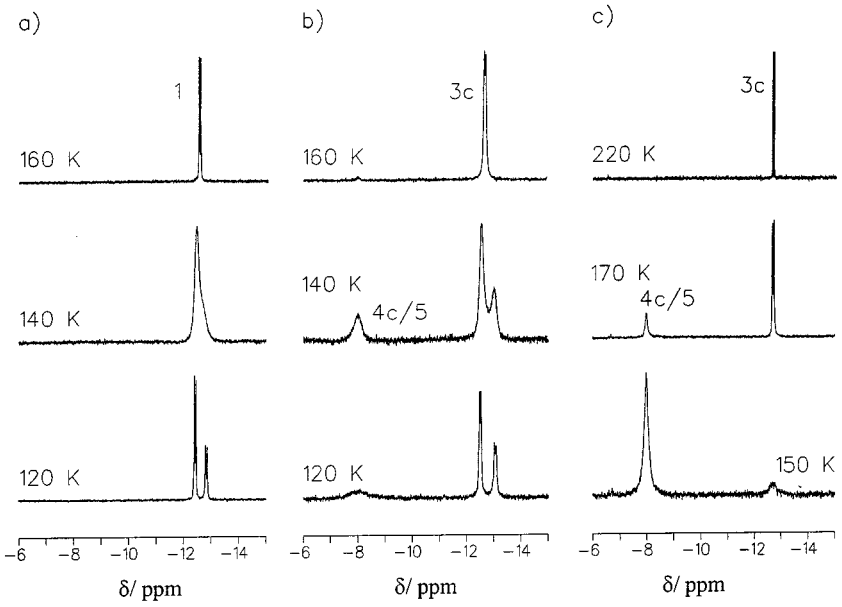

Figure 7. Hydride region of the 500-MHz ^{1}H NMR spectra of CpRu(CO)(PCy_3)H (**1**) at different temperatures in $CDClF_2/CDF_3$ (2:1) (a) without proton donor, (b) in the presence of 12 equiv. of **2c**, (c) in the presence of 100 equiv. of **2c**

of **2c** is added (Figure 6, a, b). Further increase in alcohol concentration (Figure 6, c) does not change the position of this resonance. A slight high-field shift of the hydride ligand signal ($\Delta\delta$ = 0.2 ppm) is normal for RuH···HOR bonding, and has been observed before.[11,14,19,21]

^{1}H NMR spectra of **1** without alcohol at different temperatures show that the position of the hydride signal does not change when the temperature is lowered to 150 K. Below that temperature the signal reversibly splits into two doublets with the intensity ratio 2:1 (Figure 7, a). A similar splitting was observed for Cp*$RuH_3(PCy_3)$ and is suggested to be due to the frozen motion of cyclohexyl rings.[42]

The η^2-H_2 ligand signal at $\delta = -8.0$ appears at 150 K, and increases in intensity down to 140 K in the presence of 12 equiv. of **2c** (Figure 7, b). The broadening of the signal at $\delta = -8.0$ in Figure 7 (b) could be explained by the existence of the equilibrium between forms **4c** and **5**, and fast exchange between them. This suggestion is in accordance with IR-spectroscopic data which showed the formation of ion pair **4c** for this concentration ratio. In the presence of 100 equiv. of **2c** the η^2-H_2 ligand signal of **4/5** appears already at 170 K (Figure 7, c). The increase of medium polarity could lead to partial dissociation of **4c**, and the signal becomes narrower. Full proton transfer is already observed at 150 K. At 110 K the signal of the η^2-H_2 ligand broadens into the baseline. The increase of the temperature leads to restoration of the initial spectrum revealing the reversibility of the process.

Discussion

The analysis of results obtained by low-temperature IR and NMR studies enables us to propose the stepwise mechanism of reaction between hydride **1** and proton donors **2**, resulting in the formation of the dihydrogen complex **5** according to Scheme 1. The first step of the interaction is the formation of a hydrogen bond between proton donors and hydride hydrogen atom (**3**). The determined thermodynamic characteristics of hydrogen-bonded complexes **3** showed that the ruthenium hydride **1** forms H-bonds of medium strength ($-\Delta H$ = 5.3−7.6 kcal mol^{-1}). The $-\Delta H^0$ values increase with ROH proton-donating abilities in the sequence CF_3CH_2OH (**2a**) < $(CF_3)_2CHOH$ (**2b**) < $(CF_3)_3COH$ (**2c**).

The proton-accepting ability E_j of the hydride hydrogen atom in **1** does not depend on the strength of the proton donor or on the media. It equals 1.02±0.02 and is somewhat larger than that in rhenium dihydrides $H_2Re(NO)(CO)(PR_3)_2$ (0.68−0.79).[13] The increased basicity of the hydride atom is responsible for proton transfer not only from strong proton donors such as CF_3COOH (**2d**) and HBF_4 (**2e**), but also from weaker proton donors such as $(CF_3)_2CHOH$ (**2b**) and $(CF_3)_3COH$ (**2c**) when in excess, as well as in the case of {$MeC(CH_2PPh_2)_3$}$Re(CO)_2H$ (E_j = 0.97).[19]

The next step − proton transfer from the H···H complex and generation of the dihydrogen complex − was shown to be an equilibrium process. After proton transfer, the cationic dihydrogen complex forms a contact ion pair **4**, stabilised by hydrogen bonding with the anion. The formation of ion pairs **4**, and the equilibrium between them and free cation **5** was studied using the known very high sensitivity of ν_{CO} vibrations to weak intermolecular interactions. Thus, depending on the ratio **1/2d**, only contact ion pair **4d** (ν_{CO} = 1996 cm^{-1}), only free cation **5** (ν_{CO} = 2020 cm^{-1}), or both forms can exist in solution simultaneously (Fig-

ure 3). The concentration dependence of ν_{CO} of **2d** and ν_{OCO}^{as} of **6d** anion bands confirms this conclusion. The existence of the equilibrium between free cation and ion pair $Cp^*M(CO)_2H^+\cdots{}^-OOCCF_3$ was established before for protonation of $Cp^*M(CO)_2$ (M = Rh, Ir) with CF_3COOH (**2d**),[36−38] and the spectral changes were similar to those observed here. The proton transfer to the metal atom has been shown to cause a large high-frequency shift of the ν_{CO} bands ($\Delta\nu$ = +95 to +143 cm^{-1}). Formation of ion pairs $Cp^*M(CO)_2H^+\cdots{}^-OOCCF_3$ resulted in a low-frequency shift of the ν_{CO} band of the cation in the range −20 to −50 cm^{-1}, depending on the nature of the metal atom. Moreover, the low-frequency shift of this band should also depend on the proton-accepting ability of an anion. Indeed, in the present case, the formation of the ion pair of $[Ru(\eta^2\text{-}H_2)]^+\cdots{}^-OC(CF_3)_3$ (**4c**) causes the larger low-frequency shift of the ν_{CO} band of cation **5** than that caused by the CF_3COO^- anion in **4d**. The position of ν_{CO} bands of **4c** is 1960 cm^{-1} compared to 1996 cm^{-1} for **4d**. That is in agreement with the larger proton-accepting ability of $(CF_3)_3CO^-$ compared to that of CF_3COO^-. It is noteworthy that the experimental observation of ion-paired H-complex $[Ru(\eta^2\text{-}H_2)]^+\cdots OR^-$ formation is in accordance with ion-molecular $[Ru(\eta^2\text{-}H_2)]^+\cdots OH_2$ hydrogen bonding determined in DFT calculations.[43]

Thus, the results obtained allow us to believe that proton transfer takes place within dihydrogen-bonded intermediate **3**, leading to complex **4** with a hydrogen bond between the η^2-H_2 ligand and the anion. A series of transition states of similar hydrogen-bonded structures was proposed recently by Basallote et al.[22] on the basis of inverse kinetic isotope effect data for the protonation of *cis*-$[FeH_2\{P(CH_2CH_2PPh_2)_3\}]$ with strong acids. They were, however, unable to provide experimental information on the structure of the intermediates and to elucidate the rate-determining step of the reaction. Here the sensitivity of the IR-spectral method allows us to observe different intermediates and to support such a stepwise proton transfer mechanism.

The proton transfer step appeared to be a slow process − the formation of **4c** and the settling of the equilibrium take about 30 min. Since the hydrogen bond formation is well known to be diffusion-controlled process, we assume that the *intra*-complex conversion of **3c** into **4c** is the rate-determining step in the proton transfer reaction. First-order rate constants obtained (Table 2) do not depend on the concentration of the reagents [k_{obs} = (1.6±0.2) × 10^{-3} s^{-1}] and support this idea.

Very recently,[41] studying the protonation of $\{MeC(CH_2PPh_2)_3\}Re(CO)_2H$ by $(CF_3)_3COH$ (**2c**) we suggested that the proton transfer barrier ($\Delta G^{\#}$) in this system should be about 12 kcal/mol. In the present work the value of k_{obs} obtained gives us an opportunity to estimate the barrier of proton transfer $\Delta G^{\#}$ (14.3 kcal/mol at 200 K). We can suggest that the low rate and high barrier are determined by steric hindrance of the PCy_3 ligand that embarrasses the proton transfer, as well as the accompanying complex reorganization. In this system even H···H hydrogen bonding has substantial steric hindrance and the large change of entropy (ΔS^0 = −21.6±0.6 e.u.) was determined. Such a value is near the highest values of H-complex formation entropy. The steric effects of the ligand and acid perhaps affect the proton transfer. The electronic factors determining the proton transfer barrier height were considered in the theoretical work.[43] The results of the DFT calculations for model hydride $CpRuH(CO)(PH_3)$ show that in the case of a weak proton donor such as H_2O the barrier for proton transfer from the H···H complex to the η^2-H_2 complex reaches about 40 kcal/mol, and proton transfer does not occur. When the strong proton donor H_3O^+ is used as a model the barrier drops significantly. These data are in good agreement with our results. In the case of moderate proton donors like $(CF_3)_2CHOH$ (**2b**) and $(CF_3)_3COH$ (**2c**), the barrier is high and proton transfer yielding the η^2-H_2 complex is slow. In the case of the strong acid CF_3COOH (**2d**) the barrier height becomes negligible, and protonation proceeds immediately.

Conclusions

By varying the proton donor strength, concentration, and temperature (250−140 K) we were able to find experimental evidence of a stepwise mechanism for the protonation of $CpRuH(CO)(PCy_3)$ (**1**). The spectral and thermodynamic characteristics of hydrogen bonding preceding the proton transfer and the formation of a dihydrogen complex were determined. The formation of ion pairs stabilized by hydrogen bonds between dihydrogen complex and anions [CF_3COO^-, $(CF_3)_3CO^-$] was observed in CH_2Cl_2. Low-rate constants and a high barrier of low-temperature protonation were determined for the first time. The results obtained seem to offer good experimental support for the long since suspected mechanism of protonation leading to the cationic dihydrogen complexes. Of course, further studies are required to determine the influence of solvent polarity and proton donor strength on the kinetic and thermodynamic characteristics of this interaction, and to establish the generality of mechanism suggested in this paper.

Experimental Section

$CpRuH(CO)PCy_3$ (**1**) was prepared as previously described.[25,26] IR measurements were carried out with a "Specord M82" spectrometer using 0.1-cm CaF_2 cells. For the low-temperature measurements a cryostat Carl Zeiss Jena was employed in the temperature range 190−300 K using a stream of liquid nitrogen. The accuracy of temperature adjustment was ±0.5 °C. The cell width was 0.04−0.12 cm. The reagents were mixed at low temperatures to prevent the dihydrogen evolution. The cold solution was then transferred into the cryostat pre-cooled to the required temperature. All samples were prepared under dry argon using standard Schlenk techniques. Anhydrous solvents were freshly distilled and degassed prior to use. The ^1H NMR spectra were recorded with Bruker WP-200, AMX 400, and AMX-500 spectrometers. Standard Bruker software was used for the inversion-recovery T_1 determination. The temperature was calibrated externally by a Pt100 thermo device.

The preparation of deuterated freon mixtures and of the samples using high-vacuum techniques were performed according to known procedures.[44−46]

Acknowledgments

We are extremely grateful to Prof. V. I. Bakhmutov and E. V. Vorontsov for NMR measurement in CD_2Cl_2 and C_7D_8, and for useful discussions. Thanks are expressed to P&M company (Moscow, Russian Federation) for providing the fluorinated alcohols. The authors thank RFBR-INTAS (N 95-136) and Russian Foundation for Basic Research (N 96-03-34114, 99-03-33270) for financial support.

[1] P. G. Jessop, R. H. Morris, *Coord. Chem. Rev.* **1992**, *121*, 155−284.
[2] A. J. Lough, S. Park, R. Ramachandran, R. H. Morris, *J. Am. Chem. Soc.* **1994**, *116*, 8356−8357.
[3] S. Park, R. Ramachandran, A. J. Lough, R. H. Morris, *J. Chem. Soc., Chem. Commun.* **1994**, 2201−2202.
[4] J. C. Lee, E. Peris, A. L. Rheingold, R. H. Crabtree, *J. Am. Chem. Soc.* **1994**, *116*, 11014−11019.
[5] S. Park, A. J. Lough, R. H. Morris, *Inorg. Chem.* **1996**, *35*, 3001−3006.
[6] J. C. Lee, A. L. Rheingold, B. Muller, P. S. Pregosin, R. H. Crabtree, *J. Chem. Soc., Chem. Commun.* **1994**, 1021−1022.
[7] E. Peris, J. C. Lee, J. R. Rambo, O. Eisenstein, R. H. Crabtree, *J. Am. Chem. Soc.* **1995**, *117*, 3485−3491.
[8] E. Peris, J. Wessel, B. P. Patel, R. H. Crabtree, *J. Chem. Soc., Chem. Commun.* **1995**, 2175−2176.
[9] E. Wessel, J. C. Lee, E. Peris, G. P. Yap, J.B. Fortin, J. S. Ricci, G. Sini, A. Albinati, T. F. Koetzle, O. Eisenstein, A. L. Rheingold, R. H. Crabtree, *Angew. Chem. Int. Ed. Engl.* **1995**, *34*, 2507−2508.
[10] R. H. Crabtree, P. E. M. Siegbahn, O. Eisenstein, A. L. Rheingold, T. F. Koetzle, *Acc. Chem. Res.* **1996**, *29*, 348−354.
[11] E. S. Shubina, N. V. Belkova, A. N. Krylov, E. V. Vorontsov, L. M. Epstein, D. G. Gusev, M. Niedermann, H. Berke, *J. Am. Chem. Soc.* **1996**, *118*, 1105−1112.
[12] N. V. Belkova, E. S. Shubina, A. V. Ionidis, L. M. Epstein, H. Jacobsen, A. Messmer, H. Berke, *Inorg. Chem.* **1997**, *36*, 1522−1525.
[13] N. V. Belkova, E. S. Shubina, L. M. Epstein, S. E. Nefedov, I. L. Eremenko, *J. Organomet. Chem.* **2000**, *610*, 58−70.
[14] E. S. Shubina, N. V. Belkova, A.V. Ionidis, N. S. Golubev, S. N. Smirnov, P. Schah-Mohammedi, L. M. Epstein, *Izv. Akad. Nauk, Ser. Khim.*, **1997**, 1405−1406; (*Russ. Chem. Bull.* **1997**, *44*, 1349−1350).
[15] E. S. Shubina, N. V. Belkova, L. M. Epstein, *J. Organomet. Chem.* **1997**, *536−537*, 17−29.
[16] J. A. Ayllon, S. Sabo-Etienne, B. Chaudret, S. Ulrich, H.-H. Limbach, *Inorg. Chim. Acta* **1997**, *259*, 1−4.
[17] J. A. Ayllon, C. Gervaux, S. Sabo-Etienne, B. Chaudret, *Organometallics* **1997**, *16*, 2000−2002.
[18] L. M. Epstein, E. S. Shubina, *Ber. Bunsen-Ges. Phys. Chem.* **1998**, *102*, 359−363.
[19] E. S. Shubina, N. V. Belkova, E. V. Bakhmutova, E. V. Vorontsov, V. I. Bakhmutov, A. V. Ionidis, C. Bianchini, L. Marvelli, M. Peruzzini, L. M. Epstein, *Inorg. Chim. Acta* **1998**, *280*, 302−306.
[20] E. S. Shubina, N. V. Belkova, E. V. Bakhmutova, L. N. Saytkulova, A. V. Ionidis, L. M. Epstein, *Izv. Akad. Nauk, Ser. Khim.* **1998**, 846−851; (*Russ. Chem. Bull.* **1998**, *47*, 817−822).
[21] S. Gründemann, S. Ulrich, H.-H. Limbach, N. S. Golubev, G. S. Denisov, L. M. Epstein, S. Sabo-Etienne, B. Chaudret, *Inorg. Chem.* **1999**, *38*, 2550−2551.
[22] M. G. Basallote, J. Duran, M. J. Fernandez-Trujillo, M. A. Manez, J. Rodriguez de la Torre, *J. Chem. Soc., Dalton Trans.* **1998**, 745−749.
[23] M. G. Basallote, J. Duran, M. J. Fernandez-Trujillo, M. A. Manez, *J. Chem. Soc., Dalton Trans.* **1998**, 2205−2209.
[24] M. G. Basallote, J. Duran, M. J. Fernandez-Trujillo, M. A. Manez, *Inorg. Chem.* **1999**, *38*, 5067−5071.
[25] M. S. Chinn, D. M. Heinekey, *J. Am. Chem. Soc.* **1987**, *109*, 5865−5867
[26] M. S. Chinn, D. M. Heinekey, *J. Am. Chem. Soc.* **1990**, *112*, 5166−5175.
[27] S. G. Kazarian, P. A. Hamley, M. Poliakoff, *J. Chem. Soc., Chem. Commun.* **1992**, 994−995.
[28] S. G. Kazarian, P. A. Hamley, M. Poliakoff, *J. Am. Chem. Soc.* **1993**, *115*, 9069−9079.
[29] P. A. Hamley, S. G. Kazarian, M. Poliakoff, *Organometallics* **1994**, *13*, 1767−1774.
[30] J. Murto, A. Kivinen, R. Vitala, J. Hyoemaeki, *Spectrochim. Acta* **1973**, *29A*, 1121−1138
[31] A. Barnes, J. Murto, *J. Chem. Soc., Faraday Trans. 2* **1972**, *68*, 1642−1651
[32] D. M. Heinekey, C. E. Radzewich, M. H. Voges, B. M. Schomber, *J. Am. Chem. Soc.* **1997**, *119*, 4172−4181.
[33] S. Feracin, T. Burgi, V. I. Bakhmutov, I. L. Eremenko, E. V. Vorontsov, A.V. Vymenits, H. Berke, *Organometallics* **1994**, *13*, 4194−4202.
[34] G. S. Denisov, G. S. Gusakova, A. L. Smolyansky, *J. Mol. Struct.* **1973**, *15*, 377−380.
[35] Z. Dega-Szafran, M. Grundwald-Wyspinka, M. Szafran, *Spectrochim. Acta* **1991**, *47A*, 543−550.
[36] E. S. Shubina, A. N. Krylov, D. V. Muratov, A. A. Fil'chikov, L. M. Epstein, *Izv. Akad. Nauk, Ser. Khim.*, **1993**, 2002−2004 (*Russ. Chem. Bull.* **1993**, *42*, 1919−1921).
[37] L. M. Epstein, A. N. Krylov, E. S. Shubina, *J. Mol. Struct.* **1994**, *322*, 345−352.
[38] E. S. Shubina, A. N. Krylov, A. Z. Kreindlin, M. I. Rybinskaya, L. M. Epstein, *J. Organomet. Chem.* **1994**, *465*, 259−264.
[39] A. V. Iogansen, *Theor. Experim. Khim.* **1971**, 302−320;
[40] The empirical Iogansen "rule of factors"[39] demonstrating the invariability of proton donor (P_i) and proton acceptor (E_j) properties of organic acids and bases in hydrogen bonding was obtained from a large array of spectral and colorimetric data. We used the following equation for the "rule of factors" $(-\Delta H_{ij}) = (-\Delta H_{11})P_iE_j$ where $(-\Delta H_{11})$ = enthalpy of hydrogen bonding for a standard pair: phenol−diethyl ether (P_{11} = E_{11} = 1.00) as for tungsten hydrides.[11]
[41] N. V. Belkova, E. V. Bakhmutova, E. S. Shubina, C. Bianchini, M. Peruzzini, V. I. Bakhmutov, L. M. Epstein, *Eur. J. Inorg. Chem.* **2000**, 2163−2165.
[42] S. Gründemann, N. S. Golubev, H.-H. Limbach, unpublished results.
[43] G. Orlova, S. Sheiner, *J. Phys. Chem. A* **1998**, *102*, 4813−4818.
[44] N. S. Golubev, G. S. Denisov, *J. Mol. Struct.* **1992**, *270*, 263−269.
[45] N. S. Golubev, S. N. Smirnov, V. A. Gindin, G. S. Denisov, H. Benedict, H.-H. Limbach, *J. Am. Chem. Soc.* **1994**, *116*, 12055−12056.
[46] S. N. Smirnov, N. S. Golubev, G. S. Denisov, H. Benedict, P. Schah-Mohammedi, H.-H. Limbach, *J. Am. Chem. Soc.* **1996**, *118*, 4094−4101.

Received October 26, 2000
[I00403]

Ligational Properties of Two New Phenolic Aza Cages towards Proton and Alkali Metal Ions − a Theoretical and an Experimental Approach

Paolo Dapporto,[a] Mauro Formica,[b] Vieri Fusi,*[b] Luca Giorgi,[b] Mauro Micheloni,*[b] Roberto Pontellini,[b] Paola Paoli,*[a] and Patrizia Rossi[a]

Keywords: Synthesis / Aza cages / Crystal structures / Thermodynamics / Molecular dynamics

Molecular Dynamics (MD) simulations were performed on several species (anion, zwitterion, and neutral metal complexes) of two phenolic aza cages (**L1** and **L2**) in aqueous solution. The anionic species of the smaller **L1** ligand appears to be able to selectively encapsulate Li^+, while the other alkaline metal ions tested (Na^+ and K^+) are too large to be encapsulated. The larger cage **L2** does not show any selectivity; the anion binds all the alkaline metal ions. The two aza cages **L1** and **L2** were synthesized. Both basicity and alkali metal complex formation were studied in aqueous solution at 25 °C in 0.15 mol dm^{-3} Me_4NCl, using potentiometric, UV/Vis- and NMR-spectroscopic techniques. Both cages behave as triprotic bases in the pH range investigated; $\log K_1$ = 12.15(6), $\log K_2$ = 7.39(5), $\log K_3$ = 1.4(1) for **L1** and $\log K_1$ = 11.76(5), $\log K_2$ = 8.24(5), $\log K_3$ = 2.9(2) for **L2**. The last proton cannot be removed because both compounds are strongly basic under the experimental conditions studied. Proton localization was studied by UV/Vis and NMR spectroscopy, both in water and nonaqueous solutions. The crystal structures of [H**L1**](ClO_4) and [Na**L2**](ClO_4) were determined by X-ray analysis. The crystals of [H**L1**](ClO_4) are triclinic, space group $P(\bar{1})$; cell parameters are a = 10.3628(8), b = 11.938(1), c = 12.201(4) Å, α = 117.53(1), β = 101.25(1), γ = 102.774°. The crystals of [Na**L2**](ClO_4) are monoclinic, space group $P2_1/n$; cell parameters are a = 10.6154(7), b = 17.0418(9), c = 14.9452(9) Å, β = 95.634(6)°.

Introduction

The design of macrocyclic molecules to achieve selective host recognition is a widely used synthetic strategy.[1−6] To complex small, spherical guests such as metal ions, only macropolycyclic hosts are able to provide many binding sites directed towards the guest in a convergent manner, thus making the resulting metal complex thermodynamically stable. A further advantage of cage-like hosts is that solvation inside the cavity is weaker than with hosts where the binding sites are more exposed to the solvent.[7]

Alkali and alkaline earth cations are the simplest guests; they are spherical in shape and utilize only electrostatic forces for binding. In order to achieve selectivity among the alkali metal ions the size of the cavity of the macropolycyclic host should exactly match that of the alkali metal ion.

In our laboratory we have synthesized many small aza cages,[8−22] some of which are able to selectively encapsulate the lithium ion.[11,13,15,17,18] In some cases these molecules behave as "*fast proton sponges*",[8,9,11,12,19] indicating that the smallest cation, the proton, is also selectively encapsulated. In order to gain spectroscopic information about the binding event, chromoionophores such as nitro and/or phenolic groups have been inserted into the molecular frameworks.[23−26] One of the latest small aza cages studied in our laboratories thus far is compound **L** (see Scheme 1).[27] The ligand is able to selectively encapsulate the lithium ion, a $\log K > 3$ is expected for the complexation process $Li^+ + [H_{-1}L]^- = [LiH_{-1}L]$.[27] At 300 K the molecule, both in the $[H_2L]^{2+}$ [27] and the $[H_{-1}L]^-$ species, appeared rather rigid in the MD simulations performed in aqueous solution [the solvent was mimicked by using a distance-dependent dielectric constant $\varepsilon(r) = 80r$, unpublished results]. In particular, the phenolic moiety does not change its orientation with respect to the [12]aneN_4 ring. It is almost parallel to the *trans*-dimethylated tetraazamacrocycle with the oxygen atom pointing "outside" the macrobicyclic cavity. We designed the trial molecules **L1** and **L2** (see Scheme 1) starting from this molecule, with the aim to obtain a more flexible macrobicyclic skeleton which can better accommodate the donors around the metal guest. The promising theoretical results obtained encouraged us to synthesize these two new molecules. Their ligational properties towards proton (i.e. their basicity) and alkali metal ions were investigated both in solution (by potentiometric titrations, UV/Vis and NMR spectra) and in the solid state (by

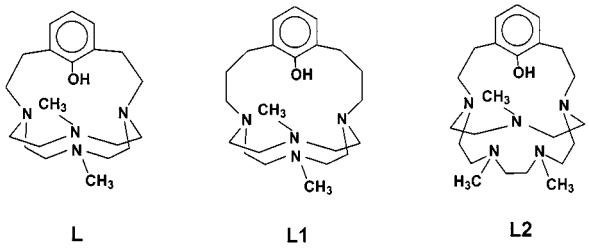

Scheme 1. Drawing of the ligands

[a] "Sergio Stecco" Department of Energy Engineering, University of Florence,
Via S. Marta No. 3, 50139 Florence, Italy
[b] Institute of Chemical Sciences, University of Urbino,
Piazza Rinascimento No. 6, 61029 Urbino, Italy
Fax: (internat.) + 39-0722/350032
E-mail: mauro@chim.uniurb.it

 © WILEY-VCH Verlag GmbH, 69451 Weinheim, 2001 1434−1948/01/0707−1763 $ 17.50+.50/0

X-ray diffraction), and then compared with the modeled behavior.

Results and Discussion

Molecular Dynamics Simulations

(i) *Anion Species*

During the MD simulation of $[H_{-1}\mathbf{L1}]^-$, the dominant conformation was found to be characterized by a phenolate group which is nearly parallel to the mean plane described by the four nitrogen atoms. In this case, the oxygen atom of the bridging unit is always directed towards the methyl moiety disposed above the *trans*-dimethylated cyclen ring. As a consequence, during the MD run at least one $-CH_3\cdots O$ intramolecular interaction (< 2.7 Å) takes place. The two *trans*-disposed methyl groups point in opposite directions with respect to the [12]aneN$_4$ mean plane, with the exception of just a few conformations. Figure 1 (a) reports the average structure from snapshots of the coordinates for $[H_{-1}\mathbf{L1}]^-$. However, during the simulation time a few conformations were observed to have the phenolate moiety almost perpendicular to the [12]aneN$_4$ ring. As expected, the propyl chains allow the phenolate ring greater conformational freedom relative to the ligand **L**. In this regard the $[H_{-1}\mathbf{L2}]^-$ anion is more rigid, with the benzene ring always in the same orientation with respect to the 15-membered ring. Thus, the lengthening of the polyaza ring does not provide greater conformational freedom of the bridging moiety. As in **L** and **L1**, the phenolate ring of **L2** is almost parallel to the N_5 mean plane and the oxygen atom is oriented towards the longer chain bearing the two methyl groups of the [15]aneN$_5$ base. The latter groups are always pointing in the opposite direction to the [15]aneN$_5$ ring, while the third methyl group is always positioned below the mean plane. Figure 1 shows the average conformation resulting from MD. Furthermore, the collected conformations show at least one intramolecular interaction between the phenolic oxygen atom and a hydrogen atom of a methyl group.

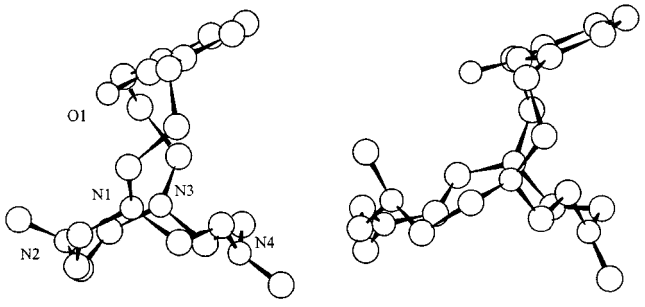

Figure 1. Average conformation from snapshots of coordinates for (a) $[H_{-1}\mathbf{L1}]^-$, (b) $[H_{-1}\mathbf{L2}]^-$

In order to evaluate the approximate size of the three-dimensional cavity inside the two macrocyclic ligands that is able to accommodate the cation, the distances between the geometric center defined by the donors and each donor atom itself were calculated throughout the simulations. Table 1 lists these average distances for the $[H_{-1}\mathbf{L1}]^-$ and $[H_{-1}\mathbf{L2}]^-$ species, as well as an estimate of the metal–donor bond lengths obtained from crystal structures of metal ($M = Li^+$, Na^+, and K^+) complexes having nitrogen and/or oxygen atoms as donors, which have been deposited at the CCDC.[28] With regard to the $[H_{-1}\mathbf{L1}]^-$ ligand, comparison between the distance values reported in Table 1 seems to indicate that the molecular cavity is too small to encapsulate the sodium and potassium ions, whereas it is well suited to the size of the Li^+ ion. On the contrary, the donors of the larger $[H_{-1}\mathbf{L2}]^-$ host appear to be suitable to bind the sodium and potassium cations, while the lighter lithium is probably too small.

Table 1. Mean X (center of donors)–donor atoms distances [Å] obtained from MD simulations and mean metal–donor bond lengths [Å] obtained from the crystal structures of the metal ($M = Li^+$, Na^+, and K^+) complexes having nitrogen and/or oxygen atoms as donors deposited at the CCDC

$[H_{-1}\mathbf{L1}]^-$	$[H_{-1}\mathbf{L2}]^-$	Li^+ donor	Na^+ donor	K^+ donor
X–O1 2.78	X–O1 2.61	Li–N 2.2	Na–N 2.5	K–N 2.8
X–N1 2.21	X–N1 2.63	Li–O 2.1	Na–O 2.4	K–O 2.8
X–N2 2.16	X–N2 2.80			
X–N3 2.15	X–N3 2.95			
X–N4 2.71	X–N4 2.72			
	X–N5 3.05			

(ii) *Neutral Species*

Both cages in their neutral form still contain one proton and are zwitterions. The acidic hydrogen atom (H1) was bound to a bridgehead nitrogen atom, as found in previous work involving similar monoprotonated cages.[29] Once again, during the MD runs the phenolate ring is almost coplanar to the N_4 and N_5 mean planes of **L1** and **L2**, respectively. However, in **L1** the propyl chains connecting the phenolate group to the [12]aneN$_4$ are more stretched out than in the anionic form. As a result, the phenolic oxygen atom is further from the mean N_4 plane in **L1** than in $[H_{-1}\mathbf{L1}]^-$ (see Figure 2, a), and the stabilization of the zwitterion can be entirely ascribed to the nitrogen atoms (vide infra). Conversely, the introduction of an acidic proton within the molecular framework of $[H_{-1}\mathbf{L2}]^-$ does not significantly affect the overall shape of the molecule, the only noteworthy difference is that the two adjacent methylated nitrogen atoms are always pointing above the N_5 mean plane (see Figure 2, b).

In order to gain some information concerning the relative basicity of both compounds in the reaction $[H_{-1}L]^- + H^+ \rightarrow L$, the inter-atomic distances of the H···donor atoms were collected during the simulations. In both zwitterions, the acidic proton appears to be involved in essentially two H-bonding interactions (see Table 2). In **L1** the acidic hydrogen atom interacts more closely with the two methylated nitrogen atoms. The interaction with the phenolic oxygen atom is weaker as it is more distant. Most conformations of the larger compound **L2**, show an N–H···O hydrogen

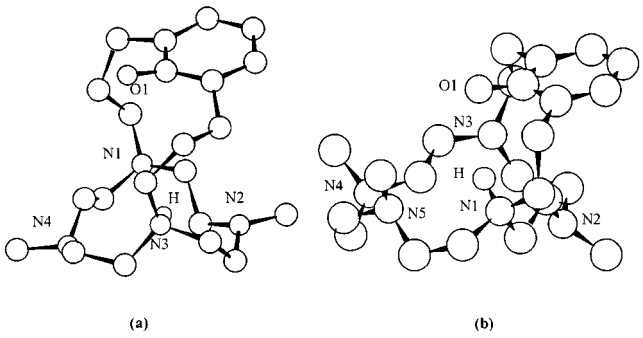

Figure 2. Average conformation from snapshots of coordinates for (a) [**L1**], (b) [**L2**]

Table 2. Mean H−donor atoms distances [Å] obtained from MD simulations

L1	**L2**
H−O1 4.15	H−O1 2.34
H−N1 3.61	H−N2 3.92
H−N2 2.41	H−N3 3.92
H−N4 2.62	H−N4 4.46
	H−N5 2.66

bond and an interaction involving the closer methylated nitrogen atom N5 belonging to the longer arm of the [15]aneN$_5$ ring. In both forms the mean H···acceptor distances are very similar; as a result, we can infer that the basicity properties of the two polyaminic bases should be similar.

(iii)−(iv) *Metal Complexes*

The results from the simulations performed in the two media studied are practically identical. Table 3 reports the average distances of the M−donors extracted from the MD simulations. In both cases [H$_{-1}$**L1**]$^-$ appears to be able to bind only the smallest alkaline cation. The sodium ion comes out from the molecular cavity, remaining close to the phenolic oxygen atom throughout the entire simulation time (mean Na−O distance 2.22 Å). The largest ion, potassium, moves away from the macrocycle very quickly, thus confirming the results of the preliminary studies concerning the cavity size of the ligands in the anionic form. The mean Li−N distances monitored during the MD run ranged from 2.09 to 2.34 Å. The phenolic oxygen atom interacts strongly with the lithium cation. The mean Li−O distance is 1.75 Å, with the Li−O bond pointing inside the molecular cavity. As a result of this interaction, the phenyl ring is almost perpendicular to the N$_4$ ring and the overall shape of the metal complex is different from that observed for the anion and the zwitterion (see Figure 3, a). The coordination geometry around the metal guest is trigonal-bipyramidal, with the bridgehead nitrogen atoms occupying the axial positions, as already found in the solid-state X-ray structures of analogous tbp macrobicycle−Li$^+$ complexes (SEKSAC[15a] and SONJAC[17] refcode). In the latter complexes, all the donor atoms were nitrogen atoms and the Li−N distances were shorter (mean 2.04 Å) than in [LiH$_{-1}$**L1**]. Furthermore, in the lithium complex with 4,7,13-trioxa-1,10-diazabicyclo[8.5.5]icosane (FENHIP[30]), whose chain lengths are comparable with those of **L2**, the coordination distances are very similar to those observed during the MD simulation of [LiH$_{-1}$**L2**] (vide infra).

Table 3. Mean M−donor atoms distances [Å] obtained from MD simulations

H$_{-1}$**L1**	LiH$_{-1}$**L2**
Li−O1 1.75	Li−O1 1.81
Li−N1 2.34	Li−N1 2.79
Li−N2 2.09	Li−N2 2.29
Li−N3 2.21	Li−N3 2.44
Li−N4 2.13	Li−N4 2.17
	Li−N5 2.90
NaH$_{-1}$L2	**KH$_{-1}$L2**
Na−O1 2.15	K−O1 2.51
Na−N1 2.66	K−N1 2.76
Na−N2 2.47	K−N2 2.72
Na−N3 2.59	K−N3 2.72
Na−N4 2.63	K−N4 2.71
Na−N5 2.44	K−N5 2.63

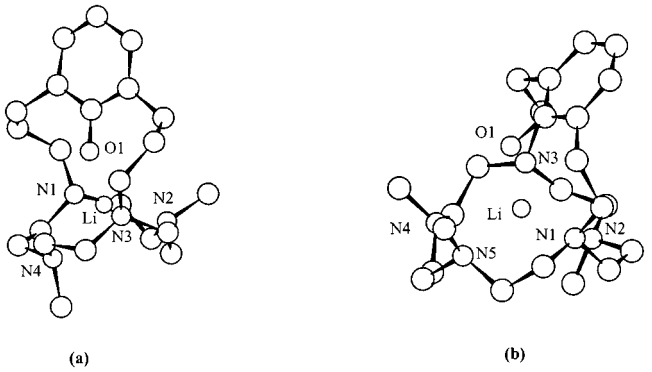

Figure 3. Average conformation from snapshots of coordinates for (a) [Li**L1**], (b) [Li**L2**]

The [H$_{-1}$**L2**] species behaved in a similar manner towards the lithium, sodium, and potassium cations. During the MD runs the cation was encapsulated within the ligand cavity in all cases. These results seem to indicate that the larger ligand is not a selective binder of the lithium ion. In the [LiH$_{-1}$**L2**] complex the mean Li−N distances range from 2.2 to 2.9 Å, with a mean Li−O bond length of 1.8 Å (see Table 3). Essentially, the molecular cavity appears to be too large to accommodate the smallest alkaline cation, while the monitored M−donor distances for the sodium and potassium complexes are in agreement with the corresponding experimental values retrieved from the CCDC. In terms of bond lengths, the coordination of the lithium ion appears to be of the 4+2 type which is in agreement with the trend observed in the solid-state structures of hexacoordinated Li$^+$−macrobicyclic complexes with nitrogen and/or oxygen donor atoms, retrieved from the CCDC.

The phenyl ring gradually changes its orientation with respect to the N_5 mean plane, in the lithium complex it is almost perpendicular, while in the potassium one it is almost coplanar (see Figure 3, b, and Figure 4).

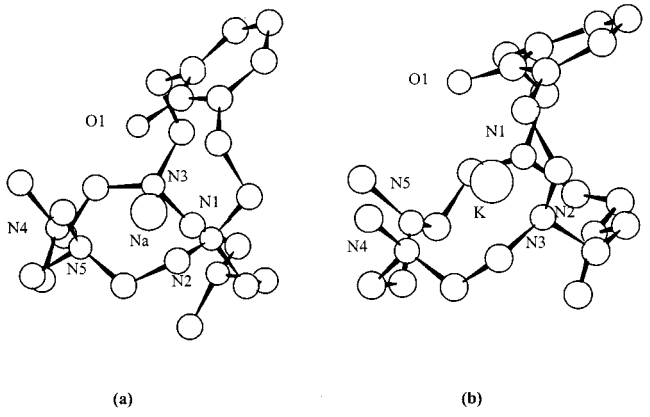

Figure 4. Average conformation from snapshots of coordinates for (a) [Na**L2**], (b) [K**L2**]

Synthesis

The cages **L1** and **L2** were prepared according to the synthetic procedures depicted in Figure 5. The two cages were obtained by following the synthetic procedure reported for the analogous phenolic aza cage **L**.[25] This procedure involves the use of a dimesyl derivative of 2,6-dimethylanisole, and of an aza crown base as the reactants to increase the 1 + 1 product in the final cyclization. In order to obtain **L2**, the new aza crown base **7** was synthesized (see Figure 6). The synthesis of **7**, according to the Richman–Atkins method, requires the use of the ditosylated polyamine **3**, obtained by the extension of *N*,*N*′-dimethylethylendiamine (**1**) with 2 equiv. of *N*-(*p*-tolylsulfonyl)aziridine (**2**). The reaction of the disodium salt of **3** with bis(2-chloroethyl)methylamine (**5**) in DMF leads to the ditosylated macrocycle **6**, which was detosylated with strong acid giving **7**. By treating the aza base **7** with methyl 2-[2-methoxy-3-(2-methylsulfonyloxyethyl)phenyl]ethanesulfonate (**16**) in acetonitrile in the presence of an alkaline carbonate base, we obtained the phenol-protected cage **18** (see Figure 5). To synthesize the cage **L1**, a longer dimesyl derivative **15** of 2,6-dimethylanisole was prepared (see Figure 7). In order to obtain reagent **10**, which is the starting material used to prepare **15**, we followed a different synthetic scheme than that reported previously,[31] thus achieving a higher reaction yield. Compound **15** was obtained from **10** using a classic elongation method of an alkyl chain. The cyclization of **15** with the macrocyclic aza base **17**, gives the phenol-protected cage **19**. For both ligands **18** and **19**, no template effect was found in the cyclization step; moreover, they were deprotected in the same way, with sodium ethanethiolate in DMF. This afforded the phenolic aza cages **L1** and **L2**, after the purification steps.

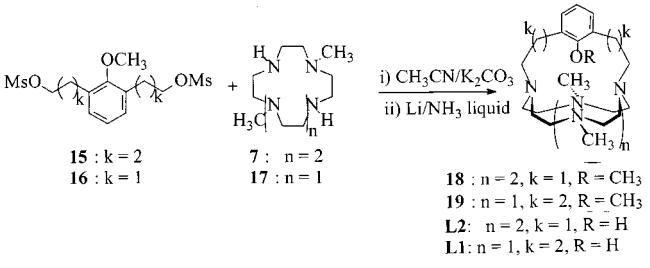

Figure 5. Synthetic pathway used to obtain compounds **L1** and **L2**

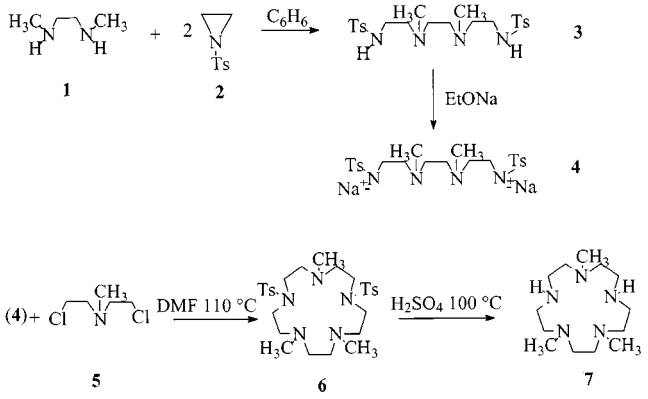

Figure 6. Synthetic procedure to obtain macrocycle **7**

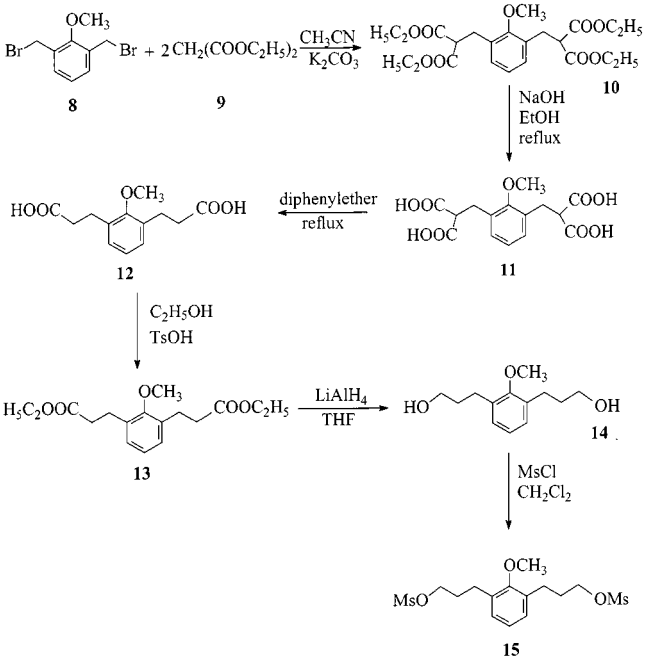

Figure 7. Synthetic procedure to obtain intermediate compounds for the synthesis of **L1**

Protonation and Complex Formation Equilibria

Table 4 reports the protonation constants of **L1** and **L2**. The ligands have a total of five and six protonation sites respectively, and all of the nitrogen atoms are tertiary. Both cages accept three protons under the experimental conditions employed. It should be noted that both cages in their neutral species still contain one proton. This proton cannot be removed in the pH range investigated because the fully deprotonated species $[H_{-1}\mathbf{L1}]^-$ and $[H_{-1}\mathbf{L2}]^-$ are strongly

basic. As expected, the molecular topology strongly influences the basicity behavior of **L1** and **L2**; both compounds are much stronger bases than both the phenolate and the polyaminic tertiary nitrogen atom.[32]

Table 4. Protonation constants of **L1** and **L2** (log *K*) determined by potentiometry in 0.15 mol dm^{-3} Me_4NCl aqueous solution at 298±0.1 K

Reaction	**L1**	**L2**
$L + H^+ = HL^+$	12.15(6)[a]	11.76(5)
$HL^+ + H^+ = H_2L^{2+}$	7.39(5)	8.24(5)
$H_2L^{2+} + H^+ = H_3L^{3+}$	1.4(1)	2.9(2)

[a] Values in parentheses are the standard deviation to the last significant figure.

In order to understand how the phenolic moiety is involved in the protonation steps, absorption electronic spectra and NMR experiments were performed on the compounds **L1** and **L2** in water and in nonaqueous solvents. For both ligands, the absorption and NMR spectra show the involvement of the phenolic group in the protonation steps. For example, the UV spectra of **L1** recorded in aqueous solution, are different in acidic and basic solution. The spectrum shows a band with λ_{max} = 272 nm ($\varepsilon_{\lambda max}$ = 950 M^{-1} cm^{-1}) in the acidic region, while at a pH value slightly over 12, where the neutral species is prevalent in solution, two bands appear in the spectra at λ_{max} = 239 ($\varepsilon_{\lambda max}$ = 5900 M^{-1} cm^{-1}) and 295 nm ($\varepsilon_{\lambda max}$ = 2600 M^{-1} cm^{-1}). This latter spectrum is also maintained at more alkaline pH values. The different behavior of the chromophore in the acidic and basic solution is due to the presence of the phenol hydroxy form at low pH values and to the phenolate form at high pH values. This spectral feature suggests that in the neutral species the ligand is in the zwitterionic form in aqueous solution, with the acidic proton located on the aza base. ^1H NMR spectra of **L1** recorded in aqueous solution, confirmed this hypothesis. The spectrum at pH = 2 in fact shows broad resonances in the aliphatic field, while the aromatic protons give rise to a doublet at δ = 7.15 integrating for two protons (the aromatic protons in *meta* position), and a triplet at δ = 7.00 integrating for one proton (the aromatic proton in *para* position). These resonances undergo an upfield shift in the spectrum recorded at pH = 12, resonating at δ = 6.86 and 6.38 for the doublet and the triplet, respectively. This indicates the deprotonation of the phenolic group at alkaline pH values. Compound **L2** shows a similar behavior with very small differences in wavelengths and in chemical shifts.

The behavior of **L1** and **L2** is different in methanol. The absorption spectra for the phenolic group do not change significantly in acidic or strong alkaline solution, the maximum wavelength and molar absorptivity remain the same [one band with λ_{max} = 276 nm (ε = 1400 M^{-1} cm^{-1})]. In other words, the phenolic group appears in its hydroxy form even in the neutral species. This behavior was also found for **L**, as already reported,[27] and can be explained by the different solvating power of the two media; the charge−charge separation in water is successful, however, in methanol it is not. Nevertheless, it was possible to record the spectrum of the $[H\mathbf{L1}]^+$ species in methanol which shows a different absorption spectrum from the previous ones. Two bands appear at λ_{max} = 236 nm ($\varepsilon_{\lambda max}$ = 4300 M^{-1} cm^{-1}) and λ_{max} = 292 nm ($\varepsilon_{\lambda max}$ = 700 M^{-1} cm^{-1}). The spectrum is similar to that recorded in aqueous solution at an alkaline pH value, highlighting the presence of the phenolate form in the $[H\mathbf{L1}]^+$ species in methanol.

^1H and ^{13}C NMR spectra were recorded to better analyze the $[H\mathbf{L1}]^+$ species in solution. The ^1H NMR spectrum of the $[H\mathbf{L1}]^+$ species, carried out in $CDCl_3$, is shown in Figure 8a. It shows a broad deshielded resonance at δ = 9.97 integrating for two protons which can be assigned to the acidic protons of the ligand. After the addition of a small amount of H_2O or CH_3OH to the chloroform solution, the signal remains. This indicates a slow exchange, on the NMR time scale, of the two protons with the mobile protons of the solvent. However, when D_2O or CD_3OD was added the resonance disappeared. These experimental data suggest that the two protons are positioned inside the macrocyclic cavity and are stabilized by a strong hydrogen-bonding network involving the donor functions. This is in agreement with the X-ray structure (vide infra). The ^1H NMR spectrum of the same species recorded in CD_3OD (Figure 8, b) reveals the disappearance of the deshielded resonance, while the pattern of the other resonances remain quite similar. The addition of Me_4NOH to the species $[H\mathbf{L1}]^+$ in CD_3OD solution (Figure 8, c) leads to a downfield shift of the triplet

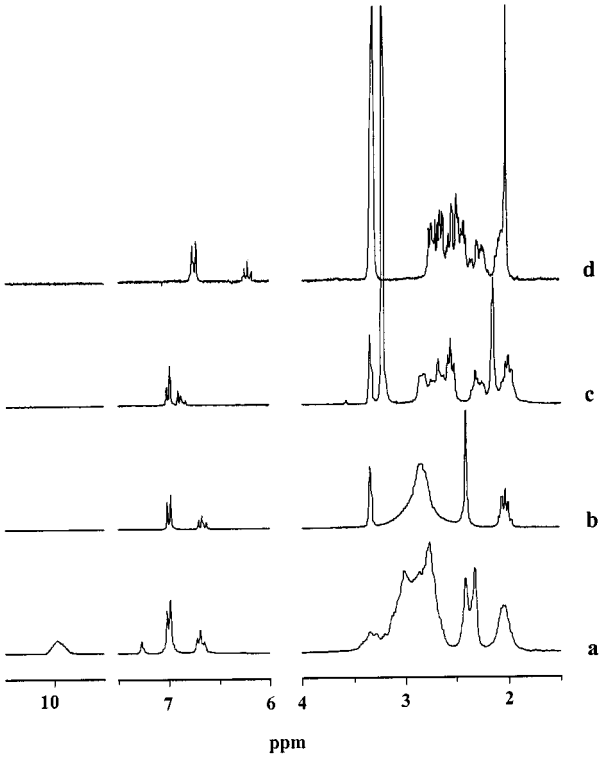

Figure 8. (a) The ^1H NMR spectrum of $[H\mathbf{L1}]^+$ in $CDCl_3$, (b) ^1H NMR spectrum of $[H\mathbf{L1}]^+$ in CD_3OD, (c) ^1H NMR spectrum after the addition of Me_4NOH, (d) ^1H NMR spectrum of $[LiH_{-1}\mathbf{L1}]$ in CD_3OD

due to the aromatic proton in the *para* position, together with an upfield shift of almost all the aliphatic resonances, thus indicating the loss of positive charge density on the amine groups and the protonation of the phenolate oxygen atom. This is in agreement with the UV spectra. In conclusion we can say that in the $[H\mathbf{L1}]^+$ species, the nature of the acidic proton, in water and in organic solvents, seems to be the same as that found in the solid state. In organic solvents the removal of one proton results in the redistribution of the last acidic proton, it is located on the oxygen atom. However, in aqueous solution the last acidic proton remains on the aza base. The ^{13}C NMR spectra recorded in the same solvents, also support this hypothesis. Moreover, **L2** and the smallest compound **L** display similar behavior.[27]

Alkali Metal Ions Complexation

The coordination of the alkali metal ions by ligands **L1** and **L2** was also investigated by ^1H, ^{13}C, and ^7Li NMR spectroscopy and by UV/Vis absorption electronic spectra in water and in organic solvents. Potentiometry was also employed to investigate the formation equilibria of alkali metal complexes (see Table 5). The equilibrium constants reported in Table 5 refer to an overall process in which the alkali metal ion M^+ is bound and, at the same time, the last proton present in the cages is removed, yielding a neutral species $MH_{-1}L$ [$M^+ + L = MH_{-1}L + H^+$]. The stability constants relative to the net complexation process $M^+ + H_{-1}L^- = MH_{-1}L$ can only be estimated since the first protonation constant for both cages **L1** and **L2** is too high to be measured under the chosen experimental conditions. The log*K* value for the first protonation step $H^+ + H_{-1}L = L$ should be greater than 12.15 and 11.76 for **L1** and **L2**, respectively. Also, log*K* > 4 and log*K* > 3 are expected for the net complexation process ($Li^+ + H_{-1}L^- =$ LiL) for **L1** and **L2**, respectively, since the values for the complexation of Li^+ (8.03 and 8.91, see Table 5) should be subtracted. For cage **L2** all three metal ions can be complexed, potentiometric studies show that the estimated stability constants are very similar (see Table 5). For ligand **L1**, the spectroscopic experiments do not reveal any complex formation with sodium and potassium ions in water or in the alcohol solution. **L1** does form a complex with the smallest ion Li^+ and the complex was also isolated in the solid state. As is often the case with aza cage lithium complexes,[11,13,15,17,18] the solid complex is soluble in organic solvents such as $CDCl_3$. The ^7Li NMR spectrum shows a sharp peak which is shifted downfield (0.53 ppm) with respect to that of the free Li^+ ion. The spectra of $[LiH_{-1}\mathbf{L1}]$ show the same signal with an approximately equal chemical shift both in water and in methanol. When an excess amount of Li^+ is added to the solution of the complex, the ^7Li NMR spectrum shows the appearance of a new sharp peak at $\delta = 0$ due to the free lithium ion, together with that of the complexed lithium ion. The simultaneous presence of two peaks in the spectrum denotes a slow exchange (on the NMR time scale) of the complexed lithium ion with the free lithium. The independence of the ^7Li chemical shift from the solvent, and the slow exchange on the NMR time scale between the free and bound lithium ion suggest that it is encapsulated inside the macrocyclic cavity and hence is quite isolated from the medium. The ^1H NMR spectrum of the $[LiH_{-1}\mathbf{L1}]$ in CD_3OD (see Figure 8 spectrum d) shows a marked upfield shift of the triplet signal due to the aromatic proton in the *para* position relative to that of the neutral species (see Figure 8 spectrum c). This suggests the deprotonation of the phenol group with lithium complexation. The ^1H NMR spectrum of the lithium complex recorded in aqueous solution shows broader signals with approximately the same chemical shifts in the resonances. The UV spectra recorded in water and in methanol of the lithium complex show the two characteristic bands of the phenolate form with an increased molar absorptivity in water with respect to the free ligand at the same pH values [λ_{max} = 241 nm ($\varepsilon_{\lambda max}$ = 8250 M^{-1} cm^{-1}), λ_{max} = 296 nm ($\varepsilon_{\lambda max}$ = 4200 M^{-1} cm^{-1})].

Table 5. Logarithms of the equilibrium constants determined in 0.15 mol dm^{-3} Me_4NCl at 298.1 K for the complexation reactions of **L1** and **L2** with Li^+, Na^+, and K^+ ions

	Li^+	Na^+	K^+
$M^+ + \mathbf{L1} = MH_{-1}\mathbf{L1} + H^+$	−8.03	–	–
$M^+ + \mathbf{L2} = MH_{-1}\mathbf{L2} + H^+$	−8.91	−8.33	−8.65

A different behavior is shown by the larger compound **L2**. No selectivity was found in aqueous solution by the spectroscopic techniques which is in agreement with the MD simulations. However, some interesting aspects were revealed. The ^7Li NMR spectra recorded in aqueous solution and in methanol show only one signal that rapidly interchanges with the free lithium ion, thus denoting the easy access of the solvent to the ion sphere, together with the poor fit of the ion in the macrocyclic cavity as previously inferred from MD simulation results. In both media, the ^1H NMR spectra of the $[MH_{-1}\mathbf{L2}]$ metal complexes reveal the lack of selectivity of the ligand; for example, the spectrum of each complex can also be obtained by adding a small excess of the metal ion to a solution of another complex. However, some interesting results were found in the case of the sodium complexes. Solution studies performed in methanol in fact reveal that the $[Na\mathbf{L2}]^+$ species, which is probably in a conformation similar to that found in the crystal structure, rapidly evolves into another species upon addition of a small amount of a base. This is well depicted by monitoring the aromatic region of the ^1H NMR spectra of $[Na\mathbf{L2}]^+$ and the UV/Vis absorption electronic spectra of these species (Figure 9). The new species corresponds to that of the $[NaH_{-1}\mathbf{L2}]$ sodium complex which is isolated in the solid state as reported in the Exp. Sect. As depicted in the aromatic part of the ^1H NMR spectrum of the $[NaH_{-1}\mathbf{L2}]$ species, there are two stable conformers on the NMR time scale that give rise to a high number of signals in the ^{13}C NMR spectra as well (see Exp. Sect.). However, in both conformers, the upfield shift of the proton located

in the *para* position, as compared with that in the $[NaL2]^+$ spectrum, suggests the deprotonation of the phenolic group of **L2** due to metal complexation. This hypothesis was confirmed by the comparison of the UV spectra of the $[NaL2]^+$ and $[NaH_{-1}L2]$ complexes, each of which has the spectral characteristics of one of the two forms of the phenol, thus suggesting a conformation of $[NaL2]^+$ in solution which is similar to that found in the solid state and leading to the deprotonation of the ligand in more basic solutions.

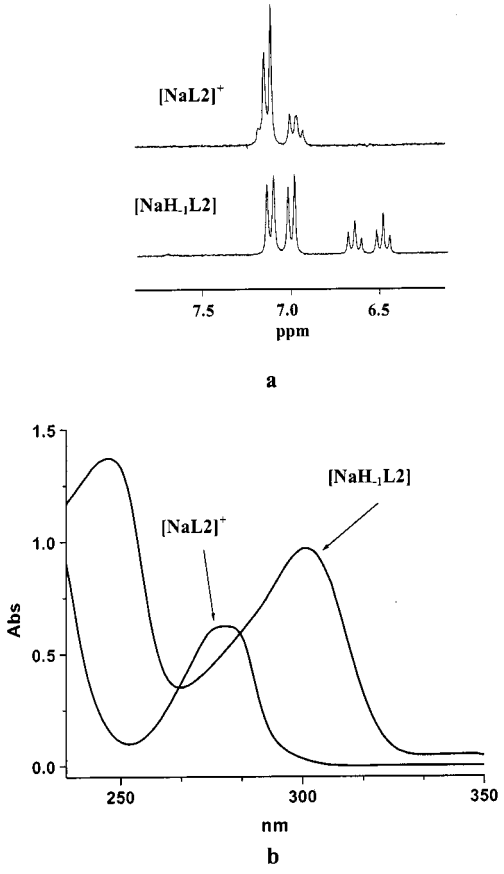

Figure 9. (a) The ^1H NMR spectra of the Na^+/**L2** system, (b) UV/Vis absorption electronic spectra of $[NaL2]^+$ and $[NaH_{-1}L2]$

X-ray Structures

$[HL1]^+(ClO_4)^-$

The crystal structure consists of $[HL1]^+$ cations and $(ClO_4)^-$ anions. Figure 10 shows an ORTEP[33] view of the $[HL1]^+$ cation with the atom labelling. Crystal and structure refinement data are reported in Table 6. With regard to the protonation sites, the two acidic hydrogen atoms are bound to the bridgehead nitrogen atoms N1 and N3 and form short hydrogen bonds with the oxygen atom O1 [H1N···O1 1.70(7), H3N···O1 1.79(6) Å]. The interactions between these hydrogen atoms and the other two donor atoms (N2 and N4) are significantly weaker than those involving the oxygen atom with distances 2.56(7) and 2.90(7) Å for [H3N···N2] and [H1N···N2], respectively, and 2.67(5) and 2.79(5) Å for [H1N···N4] and [H3N···N4], respectively. The atoms N1 and N3 are pointing toward the phenolic group. The nitrogen atoms N2 and N4 are on the opposite side of the N_4 mean plane, with their bonded methyl groups equatorial and axial with respect to the N_4 mean plane, respectively. In the crystal there are no strong intermolecular interactions. The conformation assumed by the [12]aneN$_4$ ring is of the [2424] C-corners type.[34] This is not a very common conformation for this class of compounds; in fact, the analysis of the solid-state structures collected in the Cambridge Structural Database v.5.19 revealed that the most common conformation assumed by [12]aneN$_4$ diprotonated rings is [3333].

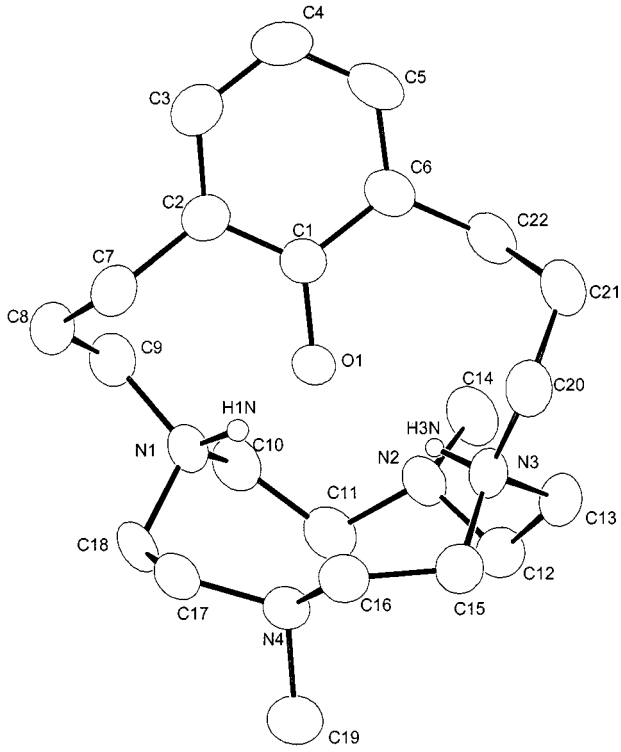

Figure 10. ORTEP view of the $[HL1]^+$ cation

Table 6. Crystal data and structure refinement for $[HL1](ClO_4)$ and $[NaL2](ClO_4)$

Empirical formula	$C_{22}H_{39}ClN_4O_5$	$C_{23}H_{41}ClN_5NaO_5$
Molecular mass	475.02	526.05
Temperature [K]	293	293
λ [Å]	1.5418	1.5418
Crystal system, space group	triclinic, $P(\bar{1})$	monoclinic, $P2_1/n$
Unit cell dimensions[Å, °]	a = 10.3628(8), α = 117.53(1) b = 11.938(1), β = 101.25(1) c = 12.201(4), γ = 102.774(9)	a = 10.6154(7) b = 17.0418(9), β = 95.634(6) c = 14.9452(9)
Volume [Å^3]	1225.9(9)	2690.6(2)
Z	2	4
Calculated density [g/cm^3]	1.287	1.299
μ [mm^{-1}]	1.706	1.763
Final R indices [$I > 2\sigma(I)$]	$R1$ = 0.0519, $wR2$ = 0.1408	$R1$ = 0.0682, $wR2$ = 0.1948
R indices (all data)	$R1$ = 0.0653, $wR2$ = 0.1564	$R1$ = 0.0848, $wR2$ = 0.2135

$[NaL2]^+(ClO_4)^-$

The structure consists of $[NaL2]^+$ cations and of $(ClO_4)^-$ anions. Figure 11 shows a perspective view of the complex cation. In Table 6 crystal and structure refinement data are reported. Selected bond lengths and angles are given in Table 7. The sodium ion is bound to the five nitrogen atoms of the ligand and to the oxygen atom of the phenol group. The coordination geometry around the sodium ion can be described as a strongly distorted pyramid having a pentagonal base, with the apex occupied by the oxygen atom. The five nitrogen atoms at the corners of the pentagonal base are not in a plane as seen by the deviations from the mean plane passing through them [minimum deviation 0.045(3) Å (N5), maximum deviation 0.750(3) Å (N3), mean deviation 0.507(3) Å]. The Na−N distances range from 2.455(3) to 2.731(3) Å. It is worthy to note that the two bridgehead nitrogen atoms are significantly further (see Table 7), perhaps because of the conformational requirements of the ethylenic chains connecting the phenol ring to the 15-membered macrocycle. The complex cation possesses a pseudo-symmetry plane crossing the phenol moiety and the bond between the C17 and C18 atoms. In this plane lie the Na, N2, and O1 atoms. An examination of the dihedral angles of the macrobicycle shows that the greatest deviation from this pseudo-symmetry is due to the N4−C17−C18−N5 fragment; the dihedral angle around N4−C17 is −175°, versus a value of 96° for the angle about the N5−C18 bond. The phenol ring forms an angle of 18.4(1)° with the N_5 mean plane. Both the methyl groups bound to N4 and N5 are pointing towards the same side of the N_5 ring, with the other methyl group (bound to N2) pointing in the opposite direction. This is in agreement with the results of MD simulations performed on the zwitterionic species. No interesting intramolecular interactions were observed, while a short intermolecular interaction between the hydrogen atom of the phenol group and an oxygen atom of the perchlorate anion was observed [O1−H10····O2 = 2.09(4) Å].

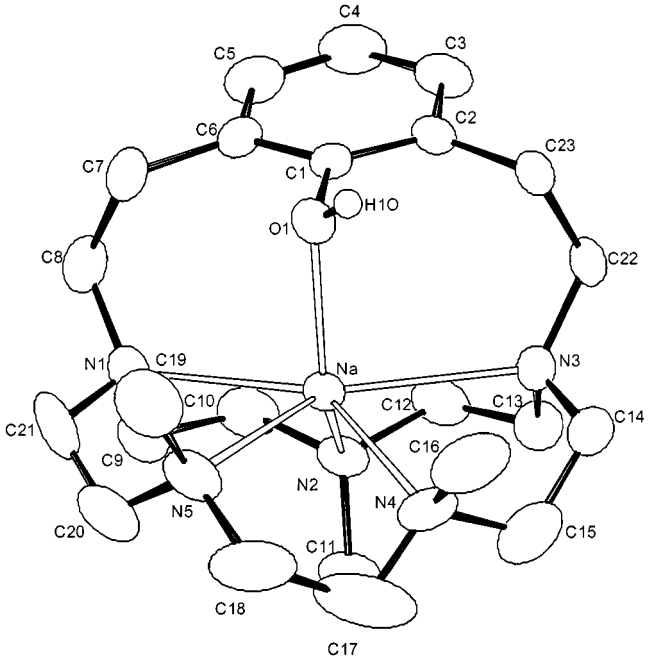

Figure 11. ORTEP view of the $[NaL2]^+$ complex

Table 7. Selected bonds lengths [Å] and angles [°] for $[NaL2]^+$

Na−O(1)	2.301(3)
Na−N(4)	2.455(3)
Na−N(2)	2.473(3)
Na−N(5)	2.504(3)
Na−N(1)	2.667(3)
Na−N(3)	2.731(3)
O(1)−Na−N(4)	109.61(11)
O(1)−Na−N(2)	132.82(10)
N(4)−Na−N(2)	108.91(12)
O(1)−Na−N(5)	94.87(12)
N(4)−Na−N(5)	73.05(16)
N(2)−Na−N(5)	121.84(13)
O(1)−Na−N(1)	91.30(11)
N(4)−Na−N(1)	141.78(14)
N(2)−Na−N(1)	74.24(12)
N(5)−Na−N(1)	73.62(15)
O(1)−Na−N(3)	93.60(10)
N(4)−Na−N(3)	72.59(13)
N(2)−Na−N(3)	73.15(11)
N(5)−Na−N(3)	145.49(15)
N(1)−Na−N(3)	139.54(13)

Experimental Section

General Remarks: ^1H, ^{13}C, and ^7Li NMR spectra were recorded with a Bruker AC-200 instrument, operating at 200.13, 50.33, and 77.78 MHz, respectively. In the ^1H NMR experiments peak positions are reported in relation to HOD ($\delta = 4.75$) and dioxane was used as the reference in the ^{13}C NMR spectra ($\delta = 67.4$). ^7Li peaks are reported in relation to free $LiClO_4$. ^1H-^1H and ^1H-^{13}C correlation experiments were performed to assign the signals. Solvents and starting products were used as purchased.

Molecular Dynamics (MD) Simulation Protocol: The studied species were the anions $[H_{-1}L1]^-$ and $[H_{-1}L2]^-$, the neutral ligands **L1** and **L2** (zwitterionic forms) and the neutral metal complexes $M[H_{-1}L1]$ and $M[H_{-1}L2]$ ($M = Li^+$, Na^+, and K^+). The MSI software programs InsightII and Discover version 98.0[35] were used for all the molecular modeling studies. Based on the good results of a previous computational study performed on monoprotonated macrocyclic compounds[29] of the same family, the Amber[36] force field was used (all the 1−4 nonbonding interactions were scaled by a factor of 0.5). Atomic charge distributions were calculated according to the ChelpG scheme at the single point 6−31G* level of theory using Guassian94 (revision D3).[37] As initial geometries for each species in vacuo, fully optimized model-built structures were used. In addition, before starting with the MD procedures the initial molecular assembly was further optimized until the convergence criterion was met (< 0.01 kcal mol^{-1}). The MD simulation temperature was set at 298 K and the Verlet leapfrog algorithm, with a time step of 1 fs, was used for integration of equations of motion in all simulations. In energy calculations 9.5 and 12.5 Å nonbonded cutoff distances (buffer width 0.5 Å) were employed for van der Waals and Coulomb terms, respectively. In a preliminary

MD study (**i**) on the $[H_{-1}\mathbf{L1}]^-$ and $[H_{-1}\mathbf{L2}]^-$ species, performed to evaluate the molecular cavity, the system was allowed to equilibrate for 8 ps, then MD simulations were run for 80 ps with snapshot conformations saved every ps, and a distance-dependent dielectric constant [$\varepsilon(r) = 80r$] was used. The dynamic behavior of the zwitterionic ligand forms, **L1** and **L2**, (**ii**) was investigated by placing the studied species in a cubic cell (25 Å edge) containing SPC model water molecules (equilibration time 8 ps, data collection time 80 ps, snapshot conformations saved every ps). The geometry of the water molecules was fixed by means of the rattle option. Periodic boundary conditions were applied. In addition, calculations on $M[H_{-1}\mathbf{L1}]$ and $M[H_{-1}\mathbf{L2}]$ were performed both by mimicking the solvent with a distance-dependent dielectric constant $\varepsilon(r) = 80r$ [equilibration time 20 ps, data collection time 200 ps, (**iii**)] and by surrounding the solute species with water molecules occupying the volume of a cube (25 Å edge) as previously reported (**iv**).

Spectrophotometric Measurements: Absorption spectra were recorded at 298 K with a Varian Cary-100 spectrophotometer, equipped with a temperature control unit.

Potentiometric Measurements: All potentiometric measurements were carried out in 0.15 mol dm^{-3} Me_4NCl at 298.0±0.1 K, in the pH range 2.4−10.5, using the fully automatic equipment that has already been described.[38] The emf data were acquired with the PASAT computer program.[38] The electrode was calibrated as a hydrogen concentration probe by titrating known amounts of HCl with CO_2-free Me_4NOH solutions and determining the equivalent point by Gran's method,[39] which gives the standard potential E° and the ionic product of water K_w. At least two to three measurements were performed for each ligand. The HYPERQUAD[40] computer programs were used to process the potentiometric data and calculate the protonation constants.

Ligand Synthesis: The precursor reagents **7** and **15** were synthesized as depicted in Figure 6 and Figure 7, respectively. Ligands **L1** and **L2** were obtained according to the synthetic procedure reported in Figure 5. *N*-(*p*-Tolylsulfonyl)aziridine (**2**),[41] bis(2-chloroethyl)methylamine (**5**),[42] 2,6-bis(bromomethyl)anisole (**8**),[43] and **16**[43] were prepared as previously described. The solvents and the starting materials not mentioned were used as purchased. All reactions were carried out under nitrogen.

4,7-Dimethyl-1,10-bis(*p*-tolylsulfonyl)-1,4,7,10-tetraazadecane (3): A solution of *N*-(*p*-tolylsulfonyl)aziridine (6.7 g, 0.034 mol) in anhydrous benzene (200 mL) was added dropwise at room temperature to a stirred solution of *N*,*N*′-dimethyl-1,2-ethylendiamine (3.0 g, 0.034 mol) in anhydrous benzene (400 mL) over a period of 7 h. The resulting solution was kept at room temperature for ca. 12 h and then a further 6.7 g (0.0034 mol) of **2** in 200 mL of benzene was added under the same experimental conditions. After 12 h, the turbid solution was filtered and concentrated under reduced pressure to give the crude compound **3** as a yellowish solid. The product was dissolved in 150 mL of ethanol and an excess of 37% HCl was added to the solution, obtaining **3** as the dihydrochloride salt. Yield: 14.7 g (78%). − $C_{22}H_{36}Cl_2N_4O_4S_2$ (555.6): calcd. C 47.56, H 6.53, N 10.08; found C 47.6, H 6.6, N 10.0. − ^{1}H NMR (D_2O, 25 °C): δ = 2.34 (s, 6 H), 2.94 (s, 6 H), 3.23 (t, 4 H), 3.36 (t, 4 H), 3.67 (s, 4 H), 7.38 (d, 4 H), 7.69 (d, 4 H). − ^{13}C NMR (D_2O, 25 °C): δ = 21.9, 38.7, 42.3, 50.6, 57.1, 128.1, 131.5, 135.1, 146.9.

1,7,10-Trimethyl-4,13-bis(*p*-tolylsulfonyl)-1,4,7,10,13-pentaazacyclopentadecane (6): A solution of sodium (0.96 g, 0.042 mol) in dry ethanol (50 mL) was added to a hot solution of **3**·2HCl (5.6 g, 0.01 mol) in dry ethanol (100 mL). The resulting suspension was refluxed for 30 min, after which time the solvent was removed under reduced pressure. The solid residue was dissolved in dry DMF (50 mL) and to the resulting solution, heated at 110 °C, a solution of bis(2-chloroethyl)methylamine (**5**) (1.6 g, 0.01 mol), dissolved in 100 mL of dry DMF, was added. The reaction mixture was stirred over a period of 4 h. It was kept at 110 °C for a further 2 h. The suspension was then cooled, filtered, and concentrated under reduced pressure to give a yellowish solid, which was chromatographed on neutral alumina using $CHCl_3$ as the eluent. The eluted fractions containing the product having $R_f = 0.77$ were collected and concentrated to dryness, affording **6** as a white solid. Yield: 3.1 g (55%). − $C_{27}H_{43}N_5O_4S_2$ (565.8): calcd. C 57.32, H 7.66, N 12.38; found C 57.5, H 7.7, N 12.5. − MS (FAB): 567 [M + H^+]. − ^{1}H NMR ($CDCl_3$, 25 °C): δ = 2.14 (s, 6 H), 2.37 (s, 3 H), 2.42 (s, 6 H), 2.54 (t, 4 H), 2.67 (t, 4 H), 2.96 (s, 4 H), 3.28 (m, 8 H) 7.28 (d, 4 H), 7.68 (d, 4 H). − ^{13}C NMR ($CDCl_3$, 25 °C): δ = 21.5, 42.5, 43.7, 46.9, 47.4, 55.6, 56.4, 58.4 127.1, 129.7, 136.7, 143.2.

1,7,10-Trimethyl-1,4,7,10,13-pentaazacyclopentadecane (7): A solution of **6** (3.0 g, 0.005 mol) was dissolved in 8 mL of 96% H_2SO_4 and the resulting solution kept at 100 °C for 72 h. The solution was cooled and added to 200 mL of diethyl ether with stirring. It gave a brown solid, which was filtered and washed with diethyl ether. The residue was dissolved in the minimum amount of water and made alkaline with concentrated aqueous NaOH. The Na_2SO_4 precipitate was filtered off and the alkaline solution was extracted with $CHCl_3$ (6 × 100 mL). The organic solutions were combined, dried with Na_2SO_4 and concentrated under reduced pressure to obtain **7** as a colorless oil. Yield: 1.2 g (88%). − $C_{13}H_{31}N_5$ (257.4): calcd. C 60.66, H 12.14, N 27.21; found C 60.5, H 12.3, N 27.0. − ^{1}H NMR ($CDCl_3$, 25 °C): δ = 2.13 (s, 6 H), 2.24 (s, 3 H), 2.41 (m, 8 H), 2.51 (t, 4 H), 2.67 (t, 4 H), 2.76 (s, 4 H),. − ^{13}C NMR ($CDCl_3$, 25 °C): δ = 42.1, 42.4, 47.1, 47.2, 55.6, 57.0, 57.5.

Diethyl 2-{3-[2,2-Bis(ethoxycarbonyl)ethyl]-2-methoxybenzyl}-malonate (10): A solution of **8** (11.8 g, 0.04 mol) in 150 mL of acetonitrile was added to a refluxing suspension of **9** (12.8 g, 0.08 mol) and K_2CO_3 (27.6 g, 0.2 mol) in 300 mL of acetonitrile over a period of 1 h. The reaction mixture was maintained under reflux for a further 3 d. The mixture was then cooled to room temperature and the resulting suspension was filtered and the solution concentrated under reduced pressure, giving the crude product, which was chromatographed on neutral alumina ($CHCl_3$). The eluted fractions ($R_f = 0.79$) were collected and concentrated to dryness, affording **10** as a colorless oil. Yield: 16.7 g (92%). − $C_{23}H_{32}O_9$ (452.5): calcd. C 61.05, H 7.13; found C 60.9, H 7.2. − ^{1}H NMR ($CDCl_3$, 25 °C): δ = 1.20 (t, 12 H), 3.22 (d, 4 H) 3.79 (t, 2 H), 3.81 (s, 3 H), 4.14 (q, 8 H), 6.92(t, 1 H), 7.08 (d, 2 H). − ^{13}C NMR ($CDCl_3$, 25 °C): δ = 13.9, 29.5, 52.1, 60.7, 60.9, 124.1, 129.6, 131.4, 157.7, 169.1.

2-[3-(2,2-Dicarboxyethyl)-2-methoxybenzyl]malonic Acid (11): A solution of **10** (9.0 g, 0.02 mol) and NaOH (12.0 g, 0.3 mol) in 100 mL of ethanol was refluxed for 7 h. The mixture was cooled, 50 mL of ethanol was added. The solution was maintained under stirring for further 12 h. Acetonitrile (80 mL) was added to the resulting deliquescent mixture until the complete precipitation of a white solid was obtained. The dried solid was dissolved in the minimum amount of water and the solution, made acidic with 37% HCl, was extracted with ethyl ether (5 × 30 mL). The organic solutions were combined, dried with Na_2SO_4 and concentrated under reduced pressure to obtain **11** as a colorless oil. Yield: 5.4 g (79%). − $C_{15}H_{16}O_9$ (340.3): calcd. C 52.95, H 4.74; found C 53.1, H 4.8. − ^{1}H NMR ($CDCl_3$, 25 °C): δ = 3.10 (d, 4 H) 3.67 (s, 3 H), 3.77 (t, 2 H), 6.92(t, 1 H), 7.00 (d, 2 H). − ^{13}C NMR ($CDCl_3$, 25 °C): δ = 30.3, 53.5, 62.3, 126.1, 130.8, 132.2, 158.2, 174.2.

3-[3-(2-Carboxyethyl)-2-methoxyphenyl]propionic Acid (12): A solution of **11** (6.8 g, 0.02 mol) and diphenyl ether (150 g) was refluxed for 2 h. The solution was cooled and 50 mL of $CHCl_3$ was added. This solution was then washed with 0.1 mol dm^{-3} NaOH (6 × 25 mL). The collected aqueous part was acidified with 96% H_2SO_4 and the solution extracted with diethyl ether (6 × 25 mL). The organic solutions were combined, dried with Na_2SO_4 and concentrated under reduced pressure to obtain **12** as a yellowish solid. Yield: 3.9 g (77%). − $C_{13}H_{16}O_5$ (252.3): calcd. C 61.90, H 6.39; found C 61.8, H 6.3. − ^{1}H NMR ($CDCl_3$, 25 °C): δ = 2.70 (t, 4 H) 2.99 (t, 4 H), 3.78 (s, 3 H), 7.08 (m, 3 H), 10.32 (b, 2 H). − ^{13}C NMR ($CDCl_3$, 25 °C): δ = 25.2, 34.5, 61.0, 124.5, 128.4, 133.4, 157.1, 179.4.

Ethyl 3-[3-(2-Ethoxycarbonylethyl)-2-methoxyphenyl]propionate (13): A solution of **12** (7.6 g, 0.03 mol) and *p*-toluenesulfonic acid (8.6 g, 0.045 mol) in 100 mL of ethanol was kept under reflux for a period of 12 h. An aqueous solution of $NaHCO_3$ was added to the reaction mixture (cooled to room temperature) until neutralization was achieved. The mixture was extracted with CH_2Cl_2 (3 × 50 mL), and the organic layer was combined, dried with Na_2SO_4 and concentrated under reduced pressure to obtain **13** as an oil. Yield: 8.2 g (89%). − $C_{17}H_{24}O_5$ (308.4): calcd. C 66.21, H 7.84; found C 66.0, H 7.9. − ^{1}H NMR ($CDCl_3$, 25 °C): δ = 1.25 (t, 6 H), 2.62 (t, 4 H), 2.98 (t, 4 H), 3.77 (s, 3 H), 4.14 (q, 4 H), 7.02 (m, 3 H). − ^{13}C NMR ($CDCl_3$, 25 °C): δ = 14.2, 25.5, 34.9, 60.4, 61.3, 124.3, 128.2, 133.8, 157.3, 173.2.

3-[3-(3-Hydroxypropyl)-2-methoxyphenyl]propanol (14): A solution of **13** (6.2 g, 0.02 mol) in 50 mL of anhydrous diethyl ether was carefully added to a suspension of $LiAlH_4$ in 100 mL of anhydrous ethyl ether. The mixture was allowed to react for 3 h at room temperature. An aqueous solution of $NaHCO_3$ was added to the mixture until excess $LiAlH_4$ was completely destroyed. The suspension was extracted with $CHCl_3$ (6 × 50 mL) and the organic solutions were combined, dried with Na_2SO_4 and concentrated under reduced pressure to obtain **14** as a yellowish oil. Yield: 4.1 g (91%). − $C_{13}H_{20}O_3$ (224.3): calcd. C 69.61, H 8.99; found C 69.7, H 9.1. − ^{1}H NMR ($CDCl_3$, 25 °C): δ = 1.87 (q, 4 H), 2.34 (s, 2 H), 2.75 (t, 4 H), 3.58 (t, 4 H), 3.78 (s, 3 H), 7.05 (m, 3 H). − ^{13}C NMR ($CDCl_3$, 25 °C): δ = 25.7, 33.5, 61.4, 61.6, 124.8, 128.3, 134.5, 156.5.

Methyl 3-[2-Methoxy-3-(3-methylsulfonyloxypropyl)phenyl]propylsulfonate (15): A solution of methylsulfonyl chloride in anhydrous CH_2Cl_2 (40 mL) was added to an ice-cold solution of **14** (4.0 g, 0.018 mol) and triethylamine in 50 mL of anhydrous CH_2Cl_2, over a period of 1 h. The solution was kept at this temperature for a further 2 h, and then washed with 5% HCl aqueous solution (3 × 50 mL), 10% $NaHCO_3$ aqueous solution (3 × 50 mL) and water (3 × 50 mL). The organic part was dried with Na_2SO_4 and concentrated under reduced pressure to give **15** as an oil. Yield: 6.5 g (95%). − $C_{15}H_{24}O_7S_2$ (380.5): calcd. C 47.35, H 6.36; found C 47.2, H 6.5. − ^{1}H NMR ($CDCl_3$, 25 °C): δ = 2.09 (q, 4 H), 2.77 (t, 4 H), 3.01 (s, 6 H), 3.74 (s, 3 H), 4.24 (t, 4 H), 7.06 (m, 3 H). − ^{13}C NMR ($CDCl_3$, 25 °C): δ = 26.0, 29.9, 37.3, 61.2, 69.6, 124.5, 128.6, 133.7, 156.7.

Cryptand 18 (18·4HCl): Amine **7** (1.3 g, 5 mmol) and Na_2CO_3 (2.65 g, 25 mmol) were suspended in refluxing CH_3CN (100 mL). To this mixture, a solution of **15** (1.8 g, 5 mmol) in CH_3CN (100 mL) was added dropwise over 6 h, after which the suspension was refluxed for 72 h and then filtered. The solution was concentrated under vacuum to yield the crude product, which was chromatographed on neutral alumina ($CHCl_3$/CH_3OH, 100:4). The eluted fractions were collected and concentrated to yield an oil, which was dissolved in ethanol and treated with 37% hydrochloride acid to give **18** as a tetrahydrochloride salt (1.2 g, 42%). − $C_{24}H_{47}Cl_4N_5O$ (**18**·4HCl: 563.5): calcd. C 51.16, H 8.41, N 12.43; found C 51.1, H 8.3, N 12.3. − MS (FAB), *m*/*z*: 419 [M + H^+]. − ^{13}C NMR: δ = 25.8, 29.7, 43.2, 43.3, 44.6, 52.3, 52.7, 53.8, 55.3, 56.1, 62.0, 64.1, 127.2, 128.3, 129.6, 131.5, 135.3, 157.5, 158.2.

Cryptand L2 (L2·4HCl): A solution of cryptand **18**·4HCl (1.1 g, 2 mmol), EtSNa (1.7 g, 20 mmol) and LiBr (0.51 g, 6 mmol) in dry DMF (50 mL) was heated at 150 °C for 6 h. The solvent was then vacuum-evaporated and the residue was suspended in CH_2Cl_2 and filtered. The organic layer was concentrated and the crude product was chromatographed on neutral alumina (CH_2Cl_2/MeOH, 100:1). The eluted fractions were collected and concentrated to dryness. The crude product was dissolved in ethanol and treated with 37% hydrochloric acid to give the **L2** tetrahydrochloride salt as a white solid (0.69 g, 63%). − $C_{23}H_{45}Cl_4N_5O$ (**L2**·4HCl: 549.5): calcd. C 50.28, H 8.25, N 12.75; found C 55.3, H 8.4, N 12.6. − ^{1}H NMR (D_2O, pH = 7): δ = 2.32 (s, 3 H) 2.63 (s, 6 H), 3.28 (b, 28 H), 6.72 (t, 1 H), 7.02 (d, 2 H). − ^{13}C NMR (D_2O, pH = 7): δ = 30.4, 41.5, 41.7, 52.1, 54.9, 55.3, 56.0, 58.8, 120.7, 129.1, 131.7, 156.5.

Cryptand 19 (19·2HClO$_4$): This compound was synthesized from amine **17** (2.0 g, 0.01 mol), Na_2CO_3 (5.3 g, 0.05 mol) and **15** (3.5 g, 0.01 mol) according to the same procedure reported for **18**. The crude product **17** was dissolved in ethanol and treated with 65% perchloric acid to give the diperchlorate salt as a white solid (2.3 g, 39%). − $C_{23}H_{42}Cl_2N_4O_9$ (**19**·2$HClO_4$: 589.5): calcd. C 48.86, H 7.18, N 9.50; found C 48.9, H 7.1, N 9.4. − MS (FAB), *m*/*z*: 390 [M + H^+]. − ^{1}H NMR (D_2O, pH = 7, 25° C): δ = 2.14 (b, 4 H), 2.36 (s, 6 H), 2.83 (b, 16 H), 3.19 (b, 4 H), 3.39 (b, 4 H), 3.80 (s, 3 H), 7.27 (m, 3 H). − ^{13}C NMR (D_2O, pH = 7, 25° C): δ = 25.2, 29.0, 43.6, 45.2, 49.4, 52.8, 53.4, 54.0, 55.6, 62.2, 127.1, 130.2, 136.1, 157.2.

Cryptand L1 (L1·3HCl): This compound was synthesized from cryptand **19**·2$HClO_4$ (1.2 g, 2 mmol), according to the same procedure reported for **L2**. The crude product **L1** was dissolved in ethanol and treated with 37% hydrochloric acid to give the trihydrochloride salt as a white solid (0.57 g, 59%). − $C_{22}H_{41}Cl_3N_4O$ (**L1**·3HCl: 484.0): calcd. C 54.60, H 8.54, N 11.58; found C 54.5, H 8.7, N 11.4. − ^{1}H NMR (D_2O, pH = 3): δ = 2.03 (m, 4 H) 2.66 (s, 6 H), 2.76 (m, 16 H), 3.16 (m, 8 H), 6.99 (t, 1 H), 7.14 (d, 2 H). − ^{13}C NMR (D_2O, pH = 3): δ = 25.7, 29.4, 44.6, 49.8, 53.7, 54.4, 124.3, 130.2, 132.6, 156.2.

Preparation of the Complexes. − [LiH$_{-1}$L1]: A solution of LiOH (10 mg, 0.44 mmol) in 15 mL of methanol was added to a solution of **L1**·3HCl_3 (48 mg, 0.1 mmol) in methanol (15 mL). The reaction mixture was stirred for 15 min and then concentrated to dryness. The solid was suspended in 20 mL of $CHCl_3$ and the mixture filtered to separate the inorganic excess. The organic solution was dried with Na_2SO_4. On addition of cyclohexane (25 mL) a white precipitate formed. Yield 31 mg (81%). − $C_{22}H_{37}LiN_4O$ (380.5): calcd. C 69.45, H 9.80, N 14.72; found C 69.3, H 9.7, N 14.6. − ^{13}C NMR ($CDCl_3$): δ = 29.9, 34.2, 43.7, 54.3, 55.5, 59.3, 119.5, 129.4, 132.7, 160.4. − **[NaL2]:** An excess of $NaClO_4$ was added to a solution of **L2**·4HCl (165 mg, 0.3 mmol) in 50 mL of water. A 0.1 mol dm^{-3} NaOH solution was added until complete precipitation of a white precipitate was obtained. The solid was then suspended in 20 mL of $CHCl_3$ and the mixture filtered. The liquid part was dried with Na_2SO_4 and concentrated to dryness. The solid was recrystallized by slow concentration of a mixture of $CHCl_3$/cyclohexane, obtaining white crystals suitable for X-ray analysis.

Yield 60 mg (38%). − $C_{23}H_{41}ClN_5NaO_5$ (526.1): calcd. C 52.51, H 7.86, N 13.31; found C 52.6, H 7.9, N 13.2. − ^{13}C NMR ($CDCl_3$): δ = 30.6, 42.7, 42.9, 55.3, 56.7, 58.3, 58.6, 63.0, 121.1, 127.4, 133.0, 153.8. − **[NaH$_{-1}$L2]:** This compound was synthesized from [Na**L2**] (53 mg, 0.1 mmol) according to the same procedure reported for [LiH$_{-1}$**L1**], giving [NaH$_{-1}$**L2**] as a white solid. Yield: 30 mg, 69%). − $C_{23}H_{40}N_5NaO$ (425.6): calcd. C 64.91, H 9.47, N 16.46; found C 64.3, H 9.3, N 16.4. − ^{13}C NMR (CD_3OD): δ = 29.1, 31.3, 41.2, 41.8, 43.1, 43.2, 52.6, 54.4, 54.5, 57.1, 57.2, 57.3, 57.5, 58.2, 59.3, 60.9, 66.7, 111.2, 114.69, 127.2, 128.7, 130.7, 132.4, 163.2, 163.4.

Cambridge Structural Database Search: The Cambridge Structural Database (CCDC) V5.19 was used to retrieve structural information about the penta- and hexacoordinated complexes of lithium, sodium and potassium by nitrogen and/or oxygen atoms. The VISTA V2.1 software was used to analyze the retrieved fragments.

X-ray Crystallographic Studies: Cell parameters and intensity data for the two structures were obtained with a Siemens P4 diffractometer, using graphite-monochromated Cu-K_α radiation (λ = 1.54184 Å). Cell parameters were determined by least-squares fitting of 25 centered reflections. The intensities of three standard reflections were measured every 60 min to check the stability of the diffractometer and the decay of the crystals. Intensity data were corrected for Lorentz and polarization effects, and an absorption correction was applied once the structure had been solved by using the Walker and Stuart method.[44] The two structures were solved using the SIR-97 program[45] and subsequently refined by the full-matrix least-squares program SHELX-97.[46] Protonation hydrogen atoms of ligand **L1** were found in difference syntheses and their positions were refined, as well as their isotropic displacement parameters. The other hydrogen atoms of the molecule were introduced in calculated positions and their coordinates refined in agreement with those of the linked atoms [overall isotropic temperature factor U = 0.048(2) Å^2]. The H10 atom of compound **L2** was found in a difference synthesis and its position was refined, as well as its thermal parameter. The other hydrogen atoms of the complex were introduced in calculated positions and their coordinates refined in agreement with those of the linked atoms [U = 0.0126(3) Å^2]. All the non-hydrogen atoms of the two structures were refined anisotropically. Atomic scattering factors and anomalous dispersion corrections for all the atoms were taken from ref.[47] Geometrical calculations were performed using PARST97.[48] The molecular plot was produced by the ORTEP program.[33] Crystallographic data (excluding structural factors) for the structures reported in this paper have been deposited at the Cambridge Crystallographic Data Centre as supplementary publication no. CCDC-152533 and -152534 for [H**L1**](ClO_4) and [Na**L2**](ClO_4), respectively. Copies may be obtained without charge from CCDC, Union Road, Cambridge CB2 1EZ, UK [Fax: (internat.) + 44-1223/336-033; E-mail: deposit@ccdc.cam.ac.uk].

Acknowledgments

Support for this research from MURST (Ministero per l'Università e la Ricerca Scientifica e Tecnologica, COFIN98) and CNR (Consiglio Nazionale delle Ricerche) is gratefully acknowledged.

[1] R. M. Izatt, J. J. Christensen, *Synthetic Multidentate Macrocyclic Ligands*, Academic Press, New York, **1978**.
[2] L. F. Lindoy, *The Chemistry of Macrocyclic Ligands Complexes*, Cambridge University Press, **1989**.
[3] A. Bianchi, M. Micheloni, P. Paoletti, *Coord. Chem. Rev.* **1991**, *101*, 17.
[4] [4a] J. S. Bradshaw, *Aza-Crown Macrocycles*, Wiley, New York, **1993**. − [4b] R. M. Izatt, K. Pawlak, J. S. Bradshaw, R. L. Bruening, *Chem. Rev.* **1991**, *91*, 1721.
[5] [5a] G. W. Gokel, "Crown Ethers and Cryptands" in *Monographs in Supramolecular Chemistry* (Ed.: J. F. Stoddart), The Royal Society of Chemistry, Cambridge, **1992**. − [5b] A. F. Sholl, I. O. Sutherland, *J. Chem. Soc., Chem. Commun.* **1992**, 1252.
[6] [6a] M. Ciampolini, N. Nardi, B. Valtancoli, M. Micheloni, *Coord. Chem. Rev.* **1992**, *120*, 223. − [6b] A. Bencini, V. Fusi, C. Giorgi, M. Micheloni, N. Nardi, B. Valtancoli, *J. Chem. Soc., Perkin Trans. 2* **1996**, 2297. − [6c] M. Formica, V. Fusi, M. Micheloni, R. Pontellini, P. Romani, *Coord. Chem. Rev.* **1999**, *184*, 347 and refs. therein.
[7] H. J. Schneider, A. Yatsimirsky, *Principles and Methods in Supramolecular Chemistry*, Wiley, Chichester, **2000**.
[8] S. Chimichi, M. Ciampolini, P. Dapporto, M. Micheloni F. Vizza, F. Zanobini, *J. Chem. Soc., Dalton Trans.* **1986**, 505.
[9] M. Ciampolini, S. Mangani, M. Micheloni, P. Orioli, F. Vizza, F. Zanobini, *Gazz. Chim. Ital.* **1986**, *116*, 189.
[10] A. Bianchi, E. Garcia-España, M. Micheloni, N. Nardi, F. Vizza, *Inorg. Chem.* **1986**, *25*, 4379.
[11] A. Bianchi, S. Chimichi, M. Ciampolini, M. Micheloni, F. Vizza, *Gazz. Chim. Ital.* **1987**, *117*, 499.
[12] A. Bianchi, M. Ciampolini, E. Garcia-España, S. Mangani, M. Micheloni, N. Nardi, J. A. Ramirez, B. Valtancoli, *J. Chem. Soc., Perkin Trans. 2* **1989**, 1131.
[13] A. Bencini, A. Bianchi, A. Borselli, M. Ciampolini, P. Dapporto, E. Garcia-España, M. Micheloni, N. Nardi, P. Paoli, J. A. Ramirez, B. Valtancoli, *Inorg. Chem.* **1989**, *28*, 4279.
[14] A. Bencini, A. Bianchi, A. Borselli, M. Ciampolini, P. Dapporto, E. Garcia-España, M. Micheloni, P. Paoli, J. A. Ramirez, B. Valtancoli, *J. Chem. Soc., Perkin Trans. 2* **1990**, 209.
[15] [15a] A. Bencini, A. Bianchi, A. Borselli, S. Chimichi, M. Ciampolini, P. Dapporto, M. Micheloni, N. Nardi, P. Paoli, B. Valtancoli, *J. Chem. Soc., Chem. Commun.* **1990**, 174 − [15b] A. Bencini, A. Bianchi, A. Borselli, S. Chimichi, M. Ciampolini, P. Dapporto, M. Micheloni, N. Nardi, P. Paoli, B. Valtancoli, *Inorg. Chem.* **1990**, *29*, 3282.
[16] M. Micheloni, N. Nardi, B. Valtancoli, *Gazz. Chim. Ital.* **1991**, *121*, 29.
[17] A. Bencini, A. Bianchi, S. Chimichi, M. Ciampolini, P. Dapporto, E. Garcia-España, M. Micheloni, N. Nardi, P. Paoli, B. Valtancoli, *Inorg. Chem.* **1991**, *30*, 3687.
[18] A. Bencini, A. Bianchi, M. Ciampolini, P. Dapporto, M. Micheloni, N. Nardi, P. Paoli, B. Valtancoli, *J. Chem. Soc., Perkin Trans. 2* **1992**, 181.
[19] C. Bazzicalupi, A. Bencini, A. Bianchi, M. Ciampolini, P. Dapporto, V. Fusi, M. Micheloni, N. Nardi, P. Paoli, B. Valtancoli, *J. Chem. Soc., Perkin Trans. 2* **1993**, 115.
[20] A. Bencini, A. Bianchi, P. Dapporto, V. Fusi, E. Garcia-España, M. Micheloni, P. Paoletti, P. Paoli, A. Rodriguez, B. Valtancoli, *Inorg. Chem.* **1993**, *32*, 2753.
[21] C. Bazzicalupi, A. Bencini, A. Bianchi, M. Ciampolini, V. Fusi, M. Micheloni, N. Nardi, P. Paoli, B. Valtancoli, *Supramolecular Chem.* **1994**, *3*, 141.
[22] A. Bencini, V. Fusi, C. Giorgi, M. Micheloni, N. Nardi, B. Valtancoli, *J. Chem. Soc., Perkin Trans. 2* **1996**, 2297.
[23] C. Bazzicalupi, A. Bencini, M. Ciampolini, V. Fusi, M. Micheloni, N. Nardi, I. Razzolini, B. Valtancoli, *Supramolecular Chem.* **1996**, 61.
[24] P. Dapporto, V. Fusi, M. Micheloni, P. Palma, P. Paoli, R. Pontellini, *Inorg. Chim. Acta* **1998**, *275*, 168.
[25] E. Bardazzi, M. Ciampolini, V. Fusi, M. Micheloni, N. Nardi, R. Pontellini, P. Romani, *J. Org. Chem.* **1999**, *64*, 1335.
[26] P. Dapporto, V. Fusi, C. Giorgi, M. Micheloni, P. Palma, P. Paoli, R. Pontellini, *Supramolecular Chem.* **1999**, *10*, 243.
[27] M. Micheloni, M. Formica, V. Fusi, P. Romani, R. Pontellini,

P. Dapporto, P. Paoli, P. Rossi, B. Valtancoli, *Eur. J. Inorg. Chem.* **2000**, 51.
[28] F. H. Allen, O. Kennard, Cambridge Structural Database, *Chem. Des. Autom. News* **1993**, *8*, 31.
[29] C. Bazzicalupi, P. Dapporto, V. Fusi, P. Paoli, N. Nardi, B. Valtancoli, *Supramolecular Chem.* **1996**, *7*, 195.
[30] A. Abou-Hamdan, A. M. Hounslow, S. F. Lincoln, T. W. Hambley, *J. Chem. Soc., Dalton Trans.* **1987**, 489.
[31] C. Meiners, M. Nieger, F. Voegtle, *Liebigs Ann.* **1996**, *2*, 297.
[32] L. D. Pettit, *IUPAC − Stability Constants Database*, Academic Software, Yorks, **1994**.
[33] C. K. Johnson, *ORTEP*, Rep. ORNL 3794, Oak Ridge National Laboratory, TN, USA, **1971**.
[34] I. Bernal (Ed.), *Stereochemical and Stereophysical Behaviour of Macrocycles*, Elsevier, Amsterdam, **1987**, p.34.
[35] Biosym/MSI, 9685 Scranton Road, San Diego, CA 92121-3752, USA.
[36] S. J. Weiner, P. A. Kollman, D. A. Case, U. C. Singh, C. Ghio, G. Alagona, S. Profeta, Jr., P. Weiner, *J. Am. Chem. Soc.* **1984**, *106*, 765.
[37] M. J. Frisch, G. W. Trucks, H. B. Schlegel, P. M. W. Gill, B. G. Johnson, M. A. Robb, J. R. Cheeseman, T. A. Keith, G. A. Petersson, J. A. Montgomery, K. Raghavachari, M. A. Al-Laham, V. G. Zakrzewski, J. V. Ortiz, J. B. Foresman, J. Cioslowski, B. B. Stefanov, A. Nanayakkara, M. Challacombe, C. Y. Peng, P. Y. Ayala, W. Chen, M. W. Wong, J. L. Andres, E. S. Replogle, R. Gomperts, R. L. Martin, D. J. Fox, J. S. Binkley, D. J. Defrees, J. Baker, J. P. Stewart, M. Head-Gordon, C. Gonzalez, J. A. Pople, Gaussian, Inc., Pittsburgh PA, **1995**.
[38] M. Fontanelli, M. Micheloni, *1st Spanish-Italian Conf. Thermodynamics of Metal Complexes*, Peñiscola, Univ. of Valencia, Spain, p. 41, June 3−6 **1990**.
[39] [39a] G. Gran, *Analyst* **1952**, *77*, 661 − [39b] F. J. Rossotti, H. Rossotti, *J. Chem. Edu.* **1996**, *43*, 1739.
[40] P. Gans, A. Sabatini, A. Vacca, *Talenta* **1996**, *43*, 1739.
[41] A. E. Martin, T. M. Ford, J. E. Bulkowski, *J. Org. Chem.* **1982**, *47*, 412.
[42] K. Ward, *J. Am. Chem. Soc.* **1935**, *57*, 914.
[43] W. Zazulak, E. Chapoteau, B. P. Czech, A. Kumar, *J. Org. Chem.* **1992**, *25*, 6720.
[44] N. Walker, D. D. Stuart, *Acta Crystallogr., Sect. A* **1983**, *39*, 158.
[45] A. Altomare, G. Cascarano, C. Giacovazzo, A. Guagliardi, M. C. Burla, M. C.; G. Polidori, M. Camalli, *J. Appl. Crystallogr.* **1994**, *27*, 435.
[46] G. M. Sheldrick, *SHELXL-97*, University of Göttingen, Germany, **1997**.
[47] *International Tables for X-ray Crystallography*, Kynoch Press, Birmingham, UK, **1974**, vol.4.
[48] M. Nardelli, *Comput. Chem.* **1983**, *7*, 95.

Received November 22, 2000
[I00443]

Metallophthalocyanines Linked to Organic Copolymers as Efficient Oxidative Supported Catalysts

Muriel Sanchez,[a] Nicolas Chap,[a] Jean-Bernard Cazaux,[b] and Bernard Meunier*[a]

Keywords: Phthalocyanines / Supported catalysts / Polymers / Oxidations

The covalent anchoring of metallo(chlorosulfonyl)phthalocyanines **1** onto the acrylic copolymers **2** and **3** has been achieved. When using H_2O_2 or $KHSO_5$ as oxidant, these supported catalysts are able to oxidize a poorly biodegradable molecule such as 2,4,6-trichlorophenol or a tannin model such as 3,5-di-*tert*-butylcatechol. The influence of the spacer and the nature of the reaction medium on the catalytic activities have been studied, as well as the recycling of these supported metallophthalocyanine catalysts.

Introduction

Metallophthalocyanines (e.g., **1** and **4**, Scheme 1) have attracted considerable interest because of their structural similarity to metalloporphyrin complexes found at the active sites of metalloenzymes.[1] These phthalocyanine complexes are often more easily prepared than synthetic metalloporphyrins, and exhibit interesting properties in areas such as sensitizers[1,2] (e.g., in photodynamic cancer therapy), catalysts[1,3] (e.g., for thiol oxidation in gasoline fractions), electrocatalysts[1,4] (e.g., for O_2 reduction in fuel cells), sensors[1][3c,5] (e.g., NO_x and O_2 gas sensors) or nonlinear optical devices.[1,6]

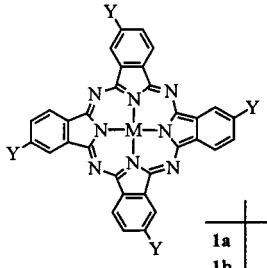

A

	Y	M
1a	SO_2Cl	Fe
1b	SO_2Cl	Co
4a	$SO_3^-Na^+$	Mn
4b	$SO_3^-Na^+$	Fe
4c	$SO_3^-Na^+$	Co

Scheme 1. Structure of the metallo[2,9,16,23-tetrakis(chlorosulfonyl) and -tetrasulfo]phthalocyanines **1** and **4**

In the field of bio-inspired oxidations, it has been shown in our laboratory that water-soluble metallo(sulfo)phthalocyanines **4** (Scheme 1) can be used as oxidation catalysts with H_2O_2 or $KHSO_5$.[7] Highly reactive metal−peroxo (e.g., $Fe^{III}-OOY$) and metal−oxo ($Fe^{IV}=O$) species are probably involved in the catalytic oxidations of poorly biodegradable molecules such as polychlorinated phenols, catechols, and polycondensed aromatics.[7] One limitation of these catalysts is the formation in solution of inactive aggregates and dimers of the metallophthalocyanine complexes, which significantly affects their catalytic properties. This aggregation phenomenon is usually depicted as a coplanar association of the aromatic rings driven by enhanced van der Waals forces and dimer formation through μ-oxo bridges.[7a,8] In solution, the monomerization of water-soluble metallophthalocyanines can be achieved by adding an organic co-solvent[7a] or a detergent.[9] Another strategy used to obtain a monomolecular dispersion of these macrocyclic complexes is based upon their heterogenization on the surface of a support. Several types of carrier have been used for this task, such as charcoal,[10] organic polymers,[11] silica,[12] zeolites,[13] and clays.[14] Among the advantages of using supported catalysts is the easy separation of the catalysts from products and the subsequent possible recycling of the catalyst.[15]

Recently, we have described the covalent attachment of the chlorosulfonyl-substituted iron-phthalocyanine **1a** (Scheme 1) to functionalized 3-aminopropyl-silica via a sulfonamide linkage.[16] This supported catalyst, when using hydrogen peroxide as oxidant, is able to degrade a recalcitrant pollutant. However, the efficiency of this catalytic system was lower than that obtained under homogeneous conditions. This probably results from diffusion-limitation effects inherent to the use of silica as support, despite the fact that mineral supports have a better reputation of chemical stability compared to organic polymers in catalytic oxidations with supported catalysts.[17]

Here, we report the preparation of new organic polymers-supported metallophthalocyanines, and their efficiency as oxidation catalysts.

Results and Discussion

Preparation of the Supported Catalysts

We have previously shown that a sulfonamide linkage used to immobilize an iron-phthalocyanine onto modified

[a] Laboratoire de Chimie de Coordination du CNRS,
205 route de Narbonne, 31077 Toulouse cedex 4, France
E-mail: bmeunier@lcc-toulouse.fr
[b] EXPANSIA,
Route d'Avignon, BP N 6, 30390 Aramon, France

 © WILEY-VCH Verlag GmbH, 69451 Weinheim, 2001 1434−1948/01/0707−1775 $ 17.50+.50/0

silica is stable under oxidative conditions.[15] Therefore, we decided to use the same type of linkage for the attachment of chlorosulfonyl-substituted phthalocyanine complexes **1** onto organic supports. The organic supports used were the acrylic copolymers Met-Expansin-NH_2® (**2**) and Met-Expansin-Piperazine (**3**), which both possess an amino-functionalized pendant arm and were prepared from Met-Expansin® (**5**) by EXPANSIA. These resins were synthesized from the polymerization of the monomer *N*-acryloylpyrrolidine (**6**), the cross-linking agent *N*,*N*′-bis(methacryloyl)-1,2-diaminoethane (**7**), and *N*-acryloyl-β-alanine methyl ester (**8**) as functionalizing agent (Patent EP 79842, 1982) (Scheme 2).

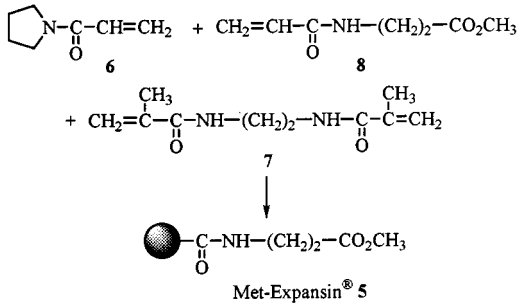

Scheme 2. Synthesis of Met-Expansin® (**5**)

The polyacrylamide **5** can be treated with ethylenediamine to afford **2** (Patent EP 81408, 1982) (Scheme 3). This resin contains 0.56 mmol-equiv. of NH_2 per gram of dry material that can be used to covalently anchor the metallo(chlorosulfonyl)phthalocyanines **1**. A spacer can also be used to increase the distance between the catalyst and the polymer surface. This modification of the tether helps to increase the solvent, substrate, and oxidant access, similar to homogeneous reaction conditions. Copolymer **3** was prepared by treating **2** with bromoacetic anhydride, followed by the addition of piperazine (Patent Fr. Dem. 9904135, 1999). It contains 0.5 mmol-equiv. of terminal NH functions per gram of dry resin.

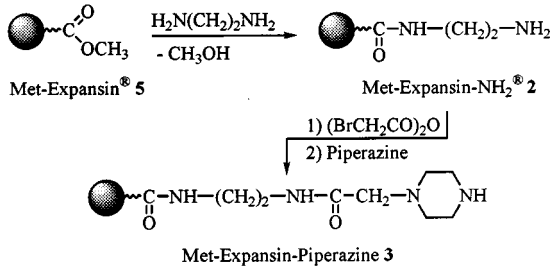

Scheme 3. Synthesis of Met-Expansin-NH_2® (**2**) and Met-Expansin-Piperazine (**3**)

The two organic copolymers **2** and **3** are insoluble in organic solvents and in aqueous media; however, these resins swell in protic solvents to form gels. This property is certainly important for the preparation of supported catalysts, because the surface area of the carrier is considerably increased making the active catalytic centers more accessible.

The immobilization of the chlorosulfonyl derivatives **1** of the iron- and cobalt-phthalocyanines was achieved by heating a mixture of resin and complex in pyridine to reflux. The supported catalysts FePc-SO_2NH-Met-Expansin (**9**) (20.0 μmol of iron per gram of dry resin), FePc-SO_2N(pip)-Met-Expansin (**10a**) (26.5 μmol Fe/g), and CoPc-SO_2N-(pip)-Met-Expansin (**10b**) (42.0 μmol Co/g) were thus obtained from the polyacrylamides **2** and **3** (Scheme 4).

After filtration, the loading of the supports was indirectly calculated by determining the amount of **1** remaining in solution by UV/Vis spectroscopy. No release of metallophthalocyanine was observed after several washings with water, dimethylformamide, and ethanol. The green color of these modified polymers obtained after the washing procedures strongly suggested that the metallophthalocyanine complexes were attached in monomeric form (μ-oxo-metallophthalocyanine dimers and aggregates are generally blue).[7a] It is important to note that no desorption of the metallophthalocyanine catalysts was detected under oxidative conditions (e.g., after addition of H_2O_2 or $KHSO_5$) according to UV/Visible measurements.

For comparison, the silica-supported catalysts FePc-SO_2NH-Silica (**11**) (42.0 μmol Fe/g) and FePc-SO_2N(pip)-Silica (**12**) (40.0 μmol Fe/g) were also prepared. The grafted polymer **11** comes from the direct fixation of **1** onto a commercially available modified silica featuring primary amine linkers, whereas **12** contains the piperazine spacer introduced by the same procedure used for the preparation of **3** from **2** (Scheme 5).

Catalytic Activities of the Grafted Complexes 9−11 for the H_2O_2 Oxidation of a Chlorinated Pollutant

2,4,6-Trichlorophenol (TCP) is produced by paper mills during the oxidative chlorine degradation of lignin in white paper manufacturing.[18] Due to its slow biodegradation by aerobic or anaerobic microorganisms and its resistance to oxidative or reductive chemical treatments, this substrate is extremely persistent in the environment. Thus, TCP is commonly used as a pollutant model. It has been shown that ligninase (a peroxidase isolated from the white-rot fungus *Phanerochaete chrysosporium*) is able to degrade TCP by an oxidative pathway, although the conversion is slow.[18b] Synthetic metalloporphyrins, which are efficient peroxidase models, are able to oxidize TCP to the corresponding quinone, but are unable to cleave the aromatic ring of TCP.[19] Using either soluble metallophthalocyanines, or the corresponding immobilized catalysts onto a support (silica or Amberlite), with H_2O_2 as a "green" oxidant, TCP has been converted in two classes of compounds: aromatic ring cleavage products (C_4 diacids, with chloromaleic acid being the major product) and oxidative coupling products (Scheme 6).[7,20]

Under the same experimental conditions [1 mM TCP solution in a mixture of 50 mM phosphate buffer (pH = 7)/acetone (80:20), 6 mM H_2O_2, and 2 mol-% of catalyst], however, the reaction was markedly faster with the iron-tetrasulfophthalocyanine catalyst **4b** under homogeneous condi-

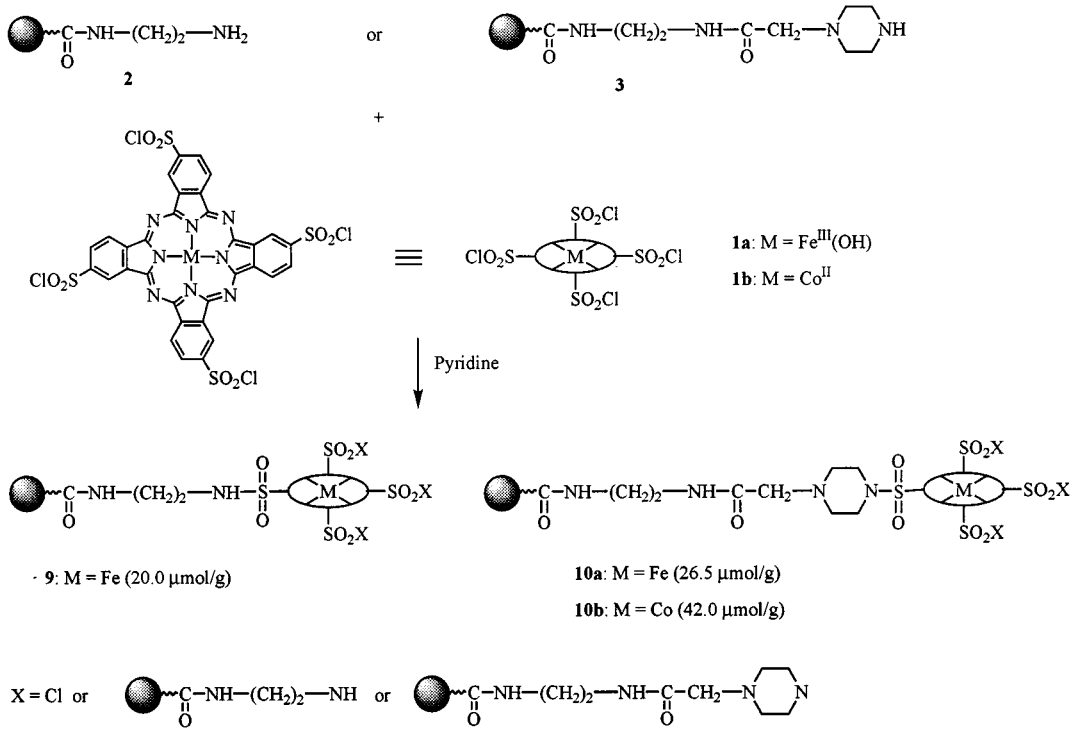

Scheme 4. Immobilization of the metallophthalocyanines **1** onto **2** and **3**

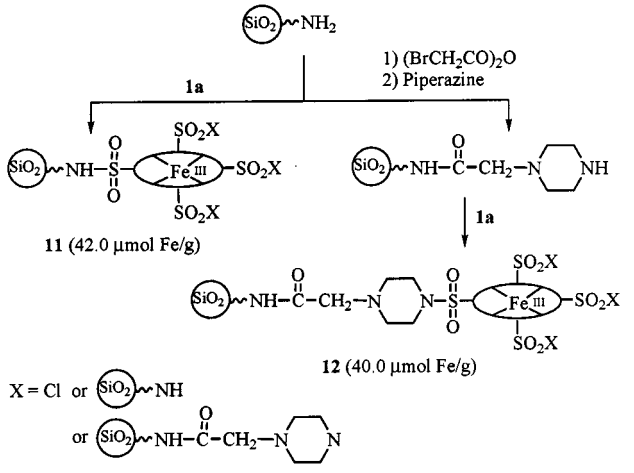

Scheme 5. Immobilization of the metallophthalocyanines **1** onto silica

tions, compared to the iron complex **11** grafted onto silica modified with primary amine linkers. Indeed, full conversion of TCP was achieved within 45 min with **4b** (Run 2, Table 1), while it took 1 h for the supported catalyst **11** to oxidize only 52% of TCP (Run 3).

The oxidative properties of the metallophthalocyanines immobilized onto the organic polymers **2** and **3** were also investigated. First, we checked that the TCP substrate was not oxidized by H_2O_2 and the support material alone, in the absence of metallophthalocyanine catalyst (Run 1). In addition, this control experiment confirmed that there is no physisorption of the substrate onto the surface of the support. In the presence of phosphate buffer, but without any organic co-solvent, the supported iron catalysts **9** and **10a** with H_2O_2 were able to degrade 85% (Run 4) and 62% (Run 10) of the TCP, respectively, within 1 h. The presence of an organic co-solvent such as ethanol or acetone, which allowed a better solubilization of the poorly water-soluble TCP substrate, improved the degradation process up to full conversion of TCP within 1 h (Runs 5, 6, 11, and 12). Also, with acetone as co-solvent, the degradation of TCP was complete after 20 min with **9** and after 25 min with **10a**. The turnover rates (based on the first 30 min of the reaction) of these two supported catalysts are 150 and 120 cycles per hour, respectively. These results are of great interest, since the catalytic activities of these new supported metallophthalocyanines are comparable to those observed under homogeneous conditions.

The recycling of **10a**, a key point for supported catalysts, was then investigated. After a first catalytic oxidation, a second portion of pollutant and oxidant was added to the reaction mixture. In this second run, 91% of TCP was converted in 15 min (Run 13) indicating that the catalytic activity of the metallophthalocyanine remained intact.

For comparison, the catalytic activity of the supported cobalt complex **10b** was also checked (Runs 14−17). The full conversion of TCP could be achieved in 30 min with 4 mol-% of **10b** and with 20% of acetone in the reaction mixture (Run 17). Although the results obtained with this supported catalyst are less impressive than with the corresponding iron(III) complex, they are also of potential commercial interest. Indeed, the (chlorosulfonyl)phthalocyanine **1b** used for the immobilization on the organic copolymer was synthesized from the readily available sulfo precursor

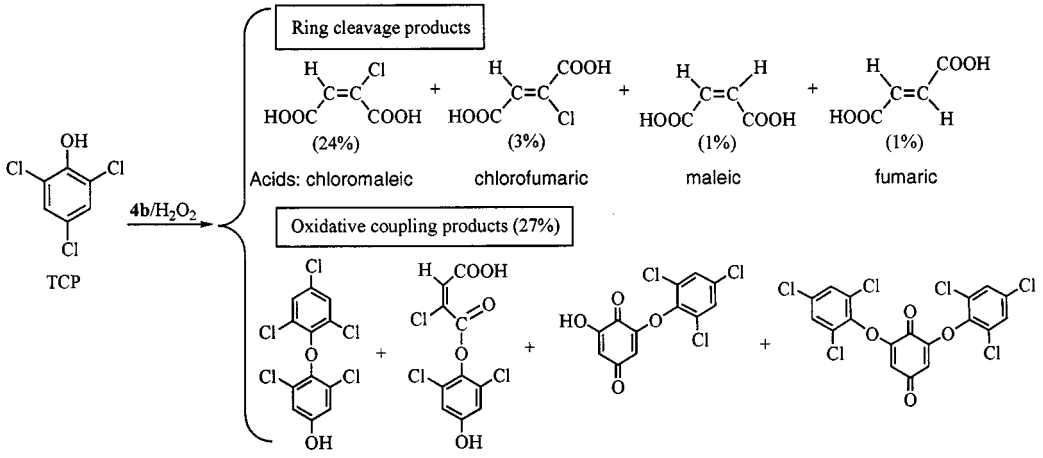

Scheme 6. Degradation products of 2,4,6-trichlorophenol by the catalytic metallophthalocyanine/H_2O_2 systems

Table 1. Oxidation of 2,4,6-trichlorophenol (TCP) catalyzed by the metallophthalocyanines/H_2O_2 systems

Run	Catalyst	Cat./TCP [mol-%]	Solvent	TCP conversion (%) 1:2 h	1 h	2 h	T.O.[a] [h^{-1}]
1	–	–	PB[b]	7	–	–	–
2	**4b**	2	PB/acetone	94	100		94
3	**11**	2	PB/acetone	39	52	69	39
4	**9**	2	PB	74	85	88	74
5	**9**	2	PB/EtOH	84	100		84
6	**9**	2	PB/acetone	100			> 100
7	**9**	2	H_2O/NaOH	43	55	56	43
8	**9**	3	H_2O/NaOH	53	65	79	35
9[c]	**9**	3	H_2O/NaOH	71	89	93	47
10	**10a**	2	PB	–	62	67	< 62
11	**10a**	2	PB/EtOH	99	100		99
12	**10a**	2	PB/acetone	100			> 100
13	**10a**	2	PB/acetone	100			> 100
				91[d] (15 min)			> 100
14	**10b**	2	PB	38	46	44	38
15	**10b**	4	PB	47	57	58	23.5
16	**10b**	4	PB/EtOH	67	94	100	33.5
17	**10b**	4	PB/acetone	100			50
18	**12**	2	PB/acetone	91	100		91
19	**12**	2	H_2O/NaOH	9	11	12	9

[a] T.O.: Turn over numbers calculated after 30 min of reaction. – [b] PB: Phosphate buffer (pH = 7). – [c] Sequential addition of H_2O_2: 4 × 1 aliquot every 10 min. – [d] Recycling of the supported catalyst: after 15 min of a first oxidation reaction, new portions of TCP and H_2O_2 were added in the same batch.

4c, which is widely used in the industrial mercaptan oxidation process (Merox) for the treatment of petroleum distillates.[3]

The covalent attachment of the metallophthalocyanines **1** onto the organic copolymers **2** and **3** proved to be suitable for the preparation of active systems for the catalytic oxidative degradation of recalcitrant pollutants such as 2,4,6-trichlorophenol. The different properties (flexibility, swelling, etc.) of these carriers make them excellent candidates for catalytic supports.

It should be noted that the behavior of **9** and **10a** are almost identical, with **9** being only slightly more efficient than the corresponding piperazine-containing polymer. These organic copolymers **2** and **3** are relatively flexible, consequently the role of an additional spacer to increase the distance between the catalyst and the support is rather limited. In contrast, with a more rigid carrier material like silica, this modification could notably change the catalytic properties of a metallophthalocyanine complex covalently linked to silica. In order to verify this hypothesis, we determined the oxidative properties of the silica-supported iron complex **12**, which features the same piperazine spacer as in **10a**.

Influence of the Piperazine Spacer

In order to determine the influence of the spacer, we compared the oxidative properties of **12** (containing 40.0 μmol of iron per gram of resin) to those of **11** with the same catalyst loading (42.0 μmol/g). In the oxidative degradation of TCP with H_2O_2, the catalytic activity of the

supported catalyst containing the piperazine spacer was 3 times higher after 30 min (Runs 3 and 18, Table 1). In addition, for the first time, it was possible to achieve a full conversion of TCP in 1 h with a metallophthalocyanine grafted onto modified silica (Run 18). *This result strongly indicates that when anchoring a large catalyst molecule like a metallophthalocyanine (a macrocyclic molecule with a diameter of ca. 25 Å) onto a rigid support such as silica, it is necessary to introduce a long spacer between the catalyst and the surface of the support.* Without this modification, the oxidative activities of the corresponding supported catalysts are reduced. These results provide further motivation to use the flexible organic copolymers **2** and **3** as supports in catalytic oxidations.

Catalytic Oxidation of TCP in Pure Aqueous Medium (without Buffer)

The experiments described above for the degradation of TCP were carried out in phosphate buffer (pH = 7) medium. Under homogeneous conditions it has been shown that this pH value is optimal for a good catalytic activity. This can be explained by the fact that the first step of TCP degradation is a one-electron oxidation of the phenolate anion [7a] (pK_a value of TCP: 6.2).[21] However, since the final aim of this work is the decontamination of industrial waste waters, the presence of phosphate ions is ecologically not appropriate.

With this in mind, we tried to degrade TCP in a pure aqueous medium, using the most active polyacrylamide- and silica-supported catalysts **9** and **12**. The pH value of the reaction mixture was adjusted to 7 with sodium hydroxide in order to have only the more oxidizable phenolate form of the substrate in solution. With a 2 mol-% ratio catalyst/TCP, the supported catalyst **9** and H_2O_2 are able to oxidize 55% of the starting TCP after 1 h (Run 7, Table 1), whereas, under the same conditions, the iron-phthalocyanine grafted onto the modified piperazine-silica **12** converted only 11% of TCP (Run 19). Since the tetrasulfophthalocyanine **4b** is totally inactive in a purely aqueous medium under homogeneous conditions,[22] these results were encouraging. The ratio catalyst/substrate was raised to 3 mol-% for **9** and the conversion of TCP increased to 65% after 1 h and to 79% after 2 h (Run 8). With a sequential addition of the oxidant in 4 aliquots, every 10 min, a quasi-complete degradation of TCP can be achieved in a purely aqueous medium within 2 h (Run 9). The sequential addition of H_2O_2 disfavors its consumption by a disproportionation reaction (leading to water and molecular oxygen) induced by the catalase-like reactivity of the metallophthalocyanine complex.[7a]

Catalytic Degradation of TCP with $KHSO_5$ as Oxidant

Potassium monopersulfate ($KHSO_5$) is an oxygen atom donor that has been shown to be highly efficient for the activation of metallophthalocyanines and metalloporphyrins.[7,19] It is commercially available as the triple salt $2KHSO_5{\cdot}KHSO_4{\cdot}K_2SO_4$, and is a classic reagent in Baeyer−Villiger oxidations.[23] An initial control experiment was made to ensure that TCP was not oxidized by $KHSO_5$ without catalyst (Run 1, Table 2) and that there was no leaching of the iron-phthalocyanine under these new oxidation conditions [8 mg of **9** suspended in 8 mL of a phosphate buffer (pH =7) with 5 equiv. of $KHSO_5$].

In a purely aqueous medium, the degradation of TCP by the catalytic **9** (2 mol-%)/$KHSO_5$ system is very fast (79% in 5 min, Run 2, Table 2). However, the conversion of TCP reached a plateau after 10 min and a bleaching of the supported catalyst was observed. The pH measurement of the solution gave a value of 2.5, which was attributed to the intrinsic acidity of $KHSO_5$. At such a low pH value, the supported catalyst is probably decomposed. In contrast, when the reaction mixture was buffered at pH = 7 using a phosphate buffer, the conversion of TCP was complete in 5 min (Run 3). Under these conditions, the turnover rate of this supported iron-(sulfonamido)phthalocyanine was 10 catalytic cycles per minute (based on the first five minutes of the reaction). With the catalytic **9**/$KHSO_5$ system, the turnover rate can be increased up to 16 cycles/min using 1 mol-% of catalyst (Run 4). In contrast, with only 0.1 mol-% of catalyst, the degradation of TCP was incomplete after 1 h (Run 5).

We also checked the possibility of recycling this supported catalyst under these strong oxidation conditions. After a first catalytic reaction, new portions of substrate and oxidant were added every 5 min (Run 6). The results were very surprising: the catalytic system was still efficient after the addition of 3 new portions of pollutant and had retained its initial catalytic activity.

We have established that the activation of metallophthalocyanines anchored onto **2** and **3** with either hydrogen peroxide or potassium monopersulfate as oxidants is an efficient method for the oxidative degradation of a notable pollutant such as TCP. Moreover, NMR studies carried out after the catalytic oxidation of TCP with H_2O_2 (as well as with $KHSO_5$) have shown the formation of ring cleavage products, which are biodegradable. For example, for the H_2O_2 oxidation of TCP catalyzed by **10a**, we observed the formation of 12% of chloromaleic acid, 3% of chlorofumaric acid, 4% of maleic acid, 3% of fumaric acid and 6% of coupling products. Thus, these catalytic systems might be useful for the oxidative treatment of industrial waste waters. However, these bio-inspired supported oxidative catalysts might also be useful as bleaching agents in a new generation of washing powders, able to operate at room temperature.

H_2O_2 Oxidative Degradation of 3,5-Di-*tert*-butylcatechol Catalyzed by 9

Catechol and its derivatives are often used as substrates for the evaluation of bleaching agents since they are considered good models of stains (catechols are the most common structure encountered in condensed tannins, which are among the main stains).[24] Under homogeneous conditions, the iron-sulfophthalocyanine **4b** in conjunction with an oxidant was able to degrade several catechols such as catechol itself, as well as its 3-methyl, 3-methoxy, 3,5-di-

Table 2. $KHSO_5$ oxidation of 2,4,6-trichlorophenol (TCP) catalyzed by **9**

Run	Cat./TCP [mol-%]	Solvent	TCP conversion (%) 5 min	10 min	15 min	30 min	60 min	T.O.[a] [min^{-1}]
1	–	PB[b]	–	–	–	0	–	–
2	2	H_2O[c]	79	88	89	92	92	7.9
3	2	PB	100					10
4	1	PB	81	96				16.2
5	0.1	PB	36	45	53	66	72	72
6[d]	2	PB	61					6.1
			97					9.7
			94					9.4
			87					8.7

[a] T.O.: Turn over numbers calculated after 5 min. – [b] PB: Phosphate buffer (pH = 7). – [c] Pure aqueous media (pH = 2.5). – [d] Recycling of the supported catalyst: after 5 min of a first oxidation reaction with 3.75 equiv. of $KHSO_5$, new portions of TCP and $KHSO_5$ were added every 5 min in the same batch.

tert-butyl, and tetrachloro derivatives.[25] The degradation products from 3,5-di-*tert*-butylcatechol (DTBC) were identified by ^1H NMR as 3,5-di-*tert*-butyl-1,2-benzoquinone, 3,5-di-*tert*-butylmuconic anhydride, and 3,5-di-*tert*-butyl-5-(carboxyhydroxymethyl)-2-furanone (Scheme 7).

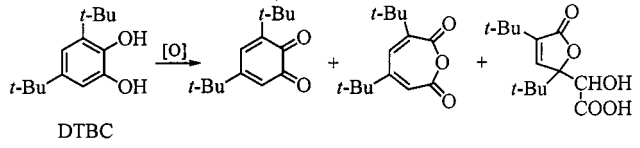

Scheme 7. Degradation products of 3,5-di-*tert*-butylcatechol catalyzed by the iron-tetrasulfophthalocyanine **4b**

When H_2O_2 was used as oxidant, the noncatalyzed reaction with DTBC was negligible (Run 1, Table 3). The oxidative properties of the **9**/H_2O_2 system were used for the catalytic degradation of DTBC. We first noted that the substrate was not physisorbed on the surface of the support. Three reaction media were then checked for the degradation of DTBC at room temperature: borate buffer (pH = 9)/CH_3CN (50:50, v/v), phosphate buffer (pH = 7)/CH_3CN (50:50, v/v) and H_2O/CH_3CN (50:50, v/v). The presence of acetonitrile is necessary as organic co-solvent for a good solubility of DTBC. With 2 mol-% of catalyst, the results for the degradation of DTBC are quite similar in the three different reaction media (Runs 2–4, Table 3). The most interesting results were obtained without buffering the reaction solution (which can be considered as an advantage), and as a result, attempts were made to optimize this reaction. By increasing the catalyst/substrate ratio to 3 mol-%, full conversion of DTBC was achieved in 1 h (Run 5, Table 3). ^1H NMR studies carried out after the catalytic oxidation of DTBC in a water/acetonitrile mixture revealed the formation of 3,5-di-*tert*-butyl-1,2-benzoquinone (50% yield, no other products could be detected).

The recycling capacity of **9** was also studied in the degradation of DTBC. In this case, this supported catalyst also showed excellent behavior without loss of its oxidative properties, as expected for an efficient long-life catalyst. In fact, after having converted 82% of DTBC in a first catalytic oxidation, the same system was still able to degrade 4 new portions of substrate (Run 6, Table 3). However, for an application in washing powders, it would be accurate and realistic to work with a water-soluble catechol such as 3,4-dihydroxybenzoic acid, current work is underway in this direction.

Table 3. H_2O_2 oxidation of 3,5-di-*tert*-butylcatechol (DTBC) catalyzed by **9**

Run	Solvent	pH	Cat./DTBC [mol-%]	TCP conversion (%) 10 min	20 min	30 min	45 min	60 min	T.O.[a] [h^{-1}]
1[b]	H_2O/CH_3CN	5.5	–	–	–	1	–	2	–
2	BB/CH_3CN[c]	9	2	23	36	61	68	78	61
3	PB/CH_3CN[d]	7	2	41	49	55	60	62	55
4	H_2O/CH_3CN	5.5	2	29	45	61	71	81	61
5	H_2O/CH_3CN	5.5	3	39	71	84	90	97	56
6[e]	H_2O/CH_3CN	5.5	3			82			55
						74			49
						70			47
						55	71	78	37

[a] T.O.: Turn over numbers calculated after 30 min. – [b] Control reaction without catalyst. – [c] BB: Borate buffer (pH = 9). – [d] PB: Phosphate buffer (pH = 7). – [e] Recycling of the supported catalyst: after 30 min of a first oxidation reaction, new portions of TCP and $KHSO_5$ were added every 30 min in the same batch.

Conclusion

The covalent anchoring of metallophthalocyanines onto the acrylic copolymers Met-Expansin-NH_2® (**2**) and Met-Expansin-Piperazine (**3**) allowed the fixation of these macrocyclic complexes in a monomolecular dispersion, resistant to oxidative conditions. These bio-inspired supported catalysts, when activated with H_2O_2 (the "green" oxidant) or $KHSO_5$ were able to fully degrade a recalcitrant pollutant such as 2,4,6-trichlorophenol. The organic carriers proved flexible enough as to eliminate the need to introduce an additional piperazine spacer between catalyst and support as observed with modified silica. Furthermore, it has been possible to use these polyacrylamide-supported catalysts in a purely aqueous medium, whilst retaining a good catalytic activity of the metallophthalocyanine complex.

These new efficient supported catalysts could easily be used for the oxidative treatment of waste water or industrial effluents. Another possible field of application could also be related to the development of bleaching agents operating at room temperature, since such catalytic systems are able to oxidize a tannin model such as 3,5-di-*tert*-butylcatechol.

Experimental Section

General Remarks: The conversions of 2,4,6-trichlorophenol (TCP) and 3,5-di-*tert*-butylcatechol (DTBC) were monitored by HPLC (Waters) equipped with a μ-Bondapak C18 column using a methanol/ammonium acetate buffer mixture [7:3, v/v; 50 mM acetate buffer (pH = 5) acidified to pH = 4 with acetic acid] with detection at 220 nm for TCP and a methanol/water mixture (8:2, v/v) with detection at 226 nm for DTBC. − The UV/Vis absorption spectra were recorded with a Hewlett Packard 8452A spectrophotometer. Met-Expansin-NH_2® (**2**) (0.56 mmol-equiv. NH_2/g) and Met-Expansin-Piperazine (**3**) (0.50 mmol-equiv. NH/g) copolymers were a gift from EXPANSIA. The 3-aminopropyl-functionalized silica gel (0.90 mmol-equiv. NH_2/g) was purchased from Aldrich.[26] The reactants bromoacetic acid, dicyclohexylcarbodiimide and piperazine are commercially available and were used without further purification. 2,4,6-Trichlorophenol was obtained from Janssen and 3,5-di-*tert*-butylcatechol from Aldrich. Hydrogen peroxide was supplied from Acros as a 35 wt-% aqueous solution. Curox® ($2KHSO_5 \cdot KHSO_4 \cdot K_2SO_4$) was a gift from Peroxid Chemie GmbH. All solvents used were of analytical grade and milliQ-water was always used to prepare aqueous solutions. Iron(III) and cobalt(II) tetrasulfophthalocyanines (**4b** and **4c**) were prepared according to previously published modifications[7a] of the method of Weber and Busch.[27]

Attachment of the Piperazine Linker on Silica: A solution of dicyclohexylcarbodiimide (0.56 g, 2.70 mmol) in CH_2Cl_2 (10 mL) was added dropwise at 0 °C to a solution of bromoacetic acid (0.75 g, 5.40 mmol) in CH_2Cl_2 (10 mL). The solution was allowed to warm to room temperature and stirred for 1 h. The dicyclohexylurea precipitate that formed was removed by filtration, the solid was washed three times with CH_2Cl_2 (3 × 20 mL), and the washings were combined. The bromoacetic anhydride solution thus obtained was directly added to the commercially available silica containing primary amine linkers (1.00 g, 0.90 mmol of NH_2 functions) and stirred for 12 h at room temperature. The modified silica was filtered, washed three times with CH_2Cl_2 (3 × 20 mL), and dried for 12 h at 50 °C. A suspension of the carrier containing CH_2Br end groups in DMF (5 mL) was added to a solution of piperazine (0.77 g, 9.00 mmol) in DMF (5 mL) and stirred 24 h at room temperature. The modified support thus obtained was isolated by filtration, washed three times with water (3 × 20 mL), ethanol (3 × 20 mL) and acetone (3 × 20 mL) prior to drying at 50 °C for 12 h. Yield: 0.78 g (78%).

General Procedure for the Immobilization of the Metallophthalocyanines: In a typical experiment, a suspension of the metallo(chlorosulfonyl)phthalocyanine **1a** or **1b** in pyridine (20 mL) and the carrier was heated at reflux for 24 h. The mixture was filtered and the solid obtained washed three times with a dimethylformamide/water mixture (80:20, v/v) (3 × 20 mL) and then ether (3 × 20 mL) prior to drying at 53 °C for 12 h. The supported metallo(sulfonamido)phthalocyanines were obtained as green powders. The contents of catalyst fixed onto the carriers were determined indirectly by calculating the amount of unchanged **1** using UV/Vis spectroscopy. The quantities used and yields obtained are given in Table 4.

Table 4. Quantities and yields for the preparation of the supported metallophthalocyanines

Product	**1**		Support		Loading	Yield
	mg	μmol	g	μmol (NH)	[μmol/g]	(%)
9	25.6	22.8	1.00	560	20.0	88
10a	50.0	44.5	1.00	500	26.5	60
10b	25.0	22.2	0.50	280	42.0	100
11	32.6	29.0	0.50	450	42.0	100
12	20.3	18.0	0.40	360	40.0	89

General Procedure for Catalytic TCP Degradation: In a typical experiment, for a catalyst/TCP ratio of 2 mol-%, 0.16 μmol of Fe^{III} or Co^{II} of the supported catalyst [i.e., 8.0 mg of **9** (loading 20.0 μmol/g), 6.0 mg of **10a** (loading 26.5 μmol/g), 3.8 mg of **10b** (loading 42.0 μmol/g), 3.8 mg of **11** (loading 42.0 μmol/g), 4.0 mg of **12** (loading 40.0 μmol/g)] and 40 μL of a 1.2 M aqueous solution of hydrogen peroxide (48.0 μmol) were added to a 1 mM TCP solution (8 mL, 8.0 μmol) in phosphate buffer 50 mM (pH = 7). The reaction mixture was stirred at room temperature and analyzed by HPLC. For the experiments carried out in the presence of an organic co-solvent, a 1 mM TCP solution was prepared in a mixture of 50 mM phosphate buffer/ethanol or acetone (80:20, v/v). Run 7 in Table 1 was carried out with a 1 mM TCP aqueous solution adjusted to pH = 7 with NaOH (final concentration of NaOH: 1 mM). When $KHSO_5$ was used as oxidant, a solution of Curox® (12.3 mg, 40.0 μmol) in water (100 μL) was added to the reaction mixture.

^{1}H NMR Analysis of the Degradation Products of TCP by the Catalytic 10a/H_2O_2 System: The supported catalyst **10a** (loading 26.5 μmol/g) (60.0 mg, 1.6 μmol) and 400 μL of a 1.2 M aqueous solution of hydrogen peroxide (480.0 μmol) were added to a 1 mM TCP solution (80 mL, 80.0 μmol) in a 50 mM phosphate buffer (pH = 7)/ethanol (80:20, v/v) mixture. The reaction mixture was stirred for 1 h at room temperature. After filtration of the supported catalyst **10a** and several washings with acetonitrile, the reaction mixture was dried under vacuum. Then 7 mL of 1 M HCl, saturated with NaCl, was added to the dry residue and the organic products were extracted with diethyl ether (3 × 60 mL). After concentration of the ether extracts, the solid residue was dissolved in deuterated dimethyl sulfoxide ([D_6]DMSO) for NMR analysis. Then 5 μL of $CHCl_3$ (62.0 μmol) was added as an internal standard to quantify the oxidation products. − ^{1}H NMR ([D_6]DMSO): δ =

6.39 (s, 2 H, maleic acid, 4%), 6.69 (s, 1 H, chloromaleic acid, 12%), 6.74 (s, 2 H, fumaric acid, 3%), 7.30 (s, 1 H, chlorofumaric acid, 3%), 7.80−8.10 (br, 2 H, coupling products, 6%). − It should be noted that these yields differ from one experiment to another, depending on the time the oxidation reaction was stopped.

General Procedure for Catalytic DTBC Degradation: In a typical experiment, for a catalyst/TCP ratio of 2 mol-%, 8.0 mg of the supported catalyst **9** (loading 20.0 μmol/g) (0.16 μmol) and 40 μL of a 1.2 M aqueous solution of hydrogen peroxide (48.0 μmol) were added to a 1 mM DTBC solution (8 mL, 8.0 μmol) in a 50 mM borate buffer (pH = 9)/acetonitrile (1:1, v/v) mixture or in 50 mM phosphate buffer (pH = 7)/acetonitrile (1:1, v/v) or in water/acetonitrile (1:1, v/v). The reaction mixture was stirred at room temperature and analyzed by HPLC.

^{1}H NMR Analysis of the Degradation Products of DTBC by the Catalytic 9/H_2O_2 System: The supported catalyst **9** (loading 20.0 μmol/g) (80.0 mg, 1.5 μmol) and 250 μL of a 1.2 M aqueous solution of hydrogen peroxide (300.0 μmol) were added to a 6.25 mM DTBC solution (8 mL, 50.0 μmol) in a water/acetonitrile (1:1, v/v) mixture. The reaction mixture was stirred for 45 min at room temperature. After filtration of the supported catalyst and several washings with acetonitrile, the reaction mixture was dried under vacuum. Then 7 mL of 1 M HCl, saturated with NaCl, was added to the dry residue and the organic products were extracted with diethyl ether (3 × 60 mL). After concentration of the ether extracts, the solid residue was dissolved in deuterated dimethyl sulfoxide ([D_6]DMSO) for NMR analysis. Then 2 μL of $CHCl_3$ (25.0 μmol) was added as an internal standard to quantify the oxidation products. − ^{1}H NMR ([D_6]DMSO): δ = 1.30 (s, 9 H, *t*Bu), 1.33 (s, 9 H, *t*Bu), 6.25 (d, *J* = 2.2 Hz, 1 H, HC=), 7.08 (d, *J* = 2.2 Hz, 1 H, HC=). − ^{13}C{^{1}H} NMR ([D_6]DMSO): δ = 27.7 (s, CH_3C), 29.1 (s, CH_3C), 35.1 (s, CH_3*C*), 35.8 (s, CH_3*C*), 121.9 (s, HC=), 133.5 (s, HC=), 149.0 (s, C=), 162.6 (s, C=), 180.0 (s, C=O), 180.6 (s, C=O).

Recycling of the Supported Catalysts in the Oxidative Degradation of TCP and DTBC

TCP Degradation by 10a and H_2O_2: The supported metallophthalocyanine **10a** [6.0 mg, loading 26.5 μmol/g (0.16 μmol of iron, 2 mol-%)] and 40 μL of a 1.2 M aqueous solution of H_2O_2 (48.0 μmol) were added to a 1 mM TCP solution (8 mL, 8.0 μmol) in a 50 mM phosphate buffer (pH = 7)/acetone (80:20, v/v) mixture. The oxidation reaction was stirred for 30 min at room temperature. A 0.16 M TCP solution (50 μL, 8.0 μmol) in acetone and 40 μL of a 1.2 M aqueous solution of H_2O_2 (48.0 μmol) were then added to the reaction mixture. The TCP conversion was monitored by HPLC analysis.

TCP Degradation by 9 and $KHSO_5$: The supported metallophthalocyanine **9** [(8.0 mg, loading 20.0 μmol/g (0.16 μmol of iron, 2 mol-%)] and 50 μL of a 0.8 M Curox® solution (40.0 μmol) in water were added to a 1 mM TCP solution (8 mL, 8.0 μmol) in 50 mM phosphate buffer (pH = 7). The oxidation reaction mixture was stirred for 5 min at room temperature. A 0.8 M TCP solution (10 μL, 8.0 μmol) in acetonitrile and 50 μL of a 0.8 M Curox® solution (40.0 μmol) were then added to the reaction mixture every 5 min. The TCP conversion was monitored by HPLC analysis.

DTBC Degradation by 9 and H_2O_2: The supported metallophthalocyanine **9** [(12.0 mg, loading 20.0 μmol/g (0.24 μmol of iron, 3 mol-%)] and 40 μL of a 1.2 M aqueous solution of H_2O_2 (48.0 μmol) were added to a 1 mM DTBC solution (8 mL, 8.0 μmol) in a water/acetonitrile (1:1, v/v) mixture. The oxidation reaction mixture was stirred for 30 min at room temperature. A 0.4 M DTBC solution (20 μL, 8.0 μmol) in acetonitrile and 40 μL of a 1.2 M aqueous solution of H_2O_2 (48.0 μmol) were then added to the reaction mixture every 30 min. The DTBC conversion was monitored by HPLC analysis.

Acknowledgments

The financial support of CNRS and Expansia is gratefully acknowledged.

[1] [1a] *Phthalocyanines: Properties and Applications* (Eds.: C. C. Leznoff, A. B. P. Lever), VCH Publishers, Inc., New York, **1989−1996**, vol. 1−4. − [1b] M. Hanack, M. Lang, *Chemtracts: Inorg. Chem.* **1996**, *8*, 45−79.
[2] [2a] R. Gerdes, D. Wöhrle, W. Spiller, G. Schneider, G. Schnurpfeil, G. Schulz-Ekloff, *J. Photochem. Photobiol.* **1997**, *111*, 65−74. − [2b] M. J. Abrams, *Platinum Met. Rev.* **1995**, *39*, 14−18. − [2c]J. E. van Lier in *Photodynamic Therapy of Neoplastic Diseases* (Ed.: D. Kessel), CRC Press, Boca Raton, FL, **1990**, vol. I.
[3] [3a] M. Kimura, Y. Yamagushi, T. Koyama, K. Hanabusa, H. Shirai, *J. Porphyrins Phthalocyanines* **1997**, *1*, 309−313. − [3b] V. Iliev, A. Ileva, *J. Mol. Catal. A* **1995**, *103*, 147−153. − [3c] B. Basu, S. Satapathy, A. K. Bhatnagar, *Catal. Rev. Sci. Eng.* **1993**, *35*, 571−609. − [3d] J. R. Salazar in *Handbook of Petroleum Processes* (Ed.: R. A. Mayers), Mc Raw Hill, New York, **1986**, part 9.
[4] J. Premkumar, R. Ramaraj, *Chem. Commun.* **1997**, 343−344.
[5] [5a] T. Kudo, M. Kimura, K. Hanabusa, H. Shirai, T. Sakaguchi, *J. Porphyrins Phthalocyanines* **1999**, *3*, 65−69. − [5b] H. Engelkamp, S. Middelbeek, R. J. M. Nolte, *Science* **1999**, *284*, 785−788.
[6] [6a] M. E. Boyle, J. D. Adkins, A. W. Snow, R. F. Cozzens, R. F. Brady Jr., *J. Appl. Polym. Sci.* **1995**, *57*, 77. − [6b] J. S. Shirk, J. R. Lindle, F. J. Bartoli, Z. H. Kafafi, A. W. Snow, M. E. Boyle, *Int. J. Nonlin. Opt. Phys.* **1992**, *1*, 699. − [6c] T. J. Marks, *Angew. Chem. Int. Ed. Engl.* **1990**, *29*, 857−879.
[7] [7a] A. Hadasch, A. Sorokin, A. Rabion, B. Meunier, *New J. Chem.* **1998**, *22*, 45−51. − [7b] A. Sorokin, B. Meunier, *Eur. J. Inorg. Chem.* **1998**, 1269−1281. − [7c] A. Sorokin, L. Fraisse, A. Rabion, B. Meunier, *J. Mol. Catal. A* **1997**, *117*, 103−114. − [7d] B. Meunier, A. Sorokin, *Acc. Chem. Res.* **1997**, *30*, 470−476. − [7e] A. Sorokin, S. De Suzzoni-Dezard, D. Poullain, J.-P. Noël, B. Meunier, *J. Am. Chem. Soc.* **1996**, *118*, 7410−7411. − [7f] A. Sorokin, B. Meunier, *Chem. Eur. J.* **1996**, *2*, 1308−1317. − [7g] A. Sorokin, J.-L. Séris, B. Meunier, *Science* **1995**, *268*, 1163−1166.
[8] V. N. Nemykin, V. YA. Chernii, S. V. Volkov, N. I. Bundina, O. L. Kaliya, V. D. Li, E. A. Lukyanets, *J. Porphyrins Phthalocyanines* **1999**, *3*, 87−98.
[9] G. Schneider, D. Wöhrle, W. Spiller, J. Stark, G. Schulz-Ekloff, *Photochem. Photobiol.* **1994**, *60*, 333−342.
[10] [10a] R. C. Sosa, R. F. Parton, P. E. Neys, O. Lardinois, P. A. Jacobs, P. G. Rouxhet, *J. Mol. Catal. A* **1996**, *110*, 141−151. − [10b] J. H. Zagal, *Coord. Chem. Rev.* **1992**, *119*, 89−136 and references therein. − [10c] D. Wöhrle, T. Buck, G. Schneider, G. Schulz-Ekloff, H. Fischer, *J. Inorg. Organomet. Polym.* **1991**, *1*, 115−130.
[11] [11a] W. T. Ford, H. El-Hamshary, I. Stefanithis, H. O. Spivey, M. Hassanein, A. Selim, *New J. Chem.* **1996**, *20*, 549−557. − [11b] E. T. W. M. Schipper, R. P. M. Pinckaers, P. Piet, A. L. German, *Macromolecules* **1995**, *28*, 2194−2200. − [11c] X. Zhang, M. Gao, X. Kong, Y. Sun, J. Shen, *J. Chem. Soc., Chem. Commun.* **1994**, 1055−1056.
[12] [12a] A. Hirth, A. K. Sobbi, D. Wöhrle, *J. Porphyrins Phthalocyanines* **1997**, *1*, 275−279. − [12b] L. T. Kubota, Y. Gushiken, J. Perez, A. A. Tanaka, *Langmuir* **1995**, *11*, 1009−1013. − [12c] Y. L. Zub, A. B. Pecheny, A. A. Chuiko, T. L. Stuchinskaya, N. N. Kundo, *Catal. Today* **1993**, *17*, 31−40.

[13] [13a] R. F. Parton, G. J. Peere, P. E. Neys, P. A. Jacobs, R. Claessens, G. V. Baron, *J. Mol. Catal. A* **1996**, *113*, 445−454. − [13b] K. J. Balkus Jr., M. Eissa, R. Levado, *J. Am. Chem. Soc.* **1995**, *117*, 10753−10754. − [13c] F. Bedioui, *Coord. Chem. Rev.* **1995**, *144*, 39−68. − [13d] R. F. Parton, I. F. J. Vankelecom, M. J. A. Casselman, C. P. Bezoukhanova, J. B. Uytterhoeven, P. A. Jacobs, *Nature* **1994**, *370*, 541−544.

[14] [14a] V. Iliev, A. Ileva, L. Bilyarska, *J. Mol. Catal. A* **1997**, *126*, 99−108. − [14b] K. A. Carrado, J. E. Forman, R. E. Botto, R. E. Winans, *Chem. Mater.* **1993**, *5*, 472−478. − [14c] M. Chiwe, T. J. Pinnavaia, *J. Chem. Soc., Chem. Commun.* **1993**, 278−280.

[15] L. Canali, D. C. Sherrington, *Chem. Soc. Rev.* **1999**, *28*, 85−93.

[16] M. Sanchez, A. Hadasch, A. Rabion, B. Meunier, *C. R. Acad. Sci. Paris*, **1999**, *IIC*, 241−250.

[17] L. Canali, D. C. Sherrington, *Chem. Soc. Rev.* **1999**, *28*, 85−93.

[18] [18a] V. B. Huynh, H. M. Chang, T. W. Joyce, T. K. Kirk, *Tappi* **1985**, *68*, 98−102. − [18b] N. Pal, G. Lewandowski, P. M. Armenante, *Biotechnol. Bioeng.* **1995**, *46*, 599−609.

[19] [19a]] G. Labat, J.-L. Séris, B. Meunier, *Angew. Chem. Int. Ed. Engl.* **1990**, *29*, 1471−1473. − [19b] B. Meunier, *Chem. Rev.* **1992**, *92*, 1411−1456.

[20] A. Hadasch, A. Sorokin, A. Rabion, L. Fraisse, B. Meunier, *Bull. Soc. Chim. Fr.* **1997**, *134*, 1025−1032.

[21] P. G. Tratnyek, J. Holgné, *Environ. Sci. Technol.* **1991**, *25*, 1596−1604.

[22] A. Hadasch, Doctoral Thesis, Univ. of Toulouse, **1999**.

[23] M. Renz, B. Meunier, *Eur. J. Org. Chem.* **1999**, 737−750.

[24] R. Hage, J. E. Iburg, J. Kershner, J. H. Koek, E. L. M. Lempers, R. J. Martens, U. S. Racherla, S. W. Russel, T. Swarthoff, M. R. P. van der Vliet, J. B. Wamaar, L. van der Wolf, B. Krijnen, *Nature* **1994**, *369*, 637−639.

[25] A. Sorokin, L. Fraisse, A. Rabion, B. Meunier, *J. Mol. Catal.* **1997**, *117*, 103−114.

[26] The 3-aminopropyl-functionnalized silica gel can also be easily prepared from silica and triethoxy- or trimethoxysilane: [26a] E. Angeletti, C. Canepa, G. Martinetti, P. Venturello, *J. Chem. Soc., Perkin Trans. 1* **1989**, 105−107. − [26b] F. Gasparrini, M. Giovannoli, D. Misiti, G. Palmieri, *Tetrahedron* **1984**, *40*, 1491−1500.

[27] M. J. H. Weber, D. H. Busch, *Inorg. Chem.* **1965**, *4*, 469−471.

Received December 4, 2000
[I00460]

Synthesis, Structure and Reactivity of a Zirconocene Dichloride with $(Me_3Si)_2NSiMe_2$ Side-Chains

Alexander Rau,*[a] Hans-Peter Dornik,[a] Helmut Paulus,[b] and Gerhard Luft[a]

Keywords: Metallocenes / Zirconium / N ligands / Structure elucidation / Cyclopentadienyl ligands

The new zirconocene $[(\eta^5\text{-}C_5H_4SiMe_2N(SiMe_3)_2]_2ZrCl_2$ (**1**) has been prepared in a convenient three-step synthesis. A crystal structure determination of **1** shows two molecules in the unit cell, one in which the $(Me_3Si)_2NSiMe_2$ groups are accommodated in a nearly synperiplanar conformation directly above and below the $ZrCl_2$ group, and one in which these groups exhibit a synclinal conformation. The reaction of **1** with a mixture of $SOCl_2/SO_2Cl_2$ leads to the formation of $[(\eta^5\text{-}C_5H_4SiMe_2Cl]_2ZrCl_2$ (**2**).

Introduction

Group 4 metallocene complexes bearing side-chains that can modify the steric and electronic properties of the metal centre have attracted growing interest in recent years due to their potential catalytic applications. The influence of alkyl groups attached to the cyclopentadienyl (Cp) unit on the structure-reactivity relation of metallocene catalysts has been intensively studied.[1−3] Metallocenes with side-chains containing NR_2, PR_2, OR and SR functions are found to have interesting catalytic properties due to intra- or intermolecular donor acceptor interactions.[4,5] Furthermore, ROSi[6−8] and ClSi[8] functions can be used for anchoring metallocene pre-catalysts *covalently* on solid surfaces.

In this paper we describe the synthesis of the new zirconocene $[(\eta^5\text{-}C_5H_4SiMe_2N(SiMe_3)_2]_2ZrCl_2$ (**1**). The influence of the bulky group attached to the Cp fragment on the molecular structure is discussed. In addition, we report on the conversion of complex **1** into $[(\eta^5\text{-}C_5H_4SiMe_2Cl]_2ZrCl_2$ (**2**).

Results and Discussion

$[(\eta^5\text{-}C_5H_4SiMe_2N(SiMe_3)_2]_2ZrCl_2$ (**1**) was prepared on a large scale by the synthetic route depicted in Scheme 1. All the synthetic steps were performed at room temperature. In the first step, potassium bis(trimethylsilyl)amide was reacted with an excess of Me_2SiCl_2 to give $(Me_3Si)_2NSiMe_2Cl$, which was obtained as a colourless oil after distillation. Reaction of $(Me_3Si)_2NSiMe_2Cl$ with CpNa in THF resulted in the new cyclopentadiene $(Me_3Si)_2NSiMe_2Cp$, which was isolated as a mixture of three isomers after distillation.[9] The target complex **1** was synthesized by deprotonation of $(Me_3Si)_2NSiMe_2Cp$ with *n*BuLi and a subsequent salt metathesis reaction of the resulting lithium cyclopentadienyl compound with $ZrCl_4$.

$$KN(SiMe_3)_2 \xrightarrow{Me_2SiCl_2} (Me_3Si)_2NSiMe_2Cl \xrightarrow{NaCp} CpSiMe_2N(SiMe_3)_2$$

$$2\ CpSiMe_2N(SiMe_3)_2 \xrightarrow[2)\ ZrCl_4]{1)\ n\text{BuLi}} [\eta^5\text{-}C_5H_4SiMe_2N(SiMe_3)_2]_2ZrCl_2$$

1

Scheme 1

Due to the lipophilic trimethylsilyl groups,[10,11] complex **1** is highly soluble in hydrocarbons, which made necessary two successive low-temperature crystallisations from the mother liquor to obtain a 58% yield of **1** as colourless crystals. The NMR spectra of **1** recorded at room temperature give no indication of a hindered rotation of the Cp moieties, as is known for related metallocenes with sterically demanding cyclopentadienyl ligands.[12] In the ^1H NMR spectrum, the Cp hydrogens appear as two multiplets centred at $\delta = 6.67$ and 6.37, and the trimethyl silyl groups appear as two sharp singlets at $\delta = 0.04$ and 0.48.

Single crystals of **1** suitable for X-ray diffraction were obtained by slow cooling of toluene solutions. Figure 1 shows the two molecular structures of **1** that are found in the unit cell in a 1:1 ratio. Both molecular structures show the expected pseudo-tetrahedral coordination of the zirconium atom. As shown in Figure 2 and listed in Table 1, the molecular structures of $(RC_5H_4)_2ZrCl_2$ compounds with bulky R groups can be divided into three distinct types with different conformations of the cyclopentadiene moieties.[10,13−15] According to the data in Table 1, the size and the degree of rotational freedom of the R groups seem to determine what type of structure is formed: compounds that contain bulky substituent groups with a fixed geometry adopt structure type I, whereas the other compounds prefer the structure types II or III. Remarkably, single crystals of complex **1** contain the structure types II and III, whereas

[a] Institut für Chemische Technologie der Technischen Universität Darmstadt,
Petersenstraße 20, 64287 Darmstadt, Germany
Fax: (internat.) + 49-6151/16-4214
E-mail: alex@bodo.ct.chemie.tu-darmstadt.de
[b] Material und Geowissenschaften der Technischen Universität Darmstadt,
Petersenstraße 23, 64287 Darmstadt, Germany

 © WILEY-VCH Verlag GmbH, 69451 Weinheim, 2001 1434−1948/01/0707−1785 $ 17.50+.50/0

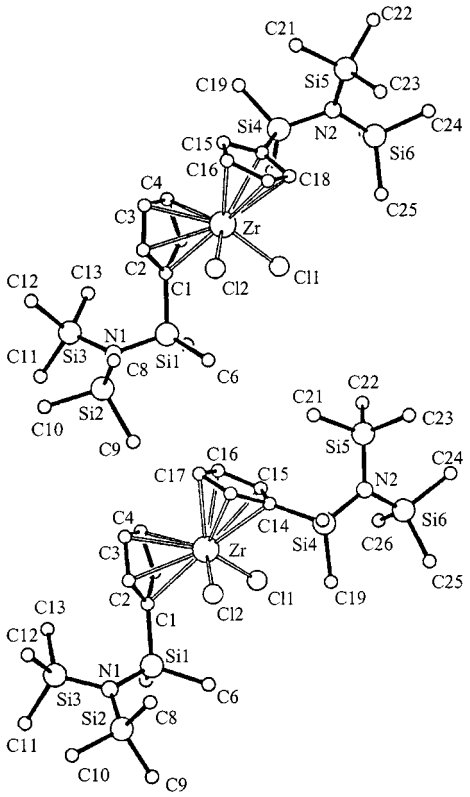

Figure 1. Molecular structures of 1 together with atomic labelling scheme

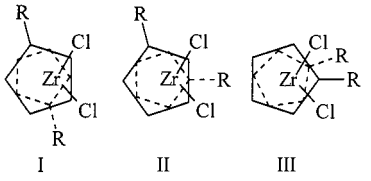

Figure 2. Structure types of $(\eta^5\text{-}RC_5H_4)_2ZrCl_2$ compounds

the unit cells of the other compounds contain only one single molecular structure.

As displayed in Table 1, the (Cp centroid)−Zr−(Cp centroid) bond angles and the Zr−(Cp centroid) bond lengths of complex **1** are in the range of other $(RC_5H_4)_2ZrCl_2$ compounds, whereas the Cl−Zr−Cl bond angles of **1** are increased relative to those of related compounds. In particular, the structure type III of **1** shows a widened Cl−Zr−Cl bond angle (105.7°). This is probably due to the steric bulk of the Cp ligands. The same trend concerning the Cl−Zr−Cl bond angle was found with $(R_2C_5H_3)_2ZrX_2$ metallocenes.[10]

Attempts to prepare the mono-cyclopentadienyl complex $[(\eta^5\text{-}C_5H_4SiMe_2N(SiMe_3)_2]ZrCl_3$ by reaction of $[(Me_3Si)_2NSiMe_2C_5H_4]Li$ with one equivalent $ZrCl_4$ failed. Even if the reaction was performed with a large excess of $ZrCl_4$, only the sandwich complex **1** could be isolated. This must be due to ligand redistribution reactions of the zirconium trichloride leading to complex **1** and $ZrCl_4$, as has already been reported by Lappert and co-workers for $(\eta^5\text{-}C_5H_4Bu^t)_2ZrCl_2$ in the presence of THF.[11] Apart from some exceptions, such as $[(\eta^5\text{-}C_5H_3(SiMe_3)_2]_2ZrCl_2$, they observed that in the absence of THF, in toluene as solvent, the redistribution reaction of $(\eta^5\text{-}C_5H_{5-n}R_n)ZrCl_2$ with $ZrCl_4$ can be directed to the monocyclopentadienyl zirconium trichlorides. However, we observed no reaction of complex **1** with $ZrCl_4$ in toluene at room temperature.

Another method for the preparation of mono-cyclopentadienyl complexes from the corresponding dichlorides has been described by Garg and co-workers.[16] They refluxed Cp_2TiCl_2 with a mixture of $SOCl_2/SO_2Cl_2$ to produce $CpTiCl_3$ in more than 90% yield. However, we found that the reaction of $[(\eta^5\text{-}C_5H_4SiMe_2N(SiMe_3)_2]_2ZrCl_2$ (**1**) in refluxing $SOCl_2/SO_2Cl_2$ leads to $(\eta^5\text{-}C_5H_4SiMe_2Cl)_2ZrCl_2$ (**2**). No trichloride products were found (Scheme 2). Complex **2** is extremely sensitive to moisture and reacts on addition of a stoichiometric amount of water to form the bridged complex $[(\eta^5\text{-}C_5H_4)SiMe_2OSiMe_2(\eta^5\text{-}C_5H_4)]ZrCl_2$,

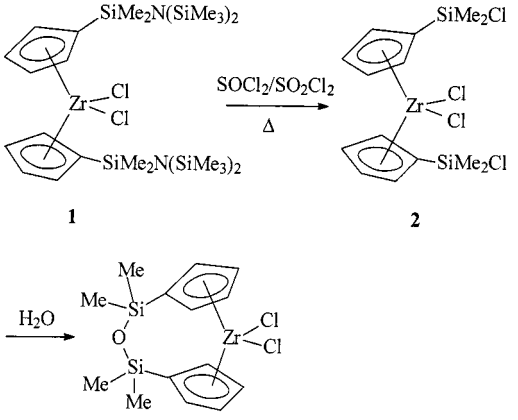

Scheme 2

Table 1. Structural parameters for some $(\eta^5\text{-}RC_5H_4)_2ZrCl_2$ compounds

Metallocene	Structure type	Cp(z)−Zr−Cp(z)[a] [°]	Zr−Cp(z) [Å]	Cl−Zr−Cl [°]	ref.
$(C_6H_5CH_2C_5H_4)_2ZrCl_2$	III	126	2.16	94.4	[13]
(Methylestratrienyl-$C_5H_4)_2ZrCl_2$	II	128.7	2.2	95.2	[14]
$(t\text{Bu}C_5H_4)_2ZrCl_2$	I	128.6	2.2	94.3	[15]
$(Me_3SiC_5H_4)_2ZrCl_2$	I	129.1	2.2	94	[10]
$[(Me_3Si)_2NSiMe_2C_5H_4]_2ZrCl_2$ (**1**)	III	126	2.2	105.7	
	II	126	2.2	99.5	

[a] Cp(z) = centroid of cyclopentadienyl rings.

as already described by Royo and co-workers for the analogous Ti and Hf complexes of **2**.[17]

Group 4 metallocenes bearing reactive groups like Me_3OSi or $ClSiMe_2$ cannot be produced by the classic salt metathesis reaction of alkali metal cyclopentadienyl compounds with transition metal chlorides.[6] Instead of this synthetic pathway, the central metal has to be introduced by the reaction of the cyclopentadiene compounds with metal amides,[6] or, if groups attached to the cyclopentadiene ring increase its acidity, by refluxing the cyclopentadiene compound in the presence of metal tetrachlorides and triethylamine.[17] As we have shown, the $(Me_3Si)_2NSiMe_2$ group is not sensitive to strong bases like *n*BuLi and, in complex **1**, is easily transformed to the $ClSiMe_2$ group, which opens up the classic synthetic pathway to zirconocenes with the $ClSiMe_2$ function.

Conclusion

The new metallocene complex $[(Me_3Si)_2NSiMe_2C_5H_4]_2ZrCl_2$ (**1**) bearing bulky, functionalized side-chains was prepared on a large scale in a convenient three-step synthesis. The X-ray analysis of **1** shows that the unit cell contains two different molecular structures in a 1:1 ratio. The structures differ from the conformation of the cyclopentadiene rings. In one of these conformations, the side-chains are positioned in a nearly synperiplanar conformation at the open side of the sandwich complex. When the molecular structures of **1** and related $(RCp)_2ZrCl_2$ compounds with bulky R groups are compared, it can be concluded that this conformation requires R groups with a certain degree of rotational freedom, which allows less steric congestion in this conformation.

The reaction of complex **1** with $SOCl_2/SO_2Cl_2$ leads to $(\eta^5\text{-}C_5H_4SiMe_2Cl)_2ZrCl_2$ (**2**) in good yields. Group 4 metallocenes with reactive side-chains containing $ClSiMe_2$ functions are interesting precursors for heterogeneous catalysts. Because of the reactive group these metallocenes cannot be produced by the classic reaction of metal chloride salts with the alkali metal derivatives of the ligand system. In one example, we have shown that the $(Me_3Si)_2NSiMe_2$ group can be used as a protecting group of the $ClSiMe_2$ function in zirconocene synthesis, which opens up the classic synthetic pathway to zirconocenes bearing the $ClSiMe_2$ group.

Experimental Section

General: All experiments with air-sensitive materials were carried out under an atmosphere of argon using standard Schlenk techniques. Solvents were dried over Na-K alloy (THF, hexane, toluene, diethyl ether) or calcium hydride (dichloromethane), followed by distillation and storage under argon. ^1H (300 MHz) and ^{13}C (75 MHz) NMR spectra were recorded on either a Bruker ARX 300 or a Bruker AC 300 spectrometer. The mass spectra were determined using a Varian MAT 311A instrument. The elemental analyses were obtained using a Perkin−Elmer CHN 240B instrument.

$(Me_3Si)_2NSiMe_2Cl$: $KN(SiMe_3)_2$ (100.82 g, 0.505 mol) and 500 mL of toluene were added to a three-necked flask equipped with a stirring device. Then, Me_2SiCl_2 (400 mL, 3.298 mol) was added dropwise within 2 h. The resulting mixture was stirred for 4 days. The volatiles were then removed in vacuo. The resulting suspension was filtered, and the residue was washed three times with 75 mL of hexane. The volatiles of the filtrate were removed in vacuo and the residue was distilled at 10^{-2} mbar. The fraction between 99 and 101 °C yielded 108.39 g (0.427 mol, 84.5%) of $(Me_3Si)_2NSiMe_2Cl$ as a colourless oil. − ^1H NMR ($CDCl_3$): δ = 0.25 (s, 18 H, $SiMe_3$), 0.55 (s, 6 H, $SiMe_2$). − MS (FI): *m*/*z* = 254 $[M]^+$, 219 $[M - Cl]^+$.

$(Me_3Si)_2NSiMe_2Cp$: $(Me_3Si)_2NSiMe_2Cl$ (107.95 g, 0.425 mol) and 100 mL of THF were placed in a flask, and then 232 mL of NaCp solution (0.464 mol, 2 M in THF) were added dropwise. The resulting mixture was stirred for 2 days. Most of the solvent was removed in vacuo and then 200 mL of hexane was added. The resulting suspension was filtered and the brown residue was washed three times with 50 mL hexane. The volatiles of the filtrate were removed in vacuo to give 106.74 g (0.376 mol) of the crude product as a brown oil, which was further purified by distillation at 10^{-2} mbar. The fraction between 148 and 150 °C yielded $(Me_3Si)_2NSiMe_2Cp$ (54.59 g, 0.193 mol, 45%) as a pale yellow oil (mixture of three isomers 10:10:1 by ^1H NMR spectroscopy). − ^1H NMR of all isomers ($CDCl_3$): δ = −0.01 (s, 6 H, $SiMe_2$), 0.13 (s, 18 H, $SiMe_3$), 0.14 (s, 6 H, $SiMe_2$), 0.23 (s, 18 H, $SiMe_3$), 0.29 (s, 18 H, $SiMe_3$), 0.30 (s, 6 H, $SiMe_2$), 2.99 (br. s, 2 H, CH_2, both main isomers), 3.64 (br. s, 1 H, CH saturated), 6.41−6.77 (m, CH, unsaturated, all isomers). − MS (FD): *m*/*z* = 283 $[M]^+$, 218 $[M - C_5H_5]^+$. − $C_{13}H_{29}NSi_3$ (283.64): calcd. C 55.05, H 10.31, N 4.94; found C 54.78, H 10.55, N 4.69.

$[(Me_3Si)_2NSiMe_2C_5H_4]_2ZrCl_2$ (1): $(Me_3Si)_2NSiMe_2Cp$ (22.08 g, 0.078 mol), 200 mL of hexane and 200 mL of toluene were placed into a flask, and then 50 mL of *n*BuLi (0.080 mol, 1.6 M in hexane) were added dropwise. The resulting solution was stirred for 18 h and then added to a suspension of $ZrCl_4$ (9.32 g, 0.040 mol) in 200 mL of toluene. Next, 150 mL of THF were slowly added dropwise to the suspension and the resulting mixture was stirred for 2 days. After sedimentation of the solids, the liquid phase was removed with a cannula, and the residue was washed with 100 mL of hexane and filtered. The resulting liquids were combined, and the volatiles were removed in vacuo to produce a brown solid residue. Crystallisation from hexane/toluene at low temperatures gave colourless crystals of **1** (22.89 g, 0.031 mol, 39.7%). From two successive crystallisations of the mother liquor, further 10.45 g (0.014 mol, 17.9%) of **1** could be isolated. − ^1H NMR ($CDCl_3$): δ = 0.08 (s, 36 H, $SiMe_3$), 0.52 (s, 18 H, $SiMe_2$), 6.41 ("t", 4 H, Cp), 6.71 ("t", 4 H, Cp). − ^{13}C NMR ($CDCl_3$): δ = 5.38 ($SiMe_2$), 5.67 ($SiMe_3$), 114.42 (CH), 127.99 (C_q), 129.06 (CH). − MS (FD): *m*/*z* = 727 $[M^+]$. − $C_{26}H_{56}Cl_2N_2Si_6Zr$ (727.38): calcd. C 42.93, H 7.76, N 3.85; found C 42.63, H 7.86, N 3.91.

X-ray Crystal Structure Analysis of 1

Crystal Data and Refinement Details: Formula $C_{26}H_{56}Cl_2N_2Si_6Zr$, M_r = 727.38, 0.35 × 0.22 × 0.18 mm, *a* = 15.032(5) Å, *b* = 17.443(6) Å, *c* = 17.962(6) Å, α = 61.49(1)°, β = 74.48(1)°, γ = 74.93(1)°, *V* = 3938.7(2) Å^3, *Z* = 4, *d* = 1.23 g cm^{-3}, triclinic, space group $P\bar{1}$, diffractometer Stoe-Stadi4, λ = 0.71069 Å (Mo-K_α), graphite, data collection mode 2Θ/ω = 1:1, range 3 < 2Θ < 45, $-16 \le h \le 16$, $-18 \le k \le 18$, $-19 \le l \le 19$, reflections measured 20561, reflections observed 7302, $I > 2\sigma(I)$, 5.99 cm^{-1}, ψ-scan, T_{min} 0.787, T_{max} 0.893. Structural analysis SHELXS-86, refinement on F^2, hydrogen positions geom., R_1 = 0.0370 and wR_2 = 0.0815. Programs used SHELXS-86 and SHELXL-93.

Crystallographic data (excluding structure factors) for the structure reported in this paper have been deposited with the Cambridge Crystallographic Data Centre as supplementary publication no. CCDC-152331. Copies of the data can be obtained free of charge on application to CCDC, 12 Union Road, Cambridge CB2 1EZ, UK [Fax: (internat.) +44-1223/336-033; E-mail: deposit@ccdc.cam.ac.uk].

$(ClMe_2SiC_5H_4)_2ZrCl_2$ (2): Compound **1** (3.40 g, 4.68 mmol) was placed in a flask and a solution of SO_2Cl_2 (5 mL, 62.24 mmol) and $SOCl_2$ (14 mL, 191.93 mmol) was added dropwise. The resulting mixture was refluxed for 2 h and then filtered. The volatiles of the filtrate were removed in vacuo to produce a light brown residue. Recrystallisation from toluene/hexane yielded **2** (1.10 g, 2.30 mmol; 50%). – ^{1}H NMR ($CDCl_3$): δ = 0.72 (s, 12 H, $SiMe_2Cl$), 6.57 (m, 4 H, C_5H_4), 6.78 (m, 4 H, C_5H_4). – ^{13}C NMR ($CDCl_3$): δ = 3.2 ($SiMe_2$), 116.7 (C_{ipso} (C_5H_4), 122.5, 126.3 [CH of (C_5H_4)]. – MS (EI): *m*/*z* = 478 $[M]^+$, 320 $[M - C_5H_4SiClMe_2]^+$, 122 $[C_5H_4SiMe_2]^+$. – $C_{14}H_{20}Cl_4Si_2Zr$ (477.52): calcd. C 35.21, H 4.22; found C 35.48, H 4.35.

$[(\eta^5\text{-}C_5H_4)SiMe_2OSiMe_2(\eta^5\text{-}C_5H_5)]ZrCl_2$: Water (35 μL) was added to a solution of **2** (810 mg, 1.69 mmol) in 25 mL of toluene. The resulting solution was stirred for 12 h at room temperature, and then the volatiles were removed in vacuo. Recrystallisation of the residue from toluene/hexane yielded $[(\eta^5\text{-}C_5H_4)SiMe_2OSiMe_2(\eta^5\text{-}C_5H_5)]ZrCl_2$ (574 mg, 1.36 mmol; 80%) as pale yellow crystals. – ^{1}H NMR ($CDCl_3$): δ = 0.36 (s, 12 H, $SiMe_2$), 6.53 ("tr", 4 H, C_5H_4), 6.84 ("tr", 4 H, C_5H_4). – ^{13}C NMR ($CDCl_3$): δ = 0.9 ($SiMe_2$), 117.2 [(C_{ipso} (C_5H_4)], 122.4, 125.7 [CH (C_5H_4)]. – MS (EI): *m*/*z* = 422 $[M]^+$, 407 $[M - CH_3]$. – $C_{14}H_{20}Cl_2OSi_2Zr$ (422.61): calcd. C 39.79, H 4.77, found C 39.76, H 5.92.

Acknowledgments

The authors wish to thank the Bundesministerium für Bildung und Forschung and the BASF AG for financial support.

[1] P. C. Möhring, N. J. Coville, *J. Mol. Catal.* **1992**, *77*, 41–50.
[2] P. Burger, K. Hortmann, H.-H. Brintziger, *Makromol. Chem. Macromol. Sym.* **1993**, *66*, 127–140.
[3] C. Janiak, K. C. H. Lange, U. Versteeg, D. Lentz, P. H. M. Budzelaar, *Chem. Ber.* **1996**, *129*, 1517–1529.
[4] For a recent review, see: C. Müller, D. Vos, P. Jutzi, *J. Organomet. Chem.* **2000**, *600*, 127–143 and references therein.
[5] A. Rau, T. Wieczorek, A. Dyroff, H.-P. Dornik, G. Luft, *J. Mol. Catal.* submitted.
[6] M. Galan-Fereres, T. Koch, E. Hey-Hawkins, M. S. Eisen, *J. Organomet. Chem.* **1999**, *580*, 145–155.
[7] H. Juvaste, T. T. Pakkanen, E. I. Iiskola, *J. Organomet. Chem.* **2000**, *606*, 169–175.
[8] P. Jutzi, T. Heidemann, B. Neumann, H.-G. Stammler, *J. Organomet. Chem.* **1995**, *472*, 27–38.
[9] For isomers and fluxionality of Cp compounds, see: P. Jutzi, *Chem. Rev.* **1986**, *86*, 983–996.
[10] A. Antinolo, M. F. Lappert, A. Singh, D. J. W. Winterborn, L. M. Engelhardt, C. L. Raston, A. H. White, A. J. Carty, N. J. Taylor, *J. Chem. Soc., Dalton Trans.* **1987**, 1463–1472.
[11] P. B. Hitchcock, M. F. Lappert, D.-S. Liu, E. Ryan, *Polyhedron* **1995**, *14*, 2745–2752.
[12] J. Okuda, *Top. Curr. Chem.* **1991**, *160*, 97–145.
[13] Y. Dusausoy, J. Protas, P. Reaut, B. Gautheron, G. Tainturier, *J. Organomet. Chem.* **1978**, *157*, 167–172.
[14] G. Erker, C. Mollenkopf, M. Grehl, B. Schönecker, *Chem. Ber.* **1994**, *127*, 2341–2345.
[15] R. A. Howie, G. P. McQuillan, D. W. Thompson, G. A. Lock, *J. Organomet. Chem.* **1986**, *303*, 213–220.
[16] K. Chandra, R. K. Sharma, N. Kumar, B. S. Garg, *Chem. and Ind.* **1980**, 288.
[17] S. Ciruelos, A. Sebastián, T. Cuenca, P. Gomez-Sal, A. Manzanero, P. Royo, *J. Organomet. Chem.* **2000**, *604*, 103–115.

Received December 14, 2000
[I00471]

New Polypodal Polycarboxylic Ligands − Complexation of Rare-Earth Ions in Aqueous Solution

Romain Viguier,[a] Guy Serratrice,*[b] Agnes Dupraz,[a] and Claude Dupuy[a]

Keywords: Lanthanides / Carboxylic acids / Thermodynamics / N ligands / NMR spectroscopy

The complexation ability of new polypodal carboxylic ligands prepared from 2,2-bis(hydroxymethyl)-1-alkanols was investigated in aqueous solution with Y^{3+} and various lanthanide ions (La^{3+}, Sm^{3+}, Eu^{3+}, Gd^{3+}, Tb^{3+}, Dy^{3+}). The values of the stability constants for ML complexes are of the order of 10^4 for the hexadentate trioxypropionates, 10^7 for the hexadentate trioxyacetates and 10^{14} for the nonadentate triaminohexaacetates. In these systems, the nitrogens of the amino groups seem to be better chelating atoms than the oxygens of the ether groups. The hydration numbers of dysprosium(III) complexes have been determined from the Dy^{III}-induced ^{17}O NMR water shifts.

Introduction

The design of polypodal ligands capable of forming stable complexes for in vivo use has received increasing interest in the past decade.[1] With a view towards the preparation of new complexing systems for yttrium and some lanthanide ions which could be used for radiotherapy or as biomedical radiolabels (^{90}Y, ^{153}Sm, ^{165}Dy), we undertook the synthesis of a series of new polypodal ligands: trioxypropionic acids (TOTP),[2] trioxytriacetic acids (TOTA)[3] and triaminohexaacetic acids (TAHA) (see Figure 1). Derivatives of these compounds for conjugation with a biomolecule (such as a monoclonal antibody or peptide) should be easier to prepare than macrocyclic ligands bearing carboxylate groups, which are well-known for their ability to complex yttrium and lanthanides ions.[1,4]

In this paper we report the stability constants of the 1:1 complexes (ML) of these ligands with yttrium(III) and a variety of lanthanide(III) cations in aqueous solution as determined potentiometrically. The ^{17}O NMR spectra in variable pH solutions of the Dy^{III} complexes are also described in order to gain information on their coordination sphere in aqueous solution. A shift of the water ^{17}O NMR signal (Dysprosium Induced Shift, DIS) is induced upon addition of dysprosium(III) complexes to water that is related to the number of coordinated water molecules in the complex.

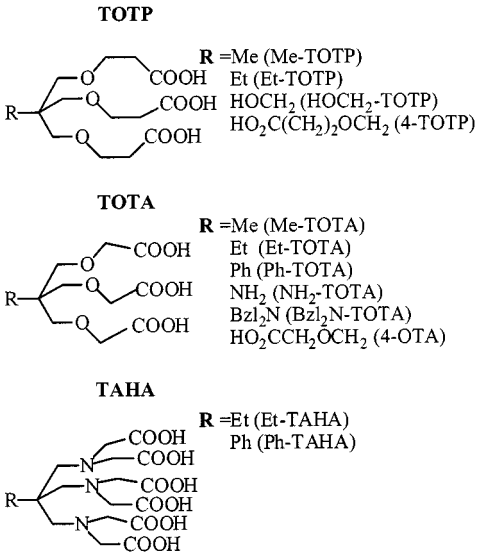

Figure 1. Structure of the ligands

Results

Ligands Synthesis

The TOTP and TOTA ligands are easily accessible from inexpensive commercial primary polyols. These preparations involve two steps: the formation of the ether linkages followed by the hydrolysis of the *tert*-butyl ester functions with formic acid. The polyetherifications were accomplished by phase-transfer catalysis[2,3] with *tert*-butyl acrylate or *tert*-butyl bromoacetate (Figure 2).

The TAHA ligands were also synthesised from primary polyols using the procedure described by Hellmann and coworkers[5] to prepare 1,1,1-tris(aminomethyl)phenylmethane (Figure 3).

Ligand Deprotonation Constants

The deprotonation constants K_a of the ligands investigated in this research were studied by potentiometric titration. Analysis of the potentiometric titration curves (see Figure 4 for examples and details in Exp. Section) by the SUPERQUAD[6] program yielded the pK_{an} values defined by Equation (1) and (2) (charges omitted for clarity):

[a] Laboratoire d'Etudes Dynamiques et Structurales de la Sélectivité, (LEDSS 4,), UMR CNRS 5616, Université Joseph Fourier,
BP 53, 38041 Grenoble Cedex 9, France
[b] Laboratoire d'Etudes Dynamiques et Structurales de la Sélectivité, (LEDSS 2), UMR CNRS 5616, Université Joseph Fourier,
BP 53, 38041 Grenoble Cedex 9, France
E-mail: Guy.Serratrice@ujf-grenoble.fr

 © WILEY-VCH Verlag GmbH, 69451 Weinheim, 2001 1434−1948/01/0707−1789 $ 17.50+.50/0

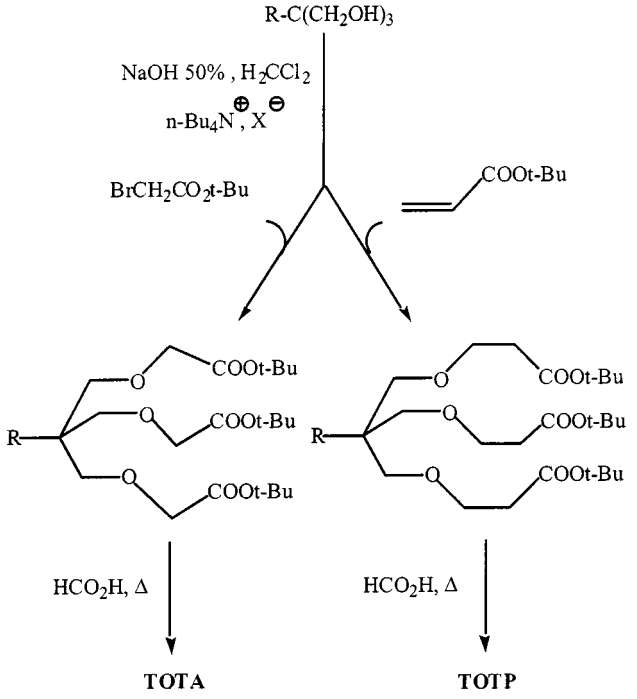

Figure 2. Synthesis of the ligands TOTP and TOTA

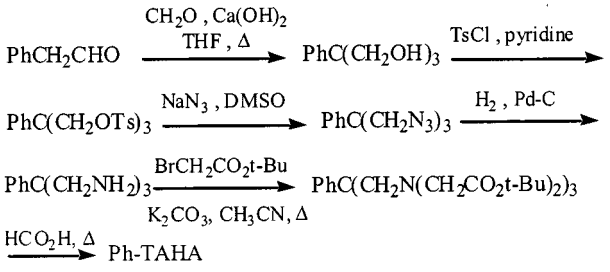

Figure 3. Synthesis of the ligand Ph-TAHA

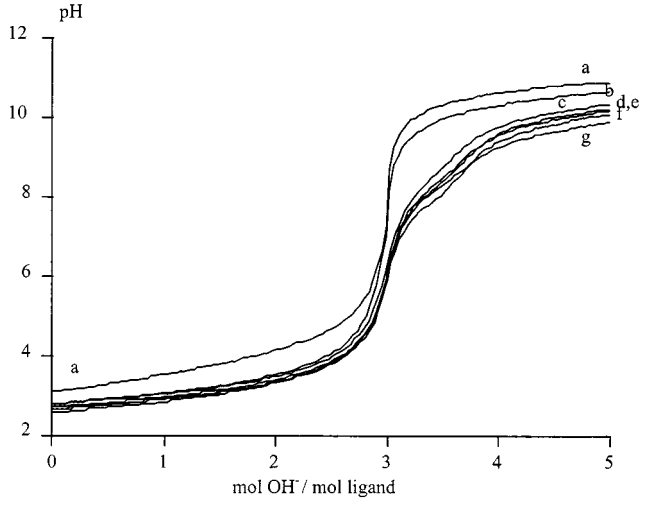

Figure 4. Potentiometric titration curves for (a) 1 mM ligand Me-TOTA and (1:1 1 mM Me-TOTA + (b) La^{3+}, (c) Sm^{3+}, (d) Eu^{3+}, (e) Tb^{3+}, (f) Gd^{3+}, (g) Y^{3+}; all solutions were at 25 °C and $I = 0.1$ M (NMe_4Cl); the data were refined by the SUPERQUAD program

$$LH_n \rightleftarrows LH_{n-1} + H^+ \quad (1)$$

$$K_{an} = [LH_{n-1}]\,[H^+]/[LH_n] \quad (2)$$

The ligands of the series TOTA and TOTP possess three carboxylic groups and the tetrapodal ligands 4-OTA and 4-TOTP four carboxylic groups. The two derivatives NH_2-TOTA and $N(Bz)_2$-TOTA have a fourth ionizable proton in an ammonium group. The pK_{an} values are listed in Table 1. For the ligand of the tri(amino)hexaacetic acid series, denoted Ph-TAHA, the pK_{an} of three carboxylic groups (three pK_{an} values are too low to be determined from potentiometric titration) and of the three ammonium groups have been determined. The values are reported in Table 2 together with literature data for tripodal ligands incorporating aminocarboxylate groups.

Table 1. Deprotonation constants of the *R*-TOTA ligands[a]

Ligand	pK_{a4}	pK_{a3}	pK_{a2}	pK_{a1}
Me-TOTA		2.89(4)	3.56(1)	4.36(1)
Et-TOTA		2.35(9)	3.40(1)	4.29(1)
Ph-TOTA		3.05(1)	3.53(1)	4.26(1)
NH_2-TOTA	2.64(5)	3.03(2)	3.96(2)	9.49(1)
$N(Bz)_2$-TOTA	2.90(5)	3.19(3)	4.08(2)	7.74(1)
4-OTA	2.71(2)	3.75(2)	3.92(1)	4.98(1)
Me-TOTP		4.02(1)	4.63(1)	5.46(1)
Et-TOTP		4.14(1)	4.64(1)	5.50(1)
$HO(CH_2)$-TOTP		4.25(1)	4.83(1)	5.85(1)
4-TOTP	3.87(2)	4.41(1)	5.00(1)	5.68(1)

[a] All values are determined at 25 °C and $I = 0.1$ M (NMe_4Cl); standard deviation of the last significant digit (95% confidence level) in parentheses.

Table 2. Deprotonation constants of the ligand Ph-TAHA and comparison with literature data

Ligand	pK_{a6}	pK_{a5}	pK_{a4}	pK_{a3}	pK_{a2}	pK_{a1}
Ph-TAHA	2.2(1)	3.36(7)	3.71(5)	4.81(5)	7.20(4)	11.17(4)
TAPHA[b]	2.0	2.42	3.52	4.3	8.26	9.88
TAMETA[c]				4.69	7.73	10.73

[a] All values are determined at 25 °C and $I = 0.1$ M (NMe_4Cl); standard deviation of the last significant digit (95% confidence level) in parentheses. – [b] 1,2,3-Triaminopropanehexaacetic acid, ref.[11] – [c] 1,1,1-Tris(aminomethyl)ethane-*N*,*N*′,*N*′′-triacetic acid, ref.[10]

Stability Constants of the Metal Complexes

The stability constants were determined from potentiometric titration of ligand/metal solutions at a molar ratio of 1:1. (for example, as shown in Figure 4). The titration curves for ligands Me, Et, Ph-TOTA and *R*-TOTP exhibit buffer regions over the pH range 7−10 owing to the formation of hydroxo complexes; however, a precipitation occurred and precluded the use of the data in refinement program. No precipitation was observed below pH 10 for ligands the NH_2, $N(Bz)_2$ and 4-OTA. Analysis of the titration curves was performed over the pH range 2.5−6 by the

SUPERQUAD program[6] yielding the K_{ML} and K_{MLH_n} constants. The best fit of the data was obtained by considering only the 1:1 species. The values are reported in Table 3 (*R*-TOTA) and Table 4 (*R*-TOTP).

served DIS represents a concentration-weighted average of the shifts of the individual species in solution. The experimental DIS was measured for different Dy^{III} concentrations. The plot of the DIS versus [Dy^{III}] gives a straight line

Table 3. Stability constants and protonation constants of lanthanide complexes[a] with TOTA ligands and pSm values[b]

Ligand	Y^{3+}	La^{3+}	Sm^{3+}	Eu^{3+}	Gd^{3+}	Tb^{3+}	pSm
Me-TOTA log *K*(ML)[c]	6.6(1)	5.7(1)	6.8(1)	6.8(1)	6.8(1)	7.0(1)	4.90
Et-TOTA log *K*(ML)	6.65(5)	6.05(6)	7.1(1)	7.0(1)	7.2(1)	7.2(1)	5.05
Ph-TOTA log *K*(ML)	6.6(1)	5.0(1)	6.7(1)		7.0(1)	7.0(1)	4.85
NH_2-TOTA log *K*(ML)	8.40(5)	8.01(7)	9.21(2)	9.15(2)	9.10(3)	9.22(1)	4.90
log K(MLH)[d]	4.12(3)	4.74(5)	3.56(2)	3.76(2)	3.85(3)	3.74(2)	
$N(Bz)_2$-TOTA log *K*(ML)	8.81(3)	7.57(3)	9.06(4)	8.69(1)	8.72(2)	8.59(1)	5.45
log *K*(MLH)	3.64(2)	4.02(3)	3.43(3)	3.31(1)	3.28(1)	3.38(1)	
4-OTA log *K*(ML)	8.13(2)	6.55(2)	8.10(2)	7.87(5)	7.42(3)	7.33(2)	5.55
log *K*(MLH)	3.77(2)	4.4 (1)	3.82(4)	3.8(1)	3.87(6)	3.88(4)	

[a] All values are determined at 25 °C and I = 0.1 M (NMe_4Cl); standard deviation of the last significant digit (95% confidence level) in parentheses. – [b] calculated for $[L]_{tot} = 10^{-3}$ M, $[Sm^{3+}]_{tot} = 10^{-3}$ M and pH = 7. – [c] $K(ML) = [ML]/[M][L]$. – [d] $K(MLH) = [MLH]/[ML][H]$.

Table 4. Stability constants and protonation constants of lanthanide complexes[a]

Ligand	Y^{3+}	La^{3+}	Sm^{3+}	Eu^{3+}	Gd^{3+}	Tb^{3+}
Me-TOTP log *K*(ML)[b]	3.65(3)	3.22(3)	3.82(8)	3.95(2)	3.72(2)	3.7(1)
log *K*(MLH)[c]	4.30(5)		4.08(6)	4.35(6)	4.20(2)	4.25(6)
Et-TOTP log *K*(ML)	3.63(5)	3.21(2)	3.88(1)	3.97(1)		3.79(1)
log *K*(MLH)	4.60(2)	4.75(2)	4.68(2)	4.61(2)		4.57(3)
$HO(CH_2)$-TOTP log *K*(ML)	4.52(2)	4.23(2)	5.04(3)	4.23(2)	4.50(4)	4.57(2)
log *K*(MLH)		4.1(1)				
4-OTP log *K*(ML)	4.7(1)	3.90(3)	5.0(1)	5.20(1)	4.9(1)	4.8(1)
log *K*(MLH)	4.95(5)	5.1(1)	5.00(5)	4.95(2)	5.01(8)	5.02(9)

[a] All values are determined at 25 °C and I = 0.1 M (NMe_4Cl); standard deviation of the last significant digit (95% confidence level) in parentheses. – [b] with TOTP ligands$K(ML) = [ML]/[M][L]$. – [c] $K(MLH) = [MLH]/[ML][H]$.

With the ligand Ph-TAHA we investigated the complexation of the cations Sm^{3+}, for comparison with the other ligands, Dy^{3+}, for comparison with the NMR study, and Ce^{3+}. No precipitation occurred above pH 7 and the titration data were refined over the pH range 2.5–8. A comparison of the titration curves of the ligand solution and of the metal-ligand solution (Figure 5) indicates that no hydroxo complexes are formed at basic pH's, which is contrary to the ligands of the TOTA and TOTP series. The stability constants are shown in Table 5.

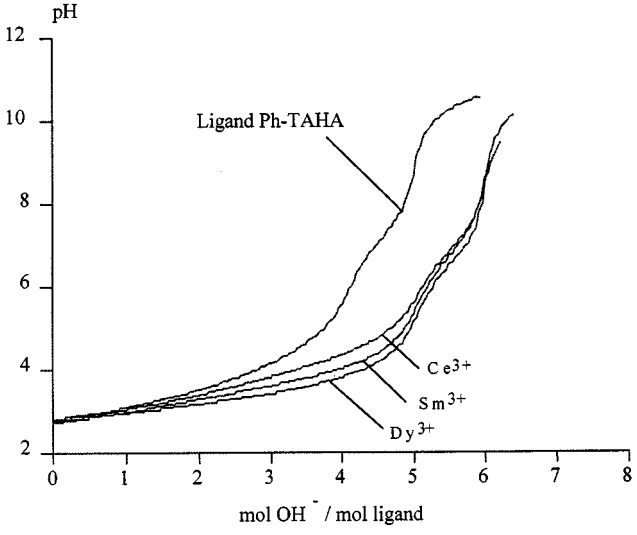

Figure 5. Potentiometric titration curves for 1 mM Ph-TAHA and Ph-TAHA + Ln^{III} (1:1; 1 mM); all solutions were at 25 °C and I = 0.1 M (NMe_4Cl); the data were refined by the SUPERQUAD program

^{17}O NMR Spectroscopy

The number of water molecules present in the lanthanide complexes was investigated by dysprosium-induced ^{17}O shift measurements. From these a qualitative picture of the lanthanide coordination sphere can be deduced. Addition of Dy^{III} complexes to water results in a shift of the water signal in the ^{17}O NMR spectrum to lower frequencies. Peters and co-workers[7] have shown that the dysprosium-induced shift of water (DIS) can be utilised to estimate the number of bound water molecules associated with the lanthanide complexes. The exchange between bound and bulk water is fast on the NMR time scale. Accordingly, the ob-

Table 5. Stability constants and protonation constants of lanthanide complexes[a] and pSm values[b] for the ligand Ph-TAHA

Ligand		Ce^{3+}	Sm^{3+}	Dy^{3+}	pSm
Ph-TAHA	log K (ML)[c]	11.14(3)	12.71(1)	14.85(7)	5.64
	log K(MLH)[d]	6.90(2)	6.62(1)	6.51(7)	
	log K(MLH_2)[d]	4.53(2)	4.17(1)	3.95(7)	
	log K(MLH_4)[e]	7.30(6)	6.88(2)	6.59(9)	

[a] All values are determined at 25 °C and I = 0.1 M (NMe_4Cl); standard deviation of the last significant digit (95% confidence level) in parentheses. – [b] calculated for $[L]_{tot} = 10^{-3}$ M, $[Sm^{3+}]_{tot} = 10^{-3}$ M and pH = 7. – [c] K(ML) = [ML]/[M][L]. – [d] $K(MLH_n) = [MLH_n]/[MLH_{n-1}][H]$. – [e] $K(MLH_4) = [MLH_4]/[MLH_2][H]^2$.

with a slope proportional to the number of bound water molecules in the complex. DIS measurements were carried out for the ligands Ph-TOTA, 4-OTP and Ph-TAHA. Following the procedure described by Peters,[7] the DIS for solutions of the hydrated cation $[Dy(H_2O)_8]^{3+}$ at pH 6.5 were measured, these results produced a slope of 358 ppm M^{-1} (Figure 6a or 7a) which is in excellent agreement with that obtained in Peters's paper (−357 ppm M^{-1}). Therefore, a value of 45 ppm M^{-1} can be calculated for one coordinated water molecule if the cation is hydrated by eight water molecules.[8] DIS measurements were also performed for solutions of the complex $[Dy(ligand)(H_2O)_q]^{3+}$ over the pH range 1−5 for Ph-TOTA, 2−5 for 4-OTP and 1−9 for Ph-TAHA. The experimental slopes p of the plots of the DIS versus $[Dy(ligand)(H_2O)_q]$ (Figure 6 and 7) were determined. The p values and the calculated water coordination numbers, q, are shown in Table 6. The q values indicate that the number of coordination positions for the ligand increase as the pH increases (Table 6) which agrees with the existence of different protonated species.

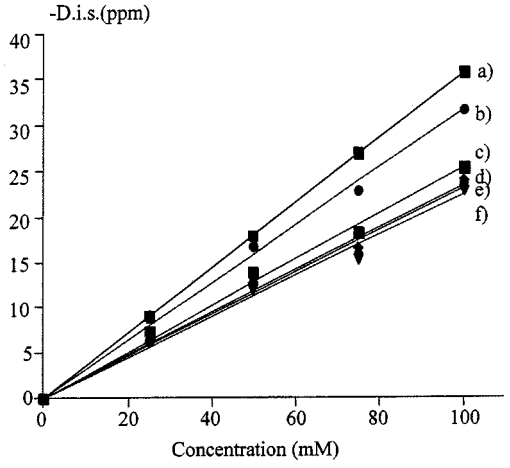

Figure 6. ^{17}O NMR shifts of water versus dysprosium complex concentration for solutions of: (a) $Dy(H_2O)_8$, (b) Dy(Ph-TOTA) at pH 1, (c) pH 2, (d) pH 3, (e) pH 4, (f) pH 5

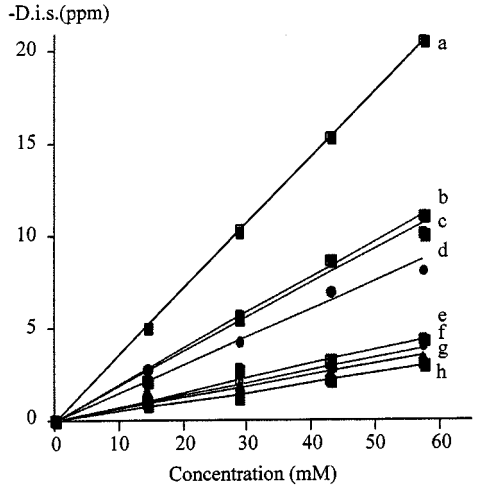

Figure 7. ^{17}O NMR shifts of water versus dysprosium complex concentration for solutions of: (a) $Dy(H_2O)_8$, (b) Dy(Ph-TAHA) at pH 1, (c) pH 2, (d) pH 3, (e) pH 4, (f) pH 5, (g) pH 6, (h) pH 9

Table 6. Values of the water coordination number q in Dy^{III} complexes derived from ^{17}O chemical shifts

Ligand	pH	p[a]	q
H_2O	6.5	−358	8
Ph-TOTA	1	−317	7.1
	2	−255	5.7
	3	−235	5.3
	4	−231	5.2
	5	−224	5.0
4-OTP	2−4	−288	6.4
Ph-TAHA	1	−195	4.4
	2	−186	4.2
	3	−152	3.4
	4	−77	1.7
	5	−68	1.5
	6	−62	1.4
	9	−51	1.1

[a] Slope of the plot of DIS versus the concentration of the complex (in ppm M^{-1}).

Discussion

Ligand Deprotonation Constants

For the ligands of the series *R*-TOTA it should be noted that the average values of the carboxylic pK_a over a range 3.21−3.61 in the tripodal ligands are close to the value of 3.31 for the analogous monodentate methoxyacetic acid.[9] For the ligands of the series TOTP the pK_{an} values are higher than those for the ligands *R*-TOTA, owing to the presence of a second methylene group which acts as an electron donor. A similar effect is observed in 3-hydroxypropionic acid (pK_a = 4.32[9]) in comparison to hydroxyacetic acid (pK_a = 3.63).[9] Furthermore, the separation of the pK_{an} values for a given ligand is in the range 0.39−1.05 [except for a value of 0.29 for $N(Bz)_2$-TOTA]. This reflects a rough statistical separation (log 3 or 0.48), which is consistent with noninteracting pendant arms. For the ligand Ph-TAHA, the three highest and the three lowest pK_a values are attributed to the ammonium and carboxylic

groups, respectively. The acidities of the ammonium groups are close to those of the ligands TAMETA [1,1,1-tris-(aminomethyl)ethane-*N*,*N*′,*N*′′-triacetic acid][10] which has a similar tripodal structure. The pK_a's of the carboxylic groups are comparable to those of the ligand TAPHA (1,2,3-triaminopropanehexaacetic acid)[11] which contains three aminodiacetic arms.

Stability Constants of the Metal Complexes

A small change in the stability constant *K*(ML) is observed on going from Sm^{3+} to Tb^{3+} and for Y^{3+}. The values for La^{3+} are smaller than those for the other cations owing to its larger size and its lower Lewis acidity. The same trend has been observed for EDTA complexes.[9] The ligands TOTP appear to be poor chelators of Ln^{III} ions, since their stability constants are two or three orders of magnitude lower than those of the TOTA series. This result shows that the presence of longer chains in TOTP than in TOTA ligands makes the complexation of Ln^{III} ions unfavorable, probably due to their higher flexibility. Furthermore, the coordination of carboxylic groups could be hindered by their weak acidity. Accordingly, the water coordination number of 6 (Table 6) (corresponding to a ligand coordination number of 2 or 3) for 4-OTP, as determined by ^{17}O NMR spectroscopy, is not unexpected even for a tetrapodal ligand. For the complex with Ph-TOTA, the value $q = 5$ suggests a coordination of three carboxylates in the ML species. These results clearly show that the ether oxygens are not involved in the coordination to the cation. The complexation constants for the lanthanides with ligands having the same backbone as the TOTA series, each arm containing one or two ethylenoxy moieties ($CH_2CH_2OCH_2CH_2CO_2H$ or $CH_2CH_2OCH_2CH_2OCH_2CH_2CO_2$ H), have also been measured (not described here).[12] These ligands were found to have stability constants *K*(ML) approximately equal to those for the *R*-TOTP ligands. This result also supports the fact that the ether oxygens are not involved in the complexation to the cations and that the carboxylate anions alone are responsible for the complexation.

Since the ligands are weak acids, proton competition occurs depending on their pK_a and the pH. The pM (= −log[M]) is thus a more reliable parameter for a comparison of ligand effectiveness under given conditions of pH, M and L concentrations: the larger the pM values, the more effective the ligand. The pM values for the cation Sm^{3+} ($[L]_{tot} = 10^{-3}$ M, $[Sm^{3+}]_{tot} = 10^{-3}$ M) over the pH range 3−7 for the ligands *R*-TOTA and 3−9 for the ligand Ph-TAHA have been calculated and are presented on the plot of pSm vs. pH in Figure 8. The values of pSm at pH 7 are reported in Table 3 and 5. For the ligands *R*-TOTA, the pSm values for R = Me, Et or Ph are very close and much higher than those for the ligands NH_2-TOTA and $N(Bz)_2$-TOTA at acidic pH. These ligands are protonated at the nitrogen and the positive charge is assumed to reduce the affinity of the ligand for the lanthanide cation. However, at pH > 6 for $N(Bz)_2$-TOTA and pH > 7 for NH_2-TOTA, this affinity is greatly enhanced. This could be ascribed to the coordination of the cation with the nitrogen of the amine. The pSm value for the ligand 4-OTA is about 0.5 units higher than those for the *R*-TOTA ligands, showing that a fourth arm increases the affinity for the cation, and is probably involved in the coordination. Furthermore, it can be seen that these three ligands prevent the precipitation of hydroxo complexes in neutral and basic mediums.

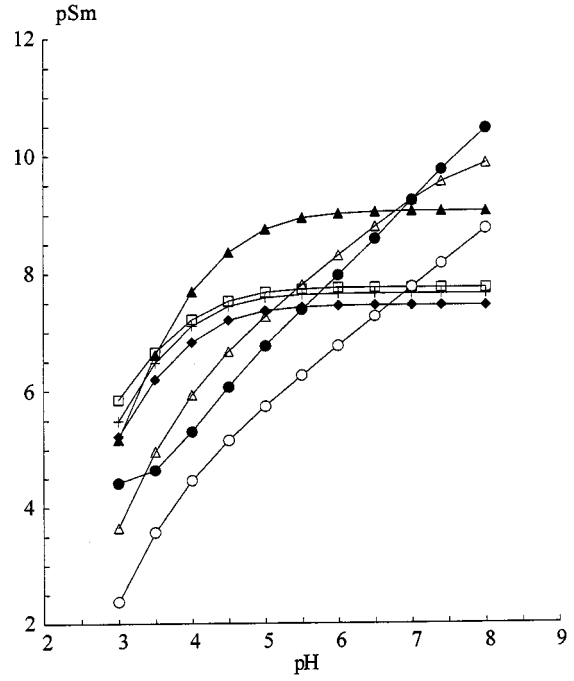

Figure 8. Plot of pSm vs. pH for the ligands; pSm was calculated for $[L]_{tot} = 10^{-3}$ M, $[Sm^{3+}]_{tot} = 10^{-3}$ M using the known constants of Me-TOTA (◆), Et-TOTA (□), Ph-TOTA (+), NH_2-TOTA (○), NBz_2-TOTA (Δ), 4-OTA (▲) and Ph-TAHA (●)

The pSm vs. pH curve indicates that the ligand Ph-TAHA is a poorer complexing agent in an acidic medium, but is more efficient at pH above 7, than the other ligands described in this paper. The obvious advantage of this ligand is much greater efficiency of complexation in basic media and an increase in the coordination number as the pH increases, as determined by the ^{17}O NMR study. The water coordination number *q* varies from a mean value of 4 over the pH range 1−3 to a mean value of 1.5 over the pH range 4−6. The latest value reflects the contribution of several species, among which [DyLH] is predominant with a hexadentate ligand. At pH 9, the *q* value of 1.1 attributed to the [DyL] species indicates that the coordination to the ligand is heptadentate with one water molecule. This suggests that the six carboxylate oxygens and one nitrogen are involved in the coordination to the cation. As a consequence, no hydroxo complexes are formed at basic pH. This reflects the low Lewis acidic character of the cation in the complex ML.

Conclusion

Our results have shown that the coordination to the lanthanides ions involves the carboxylate groups alone and not

the oxygens from the ether groups (TOTP or TOTA), while the nitrogen in similar polypodal ligands does participate in the chelation (TAHA). The presence of amino groups enhances the stability constants of the complexes, thus preventing the formation of hydroxo complexes or precipitation of metal hydroxides at pH close to or above 7. The formation of 1:1 complexes leads to a relatively high hydration number as determined by Dy^{III}-induced ^{17}O NMR water shifts. A value of 5 has been obtained for the tris(carboxylate) ligands and a value of 2 for the tris(aminocarboxylate) ligands. This hydration state is expected to provide interesting relaxivity properties for these complexes. However, the results in terms of the potentialities of these ligands in biomedical applications are still not satisfactory. With some ligands of the TOTP series, the bioconjugation with a fragment of monoclonal antibody [*anti*-ACE(F6)] has been realized.[2] A study of ^{111}In radiolabelling indicated that one ligand is linked to the $F(ab')_2$ but the complexes of these bioconjugated polypodal ligands with ^{153}Sm are not stable enough to be purified.

Experimental Section

Materials: Hydrated lanthanide chlorides were obtained from Aldrich. All other compounds were of reagent grade and were used without further purification.

Instrumentation: ^1H NMR spectra (200, 250 and 300 MHz) are referenced to TMS and recorded on Bruker AC 200, Bruker AWM 250 or Bruker AM 300 spectrometers. ^{17}O NMR spectra (natural abundance) were recorded at 54.24 MHz on a Bruker AM 300 spectrometer, using 5 mm sample tubes. Mass spectra were obtained with a NERMAGT1OC quadrupolar instrument. Infrared spectra were obtained as KBr disks for solid compounds and as pure film products between two NaCl discs for oils on a Nicolet Impact 400 spectrometer driven by the OMNIC program on a PC. Elemental analyses were performed by Le Service Central d'Analyses du CNRS in Vernaison (France). Melting points were measured on a Buchi-Tottoli apparatus and are uncorrected.

Synthesis of *R*-TOTP and *R*-TOTA: These ligands were prepared by acid hydrolysis from the corresponding polyesters, which were themselves prepared by a previously described method.[2,3]

Synthesis of Ph-TAHA

1,1,1-Tris(hydroxymethyl)phenylmethane: A solution of phenylacetaldehyde (10.75 g, 0.09 mol), paraformaldehyde (16.8 g, 0.56 mol) and $Ca(OH)_2$ (5.2 g, 0.70 mol) in THF (60 mL) was stirred at 60−65 °C for four days. After cooling to room temperature, the mixture was filtered through celite gel and the solvent was evaporated under vacuum (0.05 Torr). The residual oil was dissolved in hot ethyl acetate. Under standing at room temperature the product crystallized as a white powder (9.55 g, 58%), m.p. 80−81 °C. − $C_{10}H_{14}O_3$ (182.22): calcd. C 65.32, H 7.50; found C 65.93, H 7.69. − ^1H NMR ($CDCl_3$): δ = 3.92 (s, 6 H, CH_2OH), 7.18−7.46 (m, 5 H, aromatic CH). − ^{13}C NMR ($CDCl_3$): δ = 48.7 (C_6H_5-*C*), 65.8 (CH_2OH), 126.7, 127.2, 129.0 and 138.4 (C_6H_5).

1,1,1-Tris[(4-tolylsulfonyl)methyl]phenylmethane: *p*-Toluenesulfonyl chloride (36.5 g, 0.191 mol) was slowly added to a solution of 1,1,1-tris(hydroxymethyl)phenylmethane (8.717 g, 0.048 mol) in cold pyridine (90 mL) at a rate such that the temperature remained between 5 and 10 °C. After stirring at room temperature for half an hour, the mixture was poured into 15 mL of cold water. The product obtained was filtered, washed with diethyl ether (3 × 20 mL) and dried in vacuo for a few days to yield 27.76g (90%) of a white powder, m.p. 136 °C. − $C_{31}H_{32}O_9S_3$ (644.77): calcd. C 57.66, H 5.06; found C 57.75, H 5.00. − ^1H NMR ($CDCl_3$): δ = 2.45 (s, 9 H, CH_3), 4.18 (s, 6 H, CH_2), 6.94−7.19 (m, 5 H, C_6H_5), 7.29 and 7.32 (d, *J* = 7.13 Hz, 6 H, Tos-H^2), 7.60 and 7.62 (d, *J* = 6.34 Hz, 6 H, Tos-H^3). − ^{13}C NMR ($CDCl_3$): δ = 21.7 (CH_3), 46.0 (C_6H_5-*C*), 68.9 (CH_2), 126.1 (C_6H_5-C^4), 127.6 (Tos-C^2), 127.9 (Tos-C^3), 128.7 (C_6H_5-C^2), 130.0 (Tos-C^3), 131.6 (Tos-C^4), 134.7 (C_6H_5-C^1), 135.2 (Tos-C^1).

1,1,1-Tris(azidomethyl)phenylmethane: 1,1,1-Tris[(4-tolylsulfonyl)-methyl]phenylmethane (3.22 g, 5 mmol) and NaN_3 (2.94 g, 45 mmol) in DMSO (50 mL) were stirred at 90 °C for three hours. After cooling to room temperature the solution was poured into water (250 mL). The suspension was then extracted with ethyl acetate (250 mL). The organic fraction was washed with a saturated ammonium chloride solution, and dried with anhydrous sodium sulfate. The solution was filtered and the solvent was carefully removed under vacuum yielding 1.471 g of a crude transparent oil which was used directly in the following step. − ^1H NMR ($CDCl_3$): δ = 3.65 (s, 6 H, C−CH_2N_3), 7.22−7.40 (m, 5 H, aromatics CH). − ^{13}C NMR ($CDCl_3$): δ = 46.9 (C_6H_5-*C*), 54.3 (CH_2), 126.2, 127.8 and 128.8 (aromatics CH), 138.3 (aromatic C). − IR (NaCl disk): ν_{N_3} = 2103 cm^{-1}.

1,1,1-Tris(aminomethyl)phenylmethane: 10% Pd/C (0.500 g) was added to a solution of 1,1,1-tris(azidomethyl)phenylmethane (1.28 g, 5 mmol) in anhydrous ethanol (25 mL) under argon. The solution was stirred under H_2 for 6 hours and then filtered through Celite, which was then washed with more ethanol. The solvent was removed under vacuum to yield 0.075g (99%) of a transparent oil. − $C_{10}H_{17}N_3$ (179.26): calcd. C 66.66, H 9.86, N 23.25; C 67.00, H 9.56, N 23.44. − ^1H NMR ($CDCl_3$): δ = 3.05 (s, 6 H, CH_2), 7.19−7.42 (m, 5 H, aromatics CH). − ^{13}C NMR ($CDCl_3$): δ = 45.4 (CH_2), 48.1 (C_6H_5-C), 125.2, 127.1 and 128.4 (aromatics CH), 141.7 (aromatic C).

1,1,1-Tris[di(*tert*-butylcarboxymethyl)aminomethyl]phenylmethane: 1,1,1-Tris(aminomethyl)phenylmethane (0.803 g, 4.72 mmol) was dissolved in acetonitrile (25 mL) by warming slightly. Potassium carbonate (7.834 g, 12 equiv.) and *tert*-butyl bromoacetate (11.056g, 12 equiv.) were then added and the solution stirred for one week at 60 °C. After cooling to room temperature the organic products were extracted with ethyl acetate. The organic layer was washed with saturated NaCl solution and dried with anhydrous sodium sulfate. After filtration the solvent was removed under vacuum to yield a crude oil, which was purified by column chromatography with silica gel and a cyclohexane/ethyl acetate gradient from 10:0 to 8:2. The product was obtained as an oil (0.590 g, 14.5%). MS (D/IC, NH_3 + isobutane): *m*/*z* = 864 $[M + 1]^+$. − ^1H NMR ($CDCl_3$): δ = 1.42 (s, 54 H, CH_3), 3.23 (s, 12 H, CH_2), 3.27 (s, 6 H, CH_2), 7.14−7.40 (m, 5 H, aromatics CH). − ^{13}C NMR ($CDCl_3$): δ = 28.18 (CH_3), 48.49 (C_6H_5-*C*), 56.44 (N*C*H_2CO_2tBu), 59.29 (C*C*H_2N), 80.40 [*C*(CH_3)$_3$], 125.82, 126.61 and 128.55 (aromatics CH), 144.69 (aromatic C), 171.19 (*C*O_2tBu).

1,1,1-Tris[di(carboxymethyl)aminomethyl]phenylmethane: 1,1,1-Tris[di(*tert*-butyl)aminomethyl]phenylmethane (0.200g, 0.232 mmol) in formic acid (5 mL, 97%) was stirred for three hours at 60 °C. The solvent was removed under vacuum and the residual product was dried overnight under vacuum to yield 0.120 g (98%) of product. − $C_{22}H_{29}N_3O_{12}\cdot 3H_2O$ (581.55): calcd. C 45.14, H 5.97,

N 8.70, O 36.63; C 45.43, H 6.02, N 7.23, O 41.30. Potentiometric analysis was consistent with this molecular weight. – ^{1}H NMR (D_2O, pD = 1.0): δ = 3.45 (s, 12 H, NCH_2CO$_2$H), 3.54 (s, 6 H, CCH_2N), 7.17–7.42 (m, 5 H, aromatics CH). – ^{13}C NMR (D_2O, pD = 1.0): δ = 48.00 (C_6H_5-*C*), 58.59 (N*C*H$_2$CO$_2$H), 63.30 (C*C*H$_2$N), 128.90, 130.79 and 132.06 (aromatics CH), 140.44 (aromatic C), 175.04 (CO$_2$ H). MS (FAB): *m*/*z* = 528 [M + 1]$^+$.

Potentiometric Titrations: All the measurements were made at 25 °C and the solutions were prepared with deionized and doubly distilled water. The ionic strength was fixed at I = 0.1 M with tetramethylammonium chloride (PROLABO puriss). The potentiometric titrations were performed using an automatic titrator system, DMS 716 Titrino (Metrohm), equipped with a combined glass electrode (Metrohm, filled with NaCl saturated solution) and connected to an IBM Aptiva microcomputer. The electrodes were calibrated to read pH according to the classical method.[13] The ligand and its metal(III) complex of ca. 0.001 M were titrated with standardized 0.025 M tetramethylammonium hydroxide. Argon was bubbled through the solutions to exclude CO_2 and O_2. Tetramethylammonium hydroxide solution was standardized against potassium hydrogenphthalate. Carbonate content was checked by Gran's method. The titration data were refined by the non-linear least-squares refinement program SUPERQUAD[6] to determine the deprotonation and/or stability constants (σ_{fit} in the range 1–5). Typically, about 150 data points were collected over the pH range 2.5–10.5 for the ligand solution and 100 points over the pH range 2.5–7 for the metal-ligand solution since precipitation occurred at a pH of about 7.5. The pK_{an} values were calculated from the cumulative constants determined by the program. The values of the stability constants are the mean values calculated from two or three titrations.

NMR Measurements: ^{17}O spectra (natural abundance) were recorded at 54.24 MHz on a Bruker AM 300 using 5 mm samples tubes. The ^{17}O shifts were referenced to the external $D_2{}^{17}O$ signal. The dysprosium-induced shifts (DIS) were obtained from the observed shift by making a correction for the bulk magnetic susceptibility of the solution. The solutions of the dysprosium complexes at a Dy^{III}/ligand molar ratio of 1 were prepared in doubly distilled water containing 20% D_2O. Concentrations ranged from 0.025 to 0.1 M. The pH was adjusted with tetramethylammonium hydroxide or HCl solution and measured by a pH meter employing a combined microelectrode and calibrated with standard buffers at pH 4.01, 6.86 and 10.01 from Polylabo.

[1] For reviews see: [1a] S. Jurisson, D. Berning, W. Jia, D. Ma, *Chem. Rev.* **1993**, *93*, 1137–1156. – [1b] C. J. Anderson, M. J. Welch, *Chem. Rev.* **1999**, *99*, 2219–2234. – [1c] W. A. Volkert, T. J. Hoffman, *Chem. Rev.* **1999**, *99*, 2269–2292. – [1d] F. Renaud, C. Piguet, G. Bernardinelli, J.-C. Bünzli, G. Hopfgartner, *J. Am. Chem. Soc.* **1999**, *121*, 9326–9342.

[2] A. Dupraz, P. Guy, C. Dupuy, *Tetrahedron Lett.* **1996**, *37*, 1237–1240.

[3] C. Dupuy, R. Viguier, A. Dupraz, *Synth. Commun.* **2001**, in press.

[4] V. Alexander, *Chem. Rev.* **1995**, *95*, 273–342.

[5] K. Hellmann, S. Friedrich, L. Gade, W-S. Li, M. McParthin, *Chem. Ber.* **1995**, *128*, 29–34.

[6] P. Gans, A. Sabatini, A. Vacca, *J. Chem. Soc., Dalton Trans.* **1985**, 1195–2000.

[7] M. C. Alpoim, A. M. Urbano, C. F. G. C. Geraldes, J. A. Peters, *J. Chem. Soc., Dalton Trans.* **1992**, 463–467.

[8] C. Cossy, A. C. Barnes, J. E. Enderby, A. E. Merbach, *J. Chem. Phys.* **1989**, *90*, 3254–3260.

[9] A. E. Martell, R. M. Smith, *Critical Stability Constants*, Plenum Press, New York, **1974**.

[10] D. M. Higgins, L. J. Zompa, *J. Coord. Chem.* **1977**, *7*, 105–112.

[11] Y. Moriguchi, M. Miyazaki, K. Ueno, *Bull. Chem. Soc. Japan* **1968**, *41*, 1344–1352.

[12] R. Viguier, Thesis, Université de Grenoble 1, **1999**.

[13] A. E. Martell, R. J. Motekaitis, *Determination and Use of Stability Constants*, 2nd ed., VCH Publishers, New York, **1992**.

Received January 5, 2001
[I01005]

Catalytic Activity Enhancement of a Cyclodextrin/Water-Soluble-Rhodium Complex System Due to its Gradual Supramolecular Organization in the Interphase

Michel Dessoudeix,[a] Martine Urrutigoïty,[a] and Philippe Kalck*[a]

Keywords: Biphasic catalysis / Cyclodextrins / Hydroformylation / Rhodium

Heavy terminal alkenes can be hydroformylated at a significant rate by using the water-soluble catalyst precursor $[Rh_2(\mu\text{-}S\textit{t}Bu)_2(CO)_2(TPPTS)_2]$ and β-cyclodextrin or its dimethylated form as phase-transfer agent. A study of the recycling has shown that the aqueous phase can be directly reintroduced into catalysis and also that each new run presents a slightly higher level of activity. Careful examination of the parameters of this catalysis leads us to propose that a gradual supramolecular organization in the interphase occurs for the rhodium complex, its solvation sphere and cyclodextrin which should involve at least two molecules in a head-to-tail or head-to-head arrangement.

Introduction

Homogeneous catalysts continue to play a prominent role as efficient tools to produce fine chemicals in enantioselective catalysis.[1,2] However, the separation of the catalyst from the reaction products is still one of the main concerns of chemists.[3] Among the various methods described in the literature,[3] the use of water soluble complexes with hydrophobic organic products, needing only a decantation step for the separation and the recycling of the catalyst, is increasingly popular. Nevertheless, for heavy substrates, the contact with the catalyst in the aqueous phase becomes the rate limiting step so that the use of cyclodextrins (CD's) as inverse phase-transfer agents appears to be an elegant way which preserves some economical viability.[4] Since the first report of the use of α-cyclodextrin in the hydroformylation reaction,[5] several studies have appeared to show that the transfer phenomenon is significantly enhanced between the organic phase and the aqueous phase where the catalyst is maintained.[6] In fact, it has been shown that CD — which is soluble in water but has poor solubility in polar solvents — forms inclusion complexes with both the substrate and the products transferring them into the aqueous phase. More recently, the efficiency of this process has been attributed to the greater complexation coefficient of the CD with the substrate than with the product.[7]

We have investigated the role of β-cyclodextrin and dimethyl-β-cyclodextrin in the biphasic low-pressure hydroformylation reaction of heavy alkenes catalyzed by the water-soluble complex $[Rh_2(\mu\text{-}S\textit{t}Bu)_2(CO)_2(TPPTS)_2]$. Various alkenes have been used as representative elements of heavy molecules and they range from C_8 to C_{18}. All the parameters of this reaction have been considered and their influence on the conversion rate and the regioselectivity analyzed. Moreover, the recycling of the aqueous phase containing both the catalyst and the cyclodextrin has been studied.

[a] Laboratoire de Catalyse, Chimie Fine et Polymères, Ecole Nationale Supérieure de Chimie de Toulouse,
118, route de Narbonne, 31077 Toulouse Cédex 04, France
E-mail: pkalck@ensct.fr

Results and Discussion

The general procedure adopted in the present experiments is 5 bar for the total pressure of a 1:1 H_2/CO mixture, a temperature of 80 °C and a stirring rate, for the mechanical stirrer of the autoclave, of 1870 rpm, i.e. in a chemical regime where the conversion rate does not depend on the stirring. Thus, the mass transfer of the substrate from the organic phase to the aqueous phase in which catalysis occurs remains constant. The stirring rate was adjusted to the same value from one experiment to another so that this parameter is not involved in the following discussion and does not affect the parameters which are analyzed.

We can recall[8] that, in the absence of cyclodextrin, oct-1-ene, whose solubility in water is only 2.07×10^{-3} g/L, is slowly transformed into the corresponding C_9 aldehydes since the yield is 11% in 20 h; the selectivity of *n*-nonanal vs. 2-methyloctanal is as high as 98% and is characteristic of a catalysis in pure water. After the addition of cyclodextrin in a oct-1-ene/cyclodextrin molar ratio of 28 and a β-CD/rhodium molar ratio of 18.4, the conversion rate reaches 26%, as shown in Table 1, and the linearity decreases to 88.5%. Such a lowering of the regioselectivity indicates that the medium where the catalytic activity of the system occurs is no longer completely aqueous and is, in fact, intermediate between aqueous and purely organic, since in a pure toluene phase previous experiments have shown a 75% selectivity. In Table 1 we have examined the effects of the chain length on the conversion. For dec-1-ene, the yield decreases to 6.2%, whereas the selectivity for the linearity is 90.2%. However, for higher alkenes, the reactivity is very modest and lies between 1 and 2% for C_{18} to C_{12} alkenes.

In order to improve significantly the mass transfer, we have used dimethylated-β-cyclodextrin (DM-β-CD) which

 © WILEY-VCH Verlag GmbH, 69451 Weinheim, 2001 1434−1948/01/0707−1797 $ 17.50+.50/0

Table 1. Evolution of the yield and the linearity as a function of the number of carbon atoms of the alkene; reaction conditions: P_T = 5 bar, T = 80 °C, time = 18 h, catalyst = 0.25 mmol, P/Rh = 10, H_2O = 40 mL, alkene = 64 mmol, β-CD = 2.3 mmol, DM-β-CD = 2.6 mmol

Number of carbon atoms	β-CD		DM-β-CD	
	Yield (%)	Linear aldehyde (%)	Yield (%)	Linear aldehyde (%)
8	26.2	88.5	59.1	88.7
10	6.2	90.2	50.7	90.2
12	2.1	n. d.	30.1	93.2
14	1.6	n. d.	8.3	85.5
16	1.4	n. d.	5.3	79.1

is much more soluble in water than β-CD itself (590 and 18.5 g/L, respectively). These results are displayed in Table 1. For oct-1-ene the conversion is greatly improved since it reaches 59.1%, instead of 26% for β-CD, the linearity being unchanged. In addition dec-1-ene and dodec-1-ene are readily transformed whereas the C_{14} and C_{16} alkenes are still converted but at a lower rate. In fact, the distinct behavior between β-CD and its dimethylated form stems mainly from the differences which exist in the hydrogen-bond network and in their steric hindrance, β-CD being rigid and DM-β-CD showing a significant flexibility. In fact, it seems that the height of the CD's and the size of the cavity play a dramatic effect along the chain length for its inclusion inside the cavity to a greater or lesser extent by minimizing the hydrophobic effect. Such a fitting allows the aliphatic chain to be coiled up with mainly the carbon−carbon double bond emerging from the torus. These results show that DM-β-CD rapidly transforms various heavy alkenes as opposed to β-CD which cannot convert an alkene heavier than oct-1-ene. We have checked that, in an equimolar mixture of C_8, C_{10} and C_{12} alkenes, β-CD discriminates in favor of oct-1-ene since 70% is converted.

The influence of the quantities of the two cyclodextrins introduced has been investigated in a wide range. Table 2 displays the yields, the selectivities in linear aldehyde and the turnover frequencies when β-CD is progressively added. β-CD begins to precipitate at 2.3 mmol. Of course, beyond this value the yields remain constant.

Table 2. Influence of the quantity of β-cyclodextrin on the yield and the linearity during the hydroformylation of oct-1-ene; reaction conditions: P_T = 5 bar, T = 80 °C, time =18 h, catalyst = 0.25 mmol, P/Rh = 10, H_2O = 40 ml, oct-1-ene = 64 mmol

β-CD (mmol)	Yield (%)	Linearity (%)	TOF (h^{-1})	TOF/β-CD ($h^{-1} \times mmol^{-1}$)
0	2	98	0.6	–
0.44	6	98	1.8	4.1
0.88	10.2	97	3.0	3.4
1.32	14.1	95	4.2	3.2
1.76	19.2	93	5.7	3.3
2.20	26.2	88.5	7.8	3.5
4.41	30.1	87.2	9.0	2.0

As shown in Figure 1, variation of the yield with the amounts of added cyclodextrin occurs almost linearly until a plateau is reached beyond 2.3 mmol. Similarly, the linearity decreases slowly from 98% (in the absence of β-CD) to 88% near to the 2.3 mmol point. It occurred to us to investigate the turnover frequencies calculated per mol of CD versus the quantities of β-CD, thus expressed in h^{-1} per mol (last column in Table 2). Instead of the expected straight line, we observed that the curve decreases until it reaches a minimum near 1.5 mmol (Figure 2), then increases to a local optimum value of 2.3 mmol.

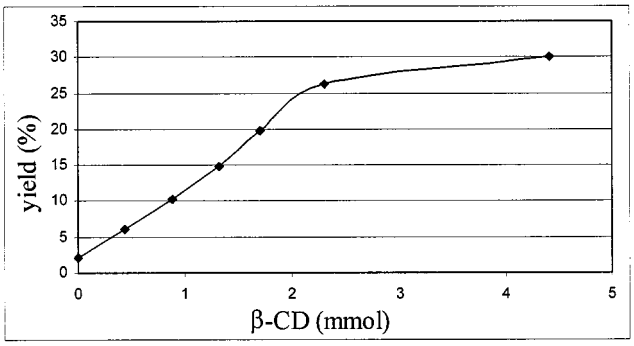

Figure 1. Variation of the yield versus quantity of β-CD

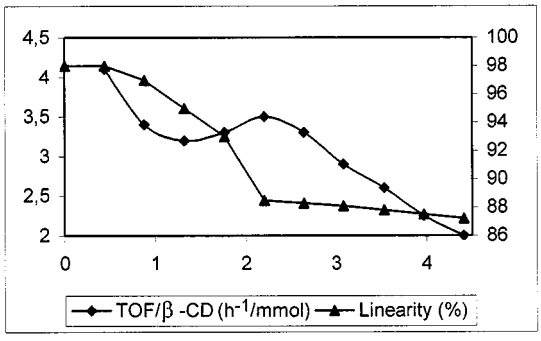

Figure 2. Curves of the TOF/β-CD and the linearity as a function of the quantity of β-CD

This phenomenon seems to be directly connected to the concentration of β-CD in the medium. An organization of the solvation sphere of the cyclodextrin should give a regular effect. We suggest that the observed effect could result from a particular arrangement of several cyclodextrin units. First, a decrease of the curve is consistent with an inhibiting effect which could be due to two CD's encapsulating one guest in a head-to-head manner.[9,10] The optimum value

Table 3. Evolution of the yield, the linearity and the TOF during recycling; reaction conditions: P_T = 5 bar,; T = 80 °C, time = 18 h, catalyst = 0.25 mmol, P/Rh = 10, H_2O = 40 mL, alkene = 64 mmol, DM-β-CD = 3.05 mmol

Recycling	Oct-1-ene			Dec-1-ene		
Yield (%)	Nonanal (%)	TOF (h^{-1})	Yield (%)	Undecanal (%)	TOF (h^{-1})	
0	65.9	85.0	19.7	65.5	89.7	19.6
1	80.0	88.6	23.9	69.1	89.3	20.6
2	87.5	86.8	26.1	73.0	88.8	21.8
3	91.1	85.7	27.2	84.7	87.6	25.3

should correspond to a peculiar arrangement of two or three β-CD's giving rise to a kind of tunnel, as already mentioned in the literature for the head-to-tail encapsulation of very large molecules.[11,12] The further decrease in the curve is due to the precipitation of β-CD (in the calculations the full quantity of β-CD has been introduced).

When the regioselectivity is considered, it is clear that the selectivity in linear aldehyde decreases dramatically for increasing amounts of β-CD. This unexpected decrease of the selectivity curve shows the role of the steric hindrance of the β-CD on the C=C double bond: in our opinion it is more and more included in the CD cavity thus providing preferential access of the terminal carbon to the hydride ligand in the step where the rhodium-alkyl species is formed (Figure 3). If the aim is to obtain the better yields of linear aldehydes, an examination of Figure 2 shows that a good compromise between the yield and the linearity lies in the range 1.76−2.20 mmol of β-cyclodextrin.

DM-β-CD shows similar trends, but for oct-1-ene, due to its too short chain length, only the inhibiting effect is observed, whereas for dec-1-ene and dodec-1-ene, the TOF/DM-β-CD versus the quantity of DM-β-CD remains constant, although a slight increase can be noted in the latter case. Here, the chain length is more adapted to the depth imposed by the arrangement of the two CD's. Except for oct-1-ene, which becomes more included inside the organophilic cavity and for which the linearity decreases as expected for an organic environment,[13] the linearity of the aldehydes formed from dec-1-ene and dodec-1-ene remains almost invariant showing once again the mutual adaptation of the two DM-β-CD's framework and these two alkenes.

Whereas recycling a catalyst produces generally either no variation in the yield or a decrease in the catalytic activity, we observed, on four successive runs, an important enhancement of the yield, with the linearity being almost the same (Table 3 and Figure 2).

Such an increase in the catalytic activity along the recycling means that the system keeps a sort of a local organization which improves the contact between the reactants. Indeed, from one run to the next, after decantation, the aqueous phase is directly recycled with no further work up. Thus, as this phase contains the cyclodextrin and the water-soluble rhodium complex, such a direct reintroduction does not disrupt the arrangement gained by the catalyst/cyclodextrin/substrate/solvent system during the previous run. The association of two cyclodextrin units, head-to-head or head-to-tail, is consistent with this hypothesis. We need also to consider how the organic/aqueous volume around the DM-β-CD/ $[Rh_2(\mu\text{-}S\textit{t}Bu)_2(CO)_2(TPPTS)_2]$ couple is organized. Indeed, the internal secondary alcohol groups inside the DM-β-CD torus are considered as hydrophobic whereas the external primary alcohol functions are compatible with the approach of water molecules. However, near the entrance of the cavity a mixed volume should be present containing toluene and water, especially at 80 °C, a temperature for which we are near the heteroazeotropic composition; the relative concentration of both solvents should vary, of course, inside this volume. The arrangement should associate the rhodium complex and the external part of the cyclodextrin(s) in the water-rich area and the alkene in the organic-rich part of this volume. Thus, such an organization could improve the transfer phenomenon from one run to the next. This system could possibly migrate more rapidly near the interface giving rise to a more efficient transfer of the alkene from the organic phase to the so-called aqueous phase. Such a view is not inconsistent with the association of two cyclodextrin units.

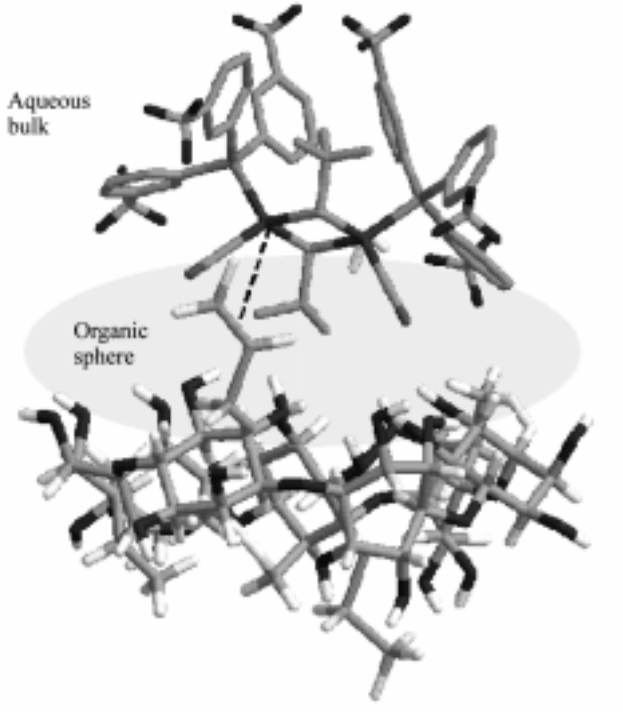

Figure 3. Scheme of the hydroformylation of oct-1-ene, using cyclodextrin, in the organic sphere

Conclusion

We can conclude that a solvation sphere is gradually organized in the volume where the cyclodextrin improves the contact between the carbon-carbon double bond and the rhodium center of the catalyst (Figure 3). This specific volume can be viewed as a supramolecular microreactor.

Experimental Section

Starting Materials: All reagents were purchased from Aldrich and used without further purification. Cyclodextrins are a generous gift from Wacker Chimie S.A. and tris(*m*-sodiumsulfonatophenyl)phosphane (TPPTS) a gift from Hoechst (Ruhrchemie). Rhodium trichloride trihydrate is a generous loan from Engelhardt-Comptoir-Lyon-Alemand-Louyot. The complex $[Rh_2(\mu\text{-}StBu)_2(CO)_2(TPPTS)_2]$ was prepared as previously described.[14]

Biphasic Catalysis: In a typical run, $[Rh_2(\mu\text{-}StBu)_2(CO)_2(TPPTS)_2]$ (0.25 mmol, 0.42 g) and TPPTS (4.5 mmol, 2.8 g) were dissolved in 40 mL of deaerated water in a Schlenk tube, and then 64 mmol of alkene was added. The reactor was evacuated and the solution introduced by suction. The reactor was then heated to 80 °C (preheated oil bath) under mechanical stirring (1870 rpm). When the temperature of 80 °C was reached, the autoclave was pressured with 5 bar of an equimolar CO/H_2 mixture. During the catalytic test, the pressure was kept constant and equal to 10 bar inside the reactor. After 18 h, the gas mixture feed was stopped and the reactor cooled to room temperature. The gas present inside the reactor was then slowly evacuated. After opening the reactor the biphasic solution was transferred by suction into a round-bottom flask and placed under nitrogen.

GPC: After catalysis the organic phases were analyzed by gas phase chromatography on a Carlo Erba HRGC 5160 apparatus equipped with a flame ionization detector and a capillary column Alltech Econocap FFAP (30m; 0.53 mm; 1.2μm), T_{det} = 200 °C, P_{H_2} = 0.5 bar.

Infrared Spectroscopy: Infrared spectra were recorded on a Perkin−Elmer 1710 FTIR apparatus.

[1] B. Cornils and W. A. Herrmann, in *Applied Homogeneous Catalysis with Organometallic Compounds − A Comprehensive Handbook in Two Volumes*, John Wiley & Sons, Chichester, **1996**.

[2] A. N. Collins, G. N. Sheldrake and J. Crosby, in *Chirality in Industry*, John Wiley & Sons, Chichester, **1997**.

[3] B. Cornils and W. A. Herrmann, in *Aqueous-Phase Organometallic Catalysis − Concept and Application*, John Wiley & Sons, Chichester, **1996**.

[4] W. Saenger, *Angew. Chem. Int. Ed. Engl.* **1980**, *19*, 344−362; K. A. Connors, *Chem. Rev.* **1997**, *97*, 1325−1357.

[5] J. R. Anderson, E. M. Campi, W. R. Jackson, *Catal. Lett.* **1991**, *9*, 55−58.

[6] E. Monflier, E. Blouet, Y. Barbaux, A. Mortreux, *Angew. Chem. Int. Ed. Engl.* **1994**, *33*, 2100−2102.

[7] E. Monflier, G. Fremy, Y. Castanet, A. Mortreux, *Angew. Chem. Int. Ed. Engl.* **1995**, *34*, 2269−2271.

[8] P. Kalck, L. Miquel, M. Dessoudeix, *Catal. Today* **1998**, *42*, 431−440.

[9] P. M. Ivanov, D. Salvatierra, C. Jaime, *J. Org. Chem.* **1996**, *61*, 7012−7018.

[10] J. Velasco, P. Guardado, C. Carmona, M. A. Muñoz, M. Balón, *J. Chem. Soc., Faraday Trans.* **1998**, *94*, 1469−1476.

[11] H. Asanuma, M. Kakazu, M. Shibata, T. Hishiya, M. Komiyama, *Chem. Commun.* **1997**, 1971−1972.

[12] M. Ceccato, P. Lo Nostro, C. Rossi, C. Bonechi, A. Donati, P. Baglioni, *J. Phys. Chem. B* **1997**, *101*, 5094−5099.

[13] Ph. Kalck, in *Organometallics in Organic Synthesis. Aspects of a Modern Interdisciplinary Field* (Eds.: A. de Meijere, H. tom Dieck), Springer, Heidelberg, **1987**, 297−320.

[14] Ph. Kalck, P. Escaffre, F. Serein-Spirau, A. Thorez, B. Besson, Y. Coleuille, R. Perron, *New J. Chem.* **1988**, *12*, 687−690.

Received June 22, 2000
[I00247]

Unique Evidence for a Rh^{III} to Rh^{I} Reduction by Deoxygenation of a Carbonate Moiety to CO_2 by an Out-of-Sphere Phosphane

Michele Aresta,[a] Angela Dibenedetto,[a] and Immacolata Tommasi*[a][‡]

Keywords: Carbon dioxide / Deoxygenation / Redox chemistry / Rhodium / Phosphanes

Rh^{III} carbonate generated from either a peroxocarbonate complex $[RhCl(CO_4)(PR_3)_3]$ or $[RhCl_3(PR_3)_3]$ and Na_2CO_3, is reduced to Rh^{I} by deoxygenation of the carbonate moiety to CO_2 by an out-of-sphere phosphane. The reaction takes place in mild conditions and is implied in the catalytic activity shown by Rh^{I} in the oxidation of styrene with O_2/CO_2 mixtures.

Introduction

Transition metal peroxo-carbonates have been known for some time.[1,2] They are usually prepared by reaction of metal dioxygen complexes with CO_2. Accordingly, Rh^{III} peroxocarbonates are easily obtained according to Equation (1). Alternatively, transition metal carbon dioxide complexes can react with dioxygen[3,4] to afford peroxocarbonates.

$$P_3RhCl + O_2 \longrightarrow P_3RhCl(O_2) \xrightarrow{CO_2} P_3RhCl(CO_4) \qquad (1)$$

By using labelled species, we have recently shown that CO_2 reacts with $Rh(\eta^2\text{-}O_2)$ complexes by insertion into the O−O bond (Scheme 1, path A), rather than by insertion into the M−O bond (Scheme 1, path B).[5] The reaction pathway has been demonstrated through coupling an IR theoretical study (calculation of the vibrational frequencies of selected bonds of the peroxocarbonate complexes) with experimental vibrational frequencies. The latter match the values calculated for the species obtained assuming CO_2 insertion into the O−O bond (± 2 cm^{-1})[5] better than those of products originating from CO_2 insertion into the M−O bond. This reaction has also been modelled using the Impulse Oscillation Model, IOM,[6−8] which assumes that the vibrations of the metal-dioxygen complex and CO_2 must be synchronised in order for the insertion reaction to occur. IOM unequivocally shows that path A is preferred (up to 92% selectivity) over path B.[9,10]

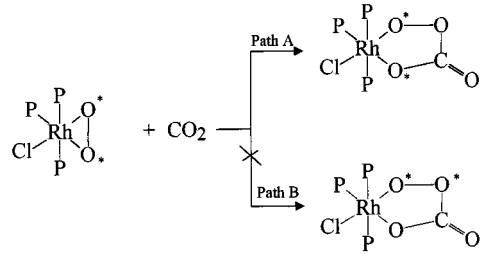

Scheme 1. Alternative pathways for CO_2 reaction with a Rh dioxygen complex

Very interestingly, the reaction of carbon dioxide metal complexes with dioxygen to afford peroxocarbonates proceeds through the substitution of coordinated CO_2 by dioxygen and subsequent insertion of CO_2 into the O−O bond of the newly formed dioxygen complex.[11]

We have also shown that peroxocarbonates may act as selective one-oxygen transfer agents to an oxophile (Scheme 2).[12−15] By using asymmetrically labelled species, we have demonstrated that the oxygen bonded to the metal is the atom of the peroxo group transferred to the oxophile.[5] The Rh peroxocarbonate is thus converted into a Rh^{III} carbonate complex.

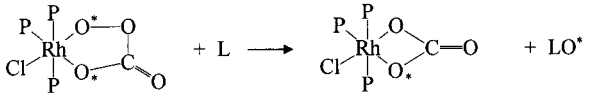

2 **3**

Scheme 2. One-oxygen transfer from the peroxocarbonate moiety to an oxophile

It should be noted that when the peroxocarbonate $[RhCl(CO_4)(PEt_2Ph)_3]$ acts as a one-oxygen transfer agent, the starting Rh^{I} complex $[RhCl(PEt_2Ph)_3]$ is found along with other compounds that undoubtedly originate from the peroxocarbonate. In principle, the Rh^{I} complex could be produced from the peroxocarbonate if the reaction in Equation (1) is reversible.

In an attempt to demonstrate if such a hypothesis holds or not, we have carefully investigated the reaction and have unequivocally shown that $[RhCl(PEt_2Ph)_3]$ originates from Rh^{III} carbonate $[RhCl(CO_3)(PEt_2Ph)_3]$, through an unprecedented carbonate deoxygenation to carbon dioxide promoted by an external phosphane. We describe in this paper some properties of Rh peroxocarbonate **2** and the reduction

[a] Dipartimento di Chimica, Università degli Studi di Bari, Campus Universitario,
Via Orabona, 4−70126 Bari, Italy
Fax: (internat.) +39-080/544-2429
E-mail: miares@tin.it
[‡] Present address: Université de Bourgogne, L.S.E.O. − UMR 5632 − Equipe V, Sciences Mirande 9,
av. Alain Savary BP 47870−21078 Dijon Cedex, France
E-mail: ada.tommasi@u-bourgogne.fr

 © WILEY-VCH Verlag GmbH, 69451 Weinheim, 2001 1434−1948/01/0707−1801 $ 17.50+.50/0

of carbonate **3** to $[RhCl(PEt_2Ph)_3]$. The latter reaction has also been performed using an external carbonate source (Na_2CO_3, Ag_2CO_3) and a Rh^{III} chloride complex.

Results and Discussion

Rh^{III} peroxocarbonate was prepared by reaction of $[RhCl(PEt_2Ph)_3(O_2)]$ with CO_2 at 240 K in toluene[4,5] according to Equation (1). The pure compound is quite stable at low temperature (below 240 K) in the solid state for several days or for several minutes at a temperature as high as 340 K (see Experimental Section). Conversely, in solution above 250 K, or in the solid state at 323 K in the presence of an external phosphane, or any other species that may interact with the Rh centre, it readily reacts and transfers one oxygen atom to an oxophile to afford the carbonate complex **3** (Scheme 2). It is worth recalling that olefins and tetrahydrofuran can be oxidised in this way under mild conditions by Rh peroxocarbonates.[13]

When pure **2** is dissolved in CH_2Cl_2 at 250 K, the ^{31}P NMR spectrum unequivocally shows the conversion of the peroxocarbonate (Figure 1, spectrum A) into a number of other species (Figure 1, spectrum B). These have all been identified by comparison with the spectra of authentic samples. Resonances a−g have been assigned as follows: (a) assigned to the $O{=}PEt_2Ph$ species; (b) and (e) assigned to the *mer*-$RhCl(CO_3)(PEt_2Ph)_3$ species; (c) and (f) assigned to the *mer*-$RhCl(CO_4)(PEt_2Ph)_3$ species; (d and g) assigned to the *mer*-$RhCl_3(PEt_2Ph)_3$ species (see Experimental Section).

It is evident from these data that **2** behaves differently whether it is pure or is in the presence of external ligands or a solvent. Moreover, the fact that a coordinated phosphane is not oxidised (we recall that pure **2** is stable up to 345 K), demonstrates that the O-transfer process is intermolecular, not intramolecular.

The reactivity in the solid state and in solution find a common basis of interpretation. However, in solution the oxygen transfer is promoted by the solvent, which causes the phosphane dissociation (Scheme 3, path a).

The out-of-sphere phosphane formed in solution attacks the peroxo group affording carbonate and phosphane oxide (Scheme 3, path a). The latter may be found free in solution or coordinated to Rh, according to the nature of solvent.

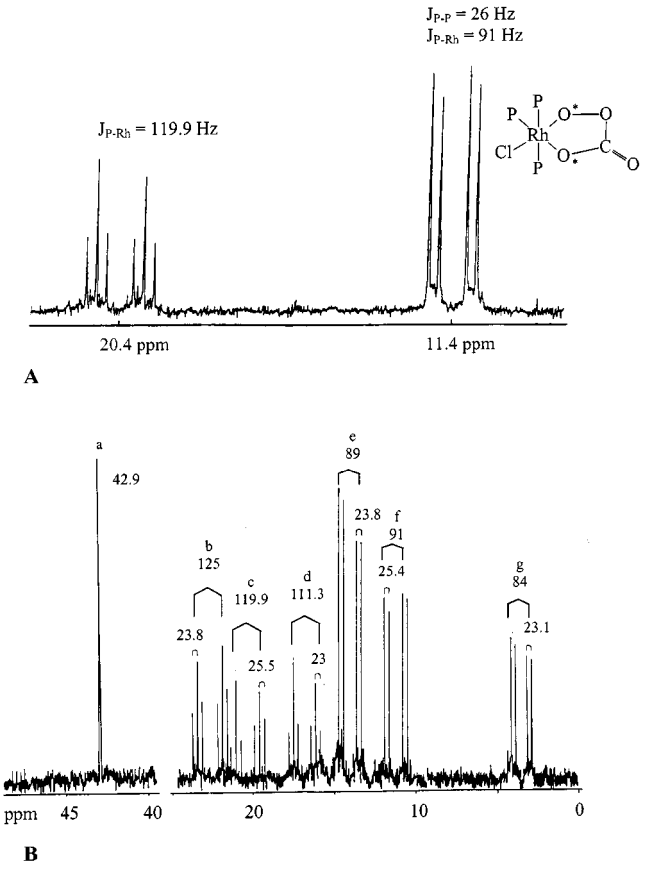

Figure 1. Spectrum A: ^{31}P NMR spectrum (213 K, CD_2Cl_2) of $[RhCl(CO_4)(PEt_2Ph)_3]$; spectrum B: ^{31}P NMR (CD_2Cl_2) spectrum of the solution from A warmed to 250 K

However, when solid Rh peroxocarbonate is warmed to 340 K with an equimolar amount of ethylene, phosphane is slowly released and then rapidly oxidised by the peroxocarbonate to Et_2PhPO (Scheme 3, path b). The selectivity of phosphane oxidation with respect to ethylene is 100%, as demonstrated by the gas-phase analysis which does not show the presence of ethylene oxidation products. The role of ethylene is therefore that of favouring the phosphane release from the Rh coordination sphere. Conversely, if more reactive olefins like styrene are used, in excess with respect to the stoichiometric ratio and under CO_2/O_2 atmosphere, they can be oxidised in solution by Rh peroxocarbonates (Scheme 4).

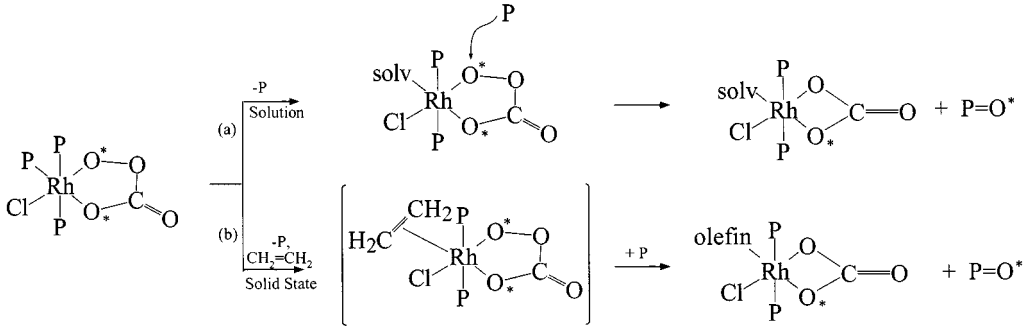

Scheme 3. Reactivity of $[RhCl(CO_4)(PR_3)_3]$ in solution (path a) and in the solid state in the presence of ethylene (path b)

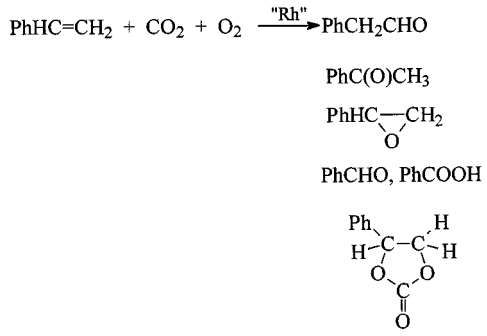

Scheme 4. Reaction of styrene with a CO_2/O_2 mixture promoted by Rh^{I}

Styrene is converted into a mixture of phenylacetaldehyde, phenylmethylketone and styrene epoxide, as major products, along with benzaldehyde which is produced by the cleavage of the styrene C−C double bond by O_2. It is worth noting that Rh peroxocarbonates and Rh dioxygen complexes show a different behaviour towards styrene oxidation.[5,13−18] While the dioxygen complex causes the cleavage of the double bond [Equation (2)], the peroxo-carbonate promotes a one-oxygen transfer to the olefin, mimicking mono-oxygenase enzymes (Scheme 4).

$$RHC{=}CH_2 + O_2 \longrightarrow RHCO + H_2CO \qquad (2)$$

The formation of the ketone and phenylacetaldehyde can be explained assuming a hydrogen shift promoted by the metal centre (Scheme 5).

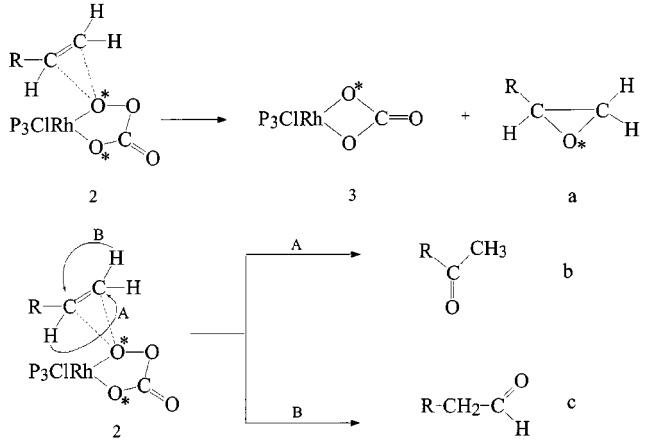

Scheme 5. Formation of ketone and terminal aldehyde by H-migration promoted by Rh^{I}

In such an oxidation reaction, if Rh complexes stabilised by monodentate P ligands are used, the catalyst has a lifetime of less than one hour. In fact, the reaction with the olefin releases the phosphane, which is easily oxidised according to Equation (3):

$$\underset{\mathbf{2}}{(PEt_2Ph)_3RhCl(CO_4)} + \text{olefin} \longrightarrow (\text{olefin})(PEt_2Ph)_2RhCl(CO_3) + P{=}O \qquad (3)$$

The phosphane oxidation can go on in the presence of an excess of olefin until complex **2** is totally converted into other species that are not active catalysts. The use of bidentate phosphanes or chelating nitrogen ligands, like dipyridyl or phenanthroline, stabilises the catalyst for up to two to three hours,[14,16] after which it has been converted into inactive species. The mechanism of deactivation of the catalyst when monodentate or bidentate ligands are used is quite different. In the case of monodentate ligands, as we have reported above, the oxidation of the dissociated phosphane causes the destruction of the catalyst [Equation (3)], whereas in the case of bidentate ligands, ligand scrambling causes the destruction of the active catalytic species as shown in Equation (4). In fact, the square-planar moiety "$Rh(L\text{-}L)_2$" (where L-L is a bidentate phosphane) is not active in catalysis as it does not promote the formation of the peroxocarbonate because two *cis*-positions are not available. Similarly, the olefin complex does not coordinate either dioxygen or CO_2.

$$2\,Rh(L\text{-}L)Cl + n\,(\text{olefin}) \longrightarrow \underset{\mathbf{5}}{Rh(L\text{-}L)_2Cl} + \underset{\mathbf{6}}{Rh(\text{olefin})_nCl} \qquad (4)$$

Compound **5** has been isolated from the reaction solution and its nature confirmed by comparison with an authentic sample. As reported above, the oxygen transfer reaction assumes a particular importance when olefins or ethers are used,[13] affording useful products. Peroxocarbonates can therefore be used to promote the transfer of a single oxygen atom of the original dioxygen molecule to an oxophile. The reaction path and products are reported in Scheme 5. In the case of an olefin, carbocation **6** could be the intermediate[13] that generates epoxides, aldehydes and ketones. The oxygen transfer reaction has been also modelled using IOM.[17,18] Very interestingly, if styrene is used (Scheme 4), the calculated distribution of products is very close to the experimental one.

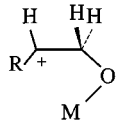

7

Scheme 6. Formula of compound **6**

When peroxocarbonates react as oxidant towards an external phosphane or, in general when they act as one-oxygen transfer agents, as reported above, the carbonate is formed, as demonstrated by spectroscopic techniques (IR, NMR). The ^{31}P NMR spectrum shows a doublet of doublets (dd) at $\delta = 14.2$ ($J_{P\text{-}P} = 23.8$ Hz, $J_{P\text{-}Rh} = 89$ Hz) and a doublets of triplets (dt) at $\delta = 22.7$ ($J_{P\text{-}Rh} = 125$ Hz). These signals are also found in the ^{31}P spectrum when a solution of **2** in CD_2Cl_2, prepared at 240 K, is heated to room temperature. Interestingly, when the oxygen transfer occurs from the peroxocarbonate to the external phosphane, the

final reaction mixture shows the presence of a ^{31}P signal that can be attributed to $[RhCl(PEt_2Ph)_3]$.[19]

The formation of this species might be explained in terms of a reversible dissociation of CO_2 from the peroxocarbonate to afford the dioxygen complex that may give back $[RhCl(PEt_2Ph)_3]$ [Equation (1)]. We have tried to prove this hypothesis by GC-MS analysis and found that dioxygen is not detected. Conversely, CO_2 is released and, if labelled O_2 is used in the synthesis of the peroxocarbonate, a semi-labelled ^{18}O species is formed. Moreover, if a phosphane is added to the Rh carbonate formed from the peroxocarbonate after oxygen-transfer to the external oxophile, phosphane oxide is formed together with $[RhCl(PEt_2Ph)_3]$ [Equation (5)].

$$\underset{\mathbf{3}}{P_3ClRh(CO_3)} + P \longrightarrow \underset{\mathbf{4}}{P_3RhCl} + P{=}O + CO_2 \qquad (5)$$

This behaviour suggests that CO_2 could originate from a mechanism in which the carbonate is implicated in the phosphane oxidation. As a matter of fact we have performed a number of reactions which have clearly demonstrated that the "Rh^{III} carbonate ion" system can transfer one oxygen atom to the phosphane with formation of phosphane oxide and CO_2. The amount of CO_2 has been evaluated by a GC of the gas phase. The GC-MS spectrum of the gas phase also shows that if the carbonate has one ^{18}O oxygen atom that is used for binding the CO_3^{2-} moiety to the metal, the resulting CO_2 has ca. 50% of ^{18}O, as does the phosphane oxide (Scheme 7).

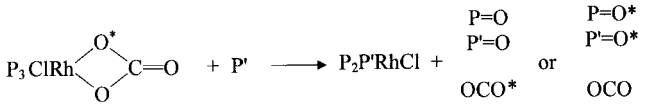

Scheme 7. Carbonate deoxygenation by an external phosphane ligand

The conversion of the carbonate to CO_2 with oxygen transfer to a substrate is reminiscent of the reaction of inorganic carbonates which form CO_2 and the metal oxide when heated at high temperature [Equation (6)].

$$MCO_3 \xrightarrow{1000\text{-}1200\ K} MO + CO_2 \qquad (6)$$
$$M = Ca, Mg$$

The release of CO_2 from coordinated carbonate complexes is not a trivial process. To the best of our knowledge, it has not been documented in the literature with phosphane as the reducing agent. It is known that hydrogen at high temperature and pressure is able to deoxygenate carbonates into carbon dioxide. In fact, $CoCO_3$ has been used for the synthesis of $Co_2(CO)_8$ with H_2 at 673 K.[20] Therefore, we decided to investigate if an external carbonate ion could itself undergo the deoxygenation reaction under mild conditions. We have thus reacted $[RhCl_3(PEt_2Ph)_3]$ with Na_2CO_3 or Ag_2CO_3 in the presence of a free phosphane. Interestingly, the reaction occurs at 353 K according to Equation (7) and (8), respectively.

$$(PEt_2Ph)_3RhCl_3 + Na_2CO_3 + P' \rightarrow (PEt_2Ph)_3RhCl + 2\,NaCl + P'{=}O + CO_2$$
$$P' = PCy_3 \qquad (7)$$

$$(PEt_2Ph)_3RhCl_3 + Ag_2CO_3 + 2\,P' \rightarrow 1/2\,[(PEt_2Ph)_2RhCl]_2 + 2\,(PEt_2Ph)AgCl + P'AgCl + P'{=}O + CO_2$$
$$P' = PEt_2Ph,\ PCy_3 \qquad (8)$$

In Equation (7), NaCl was isolated by extraction with water, and the Rh^I complex was isolated by recrystallisation from pentane. The latter has been characterised by elemental analysis, and its spectroscopic properties compared with those of an authentic sample. If PCy_3 is added as external phosphane, $O{=}PCy_3$ is the most abundant phosphane oxide, with minor amounts of $O{=}PEt_2Ph$. A limited degree of phosphane scrambling is observed (ca. 10%). Equation (7) represents a quite unique and interesting reaction, if one considers that the release of CO_2 from Na_2CO_3 requires high temperatures (>1000 K).[21] Ag_2CO_3 behaves in the same way. However, coordination to Rh lowers the decomposition temperature of the carbonate by more than 600 K. This finding rationalizes the behaviour of peroxocarbonate **2** and elucidates the reaction pathway relevant to Rh catalysis in styrene oxidation-carbonation,[12–15] allowing us to propose the cycle represented in Figure 2 for the Rh^I–Rh^{III} cyclic conversion.

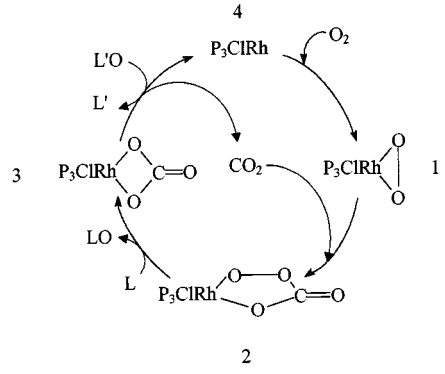

Figure 2. Double one-oxygen transfer to two different substrates from an O_2 molecule mediated by a Rh^I–Rh^{III}–Rh^I shuttle with the intermediacy of peroxocarbonate moiety; a ligand (P, L) scrambling is also observed

At the same time, the reduction of Rh^{III} to Rh^I explains the catalytic role of the metal. In fact, without reduction to Rh^I, only a stoichiometric reaction is observed in the O-transfer to the olefin from the peroxocarbonate complex. The observed turnover number. which is higher than one, can be interpreted only on the basis of a $Rh^{III} \rightarrow Rh^I$ reduction and reactivation of the catalyst.

Conclusions

The unprecedented deoxygenation of a carbonate ion to CO_2 in the presence of Rh^{III} has been observed. This finding represents an interesting new piece of chemistry demon-

strating that coordination of the carbonate anion allows the lowering of its decomposition temperature by more than 600 °C. However, this finding allows us to rationalise the catalytic role of Rh^{I} in the oxidation of styrene to styrene epoxide and other one-oxygen transfer products in an O_2/CO_2 atmosphere, with the intermediacy of peroxocarbonate−carbonate−carbon dioxide complexes.

Experimental Section

General: Unless otherwise stated, all reactions and manipulations were conducted under a dinitrogen or CO_2 atmosphere by using vacuum line techniques. All solvents were dried as described in the literature[22] and stored under dinitrogen. CO_2 (≥99.95%) and O_2 (≥99.98%) were purchased from Air Liquide Spa. The $RhCl(PR_3)_3$ complexes were prepared from $[RhCl(C_2H_4)]_2$ (Aldrich) and the corresponding phosphanes (Aldrich) according to previously reported experimental procedures.[4] The synthesis of $RhCl[^{18}O^{16}OC(^{16}O)^{18}O](PEt_2Ph)_3$ has been described previously.[5]

^{31}P NMR spectra were obtained at 81 MHz with a Varian XL-200 instrument. ^{31}P chemical shifts are referred to 85% H_3PO_4 using the high-frequency-positive convention. FTIR spectra were recorded using a Bruker 113V Fourier transform interferometer. Frequencies are accurate to ±1 cm^{-1}. Solid samples were studied as Nujol mulls (Nujol was previously dried over sodium wire and deoxygenated with argon). GC analyses were performed with a HP 5890 Series II gas chromatograph equipped with an Alltech-Heliflex AT-1000 capillary column (30 m × 0.00025 m, 0.2 μm thickness). GC-MS analysis was carried out with a gas chromatograph SHIMADZU 17 A-1000 (capillary column: 30 m × 0.00025 m, 0.25 μm thickness) detector linked to a SHIMADZU GCMS-QP 5050 mass spectrometer. GC analysis of gaseous phases was carried out with a gas chromatograph DANI equipped with a Carbowax column 3 m × 2.1 mm (ID) and TCD detector.

Study on the Thermal Stability of $(PEt_2Ph)_3RhCl(CO_4)$: a) Solid $[RhCl(CO_4)(PEt_2Ph)_3]$ (0.050 g, 0.07 mmol) was heated at 338 K for 10 min. under a dinitrogen atmosphere into Cell (a) (Figure 3) that was then connected to a GC and the gas phase analysed with a TCD. The GC analysis showed the absence of CO_2. The IR analysis of the solid showed that no reaction had occurred.
b) Analogous results were obtained when C_2H_4 was admitted into the cell and the system heated for 1−2 min. at 340 K. A longer reaction time produced a conversion of the Rh complex (see below).

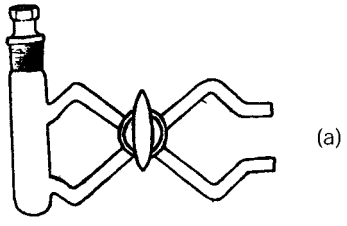

Figure 3. Apparatus used for the analysis of the gas phase in equilibrium with a solid

Conversion of $[RhCl(CO_4)(PEt_2Ph)_3]$ in CD_2Cl_2: A solution of **2** in CD_2Cl_2 was prepared at 213 K and the NMR spectrum recorded (Figure 1, spectrum A). The solution was heated to 250 K for 20 min. and the ^{31}P NMR spectrum recorded at this temperature (Figure 1, spectrum B). Heating produced the oxygen transfer to the phosphane. The following compounds were identified: *trans*-$RhCl(CO)(PEt_2Ph)_2$: δ = 26.0 (d, $J_{P\text{-}Rh}$ = 128.7 Hz); *mer*-$RhCl_3(PEt_2Ph)_3$: δ = 3.7 (dd, $J_{P\text{-}Rh}$ = 84 Hz, $J_{P\text{-}P}$ = 23.1 Hz), 16.9 (dt, $J_{P\text{-}Rh}$ = 111.3 Hz); *mer*-$RhCl(CO_3)(PEt_2Ph)_3$: δ = 14.2 (dd, $J_{P\text{-}Rh}$ = 89 Hz, $J_{P\text{-}P}$ = 23.8 Hz), 22.7 (dt, $J_{P\text{-}Rh}$ = 125 Hz); O=PEt_2Ph: δ = 42.9.

Reaction of $[RhCl(CO_4)(PEt_2Ph)_3]$ with PEt_2Ph: a) Solid **2** was heated with an equimolar amount of PEt_2Ph at 320 K under dinitrogen. The IR spectrum of the mixture showed the appearance of phosphane oxide (1150 cm^{-1}) within 4 hours and the formation of Rh^{III} carbonate (IR band at 1660 cm^{-1}), which was isolated from the mother mixture.

b) Compound **2** in CH_2Cl_2 solution was treated with an equimolar amount of PEt_2Ph at room temperature under dinitrogen. The solution was monitored at intervals of time by GC and GC/MS. The formation of phosphane oxide was clearly demonstrated to be a product of the oxidation process.

Reaction of Solid $[RhCl(CO_4)(PEt_2Ph)_3]$ with C_2H_4: Solid $[RhCl(CO_4)(PEt_2Ph)_3]$ (0.05 g, 0.07 mmol) was stirred at room temperature under a C_2H_4 atmosphere. The reaction was monitored by GC analysis of the equilibrium gas. No ethylene oxidation products were detected in the gas or solid phase, while in the solid phase phosphane oxide [^{31}P NMR: δ = 42.9 (s)] appeared after a couple of days. After a week the solid completely changed its appearance and the reaction was stopped and the solid analyzed by ^{31}P NMR spectroscopy. The residual solid was a mixture of compounds which had a ^{31}P spectrum close to that shown in Figure 1B. If an inert gas was used instead of ethylene, the complex lasted for a much longer time under the same experimental conditions.

Reaction of $(PEt_2Ph)_3RhCl(CO_4)$ with Styrene: Styrene (0.1 mL) in THF (2 mL) was added to **2** (0.100 g, 0.16 mmol) under a CO_2/O_2 atmosphere (10:1 v/v) and the solution stirred at room temperature. At intervals of 30 min., a sample was withdrawn and analysed by GC/MS. The presence of the following products was ascertained: benzaldehyde, phenylacetaldehyde, phenyl methyl ketone and styrene epoxide in a molar ratio 1:3:3:5. Benzoic acid and styrene carbonate were also present.

Reaction of $[RhCl_3(PEt_2Ph)_3]$ with Na_2CO_3: $[RhCl_3(PEt_2Ph)_3]$ (0.200 g, 0.3 mmol) was dissolved in toluene (5 mL) and a stoichiometric amount of Na_2CO_3 (0.031 g, 0.3 mmol) and free phosphane (0.050 g, 0.3 mmol) added. The reaction mixture was heated to 353 K. After 1 hour the GC analysis of the gas phase revealed the presence of CO_2 while in solution the free phosphane and phosphane oxide were detected. After 24 h, the amount of CO_2 in the gas phase increased to almost reach a CO_2/Rh ratio of 0.5. CO_2 was also present in solution. The total amount of released CO_2 allowed us to estimate when the reaction had reached completion. NaCl separated from the solution and was isolated by filtration. Its mass was 95% of the expected stoichiometric amount. From the mother solution 0.150 g of crude $[RhCl(PEt_2Ph)_3]$ was isolated, which was then crystallised from pentane. − $C_{30}H_{45}ClP_3Rh$ (636.97): calcd. C 56.57, H 7.12, Cl 5.57, P 14.59; found C 56.03, H 7.01, Cl 5.61, P 15.03.

Reaction of $(PEt_2Ph)_3RhCl_3$ with Ag_2CO_3: $[RhCl_3(PEt_2Ph)_3]$ (0.140 g, 0.2 mmol) was dissolved in CH_3CN (3 mL) and a stoichiometric amount of Ag_2CO_3 (0.050 g, 0.2 mmol) and PEt_2Ph (0.030 g, 0.2 mmol) were added. The reaction mixture was heated to 353 K. After 1 hour the GC analysis of the gas phase revealed

the presence of CO_2. After 24 h the gas phase showed an increased amount of CO_2 and from the solution a whitish-yellow solid separated, which was filtered, washed with pentane and dried in vacuo. It was analyzed as $AgCl(PEt_2Ph)$. From the solution $[RhCl(PEt_2Ph)_2]_2$ was isolated together with $O{=}PEt_2Ph$. The dimer was characterized by elemental analysis and its spectroscopic properties were compared to an authentic sample. – $C_{18}H_{33}AgClP$ (423.75): calcd. C 51.01, H 7.85, P 7.30, Cl 8.36; found C 50.85, H 7.54, P 7.10, Cl 8.16. – $C_{40}H_{60}Cl_2P_4Rh_2$ (941.54): calcd. C 51.03, H 6.42, Cl 7.53, P 13.16; found C 50.90, H 7.70, Cl 8.01, P 7.03.

In one run we used PCy_3 as the external phosphane. This was essentially totally converted into $O{=}PCy_3$. The isolated Rh complexes showed that some phosphane scrambling also took place and mixed phosphane species were obtained. The exchange did not exceed 10–15%, as demonstrated by ^{31}P NMR spectroscopy.

Acknowledgments

The MURST (Project no. 9803026360) is gratefully acknowledged. The authors thank Dr. M. Miglietta for some experimental assistance.

[1] P. J. Hayward, D. M. Blake, G. Wilkinson, C. J. Nyman, *J. Am. Chem. Soc.* **1970**, *92*, 5873–5878.
[2] L. Malatesta, R. Ugo, *J. Chem. Soc.* **1963**, 2080–2082.
[3] M. Aresta, C. F. Nobile, *J. Chem. Soc., Dalton Trans.* **1977**, 708–714.
[4] M. Aresta, E. Quaranta, A. Ciccarese, *C1 Mol. Chem.* **1985**, *1*, 267–281.
[5] M. Aresta, I. Tommasi, E. Quaranta, C. Fragale, J. Mascetti, M. Tranquille, F. Galan, M. Fouassier, *Inorg. Chem.* **1996**, *35*, 4254–4260.
[6] M. Borowiak, *J. Mol, Catal.*, **2000**, in press.
[7] COST-D3/007/94 Project: "Modelling of selective energy transfer, spatial and time coherence in catalytic reactions, tested on carbon dioxide reactions", **1998** Report.
[8] M. Aresta, E. Quaranta, I. Tommasi, J. Mascetti, M. Tranquille, M. Borowiak, in *Advances in Chemical Conversion for Mitigating Carbon Dioxide*, Studies in Surface Science and Catalysis (Eds.: T. Inui, M. Anpo, K. Izui, S. Yanagida, T. Yamaguchi), Elsevier Science B. V., **1998**, 114, 677–680.
[9] M. Aresta, E. Quaranta, I. Tommasi, *Proceedings of the 215th ACS National Meeting*, Dallas, Texas, March 29–April 2, **1998**, COLL 086.
[10] M. Aresta, M. A. Borowiak, M. G. H. Jamroz, I. Tommasi, E. Quaranta, *J. Mol. Catal. A* **2000**, in press.
[11] M. Aresta, I. Tommasi, A. Dibenedetto, M. Fouassier, J. Mascetti forthcoming paper.
[12] M. Aresta, E. Quaranta, A. Ciccarese, *J. Mol. Catal.* **1987**, *41*, 355–359.
[13] M. Aresta, C. Fragale, E. Quaranta, I. Tommasi, *J. Chem. Soc., Chem. Commun.* **1992**, 315–317.
[14] M. Aresta, A. Dibenedetto, *Proceedings of the X Congresso Brasileiro de Catalise*, 22–24 September **1999**, Salvador, Bahia, Brazil, 410–413.
[15] M. Aresta, A. Dibenedetto, *Appl. Organomet. Chem.*, in press.
[16] M. Aresta, A. Dibenedetto, I. Tommasi, *Proceedings of the International Symposium on CO_2 conversion and utilisation in refinery and chemical processing*, ACS Meeting, March 26–30, **2000**, San Francisco, 108–109.
[17] First workshop of the COST D9 Action, *Advanced Computational Chemistry of Increasingly Complex Systems*, July 2–4, **1999**, Geneva, Switzerland.
[18] J. C. Dobrowolski, M. H. Jamroz, J. K. Kazimirski, K. Bajdor, M. Borowiak, R. Larsson, *J. Mol. Struct.* **1999**, *483*, 183–187.
[19] According to the temperature and time of permanence in chlorinated solvents, $[RhCl_3(PR_3)_3]$ may also be formed, M. Aresta, M. Rossi, A. Sacco, *Inorg. Chim. Acta* **1969**, *3*, 227–231.
[20] K. Yamamoto, K. Sato Japan Pat., (mar 9, 1953); *Chem. Abstr.* **1954**, *48*, 2996.
[21] Y. A. Chang, H. Ahamad, *Thermodynamic Data on Metal Carbonates and Related Oxides*, Warrendale, Pa.: Metallurgical Society of AIME, **1982**.
[22] D. D. Perrin, W. L. Armarego, D. R. Perrin, *Purification of Laboratory Chemical* Pergamon Press, Oxford, England, **1986**.

Received September 6, 2000
[I00334]

New Mn^{II} Complexes with an N/O Coordination Sphere from Tripodal *N*-Centered Ligands − Characterization from Solid State to Solution and Reaction with Superoxide in Non-Aqueous and Aqueous Media

Clotilde Policar,*[a] Stéphanie Durot,[a] François Lambert,[a] Michèle Cesario,[b] Florence Ramiandrasoa,[a] and Irène Morgenstern-Badarau[a]

Keywords: Carboxylate ligands / Bridging ligands / Tripodal ligands / Manganese / SOD mimics

The crystal structure of a dimeric bis(μ-carboxylato)$Mn^{II}Mn^{II}$ complex (**2**) with a tetradentate *N*-centered tripodal ligand, *N*,*N*-bis[(1-methylimidazol-2-yl)methyl]glycinate, is presented. The carboxylates are bridging monodentate. This complex shows some striking differences to the previously published parent compound **1** obtained with the closely related ligand *N*-[(1-methylimidazol-2-yl)methyl]-*N*-(2-pyridylmethyl)glycinate. The carboxylato bridges in both structures are shown to be disrupted in solution. The reactivities in solution of compounds **1** and **2** toward superoxide were studied. In anhydrous DMSO solutions, a pathway involving a bis(μ-oxo)$Mn^{III}Mn^{IV}$ complex was identified. In water solutions, IC_{50} values were measured by the Fridovich test (1.7 ± 0.2 μM for **2** and 2.0 ± 0.2 μM for **1**), which showed these complexes to be good superoxide scavengers. Association constants for the complexes were estimated by means of a method based on IC_{50} measurements of the complexes under several conditions (alone and in the presence of excess ligand). They were found to be consistent with literature data.

Introduction

Superoxide ($O_2^{\cdot-}$) is the product of single-electron reduction of dioxygen. It is the first species in the dioxygen reduction cascade en route to hydrogen peroxide (H_2O_2) and the hydroxyl radical ($HO^{\cdot}$), and is known to be involved in oxidative stress.[1−5] Superoxide dismutases (SODs)[6] are metalloenzymes that actively protect cells against oxidative stress. They catalyze the dismutation of superoxide anion $O_2^{\cdot-}$ to hydrogen peroxide and oxygen. These enzymes can be classified into two major structural families, namely copper−zinc SODs and manganese or iron SODs.[1,5,7−9] SODs based on nickel have also been described,[10,11] but these have been much less well studied. Many complexes have been isolated and studied as superoxide scavengers. Such complexes contain either copper,[12−16] iron,[17−25] or manganese.[23,26−45] In our laboratory, two families of ligands have been developed with a view to obtaining iron or manganese complexes that might possibly react with superoxide. One family has been based on heptadentate polyamine hindered ligands,[19,38] while the other has been designed so as to reproduce the chemical environment of the active site in Mn and Fe SODs. In these enzymes, the first coordination sphere is a common feature, with an N_3O_1 set of ligand donors made up of three histidines and one monodentate carboxylate group, one histidine being more distant than the other ligands.[46−50] Nitrogen-centered tripodal tetradentate ligands have been synthesized with three appended moieties [two aromatic amines (pyridine or *N*-methylimidazole) and one carboxylate group], chosen in order to mimic the three closer ligands. Iron complexes have already been reported.[21,22] Manganese complexes are now being studied. Compound **1**, involving manganese(II) and *N*-[(1-methylimidazol-2-yl)methyl]-*N*-(2-pyridylmethyl)glycinate, hereafter referred to as IPG [acronym for (imidazolyl)(pyridyl)glycinate], has been described previously. It was shown to crystallize from MeOH with an infinite helical polymeric structure.[51] We describe herein the crystal structure of compound **2**, obtained from the closely related ligand *N*,*N*-bis[(1-methylimidazol-2-yl)methyl]glycinate [BIG; acronym for bis(imidazolyl)glycinate] and manganese(II). It crystallizes from water as a dinuclear bis(μ-carboxylato)-$Mn^{II}Mn^{II}$ complex. The reactivities in solution (anhydrous DMSO and aqueous buffer) of compounds **1** and **2** toward superoxide have been investigated and the results are reported herein.

[a] Laboratoire de Chimie Bio-organique et Bio-inorganique, FRE 2127, Bâtiment 420, Université Paris XI,
91405 Orsay Cedex, France
Fax: (internat.) + 33-1/69157231
E-mail: cpolicar@icmo.u-psud.fr
[b] Laboratoire de Cristallochimie, Institut de Chimie des Substances Naturelles du CNRS,
91198 Gif-sur-Yvette, France

Results

Synthesis of the Ligands

A given *N*-centered dissymmetric tripod can be synthesized by several pathways, depending on the order in which the different moieties are introduced. The yield-limiting step is usually the tertiarization of the amine. When this step is performed by reductive amination, improved yields over other synthetic methods are achieved, as previously reported in the case of *N*-[(1-methylimidazol-2-yl)methyl]-*N*-

 © WILEY-VCH Verlag GmbH, 69451 Weinheim, 2001 1434−1948/01/0707−1807 $ 17.50+.50/0

(2-pyridylmethyl)glycinate (IPG).[51] We report here a high-yielding, one-step synthesis of the ligand *N*,*N*-bis[(1-methylimidazol-2-yl)methyl]glycinate (BIG). A three-step synthesis of BIG has been published previously, which involved the preparation of *N*,*N*-bis[(1-methylimidazol-2-yl)-methyl]amine from *N*-methyl-2-carboxyimidazole and further *N*-alkylation by treatment of the secondary amine with ethyl bromoacetate.[21] The overall yield for the aldehyde to ester conversion by this new pathway was improved from 10% to 75% using a one-step reductive amination with $NaBH_3CN$ (see Scheme 1).

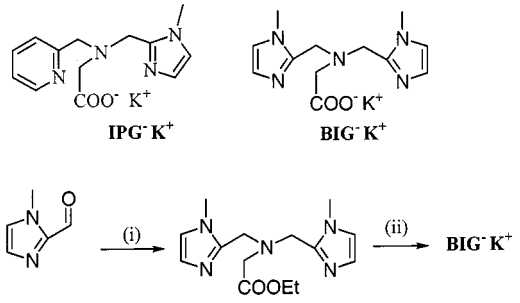

Scheme 1. Ligands IPG and BIG and the synthetic pathway leading to BIG: (i) $EtOOCCH_2NH_3Cl$, $NaBH_3CN$, anhydrous MeOH; (ii) H_2O/EtOH, K_2CO_3, room temp., 48 h

Preparation of the Complexes

Mn^{II} complexes were obtained from these two ligands with PF_6^- as the counteranion, either in anhydrous methanol or in water. With BIG, crystals were successfully grown from aqueous solution providing the dimeric compound **2**. Experimental details are given in the Exp. Sect. (see also Table 1). With IPG, as previously described, crystals suitable for X-ray analysis were slowly grown from anhydrous methanolic solution (compound **1**), providing a polymeric inorganic helix.[51]

Solid-State Characterization of Complex 2 − Comparison with Complex 1

The X-ray structure of compound **1** has been described previously. It was shown to form infinite polymeric helices in the solid state, linked through carboxylato bridges in a rather unusual *syn-anti* geometry (see Figure 1). The Mn^{II} ion is hexacoordinated. Although the two tetradentate ligands IPG and BIG are very similar (see Scheme 1), the structure of compound **2** shows drastic differences from that of compound **1**. The structure of complex **2** revealed the formation of a dinuclear complex, in which the two Mn^{II} centers are linked by two oxygen atoms of the double carboxylate monodentate bridge (μ-η^1-carboxylato) through a diamond-shaped core. In the crystal structure, the charge of the $[(BIG)Mn^{II}(\mu\text{-}OCO)_2Mn^{II}(BIG)]^{2+}$ cation is balanced by the presence of two PF_6^- anions. Selected distances and angles are presented in Table 2 and a perspective view of the structure is shown in Figure 2.

A notable structural feature of the dinuclear Mn^{II} complex is the heptacoordination of the manganese atom. The coordination environment of the metal ion consists of the three nitrogen donors N1A, N1B, N provided by the two imidazole rings and the tripodal N atom, and the oxygen atoms (O1, O2) of the carboxylate groups grafted onto the tripodal N ligand, which bridge the two metal centers. The sixth and seventh coordination sites of each metal ion are occupied by two water molecules (Figure 2). In the IR spectrum, the presence of coordinated water was confirmed by

Table 1. Summary of crystal data, intensity measurements, and structure refinement for **2**

Empirical formula	$C_{24}H_{42}F_{12}Mn_2N_{10}O_9P_2$
Molecular mass	1014.47
Crystal system	monoclinic
Space group	$P2_1/c$
a [Å]	9.240(4)
b [Å]	28.978(11)
c [Å]	15.586(6)
β [°]	95.49(4)
V [Å^3]	4154.1
Z	4
$F(000)$	2064
$D_{calcd.}$ [Mg m^{-3}]	1.622
μ (Mo-K_α) [mm^{-1}]	0.796
Crystal size [mm]	0.28 × 0.15 × 0.10
T [K]	293
No. of reflns. measd.	13461
θ range [°]	$1.41 < 2\theta < 29.07$
hkl ranges	$-9 \le h \le 10$ $-39 \le k \le 38$ $-21 \le l \le 21$
No. of unique reflns.	7525
No. of reflns. obsd. $I > 2\sigma(I)$	4729
No. of parameters/restraints	585/84
$R1$ $[I > 2\sigma(I)]$[a]	0.075
Weight	$1/[\sigma^2(F_o^2) + (0.1636P)^2 + 35.99]$[b]
$wR2$[c]	0.26
Max. Fourier diff. [e/Å^3]	0.5, −0.3

[a] $R1 = \Sigma||F_o| - |F_c||/\Sigma|F_o|$. − [b] $P = (F_o^2 + 2F_c^2)/3$. − [c] $wR2 = \{\Sigma[w(F_o^2 - F_c^2)^2/\Sigma[w(F_o^2)^2]\}1/2$.

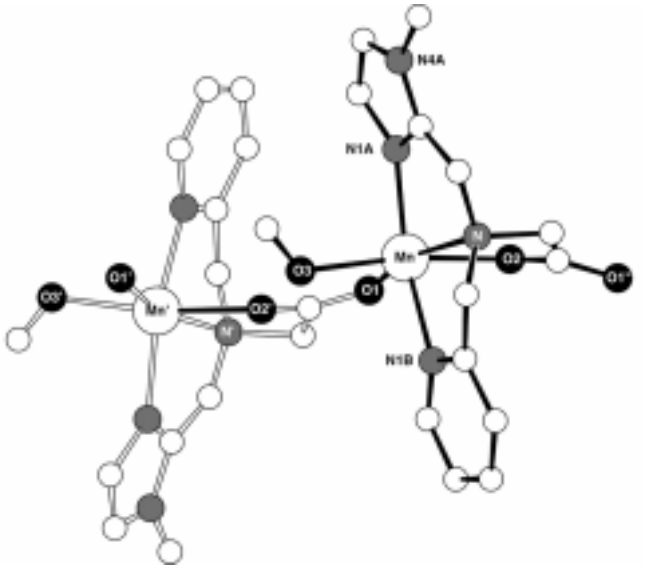

Figure 1. The polymeric association of the cationic chain of compound **1** with two adjacent monomeric units; hydrogen atoms have been omitted for clarity

Table 2. Selected bond lengths [Å] and angles [°] for **2** [the corresponding values for **1** are given in brackets; data from ref.[51]]; a) for **1**, N1A refers to the imidazole N and N1B to the pyridine N; b) O(1) refers to the closest carboxylato oxygen atom and, in the case of both **1** and **2**, it is a carboxylato group belonging to the ligand capped over Mn′

Mn−N(1A)	2.235(8)	Mn′−N(1A′)	2.204(8)	[2.13(2)]
Mn−W(2)	2.228(7)	Mn′−W(2′)	2.436(6)	
Mn−N(1B)	2.244(8)	Mn′−N(1B′)	2.253(9)	[2.23(2)]
Mn−O(1)	2.250(5)	Mn′−O(1)	2.278(6)	[2.13(2)]
Mn−O(2)	2.213(6)	Mn′−O(2)	2.272(5)	[2.18(2)]
Mn−W(1)	2.360(7)	Mn′−W(1′)	2.285(7)	
Mn−N	2.483(8)	Mn′−N′	2.519(7)	[2.36(2)]
N(1A)−Mn−W(2)	84.8(3)	N(1A′)−Mn′−W(1′)	84.4(3)	
N(1A)−Mn−N(1B)	107.7(3)	N(1A′)−Mn′−N(1B′)	108.0(3)	[147.5(6)]
W(2)−Mn−N(1B)	89.8(3)	W(1′)−Mn′−N(1B′)	94.4(3)	
N(1A)−Mn−O(1)	115.0(3)	N(1A′)−Mn′−O(2)	113.8(3)	
W(2)−Mn−O(1)	150.2(2)	W(1′)−Mn′−O(2)	148.8(2)	
N(1B)−Mn−O(1)	103.7(3)	N(1B′)−Mn′−O(2)	102.8(3)	
N(1A)−Mn−O(2)	162.6(3)	N(1A′)−Mn′−O(1)	160.3(3)	
W(2)−Mn−O(2)	82.8(2)	W(1′)−Mn′−O(1)	82.4(2)	
N(1B)−Mn−O(2)	84.5(3)	N(1B′)−Mn′−O(1)	87.6(3)	
O(1)−Mn−O(2)	72.5(2)	O(2)−Mn′−O(1)	72.7(2)	[88.3(6)]
N(1A)−Mn−W(1)	82.5(3)	N(1A′)−Mn′−W(2′)	79.8(2)	
W(2)−Mn−W(1)	84.2(2)	W(1′)−Mn′−W(2′)	83.4(2)	
N(1B)−Mn−W(1)	167.7(3)	N(1B′)−Mn′−W(2′)	171.8(2)	
O(1)−Mn−W(1)	77.2(2)	O(2)−Mn′−W(2′)	75.8(2)	
O(2)−Mn−W(1)	84.0(2)	O(1)−Mn′−W(2′)	84.3(2)	
N(1A)−Mn−N	70.5(3)	N(1A′)−Mn′−N′	70.2(3)	[75.7(6)]
W(2)−Mn−N	140.7(2)	W(1′)−Mn′−N′	143.0(2)	
N(1B)−Mn−N	70.2(3)	N(1B′)−Mn′−N′	69.7(3)	[74.0(6)]
O(1)−Mn−N	69.0(2)	O(2)−Mn′−N′	68.1(2)	[162.4(6)]
O(2)−Mn−N	126.3(2)	O(1)−Mn′−N′	127.9(2)	[75.5(6)]
W(1)−Mn−N	120.7(2)	W(2′)−Mn′−N′	116.5(2)	

the appearance of two narrow lines at 3656 and 3580 cm^{-1}.[52] These lines were absent in the IR spectrum of compound **1**, in which the Mn^{II} ions do not bear coordinated water molecules. Moreover, when compound **2** was recrystallized from D_2O, these two lines were shifted to give one composite band at 3650 cm^{-1}. This further confirms the assignment to coordinated water. The $M-N_{tripodal}$ distance is of the same order as has previously been found for similar compounds consisting of tripodal amines and Mn^{II}.[38,51,53,54] This distance is shorter than the sum of the van der Waals radii (2.82 Å), indicating that the manganese ion is linked to the $N_{tripodal}$ atom.

The bis[Mn(μ-OCO)] core is characterized by Mn−O−Mn angles of 108.4(2)° and 106.4(4)° and an Mn−Mn distance of 3.672(2) Å. This distance is of the same order of magnitude as those reported for the $Mn^{II}(\mu\text{-}OCO)_2Mn^{II}$ core with a double monodentate bridging carboxylate group [3.712(2) and 3.726(4) Å].[54] A relevant feature is the planarity of the diamond-shaped core, the four atoms Mn, O1, O2, Mn′ being rigorously coplanar (mean displacement 0.001 Å from the least-squares mean plane). A striking finding of the crystal structure determination of the dinuclear complex is a complex intra- and intermolecular hydrogen-bond network that connects the various hydrogen-bond acceptors (COO^-) and the donors/acceptors (water molecules included in the cell).

The free oxygen atoms of the carboxylate groups, O9C and O9C′, and the water molecules W1′, W2 coordinated to the metal centers Mn and Mn′ are linked by strong intramolecular hydrogen bonds (from 2.66 Å to 2.74 Å). Another strong intramolecular hydrogen bond is evident between one water molecule W1 coordinated to the Mn ion and the other water molecule W2′ linked to the second metal center Mn′. Small differences are observed for the bis(μ-OCO) bridges. Oxygen atom O9C, which is not coordinated to the metal ion, is involved in only one intramolecular hydrogen bond, while the free oxygen atom O9C′ of the second carboxylate bridge is intra- and intermolecularly hydrogen-bonded in a twofold network.

Two- or threefold connected arrangements of the four water molecules coordinated to the metal centers and the water molecule W, cocrystallized, are seen in the crystal structure. The main features of the three-dimensional hydrogen-bond scheme are reported in Table 3.

Studies in Solution: Reactivity of the Complexes Toward Superoxide

Reactivity was studied in both anhydrous media and aqueous buffer. The studies in anhydrous media were motivated by the fact that the two complexes **1** and **2** display different levels of hydration. Direct reaction of the complexes with superoxide could be monitored in anhydrous media. DMSO was chosen as it solubilizes KO_2 up to a relatively high concentration in comparison to other solvents (see Exp. Sect. for details).[55,56] In aqueous buffer, an indirect test (namely the Fridovich test) was used. In order to investigate the reactions of O_2^- with complexes **1** and **2**

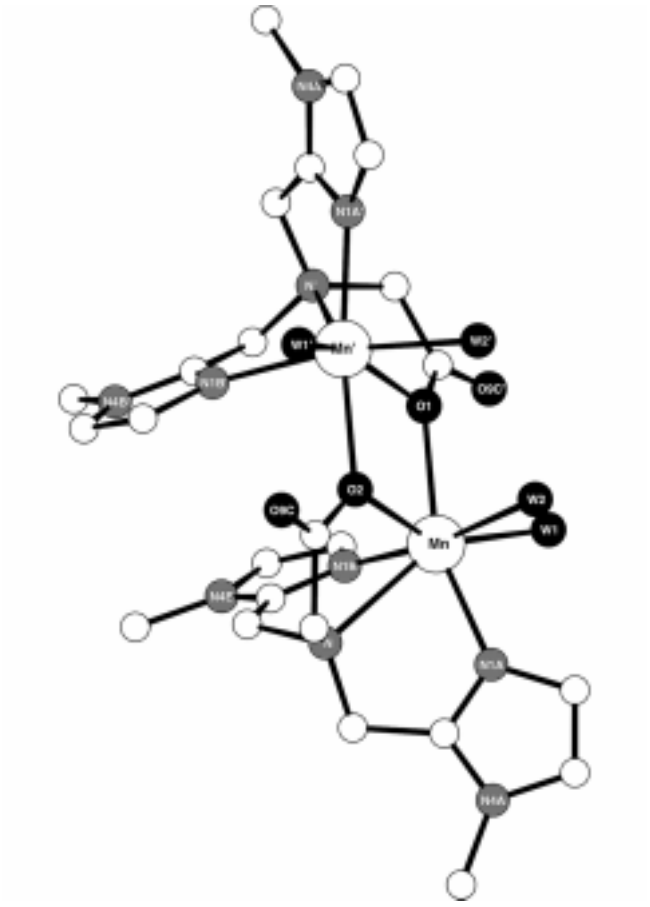

Figure 2. The molecular structure of the cation of complex **2**; hydrogen atoms have been omitted for clarity

Table 3. Details of hydrogen-bonding features related to the Mn^{II} dinuclear complex **2** (Å, °)

Intramolecular hydrogen bonds			
O9C···W1′	2.665(9)	C8C−O9C−W1′	103.1(6)
O9C′···W2	2.698(9)	C8C′−O9C′−W2	102.7(6)
W1···W2′	2.736(8)	Mn−W1−W2′	101.5(3)
		Mn′−W2′−W1	99.2(2)
Intermolecular hydrogen bonds			
W1···W2′[a]	2.768(9)	Mn−W1−W2′[b]	122.6(3)
W1′···W1[a]	2.889(9)	Mn′−W1′−W1[a]	104.1(3)
W1′···W	2.742(13)	Mn′−W1′−W	122.6(4)
W2′···O9C′[b]	2.716(9)	Mn′−W2′−O9C′[b]	103.6(3)

[a] = $-x$, $1-y$, $2-z$. − [b] = $1-x$, $1-y$, $2-z$.

in solution, their molecular properties in solution first needed to be characterized.

Anhydrous DMSO Solutions

Both complexes are soluble in DMSO. Mononuclear species are present in solution, as shown by EPR spectroscopy and mass spectrometry. The EPR spectra of **1** and **2** in DMSO (10^{-4} to 5×10^{-3} mol·dm^{-3} based on Mn^{II} content) each show the sharp, six-line signal typical of mononuclear Mn^{II} with an average separation of 102 Gauss (some smaller lines can be seen in between, which are known to be due to $\Delta m_I = \pm 1$ forbidden transitions)[57−59] (see Figure 3A). Electrospray ionization mass spectrometry (ES) showed a peak at $m/z = 392$ for **1** and at $m/z = 395$ for **2**. These peaks correspond to [(L)Mn + DMSO] (L being either IPG or BIG). For the sake of simplicity, the soluble species are referred to hereafter as MnIPG for **1** and as MnBIG for **2** and concentrations are given in terms of the Mn^{II} content.

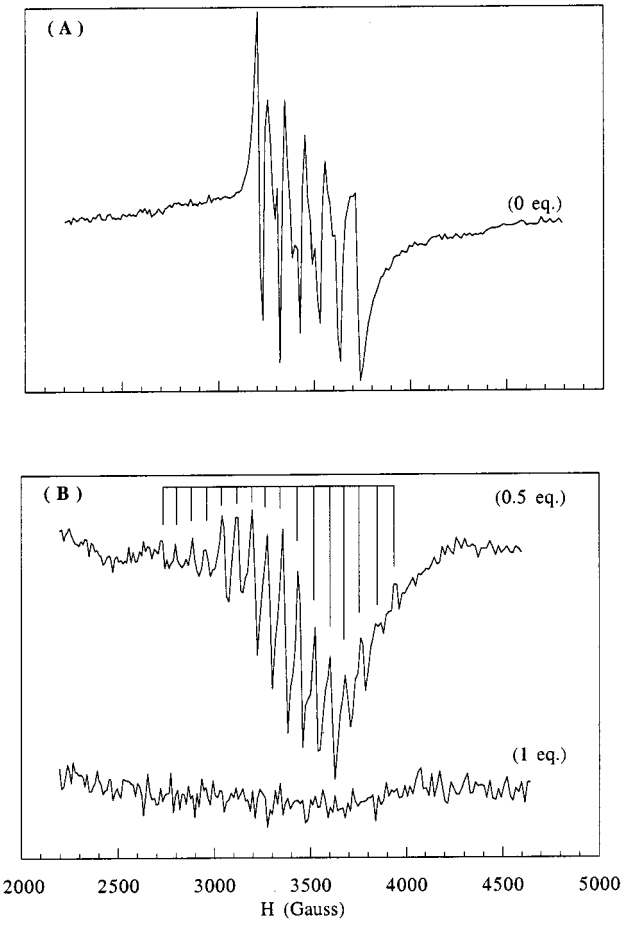

Figure 3. EPR spectra for the reaction of MnIPG (6.5×10^{-4} M based on Mn^{II} content) with potassium superoxide: A: 0 equiv. of O_2^-; B: 0.5 equiv. and 1 equiv. of O_2^- [$T = 8$ K, attenuation 44 dB (A) or 15 dB (B), modulation 5 G, gain 3.2×10^5, $t_c = 100$ ms, sweep time 200 s]

The cyclic voltammograms of both MnIPG and MnBIG in deoxygenated DMSO showed no reversible wave in the electroinactivity window of the solvent (−2.25 to 0.95 V vs. SCE), neither on platinum nor on glassy carbon working electrodes. Similarly, in acetonitrile, no wave was recorded in the range −1.8 to 1.8 V vs. SCE. Such behavior is not uncommon for Mn^{II} complexes.[38,60]

When the cyclic voltammogram of MnIPG or MnBIG in DMSO was recorded without deoxygenation, an irreversible cathodic wave was observed, corresponding to the reduction of dioxygen to superoxide. It is known that, in anhydrous DMSO, the redox couple O_2/O_2^- displays a revers-

ible wave at $E_{1/2} = -0.73$ V vs. SCE.[18,24,55,60,61] We verified that under our experimental conditions, in the absence of any complex, this reversible wave was indeed observed. Its reversibility confirmed the anhydrous nature of the solvent under the experimental conditions. The fact that the O_2/O_2^- wave became irreversible in the presence of the complexes gave a first indication that the complexes do indeed react with superoxide.

When the DMSO solution was saturated with oxygen, another reduction peak appeared at a more positive potential (+400 mV) than the O_2/O_2^- cathodic peak. Some similar pre-peaks have previously been reported for Mn^{II} complexes,[38,60] which were attributed to the reduction of dioxygen weakly bound to the metal center.[60]

Reactivity of MnIPG and MnBIG Towards Superoxide in Anhydrous DMSO

Incremental amounts of superoxide were added to an anhydrous DMSO solution containing either MnIPG or MnBIG (10^{-4} to 5×10^{-3} mol·dm^{-3} based on Mn^{II} content) and the course of the reaction at room temperature was monitored by UV/Vis spectrophotometry (room temp.), EPR (X-band) spectroscopy (100 K or 8 K), and cyclic voltammetry (room temp.). In all these experiments, special care was taken to maintain the anhydrous character of the DMSO solutions. Saturated solutions of KO_2 in DMSO were obtained as described in the Exp. Sect. Equivalents of superoxide added are given per manganese ion.

(a) Treatment of MnIPG with superoxide produced, after the addition of 1 equiv., a light-brown solution giving a typical UV/Vis spectrum as shown in Figure 4, featuring bands at 300, 360, and 510 nm. EPR spectra were recorded at 100 K and 8 K. The Mn^{II} signal intensity decreased on going from 0 to 0.5 equiv. of O_2^-. At 0.5 equiv., a small multi-line signal was observed, which appeared more clearly at 8 K (Figure 3B). On going from 0.5 to 1 equiv., this multi-line signal decreased and was no longer observed beyond 1 equiv. Above 1.5 equiv., a signal due to superoxide was recovered. The superoxide content was estimated to be approximately 0.5 equiv. and 0.9 equiv. when 1.5 equiv. and 2 equiv., respectively, of superoxide had been added (see Exp. Sect.).

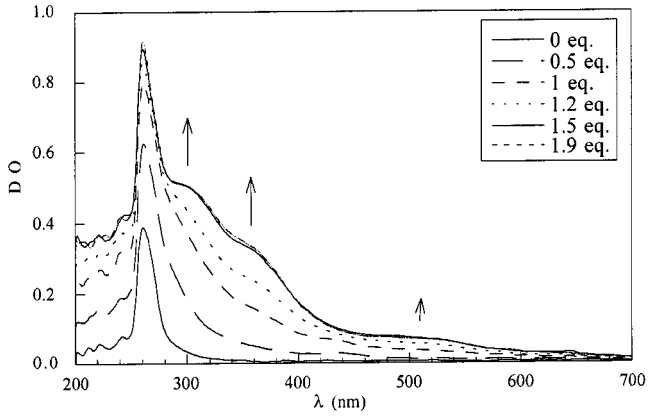

Figure 4. UV/Vis spectra for the reaction of MnIPG (10^{-4} M based on Mn^{II} content) with potassium superoxide

The reactivity of MnIPG toward superoxide was also investigated by cyclic voltammetry. This was performed by studying the evolution of the O_2/O_2^- wave.

In anhydrous DMSO, the redox couple O_2/O_2^- shows a reversible wave at $E_{1/2} = -0.73$ V vs. SCE.[18,24,55,60,61] The same reversible wave was observed from a deoxygenated 0.1 M Bu_4NPF_6/DMSO solution (15 min argon bubbling) to which a solution of KO_2 in the same electrolyte had been added (Figure 5). This wave remained stable upon further deoxygenation, indicating that it was due to superoxide and not to dioxygen that might have resulted from superoxide disproportionation. To ensure that superoxide was stable under the experimental conditions, successive amounts of superoxide in 0.1 M Bu_4NPF_6/DMSO (see Exp. Sect.) were added to a 0.1 M Bu_4NPF_6/DMSO solution in the electrochemical cell in the absence of any complex. The intensity of the anodic wave was seen to remain stable over 5−10 min and to vary linearly with the superoxide concentration.

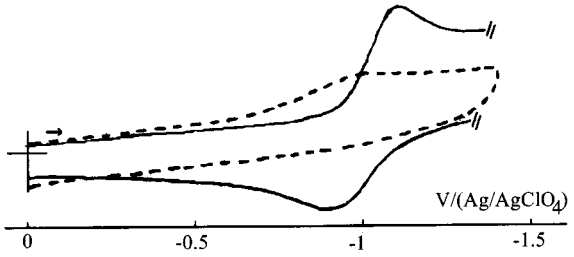

Figure 5. Cyclic voltammograms of a solution containing O_2/O_2^-; solid line: 5×10^{-4} M O_2^-; dashed line: 5×10^{-4} M MnIPG (based on Mn^{II} content) + 5×10^{-4} M O_2^-; potentials are reported vs. Ag/$AgClO_4$ in DMSO (+0.252 V vs. SCE)

When the cyclic voltammogram of MnIPG was recorded without deoxygenation of the solution, the O_2/O_2^- reduction wave became irreversible, showing no re-oxidation of superoxide at the electrode, not even at 200 mV.s^{-1}. Moreover, the O_2/O_2^- cathodic peak was slightly shifted to a more positive potential (see Figure 5), indicating an EC process. This shows that compound MnIPG reacts with superoxide produced at the electrode. When superoxide was added to the deoxygenated solution of MnIPG, no O_2/O_2^- wave was observed on going from 0.1 to 1 equiv. The superoxide wave appeared clearly after 2.5−3 equiv. of superoxide had been added.

(b) MnBIG was found to display a similar behavior upon superoxide addition, but with a different stoichiometry. The brown color and the UV band at 300 nm appeared after addition of 2 equiv. of superoxide. The multi-line EPR signal appeared after the addition of 1.5 equiv. and an EPR-silent species was obtained after the addition of a further 0.5 equiv.

In cyclic voltammetry, the O_2/O_2^- wave was absent when superoxide was added to a deoxygenated solution of **2**. After addition of 2 equiv. of superoxide, an irreversible cathodic wave appeared at 1.2 V vs. SCE, which intensified on adding further incremental amounts of superoxide. It was verified that the ligand BIG displays the same wave.

Reactivity of MnIPG and MnBIG Towards Superoxide in Aqueous Buffer

The reactivity of our complexes towards superoxide was investigated in aqueous phosphate buffer (pH = 7.8) by means of the xanthine/xanthine oxidase assay (hereafter referred to as the X/XO assay). This test, developed by Fridovich et al., is based on kinetic competition for superoxide reduction between the putative superoxide scavenger and ferricytochrome *c*.[7] The reduction of ferricytochrome *c* was monitored spectrophotometrically at 550 nm. This test requires several preliminary checks in order to improve its reliability (see Exp. Sect.).[5,35,38,62]

Compounds **1** (MnIPG) and **2** (MnBIG) in potassium phosphate buffer at pH = 7.8 were found to inhibit the reduction of ferricytochrome *c*, as shown in Figure 6. Inhibition percentages were measured for several complex concentrations and IC_{50} values were then deduced by two graphical methods (see Figure 7 and the Exp. Sect. for details).[7,35,63] The effects of chelators such as bovine serum albumin (BSA) and ethylenediaminetetraacetate (EDTA) were investigated in order to gain some insight into the stabilities of the complexes. BSA has been reported to be a powerful biological chelating agent capable of suppressing the SOD-like activity of copper complexes.[5,14] We have used it previously to test the activity of an (tris{2-[*N*-(2-pyridylmethyl)amino]ethyl}amine)Mn^{II} bis(hexafluorophosphate) (MnTPAA) in the X/XO assay. It was found that BSA (5 mg/mL) had no effect on the MnTPAA activity.[38] Similarly, BSA (5 mg/mL) showed no effect on the MnIPG activity. A small effect was observed for MnBIG in that its IC_{50} value was increased by a factor of 1.5 in the presence of BSA (5 mg/mL). The results suggest, at least for MnIPG, that as previously concluded for MnTPAA,[38] activity might be retained in vivo.

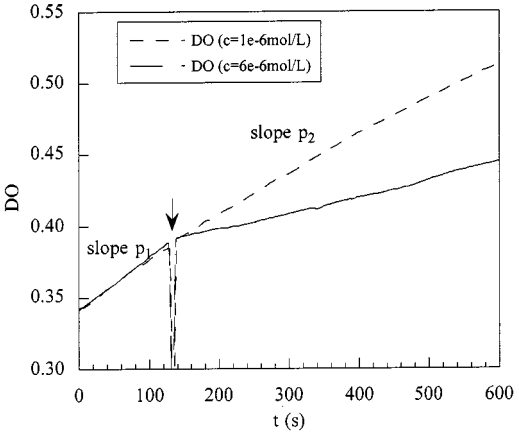

Figure 6. X/XO assay; 0−120 s: xanthine (200 μM), ferricytochrome *c* (22 μM), xanthine oxidase; after 120 s: xanthine (200 μM), ferricytochrome *c* (22 μM), xanthine oxidase, and compound MnBIG (concentration *c*, based on Mn^{II} content); the arrow indicates the addition of compound MnBIG

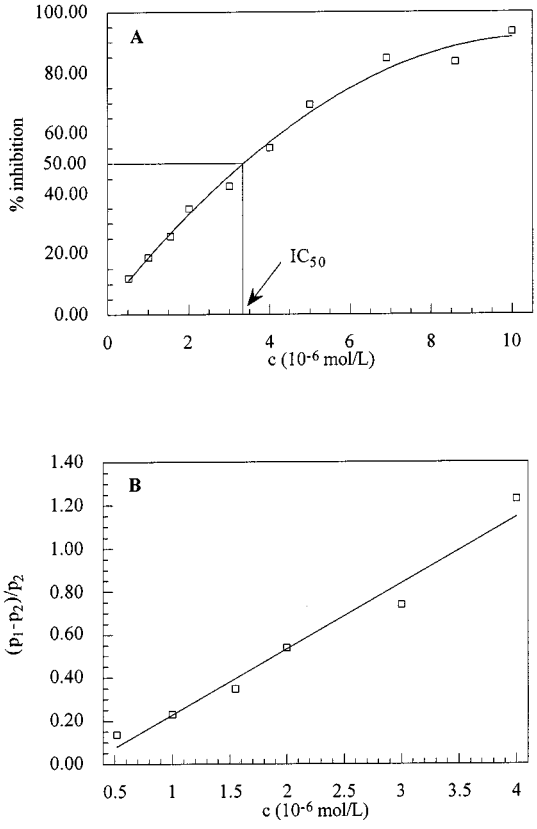

Figure 7. IC_{50} determination in the case of compound MnIPG; A: % inhibition versus concentration; B: $(p_1 - p_2)/p_2$ versus concentration

To further investigate the stabilities of the complexes, activity was measured in the presence of an excess of EDTA (3 mM, i.e. 1000 equiv.). The IC_{50} values of MnIPG and MnBIG were found to be increased by factors of 20 and 25, respectively (see Table 4), indicating low stabilities towards EDTA. Such contrasting behavior towards EDTA and BSA has previously been reported for (salen)Mn^{III} complexes. It was interpreted in terms of EDTA binding Mn from the complex rather than merely reacting with free Mn released by the complex.[5]

These experiments indicate that some decoordination might occur at concentrations in the range of the IC_{50}. Ligands IPG and BIG were tested and were found to show no activity in the X/XO assay. IC_{50} values reported so far in this article are apparent IC_{50} values (IC_{50app}) due to both

Table 4. Effect of chelators on the IC_{50} value [μM]

Compound	IC_{50app}	IC_{50} with EDTA (3 *m*M)	IC_{50} with BSA	IC_{50spe} (IC_{50} measured with excess ligand)
MnBIG	3.7 ± 0.6	90.0 ± 0.7	5.6 ± 0.1	1.7 ± 0.2
MnIPG	3.0 ± 0.5	62.3 ± 0.7	2.8 ± 0.3	2.0 ± 0.2

Table 5. IC_{50} values; comparison with literature data

Compound	IC_{50} [μM]		Ref.
	IC_{50app}	IC_{50spe}[a]	
$Mn^{II}(ClO_4)_2$ + EDTA[b]		167 ± 3	this work
Fe^{III}BIG		140	[92]
Mn^{II}TPAA[c]		50	[38]
Mn^{III}DFB[c]		10.4	[35]
$Mn^{II}(PA)_2(PAH)(H_2O)$[c]		6.5	[30]
$Mn^{II}(ClO_4)_2$		4.5 ± 0.5	this work
MnBIG[d]	3.7 ± 0.6[e]	1.7 ± 0.2[f]	this work
MnIPG[d]	3.0 ± 0.5[e]	2.0 ± 0.2[f]	this work
$Mn^{II}(OBz)(3,5\text{-}iPr_2pzH)[HB(3,5\text{-}iPr_2pzH)_3]$		0.75	[33]
Mn^{III}porphyrins		0.026 to 8	[23,43]
MnSOD *T. thermophilus*		0.0023	

[a] IC_{50spe} values were measured in the presence of excess ligand (15 equiv.). – [b] This value was measured for a sample of $Mn^{II}(ClO_4)_2$ in the presence of excess EDTA (3 mM). – [c] TPAA: tris{2-[*N*-(2-pyridylmethyl)amino]ethyl}amine; DFB: desferrioxamine B; PA: picolinato; $HB(3,5\text{-}iPr_2pzH)_3$ hydrotris(3,5-diisopropyl-1-pyrazolyl)borate. – [d] IC_{50} values are reported in terms of Mn concentration. – [e] This value is an average for three replicates performed for each of the two determination procedures. – [f] This value is an average for two replicates performed for each of the two determination procedures.

the complexes and free Mn^{II}. The IC_{50} value for $Mn(ClO_4)_2$ (4.5 μM) was found to be higher than those for the complexes under the same experimental conditions. Thus, IC_{50app} values represent an overestimation of the real IC_{50} values (specific IC_{50}) that would have been measured without decoordination. To suppress this possible free Mn^{II} contribution to the inhibition, IC_{50} values were measured in the presence of an excess of the ligand (15 equiv.), thereby providing specific IC_{50} values (IC_{50spe}). These specific IC_{50} values are reported in Table 4 and are compared with literature data in Table 5.

Discussion

The ligands IPG and BIG form two structurally distinct compounds with manganese(II). These two compounds reflect the rich structural diversity of (carboxylato)manganese complexes, as has been stressed by Iikura et al.[54] The coordination sphere about the manganese(II) ions adopts various geometries (see Table 2, Figure 1 and 2) and has various coordination numbers (6 or 7 for these two examples). This structural variety stems from the carboxylato moiety, which is μ-η^2-carboxylato-*syn-anti* in the polymeric helix adopted by **1** and μ-η^1-carboxylato in the dimeric structure of **2** in the solid state.

Reactivity in Anhydrous DMSO

Complexes **1** and **2** have different levels of hydration. In the reaction with superoxide, this hydration level is of critical importance as two protons are necessary for the superoxide reduction step producing H_2O_2. The ping-pong mechanism proposed for the enzyme suggests an inner-sphere electron-transfer, the first step being the binding of superoxide to the metal center.[49] Two concomitant pathways (inner- and outer-sphere electron transfer) have also been proposed for macrocyclic Mn^{II} derivatives.[34,37,39,44] With compound **1**, which does not have any coordinated water molecules, it is possible to test the reactivity in anhydrous media and thus, in the case of an inner-sphere mechanism, we may expect to characterize an Mn–superoxide adduct or a derivative thereof. This can be compared with the reactivity of complex **2**, as the presence of water should lead to some effective reaction with superoxide.

MnIPG reacts with 1 equiv. of superoxide, producing an EPR-silent species. After addition of 0.5 equiv., a $g = 2$, 16-line signal is observed in the EPR spectrum (see Figure 3). This indicates that a dimeric Mn–Mn $S = 1/2$ ground-state compound is obtained. This signal displays a width of 1200 G and an average spacing of 75 G. Such a spectrum is typical of bis(μ-oxo)$Mn^{III}Mn^{IV}$ complexes.[61,64–75] The conversion of Mn^{II} to bis(μ-oxo)$Mn^{III}Mn^{IV}$ species has been estimated to be 70% based on a comparison with the spectrum of a fully characterized $Mn^{III}Mn^{IV}$ compound.[76] The $Mn^{III}Mn^{IV}$ species further reacts with 0.5 equiv. of superoxide leading to an EPR-silent species, which could be either an $Mn^{III}Mn^{III}$ or an $Mn^{IV}Mn^{IV}$ species. This is consistent with the UV/Vis spectrum, as a possible assignment for the 300 and 360 nm bands is an $O \rightarrow Mn^{IV}$ LMCT.[74,77,78] Scheme 2 provides a rationalization of these experimental observations.

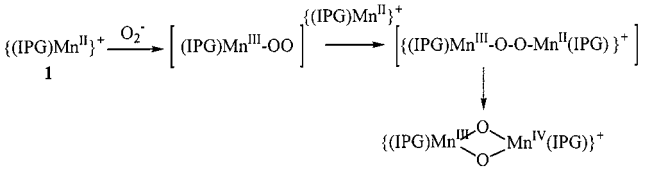

Scheme 2. Possible mechanism for bis(μ-oxo)$Mn^{III}Mn^{IV}$ dimer formation (after reaction of potassium superoxide with MnIPG)

The fact that the superoxide signal is recovered upon addition of 1.5 equiv. of superoxide shows that the silent EPR species formed at 1 equiv. of superoxide do not react with superoxide, at least in anhydrous media. A similar mechanism has previously been proposed for manganese–

porphyrins.[61] A (μ-peroxo)$Mn^{II}Mn^{III}$ species could also produce a $g = 2$, multi-line signal if the ground state had $S = 1/2$. However, as has been pointed out in the literature, a much larger spectrum would be expected.[65] Moreover, such a (μ-peroxo)$Mn^{II}Mn^{III}$ species would be expected to be unstable, whereas we found the multi-line signal to persist after the EPR tube had been left at room temperature for 5 min.

MnBIG exhibited the same pattern of spectroscopic and voltammetric characteristics, but only after 1 equiv. of superoxide per manganese ion had already been consumed. This observation has to be related to its level of hydration. The presence of water allows the production of hydrogen peroxide, either by direct reaction with superoxide or by reaction with an Mn−superoxide adduct. When the amount of superoxide was increased, an irreversible cathodic wave appeared at 1.2 V vs. SCE, which was shown to be due to the ligand BIG. This probably indicates destruction of the complex with release of the ligand.

Reactivity in Aqueous Buffer

The use of the X/XO assay to determine catalytic SOD-like activity is controversial. It has been shown, first by others, using stopped-flow techniques,[5][62] and then by us, using pulsed radiolysis,[38] that such an indirect test can give positive results both in the case of a catalytic scavenger and in the case of a stoichiometric superoxide scavenger. As a matter of fact, a small amount of superoxide is produced in the X/XO assay. For compounds displaying high IC_{50} values (in excess of 1 μM), the conditions required to probe catalytic behavior may not be fulfilled as $n_{complex} >> n_{superoxide}$ in the experiment. However, this test remains relevant for several reasons. The X/XO system provides a stationary state of superoxide of low concentration, which is closer to what is usually encountered in vivo.[14] Moreover, it provides a simple means of investigating the reactivities of complexes towards superoxide in aqueous buffers and of assessing the effect of additional compounds (e.g., chelators).[14,15,23,42,43]

The X/XO assay has proven that complexes **1** and **2** react with superoxide in aqueous solution. Experiments performed in the presence of excess chelators (BSA, EDTA) have shown that the complexes are partially decoordinated in the IC_{50} concentration range. Specific IC_{50} (IC_{50spe}) values were thus measured using an excess of the ligand. MnBIG and MnIPG show very close specific IC_{50} values, which is consistent with the two ligands being closely related. Their IC_{50spe} values fall at the low end of the range of those reported in the literature for Mn^{II} complexes (see Table 4). Much lower IC_{50} values have been reported for

Table 6. Association constants with Mn^{II} estimated for BIG and IPG and comparison with literature data; constants are given for the equilibrium Mn^{II}/L (1:1)

Ligand	Denticity	log K (T [°C]/ionic strength)	Ref.
Pyridine	monodentate	0.14 (25/0.5)	[79]
Acetic acid		0.8 (25/0.16)	[80]
2-Aminomethyl-6-methylpyridine	bidentate	1.95 (25/0.1)	[81]
D-Tartaric acid		2.49 (25/0.1)	[80]
L-2-Aminopropanoic acid (L-alanine)		2.5 (25/0.1)	[81]
Diglycolic acid		2.53 (25/0.1)	[80]
2,2′-Bipyridine		2.62 (25/0.1)	[79]
2-(Aminomethyl)pyridine		2.66 (20/0.1)	[79]
Ethylenediamine		2.67 (25/0.1)	[79]
Phthalic acid		2.74 (25/0)	[80]
Aminoacetic acid (glycine)		2.8 (25/0.1)	[81]
4-(2-Aminoethyl)imidazole (histamine)		3.0 (25/0.2)	[79]
1,10-Phenanthroline		4.0 (25/0.1)	[79]
Diethylenetriamine	tridentate	3.99 (30/0.1)	[79]
Di(2-picolyl)amine (DPA)		4.16 (25:0.1)	[79]
2,2′,2′′-Terpyridine		4.4 (25/0.002−0.1)	[81]
Oxybis(propanedioic acid)	tetradentate	4.51 (25/0.1)	[80]
Triethylenetetramine		4.9 (25/0.1)	[79]
BIG		5.3 (25/0.13)	this work
Tris(2-picolyl)amine (TPA)		5.6 (20/0.1)	[79]
Tris(2-aminoethyl)amine (TREN)		5.8 (25/0.1)	[79]
N-(2-Carboxyphenyl)iminodiacetic acid		5.85 (25/0.1)	[81]
N,*N*′-Di(2-picolyl)ethylenediamine		5.9 (25/0.1)	[79]
IPG		6.0 (25/0.13)	this work
N,*N*,*N*′,*N*′-(2-Aminoethyl)ethylenediamine	hexadentate	9.26 (25/0.1)	[79]
N,*N*,*N*′,*N*′-Tetrakis(2-picolyl)ethylenediamine (TPEN)		10.3 (20/0.1)	[79]

Mn−porphyrin compounds (see Table 4), but in these cases the manganese ion is in an Mn^{III} oxidation state. The IC_{50} value measured for MnBIG is more sensitive to the presence of chelators (EDTA, BSA, or BIG) (see Table 4). Qualitatively, this indicates that MnBIG has a smaller association constant K_{BIG} than MnIPG (K_{IPG}). Association constants could be roughly estimated from the apparent and specific IC_{50} values. Apparent IC_{50} values depend on the proportion of complex and Mn^{II} in the solution, and hence on the association constant. The apparent IC_{50} values could be approximated as the weighted average of the specific IC_{50} values for both compounds and Mn^{II}: $IC_{50app}(n) = IC_{50spe}(n)\cdot(1 - \alpha) + IC_{50spe}(Mn^{II})\cdot\alpha$ (n = MnIPG or MnBIG), α being the dissociation coefficient. This led to $K_{IPG} = 10^{6.0}$ and $K_{BIG} = 10^{5.3}$, respectively. Literature data on association constants of Mn^{II} complexes involving ligands of various denticity are reported in Table 5, together with our results from the present work.[79−81] The K_{ass} values estimated here for BIG and IPG are of the expected order of magnitude for tetradentate ligands and Mn^{II}.

As already mentioned, this X/XO assay is unable to distinguish between a catalytic and a stoichiometric scavenger for compounds showing IC_{50} values greater than 1 μM. Direct measurements of SOD activity using an excess of superoxide are necessary.[5] Pulsed-radiolysis kinetic analysis is now underway.

Conclusion

The preparation of compound **2** from Mn^{II} and *N*,*N*-bis[(1-methylimidazol-2-yl)methyl]glycinate (BIG) and its solid-state structure have been described. This compound has been shown to crystallize as an $Mn^{II}Mn^{II}$ dimer with a double carboxylato monodentate bridge (μ-η^1-carboxylato). Its geometry differs from that of compound **1**, an Mn^{II} compound prepared with the closely related ligand *N*-[(1-methylimidazol-2-yl)methyl]-*N*-(2-pyridylmethyl)-glycinate, IPG, which was previously shown to crystallize as a helical polymer.[51] Both these bridged structures are disrupted in DMSO, leading to monomeric species. In solution, compounds **1** and **2** have been shown to react with superoxide, both in anhydrous media and in aqueous buffer. They have been shown to form bis(μ-oxo) dimers in anhydrous media, such dimers being unreactive toward superoxide. IC_{50} values obtained in solution for these two compounds are among the best reported for Mn^{II} complexes, showing that the metal environment is appropriate for reaction with superoxide. However, the dimer formation, as seen under anhydrous conditions, might represent a pathway for inhibition of the activity toward superoxide in aqueous solution. We are currently working on modification of the ligand in order to prevent this possible dimerization and to enhance the stability of the complexes.

Experimental Section

General: IR spectra (KBr) were recorded with a Bruker IFS 66 FT-IR spectrometer. − ^{1}H NMR spectra were recorded with Bruker AM 200 and AM 250 spectrometers. − X-band electron paramagnetic resonance (EPR) spectra were recorded with a Bruker ER 200E spectrometer. − Cyclic voltammetry experiments were performed with an EG&G Princeton Applied Research Model 362 potentiostat connected to an Ifelec IF 2502 xy recorder. − Electronic absorption spectra were recorded with a Safas 190 DES double-mode spectrophotometer. − Chemical reagents were purchased from either Aldrich or Acros and were used without further purification. Extra-dry DMSO was purchased from Acros.[82] Xanthine oxidase and ferricytochrome *c* were purchased from Sigma.

Syntheses and Characterization

[(Ethoxycarbonyl)methyl]bis[(1-methylimidazol-2-yl)methyl]amine: Under argon at 0 °C, sodium cyanoborohydride (5 mmol, 0.32 g) was added to a deoxygenated solution of 1-methylimidazol-2-carboxaldehyde[83] (4.7 mmol, 0.52 g) and glycine ethyl ester hydrochloride ($ClNH_3CH_2COOEt$) (4.7 mmol, 0.65 g) in anhydrous MeOH (10 mL). After 2 h at 0 °C, the mixture was stirred for 12 h at room temperature. The solution was then cooled to 0 °C and acidified to pH = 5.5 with CF_3COOH, whereupon 1-methylimidazol-2-carboxaldehyde (7 mmol, 0.775 g) (in anhydrous MeOH, 2 mL) and sodium cyanoborohydride (9 mmol, 0.48 g) were added. After 2 h at 0 °C, the solution was stirred for 12 h at room temperature. It was then filtered, the methanol was evaporated, and the residual oil was extracted from the aqueous phase (pH = 8) with CH_2Cl_2. The combined organic phases were dried with Na_2SO_4 and concentrated. A yellow oil was obtained, which was purified by column chromatography (SiO_2; MeOH/CH_2Cl_2, 1:9). Yield (1.1 g, 75%). − ^{1}H NMR ($CDCl_3$): δ = 1.17 (t, 3 H, J = 7.25 Hz, CH_3CH_2COO), 3.34 (s, 2 H, NCH_2COOEt), 3.52 (s, 6 H, CH_3N_{im}), 3.80 (s, 4 H, Im-CH_2N), 4.04 (q, 2 H, J = 7.25 Hz, CH_3CH_2COO), 6.80 (d, 2 H, J = 2.25 Hz, H_{im}), 6.84 (d, 2 H, J = 2.25 Hz, H_{im}).

Potassium *N*,*N*-Bis[(1-methylimidazol-2-yl)methyl]glycinate (BIG): A solution of *N*,*N*-bis[(1-methylimidazol-2-yl)methyl]glycine ethyl ester (0.5 g) in ethanol (12 mL) was added to a solution of potassium carbonate (0.52 g) in water (35 mL). The resulting solution was stirred for 2 d at room temperature. The ethanol was then evaporated and the aqueous phase was washed with CH_2Cl_2 (2 × 10 mL). After concentration to dryness, residual K_2CO_3 was removed by extracting the carboxylate with anhydrous MeOH. Yield: 95%. − ^{1}H NMR (D_2O): δ = 3.10 (s, 2 H, NCH_2COOK), 3.45 (s, 6 H, CH_3N_{im}), 3.80 (s, 4 H, Im-CH_2N), 6.86 (d, 2 H, J = 2.25 Hz, H_{im}), 6.89 (d, 2 H, J = 2.25 Hz, H_{im}).

$[Mn(BIG)(H_2O)_2]_2\cdot 2PF_6$ (2): The pH value of a 2×10^{-3} M solution of BIG in water was adjusted to 8−8.5 by the addition of HCl. After evaporation of the water, the solid was dried overnight under reduced pressure in the presence of P_2O_5, and then KCl was removed by extraction of the ligand with anhydrous methanol. Typically, dimer crystals were obtained as follows: $MnBr_2$ (0.52 mmol, 112 mg) in deoxygenated doubly distilled water (15 mL) was added to a solution of the ligand (160 mg) in deoxygenated doubly distilled water (10 mL). The resulting mixture was allowed to stand for 2 h at 40 °C. Then, after cooling, a deoxygenated solution of NH_4PF_6 (3 equiv., 260 mg) in doubly distilled water (10 mL) was added dropwise. The resulting solution was left to stand for 3 weeks, allowing crystals to grow (see crystal data below). For further characterization and experiments, these crystals were ground and dried in vacuo over P_2O_5 for 48 h. Yield: 260 mg (55%). − $[C_{12}H_{16}N_5O_2Mn(H_2O)]_2\cdot 2PF_6$: calcd. C 30.01, H 3.78, N 14.58, F 23.74, P 6.45, Mn 11.44; found C 30.43, H 3.66, N 14.61, F 23.38, P 6.88, Mn 11.46. − IR (KBr): $\tilde{\nu}$ = 3656 and 3682 ($\nu_{linked\ water}$), 1590 (ν_{asCO}), 1382 (ν_{sCO}), 838 (PF_6), 738 ($\nu_{imid.\ deform.}$), 553 cm^{-1} (PF_6) (strong bands only).

Crystal Data for 2: $Mn_2C_{24}H_{40}N_{10}O_8{\cdot}2PF_6{\cdot}H_2O$,[84] M_r = 1014.47, monoclinic, space group $P2_1/c$, a = 9.240(4), b = 28.978(11), c = 15.586(6) Å, β = 95.49(4)°, V = 4154.1 Å^3, Z = 4, $D_{calcd.}$ = 1.622 g.cm^{-3}, λ = 0.71073 Å, T = 293(2) K, μ(Mo-K_α) = 0.796 mm^{-1}, F(000) = 2064. A prismatic crystal of dimensions 0.28 × 0.15 × 0.10 mm was mounted on an Enraf−Nonius Kappa-CCD diffractometer. A full sphere of data was collected by φ axis rotation with an increment of 1.5° over 360° and 170 s exposure per degree. "Dezingering" was accomplished by measuring each frame twice. The θ range for data collection was 1.41 to 29.07°. Data were analyzed using Kappa-CCD software.[85] Cell dimensions were refined with HKL Scalepack.[86] Data reduction was performed with Denzo.[86] Of a total of 13461 collected reflections, 7525 were independent (R_{int} = 0.046) and 4729 unique reflections had $I \geq 2\sigma(I)$. The structure was solved by direct methods (program SHELXS-86[87]) and was refined on F^2 for all reflections by least-squares methods using SHELXL-93.[88] Hydrogen atoms were included in calculated positions by using a riding model and were assigned isotropic thermal parameters 1.2 times that of the atoms to which they were bound. The asymmetric unit consists of one dimeric Mn^{II} complex, two PF_6 counteranions, and a water solvent molecule. The counteranions are subject to disorder. Two sites could be located on the difference Fourier map for each PF_6 anion. Several models for this disorder were tested. The best convergence was obtained with occupancies of 0.8 and 0.2. Refinement was pursued with restraints. The final conventional R_1 factor was found to be 0.075 for 4729 data, 84 restraints, and 585 parameters, and 0.13 for all data, wR_2 = 0.26 (all data); the largest peak and hole in the final difference map were within +0.5 and −0.3 eÅ^{-3}. A selection of bond lengths and angles is presented in Table 2. A perspective view of the Mn dimeric complex is shown in Figure 2. The hydrogen-bond network includes both intra- and intermolecular hydrogen bonds in the crystal structure, involving both the water molecules coordinated to the metal center (first coordination sphere), the noncoordinated oxygen atoms of the bis(μ-carboxylato) bridges of the dimeric complex, and the water solvent molecule included in the crystal structure. Structural data have been deposited with the Cambridge Crystallographic Data Centre (CCDC) under the depository number CCDC-150159. Copies of the data can be obtained free of charge on application to the CCDC, 12 Union Road, Cambridge CB2 1EZ, U.K. [Fax: (internat) + 44-1223/336-033; E-mail:deposit@ccdc.cam.ac.uk].

Reactivity in Anhydrous DMSO: Glassware was dried for at least one night at 125 °C and then cooled under a stream of argon. Solutions were manipulated in a Schlenk apparatus under a flow of argon and were kept under argon pressure. It was checked that superoxide disproportionation was negligible under the experimental conditions used (see below). DMSO solutions were prepared immediately prior to use. Saturated solutions of KO_2 in DMSO were obtained by stirring finely ground KO_2 in anhydrous DMSO for 1 h. The slurry was centrifuged for 10 min at 13000 g and the supernatant, which was slightly yellow, was titrated spectrophotometrically at 250 nm (ε = 2686 M^{-1}cm^{-1}).[89] Concentrations from 5 mM up to 6.5 mM were reproducibly obtained. We checked that this concentration was stable by recording UV/Vis spectra over a period of 10 min, in the course of which a decrease of less than 10% was usually recorded. This centrifugation procedure was compared with filtration and was found to provide solutions with slightly higher concentrations and improved stabilities (less decrease over 10 min). For cyclic voltammetry experiments, saturated solutions of KO_2 were prepared in 0.1 M Bu_4NPF_6 in DMSO. The same superoxide concentration was obtained.

EPR Experiments: Several concentrations of the complexes were tested (2×10^{-4} mol·dm^{-3}, 6.5×10^{-4} mol·dm^{-3}, and 1×10^{-3} mol·dm^{-3}). For each concentration, the experiment was performed in duplicate. Several Eppendorf vials were prepared containing the complex and 0−5 equiv. of superoxide with a final volume of 1 mL. Similar Eppendorf vials were prepared with superoxide alone (with quantities corresponding to 0.5−2 equiv.). These tubes were used to check that the superoxide EPR signal was observed under the experimental conditions. The intensity of the g = 2.00 signal was shown to vary linearly with superoxide concentration and could thus be used to give a rough estimate of the concentration in each experiment. After superoxide had been added, the Eppendorf vial was stirred manually. An aliquot of 100 μL was transferred to an EPR tube, immediately frozen in an EtOH/liq. N_2 bath, and kept in liq. N_2. EPR spectra were then recorded, either at 100 K or at 8 K. To estimate the conversion of Mn^{II} to $Mn^{III}Mn^{IV}$, a calibration curve was constructed. The spectra of a fully characterized bis(μ-oxo)$Mn^{III}Mn^{IV}$ compound, namely $[Mn_2O_2bispic(Me)_2en]^{3+}$,[76] at concentrations of 0.25×10^{-4} mol·dm^{-3}, 0.5×10^{-4} mol·dm^{-3}, 1×10^{-4} mol·dm^{-3}, and 1.5×10^{-4} mol·dm^{-3} in DMSO were recorded. The relative intensity of the six main peaks was plotted against concentration.

UV/Vis Experiments: Several concentrations were tested (1×10^{-4} mol·dm^{-3}, 2×10^{-4} mol·dm^{-3}, 6.5×10^{-4} mol·dm^{-3}). Successive equivalents of superoxide were directly added to the cuvette under magnetic stirring. EPR spectra of the solution from the cuvette were also recorded.

Cyclic Voltammetry Experiments: Cyclic voltammetry experiments were performed at room temperature under a stream of argon either in extra-dry DMSO containing 0.1 M Bu_4NPF_6 or in acetonitrile containing 0.1 M Bu_4NPF_6. An $Ag/AgClO_4$ electrode ($AgClO_4$ 10^{-2} M, Bu_4NPF_6 0.1 M) in DMSO was used as a reference for DMSO solutions and was separated from the solution by a glass frit. Its potential was measured as +0.252 V vs. SCE. Potentials are reported in the text vs. SCE. The working electrode was a platinum disc (2 mm diameter). Concentrations were 5×10^{-4} M and 1×10^{-3} M based on Mn^{II} content. When dioxygen-saturated electrolyte was required, dioxygen was bubbled through 0.1 M Bu_4NPF_6 in DMSO for half an hour.[55,60,90]

Xanthine/Xanthine Oxidase−Cytochrome *c* Assay: Superoxide anion was supplied to the system from the xanthine/xanthine oxidase reaction.

Reliability of the X/XO Test: To check that the tested compounds do not inhibit the production of superoxide by xanthine oxidase, the rate of conversion of xanthine to urate was determined by measuring the increase in absorbance at 290 nm over a period of 2 min in the absence and in the presence of the tested compounds. At concentrations higher than the IC_{50} values (which are of the order of 2−5 μM, see below), neither MnIPG nor MnBIG was found to inhibit this conversion. We also verified that ferricytochrome *c* was stable in the presence of both MnIPG and MnBIG. Moreover, it was important to ascertain whether the tested compounds react with H_2O_2 under the experimental conditions, as such a pathway could have led to side reactions.[62] Catalase can be added to the cuvette during the X/XO assay,[38][62] but this introduces another potential source of cross-reaction and interpretative errors.[5] Instead, we probed the H_2O_2 reaction with the complexes at a concentration in the range of the IC_{50} under the experimental conditions of the X/XO assay. The H_2O_2 concentration was found to be stable over a period of 20 min (see below).

Xanthine to Urate Assay: To measure the rate of conversion of xanthine to urate, xanthine oxidase (XO) (30 μL of 0.77 U·mL^{-1} XO)

was added to a potassium phosphate buffer solution (50 *m*M, pH = 7.8) containing 150 μM of xanthine at 25 °C to give a final volume of 1.0 mL. Urate production was monitored at 290 nm. No difference in the slope was observed in the presence or absence of the putative SOD mimics.

Reduction of Ferricytochrome *c*: The activities were measured on the basis of the ferricytochrome *c* reduction.[7,35][62] Assays were performed at 25 °C in 3 mL of reaction buffer (50 *m*M potassium phosphate buffer, pH = 7.8) containing 22 μM ferricytochrome *c*, 200 μM xanthine, and an amount of xanthine oxidase such as to give a rate of $\Delta DO_{550\ nm} = 0.025\ min^{-1}$ (about 0.01 $U{\cdot}mL^{-1}$) in the absence of any putative SOD mimic. The reduction of ferricytochrome *c* was monitored at 550 nm. After 2 min, various amounts of the relevant putative SOD mimic were added. Rates were linear for at least 8 min. The rates both in the absence and in the presence of the complex were determined for each concentration of complex added. The IC_{50} value represents the concentration of the putative SOD mimic that induces 50% inhibition of the reduction of cytochrome *c*. Values were determined as exemplified in Figure 7, where p_1 is the slope before addition of the putative SOD mimic and p_2 is the slope after its addition. The percentage inhibition is given by $\%I = (p_1 - p_2)/p_1{\cdot}100$. For each IC_{50} determination, $\%I$ was measured for several concentrations in the region of the IC_{50}. The IC_{50} value was obtained for $\%I = 50\%$. Additionally, $(p_1 - p_2)/p_2$ was also plotted against the complex concentration and the IC_{50} value was obtained for $(p_1 - p_2)/p_2 = 1$.[63] For tests with EDTA, this chelator was added to provide a final concentration of 3 *m*M in the cuvette. For tests with BSA, 30 μL of BSA (50 $mg{\cdot}mL^{-1}$) was added 4 min after the addition of xanthine oxidase and 2 min after the addition of the putative SOD mimic.

Reaction of Complexes with H_2O_2 under the X/XO Assay Conditions: H_2O_2 (10 equiv.) was added to a solution of the complex (2×10^{-6} M) in potassium phosphate (50 *m*M, pH = 7.8). The H_2O_2 concentration was determined at intervals of 5 min over half an hour by oxidation of iodide using the Ghormley method (colorimetric titration).[91]

Acknowledgments

We thank Dr. Philippe Maillard and Dr. Elodie Anxolabéhère-Mallart both for technical assistance and for discussions concerning electrochemistry, Prof. H. Toftlund for helpful suggestions, and Dr. J. P. Renault for useful discussions and comments. We also acknowledge Dr. Aurore Gref for lending us a platinum electrode. We would like to thank one of the referees for the suggestion to estimate the conversion of Mn^{II} species to the $Mn^{III}Mn^{IV}$ compound. We are grateful to Prof. J. J. Girerd's group for kindly providing us with the $Mn^{III}Mn^{IV}$ compound used as a concentration standard, in particular we would like to thank C. Hureau, Dr. G. Blondin, and Dr. P. Dorlet. We acknowledge the European Community for financial support (TMR contract FMRX-CT980174).

[1] W. R. Jakoby, D. M. Ziegler, *J. Biol. Chem.* **1990**, *265*, 20715−20718.
[2] B. Halliwell, J. M. C. Gutteridge, "Oxygen Radicals in Biological Systems" in *Methods in Enzymology* (Eds.: L. Packler, A. N. Glazer), Academic Press, New York, **1990**, 1−85.
[3] D. Mansuy, P. Battioni, "Dioxygen Activation at Heme Centers in Enzymes and Synthetic Analogs" in *Bioinorganic Catalysis*, Marcel Dekker, New York, **1995**, p. 395−423.
[4] I. Fridovich, *Ann. Rev. Biochem.* **1995**, *64*, 97−112.
[5] D. P. Riley, *Chem. Rev.* **1999**, *99*, 2573−2587.
[6] Abbreviations: SOD: superoxide dismutase; IPG: *N*-[(1-methylimidazol-2-yl)methyl]-*N*-(2-pyridylmethyl)glycinate; BIG: *N*,*N*-bis[(1-methylimidazol-2-yl)methyl]glycinate; DMSO: dimethyl sulfoxide; EPR: electron paramagnetic resonance; CV: cyclic voltammetry; SCE: saturated calomel electrode; EC process: Electrochemical-Chemical process; X/XO: xanthine/xanthine oxidase; EDTA: ethylenediaminetetraacetate; BSA: bovine serum albumine; TPAA: tris{2-[*N*-(2-pyridylmethyl)-amino]ethyl}amine; IC_{50}: 50% inhibition concentration; LMCT: ligand→metal charge transfer.
[7] J. M. McCord, I. Fridovich, *J. Biol. Chem.* **1969**, *244*, 6049−6055.
[8] S. J. Lippard, J. M. Berg, *Principles of Bioinorganic Chemistry*, University Science Books, Mill Valley, California, **1994**.
[9] I. Bertini, S. J. Gray, S. J. Lippard, J. S. Valentine, *Bioinorganic Chemistry*, University Science Books, Mill Valley, California, **1994**.
[10] H.-D. Youn, E.-J. Kim, J.-H. Roe, Y. C. Hah, S.-O. Kang, *Biochem. J.* **1996**, *318*, 889−896.
[11] I. Fridovich, *J. Exp. Biol.* **1998**, *201*, 1203.
[12] P. K. Coughlin, A. E. Martin, J. C. Dewan, E.-I. Watanabe, J. E. Bulkowski, J.-M. Lehn, S. J. Lippard, *Inorg. Chem.* **1984**, *23*, 1004−1009.
[13] E. Kimura, T. Koike, Y. Shimizu, M. Kodama, *Inorg. Chem.* **1986**, *25*, 2242−2246.
[14] J.-L. Pierre, P. Chautemps, S. Refaif, C. Beguin, A. El Marzuki, G. Serratrice, E. Saint-Aman, P. Rey, *J. Am. Chem. Soc.* **1995**, *117*, 1965−1973.
[15] J. Casanova, G. Alzuet, S. Ferrer, J. LaTorre, J. A. Ramirez, J. Borras, *Inorg. Chim. Acta* **2000**, *304*, 170−177.
[16] H. Ohtsu, Y. Shimazaki, A. Odani, O. Yamauchi, W. Mori, S. Itoh, S. Fukuzumi, *J. Am. Chem. Soc.* **2000**, *122*, 5733−5741.
[17] L. Iuliano, J. Z. Pedersen, A. Ghiselli, D. Pratico, G. Rotilio, F. Violi, *Arch. Biochem. Biophys.* **1992**, *293*, 153−157.
[18] W. S. Szulbinski, P. R. Warburton, D. H. Busch, *Inorg. Chem.* **1993**, *32*, 5368−5376.
[19] I. Morgenstern-Badarau, F. Lambert, A. Deroche, M. Cesario, J. Guilhem, B. Keita, L. Nadjo, *Inorg. Chim. Acta* **1998**, *275−276*, 234−241.
[20] T. Nagano, T. Hirano, M. Hirobe, *J. Biol. Chem.* **1989**, *264*, 9243−9249.
[21] M. C. Rodriguez, I. Morgenstern-Badarau, M. Cesario, J. Guilhem, B. Keita, L. Nadjo, *Inorg. Chem.* **1996**, *35*, 7804−7810.
[22] M. C. Rodriguez, F. Lambert, M. Cesario, I. Morgenstern-Badarau, *Inorg. Chem.* **1997**, *36*, 3525−3531.
[23] I. Batinic-Haberle, I. Spasojevic, P. Hambright, L. Benov, A. L. Crumbliss, I. Fridovich, *Inorg. Chem.* **1999**, *38*, 4011−4022.
[24] Y. Nishida, I. Watanabe, K. Unoura, *Chem. Lett.* **1991**, 1517−1520.
[25] D. L. Zhang, D. H. Busch, P. L. Lennon, R. H. Weiss, W. L. Neumann, D. P. Riley, *Inorg. Chem.* **1998**, *37*, 956−963.
[26] J. K. Howie, D. T. Sawyer, *J. Am. Chem. Soc.* **1976**, *98*, 6698−6700.
[27] J. S. Valentine, A. E. Quinn, *Inorg. Chem.* **1976**, *15*, 1997−1999.
[28] J. Stein, J. P. Fackler, G. J. McClune, J. A. Fee, L. T. Chan, *Inorg. Chem.* **1979**, *18*, 3511−3518.
[29] W. H. Koppenol, F. Levine, T. L. Hatmaker, J. Epp, J. D. Rush, *Arch. Biochem. Biophys.* **1986**, *251*, 594−599.
[30] K. S. Yamaguchi, L. Spencer, D. T. Sawyer, *FEBS Lett.* **1986**, *197*, 249−252.
[31] W. F. Beyer, I. Fridovich, *Arch. Biochem. Biophys.* **1989**, *271*, 149−156.
[32] J. D. Rush, Z. Maskos, W. H. Koppenol, *Arch. Biochem. Biophys.* **1991**, *289*, 97−102.
[33] N. Kitajima, M. Osawa, N. Tamura, Y. Moro-Oka, T. Hirano, M. Hirobe, T. Nagano, *Inorg. Chem.* **1993**, *32*, 1879−1880.
[34] D. P. Riley, R. H. Weiss, *J. Am. Chem. Soc.* **1994**, *116*, 387−388.
[35] K. M. Faulkner, R. D. Stevens, I. Fridovich, *Arch. Biochem. Biophys.* **1994**, *310*, 341−346.

[36] K. M. Faulkner, S. I. Liochev, I. Fridovich, *J. Biol. Chem.* **1994**, *269*, 23471−23476.
[37] D. P. Riley, S. L. Henke, P. J. Lennon, R. H. Weiss, W. L. Neumann, W. J. J. Rivers, K. W. Aston, K. R. Sample, H. Rahman, C.-S. Ling, J.-J. Shieh, D. H. Busch, W. Szulbinski, *Inorg. Chem.* **1996**, *119*, 5213−5231.
[38] A. Deroche, I. Morgenstern-Badarau, M. Cesario, J. Guilhem, B. Keita, L. Nadjo, C. Houée-Levin, *J. Am. Chem. Soc.* **1996**, *118*, 4567−4573.
[39] D. P. Riley, P. J. Lennon, W. L. Neumann, R. H. Weiss, *J. Am. Chem. Soc.* **1997**, *119*, 6522−6528.
[40] B. J. Day, I. Fridovich, J. D. Crapo, *Arch. Biochem. Biophys.* **1997**, *347*, 256−262.
[41] I. Batinic-Haberle, S. I. Liochev, I. Spasojevic, I. Fridovich, *Arch. Biochem. Biophys.* **1997**, *343*, 225−233.
[42] I. Batinic-Haberle, L. Benov, I. Spasojevic, I. Fridovich, *J. Biol. Chem.* **1998**, *273*, 24521−24528.
[43] R. Kachadourian, I. Batinic-Haberle, I. Fridovich, *Inorg. Chem.* **1999**, *38*, 391−396.
[44] D. P. Riley, S. L. Henke, P. J. Lennon, K. Aston, *Inorg. Chem.* **1999**, *38*, 1908−1917.
[45] D. Salvemini, Z.-Q. Wang, J. L. Zweier, A. Samouilov, H. Macarthur, T. P. Misko, M. G. Currie, S. Cuzzocrea, J. A. Sikorski, D. P. Riley, *Science* **1999**, *286*, 304−305.
[46] A. Carlioz, M. L. Ludwig, W. C. Stallings, J. A. Fee, H. M. Steinman, D. Touati, *J. Biol. Chem.* **1988**, *263*, 1555−1562.
[47] M. L. Ludwig, A. L. Metzger, K. A. Pattridge, W. C. Stallings, *J. Mol. Biol.* **1991**, *219*, 335−358.
[48] G. O. E. Borgstahl, H. E. Parge, M. J. Hickey, W. F. Beyer, R. A. Hallewell, J. A. Tainer, *Cell* **1992**, *71*, 107−118.
[49] M. S. Lah, M. M. Dixon, K. A. Pattridge, W. C. Stallings, J. A. Fee, M. L. Ludwig, *Biochem.* **1995**, *34*, 1646−1660.
[50] R. A. Edwards, H. M. Baker, M. M. Whittaker, J. W. Whittaker, G. B. Jameson, E. N. Baker, *J. Bioinorg. Chem.* **1998**, *3*, 161−171.
[51] C. Policar, F. Lambert, M. Cesario, I. Morgenstern-Badarau, *Eur. J. Inorg. Chem.* **1999**, 2201−2207.
[52] K. Nakamoto, *Infrared and Raman Spectra of Inorganic and Coordination Compounds*, J. Wiley and Sons, New York, **1978**.
[53] S. Gou, X. You, K. Yu, J. Lu, *Inorg. Chem.* **1993**, *32*, 1883−1887.
[54] H. Iikura, T. Nagata, *Inorg. Chem.* **1998**, *37*, 4702−4711.
[55] D. T. Sawyer, T. S. Calderwood, K. Yamaguchi, C. T. Angelis, *Inorg. Chem.* **1983**, *22*, 2577−2583.
[56] D. P. Riley, W. J. Rivers, R. H. Weiss, *Anal. Biochem.* **1991**, *196*, 344−349.
[57] E. Friedman, W. Low, *Phys. Rev.* **1960**, *120*, 408−410.
[58] B. Bleaney, R. S. Rubins, *Proc. Phys. Soc.* **1961**, *77*, 103−112.
[59] B. Bleaney, R. S. Rubins, *Proc. Phys. Soc.* **1961**, *78*, 778.
[60] Y. Nishida, N. Tanaka, A. Yamazaki, T. Tokii, N. Hashimoto, K. Ide, K. Iwasawa, *Inorg. Chem.* **1995**, *34*, 3616−3620.
[61] M. Perrée-Fauvet, A. Gaudemer, J. Bonvoisin, J. J. Girerd, C. Boucly-Goester, P. Boucly, *Inorg. Chem.* **1989**, *28*, 3533−3538.
[62] R. H. Weiss, A. G. Flickinger, W. J. Rivers, M. M. Hardy, K. W. Aston, U. S. Ryan, D. P. Riley, *J. Biol. Chem.* **1993**, *268*, 23049−23054.
[63] Y. Sawada, I. Yamazaki, *Biochim. Biophys. Acta* **1973**, *327*, 257−265.
[64] S. R. Cooper, G. C. Dismukes, M. P. Klein, M. Calvin, *J. Am. Chem. Soc.* **1978**, *100*, 7248−7252.
[65] G. C. Dismukes, J. E. Sheats, J. A. Smegal, *J. Am. Chem. Soc.* **1987**, *109*, 7202−7203.
[66] M. Suzuki, H. Senda, Y. Kobayashi, H. Oshio, A. Uehara, *Chem. Lett.* **1988**, 1763−1766.
[67] H. Diril, H.-R. Chang, M. J. Nilges, X. Zhang, J. A. Potenza, H. J. Schugar, S. S. Isied, D. N. Hendrickson, *J. Am. Chem. Soc.* **1989**, *111*, 5102−5114.
[68] P. A. Goodson, J. Glerup, D. Hodgson, K. Michelsen, E. Pedersen, *Inorg. Chem.* **1990**, *29*, 503−508.
[69] E. J. Larson, V. L. Pecoraro, *Introduction to Manganese Enzymes*, in *Manganese Redox Enzymes*, VCH Publishers, New York, **1992**, p. 1−28.
[70] A. Haddy, G. S. Waldo, R. H. Sands, J. E. Penner-Hahn, *Inorg. Chem.* **1994**, *33*, 2677−2682.
[71] M. Zheng, S. V. Khangulov, G. C. Dismukes, V. V. Barynin, *Inorg. Chem.* **1994**, *33*, 382−387.
[72] M. Zheng, G. C. Dismukes, *Inorg. Chem.* **1996**, *35*, 3307−3319.
[73] W. Zwyegart, R. Bittl, K. Wieghardt, W. Lubitz, *Chem. Phys. Lett.* **1996**, *261*, 272−276.
[74] Y.-M. Frapart, A. Boussac, R. Albach, E. Anxolabéhère-Mallart, M. Delroisse, J.-B. Verlhac, G. Blondin, J.-J. Girerd, J. Guilhem, M. Cesario, A. W. Rutherford, D. Lexa, *J. Am. Chem. Soc.* **1996**, 2669−2678.
[75] C. Policar, M. Knüpling, Y. M. Frapart, S. Un, *J. Phys. Chem.* **1998**, *102*, 10391−10398.
[76] C. Hureau, G. Blondin, C. Mathonière, unpublished results.
[77] K. J. Brewer, M. Calvin, R. S. Lumpkin, J. W. Otvos, L. O. Spreer, *Inorg. Chem.* **1989**, *28*, 4446−4451.
[78] D. R. Gamelin, M. L. Kirk, T. L. Stemmler, P. Samudranil, W. H. Armstrong, J. E. Penner-Hahn, E. I. Solomon, *J. Am. Chem. Soc.* **1994**, *116*, 2392−2399.
[79] A. E. Martell, R. M. Smith, *Critical Stability Constants*, Plenum Press, New York, **1975**, vol. 2.
[80] A. E. Martell, R. M. Smith, *Critical Stability Constants*, Plenum Press, New York, **1977**, vol. 3.
[81] A. E. Martell, R. M. Smith, *Critical Stability Constants*, Plenum Press, New York, **1982**, vol. 5.
[82] Extra-dry DMSO is no longer available from Acros but similar quality can be purchased from Aldrich.
[83] P. E. Iberson, H. Lund, *Acta Chem. Scand.* **1966**, *20*, 2649.
[84] Microanalysis is consistent with one water molecule per manganese ion. This discrepancy between microanalysis and X-ray data may stem from the drying of the powder in vacuo prior to microanalysis.
[85] Enraf−Nonius, Delft, The Netherlands, **1997**.
[86] Z. Otwinowski, W. Minor, "Macromolecular Crystallography, Part A", in *Methods in Enzymology*, Academic Press, London, New York, **1997**, p. 307−326.
[87] G. M. Sheldrick, *Acta Crystallogr., Sect. A* **1990**, *46*, 467.
[88] G. M. Sheldrick, University of Göttingen, Germany, **1993**.
[89] S. Kim, R. DiCosimo, J. J. San Filippo, *Anal. Chem.* **1979**, *51*, 679−681.
[90] D. T. Sawyer, J. L. Robert, *J. Electroanal. Chem.* **1966**, *12*, 90−101.
[91] A. O. Allen, C. J. Hochanadel, J. A. Ghormley, T. W. Davis, *J. Phys. Chem.* **1952**, *56*, 575−586.
[92] M. C. Rodriguez, I. Morgenstern-Badarau, unpublished results.

Received October 25, 2000
[I00402]

Olefin Epoxidation with Transition Metal η^2-Peroxo Complexes: The Control of Reactivity

Dirk V. Deubel,*[a,b] Jörg Sundermeyer,[a] and Gernot Frenking*[a]

Keywords: Density functional calculations / Epoxidations / Peroxo complexes / Transition states

The activation energies for olefin epoxidation with Mimoun-type η^2-peroxo complexes have been calculated using density functional methods. Six degrees of freedom of the complex [MOL$(O_2)$$(OER_3)$] and the olefin CH_2CHR' have been systematically modified. The calculations were based on the assumptions that the reaction follows a concerted oxygen-transfer mechanism suggested by Sharpless and that a peroxo oxygen atom *trans* to the phosphane oxide ligand is transferred. This was recently proved for the epoxidation of ethylene with the parent complex [$MoO(O_2)_2${$OP(CH_3)_3$}]. It has been found that the diperoxotungsten complexes (M = W; L = O_2) are more reactive than the diperoxomolybdenum complexes (M = Mo; L = O_2). The activation barriers for the monoperoxomolybdenum complexes (M = Mo; L = O) are significantly higher than the barriers for the corresponding diperoxo complexes (M = Mo; L = O_2), whereas equal activation energies have been predicted for both tungsten compounds (M = W; L = O_2 and O). The influence of the pnicogen oxide OER_3 on epoxidation activity is comparably small, while electron-releasing substituents R′ at the C=C bond reduce the activation barrier. The transition states for the epoxidation of alkenes with conjugated double bonds show a large extent of asymmetry, with the C–O bond at the terminal carbon atom being formed first. Additional ligands L′ coordinating to the metal center inhibit oxygen transfer. The results are in agreement with an electrophilic attack of the oxidant on the C=C double bond.

Introduction

Tremendous research efforts have focused on the epoxidation of olefins mediated by transition metal complexes,[1−7] in order to replace the chlorohydrin process which is still utilized on a million-ton-per-year scale despite its inefficiency and environmental impact.[8] Beside Herrmann-type diperoxorhenium compounds,[6] Mimoun-type diperoxo complexes of group 6 metals have been utilized as oxidants for olefins. As a promising method based on the *stoichiometric* epoxidation with Mimoun-type diperoxomolybdenum complexes [$MoO(O_2)_2(OPR_3)$] (R = NMe_2),[9] a *biphasic catalytic* system (R = *n*-dodecyl) has recently been developed[10] and patented by BASF.[11] Furthermore, *catalytic* methods in *one homogeneous phase* involving oxo- and diperoxomolybdenum compounds with the hmpa ligand (R = NMe_2)[12] and the 3-pyrazolylpyridine-*N*,*N*′ ligand[13] were reported.

In the last decade, modern computational chemistry has become an important tool in clarifying mechanisms of metal-complex-mediated epoxidations.[14−21] The long-standing controversy[22] about the mechanism of olefin epoxidation with Mimoun-type η^2-diperoxomolybdenum complexes [$MoO(O_2)_2(OPR_3)$] (**I**) has recently been settled with the help of density functional methods (Scheme 1).[16] The reaction does not follow a step-wise pathway[23] involving olefin coordination at the metal center (**II**), subsequent cycloinsertion yielding a 2,3-metalladioxolane (**III**), and cycloextrusion of the oxirane (**IV**) from the metallacycle. Although olefins coordinate with the d^0 metal center of the diperoxomolybdenum complexes (**I→II**),[24] subsequent formation of the metalladioxolane (**II→III**) does not occur; nor is a direct reaction pathway (**I→III**) from the reactants to the metallacycle energetically feasible.[16] Even if the metallacycle was formed, its decomposition would yield the carbonyl compound (**VI**) via hydrogen-migration-supported cycloreversion, rather than the epoxide (**IV**) via cycloextrusion (Scheme 2).[16] As suggested by Sharpless,[25] the oxygen atom is directly transferred from the metal peroxide to the olefin (**TS V**). Preferentially, the peroxo oxygen atom *trans*[26] to the phosphane oxide ligand is transferred and it has a *spiro* configuration in the **TS** geometry.[16] The transition state shows an anomeric effect, i.e. the O−P bond of the phosphane oxide is synperiplanar to the metal−oxygen bond being cleaved.[16,24] The concerted mechanism was also proved for olefin epoxidation with the methyloxodiperoxorhenium(VII) compound.[14] The electronic character of the oxygen transfer was clarified by Charge Decomposition Analysis (CDA)[27] of **TS V**.[20] The analysis identified donation *d* from the ethylene HOMO into the σ* orbital of the O−O bond as the predominant interaction (Figure 1). Backdonation *b*, from the oxygen lone pairs into the ethylene LUMO is significantly less important. This indicates an electrophilic attack of the metal peroxide on the olefin.[20]

Since the activation energy for the epoxidation of ethylene with [$MoO(O_2)_2${$OP(CH_3)_3$}] was calculated to be comparably high (18 kcal/mol),[16] the objective of this DFT study was to investigate the control of reactivity. A general-

[a] Fachbereich Chemie, Philipps-Universität Marburg, Hans-Meerwein-Straße, 35032 Marburg, Germany
[b] Department of Chemistry, University of Calgary, 2500 University Drive N. W., Calgary, Alberta T2N 1N4, Canada

 © WILEY-VCH Verlag GmbH, 69451 Weinheim, 2001 1434−1948/01/0707−1819 $ 17.50+.50/0

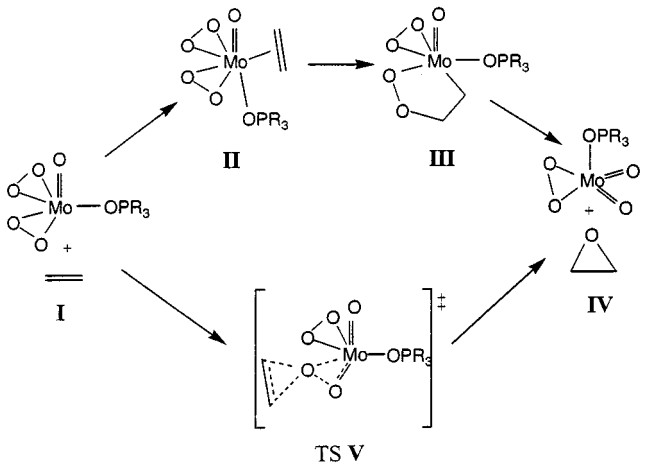

Scheme 1. The long-standing controversy about the mechanism of olefin epoxidation with Mimoun-type diperoxo complexes; the reaction follows a concerted pathway via **TS V**

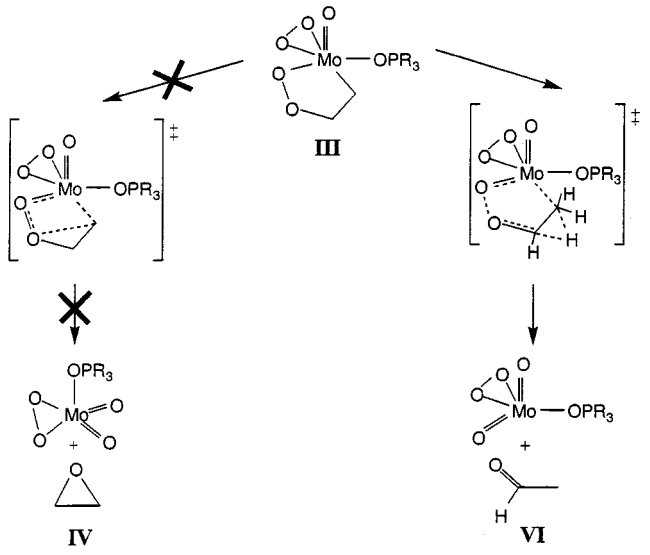

Scheme 2. Fragmentation of the metallacycle; hydrogen-migration-supported cycloreversion (**III→VI**) is favored over the cycloextrusion of oxirane (**III→IV**)

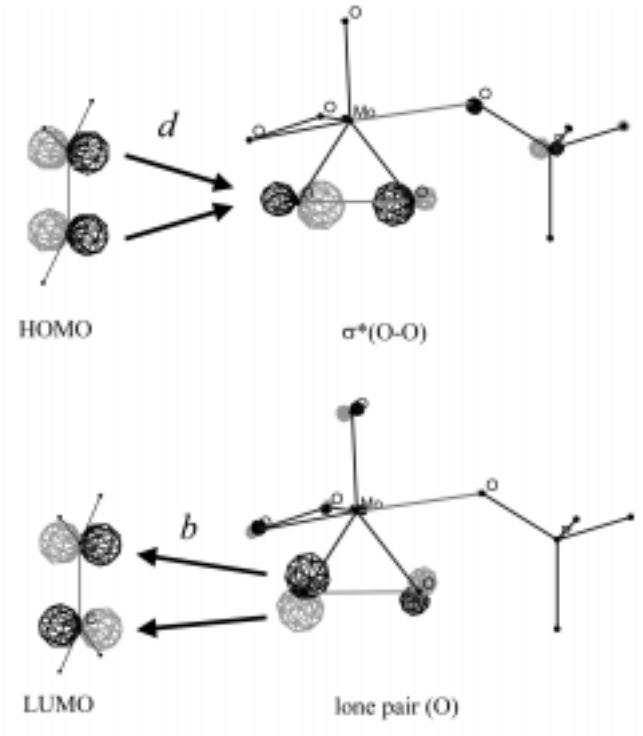

Figure 1. Predominant orbital interactions in the transition state for the epoxidation of ethylene with $[MoO(O_2)_2(OPH_3)]$; donation *d* is significantly more important than backdonation *b*

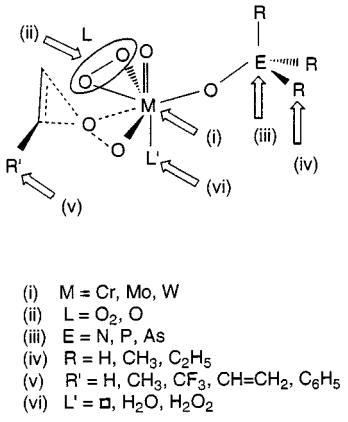

Scheme 3. Concepts for the control of reactivity of olefin oxidation with Mimoun-type peroxo complexes

ized model consisting of the metal complex $[MOL(O)_2(OER_3)L']$ and a terminal olefin CH_2CHR', contains six reactivity-determining degrees of freedom (Scheme 3) which are systematically modified in this study: (i) the metal center M, (ii) the oxo or peroxo ligand L, (iii) pnicogen E, (iv) the substituents R at the pnicogen atom, (v) the substituent R′ at the olefin, and (vi) additional ligands L′ at the metal center. The calculations were based on the assumption that the reaction follows the same concerted pathway as ethylene epoxidation with the parent complex $[MoO(O_2)_2\{OP(CH_3)_3\}]$.[16] Note that, in the catalytic systems, the coordination of the oxidant such as hydrogen peroxide, silyl peroxides, or *tert*-butyl hydroperoxide to the metal center and subsequent proton transfer can yield different species which are potentially more reactive than the parent η^2-peroxo complex.[10,13,17,21] Unless otherwise stated, transfer of the peroxo oxygen atom, which is located *trans* to the phosphane oxide, has been considered.[26]

Methods

The geometries of the molecules and transition states (**TS**) were optimized using the 3-parameter fit of the exchange potentials introduced by Becke (B3LYP).[28] Relativistic small-core ECPs[29] with a valence basis set splitting (441/2111/N1) were used for Cr (N = 4), Mo (N = 3), and W (N = 2), while 6−31G(d) all-electron basis sets were employed for the other atoms.[30] This is our standard basis set

II.[31] Vibrational frequencies and zero-point energy contributions (ZPE) were also calculated at B3LYP/II. All structures reported here are either minima (NIMAG = 0) or transition states (NIMAG = 1, **TS**) on the potential energy surface. The ZPE corrections are unscaled. Improved total energies were calculated at the B3LYP level using the same ECP and valence basis set for the metal atom, but totally uncontracted and augmented with one set of f-type polarization functions,[32] together with 6−31+G(d) basis sets for the other atoms.[33] This basis set combination is denoted III+.[34] Unless otherwise stated, the energies reported refer to the B3LYP/III+//B3LYP/II level of theory. For selected molecules, NPA atomic partial charges were calculated.[35] The computations were carried out with the program package Gaussian 98.[36]

Donor−acceptor interactions in selected transition states were examined using Charge Decomposition Analysis (CDA),[27] which is a quantitative interpretation of the Dewar−Chatt−Duncanson model.[37] The Kohn−Sham orbitals of the **TS** are expressed as a linear combination of the orbitals of the olefin and the remaining metal fragment [M] in the **TS** geometry. The orbital contributions are divided into the mixing of the occupied MOs of the olefin and the vacant orbitals of [M] (donation *d* $C_2H_3R'\rightarrow$[M]), the mixing of the vacant MOs of the olefin and the occupied orbitals of [M] (backdonation *b* $C_2H_3R'\leftarrow$[M]), and the mixing of the occupied MOs of the olefin and the occupied orbitals of [M] (repulsive polarization *r* $C_2H_3R'\rightleftarrows$[M]). A fourth term denoted as the rest term Δ gives the mixing of the unoccupied MOs of the olefin and the unoccupied MOs of [M]. The Δ term will be approximately zero if a discussion of the **TS** in terms of donor−acceptor interactions is permissible. The CDA calculations were performed using the program CDA 2.1.[38]

Results and Discussion

Tables 1−7 list the calculated activation energies for 21 systematically selected combinations (i−vi). In the tables and figures, reactants are denoted **R** and transition states are denoted **TS**. For the coordination of additional ligands L′ at the metal center (vi), stabilization energies were also calculated. The stabilized complexes are denoted **C**. The activation energies given in Table 7 refer to the stabilized complexes **C**.

(i) Influence of the Metal M

Since the patents of BASF[11] include the Mimoun-type diperoxotungsten complexes in addition to the molybdenum compounds, we are extending our study to all the group 6 metals. The reactivity of the diperoxo complexes $[MO(O_2)_2(OPR_3)]$, with M = Cr, Mo, W, with respect to ethylene epoxidation can easily be predicted. Since the oxidant attacks the olefin in an electrophilic manner,[16] the partial charges at the peroxy oxygen atoms of the free oxidants should be a measure of epoxidation activity. NPA partial charges of the three metal diperoxides are shown in Figure 2.[35] At the metal center, the charges increase from chromium to tungsten. Negative charges at the peroxo oxygen atoms of $[MO(O_2)_2(OPR_3)]$ increase in the same order; the highly negatively charged oxygen atoms of the tungsten complex are less electrophilic, and this complex should therefore be less reactive. This conclusion is supported by the reaction energies; according to the Bell−Evans−Polanyi principle,[39] a lower barrier for the chromium complex is expected due to the more exothermic reaction (Table 1). These results suggest that the activation energies increase in the order Cr < Mo < W.

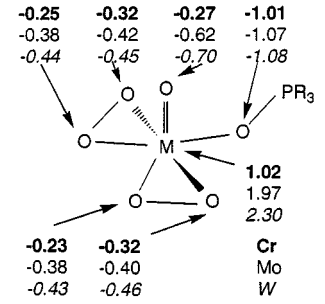

Figure 2. Calculated NPA partial charges of $[MO(O_2)_2\{OP(CH_3)_3\}]$; M = Cr (**R 1**, **bold**), Mo (**R 2**, plain), W (**R 3**, *italics*)

Table 1. O−O distances [Å] in diperoxo complexes $[MO(O_2)_2\{OP(CH_3)_3\}]$; M = Cr (**1**), Mo (**2**), W (**3**), *d*/*b* ratio in CDA of the transition states of ethylene epoxidation, reaction energies E_r [kcal/mol] and activation energies E_a [kcal/mol]; energies at the B3LYP/III+//B3LYP/II level; ZPE-corrected (B3LYP/II) values in parentheses

No.[a]	M	O−O	*d*/*b*	E_r	E_a
1	Cr	1.404	1.63[b]	−42.5 (−40.1)	21.8 (23.1)
2	Mo	1.452	1.76[c]	−37.2 (−35.4)	16.9 (17.9)
3	W	1.478	1.86[d]	−36.9 (−35.0)	14.5 (15.4)

[a] For geometry optimizations and frequency calculations, basis set STO-3G was used at the methyl groups. − [b] $d = 0.237$, $b = 0.145$, $r = -0.318$, $\Delta = -0.005$. − [c] $d = 0.237$, $b = 0.135$, $r = -0.312$, $\Delta = -0.004$. − [d] $d = 0.233$, $b = 0.125$, $r = -0.301$, $\Delta = -0.005$.

However, the calculated activation barriers show the opposite trend. Activation energies for ethylene epoxidation with $[MO(O_2)_2\{OP(CH_3)_3\}]$ decrease from chromium (23.1 kcal/mol), molybdenum (17.9 kcal/mol) to tungsten (15.4 kcal/mol, Table 1). Rösch and co-workers[19] have recently studied the epoxidation of ethylene with simpler model complexes $[MO(O_2)_2(NH_3)]$ using DFT methods. They found a similar trend for the activation energies with M = Cr, Mo, W.[40] A correlation between the σ*-orbital energy level and the activation barrier was given as an explanation.[18] This is plausible because donation from the olefin HOMO into the σ* orbital of the O−O bond being cleaved is the dominant interaction in the **TS**.[20] Furthermore, Rösch and co-workers[19] pointed out a stronger involvement of the metal d orbitals in the π* orbital of the O−O bond in the chromium compound, which increases the strength of the O−O bond and lowers the epoxidation ac-

tivity. This is also reflected by the O−O distances in the free oxidants (Table 1).

Originally, a three-membered ring transition state shown in Figure 3a was suggested.[25] If this had been true, the partial charges of the metal complexes would have led to the correct prediction of the epoxidation activity. We want to point out that the transition state is coarctate,[41] i.e. the metalladioxirane moiety is significantly involved, as schematically shown in Figure 3b. Therefore, the sum of partial charges $q(M) + q(O) + q(O)$ at the metalladioxirane moiety (Figure 2) predicts the trend of the activation barriers in relation to an electrophilic attack. A fragment-based population analysis, such as Charge Decomposition Analysis (CDA),[27] should also reflect the trend; the CDA results of the transition states are given in Table 1. The ratio donation/backdonation (d/b) is a measure of the electronic character of the oxidants. The analysis reveals that the d/b values, and therefore the electrophilicity of the oxidants increase in the order Cr < Mo < W. Since the oxidant attacks the olefin in an electrophilic manner, the reactivity of comparable oxygen-transfer agents correlates with their electrophilicity.

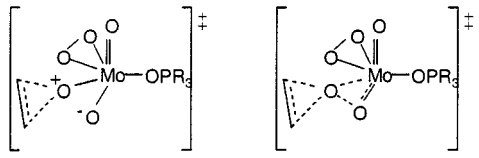

Figure 3. The nature of the transition state for olefin epoxidation with transition metal peroxo complexes: a) **TS** involving only the olefin and the oxygen atom that is transferred, b) coarctate **TS**

(ii) Reactivity of Monoperoxo Complexes

Olefin epoxidation with a diperoxo complex yields the oxirane2 and the monoperoxo complex, which might then oxidize an olefin. To highlight the reactivity of the monoperoxomolybdenum compounds, we calculated the activation energies for the epoxidation of ethylene with $[MoO(O_2)L(OPR_3)]$ (L = O_2, O; Table 2). CDA results are also given in Table 2. In contrast to the transition states presented in the other sections, both isomers of the **TS**s, i.e. for an olefin attack at the peroxo oxygen atom *cis* and *trans* to the phosphane oxide, have been considered since the preferential attack has not yet been clarified for the monoperoxo complexes. The **TS**s for a *cis* attack are denoted **c**. Figure 4 shows the optimized structures for the transition states of ethylene epoxidation with the molybdenum diperoxides $[MoO(O_2)_2(OPH_3)]$ (**TS 10** and **TS 10c**, respectively) and monoperoxides $[MoO_2(O_2)(OPH_3)]$ (**TS 12** and **TS 12c**, respectively). CDA of the diperoxo compounds indicates that the transfer of the *cis* oxygen atom is less electrophilic (**TS 10c**: $d/b = 1.60$), and therefore less reactive (E_a = 24.7 kcal/mol) than the transfer of the *trans* oxygen atom (**TS 10**: $d/b = 1.92$, E_a = 15.2 kcal/mol). The corresponding results for the monoperoxo complexes are surprising. Although the peroxo oxygen atom situated *trans* is also more electrophilic ($d/b = 2.00$ for **TS 12** versus 1.68 for **TS 12c**), the activation barriers are almost equal (17.8 and 18.0 kcal/mol, respectively). Does our simple model fail to explain the reactivity of the monoperoxo complexes? Note the optimized structures of the reactants given in Figure 5. While $[MoO(O_2)_2(OPR_3)]$ (**R 10**) has Mo−O(peroxo) bonds of equal length, the Mo−O(peroxo) bonds situated *cis* to the phosphane oxide in $[MoO_2(O_2)(OPR_3)]$ (**R 12**) are elongated. The cleavage of these bonds is already reflected by the reactant geometry, which is the reason for a moderate barrier despite its lower electrophilicity. CDA apparently describes the nature of the O−O bond rather than the metal−O(peroxo) bond. Bach and co-workers[42] pointed out for other oxidants that a prediction of activation energies based only on parameters of the O−O bond being cleaved is not always successful. In metal peroxides, the strength of the M−O bonds, reflected by their length, also has to be taken into account.

Table 2. Calculated (B3LYP/III+//B3LYP/II) activation energies E_a [kcal/mol] and CDA results of transition states of ethylene epoxidation with the diperoxo and monoperoxo complex $[MoOL(O_2)(OPH_3)]$; L = O_2 (**R 10**), O (**R 12**)

TS[a]	d $C_2H_4\rightarrow$[M]	b $C_2H_4\leftarrow$[M]	d/b	r $C_2H_4\leftrightarrow$[M]	Δ	E_a
TS 10	0.223	0.116	1.92	−0.275	−0.005	14.2 (15.2)
TS 10c	0.230	0.144	1.60	−0.332	−0.005	23.8 (24.7)
TS 12	0.230	0.115	2.00	−0.288	−0.004	17.0 (17.8)
TS 12c	0.208	0.124	1.68	−0.283	−0.005	17.0 (18.0)

[a] **TS** for an olefin attack on the peroxo oxygen atom *cis* to the phosphane oxide ligand are denoted **c**. Otherwise, the *trans* peroxo atom is attacked.

Olefin epoxidation with several (monoperoxo)Mo^{VI} complexes of the type $[X_2MoO(O_2)(H_2O)(NH_3)]$ was recently studied by Rösch and co-workers using density functional methods.[18] These monoperoxo complexes exhibit higher barriers for direct oxygen transfer to ethylene than those for the reference diperoxo complex $[MoO(O_2)_2(H_2O)(NH_3)]$.[18] The most electronegative ligands X induce the lowest barriers, which is in agreement with the concept of an electrophilic attack of the molybdenum peroxide on the olefin.

Our calculations reveal that the monoperoxomolybdenum complexes (**R 12**: E_a = 17.8 kcal/mol) are less reactive than the diperoxo complexes (**R 10**: E_a = 15.2 kcal/mol). The small reactivity of monoperoxomolybdenum compounds was supported by experiments[10,43] and a recent theoretical[18] study. However, the data provided in Table 3 reveal that the reactivities of the tungsten compounds are different. The calculated activation barriers for ethylene epoxidation with the monoperoxo- (**R 13**: E_a = 13.5 kcal/mol) and diperoxotungsten compounds (**R 11**: E_a = 12.7 kcal/mol) are almost equal, indicating that both tungsten species are active oxidants.

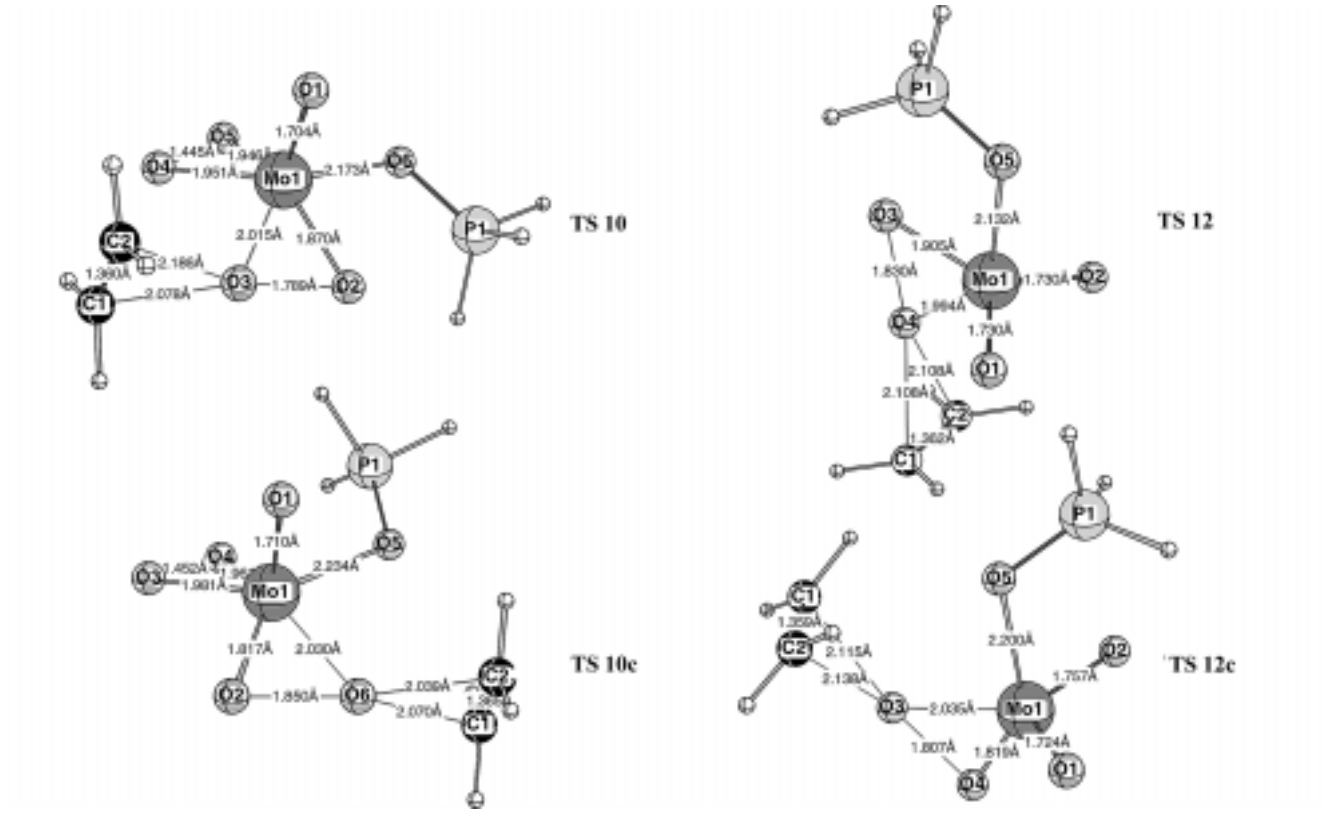

Figure 4. Optimized geometry of **TS 10**, **TS 10c**, **TS 12**, and **TS 12c** (B3LYP/II)

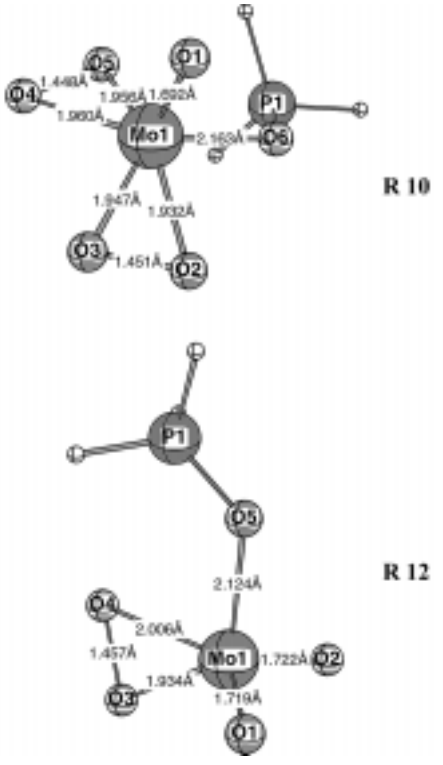

Figure 5. Optimized geometry of **R 10** and **R 12** (B3LYP/II)

(iii) Influence of the Pnicogen E

Besides amphiphilic phosphane oxide ligands, the corresponding amine and arsane oxides are used in the metal-catalyzed epoxidation under biphasic conditions.[10,11] Thus, we have investigated the reactivity of the diperoxo complexes $[MO(O_2)_2\{OE(CH_3)_3\}]$ with M = Cr, Mo, W and with E = N, P, As. The results given in Table 4 are similar for the three metals; we focus on the molybdenum compounds for which the largest differences in the activation barriers are found. The calculations show that the complexes with the phosphane oxide ligands tend to be slightly more reactive than the amine and arsane oxide complexes. Phosphane oxides are weaker donors than their N and As analogues. Therefore, the OPR_3 complexes are more electrophilic at the metalladioxirane moieties and more reactive. This is in agreement with the experimental results for stoichiometric olefin epoxidation.[10] Surprisingly, the opposite trend is found for the reaction performed under biphasic conditions. In this system, the phosphane oxide complexes are less efficient.[10] Note that the turnover frequencies depend both on the intrinsic reactivity of the oxidants and on their Nernst distribution in the two phases. Amine and arsane oxides are comparably strong donors and they can extract the catalyst more efficiently into the organic phase, where epoxidation occurs. Despite higher activation barriers, the E = N, As systems are better oxidants under biphasic conditions due to their better extracting abilities,

which leads to a larger concentration of catalyst in the organic phase.[10] Although one should not over-interpret the small calculated differences in activation energies, the theoretically predicted activation barriers reflect the experimental trends.

Table 3. Calculated (B3LYP/III+//B3LYP/II) activation energies E_a [kcal/mol] for ethylene epoxidation with mono- and diperoxo complexes [$MOL(O_2)\{OE(CH_3)_3\}$]; M = Mo, W; L = O_2, O; ZPE-corrected (B3LYP/II) values are given in parentheses

No.[a]	(i) M	(ii) L	(iii) E	(iv) R	(v) R′	(vi) L′	E_a
10	Mo	O_2	P	H	H	□	14.2 (15.2)
10c	Mo	O_2	P	H	H	□	23.8 (24.7)
11	W	O_2	P	H	H	□	11.9 (12.7)
12	Mo	O	P	H	H	□	17.0 (17.8)
12c	Mo	O	P	H	H	□	17.0 (18.0)
13	W	O	P	H	H	□	12.7 (13.5)
13c	W	O	P	H	H	□	13.4 (14.4)

[a] **TS** for an olefin attack on the peroxo oxygen atom *cis* to the phosphane oxide ligand are denoted **c**. Otherwise, the *trans* peroxo oxygen is attacked. – [b] □ = free coordination site.

Table 4. Calculated (B3LYP/III+//B3LYP/II) activation energies E_a [kcal/mol] for ethylene epoxidation with diperoxo complexes [$MO(O_2)_2\{OE(CH_3)_3\}$]; M = Cr, Mo, W; E = N, P, As; ZPE-corrected (B3LYP/II) values are given in parentheses

No.	(i) M	(ii) L	(iii) E	(iv) R[a]	(v) R′	(vi) L′	E_a
1	Cr	O_2	P	CH_3	H		21.8 (23.1)
2	Mo	O_2	P	CH_3	H		16.9 (17.9)
3	W	O_2	P	CH_3	H		14.5 (15.4)
4	Cr	O_2	N	CH_3	H		22.3 (23.3)
5	Mo	O_2	N	CH_3	H		17.8 (18.7)
6	W	O_2	N	CH_3	H		15.1 (16.0)
7	Cr	O_2	As	CH_3	H		22.0 (22.9)
8	Mo	O_2	As	CH_3	H		18.6 (19.6)
9	W	O_2	As	CH_3	H		14.4 (15.3)

[a] For geometry optimizations and frequency calculations, basis set STO-3G was used at the methyl groups. – [b] □ = free coordination site.

(iv) Influence of Substituents R at the Pnicogen Oxide

Amphiphilic pnicogen oxides with long alkyl chains *n*-C_kH_{2k+1} are used as ligands in the biphasic system. The turnover frequencies strongly depend on the chain length *k*; after increasing with increasing *k*, they remain constant from about $k = 8$.[32] The crucial question is whether the chain length has an influence on the reactivity of the complex, or only on its Nernst distribution equilibrium. Thus, we calculated activation energies for the epoxidation of ethylene by [$MoO(O_2)_2(OPR_3)$] with R = H, CH_3, C_2H_5 (Table 5). The decreasing reactivity from the phosphane oxide complexes (R = H, E_a = 15.2 kcal/mol) to the trimethylphosphane oxide complexes (R = CH_3, E_a = 17.5 kcal/mol) arises from a larger electron density at the metal center and at the peroxo oxygen atoms in the latter compound. The important result for the complex with R = C_2H_5 should be noted. The activation barrier increases by only 0.4 kcal/mol compared with that for the complex with R = CH_3. Alkyl chains longer than $k = 1$ influence the concentration of the catalyst [$MoO(O_2)_2\{OP(n\text{-}C_kH_{2k+1})_3\}$] in the organic phase rather than the reactivity. Therefore, trimethylphosphane oxide is an excellent model for the amphiphilic ligand in computational studies on the control of reactivity.[45]

Table 5. Calculated (B3LYP/III+//B3LYP/II) activation energies E_a [kcal/mol] for ethylene epoxidation with [$MoO(O_2)_2(OPR_3)$]; R = H, CH_3, C_2H_5; ZPE-corrected (B3LYP/II) values are given in parentheses

No.	(i) M	(ii) L	(iii) E	(iv) R	(v) R′	(vi) L′	E_a
10	Mo	O_2	P	H	H	□	14.2 (15.2)
2	Mo	O_2	P	CH_3 [a]	H	□	16.9 (17.9)
14	Mo	O_2	P	CH_3	H	□	16.6 (17.5)
15	Mo	O_2	P	C_2H_5	H	□	17.1 (17.9)

[a] For geometry optimizations and frequency calculations, basis set STO-3G was used at the methyl groups.

(v) Influence of Substituents R′ at the Olefin

In our quantum-chemical calculations, ethylene has been used as a model for the olefin, although the homogeneously catalytic activation of hydrogen peroxide is probably unnecessary for the industrial production of ethylene oxide. Heterogeneously catalytic epoxidation on silver surfaces with O_2 as the oxidant works perfectly for ethylene, but fails for alkyl-substituted olefins due to a chemoselectivity problem. Allylic C–H bonds of the latter substrates are preferentially oxidized.[46] Thus, we are expanding our study of epoxidation with [$MoO(O_2)_2(OPH_3)$] to olefins of the type C_2H_3R', with a variety of substituents R′ = H, CH_3, CF_3, $CH{=}CH_2$, C_6H_5. Since attempts to induce an enantioface selectivity of olefin epoxidation by the employment of chiral phosphane oxide ligands failed,[44] only one of four diastereomeric transition states was arbitrarily selected for the attack at the peroxo oxygen atom *trans* to the OPR_3 ligand, and was optimized with all substituents R′ (Scheme 3). Electron-donating substituents might lower the barrier and vice versa, because donation from the olefin HOMO into the σ*(O–O) orbital is the predominant interaction in the transition state. The data given in Table 6 confirm this hypothesis. The calculated barrier for 3,3,3-trifluoropropene (17.2 kcal/mol) is higher than for ethylene (15.2 kcal/mol), whereas propylene is oxidized faster (E_a = 12.9 kcal/mol). Additional alkyl substituents at the olefin should further accelerate the reaction.[23] π-Conjugation in *transoid*-butadiene and styrene also leads to slightly smaller activation barriers. While the orbital coefficients at the carbon atoms in the olefin HOMO decrease, the energy of this orbital increases due to conjugation.[47] The geometry of **TS 18** for *transoid*-butadiene given in Figure 6 reveals a strongly asynchronous but still concerted epoxidation of conjugated double bonds. The C–O bond at the terminal carbon atom

Table 6. Calculated (B3LYP/III+//B3LYP/II) activation energies E_a [kcal/mol] for epoxidation of olefins CH_2=CHR, R′ = H, CF_3, CH_3, CH=CH_2, C_6H_5 with [$MoO(O_2)_2(OPH_3)$]; ZPE-corrected (B3LYP/II) values are given in parentheses

No.	(i) M	(ii) L	(iii) E	(iv) R	(v) R′	(vi) L′	E_a
10	Mo	O_2	P	H	H	□	14.2 (15.2)
16	Mo	O_2	P	H	CF_3	□	16.9 (17.2)
17	Mo	O_2	P	H	CH_3	□	12.4 (12.9)
18	Mo	O_2	P	H	CH=CH_2	□	12.6 (7.4)
19	Mo	O_2	P	H	C_6H_5	□	12.0 (12.5)

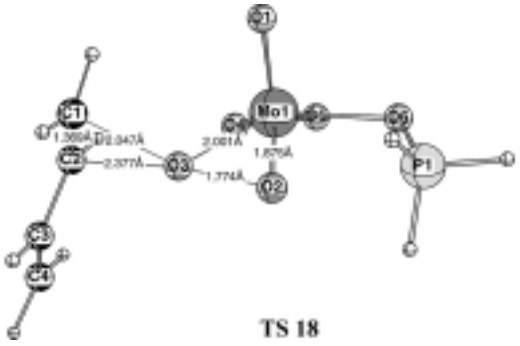

Figure 6. Optimized geometry of **TS 18** (B3LYP/II)

C1 is formed first because of the larger coefficient at C1 in the olefin HOMO.[47]

(vi) Influence of Additional Ligands L′ at the Metal Center

Due to the solubility of hydrogen peroxide in the organic phase ($CHCl_3$), epoxidation can occur in a different manner than that has been discussed for homogeneous *t*BuOOH activation:[13] Hydrogen peroxide can coordinate at the metal center, and catalytically active species might be formed in subsequent reactions.[13] In this section, we investigate the influence of an additional ligand L′ = H_2O, H_2O_2 on the stability and reactivity of diperoxo complexes [$MoO(O_2)_2(OPR_3)L'$]. The results are collected in Table 7. The coordination of an aqua and hydrogen peroxide ligand to [$MoO(O_2)_2\{OP(CH_3)_3\}$] is exothermic by −8.6 and −12.6 kcal/mol, respectively.[48,49] However, in agreement with the electrophilicity concept, the additional ligand increases the electron density at the reactive site and should therefore lower the reactivity. For the complex **C 21** with an additional H_2O_2 ligand, a corresponding transition state **TS 21** has not been optimized, because olefin attack at O3 leads to the dissociation of the hydrogen peroxide ligand. For the aqua complex **C 20**, the calculated activation energy for epoxidation increases to the comparably high value of 24.2 kcal/mol.

The coordination of a strong donor ligand inhibits the molybdenum-catalyzed epoxidation of olefins. This was already reported by Mimoun et al.[23] However, the reason for the inhibition is a lower electrophilicity of the complex rather than the blocking of a free coordination site for the olefin by the strong donor ligands at the metal center. It is interesting to note the slight influence that coordination of an aqua ligand to methyloxodiperoxorhenium(VII) compounds has on the reactivity of olefin epoxidation. Moreover, Kühn, Rösch, and co-workers[50] have recently found that Re-catalyzed olefin epoxidation is accelerated in the presence of N ligands. From the results of this section, an important conclusion for Mo-catalyzed epoxidations can be drawn. Due to the coordination of the oxidant, such as H_2O_2 or *t*BuOOH, to the metal center and due to the high activation barriers for the stabilized complexes, these catalytic processes must involve different species formed in subsequent reaction steps. Thiel and co-workers recently gave experimental[13] and theoretical[17] evidence for a potential proton transfer from an alkyl hydroperoxide ligand ROOH that is coordinated to the metal center, to an η^2-peroxo group of [$MoO(\eta^2\text{-}O_2)_2(NH_3)(ROOH)$]. During intramolecular proton transfer, the metalladioxirane moiety $M(O_2)$ is opened and species of the type [$MoO(\eta^2\text{-}O_2)(\eta^1\text{-}OOH)(NH_3)(\eta^1\text{-}OOR)$] are formed. The proton-transfer step also seems to be possible from hydroperoxide coordinating to the metal center.[21] Hence, in the presence of hydrogen peroxide, additional reaction mechanisms have to be taken into account, as suggested by Sheldon,[1,51] Sharpless[52] and Thiel,[13] for metal-complex-catalyzed epoxidations with alkyl hydroperoxides.

Conclusions

The reactivity of Mimoun-type peroxo complexes used for the epoxidation of olefins depends on six degrees of freedom of our extended model system [$MOL(O_2)(OER_3)L'$] and CH_2CHR' in the following way (see Scheme 3):

Table 7. Calculated (B3LYP/III+//B3LYP/II) stabilization energies E_s [kcal/mol] for the addition of L′ = {□, H_2O, H_2O_2} to [$MoO(O_2)(O_2)(OPR_3)$] and activation energies E_a [kcal/mol] for ethylene epoxidation with [$MoO(O_2)(O_2)(OPR_3)L'$]; ZPE-corrected (B3LYP/II) values are given in parentheses

No.	(i) M	(ii) L	(iii) E	(iv) R	(v) R′	(vi) L′	E_s	E_a
2	Mo	O_2	P	CH_3 [a]	H	□	–	16.9 (17.9)
20	Mo	O_2	P	CH_3 [a]	H	H_2O	−11.6 (−8.6)	23.8 (24.2)
21	Mo	O_2	P	CH_3 [a]	H	H_2O_2	−15.0 (−12.6)	–[b]

[a] For geometry optimizations and frequency calculations, basis set STO-3G was used at the methyl groups. – [b] The H_2O_2 ligand is removed from the metal center during olefin attack.

(i) Metal M = Cr, Mo, W: In the complexes $[MO(O_2)_2(OER_3)]$, we find the trend in the epoxidation activity to be W > Mo > Cr. While atomic partial charges and thermodynamic considerations fail to predict activation energies, Charge Decomposition Analysis (CDA) of the transition states was employed as a powerful tool to reveal the relationship between reactivity and the electrophilicity at the metalladioxirane moieties.

(ii) Diperoxo versus monoperoxo compounds; L = O_2, O: Activity O_2 > O. The monoperoxotungsten complex apparently is an active oxidant, whereas the corresponding monoperoxomolybdenum species seems to be inactive.

(iii) Pnicogen E = N, P, As: Activity P > N, As. In agreement with experimental data, complexes with the weaker donor phosphane oxide are more electrophilic and, thus more active under homogeneous conditions than their N and As counterparts. However, the better extracting ability of the latter compounds makes them superior in a biphasic protocol.

(iv) Substituents at the pnicogen R = H, CH_3, C_2H_5: Activity H > CH_3, C_2H_5. Long alkyl chains at the pnicogen oxides used as ligands in the biphasic catalytic system (BASF) have no influence on reactivity, but adjust the Nernst equilibrium, thereby favoring quantitative extraction of the catalyst.

(v) Substituents at the olefin R′ = H, CH_3, CF_3, CH=CH_2, C_6H_5: Reactivity CH_3, CH=CH_2, C_6H_5 > H > CF_3. Due to the electrophilic nature of oxygen transfer, more nucleophilic olefins react faster. The epoxidation of π-conjugated olefins is highly asynchronous; the C−O bond at the terminal carbon atom is formed first.

(vi) Additional ligands at the metal center L′ = □ (free coordination site), H_2O: Activity □ > H_2O. The reason why donor ligands, such as H_2O, inhibit oxygen transfer from the molybdenum compounds is the lower electrophilicity at the peroxo functionalities, rather than blocking the free coordination site for the activation of the olefin. Complexes of the type $[MoO(O_2)_2(OPR_3)L']$, with proton-containing ligands L′, such as H_2O and H_2O_2, can be expected to form compounds with η^1-OOH ligands via proton transfer. These species are probably more reactive than η^2-peroxo complexes.

Acknowledgments

Dirk V. Deubel thanks Jan Frunzke for helpful discussions. He thanks the Fonds der Chemischen Industrie for a Kekulé Scholarship and the Deutscher Akademischer Austauschdienst for a NATO Fellowship. This work has also been supported by the Deutsche Forschungsgemeinschaft (SFB 260 and Schwerpunktprogramm Peroxidchemie). Excellent service has been provided by the computer center of the Philipps-Universität Marburg. Additional computer resources were granted by the HLRS Stuttgart.

[1] R. A. Sheldon, in *Applied Homogeneous Catalysis with Organometallic Compounds* (Eds.: B. Cornils, W. A. Herrmann), VCH, Weinheim, **1996**, vol. 1, p. 441.
[2] J. Koller, US *3.350.422*, **1967**; *US 3.351.635*, **1967**.
[3] [3a] A. Butler, M.-J. Clague, G. Meister, *Chem. Rev.* **1994**, 94, 625 and references cited therein. − [3b] V. Conte, F. Di Furia, S. Moro, *J. Mol. Catal.* **1997**, *120*, 93.
[4] [4a] I. V. Kozhevnikov, *Chem. Rev.* **1998**, *98*, 171. − [4b] C. Venturello, R. D′Aloisio, J. C. J. Bart, M. Ricci, *J. Mol. Catal.* **1985**, *32*, 107. − [4c] Y. Ishii, M. Ogawa, in *Reviews on Heteroatom Chemistry* (Eds.: A. Ohno, N. Furukawa), MYU, Tokyo, **1990**, vol. 3, p. 121; [4d] R. Neumann, M. Cohen, *Angew. Chem.* **1997**, *109*, 1810; *Angew. Chem. Int. Eg. Engl.* **1997**, *36*, 1738. − [4e] M. Bösing, A. Nöh, I. Loose, B. Krebs, *J. Am. Chem. Soc.* **1998**, *120*, 7252.
[5] M. H. Dickman, M. T. Pope, *Chem. Rev.* **1994**, *94*, 569.
[6] [6a] C. C. Romão, F. E. Kühn, W. A. Herrmann, *Chem. Rev.* **1997**, *97*, 3197 and references cited therein. − [6b] W. Adam, C. M. Mitchell, *Eur. J. Org. Chem.* **1999**, 785. − [6c] W. A. Herrmann, D. W. Marz, W. Wagner, J. G. Kuchler, G. Weichselbaumer, R. W. Fischer (Hoechst AG), *DE 3.902.357*, **1989**; *EP 90101439.9*, **1990**.
[7] [7a] A. M. Al-Aljouni, J. H. Espenson, *J. Am. Chem. Soc.* **1995**, *117*, 9243. − [7b] A. M. Al-Aljouni, J. H. Espenson, *J. Org. Chem.* **1996**, *61*, 3969. − [7c] H. Tan, J. H. Espenson, *Inorg. Chem.* **1998**, *37*, 467.
[8] K. Weissermel, H.-J. Arpe, *Industrial Organic Chemistry*, Wiley-VCH, New York, **1997**.
[9] [9a] H. Mimoun, *Angew. Chem.* **1982**, *94*, 750; *Angew. Chem. Int. Ed. Engl.* **1982**, *21*, 734. − [9b] H. Mimoun, I. Seree de Roch, L. Sajus, *Bull. Soc. Chem. Fr.* **1969**, 1481.
[10] G. Wahl, D. Kleinhenz, A. Schorm, J. Sundermeyer, R. Stowasser, C. Rummey, G. Bringmann, C. Fickert, W. Kiefer, *Chem. Eur. J.* **1999**, *5*, 3237.
[11] [11a] M. Schulz, J. H. Teles, J. Sundermeyer, G. Wahl (BASF AG) *DE 195.33.331.4*, **1995**. − [11b] M. Schulz, J. H. Teles, J. Sundermeyer, G. Wahl (BASF AG) *WO 10054*, **1995**.
[12] E. P. Talsi, K. V. Shalyaev, K. I. Zamaraev, *J. Mol. Catal.* **1993**, *83*, 347 and references cited therein.
[13] [13a] W. R. Thiel, T. Priermeyer, *Angew. Chem.* **1995**, *107*, 1870; *Angew. Chem. Int. Ed. Engl.* **1995**, *16*, 1737. − [13b] W. R. Thiel, *Chem. Ber.* **1996**, *129*, 575. − [13c] W. R. Thiel, *J. Mol. Catal. A* **1997**, *117*, 449. − [13d] W. R. Thiel, J. Eppinger, *Chem. Eur. J.* **1997**, *3*, 696.
[14] P. Gisdakis, S. Antonczak, S. Köstlmeier, W. A. Herrmann, W. A.; N. Rösch, *Angew. Chem.* **1998**, *110*, 2333; *Angew. Chem. Int. Ed.* **1998**, *37*, 2211.
[15] I. V. Yudanov, P. Gisdakis, C. Di Valentin, N. Rösch, *Eur. J. Inorg. Chem.* **1999**, *5*, 3603.
[16] D. V. Deubel, J. Sundermeyer, G. Frenking, *J. Am. Chem. Soc.* **2000**, *122*, 10101.
[17] A. Hroch, G. Gemmecker, W. R. Thiel, *Eur. J. Inorg. Chem.* **2000**, 1107.
[18] I. V. Yudanov, C. Di Valentin, P. Gisdakis, N. Rösch, *J. Mol. Catal.* **2000**, *158*, 189.
[19] C. Di Valentin, P. Gisdakis, I. V. Yudanov, N. Rösch, *J. Org. Chem.* **2000**, *65*, 2996.
[20] D. V. Deubel, G. Frenking, H. M. Senn, J. Sundermeyer, *Chem. Commun.* **2000**, 2469.
[21] D. V. Deubel, J. Sundermeyer, G. Frenking, *Org. Lett.*, **2001**, *3*, 329.
[22] J. Sundermeyer, *Angew. Chem.* **1993**, *105*, 1195; *Angew. Chem. Int. Ed. Engl.* **1993**, *32*, 1144.
[23] H. Mimoun, I. Seree de Roch, L. Sajus, *Tetrahedron* **1970**, *26*, 37.
[24] D. V. Deubel, J. Sundermeyer, G. Frenking, *Inorg. Chem.* **2000**, *39*, 2314.
[25] K. B. Sharpless, J. M. Townsend, D. R. Williams, *J. Am. Chem. Soc.* **1972**, *94*, 295.
[26] In Figure 5, the optimized structure of the model complex $[MoO(O_2)_2(OPH_3)]$ **R 10** is shown. Atom O2 is denoted *cis*, atom O3 is denoted *trans*. The activation energy for the transfer of the *cis*-oxygen atom was theoretically predicted to be 9.5 kcal/mol larger than for the *trans*-oxygen atom (ref.[16]).
[27] S. Dapprich, G. Frenking, *J. Phys. Chem.* **1995**, *99*, 9352.
[28] A. D. Becke, *J. Chem. Phys.* **1993**, *98*, 5648.
[29] P. J. Hay, W. R. Wadt, *J. Chem. Phys.* **1985**, *82*, 299.

[30] [30a] J. S. Binkley, J. A. Pople, W. J. Hehre, *J. Am. Chem. Soc.* **1980**, *102*, 939. – [30b] W. J. Hehre, R. Ditchfield, J. A. Pople, *J. Chem. Phys.* **1972**, *56*, 2257.
[31] G. Frenking, I. Antes, M. Böhme, S. Dapprich, A. W. Ehlers, V. Jonas, A. Neuhaus, M. Otto, R. Stegmann, A. Veldkamp, S. F. Vyboishchikov, *Reviews in Computational Chemistry* (Eds.: K. B. Lipkowitz, D. B. Boyd), VCH, New York, **1996**, vol. 8, p. 63.
[32] A. W. Ehlers, M. Böhme, S. Dapprich, A. Gobbi, A. Höllwarth, V. Jonas, K. F. Köhler, R. Stegmann, A. Veldkamp, G. Frenking, *Chem. Phys. Lett.* **1993**, *208*, 111.
[33] T. Clark, J. Chandrasekhar, G. W. Spitznagel, P. v. R. Schleyer, *J. Comput. Chem.* **1983**, *4*, 294.
[34] D. V. Deubel, G. Frenking, *J. Am. Chem. Soc.* **1999**, *121*, 2021.
[35] A. E. Reed, L. A. Curtiss, F. Weinhold, *Chem. Rev.* **1988**, *88*, 899.
[36] M. J. Frisch, G. W. Trucks, H. B. Schlegel, G. E. Scuseria, M. A. Robb, J. R. Cheeseman, V. G. Zakrzewski, J. A. Montgomery, Jr., R. E. Stratmann, J. C. Burant, S. Dapprich, J. M. Millam, A. D. Daniels, K. N. Kudin, M. C. Strain, O. Farkas, J. Tomasi, V. Barone, M. Cossi, R. Cammi, B. Mennucci, C. Pomelli, C. Adamo, S. Clifford, J. Ochterski, G. A. Petersson, P. Y. Ayala, Q. Cui, K. Morokuma, D. K. Malick, A. D. Rabuck, K. Raghavachari, J. B. Foresman, J. Cioslowski, J. V. Ortiz, B. B. Stefanov, G. Liu, A. Liashenko, P. Piskorz, I. Komaromi, R. Gomperts, R. L. Martin, D. J. Fox, T. Keith, M. A. Al-Laham, C. Y. Peng, A. Nanayakkara, C. Gonzalez, M. Challacombe, P. M. W. Gill, B. Johnson, W. Chen, M. W. Wong, J. L. Andres, C. Gonzalez, M. Head-Gordon, E. S. Replogle, and J. A. Pople, *Gaussian 98, Revision A.3*, Gaussian, Inc., Pittsburgh PA, **1998**.
[37] [37a] J. S. Dewar, *Bull. Soc. Chim. Fr.* **1951**, *18*, c71. – [37b] J. Chatt, L. A. Duncanson, *J. Chem. Soc.* **1953**, 2939.
[38] CDA 2.1, S. Dapprich, G. Frenking, Marburg, **1994**. The program is available via ftp.chemie.uni-marburg.de/pub/cda
[39] F. Jensen, *Introduction to Computational Chemistry*, Wiley, Chichester, **1999**.
[40] Note that these compounds $[MO(O_2)_2(NH_3)]$ are unsuitable models for the BASF system: A complex with an olefin directly bound to the metal center was not found as a minimum on the potential-energy surface with the $[MO(O_2)_2(NH_3)]$ model (ref.[19]) but with the $[MO(O_2)_2(OPR_3)]$ model (ref.[16]).
[41] [41a] R. Herges, *Angew. Chem.* **1994**, *106*, 261. – [41b] R. Herges, *J. Chem. Inf. Comput. Sci.* **1994**, *34*, 91.
[42] R. D. Bach, M. N. Glukhovtsev, C. Canepa, *J. Am. Chem. Soc.* **1998**, *120*, 775.
[43] G. Amato, A. Arcoria, F. P. Ballistreri, G. A. Tomaselli, *J. Mol. Catal.* **1986**, *37*, 165.
[44] [44a] G. Wahl, PhD thesis, Würzburg University, Germany, **1998**. – [44b] D. Kleinhenz, PhD thesis, Marburg University, Germany, **2000**.
[45] Utilizing the STO-3G basis set instead of 6−31G* at the methyl moieties for geometry optimization and frequency calculation provides results of the subsequent total-energy calculation at the B3LYP/III+ level without loss of accuracy (see Table 5).
[46] [46a] M. A. Barteau, R. J. Madix, *The Chemical Physics of Solid Surfaces and Heterogenious Catalysis* (Eds.: D. A. King, D. P. Woodruff), Elsevier, Amsterdam, **1982**, p. 95. – [46b] R. A. Van Santen, H. P. C. E. Kuipers, *Adv. Catal.* **1987**, *35*, 265. – [46c] W. M. H. Satchler, C. Backx, R. A. Van Santen, *Catal. Rev.* **1981**, *23*, 127.
[47] I. Fleming in *Frontier Orbitals and Organic Chemical Reactions*, Wiley, New York, **1976**.
[48] Note that experimental free-enthalpy values might differ from the calculated energies. For instance, the coordination of an additional ligand L′ to the metal center is an isokinetic reaction, i.e. the entropic contribution to the free enthalpy partially compensates the enthalpic stabilization. Solvation effects were not explicitly taken into account in our study because the molecules are too large. Furthermore, there is a basis-set-superposition error (BSSE), which is, however, expected to be very small since diffuse basis functions have been employed for energy calculations.
[49] In a previous study (ref.[24]), two isomers of the complex $[MoO(O_2)_2(OPH_3)(H_2O)]$ were found on the potential-energy surface. The OPH_3 and H_2O ligands occupy one equatorial and one axial coordination site of a pentagonal bipyramid. The isomer with the stronger phoshane oxide ligand in the equatorial position is favored by 5.3 kcal/mol over the isomer with the aqua ligand in the equatorial position. Due to electronic and steric reasons, we expected an even larger preference of the former isomer when the improved model $OPMe_3$ is utilized and omitted the investigation of the latter isomer using the improved model.
[50] F. E. Kühn, A. M. Santos, P. W. Roesky, E. Herdtweck, S. Scherer, P. Gisdakis, I. V. Yudanov, C. Di Valentin, N. Rösch, *Chem. Eur. J.* **1999**, *5*, 3603.
[51] R. A. Sheldon, *Recl. Trav. Chim. Pays-Bas* **1973**, *253*, 367.
[52] A. O. Chong, K. B. Sharpless, *J. Org. Chem.* **1977**, *42*, 1587.

Received October 14, 2000
[I00427]

The EPR Pattern of [CrO(*cis*-1,2-cyclopentanediolato)$_2$]$^-$ and [CrO(*trans*-1,2-cyclopentanediolato)$_2$]$^-$

Sandra Signorella,*[a] Verónica Daier,[a] Mabel Santoro,[a] Silvia García,[a] Claudia Palopoli,[a] Juan Carlos González,[a] Lazlo Korecz,[b] Antal Rockenbauer,[b] and Luis F. Sala*[a]

Keywords: Chromates / Chromium / Redox chemistry / EPR spectroscopy

The addition of a large excess of 1,2-cyclopentanediol to a 1:1 mixture of glutathione and Cr^{VI} at pH 7.5 stabilises the intermediate Cr^V species formed by the one-electron reduction of Cr^{VI} by glutathione. The isotropic EPR parameters (g_{iso} and A_{iso}) of the Cr^V species formed with both *cis*- and *trans*-1,2-cyclopentanediol correspond to those calculated for five-coordinate oxo-Cr^V complexes with four alcoholato donors [Cr(O)(1,2-cyclopentanediolato)$_2$]$^-$. The five-coordinate oxo-Cr^V species formed with both 1,2-cyclopentanediol isomers show very similar EPR superhyperfine patterns, but differ in their stability and the conditions required for their formation due to the different chelation ability of the *cis*- vs. *trans*-1,2-diolato moiety.

Introduction

Cr^V intermediates are generated in the oxidation of a number of organic substrates by Cr^{VI} and are possibly linked to the formation of Cr-induced cancers.[1−2] The biological reduction of Cr^{VI} to lower states has been observed with a wide variety of naturally occurring cellular reductants.[3−7] Ligands that possess two oxygen atoms able to form five-membered rings about the metal ion are effective as nonenzymatic reductants and complexation agents towards hypervalent chromium and can stabilise the labile oxidation states of chromium.[8−14] Thus, it is becoming more apparent that diol ligands may play an important role in the stabilisation of Cr^V species formed during the reaction of Cr^{VI} with intracellular reductants. In particular, Cr^V-sugar species are very stable at physiological pH values and remain in solution for between several days and several months after the initiation of the reaction.[15−24]

The most common means of characterising Cr^V complexes in solution is EPR spectroscopy, where strong isotropic signals are observed at room temperature in the X-band spectra. An empirical relationship between the nature and the number of donor groups and the EPR spectral parameters of Cr^V complexes has been established.[25] Five-coordinate Cr^V species show higher g_{iso} and lower ^{53}Cr A_{iso} values than the corresponding six-coordinate species.[25−27] Thus, the assignment of the structures of new oxo-Cr^V species in solution may be made according to the isotropic EPR parameters (g_{iso} and A_{iso} values) and the superhyperfine (shf) pattern of the signal.

[a] Departamento de Química, Facultad de Ciencias Bioquímicas y Farmacéuticas, UNR,
Suipacha 531, 2000 Rosario, Argentina
E-mail: signorel@infovia.com.ar
inquibir@satlink.com
[b] Central Research Institute for Chemistry,
P. O. Box 17, Budapest, 1525, Hungary

It has been found that the multiplicity of the EPR signal of Cr^V-diolato complexes is dependent upon whether the ligand is cyclically strained or not. It was observed that in Cr^V-diolato complexes formed with linear diols all the protons are equivalent in the isotropic EPR spectra,[28] but the strain of a six-membered ring imparts inequivalence to the magnetic environment of the protons in the second coordination sphere.[29] Thus, the signals in the EPR spectra of [CrO(*cis*-1,2-cyclohexanediolato)$_2$]$^-$ and [CrO(*trans*-1,2-cyclohexanediolato)$_2$]$^-$ exhibit a triplet and a singlet, respectively, and the difference was explained by arguing that only when the protons lie in the Cr^V-ligand plane is there a maximal overlap between the proton orbital and the Cr^V orbital containing the unpaired electron density.[29]

In the present work we study the Cr^V-diolato complexes formed by reduction of Cr^{VI} by glutathione (GSH) in the presence of *cis*- or *trans*-1,2-cyclopentanediol in order to extend the analysis of the EPR shf pattern to Cr^V-diolato species formed between Cr^V and five-membered ring 1,2-diols. Our results show that [CrO(*cis*-1,2-cyclopentanediolato)$_2$]$^-$ and [CrO(*trans*-1,2-cyclopentanediolato)$_2$]$^-$ yield EPR signals of the same multiplicity, with similar shf coupling constants — an EPR pattern markedly different from that observed for Cr^V complexes formed from *cis*- and *trans*-1,2-cyclohexanediol. Thus, the present results should be useful for the interpretation of the EPR spectra of the Cr^V species formed in the reduction of Cr^{VI} by biologically relevant substrates containing a five-membered 1,2-diolate ring.

Results

The reaction of Cr^{VI} with GSH (4.5 mM; 1:1 ratio) at pH = 7.5 affords three intermediate Cr^V species with EPR signals at g_{iso} = 1.9859, 1.9771 and 1.9719 [Figure 1(a)] and

 © WILEY-VCH Verlag GmbH, 69451 Weinheim, 2001 1434−1948/01/0707−1829 $ 17.50+.50/0

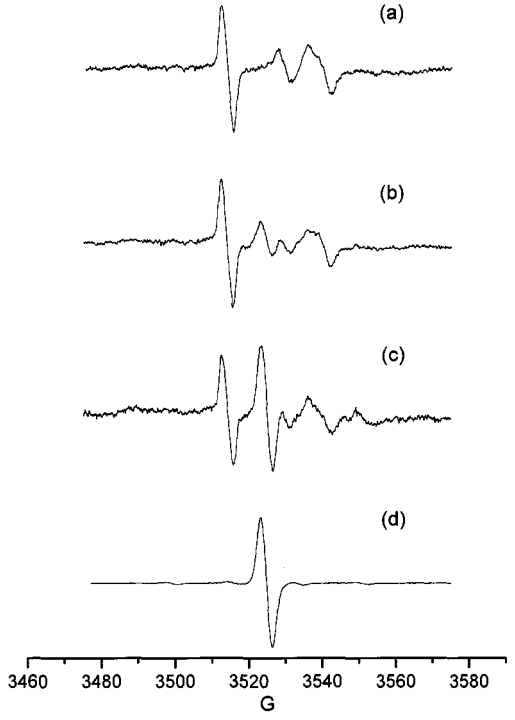

Figure 1. X-band EPR spectra of mixtures of: (a) GSH/Cr^{VI} = 1:1, [Cr^{VI}] = 4.5 mM; (b) GSH/Cr^{VI}/*trans*-diol= 1:1:100, [Cr^{VI}] = 4.5 mM; (c) GSH/Cr^{VI}/*trans*-diol = 1:1:500, [Cr^{VI}] = 1.0 mM; (d) GSH/Cr^{VI}/*trans*-diol = 1:1:5000, [Cr^{VI}] = 1.0 mM; T = 25 °C, pH = 7.5, t = 10 min., frequency = 9.7667 GHz. mod. ampl. = 4 G

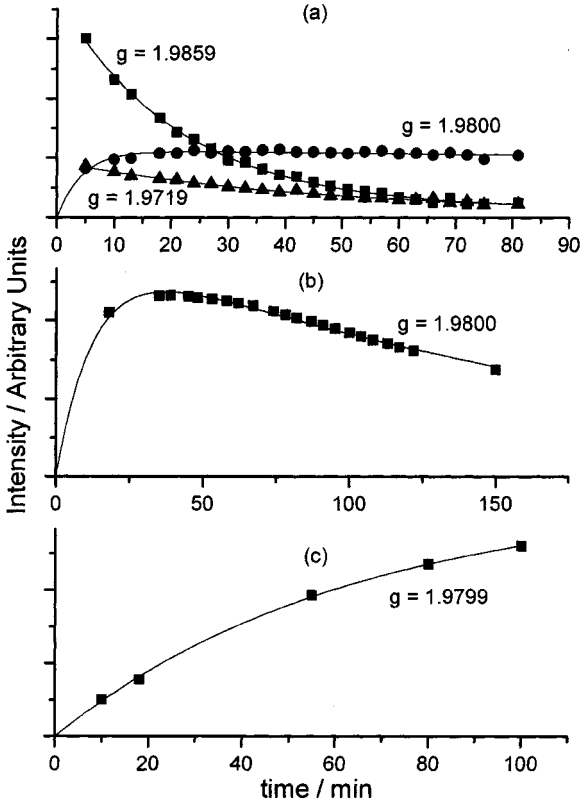

Figure 2. Time dependence of the EPR signal intensities; conditions: (a) GSH/Cr^{VI}/*trans*-diol = 1:1:100, [Cr^{VI}] = 4.5 mM; (b) GSH/Cr^{VI}/*trans*-diol = 1:1:5000, [Cr^{VI}] = 1.0 mM; (c) GSH/Cr^{VI}/*cis*-diol = 1:1:10000, [Cr^{VI}] = 0.5 mM. T = 25 °C, pH = 7.5

relative intensity 2.7:0.68:1, five minutes after the initiation of the reaction. The first signal decays twice as fast as the other two and they are no longer observed after 80 min. The same kinetic behaviour is observed for equimolar Cr^{VI}/GSH mixtures down to 0.5 mM.

When the same reaction is performed in the presence of a 100-fold excess of 1,2-*trans*-cyclopentanediol, the three signals attributed to the Cr^{V}-GSH intermediate species again decay with time and disappear 80 min. after mixing, while a fourth signal appears at g_{iso} = 1.9800 [Figure 1(b)]. This new signal reaches its maximum intensity 30 min. after mixing and decays slowly. The time-dependent variation of the intensity of this signal together with those corresponding to the decay of the Cr^{V}-GSH species at g_{iso} = 1.9859 and 1.9719 are shown in Figure 2(a).

In the presence of a 500-fold excess of *trans*-1,2-cyclopentanediol over the GSH/Cr^{VI} mixture, the EPR spectra are immediately dominated by the Cr^{V} signal at g_{iso} = 1.9800 [Figure 1(c)]. Under these conditions, this signal partially resolves into its components when the modulation amplitude is reduced to 0.4 G.

When the reaction is followed using a much larger *trans*-1,2-cyclopentanediol/Cr^{VI} ratio (5000:1), only the signal at g_{iso} = 1.9800 is observed [Figure 1(d)]. Under these conditions, this signal reaches its maximum intensity 40 min. after mixing and then decays slowly; the time-dependent trace shown in Figure 2(b). In this case, when the modulation amplitude is lowered to 0.4 G, the shf splitting of the signal resolves.

In the presence of excess *cis*-1,2-cyclopentanediol, a 100:1:1 diol/Cr^{VI}/GSH ratio is enough to afford a Cr^{V} signal at g_{iso} = 1.9799 as the only EPR feature in the spectrum. In this case a 500-fold excess of *cis*-1.2-cyclopentanediol is not enough to resolve the EPR signal [Figure 3(a)], but when a much larger excess (5000−10000:1:1 diol/Cr^{VI}/GSH) is used the multiplet resolves well [Figure 3(b)]. Under the last conditions, the rate of decay of the Cr^{V} signal is extremely slow and the signal intensity increases continuously for several hours [Figure 2(c)].

Discussion

It is well known that five-membered Cr^{V} chelates are the most stable and that the CrO^{3+} ion shows a marked preference for binding to *cis*- rather than *trans*-diol groups of cyclic diols.[15,21−24,30−32] Several observations confirm the expected higher ability of the *cis* vs. the *trans* isomer of 1,2-cyclopentanediol for binding Cr^{V}: the receiver gain required to observe the Cr^{V}-diolato signal is 1000 times higher for the *trans* than for the *cis* isomer; the excess of diol needed for the complete replacement of GSH in the Cr^{V} coordination sphere is much larger for the *trans* (5000:1) than for the *cis* (100:1) isomer; under the same experimental conditions, the rate of decay of the Cr^{V} signal is much faster for the *trans* than for the *cis* isomer of 1,2-cyclopentanediol.

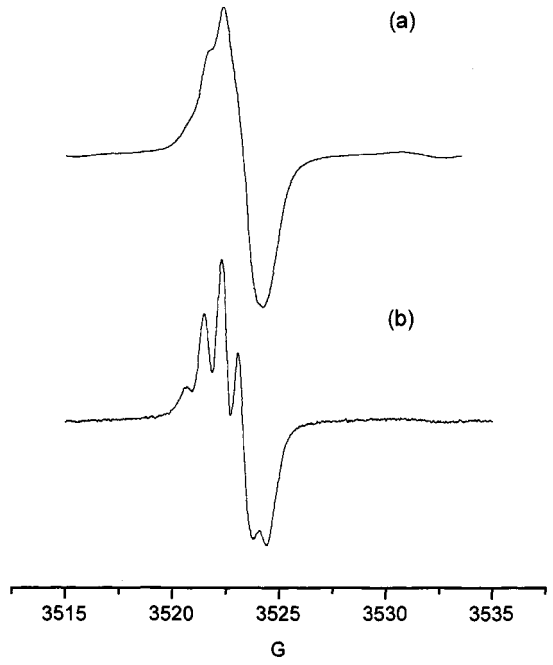

Figure 3. X-band EPR spectra of mixtures of: (a) GSH/Cr^{VI}/*cis*-diol = 1:1:500, [Cr^{VI}] = 1.0 mM; (b) GSH/Cr^{VI}/*cis*-diol = 1:1:10000, [Cr^{VI}] = 0.5 mM; T = 25 °C, pH = 7.5, t = 15 min., frequency = 9.7634 GHz. mod. ampl. = 0.04 G

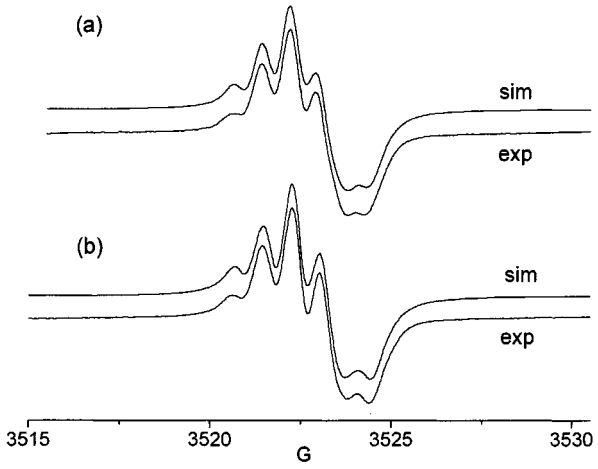

Figure 4. Experimental and simulated X-band EPR spectra of mixtures of: (a) GSH/Cr^{VI}/*trans*-diol = 1:1:5000, [Cr^{VI}] = 1.0 mM, frequency = 9.7620 GHz., mod. ampl. = 0.4 G; (b) GSH/Cr^{VI}/*cis*-diol = 1:1:5000, [Cr^{VI}] = 0.5 mM, frequency = 9.7634 GHz., mod. ampl. = 0.4 G

We used the isotropic EPR parameters g_{iso} and A_{iso} to estimate the coordination number and the nature of the donor groups of the Cr^V species formed in the reaction of Cr^{VI} with GSH in the presence of either excess *cis* or *trans* 1,2-cyclopentanediol, according to a described empirical method.[25−27] The EPR spectra were found to be composed of two Cr^V species (the signals were deconvoluted by fitting the spectra by Lorentzian derivatives). The best fit of the whole set of EPR spectra of Cr^V species formed with either the *cis* or *trans* isomer and different diol-to-Cr^{VI} ratios affords the spectral parameters listed in Table 1; the goodness-of-fit is shown in Figure 4. The spectral parameters for each Cr^V species listed in Table 1 are consistent within all simulation, with maximum deviations in the g_{iso} and ^{1}H a_{iso} values being ±0.0001 units and ±0.02 × 10^{-4} cm^{-1}, respectively. When setting all equivalent protons or pairs of equivalent protons to fit spectra, the spectral parameters were not consistent for all the simulated spectra even when some individual spectra showed a good correlation.

The g_{iso} and A_{iso} values of the Cr^V species formed with the two isomers correspond to those calculated for five-coordinate oxo-Cr^V complexes with four alcoholato donors.[25] In the presence of a large excess of either *cis*- or *trans*-1,2-cyclopentanediol, the EPR signal is a composite of two oxo-Cr^V-(diolato)$_2$ species with four (two from each chelate ring) and three carbinolic protons coupled to the Cr^V electronic spin, respectively (Table 1). In our simulations, we included values for ^{1}H a_{iso} only where the ^{1}H a_{iso} value is greater than the line width (LW) of the Cr^V species, since the signal is not significantly affected when the ^{1}H a_{iso} value is ≤ LW. Thus, the fourth carbinolic proton of the second component should be very weakly coupled to the Cr^V electronic spin resulting in a ^{1}H a_{iso} < LW. The values of ^{1}H a_{iso} of 0.41 × 10^{-4} and 0.47 × 10^{-4} cm^{-1} found for the second component of the EPR signals are just inside the lower simulation limit.

For the two protons lying in the Cr^V-ligand plane in [CrO(*cis*-1,2-cyclohexanediolato)$_2$]$^-$, the observed ^{1}H$_{eq}$ a_{iso} is approximately 0.9 × 10^{-4} cm^{-1}.[29] Measurements of isotropic and anisotropic ^{1}H ENDOR spectra of a series of oxo-Cr^V-diolato$_2$ complexes formed with linear diols showed that the shf coupling constants ^{1}H$_{eq}$ a_{iso} and ^{1}H$_{ax}$ a_{iso} are equal to 0.81 and 0.37 × 10^{-4} cm^{-1}, respectively.[33] This gives us an idea of the values of ^{1}H a_{iso} corresponding

Table 1. EPR spectral parameters

Cr^V species	g_{iso}	^{53}Cr A_{iso}/10^4 cm^{-1}	a_H/10^{4}cm^{-1}
[Cr(O)(*cis*-1,2-cyclopentanediolato)$_2$]$^-$	1.9803	15.9	0.84, 0.81,0.74, 0.64
	1.9798		0.76, 0.65, 0.41
[Cr(O)(*trans*-1,2-cyclopentanediolato)$_2$]$^-$	1.9804	15.9	0.84, 0.76, 0.72, 0.62
	1.9799		0.75, 0.64, 0.47

to the maximal and minimal overlap between the proton orbital and the Cr^V orbital containing the unpaired electron density in oxo-Cr^V-diolato$_2$ systems. Accordingly, in the present case, for the Cr^V species at g_{iso} = 1.9798/9 it is possible to differentiate two carbinolic protons with shf coupling constants intermediate between those corresponding to "pseudo-axial" and "pseudo-equatorial" protons, and two carbinolic protons close to the "pseudo-axial" orientation. While for the Cr^V species at g_{iso} = 1.9803/4, two carbinolic protons lie near the Cr^V-ligand plane and the two others form larger angles with the Cr^V-ligand plane.

The two components can be attributed to two geometric isomers of the $[Cr^V(O)(diolato)_2]^-$ moiety (Scheme 1).[29] Three different geometric isomers (I−III) are possible for $[Cr^V(O)(cis\text{-}1,2\text{-cyclopentanediolato})_2]^-$, whereas only two (IV−V) can exist for $[Cr^V(O)(trans\text{-}1,2\text{-cyclopentanediolato})_2]^-$. However, in both cases only two species are required to simulate the EPR signal. It seems reasonable to assume that the angles between the carbinolic protons and the Cr^V-ligand plane in two of the geometric isomers of $[Cr^V(O)(cis\text{-}1,2\text{-cyclopentanediolato})_2]^-$ are very similar, so we cannot distinguish between them (this should be the case for isomers I and II).

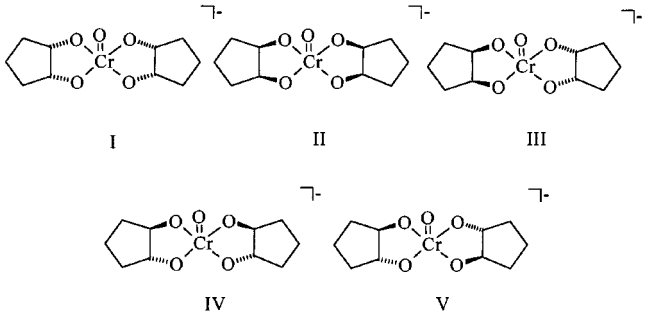

Scheme 1

For the largest diol/Cr^{VI} ratio used in this work the g_{quint}/g_{quart} ratios are 1:1.5 and 1:2.3 for Cr^V species formed with the *cis* and *trans* isomers, respectively, and are independent of the reaction time.

The shf EPR pattern observed for the $[Cr^V(O)(diolato)_2]^-$ species formed with *cis*- and *trans*-1,2-cyclopentanediol is clearly different from that reported for oxo-Cr^V-(diolato)$_2$ species formed with *cis*- and *trans*-1,2-cyclohexanediol. In the case of 1,2-cyclohexanediol, the *trans* isomer affords a singlet, while the *cis* isomer affords two triplets corresponding to two geometric isomers of $[Cr^V(O)(cis\text{-}1,2\text{-cyclohexanediolato})_2]^-$, each with two equivalent H_{eq} coupled to the Cr^V electronic spin. It seems evident that the $[Cr^V(O)(1,2\text{-cyclohexanediolato})_2]^-$ system differentiates the axially and equatorially disposed carbinolic protons, and, consequently, the resulting shf coupling corresponds to the maximal and minimal values expected for the ^1H coupled to the Cr^V electronic spin.

The situation is different for the oxo-Cr^V-(diolato)$_2$ species formed with *cis*- and *trans*-1,2-cyclopentanediol. The EPR spectra of $[Cr^V(O)(1,2\text{-cyclopentanediolato})_2]^-$ formed with both the *cis* and *trans* isomers show the same EPR spectral pattern corresponding to two Cr^V components split by nonequivalent carbinolic protons coupled to the Cr^V electronic spin: one Cr^V component with two "pseudo-equatorial" protons [^1H a_{iso} = 0.84, 0.81 × 10^{-4} cm^{-1} (*cis*-diolate) and 0.84, 0.76 × 10^{-4} cm^{-1} (*trans*-diolate)] and two protons disposed at angles in between the "pseudo-axial/equatorial" orientations, and a second Cr^V species with two "pseudo-axial" protons [^1H a_{iso} = 0.41, < LW (*cis*-diolate) and 0.47, < LW (*trans*-diolate)], and two protons protruding at intermediate angles. Thus, the strained bi-cycle arising from the two fused five-membered rings in $[Cr^V(O)(1,2\text{-cyclopentanediolato})_2]^-$ yields isotropic EPR spectra corresponding to the average conformations of two geometric isomers in which all the carbinolic protons are inequivalent.

Conclusions

Our results show that, as expected, *cis*-1,2-cyclopentanediol possesses a higher ability for binding Cr^V than *trans*-1,2-cyclopentanediol, and that the EPR spectra of Cr^V-(diolato)$_2$ species formed with either the *trans* or *cis* isomer of 1,2-cyclopentanediol exhibit a very similar EPR pattern. For both the *cis* and *trans* isomers, the EPR signal is a composite of two oxo-Cr^V-(diolato)$_2$ species split by four and three (the fourth ^1H a_{iso} is less than the line width) carbinolic protons coupled to the electronic spin, respectively. This new information on the spectral pattern of the EPR signal of Cr^V chelates formed with the *cis* and *trans* isomers of five-membered ring 1,2-diols should be useful in the interpretation of the EPR spectra of the Cr^V species formed in the reduction of Cr^{VI} by NAD(P)H[4] and nucleotides[34] by Cr^V binding to the *cis*-1,2-diolato moiety of the ribose ring and confirm the previous interpretation of the EPR spectra of Cr^V-furanosic sugar species.[21]

Experimental Section

Materials: *cis*-1,2-Cyclopentanediol (Aldrich grade), *trans*-1,2-cyclopentanediol (Aldrich grade), sodium dichromate (Mallinckrodt) and GSH (Sigma grade) were used without further purification. Water was purified by deionisation, followed by double distillation from a potassium permanganate solution. The pH of the solutions was adjusted by addition of 4-(2-hydroxyethyl)-1-piperazineethanesulfonic acid (HEPES).

Warning: Chromic acids are toxic and carcinogenic.

Methods: EPR Measurements: The EPR spectra were performed on a Bruker ESP 300 E spectrometer. The microwave frequency was generated with a Bruker 04 ER (9−10 GHz) and measured with a Racal−Dana frequency meter. The magnetic field was measured with a Bruker NMR probe gaussmeter. All of the EPR experiments were carried out at room temperature. In a typical experiment, 10μL of an aqueous solution of Cr^{VI} (0.1 M) was added to a mixture of 10μL GSH (0.1 M), 0.5030 g diol and 1 mL HEPES (0.1 M) and immediately transferred to a flat quartz cell. The EPR spectra were simulated with a program for the automatic computer simulation of EPR spectra,[35] using 100% Lorentzian lineshapes.

Acknowledgments

This work was supported by the National Research Council of Argentina (CONICET), the Third World Academy of Sciences (TWAS), the National University of Rosario (UNR), the International Foundation for Sciences (IFS), the National Agency for Sciences Promotion, ANTORCHAS Foundation and the grant HU/A98-EVI/07 (Scientific Co-operation Project between Hungary and Argentina).

[1] C. B. Klein, in *Toxicology of Metals* (Ed.: L. W. Chang), CRC-Lewis Publishers, New York, **1996**, pp. 205−220.
[2] M. Costa, *Crit. Rev. Toxicol.* **1997**, *27*, 431−442.
[3] D. H. Stearns, K. E. Wetterhahn, *Chem. Res. Toxicol.* **1994**, *7*, 219−230.
[4] K. E. Wetterhahn Jannette, *J. Am. Chem. Soc.* **1982**, *104*, 874−875.
[5] P. O'Brien, J. Barrett, F. Swanson, *Inorg. Chim. Acta* **1985**, *108*, L19−L20.
[6] P. A. Lay, A. Levina, *J. Am. Chem. Soc.* **1998**, *120*, 6704−6714.
[7] M. Ciéslak-Golonka, *Polyhedron* **1996**, *15*, 3667−3689.
[8] M. Krumpolc, B. G. de Boer, J. Rocek, *J. Am. Chem. Soc.* **1978**, *100*, 145−153.
[9] S. L. Brauer, K. E. Wetterhahn, *J. Am. Chem. Soc.* **1991**, *113*, 3001−3007.
[10] D. M. L. Goodgame, P. B. Hayman, D. E. Hathaway, *Polyhedron* **1982**, *1*, 497−499.
[11] D. M. L. Goodgame, A. M. Joy, *J. Inorg. Biochem.* **1986**, *26*, 219−224.
[12] R. Codd, P. Lay, A. Levina, *Inorg. Chem.* **1997**, *36*, 5440−5448.
[13] R. P. Farrell, P. A. Lay, A. Levina, I. A. Maxwell, R. Bramley, S. Brumby, J. Ji, *Inorg. Chem.* **1998**, *37*, 3159−3166.
[14] R. Codd, A. Levina, L. Zhang, T. W. Hambley, P. A. Lay, *Inorg. Chem.* **2000**, *39*, 990−997.
[15] L. F. Sala, S. R. Signorella, M. Rizzotto, M. I. Frascaroli, F. Gandolfo, *Can. J. Chem.* **1992**, *70*, 2046−2052.
[16] S. R. Signorella, M. I. Santoro, M. N. Mulero, L. F. Sala, *Can. J. Chem.* **1994**, *72*, 398−402.
[17] M. Rizzotto, S. Signorella, M. I. Frascaroli, V. Daier, L. F. Sala, *J. Carbohydr. Chem.* **1995**, *14*, 45−51.
[18] S. Signorella, M. Rizzotto, V. Daier, M. I. Frascaroli, C. Palopoli, D. Martino, A. Bousseksou, L. F. Sala, *J. Chem. Soc., Dalton Trans.* **1996**, 1607−1611.
[19] S. Signorella, S. García, L. F. Sala, *Polyhedron* **1997**, *16*, 701−706.
[20] S. Signorella, M. Santoro, C. Palopoli, C. Brondino, J. M. Salas-Peregrín, M. Quirós, L. F. Sala, *Polyhedron* **1998**, *17*, 2739−2749.
[21] V. Daier, S. Signorella, M. Rizzotto, M. I. Frascaroli, C. Palopoli, C. Brondino, J. M. Salas-Peregrín, L. F. Sala, *Can. J. Chem.* **1999**, *77*, 57−64.
[22] S. Signorella, V. Daier, S. García, R. Cargnello, J. C. González, M. Rizzotto, L. F. Sala, *Carbohydr. Res.* **1999**, *316*, 14−25.
[23] S. Signorella, R. Lafarga, V. Daier, L. F. Sala, *Carbohydr. Res.* **2000**, *324/2*, 127−135.
[24] S. Signorella, M. I. Frascaroli, S. García, M. Santoro, J. C. González, C. Palopoli, N. Casado, L. F. Sala, *J. Chem. Soc., Dalton Trans.* **2000**, 1617−1623.
[25] G. Barr-David, M. Charara, R. Codd, R. P. Farrell, J. A. Irwin, P. A. Lay, R. Bramley, S. Brumby, J. Y. Ji, G. R. Hanson, *J. Chem. Soc., Faraday Trans.* **1995**, *91*, 1207−1216.
[26] R. Bramley, J. Y. Ji, R. J. Judd, P. A. Lay, *Inorg. Chem.* **1990**, *29*, 3089−3094.
[27] R. P. Farrell, R. J. Judd, P. A. Lay, R. Bramley, J. Y. Ji, *Inorg. Chem.* **1989**, *28*, 3401−3403.
[28] R. Brambley, J. Y. Li, P. A. Lay, *Inorg. Chem.* **1991**, *30*, 1557−1564.
[29] R. Codd, P. A. Lay, *J. Am. Chem. Soc.* **1999**, *121*, 7864−7876.
[30] S. P. Kaiwar, M. S. S. Raghavan, C. P. Rao, *Carbohyd. Res.* **1994**, *256*, 29−40.
[31] M. Branca, G. Micera, A. Dessi, *Inorg. Chim. Acta* **1988**, *153*, 61−65.
[32] M. Branca, A. Dessi, H. Kozlowski, G. Micera, J. Swiatek, *J. Inorg. Biochem.* **1990**, *39*, 217−226.
[33] M. Branca, G. Micera, U. Segre, A. Dessi, *Inorg. Chem.* **1992**, *31*, 2404−2408.
[34] M. Rizzotto, V. Moreno, S. Signorella, V. Daier, L. F. Sala, *Polyhedron* **2000**, *19*, 417−423.
[35] A. Rockenbauer, L. Korecz, *Appl. Magn. Resonance* **1996**, *10*, 29−43.

Received November 20, 2000
[I00444]

Solvothermal Synthesis, Crystal Structure, and Thermoanalytical Investigations of the New Layered Thioantimonate(III) $[Fe(C_4H_{13}N_3)_2]Sb_6S_{10} \cdot 0.5\ H_2O$

Ralph Stähler,[a] Christian Näther,[a] and Wolfgang Bensch*[a]

Dedicated to Prof. Dr. Hk. Müller-Buschbaum on the occasion of his 70th birthday

Keywords: Thioantimonates / Solvothermal synthesis / Crystal structure / Thermoanalytical measurements

The novel thioantimonate(III) $[Fe(C_4H_{13}N_3)_2]Sb_6S_{10} \cdot 0.5\ H_2O$ was synthesised under mild hydrothermal conditions by allowing elemental Fe, Sb, and S to react in a 50% diethylenetriamine (dien) solution. The compound crystallises in the monoclinic space group $C2/c$ with a = 33.789(3), b = 8.5697(4), c = 24.620(2) Å, β = 118.411(8)°, and V = 6270.3(7) Å^3. In the crystal structure, five SbS_3 trigonal pyramids and one SbS_4 unit are interconnected by sharing common S atoms, forming Sb_2S_2, Sb_4S_4, and Sb_5S_5 heterocycles. The layered $[Sb_6S_{10}]^{2-}$ anion is formed by condensation of the rings in the order Sb_4S_4–Sb_5S_5–Sb_2S_2–Sb_5S_5–Sb_4S_4. The interconnection of the different Sb_xS_x heterocycles leads to the formation of a large $Sb_{16}S_{16}$ ring. The special geometries of the SbS_x units and their interconnection results in a new and unprecedented architecture of the four-atoms thick thioantimonate layer. The calculated bond valence sums (BVS) for the Sb atoms range from 3.07 to 3.16 v. u., indicating that the Sb atoms are formally trivalent. The $[Fe(dien)_2]^{2+}$ cations and the water molecule are located between neighbouring layers. The thermal behaviour of the compound was investigated using DTA-TG measurements. Upon heating decomposition starts at about 200 °C, which is accompanied by the removal of the organic ligands and the incorporated water molecules. In the X-ray powder pattern of the decomposition product, the three compounds Sb_2S_3, $FeSb_2S_4$, and FeS could be identified.

Introduction

In several articles published in the last few years the technologically useful properties of microporous solids have been reviewed in detail.[1−5] The syntheses of such microporous solids are typically carried out under solvothermal conditions in the presence of an organic molecule that should exert a directing effect on the crystallisation process, resulting in the formation of an open-framework inorganic material. The organic species is retained within the cavities or channels of the products. The vast majority of research work is focused on oxidic materials. But chalcogenidometallates with open frameworks have attracted considerable interest because several new compounds are semiconductors and show photoconductivity.[6,7] The syntheses and the structural features of chalcogenidometallates have been recently reviewed.[8,9] A large number of thioantimonates(III) exhibiting different degrees of condensation of the Sb_xS_y anionic fragments were reported.[10−23] In these compounds the linking of the complex anions leads to very different structures. Compounds with one-, two-, and three-dimensional structures were isolated and characterised. Despite the great differences between the thioantimonate(III) structures several structural relationships have been recognised.[9,24] For an insight into the general structural chemistry of the thioantimonates(III) new compounds must be synthesised and characterised. Here we report on the novel compound $[Fe(dien)_2]Sb_6S_{10} \cdot 0.5H_2O$, which adopts a new structure type.

Results and Discussion

The compound $[Fe(dien)_2]Sb_6S_{10} \cdot 0.5\ H_2O$ crystallises in the monoclinic space group $C2/c$ with eight formula units in the unit cell. There are two crystallographically independent Fe^{2+} cations in the asymmetric unit placed in a distorted octahedral environment of two chelating dien ligands (Figure 1: A and B). Hexacoordinated diethylenetriamine complexes of transition group elements have been known for a long time,[25,26] and the geometric isomers of the cations were intensively studied.[25,27−32] The ligand and the cation form fused five-membered rings with conformations that are expected to be different for both isomers. The two independent $[Fe(dien)_2]^{2+}$ cations in $[Fe(dien)_2]Sb_6S_{10} \cdot 0.5\ H_2O$ are meridional [Fe(1)] and *s*-facial [Fe(2)]. We note that $[Fe(dien)_2]^{2+}$ cations have not been reported until now. The Fe−N distances are between 2.185(3) and 2.257(3) Å (Table 1) and comparable with those reported in the literature.[33] The angles N−Fe−N vary between 78.1(2) and 156.2(2)°. As noted before the conformations of the two cations are significantly different and an attempt to fit the two cations onto each other results in a mean root deviation of about 1.5 Å.

Formal valence considerations suggest that all Sb atoms are trivalent. With the exception of Sb(6) each of the crystallographically unique Sb atoms is coordinated by three sulfur atoms with distances Sb−S ranging from 2.3920(8)

[a] Institut für Anorganische Chemie, Universität Kiel, Olshausenstraße 40, 24098 Kiel, Germany

 © WILEY-VCH Verlag GmbH, 69451 Weinheim, 2001 1434−1948/01/0707−1835 $ 17.50+.50/0

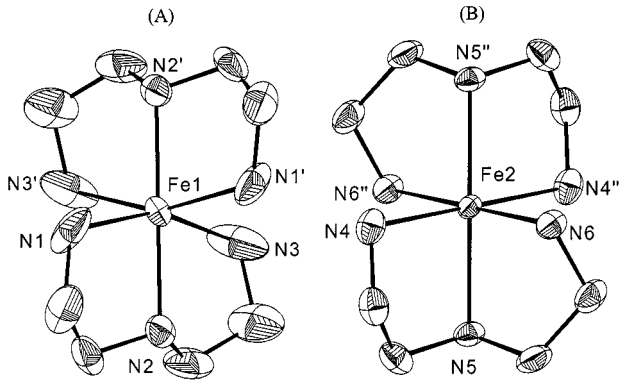

Figure 1. Structures of the two crystallographically independent $[Fe(dien)_2]^{2+}$ cations in the crystal structure of $[Fe(dien)_2]Sb_6S_{10} \cdot 0.5\ H_2O$ with labelling: (A) *mer* isomer and (B) *s-fac* isomer; note: atoms with superscripts are generated by symmetry operations

Table 1. Selected geometric parameters [Å, °] for $[Fe(dien)_2]Sb_6S_{10} \cdot 0.5\ H_2O$

Sb(1)−S(1)	2.4562(7)	Sb(1)−S(4)	2.4331(8)
Sb(1)−S(6)	2.5023(8)	Sb(2)−S(1)	2.4405(8)
Sb(2)−S(2)	2.4560(8)	Sb(2)−S(7)[a]	2.5014(8)
Sb(3)−S(5)	2.3920(8)	Sb(3)−S(3)	2.4691(9)
Sb(3)−S(2)	2.4725(7)	Sb(4)−S(10)[b]	2.4491(8)
Sb(4)−S(4)	2.4594(8)	Sb(4)−S(3)	2.5075(8)
Sb(5)−S(8)	2.3976(8)	Sb(5)−S(6)	2.4283(8)
Sb(5)−S(7)	2.5209(8)	Sb(6)−S(9)	2.4131(8)
Sb(6)−S(10)	2.4824(8)	Sb(6)−S(8)	2.7111(9)
Sb(6)−S(9)[b]	2.7522(8)	Fe(1)−N(1)	2.203(4)
Fe(1)−N(2)	2.185(3)	Fe(1)−N(3)	2.236(4)
Fe(2)−N(4)	2.257(3)	Fe(2)−N(5)	2.228(3)
Fe(2)−N(6)	2.187(3)		
S(4)−Sb(1)−S(1)	98.88(3)	S(4)−Sb(1)−S(6)	86.15(3)
S(1)−Sb(1)−S(6)	81.83(3)	S(1)−Sb(2)−S(2)	99.76(3)
S(1)−Sb(2)−S(7)[a]	88.63(3)	S(2)−Sb(2)−S(7)[a]	87.63(2)
S(5)−Sb(3)−S(3)	98.40(3)	S(5)−Sb(3)−S(2)	96.51(3)
S(3)−Sb(3)−S(2)	95.86(3)	S(10)[b]−Sb(4)−S(4)	92.37(3)
S(10)[b]−Sb(4)−S(3)	85.50(3)	S(4)−Sb(4)−S(3)	94.93(3)
S(8)−Sb(5)−S(6)	101.38(3)	S(8)−Sb(5)−S(7)	91.26(3)
S(6)−Sb(5)−S(7)	92.97(3)	S(9)−Sb(6)−S(10)	95.55(3)
S(9)−Sb(6)−S(8)	89.44(3)	S(10)−Sb(6)−S(8)	88.38(3)
S(9)−Sb(6)−S(9)[b]	88.87(3)	S(10)−Sb(6)−S(9)[b]	90.41(3)
S(8)−Sb(6)−S(9) [b]	177.81(2)	Sb(2)−S(1)−Sb(1)	106.50(3)
Sb(2)−S(2)−Sb(3)	97.65(3)	Sb(3)−S(3)−Sb(4)	97.88(3)
Sb(1)−S(4)−Sb(4)	103.58(3)	Sb(5)−S(6)−Sb(1)	98.79(3)
Sb(2)[a]−S(7)−Sb(5)	99.19(3)	Sb(5)−S(8)−Sb(6)	106.75(3)
Sb(6)−S(9)−Sb(6)[b]	91.13(3)	Sb(4)[b]−S(10)−Sb(6)	101.67(3)

Symmetry codes: [a] $1.5 - x, -0.5 + y, 1.5 - z$. − [b] $1 - x, 2 - y, 1 - z$.

to 2.5209(8) Å (Table 1). The SbS_3 units have an approximately trigonal-pyramidal geometry with angles between 81.83(3) and 106.50(3)° (Table 1). For Sb(6) only two short bonds to S atoms of 2.4131(8) and 2.4824(8) Å are observed, and two longer distances of 2.7111(9) and 2.7522(8) Å (Table 1). The latter distances are longer than expected for single bonds that vary between about 2.4 and 2.6 Å, but they are significantly shorter than the typical so-called secondary bonds with Sb−S distances above around 2.9 Å. Hence, for the further discussion the two S atoms are included in the first coordination sphere of the Sb(6) atom. We note that SbS_4 units with distances between 2.4 and 2.85 Å were reported for $Cs_2Sb_8S_{13}$,[32] $(CH_3NH_3)_2Sb_8S_{13}$,[34] or $Cs_5Sb_8S_{18}(HCO_3)$.[20] All antimony atoms complete their coordination environments with sulfur neighbours at distances between 3.0567(8) and 3.7462(9) (Table 2), which is less than the sum of the van der Waals radii (S_{vdw} + Sb_{vdw} = 3.80 Å).[35] It is noted that the presence of short and long Sb−S distances is often observed in antimony sulfides. The longer Sb−S separations link the primary building blocks yielding higher structural units.

Table 2. Additional long Sb−S bonds [Å]

Sb1−S5	3.1130(9)
Sb1−S7	3.7277(9)
Sb1−S8	3.629(1)
Sb2−S5	3.1651(8)
Sb2−S6[a]	3.5850(8)
Sb2−S6[b]	3.5355(9)
Sb3−S6[b]	3.5048(9)
Sb4−S5	3.3124(9)
Sb4−S9	3.0567(8)
Sb5−S1[c]	3.5424(8)
Sb5−S5[d]	3.3102(8)
Sb6−S4	3.3624(8)
Sb6−S5[d]	3.7462(9)

Symmetry codes: [a] $x, -1 + y, z$. − [b] $1.5 - x, -0.5 + y, 1.5 - z$. − [c] $1.5 - x, 0.5 + y, 1.5 - z$. − [d] $x, 1 + y, z$.

A way to describe the structure of the anion is based on the condensation of different Sb_xS_y heterocycles formed by the interconnection of the SbS_3 and SbS_4 units. The vertex linkage of SbS_3 pyramids involving Sb(1) to Sb(4) leads to

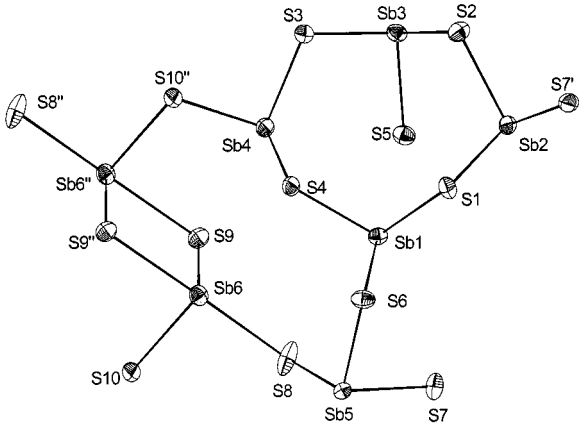

Figure 2. Condensation of the Sb_4S_4 heterocycle and the Sb_3S_8 unit generating an Sb_5S_5 ring; note: atoms denoted with superscripts are generated by symmetry operations

the formation of a puckered Sb_4S_4 ring (Figure 2). A second building-block with composition Sb_3S_8 is composed of two edge-sharing SbS_4 units [Sb(6) and Sb(6a)] being vertex-linked to the Sb(5)S_3 pyramid. The two Sb(6)S_4 units are related by a centre of symmetry forming an Sb_2S_2 ring (Figure 2).

The Sb_3S_8 unit is condensed to the Sb_4S_4 ring via two S atoms [S(6) and S(10a)], resulting in the formation of an

Sb_5S_5 ring [involving Sb(1), Sb(4), Sb(5), Sb(6), and Sb(6a)] (Figure 2). Due to the inversion centre located between the two $Sb(6)S_4$ units, a system of condensed heterocycles with the order $Sb_4S_4-Sb_5S_5-Sb_2S_2-Sb_5S_5-Sb_4S_4$ is generated (Figure 3). The assembly into the final layered anion is achieved by vertex linking of the condensed ring system via the terminal S(7) atoms. Consequently, another large heterocycle with composition $Sb_{16}S_{16}$ is present (shaded area in Figure 3). We note that the layers are four atoms thick, whereas for the overwhelming number of thioantimonates(III) two-atom thick layers are observed.

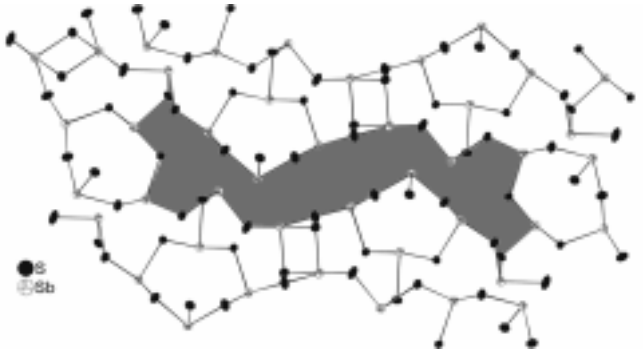

Figure 3. The layered anion with the large $Sb_{16}S_{16}$ ring (shaded area) with displacement ellipsoids drawn at the 50% probability level

The description becomes more complex when the secondary Sb−S bonds are considered. The Sb atoms in the Sb_4S_4 ring have longer Sb−S contacts [Sb(1)−S(5), Sb(1)−S(7), Sb(1)−S(8), Sb(2)−S(5), Sb(2)−S(6A), Sb(2)−S(6B), Sb(3)−S(6B), Sb(4)−S(5), Sb(4)−S(9), Sb(5)−S(1C), Sb(5)−S5(D), Sb(6)−S(4A), Sb(6)−S(5D)] ranging from 3.0567(8) to 3.7462(9) Å (Table 2), enhancing the coordination number from three to six. The atoms Sb(1) and Sb(6) have six neighbours and are in a distorted octahedral environment (Figure 4, B, F). When the s^2 lone pair is treated as a coordination site the polyhedron about Sb(3) may be described as distorted ψ-SbS_4 trigonal-bipyramid. The Sb(4) and Sb(5) atoms have two S neighbours, giving a distorted ψ-SbS_5 octahedron (Figure 4, C, D). With the enhanced coordination environments, different secondary building units can be identified (Figure 4). An Sb_3S_4 semicube (Figure 4, E) involving the two symmetry-related Sb(6) atoms and Sb(4) is formed, which is common in thioantimonates(III).[10,36−39]

The two symmetry-related $Sb(6)S_6$ octahedra share a common edge yielding an Sb_2S_{10} double-octahedron (Figure 4, F). Such a secondary building unit was found in $Cs_2Sb_8S_{13}$[36] and $(CH_3NH_3)_2Sb_8S_{13}$.[37] The three atoms Sb(1), Sb(2), and Sb(4) have secondary bonds to the S(5) atom that is located on top of the crown-like Sb_4S_5 heterocycle (Figure 4, A) thus joining the polyhedra of these Sb atoms of the ring.

The layered anions are within the (−101) plane, and are stacked onto each other parallel to the [110] plane. The cations as well as the water molecule are located between the layers (Figure 5). Six short intermolecular N−H···S distances (Table 3) with H···S distances ranging from 2.460 to 2.959 Å and N−H···S angles between 149.17° and 175.46° are observed, indicative of hydrogen bonding (Table 3).

The crystal structures of many thioantimonates(III) can be described on the basis of the condensation of different Sb_xS_y heterocycles. In the compound $[(CH_3NH_3)_{1.03}K_{2.97}]Sb_{12}S_{20}\cdot 1.34\,H_2O$,[40] in which the anionic part has the same composition when divided by two, the layered $[Sb_{12}S_{20}]^{4-}$ anion is formed by two complex rings having the same composition − $Sb_{12}S_{20}$ − and a very similar shape. Including the S atoms of the different rings (note: in the original contribution only the Sb atoms were counted) an Sb_8S_8 ring and four Sb_3S_3 rings are condensed giving the $Sb_{12}S_{20}$ complex ring system. The complex rings are interconnected into two-atom thick layers by so-called secondary bonds that are between 3.0567(8) and 3.5850(8)

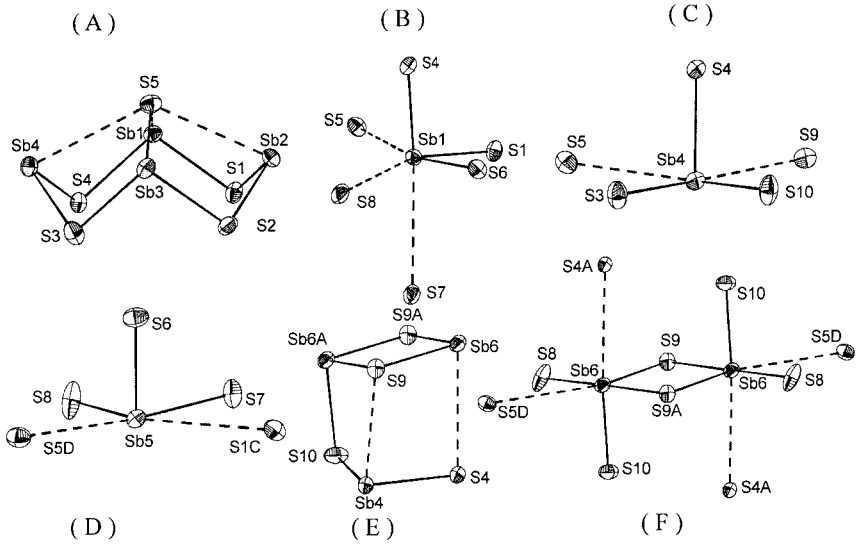

Figure 4. The environments of the Sb atoms with related long secondary bonds (dotted lines); the letters denote symmetry-related atoms (symmetry codes are given in Table 3); the probability ellipsoids are drawn at the 50% level

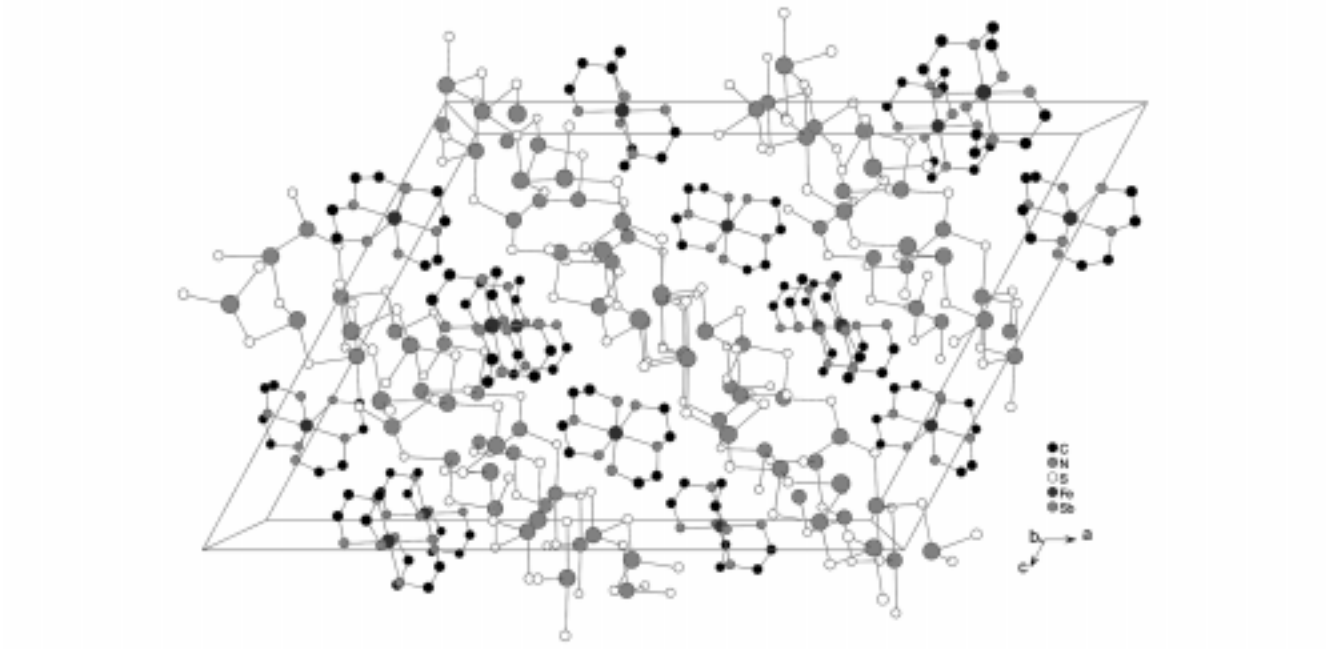

Figure 5. Arrangement of the $[Sb_6S_{10}]^{2-}$ anions and $[Fe(dien)_2]^{2+}$ cations in the crystal structure of $[Fe(C_4H_{13}N_3)_2]Sb_6S_{10} \cdot 0.5\ H_2O$ (water molecules and hydrogen atoms are omitted for clarity)

Table 3. Intermolecular N−H···S contacts and angles [Å, °]

D−H	*d*(H···A)	D−H−A	*A*	D−H	*d*(H···A)	D−H−A	*A*
N4−H6N	2.553	149.54	S2[a]	N2−H3N	2.460	175.46	S8[a]
N6−H10N	2.959	149.17	S2[a]	N1−H2N	2.573	158.67	S9[b]
N3−H5N	2.792	160.47	S3[c]	N1−H1N	2.361	161.21	O1[d]
N5−H8N	2.740	153.55	S7[d]	N3−H4N	2.185	157.36	O1[a]

Symmetry codes: [a] $-x + 3/2, -y + 3/2, -z + 1$. − [b] $-x + 1, y, -z + 3/2$. − [c] $-x + 1, -y + 1, -z + 1$. − [d] $-x + 3/2, y - 1/2, -z + 3/2$.

Å. The compound $[Ph_4P]_2Sb_6S_{10}$[41] contains also an $[Sb_6S_{10}]^{2-}$ anion, but it forms an infinite one-dimensional anionic $(Sb_6S_{10}^{2-})_n$ chain by vertex linkage of SbS_3 pyramids. The interconnection of the pyramids leads to the formation of condensed 10-membered Sb_5S_5 rings with alternating Sb and S atoms. The anionic part of this structure is similar to that reported for $Sb_3S_5{\cdot}N(C_3H_7)_4$.[23] It can be assumed that the size, shape, and charge of the cations determine the dimensionality and the condensation density of the thioantimonate(III) anion.

The Sb_3S_3 rings as well as Sb_4S_4 rings are also found in $[(CH_3CH_2CH_2CH_2NH_2CH_2)_2]_{0.5}Sb_7S_{11}$.[39] In the thioantimonates(III) $[H_3N(CH_2)_3NH_3]Sb_{10}S_{16}$,[42] $(CH_3NH_3)_2Sb_8S_{13}$,[34] $(enH_2)Sb_8S_{13}$ [43], and $(NH_4)_2Sb_4S_7$ [10], the Sb_3S_3 rings are present, and the former two compounds may be viewed as 3-dimensional framework structures when the longer Sb−S contacts are considered.

The bond valence sums (BVS) for the Sb atoms were calculated using the parameters from Brese and O'Keeffe[44] (minimum valence = 0.01). The BVS range from 3.07 to 3.16 v. u. indicating that the Sb atoms formally trivalent. Strong deviations of the calculated BVS from integer numbers are correlated to the stereoactivity of the lone electron pairs (LEP).[45,46] Applying the procedure reported in ref.[47] the BVS of the SbS_x polyhedra are plotted against a parameter $|\Phi|$, which is the length of the vector $\Phi = -\Sigma\Phi_{ij}$ with Φ_{ij} being a vector pointing from Sb_i to the coordinating atom S_j at the distance D_{ij}. The length of Φ_{ij} is given by $\exp(-D_{ij}/0.2)$. The summation is performed over all coordinating S atoms of a polyhedron. For a strong deviation of the spatial distribution of the LEP from spherical symmetry, large $|\Phi|$ values are expected. We observe higher $|\Phi|$ values for Sb(1), Sb(3), and Sb(5), indicating stronger sp^3 character of their LEP.[45] One can assume that the LEP of these Sb^{III} cations are on the opposite side of the three shortest Sb−S bonds of each SbS_3 pyramid.

Thermal Investigations

The thermal behaviour of the title compound was investigated using simultaneous difference thermal analysis and thermogravimetry experiments (Figure 6). Heating selected single crystals of $[Fe(dien)_2]Sb_6S_{10} \cdot 0.5\ H_2O$ under argon a mass loss of 16.5% is observed at T_{onset} = 240.7 °C in the TG curve, which can be attributed to the complete removal

of the dien ligands and the incorporated water molecules $\{-\Delta m_{theor.}[(dien)_2 + 0.5\ H_2O = 16.2\%]\}$. The removal of the ligands is accompanied by two endothermic events at T_P = 261.1 °C and T_P = 277.5 °C. These two peaks were always observed, irrespective of whether large single crystals or powdered samples were used. Such a splitting of the DTA peak during the loss of this organic ligand was also observed for other compounds in which metal cations are surrounded by two dien ligands.[30,47,48] For the present thermal reaction the splitting of the DTA peak is presumably due to a stepwise loss of the ligands, because both cations are in a different environment. In the X-ray powder pattern of the product, the compounds Sb_2S_3, $FeSb_2S_4$, and FeS could be identified. Spectroscopic investigations prove the loss of the organic ligands during the thermal decomposition and elemental analysis shows that only a small amount of carbon and nitrogen is present in the residue (C: 1.11%; N: 0.6%).

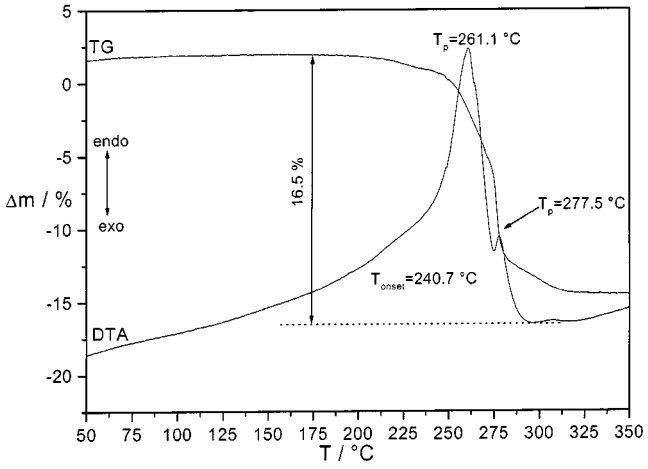

Figure 6. DTA-TG curve for $[Fe(dien)_2]Sb_6S_{10}\cdot 0.5\ H_2O$ (under argon, weight 108.5 mg, powdered crystals, T_p = peak temperature)

Experimental Section

Synthesis: $[Fe(dien)_2]Sb_6S_{10}\cdot 0.5\ H_2O$ (dien = diethylenetriamine) was prepared by treating elemental Fe, Sb, and S in an aqueous solution of dien under solvothermal conditions. In a typical synthesis, 1 mmol of Fe (0.055847 g), 1 mmol of Sb (0.121757 g), and 3 mmol of S (0.032066 g) were added to 10 mL of 50% dien solution. The mixture was heated in a Teflon-lined autoclave at 150 °C for 6 d. The reaction mixture was filtered, washed with water and acetone, and cleaned in an ultrasonic bath. The product consisted of two phases: dark-red needle-like crystals of the title compound as the major phase (yield: 90% based on Sb) and a grey microcrystalline powder as the minor phase, which was amorphous against X-ray powder diffraction. In the by-product the elements iron, sulfur, and antimony were identified with an EDAX analysis.

Structure Determination: Intensities were collected with a STOE Imaging Plate Diffraction System (IPDS) using monochromated Mo-K_α radiation (λ = 0.71073 Å). The intensities were corrected for Lorentz, polarisation, and absorption effects. Structure solution was performed using SHELXS-97.[49] Refinement was done against F^2 using SHELXL-97.[50] All heavy atoms were refined anisotropically. The hydrogen atoms were positioned with idealised geometry and refined with fixed isotropic displacement parameters using a riding model. Technical details of data acquisition and refinement results are summarised in Table 4.

Table 4. Crystallographic data for $[Fe(dien)_2]Sb_6S_{10}\cdot 0.5\ H_2O$

Empirical formula	$[Fe(C_4H_{13}N_3)_2]Sb_6S_{10}\cdot 0.5\ H_2O$
Colour, habit	red needles
Crystal size	0.3 × 0.1 × 0.1 mm
Molecular mass	1321.3 g/mol
Crystal system	monoclinic
Space group	*C*2/*c* (I. T. No. 15)
Calculated density	2.799 g/cm^3
Lattice parameters	
a [Å]	33.789(3) Å
b [Å]]	8.5697(4) Å
c [Å]	24.620(2) Å
β [°]	118.411(8)°
V [Å^3]	6270.3(7) Å^3
Z	8
Temperature	293 K
Scan range	$3.8° \le 2\theta \le 56.3°$
	$-44 \le h \le 44$
	$-9 \le k \le 10$
	$-32 \le l \le 32$
Measured reflections	25723
Independent reflections	7061
Reflections with $F_o > 4\sigma(F_o)$	6304
$R_{int.}$	0.0245
μ	6.22 mm^{-1}
Absorption correction	face-indexed
min./max. trans.	0.3101/0.5057
Extinction correction[a]	$x = 0.00029(2)$
Weight[b]	$y = 0.0377$, $z = 1.2074$
Residual electron density	max. 0.73/min. −0.77 e$^-$/Å^3
*R*1 for all $F_o > 4\sigma(Fo)$	0.0209
*R*1 for all reflections	0.0253
*wR*2 for all $F_o > 4\sigma(F_o)$	0.0508
*wR*2 for all reflections	0.0524
Goodness of fit	1.014

[a] $F^* = F_c\,(k[1 + 0.001 \cdot x \cdot F_c^2 \cdot \lambda^3/\sin(2\theta)]^{-0.25})$. — [b] $w = 1/[\sigma^2(F_o^2) + (y \cdot P)^2 + z \cdot P]$; $P = [\max(F_o^2,0) + 2 \cdot F_c^2]/3$.

Thermoanalytical Measurements: Thermoanalytical measurements were performed using a DTA-TG device STA 429 from Netzsch. All measurements were performed under argon (flow rate 50 mL min^{-1}) with Al_2O_3 crucibles and heating rates of 3 K min^{-1}).

ESEM/EDAX Investigations: Scanning electron microscopic investigations were conducted with the Environmental Scanning Electron Microscope (ESEM XL 30, Fa. Phillips) equipped with an EDAX system.

X-ray Powder Diffractometry: The X-ray powder patterns were recorded with a STOE Stadi-P diffractometer (Co-K_α radiation, λ = 1.788965 Å) in transmission geometry.

Crystallographic data (excluding structure factors) for the structure reported in this paper have been deposited with the Cambridge Crystallographic Data Centre as supplementary publication no. CCDC-151878. Copies of the data can be obtained free of charge on application to CCDC, 12 Union Road, Cambridge CB2 1 EZ, UK [Fax: (internat.) + 44-1223/336-033; E-mail: deposit@ccdc.cam.ac.uk].

Acknowledgments

Many thanks to Prof. Dr. F. Liebau for the calculations of the bond valence values. Financial support by the Deutsche Forschungsgemeinschaft and the State of Schleswig-Holstein is gratefully acknowledged.

[1] M. E. Davis, *Acc. Chem. Res.* **1993**, *26*, 111−115.
[2] M. E. Davis, *Microporous Mesoporous Mater.* **1998**, *21*, 173−182.
[3] G. A. Ozin, A. Kuperman, A. Stein, *Angew. Chem.* **1989**, *101*, 373−390; *Angew. Chem. Int. Ed. Engl.* **1989**, *28*, 59−376.
[4] J. Chen, R. H. Jones, S. Natarajan, J. M. Thomas, *Angew. Chem.* **1994**, *106*, 667−668.
[5] M. T. Weller, S. E. Dann, *Curr. Opinion Solid State Mater. Sci.* **1998**, *3*, 137−143.
[6] U. Simon, F. Schüth, S. Schunk, X. Wang, F. Liebau, *Angew. Chem.* **1997**, *109*, 1138−1142; *Angew. Chem. Int. Ed. Engl.* **1997**, *36*, 1121−1124.
[7] F. Starrost, E. E. Krasovskii, W. Schattke, J. Jockel, U. Simon, X. Wang, F. Liebau, *Phys. Rev. Lett.* **1998**, *80*, 3316−3319.
[8] W. S. Sheldrick, M. Wachhold, *Angew. Chem.* **1997**, *109*, 215−234; *Angew. Chem. Int. Ed. Engl.* **1997**, *36*, 204−224.
[9] W. S. Sheldrick, M. Wachhold, *Coordination Chem. Rev.* **1998**, *176*, 211−322.
[10] G. Dittmar, H. Schäfer, *Z. Anorg. Allg. Chem.* **1977**, *437*, 183−187.
[11] H. A. Graf, H. Schäfer, *Z. Anorg. Allg. Chem.* **1975**, *414*, 220−230.
[12] G. Dittmar, H. Schäfer, *Z. Anorg. Allg. Chem.* **1978**, *441*, 98−102.
[13] B. Eisenmann, H. Schäfer, *Z. Naturforsch., B* **1979**, *34*, 383−385.
[14] G. Cordier, H. Schäfer, C. Schwidetzky, *Z. Naturforsch., B* **1984**, *39*, 131−134.
[15] K. Volk, P. Bickert, R. Kolmer, H. Schäfer, *Z. Naturforsch., B* **1979**, *34*, 380−382.
[16] U. Müller, A. T. Mohammed, *Z. Anorg. Allg. Chem.* **1986**, *533*, 65−72.
[17] B. F. Hoskins, E. R. T. Tiekink, G. Winter, *Inorg. Chim. Acta* **1985**, *99*, 177−186.
[18] M. Schur, W. Bensch, *Z. Anorg. Allg. Chem.* **1998**, *624*, 310−314.
[19] H. Rijnberk, C. Näther, M. Schur, I. Jeß, W. Bensch, *Acta Crystallogr., Sect. C* **1998**, *54*, 920−923.
[20] G. L. Schimek, J. W. Kolis, *Inorg. Chem.* **1997**, *36*, 1689−1693.
[21] K. Volk, H. Schäfer, *Z. Naturforsch., B* **1979**, *34*, 172−175.
[22] J. B. Parise, *Science* **1991**, *251*, 293−294.
[23] J. B. Parise, Y. Ko, *Chem. Mater.* **1992**, *4*, 1446−1450.
[24] K. Tan, Y. Ko, J. B. Parise, J.-H. Park, A. Darovsky, *Chem. Mater.* **1996**, *8*, 493−496.
[25] G. H. Searle, S. F. Lincoln, F. R. Keene, S. G. Teague, D. G. Rowe, *Aust. J. Chem.* **1977**, *30*, 1221−1228.
[26] F. G. Mann, *J. Chem. Soc.* **1934**, 466−474.
[27] F. R. Keene, G. H. Searle, *Inorg. Chem.* **1972**, *11*, 148−156.
[28] Y. Yoshikawa, K. Yamasaki, *Bull. Chem. Soc. Jpn.* **1972**, *45*, 179−184.
[29] G. H. Searle, D. A. House, *Aust. J. Chem.* **1987**, *40*, 361−374.
[30] A. K. Mukherjee, S. Korner, A. Ghosh, N. R. Chaudhuri, M. Mukherjee, A. J. Welch, *J. Chem. Soc., Dalton Trans.* **1994**, 2367−2371.
[31] F. S. Stephens, *J. Chem. Soc.* **1969**, 883−890; F. S. Stephens, *J. Chem. Soc.*, **1969**, 2233−2340.
[32] K. Harada, *Bull. Chem. Soc. Jpn.* **1993**, *66*, 2889−2899.
[33] A. Zalkin, D. H. Templeton, T. Ueki, *Inorg. Chem.* **1973**, *12*, 1641−1646.
[34] X. Wang, F. Liebau, *J. Solid State Chem.* **1994**, *111*, 385−389.
[35] A. Bondi, *J. Phys. Chem.* **1964**, *68*, 441−451.
[36] K. Volk, H. Schäfer, *Z. Naturforsch., B* **1979**, *34*, 1637−1640.
[37] W. Bensch, M. Schur, *Z. Naturforsch., B* **1997**, *52*, 405−409.
[38] H.-O. Stephan, M. G. Kanatzidis, *Inorg. Chem.* **1997**, *36*, 6050−6057.
[39] A. V. Powell, S. Boissiere, A. M. Chippindale, *Chem. Mater.* **2000**, *12*, 182−187.
[40] X. Wang, A. J. Jacobson, F. Liebau, *J. Solid State Chem.* **1998**, *140*, 387−395.
[41] H. Rijnberk, C. Näther, W. Bensch, *Monatsh. Chemie* **2000**, *131*, 721−726.
[42] X. Wang, *Eur. J. Solid State Inorg. Chem.* **1995**, *32*, 303−312.
[43] K. Tan, Y. Ko, J. B. Parise, *Acta Crystallogr., Sect. C* **1994**, *50*, 1439−1442.
[44] N. Brese, M. O'Keeffe, *Acta Crystallogr., Sect. B* **1991**, *47*, 192−197.
[45] X. Wang, F. Liebau, *Acta Crystallogr., Sect. B* **1996**, *52*, 7−15.
[46] X. Wang, F. Liebau, *Z. Kristallogr.* **1996**, *211*, 437−439.
[47] S. Koner, A. Ghosh, N. R. Chaudhuri, *Trans. Met. Chem.* **1988**, *13*, 291−296.
[48] S. Koner, A. Ghosh, N. R. Chaudhuri, *Trans. Met. Chem.* **1990**, *15*, 394−398.
[49] G. M. Sheldrick, *SHELXS-97*, Universität Göttingen, **1997**.
[50] G. M. Sheldrick, *SHELXL-97*, Universität Göttingen, **1997**.

Received November 27, 2000
[I00454]

Synthesis and Structures of Boron- and Aluminum-Containing Spirocycles with P-P Units

Wolfgang Köstler[a] and Gerald Linti*[a]

Keywords: Boron / Phosphorus / Aluminum / Heterocycles / Density functional calculations

The reaction of aluminum trichloride with $(t\text{BuP})_2K_2$ affords the potassium salt of the candy-like tricylic compound $[(t\text{BuP})_8Al_2]^{2-}$ **3**.With boron trifluoride–dimethyl etherate the bicyclic spiropentane derivative $(t\text{BuP})_3(t\text{BuPMe})B$ **1** is formed. Obviously, cleavage of the dimethyl ether has occurred. The formation of **1** is accompanied by a boron-phosphorus macrocyclic compound resulting from THF cleavage. All structures have been confirmed by single crystal X-ray crystallography. BP_4R_4 compounds were investigated by DFT methods.

Introduction

The chemistry of heterocyclic compounds of phosphorus with elements of group 13 has been investigated extensively in the past decades. This is especially true for the chemistry of boron.[1] In the case of aluminum four-membered ring compounds of type $(R_2AlPR'_2)_2$ are the most common;[2] they are considered as dimeric phosphanylalanes. In recent years the monomeric phosphanylalanes[3] have attracted interest in the investigation of possible p-p(π) interactions between atoms of group 13 and 15. With $(MesAlPPh)_3$ [4] the first AlP heterocycle with three coordinated aluminum and phosphorus atoms was synthesized. Comparatively little work has been done on heterocycles of these elements with P-P groups. Only diphospaboriranes $(t\text{BuP})_2BNEt_2$ [5] and the bicyclobutane derivative $tmpBP_2Btmp$[6] (tmp = 2,2,6,6-tetramethylpiperidino) and 1,2,3,4-diphosphadiboretanes such as $(t\text{BuP})_2(BNMe_2)_2$ [7] have been structurally characterized.

On the other hand, butadiene analogues $R_2B-(PR')_2-BR_2$ have been used in the discussion on the correlation of hybridization and bond length.[8] Recently, we reported the gallium analogue $tmp_2Ga(Pt\text{Bu})_2Gatmp_2$.[9] Here we present the results of reactions of the dipotassium salt of the diphosphandiide $(t\text{BuPP}t\text{Bu})^{2-}$ [10] with halides of boron and aluminum.

Results and Discussion

Reactions

If boron trifluoride-dimethyl etherate is reacted with $(t\text{BuP})_2K_2\cdot 0.5THF$ [Equation (1)] the expected product of simple substitution of the fluoride groups at the boron center is not observed. Compound **1** is isolated instead in good yields.

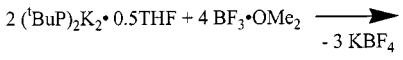

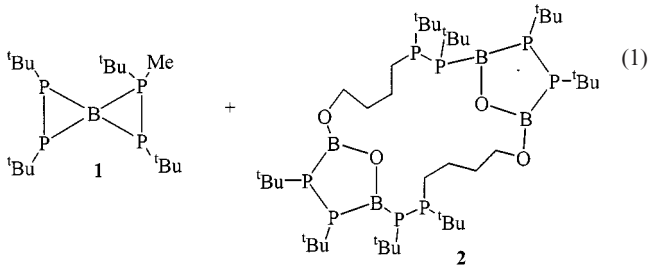

(1)

This compound is the product of the cleavage of dimethyl ether by a proposed intermediate such as $[(t\text{BuP})_4B]^-$. Neither an expected by-product of the type X_2BOMe nor the product of cleavage of Me_2O by a Lewis acidic boron compound could be observed in the reaction mixture by means of ^{11}B NMR spectroscopy. The macrocycle **2** is a minor by-product of this reaction. It is formed by cleavage of THF instead of dimethyl ether at the Lewis acidic boron centers and nucleophilic phosphorus atoms.

With aluminum trichloride and $(t\text{BuP})_2K_2$ the dianionic spirocycle **3** is obtained [Equation (2)]. No products of ether cleavage could be identified. In contrast to the BP_4

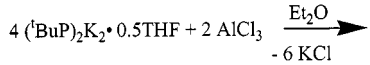

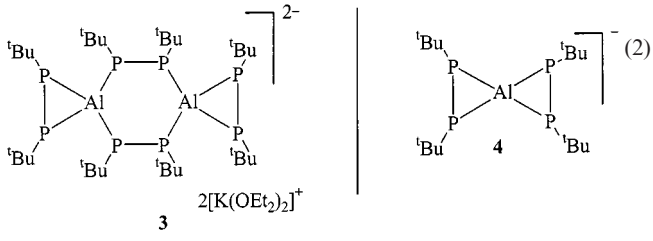

(2)

[a] Universität Heidelberg, Anorganisch-Chemisches Institut, Im Neuenheimer Feld 270, 69120 Heidelberg, Germany
Fax: (internat.) +49-6221/540-617
E-mail: gerald.linti@urz.uni-heidelberg.de

 © WILEY-VCH Verlag GmbH, 69451 Weinheim, 2001 1434–1948/01/0707–1841 $ 17.50+.50/0

derivative **1** the tricyclic Al_2P_8 compound **3** contains a six-membered AlP ring in addition to three-membered rings. Thus, **3** might be viewed as a dimer of the hypothetical AlP_4 compound **4**.

Crystal Structure Analyses

Compound **1** crystallizes in the orthorhombic crystal system, space group $P2_12_12_1$ (Table 1). The boron atom in the spirocyclic molecule (Figure 1) is coordinated in a distorted tetrahedral fashion. There is a three-membered ring formed by a $(t\text{BuP})_2$ unit and a boron atom. A second three-membered ring is made up by the boron center and a tBuP−P(Me)tBu unit. Thus, at first glance **1** may be viewed as a phosphane adduct of a trisphosphanyl borane. Both of the three-membered rings are orthogonal to one another, as is expected for a spiropentane analogue.

The boron-phosphorus bond lengths to the three-coordinate phosphorus atoms are between 194 and 198 pm. This distance is as expected for boron phosphorus bonds between tetracoordinate boron and λ^3 phosphorus atoms, for example in $(Et_2P)_2B(\mu\text{-}PEt_2)_2B(PEt_2)$.[1] The B(1)−P(4) bond (i.e. the λ^4-B−λ^4-P bond) is only 189 pm long. This is remarkable, because at the first glance this bond is expected to be the longest one. Actually, a short bond length like this is typical for bonds between three-coordinate boron and phosphorus atoms. Other examples of three-membered rings are $(t\text{BuP})_2BNEt_2$ [$d_{BP'}$ = 189 pm][5] and $(tmpB)_2P_2$ [d_{BP} = 190.5 (av.)].[6] In **1** two different P−P bond lengths are observed; the P(1)−P(2) bond [d_{PP} = 219.4(2) pm] is 4 pm longer than the P(3)−P(4) bond [d_{PP} = 215.6(2) pm]. Again, the bond involving the λ^4 phosphorus atom is the shorter one. A possible explanation may be found by inspecting the formal charges in **1**. If these are taken as real charges, the P(4)−B(1) bond is shortened by electrostatic attraction. This is discussed more precisely in the following subsection. In comparison to other compounds with P−P bonds, the P-P units in **1** show quite short bonds. For example, in $Et_2NB(Pt\text{Bu}_2)_2$ the P−P bond is longer [d_{PP} = 223 pm]. In contrast with this, even shorter P−P bonds [d_{PP} = 210 pm] are observed in open chain diboryldiphosphanes.[8]

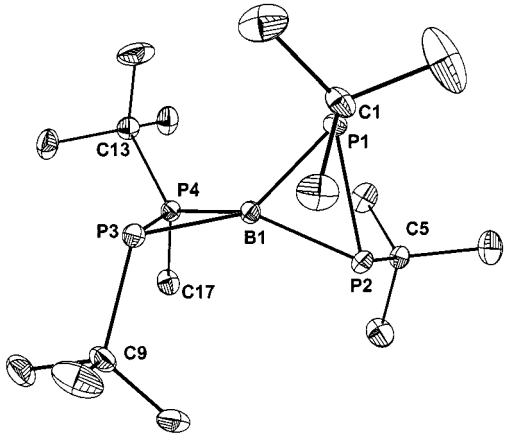

Figure 1. ORTEP view of a molecule of **1**; selected bond lengths [pm] and angles [°]: B(1)−P(1) 193.5(5), B(1)−P(2) 193.7(5), B(1)−P(3) 197.7(5), B(1)−P(4) 188.9(5), P(1)−P(2) 219.4(2), P(3)−P(4) 215.6(2); P(1)−B(1)−P(2) 69.0(2), P(3)−B(1)−P(4) 67.7(2), B(1)−P(1)−P(2) 55.5(2), B(1)−P(3)−P(4) 54.2(2), B(1)−P(4)−P(3) 58.1(1), B(1)−P(2)−P(1) 55.45(1)

Table 1. X-ray structure determination

	1	**3**
Mol. formula	$C_{17}H_{39}BP_4$	$C_{48}H_{112}Al_2K_2O_4P_8$
Cryst. size [mm]	0.2 × 0.15 × 0.15	0.6 × 0.4 × 0.4
Cryst. syst.	Orthorhombic	Monoclinic
Space group	$P2_12_12_1$	$P2_1/n$
Mol. wt.	378.2	1133.3
a [pm]	959.2(6)	1092.9(2)
b [pm]	1498.3(7)	1806.4(2)
c [pm]	1621.4(9)	1785.3(3)
β [deg]		92.95(3)
V [nm^3]	2.330(2)	3.520(1)
Z	4	2
D (calcd.), [gcm^{-3}]	1.078	1.069
F(000)	824	1232
μ [mm^{-1}]	0.320	0.374
2θ range [°]	14−48	5−45
No. of collcd. rflns	10425	6199
No. of unique rflns	3482	4580
No. of obsd. rflns [$I > 2\sigma(I)$]	3074	3115
GOF	1.178	1.003
Parameters	212	305
$wR2$(all data)	0.098	0.108
$R1$	0.052	0.040
Largest diff. peak [eÅ^{-3}]	0.273	0.298

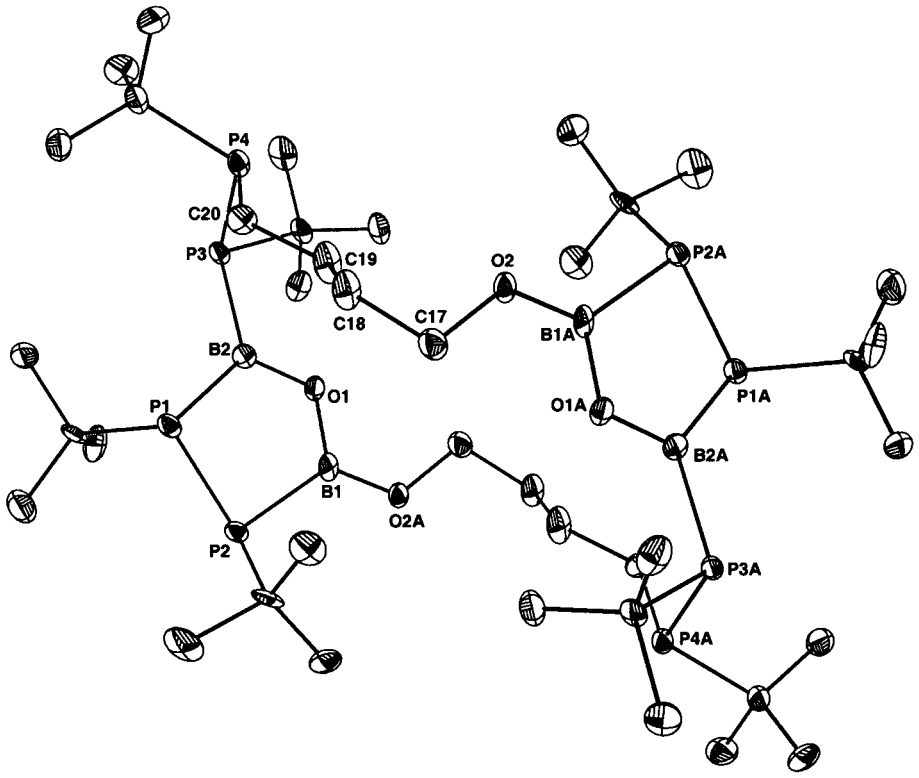

Figure 2. ORTEP view of a molecule of **2**

Compound **2** crystallizes triclinically in the space group $P\bar{1}$.[11] The molecule (Figure 2) consists of a central large 20-membered ring, consisting of four boron, four phosphorus, four oxygen and eight carbon atoms. The boron and oxygen atoms are also part of fused five-membered B_2OP_2 rings. Due to the low quality of the X-ray structure determination no bonding parameters will be discussed.

Compound **3** crystallizes in the monoclinic space group $P2_1/n$. The centrosymmetric molecule (Figure 3) consists of two three-membered and one six-membered aluminum phosphorus ring in a chair conformation. In this spirocycle, the three-membered P_2Al rings and the AlP_2 units of the six-membered ring show an interplanar angle of only 70°. The aluminum atoms reside in a distorted tetrahedral array of four phosphorus atoms. The P(3)−Al−P(4) angle within the three-membered ring is very acute [54.72(4)°]; the corresponding one, P(1)−Al−P(2)A, in which the phosphorus atoms involved are part of the six-membered ring, is near the tetrahedral angle [107.26(5)°]. Consequently, the P−Al−P angles out of the rings are wider than 109°. The central Al_2P_4 ring adopts a chair conformation. P(2) and P(3) are coordinated in a trigonal pyramidal fashion by aluminum, carbon and phosphorus centers, the sum of angles being 337.2° at P(2) and 295.0° at P(3). P(1) and P(4) have contacts to a potassium cation [d_{KP} = 322 and 323 pm]. Consequently, P(1) and P(4) have longer Al−P bonds than P(2) and P(3). The distance K−P(2) is longer by 55 pm [$d_{K-P(2)}$ = 376.7 pm]. Thus, it is longer than the sum of the van der Waals radius of a phosphorus atom (190 pm) and

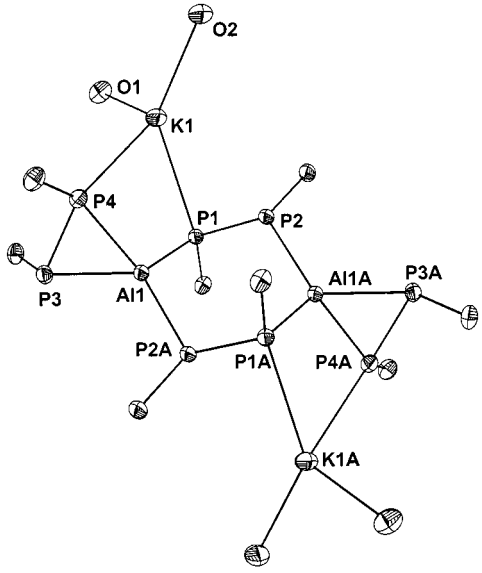

Figure 3. ORTEP view of a molecule of **3**; methyl and ethyl groups have been omitted for clarity; selected bond lengths [pm] and angles [°]: K−P(4) 322.05(14), K−P(1) 323.2(2), Al−P(1) 238.64(14), Al−P(3) 236.89(14), Al−P(2)A 237.28(14), Al−P(4) 239.1(2), P(1)−P(2) 217.05(13), P(3)−P(4) 218.8(2), P(3)−Al−P(1) 121.05(5), P(3)−Al−P(4) 54.72(4), P(1)−Al−P(4) 105.64(5), P(3)−P(4)−Al 62.12(5), P(3)−Al−P(2)A 119.48(5), P(2)A−Al−P(1) 107.26(5), P(2)A−Al−P(4) 141.68(6), P(2)−P(1)−Al 98.19(5), P(1)−P(2)−AlA 114.20(6), P(4)−P(3)−Al 63.16(4)

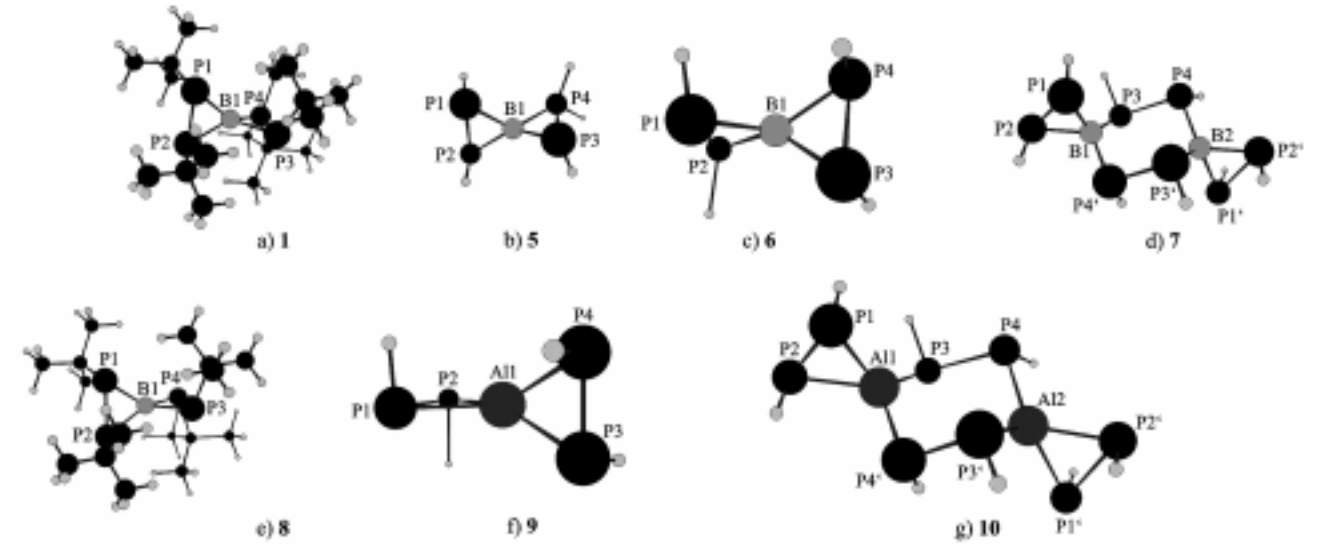

Figure 4. View of a molecule of: a) **1**, b) **5**, c) **6**, d) **7**, e) **8**, f) **9** and g) **10**, as predicted by RI-DFT calculations

Table 2. Selected DFT-calculated bond lengths [pm] for **1** (exp.) to **10**

	1 (exp·)	**5**	**6**	**7**	**8**	**9**	**10**	**3 (exp.)**
B(1)−P(1)	195.2 (193.5)	194.1	196.0−196.1	199.0−201.1	196.2−196.7	(Al−P) 236.9−237.1	239.8−241.7	236.9−239.1
B(1)−P(2)	196.0 (193.7)	195.7	−	−	−	−	−	−
B(1)−P(3)	200.1 (197.7)	196.6	−	197.8−198.3	−	−	−	−
B(1)−P(4)	191.3 (188.9)	193.2	−	−	−	−	−	−
P(1)−P(2)	223.1 (219.4)	227.1	227.7	226.5	223.2−223.7	235.5−235.6	232.4	218.8
P(3)−P(4)	220.1 (215.6)	223.1	−	227.8	−	−	227.6	217.1

the effective ionic radius of a potassium cation (150 pm). The potassium centers can be considered to be coordinated distorted tetrahedrally by two phosphorus atoms and two diethyl ether molecules. The P−P bonds in the three- and six-membered rings do not differ very much and are similar to those in **1**. The Al−P distances are between 236.9 and 239.2 pm long. This is shorter than in oligomeric phosphanylalanes $(R_2AlPR'_2)_n$ (range 243.3−247.5 pm).

Results of DFT Calculations

The most striking feature in the unusual spiropentane derivative **1** is the short λ P−B bond. Therefore, **1** and related compounds have been investigated by Density Functional methods. All calculations were done with the Turbomole program package[12] (**5a, b**) with RI approximation, the BP86 functional and SV(P) bases for all atoms.

For both, **1** and **5** a good agreement was found between the experimentally determined and the calculated structures (see Figure 4 and Table 2).

In **1** and in the all-hydrogen substituted spiropentane derivative **5** the λ^4 P−B bond is the shortest one and the other B−P bond, which is part of the same three-membered ring, is the longest one in the molecule. Obviously, steric arguments do not apply when explaining this observation. In the anionic compounds **6** and **8** four identical B−P bonds are expected and this is verified by the calculations. These B−P distances are similar to those in the $(RP)_2B$ rings in **1** and **5**.

By inspecting the atomic charges obtained from an Ahlrich−Heinzmann population analysis, a negative charge is found on the tetracoordinated boron atoms of **1** (−0.74), **5** (−0.75), **6** (−0.73) and **8** (−0.73) and a nearly equal positive charge on the tetracoordinated phosphorus atoms in **1** (+0.65) and **5** (+0.41). This is in line with the formal charges on these atoms and explains the short bond lengths. All other phosphorus atoms have very small charges (<+0.14). According to the shared electron numbers (SEN) obtained from this population analysis all B−P bonds are to be regarded as single bonds (SEN = 1.25−1.35). In particular, the short λ^4 PB bond has an SEN similar to the other B−P bonds; the longest B−P bonds in **1** and **5** have the smallest SEN, as expected. This is in line with the electrostatic interpretation of the bond shortening. The P(3)−P(4) bond in **1** and **5** is shorter than the λ^3[P(1)−P(2)] bond by 4 pm. A possible explanation may be found by inspecting the results of a natural bond orbital analysis. According to this, the P1−P2 bond acts as an electron donor into the σ*(B1P3) and σ*(B1P4) orbitals. Hereby a stabilization of 58 kJ·mol^{-1} is achieved. The P3−P4 bond is a weaker donor. By donation of electrons into the σ*(B1P1) and σ*(B1P2) orbitals a stabilization of only 36 kJ·mol^{-1} results.

The possible dimerization of **6** to afford **7** is endothermic (ΔH_{Dim} = 140 kJ·mol^{-1}). The B−P bonds in the dimer are longer than those in **6** by 4 pm. The P−P bonds are almost unaffected.

For the aluminum homologue **9**, the dimerization to **10** is also endothermic, but only by 64 kJ·mol^{-1}. Taking into account that **3** is not a free dianion as assumed for **10**, with the larger aluminum atom as spiro-center the dimeric structure is preferred over the monomer.

The Al−P bonds in **10** are similar to those in **3**, but longer than in **9**. Very striking are the long P−P bonds in **9**, which are in contrast to those in **3**. Here, the influence of substituents and the missing counterions is evident (compare P−P bond lengths in **1** and **5**−**8**). In a similar manner to **3**, the P−Al−P angles in **10** within the three-membered ring are 57.8°; within the six-membered rings they are 109.8° and 115.9°. Quantum chemical calculations are also helpful in assigning the NMR signals in **1**. For the calculated structure of **1** NMR shielding parameters can be calculated using the GIAO method[13] implemented in the Gaussian98 program. As reference points the shielding parameters for BF_3 and PH_3 were also calculated on the same level. The results, which are in good agreement with the experimentally observed data, and the assignment are summarized in Table 3. The ^{11}B NMR shift is in the typical range for tetracoordinated boron compounds. In the ^{31}P NMR spectrum a line-rich ABCX spin system is observed. The three chemically different P*t*Bu units are observed in a small range of 20 ppm as the tetracoordinated phosphorus atom is better shielded.

Table 3. ^{11}B and ^{31}P NMR shifts for **1** from GIAO calculations (BP86/6−31G*) and experimental values

	1 (DFT)	**1** (exp.)
δ^{11}B	−23.4	−25.9
δ^{31}P	−66 P(4)	−59.5
	−125 P(1)	−136.2
	−133 P(2)	−145.3
	−141 P(3)	−158.1

Conclusion

The group 13-phosphorus spirocycles **1** and **3** are new classes of heterocyclic small ring compounds. The larger covalent radius of aluminum compared to boron causes the different ring sizes in **1** and **3**.

Experimental Section

General Remarks: All experiments were performed under purified nitrogen or in vacuo with Schlenk techniques. All yields are referenced to $K_2P_2tBu_2$. Elemental analyses were performed in the microanalytical laboratory of the University of Karlsruhe. NMR: Bruker ACP200 and 250; Mass spectra: Varian MAT711; X-ray crystallography: Suitable crystals were mounted with a perfluorinated polyether oil on the tip of a glass fiber and cooled immediately on the goniometer head. Data collections were performed with Mo-K_α radiation (graphite monochromator) on a STOE STADI4 diffractometer (**2**, **3**) in a ω-scan mode or on a Siemens Bruker P4 diffractometer with CCD detector (**1**). Structures were solved and refined with the Bruker AXS Shelxtl 5.1 program package. Refinement in full-matrix against F^2. All non-hydrogen atoms were included as a riding-model with fixed isotropic U values in the final refinement. For further data see Table 1.

Crystallographic data (excluding structure factors) for the structure(s) reported in this paper have been deposited with the Cambridge Crystallographic Data Centre as supplementary publication nos. CCDC-152829 (**1**) and -152830 (**3**). Copies of the data can be obtained free of charge on application to CCDC, 12 Union Road, Cambridge CB2 1EZ, UK [Fax: (internat.) +44-1223/336-033; E-mail: deposit@ccdc.cam.ac.uk].

Quantum chemical calculations: The program packages TURBOMOL[12] and Gaussian98W[13] were used for the RI-DFT calculations[14] (BP86 functional,[15] SV(P)base), the NBO and GIAO calculations

(*t*BuP)$_2$B(P*t*Bu)P(*t*Bu)Me (1) and (2): $tBu_2P_2K_2$·0.5THF (0.48 g, 1.65 mmol) was suspended in 15 mL of diethyl ether and a solution of BF_3·OMe_2 (0.50 g; 4.40 mmol) in 25 mL diethyl ether was added dropwise at ambient temperature. After stirring for 12 h all volatiles were removed in vacuo. The residue was then taken up in 30 mL of pentane. KBF_4 (0.43 g) was separated by filtration. The solution was concentrated to a volume of 5 mL. At −30 °C colorless plates of **1** crystallized; yield: 0.14 g (45%), m.p. 72−74 °C. From the reduced mother liquor (2 mL) some colorless crystals of **2** were isolated, 0.02 g (5%).

1: ^{1}H NMR (C_6D_6): δ = 1.05 (d, $^2J_{PH}$ = 18 Hz, PMe), 1.28 (d, $^3J_{PH}$ = 12 Hz, *t*Bu), 1.40 (m, 3*t*Bu). − ^{31}P NMR(C_6D_6): δ = −158.1 (m, N = 253 Hz, P*t*Bu), −145.3 (m, N = 665.8 Hz, *t*Bu), −136.2 (m, N = 170 Hz, P*t*Bu), −59.5 (m, N = 407 Hz, PM*e*tBu). − ^{11}B NMR: δ = −25.9 ("d", $^1J_{BP}$ = 40 Hz). − MS (70 eV, EI): *m*/*z* (%) = 378 (38) [M$^+$], 321 (28) [M − *t*Bu]$^+$, 265 (30) [M − *t*Bu − C_4H_8]$^+$, 207 (100) [MeBP$_4$*t*Bu]$^+$. − $C_{17}H_{39}BP_4$ (378.2): calcd. C 53.99, H 10.39; found C 52.09, H 10.18.

Al$_2$(P*t*Bu)$_8$K$_2$·(OEt$_2$)$_4$ (3): A solution of $AlCl_3$ (0.11 g, 0.83 mmol) in 10 mL diethyl ether was added dropwise at ambient temperature to a suspension of $tBu_2P_2K_2$·0.5THF (0.36 g, 1.24 mmol) in 25 mL diethyl ether. After stirring for 1 day the mixture was filtered and the colorless solution was reduced in volume to 20 mL. On standing at ambient temperature colorless plates of **3** crystallized; yield: 0.24 g (68%, ref to $tBu_2P_2K_2$), m.p. (dec.) >90 °C. Compound **3** is extremely pyrophoric and does not redissolve in common NMR solvents. Thus, analytical data given are incomplete (a ^{31}P NMR spectrum recorded from the reaction mixture exhibited several groups of signals between δ = −220 and −10 which could not be assigned unequivocally). − MS (70 eV, EI): *m*/*z* (%) = 499 (0.1) [Al(P*t*Bu)$_5$PH]$^+$, 494 (0.1) [Al$_2$(P*t*Bu)$_5$]$^+$, 352 (5) [(P*t*Bu)$_4$]$^{+\cdot}$, 264 (7) [P*t*Bu)$_3$]$^{+\cdot}$, 57 (100) [*t*Bu]$^+$.

Acknowledgments

We are grateful to the Deutsche Forschungsgemeinschaft and the Fonds der Chemischen Industrie for the generous financial support. We also thank Dr. J. Knizek (Prof. Nöth, Munich) and E. Möllhausen (Prof. Schnöckel, Karlsruhe) for the assistance with the X-ray structure determinations.

[1] R. T. Paine, H. Nöth, *Chem. Rev.* **1995**, *95*, 343−379.
[2] A. J. Downs (Ed.), *Chemistry of Aluminium, Gallium, Indium and Thallium*, Blackie Academic, London, **1993**; As example, see the following references and prior literature cited therein: [2a] J. F. Janik, E. N. Duesler, W. F. McNamara, M. Westerhausen, R. T. Paine, *Organometallics* **1989**, *8*, 506−514. − [2b] O. T. Beachley, C. Tessier-Youngs, *Organometallics* **1983**, *2*, 796−801. − [2c] G. Fritz, G. Trenczek, *Z. Anorg. Allg. Chem.* **1964**, *331*, 206−. − [2d] S. A. Sangokoya, W. T. Pennington, G. H. Robinson, D. C. Hrncir, *J Organomet. Chem.* **1990**, *385*, 23−31.
[3] R. J. Wehmschulte, K. Ruhlandt-Senge, P. P. Power, *Inorg. Chem.* **1994**, *33*, 3205−3207.
[4] [4a] P. P. Power, *J. Organomet. Chem.* **1990**, *400*, 49−69. − [4b] D. A. Atwood, L. Contreras, A. H. Cowley, *Organometallics* **1993**, *12*, 17−18.
[5] M. Baudler, *Pure and Applied Chem.* **1980**, *52*, 755−769.
[6] P. Kölle, G. Linti, H. Nöth, K. Polborn, *J. Organomet. Chem.* **1988**, *355*, 7−18.
[7] M. Baudler, M. Hintze, *Z. Anorg. Allg. Chem.* **1985**, *522*, 184−188.
[8] D. C. Pestana, P. P. Power, *Inorg. Chem.* **1991**, *30*, 528−535.
[9] G. Linti, R. Frey, W. Köstler, H. Schwenk, *Chem. Ber./Recueil* **1997**, *130*, 663−668.
[10] M. Baudler, C. Gruner, G. Fürstenberg, B. Kloth, F. Saykowski, V. Özer, *Z. Anorg. Allg. Chem.* **1978**, *446*, 169−176.
[11] Due to the low quality and waxy consistence of all crystals examined, the crystal structure analysis of **2** can only be used for getting a rough picture of the connectivities in the macrocycle. The X-ray structural data are: space group $P\bar{1}$, a = 977.0(2), b = 1184.2(2), c = 12.646(3) pm, α = 80.09(3)°, β = 77.49(3)°, γ = 73.08(3)°, no. of refl. [$I > 4\sigma(I)$] = 3330(2299), param. = 265, R_1 = 0.160, wR_2 = 0.536.
[12] O. Treutler, R. Ahlrichs, *J. Chem. Phys.* **1995**, *102*, 346−354.
[13] Gaussian 98, Revision A.7, M. J. Frisch, G. W. Trucks, H. B. Schlegel, G. E. Scuseria, M. A. Robb, J. R. Cheeseman, V. G. Zakrzewski, J. A. Montgomery, Jr., R. E. Stratmann, J. C. Burant, S. Dapprich, J. M. Millam, A. D. Daniels, K. N. Kudin, M. C. Strain, O. Farkas, J. Tomasi, V. Barone, M. Cossi, R. Cammi, B. Mennucci, C. Pomelli, C. Adamo, S. Clifford, J. Ochterski, G. A. Petersson, P. Y. Ayala, Q. Cui, K. Morokuma, D. K. Malick, A. D. Rabuck, K. Raghavachari, J. B. Foresman, J. Cioslowski, J. V. Ortiz, A. G. Baboul, B. B. Stefanov, G. Liu, A. Liashenko, P. Piskorz, I. Komaromi, R. Gomperts, R. L. Martin, D. J. Fox, T. Keith, M. A. Al-Laham, C. Y. Peng, A. Nanayakkara, C. Gonzalez, M. Challacombe, P. M. W. Gill, B. Johnson, W. Chen, M. W. Wong, J. L. Andres, C. Gonzalez, M. Head-Gordon, E. S. Replogle, J. A. Pople, Gaussian, Inc., Pittsburgh PA, **1998**.
[14] A. D. Becke, *Phys. Rev. A* **1985**, *38*, 3098−3100; J. P. Perdew, *Phys. Rev. B* **1986**, *33*, 8822−8824.
[15] K. Eichkorn, O. Treutler, H. Ohm, M. Häser, R. Ahlrichs, *Chem. Phys. Lett.* **1995**, *242*, 652−660; K. Eichkorn, F. Weigend, O. Treutler, R. Ahlrichs, *Theor. Chem. Acc.* **1997**, *97*, 119−124.

Received December 7, 2000
[I00465]

Some New Dicationic Dihydrogen Complexes of Ruthenium

Kanak K. Majumdar,[a] H. V. Nanishankar,[a] and Balaji R. Jagirdar*[a]

Keywords: Hydrogen / Hydride ligands / NMR spectroscopy / Acidity / Ruthenium

A series of new dicationic dihydrogen complexes of ruthenium of the type *trans*-[(dppe)$_2$Ru(η^2-H$_2$)(RCN)][BF$_4$]$_2$ [dppe = Ph$_2$PCH$_2$CH$_2$PPh$_2$; R = CH$_3$, CH$_3$CH$_2$, CH$_3$CH$_2$CH$_2$, CH$_2$=CH, *p*-CH$_3$–C$_6$H$_4$–CH$_2$, C$_6$H$_5$, and (CH$_3$)$_2$N] have been prepared by the protonation reaction of the precursor hydrides, *trans*-[(dppe)$_2$Ru(H)(RCN)][BF$_4$] using HBF$_4$·OEt$_2$. The variable temperature spin-lattice relaxation times (T_1, ms) and the H, D coupling constants of the η^2-HD isotopomers indicate the intact nature of the H–H bond in these complexes. It was found that the spectroscopic and chemical properties of these derivatives are not very sensitive to the change in the *trans* nitrile ligand. The pK_a values of the dihydrogen complexes have been determined using the equilibrium: *trans*-[(dppe)$_2$Ru(H)(RCN)][BF$_4$] + HBF$_4$·OEt$_2$ ⇄ *trans*-[(dppe)$_2$Ru(η^2-H$_2$)(RCN)][BF$_4$]$_2$ + Et$_2$O by ^{1}H NMR spectroscopy.

Introduction

The dihydrogen molecule can be activated toward heterolytic cleavage when coordinated to a cationic metal center. This was first realized by Crabtree and Lavin in the deprotonation reaction of the H$_2$ ligand in [(PPh$_3$)$_2$(bq)Ir(η^2-H$_2$)H]$^+$ (bq = 7,8-benzoquinolato) in the presence of alkyllithium reagents in preference to the loss of hydride ligand.[1] The heterolysis of dihydrogen has been observed for a variety of complexes and has been shown to depend on the nature of the metal center as well as the ancillary ligand environment.[2] Lau and co-workers[2l] recently prepared and characterized various dihydrogen complexes of ruthenium with triazacyclononane, trimethyltriazacyclononane, and hydrotris(pyrazolyl)borate as ancillary ligands. They found their dicationic complexes to be more acidic than their monocationic hydrotris(pyrazolyl)borate and cyclopentadienyl counterparts. Morris et al.[2p] reported a highly acidic dicationic dihydrogen complex, *trans*-[(dppe)$_2$Ru(η^2-H$_2$)(CNH)][OTf]$_2$ that was found to be stable with respect to loss of protons or H$_2$ in the presence of strong acids like HOTf. However, it should not be implied that the dicationic dihydrogen complexes would be stronger acids than the monocationic derivatives. Harman and Taube[3] found the dicationic osmium complex, [Os(H$_2$)(NH$_3$)$_5$]$^{2+}$ to be a weak acid that is stable toward moderately strong bases such as NaOMe.

The dicationic dihydrogen complexes of transition metals reported to date are very few in number. Therefore, we sought to synthesize and characterize a series of isostructural dicationic dihydrogen complexes of ruthenium bearing bis(1,2-diphenylphosphanyl)ethane (dppe) and nitrile ligands. In addition, we also wanted to study the variation in some of the properties of dihydrogen complexes, for example, the H−H distances and the acidities with a change in the steric and the electronic properties of the nitrile ligand that is *trans* to the dihydrogen moiety.

[a] Department of Inorganic and Physical Chemistry, Indian Institute of Science,
Bangalore 560 012, India
E-mail: jagirdar@ipc.iisc.ernet.in

Supporting information for this article is available on the WWW under http://www.wiley-vch.de/home/eurjic or from the author.

Results and Discussion

Synthesis and Characterization of the New Ruthenium Hydride Complexes

The complexes *trans*-[(dppe)$_2$Ru(H)(RCN)][BF$_4$] [R = CH$_3$ (**1**), CH$_3$CH$_2$ (**2**), CH$_3$CH$_2$CH$_2$ (**3**), CH$_2$=CH (**4**), *p*-CH$_3$−C$_6$H$_4$−CH$_2$ (**5**), C$_6$H$_5$ (**6**), (CH$_3$)$_2$N (**7**)] were prepared from *trans*-[(dppe)$_2$Ru(η^2-H$_2$)(H)][BF$_4$] by the substitution of the dihydrogen ligand by the nitrile, analogous to the preparation of *trans*-[(dppe)$_2$Os(H)(CH$_3$CN)][BF$_4$] reported by Schlaf et al.[2i] [Equation (1)].

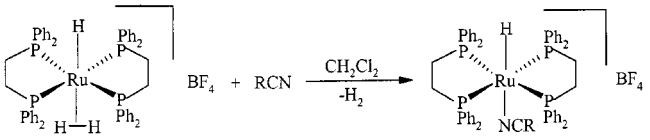

R = CH$_3$- (**1**), CH$_3$CH$_2$- (**2**), CH$_3$CH$_2$CH$_2$- (**3**), CH$_2$=CH- (**4**), *p*-CH$_3$-C$_6$H$_4$-CH$_2$- (**5**), C$_6$H$_5$- (**6**), (CH$_3$)$_2$N- (**7**)

(1)

The products were obtained in fairly good yields as summarized in Table 1. They are all colorless to off-white solids. Purification of the complexes was achieved by crystallization by slow diffusion of Et$_2$O into a CH$_2$Cl$_2$ solution containing the hydride complex and a slight excess of the appropriate nitrile. In the absence of the excess nitrile in the crystallization solution, we observed that loss of the nitrile ligand bound to ruthenium takes place due to its lability. This results in the decomposition of the hydride complex into intractable products.

 © WILEY-VCH Verlag GmbH, 69451 Weinheim, 2001 1434−1948/01/0707−1847 $ 17.50+.50/0

Table 1. Preparation and analytical data for *trans*-[$(dppe)_2Ru(H)(RCN)][BF_4]$ complexes

R	Starting materials [A][b] (mg)	[B][b] (mg)	Yield % (mg)	Analysis (%)[a] C	H	N	P[c]
CH_3 (**1**)	0.06 (59)	1.22 (50)	75 (47)	63.63 (63.15)	5.43 (5.07)	1.38 (1.36)	*n.d.*
CH_3CH_2 (**2**)	0.20 (197)	0.56 (30)	71 (149)	63.78 (63.46)	5.50 (5.19)	1.10 (1.34)	11.81 (11.92)
$CH_3(CH_2)_2$ (**3**)	0.20 (197)	0.57 (39)	70 (149)	63.83 (63.76)	5.30 (5.31)	1.00 (1.33)	*n.d.*
CH_2=CH (**4**)	0.20 (197)	0.47 (24)	73 (153)	63.12 (63.58)	5.09 (5.00)	0.98 (1.34)	11.46 (11.95)
p-$CH_3-C_6H_4-CH_2$ (**5**)	0.20 (197)	0.45 (59)	64 (140)	65.60 (65.59)	5.23 (5.19)	1.25 (1.25)	*n.d.*
C_6H_5 (**6**)	0.20 (197)	0.49 (50)	54 (119)	65.08 (65.07)	5.36 (4.96)	1.42 (1.29)	*n.d.*
$(CH_3)_2N$ (**7**)	0.20 (197)	0.49 (34)	62 (132)	62.66 (62.56)	5.40 (5.21)	2.66 (2.65)	*n.d.*

[a] Calculated values are given in parentheses. – [b] [A] = [*trans*-$[(dppe)_2Ru(H_2)(H)][BF_4]$]; [B] = [nitrile] (mmol). – [c] *n.d.* not determined.

Table 2. ^1H and $^{31}P\{^1H\}$ NMR spectroscopic data (δ) of *trans*-$[(dppe)_2Ru(H)(RCN)][BF_4]$ complexes in CD_2Cl_2

R	δ(Ru–H)	$J(H,P_{cis})$ Hz	δ(R)	δ(CH_2-CH_2)	δ(Ph)	δ[P(dppe)]
CH_3 (**1**)	–15.98 (qnt, 1 H)	20	1.58 (s, 3 H, C*H*$_3$)	2.61 (m, 4 H) 1.96 (m, 4 H)	6.65–7.54 (m, 40 H)	65.55
CH_3CH_2 (**2**)	–16.00 (qnt, 1 H)	20	1.93 (q, 2 H, C*H*$_2$) 0.69 (t, 3 H, C*H*$_3$)	2.41 (m, 4 H) 1.96 (m, 4 H)	6.69–7.27 (m, 40 H)	64.54
$CH_3(CH_2)_2$ (**3**)	–16.00 (qnt, 1 H)	20	1.9 (m, 4 H, $CH_3CH_2CH_2$) 0.69 (t, 3 H, C*H*$_3$)	2.40 (m, 4 H) 1.95 (m, 4 H)	6.66–7.5 (m, 40 H)	64.10
CH_2=CH (**4**)	–15.25 (qnt, 1 H)	20	5.8 (d, 2 H, C*H*$_2$=CH) 5.42 (t, 1 H, CH_2=C*H*)	2.38 (m, 4 H) 1.96 (m, 4 H)	6.68–7.41 (m, 40 H)	64.11
p-$CH_3-C_6H_4-CH_2$ (**5**)	–15.85 (qnt, 1 H)	20	6.83 (m, 4 H, C_6H_4) 2.22 (m, 2 H, C*H*$_2$) 1.0 (m, 3 H, C*H*$_3$)	2.33 (m, 4 H) 1.90 (m, 4 H)	6.83–7.51 (m, 40 H)	65.87
C_6H_5 (**6**)	–15.28 (qnt, 1 H)	20	6.71–7.54 (m, 5 H, C_6H_5)	2.61 (m, 4 H) 1.95 (m, 4 H)	6.71–7.54 (m, 40 H)	63.79
$(CH_3)_2N$ (**7**)	–16.60 (qnt, 1 H)	20	0.99 (s, 6 H, C*H*$_3$)	2.32 (m, 4 H) 1.98 (m, 4 H)	6.99–7.53 (m, 40 H)	65.74

The ^1H NMR spectra of the complexes show quintets for the hydride ligand confirming the coupling of the hydride with the four *cis*-phosphorus (dppe) ligands. The value of *J*(H,P) is remarkably similar in all these derivatives (20 Hz) indicating that the variation of the *trans*-nitrile ligand has no effect on the coupling constant. The $^{31}P\{^1H\}$ NMR spectra consist of only one singlet for the dppe phosphorus nuclei. This suggests that all the four phosphorus atoms are equivalent in solution. The ^1H and $^{31}P\{^1H\}$ NMR spectroscopic data for these complexes are summarized in Table 2.

In order to obtain some insight with regard to the cavity formed by the sterically encumbered $[(dppe)_2Ru(H)]^+$ fragment, we examined the X-ray crystal structure of *trans*-$[(dppe)_2Ru(H)(p\text{-}CH_3-C_6H_4-CH_2CN)][BF_4]$ (**5**). Unfortunately, the structure solution could not be achieved satisfactorily because the *p*-$CH_3-C_6H_4-CH_2CN$ group was severely disordered (the structure details can be found in the Supporting Information). Nevertheless, it is instructive to note that the nitrile should be almost *rod-shaped* in order to be accommodated *trans* to the hydride. Attempts to prepare hydride complexes with more bulky *trans* nitrile ligands failed and the starting hydride-dihydrogen complex *trans*-$[(dppe)_2Ru(\eta^2\text{-}H_2)(H)][BF_4]$ was recovered.

Preparation and Properties of the Dihydrogen Complexes

The protonation of the starting hydride complexes *trans*-$[(dppe)_2Ru(H)(RCN)][BF_4]$ with excess 54% $HBF_4{\cdot}OEt_2$ yielded the corresponding dihydrogen complexes, *trans*-$[(dppe)_2Ru(\eta^2\text{-}H_2)(RCN)][BF_4]_2$ [R = CH_3 (**1a**), CH_3CH_2 (**2a**), $CH_3CH_2CH_2$ (**3a**), CH_2=CH (**4a**), *p*-$CH_3-C_6H_4-CH_2$ (**5a**), C_6H_5 (**6a**), $(CH_3)_2N$ (**7a**)]. These reactions were carried out in CD_2Cl_2 under 1 atm. of either dihydrogen or argon. The dihydrogen complexes were characterized by NMR spectroscopy. All of these derivatives were found to be stable in solution at room temperature for periods as long as two days before undergoing decomposition into the starting hydride complex and a proton equivalent (exists as $HOEt_2^+BF_4^-$).

Table 3. ^1H and $^{31}P\{^1H\}$ NMR spectroscopic data (δ) of *trans*-$[(dppe)_2Ru(\eta^2\text{-}H_2)(RCN)][BF_4]_2$ complexes in CD_2Cl_2

R	δ[Ru(η²-H₂)]	δ(R)	δ(CH₂−CH₂)	δ(Ph)	δ[P(dppe)]
CH_3 (**1a**)	−11.2(br s, 2 H)	1.45 (s, 3 H, CH_3)	2.80 (m, 4 H) 2.28 (m, 4 H)	7.08−7.33 (m, 40 H)	55.19
CH_3CH_2 (**2a**)	−11.1(br s, 2 H)	2.54 (q, 2 H, CH_2) 0.5 (t, 3 H, CH_3)	2.84 (m, 4 H) 2.28 (m, 4 H)	6.90−7.21 (m, 40 H)	53.99
$CH_3(CH_2)_2$ (**3a**)	−11.2(br s, 2 H)	1.49 (m, 4 H, $CH_3CH_2CH_2$) 0.46 (t, 3 H, CH_3)	2.84 (m, 4 H) 2.29 (m, 4 H)	7.1−7.4 (m, 40 H)	53.99
CH_2=CH (**4a**)	−10.95(br s, 2 H)	6.4 (t, 1 H, CH_2=CH) 6.2 (d, 2 H, CH_2=CH)	2.86 (m, 4 H) 2.29 (m, 4 H)	7.0−7.2 (m, 40 H)	54.24
p-$CH_3-C_6H_4-CH_2$ (**5a**)	−11.38(br s, 2 H)	6.66−7.63 (m, 4 H, C_6H_4) 2.11 (m, 2 H, CH_2) 1.08 (m, 3 H, CH_3)	2.87 (m, 4 H) 2.32 (m, 4 H)	6.66−7.63 (m, 40 H)	54.43
C_6H_5 (**6a**)	−10.94(br s, 2 H)	6.9−7.4 (m, 5 H, C_6H_5)	2.80 (m, 4 H) 2.30 (m, 4 H)	6.9−7.4 (m, 40 H)	55.34
$(CH_3)_2N$ (**7a**)	−11.69(br s, 2 H)	1.3 (s, 6 H, CH_3)	2.82 (m, 4 H) 2.27 (m, 4 H)	7.14−7.53 (m, 40 H)	54.95

The ^1H NMR spectrum of the dihydrogen complexes shows a broad singlet in the hydride region whose line widths ($\Delta\nu_{1/2}$) are in the range 36 to 43 Hz. This signal is shifted downfield with respect to the starting hydride complex. The $^{31}P\{^1H\}$ NMR spectrum also shows a singlet for the dppe phosphorus atoms that is also shifted downfield in relation to the precursor hydride complex. The ^1H and $^{31}P\{^1H\}$ NMR spectroscopic data are summarized in Table 3.

The classification of **1a**−**7a** as dihydrogen complexes is based on variable temperature ^1H spin-lattice relaxation time (T_1, ms) measurements and the observation of H, D coupling constants of the η²-HD isotopomers **1b**−**7b**. The measured and the calculated T_1 minima data[4] as a function of temperature are given in Table 4. All of these derivatives exhibit short T_1 minima (18−21 ms) demonstrating that there is an intact H−H bond in these complexes. These values have been obtained directly from the experiments and also by fitting the equations that describe the dominant dipolar relaxation mechanism to the variable temperature T_1 data as described earlier by Morris and co-workers.[5] From the T_1 minima, the H−H distances can be calculated after appropriate corrections[6] have been made for the relaxation contributions from other nuclei in the vicinity. The analysis of T_1 data leads to three possible values for the H−H distance depending upon the relative rate at which the H_2 ligand undergoes rotation (slow, fast, and intermediate).[5,7] Table 4 also lists the H−H distances (for slow and fast rotation regimes of H_2) as determined from the T_1 minima for the complexes **1a**−**7a**. The H−H distances thus obtained fall in the range 1.12 to 0.87 Å for the slow and the fast spinning regimes, respectively.

Table 4. Observed and calculated spin-lattice relaxation times (T_1 minima; 400 MHz) and the H−H distances of the dihydrogen ligand in the complexes *trans*-$[(dppe)_2Ru(\eta^2\text{-}H_2)(RCN)][BF_4]_2$ **1a**−**7a** in CD_2Cl_2

R	T_1(obs), ms (T, K)	T_1(calc), ms	r_{HH} (Å)[a]
CH_3 (**1a**)	18.98 (283)	19.39	0.87/1.10
CH_3CH_2 (**2a**)	20.41 (273)	21.39	0.88/1.12
$CH_3(CH_2)_2$ (**3a**)	20.34 (283)	20.76	0.88/1.11
CH_2=CH (**4a**)	19.98 (273)	20.08	0.88/1.11
p-$CH_3-C_6H_4-CH_2$ (**5a**)	19.83 (283)	19.92	0.88/1.11
C_6H_5 (**6a**)	18.25 (283)	18.22	0.87/1.09
$(CH_3)_2N$ (**7a**)	20.15 (273)	20.72	0.89/1.12

[a] For fast rotation/static regimes of the H_2 ligand.

The partial incorporation of deuterium into the H_2 ligand could, in general, be accomplished by exposing the dihydrogen complex to D_2 gas or the use of deuterated acid (in the current work, $DBF_4{\cdot}OEt_2$ has been used) to deuterate the starting hydride complex. It was proposed that a combination of the lability and the acidity of the H_2 ligand is responsible for the formation of the HD isotopomers.[8] The HD isotopomers, *trans*-$[(dppe)_2Ru(\eta^2\text{-}HD)(RCN)][BF_4]_2$ [R = CH_3, CH_3CH_2, $CH_3CH_2CH_2$, CH_2=CH, *p*-$CH_3-C_6H_4-CH_2$, C_6H_5, $(CH_3)_2N$] were obtained from the starting hydride complexes by the addition of excess DBF_4 [prepared from HBF_4 and D_2O in the ratio 3:1 (v/v)] in CD_2Cl_2. The ^1H NMR spectra at room temperature exhibit a sharp triplet of quintets after nullifying the signal due to η²-H_2 from the known spin-lattice relaxation times (T_1, ms). The intensity ratio of the triplet resonance is approximately 1:1:1 with J(H,D) values in the range 26−28 Hz. Further splitting of each of the triplet signals into quintets, although not fully resolved, is due to coupling with the four dppe phosphorus atoms with a corresponding $J(H,P_{cis})$ of ca. 5 Hz. There does not seem to be a consistent trend for the J(H,D) values, which are relatively insensitive to the nature of the nitrile *trans* to the H_2. This is typical of complexes that have η²-HD bound *trans* to a strong-field π-acid ligand.[9] Figure 1 shows the hydride region of the ^1H NMR spectrum of *trans*-$[(dppe)_2Ru(\eta^2\text{-}HD)(p\text{-}CH_3-C_6H_4-CH_2-CN)][BF_4]_2$. The HD resonances of all the complexes suffer from upfield shifts from the H_2 signals (Δδ from 34 to 43 ppb) which is typical for the dihydrogen complexes reported thus far.[10] The shift that is observed in the case of H_2/HD gas is on the order of +36 ppb.[11]

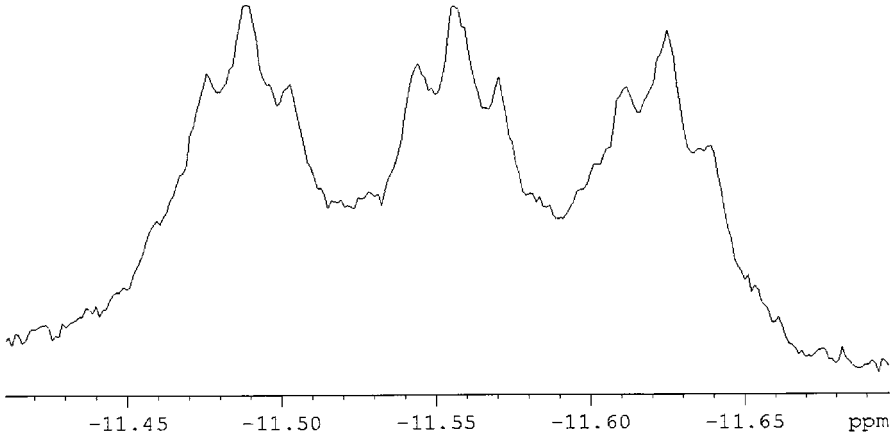

Figure 1. ^{1}H NMR spectrum (hydride region) of *trans*-[(dppe)$_2$Ru(η^2-HD)(*p*-CH$_3$−C$_6$H$_4$−CH$_2$CN)][BF$_4$]$_2$ (400 MHz, 298 K) in CD_2Cl_2; resonance due to η^2-H$_2$ ligand has been nullified

The H-H distances (r_{HH}) could be calculated from the inverse relationship between r_{HH} and J(H,D) of the HD isotopomer.[12] Thus, distances on the order of 0.96−0.97 Å have been obtained for our complexes. Gusev et al.[13] analyzed the T_1 minima and J(H,D) values of certain reported dihydrogen complexes that have $J(H,D) \geq 25$ Hz. According to this analysis, in complexes of the type *trans*-[(P-P)$_2$M(H)(η^2-H$_2$)]$^+$ (M = Fe, Ru; P-P = chelating phosphane), it is necessary to invoke the fast rotation approximation in order to obtain a reasonable H−H distance for the H$_2$ ligand. However, Morris and Wittebort[7] have shown that the rotation around M−H$_2$ in a majority of complexes is either in the fast motion regime or is a librational motion. Table 5 lists the H−H distances for the complexes **1a**−**7a** calculated from the J(H,D) values. The H−H distances obtained from the H−D coupling constants lie between the distances (slow and fast) obtained from T_1 values, suggesting that the relaxation of the dihydrogen ligand in this series of complexes is significantly dominated by libration and torsional motions as described earlier by Morris and Wittebort.[7] Many examples have been reported in the literature where such a situation has been observed.[7] The relatively long H−H distances found for these derivatives is consistent with the tight binding of H$_2$ to the ruthenium center.

Table 5. H−H Distances of *trans*-[(dppe)$_2$Ru(η^2-H$_2$)(RCN)][BF$_4$]$_2$ complexes **1a**−**7a** obtained from J(H,D)

R	J(H,D) Hz	r_{HH} (Å)
CH$_3$ (**1a**)	27	0.96
CH$_3$CH$_2$ (**2a**)	27	0.96
CH$_3$(CH$_2$)$_2$ (**3a**)	28	0.95
CH$_2$=CH (**4a**)	26	0.98
p-CH$_3$−C$_6$H$_4$−CH$_2$ (**5a**)	28	0.95
C$_6$H$_5$ (**6a**)	27	0.96
(CH$_3$)$_2$N (**7a**)	27	0.96

Acidities of the Dihydrogen Complexes

The acidities of the dihydrogen complexes have been measured on the pseudo aqueous pK_a scale.[2c][2i][2k][2l][12b,14] The equilibrium constants for the protonation of the hydride complex using an acid whose aqueous pK_a is known are determined in a nonaqueous medium. Then, the pseudo aqueous pK_a of the dihydrogen complex is calculated with respect to the aqueous pK_a of the protonating agent. The pK_a values of the dihydrogen complexes **1a**−**7a** have been estimated by studying the equilibrium shown in Equation (2) using ^{1}H NMR spectroscopy at −30 °C.

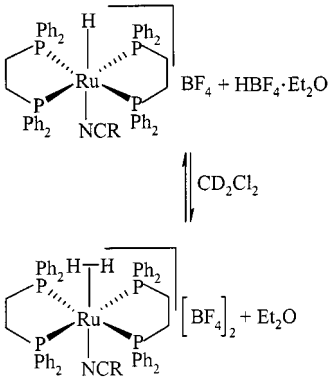

(2)

R = CH_3-, CH_3CH_2-, $CH_3CH_2CH_2$-, CH_2=CH-, *p*-CH_3-C_6H_4-CH_2-, C_6H_5-, $(CH_3)_2N$-

The relative molar concentrations of the hydrides, HBF_4·OEt_2, the dihydrogen complexes, and Et_2O were estimated from the ^{1}H NMR spectral integrations of the respective signals. As suggested earlier by Kristjánsdóttir and Norton,[15] the pK_a values of the dihydrogen complexes have been estimated from the equilibrium constants K_{eq} of Equation (2) and the pK_a of the protonating agent, here HBF_4·OEt_2 (−2.4)[16] using Equation (3).

$$pK_a[RuH_2]^{2+} = pK_a[HBF_4 \cdot Et_2O] + \log K_{eq} \quad (3)$$

$[RuH_2]^{2+}$ = *trans*-[(dppe)$_2$Ru(η^2-H$_2$)(RCN)][BF$_4$]$_2$

The pK_a values of the dicationic dihydrogen complexes **1a**−**7a** are summarized in Table 6. The magnitude of these pK_a values are very approximate and accurate values could only be obtained when the actual non-ion-paired pK_a of $HOEt_2^+BF_4^-$ in CH_2Cl_2 is determined and corrections are made for ion pairing for all of the species in solution.[17] All of these derivatives exhibit low pK_a values indicating that they are quite acidic species. At this juncture, it is quite appropriate to compare the acidity of *trans*-[(dppe)$_2$Ru(η^2-H_2)(CNH)][OTf]$_2$ reported by Morris et al.[2p] with those of ours. *trans*-[(dppe)$_2$Ru(η^2-H_2)(CNH)][OTf]$_2$ is the first member of this class of compounds. This complex was found to be highly acidic since it was only completely formed in an excess of HOTf in CH_2Cl_2. Furthermore, it was proposed that the pK_a of this complex was very near to that of HOTf in CH_2Cl_2 (the aqueous pK_a of HOTf has been estimated to be −4.9).[2k] The complexes reported in this work are less acidic in comparison to that of Morris' (compare with the pK_a of the protonating agent used, HBF_4·OEt_2 = −2.4). In general, the acidity of isostructural dihydrogen complexes decreases as ligands become more electron donating. The trend in the pK_a values of our complexes does seem to corroborate this: the greater the electrophilicity of the metal center, the greater is the activation of the dihydrogen towards heterolysis. In addition to this series of dicationic dihydrogen complexes that are quite acidic and at the same time stable at room temperature with respect to loss of H_2, several other derivatives have also been reported earlier by other groups.[2k,10d,18]

Table 6. Estimation of the acidities of *trans*-[(dppe)$_2$Ru(η^2-H_2)(RCN)][BF_4]$_2$ complexes in CD_2Cl_2

R	K_{eq} [a]	pK_a[b]
CH_3 (**1a**)	0.217	-1.7
CH_3CH_2 (**2a**)	0.011	-0.4
$CH_3(CH_2)_2$ (**3a**)	0.006	-0.2
CH_2=CH (**4a**)	0.066	-1.3
p-CH_3−C_6H_4−CH_2 (**5a**)	0.070	-1.3
C_6H_5 (**6a**)	0.713	-2.2
$(CH_3)_2N$ (**7a**)	0.461	-1.9

[a] From equilibrium shown in Equation (2); determined at 243 K. − [b] Calculated from Equation (3).

Conclusions

The complexes *trans*-[(dppe)$_2$Ru(H_2)(RCN)][BF_4]$_2$ [R = CH_3 (**1a**), CH_3CH_2 (**2a**), $CH_3CH_2CH_2$ (**3a**), CH_2=CH (**4a**), *p*-CH_3−C_6H_4−CH_2 (**5a**), C_6H_5 (**6a**), $(CH_3)_2N$ (**7a**)] are formulated as dihydrogen complexes based on their short T_1 values and the observation of H, D coupling in the corresponding HD isotopomers. All of these derivatives are stable at room temperature. The long H−H distances and the relatively nonlabile nature of the H_2 ligand shows strong M−H_2 interactions in these complexes. The pK_a values of these complexes indicate that they are quite acidic.

Experimental Section

General: All reactions except those involving the dihydrogen complexes were carried out under dry and purified nitrogen atmosphere at room temperature using standard Schlenk[19] and inert atmosphere techniques, unless otherwise specified. The manipulations involving solutions of dihydrogen complexes were carried out under an atmosphere of dihydrogen or argon gas. 1,2-Bis(diphenylphosphanyl)ethane (dppe)[20] and the complex *trans*-[(dppe)$_2$Ru(η^2-H_2)(H)][BF_4][21] were prepared according to published procedures.

The ^{1}H and ^{31}P NMR spectra were obtained on a AMX Bruker 400 MHz instrument. The shift of the residual protons of the deuterated solvent was used as an internal reference. All ^{31}P NMR spectra were proton decoupled. ^{31}P NMR chemical shifts have been measured relative to 85% H_3PO_4 in CD_2Cl_2. Variable temperature proton T_1 measurements were carried out at 400 MHz using the inversion recovery method (180°-τ-90° pulse sequence at each temperature).[22] Microanalyses were performed at the Institut für Anorganische Chemie, der Universität Göttingen, Germany and National Chemical Laboratory, Pune, India.

Preparation of *trans*-[(dppe)$_2$Ru(H)(CH_3CN)][BF_4] (1): A method similar to the preparation of the osmium analogue of (**1**) reported[2i] earlier was employed for this preparation. *trans*-[(dppe)$_2$Ru(η^2-H_2)(H)][BF_4] (60 mg, 0.06 mmol) was dissolved in 3 mL of CH_2Cl_2 under 1 atm. of dihydrogen. Acetonitrile (50 mg, 1.22 mmol) was then added with a syringe and the mixture was allowed to stir at room temperature for 12 h. Addition of 20 mL of Et_2O caused complete precipitation of the pale yellow product. Et_2O was removed with a cannula and the precipitate was dried by passing a slow stream of H_2. Yield: 47 mg (75%). The product was crystallized from a CH_2Cl_2 solution containing the hydride complex and a few drops of the nitrile by the diffusion of Et_2O at room temperature. The ^{1}H and ^{31}P{^{1}H} NMR spectroscopic data are summarized in Table 2.

The complexes, *trans*-[(dppe)$_2$Ru(H)(RCN)][BF_4] [R = CH_3CH_2 (**2**), $CH_3CH_2CH_2$ (**3**), CH_2=CH (**4**), *p*-CH_3−C_6H_4−CH_2 (**5**), C_6H_5 (**6**), $(CH_3)_2N$ (**7**)] were similarly prepared from *trans*-[(dppe)$_2$Ru(η^2-H_2)(H)][BF_4] and the corresponding nitrile as summarized in Table 1. All of these products were purified by crystallization from a solution containing the respective hydride complex and a few drops of the corresponding nitrile in CH_2Cl_2 by the diffusion of Et_2O. The ^{1}H and ^{31}P NMR spectroscopic data are summarized in Table 2.

Preparation of *trans*-[(dppe)$_2$Ru(η^2-H_2)(CH_3CN)][BF_4]$_2$ (1a): In a typical experiment, a sample (15 mg) of *trans*-[(dppe)$_2$Ru(H)(CH_3CN)][BF_4] (**1**) was placed in a 5 mm NMR tube provided with a septum. The tube was carefully evacuated and then filled with dihydrogen in three cycles. The hydride complex was then dissolved in CD_2Cl_2 (0.7 mL) and 10 μL of 54% HBF_4·OEt_2 was added. The reaction was found to be almost instantaneous and the protonation was complete within a few seconds. The solution was then analyzed by NMR spectroscopy. The ^{1}H and ^{31}P{^{1}H} NMR spectroscopic data are summarized in Table 3.

The corresponding dihydrogen complexes, *trans*-[(dppe)$_2$Ru(η^2-H_2)(RCN)][BF_4]$_2$ [R = CH_3CH_2 (**2a**), $CH_3CH_2CH_2$ (**3a**), CH_2=CH (**4a**), *p*-CH_3−C_6H_4−CH_2 (**5a**), C_6H_5 (**6a**), $(CH_3)_2N$ (**7a**) were similarly prepared and characterized. The ^{1}H and ^{31}P{^{1}H} NMR spectroscopic data of these derivatives are given in Table 3.

Decomposition Reaction of *trans*-[(dppe)$_2$Ru(η^2-H_2)(CH_3CN)][BF_4]$_2$ (1a): An NMR tube provided with a septum, loaded with *trans*-

$[(dppe)_2Ru(\eta^2\text{-}H_2)(CH_3CN)][BF_4]_2$ **(1a)** (10 mg) in CD_2Cl_2 (0.7 mL) under a hydrogen atmosphere was allowed to stand at room temperature for several days. ^1H NMR spectra were recorded periodically to monitor the stability of the dihydrogen complex. It was found that after ca. 36−72 h, the hydride complex *trans*-$[(dppe)_2Ru(H)(CH_3CN)][BF_4]$ (**1**) started to appear. This suggests that the dihydrogen complex is unstable for an extended period of time and that it undergoes decomposition to the hydride complex and a proton.

Preparation of the H−D Isotopomers of *trans*-$[(dppe)_2Ru(\eta^2\text{-}H_2)(RCN)][BF_4]_2$ [R = CH_3, CH_3CH_2, $CH_3CH_2CH_2$, CH_2=CH, *p*-$CH_3-C_6H_4-CH_2$, C_6H_5, $(CH_3)_2N$]: These derivatives were prepared in the following manner: Each of the hydride complexes (15 mg) was dissolved in 0.7 mL CD_2Cl_2 in a 5 mm NMR tube under an atmosphere of Ar followed by the addition of DBF_4 (prepared from $HBF_4{\cdot}OEt_2$ and D_2O in a 3:1 ratio). The η^2-HD signals were observed in the ^1H NMR spectrum by nullifying the signal due to η^2-H_2 by the inversion recovery method using the relationship $T_1 = \tau_{null}/\ln 2$ and the known T_1 values of the dihydrogen complexes at room temperature.[8,23,24] The J(H,D) values together with the H−H distances for these complexes are summarized in Table 5.

Acidity Measurements: In a typical experiment, a 5 mm NMR tube was charged with 20 mg of the hydride complex. It was dissolved in 0.6 mL of CD_2Cl_2 and the solution was cooled to 243 K. The ^1H and $^{31}P\{^1H\}$ NMR spectra were then recorded with the probe at 243 K. One equivalent of 54% $HBF_4{\cdot}Et_2O$ was added to the tube, shaken for some time and transferred back to the probe at 243 K. The relative concentrations of all the species [as in Equation (2)] were calculated from the integrations of the respective peaks in the ^1H NMR spectra. The pK_a values were calculated from the equilibrium depicted in Equation (2) and are summarized in Table 6.

Supporting Information Available: Observed and calculated spin-lattice relaxation time (T_1, ms; 400 MHz) data as a function of temperature of the dihydrogen ligand in the complexes *trans*-$[(dppe)_2Ru(\eta^2\text{-}H_2)(RCN)][BF_4]_2$ [R = CH_3 (**1a**), CH_3CH_2 (**2a**), $CH_3CH_2CH_2$ (**3a**), CH_2=CH (**4a**), *p*-$CH_3-C_6H_4-CH_2$ (**5a**), C_6H_5 (**6a**), and $(CH_3)_2N$ (**7a**)] and tables of crystal data, structure solution and refinement, atomic coordinates, bond lengths and angles, anisotropic thermal parameters, hydrogen atom coordinates, and an ORTEP diagram for **5**. Crystallographic data (excluding structure factors) for the structure(s) reported in the Supporting Information of this paper have been deposited with the Cambridge Crystallographic Data Centre as supplementary publication no. CCDC-159782. Copies of the data can be obtained free of charge on application to CCDC, 12 Union Road, Cambridge CB2 1EZ, UK [Fax: int. code +44-1223/336-033; E-mail: deposit@ccdc.cam.ac.uk].

Acknowledgments

Financial support from the Council of Scientific and Industrial Research of India is gratefully acknowledged. We thank the Sophisticated Instruments Facility, Indian Institute of Science for the NMR spectroscopic data and Institut für Anorganische Chemie, der Universität Göttingen, Germany and Dr. Amitabha Sarkar, National Chemical Laboratory, Pune, India, for elemental analysis data. We also thank the National Single Crystal Diffractometer Facility at the University of Hyderabad funded by the Department of Science and Technology for crystal structure data and Ms. Nisha Mathew for help with the data analysis.

[1] R. H. Crabtree, M. Lavin, *J. Chem. Soc., Chem. Commun.* **1985**, 794−795.
[2] [2a] P. J. Brothers, *Prog. Inorg. Chem.* **1981**, *28*, 1−61. − [2b] M. S. Chinn, D. M. Heinekey, *J. Am. Chem. Soc.* **1987**, *109*, 5865−5867. − [2c] G. Jia, A. J. Lough, R. H. Morris, *Organometallics* **1992**, *11*, 161−171. − [2d] M. S. Chinn, D. M. Heinekey, N. G. Payne, C. D. Sofield, *Organometallics* **1989**, *8*, 1824−1826. − [2e] J. P. Collman, J. E. Hutchison, P. S. Wagenknecht, N. S. Lewis, M. A. Lopez, R. Guildard, *J. Am. Chem. Soc.* **1990**, *112*, 8206−8208. − [2f] L. S. Van Der Sluys, M. M. Miller, G. J. Kubas, K. G. Caulton, *J. Am. Chem. Soc.* **1991**, *113*, 2513−2520. − [2g] R. H. Morris, *Inorg. Chem.* **1992**, *31*, 1471−1478. − [2h] M. Schlaf, A. J. Lough, R. H. Morris, *Organometallics* **1993**, *12*, 3808−3809. − [2i] M. Schlaf, A. J. Lough, P. A. Maltby, R. H. Morris, *Organometallics* **1996**, *15*, 2270−2278. − [2j] D. M. Heinekey, T. A. Luther, *Inorg. Chem.* **1996**, *35*, 4396−4399. − [2k] E. Rocchini, A. Mezzetti, H. Rüegger, U. Burckhardt, V. Gramlich, A. D. Del Zotto, P. Martinuzzi, P. Rigo, *Inorg. Chem.* **1997**, *36*, 711−720. − [2l] S. M. Ng, Y. Q. Fang, C. P. Lau, W. T. Wong, G. Jia, *Organometallics* **1998**, *17*, 2052−2059. − [2m] T. P. Fong, A. J. Lough, R. H. Morris, A. Mezzetti, E. Rocchini, P. Rigo, *J. Chem. Soc., Dalton Trans.* **1998**, 2111−2113 and references therein. − [2n] A. C. Ontko, J. F. Houlis, R. C. Schnabel, D. M. Roddick, T. P. Fong, A. J. Lough, R. H. Morris, *Organometallics* **1998**, *17*, 5467−5476. − [2o] J. Huhmann-Vincent, B. L. Scott, G. J. Kubas, *J. Am. Chem. Soc.* **1998**, *120*, 6808−6809. − [2p] T. P. Fong, C. E. Forde, A. J. Lough, R. H. Morris, P. Rigo, E. Rocchini, T. Stephan, *J. Chem. Soc., Dalton Trans.* **1999**, 4475−4486.
[3] W. D. Harman, H. Taube, *J. Am. Chem. Soc.* **1990**, *112*, 2261−2263.
[4] Temperature-dependent correlation time $\tau = \tau_0 e^{Ea/RT}$. Parameters used for the calculated T_1 values: (**1**), $\tau_0 = 2.16 \times 10^{-11}$ s; E_a = 2.43 kcal mol^{-1}; (**2**), $\tau_0 = 3.23 \times 10^{-11}$ s; E_a = 2.24 kcal mol^{-1}; (**3**), $\tau_0 = 2.01 \times 10^{-11}$ s; E_a = 2.34 kcal mol^{-1}; (**4**), $\tau_0 = 3.58 \times 10^{-11}$ s; E_a = 2.07 kcal mol^{-1}; (**5**), $\tau_0 = 3.15 \times 10^{-11}$ s; E_a = 2.17 kcal mol^{-1}; (**6**), $\tau_0 = 3.57 \times 10^{-11}$ s; E_a = 2.15 kcal mol^{-1}; (**7**), $\tau_0 = 1.06 \times 10^{-11}$ s; E_a = 2.65 kcal mol^{-1}.
[5] M. T. Bautista, K. A. Earl, P. A. Maltby, R. H. Morris, C. T. Schweitzer, A. Sella, *J. Am. Chem. Soc.* **1988**, *110*, 7031−7036.
[6] P. J. Desrosiers, L. Cai, Z. Lin, R. Richards, J. Halpern, *J. Am. Chem. Soc.* **1991**, *113*, 4173−4184.
[7] R. H. Morris, R. J. Wittebort, *Magn. Reson. Chem.* **1997**, *35*, 243−250.
[8] A. C. Albeniz, D. M. Heinekey, R. H. Crabtree, *Inorg. Chem.* **1991**, *30*, 3632−3635.
[9] R. H. Morris, in *The Chemistry of the Dihydrogen Ligand in Transition Metal Compounds With Sulfur-donor Ligands, in Transition Metal Sulfides. Chemistry and Catalysis* (Eds.: T. Weber, R. Prins, R. A. van Santen), Kluwer Academic Publishers: London, **1998**.
[10] [10a] J. P. Collman, P. S. Wagenknecht, J. E. Hutchison, N. S. Lewis, M. A. Lopez, R. Guilard, M. L'Her, A. A. Bothner-By, P. K. Mishra, *J. Am. Chem. Soc.* **1992**, *114*, 5654−5664. − [10b] B. Moreno, S. Sabo-Etienne, B. Chaudret, A. Rodriguez-Fernandez, F. Jalón, S. Trofimenko, *J. Am. Chem. Soc.* **1994**, *116*, 2635−2636. − [10c] T. Hasegawa, Z.-W. Li, S. Parkin, H. Hope, R. K. McMullan, T. F. Koetzle, H. Taube, *J. Am. Chem. Soc.* **1994**, *116*, 4352−4356. − [10d] T. A. Luther, D. M. Heinekey, *Inorg. Chem.* **1998**, *37*, 127−132.
[11] D. F. Evans, *Chem. Ind.* **1961**, 1960.
[12] [12a] D. M. Heinekey, T. A. Luther, *Inorg. Chem.* **1996**, *35*, 4396−4399. − [12b] P. A. Maltby, M. Schlaf, M. Steinbeck, A. J. Lough, R. H. Morris, W. T. Klooster, T. F. Koetzle, R. C. Srivastava, *J. Am. Chem. Soc.* **1996**, *118*, 5396−5407. − [12c] W. A. King, X-L. Luo, B. L. Scott, G. J. Kubas, K. W. Zilm, *J. Am. Chem. Soc.* **1996**, *118*, 6782−6783.

[13] D. G. Gusev, R. L. Kuhlman, K. B. Renkema, O. Eisenstein, K. G. Kaulton, *Inorg. Chem.* **1996**, *35*, 6775−6783.

[14] [14a] G. Jia, R. H. Morris, *Inorg. Chem.* **1990**, *29*, 581−582. − [14b] G. Jia, R. H. Morris, C. T. Schweitzer, *Inorg. Chem.* **1991**, *30*, 593−594. − [14c] G. Jia, R. H. Morris, *J. Am. Chem. Soc.* **1991**, *113*, 875−883. − [14d] E. P. Cappellani, S. D. Drouin, G. Jia, P. A. Maltby, R. H. Morris, C. T. Schweitzer, *J. Am. Chem. Soc.* **1994**, *116*, 3375−3388. − [14e] B. Chin, A. J. Lough, R. H. Morris, C. T. Schweitzer, C. D'Agostino, *Inorg. Chem.* **1994**, *33*, 6278−6288.

[15] S. S. Kristjánsdóttir, J. R. Norton, in *Transition Metal Hydrides* (Ed.: A. Dedieu), VCH, Weinheim, Germany, **1992**, Chapter 9, pp 324−334.

[16] G. Perdoncin, G. Scorrano, *J. Am. Chem. Soc.* **1977**, *99*, 6983−6986.

[17] K. Abdur-Rashid, T. P. Fong, B. Greaves, D. G. Gusev, J. G. Hinman, S. E. Landau, A. J. Lough, R. H. Morris, *J. Am. Chem. Soc.* **2000**, *122*, 9155−9171.

[18] C. E. Forde, S. E. Landau, R. H. Morris, *J. Chem. Soc., Dalton Trans.* **1997**, 1663−1664.

[19] [19a] D. F. Shriver, M. A. Drezdon, *The Manipulation of Air Sensitive Compounds*, 2nd edn., Wiley, New York, **1986**. − [19b] S. Herzog, J. Dehnert, K. Luhder, in *Technique of Inorganic Chemistry* (Ed.: H. D. Johnassen), Interscience, New York, **1969**, Vol. VII.

[20] J. Chatt, F. A. Hart, *J. Chem. Soc.* **1960**, 1378−1389.

[21] M. T. Bautista, E. P. Cappellani, S. D. Droudin, R. H. Morris, C. T. Schweitzer, A. Sella, J. Zubkowski, *J. Am. Chem. Soc.* **1991**, *113*, 4876−4887.

[22] D. G. Hamilton, R. H. Crabtree, *J. Am. Chem. Soc.* **1988**, *110*, 4126−4133.

[23] B. Chin, A. J. Lough, R. H. Morris, C. T. Schweitzer, C. D′Agostino, *Inorg. Chem.* **1994**, *33*, 6278−6288.

[24] M. S. Chinn, D. M. Heinekey, N. G. Payne, C. D. Sofield, *Organometallics* **1989**, *8*, 1824−1826.

Received December 21, 2000
[I00485]

Construction and Characterization of Organic-Inorganic Hybridized Molecules with Infinite 2D Grid Network and 1D Zigzag Chain Structures

Wei-Yin Sun,*[a] Bao-Li Fei,[a] Taka-aki Okamura,[b] Wen-Xia Tang,[a] and Norikazu Ueyama[b]

Keywords: Organic-inorganic hybrid composites / Structure elucidation / Supramolecular chemistry / Copper / N ligands

Two coordination polymers with a 2D grid network structure of $[Cu(L1)]NO_3 \cdot H_2O$ (**1**) and $[Cu(L1\text{-}2H)](AcOH)_2 \cdot (C_2H_5)_2O \cdot 4H_2O$ (**2**) were obtained by reaction of the flexible tetradentate ligand 1,2-bis(4′-pyridylmethylamino)ethane (L1) with one mol of $[Cu(CH_3CN)_4]NO_3$ or $Cu(OAc)_2 \cdot H_2O$. The syntheses of a new bridging ligand 1,2-bis(4′-pyridylmethyleneamino)ethane (L2) and its copper(I) complexes are described. When L2 reacts with $[Cu(CH_3CN)_4] \cdot ClO_4$ or $[Cu(CH_3CN)_4] \cdot NO_3$, two interesting complexes with an infinite zigzag chain-like structure $[Cu(L2)(CH_3CN)]NO_3$ (**3**) and $[Cu(L2)(CH_3CN)]ClO_4$ (**4**), involving the coordination of an acetonitrile molecule, were obtained. These coordination complexes were characterized by X-ray crystallography. The results showed that the rigidity of the ligand and the different chemical valence of the transition metal ions have a large effect on the construction of supramolecular frameworks.

Introduction

The metal-ion-directed generation of molecular entities currently provides a very efficient method for the construction of coordination frameworks. Recently, many efforts have been devoted to the investigation of the crystal engineering of one (1D), two (2D) and three-dimensional (3D) coordination polymers.[1,2] However, flexible bridging ligands have not often been employed to construct coordination polymers with transition metal ions, perhaps due to the difficulties in predicting the resulting network structures.[3,4] Previous work has demonstrated that the flexible tetradentate ligand 1,2-bis(4′-pyridylmethylamino)ethane (L1) gives 1D or 2D frameworks depending on the counter anions.[5] In the silver(I) complexes, the structure of $[Ag(L1)]NO_3$ is an infinite 1D hinged cationic chain, while in the case of the complex with a perchlorate anion, $[Ag(L1)]ClO_4 \cdot CH_3CN$ is an infinite 2D cationic network. It is clear that the counter anions play an important role in the construction of these supramolecular complexes.[5] We describe here the reaction of the flexible tetradentate ligand L1 with $[Cu(CH_3CN)_4]NO_3$ and $Cu(OAc)_2 \cdot H_2O$ with the aim of obtaining different network structures by changing the chemical valence of the metal ions.

The generation of supramolecular frameworks is influenced by factors such as the solvent system, templates, counterions, ligand geometry and sometimes the ratio between the metal salt and the ligand.[6–13] In order to add rigidity to L1, we synthesized a new tetradentate ligand 1,2-bis(4′-pyridylmethyleneamino)ethane (L2) (Scheme 1) to detect the influence of the rigidity of the ligand on the supramolecular construction progress.

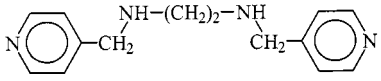

L1

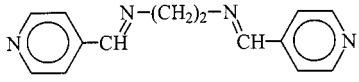

L2

Scheme 1

We report here the assembly of an infinite 2D cationic grid $[CuL1]^+$, an infinite neutral grid network $[Cu(L1\text{-}2H)](AcOH) \cdot (C_2H_5)_2O \cdot 4H_2O$ and two polymeric copper(I) complexes with infinite zigzag chain-like structures $[Cu(L2)(CH_3CN)]NO_3$ and $[Cu(L2)(CH_3CN)]ClO_4$.

Results and Discussion

Synthesis and Reactivity

In principle, supramolecular networks can be obtained by the concurrent action of both extended coordination and hydrogen bonds. We chose to react the flexible tetradentate ligand 1,2-bis(4′-pyridylmethylamino)ethane (L1) with Cu^I and Cu^{II} salts to construct networks by the formation of coordination bonds. The ligand 1,2-bis(4′-pyridylmethyleneamino)ethane (L2) is a di-Schiff base and an analogue of L1. The difference between the L1 and L2 ligands is that L2 is more rigid.

[a] Coordination Chemistry Institute, State Key Laboratory of Coordination Chemistry, Nanjing University,
Nanjing 210093, China
Fax: (internat.) +86-25/331-4502
E-mail: sunwy@netra.nju.edu.cn
[b] Department of Macromolecular Science, Graduate School of Science, Osaka University,
Toyonaka, Osaka 560, Japan

Supporting information for this article is available on the WWW under http://www.eurjic.com or from the author.

 © WILEY-VCH Verlag GmbH, 69451 Weinheim, 2001 1434–1948/01/0707–1855 $ 17.50+.50/0

The polymeric complexes $[Cu(L1)]NO_3·H_2O$ (**1**), $[Cu(L1\text{-}2H)](AcOH)_2·(C_2H_5)_2O·4H_2O$ (**2**), $[Cu(L2)(CH_3CN)]NO_3$ (**3**) and $[Cu(L2)(CH_3CN)]ClO_4$ (**4**) were readily obtained by the reaction of Cu^I or Cu^{II} salts with the ligands L1 and L2 in a molar ratio of 1:1 under mild conditions (see Exp. Section). The elemental C, H and N analysis and X-ray crystal structure analysis confirmed the chemical formulation of these complexes. The complexes **1**, **3** and **4** are stable in the solid state, but not very stable in solution. Crystals of **2** rapidly lose solvent molecules when they are isolated from the reaction mixture.

Crystal Structure Description

The structures of complexes **1**, **2**, **3** and **4** were determined by X-ray crystallography. The crystal and data collection parameters are summarized in Table 1 and selected bond lengths and angles are listed in Table 2.

As shown in Figure 1a, each copper(I) atom in the complex **1** is coordinated by two N atoms of an ethylenediamine unit of one L1, and two N atoms of a pyridyl unit from two other L1 ligands. The coordination geometry of the copper(I) atom is distorted tetrahedral with coordination angles (N−Cu−N) ranging between 85.4(2) to 124.0(3)° and an average Cu−N bond length of 2.082(6) Å (Table 2).

Table 2. Selected bond distances [Å] and angles [deg] for **1**,**2** and **3**

$[Cu(L1)]NO_3·H_2O$ **1**			
Cu(1)−N(11)	2.125(6)	Cu(1)−N(21)	2.122(6)
Cu(1)−N(12)	2.069(6)	Cu(1)−N(22)	2.014(7)
(Cu−N)av		2.082(6)	
N(11)−Cu(1)−N(12)	109.7(2)	N(11)−Cu(1)−N(21)	85.4(2)
N(11)−Cu(1)−N(22)	124.0(3)	N(12)−Cu(1)−N(21)	114.8(3)
N(12)−Cu(1)−N(22)	105.8(3)	N(21)−Cu(1)−N(22)	116.6(3)
$[Cu(L1\text{-}2H)](AcOH)_2·(C_2H_5)_2O·4H_2O$ **2**			
Cu(1)−N(1)	2.032(4)	Cu(1)−N(2)	2.008(4)
(Cu−N)av		2.020(4)	
N(1)−Cu(1)−N(1)[a]	84.2(2)	N(1)−Cu(1)−N(2)	178.4(2)
N(1)−Cu(1)−N(2)[a]	94.1 (2)	N(2)−Cu(1)−N(2)[a]	87.5(2)
$[Cu(L2)(CH_3CN)]NO_3$ **3**			
Cu(1)−N(11)	2.109(3)	Cu(1)−N(12)[b]	2.051(3)
Cu(1)−N(21)	2.044(3)	Cu(1)−N(31)	1.936(3)
(Cu−N)av		2.035(3)	
N(11)−Cu(1)−N(21)	85.0(1)	N(11)−Cu(1)−N(31)	119.5(1)
N(11)−Cu(1)−N(12)[b]	101.0(1)	N(21)−Cu(1)−N(31)	126.2(1)
N(12)[b]−Cu(1)−N(21)	115.6(1)	N(12)[b]−Cu(1)−N(31)	106.1(1)

[a] Equivalent atoms generated by $2-x, y, z$. − [b] Equivalent atoms generated by $-0.5+x, -0.5-y, z$.

Table 1. Crystallographic data for compounds **1, 2** and **3**

	1	**2**	**3**
Empirical formula	$C_{14}H_{20}CuN_5O_4$	$C_{22}H_{40}CuN_4O_9$	$C_{16}H_{17}CuN_6O_3$
M	385.89	568.13	404.89
Crystal system	Orthorhombic	Orthorhombic	Monoclinic
Space group	$P2_12_12_1$	*Cmcm*	$P2_1/a$
a [Å]	10.9975(9)	13.519(2)	9.3258(6)
b [Å]	16.951(2)	12.258(2)	20.632(1)
c [Å]	8.7615(9)	17.975(9)	9.9530(7)
β [°]			113.937(2)
V [Å^3]	1633.3(3)	2978(2)	1750.3(2)
Z	4	4	4
D_c [g·cm^{-3}]	1.569	1.267	1.536
μ [mm^{-1}]	1.376	0.783	1.277
Crystal habit, color	Orange prism	Blue platelet	Orange platelet
Crystal size [mm]	0.20 × 0.20 × 0.05	0.34 × 0.34 × 0.10	0.35 × 0.30 × 0.10
$2\theta_{max}$ [°]	60	55	55
Index range	$-14 \le h \le 14$	$0 \le h \le 17$	$-12 \le h \le 12$
	$-23 \le k \le 23$	$-15 \le k \le 8$	$-26 \le k \le 26$
	$-12 \le l \le 12$	$-23 \le l \le 13$	$-12 \le l \le 12$
Reflns. Collected	8007	2819	6967
Independent reflns.	2910	1835	3873
R_{int}	0.045	0.059	0.068
Obsd. reflns. [$I > 2\sigma(I)$]	1542	558	2653
Parameters refined	218	111	235
R (obsd. data)	0.0701	0.079	0.0467
wR (obsd. data)	0.1608[a]	0.2375[b]	0.1635[c]
Goodness of fit	1.296	0.983	1.316
Residuals [e Å^{-3}]	0.88; −1.44	0.49; −0.84	1.30; −2.67

[a] $\omega = 1/[\sigma^2(F_0)^2 + (0.0500P)^2]$, where $P = (F_0^2 + 2F_c^2)/3$. − [b] $\omega = 1/[\sigma^2(F_0)^2 + (0.1000P)^2]$, where $P = (F_0^2 + 2F_c^2)/3$. − [c] $\omega = 1/[\sigma^2(F_0)^2 + (0.0800P)^2]$, where $P = (F_0^2 + 2F_c^2)/3$.

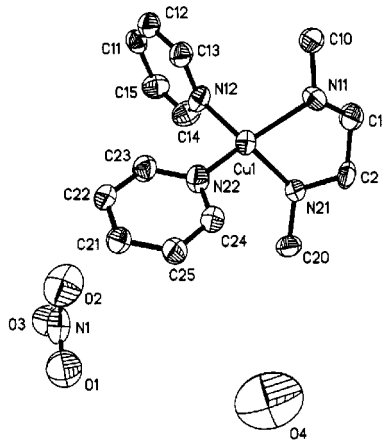

(a)

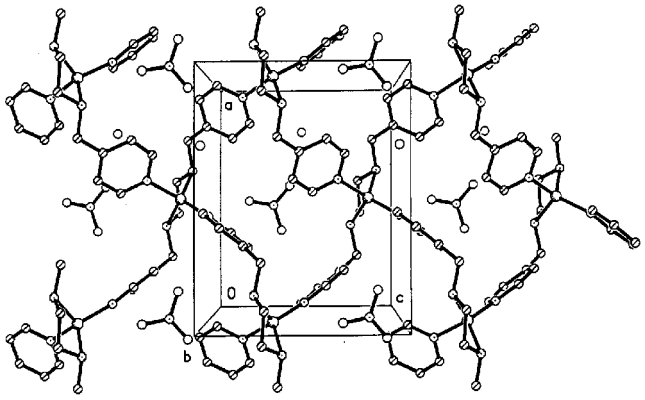

(b)

Figure 1. (a) Crystal structure of $[Cu(L1)]NO_3$ **1** with the ellipsoids drawn at the 50% probability level; (b) infinite grid structure of $[Cu^{I}(L1)]NO_3$ **1**

Complex **1** forms an infinite 2D grid network connected by Cu−N coordination bonds (Figure 1b) in which each L1 ligand has an almost linear conformation with a dihedral angle of 82.5° between the two terminal pyridyl rings of the L1 ligand.1

Complex **1** has one water molecule in the crystal in addition to the nitrate anion, as confirmed by thermogravimetric analysis: the TGA data of complex **1** showed an initial weight loss of 4.9% (calcd. 4.7%) centered at 80 °C, representing the loss of uncoordinated water molecule. The nitrate anions and water molecules are located at the vacancy between the two adjacent cationic layers through two N−H···O and three C−H···O hydrogen bonds as tabulated in Table 3. In the previously reported analog $[Cu(L1)]ClO_4$, there is only one C−H···O hydrogen bond between the ClO_4^- and pyridyl ring of the adjacent ligand.[5] In addition to these hydrogen bonds, there are T-type edge-to-face π-π interactions between pyridine rings which are similar to those of the perchlorate analog, as discussed previously.[5,14]

Table 3. Hydrogen bonds data for complexes **1**, **2** and **3**

D−H···A	Distance of D···A (Å)	Angle of D−H−A (°)
	$[Cu(L1)]NO_3·H_2O$ **1**	
N(11)−H···O(3)[a]	3.107(7)	151.8
N(21)−H···O(2)[b]	3.322(10)	164.6
C(2)−H···O(4)[c]	3.35(2)	148.0
C(10)−H···O(4)[d]	3.393(19)	148.5
C(22)−H···O(1)[e]	3.472(11)	164.1
	$[Cu(L1\text{-}2H)](AcOH)_2·(C_2H_5)_2O·4H_2O$ **2**	
C(5)−H···O(1)	3.164(8)	129.8
C(32)−H···O(4)	2.77(3)	111.9
	$[Cu(L2)(CH_3CN)]NO_3$ **3**	
C(12)−H(6)···N(31)	3.428(6)	168.6
C(14)−H(8)···O(41)[f]	3.502(6)	161.1
C(22)−H(11)···O(43)[g]	3.455(7)	156.9
C(25)−H(14)···N(31)	3.396(6)	143.4

[a] Equivalent atoms generated by $1.5 - x, -y, -0.5 + z$. − [b] Equivalent atoms generated by $0.5 + x, 0.5 - y, 1 - z$. − [c] Equivalent atoms generated by $1 + x, y, z$. − [d] Equivalent atoms generated by $1.5 - x, -y, 0.5 + z$. − [e] Equivalent atoms generated by $0.5 + x, -0.5 - y, -z$. − [f] Equivalent atoms generated by $-0.5 + x, -0.5 - y, 1 + z$. − [g] Equivalent atoms generated by $2.5 - x, 0.5 + y, -z$.

In contrast to the tetrahedral geometry of Cu^{I}, four-coordinate Cu^{II} complexes are usually square planar. After several attempts at reactions between the L1 and Cu^{II} salts with various anions, we finally succeeded in obtaining single crystals of a complex of $Cu(OAc)_2$ with L1, i.e. $[Cu(L1\text{-}2H)](AcOH)_2·(C_2H_5)_2O·4H_2O$ (**2**). The structure around the Cu^{II} atom is shown in Figure 2a, along with the atom numbering scheme. The atoms Cu(1), N(1), N(2), C(1), C(2) and C(3) are all at special positions in the crystallographic mirror plane. The ethylenediamine moiety is deprotonated since all its' atoms are completely coplanar. The existence of acetic acid rather than an acetate anion was confirmed by IR spectroscopy. Each Cu^{II} atom is coordinated by four N atoms from three L1 ligands with a square-planar coordination geometry. The bond lengths of Cu(1)−N(1) and Cu(1)−N(2) are 2.032(4) and 2.008(4) Å, respectively. Each L1 ligand coordinates to three Cu^{II} atoms. Such a coordination mode means that complex **2** forms an infinite 2D network (Figure 2b). It is obvious that the 2D sheet of **2** is different from that of complex **1**, even though they are both grids. First, the sheet of **2** is completely planar and each grid is a square (see Figure 1b and Figure S1 in the Supporting Information) while that of **1** has a corrugated and wavy network structure. In addition, the ligand forms a "V" shape to match the coordination geometry of **2**, while in the case of **1** L1 has an almost linear

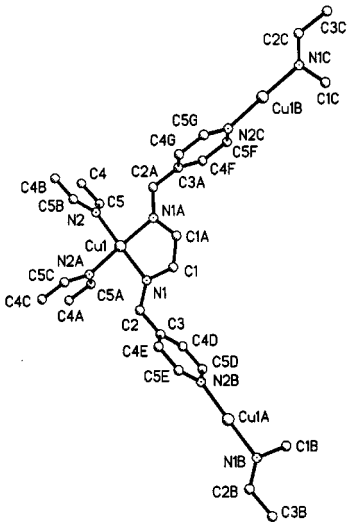

(a)

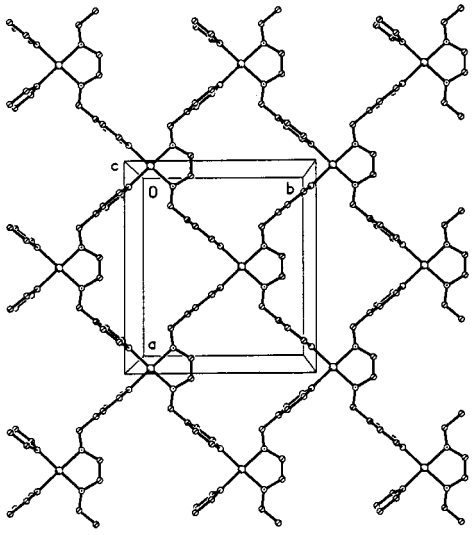

(b)

Figure 2. (a) Crystal structure of the cationic moiety of [Cu(L1-2H)]$(AcOH)_2$·$(C_2H_5)_2O$·$4H_2O$ **2** with atom numbering scheme; (b) infinite 2D grid network of [Cu(L1-2H)]$(AcOH)_2$·$(C_2H_5)_2O$·$4H_2O$ **2**

conformation. The Cu−Cu separation in the square of **2** is 9.12 Å. There are open channels in **2** since the two adjacent sheets are parallel to each other (see Figure S2 in the Supporting Information). The channels are occupied by distorted acetic acid, diethyl ether and water molecules (see Figures S1 and S2 in the Supporting Information). The Cu−Cu distance between two adjacent sheets is 9.40 Å. There are two C(5)−H···O(1) and C(32)−H···O(4) hydrogen bonds (Table 3). Complex **2** rapidly loses diethyl ether in the air; however, the presence of water and acetic acid can be confirmed by thermogravimetric analysis. The TGA data of **2** showed a loss of water and acetic acid centered at 110 and 180 °C, respectively.

We obtained two unexpected infinite zigzag chains **3** and **4** by using a readily prepared ligand L2. The very similar cell parameters of complexes **3** and **4** indicate that they are isomorphous and isostructural. Therefore, only the structure of **3** is described here. The repeat unit of the crystal structure of **3** is illustrated in Figure 3a. Each Cu^I atom is coordinated by two N atoms of the ethylenediimine unit of one L2, a pyridine group of the other L2 and one acetonitrile molecule. The coordination environment of the copper(I) atom is a distorted tetrahedron. The average Cu−N distance of 2.035(3) Å is similar to those (2.02−2.07 Å) of four-coordinate copper(I) complexes,[15] and is shorter than that of complex **1** [2.082(6) Å]. The Cu(1)−N(31) (MeCN) distance of 1.936(3) Å is in the range of reported four-coordinate copper(I) complexes with acetonitrile ligands [1.86−2.26 Å].[16−18] The Cu−Cu separation of 7.54 Å is much longer than that in Cu metal (2.56 Å), and implies no Cu^I−Cu^I interactions in the crystal. The dihedral angle between the two terminal pyridine units of the L2 ligand is 8.6° which is different from that of **1** (82.5°). It has been reported that a di-Schiff base ligand obtained from pyridine-2-carbaldehyde and ethane-1,2-diamine, when reacted with silver(I) complexes, forms a dinuclear double-stranded helical complex.[19]

It is interesting to note that one pyridine unit of the L2 ligand remains uncoordinated, with one acetonitrile molecule coordinating to the Cu^I atom instead. This phenomenon is unusual in tetradentate bridging ligands since the coordination ability of acetonitrile is weaker than that of the pyridine unit. Such a coordination mode gives an extended polynuclear Cu^I cation with a zigzag chain-like structure as illustrated in Figure 3 (b and c). It is noteworthy that each Cu^I atom in **3** is coordinated by three N atoms from two L2 ligands and, in turn, each L2 ligand connects two Cu^I atoms, while in the case of **1**, **2** and other complexes with the L1 ligand, each metal ion is coordinated by four N atoms from three L1 ligand and each L1 ligand connects three metal ions. The nitrate counter ions are located between the two chains by formation of two C−H···O hydrogen bonds between the oxygen atom and pyridyl C−H group (Table 3).

From the present and previous studies it was found that both metal ions and organic ligands have a great influence on the construction of supramolecular frameworks. The reactions between the flexible ligand L1 and Ag^I, Cu^I, Cu^{II} salts with different anions are summarized schematically in Figure 4. It has been reported that different 2D networks can be prepared by reactions of 2,1,3-benzothiadiazoles with copper(I) perchlorate and nitrate due to the different coordination ability of perchlorate and nitrate ions.[20] However, in the case of our copper(I) complexes, the same frameworks were obtained from L1 and $Cu(CH_3CN)_4ClO_4$ and $Cu(CH_3CN)_4NO_3$. This implies that there is no obvious influence of the anions on the formation of networks

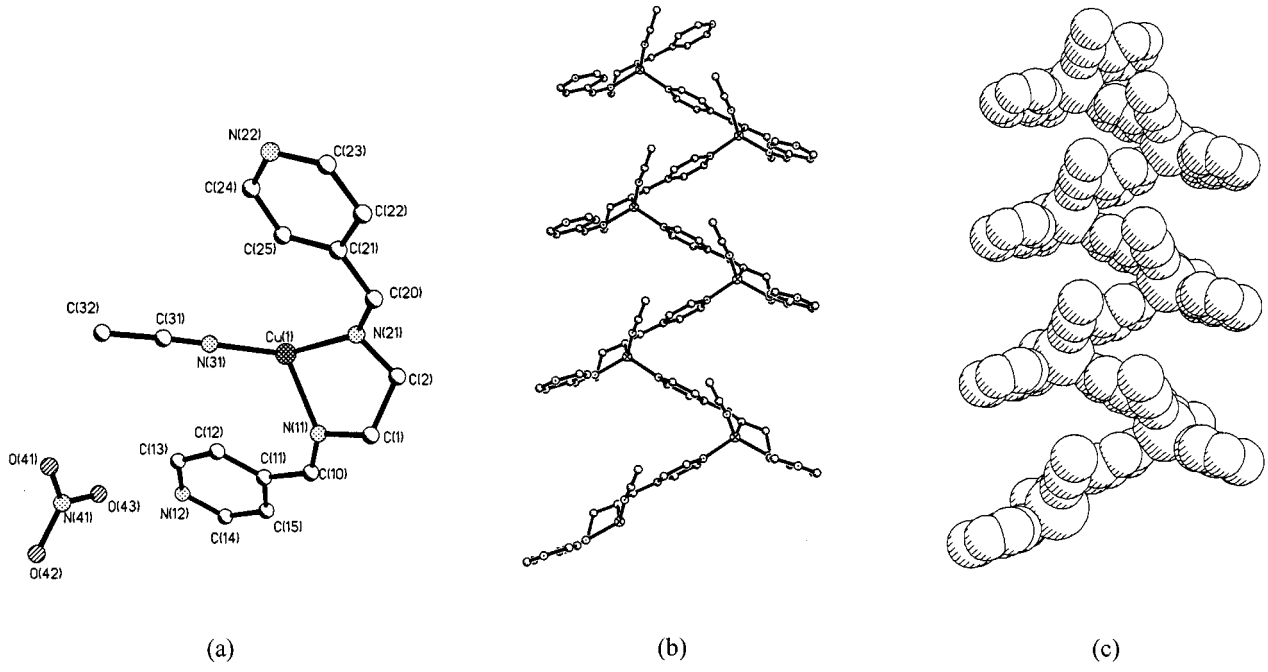

Figure 3. (a) Crystal structure of $[Cu(L2)(CH_3CN)]NO_3$ **3** with atom numbering scheme; (b) part of the single helical structure of **3**; (c) space-filling representation of **3**

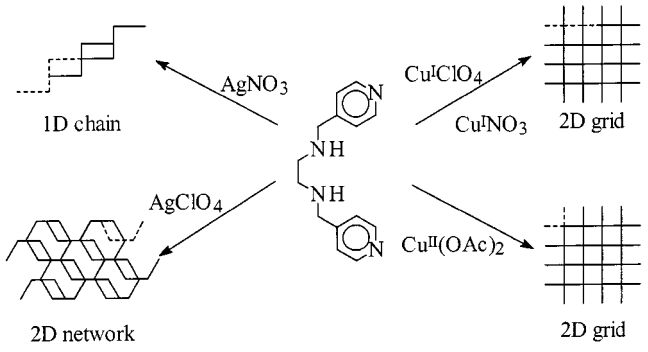

Figure 4. Schematic drawing for reactions between the L1 and Ag^I, Cu^I and Cu^{II} salts; the dashed line refers to one of the L1 ligands

in the Cu^I–L1 system; in the case of silver(I) complexes with the same L1 ligand, 1D and 2D arrays were formed by self-assembly of L1 with silver(I) nitrate and perchlorate, respectively.[5] These results imply that the assembly process is also influenced by the nature of the metal ions. The different structures of complexes **1** and **2** were considered to be caused by the different geometric needs of Cu^I and Cu^{II} ions.

Properties

Powdered samples of the Cu^{II} complex of L1 (**2**) showed photoluminescence with an emission maximum at 430 nm upon excitation at 310 nm. However, no photoluminescence was observed for the Cu^I complex **1**. Powdered **3**, with the di-Schiff base ligand, also showed photoluminescence, with an emission maximum at 391 nm upon excitation at 291 nm. These results indicate that the luminescent properties of the synthesized complexes depend on the nature of the organic ligand and the oxidation state of the metal ions.

The magnetic properties of complex **2** were studied by susceptibility measurements. The effective moment of complex **2** is 1.98 μ_B ($\mu_B \approx 9.27 \times 10^{-24}$ J T^{-1}) at 300 K and 1.73 μ_B at 75 K, which is the same as the spin-only value of 1.73 μ_B expected for isolated Cu^{II} ($S = 1/2$). The slight smooth decrease of μ_{eff} with T shows that a very weak antiferromagnetic exchange is operative due to the large intermetallic distance, as revealed by the X-ray crystal structure.

Conclusion

We have shown that the ligand L1 reacts with $[Cu(CH_3CN)_4]NO_3$ and $Cu(OAc)_2{\cdot}H_2O$ to afford two coordination networks. The two grids of complexes **1** and **2** are slightly different, the ligand in the structure of **1** is linear, whilst in **2** it is in a "V" shape. This is due to the different coordination requirement of the metal ions, which in turn is due to the different ionic radii. These results indicate that even if the same ligand is used, the assembly process may be different due to the different valence of te metal ions. To the best of our knowledge, examples of this are very rare.

The ligand L2 is similar to L1 except for the rigidity: when they react with $[Cu(CH_3CN)_4]NO_3$, the resulting sup-

ramolecular frameworks are very different. One product is an infinite chain structure and the other is a 2D grid network. In addition, complexes of **1** and **2** are stabilized by T-type edge-to-face π-π interactions, whereas no such interactions were observed in the structure of **3**. This suggests that the rigidity of a ligand may have a significant effect on the construction of complexes.

These results imply that the coordination geometry of the ligand and the coordination requirement of the transition metal ion are the primary factors in the construction of supramolecular structures.

Experimental Section

General Methods: All commercially available chemicals were of reagent grade and used as received without further purification. Acetonitrile and ethanol were dried and purified by distillation before use. L1 and $[Cu(CH_3CN)_4]NO_3$ were prepared according to literature methods.[5,21] Samples for C, H and N analyses were dried in vacuum and the analyses were made on a Perkin−Elmer 240C elemental analyzer at the analysis center of Nanjing University. ^1H NMR spectroscopy was performed on a Bruker AM-500 NMR spectrometer, using TMS ($SiMe_4$) as an internal reference at room temperature. Thermogravimetric and differential analyses were taken on a simultaneous SDT 2960 thermal analyzer under N_2 with a heating rate of 10 °C/min. Luminescence spectra were recorded on an Hitachi 850 fluorescence spectrophotometer at room temperature (25 °C). Magnetic measurements on powdered samples were carried out using a CHAN-2000 Faraday magnetometer in the 75 ≈ 300 K temperature range. The apparatus was calibrated with $[Ni(en)_3]S_2O_3$ (en = ethylenediamine). Diamagnetic corrections were made using Pascal's constants.

Synthesis of 1,2-Bis(4′-pyridylmethyleneamino)ethane (L2): 1,2-Ethanediamine (0.53 mL, 7.9 mmol) was dissolved in 30 mL of refluxing absolute methanol and pyridine-4-carbaldehyde (1.41 mL, 15.0 mmol) in 30 mL of absolute methanol was added slowly to give a clear yellowish solution. The mixture was refluxed for 3 h and stirred overnight at ambient temperature. The solvents were removed by evaporation, then 30 mL deionized water was added, and the products were extracted with chloroform (4 × 25 ml). The chloroform solution was evaporated to a syrupy residue under reduced pressure. A powder was obtained by recrystallization of the residue from chloroform and diethyl ether. Washing with diethyl ether and drying in vacuum gave L2 (1.64 g, 92%). − ES-MS: *m/z* = 239.1 $[L2 + H]^+$. − $C_{14}H_{14}N_4$ (238.29): calcd. C 70.56, H 5.92, N 23.51; found C 70.49, H 5.64, N 23.53.

Synthesis of $[Cu(L1)]NO_3·H_2O$ (1): All the procedures for synthesis and spectral measurements were carried out under an argon atmosphere. An acetonitrile solution of $Cu(CH_3CN)_4NO_3$ (0.1 mmol) was added dropwise to a solution of L1 (24.2 mg, 0.1 mmol) in acetonitrile (10 mL) at room temperature to give a clear solution. Orange single crystals (22.1 mg, 40%) suitable for X-ray diffraction were obtained by slow diffusion of diethyl ether into the clear filtrate for several days. − ^1H NMR (CD_3CN, 25 °C): δ = 2.81 (s, 4 H), 3.79 (s, 4 H), 7.36 (br, 4 H), 8.60 (br, 4 H). − $C_{14}H_{18}CuN_5O_3$ (367.87): calcd. C 45.71, H 4.93, N 19.04; found C 45.77, H 5.17, N 19.18.

Synthesis of $[Cu(L1-2H)](AcOH)_2·(C_2H_5)_2O·4H_2O$ (2): A deionized aqueous solution (1 mL) of $Cu(OAc)_2·H_2O$ (19.9 mg, 0.1 mmol) was added dropwise to an ethanol solution (10 mL) of L1 (24.2 mg, 0.1 mmol) at 50 °C and stirred for 20 min. Blue single crystals (45.2 mg, 70%) suitable for X-ray diffraction were obtained by slow diffusion of diethyl ether into the clear filtrate for several days. − $C_{18}H_{28}CuN_4O_6$ (459.99): calcd. C 47.00, H 6.14, N 12.18; found C 47.38, H 6.01, N 11.93. (The diethyl ether and part of water molecules might be lost during the drying process)

Synthesis of $[Cu(L2)(CH_3CN)]NO_3$ (3): The complex was prepared in the same way as complex **1** except that L1 was replaced by L2. Orange single crystals suitable for X-ray diffraction were obtained (25.8 mg, 64%). − $C_{16}H_{17}CuN_6O_3$ (404.89): calcd. C 47.46, H 4.23, N 20.75; found C 47.24, H 4.32, N 20.89.

Synthesis of $[Cu(L2)(CH_3CN)]ClO_4$ (4): The procedure was similar to that of complex **3** except $[Cu(CH_3CN)_4]NO_3$ was changed to $[Cu(CH_3CN)_4]ClO_4$. Orange single crystals were obtained (26.5 mg, 60%). − $C_{16}H_{17}ClCuN_5O_4$ (442.34): calcd. C 43.44, H 3.87, N 15.83; found C 43.65, H 4.19, N 15.76.

X-ray Crystal Structure Analysis for Complexes 1, 2 and 3: The intensity data were collected at −50 °C for **1** and **3** on a Rigaku RAXIS-RAPID Imaging Plate diffractometer. The data collection for **2** was performed on a Rigaku AFC7S automatic four-circle diffractometer at room temperature, using graphite-monochromated Mo-K_α radiation (λ = 0.7107 Å). The structures were solved by direct methods with SIR92,[22] and expanded using Fourier techniques.[23] All data were refined anisotropically by the full-matrix least-squares method for non-hydrogen atoms. The hydrogen atoms were generated geometrically. All calculations were carried out on SGI workstation using the teXsan crystallographic software package of Molecular Structure Corporation.[24]

Crystallographic data (excluding structure factors) for the structures reported in this paper have been deposited with the Cambridge Crystallographic Data Centre as supplementary publication nos. CCDC-154337 (**1**), CCDC-154338 (**2**) and CCDC-154339 (**3**). Copies of the data can be obtained free of charge on application to CCDC, 12 Union Road, Cambridge CB2 1EZ, UK [Fax: (internat.) +44-1223/336-033; E-mail: deposit@ccdc.cam.ac.uk].

Acknowledgments

This work was supported by National Natural Science Foundation of China.

[1] L. Carlucci, G. Ciani, D. M. Proserpio, A. Sironi, *J. Chem. Soc., Dalton Trans.* **1997**, 1801−1803.
[2] M. Munakata, L. P. Wu, T. Kuroda-Sowa, *Adv. Inorg. Chem.* **1998**, *46*, 173−303.
[3] D. M. L. Goodgame, S. Menzer, A. M. Smith, D. J. Williams, *Angew. Chem. Int. Ed. Engl.* **1995**, *34*, 574−575.
[4] P. Losier, M. J. Zaworotko, *Angew. Chem. Int. Ed. Engl.* **1996**, *35*, 2779−2782.
[5] B. L. Fei, W. Y. Sun, K. B. Yu, W. X. Tang, *J. Chem. Soc., Dalton Trans.* **2000**, 805−811.
[6] M. Munakata, L. P. Wu, T. Kuroda-Sowa, M. Maekawa, K. Moriwaki, S. Kitagawa, *Inorg. Chem.* **1997**, *36*, 5416−5418.
[7] M.-C. Hong, W.-P. Su, R. Cao, W.-J. Zhang, J.-X. Lu, *Inorg. Chem.* **1999**, *38*, 600−602.
[8] M. Munakata, L. P. Wu, T. Kurada-Sowa, *Bull. Chem. Soc. Jpn.* **1997**, *70*, 1727−1743.
[9] L. Carlucci, G. Ciani, D. W. Gudenberg, D. M. Prosperpio, A. Siraoni, *Chem. Commun.* **1997**, 631−632.
[10] L. Carlucci, G. Ciani, D. M. Prosperpio, A. Sironi, *Inorg. Chem.* **1995**, *34*, 5698−5700.

[11] M. Kasai, M. Aoyagi, M. Fujita, *J. Am. Chem. Soc.* **2000**, *122*, 2140−2141.
[12] S.-I. Noro, M. Kondo, T. Ishii, S. Kitagawa, H. Matsuzaka, *J. Chem. Soc., Dalton Trans.* **1999**, 1569−1574.
[13] Y. Suenaga, S. G. Yan, L. P. Wu, I. Ino, T. Kuroda-Sowa, M. Maekawa, M. Munakata, *J. Chem. Soc., Dalton Trans.* **1998**, 1121−1125.
[14] [14a] M. Fujita, M. Aoyagi, F. Ibukuro, K. Ogura and K. Yamaguchi, *J. Am. Chem. Soc.* **1998**, *120*, 611−612. − [14b] C. A. Hunter, J. K. M. Sanders, *J. Am. Chem. Soc.* **1990**, *112*, 5525−5534.
[15] P. J. Burke, D. R. McMillin, W. R. Robinson, *Inorg. Chem.* **1980**, *19*, 1211−1214.
[16] E. Lastra, M. P. Gamasa, J. Gimeno, M. Lanfranchi, A. Tiripicchio, *J. Chem. Soc., Dalton Trans.* **1989**, 1499−1506.
[17] J. Díez, M. P. Gamasa, J. Gimeno, A. Tiripicchio, M. T. Camellini, *J. Chem. Soc., Dalton Trans.* **1987**, 1275−1278.
[18] R. O. Gould, A. J. Lavery, M. Schröder, *Chem. Commun.* **1985**, 1492−1493.
[19] P. K. Bower, K. A. Porter, A. D. Rae, A. C. Willis, S. B. Wild, *Chem. Commun.* **1998**, 1153−1154.
[20] M. Munakata, T. Kuroda-Sowa, M. Maekawa, M. Nakamura, S. I. Akiyama, S. Kitagawa, *Inorg. Chem.* **1994**, *33*, 1284−1291.
[21] B. J. Hathaway, D. G. Holah, J. D. Postlethwaite, *J. Chem. Soc.* **1961**, 3215−3218.
[22] SIR92: A. Altomare, M. C. Burla, M. Camalli, M. Cascarano, C. Giacovazzo, A. Guagliardi, G. Polidori, *J. Appl. Cryst.* **1994**, *27*, 435.
[23] DIRDIF94: P. T. Beurskens, G. Admiraal, G. Beurskens, W. P. Bosman, R. de Gelder, R. Israel, J. M. M. Smits, 1994. The DIRFID-94 program system, Technical Report of the Crystallography Laboratory, University of Nijmegen, The Netherlands.
[24] teXsan: Crystal Structure Analysis Package, Molecular Structure Corporation, **1999**.

Received December 28, 2000
[I00487]

Control of the Microarchitecture of a Double Helix – Electrochemical Synthesis and Characterisation of a Novel Dinickel(II) Helicate with Different Groove Sizes

Miguel Vázquez,[a] Manuel R. Bermejo,*[a] Matilde Fondo,[a] Ana M. González,[a] José Mahía,[b] Lorenzo Sorace,[c] and Dante Gatteschi[c]

Dedicated to Professor Rafael Usón on the occasion of his 75th birthday

Keywords: Supramolecular chemistry / Helicates / Nickel / Schiff bases / Electrochemical synthesis

Self-assembly of nickel ions and the N_4 Schiff base **H_2PTs** [**H_2PTs**: *N,N′*-bis(2-tosylaminobenzylidene)-1,3-diaminopropane] in an electrochemical cell leads to the novel neutral double-stranded dinuclear helicate $[NiPTs]_2 \cdot CH_3CN$ (**1**). Complex **1** was fully characterised by elemental analysis, IR and EPR spectroscopy, FAB mass spectrometry, and magnetic measurements. The single X-ray crystal structure of **1** shows that both ligands are asymmetrically positioned around the Ni–Ni axis, leading to a double-helical complex that presents a major and a minor groove.

Introduction

Helicate architectures have received a great deal of attention in recent years mainly due to DNA showing double-helical arrays.[1–8] However, the similarities between the structure of nucleic acids and that of synthetic metallo-helicates are very limited, principally because in most helicates the metal binding units are usually positioned symmetrically and on opposite sides of the helix, leading to two equivalent grooves. Hence, an important challenge of supramolecular chemistry is to design ligand strands that can associate on one side of the helical axis. This should lead to the isolation of asymmetrical helicates, which could be models of DNA structure.

Furthermore, it is highly desirable that these ligands are inexpensive, readily prepared, and easily modified donors, in order to enable wider access to this field. Schiff bases seem to be suitable ligands for this proposal.

By merging these two assumptions, one should try to find direct ways of preparing helical asymmetrical compounds with different groove sizes. However, very little work involving this concept has been published. In 1984 Van Koten et al.[9] described a binuclear $[Ag_2(N_4)_2]^{2+}$ dication with helical structure, where the N_4 donors are not symmetry re lated. More recently, Fabrizzi et al.[10] prepared a bis-iminoquinoline Cu^I helical cation with a certain degree of asymmetry, due to the reciprocal positioning of the ligand strands. It was not until 1999, however, that Hannon et al.[11] emphasised the significance of such asymmetry, and reported a Schiff base silver(I) double helical complex containing a major and a minor groove.

Our studies of the first-row transition metal complexes with imine-based ligands lead us to isolate mono-, di-, or trinuclear helical species.[12–15] As a continuation of this research, and considering that π-stacking interactions between benzylidene groups may provide a suitable tool for controlling the spatial orientation of ligand strands in a double-helical structure,[11] we have designed a new symmetric N_4 Schiff base ligand (see Scheme 1). This ligand contains four acyclic N donor atoms, an acyclic flexible spacer, and terminal bulky groups that should prevent the formation of undesired mononuclear species.[16–18] Furthermore, the Schiff base presents two benzylidene rings fused to the acyclic nitrogen atoms that could give rise to π-stacking interactions, as we have previously observed.[19] This could dictate a non-equivalent wrapping of the ligands around the M···M axis. The reaction of this potential bis-bidentate and dianionic ligand with nickel under electrochemical conditions was studied, and the results achieved are reported herein.

[a] Departamento de Química Inorgánica, Facultade de Química, Universidade de Santiago de Compostela, 15706 Santiago de Compostela, Spain
Fax: (internat.) +34 981 597 525
E-mail: qimb45@usc.es
[b] Servicios Xerais de Apoio á Investigación, Universidade da Coruña, 15071 A Coruña, Spain
[c] Dipartimento di Chimica Generale, Università degli Studi di Firenze, 50144 Firenze, Italy

Results and Discussion

Design and Synthesis of the Ligand

The Schiff base **H_2PTs** [IUPAC name: *N,N′*-bis(2-tosylaminobenzylidene)-1,3-diaminopropane] has been prepared following a three-step procedure (Scheme 1) with a overall yield of 60%. The first step involves the oxidation of the

 © WILEY-VCH Verlag GmbH, 69451 Weinheim, 2001 1434–1948/01/0707–1863 $ 17.50+.50/0

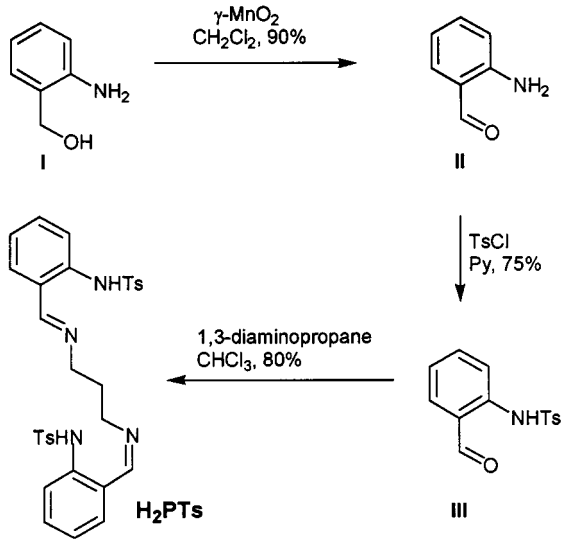

Scheme 1. Synthesis of the ligand $\mathbf{H_2PTs}$

OH group of **I** to give aldehyde **II**. Subsequently, *N*-tosylation of 2-aminobenzaldehyde **II** with tosyl chloride afforded aldehyde **III**.[20] Finally, treatment of **III** with 1,3-diaminopropane in chloroform under reflux conditions gave the N_4 Schiff base ligand $\mathbf{H_2PTs}$.

The yellow powdery solid formed was satisfactorily characterised by elemental analysis, IR, ^{1}H NMR spectroscopy, and FAB mass spectrometry. Besides, the structure of the ligand was known by X-ray diffraction studies.[21] This structure shows that the bulky terminal tosyl groups are *trans* to each other, in order to minimise the steric hindrance. Thus, it seems that the ligand should preferably act as bis-bidentate, spanning two metal centres, and preventing the formation of mononuclear species, in order to avoid the tosyl groups getting closer. In addition, the benzylidene moieties, fused to the N-atoms of different ligands, give rise to π-stacking interactions when the ligand is free. These interactions could be also present in the corresponding complexes, as has been previously observed for similar systems,[19] and could predispose the ligands to associate asymmetrically around the helical axis, leading to helicates with different groove sizes.

Electrochemical Synthesis of the Nickel Complex

Complex **1** was obtained by electrochemical oxidation of a nickel anode in an acetonitrile solution of the ligand $\mathbf{H_2PTs}$, in the presence of a small quantity of tetraethylammonium perchlorate as supporting electrolyte. The cell can be summarised as Pt(−)|H_2PTs + MeCN|Ni(+). This synthetic procedure yields the neutral $[NiPTs]_2$ complex with high purity and in high yield.[12−15,22]

The electrochemical efficiency of the cell E_f was close to 0.5 mol·F^{-1}, which is compatible with the reactions shown in Scheme 2.

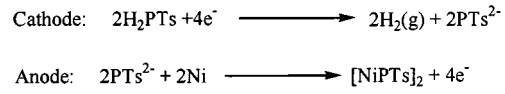

Scheme 2

The green powder nickel complex formed by this synthetic route is insoluble in water and apolar organic solvents, and soluble in common polar organic solvents. It appears to be stable both in the solid state and in solution.

Crystal Structure

Green plate single crystals of $[NiPTs]_2.CH_3CN$ (**1**), suitable for X-ray diffraction studies, were grown by vapour diffusion of diethyl ether into an acetonitrile solution of the powder $[NiPTs]_2$. An Ortep view of the structure is shown in Figure 1. Experimental details are presented in Table 3

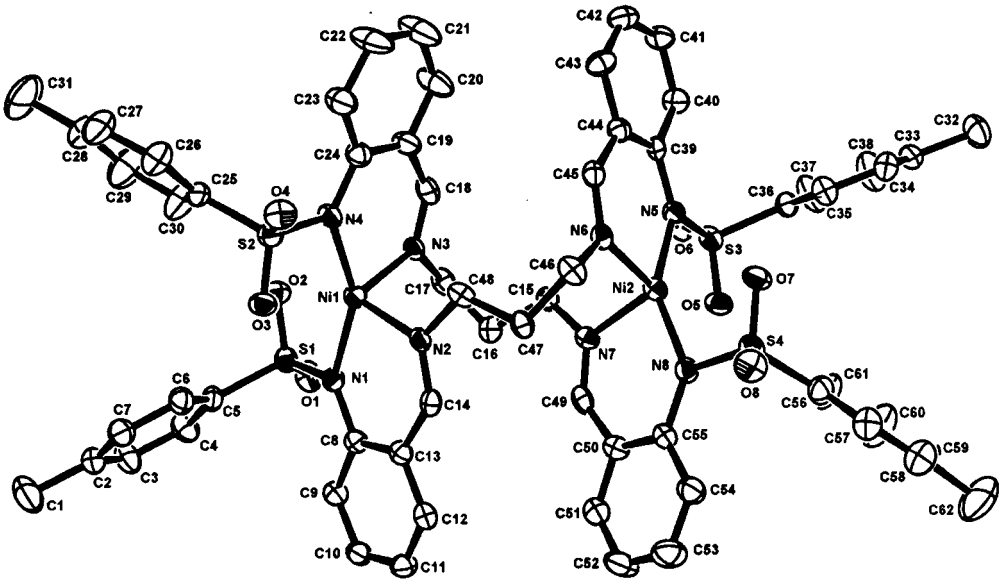

Figure 1. ORTEP view of complex **1** (thermal ellipsoids are drawn at 30% of probability level and hydrogen atoms and solvent molecules have been omitted for clarity)

Table 1. Main bond lengths [Å] for **1**

Ni(1)−N(1)	1.991(5)
Ni(1)−N(2)	1.999(6)
Ni(1)−N(3)	2.017(5)
Ni(1)−N(4)	1.985(5)
Ni(2)−N(5)	1.977(5)
Ni(2)−N(6)	2.016(6)
Ni(2)−N(7)	2.018(6)
Ni(2)−N(8)	1.971(6)

Table 2. Main bond angles [°] for **1**

N(1)−Ni(1)−N(2)	91.7(2)
N(4)−Ni(1)−N(1)	151.7(2)
N(4)−Ni(1)−N(2)	103.9(2)
N(4)−Ni(1)−N(3)	91.5(2)
N(2)−Ni(1)−N(3)	101.0(2)
N(1)−Ni(1)−N(3)	108.8(2)
N(8)−Ni(2)−N(5)	149.8(2)
N(8)−Ni(2)−N(6)	107.6(2)
N(5)−Ni(2)−N(6)	91.9(2)
N(8)−Ni(2)−N(7)	91.7(2)
N(5)−Ni(2)−N(7)	106.2(2)
N(6)−Ni(2)−N(7)	103.5(2)

and selected bond lengths and angles in Table 1 and Table 2.

The asymmetric unit contains a $[NiPTs]_2$ molecule with two acetonitrile solvates at 0.5 occupancy. The compound is a binuclear nickel complex, with the ligands spanning both metal centres, and intertwined to give a double helix. Both enantiomers (left- and right-handed) are observed in the unit cell.

Each ligand uses both nitrogen atoms of one binding moiety [N(1), N(2); N(3), N(4)] to coordinate one metal centre [Ni(1)]. The remaining imine nitrogen [N(6), N(7)] and amide nitrogen [N(5), N(8)] atoms of the second binding units of both $[PTs]^{2-}$ coordinate the second nickel atom [Ni(2)]. Thus, the environment of the metal centres can be described as distorted tetrahedral, with both ligands acting as bisbidentate N_4 donors. This distortion is shown by the angles between nitrogen and nickel atoms, which range from 91.7(2)° to 151.7(2)° for Ni(1) and from 149.8(2) to 91.7(2) for Ni(2). The longer angles [151.7(2)° and 149.8(2)°] are those between nickel and the amide nitrogen atoms, and this seems to be the result of the attempt to minimise the steric hindrance between the tosyl groups.

This tetrahedral geometry is quite unusual for dinickel helical complexes, where the nickel atom is usually six-coordinated.[13−14,23−25] Thus, in nickel complexes with imine-based ligands of the hydrazone type, composed by two bidentate arms and a spacer with a donor atom, two different possibilities of reaching the coordination number 6 have been described.[13−14,23] The most general one is the linking of two bidentate arms and two central donor atoms, which act as bridges, to the same metal atom.[13−14,23] When this type of complex is recrystallised in a donor solvent, the central bridges break and the donor atoms of the spacers are now linked to only one metal centre, acting as terminal donors. This would lead to a coordination number of six for one metal atom and to a coordination number of four for the other one. The two free coordination positions of the second nickel atom are now filled by donor solvent molecules, giving rise to a [6 + 4 + (2)] helix.[13−14]

However, when the ligand does not contain a donor atom in the spacer group, the octahedral environment with bis-bidentate Schiff bases is normally achieved by simultaneous coordination of three strands to two metal centres. Thus, the most common nickel helical complexes with Schiff bases described in literature are the dinuclear triple helical ones.[24−25] In this case study, two factors can prevent the coordination of a third [H_2PTS] ligand or solvent molecules in order to achieve a coordination number six: 1) the steric hindrance of the bulky tosyl groups; 2) the closeness of some of the tosyl oxygen atoms to Ni(1) [O(2) and O(3)] and Ni(2) [O(5) and O(7)]. These distances of ca. 2.5 Å seem to indicate that one oxygen atom of each tosyl group is weakly interacting with one metal atom. Thus, the aforementioned distances could be taken as secondary intramolecular bonds, since they are too long to be considered true coordinated bonds. This fact could have a profound influence on the adopted tetrahedral geometry, as maybe these oxygen atoms are too close to the nickel centres to allow any other ligand to complete their environment requirements.

Each ligand forms two six-membered chelate rings, one around each metal atom, which are nearly planar, with angles between the chelate rings of 85.75° and 80.18° around Ni(1) and Ni(2), respectively. The Ni−N(imine) bond lengths [Ni(1)−N(2) = 1.999(6) Å, Ni(1)−N(3) = 2.017(5) Å, Ni(2)−N(6) = 2.018(6) Å, and Ni(2)−N(7) = 2.018(6) Å] are shorter than those found for octahedral triple dinickel helicates with Schiff bases.[25] This could be a reflection of the lower coordination number in the latter complexes. The same occurs with the Ni−N(amide) bonds [Ni(1)−N(1) = 1.991(5) Å, Ni(1)−N(4) = 1.985(5) Å, Ni(2)−N(5) = 1.977(6) Å, and Ni(2)−N(8) = 1.971(6) Å], which are shorter than the Ni−Ni(amide) distances found for hexa-coordinated nickel Schiff base complexes containing the NTos radical.[26] The Ni(1)···N(2) distance of 6.207 Å is shorter than the ones reported for nickel triple helical complexes[24−25] (about 11 Å), but longer than the ones for double helical nickel complexes with hydrazone ligands,[13−14,23] as was expected.

All these distances and angles also show the non-equivalence of the environment of the nickel atoms and of both Schiff bases, giving rise to a certain degree of asymmetry. This asymmetry leads to the formation of two grooves of different size. The two distinct grooves (major and minor) seem to be exacerbated by aromatic π-stacking interactions between the benzylidene rings of the binding moieties. Two interactions of different strength can be observed between aromatic rings of different ligand strands, as is shown in Figure 2. From now we will call A and B the two benzylidene rings of the dark strand, and C and D those of the light strand. Interaction between A and D (Figure 2, left) gives

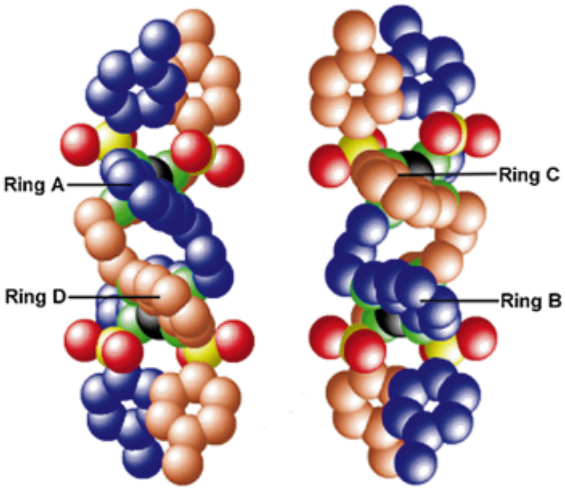

Figure 2. Space-filling representation of complex **1**, showing the minor (left) and major (right) grooves. Both representations correspond to the same enantiomer, turned 180°

rise to distances of 2.455−3.179 Å between the atoms of A and mean plane of D, with an angle between their least-square planes of 16.0°. Similarly, C overlaps with B (Figure 2, right) leading to a longer distance (2.682−3.755 Å) and to a bigger acute angle (25.2°). Thus, to the best of our knowledge, this is the first example where π-stacking interactions between aromatic rings of the binding moieties (not of the spacer group) control the micro-architecture of the helix, and lead to an asymmetrical double-stranded helicate with a major and a minor groove.

However, no specific π-stacking interactions (face-face or face-edge π-π) are identifiable between the terminal tosyl aromatic rings, which probably appear separated to minimize the steric repulsion.

Finally, the helical turn, defined as the angle subtended by the centroids of the inner benzylidene rings of the ligand along the Ni−Ni axis (helical axis), are 174.8° and 179.6° for each strand.

IR Spectroscopy and FAB Mass Spectrometry

The IR spectra of **1** shows a strong band at ca. 1625 cm^{-1} due to the imine ν(C=N) mode, which exhibit a shift of 10 cm^{-1} to lower energy from the free ligand value, indicative of coordination of the ligand to nickel. In addition, the band due to ν(C−N) mode undergoes a negative shift (1303 vs. 1340 cm^{-1} in the free ligand). This behaviour is compatible with the participation of both imine an amide nitrogen atoms in the coordination to nickel centres.[27−28]

The FAB mass spectrum of **1** presents a peak at m/z = 646 due to the fragment $[NiPTs]^+$, that confirms the coordination of the ligand to the metal centre. Besides a prominent peak at m/z = 1292 is assigned to the fragment $[NiPTs]_2^+$, which seems to indicate a dinuclear nature of complex **1**, as the X-ray structure shows.

Magnetic and EPR Characterisation

Nickel(II) tetrahedral complexes usually exhibit a large magnetic moment, due to the largely unquenched orbital momentum; this is usually observed together with a large dependence of the magnetic moment on temperature. However, distortion from ideal tetrahedral symmetry may remove the orbital degeneration of the ground state, thus reducing both the temperature dependence and the absolute value of the magnetic moment.[29−31]

The high temperature value of the magnetic moment of **1** (1.36 emu K per mol of Ni^{2+}at 280 K) is quite low for a tetrahedral nickel(II), thus indicating that, as expected from the structural data, large distortions from tetrahedral symmetry are active in reducing the orbital contribution to the magnetic moment. The temperature dependence of the product (shown in Figure 3) is quite small. In agreement with this interpretation, on lowering the temperature, χT slowly decreases to 1.20 emu K per mol of Ni^{2+} centre at 22 K. Only below this temperature does it drop until it reaches 0.32 emu K mol^{-1} at 2 K. As the two tetrahedral units of Ni^{2+} are quite far from each other (6.207 Å), and there are no bridging ligands capable of transmitting the exchange coupling interaction between them, it seems reasonable to attribute this behaviour to a large Zero Field Splitting of the $S = 1$ ground state, which is a well-known characteristic of nickel(II) complexes.

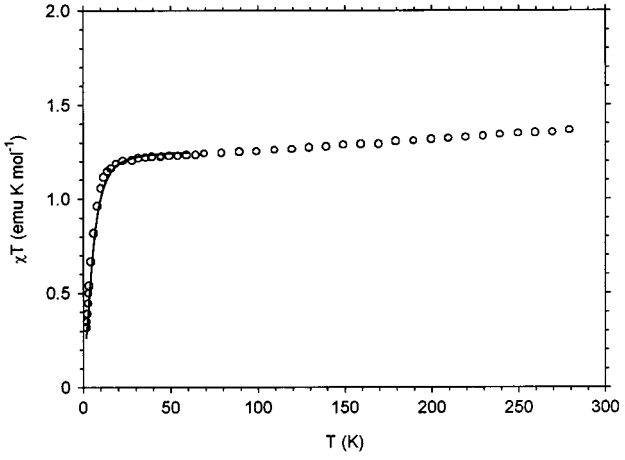

Figure 3. Plot of χT versus T for **1**, in the range 2−280 K

This hypothesis was confirmed both by the absence of any X-Band EPR signal at 4.2 K, and by the behaviour of the M vs. H curve, measured at 3 K. As shown in Figure 4, the magnetisation is slowly increasing with the field and it

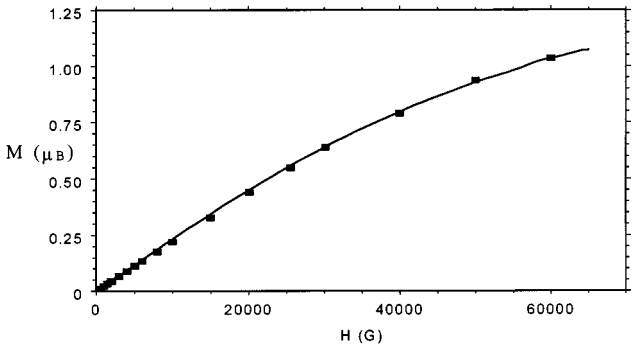

Figure 4. Magnetisation plot (M) versus H for **1**

is still far from saturation at 6.0 T (1.04 μ_B per Ni^{2+}). The magnetisation curve was fairly well reproduced (Figure 4, continuous line) assuming a D value of 13.0±0.2 cm^{-1} and a g value of 2.20±0.03, in agreement with what was expected for Ni^{2+}. Assuming the same parameters, we were then able to reproduce (Figure 3, continuous line) the low temperature part of the χT curve. The large D value may be due to the presence of low-lying excited states admixed through spin-orbit coupling. As far as the slight difference in the two tetrahedral units is concerned, it should be stressed that these parameters represent an average between the values of each single centre.

Conclusion

This work shows that careful selection and design of Schiff base ligands can yield helical nickel complexes. The presence of bulky terminal groups in the N_4 donor **H_2PTs** described herein constrains the ligand to act as binucleating. Besides, the presence of benzylidene moieties in the ligand strands seems to play a fundamental role in the asymmetrical structure of the helix. Thus, a neutral double-stranded dinickel helical complex, so scarce in literature, can be isolated by means of the electrochemical synthesis. In addition, internal π-stacking interactions between ligand binding domains control the micro-architecture of the double helix, leading to a helicate with different size grooves, reminiscent of DNA structure.

Variation of the length and rigidity of the spacer, as well as studies of further factors that can affect the spatial orientation of ligand strands in metallo-supramolecular compounds, are in progress in our laboratory.

Experimental Section

Elemental analysis was performed on a Carlo Erba EA 1108 analyser. − The NMR spectra were recorded on a Bruker WM-250 spectrometer using $CDCl_3$ as solvent. − Infrared spectra were recorded as KBr pellets on a Bio-Rad FTS 135 spectrophotometer in the range of 4000−600 cm^{-1}. − Mass spectrometry (FAB) was performed on a Micromass Autospec mass spectrometer, employing *m*-nitrobenzyl alcohol as a matrix. − The EPR spectrum of **1** was recorded using a Varian ESR9 spectrometer equipped with a ^{4}He continuous flow cryostat. − Magnetic measurements between 2 and 280 K were performed using a Cryogenics Squid magnetometer with field up to 6.5 T. The data were corrected for sample holder contribution and diamagnetism of the sample using Pascal constants.

Syntheses: All the starting materials were purchase from Aldrich and used without further purification. 2-tosylaminobenzaldehyde **III** was prepared according to a method previously reported in literature,[20] as shown in Scheme 1.

***N,N′*-Bis(2-tosylaminobenzylidene)-1,3-diaminopropane (H_2PTs):** To a solution of 2-tosylaminobenzaldehyde **III** (5.0 g, 18.2 mmol) in chloroform (150 mL) 1,3-diaminopropane (0.8 mL, 9.1 mmol) was added and the mixture was heated under reflux. The volume of the solution was reduced over a 4 h period to ca. 50 mL, using a Dean−Stark trap, and was then allowed to cool. The resultant yellow solution was concentrated to ca. 10 mL. The solid, which precipitated, was collected by filtration, washed with diethyl ether (3 mL) and dried in vacuo. Yield 4.3 g (80%). m.p.: 145 °C. − $C_{31}H_{32}N_4O_4S_2$ (588.8): calcd. C 63.24, H 5.48, N 9.52, S 10.89; found C 63.0, H 5.3, N 9.4, S 10.5. FAB-MS: m/z = 589.2 [M^+]. − ^{1}H NMR (250 MHz, $CDCl_3$, ppm): δ = 13.0 (s, 2 H), 8.4 (s, 2 H), 7.7 (d, 4 H), 7.6 (d, 2 H), 7.2 (m, 6 H), 7.1 (d, 2 H), 7.0(dt, 2 H), 3.8 (t, 4 H), 2.3 (s, 6 H), 2.2 (q, 2 H). − IR (KBr, cm^{-1}): ν(C=N) 1635 s, ν(C−N) 1340 s, $\nu_{as}(SO_2)$ 1287 s, $\nu_s(SO_2)$ 1163 s.

[NiPTs]$_2$: A solution of H_2PTs (0.2 g, 0.3 mmol) in acetonitrile (80 mL), containing 10 mg of tetramethylammonium perchlorate as supporting electrolyte, was electrolysed for 3.6 h using a current of 5 mA and 7.2 V. Concentration of the resultant solution to a third of its initial volume yielded a green solid that was washed with diethyl ether and dried in vacuo. Yield: 0.2 g (86%). − $C_{62}H_{60}N_8Ni_2O_8S_4{\cdot}CH_3CN$ (1333.9): calcd. C 57.7, H 4.7, N 9.5, S 9.6; found C 58.0, H 4.6, N 9.5, S 9.8. FAB-MS, m/z (%) = 646 (54, NiPTs), 1292 (42, Ni_2PTs_2). − IR (KBr, cm^{-1}): ν(C=N) 1625 s, ν(C−N) 1303 s, $\nu_{as}(SO_2)$ 1260 s, $\nu_s(SO_2)$ 1129 s.

Recrystallisation of the green powder in acetonitrile yields crystals of [NiPTs]$_2{\cdot}CH_3CN$ **1** suitable for X-ray diffraction studies.

CAUTION: Perchlorate salts are potentially explosive and should therefore be handled with the appropriate care.

X-ray Crystallography: Crystals of **1** suitable for X-ray diffraction studies were grown as previously detailed. X-ray data were collected on a Siemens SMART CCD area-detector diffractometer with graphite monochromated Mo-K_α radiation (λ = 0.71073 Å) operating at room temperature, using ω scans (Table 3). The structure was solved by direct methods[32] and refined by full-matrix least-squares on F^2. Absorption and incident beam corrections were applied (SADABS). All non-hydrogen atoms were refined anisotropically. All hydrogen atoms were included in the model at geometrically calculated positions and refined using a riding model.

Crystallographic data (excluding structure factors) for the structure reported in this paper have been deposited with the Cambridge Crystallographic Data Centre as supplementary publication no. CCDC-142926. Copies of the data can be obtained free of charge

Table 3. Crystal data and details of the structure determination of **1**

Empirical formula	$C_{64}H_{63}N_9Ni_2O_8S_4$
Molecular weight [g/mol]	1331.89
Crystal system	monoclinic
Space group	$P2(1)/c$
a [Å]	18.941(1)
b [Å]	24.802(1)
c [Å]	15.580(1)
β [°]	108.88°
V [A^3]	6970.2(2)
Z	4
$D_{calcd.}$ [Mg/m^3]	1.269
F(000)	2776
μ [mm^{-1}]	0.716
Crystal size [mm]	0.40 × 0.25 × 0.05
Crystal colour	green
Reflections collected/unique	24294/11983
Restraints	6
Parameters	811
Goodness-of-fit on F^2	1.006
Final $R1$, $wR2$ [$I > 2\sigma(I)$][a]	0.0692, 0.1391
Final $R1$, $wR2$ [all data]	0.1869, 0.1936

[a] $R1 = \Sigma||F_0| - |F_c||/\Sigma|F_0|$; $wR2 = \{\Sigma[w(F_0^2 - F_c^2)^2]/\Sigma[w(F_0^2)^2]\}^{1/2}$.

on application to CCDC, 12 Union Road, Cambridge CB2 1EZ, UK [Fax: (+44)1223/336-033; E-mail: deposit@ccdc.cam.ac.uk].

Acknowledgments

The authors thank Xunta de Galicia (PGIDT99PXI20903B) and 3MD EU Network (contract no. ERB 4061 PL 97-0197) for financial support. M.V. thanks the Fundación Segundo Gil Dávila for a grant. M.V. also thanks Professor Rafael Ruiz for his unselfish help during the realisation of this work.

[1] J. M. Lehn, *Supramolecular Chemistry-Concepts and Perspectives*, VCH, Weinheim, **1995**.
[2] E. C. Constable, in: *Comprehensive Supramolecular Chemistry*, vol. 9 (Eds.: J. P. Sauvage, M. W. Hosseini). Pergamon Press, Oxford, **1996**, 213−252.
[3] D. Philp, J. F. Stoddart, *Angew. Chem. Int. Ed. Engl.* **1996**, *35*, 1154−1196.
[4] C. Piguet, G. Bernarddinelli, G. Hopfgartner, *Chem. Rev.* **1997**, 2005−2062.
[5] M. Albrecht, R. Fröhlich, *J. Am. Chem. Soc.* **1997**, *119*, 1656−1661.
[6] J. S. Fleming, K. L. V. Mann, S. M. Couchman, J. C. Jeffery, J. A. McClevery, M. D. Ward, *J. Chem. Soc., Dalton Trans.* **1998**, 2047−2052.
[7] R. W. Saalfrank, I. Bernt, *Curr. Opin. Solid State Mater. Sci.* **1998**, *3*, 407−412.
[8] J. Xu, T. N. Parac, K. N. Raymond, *Angew. Chem. Int. Ed.* **1999**, *38*, 2878−2882.
[9] G. C. van Stein, G. van Koten, K. Vrieze, C. Brevard, A. L. Spek, *J. Am. Chem. Soc.* **1984**, *106*, 4486−4492.
[10] V. Amendola, L. Fabbrizzi, L. Linati, C. Mangano, P. Pallavicini, V. Pedrazzini, M. Zema, *Chem. Eur. J.* **1999**, *5*, 3679−3688.
[11] M. J. Hannon, C. L. Painting, N. W. Alcock, *Chem. Commun.* **1999**, 2023−2024.
[12] J. Sanmartín, M. R. Bermejo, A. García-Deibe. O. Piro, E. E. Castellano, *Chem. Commun.* **1999**, 1953−1954.
[13] M. R. Bermejo, M. Fondo, A. M. González, O. L. Hoyos, A. Sousa, C. A. McAuliffe, W. Hussain, R. Pritchard, V. M. Novotorsev, *J. Chem. Soc., Dalton Trans.* **1999**, 2211−2217.
[14] M. R. Bermejo, A. Sousa, M. Fondo, A. M. González, O. L. Hoyos, R. Pedrido, M. Maestro, J. Mahía, *Z. Anorg. Allg. Chem.* **2000**, *626*, 506−513.
[15] O. L Hoyos, M. R. Bermejo, M. Fondo, A. García-Deibe, A. M. González, M. Maneiro, R. Pedrido, *J. Chem. Soc., Dalton Trans.* **2000**, 3122−3127.
[16] N. A. Bailey, E. D. McKenzie, J. M. Worthington, *J. Chem. Soc., Dalton Trans.* **1974**, 1363−1366.
[17] N. A. Bailey, E. D. McKenzie, *Inorg. Chim. Acta.* **1980**, *43*, 205−210.
[18] G. Brewer, J. Jasinski, W. Mahany, L. May, S. Prytkov, *Inorg. Chim. Acta.* **1995**, *232*, 183−187.
[19] [19a] N. Aurangzeb, C. E. Hulme, C. A. McAuliffe, R. G. Pritchard, M. Watkinson, M. R. Bermejo, A. García-Deibe, J. Sanmartín, A. Sousa, *J. Chem. Soc., Chem. Commun.* **1994**, 1153−1155. − [19b] M. R. Bermejo, M. Fondo, A. García-Deibe, M. Rey, J. Sanmartín, A. Sousa, M. Watkinson, C. A. McAuliffe, R. G. Pritchard, *Polyhedron* **1996**, *15*, 4185−4194. − [19c] J. Sanmartín, M. R. Bermejo, A. M. García-Deibe, I. M. Rivas, A. R. Fernández, *J. Chem. Soc., Dalton Trans.* **2000**, 4174−4181.
[20] N. I. Chernova, Y. S. Ryabokobylko, V. G. Brudz, B. M. Bolotin, *Zh. Neorg. Khim.* **1971**, 1680−1684.
[21] J. Mahía, M. Maestro, M. Vázquez, M. R. Bermejo, J. Sanmartín, M. Maneiro, *Acta Crystallogr., Sect. C* **1999**, *55*, 1545−1547.
[22] J. Sanmartín, M. R. Bermejo, A. M. García-Deibe, A. L. Llamas-Saiz, *Chem. Commun.* **2000**, 795−796.
[23] G. Paolucci, S. Stelluto, S. Sitran, D. Ajo, F. Benetollo, A. Polo, G. Bombieri, *Inorg. Chim. Acta*, 1992, **193**, 57−75.
[24] M. J. Hannon, C. L. Painting, A. Jackson, J. Hamblin, W. Errington, *Chem. Commun.* **1997**, 1807−1808.
[25] H. Cheng, D. Chun-ying, F. Chen-jie, M. Qing-jin, *J. Chem. Soc., Dalton Trans.* **2000**, 2419−2424.
[26] M. R. Bermejo, A. Sousa, M. Fondo, M. Helliwell, *New. J. Chem.* **2000**, *24*, 33−41.
[27] K. Nakamoto in *Infrared and Raman Spectra of Inorganic and Coordination Compounds.* John Wiley & Sons, New York, **1997**.
[28] L. J. Bellamy, in: *Advances in Infrared Group Frequencies.* Methuen & Co., **1969**.
[29] A. Bencini, F. Mani, L. Sacconi, in: *Comprehensive Coordination Chemistry*, vol. 5 (Eds.: G. Wilkinson, R. D. Gillard, J. Mc Cleverty). Pergamon Press, **1987**.
[30] M. Gerloch, D. A. Cruse, *J. Chem. Soc., Dalton Trans.* **1977**, 152−159.
[31] M. Gerloch, D. A. Cruse, *J. Chem. Soc., Dalton Trans.* **1977**, 1613−1617.
[32] G. M. Sheldrick, *SHELX-97* (*SHELXS 97* and *SHELXL 97*), Programs for Crystal Structure Analyses, University of Göttingen, Germany, **1998**.

Received October 10, 2000
[I00383]

Functionalization of Cage Amines with Pendant Aromatic and Heteroaromatic Substituents

Stephen Burnet,[a] Min-Ho Choi,[b] Paul S. Donnelly,[a] Jack M. Harrowfield,*[a] Irina Ivanova,[a] Seong-Hoon Jeong,[b] Yang Kim,[b] Mauro Mocerino,[a] Brian W. Skelton,[c] Allan H. White,[c] Charlotte C. Williams,[a] and Zhi-Ling Zeng[a]

Keywords: Cage amines / Functionalization / Polymers / Electrochemistry

Structural studies have confirmed that it is possible to exploit the relatively low nucleophilicity of the "external" amino substituents on the Co^{III} complex of 1,8-diaminosarcophagine ("sarcophagine" = sar = 3,6,10,13,16,19-hexaazabicyclo[6.6.6]-icosane) in acylation and alkylation reactions leading to a variety of functionalized cage amine complexes. With the appropriate choice of solvent, all these reactions can be conducted with high efficiency, and the new complexes display properties foreshadowing the application of cage systems in, for example, electroactive polymers.

Introduction

The presence of external functional groups on the metal complexes of the very readily obtained cage amine "diaminosarcophagine" {1,8-diamino-3,6,10,13,16,19-hexaazabicyclo[6.6.6]icosane = $(NH_2)_2$sar},[1] has led to the exploration of reactions of these groups to generate derivatives offering a variety of possible applications.[2] Our interests in this area include the incorporation of $[M\{(NH_2)_2sar\}]^{n+}$ (M = metal) units into amide polymers and the use of cage complexes as electrocatalysts, and so we have been particularly interested in acylation reactions of $[M\{(NH_2)_2sar\}]^{n+}$, as well as in processes whereby potentially electroactive groups can be introduced into such complexes. A known difficulty with reactions of amino groups attached to a cationic complex ion centre is that the nucleophilicity of these groups may be strongly reduced by the proximity of the positive site.[1−6] Carboxymethylation reactions of $[Cu\{(NH_2)_2sar\}]^{2+}$, for example, proceed considerably more rapidly than those of $[Co\{(NH_2)_2sar\}]^{3+}$, although such reaction studies have also demonstrated the utility of metal ion coordination in controlling the extent and position of substitution.[6] In the present work, we explore the use of cobalt(III) complexes of cage amines in reactions that may provide models for polymer formation processes or produce materials that may be converted into polymers by electrochemical means. Thus, we have examined reactions at the external amino groups leading to the formation of amide and imide derivatives or to the attachment of groups with electropolymerizable substituents (or with substituents readily functionalized for the purpose of subsequent polymerization).

[a] Research Centre for Advanced Mineral and Materials Processing and Chemistry Department, University of Western Australia,
Nedlands, WA 6907, Australia
Fax: (internat.) +61−8 9380−1116
E-mail: jmh@chem.uwa.edu.au
[b] Department of Chemistry, Kosin University,
Yeongdo-gu, Pusan, 606−701, Korea
[c] Crystallography Centre and Department of Chemistry, University of Western Australia,
Nedlands, WA 6907, Australia

Results and Discussion

Structural studies based on X-ray crystallography were an essential component of the present work, not only for the purpose of defining the nature of the species isolated but also to characterize the mutual influences of the core cage complex and the peripheral substituents upon one another. Certain aspects of the solid-state structures are nonetheless familiar from earlier extensive studies of simpler cage amine complexes,[1−8] so that in general we comment only briefly on the cage stereochemistry and on the interactions of counteranions with coordinated NH atoms. For convenience, the Co(sarcophagine) units in all the structures determined (Figure 1) are shown in the Δ configuration, though in fact all syntheses were conducted with racemic reactants and all crystals proved to be racemic compounds. In cases where the cage substituents were acidic or basic in nature, the localization of protons was sometimes problematic and the models presented as "best" must be regarded as tentative. It is possible, of course, that the species considered to be immobilized within the solids are not those dominant in solution, though the forms of association seen in the solids, while predictable, are nonetheless useful in considering modes that may influence solution behaviour.

The rapid electron-transfer reactions and kinetic inertness in more than one oxidation state of many cage amine complexes makes the incorporation of these entities into insoluble polymers of possible interest, for example, in constructing novel rechargeable battery systems.[9] Polyamide formation from $[M\{(NH_2)_2sar\}]^{n+}$ units would seem an

 © WILEY-VCH Verlag GmbH, 69451 Weinheim, 2001 1434−1948/01/0707−1869 $ 17.50+.50/0

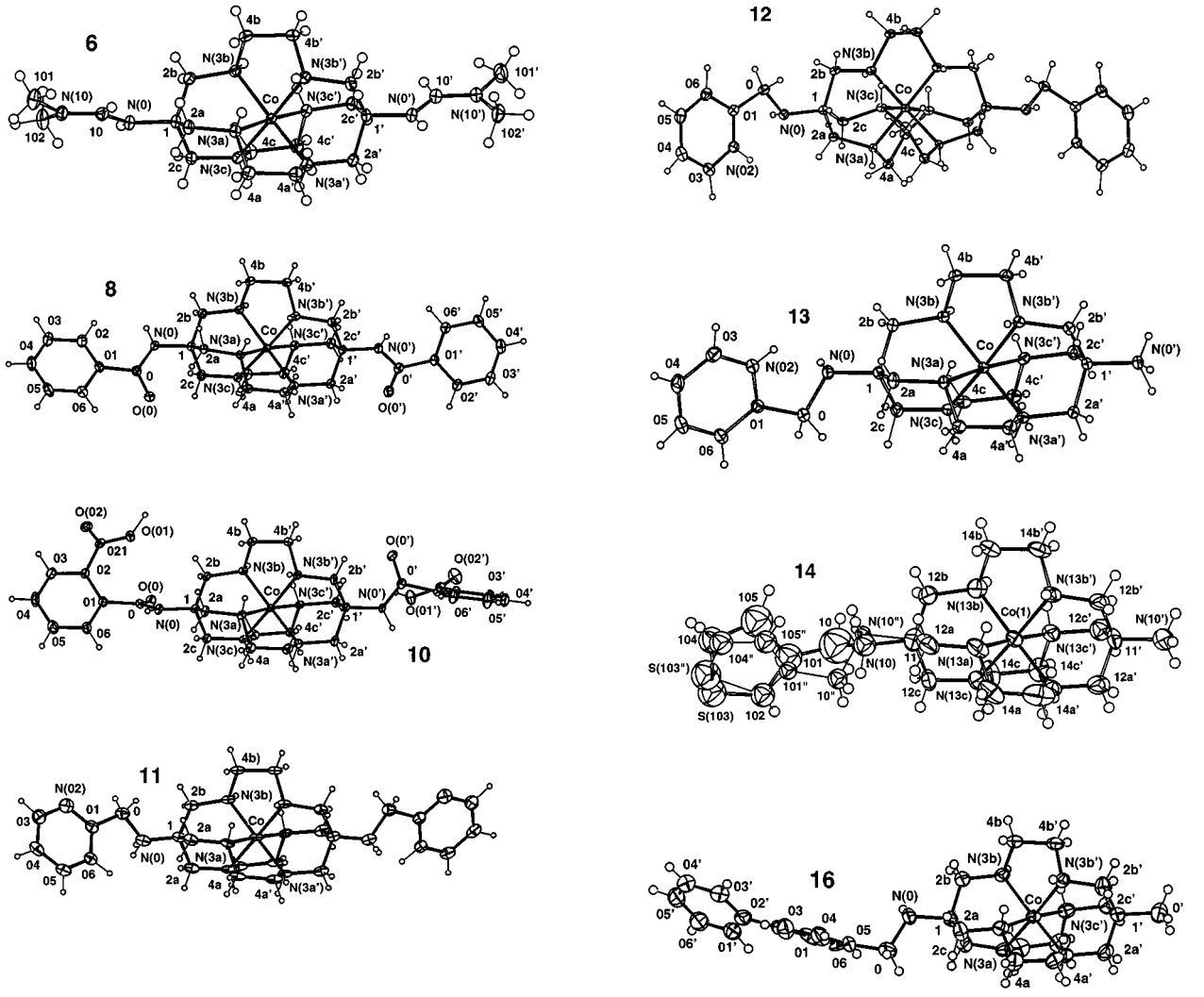

Figure 1. Projections of the cations of **6**, **8**, **10**, **11**, **12**, **13**, **14**, and **16** (cations 1 for **10**, **14**, **16**) in common orientation

obvious path to such polymers, but there is considerable flexibility in the way in which such a synthesis might be conducted. The Schotten−Baumann reaction[10] is one of the longest-known and simplest reactions for the formation of aromatic carboxamides from water-soluble amines, hence, given the fact that $[M\{(NH_2)_2sar\}]^{n+}$ complexes are typically highly water-soluble (as their chlorides, for example), this reaction was explored to see whether acceptable efficiency could be obtained even with an amine of low nucleophilicity. In the event, this was not the case, but a structure determination of the benzoylation product was of interest with regard to the possibility that the poor yields and relatively facile acid-catalysed hydrolysis might be consequences of unusual distortions of the amide resulting from its incorporation into the cage complex. The structure of hydrated $[Co\{sar(NHCOC_6H_5)_2\}]Cl_3$ (**8**, Figure 1), shows the cage Co(sar) unit to be very similar to that in the parent compound and many derivatives thereof,[1−8] with its *lel*$_3$ conformation seemingly once again stemming from the chelation of chloride counteranions by coordinated NH groups [Cl(1)···H(3a′,c) 2.49(2), 2.25(2); Cl(2)···H(3b′,a) 2.38(3), 2.29(2); Cl(3)···H(3c′,b) 2.27(3), 2.47(3) Å]. The structure is well-defined, with all hydrogens being locatable other than those in the vicinity of the partially occupied water molecule site, and both the amide NH [H(0′)···O(01) 2.22(3) Å] and O [H(01a)···O(0′) ($2 - x$, $y + 1/2$, $1\,^1/_2 - z$) 2.07(4) Å] atoms are involved in H-bonding. The amide geometry is comparable with that of benzamide itself;[11−14] benzoylation of the cage complex causes no substantial electronic distortions of the product components, though presumably the charge of the complex may facilitate attack of a polar nucleophile at the amide carbon.

A useful discovery made during efforts to use nonaqueous solvents for the acylation of $[Co\{(NH_2)_2sar\}]^{3+}$ was that the 1,8-amino groups were found to be acylated very rapidly with activated acylating agents. Thus, formation of the formamidino derivative of the cage complex appears to be complete within the time of mixing at room temperature in a benzoyl chloride/dimethylformamide medium. The presumed mechanism for this process is shown in Figure 2.

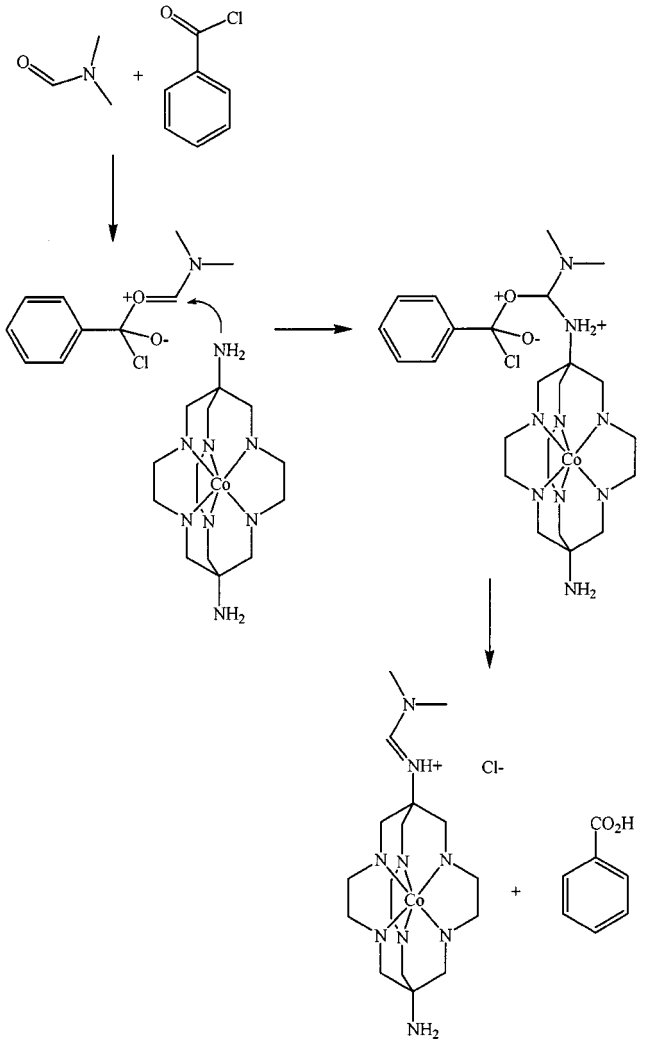

Figure 2. A possible pathway for amidine formation from dimethylformamide and $[Co\{(NH_2)_2sar\}]^{3+}$

The structure determination for $[Co\{sar[NHCHN(CH_3)_2]\}]Cl_5{\cdot}3H_2O$, **6** (Figure 1), was again sufficiently precise for hydrogen atom refinement, exemplifying yet another case of the *lel*$_3$ conformation arising from NH-bond chelation of chloride counteranions [Cl(1)···H(3c′,b) 2.34(2), 2.30(2); Cl(2)···H(3b′,a) 2.30(2), 2.29(2); Cl(3)···H(3a′,c) 2.30(2), 2.29(2) Å]. The structure confirms amidine formation, presumably as a result of the activation of DMF by acylation; both amidine groups remain sufficiently basic to be protonated in dilute HCl. Extensive H-bonding interactions are seen between the nitrogen atoms of the pendant groups and the anions and lattice water [Cl(5)···H(1) 2.31(2); O(03)···H(1′) 1.94(2) Å], and there are also direct interactions between the latter entities [Cl(3)···H(02a) 2.28(4); Cl(4)···H(02b), H(03b) ($1-x$, $-y$, $1-z$) 2.18(3), 2.33(3); Cl(5)···H(01a) (x, $y-1$, z) 2.35(3); O(2)···H(03a) (x, $y-1$, z) 1.93(3) Å]. The particular properties of dimethylformamide may be important in favouring amidine formation, as was also observed in early efforts to conduct phthaloylation reactions (see below) in this solvent; such behaviour was no longer prominent when dimethylacetamide was used as solvent. In turn, it was these observations that ultimately led to the use of dimethylacetamide in an efficient synthesis of the dibenzoylated cage complex.

As a model for reactions possibly involving the formation of a polyimide based on a cage amine and, for example, perylene dicarboximide units,[15] the formation of phthalimide derivatives of $[Co\{(NH_2)_2sar\}]^{3+}$ was examined. While the use of acetic acid as the reaction solvent appeared to result in formation of the bis(phthalimide) complex, under the conditions necessary for chromatographic purification of the reaction products ring opening to give the bis(phthalamic acid) was essentially complete. Such reactivity of the imide unit is perhaps unsurprising, given its incorporation into a highly charged cation. The use of dimethylacetamide (DMA) as a solvent for phthaloylation reactions is known[15] to favour phthalamic acid formation and, indeed, the reaction of $[Co\{(NH_2)_2sar\}]^{3+}$ with a moderate excess of phthalic anhydride in DMA led to essentially quantitative and direct formation of the "open" bis(phthalamic acid), **10**, which was structurally characterized as its chloride salt. As with the bis(benzoyl) derivative, the product did not display any anomalous structural features. The cage unit is again *lel*$_3$, once more arising from chloride anion chelation, and both the amide NH and carboxylic acid groups are involved in extended H-bonding arrays involving both water and the chloride anions. The mean bond lengths in the amide units (C−O 1.22 Å; C−N 1.35 Å) suggest some contraction of the C−O bond and elongation of the C−N bond relative to those in a simple phthalamide such as 2-phenylcarbamoylbenzoic acid,[16] although in the context of a less precise complex ion structure these differences cannot be seen as significant.

Like simpler amic acids,[15] the bis(phthalamic acid) complex could be converted into an imide form by heating in the solid state, but even under rather extreme conditions (180 °C, 5 Torr pressure, 5 h) this conversion was only ca. 20% complete. Hence, there appears to be a genuine resistance to the formation of imides, at least from $[Co\{(NH_2)_2sar\}]^{3+}$, and the hydrolytic stability seen for the bis(phthalamic acid) and, to a lesser extent, the simpler bis(benzamide) described above led us to the conclusion that the formation of polyamides should be a favourable method for the inclusion of cage units in polymers. Obviously, dimethylacetamide must currently be regarded as the solvent of choice for such reactions.

Reductive alkylations involving intermediate formation of imines between a carbonyl compound and cage amino substituents have been successfully used in the generation of a number of $[Co\{(NH_2)_2sar\}]^{3+}$ derivatives[3,5] and the work reported herein has served to extend the variety of these syntheses. We have found that the generation of imine species in reactions between aromatic aldehydes and $[Co\{(NH_2)_2sar\}]^{3+}$ in dimethyl sulfoxide can be readily monitored by ^{1}H NMR spectroscopy (most readily, through the appearance of an imine group CH resonance near $\delta = 8.5$), although in the presence of only a moderate excess of the aldehyde, conversion is slow and incomplete and, after

reduction, the product mixtures are invariably found to contain both mono- and dialkylated species. In the case of $[Co\{(CH_3)(NH_2)sar\}]^{3+}$, however, fully (mono)alkylated species are obtained more readily. In both systems, however, exhaustive chromatography of the reaction products has provided evidence of minor amounts of other (as yet, unidentified) products and the chemistry of these reactions cannot be said to be fully characterized, even though the desired products can be obtained with acceptable efficiency. Significant features of the ^1H NMR spectra of the isolated products containing groups other than 2-pyridylmethyl are summarized in Table 1. No anomalies are apparent, although it is unclear as to why the diastereotopicity of the methylene linker-group protons should be evident in some spectra (which show an AB quadruplet) and not in others.

To establish the structural influences of various cage alkylations, single-crystal structure determinations have been performed on $[Co\{(2\text{-}pyCH_2NH)_2sar\}]^{3+}$ as its monoprotonated tetranitrate **11** and its diprotonated bis(dithionate) chloride **12**, on $[Co\{(NH_2)(2\text{-}pyCH_2NH)sar\}]^{3+}$ as its diprotonated bis(dithionate) chloride **13**, and on $[Co\{(CH_3)(C_6H_5C_6H_4CH_2NH)sar\}]^{3+}$ as its mixed nitrate chloride **16** (see also the discussion of structure **14** below). The dialkylated cage structures (Figure 1) provide further examples of different conformers of a given cage complex being found in different salts;[5,6] thus, the 5+ cation of the dithionate chloride is found to be in the ob_3 form, while the 4+ cation in the tetranitrate is in the lel_3 form. This may be the only significant consequence of alkylation on the structure of the inner cage species. While there is some evidence that the preferred conformation of cages of the sarcophagine complex type may depend on the size of the 1,8-substituents,[3,5] the hydrogen atoms of the secondary N-donor atoms in the Co^{III} complexes are always involved in markedly different interactions with the counteranions and lattice solvent in the different conformers, and the availability of an H-bond acceptor capable of bridging between two NH units of different caps appears to be a significant factor favouring the lel_3 form.[3,6] Although the simple form of tris-chelation of anions as in structures **6**, **8**, and **10** does not apply for **11**, an equally elegant relative does apply (Figure 3). One of the two crystallographically independent anions is disposed with its axis (and those of its symmetry related images) approximately parallel to that of the cation, so that its three oxygen atoms interact with different cations, each O chelating two NH bonds. Thus, the relevant distances are N(3a)···O(12,13) (1/2 + x, 1/2 + y, z) 3.343(7), 3.244(6); N(3a′)···O(11,12) (1 − x, y, 1/2 − z) 3.223(6), 3.221(7); N(3b)···O(11,13) (x − 1/2, 1/2 + y, z) 3.178(7), 3.137(7) Å; from the opposite viewpoint, O(11)···N(3a′) (1 − x, y, 1/2 − z), N(3b) (1/2 + x, y − 1/2, z) 3.223(6), 3.178(7); O(12)···N(3a) (x − 1/2, y − 1/2, z), N(3a′) (1 − x, y, 1/2 − z) 3.343(7), 3.221(7); O(13)···N(3a) (x − 1/2, y − 1/2, z) 3.244(6), N(3b) (x + 1/2, y − 1/2, z) 3.137(7) Å (Figure 3).

The well-defined pendant amine hydrogen interacts with the water oxygen [H(0NA)···O(01) 2.0 (est.)], and the hydrogen of the latter is in turn coordinated by the pyridine nitrogen [N(02)···O(01) (1 − x, 1 − y, 1 − z) 2.67(1) Å]; beyond this the remainder of the structure (the other nitrate group) is disordered, with the assignment of the final hydrogen atom, as well as those of the water molecule, being dubious. The latter have four potential hydrogen-bonding interactions, two of which are presumably donor interactions [to N(02) (pyridine) (1 − x, 1 − y, 1 − z) and nitrate O(23) (disordered)], one an acceptor interaction [N(0)], and one ambiguous.

While the single proton associated with **11** appears to be bound to an amino rather than a pyridine nitrogen, in the diprotonated species **12** both protons are localized on pyridine *N* centres. Given that the acidity-enhancing effect of the adjacent Co^{III} cation should vary with distance from the metal centre,[17] it is perhaps not surprising to find a similar affinity for the two sites. In any case, protonation of the pendant groups strongly influences the nature of the H-bonding array in the solid, which in this case includes coordination of the NH units to separate H-bond acceptors [Cl···H(3b) 2.46(3), O(13)···H(3c) 2.04(4), O(22)···H(3a′) ($1\,^1/_2$ + x, y − 1/2, 1/2 − z) 2.32(4) Å] and, as in other examples of this form of H-bonding,[6] also involves the ob_3 conformation of the cage ligand. Other H-bonding interactions involve the pyridine and adjacent external amino groups [O(11)···H(0N) (x, 1 − y, z − 1/2) 2.16(5), H(02) ($1\,^1/_2$ − x, y − 1/2, −z − 1/2) 2.09(4) Å], water molecules (assumed on the basis of O···O separations, since associated protons were not located) [O(01)···O(01) (2 − x, y, 1/2 − z) 2.745(8), O(02) ($1\,^1/_2$ − x, 1/2 + y, 1/2 − z) 2.761(6); O(02)···O(03) 2.682(6); O(03)···O(03) (11/2 − x, 1/2 − y, 1 − z) 2.608(6) Å], and the dithionate anion [O(01)···O(21) 2.816(5); O(03)···O(12) (x, 1 − y, 1/2 − z) 2.744(6) Å]. The chloride environment is sparse, there being two contacts at 2.46(3) Å as above and two more to H(4cA) (x, 1 − y, 1/2 + z) (etc.) with distances of 2.74(3) Å.

That the particular choice of anions and degree of protonation are not the sole determinants of the solid-state conformation of the cage is shown by the fact that $[Co\{sar(NH_3)[NHCH_2(C_5H_4NH)]\}](S_2O_6)_2Cl\cdot 3H_2O$ (**13**), in which protonation of the pyridine nitrogen again seems preferred to that of the alkylated aliphatic nitrogen, is found in the lel_3 conformation. This is associated with a return to prominence of the tris(chelate) role of the core amine hydrogens in this compound, although with a diversity of interaction types: Cl···H(3b′,a) 2.17(4), 2.36(4) Å is conventional; H(3c′)···O(13) (x, y − 1, z), H(3b)···O(12) (x, y − 1, z) 2.31(3), 2.09(4) Å indicate a spanning of the pair of NH groups by O−S−O of one end of a dithionate anion, and in H(3a′,c)···O(03) 1.91(4), 1.95(4) Å, a water molecule oxygen is sequestered. The chloride shows a close contact to a water molecule, Cl···H(02A) 2.2 Å (est.). The terminal protonated NH_3^+ group shows contacts with a water molecule [H(0′A)···O(02) (x, y − 1, z) 1.69(7) Å] and with anionic oxygen atoms [H(0′B)···O(11) (− x, 1 − y, 1 − z) 1.88(4), H(0′c)···O(33) (x, 1/2 − y, z − 1/2) 2.09(5) Å], while at the other end the strongest interaction is found between the pyridinium hydrogen and an anionic oxygen [H(02)···O(21) 2.17(4) Å]. A limited number of the remaining anionic oxy-

Table 1. Functional group resonances in the ^{1}H NMR spectra (200 MHz, 0.1 M DCl solution) of $[Co(X)(YNH_2)sar]^{n+}$ complexes

X	Y	δ
CH_3	$C_6H_5CH_2$	CH_3 0.90 CH_2(Y) 4.13, 4.19, 4.20, 4.27 ArH 7.43
CH_3	4-$CH_3C_6H_4CH_2$	CH_3(X) 0.90 CH_3(Y) 2.31 CH_2(Y) 4.04, 4.11 (d), 4.18 ArH 7.28
CH_3	$C_6H_5CH(CH_3)CH_2$	CH_3(X) 0.89 CH_3(Y) 1.27, 1.30 ArH 7.3−7.5 (m)
CH_3	$C_6H_5C_6H_4CH_2$	CH_3 0.90 CH_2(Y) 4.10 ArH 7.41−7.53 (m), 7.66−7.73 (m)
CH_3	(4-C_5H_4N)CH_2	CH_3 0.90 CH_2(Y) 4.54, 4.59, 4.66, 4.71 ArH 8.18, 8.21 (d), 8.82, 8.86
CH_3	2-furanylCH_2	CH_3 0.85 CH_2(Y) 4.33 Furanyl-H 6.41 (m), 6.56, 6.58, 7.51 (d)
CH_3	2-thiophenylCH_2	CH_3 0.87 CH_2(Y) 4.48, 4.53, 4.56, 4.61 Thiophenyl-H 7.04, 7.05, 7.06, 7.25, 7.27, 7.50, 7.53
NH_3^+	$C_6H_5CH_2$	CH_2(Y) 3.86 ArH 7.30−7.40 (m)
NH_3^+	4-$CH_3C_6H_4CH_2$	CH_3(Y) 2.39 CH_2(Y) 3.97 ArH 7.24
NH_3^+	3-$CH_3C_6H_4CH_2$	CH_3(Y) 2.30 CH_2(Y) 4.00 ArH 7.14−7.35 (m)
NH_3^+	2-$CH_3C_6H_4CH_2$	CH_3(Y) 2.32 CH_2(Y) 4.15 ArH 7.25−7.35 (m)
NH_3^+	$C_6H_5CH(CH_3)CH_2$	CH_3 1.25, 1.28 ArH 7.29, 7.31, 7.32, 7.36, 7.39
NH_3^+	(4-C_5H_4N)CH_2	CH_2 4.58 ArH 7.16, 7.20, 8.80, 8.83
NH_3^+	2-furanylCH_2	CH_2 4.20 Furanyl H **6.4**0 (m), 6.52 (m), 7.50 (m)
NH_3^+	2-thiophenylCH_2	CH_2 4.38 Thiophenyl-H 7.00, 7.01, 7.03, 7.04, 7.17, 7.19, 7.44 (d), 7.47 (d)
NH_3^+	3-thiophenylCH_2	CH_2 4.16 Thiophenyl-H 7.02 (d), 7.35 (q), 7.44 (d)
$C_6H_5CH_2$	$C_6H_5CH_2$	CH_2 4.11, 4.17, 4.19, 4.25 ArH 7.43
4-$CH_3C_6H_4CH_2$	4-$CH_3C_6H_4CH_2$	CH_3 2.29 CH_2 4.13, 4.19, 4.21, 4.27
$C_6H_5CH(CH_3)CH_2$	$C_6H_5CH(CH_3)CH_2$	CH_3 1.28, 1.31 CH_2 **3.5**3 (br), 3.58 (br) ArH 7.31, 7.33, 7.35, 7.38, 7.41, 7.45
(4-C_5H_4N)CH_2	(4-C_5H_4N)CH_2	CH_2 4.58 ArH 7.16, 7.20, 8.80, 8.83
2-furanylCH_2	2-furanylCH_2	CH_2 4.29 Furanyl-H 6.43 (m), 6.57 (m), 7.53 (m)
3-thiophenylCH_2	3-thiophenylCH_2	CH_2 3.58 (q) Thiophenyl-H 6.88 (d), 7.10 (d), 7.24 (q)

gens are strongly hydrogen-bonded with water: O(31)···H(01A) (1 − *x*, *y* − 1/2, 1 $^1/_2$ − *z*) 1.8 (est.), O(41)···H(02B) (1 − *x*, 1/2 + *y*, 1/2 − *z*) 2.3 (est.), O(42)···H(01B), H(03B) (1 − *x*, *y* + 1/2, 1 $^1/_2$ − *z*) 2.2, 1.9 Å (est.). A strong water···water interaction [H(03A)···O(01) 1.7 (est.)] is found. In **13**, as in **12**, there is no evidence of stacking interactions of the pyridine rings, despite the fact that in **12** parallel arrays of pyridine rings from separate complex ion units may be discerned in the lattice. In **11**, however, arrays of parallel pyridine rings may be indicative of some stacking, as suggested by C···C contacts of ca. 3.7 Å.

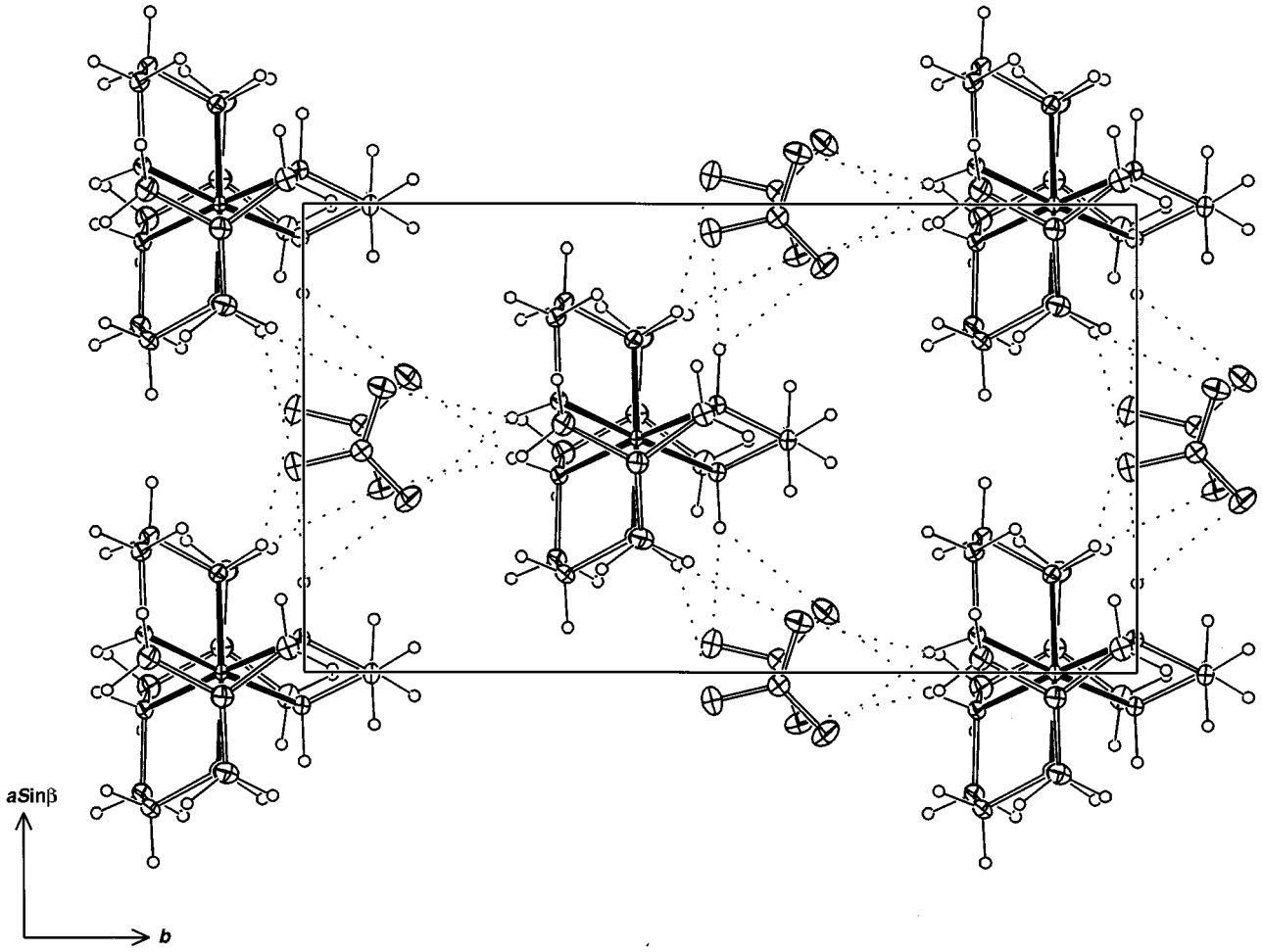

Figure 3. Section of the structure of **11**, projected down *a*, showing the cations centred at $z = 1/4$, on twofold axes, with the cage pendants being omitted so as to display the linking of cations centred on that plane by associated hydrogen-bonded nitrate ions

When a neutral aromatic unit is introduced as a substituent, as is the case with the biphenylmethyl unit in **16**, diminished charge repulsions appear to allow more significant stacking interactions, as indicated by the "herringbone" array of the biphenyl groups evident in this solid (in the projection down *a*). The cage unit adopts an lel_3 conformation, once again attributable to NH chelation of the anions, though the interactions are somewhat complicated to describe in this mixed anion species. Those of cation 1 involve the halide and a pair of nitrate groups: Cl···H(13b′,a) 2.5, 2.1; O(21)···H(13b,c′) 1.9, 2.2; O(13)···H(13a′,c) (x, 2 − y, z + 1/2) 2.2, 2.2 (est.) [also involving O(12)···H(13a′) (x, 2 − y, z + 1/2) 2.2 Å]. For cation 2, one chelate involves a water oxygen, O(06)···H(23b′,a) (x, y + 1, z) 2.3, 2.0, while the other two involve nitrate oxygens, O(41)···H(23c′,b) (x, 1 − y, z + 1/2) 2.1, 2.0; O(52,52′)···H(23c′,a) (x, y + 1, z) 2.2, 2.1; 2.30, −; O(53,53′)···H(23a′) (x, y + 1, z) 2.2, 2.3 Å (est.). Other H-bonds are formed to the pendant amino group nitrogen atom: H(10N)···O(12) 1.9, H(20N)···O(53) (x, 2 − y, z − 1/2) 2.0 Å (est.).

The introduction of aromatic substituents on cage amine complexes through the present and other means[18] is facile and is of interest in that the stability of these complexes in strongly acidic media allows functionalization of the aromatic units under simple, conventional conditions for electrophilic substitution. Such further functionalization could endow the complexes with new properties, for example, the introduction of vinyl substituents may possibly offer another route to polymer-immobilized cage complexes. As in the acylation and alkylation reactions of amino groups attached to the cages, some retardation of electrophilic attack, in this case on a pendant aromatic unit, was to be expected as a result of the cationic charge on the complex. At least in the case of $[Co\{(C_6H_5CH_2NH_2)_2sar\}]^{5+}$, however, this did not appear to be an important effect. Reaction of the complex in H_2SO_4/HNO_3 at room temperature for 5 min resulted in predominant symmetrical disubstitution at the 3-positions of the ring, with a small amount of mono-3-substituted material also being present. Reductions of these nitro compounds and reactions of the resulting aromatic amine derivatives are currently under investigation.[19]

A more direct pathway to the formation of polymers incorporating cage complex substituents is offered by complex derivatives containing electropolymerizable groups

such as furan, pyrrole, and thiophene.[20] Although reductive alkylation of $[Co\{(NH_2)_2sar\}]^{3+}$ with 2-pyrrolecarbaldehyde appeared to be successful, the product underwent acid-catalysed conversion into a "pyrrole black",[21] which was irreversibly absorbed on Dowex 50 cation-exchange resin; as yet we have not succeeded in obtaining the simple pyrrolylmethyl cage derivatives in a pure form. The furan and thiophene analogues, however, are readily obtained. As derivatives of 2-substituted heterocycles, these are not expected[20,21] to readily undergo oxidative polymerization, but they can at least be taken as putative models for the behaviour at the metal centre in a polymerized derivative. Encouragingly, electrochemical measurements have shown that the substituted Co^{III} cage complexes exhibit a quasi-reversible Co^{III}/Co^{II} couple at potentials essentially identical to those of their unsubstituted analogues. For both the thiophene and furan derivatives, a highly irreversible oxidation wave near +1.4 V may be consistent with an oxidation process at the ring, but no real evidence has been obtained for any resulting polymerization (for example, ion-exchange chromatography after extensive electrolysis or vigorous chemical oxidation only showed the presence of materials with similar elution characteristics to those of the reactants). The heterocycle oxidation wave alone has been taken as evidence for the occurrence of polymerization processes in closely related systems,[22] but in the present case measurements were made in aqueous solution and water is known to strongly inhibit oxidative polymer formation.[20]

More interesting redox properties were expected of the 3-substituted thiophene derivative, and to characterize fully the nature of the 3-thiophenyl substituent attached to a cage, the structure of $[Co\{[3\text{-}(C_4H_3S)CH_2NH_2](NH_3)sar\}]Cl_5\cdot 3H_2O$ (**14**) was determined by single-crystal X-ray crystallography. This confirmed the anticipated nature of the complex, with the cation adopting the familiar lel_3 conformation and the substituent lying in an extended position such that the cobalt cage unit clearly does not congest regions near the 2- (and 4-) positions of the thiophene ring. The cage again chelates chloride anions [(cation 1) Cl(1,1′)···H(13c′) 2.4, 2.7; Cl(1,1′)···H(13b) 2.2, 2.0; Cl(7)···H(13a′,c) (x, 1 − y, z − 1/2) 2.2, 2.1; Cl(8)···H(13b′,a) (x, 1 − y, z − 1/2) 2.3 (×2); (cation 2) Cl(6)···H(23c′,b) (1/2 + x, 1/2 + y, z) 2.3, 2.2; Cl(5)···H(23b′,a) (1 + x, y, z) 2.3, 2.1; Cl(3)···H(23a′,c) (1 + x, y, z) 2.1, 2.3 Å (all est.)], albeit with some disorder, and while the thiophene rings can be seen to form a herringbone array, there are no close inter-ring contacts. Cyclic voltammetry of the complex (in aqueous media) showed characteristics similar to those of the 2-thiophenyl analogue in that an irreversible oxidation wave near +1.4 V was apparent, but vigorous chemical oxidation in concentrated nitric acid gave contrasting results in that the product did show some properties of a large molecule. Thus, the product was of very low solubility in water and the bulk of it was irreversibly retained on both Sephadex and Dowex cation-exchange resins (it appeared possible to elute some material initially, but, on standing, even this small fraction became impossible to elute). Furthermore, the solid was a bright-yellow colour and in aqueous solution showed an absorption spectrum with an intense maximum near 420 nm, quite atypical of Co^{III} cage amine complexes, but typical of polythienyls.[20] All "solutions" were in fact perceptibly cloudy to the eye, again consistent with the solid containing high molecular weight species. The most prominent feature of the cyclic voltammogram of the solution was a strong oxidation wave near 1.4 V, with evidence for interconversion of a Co^{III}/Co^{II} couple near −0.3 V being retained. This material is currently being subjected to a more detailed investigation, one of the possible complications arising from its method of synthesis being that of nitrosation,[1,6,7] although it may be noted that simple dissolution of the dialkylated reactant complex in concentrated HNO_3 alone gives only species having the characteristics of mononuclear Co^{III} cage amine complexes.

A more conventional approach to oxidative polymerization of thiophene derivatives is to use electrochemical methods in nonaqueous solvents. Although the choice of solvent is restricted by the nature of the cage amine complex, it is possible to examine the triflate salt of the mono(3-thiophenyl) derivative in acetonitrile. Representative cyclic voltammograms for a series of measurements using a Pt working electrode and sodium triflate as the electrolyte are shown in Figure 4.

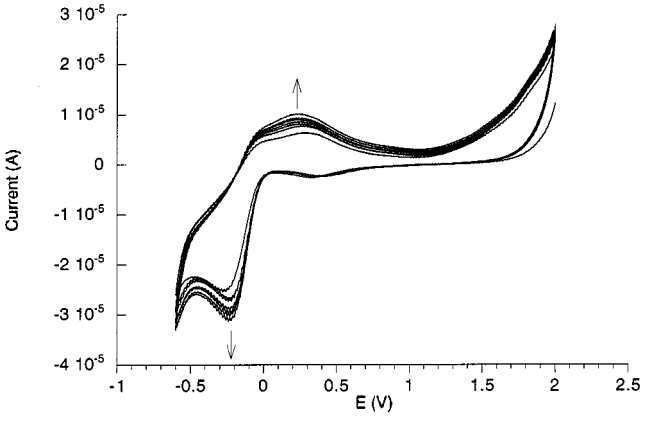

Figure 4. Electropolymerization of Co-cage thiophene conjugate

Although simple chemical experiments show the Co^{III}/Co^{II} interconversion to be reversible, it is apparently not electrochemically reversible, seemingly because of adsorption of the Co^{II} species in the present case.[23] Nevertheless, repeated scanning shows the current to increase with each consecutive scan, consistent with the deposition of a conductive material on the electrode surface. After such a series of measurements, the electrode was removed, washed well with water to remove any adhering monomeric complex, dried, and then placed in a simple acetonitrile solution of sodium triflate. Cyclic voltammograms subsequently obtained are shown in Figure 5.

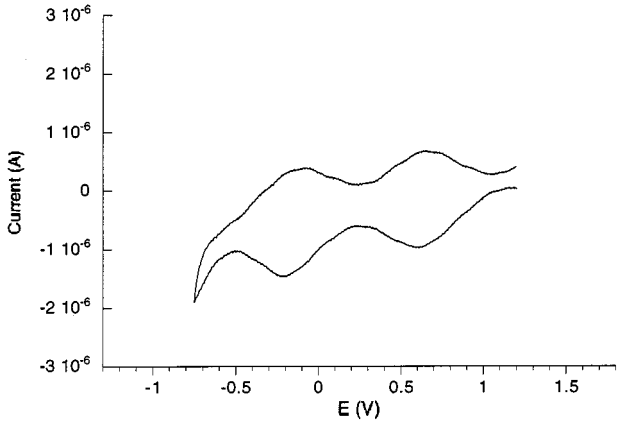

Figure 5. Cyclic voltammogram of modified electrode

Clearly, a conductive and electroactive material had been deposited on the electrode surface, and we tentatively ascribe the two waves with very small anodic/cathodic peak separations to polymer-pendant Co^{III}/Co^{II} (near −0.2 V) and polythiophene (near +0.6 V) centred processes. Obviously, there are interesting prospects here with regard to use of chiral Co^{III} monomers as sources of possible asymmetric electrocatalysts[24] and with regard to varying the electrochemical properties of the polymer by substituting the Co by other transition metals.

Conclusion

From the present and related works,[2,3,5,6] a substantial array of usefully 1,8-functionalized derivatives of the cage complex $[Co(sar)]^{3+}$ is now available. It would appear to be generally true that substitution at the 1,8-positions of this complex does not significantly modify the properties of the central unit. Correspondingly, the properties of the pendant groups do not appear to be critically modified by the presence of the nearby cationic centre. The Co^{III} should be replaceable by numerous other metals,[2,6] so that there may be many pathways to truly practical applications of cage amine complexes, such as in radiopharmaceutical agents based on Cu^{II}, for example.[25]

Experimental Section

General Remarks: NMR spectra were acquired from samples in D_2O solution on Varian Gemini 200 (^1H at 200 MHz and ^{13}C at 50.3 MHz) or Bruker ARX 500 (^1H at 500.13 MHz and ^{13}C at 125.8 MHz) spectrometers. Chemical shifts are expressed in ppm relative to an internal standard of acetone ($\delta = 2.04$ for ^1H NMR spectra and $\delta = 29.4$ for ^{13}C NMR, relative to TMS). − Ion-exchange chromatography was performed under gravity flow using Dowex 50W × 2 (H^+ form, 200−400 mesh) or SP Sephadex C25 (Na^+ form, 200−400 mesh) cation-exchange resins. All evaporations were performed at reduced pressure (ca. 20 Torr) using a Büchi rotary evaporator and a water aspirator. The Schlenk technique using high purity argon or high purity nitrogen was employed wherever it was necessary to exclude oxygen from preparative mixtures. − UV/Vis absorption spectra (200−800 nm) were recorded on a Hewlett−Packard 8452A diode-array spectrophotometer. − Cyclic voltammograms were recorded with a MacLab$\curlyvee$ potentiostat controlled by a Macintosh SE computer employing AD Instruments Echem software, using a platinum working electrode, a platinum counterelectrode, and a silver/silver chloride reference electrode. All solutions had a composition of 1−5 mM analyte in 0.1 M $NaClO_4$ solution. Water was purified using a Milli-Q ultra-pure water system. All solutions were purged with argon and were analysed at ambient temperatures. − Microanalyses for carbon, hydrogen, and nitrogen were carried out by the Australian National University Microanalytical Service. All samples were thoroughly dried in vacuo (0.1 Torr) at 50 °C for 4 h prior to their analysis.

$[Co\{(NH_3)_2sar\}]Cl_5\cdot H_2O$ was prepared as described previously.[7] Solvents from Fluka (pyridine, acetonitrile, dimethyl sulfoxide, dimethylformamide) and Eastman (dimethylacetamide) were used as received, as were reagents (phthalic anhydride, triethylamine) from Aldrich. Benzoyl chloride (Aldrich) was distilled prior to use. Aldehydes (2-pyridinecarbaldehyde, 4-pyridinecarbaldehyde, benzaldehyde, 3- and 4-methylbenzaldehyde, 2-phenylpropanal (hydratropaldehyde), biphenyl-4-carboxaldehyde, furancarbaldehyde, 2-thiophenecarbaldehyde, and 3-thiophenecarbaldehyde) from Aldrich were used as received. Various solids containing the $[Co\{(NH_2)_2sar\}]^{3+}$ cation were used as sources of this unprotonated cage complex (although equivalent results were often obtained simply by adding a base such as triethylamine to a solution of a protonated complex salt). $[Co\{(NH_2)_2sar\}]Cl_3\cdot nH_2O$ was prepared by heating (80 °C) a mixture of $[Co\{(NH_3)_2sar\}]Cl_5\cdot H_2O$ (5.7 g) and Li_2CO_3 (0.74 g) in water (5 mL) until effervescence had ceased. The deep brown-yellow solution was filtered, cooled, and gradually diluted with ethanol (50 mL) to precipitate a yellow, crystalline solid (4.5 g, 92%). − **$[Co\{(NH_2)_2sar\}]Cl_3\cdot 1.5H_2O$ (1):** calcd. C 33.18, H 7.36, N 22.11; found C 33.4, H 7.4, N 22.2. The analogous acetate salt was obtained by passing a solution of $[Co\{(NH_3)_2sar\}]Cl_5\cdot H_2O$ (5.70 g) in water (5 mL) through a column containing a tenfold excess of acetate-form Dowex 1 × 8 anion-exchange resin. The complex was washed from the column with water, the eluate was concentrated to a viscous, orange oil under reduced pressure, the residue was almost dried by twofold co-evaporation of ethanol, and finally it was crystallized from ethanol by the addition of diethyl ether. (Note that without the repeated evaporations, the solid retained some excess acetic acid.) Yield: 3.50 g, 52%. − **$[Co\{(NH_2)_2sar\}](CH_3CO_2)_3\cdot 6.5H_2O$ (2):** calcd. C 35.98, H 8.45, N 16.78; found C 35.9, H 8.5, N 16.8. To obtain the triperchlorate, perchloric acid (70%, 1 mL; CAUTION!) was added to a solution of the acetate (0.99 g) in ethanol (10 mL) to give initially a yellow, crystalline precipitate (1.13 g, 81%) of the pentaperchlorate. This was collected by filtration and washed first with ethanol/diethyl ether and then with diethyl ether. The solid rapidly underwent a colour change to red-orange on exposure to air, presumably as a result of hydration, although it did not deliquesce. − **$[Co\{(NH_3)_2sar\}](ClO_4)_5\cdot 4H_2O$ (3):** calcd. C 17.80, H 4.69, N 11.86; found C 17.9, H 5.1, N 11.9. (Note that as a possibly safer procedure, the pentaperchlorate may also be isolated from water as orange needles, although the yield is poor due to the high solubility of the compound.) The pentaperchlorate (1.40 g) and NaOH (0.11 g; one pellet) were dissolved in water (1 mL). The resulting solution took on a dark-yellow colour before copious precipitation of yellow-brown crystals commenced. Ethanol (10 mL) was then added and the mixture was cooled in ice to maximize precipitation of the solid (0.92 g, 88%), which was collected and washed with ethanol and

diethyl ether. − **[Co{$(NH_2)_2$sar}]$(ClO_4)_3$·2H_2O (4):** calcd. C 23.76, H 5.41, N 15.83; found C 23.9, H 5.7, N 15.8. Despite the apparently low solubility in water of the triperchlorate, attempts to isolate it directly from the more convenient starting material [Co{$(NH_3)_2$sar}]$Cl(ClO_4)_4$·2H_2O[6] invariably resulted in the chloride-perchlorate. Thus, [Co{$(NH_3)_2$sar}]$Cl(ClO_4)_4$·2H_2O (2.3 g) and NaOH (0.25 g) were dissolved in water (2.5 mL) to give a dark-brown solution; $NaClO_4$·H_2O (2.00 g) was added and the solution was diluted with ethanol (50 mL) to give a yellow precipitate, which was then recrystallized from hot water (5 mL) containing concentrated aqueous ammonia (2 drops) by the addition of ethanol (50 mL). Yield: 1.65 g, 100%. − **[Co{$(NH_2)_2$sar}]$Cl_2(ClO_4)$·H_2O (5):** calcd. C 29.93, H 6.46, N 19.95; found C 30.3, H 6.7, N 19.9.

Reactions of [Co{$(NH_2)_2$sar}]$^{3+}$ under Benzoylation Conditions: Attempts to react aqueous solutions of [Co{$(NH_3)_2$sar}]Cl_5·H_2O (containing sufficient base to both deprotonate the complex and neutralize the acid produced in acylation) with benzoyl chloride resulted in very low yields of (mono- and di-) benzoylated complexes, even when highly concentrated solutions (ca. 1−5 M) of the very soluble complex were used. For example, from the reaction of [Co{$(NH_3)_2$sar}]Cl_5H_2O (5.70 g, 10 mmol) in water (10 mL) with a fourfold excess of benzoyl chloride (5.60 g) in the presence of triethylamine (6.10 g), cation-exchange chromatography (SP Sephadex, 0.5 M NaCl/0.5 M $NaClO_4$ as eluent) enabled the isolation of ca. 200 mg of the monobenzoylated and ca. 20 mg of the dibenzoylated complexes. Absorption on Dowex 50W × 2 cation-exchange resin and re-elution with HCl to recover the complexes from the Sephadex column eluates led to partial hydrolysis of the benzoyl compounds, so these yields are lower estimates but not dramatically so. Attempts to use other solvents (acetonitrile, dimethyl sulfoxide, pyridine) as the reaction medium were even less successful, except in the cases of dimethylformamide and dimethylacetamide. In dimethylformamide, benzoylated products could be observed in moderate yields along with formamidino derivatives of the cage, and by varying the reaction conditions both products could be obtained quite readily.

[Co{[$(CH_3)_2$NCHNH]$_2$sar}]Cl_5·3H_2O (6): Triethylamine (0.5 mL) was added to a solution of [Co{$(NH_3)_2$sar}]$Cl(ClO_4)_4$·H_2O (0.50 g) in dimethylformamide (5 mL), which led to an appreciable darkening of the yellow solution. Under vigorous stirring, benzoyl chloride (0.70 g) was rapidly added, resulting in a lightening of the colour of the solution, followed, almost immediately, by the deposition of a yellow precipitate. After 5 min, the mixture was poured into water (50 mL) containing concentrated HCl (2 mL) and the precipitated benzoic acid was extracted into dichloromethane. The aqueous phase was passed through a column of H^+ form Dowex 50W × 2 cation-exchange resin to absorb the complex cation(s). The column was washed with water, then eluted with 1 M HCl to remove $[HN(C_2H_5)_3]^+$, and finally the yellow complex band was eluted with 3 M HCl. Although no separation was observed, ^{1}H NMR spectra of the residues obtained upon evaporation of the solvent from sequential eluate fractions indicated that at least two materials were present; resonances near δ = 7.5 and 7.9 showed a significant variation in their relative intensities through the sequence. The combined eluates were concentrated to dryness under reduced pressure and the yellow residue was redissolved in water (2 mL). Addition of ethanol (50 mL) led to precipitation of a yellow solid, which was recrystallized in a similar manner to furnish a material (0.20 g, 44%) showing only the lower field of the aforementioned two resonances in its ^{1}H NMR spectrum. A further recrystallization from water by vapour diffusion of ethanol provided clear yellow tablets suitable for X-ray crystallography. − ^{1}H NMR: δ = 2.62−2.85 (m, cage amine CH_2, 12 H), 2.92, 3.18 (two s, formamidino methyl groups, 12 H), 3.30−3.40 (m, cage amine CH_2, 12 H), 7.85 (br. s, formyl H, 2 H). − ^{13}C NMR: δ = 39.1, 46.6 (formamidino methyl), 55.5, 57.6 (cage methylene), 62.5 (cage quaternary), 156.3 (formyl). − For elemental analysis, the complex was recrystallized from 1 M HCl by the addition of ethanol; the results indicated that the complex formed as a "hydrochloride" under these conditions. − $[CoC_{20}H_{46}N_{10}]Cl_5HCl$·4$H_2O$ = $C_{20}H_{55}Cl_6CoN_{10}O_4$: calcd. C 31.14, H 7.19, N 18.16; found C 31.1, H 6.4, N 17.7.

[Co{$(C_6H_5CONH)(NH_3)$sar}]$(NO_3)_4HNO_3$·2H_2O (7): Triethylamine (0.41 g) was added to a solution of [Co{$(NH_2)_2$sar}]$(ClO_4)_3$·2H_2O (0.68 g) in dimethylformamide (1 mL), which led to a colour change from yellow-orange to dark brown. The resulting solution was cooled in ice, and then benzoyl chloride (0.56 g) was added under vigorous stirring. A yellow precipitate formed immediately and, after 5 min, precipitation was completed by the addition of ethanol (20 mL) and diethyl ether (10 mL). The solid was collected by filtration and redissolved in water (2 mL). Addition of ethanol (50 mL) precipitated a yellow powder (largely composed of the formamidino compound described above), which was filtered off, and then the filtrate was concentrated to dryness under reduced pressure. The deliquescent residue was redissolved in water (2 mL) and the yellow solution was cooled in ice. Dilute nitric acid (4 M, 2 mL) was added and the mixture was kept in the ice-bath as a crystalline precipitate formed. After 5 min, this was collected, washed with methanol and diethyl ether, and dried, giving 0.35 g (44%) of the complex. Analysis for $[CoC_{21}H_{39}N_8O](NO_3)_4$·$HNO_3$·2$H_2O$ ≡ $C_{21}H_{44}CoN_{13}O_{18}$: calcd. C 30.55, H 5.37, N 22.06; found C 30.8, H 5.3, N 22.3. − ^{1}H NMR: δ = 2.80−3.05 (m, cage amine CH_2, 12 H), 3.33−3.51 (m, cage amine CH_2, 12 H), 7.35 (m, ArH, 2 H), 7.46 (m, ArH, 1 H), 7.53 (m, ArH, 2 H). Additional very weak signals in this spectrum were possibly indicative of the presence of some mixed formamidino-benzoyl cage complex. The most efficient preparation of the dibenzoyl complex was that conducted in dimethylacetamide, after which chromatography indicated no more than trace amounts of any other product. Thus, triethylamine (0.41 g) was added to a solution of [Co{$(NH_2)_2$sar}]$(ClO_4)_3$ (0.68 g) in dimethylacetamide (1 mL), which led to a colour change from yellow-orange to dark brown. The resulting solution was cooled in ice, and then benzoyl chloride (0.56 g) was added under vigorous stirring. The colour of the solution rapidly became lighter and a yellow precipitate began to form within 10 s. After 5 min, ethanol (5 mL) was added to ensure hydrolysis of any remaining benzoyl chloride, and then diethyl ether (50 mL) was added to complete precipitation of the yellow solid. This was collected and redissolved in water (10 mL); the yellow solution was filtered and the filtrate was treated with conc. HCl (1 mL). Some precipitate formed but redissolved upon addition of ethanol (50 mL). Diethyl ether (ca. 400 mL) was then added to the point of permanent turbidity and the mixture was left to stand for 30 min to allow precipitation of fine, yellow crystals (0.37 g, 41%). Despite the intent to obtain the complex as its chloride, this procedure seemed to result in retention of the original perchlorate anion. − [Co{$(C_6H_5CONH)_2$sar}]$(ClO_4)_3$·4H_2O (**8**) ≡ $C_{28}H_{50}Cl_3CoN_8O_{18}$: calcd. C 35.32, H 5.29, N 11.77; found C 35.0, H 5.0, N 11.7. To ensure conversion into the chloride, **9**, this solid was shaken with an aqueous slurry of chloride-form Dowex 1 × 8 anion-exchange resin and the solution obtained was concentrated to dryness under reduced pressure. Crystals suitable for X-ray diffraction analysis were grown by redissolving the residual solid in hot (80 °C) water and allowing the solution to cool slowly to room temperature. − ^{1}H NMR: δ = 2.93−2.99 (br. d, cage amine CH_2,

6 H), 3.18, 3.24 (d, cage amine CH_2, 6 H), 3.57−3.67 (m, cage amine CH_2, 12 H), 7.55 (m, ArH, 2 H), 7.66 (m, ArH, 1 H), 7.73 (d, ArH, 2 H). − ^{13}C NMR: δ = 54.2, 55.5 (cage methylene), 60.6 (cage quaternary C), 129.8, 131.2, 135.1, 135.7 (ArC), 173.9 (carbonyl C).

Phthaloylation of $[Co\{(NH_2)_2sar\}]^{3+}$. − Method 1: A mixture of $[Co\{(NH_2)_2sar\}]Cl_3\cdot 2H_2O$ (1.00 g, 1.94 mmol) and phthalic anhydride (1.44 g, 9.73 mmol) in glacial acetic acid (80 mL) was heated under reflux for 2 h, in the course of which the initially orange solution darkened appreciably. The solvent was then removed under reduced pressure, the residue was extracted with water (50 mL), and the insoluble (white) material was filtered off. The filtrate was concentrated to leave an orange residue (1.10 g), which was redissolved in water (200 mL) and applied to a column (30 cm × 4 cm) of Na^+-form SP Sephadex C25 cation-exchange resin. The column was eluted with 0.5 M NaCl solution to separate four components, from which the complexes present were individually isolated by absorbing the eluate fractions on H^+-form Dowex 50W × 2 cation-exchange resin, washing the resin with water (100 mL) and 1 M HCl (100 mL), eluting the orange material with 3 M HCl, and concentrating the eluate to dryness under reduced pressure. Fraction 1 (ca. 0.20 g, 12%): ^{1}H NMR: δ = 2.50−3.95 (m, cage amine CH_2, 24 H), 7.41−8.06 (m, ArH, 8 H). − ^{13}C NMR: δ = 52.8, 55.0, 59.6, 128.7, 129.4, 131.7, 131.9, 134.3, 137.7, 171.0, 174.4. This was identified as the bis(phthalamic acid) derivative. Fraction 2 (ca. 0.60 g, 36%), as isolated, gave identical spectra to Fraction 1 except for the presence of a sharp singlet at δ = 7.84 in the ^{1}H spectrum, consistent with the presence of ca. 5% of an imide species. Fractions 3 and 4 were not well-separated and provided residues with identical spectroscopic properties, consistent with those of a mono(phthalamic acid): ^{1}H NMR: δ = 2.76−3.74 (m, cage amine CH_2, 24 H), 7.40−8.04 (m, ArH, 4 H). − ^{13}C NMR: δ = 52.6, 55.5 (cage methylene), 60.0 (cage quaternary C), 128.6, 128.8, 131.7, 131.9, 134.4, 137.8 (ArC), 170.5, 174.2 (carbonyl C).

Method 2: A mixture of $[Co\{(NH_2)_2sar\}]Cl_3\cdot 2H_2O$ (1.00 g, 1.94 mmol) and phthalic anhydride (1.44 g, 9.73 mmol) in dimethylacetamide (DMA; 70 mL) was heated at 90 °C for 17 h. After cooling the orange solution, it was diluted with diethyl ether (400 mL) and placed in a refrigerator (4 °C), whereupon orange needles slowly precipitated. The crystals were collected, washed with diethyl ether, and then redissolved in water (500 mL) to allow absorption of the complex(es) on a column (30 cm × 4 cm) of Na^+-form SP Sephadex C25 cation-exchange resin. Elution with 0.5 M NaCl produced a single band, from which the complex (1.30 g, 77%) was recovered as described above. The ^{1}H and ^{13}C NMR spectra of the residue were identical to those summarized above for the bis(phthalamic acid). The complex was recrystallized from hot water by cooling in ice to furnish orange needles. − $[CoC_{30}H_{42}N_8O_6]Cl_3\cdot 5H_2O$ (**10**) = $C_{30}H_{52}Cl_3CoN_8O_{11}$: calcd. C 41.60, H 6.05, N 12.94; found C 41.6, H 5.1, N 12.9.

Reductive Alkylation of $[Co\{(NH_2)_2sar\}]^{3+}$ and $[Co\{(CH_3)(NH_2)sar\}]^{3+}$

The following procedures, described for reactions involving 2-pyridinecarbaldehyde, were also carried out using 4-pyridinecarbaldehyde, benzaldehyde, 4-methylbenzaldehyde (*p*-tolualdehyde), 3-methylbenzaldehyde, 2-phenylpropanal (hydratropaldehyde), 4-biphenyl-4-carboxaldehyde (the product from reaction with $[Co\{(CH_3)(NH_2)sar\}]^{3+}$ ultimately being characterized by a crystal structure determination as the nitrate-chloride, **16**), furancarbaldehyde and 2-thiophenecarbaldehyde. In most cases, the relevant products were obtained in acceptable yields, though the syntheses were not optimized in each individual case and as a result some reactions of $[Co\{(NH_2)_2sar\}]^{3+}$ provided only the monoalkylation product. An efficient alternative synthesis of the product of the reaction of $[Co\{(CH_3)(NH_2)sar\}]^{3+}$ with 4-pyridinecarbaldehyde has been described in the literature.[3]

$[Co\{(2\text{-}pyCH_2NH)_2sar\}]^{3+}$ and $[Co\{(2\text{-}pyCH_2NH)(NH_2)sar\}]^{3+}$: $[Co\{(NH_3)_2sar\}]Cl_5\cdot H_2O$ (1.8 g, 3 mmol) was converted into its acetate salt by dissolution in water, passage through a column of acetate-form Dowex 1 × 8 anion-exchange resin, concentration of the eluate to a viscous oil, and crystallization of the latter by precipitation from methanol by the addition of diethyl ether. Although conversion was quantitative, the acetate prepared in this way invariably appeared to have a composition intermediate between those of $[Co\{(NH_3)(NH_2)sar\}](O_2CCH_3)_4$ and $[Co\{(NH_2)_2sar\}](O_2CCH_3)_3$, hence a base was added in the following step of the synthesis. Thus, the acetate was dissolved in dimethyl sulfoxide (30 mL) containing triethylamine (1 mL). 2-Pyridinecarbaldehyde (0.96 g, 9 mmol) was added and the resulting mixture was heated at 90 °C for 12 h under a nitrogen atmosphere. After cooling the solution to room temperature, sodium borohydride (0.50 g) was added and the mixture was stirred vigorously for 1 h. The excess borohydride was then destroyed by the slow addition of 3 M HCl (20 mL), and the solution was diluted with water (1 L) containing hydrogen peroxide (30%, 1 mL) to ensure complete conversion of Co^{II} back to Co^{III}. The orange solution thus obtained was absorbed on a column (4 × 50 cm) of H^+-form Dowex 50W × 2 cation-exchange resin and, after washing the column with water (2 L) and 0.5 M HCl (1 L), the remaining orange complexes were eluted with 3 M HCl. Three components were observed; the individual eluates were concentrated under reduced pressure and then the complexes were precipitated by the addition of ethanol. The first band contained unchanged starting material, the second (F2) contained the monosubstituted complex, and the third (F3) contained the disubstituted complex. Yield from F2: 1.13 g, 56%. − $C_{20}H_{41}Cl_5CoN_9\cdot 1.5H_2O$: calcd. C 35.81, H 6.61, N 18.79; found C 35.8, H 6.6, N 19.0. − UV/Vis (0.1 M HCl): λ_{max} = 472 nm, ε_{max} = 115 M^{-1} cm^{-1}. − ^{1}H NMR: δ = 2.76−3.60 (complex multiplet, 24 H, cage methylene), 4.41 (s, 2 H, CH_2py), 8.00, 8.02, 8.04, 8.06, 8.54, 8.58, 8.59, 8.74, 8.77 (m, 4 H, ArH). − Yield from F3: 1.18 g 53%. − $C_{26}H_{45}Cl_4CoN_{10}\cdot 2H_2O$: calcd. C 42.52, H 6.72, N 19.07; found C 42.5, H 6.3, N 19.1. − UV/Vis (0.1 M HCl): λ_{max} = 470 nm, ε_{max} = 95.4 M^{-1} cm^{-1}. − ^{1}H NMR: δ = 2.61, 2.67, 2.69 and 3.16, 3.22, 3.26 (ill-resolved multiplets, 24 H, cage methylene), 4.23 (s, 4 H, CH_2py), 7.1 (br. s, 6 H, NH), 7.73, 7.76, 7.80, 7.86, 8.30, 8.35, 8.38, 8.50, 8.54 (m, 8 H, ArH). − In seeking to obtain crystals from F3 suitable for X-ray crystallography, aqueous solutions of the chloride were treated with dilute HNO_3 and $Li_2S_2O_6$, giving, on slow evaporation of the solvent from the product solutions at room temperature, materials that were established by subsequent structure determinations (see below) to be the differently protonated species $[Co\{(2\text{-}pyCH_2NH)(2\text{-}pyCH_2NH_2)sar\}](NO_3)_4\cdot 2H_2O$ (**11**) and $[Co\{(2\text{-}pyCH_2NH_2)_2sar\}](S_2O_6)_2Cl\cdot 6H_2O$ (**12**), respectively. F2 was subsequently also crystallized by the use of dithionate to give the diprotonated dithionate-chloride $[Co\{sar(NH_3)[NHCH_2(C_5H_4NH)]\}](S_2O_6)_2Cl\cdot 3H_2O$ (**13**).

$[Co\{(2\text{-}pyCH_2NH)(CH_3)sar\}]^{3+}$: $[Co\{(CH_3)(NH_3)sar\}]Cl_4\cdot 0.5H_2O$ (1.05 g, 2 mmol) was converted into the acetate following the procedure described above. This was dissolved in dimethyl sulfoxide (30 mL) containing triethylamine (0.20 g), after which 2-pyridinecarbaldehyde (0.32 g, 3 mmol) was added and the mixture was heated at 90 °C for 10 h. Reduction with borohydride, re-oxidation of the metal, and chromatographic workup of the product mixture

were conducted as described above. In this case, only two bands were observed, the first corresponding to the reactant and the second being the desired product. Yield (F2): 1.10 g, 88%. − $C_{21}H_{41}Cl_4CoN_8{\cdot}H_2O$: calcd. C 40.40, H 6.94, N 17.95; found C 40.4, H 6.9, N 18.0. − UV/Vis (0.1 M HCl): λ_{max} = 472 nm, ε_{max} = 129 M^{-1} cm^{-1}. − ^{1}H NMR: δ = 0.98 (s, 3 H, CH_3), 2.45, 2.52, 2.71, 2.78. 2.82, 2.86, 3.06, 3.10, 3.13, 3.35, 3.39 (m, 24 H, cage methylene), 4.31 (s, 2 H, CH_2py), 7.00, 7.15 (br. s, 6 H, NH), 7.98, 8.01, 8.03, 8.05, 8.54, 8.58, 8.62, 8.75, 8.79 (m, 4 H, ArH).

Apparent Polymerization Processes

When the procedure described above for the reactions of $[Co\{(NH_3)_2sar\}]Cl_5{\cdot}H_2O$ was followed using 2-pyrrolecarbaldehyde as the substrate, all proceeded as expected until attempts were made to elute the crude reaction product from H^+-form Dowex 50W × 2 resin using 3 M HCl. The orange eluate rapidly began to darken and within a few hours appeared black. Dilution and reabsorption of the solution on the resin gave a black deposit, which could not be removed even by the use of concentrated HCl as eluent.

In the case of the product obtained from the reaction with 3-thiophenecarbaldehyde, isolation of the alkylated cage complexes was straightforward, but under strongly oxidative conditions some evidence of polymerization was obtained. Thus, 3-thiophenecarbaldehyde (0.35 g) was added to a solution of $[Co\{(NH_2)_2sar\}](ClO_4)_3$ (1.00 g) in dimethylacetamide (2 mL) and the mixture was heated on a steam bath for 20 min. Excess $NaBH_4$ (0.10 g) was added to the cooled orange solution, which led to an immediate colour change to an intense violet (presumably due to the *N*-deprotonated cage complex[7]). After 5 min, this solution was poured into 1 M HCl (50 mL) and, when the effervescence due to decomposition of the excess $[BH_4]^-$ had subsided, the orange solution was left to stand at room temperature for 12 h, in the course of which the bulk of the dialkylated product complex precipitated as fine, yellow needles. This solid (0.30 g, 26%) was filtered off, washed with ethanol, and the combined filtrate and washings were passed through a column of H^+-form Dowex 50W × 2 resin to absorb the residual soluble complexes as an orange band. The column was washed with 1 M HCl to remove Na^+, then eluted with a gradient of 3 M → 7 M HCl to reveal three orange components. The first proved to be a trace of reactant, the second consisted of the monoalkylated complex (0.26 g, 26%), and the third consisted of additional dialkylated complex (0.17 g, 14%). Note that in a similar experiment using only 0.18 g of 3-thiophenecarbaldehyde in the hope of obtaining largely the monoalkylated complex, a mixture of the same three species was obtained, although the monoalkylated complex (0.36 g, 37%) did predominate over the dialkylated (0.18 g, 15%). Analysis for the monoalkylated complex $C_{19}H_{40}Cl_5CoN_8S{\cdot}3H_2O$: calcd. C 32.47, H 6.60, N 15.94, S 4.56; found C 33.0, H 7.3, N 15.4, S 4.3; for the dialkylated complex $C_{24}H_{44}Cl_5CoN_8S_2{\cdot}5H_2O$: calcd. C 34.52, H 6.52, N 13.42, S 7.68; found C 34.8, H 6.8, N 13.5, S 7.4. − UV/Vis: monoalkylated complex (0.1 M HCl): λ_{max} = 472 nm, ε_{max} = 108 M^{-1} cm^{-1}; dialkylated complex (water): λ_{max} = 471 nm, ε_{max} = 152 M^{-1} cm^{-1}. Monoalkylated complex: ^{1}H NMR: δ = 2.80 (m), 3.42 (m, ethylene bridge AA′BB′ system), 2.91 (d), 3.32 (d, cap methylene AB systems), 4.16 (s, substituent methylene), 7.02 (d), 7.35 (q), 7.44 (d, thiophene CH). − ^{13}C NMR: δ = 40.1, 49.1, 50.3, 53.17, 53.21 (CH_2), 55.0, 60.0 (quaternary C), 126.9, 127.0, 127.1 (thiophene ArCH), 129.7 (thiophene ArC); dialkylated complex: ^{1}H NMR: δ = 2.40 (d), 3.02 (d, cap methylene AB system), 2.56 (m), 3.10 (m, ethylene bridge AA′BB′ system), 3.58 (q, substituent methylene), 6.88 (d), 7.10 (d), 7.24 (q, thiophene CH). − ^{13}C NMR: δ = 40.2, 48.1, 52.4 (CH_2), 59.7 (quaternary C), 127.0, 127.2, 127.5 (thiophene ArCH), 128.6 (thiophene ArC). Note that, as for all cage complexes with basic external substituents, chemical shift values and the overall appearance of the spectra are generally very dependent on both the concentration and pH of the solutions.[7] Crystals of the monoalkylated complex (as its pentachloride, **14**) suitable for X-ray diffraction analysis were obtained by adding ethanol to a solution of the complex in water to the point of turbidity and then allowing the mixture to stand at room temperature for 24 h. Of various attempts made to achieve chemically oxidative oligomerization of the thiophene-substituted complexes, only the following provided some evidence of success. The dialkylated complex (chloride, **15**; 100 mg) was dissolved in concentrated HNO_3 (2 mL) and this orange solution was mixed with a slurry of $[NH_4]_2[Ce(NO_3)_6]$ (80 mg) in concentrated HNO_3 (1 mL). Agitation of the mixture resulted in the rapid dissolution of all solids and a colour change of the solution to deep yellow-orange. After 5 min, water (10 mL) was added, which led to the deposition of a yellow-orange solid. The mixture was cooled in ice for 5 min and then the precipitate was collected, washed with water (2 mL), ethanol, and diethyl ether, and dried in air (74 mg). The cloudy filtrate and washings were pale-yellow in colour.

Structure Determinations

Diffraction data were acquired in a number of modes, at the specified temperature, using monochromatic Mo-K_α radiation, λ = 0.71073 Å, on all instruments. Using a single counter instrument in 2θ/θ scan mode, *N* unique reflections were measured within the specified $2\theta_{max}$ limit, N_o with $I > 3\sigma(I)$ being considered "observed", gaussian absorption corrections being applied. Data were also measured using a Bruker AXS CCD instrument ($2\theta_{max}$ = 58°), the total number of reflections, N_t, within a full sphere being merged to *N* unique, R_{int} as specified after "empirical"/multiscan absorption correction within the proprietary/preprocessing software; the "observed" criterion applied was $F > 4\sigma(F)$. Anisotropic thermal parameter forms were refined in a full-matrix context for non-hydrogen atoms, $(x, y, z, U_{iso})_H$ being constrained at estimated values. Conventional residuals *R*, R_w (statistical weights) on |*F*| are quoted at convergence. Neutral atom complex scattering factors were employed within the Xtal 3.4 program system.[24] Pertinent results are given in the Figures and below; individual variations in procedure/difficulties/idiosyncrasies are cited as "*variata*". Crystallographic data (excluding structure factors) for the structures reported in this paper have been deposited with the Cambridge Crystallographic Data Centre as supplementary publication nos. CCDC-151305−151312. Copies of the data can be obtained free of charge on application to the CCDC, 12 Union Road, Cambridge, CB2 1EZ, U.K. [Fax: (internat.) +44 (0)1223/336033; E-mail: deposit@ccdc.cam.ac.uk]. Cation projections are shown in Figure 1; common *ad hoc* crystallographic numbering is shown, carbon atoms being denoted by number only. Non-hydrogen atoms are shown with 20% (room temperature) or 50% (low temperature) probability displacement ellipsoids. Bond lengths and angles are generally as expected throughout the array and are not addressed further, the interest lying in the isomeric and conformational variations discussed in the text above and shown in the Figures.

Crystal/Refinement Data

6. $[Co\{sar[NHCHN(CH_3)_2]\}]Cl_5{\cdot}3H_2O$ ≡ $C_{20}H_{52}Cl_5CoN_{10}O_3$, $M \approx 716.9$. CCD-instrument, $T \approx 153$ K. Triclinic, space group $P\bar{1}$ (C_i^1, No.2), a = 8.902(1), b = 12.105(2), c = 16.378(2) Å, α = 70.584(2), β = 76.662(2), γ = 82.194(2)°, V = 1616.1 Å^3. $D_{calcd.}$ (Z = 2) = 1.473 g cm^{-3}. μ_{Mo} = 9.9 cm^{-1}; specimen: 0.35 × 0.20 × 0.08 mm; $T'_{min.,max}$ = 0.68, 0.89. N_t = 18312, N = 7724 (R_{int} =

0.022), $N_o = 6978$; $R = 0.027$, $R_w = 0.038$. $|\Delta\rho_{max}| = 0.51(2)$ e Å^{-3}.

Variata: $(x, y, z, U_{iso})_{HHH}$ were refined throughout.

8. [Co{sar(NHCOC$_6$H$_5$)$_2$}]Cl$_3$·1.63H$_2$O ≡ $C_{28}H_{45.26}Cl_3CoN_8O_{3.63}$, $M \approx 717.4$. Single-counter instrument, $T \approx 295$ K. Monoclinic, space group $P2_1/c$ (C_{2h}^5, No.14), $a = 16.242(8)$, $b = 13.810(4)$, $c = 16.714(16)$ Å, $\beta = 115.93(5)°$, $V = 3372$ Å^3. $D_{calcd.}$ ($Z = 4$) = 1.426 g cm^{-3}. $\mu_{Mo} = 7.9$ cm^{-1}; specimen: 0.22 × 0.65 × 0.60 mm; $T_{min.,max} = 0.62, 0.93$. $2\theta_{max} = 60°$; $N = 7728$, $N_o = 5795$; $R = 0.035$, $R_w = 0.039$. $|\Delta\rho_{max}| = 0.44$ e Å^{-3}.

Variata: Site occupancy of O(2) refined to 0.630(6); no associated hydrogen atoms were located. For all other hydrogen atoms, (x, y, z, U_{iso}) were refined.

10. [Co{sar[NHCO(*o*-C$_6$H$_4$CO$_2$H)]$_2$}]Cl$_3$·6^3/$_4$H$_2$O ≡ $C_{30}H_{55.5}Cl_3CoN_8O_{12.75}$, $M \approx 897.6$. CCD instrument, $T \approx 300$ K. Triclinic, space group $P\bar{1}$, $a = 13.433(1)$, $b = 17.434(2)$, $c = 18.997(2)$ Å, $\alpha = 97.181(2)$, $\beta = 99.057(2)$, $\gamma = 108.238(2)°$, $V = 4100$ Å^3. $D_{calcd.}$ ($Z = 4$) = 1.454 g cm^{-3}. $\mu_{Mo} = 6.8$ cm^{-1}; specimen: 0.45 × 0.35 × 0.15 mm; $'T'_{min.,max} = 0.74, 0.87$. $N_t = 47686$; $N = 19991$ ($R_{int} = 0.032$), $N_o = 7593$; $R = 0.055$, $R_w = 0.058$. $|\Delta\rho_{max}| = 0.84$ e Å^{-3}.

Variata: High "thermal motion" was evident in relation to a number of residues modelled as water molecule oxygen atoms; refinement of site occupancies suggested only that of O(14) to be seriously deviant from unity, disposed over a pair of sites 1.79(2) Å apart, its occupancies refining to ca. 0.5 and being constrained thus. Hydrogen atoms were located in difference maps as being associated with O(1)−O(7).

11. [Co{sar(NH$_2$CH$_2$C$_5$H$_4$N)(NHCH$_2$C$_5$H$_4$N)}](NO$_3$)$_4$·2H$_2$O ≡ $C_{26}H_{49}CoN_{14}O_{14}$, $M = 840.7$. Single-counter instrument, $T \approx 295$ K. Monoclinic, space group $C2/c$ (C_{2h}^6, No. 15), $a = 8.416(2)$, $b = 14.877(3)$, $c = 27.405(4)$ Å, $\beta = 95.39(1)°$, $V = 3461$ Å^3. $D_{calcd.}$ ($Z = 4$) = 1.634 g cm^{-3}. $\mu_{Mo} = 5.9$ cm^{-1}; specimen: 0.40 × 0.25 × 0.30 mm; $T_{min.,max} = 0.84, 0.96$. $2\theta_{max} = 50°$; N_t (hemisphere to 50°; sphere to 40°) = 8648, $N = 3009$ ($R_{int} = 0.079$), $N_o = 1947$; $R = 0.060$, $R_w = 0.062$. $|\Delta\rho_{max}| = 1.00$ e Å^{-3}.

Variata: Protonation as indicated is incompatible with $Z = 4$ in the centrosymmetric space group; difference map considerations suggested protonation of the "diamsar" nitrogen atoms and the proton was located thus, occupancy 0.5; other disorder, notably among one of the nitrate groups, also modelled as disposed over two sets of sites, occupancies 0.5, may be concerted with that of the protonation. Attempted refinement in a lower symmetry was (inherently) unfruitful (it has not escaped our notice that in later determinations in the series, the pyridine moiety is definitively described as protonated, rather than the NH group).

12. [Co{sar[NHCH$_2$(C$_5$H$_4$NH)]$_2$}](S$_2$O$_6$)$_2$Cl·6H$_2$O ≡ $C_{26}H_{58}ClCoN_{10}O_{18}S_4$, $M = 1021.5$. Single-counter instrument, $T \approx 295$ K. Monoclinic, space group $C2/c$, $a = 16.353(3)$, $b = 14.783(3)$, $c = 17.510(3)$ Å, $\beta = 98.38(2)°$, $V = 4188$ Å^3. $D_{calcd.}$ ($Z = 4$) = 1.620 g cm^{-3}. $\mu_{Mo} = 7.6$ cm^{-1}; specimen: 0.55 × 0.50 × 0.26 mm; $T_{min.,max} = 0.72, 0.83$. $2\theta_{max} = 55°$; N_t (hemisphere) = 7753, $N = 4813$ ($R_{int} = 0.029$), $N_o = 3694$; $R = 0.050$, $R_w = 0.066$. $|\Delta\rho_{max}| = 0.91$ e Å^{-3}.

Variata: Hydrogen atoms were not located as being associated with "water molecule oxygen atoms" O(2,3), these having apparent occupancies of unity based on refinement behaviour; (x, y, z, U_{iso}) (all other H) were refined.

13. [Co{sar(NH$_3$)[NHCH$_2$(C$_5$H$_4$NH)]}](S$_2$O$_6$)$_2$Cl·3H$_2$O ≡ $C_{20}H_{47}ClCoN_9O_{15}S_4$, $M = 876.3$. CCD instrument, $T \approx 300$ K. Monoclinic, space group $P2_1/c$ (C_{2h}^5, No. 14), $a = 14.457(1)$, $b = 9.8567(8)$, $c = 24.562(2)$ Å, $\beta = 96.990(2)°$, $V = 3474$ Å^3. $D_{calcd.}$ ($Z = 4$) = 1.675 g cm^{-3}. $\mu_{Mo} = 8.9$ cm^{-1}; specimen: 0.24 × 0.16 × 0.10 mm; $'T'_{min.,max} = 0.66, 0.93$. $N_t = 38653$, $N = 8676$ ($R_{int} = 0.038$), $N_o = 5464$; $R = 0.045$, $R_w = 0.052$. $|\Delta\rho_{max}| = 0.78$ e Å^{-3}.

Variata: (x, y, z, U_{iso}) were refined for all hydrogen atoms except those associated with the water molecules, which were located from difference maps.

14. [Co{sar(NH$_3$)(NH$_2$CH$_2$C$_4$H$_3$S)}]Cl$_5$·3H$_2$O ≡ $C_{19}H_{46}Cl_5CoN_8O_3S$, $M = 702.9$. CCD instrument, $T \approx 153$ K. Monoclinic, space group Cc (C_s^4, No. 9), $a = 19.321(3)$, $b = 19.624(3)$, $c = 16.989(2)$ Å, $\beta = 91.255(2)°$, $V = 6440$ Å^3. $D_{calcd.}$ ($Z = 8$) = 1.450 g cm^{-3}. $\mu_{Mo} = 10.5$ cm^{-1}; specimen: 0.65 × 0.17 × 0.15 mm; $'T'_{min.,max} = 0.54, 0.88$. $N_t = 17751$, $N = 4560$ ($R_{int} = 0.050$), $N_o = 4167$ ("Friedel pairs" preserved distinct); $R = 0.060$, $R_w = 0.073$; $x_{abs} = 0.06(4)$. $|\Delta\rho_{max}| = 0.70(3)$ e Å^{-3}.

Variata: The pendant residue on molecule 1 of the two independent molecules in the asymmetric unit was modelled as being disordered over two sets of sites; occupancies were set at 0.5 each after trial refinement and coalesced with a more extensive mass of disordered fragments modelled as water molecule oxygen atoms; site occupancies 0.5. Cl(1,2) were also modelled as being disordered over pairs of sites, with separations of 0.80(3), 1.49(4) Å, and occupancies refining to 0.74(2), 0.72(2); under unit totality constraint after trial refinement, these complemented the smaller fragments of the Cl; those of the other disordered non-hydrogen atoms were refined with isotropic thermal parameter forms.

16. [Co{sar(CH$_3$)(NHCH$_2$C$_6$H$_4$C$_6$H$_5$)}](NO$_3$)$_{2.5}$Cl$_{0.5}$ca. 4^1/$_8$H$_2$O ≡ $C_{28}H_{53.25}Cl_{0.5}CoN_{9.5}O_{11.625}$, $M \approx 785.7$. CCD instrument, $T \approx 153$ K. Monoclinic, space group $C2/c$, $a = 60.926(5)$, $b = 15.353(1)$, $c = 15.365(1)$ Å, $\beta = 92.410(2)°$, $V = 14360$ Å^3. $D_{calcd.}$ ($Z = 16$) = 1.454 g cm^{-3}. $\mu_{Mo} = 5.9$ cm^{-1}; specimen: 0.80 × 0.35 × 0.10 mm; $'T'_{min.,max} = 0.52, 0.86$. $N_t = 79381$, $N = 12608$ ($R_{int} = 0.10$), $N_o = 7314$; $R = 0.099$, $R_w = 0.12$. $|\Delta\rho_{max}| = 3.71(4)$ e Å^{-3}.

Variata: The anion complement was modelled in terms of a total charge of three, made up of one-half of a chloride ion and two-and-a-half nitrate ions, one of the latter being modelled as being disordered over two sets of sites, oxygen occupancies set at 0.5 after trial refinement. The molecules pack as double layers disposed on either side of the plane(s) $x = 0.125$ (etc.), interleaved by layers comprising residues modelled in terms of some anions and water molecule oxygen atoms, about the plane(s) $x = 0$ (etc.). These encompass considerable disorder with a number of site occupancies modelled being set at 0.5 after trial refinement.

Acknowledgments

This work was partially supported by the Australian Research Council and by Kosin University.

[1] G. A. Bottomley, I. J. Clark, I. I. Creaser, L. M. Engelhardt, R. J. Geue, K. S. Hagen, J. M. Harrowfield, G. A. Lawrance, P. A. Lay, A. M. Sargeson, A. J. See, B. W. Skelton, A. H. White, F. R. Wilner, *Aust. J. Chem.* **1994**, *47*, 143−179.
[2] A. M. Sargeson, *Coord. Chem. Rev.* **1996**, *151*, 89−114; *Pure Appl. Chem.* **1986**, *58*, 1511−1522.
[3] M. Gajhede, A. Hammershoi, L. K. Skov, *Acta Chem. Scand.* **1991**, *45*, 474−481.

[4] P. V. Bernhardt, J. M. Harrowfield, D. C. R. Hockless, A. M. Sargeson, *Inorg. Chem.* **1994**, *33*, 5659−5670.

[5] G. C. Yeh, A. M. Beatty, J. K. Bashkin, *Inorg. Chem.* **1996**, *35*, 3828−3835.

[6] P. S. Donnelly, J. M. Harrowfield, B. W. Skelton, A. H. White, *Inorg. Chem.* **2000**, *39*, 5817−5830.

[7] R. J. Geue, T. W. Hambley, J. M. Harrowfield, A. M. Sargeson, M. R. Snow, *J. Am. Chem. Soc.* **1984**, *106*, 5478−5488.

[8] [8a] P. Comba, L. M. Engelhardt, J. M. Harrowfield, E. Horn, A. M. Sargeson, M. R. Snow, A. H. White, *Inorg. Chem.* **1985**, *24*, 2325−2327. − [8b] I. J. Clark, I. I. Creaser, L. M. Engelhardt, J. M. Harrowfield, E. R. Krausz, G. M. Moran, A. M. Sargeson, A. H. White, *Aust. J. Chem.* **1993**, *46*, 111−126. − [8c] L. M. Engelhardt, J. M. Harrowfield, A. M. Sargeson, A. H. White, *Aust. J. Chem.* **1993**, *46*, 27−133. − [8d] I. I. Creaser, L. M. Engelhardt, J. M. Harrowfield, A. M. Sargeson, B. W. Skelton, A. H. White, *Aust. J. Chem.* **1993**, *46*, 465−476. − [8e] I. J. Clark, L. M. Engelhardt, R. J. Geue, J. M. Harrowfield, A. M. Sargeson, B. W. Skelton, A. H. White, *Aust. J. Chem.* **1993**, *46*, 1485−1505. − [8f] P. A. Brayshaw, J.-C. G. Bünzli, P. Froidevaux, J. M. Harrowfield, A. N. Sobolev, *Inorg. Chem.* **1995**, *34*, 2068−2076. − [8g] P. V. Bernhardt, R. Bramley, L. M. Engelhardt, J. M. Harrowfield, D. C. R. Hockless, B. R. Korybut-Daszkiewicz, E. R. Krausz, T. Morgan, A. M. Sargeson, B. W. Skelton, A. H. White, *Inorg. Chem.* **1995**, *34*, 3589−3599.

[9] P. Novák, K. Müller, K. S. V. Santhanam, O. Haas, *Chem. Rev.* **1997**, *97*, 207−281.

[10] I. L. Finar, *Organic Chemistry*, 3rd Edition, Longmans, 1959, p. 647.

[11] B. C. R. Penfold, J. C. B. White, *Acta Crystallogr.* **1959**, *12*, 130−133.

[12] C. C. F. Blake, R. W. H. Small, *Acta Crystallogr., Sect. B* **1972**, *28*, 2201−2206.

[13] Q. Gao, G. A. Jeffrey, J. R. Ruble, R. K. McMullan, *Acta Crystallogr., Sect. B (Str. Sci.)* **1991**, *47*, 742−745.

[14] J. R. Ruble, A. Galvao, *Acta Crystallogr., Sect. B (Str. Sci.)* **1995**, *51*, 835−838.

[15] M. K. Ghosh, K. L. Mittal, *Polyimides: Fundamentals and Applications*, Marcel Dekker, New York, **1996**.

[16] G. Smith, C. H. L. Kennard, G. F. Katekar, *Aust. J. Chem.* **1983**, *36*, 2455−2463.

[17] J. M. Harrowfield, V. Norris, A. M. Sargeson, *J. Am. Chem. Soc.* **1976**, *98*, 7282−7289.

[18] P. M. Angus, A. M. T. Bygott, R. J. Geue, B. Korybut-Daszkiewicz, A. H. W. Mau, A. M. Sargeson, M. M. Sheil, A. C. Willis, *Chem. Eur. J.* **1997**, *3*, 1283−1291 and references therein.

[19] J. M. Harrowfield, G. A. Koutsantonis, N. Lengkeek, *work in progress.*

[20] J. Roncali, *Chem. Rev.* **1992**, *92*, 711−738 and references therein.

[21] G. P. Gardini, *Adv. Heterocycl. Chem.* **1973**, *15*, 67−98.

[22] Y. Zhu, D. B. Millet, M. Wolf, S. J. Rettig, *Organometallics* **1999**, *18*, 1930−1938.

[23] A. M. Bond, G. A. Lawrance, P. A. Lay, A. M. Sargeson, *Inorg. Chem.* **1983**, *22*, 2010−2021.

[24] S. E. Denmark, E. N. Jacobsen, *Acc. Chem. Res.* **2000**, *324* and following articles.

[25] N. Di Bartolo, A. M. Sargeson, S. V. Smith, *J. Chem. Soc., Dalton Trans* **2000**, in press.

[26] "*The Xtal 3.4 User's Manual*", (Eds.: S. R. Hall, G. S. D. King, J. M. Stewart), University of Western Australia, Lamb, Perth, **1995**.

Received October 21, 2000
[I00400]

Intercalates of Vanadyl Phosphate with Branched Alcohols

Ludvík Beneš,*[a] Vítězslav Zima,[a] and Klára Melánová[a]

Keywords: Vanadium / Phosphate / Alcohols / Intercalations

Intercalates of $VOPO_4$ with several branched alcohols (2-propanol, 2-methyl-1-propanol, 3-methyl-1-butanol, 4-methyl-1-pentanol, 2-methyl-2-propanol, 2,2-dimethyl-1-propanol, 3,3-dimethylbutanol, 3-methyl-1-pentanol, 2-methyl-1-pentanol, 2-hexanol, 2-ethyl-1-butanol, 2-propyl-1-pentanol) were prepared and characterized by powder X-ray diffractometry and thermogravimetry. Only 2-propanol, 2-methyl-1-propanol and 3-methyl-1-butanol were directly intercalated into vanadyl phosphate dihydrate. The other intercalates were prepared by the displacement of 2-propanol. Gas chromatography of the solid intercalates showed that no mixed intercalates still containing the starting alcohol are formed, except the 4-methyl-1-pentanol intercalate. The arrangement of the guest molecules in the interlayer space of the host is discussed. The alcohols are anchored to the host layers by donor-acceptor bonds between their oxygen atoms and the vanadium atoms of the host structure, and by hydrogen bonding.

Introduction

A number of papers have reported attempts to find the principles governing the structure arrangements of unbranched aliphatic molecules with terminal functional groups during their intercalation into various host structures.[1,2] With this aim the intercalations of, for example, aliphatic alcohols, diols and amines into some natural silicates,[3,4] vanadyl phosphate and sulfate,[5−8] α- and γ-$Zr(HPO_4)_2{\cdot}H_2O$,[9,10] and other similar hosts were investigated.

The reaction of solid $VOPO_4{\cdot}2H_2O$ with liquid or molten 1-alkanols in a microwave field leads to intercalation compounds with the general formula $VOPO_4{\cdot}2C_nH_{2n+1}OH$ ($n = 2-18$).[8] The structure of these polycrystalline layered complexes retains the original layers of $(VOPO_4)_\infty$. The molecules of the alcohols are placed between the host layers in a bimolecular arrangement, and are anchored by donor-acceptor bonds between the oxygen atom of the OH group and the vanadium atom, as well as by hydrogen bonds. The aliphatic chains of the intercalated alcohol molecules possess an *all-trans* configuration and their axes are perpendicular to the host layers.

Little attention has been paid to the intercalation of molecules with branched alkyl chains. The intercalation of 2-butylamine, isobutylamine and neopentylamine into mixed niobyl-vanadyl phosphate was studied.[11] Smaller amounts of 2-butylamine than isobutylamine are intercalated, because of the larger cross-section area. An increase in the molecular volume (neopentylamine) also decreases the amine content. The basal spacing of these amine intercalates is close to that of 1-propylamine and their molecules are arranged in a bimolecular way with their main axis tilted at an angle of 58° with respect to the layer. 2-Propanol, 2-methyl-1-propanol and 3-methyl-1-butanol were intercalated into anhydrous vanadyl sulfate.[6] The basal spacing of these intercalates is very similar to that of the unbranched alcohol with the same length of the main alkyl chain. The content of isoalcohols in the intercalates is lower than that for 1-alkanols.

In this paper the structure of the $VOPO_4$ intercalates with several branched alcohols is discussed.

Results and Discussion

Preparation and Characterization of Intercalates

Only 2-propanol, 2-methyl-1-propanol and 3-methyl-1-butanol were directly intercalated into vanadyl phosphate dihydrate. The intercalates of vanadyl phosphate with other branched alcohols were prepared by displacement of 2-propanol. To exclude the possible formation of a mixed intercalate of 2-propanol with the branched alcohol, an analogous reaction was carried out starting from the 1-propanol intercalate as a precursor. All intercalates are yellow, indicating that vanadium(V) is not significantly reduced. The intercalates of the branched alcohols are distinctly less stable than the intercalates of 1-alkanols,[8] and rapidly decompose in air (relative humidity of 50%) and hydrate to $VOPO_4{\cdot}2H_2O$.

The intercalates prepared are crystalline solids. The diffractograms show a series of sharp (00*l*) reflections (typical diffractograms are shown in Figure 1). The *a* parameter of the tetragonal lattice was determined from the (200) and (201) diffraction lines (Table 1). The same lattice parameter *c* was obtained for the intercalates prepared by displacement of 1-propanol. Gas chromatography of the solid intercalates showed that no mixed intercalates containing starting alcohol were formed, with just one exception (see below). The stoichiometric quotient x_{exp} obtained by the thermogravimetric analysis and several checking analyses of

[a] Joint Laboratory of Solid State Chemistry of Academy of Sciences of the Czech Republic and University of Pardubice, Studentská 84, 532 10 Pardubice, Czech Republic
Fax: (internat.) + 420-40/603-6011
E-mail: ludvik.benes@upce.cz

 © WILEY-VCH Verlag GmbH, 69451 Weinheim, 2001 1434−1948/01/0707−1883 $ 17.50+.50/0

carbon and hydrogen contents are given in Table 1, together with the values of x_{calc} calculated as a ratio of the volume of alcohol intercalated and the molar volume of alcohol calculated from its density. The volume of the alcohol intercalated was calculated as a difference between the unit cell volume of the intercalate and anhydrous $VOPO_4$.

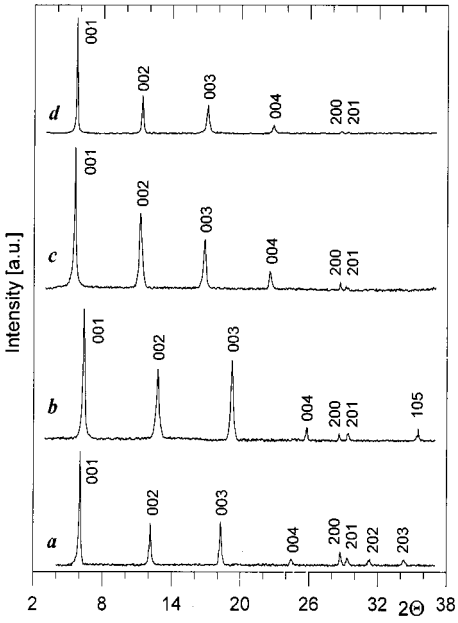

Figure 1. Diffractograms of the $VOPO_4$ intercalates with: (a) 2-methyl-1-propanol, B; (b) 2,2-dimethyl-1-propanol, K; (c) 3,3-dimethyl-1-butanol, J; (d) 2-ethyl-1-butanol, I

Table 1. Lattice parameters and composition of intercalates (mol alcohol/mol $VOPO_4$)

Alcohol	Denotation	a [Å]	c [Å]	x_{exp}	x_{calc}
2-Propanol	A	6.21	13.26	1.45	1.39
2-Methyl-1-propanol	B	6.22	14.58	1.20	1.32
3-Methyl-1-butanol	C	6.21	16.27	1.40	1.29
4-Methyl-1-pentanol	D	6.21	19.67	-	-
3-Methyl-1-pentanol	E	6.21	16.94	1.05	1.20
2-Methyl-1-pentanol	F	6.21	16.80	0.90	1.18
2-Hexanol	G	6.20	16.83	0.95	1.17
2-Propyl-1-pentanol	H	6.21	16.60	1.03	0.93
2-Ethyl-1-butanol	I	6.22	15.64	0.90	1.09
3,3-Dimethyl -1-butanol	J	6.22	15.80	1.05	1.08
2,2-Dimethyl-1-propanol	K	6.20	14.20	0.98	1.06
2-Methyl-2-propanol	L	6.21	12.80	1.00	1.07

The IR spectra of the $VOPO_4$ intercalates shows a ν(V=O) band in the region 1000−1007 cm^{-1}, overlapping the intense bands of the PO_4 tetrahedron. This indicates the presence of a donor-acceptor bond between the oxygen atom of the alcohol and the vanadium atom similar to the bond between the water or 1-alkanol molecules and the host layers.[12,13] Several broad bands in the region from 3600 to 3100 cm^{-1} were found, which could be assigned to a valence vibration of the OH group affected by the interaction of the alcohol with the host lattice.

Suggested Arrangements of Guest Molecules

A set of 12 alcohols with branched aliphatic chains was chosen so as to provide maximum information about the influence of the chain branching on the composition, basal spacing, and stability of the intercalates formed. The structures of the chains are shown in Figure 2. In the following text, the properties of these intercalates are compared with the intercalates of $VOPO_4$ with the 1-alkanols and 2-alkanols studied earlier.[8,15] The influence of the number of the carbon atoms in the main chain on properties of the intercalates is examined. A chain with increasing number of the carbon atoms in a series is considered as the main chain.

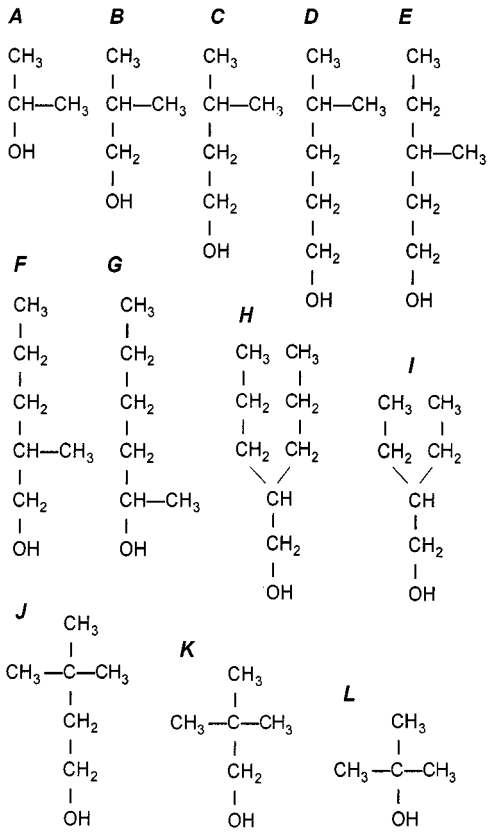

Figure 2. Structure of the guest molecules; see also Table 1

Intercalates with Isoalcohols

With increasing length of the main chain the basal spacing of the intercalates of the first three isoalcohols (A−C) changes linearly, increasing by one carbon atom (1.51 Å) at a time. This increase is equal to 1.28 Å for an unbranched alkyl *all-trans* chain placed perpendicularly to the host layers.[14] It is obvious that the molecules of these three isoalcohols form a bilayer system between the $(VOPO_4)_\infty$ sheets, and their main chains are tilted at an angle $\alpha = 36°$ to the host layers.

The experimental stoichiometric coefficient (TGA) and that calculated from the changes of the volume is ≈1.3 for these intercalates (Table 1). For 3-methyl-1-butanol, x_{exp} =

1.4 and $x_{calc} = 1.3$. The free interlayer volume available to 3-methyl-1-butanol in the intercalate is given by

$$V_i = (d - d_H) \times a^2 = 466.24 \text{ Å}^3$$

where d is the basal spacing of the intercalate, d_H is the thickness of the host layer (which is equal to the basal spacing of anhydrous $VOPO_4$), and a is the parameter of the tetragonal layer. The molecular volume of 3-methyl-1-butanol is $V_g = 180.8$ Å^3 (calculated by the ChemSketch program). The theoretical number of the guest molecules which can be placed at one vanadium site is therefore

$$x_{theor} = V_i/(V_g \times Z) = 1.29$$

where $Z = 2$ (number of formula units per cell as found for $VOPO_4 \cdot 2H_2O$).[16] To complement the coordination sphere of every vanadium atom in the host layer to an octahedron, one alcohol molecule should be bonded by a donor-acceptor bond to every vanadium atom. The rest of the alcohol molecules should be bonded by hydrogen bonds only and placed in the cavities among the donor-acceptor-bonded molecules. A similar principle of the guest arrangement was proposed for the intercalate of vanadyl phosphate with propargyl alcohol.[17]

The intercalate with 4-methyl-1-pentanol has a distinctly higher basal spacing than the other three alcohols from this group (see Table 1). Only this intercalate decomposes to a multiphase during drying carried out either by vacuum distillation at 25 °C in an evacuated ampoule or by washing with ether and subsequent blowing with dry nitrogen. The basal spacing is practically the same as that for the 1-pentanol intercalate (19.71 Å),[8] indicating that the guest molecules are roughly perpendicular to the host layers. We can assume that the intercalate prepared is in fact a cointercalate containing 2-propanol or 1-propanol (according to the precursor used) in the cavities among the methyl groups of the 4-methyl-1-pentanol molecules. The presence of 2-propanol or 1-propanol was confirmed by gas chromatography of the hydrolyzate of the wet samples after washing with 4-methyl-1-pentanol; propanol was not found in the hydrolyzate of the dry multiphase product. The decomposition of the sample during drying is connected to the release of the propanol molecules from the intercalate structure.

Intercalates with Alcohols Having Three Methyl Groups at the Terminal Carbon Atom of the Main Chain

Three alcohols were intercalated into $VOPO_4$: 2-methyl-2-propanol (*tert*-butyl alcohol, see structure L in Figure 2), 2,2-dimethyl-1-propanol (K), and 3,3-dimethylbutanol (J). As for the isoalcohols, alcohols with three terminal methyl groups change the basal spacing linearly with increasing chain length in increments of 1.50 Å per carbon atom. This implies that these alcohols are also present in the space in two layers and their main chain is tilted to the host layer at an angle of 36°. The amount of alcohol intercalated was distinctly lower than that for the isoalcohol intercalates and the stoichiometric coefficient is ≈1. This value and the value of the basal spacing allow us to propose a relatively simple arrangement of the alcohol molecules in the interlayer space as depicted in Figure 3.

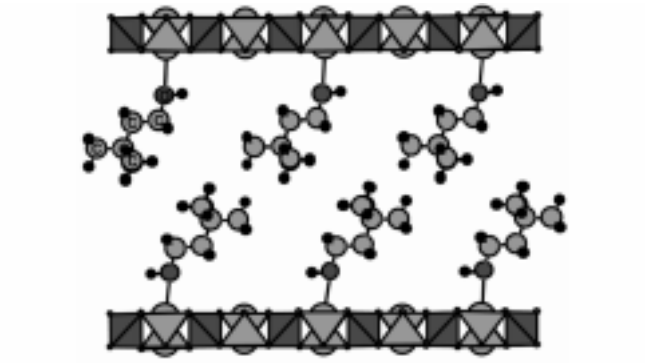

Figure 3. Proposed arrangement of 3,3-dimethyl-1-butanol between the $VOPO_4$ layers viewed in the direction of the *xy* diagonal

From a comparison of the isoalcohol intercalates with this group of intercalates we deduced that the amount of intercalated alcohol was lower for more-branched alcohols; nevertheless the basal spacing and, consequently, the orientation of the main chain with respect to the host layers remained the same.

The Effect of the Position of the Methyl Group in the Main Chain

This effect on the composition and structure was followed in the series 4-methyl-1-pentanol (see structure D in Figure 2), 3-methyl-1-pentanol (E), 2-methyl-1-pentanol (F), and 2-hexanol (which can be considered as "1-methyl-1-pentanol" in the given series, G). As mentioned above, 4-methyl-1-pentanol forms a very unstable cointercalate containing propanol and having a distinctly higher basal spacing. The other three alcohols form intercalates with roughly the same basal spacing and their stoichiometric coefficient x is equal to 1 (see Table 1). A two-layer arrangement of the guest molecules was proposed for the 2-alkanol intercalates, with the guest chain tilted with respect to the host layers at $\alpha = 25.6°$; this also applies to the 2-hexanol intercalate (see Figure 4).[15] With regard to the similar

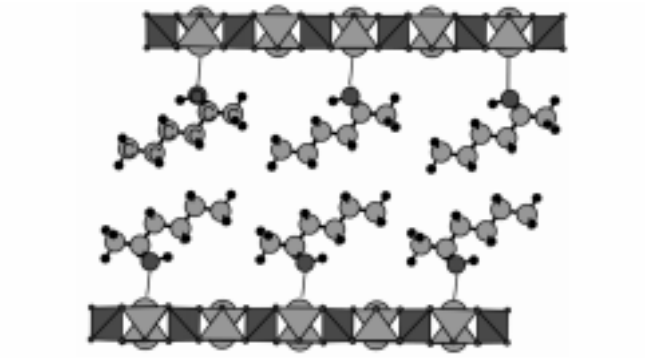

Figure 4. Proposed arrangement of the 2-hexanol molecules between the $VOPO_4$ layers viewed in the direction of the *xy* diagonal

basal spacing, it is very probable that the 2-methyl-1-pentanol and 3-methyl-1-pentanol molecules are found in the interlayer space in a similar arrangement. This means that the position of the methyl group probably does not influence the arrangement of these alcohols in the intercalates. In contrast to 1-pentanol ($x = 2$), which forms a bilayer arrangement with the chains perpendicular to the host layers, there is a significant decrease of the amount of intercalated alcohol ($x = 1$), which is connected to a distinct inclination of the carbon chain. Only a methyl group placed at the end of the long chain allows a perpendicular arrangement as inferred from the higher value of the basal spacing for the 4-methyl-1-pentanol intercalate.

Influence of the Size of Two Identical Alkyl Groups in 2,2-Dialkyl-1-ethanol

Intercalates with 2-methyl-1-propanol (B), 2-ethyl-1-butanol (H), and 2-propyl-1-pentanol (I) were prepared in this series. In contrast to the ethanol intercalate there is a distinct decrease of the stoichiometric coefficient, which is equal to one for the longer alcohols. An arrangement of the 2-propyl-1-pentanol molecules in the interlayer space is proposed in Figure 5. For this alcohol we can consider the heptane chain as a main alkyl chain in the *all-trans* configuration with a -CH_2CH_2OH group (a hydroxyethyl group) bonded to its fourth carbon atom. The hydroxyethyl group is anchored to the host layers by a donor-acceptor bond between the guest oxygen atom and the vanadium atom of $VOPO_4$. The heptane chain is oriented in the direction of the diagonal of the host sheet and is inclined to this sheet at an angle of less than 90°.

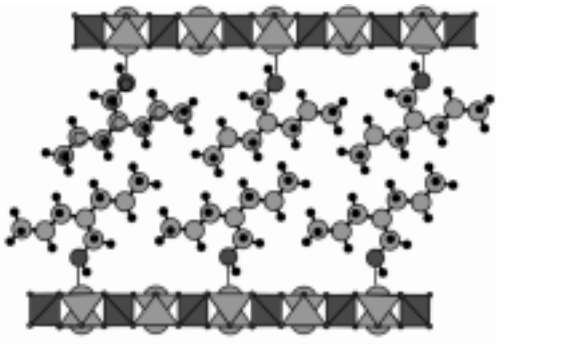

Figure 5. Proposed arrangement of the 2-propyl-1-pentanol molecules between the $VOPO_4$ layers viewed in the direction of the *xy* diagonal

Comparison of Ethanol, 2-Propanol, and *tert*-Butyl Alcohol Intercalates

Whereas the basal spacing of the intercalates of all three alcohols discussed is roughly the same, the stoichiometric coefficient decreases in the series $VOPO_4$·ethanol > $VOPO_4$·(2-propanol) > $VOPO_4$·(*tert*-butyl alcohol), with a value of $x = 1$ for the *tert*-butyl alcohol intercalate. It can be presumed that the molecules of all three alcohols are arranged in two layers in the interlayer space. The decrease of the stoichiometric coefficient with increasing branching is due to steric effects. The molecules of 2-propanol and *tert*-butyl alcohol, anchored by their oxygen atoms to the vanadium atoms of the layers, do not allow other molecules bonded only by the H bonds to fill the space between coordinated molecules as they have larger cross-sections than ethanol.

Experimental Section

Preparation: Intercalates of the isoalcohols were prepared by suspending $VOPO_4·2H_2O$ (0.3 g) in dry alcohol (7 mL) and subsequent short exposure (0.5−2 min.) to a microwave field. Intercalates of other branched alcohols were obtained by a displacement reaction. The solid 2-propanol intercalated host was prepared in advance and used as a starting material for the reactions with other alcohols. After cooling, the solid product formed was filtered off. All samples used for X-ray diffraction analyses contained small amounts of the free alcohol. The samples for TG-DTA and elemental analyses were washed with dry ether and dried in nitrogen at room temperature.

Analyses: The TGAs of the intercalates were performed with a Derivatograph MOM (Hungary), the measurements being carried out in the temperature interval of 30−600 °C in air at a heating rate of 5 °C/min. The weight of the samples was 100 mg. In some cases the composition was determined by elemental analysis (C, H).

Gas chromatography was used to check whether the intercalates contained starting alcohol (2-propanol or 1-propanol) or not. The sample was washed with an excess of the alcohol intercalated to remove 2-propanol or 1-propanol released by the intercalation. The intercalate was then hydrolyzed in a small amount of water and the hydrolysate was analyzed by GC with a Chrom4 chromatograph (Czech Republic).

X-ray Diffraction Measurements: The powder data of the intercalates with a small excess of the guest alcohol were obtained with an X-ray diffractometer (HZG-4, Germany) using Cu-$K_{\alpha 1}$ radiation ($\lambda = 1.54051$ Å) with removal of the Cu-K_β radiation by a nickel filter. The Cu-$K_{\alpha 2}$ intensities were removed from the original data. Silicon ($a = 5.43055$ Å) was used as the internal standard. Diffraction angles were measured from 1.5° to 37° (2Θ).

IR Spectroscopy: Infrared spectra of the solid intercalates were measured in Nujol suspensions in the region of 4000−400 cm^{-1} using a Perkin−Elmer 684 spectrometer.

Acknowledgments

This work was supported by the Academy of Sciences of the Czech Republic (Key Project 12).

[1] G. Lagaly, K. Beneke, *Colloid Polym. Sci.* **1991**, *269*, 1198−1211.
[2] A. Clearfield, *Intercalation Chemistry of Selected Layered Oxides and Phosphates*, in *Progress in Intercalation Research* (Eds.: W. Müller-Warmuth and R. Schöllhorn), Kluwer Academic Publishers, **1994**, pp.223−271.
[3] G. Lagaly, S. Fritz, A. Weiss, *Clays Clay Miner.* **1975**, *23*, 45−54.

[4] G. Lagaly, *Clay Miner.* **1981**, *16*, 1−21.
[5] K. Beneke, G. Lagaly, *Inorg. Chem.* **1983**, *22*, 1503−1507.
[6] L. Beneš, J. Votinský, J. Kalousová, J. Klikorka, *Inorg. Chim. Acta* **1986**, *114*, 47−50.
[7] L. Beneš, R. Hyklová, J. Kalousová, J. Votinský, *Inorg. Chim. Acta* **1990**, *177*, 71−74.
[8] L. Beneš, K. Melánová, V. Zima, J. Kalousová, J. Votinský, *Inorg. Chem.* **1997**, *36*, 2850−2853.
[9] U. Costantino, *J. Chem. Soc., Dalton Trans.* **1979**, 402−405.
[10] U. Costantino, *J. Inorg. Nucl. Chem.* **1981**, *43*, 1895−1902.
[11] A. L. Garcia-Ponce, L. Moreno-Real, A. Jimenez-Lopez, *Can. J. Chem.* **1990**, *68*, 592−596.
[12] M. Trchová, P. Čapková, P. Matějka, K. Melánová, L. Beneš, *J. Solid State Chem.* **1999**, *148*, 197−204.
[13] L. Beneš, K. Melánová, M. Trchová, P. Čapková, P. Matějka, *Eur. J. Inorg. Chem.* **1999**, 2289−2294.
[14] G. Lagaly, *Angew. Chem.* **1976**, *15*, 575−586.
[15] L. Beneš, V. Zima, K. Melánová, *J. Incl. Phenom.*, in press.
[16] M. Tachez, F. Theobald, J. Bernard, A. W. Hewat, *Rev. Chim. Miner.* **1982**, *19*, 291−300.
[17] L. Beneš, K. Melánová, V. Zima, M. Trchová, E. Uhlířová, P. Matějka, *Eur. J. Inorg. Chem.* **2001**, 713−719.

Received January 5, 2001
[I01009]

1-Oxa-3-aza-2,4-disilacyclobutanes − Synthesis, X-ray Structures, and Reactivity

Uwe Klingebiel,*[a] M. Noltemeyer[a]

Keywords: Silicon / Structure elucidation / Silanes / Small ring systems

Lithium aminodi(*tert*-butyl)silanolate reacts with F_3SiR to give the aminosiloxane $(Me_3C)_2SiNH_2–O–SiF_2R$ [**1**; R = 2,4,6-$(tBu)_3C_6H_2$]. In the reaction of **1** with BuLi a four-membered (Si–O–Si–NH) ring system **2** is formed [–$(Me_3C)_2$Si–O–SiFR–NH–]. The amino-1,3-disiloxane $RSiF_2–NH–Si(CMe_3)_2–O–SiF_2R$ (**3**) is obtained from dilithiated amino(di-*tert*-butyl)silanol and F_3SiR. Compound **1** reacts with BuLi with formation of a dimeric lithium derivative through the Li–N bond (**4**). In **4** the transannular Si···Si distance was found to be 237.2 pm, which is the shortest distance so far found between two silicon atoms contained in four-membered rings. Compound **4** reacts with $Me_3SiOSO_2CF_3$ with substitution of the lithium by the Me_3Si group to give **5**.

Introduction

In silicon chemistry it is possible to stabilize compounds with two or three OH or NH_2 groups bonded to one silicon atom, in contrast to carbon chemistry. The first silanediols and -diamines were described by Sommer and Tyler in the fifties.[1] Silanetriols and -triamines followed about thirty years later.[2−4] We succeeded in preparing stable halosilanols,[5] (e.g. chlorosilanols) from the reaction of silanediols with PCl_5, accompanied by formation of HCl and $POCl_3$. The reaction of di-*tert*-butyl-dichlorosilane with ammonia proceeds with complete cleavage of hydrogen chloride to afford the amino-di-*tert*-butylsilanol, the only aminosilanol known so far,[2,6] which is stable towards self-reaction [Equation (1)].

$$R_2Si(OH)_2 \xrightarrow[-HCl,\ -POCl_3]{+PCl_5} R_2Si(OH)Cl \xrightarrow[-NH_4Cl]{+2\ NH_3} R_2Si(OH)NH_2 \quad (1)$$

The kinetic stabilization of the aminosilanol led to the stepwise synthesis of numerous acyclic and cyclic organosilicon compounds.[7] After lithiation of the aminosilanol,[6] treatment with a halosilane always results in attachment of the new organosilicon group to the oxygen atom; aminosiloxanes are formed [Equation (2)]. Lithiation of these aminosiloxanes normally leads again to the bonding of lithium to the oxygen atom. In this case aminosilanolates of type I are formed. This means that in the lithiation reaction the silyl substituent on the oxygen atom is displaced by the Lewis acidic lithium, so that an O → N silyl group migration is observed.[8] This rearrangement can be prevented by bulky groups [Equation (2)]. Siloxaneamides of type II are then formed. Therefore the success of the substitution of the silyl groups determines which isomer is obtained.[8] In reactions with other halosilanes silylamino-1,3-disiloxanes are obtained.

In attempting to obtain cyclic products by salt elimination from isomeric lithium compounds we isolated eight-membered (Si−O−Si−N) rings [Equation (2)].[9,10] Lithium derivatives of type I are found to be very stable; they can be distilled without decomposition.[11] However, they are direct precursors of four-membered (Si−O−Si−N) rings when catalytic amounts (1−5%) of fluorosilanes are added to a solution of the lithium compounds.[8,12]

In this paper we describe the preparation of 1-[amino-1,1-di(*tert*-butyl)]-3-[2,4,6-tri(*tert*-butyl)phenyl]-3,3-difluoro-1,3-disiloxane, its cyclisation to the first (Si−NH−Si−O) four-membered ring system, and the formation of its lithium derivative.

Results and Discussions

In preparative ring chemistry bulky groups lead to the formation of small ring compounds. In order to prepare a fluoro-functionalized Si(F)−O−Si−N(H) four-membered ring system we used the bulky $Si(CMe_3)_2$ and $F_2SiC_6H_2(CMe_3)_3$ units. The lithiated aminodi(*tert*-butyl)silanol[6] reacts with 2,4,6-tri(*tert*-butyl)phenyltrifluorosilane to yield the aminosiloxane **1** [Equation (3)], which is stable against HF or NH_3 condensation.

Our attempts to isolate the lithium derivative of **1** in the reaction of **1** and BuLi were unsuccessful, LiF elimination occurred and the 1-aza-3-oxa-2,4-disilacyclobutane **2** was obtained [Equation (4)].

Crystal Structure of 2

Colorless crystals of **2** with space group $P\bar{1}$ were obtained from a saturated solution of *n*-hexane. The atoms N(1), Si(1), O(1) and Si(2) of the molecule form a planar four-membered ring, but there are some irregularities as follows. At the oxygen and the nitrogen atoms there is a slight open-

[a] Institut für Anorganische Chemie der Georg-August-Universität Göttingen,
Tammannstraße 4, 37077 Göttingen, Germany
E-mail: uklinge@gwdg.de

 © WILEY-VCH Verlag GmbH, 69451 Weinheim, 2001 1434−1948/01/0707−1889 $ 17.50+.50/0

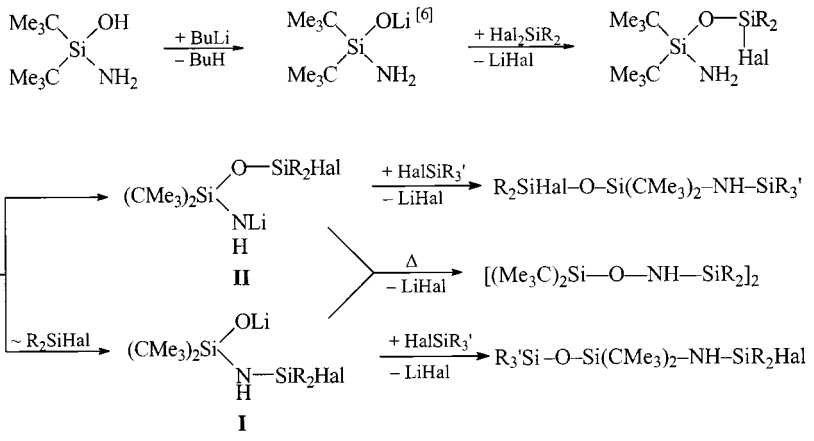

(2)

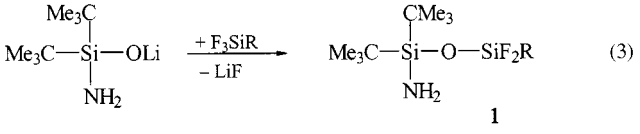

(3)

R = 2,4,6–$(CMe_3)_3C_6H_2$

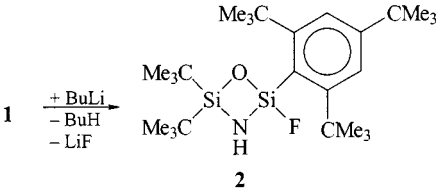

(4)

ing of the Si(1)−O(1)−Si(2) angle (93.42°) and the Si(1)−N(1)−Si(2) angle (94.03°), which is accompanied by a contraction of the angles at the other ring atoms [N(1)−Si(1)−O(1) = 87.15°; N(1)−Si(2)−O(1) = 85.4°]. The Si(1)−O(1) (167.2 pm), and the Si(2)−O(1) (170.2 pm) bond lengths are lengthened. The Si(1)−N(1) (166.6 pm) and Si(2)−N(1) (169.1 pm) bonds are short, even shorter than the Si−O bonds. In order to see if there is any O/NH split occupancy of O(1) re-refinements of O/NH occupancies were carried out on both sites. However, strong correlation with ADPS leads to unstable refinement. Also, no hydrogen atoms could be located in the difference maps and riding models had to be used throughout. The Si···Si nonbonding distance in the ring is 245.6 pm, the corresponding N···O distance is 230.1 pm. These short distances illustrate that the ring atoms in a four-membered ring as strained as this one are forced to approach each other to an extraordinary extent. The C(1) atom of the aryl group is found to have no planar environment: the sum of the angles at C(1) amounts to 355.7°. Figure 1 shows the structure of compound **2**.

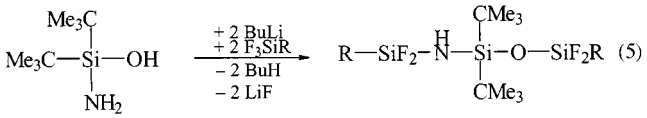

(5)

R = 2,4,6–$C_6H_2(CMe_3)_3$

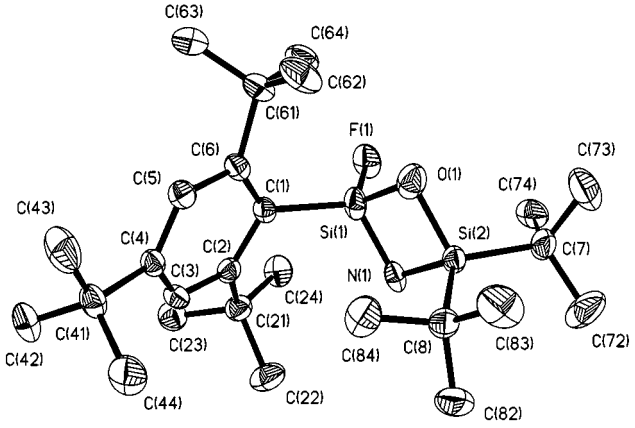

Figure 1. Structure of **2**; selected bond lengths [pm] and angles [°]: Si(1)−F(1) 158.81(13), Si(1)−N(1) 166.6(2), Si(1)−O(1) 167.2(2), Si(1)−C(1) 186.3(2), Si(1)−Si(2) 245.56(10), Si(2)−N(1) 169.1(2), Si(2)−O(1) 170.2(2), Si(2)−C(7) 188.3(2); F(1)−Si(1)−N(1) 111.17(9), F(1)−Si(1)−O(1) 111.30(8), N(1)−Si(1)−O(1) 87.15(9), F(1)−Si(1)−C(1) 114.70(8), N(1)−Si(1)−C(1) 114.73(9), O(1)−Si(1)−C(1) 114.78(9), N(1)−Si(2)−O(1) 85.40(10), Si(1)−O(1)−Si(2) 93.42(10), Si(1)−N(1)−Si(2) 94.03(10)

Disilylation of the aminosilanol is possible by starting from the dilithium derivative according to Equation (5):

Crystal Structure of 4

The lithium compound **4** is obtained in high yields [Equation (6)] from the reaction of **2** with BuLi, thus confirming the structure of **4**.

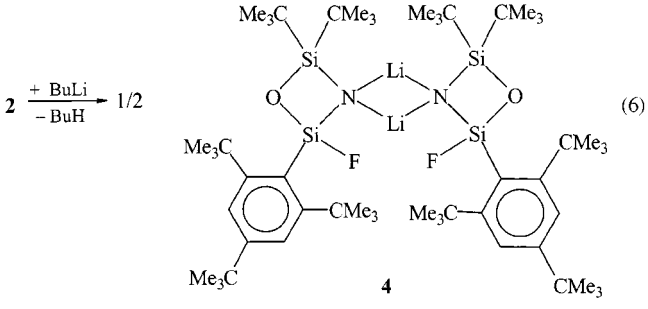

(6)

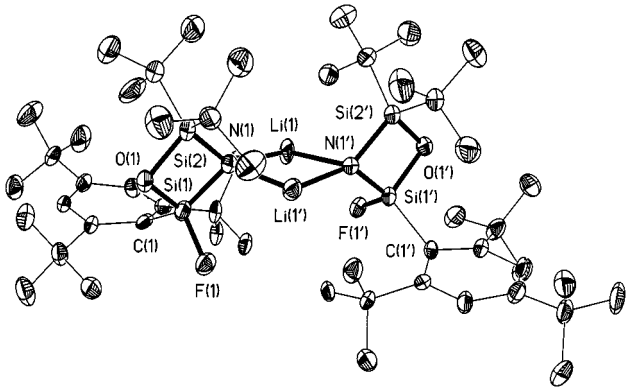

Figure 2. Structure of **4**; selected bond lengths [pm] and angles [°]: Si(1)−F(1) 161.8(4), Si(1)−O(1) 166.7(5), Si(1)−N(1) 172.1(6), Si(1)−C(1) 187.6(7), Si(1)−Si(2) 237.2(3), Si(2)−O(1) 169.6(5), Si(2)−N(1) 174.3(6), Si(2)−C(8) 190.1(8), Li(1)−N(1) 195.1(12), Li(1)−N(1′) 203.5(13), Li(1)−Li(1′) 232(2), N(1)−Li(1′) 201.5(13), Si(1′)−F(1′) 160.5(5), Si(1′)−O(1′) 166.7(5), Si(1′)−N(1′) 172.9(6), Si(1′)−Si(2′) 237.3(3), Si(2′)−O(1′) 169.8(5), Si(2′)−N(1′) 173.5(6), Li(1′)−N(1′) 195.4(12); F(1)−Si(1)−O(1) 110.8(2), F(1)−Si(1)−N(1) 109.1(2), O(1)−Si(1)−N(1) 92.6(3), O(1)−Si(1)−Li(1′) 102.1(3), N(1)−Si(1)−Li(1′) 37.9(3), O(1)−Si(2)−N(1) 90.9(3), N(1)−Li(1)−N(1′) 107.7(6), N(1)−Li(1)−Li(1′) 55.5(4), Si(1)−N(1)−Si(2) 86.4(3), Li(1)−N(1)−Li(1′) 71.5(5), Si(1)−O(1)−Si(2) 89.7(2), O(1′)−Si(2′)−N(1′) 91.1(3), N(1′)−Li(1′)−N(1) 108.4(6), Si(1′)−N(1′)−Si(2′) 86.5(3), Li(1′)−N(1′)−Li(1) 71.0(5), Si(1′)−O(1′)−Si(2′) 89.7(2)

Compound **4** crystallizes from *n*-hexane as a dimer in the space group *C*2/*c* (Figure 2) Again the crystal structure shows some irregularities. The dimer of **4** is formed from a four-membered $(Li-N)_2$ ring system, which is not entirely planar but folded by 10.7° across the Li···Li line. The Si−O−Si−N rings have an angle of 86° to the central $(LiN)_2$ ring and of 5.8° to each other. The *tert*-butyl groups and therefore the aryl group and the fluorine atom are in *cis* positions. The sum of the angles around C(1) amounts to 355.1°. In contrast to compound **2**, the Si−O distances here are shorter than the Si−N distances. Now the ring angles at Si(1) (92.6°) and Si(2) (90.9°) are above 90° and the angles at O(1) (89.7°) and N(1) (86.4°) are smaller than 90°. This brings the Si(1) and Si(2) atoms into a close approximation. The Si···Si nonbonding distance in the ring is only 237.2 pm, which as far as we are aware is the shortest nonbonding Si···Si contact found so far. The transannular O···N distance is found to be 245.1 pm. The bonding properties of such small four-membered rings containing two opposite silicon atoms have been investigated by various theoretical methods[5,13−16]. Table 1 shows examples of known rings. The presence of a transannular σ bond has been excluded, in agreement with the very small Si···Si coupling constant.[17] Grev and Schäfer have explained the short Si···Si contacts in terms of an "unsupported π bond", which lies in the plane of the ring.[15]

The bulky groups at this lithiated fluorine-containing ring system motivated us to test the possibility of a LiF elimination. In the eighties and nineties we were successful in the preparation of iminosilanes in the following reaction [Equation (7)]:

Table 1. Geometric parameters of $[R_2Si-X]_2$ four-membered rings; X = CR_2', NR′ and O

	Si−X [pm]	Si···Si [pm]
$[H_2Si-C(CMe_3)_2]_2$[a]	190.3	270.3
$[H_2Si-CH_2]_2$ [b]	188.8	259.2
$[Cl_2Si-NCMe_3]_2$[c]	171.1	245.0
$[F_2Si-NCMe_3]_2$[d]	170.6	241.3
$[Mes_2Si-O]_2$[e]	167.0	239.0
$[F_2Si-NSiMe(CMe_3)_2]_2$[f]	170.7	237.8
4[g]		237.2

[a] Crystal structure, see ref.[18] − [b] Gas-phase structure, see ref.[19] − [c] Crystal structure, see ref.[20] − [d] Gas-phase structure, see ref.[20] − [e] Crystal structure, see ref.[17] − [f] Crystal structure, see ref.[21] − [g] This work.

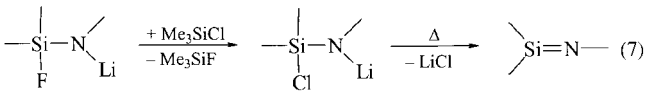

In the analogous reaction of **4** with Me_3SiCl, however, we isolated the silyl-substituted compound **5**, which was also obtained from the reaction of **4** and $Me_3Si-O-SO_2-CF_3$ [Equation (8)].

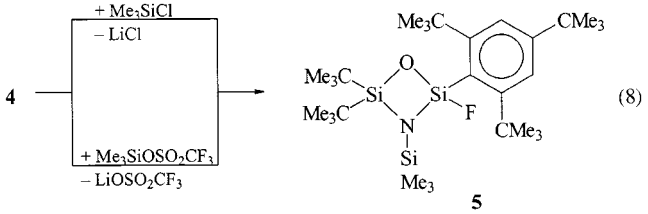

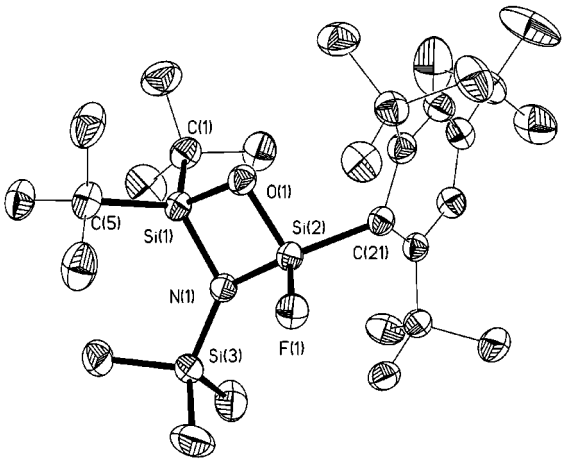

Figure 3. Structure of **5**; selected bond lengths [pm] and angles [°]: Si(1)−O(1) 167.56(12), Si(1)−N(1) 177.41(14), Si(1)−C(1) 189.9(2), Si(1)−C(5) 190.4(2), Si(1)−Si(2) 244.53(7), Si(2)−F(1) 159.38(10), Si(2)−O(1) 165.32(12), Si(2)−N(1) 175.26(14), Si(3)−N(1) 174.80(14); O(1)−Si(1)−N(1) 88.07(6), F(1)−Si(2)−O(1) 113.60(6), F(1)−Si(2)−N(1) 107.73(6), O(1)−Si(2)−N(1) 89.51(6), Si(3)−N(1)−Si(2) 137.28(8), Si(3)−N(1)−Si(1) 128.32(8), Si(2)−N(1)−Si(1) 87.79(6), Si(2)−O(1)−Si(1) 94.54(6)

Crystal Structure of 5

Crystals of **5** were obtained from a THF solution. It crystallizes in the space group *Pbcn* (Figure 3). The ring system of **5** resembles the ring system of **2**. The ring angles at the Si atoms are smaller than 90° and the angles at the N and O atoms are larger, although in **5** the Si−N bonds are much longer than in **2** and than the Si−O bonds. The transannular Si···Si distance is 244.5 pm. Compound **5** has a planar (O−Si−N−Si) four-membered ring. The sum of the angles around the N atom is 353.39°, indicating a slightly trigonal environment. The C(21) atom deviates slightly from the plane, as well [ΣC(21) = 356.26°]. The angle between the four-membered ring and Si(3) amounts 21.3°.

Experimental Section

All experiments were performed in oven-dried glassware using standard inert atmosphere and vacuum-line techniques. The NMR spectra were recorded in $CDCl_3$ (**1**, **3**) or C_6D_6 (**2**, **4**, **5**) with $SiMe_4$ and C_6F_6 (^1H, ^{13}C, ^{19}F, ^{29}Si) as internal and $MeNO_2$ (^{15}N) as external references. The progress of the reactions was monitored by ^{19}F NMR spectroscopy. The compounds were isolated analytically pure.

1-[Aminodi(*tert*-butyl)]-3-{[2,4,6-tri(*tert*-butyl)phenyl]difluoro}1,3-disiloxane (1): To a solution of $(Me_3C)_2Si(NH_2)OLi$ (5.4 g, 0.03 mol) in 50 mL THF was slowly added at room temperature 2,4,6-$(CMe_3)_3C_6H_2SiF_3$ (9.9 g, 0.03 mol) in 20 mL THF. The reaction mixture was refluxed for 1 h and cooled to room temperature. Compound **1** was separated from LiF by condensing into a cooled trap in vacuo and then distilled to give a pure sample, which crystallized. − Yield 88%, b.p. 155 °C/0.03 mbar, m.p. 88 °C. − ^1H NMR: δ = 1.00 ($SiCMe_3$), 1.35 (4-C_6CMe_3), 1.54 (2,6-C_6CMe_3), 7.44 (C_6H_2). − ^{13}C NMR: δ = 20.05 (SiC), 27.95 ($SiCC_3$), 31.36 (4-C_6CC_3) 33.45 (t, $^5J_{CF}$ = 2.7 Hz, 2,6-C_6CC_3), 34.96 (4-C_6C), 39.01 (2,6-C_6C), 117.53 (t, $^2J_{CF}$ = 23.7 Hz, F_2SiC), 123.07 (3,5-C_6), 152.05 (4-C_6), 160.81 (t, $^3J_{CF}$ = 1.3 Hz, 2,6-C_6). − ^{19}F NMR: δ = 46.7. − ^{29}Si NMR: δ = −73.50 (t, J_{SiF} = 248.9 Hz, SiF_2), −7.66 ($SiNH_2$). − MS (EI): *m*/*z* (%) = 470 (1) $[M - CH_3]^+$, 428 (28) $[M - C(CH_3)_3]^+$. − $C_{26}H_{49}F_2NOSi_2$ (485.85): calcd. C 64.28, H 10.16; found C 64.42, H 10.34.

1-Oxa-3-aza-2,4-disilacyclobutane (2): A solution of **1** (4.8 g, 0.01 mol) in a mixture of 50 mL *n*-hexane and 5 mL THF was treated with 6.25 mL of *n*BuLi (1.6 M solution in *n*-hexane, 0.01 mol). The reaction occurred at room temperature. After stirring for 2 h the solvents were condensed into a cooled trap. Compound **2** crystallized from *n*-hexane. − Yield 90%, m.p. 130 °C. − ^1H NMR: δ = 0.60 ($SiCMe_3$), 1.10 ($SiCMe_3$), 1.38 (4-C_6CMe_3), 1.45 (d, $^5J_{HF}$ = 1.0 Hz, 2,6-C_6CMe_3), 1.65 (d, $^5J_{HF}$ = 1.2 Hz, 2,6-C_6CMe_3), 7.34 (d, $^5J_{HF}$ = 1.4 Hz, 3,5-C_6H), 7.45 (d, $^5J_{HF}$ = 1.4 Hz, 3,5-C_6H). −

Table 2. Crystal data and data collections parameters for **2**, **4** and **5**

	2	**4**	**5**
Empirical formula	$C_{26}H_{48}FNOSi_2$	$C_{54}H_{98}F_2Li_2N_2O_{250}Si_4$	$C_{29}H_{56}FNOSi_3{\cdot}0.5THF$
Molecular mass [g/mol]	465.83	979.58	538.02
Temperature [K]	150(2)	150(2)	200(2)
Wave length [pm]	71.073	71.073	71.073
Crystal system	Triclinic	Monoclinic	Orthorhombic
Space group	$P\bar{1}$	*C*2/*c*	*Pbcn*
Unit cell dimensions	*a* = 1032.6(3) pm	*a* = 4182.3(28) pm	*a* = 1989.7(3) pm
	b = 1048.7(3) pm	*b* = 1368.2(9) pm	*b* = 1633.03(15) pm
	c = 1332.4(6) pm	*c* = 2968.1(17) pm	*c* = 2078.4(3) pm
	α = 89.76(3)°	α =90°	α = 90°
	β = 86.95(4)°	β = 133.97(3)°	β = 90°
	γ = 86.93(2)°	γ = 90°	γ = 90°
Volume [nm^3]	1.4387(8)	12.2245(135)	6.7532(15)
Z	2	8	8
Density (calculated) [Mg/m^3]	1.075	1.065	1.058
Absorption coefficient [mm^{-1}]	0.146	0.141	0.166
F(000)	512	4288	2368
Crystal size [mm]	1.00 × 1.00 × 1.00	0.60 × 0.50 × 0.30	0.80 × 0.70 × 0.60
θ range for data collection	3.56 to 25.00°	3.54 to 20.02°	3.64 to 25.04°
Index ranges	$-12 < h < 12$	$-32 < h < 40$	$-23 < h < 23$
	$-12 < k < 12$	$-13 < k < 13$	$-19 < k < 19$
	$-14 < l < 15$	$-28 < l < 28$	$-24 < l < 24$
Reflections collected	6545	6935	11920
Independent reflections	5042 [*R*(int) = 0.0254]	5690 [*R*(int) = 0.0631]	5960 [*R*(int) = 0.0631]
Refinement method	Full-matrix least-squares on F^2	Full-matrix least-squares on F^2	Full-matrix least-squares on F^2
Data/restraints/parameters	5037/0/295	5666/0/618	5950/0/334
Goodness-of-fit on F^2	1.057	1.061	1.061
Final *R* indices [$I > 2\sigma(I)$]	*R*1 = 0.0501	*R*1 = 0.0716	*R*1 = 0.0380
	*wR*2 = 0.1312	*wR*2 = 0.1688	*wR*2 = 0.1020
R indices (all data)	*R*1 = 0.0565	*R*1 = 0.1189	*R*1 = 0.0459
	*wR*2 = 0.1401	*wR*2 = 0.2237	*wR*2 = 0.1116
Largest diff. peak and hole	0.532 and −0.334 e.Å^{-3}	0.598 and −0.414 e·Å^{-3}	0.283 and −0.240 e·Å^{-3}

^{13}C NMR: δ = 20.94 (d, $^4J_{CF}$ = 3.6 Hz, Si*C*C$_3$), 20.97 (Si*C*C$_3$), 21.42 (SiC*C*$_3$), 26.65 (SiC*C*$_3$) 31.21 (4-C$_6$C*C*$_3$), 32.93 (d, $^5J_{CF}$ = 1.5 Hz, 2,6-C$_6$C*C*$_3$), 32.98 (d, $^5J_{CF}$ = 0.6 Hz, 2,6-C$_6$C*C*$_3$), 34.70 (4-C$_6$*C*), 38.97 (d, $^4J_{CF}$ = 1.1 Hz, 2,6-C$_6$*C*$_2$), 38.98 (d, $^4J_{CF}$ = 1.1 Hz, 2,6-C$_6$*C*), 122.35 (d, $^2J_{CF}$ = 35.3 Hz, FSiC), 122.15 (d, $^3J_{CF}$ = 1.9 Hz, 2,6-C$_6$), 123.12 (d, $^3J_{CF}$ = 1.8 Hz, 2,6-C$_6$), 151.52 (4-C$_6$), 157.90 (d, $^4J_{CF}$ = 0.4 Hz ,3,5-C$_6$), 159.78 (d, $^4J_{CF}$ = 0.3 Hz, 3,5-C$_6$). − ^{15}N NMR: δ = −339.80 (d, $^2J_{NF}$ = 3.9 Hz). − ^{19}F NMR: δ = 54.5. − ^{29}Si NMR: δ = −47.20 (d, J_{SiF} = 313.35 Hz, SiF), 9.78 (d, $^3J_{SiF}$ = 2.32 Hz). − MS (EI): *m*/*z* (%) = 465 (7) [M$^+$], 408 (100) [M − CMe$_3^+$]. − C$_{26}$H$_{48}$FNOSi$_2$ (465.85): calcd. C 67.04, H 10.39; found C 67.39, H 10.70.

1-Di(*tert*-butyl)-1-{[2,4,6-tri(*tert*-butyl)phenyl]difluorosilylamino}-3-[difluoro-2,4,6-tri(*tert*-butyl)phenyl]-1,3-disiloxane (3): To a solution of (Me$_3$C)$_2$Si(NH$_2$)OLi (1.8 g, 0.01 mol) in 50 mL THF was added 6.25 mL of *n*BuLi (1.6 M solution in *n*-hexane). The reaction mixture was heated under reflux for 1 h, cooled to room temperature and mixed with 2,4,6-(CMe$_3$)$_3$C$_6$H$_2$SiF$_3$ (6.6 g, 0.02 mol) in 20 mL THF. The mixture was heated under reflux for a further 2 h. The formation of **3** was monitored by ^{19}F NMR spectroscopy. Compound **3** was separated from LiF by condensing the product and solvents into a cooled trap in vacuo. It was then distilled in vacuo and recrystallized from *n*-hexane to give a pure sample. − Yield 75%, b.p. 210 °C/0.01 mbar, m.p. 158 °C. − ^{1}H NMR: δ = 1.12 (SiCMe$_3$), 1.30, 1.31 (4-C$_6$CMe$_3$), 1.47, 1.51 [2,6-C$_6$(CMe$_3$)$_2$] 7.38, 7.40 (C$_6$H$_2$). − ^{13}C NMR: δ = 21.09 (SiC), 27.61 (Si*C*C$_3$), 31.11, 31.30 (4-C$_6$C*C*$_3$), 33.20 (t, $^5J_{CF}$ = 2.43 Hz, 2,6-C$_6$*C*$_3$), 33.58 (t, $^5J_{CF}$ = 2.12 Hz, 2,6-C$_6$C*C*$_3$), 34.68, 34.69 (4-C$_6$*C*), 38.67, 38.99 (2,6-C$_6$*C*$_2$), 116.85 (t, $^2J_{CF}$ = 23.24 Hz, 1-C$_6$) 119.5 (t, $^2J_{CF}$ = 20.18 Hz, 1-C$_6$), 122.78, 122.95 (3,5-C$_6$), 151.73, 151.96 (4-C$_6$), 160.67 (t, $^3J_{CF}$ = 1.3 Hz, 2,6-C$_6$), 160.78 (t, $^2J_{CF}$ = 1.2 Hz, 2,6-C$_6$). − ^{19}F NMR: δ = 47.40 (OSiF$_2$), 49.37 (d, $^3J_{HF}$ = 6.45 Hz, NHSiF$_2$). − ^{29}Si NMR: δ = −74.09 (t, J_{SiF} = 250.5 Hz, OSiF$_2$), −48.32 (t, J_{SiF} = 341.4 Hz, NSiF$_2$), −5.41 (pquint, $^3J_{SiF}$ = 0.91 Hz, SiCMe$_3$). − MS (EI): *m*/*z* (%) = 795 (1) [M$^+$], 738 (100) [M − C$_4$H$_9^+$]. − C$_{44}$H$_{77}$F$_4$NOSi$_3$ (796.35): calcd. C 66.36, H 9.75; found C 66.43, H 9.87.

Lithium 4,4-di(*tert*-butyl)-2-fluoro-2-[2,4,6-tri(*tert*-butyl)phenyl]-1-oxa-3-aza-2,4-disilacyclobutane (4): A solution of **2** (4.6 g, 0.01 mol) in 30 mL *n*-hexane was treated with 6.25 mL of *n*BuLi (1.6 M solution in *n*-hexane, 0.01 mol). The lithiation occurred at room temperature, was monitored by ^{19}F NMR spectroscopy, and finished after 2 h. Compound **4** was separated from solvent in vacuo and crystallized from *n*-hexane as a dimer. − Yield 95%. − ^{1}H NMR: δ = 1.00, 1.17 (SiCMe$_3$), 1.30 (4-C$_6$CMe$_3$), 1.55, 1.57 (2,6-C$_6$CMe$_3$), 7.40 (C$_6$H$_2$). − ^{13}C NMR: δ = 20.80, 21.07 (Si*C*C$_3$), 27.90, 28.07 (SiC*C*$_3$), 31.24 (4-C$_6$C*C*$_3$), 33.81 (2,6-C$_6$C*C*$_3$), 34.59 (4-C$_6$C), 39.40 (2,6-C$_6$C$_2$), 122.60 (2,6-C$_6$), 125.26 (d, $^2J_{CF}$ = 20.72 Hz, FSiC), 150.92 (4-C$_6$), 161.22 (3,5-C$_6$). − ^{19}F NMR: δ = 60.53. − ^{29}Si NMR: δ = −52.16 (d, J_{SiF} = 248.11 Hz, SiF), −1.08 (SiC$_2$).

4,4-Di(*tert*-butyl)-2-fluoro-3-trimethylsilyl-2-[2,4,6-tri(*tert*-butyl)-phenyl]-1-oxa-3-aza-2,4-disilacyclobutane (5): Compound **4** (4.7 g, 0.01 mol) in 50 mL THF was mixed with Me$_3$SiOSO$_2$CF$_3$ (2.2 g, 0.01 mol). In an exothermic reaction LiOSO$_2$CF$_3$ and **5** were formed. LiOSO$_2$CF$_3$ was removed by filtration through a frit and **5** crystallized from the THF solution. − Yield 95%, m.p. 112 °C. − ^{1}H NMR: δ = 0.23 (SiMe$_3$), 0.58 (SiCMe$_3$), 1.13 (SiCMe$_3$), 1.26 (4-C$_6$CMe$_3$), 1.45 [d, $^6J_{HF}$ = 1.13 Hz, 2,6-C$_6$(CMe$_3$)$_2$], 7.26 (C$_6$H$_2$). − ^{13}C NMR: δ = 4.75 (SiC$_3$), 21.80 (d, $^4J_{CF}$ = 3.48 Hz, Si*C*C$_3$), 22.74 (Si*C*C$_3$), 26.88 (SiC*C*$_3$), 27.85 (SiC*C*$_3$), 31.10 (4-C$_6$C*C*$_3$), 33.25 [d, $^5J_{CF}$ = 1.46 Hz, 2,6-C$_6$(C*C*$_3$)], 34.42 (4-C$_6$C), 39.19 (d, $^4J_{CF}$ = 1.15 Hz, 2,6-C$_6$*C*$_2$), 121.43 (d, $^2J_{CF}$ = 36.20 Hz, FSiC), 121.64 (d, $^3J_{CF}$ = 1.2 Hz, 2,6-SiC$_6$), 150.80 (4-C$_6$), 159.67 (3,5-C$_6$). − ^{19}F NMR: δ = 57.10. − ^{29}Si NMR: δ = −49.03 (d, J_{SiF} = 326.9 Hz, SiF), −4.34 (d, $^3J_{SiF}$ = 1.5 Hz, SiMe$_3$), 12.85 (d, $^3J_{SiF}$ = 2.0 Hz, SiCMe$_3$). − MS (EI): *m*/*z* (%) = 537 (12) [M$^+$], 480 (100) [M − CMe$_3^+$]. − C$_{29}$H$_{55}$FNOSi$_3$ (537.02): calcd. C 64.86, H 10.32; found C 64.69, H 10.02.

X-ray Structure Determination of 2, 4 and 5: The data in Table 2 were collected on a STOE AED2 four circle diffractometer with Mo-K_α radiation. The structures were solved and refined using the SHELX program suite.[22] The data of **4** were measured only to a resolution of Θ = 20 degrees.

Crystallographic data (excluding structure factors) for the structures reported in this paper have been deposited with the Cambridge Crystallographic Data Centre as supplementary publication nos. CCDC-151335 (**2**), -151336 (**4**) and -151337 (**5**). Copies of the data can be obtained free of charge on application to CCDC, 12 Union Road, Cambridge CB2 1EZ, UK [Fax: (internat.) +44-1223/336-033, E-mail: deposit@ccdc.cam.ac.uk].

Acknowledgments

We are grateful to the Deutsche Forschungsgemeinschaft and Fonds der Chemischen Industrie for support of this work.

[1] L. H. Sommer, L. J. Tyler, *J. Am. Chem. Soc.* **1954**, *76*, 1030−1034.
[2] P. D. Lickiss, *Adv. Inorg. Chem.* **1995**, *42*, 147−262.
[3] K. Ruhlandt-Senge, R. A. Bartlett, M. M. Olmstead, P. P. Power, *Angew. Chem.* **1993**, *105*, 459−461; *Angew. Chem. Int. Ed. Engl.* **1993**, *32*, 425−427.
[4] R. Murugavel, M. Bhattadarjee, H. W. Roesky, *Appl. Organomet. Chem.* **1999**, *13*, 227−243.
[5] O. Graalmann, U. Klingebiel, *J. Organomet. Chem.* **1984**, *275*, C1−C4.
[6] O. Graalmann, U. Klingebiel, W. Clegg, M. Haase, G. M. Sheldrick, *Angew. Chem.* **1984**, *96*, 904−905; *Angew. Chem. Int. Ed. Engl.* **1984**, *23*, 891−892.
[7] U. Klingebiel, S. Schütte, D. Schmidt-Bäse, in *The Chemistry of Inorganic Ring Systems* (Ed.: R. Steudel), Elsevier, Amsterdam, **1992**, 75−99.
[8] D. Schmidt-Bäse, U. Klingebiel, *J. Organomet. Chem.* **1989**, *364*, 313−321.
[9] E. Egert, M. Haase, U. Klingebiel, C. Lensch, D. Schmidt, G. M. Sheldrick, *J. Organomet. Chem.* **1986**, *315*, 19−25.
[10] O. Graalmann, U. Klingebiel, M. Meyer, *Chem. Ber.* **1986**, *119*, 872−877.
[11] S. Walter, U. Klingebiel, M. Noltemeyer, *Chem. Ber.* **1992**, *125*, 783−788.
[12] K. Dippel, U. Klingebiel, G. M. Sheldrick, D. Stalke, *Chem. Ber.* **1987**, *120*, 611−616.
[13] Y. Appeloig, in *The Chemistry of Organic Silicon Compounds* (Eds.: S. Patai and Z. Rappaport), Part 1, Wiley, Chichester, **1989**, p. 1213.
[14] M. O′Keefe, G. V. Gibbs, *J. Phys. Chem.* **1985**, *89*, 4574.
[15] R. S. Grev, H. F. Schäfer, III, *J. Am. Chem. Soc.* **1987**, *109*, 6577.
[16] A. Savin, H. J. Flad, H. W. Preuss, H. G. von Schnering, *Angew. Chem.* **1992**, *104*, 185−186; *Angew. Chem. Int. Ed. Engl.* **1992**, *31*, 185−186.
[17] R. West, *Angew. Chem.* **1987**, *99*, 1231−1241; *Angew. Chem. Int. Ed. Engl.* **1987**, *26*, 1201−1211.

[18] M. Jendras, Dissertation Univ. Göttingen, **2000**.
[19] B. Rempfer, G. Pfafferott, H. Oberhammer, N. Auner, J. E. Boggs, *Acta Chem. Scand., Ser. A* **1988**, *42*, 352.
[20] C. Brönnecke, R. Herbst-Irmer, U. Klingebiel, P. Neugebauer, M. Schäfer, H. Oberhammer, Chem. Ber.„/*Recueil* **1997**, *130*, 835−837.
[21] B. Tecklenburg, U. Klingebiel, M. Noltemeyer, D. Schmidt-Bäse, *Z. Naturforsch. B: Chem. Sci.* **1992**, *47*, 855−860.
[22] G. M. Sheldrick, The SHELX-97 manual, Universität Göttingen, **1997**.

Received October 3, 2000
[I00401]

Synthesis, Structures and Ethylene Polymerisation Behaviour of Low Valent β-Diketiminato Chromium Complexes

Vernon C. Gibson,*[a] Claire Newton,[a] Carl Redshaw,[a] Gregory A. Solan,[a] Andrew J. P. White,[a] and David J. Williams[a]

Keywords: Chromium / N ligands / Ethylene / Polymerisation

The preparation, reaction chemistry and ethylene polymerisation behaviour of low valent β-diketiminato chromium complexes are described. $[(DDP)CrCl(\mu\text{-}Cl)]_2$ (**1**) [DDPH = 2-{(2,6-diisopropylphenyl)amino}-4-{(2,6-diisopropylphenyl)imino}-pent-2-ene] is formed by treatment of $CrCl_3(THF)_3$ with LiDDP. Alkylation of **1** with $AlMe_3$ results in the formation of the binuclear dimethyl complex $[(DDP)CrMe(\mu\text{-}Cl)]_2$ (**2**). In contrast, the attempted alkylation of **1** with benzylmagnesium chloride results in reduction to form the dichromium(II) complex $[(DDP)Cr(\mu\text{-}Cl)]_2$ (**3**). Depending on the conditions of crystallisation, **3** can be obtained as the THF adduct [**3(THF)$_2$·THF**] or co-crystallised with a molecule of dibenzyl [**3·Bz-Bz**]. Cleavage of the dimeric unit in **1** can be achieved by the addition of carboxylates or β-diketonates to give $[(DDP)CrCl(O_2CR)(THF)]$ (R = Me **4a**, Ph **4b**) and $[(DDP)CrCl(\{O(R)C\}_2CH)]$ (R = Me **5a**, Ph **5b**), respectively. Single crystal X-ray diffraction studies have been performed on **1**, **2**, **3(THF)$_2$·THF**, **3·Bz-Bz**, **4a**, and **5b**. Complexes **1**, **2** and **3(THF)$_2$·THF** are dimeric and have molecular C_{2h} symmetry. Complex **3·Bz Bz** is also dimeric but has its potential C_{2h} symmetry removed by a significant tetrahedral distortion of the chromium coordination geometry. Compound **4a** has an octahedral chromium centre coordinated to a single bidentate diketiminate ligand, a bidentate acetate, a chloride and a THF molecule. Complex **5b** has a square pyramidal chromium with apical chloride and basal η^2 diketiminate and diketonate ligands. The complex contains strong intramolecular C–H···π stabilising interactions. All the complexes are active in ethylene polymerisation on treatment with suitable aluminium activators, affording high molecular weight polyethylene.

Introduction

Supported chromium catalysts play a key role in the worldwide production of polyethylene, and much effort has been directed towards developing an understanding of these systems from a surface science/heterogeneous catalysis point of view.[1,2] A complementary approach is to develop homogeneous model systems, not only to gain understanding of the chromium-centred chemistry of the supported systems, but also to advance chromium olefin polymerisation catalysis into an era of well-defined, single-site catalysts. To date, the majority of reports of homogeneous chromium catalysts for olefin polymerisation have been on half-sandwich chromium systems.[3−4] However, more recently there has been growing interest in non-cyclopentadienyl chromium catalysts.[5,6]

In this paper we are concerned with chemistry of low-valent chromium compounds containing the monoanionic *N,N*-chelate β-diketiminato ligand, $[ArNC(Me)CHC(Me)NAr]^-$ (Ar = 2,6-*i*$Pr_2C_6H_3$, DDP). This ligand (DDP) and members of the general family, $[ArNC(R)CHC(R)NAr]^-$, have been the subject of intense interest in recent years and complexes incorporating early[7] and late[8] transition metals, main group metals[9] and lanthanides have been reported.[10] Their ease of preparation, facility for aryl (Ar) and R group variation and variability in bonding mode,[7c] are particularly attractive features.

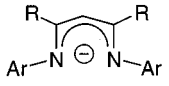

DDP (Ar = 2,6-^{i}Pr$_2$C$_6$H$_3$, R = Me)

In independent studies, Theopold and this group have communicated chromium(III) (d^3) complexes supported by β-diketiminato ligands, albeit with different aryl groups, as olefin polymerisation catalysts.[6h,6i] Herein we report, as part of a general study of the olefin polymerisation capability of non-cyclopentadienyl-containing chromium complexes,[6b−6h] our findings on a range of DDP-supported chromium(II) and -(III) systems (Scheme 1).

Results and Discussion

The protonated β-diketiminato ligand, 2-[(2,6-diisopropylphenyl)amino]-4-[(2,6-diisopropylphenyl)imino]pent-2-ene (DDPH) was prepared using a method similar to that reported for related ligands[11] and more recently by Feldman for DDPH itself.[8b] The lithium salt of DDPH was prepared by addition of one equivalent of *n*BuLi to a THF solution of DDPH at −78 °C and used without isolation.

Addition of one equivalent of $CrCl_3(THF)_3$ to LiDDP in THF gave $[(DDP)CrCl(\mu\text{-}Cl)]_2$ (**1**) as a green solid in good yield upon workup (Scheme 1). Crystals of **1** suitable for an X-ray structure determination were grown from a concentrated pentane solution at −20 °C. The structure is dimeric

[a] Department of Chemistry, Imperial College, South Kensington, London SW7 2AY, U.K.
E-mail: V.Gibson@ic.ac.uk

 © WILEY-VCH Verlag GmbH, 69451 Weinheim, 2001 1434−1948/01/0707−1895 $ 17.50+.50/0

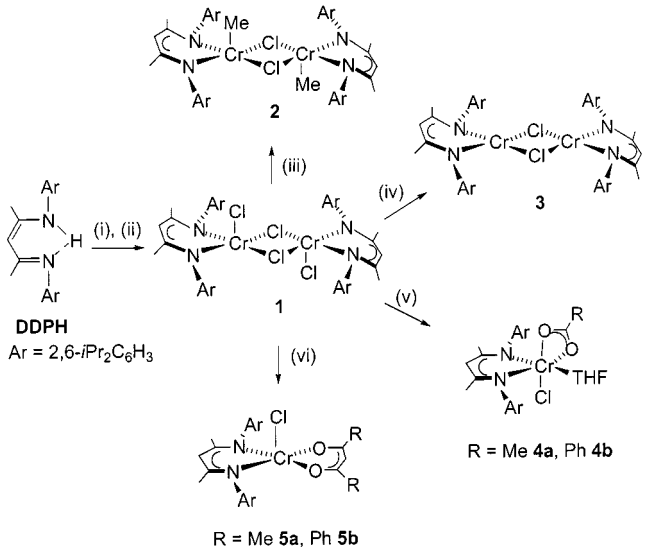

Scheme 1. Reagents and conditions: (i) *n*BuLi, THF, −78 °C; (ii) $CrCl_3(THF)_3$, THF, −78 °C; (iii) $AlMe_3$, THF, 20 °C; (iv) BzMgCl, THF, −78 °C; (v) NaO_2CR, THF, −78 °C; (vi) Li[{O(R)C}$_2$CH], THF, −78 °C

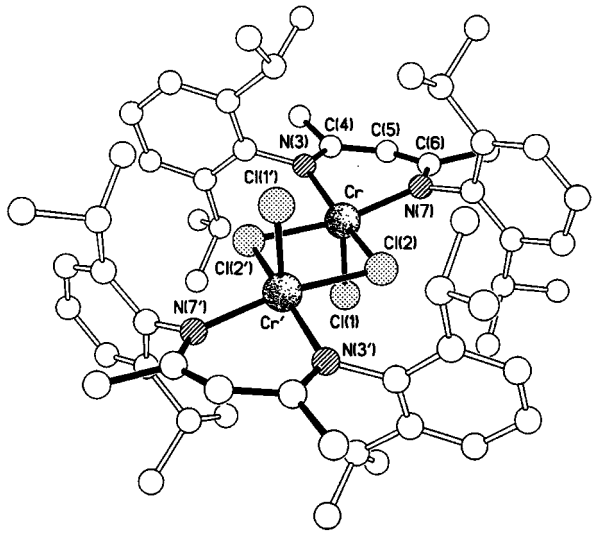

Figure 1. The molecular structure of **1**

(Figure 1) and has non-crystallographic C_{2h} symmetry about an axis passing through the two bridging chlorine atoms (the crystallographic symmetry is C_i). The geometry at chromium is distorted square pyramidal with the chromium atom being displaced by 0.35 Å out of the basal plane in the direction of Cl(1). Although the bridging Cr−Cl distances are identical within the errors of the structure determination, there is a marked asymmetry in the apical/basal Cr−Cl distances, with the apical bond being ca. 0.17 Å shorter than its basal counterparts (Table 1). The Cr−N distances are unexceptional. The nonbonded Cr···Cr separation (3.69 Å) is long, and extends outside the range found in a number of other chloride-bridged chromium(III) complexes.[12−15] This distance may in part be due to the steric repulsion between the bulky aryl ligands. The six-membered chelate ring has a boat conformation with the chromium and C(5) atoms lying 0.60 and 0.13 Å, respectively, out of the N(3)−C(4)−C(6)−N(7) plane (which is coplanar to within 0.01 Å). There is a pronounced pattern of delocalisation in the bond lengths of the N(3) to N(7) linkages. All four 2,6-diisopropylphenyl rings are oriented essentially orthogonally (84 and 87°) to their respective chelate C−N−Cr planes, a geometry that is stabilised by pairs of C−H···N(p_π) interactions[16] between N(3) and N(7) and their proximal isopropyl methine hydrogen atoms; the H···N distances are in the range 2.42 to 2.54 Å with associated C···N distances of between 2.89 and 3.00 Å. There are no intermolecular packing interactions of note.

It is noteworthy that substitution of the 2,6-diisopropylphenyl groups in DDP for phenyl groups results in a mononuclear six-coordinate chromium(III) dichloride complex in which the coordination sphere is completed by THF molecules.[6i] The preference of complexes coordinated by β-diketiminato ligands, with bulky groups on the 2,6-positions of the aryl substituents, to exhibit low coordination

Table 1. Selected bond lengths (Å) and angles (°) for **1** (apical = Cl) and **2** (apical = Me)

	1	**2**[a]	
Cr−apical	2.233(2)	2.037(7)	2.042(8)
Cr−Cl(2)	2.403(2)	2.3951(13)	2.3925(13)
Cr−Cl(2′)	2.397(2)	2.3951(13)	2.3925(13)
Cr−N(3)	1.986(5)	2.028(4)	2.031(4)
Cr−N(7)	1.990(5)	2.028(4)	2.031(4)
N(3)−C(4)	1.349(8)	1.328(6)	1.324(7)
C(4)−C(5)	1.395(9)	1.400(6)	1.397(6)
C(5)−C(6)	1.379(9)	1.400(6)	1.397(6)
C(6)−N(7)	1.349(8)	1.328(6)	1.324(7)
N(3)−Cr−N(7)	91.4(2)	91.3(2)	90.8(2)
N(3)−Cr−Cl(1)	99.6(2)	95.4(2)	96.8(2)
N(7)−Cr−Cl(1)	99.5(2)	95.4(2)	96.8(2)
N(3)−Cr−Cl(2′)	91.2(2)	92.68(11)	92.68(12)
N(7)−Cr−Cl(2′)	160.1(2)	165.73(12)	165.41(12)
Cl(1)−Cr−Cl(2′)	99.49(7)	97.8(2)	96.8(2)
N(3)−Cr−Cl(2)	160.34(14)	165.73(12)	165.41(12)
N(7)−Cr−Cl(2)	91.9(2)	92.68(11)	92.68(12)
Cl(1)−Cr−Cl(2)	98.91(7)	97.8(2)	96.8(2)
Cl(2)−Cr−Cl(2′)	79.34(6)	80.31(7)	80.62(7)
Cr−Cl(2)−Cr′	100.66(6)	99.69(7)	99.38(7)

[a] The two sets of values refer to the two crystallographically independent molecules.

numbers has also recently been observed by Budzelaar and co-workers.[8a]

The *N,N*-β-diketiminato chromium derivatives **2**−**5** have been prepared by in situ formation of **1** followed by treatment with the reagents shown in Scheme 1. The reaction with $AlMe_3$ affords a dark oily residue. Extraction of this residue into pentane and cooling to −20 °C gives crimson needles of [(DDP)CrMe(μ-Cl)]$_2$ (**2**) in good yield. A crystal prepared in this manner was used for a single crystal X-ray diffraction study. Complex **2** crystallises with two independent molecules in the asymmetric unit. Both have crystallographic C_{2h} symmetry and essentially identical conforma-

tions — the maximum deviation of the best fit of the two molecules (excluding the isopropyl methyl groups) is 0.08 Å. Replacement of the apical chloride in **1** by a methyl group to give **2** has virtually no effect on the geometry of **2**, the central core (including the two chelate rings) fitting to within 0.1 Å of that in **1**, though the Cr−N distances are noticeably increased by ca. 0.04 Å (Table 1). The Cr−Me distances in the two independent molecules are 2.037(7) and 2.042(8) Å. The displacement of the chromium atom out of the basal plane in the direction of the apical methyl group (ca. 0.25 Å) is noticeably less than that towards the chloride in **1**. The nonbonded Cr···Cr separation is slightly reduced (ca. 3.66 Å). Within the chelate ring Cr and C(2) lie 0.52 and 0.14 Å out of the N(3)−C(4)−C(6)−N(7) plane (see Figure 1) in one independent molecule and 0.55 and 0.15 Å, respectively, in the other. Each of the 2,6-diisopropylphenyl rings are rotated by ca. 85° out of their respective chelate C−N−Cr planes, a conformation again stabilised by pairs of C−H···N(p_π) interactions; the C···N distances are in the range 2.87 to 3.00 Å with associated H···N distances of between 2.40 and 2.52 Å. As with **1**, there are no noteworthy intermolecular packing interactions.

Attempted alkylation of **1** with benzyl Grignard reagent, however, results in the reduction of **1** to give [(DDP)Cr(μ-Cl)]$_2$ (**3**) as a green solid in high yield. Recrystallisation of this solid from THF gives **3(THF)$_2$·THF** while from pentane **3·Bz-Bz** is obtained. Single crystals of both forms of **3** were obtained by cooling the corresponding solutions to −20 °C overnight. The X-ray analysis showed **3(THF)$_2$·THF** to be structurally related to **2**, having crystallographic C_{2h} symmetry (Figure 2) but with the apical methyl ligand replaced by a weakly bound THF molecule [Cr−O(20) = 2.442(3) Å, Table 2] which is disordered about the mirror plane which passes through Cr, Cr′, O(20) and O(20′). The geometry at chromium is still square pyramidal with the chromium atom lying 0.13 Å out of the basal plane. The Cr−N distance [2.071(2) Å] is increased relative to that in **2** [av. 2.030 Å], although it still lies within the range observed for Cr−N bonds in the literature. The chelate rings retain a boat conformation with Cr and C(2) lying 0.43 and 0.12 Å, respectively, out of the N−C(1)−N′−C(1′) plane. The non-bonded Cr···Cr separation is 3.67 Å and lies at the top end of the range reported for chloride-bridged dichromium(II) complexes.[17,18] The 2,6-diisopropylphenyl rings are rotated by ca. 85° out of their respective chelate C−N−Cr planes, a conformation again stabilised by pairs of C−H···N(p_π) interactions; the C···N distances are in the range 2.91 to 2.94 Å with associated H···N distances of between 2.41 and 2.50 Å. There are no significant intermolecular close contacts between the complexes or the included THF solvent molecule.

In the structure of **3·Bz-Bz**, where there is an absence of apical substituents on the chromium centres, the geometry at chromium is square planar (Figure 3), although with a marked tetrahedral distortion, the N−N−Cr and Cr−Cl−Cl planes being inclined by 18°. The complex has crystallographic C_i symmetry and symmetric Cr−Cl bridges (Table 3). The Cr−N bond lengths are the same as

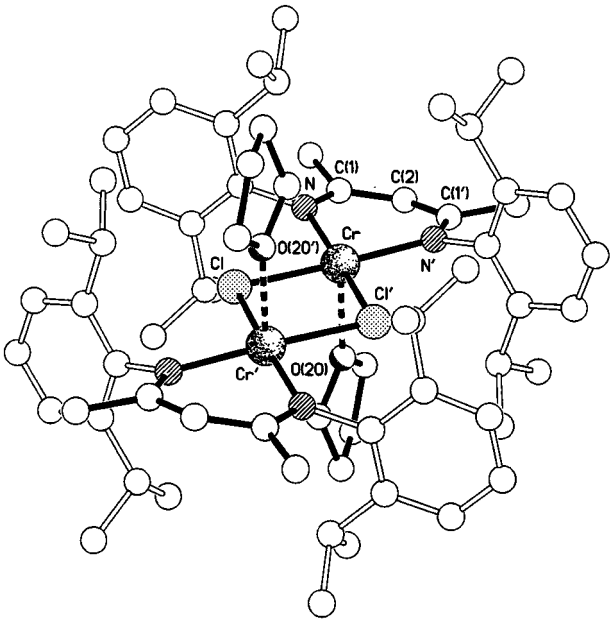

Figure 2. The molecular structure of the metal complex in **3(THF)$_2$·THF**

Table 2. Selected bond lengths (Å) and angles (°) for **3(THF)$_2$·THF**

Cr−Cl′	2.4182(6)	Cr−Cl	2.4182(6)
Cr−N	2.071(2)	Cr−N′	2.071(2)
Cr−O(20)	2.442(3)	N−C(1)	1.336(3)
N−Ar	1.450(3)	C(1)−C(2)	1.400(3)
C(2)−C(1′)	1.400(3)		
N−Cr−N′	91.26(10)	N−Cr−Cl′	171.58(6)
N′−Cr−Cl′	93.37(5)	N−Cr−Cl	93.37(5)
N′−Cr−Cl	171.58(6)	Cl′−Cr−Cl	81.21(3)
N−Cr−O(20)	92.39(7)	N′−Cr−O(20)	92.39(7)
Cl′−Cr−O(20)	94.44(5)	Cl−Cr−O(20)	94.44(5)
Cr−Cl−Cr′	98.79(3)		

in **2**. The non-bonded Cr···Cr separation here is 3.60 Å, noticeably shorter than in **1**, **2** and **3(THF)$_2$·THF**. The chelate ring, whilst still having a boat conformation, is distinctly flattened in comparison to **1**, **2** and **3(THF)$_2$·THF**, with Cr and C(3) lying 0.30 and 0.09 Å, respectively, out of the N(1)−C(2)−C(4)−N(5) plane. The 2,6-diisopropylphenyl rings are rotated by 85 and 88° out of their respective chelate C−N−Cr planes, with associated C−H···N(p_π) interactions (C···N distances in the range 2.87 to 2.92 Å, H···N distances between 2.39 and 2.50 Å). There are no notable intermolecular packing interactions involving either the complex or the co-crystallised dibenzyl molecules.

It is noteworthy that complex **3(THF)$_2$·THF** can also be prepared more directly by treating $CrCl_2$·THF with one equivalent of LiDDP in THF.

The pathway by which **3** is formed from **1** is uncertain. However, it would seem possible that benzylation of the apical *trans* sites in **1** occurs initially to give the benzyl analogue of **2** in a manner similar to the benzylation of [Cp*CrCl(μ-Cl)]$_2$,[13e] followed by isomerisation to the *cis* isomer and reductive coupling of benzyl groups to give **3** and di-

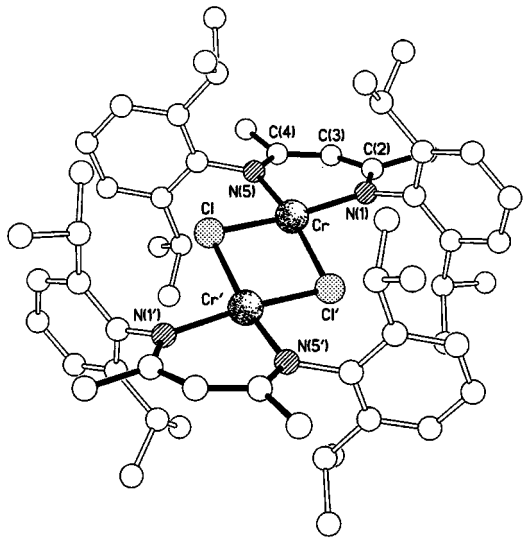

Figure 3. The molecular structure of the chromium-containing species in **3·Bz-Bz**

Table 3. Selected bond lengths (Å) and angles (°) for **3·Bz-Bz**

Cr−Cl	2.3877(9)	Cr−Cl′	2.3851(9)
Cr−N(1)	2.036(2)	Cr−N(5)	2.031(2)
N(1)−C(2)	1.331(4)	C(2)−C(3)	1.393(4)
C(3)−C(4)	1.400(4)	C(4)−N(5)	1.335(4)
N(5)−Cr−N(1)	90.93(10)	N(5)−Cr−Cl′	168.04(8)
N(1)−Cr−Cl′	94.54(7)	N(5)−Cr−Cl	95.21(7)
N(1)−Cr−Cl	165.75(8)	Cl−Cr−Cl′	81.95(3)
Cr−Cl−Cr′	98.05(3)		

benzyl (Scheme 2). It is noteworthy that Theopold has recently postulated a related *trans-cis* isomerisation of the related complex $[Cp^*CrMe(\mu\text{-}Cl)]_2$.[13a] However, we cannot rule out Wurtz coupling occurring independently of the transition metal centre in a way that is often observed during the preparation of benzylic Grignard reagents.[19,20]

Whilst reaction of **1** with either $AlMe_3$ or BzMgCl results in preservation of the dimeric core, interaction with carboxylates or β-diketonates results in cleavage of the dimer to give discrete mononuclear chromium(III) complexes. For example, treatment of **1** with NaO_2CR (R = Me, Ph) at −78 °C gives the complexes [(DDP)CrCl(O_2CR)(THF)] (R = Me **4a**, Ph **4b**) in high yield. Both **4a** and **4b** can be recrystallised from a concentrated pentane solution at −20 °C. A single crystal of **4a** was subjected to an X-ray diffraction study. The structure of **4a** consists of an octahedral chromium centre with the oxygen atom of the THF ligand and one of the oxygen atoms of the acetate ligand in the same plane as the nitrogen atoms of the bidentate ligand; the remaining oxygen atom of the η^2-chelating acetate group occupies a site *trans* to the chloride ligand (Figure 4). The structure of **4a** thus resembles that of the less sterically demanding diphenyl β-diketiminato complex [{PhNC(Me)CHC(Me)NPh}$CrCl_2$-$(THF)_2$],[6i] with a THF and a chloride ligand effectively replaced by an acetate group. In **4a** the geometry at chromium is distorted with *cis* angles in the range 63.7(1) to 101.9(1)°, the acute angle being associated with the bite of the acetate ligand. The Cr−N distances (Table 4) are the same as in **2** and **3·BzBz**, and the Cr−Cl distance [2.295(1) Å] is similar to that to the terminal chloride in **1**. The Cr−O(THF) distance [2.119(3) Å] is consistent with the presence of a formal σ-bond, similar to that to the loosely associated apical ligand in **3(THF)$_2$·THF** [2.442(3) Å]. The six-membered chelate ring has a distinctive boat conformation with the chromium and C(3) lying 0.60 and 0.11 Å, respectively, out of the N(1)−C(2)−C(4)−N(5) plane. There are characteristic orthogonal orientations (83 and 87°) of the 2,6-diisopropylphenyl ring systems to the chelate ring. Stabilisation of this conformation is again by weak C−H···N(p_π) interactions (C···N distances in the range 2.89 to 2.98 Å, H···N distances between 2.41 and 2.50 Å). The packing is normal van der Waals.

Compound **4b** is presumed to possess a similar structure to **4a**. Unlike the reactions of **1** with carboxylates, treatment of **1** with the more sterically demanding β-diketonates, {CH[C(R)O]$_2$}$^-$ [R = Me (acac), Ph (dbm)], results in the five-coordinate complexes [(DDP)CrCl({O(R)C}$_2$CH)] (R = Me **5a**, Ph **5b**). Both **5a** and **5b** can be recrystallised from pentane at −20° C. Compound **5b** has been the subject of a single crystal X-ray diffraction study. This study shows **5b** to have a square pyramidal coordination geometry at chromium (Figure 5), with the basal sites occupied

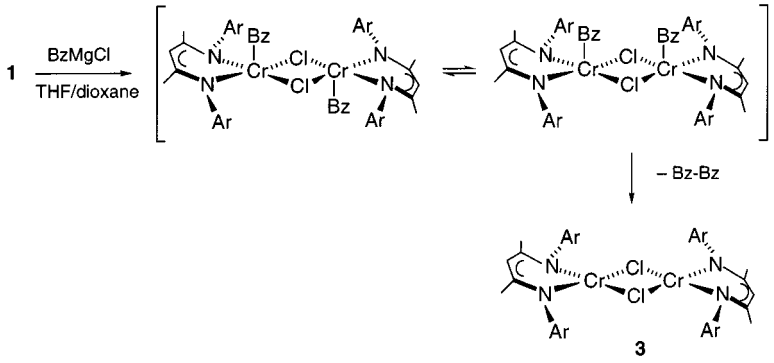

Scheme 2. Plausible pathway for the formation of **3** from **1**

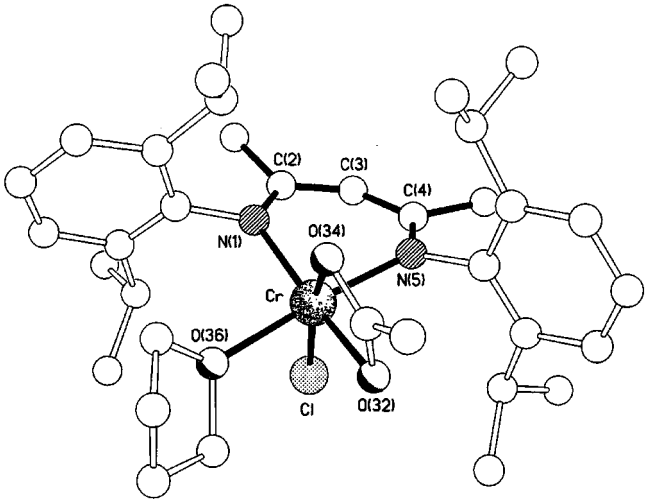

Figure 4. The molecular structure of **4a**

Table 4. Selected bond lengths (Å) and angles (°) for **4a**

Cr−Cl	2.2947(12)	Cr−N(1)	2.029(3)
Cr−N(5)	2.023(3)	Cr−O(32)	2.059(3)
Cr−O(34)	2.043(3)	Cr−O(36)	2.119(3)
N(1)−C(2)	1.330(5)	C(2)−C(3)	1.409(5)
C(3)−C(4)	1.383(5)	C(4)−N(5)	1.323(5)
N(5)−Cr−N(1)	90.37(12)	N(5)−Cr−O(34)	90.70(12)
N(1)−Cr−O(34)	101.90(12)	N(5)−Cr−O(32)	91.06(12)
N(1)−Cr−O(32)	165.52(12)	O(34)−Cr−O(32)	63.67(12)
N(5)−Cr−O(36)	174.12(12)	N(1)−Cr−O(36)	95.14(11)
O(34)−Cr−O(36)	86.16(12)	O(32)−Cr−O(36)	83.10(11)
N(5)−Cr−Cl	93.10(9)	N(1)−Cr−Cl	93.23(9)
O(34)−Cr−Cl	164.38(9)	O(32)−Cr−Cl	101.08(10)
O(36)−Cr−Cl	88.65(9)		

by the two η^2 ligands and the apical site by a chloride ligand. The metal atom lies 0.32 Å out of the basal plane (which is planar to within 0.002 Å) in the direction of the chloride ligand [Cr−Cl 2.229(1) Å]. The Cr−N distances (Table 5) are the same as in **2**, **3·Bz-Bz** and **4a**. The diketiminate chelate ring has, as in all the other complexes, a boat conformation with the chromium and C(3) lying 0.43 and 0.11 Å, respectively, out of the N(1)−C(2)−C(4)−N(5) plane. The Cr(dbm) chelate ring is much flatter, with the chromium and C(8) lying 0.23 and 0.02 Å, respectively, out of the O(6)−C(7)−C(9)−O(10) plane. The 2,6-diisopropylphenyl ring systems are, as usual, oriented orthogonally (83 and 86°) to the chelate ring, with C−H···N(p_π) stabilisation (C···N distances in the range 2.90 to 2.98 Å, H···N distances between 2.38 and 2.49 Å). In contrast, the planes of the two phenyl rings of the dbm ligand lie close to that of their chelate ring (twists of ca. 10 and 20°) and as a consequence direct one of their *ortho* C−H hydrogen atoms into the faces of their proximal 2,6-diisopropylphenyl rings of the diketiminate ligand; the H···π distances are short at 2.40 and 2.53 Å and have associated C−H···π angles of 168 and 160°, respectively. Accompanying this interaction is a noticeable contraction of both the O(6)−C(7)−C(42) and O(10)−C(9)−C(48) angles [115.8(3) and 116.2(3)°, respectively], and to a lesser extent also those for C(7)−C(42)−C(37) and C(9)−C(48)−C(47) [117.3(2) and 118.0(2)°, respectively], from normal trigonal values. These interactions are directly analogous to those present between the *ortho* hydrogen atoms of a dbm ligand coordinated to iridium and the phenyl rings of a pair of triphenylphosphane ligands coordinated to the same metal centre.[21] There are no packing interactions of note.

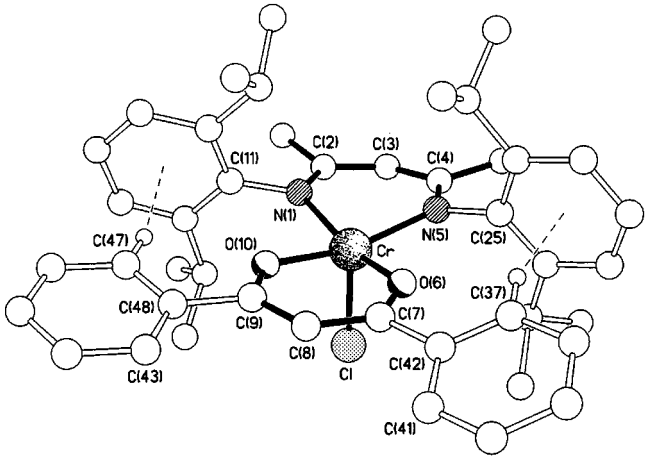

Figure 5. The molecular structure of **5b**, showing also the weak intramolecular C−H···π stabilising interactions

Table 5. Selected bond lengths (Å) and angles (°) for **5b**

Cr−Cl	2.2294(14)	Cr−N(1)	2.020(3)
Cr−N(5)	2.032(3)	Cr−O(6)	1.958(3)
Cr−O(10)	1.961(3)	N(1)−C(2)	1.341(5)
C(2)−C(3)	1.387(6)	C(3)−C(4)	1.391(6)
C(4)−N(5)	1.329(5)		
O(6)−Cr−O(10)	86.89(11)	O(6)−Cr−N(1)	161.27(13)
O(10)−Cr−N(1)	87.83(12)	O(6)−Cr−N(5)	88.85(13)
O(10)−Cr−N(5)	161.63(13)	N(1)−Cr−N(5)	90.54(13)
O(6)−Cr−Cl	96.18(10)	O(10)−Cr−Cl	96.02(10)
N(1)−Cr−Cl	102.25(11)	N(5)−Cr−Cl	102.20(10)

Examples of mononuclear five-coordinate Cr^{III} complexes are rare, due to the significant ligand-field stabilisation of the d^3 configuration in an octahedral geometry.[20] **5a** is presumed to possess a similar structure to **5b**.

All the complexes are paramagnetic, affording broad uninformative ^{1}H NMR spectra. The mononuclear complexes **4** and **5** exhibit magnetic moments between 3.8 and 4.1 BM (Evans Balance at ambient temperature) consistent with three unpaired electrons (d^3) while the dimeric chromium(III) complexes **1** and **2** display magnetic moments of 3.5 and 3.6 BM characteristic of antiferromagnetically coupled $S = 3/2$ chromium(III) centres.[7f,23] In addition, the X-band EPR spectra of all the Cr^{III} complexes in toluene at ambient temperature all support the complexes being assigned Cr^{III} with sharp signals corresponding to g values of ca. 1.98 with no observable hyperfine coupling.[24]

The FAB mass spectra of the mononuclear complexes **4** and **5** give molecular ion peaks and/or peaks corresponding

to fragmentation peaks. For the dimeric complexes **1**−**3** fragmentation of the dinuclear unit must readily occur in the instrument as only peaks attributable to mononuclear fragments are observed. This observation is consistent with the ready cleavage of the dimeric assembly in the presence of carboxylates or β-diketonates (see complexes **4** and **5**) leading to the prospect that **1**−**3** can be regarded as loosely associated monomers.

The results of Schlenk-scale ethylene polymerisation screening tests at 1 bar/25 °C using dual-component catalyst systems (**1**−**5** + cocatalyst) are collected in Table 6. Three types of aluminium co-catalyst have been employed to activate pre-catalysts **1**−**5**, namely methylaluminoxane (MAO), diethylaluminium chloride (DEAC) and dimethylaluminium chloride (DMAC) (see Table 6; runs 1−19). The results reported in Table 6 were reproduced several times, though not optimised beyond the conditions reported.

Table 6. Results of ethylene polymerisation runs using precatalysts **1**−**5**[a]

Run	Precatalyst (mmol)	Activator[b] (mmol/ equiv.)	Yield PE (g)[c]	Activity (g/mmol·h·bar)
1	**1** (0.015)	MAO (6.0/400)	0.12	4[d]
2	**1** (0.015)	DEAC (0.45/30)	2.25	75[d]
3	**2** (0.015)	MAO (6.0/400)	0.30	10[d]
4	**2** (0.015)	DEAC (0.45/30)	1.60	54[d]
5	**3** (0.015)	MAO (6.0/400)	0.24	8[d]
6	**3** (0.015)	DEAC (0.45/30)	2.16	72[d]
7	**3** (0.015)	DMAC (0.45/30)	2.37	79[d]
8	**4a** (0.015)	MAO (6.0/400)	0.05	3
9	**4a** (0.015)	DEAC (0.45/30)	1.77	118[e]
10	**4a** (0.015)	DMAC(0.45/30)	1.05	70
11	**4b** (0.01)	MAO (4.0/400)	0.13	13
12	**4b** (0.01)	DEAC (0.3/30)	0.85	85
13	**4b** (0.01)	DMAC (0.3/30)	0.93	93
14	**5a** (0.015)	MAO (6.0/400)	0.30	20
15	**5a** (0.015)	DEAC (0.45/30)	1.48	49
16	**5a** (0.015)	DMAC (0.45/30)	1.61	54
17	**5b** (0.015)	MAO (6.0/400)	0.15	10
18	**5b** (0.015)	DEAC (0.45/30)	0.84	56
19	**5b** (0.015)	DMAC (0.45/30)	1.20	80

[a] *General conditions*: 1 bar ethylene Schlenk test carried out in toluene (40 mL) at 25 °C, over 60 min., reaction quenched with dil HCl and the solid washed with methanol (50 cm^3) and dried in a vacuum oven at 40 °C. – [b] MAO = methylaluminoxane. – [c] Solid polyethylene. – [d] Activity reported per chromium centre. – [e] As a representative example, GPC analysis of the polyethylene afforded M_w = 925000, M_n = 110000, M_w/M_n = 8.4. Care should be taken in the interpretation of these values, however, since, in general, the polymers derived from these polymerizations are not fully soluble in the 1,2,4-trichlorobenzene GPC solvent, even upon heating at 160 °C for several hours.

On analysis of Table 6 several points emerge. Firstly, all DDP-supported chromium complexes are active in the presence of alkylaluminum activator, converting ethylene to high molecular weight polyethylene. In no case has polyethylene been obtained using **1**−**5** in the absence of an aluminium activator, nor has there been any evidence for low molecular weight oligomers (by GCMS). Secondly, the most active systems (runs 9 and 13) comprise a combination of one equivalent of chromium complex to thirty equivalents of alkylaluminium chloride activator. We have found that activities start to fall with a greater or lower concentration of activator. Notably, MAO (400 equiv.) results in lower activities (runs 1, 3, 5, 8, 11, 14, 17). Thirdly, the similar activities [*cf.* 75 (run 2), 72 g/mmol·h·bar (run 6)] observed employing the DDP-supported Cr^{III}- and Cr^{II}-chloride complexes **1** and **3**, and the purple colour of the active catalyst (in both cases), suggest a common active species.

The mechanism by which these dual component systems operate is uncertain. The fact that the most active systems combine an alkylaluminium chloride rather than MAO rather suggests that alkyl abstraction to form a cationic species is not occurring here. This may account for the generally lower activities observed by comparison with the Cp-amine systems reported by Jolly where a cationic active centre is believed to operate. The identity of the active oxidation state is uncertain but the similarity in productivities and reactivity involving the Cr^{II} and Cr^{III} complexes **1** and **3**, coupled with the ready reduction of **1** on benzylation, lends some support for a Cr^{II} species.

Conclusions

The chemistry of the sterically demanding β-diketiminato ligand DDP on low valent chromium has been explored. Complexation of DDP with $CrCl_3(THF)_3$ leads to a readily derivatisable coordinatively unsaturated dimeric species **1**. Preservation of the dimeric core occurs on alkylation or reduction of **1**, while addition of chelating carboxylate or β-diketonate ligands to **1** causes fragmentation to give discrete mononuclear complexes. Notably, only in the case of **4** is the more common octahedral geometry of Cr^{III} achieved. All the complexes polymerise ethylene on addition of aluminium activators to give high molecular weight polyethylene.

Experimental Section

General: All manipulations were carried out under an atmosphere of nitrogen using standard Schlenk and cannula techniques or in a conventional nitrogen-filled glove-box. Solvents were refluxed over an appropriate drying agent, and distilled and degassed prior to use. Elemental analyses were performed by the microanalytical services of the Department of Chemistry at Imperial College and Medac Ltd. NMR spectra were recorded on a Bruker spectrometer at 250 MHz (^1H) and 62.9 MHz (^{13}C) at room temperature; chemical shifts are referenced to the residual protonated impurity of the deuterated solvent. IR spectra (nujol mulls, KBr/CsI windows) were recorded on Perkin−Elmer 577 and 457 grating spectrophotometers. Mass spectra were obtained using fast atom bombardment (FAB). Gel permeation chromatographs (GPC) were obtained using a Waters 150CV [columns are supplied by Shodex (807, 806 & 804) BP Chemicals Ltd.]. Magnetic Susceptibility studies were performed using an Evans Balance at room temperature. Diamagnetic corrections for the samples were determined from Pascal's constants and literature values.[25]

$CrCl_3(THF)_3$ [26] and DDPH[8b] were prepared according to the established procedures. The reagents $AlMe_3$ (2.0 M solution in toluene), Et_2AlCl (1.8 M solution in toluene), Me_2AlCl (1.0 M solution in hexane), MAO (10% solution in toluene) and BzMgCl (2.0 M solution in THF) were purchased from Aldrich Chemical Co. All other chemicals were obtained commercially and used as received unless stated otherwise.

Preparation of [(DDP)CrCl(μ-Cl)]$_2$ (1): $CrCl_3(THF)_3$ (1.00 g, 2.67 mmol) was loaded into a Schlenk flask containing one equivalent of the lithium salt of DDPH (1.13 g, 2.67 mol) in THF (40 mL) at −78 °C. The solution was stirred overnight at room temperature giving an olive green solution. The volatiles were removed under reduced pressure and pentane (50 mL) added. Filtration of the lithium salts gave the crude product which was recrystallised by standing at −20 °C overnight to give **1** (1.08 g, 75%). FAB-MS: m/z = 504 [$M^+/2$]. − $C_{58}H_{82}Cl_4Cr_2N_4$ (1081.1): calcd. C 64.44, H 7.59, N 5.19; found C 64.65, H 7.81, N 5.41. − μ_{eff} = 3.60 BM.

Preparation of [(DDP)CrMe(μ-Cl)]$_2$ (2): A THF (40 mL) solution of **1** was formed as above by stirring $CrCl_3(THF)_3$ (1.00 g, 2.67 mmol) and LiDDP (1.13 g, 2.67 mol) together overnight. $AlMe_3$ (2.5 mL, 5.0 mmol) was introduced to the green solution with a syringe at room temperature. After stirring overnight the solution was taken to dryness to give a dark oily residue. Extraction with pentane (60 mL) followed by filtration gave a dark purple solution. Concentration of the solution to half volume and standing at −20 °C gave **2** as crimson needles (0.94 g, 68%). FAB-MS: m/z = 469 [$M^+/2$ − Me − Cl]. − $C_{60}H_{88}Cl_2Cr_2N_4$ (1040.3): calcd. C 69.30, H 8.47, N 5.39; found C 69.41, H 8.81, N 5.82. − μ_{eff} = 3.50 BM.

Preparation of [(DDP)Cr(μ-Cl)]$_2$ (3): A THF (40 mL) solution of **1** was formed as above by stirring $CrCl_3(THF)_3$ (1.00 g, 2.67 mmol) and LiDDP (1.13 g, 2.67 mol) together overnight. Benzylmagnesium chloride (2.67 mL, 5.34 mmol) was added to the green solution at −78 °C with a syringe and the solution allowed to warm to room temperature to give an apple green solution. Dioxane (2 mL) was added to the solution after 12 h, stirred for a further 2 h and filtered to give an apple green solution. The complex **3(THF)$_2$·THF** (1.09 g, 71%) could be isolated as lime green crystals by cooling the apple green THF/dioxane solution to −20 °C. Alternatively, **3·Bz-Bz** (1.03 g, 65%) could be isolated as green crystals by stripping the volatiles from the reaction mixture and extracting the residue with pentane and cooling the solution to −20 °C.

3(THF)$_2$·THF: $C_{66}H_{98}Cl_2Cr_2N_4O_2$ (1154.4): calcd. C 68.69, H 8.50, N 4.86; found C 68.81, H 8.70, N 4.69. − FAB-MS: m/z = 469 [$M^+/2$ − Cl − THF].

3·Bz-Bz: $C_{72}H_{96}Cl_2Cr_2N_4$ (1192.5): calcd. C 72.54, H 8.06, N 4.70; found C 72.71, H 8.34, N 4.69. − FAB-MS: m/z = 469 [$M^+/2$ − Cl − $C_6H_5CH_2$].

Preparation of [(DDP)CrCl(O$_2$CR)(THF)] (R = Me 4a, Ph 4b): To a THF (40 mL) solution of the lithium salt of DDPH (1.13 g, 2.67 mmol) at −78 °C was added $CrCl_3(THF)_3$ (1.00 g, 2.67 mmol). The solution was allowed to warm to room temperature and stirred for 3 h before the addition of sodium acetate (0.22 g, 2.67 mmol) or sodium benzoate (0.38 g, 2.67 mmol) at −78 °C. The solutions were allowed to warm to room temperature and stirred for a further 12 h. After removal of the solvent under reduced pressure, pentane (60 mL) was introduced and the lithium salts filtered. Concentration of the filtrates to half volume and cooling to −20 °C overnight gave **4a** (0.68 g, 45%) and **4b** (0.85 g, 49%) as green crystals.

4a: FAB-MS: m/z = 563 [M^+ − THF], 528 [M^+ − Cl − THF], 467 [M^+ − Cl − THF − O_2CMe]. − $C_{35}H_{52}ClN_2O_2$ (568.26): calcd. C 66.09, H 8.18, N 4.41; found C 66.12, H 8.41, N 4.29. − μ_{eff} = 3.80 BM.

4b: FAB-MS: m/z = 696 [M^+], 590 [M^+ − Cl − THF], 467 [M^+ − Cl − THF − O_2CPh]. − $C_{40}H_{54}ClCrN_2$ (650.33): calcd. C 68.82, H 7.74, N 4.01; found C 68.91, H 7.89, N 3.98. − μ_{eff} = 3.74 BM.

Preparation of [(DDP)CrCl({O(R)C}$_2$CH)] (R = Me 5a, Ph 5b): To a THF (40 mL) solution of the lithium salt of DDPH (1.13 g, 2.67 mmol) at −78 °C was added $CrCl_3(THF)_3$ (1.00 g, 2.67 mmol). The solution was allowed to warm to room temperature and stirred for 3 h before the addition of the lithium salts of either 2,4-pentanedione (0.28 g, 2.67 mmol) or dibenzoylmethane (0.61 g, 2.67 mmol) at −78 °C. The solutions were allowed to warm to room temperature and stirred for a further 12 h. After removal of the solvent under reduced pressure pentane (60 mL) was introduced and the lithium salts filtered. Concentration of the filtrates to half volume and cooling to −20 °C overnight gave **5a** (0.72 g, 45%) and **5b** (0.99 g, 51%) as red crystals.

5a: FAB-MS: m/z = 568 [M^+ − Cl], 419 [M^+ − Cl − {O(Me)C}$_2$CH − Cr]. − $C_{34}H_{48}ClCrN_2O_2$ (604.21): calcd. C 67.61, H 7.95, N 4.64; found C 67.30, H 8.01, N 4.44. − μ_{eff} = 4.06 BM.

5b: FAB-MS: m/z = 692 [M^+ − Cl], 419 [M^+ − Cl − {O(Ph)C}$_2$CH − Cr]. − $C_{44}H_{52}ClCrN_2O_2$ (728.36): calcd. C 72.58, H 7.15, N 3.85; found C 73.71, H 6.99, N 3.78. − μ_{eff} = 3.80 BM.

Polymerisation Procedure: Results of Schlenk-line tests (1 bar) are listed in Table 6; the polymerisation procedure is as follows: The precatalyst (0.01−0.015 mmol of **1**−**5**) was dissolved in toluene (40 mL) and the co-catalyst (MAO, DEAC or DMAC) added. The Schlenk tube was purged with ethylene and the contents magnetically stirred and maintained under ethylene (1 bar) for the duration of the polymerisation. After 1 h the polymerisation was terminated by the addition of dil. HCl/MeOH. The solid polyethylene was recovered by filtration, washed with methanol (50 mL) and dried (vacuum oven at 50 °C).

X-ray Crystal Structure Determinations of 1, 2, 3(THF)$_2$.THF, 3·Bz-Bz, 4a, and 5b: Table 7 provides a summary of the crystal data, data collection, and refinement parameters for compounds **1**, **2**, **3(THF)$_2$·THF**, **3·Bz-Bz**, **4a** and **5b**.

The structures were solved by direct methods, and the major occupancy non-hydrogen atoms were refined anisotropically using full-matrix, least-squares based on F^2. In **1**, **2**, **3(THF)$_2$·THF** and **4a** disorder was found in the solvent molecules; in each case two partial occupancy orientations were identified with, in **1**, **3(THF)$_2$·THF** and **4a**, the major occupancy non-hydrogen atoms refined anisotropically and the minor occupancy non-hydrogen atoms refined isotropically, and in **2** all the disordered non-hydrogen atoms refined anisotropically. Throughout all six structures the C−H hydrogen atoms of methyl groups bound to sp^2 centres were located from ΔF maps, idealised, assigned isotropic thermal parameters [U(H) = 1.5U_{eq}(C)] and allowed to ride on their parent atoms. The remaining hydrogen atoms were placed in calculated positions, assigned isotropic thermal parameters [U(H) = 1.2U_{eq}(C); U(H) = 1.5U_{eq}(C-Me)], and allowed to ride on their parent atoms. All computations were carried out using the SHELXTL PC program system.[27]

Crystallographic data (excluding structure factors) have been deposited with the Cambridge Crystallographic Data Centre as supplementary publication no's: CCDC-150447−150452 for structures **1**−**5b**, respectively (Table 7). Copies of the data can be obtained free of charge on application to CCCD, 12 Union Road, Cambridge CB2 1EZ, U.K. [Fax: (internat.) +44-1223/336-033: E-mail: deposit@ccdc.cam.ac.uk].

Table 7. Crystal data, data collection and refinement parameters for compounds **1**, **2**, **3(THF)$_2$·THF**, **3·Bz-Bz**, **4a** and **5b**[a]

	1	**2**	**3(THF)$_2$·THF**	**3·Bz-Bz**	**4a**	**5b**
Formula	$C_{58}H_{82}N_4Cl_4Cr_2$	$C_{60}H_{88}N_4Cl_2Cr_2$	$C_{58}H_{82}N_4Cl_2Cr_2$	$C_{58}H_{82}N_4Cl_2Cr_2$	$C_{35}H_{52}N_2O_3ClCr$	$C_{44}H_{52}N_2O_2ClCr$
Solvent	C_5H_{12}	$0.5C_5H_{12}$	$3C_4H_8O$	$PhCH_2CH_2Ph$	–	–
Molecular weight	1153.2	1076.3	1226.5	1192.4	636.2	728.3
Colour, habit	black blocks	crimson prismatic needles	green octahedra	green blocks	red prismatic needles	orange/red prisms
Crystal size/mm	0.23 × 0.10 × 0.07	0.33 × 0.17 × 0.13	0.73 × 0.67 × 0.67	0.67 × 0.50 × 0.33	0.90 × 0.27 × 0.27	0.57 × 0.40 × 0.23
Crystal system	monoclinic	monoclinic	tetragonal	triclinic	monoclinic	triclinic
Space group	$P2_1/c$ (no. 14)	$C2/m$ (no. 12)	$P4_2/m$ (no 84)	$P\bar{1}$ (no. 2)	$P2_1/c$ (no. 14)	$P\bar{1}$ (no. 2)
T/K	203	203	203	183	203	203
a/Å	13.581(3)	19.434(3)	13.036(2)	12.034(1)	8.935(2)	11.140(1)
b/Å	13.547(3)	21.764(2)	–	12.564(1)	17.001(2)	12.780(2)
c/Å	17.553(2)	15.098(2)	20.134(2)	13.637(1)	23.258(2)	14.712(3)
α/deg	–	–	–	97.37(1)	–	76.52(1)
β/deg	104.28(2)	90.58(1)	–	114.72(1)	97.66(1)	84.97(1)
γ/deg	–	–	–	110.28(1)	–	80.50(1)
V/Å^3	3130(1)	6386(1)	3421.3(7)	1663.9(1)	3501.2(8)	2006.2(5)
Z	2[b]	4[c]	2[d]	1[b]	4	2
D_c/g cm^{-3}	1.224	1.120	1.191	1.190	1.207	1.206
F(000)	1232	2316	1320	638	1364	774
Radiation used	Cu-K_α [e]	Cu-K_α [e]	Mo-K_α	Cu-K_α [e]	Mo-K_α	Mo-K_α
μ/mm^{-1}	4.73	3.85	0.44	3.75	0.44	0.39
θ range/deg	3.4–58.0	2.9–60.0	1.9–30.0	6.3–63.0	1.8–25.0	1.9–25.0
No. of unique reflections						
measured	4293	4866	5101	5228	6111	6954
observed, $\|F_o\| > 4\sigma(\|F_o\|)$	2823	3370	3603	4547	3963	4296
Absorption correction	semi-empirical	–	–	semi-empirical	semi-empirical	–
Max., min. transmission	0.58, 0.41	–	–	0.35, 0.21	0.90, 0.83	–
No. of variables	353	340	245	350	383	427
R_1, wR_2 [f]	0.067, 0.153	0.065, 0.164	0.056, 0.128	0.056, 0.142	0.054, 0.109	0.058, 0.112

[a] Details in common: graphite monochromated radiation, ω-scans, Siemens P4 diffractometer, refinement based on F^2. – [b] The molecule has crystallographic C_i symmetry. – [c] There are two crystallographically independent C_{2h} symmetric molecules in the asymmetric unit. – [d] The molecule has crystallographic C_{2h} symmetry. – [e] Rotating anode source. – [f] $R_1 = \Sigma||F_o| - |F_c||/\Sigma|F_o|$; $wR_2 = [\Sigma\, w(F_o^2 - F_c^2)^2/\Sigma w(F_o^2)^2]^{1/2}$; $w^{-1} = \sigma^2(F_o^2) + (aP)^2 + bP$.

Acknowledgments

BP-Amoco Chemicals Ltd is thanked for financial support. Drs. J. Boyle and G. Audley are thanked for NMR and GPC measurements, respectively.

[1] [1a] F. J. Karol, G. L. Garapinka, C. Wu, A. W. Dow, R. N. Johnson, W. I. Carrick, J. Polym. Sci., *Part A* **1972**, *10*, 2621–2637. – [1b] J. P. Hogan, J. Polym. Sci., *Part A* **1972**, *8*, 2637–2652.

[2] [2a] M. P. McDaniel, *Adv. Catal.* **1985**, *33*, 47–98. – [2b] J. A. N. Ajjou, S. L. Scott, V. Paquet, *J. Am. Chem. Soc.* **1998**, *120*, 415–416.

[3] For recent reviews, see: K. H. Theopold, *Chem. Eur. J.* **1998**, *3*, 15–24; K. H. Theopold, *CHEMTECH* **1997**, *27*, 26–32.

[4] [4a] R. Emrich, O. Heinemann, P. W. Jolly, C. Krüger, G. P. J. Verhovnik, *Organometallics* **1997**, *16*, 1511–1513. – [4b] D. A. Gohre, P. W. Jolly, B. Kryger, J. Rust, G. P. J. Verhovnik, *Organometallics* **2000**, *19*, 388–402. – [4c] V. R. Jensen, K. Angermund, P. W. Jolly, K. J. Borve, *Organometallics* **2000**, *19*, 403–410.

[5] G. J. P. Britovsek, V. C. Gibson, D. F. Wass, *Angew. Chem. Int. Ed.* **1999**, *38*, 428–447, and references therein.

[6] [6a] F. J. Feher, R. L. Blanski, *J. Chem. Soc., Chem. Commun.* **1990**, 1614–1616. – [6b] M. P. Coles, V. C. Gibson, *Polym. Bull.* **1994**, *33*, 529–533. – [6c] M. P. Coles, C. I. Dalby, V. C. Gibson, W. Clegg and M. R. J. Elsegood, *J. Chem. Soc., Chem. Commun.* **1995**, 1709–1711. – [6d] M. P. Coles, C. I. Dalby, V. C. Gibson, I. R. Little, E. L. Marshall, M. H. R. da Costa, S. Mastroianni, *J. Organomet. Chem.* **1999**, *591*, 78–87. – [6e] V. C. Gibson, C. Newton, C. Redshaw, G. A. Solan, A. J. P. White, D. J. Williams, *J. Chem. Soc., Dalton Trans.* **1999**, 827–829. – [6f] V. C. Gibson, S. Mastroianni, C. Newton, C. Redshaw, G. A. Solan, A. J. P. White, D. J. Williams, *J. Chem. Soc., Dalton Trans.* **2000**, 1969–1971. – [6g]V. C. Gibson, C. Newton, G. A. Solan (BP Chemicals Ltd.), WO 99/19335, **1999** [*Chem. Abstr.* **1999**, *130*, 297099p]. – [6h]V. C. Gibson, P. J. Maddox, C. Newton, C. Redshaw, G. A. Solan, A. J. P. White and D. J. Williams, *Chem. Commun.* **1998**, 1651–1652. – [6i] W.-K. Kim, M. J. Fevola, L. M. Liable-Sands, A. L. Rheingold, K. H. Theopold, *Organometallics* **1998**, *17*, 4541–4543. – [6j] R. D. Köhn, M. Haufe, S. Mihan and D. Lilge, *Chem. Commun.* **2000**, 1927–1928.

[7] [7a] B. Qian, W. J. Scanlon, M. R. Smith, III, *Organometallics* **1999**, *18*, 1693–1698. – [7b] P. H. M. Budzelaar, A. B. van Oort, A. G. Orpen, *Eur. J. Inorg. Chem.* **1998**, 1485–1494. – [7c] M. Rahim, N. J. Taylor, S. Xin, S. Collins, *Organometallics* **1998**, *17*, 1315–1323. – [7d] M. F. Lappert, D. S. Liu, *J. Organomet. Chem.* **1995**, *500*, 203–217. – [7e] P. B. Hitchcock, M. F. Lappert, S. D. Liu, *J. Chem. Soc., Chem. Commun.* **1994**, 2637. – [7f] D. S. Richeson, J. F. Mitchell, K. H. Theopold, *Organometallics* **1989**, *8*, 2570–2577. – [7g] J. E. Bercaw, D. L. Davies, P. T. Wolczanski, *Organometallics* **1986**, *5*, 443–450.

[8] [8a] P. H. M. Budzelarr, R. de Gelder, A. W. Gal, *Organometallics* **1998**, *17*, 4121–4123. – [8b] J. Feldman, S. J. McLain, A. Parthasarathy, W. J. Marshall, J. C. Calabrese, S. D. Arthur, *Organometallics* **1997**, *16*, 1514–1516.

[9] [9a] F. Cosledan, P. B. Hitchcock, M. F. Lappert, *Chem. Commun.* **1999**, 705–706. – [9b] C. E. Radzewich, M. P. Coles, R. F. Jordan, *J. Am. Chem. Soc.* **1998**, *120*, 9384–9385. – [9c] B.

Qian, D. L. Ward, M. R. Smith, III, *Organometallics* **1998**, *17*, 3070−3076. − [9d] M. Cheng, E. B. Lobkovsky, G. W. Coates, *J. Am. Chem. Soc.* **1998**, *120*, 11018−11019. − [9e] V. C. Gibson, J. A. Segal, A. J. P. White, D. J. Williams, *J. Am. Chem. Soc.* **2000**, *122*, 7120−7121.

[10] D. Dress, J. Magull, *Z. Anorg. Allg. Chem.* **1994**, *620*, 814−818.

[11] [11a] S. G. McGeachin, *Can. J. Chem.* **1968**, *46*, 1903−1912. − [11b] J. E. Parks, R. H. Holm, *Inorg, Chem.* **1968**, *7*, 1408−1416.

[12] Range for $Cr^{III}\cdots Cr^{III}$ distances for $Cr(\mu\text{-}Cl)_2Cr$ complexes: 3.64−3.23 Å. See, for example, refs.[13−15]

[13] [13a] R. A. Heintz, S. Leelasubcharoen, L. M. Liable-Sands, A. L. Rheingold, K. H. Theopold, *Organometallics* **1998**, *17*, 5477−5485. − [13b] D. S. Richeson, S.-W. Hsu, N. H. Fredd, G. Van Duyne, K. H. Theopold, *J. Am. Chem. Soc.* **1986**, *108*, 8273−8274. − [13c] W. A. Hermann, W. R. Thiel, E. Herdtweck, *J. Organomet. Chem.* **1988**, *353*, 323−336. − [13d] G. Bhandari, Y. Kim, J. M. McFarland, A. L. Rheingold, K. H. Theopold, *Organometallics* **1995**, *14*, 738−745. − [13e] F. A. Cotton, J. L. Eglin, R. L. Luck, K.-A. Son, *Inorg. Chem.* **1990**, *29*, 1802−1806.

[14] O. Heinemann, P. W. Jolly, C. Krüger, G. P. J. Verhovnik, *J. Organomet. Chem.* **1998**, *553*, 477−479.

[15] F. H. Koehler, R. de Cao, K. Ackermann, J. Sedlmaier, *Z. Naturforsch., Teil B* **1983**, *38*, 1406−1411.

[16] P. N. Jagg, P. F. Kelly, H. S. Rzepa, D. J. Williams, J. D. Woollins, W. Wylie, *J. Chem. Soc., Chem. Commun.* **1991**, 942−944.

[17] Range for $Cr^{II}\cdots Cr^{II}$ distances for $Cr(\mu\text{-}Cl)_2Cr$ complexes: 3.817−2.642 Å. See ref.[18]

[18] [18a] A. R. Hermes, G. S. Girolami, *Inorg. Chem.* **1988**, *27*, 1775. − [18b] F. A. Cotton, R. L. Luck, K.-A. Son, *Inorg. Chim. Acta* **1990**, *168*, 3−4. − [18c] M. D. Fryzuk, D. B. Leznoff, S. J. Rettig, R. C. Thompson, *Inorg. Chem.* **1994**, *33*, 5528−5534. − [18d] R. A. Hermtz, R. L. Ostrander, A. L. Rheingold, K. H. Theopold, *J. Am. Chem. Soc.* **1994**, *116*, 11387. − [18e] B. Bachmann, J. Heck, F. Hahn, W. Massa, J. Pebler, *Z. Anorg. Allg. Chem.* **1995**, *621*, 2061−2064.

[19] H. R. Rogers, C. L. Hill, Y. Fujiwara, R. J. Rogers, H. L. Mitchells, G. M. Whitesides, *J. Am. Chem. Soc.* **1980**, *102*, 217−226.

[20] [20a]Y. Liang, G. P. A. Yap, A. L. Rheingold, K. H. Theopold, *Organometallics* **1996**, *15*, 5284−5286. − [20b] P. T. Greene, B. J. Russ, J. S. Wood, *J. Chem. Soc. A* **1971**, 3636−3638. − [20c] M. D. Fryzuk, D. B. Leznoff, S. J. Rettig, *Organometallics* **1997**, *16*, 5116−5119. − [20d] F. A. Cotton, J. Czuchajowska, L. R. Falvello, X. Feng, *Inorg. Chim. Acta* **1990**, *172*, 135−136.

[21] M. Cowie, M. D. Gauthier, S. J. Loeb, I. R. McKeer, *Organometallics* **1983**, *2*, 1057−1059.

[22] F. A. Cotton, G. Wilkinson, *Advanced Inorganic Chemistry* 5th ed.; Wiley: New York, **1988**; p 689.

[23] C. J. Cairns, D. H. Busch, *Coord. Chem. Rev.* **1986**, *69*, 1−55.

[24] C. Redshaw, G. Wilkinson, B. Hussain-Bates, M. B. Hursthouse, *J. Chem. Soc., Dalton Trans.* **1992**, 1803−1811 and refs. therein.

[25] [25a] C. J. O'Connor, *Prog. Inorg. Chem.* **1982**, *29*, 203. − [25b] *Handbook of Chemistry and Physics* (Ed.: R. C. Weast), CRC Press, Boca Raton, FL, 70th edn., **1990**, p. E134.

[26] J. Shamir, *Inorg. Chim. Acta* **1989**, *156*, 163−164.

[27] SHELXTL PC version 5.03, Siemens Analytical X-ray Instruments, Inc., Madison, WI, **1994**.

Received November 20, 2000
[I00438]

Palladacycles − An Old Organometallic Family Revisited: New, Simple, and Efficient Catalyst Precursors for Homogeneous Catalysis

Jairton Dupont,[a] Michel Pfeffer,*[b] and John Spencer[c]

Dedicated to the memory of Professor John Osborn

Keywords: Metallacycles / Palladium / Homogeneous catalysis / C−C coupling / Hydrogenations

Nitrogen-, phosphorus-, and sulfur-containing palladacycles, typically containing four- or six-electron donor anionic metallated ligands, are emerging as a new family of organometallic catalyst precursors. These thermally and air-stable complexes are easy to handle and their synthesis is often straightforward. Palladacycles are now being successfully exploited in catalytic reactions ranging from classical hydrogenations to enantioselective aldol-type condensations. The main recent achievements pertaining to their use in homogeneous organometallic catalysis are outlined herein.

Introduction

Palladacycles are a popular and thoroughly investigated class of organopalladium compounds. The vast majority of these complexes possess anionic four-electron (bidentate) or six-electron (tridentate) donor ligands, with five-membered nitrogen-containing rings being the most common (Scheme 1).[1] Such systems have been known since the 1960s.[2]

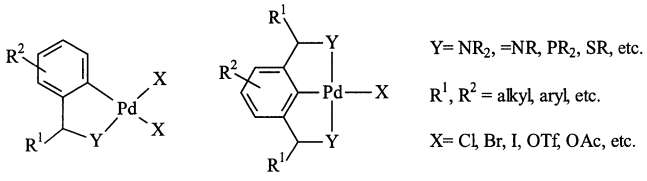

Scheme 1. Examples of palladacycles

Their synthesis is facile and it is possible to modulate their electronic and steric properties simply by changing (i) the size of the metallacyclic ring (3−10 membered), (ii) the

[a] Laboratory of Molecular Catalysis − IQ − UFRGS, Av. Bento Gonçalves, 9500 Porto Alegre 91501-970 RS, Brazil
[b] Laboratory of Metal-Mediated Synthesis, ULP, 4, Rue Blaise Pascal, 67000 Strasbourg, France
[c] Thrombosis Research Institute, Emmanuel Kaye Building, Manresa Road, London SW3 6LR, U.K.

Jairton Dupont was born in 1958 in Farroupilha (Brazil). He studied chemistry at the PUCRS (Brazil) and received his Ph.D. in 1988 under the guidance of Dr. M. Pfeffer at the Université Louis Pasteur in Strasbourg. After a postdoctoral position (1988−1990) with Prof. S. G. Davies at the Dyson Perrins Laboratory, University of Oxford (U.K.), he began to work as a visiting scientist (1990−1992) at the Institute of Chemistry, UFRGS (Brazil). In 1992, he became a Professor of Organic Chemistry at the same Institute. His research interests are centered around synthetic organometallic chemistry with a special emphasis on homogeneous catalysis in biphasic media. He is the author of around 60 scientific publications and 7 patents.

Michel Pfeffer was educated at the University of Strasbourg, where he obtained his Ph.D. in 1975 in the Laboratoire de Chimie de Coordination with Prof. Jean Dehand. He then spent one year with Prof. F. G. A. Stone at the University of Bristol as a postdoctoral student. Since 1973, he has held a position in the CNRS at the UniversitéLouis Pasteur in Strasbourg, where he became Directeur de recherche in 1985. His current research interests lie at the interface of inorganic, organometallic, and organic chemistry, with an emphasis on metal-mediated functionalization of C−H bonds through reactions aimed at producing new carbon−carbon or carbon−heteroatom bonds.

John Spencer obtained a B.Sc. (1st class, Hon.) at Sussex University in Chemistry with European Studies in 1990 before studying for a Ph.D. under the supervision of Michel Pfeffer, Strasbourg (1990−1994). After a postdoctoral stay with Antonio Togni at the ETH, Zurich, he returned to England where he first worked in the pharmaceutical industry (Xenova, Cerebrus). He then took up his current position at the Thrombosis Research Institute (London), where he is now a Senior Research Scientist. He is a co-author of over a dozen papers and patents and his research interests include organopalladium and organoboron chemistry, as well as asymmetric catalysis.

MICROREVIEWS: This feature introduces the readers to the authors' research through a concise overview of the selected topic. Reference to important work from others in the field is included.

 © WILEY-VCH Verlag GmbH, 69451 Weinheim, 2001 1434−1948/01/0808−1917 $ 17.50+.50/0

nature of the metallated carbon atom (aliphatic, aromatic, vinylic, etc.), (iii) the type of donor group (N-, P-, S-, O-containing group, etc.) and its substituents (alkyl, aryl, etc.), or (iv) the nature of the X ligands (halide, triflate, or solvent, e.g. THF, H_2O). These factors determine whether the complex is dimeric, monomeric, neutral, or cationic. This flexibility confers a plethora of potential applications upon this class of compounds.

In the following applications, palladacycles can be further subdivided into two classes of compounds: one in which the Pd−C bond remains intact, i.e. the cyclopalladated unit is used as an ancillary ligand, and a second class where the palladated carbon atom is functionalized (mainly for organic synthesis). Indeed, these complexes have been used as intermediates for organic synthesis,[3] as new materials[4] (in liquid crystals, nonlinear optics, etc.), in bioorganometallic chemistry,[5] and, much more recently, they have undergone a renaissance as a result of their increasingly impressive applications in organometallic homogeneous catalysis.

The catalytic properties of cyclopalladated complexes were investigated more than a decade ago,[6] although previous reviews have tended to focus on the synthesis of palladacycles and their applications in mainly stoichiometric processes with scant progress being achieved in the area of catalytic applications. It is only recently that the true potential of palladacycles in organometallic catalysis has been recognized. There are two intriguing aspects regarding this last point: (i) the Pd−C bond in the majority of palladacycles is reactive towards a wide range of nucleophilic and electrophilic reagents exploited in catalysis, and (ii) the palladacycle can often be recovered unchanged following catalysis and can sometimes even be recycled. Mechanistic studies aimed at ascertaining the actual role of the palladium atom in these catalytic systems are a matter of intense current discussion since, besides the classical Pd^0/Pd^{II} catalytic cycles, several studies are now pointing to the involvement of Pd^{II}/Pd^{IV} cycles. However, no definitive argument in favour of one or other of these hypotheses has yet been presented.

Palladacycles are now emerging as a new family of catalyst precursors for a host of reactions. These derivatives easily fall into the current paradigm for homogeneous catalysis; they are often easily prepared in high yields through a C−H activation process, are often air- and moisture-stable, and, once catalytically active (usually above 100 °C), can attain high turnover numbers (TONs). Their applications in mainly Heck-type reactions were recently reviewed by Herrmann and co-workers;[7] this review covered complexes derived from the palladation of tris(*o*-tolylphosphane) developed in their laboratory. However, as already mentioned, palladacycles offer a much wider variety of catalytic applications and several new and efficient complexes based on different ligand backbones have since been reported. This brief overview will concentrate on recent examples involving the use of genuine, well-characterized palladacycles as catalyst precursors, in particular for catalytic C−C bond-forming reactions.

Hydrogenations

The use of palladacycles as catalyst precursors for hydrogenations represents one of the first applications of this class of compounds in catalysis. It was demonstrated that cyclopalladated triphenyl phosphite was effective in promoting the hydrogenation of C=C bonds, whereas its non-*ortho*-palladated analogue decomposed under the catalytic conditions and did not promote the reduction reaction (Scheme 2).[6]

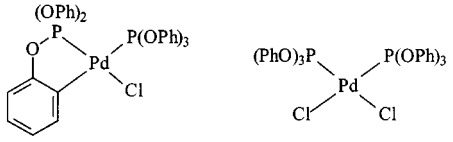

Scheme 2. Palladated and nonpalladated triphenyl phosphite ligands

The presence of a Pd−C bond in hydrogenation catalyst precursors, derived from the *ortho*-palladation of azobenzenes, hydrazobenzenes, or *N*,*N*-dimethylbenzylamine, was also found to be essential to effectively promote the selective reduction of nitroaromatic compounds, nitroalkenes, nitriles, alkynes, alkenes, and aromatic carbonyl compounds.[8] Surprisingly, however, despite the report of these very promising results, the use of palladacycles in reduction processes has not been further explored.

Heck Coupling Reactions

The arylation of C=C double bonds (Heck reaction)[9] is mediated by a variety of Pd^{II} and Pd^0 catalyst precursors (Scheme 3).

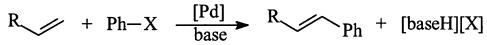

Scheme 3. Heck coupling reaction

In this context, phosphorus-,[7,10−21] nitrogen-,[22−27] and sulfur-containing[28−30] palladacycles are among the most active catalyst precursors for the promotion of such reactions reported to date (Scheme 4).

All of the palladacycles shown in Scheme 4 promote the Heck reaction of aryl iodides with acrylic esters (Table 1). In this reaction, the highest catalytic activity observed to date was achieved with the palladacycle **6** (Table 1, Entry 9). It is interesting to note that this palladacycle only promotes the Heck reaction between aryl iodides and acrylic esters. However, it should be pointed out that almost any Pd^{II} or Pd^0 derivative, irrespective of whether it is associated with stabilizing ligands, is capable of promoting Heck reactions involving aryl iodides or aryl bromides substituted with electron-withdrawing groups. In contrast, only a few palladacycles are active catalyst precursors for electron-rich aryl bromides (Table 1). Moreover, in the case of aryl chlorides, complexes **1**, **7**, **8**, and **11** were found to be the only active palladacycles (Entries 23−30, Table 1). In particular, **7** promotes the Heck reaction of electron-rich aryl chlorides, such as 4-chloroanisole (Entry 29, Table 1).[21]

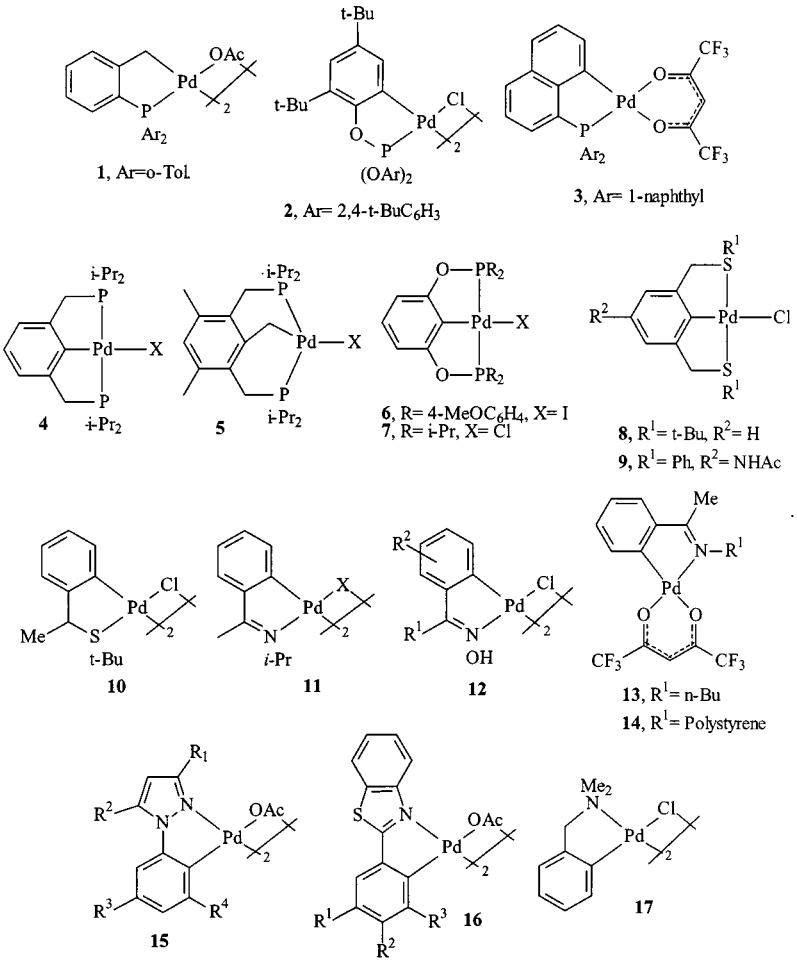

Scheme 4. Palladacyclic catalyst precursors for the Heck reaction

It was recently demonstrated that cationic derivatives of binuclear conjugated palladacycles (Scheme 5) are also highly active catalyst precursors for the Heck reaction of iodobenzene with styrene or methyl acrylate.[31]

Palladacycles can also be involved in recyclable catalytic systems, e.g. by running the reaction of phosphapalladacycle **1**[32,33] in ionic liquids,[34] or by employing the polyethylene glycol bound sulfur-containing palladacycle **9**[28] or the polystyrene-bound imine-containing palladacycle (see later).[26] Moreover, trifluoroacetate-bridged derivatives of **1** have been shown to catalyse Heck reactions in supercritical carbon dioxide.[35,36]

Palladacycle **1** has also been successfully used as a catalyst precursor for an intramolecular Heck-type reaction generating six-membered ring D analogues of the pentacyclic alkaloid cephalotaxine in high yields (Scheme 6).[37]

Benzothiazole palladacycles such as **16** have been used as catalysts in a three-component cascade process (Scheme 7) yielding 1-substituted styrenes in high yields (82−92%) under relatively mild reaction conditions (80 °C, 10 h).[27]

Optically active sulfur-containing palladacycle **10** promotes the arylation of 3,4-dihydro-2*H*-pyran under mild reaction conditions, albeit without any asymmetric induction (Scheme 8). This suggests that the palladacyclic moiety is probably not present in the catalytically active species.[38]

It is often assumed that the mechanism[39] of the Heck reaction involves the in situ generation of a Pd^0 species, which undergoes oxidative addition of the aryl halide yielding a Pd^{II}−aryl intermediate. Coordination of the olefin and its migratory insertion into the Pd−aryl bond leads to a Pd^{II}−alkyl complex. β-Hydrogen elimination affords the arylated olefin and a Pd−H species, which, through reductive elimination, regenerates the Pd^0 catalytically active species.[9]

The cyclopalladated moiety could sometimes be isolated unchanged after catalysis and in certain cases it was recycled.[22,28] It has also been observed that the Pd−C bond of these palladacycles is usually unreactive towards C=C units. Hence, no reduction of Pd^{II} to Pd^0 should occur through, for instance, a reductive elimination of HX following the β-elimination process of the cyclopalladated ligand coupled with the olefin. Moreover, since in most of these cases no formation of metallic palladium was noted, an alternative mechanism involving Pd^{II}/Pd^{IV} has recently been proposed by Shaw[19] and has been adapted for phosphorus-containing palladacycles such as **7**.[21] The key step in this mechanism is a reversible nucleophilic attack on the Pd^{II}−olefin complex by acetate or halide anions generating an electron-rich Pd^{II} species, which then undergoes oxidative addition of the aryl halide. Loss of the nucleophile fol-

Table 1. Palladacycles which promote the Heck arylation reaction (Scheme 3)

Entry	Pd compd.	R	X	T [°C]	t [h]	Base	Conv. (%)	TON (10^3)	TOF [h^{-1}]	Ref.
1	**1**	CO_2Bu	Br	140	48	NaOAc	99	9.8	204	[12]
2	**2**	CO_2Bu	Br	140	18	NaOAc	51	0.25	14	[16]
3	**3**	CO_2Me	I	95	312	NBu_3	56	1120	3590	[13]
4	**3**	Ph	I	120	120	NBu_3	65	650	5417	[13]
5	**3**	Ph	Br	115	30	NBu_3	77	0.77	26	[13]
6	**4**	CO_2Me	I	140	350	Na_2CO_3	91	520	1487	[17]
7	**5**	CO_2Me	I	140	40	Na_2CO_3	95	529	13217	[17]
8	**5**	CO_2Me	Br	140	63	Na_2CO_3	93	133	2109	[17]
9	**6**	CO_2Bu	I	180	22	Na_2CO_3	89	8900	404500	[15]
10	**8**	CO_2Me	I	140	24	NEt_3	90	45	1875	[29]
11	**9**	CO_2Me	I	80	60	NEt_3	–	70	1167	[28]
12	**10**	CO_2Me	I	140	1	NEt_3	94	47	47000	[29]
13	**10**	CO_2Me	Br	170	8	NEt_3	75	37	46875	[29]
14	**11**	CO_2Me	I	140	18	NEt_3	100	1429	79389	[22]
15	**11**	CO_2Me	Br	140	130	Na_2CO_3	93	133	1022	[22]
16	**12**	CO_2Me	I	110	12	NEt_3	99	100	8333	[24]
17	**12**	Ph	Br	150	1	K_2CO_3	96	0.48	483	[25]
18	**13**	Ph	I	140	120	N^nPr_3	91	91	758	[26]
19	**14**	Ph	I	140	11	N^nPr_3	100	15.6	1420	[26]
20	**15**	CO_2Bu	I	110	48	K_2CO_3	100	2000	41667	[27]
21	**16**	CO_2Bu	I	90	48	K_2CO_3	90	100	2083	[27]
22	**17**	CO_2Et	Br	130	34	K_2CO_3	90	90	2647	[25]
23	**1**	CO_2Bu	[a]	140	48	NaOAc	93	0.087	1.8	[10]
24	**10**	CO_2Bu	[a]	170	6	NaOAc	61	30500	5082	[29]
25	**1**	CO_2Bu	[b]	130	24	NaOAc	90	80.1	34	[12]
26	**10**	CO_2Bu	[c]	170	2	NaOAc	49	490	245	[29]
27	**7**	Ph	[b]	180	24	CsOAc	81	122	5.1	[21]
28	**7**	Ph	Cl	180	24	CsOAc	99	149	6.2	[21]
29	**7**	Ph	[d]	180	24	CsOAc	86	129	5.4	[21]
30	**12**	Ph	[c]	150	42	K_2CO_3	71	70	1166	[25]

[a] 4-Bromoanisole. – [b] 4-Chlorobenzaldehyde. – [c] 4-Nitrochlorobenzene. – [d] 4-Chloroanisole.

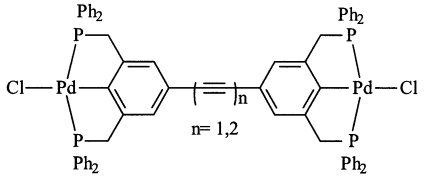

Scheme 5. A binuclear phosphapalladacycle

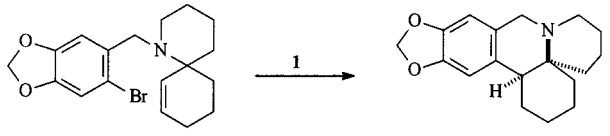

Scheme 6. Palladacycle **1** mediated intramolecular Heck reaction

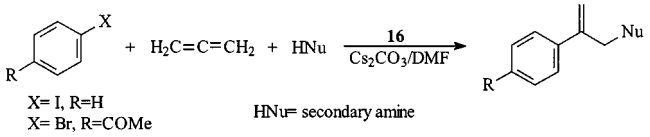

Scheme 7. A three-component cascade process

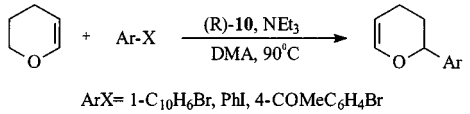

Scheme 8. Arylation of 3,4-dihydro-2*H*-pyran

lowed by migratory insertion of the thus generated C=C bond into the Pd^{IV}–aryl bond, β-hydrogen elimination, and reductive elimination of HX then produces the arylated olefin and regenerates the Pd^{II} catalyst. However, one important feature disfavouring this suggestion is the lack of precedence for observing the oxidative addition of aryl halides to Pd^{II} as compared to the now well-known oxidative addition of alkyl halides to organopalladium(II) species.[40] Nevertheless, it would seem that a Pd^{IV} intermediate has recently been isolated in the arylation of norbornene (see later).[41] In the case of palladacycles of type **1**, Herrmann et al. have suggested that they constitute a reservoir of highly active Pd^0 species, which are generated by heterolytic cleavage of the Pd–C bond with subsequent reduction to Pd^0.[7] Very recently, in the case of cyclopalladated imine complexes such as **13** and **14** (Scheme 4), the involvement of Pd^0 nanoparticles originating from the immobilized palladacycles has been proposed.[26] It is unclear as to which mechanism is the most likely to be operative. Further studies to strengthen one or other of the proposals are still required.

Suzuki and Stille Cross-Coupling Reactions

The cross-coupling of aryl halides with organoboron compounds (Suzuki cross-coupling reaction)[42] or or-

ganotin compounds (Stille cross-coupling reaction)[43] is mediated by a variety of palladium catalyst precursors, the latter usually bearing phosphane ligands.

Suzuki and Stille cross-couplings have only been investigated with a few palladacycles (Table 2).

Table 2. Suzuki and Stille cross-couplings catalysed by palladacycles (ArX + PhM → ArPh + MX)

Entry	Pd compd. (%)	M	Ar	X	base	*T* [°C]	*t* [h]	Yield (%)	Ref.
1	**1** (10^{-3})	$B(OH)_2$	4-$MeCOC_6H_4$	Br	K_2CO_3	130	20	74	[20]
2	**1** (10^{-1})	$B(OH)_2$	Ph	Br	K_2CO_3	130	20	99	[20]
3	**1** (10^{-2})	$B(OH)_2$	4-$MeOC_6H_4$	Br	K_2CO_3	130	20	76	[20]
4	**1** (10^{-1})	$B(OH)_2$	4-$MeCOC_6H_4$	Cl	K_2CO_3	130	20	82	[20]
5	**12** (10^{-1})	$B(OH)_2$	4-$MeCOC_6H_4$	Br	K_2CO_3	110	0.5	97	[24]
6	**11** (10^{-6})	$B(OH)_2$	4-$MeCOC_6H_4$	Br	K_2CO_3	130	16	84	[23]
7	**11** (5×10^{-6})	$B(OH)_2$	Ph	Br	K_2CO_3	130	3	90	[23]
8	**11** (5×10^{-6})	$B(OH)_2$	4-$MeOC_6H_4$	Br	K_2CO_3	130	3	60	[23]
9	**10** (0.5)	$B(OH)_2$	4-$MeOC_6H_4$	Br	K_3PO_4	130	4	90	[30]
10	**10** (0.5)	$B(OH)_2$	4-$MeOC_6H_4$	Br	K_3PO_4	25	38	95	[30]
11	**6** (10^{-2})	$B(OH)_2$	4-$MeOC_6H_4$	Br	K_2CO_3	130	18	87	[44]
12	**10** (0.5)	$B(OH)_2$	4-NCC_6H_4	Cl	K_3PO_4	25	16	92	[30]
13	**10** (0.5)	$B(OH)_2$	Ph	Cl	K_3PO_4	130	22	46	[30]
14	**6** (10^{-2})	$B(OH)_2$	4-$NO_2C_6H_4$	Cl	K_2CO_3	130	18	43	[44]
15	**1** (2.0)	$SnMe_3$	Ph	Br	−	110	24	97	[7]
16	**1** (5.0)	$SnMe_3$	4-$MeCOC_6H_4$	Br	−	100	4	96	[45]
17	**12** (3.0)	$SnMe_3$	4-$MeCOC_6H_4$	Br	−	110	5	95	[24]

Phospha- and nitrogen-palladacycles effectively promote the Suzuki cross-coupling of aryl bromides, albeit only at elevated temperatures (100−130 °C). It is important to note that $Pd(OAc)_2$ has also been shown to catalyse the Suzuki cross-coupling reaction of aryl bromides with high turnovers, and consequently these substrates (in particular 4-bromoacetophenone) are not useful benchmarks for testing new catalysts in Suzuki couplings.[46] Palladacycle **12** was only tested in the coupling of 4-bromoacetophenone with phenylboronic acid at 110 °C.[24] However, sulfur-containing palladacycles catalyse these couplings at room temperature (see Table 2, Entries 10 and 12) and, moreover, they also promote the reaction of less reactive aryl chlorides, although higher reaction temperatures are required in the latter cases. This system represents the most effective phosphane-free catalyst system for the room temperature Suzuki cross-coupling reported to date.[47]

Mechanistic insights into the Stille coupling have been obtained by monitoring the reaction of palladacycle **1** with Me_3SnPh by NMR spectroscopy. The investigators observed the formation of free and palladium-ligated arylated phosphane and P(*o*Tol)$_3$ ligands (Scheme 9).[37]

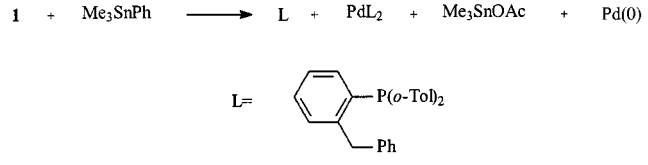

Scheme 9. The formation of Pd^0 catalytically active species

These observations suggested that the catalytically active species in the Stille and Suzuki couplings possess either P(*o*-Tol)$_3$ or modified PAr(*o*Tol)$_2$ ligands, or a combination of the two, associated with Pd^0. In these cases, the palladacycle may act as a reservoir of catalytically active Pd^0 species.

Phosphapalladacycle **1** has also been shown to catalyse the coupling of functionalized bromoarenes to a polystyrene-bound aryl tributylstannane. This reaction provides a convenient method for the synthesis of several biaryl compounds on resins.[48]

The phosphapalladacycle **1** is also an effective catalyst precursor for other coupling reactions, such as Grignard and Negishi-type protocols.[7] Very recently, it was reported that cyclopalladated oximes such as **12** also promote the Ullmann homo-coupling reaction of 4-iodo- and 4-bromoacetophenone with modest TONs (up to 50).[24] In contrast, sulfur-containing palladacycles such as **10** (Scheme 4) efficiently catalyse the homo-coupling of various aryl iodides and bromides in high yields (> 90%, Scheme 10).[49]

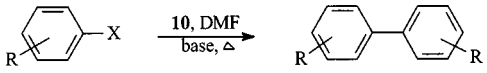

R= H, Me, COMe, OMe, NO_2, etc.; X= Br, I.

Scheme 10. Ullmann homo-coupling promoted by palladacycle **10**

Palladacycle **1** has been shown to be one of the most efficient of the classical Pd catalysts for a Suzuki-like reaction between Ar−N_2BF_4 and Ar′−BF_3K affording the expected biphenyl Ar−Ar′ as a result of a cross-coupling (Scheme 11).[50]

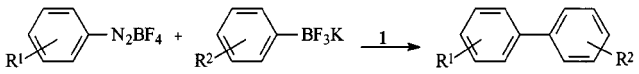

Scheme 11. Cross-coupling of organotrifluoroborates

The catalyst is usually active at low concentrations (0.1%) and the reactions proved successful with substrates bearing either electron-withdrawing or electron-donating substituents. The same catalyst was also effectively used in the formation of styrene and stilbene derivatives by the reac-

tions of $Ar-N_2BF_4$ with vinyl and styryl trifluoroborates, respectively.

Palladacycle **1** was also used in the sixfold alkenylation of hexabromobenzene through Suzuki and Stille couplings (Scheme 12), generating hexakis(3,3-dimethyl-1-butenyl)-benzene in good yields.[51]

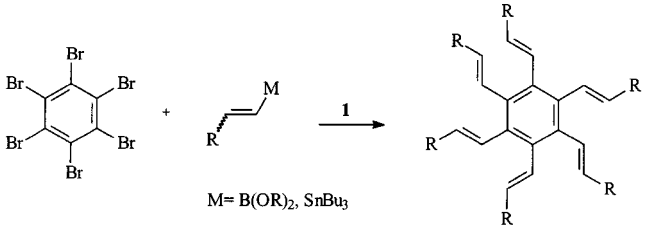

Scheme 12. Sixfold coupling of hexabromobenzene catalysed by palladacycle **1**

Hydroarylation of Olefins

Cyclopalladated aminophosphane-based ligand systems (Scheme 13) are highly efficient catalysts for the hydroarylation of norbornene, giving rise to exceptionally high TONs. Indeed, the latter can reach an incredible and unprecedented 10^{10}, corresponding to a catalyst loading of as little as 5×10^{-9} mol-%.[41,52]

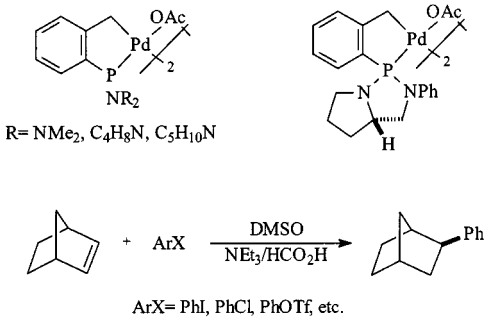

Scheme 13. Hydroarylation of norbornene catalysed by a phosphapalladacycle

An enantioselective variant has been developed, giving modest *ee* values (up to 25%) in the hydroarylation of norbornene with phenyl triflate.[41] By treating the phosphapalladacycle with iodobenzene, the authors isolated a rather strange organopalladium species (Scheme 14).

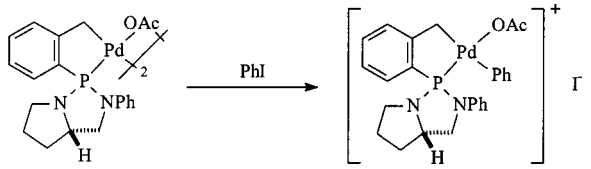

Scheme 14. The formation of a Pd^{IV} intermediate

Its crystal structure suggested the presence of a cationic tetracoordinate Pd^{IV} species having an iodide as a counterion. Although no details have been given concerning the behaviour of this product, confirmation of this preliminary result would provide a strong argument for the existence of a $Pd^{II}-Pd^{IV}$ pathway in, for example, the Heck reaction.

Sonogashira Reaction

The palladium-catalysed coupling of aryl iodides and bromides with terminal alkynes is a well-established method for the preparation of disubstituted alkynes (Scheme 15).[53] A wide variety of palladium catalyst precursors efficiently promote this reaction, usually in the presence of CuI as a co-catalyst. Not surprisingly, phosphorus-,[54] nitrogen-,[23] and sulfur-containing [55] palladacycles mediate this coupling reaction. However, in the case of palladacycle **1**, the reaction is catalysed in the absence of a co-catalyst and using a very low catalyst loading. Turnover numbers up to 8000 have been reported in the coupling of 4-bromoacetophenone with phenylacetylene.[54]

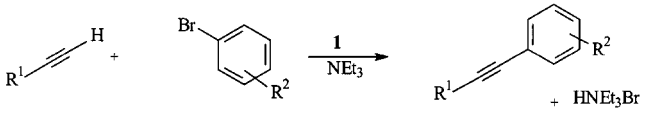

Scheme 15. The Sonogashira coupling reaction

Here also, a mechanism involving Pd^{IV} species has been postulated as being operative in the case of palladacycle **1**.

Amination of Aryl Halides[56,57]

Phosphapalladacycles were among the first palladium catalyst precursors to be used to promote the amination of aryl halides leading to substituted anilines (Scheme 16).[37,58] The reactions of secondary amines with bromoarenes and activated chloroarenes are efficiently catalysed by palladacycle **1** using NaO*t*Bu or KO*t*Bu as a base at temperatures in the range 100−130 °C.[58]

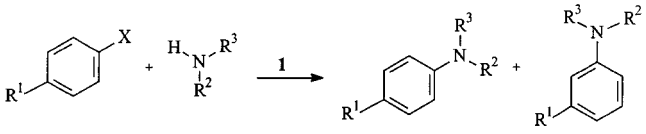

X= Br, R^1= COMe, CN, F, Me, H, OMe; amine= piperidine, $HNBu_2$, $HNPh_2$, $HNiPr_2$

X= Cl, R^1= CF_3, COPh; amine= piperidine, $HNBu_2$, $HNPh_2$, $HNiPr_2$, etc.

Scheme 16. Amination of aryl halides promoted by palladacycle **1**

It is interesting to note that the *meta* isomer was also obtained, and that a side mechanism involving aryne intermediates was shown to be operative by running the reaction in the absence of a catalyst. Elegant studies showed that in these cases the palladacycle **1** again serves as a reservoir of catalytically active Pd^0−phosphane species. The latter are probably formed through a β-hydrogen elimination followed by a reductive elimination process from a palladium amide complex (Scheme 17).

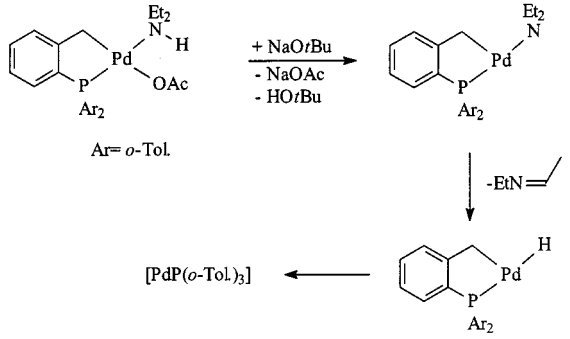

Scheme 17. Postulated mechanism for the generation of Pd^0 species from palladacycle **1** in the presence of $HNEt_2$

Hetero- and Carbo-Annulation Reactions

Palladacycles are also effective catalyst precursors for the preparation of *N*-methylbenzo[*d*,*e*]quinolines,[59] *N*-methyldibenzo[*d*,*e*,*g*]quinolines,[60] and 2,3-diphenylindenone.[7] Cyclopalladated (dimethylamino)naphthalene (Scheme 18) and -phenanthrene complexes (Scheme 19) were shown to mediate the reaction of internal alkynes with (dimethylamino)iodonaphthalene and -phenanthrene derivatives, respectively, leading to quinolines in reasonable to good yields (Schemes 18 and 19).

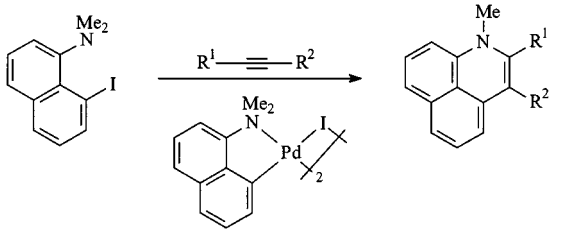

Scheme 18. Nitrogen palladacycle catalysed quinoline synthesis

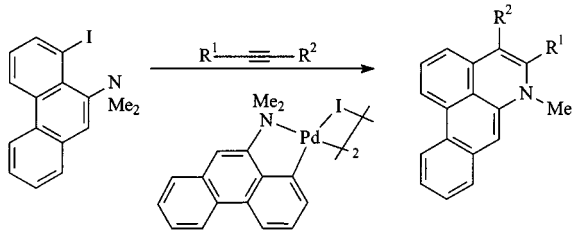

Scheme 19. Pd-catalysed construction of the B-fragment of the Aporphine skeleton

It has recently been shown that 2,3-diphenylindenone can be prepared by the reaction of 2-bromobenzaldehyde with diphenylacetylene in the presence of 0.1 mol-% of palladacycle **1** (Scheme 20).[7]

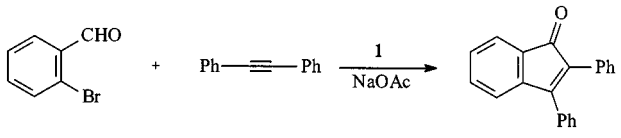

Scheme 20. Synthesis of a substituted indenone catalysed by **1**

Palladacycles of type **16** (Scheme 4) have been used to generate catalytically active Pd^0 species for the intramolecular nucleophilic addition of allylic intermediates, generated from allene, to 2-bromoaryl aldehydes or ketones (Scheme 21).[61]

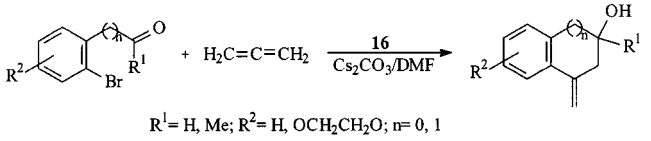

Scheme 21. Carbopalladation of allenes

Despite the high potential of this method for the synthesis of carbo- and heterocycles, which starts from easily accessible substrates, few examples of these types of reactions have appeared. Nevertheless, many related processes are mediated by catalytic systems based on palladium acetate.[62]

Telomerization of Dienes

Cyclopalladated phosphane enolates bearing *N*,*N*-dimethylbenzylamine ligands (Scheme 22) have been shown to be reversible CO_2 carriers at room temperature.[63]

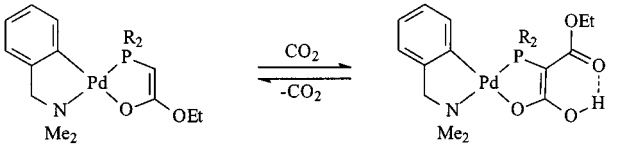

Scheme 22. Phosphane enolate palladacycles as reversible CO_2 carriers (R = Ph, Cy)

These complexes catalyse the telomerization of butadiene with CO_2 under relatively mild reaction conditions (20 bar CO_2, 90 °C) to furnish the lactone 2-ethylidene-6-hepten-5-olide with good selectivity (up to 93%) (Scheme 23).[64]

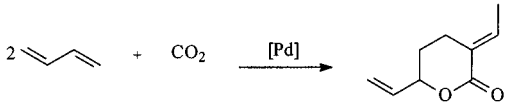

Scheme 23. Telomerization of butadiene with CO_2

These complexes were the first examples of CO_2 carriers showing catalytic activity towards CO_2. It is also interesting to note that the cyclopalladated unit was isolated intact after catalysis, demonstrating its ancillary behaviour.

Not surprisingly, nitrogen-containing palladacycles, such as those derived from amines, imines, and quinolines (Scheme 24), promote the selective telomerization of 1,3-dienes with alcohols.[65,66]

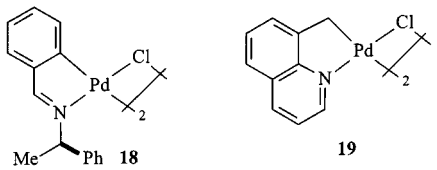

Scheme 24. Palladacycle catalyst precursors for the telomerization of 1,3-dienes

The cationic palladacycles derived from **17**−**19** mediate the telomerization of butadiene with methanol giving telomers containing 2−6 diene units (Scheme 25).

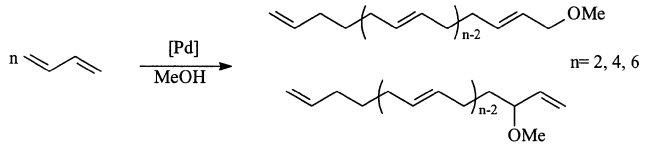

Scheme 25. Palladacycle-catalysed telomerization of butadiene with methanol

The selectivity was found to be strongly influenced by the nature of the palladacycle catalyst precursor, suggesting that the ligands it bears are present in the catalytically active species. Selectivities of up to 61% in high telomers (4 and 6 monomeric units) could be achieved using palladacycle **17**.[66] This selectivity is superior to that obtained with other palladium catalysts such as π-allyl complexes.[67] Palladacycle **16** was also shown to be effective in the generation of catalytic species for the telomerization of isoprene with methanol, yielding 1-methoxy-2,6-dimethyl-2,7-octadiene with selectivities of up to 67% (Scheme 26).[65]

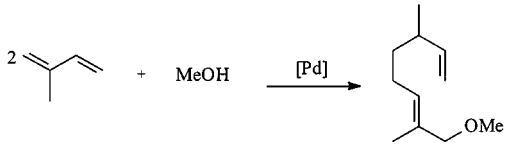

Scheme 26. Telomerization of isoprene with methanol

Aldol-Type Reactions[68−70]

Cyclopalladated complexes containing PCP and NCN ligands have recently been utilized in asymmetric aldol-type reactions (Scheme 27).

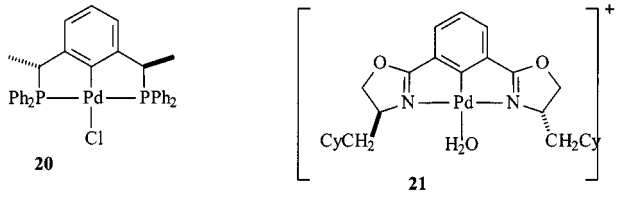

Scheme 27. Palladacycles used as catalyst precursors for aldol-type reactions

The rationale behind the deployment of such complexes stemmed from the observation that classical ligands, including BINAP and DIOP, led to poor selectivities in these reactions, which was attributed to the fact that the key enantioselective step occurred too far away from the chiral pocket. PCP and NCN ligand-based systems offer a deeper chiral pocket, leading to some enantio-discrimination without the need for pendant groups designed for secondary interactions.[71]

To carry out the aforementioned reaction using methyl isocyanoacetate and various aldehydes (Scheme 28), it was found that the cyclopalladated complex had to be activated by halide abstraction with a silver salt.

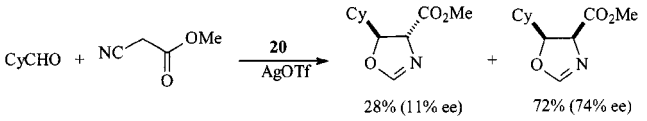

Scheme 28. Asymmetric aldol reaction catalysed by a cyclopalladated PCP complex

Some pertinent observations were made regarding this system:

(i) Palladium complexes are more effective than their platinum congeners. Moreover, *cis* selectivity is higher than that with similar related platinum complexes.[72]

(ii) THF is the solvent of choice; other variations, such as the order of addition of the reactants or the nature of the base used, have little effect on the reaction outcome.

Cyclopalladated NCN ligands were found to be ineffective in the above reaction and also in Diels−Alder reactions. However, they were found to be effective in the formation of a quaternary centre through chiral Michael addition (Scheme 29).

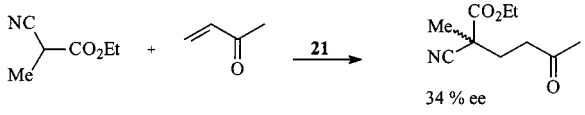

Scheme 29. Asymmetric Michael addition mediated by an NCN palladacycle

For these reactions, selectivities were found to be higher in toluene and increased when bulky substituents were present on the oxazoline ligands, although reaction times were often longer. The reaction is presumed to proceed through a Pd^{II} intermediate acting as a Lewis acid. An immobilized catalyst system is envisaged as offering an improvement in the near future.

Cyclopropanation

Recent reports have shown that neutral acetylacetonato and amino acid chelated cyclopalladated complexes (Scheme 30) are capable of catalysing cyclopropanation reactions.[73]

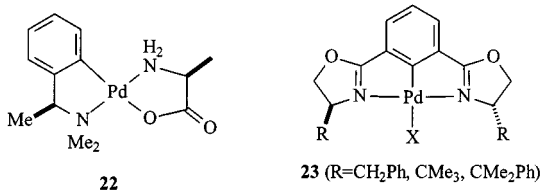

Scheme 30. Chiral palladacyclic catalyst precursors used in cyclopropanation reactions

The enantioselectivities achieved with these palladacycles are poor, with the highest *ee* values being less than 10%. Diastereoselectivities reached 20% when a menthol-con-

taining diazoacetate derivative was used as a chiral starting material (Scheme 31).

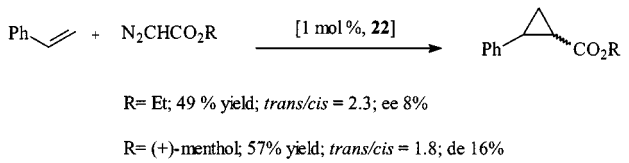

Scheme 31. Cyclopropanation catalysed by a nonracemic benzylamine amino acid palladacycle

Non-racemic aryloxazoline palladacycles such as **21** have been shown to efficiently promote the diazomethane-based cylopropanation reaction (Scheme 32), but all the obtained products were racemic.[74]

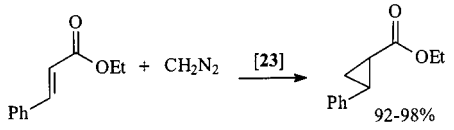

Scheme 32. Cyclopropanation catalysed by aryloxazoline palladacycles

Allylic Substitution and Rearrangement[75]

Archetypal allylic substitutions of 1,3-diphenylprop-2-enyl acetate were investigated with PCP ligands such as that used in palladacycle **18** and modest enantioselectivities were achieved (Scheme 33).[76] Here though, when associated with π-allylpalladium complexes, the ligands are likely to adopt a bidentate PP-type coordination mode, taking them beyond the scope of this review.

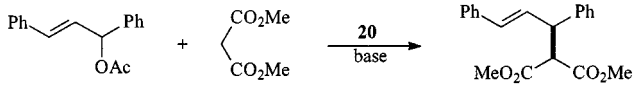

Scheme 33. Allylic substitution reaction

Functionalized allylic alcohols can be converted into chiral allylic amine derivatives by a palladium-catalysed 3,3-sigmatropic rearrangement.[77] The achiral version of this reaction is effected by $PdCl_2(PhCN)_2$ and the authors chose palladium complexes containing an anionic ligand as a "chiral mimic" of the aforementioned complex.[78] Planar chiral ferrocene derivatives (Scheme 34) proved to be the most effective catalysts, affording excellent enantioselectivities with good reaction rates and yields, whilst avoiding side products due to 1,3-rearrangements (e.g. hexadienes).

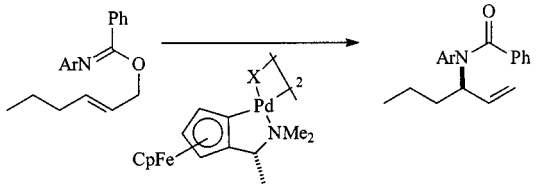

Scheme 34. Chiral planar ferrocenyl palladacycle mediated allylic rearrangements

Conclusions and Perspectives

It is quite fitting that the majority of the work cited herein has been published during the last five years as our goal has been to demonstrate that the chemistry of cyclopalladated complexes, which is still in its infancy in terms of catalytic applications, will undoubtedly have a lot more to offer in the near future.

It is clear from the state of the art that further detailed mechanistic studies will have to be performed in order to unambiguously determine whether or not the cyclopalladated ligand is indeed attached to the catalytically active Pd species or whether these compounds are merely powerful sources of ligand-stabilized Pd^0 in which the Pd−C bond has been cleaved. This will aid the rational design of ligands and complexes, thereby leading to even more efficient palladium-containing catalysts. With TONs reaching 10^5 and even 10^{10} in some cases, more applied synthetic (e.g. natural products) and industrial applications can soon be anticipated. Palladacycles such as **1** are now commercially available and general procedures for their preparation are part of classical organometallic procedures.[79]

Acknowledgments

This work was supported in part by the CNPq and FAPERGS (Brazil), the CNRS (France), and the Thrombosis Research Institute (UK).

[1] [1a] G. W. Parshall, *Acc. Chem. Res.* **1970**, *3*, 139−144. − [1b] J. Dehand, M. Pfeffer, *Coord. Chem. Rev.* **1976**, *18*, 327−352. − [1c] M. I. Bruce, *Angew. Chem. Int. Ed. Engl.* **1977**, *16*, 73−86. − [1d] I. Omae, *Chem. Rev.* **1979**, *79*, 287−321. − [1e] I. Omae, *Coord. Chem. Rev.* **1979**, *28*, 97−115. − [1f] I. Omae, *Coord. Chem. Rev.* **1980**, *32*, 235−271. − [1g] I. Omae, *Coord. Chem. Rev.* **1982**, *42*, 245−257. − [1h] E. C. Constable, *Polyhedron* **1984**, *3*, 1037−1057. − [1i] I. P. Rothwell, *Polyhedron* **1985**, *4*, 177−200. − [1j] G. R. Newkome, W. E. Puckett, V. R. Gupta, G. E. Kiefer, *Chem. Rev.* **1986**, 451−489. − [1k] P. Steenwinkel, R. A. Gossage, G. van Koten, *Chem. Eur. J.* **1998**, *4*, 759−762. − [1l] G. Dyker, *Angew. Chem. Int. Ed.* **1999**, *38*, 1698−1712.

[2] A. C. Cope, E. C. Friedrich, *J. Am. Chem. Soc.* **1968**, *90*, 909−911.

[3] [3a] A. D. Ryabov, *Synthesis* **1985**, 233−252. − [3b] M. Pfeffer, *Recl. Trav. Chim. Pays-Bas* **1990**, *109*, 567−576. − [3c] M. Pfeffer, *Pure Appl. Chem.* **1992**, *64*, 335−342.

[4] [4a] P. Espinet, M. A. Esteruelas, L. A. Oro, J. L. Serrano, E. Sola, *Coord. Chem. Rev.* **1992**, *117*, 215−274. − [4b] M. Beley, S. Chodorowski-Kimmes, J. P. Collin, J. P. Sauvage, *Tetrahedron Lett.* **1993**, *34*, 2933−2936. − [4c] A. El-Ghayourry, L. Douce, A. Skoulios, R. Ziessel, *Angew. Chem. Int. Ed.* **1998**, *37*, 1255−1258.

[5] C. Navarro-Ranninger, I. Lopez-Solera, J. M. Perez, J. R. Masaguer, C. Alonso, *Appl. Organomet. Chem.* **1993**, *7*, 57−61.

[6] L. N. Lewis, *J. Am. Chem. Soc.* **1986**, *108*, 743−749.

[7] W. A. Herrmann, V. P. W. Böhm, C.-P. Reisinger, *J. Organomet. Chem.* **1999**, *576*, 23−41.

[8] [8a] P. K. Santra, C. R. Saha, *J. Mol. Catal.* **1987**, *39*, 279−292. − [8b] A. Bose, C. R. Saha, *J. Mol. Catal.* **1989**, *49*, 271−283.

[9] [9a] W. A. Herrmann in *Applied Homogeneous Catalysis with Organometallic Compounds* (Eds.: B. Cornils, W. A. Herrmann), Wiley-VCH, Weinheim, **2000**, p. 712−732. − [9b] S. Bräse, A. de Meijere in *Metal-Catalyzed Cross-Coupling Reactions* (Eds.: F. Diederich, P. J. Stang), Wiley-VCH, Weinheim, **1998**, p. 99−167. − [9c] A. de Meijere, S. Bräse, *J. Organomet. Chem.* **1999**, *576*, 88−110. − [9d] I. P. Beletskaya, A. V. Cheprakov, *Chem. Rev.* **2000**, *100*, 3009−3066.

[10] W. A. Herrmann, C. Brossmer, C.-P. Reisinger, T. H. Riermeier, K. Öfele, M. Beller, *Chem. Eur. J.* **1997**, *3*, 1357−1364.

[11] M. Beller, T. H. Riermeier, *Eur. J. Inorg. Chem.* **1998**, 29−35.

[12] W. A. Herrmann, C. Brossmer, K. Öfele, C.-P. Reisinger, T. Riermeier, M. Beller, H. Fischer, *Angew. Chem. Int. Ed. Engl.* **1995**, *34*, 1844−1848.

[13] B. L. Shaw, S. D. Perera, E. A. Staley, *Chem. Commun.* **1998**, 1361−1362.

[14] D. A. Albisson, R. B. Bedford, S. E. Lawrence, P. N. Scully, *Chem. Commun.* **1998**, 2095−2096.

[15] F. Miyazaki, K. Yamaguchi, M. Shibasaki, *Tetrahedron Lett.* **1999**, *40*, 7379−7383.

[16] D. A. Albisson, R. B. Bedford, P. N. Scully, *Tetrahedron Lett.* **1998**, *39*, 9793−9796.

[17] M. Ohff, A. Ohff, M. E. van der Boom, D. Milstein, *J. Am. Chem. Soc.* **1997**, *119*, 11687−11688.

[18] M. Beller, T. H. Riermeier, *Tetrahedron Lett.* **1996**, *37*, 6535−6538.

[19] B. L. Shaw, *New J. Chem.* **1998**, 77−79.

[20] M. Beller, H. Fischer, W. A. Herrmann, K. Öfele, C. Brossmer, *Angew. Chem. Int. Ed. Engl.* **1995**, *34*, 1848−1849.

[21] D. Morales-Morales, R. Redón, C. Yung, C. M. Jensen, *Chem. Commun.* **2000**, 1619−1670.

[22] M. Ohff, A. Ohff, D. Milstein, *Chem. Commun.* **1999**, 357−358.

[23] H. Weissman, D. Milstein, *Chem. Commun.* **1999**, 1901−1902.

[24] D. A. Alonso, C. Nejera, M. C. Pacheco, *Org. Lett.* **2000**, *2*, 1823−1826.

[25] S. Iyer, C. Ramesh, *Tetrahedron Lett.* **2000**, *41*, 8981−8984.

[26] M. Nowotny, U. Hanefeld, H. van Koningsveld, T. Maschmeyer, *Chem. Commun.* **2000**, 1877−1878.

[27] X. Gai, R. Grigg, M. I. Ramzan, V. Sridharan, S. Collard, J. E. Muir, *Chem. Commun.* **2000**, 2053−2054.

[28] [28a] D. E. Bergbreiter, P. L. Osburn, Y.-S. Liu, *J. Am. Chem. Soc.* **1999**, *121*, 9531−9538. − [28b] D. E. Bergbreiter, P. L. Osburn, A. Wilson, E. M. Sink, *J. Am. Chem. Soc.* **2000**, *122*, 9058−9064.

[29] A. S. Gruber, D. Zim, G. Ebeling, A. L. Monteiro, J. Dupont, *Org. Lett.* **2000**, *2*, 1287−1290.

[30] D. Zim, A. S. Gruber, G. Ebeling, J. Dupont, A. L. Monteiro, *Org. Lett.* **2000**, *2*, 2881−2884.

[31] I. P. Beletskaya, A. V. Chuchurjukin, H. P. Dijkstra, G. P. M. van Klink, G. van Koten, *Tetrahedron Lett.* **2000**, *41*, 1075−1079.

[32] W. A. Herrmann, V. P. W. Böhm, *J. Organomet. Chem.* **1999**, *572*, 141−145.

[33] V. P. W. Böhm, W. A. Herrmann, *Chem. Eur. J.* **2000**, *6*, 1017−1025.

[34] For reactions in ionic liquids, see, for example: [34a] T. Welton, *Chem. Rev.* **1999**, *99*, 2071−2083. − [34b] J. Dupont, C. S. Consorti, J. Spencer, *J. Braz. Chem. Soc.* **2000**, *11*, 337−344. − [34c] P. Wasseerscheid, W. Keim, *Angew. Chem. Int. Ed.* **2000**, *39*, 3772−3789.

[35] N. Shezard, R. S. Oakes, A. A. Clifford, C. M. Rayner, *Tetrahedron Lett.* **1999**, *40*, 2221−2224.

[36] For a recent review on the use of supercritical carbon dioxide, see: P. G. Jessop, T. Ikariya, R. Noyori, *Chem. Rev.* **1999**, *99*, 475−493.

[37] L. F. Tietze, H. Schirok, M. Wöhrmann, K. Schrader, *Eur. J. Org. Chem.* **2000**, 2433−2444.

[38] J. Dupont, A. S. Gruber, G. S. Fonseca, A. L. Monteiro, G. Ebeling, R. A. Burrow, *Organometallics* **2001**, *20*, 171−176.

[39] For a recent discussion on the mechanism of Pd-mediated cross-coupling reactions, see: C. Amatore, A. Jutand, *Acc. Chem. Res.* **2000**, *33*, 314−321.

[40] [40a] A. J. Canty in *Handbook of Organopalladium Chemistry for Organic Synthesis* (Ed.: E.-I. Negishi), chapter II, in press. − [40b] A. Bayler, A. J. Canty, J. H. Ryan, B. W. Skelton, A. H. White, *Inorg. Chem. Commun.* **2000**, *3*, 575−578. − [40c] A. J. Canty, J. L. Hoare, B. W. Skelton, A. H. White, G. van Koten, *J. Organomet. Chem.* **1998**, *552*, 23−29. − [40d] A. J. Canty, *Acc. Chem. Res.* **1992**, *25*, 83−90.

[41] J. M. Brunel, M.-H. Hirlemann, A. Heumann, G. Buono, *Chem. Commun.* **2000**, 1869−1870.

[42] A. Suzuki in *Metal-Catalyzed Cross-Coupling Reactions* (Eds.: F. Diederich, P. J. Stang), Wiley-VCH, Weinheim, **1998**, pp. 49−97.

[43] [43a] D. Milstein, J. K. Stille, *J. Am. Chem. Soc.* **1979**, *101*, 4992−4998. − [43b] V. Farina, V. Krishnamurthy, W. J. Scott, *The Stille Reaction*, J. Wiley, New York, **1998**.

[44] R. B. Bedford, S. M. Draper, P. N. Scully, S. L. Welch, *New J. Chem.* **2000**, *24*, 745−747.

[45] J. Louie, J. F. Hartwig, *Angew. Chem. Int. Ed.* **1996**, *35*, 2359−2361.

[46] [46a] J. P. Wolfe, R. A. Singer, B. H. Yang, S. L. Buchwald, *J. Am. Chem. Soc.* **1999**, *121*, 9550−9561. − [46b] D. Zim, A. L. Monteiro, J. Dupont, *Tetrahedron Lett.* **2000**, *41*, 8199−8202.

[47] Palladium complexes associated with electron-rich and bulky phosphanes also promote the cross-coupling at room temperature; see, for example: [47a] J. P. Wolfe, S. L. Buchwald, *Angew. Chem. Int. Ed.* **1999**, *38*, 2413−2416. − [47b] A. F. Litke, C. Y. Dai, G. C. Fu, *J. Am. Chem. Soc.* **2000**, *122*, 4020−4028. − [47c] A. Zapf, A. Ehrentraut, M. Beller, *Angew. Chem. Int. Ed.* **2000**, *39*, 4153−4155.

[48] M. S. Brody, M. G. Finn, *Tetrahedron Lett.* **1999**, *40*, 415−418.

[49] J. Dupont, A. L. Monteiro, unpublished results.

[50] S. Darses, G. Michaud, J.-P. Genêt, *Eur. J. Org. Chem.* **1999**, 1875−1883.

[51] P. Prinz, A. Lansky, T. Haumann, R. Boese, M. Noltemeyer, B. Knieriem, A. de Meijere, *Angew. Chem. Int. Ed. Engl.* **1997**, *36*, 1289−1292.

[52] J. M. Brunel, A. Heumann, G. Buono, *Angew. Chem. Int. Ed.* **2000**, *39*, 1946−1949.

[53] K. Sonogashira in *Comprehensive Organic Synthesis* (Eds.: B. M. Trost, I. Fleming), Pergamon, Oxford, **1990**, vol. 3, pp. 521.

[54] W. A. Herrmann, C.-P. Reisinger, K. Öfele, C. Brosmer, M. Beller, H. Fischer, *J. Mol. Catal. A: Chem.* **1996**, *108*, 51−56.

[55] G. Fonseca, G. Ebeling, A. L. Monteiro, J. Dupont, manuscript in preparation.

[56] A. S. Guram, R. A. Rennels, S. L. Buchwald, *Angew. Chem. Int. Ed. Engl.* **1995**, *34*, 1348−1350.

[57] J. Louie, J. F. Hartwig, *Tetrahedron Lett.* **1995**, *36*, 3609−3612.

[58] M. Beller, T. H. Riermeier, C.-P. Reisinger, W. A. Herrmann, *Tetrahedron Lett.* **1997**, *38*, 2073−2074.

[59] N. Beydoun, M. Pfeffer, *Synthesis* **1990**, 729−731.

[60] A.-E. Gies, M. Pfeffer, C. Sirlin, J. Spencer, *Eur. J. Org. Chem.* **1999**, 1957−1961.

[61] X. Gai, R. Grigg, S. Collard, J. E. Muir, *Chem. Commun.* **2000**, 1765−1766.

[62] [62a] J. Spencer, M. Pfeffer, in: *Advances in Metal-Organic Chemistry* (Ed. L. S. Liebeskind), JAI Press, London **1998**, vol. 6, p. 103−144. − [62b] R. C. Larock, E. K. Yum, M. D. Refvik, *J. Org. Chem.* **1998**, *63*, 7652−7662.

[63] P. Braunstein, D. Matt, Y. Dusausoy, J. Fischer, A. Mitschler, L. Ricard, *J. Am. Chem. Soc.* **1981**, *103*, 5115−5125.
[64] P. Braunstein, D. Matt, D. Nobel, *J. Am. Chem. Soc.* **1988**, *110*, 3207−3212.
[65] P. Dani, J. Dupont, A. L. Monteiro, *J. Braz. Chem. Soc.* **1996**, *7*, 15−18.
[66] M. Camargo, P. Dani, J. Dupont, R. F. de Souza, M. Pfeffer, I. Tkatchenko, *J. Mol. Catal. A: Chem.* **1996**, *109*, 127−131.
[67] P. Grenouillet, D. Neibecker, J. Poirier, I. Tkatchenko, *Angew. Chem. Int. Ed. Engl.* **1982**, *21*, 767−769.
[68] J. M. Longmire, X. Zhang, M. Shang, *Organometallics* **1998**, *17*, 4374−4379.
[69] M. A. Stark, C. J. Richards, *Tetrahedron Lett.* **1997**, *38*, 5881−5884.
[70] M. A. Stark, G. Jones, C. J. Richards, *Organometallics* **2000**, *19*, 1282−1291.
[71] Y. Ito, M. Sawamura, T. Hayashi, *J. Am. Chem. Soc.* **1986**, *108*, 6405−6406.
[72] F. Gorla, A. Togni, L. M. Venanzi, A. Albertini, F. Lianza, *Organometallics* **1994**, *13*, 1607−1616.
[73] R. Navarro, E. P. Urriolabeitia, C. Cativiela, M. D. Diaz-de-Villegas, M. P. Lopez, E. Alonso, *J. Mol. Catal. A: Chem.* **1996**, *105*, 111−116.
[74] S. E. Denmark, R. A. Stavenger, A.-M. Faucher, J. P. Edwards, *J. Org. Chem.* **1997**, *62*, 3375−3389.
[75] M. Beller, T. H. Riermeier, A. Zapf, *Top. Catal.* **1997**, *4*, 301−309.
[76] J. M. Longmire, X. Zhang, *Tetrahedron Lett.* **1997**, *38*, 1725−1728.
[77] M. Calter, T. K. Hollis, L. E. Overman, J. Ziller, G. G. Zipp, *J. Org. Chem.* **1997**, *62*, 1449−1456.
[78] T. K. Hollis, L. E. Overman, *Tetrahedron Lett.* **1997**, *38*, 8837−8840.
[79] M. Pfeffer, A. B. Goel, *Inorg. Synth.* **1989**, *26*, 211−215.

Received October 12, 2000
[I00387]

The Crystal Structure of a Phosphite Ozonide, $C_2H_5C(CH_2O)_3PO_3$

Anton Dimitrov[a] and Konrad Seppelt*[a]

Keywords: Ozone / Phosphorus / Ozonolysis

The crystal structure of $C_2H_5C(CH_2O)_3PO_3$ shows that this ozonide contains a symmetric, almost planar, four-membered PO_3 ring with two crystallographically different, but otherwise essentially equal, molecules in the asymmetric unit cell.

Generally, ozonides are salts containing the O_3^- anion[1] or the reaction products of ozone with unsaturated organic materials. In the latter case it is common to distinguish between primary ozonides having a 1,2,3-trioxacyclopentane ring and secondary ozonides with a 1,2,4-trioxacyclopentane ring. The organic ozonides are thought to be formed by a sequence of [2 + 3] addition and reversion reactions ("Criegee mechanism"), and there is abundant evidence for this mechanism.[2]

Ozone also adds across the 9,10 position of a substituted anthracene, and this "primary" ozonide is the first one that is stable enough to be characterized by a single-crystal structure determination.[3] From this it is evident, in spite of some disorder in the structure, that the O_3 molecule has simply added across the central carbon atoms of the anthracene molecule, a reaction that, at least formally, can be described as a [3 + 4] addition reaction.

There is yet another class of ozonides, the phosphite ozonides, which could be classified as inorganic covalent ozonides. They were first observed in 1961.[4] They are formed in the reaction between organic phosphites and ozone at low temperatures. There is abundant work on triphenylphosphite ozonide.[4−15] The thermal stability of some phosphite ozonides reach almost room temperature, especially if cyclic and polycyclic phosphite ozonides are considered.[16−26]

Phosphite ozonides are very convenient precursors of singlet oxygen, since they all tend to evolve singlet oxygen with simultaneous formation of the stable phosphates. These ozonides are assumed to have a four-membered, λ^5-PO_3 ring. In this context a high resolution ^{17}O NMR spectrum could be informative; however, the results are not conclusive (see below).

Of particular interest would be the detailed structure of such a phosphite ozonide. This could finally answer the questions as to whether these ozonides definitely contain a four-membered PO_3 ring, whether this ring is C_{2v} symmetric (planar and with equal bond lengths), and what is the general coordination around the five-coordinate phosphorous atom.

[a] Institut für Chemie, Freie Universität Berlin,
Fabeckstraße 34−36, 14195 Berlin, Germany
Fax: (internat.) +49-30/838-54289
E-mail: seppelt@chemie.fu-berlin.de

In the following sections we will describe the crystal structure of a well-selected phosphite ozonide to address these questions. At this point the remarkable formation of a PO_2 three-membered ring (dioxaphosphirane) from a three-valent phosphorus precursor and molecular oxygen should be noted.[27]

Results

At the beginning of this survey we had to select one of the more stable phosphite ozonides. The candidates were triphenylphosphite ozonide (**1**), 4-ethyl-1-phospha-2,6,7-trioxabicyclo[2.2.2]octane ozonide (**2**),[16,23] or 1-phospha-2,8,9-trioxaadamantane ozonide (**3**).[18,23] We have chosen **2** as a compromise between stability of **3** and ease of preparation of **1**. After all, the triol starting material for the preparation of **2** is commercially available and **2** is said to be stable below −15 °C. Such temperatures can easily be maintained for preparation, crystal growth, and single-crystal structure determination.

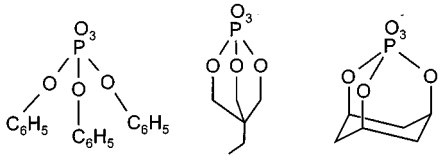

1 **2** **3**

The preparation of **2** followed the published procedures. Crystal growth was monitored by ^{31}P NMR spectroscopy, which readily helps to analyze the amounts of starting material phosphite, product phosphite ozonide, and phosphate as the major decomposition product. Obtaining suitable single crystals was, however, not trivial. Compound **2** of about 90% purity did not recrystallize from various solvents at all, or it formed microcrystalline powders. Single crystals were, however, obtained from CH_2Cl_2 solution.

In the first and reproducibly monoclinic crystalline modification the organic part of the molecule is at least twofold, possibly even threefold, disordered, whereas the environment around the phosphorous is reasonably well resolved. The four-membered PO_3 ring looks very much the same as in the crystallographic determination of modification 3. Therefore, and also because the criteria for a good crystal

 © WILEY-VCH Verlag GmbH, 69451 Weinheim, 2001 1434−1948/01/0808−1929 $ 17.50+.50/0

Table 1. Crystal and structure refinement data for **2** [{$2C_2H_5C(CH_2O)\}_3PO_3$]·$3CHFCl_2$

	Modification 1	Modification 2	Modification 3
Mol. form.	$C_2H_5C(CH_2O)_3PO_3C_6H_{11}O_6P$	$C_2H_5C(CH_2O)PO_3$	$2C_2H_5C(CH_2O)_3PO_3{\cdot}3CHFCl_2$
Mol. wt.	210.12	210.12	728.99
a[pm]	757.9(1)	883.2(2)	877.1(3)
b[pm]	660.7(1)	1008.3(2)	1064.5(4)
c[pm]	1706.1(2)	1009.3(2)	1543.9(6)
α[°]	90	97.189(3)	93.37(1)
β[°]	91.548(2)	104.025(4)	95.19(1)
γ[°]	90	96.797(4)	97.62(1)
Vol. [10^6 pm^3]	854.1	854.8	1419.3
Z	4	4	2
Space group	$P2_1/c$	$P\bar{1}$	$P\bar{1}$
Density, calcd. [Mg m^{-3}]			1.706
Absorption coefficient [mm^{-1}]			0.792
F(000)			740
Crystal size [mm]			0.3 × 0.3 × 0.2
Color			colorless
θmin, max [°]			1.9, 26.37
Index range			$-10 \le h \le 10$ $-13 \le k \le 13$ $-19 \le l \le 19$
Reflections collected/unique			13150/5772
R_{int}			0.076
Completeness to 2θ = 52.7°			99.7%
Refinement method			Full-matrix least-squares on F^2
Data/parameters			5772/343
Goodness of fit			1.025
Final *R* values [$I > 2\sigma(I)$]			$R_1 = 0.0777$, $wR_2 = 0.2114$
All data			$R_1 = 0.0925$, $wR_2 = 0.2279$
Largest difference peak, hole			0.951, $-1.007{\cdot}10^{-6}$ e pm^{-3}

structure are only modestly met, we include in Table 1 only the lattice constants of this modification. In a second modification, which has been obtained only once, there was no disorder, but the crystallographic criteria are even worse than in the first modification, due to an imperfect crystal.

Acceptable results were obtained by recrystallization from $CHFCl_2$ solution. These crystals also contain solvent molecules. The crystal structure data are also summarized in Table 1 and detailed bond distances and bond lengths are collected in Table 2. The asymmetric unit of the cell contains two molecules of **2** along with three molecules of $CHFCl_2$. The two crystallographic different molecules of **2** differ significantly only in the orientation of the terminal ethyl group with respect to the PO_3 ring plane.

The coordination polyhedron around the phosphorous atoms is clearly a tetragonal pyramid (Figure 1). The O3 and O23 atoms are considered as apexes and have bond angles of 102−105° to the other four oxygen atoms bonded to phosphorous. The apical P−O bond is, as expected, the shortest of the P−O bonds. The PO_2 angles within the basal part are strongly influenced by the four-membered PO_3 ring, since the PO_2 inner-ring angle is only 78°. All other inner ring angles are slightly above 90° so that an inner-ring-angle sum of 360° is obtained, indicating near planarity of the ring. The dihedral angles of the four-membered rings are about 7°.

The distances within the four-membered ring are pairwise about equal. The O−O bond lengths of 146 pm indicate the single-bond character of these bonds, in contrast to the bond lengths of 127 pm in free ozone. The O−O bond lengths compare nicely with those in $F_3-O-O-O-CF_3$ [143.7(2) crystal, 145.2(5) gas],[28] but not so well with 9-*tert*-butyl-10-methylanthracene 9,10-ozonide [136.1(6) and 142.8(6) pm]. In the latter, however, the central oxygen atom is disordered over two symmetrically equivalent positions, and, strictly speaking, all the other atoms as well, so that the estimated standard deviations may be much larger than given. This also holds for the O−O−O bond angle of 113.3(4)°. This is found to be 106.4(1)° in $CF_3-O-O-O-CF_3$,[28] but only 92° in **2**.

The NMR spectra are inconclusive for the structure of **2**. While the ^{31}P resonance shows the expected septets due to ^{1}H-^{31}P coupling, the ^{17}O resonance of **2** made from ^{17}O enriched ozone exhibits a broad line at δ = 411.7 with a shoulder at δ = 470.6, which can be assigned to the phosphorous-bonded oxygen atoms of the O_3 unit and the cent-

Table 2. Selected bond lengths (pm), angles, and dihedral angles [°] of **2**

Molecule I		Molecule II	
P1−O1	160.8(2)	P2−O21	160.9(3)
P1−O2	161.8(3)	P2−O22	161.6(2)
P1−O3	157.6(3)	P2−O23	157.0(3)
P1−O4	166.7(3)	P2−O24	167.1(8)
P1−O5	167.0(3)	P2−O25	167.8(3)
O4−O6	146.2(4)	P2−O26	145.8(4)
O5−O6	146.3(4)	P2−O21	145.6(4)
O1−P1−O2	98.1(1)	O21−P2−O22	98.2(1)
O1−P1−O3	102.7(1)	O21−P2−O23	102.8(1)
O1−P1−O4	85.7(1)	O21−P2−O24	85.5(1)
O1−P1−O5	149.7(1)	O21−P2−O25	150.8(2)
O2−P1−O3	102.7(1)	O22−P2−O23	103.5(1)
O2−P1−O4	150.7(1)	O22−P2−O24	149.3(1)
O2−P1−O5	84.6(1)	O22−P2−O25	85.1(1)
O3−P1−O4	104.7(1)	O23−P2−O24	105.4(2)
O3−P1−O5	105.5(1)	O23−P2−O25	104.6(1)
O4−P1−O5	78.2(1)	O24−P2−O25	77.7(1)
P1−O4−O6	94.4(2)	P2−O24−O26	94.6(2)
P1−O5−O6	94.6(2)	P2−O25−O26	94.4(2)
O4−O6−O5	92.1(2)	O24−O26−O25	92.3(2)
O5−P1−O4−O6	6.3(2)	O25−P2−O24−O26	−7.1(2)

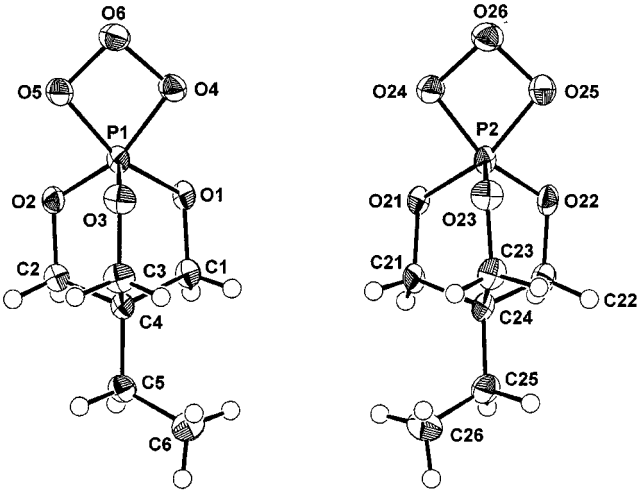

Figure 1. The crystallographically different molecules of **2**; ORTEP representation with 50% probability ellipsoids

ral oxygen atom. In $CF_3-O-O-O-CF_3$ the chemical shift values for the corresponding oxygen atoms are δ = 321 and 479.[29] In ozone, extremely high shifts of δ = 1590 and 1020 are observed.[30]

Experimental Section

General: All chemicals and solvents were dried prior to use and handled in a glove box and/or glass vacuum line. NMR spectra: JEOL multinuclear instrument at 400 MHz for ^1H. Spectra are recorded relative to $H_3{}^{31}PO_4$, ^{13}C-TMS, and $H_2{}^{17}O$ as external standards. Raman spectra: Bruker RPS 100 S instrument with Nd: YAG laser excitation, λ = 1064 nm. Samples were kept in glass tubes, and Raman scattering of the tubes was subtracted digitally. Crystal structures: A suitable crystal was fixed on the tip of a glass needle with the help of a special cooling device[31] and mounted on the Bruker SMART CCD 1000 TU diffractometer equipped with Mo-K_α irradiation, a graphite monochromator. The data set was measured in steps of 0.3° in ω, and 3 times 600 scans in ψ = 0°, 90°, and 240°, with exposure times of 10 sec/frame and a detector to crystal distance of 4.0 cm. A full shell of data up to 2θ = 53° was measured. Data were reduced to intensities and corrected for background (SAINT). The structures were solved[32] and refined[33] with the SHELTL program suite.

Crystallographic data (excluding structure factors) for the structure reported in this paper have been deposited with the Cambridge Crystallographic Data Centre as supplementary publication no. CCDC-155612. Copies of the data can be obtained free of charge on application to CCDC, 12 Union Road, Cambridge CB2 1EZ, UK [Fax: (internat.) +44-1223/336-033; E-mail: deposit@ccdc.cam.ac.uk].

Preparation of 4-Ethyl-1-phospha-2,6,7-trioxabicyclo[2.2.2]octane: This compound was prepared according to the literature procedure from $CH_3CH_2C(CH_2OH)_3$ and PCl_3,[34] and recrystallized from n-pentane. M.p. 55.7 °C, ^{31}P NMR ($CDCl_3$): δ = 93.1 ($^3J_{P,H}$ = 1.9 Hz). − ^1H NMR ($CDCl_3$): δ = 0.75 (^3J = 7.8 Hz, CH_3), 1.11 (CH_3-CH_2), 3.92 ($^3J_{H,P}$ = 1.9 Hz, CH_2O). − ^{13}C NMR ($CDCl_3$): δ = 6.79 (CH_3), 24.40 ($^4J_{C,P}$ = 5.4 Hz, CH_3-CH_2), 34.39 ($^3J_{C,P}$ = 22.1 Hz, C), 70.49 (CH_2O).

Preparation of 4-Ethyl-1-phospha-2,6,7-trioxabicyclo [2.2.2]octane Ozonide(2):[16,17] The phosphite (100 mg) was dissolved in 4 mL of CH_2Cl_2 or $CHFCl_2$ in a 10 mm-diameter glass tube. This was connected via a septum and two 1.5 mm-diameter inlet and outlet tubes of PFA (perfluoroether-tetrafluoroethylene copolymer) with an ozone generator. At −78 °C an O_3/O_2 stream was bubbled through the solution until it turned blue due to dissolved ozone at the end of the reaction. The excess of ozone and about half of the solvent were pumped out at −78 °C on the vacuum line. In the case of $CHFCl_2$ as a solvent the tube was sealed. In case of CH_2Cl_2 as a solvent, about 1 mL of $CFCl_3$ was added to the concentrated solution of the ozonide before sealing the tube. Suitable single crystals for X−ray diffraction were grown at −85 °C.

For experimental details of the crystal structures see Table 1; for numerical values of the structure see Table 2.

The purity of the samples was monitored by recording ^{31}P NMR spectra: ^{31}P NMR: δ = −43.1. ($^3J_{H,P}$ = 8.9 Hz; ref.[17] −43.6). At −78 °C only the signal of the ozonide and at room temperature only those of the phosphate were present: Raman spectrum (solid), bands below 1500 cm^{-1}: $\tilde{\nu}$ = 1474(30), 1446(10), 1345(3), 1286(9), 1256(11), 1156(15), 1088(10), 1047(15), 981(4), 964(6), 905(8)*, 887(50)*, 867(25)*, 853(35), 838(4), 820(3), 792(70), 776(2), 762(8), 727(7), 671(100), 629(3), 598(3), 516(9), 488(12), 471(6), 458(25), 443(2), 409(20), 388(25), 367(4), 325(30), 307(4), 280(6), 217(4), 193(1), 160(4), 116(10) cm^{-1}. The bands marked with an asterisk are not present in the phosphite starting material or the phosphate decomposition product and are therefore assigned to the PO_3 ring vibrations.

For ^{17}O NMR measurements, the ozonide was synthesized using ozone prepared by the discharge method in a closed system[35] with oxygen enriched to 35% ^{17}O. CD_2Cl_2 (3 mL) in a 10 mm-diameter glass tube was saturated at −78 °C with the labeled ozone. An aliquot of a 0.2 M solution of the phosphite in CD_2Cl_2 was added slowly from a precooled syringe connected to a 1.5 mm-diameter

inlet tube of FEP into the O_3 solution until only a pale blue color of dissolved ozone remained (typically 1−2 mL of the solution were needed). After the addition was complete, the excess ozone and part of the solvent were pumped out at −78 °C. The remaining solution was transferred into an NMR tube and the tube sealed. According to the ^{31}P NMR spectra some phosphate was always formed.

^{17}O NMR spectra were recorded at −70, −40, −20, 0 °C and at room temperature. At −70 °C two broad signals at δ = 470.6 (the smaller one probably belonging to the central oxygen of the trioxaphosphetane ring of the ozonide) and at δ = 411.6 (main signal, probably due to the two terminal oxygens of the trioxaphosphetane ring) were observed. Upon raising the temperature the signals broadened. At −20 °C the low-field signal was no longer observable, and the remaining signal at δ = 412 had a Δν1/2 value of 928 Hz.

At room temperature these signals disappeared and the signal of the labeled P=^{17}O part of the phosphate increased: ^{17}O NMR (CD_2Cl_2): δ = 65.75 (d, $^1J_{P,O}$ = 153 Hz).

Acknowledgments

We thank the Deutsche Forschungsgemeinschaft and the Fonds der Chemischen Industrie for financial support.

[1] W. Hesse, M. Jansen, W. Schnick, *Prog. Solid State Chem.* **1989**, *19*, 47−110.
[2] R. L. Kuczkowski, *Acc. Chem. Res.* **1983**, *16*, 42−47.
[3] Y. Ito, A. Matsuura, R. Otani, T. Matsuura, *J. Am. Chem. Soc.* **1983**, *105*, 5699−5700.
[4] Q. E. Thompson, *J. Am. Chem. Soc.* **1961**, *83*, 846−851.
[5] R. W. Murray, M. L. Kaplan, *J. Am. Chem. Soc.* **1968**, *90*, 537−538.
[6] E. Wasserman, R. W. Murray, M. L. Kaplan, W. A. Yager, *J. Am. Chem. Soc.* **1968**, *90*, 4160−4161.
[7] R. W. Murray, M. L. Kaplan, *J. Am. Chem. Soc.* **1963**, *91*, 5358−5364.
[8] P. D. Bartlett, G. D. Mendenhall, *J. Am. Chem. Soc.* **1970**, *92*, 210−211.
[9] R. W. Murray, R. D. Smetana, E. Block, *Tetrahedron Lett.* **1971**, *4*, 299−302.
[10] E. Koch, *Anal. Chem.* **1973**, *45*, 2120−2124.
[11] P. D. Bartlett, G. D. Mendenhall, D. L. Durham, *J. Org. Chem.* **1980**, *45*, 4269−4271.
[12] P. D. Bartlett, H.-K. Chu, *J. Org. Chem.* **1980**, *45*, 3000−3004.
[13] W. A. Pryer, C. K. Govindan, *J. Org. Chem.* **1981**, *46*, 4679−4682.
[14] P. D. Bartlett, C. M. Lonzetta, *J. Am. Chem. Soc.* **1983**, *105*, 1984−1988.
[15] G. D. Mendenhall, D. B. Priddy, *J. Org. Chem.* **1999**, *64*, 5783−5789.
[16] M. E. Breunan, *J. Chem. Soc., Chem. Commun.* **1970**, 956−957.
[17] L. M. Stephenson, D. E. Mc Clure, *J. Am. Chem. Soc.* **1973**, *95*, 3074−3076.
[18] A. P. Schaap, K. Kees, A. L. Thayer, *J. Org. Chem.* **1977**, *40*, 1185−1186.
[19] M. Koenig, F. El Khatib, A. Munoz, R. Wolf, *Tetrahedron Lett.* **1982**, *23*, 421−424.
[20] A. M. Caminade, F. El Khatib, M. Koenig, *Phosphorus & Sulfur* **1983**, *18*, 97−100.
[21] G. D. Mendenhall, R. F. Kessick, M. Dobrzelewski, *J. Photochem.* **1984**, *25*, 227−243.
[22] F. El Khatib, A. M. Caminade, M. Koenig, *Phosphorus & Sulfur* **1984**, *20*, 55−60.
[23] S. M. Ramos, J. C. Owrutsky, P. M. Keehn, *Tetrahedron Lett.* **1985**, *26*, 5895−5899.
[24] F. El Khatib, C. Tachon, A.-M. Caminade, M. Koenig, *Tetrahedron Lett.* **1985**, *26*, 3007−3010.
[25] A. M. Caminade, F. El Khatib, M. Koenig, J. M. Anbry, *Can. J. Chem.* **1985**, *63*, 3203−3209.
[26] V. V. Shereshovets, F. F. Khizbullin, R. K. Yanbaev, N. M. Koroteva, M. M. Khozanowskaya, N. A. Mukmeneva, V. D. Komissavov, S. A. Tolstikov, *J. Org. Chem. USSR (Engl.)* **1996**, *26*, 534−537.
[27] M. Nakamoto, K. Akiba, *J. Am. Chem. Soc.* **1999**, *121*, 6958−6959.
[28] K. I. Gobbato, M. F. Klapdor, D. Mootz, W. Poll, S. E. Ulic, H. Willner, H. Oberhammer, *Angew. Chem.* **1995**, *107*, 2433−2434; *Angew. Chem. Int. Ed. Engl.* **1995**, *34*, 2244−2245.
[29] I. J. Solomon, A. J. Kacmarek, W. K. Sumida, J. K. Ranay, *Inorg. Chem.* **1972**, *11*, 195−196.
[30] A. Dimitrov, K. Seppelt, D. Scheffler, H. Willner, *J. Am. Chem. soc.* 120, *34*, 8711−8714.
[31] H. Schumann, W. Genthe, E. Hahn, M.-B. Hossein, D. v. d. Helm, *J. Organomet. Chem.* **1986**, *299*, 67−84.
[32] G. Sheldrick, SHELXS, *Program for Crystal Structure Solution*, Göttingen, **1986**.
[33] G. Sheldrick, SHELXL-97, *Program for Crystal Structure Refinement*, Göttingen, **1997**.
[34] W. S. Wachsworth, W. D. Emmons, *J. Am. Chem. Soc.* **1962**, *84*, 610−617.
[35] M. Griggs, S. Kaye, *Rev. Sci. Instrum.* **1968**, *39*, 1685−1686.

Received January 25, 2001
[I01034]

Rearrangement of a Titanium Alkoxide Cluster upon Substitution of the Alkoxide Groups by Carboxylate Ligands − Synthesis of $[Ti_6O_4(OEt)_{14}(OOCPh)_2]$ from $[Ti_7O_4(OEt)_{20}]$

Ivan Mijatovic,[a] Guido Kickelbick,[a] and Ulrich Schubert*[a]

Keywords: Titanium / Cluster compounds / X-ray diffraction / Polyoxometalates / Carboxylate ligands

Reaction of $[Ti_7O_4(OEt)_{20}]$ with benzoic acid results in the formation of the new cluster $[Ti_6O_4(OEt)_{14}(OOCPh)_2]$ with concomitant rearrangement of the cluster structure. The molecular structure of the new cluster was determined by single-crystal X-ray diffraction and can be represented by the extended formula $[Ti_6(\mu_4\text{-}O)_2(\mu_2\text{-}O)_2(\mu_2\text{-}OEt)_6(\mu_2\text{-}benzoate)_2(\mu_1\text{-}OEt)_8]$.

Introduction

Metal oxide clusters capped by reactive organic groups are interesting building blocks for the synthesis of inorganic-organic hybrid materials due to their well-defined shape and their size in the lower nanometer range.[1] A key issue for the preparation of organically modified transition metal oxide clusters (OMTOCs) is the attachment of suitable organic groups to the metal atoms at the cluster surface. The introduction of organic groups can often be achieved with bi- (or multi)dentate (chelating or bridging) groups, such as carboxylates, sulfonates, phosphonates, β-diketonates, etc. These groups may also carry organic functionalities, such as polymerizable double bonds.

OMTOCs can be prepared by two strategies. The multidentate groups can either be grafted to a pre-formed cluster ("surface modification" method) or introduced during the cluster synthesis ("in situ" method). The latter method has been used successfully for the preparation of carboxylate- or β-diketonate-substituted metal oxide clusters by reaction of metal alkoxides with carboxylic acids or β-diketones,[1,2] where concomitant ester formation results in the formation of oxo and hydroxo ligands. There are also well-established routes for the preparation of a variety of neutral or (mostly) charged metal oxide clusters. The subsequent modification of their surface by organic groups requires: (i) reactive groups, such as OH, Cl or OR, bonded to the surface metal atoms, and (ii) the simultaneous balancing of charges and coordination numbers upon substitution of these groups. The latter is only possible without major difficulties if both the number of the occupied coordination sites and the charges of the entering ligands are the same as those of the leaving groups. For example, when $[Ti_{16}O_{16}(OEt)_{32}]$ was reacted with small amounts of carboxylic acids, a few of the bridging OEt groups were replaced by bridging carboxylate groups (for higher carboxylate:Ti proportions, the cluster core was cleaved).[3]

[a] Institut für Anorganische Chemie, Technische Universität Wien,
Getreidemarkt 9, 1060 Wien, Austria

The substitution of mono-anionic, *mono*dentate groups (OR, OH, Cl etc.) by mono-anionic, *bi*dentate ligands (carboxylates, β-diketonates, etc.) requires either rearrangement of the cluster or a change of the coordination modes of the bridging groups (e.g., bridging OR or OH to terminal, or μ_3 oxygens to μ_2 oxygens) to make additional coordination sites available. Reaction of the clusters with bidentate ligands may even lead to the complete degradation to monomeric compounds; for example, $[Zr(acac)_2(OMc)_2]$ (OMc = methacrylate, acac = acetylacetonate) was obtained from the reaction of $[Zr_4O_2(OMc)_{12}]$ with acetylacetone.[4]

Results and Discussion

In this paper we describe the rearrangement of a titanium oxoalkoxide cluster upon partial substitution of alkoxide groups by carboxylate groups. Among the many structurally characterised titanium polyoxoalkoxides with compositions ranging from $[Ti_3O(OR)_{10}]$ to $[Ti_{18}O_{27}(OR)_{18}]$[5] we have selected $[Ti_7O_4(OEt)_{20}]$ (**1**) as a model compound.[6,7] When **1** was reacted with a 1.5-molar excess of benzoic acid in benzene solution at ambient temperature [Equation (1); monitored by ^{13}C NMR spectroscopy], both starting compounds were completely consumed (more than 1.5 equivalents of benzoic acid results in the formation of increasing amounts of a poorly soluble precipitate). The NMR spectra of the reaction solution indicated the presence of a single cluster. When the volatile compounds were removed and the resulting residue was dissolved in heptane, the ^{13}C NMR spectrum was still that of the initially formed cluster. From this solution, crystals of $[Ti_6O_4(OEt)_{14}(OOCPh)_2]$ (**2**) precipitated at −20 °C. The ^{13}C NMR spectra of the initially formed cluster (the composition and structure of which is still unknown) and **2** are very similar, but can be clearly distinguished. The main difference is that **2** shows more signals in the CH_2 and CH_3 region than the initially formed cluster. The formation of **2** from the initial cluster is reversible, i.e. if the crystals are redissolved in the mother

 © WILEY-VCH Verlag GmbH, 69451 Weinheim, 2001 1434−1948/01/0808−1933 $ 17.50+.50/0

liquid, the spectrum of the initial cluster is again observed. This indicates that **2** is in equilibrium with the initial cluster. Once **2** was isolated analytically pure and dissolved in heptane, it did not reconvert into the initial cluster. We can exclude that the formation of both the initial cluster and **2** is due to the presence of water — which might be produced by ester formation between benzoic acid and the cleaved ethanol — because both the initial cluster and **2** (precipitating from its solution) were observed when **1** was reacted with acetic benzoic anhydride instead of benzoic acid. In the latter reaction, ethyl acetate was formed as a by-product.

$$[Ti_7O_4(OEt)_{20}]\ (\mathbf{1}) + 1.5\ PhCOOH \rightarrow [Ti_6O_4(OEt)_{14}(OOCPh)_2]\ (\mathbf{2}) + ... \quad (1)$$

The structure of **2** was determined by a single crystal X-ray structure analysis (Figure 1). The composition of **2** formally differs from that of **1** by a $Ti(OEt)_4$ unit and the substitution of two of the remaining ethoxide ligands by benzoate ligands. An inspection of the molecular structures shows, however, that this is accompanied by an extensive structural rearrangement. The titanium atoms are octahedrally coordinated in both clusters. The total 42 coordination sites in **1** (general formula $Ti_7O_4X_{20}$, X = mono-anionic ligand) are occupied by two μ_4-O, two μ_3-O, eight bridging OEt and twelve terminal OEt {i.e., $[Ti_7(\mu_4\text{-}O)_2(\mu_3\text{-}O)_2(\mu_2\text{-}OEt)_8(\mu_1\text{-}OEt)_{12}]$}.[7,8] In the resulting Ti_6 cluster **2**, only 36 coordination sites are available for the ligands. Thus, when two bridging OEt ligands are formally replaced by two bridging benzoate ligands, other ligands must change their coordination mode in order to adjust for the smaller number of available coordination sites. As a matter of fact, two of the bridging oxygen atoms in **2** are μ_2 coordinated, rather than μ_3 in **1**, i.e. the extended formula of **2** is $[Ti_6(\mu_4\text{-}O)_2(\mu_2\text{-}O)_2(\mu_2\text{-}OEt)_6(\mu_2\text{-benzoate})_2(\mu_1\text{-}OEt)_8]$. The changing of the two oxygen atoms from a μ_3 coordination mode to μ_2 necessarily implies that the titanium octahedra in **1** and **2** are connected in a different way (Figure 2).

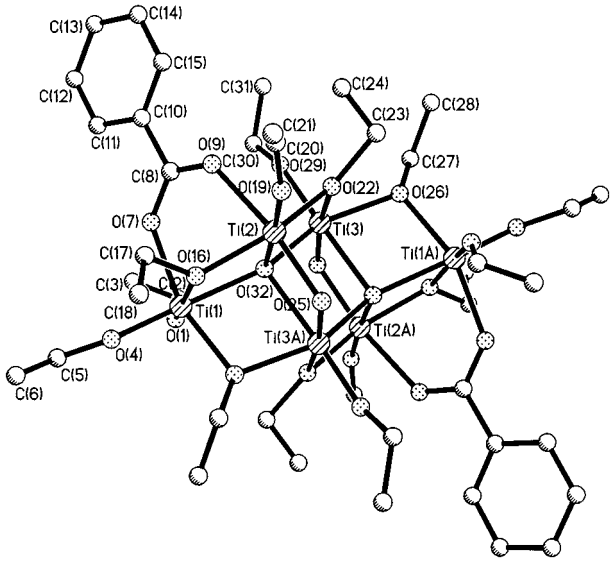

Figure 1. Molecular structure of $[Ti_6O_4(OEt)_{14}(OOCPh)_2]$ (**2**); selected distances (in pm) and bond angles (in °): Ti(1)−O(1) 177.3(4), Ti(1)−O(4) 177.4(4), Ti(1)−O(7) 204.3(4), Ti(1)−O(16) 208.9(4), Ti(1)−O(26) 201.1(4), Ti(1)−O(32) 208.2(3), Ti(2)−O(9) 216.6(4), Ti(2)−O(19) 177.0(4), Ti(2)−O(16) 196.2(4), Ti(2)−O(22) 193.9(4), Ti(2)−O(25) 183.2(4), Ti(2)−O(32) 208.6(3), Ti(3)−O(22) 208.5(4), Ti(3)−O(26) 201.5(4), Ti(3)−O(25) 183.9(3), Ti(2)−O(29) 176.9(4), Ti(3)−O(32) 196.6(3), Ti(3)−O(32)* 214.2(3). Ti(1)−O(16)−Ti(2) 102.0(2), Ti(2)−O(22)−Ti(3) 103.6(2), Ti(2)−O(25)−Ti(3)* 109.9(2), Ti(1)−O(32)−Ti(2) 98.2(1), Ti(1)−O(32)−Ti(3) 150.6(1), Ti(2)−O(32)−Ti(3) 102.7(2), Ti(3)−O(32)−Ti(3)* 100.6(2), Ti(1)−O(32)−Ti(3)* 99.6(1), Ti(2)−O(32)−Ti(3)* 90.6(1); *symmetry-equivalent atoms

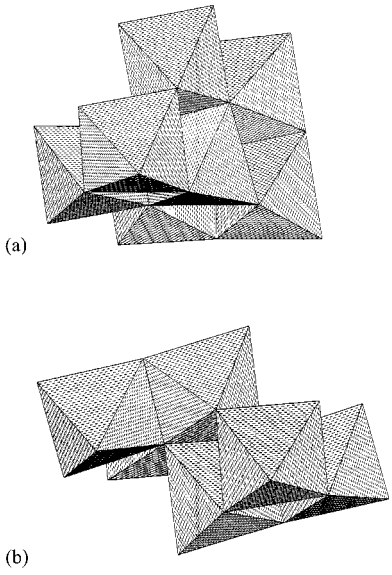

Figure 2. Arrangement of the Ti octahedra in **1** (a)[6,7] and **2** (b)

Several types of carboxylate-substituted titanium polyoxoalkoxides have been obtained by reaction of $Ti(OR)_4$ with carboxylic acids,[9−11] with the degree of substitution by carboxylate groups (r = carboxylate/Ti ratio) ranging from 1.78 in $[Ti_9O_8(OR)_4(OOCR')_{16}]$ to 0.5 in $[Ti_4O_2(OR)_{10}(OOCR')_2]$. Compared with the known clusters, **2** is exceptional in two respects: (i) it is the only cluster prepared by substitution of a pre-formed polyoxoalkoxide (with concomitant rearrangement of the cluster core), and (ii) it has the lowest degree of substitution (r = 0.33). Interestingly, only the two clusters with the lowest degree of substitution, $[Ti_4O_2(OR)_{10}(OOCH)_2]$[10] and **2**, contain μ_4-oxygens, while the other clusters are less condensed with only μ_2- and μ_3-oxygens. For example, in the other known cluster with the general composition $Ti_6O_4X_{16}$, $[Ti_6O_4(O\textit{i}Pr)_{12}(OOCMe)_4]$,[11] the two additional carboxylate groups (compared to **2**) do not replace two μ_2-OR groups; instead, the coordination mode of both the μ_4-oxygens in **2** is changed to μ_3 in order to accommodate the two bridging ligands {i.e., the extended formula is $[Ti_6(\mu_3\text{-}O)_2(\mu_2\text{-}O)_2(\mu_2\text{-}O\textit{i}Pr)_6(\mu_2\text{-acetate})_4(\mu_1\text{-}O\textit{i}Pr)_6]$}.

Experimental Section

All operations were carried out in Schlenk tubes under an argon atmosphere.

$Ti_6O_4(OEt)_{14}(OOCPh)_2$ (2): A solution of benzoic acid (64 mg, 0.52 mmol) in 5 mL of benzene was added dropwise at room temperature to a solution of $Ti_7O_4(OEt)_{20}$ [**1**: ^{13}C NMR δ = 18.5, 18.8, 19.0, 19.2, 19.6, 19.67, 19.74 (CH_3), 66.0, 70.4, 70.8, 70.9, 71.4, 71.5, 71.6, 71.8 (CH_2)] (450 mg, 0.35 mmol) in 5 mL of benzene. The solution was stirred for 12 h at 25 °C. After removal of all volatiles and addition of heptane (5 mL) the following ^{13}C NMR spectrum was observed: δ = 18.4, 18.9, 19.3 (CH_3), 69.1, 71.0, 71.5, 72.6, 72.8 (CH_2), 128.2, 130.2, 131.9, 135.0 (Ph), 172.2 (COO). From this solution, cluster **2** crystallized at −20 °C during 12 h. Yield 304 mg (0.25 mmol; yield: 61% relative to Ti, 93% relative to benzoic acid). Selected spectroscopic and analytic data of **2**: $C_{42}H_{80}O_{22}Ti_6$ calcd. C 41.2, H 6.6, Ti 23.5; found C 41.0, H 6.2, Ti 23.6. − ^{13}C NMR δ = 17.8, 17.9, 18.2, 18.4, 18.9, 19.3, 19.4 (CH_3), 69.1, 69.6, 71.1, 71.6, 73.0, 73.3, 74.3 (CH_2), 128.3, 130.4, 132.0, 135.2 (Ph), 172.3 (COO). − IR (KBr): $\tilde{\nu}$ = 841 (w), 890 (s), 924 (s), 1069 (vs), 1124 (vs), 1352 (s), 1375 (s), 1401 (s, COO sym), 1447 (vs), 1469 (m), 1493 (m), 1552 (s), 1595 (s, COO asym), 1821 (w), 1934 (w), 2697 (w), 2858 (vs), 2924 (vs), 2968 (vs), 3065 (w).

X-ray Structure Analysis of 2. A selected crystal (0.54 × 0.32 × 0.22 mm) was mounted on a Siemens SMART diffractometer with a CCD area detector. Graphite-monochromated Mo-K_α radiation (71.073 pm) was used for all measurements. The crystal-to-detector distance was 4.40 cm. A hemisphere of data was collected by a combination of three sets of exposures at 294 K. Each set had a different φ angle for the crystal, and each exposure took 20 s and covered 0.3° in ω. 12010 reflections were collected. The data were corrected for polarization and Lorentz effects, and an empirical absorption correction (SADABS) was applied. The cell dimensions were refined with all unique reflections. Crystal data: M = 1224.29, monoclinic, Z = 2, a = 1245.8(2), b = 1780.9(3), c = 1417.7(3) pm, β = 108.351(4), U = 2985.4(9)·10^6 pm^3, space group $P2_1/n$, D_{calc} = 1.362 gcm^{-3}, μ(Mo-K_α) = 8.31 cm^{-1} The structure was solved by direct methods (SHELXS-86). Refinement was carried out with the full-matrix least-squares method based on F^2 (SHELXL-93) with anisotropic thermal parameters for all non-hydrogen atoms using 3631 unique reflections. Hydrogen atoms were inserted in calculated positions and refined riding with the corresponding atom. R_1 = 0.042 [$I > 2\sigma(I)$], R_2 = 0.121, GOF = 1.013. Crystallographic data (excluding structure factors) for the structure of **2** have been deposited at the Cambridge Crystallographic Data Centre as supplementary publication no. CCDC 157 873. Copies of the data can be obtained free of charge on application to CCDC, 12 Union Road, Cambridge CB2 1EZ, UK [Fax: (internat.) +44-1223/336-033; E-mail: deposit@ccdc.cam.ac.uk].

Acknowledgments

We thank the Fonds zur Förderung der wissenschaftlichen Forschung, Vienna, (FWF) for their support of this work.

[1] Review articles: G. Kickelbick, U. Schubert, *Monatsh. Chem.* **2001**, *132*, 13; U. Schubert, *Chem. Mater.*, in press.
[2] Review article: U. Schubert, N. Hüsing, A. Lorenz, *Chem. Mater.* **1995**, *7*, 2010.
[3] G. J. de A. A. Soler-Illia, L. Rozes, M. K. Boggiano, C. Sanchez, C.-O. Turrin, A.-M. Caminade, J.-P. Majoral, *Angew. Chem. Int. Ed.* **2000**, *39*, 4248; G. J. de A. A. Soler-Illia, E. Scolan, A. Loius, P.-A. Albouy, C. Sanchez, *New J. Chem.* **2001**, *25*, 156.
[4] B. Moraru, G. Kickelbick, M. Batistella, U. Schubert, *J. Organomet. Chem.* in press.
[5] C. F. Campana, Y. Chen, V. W. Day, W. G. Klemperer, R. A. Sparks, *J. Chem. Soc., Dalton Trans.* **1996**, 691, and references cited therein.
[6] K. Watenpaugh, C. N. Caughlan, *J. Chem. Soc., Chem. Commun.* **1967**, 76.
[7] V. W. Day, T. A. Eberspacher, W. G. Klemperer, C. W. Park, F. S. Rosenberg, *J. Am. Chem. Soc.* **1991**, *113*, 8190.
[8] R. Schmid, A. Mosset, J. Galy, *J. Chem. Soc., Dalton Trans.* **1991**, 1999.
[9] I. Gautier-Luneau, A. Mosset, J. Galy, *Z. Kristallogr.* **1987**, *180*, 83; S. Doeuff, Y. Dromzee, F. Taulelle, C. Sanchez, *Inorg. Chem.* **1989**, *28*, 4439; S. Doeuff, Y. Dromzee, C. Sanchez, *C. R. Acad. Sci. Sect. 2* **1989**, *308*, 1409; I. Laaziz, A. Larbot, C. Guizard, J. Durand, L. Cot, *Acta Crystallogr., Sect. C* **1990**, *46*, 2332; U. Schubert, E. Arpac, W. Glaubitt, A. Helmerich, C. Chau, *Chem. Mater.* **1992**, *4*, 291; X. Lei, M. Shang, T. P. Fehlner, *Organometallics* **1996**, *15*, 3779; G. Kickelbick, U. Schubert, *Eur. J. Inorg. Chem.* **1998**, 159; R. Papiernik, L. G. Hubert-Pfalzgraf, J. Vaissermann, M. C. H. P. Goncalves, *J. Chem. Soc., Dalton Trans.* **1998**, 2285.
[10] T. J. Boyle, T. M. Alam, C. J. Tafoya, B. L. Scott, *Inorg. Chem.* **1998**, *37*, 5588.
[11] N. Steunou, F. Robert, K. Boubekeur, F. Ribot, C. Sanchez, *Inorg. Chim. Acta* **1998**, *279*, 144.

Received March 23, 2001
[I01106]

Complexes of Manganese, Iron, Zinc, and Molybdenum with a Superbasic Tris(guanidine) Derivative of Tris(2-ethylamino)amine (Tren) as a Tripod Ligand

Harald Wittmann,[a] Volker Raab,[a] Andrea Schorm,[a] Jörn Plackmeyer,[a] and Jörg Sundermeyer*[a]

Dedicated to Professor Herbert Roesky on the occasion of his 65th birthday

Keywords: Ligand design / N ligands / Tripodal ligands / Coordination chemistry / Manganese / Iron / Zinc / Molybdenum

The synthesis of the novel tripod ligand $N[CH_2CH_2N{=}C(NMe_2)_2]_3$, based on the tris(2-ethylamino)amine (tren) backbone and having a set of three superbasic tetramethylguanidine (TMG) donor atoms instead of the primary amine functionalities, is described. This ligand has been prepared by treating tren with the Vilsmeyer salt $[(Me_2N)_2CCl]Cl$ in the presence of triethylamine as an auxiliary base and NaOH. Complexes of manganese(II), iron(II), and zinc(II) as biologically relevant transition metal ions as well as of molybdenum(0) have been synthesized and spectroscopically and structurally characterized. The electrochemical properties of selected complexes have been studied.

Introduction

Peralkylguanidines belong to the strongest neutral organic bases known.[1] They are several orders of magnitude more basic than tertiary amines due to the excellent stabilization of the positive charge over their resonance-stabilized cations.[2] This trend is illustrated by the pK_{BH^+} values (MeCN) of the 1,2,2,6,6-pentamethylpiperidinium cation (18.62), the parent guanidinium cation (23.00), and the pentamethylguanidinium cation (25.00).[2c] Therefore, in aqueous media, guanidines exist almost exclusively in the protonated form.[3] Guanidines are currently attracting attention as anion receptors,[4] both in enzymes and in model systems. Due to their hydrophilic nature, they also play an important role in the mediation of solubility of natural products[5] and in the stabilization of protein conformations through hydrogen bonding.[5–7] However, surprisingly little is known about the coordination chemistry of guanidines. There is some indication that the guanidine functionality of arginine may play a role as a neutral donor towards various metal cations in the hydrophobic domains of cytochrome *c* enzymes and other such systems.[2,5,6,8] There have been a few reports on coordination compounds of monoguanidines $HN{=}C(NRR')_2$.[5,6,8,9] The first complexes of chelating bis(guanidine)s have recently been reported by Kuhn[10] and ourselves.[11a] We became interested in the coordination chemistry of bis-, tris-, and oligoguanidines because of the marked tendency of biguanides to stabilize unusually high oxidation states of metals, e.g. in Ag^{III} [12] and Ni^{III} [13] complexes (Scheme 1).

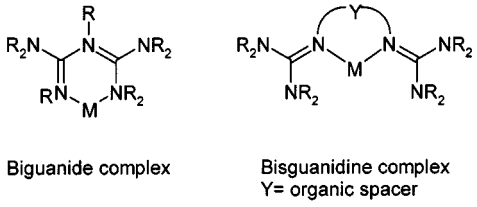

Scheme 1. Guanidine-based complexes

The focus of this investigation is the evaluation of the donor capabilities of tetradentate pentaalkylguanidine derivatives. The basicities of these neutral ligands are intermediate between those of tertiary amines and amido ligands, but the question remains as to how well they interact with Lewis acids. Indeed, the question arises as to whether, in addition to their strong σ-donor interaction sp^2-N→M, guanidines may also be π-acidic like Schiff bases or π-basic like amido ligands. Various aspects of guanidine coordination chemistry remain unexplored, such as the fine tuning of the basicity, donor strength, steric demand, and control of the solubility by variation of the substituents at the guanidine function. Following our study on guanidine derivatives of the tmeda and tame backbones,[11a] we wish to report our first results on the synthesis and coordination chemistry of guanidine derivatives of the tren ligand family (Scheme 2). The target molecule 1,1,1-tris{2-[N^2-(1,1,3,3-tetramethylguanidino)]ethyl}amine (**1**) (TMG_3tren) is structurally related to known Schiff bases,[14] tris(pyridylmethyl)amine (tmpa),[15] and other tripodal ligands[16] based on the well-known tren backbone (Scheme 2).

[a] Fachbereich Chemie, Philipps-Universität Marburg, Hans-Meerwein-Straße, 35032 Marburg, Germany
Fax: (internat.) + 49-6421/28-28917
E-mail: jsu@chemie.uni-marburg.de

 © WILEY-VCH Verlag GmbH, 69451 Weinheim, 2001 1434–1948/01/0808–1937 $ 17.50+.50/0

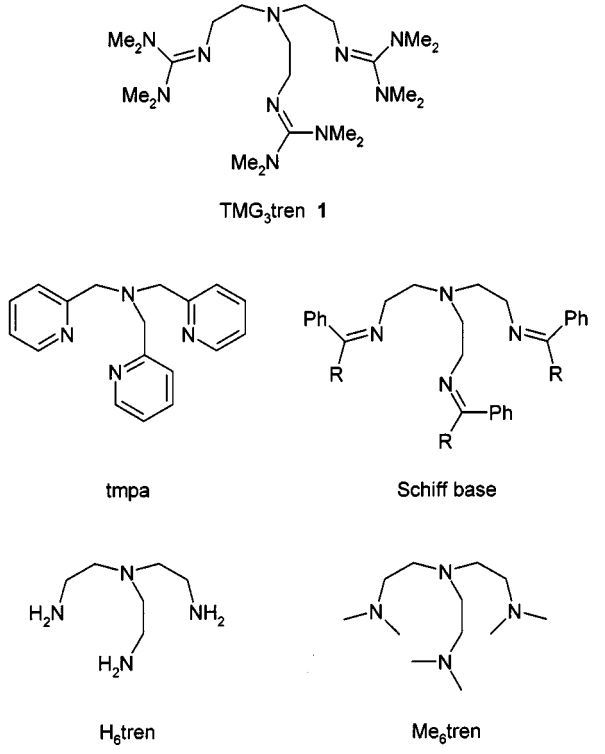

Scheme 2. Structural relationship between the target ligand **1** and known tripods of the tren ligand family

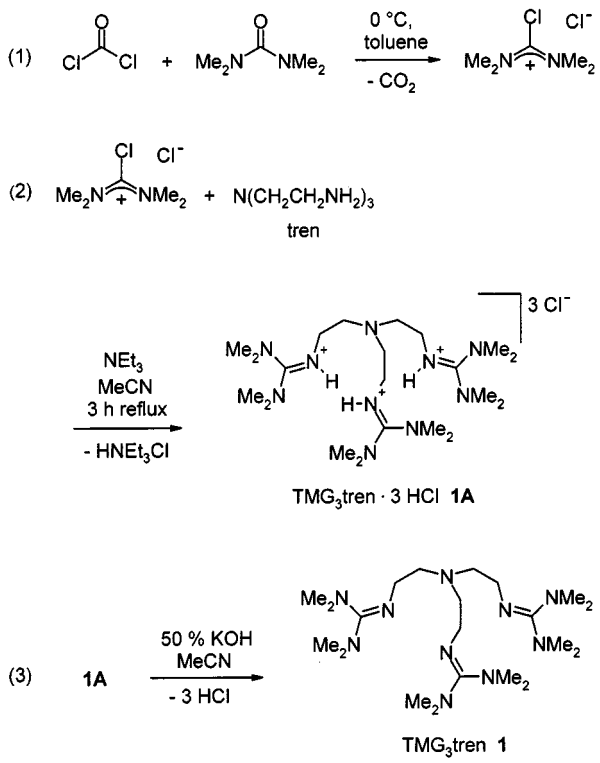

Scheme 3. Preparation of peralkylated oligoguanidines

Results and Discussion

Ligand Synthesis

The synthesis of the target ligand **1** was accomplished following our general procedure that allows the transformation of primary bis-, tris-, or polyamines into the corresponding tetramethylguanidino derivatives.[11] The main problem associated with this synthesis is that polyguanidines as well as their hydrochlorides are extremely hygroscopic. Typically, they cannot be distilled/sublimed without decomposition and may not be purified by column chromatography on polar phases (SiO_2, Al_2O_3). Because of these purification difficulties, it was imperative that the synthesis involved selective reactions. A nearly quantitative transformation of a primary amine functionality into the guanidine may be accomplished by reaction with the Vilsmeyer salt $[(Me_2N)_2CCl]Cl$, a method first described by Eilingsfeld and Seefelder[17] and later improved by Kantlehner et al.[18] for *mono*guanidines. The Vilsmeyer salt is obtained by reaction of tetramethylurea with phosgene[19] or oxalyl chloride in toluene.[20] Reaction of the latter with tren in the presence of triethylamine as an auxiliary base leads to the corresponding hydrochloride **1A** (Scheme 3). Separation from the by-product Et_3NHCl is accomplished by adding 1 equiv. of NaOH per guanidine functionality and removing the resulting Et_3N and NaCl by crystallization from acetonitrile/diethyl ether. In the present case, the free base **1** was obtained in an overall yield of up to 86% by deprotonation of the tris(hydrochloride) using a two-phase system of MeCN/50% aqueous KOH.

The spectroscopic features of the protonated ligand **1A** are very similar to those of the free guanidine base **1**. A difference can be seen in the IR spectra, where TMG_3tren shows a single absorption at $\nu(C{=}N) = 1620\ cm^{-1}$ while the corresponding absorption of the tris(hydrochloride) is split into two separate bands at 1627 and 1584 cm^{-1}. This splitting is a typical feature due the decreased molecular symmetry in guanidinium cations. It is also observed for the hexamethylguanidinium cation.[21] In order to avoid steric interactions, the Me_2N substituents adopt a mutually twisted propeller-like conformation[21,22] rather than a coplanar one. The UV/Vis spectrum of **1** in MeCN shows an absorption at 216 nm with a molar extinction coefficient ε of approximately $1{\cdot}10^4$ for each guanidinium unit, attributable to the $\pi{\rightarrow}\pi^*$ transition of the C=N bond.[23] The ^1H NMR spectrum of **1** features only one signal due to the methyl groups, while the ^{13}C NMR spectrum reveals the presence of two chemically non-equivalent methyl groups. It is known from the literature that the barrier to rotation about the C=N double bond of pentaalkylguanidines (Scheme 4) leading to a *syn-anti* isomerization[2b,24] is markedly lowered by protonation or by increased steric demand of the alkyl groups. The bulkiness of the tren backbone leads to a lower barrier, which is manifested in the equivalence seen in the ^1H NMR spectrum.

Scheme 4. The *syn-anti* isomerization of pentasubstituted guanidines

Synthesis of the Metal Complexes

The free guanidine base **1** is moderately stable in D_2O. Due to slow hydrolysis, tetramethylurea is formed over a period of several days by decomposition of the guanidinium hydroxide. In contrast, the hydrochloride **1A** is perfectly stable in D_2O. In order to avoid side reactions due to hydrolysis of the ligand and of the metal salts, the latter were dehydrated by the orthoester method[25] prior to complexation. The complexes were synthesized in good yields by combining the dehydrated metal salts with 1.05 equiv. of TMG_3tren (**1**) in dry acetonitrile and stirring for 30 min (Scheme 5). The resulting ionic complexes **2**–**5** proved to be soluble in polar aprotic media such as MeCN, CH_2Cl_2, or acetone, but insoluble in diethyl ether and hydrocarbons.

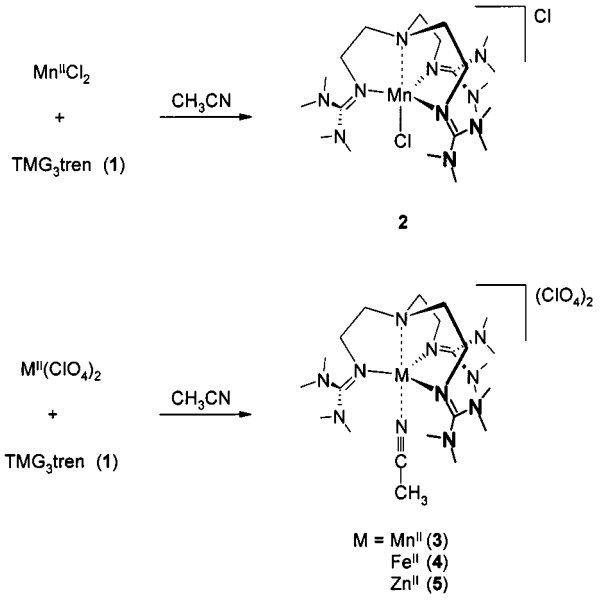

Scheme 5. Complexation of M^{2+} salts with TMG_3tren

The spectroscopic properties of the complexes resemble those of the protonated ligand (**1A**). For example, two IR absorptions are seen in the 1600 cm^{-1} region due to ν(C=N). The UV/Vis maxima are shifted 5–10 nm to lower wavelengths. While the zinc(II) complex (**5**) is diamagnetic, the manganese(II) (**2**, **3**) and iron(II) (**4**) complexes are paramagnetic with spin-only values of the order expected for d^5 and d^6 high-spin complexes[26] comparable to those of known complexes: μ_{eff}[Mn(Me_6tren)Br]Br: 6.01 B.M.; μ_{eff}[Fe(Me_6tren)Br]Br: 5.34 B.M.;[27] μ_{eff}[Mn(ntb)Cl]Cl [ntb = tris(2-benzimidazolylmethyl)amine]: 5.83 B.M.[28] Their magnetic susceptibilities, μ_{eff}(**2**): 5.9 B.M.; μ_{eff}(**3**): 5.8 B.M.; μ_{eff}(**4**): 5.4 B.M., all with an uncertainty of ±0.1, were determined by the Evans method.[29]

Attempts to prepare well-defined complexes of **1** with Fe^{III} and Mn^{III} salts have hitherto proved unsuccessful. It seems that, due to steric repulsion, the bite of the ligand is better matched with larger ions than with smaller, highly charged ions. This interpretation is in accordance with the electrochemical results discussed below, which reveal the rapid decomposition of the oxidized iron species.

The stabilities of compounds **2**–**5** towards hydrolysis were examined. All the complexes were found to be sensitive to air and moisture, despite the extreme steric shielding provided by the ligand. In general, it was observed that metal hydroxides along with the protonated ligand were formed when **2**–**5** were exposed to aqueous solvent mixtures. These findings may be explained by the extremely high proton affinity of guanidines. Deprotonation of an aqua ligand irreversibly induces the hydrolytic cleavage of the metal–nitrogen bond, a pattern that is also typical for amido complexes (Scheme 6).

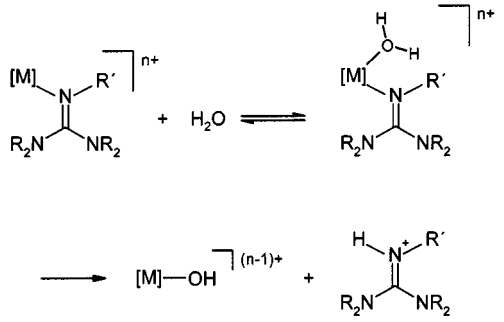

Scheme 6. Hydrolytic cleavage of the metal–nitrogen bond

Structural Characterization

Single crystals of all the ionic complexes suitable for X-ray crystallography were grown by slow diffusion of diethyl ether into acetonitrile solutions. The results of the structure analyses are presented in Figures 1–6, while selected bond lengths and angles are collected in Table 1 and parameters relating to the data collection and refinement are listed in Tables 7 and 8. Complexes **2** (Figures 1 and 2), **3** (Figure 3), **4** (Figure 4), and **5** (Figure 5) each possess a nearly C_3-symmetrical trigonal-bipyramidal molecular geometry, with the amine nitrogen atom located in one of the axial positions, and *N*-coordinated acetonitrile (**3**, **4**, **5**) or chloride ion (**2**) occupying the other.

The imino nitrogen atoms of the guanidine groups define the equatorial plane. The metal atom is slightly axially distorted from the equatorial plane towards the acetonitrile molecule. As is evident from Table 2, this deviation is accompanied by a change in the ionic radius of the metal center. It also has an effect on the bond lengths between the amine and guanidine nitrogen atoms and the metal ion, whereas the distance to the acetonitrile nitrogen atom remains essentially the same. Other compounds containing Mn, Fe, and Zn in similar tren ligand coordination spheres are included in the table in order to correlate our results.

Table 1. Selected bond lengths [pm] and bond angles [°] in complexes **2**−**6**, with standard deviations in parentheses

		$[Mn^{II}(TMG_3tren)Cl]Cl$ (**2**)			
Mn(1)−N(1)	218.2(2)	Mn(1)−N(4)	217.7(1)	Mn(1)−N(7)	219.1(2)
Mn(1)−N(10)	237.8(1)	Mn(1)−Cl(1)	243.0(1)		
av.(N_{eq}−Mn−N_{eq})	114.63(6)	av.(N_{ax}−Mn−N_{eq})	76.38(5)	N(10)−Mn(1)−Cl(1)	177.57(4)
		$[Mn^{II}(TMG_3tren)NCMe](ClO_4)_2$ (**3**)			
Mn(1)−N(2)	212.7(3)	Mn(1)−N(5)	214.8(3)	Mn(1)−N(8)	213.1(3)
Mn(1)−N(1)	232.8(3)	Mn(1)−N(11)	221.5(3)		
av.(N_{eq}−Mn−N_{eq})	115.79(11)	av.(N_{ax}−Mn−N_{eq})	78.00(10)	N(1)−Mn(1)−N(11)	175.64(11)
		$[Fe^{II}(TMG_3tren)NCMe](ClO_4)_2$ (**4**)			
Fe(1)−N(2)	207.3(3)	Fe(1)−N(5)	206.1(4)	Fe(1)−N(8)	208.4(4)
Fe(1)−N(1)	225.4(3)	Fe(1)−N(11)	215.1(4)		
av.(N_{eq}−Fe−N_{eq})	116.95(14)	av.(N_{ax}−Fe−N_{eq})	79.85(14)	N(1)−Fe(1)−N(11)	176.62(14)
		$[Zn^{II}(TMG_3tren)NCMe](ClO_4)_2$ (**5**)			
Zn(1)−N(2)	203.4(2)	Zn(1)−N(5)	203.4(2)	Zn(1)−N(8)	205.1(3)
Zn(1)−N(1)	226.9(2)	Zn(1)−N(11)	218.7(3)		
av.(N_{eq}−Zn−N_{eq})	117.46(10)	av.(N_{ax}−Zn−N_{eq})	80.74(9)	N(1)−Zn(1)−N(11)	177.25(9)
		$[Mo^0(TMG_3tren)(CO)_3]$ (**6**)			
Mo(1)−N(1)	235.4(2)	Mo(1)−N(2)	233.6(2)	Mo(1)−N(5)	231.9(2)
Mo(1)−C(22)	193.0(3)	Mo(1)−C(23)	192.4(3)	Mo(1)−C(24)	192.4(3)
N(2)−C(3)	131.7(3)	C(3)−N(3)	136.4(4)	C(3)−N(4)	137.7(4)
N(5)−C(10)	131.1(3)	C(10)−N(6)	137.2(4)	C(10)−N(7)	137.2(4)
N(8)−C(17)	127.6(4)	C(17)−N(9)	139.6(4)	C(17)−N(10)	137.8(4)
N(1)−Mo(1)−C(23)	175.64(10)	N(2)−Mo(1)−C(24)	174.64(10)	N(5)−Mo(1)−C(22)	167.41(10)

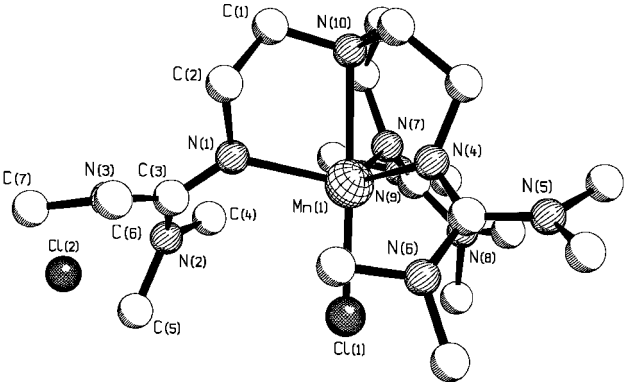

Figure 1. Molecular structure of **2**[44]

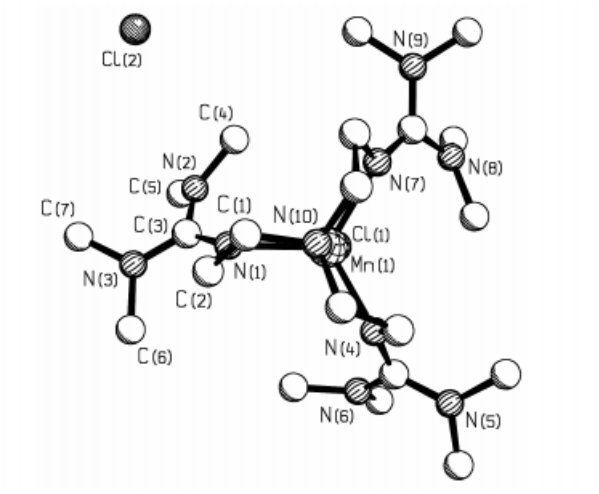

Figure 2. Molecular structure of $[Mn^{II}(TMG_3tren)Cl]Cl$ (**2**); SCHAKAL plot of a projection along the local C_3 axis[44]

However, an absolute comparison remains difficult because the ligand properties differ significantly, e.g. in terms of steric hindrance or considering the different neutral and anionic coligands, which lead to different effective charges at the metal atoms and hence to different bond lengths to the equatorial nitrogen atoms.[30]

Comparing complex **2**, which bears an anionic chloro ligand, with dicationic **3**, which has a neutral acetonitrile ligand instead, the increased contraction of the TMG_3tren ligand can be directly attributed to the higher effective charge at the metal center. As expected, the axial distortion decreases with decreasing ion radius of the central atom.

A comparison of **2** with $[Mn^{II}(Me_6tren)Br]Br$ [48] (**A**) as regards the relative donor abilities of the amine and guanidine ligands is made difficult by the different steric requirements of the two ligand regimes. In the case of **1**, steric repulsion is greatest at the periphery. Since donor ability incorporates both basicity and steric hindrance, the TMG_3tren ligand can be estimated to be superior to Me_6tren in its donor ability. The guanidine sp^2-nitrogen atom is much more basic than the amine sp^3-nitrogen atom of Me_6tren and is also sterically less hindered. The net result is that the average bond length between the equatorial guanidine nitrogen atoms and the metal center is much smaller (218 pm) than the corresponding amine−metal distance in $[Mn^{II}Br(Me_6tren)]Br$ (**A**) (227 pm). A stronger donor component of the equatorial guanidines is also consistent with the longer distance to the axial amine in **2** (238 pm) compared to that in the corresponding Me_6tren

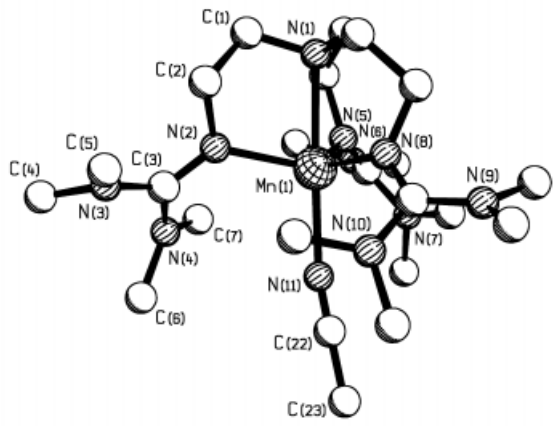

Figure 3. Molecular structure of **3**[44]

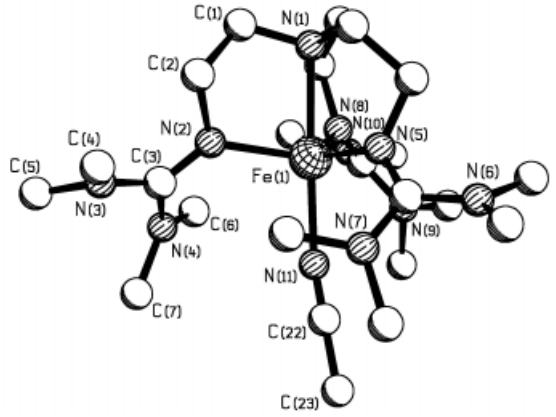

Figure 4. Molecular structure of **4**[44]

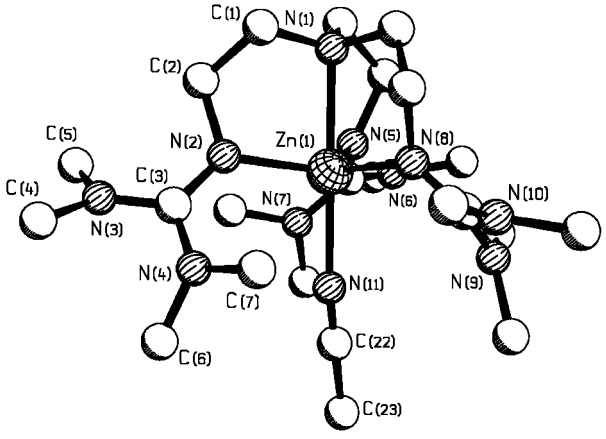

Figure 5. Molecular structure of **5**[44]

complex **A** (219 pm). In the latter donor−acceptor complex, the axial amine has to provide more electron density towards the overall charge compensation. As a consequence, the displacement of the manganese cation out of the equatorial plane is significantly greater in **2** (51 pm) compared to that in $[Mn^{II}(Me_6tren)Br]Br$ (**A**) (36 pm).

A characteristic structural feature of all the complexes **2**−**5** is shown in Figure 2. In order to reduce steric repulsion, the guanidine dimethylamino units are twisted by approximately 40° into a propeller-like conformation. The dimethylamino groups are not coplanar within the planar guanidine CN_3 unit but show out-of-plane torsion angles of 20−45° (Table 3). A similar distortion has been found for the hexamethylguanidinium cation in its ground state.[31]

In spite of these steric limitations to perfect π-conjugation in the outer ligand sphere, the superbasic tripod **1** efficiently stabilizes dicationic complexes by delocalizing the charge over the three perfectly planar guanidinium cations (sum of angles in representative **2**: see Table 5).

According to a CCDC search,[32] no structurally characterized complexes of iron and manganese with pentacoordination by five neutral N donor ligands have hitherto been reported. On the other hand, for d^{10} Zn^{2+},[33] Cd^{2+},[34] Ag^{+},[35] and d^9 Cu^{2+},[36] this coordination mode is more common. Just a few representatives involving the tren ligand or its *N*-methyl derivatives and an anionic ligand have been reported, for example the halide complexes of Di Vaira et al.[48] and Templeton et al.,[50] and the pseudohalide (OCN^- and SCN^-) complexes investigated by Laskowski and co-workers.[37]

The Question of π-Bonding Contributions of Guanidine Ligands

Because the C=N valence vibrations of coordinated guanidines do not seem to give a reliable measure of the donor and acceptor qualities of TMG_3tren, we set out to synthesize a complex containing CO as an indicator ligand for electronic interactions of the coligands. The tris(acetonitrile) complex $[Mo(CH_3CN)_3(CO)_3]$ was found to react cleanly with **1** to give compound **6** in 79% yield (Scheme 7). The IR spectrum of **6** features more than two ν(C=N) absorptions in the region 1515−1580 cm^{-1}, while in the ^{13}C NMR spectrum two resonances due to guanidine CN_3 moieties are observed. Complex **6** proved to be stable under atmospheric conditions for a short period of time, but ultimately turned from yellow to brown. It showed a similar sensitivity to oxidation in solution. While the TMG_3tren ligand is able to displace even an anionic chloro ligand from **2**, it is incapable of displacing more than three carbon monoxide ligands from $[Mo(CO)_6]$ or derivatives thereof. It bonds in a facial manner, leaving one guanidine functionality as a dangling arm. This may be taken as an indication that **1** is not a good π-acceptor, and furthermore that it is a ligand of constrained geometry, not being able to stabilize geometries other than trigonal-bipyramidal in its tripodal coordination mode. Figure 6 shows the results of an X-ray analysis of single crystals of **6** obtained from acetonitrile/diethyl ether.

The molecule of **6** exhibits local C_s symmetry in the crystalline state with a mirror plane defined by Mo, N(1), C(23), and C(24). The molybdenum atom is coordinated in a distorted octahedral manner. The inner ligand core is defined by three facial carbonyl ligands, one amine, and two guanidine ligands. One dangling guanidine arm points away from the inner core. The amine is bonded with a slightly longer Mo−N(1) distance [235.4(2) pm] than the two guanidines Mo−N(2) [233.6(2) pm] and Mo(1)−N(5) [231.9(2) pm]. However, this difference in bonding is not reflected in specific bonding differences of the *trans*-CO ligands. On the

Table 2. Ionic radii of Mn, Fe, and Zn; structural features of complexes **2**−**5** and literature counterparts

Complex	Metal atom	Ion radius[47] [pm]	Axial distortion[a] [pm]	d(M−N_{ax}) [pm]	d(M−N_{eq})[b] [pm]	d(M−L_{ax}) [pm]
A	$[L^1Mn^{II}-Br]^+$ [48]	89	36	219	227	249
A′	$[L^2Mn^{II}-Cl]^+$ [28]	89	63	252	216	236
B	$[L^1Fe^{II}-Br]^+$ [48]	85	32	221	215	248
C	$[L^1Zn^{II}-Br]^+$ [48]	82	27	219	211	245
C′	$[L^2Zn^{II}-Cl]^+$ [49]	82	64	248	205	225
C′′	$[L^3Zn^{II}-Cl]^+$ [50]	82	39	232	206	231
2	$[(\mathbf{1})Mn^{II}-Cl]^+$	89	51	237.8(1)	218.3(2)	243.0(1)
3	$[(\mathbf{1})Mn^{II}(NCMe)]^{++}$	89	44	232.8(3)	213.5(3)	221.5(3)
4	$[(\mathbf{1})Fe^{II}(NCMe)]^{++}$	85[c]	37	225.4(3)	207.3(4)	215.1(4)
5	$[(\mathbf{1})Zn^{II}(NCMe)]^{++}$	82	33	226.9(2)	204.0(2)	218.7(3)

[a] Distance of M from the equatorial plane defined by the three equatorial nitrogen atoms. − [b] Average distance of the three equatorial nitrogen atoms from the metal center. − [c] Average radius of Fe^{2+} for coordination numbers of 4 and 6 (high spin).[47] Standard deviations in parentheses. L^1 = Me_6tren, L^2 = tris(2-benzimidazolylmethyl)amine (ntb), L^3 = $_6$tren.

Table 3. Torsion angles [°] in complex $[Mn^{II}(TMG_3tren)Cl]Cl$ (**2**)

Mn(1)−N(1)−C(3)−N(2/3)	−42.7/140.3
N(1)−C(3)−N(2)−C(4/5)	−22.4/139.9
N(1)−C(3)−N(3)−C(6/7)	−40.6/147.2

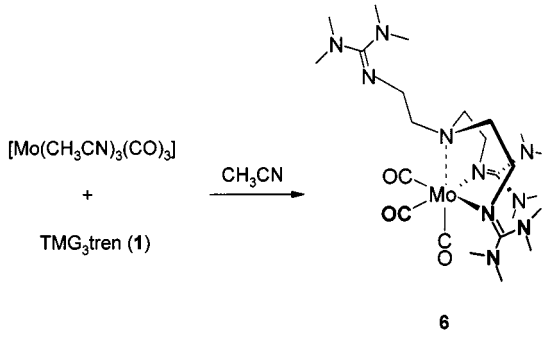

Scheme 7. Facial coordination of TMG_3tren to $[Mo(CO)_3]$ in **6**

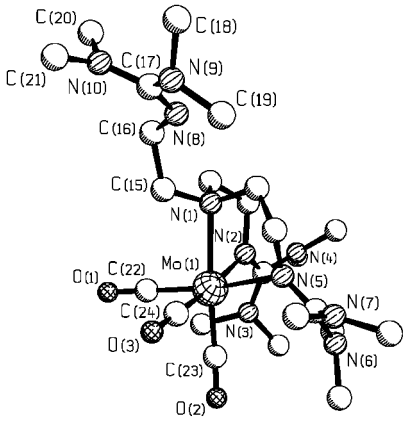

Figure 6. Molecular structure of **6**[48]

other hand, a comparison of the structural parameters of the closely related complexes **6** and $[Mo(CO)_3(dien)]$,[38] in which *cis*-diethylenetriamine (dien) acts as a pure σ-donor, indicates slightly stronger donation by the guanidine ligand. Back-donation in **6** is slightly stronger; the Mo−C bonds tend to be shorter and the C−O bonds tend to be slightly longer as compared to those in the amine complex $[Mo(CO)_3(dien)]$ (Table 4).

Table 4. Comparison of bond lengths in **6** and $[Mo(CO)_3(dien)]$; dien = *cis*-diethylenetriamine

	6	$[Mo(CO)_3(dien)]$[38]
av.(Mo−N_{amine}) [pm]	235.4	232.3
av.(Mo−N_{imine}) [pm]	232.7	−
av.(Mo−C) [pm]	192.6	194.3
av.(C−O) [pm]	117.8	115.3
av.(C−Mo−C) [°]	84.8	85.3

Carbonyl stretching frequencies are often used as an additional criterion for evaluating the donor/acceptor qualities of coligands. There is no clear trend when guanidine **6** (1883 cm^{-1}) is compared to complexes of amines that act as pure σ-donors such as $[Mo(CO)_3(tacn)]$ (1850 cm^{-1})[39] or $[Mo(CO)_3(dien)]$ (1887 cm^{-1}).[38] On the basis of structural and IR spectroscopic evidence, it appears that there is no π-interaction between the metal center and ligand **1**.

Finally, the comparison of C−N bond lengths in guanidines, guanidinium hydrochlorides, and guanidine complexes (Lewis acid adducts) allows us to estimate the extent of electron density donation to a proton or a Lewis acid, respectively. The greater the donation, the more the imino nitrogen−carbon bond length should become equivalent to the peripheral C−NMe_2 bond lengths. In the dangling guanidine group of **6**, a short C−$N_{guanidine}$ bond [127.6(4) pm] and two long bonds to the peripheral C−NMe_2 groups [139.6(4) and 137.8(4) pm] are observed. The differences between these three guanidine C−N bond lengths become much smaller when the guanidine is coordinated to a Lewis acid (e.g. **2**), and become negligible upon protonation as a result of complete charge delocalization (Table 5).

Cyclic Voltammetric Measurements

In order to gain additional information about the synthesized compounds, cyclic voltammetry experiments were carried out. A reversible $Mn^{+3/+2}$ couple could be observed for **2** ($E_{1/2}$ = +0.47 V, $\Delta E_{1/2}$ = 0.11 V, i_a/i_c = 1), along with

Table 5. Bond angle sums [°] and selected guanidine C−N distances [pm] in the non-coordinated guanidine of **6**, the coordinated guanidine in **2**, and the protonated guanidine in bis(tetramethylguanidino)ethane hydrochloride

		[Mo(TMG$_3$tren)(CO)$_3$] (**6**)			
Σ° N(8)	–	Σ° N(9/10)	344.5/358.8	Σ° C(17)	359.9
C(17)−N(8)	127.6(4)	C(17)−N(9)	139.6(4)	C(17)−N(10)	137.8(4)
		[Mn^{II}(TMG$_3$tren)Cl]Cl (**2**)			
Σ° N(1)	359.4	Σ° N(2/3)	357.8/359.6	Σ° C(3)	359.9
C(3)−N(1)	131.9(2)	C(3)−N(2)	135.5(2)	C(3)−N(3)	136.9(2)
		TMG$_2$en·2HCl[11a]			
Σ° N(3)	358.1	Σ° N(1/2)	359.9/359.9	Σ° C(5)	360.0
C(5)−N(3)	133.6(2)	C(5)−N(1)	134.2(2)	C(5)−N(2)	133.8(2)

an additional wave ($E_{1/2}$ = +0.92 V, $\Delta E_{1/2}$ = 0.22 V, i_a/i_c = 4) for the couple $Mn^{+4/+3}$. The latter was irreversible, pointing to rapid decomposition of the oxidized species (Figure 7).

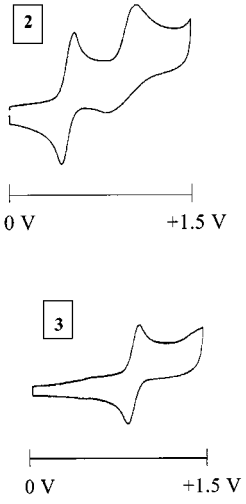

Figure 7. Cyclic voltammograms of **2** and **3** (CH_3CN/TBAP, 2 mm glassy carbon/SCE/Pt, v = 100 mV s^{-1}, 20 °C)

Complex **3** shows only a single wave in the anodic region at $E_{1/2}$ = +0.88 V ($\Delta E_{1/2}$ = 0.09 V, i_a/i_c = 1), corresponding to the reversible couple $Mn^{+3/+2}$. The $Mn^{II} \rightarrow Mn^{III}$ transition for compound **2** was found to occur at a lower oxidation potential than the corresponding step for **3** owing to the presence of the anionic chloro ligand, which facilitates the oxidation of **2**. The oxidation potential of $Mn^{III} \rightarrow Mn^{IV}$ does not lie within the window of 0 to 1.5 V.

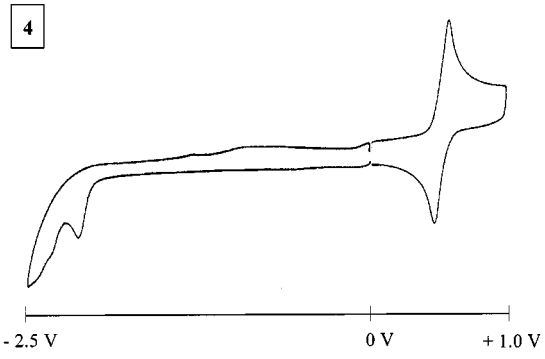

Figure 8. Cyclic voltammogram of **4** (CH_3CN/TBAP, 2 mm glassy carbon/SCE/Pt, v = 100 mV s^{-1}, 20 °C)

Complex **4** displays a potential of $E_{1/2}$ = +0.52 V ($\Delta E_{1/2}$ = 0.11 V) for the $Fe^{II} \rightarrow Fe^{III}$ electron transfer, i_a/i_c = 1 (Figure 8). The irreversible wave in the cathodic region (− 2.09 V) can only cautiously be assigned to an $Fe^{II} \rightarrow Fe^{I}$ reduction because of its low intensity and position near the border of the electrochemical window.

The values of the normal potentials can only be compared indirectly due to the different recording conditions (solvent, temperature) but can still be used to draw qualitative conclusions. All the complexes display lower oxidation potentials compared to the redox potentials of the aqua complexes Mn (II → III): +1.54 V; Fe (II → III): +0.77 V[40] as a result of the electron-donating TMG$_3$tren ligand. As expected, the monocationic complex **2** is more easily oxidized than the dicationic compound **3** (Table 6).

Table 6. Selected redox potentials

Metal complex	$E_{1/2}$[40] [V]
$[Mn(H_2O)_6]^{2+}$ (+3/+2)[a]	+1.54
[(**1**)Mn(NCMe)]$^{2+}$ (+3/+2)[b]	+0.88
[(**1**)Mn−Cl]$^{+}$ (+3/+2)[b]	+0.47
$[Fe(H_2O)_6]^{2+}$ (+3/+2)[a]	+0.77
[(**1**)Fe(NCMe)]$^{2+}$ (+3/+2)[b]	+0.52

[a] Recorded in H_2O. − [b] Recorded in MeCN.

Besides the inherent donor abilities of a given ligand, steric factors cannot be neglected with regard to the resulting oxidation potential and stability of the oxidized species.[41] This statement is related to the investigations of Ray[42] and Schrock,[43] who commented on the oxidation potentials of various transition metal complexes with tren-like amido ligands possessing varying degrees of steric strain. We believe that the instability of our oxidized complexes is due to the steric strain of the ligand periphery imposed by the reduced radius of the cation in its oxidized form.

Conclusions

Peralkyloligoguanidines are an unexplored class of multidentate nitrogen ligands within the large family of chelating N-donors typically containing amines, imines (Schiff bases), and azaaromatic building blocks. The novel tripod ligand TMG_3tren (**1**), a derivative of tren with three superbasic pentaalkylguanidine donor functions and a geometry constrained to coordinate metal ions preferably in a trigonal-bipyramidal mode, has been introduced. Due to its ability to delocalize positive charge over the three guanidinium moieties, **1** stabilizes cationic and even dicationic complexes, which are not so common for the corresponding parent compounds with tren ligands. However, increasing steric strain on the ligand periphery as a consequence of the decreased ionic radii of highly oxidized metal cations seems to limit the stability of such high-valent species. Initial evidence that larger cations are coordinated more favourably than smaller ones was provided by the bite angle and steric constraints of the tripodal ligand sphere of **1**. Our current interest is focused on the Lewis acid activation of small molecules other than acetonitrile and their transformations in the molecular pocket imposed by the guanidine ligand environment. Furthermore, we are extending our investigation of this class of ligands to other metals and other guanidine building blocks.

Experimental Section

Materials and Methods: All experiments were carried out in glassware that was assembled while hot and cooled under vacuum. Inert gas argon 4.8 was dried with granulated P_4O_{10}. Solvents were purified according to literature procedures and were also kept under an inert gas. Tris(2-aminoethyl)amine and the metal salts were used as purchased from Fluka. Triethylamine was freshly distilled and stored under argon prior to use. Substances sensitive to air and moisture were kept in a nitrogen-flushed glove-box (Braun, Type MB 150 BG-1). − Spectra were recorded with the following spectrometers: NMR: Bruker AM 400 (^{13}C: gated-decoupled). − IR: Bruker IFS 88 FT. − MS (EI, 70 eV): Varian MAT CH-7a. − Elemental analysis: Heraeus CHN-Rapid. − Melting points: Büchi MP B-540 apparatus (uncorrected values). − X-ray crystallography: Enraf−Nonius CAD4 and Siemens P4. − Magnetic susceptibility: Momentum apparatus, using the Evans method.[29]

Electrochemical Measurements: Cyclic voltammetry (CV) was performed with electrochemical equipment from AMEL (Milano) consisting of a Model 552 potentiostat, a Model 563 multipurpose unit, a Nicolet Model 3091 storage oscilloscope, and a Kipp & Zonen Model BD 90 x/y recorder. The electrochemical cell was operated under argon, with glassy carbon, platinum rod, and saturated calomel (SCE) serving as working, counter, and reference electrodes, respectively. For temperature control, the cell was immersed in a thermostatted cooling bath. CV curves were obtained at a scan rate of 100 mV s^{-1} working at 20 °C in MeCN/0.1 M nBu$_4$NClO$_4$.

Caution! Phosgene is a severe toxic agent that can cause pulmonary embolism and in cases of heavy exposure may be lethal. It should only be used in a well-ventilated fume hood. Perchlorate salts are potentially explosive and should be handled with care.

Chlorotetramethylformamidinium Chloride:[19] In a flask fitted with a reflux condenser cryostatted at −30 °C, phosgene was passed through a solution of tetramethylurea (50.00 g, 430 mmol) in toluene (200 mL) kept at 0 °C for 2 h. The phosgene inlet was then closed and the solution was allowed to warm to room temperature under stirring for a period of 24 h, with the reflux condenser being maintained at −30 °C. The precipitate formed was collected by filtration, washed three times with dry diethyl ether, and dried in vacuo. Yield ca. 95%.

1,1,1-Tris{2-[*N*^{2}-(1,1,3,3-tetramethylguanidino)]ethyl}amine (1): To a solution of tris(2-aminoethyl)amine (14.62 g, 100 mmol) and triethylamine (30.36 g, 41.6 mL, 300 mmol) in acetonitrile (50 mL), a solution of $[(Me_2N)_2CCl]Cl$ (51.32 g, 300 mmol) in acetonitrile (150 mL) was slowly added under cooling in an ice bath. After the exothermic reaction had occurred, the mixture was refluxed for 3 h, in the course of which a clear solution was produced. NaOH (12.00 g, 300 mmol) in water (30 mL) was subsequently added under vigorous stirring in order to deprotonate the Et_3NHCl. After evaporation of the solvents and excess NEt_3, TMG_3tren (**1**) was obtained by deprotonation of **1A** [tris(hydrochloride)] with 50% KOH (50 mL) and extracting the aqueous phase with MeCN (3 × 50 mL). The combined extracts were concentrated to dryness and the residue was taken up in warm hexane. The resulting solution was dried with $MgSO_4$, stirred with activated charcoal while still warm to eliminate impurities, and then filtered through Celite. Finally, removal of the solvent and drying of the residue in vacuo gave TMG_3tren (**1**) as a pale-yellow slowly crystallizing oil in 86% yield (38.03 g, 86 mmol). − M.p. 59−60 °C. − ^{1}H NMR (200.1 MHz, $CDCl_3$, 25 °C, $CDCl_3$): δ = 3.23 (m, 6 H, CH_2), 2.84−2.59 (m, 42 H, CH_2 + CH_3). − ^{13}C NMR (50.3 MHz, $CDCl_3$, 25 °C, $CDCl_3$): δ = 160.4 (CN_3), 58.2, 48.3 (CH_2), 39.6, 38.8 (CH_3). − IR (film): $\tilde{\nu}$ = 2880 s, 2839 sh, 1620 s [ν(C=N)], 1495 m, 1453 w, 1364 s, 1236 w, 1130 m, 1062 w, 989 w cm^{-1}. − UV/Vis (MeCN): λ_{max} (ε) = 216 nm (24000 mol^{-1} dm^3 cm^{-1}). − MS (70 eV, EI): *m/z* (%) = 439.0 (1) $[M - H]^+$, 312.0 (100) $[C_{15}H_{34}N_7]^+$, 210.0 (73) $[C_{11}H_{22}N_4]^+$, 142.0 (43) $[C_7H_{16}N_3]^+$, 128.0 (54) $[C_6H_{14}N_3]^+$, 85.0 (82) $[C_4H_9N_2]^+$, 72.0 (26) $[C_3H_8N_2]^+$, 58.0 (80) $[C_2H_6N_2]^+$. − $C_{21}H_{48}N_{10}$ (440.7): calcd. C 57.24, H 10.98, N 31.78; found C 56.87, H 10.83, N 31.45.

1,1,1-Tris{2-[*N*^{2}-(1,1,3,3-tetramethylguanidinium)]ethyl}amine Trichloride (1A; 1·3HCl): The hydrochloride salt could be obtained by treating the free oligoguanidine base (0.57 g, 1.13 mmol) dissolved in EtOH (10 mL) with the requisite amount of 1 M HCl (3.5 mL). Recrystallization from EtOH/Et_2O gave strongly hygroscopic, colorless crystals that analyzed as the trihydrate. Yield 0.51 g (0.84 mmol, 74%). Following our synthesis of **1**, the TMG_3tren tris(hydrochloride) **1A** could also be obtained without isolation of the free base. After deprotonation of Et_3NHCl with an equimolar amount of NaOH dissolved in the minimum volume of water and removing all volatiles in vacuo, the crude tris(hydrochloride) was redissolved in warm MeCN. The resulting solution was dried with $MgSO_4$, treated with activated charcoal, passed through Celite, and the solvent was evaporated. The residue was washed with dry diethyl ether and dried in vacuo to yield the tris(hydrochloride) **1A** as a colorless, strongly hygroscopic solid that analyzed as the trihydrate. − M.p. 153 °C (dec.). − ^{1}H NMR (200.1 MHz, CD_3CN, 25 °C, CD_3CN): δ = 8.91 (br. s, 3 H, NH), 3.76 (br., 12 H, CH_2), 2.92 (s, 36 H, CH_3), 2.55 (br., 6 H, H_2O). − ^{13}C NMR (50.3 MHz, CD_3CN, 25 °C, CD_3CN): δ = 161.3 (CN_3), 51.7 (CH_2), 39.5 (CH_3), 39.3 (CH_2). − IR (KBr): $\tilde{\nu}$ = 3431 s, 1627 s, 1584 s [ν(C=N)], 1457 m, 1406 s, 1311 w, 1233 w, 1176 w, 1136 w, 1067 w, 900 m, 668 br cm^{-1}. − UV/Vis (H_2O): λ_{max} (ε) = 213 nm (34000 mol^{-1} dm^3

cm^{-1}). − MS (70 eV, EI): *m/z* (%) = 440.0 (1) $[M - 3\,HCl]^+$, 312.0 (95) $[C_{15}H_{34}N_7]^+$, 255.0 (28) $[C_{12}H_{27}N_6]^+$, 222.0 (17) $[C_{10}H_{18}N_6]^+$, 210.0 (67) $[C_{11}H_{22}N_4]^+$, 197.0 (28) $[C_{10}H_{21}N_4]^+$, 142.0 (91) $[C_7H_{16}N_3]^+$, 128.0 (94) $[C_6H_{14}N_3]^+$, 97.0 (45) $[C_6H_{11}N]^+$, 85.0 (94) $[C_4H_9N_2]^+$, 71.0 (64) $[C_3H_7N_2]^+$, 58.0 (95) $[C_2H_6N_2]^+$, 36.0 (100) $[HCl]^+$. − $C_{21}H_{51}Cl_3N_{10}\cdot 3H_2O$ (604.1): calcd. C 41.75, H 9.51, N 23.19; found C 41.69, H 9.86, N 22.83.

General Procedure for the Synthesis of the TMG_3tren Complexes: The metal salts were first dehydrated by the orthoester method.[25] Thus, the hydrated salts were stirred in dry EtOH containing twice the molar amount, with respect to the water present in the salt, of triethyl orthoformate at 60 °C for 1 h. Equimolar amounts of the dehydrated metal salt and **1** were separately dissolved in 5-mL portions of dry MeCN under argon. These solutions were then combined and the resulting mixture was stirred for 30 min. at 40−50 °C, filtered through Celite, and concentrated to a volume of ca. 3 mL. The complex was then precipitated by the addition of dry diethyl ether (10 mL), washed with absolute diethyl ether, and dried in vacuo. Single crystals suitable for X-ray analysis could be grown by slow diffusion of diethyl ether into the respective acetonitrile solutions.

Chloro{1,1,1-tris[N^2-(1,1,3,3-tetramethylguanidino)ethyl]amine}manganese(II) Chloride (2): The general procedure was followed using $MnCl_2$ (0.15 g, 1.12 mmol) and **1** (0.66 g, 1.15 mmol). Yield 0.59 g (1.04 mmol, 93%) as colorless crystals. − M.p. 230 °C (dec.). − IR (KBr): $\tilde{\nu}$ = 2947 m, 2881 m, 1618 s, 1573 s [ν(C=N)], 1553 vs, 1427 m, 1395 m, 1342 w, 1164 sh, 1151 s, 1075 m, 891 m, 764 m cm^{-1}. − UV/Vis (MeCN): λ_{max} (ε) = 226 nm (49000 mol^{-1} dm^3 cm^{-1}). − MS (70 eV, EI): *m/z* = 312.0 (60) $[C_{15}H_{34}N_7]^+$, 210.0 (33) $[C_{11}H_{22}N_4]^+$, 142.0 (32) $[C_7H_{16}N_3]^+$, 128.0 (43) $[C_6H_{14}N_3]^+$, 85.0 (100) $[C_4H_9N_2]^+$, 71.0 (31) $[C_3H_7N_2]^+$, 58.0 (74) $[C_2H_6N_2]^+$, 28.0 (80) $[CH_2N]^+$. − μ_{eff} (Evans method, 5% [D6]benzene in CD_3CN, 25 °C): μ_B/mol = 5.9±0.1. − CV (MeCN/TBAP, 2 mm GC/SCE/Pt, *v* = 100 mV s^{-1}, 20 °C): $E_{1/2}(+3/+2)$ = 0.47 V, $\Delta E_{1/2}(+3/+2)$ = 0.11 V, $I_{pa/pc}$ = 1; $E_{1/2}(+4/+3)$ = 0.92 V, $\Delta E_{1/2}(+4/+3)$ = 0.22 V, $I_{pa/pc}$ = 4. − $C_{21}H_{48}Cl_2MnN_{10}$ (566.5): calcd. C 44.52, H 8.54, N 24.72; found C 44.06, H 8.53, N 23.73.

Acetonitrile(1,1,1-tris{2-[N^2-(1,1,3,3-tetramethylguanidino)]-ethyl}amine)manganese(II) Diperchlorate (3): The general procedure was followed using $Mn(ClO_4)_2$ (0.47 g, 1.86 mmol) and **1** (0.84 g, 1.90 mmol). Yield 1.30 g (1.77 mmol, 95%) as colorless crystals. − IR (KBr): $\tilde{\nu}$ = 2893 m, 2275 w [ν(C≡N)], 1616 sh, 1565 vs, 1535 s [ν(C=N)], 1463 m, 1427 m, 1398 s, 1346 w, 1257 w, 1164 m, 1092 vs [ν(Cl=O)], 906 w, 892 w, 769 m, 624 s cm^{-1}. − MS (70 eV, EI): *m/z* (%) = 128.0 (24) $[C_6H_{14}N_3]^+$, 85.0 (100) $[C_4H_9N_2]^+$, 71.0 (25) $[C_3H_7N_2]^+$, 44.0 (46) $[C_2H_6N]^+$. − μ_{eff} (Evans method, 5% [D6]benzene in CD_3CN, 25 °C): μ_B/mol = 5.8±0.1. − CV (MeCN/TBAP, 2 mm GC/SCE/Pt, *v* = 100 mV s^{-1}, 20 °C): $E_{1/2}(+3/+2)$ = 0.88 V, $\Delta E_{1/2}(+3/+2)$ = 0.09 V, $I_{pa/pc}$ = 1. − $C_{23}H_{51}Cl_2MnN_{11}O_8$ (735.6): calcd. C 37.56, H 6.99, N 20.95; found C 37.42, H 6.95, N 20.62

Table 7. Crystal data and details of the structure refinement for **2**, **3**, and **4**

Complex	$[Mn^{II}(TMG_3tren)Cl]Cl$ (**2**)	$[Mn^{II}(TMG_3tren)NCMe](ClO_4)_2$ (**3**)	$[Fe^{II}(TMG_3tren)NCMe](ClO_4)_2$ (**4**)
Empirical formula	$C_{21}H_{48}Cl_2MnN_{10}$	$C_{23}H_{51}Cl_2MnN_{11}O_8$	$C_{23}H_{51}Cl_2FeN_{11}O_8$
Molecular mass [g mol^{-1}]	607.59	735.59	736.50
Temperature [K]	223(2)	198(2)	198(2)
Crystal system	triclinic	monoclinic	monoclinic
Space group	$P\bar{1}$	$P2_1/c$	$P2_1/c$
a [pm]	1174.6(3)	1619.1(1)	1614.4(1)
b [pm]	1227.4(2)	1333.6(1)	1329.3(1)
c [pm]	1298.1(2)	1651.1(1)	1641.7(1)
α [°]	92.451(9)	90	90
β [°]	96.182(10)	94.669(10)	94.460(10)
γ [°]	117.907(10)	90	90
Volume [Å^3]	1635.1(5)	3553.1(5)	3512.7(4)
Z	2	4	4
ρ [Mg m^{-3}]	1.234	1.375	1.393
μ [mm^{-1}]	0.598	0.580	0.640
F(000)	650	1556	1560
Crystal size [mm]	0.40 × 0.30 × 0.20	0.39 × 0.33 × 0.15	0.28 × 0.21 × 0.10
Diffractometer	Siemens P4	Enraf Nonius CAD4	Enraf Nonius CAD4
Scan technique	ω-scan	ω-scan	ω-scan
θ range for data collection [°]	1.89−27.71	2.48−24.99	3.06−24.98
Index ranges	$0 \le h \le 13$	$0 \le h \le 19$	$-19 \le h \le 0$
	$-14 \le k \le 14$	$0 \le k \le 15$	$-15 \le k \le 0$
	$-14 \le l \le 14$	$-19 \le l \le 19$	$-19 \le l \le 19$
Reflections collected	5996	6462	6379
Independent reflections	5720	6227	6150
R_{int}	0.0461	0.0169	0.0309
Observed reflections [$F \ge 4\sigma(F)$]	5230	5272	3741
Data/restraints/parameters	5720/0/366	6227/0/430	6150/0/430
Goodness of fit on F^2	1.033	1.106	1.032
*R*1 [$F_0 \ge 4\sigma(F)$][a]	0.0327	0.0487	0.0599
wR_2 (all data)[a]	0.0916	0.1655	0.1490
Transmission (min./max.)	0.8898/0.7959	0.9181/0.0855	0.9388/0.8412
Largest diff. peak and hole [eÅ^{-3}]	0.364/−0.316	0.532/−0.448	0.529/−0.364

[a] $R_1 = \Sigma||F_o| - |F_c||/\Sigma|F_o|$; $wR_2 = \{\Sigma[w(F_o^2 - F_c^2)^2]/\Sigma[w(F_o^2)^2]\}^{1/2}$.

Acetonitrile(1,1,1-tris{2-[N^2-(1,1,3,3-tetramethylguanidino)]ethyl}amine)iron(II) Diperchlorate (4): The general procedure was followed using $Fe(ClO_4)_2$ (0.32 g, 1.26 mmol) and **1** (0.57 g, 1.30 mmol). Yield 0.83 g (1.13 mmol, 89%) as light-yellow crystals. − IR (KBr): $\tilde{\nu}$ = 2893 m, 2270 w [ν(C≡N)], 1614 sh, 1558 vs, 1533 sh [ν(C=N)], 1463 m, 1427 m, 1399 s, 1346 m, 1257 w, 1166 m, 1090 vs [ν(Cl=O)], 908 w, 894 m, 772 m, 623 s cm^{-1}. − μ_{eff} (Evans method, 5% [D_6]benzene in CD_3CN, 25 °C): μ_B/mol = 5.4±0.1. − CV (MeCN/TBAP, 2 mm GC/SCE/Pt, v = 100 mV s^{-1}, 20 °C): $E_{1/2}(+3/+2)$ = 0.52 V, $\Delta E_{1/2}(+3/+2)$ = 0.11 V, $I_{pa/pc}$ = 1, $E_{1/2}(+2/+1)$ = −2.09 V. − $C_{23}H_{51}Cl_2FeN_{11}O_8$ (736.5): calcd. C 37.51, H 6.98, N 20.92; found C 36.90, H 7.03, N 20.52.

Acetonitrile(1,1,1-tris{2-[N^2-(1,1,3,3-tetramethylguanidino)]ethyl}amine)zinc(II) Diperchlorate (5): The general procedure was followed using $Zn(ClO_4)_2$ (0.41 g, 1.54 mmol) and **1** (0.71 g, 1.60 mmol). Yield 0.96 g (1.29 mmol, 84%) as colorless crystals. − ^{1}H NMR (200.1 MHz, $CDCl_3$, 25 °C, $CDCl_3$): δ = 3.02−2.77 (br. m, 48 H, CH_3 + CH_2), 2.04 (s, 3 H, $NCCH_3$). − ^{13}C NMR (50.3 MHz, $CDCl_3$, 25 °C, $CDCl_3$): δ = 165.9 (CN_3), 53.8 (CH_2), 46.6 (CH_2), 39.3 (CH_3). − IR (KBr): $\tilde{\nu}$ = 2948 w, 2894 w, 2251 w [ν(C≡N)], 1620 sh, 1571 s, 1555 s [ν(C=N)], 1463 w, 1427 m, 1398 s, 1348 w, 1250 w, 1165 m, 1146 m, 1096 vs [ν(Cl=O)], 894 w, 766 w, 625 m cm^{-1}. − MS (70 eV, EI): m/z (%) = 85.0 (100) $[C_4H_9N_2]^+$, 71.0 (33) $[C_3H_7N_2]^+$, 44.0 (60) $[C_2H_6N]^+$. − $C_{23}H_{51}Cl_2N_{11}O_8Zn$ (746.0): calcd. C 37.03, H 6.89, N 20.65; found C 36.88, H 7.09, N 20.53.

Tricarbonyl(*fac*-tris{2-[N^2-(1,1,3,3-tetramethylguanidino)]ethyl}amine)molybdenum(0) (6): The general procedure was followed using $[Mo(CH_3CN)_3(CO)_3]$ (0.42 g, 1.40 mmol) and **1** (0.88 g, 2.00 mmol). Yield 0.69 g (1.11 mmol, 79%) as a yellow powder. − ^{1}H NMR (300.1 MHz, CD_3CN, 25 °C, CD_3CN): δ = 3.50 (m, 2 H, CH_2), 3.16 (m, 6 H, CH_2), 2.70 (m, 40 H, CH_3 + CH_2). − ^{13}C NMR (75.5 MHz, CD_3CN, 25 °C, CD_3CN): δ = 232.7, 230.1 (CO), 166.5 (CN_3, coordinated TMG), 160.8 (CN_3, free TMG), 66.1, 57.2, 50.7, 46.2 (CH_2), 39.8, 39.3 (CH_3). − IR (KBr): $\tilde{\nu}$ = 2889 s, 1883 s, 1740 vs, 1730 sh [ν(C=O)], 1619 s, 1577 s, 1553 sh, 1515 s [ν(C=N)], 1455 m, 1424 w, 1390 s, 1236 m, 1142 m, 1060 w, 1026 w, 976 w, 895 w, 763 w cm^{-1}. − MS (70 eV, EI): m/z (%) = 621.0 (1) $[M]^+$, 594.0 (2) $[M - CO]^+$, 312.0 (98) $[C_{15}H_{34}N_7]^+$, 255.0 (17) $[C_{11}H_{25}N_7]^+$, 210.0 (52) $[C_{11}H_{22}N_4]^+$, 142.0 (60) $[C_7H_{16}N_3]^+$, 128.0 (64) $[C_6H_{14}N_3]^+$, 101.0 (40) $[C_5H_{13}N_2]^+$, 85.0 (96) $[C_4H_9N_2]^+$, 72.0 (53) $[C_3H_8N_2]^+$, 58.0 (100) $[C_2H_6N_2]^+$, 44.0 (37) $[C_2H_6N]^+$, 28.0 (72) $[CH_2N]^+$. − $C_{21}H_{48}MoN_{10}O_3$ (620.7): calcd. C 46.45, H 7.80, N 22.57; found C 45.89, H 8.07, N 22.29.

X-ray Structure Analysis: Crystal data and experimental conditions are listed in Tables 7 and 8. The molecular structures are illustrated as SCHAKAL[44] plots in Figures 1−6. Selected bond lengths and angles with standard deviations in parentheses are presented in Table 1. Intensity data were collected with graphite-monochromated Mo-K_α radiation (λ = 71.069 pm). The collected reflections were corrected for Lorentz and polarization effects. The structures

Table 8. Crystal data and details of the structure refinement for **5** and **6**

Complex	$[Zn^{II}(TMG_3tren)NCMe](ClO_4)_2$ (**5**)	$[Mo^0(TMG_3tren)(CO)_3]$ (**6**)
Empirical formula	$C_{23}H_{51}Cl_2N_{11}O_8Zn$	$C_{21}H_{48}MoN_{10}O_3$
Molecular mass [g mol^{-1}]	746.02	661.72
Temperature [K]	193(2)	223(2)
Crystal system	monoclinic	triclinic
Space group	$P2_1/c$	$P\bar{1}$
a [pm]	1618.2(10)	1006.0(2)
b [pm]	1320.4(9)	1259.5(2)
c [pm]	1634.3(6)	1529.3(2)
α [°]	90	66.470(12)
β [°]	94.63(4)	75.237(9)
γ [°]	90	76.840(15)
Volume [Å^3]	3481(3)	1700.3(5)
Z	4	2
ρ [Mg m^{-3}]	1.424	1.292
μ [mm^{-1}]	0.918	0.429
F(000)	1576	700
Crystal size [mm]	0.25 × 0.25 × 0.25	0.45 × 0.35 × 0.25
Diffractometer	Enraf Nonius CAD4	Siemens P4
Scan technique	ω-scan	ω-scan
θ range for data collection [°]	2.30−26.01	1.78−25.04
Index ranges	$-19 \le h \le 19$	$0 \le h \le 11$
	$-16 \le k \le 0$	$-13 \le k \le 13$
	$0 \le l \le 20$	$-14 \le l \le 14$
Reflections collected	7086	5789
Independent reflections	6834	5483
R_{int}	0.0194	0.0281
Observed reflections [$F \ge 4\sigma(F)$]	5251	4982
Data/restraints/parameters	6834/0/418	5483/0/403
Goodness of fit on F^2	1.038	1.010
$R1$ [$F_0 \ge 4\sigma(F)$][a]	0.0418	0.0334
wR_2 (all data)[a]	0.1192	0.0907
Transmission (min./max.)	0.8030/0.8030	0.9004/0.8305
Largest diff. peak and hole [eÅ^{-3}]	0.595/−0.537	0.722/−0.619

[a] $R_1 = \Sigma||F_o| - |F_c||/\Sigma|F_o|$; $wR_2 = \{\Sigma[w(F_o^2 - F_c^2)^2]/\Sigma[w(F_o^2)^2]\}^{1/2}$.

of **2**, **5**, and **6** were solved by direct methods and refined by full-matrix least-squares methods on F^2, while those of **3** and **4** were solved using SIR-92.[45] Hydrogen atom positions were calculated and isotropically refined except for those of H23A, B, C of **3** and **4**, which were found and then isotropically refined. An empirical absorption correction based on the ψ-scans of 9 reflections (T_{min} = 0.4508, T_{max} = 0.5098) was performed for **4**.[46]

Acknowledgments

Financial support from the Deutsche Forschungsgemeinschaft, the Fonds der Chemischen Industrie, BASF AG Ludwigshafen, Dr. A. Hettche, and Dr. A. Oftring is gratefully acknowledged. We thank Prof. Ch. Elschenbroich for his kind support and for discussions with regard to the CV measurements.

[1] [1a] G. Wieland, G. Simchen, *Liebigs Ann. Chem.* **1985**, 2178−2193. − [1b] D. H. R. Barton, J. D. Elliot, S. D. Géro, *J. Chem. Soc., Perkin Trans. 1* **1982**, 2085−2090. − [1c] D. H. R. Barton, J. K. Kervagoret, S. Z. Zard, *Tetrahedron* **1990**, *46*, 7587−7598.

[2] [2a] P. A. S. Smith, in: *The Chemistry of Open-Chain Organic Nitrogen Compounds*, vol. 1, W. A. Benjamin, Inc. New York, **1965**, pp. 277−290. − [2b] Y. Yamamoto, S. Kojima, in: *The Chemistry of Amidines and Imidates*, vol. 2, J. Wiley & Sons, Chichester, **1991**, pp. 485−526. − [2c] R. Schwesinger, *Nachr. Chem. Tech. Lab.* **1990**, *38*, 1214−1226.

[3] H. Dugas, C. Penney, in: *Bioorganic Chemistry*, Springer, New York, **1981**, p. 15.

[4] Representative examples: [4a] M. S. Muche, M. W. Göbel, *Angew. Chem.* **1996**, *108*, 2263−2265; *Angew. Chem. Int. Ed. Engl.* **1996**, *35*, 2126−2129 and references cited therein. − [4b] G. Deslongchamps, A. Galán, J. de Mendoza, J. Rebek, Jr., *Angew. Chem. Int. Ed. Engl.* **1992**, *31*, 61−63 and references cited therein.

[5] E. M. A. Ratilla, B. K. Scott, M. S. Moxness, N. M. Kostic, *Inorg. Chem.* **1990**, *29*, 918−926.

[6] [6a] A. Hessler, O. Stelzer, H. Dibowski, K. Worm, F. P. Schmidtchen, *J. Org. Chem.* **1997**, *62*, 2362−2369. − [6b] F. P. Schmidtchen, M. Berger, *Chem. Rev.* **1997**, *97*, 1609−1646.

[7] [7a] P. D. Beer, D. K. Smith, *Prog. Inorg. Chem.* **1997**, *46*, 1−96. − [7b] J. S. Albert, M. W. Peczuh, A. D. Hamilton, *Bioorg. Med. Chem.* **1997**, *5*, 1455−1467. − [7c] C. Schmuck, *Chem. Eur. J.* **2000**, *6*, 709−718.

[8] [8a] E. M. A. Ratilla, N. M. Kostic, *J. Am. Chem. Soc.* **1988**, *110*, 4427−4428. − [8b] A. E. Przybyla, J. Robbins, N. Menon, H. D. Peck, Jr., *FEMS Microbiol. Rev.* **1992**, *88*, 109−136. − [8c] D. P. Fairlie, W. G. Jackson, B. W. Skelton, H. Wen, A. H. White, W. A. Wickramasinghe, T. C. Woon, H. Taube, *Inorg. Chem.* **1997**, *36*, 1020−1028.

[9] [9a] R. Longhi, R. S. Drago, *Inorg. Chem.* **1965**, *4*, 11−14. − [9b] R. Snaith, K. Wade, B. K. Wyatt, *J. Chem. Soc. A* **1970**, 380−383. − [9c]R. C. Mehrotra, in: *Comprehensive Coordination Chemistry*, vol. 2, Pergamon, Oxford, **1987**, pp. 269−291. − [9d]N. de Vries, C. E. Costello, A. G. Jones, A. Davison, *Inorg. Chem.* **1990**, *29*, 1348−1352. − [9e] W. P. Fehlhammer, R. Metzner, W. Sperber, *Chem. Ber.* **1994**, *127*, 829−833. − [9f] P. J. Bailey, K. J. Grant, S. Pace, S. Parsons, L. J. Stewart, *J. Chem. Soc., Dalton Trans.* **1997**, 4263−4266. − [9g] W. Schneider, A. Bauer, A. Schier, H. Schmidbaur, *Chem. Ber./Recueil* **1997**, *130*, 1417−1422.

[10] N. Kuhn, M. Grathwohl, M. Steimann, G. Henkel, *Z. Naturforsch., B* **1998**, *53*, 997−1003.

[11] [11a] H. Wittmann, A. Schorm, J. Sundermeyer, *Z. Anorg. Allg. Chem.* **2000**, *626*, 1583−1590. − [11b] H. Wittmann, Ph. D. thesis, Philipps-Universität Marburg, **1999**.

[12] M. L. Simms, J. L. Atwood, D. A. Zatko, *J. Chem. Soc., Chem. Commun.* **1973**, 46.

[13] D. Sen, C. Saha, *J. Chem. Soc., Dalton Trans.* **1976**, 776.

[14] S. Djebbar-Sid, O. Benali-Baitich, J. P. Deloume, *Transition Met. Chem.* **1998**, *23*, 443−447.

[15] [15a] Y. Gultneh, A. Farooq, K. D. Karlin, S. Liu, J. Zubieta, *Inorg. Chim. Acta* **1993**, *211*, 171−175. − [15b] S. Fox, A. Nanthakumar, M. Wikstrom, K. D. Karlin, N. J. Blackburn, *J. Am. Chem. Soc.* **1996**, *118*, 24−34. − [15c] T. D. Ju, R. A. Ghiladi, D.-H. Lee, G. P. F. Van Strijdonck, A. S. Woods, R. J. Cotter, V. G. Young, K. D. Karlin, *Inorg. Chem.* **1999**, *38*, 2244−2245.

[16] [16a] M. Pascaly, M. Duda, A. Rompel, B. H. Shift, W. Meyer-Klaucke, B. Krebs, *Inorg. Chem.* **1999**, *291*, 289. − [16b] M. Duda, M. Pascaly, B. Krebs, *Chem. Commun.* **1997**, 835.

[17] [17a] H. Eilingsfeld, M. Seefelder, H. Weidinger, *Angew. Chem.* **1960**, *72*, 836−845. − [17b] H. Eilingsfeld, G. Neubauer, M. Seefelder, H. Weidinger, *Chem. Ber.* **1964**, *97*, 1232−1245.

[18] W. Kantlehner, E. Haug, W. W. Mergen, P. Speh, T. Maier, J. J. Kapassakalidis, H.-J. Bräuner, H. Hagen, *Liebigs Ann. Chem.* **1984**, 108−126.

[19] I. A. Cliffe, in: *Comprehensive Organic Functional Group Transformations*, vol. 6, Elsevier Science Ltd., Oxford, **1987**, pp. 639−675.

[20] R. Knorr, A. Trzeciak, W. Bannwarth, D. Gillessen, *Tetrahedron Lett.* **1989**, *30*, 1927−1930.

[21] [21a] A. J. Papa, *J. Org. Chem.* **1966**, *31*, 1426−1430. − [21b] W. Petz, *J. Organomet. Chem.* **1975**, *90*, 223−226.

[22] A. V. Santoro, G. Mickevicius, *J. Org. Chem.* **1979**, *44*, 117−120.

[23] M. Hesse, H. Meier, B. Zeeh, in: *Spektoskopische Methoden in der organischen Chemie*, 4th ed., Thieme, Stuttgart, **1991**, p. 9.

[24] H. Kessler, D. Leibfritz, *Tetrahedron* **1970**, *26*, 1805−1820.

[25] P. W. N. M. van Leeuwen, W. L. Groeneveld, *Inorg. Nucl. Chem. Lett.* **1967**, *3*, 145−146.

[26] E. Riedel, *Anorganische Chemie*, 2nd ed., W. de Gruyter, Berlin, New York, **1990**, p. 586.

[27] M. Ciampolini, N. Nardi, *Inorg. Chem.* **1966**, *5*, 1150−1154.

[28] M. S. Lah, H. Chun, *Inorg. Chem.* **1997**, *36*, 1782−1785.

[29] [29a] D. F. Evans, *J. Chem. Soc.* **1953**, 2003−2005. − [29b] H. P. Fritz, K.-E. Schwarzhans, *J. Organomet. Chem.* **1964**, *1*, 208−211. − [29c] T. H. Crawford, J. Swanson, *J. Chem. Educ.* **1971**, *48*, 382−386. − [29d] J. Löliger, R. Scheffold, *J. Chem. Educ.* **1972**, *49*, 646−647. − [29e] D. H. Grant, *J. Chem. Educ.* **1995**, *72*, 39−40.

[30] R. J. Deeth, M. Gerloch, *Inorg. Chem.* **1985**, *24*, 4490−4493.

[31] A. Gobbi, G. Frenking, *J. Am. Chem. Soc.* **1993**, *115*, 2362−2372.

[32] CCDC search, September **2000**.

[33] Representative examples: [33a] K. R. Adam, S. P. H. Arshad, D. S. Baldwin, P. A. Duckworth, A. J. Leong, L. F. Lindoy, B. J. McCool, M. McPartlin, B. A. Tailor, P. A. Tasker, *Inorg. Chem.* **1994**, *33*, 1194−1200. − [33b] N. W. Alcock, F. McLaren, P. Moore, G. A. Pike, S. M. Roe, *J. Chem. Soc., Chem. Commun.* **1989**, 629−632. − [33c] L. Casella, M. E. Silver, J. A. Ibers, *Inorg. Chem.* **1984**, *23*, 1409−1418.

[34] M. G. B. Drew, S. Hollis, S. G. McFall, S. M. Nelson, *J. Inorg. Nucl. Chem.* **1978**, *40*, 1595−1596.

[35] S. M. Nelson, S. G. McFall, M. G. B. Drew, A. H. bin Othman, *J. Chem. Soc., Chem. Commun.* **1977**, 370−371.

[36] [36a] M. Duggan, N. Ray, B. Hathaway, G. Tomlinson, P. Brint, K. Pelin, *J. Chem. Soc., Dalton Trans.* **1980**, 1342−1348. − [36b] L. Raehm, J. M. Kern, J.-P. Sauvage, *Chem. Eur. J.* **1999**, *5*, 3310−3317.

[37] E. J. Laskowski, D. N. Hendrickson, *Inorg. Chem.* **1978**, *17*, 457−470.

[38] F. A. Cotton, R. M. Wing, *Inorg. Chem.* **1965**, *4*, 314−317.

[39] P. Chaudhuri, K. Wieghardt, Y.-H. Tsai, C. Krüger, *Inorg. Chem.* **1984**, *23*, 427−432.

[40] *Handbook of Chemistry and Physics*, 1st student ed., CRC Press, Boca Raton, **1988**.

[41] M. G. B. Drew, C. J. Harding, V. McKee, G. G. Morgan, J. Nelson, *Chem. Commun.* **1995**, 1035−1038.

[42] [42a] M. Ray, B. S. Hammes, G. P. A. Yap, A. L. Rheingold, A. S. Borovik, *Inorg. Chem.* **1998**, *37*, 1527−1532. − [42b] M. Ray, A. P. Golombek, M. P. Hendrich, V. G. Young Jr., A. S. Borovik, *J. Am. Chem. Soc.* **1996**, *118*, 6084−6085. − [42c] M. Ray, G. P. A. Yap, A. L. Rheingold, A. S. Borovik, *J. Chem. Soc., Chem. Commun.* **1995**, 1777−1778.

[43] [43a] C. C. Cummins, J. Lee, R. R. Schrock, W. M. Davis, *Angew. Chem.* **1992**, *104*, 1510−1512; *Angew. Chem. Int. Ed. Engl.* **1992**, *31*, 1501−1503. − [43b] J. S. Freundlich, R. R. Schrock, C. C. Cummins, W. M. Davis, *J. Am. Chem. Soc.* **1994**, *116*, 6476−6477. − [43c] R. R. Schrock, C. C. Cummins, T. Wilhelm, S. Lin, S. M. Reid, M. Kol, W. M. Davis, *Organometallics* **1996**, *15*, 1470−1476.

[44] E. Keller, *SCHAKAL-97, Program for the Graphic Representation of Molecule and Crystallographic Models*, Universität Freiburg, **1997**.

[45] [45a] G. M. Sheldrick, *SHELXS-97* (resolution), University of Göttingen, **1997**; *SHELXL-97* (refinement), University of Göttingen, **1997**; *SHELXTL 5.06*, Siemens Analytical X-ray Instruments Inc., Madison, WI, USA, **1995**. − [45b] C. Giacovazzo, *SIR-92* (resolution) University of Bari, **1992**.

[46] Crystallographic data (excluding structure factors) for the structures reported in this paper have been deposited with the Cambridge Crystallographic Data Centre as supplementary publication nos. CCDC-148696 (**2**), -148700 (**3**), -148699 (**4**), -148698 (**5**), and -148697 (**6**). Copies of the data can be obtained free of charge on application to the CCDC, 12 Union Road, Cambridge CB2 1EZ, U.K. [Fax: (internat.) + 44-1223/336-033; E-mail: deposit@ccdc.cam.ac.uk].

[47] [47a] J. E. Huheey, E. A. Keiter, R. L. Keiter, in: *Inorganic Chemistry*, 4th ed., Harper Collins, New York, **1993**. − [47b] U. Müller, in: *Anorganische Strukturchemie*, 3rd ed., Teubner, Stuttgart, **1996**.

[48] M. Di Vaira, P. L. Orioli, *Acta Crystallogr., Sect. B* **1968**, *24*, 1269−1272.

[49] R. Gregorzik, U. Hartmann, H. Vahrenkamp, *Chem. Ber.* **1994**, *127*, 2117−2122.

[50] R. J. Sime, R. P. Dodge, A. Zalkin, D. H. Templeton, *Inorg. Chem.* **1971**, *10*, 537−541.

Received December 19, 2000
[I00478]

Reductions of 1,3,5-Triboracyclohexanes and Related 1,3,5-Triboraalkanes with Alkali Metals to Trishomoaromatic Aggregates — Tetrameric Lithium and Sodium, and Polymeric Sodium and Potassium Trishomoaromatic Cyclotriborate Compounds

Wolfgang Lößlein,[a] Hans Pritzkow,[a] Paul von Ragué Schleyer,*[b] Lawrence R. Schmitz,[c] and Walter Siebert*[a]

Dedicated to Prof. Kurt Dehnicke on the occasion of his 70th birthday

Keywords: Boron / Aromaticity / NMR spectroscopy / Alkali metals

Hexamethyl-1,3,5-triboracyclohexane can be reduced by alkali metals in donor solvents. Two electrons are added to the combination of p-orbitals at the boron centers forming trishomoaromatic dianions. X-ray structure analyses show a variety of arrangements, depending on the alkali metal: Tetrameric aggregates with lithium, a polymeric, meander-like chain or a complex tetramer with sodium, and a zigzag-chain polymer with potassium. The set of dianions show characteristic NMR chemical shifts in the high-field region, but do not obey a monotonous order with the counterions Li^+ to Cs^+. Lithium is out of line because of its exceptionally low electronegativity. IGLO chemical shift calculations agree very well with the experimentally observed data. The computed Nucleus-Independent Chemical Shift (NICS) values prove the strong homoaromatic character of the reduced triboraheterocycles. Compared with isoelectronic analogues the reduced triboraheterocycle shows a remarkable stabilization energy towards the corresponding, non-aromatic species.

Introduction

Reduction of unsaturated boron heterocycles in donor solvents by alkali metals leads to the formation of aromatic anions.[1] Remarkable results such as the synthesis of the doubly-aromatic anion **1** with σ and π 3c,2e bonding have been reported by Berndt et al.[2,3] Recently we obtained the new, trishomoaromatic system **3** by reducing 1,3,5-triboracyclohexanes **2** with lithium.[4,5] The empty p-orbitals of **2** are able to accept two electrons to form the dianion **3**, which is isoelectronic with the trishomocyclopropenylium cation **6**.[6] We now describe the reactions of the hexamethyl derivative **2** with various alkali metals and the influence of these metals on the structures and on the NMR chemical shifts of the trishomoaromatic dianions **3**. Our investigations are supported by computational studies on the stabilization and on the Nucleus-Independent Chemical Shifts (NICS)[7] of the isoelectronic, parent trishomoaromatic set **4**, **5**, and **6**.

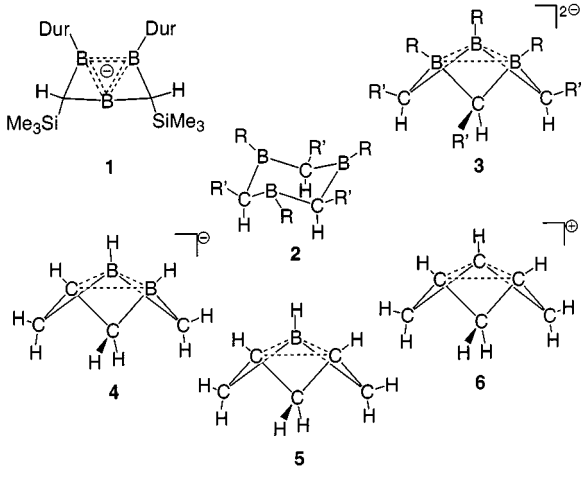

Results and Discussion

Formation and X-ray Structure Analyses of Trishomoaromatic Dianions

Hexamethyl-1,3,5-triboracyclohexane (**2**) reacted with Li powder at 0 °C in both Et_2O and THF (Scheme 1) to give yellow-orange solutions after filtration. Removal of the solvent gave only amorphous products $\{\mathbf{3}[(Li^+)_2(OEt_2)_{2n}]\}_m$ and $\{\mathbf{3}[(Li^+)_2(thf)_{2n}]\}_m$ of unknown structure.

[a] Anorganisch Chemisches Institut der Universität, Im Neuenheimer Feld 270, 69120 Heidelberg
[b] Computational Chemistry Annex, Department of Chemistry, University of Georgia, Athens, GA, 30602 USA
[c] Marshall University, 400 Hal Greer Blvd, Huntington, WV, 25755 USA

 © WILEY-VCH Verlag GmbH, 69451 Weinheim, 2001 1434−1948/01/0808−1949 $ 17.50+.50/0

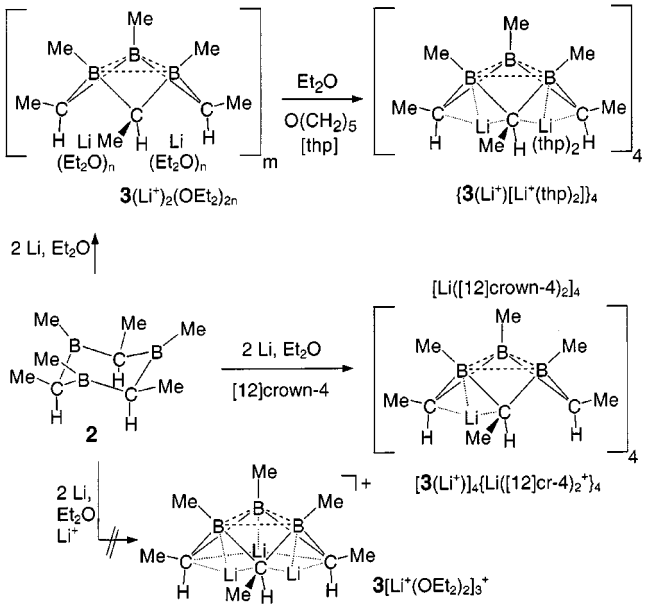

Scheme 1

Very air- and moisture-sensitive crystals were obtained by adding tetrahydropyran (thp) or [12]crown-4 to THF solutions of reduced **2**. Surprisingly, the X-ray structures (see below) revealed tetrameric aggregates for $\{\mathbf{3}(Li^+)[Li(thp)_2^+]\}_4$ and for $[\mathbf{3}(Li^+)]_4\{Li([12]cr\text{-}4)_2^+\}_4$. The low solubility of both these compounds precluded spectroscopic characterization. An attempt to obtain $\mathbf{3}[Li(OEt_2)_2]_3^+$ by reducing **2** with lithium in Et_2O in the presence of LiCl failed to give any monomeric product.

To study the reaction with the other alkali metals **2** was treated with sodium, potassium, rubidium, or cesium as described above (Scheme 2−4). The initially formed amorphous reduction products were soluble in $[D]_8THF$.

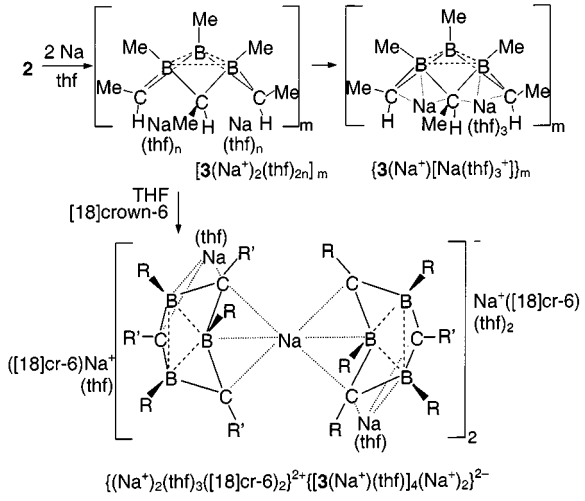

$\{(Na^+)_2(thf)_3([18]cr\text{-}6)_2\}^{2+}\{[\mathbf{3}(Na^+)(thf)]_4(Na^+)_2\}^{2-}$

Scheme 2. Reduction of **3** with sodium; in the formula of $\{(Na^+)_2(thf)_3([18]cr\text{-}6)_2\}^{2+}\{[\mathbf{3}(Na^+)(thf)]_4(Na^+)_2\}^{2-}$ the hydrogen atoms are omitted

The reduction of **2** with sodium or potassium gave crystals in addition to the amorphous products. X-ray structure analyses revealed a polymeric aggregation of $\mathbf{3}(Na^+)_2(THF)_3$ and, in the presence of [18]crown-6, an interesting tetramer. In contrast the potassium structure forms only a zigzag polymer (see below). The X-ray structures of all the reduced **2** products reveal that they adopt *nido* arrangements with axial methine hydrogens and equatorial CH_3 groups.

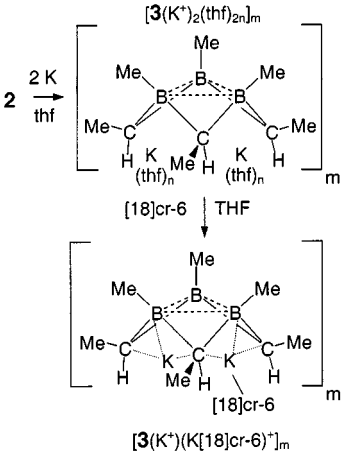

Scheme 3

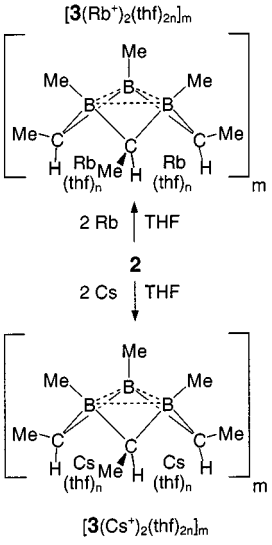

Scheme 4

For $[\mathbf{3}(Li^+)Li(thp)_2]_4$ only a very limited data set ($2\theta_{max} = 30°$) was obtained. However, the structure could be solved and showed severe disorder of the thp ligands; a gross description of the structure (Figure 1) can therefore be given. The structure of $[\mathbf{3}(Li^+)]_4\{Li([12]cr\text{-}4)_2^+\}_4$ with [12]crown-4 as ligand refined well (Figure 2). In both structures four $(MeCH)_3(MeB)_3$ units in the cyclic tetramer are connected by Li cations. While the second Li of each dianion in $\{\mathbf{3}(Li^+)[Li(thp)_2^+]\}_4$ complexed by two thp is capping the third C_2B plane, in $[\mathbf{3}(Li^+)]_4\{Li([12]cr\text{-}4)_2^+\}_4$ the second Li is completely separated from the dianion **3** by two crown ether ligands leaving the third C_2B plane uncoordinated. The boron−boron distances in the B_3 ring are larger than 2c,2e B−B bonds and differ somewhat [1.825(5) Å when both B atoms coordinate to Li's, vs. 1.851(5) and

1.848(5) Å, when only one B coordinates to Li]. The Li···B contacts are long [2.239(6) and 2.251(6) Å] and the B−C bond lengths are normal for a single bond [between 1.603(5) and 1.632(4) Å]. In $[\mathbf{3}(Li^+)]_4\{Li([12]cr\text{-}4)_2{}^+\}_4$ the axial hydrogen substituents could be located.

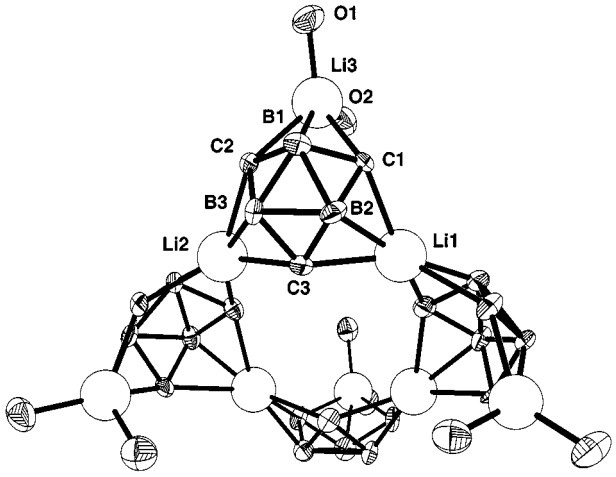

Figure 1. Structure of $\{\mathbf{3}(Li^+)[Li(thp)_2{}^+]\}_4$ in the crystal [the $(CH_2)_4$ chain of the thp ligands and the methyl groups are omitted for clarity]

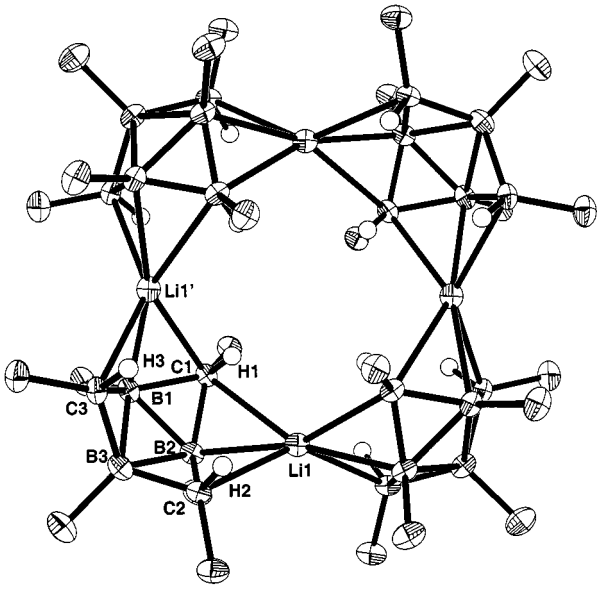

Figure 2. Molecular structure of the tetrameric anion in $\{\mathbf{3}(Li^+)[(Li[12]cr\text{-}4)_2{}^+]\}_4$ in the crystal; selected distances [Å] and angles [°]: B1−B2 1.825(5), B1−B3 1.851(5), B2−B3 1.848(5), Li1−C1 2.456(6), Li1′−C1 2.354(6), Li1′−C3 2.285(6), Li1−C2 2.247(6), Li1′−B1 2.239(6), Li1−B2 2.251(6); B2−B1−B3 60.4(2), B1−B2−B3 60.5(2), B1−B3−B2 59.1(2), B1−C1−B2 68.6(2), B2−C2−B3 70.0(2), B1−C3−B3 69.8(3) (symmetry operation for ′: y, 3/2 − x, 1/2 − z)

Air- and moisture-sensitive crystals of $\{\mathbf{3}[(Na^+)_2(thf)_3]\}_m$ were obtained after partial removal of the THF solvent. Surprisingly, the X-ray structure analysis (Figure 3a,b) revealed a polymeric arrangement of $\{\mathbf{3}(Na^+)[Na(thf)_3{}^+]\}_m$, consisting of a two-dimensional, meander-like chain pattern. There is no contact between individual chains. Half of the sodium centers bridge the **3** units through C_2B interactions and are solvent free; the other sodium centers in the terminal positions are coordinated by three THF ligands.

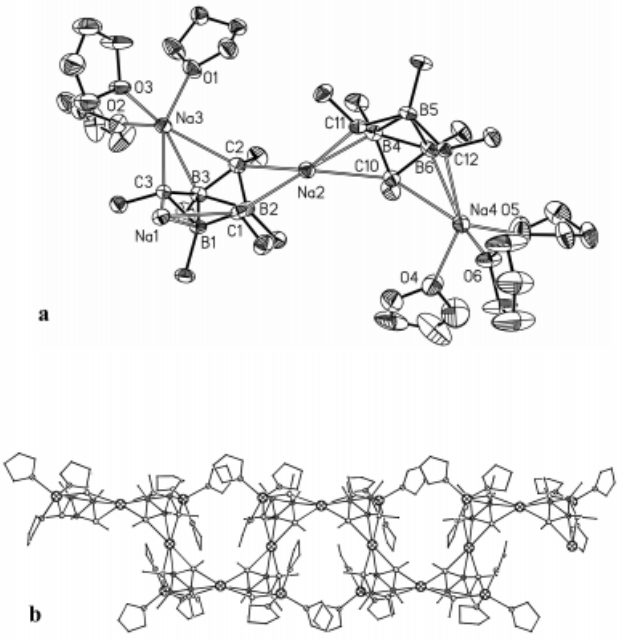

Figure 3. (a) Structure of two units of $\{\mathbf{3}(Na^+)[Na(thf)_3{}^+]\}_m$ in the crystal; selected distances [A] and angles [°]: B−B 1.827−1.846(6), Na1(2)−B 2.447−2.471(5), Na1(2)−C 2.621−2.764(5), Na3−B3 2.595(5), Na4−B6 2.601(6), Na3−C 2.673(4), 2.827(5), Na4−C 2.689(4), 2.768(5), Na3(4)−O 2.316−2.360(4); B−B−B 59.6−60.7(3), B−C−B 68.2−69.5(3); (b) structure of the meander-like chain of $\{\mathbf{3}(Na^+)[Na(thf)_3{}^+]\}_m$ in the crystal

A few crystals could be obtained when an excess of [18]crown-6 was added to the solution of the Na-reduced ring. An X-ray structure analysis showed tetrahedral aggregation of four units of **3** around an octahedron of six sodium ions, each connecting two C_2B faces of adjacent dianions of **3**. Four of the six sodium ions are complexed by a THF ligand, while the remaining two *trans*-oriented Na^+ ions have no other contacts than to the two adjacent C_2B units in **3**. In the crystal these two Na ions are shielded by a $\{(thf)_2Na([18]cr\text{-}6)\}^+$ unit and a $\{(thf)Na([18]cr\text{-}6)\}^+$ unit, which balance the charge of the tetrameric dianion (Figure 4 and 5).

Unfortunately, no NMR spectroscopic data could be obtained. The "vacant" coordination site of $\{(thf)Na^+([18]cr\text{-}6)\}^+$ is involved in an agostic interaction with a methyl group of **3** (dashed line in Figure 5). Disorder decreases the quality of the X-ray structure analysis.

The addition of [18]crown-6 after reduction of **2** with potassium yielded crystals. One of the K^+ ions bridges the C_2B faces of two adjacent units **3** resulting in a zigzag chain (Figure 6 and 7). The other K^+ ion occupies the third face of **3** and is coordinated by [18]cr-6.

In the structures the bond lengths and angles within **3** are almost identical. Due to the growing ionic radii from Li^+ to K^+ the distances of the cations to the C_2B faces

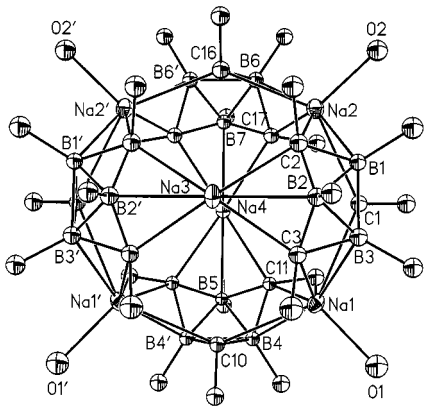

Figure 4. Structure of the dianion of compound $\{(thf)_2Na([18]cr-6)\}^+\{[\mathbf{3}(Na^+)(thf)]_4(Na^+)_2\}^{2-}\{(thf)Na([18]cr-6)\}^+$ in the crystal (symmetry operation for ′: $x, y, -z$)

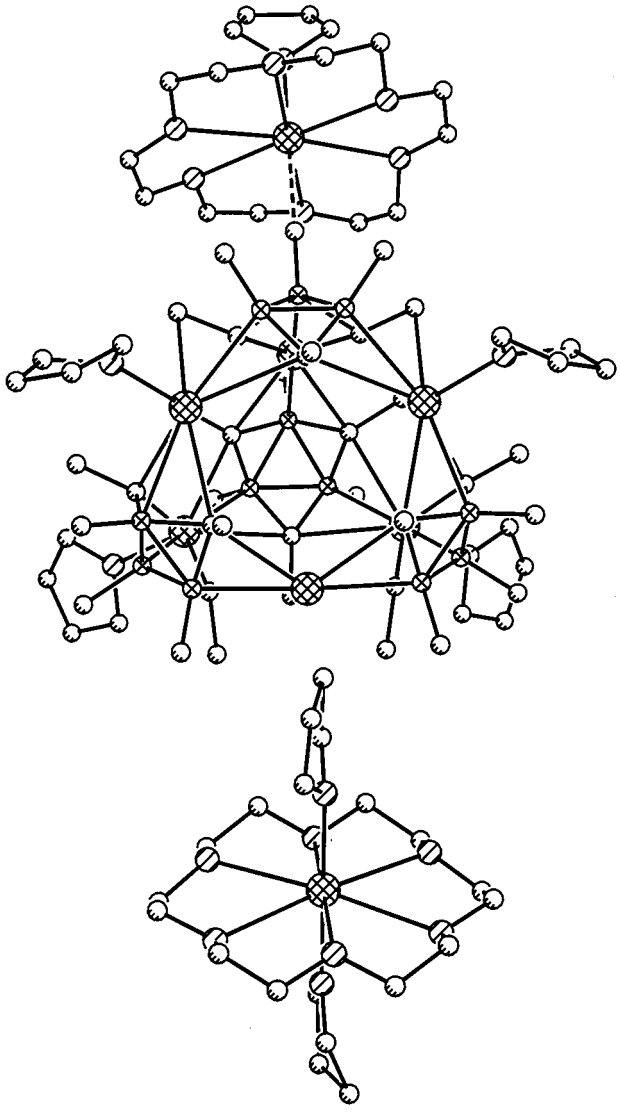

Figure 5. Molecular structure of $\{(thf)_2Na([18]cr-6)\}^+\{[\mathbf{3}-(Na^+)(thf)]_4(Na^+)_2\}^{2-}\{(thf)Na([18]cr-6)\}^+$ in the crystal

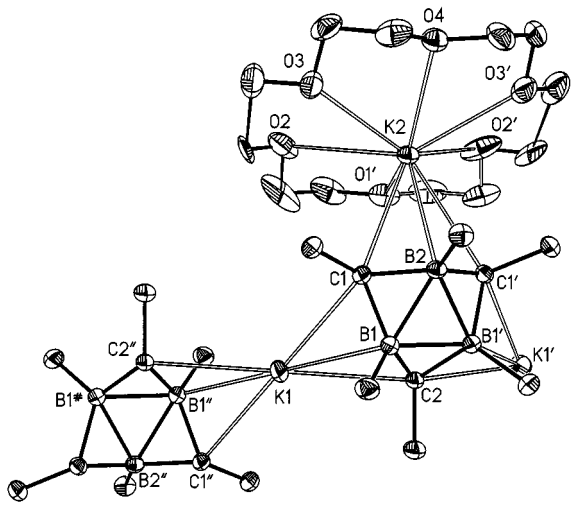

Figure 6. Structure of two units of $[\mathbf{3}(K^+)(K[18]crown-6)^+]_m$ in the crystal (one $(K^+([18]cr-6)$ unit omitted for clarity); selected distances [A] and angles [°]: B1−B2 1.868(4), B1−B1′ 1.831(5), K1−B1 2.798(3), K2−B2 3.147(3), K1−C1 2.944(2), K1−C2 2.978(1), K2−C1 3.164(2), K2−O 2.893−3.002(5); B1′−B1−B2 60.7(1), B1′−B2−B1 58.7(2), B2−C1−B1 70.5(2), B1−C2−B1′ 68.5(2). (symmetry operation for ′: x, 1/2 − y, z; for ″: $-x$, $-y$, 1 − z; for #: $-x$, y − 1/2, 1 − z)

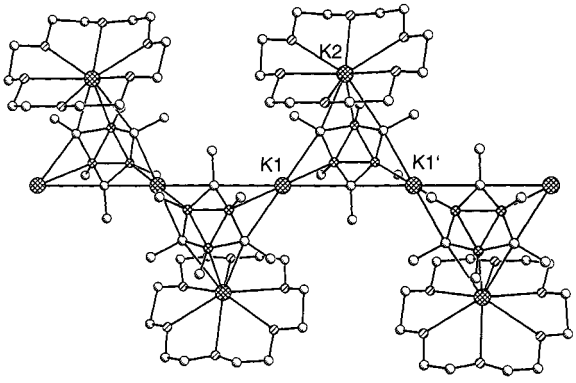

Figure 7. Structure of $[\mathbf{3}(K^+)(K[18]crown-6)^+]_m$ in the crystal showing segments of the polymer chain

increase. For a comparison with the structures of other organoalkali metal compounds see ref.[8]

NMR spectroscopic Characterization

Two broad ^1H NMR signals at $\delta = -3.2$ and -3.4 are assigned to the methine protons of the initial reduction product $\{\mathbf{3}[(Li^+)_2(thf)_{2n}]\}_m$ in $[D]_8THF$ solution. Since the reduction yielded a mixture of diastereomers with different axial/equatorial C−Me orientations, three B−Me and two C−Me signals were found. This had already been observed by NMR spectroscopy and by X-ray crystal analysis for $(MeCH)_3(ClB)_3$, the precursor of **2**.[5] The ^{11}B NMR signal of reduced **2** at $\delta = -29.2$ is at extremely high-field (neutral **2**: $\delta = 84.3$), and indicates the increased connectivity of the boron atoms.

The NMR signals could be assigned to a mixture of two diastereomers — one form with all the methine protons in axial configurations and the other with one equatorial and two axial methine protons. The ratio of diastereomers varies, but the all-axial form always dominates.

The reduction products show a pronounced high-field shift in their ^{11}B NMR spectra (Table 1), although there are quantitative differences showing two trends of opposite direction. The ^{11}B NMR chemical shifts decrease monotonously in absolute value within the alkali metal group, but only from Na to Cs, from $\delta = -35.3$ for $\{\mathbf{3}[(Na^+)_2(thf)_{2n}]\}_m$ to $\delta = -29.8$ for $\{\mathbf{3}[(Cs^+)_2(thf)_{2n}]\}_m$; the Li-reduced product $\{\mathbf{3}[(Li^+)_2(thf)_{2n}]\}_m$ ($\delta = -29.2$) does not seem to fit this trend. The same ordering occurs in the ^{13}C NMR spectra for the C−Me groups and the methine carbon atoms, again with $\{\mathbf{3}[(Li^+)_2(thf)_{2n}]\}_m$ as the exception. In contrast the ^1H NMR spectra show a trend to higher-field methine proton chemical shifts.

The special behavior of the Li-reduced species can be attributed to the decreased electronegativity (EN) of lithium.[9,10] This is due to the smaller effective charge of the Li nucleus. From sodium to cesium the EN decreases monotonously and the C−H and C−Me proton shifts appear at increasingly higher fields (see Table 1).

Computational Results

IGLO ^{11}B NMR shift calculations[7,11] of the C_{3v} model of $[(CH_2)_3(BH)_3Li_3]^+$ $\{[(Li^+)_3\mathbf{3}]^+\}$ gave $\delta^{11}{}_B = -31.8$, in very good agreement with the experimental value. The NICS values,[7] $\delta = -28.5$ at the center of all the C and B atoms and $\delta = -42.3$ at the center of the three boron atoms, also indicate pronounced homoaromatic character (see below). Comprehensive computations on the various possible monomeric minima $[(CH_2)_3(BH)_3Li_3]^+$ $\{[(Li^+)_3\mathbf{3}]^+\}$, $(CH_2)_3(BH)_3Li_2$ $[(Li^+)_2\mathbf{3}]$ and $[(CH_2)_3(BH)_3Li]^-$ $\{[(Li^+)\mathbf{3}^-]\}$, reveal that Li attachment at the B_3 face is preferred over a C_2B unit in all cases $\{[(Li^+)\mathbf{3}^-]$: C_{3v} (B-face); $[(Li^+)_2\mathbf{3}]$: C_s; $[(Li^+)_3\mathbf{3}]^+$: $C_{2v}\}$. The lithium bonding is predominantly electrostatic, but small covalent contributions to the interactions between the Li^+ centers and nearby H, B and C atoms are present. The C_2B-face coordination observed experimentally for $\{\mathbf{3}(Li^+)[Li(thp)_2^+]\}_4$ and $\{\mathbf{3}(Li^+)[(Li[12]cr\text{-}4)_2^+]\}_4$ may be attributed to the combined effects of the steric influences of the methyl groups at the B_3 face and to the electrostatic advantages of the tetrameric association.

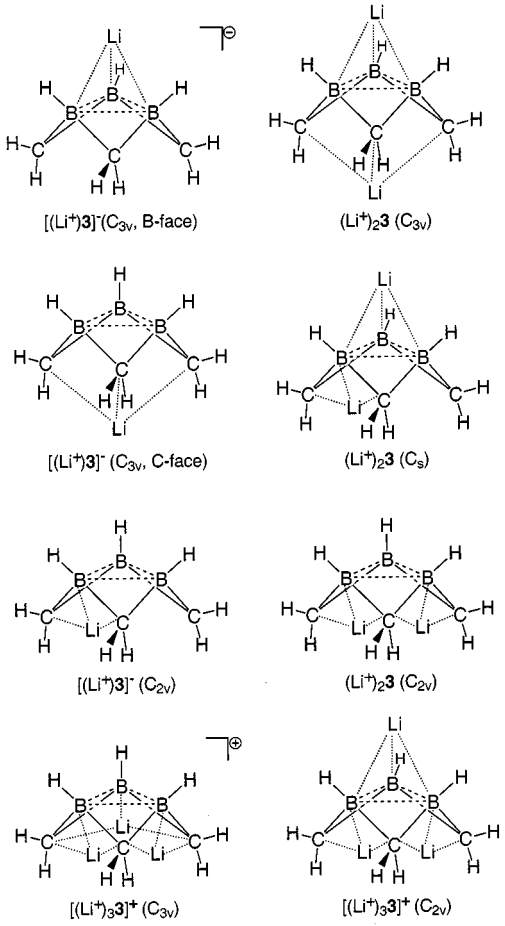

Most surprising is the remarkable homoaromatic stabilization energy[3] of the $[(CH_2)_3(BH)_3]^{2-}$ dianion (**3**, R =

Table 1. NMR chemical shifts of reduced **2**, depending on the alkali metal

	Li	Na	K	Rb	Cs
^{11}B	−29.2	−35.3, −37.1	−32.4	−31.5	−29.8
^1H					
$(CH_3CH_{ax})_3$	−3.42 (m)	−3.34 (q)	−3.64 (q)	−3.78 (q)	−3.89 (q)
$(CH_3CH_{ax})_2$	−3.23 (m)	−3.03 (q)	−3.34 (q)	−3.46 (q)	−3.64 (q)
$(CH_3CH_{ax})_1$	−1.66 (m)	−1.57 (q)	−1.80 (q)	−1.84 (q)	−1.89 (q)
BCH_3	−0.59 (s, br)	−0.59 (s, br)	−0.71 (s, br)	−0.73 (s, br)	−0.76 (s, br)
BCH_3	−0.52 (s, br)		−0.65 (s, br)	−0.64 (s, br)	−0.72 (s, br)
$CHCH_3$(ax)	0.81 (d)	0.82 (d)	0.82 (d)	0.84 (d)	0.82 (d)
$CHCH_3$ (eq)	1.23 (d)	1.05 (d)	1.03 (d)	0.93 (d)	0.91 (d)
$CHCH_3$ (eq)	1.35 (d)	1.16 (d)	1.09 (d)	1.05 (d)	1.01 (d)
^{13}C					
$CHCH_3$	15.4	15.2	15.5	16.1	16.1
$CHCH_3$	−4.0	−3.9	−2.1	−1.3	−1.3
BCH_3	15.6	15.4	16.0	17.8	17.8

Table 2. Stabilization energies (kcalmol^{-1} at //B3LYP/6−311+G**) and NICS values (at PW91/IGLO III)[4] for the trishomoaromatic systems **3**−**6**

Trishomoaromatic system	Isodesmic reaction[a]	vs. boat form[b]	NICS(0)[c]	NICS(rc)[d]
$[(CH_2)_3(BH)_3]^{2-}$ (**3**)	−41.05	−32.35	−35.4	−22.5
$[(CH_2)_3(CH)(BH)_2]^{-}$ (**4**)	−19.63	−16.11	−37.1	−21.4
$[(CH_2)_3(CH)_2(BH)]$ (**5**)	+5.55	+6.55	−34.8	−16.7
$[(CH_2)_3(CH)_3]^{+}$ (**6**)	−8.73	−12.54	−46.4	−22.7

[a] The isodesmic equations (Scheme 5) involve cyclohexane and **3**−**6** as product pairs. The reactants are cyclohexyl cation (for **6**) and boracyclohexane (for **3**−**5**), as well as bicyclo[3.1.0]hexane (for **5** and **6**) and its 1-(B^-) (for **4**) and 1,5-(B^-)$_2$ (for **3**) counterparts. − [b] Energy differences between **3**−**6** and their boat-form conformers which lack 3c,2e bonding (see ref.[7f] for a prior use of this method). − [c] Computed at the mass unweighted centers of the 6-rings. − [d] The ring current contributions (localized by the IGLO method) computed at the centers of the three C/B atom triangles involved in 3c,2e bonding.

R′ = H), which is larger than all three of the isoelectronic counterparts **4**−**6** (Table 2), even when evaluated by two different methods.[12] These stabilization energies are based on the isodesmic reactions in Scheme 5 and the chair (delocalized)−boat (localized) energy differences. This is caused by the reduced coulombic interaction between the two negative charges when they are delocalized over the B_3 triangle. In contrast, the electron repulsion in the classic reference species is high because of two adjacent B^- units. The positive stabilization energies of the neutral analog **5** reflect the ring strain required to achieve the chair conformation (which is greater than the stabilization to be gained). This situation is discussed in ref.[12] The NICS(0) values, based on total NMR shieldings in the six-membered ring centers, and the NICS(rc) values in the 3c,2e ring centers (also given in Table 2) measure the current contributions. Malkin's implementation[7b] of Kutzelnigg's IGLO program[11] provides a detailed breakdown of the total shieldings in terms of all the localized orbital contributions.

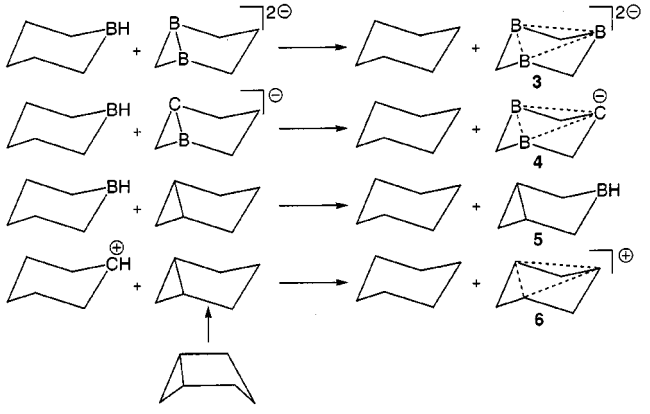

Scheme 5

Of greatest interest are the diatropic effects due to the cyclic electron delocalization [i.e., the magnetic evaluation of the 3c,2e "aromatic" bonding given by NICS(rc)]. These values are augmented by the local diatropic shielding contributions of nearby C−C, C−H and B−H bonds. Hence, the NICS(0) values are displaced further upfield. (The local induced circulations of the sigma C−C bonds in benzene, in contrast, are paratropic and reduce the NICS(0) value to ca −10.) The benzene NICS(rc, i.e. π) of about −22 at the ring center is quite similar to the 3c,2e data above.

Conclusion

The reaction of **2** with lithium gave tetrameric aggregates of the trishomoaromatic compounds $\{\mathbf{3}(Li^+)[Li(thp)_2^+]\}_4$ and $[\mathbf{3}(Li^+)]_4\{Li([12]cr\text{-}4)_2^+\}_4$ in the solid state. The expected monomeric dianion **3** (R = R′ = Me) and the cation $\mathbf{3}[(Li^+)(thf)_2]_3^+$ as electronic analogues to the trishomocyclopropenylium cation **6**[6] could not be isolated. Alternatively, the monomeric unit $\mathbf{3}[(Li^+)(thf)_2]_3^+$, with two donor molecules at each of the three Li centers, may be described as a hypho cluster with 26 skeleton electrons.[13]

The reduction product of **2** with sodium crystallizes as a polymeric, meander-like chain, in which the trishomoaromatic units are bridged at C_2B faces by half of the sodium ions, with the other half connected in terminal positions to one C_2B face and three THF ligands. A tetramer of **3** with an unusual structure was obtained in the presence of [18]crown-6. The linear polymer $[\mathbf{3}(K^+)(K[18]cr\text{-}6)^+]_m$ is formed with potassium as the electron donor. NMR spectroscopic data show that reduction with rubidium and with cesium also led to the doubly reduced ring systems.

The NMR spectra of all the Li-reduced compound $\{\mathbf{3}[(M^+)_2(thf)_{2n}]\}_m$ show regular trends of chemical shifts from Na to Cs, but the Li values are often out of line due to the exceptional electronegativity of lithium. The trishomoaromatic delocalized three center, two electron bonding in the reduced 1,3,5-triboracyclohexanes (**3**), as well as in the isoelectronic series **3**−**5**, is demonstrated by the highly negative NICS values computed inside the rings. These indicate the presence of large induced diatropic ring currents in all these systems. In addition, the stabilization energies due to the 3c,2e delocalization are quite large.

Experimental Section

General: All reactions were carried out under dry argon or nitrogen using standard Schlenk techniques. Solvents were dried, distilled,

and saturated with nitrogen. Glassware was dried with a heat-gun under high vacuum. The alkali metals were washed with *n*-hexane and THF, heated in THF for 2 h under reflux and filtered. Lithium was used as a powder, and sodium, potassium, rubidium and cesium as blocks. – ^{1}H, ^{13}C and ^{11}B NMR: Bruker DRX 200 spectrometer, NMR references are $(CH_3)_4Si$ and $Et_2O{\cdot}BF_3$.

General Procedure for the Reduction of the Triboraheterocycles: A suspension of excess alkali metal in THF or Et_2O was cooled to 0 °C. The boron heterocycle was added and stirred overnight while warming to room temperature. Separation of the unreacted alkali metal by filtration through a glass filter of G III porosity led to clear yellow-orange solutions. Removal of the solvent gave amorphous residues of $[\mathbf{3}(M^+)_2(thf_2)_{2n}]_m$ and $[\mathbf{3}(M^+)_2(OEt_2)_{2n}]_m$, which are soluble in [D$_8$]THF.

Reduction of 2 with Lithium: Amounts: diethyl ether (20 mL), **2** (200 mg, 1.23 mmol). For crystallization the solution was concentrated to 1−2 mL by vacuum evaporation and THP or [12]crown-4 (0.2 mL) was added to yield $[\mathbf{3}(Li^+)]_4[Li(thp)_2{}^+]_4$ (28 mg, 7%) or $[\mathbf{3}(Li^+)]_4\{Li([12]cr\text{-}4)_2{}^+\}_4$ (12 mg, 3%). NMR spectroscopic data of the initial reduction product $[\mathbf{3}(Li^+)_2(OEt_2)_{2n}]_m$: ^{1}H NMR (200 MHz, [D$_8$]THF): δ = −3.42 [q, ^3J(H,H) = 3 Hz, 3 H, CH_{ax}], −3.2 (br. m, 2 H, CH_{ax}), −1.7 (br. m, 1 H, CH_{eq}], −0.6 (br. s, 9 H, BCH_3), −0.5 (br. s, 6 H, BCH_3), −0.5 (br. s, 3 H, BCH_3), 0.81 [d, ^3J(H,H) = 3 Hz, 3 H, $C(CH_3)_{ax}$], 1.23 [d, ^3J(H,H) = 3 Hz, 6 H, $C(CH_3)_{eq}$], 1.35 [d, ^3J(H,H) = 3 Hz, 9 H, $C(CH_3)_{eq}$]. – ^{13}C NMR (50 MHz, [D$_8$]THF): δ = −4.0 (CH), 15.4 (CCH_3), 15.6 (BCH_3). – ^{11}B NMR (64 MHz, [D$_8$]THF): δ = −29.2.

Reduction of 2 with Sodium: Amounts: THF (40 mL), **2** (150 mg, 0.93 mmol). Crystallization from the filtered solution after solvent removal to ca. 1 mL gave $\{\mathbf{3}(Na^+)[Na(thf)_3{}^+]\}_m$ (95 mg, 0.22 mmol, 24%). After addition of [18]crown-6 (420 mg) to the filtered solution, crystallization occurred after solvent evaporation to 1 mL to give $\{(thf)_2Na([18]cr\text{-}6)\}^+\{[\mathbf{3}(Na^+)\text{-}(thf)]_4(Na^+)_2\}^{2-}\{(thf)Na([18]cr\text{-}6)\}^+$ (43 mg, 0.02 mmol, 9%). NMR spectroscopic data of the initial reduction product $[\mathbf{3}(Na^+)_2(thf)_{2n}]_m$ (ratio of diastereomers $(CH_{ax})_3/(CH_{ax})_2(CH_{eq})$ = 3:1): ^{1}H NMR (200 MHz, [D$_8$]THF): δ = −3.34 [q, ^3J(H,H) = 3 Hz, 3 H, CH_{ax}], −3.03 [q, ^3J(H,H) = 3 Hz, 2 H, CH_{ax}], −1.57 [q, ^3J(H,H) = 3 Hz, 1 H, CH_{eq}], −0.6 (br. s, 9 H, BCH_3), 0.82 [d, ^3J(H,H) = 3 Hz, 3 H, $C(CH_3)_{ax}$], 1.05 [d, ^3J(H,H) = 3 Hz, 6 H, $C(CH_3)_{eq}$], 1.16 [d, ^3J(H,H) = 3 Hz, 9 H, $C(CH_3)_{eq}$]. – ^{13}C NMR (50 MHz, [D$_8$]THF): δ = −3.9 (CH), 15.2 (CCH_3), 15.4 (BCH_3). – ^{11}B NMR (64 MHz, [D$_8$]THF): δ = −35.3 and −37.1.

Reduction of 2 with Potassium: Amounts: THF (40 mL), **2** (140 mg, 0.86 mmol). After reaction and filtration, [18]crown-6 (350 mg) was added to the solution. The solvent was partially removed in vacuum and $[\mathbf{3}(K^+)(K[18]cr\text{-}6)^+]_m$ (56 mg, 0.11 mmol, 12%) crystallized. NMR spectroscopic data of the initial reduction product $[\mathbf{3}(K^+)_2(thf)_{2n}]_m$ (ratio of diastereomers $(CH_{ax})_3/(CH_{ax})_2(CH_{eq})$ = 6:1): ^{1}H NMR (200 MHz, [D$_8$]THF): δ = −3.64 [q, ^3J(H,H) = 3 Hz, 3 H, CH_{ax}], −3.34 [q, ^3J(H,H) = 3 Hz, 2 H, CH_{ax}], −1.80 [q, ^3J(H,H) = 3 Hz, 1 H, CH_{eq}], −0.7 (br. s, 9 H, BCH_3), −0.6 (br. s, 6 H, BCH_3), 0.82 [m, 3 H, $C(CH_3)_{ax}$], 1.03 [d, ^3J(H,H) = 3 Hz, 6 H, $C(CH_3)_{eq}$], 1.09 [d, ^3J(H,H) = 3 Hz, 9 H, $C(CH_3)_{eq}$]. – ^{13}C NMR (50 MHz, [D$_8$]THF): δ = −2.1 (CH), 15.5 (CCH_3), 16.0 (BCH_3). – ^{11}B NMR (64 MHz, [D$_8$]THF): δ = −32.4.

Reduction of 2 with Rubidium: Amounts: THF (50mL), **2** (200 mg, 1.23 mmol). NMR spectroscopic data of the amorphous reduction

Table 3. Crystal data and structure refinement of $\{\mathbf{3}(Li^+)[Li(thp)_2{}^+]\}_4$, $[\mathbf{3}(Li^+)_2([12]cr\text{-}4)_2]_4$, $\{\mathbf{3}(Na^+)[Na(thf)_3{}^+]\}_m$, $\{(thf)_2Na([18]cr\text{-}6)\}^+\{[\mathbf{3}(Na^+)(thf)]_4(Na^+)_2\}^{2-}\{(thf)Na([18]cr\text{-}6)\}^+$and $[\mathbf{3}(K^+)(K[18]crown\text{-}6)^+]_m$

	$[\mathbf{3}(Li^+)]_4\{Li([12]cr\text{-}4)_2{}^+\}_4$	$\{\mathbf{3}(Na^+)[Na(thf)_3{}^+]\}_m$	Octahedral Na_6 compd. (Fig. 4)[a]	$[\mathbf{3}(K^+)(K[18]cr\text{-}6)^+]_m$
Empirical formula	$C_{25}H_{53}B_3Li_2O_8$	$C_{21}H_{45}B_3Na_2O_3$	$C_{96}H_{204}B_{12}Na_8O_{21}$	$C_{29}H_{61}B_3K_2O_8$
Molecular weight	527.98	423.98	2008.23	648.41
Crystal system	Tetragonal	Orthorhombic	Orthorhombic	Monoclinic
Space group	$P4_2/n$	$P2_12_12_1$	$Pnnm$	$P2_1/m$
a [Å]	20.156(11)	11.0551(3)	22.142(5)	11.746(2)
b [Å]	20.156(11)	15.9133(4)	28.468(5)	11.372(2)
c [Å]	14.937(8)	29.9410(8)	19.154(3)	13.988(2)
α [°]	90	90	90	90
β [°]	90	90	90	97.37(1)
γ [°]	90	90	90	90
V [Å^3]	6068(6)	5267.3(2)	12073(4)	1853.0(5)
Z	8	8	4	2
Calcd. density [g/cm^3]	1.156	1.07	1.11	1.16
Absorp. coeff. [mm^{-1}]	0.080	0.09	0.10	0.30
F(000)	2304	1856	4384	704
Crystal size [mm]	0.80 × 0.50 × 0.35	0.32 × 0.44 × 0.45	0.15 × 0.15 × 0.25	0.09 × 0.35 × 0.46
Θ_{max} [°]	25.1	25.1	18.0	28.3
Index ranges	0/23, 0/23, 0/17	−13/13, 0/18, 0/35	0/19, 0/24, 0/16	−14/15, −12/15, −18/18
Unique reflections	5341	9324	4331	4688
Observed [$I > 2\sigma I$)	2790	6794	2469	3700
Parameters	364	544	407	299
Final R indices				
$R1$ [$I > 2\sigma(I)$]	0.060	0.088	0.117	0.071
$wR2$	0.141	0.265	0.356	0.218
Largest diff. peak/hole[e/Å^3]	0.191/ −0.185	0.61/−0.26	0.61/−0.63	0.89/−0.68

[a] $\{(thf)_2Na([18]cr\text{-}6)\}^+\{[\mathbf{3}(Na^+)(thf)]_4(Na^+)_2\}^{2-}\{(thf)Na([18]cr\text{-}6)\}^+$.

product $[\mathbf{3}(Rb^+)_2(THF)_{2n}]_m$ (ratio of diastereomers $(CH_{ax})_3/(CH_{ax})_2(CH_{eq}) = 9:1$): ^1H NMR (200 MHz, [D$_8$]THF): δ = −3.78 [q, $^3J(H,H)$ = 3 Hz, 3 H, CH_{ax}], −3.46 [q, $^3J(H,H)$ = 3 Hz, 2 H, CH_{ax}], −1.84 [q, $^3J(H,H)$ = 3 Hz, 1 H, CH_{eq}], −0.7 (br. s, 9 H, BCH_3), −0.6 (br. s, 6 H, BCH_3), 0.84 [m, 3 H, $C(CH_3)_{ax}$], 0.93 [d, $^3J(H,H)$ = 3 Hz, 6 H, $C(CH_3)_{eq}$], 1.05 [d, $^3J(H,H)$ = 3 Hz, 12 H, $C(CH_3)_{eq}$]. − ^{13}C NMR (50 MHz, [D$_8$]THF): δ = −1.3 (CH), 16.1 (CCH_3), 17.8 (BCH_3). − ^{11}B NMR (64 MHz, [D$_8$]THF): δ = −31.5.

Reduction of 2 with Cesium: Amounts: THF (50mL), **2** (190 mg, 1.17 mmol). NMR spectroscopic data of the amorphous reduction product $[\mathbf{3}(Cs^+)_2(THF)_{2n}]_m$ (ratio of diastereomers $(CH_{ax})_3/(CH_{ax})_2(CH_{eq}) = 12:1$): ^1H NMR (200 MHz, [D$_8$]THF): δ = −3.89 [q, $^3J(H,H)$ = 3 Hz, 3 H, CH_{ax}], −3.64 [q, $^3J(H,H)$ = 3 Hz, 2 H, CH_{ax}], −1.89 [q, $^3J(H,H)$ = 3 Hz, 1 H, CH_{eq}], −0.8 (br. s, 9 H, BCH_3), −0.7 (br. s, 6 H, BCH_3), 0.82 [d, $^3J(H,H)$ = 3 Hz, 3 H, $C(CH_3)_{ax}$], 0.91 [d, $^3J(H,H)$ = 3 Hz, 6 H, $C(CH_3)_{eq}$], 1.01 [d, $^3J(H,H)$ = 3 Hz, 9 H, $C(CH_3)_{eq}$]. − ^{13}C NMR (50 MHz, [D$_8$]THF): δ = −1.3 (CH), 16.1 (CCH_3), 17.8 (BCH_3). − ^{11}B NMR (64 MHz, [D$_8$]THF): δ = −29.8.

X-ray Structure Determinations of $\{3(Li^+)[Li(thp)_2^+]\}_4$, $[3(Li^+)]_4\{Li([12]cr\text{-}4)_2^+\}_4$, $\{3(Na^+)[Na(thf)_3^+]\}_m$, $\{(thf)_2Na([18]cr\text{-}6)\}^+\{[3(Na^+)(thf)]_4(Na^+)_2\}^{2-}\{(thf)Na([18]cr\text{-}6)\}^+$ and $[3(K^+)(K[18]cr\text{-}6)^+]_m$: Crystal data and details of the structure determinations are listed in Table 3. Intensity data for $\{3(Li^+)[Li(thp)_2^+]\}_4$ and $[3(Li^+)]_4\{Li([12]cr\text{-}4)_2^+\}_4$ were collected at 210 K with a Siemens Stoe AED2 diffractometer, and for $\{3(Na^+)[Na(thf)_3^+]\}_m$, $\{(thf)_2Na([18]cr\text{-}6)\}^+\{[3(Na^+)(thf)]_4(Na^+)_2\}^{2-}\{(thf)Na([18]cr\text{-}6)\}^+$ and $[3(K^+)(K[18]cr\text{-}6)^+]_m$ at 173 K with a Bruker AXS Smart 1000 (Mo-K_α radiation, λ = 0.71073 Å, graphite monochromator, ω-scan). The structures were solved by direct methods and refined by least-squares methods based on F^2 with all measured reflections (SHELXL-97).[14] Non-hydrogen atoms were refined anisotropically (in $\{(thf)_2Na([18]cr\text{-}6)\}^+\{[3(Na^+)(thf)]_4(Na^+)_2\}^{2-}\{(thf)Na([18]cr\text{-}6)\}^+$ only the Na atoms). Most of the hydrogen atoms were inserted in their calculated positions. The THF and crown ligands are in some cases severely disordered. The crystal structure of $\{(thf)_2Na([18]cr\text{-}6)\}^+\{[3(Na^+)(thf)]_4(Na^+)_2\}^{2-}\{(thf)Na([18]cr\text{-}6)\}^+$ is not very precise, due to the very limited data set.

Crystallographic data (excluding structure factors) for the structures reported in this paper have been deposited with the Cambridge Crystallographic Data Center as supplementary publication nos. CCDC-133326 ($[\mathbf{3}(Li^+)_2([12]cr\text{-}4)_2]_4$), -156933 ($\{\mathbf{3}(Na^+)[Na(thf)_3^+]\}_m$), -156934 ($\{(thf)_2Na([18]cr\text{-}6)\}^+\{[3(Na^+)(thf)]_4(Na^+)_2\}^{2-}\{(thf)Na([18]cr\text{-}6)\}^+$) and -156935 ($[\mathbf{3}(K^+)(K[18]cr\text{-}6)^+]_m$). Copies of the data can be obtained free of charge upon application to CCDC, 12 Union Road, Cambridge CB2 1EZ, UK [Fax: (internat.) +44-1223/336-033; E-mail: deposit@ccdc.cam.ac.uk].

Acknowledgments

This work was supported by the Deutsche Forschungsgemeinschaft (Schwerpunkt Polyeder) and the Fonds der Chemischen Industrie.

[1] G. E. Herberich, in *Comprehensive Organometallic Chemistry* (Eds. G. Wilkinson, F. G. A. Stone, E. W. Abel), Pergamon Press **1982**, vol. 1, pp. 381−408.
[2] M. Unverzagt, G. Subramanian, M. Hofmann, P. v. R. Schleyer, S. Berger, K. Harms, W. Massa, A. Berndt, *Angew. Chem.* **1997**, *109*, 1567−1568; *Angew. Chem. Int. Ed. Engl.* **1997**, *36*, 1469−1472.
[3] D. Scheschkewitz, A. Ghaffari, P. Amseis, M. Unverzagt, G. Subramanian, M. Hofmann, P. v. R. Schleyer, H. F. Schaefer III, G. Geiseler, W. Massa, A. Berndt, *Angew. Chem.* **2000**, *112*, 1329−1333; *Angew. Chem. Int. Ed.* **2000**, *39*, 1272−1276.
[4] W. Lösslein, H. Pritzkow, P. von R. Schleyer, L. R. Schmitz, W. Siebert, *Angew. Chem.* **2000**, *112*, 1333−1336; *Angew. Chem. Int. Ed.* **2000**, *39*, 1276−1280.
[5] T. Deforth, M. Kaschke, H. Stock, H. Pritzkow, W. Siebert, *Z. Naturforsch.* **1997**, *52b*, 823−830.
[6] [6a] S. Winstein, J. Sonnenberg, L. de Vries, *J. Am. Chem. Soc.* **1959**, *81*, 6523−6524. − [6b] S. Winstein, *J. Am. Chem. Soc.* **1959**, *81*, 6524−6525. − [6c] S. Masamune, M. Sakai, A.V. Kemp-Jones, T. Nakashima, *Can. J. Chem.* **1974**, *52*, 855−857. − [6d] K. J. Szabo, E. Kraka, D. Cremer, *J. Org. Chem.* **1996**, *61*, 2783−2800.
[7] [7a] P. v. R. Schleyer, C. Maerker, A. Dransfeld, H. Jiao, N. J. R. van Eikema Hommes, *J. Am. Chem. Soc.* **1996**, *118*, 6317−6318. − [7b] P. v. R. Schleyer, H. Jiao, N. J. R. van Eikema Hommes, V. G. Malkin, O. L. Malkina, *J. Am. Chem. Soc.* **1997**, *119*, 12669−12670. − [7c] P. v. R. Schleyer, G. Subramanian, H. Jiao, K. Najafian, M. Hofmann, in *Advances in Boron Chemistry* (Ed.: W. Siebert), The Royal Society of Chemistry, Cambridge, UK, **1997**, pp. 3−14. − [7d] P. v. R. Schleyer, K. Najafian, *Inorg. Chem.* **1998**, *37*, 3454−3470. − [7e] P. v. R. Schleyer, K. Najafian, A. M. Mebel, *Inorg. Chem.* **1998**, *37*, 6765−6772. − [7f] M. Hofmann, D. Scheschkewitz, A. Ghaffari, G. Geiseler, W. Massa, H. F. Schaefer, A. Berndt, *J. Mol. Model.*, submitted.
[8] [8a] M. Geissler, J. Kopf, B. Schubert, E. Weiss, W. Neugebauer, P. v. R. Schleyer, *Angew. Chem.* **1987**, *99*, 569−570. − [8b] C. Schade, P. v. R. Schleyer, M. Geissler, E. Weiss, *Angew. Chem.* **1986**, *98*, 922−924; *Angew. Chem. Int. Ed. Engl.* **1986**, *25*, 902−904. − [8c] C. Schade, P. v. R. Schleyer, *Adv. Organomet. Chem.* **1987**, *27*, 169−278.
[9] C. Lambert, P. v. R. Schleyer, *Angew. Chem.* **1994**, *106*, 1187−1199; *Angew. Chem. Int. Ed. Engl.* **1994**, *33*, 1129−1140.
[10] C. Lambert, M. Kaupp, P. v. R. Schleyer, *Organometallics* **1993**, *12*, 853−859.
[11] W. Kutzelnigg. U. Fleischer, M. Schindler, in *NMR: Basic Principles and Progress*, Springer Verlag Berlin, **1990**, Vol. *23*, 165.
[12] J. M. Schulman, R. L. Disch, P. v. R. Schleyer, M. Bühl, M. Bremer, W. Koch, *J. Am. Chem. Soc.* **1992**, *114*, 7897−7901.
[13] [13a] K. Wade, *Adv. Inorg. Chem. Radiochem.* **1976**, *18*, 1−66. − [13b] D. M. P. Mingos, *Adv. Organomet. Chem.* **1977**, *15*, 1−51.
[14] G. M. Sheldrick, SHELXTL NT5.10, Bruker AXS, Madison, WI., **1999**.

Received January 17, 2001
[I01022]

Vinylidene, Vinyl, and Carbene Ruthenium Complexes with Chelating Diphosphanes as Ligands

Helmut Werner,*[a] Stefan Jung,[a] Pablo González-Herrero,[a] Kerstin Ilg,[a] and Justin Wolf[a]

Dedicated to Professor Wolfgang Kiefer on the occasion of his 60th birthday

Keywords: Ruthenium / Carbene ligands / Vinylidene ligands / Chelates / Phosphanes

The ruthenium vinylidenes $[RuCl_2(=C=CHR)(PR'_3)_2]$ (**1**, **2**) react with 1,2-$C_2H_4(PCy_2)_2$ (**3**) to give the chelate complexes $[RuCl_2(=C=CHR)(\kappa^2\text{-}\mathbf{3})]$ (**4**, **5**) by displacement of the two monodentate phosphane ligands. In contrast, the reaction of the hydrido compound $[RuHCl(=C=CH_2)(PCy_3)_2]$ (**6**) with excess **3** proceeds by migration of the hydride to the Cα carbon atom of the vinylidene unit and affords the six-coordinate vinyl complex *trans*-$[RuCl(CH=CH_2)(\kappa^2\text{-}\mathbf{3})_2]$ (**7**). Protonation of **7**, followed by addition of NH_4PF_6, yields the cationic ruthenium carbene *trans*-$[RuCl(=CHCH_3)(\kappa^2\text{-}\mathbf{3})_2]PF_6$ (**8**), together with small quantities of the hydrido compound $[RuH(\kappa^2\text{-}\mathbf{3})_2]PF_6$ (**9**). The Grubbs catalyst $[RuCl_2(=CHPh)(PCy_3)_2]$ (**10**) reacts with both **3** and $[Fe(\eta^5\text{-}C_5H_4PPh_2)_2]$ (**11**), also by ligand substitution, to give the corresponding chelate complexes $[RuCl_2(=CHPh)(\kappa^2\text{-}\mathbf{3})]$ (**12**) and $[RuCl_2(=CHPh)(\kappa^2\text{-}\mathbf{11})]$ (**13**); the latter has been characterized by X-ray crystal structure analysis.

Introduction

Recently, we reported that the reaction of the hydrido compound $[RuHCl(=C=CH_2)(PCy_3)_2]$ with acids HA, having a non-coordinating anion A^- such as BF_4^- or $B(Ar_f)_4^-$ [Ar_f = 3,5-$C_6H_3(CF_3)_2$], affords, in the presence of a donor solvent S, the six-coordinate carbyne(hydrido) complexes $[RuHCl(\equiv CCH_3)(PCy_3)_2(S)]A$ instead of the anticipated five-coordinate vinylideneruthenium derivatives $[RuCl(=C=CH_2)(PCy_3)_2(S)]A$.[1] Although the carbyne(hydrido) cations are highly efficient catalysts for the ring-opening metathesis polymerization (ROMP) of cyclooctene as well as for the cross-olefin metathesis of cyclopentene with methylacrylate, their lifetime is rather limited and significantly shorter than that of the corresponding ruthenium carbene $[RuCl_2(=CHCH_3)(PCy_3)_2]$.[2,3] This unfavorable aspect prompted us to prepare five-coordinate vinylideneruthenium complexes with chelating diphosphanes as ligands, which, we hoped, would be more suitable starting materials for the synthesis of stable cationic ruthenium carbynes. In this context it has to be mentioned that during the progress of this work, Hofmann et al. described the preparation and structural characterization of the carbeneruthenium compounds $[RuCl_2(=CHR)\{\kappa^2\text{-}tBu_2P(CH_2)_nPtBu_2\}]$ (n = 1 and 2) which, in the presence of trimethylsilyl triflate, catalyze the ring-opening metathesis polymerization (ROMP) of strained cycloolefins such as cyclooctene or norbornene.[4,5]

Results and Discussion

The reaction of the dichlororuthenium compound **1**[6] with an excess of the sterically demanding diphosphane **3** in ether results in the displacement of the two monodentate phosphane ligands and the formation of the chelate complex **4**, which precipitated as a yellow solid and was isolated in 94% yield (Scheme 1). The synthesis of the related complex **5** could only be achieved using **2** as the starting material since the bis(tricyclohexylphosphane)ruthenium counterpart $[RuCl_2(=C=CHPh)(PCy_3)_2]$[6,7] does not react with **3** by substitution of the PCy_3 units. The yield of **5** is relatively low (31%) due to the formation of an insoluble (probably polymeric) by-product. Both **4** and **5** are quite stable in the solid state but slowly decompose in solution. The ^1H NMR spectra of **4** and **5** display a triplet at δ = 3.26 (**4**) and 4.62 (**5**), which is assigned to the =C*H*R proton of the vinylidene ligand. The ^{13}C NMR spectra show the resonance for the Cα carbon atom of the Ru=C=CHR unit at δ = 353.0 (**4**) and 355.4 (**5**), the low-field chemical shift

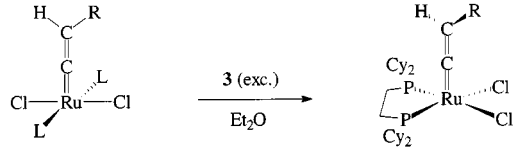

	L	R
1	PCy_3	*t*Bu
2	$PiPr_3$	Ph

	R
4	*t*Bu
5	Ph

Scheme 1

[a] Institut für Anorganische Chemie der Universität Würzburg, Am Hubland, 97074 Würzburg, Germany

 © WILEY-VCH Verlag GmbH, 69451 Weinheim, 2001 1434−1948/01/0808−1957 $ 17.50+.50/0

being in good agreement with the data observed for other mononuclear ruthenium vinylidenes.[6–8]

The most important feature of the NMR spectroscopic data of **4** and **5**, however, is the appearance of *two* signals at δ = 74.9, 73.5 (**4**) and 76.9, 74.5 (**5**) in the ^{31}P NMR spectra that are part of an AB system. The conclusion is that the chelating five-coordinate vinylidene complexes do not possess any plane of symmetry and, as found in the crystal structure of **1**,[6] the C–R bond lies parallel to one of the Ru–Cl bonds. Moreover, the rotation around the Ru=C=C axis must be significantly hindered, possibly due to the steric requirements of the four cyclohexyl groups.

Both **4** and **5** can be protonated with $HBF_4{\cdot}OEt_2$. While the protonation of **4** requires only one equivalent of the acid, the corresponding reaction of **5** requires an excess. In both cases a mixture of two products is formed of which one, according to the ^1H and ^{31}P NMR spectroscopic data, is the expected cationic ruthenium carbyne. Unfortunately, all attempts to separate the two compounds by fractional crystallization failed. The protonation is reversible and thus, upon addition of ether to a solution of the products in CH_2Cl_2, the ruthenium vinylidenes **4** and **5** are regenerated.

In contrast to **1**, which upon treatment with **3** affords the vinylidene compound **4**, the reaction of the chloro(hydrido) derivative **6** with a sixfold excess of **3** gives the vinylruthenium(II) complex **7** in 75% isolated yield (Scheme 2). A similar conversion of a RuH(=C=CHR) to a Ru(CH=CHR) moiety was recently reported by Caulton et al. who prepared the cationic vinyl compound [Ru(CH=CHSiMe$_3$)(CNMe)$_3$(P*t*Bu$_2$Me)$_2$]I from [RuHI(=C=CHSiMe$_3$)(P*t*Bu$_2$Me)$_2$] and methyl isocyanide.[9] With regard to the structure of **7**, we assume that the two chelating diphosphane ligands are *trans* disposed which is consistent with the single resonance in the ^{31}P NMR spectrum at δ = 53.2.

In analogy to the five-coordinate vinyl complex [Ru(CH=CH$_2$)(CH$_3$CN)$_2$(PCy$_3$)$_2$]BF$_4$, which reacts with HBF_4 in ether to generate the dicationic ruthenium carbene [Ru(=CHCH$_3$)(CH$_3$CN)$_2$(PCy$_3$)$_2$](BF$_4$)$_2$,[10] treatment of **7** with ethereal HBF_4, followed by addition of NH_4PF_6, gives the monocationic, six-coordinate carbene compound **8** in moderate yield. The hydrido complex **9** is formed (yield 10%) as a by-product; it was previously obtained by Winter and Hornung from [RuCl$_2$(DMSO)$_4$], **3** and NH*i*Pr$_2$ in the presence of NH_4PF_6.[11] Typical spectroscopic features of **8** are the signal for the RuC*H* proton at δ = 16.48 in the ^1H NMR spectrum and the multiplet for the carbene carbon atom at δ = 342.9 in the ^{13}C NMR spectrum; the latter appears as a singlet after $^{13}C\{^{31}P\}$ decoupling. Similarly to **4** and **5**, the ^{31}P NMR spectrum of **8** displays two resonances at δ = 80.3 and 78.9, corresponding to an AB system, which illustrates that the PCy$_2$ units are pairwise inequivalent.

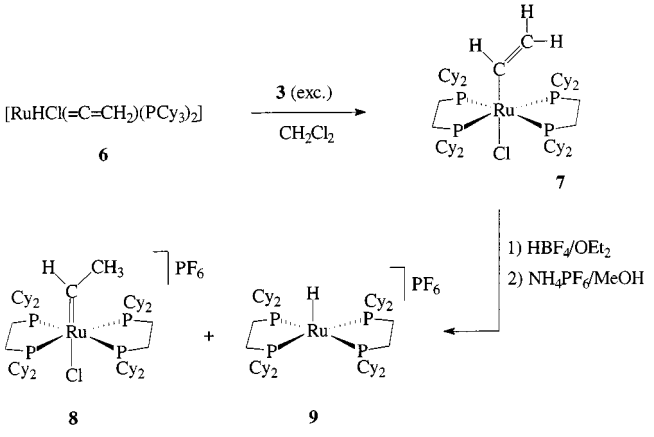

Scheme 2

In order to compare the reactivity of the five-coordinate ruthenium vinylidenes **1** and **2** with that of related ruthenium carbenes, the Grubbs catalyst **10** was also treated with **3** as well as with 1,1′-bis(diphenylphosphanyl)ferrocene (**11**). In both cases the monodentate PCy$_3$ ligands are readily displaced and the chelate compounds **12** and **13** (Scheme 3) are isolated in nearly quantitative yield. Both **12** and **13** can be stored under argon for weeks without decomposition, and they are also significantly more stable in solution than their vinylidene counterparts **4** and **5**. The ^1H NMR spectra of **12** and **13** show the expected triplet resonance for the Ru=C*H*Ph proton at δ = 14.68 (**12**) and 17.18 (**13**), while the signal for the carbene carbon atom is observed in the ^{13}C NMR spectra at δ = 282.6 (**12**) and 364.3 (**13**). Consistent with the results obtained by Hofmann and co-workers,[4,5] the ruthenium carbenes **12** and **13** are inactive in the ROMP of cyclooctene, but become good catalysts for olefin metathesis upon addition of trimethylsilyl triflate.

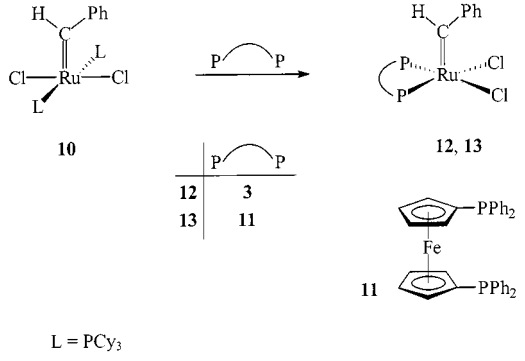

Scheme 3

The molecular structure of **13** is shown in Figure 1. In contrast to the ruthenium vinylidene [RuCl$_2$(=C=CHPh)(PCy$_3$)$_2$][7] and the related ruthenium carbenes [RuCl$_2$(=CHCH=CMe$_2$)(κ^2-*t*Bu$_2$PCH$_2$P*t*Bu$_2$)][4] and [RuCl(=CHPh)(κ^2-*t*Bu$_2$PCH$_2$CH$_2$-P*t*Bu$_2$)],[5] the geometry around the metal center is not square-pyramidal but distorted trigonal-bipyramidal. The P1–Ru–Cl2 axis, connecting the ligand atoms in the apical positions, is somewhat bent [167.23(5)°] which could be due to the steric hindrance between the two phenyl rings containing the carbon atoms C30–C35 and C2–C7. While the angle C1–Ru–P2 is near to 90°, the two other bond angles in the basal plane of the molecule are considerably larger [123.93(14)° and 146.96(5)°, respectively]. Owing to the che-

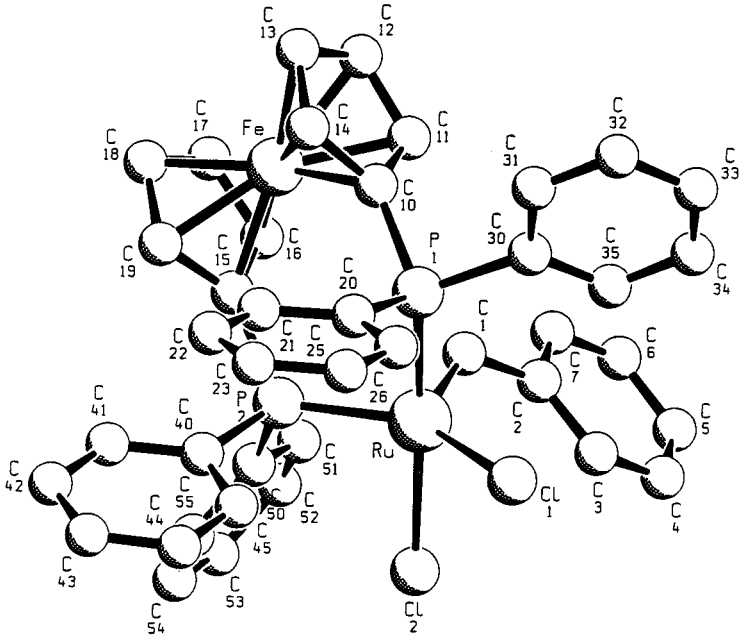

Figure 1. Molecular structure (SCHAKAL plot) of **13**; four of the five phenyl rings are reduced in size and the hydrogen atoms are omitted for clarity; selected bond lengths [Å] and angles [°]: Ru−C1 1.860(5), Ru−P1 2.3151(14), Ru−P2 2.2718(12), Ru−Cl1 2.3949(13), Ru−Cl2 2.4115(14), C1−C2 1.470(7); P1−Ru−P2 95.32 (5), P1−Ru−C1 90.46(16), P1−Ru−Cl1 84.07(5), P1−Ru−Cl2 167.23(5), P2−Ru−C1 89.07(14), P2−Ru−Cl1 146.96(5), P2−Ru−Cl2 87.13(5), Cl1−Ru−Cl2 86.93(5), C1−Ru−Cl1 123.93(14), C1−Ru−Cl2 102.09(16), Ru−C1−C3 125.3(4)

lating coordination of **11**, the cyclopentadienyl rings are not parallel to each other, the two planes C10−C11−C12−C13−C14 and C15−C16−C17−C18−C19 forming a dihedral angle of 37.7(3)°. The Ru−C1 bond length [1.860(5) Å] is almost identical to that of the Hofmann compounds [$RuCl_2(=CHCH=CMe_2)(\kappa^2$-$t Bu_2PCH_2Pt Bu_2)$] [1.858(2) Å][4] and [$RuCl_2(=CHPh)(\kappa^2$-$t Bu_2PCH_2CH_2Pt Bu_2)$] [1.836(3) Å][5] and differs only slightly from that of the bis(tricyclohexylphosphane) complexes [$RuCl_2(=CH$-p-$C_6H_4Cl)(PCy_3)_2$] [1.839(3) Å][2] and [$RuCl(CN)(=CHCH_3)(PCy_3)_2$] [1.810(6) Å].[12] The Ru−P distances of **13** are in the expected range and that is also true for the Ru−Cl bond lengths.

Experimental Section

All operations were carried out under argon using Schlenk techniques. The starting materials **1**,[6] **2**,[7] **3**,[13] **6**,[3] and **10**[2] were prepared as described in the literature. Compound **11** was a product from Aldrich. − NMR: Bruker AC 200 and AMX 400 [dvt = doublet of virtual triplets; $N = {}^3J(PH) + {}^5J(PH)$ or ${}^2J(PC) + {}^4J(PC)$]. − MS: Finnigan 90 MAT. − Melting points determined by DTA.

Preparation of [$RuCl_2(=C=CHt Bu)(\kappa^2$-3)] (4): A solution of **1** (1.13 g, 1.39 mmol) in 60 mL of ether was treated with **3** (878 mg, 2.08 mmol) and stirred for 7.5 h at room temperature. A yellow solid precipitated, which was separated from the mother liquor, washed with ether (2 × 10 mL) and recrystallized from CH_2Cl_2/pentane (1:10) (−20 °C); yield 884 mg (94%); m.p. 174 °C (dec.). − IR (KBr): ν(C=C) = 1648 cm^{-1}. − ^1H NMR (400 MHz, $CDCl_3$): δ = 3.26 [t, J(PH) = 3.8 Hz, 1 H, =C*H*R], 2.59−1.26 (br. m, 48 H, CH_2 and C_6H_{11}), 1.20 (s, 9 H, CCH_3). − $^{13}C\{^1H,^{31}P\}$ NMR (100.6 MHz, $CDCl_3$): δ = 353.0 (Ru=C), 118.9 (=*C*HR), 40.2, 39.9, 39.3, 38.3 (CH of C_6H_{11}), 33.1 (CCH_3), 32.1 (CCH_3), 30.4, 30.0, 29.9, 29.6, 28.8, 28.7, 28.2, 27.7, 27.5, 27.4, 26.9, 26.1, 26.0 (CH_2 of C_6H_{11}), 21.5, 20.1 (CH_2 of **3**). − $^{31}P\{^1H\}$ NMR (162.0 MHz, $CDCl_3$): δ = 74.9, 73.5 (AB system, J = 13.5 Hz). − $C_{32}H_{58}Cl_2P_2Ru$ (676.7): calcd. C 56.97, H 8.64; found C 56.60, H 8.22.

Preparation of [$RuCl_2(=C=CHPh)(\kappa^2$-3)] (5): A solution of **2** (347 mg, 0.58 mmol) in 20 mL of ether was treated with **3** (438 mg, 1.04 mmol) and stirred for 2.5 h at room temperature. A pink solid slowly precipitated which was separated from the mother liquor, washed with ether (2 × 10 mL) and suspended in 8 mL of CH_2Cl_2. A color change from pink to yellow occurred upon stirring this suspension for 4.5 h at room temperature. The suspension was filtered to remove the insoluble by-product, the filtrate was concentrated to ca. 3 mL in vacuo and 20 mL of ether was added. A greenish-yellow precipitate was formed which was recrystallized from CH_2Cl_2/ether (1:10) (−20 °C): yield 127 mg (31%); m.p. 128 °C (dec.). − IR (KBr): ν(C=C) = 1626 cm^{-1}. − ^1H NMR (400 MHz, $CDCl_3$): δ = 7.20, 7.02 (both m, 5 H, C_6H_5), 4.62 [t, J(PH) = 3.5 Hz, 1 H, =C*H*Ph], 2.69−0.90 (br. m, 48 H, CH_2 and C_6H_{11}). − $^{13}C\{^1H,^{31}P\}$ NMR (100.6 MHz, $CDCl_3$): δ =355.4 (Ru=C), 128.5, 127.9, 126.8, 125.9 (all C_6H_5), 112.3 (=*C*HPh), 40.9, 40.0, 39.5, 38.0 (CH of C_6H_{11}), 30.2, 30.0, 29.3, 28.9, 28.6, 28.4, 27.5, 27.2, 27.1, 27.0, 26.9, 26.6, 26.0, 25.9, 25.5, 25.4 (CH_2 of C_6H_{11}), 22.3, 20.4 (CH_2 of **3**). − $^{31}P\{^1H\}$ NMR (162.0 MHz, $CDCl_3$): δ = 76.9, 74.5 (AB system, J = 15.3 Hz). − $C_{34}H_{54}Cl_2P_2Ru$ (696.8): calcd. C 58.61, H 7.81; found C 58.25, H 7.44.

Preparation of *trans*-[$RuCl(CH=CH_2)(\kappa^2$-3)$_2$] (7): A solution of **6** (350 mg, 0.48 mmol) in 25 mL of CH_2Cl_2 was treated with a solution of **3** (1.21 g, 2.85 mmol) in 15 mL of CH_2Cl_2 and stirred for 1 h at room temperature. The solvent was evaporated in vacuo, and the off-white solid was washed with pentane (2 × 10 mL) and dried: yield 365 mg (75%); m.p. 54 °C (dec.). − IR (KBr): ν(C=C) = 1528 cm^{-1}. − ^1H NMR (300 MHz, CD_2Cl_2): δ = 6.74 (m,

1 H, RuCH), 4.67 [d, *J*(HH) = 7.2 Hz, 1 H, one H of CH_2 *cis* to =CH], 3.91 [d, *J*(HH) = 15.3 Hz, 1 H, one H of CH_2 *trans* to =CH], 2.43−1.14 (br. m, 96 H, CH_2 of **3** and C_6H_{11}). − $^{13}C\{^1H\}$ NMR (75.5 MHz, CD_2Cl_2): δ = 146.8 (m, RuCH), 120.1 (m, $=CH_2$), 39.3, 35.5 (both m, CH of C_6H_{11}), 30.5, 29.9, 29.6, 29.1, 28.0, 27.7, 27.4, 27.3, 26.1, 26.0 (all s, CH_2 of C_6H_{11}), 18.0 (m, CH_2 of **3**). − $^{31}P\{^1H\}$ NMR (162.0 MHz, CD_2Cl_2): δ = 53.2 (s). − $C_{54}H_{99}ClP_4Ru$ (1008.8): calcd. C 64.29, H 9.89; found C 64.13, H 9.88.

Preparation of *trans*-[RuCl(=CHCH$_3$)(κ^2-3)$_2$]PF$_6$ (8): A solution of **7** (309 mg, 0.31 mmol) in 20 mL of CH_2Cl_2 was treated at −78 °C with 0.4 mL of a 1.6 M solution of HBF_4 (0.64 mmol) in ether. After stirring the solution 30 min. at −78 °C, the solvent was evaporated in vacuo and the residue washed with ether (2 × 10 mL). The brownish yellow solid, which according to the ^1H NMR spectrum consists of a mixture of the BF_4^- salts of the cations $[RuCl(=CHCH_3)(\kappa^2\text{-}\mathbf{3})_2]^+$ and $[RuH(\kappa^2\text{-}\mathbf{3})_2]^+$, was suspended in 15 mL of methanol and the suspension was treated dropwise with a solution of NH_4PF_6 (340 mg, 2.09 mmol) in 10 mL of methanol. Stirring the reaction mixture for 25 min. at room temperature led to the formation of a pink precipitate of **8**, which was separated from the mother liquor, washed with methanol (2 × 15 mL) and dried: yield 111 mg (39%). From the mother liquor and the combined washings a yellow solid slowly precipitated which was identified as $[RuH(\kappa^2\text{-}\mathbf{3})_2]PF_6$ (**9**) by comparison with reference data.[11]

8: m.p. 92 ° C (dec.). − Λ(CH_3NO_2) = 53.4 cm$^2\Omega^{-1}$ mol^{-1}. − ^1H NMR (400 MHz, CD_2Cl_2): δ = 16.48 [m; in $^1H\{^{31}P\}$: q, *J*(HH) = 6.0 Hz, 1 H, =CH], 2.94 [d, *J*(HH) = 6.0 Hz, 3 H, CH_3], 2.81, 2.66, 2.44−0.90 (all m, 96 H, CH_2 and C_6H_{11}). − $^{13}C\{^1H\}$ NMR (100.6 MHz, CD_2Cl_2): δ = 342.9 [quin, *J*(PC) = 14.5 Hz, Ru=C], 49.5 (s, CH_3), 39.9 [d, *J*(PC) = 21.6 Hz, CH of C_6H_{11}], 38.0 [d, *J*(PC) = 24.2 Hz, CH of C_6H_{11}], 37.6 [d, *J*(PC) = 22.9 Hz, CH of C_6H_{11}], 37.5 [d, *J*(PC) = 25.4 Hz, CH of C_6H_{11}], 29.9, 29.4, 29.3 (all s, CH_2 of C_6H_{11}), 28.9 [d, *J*(PC) = 2.6 Hz, CH_2 of C_6H_{11}], 28.6 [d, *J*(PC) = 6.4 Hz, CH_2 of C_6H_{11}], 28.5 [d, *J*(PC) = 5.1 Hz, CH_2 of C_6H_{11}], 27.8−27.1 (m, CH_2 of C_6H_{11}), 26.7 [d, *J*(PC) = 11.4 Hz, CH_2 of C_6H_{11}], 26.4, 26.2, 26.1 (all s, CH_2 of C_6H_{11}), 20.0, 19.4 [both dd, *J*(PC) = 29.2 and 8.9 Hz, CH_2 of **3**]. − $^{31}P\{^1H\}$ NMR (162.0 MHz, CD_2Cl_2): δ = 80.3, 78.9 (AB system, *J* = 21.8 Hz), −144.4 [sept, *J*(PF) = 710.7 Hz, PF_6^-]. − $C_{54}H_{100}ClF_6P_5Ru$ (1154.8): calcd. C 56.17, H 8.73; found C 55.88, H 8.27.

Preparation of *trans*-[RuCl$_2$(=CHPh)(κ^2-3)] (12): A solution of **10** (202 mg, 0.25 mmol) in 8 mL of CH_2Cl_2 was treated with a solution of **3** (129 mg, 0.31 mmol) in 5 mL of CH_2Cl_2 and stirred for 3.5 h at room temperature. The solvent was evaporated in vacuo, the remaining greenish solid was washed with pentane (3 × 10 mL) and ether (2 × 8 mL) and then dried: yield 160 mg (92%); m.p. 76 °C (dec.). − ^1H NMR (400 MHz, CD_2Cl_2): δ = 14.68 [t, *J*(PH) = 16.1 Hz, 1 H, =C*H*Ph], 8.41, 7.70−7.34 (both m, 5 H, C_6H_5), 2.30−0.86 (m, 48 H, CH_2 and C_6H_{11}). − $^{13}C\{^1H\}$ NMR (100.6 MHz, CD_2Cl_2): δ = 292.6 [t, *J*(PC) = 16.5 Hz, Ru=C], 148.7 (s, *ipso*-C of C_6H_5), 131.5, 130.5, 128.8 (all s, C_6H_5), 38.1, 36.3 (both m, CH of C_6H_{11}), 30.1, 28.8, 28.4, 28.2 (all s, CH_2 of C_6H_{11}), 27.5−26.5 (m, CH_2 of C_6H_{11}), 26.4, 26.0 (both s, CH_2 of C_6H_{11}), 20.1 [dd, *J*(PC) = 20.4 and 16.5 Hz, CH_2 of **3**]. − $^{31}P\{^1H\}$ NMR (162.0 MHz, CD_2Cl_2): δ = 81.7 (s). − $C_{33}H_{54}Cl_2P_2Ru$ (684.7): calcd. C 57.89, H 7.95; found C 57.65, H 7.57.

Preparation of *trans*-[RuCl$_2$(=CHPh)(κ^2-11)] (13): A solution of **10** (492 mg, 0.60 mmol) in 15 mL of CH_2Cl_2 was treated with a solution of **11** (398 mg, 0.72 mmol) in 10 mL of CH_2Cl_2 and stirred for 7 h at room temperature. The solvent was evaporated in vacuo, the remaining olive-green solid was washed with acetone (2 × 5 mL) and pentane (2 × 6 mL) and then dried: yield 430 mg (88%); m.p. 176 °C (dec.). − ^1H NMR (200 MHz, CD_2Cl_2): δ = 17.18 [t, *J*(PH) = 18.2 Hz, 1 H, =C*H*Ph], 7.88−7.02 (br. m, 25 H, C_6H_5), 4.78, 4.59, 4.47, 4.36 (all s, 8 H, C_5H_4). − $^{13}C\{^1H\}$ NMR (100.6 MHz, CD_2Cl_2): δ = 364.3 [t, *J*(PC) = 21.0 Hz, Ru=C], 150.5 (s, *ipso*-C of C_6H_5), 135.7, 133.5 [both t, *J*(PC) = 5.1 Hz, C_6H_5], 132.7, 131.0, 130.7, 129.6, 129.5 (all s, C_6H_5), 127.9, 127.2 [both t, *J*(PC) = 5.1 Hz, C_6H_5], 74.6 [t, *J*(PC) = 5.1 Hz, C_5H_4], 74.5 (s, C_5H_4), 72.5 [t, *J*(PC) = 5.1 Hz, C_5H_4], 69.3 (s, C_5H_4). − $^{31}P\{^1H\}$ NMR (162.0 MHz, CD_2Cl_2): δ = 50.9 (s). − MS (FAB): *m*/*z* = 816 [M$^+$]. − $C_{41}H_{34}Cl_2FeP_2Ru$ (816.5): calcd. C 60.31, H 4.20, Ru 12.38; found C 59.95, H 4.64, Ru 11.77.

Determination of the X-ray Crystal Structure of 13: Single crystals were grown upon cooling of a saturated solution of **13** in CH_2Cl_2 from 25 °C to −20 °C. Crystal data (from 5000 reflections, 2.34° < Θ < 25.00°): triclinic; space group $P2_1/c$ (No. 14); *a* = 13.998(2), *b* = 14.7459(16), *c* = 20.125(3) Å, β = 98.417(18)°; *V* = 4109.3(10) Å^3, *Z* = 4; $d_{calcd.}$ = 1.593 g·cm^{-3}; μ(Mo-K_α) = 1.220 mm^{-1}; crystal size 0.18 × 0.18 × 0.12 mm; IPDS (STOE), Mo-K_α radiation (0.71073 Å), graphite monochromator; *T* = 173(2) K; -scans, max. 2θ = 50.00°; 32351 reflections measured, 7226 independent ($R_{int.}$ = 0.0530), 4891 with $I > 2\sigma(I)$. Intensity data were corrected for Lorentz and polarization effects. The structure was solved by direct methods (SHELXS-97).[14] Atomic coordinates and the anisotropic thermal parameters of non-hydrogen atoms were refined by full-matrix least-squares on F^2 (SHELXL-97).[15] The positions of all hydrogen atoms were calculated according to ideal geometry and refined by using the riding method. The asymmetric unit includes two molecules of CH_2Cl_2 which were refined anisotropically with restraints. One of them was found to be disordered and two positions were refined with occupancy factors of 0.85 and 0.15, respectively. Conventional *R* = 0.0403 [for 4891 reflections with $I > 2\sigma(I)$], and weighted wR_2 = 0.1041 for all 7226 located reflections; reflection/parameter ratio 14.5; residual electron density +0.121/−0.067 eÅ^{-3}.

Crystallographic data (excluding structure factors) for **13** have been deposited with the Cambridge Crystallographic Data Centre as supplementary publication no. CCDC-159684. Copies of the data can be obtained free of charge on application to CCDC, 12 Union Road, Cambridge CB2 1EZ, UK [Fax: (internat.) +44-1223/336-033; E-mail: deposit@ccdc.cam.ac.uk].

Acknowledgments

This work was supported by the Deutsche Forschungsgemeinschaft (SFB 347), the BASF AG, and the Fonds der Chemischen Industrie. We are grateful to the latter in particular for a Ph. D. grant (to K. I.) and also thank the European Commission under the Training and Mobility of Researchers program for a Marie Curie Fellowship (to P. G.-H.). Moreover, we thank Dr. W. Buchner and Mrs. M.-L. Schäfer for NMR measurements, Mrs. R. Schedl and Mr. C. P. Kneis for elemental analyses and DTA measurements, and Dr. G. Lange and Mr. F. Dadrich for mass spectra.

[1] W. Stüer, J. Wolf, H. Werner, P. Schwab, M. Schulz, *Angew. Chem.* **1998**, *110*, 3603−3606; *Angew. Chem. Int. Ed.* **1998**, 37, 3421−2423.

[2] [2a] P. Schwab, M. B. France, J. W. Ziller, R. H. Grubbs, *Angew. Chem.* **1995**, *107*, 2179−2181; *Angew. Chem. Int. Ed. Engl.* **1995**, *34*, 2039−2041. − [2b] P. Schwab, R. H. Grubbs, J. W. Ziller, *J. Am. Chem. Soc.* **1996**, *118*, 100−110.

[3] J. Wolf, W. Stüer, C. Grünwald, H. Werner, P. Schwab, M. Schulz, *Angew. Chem.* **1998**, *110*, 1165−1167; *Angew. Chem. Int. Ed.* **1998**, *37*, 1124−1126.

[4] [4a] S. M. Hansen, M. A. O. Volland, F. Rominger, F. Eisenträger, P. Hofmann, *Angew. Chem.* **1999**, *111*, 1360−1364; *Angew. Chem. Int. Ed.* **1999**, *38*, 1273−1276. − [4b] S. M. Hansen, F. Rominger, M. Metz, P. Hofmann, *Chem. Eur. J.* **1999**, *5*, 557−566.
[5] M. A. O. Volland, B. F. Straub, I. Gruber, F. Rominger, P. Hofmann, *J. Organomet. Chem.* **2001**, *617−618*, 288−291.
[6] H. Katayama, F. Ozawa, *Organometallics* **1998**, *17*, 5190−5196.
[7] J. Wolf, W. Stüer, C. Grünwald, O. Gevert, M. Laubender, H. Werner, *Eur. J. Inorg. Chem.* **1998**, 1827−1834.
[8] [8a] M. I. Bruce, A. G. Swincer, *Adv. Organomet. Chem.* **1983**, *22*, 59−128. − [8b] M. I. Bruce, *Chem. Rev.* **1991**, *91*, 197−257. − [8c] Y. Wakatsuki, H. Yamazaki, N. Kumegawa, T. Satoh, J. Y. Satoh, *J. Am. Chem. Soc.* **1991**, *113*, 9604−9610. − [8d] H. Werner, A. Stark, M. Schulz, J. Wolf, *Organometallics* **1992**, *11*, 1126−1130. − [8e] H. Werner, P. Steinert, C. Grünwald, J. Wolf, *Chem. Ber.* **1995**, *128*, 49−62. − [8f] M. Martin, O. Gevert, H. Werner, *J. Chem. Soc., Dalton Trans.* **1996**, 2275−2283.
[9] M. Oliván, E. Clot, O. Eisenstein, K. G. Caulton, *Organometallics* **1998**, *17*, 3091−3100.
[10] S. Jung, K. Ilg, J. Wolf, H. Werner, submitted for publication.
[11] R. F. Winter, F. M. Hornung, *Inorg. Chem.* **1997**, *36*, 6197−6204.
[12] B. Weberndörfer, Dissertation, Universität Würzburg, **2001**.
[13] K. Issleib, K. Krech, K. Gruber, *Chem. Ber.* **1963**, *96*, 2186−2192.
[14] G. M. Sheldrick, *Acta Crystallogr., Sect. A* **1990**, *46*, 467−473.
[15] G. M. Sheldrick, *A Program for Crystal Structure Refinement*, University of Göttingen, **1993.**

Received March 8, 2001
[I01089]

Diastereoselectivity of Octahedral Cobalt(II) Pybox Complexes

Christophe Provent,[a] Gérald Bernardinelli,[b] Alan F. Williams,*[a] and Nathalie Vulliermet[c]

Keywords: Cobalt / Chirality / N ligands / Coordination chemistry

The cobalt(II) complexes prepared with a series of enantiopure ligands (**1**–**3**) containing the bis(oxazolinyl)pyridine unit have been studied. The ligands form high spin octahedral complexes as shown by the X-ray crystal structure of the homochiral complex $[Co(R,R\text{-}\mathbf{1})_2](ClO_4)_2(CH_3CN)_3$. The diastereoselectivity of complex formation has been studied: equimolar mixtures of *RR* and *SS* ligands show mixtures of homochiral and heterochiral complexes for **2** and **3**, but the phenyl-substituted ligand **1** shows exclusive formation of the heterochiral species. This selectivity is correlated with structural and electronic properties of the complexes.

Introduction

The use of chiral ligands in coordination chemistry is becoming increasingly important.[1] When two or more chiral ligands are bound to the same ligand, diastereomers may be formed, and the selectivity for one or other diastereomer may be studied.[2–7] The bis(oxazolinyl)pyridine (pybox) family of ligands (Scheme 1) were first developed by Nishiyama and co-workers for enantioselective homogeneous catalysis,[8,9] and have also been used to generate chiral Lewis acid catalysts.[10] We have recently used these ligands for the enantioselective synthesis of helical complexes.[11] During this work it was observed that the phenyl derivative **1** showed significantly different behavior from the other ligands **2** and **3**, forming a cyclic trinuclear helicate rather than a linear dinuclear helicate. This difference could be attributed to intramolecular attractions between the phenyl substituents and the pyridine moiety.[12] It therefore seemed of interest to study the chemistry of simple, mononuclear octahedral complexes of the type $[ML_2]$ to see if these substituent effects were also observed in these simple systems. In this paper we report on the remarkable difference in diastereoselectivity observed with the three different ligands with cobalt(II).

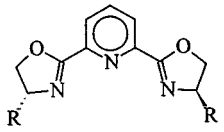

1 R = Ph
2 R = Me
3 R = Bzl

Scheme 1. Ligands used in this work

Results

Synthesis of Complexes

The cobalt(II) complexes were prepared by adding two equivalents of ligand in acetonitrile to a solution of one equivalent of cobalt(II) perchlorate in acetonitrile at 20 °C (the heterochiral complex synthesis was carried out by mixing one equivalent of *R*,*R* ligand, one equivalent of *S*,*S* ligand and one equivalent of cobalt salt). The solutions were stirred for 30 minutes and then concentrated, before crystallization by diffusion of diethyl ether or *tert*-butyl methyl ether. The crystals prepared with $[Co(R,R\text{-}\mathbf{1})_2]^{2+}$ were of suitable quality for an X-ray structure determination. The complexes were characterized in solution by electrospray mass spectrometry (ESMS) and ^{1}H NMR spectroscopy. ESMS showed the exclusive formation of $[CoL_2]^{2+}$ with the base peak due to $[CoL_2]^{2+}$ and a weaker peak due to $\{[CoL_2](ClO_4)\}^+$. The ^{1}H NMR spectra are discussed below.

Crystal Structure of $[Co(R,R\text{-}\mathbf{1})_2](ClO_4)_2(CH_3CN)_3$

The X-ray crystal structure analysis of the orange crystals of $[Co(RR\text{-}\mathbf{1})_2](ClO_4)_2(CH_3CN)_3$ shows the expected octahedral ML_2 structure with the ligand acting as a meridional tridentate ligand (Figure 1). The cobalt(II) cation is coordinated by two pyridine-N atoms and four oxazoline-N atoms [av. Co-N(oxazoline) distance: 2.15 Å; av. Co-N(pyridine) distance: 2.06 Å]. The chelate bite angles are similar and close to 76°. The small bite angle results in considerable deviation of the angles at the cobalt atom from 90°, but the two pyridine rings are inclined at 93.2(8)°, close to the ideal value.

[a] Département de Chimie minérale, analytique, et appliquée, Université de Genève,
30 quai Ernest Ansermet, 1211 Genève 4, Switzerland
Fax: (internat.) + 41-22/702-6069
E-mail: Alan.Williams@chiam.unige.ch
[b] Laboratoire de Cristallographie aux rayons-X, Université de Genève,
24 quai Ernest Ansermet, 1211 Genève 4, Switzerland
[c] Département de Chimie physique, Université de Genève,
30 quai Ernest Ansermet, 1211 Genève 4, Switzerland

 © WILEY-VCH Verlag GmbH, 69451 Weinheim, 2001 1434–1948/01/0808–1963 $ 17.50+.50/0

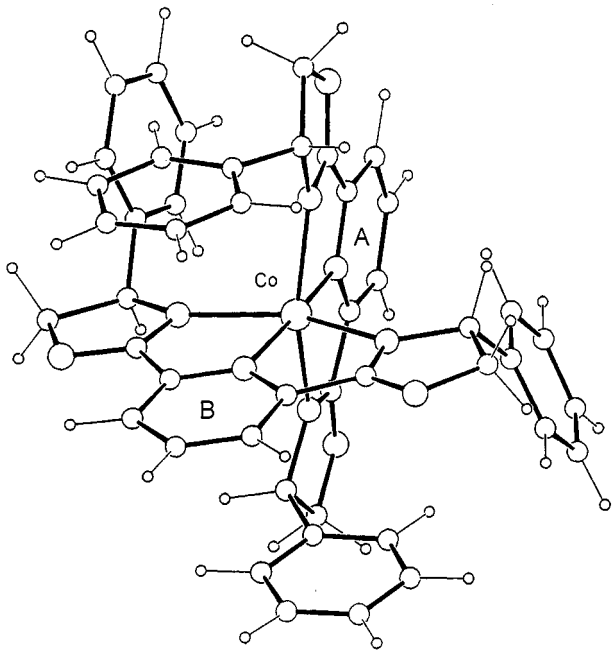

Figure 1. Structure of the cation $[Co(R,R\text{-}\mathbf{1})_2]^{2+}$; the stacking interaction is observed between the pyridine of ligand B and the phenyls of ligand A

The two ligands differ in the conformation of the phenyl substituents. Ligand A has the two phenyl rings oriented at roughly 90° to the oxazoline plane, in such a way as to lie almost parallel to the pyridine of ligand B [interplane angles: 3.7(7) and 3.0(7)°; interplane distances: 3.55(7) and 3.66(6) Å] indicating a stacking interaction similar to that observed in the circular trinuclear helicate.[11] The phenyl groups of ligand A are offset with respect to the coordinated pyridine of ligand B, as expected according to the model of Hunter and Sanders.[13] This orientation of ligand A, however, brings the phenyl rings close to those of ligand B. The geometry of this phenyl−phenyl interaction cannot be regarded as an edge-to-face interaction[14] since the hydrogen atoms are not directed toward the phenyl carbons. It may therefore be considered as a repulsion that prevents the phenyls of B from stacking with the pyridine of A. The phenyls of B are inclined at 17.9(9) and 31.1(1)° with respect to the pyridine of A, the interplane distances are longer, and the overlap is poor. The steric repulsion between the phenyls is shown by a CPK representation of the cation and by the slight deviations of the bis(oxazoline)pyridine units from planarity. The presence of the stacking interaction in one direction but not in the other reduces the molecular symmetry from D_2 to C_2.

Properties in Solution

Table 1 summarizes the electronic and CD transitions associated with the d-d bands in acetonitrile solution. The values are typical of high spin octahedral cobalt(II) with spin-allowed bands around 1100 nm and 470 nm. The ligand field as estimated by the d-d band positions decreases in the series **1** > **2** > **3**. The CD spectrum shows negative bands associated with the spin-allowed d-d bands for the *R*,*R* enantiomer of the ligand, although only the higher energy band falls completely within the range of the instrument. Two other weak CD bands are observed around 520 and 620 nm and are assumed to be associated with spin-forbidden or two-electron excitations. MLCT bands are observed around 340 nm as shoulders on ligand-based absorptions, at slightly higher energy than a strong CD signal (negative for the *R*,*R* isomer). The CD spectra of complexes of the *S*,*S* enantiomers of the ligands are the inverse of those of the *R*,*R* enantiomers.

The fast electronic relaxation times of high spin cobalt(II) allow the ^{1}H NMR spectra to be recorded at 20 °C in acetonitrile (Figure 2). The proton α to the nitrogen of the oxazoline lies closest to the metal center and has an NMR shift of δ = 86.3. The other peaks lie between δ = 0 and 40. The spectra show the two ligands to be equivalent and symmetric. The ^{1}H NMR spectra allow the investigation of the diastereoselectivity of complex formation. If an enantiopure ligand is used, only the homochiral complex is obtained, but if a racemic mixture of *R*,*R* and *S*,*S* ligands is used then the heterochiral *meso*-complex $[Co(R,R\text{-}\mathbf{L})(S,S\text{-}\mathbf{L})]^{2+}$ may also be formed. The two enantiomers of the homochiral complexes have identical spectra, but the heterochiral complex shows a different spectrum. Reaction of cobalt(II) with an equimolar amount of *R*,*R* and *S*,*S* ligands may thus be used to study the diastereoselectivity. The three ligands show very different behavior. Ligand **1** shows exclusive formation of the heterochiral complex $[Co(R,R\text{-}\mathbf{1})(S,S\text{-}\mathbf{1})]^{2+}$ with a spectrum totally different from $[Co(R,R\text{-}\mathbf{1})_2]^{2+}$ and no trace of the homochiral complex. Ligands **2** and **3**, on the other hand, show the presence of

Table 1. d-d absorption bands and circular dichroism of complexes in acetonitrile solution

	$[Co(R,R\text{-}\mathbf{1})_2]^{2+}$	$[Co(R,R\text{-}\mathbf{2})_2]^{2+}$	$[Co(R,R\text{-}\mathbf{3})_2]^{2+}$	$[Co(R,R\text{-}\mathbf{1})(S,S\text{-}\mathbf{1})]^{2+}$
d-d spectra: λ_{max}, ε				
$^4T_2(F) \leftarrow {}^4T_1$	1100(15)	1117(15)	1147(13)	1068(16)
$^4T_2(P) \leftarrow {}^4T_1$	463(56)	472(47)	475(36)	470(54)
CD spectra: λ_{max}, Δε				
	622(−0.053)	607(−0.03)	624(−0.07)	
	518(0.31)	527(0.09)	561(0.04)	
	459(−0.31)	468(−0.29)	472(−0.43)	
	368(−1.16)	365(−0.70)	359(−1.54)	

both complexes, with a heterochiral/homochiral ratio of 2 for **2** and 1 for **3**.

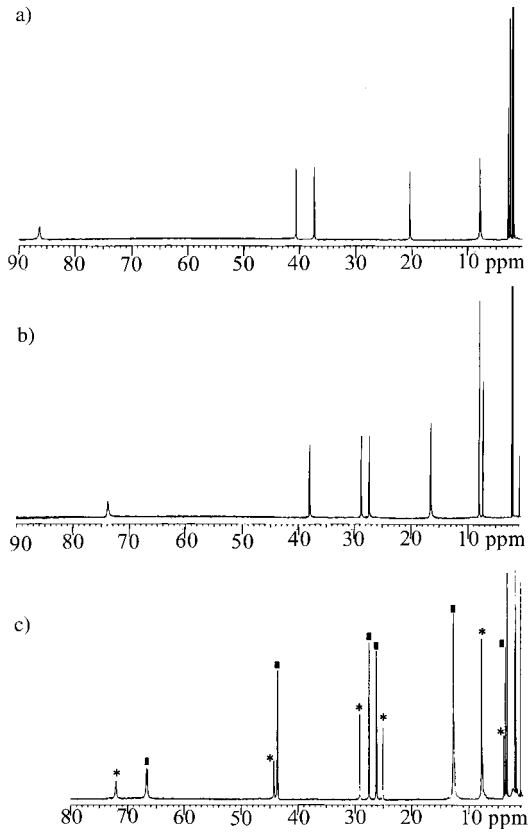

Figure 2. ^{1}H NMR spectra in [D$_3$]acetonitrile of (a) [Co(*R*,*R*-**1**)$_2$]$^{2+}$, (b) [Co(*R*,*R*-**1**) (*S*,*S*-**1**)]$^{2+}$, and (c) an equimolar mixture of cobalt(II), *R*,*R*-**2**, and *S*,*S*-**2**; the peaks due to the homochiral complex are marked with an asterisk, those of the heterochiral complex with a block

Cyclic voltammetry of [Co(*R*,*R*-**1**)$_2$]$^{2+}$ in acetonitrile showed three redox waves, two assigned to ligand reduction at −1.30 and −0.45 V, and a peak at +1.15V assigned to the Co^{III}/Co^{II} couple. This latter value is quite high, but may be understood in terms of the low donor strength of the oxazoline ligands, the π-acceptor properties of the ligand, and possible steric hindrance which prevents the shortening of the Co−N bond lengths associated with oxidation of Co^{II}.[15] The voltammogram for [Co(*R*,*R*-**2**)$_2$]$^{2+}$ is essentially identical, although for [Co(*R*,*R*-**3**)$_2$]$^{2+}$ no oxidation of Co^{II} was observed. For the heterochiral complex [Co(*R*,*R*-**1**)(*S*,*S*-**1**)]$^{2+}$ the ligand reduction potentials were unchanged but the Co^{III}/Co^{II} potential was significantly lower (+1.01 V) than for the homochiral complex.

Discussion

The three ligands studied here all form octahedral complexes of the type ML$_2$ with cobalt(II), but show significant differences in their physical and chemical properties arising from the different substituents on the oxazoline ring. We assume that these effects are due to the size and shape of these substituents rather than from inductive electronic effects. The results suggest that the benzyl group of ligand **3** provides the greatest hindrance, resulting in the lowest ligand field strength and the absence of oxidation of Co^{II}. Logically one would expect the phenyl group to exert a steric effect similar to the benzyl, but it is in fact ligand **2** with a methyl substituent that is closer to the benzyl group in ligand field strength, although in this case oxidation to Co^{III} may be observed. The phenyl-substituted ligand **1** shows the strongest ligand field of the homochiral complexes. Furthermore, ligand **1** is unique in its diastereoselectivity, forming the heterochiral complex exclusively whereas **2** and **3** give mixtures, that for ligand **3** being essentially statistical.

Two features render the phenyl substituent unique: firstly, all atoms of the phenyl group lie in the same plane, and it is therefore possible to orient the substituent so that it lies parallel to the bisoxazolinyl plane of the second ligand in the complex of [Co(*R*,*R*-**1**)$_2$]$^{2+}$, as shown in Figure 1. Attempts to grow crystals of the other complexes were unfortunately unsuccessful, but modeling studies show that in the benzyl and methyl complexes the methylene hydrogens of the substituent must be directed towards the second ligand: this is not the case for the phenyl substituent. Secondly, the phenyl groups can actually give an attractive interaction with the pyridine of the second ligand. This was clearly established in the trinuclear silver complex,[11] and, on the basis of the crystal structure, appears to be the case here. The lesser interligand repulsion of **1** compared to **2** and **3** can therefore explain the higher ligand field. Intramolecular stacking interactions have previously been reported as enhancing the stability of 2:1 complexes.[16]

The diastereoselectivity may also be understood from an examination of the crystal structure of [Co(*R*,*R*-**1**)$_2$](ClO$_4$)$_2$. If we look along the pyridine−cobalt−pyridine axis, the ligand planes form a cross, with the substituents at right angles to the arms of the cross. In the homochiral complex, the substituents are directed into two diagonally opposed quadrants of the cross, and consequently may repel each other. In the heterochiral complex each substituent is directed into a different quadrant, and repulsion is avoided. It is now possible to obtain four π-stacking interactions between the pyridine and the phenyl groups. In consequence, the ligand field increases, and the cobalt(II) oxidation potential is lowered. Indeed, the first d-d band of the heterochiral complex moves to higher energy relative to the homochiral complex. This diastereoselectivity will be most marked for the phenyl-substituted ligand **1**, since it projects far enough out of the ligand plane for the substituents to repel each other in the homochiral complex (Scheme 2). For the smaller methyl-substituted ligand the extension is not sufficient, and the benzyl group is sufficiently flexible to be able to bend away from the other ligand.

This effect has been observed previously by Evans[10] for complexes of **1** with copper(II): the crystal structures of [Cu(*S*,*S*-**1**)$_2$]$^{2+}$ and [Cu(*R*,*R*-**1**)(*S*,*S*-**1**)]$^{2+}$, although they are affected by a Jahn−Teller distortion, show the repulsion of the phenyls in the homochiral complex that is absent in the

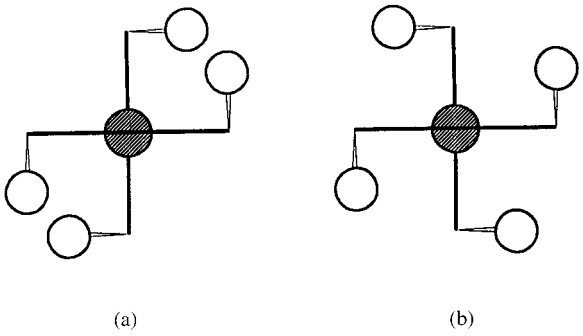

Scheme 2. Intraligand repulsion between substituents in the homochiral complex (a) and the heterochiral complex (b)

heterochiral complex. The greater stability of the heterochiral complex was shown by the nonlinear response of the enantioselectivity of reactions catalyzed by $[Cu(\mathbf{1})]^{2+}$ to the enantiomeric purity of ligand **1**: the selective formation and precipitation of $[Cu(R,R\text{-}\mathbf{1})(S,S\text{-}\mathbf{1})]^{2+}$ resulted in an enrichment of one enantiomer of the catalytically active species $[Cu(\mathbf{1})]^{2+}$ in solution. A similar nonlinear effect has been observed in other reactions catalyzed by oxazoline ligands.[17,18]

The remarkable difference in diastereoselectivity may thus be explained in terms of the properties of the substituent. The phenyl group which stood apart from the others in helicate chemistry[11] also shows different behavior in simple octahedral complexes. It is reasonable to suppose that this effect might influence the enantioselectivity of catalytic reactions using these ligands, and, indeed, Evans and coworkers[10] did observe that the enantioselectivity was highest for the phenyl-substituted ligand when compared with benzyl, isopropyl and *tert*-butyl substituents.

Experimental Section

General: The ligands were prepared according to the literature.[8,11,12] Diethyl ether was purified according to standard procedures. Other solvents (Fluka p.a.) were used without further purification. Hexaaquacobalt(II) perchlorate (Fluka) was used without purification. ^{1}H NMR spectra were recorded on a Varian Gemini-300 (at 300 MHz); shifts are given with reference to TMS. NMR solvents ([D$_3$]acetonitrile): Dr. Glaser AG Basel, isotopic purity > 99.80 atom%D. UV/visible spectra were recorded on a Cary/Varian spectrometer; 0.1 or 1 cm cell; 22 °C. CD spectra were recorded on a Jasco J-715 spectropolarimeter; 1 cm cell; 22 °C.

Cyclic Voltammetry: Electrochemical measurements were performed with a three-electrode system consisting of a platinum working electrode, a platinum counter-electrode and an Ag/AgCl reference electrode. All measurements were carried out under N_2 in degassed, freshly distilled solvent (acetonitrile), using 0.1 M nBu$_4$NPF$_6$ as supporting electrolyte. Before measurement, the system was standardized with the Ru(bipy)$_3$(ClO$_4$)$_2$ complex and potentials are given with respect to the normal hydrogen electrode. A Bioanalytical System Model CV-50 W was used to record and process the data.

General Procedure for Complex Synthesis: An acetonitrile/dichloromethane solution (4:1) of enantiopure ligand (4.08×10^{-4} mol) was added dropwise to a solution of 2.04×10^{-4} mol of metal salt [Co(ClO$_4$)$_2$·6H$_2$O] in acetonitrile. The solution was stirred for 30 minutes at room temperature and then concentrated to 1−2 mL. The complex was crystallized from the acetonitrile solution by diffusion of diethyl ether or *tert*-butyl methyl ether. Yields were typically 75%. For the synthesis of heterochiral species, the acetonitrile/dichloromethane solution contained 2.04×10^{-4} mol of the *R*,*R* enantiomer and 2.04×10^{-4} mol of the *S*,*S* enantiomer.

[Co(*R*,*R*-1)$_2$(ClO$_4$)$_2$]: Yield 76%. $C_{46}H_{38}Cl_2CoN_6O_{10}.1/2H_2O$: calcd. C 54.94, H 3.91, N 8.36; found C 54.95, H 3.97, N 8.34. − ^{1}H NMR (300 MHz, [D$_3$]acetonitrile, TMS): δ = 0.10 (2 H), 2.54 (8 H), 2.90 (4 H), 7.82 (8 H), 20.29 (4 H), 37.29 (4 H), 40.53 (4 H), 86.32 (4 H). − ES-MS (acetonitrile): *m*/*z* (%) = 399.0 (100) $[Co(\mathbf{1})_2]^{2+}$, 896.0 (15) $[Co(\mathbf{1})_2ClO_4]^+$. Very small peaks corresponding to the ligand and to the (complex + acetonitrile) were also observed. These last peaks are attributable to fragmentation in the spectrometer. Cyclic voltammetry: +1.14 V (Δ*E* = 105 mV), −0.43 V (Δ*E* = 75 mV), −1.30 V (Δ*E* = 80 mV).

[Co(*S*,*S*-1)$_2$](ClO$_4$)$_2$: Yield 69%. $C_{46}H_{38}Cl_2CoN_6O_{10}·H_2O$: calcd. C 54.45, H 3.97, N 8.28; found C 54.51, H 3.81, N 8.27. ^{1}H NMR spectrum and electrochemical data identical to [Co(*R*,*R*-1)$_2$(ClO$_4$)$_2$].

[Co(*R*,*R*-1)(*S*,*S*-1)](ClO$_4$)$_2$: Yield 75%. $C_{46}H_{38}Cl_2CoN_6O_{10}·H_2O$: calcd. C 54.45, H 3.97, N 8.28; found C 54.25, H 3.88, N 8.24. − ^{1}H NMR (300 MHz, [D$_3$]acetonitrile, TMS): δ = 0.80 (2 H), 7.31 (4 H), 7.96 (8 H), 16.44 (8 H), 27.30 (4 H), 28.80 (4 H), 37.97 (4 H), 73.84 (4 H). − Cyclic voltammetry: +1.01 V (Δ*E* = 150 mV), −0.46 V (Δ*E* = 70 mV), −1.35 V (Δ*E* = 60 mV).

[Co(*R*,*R*-2)$_2$](ClO$_4$)$_2$: Yield 79%. $C_{26}H_{30}Cl_2CoN_6O_{10}$ (716.39): calcd. C 41.73, H 4.04, N 11.23; found C 41.14, H 4.11, N 11.08. − ^{1}H NMR (300 MHz, [D$_3$]acetonitrile, TMS): δ = 3.96 (2 H), 7.80 (12 H), 25.08 (4 H), 29.20 (4 H), 44.18 (4 H), 72.20 (4 H). − ES-MS (acetonitrile): *m*/*z* (%) = 274.5 (100) $[Co(\mathbf{2})_2]^{2+}$, 648 (48) $[Co(\mathbf{2})_2ClO_4]^+$. − Cyclic voltammetry: +1.15 V (Δ*E* = 110 mV), −0.46 V (Δ*E* = 70 mV), −1.31 V (Δ*E* = 70 mV).

[Co(*S*,*S*-2)$_2$](ClO$_4$)$_2$: Yield 72%. $C_{26}H_{30}Cl_2CoN_6O_{10}$ (716.39): calcd. C 41.73, H 4.04, N 11.23; found C 41.36, H 3.97, N 11.14. − ^{1}H NMR spectrum and electrochemical data identical to [Co(*R*,*R*-2)$_2$](ClO$_4$)$_2$.

Equimolar mixture of Co(ClO$_4$)$_2$·6H$_2$O, *R*,*R*-2 and *S*,*S*-2: ^{1}H NMR (300 MHz, [D$_3$]acetonitrile, TMS): two species. 33% of homochiral complex: δ = 3.96 (2 H), 7.80 (12 H), 25.08 (4 H), 29.20 (4 H), 44.18 (4 H), 72.20 (4 H). 66% of heterochiral complex: δ = 3.73 (2 H), 12.69 (12 H), 26.18 (4 H), 27.48 (4 H), 43.66 (4 H), 66.70 (4 H).

[Co(*R*,*R*-3)$_2$](ClO$_4$)$_2$ and [Co(*S*,*S*-3)$_2$](ClO$_4$)$_2$: Yield 80%. ^{1}H NMR (300 MHz, [D$_3$]acetonitrile, TMS): δ = 0.24 (8 H), 3.96 (12 H), 5.64 (4 H), 16.52 (2 H), 17.40 (4 H), 22.89 (4 H), 30.10 (4 H, broad), 49.69 (4 H, broad), 66.00 (4 H). − Cyclic voltammetry: −0.43 V (Δ*E* = 73 mV), −1.24 V (Δ*E* = 74 mV). − ES-MS (acetonitrile): *m*/*z* (%) = 426.7 (100) $[Co(\mathbf{3})_2]^{2+}$, 952.0 (16) $[Co(\mathbf{3})_2ClO_4]^+$.

Equimolar Mixture of Co(ClO$_4$)$_2$·6H$_2$O, *R*,*R*-3 and *S*,*S*-3: ^{1}H NMR (300 MHz, [D$_3$]acetonitrile, TMS): two species. ≈50% of homochiral complex: δ = 0.49 (8 H), 3.94 (12 H), 6.13 (4 H), 16.48 (2 H), 17.63 (4 H), 22.96 (4 H), 29.68 (4 H, broad), 50.58 (4 H, broad), 65.75 (4 H). ≈50% of heterochiral complex: δ = 5.66 (12 H), 6.79 (8 H), 6.89 (2 H), 17.13 (4 H), 20.91 (4 H, broad), 24.92 (4 H), 26.07 (4 H), 50.18 (4 H), 63.29 (4 H, broad).

Crystal Structure of $[Co(R,R\text{-}1)_2](ClO_4)_2\cdot 3MeCN$, $Co(C_{22}H_{19}N_3O_2)_2(ClO_4)_2(CH_3CN)_3$: Molecular mass = 1119.8, orange crystal 0.22 × 0.22 × 0.23 mm, monoclinic, $P2_1$, a = 10.907(1) Å, b = 21.717(3) Å, c = 11.879(1) Å, β = 112.768(8)°, V = 2594.5(5) (Å)^3, Z = 2, D_x = 1.43 g·cm^{-3}. Data collection, Stoe STADI4, Cu-K_α, graphite monochromator, T = 200 K, ω-2θ scan, 3° < 2θ < 110°, −11 < h < 11; 0 < k < 22; 0 < l < 12 and all antireflections of these. 6557 reflections measured, 6344 unique, 5159 observed ($|F_o| > 4\sigma(F_0)$], μ = 4.147 mm^{-1}, spherical absorption correction A* min., max = 1.862, 1.954. Structure solved by direct methods,[19] and refined by full-matrix least-squares with hydrogens in calculated positions using 687 parameters for 5159 reflections.[20] Final R value 0.057, R_w = 0.048, Flack absolute structure parameter = 0.00(1).[21,22]

Crystallographic data (excluding structure factors) for the structure included in this paper have been deposited with the Cambridge Crystallographic Data Centre as supplementary publication no. CCDC-149396. Copies of the data can be obtained free of charge on application to CCDC, 12 Union Road, Cambridge CB2 1EZ, UK [Fax: (internat.) +44-1223/336-033; E-mail: deposit@ccdc.cam.ac.uk].

Molecular Modeling: Calculations were carried out using the Universal force field 1.02[23] with charge equilibration.[24] A reasonable agreement between calculated structure and that observed for $[Co(RR\text{-}1)_2]^{2+}$ was obtained as judged by superposition of the structures, although the optimized Co−N bond lengths were too short (1.811 Å compared with the experimental average of 2.1190 Å).

Acknowledgments

This work was supported by the Swiss National Science Foundation. We thank Werner Kloeti (University of Geneva) for recording electrospray mass spectra.

[1] U. Knof, A. von Zelewsky, *Angew. Chem. Int. Ed.* **1999**, *38*, 302−322.
[2] K. Bernauer, S. Bourqui, D. Hugi-Cleary, R. Warmuth, *Helv. Chim. Acta* **1992**, *75*, 1288−1296.
[3] K. Bernauer, F. Gretillat, H. Stoeckli-Evans, R. Warmuth, *Helv. Chim. Acta* **1993**, *76*, 545−556.
[4] E. C. Constable, T. Kulke, M. Neuburger, M. Zehnder, *Chem. Commun.* **1997**, 489−490.
[5] G. Baum, E. C. Constable, D. Fenske, C. E. Housecroft, T. Kulke, *Chem. Eur. J.* **1999**, *5*, 1862−1873.
[6] E. J. Enemark, T. D. P. Stack, *Angew. Chem. Int. Ed. Engl.* **1995**, *34*, 996−998.
[7] J. M. Vincent, C. Philouze, I. Pianet, J.-B. Verlhac, *Chem. Eur. J.* **2000**, *6*, 3595−3599.
[8] H. Nishiyama, M. Kondo, T. Nakamura, K. Itoh, *Organometallics* **1991**, *10*, 500−508.
[9] H. Nishiyama, T. Nitoh, Y. Motoyama, K. Aoki, *Chem. Eur. J.* **1999**, *5*, 3509−3513.
[10] D. A. Evans, M. C. Kozlowski, J. A. Murry, C. S. Burgey, K. R. Campos, B. T. Connell, R. J. Staples, *J. Am. Chem. Soc.* **1999**, *121*, 669−685.
[11] C. Provent, S. Hewage, G. Brand, G. Bernardinelli, L. J. Charbonnière, A. F. Williams, *Angew. Chem. Int. Ed. Engl.* **1997**, *36*, 1287−1289.
[12] C. Provent, E. Rivara-Minten, S. Hewage, G. Brunner, A. F. Williams, *Chem. Eur. J.* **1999**, *5*, 3487−3494.
[13] C. A. Hunter, J. K. M. Sanders, *J. Am. Chem. Soc.* **1990**, *112*, 5525−5534.
[14] S. K. Burley, G. A. Petsko, *Science* **1985**, *229*, 23−28.
[15] C. Piguet, G. Bernardinelli, B. Bocquet, O. Schaad, A. F. Williams, *Inorg. Chem.* **1994**, *33*, 4112−4121.
[16] R. Wietzke, M. Mazzanti, J.-M. Latour, J. Pécaut, *Chem. Commun.* **1999**, 209−210.
[17] S. Kanemasa, Y. Oderaotoshi, S. Sakaguchi, H. Yamamoto, J. Tanaka, E. Wada, D. P. Curran, *J. Am. Chem. Soc.* **1998**, *120*, 3074−3088.
[18] S. Crosignani, G. Desimoni, G. Faita, S. Filippone, A. Mortoni, P. Righetti, M. Zema, *Tetrahedron Lett.* **1999**, *40*, 7007−7010.
[19] P. Main, S. J. Fiske, S. E. Hull, L. Lessinger, D. Germain, J. P. Declercq, M. M. Woolfson, Universities of York (England) and Louvaine-La-Neuve (Belgium) 1987.
[20] S. R. Hall, H. D. Flack, J. M. Stewart, *XTAL 3.2 User's Manual*, Universities of Western Australia, Geneva and Maryland **1992**.
[21] H. D. Flack, *Acta Crystallogr., Sect. A* **1983**, *39*, 876−881.
[22] H. D. Flack, G. Bernardinelli, *Acta Crystallogr., Sect. A* **1999**, *A55*, 908−915.
[23] A. K. Rappe, C. J. Casewit, K. S. Colwell, W. A. Goddard III, W. M. Skiff, *J. Am. Chem. Soc.* **1992**, *114*, 10024−10035.
[24] A. K. Rappe, W. A. Goddard III, *J. Phys. Chem.* **1991**, *95*, 3358.

Received October 13, 2000
[I00390]

σ-Donor versus η⁶-π-Arene Interactions in Monomeric Europium(II) and Ytterbium(II) Thiolates − An Experimental and Computational Study

Mark Niemeyer[a]

Dedicated to Professor Glen B. Deacon on the occasion of his 65th birthday

Keywords: Ab initio calculations / Lanthanides / π interactions / S ligands / Ytterbium

The base-free, hydrocarbon-soluble complexes $M(SAr^*)_2$ (**4a**: M = Eu, orange; **4b**: M = Yb, purple; Ar^* = 2,6-$Trip_2C_6H_3$; Trip = 2,4,6-$i Pr_3C_6H_2$) have been prepared by a protolysis reaction of the Grignard-analogous compound RLnI (R = 2-$F_3CC_6H_4$) with $HSAr^*$. Compound **4b** has been characterized by melting point, elemental analysis, ^1H, ^{13}C, and ^{171}Yb NMR, IR spectroscopy, UV/Vis spectrophotometry, mass spectrometry, and X-ray crystallography. Additionally, the purple Yb^{III} complex $YbI_2(SAr^*)(THF)_3$ (**3**) and the yellow DME adduct $Yb(SAr^*)_2(dme)_2$ (**5**) have been synthesized and characterized by X-ray crystallography. The solid-state structures of **4a** and **4b** (as THF or benzene hemisolvates) show monomeric units with the metal atom bonded to two terminal thiolate ligands [av. M–S: 281.7 pm (**4a**)/269.1 pm (**4b**)]. Additional η⁶-π-arene interactions are observed to two C_6H_2 rings of the Trip substituents [av. M···C: 306.5 pm (**4a**)/297.3 pm (**4b**)]. The binding energy for these interactions has been determined by variable-temperature ^1H NMR spectroscopy to be 54.3 kJ mol^{-1} (in methylcyclohexane) and 57.1 kJ mol^{-1} (in toluene). The nature and strength of the η⁶-π-arene bonding has been studied by ab initio calculations on the model systems $[M(arene)]^{2+}$ (arene = C_6H_6, C_6F_6, 1,3,5-$Me_3C_6H_3$, 1,3,5-$i Pr_3C_6H_3$) and $Yb(SH)_2(C_6H_6)_n$ (n = 1, 2). The results are compared with the binding energies in the σ-donor adducts $[M(THF)]^{2+}$, $[M(dme)]^{2+}$, and $[M(imidazol\text{-}2\text{-}ylidene)]^{2+}$.

Introduction

The use of charged π-donor ligands and the principle of steric saturation by associated neutral σ-donors or the addition of anionic ligands have dominated organolanthanoid[1] chemistry over the past decades. More recently, however, there has been a growing interest in low-coordinate σ-bonded lanthanoid complexes with bulky substituted organyls,[2,3] Group 14, Group 15, or Group 16 heteroelements.[4] Moreover, the avoidance of coordinating solvents often leads to novel structures and unusual lanthanoid−ligand interactions. Examples of the latter include agostic-type interactions[5] with alkyl-substituted ligands[6−11] or metal−π-arene interactions[12−15] in aryl-substituted ligand systems. In this paper, the synthesis and characterization of the *m*-terphenyl-based[16] metal thiolates $YbI_2(SAr^*)(THF)_3$ (**3**) (Ar^* = 2,6-$Trip_2C_6H_3$; Trip = 2,4,6-$i Pr_3C_6H_2$), $M(SAr^*)_2$ [M = Eu (**4a**), Yb (**4b**)], and $Yb(SAr^*)_2(dme)_2$ (**5**) are described. The σ-donor-free compounds **4a** and **4b** show two metal−η⁶-π-arene interactions in the solid state. According to NMR-spectroscopic results, these interactions persist in solution. The nature and strength of these interactions has been studied by ab initio calculations on simple model systems.

[a] Institut für Anorganische Chemie der Universität Stuttgart, Pfaffenwaldring 55, 70569 Stuttgart, Germany
Fax: (internat.) + 49-(0)711/685-4241
E-mail: niemeyer@iac.uni-stuttgart.de

Results and Discussion

Syntheses

The syntheses of compounds **1**−**5** are summarized in Scheme 1. Initially, the ytterbium(II) thiolate **4b** was obtained from the reaction of $Yb[N(SiMe_3)_2]_2$ with $HSAr^*$. Mixing the two compounds in *n*-pentane resulted in a color change from orange to purple. Removal of the solvent followed by recrystallization of the residue from a mixture of *n*-heptane and benzene gave **4b** as an extremely air-sensitive crystalline material. However, a much easier route to **4b**, which circumvents the somewhat cumbersome preparation[17] of donor-free $Yb[N(SiMe_3)_2]_2$, is a direct synthesis starting from ytterbium metal and 2-iodobenzotrifluoride. The reaction of lanthanide metals with organyl iodides to give Grignard-analogous compounds RLnI (Ln = Sm, Eu, Yb) has been known for some time.[18] The isolation and structural characterization of such compounds has, however, only recently been achieved.[15,19−21] The initially formed arylytterbium(II) iodide **1b** is instantly protolysed by the thiol $HSAr^*$ to give the mixed (thiolato)ytterbium(II) iodide **2b**. Replacing THF by *n*-pentane as the solvent causes the precipitation of $YbI_2(THF)_4$.[22] After removal of the solvent and recrystallization of the residue from an *n*-heptane/toluene mixture, purple **4b** is obtained in 66% yield. The preparation of the donor-free europium(II) thiolate $Eu(SAr^*)_2$ **4a** was accomplished in a similar manner. Attempts to isolate the intermediate mixed (thiolato)-lanthanide(II) iodides **2a** and **2b** did not prove to be successful. Thus, in the case of the ytterbium derivative, crystalliza-

 © WILEY-VCH Verlag GmbH, 69451 Weinheim, 2001 1434−1948/01/0808−1969 $ 17.50+.50/0

tion at −15 °C only afforded $YbI_2(THF)_4$. Nevertheless, the formation of **2b** was confirmed by its ^{171}Yb NMR signal. Moreover, it was possible to synthesize the diiodo(thiolato)ytterbium(III) complex **3** in good yield by oxidation of **2b** with iodine. A remarkable feature of the preparation of **4a** and **4b** is the ease with which the coordinated tetrahydrofuran can be removed. Although in the case of **4b** coordination of THF is observed at low temperatures (vide infra), it can be completely removed by pumping at 10^{-3} mbar at ambient temperature. In the case of the europium compound, it is even possible to crystallize donor-free **4a** from an *n*-heptane/THF mixture to give the packing complex **4a**·$(THF)_{0.5}$, in which no Eu−O(THF) interactions are observed. This unusual behavior is in contrast to the preparation of other unsolvated lanthanide(II) compounds, e.g. $LnCp^*_2$ or $Ln(OAr)_2$, from solvated complexes, which normally requires repeated sublimation at elevated temperatures.[23] Using dimethoxyethane as a more strongly chelating ligand, it is possible to synthesize the more stable yellow complex $Yb(SAr^*)_2(dme)_2$ (**5**). Even in this case, complete removal of the coordinated solvent can be achieved by pumping overnight at 20 °C/10^{-3} mbar.

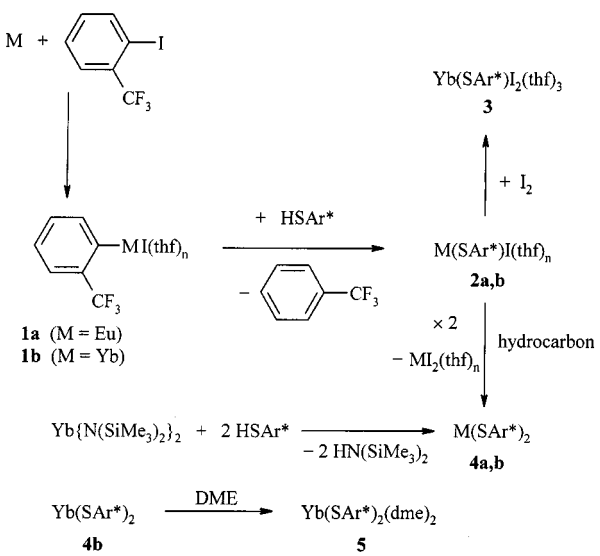

Scheme 1. Syntheses of compounds **1**−**5**

The protolysis of the aryllanthanide(II) iodides **1a** and **1b** seems to be of general interest for the preparation of other lanthanide(II) complexes. In contrast, the usual metathesis reactions often lead to alkali metal halide contaminated products or to the formation of unwanted ate complexes, while the related one-pot transmetallation/protolysis route of Deacon et al.[17] relies on poisonous Ph_2Hg. Using our method, we were able to synthesize the known compounds[23] $Yb[N(SiMe_3)_2]_2(THF)_2$, $Yb(OAr')_2(THF)_2$ (Ar′ = 2,6-*t*Bu_2-4-MeC_6H_2), and $YbCp^*_2(THF)_2$ in pure form and good yields.[24] Although the 2-iodobenzotrifluoride used here can be replaced by other aryl iodides, we have found it to be superior, giving shorter reaction times and improved purity of the products.[24]

X-ray Crystal Structures

Compounds **3**, **4a**, **4b**, and **5** were examined by X-ray crystallography. Their molecular structures are shown in Figures 1, 2, 3 and 4, while salient structural parameters are given in Tables 1, 2 and 3. The solid-state structure of purple $YbI_2(SAr^*)(THF)_3$ (**3**) consists of monomeric units (Figure 1). The central Yb atom shows a distorted octahedral coordination with two iodo ligands in apical positions [I(1)−Yb−I(2) = 176.74(3)°]. Despite the presence of the sterically crowded SAr* ligand, the Yb−S bond length of 258.1(2) pm seems to be the shortest ytterbium−sulfur distance yet reported for a molecular ytterbium compound.[4] It may be compared with the average Yb−S bond lengths in the six-coordinate complexes $Yb(STrip)_3(py)_3$ and *mer*-$Yb(SPh)_3(py)_3$, which were determined as 264.8 pm and 264.7 pm, respectively (Table 4). The shortest Yb−S distance of 260.9(4) pm is found *trans* to one pyridine ligand in the latter. In **3**, the Yb−I bond lengths of 291.0(1) pm [Yb−I(1)] and 298.4(1) pm [Yb−I(2)] are close to the values seen in the previously reported dimeric complex $[(\mu\text{-}OMe)YbI_2(dme)]_2$ (av. 293.2 pm)[25] and the formally eight-coordinate compound $Yb(Cp)_2I(THF)$ (293.2 pm).[26] The different Yb−I bond lengths in **3** can be attributed to the significant deviation of the Yb atom from the S−O(41)−O(51)−O(61) plane by 10.6 pm (Table 1). A notable feature of the structure of **3** is that the Yb−O distances to the coordinated THF ligands are rather different. With a value of 239.0(6) pm, the Yb−O(41) bond *trans* to the SAr* group is unusually long, whereas the others (av. Yb−O = 227.3 pm) are in the normal range for Yb^{III} complexes with six-coordinate metal centers.[27] The long Yb−O(41) bond may be compared with the average Yb−O distance of 239.5 pm *trans* to the C_6H_5 groups in *fac*-$YbPh_3(THF)_3$.[28] The *trans* influence of THF ligands in lanthanoid(III) chemistry has been noted previously.[29]

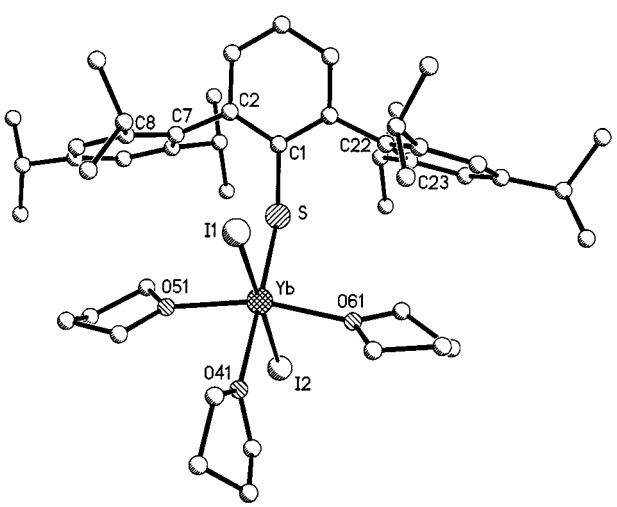

Figure 1. Molecular structure of **3**, showing the atom numbering scheme; hydrogen atoms have been omitted for clarity

Because of their very similar features, the solid-state structures of the compounds $Eu(SAr^*)_2$ [**4a**·$(THF)_{0.5}$] and $Yb(SAr^*)_2$ [**4b**·$(C_6H_6)_{0.5}$] will be discussed together. Both complexes crystallize as monomers. Their molecular struc-

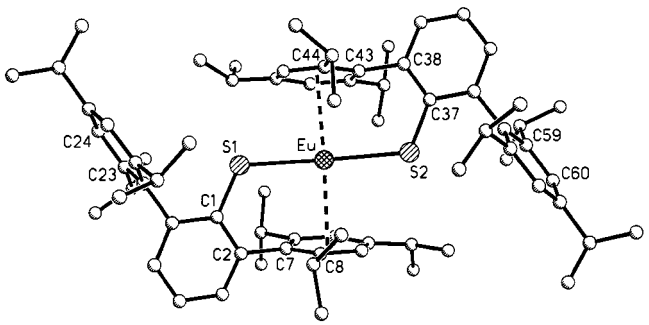

Figure 2. Molecular structure of **4a**, showing the atom numbering scheme for **4a** and **4b**; hydrogen atoms, the minor parts of the disordered isopropyl groups, and the co-crystallized THF molecule have been omitted for clarity

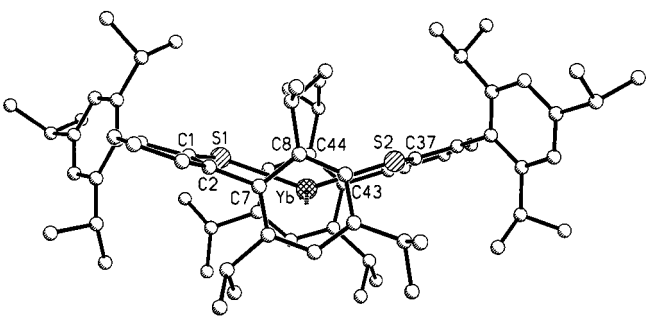

Figure 3. Molecular structure of **4b**, showing the two η⁶-coordinated arene rings and part of the atom numbering scheme; hydrogen atoms, the minor parts of the disordered isopropyl groups, and the co-crystallized benzene molecule have been omitted for clarity

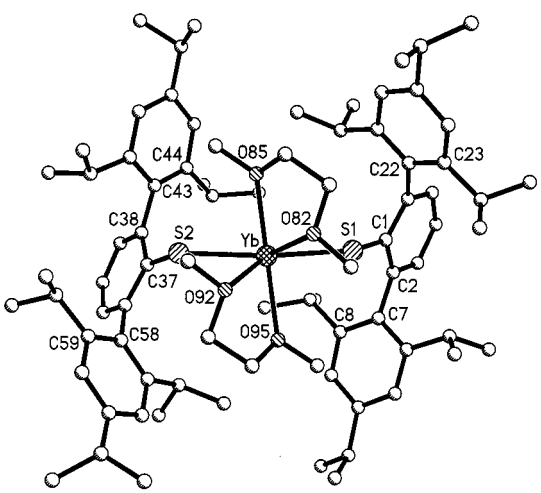

Figure 4. Molecular structure of **5**, showing the atom numbering scheme; hydrogen atoms and the minor parts of the disordered isopropyl groups have been omitted for clarity

tures are illustrated in Figure 2 (**4a**) and Figure 3 (**4b**), while salient bond parameters are listed in Table 2. Despite the difference in the ionic radii of europium(II) and ytterbium(II), both complexes crystallize in isomorphous cells. They differ in the type of solvent that is packed in the cavities of the structure. There are, however, no significant interactions between the metal centers and the co-crystallized tetrahydrofuran or benzene molecules. Each metal atom is coordinated to the sulfur atoms of the thiolate ligands with S−M−S angles of 141.89(4)° (**4a**) and 142.73(8)° (**4b**), respectively. The most striking structural features of **4a** and **4b** are the additional η⁶-π-interactions to two *ortho*-2,4,6-triisopropylphenyl rings of the terphenyl groups (Figure 3). Although the occurrence of two η⁶-π-bonded arene rings is unprecedented for structurally authenticated di- or trivalent lanthanide species,[12] such interactions are well-known in some bis(arene)lanthanide(0) derivatives. Structurally characterized examples include the compounds M(η⁶-1,3,5-tBu$_3$C$_6$H$_3$)$_2$ (M = Y, Gd, Ho).[30] It should be noted that the cyclometallated scandium(II) complex ScH(η⁶-tBu$_3$C$_6$H$_3$)[η⁶,η¹-(CH$_2$CMe$_2$)tBu$_2$C$_6$H$_3$], which was formed by C−H insertion from Sc(η⁶-1,3,5-tBu$_3$C$_6$H$_3$)$_2$, may also possess two metal−π-arene interactions, although this was based purely on ESR evidence.[31]

The two terphenylthiolate ligands in **4a** and **4b** are orientated in such a way that the most favorable η⁶-π-arene bonding is maximized. In effect, the interplanar angles between the M−S−C planes and the central 2,6-substituted phenyl rings, i.e. A/D and E/H (Table 2), are in the range 0.3° to 6.7°. Together with the perpendicular arrangement of the *ortho*-Trip groups (A/B, A/C, E/F, E/G = 82.0−89.5°), an almost parallel orientation of the C(7)−C(12) and C(43)−C(48) rings to the central S(1)−M−S(2) plane is achieved (B/I, F/I = 6.3−13.6°). Despite the formal coordination number of eight, the observed europium−sulfur and ytterbium−sulfur distances are surprisingly short. In fact, they are ca. 8−13 pm (**4a**) and 7−19 pm (**4b**) pm shorter than the metal−sulfur distances reported for other europium(II) and ytterbium(II) thiolates (Table 4). In **4a**, the europium ion interacts essentially equally with both Trip rings with Eu−C distances in the relatively narrow range of 298.8(3)−315.0(3) pm for C(7)−C(12) and 296.7(3)−316.1(3) pm for C(43)−C(48), with average values of 307.0 pm and 305.9 pm, respectively. In **4b**, the Yb−C interactions to the C(7)−C(12) ring were found to have distances between 287.0(8) and 305.2(8) pm (av. 296.3 pm), with a somewhat greater variation of 282.4(8)−313.9(8) pm (av. 298.3) for the bonding to the second C(43)−C(48) arene ring. The average metal−centroid distances are 272.8 pm (**4a**) and 263.7 pm (**4b**), whereas the X(1)−M−X(2) angles, where X(1) and X(2) define the centroids of the coordinated arene rings, are 166.9° and 164.5° respectively. Salient structural parameters in known compounds with europium− and ytterbium−η⁶-π-arene coordination are summarized in Table 5. The Yb−C interactions in **4b** are comparable to the reported average Yb^{II}−C distances, which fall in the range 296−304 pm. In accordance with the smaller radius of Yb^{III}, the complex Yb(C$_6$Me$_6$)(AlCl$_4$)$_3$ shows shorter Yb−C distances of 286 pm (av.). The nine-coordinate Eu center in the tetrameric compound [Eu(C$_6$Me$_6$)(AlCl$_4$)$_2$]$_4$ exhibits an average Eu−C interaction of 300 pm. The shortening by 6−7 pm compared to **4a** may be explained in terms of a stronger polar attraction between the Eu ion and the arene ring caused by the more electronegative AlCl$_4^-$ ligands.

The molecular structure of the yellow complex Yb(SAr*)$_2$(dme)$_2$ (**5**) is shown in Figure 4. The Yb atom has a distorted octahedral coordination, in which the thiolate groups and each DME ligand occupy a *cis* position. The

Table 1. (a) Selected interatomic distances [pm], (b) angles [°], (c) distances from least-square planes [pm], and (d) interplanar angles [°] in $YbI_2(SAr^*)(THF)_3$ (**3**)

(a)								
Yb−S		258.1(2)		Yb−O(51)		227.0(6)		
Yb−I(1)		291.00(9)		Yb−O(61)		227.5(6)		
Yb−I(2)		298.40(10)		S−C(1)		177.8(9)		
Yb−O(41)		239.0(6)						
(b)								
I(1)−Yb−I(2)		176.74(3)		I(2)−Yb−O(51)		86.2(2)		
S−Yb−O(41)		175.9(2)		I(2)−Yb−O(61)		87.5(2)		
S−Yb−O(51)		93.7(2)		O(41)−Yb−O(51)		83.9(2)		
S−Yb−O(61)		100.0(2)		O(41)−Yb−O(61)		81.9(2)		
S−Yb−I(1)		96.81(6)		O(51)−Yb−O(61)		164.5(2)		
S−Yb−I(2)		86.45(6)		Yb−S−C(1)		125.1(3)		
I(1)−Yb−O(41)		86.8(2)		S−C(1)−C(6)		120.9(7)		
I(1)−Yb−O(51)		93.6(2)		S−C(1)−C(2)		120.2(7)		
I(1)−Yb−O(61)		91.9(2)		C(1)−C(2)−C(7)		124.8(8)		
I(2)−Yb−O(41)		90.0(2)		C(1)−C(6)−C(22)		124.5(8)		
(c)[a]								
C(1)*	C(2)*	C(3)*	C(4)*	C(5)*	C(6)*	S	C(7)	C(22)
+2.1	−0.6	−1.0	+1.1	+0.4	−2.0	−14.6	−14.1	−12.4
S*	O(41)*	O(51)*	O(61)*	Yb	I(1)	I(2)		
+2.4	+3.3	−2.9	−2.8	+10.6	+300.4	−287.7		
(d)[b]								
A/B	74.5	A/C	73.0	A/D	88.8			

[a] Atoms marked with an asterisk define the least-square plane. − [b] Least-square planes defined by the following atoms: A: C(1) to C(6); B: C(7) to C(12); C: C(22) to C(27); D: C(1), S, Yb.

rather different S(1)−Yb−S(2), O(82)−Yb−O(85), and O(92)−Yb−O(95) angles of 141.3(1)°, 64.8(2)°, and 65.1(2)°, respectively, reveal a severe distortion from the ideal octahedral environment. The Yb−S bond length of 273.9 pm and the average Yb−O distances of 248.0 pm may be compared with the corresponding values of 275.6(8) pm and 253.5 pm in the related complex $Yb(SMes^*)_2(dme)_2$.[32] Apparently, the slightly shorter distances in **5** are compensated by the more acute S−Yb−S angle of 124.4(2)° in the latter.

Although the Ar* and Mes* substituents are of similar size, they often induce different oligomerization and solvent complexation behavior, as has been noted previously.[16] In contrast to the structures of **4a** and **4b**, the interplanar angles between the M−S−C planes and the central C_6H_3 arene rings, i.e. A/D and E/H (Table 3), are close to 90°, which is a consequence of repulsive forces between the DME ligands and the *ortho*-Trip groups.

It is interesting to compare the molecular structures of **3**, **4a**, **4b**, and **5** in terms of the different degrees of steric crowding. Thus, the average M−S−C angle increases from 115° and 116° in **4b** and **4a**, through 125° in **3**, up to 146° in **5**. Furthermore, the average displacement of the *ipso*-Trip carbon atoms [i.e. C(7), C(22), C(43), and C(58)] from the central C_6H_3 plane increases in the order **4a** (8.2 pm), **4b** (9.6 pm), **3** (13.3 pm), and **5** (22.9 pm). Apparently, the maximum steric congestion is observed for compound **5**.

Spectroscopic Characterization

The diamagnetic complexes **4b** and **5** have been characterized by ^1H and ^{13}C NMR spectroscopy. In addition, compounds **2b**, **4b**, and **5** have been examined by ^{171}Yb NMR spectroscopy (Table 6). The ^{171}Yb NMR spectrum of an in situ prepared solution of **2b** in $[D_8]THF$ shows a main signal at $\delta = 351$. Smaller resonances of equal height at $\delta = 281$ and $\delta = 457$ can be assigned to the dithiolato species $Yb(SAr^*)_2(THF)_x$ (**6**) and solvated ytterbium(II) iodide $YbI_2(THF)_4$ (**4b**).[33] In the ^{171}Yb NMR spectrum of **4b** in $[D_8]$toluene or $[D_6]$benzene, a sharp resonance is observed at $\delta = 768$. A different chemical shift is found if the aromatic solvent is replaced by an alkane. Thus, a ^{171}Yb NMR signal at $\delta = 837$ is observed in $[D_{14}]$methylcyclohexane at 233 K, whereas no ^{171}Yb resonance is detectable at ambient temperature. The reaction of purple **4b** with more strongly coordinating solvents such as THF or DME results in a color change to yellow. In the ^{171}Yb NMR spectrum, a shift to higher field is observed with resonances at $\delta = 204$ (at 233 K) and $\delta = 281$ for the solvated complexes $Yb(SAr^*)_2(dme)_2$ **5** and $Yb(SAr^*)_2(THF)_x$ **6**, respectively. These values may be compared with the ^{171}Yb NMR chemical shifts of the ytterbium(II) thiolate $Yb(SMes^*)_2(dme)_2$ and related selenolates and tellurolates, which are found at lower field, specifically at $\delta = 485$[32] and $\delta = 430-526$,[34] respectively. It is notable that no ^{171}Yb NMR signal can be detected for **5** at ambient temperature. Apparently, dynamic processes such as solvent exchange, intermolecular arene coordination, or equilibria due to hindered rotation complicate the interpretation of solution NMR-spectroscopic data for compounds **4b** and **5**. In order to gain more insight into these different processes, variable-temperature ^1H NMR experiments were performed. At room temperature, the ^1H NMR spectrum of **4b** in $[D_8]$toluene shows only one type of thiolate ligand environment with equivalent Trip

Table 2. (a) Selected interatomic distances [pm], (b) angles [°], (c) distances from least-square planes [pm], (d) and interplanar angles [°] in Eu(SAr*)$_2$ (**4a**) and Yb(SAr*)$_2$ (**4b**)

	4a·(THF)$_{0.5}$		**4b**·(C$_6$H$_6$)$_{0.5}$	
(a)				
M−S(1)	281.6(1)		268.5(2)	
M−S(2)	281.8(1)	{281.7}[a]	269.6(2)	{269.1}
M···C(7)	303.7(3)		292.2(8)	
M···C(8)	309.4(3)		297.1(8)	
M···C(9)	312.8(3)		302.8(8)	
M···C(10)	315.0(3)		305.2(8)	
M···C(11)	302.4(3)		293.3(9)	
M···C(12)	298.8(3)	{307.0}	287.0(8)	{296.3}
M···C(43)	301.1(3)		287.7(8)	
M···C(44)	306.9(3)		311.8(8)	
M···C(45)	311.1(3)		313.9(8)	
M···C(46)	316.1(3)		301.7(8)	
M···C(47)	303.3(3)		292.3(8)	
M···C(48)	296.7(3)	{305.9}	282.4(8)	{298.3}
M···X(1)[b]	273.4		262.3	
M···X(2)	272.2	{272.8}	265.0	{263.7}
(b)				
S(1)−M−S(2)	141.89(4)		142.73(8)	
Yb−S(1)−C(1)	115.85(11)		115.7(3)	
Yb−S(2)−C(37)	115.40(11)		115.0(3)	
X(1)−M−X(2)	166.9		164.5	
S(1)−C(1)−C(2)	122.3(2)		121.7(6)	
S(1)−C(1)−C(6)	119.5(2)		119.7(6)	
S(2)−C(37)−C(38)	122.3(3)		120.4(6)	
S(2)−C(37)−C(42)	120.4(2)		121.2(6)	
C(1)−C(2)−C(7)	120.3(3)		119.4(7)	
C(1)−C(6)−C(22)	119.6(3)		120.4(7)	
C(37)−C(38)−C(43)	119.9(3)		120.9(7)	
C(37)−C(42)−C(58)	119.6(3)		121.1(7)	

(c)[c]

	C(1)*	C(2)*	C(3)*	C(4)*	C(5)*	C(6)*	S(1)	C(7)	C(22)
4a:	+3.0	−0.9	−1.7	+2.2	+0.0	−2.6	+15.0	−2.8	−16.2
4b:	+3.2	−1.5	−1.7	+3.1	−1.3	−1.9	+17.5	−10.8	−20.1
	C(37)*	C(38)*	C(39)*	C(40)*	C(41)*	C(42)*	S(2)	C(43)	C(58)
4a:	+1.4	−0.7	−0.6	+1.1	−0.4	−0.9	+3.0	−7.6	−6.2
4b:	+1.4	−1.5	+0.4	+0.7	−0.8	−0.2	+1.0	−1.1	−6.3

(d)[d]

	A/B	A/C	E/F	E/G	B/I	F/I	B/F	A/D	E/H
4a:	83.6	89.5	85.2	85.0	11.5	6.3	16.0	4.7	1.7
4b:	82.0	89.0	84.2	82.7	13.6	7.3	19.5	6.7	0.3

[a] Average values are given in brackets. − [b] X(1) and X(2) define the centroids of the C(7) to C(12) and C(43) to C(48) arene rings, respectively. − [c] Atoms marked with an asterisk define the least-square plane. − [d] Least-square planes defined by the following atoms: A: C(1) to C(6); B: C(7) to C(12); C: C(22) to C(27); D: C(1), S(1), M; E: C(37) to C(42); F: C(43) to C(48); G: C(58) to C(63); H: C(37), S(2), M; I: S(1), M, S(2).

substituents, although the signals are very broad. If the temperature is gradually increased, the linewidth decreases and sharp signals are observed at 358 K. At lower temperatures, two coalescence points were detected at 284 K and 227 K, corresponding to energy barriers of 57.1 kJ mol^{-1} and 46.5 kJ mol^{-1}, respectively. A full interpretation of the low-temperature ^{1}H NMR spectra has not yet been possible due to their complex nature and overlapping signals. It is clear, however, that below 284 K two different Trip substituent environments exist, as is evident from the appearance of two different resonances for the *m*-Trip protons. This observation can be interpreted in terms of hindered rotation about the S(1)−C(1) or S(2)−C(37) bonds and hence the persistence of the metal−π-arene interactions in solution. In order to exclude additional interactions with the aromatic solvent toluene, further low-temperature ^{1}H NMR experiments were performed in [D$_{14}$]methylcyclohexane. In this solvent, a single energy barrier of 54.3 kJ mol^{-1} is found and two signals due to the aromatic protons of the Trip substituents are observed below 263 K. In contrast, the ^{1}H NMR spectrum of **5** shows only one set of signals due to the Trip substituents and the coordinated DME molecules in the temperature range 223−300 K.

The weak tendency of **4b** to coordinate THF was examined by additional ^{171}Yb NMR experiments. As mentioned above, a yellow solution of **4b** in neat [D$_8$]THF shows a

Table 3. (a) Selected interatomic distances [pm], (b) angles [°], (c) distances from least-square planes [pm], and (d) interplanar angles [°] in $Yb(SAr^*)_2(dme)_2$ (**5**)

(a)			
Yb−S(1)	2.739(2)	Yb−O(85)	2.477(5)
Yb−S(2)	2.739(3)	Yb−O(92)	2.510(6)
Yb−O(82)	2.478(6)	Yb−O(95)	2.461(5)
(b)			
S(1)−Yb−S(2)	141.25(11)	O(85)−Yb−O(92)	91.9(2)
S(1)−Yb−O(82)	77.18(16)	O(92)−Yb−O(95)	65.1(2)
S(1)−Yb−O(85)	100.22(13)	Yb−S(1)−C(1)	149.0(4)
S(1)−Yb−O(92)	136.93(17)	Yb−S(2)−C(37)	142.8(3)
S(1)−Yb−O(95)	88.61(13)	S(1)−C(1)−C(6)	121.0(6)
S(2)−Yb−O(82)	138.08(14)	S(1)−C(1)−C(2)	120.9(6)
S(2)−Yb−O(85)	87.19(14)	S(2)−C(37)−C(42)	120.4(6)
S(2)−Yb−O(92)	79.95(14)	S(2)−C(37)−C(38)	120.9(6)
S(2)−Yb−O(95)	102.00(14)	C(1)−C(2)−C(7)	122.6(7)
O(82)−Yb−O(85)	64.8(2)	C(1)−C(6)−C(22)	121.5(7)
O(82)−Yb−O(92)	71.1(2)	C(37)−C(38)−C(43)	124.1(7)
O(82)−Yb−O(95)	92.7(2)	C(37)−C(42)−C(58)	122.6(7)
O(85)−Yb−O(95)	152.8(2)		

(c)[a]

C(1)*	C(2)*	C(3)*	C(4)*	C(5)*	C(6)*	S(1)	C(7)	C(22)
−3.1	+2.0	+0.7	−2.4	+1.2	+1.6	−1.7	+22.1	+21.1
C(37)*	C(38)*	C(39)*	C(40)*	C(41)*	C(42)*	S(2)	C(43)	C(58)
+5.1	−3.5	−1.5	+4.7	−3.2	−1.8	+11.1	−27.6	−20.9

(d)[b]

A/B	A/C	E/F	E/G	A/D	E/H
89.6	89.1	71.7	78.6	82.1	87.3

[a] Atoms marked with an asterisk define the least-square plane. – [b] Least-square planes defined by the following atoms: A: C(1) to C(6); B: C(7) to C(12); C: C(22) to C(27); D: C(1), S(1), Yb; E: C(37) to C(42); F: C(43) to C(48); G: C(58) to C(63); H: C(37), S(2), Yb.

Table 4. Salient structural parameters for selected europium and ytterbium thiolates

Compound	Oxid.	c. n.[a]	av. Yb−S [pm]	av. Yb−S−C [°][b]	Ref.
$Eu_2(STrip)_4(THF)_6$	+II	6	289.8[c]/301.6[d]	125[c]	[55]
$Eu(SC_5H_4N\text{-}2)_2(py)_4$	+II	8	304.6		[56]
$Eu(SC_5H_4N\text{-}2)_2(THF)_2(bipy)$	+II	8	300.6		[56]
4a	+II	2 (+ 6)	281.7	116	
$Yb(SMes^*)_2(dme)_2$	+II	6	275.6	125	[32]
$Yb(SPh)_2(py)_4$	+II	6	282.7	102	[57]
$[Yb(\mu\text{-}SPh)(\eta^5\text{-}C_4Me_4P)(THF)_2]_2$	+II	7	282.6		[58]
$Yb(SC_5H_4N\text{-}2)_2(py)_3$	+II	7	288.4		[59]
5	+II	6	273.9	146	
4b	+II	2 (+ 6)	269.1	115	
$Yb(SPh)_3(py)_3$	+III	6	264.7		[56]
$Yb(STrip)_3(py)_3$	+III	6	264.8	117	[55]
$Yb_2(S\mathit{t}Bu)_6(bipy)_2$	+III	6	262.3[c]/274.7[d]	124	[60]
$Yb(SC_5H_4N\text{-}2)_3(py)_2$	+III	8	276.1		[59]
3	+III	6	258.1	125	

[a] Coordination number. – [b] Selected values for monomeric compounds with monodentate ligands. – [c] Terminal ligand. – [d] Bridging ligand.

^{171}Yb NMR resonance of δ = 281. In contrast, there is no detectable signal in the ^{171}Yb NMR spectrum at ambient temperature if a 4:1 mixture of toluene and THF is used as solvent. However, if this purple solution is cooled to 253 K, a color change to yellow is observed and a broad resonance appears at δ = 316 ($w_{1/2}$ = 700 Hz). At 233 K, the signal is shifted to δ = 336 and the linewidth is reduced to 180 Hz. Apparently, if the concentration of THF is too low, the solvated complex $Yb(SAr^*)_2(THF)_x$ (**6**) is only stable at low temperatures. The temperature dependence of the chemical shift for **6** (−0.85 ppm K^{-1}) may be compared with other reported values, which typically vary between +2 and −0.5 ppm K^{-1}.[34]

In the mass spectra of **4a** and **4b**, intense signals due to the molecular ions were found (base peak for **4b**; rel. intensity of 48% for **4a**). In addition, solutions of **4b** in *n*-pentane (purple) and THF (yellow) were studied by UV/Vis spectro-

Table 5. Salient structural parameters for compounds with europium and ytterbium η⁶-π-arene coordination

Compound	Oxid.	Yb−C [pm][a]	Yb−X [pm][b]	Ref.
$[Eu(C_6Me_6)(AlCl_4)_2]_4$	+II	292(2)−307(2) {300}	{267}	[61]
4a	+II	298.8(3)−315.0(3) {307}	273	
		296.7(3)−316.1(3) {306}	272	
$Yb(C_6Me_6)(AlCl_4)_3$	+III	274(4)−301(5) {286}	248	[62]
$Yb(ODpp)_3$ [c]	+III	281.4(4)−314.8(6) {296}	263	[63]
$Yb_2(ODpp)_4$ [d]	+II	275(3)−318(4) {296}		[14]
$[Yb_2(ODpp)_3]^+$	+II	294(1)−315(1) {304}	270	[14]
		287(1)−306(1) {297}	263	
4b	+II	287.0(8)−305.2(8) {296}	262	
		282.4(8)−313.9(8) {298}	265	

[a] {Av. values}. − [b] X defines the centroid of the arene rings. − [c] Dpp = 2,6-$Ph_2C_6H_3$. − [d] Av. values for two independent molecules.

Table 6. ^{171}Yb NMR parameters for compounds **1b**, **2b**, **4b**, and **5**

Compound	Solvent	T [K]	δ [ppm]	$w_{1/2}$ [Hz]
1b	$[D_8]$THF	298	[a]	
2b	$[D_8]$THF	298	351[b]	28
4b	$[D_6]$benzene	298	768	8
4b	$[D_{14}]$methylcyclohexane	298	[c]	
	$[D_{14}]$methylcyclohexane	233	837	70
4b	$[D_6]$toluene (80%) + $[D_8]$THF (20%)	298	[c]	
	$[D_6]$toluene (80%) + $[D_8]$THF (20%)	253	316	700
	$[D_6]$toluene (80%) + $[D_8]$THF (20%)	233	336	180
4b	$[D_8]$THF	298	281	50
5	$[D_{10}]$DME	298	[c]	
	$[D_{10}]$DME	233	204	75

[a] No ^{171}Yb NMR signal besides the resonance for $YbI_2(THF)_4$ (δ = 457) detectable. − [b] Additional smaller signals for the homoleptic species $YbI_2(THF)_4$ (δ = 457, $w_{1/2}$ = 40 Hz) and $Yb(SAr^*)_2(THF)_x$ (δ = 281, $w_{1/2}$ = 70 Hz) were observed. − [c] No ^{171}Yb NMR signal detectable.

photometry. Absorption maxima were observed at 475/546 nm and 369/417 nm, respectively.

It is know from studies on dimeric lanthanide and actinide aryl oxide complexes $M_2(OAr)_6$ (Ar = 2,6-*i*$Pr_2C_6H_3$; M = La, Nd, Sm, Er, U) that infrared spectroscopy is a valuable tool for the identification of η⁶-arene-bridged dimeric structures.[35−37] IR spectroscopy shows distinct differences in the aromatic C=C vibrational modes for the π-bound and *O*-bridged phenoxide ligands in these compounds. Table 7 shows the IR vibrational frequencies for the aromatic stretching modes in compounds **3**, **4a**, **4b**, **5** and the thiol Ar*SH, recorded as Nujol mulls. Two bands in the regions 1604−1606 cm^{-1} and 1565−1569 cm^{-1} are common to all the spectra. Additional stretching modes at 1591/1545 cm^{-1} (**4a**) and 1592/1544 cm^{-1} (**4b**) are observed only in the IR spectra of the donor-free compounds. The latter clearly indicate a weakening of the aromatic C=C bonds, consistent with the presence of π-arene interactions, as observed by X-ray crystallography.

Table 7. Infrared vibrational wavenumbers [cm^{-1}] for the ν(C=C) stretching modes in compounds **3**, **4a**, **4b**, and **5** and the thiol Ar*SH

Compound	ν(C=C)			
3	1605		1565	
4a	1606	1591	1569	1545
4b	1606	1592	1568	1544
5	1604		1566	
Ar*SH	1605		1567	

Ab initio Calculations

Previous theoretical studies of lanthanide bonding to arenes have been mainly limited to complexes of the zero-valent metals.[38,39] To gain more insight into the Eu^{2+}− or Yb^{2+}−arene interactions present in **4a** and **4b**, ab initio calculations on suitable model systems were performed. Quasi-relativistic pseudo-potentials of the Stuttgart/Bonn group were employed for atoms heavier than sulfur.

(a) [Ln(donor)]$^{2+}$ Species

In order to test the influence of different substituents and to gain a qualitative impression of the magnitude of the Ln^{2+}−η⁶-arene interaction, the simple complexes $[Ln(arene)]^{2+}$ (Ln = Eu, Yb; arene = C_6H_6, C_6F_6, 1,3,5-$Me_3C_6H_3$, 1,3,5-*i*$Pr_3C_6H_3$) were first examined. For comparison, the coordination of Eu^{2+} and Yb^{2+} to the strong σ-donors tetrahydrofuran, dimethoxyethane, and the Arduengo-type carbene imidazol-2-ylidene was also investigated. Table 8 summarizes the results of these calculations,

Table 8. B3LYP/6−31G*-optimized bond lengths [pm] and binding energies [kJ mol^{-1}] for [Ln(arene)]$^{2+}$, [Ln(THF)]$^{2+}$, [Ln(dme)]$^{2+}$, and [Ln(imidazol-2-ylidene)]$^{2+}$ species (Ln = Eu, Yb)

Compound	Symm.	Yb−C/O	C−C[a]	ΔE_e	ΔE_{ZPE}	ΔH_0
$[Eu(C_6H_6)]^{2+}$	C_{6v}	298.9	141.0	−277.1	3.8	−273.3
$[Eu(C_6F_6)]^{2+}$	C_{6v}	308.5	141.2	−115.6	2.1	−113.5
$[Eu(1,3,5\text{-}Me_3C_6H_3)]^{2+}$	C_3	{293.1}[b]	{141.6}	−334.4	3.8	−330.6
$[Eu(1,3,5\text{-}i Pr_3C_6H_3)]^{2+}$	C_3	{290.9}	{141.3}	−382.3	−1.0	−383.3
$[Eu(THF)]^{2+}$	C_2	231.2		−297.0	2.3	−294.7
$[Eu(dme)]^{2+}$	C_2	241.0		−428.3	5.1	−423.2
[Eu(imidazol-2-ylidene)]$^{2+}$	C_{2v}	258.8		−386.2	6.5	−379.7
$[Yb(C_6H_6)]^{2+}$	C_{6v}	287.9	141.1	−305.3	3.6	−301.7
$[Yb(C_6F_6)]^{2+}$	C_{6v}	297.1	141.4	−134.2	1.9	−132.3
$[Yb(1,3,5\text{-}Me_3C_6H_3)]^{2+}$	C_3	{282.6}	141.7	−366.4	3.6	−362.8
$[Yb(1,3,5\text{-}i Pr_3C_6H_3)]^{2+}$	C_3	{280.7}	141.3	−420.7	−1.4	−422.1
$[Yb(THF)]^{2+}$	C_2	222.5		−325.8	2.4	−323.4
$[Yb(dme)]^{2+}$	C_2	231.6.0		−470.2	5.4	−464.8
[Yb(imidazol-2-ylidene)]$^{2+}$	C_{2v}	249.1		−425.7	6.5	−419.2

[a] For the isolated arenes, the following C−C distances were obtained at the B3LYP/6−31G* level of theory: 139.7 (C_6H_6), 139.4 (C_6F_6), {139.9} (1,3,5-$Me_3C_6H_3$) {140.0} (1,3,5-$iPr_3C_6H_3$). − [b] {Av. values}.

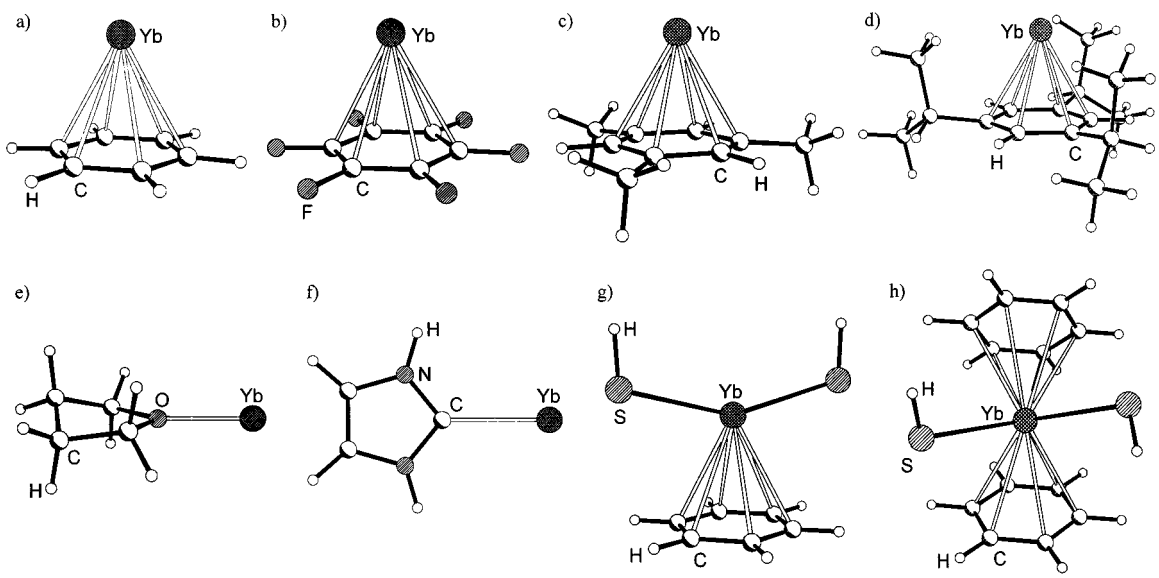

Figure 5. Optimized structures for the model compounds (a) $[Yb(C_6H_6)]^{2+}$, (b) $[Yb(C_6F_6)]^{2+}$, (c) $[Yb(1,3,5\text{-}Me_3C_6H_3)]^{2+}$, (d) $[Yb(1,3,5\text{-}iPr_3C_6H_3)]^{2+}$, (e) $[Yb(THF)]^{2+}$, (f) [Yb(imidazol-2-ylidene)]$^{2+}$, (g) $[Yb(SH)_2(C_6H_6)]$, and (h) $[Yb(SH)_2(C_6H_6)_2]$; calculations were either performed at the B3LYP/6−31G* [(a)−(f)] or the MP2/6−31G* [(g), (h)] level of theory

which were performed at the B3LYP/6−31G* level of theory. The optimized structures of the Yb^{2+} adducts are shown in Figure 5 (a)−(f). Obviously, the binding energy largely depends on the electron-withdrawing or -donating ability of the substituents on the arene rings, as would be expected for a cation−arene interaction dominated by electrostatics. Therefore, as a result of the strong $-I$ effect of the fluorine atoms, the smallest binding energy (ΔH_0) of −113.5 kJ mol^{-1} is calculated for the compound $[Eu(C_6F_6)]^{2+}$, whereas a value of −273.3 kJ mol^{-1} is calculated for the benzene complex $[Eu(C_6H_6)]^{2+}$. The introduction of electron-donating alkyl groups leads to a substantial increase in ΔH_0 from −330.6 kJ mol^{-1} for $[Eu(1,3,5\text{-}Me_3C_6H_3)]^{2+}$ to −383.3 kJ mol^{-1} for $[Eu(1,3,5\text{-}iPr_3C_6H_3)]^{2+}$. With a value of 297 kJ mol^{-1}, the dissociation energy of the adduct $[Eu(THF)]^{2+}$ is intermediate between the values for $[Eu(C_6H_6)]^{2+}$ and $[Eu(1,3,5\text{-}Me_3C_6H_3)]^{2+}$. This is in accordance with the experimental observation that intramolecular arene binding in **4a** and **4b** is favored over the coordination of THF. It is notable that the binding energy for the interaction of Eu^{2+} with the Arduengo-type carbene imidazol-2-ylidene is substantially larger than that for the coordination of THF and comparable to that for coordination of the arene 1,3,5-$iPr_3C_6H_3$. Therefore, it should be possible to obtain adducts of **4a** or **4b** with substituted carbenes of the imidazol-2-ylidene type. As one might expect, the greatest dissociation energy of 423 kJ mol^{-1} is found for the compound $[Eu(dme)]^{2+}$. This is in agreement with the isolation of the bis(DME) adduct **5**. Compared to the corresponding Eu^{2+} compounds, the binding energies of the Yb^{2+} complexes are increased by 9−14%, which is attributable to the smaller ionic radius of

Table 9. Calculated bond lengths [pm], bond angles [°], torsion angles [°], and energies [Hartree] for $Yb(SH)_2$ species (see below) at different levels of theory

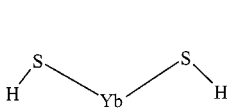

anti,anti (C_{2v})

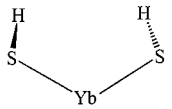

syn,syn (C_2)

Compound	Symm.	Yb−S	S−Yb−S	S−H	H−S−Yb	H−S−Yb−S	E_e	E_{ZPE}
	B3LYP/6−31G*							
$Yb(SH)_2$ *anti*/*anti*	C_{2v}	270.5	132.1	135.7	96.7	180	−830.601965	0.015359
$Yb(SH)_2$ *syn*/*syn*	C_2	269.0	128.5	135.4	98.4	3.4	−830.604450	0.015495
	B3LYP/6−31+G**							
$Yb(SH)_2$ *anti*/*anti*	C_{2v}	270.8	133.9	135.3	95.9	180	−830.612178	0.015359
$Yb(SH)_2$ *syn*/*syn*	C_2	269.2	128.8	135.0	97.8	3.5	−830.614476	0.015489
	MP2/6−31G*							
$Yb(SH)_2$ *anti*/*anti*	no minimum							
$Yb(SH)_2$ *syn*/*syn*	C_2	270.6	149.7	134.5	101.7	20.2	−829.238995	0.015563
	MP2/6−31+G**							
$Yb(SH)_2$ *syn*/*syn*	C_2	271.3	152.1	133.6	97.2	34.3	−829.267290	0.015833

the latter. In accordance with the electronic properties of the various arene ligands, the metal···C(arene) distances also vary considerably by 16−17 pm, being shortest in $[M(1,3,5\text{-}iPr_3C_6H_3)]^{2+}$ and longest in $[M(C_6F_6)]^{2+}$. A notable feature of the calculated $[M(1,3,5\text{-}iPr_3C_6H_3)]^{2+}$ structures is the presence of three agostic-type M···H interactions to C−H bonds of the isopropyl groups (Eu···H: 296.2 pm; Yb···H: 285.5 pm). The shortest experimentally determined M···H distances in **4a** and **4b** are 303 pm and 301 pm, respectively.

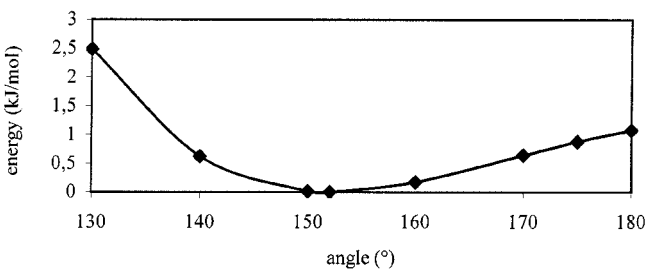

Figure 6. Bending potential curve for *syn*/*syn* $Yb(SH)_2$ at the MP2/6−31+G** level of theory

(b) $Yb(SH)_2$

DFT calculations with two different basis sets revealed at least two stable conformers (Table 9). The U-shaped *syn*,*syn* species with C_2 symmetry is energetically favored by ca. 6 kJ mol^{-1} over the W-shaped *anti*,*anti* conformer (C_{2v}). According to MP2 results, only the former is a minimum on the potential-energy surface. The bending angle at the Yb center and the Yb−S distance were computed at MP2/6−31+G** level to be 152.1° and 271.3 pm, respectively. The DFT calculations showed slightly shorter Yb−S bonds and a more acute S−Yb−S angle of ca. 130° for both conformers. The occurrence of bent equilibrium geometries for some lanthanide MX_2 species[40,41] and related compounds of the heavier alkaline earth elements[42,43] is now well established. This bending can be explained by the presence of small σ-bonding contributions (involving metal d orbitals) and/or the polarization of the metal cation by the ligands. According to Kaupp et al., the MX_2 compounds can be divided into molecules with genuinely bent structures [for example, EuF_2, $Ba(CH_3)_2$] and molecules with quasi-linear equilibrium geometries (for example, $SmCp_2$, CaF_2). The latter show almost no energy change (< 1−2 kJ mol^{-1}) when the equilibrium angle is increased to 180°, whereas the former exhibit considerable linearization energies of up to 33 kJ mol^{-1}.

Figure 6 shows the rather shallow bending potential curve for *syn*/*syn* $Yb(SH)_2$ calculated at the MP2/6-31+G** level of theory. With a linearization energy of 1.1 kJ mol^{-1}, it can be classified as a quasi-linear molecule.

(c) $Yb(SH)_2(C_6H_6)_n$ Complexes (n = 1, 2)

Calculated bond parameters and binding energies for $Yb(SH)_2(C_6H_6)$ and $Yb(SH)_2(C_6H_6)_2$ species, both of which were computed at the B3LYP and MP2 levels of theory using the 6−31G* basis set, are summarized in Table 10. The MP2-optimized structures are shown in Figure 5 (g) and (h). Compared to the experimentally determined distances in complex **4b**, the calculated Yb−S bond lengths for the model compound $Yb(SH)_2(C_6H_6)_2$ are overestimated by 5.1 pm (MP2) and 7.1 pm (B3LYP), respectively. The difference between the DFT-computed and observed Yb···C distances is quite substantial, amounting to +22.3 pm. A much better description is provided by the MP2 calculation, which overestimates the distance of the Yb···arene interaction by only 5.6 pm. Replacing the coordinated benzene in $Yb(SH)_2(C_6H_6)_2$ by the substituted arene 1,3,5-$iPr_3C_6H_3$ can be expected to result in a further reduction in the Yb···C distances, which might, however, be partly compensated by repulsion between the isopropyl groups. The dissociation enthalpy corresponding to the reaction

Table 10. Calculated bond lengths [pm], bond angles [°], torsion angles [°], and binding energies [kJ mol^{-1}] for $Yb(SH)_2(C_6H_6)$ and $Yb(SH)_2(C_6H_6)_2$ species at different levels of theory

Compound[a]	Symm.	Yb−C[b]	Yb−S	S−Yb−S	H−S−Yb−S	ΔE_e	ΔE_{ZPE}	ΔH_0 [c]
	B3LYP/6−31G*							
$Yb(SH)_2(C_6H_6)$	C_2	{310.5}	272.9	139.1	0.4	−70.8	+4.4	−66.4
$Yb(SH)_2(C_6H_6)_2$	C_2	{319.6}	276.2	124.5	44.0	−105.2	+7.3	−97.9
	MP2/6−31G*							
$Yb(SH)_2(C_6H_6)$	C_2	{298.1}	271.8	149.9	0.02	−108.3	+4.6[d]	−103.7
$Yb(SH)_2(C_6H_6)_2$	C_2	{302.9}	274.2	126.6	52.4	−185.4	+7.8[d]	−177.6

[a] *syn*/*syn* isomers only. − [b] {Av. values}. − [c] According to the reaction $Yb(SH)_2 + n\ C_6H_6 \rightarrow Yb(SH)_2(C_6H_6)_n$. − [d] E_{ZPE} was taken from the DFT calculation above.

$Yb(SH)_2(C_6H_6)_2 \rightarrow Yb(SH)_2(C_6H_6) + C_6H_6$ was estimated to be 31.5 kJ mol^{-1} (B3LYP) and 73.9 kJ mol^{-1} (MP2). These values may be compared with the NMR-spectroscopically determined energy barriers of 57.1 kJ mol^{-1} and 54.3 kJ mol^{-1} found for solutions of **4b** in [D_8]toluene or [D_{14}]methylcyclohexane.

Conclusion

The use of the very bulky *m*-terphenyl-substituted Ar*S ligand has permitted the synthesis of the first monomeric σ-donor-free lanthanide(II) thiolates. In the solid state, steric saturation of the europium and ytterbium centers is achieved by two η^6-π-arene interactions, as has been demonstrated by X-ray structural analysis and IR spectroscopy. Evidence that these interactions also persist in solution has been provided by variable-temperature NMR experiments, which show an energy barrier of 54.3 kJ mol^{-1} for **4b** in methylcyclohexane solution. In contrast, the ^{1}H NMR spectrum of the bis(DME) adduct **5** shows no dynamic character in the temperature range 223−300 K, despite the more crowded environment of the Yb center. From ab initio calculations on the model system $Yb(SH)_2(C_6H_6)_2$, it has been estimated that the dissociation of one molecule of benzene requires between 31.5 and 73.9 kJ mol^{-1} depending on the method used.

Experimental Section

General: All manipulations were performed using standard Schlenk techniques under purified argon. Solvents were freshly distilled under argon from Na wire or $LiAlH_4$. The compounds $Yb[N(SiMe_3)_2]_2$ [17] and Ar*SH[44] were synthesized according to known literature procedures. − NMR spectra were recorded with Bruker AM 200, AC250, and AM 400 instruments and were referenced to solvent resonances (^{1}H, ^{13}C) or $YbCp^*_2(THF)_2$ [34] (^{171}Yb). − UV spectra were recorded with a Bruins Omega 10 spectrophotometer. − IR spectra were recorded in the range 4000−200 cm^{-1} with a Perkin−Elmer Paragon 1000 PC spectrometer. − Mass spectra were measured with a Varian MAT711 instrument. − Melting points were determined under Ar in sealed glass tubes.

$Yb(SAr^*)I_2(THF)_3$ (3): A solution of **2b** was prepared from Ar*SH (1.76 g, 3.41 mmol), Yb chips (0.59 g, 3.41 mmol), and 2-iodobenzotrifluoride (0.48 mL, 3.41 mmol) as described below for the synthesis of **4b**. With stirring, a solution of iodine (0.42 g, 3.31 mmol) in THF was added dropwise at 0 °C. The mixture was allowed to warm to ambient temperature and ca. 30 mL of *n*-heptane was added. After filtration through a glass filter frit, the resulting purple solution was concentrated until crystallization commenced and then stored in a freezer at ca. −25 °C for 2 d to give **3** as purple crystals (2.25 g, 57%); m.p. 120−240 °C (dec., compound gradually decolorizes). − IR (CsBr, Nujol): $\tilde{\nu}$ = 1605 ms, 1565 m, 1358 s, 1345 sh, 1315 ms, 1299 s, 1247 m, 1166 ms, 1154 mw, 1130 mw, 1115 m, 1098 m, 1068 ms, 1037 s, 1000 vs, 954 w, 940 m, 916 m, 878 s, 851 sh, 835 vs, 800 s, 774 s, 745 s, 732 s, 674 m, 663 mw, 650 ms, 608 w, 590 w, 526 m, 508 w, 427 mw, 410 cm^{-1} w. − $C_{48}H_{73}I_2O_3SYb$ (1157.0): calcd. C 49.83, H 6.36; found C 49.50, H 6.38.

$Eu(SAr^*)_2$ (4a): At 0 °C, an Eu ingot (3.9 g, 25.7 mmol) was added to a stirred solution of Ar*SH (1.08 g, 2.10 mmol) and 2-iodobenzotrifluoride (0.48 mL, 3.41 mmol) in THF (60 mL). Stirring was continued for 1 h at 0 °C and for a further 1 h at 20 °C, whereupon the resulting light-orange solution was carefully decanted from the excess Eu metal. The volume of the solution was reduced to ca. 5 mL and *n*-heptane (ca. 20 mL) was added. After separation from the precipitated $EuI_2(THF)_5$, the remaining solution was concentrated in vacuo until crystallization commenced. Storage in a freezer at 5 °C overnight afforded **4a**·$(THF)_{0.5}$ as orange crystals (0.89 g, 70%); m.p. 289−292 °C (compound softens > 216 °C). − IR (CsBr, Nujol): $\tilde{\nu}$ = 1606 m, 1591 m, 1569 ms, 1545 m, 1411 m, 1363 s, 1336 m, 1314 ms, 1249 ms, 1167 ms, 1150 m, 1110 ms, 1081 m, 1069 ms, 1049 vs, 1003 m, 939 ms, 922 m, 886 vs, 870 s, 850 w, 791 s, 775 m, 756 m, 738 vs, 733 vs, 649 ms, 612 w, 587 m, 562 w, 519 ms, 426 w, 360 cm^{-1} m. − EI-MS (70 eV): *m*/*z* (%) = 1179.7 (48) [$Eu(SAr^*)_2^+$], 666.3 (100) [$EuSAr^{*+}$], 514.4 (77) [SAr^{*+}]. − $C_{74}H_{102}EuO_{0.5}S_2$ (1215.7): calcd. C 73.11, H 8.46; found C 72.91, H 8.72.

$Yb(SAr^*)_2$ (4b). − Method A: Ar*SH (0.26 g, 0.50 mmol) was added through a solid-addition tube to a stirred solution of $Yb[N(SiMe_3)_2]_2$ (0.12 g, 0.24 mmol) in *n*-pentane (ca. 15 mL). The reaction mixture was stirred for a further 30 min and then the solvent was removed under reduced pressure. The intensely colored residue was redissolved in a mixture of *n*-heptane and a small amount of benzene. Cooling in a freezer at 5 °C afforded **4b**·$(C_6H_6)_{0.5}$ as purple crystals (0.19 g, 64%), which were suitable for X-ray crystallographic studies. The solvate-free compound **1** was obtained by pumping at 10^{-3} mbar for 2 h. − **Method B:** Ar*SH (2.06 g, 4.00 mmol) and Yb chips (1.1 g, 6.36 mmol) were suspended in THF (60 mL) at 0 °C. With stirring, 2-iodobenzotrifluoride (0.56 mL, 4.00 mmol) was added dropwise and after a short induction period a color change to orange was observed. Stirring was con-

tinued for 2 h, whereupon the resulting maroon solution was carefully decanted from the unchanged excess Yb metal. Most of the solvent was removed under reduced pressure and the concentrate was treated with *n*-pentane (50 mL). The solution was separated from the precipitated greenish-yellow $YbI_2(THF)_4$ and all volatile materials were distilled off in vacuo. Recrystallization of the purple-brown residue from *n*-heptane/toluene (20:1) followed by pumping at 10^{-3} mbar for 2 h gave pure **4b** as a purple powder (1.58 g, 66%); m.p. 263−265 °C (compound softens > 220 °C). − ^{1}H NMR (250.1 MHz, [D$_8$]toluene, 85 °C): δ = 1.06 [d, $^3J_{HH}$ = 6.9 Hz, 24 H, *o*/*p*-CH(CH_3)$_2$], 1.24 [d, $^3J_{HH}$ = 6.9 Hz, 24 H, *o*/*p*-CH(CH_3)$_2$], 1.31 [d, $^3J_{HH}$ = 6.9 Hz, 24 H, *o*/*p*-CH(CH_3)$_2$], 2.89 [sept, $^3J_{HH}$ = 6.9 Hz, 8 H, *o*-CH(CH$_3$)$_2$], 3.07 [sept, $^3J_{HH}$ = 6.9 Hz, 4 H, *p*-CH(CH$_3$)$_2$], 6.86 (m, 6 H, *m*/*p*-C$_6$H$_3$), 7.17 (s, 8 H, *m*-Trip). − ^{13}C NMR (62.9 MHz, [D$_8$]toluene, 85 °C): δ = 23.8, 24.3, 24.8 [*o*/*p*-CH(*C*H$_3$)$_2$], 31.2 [*o*-*C*H(CH$_3$)$_2$], 34.0 [*p*-*C*H(CH$_3$)$_2$], 120.6 (*p*-C$_6$H$_3$), 122.0 (*m*-Trip), 129.0 (*m*-C$_6$H$_3$), 141.6, 142.7 (*i*-Trip, *o*-C$_6$H$_3$), 148.3 (*o*-Trip), 149.3 (*p*-Trip), 152.5 (*i*-C$_6$H$_3$). − ^{171}Yb NMR (70.1 MHz, [D$_6$]benzene, 25 °C): δ = 768 ($w_{1/2}$ = 8 Hz) − IR (CsBr, Nujol): $\tilde{\nu}$ = 1606 m, 1592 m, 1568 m, 1544 m, 1314 ms, 1249 ms, 1168 ms, 1150 m, 1110 ms, 1082 m, 1069 m, 1049 s, 1004 w, 939 s, 920 m, 886 vs, 869 vs, 849 w, 791 vs, 774 m, 755 ms, 740 vs, 733 vs, 650 s, 611 w, 587 m, 519 s, 425 w, 363 m, 306 cm^{-1} w. − EI-MS (70 eV): *m*/*z* (%) = 1200.7 (100) [Yb(SAr*)$_2^+$], 687.3 (32) [YbSAr*$^+$], 514.4 (19) [SAr*$^+$]. − $C_{72}H_{98}S_2Yb$ (1200.74): calcd. C 72.02, H 8.23; found C 71.41, H 8.36. − UV/Vis (*n*-pentane): λ_{max} (ε) = 475 nm (110 M^{-1} cm^{-1}), 546 (90). − UV/Vis (THF): λ_{max} (ε) = 369 nm (480 M^{-1} cm^{-1}), 417 (250).

Yb(SAr*)$_2$(THF)$_x$ (6): ^{1}H NMR (200.13 MHz, [D$_8$]THF, 25 °C): δ = 0.95 [d, $^3J_{HH}$ = 6.8 Hz, 24 H, *o*/*p*-CH(CH_3)$_2$], 1.16 [d, $^3J_{HH}$ = 6.8 Hz, 24 H, *o*/*p*-CH(CH_3)$_2$], 1.26 [d, $^3J_{HH}$ = 6.8 Hz, 24 H, *o*/*p*-CH(CH_3)$_2$], 2.86 [sept, $^3J_{HH}$ = 6.8 Hz, 4 H, *p*-CH(CH$_3$)$_2$], 2.95 [sept, $^3J_{HH}$ = 6.8 Hz, 8 H, *o*-CH(CH$_3$)$_2$], 6.67 (m, 6 H, *m*/*p*-C$_6$H$_3$), 6.93 (s, 8 H, *m*-Trip). − ^{13}C NMR (50.33 MHz, [D$_8$]THF, 25 °C): δ = 24.5, 24.5, 25.8 [*o*/*p*-CH(*C*H$_3$)$_2$], 31.2 [*o*-*C*H(CH$_3$)$_2$], 34.9 [*p*-*C*H(CH$_3$)$_2$], 119.3 (*p*-C$_6$H$_3$), 121.1 (*m*-Trip), 129.9 (*m*-C$_6$H$_3$), 142.9, 144.4 (*i*-Trip, *o*-C$_6$H$_3$), 146.3 (*p*-Trip), 147.3 (*o*-Trip), 152.5 (*i*-C$_6$H$_3$). − ^{171}Yb NMR (70.1 MHz, [D$_8$]THF, 25 °C): δ = 281 ($w_{1/2}$ = 50 Hz). − ^{171}Yb NMR {70.1 MHz, [D$_8$]toluene (ca. 80%) + [D$_8$]THF (ca. 20%), −40 °C}: δ = 336 ($w_{1/2}$ = 180 Hz).

Yb(SAr*)$_2$(dme)$_2$ (5): In a Schlenk tube, purple **4b** (0.35 g, 0.29 mmol) was treated with two drops of DME, which immediately gave **5** as a yellow, microcrystalline material in quantitative yield. The excess DME was carefully removed in vacuo at 0 °C. Prolonged pumping at 10^{-3} mbar overnight gave **4b** once more. Crystals of **5** suitable for X-ray crystallographic studies were obtained from an *n*-pentane/DME mixture (5:1) at −25 °C; m.p.: compound darkens > ca. 110 °C and melts to a purple-brown liquid between 265 and 270 °C. After cooling to ambient temperature and standing for 1 h, the upper crust of the solid turns yellow again. − ^{1}H NMR (250.1 MHz, [D$_{10}$]DME, 25 °C): δ = 0.97 [d, $^3J_{HH}$ = 6.8 Hz, 24 H, *o*/*p*-CH(CH_3)$_2$], 1.18 [d, $^3J_{HH}$ = 6.8 Hz, 24 H, *o*/*p*-CH(CH_3)$_2$], 1.25 [d, $^3J_{HH}$ = 6.8 Hz, 24 H, *o*/*p*-CH(CH_3)$_2$], 2.87 [m, 12 H, *o*- + *p*-CH(CH$_3$)$_2$], 3.27 (s, 12 H, OCH$_3$), 3.43 (s, 8 H, OCH$_2$) [these two signals correspond to the coordinated non-deuterated DME; another set of signals is observed for the perdeuterated solvent], 6.67 (m, 6 H, *m*- + *p*-C$_6$H$_3$), 6.88 (s, 8 H, *m*-Trip). − ^{171}Yb NMR (70.1 MHz, [D$_{10}$]DME, −40 °C): δ = 204 ($w_{1/2}$ = 75 Hz). − IR (CsBr, Nujol): $\tilde{\nu}$ = 1604 m, 1566 ms, 1358 s, 1315 ms, 1276 w, 1243 ms, 1209 w, 1190 m, 1168

Table 11. Selected crystallographic data for compounds **3**, **4a**, **4b**, and **5**

Compound[a]	**3**	**4a**·(THF)$_{0.5}$	**4b**·(C$_6$H$_6$)$_{0.5}$	**5**
Empirical formula	$C_{48}H_{73}I_2O_3SYb$	$C_{74}H_{102}S_2Eu$	$C_{75}H_{101}S_2Yb$	$C_{80}H_{118}O_4S_2Yb$
Molecular mass	1157.0	1215.6	1239.7	1380.9
Color, habit	purple, plate	deep orange, block	purple, block	yellow, needle fragment
Crystal size [mm]	0.45 × 0.20 × 0.05	0.70 × 0.40 × 0.35	0.75 × 0.65 × 0.60	0.40 × 0.30 × 0.30
Crystal system	orthorhombic	triclinic	triclinic	monoclinic
Space group	$P2_12_12_1$	$P\bar{1}$	$P\bar{1}$	$P2_1$
a [Å]	13.543(3)	13.278(2)	13.028(5)	13.905(3)
b [Å]	15.984(3)	14.537(3)	14.270(6)	18.837(4)
c [Å]	23.448(5)	18.804(4)	18.681(8)	15.329(3)
α [°]	90	105.60(2)	106.63(3)	90
β [°]	90	95.18(1)	96.02(2)	107.56(2)
γ [°]	90	97.80(1)	96.61(2)	90
V [Å^3]	5076(2)	3433(1)	3271(2)	3828(1)
Z	4	2	2	2
$d_{calcd.}$ [g cm^{-3}]	1.514	1.176	1.259	1.198
μ [cm^{-1}]	31.35	10.13	15.34	13.21
2θ range [°]	3−54	4−54	4−50	3−54
Unique data/R_{int}	6727/0.0630	14752/0.0373	11176/0.0652	9449/0.0466
Data with $I > 2\sigma(I)$ (N_o)	5499	11454	8311	7449
Parameters (N_p)	527	832	828	829
*R*1 [$I > 2\sigma(I)$][b]	0.0436	0.0419	0.0671	0.0479
*wR*2 (all data)[c]	0.0848	0.1018	0.1818	0.1033
GoF[d]	1.213	0.956	1.225	1.206
Largest diff. peak and hole [e·Å^{-3}]	0.62/−0.83	1.10/−0.83	1.78/−1.62	1.19/−0.60

[a] All data were collected at 173 K using Mo-K_α (λ = 0.71073 Å) radiation. − [b] $R1 = (||F_o| - |F_c||)/|F_o|$. − [c] $wR2 = \{[w(F_o^2 - F_c^2)^2]/[w(F_o^2)^2]\}^{1/2}$. − [d] GoF = $\{[w(F_o^2 - F_c^2)^2]/(N_o - N_p)\}$.

m, 1128 w, 1111 ms, 1059 vs, 1051 sh, 1025 ms, 1005 m, 954 w, 941 m, 920 w, 875 s, 872 s, 868 s, 860 s, 831 m, 794 s, 775 m, 755 w, 742 vs, 736 vs, 650 ms, 608 w, 588 w, 567 w, 520 m, 425 mw, 379 cm^{-1} mw. − $C_{80}H_{118}O_4S_2Yb$ (1381.0): calcd. C 69.58, H 8.61; found C 69.42, H 8.71.

X-ray Crystallography: X-ray-quality crystals were obtained as described above. Crystals were removed from Schlenk tubes and immediately covered with a layer of viscous hydrocarbon oil (Paratone N, Exxon). A suitable crystal was selected, attached to a glass fibre, and instantly placed in a low-temperature N_2 stream.[45] All data were collected at 173 K using either a Syntex $P2_1$ (**3**, **5**) or a Siemens P4 (**4a**, **4b**) diffractometer. Crystal data are given in Table 11. Calculations were carried out with the SHELXTL PC 5.03[46] and SHELXL-97[47] program systems installed on a local PC. The structures were solved by direct methods and refined against F_o^2 by full-matrix least-squares techniques. An absorption correction was applied by using semiempirical ψ-scans (**5**) or the program XABS2[48] (**3**, **4b**). For **4a**, no absorption correction was used. Anisotropic thermal parameters were included for all non-hydrogen atoms with the exception of the co-crystallized THF molecule, which was refined with a common isotropic U value. The methyl carbon atoms of two (**5**) or four (**4a**, **4b**) disordered isopropyl groups were refined with split positions. The geometries of the disordered isopropyl groups and the co-crystallized benzene molecule (**4b**) were restrained with SADI and DFIX commands. H atoms were placed in geometrical positions and were refined using a riding model that included free rotation of the methyl groups. Their isotropic thermal parameters were either allowed to refine or were constrained to 1.2 (aryl H) or 1.5 (methyl groups) times U_{eq} of the carbon atom to which they were bound. Final R values are listed in Table 11. Salient bond lengths and angles are given in Tables 1−3. Crystallographic data (excluding structure factors) for the structures reported in this paper have been deposited with the Cambridge Crystallographic Data Centre as supplementary publication nos. CCDC-150909 (**3**), -150907 (**4a**), -150908 (**4b**), and -150910 (**5**). Copies of the data can be obtained free of charge on application to the CCDC, 12 Union Road, Cambridge CB2 1EZ, U.K. [Fax: (internat.) + 44-1223/336-033; E-mail: deposit@ccdc.cam.ac.uk].

Computational Details: The Gaussian 98[49] package was used for all energy and frequency calculations. The geometries of the molecules were optimized using either density functional theory (DFT) with the functional B3LYP or second-order Møller−Plesset perturbation theory (MP2). Quasi-relativistic 11- or 10-valence-electron pseudo-potentials of the Stuttgart/Bonn group were employed for the heavy atoms Sc,[50] Eu, and Yb.[51,52] The corresponding (8s7p6d1f)/[6s5p3d1f] valence basis set for Sc was taken from the literature, whereas the (7s6p5d)/[5s4p3d] valence basis sets for Eu and Yb were augmented by one set of f-functions. The basis sets for C, H, F, and S were either 6−31G* or 6−31+G** [$Yb(SH)_2$ species only]. Frequency calculations were carried out to verify that the geometries were true minima on the potential-energy surface and to obtain the zero-point energy (E_{ZPE}). The sum of the electronic energy (E_e) and the zero-point energy was used to calculate differences interpreted as reaction enthalpies (ΔH_0) at 0 K. For calibration purposes, test calculations were performed to compute the cation−ring binding energy of $[Sc(C_6H_6)]^+$, which was determined experimentally as -222 ± 21 kJ mol^{-1}.[53,54] The results of B3LYP and MP2 calculations with the 6−31+G** basis set fall within the experimental error bars. The binding energy was found to be overestimated by 9−16% using the 6−31G* or 6−311+G** basis sets.

Acknowledgments

Support of this work by the Fonds der Chemischen Industrie is gratefully acknowledged. The author also wishes to thank Prof. G. Becker for generous support.

[1] M. N. Bochkarev, L. N. Zakharov, G. S. Kalinina, *Organoderivatives of Rare Earth Elements*, Kluwer Academic Press, Dordrecht, **1995**.
[2] F. T. Edelmann, *Angew. Chem.* **1995**, *107*, 2647−2669; *Angew. Chem. Int. Ed. Engl.* **1995**, *34*, 2466−2488.
[3] S. A. Cotton, *Coord. Chem. Rev.* **1997**, *160*, 93−127.
[4] F. Nief, *Coord. Chem. Rev.* **1998**, *178−180*, 13−81.
[5] J. M. Boncella, R. A. Andersen, *Organometallics* **1985**, *4*, 205−206.
[6] P. B. Hitchcock, M. F. Lappert, R. G. Smith, R. A. Bartlett, P. P. Power, *J. Chem. Soc., Chem. Commun.* **1988**, 1007−1009.
[7] P. B. Hitchcock, J. A. K. Howard, M. F. Lappert, S. Prashar, *J. Organomet. Chem.* **1992**, *437*, 177−189.
[8] W. J. Evans, R. Anwander, J. W. Ziller, *Inorg. Chem.* **1995**, *34*, 5927−5930.
[9] M. Westerhausen, M. Hartmann, W. Schwarz, *Inorg. Chim. Acta* **1998**, *269*, 91−100.
[10] W. T. Klooster, R. S. Lu, R. Anwander, W. J. Evans, T. F. Koetzle, R. Bau, *Angew. Chem.* **1998**, *110*, 1326−1329; *Angew. Chem. Int. Ed.* **1998**, *37*, 1268−1270.
[11] W. T. Klooster, L. Brammer, C. J. Schaverien, P. H. M. Budzelaar, *J. Am. Chem. Soc.* **1999**, *121*, 1381−1382.
[12] G. B. Deacon, Q. Shen, *J. Organomet. Chem.* **1996**, *506*, 1−17.
[13] M. Niemeyer, S.-O. Hauber, *Z. Anorg. Allg. Chem.* **1999**, *625*, 137−140.
[14] G. B. Deacon, C. M. Forsyth, P. C. Junk, B. W. Skelton, A. H. White, *Chem. Eur. J.* **1999**, *5*, 1452−1459.
[15] G. Heckmann, M. Niemeyer, *J. Am. Chem. Soc.* **2000**, *122*, 4227−4228.
[16] B. Twamley, S. T. Haubrich, P. P. Power, *Adv. Organomet. Chem.* **1999**, *44*, 1−65.
[17] G. B. Deacon, G. D. Fallon, C. M. Forsyth, H. Schumann, R. Weimann, *Chem. Ber./Recueil* **1997**, *130*, 409−415.
[18] D. F. Evans, G. V. Fazakerley, R. F. Phillips, *J. Chem. Soc. A* **1971**, 1931−1934.
[19] C. Eaborn, P. B. Hitchcock, K. Izod, Z.-R. Lu, J. D. Smith, *Organometallics* **1996**, *15*, 4783−4790.
[20] C. Eaborn, P. B. Hitchcock, K. Izod, J. D. Smith, *J. Am. Chem. Soc.* **1994**, *116*, 12071−12072.
[21] M. Niemeyer, *Z. Anorg. Allg. Chem.* **2000**, *626*, 1027−1029.
[22] The precipitated $YbI_2(THF)_4$ was identified by ^{171}Yb NMR and UV/Vis spectroscopy. The latter method also showed the absence of Yb^{III} impurities.
[23] F. T. Edelmann, *Lanthanides and Actinides* in *Synthetic Methods of Organometallic and Inorganic Chemistry (Hermann/Brauer)* (Ed.: W. A. Hermann), Georg Thieme Verlag, Stuttgart, **1997**.
[24] M. Niemeyer, unpublished results.
[25] D. J. Duncalf, P. B. Hitchcock, G. A. Lawless, *Chem. Commun.* **1996**, 269−271.
[26] G. B. Deacon, S. C. Harris, G. Meyer, D. Stellfeldt, D. L. Wilkinson, G. Zelesny, *J. Organomet. Chem.* **1996**, *525*, 247−254.
[27] A search of the CCDC database (Vers. April 2000) for Yb^{III}−O(THF) distances with a six-coordinate metal center gave 23 hits in the range 225.5 to 240.9 pm (av. 231.9 pm). A search for the *trans*-O(THF)−Yb^{III}−O(THF) fragment resulted in seven hits with an average distance of 226.9 pm.
[28] L. N. Bochkarev, T. A. Zheleznova, A. V. Safronova, M. S. Drozdov, S. F. Zhiltsov, L. N. Zakharov, G. K. Fukin, S. Y. Khorshev, *Russ. Chem. Bull.* **1998**, *47*, 165−168.
[29] G. B. Deacon, T. C. Feng, B. W. Skelton, A. H. White, *Aust. J. Chem.* **1995**, 741−756.
[30] F. G. N. Cloke, *Chem. Soc. Rev.* **1993**, 17−24.

[31] F. G. N. Cloke, K. Khan, R. N. Perutz, *J. Chem. Soc., Chem. Commun.* **1991**, *48*, 1372−1373.
[32] B. Cetinkaya, P. B. Hitchcock, M. F. Lappert, R. G. Smith, *J. Chem. Soc., Chem. Commun.* **1992**, 932−934.
[33] J. R. van den Hende, P. B. Hitchcock, S. A. Holmes, M. F. Lappert, W. P. Leung, T. C. W. Mak, S. Prashar, *J. Chem. Soc., Dalton Trans.* **1995**, 1427−1433.
[34] J. M. Keates, G. A. Lawless, *^{171}Yb NMR Spectroscopy* in *Advanced Applications of NMR to Organometallic Chemistry* (Eds.: M. Gielen, R. Willem, B. Wrackmeyer), Wiley, Chichester, **1996**, chapter 12.
[35] W. G. van der Sluys, C. J. Burns, J. C. Huffman, A. P. Sattelberger, *J. Am. Chem. Soc.* **1988**, *110*, 5924−5925.
[36] D. M. Barnhart, D. L. Clark, J. C. Gordon, J. C. Huffman, R. L. Vincent, J. G. Watkin, B. D. Zwick, *Inorg. Chem.* **1994**, *33*, 3487−3497.
[37] R. J. Butcher, D. L. Clark, S. K. Grumbine, R. L. Vincent-Hollis, B. L. Scott, J. G. Watkin, *Inorg. Chem.* **1995**, *34*, 5468−5476.
[38] W. A. King, S. Di Bella, G. Lanza, K. Khan, D. J. Duncalf, F. G. N. Cloke, I. L. Fragala, T. J. Marks, *J. Am. Chem. Soc.* **1996**, *118*, 627−635.
[39] G. Hong, F. Schautz, M. Dolg, *J. Am. Chem. Soc.* **1999**, *121*, 1502−1512.
[40] M. Dolg, H. Stoll, H. Preuss, *J. Mol. Struct. (Theochem)* **1991**, *235*, 67−79.
[41] M. Kaupp, P. v. R. Schleyer, M. Dolg, H. Stoll, *J. Am. Chem. Soc.* **1992**, *114*, 8202−8208.
[42] M. Kaupp, P. v. R. Schleyer, *J. Am. Chem. Soc.* **1992**, *114*, 491−497.
[43] R. Blom, K. Faegri, Jr., H. V. Volden, *Organometallics* **1990**, *9*, 372−379.
[44] M. Niemeyer, P. P. Power, *Inorg. Chem.* **1996**, *35*, 7264−7272.
[45] H. Hope, *Handling of Reactive Compounds for X-ray Structure Analysis* in *Experimental Organometallic Chemistry: A Practicum in Synthesis and Characterization* (Eds.: A. L. Wayda, M. Y. Darensbourg), American Chemical Society, Washington DC, **1987**, chapter 10.
[46] *SHELXTL PC 5.03*, Siemens Analytical X-ray Instruments Inc., Madison, WI, **1994**.
[47] G. M. Sheldrick, *Program for Crystal Structure Solution and Refinement*, Universität Göttingen, **1997**.
[48] S. Parkin, B. Moezzi, H. Hope, *J. Appl. Crystallogr.* **1995**, *28*, 53−56.
[49] M. J. Frisch, G. W. Trucks, H. B. Schlegel, G. E. Scuseria, M. A. Robb, J. R. Cheeseman, V. G. Zakrzewski, J. A. Montgomery, Jr., R. E. Stratmann, J. C. Burant, S. Dapprich, J. M. Millam, A. D. Daniels, K. N. Kudin, M. C. Strain, O. Farkas, J. Tomasi, V. Barone, M. Cossi, R. Cammi, B. Mennucci, C. Pomelli, C. Adamo, S. Clifford, J. Ochterski, G. A. Petersson, P. Y. Ayala, Q. Cui, K. Morokuma, D. K. Malick, A. D. Rabuck, K. Raghavachari, J. B. Foresman, J. Cioslowski, J. V. Ortiz, A. G. Baboul, B. B. Stefanov, G. Liu, A. Liashenko, P. Piskorz, I. Komaromi, R. Gomperts, R. L. Martin, D. J. Fox, T. Keith, M. A. Al-Laham, C. Y. Peng, A. Nanayakkara, C. Gonzalez, M. Challacombe, P. M. W. Gill, B. Johnson, W. Chen, M. W. Wong, J. L. Andres, C. Gonzalez, M. Head-Gordon, E. S. Replogle, J. A. Pople, *Gaussian 98, Rev. A.7*, Gaussian, Inc., Pittsburgh PA, **1998**.
[50] M. Dolg, U. Wedig, H. Stoll, H. Preuss, *J. Chem. Phys.* **1987**, *86*, 866−872.
[51] M. Dolg, H. Stoll, A. Savin, H. Preuss, *Theor. Chim. Acta* **1989**, *75*, 173−194.
[52] M. Dolg, H. Stoll, H. Preuss, *Theor. Chim. Acta* **1993**, *85*, 441−450.
[53] L. M. Lech, B. S. Freiser, *Organometallics* **1988**, *7*, 1948−1957.
[54] C. W. Bauschlicher Jr., H. Partridge, S. R. Langhoff, *J. Phys. Chem.* **1992**, *96*, 3273−3278.
[55] K. Mashima, Y. Nakayama, H. Fukumoto, N. Kanehisa, Y. Kai, A. Nakamura, *J. Chem. Soc., Chem. Commun.* **1994**, 2523−2524.
[56] M. Berardini, J. G. Brennan, *Inorg. Chem.* **1995**, *34*, 6179−6185.
[57] M. Brewer, D. Khasnis, M. Buretea, M. Berardini, T. J. Emge, J. G. Brennan, *Inorg. Chem.* **1994**, *33*, 2743−2747.
[58] F. Nief, L. Ricard, *J. Chem. Soc., Chem. Commun.* **1994**, 2723−2724.
[59] M. Berardini, J. Lee, D. Freedman, J. Lee, T. J. Emge, J. G. Brennan, *Inorg. Chem.* **1997**, *36*, 5772−5776.
[60] H. C. Aspinall, S. A. Cunningham, P. Maestro, P. Macaudiere, *Inorg. Chem.* **1998**, *37*, 5396−5398.
[61] H. Liang, Q. Shen, S. Jin, Y. Lin, *J. Chem. Soc., Chem. Commun.* **1992**, 480−481.
[62] H. Liang, Q. Shen, J. Guan, Y. Lin, *J. Organomet. Chem.* **1994**, *474*, 113−116.
[63] G. B. Deacon, S. Nickel, P. MacKinnon, E. R. T. Tiekink, *Aust. J. Chem.* **1990**, *43*, 1245−1257.

Received October 17, 2000
[I00395]

Synthesis and Structural Studies of Pyridine-2-selenolates − Reactions with Electrophilic Phosphorus(III) Compounds and Related Complex Chemistry

Jörg Laube,[a] Stefan Jäger,[a] and Carsten Thöne*[a]

Dedicated to Professor Henning Hopf on the occasion of his 60th birthday

Keywords: Selenium / P ligands / Molybdenum / Metallacycles / Coinage-metal complexes

The reaction intermediates in the synthesis of 2,2′-bis(pyridyl) diselenide (2,2′-Py_2Se_2) have been determined. The reaction of Na_2Se_2 with 2-BrC_5H_4N (2-BrPy) leads to a tautomeric mixture of pyridine-2-selenol (2-PySeH) and pyridine-2(1*H*)-selone (2-PyHSe), which have been investigated by spectroscopic means. Additionally, the crystal structure of the latter has been determined. Reductive cleavage of the Se–Se bond in 2,2′-Py_2Se_2 with K*B*s*Bu*$_3$H leads to K-2-SePy, which was trapped, either as [(18-crown-6)K]$^+$[2-PySe]$^-$, whose structure contains polymeric cation–anion chains, or as [Et_4N]$^+$[2-PySe]$^-$. Reactions of K-2-SePy or [Et_4N]$^+$[2-PySe]$^-$ with Ph_2PCl, *t*Bu_2PCl, or *t*$BuPBr_2$ lead to the corresponding, extremely air-sensitive (pyridyl)selenophosphanes Ph_2P-2-SePy, *t*Bu_2P-2-SePy, and *t*BuP(2-SePy)$_2$. The latter was trapped as *t*BuP(O)(2-SePy)$_2$, whose crystal structure has been determined. Metal complexes of these (pyridyl)selenophosphanes have been prepared starting from the phosphane and CuBr, AgBr, (tht)AuCl (tht = tetrahydrothiophene), or [(η^6-C_7H_8)Mo(CO)$_3$], in one-pot syntheses. All crystal structures of the resulting metallacycles [({(C$_5$H$_4$N-2-Se)*t*Bu_2P}-*N,P*)Cu(μ-Br)]$_2$, [({(C$_5$H$_4$N-2-Se)*t*Bu_2P}-*N,P*)Ag(μ-Br)]$_2$, [({(C$_5$H$_4$N-2-Se)*t*Bu_2P}-*P*)AuCl], and [({(C$_5$H$_4$N-2-Se)$_2$*t*BuP}-*N,N′,P*)Mo(CO)$_3$], were determined. Additionally, comprehensive spectroscopic investigations are presented.

Introduction

Recent research in our laboratory has shown that 2,2′-bis(pyridyl) diselenide (Py_2Se_2) is a useful starting material for the preparation of (pyridyl-2-selenolato)metal complexes.[1] The most common reaction mechanisms comprise oxidative addition of Py_2Se_2 to unsaturated metal centres and reductive cleavage of the Se−Se bond with organoboron hydrides, and subsequent reactions of the formed $PySe^-$ anion with halometal complexes. Additionally, oxidative addition of Py_2Se_2 to finely divided elemental metals could be employed, as shown for In.[2]

Apart from homoleptic (pyridineselenolato)metal complexes, which can serve as volatile starting materials for the preparation of thin metal selenide layers,[3] the coordination chemistry of ligands that contain the soft/hard Se/N donor set is surprisingly unexplored,[4] although Py_2Se_2 was first synthesized in 1962,[5] and its use in organic syntheses[6] and biochemistry[7] is well documented. The mechanism of Py_2Se_2 formation from Na_2Se_2 and 2-BrPy under acidic conditions is also not well understood. Py_2Se_2 is usually synthesized by oxidation of Py-2-SeH with various oxidising agents, but the reported syntheses of Py-2-SeH are often unreliable for different reasons.[3a,5][7c,8] In the first part of this paper, we report on the synthesis and characterization of Py-2-SeH and its tautomeric form pyridine-2(1*H*)-selone PyH-2-Se, together with the synthesis of the useful starting material in pyridineselenolate chemistry, [Et_4N][2-PySe]. We also report the crystal structure of PyH-2-Se and [(18-crown-6)K][2-PySe].

(Organoseleno)phosphanes are relatively rare in the literature, and apart from $P(SePh)_3$, no crystal structure has been published.[9] Heteroatom-substituted phosphanes were shown to be useful ligands that display enhanced catalytic activities,[10] as described for the reaction of ketones with propane-2-ol to form corresponding alcohols with [$RuCl_2(PPh_3)_3$] or [$RuCl_2(PPh_3)$(N,P,N)] [N,P,N = bis(2-oxazoline-2-yl-methyl)(phenyl)phosphane] as catalyst.[11] One possibility for controlling the reaction pathways and the selectivity of phosphane-containing catalysts is the modification of the surrounding phosphane by varying the donor atom sets, which are usually C, N, and P. The introduction of selenium offers different coordination modes with hard and soft metal centres. In the second part of the paper, we therefore describe the syntheses of (pyridylseleno)-phosphanes and related metal complexes, together with the crystal structures of *t*BuP(O)(2-SePy)$_2$, [({(C$_5$H$_4$N-2-Se)*t*Bu_2P}-*N,P*)Cu(μ-Br)]$_2$, [({(C$_5$H$_4$N-2-Se)*t*Bu_2P}-*N,P*)Ag-(μ-Br)]$_2$, [({(C$_5$H$_4$N-2-Se)*t*Bu_2P}-*P*)AuCl], and [({(C$_5$H$_4$N-2-Se)$_2$*t*BuP}-*N,N′,P*)Mo(CO)$_3$].

Results and Discussion

Pyridine-2-selenol (1), Pyridine-2(1*H*)-selone (2), and Related Selenolates

Our previously described synthesis of Py-2-SeH is strongly dependent on the reaction conditions.[1a] All attempts to repeat the synthesis at slightly different temper-

[a] Institut für Anorganische und Analytische Chemie der Technischen Universität,
Hagenring 30, 38106 Braunschweig, Germany
E-mail: c.thoene@tu-bs.de

 © WILEY-VCH Verlag GmbH, 69451 Weinheim, 2001 1434−1948/01/0808−1983 $ 17.50+.50/0

atures or pH values have been unsuccessful. This prompted us to examine this reaction in more detail. The results are shown in Scheme 1.

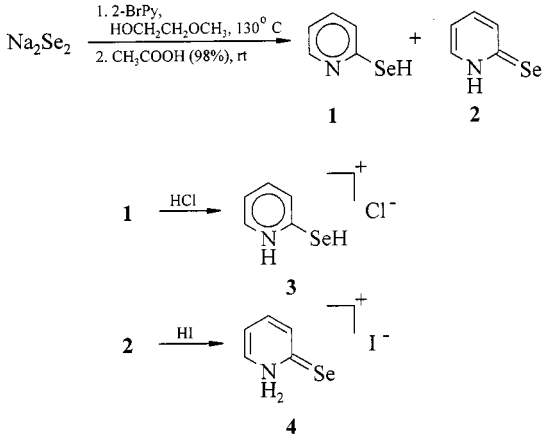

Scheme 1. Synthesis of 2-pyridineselenol (**1**) and pyridine-2(1*H*)-selone (**2**) and their reactions with HCl and HI

The acidification of the reaction mixture Na_2Se_2/2-BrPy, after refluxing it for 24 h in glycol monomethyl ether, with glacial acetic acid, leads to a mixture of Py-2-SeH (**1**) and PyH-2-Se (**2**) (ratio 1:6). These could be easily separated, since **1** and **2** have different physical properties: **1** is a light-yellow air-sensitive powder, soluble in polar solvents (alcohols, H_2O), but only sparingly soluble in CH_2Cl_2; **2** is a dark-yellow to orange air-stable and crystalline solid, soluble in polar solvents, but only sparingly soluble in H_2O. Once separated, **2** does not equilibrate to **1** in polar solvents. However, the mixture of **1** and **2** does not have to be separated for the synthesis of Py_2Se_2. The tautomerism of **1** and **2** was examined by spectroscopic means. It was shown that the UV/Vis spectrum of **2** is similar to the corresponding spectrum of 1-methylpyridine-2(1*H*)-selone, which gives a first hint of the selone structure.[5,12] Additional measurements of the dipole moment suggest the selone to be dimeric and resonance-stabilized (Scheme 2).

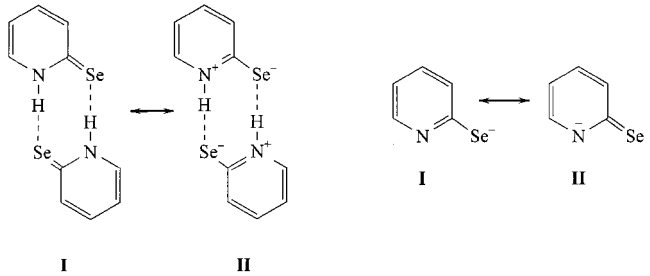

Scheme 2. Resonance forms of the dimeric pyridine-2(1*H*)-selone (**2**) and the 2-$PySe^-$ anion

The zwitterionic form **II** contributes markedly, since the dipole moment is relatively high and strongly solvent-dependent. ^{1}H NMR spectroscopic data show that the SeH signal of **1** (δ = 8.53) is shifted to low field in comparison with other organic selenols [PhSeH: δ = 1.36 (m); 2,4,6-$(CF_3)_3C_6H_2$SeH: δ = 2.36].[13] The tautomeric forms **1** and **2** are therefore easily distinguishable, since **2** displays a corresponding ^{1}H NMR resonance at a lower field (δ = 12−14; depending on the solvent and concentration). Further experiments showed that **1** and **2** react with acids to produce, e.g., the corresponding pyridinium hydrochloride and hydroiodide **3** and **4**. Protonation occurs exclusively at the nitrogen atom, and again the ^{1}H NMR spectroscopic data allow a clear distinction. Thus, the resonance for SeH of **3** appears at δ = 4.96, with an H−Se coupling constant of 14 Hz, derived from ^{77}Se satellites. The corresponding resonance of the amine proton is shifted to lower field (δ = 11.93). The ^{1}H NMR spectrum of **4** displays a resonance for the equivalent amine protons at δ = 8.88 (av. value of three measurements).

To confirm the NMR results, an X-ray structure analysis of **2** was performed (Figure 1). Alternative positions of the pyridine N atom and the *o*-carbon atom C2 were refined to establish the exact connectivity (see Exp. Sect.).

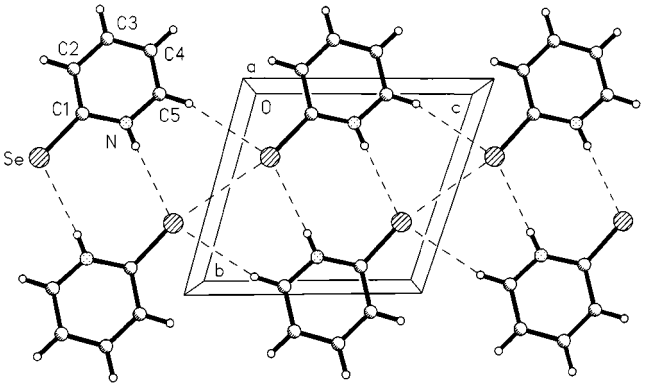

Figure 1. Molecular structure of PyH-2-Se (**2**) displaying intermolecular hydrogen bonding and weak Se−Se interactions (ellipsoids drawn at 50% probability level); selected bond lengths [pm] and angles [°]: Se−C1 184.6(8), N−C1 135.4(10), N−C5 133.8(10), N···Se^{i} 336.2(6), C5···Se^{ii} 386.0(8), Se···Se^{iii} 353.9(2); Se−C1−N 120.5(5), Se−C1−C2 124.8(6), C1−N−C5 125.5(7), N−C1−C2 114.7(7), N−H1···Se^{i} 164(8), C5−H5···Se^{ii} 163.7, C1−Se···Se^{iii} 167.7(2); *i*: x, y + 1, z; *ii*: x, y + 1, z + 1; *iii*: x, y + 1, z − 1

The crystal structure consists of dimeric pyridine-2(1*H*)-selones with planar monomeric units (max. dev. 8 pm for the N−H proton H1), connected via N−H···Se hydrogen bonds. The C=Se bond length of 184.6(8) pm is attributable to a resonance-stabilized C−Se double bond (Scheme 2). In selones not stabilized by resonance, the C=Se bonds are significantly shorter {1,5-dimethyl-3,7-dithiabicyclo[3.3.1]nonane-9-selone 177.4(6) pm; 4,4′-dimethoxyselenobenzophenone 179.0(4) pm; calculated value for selenoformaldehyde 173.9 pm}.[14] All other bond lengths are similar to those in pyridine.[15] Figure 2 shows the packing of **2**. The dimeric units are linked by weak Se···Se contacts of 353.9(2) pm and non-classical C−H···Se hydrogen bonds of C···Se 386.0(8) pm and H···Se 294 pm to form planar tapes, parallel to the *c* axis.

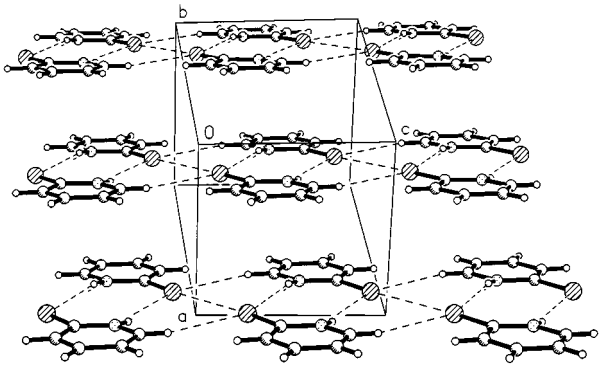

Figure 2. Packing diagram of (**2**) displaying the planar ribbons parallel to the *c* axis; radii are arbitrary; dashed lines correspond to N−H···Se hydrogen bonds, Se···Se contacts, and C−H···Se hydrogen bonds

To exploit the synthetic potential of the strongly nucleophilic 2-$PySe^-$ anion, it was necessary to introduce a new starting material with suitable properties, since many known syntheses of $PySe^-$ often suffer from a lack of reliability. One possible starting material is the pale-yellow compound $[Et_4N][2\text{-SePy}]$ (**7**), which can be easily prepared as described in Scheme 3.

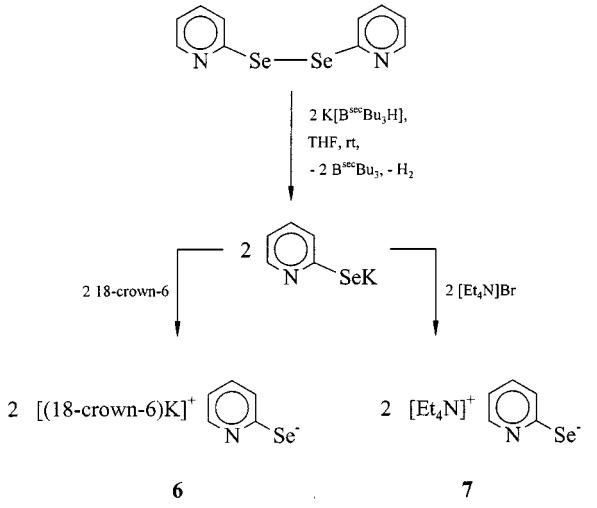

Scheme 3. Synthesis of the stable pyridine-2-selenolates [(18-crown-6)K][2-SePy] (**6**) and $[Et_4N][2\text{-SePy}]$ (**7**)

The synthesis strongly depends on the reducing agent for 2,2′-Py_2Se_2 (**5**). Usually, reactions with 2-$PySe^-$ are performed in situ with Na, NaH, or MBR_3H (M = Li, Na) as reducing agents for **5**. The disadvantages of such procedures are as follows: (i) an excess of Na or NaH is difficult to remove from the reaction mixture, and can lead to undesired side-reactions if the reactants are redox-sensitive; (ii) the concentration of commercially available MBR_3H solutions is neither stable nor easy to monitor. In the case of **7**, these problems do not occur, since K*B*s*Bu*$_3$H solutions can be used in excess, and $[Et_4N]Br$ is not redox-sensitive. Additional advantages are the low solubility of $[Et_4N]Hal$ (Hal = Cl^-, Br^-) in many organic solvents, which can be regarded as the driving force in reactions of **7** with halogen derivatives, and the easy handling of the less air-sensitive **7**, which can be weighed in air.

A second possibility for stabilizing the 2-$PySe^-$ anion is the reaction of K-2-SePy with 18-crown-6 ether. The colourless oily product [(18-crown-6)K][2-SePy] (**6**) could be crystallised from ethanol/diethyl ether in moderate yield. The resonances in the ^{77}Se NMR spectra appear at low field [**2**: δ = 314.0 ($CDCl_3$), δ = 214.9 (H_2O); **6**: δ = 441.8 (CD_3OD); **7**: δ = 359.6 (CD_3OD)]. The values for **6** and **7** indicate a strong contribution of the ionic and the amide mesomeric form, as depicted in Scheme 2. This is in agreement with the shift of the resonance of **2** to higher field, when changing the solvent to H_2O, in which the ionic mesomeric form is more favoured. In systems where mesomeric forms display markedly different contributions, the resonances of the selenolates are usually shifted to higher field, compared with the corresponding selenols.[16] Unfortunately, appropriate data for **1** are not available.

The crystal structure of **6** is shown in Figure 3. It consists of cation−anion pairs with the potassium ion 82.8(3) pm outside the ideal plane through the oxygen atoms, linked by short K···N and K···Se contacts of 276.5(6) and 348.5(2) pm, respectively. Comparable, slightly smaller values for K···Se contacts were observed in $\{K[Ph_2P(Se)NSiMe_3]\cdot THF\}_2$ [336.6(5) and 338.9(4) pm] and 2-$MeOC_6H_4COSeK$ [330.9(1) pm].[17] In all such compounds, the negative charge at the selenium atom is delocalized; crystal structures with the negative charge centred at the selenium atom are unknown. Weak non-classical C−H···O hydrogen bonds of 264.4 and 255.5 pm (H···O) link the cation−anion pairs to infinite chains along the *a* axis. The Se−C bond, at 186.6(6) pm, is only slightly longer than the corresponding one in **2**, and can therefore also be described as a resonance-stabilized C−Se double bond (Scheme 3). Similar

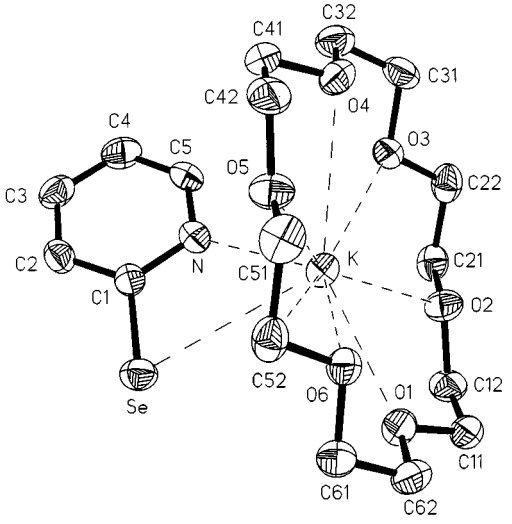

Figure 3. Molecular structure of $[(18\text{-crown-6})K]^+[2\text{-PySe}]^-$ (**6**) (ellipsoids drawn at 50% probability level): H atoms omitted for clarity; selected bond lengths [pm] and angles [°]: Se−C1 186.6(6), N−C1 136.1(8), N−C5 133.6(8), K−O 280.3(4) to 314.1(4), K···Se 348.5(2), K···N 276.5(6); C1−N−C5 117.5(6), N−C1−C2 120.0(6), N−C5−C4 125.3(6), N−C1−Se 118.3(5)

bonding patterns were detected in the corresponding thiolate [(18-crown-6)K][2-SPy] with a K···N contact of 285.4(3) and a K···S contact of 325.58(1) pm.[18]

(2-Pyridylseleno)phosphanes and Related Complexes

K-2-SePy and [Et_4N][2-SePy] (**7**) are useful starting materials for introducing 2-$PySe^-$ into phosphanes (Scheme 4).

The nature of the products in such reactions is strongly dependent on the nucleophilicity of the starting material used, as shown for the reaction of Ph_2PCl with NaSePh, which leads quantitatively to Ph_3PSe even at low temperatures.[19] Apart from *t*Bu_2P(2-SePy) (**9**), which can be crystallised as an analytically pure yellow compound at low temperatures, the resulting yellow (2-pyridylseleno)phosphanes Ph_2P(2-SePy) (**8**) and *t*BuP(2-SePy)$_2$ (**10**) are extremely air-sensitive and oily compounds. Therefore, reactions with **8** and **10** should be performed in situ. The synthesis of **10** cannot be performed with **7** as starting material, since the nucleophilicity is not sufficient at room temperature. Performing the reaction at higher temperatures leads to an inseparable mixture of phosphorus-containing compounds. During the synthesis of **10** with K-2-SePy at room temperature, KCl forms an emulsion, which leads to difficulties in the workup procedure. Attempts to remove KCl resulted in complete oxidation of **10** to the corresponding phosphane oxide *t*BuP(O)(2-SePy)$_2$ **11**, whose crystal structure was determined (vide infra).

Compounds **9** and **11** have been fully characterized, whereas **8** and **10** have only been characterized by ^{31}P NMR spectroscopy. All (2-pyridylseleno)phosphanes and the phosphane oxide derivative display singlets in the ^{31}P NMR spectra in the range $\delta = +20$ to $+110$. The ^{31}P-^{77}Se coupling constants derived from ^{77}Se satellites (219−236 Hz for **8**, **9**, and **10**; 413 Hz for **11**) are typical values for P−Se single bonds, and the greater magnitude of the value for **11** shows the typical influence of the oxidation state change from P^{III} to P^{V}, accompanied by the introduction of an electron-withdrawing substituent.[16] Similar values of the chemical shift and the ^{31}P-^{77}Se coupling constant were found in Me_2PSeMe ($\delta = 0.8$, 218 Hz), $(CF_3)_2$PSeMe ($\delta = 27.9$, 294 Hz), and [Ph_2PSePPh_2Cr(CO)$_5$] [$\delta = 25.7$ with 244 Hz (λ^3-P), $\delta = 78.6$ with 312 Hz (λ^4-P)].[20] The corresponding resonance signals in the ^{77}Se NMR spectra appear at $\delta = +271$ for **9** and $\delta = +437.8$ for **11**, as doublets with coupling constants of the same magnitude.

The crystal structure of **11** is shown in Figure 4. It consists of loose dimers, linked by non-classical C−H···O hydrogen bonds with H···O = 259 pm. Additionally, intramolecular C−H···O hydrogen bonds with H···O = 245 pm are observed. The angles at the selenium atom differ considerably with values of 95.28(12)° and 104.92(12)°, probably associated with the intramolecular hydrogen bond. The observed P−Se bond lengths of 224.68(11) and 225.62(12) pm are attributable to P−Se single bonds and similar to the central P−Se bonds in [*t*BuP(Se)(μ-Se)]$_2$ with 226.9(2) pm.[21]

The (pyridylseleno)phosphanes **9** and **10** were treated with unsaturated metal complexes in order to examine which binding site of the potentially three- or five-atom donor set could be used for complexation reactions (Scheme 5, Scheme 6, and Scheme 7).

In the case of Cu^I and Ag^I, the doubly bromo-bridged dinuclear complexes [({(C_5H_4N-2-Se)*t*Bu_2P}-*N*,*P*)Cu(μ-Br)]$_2$ (**12**) and [({(C_5H_4N-2-Se)*t*Bu_2P}-*N*,*P*)Ag(μ-Br)]$_2$ (**13**) were formed in almost quantitative yield as air-stable pale-yellow to colourless solids. The reaction of **9** with (tht)AuCl

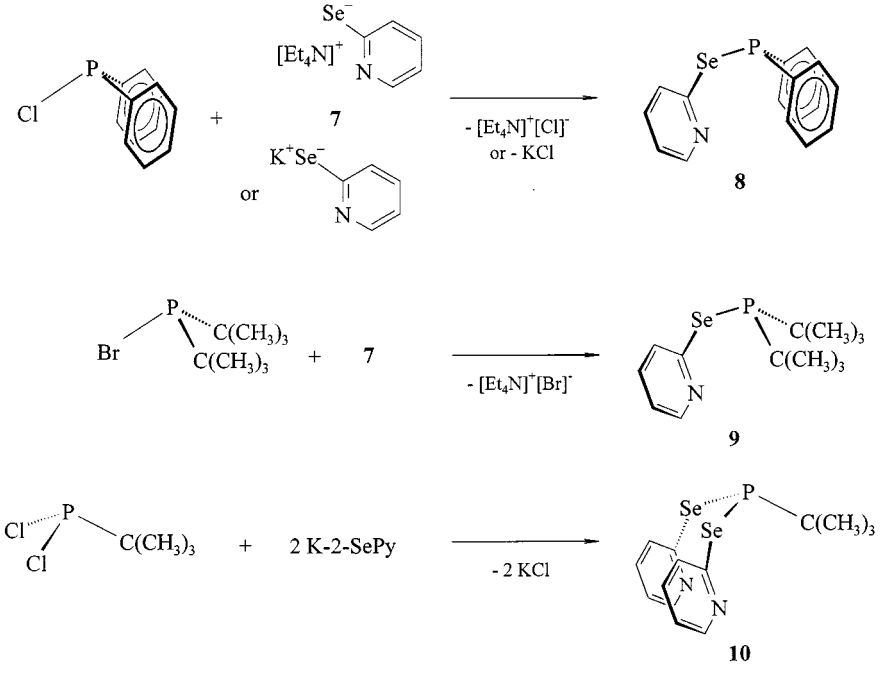

Scheme 4. Synthesis of the (2-pyridylseleno)phosphanes **8**−**10**

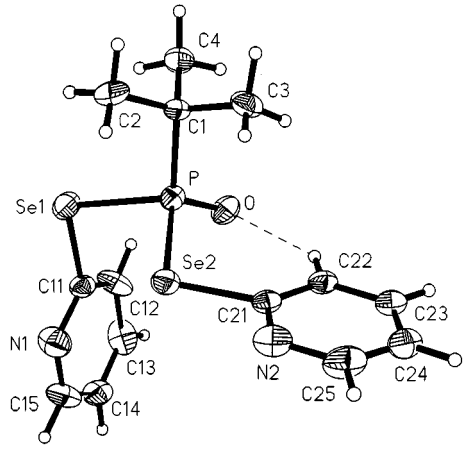

Figure 4. Molecular structure of *t*BuP(O)(2-SePy)$_2$ (**11**) (ellipsoids drawn at 50% probability level); selected bond lengths [pm] and angles [°]: P−Se1 224.68(11), P−Se2 225.62(12), P−O 147.0(3), Se1−C11 193.3(4), Se2−C21 195.1(4), C22···O 325.0(5), C23···O^{i} 317.7(5); O−P−C1 113.80(2), O−P−Se1 116.19(12), O−P−Se2 114.46(12), C1−P−Se1 103.82(13), C1−P−Se2 109.05(13), Se1−P−Se2 97.94(4), P−Se1−C11 95.28(12), P−Se2−C21 104.92(12); *i*: $-x + 1$, y, $-z + 0.5$

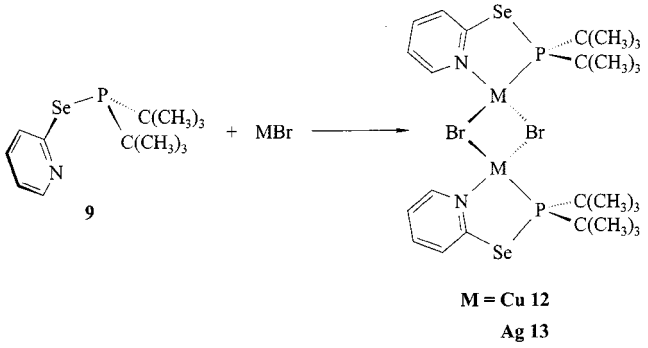

Scheme 5. Syntheses of the Cu^{I} and Ag^{I} complexes **12** and **13**

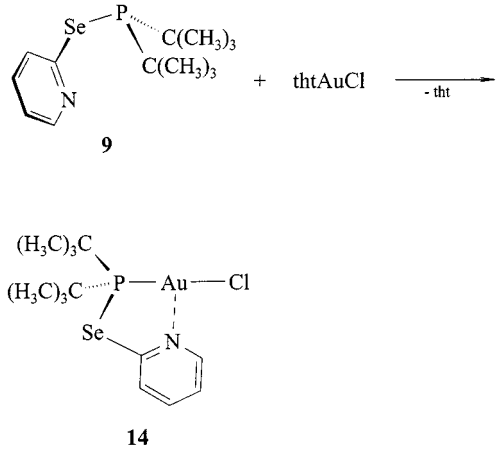

Scheme 6. Synthesis of the Au^{I} complex **14**

(tht = tetrahydrothiophene) leads in contrast to the mononuclear complex [({(C$_5$H$_4$N-2-Se)*t*Bu$_2$P}-*P*)AuCl] (**14**). Finally, the reaction of the bis(pyridylseleno)phosphane **10** with [(η^6-C$_7$H$_8$)Mo(CO)$_3$] leads to the deep-red mononuclear complex [({(C$_5$H$_4$N-2-Se)$_2$*t*BuP}-

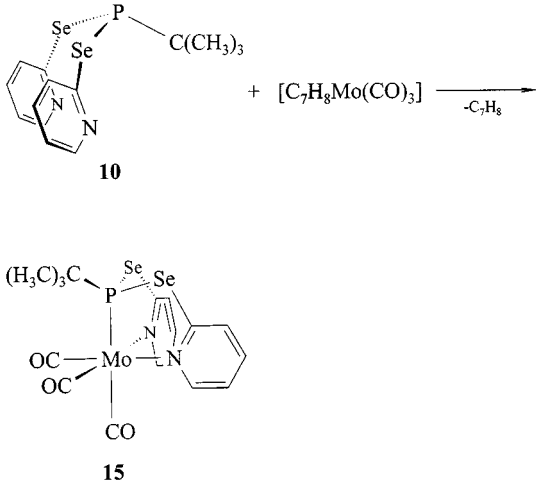

Scheme 7. Synthesis of the Mo^{0} complex **15**

N,*N*′,*P*)Mo(CO)$_3$] (**15**) in moderate yield. All complexes were fully characterized, including crystal structure analyses.

The resonances in the ^{31}P NMR spectra show a shift to lower field, going from the Cu^{I} complex **12** to the Au^{I} complex **14**, with values of δ = 72.4 (**12**), δ = 84.7 (**13**), and δ = 117.3 (**14**) (chemical shift for **9**: δ = 90.3). By contrast, generally the opposite tendency is observed, caused by an increasing electron density from Cu to Au. This observation could be explained in terms of metal−nitrogen bonds of different strengths. The strongest metal−nitrogen bond in this row can be apparently found in **12**, leading to an increased electron density at Cu^{I}, whereas the Au^{I}−N bond in **14** must be considered as weak. This results in a stronger metal−phosphorus back donation, which explains the shift of the ^{31}P NMR resonances of **12** and **13** to higher field, compared with the uncomplexed phosphane. The explanation of the corresponding resonances in the ^{77}Se NMR spectra with values of δ = +520 (**12**), δ = +470 (**13**), and δ = +501 (**14**) (chemical shift for **9**: δ = +271) seems to be more complicated, since a clear tendency cannot be observed. Even the ^{77}Se-^{31}P coupling constants (240 to 322 Hz) are similar to that of the uncomplexed phosphane (235 Hz), so that the interpretation of the electron densities in the examined nuclei, as derived from ^{77}Se NMR spectroscopic data, is not reasonable. In the case of the Mo^{0} complex **15**, the ^{31}P NMR resonance with δ = 155.9 is strongly shifted to lower field, compared with the corresponding value for **10** (δ = 101). Additionally, the equivalent Se atoms display a chemical shift in the ^{77}Se NMR spectrum at extremely low field (δ = +761.1). Unfortunately, the corresponding data for **10** are not available, since its instability does not permit ^{77}Se NMR experiments. Since **12** and **13** are isostructural, their crystal structures are discussed together (Figure 5).

The common feature in both structures is that two monomeric units are doubly bridged by bromide to form dinuclear complexes. The resulting central four-membered M$_2$Br$_2$ rings are folded across the M···M vector, with corresponding interplanar angles of 20.25(5)° for **12** and 24.62(3)° for

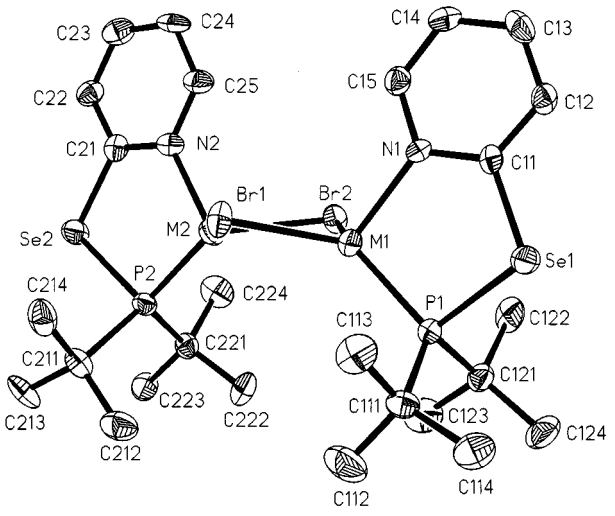

Figure 5. Molecular structures of [({$(C_5H_4N$-2-Se)tBu$_2$P}-*N*,*P*)M(μ-Br)]$_2$ [M = Cu (**12**), Ag (**13**)] (ellipsoids drawn at 50% probability level); H atoms omitted for clarity; selected bond lengths [pm] and angles [°] (the second value corresponds to the silver complex **13**): M1−N1 210.9(4)/245.6(3), M2−N2 210.4(5)/248.8(3), M1−P1 220.15(17)/241.16(11), M2−P2 220.09(17)/241.76(11), M1−Br1 245.96(10)/263.12(6), M1−Br2 249.77(10)/270.17(6), M2−Br1 248.43(10)/265.32(7), M2−Br2 247.73(10)/267.84(6), P1−Se1 226.41(17)/225.45(12), P2−Se2 226.92(17)/225.37(12), Se1−C11 191.8(6)/194.5(4), Se2−C21 192.7(6)/194.3(4), M1···M2 314.30(11)/313.33(6), Br1···Br2 377.66(10)/421.53(8); N1−M1−P1 95.11(14)/85.14(8), M1−P1−Se1 101.07(7)/105.33(5), P1−Se1−C11 99.31(17)/100.98(12), Se1−C11−N1 119.7(4)/119.2(3), C11−N1−M1 121.8(4)/122.9(3), N2−M2−P2 94.74(14), M2−P2−Se2101.52(7)/106.76(5), P2−Se2−C21 99.6(2)/101.66(13), Se2−C21−N2 120.1(4)/120.5(3), C21−N2−M2 123.2(4)/124.5(3)

13, which leads to relatively short metal−metal contacts of 314.30(11) and 313.33(6) pm, respectively. These values and corresponding bonding parameters are often found in Cu_2Br_2 and Ag_2Br_2 rings.[22] The (2-pyridylseleno)phosphane ligands act as chelates and are bound through the phosphorus and nitrogen atoms. The P−Se bond lengths in both complexes are 226.41(17) and 226.92(17) pm for **12**, and 225.45(12) and 225.37(12) pm for **13**, which correspond to P−Se single bonds. The strength of the metal−nitrogen bond may be assumed to be greater in **12** [210.9(4), 210.4(5) pm] than in **13** [245.6(3), 248.8(3) pm], consistent with the greater hardness of Cu^I centres compared with Ag^I centres. The molecular structure of the Au^I complex **14** is shown in Figure 6.

In contrast to the dimeric complexes **12** and **13**, complex **14** forms a simple monomer with a semi-chelating (2-pyridylseleno)phosphane ligand and essentially linear bonding at Au. An additional Au···N contact of 282.8(7) pm, which is too long for a bonding interaction is also formed. Normal Au−N single bonds in Au^I−amine complexes are much shorter (ca. 200 pm).[23] The P−Se bond length of 225.3(2) pm is again assignable to a P−Se single bond. In the molecular structure of the Mo^0 complex **15**, the bis(2-pyridylseleno)phosphane **10** acts as a tridentate chelating ligand (Figure 7).

Complex **15** crystallized with one disordered CH_2Cl_2 molecule per asymmetric unit, which was refined in two alternative positions. The coordination sphere of the molybdenum centre is slightly distorted octahedral, with angles ranging from 82.91(8) to 96.77(13)° and 175.26(13) to 177.08(13)°. The ligand is exclusively bound through both nitrogen and phosphorus atoms in a *fac* arrangement, and shows a strong *trans* influence with Mo−C bond lengths of 194.2(4) pm (av. value, carbonyl groups *cis* to the P atom) and 200.9(4) pm (carbonyl group *trans* to the P atom). The P−Se bond lengths of 226.59(10) and 227.12(10) pm match the observed values in **12**, **13**, and **14**, and therefore again correspond to P−Se single bonds. All other bonding para-

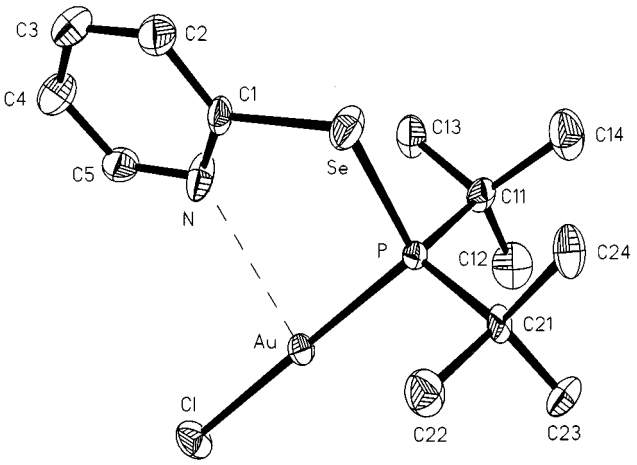

Figure 6. Molecular structure of [({$(C_5H_4N$-2-Se)tBu$_2$P}-*P*)AuCl] (**14**) (ellipsoids drawn at 50% probability level); H atoms omitted for clarity; selected bond lengths [pm] and angles [°]: Au−P 223.7(2), Au−Cl 230.2(2), P−Se 225.3(2), Se−C1 194.0(7), Au···N 282.8(8); P−Au−Cl 179.63(9), Au−P−Se 110.93(8), P−Se−C1 101.9(3), N···Au−Cl 101.02(14), N···Au−P 79.22(14)

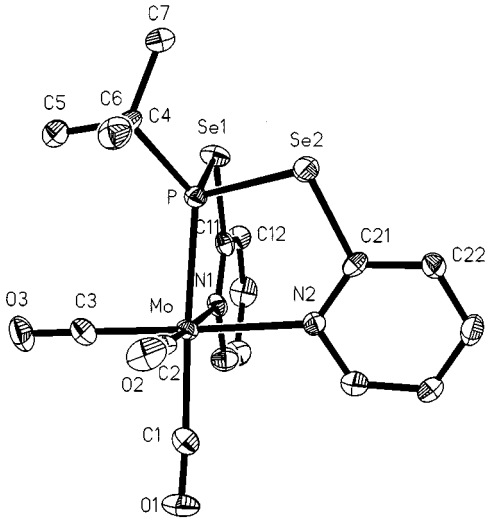

Figure 7. Molecular structure of [({$(C_5H_4N$-2-Se)$_2t$BuP}-*N*,*N*′,*P*)Mo(CO)$_3$] (**15**) (ellipsoids drawn at 50% probability level); H atoms and CH_2Cl_2 molecule omitted for clarity; selected bond lengths [pm] and angles [°]: Mo−P 239.24(10), Mo−N1 230.3(3), Mo−N2 230.1(3), P−Se1 226.59(10), P−Se2 227.12(10), Se1−C11 191.7(4), Se2−C21 192.2(4); P−Mo−N1 84.17(8), P−Mo−N2 82.91(8), N1−Mo−N2 84.78(10), Mo−P−C4 132.32(12), Mo−P−Se1 108.01(4), Mo−P−Se2 106.21(4), Se1−P−Se2 105.04(4), Se1−P−C4 101.31(12), Se2−P−C4 101.26(12), P−Se1−C11 97.79(11), P−Se2−C21 96.28(11)

meters in the complexes **12** to **15** are consistent with the usually observed values.

Experimental Section

General Techniques: All reactions were performed under dry dinitrogen using conventional Schlenk techniques. Solvents were dried and degassed using standard procedures prior to use. − NMR spectra were recorded with a Bruker AC 200 at room temperature [^{1}H: 200.1 MHz; ^{13}C: 50.32 MHz; ^{31}P: 81.0 MHz; ^{77}Se: 38.2 MHz; standards Me_4Si (^{1}H, ^{13}C); 85% H_3PO_4 (^{31}P); 100% Me_2Se (^{77}Se)]. − IR spectra were recorded in KBr with a Biorad FTS 165 spectrometer. − UV/Vis spectra were recorded with a Perkin−Elmer Lambda 15 spectrometer using quartz cuvettes with a diameter of 1 cm. − MS: Finnigan MAT 8430 at 70 eV. − Elemental analyses of the isolated products were performed by the analytical laboratory of this Institute. − (2,2′-Bispyridyl) diselenide was prepared according to a literature procedure.[1a] All other commercial-grade chemicals were used without further purification.

Py-2-SeH (1) and PyH-2-Se (2): Na_2Se_2 was prepared according to the procedure of Klayman et al. starting from grey selenium (30 g, 0.38 mol) and $NaBH_4$ (10 g, 0.27 mol) in 500 mL of ethanol.[24] After the reaction was complete, the solvent was removed in vacuo at 50 °C. Ethylene glycol monomethyl ether (500 mL) was added to the grey-violet solid, affording a dark-red solution. To this solution was added 2-BrPy (20.1 g, 0.127 mol), and the reaction mixture was allowed to reflux for 24 h. The resulting yellow-brown solution was filtered and concentrated, and H_2O (320 mL, degassed) was added. After addition of glacial acetic acid (80 mL) with stirring, red selenium precipitated, which was removed by filtration after 1 h of stirring at ambient temperature. The yellow filtrate was concentrated at 80 °C and the resulting yellow solid was extracted with CH_2Cl_2 (500 mL) using a Soxhlet apparatus. Concentration of the yellow extract afforded pale-yellow **1** (1.7 g, 9%). Subsequent evaporation of the solvent and storage at −30 °C afforded dark-yellow **2** (12 g, 60%) as a crystalline product. Suitable crystals of **2** for an X-ray structure analysis were obtained from liquid-liquid diffusion of hexanes into a CH_2Cl_2 solution. **1:** ^{1}H NMR ([D$_6$]DMSO): δ = 6.96 (m, 1 H, *p* to CSeH), 7.43 (m, 1 H, *p* to N), 7.61 (m, 1 H, *o* to N), 7.80 (m, 1 H *o* to CSeH), 8.53 (s, br, 1 H, SeH); ref.[1a] ($CDCl_3$): δ = 6.98, 7.38, 7.71, 7.86, 8.41. − **2:** M.p.: 137 °C. − C_5H_5NSe (158.06): calcd. C 37.99, H 3.19, N 8.86; found C 38.05, H 3.16, N 8.86. − IR (CH_2Cl_2, $\tilde{\nu}$ [cm^{-1}]): 1607 (m, br), 1572 (st), 1561 (st), 1420 (st, br), 1271 (st), 1244 (st), 1107 (m), 1078 (m), 1044 (w), 893 (vs), 774 (vs, br), 685 (vs, br). − ^{1}H NMR ($CDCl_3$): δ = 6.96 (m, 1 H, *p* to C=Se), 7.38 (m, 1 H, *p* to NH), 7.73 (m, 1 H, *o* to NH), 7.85 (m, 1 H, *o* to C=Se), 13.44 (s, br, 1 H, NH, av. value of six measurements with values of δ = 12.03 to 14.07). − ^{13}C NMR ($CDCl_3$): δ = 118.6 (s, *p* to C=Se), 131.3 (s, *o* to C=Se), 137.8 (s, *p* to NH), 143.4(s, *o* to NH), 162.0 (s, *C*=Se). − ^{77}Se NMR ($CDCl_3$): δ = 314.0 s; (H_2O with C_6D_6 capillary): δ = 214.9 s. − UV/Vis (10^{-3} M in H_2O, λ_{max} [nm]): 228, 283, 357; ref.[5] (H_2O, pH = 5.7): 227, 285, 358.

[HPy-2-SeH]$^+$Cl$^-$ (3): A suspension of **1** (500 mg, 3.16 mmol) in 40 mL of THF was treated with Ph_2PCl (698 mg, 3.16 mmol) at room temperature. A clear yellow solution was formed immediately. After 3 h of stirring, a pale yellow precipitate had formed, which was filtered off and dried in vacuo (370 mg, 60%). − ^{1}H NMR ([D$_6$]DMSO): δ = 4.96 [s, 1 H, Se*H*, ^{77}Se satellites, *J*(H,Se) = 14.2 Hz], 7.39 (m, 1 H, *p* to CSeH), 7.82 (m, 2 H, *o* and *p* to NH), 8.57 (m, 1 H, *o* to CSeH), 11.93 (s, br, 1 H, N*H*).

[H$_2$Py-2-Se]$^+$I$^-$ (4): A 57% HI solution in H_2O (3 mL) was added to a suspension of **2** (500 mg, 3.16 mmol) in 20 mL of H_2O. A clear yellow solution formed immediately. Removal of H_2O in vacuo gave **4** as a pale yellow solid in quantitative yield. Compound **4** decomposes in neutral H_2O, and is sparingly soluble in $CHCl_3$ and acetone. Solutions of **4** in methanol or DMSO are dark-yellow. − C_5H_6INSe (285.97): calcd. C 21.00, H 2.11, N 4.90; found C 20.81, H 2.11, N 4.72. − ^{1}H NMR ([D$_6$]DMSO): δ = 7.30 (m, 1 H, *p* to C=Se), 7.79 (m, 2 H, *o* and *p* to NH_2), 8.43 (m, 1 H, *o* to C=Se), 8.88 (s, br, 2 H, NH_2, av. value of two measurements with values of δ = 8.64 and 9.12).

[(18-crown-6)K]$^+$[2-PySe]$^-$ (6): A solution of KB*s*Bu$_3$H (6.33 mL of a 1 M solution in THF, 6.33 mmol) was added to a solution of 2,2′-Py_2Se_2 (**5**; 1 g, 3.16 mmol) in 40 mL of THF. Gas evolution occurred and a pale yellow solid precipitated, leaving a colourless supernatant solution. After 1 h of stirring at ambient temperature, the solvent was removed in vacuo and 20 mL of ethanol and solid 18-crown-6 ether (1.67 g, 6.33 mmol) was added. After 30 min, the product was crystallized with diethyl ether at −30 °C (450 mg, 15%). − M.p.: 152 °C. − $C_{17}H_{28}KNO_6Se$ (460.47): calcd. C 44.34, H 6.13, N 3.04; found C 44.72, 3.03, 6.19. − ^{1}H NMR (CD_3OD): δ = 3.66 (s, 24 H, CH_2), 6.92 (m, 1 H, *p* to CSe), 7.26 (m, 1 H, *p* to N), 7.71 (m, 1 H, *o* to N), 8.10 (m, 1 H, *o* to CSe). − ^{13}C NMR (CD_3OD): δ = 71.3 (s, *C*H$_2$), 118.6 (s, *p* to CSe), 132.7 (s, *o* to CSe), 135.8 (s, *p* to N), 148.9 (s, *o* to N), 164.5 (s, *C*Se). − ^{77}Se NMR (CD_3OD): δ = 441.8 s. − MS (FAB): *m*/*z* (%) = 303 (100) [(18-crown-6)K]$^+$, 158 (100) [2-PySe]$^-$.

[Et$_4$N]$^+$[2-PySe]$^-$ (7): K-2-SePy was prepared in the same manner as described for **6**, starting from 25.3 mL of a 1 M KB*s*Bu$_3$H solution in THF (25.3 mmol) and **5** (4 g, 12.65 mmol) in 100 mL of THF. The pale yellow solid was dissolved in 100 mL of ethanol and Et_4NBr (5.32 g, 25.31 mmol) was added. After 15 min of stirring at ambient temperature, the solvent was removed in vacuo and the remaining solid was suspended in 200 mL of acetone. The workup procedure comprised filtration and washing of the solid for several times with 20 mL of acetone until the filtrate became colourless. The combined acetone extracts were concentrated, washed with diethyl ether and dried in vacuo, leaving a pale yellow solid of **7** (5.98 g, 82%), soluble in polar organic solvents such as CH_3CN, DMSO or alcohols. − M.p.: 108 °C. − $C_{13}H_{24}N_2Se$ (287.31): calcd. C 54.35, H 8.42, N 9.75; found C 53.28, H 8.37, N 9.52. − ^{1}H NMR ([D$_6$]DMSO): δ = 1.15 [t, 12 H, CH_3, ^{3}*J*(H,H) = 7.2 Hz], 3.21 [q, 8 H, CH_2, ^{3}*J*(H,H) = 7.2 Hz], 6.49 (m, 1 H, *p* to CSe), 6.78 (m, 1 H, *p* to N), 7.26 (m, 1 H, *o* to N), 7.84 (m, *o* to CSe). − ^{13}C NMR ([D$_6$]DMSO): δ = 7.1 (s, *C*H$_3$), 51.4 (s, *C*H$_2$), 113.7 (s, *p* to CSe), 131.8 (s, *o* to CSe), 132.6 (s, *p* to N), 147.7 (s, *o* to N), 172.7 (s, *C*Se). − ^{77}Se NMR (CD_3OD): δ = 359.6 s. − UV/Vis (10^{-3} M in H_2O, λ_{max} [nm]): 233, 277, 352.

Ph$_2$P-2-SePy (8). − Route A: To a solution of K-2-SePy, prepared from a solution of **5** (1 g, 3.16 mmol) in 40 mL of diethyl ether and 6.33 mL of a 1 M KB*s*Bu$_3$H solution in THF at −70 °C, was added Ph_2PCl (1.41 g, 6.37 mmol) dropwise via a syringe. The reaction mixture was allowed to warm to room temperature within 1 h, and was stirred for additional 2 h at 25 °C and then filtered, leaving a dark-yellow filtrate. − **Route B:** Ph_2PCl (195 mg, 0.88 mmol) was added dropwise via a syringe to a solution of **7** (254 mg, 0.88 mmol) in 20 mL of CH_3CN at 0 °C. After 2 h of additional stirring, the mixture was filtered, leaving a dark-yellow filtrate (quantitative yield, monitored by ^{31}P NMR means). **8** was completely oxidized during the workup, leading to various unidentified products, but it is stable in solution under N_2. − ^{31}P NMR (THF

solution, C_6D_6 capillary): δ = 22.40 [s, ^{77}Se satellites, J(P,Se) = 219 Hz].

***t*Bu$_2$P-2-SePy (9):** A solution of *t*Bu$_2$PBr (1.21 g, 5.35 mmol) in 60 mL of CH_3CN was added dropwise to a solution of **7** (1.54 g, 5.35 mmol in 60 mL of CH_3CN). The reaction mixture was stirred for 3 h at room temperature, to leave a colourless solution. The workup procedure comprised removal of the solvent in vacuo, addition of 10 mL of diethyl ether, filtration of Et_4NBr and removal of the diethyl ether, leaving a pale yellow oil that crystallized upon standing at −30 °C in nearly quantitative yield. Compound **9** is soluble in nearly all common organic solvents. − M.p.: 28 °C. − $C_{13}H_{22}NPSe$ (302.26): calcd. C 51.66, H 7.34, N 4.63; found C 51.74, H 7.35, N 4.44. − ^{1}H NMR ([D$_6$]acetone): δ = 1.34 [d, 18 H, CH_3, ^3J(H,P) = 12 Hz], 7.13 (m, 1 H, *p* to CSe), 7.59 (m, 1 H, *p* to N), 7.91 (m, 1 H, *o* to N), 8.36 (m, 1 H, *o* to CSe). − ^{13}C NMR ($CDCl_3$): δ = 30.3 [d, *C*H$_3$, ^2J(C,P) = 15 Hz], 34.8 [d, *C*(CH$_3$)$_3$, J(C,P) = 32.9 Hz], 120.5 (s, *p* to CSe), 126.5 [d, *o* to CSe, ^3J(C,P) = 12.9 Hz], 136.3 (s, *p* to N), 149.6 [d, *o* to N, ^4J(C,P) = 2.4 Hz], 156.8 [d, *C*Se, ^2J(C,P) = 17.5 Hz]. − ^{31}P NMR ($CDCl_3$): δ = 90.33 [s, ^{77}Se satellites, J(P,Se) = 235.5 Hz]. − ^{77}Se NMR ($CDCl_3$): δ = 271 [d, J(Se,P) = 235.1 Hz]. − MS (EI): *m*/*z* (%): 303 (2) [M]$^+$, 246 (100) [M − *t*Bu]$^+$.

***t*BuP(2-SePy)$_2$ (10) and *t*BuP(O)(2-SePy)$_2$ (11):** K-2-SePy was prepared from **5** (1.74 g, 5.51 mmol) in 40 mL of THF and 11.01 mL of a 1 M K*B*s*Bu*$_3$H solution (11.01 mmol) in THF. A solution of *t*BuPCl$_2$ (876 mg, 5.51 mmol) in 20 mL of THF was added over 30 min. The yellow reaction mixture was stirred for additional 2 h, and contained **10** and KCl as an emulsion. − ^{31}P NMR (THF, C_6D_6 capillary): δ = 101.0 [s, ^{77}Se satellites, J(P,Se) = 228.4 Hz]. − Removal of the solvent in vacuo led to an oily solid mixture, which was then suspended in 50 mL of CH_2Cl_2 and filtered through silica. The dark-yellow filtrate was reduced to 10 mL and crystallized by addition of hexanes and storage at −30 °C (1.43 g, 62%, yellow prisms). − M.p.: 85 °C. − $C_{14}H_{17}N_2OPSe_2$ (418.20): calcd. C 40.21, H 4.10, N 6.70; found C 39.83, H 4.12, N 6.59. − ^{1}H NMR ([D$_6$]acetone): δ = 1.30 [d, 9 H, CH_3, ^3J(H,P) = 21.7 Hz], 7.36 (m, 2 H, *p* to CSe), 7.73 (m, 2 H, *p* to N), 7.94 (m, 2 H, *o* to N), 8.48 (m, 2 H, *o* to CSe). − ^{13}C NMR ($CDCl_3$): δ = 25.0 [d, *C*H$_3$, ^2J(C,P) = 1.4 Hz], 46.0 [d, *C*(CH$_3$)$_3$, J(C,P) = 49 Hz], 123.2 (s, *p* to CSe), 131.6 [d, *o* to CSe, ^3J(C,P) = 1.7 Hz], 137.0 (s, *p* to N), 150.3 (s, *o* to N), 151.2 [d, *C*Se, ^2J(C,P) = 5.7 Hz]. − ^{31}P NMR ([D$_6$]acetone): δ = 72.1 [s, ^{77}Se satellites, J(P,Se) = 412.5 Hz]. − ^{77}Se NMR ($CDCl_3$): δ = 437.8 [d, J(Se,P) = 417.8 Hz]. − MS (CI): *m*/*z* (%): 376 (100) [M − *t*Bu]$^+$, 262 (2) [M − SePy]$^+$.

[({(C$_5$H$_4$N-2-Se)*t*Bu$_2$P}-*N*,*P*)Cu(μ-Br)]$_2$ (12), [({(C$_5$H$_4$N-2-Se)*t*Bu$_2$P}-*N*,*P*)Ag(μ-Br)]$_2$ (13), and [({(C$_5$H$_4$N-2-Se)*t*Bu$_2$P}-*P*)AuCl] (14): Complex **12** was prepared from CuBr (176 mg, 1.23 mmol) and **9** (371 mg, 1.23 mmol), complex **13** from AgBr (391 mg, 2.08 mmol) and **9** (629 mg, 2.08 mmol), and complex **14** from thtAuCl (774 mg, 2.41 mmol) (tht = tetrahydrothiophene) and **9** (730 mg, 2.41 mmol), by addition of a solution of the metal halide to a solution of **9** (in the case of **12**), or addition of a solution of **9** to a solution of the metal halide (in the case of **13**, **14**) in CH_3CN (60 mL), and stirring for 3 h at room temperature under exclusion of light. The solvent was removed in vacuo, and crystallisation from a CH_2Cl_2 solution by layering with hexanes afforded colourless (**13**) to pale-yellow (**12**, **14**) solids. Single crystals suitable for an X-ray analysis were obtained directly from the reaction mixture in all cases.

12: Nearly quantitative yield, M.p.: 233 °C. − $C_{26}H_{44}Br_2Cu_2N_2P_2Se_2$ (891.42): calcd. C 35.03, H 4.98, N 3.03; found C 35.09, H 4.98, N 3.03. − ^{1}H NMR ($CDCl_3$): δ = 1.45 [d, 36 H, CH_3, ^3J(H,P) = 15.4 Hz], 7.20 (m, 2 H, *p* to CSe), 7.52 (m, 4 H, *o* and *p* to N), 8.87 (m, 2 H, *o* to CSe). − ^{13}C NMR (CD_2Cl_2): δ = 30.4 [d, *C*H$_3$, ^2J(C,P) = 9.8 Hz], 37.0 [d, *C*(CH$_3$)$_3$, J(C,P) = 4.5 Hz], 122.3 [d, *p* to CSe, ^5J(C,P) = 1.9 Hz], 126.2 (s, *o* to CSe), 137.6 [d, *p* to N, ^4J(C,P) = 1.5 Hz], 151.1 [d, *o* to N, ^4J(C,P) = 2.5 Hz], 155.4 [d, *C*Se, ^2J(C,P) = 6.5 Hz]. − ^{31}P NMR ($CDCl_3$): δ = 72.4 (s, br). − ^{77}Se NMR (CD_2Cl_2): δ = 520.4 [d, J(Se,P) = 240 Hz]. − MS (EI): *m*/*z* (%) {monomer = [M]$^+$}: 445 (31) [M]$^+$, 246 (100) [2-SePyP*t*Bu]$^+$.

13: 882 mg, 87%, M.p.: 189 °C. − $C_{26}H_{44}Ag_2Br_2N_2P_2Se_2$ (980.07): calcd. C 31.86, H 4.53, N 2.86; found C 31.87, H 4.52, N 2.84. − ^{1}H NMR ($CDCl_3$): δ = 1.43 [d, 36 H, CH_3, ^3J(H,P) = 15.8 Hz], 7.16 (m, 2 H, *p* to CSe), 7.47 (m, 4 H, *o* and *p* to N), 8.77 (m, 2 H, *o* to CSe). − ^{13}C NMR (CD_2Cl_2): δ = 30.4 [d, *C*H$_3$, ^2J(C,P) = 11 Hz], 37.2 [d, *C*(CH$_3$)$_3$, J(C,P) = 8.8 Hz], 122.4 [d, *p* to CSe, ^5J(C,P) = 1.5 Hz], 127.1 (s, *o* to CSe), 137.6 [d, *p* to N, ^4J(C,P) = 1.4 Hz], 151.7 (s, *o* to N), 152.0 [d, *C*Se, ^2J(C,P) = 2.6 Hz]. − ^{31}P NMR ($CDCl_3$): δ = 84.7 (s, br). − ^{77}Se NMR (CD_2Cl_2): δ = 470.2 [d, J(Se,P) = 273.8 Hz]. − MS (EI): *m*/*z* (%): 246 (100) [2-SePyP*t*Bu]$^+$.

14: 1.16 g, 90%, M.p.: > 126 °C (dec.). − $C_{13}H_{22}AuClNPSe$ (534.68): calcd. C 29.20, H 4.15, N 2.62; found C 29.00, H 4.19, N 2.48. − ^{1}H NMR (CD_2Cl_2): δ = 1.49 (d, 18 H, CH_3, ^3J(H,P) = 17.2 Hz), 7.30 (m, 1 H, *p* to CSe), 7.60 (m, 1 H, *p* to N), 7.75 (m, 1 H, *o* to N), 8.50 (m, 1 H, *o* to CSe). − ^{13}C NMR (CD_2Cl_2): δ = 30.0 [d, *C*H$_3$, ^2J(C,P) = 6.5 Hz], 40.1 [d, *C*(CH$_3$)$_3$, J(C,P) = 14 Hz], 123.8 (s, *o* to N), 131.4 [d, *o* to CSe, ^3J(C,P) = 2.2 Hz], 137.8 (s, *p* to N), 151.0 (s, *o* to N), 151.8 (s, CSe). − ^{31}P NMR (CD_2Cl_2): δ = 117.3 [s, ^{77}Se satellites, J(P,Se) = 319.8 Hz]. − ^{77}Se NMR (CD_2Cl_2): δ = 501.0 [d, J(Se,P) = 322.3 Hz]. − MS (EI): *m*/*z* (%): 535 (31) [M]$^+$, 246 (100) [2-SePyP*t*Bu]$^+$.

[({(C$_5$H$_4$N-2-Se)$_2$*t*BuP}-*N*,*N*′,*P*)Mo(CO)$_3$] (15): The yellow reaction mixture of **10** (5.1 mmol) was concentrated to dryness, and the remaining solid was suspended in 40 mL of toluene. A solution of [(η^6-C$_7$H$_8$)Mo(CO)$_3$] (1.38 g, 5.1 mmol) in 50 mL of toluene was added dropwise at room temperature under exclusion of light to the reaction mixture. After 12 h of stirring at room temperature, the solvent was removed in vacuo. The workup procedure comprised addition of 60 mL of CH_2Cl_2, filtration through silica, and column chromatography on silica (40 × 3 cm; eluent: CH_2Cl_2/hexanes, 75:25). After four fractions (yellow, orange, brown, red) that contained traces of unidentified by-products, the deep-red main fraction of **15** eluted. Crystals of the CH_2Cl_2 hemisolvate were obtained by layering a CH_2Cl_2 solution (20 mL) with hexanes (150 mL) at room temperature. − Yield: 1.15 g, 34%, M.p.: > 125 °C (dec.). − $C_{17.5}H_{18}ClMoN_2O_3PSe_2$ (624.63): calcd. C 33.65, H 2.90, N 4.48; found C 33.56, H 2.89, 4.39. − IR (CH_2Cl_2, ṽ [cm^{-1}]): 1931 vs, 1838 st, br, 1815 st, br (Mo−*CO*). − ^{1}H NMR ([D$_6$]acetone): δ = 1.67 [d, 9 H, CH_3, ^3J(H,P) = 17.7 Hz], 5.62 (s, 1 H, CH_2Cl_2), 7.18 (m, 2 H, *p* to CSe), 7.61 (m, 2 H, *p* to N), 7.75 (m, 2 H, *o* to N), 9.49 (m, 2 H, *o* to CSe). − ^{13}C NMR ([D$_6$]acetone): δ = 28.6 [d, *C*H$_3$, ^3J(C,P) = 6.2 Hz], 41.5 [d, *C*(CH$_3$)$_3$, J(C,P) = 10.9 Hz], 54.9 (s, *C*H$_2$Cl$_2$), 122.8 (s, *p* to CSe), 127.6 [d, *o* to CSe, ^3J(C,P) = 2.7 Hz], 138.0 (s, *p* to N), 154.4 [d, *o* to N, ^4J(C,P) = 5.6 Hz], 163.3 [d, *C*Se, ^2J(C,P) = 10.8 Hz], 222.8, 227.2, 227.3 (s, Mo*C*O). − ^{31}P NMR ([D$_6$]acetone): δ = 155.9 [s, ^{77}Se satellites, J(P,Se) = 257.1 Hz]. − ^{77}Se NMR ([D$_6$]acetone): δ = 761.1 [d, J(Se,P) = 258.8 Hz]. − MS (EI): *m*/*z* (%): 582 (1) [M]$^+$, 246 (32) [PySeP*t*Bu]$^+$, 57 (100) [*t*Bu]$^+$.

Crystal Structure Analyses: The crystal structures for **2**, **6**, **11**, **12**, **13**, **14**, and **15** were performed with a Siemens P4 diffractometer

Table 1. Crystal data for the compounds **2**, **6**, and **11**

	2	**6**	**11**
Empirical formula	C_5H_5NSe	$C_{17}H_{28}KNO_6Se$	$C_{14}H_{17}N_2OPSe_2$
Molecular mass [gmol^{-3}]	158.06	460.46	418.19
Crystal size [mm]	0.26 × 0.20 × 0.14	0.30 × 0.16 × 0.12	0.40 × 0.32 × 0.24
Space group	$P\bar{1}$ (No. 2)	$P1$ (No. 1)	$C2/c$ (No. 15)
Crystal system	triclinic	triclinic	monoclinic
a [pm]	660.2(2)	827.9(3)	1718.7(2)
b [pm]	685.6(2)	834.4(3)	755.90(8)
c [pm]	693.6(2)	900.5(2)	2470.0(3)
α [°]	103.93(2)	74.10(2)	90
β [°]	94.61(2)	66.52(2)	97.509(8)
γ [°]	111.98(2)	63.97(3)	90
V [nm^3]	0.2775(1)	0.5090(3)	3.1814(7)
Z	2	1	8
$d_{calcd.}$ [gcm^{-3}]	1.892	1.502	1.746
μ [cm^{-1}]	66.24	20.80	47.46
$2\Theta_{max}$	50	50	50
Data (total)	1882	3522	4190
Data (independent)	948	3290	2753
Restraints	0	3	0
Parameters	68	235	184
S (F^2)	1.004	1.045	0.858
R_1	0.0629	0.0459	0.0326
wR_2	0.1585	0.1107	0.0651

Table 2. Crystal data for the compounds **12**, **13**, **14**, and **15**

	12	**13**	**14**	**15**·0.5 CH_2Cl_2
Empirical formula	$C_{26}H_{44}Br_2Cu_2N_2P_2Se_2$	$C_{26}H_{44}Ag_2Br_2N_2P_2Se_2$	$C_{13}H_{22}AuClNPSe$	$C_{17.5}H_{18}ClMoN_2O_3PSe_2$
Molecular mass [gmol^{-3}]	891.42	980.05	534.66	624.62
Crystal size [mm]	0.26 × 0.18 × 0.16	0.30 × 0.24 × 0.24	0.24 × 0.20 × 0.20	0.50 × 0.30 × 0.20
Space group	$P\bar{1}$ (No. 2)	$P\bar{1}$ (No. 2)	$P2_1/c$ (No. 14)	$P2_1/c$ (No. 14)
Crystal system	triclinic	triclinic	monoclinic	monoclinic
a [pm]	968.71(12)	990.34(10)	1367.8(2)	1591.15(14)
b [pm]	1223.32(14)	1245.15(14)	1220.6(2)	1164.74(14)
c [pm]	1493.14(18)	1483.4(2)	1040.3(2)	1197.08(10)
α [°]	92.497(10)	93.551(10)	90	90
β [°]	93.076(10)	94.787(10)	105.95(2)	102.496(6)
γ [°]	106.182(10)	104.200(8)	90	90
V [nm^3]	1.6937(4)	1.7604(4)	1.6699(5)	2.1660(4)
Z	2	2	4	4
d_c [gcm^{-3}]	1.748	1.849	2.127	1.915
μ [cm^{-1}]	58.76	55.58	112.30	41.84
$2\Theta_{max}$	50	50	50	50
Data (total)	6268	10239	5956	3998
Data (independent)	5965	6195	2929	3799
Restraints	0	0	0	146
Parameters	337	338	169	265
S (F^2)	0.758	0.856	0.761	0.873
R_1	0.0376	0.0287	0.0279	0.0280
wR_2	0.0563	0.0546	0.0488	0.0537

(graphite-monochromated Mo-K_α radiation, λ = 71.073 pm) at −100 °C in the ω-scan mode (Table 1 and Table 2). Cell parameters were refined from setting angles at 2Θ = 20−24°. Absorption corrections based on Ψ-scans were applied. The structures were solved by direct methods using SHELXS-86/97,[25] and subjected to full-matrix least-squares refinement on F^2 using SHELXL-93/97,[26] with anisotropic displacement parameters for non-H atoms. Correct positions for nitrogen and carbon atoms in the crystal structure of **2** were established from the refinement of alternative positions and subsequent comparison of the R values and the final electron density ($wR2$: 0.1585 vs. 0.1703, ρ_{max} 1.28·10^{-6} e pm^{-3}). Methyl groups were treated as rigid groups and N-bonded hydrogen atoms were refined freely. All other hydrogen atoms were included using a riding model. Crystallographic data (excluding structure factors) for the structures reported in this paper have been deposited with the Cambridge Crystallographic Data Centre as supplementary publications no. CCDC-150945 (**2**), -150946 (**6**), -150947 (**11**), -150948 (**12**), -150949 (**13**), -150950 (**14**), and -150951 (**15**). Copies

of the data can be obtained free of charge on application to CCDC, 12 Union Road, Cambridge CB2 1EZ, UK [Fax: (internat.) + 44-1223/336-033; E-mail: deposit@ccdc.cam.ac.uk].

Acknowledgments

We thank the Fonds der Chemischen Industrie and the Braunschweigischer Hochschulbund for financial support and Prof. Peter G. Jones for helpful discussions. Diffractometer maintenance by Andreas Weinkauf is gratefully acknowledged.

[1] [1a] C. O. Kienitz, C. Thöne, P. G. Jones, *Inorg. Chem.* **1996**, *35*, 3990−3997. − [1b] C. O. Kienitz, C. Thöne, P. G. Jones, *Z. Naturforsch., B* **2000**, *55*, 587−596.

[2] [2a] Y. Cheng, T. J. Emge, J. G. Brennan, *Inorg. Chem.* **1996**, *35*, 7339−7344. − [2b] J. Romero, M. L. Duran, J. A. Garcia-Vazquez, A. Castiñeiras, A. Sousa, L. Christaens, J. Zubieta, *Inorg. Chim. Acta* **1997**, *255*, 307−311.

[3] [3a] Y. Cheng, T. J. Emge, J. G. Brennan, *Inorg. Chem.* **1994**, *33*, 3711−3714. − [3b] D. V. Khasnis, M. Buretea, T. J. Emge, J. G. Brennan, *J. Chem. Soc., Dalton Trans.* **1995**, 45−48. − [3c] A. Khanna, A. Bala, B. L. Khandelwal, *J. Organomet. Chem.* **1995**, *494*, 199−204. − [3d] Y. Cheng, T. J. Emge, J. G. Brennan, *Inorg. Chem.* **1996**, *35*, 342−346. − [3e] S. Narayan, V. K. Jain, B. Varghese, *J. Chem. Soc., Dalton Trans.* **1998**, 2359−2366.

[4] [4a] S. Patai, Z. Rappoport (Eds.), *The chemistry of organic selenium and tellurium compounds*, J. Wiley & Sons, New York, **1986**, vol. 1 and 2. − [4b] F. H. Allen, O. Kennard, "Cambridge Structural Database CCDC, version April **2000**", *Chem. Des. Autom. News* **1993**, *8*, 31−37.

[5] H. G. Mautner, S.-H. Chu, C. M. Lee, *J. Org. Chem.* **1962**, *27*, 3671−3673.

[6] [6a] A. Toshimitsu, H. Owada, S. Uemura, M. Okano, *Tetrahedron Lett.* **1982**, *23*, 2105−2108. − [6b] A. Toshimitsu, H. Owada, K. Terao, S. Uemura, M. Okano, *J. Org. Chem.* **1984**, *49*, 3796−3800. − [6c] A. Toshimitsu, H. Owada, K. Terao, S. Uemura, M. Okano, *J. Chem. Soc., Perkin Trans. 1* **1985**, 373−378. − [6d] D. H. R. Barton, D. Crich, *Tetrahedron* **1985**, *41*, 4359−4364. − [6e] A. Toshimitsu, G. Hayashi, K. Terao, S. Uemura, *J. Chem. Soc., Perkin Trans. 1* **1988**, 2113−2117.

[7] [7a]H. Takadu, Y. Shimida, Y. Nakajima, T. Hata, *Nucleic Acids Res.* **1976**, *3*, 1233. − [7b] H. Takadu, T. Konishi, T. Hata, *Chem. Lett.* **1977**, *6*, 655. − [7c] H. Takadu, T. Yamazaki, *Nucleic Acid Chem.* **1978**, *2*, 869. − [7d] H. Takadu, M. Kato, M. Yoshida, R. Yamaguchi, *J. Org. Chem.* **1980**, *45*, 3347−3350.

[8] Py-2-SeH equilibrates easily with its tautomeric form pyridine-2(1*H*)-selone PyH-2-Se.[8a] L. E. Overman, D. Matzinger, E. M. O'Connor, J. D. Overman, *J. Am. Chem. Soc.* **1974**, *96*, 6081−6089. − [8b] T. Kamiyama, S. Enomoto, M. Inoue, *Chem. Pharm. Bull.* **1985**, *33*, 5184.

[9] N. L. Leder, R. K. Shibao, H. Eckert, *Acta Crystallogr., Sect. C* **1992**, *48*, 1670−1671.

[10] [10a] J. P. Collman, L. S. Hegedus, J. R. Norton, R. G. Finke, *Principles and Applications of Organotransition Metal Chemistry*, University Science Book, CA, **1987**. − [10b] A. Togni, L. M. Venanzi, *Angew. Chem. Int. Ed. Engl.* **1994**, *33*, 497−527. − [10c] H. A. Mayer, W. C. Kaska, *Chem. Rev.* **1994**, *94*, 1239−1272.

[11] [11a] R. Chowdury, J.-E. Bäckväll, *J. Chem. Soc., Chem. Commun.* **1991**, 1063−1064. − [11b] P. Braunstein, M. D. Fryzuk, F. Naud, S. J. Rettig, *J. Chem. Soc., Dalton Trans.* **1999**, 589−594.

[12] M. H. Krackov, C. M. Lee, H. G. Mautner, *J. Am. Chem. Soc.* **1965**, *87*, 892−896.

[13] [13a] M. Miyoshi, H. Ishii, K. Kondo, Sh. Murai, N. Sonoda, *Synthesis* **1979**, 300−301. − [13b] D. Labahn, F. M. Bohnen, R. Herbst-Irmer, E. Pohl, D. Stalke, H.-W. Roesky, *Z. Anorg. Allg. Chem.* **1994**, *620*, 41−47.

[14] [14a] P. R. Brooks, J. A. Counter, R. Bishop, E. R. T. Tiekink, *Acta Crystallogr., Sect. C* **1991**, *47*, 1939−1940. − [14b] K. Okuma, K. Kojima, I. Kaneko, Y. Tsujimoto, H. Ohta, Y. Yokomori, *J. Chem. Soc., Perkin Trans. 1* **1994**, 2151−2159. − [14c] S. Collins, T. G. Back, A. Rauk, *J. Am. Chem. Soc.* **1985**, *107*, 6589−6592.

[15] D. Mootz, H.-G. Wussow, *J. Chem. Phys.* **1981**, *75*, 1517−1522.

[16] H. Duddeck, *Progr. NMR Spectrosc.* **1995**, *27*, 1−323.

[17] [17a] T. Chivers, M. Parvez, M. A. Seay, *Inorg. Chem.* **1994**, *33*, 2147−2150. − [17b] O. Niyomura, S. Kato, T. Kanda, *Inorg. Chem.* **1999**, *38*, 507−518.

[18] S. Chadwick, K. Ruhlandt-Senge, *Chem. Eur. J.* **1998**, *4*, 1768−1780.

[19] R. A. McLean, *Inorg. Nucl. Chem. Lett.* **1969**, *5*, 745−747.

[20] [20a] J. Grobe, M. Kohne-Wachter, Duc Le Van, *Z. Anorg. Allg. Chem.* **1984**, *519*, 67−74. − [20b] K. Merzweiler, H.-J. Kersten, *Z. Naturforsch., B* **1991**, *46*, 1025−1030.

[21] J. T. Shore, W. T. Pennington, M. C. Noble, A. W. Cordes, *Phosphorus Sulfur Silicon* **1988**, *39*, 153−157.

[22] Numerous examples for Cu_2Br_2 and Ag_2Br_2 rings in phosphane-containing complexes are known. See for example Cu:[22a] L. M. Engelhardt, P. C. Healy, J. D. Kildea, A. H. White, *Aust. J. Chem.* **1989**, *42*, 913−922. − [22b] G. A. Bowmaker, J. V. Hanna, R. D. Hart, P. C. Healy, A. H. White, *J. Chem. Soc., Dalton Trans.* **1994**, 2621−2629; G. A. Bowmaker, J. V. Hanna, R. D. Hart, P. C. Healy, A. H. White, *Aust. J. Chem.* **1994**, *47*, 25−45. − Ag: [22c] P. C. Healy, N. K. Mills, A. H. White, *J. Chem. Soc., Dalton Trans.* **1985**, 111−116. − [22d] S. Gotsis, L. M. Engelhardt, P. C. Healy, J. D. Kildea, A. H. White, *Aust. J. Chem.* **1989**, *42*, 923−931. − [22e] G. A. Bowmaker, Effendy, J. V. Hanna, P. C. Healy, B. W. Skelton, A. H. White, *J. Chem. Soc., Dalton Trans.* **1993**, 1387−1397.

[23] [23a] B. Ahrens, PhD thesis, Technical University of Braunschweig, Germany, **1998**. − [23b] B. Ahrens, S. Friedrichs, R. Herbst-Irmer, P. G. Jones, *Eur. J. Inorg. Chem.* **2000**, 2017−2029.

[24] D. L. Klayman, T. S. Griffin, *J. Am. Chem. Soc.* **1973**, *95*, 197−200.

[25] G. M. Sheldrick, *SHELXS-86/97, A program for solving crystal structures*, University of Göttingen, **1997**.

[26] G. M. Sheldrick, *SHELXL-93/97, A program for refining crystal structures*, University of Göttingen, **1997**.

Received November 2, 2000
[I00418]

Bi-Layer Complexes Incorporating Large Organic Cations and Anionic Tetra-*p*-Sulfonated Calix[4]arene Capsules

Timothy Ness,[b] Peter J. Nichols,[b] and Colin L. Raston*[a]

Keywords: Supramolecular chemistry / Calixarenes / Crown compounds / Macrocycles

H_4TMTAA^{2+}/18-crown-6, H_4TMTAA^{2+}/2-hydroxybenzimidazole and $cyclamH_4^{4+}$ self-assemble with sodium tetra-*p*-sulfonated calix[4]arene to form capsules within overall bilayer structures. $[H_4TMTAA^{2+}]_2$[*trans*-{$Na^+\subset$(18-crown-6)$(H_2O)_2$}$\subset$ {(*p*-O_3S-calix[4]arene)$_2$} + $3H^+$]·$17H_2O$ crystallises in the triclinic space group $P\bar{1}$ and contains the "Russian Doll" assembled superanion capsule, {$Na^+\subset$(18-crown-6)$(OH_2)_2$}$\subset${(*p*-O_3S-calix[4]arene)$_2$}$^{7-}$. $[H_4TMTAA^{2+}]_2[(C_7N_2OH_7^+)_2\subset$ {(*p*-O_3S-calix[4]arene)$_2$} + $2H^+$]·$17H_2O$ also crystallises in the triclinic space group $P\bar{1}$ and also contains a superanion capsule with two 2-hydroxybenzimidazolium cations as the capsule core. [$cyclamH_4^{4+}$][{$cyclamH_4^{4+}\subset$ {(*p*-O_3S-calix[4]-arene)$_2$}]·$18H_2O$ crystallises in the space group $P2_1/n$ and is an example of a slipped capsule, with the slight "mismatch" allowing stronger internal capsule H-bonding. The cations influence the spacing between the bilayers and can span the calixarene layers.

Introduction

Capsules based on two *p*-sulfonatocalix[n]arenes shrouding other molecules including 18-crown-6[1−4] and protonated cylam[5] (n = 4) and H_2SO_4 (n = 5),[6] have recently been established. In the solid state these capsules (n = 4) have host-guest hydrophobic complementarity and hydrogen bonding mediated by a variety of inorganic cationic species including lanthanide cations,[7] aluminium(III)/Keggin ions,[3] chromium(III)[1,4] and rhodium(III)[3] polynuclear oxo/hydroxo cations. Some of these complexes take on a bi-layer structure with an adjacent calix[4]arene from different capsules, with alternating H-bonding and π-stacking in opposite directions, as shown in cartoon form for *trans*-{$Na^+\subset$(18-crown-6)$(H_2O)_2$} in Figure 1.[1,8a−8g] Other examples of the bilayer structures represent "slipped" capsules (a misalignment of the calixarenes), which in some cases allows one sulfonate group to be in or over the cavity of the other calixarene, and vice versa, through to a complete mismatch of the calixarenes in opposing layers. Generally the inorganic ions stabilise the capsule by H-bonding and reside in the hydrophilic layers in the complexes. The 18-crown-6-containing capsules held together by the dimeric and trimeric oxo-chromium cations are located in a considerably distorted bilayer arrangement.[2] The Keggin ion complexes completely disrupt the bilayer structure with the presence of two types of calixarenes.[4] The large cation, La^{3+}, also completely disrupts the bi-layer structure.[7] Herein we report the use of large organic cations, H_4TMTAA^{2+} (TMTAAH$_2$ = 5,7,12,14-tetramethyldibenzo[*b,i*][1,4,8,11]tetraazacyclotetradecane) and $cyclamH_4^{4+}$, tetra-protonated 1,4,8,11-tetraazacyclotetradecane, to assembly a variety of capsules based on the assembly of two tetra-*p*-sulfonatocalix[4]arenes.

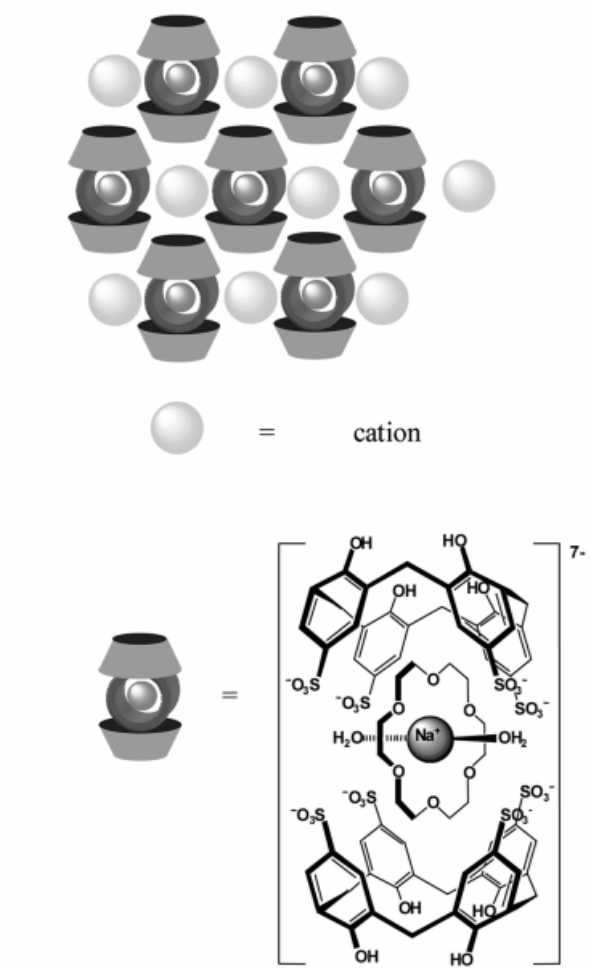

Figure 1. Cartoon of the bi-layer assembly of *p*-sulfonatocalix[4]-arene capsules

[a] School of Chemistry, University of Leeds, Woodhouse Lane, Leeds LS2 9JT, UK
Fax: (internat.) +44-113/233-6401
E-mail: c.l.raston@chem.leeds.ac.uk
[b] School of Chemistry, Monash University, Melbourne, Victoria 3800, Australia

 © WILEY-VCH Verlag GmbH, 69451 Weinheim, 2001 1434−1948/01/0808−1993 $ 17.50+.50/0

Results and Discussion

The synthesis of the new capsule-type complexes (Figure 2) is summarised in Scheme 1. For compounds $[H_4TMTAA^{2+}]_2[trans\text{-}\{Na^+\subset(18\text{-crown-}6)(H_2O)_2\}\subset\{(p\text{-}O_3S\text{-calix[4]arene})_2\} + 3H^+]\cdot 17H_2O$ (**1**) and $[H_4TMTAA^{2+}]_2[(C_7N_2OH_7^+)_2\subset\{(p\text{-}O_3S\text{-calix[4]arene})_2\} + 2H^+]\cdot 17H_2O$ (**2**), the products are also contaminated with 2,4-dimethyl-1,5-benzodiazepinium chloride due to acid decomposition of H_4TMTAA^{2+}. Compound **1** crystallises in the triclinic space group $P\bar{1}$ and contains the "Russian Doll"-assembled superanion capsule $\{Na^+\subset(18\text{-crown-}6)(OH_2)_2\}\subset\{(p\text{-}O_3S\text{-calix[4]arene})_2\}^{7-}$. The capsule has internal H-bonding (axially bound water molecules; sulfonate to water O···O distance: 2.78 Å) and external H-bonding through H_4TMTAA^{2+} interactions (sulfonate to imine O···N distance: 2.77 Å) as well as H-bonding through waters of crystallisation (O···O distance: 2.82 Å).

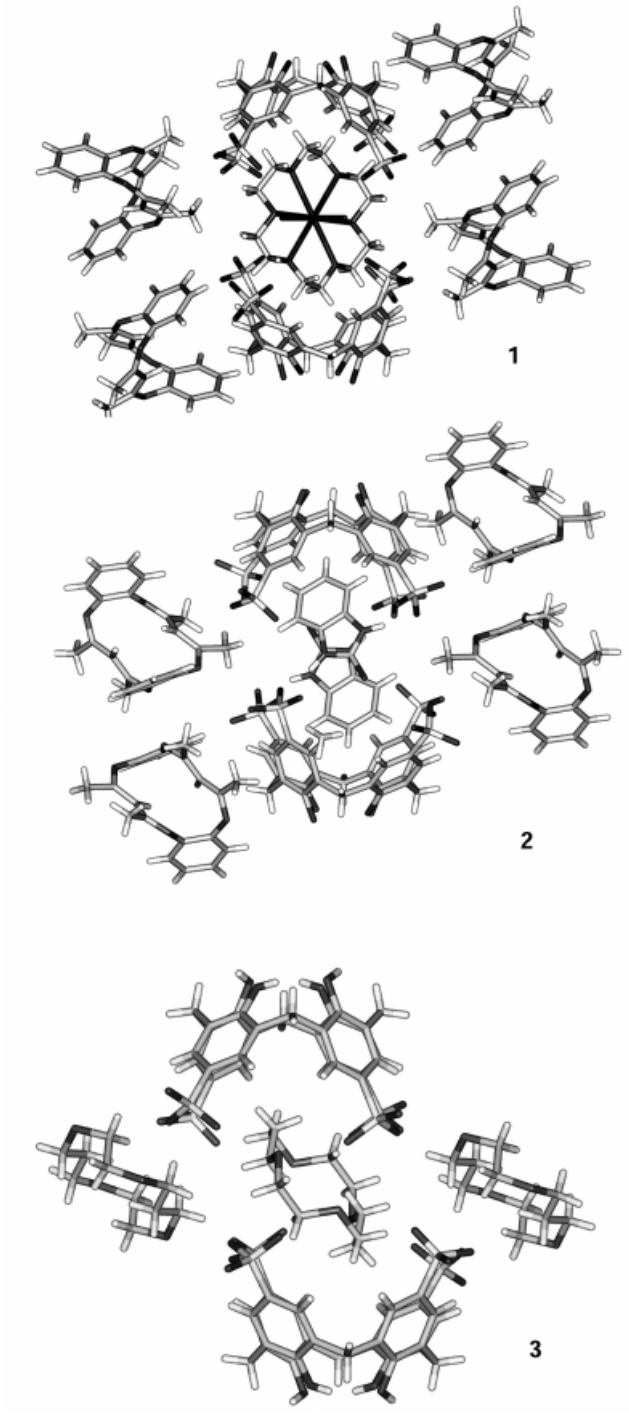

Figure 2. Comparison of the structures of compounds **1**–**3**

Remarkably a bilayer structure is formed in the presence of the large organic cation H_4TMTAA^{2+}, which has similar dimensions to p-O_3S-calix[4]arene and essentially substitutes alternate calix[4]arenes in the usual bilayer found in p-O_3S-calix[4]arene^{4-} complexes that consist of columns of "up"/"down" calix[4]arenes.[8a–8g] Within each column an "up" calix[4]arene is in close proximity to two other "down" calix[4]arenes with each interacting through aromatic ring π-stacking and two sulfonate-to-hydroxy H-bonds associated with the stacked rings. Four other calix[4]arene molecules in the two adjacent columns are then associated through sulfonate-to-sulfonate H-bonds possibly mediated by water. In the present structure, H_4TMTAA^{2+} cations are interspersed between columns of "up"/"down" calix[4]arenes. Within each calix[4]arene column an "up" calix[4]arene is in close proximity to two other "down" calix[4]arenes with each interacting through aromatic ring π-stacking (offset, coplanar with shortest C···C contacts of 3.40 Å) and two sulfonate-to-hydroxy H bonds (O···O distance: 3.02 Å) associated with the stacked rings. The H_4TMTAA^{2+} cations interact with calix[4]arenes through a non-classical H bond (a methyl hydrogen pointing to the centre of the calix[4]arene aromatic ring; methyl carbon to ring carbons: C···C distances = 3.54–3.62 Å, with a C···ring centroid distance of 3.31 Å) and the imine hydrogen to sulfonate H bond described above. Two other H_4TMTAA^{2+} cations pack close to each calix[4]arene with no obvious interactions: the phenyl- or methyl-lined concave surfaces are seemingly two steep to accommodate the concave-convex supramolecular interaction seen in many Ni(TMTAA) complexes.[9a–9e] Water also permeates the H_4TMTAA^{2+} and calix[4]arene layer, with H-bonding to both calix[4]arenes and H_4TMTAA^{2+} cations.

The hydrophilic layer consists of the di-aqua sodium/18-crown-6 complex and water of crystallisation, with the 18-crown-6 complex within the capsule thus spanning the layers. H_4TMTAA^{2+} cations form "up"/"down" columns perpendicular to the calix[4]arene columns and interacting across the layers through aromatic ring π-stacking. Within the calix[4]arene layer there are offset, coplanar aromatic rings with shortest C···C distances of 3.42 Å. Within the hydrophilic layer there are offset, coplanar aromatic rings with shortest C···C distances of 3.31 Å. The calix[4]arene separation across the capsules (or layers) is characterised by pairs of sulfonate groups with a shortest O···O distance of 4.27 Å.

Compound **2** also crystallises in the triclinic space group $P\bar{1}$ and also contains a superanion, $\{(C_7N_2OH_7^+)_2\subset\{(p\text{-}O_3S\text{-calix[4]arene})_2\}^{6-}$. The capsule also has internal H-bonding (2-hydroxybenzimidazol-N and -O to sulfonate

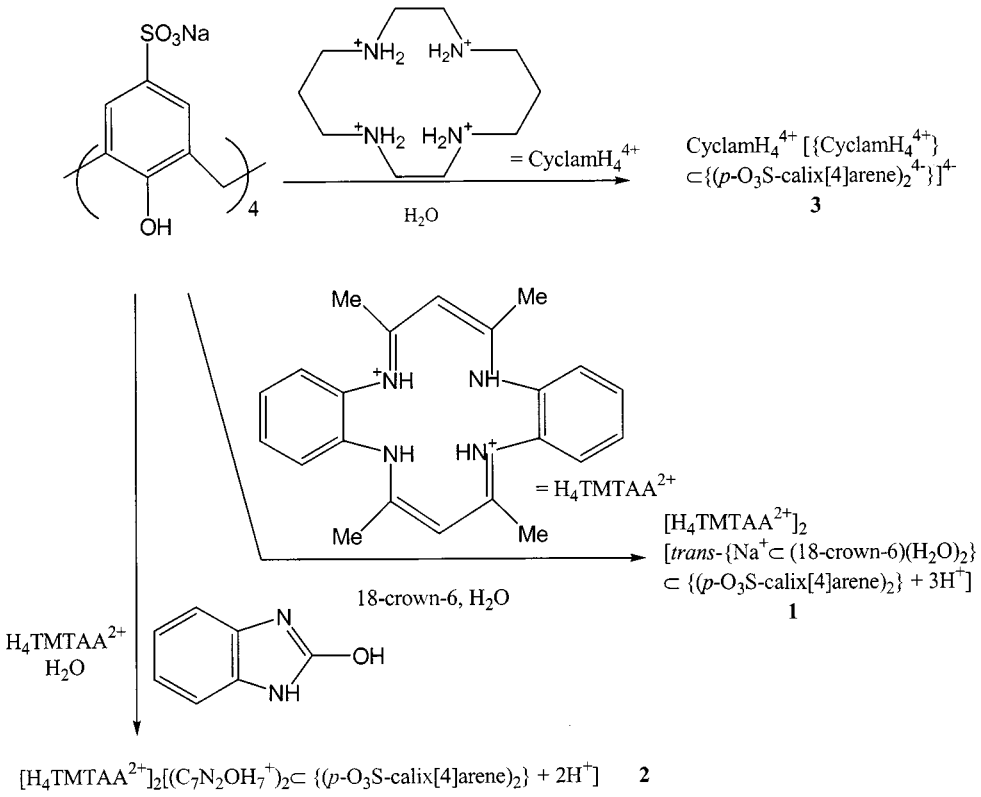

Scheme 1

oxygen interactions: N···O = 2.75, 2.81 Å; O···O = 3.36, 3.44 Å) and external H-bonding through waters of crystallisation (distances 2.61 Å). H-bonding for H_4TMTAA^{2+} to calix[4]arene in this complex is weaker than in compound **1** (sulfonate to imine: O···N distance = 3.10 Å). The guest molecules form an aromatic ring π-stacked dimer (coplanar; closest contacts: O···C = 3.42 Å; C···N = 3.41 Å; C···C = 3.37 Å) with the monomers *anti* to each other.

The calix[4]arene layer again consists of H_4TMTAA^{2+} interspersed between columns of calix[4]arenes. The "up"/"down" calix[4]arene columns exhibiting the usual sulfonated phenol π-stacking/H-bonding interactions (coplanar rings: C···C distances = 3.61−3.64 Å; sulfonate oxygen to phenolic oxygen distance: 3.22 Å). Across the columns the calix[4]arenes interact with H_4TMTAA^{2+} through "non-classical" H-bonding interactions (C···ring centroid = 3.46 Å). Columns of H_4TMTAA^{2+} cations, perpendicular to the calix[4]arene columns, again transverse the calix[4]arene layer. The H_4TMTAA^{2+} columns therefore span the bilayer by aromatic ring π-stacking (well aligned; coplanar aromatic rings with C···C distances of 3.40−3.58 Å and 3.55−3.62 Å for the stacking in and out of the hydrophilic layer, respectively). The calix[4]arene separation across the capsules (or layers) is characterised by sulfur-to-sulfur distances of 5.42 and 6.70 Å (closest O···O contact: 4.00 Å).

$[cyclamH_4^{4+}][\{cyclamH_4^{4+}\}\subset\{(p\text{-}O_3S\text{-calix[4]arene})_2\}]\cdot 18H_2O$ (**3**) crystallises in the space group $P2_1/n$ and is an example of a slipped capsule, with the slight "mismatch" allowing stronger internal H-bonding interactions. A similar capsule has been observed in $[Cr_2(OH)_2(H_2O)_8][\{cyclamH_4^{4+}\}\subset\{(p\text{-}O_3S\text{-calix[4]arene})_2\}]$.[4] The capsule in compound **3** is characterised by internal H bond interactions (N···O distances: 2.73, 2.78 and 2.90 Å) with the shortest O···O calix[4]arene separations at 5.21 Å. The capsule also features external H-bonding through the *exo*-$cyclamH_4^{4+}$ interactions (N···O distance: 2.79 Å) as well as H-bonding through waters of crystallisation (shortest O···O distance: 2.58 Å).

The overall structure is characterised by the bilayer arrangement with the cyclam cations located in the hydrophilic layer. Each calix[4]arene molecule is in close proximity to two other calix[4]arenes through sulfonated phenol π-stacking/H-bonding interactions (coplanar rings; C···C distances: 3.67−3.79 Å; sulfonate oxygen to phenolic oxygen distance: 3.16 Å). Four other calix[4]arene molecules in the two adjacent columns are associated through sulfonate-to-sulfonate O···H bonds, some mediated by water. The cyclam cations are well separated (shortest C···C distance: 4.03Å) but are H-bonded to water molecules in the hydrophilic layer.

Conclusion

The sulfonated phenol π-stacking/H-bonding interaction in tetra-*p*-sulfonatocalix[4]arene complexes leading to columns of alternating "up"/"down" calix[4]arenes dominates in the overall assembly of calix[4]arene complexes. As seen

in the results presented in this study, the presence of charge-balancing cations *exo* and *endo* to the calix[4]arenes can influence the overall structures in two major ways: they can determine the calix[4]arene layer separation and they can act to separate columns of calix[4]arenes within the calix[4]arene layer. The alignment of calix[4]arene columns to allow capsule formation and the subsequent efficient internal and external H-bonding leads to more tightly bound structures. The encapsulation of guest molecules within the superanions offers the possibility of arranging molecules to permit subsequent stereospecific reaction, and, in view of the dimer observed in the 2-hydroxybenzimidazole capsule, offers the possibility to study π-stacking in amino acid pairs. The H_4TMTAA^{2+} complexes contain columns of the cations running transverse to the columns of the calix[4]-arene anions and thus spanning the calix[4]arene layers, which is of current interest with respect to understanding transport across bilayer structures.[8b]

Experimental Section

Synthesis of $[H_4TMTAA^{2+}]_2[$*trans*-{$Na^+\subset$(18-crown-6)-$(H_2O)_2$}$\subset${(*p*-O_3S-calix[4]arene)$_2$} $+3H^+]\cdot 17H_2O$ (1): Equimolar amounts of $TMTAAH_2$, 18-crown-6 and tetrasodium tetra-*p*-sulfonatocalix[4]arene (0.038 mmol) were mixed in a 50/50 mix of water and ethanol (overall 20 mL) to which 4 mL of 1 M HCl had been added. The solution soon changed from colourless to orange. On slow evaporation crystalline material deposited, the bulk of which (ca. 48 mg; 90%) consisted of clear, colourless crystals of $[H_4TMTAA^{2+}]_2[$*trans*-{$Na^+\subset$(18-crown-6)$(H_2O)_2$}$\subset${(*p*-O_3S-calix[4]arene)$_2$} + $3H^+]\cdot 17H_2O$ (**1**). Purple/yellow dichroic crystals of 2,4-dimethyl-1,5-benzodiazepinium chloride were also present. The colour change on mixing and subsequent isolation of the 2,4-dimethyl-1,5-benzodiazepinium chloride are a result of the aqueous-acid instability of $TMTAAH_2$. The presence of multiple products in these reactions as well as the general rapid loss of water from the complex hydrates meant that good microanalyses could not be obtained.

Synthesis of $[H_4TMTAA^{2+}]_2[(C_7N_2OH_7^+)_2\subset${(*p*-$O_3$S-calix-[4]arene)$_2$} + $2H^+]\cdot 17H_2O$ (2): Reaction of equimolar amounts of $TMTAAH_2$, tetrasodium tetra-*p*-sulfonatocalix[4]arene and 2-hydroxybenzimidazole (0.038 mmol) in acidic aqueous acid solution resulted in a coloured solution which, on evaporation of the solvents, gave $[H_4TMTAA^{2+}]_2[(C_7N_2OH_7^+)_2\subset${(*p*-$O_3$S-calix[4]arene)$_2$} + $2H^+]\cdot 17H_2O$ (**2**; ca. 38 mg; 72%) and 2,4-dimethyl-1,5-benzodiazepinium chloride. The presence of multiple products in these reactions as well as the rapid loss of water from the complex hydrates meant that good microanalyses could not be obtained.

Synthesis of $[cyclamH_4^{4+}][\{cyclamH_4^{4+}\}\subset\{$(*p*-$O_3$S-calix-[4]arene)$_2\}]\cdot 18H_2O$ (3): Reaction of cyclam (6.3 mg, 0.031 mmol), tetrasodium tetra-*p*-O_3S-calix[4]arene (6.3 mg, 0.076 mmol) and $Fe(NO_3)_3\cdot 9H_2O$ (7.0 mg, 0.17 mmol) in aqueous solution, with the pH adjusted to 0.99 using $HClO_4$, followed by slow evaporation of the yellow solution gave pale yellow crystals of $[cyclamH_4^{4+}][\{cyclamH_4^{4+}\}\subset\{$(*p*-$O_3$S-calix[4]arene)$_2\}]\cdot 18H_2O$, (ca. 20 mg; 60%). Due to loss of solvent from the crystals, satisfactory results from microanalysis were unobtainable.

X-ray Crystallographic Study: Crystals were mounted onto glass capillaries under oil. X-ray data were collected at 123(1) K on an Enraf−Nonius KappaCCD single crystal diffractometer with Mo-K_α radiation (λ = 0.71073 Å). Data was corrected for Lorentzian and polarisation effects, but not absorption. The non-hydrogen atoms (except oxygen atoms in waters of crystallisation) were refined anisotropically and hydrogen atoms were included at geometrically estimated positions but not refined.

1: Colourless, prismatic crystal of dimensions 0.20 × 0.20 × 0.15 mm. The structure was solved using direct methods (teXsan[10]) and refined by full-matrix least-squares on F (teXsan[10]): $C_{112}H_{157}N_8Na_1O_{57}S_8$, M_r = 2806.96 g mol^{-1}, triclinic, $P\bar{1}$ (no. 2), a = 14.3711(5), b = 17.3467(6), c = 17.5191(4) Å, α = 115.261(1)°, β = 95.759(2)°, γ = 112.623(1)°, V = 3498.0(0.2) Å^3, ρ_{calc} = 1.36 gdm^{-3}, μ = 2.24 cm^{-1} (no correction), Z = 1, 50839 reflections (17557 unique), $2\theta_{max}$ = 60.2° [9102 observed, $I > 2\sigma(I)$, R = 0.148, Rw = 0.155].

2: Clear, orange, prismatic crystal of dimensions 0.25 × 0.20 × 0.15 mm. The structure was solved using direct methods (teXsan[10]) and refined by full-matrix least-squares on F (teXsan[10]): $C_{57}H_{78}N_6O_{25.5}S_4$, M_r = 1383.51 g mol^{-1}, triclinic, $P\bar{1}$ (no. 2), a = 14.6516(5), b = 15.8265(6), c = 16.3448(4) Å, α = 108.430(2)°, β = 105.402(2)°, γ = 108.984(1)°, V = 2929.9(0.1) Å^3, ρ_{calc} = 1.475 gdm^{-3}, μ = 2.44 cm^{-1} (no correction), Z = 2, 45397 reflections (15658 unique), $2\theta_{max}$ = 60.0° [8516 observed, $I > 2\sigma(I)$, R = 0.090, Rw = 0.070].

3: Prismatic crystal of dimensions 0.5 × 0.3 × 0.2 mm. The structure was solved using direct methods (XSEED/SHELXL-97[10]) and refined by full-matrix least-squares on F^2 (XSEED/SHELXL-97[10]): $C_{76}H_{80}N_8O_{50}S_8$, M_r = 2161.96 g mol^{-1}, monoclinic, $P2_1/n$ (No. 14), a = 10.841(2), b = 28.092(6), c = 15.740(3) Å, β = 96.29(3)°, V = 4764.6(1.6) Å^3, ρ_{calc} = 1.507 gdm^{-3}, μ = 2.92 cm^{-1} (no correction), Z = 2, 29563 reflections (11988 unique), $2\theta_{max}$ = 52° [8088 observed, $I > 2\sigma(I)$, R = 0.060, Rw = 0.127].

Crystallographic data (excluding structure factors) for the structures reported in this paper have been deposited with the Cambridge Crystallographic Data Centre as supplementary publication no. CCDC-149551 (**1**), CCDC-149552 (**2**), and CCDC-149553 (**3**). Copies of the data can be obtained free of charge on application to CCDC, 12 Union Road, Cambridge CB2 1EZ, UK [Fax: (internat.) +44-1223/336-033; E-mail: deposit@ccdc.cam.ac.uk].

Acknowledgments

This work is supported by the Australian Research Council.

[1] A. Drljaca, M. J. Hardie, C. L. Raston, L. Spiccia, *Chem. Eur. J.* **1999**, *5*, 2295−2299.
[2] A. Drljaca, M. J. Hardie, T. Ness, C. L. Raston, *Eur. J. Inorg. Chem.* **2000**, 2221−2229.
[3] A. Drljaca, M. J. Hardie, C. L. Raston, *J. Chem. Soc., Dalton Trans.* **1999**, 3639−3642.
[4] S. Airey, A. Drljaca, M. J. Hardie, C. L. Raston, *Chem. Commun.* **1999**, 1137−1138.
[5] M. J. Hardie, M. Makha, C. L. Raston, *Chem. Commun.* **1999**, 2409−2410.
[6] M. J. Hardie, C. L. Raston, *J. Chem. Soc., Dalton Trans.* **2000**, 2483−2492.
[7] A. Drljaca, M. J. Hardie, J. A. Johnson, C. L. Raston, H. R. Webb, *Chem. Commun.* **1999**, 1135−1136.

[8] [8a] G. W. Orr, L. J. Barbour, J. L. Atwood, *Science* **1999**, *285*, 1049−1052. − [8b] M. Selkti, A. W. Coleman, I. Nicolis, N. Douteau-Guevel, F. Villain, A. Tomas, C. de Rango, *Chem. Commun.* **2000**, 161−162. − [8c] J. L. Atwood, L. J. Barbour, E. S. Dawson, P. C. Junk, J. Kienzle, *Supramol. Chem.* **1996**, *7*, 271−274. − [8d] P. C. Leverd, P. Berthault, M. Lance, M. Nierlich, *Eur. J. Org. Chem.* **2000**, 133−139. − [8e] J. W. Steed, C. P. Johnson, C. L. Barnes, R. K. Juneja, J. L. Atwood, S. Reilly, R. L. Hollis, P. H. Smith, D. L. Clark, *J. Am. Chem. Soc.* **1995**, *117*, 11426−11433. − [8f] A. W. Coleman, S. G. Bott, S. D. Morley, C. M. Means, K. D. Robinson, H. Zhang, J. L. Atwood, *Angew. Chem. Int. Ed. Engl.* **1988**, *27*, 1361−1362. − [8g] J. L. Atwood, A. W. Coleman, H. Zhang, S. G. Bott, *J. Incl. Phenom.* **1989**, *7*, 203−206.

[9] [9a] P. C. Andrews, J. L. Atwood, L. J. Barbour, P. J. Nichols, C. L. Raston, *Chem. Eur. J.* **1998**, *4*, 1384−1387. − [9b] P. D. Croucher, J. M. E. Marshall, P. J. Nichols, C. L. Raston, *Chem. Commun.* **1999**, 193−194. − [9c] P. D. Croucher, P. J. Nichols, C. L. Raston, *J. Chem. Soc., Dalton Trans.* **1999**, 279−284. − [9d] P. C. Andrews, J. L. Atwood, L. J. Barbour, P. D. Croucher, P. J. Nichols, N. O. Smith, B. W. Skelton, A. H. White, C. L. Raston, *J. Chem. Soc., Dalton Trans.* **1999**, 2927−2932. − [9e] P. J. Nichols, K. Baranyai, C. L. Raston, *Angew. Chem. Int. Ed.* **2000**, *39*, 1842−1845.

[10] teXsan: Crystal Structure Analysis Package, Molecular Structure Corporation (**1985** and **1992**); SHELXS-97, Program for the Solution of Crystal Structures, G. M. Sheldrick, **1997**, Gottingen, Germany; Xseed, a graphical interface to the SHELX program suite, L. J. Barbour, **1999**, University of Missouri, USA.

Received February 9, 2001
[I01047]

The First Transition Metal Complexes of 15-Membered Triolefinic Macrocycles: (*E,E,E*)-1,6,11-Tris(arenesulfonyl)-1,6,11-triazacyclopentadeca-3,8,13-triene Complexes of Palladium(0), Platinum(0), and Silver(I)

Silvia Cerezo,[a] Jordi Cortès,[a] Elena Lago,[b] Elies Molins,[b] Marcial Moreno-Mañas,*[a] Teodor Parella,[c] Roser Pleixats,[a] Javier Torrejón,[a] and Adelina Vallribera[a]

Keywords: Palladium / Platinum / Silver / Macrocyclic ligands / Heterocycles

(*E,E,E*)-1,6,11-Tris(arenesulfonyl)-1,6,11-triazacyclopentadeca-3,8,13-trienes (**1**) form very stable complexes with Pd^0 and Pt^0, and moderately stable complexes with Ag^I. The three olefins in the macrocycle are responsible for the complexation. The X-ray structures of two complexes of Pd^0 and Pt^0 are presented; both complexes are planar trigonal.

Introduction

Nitrogen-containing 15-membered macrocycles are commonplace.[1,2] However, nitrogen-containing 15-membered macrocycles featuring internal olefinic double bonds are exceptional. The few known examples contain only one double bond, and metathesis is the key step for their preparation.[3] In 1998 we described the serendipitous formation of (*E,E,E*)-1,6,11-tris(arenesulfonyl)-1,6,11-triazacyclopentadeca-3,8,13-trienes (**1**) and the complex **2b-Pd^0** (Scheme 1) by nonselective palladium(0)-catalyzed Tsuji−Trost allylation of arenesulfonamides with *cis*-2-butene-1,4-diol dicarbonate.[4] The macrocycle **1b** affords the complex **2b-Pd^0** by treatment with sources of Pd^0. This complex is very stable, catalyses certain Suzuki-type cross-coupling reactions, and is easily recovered after catalysis.[5] Later we published the optimized preparations of macrocycles **1** featuring a vast array of substituents at the arenesulfonyl moieties.[6]

The complexes $Pd_2(dba)_3$-solvent and $Pd_2(dba)_4$ [7] are very well-known and their catalytic effect has been recognized. Many other complexes of olefins with palladium(0) and platinum(0) have been described.[8−10] However, only a few complexes of transition metals with triolefinic macrocycles are known. Thus, the diverse configurational isomers of the 12-membered carbocycle cyclododeca-1,5,9-triene have a rich coordination chemistry, and their Ni^0 complexes have played a fundamental role in catalysis and in organonickel chemistry.[11] X-ray diffraction data of the (*E,E,*E) isomer show that the complex is planar trigonal.[11b] Other metals form complexes with cyclododecatrienes: Cu^I,[12] Pd^{II},[13] Ag^I,[14] Rh^{III},[15] and Ru^{II}.[16] Related 12-membered carbocycles also form nickel(0) complexes.[17] At the upper limit of ring size, 13-membered (*Z,E,Z*)-cyclotrideca-1,5,9-triene forms a complex with Ag^I.[18] A special case is the complexation of Ag^I by [2.2.2]paracyclophanes, which occurs in an η^2 manner at each of the three benzene rings.[19] The related [2_6](1,2,4,5)cyclophane (deltaphane) presents the same behavior.[19b] In contrast, (*Z,Z,Z*)-tribenz[12]annulene, the triunsaturated analogue of [2.2.2]orthocyclophane coordinates Ag^I through the three olefins.[20] Metal complexes of macrocyclic triolefins higher than 13-membered are unknown.

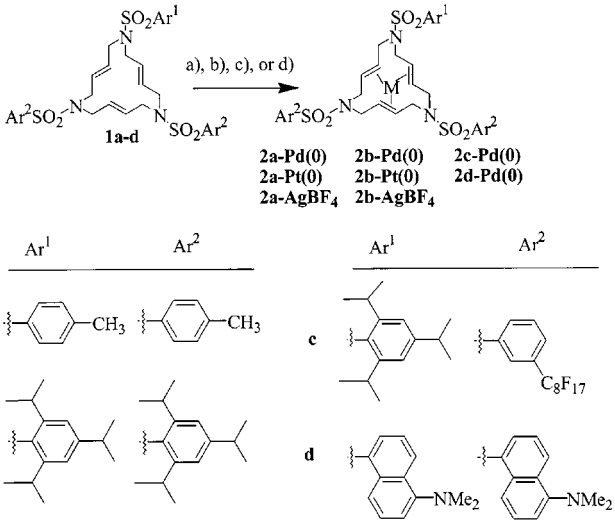

Scheme 1. Preparation of complexes **2**: a) $Pd(PPh_3)_4$ in THF for **2a-Pd^0** and **2b-Pd^0**; b) $Pd(dba)_2$ in THF for **2c-Pd^0** and **2d-Pd^0**; c) $Pt(PPh_3)_4$ in THF for **2a-Pt^0** and in DMF for **2b-Pt^0**; d) $AgBF_4$ in acetone for **2a-Ag^{I}BF$_4$** and **2b-Ag^{I}BF$_4$**

[a] Department of Chemistry, Universitat Autònoma de Barcelona, Cerdanyola,
08193 Barcelona, Spain
Fax: (internat.) +34-93/581-1265
E-mail: marcial.moreno@uab.es
[b] Institut de Ciència de Materials de Barcelona (CSIC), Campus de la UAB,
08193 Cerdanyola, Spain
[c] Servei de RMN, Universitat Autònoma de Barcelona, Cerdanyola,
08193 Barcelona, Spain

 © WILEY-VCH Verlag GmbH, 69451 Weinheim, 2001 1434−1948/01/0808−1999 $ 17.50+.50/0

Spurred on by these findings we decided to study the complexing ability of macrocycles **1** towards transition metals.

Results and Discussion

Complexes **2** were very easily prepared by the reaction of macrocycles **1** with familiar sources of the corresponding metals. Both tetrakis(triphenylphosphane)palladium(0) and $Pd(dba)_2$ gave excellent results as Pd sources, whereas only tetrakis(triphenylphosphane)platinum(0) was tested for platinum (Scheme 1). Silver tetrafluoroborate was used for the formation of the silver complexes. These complexes are much less stable than those of Pd^0 and Pt^0. Strong evidence for the structures was secured by X-ray diffraction for **2a-Pd^0** (Figure 1 and 2) and **2a-Pt^0** (Figure 3 and 4) and in all cases by MALDI-TOF mass spectrometry.

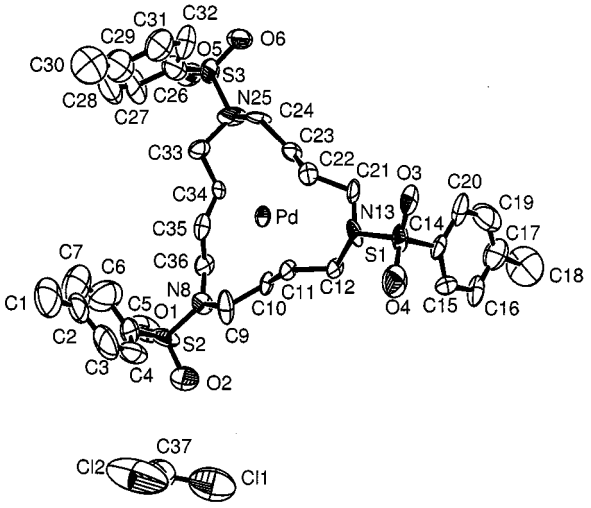

Figure 1. Perspective view of the **2a-Pd^0** molecule with the crystallographic atom numbering; atoms are represented as their thermal vibration ellipsoids (50% probability)

Complexes **2a-Pd^0** and **2a-Pt^0** are planar trigonal, with the distances from the metal atoms to the plane defined by the central points of the three olefin bonds being 0.018 and 0.015 Å, respectively. The complexes crystallize with one molecule of dichloromethane. They are not symmetrical, and in particular they lack a C_3 axis of symmetry. Two C=C bonds are longer than in the corresponding free ligand **1a**[6] (see Table 1). However, the third C=C bond is shorter than the other two in both complexes, and is close to the distance in the free ligand. These facts suggest that complexation by one olefin is weaker than complexation by the other two, a feature that is also evident in solution from NMR spectroscopic data.

The ^{13}C NMR spectrum of **2a-Pd^0** shows three signals of about the same intensity for three different types of CH_2 groups at δ = 45.1, 48.2, and 49.5 (Table 2). Also, three different signals appear, again of similar intensities, for three different types of olefinic CH groups, at δ = 78.5, 78.7, and 82.8. Moreover, the signals of the aromatic pro-

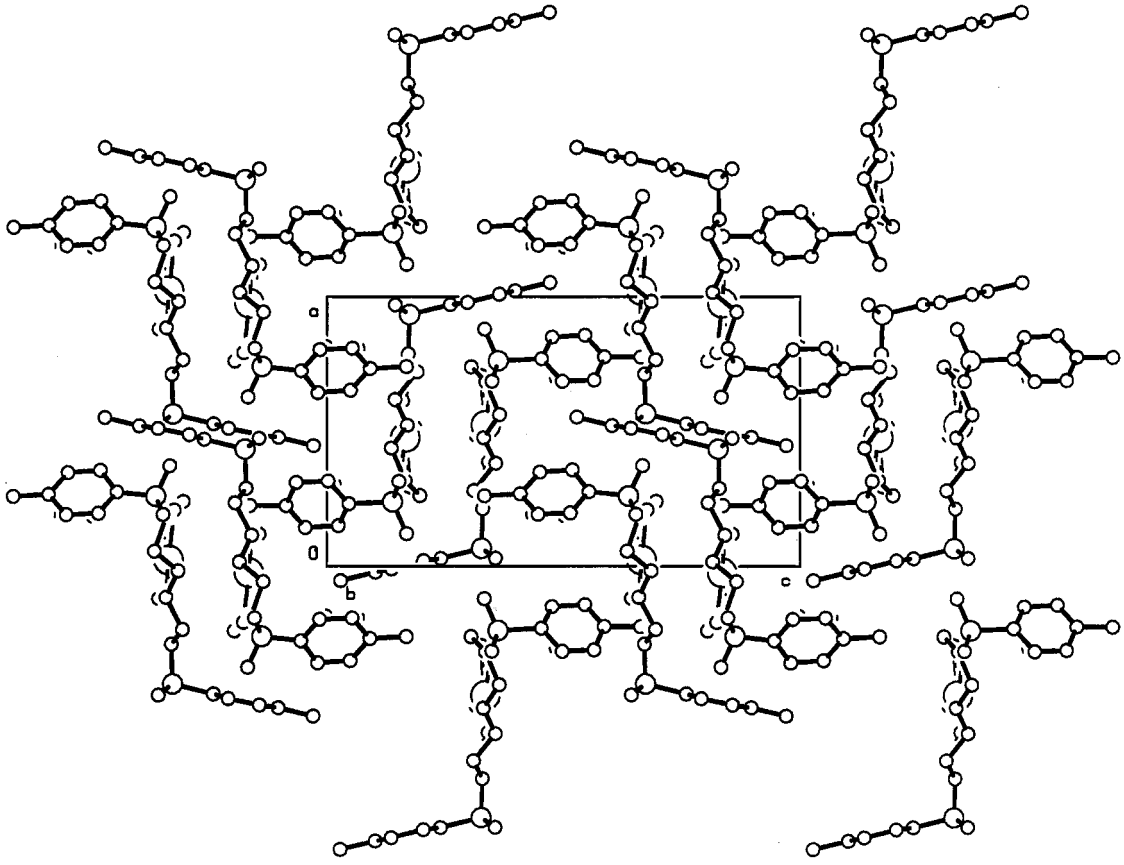

Figure 2. Perspective view of the unit cell of **2a-Pd^0**

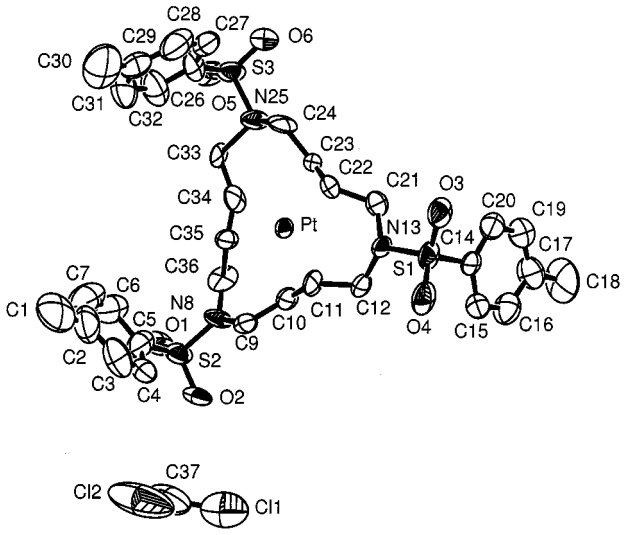

Figure 3. Perspective view of the **2a-Pt^0** molecule with the crystallographic atom numbering; atoms are represented as their thermal vibration ellipsoids (50% probability)

tons appear in two sets, one set of signals being about twice the intensity of the other, confirming that two olefins behave the same both in the ^{1}H NMR and ^{13}C NMR spectra and the third behaves differently. This is a general behavior for complexes **2-Pd^0** and **2-Pt^0**, and can only be compatible with an averaged plane of symmetry rather than with a C_3 symmetry axis. The ^{1}H NMR spectra were further complicated by the fact that the protons pertaining to the same methylene group are not averaged, due to conformational rigidity. These methylenic protons are in different environments and therefore they give signals at very different chemical shifts. Selective 1D TOCSY experiments performed on complexes **2a-Pd^0**, **2a-Pt^0**, and **2b-Pd^0** permitted the determination of the chemical shifts and coupling constants indicated in Table 2. Thus, the pairs of positions C2−C15, C3−C14, C4−C13, and C5−C12 are connected by an averaged plane of symmetry, as are the pairs C7−C10 and C8−C9 (see Scheme 2 for numbering). A simplified representation of the equilibrium causing this averaged response is shown in Scheme 2. As a consequence, the olefinic carbon atoms (and their corresponding hydrogen atoms) in positions C3 and C14 give the same signals, which are different from the signals due to the other bound carbons (positions C4 and C13). Moreover, the third double bond at positions C8 and C9 is different from the others, and positions C8 and C9 give the same signal. In other words the NMR spectroscopic data show that, in solution, two olefins complex the metal with the same strength, and the third one complexes differently, as already shown in the solid phase by X-ray diffraction studies.

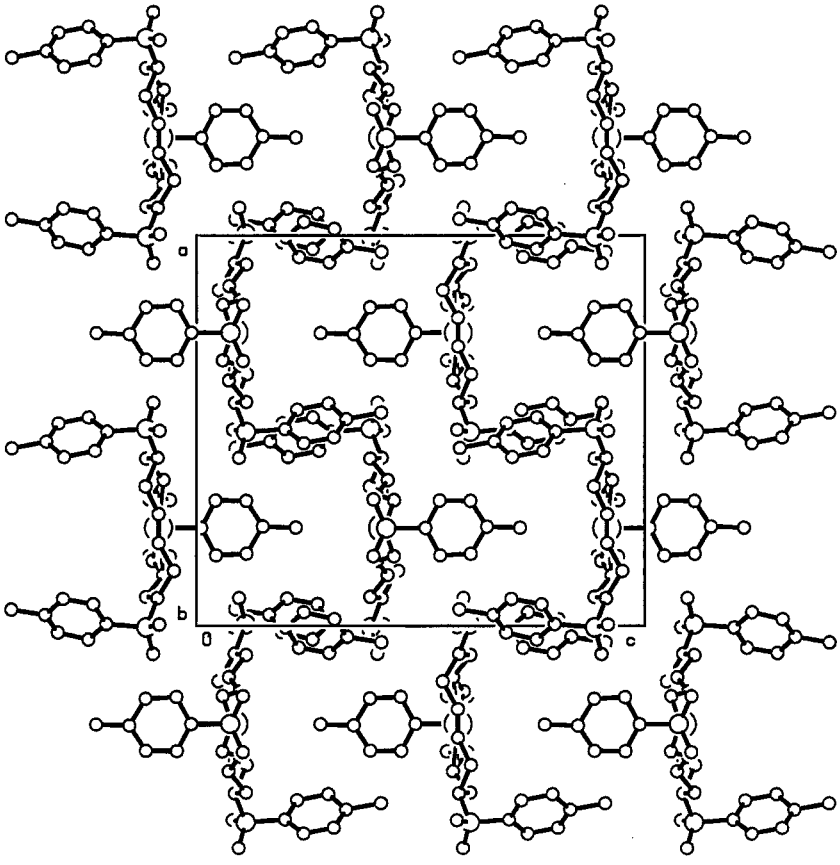

Figure 4. Perspective view of the unit cell of **2a-Pt^0**

Table 1. Selected bond lengths and angles found in **2a-Pd^0** and **2a-Pt^0**

	Pd−olefin distances (Å)		Bond lengths (Å)		Torsion angles (°)	
2a-Pd^0	Pd−C10	2.142(6)	C10−C11	1.301(7)	H10−C10−C11−H11	148.1(9)
	Pd−C11	2.244(6)				
2a-Pd^0	Pd−C22	2.186(6)	C22−C23	1.368(7)	H22−C22−C23−H23	146.7(9)
	Pd−C23	2.261(6)				
2a-Pd^0	Pd−C34	2.167(5)	C34−C35	1.368(7)	H34−C34−C35−H35	147.9(9)
	Pd−C35	2.234(6)				
2a-Pt^0	Pt−C10	2.128(15)	C10−C11	1.365(14)	H10−C10−C11−H11	146.4(12)
	Pt−C11	2.146(12)				
2a-Pt^0	Pt−C22	2.145(11)	C22−C23	1.389(14)	H22−C22−C23−H23	145.6(12)
	Pt−C23	2.154(15)				
2a-Pt^0	Pt−C34	2.135(11)	C34−C35	1.274(15)	H34−C34−C35−H35	162.6(12)
	Pt−C35	2.152(11)				
1a[6]			C10−C11	1.292(7)		
			C22−C23	1.291(7)		
			C34−C35	1.277(7)		

Table 2. NMR spectroscopic data for Complexes **2a-Pd^0**, **2b-Pd^0**, and **2a-Pt^0**

Positions	**2a-Pd^0** [a] ^{1}H NMR	**2a-Pd^0** ^{13}C NMR	**2b-Pd^0**[b] ^{1}H NMR	**2b-Pd^0** ^{13}C NMR	**2a-Pt^0**[a] ^{1}H NMR	**2a-Pt^0** ^{13}C NMR
2 and 15 (−CH_2−)	3.07 (dd, J = 14.2, 11.3)	45.1	3.05 (dd, J = 12.6, 12.4)	43.8	2.98 (dd, J = 13.6, 11.5)	44.3
	4.78 (d, J = 14.3)		4.55 (d, J = 12.6)		5.02 (d, J = 12.7)	
3 and 14 (=CH−)	2.79 (t, J = 11.7)	82.8	2.80 (t, J = 12.4)	83.7	2.07 (td, J = 13.3, 2.3)	69.0
4 and 13 (=CH−)	3.93−4.03 (m)	78.7	4.10 (dd, J = 12.4, 11.1)	79.3	3.41 (td, J = 11.6, 3.8)	63.2
5 and 12 (−CH_2−)	1.63 (dd, J = 14.3, 10.7)	49.5	1.52 (dd, J = 15.6, 11.1)	47.9	1.34 (dd, J = 14.0, 10.9)	48.5
	4.62 (d, J = 14.3)		4.22 (dd, J = 15.6, 3.2)		4.58 (dd, J = 14.0, 3.8)	
7 and 10 (−CH_2−)	1.50−1.80 (m)	48.2	1.58 (dd, J = 15.3, 9.5)	46.5	1.35−1.46 (m),	47.2
	4.64 (d, J = 14.3)		4.30 (d, J = 15.3)		4.62 (d, J = 12)	
8 and 9 (=CH−)	3.75 (m)	78.5	3.85 (d, J = 9.5)	79.2	3.22−3.25 (m)	62.7

[a] ^{1}H and ^{13}C NMR spectra for **2a-Pd^0** and **2a-Pt^0** were recorded in $CDCl_3$. − [b] ^{1}H and ^{13}C NMR spectra for **2b-Pd^0** were recorded in [D_8]toluene.

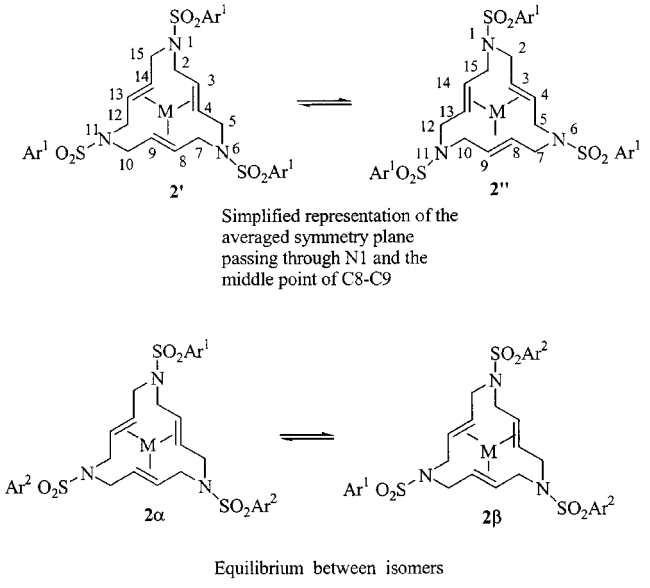

Scheme 2. Averaged plane of symmetry and equilibrium between isomers in complexes **2**

In the case of different N-substituents, as for **2c-Pd^0**, two different isomers are expected depending on which substituent occupies the position opposite to the singular olefin. Although no attempts have been performed to separate these possible isomers, the ^{13}C NMR spectrum for **2c-Pd^0** confirms this situation in solution. Thus, the **2α** isomer (Scheme 2) has the unique (2,4,6-triisopropyl)phenylsulfonyl group opposite the singular olefin, and therefore it has an averaged plane of symmetry and three different signals are predicted for the olefinic protons and for the ring methylene protons, whereas the **2β** isomer has no symmetry whatsoever, and therefore six different signals are predicted for the olefinic protons and for the methylenic protons. The experimental result is that **2c-Pd^0** has nine signals in the olefinic region between δ = 77.6 and 88.4 and eight signals in the CH_2 region between δ = 43.7 and 49.5. Efforts are presently being made to prepare crystals of different N-substituted macrocycles.

The silver complexes were not stable and could not be studied in depth.

Conclusion

Preparations of the first Pd^0, Pt^0, and Ag^I complexes of 15-membered macrocyclic triolefins are described. X-ray analysis and NMR spectroscopic data indicate that the complexes have an averaged plane of symmetry rather than a C_3 axis.

Experimental Section

General: Macrocycles **1** were prepared as described previously.[5,6] Melting points were determined with a Kofler apparatus and are uncorrected. − IR spectra were recorded with a Nicolet FT-IR 510 ZDX. − NMR spectra were recorded with a Bruker-Analytik AC250. ^{1}H NMR (250 MHz) chemical shifts are reported relative to $CHCl_3$ at δ = 7.26 or tetramethylsilane at δ = 0.00. Coupling constants are reported in Hz. ^{13}C NMR (62.5 MHz) chemical shifts are expressed relative to $CDCl_3$ at δ = 77.00 or tetramethylsilane at δ = 0.00. Mass spectra (EIMS) were obtained with a Hewlett−Packard 5989A spectrometer and determined at an ionizing voltage of 70 eV. MALDI-TOF spectra were recorded on a BIFLEX spectrometer (Bruker−Franzen Analytik) equipped with a pulsed nitrogen laser (337 nm), operating in positive-ion reflector mode, and using 19 kV acceleration voltage. Matrices (α-cyanocinnamic acid) were prepared at 5 mg/mL in THF. Analytes were dissolved at concentrations between 0.1 and 5 mg/mL in THF or chloroform. − Elemental analyses were determined at the Servei d′Anàlisi Química de la Universitat Autònoma de Barcelona.

(*E,E,E*)-1,6,11-Tris[(4-methylphenyl)sulfonyl]-1,6,11-triazacyclopentadeca-3,8,13-trienepalladium(0) (2a-Pd^0): A solution of macrocycle **1a** (0.150 g, 0.125 mmol) and tetrakis(triphenylphosphane)palladium(0) (0.100 g, 0.150 mmol) in tetrahydrofuran (4 mL) was refluxed for 24 h. More tetrakis(triphenylphosphane)palladium(0) (0.50 g, 0.75 mol) was then added and the reflux continued for a further 24 h. The solvent was then evaporated and the residue was passed through a silica gel column with hexane/ethyl acetate/dichloromethane (2:1:1) as eluent to afford **2a-Pd^0** (0.164 g, 95%) as a solid, m.p. 237−240 °C (dec). − IR (KBr): $\tilde{\nu}$ = 1340, 1162, 1094, 904, 657 cm^{-1}. − ^{1}H NMR (250 MHz, $CDCl_3$): δ = 1.60 (m, 2 H), 1.63 (dd, *J* = 14.3 and 10.7 Hz, 2 H), 2.39 (s, 9 H), 2.79 (t, *J* = 11.7 Hz, 2 H), 3.07 (dd, *J* = 14.2 and 11.3 Hz, 2 H), 3.75 (d, *J* = 8.9 Hz, 2 H), 3.93−4.03 (m, 2 H), 4.62 (d, *J* = 14.0 Hz, 2 H), 4.64 (d, *J* = 14.3 Hz, 2 H), 4.78 (d, *J* = 14.3 Hz, 2 H), 7.28 (d, *J* = 8.2, 6 H), 7.64 (d, *J* = 8.2 Hz, 4 H), 7.71 (d, *J* = 8.2 Hz, 2 H). − ^{13}C NMR (62.5 MHz, $CDCl_3$): δ = 21.5, 45.1, 48.2, 49.5, 78.5, 78.7, 82.8, 127.0, 127.2, 129.8, 135.2, 136.1, 143.4, 143.6. − MALDI-TOF MS: *m/z* (%) = 774.9 [M]$^+$, 798.1 [M + Na]$^+$, 813.9 [M + K]$^+$. − $C_{33}H_{39}N_3O_6PdS_3{\cdot}CH_2Cl_2$ (861.2): calcd. C 47.42, H 4.80, N 4.88, S 11.15; found C 47.47 and 47.46, H 4.82 and 4.80, N 4.71 and 4.67, S 10.76 and 10.89.

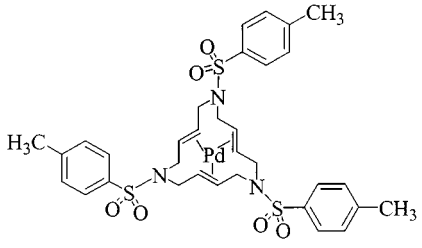

2a-Pd(0)

(*E,E,E*)-1,6,11-Tris[(4-methylphenyl)sulfonyl]-1,6,11-triazacyclopentadeca-3,8,13-trieneplatinum(0) (2a-Pt^0): A solution of macrocycle **1a** (0.186 g, 0.149 mmol) and tetrakis(triphenylphosphane)platinum(0) (0.186 g, 0.149 mmol) in tetrahydrofuran (6 mL) was refluxed for 144 h. The solvent was then evaporated and the residue was passed through a silica gel column with hexane/ethyl acetate/dichloromethane (2:1:1) as eluent to afford **2a-Pt^0** (0.078 g, 60%) as a solid, m.p. 260−263 °C (dec., change of crystalline structure at 168−172 °C). − IR (KBr): $\tilde{\nu}$ = 1340, 1162, 1092, 909, 661 cm^{-1}. − ^{1}H NMR (250 MHz, $CDCl_3$): δ = 1.34−1.46 (m, 4 H), 2.07 (td, *J* = 13.3 and 2.3 Hz, 2 H), 2.40 (s, 9 H), 2.98 (dd, *J* = 13.6 and 11.5 Hz, 2 H), 3.22−3.25 (m, 2 H), 3.41 (td, *J* = 11.6 and 3.8 Hz, 2 H), 4.58 (dd, *J* = 13.6 and 3.8 Hz, 2 H), 4.62 (d, *J* = 12.0 Hz, 2 H), 5.02 (d, *J* = 12.7 Hz, 2 H), 7.26 (d, *J* = 8.2 Hz, 6 H), 7.62 (d, *J* = 8.2 Hz, 4 H), 7.65 (d, *J* = 8.2 Hz, 2 H). − ^{13}C NMR (62.5 MHz, $CDCl_3$): δ = 21.5, 44.3, 47.2, 48.5, 62.7, 63.2, 69.0, 127.0, 127.2, 129.8, 135.0, 136.0, 143.4, 143.6. − MALDI-TOF MS: *m/z* (%) = 864.9 [M]$^+$, 887.9 [M + Na]$^+$, 903.9 [M + K]$^+$. − $C_{33}H_{39}N_3O_6PtS_3{\cdot}CH_2Cl_2$ (949.9): calcd. C 43.00, H 4.35, N 4.42, S 10.11; found C 43.57, H 4.07, N 4.15, S 9.73.

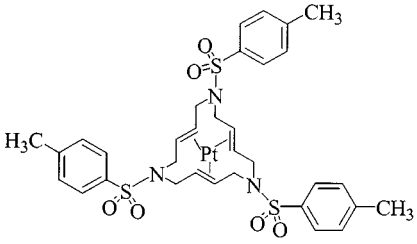

2a-Pt(0)

(*E,E,E*)-1,6,11-Tris[(4-methylphenyl)sulfonyl]-1,6,11-triazacyclopentadeca-3,8,13-trienesilver(I) Tetrafluoroborate (2a-Ag^{I}BF$_4$): A solution of macrocycle **1a** (0.300 g, 0.45 mmol) and silver tetrafluoroborate (0.216 g, 0.90 mmol) in acetone (12 mL) was stirred for 5 min. at room temperature and the mixture was then left for 20 h. The formed precipitate was filtered off to afford **2a-Ag^{I}BF$_4$** as a white solid (0.200 g, 54%), m.p. 206−208 °C (dec). − IR (KBr): $\tilde{\nu}$ = 1700, 1392, 1349, 1165, 1092, 1058, 1009, 939, 904, 815, 754, 659 cm^{-1}. − ^{1}H NMR (250 MHz, $CDCl_3$): δ = 2.44 (s, 9 H), 3.75 (s, 12 H), 5.74 (s, 6 H), 7.33 (d, *J* = 7.9 Hz, 6 H), 7.66 (d, *J* = 7.9 Hz, 6 H). − MALDI-TOF MS: *m/z* (%) = 776.1 [M of cation]$^+$, 692.2 [M − Ag + Na]$^+$. − $C_{33}H_{39}AgBF_4N_3O_6S_3{\cdot}CH_3COCH_3$ (922.6): calcd. C 46.87, H 4.92, N 4.55, S 10.42; found C 46.91 and 46.90, H 4.98 and 4.89, N 4.71 and 4.60, S 10.52 and 10.48.

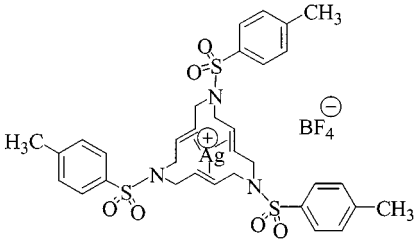

2a-Ag(I)BF$_4$

(*E,E,E*)-1,6,11-Tris[(2,4,6-triisopropylphenyl)sulfonyl]-1,6,11-triazacyclopentadeca-3,8,13-trienepalladium(0) (2b-Pd^0): This compound was prepared as for **2a-Pd^0** according to ref.[5]

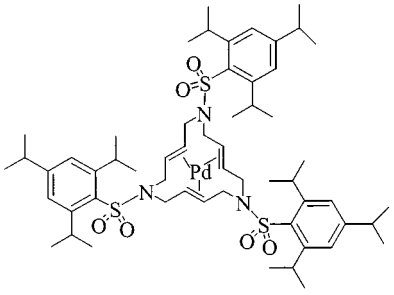

2b-Pd(0)

(*E,E,E*)-1,6,11-Tris[(2,4,6-triisopropylphenyl)sulfonyl]-1,6,11-triazacyclopentadeca-3,8,13-trieneplatinum(0) (2b-Pt^0): A solution of macrocycle **1b** (0.083 g, 0.08 mmol) and tetrakis(triphenylphosphane)platinum(0) (0.200 g, 0.17 mmol) in DMF (2.5 mL) was heated at 130 °C for four days. The solvent was then distilled off at reduced pressure and the residue was passed through a column of silica gel with hexane/ethyl acetate (5:1) as eluent to afford **2b-Pt^0** (0.07 g, 70%) as a white solid, m.p. 286−287 °C (dec). − IR (KBr): $\tilde{\nu}$ = 2960, 1601, 1461, 1427, 1363, 1315, 1262, 1151, 1103, 1047 cm^{-1}. − ^{1}H NMR (250 MHz, $CDCl_3$): δ = 1.20−1.26 (m, 54 H), 1.84 (m, 4 H), 2.49 (t, *J* = 11.1 Hz, 2 H), 2.89 (septet, *J* = 6.9 Hz, 3 H), 3.14 (t, *J* = 11.1 Hz, 2 H), 3.38 (d, *J* = 8.6 Hz, 2 H), 3.58 (dt, *J* = 12.5 and 3.8 Hz, 2 H), 4.17 (septet, *J* = 6.8 Hz, 6 H), 4.36−4.40 (m, 2 H), 4.45 (d, *J* = 14.7 Hz, 2 H), 4.82 (d, *J* = 12.4 Hz, 2 H), 7.16 (s, 6 H). − ^{13}C NMR (62.5 MHz, $CDCl_3$): δ = 23.5, 24.8, 29.3, 34.2, 43.1, 45.6, 47.0, 62.9, 63.4, 69.7, 123.9, 131.3, 151.4, 153.2. − MALDI-TOF MS: *m/z* (%) = 1201.3 $[M]^+$, 935.1 $[M - SO_2Ar]^+$, 667.6 $[M - 2SO_2Ar]^+$. − $C_{57}H_{87}N_3O_6PtS_3$ (1201.6): calcd. C 56.98, H 7.30, N 3.50, S 8.00; found C 56.97 and 56.91, H 7.18 and 7.27, N 3.52 and 3.48, S 7.85 and 7.83.

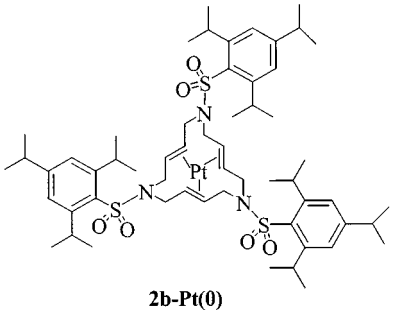

2b-Pt(0)

(*E,E,E*)-1,6,11-Tris[(2,4,6-triisopropylphenyl)sulfonyl]-1,6,11-triazacyclopentadeca-3,8,13-trienesilver(I) Tetrafluoroborate (2b-Ag^{I}BF$_4$): A solution of macrocycle **1b** (0.100 g, 0.1 mmol) and silver tetrafluoroborate (0.020 g, 0.1 mmol) in acetone (0.5 mL) was refluxed for 5 h in a round-bottomed flask kept in the dark. The solvent was eliminated by passing a stream of nitrogen though the flask to afford complex **2b-Ag^{I}BF$_4$** quantitatively: This compound was not stable to further purification procedures. M.p. 213−216 °C (dec). − IR (KBr): $\tilde{\nu}$ = 2960, 1602, 1464, 1428, 1364, 1322, 1154, 1108, 1041, 997 cm^{-1}. − ^{1}H NMR (250 MHz, $CDCl_3$, at 328 K): δ = 1.22 (m, 54 H), 2.87 (septet, *J* = 7.0, 3 H), 3.75−4.10 (m, 18 H), 6.06 (br. s, 6 H), 7.15 (s, 6 H). − ^{13}C NMR (62.5 MHz, $CDCl_3$): δ = 23.5, 24.7, 29.4, 34.2, 47.3, 123.7, 123.9, 124.2, 130.1, 151.6, 153.8. − MALDI-TOF MS: *m/z* (%) = 1112.5 [M of cation]$^+$.

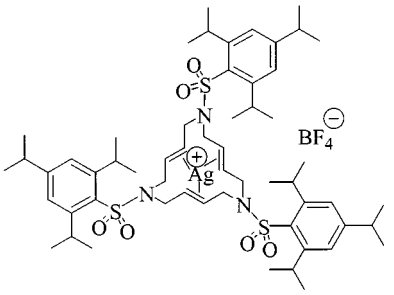

2b-Ag(I)BF$_4$

(*E,E,E*)-1,6-Bis[(3-perfluorooctylphenyl)sulfonyl]-11-[(2,4,6-triisopropylphenyl)sulfonyl]-1,6,11-triazacyclopentadeca-3,8,13-trienepalladium(0) (2c-Pd^0): A solution of macrocycle **1c** (1.920 g, 1.21 mmol) and bis(dibenzylideneacetone)palladium(0) (0.760 g, 1.33 mmol) in tetrahydrofuran (60 mL) was maintained at room temperature for 24 h. The mixture was filtered, the solvent was removed from the filtrate in vacuo and the residue was washed with hexane and passed through a silica gel column with hexane/ethyl acetate (10:1) as eluent to afford **2c-Pd^0** (1.95 g, 95%) as a solid, m.p. 141−142 °C (dec). − IR (KBr): $\tilde{\nu}$ = 1351, 1240, 1212, 1162, 1117, 908, 658 cm^{-1}. − ^{1}H NMR (250 MHz, $CDCl_3$, α+β forms): δ = 1.21 (m, 18 H), 1.5−1.9 (m, 2 H), 1.95−2.2 (m, 2 H), 2.72 (bt, *J* ≈ 12.4 Hz), 2.85−3.00 (m) and 3.0−3.3 (m) (the three groups of signals, 6 H), 3.7−4.0 (m, 2 H), 4.0−4.3 (m, 3 H), 4.47 (bt, *J* ≈ 15 Hz, 2 H), 4.68 (bt, *J* ≈ 14 Hz, 2 H), 4.83 (bd, *J* ≈ 15 Hz, 2 H), 7.07, 7.12, and 7.19 (three s, 2 H), 7.40−7.45 (m, 2 H), 7.6−7.85 (m, 4 H), 7.95−8.1 (m, 2 H). − ^{13}C NMR (62.5 MHz, $CDCl_3$, α+β forms): δ = 23.5, 24.7, 24.8, 29.3, 34.1, 43.7, 45.2, 45.4, 46.3, 47.6, 48.2, 49.3, 49.5, 77.6, 77.9, 78.6, 78.8, 79.7, 79.9, 81.9, 82.8, 84.4, 123.9−153.4 (m). − MALDI-TOF MS: *m/z* (%) = 1695.1 $[M]^+$, 1718.1 $[M + Na]^+$, 1734.1 $[M + K]^+$. − $C_{55}H_{49}F_{34}N_3O_6PdS_3$ (1696.6): calcd. C 38.94, H 2.91, N 2.48, S 5.67; found C 39.03 and 39.02, H 3.18 and 3.30, N 2.45 and 2.44, S 5.47 and 5.42.

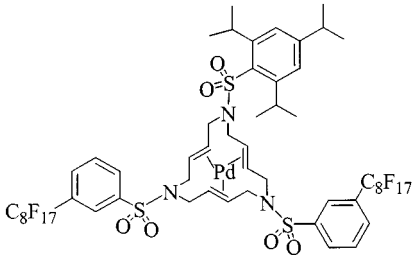

2c-Pd(0)

(*E,E,E*)-1,6,11-Tris[(5-dimethylaminonaphthyl)sulfonyl]-1,6,11-triazacyclopentadeca-3,8,13-trienepalladium(0) (2d-Pd^0): A solution of macrocycle **1d** (0.180 g, 0.20 mmol) and bis(dibenzylideneacetone)-palladium(0) (0.127 g, 0.22 mmol) in tetrahydrofuran (10 mL) was refluxed for 5 h. The mixture was filtered, the solvent was removed from the filtrate in vacuo and the solid residue (0.270 g) was passed through a silica gel column with hexane/ethyl acetate (8:2) as eluent to afford dibenzylideneacetone (0.054 g) and **2d-Pd^0** (0.180 g, 89%) as a solid, m.p. 167−169 °C (hexane/ethyl acetate). − IR (KBr): $\tilde{\nu}$ = 2940, 2832, 1574, 1457, 1401, 1322, 1144, 1068, 938, 903, 833, 789, 750 cm^{-1}. − UV/Vis (THF): λ (log ε) = 340 (4.11), 254 (4.61). − ^{1}H NMR (250 MHz, $CDCl_3$): δ = 1.86−2.02 (m, 4 H), 2.85−2.86 (two s, 18 H), 2.93−2.98 (m, 2 H), 3.18 (dd, *J* = 14.0 and 10.7 Hz, 2 H), 3.79−3.82 (m, 2 H), 4.01−4.12 (m, 2 H), 4.63 (t, *J* ≈ 13.5 Hz, 4 H), 4.89 (d, *J* ≈ 13.5 Hz, 2 H), 7.15 (dd, *J* = 7.5

Table 3. The crystal data and structure refinement for **2a-Pd^0** and **2a-Pt^0**

	2a-Pd^0	**2a-Pt^0**
Formula	$C_{34}H_{41}Cl_2N_3O_6PdS_3$	$C_{34}H_{41}Cl_2N_3O_6PtS_3$
Molecular weight	861.18	949.87
Crystal size [mm]	0.53 × 0.23 × 0.21	0.39 × 0.16 × 0.07
Crystal system	Orthorhombic	Monoclinic
Space group	$P2_12_12_1$	$P2_1/c$
a [Å]	11.1844 (13)	17.15 (9)
b [Å]	17.1818(12)	11.199 (10)
c [Å]	19.713(3)	19.74 (4)
β [°]	–	90.03 (2)
V [Å^3]	3788 (2)	3793 (2)
Z	4	4
ρ_{calc} [Mg m^{-3}]	1.510	1.663
Temperature [K]	293 (2)	293 (2)
F(000)	1768	1896
Wavelength [Å]	Mo-K_α, 0.710739	Mo-K_α, 0.710739
Absorption coefficient [mm^{-1}]	0.843	4.052
hkl range	−13/13, 0/20, 0/23	−20/20, 0/13, 0/23
Reflections collected	6633	6658
Data/restraints/parameters	6633 / 69/442	6658/5/460
Goodness of fit on F^2	1.087	0.976
Final R indices [$I > 2\sigma(I)$]	$R1$ = 0.0667	$R1$ = 0.0622
	$wR2$ = 0.1831	$wR2$ = 0.1091
R indices (all data)	$R1$ = 0.0956	$R1$ = 0.1370
	$wR2$ = 0.2018	$wR2$ = 0.1228
Largest diff. peak and hole	1.378/−0.861	0.838/−1.220

and 5.7 Hz, 3 H), 7.48−7.56 (m, 6 H), 8.19 (dd, J = 7.5 and 1.4 Hz, 3 H), 8.24−8.31 (m, 3 H), 8.53 (br. d, J = 8.2 Hz, 3 H). – ^{13}C NMR (62.5 MHz, $CDCl_3$): δ = 14.5, 22.7, 34.5, 45.1, 45.8, 48.0, 49.2, 79.6, 79.8, 83.9, 115.7, 119.6, 123.6, 128.6, 130.3, 130.4, 130.8, 131.0, 134.9, 152.3. – MALDI-TOF MS: m/z (%) = 1012.5 [M]$^+$, 929.7 [M − Pd + Na]$^+$. – $C_{48}H_{54}N_6O_6PdS_3$ (1013.6): calcd. C 56.88, H 5.37, N 8.29; found C 57.34 and 57.31, H 5.38 and 5.49, N 7.96 and 8.19.

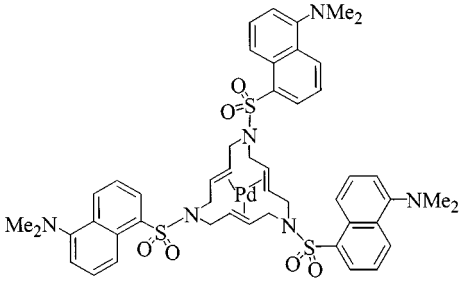

2d-Pd(0)

X-ray Analysis of 2a-Pd^0 and 2a-Pt^0. Data Collection and Processing: Crystal data and experimental conditions for the two complexes are listed in Table 3. The collected reflections were corrected for Lorentz, polarization and absorption effects [empirical Difabs, max. and min. transmission were 0.8669−0.3950 for **2a-Pd^0**, and 0.5907−0.3170 for **2a-Pt^0**]. The lattice constants were determined by least-squares fitting of the setting angles of 25 reflections. Data were recorded using the ω-2θ scan mode up to a 2θ of 49.98 for **2a-Pd^0** and 50.02 for **2a-Pt^0**.

The structure was solved by direct methods using SHELXS-97 and refined by full-matrix least-squares methods on F^2 over the complete set of data using SHELXL-97. Anisotropic thermal parameters were refined for the non-hydrogen atoms and the hydrogen atoms were introduced in calculated positions.

Crystallographic data (excluding structure factors) for the structures reported in this paper have been deposited with the Cambridge Crystallographic data center as supplementary publications nos. CCDC-150655 and -150656 for **2a-Pd^0** and **2a-Pt^0**, respectively. Copies of the data can be obtained free of charge on application to CCDC, 12 Union road, Cambridge CB2 1EZ, UK [Fax: (internat.) +44-1223/336-033; E-mail: deposit@ccdc.cam.ac.uk].

Acknowledgments

Financial support from MEC of Spain (projects PB93−0896 and PB98−0902), and from CIRIT-Generalitat de Catalunya (projects 98SGR0056 and 2000SGR0062, and predoctoral scholarships to J. C., S. C., and J. T.) is gratefully acknowledged.

[1] For a general monograph on macrocyclic compounds, see: B. Dietrich, P. Viout, J.-M. Lehn, *Aspects de la Chimie des Composés Macrocycliques*, InterEditions/Editions de CNRS, Paris, **1991**.

[2] For a review on nitrogen-bridged macrocycles, see: H. Takemura, T. Shinmyozu, T. Inazu, *Coord. Chem. Rev.* **1996**, *156*, 183−200.

[3] [3a] A. S. Ripka, R. S. Bohacek, D. H. Rich, *Bioorg. Med. Chem. Lett.* **1998**, *8*, 357−360. – [3b] W. P. D. Goldring, L. Weiler, *Org. Lett.* **1999**, *1*, 1471−1473.

[4] S. Cerezo, J. Cortès, J.-M. López-Romero, M. Moreno-Mañas, T. Parella, R. Pleixats, A. Roglans, *Tetrahedron* **1998**, *54*, 14885−14904.

[5] J. Cortès, M. Moreno-Mañas, R. Pleixats, *Eur. J. Org. Chem.* **2000**, 239−243.

[6] S. Cerezo, J. Cortès, D. Galvan, E. Lago, C. Marchi, E. Molins, M. Moreno-Mañas, R. Pleixats, J. Torrejón, A. Vallribera, *Eur. J. Org. Chem.* **2001**, 329−337.

[7] [7a] Y. Takahashi, T. Ito, S. Sakai, Y. Ishii, *Chem. Commun.* **1970**, 1065−1066. − [7b] K. Moseley, P. M. Maitlis, *Chem. Commun.* **1971**, 982−983. − [7c] T. Ukai, H. Kawazura, Y. Ishii, J. J. Bonnet, J. A. Ibers, *J. Organomet. Chem.* **1974**, *65*, 253−266. − [7d] C. G. Pierpont, M. C. Mazza, *Inorg. Chem.* **1974**, *13*, 1891−1895.

[8] For silver: [8a] G. van Kotten, J. G. Noltes, in *Comprehensive Organometallic Chemistry I, Vol. 2* (Eds.: E. W. Abel, F. G. A. Stone, and G. Wilkinson), Pergamon Press, New York, **1982**, pp. 709−763. − [8b] G. van Koten, S. L. James, J. T. B. H. Jastrzebski, in *Comprehensive Organometallic Chemistry II, Vol. 3* (Eds.: E. W. Abel, F. G. A. Stone, and G. Wilkinson), Pergamon Press, New York, **1995**, pp. 57−133. For palladium: [8c] P. M. Maitlis, P. Espinet, M. J. H. Russell, in *Comprehensive Organometallic Chemistry I, Vol. 6*, pp. 243−263. − [8d] J. A. Davies, in *Comprehensive Organometallic Chemistry II, Vol. 9*, pp. 291−390. For platinum: [8e] F. R. Hartley, in *Comprehensive Organometallic Chemistry I, Vol. 6*, pp. 471−762. − [8f] G. Brent-Young, in *Comprehensive Organometallic Chemistry II, Vol. 6*, pp. 533−588.

[9] For a recent example, see: S. Porth, J. W. Bats, D. Trauner, G. Giester, J. Mulzer, *Angew. Chem.* **1999**, *111*, 2159−2161; *Angew. Chem. Int. Ed.* **1999**, *38*, 2015−2016.

[10] For a recent general preparation of palladium(0) complexes of 1,6-dienes, see: J. Krause, G. Cestaric, K.-J. Haack, K. Seevogel, W. Storm, K.-R. Pörschke, *J. Am. Chem. Soc.* **1999**, *121*, 9807−9823.

[11] [11a] G. Wilke, *Angew. Chem.* **1988**, *100*, 189−211; *Angew. Chem. Int. Ed. Engl.* **1988**, *27*, 185−206. − [11b] D. J. Brauer, C. Krüger, *J. Organomet. Chem.* **1972**, *44*, 397−402. − [11c] R. Pörschke, W. Kleimann, Y.-H. Tsay, C. Krüger, G. Wilke, *Chem. Ber.* **1990**, *123*, 1267−1273. − [11d] R. Taube, S. Wache, J. Sieler, R. Kempe, *J. Organomet. Chem.* **1993**, *456*, 131−136. − [11e] R. Taube, S. Wache, J. Sieler, *J. Organomet. Chem.* **1993**, *459*, 335−347. − [11f] D. J. Brauer, C. Krüger, J. C. Sekutowski, *J. Organomet. Chem.* **1979**, *178*, 249−260.

[12] [12a] R. G. Salomon, J. K. Kochi, *J. Organomet. Chem.* **1972**, *43*, C7−C10. − [12b] R. G. Salomon, J. K. Kochi, *J. Chem. Soc., Chem. Commun.* **1972**, 559−560. − [12c] R. G. Salomon, J. K. Kochi, *J. Am. Chem. Soc.* **1973**, *95*, 1889−1897. − [12d] R. G. Salomon, J. K. Kochi, *J. Organomet. Chem.* **1974**, *64*, 135−143. − [12e] Y. L. Chow, X. Cheng, G. E. Buono-Core, *Organometallics* **1987**, *6*, 1126−1129.

[13] E. Balbolov, S. D. Dimitrov, *React. Kinet. Catal. Lett.* **1997**, *62*, 305−311.

[14] G. S. Lewandos, D. K. Gregston, F. R. Nelson, *J. Organomet. Chem.* **1976**, *118*, 363−374.

[15] E. A. Zuech, US. Patent 3,956,177, **1976** [*Chem. Abst.* **1976**, *85*, 37669].

[16] K. Ishimi, M. Iwase, E. Tanaka, M. Idai, Y. Uchida, *Yukagaku* **1974**, *23*, 408−411 [*Chem. Abst.* **1974**, *81*, 169878].

[17] [17a] J. D. Ferrara, C. Tessier-Youngs, W. J. Youngs, *J. Am. Chem. Soc.* **1985**, *107*, 6719−6721. − [17b] J. D. Ferrara, A. A. Tanaka, C. Fierro, C. A. Tessier-Youngs, W. J. Youngs, *Organometallics* **1989**, *8*, 2089−2098.

[18] R. Faure, H. Loiseleur, G. Haufe, H. Trauer, *Acta Crystallogr., Sect. C* **1985**, *41*, 1593−1595.

[19] [19a] C. Cohen-Addad, P. Baret, P. Chautemps, J.-L. Pierre, *Acta Crystallogr., Sect. C* **1983**, *39*, 1346−1349. − [19b] H. C. Kang, A. W. Hanson, B. Eaton, V. Boekelheide, *J. Am. Chem. Soc.* **1985**, *107*, 1979−1985. − [19c] F. R. Heirtzler, H. Hopf, P. G. Jones, P. Bubenitschek, *Tetrahedron Lett.* **1995**, *36*, 1239−1242. − [19d] F. R. Heirtzler, H. Hopf, P. G. Jones, P. Bubenitschek, *Chem. Ber.* **1995**, *128*, 1079−1082. − [19e] P. G. Jones, P. Bubenitschek, F. Heirtzler, H. Hopf, *Acta Crystallogr., Sect. C* **1996**, *52*, 1380−1384. − [19f] P. G. Jones, F. Heirtzler, H. Hopf, *Acta Crystallogr., Sect. C* **1996**, *52*, 1384−1388.

[20] M. Iyoda, Y. Kuwatani, T. Yamauchi, M. Oda, *J. Chem. Soc., Chem. Commun.* **1988**, 65−66.

Received February 26, 2001
[I01067]

Synthesis and Properties of 1,2-Dichlorodisilane and 1,1,2-Trichlorodisilane

Andreas Gupper[a] and Karl Hassler*[a]

Keywords: Silanes / NMR spectroscopy / IR spectroscopy / Raman spectroscopy / Isomers

The previously unknown disilanes 1,1,2-trichlorotri(1-naphthyl)disilane and 1,2-dichlorotetra(1-naphthyl)disilane were prepared by the reaction of 1-lithionaphthalenide with hexachlorodisilane. Reduction with $LiAlH_4$ afforded 1,1,2-tri(1-naphthyl)disilane. Treatment of 1,2-di(1-naphthyl)disilane and 1,1,2-tri(1-naphthyl)disilane with liquid hydrogen chloride gave ClH_2SiSiH_2Cl and $ClH_2SiSiHCl_2$ in quantitative yields, along with naphthalene. The chlorodisilanes were easily separated and purified by fractional condensation. Both disilanes are stable for weeks at room temperature, but undergo rapid H/Cl exchange reactions and SiSi cleavage upon the addition of traces of catalysts such as $AlCl_3$. The ^{29}Si chemical shifts and $J(^{29}Si,^{1}H)$ coupling constants, including those of ClH_2SiSiH_3 and $Cl_2HSiSiH_3$, are reported. The infrared and Raman vibrational spectra clearly prove that both chlorodisilanes comprise mixtures of *gauche* and *anti* rotamers in the liquid state.

Introduction

The chemical properties of hydridohalodisilanes $Si_2H_nX_{6-n}$ (X = F, Cl, Br and I) differ considerably from those of their carbon analogues $C_2H_nX_{6-n}$. First, the polarities of the SiH and CH bonds are opposite ($Si^{\delta+}H^{\delta-}$ vs. $C^{\delta-}H^{\delta+}$), and second the silicon atom easily forms transition states with coordination numbers >4 because of its larger size. Therefore, hydridohalosilanes easily react with water forming Si−O−Si linkages and hydrogen halides HX. In contrast to the halogenated ethanes, the activation energy for the reaction of halosilanes with oxygen is very low, making them spontaneously inflammable on contact with air. In addition, they are very prone to undergo halogen/hydrogen exchange reactions, which is not the case for the haloethanes.

The combination of these properties makes the synthesis and the handling of the compounds a difficult task. Earlier attempts focused on the reaction of disilane Si_2H_6 with various halogenating agents. For chlorodisilanes, HCl,[1−3] Cl_2,[4] BCl_3,[5−8] AgCl[3] or $SnCl_4$ [9] were used. Not unexpectedly, mixtures of chlorodisilanes were obtained that were difficult or even impossible to separate. Methods which avoided Si_2H_6 as a starting material comprised the reaction of monoiododisilane with AgCl,[10] the reaction of $SiCl_2H_2$ in an electrical discharge[11,12] or the electrophilic cleavage of the Si-phenyl bonds of tetraphenyldisilane (and other phenyldisilanes) with HCl/$AlCl_3$.[13] By these procedures, only Si_2H_5Cl could be obtained in pure form and in preparative quantities. The reaction of tetraphenyldisilane with HCl/$AlCl_3$ [13] had the disadvantage that the benzene which formed simultaneously could not be separated from the tetrachlorodisilane. In 1979, the isolation of pentachlorodisilane from a mixture of chlorosilanes obtained as a by-product of the thermal decomposition of $HSiCl_3$ for the generation of ultrapure semiconductor-grade silicon was reported.[14]

HBr and HI,[15,2,16] Br_2 [4] and I_2,[17,18] as well as BBr_3 and BI_3,[8,19] have all been used for the bromination or iodination of disilane. Monobromodisilane and monoiododisilane could be successfully prepared and purified, but not disilanes with a number of halogen atoms exceeding one.

Synthetic strategies for the preparation of fluorodisilanes comprised reactions of difluorosilylene SiF_2 with H_2S,[20] B_2H_6,[21] HBr[22] or PH_3,[23] as well as the selective reduction of bromofluorodisilanes such as $F_3SiSiHBr_2$ with Me_3SnH[24] or halogen exchange with SbF_3 [8] or ZnF_2.[25] So far, FSi_2H_5,[26] F_3SiSiH_3,[21,24] F_5Si_2H[22] and $F_2HSiSiHF_2$ [25] have been synthesised by these procedures.

In our group we have focused on the electrophilic cleavage of silicon-aryl bonds by HCl, HBr or HI:

$$\text{Si-Aryl} + HX \rightarrow Si{-}X + \text{ArylH} \quad (1)$$

Under appropriate conditions, SiH functionalities are not attacked and the method can be used for the synthesis of a variety of bromo- and iododisilanes $X_nSi_2H_{6-n}$,[27] as well as bromo- and iodotrisilanes $X_nSi_3H_{8-n}$.[28] If the boiling points of the disilanes and trisilanes differ considerably from that of benzene, hydridophenyldisilanes and -trisilanes can be used as starting materials as their synthesis poses the least problems.[29] In all other cases, the introduction of larger aryl groups such as mesityl or naphthyl seems indispensable. For instance, 1,1,2,2-tetrachlorodisilane can be prepared from 1,1,2,2-tetramesityldisilane,[25] and 1,2-dibromodisilane from 1,2-di(1-naphthyl)disilane.[30] The disilanes can then be purified simply by distillation or fractional condensation. The disadvantage with this approach is that for the preparation of naphthyldisilanes and naphthyltrisilanes the coupling reaction of chloronaphthylmonosilanes with alkali metals is not an appropriate method due to side

[a] Institute of Inorganic Chemistry, Technical University, Stremayrgasse 16, 8010 Graz, Austria
Fax: (internat.) +43-316/873-8701
E-mail: hassler@anorg.tu-graz.ac.at

 © WILEY-VCH Verlag GmbH, 69451 Weinheim, 2001 1434−1948/01/0808−2007 $ 17.50+.50/0

reactions at the aryl group. Similar problems are encountered with mesityl groups due to their increased bulkiness.

In a previous paper we reported on the synthesis of pentachloro(1-naphthyl)disilane and tetrachloro-1,2-di(1-naphthyl)disilane from hexachlorodisilane and naphthyllithium.[31] This method can be expanded for the preparation of tri- and tetranaphthyldisilanes as well, which in turn can be used for the preparation of the title hydridochlorodisilanes.

Results and Discussion

(1-Naphthyl)disilanes

The two most convenient methods for the preparation of arylated disilanes are the reductive coupling of the appropriate arylhalomonosilanes with Li, Na, K and Mg and the reaction of silyllithium, -sodium or -potassium compounds with arylhalosilanes. Unfortunately, neither method can be used for the synthesis of naphthyldisilanes as the naphthyl group easily reacts with alkali metals leading to a large number of badly defined products.

These difficulties can be circumvented by the use of naphthyllithium which, under appropriate conditions, reacts with hexachlorodisilane (although not without appreciable Si−Si bond cleavage) to form naphthylpentachlorodisilane and 1,2-dinaphthyltetrachlorodisilane:[31]

$$Si_2Cl_6 + LiC_{10}H_7 \rightarrow (C_{10}H_7)Cl_2SiSiCl_3 \quad (2)$$

$$Si_2Cl_6 + 2\,LiC_{10}H_7 \rightarrow (C_{10}H_7)Cl_2SiSiCl_2(C_{10}H_7) \quad (3)$$

Increasing the stoichiometric ratio of $LiC_{10}H_7$ vs. Si_2Cl_6 allows the preparation of 1,1,2-trichlorotrinaphthyldisilane and 1,2-dichlorotetranaphthyldisilane in moderate yields. Appreciable quantities of trichloronaphthylsilane are formed as a by-product due to increased Si−Si bond cleavage by $LiC_{10}H_7$. Both disilanes can be separated from the reaction mixture by distillation and can be purified by fractional crystallization. They are easily reduced with lithium aluminum hydride to give the corresponding naphthylhydridosilanes in nearly quantitative yields.

Chlorodisilanes

The arylated disilanes $Ar_nSi_2H_{6-n}$ are the most suitable precursors for the preparation of the halodisilanes $X_nSi_2H_{6-n}$ as the aryl groups are easily replaced by halogen atoms X (X = Cl, Br and I) upon reaction with either the liquefied hydrogen halides HX or solutions of HX in benzene. The latter method has the disadvantage that small quantities of $AlCl_3$ have to be used as a catalyst and this cannot usually be removed completely from the halodisilane. Furthemore, traces of $AlCl_3$ also catalyse halogen/hydrogen exchange reactions and Si−Si bond cleavage, thereby leading to a rapid decomposition of the disilanes. With iodine and bromine these reactions are quite slow and the disilanes can be stored at −70 °C for several weeks without any appreciable decomposition. For chlorodisilanes, disproportionation occurs quickly. Therefore, the chlorodisilanes described herein were prepared by the reaction of the naphthyldisilanes with liquefied HCl in a sealed tube. For instance, ClH_2SiSiH_2Cl prepared this way can be stored for weeks at room temperature without any decomposition.

^{29}Si NMR spectra

Table 1 and 2 summarize the ^{29}Si chemical shifts (ppm against tetramethylsilane) and $J(^{29}Si,^{1}H)$ coupling constants (Hz) for the naphthyldisilanes and chlorodisilanes, respectively. The data for 1,1,1,3-tetrachlorodinaphthyldisilane and 1,1-dichlorodisilane have been included as these molecules were also identified in the reaction mixtures. Chlorodisilane ClH_2SiSiH_3 was also prepared for NMR spectroscopic purposes; the chemical shifts and coupling constants for related disilanes described elsewhere have been included, too.

Table 1. ^{29}Si NMR chemical shifts (δ_{Si} vs. TMS) and $J(^{29}Si,^{1}H)$ coupling constants (Hz) of (1-naphthyl)chlorodisilanes and (1-naphthyl)disilanes

Disilane	δSi	δSi′	$^{1}J_{SiH}$	$^{1}J_{Si'H}$	$^{3}J_{SiH}$	$^{3}J_{Si'H}$
$NaphCl_2SiSi'Cl_3$ [a]	1.8	0.6			9.6	
$Naph_2ClSiSi'Cl_3$	−1.5	7.6			7.8	
$NaphCl_2SiSiCl_2Naph$[a]	6.3				9.1	
$Naph_2ClSiSi'Cl_2Naph$	−0.5	11.8			8.7	10.8
$Naph_2ClSiSiClNaph_2$	1.2				8.0	
$NaphH_2SiSi'H_3$ [a]	−65.8	−99.4	196.2	195.7		
$Naph_2HSiSi'H_3$	−40.9	−97.6	189.7	193.0	8.9	6.0
$NaphH_2SiSiH_2Naph$[a]	−63.4		194.2		7.2	
$Naph_2HSiSi'H_2Naph$	−39.9	−61.7	190.4	191.9	7.0	7.9

[a] Taken from ref.[31]

Table 2. ^{29}Si NMR chemical shifts (δ_{Si} vs. TMS) and $J(^{29}Si,^{1}H)$ coupling constants (Hz) of chlorodisilanes

Disilane	δSi	δSi′	$^{1}J_{SiH}$	$^{1}J_{Si'H}$	$^{2}J_{SiH}$	$^{2}J_{Si'H}$
$H_3SiSi'H_2Cl$	−95.1	−27.9	203.7	226.3	12.8	6.6
$H_3SiSi'HCl_2$	−88.9	8.3	210.5	267.3	23.4	8.9
ClH_2SiSiH_2Cl	−30.3		233.4		15.8	
$Cl_2HSiSi'H_2Cl$	−0.2	−32.1	277.7	242.2	19.8	29.3
$Cl_2HSiSiHCl_2$[a]	−5.9		287.2		36.7	
$Cl_3SiSi'HCl_2$[b]	−2.2	−8.2		294.0	45.6	
$Cl_3SiSiCl_3$[c]	−6.1					

[a] Taken from ref.[25]. – [b] Taken from ref.[13] – [c] Taken from ref.[32]

Figure 1 displays the proton coupled ^{29}Si NMR spectra of chlorodisilane and 1,2-dichlorodisilane exemplifying the quality of the spectra that have been obtained. The inter-

pretation of the spectra is straightforward as all couplings are first order.

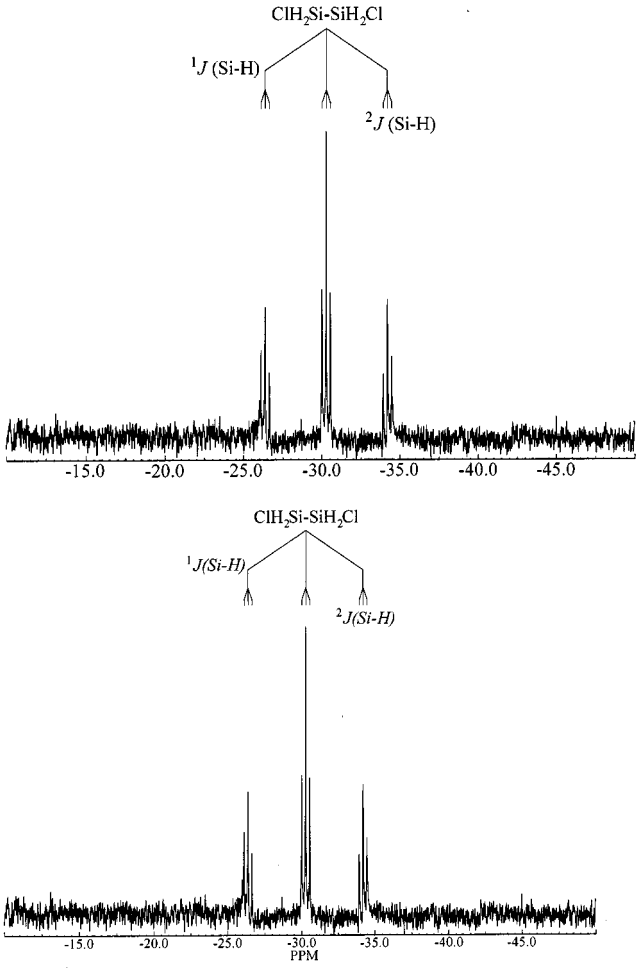

Figure 1. Proton coupled ^{29}Si NMR spectra of 1,2-dichlorodisilane (top) and chlorodisilane (bottom)

Figure 2 presents the spectrum of 1,1,2-trichlorodisilane in the range $\delta = +10$ to -40 after equilibration upon addition of $AlCl_3$. Interestingly, no 1,2-dichlorodisilane is formed. 1,1-Dichlorodisilane and 1,1,2,2-tetrachlorodisilane are readily detected, along with monosilanes such as H_3SiCl, H_2SiCl_2 and $HSiCl_3$.

From mixtures of chlorodisilanes, Söllradl and Hengge[13] deduced NMR parameters for all possible chlorodisilanes. The data presented here agree quite well with theirs.

Infrared and Raman Vibrational Spectra

Infrared and Raman vibrational spectra were recorded for 1,2-dichlorodisilane and 1,1,2-trichlorodisilane. The spectra at ambient temperatures possess more lines than predicted by the selection rules based on symmetry arguments, a clear indication for rotational isomerism. The raman spectra at low temperatures confirm this prediction, as the intensity ratio of a number of pairs of bands changes with temperature. Table 3 summarizes the data that have been obtained for the gases (IR) and the liquids (Raman).

Figure 3 illustrates the effect of temperature on the Raman spectrum of 1,1,2-trichlorodisilane. For instance, the relative intensities within the line triple at 396/407/424 cm^{-1}, and of the line pairs at 209/216, 517/525 and 550/571

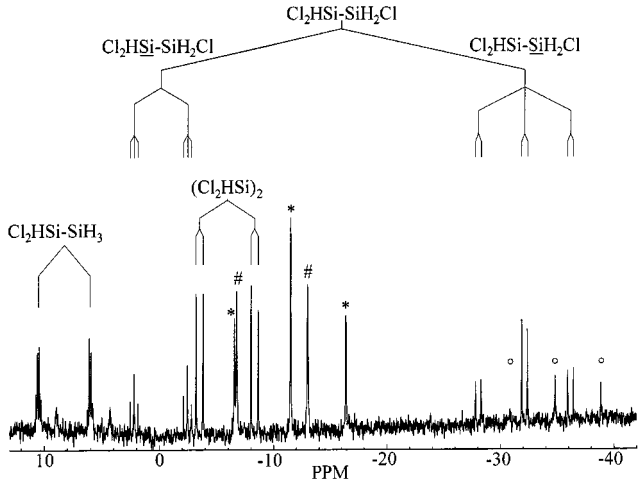

Figure 2. Proton coupled ^{29}Si NMR spectrum of 1,1,2-trichlorodisilane in the range from $\delta = +10$ to -40 after equilibration with $AlCl_3$; lines marked with ○, * and # are due to H_3SiCl, H_2SiCl_2 and $HSiCl_3$, respectively

Table 3. Absorption frequencies and assignments in the infrared spectra (gas, 2200−280 cm^{-1}) and Raman spectra (liquid, 2200−150 cm^{-1}) of 1,2-dichlorodisilane and 1,1,2-trichlorodisilane

ClH_2SiSiH_2Cl		$ClH_2SiSiHCl_2$		Assignment
IR (gas)	Raman (l)	IR (gas)	Raman (l)	
2193 s		2200 vs	2193 vs,sh	SiH stretch
2181 vs		2192 vs	2180 vs	SiH stretch
2170 s	2171 vs			SiH stretch
949 s				SiH_2 deformation
935 s	933 m	928 m	924 m,br	SiH_2 deformation
	921 m			SiH_2 deformation
	908 w			SiH_2 deformation
884 m		883 w		SiH_2 deformation
876 m	870 vw	876 s		SiH_2 deformation
843 vw	840 vw			ClSiH deformation
835 vw	832 vw	835 m	832 vw	ClSiH deformation
812 s		815 m	815 vw	ClSiH deformation
800 vs	782 vw	783 s	791 m	ClSiH deformation
766 s	757 vw		760 vw	SiH_2 twist
	702 m,b			SiH_2 twist
	691 w,sh	682 vw	688 m,br	SiH_2 twist
677 vw		621 m		SiH_2 twist
	567 vw, sh	582 vs	571 m,sh	SiCl stretch
540 m,br	540 m,br		550 s	SiCl stretch
	514 w,sh	528 s	525 w	SiCl stretch
			517 vw	SiH_2 rock
		495 vw	495 m	SiCl stretch
	441 s		424 m,sh	SiSi stretch
404 vw	411 m, sh	406 w	407 vs	SiSi stretch
	399 vs		396 vs, sh	SiSi stretch
358 w				SiH_2 rock
	308 vw			
			248 w	$SiCl_2$ deformation
			216 w,sh	$SiCl_2$ deformation
	195 vw		209 m	ClSiSi deformation
			180 m	$SiCl_2$ deformation
	157 m,br		151 s	ClSiSi deformation

cm^{-1} are clearly temperature dependent. Similar effects are observed for 1,2-dichlorodisilane. As it is impossible to accurately assign the spectra of the conformers without the help of ab initio calculations of harmonic frequencies, only approximate descriptions of the modes are given in Table 3 without any reference to individual rotamers.

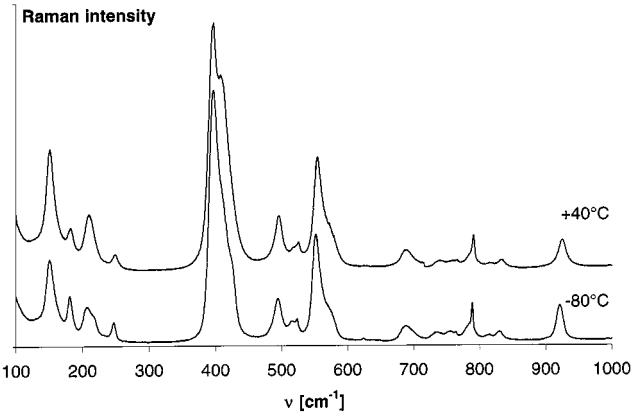

Figure 3. Raman spectra in the range $\tilde{\nu} = 100-1000\ cm^{-1}$ of 1,1,2-trichlorodisilane at two different temperatures

So far, the rotational isomerism of 1,1,2,2-tetrachlorodisilane has been examined by electron diffraction[33] and variable temperature Raman spectroscopy[34] with the result that the *gauche* conformer is found to be more stable in both the gas and the liquid phase. Ab initio calculations at various levels of theory predict the *anti* rotamer as the low energy conformer. We will report on detailed investigations of the rotational isomerism of the title molecules, including spectra of the deuterated isotopomers as well as electron diffraction experiments, in a forthcoming publication.

Experimental Section

General: Most chlorinated organosilanes are sensitive towards moisture with the formation of Si−O−Si bonds and hydrogen chloride. Furthermore, hydridochlorosilanes are also sensitive towards oxygen, many of them igniting spontaneously on contact with air. All manipulations were therefore carried out under an atmosphere of dry, oxygen-free nitrogen. All solvents were dried by distillation from potassium prior to use.

Raman spectra were recorded with a T64000 spectrometer from Jobin-Yvon, equipped with a triple monochromator. The spectra were excited with the green line (514 nm) of an Ar laser. The chlorodisilanes were condensed into 1 mm capillary glass tubes which were sealed under an inert N_2 atmosphere.

The gas-phase infrared spectra of the hydridochlorodisilanes were recorded with a Perkin−Elmer 883 spectrometer using a Perkin−Elmer gas cell with a path length of 10 cm.

NMR spectra were recorded with a Bruker MSL 300 spectrometer as solutions in mesitylene (hydridochlorodisilanes) or toluene (naphthlydisilanes) using a capillary with D_2O as an external standard. Standard pulse sequences such as INEPT were employed.

Synthesis of 1,1,2-trichlorotrinaphthyldisilane: A solution of hexachlorodisilane (45.0 g, 167.4 mmol) in 100 mL of toluene was added dropwise to a suspension of naphthyllithium in toluene [594.0 mmol; prepared from 1-bromonaphthalene (123.0 g, 594.0 mmol) and *n*-butyllithithum]. A temperature of −20 °C was maintained throughout the procedure. Upon completion, the reaction mixture was refluxed for three hours. The salts were then separated by filtration and the solvent removed by evaporation in vacuo. The liquid residue was fractionated in vacuo. All volatile products up to a temperature of 120 °C (0.01 Torr) were collected. They comprised a mixture of naphthyltrichlorosilane, pentachloronaphthyldisilane and tetrachlorodinaphthyldisilane. The residue that solidified at room temperature was found to be a mixture of 1,1,2-trichlorotrinaphthyldisilane and 1,2-dichlorotetranaphthyldisilane. Crystallization from toluene/petroleum ether (1:5) afforded 34.8 g (38%) of pure trichlorotrinaphthyldisilane. − $C_{30}H_{21}Cl_3Si_2$ (544.0): calcd. C 66.23, H 3.89; found C 66.45, H 3.86.

Synthesis of 1,1,2-Trinaphthyldisilane: The hydridodisilane was obtained in quantitative yields by standard reduction of the trichlorotrinaphthyldisilane with $LiAlH_4$ in diethyl ether. After addition of a solution of lithium aluminum hydride to the solution of the chlorodisilane at 0 °C, the reaction mixture was refluxed for several hours. Subsequently, it was added dropwise to 2 N H_2SO_4 at a temperature of 0 °C. The organic layer was then separated and the diethyl ether removed in vacuo. The residue was recrystallized from petroleum ether giving the desired product as colorless crystals. − $C_{30}H_{24}Si_2$ (440.7): calcd. C 81.76, H 5.49; found C 81.75, H 5.59.

Synthesis of 1,2-Dichlorodisilane: 1,2-Dinaphthyldisilane[31] (5.0 g) or the equivalent amount of 1,2-dimesityldisilane[35] was placed in a thick-walled glass tube. A large excess of hydrogen chloride was then condensed into the tube, which was sealed carefully. The reaction mixture was cooled to −70 °C for five hours. The glass tube was then transferred to a vacuum line and the unreacted hydrogen chloride removed very carefully. 1,2-Dichlorodisilane was then separated from naphthalene (or mesitylene) by fractional condensation, as a colorless liquid. The yield was quantitative.

Synthesis of 1,1,2-Trichlorodisilane: In a procedure completely analogous to the synthesis of 1,2-dichlorodisilane, 1,1,2-trichlorodisilane was obtained in quantitative yields from 1,1,2-trinaphthyldisilane and liquid HCl. It was purified by fractional condensation.

Acknowledgments

The authors thank the Austrian Fonds zur Förderung der wissenschaftlichen Forschung for financial support (project P-11878-CHE).

[1] A. Stock, K. Somieski, *Ber. Dtsch. Chem. Ges.* **1920**, *53*, 759−769.
[2] M. Abedini, C. H. Van Dyke, A. G. MacDiarmid, *J. Inorg. Nucl. Chem.* **1963**, *25*, 307−308.
[3] R. P. Hollandsworth, M. A. Ring, *Inorg. Chem.* **1968**, *7*, 1635−1637.
[4] F. Feher, P. Plichta, R. Guillery, *Inorg. Chem.* **1971**, *10*, 606−608.
[5] C. H. VanDyke, A. G. MacDiarmid, *J. Inorg. Nucl. Chem.* **1963**, *25*, 1503−1506.
[6] J. E. Drake, N. Goddard, *Inorg. Nucl. Chem. Lett.* **1968**, *4*, 385−388.
[7] J. E. Drake, N. Goddard, C. Riddle, *J. Chem. Soc. A* **1969**, 2704−2709.
[8] J. E. Drake, N. Goddard, *J. Chem. Soc. A* **1970**, 2587−2590.
[9] J. E. Bentham, S. Cradock, E. A. V. Ebsworth, *Inorg. Nucl. Chem. Lett.* **1971**, *7*, 1077−1079.

[10] A. D. Craig, J. V. Urenovitch, A. G. MacDiarmid, *J. Chem. Soc.* **1962**, 548−553.
[11] J. E. Drake, N. P. C. Westwood, *J. Chem. Soc. A* **1971**, 3300−3304.
[12] J. E. Drake, N. P. C. Westwood, *Chem. Ind.* **1969**, 24.
[13] H. Söllradl, E. Hengge, *J. Organomet. Chem.* **1983**, *243*, 257−269.
[14] W. Raml, E. Hengge, *Z. Naturforsch.* **1979**, *34b*, 1457−1458.
[15] A. Stock, K. Somiesky, *Ber. Dtsch. Chem. Ges.* **1920**, *53*, 759−769.
[16] L. G. L. Ward, A. G. MacDiarmid, *J. Am. Chem. Soc.* **1960**, *82*, 2151−2153.
[17] F. Feher, P. Plichta, R. Guillery, *Chem. Ber.* **1970**, *103*, 3028−3033.
[18] F. Feher, B. Mostert, A. G. Wronka, G. Betzen, *Monatsh. Chem.* **1972**, *103*, 959−965.
[19] J. E. Drake, J. Simpson, *Inorg. Nucl. Chem. Lett.* **1966**, *2*, 219−221.
[20] K. G. Sharp, J. L. Margrave, *Inorg. Chem.* **1969**, *8*, 2655−2658.
[21] D. Solan, A. B. Burg, *Inorg. Chem.* **1972**, *11*, 1253−1258.
[22] J. F. Bald, Jr., K. G. Sharp, A. G. MacDiarmid, *J. Fluorine Chem.* **1973/74**, *3*, 433−435; K. G. Sharp, J. F. Bald, Jr., *Inorg. Chem.* **1975**, *14*, 2553−2556.
[23] J. C. Thompson, A. P. G. Wright, *Can. J. Chem.* **1979**, *57*, 994−998; G. R. Langford, D. C. Moody, J. D. Odom, *Inorg. Chem.* **1975**, *14*, 134−136.
[24] J. J. D'Errico, K. G. Sharp, *J. Chem. Soc., Dalton Trans.* **1989**, 1879−1881.
[25] K. Hassler, W. Köll, *J. Organomet. Chem.* **1995**, *487*, 223−226.
[26] M. Abedini, A. G. MacDiarmid, *Inorg. Chem.* **1963**, *2*, 608−613.
[27] K. Hassler, G. Bauer, *J. Organomet. Chem.* **1993**, *460*, 149−153.
[28] K. Hassler, W. Köll, *J. Organomet. Chem.* **1997**, *540*, 113−118.
[29] K. Hassler, W. Köll, *J. Organomet. Chem.* **1997**, *538*, 145−150.
[30] K. Hassler, K. Schenzel, *J. Mol. Struct.* **1995**, *348*, 353−356.
[31] K. Hassler, *Monatsh. Chem.* **1990**, *121*, 361−363.
[32] H. C. Marsmann in *NMR Basic Principles and Progress*, Vol. 17, Springer Verlag, Berlin, Heidelberg, New York, **1981**.
[33] T. H. Johansen, K. Hagen, R. J. Stolevik, *J. Mol. Struct.* **1999**, *485*, 121−133.
[34] M. Ernst, K. Schenzel, A. Jähn, W. Köll, K. Hassler, *J. Raman Spectrosc.* **1997**, *28*, 589−597.
[35] M. Söldner, M. Sandor, A. Schier, H. Schmidbaur, *Chem. Ber./Recueil* **1997**, *130*, 1671−1676.

Received January 15, 2001
[I01020]

Heteronuclear Complexes Containing $\{Au_2Rh\}$, $\{Au_2Ir\}$ and $\{AuIr\}$ Cores with a Dithiolate Ligand Bridging the Metal Centres − X-ray Structures of $[Au_2Ir(\mu\text{-}S_2C_6H_4)(cod)(PPh_3)_2]BF_4$ and $[AuIr(\mu\text{-}S_2C_6H_3CH_3)(cod)(PPh_3)]$

Inmaculada del Rio,[a] Raquel Terroba,[b] Elena Cerrada,[b] Michael B. Hursthouse,[c] Mariano Laguna,*[b] Mark E. Light,[c] and Aurora Ruiz*[a]

Dedicated to Professor Rafael Usón on the occasion of his 75th birthday

Keywords: Gold / Rhodium / Iridium / S ligands / Hydrogenation

The use of dinuclear gold derivatives $[Au_2(\mu\text{-}S\text{-}S)(PR_3)_2]$ (S-S = benzenedithiolate, toluenedithiolate; PR_3 = PPh_3, PPh_2Me) as S-donor ligands, with rhodium and iridium complexes $[M(cod)_2]BF_4$ (M = Rh, Ir; cod = cyclooctadiene) affords new heteronuclear compounds containing the $\{Au_2M\}$ core, with the general formulation $[Au_2M(\mu\text{-}S\text{-}S)(cod)(PR_3)_2]BF_4$. One of these decomposes upon heating to give $[AuIr(\mu\text{-}S_2C_6H_4CH_3)(cod)(PPh_3)]$. The crystal structure of the former and $[Au_2Ir(\mu\text{-}S_2C_6H_4)(cod)(PPh_3)_2]BF_4$ have been established by X-ray diffraction. The sulfur atoms from the dithiolene ligands bridge two different metal centres.

Introduction

Until recently, gold and its compounds were thought to be catalytically inactive.[1] In recent years, however, gold complexes have been used as homogeneous catalysts, mainly in the addition of water and alcohols to alkynes,[2] and in the use of luminescent compounds as photocatalysts.[3]

Heteropolynuclear complexes are particularly attractive because of their interesting structural and reactive features and their potential applications in catalysis.[4] In these complexes, two or more different metal atoms or ions are present in the same molecule and may cooperate in some reactions that could not be handled by a single metal centre. This leads to new types of reactions and affords new opportunities for catalytic processes.[5] Thus, heteropolynuclear complexes containing gold and other metal centres more commonly used in homogeneous catalysis, such as rhodium and iridium, can enhance the catalytic properties of the monometallic complexes.

Different approaches can be taken to the preparation of heterometallic derivatives. The tendency of thiolate ligands to act as bridges is a good starting point for the synthesis of polynuclear compounds, and several dinuclear thiolate complexes of rhodium and iridium are active in homogeneous catalytic hydrogenation reactions.[6] Some complexes containing gold and rhodium or iridium with thiolate ligands acting as a bridge between the metal centres have been reported, such as $[Cp^*M(\mu\text{-}SR)_2AuCl_2]Cl$ (M = Rh, Ir), but their crystal structures are at present unknown.[7]

In this paper we present the synthesis of heterometallic complexes containing iridium or rhodium with dithiolene-gold compounds as ligands. The new derivatives have the general formula $[Au_2M(\mu\text{-}S\text{-}S)(cod)(PR_3)_2]BF_4$ (M = Rh, Ir; S-S = benzenedithiolate, toluenedithiolate; cod = cyclooctadiene; PR_3 = PPh_3, PPh_2Me) and $[AuIr(\mu\text{-}S_2C_6H_4CH_3)(cod)(PPh_3)]$. The crystal structures of two gold-iridium complexes have been determined by X-ray diffraction and show short iridium−gold contacts ranging

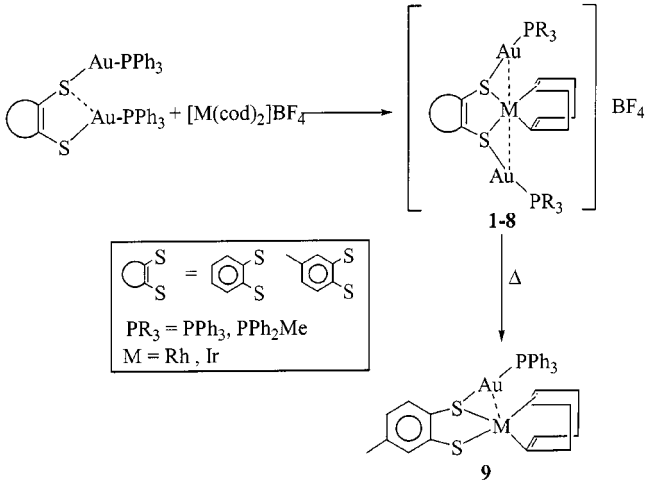

Scheme 1. Synthesis of complexes **1−9**

[a] Departamento de Química Fisica i Inorgánica. Facultad de Química. Universitat Rovira i Virgili,
Pça. Imperial Tarraco 1, 43005 Tarragona, Spain
[b] Departamento de Química Inorgánica, Instituto de Ciencia de Materiales de Aragón, Universidad de Zaragoza-C.S.I.C.,
50009 Zaragoza, Spain
E-mail mlaguna@posta.unizar.es
[c] Department of Chemistry, University of Southampton,
Highfield, Southampton SO17 1BJ, UK

 © WILEY-VCH Verlag GmbH, 69451 Weinheim, 2001 1434−1948/01/0808−2013 $ 17.50+.50/0

from 2.8544(4) to 2.9120(8) Å. Their reactivity with H_2 and CO has been investigated.

Results and Discussion

Synthesis of Polynuclear Compounds $[Au_2M(\mu\text{-S-S})(cod)(PR_3)_2]BF_4$

The polynuclear compounds **1**−**8** were prepared by the reaction of $[Au_2(\mu\text{-S-S})(PR_3)_2]$ (S-S = benzenedithiolate or toluenedithiolate; PR_3 = PPh_3, PPh_2Me) with the corresponding $[M(cod)_2]BF_4$ (M = Rh, Ir) derivative (Scheme 1).

The compounds $[Au_2(\mu\text{-S-S})(PR_3)_2]$ have a dithiolate ligand bridging the two gold centres in a μ_2 fashion. The crystal structures of several of these complexes, with different dithiolenes and different phosphane ligands, have been determined by X-ray diffraction.[8,9] In these structures, in addition to the typical gold−gold interactions, there is also one weak interaction between S and Au. This interaction points to the possibility of further coordination to another metal centre through the sulfur atoms. We therefore tested the reactivity of these dinuclear gold compounds towards the incorporation of another gold atom giving rise to $[Au_3(\mu\text{-S-S})(PR_3)_3]ClO_4$.[8] This positive result and the recent reports regarding the activity of gold complexes as catalysts,[2] have encouraged us to synthesise complexes with these digold ligands and rhodium or iridium fragments. These two metals are well known in the homogeneous catalyst area, and, in particular, some dinuclear thiolate complexes of these metals have been shown to be active in catalytic hydrogenation reactions.[6]

$[M(cod)_2]^+$ (M = Rh, Ir) derivatives are used as starting materials, with the expectation that our gold-containing compounds could substitute one of the cyclooctadiene ligands, giving the corresponding heteronuclear products. The reactions were carried out in dichloromethane. Unknown yellow solids precipitated in this solvent and were filtered off. Little information about the yellow solids has at present been obtained, due to their insolubility in all the common solvents. Their elemental analyses indicate a low percentage of carbon, which would correspond to polynuclear species with high metallic content. From the remaining dichloromethane solutions, the new products **1**−**8** were obtained, together with $[Au(PR_3)_2]BF_4$, after addition of diethyl ether. Different solvents were tried to separate the complexes **1**−**8** from the bis(phosphane)gold(I) salts, with the best results being obtained by recrystallization from $CHCl_3$/diethyl ether. The final yields were quite poor (around 20%) due to the similar solubility of both compounds.

The IR spectra show an absorption corresponding to tetrahedral BF_4^-. From the two active vibration modes only the asymmetric tension vibration (ν_a) at ≈1050 cm^{-1} can be assigned. The asymmetric deformation vibration (∂_a) at ≈ 530 cm^{-1} is coincident with the phosphane vibration zone and it cannot be differentiated.

The $^{31}P\{^1H\}$ NMR spectra show a singlet due to the phosphanes for all the compounds (Table 1). In the new complexes **1**−**8**, after the metal coordination, the sulfur atoms become asymmetric centres. Therefore, the Au−PR_3 group can adopt an *anti* or a *syn* configuration. In both cases, only one singlet should appear in the ^{31}P NMR spectrum. NMR experiments at low temperature (193 K) still show the presence of only one singlet. This indicates that either there is only one diastereoisomer in solution or there is a very rapid interchange between the *anti* and the *syn* configuration. The singlets corresponding to the Rh complexes **1**−**4** appear at lower fields than those in the gold starting materials, whilst the singlets of the Ir complexes **5**−**8** are displaced to higher field, although in both cases the magnitude is about $\Delta\delta = 1$. It is worth noting that complexes with toluendithiolate (**2**, **4**, **6** and **8**) do not show the predicted two resonances for the phosphorous due to the asymmetric nature of the ligand: only one singlet is present in their spectra, even at low temperature, as in the gold starting materials $[Au_2(\mu\text{-}S_2C_6H_3CH_3)(PR_3)_2]$.[8] A fast interchange of $AuPPh_3$ fragments should be present in solution.

Crystal Structure of $[Au_2Ir(S_2C_6H_4)(cod)(PPh_3)_2]BF_4$ (5)

The molecular structure of the complex $[Au_2Ir(S_2C_6H_4)(cod)(PPh_3)_2]BF_4$ (**5**) has been established by X-ray diffraction and the cation is shown in Figure 1. General information is given in Table 2 and selected bond lengths and angles in Table 3. The cation of **5** consists of a benzenedithiolate ligand bridging two $AuPPh_3^+$ and one $Ir(cod)^+$ fragments, in a similar arrangement to $[Au_3(S_2C_6H_3CH_3)(PPh_3)_3]ClO_4$.[8] The dithiolene and cod ligands are chelated to the iridium centre. The average Ir−S distance is 2.32 Å and the average Ir−C distance 2.15 Å. These bond lengths are similar to the ones found in the Ir^I dimers $[Ir(\mu\text{-SR})(cod)]_2$.[10]

The iridium−gold distances are Ir−Au(1) = 2.9208(9) and Ir−Au(2) = 2.9120(8) Å. These distances are longer than the corresponding single Ir−Au bond, which are in the range 2.59−2.81 Å[11] and are similar to the reported metal−metal interactions in other iridium-gold complexes.[12] There is probably a considerable similarity be-

Table 1. $^{31}P\{^1$ Rp NM^r in $CDCl_3$ (δ in ppm)

S-S	PR_3	$[Au_2(\mu\text{-S-S})(PR_3)_2]$[8]	$[Au_2Rh(\mu\text{-S-S})(cod)(PR_3)_2]BF_4$	$[Au_2Ir(\mu\text{-S-S})(cod)(PR_3)_2]BF_4$
$S_2C_6H_4$	PPh_3	35.9	36.9 (**1**)	35.2 (**5**)
$S_2C_6H_4$	PPh_2Me	20.3	21.3 (**2**)	19.5 (**6**)
$S_2C_6H_3Me$	PPh_3	36.0	37.1 (**3**)	35.3 (**7**)
$S_2C_6H_3Me$	PPh_2Me	20.3	21.4 (**4**)	19.5 (**8**)

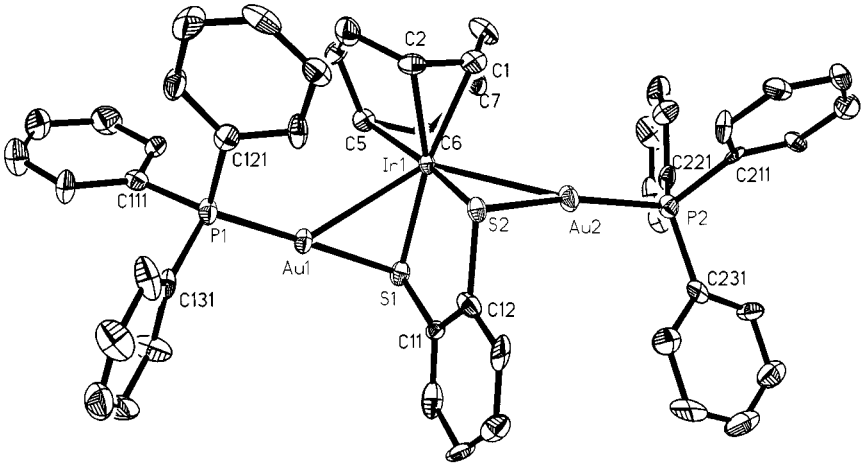

Figure 1. Molecular structure of **5** showing the cation; thermal ellipsoids are drawn at the 50% probability level and H atoms have been omitted for clarity

Table 2. Details of data collection and structure refinement for the complexes **5** and **9**

	5	**9**
Chemical formula	$C_{50}H_{46}Au_2BF_4IrP_2S_2$	$C_{33}H_{33}AuIrPS_2$
M	1443.87	913.85
Crystal system	Triclinic	Monoclinic
Space group	$P\bar{1}$	$P2_1/c$
a [Å]	11.0590(10)	10.8676(2)
b [Å]	14.528(2)	18.7639(6)
c [Å]	15.634(2)	14.7198(4)
α [°]	93.78(2)	90
β [°]	102.210(10)	102.9159(18)
γ [°]	106.550(10)	90
V [Å^3]	2331.9(5)	2925.70(13)
Z	2	4
Dc (Mg m^{-3})	2.056	2.075
F(000)	1366	1736
Crystal size	0.20 × 0.16 × 0.14	0.25 × 0.18 × 0.1
T [K]	293(2)	293(2)
μ (Mo-K_α) [mm^{-1}]	9.101	9.772
θ range [°]	1.86 to 24.94	3.03 to 25.02
Reflections collected	10011	18537
Independent reflections	4526 [*R*(int) = 0.069]	5826 [*R*(int) = 0.0516]
Data/restraints/parameters	10011/6/559	5826/0/345
Quality of fit	0.999	1.161
*R*1[a]	0.0344	0.0385
*wR*2[b]	0.1010	0.0839
Residual ρ/eÅ^{-3}	1.290, −1.460	1.445, −2.011

[a] $R1\ (F) = \sum||F_o| - |F_c|| / \sum|F_o|$. − [b] $wR2\ (F^2) = [\{\sum w(F_o^2 - F_c^2)^2\} / \{\sum w(F_o^2)^2\}]^{0.5}$.

tween the Au−Ir interaction in **5** and the numerous examples of short Au−Au contacts shown in Au^I complexes,[13] or in the case of $[Au_3(S_2C_6H_3CH_3)(PPh_3)_3]ClO_4$ [8] [2.9624(12) and 3.1966(14) Å]. The two $AuPPh_3$ units are in an up/down configuration either side of the Ir(S-S)(cod) square planar fragment. Therefore, taking into account these two gold−iridium interactions, the coordination around the iridium can be regarded as a heavily distorted octahedron.

Despite the presence of gold−iridium interactions, the gold atoms are almost linearly coordinated considering the P−Au−S arrangement, the most frequent type of configuration for gold(I) complexes, with angles P(1)−Au(1)−S(1) = 176.07(13)° and P(2)−Au(2)−S(2) = 161.33(12)°. These gold centres lie out of the plane formed by P−S−Ir by 0.079 Å for Au(1) and 0.042 Å for Au(2). The gold−sulfur bond lengths are Au(1)−S(1) = 2.372(3) and Au(2)−S(2) = 2.392(3) Å, and are a little longer than in the previously reported complex $[Au_3(S_2C_6H_3CH_3)(PPh_3)_3]ClO_4$ [8] [2.315(5) and 2.332(4) Å for the external gold atoms]. The gold−phosphorus distances are Au(1)−P(1) = 2.257(3) and Au(2)−P(2) = 2.248(3), and are similar to the values found in other Ir−Au phosphane complexes (2.199−2.292 Å).[14]

Table 3. Bond lengths [Å] and angles [°] for **5**

Au(1)−P(1)	2.257(3)
Au(1)−S(1)	2.372(3)
Au(1)−Ir(1)	2.9208(9)
Au(2)−P(2)	2.248(3)
Au(2)−S(2)	2.392(3)
Au(2)−Ir(1)	2.9120(8)
Ir(1)−C(2)	2.109(14)
Ir(1)−C(6)	2.144(14)
Ir(1)−C(5)	2.158(12)
Ir(1)−C(1)	2.201(14)
Ir(1)−S(2)	2.317(3)
Ir(1)−S(1)	2.318(4)
P(1)−Au(1)−S(1)	176.07(13)
P(1)−Au(1)−Ir(1)	129.21(10)
S(1)−Au(1)−Ir(1)	50.65(9)
P(2)−Au(2)−S(2)	161.33(12)
P(2)−Au(2)−Ir(1)	147.83(10)
S(2)−Au(2)−Ir(1)	50.66(8)
C(2)−Ir(1)−S(2)	93.6(4)
C(6)−Ir(1)−S(2)	155.4(4)
C(5)−Ir(1)−S(2)	165.9(4)
C(1)−Ir(1)−S(2)	94.7(4)
C(2)−Ir(1)−S(1)	157.0(4)
C(6)−Ir(1)−S(1)	91.2(4)
S(2)−Ir(1)−S(1)	87.89(12)
C(5)−Ir(1)−Au(2)	140.7(3)
S(2)−Ir(1)−Au(2)	52.96(8)
S(1)−Ir(1)−Au(2)	92.49(8)
S(2)−Ir(1)−Au(1)	88.05(8)
S(1)−Ir(1)−Au(1)	52.32(8)
Au(2)−Ir(1)−Au(1)	130.47(3)
C(11)−S(1)−Ir(1)	106.0(5)
C(11)−S(1)−Au(1)	97.1(4)
Ir(1)−S(1)−Au(1)	77.02(11)
C(12)−S(2)−Ir(1)	105.3(5)
C(12)−S(2)−Au(2)	94.4(4)
Ir(1)−S(2)−Au(2)	76.38(10)

The coordination plane for the Ir centre forms a dihedral angle of 176° with the dithiolene plane. The Au−PPh_3 groups are in an *anti* configuration, giving an *R*-configuration for both sulfur atoms.

Reactivity and Catalytic studies

We have studied the reactivity of the complexes [$Au_2M(\mu$-$S_2C_6H_4)(cod)(PPh_3)_2]BF_4$ (M = Rh **1**, Ir **5**). Dichloromethane solutions of both products were treated with H_2 and CO at room temperature and pressure. While we did not observe any reaction with H_2, both compounds react with CO. The dichloromethane solutions change from yellow to green and two new absorptions are observed in the IR spectra at 1993 and 2019 cm^{-1}, corresponding to terminal ν_{CO} vibrations due to the coordination of two CO molecules to the metal centres, replacing the cod ligand.[15] Evaporation of the solvent gives green solids that do not contain absorptions in the CO region, showing that the proposed dicarbonyl complex is not stable under these conditions.

Studies testing the catalytic activity of these complexes in the hydroformylation and hydrogenation of styrene were performed. The hydroformylation test was performed at 353 K and P_{CO/H_2} (1:1) = 5 atm., in dichloroethane, using complex **1** as the catalyst precursor. The catalytic test for the hydrogenation was performed at 298 K and P_{CO/H_2} = 5 atm., in dichloromethane. The catalyst precursor for the hydrogenation run was complex **5**. Both reactions were followed by gas chromatography, but neither hydroformylation nor hydrogenation were observed. The final reaction mixtures were green solutions with black solids in suspension. The black solids may correspond to the formation of reduced metals due to the presence of hydrogen pressure and/or higher temperatures.

Preparation and Crystal Structure of [AuIr(μ-$S_2C_6H_3CH_3$)(cod)(PPh_3)]

Since complex **1** decomposed in the hydroformylation and hydrogenation reactions, we studied the behaviour of complexes **1**−**8** at the temperature of refluxing acetone in order to test their thermal stability. All the complexes give insoluble black solids and [$Au(PR_3)_2]BF_4$, as confirmed by ^{31}P NMR spectroscopy. Only in the case of [$Au_2Ir(\mu$-$S_2C_6H_3CH_3)(cod)(PPh_3)_2]BF_4$ (**7**) was one diethyl ether soluble complex isolated in quite good yield and characterized as [AuIr(μ-$S_2C_6H_3CH_3$)(cod)(PPh_3)] (**9**). It shows a similar ^{31}P NMR spectrum to that of **7** with only one signal at δ = 35.1, although with toluenedithiolate several isomers should be present. The ^1H NMR spectrum shows different resonances for the cod protons, pointing to the presence of a nonsymmetrical coordination for the diolefinic ligand. In addition, the integration of the phenyl protons suggests that only one $AuPPh_3$ group is present for each cod ligand. The elemental analysis and the IR spectrum, with the lack of absorptions corresponding to a BF_4 anion, confirm the proposed stoichiometry for **9**.

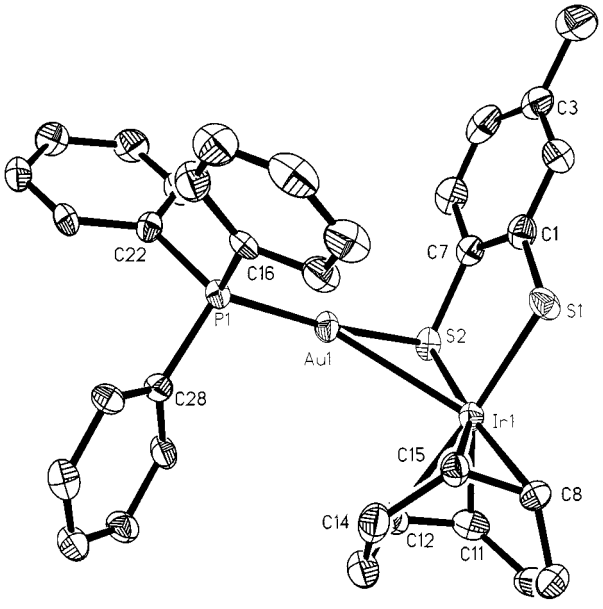

Figure 2. Molecular structure of **9**; thermal ellipsoids are drawn at the 50% probability level and H atoms have been omitted for clarity

The dinuclear structure of **9** was confirmed by X-ray analysis (Figure 2). General information is given in Table 2 and selected bond lengths and angles in Table 4. The molecule can be described as a toluenedithiolate ligand bridging one $AuPPh_3^+$ and one $Ir(cod)^+$ fragment, in a similar arrangement to that present in $[Au_2Ir(S_2C_6H_4)(cod)(PPh_3)_2]BF_4$ (**5**). In fact, the structure of **9** is very similar to **5** with the addition of a methyl group, the lack of the BF_4 anion and the presence of only one $AuPPh_3$ fragment. Complex **9** retains the planarity of the Ir(S-S)(cod) fragment and the pseudo linearity of $SAu(PPh_3)$ skeleton. The Ir−S, Au−S, Ir−C and Au−P distances are nearly identical in **5** and **9**. Only the Ir(1)−S(1) distance with the nonbridging sulfur is slightly shorter than either the Ir(1)−S(2) in complex **9** or any of the Ir−S distances in complex **5**. In addition only one iridium−gold distance in **9** [2.8544(4) Å] is shorter than the two Ir−Au contacts in **5**, showing that the interaction between the two metals is now stronger than in the trinuclear complex, although this value it is not short enough to be considered a real metal−metal bond.[11,12]

Table 4. Bond lengths [Å] and angles [°] for **9**

Au(1)−P(1)	2.2496(19)
Au(1)−S(2)	2.3829(18)
Au(1)−Ir(1)	2.8544(4)
Ir(1)−C(11)	2.133(8)
Ir(1)−C(15)	2.151(7)
Ir(1)−C(8)	2.151(7)
Ir(1)−C(12)	2.205(8)
Ir(1)−S(1)	2.2819(19)
Ir(1)−S(2)	2.3168(18)
P(1)−Au(1)−S(2)	171.82(7)
P(1)−Au(1)−Ir(1)	136.23(5)
S(2)−Au(1)−Ir(1)	51.56(4)
C(11)−Ir(1)−C(15)	98.0(3)
C(11)−Ir(1)−C(8)	81.0(3)
C(15)−Ir(1)−C(8)	39.1(3)
C(11)−Ir(1)−C(12)	38.6(3)
C(15)−Ir(1)−C(12)	80.7(3)
C(8)−Ir(1)−C(12)	88.8(3)
C(11)−Ir(1)−S(1)	147.7(2)
C(15)−Ir(1)−S(1)	95.2(2)
C(8)−Ir(1)−S(1)	91.1(2)
C(12)−Ir(1)−S(1)	173.5(2)
C(11)−Ir(1)−S(2)	94.3(2)
C(15)−Ir(1)−S(2)	151.2(2)
C(8)−Ir(1)−S(2)	169.7(2)
C(12)−Ir(1)−S(2)	93.2(2)
S(1)−Ir(1)−S(2)	88.05(7)
C(11)−Ir(1)−Au(1)	115.4(2)
C(15)−Ir(1)−Au(1)	97.6(2)
C(8)−Ir(1)−Au(1)	136.6(2)
C(12)−Ir(1)−Au(1)	83.9(2)
S(1)−Ir(1)−Au(1)	91.75(5)
S(2)−Ir(1)−Au(1)	53.66(5)
C(28)−P(1)−Au(1)	110.5(2)
C(16)−P(1)−Au(1)	112.5(2)
C(22)−P(1)−Au(1)	113.5(2)
C(7)−S(2)−Ir(1)	105.3(2)
C(7)−S(2)−Au(1)	96.5(2)
Ir(1)−S(2)−Au(1)	74.78(5)
C(1)−S(1)−Ir(1)	105.7(3)
C(15)−C(8)−Ir(1)	70.4(4)
C(9)−C(8)−Ir(1)	113.4(6)
C(12)−C(11)−Ir(1)	73.4(5)
C(10)−C(11)−Ir(1)	110.3(6)
C(8)−C(15)−Ir(1)	70.5(4)
C(14)−C(15)−Ir(1)	109.4(5)
C(11)−C(12)−Ir(1)	68.0(4)
C(13)−C(12)−Ir(1)	112.3(5)

In summary, we have prepared new polynuclear complexes with Au_2Rh, Au_2Ir, and AuIr cores using dithiolate ligands to bridge the metal centres. The crystal structures of $[Au_2Ir(\mu\text{-}S_2C_6H_4)(cod)(PPh_3)_2]BF_4$ (**5**) and $[AuIr(\mu\text{-}S_2C_6H_3CH_3)(cod)(PPh_3)]$ (**9**) show that there are gold−iridium interactions ranging from 2.9208(9) in the former to 2.8544(4) Å in the latter. The new complexes are not active precursors for either the hydroformylation or hydrogenation of styrene. This inactivity may be due to the instability of the complexes either at high P_{CO/H_2} or at high temperature.

Experimental Section

General: IR spectra were recorded on a Perkin−Elmer 883 spectrophotometer, over the range 4000−200 cm^{-1}, as Nujol mulls between polyethylene sheets. ^1H and ^{31}P NMR spectra were recorded on a Varian GEMINI 300 in $CDCl_3$ solution; chemical shifts are quoted relative to $SiMe_4$ (^1H) or H_3PO_4 (external ^{31}P). The C,H,N and S analyses were performed with a Perkin−Elmer 2400 microanalyser. Mass spectra were recorded on a VG Autospec, by liquid secondary ion mass spectrometry (LSIMS +) using nitrobenzyl alcohol as matrix and a caesium gun. Gas chromatography was performed on a Hewlett−Packard 5840A chromatograph with a flame ionisation detector using an Ultra-2 (5% diphenylsilicone/95% dimethylsilicone) capillary column (25 m × 0.2 mm Ø).

Materials: The starting materials $[Au_2(\mu\text{-}S_2C_6H_4)(PPh_3)_2]$,[8] $[Au_2(\mu\text{-}S_2C_6H_4)(PPh_2Me)_2]$,[8] $[Au_2(\mu\text{-}S_2C_6H_3Me)(PPh_3)_2]$,[8] $[Au_2(\mu\text{-}S_2C_6H_3Me)(PPh_2Me)_2]$,[8] $[Rh(cod)_2]BF_4$ [16] and $[Ir(cod)_2]BF_4$ [16] were prepared as previously described. All other reagents were commercially available, and all the reactions were carried out under an argon atmosphere. All the synthesised complexes were isolated as air-stable solids.

Preparation of Complexes 1−8: To a solution of $[Au_2(\mu\text{-}S\text{-}S)(PR_3)_2]$ [S-S = $S_2C_6H_4$, PR_3 = PPh_3 (0.106 g, 0.1 mmol), PPh_2Me (0.093 g, 0.1 mmol); S-S = $S_2C_6H_3Me$, PR_3 = PPh_3 (0.107 g, 0.1 mmol), PPh_2Me (0.095 g, 0.1 mmol)] in CH_2Cl_2 was added $[M(cod)_2]BF_4$ [M = Rh (0.041 g, 0.1 mmol), Ir (0.050 g, 0.1 mmol)]. After stirring for 1 h a yellow solid was filtered off. The solutions were concentrated in vacuum; addition of cold diethyl ether, resulted in the precipitation of yellow solids, which were filtered off, washed with cold diethyl ether and vacuum dried. These solids contained complexes **1−8** with $[Au(PR_3)_2]BF_4$. Recrystallization from chloroform/diethyl ether afforded the new compounds as yellow solids. Only the initial batch of crystals were collected as later fractions were found to be contaminated with bis(phosphane)gold(I) tetrafluoroborate.

1: Yield: 28 mg (20%). − $C_{50}H_{46}Au_2BF_4P_2RhS_2$: calcd. C 44.3, H 3.4, S 4.7; found C 44.7, H 3.4, S 4.4. − ^1H NMR: δ = 1.8 (m, 4 H, -$CH_{2\text{-}endo}$-, cod), 1.9 (m, 4 H, -$CH_{2\text{-}exo}$-, cod), 4.7 (m, 4 H, -CH=CH-, cod), 7.2−7.7 (m, 30 H, Ph + 2 H, C_6H_4), 7.9 (m, 2 H, C_6H_4). − IR (Nujol mull): ν_{BF} = 1056 cm^{-1}. − MS: *m/z* (%) = 1269 (10) $[M - BF_4]^+$.

2: Yield: 34 mg (27%). − $C_{40}H_{42}Au_2BF_4P_2RhS_2$: calcd. C 39.0, H 3.4, S 5.2; found C 39.3, H 3.7, S 4.9. − ^{1}H NMR: δ = 1.9 (m, 8 H, -CH_2-, cod), 2.2 (d, $^2J_{P-H}$ = 11.5 Hz, 6 H, PPh_2*Me*), 4.7 (m, 4 H, -CH=CH-, cod), 7.3−7.8 (m, 20 H, Ph + 2 H, C_6H_4), 7.9 (m, 2 H, C_6H_4). − IR (Nujol mull): ν_{BF} = 1057 cm^{-1}. − MS: *m*/*z* (%) = 1145 (5) [M − BF_4]$^+$.

3: Yield: 35 mg (25%). − $C_{51}H_{48}Au_2BF_4P_2RhS_2$: calcd. C 44.7, H 3.5, S 4.7; found C 44.3, H 3.6, S 4.2. − ^{1}H NMR: δ = 1.8 (m, 4 H, -CH_2-$_{endo}$, cod), 1.9 (m, 4 H, -CH_2-$_{exo}$, cod), 2.4 (s, 3 H, C_6H_3*Me*), 4.7 (m, 4 H, -CH=CH-, cod), 7.1 (dd, 1 H, C_6H_3Me), 7.3−7.7 (m, 30 H, Ph), 7.7 (m, 1 H, C_6H_3Me), 7.8 (d, $^3J_{H-H}$ = 7.7 Hz, 1 H, C_6H_3Me). − IR (Nujol mull): ν_{BF} = 1057 cm^{-1}. − MS: *m*/*z* (%) = 1283 (29) [M − BF_4]$^+$.

4: Yield: 33 mg (26%). −$C_{41}H_{44}Au_2BF_4P_2RhS_2$: calcd. C 39.5, H 3.5, S 5.1; found C 39.6, H 3.8, S 5.0. − ^{1}H NMR: δ = 1.9 (m, 8 H, -CH_2-, cod), 2.1 (d, $^2J_{P-H}$ = 11.8 Hz, 6 H, PPh_2*Me*), 2.4 (s, 3 H, C_6H_3*Me*), 4.7 (m, 4 H, -CH=CH-, cod), 7.1 (dd, 1 H, C_6H_3Me), 7.3−7.7 (m, 20 H, Ph), 7.7 (m, 1 H, C_6H_3Me), 7.8 (m, 1 H, C_6H_3Me). − IR (Nujol mull): ν_{BF} = 1060 cm^{-1}. − MS: *m*/*z* (%) = 1159 (18) [M − BF_4]$^+$.

5: Yield: 32 mg (22%). − $C_{50}H_{46}Au_2BF_4IrP_2S_2$: calcd. C 41.5, H 3.2, S 4.4; found C 41.0, H 3.2, S 4.3. − ^{1}H NMR: δ = 1.6 (m, 4 H, -CH_2-$_{endo}$, cod), 1.8 (m, 4 H, -CH_2-$_{exo}$, cod), 4.4 (m, 4 H, -CH=CH-, cod), 7.1−7.7 (m, 30 H, Ph + 2 H, C_6H_4), 8.1 (m, 2 H, C_6H_4). − IR (Nujol mull): ν_{BF} = 1055 cm^{-1}. − MS: *m*/*z* (%) = 1359 (12) [M − BF_4]$^+$

6: Yield: 40 mg (30%). − $C_{40}H_4Au_2BF_4Ir_2P_2S_2$: calcd. C 36.3, H 3.2, S 4.8; found C 36.8, H 3.5, S 4.9. − ^{1}H NMR: δ = 1.8 (m, 4 H, -CH_2-$_{endo}$, cod), 1.9 (m, 4 H, -CH_2-$_{exo}$, cod), 2.1 (m, 6 H, PPh_2*Me*), 4.4 (m, 4 H, -CH=CH-, cod), 7.8−7.2 (m, 20 H, Ph, 2 H, C_6H_4), 8.1 (m, 2 H, C_6H_4). − IR (Nujol mull): ν_{BF} = 1060 cm^{-1}. − MS: *m*/*z* (%) = 1235 (4) [M − BF_4]$^+$.

7: Yield: 34 mg (23%). − $C_{51}H_{48}Au_2BF_4IrP_2S_2$: calcd. C 41.9, H 3.3, S 4.4; found C 41.7, H 3.5, S 4.2. − ^{1}H NMR: δ = 1.6 (m, 4 H, -CH_2-$_{endo}$, cod), 1.8 (m, 4 H, -CH_2-$_{exo}$, cod), 2.5 (s, 3 H, C_6H_3*Me*), 4.4 (m, 4 H, -CH=CH-, cod), 7.1 (dd, 1 H, C_6H_3Me), 7.7−7.2 (m, 30 H, Ph), 7.7 (d, $^4J_{H-H}$ = 1.2 Hz, 1 H, C_6H_3Me), 7.9 (d, $^3J_{H-H}$ = 7.7 Hz, 1 H, C_6H_3Me). − IR (Nujol mull): ν_{BF} = 1056 cm^{-1}. − MS: *m*/*z* (%) = 1373(21) [M − BF_4]$^+$.

8: Yield: 27 mg (20%). $C_{41}H_{44}Au_2IrBF_4P_2S_2$: calcd. C 36.8, H 3.3, S 4.8; found C 36.9, H 3.7, S 4.5. − ^{1}H NMR: δ = 1.7 (m, 4 H, -CH_2-$_{endo}$, cod), 1.9 (m, 4 H, -CH_2-$_{exo}$, cod), 2.1 (d, $^2J_{P-H}$ = 10.2 Hz, 6 H, PPh_2*Me*), 2.5 (s, 3 H, C_6H_3*Me*), 4.4 (m, 4 H, -CH=CH-, cod), 7.1 (dd, 1 H, C_6H_3Me), 7.7−7.3 (m, 20 H, Ph), 7.8 (d, $^4J_{H-H}$ = 3.6 Hz, 1 H, C_6H_3Me), 7.9 (d, $^3J_{H-H}$ = 10.8 Hz, 1 H, C_6H_3Me). − IR (Nujol mull): ν_{BF} = 1059 cm^{-1}. − MS: *m*/*z* (%) = 1249 (16) [M − BF_4]$^+$.

[AuIr(μ-$S_2C_6H_3$Me)(cod)(PPh_3)$_2$] (9): A solution of **7** (0.073 g, 0.05 mmol) in acetone (20 mL) was refluxed for 3 h. After removal of the solvent to ca. 5 mL and addition of diethyl ether (20 mL) a white solid was formed, which was characterized as [Au(PPh_3)$_2$]BF_4. Partial evaporation of the solution and addition of hexane gave a yellow solid. Yield: 26 mg (57%). − $C_{33}H_{33}AuIrPS_2$: calcd. C 43.4, H 3.6, S 7.0; found C 43.8, H 3.7, S 6.6. − ^{1}H NMR: δ = 1.6 (m, 4 H, -CH_2-$_{endo}$, cod), 1.8 (m, 4 H, -CH_2-$_{exo}$, cod), 2.4 (s, 3 H, C_6H_3*Me*), 4.0 (m, 2 H, -CH=CH-, cod), 4.1 (m, 2 H, -CH=CH-, cod), 6.7 (d, 1 H, C_6H_3Me), 7.3−7.1 (m, 15 H, Ph), 7.4 (s, 1 H, C_6H_3Me), 7.5 (d, $^3J_{H-H}$ = 9.0 Hz, 1 H, C_6H_3Me) − ^{31}P{^{1}H} NMR: δ = 35.1 (s, PPh_3). − MS: *m*/*z* (%) = 913 (20) [M]$^+$.

Crystallography: Single crystals were grown by diffusing hexane into dichloromethane solutions of [Au_2Ir(μ-$S_2C_6H_4$)-(cod)(PPh_3)$_2$]BF_4 (**5**) and [AuIr(μ-$S_2C_6H_3$Me)(cod)(PPh_3)] (**9**). They were mounted at low temperature in inert oil. Crystal data and data collection parameters are summarised in Table 4. Data were collected on a Delft Instruments FAST TV area detector diffractometer positioned at the window of a rotating-anode generator with graphite monochromated Mo-K_α radiation (λ = 0.71069 Å), following procedures described elsewhere.[17]

Structure Solution and Refinement: The structures were solved using SHELXS-86 and SHELXS-97,[18] and refined by full-matrix least-squares on F_o^2, using the programs SHELXL-93 and SHELXL-97.[19] In the case of **5** the data were corrected with the program DIFABS,[20] and for **9** with the program SORTAV.[21] The non-hydrogen atoms were refined with anisotropic thermal parameters. All hydrogen atoms were included in idealized positions.

Crystallographic data (excluding structure factors) for the structure(s) included in this paper have been deposited with the Cambridge Crystallographic Data Centre as supplementary publication no. CCDC-157923 (**5** and **9**). Copies of the data can be obtained free of charge on application to CCDC, 12 Union Road, Cambridge CB2 1EZ, UK [Fax: (internat.) + 44-1223/336-033; Email: deposit@ccdc.cam.ac.uk].

Hydrogenation Procedure: The reaction was carried out in a small home-made autoclave. The styrene (0.92 cm^3, 8 mmol) and catalyst precursor **5** (57.8 mg, 0.04 mmol) were dissolved in dichloromethane (6 cm^3) and shaken under 5 atm. of H_2 at 298 K for 24 h. The conversion was measured by gas chromatography.

Hydroformylation Procedure: The catalyst precursor **1** (68.1 mg, 0.05 mmol) and styrene (1.15 cm^3, 10 mmol) were dissolved in 7.5 cm^3 of dichloromethane. This solution was transferred to the evacuated autoclave, which was then pressurised with *syn*-gas to about 80% of the reaction pressure (5 atm.). The preheated water circuit was connected to the autoclave jacket, and when thermal equilibrium was reached (5−10 minutes) more gas mixture was introduced until the required pressure was achieved. At the end of the reaction the autoclave was cooled to room temperature and depressurised. The sample was analysed by gas chromatography.

Acknowledgments

The Spanish authors thank the Dirección General de Enseñanza Superior (PB98- 0542 and PB97−0407-C05−01) for financial support, the Ministerio de Educación y Cultura for a grant (to R.T.), and the Generalitat de Catalunya (CIRIT) for a grant (to I del R.). M.B.H. thanks the Engineering and Physical Sciences Research Council for support of the X-ray facilities.

[1] [1a] R J. Puddephatt, *The Chemistry of Gold*, Elsevier, The Netherlands, **1978**.

[2] [2a] H. Schmidbaur, *Gold progress in Chemistry, Biochemistry and Technology*, John Wiley and Sons. New York, **1999**. − [2b] G. C. Bond, D. T. Thompson, *Gold Bull.* **2000**, *33*, 41−50. − [2c] J. H. Teles, S. Brode, M. Chabanas, *Angew. Chem. Int. Ed.* **1998**, *37*, 1415−1418; *Angew. Chem.* **1998**, *110*, 1475−1478. − [2d] Q. Xu, Y. Imamura, M. Fujiwara, Y. Souma, *J. Org. Chem.* **1997**, *62*, 1594−1598. − [2e] S. Komiya, Y. Sone, T. Usui, M. Hirano, A. Fukuoka, *Gold Bull.* **1996**, *29*, 131−136. − [2f] D. A. Krogstad, W. V. Konze, L. H. Pignolet, *Inorg. Chem.* **1996**, *35*, 6763−6771. − [2g] Y. Fukuda, K. Utimoto, *J Org. Chem.* **1991**, *56*, 3729−3731. − [2h] K. Fukuda, Y. Utimoto, *Bull. Chem. Soc. Jpn.* **1991**, *64*, 2013−2015. − [2i] K. Fukuda, Y. Utimoto, *Synthesis* **1991**, 975−978. − [2j] K. Fukuda, Y. Utimoto, K. Nozaki, *Heterocycles* **1987**, *25*, 297−301. − [2k] Y. Ito,

M. Sawamura, T. Hayashi, *J. Am. Chem. Soc.* **1986**, *108*, 6405−6406.

[3] [3a] A. Grohmann, H. Schmidbaur, *Comprehensive Organometallic Chemistry II* (Eds. G. Wilkinson, F. G. A. Stone, E. W. Abel), vol 3, Pergamon, **1995**. − [3b] F. Gaspassini, M. Giovannoli, D. Misiti, G. Natile, G. Palmieri, L. Maresca, *J. Am. Chem. Soc.* **1993**, *115*, 4401−4402. − [3c] A. W. Olsen, Z. H. Kafafi, *J. Am. Chem. Soc.* **1991**, *113*, 7758−7760. − [3d] Y. Hori, A. Musata, K. Kikuchi, *J. Chem. Soc., Chem. Commun.* **1987**, 728−729.

[4] B. Chaudret, B. Delavaux, R. Poilblanc, *Coord. Chem. Rev.* **1988**, *86*, 191−243.

[5] D. W. Stephan, *Coord. Chem. Rev.* **1989**, *95*, 41−107.

[6] [6a] H. Schumann, H. Hemling, N. Goren, J. Blum, *J. Organomet. Chem.* **1995**, *485*, 209−213. − [6b] H. Schumann, B. Gorella, M. Eisen, J. Blum, *J. Organomet. Chem.* **1991**, *412*, 251−258. − [6c] M. Eisen, P. Weitz, S. Shtelzer, J. Blum, H. Schumann, B. Gorella, F. H. Görlitz, *Inorg. Chim. Acta* **1991**, *188*, 167 176. − [6d] M. Eisen, J. Blum, H. Schumann, B. Gorella, *J. Mol. Cat.* **1989**, *56*, 329−337. − [6e] P. Kalck, R. Poilblanc, R. P. Martin, A. Lovera, A. Gaset, *J. Organomet. Chem.* **1980**, *195*, C9−C12.

[7] J. J. García, M. L. Hernández, H. Torrens, A. Gutierrez, F. del Río, *Inorg. Chim. Acta* **1995**, *230*, 173−176.

[8] M. C. Gimeno, P. G. Jones, A. Laguna, M. Laguna, R. Terroba, *Inorg. Chem.* **1994**, *33*, 3932−3938.

[9] [9a] R. M. Dávila, A. Elduque, T. Grant, R. J. Staples, J. P. Fackler Jr., *Inorg. Chem.* **1993**, *32*, 1749−1755. − [9b] M. Nakamoto, H. Koijman, M. Paul, W. Hiller, H. Schmidbaur, *Z. Anorg. Allg. Chem.* **1993**, *619*, 1341−1346. − [9c] M. Nakamoto, A. Schier, H. Schmidbaur, *J. Chem. Soc., Dalton Trans.* **1993**, 1347−1348

[10] [10a] E. Fernández, A. Ruiz, S. Castillón, C. Claver, J. F. Pinella, A. Alvarez-Larena, G. Germain, *J. Chem. Soc., Dalton Trans.* **1995**, 2137−2142. − [10b] F. A. Cotton, P. Lahuerta, J. LaTorre, M. Sanasí, I. Solana, W. Schwotzer, *Inorg. Chem.* **1988**, *27*, 2131−2135.

[11] A. L. Balch, V. J. Catalano, *Inorg. Chem.* **1991**, *30*, 1302−1308.

[12] [12a] A. L. Balch, V. J. Catalano, *Inorg. Chem.* **1992**, *31*, 2730−2734. − [12b] A. L. Balch, V. J. Catalano, B. C. Noll, M. M. Olmstead, *J. Am. Chem. Soc.* **1990**, *112*, 7558−75566. − [12c] A L. Balch, V. J. Catalano, M. M. Olmstead, *J. Am. Chem. Soc.* **1990**, *112*, 2010−2013. − [12d] A. L. Balch, V. J. Catalano, M. M. Olmstead, *Inorg Chem.* **1990**, *29*, 585−586. − [12e] B. D. Alexander, P. D. Boyle, B. J. Johnson, J. A. Casalnuovo, S. M. Johnson, A. M. Mueting, L. H. Pignolet, *Inorg. Chem.* **1987**, *26*, 2547−2551.

[13] P. G. Jones, *Gold Bull.* **1981**, *14*, 102−118; **1983**, *16*, 114−124; **1986**, *19*, 46−57.

[14] [14a] C. Bianchini, A. Meli, M. Peruzzini, A. Vacca, F. Vizza, A. Albinati, *Inorg. Chem.* **1992**, *31*, 3841−3850. − [14b] A. G. Sykes, K. R. Mann, *J. Am. Chem. Soc.* **1990**, *112*, 7247−7254. − [14c] A. Albinati, F. Demartin, P. Jansen, L. F. Rhodes, L. M. Venanzi, *J. Am. Chem. Soc.* **1989**, *111*, 2115−2125. − [14d] A. Albinati, C. Ankin, P. Jansen, H. Lehner, D. Matt, P. S. Pregosin, L. M. Venanzi, *Inorg. Chem.* **1989**, *28*, 1105−1111.

[15] [15a] A. Ruiz, C. Claver, J. C. Rodriguez, M. Aguiló, X. Solans, M. Font-Altaba, *J. Chem. Soc., Dalton Trans.* **1984**, 2665−2669. − [15b] R. Usón, L. A. Oro, C. Claver, M. A. Garralda, *J. Organomet. Chem.* **1976**, *105*, 365−370.

[16] [16a] J. L. Herde, J. C. Lambert, C. V. Senoff, M. A. Cushing, *Inorg. Synth.* **1974**, *15*, 18−21. − [16b] R. Usón, L. A. Oro, F. Ibañez, *Rev. Acad. Ciencias Zaragoza* **1975**, *31*, 169.

[17] J. A. Darr, S. R. Drake, M. B. Hursthouse, K. M. Abdulmalik, *Inorg. Chem.* **1994**, *32*, 5704−5708.

[18] G. M. Sheldrick, SHELXS-86 and SHELXS-97, *Acta Crystallogr., Sect. A* **1990**, *46*, 467.

[19] G. M. Sheldrick, SHELXL-93 and SHELXL-97, *Program for Crystal Structure Refinement*, University of Göttingen, **1993**.

[20] N. P. C. Walker, D. Stuart, *Acta Crystallogr., Sect. A* **1983**, *39*, 158 (adapted for FAST geometry by A. Karaulov, University of Wales, Cardiff, **1991**).

[21] [21a] R. H. Blessing, *Acta Crystallogr., Sect. A* **1995**, *51*, 33−37. − [21b] R. H. Blessing, *J. Appl. Cryst.* **1997**, *30*, 421−426.

Received February 12, 2001
[I01049]

Reactions of *t*Bu-Calix[6]arene with Lanthanide Triflates: Synthesis and Crystal Structure Determination of Novel Bimetallic Calixarene Complexes of La, Sm and Yb

Pascal C. Leverd,*[a] David Rinaldo,[a] and Martine Nierlich[a]

Keywords: O ligands / Calixarenes / Lanthanides / N ligands

The reactions of *t*Bu-calix[6]arene (H_6L) with $Ln(O_3SCF_3)_3$ (Ln = La, Sm, Yb) were used to isolate $[\{La(O_3SCF_3)(pyridine)_7\}_2H_2L]$ (**1**), $[\{Sm(O_3SCF_3)(pyridine)_4\}_2H_2L]$ (**2**) and $[\{Yb(O_3SCF_3)(terpyridine)(pyridine)\}_2H_2L]$ (**3**), three novel bimetallic calixarene complexes of the lanthanides. The solid state structures of **2** and **3** were determined by X-ray crystallography revealing compounds where the two metal cations are anchored on both sides of the macrocycle in the 1,2,3-alternate conformation. Compounds **1**–**3** are the first bis-alkoxy triflate species $\{M(OR)_2(O_3SCF_3)\}$ to be characterized in lanthanide coordination chemistry.

Introduction

Calixarenes consist of phenolic units linked by methylene bridges into a macrocyclic arrangement. These molecules, and their various substituted derivatives, make up one of the most important families of supramolecular chemistry.[1] From a coordination chemistry point of view, the parent unsubstituted calixarenes can be considered as large, flexible polyalkoxide ligands whose size and flexibility vary with the number of their phenolic units.[2] The interest and fascinating potential of this class of molecules for the design of new metal complexes is well illustrated by calix[6]arene, which has already been used for the synthesis of compounds containing one,[3] two,[4] three,[5] and even five[6] metal cations. Moreover, like all calix[$n > 5$]arenes, it has a tendency to act as a "cluster keeper"[2c,7] and has been used to stabilise polymetallic species of uranium,[2c] titanium[8] and potassium.[9]

Although the donor properties of the calixarenes have long prompted the interest of coordination chemists in their search for new ligands well-suited for the large and hard cations of the f-elements,[2d] it seems that the coordination chemistry of calix[6]arene as a ligand for the lanthanide family has not yet been investigated in detail. In fact the europium complex $[Eu(H_4L)(OH)(dmf)_6]$ (H_6L = *t*Bu-calix[6]arene) is the only 4f-metal complex of a calix[6]arene derivative whose crystal structure has been solved.[3a] This is all the more surprising, as the supposed most usual 1,2,3-alternate conformation of this macrocycle suggests that it should be an ideal platform for the complexation of two trivalent cations on both sides of the inverted cone (Figure 1). The only example of a calix[6]arene derivative complexing two metal cations is the dimeric $[UO_2(H_2L)]_2$,[4] where the uranyl units (UO_2^{2+}) are sandwiched between the two organic macrocycles in a distorted pinched-cone conformation.

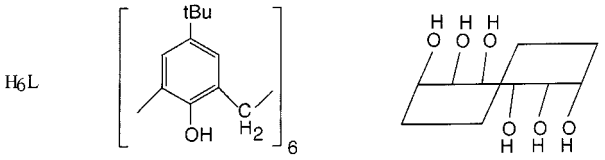

Figure 1. Schematic representation of the 1,2,3-alternate conformation of H_6L

In order to improve the knowledge of the use of H_6L as a ligand towards the lanthanides and to test the possibility of complexing two metal cations on both its coordination sites, we set out to study the reactions of H_6L with lanthanide triflates. We report herein the synthesis of $[\{La(O_3SCF_3)(pyridine)_7\}_2H_2L]$ (**1**), $[\{Sm(O_3SCF_3)(pyridine)_4\}_2H_2L]$ (**2**) and $[\{Yb(O_3SCF_3)(terpyridine)(pyridine)\}_2H_2L]$ (**3**). The solid state structures of **2** and **3** have been determined by X-ray crystallography. Compounds **1**–**3** are the first bis-alkoxy triflate species $\{M(OR)_2(O_3SCF_3)\}$ to be characterized in lanthanide coordination chemistry.

Results and Discussion

Treatment of $Ln(O_3SCF_3)_3$ with H_6L in pyridine led to the formation of a pale-yellow solution of $[\{Ln(O_3SCF_3)(pyridine)_n\}_2H_2L]$ [Scheme 1; Ln = La (**1**), Sm (**2**)]. In the case of ytterbium, an insoluble yellow powder, probably closely related to **1** and **2**, was instantly formed by the reaction. This precipitate was insoluble in hot pyridine and had a tendency to decompose in the other organic solvents.[10] However, it could be successfully dissolved in a mixture of terpyridine and pyridine to afford a bright orange solution of the complex $[\{Yb(O_3SCF_3)(terpyridine)(pyridine)\}_2H_2L]$ (**3**). The synthesis of **3** can

[a] CEA-Saclay, Service de Chimie Moléculaire, Bât. 125, 91191 Gif sur Yvette, France
Fax: (internat.) +33-1/6908-6640
E-mail: leverd@drecam.cea.fr

 © WILEY-VCH Verlag GmbH, 69451 Weinheim, 2001 1434–1948/01/0808–2021 $ 17.50+.50/0

easily be achieved from the addition of stoichiometric amounts of the three reagents in pyridine.

$$2\,Ln(O_3SCF_3)_3 + H_6L \xrightarrow{\text{pyridine}}$$

$$[\{Ln(O_3SCF_3)(pyridine)_x\}_2H_2L] + 4\,[HNC_5H_5][O_3SCF_3]$$

(Ln = **L**a, Sm, x = 7, 4)

$$2\,Yb(O_3SCF_3)_3 + H_6L + terpyridine \xrightarrow{\text{pyridine}}$$

$$[\{Yb(O_3SCF_3)(pyridine)(terpyridine)\}_2H_2L] + 4\,[HNC_5H_5][O_3SCF_3]$$

Scheme 1

One difficulty we had to circumvent in order to fully characterise complexes **1**–**3** was their rapid decomposition when isolated as solids. Although the solutions of the complexes in pyridine can be kept long enough to proceed with crystallisation experiments and analyses, in the form of microcrystalline powders they invariably turned to dark green after a few hours under argon or N_2,[11] even when the samples were kept in the dark to prevent light-induced reactions. No further complexes could be isolated from this stage. This transformation, which has not yet been understood, affects **2** and **3** completely within a few hours, but is slower for **1**. This somewhat puzzling behaviour (air-sensitive complexes are usually less sensitive in the solid state than in solution) could be due to the displacement of coordinated pyridine molecules under vacuum, leading to an increased reactivity with even traces of water or air, or to a redox process leading to the degradation of the calixarene, possibly into its quinone form. As a result, all elemental analysis had to be performed on freshly isolated samples. Compared to its Sm and Yb counterparts, **1** is highly soluble in pyridine thus we did not manage to grow single crystals suitable for an X-ray analysis.[12] The exact stoichiometry of complex **1** had to be determined by mass spectrometry. The solubility of **1** in pyridine, combined with its decomposition in the other usual organic solvents, was a hindrance to its complete purification.[10] In the end, we did not manage to synthesize **1** in its elementally pure form, but only as a triflic acid containing mixture. Solutions of **2** and **3** were allowed to stand and, after a few days, crystals suitable for X-ray crystallography could be recovered. The crystal structures were solved and revealed that in both **2** and **3**, *t*Bu-calix[6]arene acts as a double-bidentate ligand that is able to bind a metal cation on its two symmetry-related coordination sites (Figure 2 and 3).

The molecular structures of **2** and **3** present similarities in the way the trivalent cations are bound to the macrocycle. The metal centres are coordinated by seven donor atoms, the coordination geometry being a distorted, capped trigonal prism.[13] Two σ-bonds are made with phenolate groups of the calixarene. The mean M–O distances are equal to 2.179(5) Å in **2** and 2.07(2) Å in **3**, in good agreement with similar bond lengths found in the literature.[14] The crystal structures of samarium and ytterbium complexes of calixarene derivatives containing an aryloxide bond have only been reported on two occasions but never yet for the parent calixarenes.[15] One unchanged triflate group makes the last σ-bond to the metal. The M–O(triflate) bonds are significantly longer than the alkoxide one and equal to 2.449(4) Å in **2** and to 2.30(1) Å in **3**. Although only a few triflate complexes of Sm and Yb have been characterized crystallographically,[16] bond lengths of that order of magnitude are to be expected from this fairly labile ligand. The rest of the coordination sphere is occupied by nitrogen ligands coming from four pyridine molecule in **2** and from one pyridine molecule and one ter-

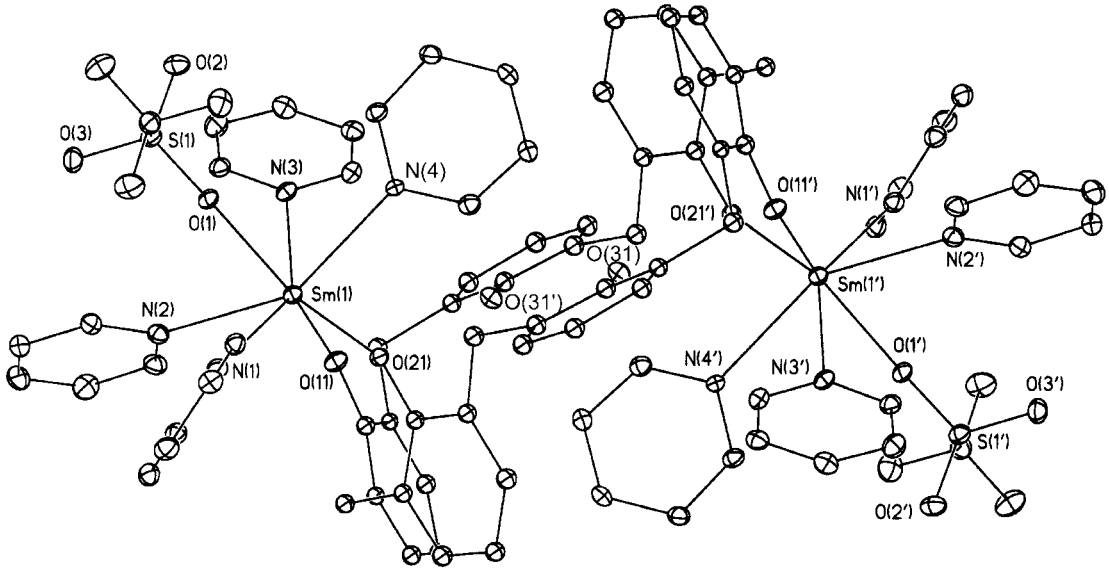

Figure 2. X-ray structure of complex **2** showing partial atom labelling; all *t*Bu groups and hydrogen atoms have been omitted for clarity; selected bond lengths [Å] and angles [°]: Sm(1)–O(1) 2.449(4), Sm(1)–O(11) 2.184(5), Sm(1)–O(21) 2.174(4), Sm(1)–N(1) 2.610(5), Sm(1)–N(2) 2.629(6), Sm(1)–N(3) 2.672(5), Sm(1)–N(4) 2.604(5)

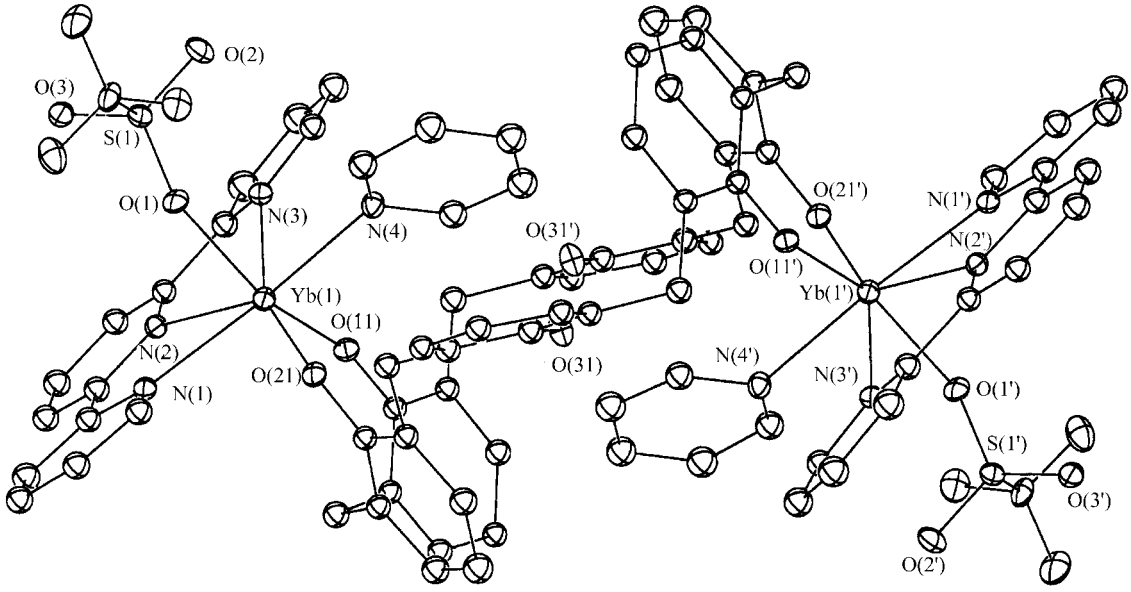

Figure 3. X-ray structure of complex **3** showing partial atom labelling; all *t*Bu groups and hydrogen atoms have been omitted for clarity; selected mean bond lengths [Å] and angles [°]: Yb(1)−O(1) 2.301(4), Yb(1)−O(11) 2.071(6), Yb(1)−O(21) 2.081(9), Yb(1)−N(1) 2.48(2), Yb(1)−N(2) 2.49(2), Yb(1)−N(3) 2.508(5), Yb(1)−N(4) 2.472(4)

pyridine ligand in **3**. The mean M−N bond lengths for the pyridine ligand are 2.63(3) Å in **2** and 2.472(4) Å in **3**, and 2.49(2) Å for the terpyridine ligand in **3**. All M−N distances are unremarkable when compared to literature data.[17] Along the series **1−3**, the number and type of N donor ligands adapt to the decreasing size of the lanthanide cation: whereas seven pyridine molecules are bound to the large La cation in **1**, only four remain on the Sm complex **2** and one in the Yb complex **3,** where the coordination sphere of the cation is completed by a terpyridine molecule. Interestingly, the replacement of three pyridine ligands in **2** by a terpyridine molecule in **3** does not lead to major differences in the coordination geometry of the two complexes, probably because the smaller bite angle imposed by the chelating ligand is balanced by the ionic radius of the smaller cation [N(1)−M−N(3) angles are equal to 147.0(1)° and 126.3(4)° in **2** and **3**, respectively]. The main crystallographic difference between **2** and **3** is the presence of two independent molecules in the asymmetric unit of **3**, both sitting on an inversion centre, thus resulting in a larger cell volume.

The organic macrocycles in **2** and **3** are deprotonated four times and both adopt the same distorted 1,2,3-alternate conformation. The presence of a hydrogen bond between O(31) and O(11′) in **2**, which is absent in **3** [O(31)−O(11′) bond lengths equal to 2.976(5) Å and 3.85(2) Å in **2** and **3**, respectively], could be one reason for the differences that can be observed in the torsion angles φ and χ[1a] of the two complexes.[18] Interestingly, the pyridine ligand bearing N(4) is located within the macrocycle in a niche that is delimited by the aromatic faces bearing O(11′) and O(21′), their methylene bridge and *t*Bu groups.[19] In this respect, the calixarene is both a first- and a second-sphere ligand of the lanthanide cation.[20]

As far as we are aware, such bis-alkoxy triflate species {$M(OR)_2$(triflate)} as **1−3** have not yet been encountered in the coordination chemistry of terminal lanthanide alkoxides. This new combination of ligands, where a metal is anchored by two strong alkoxide bonds to an organic platform but retains a reactive site, could be of interest especially in the field of catalysis in which f-metal alkoxides have long been renowned for their activity.[21] In this respect, calix[4]arene complexes were successfully used as models of d-metal oxide surfaces.[22] The synthesis of **1−3** further reinforces the ideas that large polyalkoxide ligands, such as calixarenes, are appropriate for the design of new metal-complex architectures, and that a rich chemistry can be built at the boundary between macrocyclic, supramolecular and coordination chemistries.

Experimental Section

General: All NMR spectra were performed on a Bruker DPX-200. ^{19}F NMR spectra were referenced internally by addition of $CFCl_3$. Elemental analyses were performed at Service de Microanalyse, I.C.S.N., C.N.R.S., 91198 Gif sur Yvette, France. All reactions were performed in a glove box under a dry N_2 atmosphere. All chemicals were purchased by Aldrich and used without further purification. H_6L was dried under vacuum for 12 hours at 323 K. Pyridine was dried on Na (CAUTION!) and distilled prior use. The mass spectrum of **1** was recorded on a ZAB HF VG-analytical F.A.B. mass spectrometer.

Synthesis of 1: [$La(O_3SCF_3)_3$] (0.150 g, 0.256 mmol) was treated with H_6L[6] (0.125 g, 0.128 mmol) in pyridine (20 mL) at 293 K for 2 hours. The colourless solution obtained was filtered, concentrated under vacuum to 5 mL and toluene was then added (5 mL). After 45 days at 253 K, the yellow powder that had deposited was separated by filtration, washed with toluene and dried under vacuum

to afford $[\{La(NC_5H_5)_2(O_3SCF_3)\}_2(H_2L)]\cdot 2.7(HO_3SCF_3)$ (0.172 g, 0.076 mmol, 30%). – ^{1}H NMR: δ = 0.74 (s, 18 H, *t*Bu), 1.29 (s, 36 H, *t*Bu), 2.82 (d, *J* = 11 Hz, 2 H, Ar–CH_2–Ar), 4.27 (d, *J* = 13 Hz, 4 H, Ar–CH_2–Ar), 4.28 (d, *J* = 13 Hz, 4 H, Ar–CH_2–Ar), 4.36 (d, *J* = 11 Hz, 2 H, Ar–CH_2–Ar), 7.12 (s, 12 H, ArH), 15.35 (br., 2 H, OH). – ^{19}F NMR: δ = –6.56 ($CFCl_3$) – $C_{90.7}H_{102.7}F_{14.1}La_2N_4O_{20.1}S_{4.7}$ (2267.02): calcd. C 48.05, H 4.57, 2.47; found C 48.09, H 4.76, N 2.49.[23] During the course of the reaction an aliquot of the pyridine solution was taken and sent to the mass analysis: *m*/*z* = 2653.94 ($[\{La(O_3SCF_3)(pyridine)_7\}_2H_2L]$).

Synthesis of 2: $[Sm(O_3SCF_3)_3]$ (0.150 g, 0.251 mmol) was treated with H_6L[6] (0.122 g, 0.125 mmol) in pyridine (20 mL) at 293 K for 2 hours. The pale-yellow solution obtained was filtered and concentrated under vacuum to 10 mL. It was then left standing for two days to afford a colourless microcrystalline powder that was filtered off, washed with cold pyridine and dried in vacuo to afford $[\{Sm(NC_5H_5)_6(O_3SCF_3)\}_2(H_2L)]\cdot 0.5(HO_3SCF_3)$ (0.204 g, 0.096 mmol, 77%). – $C_{98.5}H_{110.5}F_{7.5}N_6O_{13.5}S_{2.5}Sm_2$ (2117.87): calcd. C 55.86, H 5.26, N 3.97; found C 55.78, H 4.83, N 3.95. Several recrystallizations from pyridine enabled us to separate $[\{Sm(NC_5H_5)_3(O_3SCF_3)\}_2(H_2L)]$ from residual triflic acid (0.062 g, 0.030 mmol, 24%) – $C_{98}H_{110}F_6N_6O_{12}S_2Sm_2$ (2042.83): calcd. C 57.62, H 5.43, N 4.11; found C 58.17, H 5.62, N 3.88.[23]

Synthesis of 3: $[Yb(O_3SCF_3)_3]$ (0.150 g, 0.242 mmol) was treated with H_6L[6] (0.118 g, 0.121 mmol) and terpyridine (0.057 g, 0.244 mmol) in pyridine (20 mL) at 293 K for 2 hours. The orange microcrystalline powder that formed was filtered off, washed with pyridine and dried in vacuo to afford $[\{Yb(N_3C_{15}H_{11})(O_3SCF_3)\}_2(H_2L)]\cdot(NC_5H_5)$ (0.171 g, 0.079 mmol, 65%). – $C_{103}H_{107}F_6N_7O_{12}S_2Yb_2$ (2159.23): calcd. C 57.30, H 5.00, N 4.54; found C 56.98, H 5.01, N 4.68.[23]

X-ray Crystallographic Studies: Crystal data collection was performed on a Nonius Kappa-CCD diffractometer equipped with a fibre glass collimator.

Crystal Data of 2·4(NC_5H_5): $C_{128}H_{140}F_6N_{12}O_{12}S_2Sm_2$ (2517.34), 0.14 × 0.12 × 0.10 mm^3, triclinic, $P\bar{1}$, *Z* = 1, *a* = 14.852(3), *b* = 15.160(3), *c* = 15.364(4) Å, α = 91.17(3)°, β = 118.85(3), γ = 92.55(3)°, *V* = 3023(2) Å^3, $\rho_{calcd.}$ = 1.382 g·cm^{-3}, *F*(000) = 1298, $2\theta_{max}$ = 51.42°, graphite-monochromated Mo-K_α radiation (λ = 0.71073 Å), μM_o = 1.070 cm^{-1}, *T* = 100 K. The structure was solved by direct methods[24] and refined on F^2.[25] Of the 20805 reflections measured, 10577 were found to be independent (R_{int} = 0.113), 6735 of which were considered as observed [$I > 2\sigma(I)$]. All reflections were used in the refinement of the 611 parameters, leading to a final R_1 of 0.0625 and an R_{all} of 0.1205. wR_{obs} and wR_2 were equal to 0.1134 and 0.1343, respectively. All atoms were considered anisotropic with the exception of the carbon atoms of the calixarene core, which were kept isotropic in order to keep a reasonable data/parameter ratio. Hydrogen atoms were introduced in the calculation as riding on their parent atom. The goodness-of-fit parameter *S* was 0.983 and the maximum residual density 0.620 eÅ^{-3}. Two other cells corresponding to different solvates were found for the monocrystals of **1** recrystallised from pyridine: **1**·3(NC_5H_5): *a* = 14.84(1), *b* = 15.15(1), *c* = 15.34(1) Å, α = 86.45(3)°, β = 61.15(3), γ = 87.53(3)°, *V* = 3014(7) Å^3; **1**: *a* = 14.929(3), *b* = 13.799(3), *c* = 28.128(5) Å, β = 94.62(3), *V* = 5776(4) Å^3.

Crystal Data of 3·4.5(NC_5H_5): $C_{130.5}H_{134.5}F_6N_{12.5}O_{12}S_2Yb_2$ (2594.21), 0.14 × 0.12 × 0.12 mm^3, triclinic, $P\bar{1}$, *Z* = 2, *a* = 15.679(3), *b* = 15.917(3), *c* = 26.833(4) Å, α = 102.52(3)°, β = 93.12(3), γ = 107.18(3)°, *V* = 6195(2) Å^3, $\rho_{calcd.}$ = 1.391 g.cm^{-3}, *F*(000) = 2654, $2\theta_{max}$ = 51.56°, graphite-monochromated Mo-K_α radiation (λ = 0.71073 Å), μM_o = 1.607 cm^{-1}, *T* = 100 K. The structure was solved by direct methods[24] and refined on F^2.[25] Of the 32794 reflections measured, 19393 were found to be independent (R_{int} = 0.124), 8349 of which were considered as observed [$I > 2\sigma(I)$]. All reflections were used in the refinement of the 864 parameters, leading to a final R_1 of 0.0884 and an R_{all} of 0.2199. wR_{obs} and wR_2 were equal to 0.1830 and 0.2444, respectively. Solvent pyridine molecules were constrained to regular hexagons. All non-carbon atoms were considered anisotropic, with the exception of the nitrogen atoms of the solvated pyridine molecules. Hydrogen atoms were introduced in the calculation as riding on their parent atoms. The goodness-of-fit parameter *S* was 0.970 and the maximum residual density 0.943 eÅ^{-3}.

Crystallographic data (excluding structure factors) for the structure(s) included in this paper have been deposited with the Cambridge Crystallographic Data Centre as supplementary publication no. CCDC-150779 [**2·4(NC_5H_5)**] and -150780 [**3·4.5(NC_5H_5)**]. Copies of the data can be obtained free of charge on application to CCDC, 12 Union Road, Cambridge CB2 1EZ, UK [Fax: (internat.) +44-1223/336-033; Email: deposit@ccdc.cam.ac.uk].

Acknowledgments

We would like to thank Dr. Jacques Vicens for helpful discussions throughout the work.

[1] [1a] C. D. Gutsche, in *Calixarenes Revisited* (Ed. J. F. Stoddart), *Monographs in Supramolecular Chemistry* **1998**, Royal Society of Chemistry, Cambridge. – [1b] A. Ikeda, S. Shinkai, *Chem. Rev.* **1997**, 1713–1734. – [1c] V. Böhmer, *Angew. Chem. Int. Ed. Engl.* **1995**, *34*, 713–745.

[2] [2a] C. Wieser, C. B. Dieleman, D. Matt, *Coord. Chem. Rev.* **1997**, *165*, 93–161. – [2b] J.-C. Bünzli, J. M. Harrowfield, in *Calixarenes, A Versatile Class of Macrocyclic Compounds* (Eds.: J. Vicens, V. Böhmer), Kluwer Academic Publishers, Dordrecht, **1991**, pp. 211–231. – [2c] J. M. Harrowfield, *Gazz. Chim. Ital.* **1997**, *127*, 663–671. – [2d] P. Thuéry, M. Nierlich, J. Harrowfield, M. Ogden, in *Calixarene 2001* (Eds.: Z. Asfari, V. Böhmer, J. Harrowfield, J. Vicens), Kluwer Academic Publishers, Dordrecht, in press.

[3] [3a] L. M. Engelhardt, B. M. Furphy, J. M. Harrowfield, D. L. Kepert, A. H. White, F. R. Wilner, *Aust. J. Chem.* **1988**, *41*, 1465–1476.[3b] P. C. Leverd, M. Nierlich, *Eur. J. Inorg. Chem.* **2000**, 1733–1738.

[4] P. Thuéry, M. Lance, M. Nierlich, *Supramol. Chem.* **1996**, *7*, 183–185.

[5] P. C. Leverd, P. Berthault, M. Lance, M. Nierlich, *Eur. J. Inorg. Chem.* **1998**, 1859–1862.

[6] J. M. Smith, S. G. Bott, *Chem. Commun.* **1996**, 377–378.

[7] [7a] P. C. Leverd, I. Dumazet-Bonnamour, R. Lamartine, M. Nierlich, *Chem. Commun.* **2000**, 493–494. – [7b] P. Thuéry, M. Nierlich, B. Souley, Z. Asfari, J. Vicens, *J. Chem. Soc., Dalton Trans.* **1999**, 2589–2594.

[8] G. D. Andreetti, G. Calestani, F. Ugozzoli, A. Arduini, E. Ghidini, A. Pochini, R. Ungaro, *J. Incl. Phenom.* **1987**, *5*, 123–126.

[9] K. Murayama, K. Aoki, *Inorg. Chim. Acta* **1998**, *281*, 36–42.

[10] With the exception of pyridine and for **1** of the 1:1 mixture of toluene/pyridine, compounds **1–3** decompose in more or less all the solvents or mixtures of solvents we tried to dissolve them in. They were too reactive to survive in solution containing anhydrous pentane, diethyl ether, tetrahydrofuran or toluene for a long time.

[11] The change of colour from pale-yellow or orange to a dark green was observed for the microcrystalline powders of **1**−**3** even when kept in closed tubes in N_2 or argon atmosphere glove boxes ($O_2 < 1$ ppm). In the end, the complexes had to be kept in glass tubes sealed under vacuum to prevent decomposition.

[12] Concentrated solutions of **1** (0.5 g, 2−5 mL) in pyridine and in mixtures of pyridine and toluene were left standing at room temperature and in the fridge (253 K) for several months but never grew any single crystal suitable for an X-ray analysis.

[13] The geometry around the metal centre is a distorted, capped trigonal prism in both **2** and **3**. O(11)−O(21)−N(1) and N(4)−N(3)−O(1) define the faces of the prism and N(2) caps the O(11)−N(3)−O(1)−N(1) face.

[14] [14a] Z. Hou, A. Fujita, T. Miyano, H. Yamazaki, Y. Wakatsuki, *J. Am. Chem. Soc.* **1998**, *120*, 754−766. − [14b] Y. Yao, Q. Shen, J. Sun, F. Xue, *Acta Crystallogr., Sect. C* **1998**, 625−627. − [14c] G. B. Deacon, T. Feng, S. Nickel, M. I. Ogden, A. H. White, *Aust. J. Chem.* **1992**, *45*, 671−683. − [14d] D. L. Clark, J. C. Gordon, J. G. Watkin, J. C. Huffman, B. D. Zwick, *Polyhedron* **1996**, *15*, 2279−2289.

[15] [15a] P. D. Beer, M. G. B. Drew, M. Kan, P. B. Leeson, M. I. Ogden, G. Williams, *Inorg. Chem.* **1996**, *35*, 2202−2211. − [15b] P. Thuéry, M. Nierlich, J. Vicens, H. Takemura, *Polyhedron* in press.

[16] [16a] M. Nishiura, Y. Yamanoi, H. Tsuruta, K. Yamaguchi, T. Imamoto, *Bull. Soc. Chim. Fr.* **1997**, *134*, 411−420. − [16b] J. Stern, R. D. Fisher, *J. Organomet. Chem.* **1992**, *430*, C1−C4. − [16c] P. H. Smith, K. N. Raymond, *Inorg. Chem.* **1985**, *24*, 3469−3477.

[17] [17a] N. Froelich, P. B. Hitchcock, J. Hu, M. F. Lappert, J. R. Dilworth, *J. Chem. Soc., Dalton Trans.* **1996**, 1941−1946. − [17b] J. Lee, D. Freedman, J. H. Melman, M. Brewer, L. Sun, T. J. Emge, F. H. Long, J. G. Brennan, *Inorg. Chem.* **1998**, *37*, 2512−2519. − [17c] M. Berardini, J. Lee, D. Freedman, J. Lee, T. J. Emge, J. G. Brennan, *Inorg. Chem.* **1997**, *36*, 5772−5776. − [17d] C. J. Kepert, L. Weimin, B. W. Skelton, A. H. White, *Aust. J. Chem.* **1994**, *47*, 365−384.

[18] Listing of the pairs of torsion angles φ and χ in **1**: +81.6 −89.6, +10.7 −86.0, −127.2 +69.2, and in the two molecules of **2**: +86.7 −76.9, +14.4 −123.9, −103.2 +40.9 and +96.6 −71.9, +32.5 −130.4, −95.7 +38.7. This succession of angles designates the conformation as C_i + −, + −, − +, − +, − +, + −, expect for the distorted 1,2,3-alternate conformation.[1a]

[19] The six atoms of the pyridine molecule bearing N(4), the lanthanide cation and the methylene bridge between the aromatic faces bearing O(11′) and O(21′) are found within a plane (standard deviation ±0.12 Å in **2** and ±0.27 Å in **3**). In both molecular structures, the carbon atom in the *para* position on the pyridine molecule is located at a distance inferior to 3.60 Å to the centroid of the aromatic face bearing O(11′) and also at a distance inferior to 4.00 Å to the carbon atoms of the *t*Bu groups and to at least two carbon atoms belonging to each of the aromatic rings bearing O(11′) and O(21′).

[20] J. L. Atwood, G. William Orr, K. D. Robinson, *Supramol. Chem.* **1994**, *3*, 89−91.

[21] [21a] S. J. McLain, N. E. Drysdale, *Polym. Prep.* **1992**, *33*, 174−175. − [21b] H. Abe, S. Inoue, *J. Chem. Soc., Chem. Commun.* **1994**, 1197−1198. − [21c] H. Sasai, T. Suzuki, N. Itoh, K. Tanaka, T. Date, K. Okamura, M. Shibasaki, *J. Am. Chem. Soc.* **1993**, *115*, 10372−10373. − [21d] C. Quian, C. Zhu, T. Huang, *J. Chem. Soc., Perkin Trans.* **1998**, 2131−2132.

[22] L. Giannini, G. Guillemot, E. Solari, C. Floriani, N. Re, A. Chiesi-Villa, C. Rizzoli, *J. Am. Chem. Soc.* **1999**, 2797−2807.

[23] Once the drying under vacuum was completed, the powder of the complexes was immediately brought to the microanalysis laboratory and the analyses performed within two hours.

[24] G. M. Sheldrick, *SHELXS-86, A Program for the Solution of Crystal Structures*, University of Göttingen, Germany, **1990**.

[25] G. M. Sheldrick, *SHELXL-90, A Program for the Refinement of Crystal Structures*, University of Göttingen, Germany, **1993**.

Received October 19, 2000
[I00396]

Dinuclear Cobalt(II) Complexes of an Acyclic Phenol-Based Dinucleating Ligand with Four Methoxyethyl Chelating Arms − First Magnetic Analyses in an Axially Distorted Octahedral Field

Hiroshi Sakiyama,*[a] Rie Ito,[a] Hitoshi Kumagai,[b] Katsuya Inoue,[b] Masatomi Sakamoto,[a] Yuzo Nishida,[a] and Mikio Yamasaki[c]

Keywords: Dinuclear cobalt(II) complex / Dinucleating ligand / Crystal structure / Magnetic properties

An end-off type acyclic ligand with four methoxyethyl chelating arms, 2,6-bis[bis(2-methoxyethyl)aminomethyl]-4-methylphenol [H(bomp)], formed dinuclear cobalt(II) complexes $[Co_2(bomp)(MeCO_2)_2]BPh_4$ (**1**) and $[Co_2(bomp)(PhCO_2)_2]BPh_4$ (**2**). X-ray analysis revealed that complex **1**·$CHCl_3$ contains two cobalt ions bridged by a phenolic oxygen and two acetate groups, forming a μ-phenoxo-bis(μ-acetato)dicobalt(II) core. Magnetic susceptibility was measured for **1** and **2** over the temperature range 1.8–300 K. The data were successfully analyzed using a new theoretical method assuming an axially distorted octahedral field (Δ = 753 and 775 cm^{-1}, respectively) for each cobalt(II) ion to reveal weak antiferromagnetic interactions (J = −0.96 and −1.74 cm^{-1}, respectively).

Introduction

Dinuclear cobalt complexes have attracted our interest since the active site structure of methionine aminopeptidase (MAP, EC 3.4.11.18) was revealed to contain a bis(μ-carboxylato)dicobalt(II,II) core.[1] From the point of view of coordination chemistry, it is interesting and invaluable to study the relationship between dinuclear structures and their properties and functions. In order to synthesize the dinuclear metal complexes systematically, the development of multinucleating ligands is of importance. We have developed an acyclic dinucleating ligand 2,6-bis[bis(2-methoxyethyl)aminomethyl]-4-methylphenol [H(bomp)].[2] The dinuclear zinc(II) complexes[2] and dinuclear manganese(II) complexes[3] of this ligand have been reported. The ligand consists of a phenolate head unit, two aminomethyl shoulders, and four methoxyethyl arms, providing two NO_3 coordination sites. The dizinc(II) complexes have been shown to possess an aminopeptidase function in removing *N*-terminal amino acids from substrates, and the dimanganese(II) complexes have been demonstrated to have a catalytic catalase function in the disproportionation of hydrogen peroxide into water and molecular oxygen.

We are also interested in the magnetism of dinuclear cobalt(II,II) complexes. The lowest orbital state of the free cobalt(II) ion is $^4F_1$, and the second lowest $^4P_1$ is more than 10^4 cm^{-1} higher. In the week field of O_h symmetry,[4] the $^4F_1$ term sprits into $^4T_{1g}$, $^4T_{2g}$, and $^4A_{2g}$ terms, in that order, whereas the $^4P_1$ term is not split and remains in the $^4T_{1g}$ state. As the ground state of the high-spin cobalt(II) is $^4T_{1g}$,

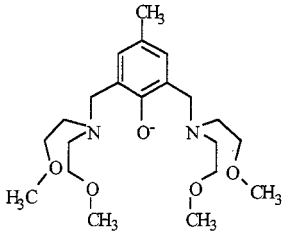

Scheme 1

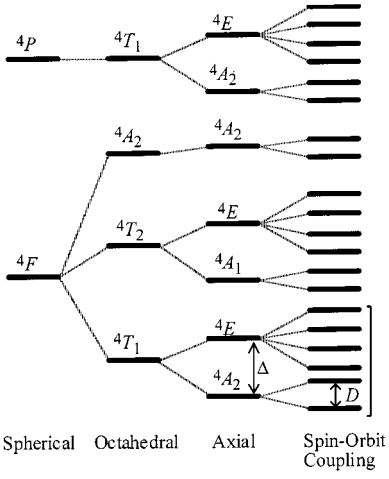

Scheme 2. Energy diagram for a high-spin cobalt(II) ion in an axially distorted octahedral environment

[a] Department of Material and Biological Chemistry, Faculty of Science, Yamagata University,
Kojirakawa, Yamagata 990−8560, Japan
Fax: (internat.) +81−23−628−4591
E-mail: Saki@sci.kj.yamagata-u.ac.jp
[b] Institute for Molecular Science,
Myodaiji, Okazaki 444−8585, Japan
[c] X-ray Research Laboratory, Rigaku Corporation,
Matsubara 3-9-12, Akishima, Tokyo 196−8666, Japan

Supporting information for this article is available on the WWW under http://www.wiley-vch.de/home/eurjic or from the author.

 © WILEY-VCH Verlag GmbH, 69451 Weinheim, 2001 1434−1948/01/0808−2027 $ 17.50+.50/0

under pure O_h symmetry, the contribution of the orbital momentum cannot be ignored, and it is the most significant one among 3d transition elements.[5] The orbital momentum complicates the magnetic equations, a difficulty that has prevented many coordination chemists from analyzing the magnetic data of the cobalt(II) complexes.

As long ago as 1963, Lines introduced a calculation method for $^4T_{1g}$-ground-state magnetism[6] in an axially distorted octahedral field, considering the axial field splitting and the spin-orbit coupling. In the 1960s, Figgis also introduced a method considering the axial field for $^2T_{1g}$,[7] $^3T_{1g}$,[8] $^5T_{1g}$,[9] and $^4T_{1g}$,[10] showing that the axial field treatment is useful for analyzing cryomagnetic data of mononuclear cobalt(II) complexes. This successful study corresponded to a mononuclear case, but, in 1971, Lines reported a theory for the analysis of the magnetic coupling between two high-spin cobalt(II) ions of pure O_h symmetry using temperature-dependent Hamiltonian.[11] This remarkable theory enabled the analysis of the magnetic data of some dinuclear cobalt(II) complexes,[12] but it was limited to only highly symmetrical cases.

In this study, we have synthesized new dicobalt(II) complexes using the dinucleating ligand bomp$^-$, and their cryomagnetic data have been analyzed using a newly obtained set of magnetic equations for dinuclear cobalt(II) complexes in lower symmetry. In this method, the axial splitting parameter Δ is adopted according to Figgis and Lines, avoiding overparameterization, to describe the axial distortion. The axial splitting parameter Δ is defined as the splitting of the orbital degeneracy of the $^4T_{1g}$ term by the asymmetric ligand component, in the absence of any spin-orbit coupling, and is taken to be positive when the orbital singlet is lowest. This enables us to analyze the data using only four variables, the axial splitting parameter Δ, the spin-orbit coupling λ, the orbital reduction factor κ, and the coupling constant J. The axial zero-field splitting parameter D and the anisotropic g-factors, g_z and g_x, can be calculated using the four variables. To the best of our knowledge, this is the first standard analytic method for the magnetism of dinuclear high-spin cobalt(II) complexes in lower symmetry, except for the specific low-temperature study,[13] and these complexes are the first examples whose cryomagnetic data are analyzed in the whole temperature range using the method in lower symmetry.

Results and Discussion

X-ray Crystal Structure of Complex 1·CHCl$_3$

The crystal structure consists of $[Co_2(bomp)(MeCO_2)_2]^+$ complex cations, tetraphenylborate anions, and chloroform molecules in a 1:1:1 molar ratio. The structure of the complex cation is depicted in Figure 1. Selected distances and angles with their estimated standard deviations are listed in Tables 1 and 2. The complex cation consists of one dinucleating ligand bomp$^-$, two cobalt(II) ions, and two acetate groups. The two cobalt ions are bridged by the one phenolic oxygen of bomp$^-$ and the two acetate ions, forming a μ-phenoxo-bis(μ-acetato)dicobalt(II) core structure. The Co(1)···Co(2) separation is 3.3360(3) Å.

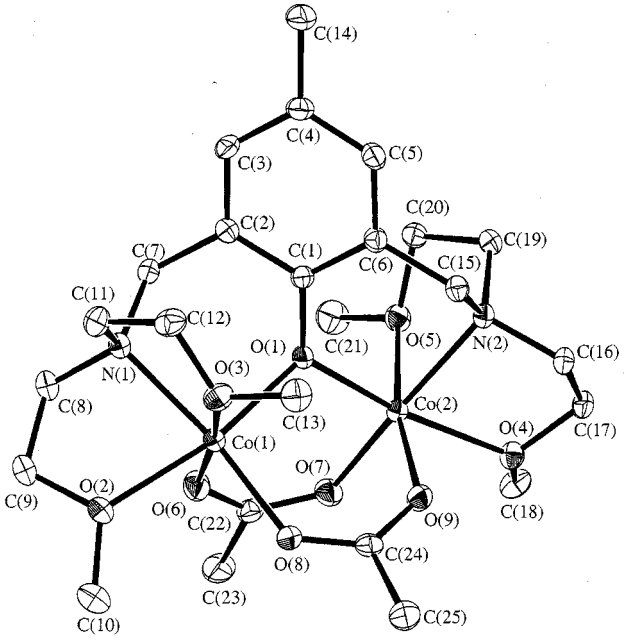

Figure 1. ORTEP[14] view of complex cation $[Co_2(bomp)(MeCO_2)_2]^+$ with the atom numbering scheme

Table 1. Selected distances (Å) for complex **1**·CHCl$_3$

atom	atom	distance	atom	atom	distance
Co(1)	O(1)	1.995(1)	Co(2)	O(1)	2.005(1)
Co(1)	O(2)	2.160(1)	Co(2)	O(4)	2.156(1)
Co(1)	O(3)	2.200(1)	Co(2)	O(5)	2.229(1)
Co(1)	O(6)	2.069(2)	Co(2)	O(7)	2.028(2)
Co(1)	O(8)	2.027(1)	Co(2)	O(9)	2.084(1)
Co(1)	N(1)	2.141(2)	Co(2)	N(2)	2.144(2)
Co(1)	Co(2)	3.3360(3)			

Table 2. Selected angles (°) for complex **1**·CHCl$_3$

atom	atom	atom	angle	atom	atom	atom	angle
O(1)	Co(1)	O(2)	166.04(6)	O(1)	Co(2)	O(4)	170.53(5)
O(1)	Co(1)	O(3)	93.73(6)	O(1)	Co(2)	O(5)	95.77(5)
O(1)	Co(1)	O(6)	92.46(6)	O(1)	Co(2)	O(7)	99.00(6)
O(1)	Co(1)	O(8)	100.27(6)	O(1)	Co(2)	O(9)	92.57(5)
O(1)	Co(1)	N(1)	92.07(6)	O(1)	Co(2)	N(2)	90.81(6)
O(2)	Co(1)	O(3)	91.23(6)	O(4)	Co(2)	O(5)	84.68(5)
O(2)	Co(1)	O(6)	82.16(6)	O(4)	Co(2)	O(7)	90.45(5)
O(2)	Co(1)	O(8)	92.90(6)	O(4)	Co(2)	O(9)	86.17(5)
O(2)	Co(1)	N(1)	76.20(6)	O(4)	Co(2)	N(2)	80.06(6)
O(3)	Co(1)	O(6)	173.29(6)	O(5)	Co(2)	O(7)	89.99(6)
O(3)	Co(1)	O(8)	88.47(6)	O(5)	Co(2)	O(9)	169.92(5)
O(3)	Co(1)	N(1)	78.02(6)	O(5)	Co(2)	N(2)	77.12(6)
O(6)	Co(1)	O(8)	92.98(6)	O(7)	Co(2)	O(9)	94.30(6)
O(6)	Co(1)	N(1)	99.17(6)	O(7)	Co(2)	N(2)	164.57(6)
O(8)	Co(1)	N(1)	162.30(6)	O(9)	Co(2)	N(2)	97.15(6)

Co(1) has a distorted octahedral geometry with O(1), O(2), O(3), and N(1) of bomp$^-$ and O(6) and O(8) of the two acetate groups. Coordination geometry around Co(2) is also distorted octahedral with O(1), O(4), O(5), and N(2) of bomp$^-$ and O(7) and O(9) of the two acetate groups. The geometries around Co(1) and Co(2) are very similar to each other, and the complex cation has a pseudo C_2 axis along C(14), C(4), C(1), and O(1). The least-squares plane of the aromatic ring of bomp$^-$ and the plane defined by Co(1), Co(2), and O(1) are twisted with a dihedral angle of 46.0°. The bond lengths between the cobalt atoms and axial ether oxygen atoms [2.200(1)−2.229(1) Å] are longer than those between cobalt atoms and equatorial ether oxygen atoms [2.156(1)−2.160(1) Å] (Figure 2). This tendency has also been observed in the related dizinc(II) complexes with acetate bridges.[2] However, in the dimanganese(II) complexes with benzoate bridges, all the manganese-oxygen(ether) bonds have almost the same length.[3] This may be explained by the steric repulsion between the two bridging benzoate ions and methoxy groups of the dinucleating ligand bomp$^-$. Thus, the symmetry around the metal ions in the benzoate-bridged complex cations is higher than that of the acetate complexes.

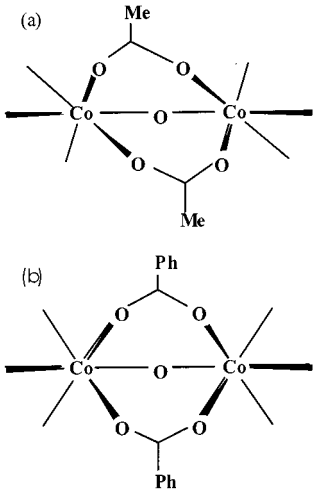

Figure 2. Schematic drawing of dinuclear cobalt(II) cores for (a) complex **1** and (b) complex **2**

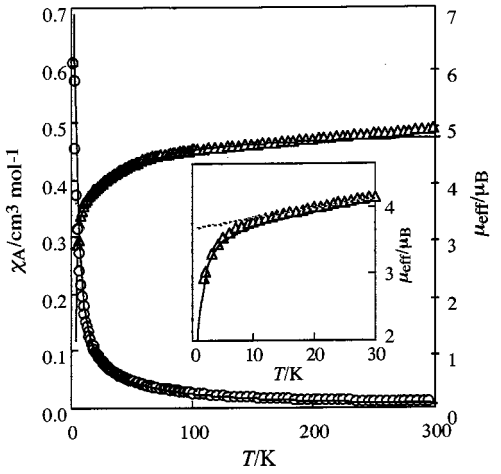

Figure 3. Temperature dependence of χ_A (O) and μ_{eff} (Δ) of the complex **1**. Dashed curves are based on equations (2a) in the text, using $\kappa = 0.96$, $\lambda = -140$ cm^{-1}, and $\Delta = 753$ cm^{-1}. Solid curves are based on a set of equations in the supplementary material section, using $\kappa = 0.96$, $\lambda = -140$ cm^{-1}, $\Delta = 753$ cm^{-1}, and $J = -0.96$ cm^{-1}

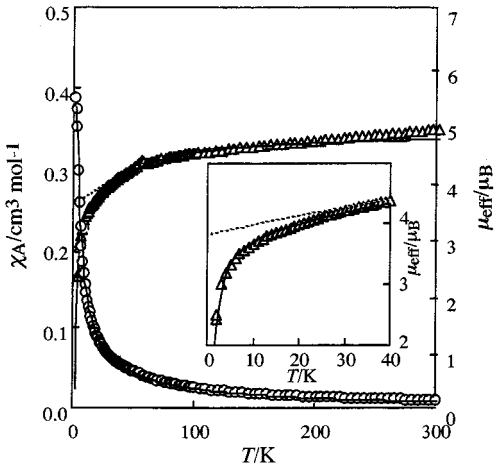

Figure 4. Temperature dependence of χ_A (O) and μ_{eff} (Δ) of the complex **2**. Dashed curves are based on equations (2a) in the text, using $\kappa = 0.92$, $\lambda = -156$ cm^{-1}, and $\Delta = 775$ cm^{-1}. Solid curves are based on a set of equations in the supplementary material section, using $\kappa = 0.92$, $\lambda = -156$ cm^{-1}, $\Delta = 775$ cm^{-1}, and $J = -1.74$ cm^{-1}

Magnetic Susceptibility of Complexes 1 and 2

Magnetic susceptibility measurements for cobalt complexes **1** and **2** were made on polycrystalline samples in the temperature range 1.8−300 K. The temperature dependence of χ_A and μ_{eff} per Co for **1** and **2** is shown in Figures 3 and 4. The μ_{eff} values per Co^{II} of the complexes at room temperature are 4.93 and 4.90 μ_B, respectively. These values are larger than the spin-only value of high-spin cobalt(II) (3.87 μ_B; $\mu_{SO} = [4S(S + 1)]^{1/2}$; $S = 3/2$), but close to the value expected when the spin momentum and the orbital momentum exist independently [5.20 μ_B; $\mu_{LS} = [L(L + 1) + 4S(S + 1)]^{1/2}$; $L = 3$, $S = 3/2$]. This indicates a contribution of the orbital momentum typical for the $^4T_{1g}$ ground state. The magnetic moments decrease with decreasing temperature, and three factors are considered to elucidate this phenomenon; (1) the contribution of the orbital momentum, (2) an intramolecular antiferromagnetic coupling between two Co^{II} centers, and (3) an intermolecular antiferromagnetic coupling. However, we neglect the intermolecular coupling in this study since the X-ray analysis shows the dinuclear cobalt(II) centers to be well separated from each other. In order to evaluate the two remaining effects, we first tried to analyze the experimental cryomagnetic data using the isotropic one-ion approximation with the spin-orbit coupling in pure O_h symmetry, $\boldsymbol{H} = -(3/2)\kappa\,\lambda\,\boldsymbol{L}\cdot\boldsymbol{S} + \beta[-(3/2)\kappa\,\boldsymbol{L} + g_e\boldsymbol{S}]\cdot H$. A magnetic susceptibility equation was obtained as follows;[5,10]

$$\chi_A = \frac{N\beta^2}{kT}\frac{F_1}{F_2} \quad (1a)$$

$$F_1 = \frac{63}{20}(-2+\kappa)^2 x + \frac{2(4+3\kappa)^2}{25\kappa} + [\frac{2}{45}(11-3\kappa)^2 x + \frac{88(4+3\kappa)^2}{2025\kappa}]\exp(-\frac{15\kappa}{4}x) + [\frac{1}{36}(10+3\kappa)^2 x - \frac{10(4+3\kappa)^2}{81\kappa}]\exp(-6\kappa x) \quad (1b)$$

$$F_2 = x[3 + 2\exp(-\frac{15\kappa}{4}x) + \exp(-6\kappa x)] \quad (1c)$$

where $x = \lambda/(k\ T)$, λ is the spin-orbit coupling, κ is the orbital reduction factor, and other symbols have their usual meanings. The cryomagnetic data could not be explained by this equation. The magnetic interaction between intramolecular two cobalt(II) ions has also been taken into consideration using Lines' isotropic theory,[11] but the simulation was not successful. This is probably due to the trigonal distortion around the cobalt(II) centers.

Secondly, we considered the distortion around the cobalt(II) ions for the magnetic data analysis introducing the axial splitting parameter Δ. It has been shown that the axial parameter Δ can be used in both the trigonal and the tetragonal field.[7,8] In the higher temperature range ($k\ T >> |J|$), one-ion approximation is available, and a magnetic susceptibility equation for a mononuclear model was obtained[5,6,10] using the van Vleck formula[15] as follows;

$$\chi_A = \frac{\chi_z + 2\chi_x}{3} \quad (2a)$$

$$\chi_{z(x)} = N\frac{\sum_n (\frac{E^{(1)}_{z(x),n}}{kT})^2 - 2E^{(2)}_{z(x),n})\exp[\frac{-E^{(0)}_n}{kT}]}{\sum_n \exp[\frac{-E^{(0)}_n}{kT}]} \quad (2b)$$

Energies $E^{(0)}_n$, $E^{(1)}_{n,z(x)}$, and $E^{(2)}_{n,z(x)}$ ($n = \pm1-\pm6$) were calculated by solving the 12×12 secular matrix,[5,6] and the resulting energy equations are shown in the supplementary material section. An important feature of this method is that only three parameters, namely, κ, λ, and Δ, are required for analyzing the cryomagnetic data in an axially distorted octahedral field. The data were well simulated in the temperature range 50−300 K for each complex, and calculated curves are also shown in Figure 3 and 4. Fitting parameters were $\kappa = 0.96$, $\lambda = -140$ cm^{-1}, and $\Delta = 753$ cm^{-1} for complex **1**, and $\kappa = 0.92$, $\lambda = -156$ cm^{-1}, and $\Delta = 775$ cm^{-1} for **2**. The g values were calculated as $g_z = 2.18$ and $g_x = 4.97$ for **1** and $g_z = 2.20$ and $g_x = 4.93$ for **2**. Agreement factors defined as $R = \Sigma(\chi_A^{calcd.} - \chi_A^{obs})^2/\Sigma(\chi_A^{obs})^2$ were 1.4×10^{-4} and 3.6×10^{-4}, respectively.

The spin-orbit coupling λ for cobalt(II) ion is theoretically expected to be -172 cm^{-1}. The λ value for the complex **2** is slightly smaller than this, and the value for complex **1** is much smaller. The orbital reduction factor κ means the reduction of the orbital momentum caused by the delocalization of the unpaired electrons, but it also contains the admixture of the upper $^4T_{1g}(^4P_1)$ state into the $^4T_{1g}(^4F_1)$ ground state. In the free cobalt(II) ion, $\kappa_{free\ ion}$ is known to be ≈0.93,[11,16] but smaller values such as ≈0.75 are also obtained when the physical distortion is large.[11] Known values of the axial splitting Δ are in the range ≈200−≈800 cm^{-1}.[10] The three parameters obtained for complex **2** are normal, while the parameters for **1** deviate slightly from the normal values. This can be explained by the fact that the symmetry of complex **1** is lower than that of **2**. Thus, the axial approximation is adequate for **2**, but not so much for **1**. In any case, in the low-temperature range, the observed data for both complexes were smaller than the calculated values in one-ion approximation, indicating antiferromagnetic interaction between two cobalt(II) ions in the complex cation.

Finally, the interaction between two cobalt(II) ions is introduced to the axial mononuclear model as a perturbation; $\boldsymbol{H} = -(3/2)\kappa\ \lambda\ \boldsymbol{L}\cdot\boldsymbol{S} + \beta[-(3/2)\kappa\ \boldsymbol{L} + g_e\boldsymbol{S}]\cdot H - J\ \boldsymbol{S}_1\cdot\boldsymbol{S}_2$. When Δ values are in the range 700−800 cm^{-1}, the energy separation between the lowest and the second lowest Kramers doublets, which corresponds to the axial zero-field splitting D, is estimated to be 120−200 cm^{-1}. The magnitude of the coupling constant J is expected to be smaller than 2 cm^{-1} ($|J| < 2$ cm^{-1}) since the susceptibility maximum was not observed[5] in either complex. In these cases ($|J| << |D|$), the perturbation of the magnetic coupling is effective only in the lowest doublet. In other words, upper states can be ignored when the magnetic interaction is observed in the lower-temperature range ($|J| \approx k\ T << |D|$), while the magnetic interaction can be neglected when the second lowest state is thermally populated in the higher-temperature range ($|J| << |D| \approx k\ T$). The same one-ion energy equations can be used, but the susceptibility equations were slightly modified (see supplementary material section). The data were well simulated in the whole temperature range using four parameters, namely, κ, λ, Δ, and J. The best-fitting parameters were $\kappa = 0.96$, $\lambda = -140$ cm^{-1}, $\Delta = 753$ cm^{-1}, $J = -0.96$ cm^{-1}, $g_z = 2.18$, and $g_x = 4.97$, and $R = 5.3 \times 10^{-4}$ for complex **1**. The corresponding parameters for complex **2** were $\kappa = 0.92$, $\lambda = -156$ cm^{-1}, $\Delta = 775$ cm^{-1}, $J = -1.74$ cm^{-1}, $g_z = 2.20$, $g_x = 4.93$, and $R = 3.6 \times 10^{-4}$ (Table 3). In order to ascertain the resulting parameters, the low-temperature data ($T < 30$) were also analyzed by the method considering only the ground Kramers doublet,[13] using the g-factors obtained above. The results were $J = -0.85$ cm^{-1}, $g_z = 2.18$, $g_x = 4.97$, $N\alpha = 0.35$ cm^{3}mol^{-1}, $R = 7.5 \times 10^{-5}$ for **1** and $J = -1.54$ cm^{-1}, $g_z = 2.20$, $g_x = 4.93$, $N\alpha = 0.24$ cm^{3}mol^{-1}, $R = 3.9 \times 10^{-4}$ for **2**. The J value obtained previously for each complex is in good agreement with the corresponding value obtained from the low-temperature data.

Table 3. Magnetic data for complexes **1** and **2**

Complex	κ	λ/cm^{-1}	Δ/cm^{-1}	J/cm^{-1}	g_z	g_x	D/cm^{-1}	$R/10^{-4}$
1	0.96	-140	753	-0.96	2.18	4.97	125	5.3
2	0.92	-156	775	-1.74	2.20	4.93	138	3.6

Limitations of Our New Theoretical Method

In this study, we have developed a new equation set for analyzing the magnetism of dinuclear high-spin cobalt(II) complexes in lower symmetry. Axial symmetry has been assumed for each cobalt(II) ion; thus, the theory is available for a trigonally-distorted octahedral field and a tetragonally-distorted one. When the symmetry around the cobalt(II) ions is rhombic and cannot be approximated by the axial field, this method is no longer useful. When the magnetic coupling between any cobalt(II) ions is negligible ($J = 0$), the magnetic equation set is completely the same as that of the axially distorted mononuclear model of Figgis and Lines. In the present theory, magnetic coupling was considered only for the lowest doublet. This approximation is valid when the coupling constant J is much smaller than the axial zero-field splitting D ($|J| << |D|$). It has been reported that the axial splitting Δ of the cobalt(II) ions in normal mononuclear cobalt(II) complexes is in the range 200−800 cm^{-1},[10] and the axial zero-field splitting is in the range 120−330 cm^{-1}. Usually, the magnitude of the coupling constant J is smaller than 10 cm^{-1} ($|J| < 10$ cm^{-1}); thus, the approximation we used in this study is expected to be useful for most dinuclear high-spin cobalt(II) complexes. However, it should be emphasized again that there is a limit in the symmetry around the cobalt(II) ion. (1) If the symmetry is isotropic ($\Delta \approx 0$), Lines' theory[11] would be preferable for the estimation of the J value. (2) If the symmetry is axial, the method we have shown in this study may be more useful than Lines' theory. (3) If the symmetry is rhombic, no method is useful at this moment, to the best of our knowledge.

Conclusion

In this study, two dinuclear cobalt(II) complexes (**1** and **2**) were made using the dinucleating ligand, $bomp^-$, and the crystal structure of complex **1** was determined. For the purpose of analyzing the cryomagnetic data, a new theoretical method was developed assuming an axially distorted octahedral field, and the experimental data were analyzed. This is the first successful magnetic analysis for dinuclear high-spin cobalt(II) complexes in an axially distorted octahedral field.

Experimental Section

Measurements: Elemental analyses were obtained at the Elemental Analysis Service Centre of Kyushu University. − Infrared (IR) spectra were recorded on a Hitachi 270−50 spectrophotometer. − Fast atom bombardment (FAB) mass spectra were measured on a Fisons ZabSpec Q mass spectrometer in *N*,*N*-dimethylformamide (DMF) with a glycerol matrix. − Molar conductances were measured on a DKK AOL-10 conductivity meter at room temperature. − Electronic spectra were recorded on a Shimadzu UV-240 spectrophotometer. − Magnetic susceptibility was measured between 1.8 and 300 K by using a Quantum Design SQUID magnetometer MPMS-5S in fields up to 5 T. All the magnetic calculations were made using the MagSaki[17] magnetic software program of our laboratory.

Materials: All chemicals were commercial products, and were used as supplied. The ligand Na(bomp) was prepared by the method reported previously.[2]

Synthesis of $[Co_2(bomp)(MeCO_2)_2]BPh_4$ (1): To a methanolic solution (15 mL) of Na(bomp) (1.0 mmol, 0.42 g) was added cobalt(II) acetate dihydrate (2.0 mmol, 0.50 g), and the resulting solution was heated under reflux for 1 h to give a pink solution. The addition of sodium tetraphenylborate (1.0 mmol, 0.34 g) resulted in the precipitation of pink microcrystals. The compound was recrystallized from a mixture of acetonitrile and 2-propanol. Yield: 0.23 g (24%). − $C_{49}H_{63}BCo_2N_2O_9$: calcd. C 61.75, H 6.65, N 2.95, Co 12.4; found C 61.60, H 6.65, N 2.90, Co 12.4. − Selected IR data (KBr): $\tilde{\nu}$ = 3050−2900, 1600, 1410, 1090, 730, 700 cm^{-1}. − FAB mass spectrum: m/z = 633 $[Co_2(bomp)(MeCO_2)_2]^+$. − Molar conductance [in DMF] = 46 Λ_M/Scm^2mol^{-1}. − UV/Vis: λ_{max} (ε/$dm^3cm^{-1}mol^{-1}$, in DMF) = 485 (30), 512 (35) nm.

Synthesis of $[Co_2(bomp)(PhCO_2)_2]BPh_4$ (2): This was prepared as pink microcrystals by a method similar to that of **1**, using cobalt(II) benzoate instead of cobalt (II) acetate tetrahydrate. Yield: 0.24 g (23%). − $C_{59}H_{67}BCo_2N_2O_9$: calcd. C 65.80, H 6.25, N 2.60, Co 11.0; found C 65.80, H 6.25, N 2.60, Co 10.9. − Selected IR data (KBr): $\tilde{\nu}$ = 3050−2900, 1610, 1400, 1085, 730, 700 cm^{-1}. − FAB mass spectrum: m/z = 757 $[Co_2(bomp)(PhCO_2)_2]^+$. − Molar conductance (in DMF) = 43 Λ_M/Scm^2mol^{-1}. − UV/Vis λ_{max} (ε/$dm^3cm^{-1}mol^{-1}$, in DMF) = 480 (40), 510 (45) nm.

Single Crystal X-ray Analysis of Complex 1·$CHCl_3$: Crystal data: $C_{50}H_{64}BCo_2Cl_3N_2O_9$, M = 1072.10, a = 13.2229(6), b = 14.5043(9), c = 16.0204(8) Å, α = 68.8982(6), β = 82.022(1), γ = 64.279(2)°, V = 2581.9(2) $Å^3$, Z = 2, $d_{calcd.}$ = 1.379 g cm^{-3}, triclinic, space group $P\bar{1}$ (no. 2), $F(000)$ = 1120.00. − Data collection: A purple prismatic crystal of **1**·$CHCl_3$ having approximate dimensions of 0.40 × 0.40 × 0.30 mm was mounted in a loop. All measurements were made on Rigaku/MSC Mercury CCD diffractometer with graphite monochromated Mo-K_α radiation (λ = 0.71069 Å). The ω scan was made to a maximum 2θ value of 54.6° at −170 ± 1 °C. Of the 29279 reflections, 11541 were unique (R_{int} = 0.019), and $I > 2.0\,\sigma(I)$ data were used. The linear absorption coefficient μ(Mo-K_α) was 8.53 cm^{-1}. A symmetry-related absorption correction was applied, which resulted in transmission factors ranging from 0.62 to 0.77. The data were corrected for Lorentz and polarization effects. − Structural analysis and refinement: The structure was solved by direct methods,[18] and expanded using Fourier techniques.[19] The non-hydrogen atoms were refined anisotropically. Hydrogen atoms were refined isotropically. The final cycle of full-matrix least-squares refinement was based on 11541 observed reflections. The final values of R and R_w were 0.065 and 0.147, respectively ($R = \Sigma||Fo| - |Fc||/\Sigma\,|Fo|$, $R_w = \{\Sigma w(|Fo| - |Fc|)^2/\Sigma\ wFo^2\}^{1/2}$). All calculations were performed using the teXsan[20] crystallographic software package of Molecular Structure Corporation.

Crystallographic data (excluding structure factors) for the structure(s) included in this paper have been deposited with the Cambridge Crystallographic Data Centre as supplementary publication no. CCDC-151304. Copies of the data can be obtained free of charge on application to CCDC, 12 Union Road, Cambridge CB2 1EZ, UK [Fax: (internat.) +44-1223/336-033; E-mail: deposit@ccdc.cam.ac.uk].

Acknowledgments

The author thanks Professor Hisashi Okawa for his encouragement.

[1] S. L. Roderick, B. W. Matthews, *Biochemistry* **1993**, *32*, 3907−3912.
[2] H. Sakiyama, R. Mochizuki, A. Sugawara, M. Sakamoto, Y. Nishida, M. Yamasaki, *J. Chem. Soc., Dalton Trans.* **1999**, 997−1000.
[3] H. Sakiyama, A. Sugawara, M. Sakamoto, Y. Nishida, K. Inoue, M. Yamasaki, *Inorg. Chim. Acta* **2000**, *310*, 163−168.
[4] B. N. Figgis, M. A. Hitchman, *Ligand Field Theory and its Applications*, Wiley-VCH, **2000**.
[5] O. Kahn, *Molecular Magnetism*, VCH, **1993**.
[6] M. E. Lines, *Phys. Rev.* **1963**, 546−555.
[7] B. N. Figgis, *Trans. Faraday Soc.* **1961**, *57*, 198−203.
[8] B. N. Figgis, J. Lewis, F. E. Mabbs, G. A. Webb, *J. Chem. Soc. A* **1966**, 1411−1421.
[9] B. N. Figgis, J. Lewis, F. E. Mabbs, G. A. Webb, *J. Chem. Soc. A* **1967**, 442−447.
[10] B. N. Figgis, M. Gerloch, J. Lewis, F. E. Mabbs, G. A. Webb, *J. Chem. Soc. A* **1968**, 2086−2093.
[11] M. E. Lines, *J. Chem. Phys.* **1971**, *55*, 2977−2984.
[12] G. D. Munno, M. Julve, F. Lloret, J. Faus, A. Caneschi, *J. Chem. Soc., Dalton Trans.* **1994**, 1175−1183.
[13] E. Coronado, M. Drillon, P. R. Nugteren, L. J. de Jongh, D. Beltran, *J. Am. Chem. Soc.* **1988**, *110*, 3907−3913.
[14] C. K. Johnson, *ORTEP*, Oak Ridge National Laboratory, **1976**.
[15] J. H. Van Vleck, *The Theory of Electronic and Magnetic Susceptibilities*, Oxford University Press, Oxford, **1932**.
[16] W. Low, *Phys. Rev.* **1958**, *109*, 256−265.
[17] H. Sakiyama, *MagSaki*, Sakiyama Laboratory, **2000**.
[18] A. Altomare, M. C. Burla, M. Camalli, G. L. Cascarano, C. Giacovazzo, A. Guagliardi, A. G. G. Moliterni, G. Polidori, R. Spagna, *J. Appl. Cryst.* **1999**, *32*, 115−119.
[19] P. T. Beurskens, G. Admiraal, G. Beurskens, W. P. Bosman, R. de Gelder, R. Israel, J. M. M. Smits, *DIRDIF-94*, University of Nijmegen, **1994**.
[20] Crystal Structure Analysis Package, Molecular Structure Corporation, **1985**, **1999**.

Received November 6, 2000
[I00420]

Conformational Preferences of Racemic Ethylene-Bridged Bis(indenyl)-Type Zirconocenes: An ab initio Hartree−Fock Study

Mikko Linnolahti,*[a] Tapani A. Pakkanen,*[a] Reko Leino,[b] Hendrik J. G. Luttikhedde,[b][‡] Carl-Eric Wilén,[b] and Jan H. Näsman[b][†]

Keywords: Ab initio calculations / Conformational analysis / Metallocenes / Polymerization catalysts / Zirconium

The ab initio Hartree–Fock method has been utilized to rationalize the conformational preferences of racemic ethylene-bridged bis(indenyl)-type zirconocenes in dichloride and cationic methyl forms. This group of catalysts is characterized by conformational isomerism due to fluxionality of the ethylene bridge resulting in two distinct orientations of the indenyl ligands, indenyl-forward (Π) and indenyl-backward (Y). A systematic investigation of the influence of methyl and trialkylsiloxy substitution on the relative stabilities of Π and Y conformations was performed. For the dichloride catalyst precursors the stabilities and orientations of the equilibrium structures are determined on the basis of repulsive interactions within the ligand framework. In the cationic methyl intermediates of the olefin polymerization catalytic cycle, the electron-rich indenyl ligand appears to reduce the electron deficiency of the cation by tilting towards the metal.

Introduction

Homogeneous olefin polymerization catalysis currently represents the most significant application of metallocenes.[1] The field has been extensively studied by experimental techniques[2−4] and, during the last decade, also by theoretical approaches.[5−120] Undoubtedly, the most influential breakthroughs have been the discoveries of isospecific polymerization of propylene by C_2-symmetric racemic *ansa*-metallocenes,[121] together with the activation of metallocene catalyst precursors with methylaluminoxane (MAO) co-catalyst.[122]

A distinct characteristic of two-atom bridged metallocenes is the conformational freedom of their five-membered metallacycles. The combination of an ethylene bridge with bis(indenyl)- or bis(tetrahydroindenyl)-based ancillary ligands results in two limiting conformations, indenyl-forward (Π) and indenyl-backward (Y) (Figure 1). If the barrier for transformation is small, the interconversion between the conformers may be rapid. In such case both conformations exist in solution and the crystal structure solely is inadequate to describe the structure of the catalyst precursor. Furthermore, notwithstanding the maintenance of C_2 symmetry, the polymerization properties, especially the stereoregulating ability of the catalytically active species formed from these two catalyst precursors have been proposed to be different.[123]

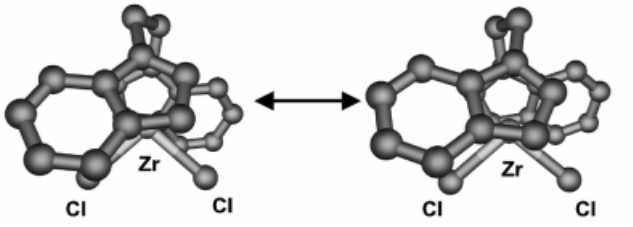

Figure 1. Top view of indenyl-forward (Π) and indenyl-backward (Y) conformations of bis(indenyl)zirconocene dichlorides

In most cases, racemic ethylene-bridged bis(indenyl)-type metallocenes crystallize in the Π conformation,[123−127] apparently due to larger nonbonding interactions within the ligand in the Y conformation.[128] The less favorable Y conformation has been observed for at least some group-IV bis(indenyl) and bis(tetrahydroindenyl) adducts and amido complexes,[129−132] but also for 2,4,7-Me_3-substituted ethylenebis(indenyl)zirconium dichloride[133] as well as for the majority of trialkylsiloxy-substituted metallocenes.[134−138] Hence, the role of ligand substituents in determination of the preferred conformation seems apparent. The aim of the present study is to clarify the relationship between the degree of ligand substitution and the preferred conformation for both dichloride precursors and cationic intermediates of olefin polymerization process.

Computational Details

Calculations were carried out with a Gaussian 94 program package,[139] using the restricted Hartree−Fock method with a standard double-zeta basis set, 3-21G*. Earlier work based on a data set of 62 bridged zirconocene dichlorides demonstrated that the HF/3-21G* method pro-

[a] Department of Chemistry, University of Joensuu, P. O. Box 111, 80101 Joensuu, Finland
Fax: (internat.) + 358-13/251-3344,
E-mail: Tapani.Pakkanen@joensuu.fi
[b] Laboratory of Polymer Technology, Åbo Akademi University, 20500 Åbo, Finland
[‡] Present address: Raisio Chemicals Ltd., P. O. Box 101, 21201 Raisio, Finland
[†] Deceased

 © WILEY-VCH Verlag GmbH, 69451 Weinheim, 2001 1434−1948/01/0808−2033 $ 17.50+.50/0

vides reliable structures for zirconocenes, the accuracy being comparable to the more expensive BLYP,[140,141] B3LYP,[141,142] and MP2 calculations with larger basis sets.[118] The good performance of the HF/3-21G* method is apparently due to small near-degeneracy and relativistic effects in several complexes of zirconium,[143,144] including zirconocenes. Furthermore, the Hartree−Fock method should be reasonable for conformational energetics[145] regardless of the lack of electron correlation, since its influence on rotational barriers is insignificant.[146]

The interconversion barrier between the Π and Y conformations was studied by systematic modification of the torsion angle of the ethylene bridge. The torsion angle was specified to a certain value while the rest of the molecule was fully optimized. The specified torsion angle was changed with intervals of 10°, after which the new constrained structure was optimized. In order to obtain the structures and energies for the local minima, the bridge constraints of the nearest intermediate structures were relieved and a full geometry optimization without symmetry constraints was performed. In order to confirm the local minima and to obtain zero-point corrections to the total energy, frequency calculations were carried out.[147] The influences of zero-point corrections on relative stabilities of the conformers are very small, on average 0.4 kJ/mol and at maximum 0.9 kJ/mol, and are therefore omitted in the interpretation of the calculations.

As a result of the procedure, the structures of the limiting Π and Y conformations and the relative stabilities of the Π−Y transformations were obtained as a function of the ethylene bridge torsion. It should be noted that the relative stability alone does not determine the preferred conformation. Crystal packing effects may be a contributory cause, since the molecules must be accommodated in the crystal lattice.

Results and Discussion

Π−Y Transformation in Dichloride Precursors

Schematic structures of the studied racemic zirconocenes are presented in Figure 2. In addition to unsubstituted bis(indenyl) (**1**) and bis(tetrahydroindenyl) (**2**) complexes, various methyl- (**3**) and siloxy-substituted (**4**) complexes were investigated. A detailed interpretation of the results follows.

Unsubstituted Ligands

The energetics for the Π−Y transformation of **1** and **2** are shown in Figure 3. The barriers for rotation are low, as verified experimentally for **1** by NMR at room temperature,[123] suggesting a feasible interconversion between the conformers. The orientation of the ethylene bridge in the Π and Y conformations corresponds to the *gauche* conformation of butane. The rotation barriers of approximately 20 kJ/mol are close to the butane *gauche-cis* energy difference of 22 kJ/mol at the HF/3-21G* level. The limit conformations are somewhat distorted from the optimal *gauche* conformation of 67° due to strain of the metallacycle and nonbonding repulsions between the indenyl ring and the ethylene bridge (Figure 4). In the Π conformation the orientation determining repulsion occurs between the bridge and H(2), whereas the orientation of the Y conformation is limited by H(7)−ethylene bridge interaction.

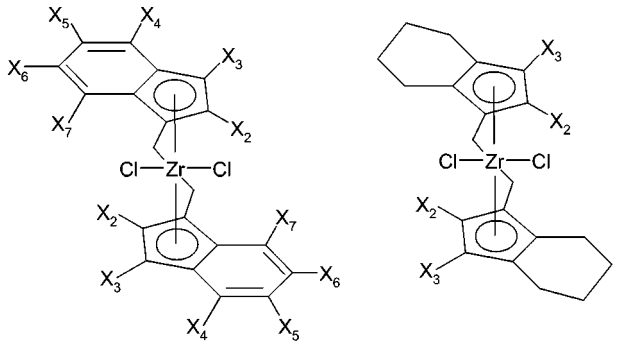

Figure 2. Schematic structures of the studied zirconocene dichlorides; X = H, unless otherwise mentioned

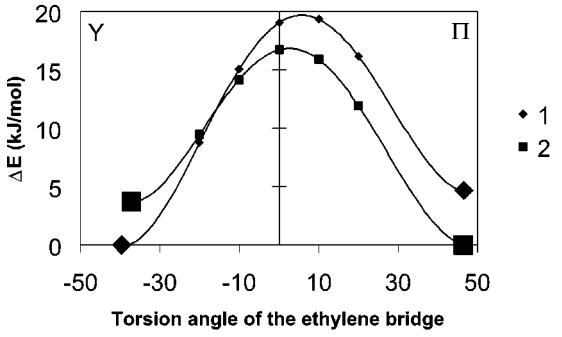

Figure 3. The Π−Y rotation energetics for bis(indenyl)- (**1**) and bis(tetrahydroindenyl)zirconocene dichlorides (**2**); the limiting Π and Y conformations are indicated by larger labels

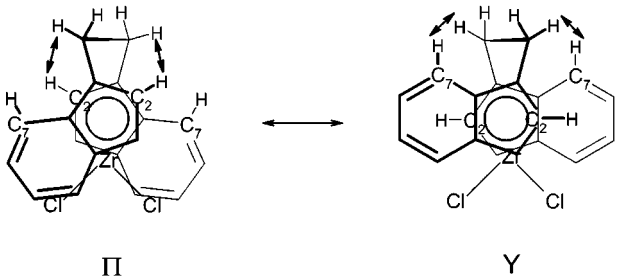

Figure 4. Orientation-determining intramolecular interactions

Both complexes crystallize in the Π conformation,[123,148] apparently due to stronger H(7)−bridge interactions[128] rather than the balancing H(2)−bridge repulsion. The calculations suggest almost identical stabilities for the conformers, in accordance with the earlier molecular mechanics calculations on complex **1**.[133] The small energy differences of approximately 4 kJ/mol are apparently beyond the quantitative accuracy of the method.

Methyl Substituents

The Π−Y transformation energies of monomethyl-substituted bis(indenyl)zirconocene dichlorides are presented in Figure 5. Due to the absence of additional substituent−bridge interactions, the energetics of **3b**−**3e** are nearly identical, also being very similar to the unsubstituted complex **1**. Supposing that the qualitative trends are correct and crystal packing effects are insignificant, **3b**−**3e** should crystallize in the Π conformation similar to **1**, which is true for **3b**, at least.[125] The energetics for **3a** and **3f** are quite different because of a small distance between the substituent and the bridge. The repulsion between the C(2) and the ethylene bridge is the orientation-determining interaction in the Π conformation of **3a**, whereas the Y conformation of **3f** is limited by the C(7)−bridge repulsion.

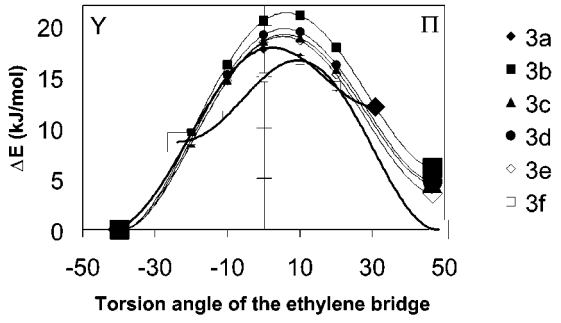

Figure 5. The Π−Y rotation energetics for monomethyl-substituted bis(indenyl)zirconocene dichlorides

Relative stabilities of **3a**−**3f** are given in Table 1. The substituent−bridge repulsion destabilizes the Π conformation of **3a**, while both limit conformations of **3f** become strongly destabilized. This suggests stronger interactions for the latter, hence supporting the earlier proposals.[123,128] Intuitively, it could be assumed that whenever several substituents are simultaneously present, the role of 7-substituent (prefers Π) is the most important, followed by 2-substituent (prefers Y), and that the role of 3-, 4-, 5- and 6-substituents is insignificant.

Table 1. Relative stabilities [kJ/mol] of ethylene-bridged methyl-substituted bis(indenyl)zirconocene dichlorides

	Π	Y
3a	22	10
3b	13	7
3c	5	0
3d	15	11
3e	14	11
3f	39	48

The Π−Y transformation energies are presented in Figure 6 for 2,4-Me_2- (**3g**), 2,7-Me_2- (**3h**), 4,7-Me_2- (**3i**), and 2,4,7-Me_3-substituted (**3j**) complexes. Due to the orientation of 4-methyl groups away from the bridge, the energetics of **3g** and **3i** are identical with the corresponding monomethyl-substituted **3a** and **3b**, respectively. The crystal structure of **3i** is Π,[126] which, as suggested by the calculations, is the more stable conformer due to C(7)−bridge repulsion. This is in accordance with the earlier proposals by Resconi et al.[126]

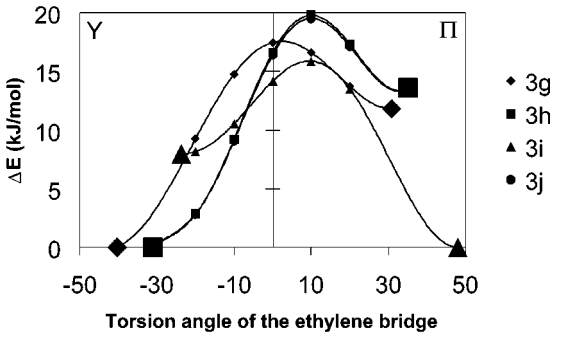

Figure 6. Π−Y rotation energetics for the studied di- and trimethyl-substituted bis(indenyl)zirconocene dichlorides

The presence of both 2- and 7-substituents (**3h** and **3j**) restricts the fluxionality of the ethylene bridge to a narrower area due to methyl−bridge interactions in both conformations. The significant stabilization of the Y conformation despite of generally stronger influence of 7-substituent is not apparent. The explanation is, in fact, further destabilization of the Π conformation, rather than stabilization of the Y conformation. The 2-methyl substituent is forced to interact with the opposite 7-methyl group, and the interaction is much stronger in the Π conformation [see Figure 4 and consider changing the hydrogen atoms of C(2) and C(7) to methyl groups]. Overall, the Y conformation is destabilized due to close contact between 7-Me and the bridge, but the Π conformation is destabilized even more because of the presence of both 2-Me−bridge interactions and the repulsion of the opposite 2-Me and 7-Me substituents. The 4-methyl substituent of **3j** has no relevance. Therefore, as suggested by the calculations, **3j** crystallizes in the Y conformation.[133] This was observed by molecular mechanics calculations as well, even though the local minimum of the unstable Π conformation was not detected.[133]

Siloxy Substituents

Siloxy-substituted zirconocenes represent a uniform group of heteroatom-functionalized group-IV metallocene complexes, showing high activities at reduced co-catalyst concentrations. In the present context, siloxy-substituted zirconocene dichlorides are particularly interesting for two reasons. First, a number of crystal structures are available, making comparisons between stabilities of the limit conformations and identities of the crystal structures possible.

Secondly, most of the crystallographically characterized siloxy-substituted metallocenes favor the generally less common Y conformation. Therefore, the role of the siloxy substituent in determining the preferred conformation deserves a detailed computational investigation.

Five crystallographically characterized siloxy-substituted zirconocenes (**4a**−**4e**) were selected for the study. Depending on the size and position of the substituents, the following classifications can be made. The attached groups are either *tert*-butyldimethylsiloxy groups (**4a**−**4c**) or triisopropylsiloxy groups (**4d**−**4e**), referred to as TBDMS and TIPS, respectively. Depending on the position of the siloxy group, the molecules are denoted 2-siloxy (**4a**, **4b**, **4d**, **4e**) or 1-siloxy (**4c**). The Π−Y transformation energies are presented in Figure 7.

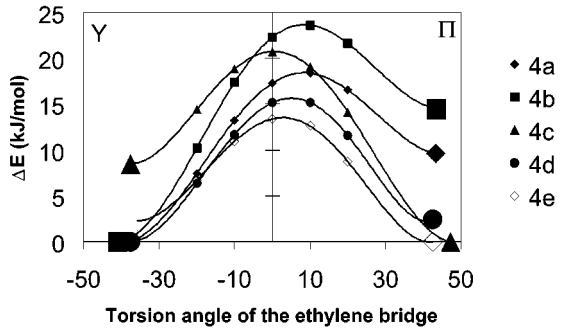

Figure 7. Π−Y rotation energetics for siloxy-substituted zirconocene dichlorides

The 2-TBDMS-substituted complexes (**4a** and **4b**) favor the Y conformation because of repulsions due to the siloxy groups. Each siloxy substituent participates in three close repulsive interactions, namely with one chlorine ligand and with both bridge carbon atoms (Figure 8). However, since the distance between the siloxy substituent and C(1) is constant in both limit conformations, only the repulsions with the oxygen atom and C(2) are orientation-determining. The Cl−O distance of 3.7 Å for the Y conformations and 4.0 Å for the Π conformations indicate smaller repulsions for the latter. On the other hand, the C(2)−O distance is 1.0 Å shorter in the Π conformation. Apparently, the repulsions at the bridge side are more significant than the balancing siloxy−chlorine repulsions. The calculations are in good agreement with experimental observations, since both **4a**[134] and **4b**[135] crystallize in the energetically favored Y conformation.

Increasing the size of the 2-siloxy substituent (TBDMS → TIPS) results in substantial repulsive interactions between the chlorine atom and the carbon atoms of the siloxy group. The Π conformation has more space to accommodate the bulky substituent, as suggested by longer Cl−C(3) distances (Figure 8). Consequently, both limit conformations become destabilized: Π due to the presence of the 2-substituent and Y because of its bulkiness. The destabilization of both conformers leads to lower rotation barriers and to almost equal stabilities. Consequently, **4d**[136] crystallizes

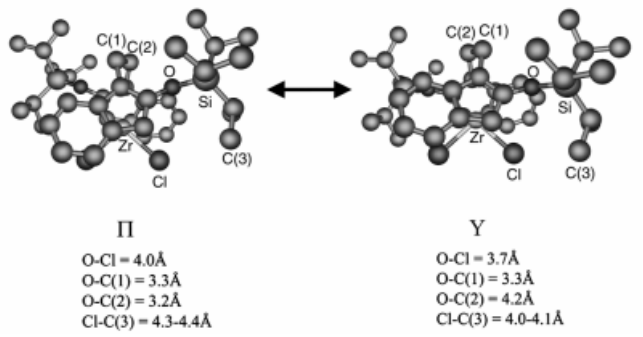

Figure 8. Orientation-determining repulsions in 2-siloxy-substituted zirconocene dichlorides

in the Π conformation while **4e**[136] crystallizes in the Y conformation.

Due to the absence of substituent−bridge interactions, these interpretations are not valid for the 1-siloxy-substituted complex **4c**, in which the siloxy group is directed towards the chlorine atoms. Repulsions with the chlorine atoms are relevant, but constant. Hence, the 1-siloxy substituent has a marginal effect on the preferred limit conformation, and Π is preferred because of its general preference over the Y conformation. This is in agreement with the experimentally determined crystal structure of **4c** (Π).[138]

Cationic Methyl Intermediates

Cationic methyl complexes represent the simplest approximations of the active species. Since the catalytic system is influenced by a number of other components, such as co-catalyst, an accurate consideration of all effects present is not quantitatively feasible. Whenever quantitative accuracy is unattainable, qualitative observations are generally useful. After all, many of the molecular properties are not influenced by the counter ion. In large co-catalyst molecules the negative charge is evenly distributed to a large space. The resulting complex is not a tight ion pair, but can be regarded as a positive complex surrounded by a uniform cloud of negative charge. The structure of such a cation is primarily determined by the internal bonding, which could be qualitatively modeled by the cation itself. It was thus decided to start from the simplest approximation, i.e., the cationic monomethyl metallocene.

Schematic structures of the studied cationic methyl intermediates are presented in Figure 9. The barriers for Π−Y transformation (Figure 10) are slightly lower than for the corresponding dichloride forms. The Π conformation is generally favored, even by the 2-substituted compounds **7** and **8**, despite of substituent−bridge repulsions.

The equilibrium structures of **5** and **6** are presented in Figure 11. In **5Π** the electron deficiency is reduced by electron donation from the indenyl ring to the metal center, resulting in "bending" of the indenyl ring. A similar type of stabilizing interaction has been recently observed in benzyl-substituted zirconocenes.[149,150] The indenyl−metal interaction is less significant in the Y conformation due to closeness of the opposite cyclopentadienyl ring, and espe-

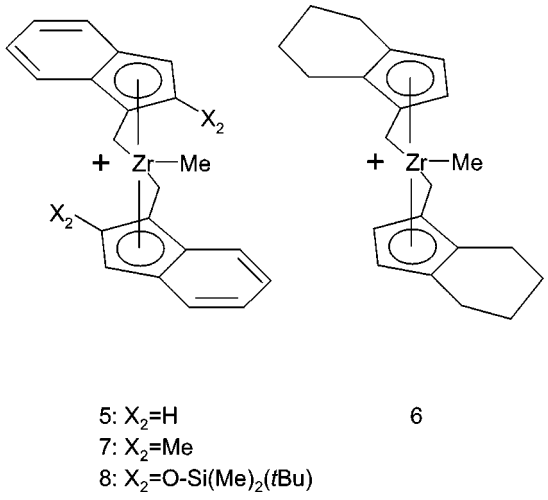

Figure 9. Schematic structures of the studied cationic zirconocenes

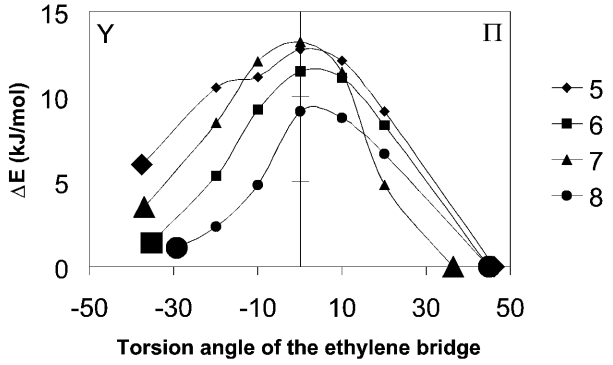

Figure 10. The Π−Y transformation energies for cationic methyl complexes

cially the carbon atom in position 2. The electron donation to the metal ion is absent in **6** as well, due to the saturated tetrahydroindenyl ligand.

By bending towards the metal ion, the quaternary carbon atoms connecting the five- and six-membered rings must distort from the optimal sp^2 hybridization. A number of crystal structures for strained metallocenes showing such distortion are available.[151−157] A direct consequence of the distortion is destabilization of the structure, which in the case of cationic **5Π** is cancelled by greater stabilization due to carbon−metal interaction. In order to verify the relevance of the phenomenon, the energy required for bending of the ring was calculated for the anionic indenyl fragment. The degree of bending, 26°, that was observed for **5Π** leads to destabilization of the structure by 34 kJ/mol. Considering the energy of approximately 80 kJ/mol gained by coordination of C=C double bond of the monomer to the metal center, the tilting of the aromatic ligand seems relevant. Apparently, the degree of bending in **5Π** represents an optimal compromise between destabilization due to distortion from the sp^2 hybridization and stabilization due to electron donation from indenyl to the electron-deficient metal ion.

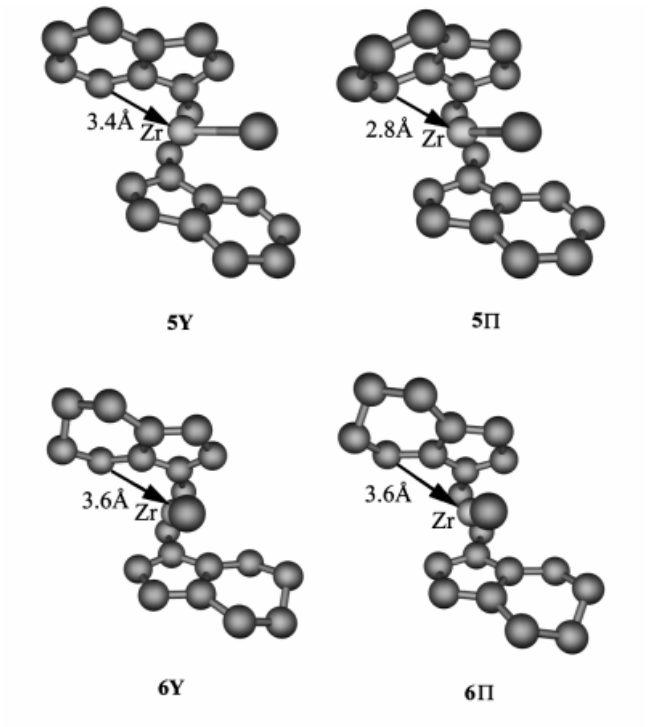

Figure 11. Optimized equilibrium structures of **5** and **6**

The influences of the selected 2-substituents on capability for indenyl bending were studied as well (Figure 12). The stabilization due to ligand−metal interaction is the least significant for unsubstituted **5**, followed by methyl-substituted **7**. The coordination energies for **5** and **7** are very small, less than 5 kJ/mol, and therefore hardly affect the coordination of the incoming monomer. Instead, the coordination energies for siloxy-substituted **8** are much larger, more than 10 kJ/mol for the Π conformation. The presence of indenyl−metal interaction in a real catalytic system would affect the polymerization process in many ways. In addition to minor blocking of the metal center, such interaction would stabilize the cation resulting in higher concentration of cationic metal centers available for the incoming monomer. Possibly, the ligand−metal interaction in combination with the electron-donating siloxy substituent[119] results in an unusually stable active species,[117] as indicated by high catalytic activities at low MAO concentrations.[135,137,158] A third possible consequence could be the increase in the number of different active species with potentially different stereoregulating abilities, possibly resulting in broadening of the molecular weight distributions of the produced polymers.[159]

Conclusion

The indenyl-forward (Π) and indenyl-backward (Y) conformations are relatively similar in energy. Furthermore, the interconversion between the conformers is rapid as also verified experimentally by Resconi et al.[123] Consequently, both conformations can be readily available in the solution,

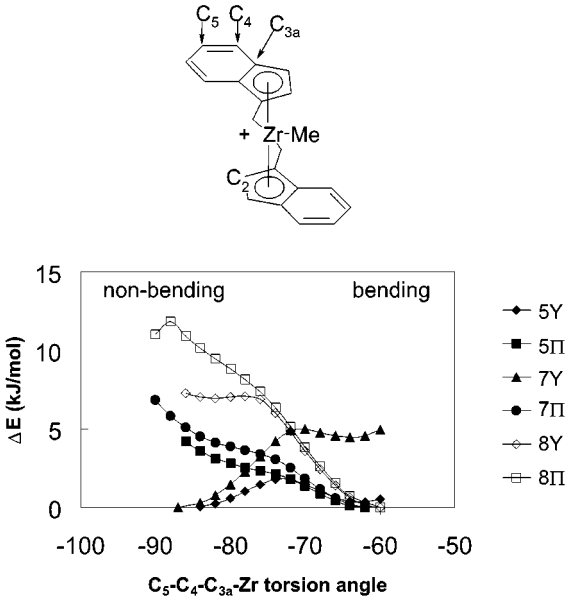

Figure 12. Energetics for the indenyl ring bending

making the crystal structure of the complex alone an inadequate representation for the structure of the precatalyst.

Conformational freedom of dichloride precursors is limited mainly by repulsions within the ligand. In the Π conformation, the most significant repulsion occurs between the bridge and the 2-substituent of the indenyl ring. In the Y conformation, the strongest repulsion can be observed between the bridge and the 7-substituent. These particular repulsions determine the orientations of the ethylene bridge in the limit conformations.

The identities and relative stabilities of the Π and Y conformations are notably changed when the corresponding cationic methyl intermediates of the olefin polymerization catalyst cycle are considered. The electron-rich indenyl ligand donates electrons to the electron-deficient metal ion by tilting towards it. The coordination is less significant for the Y conformation, resulting in general preference of the Π conformation for cations. The strength of the interaction can be controlled by substituents attached to 2-position of the indenyl ligand. The coordination energies are low with hydrogen and methyl substituents, but increase significantly by the introduction of a siloxy group.

Acknowledgments

Financial support from the Finnish Technology Development Center (TEKES) is gratefully acknowledged.

[1] N. J. Long, *Metallocenes*, Blackwell Science Ltd., Oxford, **1998**.
[2] H. H. Brintzinger, D. Fischer, R. Mülhaupt, B. Rieger, R. M. Waymouth, *Angew. Chem. Int. Ed. Engl.* **1995**, *34*, 1143−1170.
[3] C. Janiak, in: *Metallocenes: Synthesis, reactivity, applications* (Eds.: A. Togni, R. L. Halterman), Wiley-VCH, Weinheim, Germany, **1998**, p. 547−623.
[4] L. Resconi, L. Cavallo, A. Fait, F. Piemontesi, *Chem. Rev.* **2000**, *100*, 1253−1345.
Ref.[5−30]: ethylene polymerization by group-IV metallocenes; ref.[31−52]: propylene polymerization by group-IV metallocenes; ref.[53−58]: polymerization studies on higher olefins, functional monomers or copolymerization by group-IV metallocenes; ref.[59−66]: studies on metallocene−cocatalyst interactions; ref.[67−84]: related studies on other transition metal complexes than group-IV metallocenes; ref.[85−89]: publications covering two or more of the categories above; ref.[90−119]: other closely related studies not exactly matching the categories above.
[5] C. A. Jolly, D. S. Marynick, *J. Am. Chem. Soc.* **1989**, *111*, 7968−7974.
[6] M.-H. Prosenc, C. Janiak, H.-H. Brintzinger, *Organometallics* **1992**, *11*, 4036−4041.
[7] C. Janiak, *J. Organomet. Chem.* **1993**, *452*, 63−73.
[8] H. Weiss, M. Ehrig, R. Ahlrichs, *J. Am. Chem. Soc.* **1994**, *116*, 4919−4928.
[9] R. J. Meier, G. H. J. van Doremaele, S. Iarlori, F. Buda, *J. Am. Chem. Soc.* **1994**, *116*, 7274−7281.
[10] R. Fusco, L. Longo, *Macromol. Theory Simul.* **1994**, *3*, 895−904.
[11] T. K. Woo, L. Fan, T. Ziegler, *Organometallics* **1994**, *13*, 432−433.
[12] T. K. Woo, L. Fan, T. Ziegler, *Organometallics* **1994**, *13*, 2252−2261.
[13] J. C. W. Lohrenz, T. K. Woo, T. Ziegler, *J. Am. Chem. Soc.* **1995**, *117*, 12793−12800.
[14] J. C. W. Lohrenz, T. K. Woo, L. Fan, T. Ziegler, *J. Organomet. Chem.* **1995**, *497*, 91−104.
[15] R. Fusco, L. Longo, *Macromol. Symp.* **1995**, *89*, 197−202.
[16] T. Yoshida, N. Koga, K. Morokuma, *Organometallics* **1995**, *14*, 746−758.
[17] L. Fan, D. Harrison, T. K. Woo, T. Ziegler, *Organometallics* **1995**, *14*, 2018−2026.
[18] P. Margl, J. C. W. Lohrenz, T. Ziegler, P. E. Blöchl, *J. Am. Chem. Soc.* **1996**, *118*, 4434−4441.
[19] K. T. Woo, P. M. Margl, J. C. W. Lohrenz, P. E. Blöchl, T. Ziegler, *J. Am. Chem. Soc.* **1996**, *118*, 13021−13030.
[20] G. H. J. van Doremaele, R. J. Meier, S. Iarlori, F. Buda, *J. Mol. Struct.: Theochem* **1996**, *363*, 269−278.
[21] J. A. Støvneng, E. Rytter, *J. Organomet. Chem.* **1996**, *519*, 277−280.
[22] L. Cavallo, G. Guerra, *Macromolecules* **1996**, *29*, 2729−2737.
[23] S. Iarlori, F. Buda, R. Meier, G. H. J. van Doremaele, *Mol. Phys.* **1996**, *87*, 801−815.
[24] V. L. Cruz, A. Muñoz-Escalona, J. Martinez-Salazar, *Polymer* **1996**, *37*, 1663−1667.
[25] T. K. Woo, P. M. Margl, T. Ziegler, P. E. Blöchl, *Organometallics* **1997**, *16*, 3454−3468.
[26] P. M. Margl, T. K. Woo, T. Ziegler, *Organometallics* **1998**, *17*, 4997−5002.
[27] L. Petitjean, D. Pattou, M. F. Ruiz-López, *J. Phys. Chem. B* **1999**, *103*, 27−35.
[28] J. Ramos, V. Cruz, A. Munoz-Escalona, J. Martinez-Salazar, *Polymer* **2000**, *41*, 6161−6169.
[29] I. E. Nifant'ev, L. Y. Ustynyuk, D. N. Laikov, *Russ. Chem. Bull.* **2000**, *49*, 1164−1173.
[30] A. Munoz-Escalona, J. Ramos, V. Cruz, J. Martinez-Salazar, *J. Polym. Sci., Part A: Polym. Chem.* **2000**, *38*, 571−582.
[31] V. Venditto, G. Guerra, P. Corradini, R. Fusco, *Polymer* **1990**, *31*, 530−537.
[32] L. Cavallo, G. Guerra, M. Vacatello, P. Corradini, *Macromolecules* **1991**, *24*, 1784−1790.
[33] L. Cavallo, P. Corradini, G. Guerra, M. Vacatello, *Polymer* **1991**, *32*, 1329−1335.
[34] P. Corradini, G. Guerra, *Prog. Polym. Sci.* **1991**, *16*, 239−257.
[35] L. A. Castonguay, A. K. Rappé, *J. Am. Chem. Soc.* **1992**, *114*, 5832−5842.

[36] H. Kawamura-Kuribayashi, N. Koga, K. Morokuma, *J. Am. Chem. Soc.* **1992**, *114*, 8687−8694.
[37] P. Corradini, V. Busico, L. Cavallo, G. Guerra, M. Vacatello, V. Venditto, *J. Mol. Catal.* **1992**, *74*, 433−442.
[38] J. R. Hart, A. K. Rappé, *J. Am. Chem. Soc.* **1993**, *115*, 6159−6164.
[39] G. Guerra, L. Cavallo, G. Moscardi, M. Vacatello, P. Corradini, *J. Am. Chem. Soc.* **1994**, *116*, 2988−2995.
[40] Z. Yu, J. C. W. Chien, *J. Polym. Sci., Part A: Polym. Chem.* **1995**, *33*, 125−135.
[41] Z. Yu, J. C. W. Chien, *J. Polym. Sci., Part A: Polym. Chem.* **1995**, *33*, 1085−1094.
[42] G. Guerra, P. Corradini, L. Cavallo, M. Vacatello, *Macromol. Symp.* **1995**, *89*, 307−319.
[43] L. Cavallo, G. Guerra, P. Corradini, *Gazz. Chim. Ital.* **1996**, *126*, 463−467.
[44] G. Guerra, L. Cavallo, G. Moscardi, M. Vacatello, P. Corradini, *Macromolecules* **1996**, *29*, 4834−4845.
[45] T. Yoshida, N. Koga, K. Morokuma, *Organometallics* **1996**, *15*, 766−777.
[46] L. Cavallo, P. Corradini, G. Guerra, L. Resconi, *Organometallics* **1996**, *15*, 2254−2263.
[47] van derY. Leek, K. Angermund, M. Reffke, R. Kleinschmidt, R. Goretzki, G. Fink, *Chem. Eur. J.* **1997**, *3*, 585−591.
[48] G. Guerra, P. Longo, L. Cavallo, P. Corradini, L. Resconi, *J. Am. Chem. Soc.* **1997**, *119*, 4394−4403.
[49] M. Toto, L. Cavallo, P. Corradini, G. Moscardi, L. Resconi, G. Guerra, *Macromolecules* **1998**, *31*, 3431−3438.
[50] R. D. J. Froese, D. G. Musaev, K. Morokuma, *J. Mol. Struct.: Theochem* **1999**, *461−462*, 121−135.
[51] J. C. W. Lohrenz, M. Buhl, M. Weber, W. Thiel, *J. Organomet. Chem.* **1999**, *592*, 11−21.
[52] S. Lieber, M.-H. Prosenc, H.-H. Brintzinger, *Organometallics* **2000**, *19*, 377−387.
[53] G. Guerra, L. Cavallo, P. Corradini, R. Fusco, *Macromolecules* **1997**, *30*, 677−684.
[54] A. Peluso, R. Improta, A. Zambelli, *Macromolecules* **1997**, *30*, 2219−2227.
[55] V. L. Cruz, A. Muñoz-Escalona, J. Martinez-Salazar, *J. Polym. Sci., Part A: Polym. Chem.* **1998**, *36*, 1157−1167.
[56] L. Ahjopalo, B. Löfgren, K. Hakala, L.-O. Pietilä, *Eur. Polym. J.* **1999**, *35*, 1519−1528.
[57] G. Guerra, P. Longo, P. Corradini, L. Cavallo, *J. Am. Chem. Soc.* **1999**, *121*, 8651−8652.
[58] R. Sustmann, W. Sicking, F. Bandermann, M. Ferenz, *Macromolecules* **1999**, *32*, 4204−4213.
[59] R. Fusco, L. Longo, F. Masi, F. Garbassi, *Macromol. Rapid Commun.* **1997**, *18*, 433−441.
[60] R. Fusco, L. Longo, F. Masi, F. Garbassi, *Macromolecules* **1997**, *30*, 7673−7685.
[61] G. Lanza, I. L. Fragalà, T. J. Marks, *J. Am. Chem. Soc.* **1998**, *120*, 8257−8258.
[62] R. Fusco, L. Longo, A. Proto, F. Masi, F. Garbassi, *Macromol. Rapid Commun.* **1998**, *19*, 257−262.
[63] S. Yao, T. Shoji, Y. Iwamoto, E. Kamei, *Comput. Theor. Polym. Sci.* **1999**, *9*, 41−46.
[64] M. S. W. Chan, K. Vanka, C. C. Pye, T. Ziegler, *Organometallics* **1999**, *18*, 4624−4636.
[65] A. Klesing, S. Bettonville, *Phys. Chem. Chem. Phys.* **1999**, *1*, 2373−2377.
[66] K. Vanka, M. S. W. Chan, C. C. Pye, T. Ziegler, *Organometallics* **2000**, *19*, 1841−1849.
[67] P. E. M. Siegbahn, S. Strömberg, K. Zetterberg, *Organometallics* **1996**, *15*, 5542−5550.
[68] M. Svensson, T. Matsubara, K. Morokuma, *Organometallics* **1996**, *15*, 5568−5576.
[69] D. G. Musaev, R. D. J. Froese, M. Svensson, K. Morokuma, *J. Am. Chem. Soc.* **1997**, *119*, 367−374.
[70] L. Deng, P. Margl, T. Ziegler, *J. Am. Chem. Soc.* **1997**, *119*, 1094−1100.
[71] L. Deng, T. K. Woo, L. Cavallo, P. M. Margl, T. Ziegler, *J. Am. Chem. Soc.* **1997**, *119*, 6177−6186.
[72] R. D. J. Froese, D. G. Musaev, T. Matsubara, K. Morokuma, *J. Am. Chem. Soc.* **1997**, *119*, 7190−7196.
[73] T. K. Woo, P. M. Margl, P. E. Blöchl, T. Ziegler, *J. Phys. Chem. B* **1997**, *101*, 7877−7880.
[74] V. R. Jensen, K. J. Børve, *Organometallics* **1997**, *16*, 2514−2522.
[75] R. D. J. Froese, D. G. Musaev, K. Morokuma, *J. Am. Chem. Soc.* **1998**, *120*, 1581−1587.
[76] F. Bernandi, A. Bottoni, I. Rossi, *J. Am. Chem. Soc.* **1998**, *120*, 7770−7775.
[77] B. B. Coussens, F. Buda, H. Oevering, R. J. Meier, *Organometallics* **1998**, *17*, 795−801.
[78] D. G. Musaev, R. D. J. Froese, K. Morokuma, *Organometallics* **1998**, *17*, 1850−1860.
[79] L. Deng, T. Ziegler, T. K. Woo, P. Margl, L. Fan, *Organometallics* **1998**, *17*, 3240−3253.
[80] L. Deng, P. Margl, T. Ziegler, *J. Am. Chem. Soc.* **1999**, *121*, 6479−6487.
[81] R. D. J. Froese, D. G. Musaev, K. Morokuma, *Organometallics* **1999**, *18*, 373−379.
[82] A. Michalak, T. Ziegler, *Organometallics* **1999**, *18*, 3998−4004.
[83] N. Koga, *Theor. Chem. Acc.* **1999**, *102*, 285−292.
[84] D. Musaev, K. Morokuma, *Top. Catal.* **1999**, *7*, 107−123.
[85] D. G. Musaev, R. D. J. Froese, K. Morokuma, *New J. Chem.* **1997**, *21*, 1269−1282.
[86] P. Margl, L. Deng, T. Ziegler, *J. Am. Chem. Soc.* **1998**, *120*, 5517−5525.
[87] P. Margl, L. Deng, T. Ziegler, *Organometallics* **1998**, *17*, 933−946.
[88] P. Margl, L. Deng, T. Ziegler, *J. Am. Chem. Soc.* **1999**, *121*, 154−162.
[89] P. Margl, L. Deng, T. Ziegler, *Top. Catal.* **1999**, *7*, 187−280.
[90] H. Fujimoto, T. Yamasaki, H. Mizutani, N. Koga, *J. Am. Chem. Soc.* **1985**, *107*, 6157−6161.
[91] L. M. Hansen, D. S. Marynick, *Organometallics* **1989**, *8*, 2173−2179.
[92] I. Hyla-Kryspin, R. Gleiter, C. Krüger, R. Zwettler, G. Erker, *Organometallics* **1990**, *9*, 517−523.
[93] G. Erker, R. Zwettler, C. Krüger, I. Hyla-Kryspin, R. Gleiter, *Organometallics* **1990**, *9*, 524−530.
[94] H. Kawamura-Kuribayashi, N. Koga, K. Morokuma, *J. Am. Chem. Soc.* **1992**, *114*, 2359−2366.
[95] J. Endo, N. Koga, K. Morokuma, *Organometallics* **1993**, *12*, 2777−2787.
[96] R. Gleiter, I. Hyla-Kryspin, S. Niu, G. Erker, *Organometallics* **1993**, *12*, 3828−3836.
[97] L. Fan, D. Harrison, L. Deng, T. K. Woo, D. Swerhone, T. Ziegler, *Can. J. Chem.* **1995**, *73*, 989−998.
[98] E. P. Bierwagen, J. E. Bercaw, W. A. Goddard III, *J. Am. Chem. Soc.* **1994**, *116*, 1481−1489.
[99] H. J. R. de Boer, B. W. Royan, *J. Mol. Catal.* **1994**, *90*, 171−175.
[100] F. U. Axe, J. M. Coffin, *J. Phys. Chem.* **1994**, *98*, 2567−2570.
[101] V. R. Jensen, K. J. Børve, M. Ystenes, *J. Am. Chem. Soc.* **1995**, *117*, 4109−4117.
[102] I. Hyla-Kryspin, S. Niu, R. Gleiter, *Organometallics* **1995**, *14*, 964−974.
[103] V. R. Jensen, K. J. Børve, N. Westberg, M. Ystenes, *Organometallics* **1995**, *14*, 4349−4358.
[104] M.-H. Prosenc, H.-H. Brintzinger, *Organometallics* **1997**, *16*, 3889−3894.
[105] E. A. H. Griffiths, I. R. Gould, S. Ramdas, *Chem. Commun.* **1998**, 2177−2178.
[106] P. M. Margl, T. K. Woo, P. E. Blöchl, T. Ziegler, *J. Am. Chem. Soc.* **1998**, *120*, 2174−2175.
[107] L. Cavallo, G. Guerra, P. Corradini, *J. Am. Chem. Soc.* **1998**, *120*, 2428−2436.

[108] E. D. Jemmis, K. T. Giju, *J. Am. Chem. Soc.* **1998**, *120*, 6952−6964.
[109] R. Improta, C. Garzillo, A. Peluso, *J. Mol. Struct.: Theochem* **1998**, *426*, 249−255.
[110] F. Bernardi, A. Bottoni, G. P. Miscione, *Organometallics* **1998**, *17*, 16−24.
[111] W. A. King, S. Di Bella, A. Gulino, G. Lanza, I. L. Fragala, C. L. Stern, T. J. Marks, *J. Am. Chem. Soc.* **1999**, *121*, 355−366.
[112] F. U. Axe, J. W. Andzelm, *J. Am. Chem. Soc.* **1999**, *121*, 5396−5402.
[113] M. C. Chang, *Bull. Korean Chem. Soc.* **1999**, *20*, 1269−1276.
[114] Y. A. Ustynyuk, L. Y. Ystynyuk, D. N. Laikov, V. V. Lunin, *J. Organomet. Chem.* **2000**, *597*, 182−189.
[115] J.-G. Lee, H. Y. Jeong, Y. H. Ko, J. H. Jang, H. Lee, *J. Am. Chem. Soc.* **2000**, *122*, 6476−6487.
[116] D. R. Armstrong, K. W. Henderson, I. Little, C. Jenny, A. R. Kennedy, A. E. McKeown, R. E. Mulvey, *Organometallics* **2000**, *19*, 4369−4375.
[117] M. Linnolahti, T. A. Pakkanen, *Macromolecules* **2000**, *33*, 9205−9214.
[118] M. Linnolahti, P. Hirva, T. A. Pakkanen, *J. Comput. Chem.* **2001**, *22*, 51−64.
[119] N. Mäkelä, H. R. Knuuttila, M. Linnolahti, T. A. Pakkanen, *J. Chem. Soc., Dalton Trans.* **2001**, 91−95.
[120] For a recent review, see: A. K. Rappé, W. M. Skiff, C. J. Casewit, *Chem. Rev.* **2000**, *100*, 1435−1456.
[121] W. Kaminsky, K. Külper, H. H. Brintzinger, F. R. W. P. Wild, *Angew. Chem. Int. Ed. Engl.* **1985**, *24*, 507−508.
[122] A. Andresen, H. G. Cordes, J. Herwig, W. Kaminsky, A. Merck, R. Mottweiler, J. Pein, H. Sinn, H. J. Vollmer, *Angew. Chem.* **1976**, *88*, 689−690.
[123] F. Piemontesi, I. Camurati, L. Resconi, D. Balboni, A. Sironi, M. Moret, R. Zeigler, N. Piccolrovazzi, *Organometallics* **1995**, *14*, 1256−1266.
[124] S. Collins, B. A. Kuntz, N. J. Taylor, D. G. Ward, *J. Organomet. Chem.* **1988**, *342*, 21−29.
[125] J. A. Ewen, M. J. Elder, R. L. Jones, L. Haspeslagh, J. L. Atwood, S. G. Bott, K. Robinson, *Makromol. Chem. Macromol. Symp.* **1991**, *48/49*, 253−295.
[126] L. Resconi, F. Piemontesi, I. Camurati, D. Balboni, A. Sironi, M. Moret, H. Rychlicki, R. Zeigler, *Organometallics* **1996**, *15*, 5046−5059.
[127] H. J. G. Luttikhedde, R. P. Leino, C.-E. Wilen, J. H. Näsman, M. J. Ahlgren, T. A. Pakkanen, *Organometallics* **1996**, *15*, 3092−3094.
[128] S. Collins, Y. Hong, R. Ramachandran, N. J. Taylor, *Organometallics* **1991**, *10*, 2349−2356.
[129] A. Schäfer, E. Karl, L. Zsolnai, G. Huttner, H.-H. Brintzinger, *J. Organomet. Chem.* **1987**, *328*, 87−99.
[130] H. H. Brintzinger, in: *Transition Metals and Organometallics as Catalysts for Olefin Polymerization* (Eds.: W. Kaminsky, H.-J. Sinn), Springer-Verlag, Berlin, **1988**, p. 249−256.
[131] R. F. Jordan, R. E. LaPointe, N. Baenziger, G. D. Hinch, *Organometallics* **1990**, *9*, 1539−1545.
[132] G. M. Diamond, R. F. Jordan, J. L. Petersen, *Organometallics* **1996**, *15*, 4030−4037.
[133] W. Kaminsky, O. Rabe, A.-M. Schauwienold, G. U. Schupfner, J. Hanss, J. Kopf, *J. Organomet. Chem.* **1995**, *497*, 181−193.
[134] R. Leino, H. Luttikhedde, C.-E. Wilén, R. Sillanpää, J. H. Näsman, *Organometallics* **1996**, *15*, 2450−2453.
[135] R. Leino, H. J. G. Luttikhedde, P. Lehmus, C.-E. Wilén, R. Sjöholm, A. Lehtonen, J. V. Seppälä, J. H. Näsman, *Macromolecules* **1997**, *30*, 3477−3483.
[136] H. J. G. Luttikhedde, R. Leino, A. Lehtonen, J. H. Näsman, *J. Organomet. Chem.* **1998**, *555*, 127−134.
[137] R. Leino, H. J. G. Luttikhedde, P. Lehmus, C. E. Wilen, R. Sjöholm, A. Lehtonen, J. V. Seppälä, J. H. Näsman, *J. Organomet. Chem.* **1998**, *559*, 65−72.
[138] R. Leino, H. J. G. Luttikhedde, A. Lehtonen, P. Ekholm, J. H. Näsman, *J. Organomet. Chem.* **1998**, *558*, 181−188.
[139] M. J. Frisch, G. W. Trucks, H. B. Schlegel, P. M. W. Gill, B. G. Johnson, M. A. Robb, J. R. Cheeseman, T. Keith, G. A. Petersson, J. A. Montgomery, K. Raghavachari, M. A. Al-Lahman, V. G. Zakrzewski, J. V. Ortiz, J. B. Foresman, J. Cioslowski, B. B. Stefanov, A. Nanayakkara, M. Challacombe, C. Y. Peng, P. Y. Ayala, W. Chen, M. W. Wong, J. L. Andres, E. S. Replogle, R. Gomperts, R. L. Martin, D. J. Fox, J. S. Binkley, D. J. Defrees, J. Baker, J. P. Stewart, M. Head-Gordon, C. Gonzales, J. A. Pople, Gaussian 94, Gaussian, Inc., Pittsburgh, PA, **1995**.
[140] A. D. Becke, *Phys. Rev. A* **1988**, *38*, 3098−3100.
[141] C. Lee, W. Yang, R. G. Parr, *Phys. Rev. B* **1988**, *37*, 785−789.
[142] A. D. Becke, *J. Chem. Phys.* **1993**, *98*, 5648−5652.
[143] P. E. M. Siegbahn, *Adv. Chem. Phys.* **1996**, *93*, 333−387.
[144] P. Pyykkö, *Chem. Rev.* **1988**, *88*, 563−594.
[145] See for example: W. J. Hehre, J. Yu, P. E. Klunzinger, L. Lou, *A Brief Guide to Molecular Mechanics and Quantum Chemical Calculations*, Wavefunction, Inc., Irvine, CA, **1998**.
[146] W. J. Hehre, L. Radom, P. v. R. Schleyer, J. A. Pople, *Ab initio Molecular Orbital Theory*, John Wiley & Sons, New York, **1986**, p. 266.
[147] In a few cases, a very small imaginary frequency of around 0−10 cm^{-1} was obtained, suggesting a slight distortion form the local minimum conformation. A test calculation using tighter convergence criteria at the cost of increased resource usage resulted in disappearance of the imaginary frequency. However, neither the structure of the molecule nor its energy was affected.
[148] F. R. W. P. Wild, M. Wasiucionek, G. Huttner, H. H. Brintzinger, *J. Organomet. Chem.* **1985**, *288*, 63−67.
[149] L. H. Doerrer, M. L. H. Green, D. Häußinger, J. Saßmannshausen, *J. Chem. Soc., Dalton Trans.* **1999**, 2111−2118.
[150] M. Gustafsson, T. Repo, M. Linnolahti, T. A. Pakkanen, K. Lappalainen, K. Kervinen, E. Aitola, M. Klinga, M. Leskelä, to be published.
[151] J. A. Smith, J. Von Seyerl, G. Huttner, H. H. Brintzinger, *J. Organomet. Chem.* **1979**, *173*, 175−185.
[152] A. Razavi, J. Ferrara, *J. Organomet. Chem.* **1992**, *435*, 299−310.
[153] M. L. H. Green, N. J. Ishihara, *J. Chem. Soc., Dalton Trans.* **1994**, 657−665.
[154] A. Cano, T. Cuenca, P. Gomez-Sal, B. Royo, P. Royo, *Organometallics* **1994**, *13*, 1688−1694.
[155] R. M. Shaltout, J. Y. Corey, N. P. Rath, *J. Organomet. Chem.* **1995**, *503*, 205−212.
[156] W. J. Gauthier, J. F. Corrigan, N. J. Taylor, S. Collins, *Macromolecules* **1995**, *28*, 3771−3778.
[157] V. A. Dang, L. C. Yu, D. Balboni, T. Dall'Occo, L. Resconi, P. Mercandelli, M. Moret, A. Sironi, *Organometallics* **1999**, *18*, 3781−3791.
[158] P. Lehmus, E. Kokko, O. Härkki, R. Leino, H. J. G. Luttikhedde, J. H. Näsman, J. V. Seppälä, *Macromolecules* **1999**, *32*, 3547−3552.
[159] B. Rieger, X. Mu, D. T. Mallin, M. D. Rausch, J. C. W. Chien, *Macromolecules* **1990**, *23*, 3559−3567.

Received November 28, 2000
[I00452]

Tetranuclear Complexes Containing Bimetallic Tetracarboxylates and Ferrocene − Models for Subunits of One-Dimensional Organometallic Polymers

Wen-Mei Xue[a] and Fritz E. Kühn*[a]

Keywords: Metal-metal interactions / Molybdenum / Polymers / Rhodium / Ferrocene

The tetranuclear compounds $M_2(O_2C\text{-}R)_4L_2$ [M = Rh, R = nC_7H_{15}, L = ferrocenyl-4-pyridylacetylene (FPA) (**1a**); M = Rh, R = CH_3, L = FPA (**1b**); M = Mo, R = CF_3, L = FPA (**2b**); M = Rh, R = nC_7H_{15}, L = 4-ferrocenylpyridine (FP) (**3a**); M = Rh, R = CH_3, L = FP (**3b**); M = Mo, R = nC_7H_{15}, L = FP (**4a**); M = Mo, R = CF_3, L = FP (**4b**)] have been synthesized by the reaction of bimetallic tetracarboxylates with L in a 1:2 ratio, in a noncoordinating solvent. The reaction of $Mo_2(O_2C\text{-}nC_7H_{15})_4$ with FPA in a 1:2 molar ratio leads to a trinuclear compound $Mo_2(O_2C\text{-}nC_7H_{15})_4$(FPA) (**2a**). A soluble oligomer $[Rh_2(O_2C\text{-}nC_7H_{15})_4(BPEF)]_n$ [**5**, BPEF = 1,1′-bis(4-pyridylethynyl)ferrocene] is obtained by the reaction of $Rh_2(O_2C\text{-}nC_7H_{15})_4$ with BPEF in a 1:1 ratio in CH_2Cl_2 or $CHCl_3$, whereas the reaction of $Mo_2(O_2C\text{-}nC_7H_{15})_4$ with BPEF leads to a pentanuclear compound $[Mo_2(O_2C\text{-}nC_7H_{15})_4]_2$(BPEF) (**6**), even when BPEF is in excess. ^{1}H NMR, Raman, UV/Vis absorption spectroscopy and cyclic voltammetry indicate that the metal-metal bonds are weakened by the metal-axial ligand interaction and the donor-acceptor interactions occurring between the building blocks of the multinuclear compounds and oligomers. The interaction between the bimetallic centers and the ferrocene moiety is enhanced by shortening the distances between them. This shortening is achieved by modification of the axial ligand from FPA to FP. A significant electronic communication between the ferrocene units is not observed.

Introduction

Since Cotton's recognition of metal-metal bonds in 1964, the field of multiple bonds between metal atoms has been an active area of research in modern coordination chemistry. Oligomers and polymers containing metal-metal bonds in the backbone may display novel optical and magnetic properties.[1] Two general types of one-dimensional polymers can be envisaged, and these are shown in Scheme 1.[2a]

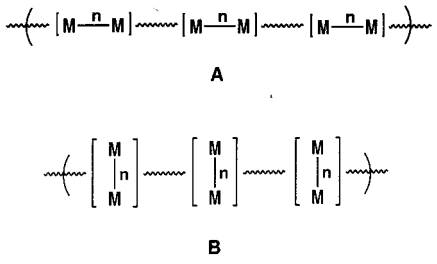

Scheme 1

In **A**, the M−M axis associated with the M−M bond is parallel to the propagating axis, whereas in **B** the M−M axis is perpendicular. Examples of the latter type are oligomers composed of $Mo_2(O_2C\text{-}tBu)_2$ and $^-OOC-R-COO^-$ units, which have been reported by Chisholm et al.[2] Polymers of type **A** can be constructed by axial coordination of the linking ligands to the bimetallic complexes. A number of bimetallic tetracarboxylates have been linked by bidentate organic axial ligands, resulting in polymeric species.[3] These types of polymers have the advantage of being readily accessible. A wide diversity of bimetallic centers, equatorial ligands and axial linkages can be used. As a result the polymer properties, such as solubility, strength of metal-axial ligand interaction, electronic and electrochemical behaviors, can be easily tuned. However, to the best of our knowledge, examples of these types of oligomers and polymers with organometallic spacing groups are very rare.[4] Nevertheless, organometallic linkers are interesting alternatives to organic linkers. Several of these organometallic complexes can be quite easily obtained and can be modified to a significant degree by well-established synthetic strategies. A much broader variety of potential product molecules are available than with simple organic molecules.

We attempted to incorporate bimetallic units into one-dimensional organometallic polymers of type **A**.[4] As this area of chemistry is relatively new, we chose to work with dimolybdenum(II) and dirhodium(II) tetracarboxylates since their molecular and electronic structures have been extensively studied.[1] Conjugated ligands containing a ferrocene moiety were selected as bridging ligands, due to the favorable electrochemical properties of ferrocene, and the comparatively easy accessibility and high synthetic yields of these complexes.

We recently reported oligomers with backbones containing 1,1′-bis(4-pyridylethynyl)ferrocene (BPEF) and bimetallic tetracarboxylates. However, it was found that these oligomers are insoluble in noncoordinating solvents, and the use of strongly coordinating solvents, such as CH_3CN

[a] Anorganisch-Chemisches Institut der Technischen Universität München,
Lichtenbergstraße 4, 85747 Garching bei München, Germany
Fax: (internat.) +49−(0)89/289-13473
E-mail: fritz.kuehn@ch.tum.de

 © WILEY-VCH Verlag GmbH, 69451 Weinheim, 2001 1434−1948/01/0808−2041 $ 17.50+.50/0

and THF, resulted in the destruction of the polymer chain due to replacement of the comparatively weakly coordinating BPEF ligands by solvent molecules.[4a] The poor solubility hinders complete characterization and detailed examination of their properties. An important step forward is to make the oligomers and polymers soluble in both coordinating and noncoordinating solvents. In this work we report on how this can be achieved. Furthermore, the axial ligands for the model compounds are modified from ferrocenyl-4-pyridylacetylene (FPA) to 4-ferrocenylpyridine (FP), in order to investigate the effect on the electronic coupling between the two ferrocene units resulting from the decreased distance between them.

Results and Discussion

Preparation and Characterization

The reactions of the bimetallic tetracarboxylates with the monodentate ligands FPA or FP, in a 1:2 molar ratio, led to the formation of the tetranuclear complexes **1a**, **1b**, **2b**, **3a, 3b**, **4a** and **4b** (Scheme 2). Compound **2a** has only one axial ligand due to the relatively weak metal-axial ligand interaction between $Mo_2(O_2C\text{-}nC_7H_{15})_4$ and FPA. Similarly, the reaction of $Mo_2(O_2C\text{-}nC_7H_{15})_4$ with a bidentate ligand BPEF in a 1:1 molar ratio gave a pentanuclear complex **6**, whereas BPEF with $Rh_2(O_2C\text{-}nC_7H_{15})_4$ formed the oligomeric compound **5**.

While the dirhodium complexes **1a**, **1b**, **3a**, **3b**, and **5** are air-stable, the dimolybdenum complexes **2a**, **2b**, **4a**, **4b**, and **6** decomposed when exposed to air for a few hours in the solid state, and within a couple of minutes in solution. The bimetallic compounds containing long-chain carboxylates are very soluble. The oligomer **5** is soluble in some noncoordinating solvents such as CH_2Cl_2 and $CHCl_3$, in contrast to the previously reported oligomers $[Rh_2(O_2CCH_3)_4(BPEF)]_n$, $[Rh_2(O_2CCF_3)_4(BPEF)]_n$, and $[Mo_2(O_2CCF_3)_4(BPEF)]_n$ which are insoluble in any noncoordinating solvent and decompose in coordinating solvents.[4]

The complexes were characterized by elemental analysis, NMR, solid state IR and Raman spectroscopies. Selected spectroscopic data are listed in Table 1.

The resonance signals for the pyridyl protons of the dirhodium complexes **1a**, **1b**, **3a**, **3b** and **5** appear at a lower field than those of the respective free ligands FPA, FP and BPEF. In contrast, upfield shifts of the pyridyl protons are observed in the dimolybdenum complexes. The coordination of the pyridyl ligands used here to form complexes with $Rh_2(O_2CCH_3)_4$ and $Rh_2(O_2C\text{-}nC_7H_{15})_4$, leads to a comparable downfield shift of the α-pyridyl protons ($\Delta^1H \approx 0.6-0.8$ ppm), reflecting the tendency of dirhodium(II) centers to bind axial ligands. The chemical shifts of the α-pyridyl protons of **2b** ($\delta = 8.03$) and **4b** ($\delta = 7.90$) differ significantly from those of the respective free ligands FPA ($\delta = 8.53$) and FP ($\delta = 8.45$), as a result of the relatively strong Lewis acidity of $Mo_2(O_2CCF_3)_4$. However, those of **2a** ($\delta = 8.30$) and **4a** ($\delta = 8.21$) differ from the free ligands by only

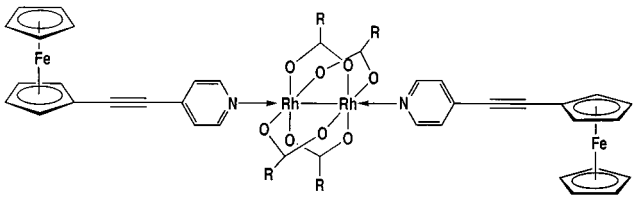

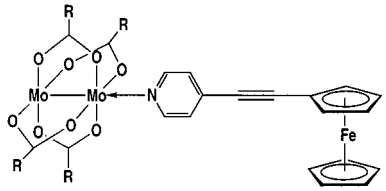

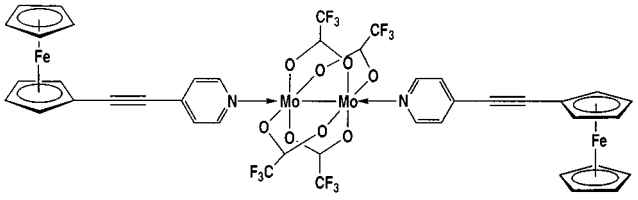

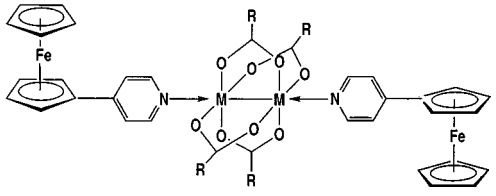

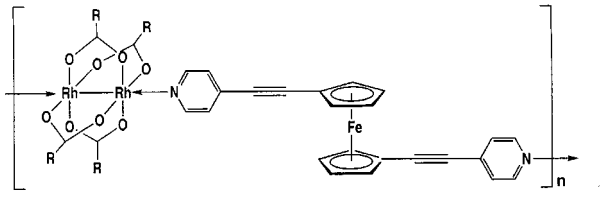

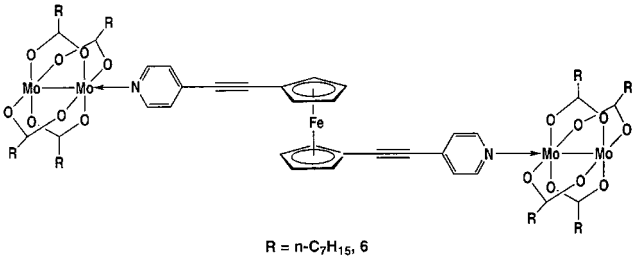

Scheme 2

Table 1. Selected characterization data of the compounds and their precursors

Compound[a]	δ(^{1}H)C_5H_4N(α)	δ(^{1}H)C_5H_4N(β)	δ(^{1}H)C_5H_4(α)	δ(^{1}H)C_5H_4(β)	δ(^{1}H)C_5H_5	δ(^{1}H)CH_2(2)	δ(^{1}H)CH_2(3)	ν(C≡C) cm^{-1}	ν(M−M) cm^{-1}
1a	9.24 s, br.	7.69 s, br.	4.60 s	4.33 s	4.29 s	2.10 t	1.42 m	2207	339
1b	9.11 s, br.	7.72 d	4.63 t	4.38 t	4.31 s	−	−	2205	341
2a	8.30 s, br.	7.22 s, br.	4.50 s	4.28 s	4.22 s	2.92t	1.85 m	2202	397
2b	8.03 d	7.24 d	4.53 t	4.33 t	4.23 s	−	−	2207	362
FPA	8.53 d	7.32 d	4.54 t	4.31 t	4.25 s	−	−	2210	−
3a	9.13 d	7.67 d	4.86 t	4.50 t	4.14 s	2.12 t	1.45 m	−	324
3b	9.21 d	7.70 d	4.87 t	4.51 t	4.14 s	−	−	−	320
4a	8.21 d	7.21 d	4.66 t	4.40 t	4.00 s	2.96 t	1.87 m	−	400
4b	7.90 d	7.19 d	4.64 t	4.42 t	3.99 s	−	−	−	360
FP	8.45 d	7.30 d	4.71 t	4.41 t	4.03 s	−	−	−	−
5	9.26 d	7.72 d	4.71 s	4.50 s	−	2.11 t	1.43 m	2211	342
6	8.31 d	7.15 d	4.54 t	4.35 t	−	2.90 t	1.83 m	2207	397
BPEF	8.46 d	7.19 d	4.57 t	4.37 t	−	−	−	2208	−
$Rh_2(O_2C$-$nC_7H_{15})_4$	−	−	−	−	−	2.34 t	1.54 m	−	344
$Mo_2(O_2C$-$nC_7H_{15})_4$	−	−	−	−	−	2.82 t	1.80 m	−	401

ca. δ = 0.23, reflecting a rather weak metal-axial ligand interaction in the $Mo_2(O_2C$-$nC_7H_{15})_4$ derivatives. The ^{1}H NMR signal of the CH_3CO_2 group is shifted downfield from δ = 1.76 in the axial-ligand free $Rh_2(O_2CCH_3)_4$, to δ = 1.88 in the FPA-coordinated complex **1b** and to δ = 1.93 in the FP ligated complex **3b**. This demonstrates that electron density must be donated back to the axial ligands. In the cases of the tetraoctanoate bimetallic derivatives, the chemical shifts of only the CH_2(2) and CH_2(3) protons are affected by the coordination of axial ligands. The resonances of the CH_2(2) moiety are shifted upfield from δ = 2.34 in the axial-ligand free $Rh_2(O_2C$-$nC_7H_{15})_4$ to ca. δ = 2.11 in the complexes **1a**, **3a** and **5**. The signals of CH_2(3) are shifted from δ = 1.54 to ca. δ = 1.43. The resonances of CH_2(2) and CH_2(3) in the cases of the dimolybdenum complexes **2a**, **4a** and **6**, are shifted downfield from δ = 2.82 [$Mo_2(O_2C$-$nC_7H_{15})_4$] to δ = 2.90−2.96 [CH_2(2)] and from δ = 1.80 to δ = 1.83−1.87 [CH_2(3)]. The ferrocene proton resonances in the FPA-coordinated complexes do not show a significant difference relative to those of the free ligand (Table 1). However, the ferrocene protons of the FP derivatives, especially the dirhodium complexes, differ notably in their chemical shifts from the free ligand as a result of the shortened distance between the ferrocene moiety and the M_2 center, thus enhancing their electronic interaction. It is also interesting to note that the ferrocene proton resonances of oligomer **5** [$\delta(H_\alpha)$ = 4.71, $\delta(H_\beta)$ = 4.50] are shifted downfield from those of the free ligand BPEF [$\delta(H_\alpha)$ = 4.57, $\delta(H_\beta)$ = 4.37], whereas the signals of its tetranuclear model complex **1a** [$\delta(H_\alpha)$ = 4.60, $\delta(H_\beta)$ = 4.33] are quite similar to the free ligand FPA [$\delta(H_\alpha)$ = 4.54, $\delta(H_\beta)$ = 4.31]. This might indicate a better electronic delocalization in the oligomer than in the tetranuclear model compound.

As demonstrated previously, Raman spectroscopy is more informative than single-crystal X-ray analysis with regard to metal-metal interactions.[5] The strong Raman band centered at 324 cm^{-1} for complex **3a** is unambiguously assigned to the stretching frequency of the Rh−Rh bond, which is shifted 20 cm^{-1} lower in energy relative to the axial-ligand free complex $Rh_2(O_2C$-$nC_7H_{15})_4$ [ν(Rh−Rh) = 344 cm^{-1}]. This observation is probably due to the fact that coupling between the Rh−Rh stretching mode and the Rh-axial ligand stretching mode leads to a weakening of the Rh−Rh interaction. However, the coupling between the dirhodium center and the axial ligands in the cases of the FPA and BPEF derivatives is weaker than in the FP-coordinated compound **3a**, as indicated by the fact that the Rh−Rh vibration frequencies of compounds **1a** (339 cm^{-1}) and **5** (342 cm^{-1}) are very similar to that of the parent precursor. The same behavior has also been observed in the cases of the $Rh_2(O_2CCH_3)_4$ derivatives. The compound $Rh_2(O_2CCH_3)_4(FP)_2$ shows a Rh−Rh vibration at 320 cm^{-1}, which is 31 cm^{-1} lower in energy than the parent compound $Rh_2(O_2CCH_3)_4$ (ν(Rh−Rh) = 351 cm^{-1}). However, compounds **1b** and $[Rh_2(O_2CCH_3)_4(BPEF)]_n$ display their Rh−Rh vibrations at 341 and 343 cm^{-1}, respectively, with a deviation of about 10 cm^{-1} from the vibration of the parent precursor. These observations also demonstrate that $Rh_2(O_2CCH_3)_4$ and $Rh_2(O_2C$-$nC_7H_{15})_4$ have a similar tendency to bind axial ligands, the weakening of the metal-metal bond is mainly dependent on the donor strength of the axial ligands. Since $Mo_2(O_2C$-$nC_7H_{15})_4$ is only weakly bonded to the axial ligands, the Mo-Mo vibrations of complexes **2a**, **4a** and **6** display their bands at 397, 400 and 397 cm^{-1}, respectively, with a deviation within the measurement error range from that of the free precursor (401 cm^{-1}). Due to the relatively strong metal-axial ligand interaction in the cases of the $Mo_2(O_2CCF_3)_4$ derivatives, the Mo−Mo vibration is shifted to lower energies (ca. 27−33 cm^{-1} relative to the precursor).

In order to demonstrate an oligomer chain growth in solution, ^{1}H NMR investigations were performed on a mixture of $Rh_2(O_2C$-$nC_7H_{15})_4$ and BPEF, in different molar ratios in $CDCl_3$. The concentrations of the compounds in solution were in the range of 2×10^{-3} to 4×10^{-3} M. The measurements were performed after the solution was stirred at room temperature for 1 h. The results of this ^{1}H NMR study are summarized in Table 2, the data for oligomer **5**

Table 2. ^{1}H NMR spectroscopic data of mixtures of BPEF (A) and $Rh_2(O_2C\text{-}nC_7H_{15})_4$ (B) in $CDCl_3$ at room temperature

Sub-stance[a]	$C_5H_4N(\alpha)$		$C_5H_4N(\beta)$		$C_5H_4(\alpha)$		$C_5H_4(\beta)$		$CH_2(2)$		$CH_2(3)$		$CH_2(4-7)$		CH_3	
	δ(^{1}H)	I[b]	δ(^{1}H)	I[b]	δ(^{1}H)	I[b]	δ(^{1}H)	I[b]	δ(^{1}H)	I[b]	δ(^{1}H)	I[b]	δ(^{1}H)	I[b]	δ(^{1}H)	I[b]
A_1B_2	9.09 s, br.	3.8 (4)	7.72 d	4.0 (4)	4.71 s	3.9 (4)	4.50 s	4.0 (4)	2.13 t	15 (16)	1.39−1.46 m	18 (16)	1.08−1.26 m	63 (64)	0.84 t	23 (24)
A_2B_3	9.17 s, br.	7.5 (8)	7.73 d	8.0 (8)	4.71 s	7.9 (8)	4.51 s	7.6 (8)	2.13 t	24 (24)	1.39−1.46 m	28 (24)	1.10−1.26 m	102 (96)	0.84 t	38 (36)
A_3B_4	9.23 s	12 (12)	7.73 d	12 (12)	4.72 s	12 (12)	4.50 s	12 (12)	2.12 t	31 (32)	1.39−1.46 m	34 (32)	1.11−1.27 m	130 (128)	0.84 t	48 (48)
A_4B_5	9.23 s	16 (16)	7.71 d	16 (16)	4.71 s	16 (16)	4.50 s	16 (16)	2.11 t	38 (40)	1.39−1.47 m	42 (40)	1.11−1.25 m	152 (160)	0.85 t	54 (60)
A_5B_6	9.26 d	20 (20)	7.73 d	20 (20)	4.72 s	20 (20)	4.50 s	20 (20)	2.12 t	45 (48)	1.39−1.47 m	50 (48)	1.10−1.26 m	195 (192)	0.85 t	72 (72)
5	9.26 d	4 (4)	7.72 d	4 (4)	4.71 s	4 (4)	4.50 s	4 (4)	2.11 t	8.9 (8)	1.39−1.47 m	9.0 (8)	1.10−1.27 m	38 (32)	0.85 t	13 (12)
A	8.46 d	4	7.19 d	4	4.57 t	4	4.37 t	4	−	−	−	−	−	−	−	−
B	−	−	−	−	−	−	−	−	2.34 t	8	1.54 m	8	1.18 m	32	0.82 t	12

[a] A_mB_n represents the molar ratio of BPEF to $Rh_2(O_2C\text{-}nC_7H_{15})_4$ which is *m*:*n*; the concentration of subunit is in the range of 2×10^{-3} to 4×10^{-3} M. − [b] I = integration, the calculated data are in parenthesis.

and the precursors $Rh_2(O_2C\text{-}nC_7H_{15})_4$ and BPEF are also included for comparative purposes. It is interesting to note that the species present in solution depends on the molar ratio of the two precursor complexes. The oligomer chain grows as the molar ratio of BPEF:$Rh_2(O_2C\text{-}nC_7H_{15})_4$ (A:B) increases. The spectrum of the solution containing BPEF and $Rh_2(O_2C\text{-}nC_7H_{15})_4$ in a 5:6 ratio is quite similar to that of the isolated oligomer **5**. This observation suggests that the repeating unit of oligmer **5** is at least 5, and its molecular weight is not lower than 5832 amu.

Electronic Absorption Spectra

The electronic absorption spectroscopic data of the complexes and their precursors are given in Table 3. Figure 1 presents a comparison of the UV/Vis spectra of oligomer **5** and its precursors. The characteristic absorptions of the product complexes are similar to those of the ferrocenyl pyridine precursors. In general, a peak at ca. 330−370 nm and a broad band centered at ca. 420−480 nm are assigned to d−d transitions in the ferrocene unit.[4,6] The fairly intense bands at λ = 320 nm are assigned to a π→π* pyridyl transition. A comparison of the lowest energy d−d transition band between compounds **1a**, **1b**, **2a**, **2b** and their axial ligand FPA, reveals that the coordination of FPA does not noticeably disturb the d−d transition energy in the ferrocene unit. This is probably due to the relatively weak metal-axial ligand interaction, weak donor ability of FPA and the long distance between the ferrocene moiety and the

Table 3. UV/Vis absorption spectroscopic data and cyclic voltammetric data of the compounds and their precursors

Material	λ_{max}/nm (ε/M^{-1} cm^{-1})[a]	$E(\Delta E_p)$, $Fe^{3+/2+}$/V[a][b]	$E(\Delta E_p)$, $[M_2]^{5+/4+}$/V[a] [b]
1a	268 (32900), 308 (30900), 365 (10700), 450 (2620)	0.18 (75)	0.49 (114)
1b	267 (35200), 308 (32800), 365 (13600), 451 (3040)	0.18 (61)	0.52 (82)
2a	261 (19500), 303 (14700), 450 (1030)	0.23 (80)	0.04 (73)
2b	254 (31800), 305 (37400), 451 (23400)	0.17 (80)	
FPA	252 (13700), 304 (12800), 352 (2320), 449 (760)	0.12 (72)	−
3a	283 (41500), 348 (11500), 456 (br., 2160)	0.15 (83)	0.44 (73)
3b	284 (30000), 341 (9290), 458 (br., 1930)	0.15 (74)	0.48 (69)
4a	289 (26000), 364 (sh, 3900), 476 (br., 2000)	0.28 (85)	0.05 (115)
4b	284 (33900), 330 (sh, 11700), 463 (br., 2250)	0.30 (92)	
FP	279 (12400), 340 (2110), 454 (630)	0.13 (104)	−
5	269 (33500), 317 (24700), 362 (11600), 450 (2130)[d]	0.33 (110)[c]	
6	261 (35300), 300 (26100), 420 (4470)	[e]	
BPEF	261 (26100), 281 (20900), 311 (19600), 350 (sh, 4160), 457 (1040)	0.28 (110)	−
$Rh_2(O_2CCH_3)_4$	434 (170, 551 (230)[f]	−	0.90 (78)
$Rh_2(O_2C\text{-}nC_7H_{15})_4$	253 (9390), 420 (200), 657 (270)	−	0.81 (102)
$Mo_2(O_2C\text{-}nC_7H_{15})_4$	261 (7800), 289 (7570), 420 (280)	−	0.04 (107)

[a] Measured in deoxygenated CH_2Cl_2 solutions except if otherwise stated. − [b] The typical concentration of the complexes is 10^{-3} M. Potentials are vs. the ferrocenium/ferrocene couple (0.00V with ΔE_p = 95 mV); scan rate is 50 mV/s; $\Delta E_p = E_{pa} - E_{pc}$ (mV). − [c] Measured in $CDCl_3$. It is not assigned with surety. − [d] Molarity is based on the repeating unit. − [e] Measurement is not successful. − [f] Measured in CH_3CN.

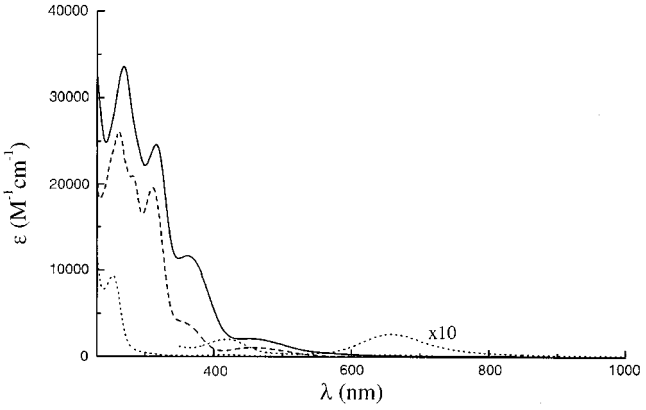

Figure 1. UV/Vis absorption spectra of $[Rh_2(O_2C\text{-}nC_7H_{15})_4\text{-}(BPEF)]_n$ (**5**, solid line), $Rh_2(O_2C\text{-}nC_7H_{15})_4$ (dotted line) and BPEF (dashed line) in CH_2Cl_2 at room temperature

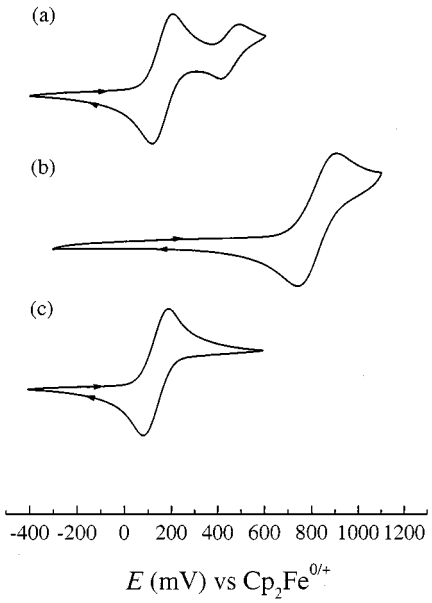

Figure 2. Cyclic voltammograms of (a) $Rh_2(O_2C\text{-}nC_7H_{15})_4(FP)_2$ (**3a**), (b) $Rh_2(O_2C\text{-}nC_7H_{15})_4$ and (c) FP at the same scan rate of 50 mV/s in CH_2Cl_2 with 0.1 M TBAH at room temperature

dimetallic centers. The ^1H NMR spectroscopic data described above are also in good agreement with this observation. However, in the cases of the FP derivatives, the lowest energy d−d transition band is shifted from 454 nm in FP to 456 nm in **3a**, 458 nm in **3b**, 463 nm in **4b** and 476 nm in **4a**. This again demonstrates that the shortening of the distance between the ferrocene unit and the bimetallic centers increases the electronic interaction between the building blocks. Even though the bathochromic shifts of the respective UV/Vis transitions are not quite pronounced, the stronger extinction coefficients of the products vs. their precursors probably indicate a better electronic delocalization. However, a metal-to-metal (ferrocene to dimetallic center) charge transfer (MM′CT) band is not found in the electronic absorption spectra (200−1100 nm).

Electrochemical Properties

As depicted in Figure 2, the cyclic voltammogram of complex **3a** in CH_2Cl_2 exhibits two subsequently reversible anodic couples. The first oxidation with $E_{1/2} = 0.15$ V is assigned to the oxidation of the two ferrocene units, whereas the second with $E_{1/2} = 0.44$ V is due to the oxidation process of the $[Rh_2]^{5+/4+}$ couple. The coordination of dirhodium(II) by FP results in a pronounced cathodic shift of the $[Rh_2]^{5+/4+}$ couple from the parent $Rh_2(O_2C\text{-}nC_7H_{15})_4$ (0.81 V), but a weak anodic shift of the $Fe^{3+/2+}$ couple from the free ligand FP (0.13 V). The same results were obtained when comparing the electrochemical behavior of the product molecules **1a**, **1b** and **3b** with their respective precursors (Table 3). The fact that the oxidation potentials of the $Fe^{3+/2+}$ couple for the above mentioned complexes are close to ones of the free ligands testifies the low electronic perturbation of the ferrocene unit caused by the linkage to the dirhodium centers. However, the $[Rh_2]^{5+/4+}$ oxidation potential is significantly shifted by the electron-donor effect of the pyridyl ligands.

The electrochemical experiments performed with the oligomer **5** were not very successful, only one reversible oxidation couple with $E_{1/2} = 0.33$ V is observed. We are not able to assign this to the oxidation process of the $[Rh_2]^{5+/4+}$ or $Fe^{3+/2+}$ couple without any doubt. Nonetheless, all the tetranuclear model complexes show a single oxidation process for the ferrocene units. We believe that the absence of electronic communication in the tetranuclear model complexes excludes the possibility of electronic communication in the corresponding polymers.

Conclusions

One-dimensional organometallic oligomers with a backbone consisting of bimetallic tetracarboxylates and π-conjugated ferrocene derivatives are generated by mixing the precursor compounds in noncoordinating solvents at room temperature. The solubility of the oligomers in noncoordinating solvents is enhanced by using octanoates as equatorial ligands. These complexes are soluble in both noncoordinating and coordinating solvents, thus enabling a complete characterization and a more detailed examination of their properties than was possible for related complexes previously examined. The electronic and electrochemical investigations of the tetranuclear model compounds indicate that the ferrocene units are electronically noncommunicating, despite the fact that the axial ligands are modified from FPA to FP which remarkably shortens the distance between the two ferrocene units. However, especially in the case of complexes consisting of Rh−Rh units and FP as the axial ligands, the Rh−Rh interaction is significantly influenced (weakened) by the coordinating ligands.

Experimental Section

General: The preparations and manipulations were carried out under an oxygen- and water-free argon atmosphere using the standard

Schlenk techniques. Solvents were dried by standard procedures, distilled, and kept under argon over molecular sieves. The syntheses of the ligands ferrocenyl-4-pyridylacetylene (FPA), 1,1′-bis(4-pyridylethynyl)ferrocene (BPEF), and the tetranuclear complexes $Rh_2(O_2CCH_3)_4(FPA)_2$ (**1b**), $Mo_2(O_2CCF_3)_4(FPA)_2$ (**2b**) have been described previously.[4] 4-Ferrocenylpyridine (FP) was prepared by a literature method.[7]

Elemental analyses were performed in the Mikroanalytisches Labor of the TU München in Garching. − ^1H, ^{13}C and ^{19}F NMR spectra were obtained with Joel JNM GX-400 spectrometers. − IR spectra were recorded on a Perkin−Elmer FT-IR spectrometer using KBr pellets as the IR matrix. − Raman spectra of the solid samples were measured on a Bio-Rad FTS 575C spectrometer using a 1064 μm excitation of the Nd:YAG laser. − Electronic absorption spectra were obtained by using a Perkin−Elmer Lambda 2 UV/Vis spectrometer. − Cyclic voltammograms were recorded with a computer-controlled Model 173 Potentiostat/galvanostat (EG&G Princeton Applied Research) in argon-saturated dried solutions, with tetrabutylammonium hexafluorophosphate (TBAH, 0.1 M) as the supporting electrolyte. The working electrode was platinum and the reference electrode was silver. Potentials are quoted vs. the ferrocene-ferrocenium couple as an internal standard.

$Rh_2(O_2C$-*n*$C_7H_{15})_4$: Prepared by ligand exchange reaction between $Rh_2(O_2CCH_3)_4$ and $CH_3(CH_2)_6COOH$ according to a literature method.[8] − $C_{32}H_{60}O_8Rh_2$ (778.24): calcd. C 49.34, H 7.77; found C 48.74, H 7.80. − IR (KBr): $\tilde{\nu}$ = 2954 s, 2922 s, 2851 s, 1568 vs, 1522 m, 1467 m, 1433 s, 1412 s, 1312 m, 740 m, 679 m cm^{-1}. − ^1H NMR ($CDCl_3$, room temp.): δ = 0.82 (t, 12 H, CH_3), 1.18 [m, 32 H, $CH_2(4-7)$], 1.54 [m, 8 H, $CH_2(3)$], 2.34 [t, 8 H, $CH_2(2)$]. − ^{13}C NMR ($CDCl_3$, room temp.): δ = 14.0 (CH_3), 22.6, 26.2, 29.1, 31.8, 37.5 (CH_2), 194.5 (CO_2).

$Mo_2(O_2C$-*n*$C_7H_{15})_4$: Prepared by a literature method.[9] − $C_{32}H_{60}Mo_2O_8$ (764.70): calcd. C 50.26, H 7.91; found C 50.77, H 8.10. − IR (KBr): $\tilde{\nu}$ = 2956 vs, 2929 vs, 2852 vs, 1506 vs, 1468 s, 1430 vs, 1412 vs, 1306 m, 1177 m, 1110 m, 802 m, 718 m, 657 m, 466 m cm^{-1}. − ^1H NMR ($CDCl_3$, room temp.): δ = 0.88 (t, 12 H, CH_3), 1.30 [m, 32 H, $CH_2(4-7)$], 1.80 [m, 8 H, $CH_2(3)$], 2.82 [t, 8 H, $CH_2(2)$]. − ^{13}C NMR ($CDCl_3$, room temp.): δ = 14.1 (CH_3), 22.7, 26.7, 29.1, 29.2, 31.9, 37.0 (CH_2), 185.7 (CO_2).

$Rh_2(O_2C$-*n*$C_7H_{15})_4(FPA)_2$ (1a): $Rh_2(O_2C$-*n*$C_7H_{15})_4$ (60 mg, 0.077 mmol) dissolved in 15 mL of CH_2Cl_2, was added to a 10 mL CH_2Cl_2 solution of FPA (49 mg, 0.17 mmol). After stirring at room temperature for 2 h, the solution was evaporated to dryness under vacuum and the residue was washed with *n*-hexane. The crude product obtained was purified by recrystallization from diethyl ether to give an orange powder. Yield: 90 mg, 86%. − $C_{66}H_{86}Fe_2N_2O_8Rh_2$ (1352.32): calcd. C 58.57, H 6.41, N 2.07; found C 58.22, H 6.80, N 2.03. − IR (KBr): $\tilde{\nu}$ = 2954 s, 2924 s, 2854 s, 2207 s, 1600 vs, 1587 vs, 1500 m, 1456 m, 1413 vs, 1314 m, 1214 m, 1170 m, 1107 m, 1011 m, 924 m, 826 m, 725 m, 677 m, 600 m, 540 m, 500 m, 486 m, 446 m cm^{-1}. − ^1H NMR ($CDCl_3$, room temp.): δ = 0.86 (t, 12 H, CH_3), 1.19 [m, 32 H, $CH_2(4-7)$], 1.42 [m, 8 H, $CH_2(3)$], 2.10 [t, 8 H, $CH_2(2)$], 4.29 (s, 10 H, C_5H_5), 4.33 [s, 4 H, $C_5H_4(\beta)$], 4.60 [s, 4 H, $C_5H_4(\alpha)$], 7.69 [s, br., 4 H, $C_5H_4N(\beta)$], 9.24 [s, br., 4 H, $C_5H_4N(\alpha)$]. − ^{13}C NMR ($CDCl_3$, room temp.): δ = 14.1 (CH_3), 22.6, 25.9, 28.9, 29.0, 31.7, 37.3 (CH_2), 63.5, 69.6, 70.2, 71.9 (C_5H_4 & C_5H_5), 83.8 [C≡*C*C_5H_4), 95.5 (NC_5H_4C≡C), 126.5 [$C_5H_4N(\beta)$], 133.1 [$C_5H_4N(\gamma)$], 150.8 [$C_5H_4N(\alpha)$], 194.2 (CO_2).

$Mo_2(O_2C$-*n*$C_7H_{15})_4$(FPA) (2a): A 20 mL diethyl ether solution containing $Mo_2(O_2C$-*n*$C_7H_{15})_4$ (122 mg,0.16 mmol) was added to a 20 mL diethyl ether solution of FPA (100 mg, 0.35 mmol). After stirring at room temperature for 2 h, the solution was evaporated to dryness under vacuum and the residue was washed with small portions of *n*-hexane. The orange product was obtained in a 65% yield (110 mg). − $C_{49}H_{73}FeMo_2NO_8Rh_2$ (1050.84): calcd. C 55.96, H 6.95, N 1.33; found C 55.32, H 7.10, N 1.28. − IR (KBr): $\tilde{\nu}$ = 2955 s, 2924 vs, 2853 s, 2202 s, 1601 s, 1507 vs, 1458 m, 1423 s, 1376 m, 1316 m, 1261 w, 1218 m, 1171 m, 1107 m, 1000 m, 928 m, 828 m, 801 m, 724 w, 645 w, 595 w, 542 w, 500 m, 446 w cm^{-1}. − ^1H NMR ($CDCl_3$, room temp.): δ = 0.88 (t, 12 H, CH_3), 1.29 [m, 32 H, $CH_2(4-7)$], 1.85 [m, 8 H, $CH_2(3)$], 2.92 [t, 8 H, $CH_2(2)$], 4.22 (s, 5 H, C_5H_5), 4.28 [s, 2 H, $C_5H_4(\beta)$], 4.50 [s, 2 H, $C_5H_4(\alpha)$], 7.22 [s, br., 2 H, $C_5H_4N(\beta)$], 8.30 [s, br., 2 H, $C_5H_4N(\alpha)$]. − ^{13}C NMR ($CDCl_3$, room temp.): δ = 14.1 (CH_3), 22.7, 26.7, 29.1, 29.2, 29.7, 31.8, 37.0 (CH_2), 63.4, 69.5, 70.1, 71.8 (C_5H_4 & C_5H_5), 83.3 (C≡*C*C_5H_4), 95.1 (NC_5H_4C≡C), 125.3 [$C_5H_4N(\beta)$], 132.9 [$C_5H_4N(\gamma)$], 149.4 [$C_5H_4N(\alpha)$], 185.4 (CO_2).

$Rh_2(O_2C$-*n*$C_7H_{15})_4(FP)_2$ (3a): $Rh_2(O_2C$-*n*$C_7H_{15})_4$ (100 mg, 0.13 mmol) and FP (74 mg, 0.28 mmol) were dissolved in 15 mL CH_2Cl_2. The solution was stirred at room temperature for 2 h, and evaporated to dryness under vacuum. The residue was washed with *n*-hexane and recrystallized in CH_2Cl_2/*n*-hexane. The orange product was obtained in a 71% yield (120 mg). − $C_{62}H_{86}Fe_2N_2O_8Rh_2$ (1304.88): calcd. C 57.07, H 6.64, N 2.15; found C 56.83, H 6.68, N 2.06. − IR (KBr): $\tilde{\nu}$ = 2954 m, 2924 s, 2854 m, 1605 s, 1585 vs, 1516 s, 1412 s, 1216 m, 1107 m,1034 w, 1017 m, 828 m, 687 m, 530 w, 498 m cm^{-1}. − ^1H NMR ($CDCl_3$, room temp.): δ = 0.86 (t, 12 H, CH_3), 1.20 [m, 32 H, $CH_2(4-7)$], 1.45 [m, 8 H, $CH_2(3)$], 2.12 [t, 8 H, $CH_2(2)$], 4.14 (s, 10 H, C_5H_5), 4.50 [t, 4 H, $C_5H_4(\beta)$], 4.86 [t, 4 H, $C_5H_4(\alpha)$], 7.67 [d, 4 H, $C_5H_4N(\beta)$], 9.93 [d, 4 H, $C_5H_4N(\alpha)$]. − ^{13}C NMR ($CDCl_3$, room temp.): δ = 14.1 (CH_3), 22.7, 25.9, 29.0, 29.1, 31.8, 37.3 (CH_2), 67.1, 70.1, 70.4, 81.0 (C_5H_4 & C_5H_5), 121.6, 149.8, 150.7 (C_5H_4N), 194.2 (CO_2).

$Rh_2(O_2CCH_3)_4(FP)_2$ (3b): A THF solution (20 mL) containing $Rh_2(O_2CCH_3)_4$ (57 mg, 0.13 mmol) and FP (75 mg, 0.28 mmol) was stirred at room temperature for 2 h, which led to an orange precipitate. The solvent was reduced to ca. 5 mL in vacuum, to which 20 mL of diethyl ether was added. The precipitate was collected and washed with 3 × 20 mL of diethyl ether. The orange product was purified by recrystallization in CH_2Cl_2/Et_2O. Yield: 110 mg (87%). − $C_{38}H_{38}Fe_2N_2O_8Rh_2$ (968.23): calcd. C 47.17, H 3.96, N 2.89; found C 47.63, H 4.17, N 2.63. − IR (KBr): $\tilde{\nu}$ = 3093 w, 2931 w, 1605 vs, 1590 vs, 1518 m, 1429 vs, 1343 m, 1290 w, 1223 m, 1108 m, 1016 m, 890 w, 836 m, 820 m, 694 m, 644 w, 627 w, 529 m, 518 m, 500 m, 434 w cm^{-1}. − ^1H NMR ($CDCl_3$, room temp.): δ = 1.93 (s, 12 H, CH_3), 4.14 (s, 10 H, C_5H_5), 4.51 [t, 4 H, $C_5H_4(\beta)$], 4.87 [t, 4 H, $C_5H_4(\alpha)$], 7.70 [d, 4 H, $C_5H_4N(\beta)$], 9.21 [d, 4 H, $C_5H_4N(\alpha)$]. − ^{13}C NMR ($CDCl_3$, room temp.): δ = 23.9 (CH_3), 67.2, 70.1, 70.5, 80.7 (C_5H_4 & C_5H_5), 121.7, 150.2, 150.6 (C_5H_4N), 191.9 (CO_2).

$Mo_2(O_2C$-*n*$C_7H_{15})_4(FP)_2$ (4a): $Mo_2(O_2C$-*n*$C_7H_{15})_4$ (100 mg, 0.13 mmol) and FP (69 mg, 0.26 mmol) were dissolved in 15 mL of CH_2Cl_2. The solution was stirred at room temperature for 2 h, and evaporated to dryness under vacuum. The residue was washed with *n*-hexane and recrystallized in CH_2Cl_2/*n*-hexane. The orange product was produced in a 53% yield (90 mg). − $C_{62}H_{86}Fe_2N_2O_8Mo_2$ (1304.88): calcd. C 57.07, H 6.64, N 2.15; found C 56.83, H 6.68, N 2.06. − IR (KBr): $\tilde{\nu}$ = 2955 s, 2919 s, 2852 s, 1506 vs, 1468 m, 1431 s, 1412 vs, 1315 w, 1109 m, 1031 w, 828 m, 718 m, 658 m, 466 m cm^{-1}. − ^1H NMR ($CDCl_3$, room temp.): δ = 0.88 (t, 12 H, CH_3), 1.30−1.41 [m, 32 H, $CH_2(4-7)$], 1.87 [m, 8 H, $CH_2(3)$], 2.96 [t, 8 H, $CH_2(2)$], 4.00 (s, 10 H, C_5H_5), 4.40 [t, 4 H, $C_5H_4(\beta)$], 4.66

[t, 4 H, C_5H_4(α)], 7.21 [d, 4 H, C_5H_4N(β)], 8.21 [d, 4 H, C_5H_4N(α)]. − ^{13}C NMR ($CDCl_3$, room temp.): δ = 14.1 (CH_3), 22.7, 26.7, 29.0, 29.1, 29.2, 31.8, 37.1 (CH_2), 66.9, 70.0, 70.3, 80.6 (C_5H_4 & C_5H_5), 120.5, 149.6 (C_5H_4N), 185.4 (CO_2).

$Mo_2(O_2CCF_3)_4(FP)_2$ (4b): $Mo_2(O_2CCF_3)_4$ (102 mg, 0.16 mmol) and FP (91 mg, 0.35 mmol) were dissolved in 15 mL of CH_2Cl_2. The solution was stirred at room temperature for 2 h, and evaporated to dryness under vacuum. The residue was washed with *n*-hexane and recrystallized in CH_2Cl_2/*n*-hexane. The orange product was obtained in a 96% yield (180 mg). − $C_{38}H_{26}F_{12}Fe_2Mo_2N_2O_8$ (1170.19): calcd. C 39.00, H 2.24, N 2.39; found C 39.20, H 2.52, N 2.51. − IR (KBr): $\tilde{\nu}$ = 1684 m, 1631m, 1603 vs, 1520 m, 1428 m, 1194 vs, 1160 s, 1108 w, 1031 w, 1014 m, 1003 m, 856 m, 822 m, 778 w, 730 s, 684 m, 527 m, 496 m cm^{-1}. − ^{1}H NMR ($CDCl_3$, room temp.): δ = 3.99 (s, 10 H, C_5H_5), 4.42 [t, 4 H, C_5H_4(β)], 4.64 [t, 4 H, C_5H_4(α)], 7.19 [d, 4 H, C_5H_4N(β)], 7.90 [d, 4 H, C_5H_4N(α)]. − ^{13}C NMR ($CDCl_3$, room temp.): δ = 67.0, 70.1, 70.7, 79.8 (C_5H_4 & C_5H_5), 114.9 (CF_3), 124.2, 148.7, 151.1 (C_5H_4N), 166.1 (CO_2). − ^{19}F NMR ($CDCl_3$, room temp.): δ = −9.29.

$[Rh_2(O_2C\text{-}nC_7H_{15})_4(BPEF)]_n$ (5): A mixture of $Rh_2(O_2C\text{-}nC_7H_{15})_4$ (117 mg, 0.15 mmol) and BPEF (58 mg, 0.15 mmol) was dissolved in 25 mL of dichloromethane. The solution was stirred at room temperature overnight, and then filtered to remove traces of the precipitate. The filtrate was then evaporated to dryness under vacuum. The crude product was washed with diethyl ether and recrystallized by diffusion of diethyl ether into its dichloromethane solution. The deep orange product was obtained in a 86% yield (150 mg). − $[C_{56}H_{76}FeN_2O_8Rh_2]_n$ ($n \times$ 1166.31): calcd. C 57.62, H 6.57, N 2.40; found C 57.38, H 6.30, N 2.43. − IR (KBr): $\tilde{\nu}$ = 2955 s, 2925 s, 2853 s, 2211 s, 1600 s, 1588 vs, 1500 m, 1458 m, 1413 s, 1314 m, 1215 m, 1172 w, 1010 m, 925 w, 826 m, 730 w, 669 w, 601 w, 550 w, 496 m cm^{-1}. − ^{1}H NMR ($CDCl_3$, room temp.): δ = 0.85 (t, 12 H, CH_3), 1.19 [m, 32 H, CH_2(4−7)], 1.43 [m, 8 H, CH_2(3)], 2.11 [t, 8 H, CH_2(2)], 4.50 [s, 4 H, C_5H_4(β)], 4.71 [s, 4 H, C_5H_4(α)], 7.72 [d, 4 H, C_5H_4N(β)], 9.26 [d, 4 H, C_5H_4N(α)]. − ^{13}C NMR ($CDCl_3$, room temp.): δ = 14.1 (CH_3), 22.6, 25.9, 29.0, 31.7, 37.3 (CH_2), 65.1, 72.5, 73.5 (C_5H_4), 84.5 (C≡*C*C_5H_4), 94.3 (NC_5H_4*C*≡C), 126.5 [C_5H_4N(β)], 132.8 [C_5H_4N(γ)], 150.9 [C_5H_4N(α)], 194.2 (CO_2).

$[Mo_2(O_2C\text{-}nC_7H_{15})_4]_2(BPEF)$ (6): A mixture of $Mo_2(O_2C\text{-}nC_7H_{15})_4$ (128 mg, 0.17 mmol) and BPEF (65 mg, 0.17 mmol) was dissolved in 20 mL of dichloromethane. The solution was stirred at room temperature overnight, and the solvent was then evaporated to dryness under vacuum. The residue was washed with one portion of 5 mL of diethyl ether and several portions of *n*-hexane. The pale-orange powder was recrystallized from CH_2Cl_2/*n*-hexane. Yield: 80 mg, 49% yield based on $Mo_2(O_2C\text{-}nC_7H_{15})_4$. − $C_{88}H_{136}FeMo_4N_2O_{16}$ (1917.66): calcd. C 55.12, H 7.15, N 1.46; found C 54.78, H 6.80, N 1.60. − IR (KBr): $\tilde{\nu}$ = 2956 vs, 2920 vs, 2852 vs, 2207 m, 1596 m, 1506 vs, 1458 m, 1430 s, 1412 vs, 1315 m, 1257 w, 1213 w, 1177 m, 1110 m, 1026 w, 928 w, 874 w, 816 m, 718 m, 657 m, 541 w, 489 m, 466 m, 444 m cm^{-1}. − ^{1}H NMR ($CDCl_3$, room temp.): δ = 0.88 (t, 24 H, CH_3), 1.29 [m, 64 H, CH_2(4−7)], 1.83 [m, 16 H, CH_2(3)], 2.90 [t, 16 H, CH_2(2)], 4.35 [t, 4 H, C_5H_4(β)], 4.54 [t, 4 H, C_5H_4(α)], 7.15 [d, 4 H, C_5H_4N(β)], 8.31 [d, 4 H, C_5H_4N(α)]. − ^{13}C NMR ($CDCl_3$, room temp.): δ = 14.1 (CH_3), 22.7, 26.7, 29.1, 29.2, 31.8, 37.0 (CH_2), 65.4, 71.8, 73.4 (C_5H_4), 84.2 (C≡*C*C_5H_4), 125.2 [C_5H_4N(β)], 132.6 [C_5H_4N(γ)], 149.4 [C_5H_4N(α)], 185.6 (CO_2).

Acknowledgments

W. M. X. thanks the Bayerische Forschungsstiftung for a postdoctoral research associate fellowship. Professor W. A. Herrmann is acknowledged for the continuous support of our work. The authors are also grateful to the Fonds der Chemischen Industrie for financial support. Dr. É. S. Bencze is acknowledged for recording the vibrational spectra.

[1] F. A. Cotton, R. A. Walton, *Multiple Bonds between Metal Atoms*, 2nd edn., Oxford University Press, London, **1993** and references therein.

[2] [2a] M. H. Chisholm, *Acc. Chem. Res.* **2000**, *33*, 53−61. − [2b] R. H. Cayton, M. H. Chisholm, J. C. Huffman, E. B. Lobkovsky, *J. Am. Chem. Soc.* **1991**, *113*, 8709−8724. − [2c] F. A. Cotton, C. Lin, C. A. Murillo, *J. Chem. Soc., Dalton Trans.* **1998**, 3151−3153.

[3] [3a] F. A. Cotton, J. G. Norman, *J. Coord. Chem.* **1971**, *1*, 161. − [3b] B. Morosin, R. C. Hughes, Z. G. Soos, *Acta Crystallogr.* **1975**, *B31*, 762−770. − [3c] F. A. Cotton, T. R. Felthouse, *Inorg. Chem.* **1980**, *19*, 328−331. − [3d] F. A. Cotton, T. R. Felthouse, *Inorg. Chem.* **1981**, *20*, 600−608. − [3e] M. Handa, K. Kasamatsu, K. Kasuge, M. Mikuriya, T. Fujii, *Chem. Lett.* **1990**, 1753−1756. − [3f] M. C. Kerby, B. W. Eichhorn, J. A. Creighton, K. P. C. Vollhardt, *Inorg. Chem.* **1990**, *29*, 1319−1323. − [3g] F. A. Cotton, Y. Kim, T. Ren, *Inorg. Chem.* **1992**, *31*, 2723−2726. − [3h] X. Ouyang, C. Campana, K. R. Dunbar, *Inorg. Chem.* **1996**, *35*, 7188−7189. − [3i] J. L. Wesemann, M. H. Chisholm, *Inorg. Chem*. **1997**, *36*, 3258−3267. − [3j] M. Handa, H. Matsumoto, D. Yashioka, R. Nukada, M. Mikuriya, I. Hiromitsu, K. Kasuge, *Bull. Chem. Soc. Jpn.* **1998**, *71*, 1811−1816. − [3k] M. Handa, M. Watanabe, D. Yashioka, S. Kawabata, R. Nukada, M. Mikuriya, H. Azuma, K. Kasuge, *Bull. Chem. Soc. Jpn.* **1999**, *72*, 2681−2686. − [3l] Y. Ding, S. S. Lau, P. E. Fanwick, R. A. Walton, *Inorg. Chim. Acta* **2000**, *300−302*, 505−511. − [3m] T. Ren, G. Zou, J. C. Alvarez, *Chem. Commun.* **2000**, 1197−1198. − [3n] K.-T. Wong, J.-M. Lehn, S.-M. Peng, G.-H. Lee, *Chem. Commun.* **2000**, 2259−2260.

[4] [4a] W.-M. Xue, F. E. Kühn, E. Herdtweck, Q. Li, *Eur. J. Inorg. Chem.* **2001**, 213−221. − [4b] A. M. Santos, F. E. Kühn, W.-M. Xue, E. Herdtweck, *J. Chem. Soc., Dalton Trans.* **2000**, 3570−3574.

[5] [5a] W.-M. Xue, F. E. Kühn, G. Zhang, E. Herdtweck, *J. Organomet. Chem.* **2000**, *596*, 177−182. − [5b] W.-M. Xue, F. E. Kühn, G. Zhang, E. Herdtweck, G. Raudaschl-Sieber, *J. Chem. Soc., Dalton Trans.* **1999**, 4103−4110.

[6] T. H. Barr, W. E. Watts, *J. Organomet. Chem.* **1968**, *15*, 177−185.

[7] T. M. Miller, K. J. Ahmed, M. S. Wrighton, *Inorg. Chem.* **1989**, *28*, 2347−2355.

[8] A.-M. Girond-Godquin, J.-C. Marchon, *J. Phys. Chem.* **1986**, *90*, 5502−5503.

[9] R. H. Cayton, M. H. Chisholm, F. D. Darrington, *Angew. Chem. Int. Ed. Engl.* **1990**, *29*, 1481−1483.

Received November 30, 2000
[I00457]

Di-, Tri-, and Tetranuclear Complexes of Ni, Pd, and Zn with Oxalamidinato Bridges: Syntheses, Structures and Catalytic Reactions

Dirk Walther,*[a] Thomas Döhler,[a] Nils Theyssen,[a] and Helmar Görls[a]

Keywords: Nickel / N ligands / Oligomerizations / Palladium / Polymerizations

The reaction of oxalic amidines $R^1N{=}C(NHR^2){-}C(NHR^2){=}NR^1$ ($oxamH_2$) with 2 equiv. $(allyl)_2M$ or $(acac)_2M$ (M: Ni, Pd) results in the formation of dinuclear complexes [(**T**)M(oxam)M(**T**)] containing dianionic bridging oxalamidinate and η^3-allyl or acac as terminal ligands **T**. The complexes were characterized by elemental analyses, mass spectrometry, and ^1H and ^{13}C NMR spectroscopy. In addition, the solid-state structures of **1** (M: Ni; **T**: η^3-allyl; R^1 = *p*-tolyl; R^2 = mesityl), **2** (M: Ni; **T**: η^3-allyl; $R^1 = R^2$ = mesityl), **9** (M: Pd; **T**: acac; R^1 = phenyl; R^2 = *p*-tolyl), and **10** (M: Pd; **T**: acac; $R^1 = R^2$ = *p*-tolyl) were determined by X-ray single-crystal diffraction analyses. All complexes contain the metal ions in a square-planar environment. Furthermore, in the η^3-allyl complexes two isomers are found in which the two allyl groups are oriented in *syn* and *anti* positions. Trinuclear complexes of the composition [(**T**)M(oxam)M^1(oxam)M(**T**)] (M^1: Zn; M: Ni or Pd) are obtained by treating Et_2Zn with 2 equiv. of an oxalic amidine in toluene, followed by addition of 2 equiv. $M(acac)_2$ or $Pd(allyl)_2$. The synthesis and solid-state X-ray analysis of the tetranuclear complex [(**T**)M(oxam)M^1(oxam)M^1(oxam)M(**T**)] (**16**: M = M^1: Zn; oxam: R^1 = *p*-tolyl; R^2 = mesityl) is also described. A number of Ni^{II} complexes oligomerize or polymerize ethylene upon activation with MAO or Et_3Al. The catalyses can be adjusted by the bulkiness of the nitrogen substituents, the nature of the cocatalyst, and the nuclearity of the complexes. The most active and selective polymerization catalyst is the heterotrinuclear NiZnNi complex **12** which contains two tetramesityloxalamidinato bridges and acac as terminal ligands **T**. Complex **12** can be activated by using only 2 equiv. Et_3Al per Ni. Initial efforts show that the palladium complexes are catalysts for the Heck coupling.

Introduction

Transition metal complexes with oxalic acid amidinato bridging ligands (“oxam“) have, surprisingly, attracted little attention. Complexes of this type should be interesting candidates for a number of attractive applications, such as the construction of well-defined linear oligonuclear complexes or the synthesis of coordination polymers starting from dinuclear complexes which contain labile terminal ligands **T**. Moreover, linear oligometal complexes with tuneable catalytic properties at peripheral positions, adjusted by inner metal ions, should offer new possibilities for catalytic reactions.

Since oxalamidinato complexes have the tendency to form ill-defined polymeric amorphous complexes[1,2] only a few structurally characterized complexes are known. The first dinuclear complex $Cp_2Ti(oxam)TiCp_2$ has been synthesized by Floriani in the 1970s.[3] Döring and Beckert prepared a number of mono- and dinuclear complexes containing for example $M(CO)_4-$ and/or the Cp_2Ti- fragments and investigated the organic chemistry of these complexes.[4−7]

We have found that mono- and dinuclear ruthenium complexes containing bpy derivatives as additional supporting ligands form stable compounds which are non-luminescent.[8] Furthermore, we have prepared the first example of dinuclear magnesium oxalamidinates. These compounds reacted with carbon dioxide to form trimeric carbamato complexes which can be considered as structural models for rubisco.[9]

In a preliminary paper we have recently communicated that dinuclear nickel complexes of the type [(acac)Ni(oxam)-Ni(acac)] can readily be synthesized by treating free oxalic amidines with $Ni(acac)_2$. Additionally, the first linear tri- and tetranuclear complexes could be isolated.[10] Some of the complexes were found to be catalytically active in ethylene oligomerization or polymerization upon activation with MAO. Apart from our preliminary communication there exists no report of oxalamidinato complexes having been used in catalytic C−C linkage reactions. From a general point of view we can consider oxalic amidinato complexes as members of a general range of the following composition in which each oxam ligand bridges two metal fragments.

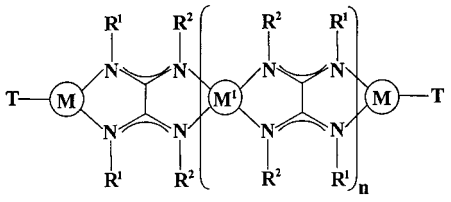

In this paper we describe the construction of well-defined di- or oligometal Ni, Pd, and Zn complexes of the above range, and investigate their catalytic behaviour in the oligomerization/polymerization of ethylene. Furthermore, initial

[a] Institut für Anorganische und Analytische Chemie der Universität Jena,
August-Bebel-Straße 2, 07743 Jena, Germany

 © WILEY-VCH Verlag GmbH, 69451 Weinheim, 2001 1434−1948/01/0808−2049 $ 17.50+.50/0

investigations of the use of some of the complexes in the Heck coupling are communicated.

Results and Discussion

Dinuclear Complexes Containing Ni, Pd, or Zn

Table 1 shows the dinuclear complexes **1**−**11** containing η^3-allyl or acetylacetonato ligands as terminal groups which were used in both the catalytic ethylene conversion and as catalysts in the Heck reaction. Complexes **6**−**8** were already described in a preliminary paper.[10]

Table 1. Di- and trinuclear oxalamidinato complexes (according to Schemes 1 and 3)

Compd.	M	Terminal ligand **T**	R^1	R^2
Dinuclear complexes of the type (**T**)M(oxam)M(**T**)				
1	Ni	η^3-allyl	*p*-tolyl[a]	mesityl[a]
2	Ni	η^3-allyl	mesityl	mesityl
3	Pd	η^3-allyl	phenyl	*p*-tolyl
4	Pd	η^3-allyl	*p*-tolyl	*p*-tolyl
5	Pd	η^3-allyl	*p*-tolyl	mesityl
6	Ni[10]	acac	*p*-tolyl	*p*-tolyl
7	Ni[10]	acac	*p*-tolyl[b]	mesityl[b]
8	Ni[10]	acac	mesityl	mesityl
9	Pd	acac	phenyl[c]	*p*-tolyl[c]
10	Pd	acac	*p*-tolyl	*p*-tolyl
11	Ni/Zn	acac	mesityl	mesityl
Trinuclear complexes of the type (**T**)M(oxam)Zn(oxam)M(**T**)				
12	Ni	acac	mesityl	mesityl
13	Pd	acac	*p*-tolyl	*p*-tolyl
14	Pd	η^3-allyl	*p*-tolyl	*p*-tolyl

[a] (*E*) arrangement of R^1 and R^2 (Scheme 2, **A** and **B**). − [b] (*Z*) arrangement of R^1 and R^2 (Scheme 2, **C** with acac instead of allyl). − [c] (*E*) arrangement of R^1 and R^2 (Scheme 2, **A** with acac instead of allyl).

A variety of dinuclear η^3-allyl complexes of Ni^{II} and Pd^{II} could be prepared by the reaction of the corresponding bis(η^3-allyl)metal complexes with the oxalic amidine (molar ratio 2:1, Scheme 1). In these reactions propene was eliminated resulting in neutral complexes of the type [(allyl)M-(oxam)M(allyl)] which are the first members of the above-mentioned homologous range (with $n = 0$).

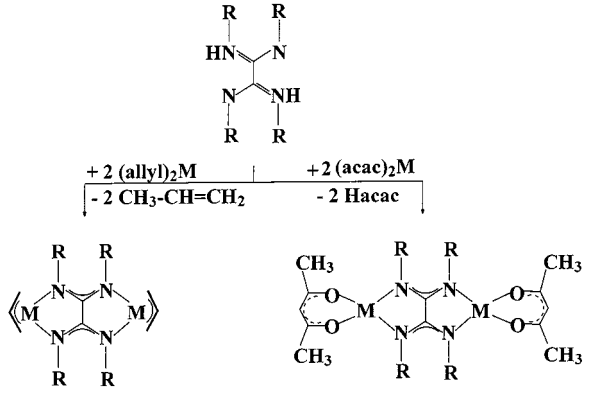

Scheme 1. Syntheses of dinuclear complexes **1**−**10**

Analogous dinuclear oxalamidinato complexes **6**−**10** containing acetylacetonato groups as terminal ligands were obtained in good yields starting from the corresponding bis(acetylacetonato)metal(II) complexes and oxalamidines (molar ratio 2:1). After workup, complexes of the type [(acac)M(oxam)M(acac)] (**6**−**10**) were isolated as crystalline compounds. The formation of coordination polymers was not observed in this reaction, due to the stable bonding of the terminal acetylacetonates in **6**−**10**. On the other hand, the complexes can easily react with organoaluminium compounds to form dinuclear Ziegler−Natta catalysts.

The synthesis of the heterodinuclear compound **11** required another preparative route: Reaction of $ZnEt_2$ with acetylacetone (molar ratio 1:1) in toluene resulted in the dimeric complex $[(acac)Zn(Et)]_2$ (**17**) which was used as starting product for **11**. Colorless crystals of compound **17** were obtained from toluene. Due to the insufficient quality of the crystals, only the structure motif could be determined by an X-ray diffraction analysis (Figure 1).

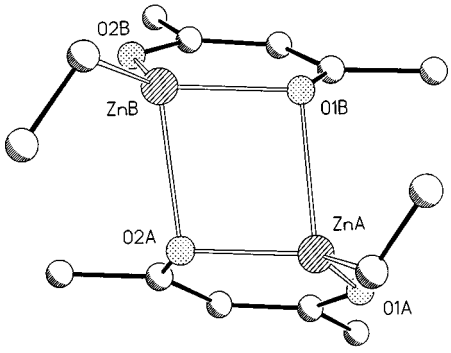

Figure 1. Structure motif of complex **17**

Complex **17** is a dimer in which the two Zn^{II} ions are held together by two bridging oxygen atoms of the acetylacetonate ligands yielding a four-membered Zn_2O_2 ring. Each Zn^{II} centre is tetrahedrally surrounded by three oxygen atoms of the acetylacetonato ligands and one ethyl group. Reaction of **17** with the oxalic amidine in THF (1:1 molar ratio) followed by treatment of the reaction mixture with 1 equiv. $Ni(acac)_2$ resulted in the formation of **11**. Upon recrystallization from toluene, **11** was isolated in 95% purity.

Structures of Dinuclear Complexes

The dinuclear complexes **1**−**11** were characterized by elemental analyses, mass spectrometry, and ^1H and ^{13}C NMR spectroscopy. In addition, the solid-state structures of **1**, **2**, **9**, and **10** were elucidated by X-ray single-crystal diffraction analyses. In principle, dinuclear η^3-allyl complexes containing oxalamidinates with different nitrogen substituents R^1, R^2 can exist in four isomers (Scheme 2), since the oxalamidinato bridge can bind either as the (*E*) isomer or as the

(*Z*) isomer; furthermore, the two η^3-allyl groups can assume *anti* or *syn* positions to each other (Scheme 2, **A**–**D**).

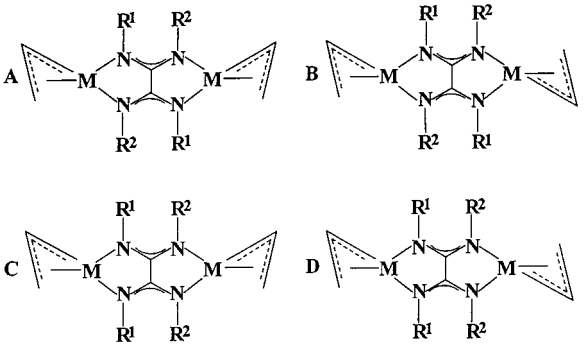

Scheme 2. Possible isomeric allylmetal complexes with bridging oxalamidinato ligands

The mass spectra of the Ni complexes **1** and **2** are typical for dinuclear oxalamidinato allylmetal complexes exhibiting the molecular ion peaks at $m/z = 698$, and 734, respectively, and peaks of smaller fragment ions due to successive loss of the allyl group giving the basic peak, and the (allyl)Ni fragment etc.

Single crystals of complex **1**, grown from *n*-hexane were used to determine its solid-state structure by an X-ray diffraction analysis. The molecular structure of **1** containing an oxalamidinato ligand with two different nitrogen substituents shows that **1** consists of a dimetallic centrosymmetric unit in which the oxalamidinato ligand acts in a bis(chelating) fashion bridging two nickel(II) ions (Figure 2).

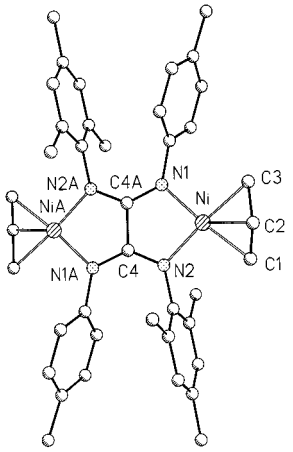

Figure 2. Molecular structure of complex **1**; for clarity the disordered allyl group is omitted; selected bond lengths [Å] and bond angles [°]: Ni–N1 1.912(2), Ni–N2 1.907(2), Ni–C1 1.988(3), Ni–C2 1.970(7), Ni–C3 1.992(3), N1–C4A 1.321(3), N2–C4 1.322(3), C4–C4A 1.522(5); N1–Ni–N2 84.49(9), N1–Ni–C1 174.8(1), N2–Ni–C3 174.0(1), N2–Ni–C1 100.6(1), C1–Ni–C3 73.8(1), Ni–N1–C4A 113.9(2), N1–C4A–C4 113.4(3), C4A–C4–N2 113.2(3), C4–N2–Ni 114.2(2); symmetry transformations used to generated equivalent atoms: A $-x + 1$, $-y + 1$, $-z + 1$

Each metal ion is in a planar environment created by two N atoms from the bridging ligand and the η^3-allyl ligand. The double chelate ring containing the CN_2 units is essentially planar. All C–N bonds are equivalent with a high double-bond character indicating a complete electron delocalization over the two CN_2 units. The C1–C1A bond length between the CN_2 units is that of a single bond [1.522(5) Å]. Other selected bond lengths and angles are listed in Figure 2. The C3, C3A atoms of the allyl groups are disordered and distributed in two positions with equal occupancy factors. Furthermore, the oxalamidinate bridging ligand is coordinated in the (*E*) form. In other words, both isomeric forms **A** and **B** (Scheme 2) are present in the solid state. The Ni–C distances in the allylnickel fragment are identical within the experimental error; furthermore, the aromatic substituents are orientated to the plane of the oxalamidinato bridge at an angle of 82.3 and 78.8°, respectively.

The solid-state structure of complex **2** is very similar to that of **1** (Figure 3). The η^3-allyl groups are also disordered, according to the presence of the *syn* and the *anti* isomer (**A** and **B**, Scheme 2) in the solid state. Bond lengths and angles are very close to those of **1** and need no further discussion.

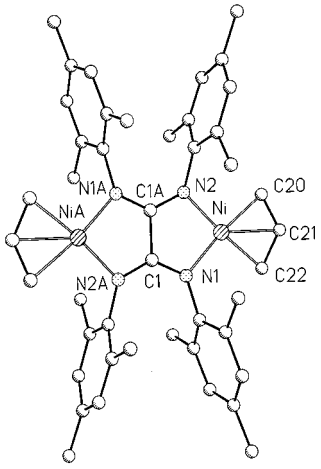

Figure 3. Molecular structure of complex **2**; for clarity the disordered allyl group is omitted; selected bond lengths [Å] and bond angles [°]: Ni–N1 1.919(2), Ni–N2 1.918(2), Ni–C20 2.005(3), Ni–C21 1.986(5), Ni–C22 2.005(3), N1–C1 1.327(3), N2–C1A 1.336(3), C1–C1A 1.525(4); N1–Ni–C20 173.4(1), N1–Ni–N2 85.18(7), N1–Ni–C22 100.5(1), N2–Ni–C20 101.3(1), N2–Ni–C22 174.3(1), C20–Ni–C22 73.1(1), Ni–N1–C1 113.5(1), N1–C1–C1A 114.2(2), C1–C1A–N2 113.3(2), C1A–N2–Ni 113.7(1); symmetry transformations used to generate equivalent atoms: A $-x + 2$, $-y$, $-z + 1$

The NMR-spectroscopic data confirm the presence of both the *syn*- and *anti*-allyl isomers in solution (see Exp. Sect.). The NMR spectra of **2** are relatively complicated. In the ^{1}H NMR spectrum, in [D_8]toluene at room temperature, two doublets of doublets for the CH_2 protons of the terminal allylic group are observed whilst the *meso*-CH protons give a multiplet at $\delta = 5.07$–5.17. These data are in agreement with the existence of two isomers in solution (Scheme 2, **A** and **B**) in which the sterically demanding mesityl groups are unsymmetrically bound giving rise to four different signals for the *o*-mesityl groups as well as for the *p*-methyl groups.

The relatively simple NMR spectra of complex **4** allow a deeper insight into the structure of the complex in $CDCl_3$ solution. In the ^1H NMR spectrum at room temperature only one signal for the protons of the methyl groups of the four *p*-tolyl substituents is observed at δ = 2.06 (relative intensity: 12). The aromatic protons of the CH groups resonate at δ = 6.50 and 6.56. Furthermore, two doublets for the 1-H/1′-H and 2-H/2′-H protons of the allyl groups of C-1 and C-1′, which each integrated for 4 H, are observed.

The most characteristic signals are the resonances of the *meso*-allylic protons, observed at δ = 5.28 and δ = 5.30, both as triplets of triplets integrated for 2 H. This clearly indicates the presence of two isomers in solution, which can be attributed to be the *syn* and the *anti* isomers **A** and **B** (with $R^1 = R^2$, Scheme 2). The molar ratio **A/B** is about 1:1. Consequently, in the ^{13}C NMR spectrum of **4** two resonances for the CH_2 carbon atoms of the allyl groups (at δ = 60.0, and 59.9) are observed. Furthermore, the carbon atoms of the aromatic ring show a double signal set. Additionally, the carbon atoms of the oxalamidinato bridge give rise to two signals at δ = 165.7 and 165.7. This also strongly supports the existence of both **A** and **B** in solution.

The palladium complex **5** contains two different nitrogen substituents and can therefore form four isomers **A**−**D** (Scheme 2). The exact orientation of the nitrogen substituents in the solid state as well as in solution is, however, still unknown.

The solid-state structures of the dinuclear (acetylacetonato)palladium(II) complexes **9** and **10** have also been fully characterized by X-ray diffraction. Figure 4 shows a view of the structure of **9** with the atom-numbering scheme and selected bond lengths and angles.

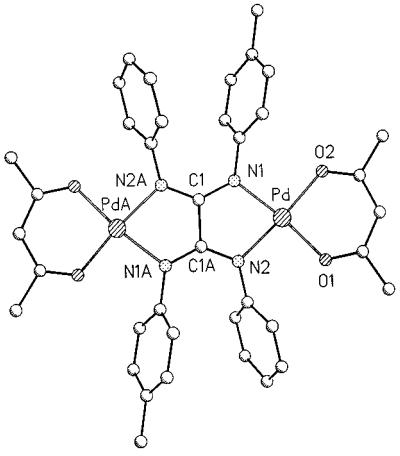

Figure 4. Molecular structure of complex **9**; selected bond lengths [Å] and bond angles [°]: Pd−O1 2.007(2), Pd−O2 2.015(2), Pd−N1 2.015(3), Pd−N2 2.024(3), N1−C1 1.332(4), N2−C1A 1.332(4), C1−C1A 1.522(6); N1−Pd−N2 80.9(1), N1−Pd−O1 173.9(1), N1−Pd−O2 94.3(1), N2−Pd−O1 93.0(1), N2−Pd−O2 174.7(1), O1−Pd−O2 91.79(9), Pd−N1−C1 115.4(2), N1−C1−C1A 114.2(3), C1−C1A−N2 114.5(3), C1A−N2−Pd 115.0(2); symmetry transformations used to generate equivalent atoms: A $-x + 2, -y + 1, -z + 2$

As expected, the coordination around the palladium centre is square-planar. The bond lengths and angles are quite normal and comparable with those of the other dinuclear oxalamidinato complexes. The substituents R^1 and R^2 at the oxalamidinate ligand assume the (*E*) form. In the ^1H NMR spectrum, in $CDCl_3$, complex **9** shows the expected number of resonances for the protons in the aromatic region and for the CH_3 and the CH protons of the acac ligand having the expected intensities.

Complex **10** containing four *p*-tolyl substituents has the same molecular structure in the solid state as **9** (not depicted). Furthermore, the bond lengths and angles are very close to those found in complex **9**. Consequently, the ^1H NMR spectrum of **10** in $[D_8]THF$ at room temperature shows the expected simple pattern for a symmetrical structure: The number of signals of the oxalamidinato and acetylacatonato ligands (δ = 1.43 for the methyl protons of the acac ligand; δ = 2.05 for the *p*-methyl groups; δ = 5.04 for the *meso* proton of acac; δ = 6.52 and 6.59 for the aromatic protons) and their integration confirm the equivalence of the two halves of the complex, as already observed in the solid state. As expected for a symmetrical structure, nine signals were found in the ^{13}C NMR spectrum of **10**.

Tri- and Tetranuclear Complexes Containing Zinc(II) in the Inner Part

The synthesis of oligometal complexes with Zn^{II} as the inner metal ion ("structural" metal) was carried out as follows: According to Scheme 3, 1 equiv. $ZnEt_2$ was very slowly treated with a solution of 2 equiv. of the free oxalamidine. Once the formation of ethane was finished, the in situ formed bis(oxalamidinato)Zn^{II} complex, containing two monoanionic oxalamidinates, was treated with $M(acac)_2$ or with $(allyl)_2Pd$ resulting in the elimination of acetylacetone or propene. Upon workup, the crystalline heterotrinuclear complexes **12**−**14** were isolated (Scheme 3).

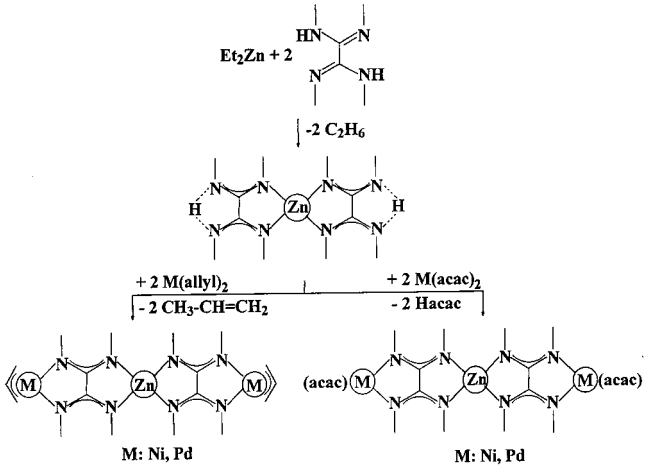

Scheme 3. Formation reaction of the heterotrinuclear complexes **12**−**14** [**12**: Ni(acac), tetramesityloxalic amidinate as bridge; **13**: Pd(acac), tetrakis(*p*-tolyl)oxalic amidinate as bridge; **14**: (allyl)Pd, tetrakis(*p*-tolyl)oxalic amidinate as bridge]

The NMR spectra of **12** and **13** are very similar. Since the Pd complex **13** contains two different types of nitrogen-

bound *p*-tolyl substituents (coordinating either at Pd or at Zn), the ^{1}H NMR spectrum ([D$_8$]THF) displays two resonances at δ = 2.02 and 2.09 for the methyl protons of the *p*-tolyl groups, a singlet for the methyl protons of the acac ligands at δ = 1.54, a singlet for the *meso*-CH group of acac at δ = 5.10, and a multiplet for the aromatic protons between δ = 6.49 and 6.55. The relative intensities of these proton signals (12:12:12:2:32) are in agreement with the trinuclear structure of **13**.

Two different resonances for the methyl protons were also found in the trinuclear η^3-allyl−Pd−Zn−Pd complex **14**. Furthermore, in the region of the CH$_2$ protons of the η^3-allyl groups four signals between δ = 2.66 and 2.44 are observed indicating the presence of two stereoisomers in solution. The ^{13}C NMR spectrum of **14** in CDCl$_3$ at room temperature confirms this. Two signals are indicated for both the carbon atoms of the CH$_2$ group (at δ = 20.52 and 20.58) and the CH group (at δ = 59.9 and 60.5) of the allyl ligands.

The tetranuclear complexes **15** and **16** were formed as follows: In the first step the inner Zn^{II} part was built up in situ by treating 2 equiv. of ZnEt$_2$ with 3 equiv. of the oxalamidine to form a reactive intermediate "[(H-oxam)Zn(oxam)Zn(oxam-H)]", which was able to act as a "metalloligand" using two N−H functions at the periphery for the reaction with 2 equiv. Ni(acac)$_2$. Upon elimination of acetylacetone, **15** crystallized at 0 °C. Alternatively, the above Zn$_2$ intermediate can undergo a reaction with ZnEt$_2$ or [(Et)Zn(acac)]$_2$ (**17**) resulting in the formation of the Zn$_4$ complex **16**.

Both complexes **15** and **16** contain two inner metal ions (Zn) and two peripheral metal ions (Ni or Zn). The single-crystal study of **16** reveals a tetrameric molecule that possesses two acetylacetonate ligands bound to each peripheral Zn ion. The four Zn ions adopt distorted tetrahedral coordination geometries with two ZnN$_4$ donor sets in the middle and two ZnN$_2$O$_2$ donor sets at the periphery. The structure of **16** is depicted in Figure 5. This molecule has no imposed symmetry. The relevant bond lengths and angles are collected in the figure captions. The Zn−N distances of the four Zn-containing tetrahedrons are statistically indistinguishable. Each of the acetylacetonate ligands is bound to Zn in a symmetrical bidentate manner. The Zn(acac) moieties are associated with average Zn−O distances of 1.952(5) Å.

The most interesting finding is, that the bis(mesityl)bis(*p*-tolyl)oxalamidinate ligands coordinate in different forms. The two peripheral oxam ligands assume the (*Z*) configuration with the two mesityl groups situated in peripheral positions. This may be due to the bulkiness of the mesityl groups. In the oxalamidinato bridge in the middle, however, the nitrogen substituents assume the (*E*) configuration. Consequently, the two inner Zn ions are surrounded by three *N*-tolyl groups and one *N*-mesityl group.

The only remarkable difference to the molecular structure of the Ni$_2$Zn$_2$ complex **15** is, that in **15** the peripheral Ni^{II} centres are in a square-planar environment,[10] whereas the inner part adopts the same coordination of the Zn

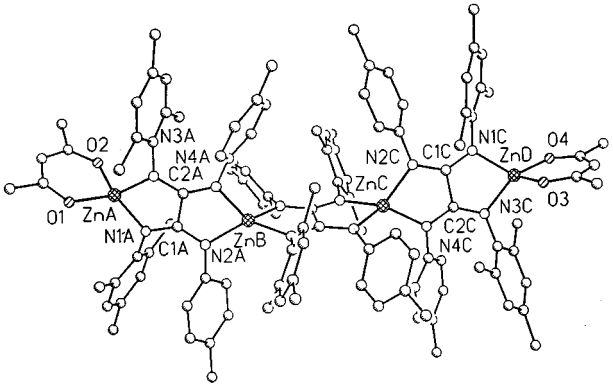

Figure 5. Molecular structure of complex **16**; selected bond lengths [Å] and bond angles [°]: ZnA−O1 1.949(4), ZnA−O2 1.963(5), ZnA−N1A 1.970(5), Zn−N3A 1.990(5), N1A−C1A 1.340(7), N2A−C1A 1.331(7), N3A−C2A 1.338(7), N4A−C2A 1.331(7), C1A−C2A 1.553(9), ZnB−N2A 1.996(5), ZnB−N4A 2.002(5), ZnB−N1B 1.995(5), ZnB−N3B 1.995(5), N1B−C1B 1.324(7), N2B−C1B 1.341(7), N3B−C2B 1.311(7), N4B−C2B 1.347(7), C1B−C2B 1.573(7), ZnC−N2B 1.992(5), ZnC−N4B 1.992(5), ZnC−N2C 2.006(5), ZnC−N4C 1.994(5), N1C−C1C 1.322(8), N2C−C1C 1.341(8), N3C−C2C 1.333(7), N4C−C2C 1.332(8), C1C−C2C 1.571(8), ZnD−N1C 1.978(5), ZnD−N3C 1.986(5), ZnD−O3 1.955(5), ZnD−O4 1.940(5); O1−ZnA−O2 95.3(2), O1−ZnA−N1A 126.1(2), O1−ZnA−N3A 119.7(2), O2−ZnA−N1A 120.6(2), O2−ZnA−N3A 112.7(2), N1A−ZnA−N3A 84.2(2), N2A−ZnB−N4A 83.1(2), N2A−ZnB−N1B 132.0(2), N2A−ZnB−N3B 120.6(2), N4A−ZnB−N1B 121.4(2), N4A−ZnB−N3B 122.6(2), N2B−ZnC−N4B 83.5(2), N2B−ZnC−N2C 120.4(2), N2B−ZnC−N4C 119.4(2), N4B−ZnC−N2C 120.4(2), N4B−ZnC−N4C 133.0(2), N2C−ZnC−N4C 83.1(2), O3−ZnD−O4 95.9(2), O3−ZnD−N1C 115.9(2), O3−ZnD−N3C 117.2(2), O4−ZnD−N1C 123.5(2), O4−ZnD−N3C 122.1(2), N1C−ZnD−N3C 84.4(2)

atoms as in **16**. The relevant bond lengths and angles in **16** are also very close to those in **15**. Since complex **16** has limited solubility in common solvents, its ^{13}C NMR spectrum could not be recorded. The ^{1}H NMR spectrum of **16** consists of six signals for the different methyl groups, one resonance for the CH proton of acac, and the signals for the aryl protons.

Catalytic Reactions

Catalytic Oligomerization/Polymerization of Ethene

Although the catalytic polymerization/oligomerization of ethylene is a well-known reaction[11−13] selective catalysts for the polymerization based on Ni^{II} or other late transition metals are very rare. Recently, Brookhart and co-workers described cationic diimine−Ni and −Pd catalysts as highly active for ethylene polymerization.[14−18] Independently, Brookhart,[19] and Gibson[20] developed cationic Fe^{II} catalysts with tridentate pyridiniminato ligands as efficient catalysts. Very recently, Grubbs and co-workers demonstrated that salicylaldiminatophenyl−Ni^{II} complexes are highly active single-site catalysts for the polymerization of 1-olefins.[21,22] Our initial investigations have shown that some dinuclear (oxalamidinato)Ni^{II} complexes are able to

act as catalysts for the oligomerization or for the polymerization of ethylene.[10]

Here we describe a study of the catalytic behaviour of di- and oligonuclear oxalamidinato complexes towards ethylene with the aim to rationalize the influence of the following three factors: bulkiness of the ligands, nature of the cocatalyst, and effect of the inner metal ion (Zn) on the catalytic activity and selectivity of the peripheral Ni^{II} ions.

The results of ethylene oligomerization/polymerization experiments are listed in Tables 2 and 3, respectively. Several features are noteworthy. In general, the catalysts are moderately active. When the catalytic reactions were carried out under an initial pressure of 10 atm in a sealed autoclave (containing 4000 mol of ethylene per mol catalyst) at 25 °C, the reactions could be used to determine the activities of the catalysts dependent on the above mentioned parameters.

The activities of the catalysts for the oligomerization were calculated from the GC traces, using extrapolated values for C_4-C_8; The catalytic activities for the polymerization were calculated from the amount of the isolated and dried polymer (see Exp. Sect.). Typically, the molecular weights of the polymers formed were around $1.2-6.7 \times 10^5$ g/mol (M_W) with $M_w/M_n = 1.4-2.0$ (Table 2).

Clearly, steric protection of the active sites is a crucial factor in controlling the selectivity and activity (Entries 4−6, Table 2). Upon activation with MAO or Et_3Al complex **8**, containing four sterically demanding mesityl substituents, is a polymerization catalyst. The reduced bulkiness of the four *p*-tolyl substituents on the nitrogen donor atoms in **6** leads to an oligomerization catalyst. In this case only C_4-C_8 olefins, and traces of C_{10} compounds are formed. Complex **7**, possessing both two *p*-tolyl groups and two mesityl groups in a (*Z*) arrangement in the oxam bridge,[10] catalyzes the oligomerization (to form C_4-C_8 olefins) as well as the polymerization reaction (Entry 6, Table 2). From this finding we can conclude that in complex **7** *both* Ni centres are catalytically active: One Ni^{II} centre, surrounded by the bulky mesityl group catalyzes the polymerization of ethylene. The other Ni^{II} centre on the opposite side, coordinating two sterically less demanding nitrogen-bound *p*-tolyl donor groups catalyzes the oligomerization of ethylene to yield C_4-C_8 oligomers.

This conclusion is supported by comparing the catalytic activity of the heterodinuclear Zn−Ni complex **11** with that of the homodinuclear Ni complex **8**. Both **8** and **11** contain

Table 2. Influence of the nitrogen substituents, the nuclearity, and the cocatalyst on the catalytic conversion of ethylene

Entry[a]	Compd.	[Al]/[Ni]	Oligomers C_4	C_6	C_8	Σ oligomers[b] g	TON[c]	Polymer g	TON[c]	M_w	$D = M_w/M_n$
1	**8**	1	−	−	−	−	−	0.13	160	3.57	1.46
2	**8**	3	−	−	−	−	−	0.85	960	4.51	1.49
3	**8**	10	0.06	0.01	−	0.07	80	1.46	1680	4.91	2.66
4	**8**	150	0.20	0.09	−	0.29	340	2.55	2960	1.57	1.78
5	**6**	150	0.83	0.33	0.11	1.27	1470	−	−	−	−
6	**7**	150	0.38	0.16	0.08	0.55	640	0.57	640	2.37	2.02
7[d]	**8**	25	−	−	−	−	−	1.69	1960	−	−
8[d]	**11**	25	−	−	−	−	−	0.86	1000	−	−
9	**12**	150	0.24	−	−	0.24	280	2.83	3280	1.89	1.43
10	**15**	150	0.86	0.40	0.14	1.40	1620	−	−	−	−
11	**8**	1	0.14	−	−	0.14	160	0.90	1040	−	−
12	**8**	2	0.04	−	−	0.04	45	1.06	1240	−	−
13	**8**	3	0.02	−	−	0.02	23	2.14	2480	−	−
14	**8**	10	0.17	0.06	−	0.23	270	2.21	2560	−	−
15	**8**	150	0.18	0.07		0.25	290	2.14	2480	2.46	1.49
16	**6**	150	0.05	0.02	−	0.07	80	−	−	−	−
17	**7**	150	0.03	−	−	0.03	35	−	−	−	−
18	**15**	150	0.03	−	−	0.03	35	−	−	−	−

[a] Solvent: toluene (20 mL); catalysts: 0.031 mmol; ethylene: 0.123 mol in the sealed reactor, ca. 4000 mol ethylene/mol catalyst (ethylene pressure 10 atm); Entries 1−10: MAO as cocatalyst; Entries 11−18: Et_3Al as cocatalyst; reaction time: 16 h (except Entries 7, and 8); reaction temperature 25 °C. − [b] Σ oligomers = g dimers + g trimers + g tetramers (see Exp. Sect.). − [c] TON: turnover number = mol of ethylene consumed/mol of Ni catalyst. − [d] Reaction time 0.5 h.

Table 3. Comparison of the catalytic polymerization of ethylene using **8** and **12** as catalytic precursers: influence of the cocatalyst

Entry[a]	Compd.	Al compd.	Equiv. Al/Ni	h	g polymer	TON[b]
1	**8**	Et_3Al	150:1	1	1.38	1600
2	**12**	Et_3Al	150:1	16	2.51	2920
3	**8**	MAO	150:1	1	2.55	2960
4	**12**	MAO	150:1	16	2.83	3280
5	**8**	Et_3Al	1:1	16	0.90	1040
6	**12**	Et_3Al	1:1	16	2.62	3040
7	**8**	Et_3Al	2:1	16	1.07	1240
8	**12**	Et_3Al	2:1	16	ca. 3.4	ca. 3960
9	**8**	Et_3Al	3:1	16	2.14	2480
10	**12**	Et_3Al	3:1	16	3.00	3480
11	**8**	Et_3Al	150:1	16	2.15	2480
12	**12**	Et_3Al	150:1	16	2.14	2480
13	**8**	Et_2AlCl	150:1	16	2.55	2960

[a] Solvent: toluene (20 mL); catalysts: 0.031 mmol; ethylene: 0.123 mol in the sealed reactor = ca. 4000 mol ethylene/mol catalyst (ethylene pressure: 10 atm); reaction temperature 25 °C. − [b] TON: turnover number = mol of ethylene consumed/mol of Ni catalyst.

four bulky mesityl substituents and therefore act as polymerization catalysts in the presence of MAO. However, **8** contains *two* catalytically active Ni^{II} centres which produce the twofold amount of polyethylene as **11**, in which only *one* Ni^{II} is present while the opposite side of the oxalamidinato bridge is coordinated by Zn^{II} which is inactive (Entries 7 and 8, Table 2).

To examine the role of the cocatalyst in the polymerization we carried out several tests in which the cocatalysts as well as the ratio cocatalyst/Ni were varied. Table 3 lists the results. Upon activation with MAO, **8** is a polymerization catalyst, however a large excess of the cocatalyst is necessary for high turnover numbers (Entry 4, Table 2; Entry 3, Table 3). In contrast, Et_3Al activates the precatalyst **8** which is already at low ratios [Al]/[Ni]: Only 3 equiv. of this cocatalyst per Ni produce an active and selective polymerization catalyst (Entry 9, Table 3) while a large excess does not significantly increase the activity. These results are in agreement with the assumption that in the case of the oxalamidinato complexes bearing dianionic oxalamidinato bridges cationic species are responsible for the catalytic activity. Furthermore, Et_3Al only activates the "polymerization site" of complex **7**, since no oligomerization products were obtained.

To test the influence of the inner metal ion Zn on the catalytic activity we compared the catalytic behavior of the dinuclear complex **8** with that of the trinuclear $ZnNi_2$ complex **12**. Both complexes contain only bulky mesityl substituents and are therefore polymerization catalysts. Table 3 clearly demonstrates that a high excess of MAO ([Al]/[Ni] = 150:1) activates the polymerization of ethylene; however, the Zn-containing complex **12** is significantly more active (Entries 1−4, Table 3). On the other hand, Et_3Al is also a powerful cocatalyst for both complexes; in this case much lower concentrations are required (Entries 5−12, Table 3). The most important finding is, however, that **12** is much more active than **8** when Et_3Al is used. Remarkably, only 2 equiv. Et_3Al per Ni are necessary to establish a highly active system (Entry 8, Table 3). In conclusion, all results of Table 3 clearly demonstrate that the inner Zn ion significantly increases the catalytic activity.

The tetranuclear complex **15** is an oligomerization catalyst, although the two peripheral Ni atoms are surrounded by two bulky *N*-mesityl groups similar to both the catalysts **8** and **12**, which are active in polymerization. The reason for this difference may be seen in the additional influence of the inner coordination polyhedra on the peripheral active Ni^{II} centres. In **8** and **12**, all nitrogen donor groups bear bulky mesityl substituents, while the inner part in **15** contains less bulky *p*-tolyl groups. This difference might be responsible for switching the polymerization activity found for both **8** and **12** to oligomerization activity observed for **15** (Entries 3 and 4, Table 3 versus Entry 18, Table 2). As expected, the Zn_4 complex **16** is catalytically inactive. Furthermore, both the η^3-allyl complexes, and the Pd complexes are inactive.

In order to test the productivity of a typical polymerization catalyst at higher pressure we carried out the catalytic reaction with the system **8**/MAO (1:300) using an initial pressure of 50 bar ethylene at 60 °C. Under these conditions a waxy polymer was formed in a selective polymerization reaction with a turnover frequency of approximately 10^5 mol ethylene consumed/(Ni × h × bar ethylene). This polymer contained about 140 methyl groups per 1000 CH_2 groups, determined by ^1H NMR spectroscopy.

In conclusion, the catalytic activity and selectivity of oligonuclear (oxalamidinato)nickel(II) complexes can be tuned by the bulkiness of the nitrogen substituents (sterically demanding substituents increase the polymerization activity), the nature of the cocatalyst (Et_3Al in low molar ratios is the best cocatalyst), and the nuclearity of the complexes (the inner Zn ion in complexes with bulky nitrogen substituents increases significantly the polymerization activity).

Catalytic Heck Reaction

The Heck coupling is a very useful method for the formation of substituted arylated olefins starting with Ar−X and the substituted olefins, which is catalyzed by a variety of palladium complexes with different controlling ligands.[23,24] Among the most active catalysts are palladacycles with C,P coordination [25−27] and (carbene)palladium complexes.[28−32]

To test the ability for catalyzing the Heck coupling we used, in initial catalytic experiments, some di- and trinuclear palladium complexes as homogeneous catalysts for the coupling of bromoacetophenone with *n*-butyl acrylate. Table 4 shows that most of the coupling reactions were fast and selective, when the catalytic reactions were carried out at 120 °C in dimethylacetamide as solvent using sodium acetate as base. The main product is *n*-butyl (*E*)-4-acetylcinnamate. A deposit of palladium was not observed when the reactions were carried out below 125 °C.

The experimental data clearly show that the influence of different nitrogen substituents is low (Entries 1−4, Table 4). On the other hand, the inner metal ion (Zn) increases the selectivity of the catalytic reaction (Entries 5−8, Table 4). With the heterotrinuclear Pd_2Zn complex **14** turnover numbers of 285000 (after 5 h) and 435000 can be achieved (Entry 8 after 27 h). This corresponds with an average turnover frequency (TOF) of about 57000 mol converted substrate/mol catalyst per hour in the first 5 h and a TOF of about 16100 over the next 27 h. These results clearly demonstrate the catalytic potential of the (oxalamidinato)palladium complexes and give evidence for the activating effects of the inner "structural metal ion" (Zn) on the catalytic behavior of the peripheral "functional" metal ions.

Experimental Section

General: The oxalic amidine ligands were prepared according to literature procedures. CH_3MgBr and CH_3MgCl (3 M in diethyl ether), purchased from Aldrich were used without additional purification. All reactions were carried out under argon and the solvents used were dried by means of standard Schlenk techniques. −

Table 4. Catalytic Heck coupling between bromoacetophenone and *n*-butyl acrylate with di- and trinuclear palladium-based catalysts

Entry[a]	Catalyst	Selectivity (%) [(*E*) product][b]	Conversion (%) 1 h	5 h	22 h	TON 1 h	5 h
1	**3**	92	63	100	100	3150	> 5000
2	**4**	82	64	100	100	3200	> 5000
3	**5**	89	17	70	85	850	> 3500
4	**9**	88	62	100	100	3100	> 5000
5	**13**	96	70	81	85	3500	> 4050
6	**14**	97	64	100	100	3200	> 5000
7	**14**	98	32	70	81	16000	> 35000
8	**14**	96	17	57	85	85000	285000

[a] Conditions: 6.25 mmol *p*-bromoacetophenone, 6.75 mmol *n*-butylacrylate, solvent *N*,*N*-dimethylacetamide (8 mL), 7 mmol CH_3COONa as base, molar ratio substrate/catalyst Entries 1−6: 5000:1; Entry 7: 50000:1; Entry 8: 500000:1; reaction temperature: 120 °C. − [b] *n*-Butyl (*E*)-4-acetylcinnamate.

^1H and ^{13}C NMR spectra were recorded at ambient temperature, unless otherwise stated, with a Bruker AC 200-MHz spectrometer. Numbering for the η^3-allyl groups in the ^1H NMR spectra: CH_2-allyl: 1-H, and 2-H; *meso*-CH-allyl: 3-H. All spectra were referenced to TMS or deuterated solvent as an internal standard. − FAB mass spectra were obtained with a Finnigan MAT SSQ 710 spectrometer (2,4-dimethoxybenzyl alcohol as matrix). − IR measurements were carried out with a Perkin−Elmer System 2000 FT-IR. − Elemental analyses (C, H, and N) were carried out at the Microanalytical Laboratory of the Friedrich-Schiller-Universität Jena. For the determination of the metals, the organic material of the complexes were oxidized using hot concentrated perchloric acid (***CAUTION: Explosions are possible!***) followed by distillation of most of the acid, and slow addition of water to the cold solutions. Metals were determined by complexometric titrations. − The syntheses of the oxalamidinato complexes **6−8**, **11**, and **15** were recently described in a preliminary communication.[10] Oxalic amidines,[33] $(\eta^3\text{-allyl})_2Ni$,[34] and $[\eta^3\text{-allylPdCl}]_2$,[35] were prepared as described. − $(\eta^3\text{-allyl})_2Pd$ was prepared by the following modified method:[36] Bis[(η^3-allyl)chloropalladium(II)] (0.5 g, 1.37 mmol), dissolved in 40 mL of THF, was cooled to −60 °C. To the clear yellow solution allylmagnesium chloride (2.74 mmol of a 2 M solution in THF) was added dropwise under stirring. Then the reaction mixture was allowed to warm very slowly to −30 °C, followed by evaporation of the solvent from the brown solution at −25 °C in vacuo. The solid reaction product was washed twice with 10 mL of *n*-pentane at 18 °C (decomposition at 20 °C), the yellow *n*-pentane solution was cooled to −50 °C. At this temperature the solvent was removed in vacuo.The last step was the sublimation of the reaction product in vacuo at −25 °C to form the very pure complex. Yield 180 mg (70%).

Complex 1: Bis[η^3-allyl(chloro)nickel(II)] (0.263 g, 0.97 mmol) was dissolved in 60 mL of THF. At −78 °C allylmagnesium chloride (1.945 mmol of a 2 M solution in THF) was added very slowly to the stirred solution. Then the yellow reaction mixture was allowed to warm to −20 °C. Slow addition of bis(mesityl)bis(*p*-tolyl)oxalamidine (0.490 g, 0.97 mmol), dissolved in 20 mL of THF, to the stirred solution resulted in a deep yellow solution. After 12 h of stirring at −5 °C, the reaction mixture was warmed to room temperature. After 2 h, the solvent was removed in vacuo. The residue was extracted with *n*-pentane and the solution filtered. At 5 °C yellow crystals of complex **1** formed. Single crystals of **1** were obtained by recrystallization from *n*-pentane or *n*-hexane. Yield 560 mg (82%). − $C_{40}H_{46}N_4Ni_2$ (700.2): calcd. C 68.62, H 6.62, N 8.00, Ni 16.76; found C 68.50, H 6.40, N 7.60, Ni 17.21. − ^1H NMR ([D$_8$]THF, 298 K, 400 MHz): δ = 1.14 (dd, CH_2-allyl, 2 H), 1.35 (dd, CH_2-allyl, 2 H), 1.45 (dd, CH_2-allyl, 2 H), 1.60 (dd, CH_2-allyl, 2 H), 2.00, 2.04 (2 × s, *p*-CH_3 of mesityl, 12 H), 2.16, 2.19, 2.25, 2.27, 2.41, 2.51 (each s, *o*-CH_3 of mesityl, each 3 H), 5.28 (m, CH of allyl, 2 H), 6.47, 6.48 (AA′BB′, CH-tolyl) 6.62 (broad, CH of mesityl, Σ aryl-H = 12 H) − ^{13}C NMR ([D$_8$]THF, 298 K, 100.6 MHz): δ = 18.4, 18.45, 18.54 (*o*-CH_3 of mesityl), 19.7 (2 signals, *p*-CH_3 of tolyl and mesityl), 54.58, 54.60 (CH_2 allyl), 109.9, 110.0, 110.47, 110.53 (CH-allyl), 123.1 (aromatic CH, several signals), 126.9, 127.1, 127.4 (aromatic CH). − IR (nujol): $\tilde{\nu}$ = 1562, 1611 cm^{-1} (C=C_{aromat}, CN). − MS (EI): *m*/*z* (%) = 698 [M^+] (23), 657 [$M^+ - C_3H_5$] (5), 540 [$M^+ - C_3H_6Ni_2$] (0.5), 502 [$M^+ - C_6H_8Ni_2$], 249.42 (basis peak) [$M^+ - C_{37}H_{40}N_4Ni_2$].

Complex 2: The reaction was carried out as described for **1**. Due to the low solubility no ^{13}C NMR spectrum could be obtained. Yield 579 mg (79%). − $C_{44}H_{54}N_4Ni_2$ (757.3): calcd. C 69.88, H 7.20, N 7.41, Ni 15.52; found C 69.22, H 7.81, N 7.1, Ni 14.83. − ^1H NMR ([D$_8$]toluene, 298 K, 200 MHz): δ = 1.34, 1.38, (each dd, CH_2-allyl, 4 H), 1.51, 1.58 (each dd, CH_2-allyl, 4 H), 2.07, 2.08 (2 × s, *p*-CH_3 of mesityl, 12 H), 2.10, 2.11 (2 × s, *p*-CH_3, 12 H) 2.30, 2.39 (2 × s, *o*-CH_3, 12 H, 2.55, 2.64 (2 × s, *o*-CH_3, 12 H), 5.07-5.17 (m, CH of allyl, 2 H), 6.39, 6.41, 6.42, 6.45 (4 × s, CH aromat) − IR (nujol): $\tilde{\nu}$ = 1591, 1613 cm^{-1} (C=C_{aromat}, CN). − MS (EI): *m*/*z* (%) = 754 [M^+] (27), 713 [$M^+ - C_3H_5$] (5), 656 (basis peak) [$M^+ - C_3H_4Ni_2$], 641 [$M^+ - C_6H_8Ni_2$] (42), 614 [$M^+ - C_6H_{10}Ni$].

Complexes 3−5 (General Preparation Procedure): The oxalic amidine (1 mmol) was dissolved in THF and cooled to −30 °C. Then this solution was added at −30 °C to bis([η^3-allyl)palladium(II)] (2.2 mmol in THF). The reaction mixture was allowed to warm to room temperature, followed by distillation of the solvent at −30 °C in vacuo. To remove the excess of bis([η^3-allyl)palladium(II)] the solid was washed three times with 10 mL of *n*-pentane at room temperature.

Complex 3: The crude material was extracted with cyclohexane to remove impurities, washed with *n*-pentane and dried in vacuo. Upon recrystallization from THF yellow crystals were isolated. Yield 640 mg (90%). − $C_{34}H_{34}N_4Pd_2$ (711.5): calcd. C 57.39, H 4.82, N 7.90; found C 56.72, H 4.68, N 7.81. − ^1H NMR (298 K, 200 MHz): δ = 2.04, 2.06 (2 × s, *p*-CH_3, 6 H), 2.51 (m, CH_2-allyl, 8 H), 5.29 (m, CH-allyl, 2 H), 6.56, 6.71 (2 × m, CH aromat, 18 H) − ^{13}C NMR ($CDCl_3$, 298 K, 50.3 MHz): δ = 20.6 (*p*-CH_3), 60.0 (CH_2-allyl), 114.2 (CH-allyl), 121.3, 124.6, 124.9, 127.0, 127.1, 127.4, 127.6, 130.8, 150.2, 152.9 (C-aromat + CH-aromat), 165.74 (C of the oxam bridge). − IR (nujol): $\tilde{\nu}$ = 1591, 1613 cm^{-1} (C=C_{aromat}, CN). − MS (EI): *m*/*z* (%) = 711 [M^+] (4), 563 [$M^+ - C_3H_5Pd$] (1), 418 (2) [$M^+ - C_6H_{10}Pd_2$].

Complex 4: Purification of the crude material was carried out as described for **3**. Yield 629 mg (85%). − $C_{36}H_{38}N_4Pd_2$ (739.5): calcd. C 58.46, H 5.18, N 7.58; found C 58.52, H 5.24, N 7.62. − ^{1}H NMR (298 K, 400 MHz): δ = 2.06 (s, *p*-CH_3, 12 H), 2.45 + 2.47 (d, CH_2-allyl, $^3J_{3,2} = {}^3J_{3',2'}$ = 6.8 Hz, 4 H), 2.56 + 2.58 (d, CH_2-allyl, $^3J_{3,1} = {}^3J_{3',1'}$ = 12.2 Hz, 4 H), 5.28 + 5.30 (2 × tt, *meso*-allyl-CH, $^3J_{1,3} = {}^3J_{1,'3'} = {}^3J_{3',2'}$ = 6.8 Hz, 2 H), 6.50, 6.56 (AA′BB′, CH aromat, $^3J_{AB}$ = 7.8 Hz., 16 H) − ^{13}C NMR ($CDCl_3$, 298 K, 100.6 MHz): δ = 20.6 (*p*-CH_3), 59.95, 59.98 (CH_2-allyl), 114.2 (CH-allyl), 124.47, 124.56, 124.58 (CH aromat), 130.6, 150.26, 150.29 (C-aromat), 165.71, 165.74 (C of the oxam bridge). − IR (nujol): $\tilde{\nu}$ = 1557, 1607, 1639 cm^{-1} (C=C_{aromat}, CN). − MS (EI): *m*/*z* (%) = 738 [M^+] (6), 445 (3) [$M^+ - C_6H_{10}Pd_2$].

Complex 5: The crude material was extracted with diethyl ether at room temperature. Colorless crystals were isolated at 4 °C. Yield 716 mg (90%). − $C_{40}H_{46}N_4Pd_2$ (795.6): calcd. C 60.38, H 5.83, N 7.04; found C 59.68, H 5.51, N 6.84. − ^{1}H NMR ($CDCl_3$, 298 K, 400 MHz): δ = 1.96, 2.01, 2.04, 2.17, 2.19, 2.22, 2.24, 2.25, 2.27, 2.29 (m, CH_3, 24 H), 2.31, 2.33, 2.36, 2.38, 2.44 (m CH_2-allyl, 8 H), 5.22 (m, CH-allyl), 6.32 (broad, CH-aromat, 4 H), 6.48, 6.62 (AA′BB′, $^3J_{AB}$ = 8.1 Hz, CH aromat, 4 H + 4 H). − ^{13}C NMR ([D_8]THF, 298 K, 50.3 MHz): δ = 19.4, 20.6 (CH_3), 57.5, 59.0 (CH_2-allyl), 114.4, 114.5, 114.6 (CH-allyl), 123.5, 123.6, 127.7, 128.2, 128.3 (CH aromat), 129.9, 130.3, 130.4, 131.7, 132.0 (C aromat), 148.8, 150.7 (*ipso*-C of *p*-tolyl, mesityl), 164.4 (C of the oxam bridge). − IR (nujol): $\tilde{\nu}$ = 1539, 155 8, 1609 cm^{-1} (C=C_{aromat}, CN). − MS (EI): *m*/*z* (%) = 794 (31) [M^+], 647 [$M^+ - C_3H_5Pd$].

Complex 9: Bis(phenyl)bis(*p*-tolyl)oxalamidine (418 mg, 1 mmol) and bis(acetylacetonato)palladium(II) 710 mg, 2 mmol), suspended in 20 mL of toluene, were refluxed for 3 h to give a clear solution. Upon distillation of 15 mL of the solvent at normal pressure the solid was filtered from the warm solution and washed first with toluene at room temperature, and then three times with diethyl ether. Recrystallization from hot benzene gave red crystals, suitable for an X-ray analysis. Compound **9** is sparingly soluble in $CHCl_3$, THF, and toluene, and practically insoluble in *n*-pentane. Yield 745 mg (90%). − $C_{38}H_{38}N_4O_4Pd_2$ (827.6): calcd. C 55.15, H 4.63, N 6.77; found C 55.62, H 4.60, N 6.31. − ^{1}H NMR ($CDCl_3$, 298 K, 400 MHz): δ = 1.41, 1.43 (2 × s, CH_3-acac, 12 H), 2.01 (s, CH_3-*p*-tolyl, 6 H), 5.04 (s, CH-acac, 2 H), 6.54−6.60, 6.70 (2 × m, CH-aromat, 16 H). − ^{13}C NMR ([D_8]THF, 298 K, 50.3 MHz): δ = 20.8 (CH_3-*p*-tolyl), 25.2 (CH_3-acac), 100.4 (CH-acac), 123.8, 127.3, 127.4, 128.0, 128.3, 133.4, 142.4, 145.2 (CH-aromat), 169.7 (C, oxam bridge). − IR (nujol): $\tilde{\nu}$ = 1506, 1539, 1578 cm^{-1} (C=C_{aromat}, CN, C=O). − MS (EI): *m*/*z* (%) = 828 (10) [M^+], 728 (4) [M^+ − acac], 621 (1) [M^+ − acacPd], 415 (4) [M+ − $acac_2Pd_2$].

Complex 10: The reaction was carried out as described for **9** using tetrakis(*p*-tolyl)oxalic amidine (440 mg, 0.98 mmol). Yield 755 mg (90%). − $C_{40}H_{42}N_4O_4Pd_2$ (855.6): calcd. C 56.15, H 4.95, N 6.55; found C 55.71, H 4.68, N 6.30. − ^{1}H NMR ($CDCl_3$, 298 K, 400 MHz): δ = 1.43 (s, CH_3-acac, 12 H), 2.05 (s, CH_3-*p*-tolyl, 12 H), 5.04 (s, CH-acac, 2 H), 6.52, 6.59 (AA′BB′, $^3J_{AB}$ = 8.5 Hz, CH-aromat, 12 H). − ^{13}C NMR ($CDCl_3$, 298 K, 50.3 MHz): δ = 20.8 (CH_3-*p*-tolyl), 25.4 (CH_3-acac), 100.3 (CH-acac), 127.1, 127.3, 132.9, 141.4 (CH-aromat), 169.4 (C, oxam bridge), 185.8 (CH-acac). − IR (nujol): $\tilde{\nu}$ = 1506, 1522, 1540, 15744 cm^{-1} (C=C_{aromat}, CN, C=O). − MS (EI): *m*/*z* (%) = 856 (3) [M^+], 756 (4) [M^+ − acac], 657 (4) [M^+ − 2 acac], 649 (3) [M^+ − acacPd], 550 (4) [M^+ − $acac_2Pd$], 443 (7) [M^+ − $acac_2Pd_2$].

Complex 12: Tetramesityloxalic amidine (2 mmol, 1.12 g) was dissolved in 50 mL of THF, and dropwise treated with $ZnEt_2$ (1.1 M solution in toluene, 0.91 mL) at room temperature. After stirring and heating for about 30 min, a solution of bis(acetylacetonato)-nickel(II) (0.51 g, 2 mmol in 10 mL of THF) was added. The color turned red within a few minutes. After stirring overnight, a red microcrystalline substance precipitated. The precipitate was filtered and washed with 10 mL of diethyl ether. Yield about 0.90 g (30%). − $C_{86}H_{102}N_8Ni_2O_4Zn$ (1494.6): calcd. C 69.11, H 6.88, N 7.50, Ni 7.85, Zn 4.38; found C 69.42, H 6.51, N 7.20, Ni 7.24, Zn 4.23. − ^{1}H NMR ([D_8]THF, 298 K, 200 MHz): δ = 1.05, 1.13 (m, CH_3-acac, 12 H), 1.69 (s, CH_3-mesityl, 12 H), 1.93, 1.95 (s, CH_3-mesityl, 12 H), 2.14 (s, CH_3-mesityl, 12 H), 2.50, 2.53, (s, CH_3-mesityl, 36 H), 4.98, 5.05 (s, CH-acac, 2 H), 6.25−6.34 (m, CH-aromat, 16 H). − ^{13}C NMR ([D_8]THF, 298 K, 50.3 MHz): δ = 19.7, 20.5, 20.6, 21.0 (CH_3-aromat), 24.9 (CH_3-acac), 100.3, 100.7 (CH-acac), 127.7, 127.9, 128.4, 131.9, 132.3, 132.9, 133.1, 134.55, 134.63, 140.64, 141.3, 143.1 (C-aromat), 162.6, 166.4 (C_{tert}-bridge), 186.8, 194.6 (CO-acac).

Complex 13: To a stirred solution of tetrakis(*p*-tolyl)oxalic amidine (440 mg, 0.98 mmol) in 30 mL of toluene, $ZnEt_2$ (0.49 mmol), dissolved in 20 mL of toluene, was slowly added dropwise, followed by 15 min of stirring. At room temperature a suspension of bis(acetylacetonato)palladium(II) (300 mg, 0.98 mmol) in 20 mL of toluene was added and the mixture was refluxed for 1 h. The solvent was then removed in vacuo, and the orange residue was washed four times with 10-mL portions of *n*-pentane. The residue was dissolved in 50 mL of diethyl ether under 15 min of stirring and filtered. The solvent was very slowly removed. In a first fraction Pd(acac)$_2$ crystallized from the solution, while **15** crystallized later. Upon dissolution of impure **15** in diethyl ether this procedure was repeated. Orange crystals of **15** were isolated, which are soluble in THF, toluene, and diethyl ether, and practically insoluble in *n*-pentane. Yield 602 mg (45%). − $C_{70}H_{70}N_8O_4Pd_2Zn$ (1365.6): calcd. C 61.57, H 5.17, N 8.21; found C 61.3, H 5.22, N 7.66. − ^{1}H NMR ($CDCl_3$, 298 K, 400 MHz): δ = 1.54 (s, CH_3-acac, 12 H), 2.09, 2.20 (2 × s, CH_3-*p*-tolyl, 24 H), 5.10 (s, CH-acac, 2 H), 6.25−6.55 (m CH-aromat, 32 H). − ^{13}C NMR ($CDCl_3$, 298 K, 50.3 MHz): δ = 20.7, 20.8 (CH_3-*p*-tolyl), 24.6 (CH_3-acac), 100.4 (CH-acac), (CH-aromat), 162.1 (C, oxam bridge), 186.4 (CH-acac). − IR (nujol): $\tilde{\nu}$ = 1507, 1540, 1572, 110 cm^{-1} (C=C_{aromat}, CN, C=O). − MS (ESI, THF/CH_3OH/$CHCl_3$ as solvent mixture): *m*/*z* (%) = 1159 (1) [M^+ − acacPd], 475 (100) [M^+ − $acac_2Pd_2$], 444 [M^+ − $acac_2Pd_2$ − Zn].

Complex 14: The reaction was carried out as described for **13** using bis([η^3-allyl)palladium(II)] at 0 °C. Upon distillation of the solvent in vacuo the residue was washed four times with *n*-pentane. Recrystallization from diethyl ether yielded yellow crystals soluble in THF, toluene, and diethyl ether. Compound **14** contains 1 equiv. diethyl ether/mol complex (GC). Yield 480 mg (36%). − $C_{70}H_{76}N_8OPd_2Zn$ (1323.6): calcd. C 63.35, H 5.74, N 8.47, Zn 4.94; found C 63.73, H 5.60, N 8.21, Zn 4.70. − ^{1}H NMR ($CDCl_3$, 298 K, 200 MHz): δ = 2.03, 2.06 (s, CH_3-*p*-tolyl, 24 H), 2.44, 2.47, 2.54 (3 × d, CH_2-allyl, $^3J_{3,2}$ = 3.4 Hz, 3 H), 2.66 (m, CH_2-allyl, 5 H), 5.31 (m, CH-allyl, 2 H), 6.16−6.51 (m, CH-aromat, 32 H). − ^{13}C NMR ($CDCl_3$, 298 K, 50.3 MHz): δ = 20.52, 20.58 (CH_3-*p*-tolyl), 59.9, 60.5 (CH_2-allyl) 114.1, 114.3 (CH-allyl), 123.97, 123.01, 124.2, 124.6, 127.47, 127.51, 127.66, 127.71, 130.48, 130.51, 130.99, 131.02 (CH-aromat), 143.77, 143.82, 150.0, 150.3 (C-aromat), 160.7, 160.8 (C oxam bridge). − IR (nujol): $\tilde{\nu}$ = 1506, 1609 cm^{-1} (C=C_{aromat}, CN). − MS (EI): *m*/*z* (%) = 1248 (< 1) [M^+], 740 (5) [M^+ − oxamZn], 591 (2) [M^+ − allylPd − oxamZn].

Complex 16: Bis(mesityl)bis(*p*-tolyl)oxalic amidine (1 mmol, 0.50 g) was dissolved in 38 mL of THF, and treated dropwise with 2 mmol

of $ZnEt_2$ (1.1 M solution in toluene, 1.8 mL) at room temperature. After 5 min of heating, the solution was stirred for 20 min and then treated with bis(mesityl)bis(*p*-tolyl)oxalic amidine (2 mmol, 1.0 g, dissolved in 12 mL of THF). This solution was refluxed for 3 min, cooled and treated with bis(acetylacetonato)(ethyl)zink(II) complex **19** (2 mmol, 0.387 g, dissolved in 10 mL of THF). Standing at room temperature for 2 d resulted in the crystallization of pure, colorless crystals of **16**, crystallizing with 2.5 equiv. THF, suitable for an X-ray analysis. Yield 290 mg (45%). − $C_{112}H_{122}N_{12}O_4Zn_4 \times 2.5$ C_4H_8O (2142.1): calcd. C 68.41, H 6.68, N 7.85; found C 67.0 H, 6.55, N 7.42. − ^{1}H NMR ($CDCl_3$, 298 K, 400 MHz): δ = 1.49, 1.64, 1.77, 1.91, 2.01, 2.08 (s, CH_3-acac, CH_3-*p*-tolyl, CH_3-mesityl, 84 H), 5.01 (s, CH-acac, 2 H), 6.1−6.54 (CH-aromat, 36 H). − MS (ESI in CH_3OH/THF): *m*/*z* (%) = 1067 (4) [$Zn(oxam)_2$].

Complex 17: Acetylacetone (10 mmol, 1.001 g), dissolved in 10 mL of toluene, was slowly treated with $ZnEt_2$ (10 mmol, 1.1 M toluene solution) at room temperature. After all the ethane was released, the solution was kept at −18 °C and colorless crystals were isolated. Yield 2.11 g (55%). − $C_{14}H_{24}O_4Zn_2$ (387.1): calcd. C 43.43, H 6.25; found C 43.64, H 6.11. − ^{1}H NMR ([D_8]toluene, 298 K, 200 MHz): δ = 0.52 (q, CH_2-ethyl, 2 H), 1.44 (t, CH_3-ethyl, 3 H), 1.75 (s, CH_3-acac, 6 H), 5.01 (s CH-acac 1 H). − ^{13}C NMR ([D_8]toluene, 298 K, 50.3 MHz): δ = − 0.03 (CH_2-ethyl), 12.8 (CH_3-methyl), 28.1 (CH_3-acac), 101.8 (CH-acac). − MS (EI): *m*/*z* (%) = 262 (61) [$Zn(acac)_2$], 192 (6) [M^+/2], 163 (68) [M^+/2 − 2 Et].

Catalytic Polymerization/Oligomerization: A 200-mL stainless steel autoclave was heated in vacuo for 2 h at approximately 100 °C and subsequently cooled to 25 °C. A solution of 0.031 mol of the catalyst precursor, dissolved in toluene, was treated either with MAO (5 M solution in toluene) or with Et_3Al (1.9 M solution in toluene). The total volume of the added solutions was 20 mL. After the autoclave was charged with this solution, catalytic reactions were carried out at 25 °C in the sealed autoclave whilst stirring (initial pressure of ethylene: 10 atm = 0.123 mol ethylene). No further ethylene was added during the reaction. After the desired reaction time (Tables 2 and 3) the reaction mixture was cooled to 0 °C. The ethylene pressure was then released, and the cooled reaction mixture was treated with a small amount of dilute hydrochloric acid at 0 °C to inactivate the catalyst, followed by addition of 1.18 mL (0.87 g) of *n*-decane as standard for GC measurements.

Analysis of the Ethylene Oligomers: An aliquot (1 mL) of the reaction mixture was very slowly treated with dilute hydrochloric acid at 0 °C, followed by separation of the organic layer. After drying the organic phase with solid Na_2CO_3, the oligomers were analyzed by GC/MS using a methylsilicon column (CPSIL 5 CB), injector temperature 40 °C, with the following temperature program: 20 °C/min up to 300 °C (15 min). The individual products were identified by MS and integrated, using *n*-decane as the internal standard (comparison with GC calibration experiments). The turnover numbers (TON) were calculated as follows:

mol ethylene consumed = g oligomers/mol weight of ethylene = g oligomers/28 $gmol^{-1}$

TON = mol of ethylene consumed/mol catalyst = mol of ethylene consumed/$0.031 \cdot 10^{-3}$ mol catalyst.

In a typical example the following C_6 olefins from the catalysis with the oligomerization catalyst **6** (Entry 5, Table 2) were characterized by GC/IR (comparison with authentic samples): overall amount of C_6 olefins = 0.33 g (100%); 4-methylpentene: 2.1%; 2,3-dimethylbutene 3.2%; 1-hexene: 53%; *trans*-3-hexene: 21%; *trans*-2-hexene: 3.2%. Retention times under the analytical conditions used were as follows: butenes: 1.238 min; 4-methylpentene: 1.478 min; 2,3-dimethylbutene: 1.584 min; 1-hexene: 1.644 min; *trans*-3-hexene: 1.69 min; *trans*-2-hexene: 1.72 min. − In most of the catalytic reactions (Tables 2 and 3) only C_4 and C_6 olefins were found. Small amounts of C_8 olefins were found in a few of the catalytic reactions (Entries 5, 6, and 10, Table 2). C_{10} oligomers were detected only in traces (Entry 5, Table 2).

Analysis of the Polymer: An aliquot of the above solution was treated with a mixture of 500 mL of methanol and 20 mL of hydrochloric acid while stirring to precipitate the polymer. After the methanol/hydrochloric acid mixture was decanted, the polymer was washed with methanol (3 × 50 mL), and dried at 70 °C in vacuo. Yields and molecular weights can be found in Tables 2 and 3. The TONs for the polymerization were determined analogously with the above calculation (see Tables 2 and 3). The polymers were analyzed by GPC using THF as a solvent and polystyrene standards. Columns were packed with styrene−divinylbenzene copolymer; column temperature: 30 °C; flow rate: 1.00 mL/min; detector 1: UV 975 (Fa. Jasco); detector 2: RI 930 (Fa. Jasco). − Typically, M_w was around $1.57 \cdot 10^5$ to $6.73 \cdot 10^5$ with polydispersity indices between 1.46 and 2.66 (Table 2).

Polymerization at Higher Pressure: A typical experiment proceeded as follows: 0.031 mmol of complex **8** and $0.93 \cdot 10^{-2}$ mol of MAO ([Ni]/[Al] = 1:150) were dissolved in 20 mL of toluene. The catalysis was carried out at 55 bar ethylene pressure at 60 °C and stirring of the reaction mixture for 10 min. The isolation of the polymer followed the above procedure. Yield 9.1 g; turnover frequency (TOF): approximately 55 g/mmol cat × bar × h. In this case a waxy polymer was obtained. According to the integration of the CH, CH_2, and CH_3 protons in the ^{1}H NMR spectrum ([D_8]toluene, 298 K, 200 MHz) approximately 140 branches/1000 ethylene units were present.

Heck Coupling: In a typical run, a 25-mL Schlenk tube was charged with an aryl halide (6.25 mmol), anhydrous sodium acetate (7 mmol) and put under argon followed by addition of *N*,*N*-dimethylacetamide (8 mL) and *n*-butyl acrylate (6.75 mmol) The solution was heated to 120 °C before the catalyst, dissolved in toluene, was added. After the reaction time, the reaction mixture was cooled and analyzed by gas chromatography.

Crystal Structure Determination: The intensity data for the compounds were collected with a Nonius KappaCCD diffractometer, using graphite-monochromated Mo-K_α radiation. Data were corrected for Lorentz and polarization effects, but not for absorption.[37,38] The structures were solved by direct methods (SHELXS[39]) and refined by full-matrix least-squares techniques against F_o^2 (SHELXL-97[40]). Since the quality of the data of compound **17** is too bad, only the conformation of the molecule and the crystallographic data are communicated. Furthermore, this data will not be published in the Cambridge Crystallographic Data Centre. The allyl groups of **1** and **2** are disordered. The disorder could be solved. The hydrogen atoms were included at calculated positions with fixed thermal parameters. All non-hydrogen atoms were refined anisotropically.[41] XP (SIEMENS Analytical X-ray Instruments, Inc.) was used for structure representations.

Crystal Data for 1:[41] $C_{40}H_{46}N_4Ni_2$, M_r = 700.23 g·mol^{-1}, gold-yellow prism, size 0.20 × 0.20 × 0.10 mm, triclinic, space group $P\bar{1}$, *a* = 8.8877(4), *b* = 9.2005(5), *c* = 11.8562(5) Å, α = 107.550(3), β = 95.843(3), γ = 98.779(3)°, *V* = 902.23(7) Å^3, *T* = −90 °C, *Z* = 1, $\rho_{calcd.}$ = 1.289 gcm^{-3}, μ(Mo-K_α) = 10.76 cm^{-1}, *F*(000) = 370, 6624 reflections in *h*(−11/11), *k*(−11/11), *l*(−15/14), measured in the range 3.19° ≤ Θ ≤ 27.53°, completeness Θ_{max} = 98.7%, 4104 independent reflections, R_{int} = 0.028, 3353 reflections with $F_o > 4\sigma(F_o)$, 218 parameters, 0 restraints, $R1_{obs}$ = 0.053, wR^2_{obs} = 0.101,

$R1_{all}$ = 0.075, wR^2_{all} = 0.108, GOOF = 1.073, largest difference peak and hole: 0.388/−0.358 e·Å^{-3}.

Crystal Data for 2:[41] $C_{44}H_{54}N_4Ni_2$, M_r = 757.33 g·mol^{-1}, gold-yellow prism, size 0.20 × 0.20 × 0.08 mm, triclinic, space group $P\bar{1}$, a = 8.4970(3), b = 10.5059(6), c = 12.4798(6) Å, α = 65.704(2), β = 87.798(3), γ = 76.103(3)°, V = 983.36(8) Å^3, T = −90 °C, Z = 1, $\rho_{calcd.}$ = 1.277 gcm^{-3}, μ(Mo-K_α) = 9.92 cm^{-1}, F(000) = 370, 7625 reflections in h(−11/11), k(−13/13), l(−16/16), measured in the range 4.33° ≤ Θ ≤ 27.49°, completeness Θ_{max} = 98.4%, 4442 independent reflections, R_{int} = 0.038, 3592 reflections with $F_o > 4\sigma(F_o)$, 300 parameters, 0 restraints, $R1_{obs}$ = 0.043, wR^2_{obs} = 0.091, $R1_{all}$ = 0.063, wR^2_{all} = 0.098, GOOF = 1.025, largest difference peak and hole: 0.357/−0.341 e·Å^{-3}.

Crystal Data for 9:[41] $C_{38}H_{38}N_4O_4Pd_2$, M_r = 827.62 g·mol^{-1}, light yellow prism, size 0.20 × 0.18 × 0.12 mm, monoclinic, space group $P2_1/c$, a = 12.5830(4), b = 8.8054(5), c = 15.9510(9) Å, β = 91.319(3)°, V = 1766.9(1) Å^3, T = −90 °C, Z = 2, $\rho_{calcd.}$ = 1.555 gcm^{-3}, μ(Mo-K_α) = 10.63 cm^{-1}, F(000) = 836, 12946 reflections in h(−16/14), k(−11/10), l(−20/17), measured in the range 3.45° ≤ Θ ≤ 27.51°, completeness Θ_{max} = 98.4%, 3996 independent reflections, R_{int} = 0.051, 3228 reflections with $F_o > 4\sigma(F_o)$, 226 parameters, 0 restraints, $R1_{obs}$ = 0.041, wR^2_{obs} = 0.086, $R1_{all}$ = 0.061, wR^2_{all} = 0.092, GOOF = 1.030, largest difference peak and hole: 0.526/−0.904 e·Å^{-3}.

Crystal Data for 10:[41] $C_{40}H_{42}N_4O_4Pd_2$, M_r = 855.58 gmol^{-1}, light yellow prism, size 0.12 × 0.12 × 0.10 mm, monoclinic, space group $P2_1/c$, a = 12.6868(9), b = 8.7318(6), c = 16.393(1) Å, β = 92.982(4)°, V = 1813.5(2) Å^3, T = −90 °C, Z = 2, $\rho_{calcd.}$ = 1.567 gcm^{-3}, μ(Mo-K_α) = 10.38 cm^{-1}, F(000) = 868, 11592 reflections in h(−16/14), k(−11/10), l(−21/16), measured in the range 3.13° ≤ Θ ≤ 27.50°, completeness Θ_{max} = 99.1%, 4126 independent reflections, R_{int} = 0.087, 2828 reflections with $F_o > 4\sigma(F_o)$, 226 parameters, 0 restraints, $R1_{obs}$ = 0.062, wR^2_{obs} = 0.105, $R1_{all}$ = 0.108, wR^2_{all} = 0.119, GOOF = 1.024, largest difference peak and hole: 1.126/−0.797 e·Å^{-3}.

Crystal Data for 16:[41] $C_{112}H_{122}N_{12}O_4\ Zn_4 \times 2.5\ C_4H_8O$, M_r = 2142.1 g·mol^{-1}, colourless prism, size 0.24 × 0.22 × 0.10 mm, triclinic, space group $P\bar{1}$, a = 16.7787(5), b = 16.9800(5), c = 23.1886(7) Å, α = 102.894(2), β = 98.691(2), γ = 105.365(2)°, V = 6052.4(3) Å^3, T = −90 °C, Z = 2, $\rho_{calcd.}$ = 1.171 gcm^{-3}, μ(Mo-K_α) = 8.38 cm^{-1}, F(000) = 2244, 45031 reflections in h(−21/19), k(−21/22), l(−30/30), measured in the range 2.98° ≤ Θ ≤ 27.51°, completeness Θ_{max} = 98.6%, 27436 independent reflections, R_{int} = 0.088, 16443 reflections with $F_o > 4\sigma(F_o)$, 1237 parameters, 0 restraints, $R1_{obs}$ = 0.111, wR^2_{obs} = 0.224, $R1_{all}$ = 0.187, wR^2_{all} = 0.259, GOOF = 1.080, largest difference peak and hole: 1.220/−0.995 e·Å^{-3}.

Crystal Data for 17: $C_{14}H_{24}O_4Zn_2$, M_r = 387.07 g·mol^{-1}, colourless prism, size 0.32 × 0.30 × 0.28 mm, orthorhombic, space group $Pbca$, a = 12.795(2), b = 15.865(2), c = 17.637(3) Å, V = 3580.2(9) Å^3, T = −90 °C, Z = 8, $\rho_{calcd.}$ = 1.436 gcm^{-3}, μ(Mo-K_α) = 26.87 cm^{-1}, F(000) = 1600, 10076 reflections in h(−16/16), k(−20/20), l(−22/22), measured in the range 3.09° ≤ Θ ≤ 27.43°, completeness Θ_{max} = 94.1%, 3853 independent reflections, R_{int} = 0.182.

Acknowledgments

Financial support for this work from the Deutsche Forschungsgemeinschaft, the VW-Stiftung and the Fonds der Chemischen Industrie is gratefully acknowledged.

[1] W. E. Hofman, *Proc. Indiana Acad. Sci.* **1969**, *79*, 129; *Chem. Abstr.* **1970**, *73*, 126513r.
[2] E. Papavil, *Anal. Stiint. Univ. Jasi, Sect. 110* **1964**, 115; *Chem. Abstr.* **1965**, *63*, 14351h.
[3] M. Pasquali, C. Floriani, A. Chiesi-Villa, C. Guastini, *J. Am. Chem. Soc.* **1979**, *101*, 4740.
[4] P. Fehling, M. Döring, F. Knoch, R. Beckert, H. Görls, *Chem. Ber.* **1995**, *128*, 405.
[5] M. Döring, H. Görls, R. Beckert, *Z. Anorg. Allg. Chem.* **1994**, *620*, 551.
[6] R. Beckert, S. Vorwerk, D. Lindauer, M. Döring, *Z. Naturforsch., Teil B* **1993**, *48*, 1186.
[7] M. Döring, P. Fehling, H. Görls, W. Imhof, R. Beckert, D. Lindauer, *J. Prakt. Chem.* **1999**, *341*, 748.
[8] M. Ruben, S. Rau, A. Skirl, K. Krause, H. Görls, D. Walther, J. G. Vos, *Inorg. Chim. Acta* **2000**, *303*, 206
[9] M. Ruben, D. Walther, R. Knake, H. Görls, R. Beckert, *Eur. J. Inorg. Chem.* **2000**, 1055.
[10] T. Döhler, H. Görls, D. Walther, *Chem. Commun.* **2000**, 945.
[11] For recent reviews see: G. J. P. Britovsek, V. C. Gibson, *Angew. Chem.* **1999**, *111*, 448; *Angew. Chem. Int. Ed.* **1999**, *38*, 428.
[12] K. A. O. Starzewski, W. M. Kelly, A. Stump, D. Freitag, *Angew. Chem.* **1999**, *111*, 2588; *Angew. Chem. Int. Ed.* **1998**, *38*, 2439.
[13] H. H. Brintzinger, D. Fischer, R. Mühlhaupt, B. Rieger, R. M. Waymouth, *Angew. Chem.* **1995**, *107*, 1255; *Angew. Chem. Int. Ed. Engl.* **1995**, *34*, 1143.
[14] L. K. Johnson, C. M. Killian, S. D. Arthur, J. Feldman, E. F. McCord, S. J. McLain, K. Kreutzer, M. A. Bennett, E. B. Coughlin, S. D. Ittel, A. Parthasarathy, D. J. Tempel, M. S. Brookhart (DuPont), WO-A 96/231010, **1996** [*Chem. Abstr.* **1996**, *125*, 222773t].
[15] L. K. Johnson, C. M. Killian, M. S. Brookhart, *J. Am. Chem. Soc.* **1995**, *117*, 6414.
[16] C. M. Killian, D. J. Tempel, L. K. Johnson, M. S. Brookhart, *J. Am. Chem. Soc.* **1996**, *118*, 11664.
[17] S. Mecking, L. K. Johnson, M. Brookhart, *J. Am. Chem. Soc.* **1996**, *118*, 267.
[18] S. Mecking, L. K. Johnson, L. Wang, M. Brookhart, *J. Am. Chem. Soc.* **1998**, *120*, 888.
[19] B. L. Small, M. Brookhart, A. M. A. Bennett, *J. Am. Chem. Soc.* **1998**, *120*, 4049.
[20] G. J. P. Britovsek, V. C. Gibson, B. S. Kimberley, P. J. Maddox, S. J. McTauish, G. A. Solan, A. J. P. White, D. J. Williams, *Chem. Commun.* **1998**, 849.
[21] T. R. Younkin, E. F. Connor, J. I. Henderson, S. K. Friedrich, R. H. Grubbs, D. A. Bansleben, *Science* **2000**, *287*, 460.
[22] C. Wang, S. Friedrich, T. R. Younkin, R. T. Li, R. H. Grubbs, D. A. Bansleben, M. W. Day, *Organometallics* **1998**, *17*, 3149.
[23] A. de Meijere, F. Meyer, *Angew. Chem.* **1994**, *106*, 2473; *Angew. Chem. Int. Ed. Engl.* **1994**, *33*, 2379.
[24] V. V. Grushin, H. Alper, *Chem. Rev.* **1994**, *106*, 2473; W. Cabri, I. Caudiani, *Acc. Chem. Res.* **1995**, *28*, 2.
[25] W. A. Herrmann, C. Broßmer, K. Öfele, C.-P. Reisinger, T. Priermeier, M. Beller, H. Fischer, *Angew. Chem.* **1995**, *107*, 1989; *Angew. Chem. Int. Ed. Engl.* **1995**, *28*, 1844.
[26] W. A. Herrmann, V. Böhm, *J. Organomet. Chem.* **1999**, *572*, 141.
[27] W. A. Herrmann, V. Böhm, C.-P. Reisinger, *J. Organomet. Chem.* **1999**, *576*, 23.
[28] W. A. Herrmann, M. Elison, J. Fischer, C. Köcher, G. R. J. Artus, *Angew. Chem.* **1995**, *107*, 2602; *Angew. Chem. Int. Ed. Engl.* **1995**, *34*, 2371.
[29] W. A. Herrmann, C.-P. Reisinger, M. J. Spiegler, *J. Organomet. Chem.* **1998**, *557*, 93.
[30] W. A. Herrmann, Th. Weskamp, V. P. W. Böhm, *J. Organomet. Chem.* **1999**, *585*, 348.
[31] W. A. Herrmann, V. Böhm, *Chem. Eur. J.* **2000**, *6*, 1017.
[32] D. S. McGuiness, K. J. Cavell, *Organometallics* **2000**, *19*, 741.

[33] R. Bauer, *Ber. Dtsch. Chem. Ges.* **1907**, *40*, 2650.
[34] G. Wilke, B. Bogdanovic, *Angew. Chem.* **1961**, *23*, 756.
[35] J. Smidt, W. Hafner, *Angew. Chem.* **1959**, *71*, 284.
[36] G. Wilke, Belg. Patent, **1963**, 631172.
[37] COLLECT, Data Collection Software, Nonius B. V., Netherlands, **1998**.
[38] Z. Otwinowski, W. Minor, *Processing of X-ray Diffraction Data Collected in Oscillation Mode*, in: *Methods in Enzymology*, vol. 276, Macromolecular Crystallography, Part A (Ed.: C. W. Carter, R. M. Sweet), pp. 307−326, Academic Press, San Diego, **1997**.
[39] G. M. Sheldrick, *Acta Crystallogr., Sect. A* **1990**, *46*, 467−473.
[40] G. M. Sheldrick, *SHELXL-97*, University of Göttingen, Germany, **1993**.
[41] Further details of the crystal structure investigations are available on requests from the Cambridge Crystallographic Data Centre, 12 Union Road, Cambridge CB2 1 EZ, UK, on quoting the depository numbers CCSD-152478 (**1**), -152482 (**2**), -152479 (**9**), -152480 (**10**), and -152481 (**16**), the names of the authors, and the journal citation.

Received December 6, 2000
[I00464]

A Novel Salt Formed by Mixed-Valence Vanadium(IV, V) $[(VO)_2O(bpy)_2(C_2O_4)_2]$ Anions and Ferromagnetic $[Cu_2(bpy)_4(C_2O_4)]$ Cations: Structure, Spectroscopic Characterization and Magnetic Properties

Otilia Costisor,*[a] Maria Brezeanu,[a] Yves Journaux,[b] Kurt Mereiter,[c] Peter Weinberger,[d] and Wolfgang Linert[d]

Keywords: Vanadium / Copper / Oxalate ligands / Magnetic properties

The new heterometallic, mixed-valence compound $[Cu_2(bpy)_4(C_2O_4)][(VO)_2O(bpy)_2(C_2O_4)_2]_2 \cdot 10H_2O$ has been synthesized, its crystal structure determined and its spectroscopic characterization accomplished by means of solid-state vibrational (far and mid FTIR) spectroscopy. The title compound crystallises in the triclinic system, space group $P\bar{1}$ (No. 2) [a = 13.488(5) Å, b = 14.160(6) Å, c = 15.829(9) Å, α = 87.22(2)°, β = 66.33(2)°, γ = 64.49(2)°, V = 2471(2) Å^3, Z = 1]. The compound consists of the cationic binuclear copper(II) complex $[Cu_2(bpy)_4(C_2O_4)]^{2+}$, two anionic binuclear mixed valence vanadium(IV)–vanadium(V) complexes $[(VO)_2O(bpy)_2(C_2O_4)_2]^-$, and ten uncoordinated water molecules. The copper atom exhibits a Jahn–Teller-distorted octahedral coordination. The vanadium atoms adopt a strongly distorted octahedral coordination and form a characteristic O=V–O–V=O moiety with a significantly bent V–O–V link. The temperature dependence of the magnetic susceptibilities has been investigated in the temperature range 2–300 K and explained in terms of the ferromagnetic interaction between Cu^{II} ions giving J = 22.7 yJ (1.14 cm^{-1}) and g = 2.014.

Introduction

Homo- and heterometallic systems involving oxalate ions (ox) as bridging ligands have been intensively studied since these ligands are very effective in transmitting exchange interactions.[1−3] Homopolynuclear copper(II) complexes consisting of both dinuclear and chain structures[4−6] have been studied, and in order to tune the dimension of spin coupling, complexes with terminal ligands such as tetramethyl-1,2-ethanediamine,[7] 1,2-ethanediamine,[8] 1,10-phenanthroline[9] or 2,2′-bipyridine[10] (bpy) have been synthesized so far. Complexes of VO^{3+} or VO^{2+} containing the oxalate ion as a bidentate ligand are also known, but they have not been studied that extensively.[11−13] Heterodimetallic copper(II)−oxovanadium(IV) oxalates, $[(terpy)Cu(ox)VO(ox)(H_2O)]\cdot H_2O$ and $[(terpy)_2Cu_2(ox)_2VO(H_2O)](ClO_4)_2\cdot H_2O$ (terpy = 2,2′:6′,2′′-terpyridine), have been the subject of recent studies[14] with the aim of elucidating the mechanism of spin coupling between paramagnetic ions through the bridging oxalate ligand. Bimetallic oxalate complexes in the copper(II)−oxovanadium(IV) system have been synthesized[15] and their ability to act as catalysts for the autoxidation of aliphatic aldehydes has been proved. As part of our continuing work in this field[16] this paper presents the structural and spectroscopic characterisation of a new heterometallic, mixed-valence compound obtained in the system vanadium/copper/oxalate which turned out to be $[Cu_2(bpy)_4(C_2O_4)][(VO)_2O(bpy)_2(C_2O_4)_2]_2\cdot 10H_2O$.

[a] Inorganic Chemistry Laboratory, Romanian Academy of Sciences, Timisoara Branch,
Bul. Mihai Viteazul 24, 1900 Timisoara, Romania
E-mail: ocostisor@acad-tim.utt.ro
[b] Laboratoire de Chimie Inorganique, bat 420, Université de Paris-Sud,
91405 Orsay, France
[c] Institute for Mineralogy, Crystallography and Structural Chemistry, Vienna University of Technology,
Getreidemarkt 9/171, 1060 Vienna, Austria
[d] Institute for Inorganic Chemistry, Vienna University of Technology,
Getreidemarkt 9/153, 1060 Vienna, Austria

Results and Discussion

Synthesis

The synthesis of the title compound was performed in a basic aqueous solution of Na_2S. Some experimental parameters, including the Cu:V molar ratio, were varied, but the resulting products remained the same. Finally, a copper/vanadium ratio of 1:2 was used. Although the crystals formed from an aqueous solution, their solubility in pure water was low. The crystals are insoluble in common organic solvents (i.e. DMSO, DMF, C_1-C_5 alcohols, acetone, acetonitrile, and chloroform).

Crystal Structure

$[Cu_2(bpy)_4(C_2O_4)][(VO)_2O(bpy)_2(C_2O_4)_2]_2\cdot 10H_2O$ crystallises in the triclinic system, space group $P\bar{1}$, with a unit cell content of one formula unit. It consists of a cationic, dinuclear copper(II) complex (Figure 1), an anionic, dinuclear mixed-valence vanadium(IV)−vanadium(V) complex (Figure 2), and water molecules filling large voids of the structure (Figure 3). The $[Cu_2(bpy)_4(C_2O_4)]^{2+}$ complex is centrosymmetric with the centre of inversion halfway between the carbon atoms C(1) and C(1A) of the bridging

 © WILEY-VCH Verlag GmbH, 69451 Weinheim, 2001 1434−1948/01/0808−2061 $ 17.50+.50/0

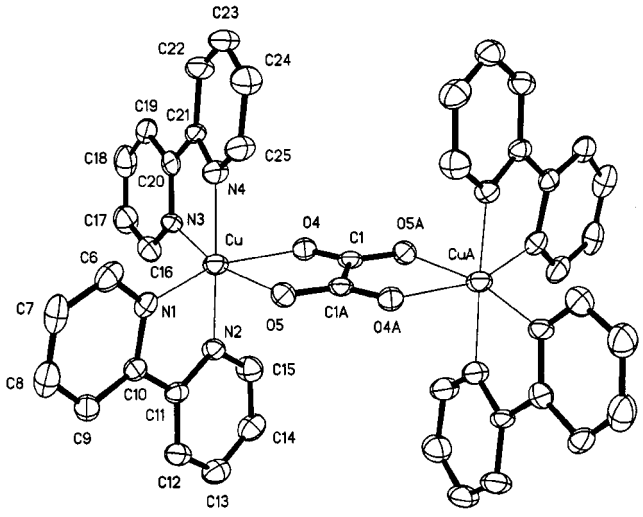

Figure 1. Thermal ellipsoid plot (20% ellipsoids) of the cationic dinuclear copper(II) complex $[Cu_2(bpy)_4(C_2O_4)]^{2+}$

bis-bidentate oxalate anion (Figure 1). The complex, including the bpy moieties, approaches quite well a noncrystallographic 2/*m* symmetry with the twofold axis passing through the two Cu atoms.

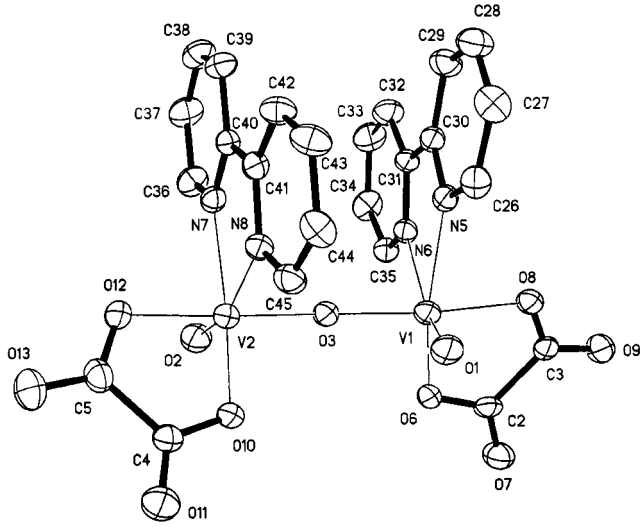

Figure 2. Thermal ellipsoid plot (20% ellipsoids) of the anionic mixed valence vanadium(IV, V) complex $[(VO)_2O(bpy)_2(C_2O_4)_2]^-$

Copper exhibits a moderately distorted octahedral coordination to two O atoms and four N atoms. A relatively weak Jahn–Teller distortion of the CuO_2N_4 polyhedron towards an elongated octahedron with four short equatorial bonds to N(1), N(2), N(4), and O(4) (Cu–N: 1.981– 2.059 Å; Cu–O: 2.141 Å) and two slightly longer axial bonds to N(3) and O(5) (Cu–N: 2.125Å; Cu–O: 2.237 Å) can be noted. The bond angles in the CuO_2N_4 octahedron are clearly controlled by the chelating bidentate ligands oxalate and 2,2′-bipyridine (O–Cu–O: 75.4 °; chelating N–Cu–N

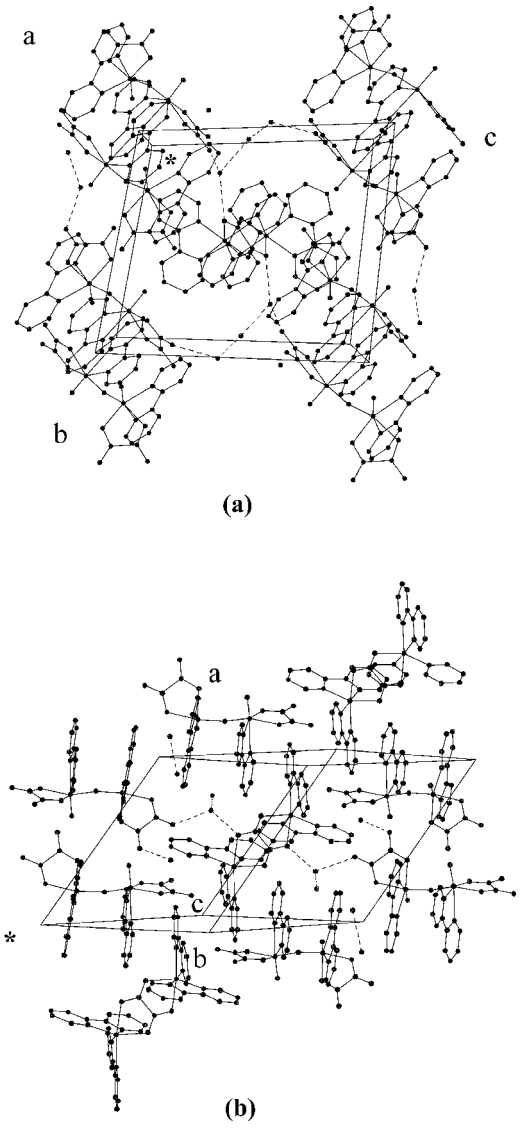

Figure 3. Packing diagram of $[Cu_2(bpy)_4(C_2O_4)][(VO)_2O(bpy)_2(C_2O_4)_2]_2 \cdot 10H_2O$ (a) viewed down the *a* axis; and (b) view approximately perpendicular to $(0\bar{1}1)$ showing the π-stacking most clearly (see text)

angles: 78.8–80.2°) whereas the remaining angles vary in the ranges 83.7–108.0° and 157.4–175.7°. Similar weak Jahn–Teller distortions were found for CuO_2N_4 octahedra in related complexes.[17,18] While the title compound represents the first example of a binuclear oxalato-bridged Cu complex with Cu:bpy = 1:2, such complexes with Cu:bpy in a 1:1 ratio have been observed before in several cases. However, they differ from the title compound by having either a square planar or a square pyramidal coordination for Cu, for example in $[Cu_2(bpy)_2(ox)(H_2O)_2][Cu(bpy)(ox)](BF_4)_2$.[19]

The dinuclear mixed-valence vanadium(IV)–vanadium(V) complex $[(VO)_2O(bpy)_2(C_2O_4)_2]^-$ is built up from two crystallographically independent vanadium atoms in distorted octahedral coordinations, each with four O and two N atoms. Each of the two vanadium atoms forms a typ-

ical vanadyl group (V=O) with a terminal oxo oxygen strongly bonded [V(1)−O(1) = 1.588 Å and V(2)−O(2) = 1.586 Å]. The second shortest V−O bonds are towards the bridging oxo oxygen O(3), with V(1)−O(3) = 1.814 Å, V(2)−O(3) = 1.796 Å and V(1)−O(3)−V(2) = 164.8°. This oxygen O(3), the V-bonded oxygen atoms of the chelating oxalate groups and the nitrogen atoms N(5) and N(7) define, with intermediate bond lengths, the slightly pyramidal equatorial coordination environments around the V(1)−O(1) and V(2)−O(2) groups. The significantly longest bonds are those to the nitrogen atoms N(6) and N(8) *trans* to O(1) and O(2). The mean V−O,N bond lengths of the two VO_4N_2 octahedra are 1.975 Å for V(1) and 1.969 Å for V(2). This, and the similarity in V−O(3) bond lengths, suggests that tetra- and pentavalent vanadium is approximately equally distributed over the two crystallographic metal sites. A further support for this view is that the complex exhibits a clear-cut noncrystallographic twofold pseudosymmetry with the twofold pseudoaxis passing approximately parallel to the V-bonded bpy's and through the bridging O(3) (Figure 2). The dimensions of the V coordination polyhedra in the title compound are in good agreement with many other oxo-bridged vanadium(IV,V) compounds. Of particular interest is the geometry of the O(1)=V(1)−O(3)−V(2)=O(2) fragment with respect to V−O−V bond angle, as well as to the O=V···V=O torsion angle. Whereas in many compounds[20−22] these quantities are exactly, or close to, 180°, in the title compound they are 164.8(3)° and 141.6(2)° and thus are close to the values for the compound of Chakravarty et al.[23] (142.0 and 160.8°) which has vanadium(V) in a square-pyramidal coordination.

The spatial arrangement of the Cu and V complexes in the title compound is shown in a view down the *a*-axis (Figure 3, a). Layer-like arrangements of the Cu and V complexes parallel to the $(0\bar{1}1)$ plane can be clearly seen in this view. Between the layers there are large open channels extending parallel to *a* which are occupied by the 10 water molecules per formula unit (5 independent molecules per asymmetric unit). These molecules are anchored in the structure mainly through hydrogen bonds to oxalate oxygen atoms with five independent O(w)···O(ox) distances to four different O(w) below 3.0 Å. Further hydrogen bonds appear to exist between the water molecules themselves, as indicated by the eight independent O(w)···O(w) distances below 3.0 Å. Among them O(3w) stands out in having only three contacts to O(w) but none to oxalate oxygen atoms. Figure 3 (b) shows another view of the structure approximately perpendicular to $(0\bar{1}1)$. This view is interesting because it indicates that the crystal structure owes much of its stability to π-stacking of the bpy molecules, in particular the molecules 2 (Cu-bonded), and 3 and 4 (V-bonded), which have their main planes all aligned approximately in the view direction and exhibit mean plane-separations of about 3.5−3.7 Å. These interactions may be considered to stabilize a structure that suffers from a destabilizing effect due to the large number of noncoordinated water molecules.

The question may arise as to whether the title compound might be a stoichiometrically H^+-bearing vanadium(IV) dimer rather than a mixed valence vanadium(IV, V) compound without additional H^+ as described above. This hypothesis was rejected for the following reasons:

(1) Bond valence calculations according to Brese and O'Keefe[24] show that the assignments of O(1), O(2) and O(3) to oxide oxygen atoms is beyond doubt (bond valence sums between 1.7 and 2.0 indicating that no OH group is present).

(2) H^+ atoms in the hydrate structure or at terminal oxalate oxygen atoms have to be accompanied by outstandingly short hydrogen bond O···O distances (2.4−2.6 Å). Since all O···O distances outside the cation coordination polyhedra are longer than 2.73 Å this possibility can be ruled out as well.

Vibrational Spectroscopy

The solid-state far- and mid-FTIR spectra are given in Figure 4 and 5. The spectra were checked with respect to reproducibility and several measurements of different samples yielded identical results.

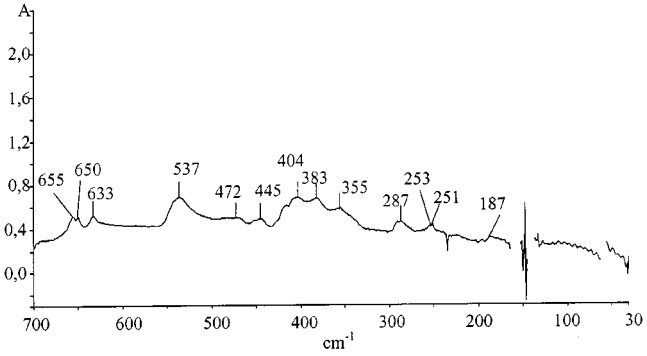

Figure 4. Solid-state far-IR spectrum of $[Cu_2(bpy)_4(C_2O_4)][(VO)_2O(bpy)_2(C_2O_4)_2]_2{\cdot}10H_2O$

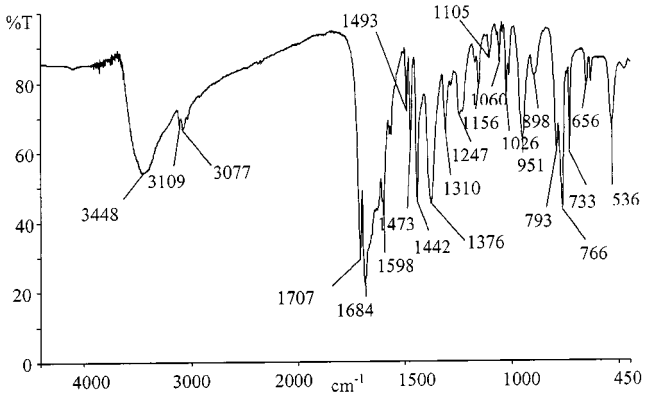

Figure 5. Solid-state mid-IR spectrum of $[Cu_2(bpy)_4(C_2O_4)][(VO)_2O(bpy)_2(C_2O_4)_2]_2{\cdot}10H_2O$

In the far IR the prominent absorption at 537 cm^{-1} is attributable to combinations of V−O(oxalate) with oxalate C−C stretching vibrations.[25] The equal prominent peak at 383 cm^{-1} is assigned to the V−N(bpy) stretching vibrations.[26] The weaker peak at 355 cm^{-1} is considered as being due to combinations of V−O(oxalate) stretching vibra-

tions with V-oxalate chelate ring deformation vibrations.[27] The rather weak absorption at 287 cm^{-1} is due to the symmetric stretching mode ν_{Cu-N} of the Cu−N(bpy) moieties.[28]

The sharp and strong absorption at 1707 cm^{-1} can be assigned to the asymmetric in-phase stretching vibration $\nu_{C=O}$ of the four terminal carbonyl groups C2−O7, C3−O9 and C4−O11, C5−O13 of the two vanadium-bonded oxalate groups. In accordance with literature data the broad and strong absorption at 1685 cm^{-1} is considered as a superposition of two asymmetric out-of-phase stretching vibrations of the carbonyl groups of the same oxalates. The strong absorption at 1376 cm^{-1} is attributed to a mode coupling of the symmetric stretching vibrations of the bridging carbonyls C2−O6, C3−O8 and C4−O10, C5−O12 with the C−C stretching vibrations of the C2−C3 and the C4−C5 bonds, respectively. The slightly weaker peak at 1247 cm^{-1} is due to a combination of the symmetric stretching vibration of the binding carbonyls C2−O6, C3−O8 and C4−O10, C5−O12, with the out-of-plane bending vibrations $\delta_{O-C=O}$ of the oxalates bound to the vanadium atoms. The very prominent absorption at 952 cm^{-1} is characteristic for the vanadyl stretching mode $\nu_{V=O}$ of the V1−O1 and V2−O2 bonds.[29] The fact that only one sharp peak is observed supports the explanation that the two vanadyl groups are indistinguishable, and is consistent with the almost identical V−O bond lengths (see Table 1). The V=O(vanadyl) stretching vibration in mixed-valence vanadium(IV, V) is detected within the range of 947 cm^{-1} (see Nishizawa et al.[30]), 980 cm^{-1} (see Pessoa et al.[31]) and 995 cm^{-1} (see Chakravarty et al.[23]), whereas the V=O(vanadyl) stretching vibration of vanadium(IV) compounds is observed at 975 cm^{-1} and at 890−920 cm^{-1} for vanadium(V) compounds (see Nishizawa et al.[30]). The strong peak at 794 cm^{-1} represents the combination mode consisting of the bending vibration $\delta_{O-C=O}$ and the stretching vibration ν_{V-O}. The rather weak absorption at 898 cm^{-1} could be the stretching vibration of V−O−V. Thus, according to the classification of Robin and Day,[32] the mixed valence vanadium(IV, V) complex of the title compound should belong to type II, where the two metal ions are in inequivalent positions with the unpaired electron shared equally between them.

Table 1. Selected geometric data for $[Cu_2(bpy)_4(C_2O_4)][(VO)_2O(bpy)_2(C_2O_4)_2]_2 \cdot 10H_2O$

N(2)−Cu−N(4)	175.7(2)	Cu−N(2)	1.981(5)
N(2)−Cu−N(1)	80.2(2)	Cu−N(4)	2.025(6)
N(2)−Cu−N(3)	96.9(2)	Cu−N(1)	2.059(5)
N(2)−Cu−O(4)	91.5(2)	Cu−N(3)	2.125(6)
N(2)−Cu−O(5)	91.0(2)	Cu−O(4)	2.141(4)
N(4)−Cu−N(1)	101.6(2)	Cu−O(5)	2.237(5)
N(4)−Cu−N(3)	78.8(3)		
N(4)−Cu−O(4)	88.3(2)	V(1)−O(1)	1.588(4)
N(4)−Cu−O(5)	93.1(2)	V(1)−O(3)	1.814(4)
N(1)−Cu−N(3)	108.0(2)	V(1)−O(6)	1.972(4)
N(1)−Cu−O(4)	157.4(2)	V(1)−O(8)	2.018(4)
N(1)−Cu−O(5)	83.7(2)	V(1)−N(5)	2.156(5)
N(3)−Cu−O(4)	93.8(2)	V(1)−N(6)	2.301(4)
N(3)−Cu−O(5)	166.8(2)		
O(4)−Cu−O(5)	75.4(2)	V(2)−O(2)	1.586(4)
O(1)−V(1)−O(3)	102.2(2)	V(2)−O(3)	1.796(4)
O(1)−V(1)−O(6)	104.5(2)	V(2)−O(10)	1.976(4)
O(1)−V(1)−O(8)	100.2(2)	V(2)−O(12)	2.051(4)
O(1)−V(1)−N(5)	89.5(2)	V(2)−N(7)	2.128(4)
O(1)−V(1)−N(6)	161.5(2)	V(2)−N(8)	2.279(5)
O(3)−V(1)−O(6)	90.6(2)		
O(3)−V(1)−O(8)	157.2(2)		
O(3)−V(1)−N(5)	98.9(2)		
O(3)−V(1)−N(6)	79.9(2)		
O(6)−V(1)−O(8)	79.9(2)		
O(6)−V(1)−N(5)	161.1(2)		
O(6)−V(1)−N(6)	93.8(2)		
O(8)−V(1)−N(5)	85.3(2)		
O(8)−V(1)−N(6)	80.2(2)		
N(5)−V(1)−N(6)	72.1(2)		
O(2)−V(2)−O(3)	103.0(2)		
O(2)−V(2)−O(10)	106.0(2)		
O(2)−V(2)−O(12)	94.9(2)		
O(2)−V(2)−N(7)	91.9(2)		
O(2)−V(2)−N(8)	163.7(2)		
O(3)−V(2)−O(10)	93.0(2)		
O(3)−V(2)−O(12)	161.9(2)		
O(3)−V(2)−N(7)	93.9(2)		
O(3)−V(2)−N(8)	82.8(2)		
O(10)−V(2)−O(12)	79.3(2)		
O(10)−V(2)−N(7)	158.8(2)		
O(10)−V(2)−N(8)	88.7(2)		
O(12)−V(2)−N(7)	88.1(2)		
O(12)−V(2)−N(8)	80.7(2)		
N(7)−V(2)−N(8)	72.3(2)		

Magnetochemical Investigations

The magnetic properties of $[Cu_2(bpy)_4(C_2O_4)][(VO)_2O(bpy)_2(C_2O_4)_2]_2 \cdot 10H_2O$ (SQUID, 2−100 K) are depicted in Figure 6. At 100 K, $\chi_M T$ is equal to 19.2 10^{-6} m^3 mol^{-1} K (1.53 cm^3 mol^{-1} K). This value is equal to that expected for two vanadyl ions and two noninteracting copper centres. The expected behaviour for the two mixed-valence vanadium dimers is a Curie law for two uncoupled $S = 1/2$. Therefore, all the variation of the $\chi_M T$ value with temperature is due to the $[Cu_2(bpy)_4(C_2O_4)]$ entity. Upon cooling, $\chi_M T$ increases smoothly showing that the dominant interaction between the Cu^{II} ions is ferromagnetic. The best fit is obtained using the following parameters $J = 22.7$ yJ (1.14 cm^{-1}) and an average g value for the copper and vanadyl ions of $g = 2.014$. The individual g factor for the copper and the vanadium cannot be determined from the magnetic data nor from EPR spectrum. The agreement factor R is then equal to $3.4 \cdot 10^{-6}$. Many binuclear Cu^{II} complexes with an oxalato bridging ligand have been structurally and magnetically characterized. Most of them are antiferromagnetically coupled, but the coupling constants depend strongly on the coordination sphere around the copper ions. The experimental coupling constants are in the −7950 to 22.8 yJ (−400 to +1.2 cm^{-1}). The largest interaction is observed for the so-called coplanar arrangement **1a**,[33] intermediate interactions are measured in the case of the perpendicular geometry **1b**,[34] and finally rare cases of ferromagnetic interactions are observed for the parallel geometry **1c**.[34,35] All these behaviours have recently been rationalized by theoretical DFT calculations.[36]

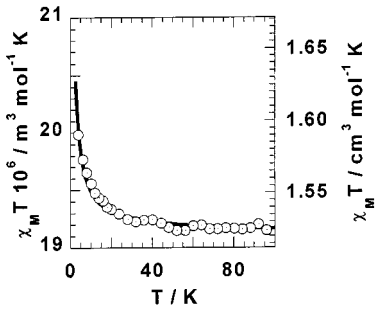

Figure 6. Plot of $\chi_M T$ vs. T for $[Cu_2(bpy)_4(C_2O_4)][(VO)_2O(bpy)_2(C_2O_4)_2]_2 \cdot 10H_2O$

The binuclear copper unit in $[Cu_2(bpy)_4(C_2O_4)][(VO)_2O(bpy)_2(C_2O_4)_2]_2 \cdot 10H_2O$ belongs to the **1c** family (see Scheme 1) with the equatorial planes of elongated octahedra perpendicular to the oxalato bridge. It is therefore not surprising to find a ferromagnetic interaction. Furthermore, the magnitude of the coupling observed for $[Cu_2(bpy)_4(C_2O_4)][(VO)_2O(bpy)_2(C_2O_4)_2]_2 \cdot 10H_2O$ is in the same range as the previous examples.

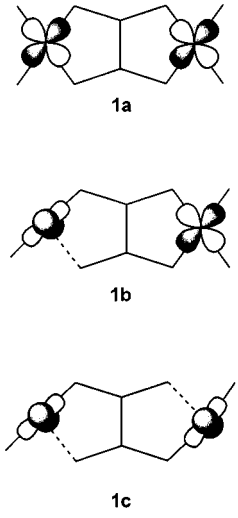

Scheme 1

Conclusion

The heterodimetallic compound $[Cu_2(bpy)_4(C_2O_4)][(VO)_2O(bpy)_2(C_2O_4)_2]_2 \cdot 10H_2O$ was synthesized and the structure was determined by crystallographic analysis. The anions consist of binuclear mixed-valence vanadium(IV)−vanadium(V) complexes in which: (*i*) the metal centres lie at almost equal distance to the bridging oxo oxygen, (*ii*) the unpaired electron is equally shared, and (*iii*) no magnetic interactions occur between the paramagnetic centres. Ferromagnetic interactions occur at low temperature between the copper(II) centres as a result of the orthogonality of the neighbouring magnetic orbitals on the oxalato bridge.

Experimental Section

General: All reagents were purchased from commercial sources (Fluka).

$[Cu_2(bpy)_4(C_2O_4)][(VO)_2O(bpy)_2(C_2O_4)_2]_2 \cdot 10H_2O$: $Cu(CH_3COO)_2 \cdot H_2O$ (0.5 g, 2.5 mmol) was mixed with 2,2′-bipyridine (0.78 g, 5 mmol) in 20 cm^3 water and the blue solution thus obtained was poured into 60 cm^3 of a solution containing 5 mmol $VO(C_2O_4)$ (stock solution) with vigorous stirring. The suspension formed was treated after a few minutes with a solution of Na_2S (0.08 g, 2.5 mmol) in 5 mL water. The obtained mixture was heated to 80 °C for one hour. After cooling to room temperature the solution was filtered. While keeping the clear solution in darkness at 5 °C (refrigerator) for a period of 2−3 weeks green crystals of the novel compound formed as a by-product, as our intention was to obtain copper-vanadium compounds with sulfide as ligand. − $C_{90}H_{84}Cu_2N_{16}O_{36}V_4$ (2296.6): calcd. C 47.07, H 3.69, N 9.76, Cu 5.53, V 8.87; found C 46.98, H 3.72, N 9.68, Cu 5.58, V 8.94.

Vibrational Spectroscopy: The dark-green powdered sample was characterised by far and mid-range FTIR spectroscopy. The solid state far-IR measurements were performed on a Perkin−Elmer System 2000 FT spectrometer with polyethylene as the matrix. To accomplish a good signal-to-noise ratio 1000 cycles, each cycle consisting of one reference scan (pure polyethylene), four sample scans and again one reference scan, were summed. During the measurement the spectrometer (optical bench including the sample chamber and the detector) was purged with nitrogen gas of purity >99.99%. The mid-range FTIR was recorded on a Perkin−Elmer 16 PC spectrometer. For good signal-to-noise ratio 64 scans in KBr as matrix were summed. During the measurement the spectrometer was also purged with nitrogen gas (>99.99%).

Magnetochemical Investigations: Magnetic measurements were performed on a Quantum Design SQUID MPMS5 magnetometer. The data were collected in the range 2−300 K for powered microcrystalline samples of $[Cu_2(bpy)_4(C_2O_4)][(VO)_2O(bpy)_2(C_2O_4)_2]_2 \cdot 10H_2O$ at 0.5 T. Diamagnetic corrections were applied based on Pascal's constant. This paper uses the SI units. The molar magnetic susceptibility χM is expressed in $m^3 \cdot mol^{-1}$. The conversion factor to the irrational emu quantity χM(ir) is $106/4\pi$. The energies are expressed in 10^{-24} Joule. The submultiple prefix for 10^{-24} is yocto, its symbol is y. Therefore 1 yJ means 10^{-24} Joule. The conversion factor to cm^{-1} is $5.034 \cdot 10^{-2}$ (1 $cm^{-1} \approx 20$ yJ).

X-ray Crystallographic Study

Crystal Data: formula $C_{90}H_{84}Cu_2N_{16}O_{36}V_4$, molecular mass 2296.58 amu, triclinic, $P\bar{1}$ (No. 2), a = 13.488(5), b = 14.160(6), c = 15.829(9) Å, α = 87.22(2)°, β = 66.33(2)°, γ = 64.49(2)°, V = 2471(2) $Å^3$, Z = 1, d = 1.544 $g \cdot cm^{-3}$, μ = 0.88 mm^{-1}, T = 301 K.

Data Collection: All available crystals were of relatively small size, poor quality and gave only low X-ray intensities. Data collection was therefore restricted to θ_{max} = 23°. X-ray data were harvested with a Siemens/Bruker SMART 3-circle diffractometer with a CCD area detector (sealed X-ray tube, Mo-K_α radiation, graphite monochromator) using ω-scan frames with Δω = 0.3° and 20 seconds per frame to cover a complete sphere of the reciprocal space by 4 × 606 frames. Absorption and crystal decay were corrected semi-empirically by equivalents.[37] Measured reflections 27550, unique reflections 6859, completeness of data 99.6%.

Structure Analysis and Refinement: The structure was solved by direct methods.[38] All non-hydrogen atoms were refined anisotropically. The hydrogen atoms of the bpy moieties were introduced in calculated positions and refined using a riding model. The hydro-

gen atoms of the water molecules could not be located with acceptable reliability and were therefore left out. The structure was refined against F^2 with the program SHELXL-97.[39] Final agreement indices were $R1 = 0.058$ [4094 $F_o > 4\sigma(F_o)$] and 0.106 for all 6859 data, $wR2 = 0.172$, $GOF = 0.98$, 667 parameters.

Crystallographic data (excluding structure factors) for the structure reported in this paper have been deposited with the Cambridge Crystallographic Data Centre as supplementary publication no. CCDC-154154. Copies of the data can be obtained free of charge on application to CCDC, 12 Union Road, Cambridge CB2 1EZ, UK [Fax: (internat.) +44-1223/336-033; E-mail: deposit@ccdc.cam.ac.uk].

Acknowledgments

Thanks for financial support are due to the Austrian Science Foundation ("Fonds zur Förderung der Wissenschaftlichen Forschung in Österreich") project P-5048 CHE, the Training and Mobility of Researchers Network (TMR) project "Thermal and Optical Spin-State Switching" (TOSS) supported by the European Union under the contract number ERB-FMRX-CT98-0199 and to the European Science Foundation under the project "Molecular Magnets". This work was supported by an exchange convention between the Romanian Academy and CNRS.

[1] See, for example: [1a] O. Kahn, *Molecular Magnetism*, VCH, New York, **1993**. – [1b] O. Kahn, *Adv. Inorg. Chem.* **1995**, *43*, 179–259 and references therein. – [1c] C. Ruiz-Perez, M. Hernandez-Molina, P. Lorenzo-Luiz, F. Lloret, J. Cano, M. Julve, *Inorg. Chem.* **2000**, *39*, 3845–3852. – [1d] J. Y. Lu, M. A. Lawandy, T. Yuen, C. L. Lin, *Inorg. Chem.* **1999**, *38*, 2695–2704.

[2] See for example: [2a] S. Decurtins, H. W. Schmalle, P. Schneuwly, J. Ensling, P. Gütlich, *J. Am. Chem. Soc.* **1994**, *116*, 9521–9528; [2b] L. Martin, S. S. Turner, P. Day, K. M. A. Malik, S. J. Coles, M. B. Hursthouse, *Chem. Commun.* **1999**, 513–517. – [2c] E. Coronado, J. R. Galán-Mascarós, C. J. Gómez-García, J. M. Martinez-Agudo, *Inorg. Chem.* **2001**, *40*, 113–120

[3] [3a] M. Ohba, H. Tamaki, N. Matsumoto, H. Okawa, *Inorg. Chem.* **1993**, *32*, 5385–5390. – [3b] G. Marinescu, M. Andruh, R. Lescouëzec, M. C. Muñoz, J. Cano, F. Lloret, M. Julve, *New J. Chem.* **2000**, *24*, 527–536.

[4] A. Michalowicz, J. J. Girerd, J. Goulon, *Inorg. Chem.* **1979**, *18*, 3004–3014.

[5] J. J. Girerd, O. Kahn, M. Verdaguer, *Inorg. Chem.* **1980**, *19*, 274–276.

[6] M. Julve, M. Verdaguer, O. Kahn, A. Gleizes, M. Philoche-Levisalles, *Inorg. Chem.* **1983**, *22*, 368–370.

[7] M. F. Charlot, M. Verdaguer, Y. Journaux, P. de Loth, J. P. Daudey, *Inorg. Chem.* **1984**, *23*, 3802–3808.

[8] H. Oshio, U. Nagashima, *Inorg. Chem.* **1992**, *31*, 3295–3301.

[9] A. Bencini, A. C. Fabretti, C. Zanchini, P. Zannini, *Inorg. Chem.* **1987**, *26*, 1445–1449.

[10] M. Julve, J. Faus, M. Verdaguer, A. Gleizes, *J. Am. Chem. Soc.* **1984**, *106*, 8306–8308.

[11] W. R. Scheidt, C. Tsai, J. L. Hoard, *J. Am. Chem. Soc.* **1971**, *93*, 3867–3871.

[12] J. Salta, C. J. O'Connor, L. Sichu, J. Zubieta, *Inorg. Chim. Acta.* **1996**, *250*, 303–310.

[13] H. Reiskamp, P. Gietz, R. Mattes, *Chem. Ber.* **1976**, *1098*, 2090–2096.

[14] R. Cortes, M. K. Urtiaga, L. Lezama, M. I. Arriortua, T. Rojo, *Inorg. Chem.* **1994**, *33*, 829–832.

[15] O. Costisor, M. Brezeanu, *Rev. Roum. Chim.* **1992**, *37*, 731–738.

[16] O. Costisor, C. Stanescu, S. Policec, P. Weinberger, J. Zhang, W. Linert, *Orient. J. Chem.* **1997**, *13*, 197–202.

[17] N. W. Alcock, P. Moore, H. A. A. Omar, *Acta Crystallogr., Sect. C* **1987**, *43*, 2074–2076

[18] J. Glerup, P. A. Goodson, D. J. Hodgson, K. Michelson, *Inorg. Chem.* **1995**, *34*, 6255–6264.

[19] A. Gleizes, M. Julve, M. Verdaguer, J. A. Real, J. Faus, X. Solans, *J. Chem. Soc., Dalton Trans.* **1992**, 3209–3216.

[20] R. A. Holwerda, B. R. Whittlesey, M. J. Nilges, *Inorg. Chem.* **1998**, *37*, 64–68.

[21] Wu Da-Xu, Lei Xin-Jian, Cao Rong, Hong Mao-Chun, *Chin. J. Struct. Chem.* **1993**, *12*, 79–84.

[22] M. Mahroof-Tahir, A. D. Keramidas, R. B. Goldfarb, O. P. Anderson, M. M. Miller, D. C. Crans, *Inorg. Chem.* **1997**, *36*, 1657–1668.

[23] J. Chakravarty, S. Dutta, A. Chakravorty, *J. Chem. Soc., Dalton Trans.* **1993**, 2857–2858.

[24] N. E. Brese, M. O'Keefe, *Acta Crystallogr., Sect. B* **1991**, *47*, 192–197.

[25] J. Fujita, A. E. Martell, K. Nakamoto, *J. Chem. Phys.* **1962**, *36*, 324–331.

[26] Y. Saito, J. Takemoto, B. Hutchinson, K. Nakamoto, *Inorg. Chem.* **1972**, *11*, 2003–2011.

[27] R. D. Hancock, D. A. Thornton, *J. Mol. Struct.* **1970**, *6*, 441–446.

[28] R. Wilde, T. K. K. Srinivasan, N. Ghosh, *J. Inorg. Nucl. Chem.* **1973**, *35*, 1017–1021.

[29] M. R. Caira, J. M. Haigh, L. R. Nassimbeni, *J. Inorg. Nucl. Chem.* **1972**, *34*, 3171–3176.

[30] M. Nishizawa, K. Hirotsu, S. Ooi, K. Saito, *J. Chem. Soc., Chem. Commun.* **1979**, 707–708.

[31] J. C. Pessoa, J. A. L. Silva, A. L. Vieira, L. Vilas-Boas, P. O'Brien, P. Thornton, *J. Chem. Soc., Dalton Trans.* **1992**, 1745–1749.

[32] M. B. Robin, P. Day, *Adv. Inorg. Chem. Radiochem.* **1967**, *10*, 248–422.

[33] M. Julve, M. Verdaguer, A. Gleizes, P.-L. Michelle, O. Kahn, *Inorg. Chem.* **1984**, *23*, 3808–3818.

[34] H. Oshio, U. Nagashima, *Inorg. Chem.* **1992**, *31*, 3295–3301.

[35] J. Suárez-Varela, J. Dominguez-Vera, E. Colacio, J. C. Avila-Róson, M. A. Hidalgo, D. Martin-Ramos, *J. Chem. Soc., Dalton Trans.* **1995**, 2143–2146.

[36] J. Cano, P. Alemany, S. Alvarez, M. Verdaguer, E. Ruiz, *Chem. Eur. J.* **1998**, *4*, 476–484.

[37] G. M. Sheldrick, Program *SADABS* **1996.**

[38] G. M. Sheldrick, *SHELXS-86*, University of Göttingen, **1986.**

[39] G. M. Sheldrick, *SHELXL-93*, University of Göttingen, **1993**.

Received December 13, 2000
[I00470]

Synthesis and Reactions of (1,1′-Bi-1*H*-phosphirene)iron Complexes − Crystal Structure of a Bridged (1-Phosphaallyl-1*H*-phosphirene)diiron(*Fe*−*Fe*) Complex[‡]

Jürgen Simon,[a] Guido J. Reiß,[a] Uwe Bergsträßer,[a] Heinrich Heydt,*[a] and Manfred Regitz*[a]

Keywords: Iron / Phosphorus heterocycles / P ligands / Valence isomerization / Twinning

The reactions of 1-chloro-1*H*-phosphirenes **5** with disodium tetracarbonlyferrate lead to the selective formation of the mono complexed bi-1*H*-phosphirenes **7**, which are converted into the doubly complexed species **9** upon treatment with diiron nonacarbonyl. Photochemical opening of one of the two three-membered ring systems in **9** furnishes the bridged complexes **10** containing phosphirene and phosphaallyl units together with an iron-iron σ-bond.

Introduction

Since the 1960's investigations on the synthesis and reactivity of phosphinines and their valence isomers have played a significant role in the development of the chemistry of low-coordinated phosphorus compounds.[2−5] In contrast, the only known representatives of diphosphinines are the 1,3[6] and 1,4 derivatives[7] **1** and **2** (Scheme 1). Recently, an access to valence isomers of the 1,3-diphospha-Dewarbenzene **3** and diphosphabenzvalene **4** types was established using specific trapping reactions of a short-lived 1,3-diphosphacyclobutadiene with suitably substituted alkynes.[8] 1,3-Diphosphinines **1** are also able to undergo a valence isomerization to the Dewar isomers on prolonged heating.[6c]

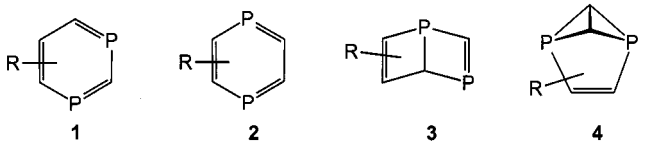

Scheme 1

In the present report, we described the synthesis of the iron complexed 1,1′-bi-1*H*-phosphirenes **7** and **9** as a further, previously unknown class of valence isomers of the diphosphinines.[9] Very recently, the corresponding 1,1′-bisilacyclopropenes, the valence isomers of 1,4-disilabenzenes, have also been synthesized.[10]

Results and Discussion

Synthesis of the (1,1′-Bi-1*H*-phosphirene)iron Complexes 7a and 7b

In the reactions of the 1-chloro-1*H*-phosphirenes **5** with disodium tetracarbonylferrate, the mono η^1 complexed 1,1′-bi-1*H*-phosphirenes **7a** and **7b** (58 and 60%) are formed highly selectively (Scheme 2), instead of the expected $\eta^{3:3}$-(bisphosphirenylium)dicarbonyliron complexes **6**.

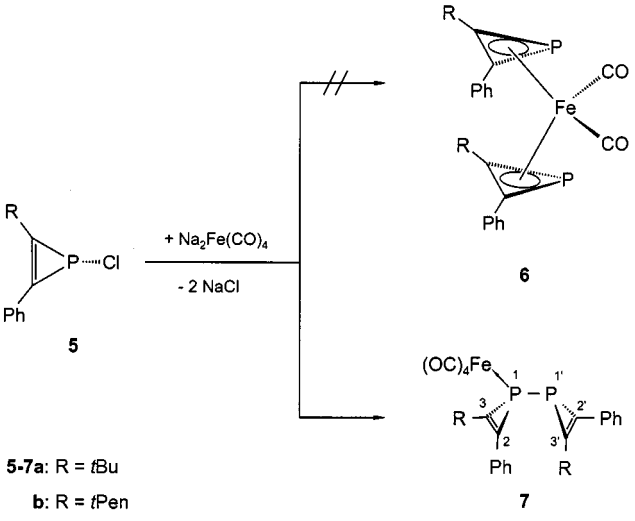

Scheme 2

Elemental analysis and mass spectroscopic data unequivocally demonstrate that the complexes **7a** and **7b** are 2:1 adducts of the 1-chloro-1*H*-phosphirenes **5a** and **5b** with Collman's reagent, formed under concomitant loss of two molecules of sodium chloride.

Mixtures of two diastereomers that cannot be separated by column chromatography are obtained. One diastere-

[‡] Organophosphorus Compounds, 154. − Part 153: Ref.[1]

[a] Fachbereich Chemie der Universität Kaiserslautern, Erwin-Schrödinger-Straße, 67663 Kaiserslautern, Germany
Fax: (internat.) +49 (0)631 205 3921
E-mail: heydt@chemie.uni-kl.de

 © WILEY-VCH Verlag GmbH, 69451 Weinheim, 2001 1434−1948/01/0808−2067 $ 17.50+.50/0

omer, however, can be enriched up to a ratio of 8:1 (**7a**) or 4:1 (**7b**) (as determined by ^{1}H NMR spectroscopy) by crystallization. The NMR spectroscopic data provide diagnostic information for the structure elucidation, as discussed below for the example of **7a** (major diastereomer; R = *t*Bu).

The formation of this product is demonstrated by its ^{31}P NMR spectrum, which reveals a significant, large $^1J_{P,P}$ coupling constant of 427.3 Hz. The signal at δ = −88.1 is assigned to the iron complexed phosphorus atom P-1 by comparison with the published values for iron complexed 1*H*-phosphirenes[11], while the signal at higher field (δ = −134.2) originates from the non-complexed phosphirene unit.

A conspicuous feature of the ^{13}C NMR spectrum of **7a** is a drastic reduction of the intracyclic carbon/phosphorus coupling constants in the complexed three-membered ring ($^1J_{C,P}$ = 22.0 and 27.1 Hz) in comparison with those of the non-complexed three-membered ring ($^1J_{C,P}$ = 50.8 and 57.7 Hz). This is a generally observed phenomenon on going from three- to four-coordinated 1*H*-phosphirenes.[12] The chemical shifts of the alkyl- and aryl-substituted ring carbon atoms are also in agreement with literature data.[13] The resonance signals at lower field (δ = 140.5 and 138.5) are attributed to the alkyl-substituted carbon atoms C-3 and C-3′ while the phenyl-substituted C atoms C-2 and C-2′ give rise to the signals at markedly higher field (δ = 124.8 and 120.3).

The formation of **7a** and **7b** must proceed through a multi-step sequence, although ^{31}P NMR monitoring of the reaction mixture did not provide any indications for the existence of intermediates (Scheme 3).

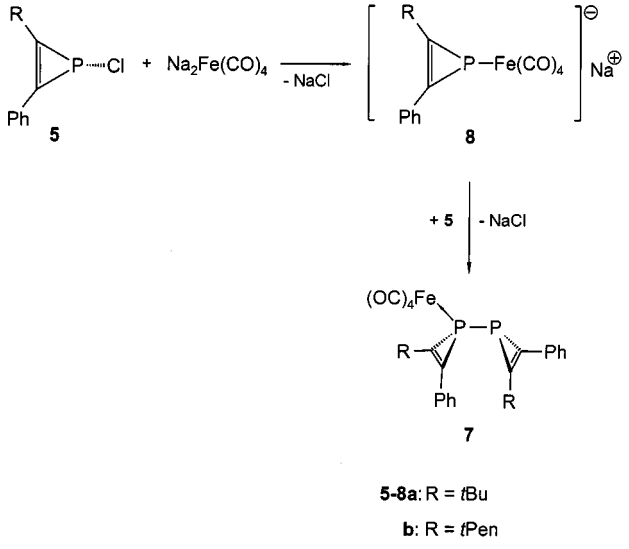

Scheme 3

A plausible mechanism involves the substitution of the chlorine atom in **5** by an anionic tetracarbonyliron fragment to afford the anionic 1*H*-phosphirene complex **8**. This complex then undergoes an immediate nucleophilic substitution with a further molecule of **5** to afford the mono complexed 1,1′-bi-1*H*-phosphirenes **7**.

Further Complexation of (1,1′-Bi-1*H*-phosphirene)iron Complexes 7a and 7b with Diironnonacarbonyl To Afford (1,1′-Bi-1*H*-phosphirene)diiron Complexes 9a and 9b

The additional complexation of the free phosphorus atom provides a possibility to improve the crystallization properties of the novel diphosphinine valence isomers **7**. Reactions of **7** with a slight excess of diiron nonacarbonyl proceed selectively to afford the (1,1′-bi-1*H*-phosphirene)-diiron complexes **9** carrying two tetracarbonyliron fragments (Scheme 4). After workup by column chromatography and subsequent recrystallization from *n*-pentane the binuclear complexes **9a** and **9b** are obtained in good yields (63% and 54%, respectively) in the form of yellow-orange crystals.

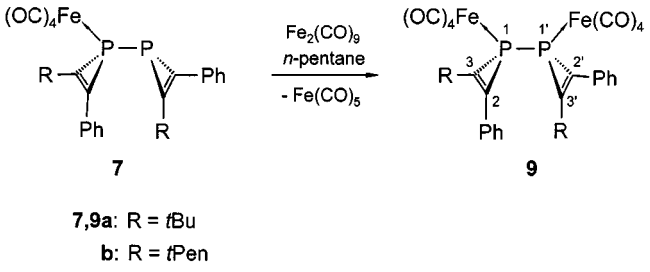

Scheme 4

Elemental analysis and mass spectroscopic data unequivocally confirm the presence of two $Fe(CO)_4$ fragments in **9a** and **9b**. The NMR spectroscopic data of these complexes are highly simplified, and discussed for the example of the main diastereomer **9a**.

The magnetically equivalent phosphorus atoms P-1 and P-1′ in **9a** give rise to a singlet signal in the ^{31}P NMR spectrum at δ = −69.3. In comparison to the spectrum of **7a** the additional complexation results in a pronounced deshielding by 64.9 ppm of the ^{31}P NMR signals of the formerly non-coordinated phosphorus.

The ^{13}C NMR spectrum of **9a** reflects the double complexation by the appearance of pseudo-triplet signals for the carbonyl and ring carbon atoms. Furthermore, the intracyclic phosphorus-carbon coupling constants of the 1*H*-phosphirene unit that was not complexed in **7a** are, as expected, drastically reduced as a result of the complexation with the second tetracarbonyliron fragment. In analogy with compound **7**, the signals for the ring carbon atoms seen at lower field are assigned to the alkyl-substituted carbon atoms C-3 and C-3′ (δ = 142.2). Similar to the ^{31}P NMR spectroscopic data of **9a** and **9b**, the ^{13}C NMR signals of the ring carbon atoms also experience a clear shift to lower field as a result of the additional complexation.

Final confirmation of the structure of the iron complexed 1,1′-bi-1*H*-phosphirene **9a** was obtained by X-ray crystallography.[9]

Photolyses of the (1,1′-Bi-1*H*-phosphirene)diiron Complexes 9a and 9b To Give the (1-Phosphaallyl-1*H*-phosphirene)-diiron(*Fe*−*Fe*) Complexes 10a and 10b

Previously, only a single example of a photochemically induced rig opening reaction of a complexed 1*H*-phosphirene was known.[14] When a solution of the doubly complexed 1,1′-bi-1*H*-phosphirenes **9a** or **9b** in C_6D_6 is irradiated in an NMR tube using a 125 W high-pressure mercury lamp, ^{31}P NMR monitoring of the mixture reveals a relatively unselective reaction sequence (Scheme 5). After workup by column chromatography and subsequent recrystallization from *n*-pentane/diethyl ether, the pure compounds **10a** or **10b** are isolated only in low yields (5 and 6%, respectively).

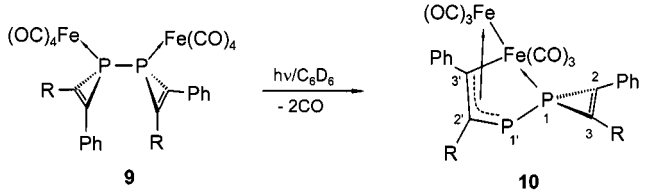

9 **10**

9,10a: R = *t*Bu
b: R = *t*Pen

Scheme 5

Elemental analysis and mass spectroscopic data unambiguously demonstrate the cleavage of two carbonyl groups from **9a** and **9b**. The NMR spectroscopic data also provide diagnostic information on the constitutions of compounds **10a** and **10b**.

The ^{31}P NMR spectra, discussed here for the example of **10a**, contains two doublets at δ = −1.6 and −70.4. Of these, the signal at higher field is only shifted slightly in comparison to that of the starting compound **9a**, thus confirming the retention of one of the two 1*H*-phosphirene units. On the other hand, the low-field shift of the other doublet indicates that the second three-membered ring unit has been opened. This signal can be assigned to a (1-phosphaallyl)iron complex by comparison with published values for structural increments of this type.[15]

The $^{13}C\{^1H\}$ NMR spectrum of **10a** is in agreement with the proposed structure, and contains 8 different signals in addition to those of the aryl and alkyl substituents. Although only one doublet at δ = 212.4 with a coupling constant of 6.8 Hz is observed for one of the two $Fe(CO)_3$ groups, a doublet signal with an appreciably larger carbon-phosphorus coupling constant of 27.1−28.8 Hz is found for each CO ligand of the second transition metal fragment. The occurrence of different signals for the carbonyl ligands of this $Fe(CO)_3$ group confirms a hindered exchange between the axial and equatorial positions of the carbonyl ligands. Since the η^3-coordination of the 1-phosphaallyl fragment creates high steric demands, these signals may safely be assigned to the tricarbonyliron fragment of this structural increment.

The carbon atoms C-2′ and C-3′of the 1-phosphaallyl element give rise to signals at δ = 191.2 and 153.9. Since the signal at lower field is split into a double doublet it is assigned to the C-2′ atom directly bonded to phosphorus. The extremely low-field position of this signal is also characteristic for a P=C double bond system. The bridging carbon atom C-3′ of **10a**, on the other hand, gives a signal at appreciably higher field. A comparison of the chemical shift of this carbon atom (C-3′; δ = 153.9) with the published values for bridged allyl complexes[16] provides further support for this structure. The signals of the ring carbon atoms C-2 and C-3 are found at δ = 150.6 (C-3) and δ = 124.6 (C-2) in the region typical for 1*H*-phosphirenes with this substitution pattern. The chemical shifts have been assigned analogously to those for compounds **7** and **9**. Although the $^{13}C\{^1H\}$ NMR signals of the phenyl substituents cannot be assigned individually, this is possible for the alkyl substituents. As expected, two sets of signals are observed for the two *tert*-butyl groups, with one of the signal sets being markedly shifted to lower field. By comparison with the values for other allyl complexes,[15] the signals at lower field are attributed to the alkyl substituents at C-2′.

This low-field signal shift of the substituents of the phosphaallyl unit is also observed in the ^1H NMR spectrum of **10a**. Thus, the *tert*-butyl group at C-2′ gives rise to a signal at δ = 1.42, while the alkyl substituent of the phosphirene ring produces a signal at δ = 1.16. The signals of the protons of the phenyl groups overlap, resulting in the observation of only a multiplet in the typical aromatic proton region.

The structure of **10a** was finally and irrevocably confirmed by X-ray crystallography (Figure 1).

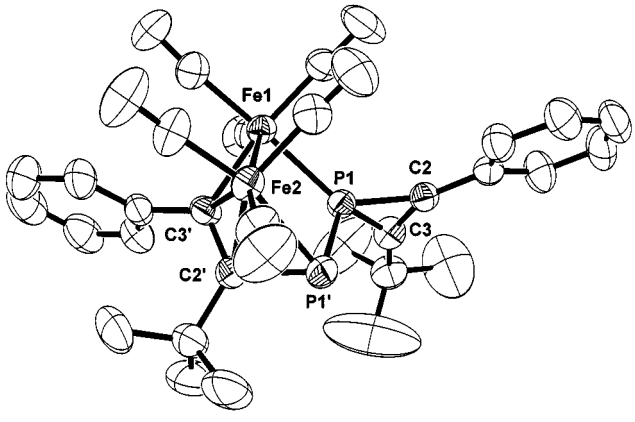

Figure 1. Molecular structure of **10a**. Selected bond lengths [Å] and angles [°]: Fe(1)−C(3′) 2.037(3), Fe(1)−P(1) 2.2078(9), Fe(1)−Fe(2) 2.6493(6), Fe(2)−C(3′) 2.102(3), Fe(2)−C(2′) 2.135(3), Fe(2)−P(1′) 2.3684(12), P(1)−C(2) 1.773(3), P(1)−C(3) 1.795(3), P(1)−P(1′) 2.1597(11), P(1′)−C(2′) 1.811(3), C(2)−C(3) 1.341(4), C(2′)−C(3′) 1.445(4); C(3′)−Fe(1)−P(1) 83.08(10), C(3′)−Fe(2)−C(2′) 39.87(12), C(3′)−Fe(2)−P(1′) 76.14(10), C(2′)−Fe(2)−P(1′) 47.07(8), C(2)−P(1)−C(3) 44.16(14), C(2)−P(1)−P(1′) 115.28(10), C(3)−P(1)−P(1′) 118.56(11), C(2′)−P(1′)−P(1) 92.56(10), C(3)−C(2)−P(1) 68.82(18), C(2)−C(3)−P(1) 67.0(2), C(3′)−C(2′)−P(1′) 115.8(2), C(2′)−C(3′)−Fe(1) 125.2(2)

The resultant ORTEP plot clearly reveals the opening of one of the two phosphirene rings with formation of an η^3 complexed 1-phosphaallyl system. The crystal structure analysis also confirms the formation of an iron-iron single bond (see below), as well as the retention of the second phosphirene ring. The Fe1−P1 bond length of 2.208(9) Å is in the typical range for an iron complexed phosphane,[17] and is comparable with the iron-phosphorus bond length in **9a**. On the other hand, the Fe−P1′ bond length in the 1-phosphaallyl unit of 2.368(1) Å is appreciably stretched in comparison with those of other η^3-phosphaallyl-iron complexes.[15] This is readily explained by the steric requirements of the substituents that force the $Fe(CO)_3$ fragment away from the 1-phosphaallyl unit. The iron-carbon separations in this structural increment are almost identical to those in a comparable compound formed by the reaction the μ_3-RP bridged cluster $(\mu_3\text{-RP})Fe_3(CO)_{10}$ with terminal alkynes.[15] The bond lengths in the phosphaallyl unit of 1.811(3) Å (P1′−C2′) and 1.445(4) Å (C2′−C3′) are clearly lengthened, and are of magnitudes typical for single bonds. This is probably due to the enormous spatial requirements of the substituents. The iron−iron bond length of 2.6493(6) Å in **10a** is also of a typical magnitude for this type of single bond.[15] The P1−P1′-bond length of 2.159(1) Å is considerably shortened in comparison with those of uncomplexed phosphanes or that of **9a**.[18] This observation can be rationalized by the ring-bracketing effect of the Fe−C-3′ bond. The intracyclic bonding parameters of the intact phosphirene ring of **10a** are in the typical ranges for a transition-metal complexed 1*H*-phosphirene.[12]

On the basis of $^{31}P\{^1H\}$ NMR monitoring of the photolysis reaction of **9a** a multi-step sequence can be assumed. By comparison of the resonance signals of the various intermediates with those of known compounds, the following mechanism can be proposed:

The initial step in the formation of **10** could be the insertion of one of the two $Fe(CO)_4$ fragments into a P−C bond of the coordinatively attached three-membered ring systems. This results in the intermediate **11**, in which a metallaphosphacyclobutene system is linked to a complexed phosphirene system (Scheme 6). The signal for the phosphorus atom in the three-membered ring of **11a** appears in the $^{31}P\{^1H\}$ NMR spectrum of the reaction solution as a doublet at $\delta = -99.5$ ($^1J_{P,P} = 322.4$ Hz). A further doublet with the same coupling constant is seen at $\delta = 56.0$. This chemical shift value is typical for a compound with a metallaphosphacyclobutene skeleton as revealed by a comparison with an analogous rhodium complex.[19] The subsequent cleavage of a carbonyl ligand from the $Fe(CO)_4$ fragment of the four-membered ring then initiates the conversion of the η^2-coordinated complex **11** with ring opening to the 16-valence electron carbene complex **12**. The P=C double bond of the phosphaalkene system in **12a** gives rise to a $^{31}P\{^1H\}$ NMR signal at $\delta = 282.1$. This value is in the typical range for a phosphaalkene. Since the 16-VE fragment in **12** is coordinatively unsaturated and thus possesses only a low stability, subsequent rearrangement occurs with cleavage of a CO ligand and formation of an Fe−C σ-bond and the Fe−Fe single bond.

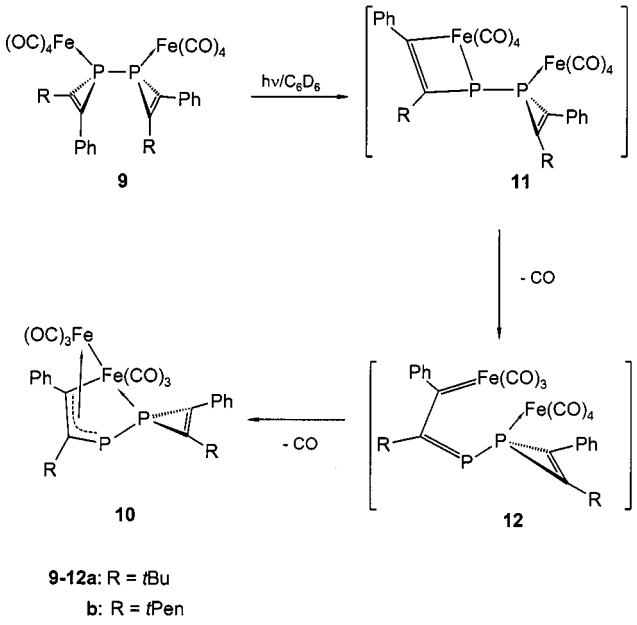

Scheme 6

Experimental Section

General Remarks: The reactions were carried out under an atmosphere of argon (purity > 99.998%) in a previously baked-out and evacuated apparatus (Schlenk techniques). The solvents were dried by standard procedures (*n*-pentane and diethyl ether: Na/K alloy), distilled and stored under argon. − Melting points: Mettler FP 61 (heating rate: 3 °C/min). − FT-IR spectra: Perkin−Elmer infrared-spectrometer 16PC. − Mass spectra: Finnigan MAT 90 spectrometer. − NMR spectra: Bruker AMX 400 (^{1}H: 400 MHz, ^{13}C: 101 MHz) and Bruker AC 200 (^{1}H: 200 MHz, ^{13}C: 50 MHz, ^{31}P: 81 MHz) spectrometers, solvent as internal standard (^{1}H and ^{13}C); the chemical shifts for ^{31}P are relative to external 85% orthophosphoric acid. − Compounds **5a** and **5b** were prepared by published methods.[13] Disodium tetracarbonylferrate was purchased from Aldrich and used without further purification.

Column chromatography was formed in water-cooled glass tubes with a positive pressure of argon on the column. Silica gel and neutral aluminum oxide were heated for 5 h under vacuum and then deactivated with 4% water.

Synthesis of the (1,1′-Bi-1*H*-phosphirene)iron Complexes 7a and 7b. − General Procedure: To a suspension of disodium tetracarbonylferrate in diethyl ether (30 mL) was added dropwise with stirring at −78 °C a solution of two equivalents of the corresponding 1-chloro-1*H*-phosphirene **5** in diethyl ether (20 mL). The reaction mixture was allowed to warm up to room temp. with stirring. The mixture was then evaporated under vacuum and the residue purified by column chromatography on silica gel with *n*-pentane/diethyl ether [40:1 (**7a**), 100:1 (**7b**)] as eluent. The yellow eluate was evaporated to dryness and the resulting red solid was recrystallized from *n*-pentane at −28 °C to yield pure **7** as orange-yellow crystals.

[3,3′-Bis(1,1-dimethylethyl)-2,2′-diphenyl-1,1′-bi-1*H*-phosphirene-κ*P*^{1}]tetracarbonyliron (7a): Starting materials: 791 mg (3.52 mmol)

1-chloro-3-(1,1-dimethylethyl)-2-phenyl-1*H*-phosphirene (**5a**), 609 mg (1.76 mmol) disodium tetracarbonylferrate. − Yield 560 mg (58%), orange-yellow crystals, mixture of two diastereomers (ratio 8:1). − m.p.: 97 − 99 °C. − IR (CCl_4, cm^{-1}): $\tilde{\nu}$ = 2966 (w), 2042 (s, CO), 1971 (m, CO), 1939 (vs, CO), 1474 (w), 1072 (m), 1008 (m), 620 (s). − $^{31}P\{^1H\}$ NMR ($CDCl_3$): *major diastereomer*: δ = −88.1 (d, $^1J_{P,P}$ = 427.3 Hz, P-1), −134.2 (d, $^1J_{P,P}$ = 427.3 Hz, P-1′); *minor diastereomer*: δ = −86.8 (d, $^1J_{P,P}$ = 427.1 Hz, P-1), −132.6 (d, $^1J_{P,P}$ = 427.1 Hz, P-1′). − ^1H NMR ($CDCl_3$): *major diastereomer*: δ = 1.44 [s, broad, 18 H, $C(CH_3)_3$]; *minor diastereomer*: δ = 1.50 [s, broad, 18 H, $C(CH_3)_3$]. − $^{13}C\{^1H\}$ NMR ($CDCl_3$): not all signals could be assigned because of overlapping effects: *major diastereomer:* δ = 29.2 [d, $^3J_{C,P}$ = 1.7 Hz, $C(CH_3)_3$], 29.5 [s, $C(CH_3)_3$], 33.9 [dd, $^2J_{C,P}$ = 6.4 Hz, $^3J_{C,P}$ = 3.0 Hz, $C(CH_3)_3$], 34.2 [d, $^2J_{C,P}$ = 6.8 Hz, $C(CH_3)_3$], 120.3 (d, $^1J_{C,P}$ = 50.8 Hz, C-2′), 124.8 (dd, $^1J_{C,P}$ = 22.0 Hz, $^2J_{C,P}$ = 4.2 Hz, C-2), 127.3 (d, $J_{C,P}$ = 7.6 Hz, Ph), 128.6 (s, Ph), 128.9 (s, Ph), 129.7 (d, $J_{C,P}$ = 5.1 Hz, Ph), 130.4 (d, $J_{C,P}$ = 4.2 Hz, Ph), 131.3 (s, Ph), 138.5 (d, $^1J_{C,P}$ = 57.7 Hz, C-3′), 140.5 (dd, $^1J_{C,P}$ = 27.1 Hz, $^2J_{C,P}$ = 5.1 Hz, C-3), 213.9 (d, $^2J_{C,P}$ = 19.5 Hz, CO); *minor diastereomer*: δ = 29.2 [s, $C(CH_3)_3$], 29.4 [d, $^3J_{C,P}$ = 2.5 Hz, $C(CH_3)_3$], 34.3 [d, $^2J_{C,P}$ = 5.9 Hz, $C(CH_3)_3$], 121.3 (dd, $^1J_{C,P}$ = 48.9 Hz, $^2J_{C,P}$ = 2.6 Hz, C-2′), 125.0 (dd, $^1J_{C,P}$ = 33.7 Hz, $^2J_{C,P}$ = 3.4 Hz, C-2), 127.2 (d, $J_{C,P}$ = 11.0 Hz, Ph), 128.6 (s, Ph), 129.7 (d, $J_{C,P}$ = 5.1 Hz, Ph), 130.3 (d, $J_{C,P}$ = 4.2 Hz, Ph), 131.2 (s, Ph), 135.6 (d, $^1J_{C,P}$ = 56.2 Hz, C-3′), 141.8 (dd, $^1J_{C,P}$ = 26.3 Hz, $^2J_{C,P}$ = 4.2 Hz, C-3), 214.2 (d, $^2J_{C,P}$ = 18.7 Hz, CO). − MS (EI, 70 eV): *m/z* (%) = 546 (8) [M^+], 434 (41) [M^+ − 4CO], 276 (100) [M^+ − 4CO − $C_{12}H_{14}$], 98 (43) [$C_2P_2Fe(CO)_2^+$], 189 (68) [$C_{12}H_{14}P^+$], 143 (26) [$C_{11}H_{11}^+$]. − $C_{28}H_{28}FeP_2O_4$ (546.32 g/mol): calcd. C 61.56, H 5.17; found C 60.90, H 5.07. − HR-MS (EI, 70 eV); [M^+]: calcd. 546.0813; found 546.0813.

[3,3′-Bis(1,1-dimethylpropyl)-2,2′-diphenyl-1*H*-phosphirene-κ*P*^{1}]-tetracarbonyliron (7b): Starting materials: 649 mg (2.72 mmol) 1-chloro-3-(1,1-dimethylpropyl)-2-phenyl-1*H*-phosphirene (**5b**), 471 mg (1.36 mmol) disodium tetracarbonylferrate. − Yield 470 mg (60%), orange-yellow solid, mixture of two diastereomers (ratio 4:1). − IR (KBr, cm^{-1}): $\tilde{\nu}$ = 2967 (s), 2934 (w), 2039 (vs, CO), 1963 (s, CO), 1938 (vs, CO), 1636 (m), 1464 (m), 1074 (s), 620 (s). − $^{31}P\{^1H\}$ NMR ($CDCl_3$): *major diastereomer*: δ = −90.6 (d, $^1J_{P,P}$ = 427.6 Hz, P-1), −132.2 (d, $^1J_{P,P}$ = 427.6 Hz, P-1′); *minor diastereomer*: δ = −88.3 (d, $^1J_{P,P}$ = 426.6 Hz, P-1), −132.3 (d, $^1J_{P,P}$ = 426.6 Hz, P-1′). − ^1H NMR ($CDCl_3$): *major diastereomer:* δ = 0.96 (t, 3 H, $^3J_{H,H}$ = 7.6 Hz, CH_2-CH_3), 1.12 (t, 3 H, $^3J_{H,H}$ = 7.0 Hz, CH_2-CH_3), 1.42, 1.43, 1.46, 1.47 [each s, 12 H, $C(CH_3)_2CH_2$], 1.63 − 1.92 (m, 4 H, CH_2-CH_3; *minor diastereomer:* the signals could not be assigned because of overlapping effects. − $^{13}C\{^1H\}$ NMR ($CDCl_3$): not all signals could be assigned because of overlapping effects: *major diastereomer:* δ = 8.7 (d, $^4J_{C,P}$ = 6.3 Hz, CH_2-CH_3), 9.1 (d, $^4J_{C,P}$ = 4.5 Hz, CH_2-CH_3), 25.7 [s, $C(CH_3)_2$], 26.2 [d, $^3J_{C,P}$ = 5.4 Hz, $C(CH_3)_2$], 26.5 [s, $C(CH_3)_2$], 26.9 [s, $C(CH_3)_2$], 34.4 (d, $^3J_{C,P}$ = 5.4 Hz, CH_2-CH_3), 34.4 (s, CH_2-CH_3), 37.0 [s, $C(CH_3)_2Et$], 37.7 [d, $^2J_{C,P}$ = 5.4 Hz, $C(CH_3)_2Et$], 120.9 (d, $^1J_{C,P}$ = 51.2 Hz, C-2′), 125.1 (d, $^1J_{C,P}$ = 22.4 Hz, C-2), 127.0 (d, $^3J_{C,P}$ = 8.3 Hz, *o*-Ph), 127.2 (d, $^3J_{C,P}$ = 7.2 Hz, *o*-Ph), 128.3 (s, Ph), 128.6 (s, Ph), 129.4 (d, $^2J_{C,P}$ = 16.2 Hz, *i*-Ph), 129.5 (d, $^2J_{C,P}$ = 14.4 Hz, *i*-Ph), 130.1 (s, Ph), 131.2 (s, Ph), 138.3 (d, $^1J_{C,P}$ = 57.5 Hz, C-3′), 141.4 (dd, $^1J_{C,P}$ = 28.3 Hz, $^2J_{C,P}$ = 4.0 Hz, C-3), 213.7 (d, $^2J_{C,P}$ = 18.0 Hz, CO); *minor diastereomer*: δ = 34.2 (s, CH_2-CH_3), 35.8 [s, $C(CH_3)_2Et$], 125.0 (d, $^1J_{C,P}$ = 21.5 Hz, C-2), 128.3 (s, Ph), 128.6 (s, Ph), 130.0 (s, Ph), 130.9 (s, Ph), 134.8 (d, $^1J_{C,P}$ = 59.2 Hz, C-3′), 139.9 (d, $^1J_{C,P}$ = 27.8 Hz, C-3), 214.1 (d, $^2J_{C,P}$ = 18.0 Hz, CO). − MS (EI, 70 eV): *m/z* (%) = 574 (1) [M^+], 462 (7) [M^+ − 4CO], 172 (28) [$C_{13}H_{16}^+$], 157 (14) [$C_{12}H_{13}^+$], 143 (100) [$C_{11}H_{11}^+$], 128 (23) [$C_{10}H_8^+$]. − HR-MS (EI, 70 eV); [M^+]: calcd. 574.1135; found 574.1130.

Synthesis of the (1,1′-Bi-1*H*-phosphirene)diiron Complexes 9a, b. − General Procedure: A mixture of the diastereomers of the corresponding mono complexed 1,1′-bi-1*H*-phosphirenes **7** was dissolved in *n*-pentane and treated with an excess of nonacarbonyldiiron. The suspension was stirred at room temp. for 24 h. The resulting dark red reaction solvents were evaporated to dryness. The brown residue was purified by column chromatography on neutral aluminum oxide with *n*-pentane as eluent. Recrystallization from *n*-pentane gave products **9a** and **9b** as yellow crystals.

[μ-[3,3′-Bis(1,1-dimethylethyl)-2,2′-diphenyl-1*H*-phosphirene-κ*P*^{1}:κ*P*$^{1'}$]]octacarbonyldiiron (9a): Starting materials: 404 mg (0.74 mmol) **7a**, 538 mg (1.48 mmol) nonacarbonyldiiron. − Yield 330 mg (63%), yellow crystals, mixture of two diastereomers (ratio 10:1). − m.p.: 135 °C (decomposition). − IR (KBr, cm^{-1}): $\tilde{\nu}$ = 2968 (m), 2930 (w), 2060 (s, CO), 2044 (s, CO), 1948 (vs, CO), 1938 (vs), 1098 (w), 1026 (w), 798 (w), 622 (m), 610 (m). − $^{31}P\{^1H\}$ NMR ($CDCl_3$): *major diastereomer*: δ = −69.3 (s); *minor diastereomer*: δ = −66.8 (s). − ^1H NMR ($CDCl_3$): *major diastereomer*: δ = 1.52 [s, 18 H, $C(CH_3)_3$]; *minor diastereomer*: δ = 1.49 [s, 18 H, $C(CH_3)_3$]. − $^{13}C\{^1H\}$ NMR ($CDCl_3$): not all signals could be assigned because of overlapping effects: *major diastereomer:* δ = 29.3 [pseudo-t, $|^3J_{C,P} + {}^4J_{C,P}|$ = 4.2 Hz, $C(CH_3)_3$], 34.8 [pseudo-t, $|^2J_{C,P} + {}^3J_{C,P}|$ = 3.4 Hz, $C(CH_3)_3$], 126.1 (pseudo-t, $|^3J_{C,P} + {}^4J_{C,P}|$ = 3.4 Hz, *o*-Ph), 128.5 (pseudo-t, $|^1J_{C,P} + {}^2J_{C,P}|$ = 15.2 Hz, C-2−C-2′), 128.9 (s, *m*-Ph), 130.4 (pseudo-t, $|^2J_{C,P} + {}^3J_{C,P}|$ = 5.9 Hz, *i*-Ph), 130.6 (d, $^5J_{C,P}$ = 1.7 Hz, *p*-Ph), 142.2 (pseudo-t, $|^1J_{C,P} + {}^2J_{C,P}|$ = 22.0 Hz, C-3−C-3′), 213.1 (pseudo-t, $|^2J_{C,P} + {}^3J_{C,P}|$ = 17.0 Hz, CO); *minor diastereomer*: δ = 29.7 [pseudo-t, $|^3J_{C,P} + {}^4J_{C,P}|$ = 5.0 Hz, $C(CH_3)_3$], 34.7 [pseudo-t, $|^2J_{C,P} + {}^3J_{C,P}|$ = 3.4 Hz, $C(CH_3)_3$], 126.0 (pseudo-t, $|^3J_{C,P} + {}^4J_{C,P}|$ = 3.4 Hz, *o*-Ph), 142.3 (pseudo-t, $|^1J_{C,P} + {}^2J_{C,P}|$ = 20.4 Hz, C-3−C-3′), 213.2 (pseudo-t, $|^2J_{C,P} + {}^3J_{C,P}|$ = 17.8 Hz, CO). − MS (EI, 70 eV): *m/z* (%) = 714 (0.02) [M^+], 490 (72) [M^+ − 8CO], 434 (14) [M^+ − Fe − 8CO], 332 (100) [M^+ − 8CO − $C_{12}H_{14}$], 287 (24) [M^+ − 8CO − $C_{12}H_{14}$ − $3CH_3$], 276 (49) [M^+ − Fe − 8CO − $C_{12}H_{14}$], 158 (36) [$C_{12}H_{14}^+$], 143 (96) [$C_{11}H_{11}^+$]. − $C_{32}H_{28}Fe_2P_2O_8$ (714.21 g/mol): calcd. C 53.82, H 3.95; found C 53.12, H 4.20.

μ-[3,3′-Bis(1,1-dimethylpropyl)-2,2′-diphenyl-1*H*-phosphirene-κ*P*^{1}:κ*P*$^{1'}$]octacarbonyldiiron (9b): Starting materials: 471 mg (0.82 mmol) **7b**, 597 mg (1.64 mmol) nonacarbonyldiiron. − Yield 330 mg (54%), mixture of two diastereomers (ratio 6:1). − IR (KBr, cm^{-1}): nu(tide) = 2970 (w), 2044 (s, CO), 1982 (m, CO), 1936 (vs, CO), 1468 (w), 1444 (w), 760 (m). − $^{31}P\{^1H\}$ NMR ($CDCl_3$): *major diastereomer*: δ = −70.5 (s); *minor diastereomer*: δ = −67.4 (s). − ^1H NMR ($CDCl_3$): *major diastereomer*: δ = 0.90 (t, $^3J_{H,H}$ = 7.2 Hz, 6 H, CH_2-CH_3), 1.42, 1.45 [each s, 12 H, $C(CH_3)_2CH_2$], 1.80 (q, $^3J_{H,H}$ = 7.2 Hz, 4 H, CH_2-CH_3); *minor diastereomer*: the signals could not be assigned because of overlapping effects and low intensity signals. − $^{13}C\{^1H\}$ NMR ($CDCl_3$): *major diastereomer:* δ = 8.8 (d, $^4J_{C,P}$ = 8.8 Hz, CH_2-CH_3), 26.0 [s, $C(CH_3)_2Et$], 26.2 [s, $C(CH_3)_2Et$], 34.2 (d, $^3J_{C,P}$ = 10.4 Hz, CH_2-CH_3), 38.3 [d, $^2J_{C,P}$ = 14.5 Hz, $C(CH_3)_2Et$], 126.3 (d, $^1J_{C,P}$ = 20.0 Hz, C-2−C-2′), 128.9 (s, *m*-Ph), 129.9 (pseudo-t, $|^2J_{C,P} + {}^3J_{C,P}|$ = 7.2 Hz, *i*-Ph), 130.4 (d, $^3J_{C,P}$ = 6.4 Hz, *o*-Ph), 130.5 (d, $^5J_{C,P}$ = 3.2 Hz, *p*-Ph), 141.6 (pseudo-t, $|^1J_{C,P} + {}^2J_{C,P}|$ = 12.0 Hz, C-3−C-3′), 213.7 (d, $^2J_{C,P}$ = 4.8 Hz, CO); *minor diastereomer*: the signals could not be assigned because of overlapping effects and low intensity signals. − MS (EI, 70 eV): *m/z* (%) = 742 (0.04) [M^+], 518 (24) [M^+ − 8CO], 346 (38) [M^+ − 8CO − $C_{13}H_{16}$], 290 (29) [M^+ − Fe − 8CO − $C_{13}H_{16}$],

143 (100) [$C_{11}H_{11}^+$], 128 (20) [$C_{10}H_8^+$]. − $C_{34}H_{32}Fe_2P_2O_8$ (742.26 g/mol): calcd. C 55.02, H 4.35; found C 53.95, H 4.10.

Photolysis of the (1,1′-Bi-1*H*-phosphirene)diiron Complexes 9a and 9b. − General Procedure: A solution of **9a** or **9b** in C_6D_6 (1 − 2 mL) was irradiated with a high-pressure mercury lamp ($\lambda \leq$ 280 nm) and the reaction was monitored by ^{31}P NMR spectroscopy (7 − 9 h). After evaporation of the solvent under vacuum the residue was purified by column chromatography on neutral aluminum oxide with *n*-pentane/diethyl ether (1:1) as eluent. Recrystallization from *n*-pentane/diethyl ether (1:1) gave **10a** and **10b** as red crystals.

Hexacarbonyl-μ-[η¹:η³-{1-[2′-(1,1-Dimethylethyl)-3′-phenyl-1′-phosphapropenyl-κ*P*¹′:κ*C*²′:κ*C*³′]-3-(1,1-dimethylethyl)-2-phenyl-1*H*-phosphirene-κ*P*¹}]diiron(*Fe*−*Fe*) (10a): Starting material: 471 mg (0.66 mmol) (**9a**). − Yield 20 mg (5%), red crystals. − $^{31}P\{^1H\}$ NMR ($CDCl_3$): δ = −1.6 (d, $^1J_{P,P}$ = 312.2 Hz, P-1′), −70.4 (d, $^1J_{P,P}$ = 312.2 Hz, P-1). − ^1H NMR ($CDCl_3$): δ = 1.16, 1.42 [each s, 18 H, $C(CH_3)_3$]. − $^{13}C\{^1H\}$ NMR ($CDCl_3$): δ = 29.7 [d, $^3J_{C,P}$ = 2.6 Hz, $C(CH_3)_3$], 34.1 [d, $^3J_{C,P}$ = 2.6 Hz, $C(CH_3)_3$], 34.5 [d, $^2J_{C,P}$ = 5.1 Hz, $C(CH_3)_3$], 41.0 [dd, $^2J_{C,P}$ = 16.1 Hz, $^3J_{C,P}$ = 1.7 Hz, $C(CH_3)_3$], 124.6 (d, $^1J_{C,P}$ = 16.9 Hz, C-2), 126.6 (s, Ph), 127.1 (d, $J_{C,P}$ = 6.8 Hz, Ph), 127.6 (s, Ph), 129.1 (s, Ph), 130.0 (s, Ph), 130.5 (s, Ph), 130.9 (d, $J_{C,P}$ = 5.1 Hz, Ph), 134.2 (s, Ph), 134.5 (s, Ph), 150.6 (d, $^1J_{C,P}$ = 41.5 Hz, C-3), 153.9 (d, $^2J_{C,P}$ = 2.5 Hz, C-3′), 191.2 (dd, $^1J_{C,P}$ = 11.0 Hz, $^2J_{C,P}$ = 5.1 Hz, C-2′), 205.4 [d, $^2J_{C,P}$ = 27.6 Hz, $Fe(CO)_3$], 209.2 [d, $^2J_{C,P}$ = 27.1 Hz, $Fe(CO)_3$], 211.4 [d, $^2J_{C,P}$ = 28.8 Hz, $Fe(CO)_3$], 212.4 [d, $^2J_{C,P}$ = 6.8 Hz, $Fe(CO)_3$]. − MS (EI, 70 eV): *m*/*z* (%) = 658 (0.06) [M^+], 490 (20) [M^+ − 6CO], 332 (34) [M^+ − 6CO − $C_{12}H_{14}$], 158 (80) [$C_{12}H_{14}^+$], 143 (100) [$C_{11}H_{11}^+$], 128 (31) [$C_{10}H_8^+$]. − $C_{30}H_{28}Fe_2P_2O_6$ (658.187 g/mol): calcd. C 54.75, H 4.29; found C 54.49, H 4.31.

Hexacarbonyl-μ-[η¹:η³-{1-[2′-(1,1-Dimethylpropyl)-3′-phenyl-1′-phosphapropenyl-κ*P*¹′:κ*C*²′:κ*C*³′]-3-(1,1-dimethylpropyl)-2-phenyl-1*H*-phosphirene-κ*P*¹}]diiron(*Fe*−*Fe*) (10b): Starting material: 401 mg (0.54 mmol) **9b**. − Yield 20 mg (6%), red crystals. − $^{31}P\{^1H\}$ NMR ($CDCl_3$): δ = 4.2 (d, $^1J_{P,P}$ = 315.2 Hz, P-1′), −69.5 (d, $^1J_{P,P}$ = 315.2 Hz, P-1). − ^1H NMR ($CDCl_3$): δ = 0.80 − 1.02 (m, 6 H, CH_2-CH_3), 1.17 [s, 3 H, $C(CH_3)_2CH_2$], 1.38 [s, 9 H, $C(CH_3)_2CH_2$], 1.74 (m, 4 H, CH_2-CH_3). − $^{13}C\{^1H\}$ NMR ($CDCl_3$): δ = 9.7 (s, CH_2-CH_3), 10.1 (s, CH_2-CH_3), 27.2 [d, $^3J_{C,P}$ = 2.5 Hz, $C(CH_3)_2Et$], 27.3 [d, $^3J_{C,P}$ = 2.5 Hz, $C(CH_3)_2Et$], 31.8 [s, $C(CH_3)_2Et$], 34.8 (d, $^3J_{C,P}$ = 1.7 Hz, CH_2-CH_3), 37.7 (d, $^3J_{C,P}$ = 0.9 Hz, CH_2-CH_3), 38.3 [d, $^2J_{C,P}$ = 4.2 Hz, $C(CH_3)_2Et$], 43.8 [d, $^2J_{C,P}$ = 14.4 Hz, $C(CH_3)_2Et$], 124.6 (d, $^1J_{C,P}$ = 18.7 Hz, C-2), 126.1 (s, Ph), 126.7 (s, Ph), 128.2 (s, Ph), 128.4 (s, Ph), 128.7 (s, Ph), 129.0 (s, Ph), 129.1 (s, Ph), 129.4 (s, Ph), 130.1 (d, $J_{C,P}$ = 21.2 Hz, Ph), 130.7 (d, $J_{C,P}$ = 4.2 Hz, Ph), 150.4 (d, $^1J_{C,P}$ = 44.1 Hz, C-3), 153.8 (d, $^2J_{C,P}$ = 0.9 Hz, C-3′), 192.9 (dd, $^1J_{C,P}$ = 17.0 Hz, $^2J_{C,P}$ = 7.6 Hz, C-2′), 205.0 [d, $^2J_{C,P}$ = 30.6 Hz, $Fe(CO)_3$], 205.6 [d, $^2J_{C,P}$ = 27.1 Hz, $Fe(CO)_3$], 209.3 [d, $^2J_{C,P}$ = 25.4 Hz, $Fe(CO)_3$], 212.5 [d, $^2J_{C,P}$ = 5.1 Hz, $Fe(CO)_3$]. − MS (EI, 70 eV): *m*/*z* (%) = 686 (0.4) [M^+], 346 (18) [M^+ − 6 CO − $C_{13}H_{16}$], 172 (25) [$C_{13}H_{16}^+$], 143 (100) [$C_{11}H_{11}^+$], 128 (23) [$C_{10}H_8^+$].

Crystallographic Data for 10a: Crystallization of **10a** from different solvents and inspection of the crystals by preliminary X-ray crystallographic studies, showed that all investigated specimens were twinned. The twinning element was in all cases a twofold axis along [100]. According to the metrical peculiarity of the monoclinic lattice constants [*a* = 14.045(1), *b* = 11.127(1), *c* = 20.109(2) Å, β = 99.077(10)°, *V* = 3103.3(5) Å³, *Z* = 4] all reflections *hkl* with *h* = 0, 9, 11, −9, −11 overlap nearly exactly, while the reflections of all other layers, depending on the resolution of the diffractometer setting, are more or less separated (twinning by reticular meohedry). The twin matrix evaluated from the orientation matrices of both twin components was calculated to (1 0 0, 0 −1 0, −0.4526 0 −1). Data collection on an IPDS-diffractometer has been performed using a light yellow crystal with the dimensions 0.30 × 0.25 × 0.20 mm³.

The standard integration and data reduction methods[20] results in data sets, that only contain non-overlapped reflections. Structure solution by direct methods and completion of the structure model by difference Fourier synthesis using only these non-overlapping reflections succeeded in the space group $P2_1/n$. For a twin refinement in SHELXL-97[21] by the method of Pratt, Coyle, and Ibers[22] for the overlapped reflections the sum of F_c^2 values of the individual twin components, each multiplied by its fraction contribution, was fitted to the F_o^2 value and its fraction contribution. Hence, the diffractometer output has to be reformatted according to the abovementioned twin law, and all reflections that neither overlap exactly nor can be resolved properly have been discarded. A simultaneous refinement of both twin components converged to a twin ratio of 0.3957/0.6043(5). All hydrogen atoms were included in the last stages of refinement in geometrically calculated positions, and their U_{iso} values were set to 1.2 and 1.5 times the U_{eq} value of the corresponding aromatic and methyl carbon atoms, respectively. Refinement of 410 parameters based on 9292 reflections converged to $wR2(F^2)$ = 0.0781, R1(*F*) = 0.0353 [for 6237 reflections with $F_o^2 > 2\sigma(F_o^2)$], GoF = 1.029, $\Delta\rho_{min}/\Delta\rho_{max}$ = −0.198/0.231 e/Å³, $(\Delta/\sigma)_{max}$ = 0.045.

Crystallographic data (excluding structure factors) for the structure included in this paper have been deposited with the Cambridge Crystallographic Data Centre as supplementary publication no. CCDC-157268. Copies of the data can be obtained free of charge on application to CCDC, 12 Union Road, Cambridge CB2 1EZ, UK [Fax: (internat.) +44−1223/336-033; E-mail: deposit@ccdc.cam.ac.uk].

Acknowledgments

We thank the Landesregierung of Rheinland-Pfalz for a graduate grant (to J. S.) and the Fonds der Chemischen Industrie for generous financial support.

[1] C. Peters, S. Stutzmann, H. Disteldorf, S. Werner, U. Bergsträßer, C. Krüger, P. Binger, M. Regitz, *Synthesis* **2000**, 529.
[2] M. Regitz, in: *Multiple Bonds and Low Coordination in Phosphorus Chemistry*, (Eds. M. Regitz, O. J. Scherer), Thieme, Stuttgart, **1990**, p. 77−83.
[3] G. Märkl, in: *Multiple Bonds and Low Coordination in Phosphorus Chemistry*, (Eds. M. Regitz, O. J. Scherer), Thieme, Stuttgart, **1990**, p. 220−249.
[4] J. Fink, W. Rösch, U.-J. Vogelbacher, M. Regitz, *Angew. Chem.* **1986**, *98*, 265−266; *Angew. Chem. Int. Ed. Engl.* **1986**, *25*, 280−282.
[5] K. Blatter, W. Rösch, U.-J. Vogelbacher, J. Fink, M. Regitz, *Angew. Chem.* **1987**, *99*, 67−68; *Angew. Chem. Int. Ed. Engl.* **1987**, *26*, 85−86.
[6] [6a] D. Böhm, F. Knoch, S. Kummer, U. Schmidt, U. Zenneck, *Angew. Chem.* **1995**, *107*, 251−254; *Angew. Chem. Int. Ed. Engl.* **1995**, *34*, 198−201. − [6b] N. Avarvari, L. Ricard, F. Mathey, P. Le Floch, O. Löber, M. Regitz, *Eur. J. Org. Chem.* **1998**, 2039−2045. − [6c] M. Hofmann, H. Heydt, M. Regitz, *Synthesis* **2001**, 463−467.
[7] [7a] G. Märkl, in: *Multiple Bonds and Low Coordination in Phosphorus Chemistry*, (Eds. M. Regitz, O. J. Scherer), Thieme, Stuttgart, **1990**, p. 252−253. − [7b] Y. Kobayashi, I. Kumadaki,

A. Ohsawa, H. Hamana, *Tetrahedron Lett.* **1976**, 3715−3716. [7c] Y. Kobayashi, H. Hamana, S. Fujino, A. Ohsawa, I. Kumadaki, *J. Am. Chem. Soc.* **1980**, *102*, 252−255.

[8] [8a] A. Mack, F. Tabellion, C. Peters, A. Nachbauer, U. Bergsträßer, F. Preuss, M. Regitz, *Phosphorus, Sulfur and Silicon* **1999**, *144*/*146*, 261−264. [8b] A. Mack, M. Regitz, in: *Advances in Strained and Interesting Organic Molecules* (Ed.: B. Halton), Suppl. 1, JAI Press Inc., Cambridge, Conn., **1999**, p. 199−221.

[9] Short communication: J. Simon, U. Bergsträßer, M. Regitz, *Chem. Commun.* **1998**, 867−868.

[10] Y. Kabe, K. Ohkubo, H. Ishikawa, W. Ando, *J. Am. Chem. Soc.* **2000**, *122*, 3775−3776.

[11] A. Marinetti, F. Mathey, J. Fischler, A. Mitschler, *J. Chem. Soc., Chem. Commun.* **1984**, 45−46.

[12] [12a] H. Heydt, in: *Science of Synthesis, Vol. 9* (Eds. G. Maas, M. Regitz), Thieme, Stuttgart, **2000**, p. 85−124. − [12b] F. Mathey, M. Regitz, in: *Comprehensive Heterocyclic Chemistry II, Vol. 1A* (Eds. A. R. Katritzky, C. W. Rees), Pergamon, Oxford, **1996**, p. 227−304. − [12c]F. Mathey, *Chem. Rev.* **1990**, *90*, 997−1025.

[13] [13a] O. Wagner, M. Ehle, M. Regitz, *Angew. Chem.* **1989**, *101*, 227−229; *Angew. Chem. Int. Ed. Engl.* **1989**, *28*, 225−226. − [13b] O. Wagner, M. Ehle, M. Birkel, J. Hoffmann, M. Regitz, *Chem. Ber.* **1991**, *124*, 1207−1213. − [13c] H. Heydt, M. Ehle, S. Haber, J. Hoffmann, O. Wagner, A. Göller, T. Clark, M. Regitz, *Chem. Ber.*/*Recueil* **1997**, *130*, 711−723.

[14] A. Marinetti, F. Mathey, *J. Am. Chem. Soc.* **1985**, *107*, 4700−4706.

[15] [15a] K. Knoll, O. Orama, G. Huttner, *Angew. Chem.* **1984**, *96*, 989; *Angew. Chem. Int. Ed. Engl.* **1984**, *23*, 976. −[15b] K. Knoll, G. Huttner, T. Fässler, L. Zsolnai, *J. Organomet. Chem.* **1987**, *327*, 255−267.

[16] [16a] C. E. Sumner, Jr., J. A. Collier, R. Petitt, *Organometallics* **1982**, *1*, 1350−1360. − [16b] T. E. Snead, C. A. Mirkin, K.-L. Lu, H. L. Beckman, G. L. Geoffroy, *Organometallics* **1992**, *11*, 942−954.

[17] [17a] F. W. B. Einstein, R. D. G. Jones, *J. Chem. Soc., Dalton Trans.* **1972**, 442−446. − [17b] R. E. Riley, R. E. Davis, *Inorg. Chem.* **1980**, *19*, 159−165. − [17c] R. L. Keiter, A. L. Rheingold, J. J. Hamerski, C. K. Castle, *Organometallics* **1983**, *2*, 1635−1639.

[18] D. G. Gilheany, in: *The Chemistry of Organophosphorus Compounds, Vol. 1* (Eds. S. Patai, F. R. Hartley), Wiley, Chichester, **1990**, p. 9−50.

[19] F. A. Ajulu, D. Carmichael, P. B. Hitchcock, F. Mathey, M. F. Meidine, J. F. Nixon, L. Ricard, M. L. Riley, *J. Chem. Soc., Chem. Commun.* **1992**, 750−752.

[20] Stoe & Cie., *IPDS-Software*, Vers. 2.87, Stoe & Cie. GmbH, Darmstadt, **1998**.

[21] G. M. Sheldrick, *SHELXL-97*, Program for the refinement of crystal structure, Universität Göttingen, **1997**.

[22] [22a] C. N. Pratt, B. A. Coyle, J. A. Ibers, *J. Chem. Soc. (A)* **1971**, 2146−2151. [22b] G. B. Jameson, *Acta Crystallogr., Sect. A* **1982**, *38*, 817−820.

Received December 18, 2000
[I00476]

Pyrazolylcyclohexanol Complexes of Vanadium − A Temperature- and Solvent-Dependent Monomer−Dimer Equilibrium

Holger Glas,[a] Klaus Köhler,[a] Eberhardt Herdtweck,[a] Peter Maas,[a] Michael Spiegler,[a] and Werner R. Thiel*[b]

Keywords: Catalysis / Oxidation / Chelates / Vanadium

The reaction of $VOCl_3$ with tridentate *rac-trans*-[1-pyrazolyl-3-(2-pyridyl)]cyclohexanol in the presence of K_2CO_3 generates a mononuclear six-coordinate V^V complex. With the bidentate ligand *rac-trans*-2-(pyrazol-1-yl)cyclohexan-1-ol, reduction of V^V to V^{IV} takes place to give a dinuclear complex with bridging alkoxo units; this compound is also accessible starting directly from the V^{IV} precursor $VOSO_4$ and LiCl. Both complexes were characterized spectroscopically and by X-ray diffraction. The dimeric V^{IV} complex is in equilibrium with its monomeric counterpart; this temperature- and solvent-dependent equilibrium was followed by EPR spectroscopy.

Introduction

Vanadium compounds are widely used in catalytic oxidation reactions.[1−3] However, the molecular structures of the actual catalytically active species are often unknown.[4] In a project on vanadium-catalyzed olefin epoxidation, our group has investigated structurally well-defined vanadium(V) complexes bearing bidentate pyrazolylpyridine ligands equipped with alkyl and ester side chains.[5] Owing to this feature, these ligands increase the solubility of the derived metal complexes in nonpolar organic solvents and therefore should allow detailed mechanistic investigations on the oxygen-transfer processes. They are active catalysts for the epoxidation of olefins as well as for the oxidation of aromatic alcohols, giving the corresponding aldehydes in high yield. However, when unfunctionalized olefins are used instead of allylic alcohols, complete conversion of the substrate has never been reached owing to catalyst deactivation, which might be due to ligand dissociation. In the present paper, the synthesis of a V^V complex bearing a tridentate pyrazolylpyridine cyclohexanolato ligand is described. Additionally, the reaction of bidentate pyrazolylcyclohexanol with $VOCl_3$ in the presence of a base was investigated, leading to a new dinuclear V^{IV} complex, which is also accessible by reacting $VOSO_4{\cdot}(H_2O)_3$ with pyrazolylcyclohexanol and LiCl in CH_3CN.

Results and Discussion

Our group has been interested in 1,3-amino alcohols bearing aromatic pyrazolyl N-donor fragments, where both donor sites are attached to a rigid cycloalkane backbone, for some time.[6−9] Such ligands can be obtained by nucleophilic attack of a pyrazole derivative on an epoxycycloalkane, giving the corresponding 1,2-*trans* configured cycloalkanols. Following this procedure, the ligands **1a,b** have been synthesized (Scheme 1, only one of the two stereoisomers is presented, as is the case in the following schemes).[8]

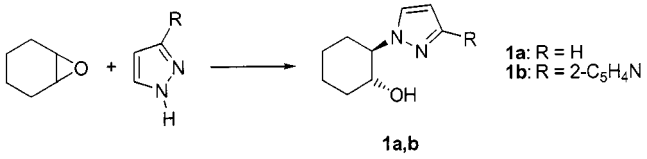

Scheme 1

The V^V oxoalkoxo complex **2** is accessible by reacting racemic *trans*-[1-pyrazolyl-3-(2-pyridyl)]cyclohexanol (**1b**) with $VOCl_3$ in the presence of K_2CO_3 (Scheme 2, only one of the two stereoisomers is shown). Owing to the tridentate ligand, the position of the oxo ligand is fixed *trans* to pyrazole, which is confirmed by a single ^{51}V NMR resonance and one set of resonances in the ^1H NMR spectrum. This is in contrast to the behavior of oxoalkoxo V^V complexes of bidentate pyrazolylpyridines,[5] which exist as mixtures of two isomers differing in the orientation of the oxo and alkoxo ligands relative to the *N*,*N*′-donor.

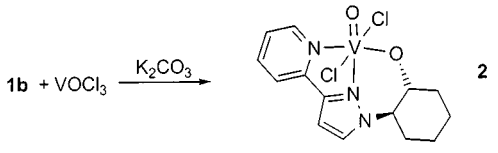

Scheme 2

As expected, the tridentate ligand enhances the stability of the V^V complex relative to the V^V complexes of bidentate pyrazolylpyridines. Unfunctionalized olefins like cyclooctene are thus efficiently converted into the corresponding epoxides (yield: 80−95%; reaction conditions: **2**/olefin/

[a] Anorganisch-chemisches Institut, Technische Universität München,
Lichtenbergstraße 4, 85747 Garching, Germany
[b] Institut für Chemie, Technische Universität Chemnitz,
Straße der Nationen 62, 09111 Chemnitz, Germany
E-mail: werner.thiel@chemie.tu-chemnitz.de

 © WILEY-VCH Verlag GmbH, 69451 Weinheim, 2001 1434−1948/01/0808−2075 $ 17.50+.50/0

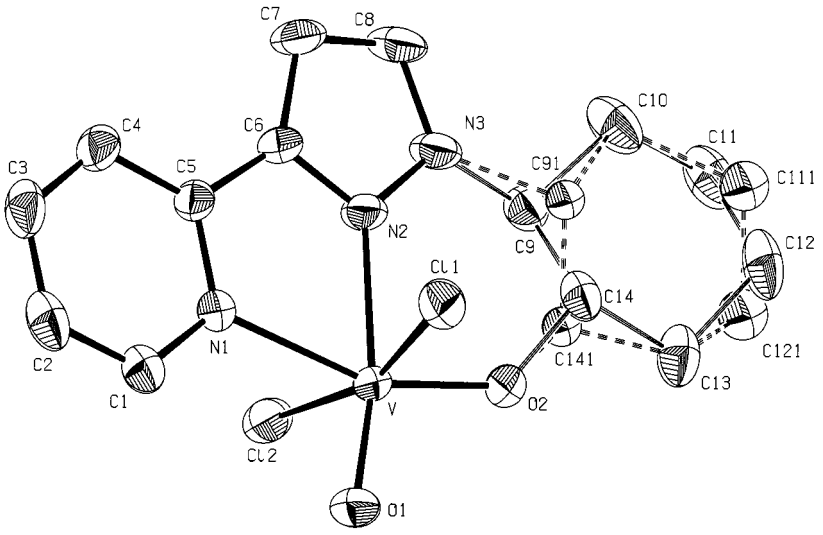

Figure 1. ORTEP[10] drawing of the molecular structure of **2** in the solid state; thermal ellipsoids are at the 50% probability level and hydrogen atoms are omitted for clarity

*t*BuOOH = 0.01:1:1, 24 h at 55 °C, solvent: $CHCl_3$). However, the vanadium complex bearing an enantiomerically pure (1*S*,2*S*)-*trans*-[1-pyrazolyl-3-(2-pyridyl)]cyclohexanol ligand[8] does not induce any enantioselectivity in the epoxidation of prochiral olefins such as 1,2-dihydronaphthalene or allylic and homoallylic alcohols.

Compound **2** crystallizes from acetone in the centrosymmetric monoclinic space group $P2_1/n$ with 0.5 equiv. of the solvent. Figure 1 shows the molecular structure of **2** in the solid state, and a selection of characteristic bond lengths and angles is given in Table 1.

Table 1. Selected bond distances (Å) and angles (°) for **2**

Bond Distances			
V−Cl1	2.3234(8)	V−O2	1.762(2)
V−Cl2	2.3412(7)	V−N1	2.167(2)
V−O1	1.597(2)	V−N2	2.145(2)
Bond Angles			
Cl1−V−Cl2	163.96(3)	O1−V−O2	105.31(8)
Cl1−V−O1	95.87(7)	O1−V−N1	97.49(8)
Cl1−V−O2	93.40(6)	O1−V−N2	169.51(8)
Cl1−V−N1	81.73(5)	O2−V−N1	157.07(7)
Cl1−V−N2	84.82(6)	O2−V−N2	85.08(8)
Cl2−V−O1	94.02(7)	N1−V−N2	72.21(7)
Cl2−V−O2	96.13(6)	V−O2−C14	132.6(2)
Cl2−V−N1	84.49(5)	O2−C14−C9	115.0(3)
Cl2−V−N2	83.18(6)		

The three ring systems (pyridine, pyrazole, cyclohexane) of the N,N,O ligand and the V=O unit are found in an almost coplanar orientation, while the chloro ligands complete the distorted octahedral coordination geometry at vanadium. Despite the crystallographic disordering in the individual crystal that was used for the structure determination, a satisfactory solution of the structure could be performed. While the V=O [1.597(2) Å] and V−O distances [1.762(2) Å] in **2** are only a few pm longer than the distances found in the isostructural oxoalkoxo vanadium(V) complexes bearing bidentate pyrazolylpyridine ligands [V=O = 1.575(3) and 1.579(2) Å; V−O = 1.740(2) and 1.735(2) Å],[5] the V−N distances in **2** are drastically shortened due to the tridentate ligand system. Usually, the M−N bonds (N = *N*-donor ligand) in the *trans* position to strong σ-donor ligands (e.g. oxo) are found to be about 10−15 pm longer than those in the *trans* position to alkoxo ligands. This is no longer true for **2**: here V−N2 [2.145(2) Å] is slightly shorter than V−N1 [2.167(2) Å], which means that the V−N bond *trans* to the oxo ligand is about 17 pm shorter when a tridentate ligand is coordinated instead of a bidentate ligand [V−N2 = 2.310(3) and 2.338(2) Å] with analogous donor properties.

Since there was no chiral induction in the epoxidation of prochiral olefins with (1*S*,2*S*)-**2**, the reaction of the bidentate ligand *trans*-2-pyrazol-1-ylcyclohexanol (**1a**) with $VOCl_3$ was investigated in order to open up an additional coordination site at the vanadium center for interaction with the substrates. Performing this reaction as for the synthesis described for **2** gives a deep orange-brown solution. However, the primary product is not stable even at −20 °C and decomposes in solution and in the solid state, leading to a black and oily precipitate, which was not investigated further, and a small amount of deep blue crystals. X-ray analysis of these crystals proved that reduction of V^V had taken place, and a dinuclear V^{IV} complex **3**, bearing one chelate, one oxo and one chloro ligand per vanadium center was formed. With this information in mind, a high yield synthesis of **3** starting from *trans*-2-pyrazol-1-ylcyclohexanol (**1a**), $VOSO_4 \cdot (H_2O)_3$ and LiCl was established (Scheme 3). Among a series of solvents (THF, CH_2Cl_2, $CHCl_3$, MeOH) which were examined for this reaction, acetonitrile proved to be the best.

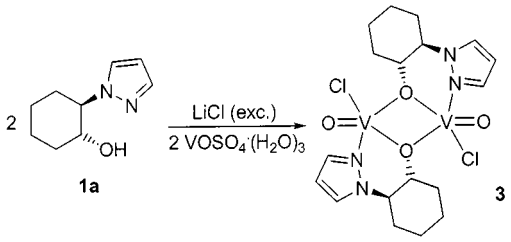

Scheme 3

Catalytic tests with compound **3** showed that the blue color of the complex vanishes after the addition of *t*BuOOH to give an orange-colored solution, indicating the oxidation of V^{IV} to V^{V}. However, it has not been possible up to now to characterize the V^{V} compound(s) formed here due to rapid decomposition. The catalytic activity of these solutions is about 20% of the activity of compound **2**.

Compound **3** crystallizes from $CHCl_3/Et_2O$ in the centrosymmetric monoclinic space group $P2_1/n$. Figure 2 shows the molecular structure of **3** in the solid state, and a selection of characteristic bond lengths and angles is given in Table 2.

In the solid state structure of **3**, the two V^{IV} centers V1 and V2, which are not equivalent in terms of crystal symmetry, are bridged by the alcoholato moieties of the chelate ligands leading to the formation of a planar V_2O_2 ring with V−O distances of about 2.0 Å. The distance V1···V2 is 3.125(1) Å, which excludes a V−V single bond. The oxo ligands O1 and O3 are found in a *cis* orientation, which has been observed in only a few V^{IV} complexes before.[11−15] Two homochiral chelate ligands are coordinated at the vanadium centers, which leads to a dimeric structure with nearly C_2 symmetry. The square-pyramidal coordination of the V^{IV} centers is completed by the chloro ligands. Complex **3** can be best compared with $[VO(THFfo)Cl]_2$ (THFfo = tetrahydrofurfuryl alcoholate), obtained from $VOCl_2$ and Na(THFfo), wherein the alcoholato moieties are also bridging the two V^{IV} centers.[13] Owing to the five-membered chelate rings formed by the THFfo ligands, the V−O distances in the V_2O_2 ring are shortened, which causes the V−V distance in $[VO(THFfo)Cl]_2$ [3.070(1) Å] to shrink slightly, compared to **3**.

Table 2. Selected bond distances (Å) and angles (°) for **3**

Bond Distances			
V1−V2	3.1250(5)		
V1−Cl1	2.3091(6)	V2−Cl2	2.3117(6)
V1−O1	1.581(2)	V2−O3	1.579(1)
V1−O2	1.968(1)	V2−O2	1.980(1)
V1−O4	1.984(1)	V2−O4	1.965(1)
V1−N2	2.087(2)	V2−N4	2.079(2)
O2−C9	1.437(2)	O4−C18	1.439(2)
Bond Angles			
Cl1−V1−O1	106.86(6)	Cl2−V2−O3	107.81(6)
Cl1−V1−O2	144.71(5)	Cl2−V2−O4	144.94(4)
Cl1−V1−O4	90.87(4)	Cl2−V2−O2	90.09(4)
Cl1−V1−N2	89.04(5)	Cl2−V2−N4	87.68(5)
O1−V1−O2	108.37(7)	O3−V2−O4	107.12(7)
O1−V1−O4	110.09(7)	O2−V2−O3	109.94(7)
O1−V1−N2	103.13(7)	O3−V2−N4	106.16(7)
O2−V1−O4	75.14(5)	O2−V2−O4	75.30(5)
O2−V1−N2	85.16(6)	O4−V2−N4	85.52(6)
O4−V1−N2	145.25(6)	O2−V2−N4	142.69(6)
V1−O2−V2	104.69(6)	V1−O4−V2	104.62(6)
V1−O2−C9	129.01(11)	V2−O2−C9	126.07(11)
V1−O4−C18	127.88(11)	V2−O4−C18	127.17(11)
Torsion Angles			
N1−C4−C9−O2	58.4(2)	N3−C13−C18−O4	57.2(2)

Compound **3** shows an interesting dynamic behavior in solution. When a deep-blue solution of **3** in $CHCl_3$ is treated with MeOH or EtOH, the color turns to green within a few hours at room temp. Decreasing the temperature of the mixture to 0 °C brings back the original blue color. This procedure can be repeated several times, which

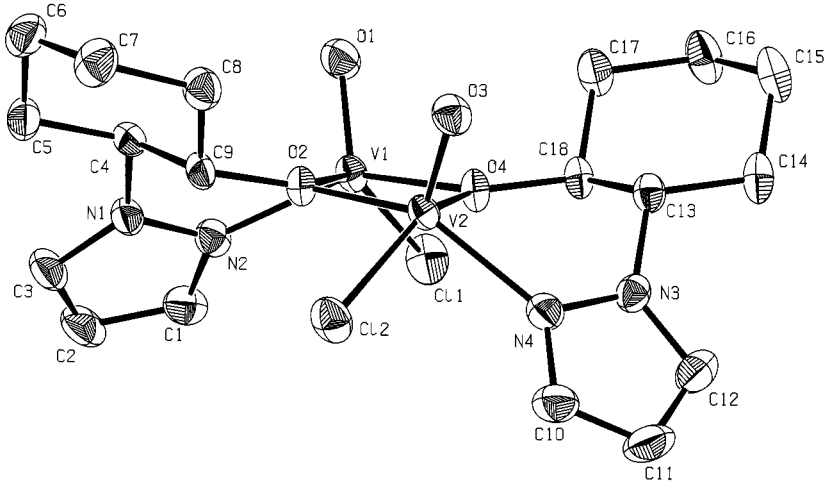

Figure 2. ORTEP[10] drawing of the molecular structure of **3** in the solid state; thermal ellipsoids are at the 50% probability level and hydrogen atoms are omitted for clarity

indicates a reversible reaction, for example a monomer ⇄ dimer equilibrium. When pyridine or THF are added to a solution of **3** in $CHCl_3$, an intense green color is observed, which persists even at low temperatures. However, when the solvents are removed in vacuum, blue microcrystalline **3** is recovered. For a deeper insight into these processes, EPR experiments were carried out.

The monomer ⇄ dimer equilibrium is illustrated in Figure 3 by the EPR spectra of complex **3** in $CHCl_3$ solution with and without addition of pyridine as donor.

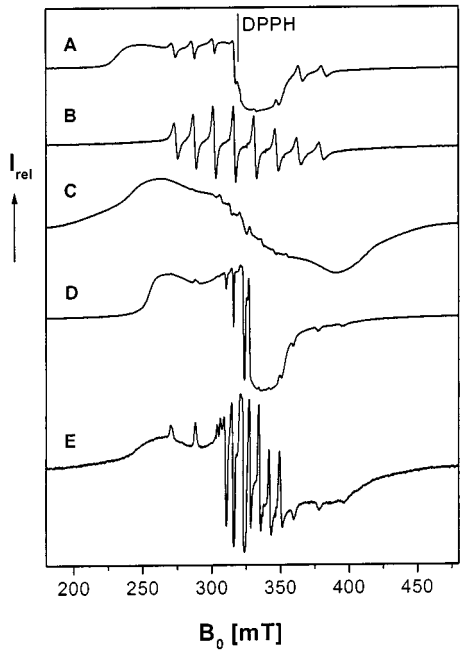

Figure 3. Liquid (A, B; T = 293 K) and frozen (C-E; T = 130 K) solution EPR spectra of the vanadium complex **3** in $CHCl_3$ ($5\cdot10^{-3}$ M) before (A and C) and after addition of pyridine (B and E: excess pyridine, D: few drops of pyridine)

The broad sigmoid EPR resonance line at $g \approx 1.97$ (line width $\Delta B_{pp} \approx 130$ mT; Figure 3 A, C−E) results from a weak magnetic interaction of the two unpaired spins in the dimeric vanadium complex (no resonance was observed at ''half-field'', i.e. no $\Delta M_S = 2$ transition). Similar EPR spectra (partially with better resolution) have been reported in the literature for dinuclear vanadium(IV) complexes.[13,16,17] The vanadium centers of **3** are weakly coupled both at room temperature in solution (Figure 3 A) and in a frozen glass (T = 30 K, Figure 3 C, D). In all cases at least a residual amount of a monomeric vanadium(IV) species is present depending on the temperature. This is reflected by the superposition of a well-resolved line octet which results from the hyperfine interaction of the unpaired electron with the nuclear spin of ^{51}V ($I = 7/2$).

The addition of pyridine at room temperature changed the color of the solution to green. An excess of pyridine provides an EPR spectrum of the monomer only at room temperature [Figure 3 B; $g_0 = 1.974$ (±0.001); $a_0 = 15.1$ (±0.03) mT]. Figure 3 C−E illustrate the effect of the stepwise addition of pyridine. Figure 3 E shows a well-resolved frozen solution EPR spectrum of the monomer superimposed on the residual dimeric species. The parameters of the former are typical for a single $S = 1/2$ VO^{2+} complex with a square-pyramidal coordination sphere of mixed donor atoms (N, O, Cl)[13] $g_{\|} = 1.952$; $g_{\perp} = 1.983$ (±0.001); $A_{\|}(^{51}V) = 18$ mT; $A_{\perp}(^{51}V) = 6.45$ mT (±0.05 mT); $B_{pp} = 1.5(_{\perp}) - 2.0(_{\|})$ mT. According to the EPR results, a monomer ⇄ dimer equilibrium can be postulated, which is influenced by the addition of donor molecules (D) (as shown in Scheme 4) and also by the variation of the temperature.

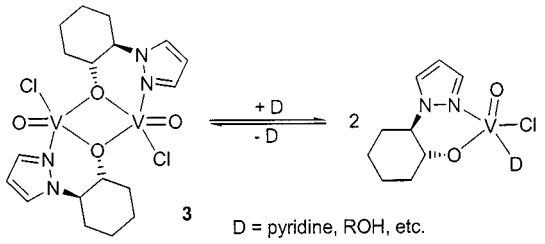

Scheme 4

Conclusion

It could be shown that using a monoanionic tridentate ligand instead of a neutral bidentate ligand enhances the catalytic performance of the V^V catalyst in the olefin epoxidation and in the oxidation of benzylic alcohol due to a reduced tendency for catalyst decomposition. However, this strategy prevents enantioselective epoxidation. Cleaving one of the neutral N-donor sites destabilizes the V^V complex and leads to a formally five-coordinate V^{IV} system, which undergoes dimerization through the alcoholato ligands. This dimerization is a reversible process as shown by EPR spectroscopy.

Experimental Section

All syntheses were performed under an atmosphere of nitrogen; solvents were dried, distilled and degassed before use. The ^1H NMR spectrum of **2** is assigned according to Scheme 5.[18]

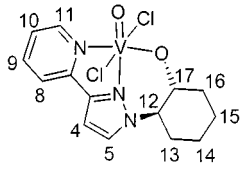

Scheme 5

Dichlorooxo{*rac-trans*-[1-pyrazolyl-3-(2-pyridyl)]cyclohexyloxy}-vanadium(V) (2): K_2CO_3 (0.50 g, 3.62 mmol) was dried for 10 min. at 300 °C in a 100 mL flask under vacuum. After cooling to room temperature, a solution of *rac-trans*-[1-pyrazolyl-3-(2-pyridyl)]cyclohexanol[8] (**1b**; 0.30 g, 1.24 mmol) in CH_2Cl_2 (40 mL) was added and the mixture was cooled to 0 °C. A solution of $VOCl_3$ (0.12 mL, 1.24 mmol) in CH_2Cl_2 (10 mL) was added dropwise and the mixture was stirred for 1 h at 0 °C and for 2 h at room temp. The

precipitate was removed by filtration, the solvent was removed in vacuum and the orange-red colored residue was dissolved in acetone (20 mL). After 7 days at −18 °C, **2** (0.16 g, 33%) was obtained as dark red crystals, containing 0.5 equiv. of acetone. Concentration of the mother liquor gave rise to further crystallization (0.113 g, 24%). − $(C_{14}H_{16}Cl_2N_3O_2V)_2{\cdot}C_3H_6O$ (818.35): calcd. C 45.50, H 4.68, N 10.27; found C 45.20, H 4.78, N 10.13. − IR (KBr): $\tilde{\nu}$ = 1018 vs ($\nu_{V=O}$) cm^{-1}. − ^1H NMR (400 MHz, 25 °C, $CDCl_3$): δ = 9.51 (d, $^3J_{10,11}$ = 5.5 Hz, 1 H, 11-H), 8.01 (t, $^3J_{9,10}$ = 6.5 Hz, 1 H, 9-H), 7.80 (d, $^3J_{8,9}$ = 7.5 Hz, 1 H, 8-H), 7.73 (d, $^3J_{4,5}$ = 2.5 Hz, 1 H, 5-H), 7.52 (dd, 1 H, 10-H), 6.83 (d, 1 H, 4-H), 4.34 (ddd, $^3J_{12,17}$ = 13.0 Hz, $^3J_{16,17}$ = 4.5 Hz, $^3J_{16',17}$ = 9.0 Hz, 1 H, 17-H), 2.69 (m, 1 H, 12-H), 2.27 (m, 2 H, CH_2), 1.97−1.24 (m, 6 H, CH_2). − ^{51}V NMR (105.2 MHz, 25 °C, $CDCl_3$): δ = −394.9.

Bis[chlorooxo(*rac-trans*-2-pyrazol-1-ylcyclohexyloxy)vanadium(IV)] (3): $VOSO_4{\cdot}(H_2O)_3$ (0.22 g, 1.00 mmol), *rac-trans*-2-(pyrazol-1-yl)-cyclohexan-1-ol[9] (**1a**; 0.17 g, 1.00 mmol) and LiCl (0.06 g, 1.50 mmol) were dissolved in acetonitrile (40 mL) and heated to 60 °C for 4 h. The resulting blue mixture was filtered and the solvent was removed in vacuum. The blue residue was dissolved in $CHCl_3$ (10 mL) and diethyl ether was condensed slowly into the solution. After a few days, deep blue crystals of **3** (0.36 g, 67%) were obtained. − $C_{18}H_{26}Cl_2N_4O_4V_2$ (535.21): calcd. C 40.39, H 4.90; N 10.47; found C 40.18, H 4.88, N 10.40. − IR (KBr): $\tilde{\nu}$ = 1014 s, 1003 vs ($\nu_{V=O}$) cm^{-1}. − EPR: see text.

X-ray Crystal Structure Determination: The complexes were crystallized from acetone (**2**) or by slow diffusion of diethyl ether into a chloroform solution (**3**). The intensity data were obtained with graphite monochromated Mo-K_α radiation on an imaging plate diffraction system (IPDS; STOE & CIE GmbH) equipped with a rotating anode (NONIUS FR591; 50 kV; 60/80 mA; 3.0/4.0 kW). Both structures were solved by a combination of direct methods and difference-Fourier syntheses. Full-matrix least-squares refinements on 307/375 parameters were carried out by minimizing $\Sigma w(F_o^2 - F_c^2)^2$ with SHELXL-97 weighting scheme and stopped at shift/err < 0.001/0.003. Neutral-atom scattering factors for all atoms and anomalous dispersion corrections for the non-hydrogen atoms were taken from the International Tables for X-ray Crystallography.[19] All calculations were performed on a DEC 3000 AXP workstation and an Intel Pentium II PC with the STRUX-V system,[20] including the programs PLATON,[10] SIR92,[21] and SHELXL-97.[22] Additional crystal data, intensity collection data and refinement parameters are presented in Table 3.

Data Collection, Structure Solution and Refinement for Complex 2: Data collection was performed within the Θ range of 2.84°< Θ < 24.65° with an exposure time of 600 seconds per image (oscillation scan modus from Θ = 0° to 270° with ΔΘ = 1.0°). A total number of 16128 reflections were collected. 273 Systematic absent reflections were rejected from the original data set. Data were corrected for Lorentz, polarization, decay and absorption effects with the DECAY algorithm.[23] Two different modes of disordering had to be included in the refinement process. At first, the positions of the chiral vanadium complex were occupied by the two stereoisomers in a 79:21 ratio. This resulted in a disordering model for the cyclohexan-1,2-diyl units wherein the positions of the carbon atoms 10 and 13 were identical for both six-membered rings. All non-hydrogen atoms of the vanadium complex were refined anisotropically with the exception of the disordered cyclohexandiyl carbon atoms of the minor species. Half an equivalent of acetone is disordered at an inversion center of the crystal system. All acetone non-hydrogen atoms were refined anisotropically. All hydrogen atoms of the major stereoisomer were found in the difference-Fourier map and refined with isotropic thermal displacement parameters. All hydrogen atoms of the minor stereoisomer and of the acetone were calculated in ideal positions (riding model; U_H = 1.2·U_C).

Data Collection, Structure Solution and Refinement for Complex 3: Data collection was performed within the Θ range of 3.15°< Θ < 25.65° with an exposure time of 180 seconds per image (oscillation scan modus from Θ = 0° to 135° with ΔΘ = 1.0°). A total number of 11436 reflections were collected. 460 Systematic absent reflections were rejected from the original data set. Data were corrected for Lorentz, polarization, decay and absorption effects, with the DECAY algorithm.[23] All non-hydrogen atoms of the vana-

Table 3. Crystal data, summary of intensity collection data and structure refinement data of **2** and **3**

	2	**3**
Chem formula	$(C_{14}H_{16}Cl_2N_3O_2V)_2{\cdot}C_3H_6O$	$C_{18}H_{26}Cl_2N_4O_4V_2$
Mol. wt.	818.35	535.21
Cryst system	Monoclinic	Monoclinic
Space group	$P2_1/n$ (No. 14)	$P2_1/n$ (No. 14)
a /Å	7.5926(4)	14.9428(9)
b /Å	18.8462(9)	8.3622(4)
c /Å	12.7320(6)	18.5264(13)
β /deg	105.488(5)	103.527(7)
V /Å^3	1755.7(2)	2250.7(2)
Z	2	4
ρ_{calcd}/g cm^{-3}	1.548	1.579
μ/mm^{-1}	0.885	1.100
T/K	163	193
No. of indep. rflns [$I_o > 2\sigma(I_o)$/all data]	2634/2908	3248/3839
*R*1[a] [$I_o > 2\sigma(I_o)$/all data]	0.0323/0.0364	0.0275/0.0330
*wR*2[b]	0.0788	0.0736
GOF[c]	1.066	0.986
Weights *a*/*b*[d]	0.0317/1.7352	0.0561/0.0
$\Delta\rho_{max/min}$ (e Å^{-3})	0.46/−0.52	0.45/−0.37

[a] $R1 = \Sigma(||F_o| - |F_c||)/\Sigma|F_o|$. − [b] $wR2 = [\Sigma w(F_o^2 - F_c^2)^2/\Sigma w(F_o^2)^2]^{1/2}$. − [c] $GOF = [\Sigma w(F_o^2 - F_c^2)^2/(NO - NV)]^{1/2}$. − [d] $w = 1/[\sigma^2(F_o^2) + (aP)^2 + bP]$, with $P = [\max(0 \text{ or } F_o^2) + 2F_c^2]/3$.

dium complex were refined anisotropically. All hydrogen atoms were found in the difference-Fourier map and refined with isotropic thermal displacement parameters.

Crystallographic data (excluding structure factors) for the structures included in this paper have been deposited with the Cambridge Crystallographic Data Centre as supplementary publication nos. CCDC-159418 (**2**) and -159419 (**3**). Copies of the data can be obtained free of charge on application to CCDC, 12 Union Road, Cambridge CB2 1EZ, UK [Fax: (internat.) +44-1223/336-033; E-mail: deposit@ccdc.cam.ac.uk].

Acknowledgments

We thank the Deutsche Forschungsgemeinschaft and the Fonds der Chemischen Industrie for support of this work.

[1] *Ullmann's Encyclopedia of Industrial Chemistry*, vol. A25, p. 644ff, VCH, Weinheim, **1994**.
[2] *Ullmann's Encyclopedia of Industrial Chemistry*, vol. A20, p. 183ff, VCH, Weinheim, **1992**.
[3] K. B. Sharpless, R. C. Michaelson, *J. Am. Chem. Soc.* **1973**, *95*, 6136−6137.
[4] D. J. Berrisford, C. Bolm, K. B. Sharpless, *Angew. Chem.* **1995**, *107*, 1159−1171; *Angew. Chem. Int. Ed. Engl.* **1995**, *34*, 1059−1070.
[5] H. Glas, E. Herdtweck, G. R. J. Artus, W. R. Thiel, *Inorg. Chem.* **1998**, *37*, 3644−3646.
[6] H. Glas, E. Herdtweck, M. Spiegler, W. R. Thiel, *J. Organometal. Chem.* in press.
[7] A.-K. Pleier, H. Glas, M. Grosche, P. Sirsch, W. R. Thiel, *Synthesis* **2001**, 55−62.
[8] H. Glas, M. Spiegler, W. R. Thiel, *Eur. J. Inorg. Chem.* **1998**, *1*, 275−281.
[9] M. Barz, E. Herdtweck, W. R. Thiel, *Tetrahedron: Asymmetry* **1996**, *7*, 1717−1722.
[10] A. L. Spek, *PLATON, A Multipurpose Crystallographic Tool*, Utrecht University, Utrecht, The Netherlands, **1999**.
[11] G. Foulon, J.-D. Foulon, N. Hovnanian, *Polyhedron* **1993**, *12*, 2507−2511.
[12] M. Mikuriya, M. Fukuya, *Bull. Chem. Soc. Jpn.* **1996**, *69*, 679−683.
[13] R. Das, K. K. Nanda, A. K. Mukherjee, M. Mukherjee, M. Helliwell, K. Nag, *J. Chem. Soc., Dalton Trans.* **1993**, 2241−2246.
[14] C. J. Carrano, C. M. Nunn, R. Quan, J. A. Bonadies, V. L. Pecoraro, *Inorg. Chem.* **1990**, *29*, 944−951.
[15] Z. Jonas, P. Sobota, S. Klimowicz Szafert, K. Szczegot, L. B. Jerzykiewicz, *J. Chem. Soc., Dalton Trans.* **1997**, 3897−3902.
[16] F. A. Cotton, G. E. Lewis, G. N. Mott, *Inorg. Chem.* **1983**, *22*, 378−382.
[17] C. W. Hahn, P. G. Rasmussen, J. C. Bayon, *Inorg. Chem.* **1992**, *31*, 1963−1969.
[18] ^{13}C NMR spectroscopic data of **2** can be obtained free of charge from the authors.
[19] *International Tables for Crystallography*, Vol. C, Tables 6.1.1.4 (pp. 500−502), 4.2.6.8 (pp. 219−222), and 4.2.4.2 (pp. 193−199), Ed. A.J.C. Wilson, Kluwer Academic Publishers, Dordrecht, The Netherlands, **1992**.
[20] G. R. J. Artus, W. Scherer, T. Priermeier, E. Herdtweck, *STRUX-V, A Program System to Handle X-ray Data*, TU München, Germany, **1997**.
[21] A. Altomare, G. Cascarano, C. Giacovazzo, A. Guagliardi, M. C. Burla, G. Polidori, M. Camalli, *J. Appl. Cryst.* **1994**, *27*, 435−436.
[22] G. M. Sheldrick, *SHELXL-97*, University of Göttingen, Göttingen, Germany, **1998**.
[23] *IPDS Operating System Version 2.8.* STOE&CIE GmbH, Darmstadt, Germany, **1997**.

Received January 8, 2001
[I01007]

Kinetic and Equilibrium Study on the Axial-Ligand Substitution Reaction of the Head-to-Tail α-Pyridonate-Bridged *cis*-Diammineplatinum(III) Dinuclear Complex: *trans* Effect of the Axial Ligand through the Pt−Pt Bond to the Opposite Axial Ligand

Nami Saeki,[a] Yuji Hirano,[a] Yasunari Sasamoto,[a] Ichiro Sato,[a] Tsuyoshi Toshida,[a] Sousei Ito,[a] Noriko Nakamura,[a] Koji Ishihara,*[a] and Kazuko Matsumoto*[a]

Keywords: Platinum / Pt^{III} dimer / Kinetics / Reaction mechanisms / α-Pyridone

Acid dissociation constant of the axial aqua ligand in the Head-to-Tail (HT) α-pyridonate-bridged *cis*-diammineplatinum(III) dimer complex $\{[(H_2O)Pt(NH_3)_2(\mu\text{-}C_5H_4NO)_2Pt(NH_3)_2(H_2O)]^{4+}\}$ was determined spectrophotometrically to be $-\log(K_{h1}/M) = 1.98\pm0.01$ at 25 °C and $I = 2.00$ M. Successive substitution reaction of the HT dimer with halide ions X^- (X^- = Cl^- and Br^-) at the two axial sites to give monohalo and dihalo complexes was studied kinetically:

$[(H_2O)Pt(NH_3)_2(\mu\text{-}C_5H_4NO)_2Pt(NH_3)_2(H_2O)]^{4+} + X^- \rightleftarrows$
$[(H_2O)Pt(NH_3)_2(\mu\text{-}C_5H_4NO)_2Pt(NH_3)_2(X)]^{3+} + H_2O$ (k_{obs1})
$[(H_2O)Pt(NH_3)_2(\mu\text{-}C_5H_4NO)_2Pt(NH_3)_2(X)]^{3+} + X^- \rightleftarrows$
$[(X)Pt(NH_3)_2(\mu\text{-}C_5H_4NO)_2Pt(NH_3)_2(X)]^{2+} + H_2O$ (k_{obs2})

Formation constants of the monohalo and dihalo complexes were determined spectrophotometrically to be $\log(K_1^{Cl}/M^{-1}) = 5.27\pm0.02$ and $\log(K_2^{Cl}/M^{-1}) = 3.83\pm0.01$ for the reaction with Cl^-, and $\log(K_1^{Br}/M^{-1}) = 5.33\pm0.03$ and $\log(K_2^{Br}/M^{-1}) = 4.44\pm0.02$ for the reaction with Br^-. In the HT dimer having two equivalent platinum atoms, the deprotonation occurs to the water molecule on one of the two Pt atoms, whereas the first nucleophilic substitution with X^- occurs to the other Pt atom. Substitution of the second water ligand with Cl^- proceeds by a simple substitution path, whereas the second substitution with Br^- proceeds by two parallel paths: one includes the dissociation of the axially coordinated water molecule followed by the Br^- coordination, and the other is the simple one-step substitution path. The difference of the reaction paths is reasonably explained by the different *trans* effect of the halide ions exerted through the Pt–Pt bond to the other terminal Pt atom in the monohalo complexes.

Introduction

There are a substantial number of diplatinum(III) complexes that involve metal−metal bonding between two d^7 platinum atoms.[1−10] They are classified into two groups: the first group involves symmetrical bridging ligands with identical coordinating atoms at both ends of the bridge, such as pyrophosphate-*P,P*, sulfate-*O,O*, and hydrogen phosphate-*O,O* ligands, and the complexes have the "lantern" structure with four symmetrically bridging ligands. The second group, which we will deal with in this report, involves complexes having asymmetrical bridging ligands with different coordinating atoms, such as α-pyrrolidonate-*N,O*, α-pyridonate-*N,O*, and acetamidate-*N,O*. These bridging ligands also appear in a class of multinuclear mixed-valent complexes called "platinum blues".[11−20] The complexes in the second group, Head-to-Head (HH) dinuclear Pt^{III} complexes $[Pt_2(NH_3)_4(N^{\cap}O)_2(X)_2]^{n+}$ ($N^{\cap}O$ = amidate, X = NO_3^-, NO_2^-, H_2O, or Cl^-, n = 2 or 4) are formed by the oxidation of "platinum blues". The two platinum atoms in the HH form are not equivalent, as shown by Scheme 1. The other isomer, head-to-tail (HT) is also known for this class of compounds, however isomerization between HH and HT of the Pt^{III} dimers does not occur in aqueous solution. The HH to HT or vice versa isomerization takes place only for the Pt^{II} dimer complexes.

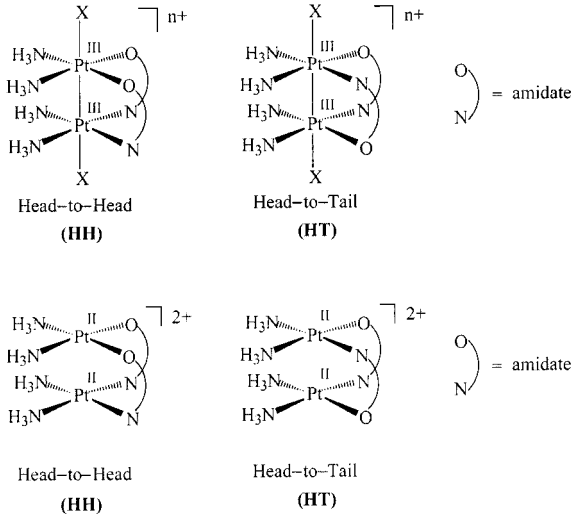

Scheme 1

As an exception, an isomerization reaction has been reported for the Pt^{III} dimer complex HH-$[Pt_2^{III}(CH_3)_4$(2-hy-

[a] Department of Chemistry, School of Science and Engineering, Waseda University,
Okubo, Shinjuku-ku, Tokyo 169−8555, Japan
Fax: (internat.) +81-3-3208-2735
E-mail: ishi3719@mn.waseda.ac.jp and
kmatsu@mn.waseda.ac.jp

Supporting information for this article is available on the WWW under http://www.wiley-vch.de/home/eurjic or from the author.

 © WILEY-VCH Verlag GmbH, 69451 Weinheim, 2001 1434−1948/01/0808−2081 $ 17.50+.50/0

droxy-6-fluoropyridonato)$_2$Py], which isomerizes to the head-to-tail (HT) isomer, HT-[$Pt_2^{III}(CH_3)_4$(2-hydroxy-6-fluoropyridonato)$_2$(Py)$_2$], when the former reacts with pyridine in chloroform.[21] Such HH to HT isomerization has been reported for several Pt^{II} dimer complexes with similar bridging amidate ligands,[22] but for Pt^{III} dimer complexes, the above-mentioned reaction represents the only example of this isomerization reported so far. Unlike their reduced forms, i.e., the Pt^{II} dimers $[Pt_2(NH_3)_4(N^{\cap}O)_2]^{2+}$, the Pt^{III} dimer complexes have axial ligands at both ends of the Pt−Pt axis, and these axial ligands play an important role in determining the chemical properties of the complex in solution. In spite of this fact, there are few kinetic studies on the axial ligand substitution reactions for the Pt^{III} dimer complexes; only a few kinetic studies have been reported for Pt^{III} dimers of the first group,[23,24] and even the reports on the simplest yet fundamentally important equilibrium parameters such as the acidity constant of the axially coordinated water are limited.[8,25]

In this paper we report the kinetic and equilibrium study on the axial aqua ligand substitution by halide ligands on the HT α-pyridonate-bridged Pt^{III} dinuclear complex, HT-$[(H_2O)Pt(NH_3)_2(\mu\text{-}C_5H_4NO)_2Pt(NH_3)_2(H_2O)]^{4+}$. Halide ions were selected as ligands rather than NO_2^-, SO_4^{2-}, etc., in order to avoid the problem of so-called "proton ambiguity" in kinetics,[26] since the dinuclear Pt^{III} complexes are found to be hydrolyzed even in highly acidic aqueous solution.

Results and Discussion

Preliminary ^{1}H NMR measurements were done, as is shown in Figure 1. When a small amount of Cl^- was added to the HT dimer solution, new peaks appeared at δ = 8.15 and 8.63 (Figure 1, b and c). Another peak was enhanced at δ = 8.7 with a decrease of the peaks at δ = 8.15 and 8.63, as [Cl^-] was increased. The peaks at δ = 8.15 and 8.63, and δ = 8.7 are assigned to the monochloro and dichloro complexes, respectively, and show that only one monochloro complex is formed and is converted to the dichloro complex.

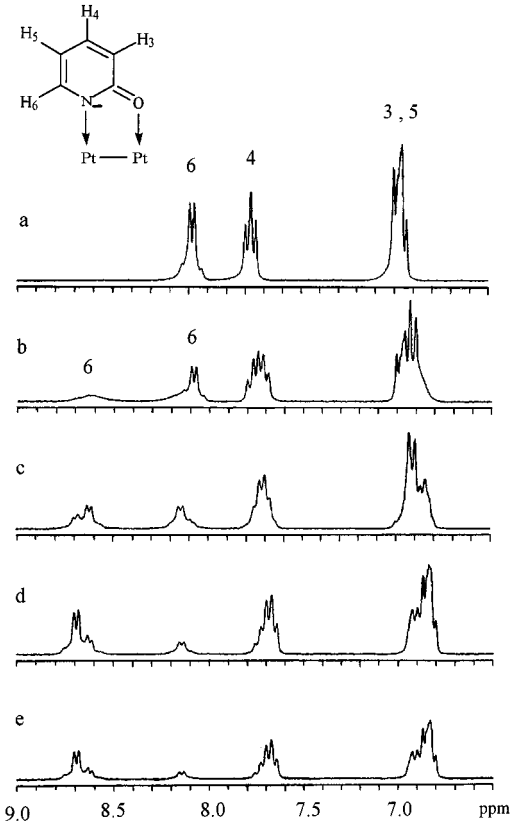

Figure 1. The ^{1}H NMR spectra of the HT dimer in acidic D_2O solution with different C_{Cl^-} at room temperature; [$DClO_4$] = 1.3 M, [HT] = 1.9×10^{-2} M, [Cl^-]/[HT] = 0 (a), 0.5 (b), 1.0 (c), 1.5 (d), 2.0 (e); solid began to precipitate at (d)

Acid Dissociation Constant of the HT Dimer

The X-ray crystallography study shows[4] that two nitrate ions cap axial positions of the HT-[$Pt_2^{III}(NH_3)_4$(α-pyridonato)$_2$(NO_3)$_2$]$^{2+}$ in solid state. Both axial nitrate ions are completely replaced by H_2O or OH^- on dissolution, since no spectral change was observed when sodium nitrate was added up to 0.020 M (mol dm^{-3}) to the aqueous solutions of the HT dimer (5.0×10^{-5} M). When the acidity of the solution was varied, an isosbestic point was observed at 244 nm (Figure SI-1, see Supporting Information). The HT dimer is stable in strongly acidic aqueous solution, and no decomposition was observed by acidification at least for several hours. The spectral change (Figure SI-1, see Supporting Information) is pH-dependent and the change can be reversed by pH adjustment. The spectral change corresponds to deprotonation of the coordinated axial water molecule as expressed in Equation (1). The deprotonation occurs to either one of the two equivalent water molecules in the HT isomer.

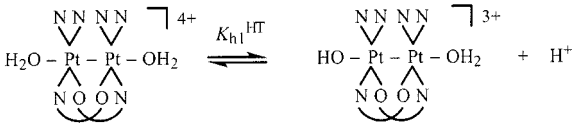

(1)

$[H_2O{-}Pt(N_3O){-}Pt(N_3O){-}OH_2]^{4+}[HO{-}Pt(N_3O){-}Pt(N_3O){-}OH_2]^{3+}$

The apparent molar absorption coefficient ε is expressed as $\varepsilon = (\varepsilon_1 + \varepsilon_2 K_{h1}[H^+]^{-1})(1 + K_{h1}[H^+]^{-1})^{-1}$, where ε_1 and ε_2 are the molar absorption coefficients of the undissociated dimer $H_2O{-}Pt(N_3O){-}Pt(N_3O){-}OH_2$ and the deprotonated dimer $H_2O{-}Pt(N_3O){-}Pt(N_3O){-}OH$, respectively, and K_{h1} is the first acid dissociation constant of the diaqua complex. The ε values at 250, 255, 260, 270, and 280 nm were analyzed simultaneously as a function of [H^+] by using a nonlinear least-squares fitting method. The K_{h1} values obtained at I = 2.00 M are as follows: $-\log(K_{h1}/M)$ = 1.98±0.01 (25.0 °C), 1.68±0.02 (35.0 °C). The value of K_{h1} for the present HT dimer is more than 1 order of magnitude larger than that of the related Pt^{III} dimer complex with dif-

ferent bridging ligands: $-\log(K_{h1}/M) = 3.49$ for the 1-methyluracilate-bridged HT dimer.[8] This difference can be explained by the less-donating α-pyridonate coordination, as compared to methyluracilate. Because of the weaker donation, the Pt^{III} atom in the α-pyridonate complex would be more electron withdrawing.

Formation Constants of the Monohalo and Dihalo Complexes

The absorption spectra were measured at $I = 2.00$ M, $[H^+] = 1.27$ M, and 25 °C, under various C_X^-/C_{HT} for a fixed C_{HT}. The results are shown in Figure 2 for both reactions with Cl^- and Br^-, in which two distinct isosbestic points are observed at 251 and 273 nm, and at 256 and 295.5 nm, respectively.

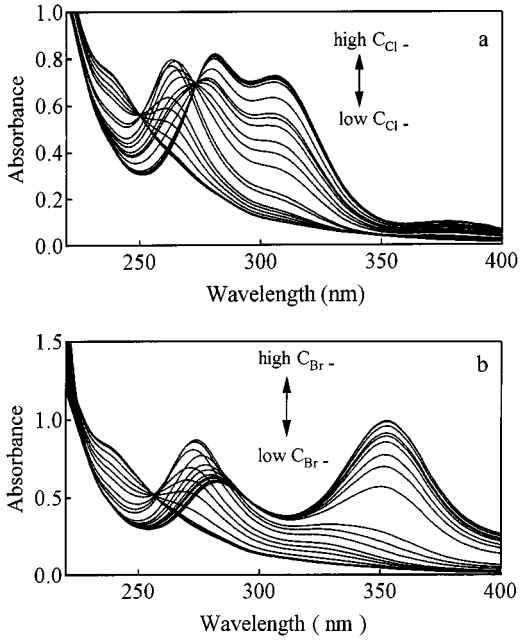

Figure 2. The UV/Vis spectra of the HT dimer in acidic aqueous solution with different C_{Cl}^- (a) and C_{Br}^- (b) at 25 °C and $I = 2.00$ M. $[H^+] = 1.27$ M; $C_{Cl}^- = (0-1.35) \times 10^{-2}$ M (a); $C_{Br}^- = (0-1.20) \times 10^{-2}$ M (b); $C_{HT} = 2.5\times10^{-5}$ M (a), 2.8×10^{-5} M (b)

Plots of the absorbance at the isosbestic point of the longer wavelength (273 nm, 295.5 nm) against C_X^-/C_{HT} showed a clear inflection point at $C_X^-/C_{HT} = 1$, however, another inflection point corresponding to $C_X^-/C_{HT} = 2$ was obscured, probably because of the smaller formation constant of the dihalo complex. The formation of the dichloro complex has also been confirmed by X-ray crystallography for the dichloro HH α-pyrrolidonate-bridged dimer,[26] in addition to the ^1H NMR results mentioned above. Therefore, the observed spectral change in Figure 2 corresponds to the following reactions.

$$[(H_2O)Pt(NH_3)_2(\mu\text{-}C_5H_4NO)_2Pt(NH_3)_2(H_2O)]^{4+} + X \xrightleftharpoons{K_1^X} [(H_2O)Pt(NH_3)_2(\mu\text{-}C_5H_4NO)_2Pt(NH_3)_2(X)]^{3+} + H_2O \quad (2)$$

$$[(H_2O)Pt(NH_3)_2(\mu\text{-}C_5H_4NO)_2Pt(NH_3)_2(X)]^{3+} + X \xrightleftharpoons{K_2^X} [(X)Pt(NH_3)_2(\mu\text{-}C_5H_4NO)_2Pt(NH_3)_2(X)]^{2+} + H_2O \quad (3)$$

The K_1^X and K_2^X values were obtained at $I = 2.00$ and 25 °C, by simultaneously analyzing the absorbance at twelve different wavelengths between 235 nm and 305 nm, and are given in Table 1 together with K_{h1} values. The K_1^{Cl} and K_2^{Cl} values are comparable to those reported for the HH α-pyrrolidonate-bridged cis-diammineplatinum(III) dimer with Cl^-.[25]

Table 1. Equilibrium constants for the reaction of the HT α-pyridonate-bridged *cis*-diammineplatinum(III) dimer with halides determined at $I = 2.00$ M ($[H^+] = 1.27$ M) and 25 °C spectrophotometrically

$-\log K_{h1}$ [mol L^{-1}]	$\log K_1^{Cl}$ [L mol^{-1}]	$\log K_2^{Cl}$ [L mol^{-1}]	$\log K_1^{Br}$ [L mol^{-1}]	$\log K_2^{Br}$ [L mol^{-1}]
1.98±0.01	5.27±0.02	3.83±0.01	5.33±0.03	4.44±0.02
3.49[a]				

[a] For HT 1-methyluracilate-bridged *cis*-diammineplatinum(III) dimer.[8]

Kinetics for the Formation of the Monohalo Complexes

Under the conditions of $C_{HT} >> C_X^-$ and $[H^+] = 0.10-0.82$ M, reactions of the HT dimer with X^- were first order and monophasic, i.e., only reaction (2) was observed. The formation rate of the monohalo complex (Pt_2X) is given by Equation (4), where $[X^-]$ is the concentration of the free halide ion. The conditional first-order rate constant, k_{obs1} was found to involve the dimer concentration and $[H^+]$.

$$d[Pt_2X]/dt = k_{obs1}[X^-] \quad (4)$$

Since k_{obs1} was linearly dependent on C_{HT} at a given $[H^+]$ as shown in Figure 3 (a), k_{obs1} is expressed as Equation (5), where k_{f1} is the second order rate constant.

$$k_{obs1} = k_{f1}C_{HT} \quad (5)$$

The two Pt atoms in the HT dimer are equivalent, and deprotonation occurs to either one of the two axial water molecules. Since the deprotonated water molecule in the octahedral aquahydroxo complexes is generally not easily replaced by other ligands, the halide substitution would take place at the other water molecule on the opposite Pt atom, $Pt(N_3O)$. That is, the deprotonation [Equation (1)] and the first substitution reaction with halide [Equation (2)] would occur to the opposite axial sites of the Pt^{III} dimer.

Therefore, two reaction pathways shown in Scheme 2 should be considered under the present condition for the

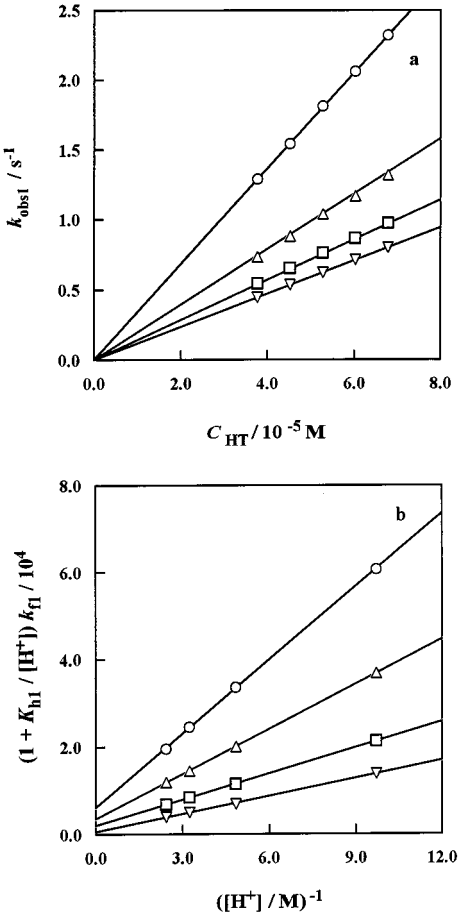

Figure 3. (a) The dependence of k_{obs1} on C_{Pt2} for the reaction of the HT dimer with bromide ion in acidic aqueous solution at 20 °C and I = 2.00 M. [H$^+$] = 0.103 (O); 0.206 (Δ); 0.309 (□); 0.412 (▽) M. $C_{Br^-} = 8.75\times10^{-7}$ M. (b) Plot of $(1 + K_{h1}/[H^+])k_{f1}$ against 1/[H$^+$] for the reaction of the HT dimer with bromide ion at 20 °C and I = 2.00 M; T = 25.0 (O); 20.0 (Δ); 15.0 (□); 10.6 (▽) °C

monohalo complex formation. For the reaction pathways in Scheme 2, the rate constant k_{obs1} is given by Equation (6).

$$k_{obs1} = \frac{k_1 + \frac{k_1^{\#}K_{h1}}{[H^+]}}{1 + \frac{K_{h1}}{[H^+]}} C_{HT} \quad (6)$$

Comparison of Equation (5) with Equation (6) gives Equation (7).

$$\left(1 + \frac{K_{h1}}{[H^+]}\right) k_{f1} = k_1 + \frac{k_1^{\#}K_{h1}}{[H^+]} \quad (7)$$

The plots of the left-hand side of Equation (7) against $[H^+]^{-1}$ were linear as shown in Figure 3 (b).

The values of k_1 and $k_1^{\#}$ were obtained by applying a nonlinear least-squares fitting to Equation (7), and are listed in Table 2. The K_{h1} values at each temperature are given as Supporting Information and were used for the calculation of k_1 and $k_1^{\#}$.

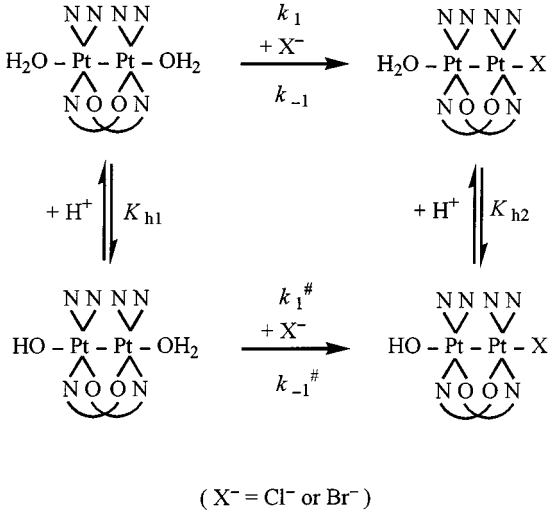

Scheme 2

Table 2. The rate constants (25 °C) and activation parameters for the first steps of the reactions of the HT dimer with halides

ligand	path	k [M^{-1}s^{-1}]	$\Delta H^{\#}$ [kJ mol^{-1}]	$\Delta S^{\#}$ [J mol^{-1}K^{-1}]
Cl$^-$	k_1	2.4×10^3 1.2×10^3 [a]	87.8±21.0	114±72
	$k_1^{\#}$	6.6×10^5 3.3×10^5 [a]	11.9±1.5	−93.7±5.3
Br$^-$	k_1	6.5×10^3 3.3×10^3 [a]	79.7±1.0	95.3±3.0
	$k_1^{\#}$	5.3×10^5 2.7×10^5 [a]	23.1±0.7	−57.9±2.0

[a] Statistical factor was taken into account (see text).

In the following discussion, half of k_1 was considered, since X$^-$ can replace both aqua ligands with an equal probability. Interestingly, the k_1 value for the reaction with Br$^-$ is larger than that with Cl$^-$; this relation is the same as that for the reactions of mononuclear Pt^{II} complexes, where the heavier halides with higher polarizability react faster. On the contrary, the $k_1^{\#}$ value is larger for Cl$^-$ than Br$^-$, which may reflect the decreased polarizability of the Pt(N$_3$O) in the HT dimer due to the deprotonation of the water molecule on the opposite axial site. We concluded that the ligand substitution rates on the axial sites of the HT dimer are sensitive to the nature of the ligands on the opposite axial site.

It is noteworthy that the rate constants k_1 and $k_1^{\#}$ in Table 2 are much larger than those for the direct substitution paths of the square planar Pt^{II} Werner-type complexes, which are of the order of 10^{-3} M^{-1}s^{-1}. A linear relationship was observed between $\Delta H^{\#}$ and $\Delta S^{\#}$ as shown in Figure SI-2 (Supporting Information, see footnote on the first page of this article), which suggests that both k_1 and $k_1^{\#}$ paths are via the same mechanism.[27,28]

For many octahedrally coordinated metal ions $[M(H_2O)_6^{n+}]$, substitution rate constants on the hexaaqua metal ions are smaller by 2−3 orders of magnitude than those of the corresponding pentaaquahydroxo metal ions $[M(H_2O)_5(OH)^{(n-1)+}]$.[29] The k_1 and $k_1^{\#}$ values in Table 2 show that the same tendency holds even through the present complexes having metal−metal bonds.

The values of k_1 and $k_1^{\#}$ in Table 2 are much larger than the rate constants of the axial ligand substitution (k_1 = 0.9 and 0.3 $M^{-1}s^{-1}$, k_2 = 0.8 and 0.4 $M^{-1}s^{-1}$ for X = Cl^- and Br^-, respectively) for the following $Pt^{III}-Pt^{III}$ system.[1]

$$Pt_2(\mu\text{-}PO_4H)_4(H_2O)_2^{2-} \underset{}{\overset{k_1}{\underset{+X^-}{\rightleftharpoons}}} Pt_2(\mu\text{-}PO_4H)_4X(H_2O)^{3-} \overset{k_2}{\underset{+X^-}{\rightleftharpoons}} Pt_2(\mu\text{-}PO_4H)_4X_2^{4-} \quad (8)$$

The large difference in the k_1 values would come from the difference of the bridging ligand, as well as the affinity difference of the halide ions for the positively charged amidate-bridged complex and for the negatively charged complex in Equation (8).

The effect of ion pairing was not observed for both reactions (2) and (3), in spite of the highly positive charge of the complexes (4+ or 3+). This is probably because the rate constants were measured at high ionic strength (2 M), where an ion-paring effect is attenuated, and the formal charge would be delocalized over the dinuclear complexes. The rate constant for reaction (2), k_{obs1}, was measured at low C_{HT} (10^{-4} M > C_{HT} >> C_X-).

Kinetics for the Formation of the Dihalo Complexes

Under the conditions of C_{HT} << C_X^- and $[H^+]$ = 0.11−1.3 M, the reaction of the HT dimer was biphasic as shown in Figure 4. The rate constant was calculated only for the slower reaction by assuming two consecutive first-order reactions.

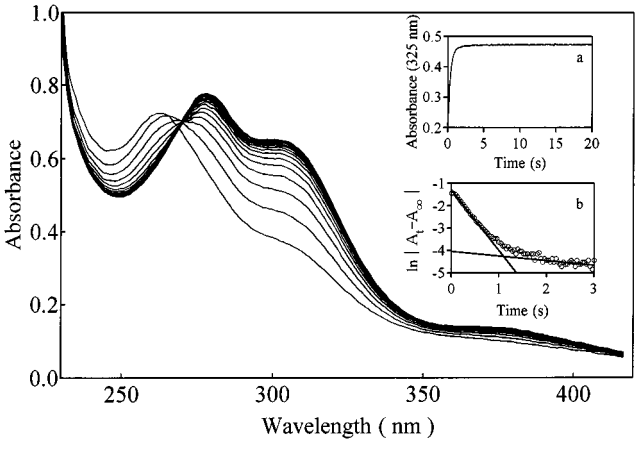

Figure 4. The UV/Vis spectra for the reaction of the HT dimer with chloride ion in acidic aqueous solution at 25 °C and I = 2.00 M. Measurement every 80 ms, C_{Cl^-} = 8.0×10^{-4} M, C_{HT} = 2.0×10^{-5} M, $[H^+]$ = 0.102 M. The inserted figure (a) shows the time dependence of the absorbance at 325 nm, and the semi-log plot (b) of the data in (a) shows clearly that the reaction is biphasic

The formation rate of the dihalo complex (Pt_2X_2) is expressed as Equation (9), where [HT−X] is the concentration of the monohalo-HT dimer.

$$d[Pt_2X_2] / dt = k_{obs2}[HT\text{-}X] \quad (9)$$

For the reaction with Cl^-, k_{obs2} was linear with respect to C_{Cl^-} at a given $[H^+]$ as shown in Figure 5 (a). The straight lines correspond to Equation (10), where k_{f2} and k_{d2} are the slope and the intercept in Figure 5 (a), respectively.

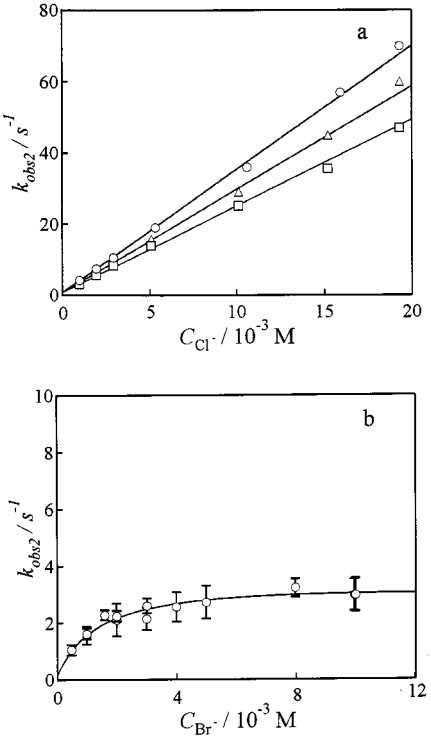

Figure 5. The dependence of k_{obs2} on C_X^- in acidic aqueous solution at 25 °C and I = 2.00 M. (a) for the reaction of the HT dimer with chloride ion, C_{HT} = 2.0×10^{-5} M, $[H^+]$ = 1.27 (□), 0.424 (Δ), 0.106 (O) M; (b) for the reaction of the HT dimer with bromide ion, C_{HT} = 2.0×10^{-5} or 4.0×10^{-5} M, $[H^+]$ = 0.4−1.6 M. The solid lines were drawn by applying a linear or non-linear least-squares fitting

$$k_{obs2} = k_{f2} C_{Cl^-} + k_{d2} \quad (10)$$

It is obvious from Figure 5a that k_{obs2} varies with $[H^+]$ in the same way as in Figure 3 (a), that is, k_{f2} in Equation (10) decreases with increasing $[H^+]$, whereas k_{d2} does not depend on $[H^+]$. For the second Cl^- substitution reaction, the reaction path in Scheme 3 was postulated, for which Equation (11) was derived.

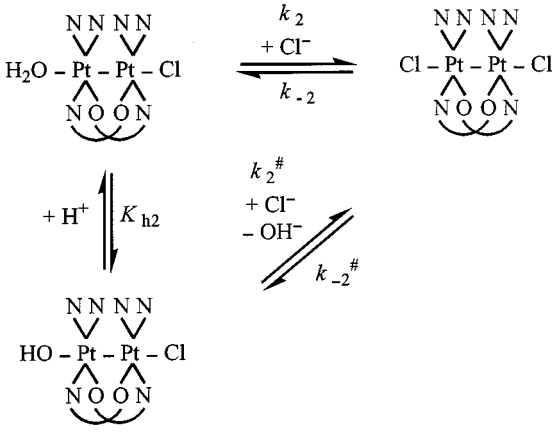

Scheme 3

$$k_{obs\,2} = \frac{k_2 + \frac{k_2^{\#} K_{h2}}{[H^+]}}{1 + \frac{K_{h2}}{[H^+]}} C_{Cl^-} + k_{-2} + \frac{k_{-2}^{\#} K_w}{[H^+]} \qquad (11)$$

The observed dependence of k_{f2} on $[H^+]$ corresponds to the coefficient of C_{Cl^-} in Equation (11). In Scheme 3, it was assumed that the coordinated OH^- is replaced by X^-. If the OH^- in the hydrolyzed species (the chlorohydroxo dimer in Scheme 3) is unreactive towards Cl^-, then $k_{obs2} = k_2[H^+][Cl^-]/([H^+] + K_{h2}) + k_{-2}$ is obtained. This equation does not correspond with the experimental observation that k_{obs2} decreases with increasing $[H^+]$. Thus, the $k_2^{\#}$ path, in which OH^- in the [HO−Pt−Pt−X] is replaced by X^-, must be involved in the HT + Cl^- system. This is unusual, considering the usual inertness of OH^- in $M(H_2O)_5(OH)^{(n-1)+}$. In HH α-pyridonate-dibridged complexes, HH-[Cl−Pt(N_2O_2)−Pt(N_4)−X], when X^- is changed from less donating NO_3^- to more donating Cl^-, the opposite (N_2O_2)Pt−Cl distance (236.0 pm → 245.5 pm) as well as the Pt−Pt length (262.4 pm → 263.7 pm) are elongated.[30] Such significant trans influence of Cl^- on the opposite axial ligand suggests that the Pt−OH distance in the HT-[HO−Pt−Pt−Cl] can be longer than usual, and OH^- in the HT-[HO−Pt−Pt−Cl] may be replaced by Cl^-. The third term in Equation (11) is negligible under the present conditions ($[H^+]$ = 0.11−1.3 M), that is, k_{d2} is virtually equal to k_{-2}.

The conditional formation constant (k_{f2}/k_{d2}) for the dichloro complex of the HT dimer can be calculated from the slope (k_{f2}) and the intercept (k_{d2}) at a given $[H^+]$. The obtained $\log(k_{f2}/k_{d2})$ value (3.64) at $[H^+]$ = 1.27 M agrees with $\log K_2^{Cl}$ listed in Table 1, within the experimental error.

On the other hand, for the reaction with Br^-, k_{obs2} increases linearly with $[Br^-]$ at lower $[Br^-]$, and at higher $[Br^-]$ it also increases linearly, but with a different slope as shown in Figure 5 (b). In both non-Werner Pt^{II} complexes and octahedral Pt^{IV} complexes, e.g., $Pt^{II}R_2S_2$ (R = Me, Ph; S = Me_2S, Me_2SO) or $Pt^{IV}Me_4(Me_2S)_2$, a dissociative mechanism has been proposed for the solvolysis reactions, and this is because of the strong *trans* labilizing effect of Me and Ph groups.[31−34] The trans effect is also observed through the Pt−Pt bond for the present HT dimer as mentioned above. It is reported that there is virtually no axial ligand on the Pt(N_4) in the HH pivalamidate-bridged Pt^{III} dimer with the alkyl ligand (R) on the Pt(N_2O_2), i.e., [Pt^{II}(N_4)−Pt^{IV}(N_2O_2)−R].[24] On the basis of these findings, it seems that reaction (3) proceeds also through a dissociative path via a coordinatively unsaturated complex as depicted in Scheme 4. It is also notable that k_{obs2} is almost independent of $[H^+]$. If the steady-state approximation is applied to the monohalo dimer without an axial ligand at the opposite site in Scheme 4, Equation (12a) involving the three terms is obtained. The first and second terms in Equation (12a) are related to the k_2 path, and the third is to the k_3 path. The $k_2^{\#}$ path in Scheme 3 is irrelevant in Scheme 4, since k_{obs2} does not vary with $[H^+]$ for the (HT + Br^-) system.

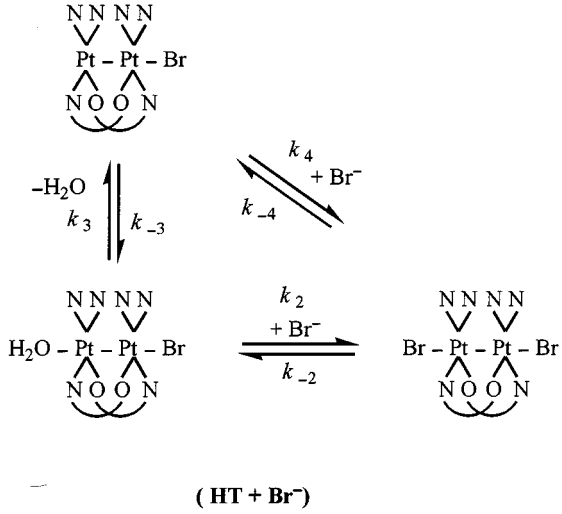

Scheme 4

$$k_{obs2} = k_2[Br^-] + k_{-2} + \frac{k_3 k_4 [Br^-] + k_{-3} k_{-4}}{k_{-3} + k_4 [Br^-]} \qquad (12a)$$

The following values were estimated from the data in Figure 5 (a, b) by applying a non-linear least-squares fitting to Equation (11) or Equation (12b) derived from Equation (12a), assuming that $k_{-2}^{\#} K_W/[H^+] = 0$ in Equation (11), and $k_{-2} = 0$ and $k_{-3}k_{-4}/k_4 = 0$ in Equation (12b): k_2 = 2490±40 $M^{-1}s^{-1}$, $k_2^{\#}K_{h2}$ = 115±5 s^{-1}, and k_{-2} = 0.59±0.38 s^{-1} for Figure 5 (a); k_2 = −25±29 $M^{-1}s^{-1}$, k_3 = 3.7±0.4 s^{-1}, and k_{-3}/k_4 = (1.4±0.2) ×10^{-3} M for Figure 5 (b) (k_2 could not be determined accurately because of the large error in k_{obs2}).

$$k_{obs2} = k_2[Br^-] + k_{-2} + \frac{k_{-3}[Br^-] + k_{-3}k_{-4}/k_4}{k_{-3}/k_4 + [Br^-]} \quad (12b)$$

The data in Figure 5 (b) were also analyzed by assuming a mechanism that involves ion pair formation. However, the fit was very poor, and the ratio of the resulting rate constants, k_2/k_{-2}, did not agree at all with K_2 obtained from the spectrophotometry, and so the ion pair formation is negligible under the present conditions.

The *trans* influence and/or the *trans* effect through the Pt−Pt bond seems to determine the reaction paths (see Schemes 3 and 4). In the aquachloro HT dimer, [H_2O−Pt−Pt−Cl], the axial aqua ligand is more acidic than that in the corresponding monobromo HT complex because of the weaker trans influence of chloride, but yet the trans effect of the axial chloride ligand is strong enough to replace the OH^- with Cl^- in the chlorohydroxo HT dimer, as is the case in Scheme 3. On the other hand, the increased *trans* influence and *trans* effect of the bromide lengthen and labilize the H_2O−Pt bond in the aquabromo HT complex, which promotes the dissociation of H_2O to produce the monohalo dimers without an axial ligand at the opposite site. This is the case in Scheme 4.

The mechanistic difference between the HT-[H_2O−Pt−Pt−Cl] and HT-[H_2O−Pt−Pt−Br] systems would reflect the relative extent of the electron donor ability of Cl^- and Br^-, that is, softer Br^- donates more electrons to the H_2O−Pt atom through the Pt−Pt bond, which enhances more the electron delocalization in the dimer (such as [H_2O−Pt^{II}−Pt^{IV}−Br]).

Conclusion

The first deprotonation occurs on one of the water molecules on the two equivalent Pt atoms and the first nucleophilic substitution with X^- occurs to the other Pt atom in the HT dimer. The formation of the HT dichloro complex from the aquachloro complex proceeds through two pathways: by a direct substitution of the aqua ligand and by a path involving OH^- substitution in the chlorohydroxo complex. The formation of the dibromo complex from the aquabromo complex, on the other hand, proceeds through a dissociative path by a coordinatively unsaturated complex as well as through a direct substitution path. The ligand substitution rates on the axial sites of the HT dimer are very sensitive to the nature of the ligands on the opposite axial sites. The mechanistic difference of the ligand substitution on the aquahalo complexes is reasonably explained by the different electron donor ability of Cl^- and Br^-.

Experimental Section

Reagents: The *cis*-[$PtCl_2(NH_3)_2$] (N.E. Chemcat) was purchased and was used without purification. Reagent grade α-pyridone (Kanto Chemical Co. Inc., Tokyo) was recrystallized once from benzene. Sodium chloride (99.99%, Kanto), sodium bromide (99.99%, Aldrich), and perchloric acid (60% UGR for trace analysis, Kanto) were used as received. Sodium perchlorate was prepared and purified according to the literature.[35] Head-to-tail [$(NO_3)Pt(NH_3)_2(\mu\text{-}C_5H_4NO)_2Pt(NH_3)_2(NO_3)](NO_3)_2\cdot 0.5H_2O$ (HT isomer) were prepared according to the literature method.[4]

Measurements: Ionic strength was maintained at 2.00 M with perchloric acid and sodium perchlorate. All the sample solutions were prepared by using water twice distilled just before measurement. Spectrophotometric measurements were performed with a rapid-scan/stopped-flow spectrophotometer USP-500 (Unisoku Scientific Instruments, Osaka) and spectrophotometers UV-160A (Shimadzu, Kyoto), UV-2200 (Shimadzu), and UV-2400 (Shimadzu). The NMR spectra were recorded on a JEOL Lambda 270 spectrometer, operating at 270 MHz for ^1H. Chemical Shifts are reported relative to TMS (tetramethylammonium perchlorate, 3.190 ppm to TMS). Under the present experimental conditions with the concentration of sodium halide (C_{X^-}, X^- = Cl^- or Br^-) in large excess over that of the HT dimer (C_{HT}), the reaction was biphasic as shown in Figure 4, and is expressed by the equation: $A_t = A_e + \alpha\exp(-k_{obs1}t) + \beta\exp(-k_{obs2}t)$, where A_t and A_e are the absorbances at time t and ∞, respectively, and α and β are composite parameters.[28] Though it is possible to estimate k_{obs1} and k_{obs2} simultaneously under the condition $C_{HT} << C_{X^-}$, k_{obs1} was determined independently under the conditions $C_{HT} >> C_{X^-}$ in order to obtain more accurate values. Rate constants were measured by monitoring the absorbance change at 265 nm for the reaction of the HT dimer with Cl^-, and at 270 nm with Br^- for k_{obs1}, at 250 nm for the reaction of the HT dimer with Cl^-, and at 265 or 350 nm for the reaction of the HT dimer with Br^- for k_{obs2}, as a function of time after mixing the solutions of the dimer and sodium halide. For the reaction with Br^-, the dependence of k_{obs2} on C_{Br^-} was not straightforward (see Results). The acid dissociation constant (K_{h1}) of the HT dimer and the formation constants (K_1^X and K_2^X) of the monohalo and the dihalo complexes were determined spectrophotometrically under the following conditions: C_{HT} = (5−6) $\times 10^{-5}$ M, $[H^+] = 1.00\times 10^{-3}$ to 0.501 M for K_{h1}; $C_{HT} = 2.48\times 10^{-5}$ M, $[H^+]$ = 1.27 M, $C_{Cl^-} = 0-1.3\times 10^{-2}$ M for K_1^{Cl} and K_2^{Cl}; $C_{HT} = 2\times 10^{-5}$ M, $[H^+]$ = 1.27 M, $C_{Br^-} = (0-4)\times 10^{-2}$ M for K_1^{Br} and K_2^{Br}. The values of K_2^{Br} was determined by using the spectroscopic data obtained only for $C_{Br^-} < 1.2\times 10^{-2}$ M, since the spectra changed differently with a different isosbestic point at higher C_{Br^-}, probably due to the reduction of the Pt^{III} dimers by water.[19]

[1] R. El-Mehdawi, S. A. Bryan, D. M. Roundhill, *J. Am. Chem. Soc.* **1985**, *107*, 6282 and references cited therein.
[2] S. Bryan, M. K. Dickson, D. M. Roundhill, *Inorg. Chem.* **1987**, *26*, 3878, and references cited therein.
[3] R. Faggiani, B. Lippert, C. J. L. Lock, R. A. Speranzini, *J. Am. Chem. Soc.* **1981**, *103*, 1111.
[4] L. S. Hollis, S. J. Lippard, *Inorg. Chem.* **1983**, *22*, 2605.
[5] L. S. Hollis, M. M. Roberts, S. J. Lippard, *Inorg. Chem.* **1983**, *22*, 3637.
[6] T. V. O'Halloran, M. M. Roberts, S. J. Lippard, *Inorg. Chem.* **1986**, *25*, 957.
[7] B. Lippert, H. Schoellhorn, U. Thewalt, *Inorg. Chem.* **1986**, *25*, 407.
[8] H. Schoellhorn, P. Eisenmann, U. Thewalt, B. Lippert, *Inorg. Chem.* **1986**, *25*, 3384.
[9] B. Lippert, H. Schoellhorn, U. Thewalt, *J. Am. Chem. Soc.* **1986**, *108*, 525.

[10] [10a] T. Abe, H. Moriyama, K. Matsumoto, *Chem. Lett.* **1989**, 1857. – [10b] T. Abe, H. Moriyama, K. Matsumoto, *Inorg. Chem.* **1991**, *30*, 4198.
[11] J. K. Barton, H. N. Rabinowitz, D. J. Szalda, S. J. Lippard, *J. Am. Chem. Soc.* **1977**, *99*, 2827.
[12] J. K. Barton, D. J. Szalda, H. N. Rabinowitz, J. V. Waszczak, S. J. Lippard, *J. Am. Chem. Soc.* **1978**, *100*, 1434.
[13] J. K. Barton, C. Caravana, S. J. Lippard, *J. Am. Chem. Soc.* **1979**, *101*, 7269.
[14] L. S. Hollis, S. J. Lippard, *J. Am. Chem. Soc.* **1981**, *103*, 1230.
[15] K. Matsumoto, K. Fuwa, *J. Am. Chem. Soc.* **1982**, *104*, 897.
[16] K. Matsumoto, H. Takahashi, K. Fuwa, *Inorg. Chem.* **1983**, *22*, 4086.
[17] K. Matsumoto, K. Fuwa, *Chem. Lett.* **1984**, *569*.
[18] K. Matsumoto, K. Fuwa, *J. Am. Chem. Soc.* **1984**, *106*, 2049.
[19] K. Matsumoto, *Chem. Lett.* **1984**, 2061.
[20] K. Matsumoto, *Bull. Chem. Soc. Jpn.* **1985**, *58*, 651.
[21] E. S. Peterson, D. P. Bancroft, D. Min, F. A. Cotton, E. A. Abbott, *Inorg. Chem.* **1990**, *29*, 229.
[22] T. V. O′Halloran, S. J. Lippard, *Inorg. Chem.* **1989**, *28*, 1289.
[23] K. Matsumoto, K. Mizuno, T. Abe, J. Kinoshita, H. Shimura, *Chem. Lett.* **1994**, 1325.
[24] K. Matsumoto, Y. Nagai, J. Matsunami, K. Mizuno, T. Abe, R. Somazawa, J. Kinoshita, H. Shimura, *J. Am. Chem. Soc.* **1998**, *120*, 2900.
[25] K. Sakai, Y. Tsuchiya, T. Tsubomura, *Technol. Rep. Seikei Univ.* **1992**, *54*, 77.
[26] R. B. Jordan, *Reaction Mechanisms of Inorganic and Organometallic Systems*, Oxford, **1991**, p. 77−80.
[27] C. P. Brink, A. L. Crumbliss, *Inorg. Chem.* **1984**, *23*, 4708.
[28] R. G. Wilkins, *Kinetics and Mechanism of Reactions of Transition Metal Complexes*, 2nd ed., VCH, **1991**.
[29] A. E. Martell (Ed.), *Coordination Chemistry*; Vol. 2, ACS Monogr. No. 174, **1978**, p. 106.
[30] K. Sakai, Y. Tanaka, Y. Tsuchiya, K. Hirata, T. Tsubomura, S. Iijima, A. Bhattacharjee, *J. Am. Chem. Soc.* **1998**, *120*, 8366.
[31] R. Romeo, *Comments Inorg. Chem.* **1990**, *11*, 21.
[32] G. Alibrandi, L. M. Scolaro, R. Romeo, *Inorg. Chem.* **1991**, *30*, 4007.
[33] K. Nakayama, Y. Kondo, K. Ishihara, *Can. J. Chem.* **1998**, *76*, 62.
[34] J. D. Atwood, *Inorganic and Organometallic Reaction Mechanisms*, 2nd ed., VCH-Verlagsgesellschaft, Weinheim, **1997**, p. 59.
[35] S. Funahashi, K. Haraguchi, M. Tanaka, *Inorg. Chem.* **1977**, *16*, 1349.

Received January 6, 2001
[I01018]

Tripodal Iminophenolate Ligand Complexes of Gallium(III), Indium(III), and Thallium(III)

Mélanie Figuet,[a] Marie Thérèse Averbuch-Pouchot,[a] Amaury du Moulinet d'Hardemare,[a] and Olivier Jarjayes*[a]

Keywords: Coordination chemistry / Gallium / Tripodal ligands / Schiff bases / Isotope effects

The polydentate tripodal Schiff base ligand **H_3L** has been prepared by treating a methanolic solution of tris(aminoethyl)-amine and 5-bromosalicylaldehyde. This ligand, and its complexes with group-13 metal ions (Ga^{III}, In^{III}, and Tl^{III}) have been characterized by elemental analysis, NMR spectroscopy, FAB$^+$-MS, and X-ray diffraction analysis. The ligand, not preorganized in the solid state, acts as a hexadentate N_3O_3 ligand in all cases to form octahedral structures, the apical nitrogen not being involved in the chelation even for the [Tl(**L**)] complex. NMR studies reveal that the intact and rigid structures of the complexes are maintained in solution. For the [Tl(**L**)] complex, long-range thallium isotope effect on the chemical shift (δ_H and δ_C) and on the coupling constants ($J_{Tl\text{-}H}$ and $J_{Tl\text{-}C}$) has been observed, confirming a strong and stable bond between Tl^{III} and **H_3L**.

Introduction

Single photon emission computed tomography (SPECT) imaging with ^{99m}Tc radionuclide is the most widely used method for routine diagnostic in nuclear medicine. If technetium-99m holds the foremost rank, this is due to its favorable nuclear characteristics (half-life 6.02 h, γ 140 keV), availability, and low cost. But when the pharmacokinetics of the radiopharmaceuticals are not well matched with the physical half-life of ^{99m}Tc, the preferred radionuclides for imaging are ^{111}In (half-life 67.4 h) or ^{67}Ga (half-life 78.1 h). Despite the great potential of the group-13 metal radionuclides in diagnostics, there are still few ligands devoted to the complexation of such radioactive ions. The most popular one, especially for In^{III} is diethylenetriaminetetraacetic acid (DTPA)[1] and its derivatives, in which one carboxylate group is often engaged to link the chelate moiety and the receptor-binding motif. However, the decreased denticity of such DTPA derivatives lower the stability of the formed complexes.[2] Thus, studying other chelation systems for the group-13 metal ions constitutes an important strategy for enhanced labelling efficiency of molecules of biological interest like peptides and monoclonal antibodies. Our laboratory is involved in the search and the synthesis of new radiopharmaceuticals for diagnostic or therapeutic applications. This led us to investigate the coordination chemistry of Ga, In, and to a lesser extent Tl (which have fewer biomedical applications). It might be worthwhile considering that, like [DTPA−In], numerous indium- or gallium-based radiopharmaceuticals are not fully chemically characterized. It is, however, of prime interest to determine the actual structure that is essential for obtaining a satisfactory comprehension of the properties of the complexes. Since group-13 (M^{III}) metal ions are usually hexacoordinated, we have investigated the chelating pattern of the tripodal imine ligand **H_3L**, derived from triethylenetriamine (*tren*) and 5-bromosalicyladehyde. Complexes of lanthanides and imine ligands derived from *tren* and salicylaldehyde[3,4] or aromatic ketones have already been described by Orvig et al.[5,6] These complexes where very unstable to moisture, and this property was attributed to the imine function, presumably hydrolyzed in water with the assistance of the acidic Ln^{III} ion. This observation led the author to study the complexation of lanthanides[7] and some group-13 metal ions (Al, Ga, and In)[8] with the saturated **H_3L**, where the imine double −N=CH− bond has been reduced to the much more stable amine −NH−CH_2− bond. The capability of the imine **H_3L** ligand to chelate Ga, In, or Tl has not been previously reported. This situation could be due to the reluctance of chemists to work with the so-called acid-sensitive imine-derived ligands. We report here the synthesis and the spectroscopic and structural characterizations of the whole post-transition group-13 metal complexes with **H_3L**.

Results and Discussion

Preparation

The one-pot complexation of M^{III} ions is not an effective method. Indeed, mixing a methanolic solution of *tren* and 5-bromosalicylaldehyde followed by the appropriate metal salt, results in the formation of a crystalline product, which was identified as the bicyclic acetal **A** shown in Scheme 1.

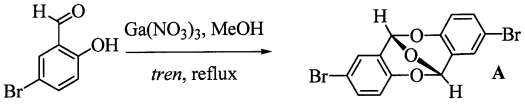

Scheme 1. Self-acetalization of 5-bromosalicylaldehyde

[a] Laboratoire d'Etudes Dynamiques et Structurales de la Sélectivité, Université Joseph Fourier, UMR CNRS 5616, 301 Rue de la Chimie, BP 53, 38041 Grenoble Cedex 09, France
Fax: (internat.) + 33-4/76514927
E-mail: Olivier.Jarjayes@ujf-grenoble.fr

 © WILEY-VCH Verlag GmbH, 69451 Weinheim, 2001 1434−1948/01/0808−2089 $ 17.50+.50/0

The recovery of this product is very likely due to the high Lewis acidity of the tricationic oxidation state of the group-13 metal ions, which are able to catalyze the self condensation of the bromosalicyladehyde. The strong acidic character of M^{III} is also confirmed by the formation of the nitrate salt of *tren*, also recovered under these conditions. Curiously, the more expected dimethoxyacetal, resulting from the reaction of the solvent (MeOH) and the aldehyde, is not isolated. This fact could be explained by a competition between the two reactions of acetalization that are chemically in equilibrium; but since **A** is less soluble in methanol than the dimethoxyacetal, the precipitation of the former shifts the equilibrium to its formation.

We can infer these observations to the lack of stability of the imine functions of the ligand in strongly acidic solutions. In other respects it is preferable to purify the ligand **H_3L** before complexation, otherwise poorer purity of the chelates results. Thus, a two-step synthesis was preferred. As depicted in Scheme 2, the tripodal **H_3L** ligand was synthesized according to Liu et al.[7] and purified by recrystallization in ethanol. It is of prime necessity to neutralize the acidic phenol functions of the ligand with a methanolic solution of NaOH (3 equiv.) prior to the introduction of a methanolic solution of the selected M^{III} salts in order to isolate the desired complexes. By this way, the result is a high recovery of the chelates (the yields ranging from 75 to 95%).

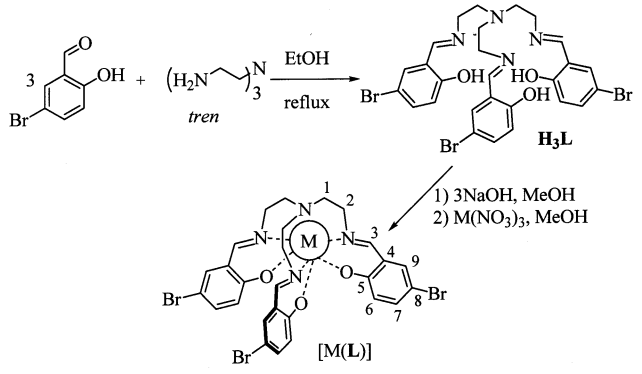

Scheme 2. Preparation scheme of **H_3L** ligand and [M(**L**)] complexes where M = Ga^{III}, In^{III} or Tl^{III}

The complexes are air-stable under neutral conditions both in the solid state and in solution in MeOH, $CHCl_3$, or DMSO, allowing their NMR characterization {exception [In(**L**)], scarcely soluble}. These results point out that once isolated, the imine complexes are not subject to hydrolysis as was written by Orvig et al.[7] Thus, the experimental preparation process is the key point for hydrolysis to occur. It happens only at low pH values if the acidity released during the complexation is not neutralized with a base. Our results are in accordance with those of Costes et al.,[9] and Kocian et al.[10] In this latter case, triethylamine proves to be too weak to allow the recovering of imine-phenole Gd^{III} complexes, only a strong base like hydroxide or methoxide ion permits the preparation of the desired chelates.

All our complexes gave satisfactory elemental analyses. The FAB^+ mass spectra obtained in a 3-nitrobenzyl alcohol matrix show the molecular ion peaks at $[M + H]^+$ (100% intensity) and the IR data show a characteristic strong band near 1625 cm^{-1} that confirms the presence of the imine function. Furthermore, no band was detected in the range 3500−3000 cm^{-1}, indicating the complete deprotonation of the phenol groups by NaOH and the absence of the N−H bond. This later remark also strongly supports the stability of the imine function in the complexes. Indeed, as a possible event, hydrolysis of the imine should result in the formation of such an N−H bond. All these data are consistent with the proposed formulation $[M(\mathbf{L})]^0$. Slow concentration of diluted methanolic solution gave crystalline material suitable for X-ray crystallographic study.

Crystallographic Studies

An ORTEP drawing of **H_3L** is illustrated in Figure 1 and details of the structure determination are collected in Table 1.

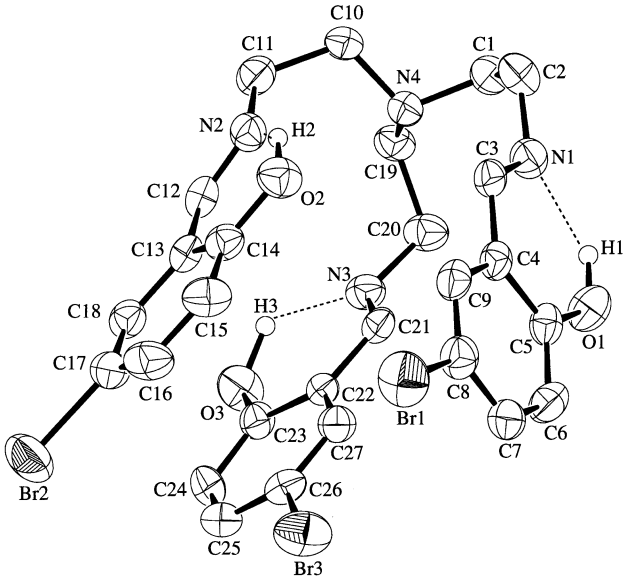

Figure 1. Structural representation of **H_3L**; hydrogen atoms are omitted for clarity

There are two **H_3L** molecules in each triclinic unit cell. All the interatomic distances and bond angles for the organic part are in the range of those given by Allen et al.[15] There is a strong hydrogen bond connecting the hydroxy hydrogen atoms and the imine nitrogen atoms (O1−H1···N1 1.89 Å, O2−H2···N2 1.67 Å, O3−H3···N3 1.79 Å) thus forming an almost planar six-membered ring. No interstrand bonds are detected, and contrary to what it is observed for other tripodal ligands,[16,17] there is no preorganization of **H_3L** in the solid state. The formation of a three-dimensional cavity with a specific spatial arrangement of the donor atoms is only achieved in the presence of the metal ions.

An ORTEP drawing of [Ga(**L**)] is illustrated in Figure 2. All the complexes are neutral with a triply deprotonated N_3O_3 imine phenol ligand completely encapsulating the M^{III} ions. The In^{III} and Tl^{III} compounds are isostructural.

Table 1. Summary of crystallographic data and structure refinement for **H_3L**, [Ga(**L**)], [In(**L**)], and [Tl(**L**)]

Compound	**H_3L**	[Ga(**L**)]	[In(**L**)]	[Tl(**L**)]
Empirical formula	$C_{27}H_{27}Br_3N_4O_3$	$C_{27}H_{24}Br_3GaN_4O_3{\cdot}CH_3OH$	$C_{27}H_{24}Br_3InN_4O_3$	$C_{27}H_{24}Br_3N_4O_3Tl$
Molecular mass	695.25	793.99	807.04	896.59
F(000)	692	784	784	848
Color/habit	pale yellow/triclinic prism	pale yellow/triclinic prism	pale yellow/triclinic prism	pale yellow/triclinic prism
Crystal size [mm]	0.24 × 0.22 × 0.21	0.18 × 0.16 × 0.16	0.22 × 0.20 × 0.19	0.17 × 0.16 × 0.16
a [Å]	9.957(1)	9.632(3)	10.366(1)	10.437(1)
b [Å]	11.970(1)	11.766(4)	11.852(4)	11.808(1)
c [Å]	13.347(1)	13.240(2)	12.899(4)	12.844(1)
α [°]	89.36(1)	101.67(2)	114.15(3)	113.69(1)
β [°]	77.21(1)	101.41(2)	95.62(2)	95.75(1)
γ [°]	67.19(1)	89.12(2)	102.18(3)	100.89(1)
V [Å^3], Z	1425.0(3), 2	1440.0(7), 2	1383.0(9), 2	1395.8(3), 2
Space group	$P\bar{1}$	$P\bar{1}$	$P\bar{1}$	$P\bar{1}$
$d_{calcd.}$ [g/cm^3]	1.620	1.831	1.938	2.133
Wavelength [Å]	0.5608 (Ag-K_α)	0.7107 (Mo-K_α)	0.7107 (Mo-K_α)	0.5608 (Ag-K_α)
μ [cm^{-1}]	22.96	51.72	52.37	54.80
Diffractometer	Enraf−Nonius Kappa CCD	Enraf−Nonius Cad-4	Enraf−Nonius Cad-4	Enraf−Nonius Kappa CCD
Scan type	φ	φ	ω	ω
2θ max [°]	36.3	59.9	60.0	51.5
No. of reflections measured/unique	7381/3925	8563/8323	8387/8040	14978/7964
with $F_o > n\sigma(F_o)$	2669 (n = 2)	4674 (n = 2)	5375 (n = 2)	6410 (n = 3)
Decay (%), correction	−	4.04, applied	0.22, none	−
Data reduction software	DENZO[a]	TEXSAN[b]	TEXSAN[b]	DENZO[a]
No. of variables	334	433	415	415
Structure solution software	TEXSAN[b]	TEXSAN[b]	TEXSAN[b]	TEXSAN[b]
Refinement (F)	full-matrix	full-matrix	full-matrix	full-matrix
H (from difference Fourier)	not refined	refined with riding model	refined with riding model	refined with riding model
Weighting scheme	$w = [\sigma^2(F_o) + p^2/4\|F_o\|^2]^{-1}$	$w = [\sigma^2(F_o) + p^2/4\|F_o\|^2]^{-1}$	$w = [\sigma^2(F_o) + p^2/4\|F_o\|^2]^{-1}$	$w = [\sigma^2(F_o) + p^2/4\|F_o\|^2]^{-1}$
Fudge factor (p)	0	0.021	0.020	0
Extinction correction	none	none	none	none
Absorption correction	none	ψ scan[c]	ψ scan[c]	multiscan[d]
T_{max}/T_{min}		0.999/0.835	0.999/0.822	0.999/0.880
Max. resid. dens. [e$^-$/Å^3]	−0.51/0.47	−0.67/1.00	−1.30/1.25	−1.29/1.22
Goodness of fit	1.514	1.881	1.955	1.286
Max shift/error	0.02	0.02	0.02	0.02
R/R_w	0.049/0.039	0.048/0.041	0.044/0.039	0.029/0.037

[a] Ref.[11] — [b] Ref.[12] — [c] Ref.[13] — [d] Ref.[14]

In the three complexes, the cations have an octahedral environment where the ligand occupies all six coordination sites around the metal ion by bonding through the lone pairs of the three imino nitrogen atoms and the three deprotonated phenolic oxygen atoms, leading to a three-fold axis passing through the metal ion and the tertiary amine function.

Despite the larger size of In^{III} and Tl^{III}, the coordination of all seven donor atoms is not observed. Indeed, the apical nitrogen atom of the *tren* part, being in all cases at much longer distances from the metal center [Tl: 2.759(3) Å; In: 2.828(3) Å; and Ga: 3.342(3) Å] does not participate in the chelation of group-13 metal ions. Each N_3 and O_3 donor set coordinates to the M^{III} ions in a facial way to form a distorted octahedral geometry as shown in Table 2.

The TlO_3N_3 and InO_3N_3 octahedra are more distorted than the GaO_3N_3 one. For [Tl(**L**)], the distortion of the coordination sphere is most evident in the compression of O−Tl−O (average 85.76°) and expansion in the N−Tl−O angles (average 106.77°) from 90°. As a result, the three

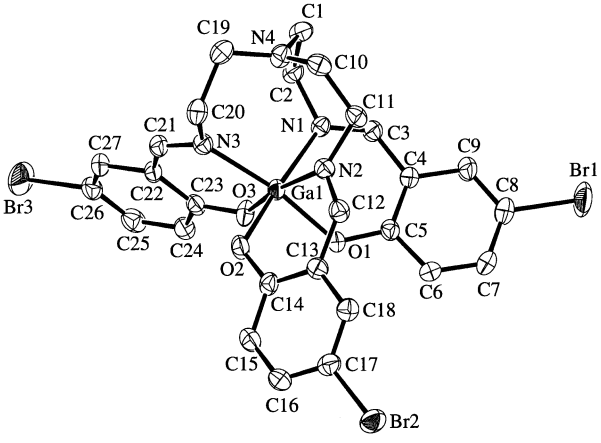

Figure 2. Structural representation of [Ga(**L**)]; hydrogen atoms are omitted for clarity

trans-O−Tl−N angles have an average value of 163.08°. If one considers the angles, those of the GaO_3N_3 octahedron are closer to regular values.

Table 2. Main bond angles [°] in the GaO_3N_3, InO_3N_3 and TlO_3N_3 entities; standard deviations are given in parentheses

[Ga(**L**)]		[In(**L**)]		[Tl(**L**)]	
O1−Ga1−O2	89.4(1)	O1−In1−O2	86.97(9)	O1−Tl1−O2	85.72(9)
O1−Ga1−O3	85.3(1)	O1−In1−O3	90.01(9)	O1−Tl1−O3	88.73(9)
O2−Ga1−O3	96.4(1)	O2−In1−O3	84.84(9)	O2−Tl1−O3	82.84(8)
O1−Ga1−N1	89.1(1)	O1−In1−N1	82.59(9)	O1−Tl1−N1	81.17(9)
O1−Ga1−N2	85.7(1)	O1−In1−N2	84.27(9)	O1−Tl1−N2	85.04(9)
O1−Ga1−N3	171.1(1)	O1−In1−N3	167.2(1)	O1−Tl1−N3	164.3(1)
O2−Ga1−N1	174.8(1)	O2−In1−N1	165.73(9)	O2−Tl1−N1	163.92(9)
O2−Ga1−N2	86.4(1)	O2−In1−N2	81.13(9)	O2−Tl1−N2	78.83(9)
O2−Ga1−N3	83.9(1)	O2−In1−N3	82.9(1)	O2−Tl1−N3	82.70(9)
O3−Ga1−N1	88.5(1)	O3−In1−N1	85.5(1)	O3−Tl1−N1	87.59(9)
O3−Ga1−N2	170.6(1)	O3−In1−N2	165.09(9)	O3−Tl1−N2	161.01(9)
O3−Ga1−N3	89.6(1)	O3−In1−N3	81.35(9)	O3−Tl1−N3	79.33(9)
N1−Ga1−N2	88.5(1)	N1−In1−N2	107.3(1)	N1−Tl1−N2	109.1(1)
N1−Ga1−N3	98.1(1)	N1−In1−N3	105.9(1)	N1−Tl1−N3	108.2(1)
N2−Ga1−N3	99.7(1)	N2−In1−N3	101.78(9)	N2−Tl1−N3	103.01(9)

The coordination behavior of **H_3L** is not dependent on the size of the coordinated metal ion. This ligand presents a roughly invariable coordination cavity. Indeed, the three metal ions (Ga^{III}, In^{III}, and Tl^{III}) are bonded in a similar way by an N_3O_3 donor set, which leads us to consider that **H_3L** is well tailored for six-coordinated neutral group-13 and lanthanide metal ion complexes. This cavity seems to fit to these three metal ions, with no significant strain on the coordinated ligand framework, contrary to the tripodal N_4O_3 amine phenol ligand where the coordination mode is metal-dependent: for large lanthanide ions, homodinuclear dimers are formed, while cationic mononuclear complexes are obtained with Al^{III} and Ga^{III}.[7,18] Selected bond lengths and angles are listed in Table 3 for the three complexes.

Table 3. Main interatomic distances [Å] for [Ga(**L**)], [In(**L**)], and [Tl(**L**)]

[Ga(**L**)]		[In(**L**)]		[Tl(**L**)]	
Ga1−O1	1.932(2)	In1−O1	2.125(2)	Tl1−O1	2.235(2)
Ga1−O2	1.922(2)	In1−O2	2.131(2)	Tl1−O2	2.243(2)
Ga1−O3	1.931(2)	In1−O3	2.148(2)	Tl1−O3	2.252(2)
Ga1−N1	2.077(3)	In1−N1	2.245(3)	Tl1−N1	2.295(3)
Ga1−N2	2.190(3)	In1−N2	2.271(3)	Tl1−N2	2.343(3)
Ga1−N3	2.090(3)	In1−N3	2.280(3)	Tl1−N3	2.328(3)

Comparison of the bond lengths shows that M^{III}−N and M^{III}−O increase on going from Ga^{III} to Tl^{III}. This trend is consistent with the larger ionic radius of the Tl^{III} ion in an octahedral environment. Ga−O and Ga−N, In−O and In−N distances are very similar to those found in other tripodal amine phenol N_4O_3 and N_3O_3 complexes[18,19] and imine phenol N_3O_3 complexes.[20]

It has been postulated that complex stability is closely related to the size of the chelate rings, and to the size of metal ion.[21] As chelate ring size increases from five to six, stability of metal complexes generally decreases. The larger the coordinated metal ion, the greater the destabilization in the metal complex as the chelate ring size increases from five to six. However, despite this general trend, we have been able to synthesize and characterize the three [M(**L**)] complexes.

NMR Studies

^{1}H NMR spectra of the ligand **H_3L** and the three complexes are shown in Figure 3. The ^{1}H NMR spectrum of the ligand in $CDCl_3$ at 400 MHz is relatively simple, with three aromatic proton signals at δ = 6.49, δ = 6.83, and δ = 7.32. The imine proton resonates at δ = 7.80 and the two methylene groups giving an AA′XX′ splitting pattern at δ = 2.83 and δ = 3.55. The proton signals were assigned using homonuclear 2D techniques (COSY) and are consistent with literature results.[7,17]

^{1}H and ^{13}C NMR spectra of the Ga^{III} and In^{III} complexes were recorded in $CDCl_3$ while the Tl^{III} complex was recorded in [D_6]DMSO. However, they both show similar features. Only one set of ^{1}H NMR resonance signals proved that the three chelating arms of the ligand remained chemically equivalent upon coordination. This is in contrast with amine phenol Al, Ga, and In complexes described by Orvig et al.,[8] in which the Ga atom is coordinated by an N_4O_2 donor set from the N_4O_3 amine phenol ligand, with one of the three phenolate oxygen atoms remaining noncoordinating and protonated.

For the [Ga(**L**)] complex, the ethylenic hydrogen atoms form an AA′BB′ spin system consisting of a distinct resonance corresponding to each of the four hydrogen atoms. This is a pattern already described for similar systems[22,23] and small heterocyclic ring structures,[24] whereby the ethylenic hydrogen atoms are locked in an axial/equatorial-type conformation.

From the crystallographic data, the angles and dihedral angles between the four different protons are available. The schematic Newman representation depicted in Figure 3 is drawn from these values. The angles between H_A and $H_{A'}$, H_A and H_B, and H_B and $H_{B'}$ are 70°, −61°, and 169°, respectively. According to the literature,[25] the coupling constants $J_{BB'} = J_{trans}$ lie in the range of 10 to 13 Hz, while the geminal coupling constants J_{AB} and $J_{A'B'}$ or J_{gem} have aver-

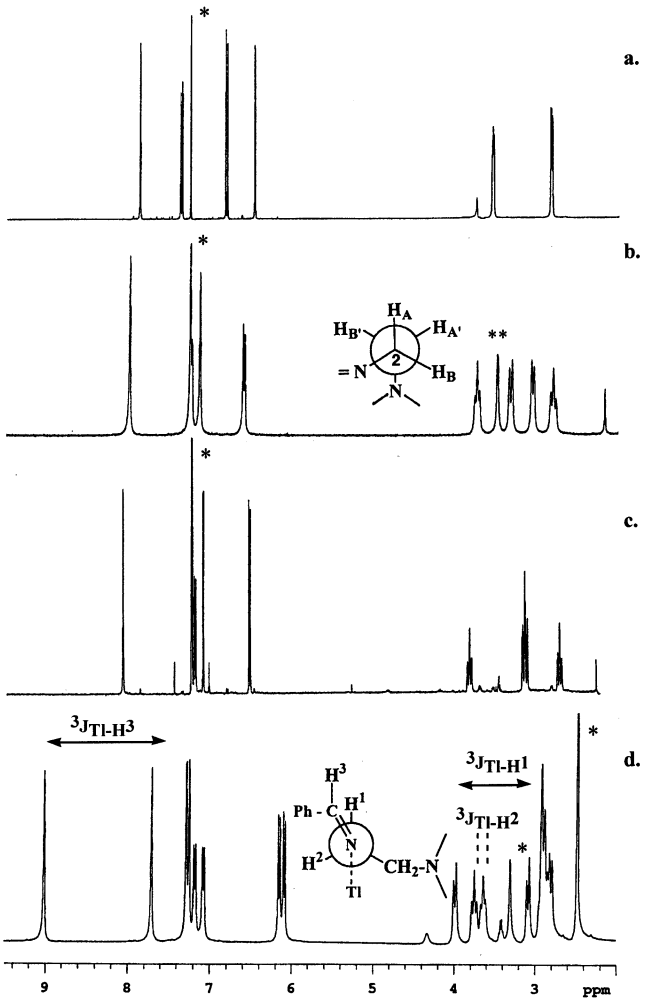

Figure 3. ^{1}H NMR spectra of a: $\mathbf{H_3L}$, b: [Ga(**L**)], c: [In(**L**)], in $CDCl_3$ and d: [Tl(**L**)] in DMSO; the asterisks (*) represent residual solvent peaks and methanol (**)

age values of −10 to −16 Hz. Moreover, if we take into account the model of Karplus, the $J_{AA'}$ and $J_{BA'}$ values must be very small or equal to zero. Finally, considering all of these data, the AA′BB′ part of the spectrum can be simulated and compared to the experimental spectrum. Using an iteration method, one can obtain a simulated spectrum for the [Ga(**L**)] complex superimposed on the experimental one, for the values of $J_{BB'}$, J_{AB}, and $J_{A'B'}$ equal to 13.3 Hz, −11.3 Hz, and −13.2 Hz, respectively. Similarly, the $J_{A'B}$, $J_{AB'}$ and $J_{AA'}$ values are 0.2 Hz, 0.1 Hz, and 0.2 Hz, respectively. In this case, the two protons H_A and $H_{A'}$ appear as two doublets at δ = 3.05 and δ = 3.32, respectively, while the two protons H_B and $H_{B'}$ appear as two pseudo triplets at δ = 3.73 and δ = 2.80, respectively. The same analysis has been ruled out for the [In(**L**)] complex, and the experimental spectrum could be simulated. The only difference to note with [Ga(**L**)] is the overlap of the two doublets of protons A and A′ giving rise to another pseudo triplet with an intensity of two. These observations clearly demonstrate that the rigid structures of the complexes are consistent with the determined structures by X-ray diffraction.

The $^{13}C\{^1H\}$ NMR spectrum consist for the [Ga(**L**)] complex of nine resonances. The complete assignment was made with the aid of 2D homonuclear (COSY) and heteronuclear (HMQC and HMBC) experiments. The aromatic carbon signals all appear in the range of δ = 105−168. The ethylenic carbon signals appear at δ = 57−61, while the imine carbon signal lies at δ = 170. The analysis of this spectrum also supports the structure of the complex shown in Figure 2 in which the metal ion is bound to the N_3O_3 core in a facial arrangement. The solubility of the [In(**L**)] complex was so poor in most of the common NMR solvents that recording the ^{13}C spectrum was excluded.

The [Tl(**L**)] complex has also been studied in solution in [D_6]DMSO. The ^{1}H NMR spectrum characterizing the complex is reported in Figure 3, and is very similar to the two previous complexes [Ga(**L**)] and [In(**L**)]. All three arms are equivalent as a result of the symmetric binding of the ligand to the metal center. Indeed, the observation of the relative simplicity of the ^{1}H and ^{13}C spectra implies that a C_3 symmetry axis is present for [M(**L**)] in solution. $^{205,203}Tl-^1H$ couplings are noticeable for most of the protons of the complex. The largest coupling constant ($^3J_{Tl-H3}$ = 523 Hz) is observed for the imine proton. A value of 709 Hz has also recently been given for a macrobicyclic complex of Tl^{III}.[26] Aromatic protons also show small coupling constants with Tl^{III} ranging from 13 to 41 Hz for ^4J and ^5J. The ethylenic protons H^1 and H^2 of the complex also form a part of an AA′BB′ spin system, but are split by the presence of the Tl^{III} ion. Assuming that a Karplus-like relationship[27,28] is also valid for this kind of vicinal coupling between Tl and the protons, the larger value of $^3J_{Tl-H}$ is indicative of a *trans* position between H^1 and Tl, while the smaller one ($^3J_{Tl-H2}$ = 45 Hz) is interpreted as resulting from a torsional angle smaller than 90°, where a minimum in the Karplus function is expected. These considerations are supported by the crystallographic data. Indeed, in the solid state, the dihedral angle values between Tl and H^1, and Tl and H^2 are −171° and 62°, respectively. Moreover, the dihedral angle value between the imine proton (H^3) and Tl is −167°, which explains the large value of this coupling. The $^3J_{Tl-H}$ can thus be seen as a stereochemically sensitive parameter, as described for [Tl−EDTA] complexes.[29] Once formed, the neutral complex is stable, and even in DMSO, a good coordinating solvent, the spectroscopic behavior of [Tl(**L**)] is in complete agreement with the solid-state data. The stability in DMSO of such complexes has also been noted for tripodal Ln complexes derived from 3-methoxysalicylaldehyde, only if deprotonation of the ligands is made with a strong base prior to the addition of Ln^{III} ions.[30]

In order to examine the fluxionality of the complexes in organic solvents ($CDCl_3$ and [D_6]DMSO), the variable-temperature (298−355 K) ^{1}H NMR spectra were recorded for [Ga(**L**)] and [Tl(**L**)], since all the complexes have very similar structures, the behavior of the In species must be very similar. No significant changes in the spectral parameters were noticed, except for minor shifts probably caused by

the thermal vibrations of the coordinated ligand framework. This clearly shows that all the complexes remain unchanged in solution in this temperature range. Therefore, the intact and rigid structure of these complexes in solution is demonstrated.

Finally, a specificity interesting to notice is that natural thallium consists of two spin 1/2 isotopes, ^{203}Tl and ^{205}Tl present in the relative abundance of 0.295 and 0.705, respectively. Spin-spin coupling constants between Tl and ^{1}H, and Tl and ^{13}C are thus observable. Moreover, one can observe a $^{205/203}$Tl isotope effect on ^{1}H and ^{13}C in the NMR spectra as shown in Figure 4.

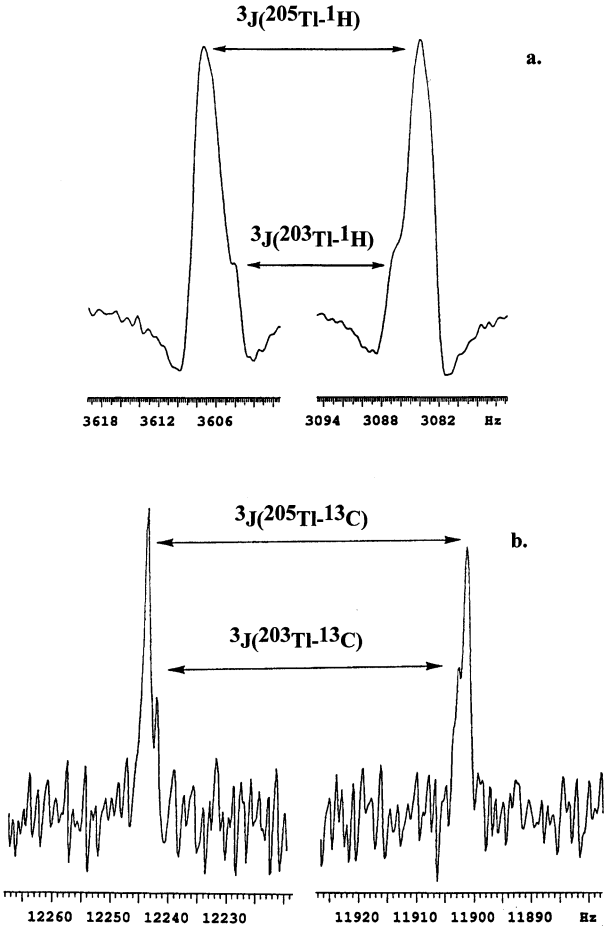

Figure 4. NMR spectra of [Tl(**L**)] in DMSO showing the isotope effect in a. on H^3 and in b. on C^4

The presence of the two thallium isotopes induces a secondary isotope effect on ^{1}H and ^{13}C in the NMR spectra, which is also called isotope shift. This secondary isotope effect on nuclear shielding is defined as the difference (Δ) in the chemical shift (δ) of a nucleus N in the isotopomer with the heavier isotope ^{k}X relative to the isotopomer with the lighter isotope ^{l}X at a site *n* bonds away and expressed by[31]

$$^{n}\Delta\delta N(^{k/l}X) = \delta N(^{k}X) - \delta N(^{l}X)$$

The superscript *n* is the number of bonds between nuclei N and X. In most cases,[32] the chemical shift for the higher isotope is at a lower frequency, thus $^{n}\Delta\delta N(^{k/l}X)$ is negative. This means that the heavier isotope causes increased shielding. In this study, the contrary is observed. Positive values of 0.625 ppb and 2.780 ppb are obtained for $^{3}\Delta\delta H(^{205/203}Tl)$ and $^{3}\Delta\delta C(^{205/203}Tl)$, respectively. It is very difficult to comment on these data because to the best of our knowledge no such $^{3}\Delta\delta H$ and $^{3}\Delta\delta C$ are available in the literature for coordination compounds. However, similar values lying in the range -1.76 to -0.88 ppb are observed for $^{3}\Delta\delta F$ in chlorofluorocarbons.[33]

For spin-spin coupling constants, the magnitude of the interaction *J*(YZ), expressed in Hz, also depends on the magnetogyric ratio of the Y and Z nuclei, and when a nucleus ^{m}Y is replaced by an isotopic species ^{n}Y, the ratio $J(^{m}YZ)/J(^{n}YZ)$ is equal to $\gamma(^{m}Y)/\gamma(^{n}Y)$. According to Figure 4, the ratios $^{3}J(^{203}Tl-^{1}H)/^{3}J(^{205}Tl-^{1}H)$ and $^{3}J(^{203}Tl-^{13}C)/^{3}J(^{205}Tl-^{13}C)$ are equal to 0.9886 and 0.9915, respectively, while $\gamma(^{203}Tl)/\gamma(^{205}Tl) = 0.9902$ confirming thus an isotope effect on coupling constants. If the isotopically substituted nucleus Y (^{m}Y/^{n}Y substitution) is involved in spin-spin interaction, one can measure a primary isotope effect on the coupling constant[32] defined as

$$^{p,q}\Delta J_X = \frac{\gamma(^{m}Y)}{\gamma(^{n}Y)} J(^{r}X^{n}Y) - J(^{r}X^{m}Y) \qquad \text{with } n > m$$

where *p* and *q* denote the number of bonds separating the site of isotopic substitution and each of the two nuclei involved in spin-spin coupling. From ^{1}H and ^{13}C NMR spectra, $^{0,3}\Delta J_H$ and $^{0,3}\Delta J_C$ values of 0.86 Hz and -0.43 Hz, respectively, are obtained only from the imine proton H^3, and the carbon atom C^4, these two atoms having the largest coupling constant with Tl^{III}. These rather low $^{0,3}\Delta J_H$ and $^{0,3}\Delta J_C$ values, which do not exceed 0.2% of the coupling constants, represent an effect through three bonds. Data on isotope effects for the coupling constants between heavy isotopes other than protons are more documented for organic compounds,[32,34] but nonexistent in coordination chemistry. However, the largest $^{1}J(^{13}C-Tl)$ values have been measured for mono- and dicyano complexes of Tl^{III}, with $^{0,1}\Delta J$ visualized in the spectra,[35] but not investigated. Any discussion of these isotope effect values would require theoretical developments.[34] Yet, what can be said is that the observation of an isotope effect implies a strong Tl−ligand coordination bond.

Conclusion

We have shown that tripodal Schiff base phenol complexes derived from salicylaldehyde, *tren* and the acidic Ga^{III}, In^{III}, and Tl^{III} metal ions could be easily prepared without noticeable imine hydrolysis. The accurate structure of all the complexes show a constant coordinating pattern

of the tripodal ligand that acts as a hexadentate ligand, giving isostructural species from Ga^{III} to Tl^{III}. Further, NMR-spectroscopic data strongly support that the rigid structure in the solid state is maintained in DMSO or $CDCl_3$ solutions. Consequently, these facts involve a strong coordination of the metal ions. This characteristic is very favorable for biomedical applications. Investigations concerning this topic are currently underway and the results will be described elsewhere.

Experimental Section

General Remarks: Tris(aminoethyl)amine (*tren*) and hydrated metal salts [$Ga(NO_3)_3$, $In(NO_3)_3$ and $Tl(NO_3)_3$] were obtained from Acros. 5-Bromosalicylaldehyde was obtained from Lancaster. All chemicals were used without further purification. Thallium is highly poisonous and should be handled with caution.[36] – NMR spectra were recorded with a Varian U400 spectrometer (operating at 100.58 MHz for ^{13}C). Each spectrum was referenced to the solvent used at room temperature. – Mass spectrometry (FAB^+ mode) experiments were run in a 3-nitrobenzyl alcohol matrix with a Nermag R10 spectrometer. – Infrared spectra were recorded as KBr disks in the range 400−4000 cm^{-1} with a Nicolet Impact 400 spectrometer. – Elemental analysis for C, H and N were performed by the Service Central d'Analyses (CNRS) at Vernaison (France).

Synthesis of Tris[(5-bromosalicylidene)aminoethyl]amine (H_3L): The ligand tris[(5-bromosalicylidene)aminoethyl]amine (**H_3L**) was prepared according to the method reported in the literature.[7] To a warm solution of 5-bromosalicyladehyde (6.03 g, 30 mmol) in absolute ethanol (100 mL) was added a solution of tris(aminoethyl)amine (1.46 g, 10 mmol) in EtOH (40 mL). After the addition was complete, the resulting bright yellow suspension was heated at reflux for 20 min and then stirred at room temperature for 0.5 h. The mixture was cooled in an ice bath for 15 min, and the yellow microcrystals were collected by filtration, washed with cold EtOH (40 mL) and Et_2O. The solid was dried under vacuum. Yield 5.36 g (77%). M.p. 145−146 °C (ref.[7] 144−145 °C). Slow evaporation of the solvent from the filtrate yielded suitable crystals for X-ray diffraction studies.

Synthesis of the Complexes, General Procedure: [M(**L**)] complexes were prepared as follows. To a suspension of the ligand **H_3L** (1 mmol) in methanol (25 mL), was added NaOH (0.12 g, 3 mmol in 10 mL of MeOH). To this homogeneous solution was added the metal nitrate in methanol (1 mmol in 25 mL). A precipitate formed immediately. The mixture was stirred at reflux for 15 min and then cooled to room temperature. The solid was filtered off; washed with methanol (2 × 20 mL) and diethyl ether (2 × 10 mL), and then dried in vacuum. Slow concentration of the filtrate over a period of two weeks yielded suitable crystals for X-ray diffraction studies.

[Ga(L)] (1): Yield: 0.720 g, 94%. – $C_{27}H_{24}Br_3GaN_4O_3$: calcd. C 42.56, H 3.17, N 7.35; found C 42.55, H 3.51, N 7.08. – ^{13}C NMR ($CDCl_3$, room temp.): δ = 57.2 (C^1), 61.7 (C^2), 105.1 (C^8), 118.4 (C^4), 125.2 (C^6) 135.8 (C^9), 137.5 (C^7), 167.9 (C^5), 169.6 (C^3). – IR (KBr): $\tilde{\nu}$ = 3047 (weak, C−H phenyl), 2877, 2840 (s, C−H aliphatic), 1622 (very strong, C=N imine), 1182 (s, C−O) cm^{-1}. – MS (FAB^+): *m/z* (%) = 763 (100) $[M + H]^+$.

[In(L)] (2): Yield: 0.605 g, 75%. – $C_{27}H_{24}Br_3InN_4O_3$: calcd. C 40.18, H 3.00, N 6.94; Br, 29.70; found C 39.71, H 2.94, N 6.77; Br, 29.36. – IR (KBr): $\tilde{\nu}$: = 3048 (weak, C−H phenyl), 2908, 2846 (s, C−H aliphatic), 1627 (very strong, C=N imine), 1169 (s, C−O) cm^{-1}. – MS (FAB^+): *m/z* (%) = 807 (100) $[M + H]^+$.

[Tl(L)] (3): Yield: 0.848 g, 95%. – $C_{27}H_{24}Br_3TlN_4O_3$: calcd. C 36.17, H 2.70, N 6.25; Br, 26.74; found C 35.76, H 2.77, N 6.18; Br, 26.53. – ^{13}C NMR ([D_6]DMSO, room temp.): δ = 55.2 (C^1), 55.7 (C^2, ^2J = 193.03 Hz), 102.1 (C^8, ^5J = 32.59 Hz), 120.0 (C^4, ^3J = 342.05 Hz), 125.2 (C^6, ^3J = 160.10 Hz), 135.1 (C^9, ^4J = 10.44 Hz), 136.5 (C^7, ^4J = 40.19 Hz), 170.2 (C^3, ^2J = 93.96 Hz), 172.1 (C^5, ^2J = 195.85 Hz). – IR (KBr): $\tilde{\nu}$ = 3047 (weak, C−H phenyl), 2877, 2840 (s, C−H aliphatic), 1622 (very strong, C=N imine), 1182 (s, C−O) cm^{-1}. – MS (FAB): *m/z* (%) = 897 (100) $[M + H]^+$.

X-ray Crystallographic Study: The main crystallographic features, the strategy used for the crystal structure determination, and its results are gathered in Table 1. Data collections were carried out at room temperature. The U_{iso} values of the H atoms have been fixed to 1.2 × $U_{equiv.}$ of the C atoms they are attached to. The structures were solved by direct methods (SIR92).[37] Crystallographic data (excluding structure factors), for the structures reported in this paper have been deposited with the Cambridge Crystallographic Data Centre as supplementary publication no. CCDC-152917, -152918, -152919, -152920 for [Tl(**L**)], [In(**L**)], [Ga(**L**)] and **H_3L**, respectively. Copies of the data can be obtained free of charge on applicaton to CCDC, 12 Union Road, Cambridge CB2 1EZ, UK [Fax: (internat.) + 44-1223/336-033; E-mail: deposit@ccdc.cam.ac.uk.

Acknowledgments

We are very grateful to Prof. C. G. Béguin for fruitful discussions and a careful reading of the manuscript.

[1] H. M. Chilton, R. J. Cowan, *Pharmaceuticals in Medical Imaging* (Eds.: D. P. Swanson, H. M. Chilton, J. H. Thrall), MacMillan Publishing Co., New York, **1990**, p. 330−342.
[2] M. W. Brechbiel, O. A. Gansow, R. W. Atcher, J. Schlom, J. Esteban, D. E. Simpson, D. Colcher, *Inorg. Chem.* **1986**, *25*, 2772−2781.
[3] M. Kanesato, T. Yokoyama, T. M. Suzuki, *Chem. Lett.* **1997**, 93−94.
[4] U. Casellato, S. Tamburini, P. Tomasin, P. A. Vigato, M. Botta, *Inorg. Chim. Acta* **1996**, *247*, 143−145.
[5] A. Smith, S. J. Rettig, C. Orvig, *Inorg. Chem.* **1988**, *27*, 3929−3934.
[6] D. J. Berg, S. T. Rettig, C. Orvig, *J. Am. Chem. Soc.* **1991**, *113*, 2528−2532.
[7] S. Liu, L. Gelmini, S. T. Rettig, R. C. Thompson, C. Orvig, *J. Am. Chem. Soc.* **1992**, *114*, 6081−6087.
[8] S. Liu, S. T. Rettig, C. Orvig, *Inorg. Chem.* **1992**, *31*, 5400−5407.
[9] J. P. Costes, F. Dahan, A. Dupuis, S. Lagrave, J. P. Laurent, *Inorg. Chem.* **1998**, *37*, 153−155.
[10] O. Kocian, K. W. Chiu, R. Demeure, B. Gallez, C. J. Jones, J. R. Thornback, *J. Chem. Soc., Perkin Trans. 1* **1994**, 527−535.
[11] DENZO-SMN, Data processing software, Nonius, Delft, The Netherlands, **1998**.
[12] TEXSAN, Single Crystal Structure Analysis Software, Version 1.7, Molecular Structure Corporation (MSC), 3200 Research Forest Drive, The Woodlands, TX 77381, USA, **1992−1997**.
[13] A. C. T. North, D. C. Philips, F. S. Mathews, *Acta Crystallogr., Sect. A* **1968**, *24*, 351−359.
[14] R. H. Blessing, *Acta Crystallogr., Sect. A* **1995**, *51*, 33−38.
[15] F. H. Allen, O. Kennard, D. G. Watson, L. Brammer, A. G. Orpen, R. Taylor, *J. Chem. Soc., Perkin Trans. 2* **1987**, S1−S19.
[16] S. Liu, E. Wong, S. J. Rettig, C. Orvig, *Inorg. Chem.* **1993**, *32*, 4268−4276.

[17] N. Gündüz, T. Gündüz, M. B. Hursthouse, H. G. Parkes, L. S. Shaw, R. A. Shaw, M. Tüzün, *J. Chem. Soc., Perkin Trans. 2* **1985**, 899−902.
[18] S. Liu, S. J. Rettig, C. Orvig, *Inorg. Chem.* **1992**, *31*, 5400−5407.
[19] S. Liu, E. Wong, V. Karunaratne, S. J. Rettig, C. Orvig, *Inorg. Chem.* **1993**, *32*, 1756−1765.
[20] M. A. Green, M. J. Welch, J. C. Huffman, *J. Am. Chem. Soc.* **1984**, *106*, 3689−3691.
[21] R. D. Hancock, A. E. Martell, *Chem. Rev.* **1989**, *89*, 1875−1914.
[22] M. P. Lowe, S. J. Rettig, C. Orvig, *J. Am. Chem. Soc.* **1996**, *118*, 10446−10456.
[23] G. Serratrice, H. Boukhalfa, C. Béguin, P. Baret, C. Caris, J. L. Pierre, *Inorg. Chem.* **1997**, *36*, 3898−3910.
[24] H. Günther, *NMR Spectroscopy*, 3rd ed., J. Wiley and Son, New York, **1985**, chapter 5.
[25] M. L. Martin, J. J. Delpuech, G. J. Martin, *Practical NMR Spectroscopy*, Heyden and Sons Ltd., London, **1980**.
[26] M. G. B. Dew, O. W. Howarth, N. Martin, G. G. Morgan, J. Nelson, *J. Chem. Soc., Dalton Trans.* **2000**, 1275- 1278.
[27] M. Karplus, *J. Chem. Phys.* **1959**, *60*, 11−25.
[28] C. A. G. Haasnoot, F. A. A. M. de Leew, C. C. Altona, *Tetrahedron* **1980**, *36*, 2783−2787.
[29] S. Musso, G. Anderegg, H. Rüegger, C. W. Schläpfer, V. Gramlich, *Inorg. Chem.* **1995**, *34*, 3329−3338.
[30] J. P. Costes, A. Dupuis, G. Commenges, S. Lagrave, J. P. Laurent, *Inorg. Chim. Acta* **1999**, *285*, 49−54.
[31] C. J. Jameson, in *Isotopic applications in NMR studies*, vol. 2 (Isotopes in the physical and biochemical sciences) (Ed.: J. Buncel, Jr.), Elsevier, Amsterdam, **1991**, chapter 1.
[32] N. M. Sergeyev, *NMR Basic Princ. Prog.* **1990**, *22*, 31−80.
[33] M. Tordeux, C. Wakselman, O. Jarjayes, C. G. Béguin, *Magn. Res. Chem.*, **2001**, *39*, 301−310.
[34] C. J. Jameson, in *Encyclopedia of NMR* (Eds.: D. M. Grant, R. K. Harris) Wiley, Chichester, **1996**, p. 2638−2655.
[35] J. Blixt, B. Györi, J. Glaser, *J. Am. Chem. Soc.* **1989**, *20*, 7787−7791.
[36] H. G. Seiler, H. Sigel, A. Sigel, *Handbook on Toxicity of Inorganic Compounds*, M. Dekker Inc., New York, Basel, **1988**.
[37] A. Altomare, A. Cascarano, G. Giacovazzo, A. Guagliardi, *J. Appl. Crystallogr.* **1993**, *26*, 343−350.

Received January 19, 2001
[I01026]

Conformational Features of Group-4 *ansa*-Metallocenes with Long $-(CH_2)_n-$ Chains Connecting Their Cyclopentadienyl Ligands

Tim Jödicke,[a][‡] Frederik Menges,[a] Gerald Kehr,[a] Gerhard Erker,*[a] Udo Höweler,[a][‡] and Roland Fröhlich[a][‡‡]

Keywords: Metallocenes / Zirconium / Conformation analysis / Density functional calculations / Polymerization

Treatment of 1,9-bis(lithiocyclopentadienyl)nonane (**8b**) with $ZrCl_4(THF)_2$, in dilute solution, gave the crystalline mononuclear "large" *ansa*-metallocene **3b** (7% isolated). The X-ray crystal structure analysis of **3b** revealed a metallocene conformation where the nonamethylene bridge is oriented toward the lateral sector of the bent metallocene wedge. An analogous structure of **3b** is probable in solution, as shown by dynamic ^1H NMR spectroscopy. The activation barrier for the metallocene conformational equilibration process of **3b** was determined as $\Delta G^{\ddagger}_{rot}$ (203 K) = 8.8 ± 0.3 kcal/mol in [D_8]toluene. A combination of force-field and DFT calculations revealed similar conformational minima for **3b** and a series of related "large" *ansa*-metallocene complexes in the gas phase. The corresponding complex $[(CH_2)_{12}(C_5H_4)_2]ZrCl_2$ (**3d**) was also prepared. When activated by treatment with methylalumoxane, both complexes **3b** and **3d** give very active metallocene Ziegler–Natta catalysts for the polymerization of ethene and the oligomerization of propene.

Introduction

A specific section of the many possible group-4 *ansa*-metallocenes has become of great importance in homogeneous catalysis. These systems usually exhibit small bridges (i.e. R_2Si, R_2C or $-CH_2-CH_2-$) between a pair of Cp, indenyl, or related ligands. They have formed the basis for the generation of homogenous Ziegler−Natta-type catalysts, which often show extraordinary reactivity/selectivity features.[1] Such systems are conformationally rigid with the "*ansa* bridge" strictly located at the narrow back side of the bent metallocene wedge. This seems to be a key factor for their controlling abilities in the actual catalytic process.[2,3] Open, non-bridged group-4 metallocenes have also been shown to lead to active Ziegler−Natta catalysts. Here, control of the stereoselectivity of polyolefin formation is sometimes achieved, based on the specific dynamic conformational properties of the alkyl- or aryl-substituted bent metallocene system.[4,5]

"Large" *ansa*-metallocenes, which have their cyclopentadienyl or indenyl ligands connected by long $-(CH_2)_n-$ chains ($n \geq$ ca. 8), comprise an interesting class of compounds. It is possible that some members of this group form stable global (or kinetically protected local) conformational minima that have the oligomethylene chain located at specific sectors of the bent metallocene wedge, where they may actively shield the active sites at the central metal center, or may get involved in reactions taking place at the activated group-4 metal inside this arrangement.[6] A long bridging $-(CH_2)_n-$ chain in a "large" *ansa*-metallocene could, for instance, be located symmetrically at the front of the bent metallocene wedge and spatially separate the space in front of the activated metal center. This may potentially alter the catalytic action in such a system relative to a less-restricted non-bridged metallocene or a conventional "small" *ansa*-metallocene system.

To the best of our knowledge, only two examples of such "large" *ansa*-metallocenes have been characterized by X-ray diffraction so far, and these show very different conformational features. Mach et al. have described the structure of $[(CH_2)_8Cp^*_2]TiCl_2$ (**1**, see Figure 1) which has the bridging octamethylene chain located at the narrow back side, almost like a "small" *ansa*-metallocene.[7] In contrast, in *rac*-$[(CH_2)_{12}(1\text{-indenyl})_2]ZrCl_2$ (*rac*-**2c**), the other previously described example, the bridging hydrocarbyl chain is C_2-symmetrically located at the front of the bent metallocene wedge.[8] This bisects the Cl−Zr−Cl angle as shown in the bottom projection in Figure 1.

From the static solid-state structures it is not clear whether these two forms represent the respective global conformers of these bent metallocenes, or if they are just local conformational minima that have been stabilized by specific solid-state features under these experimental conditions. Thus, we have characterized several representative "large" *ansa*-metallocenes, i.e. $(CH_2)_n$-bridged bis(cyclopentadienyl) or bis(indenyl) complexes of zirconium (and in one case titanium) with the number of bridging methylene units ranging from eight to twelve, by computational chemistry using force-field and DFT methods. We have found a remarkable dependence of the thermodynamically favored metallocene conformations on the length of the oligomethylene bridge. These results were complemented experimentally by the synthesis of two representative "large" *ansa*-zirconocene dichlorides, the investigation of their respective

[a] Organisch-Chemisches Institut der Universität Münster, Corrensstraße 40, 48149 Münster, Germany
[‡] Theoretical work.
[‡‡] X-ray crystal structure analysis.
Supporting information for this article is available on the WWW under http://www.wiley-vch.de/home/eurjic or from the author.

 © WILEY-VCH Verlag GmbH, 69451 Weinheim, 2001 1434−1948/01/0808−2097 $ 17.50+.50/0

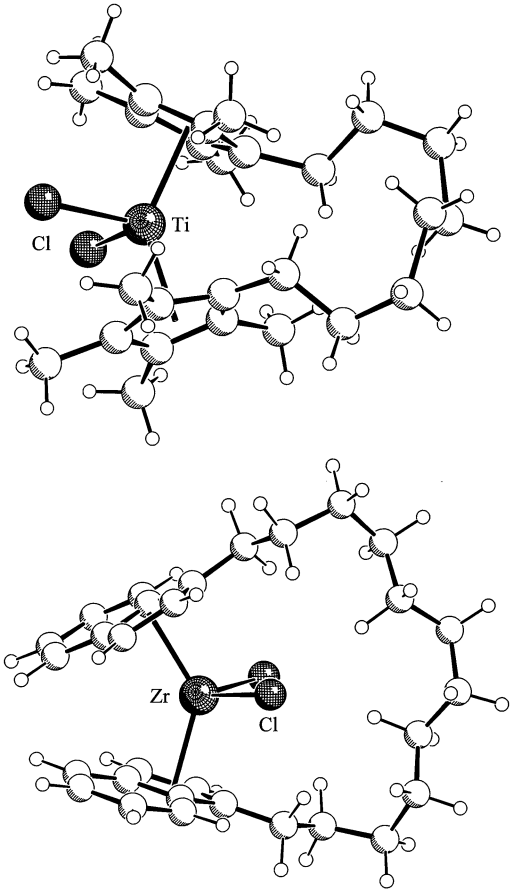

Figure 1. SCHAKAL plots of the "large" *ansa*-metallocenes **1** (top) and *rac*-**2c** (bottom), that were previously described in the literature[7,8]

dynamic conformational interconversion in solution, and the structural characterization of one example by X-ray diffraction. This has provided us with a much more detailed picture of the conformational properties of the interesting group-4 "large" *ansa*-metallocene complexes, relative to the selected views derived from previous descriptions based only on a limited number of experimental observations.

Results and Discussion

Computational Studies

The various local conformational minima of a series of $[(CH_2)_n(C_5H_4)_2]ZrCl_2$ complexes **3a**−**d** (n = 8, 9, 10, and 12) were determined and optimized using a metallocene-adapted force-field method that we had described and applied previously (see Scheme 1).[9] Relative energies of the located conformers were determined. These geometries were then used in the DFT calculation to give the respective single-point energies on the B3LYP level[10] for comparative purposes. We made sure that the conformational characteristics were predominately determined by the bent metallocene framework itself and not by the σ-substituents attached at the zirconium atom. This was done by investigating several corresponding $[(CH_2)_n(C_5H_4)_2]Zr(CH_3)_2$ complexes **4a**−**d** with the same number of bridging methylene groups. The Zr−C(sp^3) parameterization of the organometallic molecular modeling/force-field program was carried out in the course of this study (see Exp. Sect.). In addition, a similar series of *rac*- and *meso*-$[(CH_2)_n(1\text{-indenyl})_2]ZrCl_2$ complexes (*rac*-/*meso*-**2a**−**c**, n = 8, 10, and 12) was investigated by this combination of force-field/DFT calculations, and the Ti-based system **1** recently described by K. Mach et al. (see above),[7] was included in the study for comparison.

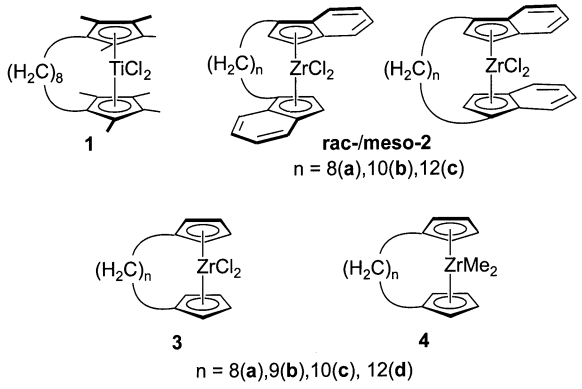

Scheme 1. "Large" *ansa*-metallocene complexes calculated by force-field and DFT methods in this study

For clarity and simplicity we want to characterize the metallocene conformations using a grid (see Figure 2) that is superimposed on a projection of the bent metallocene from the top. In this projection, the bent metallocene opens towards the right, with its σ-substituents directed toward the "east" position. In the center of that position we will place the origin of the conformational designation (i.e. 0°), we will then proceed clockwise through the "south" (90°), "west" (180°), and "north" (−90°) positions back to the origin. In the designation of a specific metallocene conformation (denoted by *mc*), we will first note the position of the Cp−CH_2− vector of the upper substituted cyclopentadienyl (or indenyl) ligand, followed by that of the lower C(Cp)−CH_2− position in degrees in this reticule, which has its center (idealized) position superimposed with the Cp(centroid)−Cp(centroid) vector. The structurally characterized examples **1** and *rac*-**2c** (see Figure 1) are thus characterized by the metallocene conformational descriptors *mc* 159/−159 (M = Ti, n = 8) and *mc* 16/−18 (M = Zr, n = 12).

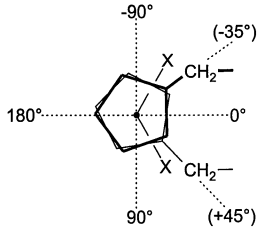

Figure 2. Reticule used for the characterization of the bent metallocene conformers; the specific example depicted would be termed as the *mc* −35/45 conformation

The molecular mechanics calculation has revealed that *rac*-**2c** is characterized by a very shallow conformational hypersurface. A variety of metallocene conformations with very similar energies were found that represent local minima on the conformational surface. The local minima of *rac*-**2c** with the lowest energies, exhibiting the oligomethylene chain predominantly in the "front", "lateral" or "back" sector of the bent metallocene wedge are listed in Table 1. The force-field calculations locate the global minimum conformation (*mc* 9/−9) with an orientation that is very close to the experimental X-ray structure of *rac*-**2c** (see Figure 1), with a structurally even closer conformation (*mc* 16/−16) close by. However, it must be noted that several other structurally different conformational minima of *rac*-**2c**, with only slightly higher energies, were found in this calculation (see Table 1). The overall picture is supported by the result of the DFT calculation. An optimized global minimum structure (*mc* 19/−19) is calculated (see Table 1), that is structurally marginally different from the observed experimental structure of *rac*-**2c**.

The situation changes systematically when the oligomethylene chain is shortened. The decamethylene-bridged system *rac*-**2b** exhibits a set of preferred "lateral" conformations as the global minimum (e.g. *mc* 74/137), whereas the orientation of the $-(CH_2)_{10}-$ bridge at the "front" side is markedly disfavored for the hypothetical system *rac*-**2b** according to this force-field calculation. This situation becomes consistently more pronounced on further shortening of the oligomethylene chain. In *rac*-**2a**, the $-(CH_2)_8-$ chain is preferentially located laterally (global minimum *mc* 85/

Table 1. Calculated metallocene conformations of the *rac*- and *meso*-[$(CH_2)_n$(1-indenyl)$_2$]$ZrCl_2$ complexes **2**

Compound	*n*	Conformation type	Relative energy MM[a]	Relative energy (*mc*)	Relative energy DFT[b]	Relative energy (*mc*)
rac-**2a**	8	"lateral"	0.0	(97/128)	0.0	(85/123)
			1.4	(82/113)	0.8	(85/128)
			1.9	(78/81)	3.3	(85/89)
		"back"	5.0	(140/−143)		[c]
		"front"	22.6	(4/−19)	17.5	(4/−21)
rac-**2b**	10	"lateral"	0.0	(74/137)	0.0	[d]
			0.1	(77/115)	−0.2	[d]
			0.2	(50/75)	0.7	[d]
		"back"	2.4	(109/−146)	5.2	[d]
			3.7	(142/−142)	4.3	[d]
		"front"	7.5	(10/21)	11.0	[d]
			4.7	(1/−11)	7.7	[d]
rac-**2c**	12	"lateral"	0.0	(85/111)	0.0	(83/116)
			0.0	(42/130)	1.1	(79/119)
			0.1	(39/123)	0.9	(57/89)
			0.1	(40/133)	0.1	(58/80)
		"back"	0.4	(105/−129)	3.2	(97/−134)
		"front"	−1.1	(9/−9)	−2.3	(19/−19)
			−0.3	(16/−16)	−1.8	(24/−24)
		"gauche"	−0.2	(2/93)	0.8	(5/88)
rac-**2c**	12	experiment:[e]		(16/−18)	–	–
meso-**2a**	8	"lateral"	0.0	(97/128)	0.0	(89/129)
			0.7	(65/91)	3.4	(73/96)
			1.9	(78/81)	3.3	(85/89)
		"back"	13.7	(140/−143)	14.4	(124/−151)
		"front"	17.0	(0/−27)	18.9	(10/−17)
			22.8	(6/29)	19.2	(3/7)
meso-**2b**	10	"lateral"	0.0	(72/105)	0.0	[d]
			0.2	(46/81)	2.4	[d]
			0.3	(50/75)	0.0	[d]
		"back"	7.2	(132/176)	9.4	[d]
			7.6	(141/−151)	8.8	[d]
			6.2	(134/−145)	6.3	[d]
		"front"	7.9	(17/−23)	8.5	[d]
			6.2	(10/−29)	7.4	[d]
meso-**2c**	12	"lateral"	0.0	(36/78)	0.0	(50/85)
			0.3	(83/139)	1.0	(80/122)
			0.4	(42/130)	1.9	(49/136)
		"back"	0.8	(111/−110)	1.5	(95/−133)
		"front"	2.0	(9/−32)	1.0	(22/−24)
			1.4	(12/−27)	0.0	(22/−25)
		"gauche"	0.1	(−2/93)	−0.6	(−6/88)

[a] Energy relative to the most stable "lateral" conformation, metallocene force field [kcal mol^{-1}]. – [b] B3LYP-optimized [kcal mol^{-1}]. – [c] No minimum found. – [d] B3LYP single point energies [kcal mol^{-1}] of the calculated force-field structure. – [e] From ref.[8]

123 by the B3LYP-DFT calculation, *mc* 97/128 by our metallocene force-field method), and the "front" orientation is strongly disfavored (see Table 1). A similar picture is found in the force-field and DFT calculations of the corresponding *meso*-[−$(CH_2)_n$−(1-indenyl)$_2$]$ZrCl_2$ systems, *meso*-**2a**−**c** (n = 8, 10, 12, see Table 1).

These results showed that the DFT calculations are very good at predicting the preferred conformations of "large" *ansa*-metallocenes. Furthermore, the much simpler metallocene force-field investigation gave quite acceptable results. Therefore, we used both methods for a priori characterization of the preferred metallocene conformations of the parent [$(CH_2)_n(\eta^5$-$C_5H_4)_2$]$ZrCl_2$ "large" *ansa*-zirconocene dichloride complexes **3a**−**d** (n = 8, 9, 10, and 12). A similar trend as in the *rac*-/*meso*-**2** series of complexes is observed here. The smaller members of the series [**3a** (n = 8), **3b** (n = 9), **3c** (n = 10)] all favor metallocene conformations that exhibit a "lateral" orientation of the oligomethylene bridge. However, the difference in energy between the preferred "lateral" conformation and the less favored "back" and "front" arrangements decreases progressively from **3a** to **3c**. Eventually, the cross-over point is reached with complex **3d** (n = 12), where the energy difference between the "front" and "lateral" arrangements becomes marginal (actually, the "front" orientation of the −$(CH_2)_{12}$− chain is slightly favored by the DFT calculation, see Table 2).

The complex **3b** (n = 9) has been synthesized and its molecular structure in the crystal has been determined (see below). The experimentally observed "lateral" orientation of the bridging nonamethylene chain is characterized by the metallocene conformational descriptor *mc* 83/83 (see Figure 2). The force-field-calculated global-minimum structure has an *mc* of 78/81, the DFT (B3LYP) global minimum has an *mc* of 77/83. This is a remarkably accurate structural coincidence in such a flexible conformational system. This result highlights the high predictive potential of both computational chemistry methods used in this investigation.[11]

We have also characterized the preferred metallocene conformations of the members of the corresponding series of [$(CH_2)_n(\eta^5$-$C_5H_4)_2$]$Zr(CH_3)_2$ complexes **4a**−**d** (n = 8, 9, 10, and 12), using our newly parameterized metallocene force-field program. The structural preferences were very similar to the [$(CH_2)_n(\eta^5$-$C_5H_4)_2$]$ZrCl_2$ series (see above). We therefore refer to the Supporting Information for the details of this study.

Finally, we have analyzed the titanium system **1**. It can be seen from Table 3 that in this case the force-field method does not reproduce the observed metallocene conformation.

Table 2. Calculated metallocene conformations of the [$(CH_2)_n(\eta^5$-$C_5H_4)_2$]$ZrCl_2$ complexes **3**

Compound	n	Configuration type	Relative energy MM[a]	(*mc*)	Relative energy DFT[b]	(*mc*)
3a	8	"lateral"	0.0	(64/90)	0.3	(70/96)
			0.1	(89/115)	0.0	(84/115)
			0.9	(77/81)	0.1	(82/89)
		"back"	6.2	(137/−144)		[c]
			6.6	(149/−149)	7.3	(147/−147)
		"front"	18.4	(0/−25)	16.0	(6/−19)
3b	9	experiment:[d]		(83/83)	–	–
3b	9	"lateral"	0.0	(78/81)	0.0	(77/83)
			0.1	(69/108)	1.3	(72/113)
			0.1	(78/102)	1.7	(72/93)
			0.9	(76/104)	2.3	(81/106)
		"back"	5.2	(97/−177)	5.1	(66/127)
			5.2	(139/−143)	6.0	(125/−155)
		"front"	12.0	(2/−30)	11.9	(7/−26)
			14.1	(28/28)	12.2	(19/19)
			9.7	(2/2)	10.5	(7/7)
3c	10	"lateral"	0.0	(68/105)	0.0	(70/104)
			0.0	(45/106)	1.8	(62/115)
			0.1	(77/104)	1.4	(79/101)
			0.2	(76/104)	0.6	(81/106)
		"back"	2.3	(109/−145)	2.3	(63/151)
			2.6	(113/−145)	1.7	(60/139)
			3.7	(109/−144)	2.5	(76/142)
		"front"	6.7	(1/9)	6.2	(3/15)
3d	12	"lateral"	0.0	(82/111)	1.8	(88/121)
			0.0	(75/99)	0.0	(73/98)
			0.2	(77/84)	0.0	(76/92)
		"back"	0.1	(111/−115)	0.7	(92/−142)
		"front"	0.2	(21/−21)	−3.2	(24/−23)
			0.4	(9/−9)	−3.3	(16/−17)
		"gauche"	0.2	(3/82)	−2.6	(27/85)

[a] See footnote in Table 1. − [b] See footnote in Table 1. − [c] See footnote in Table 1. − [d] This work, see below.

Furthermore, the DFT calculation is not decisive, it reveals that the highly methyl-substituted "large" *ansa*-titanocene complex **1** is probably characterized by a very shallow conformational hypersurface. It is likely that the observed structure of **1** does not represent the global conformational minimum of the system, but rather one of the many metallocene conformations that are similar in energy, which has been stabilized by crystal packing forces in the solid state.

Table 3. Calculated and observed metallocene conformations of the "large" *ansa*-titanocene complex $[(CH_2)_8(\eta^5\text{-}C_5Me_4)_2]TiCl_2$ (**1**)

Configuration type	Relative energy MM[a]	(*mc*)	Relative energy DFT[b]	(*mc*)
"lateral"	0.0	(89/114)	0.0	(98/126)
	1.4	(63/86)	2.9	(72/95)
"back"	0.7	(126/151)	−0.5	(139/177)
	5.8	(141/−173)	1.4	(157/−158)
	16.3	(156/−153)	[c]	
"front"	15.5	(2/−34)	13.0	(2/−20)
experiment:	[d]	(159/−159)	–	–

[a] See footnote in Table 1. − [b] See footnote in Table 1. − [c] See footnote in Table 1. − [d] From ref.[7]

Experimental Studies

Previously, we and others had tried to prepare "large" *ansa*-metallocenes by coupling reactions, by means of intramolecular metallacyclopentane formation[12] using pendant alkenyl groups attached at the Cp ligands.[6,7] The metallacyclopentane formation is not problematic, but the necessary subsequent cleavage by e.g. HCl, appears to lead to the expected "large" *ansa*-metallocene product only in a limited number of cases. Mach's peralkylated *ansa*-titanocene complex **1** was actually synthesized in that way.[7] Even in the titanium systems, competing pathways leading to ring-opened acyclic products were observed. This completely dominated the protolytic cleavage in the case of the corresponding zirconocene examples, as we had recently shown.[6]

Therefore, we have chosen to synthesize the "large" *ansa*-metallocene examples used in this study using a different pathway. Starting materials were 1,9-dihydroxynonane (**5b**) or 1,12-dihydroxydodecane (**5d**), respectively. These compounds were converted into their respective dimesylates **6b** and **6d** by treatment with methanesulfonyl chloride in pyridine. Subsequent treatment with an excess of lithium cyclopentadienide resulted in clean, twofold substitution reactions, with carbon−carbon bond formation in each case, yielding 1,9- and 1,12-bis(cyclopentadienyl)nonane (**7b**, ca. 60% isolated) and -dodecane (**7d**, 86%), respectively (see Scheme 2). These two products were then deprotonated twice by treatment with *n*-butyllithium in ether. The corresponding α,ω-bis(lithiocyclopentadienyl)alkanes **8b** and **8d** were obtained almost quantitatively, as extremely insoluble solids. These dianion equivalents were only characterized by elemental analysis and by hydrolysis and deuteriolysis experiments, and then directly employed as reagents for the metathetical reaction with zirconium tetrachloride.

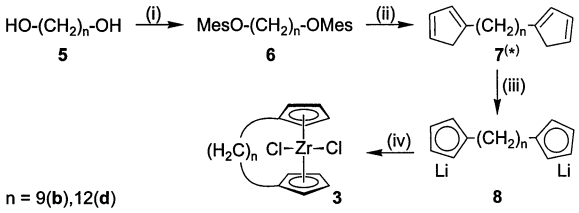

(i) CH_3SO_2Cl/pyridine; (ii) CpLi/THF; (iii) n-BuLi/Et_2O; (iv) $ZrCl_4(thf)_2$/toluene
(*) mixture of double bond isomers

Scheme 2. Syntheses of the *ansa*-metallocene complexes **3**

The reaction involving the poorly soluble $[Cp-(CH_2)_9-Cp]^{2-}(Li^+)_2$ (**8b**) was carried out with $ZrCl_4(THF)_2$ suspended in toluene. Under these circumstances, similar conditions to those used in typical high-dilution techniques[13] were obtained. The resulting product mixture nevertheless apparently contained oligomeric metallocene materials, which were highly insoluble, as the major components. Soxhlet extraction with pentane over 60 h eventually gave a soluble fraction of 1,1′-nonamethylenebis(cyclopentadienyl)zirconium dichloride (**3b**), which was obtained pure after subsequent recrystallization from toluene at −30 °C, in a 7% yield. 1,1′-Dodecamethylenebis-(cyclopentadienyl)zirconium dichloride (**3d**) was prepared analogously by treatment of the reagent **8d** with $ZrCl_4(THF)_2$, and isolated with a yield of 18%.

Crystals of complex **3b**, that were suitable for X-ray crystal structure analysis, were obtained from a benzene solution over a period of several weeks. In the solid state the nonamethylene-bridged system **3b** exhibits an eclipsed metallocene conformation that has the large *ansa* bridge oriented almost perfectly toward one lateral sector. The specific metallocene conformation can be described by the experimental metallocene conformational descriptor *mc* 83/83 (see Figure 2 and Figure 3). The chlorine atom Cl1 is disordered over two positions, therefore bonding parameters involving this atom will not be discussed in detail. The Cp(centroid)−Zr−Cp(centroid) angle in **3b** is equal to 130.6° and the averaged Cp(centroid)−Zr distance is 2.194 Å; both values are in a very typical zirconocene range {for comparison: Cp_2ZrCl_2 (129.3°/2.203 Å),[14] $[(CH_2)_3(C_5H_4)_2]ZrCl_2$ (129.5°/2.193 Å),[15] Cp_2TiCl_2 (131.0°/2.059 Å)}.[16] Only large substituents at the Cp rings result in noticeable distortions toward larger "bite angles" (and consequently smaller Cp(centroid)−Zr−Cp(centroid) angles $[(Me_3SiC_5H_4)_2ZrCl_2$ (125.4°/2.197 Å),[17] $(Me_3CC_5H_4)_2ZrCl_2$ (116.6°/2.192 Å)].[18] The opposite effect is observed for the pair of "large" *ansa*-metallocenes *rac*-**2c** [Cp(centroid)−Zr−Cp(centroid) angle 133.8°, Cp(centroid)−Zr distance 2.242 Å[8]] and **1** (137.9°/2.140 Å,[7] see Figure 1).

Thus, it appears that the $[(CH_2)_9(C_5H_4)_2]ZrCl_2$ system **3b** represents an unstrained system within the family of the "large" *ansa*-metallocenes, that can attain a normal bent metallocene core with almost no structural distortion, sim-

ilar to ordinary non-bridged $(RCp)_2MX_2$-type group-4 bent metallocene complexes. The $-(CH_2)_9-$ chain in **3b** adopts a crown-shaped cycloalkane conformation, similar to that found in many medium- and large-ring cycloalkanes (Figure 3).[19] The experimentally observed conformer of **3b** obtained in the solid state by X-ray diffraction (*mc* 83/83) is not completely identical but very similar to the probable global-minimum gas-phase structure as calculated by the force-field method (*mc* 78/81) and the DFT calculation (*mc* 77/83, see Table 2).

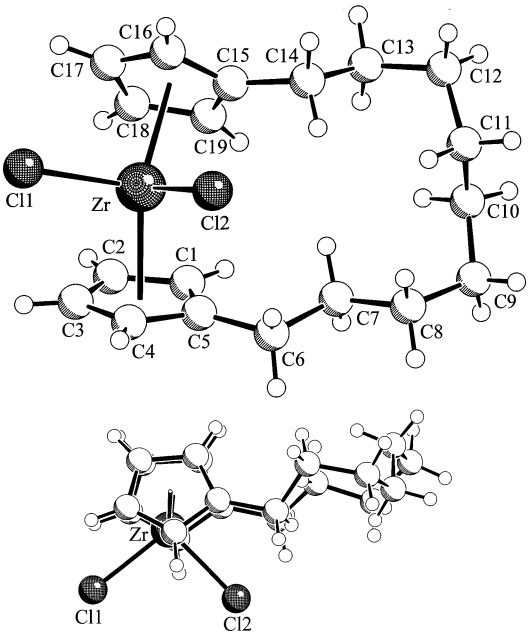

Figure 3. Two views of the molecular structure of the "large" *ansa*-metallocene **3b** in the crystal; selected bond lengths [Å], angles [°] and dihedral angles [°]: Zr−Cl1 2.424(1), Zr−Cl2 2.431(1), C1−C2 1.412(6), C1−C5 1.399(7), C2−C3 1.385(8), C3−C4 1.394(8), C4−C5 1.408(8), C5−C6 1.503(7), C6−C7 1.508(7), C7−C8 1.518(6), C8−C9 1.523(7), C9−C10 1.525(6), C10−C11 1.495(7), C11−C12 1.516(6), C12−C13 1.533(7), C13−C14 1.501(8), C14−C15 1.506(7), C15−C16 1.400(7), C15−C19 1.396(7), C16−C17 1.389(8), C17−C18 1.382(8), C18−C19 1.412(7); Cl1−Zr−Cl2 95.60(5), C5−C6−C7 113.4(4), C6−C7−C8 113.9(4), C7−C8−C9 113.2(4), C8−C9−C10 114.7(4), C9−C10−C11 114.7(4), C10−C11−C12 114.1(5), C11−C12−C13 113.9(4), C12−C13−C14 113.3(5), C13−C14−C15 114.2(5); C5−C6−C7−C8 168.3(5), C6−C7−C8−C9 173.6(4), C7−C8−C9−C10 53.9(6), C8−C9−C10−C11 65.2(6), C9−C10−C11−C12 −169.1(4), C10−C11−C12−C13 64.4(7), C11−C12−C13−C14 63.4(7), C12−C13−C14−C15 −175.0(4)

The conformational behavior of $[(CH_2)_9(C_5H_4)_2]ZrCl_2$ in solution was characterized by dynamic NMR spectroscopy. In a $[D_8]$toluene solution, complex **3b** reveals spectroscopic data of apparent C_{2v} symmetry at ambient temperature, which is caused by a rapid conformational equilibrium on the NMR-spectroscopic time scale. At ambient temperature this leads to five $-CH_2-$ ^{13}C NMR resonances assigned to the *ansa* bridge at δ = 28.6, 26.6, 25.6, 24.6 and 23.7. The intensity of the latter signal is half that of the other signals. Under these conditions there are three Cp resonances at δ = 137.9 (*ipso*-C), δ = 111.7 and 115.7. The ^1H NMR spectrum (600 MHz) at "high" temperature (298 K) is similar, exhibiting methylene signals at δ = 2.40 (α-CH_2), 1.24 (8 H), 1.18 (2 H), and 1.13 (4 H) in addition to Cp methine signals at δ = 5.65 and 5.93. Lowering of the temperature eventually results in a freezing of the dynamic conformational equilibration process on the ^1H-NMR-spectroscopic time scale. Below 203 K (at 600 MHz), the well-separated ^1H NMR resonance of the methylene group in the α-position to the Cp ring system, begins to split into two signals of equal intensity that eventually appear at δ = 2.74 and 2.07 at 183 K. Under these static conditions the hydrogen atoms at the α-CH_2 group have thus become diastereotopic. Their nonequivalence indicates the presence of a single metallocene conformational minimum that is non-C_{2v}-symmetric. The remaining apparent C_s symmetry of the spectroscopically observed system may be real, or may be caused by a remaining very rapid local conformational symmetrization effect being operative in the medium-sized annelated nonamethylene ring system. In principle, a bis(lateral) conformation of **3b** in solution, similar to that observed in the crystal seems likely. Consequently, the pair of Cp ^1H NMR resonances broadens with decreasing temperature (Figure 4). Decoalescence is observed at ca. 203 K which results in the formation of two pairs of α,α′- and β,β′-C_5H_4 ^1H NMR resonances of equal intensity, at δ = 6.47/6.09 (3-H, 4-H) and δ = 5.09/4.92 (2-H/5-H). From these values a Gibbs activation energy of $\Delta G^{\ddagger}_{rot}(203\ K) = 8.8 \pm 0.3$ kcal/mol was obtained[20] for the conformational equilibration process of the "large" *ansa*-metallocene complex **3b** in $[D_8]$toluene. The conformational barrier is apparently not solvent-dependent. In the more polar solvent $CDFCl_2/CDF_2Cl$ (1:1),[21] a similar dynamic behavior was observed and an activation barrier of $\Delta G^{\ddagger}_{rot}(184\ K) = 8.5 \pm 0.3$ kcal/mol was obtained for the conformational equilibration process.

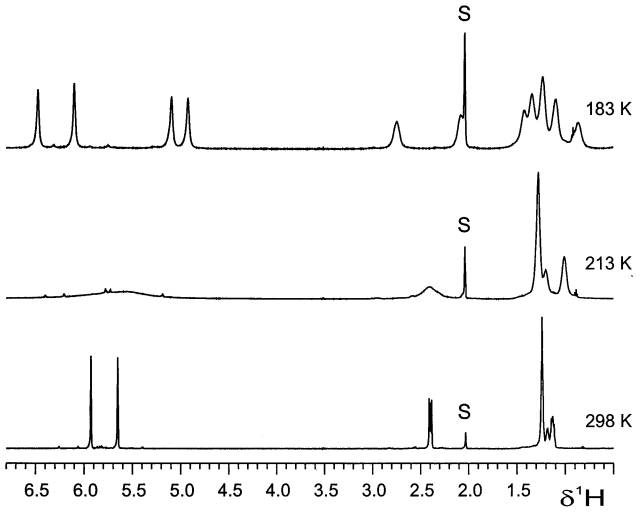

Figure 4. Dynamic ^1H NMR spectra (600 MHz) of **3b** in $[D_8]$toluene

From the dynamic NMR spectra it cannot be determined whether the C_9-oligomethylene chain moves through the front or back sector of the bent metallocene wedge during this conformational automerization process. From the computational energies of the $[(CH_2)_9(C_5H_4)_2]ZrCl_2$ system **3b**

that are compiled in Table 2, it appears that the nonamethylene chain may be accommodated slightly better at the back of the metallocene during such a migration process, although the respective ground-state energy differences are not prohibitively large and the transition-state energies were not calculated.

It can be assumed that steric interactions decrease for the dodecamethylene-bridged system $[(CH_2)_{12}(C_5H_4)_2]ZrCl_2$ (**3d**). Indeed, a similar 600-MHz ^{1}H NMR spectrum of **3d** was obtained at ambient temperature. In this case the conformational equilibration process of the "large" *ansa*-metallocene framework could not be frozen on the 600-MHz ^{1}H-NMR-spectroscopic time scale, even when the lowest temperature, 133 K, was reached (for spectroscopic details see the Exp. Sect.). It appears that the "large" *ansa*-metallocene complex **3d** exhibits dynamic properties similar to those of simple open, non-bridged alkyl-substituted group-4 bent metallocene complexes $[(prim.\text{-}alkyl)C_5H_4]_2ZrCl_2$ that are characterized by very low activation barriers for the conformational equilibration process.[22]

Olefin Polymerization Reactions

The combined conformational studies have shown that the complexes $[(CH_2)_9(C_5H_4)_2]ZrCl_2$ (**3b**) and $[(CH_2)_{12}(C_5H_4)_2]ZrCl_2$ (**3d**) attain favored conformations that have their long bridging oligomethylene chains oriented toward a lateral sector of the bent metallocene wedge, or that they are conformationally labile and may very easily turn away from the front sector. In any case, an active Ziegler−Natta catalytic system could be derived from such a singly bridged "large" *ansa*-metallocene that will allow for the unrestricted approach of reagents at the front sector of the bent metallocene wedge. This is essential for the catalyst's action, and we thus would expect that the systems **3b** and **3d** might lead to very active olefin polymerization catalysts on activation. This is indeed observed.

Activation of $[(CH_2)_9(C_5H_4)_2]ZrCl_2$ (**3b**) with methylalumoxane (MAO)[23] in toluene (Al/Zr ratio ca. 1800) at room temperature gave a very active homogeneous Ziegler−Natta catalyst for ethene polymerization. Polyethylene (m.p. 127 °C) was formed with an activity of $a \approx 2500$ kg polymer/mol [Zr]·h·bar (at 40 °C and 2 bar ethene pressure). The catalyst derived from complex $[(CH_2)_{12}(C_5H_4)_2]ZrCl_2$ (**3d**) was equally active in ethene polymerization under similar conditions ($a \approx 2400$). Both catalysts are also active in propene polymerization. Activation of **3b** was again achieved by treatment with a large excess of MAO (Al/Zr ≈ 1450). Polymerization at 40 °C (2 bar propene pressure) yielded ca. 21 g of an oily polypropylene with an activity of $a \approx$ 450 kg polypropylene/mol [Zr]·h·bar. The ^{1}H-NMR-spectroscopic analysis revealed that a low molecular weight oligomer was formed under these conditions. End-group analysis by ^{1}H NMR spectroscopy showed that an average 14-mer was obtained. The catalyst derived from the C_{12}-bridged "large" *ansa*-metallocene produced a similar propene oligomer (oligomerization degree of ca. 10 according to the NMR $H_2C{=}C(CH_3)-$ end group analysis)[24] with a catalyst activity of $a = 330$. The ^{13}C NMR pentade analysis showed that both polymers were atactic. The polypropylene formed at the **3b**/MAO-derived catalyst shows an mmmm ^{13}C NMR methyl pentade intensity of 6.7%, the material obtained at the **3d**/MAO catalyst 5.5% mmmm.

We conclude that the singly bridged "large" *ansa*-metallocenes studied in this work exhibit favored specific metallocene conformations if the bridging oligomethylene chains are small enough. Most often these chains are then found oriented toward lateral positions. Complexes with chain lengths of C_{12} or longer seem to be similar to non-bridged complexes.[25] The metal center in such monobridged systems is rather open and can easily be approached by external reagents. This results in rather active but stereochemically unselective Ziegler−Natta catalysts on activation with, for example, methylalumoxane. Bridge-specific effects will probably require a covalent fixation of a given metallocene conformation by the introduction of a second bridge.[6] It will be interesting to see how fixing a large $-(CH_2)_n-$ bridge in front of the bent metallocene alters the zirconocene behavior in an activated system. Such investigations and syntheses are actively being pursued in our laboratory.

Experimental Section

Computational Study: The force-field calculations were carried out with the program MAXIMOBY[26] using parameters based on the AMBER force field.[27] The parameters for the description of zirconium and its ligands in the $[Zr]Cl_2$ complexes were used as previously described by us.[9] A new set of parameters was deduced for the Zr−(sp^3-C) bond (carbon atom type MC) using 12 representative metallocene structures from the Cambridge Structural Database (details are provided with the Supporting Information). The following force-field data for the "new" carbon atom type MC were used (force constant in kcal mol^{-1}, reference values in Å or °): ZR−MC (110/2.275), HC−MC (330/1.09), MC−ZR−MC (80/95.5), MP−ZR−MC (80/104.2), XC−MC−ZR (5/109.5), HC−MC−ZR (40/109.5), −ZR−MC− (0/180.0, threefold) [MP denotes the artificial Cp(centroid) atom used in the metallocene force-field calculation and XC is the sp^2-carbon atom that is common to both the five- and six-membered ring of the indenyl ligand]. The starting geometries for the optimization were prepared using the visualization tool MOBY.[28] New conformations were generated within the MAXIMOBY program by breaking the central (sp^3-C)−(sp^3-C) bond of the oligomethylene chain, followed by changing the torsional angles successively by a 120° increment. Every new conformation was then optimized under the constraint that the ends of the resulting carbon chains formed initially after changing the torsion angles were not more than 6 Å apart to speed up the calculations. In addition the orientation of the ligands was changed systematically to provide different starting points for the force-field optimization procedures. The obtained results are listed in Tables 1−3. For additional information see the Supporting Information. − The validity of the force-field calculation was checked by a correlation with respective ab initio energies and ab initio conformational minimum structures. This was achieved by single-point calculations of all local minima of the obtained force-field structures by the DFT method B3LYP,[10] using the LAN L2DZ basis set. It contains a double-ζ valence basis set (8s6p4d)/[3s3p2d] with Hay and Wadt "effective core potentials" that substitute the Zr

electrons up to the 3d level,[29] and the Huzinaga−Dunning "double-ζ valence" basis set for the remaining atoms.[30] Resulting single-point energies and structures are provided in the Supporting Information. Results from the DFT optimizations are contained in Tables 1−3, and additional information (energies) are included in the Supporting Information. For details about the ZR-MC force-field parameterization, the force field and the DFT calculations see Supporting Information.

Synthetic Work. − General Information: Reactions with organometallic compounds were carried out under argon using Schlenk-type glassware or in a glove-box. Solvents (including deuterated solvents used for spectroscopic measurements) were dried and distilled prior to use. For additional general information, including a list of spectrometers used, see ref.[6] $ZrCl_4(THF)_2$,[31] 1,9-nonanediylbis(methanesulfonate) (**6b**),[32] and 1,12-dodecanediylbis(methanesulfonate) (**6d**)[33] were synthesized according to literature preparations. 1,9-Bis(cyclopentadienyl)nonane (**7b**) and 1,12-bis(cyclopentadienyl)dodecane (**7d**) were both obtained by procedures analogous to the literature preparations[34] of these compounds.

Preparation of 1,9-Bis(cyclopentadienyl)nonane (7b): Cyclopentadiene (4.10 mL, 49.4 mmol) was dissolved in 100 mL of THF at −15 °C. *n*-Butyllithium (28.5 mL of a 1.6 M solution in *n*-hexane, 45.6 mmol) was added dropwise, while stirring, over 1 h. The mixture was stirred for 3 h at 0 °C. A solution of 1,9-nonanediylbis(methanesulfonate) (**6b**) (6.00 g, 19.0 mmol) in 100 mL of THF was added dropwise at 0 °C (ice bath). The mixture was allowed to slowly warm to room temperature with stirring over a period of 12 h. Diethyl ether (75 mL) and a saturated aqueous sodium chloride solution (75 mL) was added, the organic phase separated and washed with water. The aqueous phase was extracted with ether (3×). The combined organic solutions were dried with anhydrous magnesium sulfate, filtered and concentrated in vacuo. Purification of the product was achieved by precipitation from acetone at −25 °C and gave **7b** as a pale yellow oil, as a mixture of isomers that exhibit the side chains at the 2- and 3-positions of the cyclopentadienyl rings. Yield of **7b**: 2.84 g (59%). − ^{1}H NMR (200.1 MHz, [D$_6$]benzene, 300 K): δ = 6.45 (m, 2 H, =CH), 6.34 (m, 1 H, =CH), 6.18 (m, 2 H, =CH), 5.92 (m, 1 H, =CH), 2.78, 2.68 (m, each 2 H, CH_2 of C_5H_5 of the two isomers), 2.38−2.26 (m, 4 H, 1-H, 9-H of the chain), 1.54−1.10 (m, 16 H, 2-H to 8-H of the chain). − ^{13}C NMR (50.3 MHz, [D$_6$]benzene, 300 K): δ = 149.7, 147.6 (C-1/C-2 of C_5H_5, two isomers), 135.1, 133.7, 132.8, 130.4, 126.8, 126.0 (=CH of C_5H_5, two isomers), 43.4, 41.4 (CH_2 of C_5H_5), 31.1, 30.3, 29.9 (double intensity), 29.3 (C1−C9).

1,12-Bis(cyclopentadienyl)dodecane (7d): The synthesis was carried out analogously as described above by treatment of cyclopentadiene (9.6 mL, 116.0 mmol) in 300 mL of THF with *n*-butyllithium (68.8 mL of a 1.6 M solution in *n*-hexane, 110.0 mmol) at −15 °C, followed by addition of a solution of 1,12-dodecanediylbis(methane sulfonate) (**6d**) (16.0 g, 53.6 mmol) in 200 mL of THF to give a ca. 1:1 mixture of two isomers of **7d** as an oil. Yield: 13.7 g (86%). − ^{1}H NMR (200.1 MHz, [D$_6$]benzene, 300 K): δ = 6.46 (m, 2H =CH), 6.33 (m, 1 H, =CH), 6.19 (m, 2 H, =CH), 5.97 (m, 1 H, =CH), 2.79, 2.70 (m, each 2 H, CH_2 of C_5H_5, two isomers), 2.39−2.27 (m, 4 H, 1-H, 12-H of the chain), 1.60−1.15 (m, 20 H, 2-H to 11-H of the chain). − ^{13}C NMR (50.3 MHz, [D$_6$]benzene, 300 K): δ = 149.2, 147.6 (C-1/C-2 of C_5H_5, two isomers), 135.1, 133.7, 132.6, 130.4, 126.8, 125.9 (=CH of C_5H_5, two isomers), 43.4, 41.1 (CH_2 of C_5H_5), 31.1, 30.3, 30.1, 30.0, 29.9, 29.4 (C-1−C-12).

1,9-Bis(lithiocyclopentadienyl)nonane (8b): *n*-Butyllithium (11.9 mL of a 1.6 M solution in *n*-hexane, 19.2 mmol) was added dropwise to a solution of 1,9-bis(cyclopentadienyl)nonane (**7b**) (2.08 g, 8.09 mmol) in 50 mL of diethyl ether at 0 °C. The mixture was stirred for 4 h at ambient temperature. The resulting white precipitate was collected by filtration, washed with ether (2 × 20 mL) and dried in vacuo to yield 2.02 g (93%) of **8b**, m.p. 176 °C (decomp.). − IR (KBr): $\tilde{\nu}$ = 3077 (w), 2926 (vs), 2853 (vs), 1463 (m), 1443 (m), 1077 (w), 1060 (m), 1041 (m), 1026 (m), 818 (s), 755 (vs) cm^{-1}. − $C_{19}H_{24}Li_2{\cdot}C_4H_{10}O$ (340.4): calcd. C 80.68, H 10.60; found C 80.98, H 9.90. − The product **8b** is insoluble in the usual solvents, even in the presence of 12-crown-4 crown ether. For further characterization it was therefore hydrolyzed with H_2O (a) or D_2O (b) and the resulting respective hydrocarbon products analyzed. − MS (70 eV): *m*/*z* (a) = 256 [M$^+$]; *m*/*z* (b) = 258 [M$^+$].

1,12-Bis(lithiocyclopentadienyl)dodecane (8d): The preparation was carried out analogously as described above by treatment of 1,12-bis(cyclopentadienyl)dodecane (**7d**), (9.18 g, 30.8 mmol) in 150 mL of diethyl ether with a solution of *n*-butyllithium (38.0 mL of a 1.6 M solution in *n*-hexane, 61.6 mmol), to yield 9.01 g (94%) of **8d**, m.p. 189 °C (decomp.) as an insoluble material. − IR (KBr): $\tilde{\nu}$ = 3079 (w), 2924 (vs), 2853 (vs), 1464 (m), 1367 (w), 1261 (w), 1089 (m), 1060 (m), 1041 (m), 1026 (m), 818 (s), 755(vs) cm^{-1}. − $C_{22}H_{30}Li_2{\cdot}2(C_4H_{10}O)$ (456.6): calcd. C 78.57, H 11.43; found C 78.75, H 11.13. − Hydrolysis with H_2O (a) or D_2O (b) was carried out analogously as described above to yield the respective hydrolysis products. − MS (70 eV): *m*/*z* (a) = 298 [M$^+$]; *m*/*z* (b) = 300 [M$^+$].

[1,9-Nonanediylbis(η^5-cyclopentadienyl)]zirconium Dichloride (3b): A suspension of $ZrCl_4(THF)_2$ (6.32 g, 16.8 mmol) in 100 mL of toluene was cooled to −78 °C and then slowly added to a cold (−78 °C) suspension of 1,9-bis(lithiocyclopentadienyl)nonane (**8b**) (4.50 g, 16.8 mmol) in 300 mL of THF. The mixture was allowed to warm to room temperature overnight, with stirring. The solvent was removed in vacuo. The orange colored residue was Soxhlet-extracted with pentane for 60 h to give **3b** as a grayish powder. Recrystallization from toluene at −30 °C gave **3b** as white crystals, yield 457 mg (7%), m.p. 198 °C. − $C_{19}H_{26}Cl_2Zr$ (416.5): calcd. C 54.79, H 6.29; found C 54.15, H 6.65. − IR (KBr): $\tilde{\nu}$ = 3100 (m), 2931 (vs), 2852 (s), 1487 (m), 1458 (m), 1439 (w), 1261 (m), 1096 (m), 1071 (m), 1053 (m), 1039 (m), 1029 (m), 875 (w), 853 (w), 818 (s), 732 (w) cm^{-1}. − The NMR assignments were supported by a series of 2D experiments (GHSQC, GHMBC, GCOSY);[35] the dynamic behavior of complex **3b** was examined by ^{1}H/^{13}C 1D and 2D NMR spectroscopy[20] in [D$_8$]toluene in a temperature range between 298 K and 183 K and by ^{1}H NMR in $CDFCl_2/CDF_2Cl$ (1:1)[21] between 253 K and 133 K. − ^{1}H NMR (599.9 MHz, [D$_8$]toluene, 298 K): δ = 5.93 (pseudo-t, 4 H, 3-H, 4-H of C_5H_4), 5.65 (pseudo-t, 4 H, 2-H, 5-H of C_5H_4), 2.40 (m, 4 H, 1-/9-H), 1.24 (m, 8 H, 2-/8-H and 4-/6-H), 1.18 (m, 2 H, 5-H), 1.13 (m, 4 H, 3-/7-H). − ^{13}C NMR (150.8 MHz, [D$_8$]toluene, 298 K): δ = 137.9 (C-1 of C_5H_4), 115.7 (C-3/C-4 of C_5H_4), 111.7 (C-2/C-5 of C_5H_4), 28.6 (C-1/C-9), 26.6 (C-2/C-8), 25.6 (C-3/C-7), 24.6 (C-4/C-6), 23.7 (C-5). − ^{1}H NMR (599.9 MHz, [D$_8$]toluene, 183 K): δ = 6.47 and δ = 5.09 (br., each 2 H, 3-H and 4-H of C_5H_4), 6.09 and 4.92 (br., each 2 H, 2-H and 5-H of C_5H_4), 2.74 and 2.07 (br., each 2 H, 1-H,H′ and 9-H,H′), 1.65−0.85 (m, 14 H, 2-H to 8-H). − Coalescence of 1-H,H′/9-H,H′ of the nonamethylene chain at ca. 203 K: Δν (183 K) = 399 Hz, $\Delta G^{\ddagger}_{rot}$ (203 K) = 9.0 ± 0.3 kcal mol^{-1}. Coalescence of the two groups of C_5H_4 proton resonances at ca. 203 K: Δν (183 K) = 701 Hz, $\Delta G^{\ddagger}_{rot}$ (203 K) = 8.8 ± 0.3 kcal mol^{-1}; Δν (183 K) = 828 Hz, $\Delta G^{\ddagger}_{rot}$ (203 K) = 8.7 ± 0.3 kcal mol^{-1}; averaged value in [D$_8$]toluene: $\Delta G^{\ddagger}_{rot}$ (203 K) = 8.8 ± 0.3 kcal mol^{-1}. − GHSQC NMR (599.9 MHz, [D$_8$]toluene, 183 K): δ (^{1}H)/(^{13}C) = 6.47/125.6, 6.09/115.6, 5.09/106.2, 4.92/106.5 (C_5H_4), 2.74/28.2,

Table 4. Ethene and propene polymerization reactions at the **3b**/MAO and **3d**/MAO catalysts

Precursor	Monomer[a]	mg (μmol) [Zr]	g (mmol) [Al]	Al/Zr ratio	Reaction time [min]	PE/PP[b] [g]	Activity[c]	m.p. (PE) n[d] (PP)
3b	E	8.0 (19.2)	2.1 (34.5)	1800	5	8.1	2540	127
3d	E	9.7 (21.2)	2.1 (34.5)	1630	5	8.6	2420	127
3b	P	9.8 (21.5)	2.1 (34.5)	1470	60	21.5	456	14
3d	P	10.1 (22.0)	2.1 (34.5)	1570	60	14.6	332	10

[a] All reactions were carried out at 2 bar monomer pressure at 40 °C. − [b] E = ethene, P = propene, PE = polyethylene, PP = polypropylene. − [c] Polymerization activity in kg (polymer)/mol [Zr]·h·bar. − [d] Oligomerization degree, determined by ^{1}H NMR end group analysis.

2.07/28.2, 1.45/23.5, 1.36/25.7, 1.36/22.3, 1.25/25.8, 1.24/23.5, 1.13/25.4, 1.10/22.3, 0.88/25.3 (CH_2). − ^{1}H NMR (599.9 MHz, $CDFCl_2/CDF_2Cl$, 253 K): δ = 6.45 (pseudo-t, 4 H, 3-H, 4-H of C_5H_4), 6.26 (pseudo-t, 4 H, 2-H, 5-H of C_5H_4), 2.67 (m, 4 H, 1-H, 9-H), 1.55−1.25 (m, 14 H, 2-8-H). − ^{1}H NMR (599.9 MHz, $CDFCl_2/CDF_2Cl$), 133 K): δ = 6.63 (br., 2 H), 6.36 (br., 4 H) and 6.30 (br., 2 H, C_5H_4), 2.68 and 2.46 (br., each 2 H, 1-H,H′, 9-H,H′), 1.38 (m, 14 H, 2-8-H). − 1-H,H′/9-H,H′ coalescence at ca. 183 K: Δν (133 K) = 132 Hz, $\Delta G^{\ddagger}_{rot}$ (183 K) = 8.5 ± 0.3 kcal mol^{-1}; coalescence of one group of C_5H_4 resonances at ca. 188 K: Δν (133 K) = 200 Hz, $\Delta G^{\ddagger}_{rot}$ (188 K) = 8.6 ± 0.3 kcal mol^{-1}. Averaged value in $CDFCl_2/CDF_2Cl$: $\Delta G^{\ddagger}_{rot}$(188 K) = 8.5 ± 0.3 kcal mol^{-1}.

X-ray Crystal Structure Analysis of 3b: Single crystals of complex **3b** were obtained by slow evaporation of solvent from a solution in benzene. Empirical formula $C_{19}H_{26}Cl_2Zr\cdot 1/2\ C_6H_6$, M = 455.57, colorless crystal 0.30 × 0.20 × 0.10 mm, a = 39.555(2), b = 6.512(1), c = 16.689(1) Å, β = 102.57(1)°, V = 4195.8(7) Å^3, $\rho_{calcd.}$ = 1.442 g cm^{-3}, μ = 7.81 cm^{-1}, empirical absorption correction via SORTAV (0.799 ≤ T ≤ 0.926), Z = 8, monoclinic, space group $C2/c$ (No. 15), λ = 0.71073 Å, T = 198 K, ω and φ scans, 19815 reflections collected (±h, ±k, ±l), [(sinθ)/λ] = 0.65 Å^{-1}, 4795 independent (R_{int} = 0.054) and 3448 observed reflections [I ≥ 2 σ(I)], 226 refined parameters, R = 0.054, wR^2 = 0.117, max. residual electron density 1.54 (−1.58) e Å^{-3} close to Cl1, Cl1 disordered over two positions, no disorder model used in the final refinement, hydrogen positions calculated and refined as riding atoms. Data set was collected with a Nonius KappaCCD diffractometer, equipped with a rotating anode generator Nonius FR591. Programs used: data collection COLLECT (Nonius B. V., **1998**), data reduction Denzo-SMN (Z. Otwinowski, W. Minor, *Methods Enzymol.* **1997**, *276*, 307−326), absorption correction SORTAV (R. H. Blessing, *Acta Crystallogr.* **1995**, *A51*, 33−37; R. H. Blessing, *J. Appl. Crystallogr.* **1997**, *30*, 421−426), structure solution SHELXS-97 (G. M. Sheldrick, *Acta Crystallogr.* **1990**, *A46*, 467−473), structure refinement SHELXL-97 (G. M. Sheldrick, Universität Göttingen, **1997**), graphics SCHAKAL (E. Keller, Universität Freiburg, **1997**). − Crystallographic data (excluding structure factors) for the structures reported in this paper have been deposited with the Cambridge Crystallographic Data Centre as supplementary publication CCDC-156106. Copies of the data can be obtained free of charge on application to CCDC, 12 Union Road, CambridgeCB2 1EZ, UK [Fax: (internat.) + 44-1223/336-033, E-mail: deposit@ccdc.cam.ac.uk].

[1,12-Dodecanediylbis(η^5-cyclopentadienyl)]zirconocene Dichloride (3d): A cold (−78 °C) suspension of $ZrCl_4(THF)_2$ (9.64 g, 25.6 mmol) in 250 mL of toluene was added to a suspension of the reagent **8d** (8.00 g, 25.8 mmol) in 600 mL of THF at −78 °C. The mixture was allowed to warm to room temperature overnight and then kept for 4 h at 60 °C. The solvent was removed in vacuo and the residue extracted (Soxhlet) with pentane for 60 h to give 2.06 g (18%) of **3d**, m.p. 144 °C. − $C_{22}H_{32}Cl_2Zr$ (458.6): caldc. C 57.62, H 7.03; found C 57.48, H 7.22. − IR (KBr): $\tilde{\nu}$ = 3102 (m), 2927 (vs), 2855 (s), 1488 (m), 1458 (m), 1439 (w), 1261 (w), 1094 (w), 1074 (w), 1052 (w), 1034 (m), 852 (m), 847 (m), 817 (s) cm^{-1}. − NMR assignments in [D_8]toluene were supported by GHSQC and GHMBC 2D NMR experiments[35] at 298 K. − ^{1}H NMR (599.9 MHz, [D_8]toluene, 298 K): δ = 5.85 (pseudo-t, 4 H, 3-H, 4-H of C_5H_4), 5.71 (pseudo-t, 4 H, 2-H, 5-H of C_5H_4), 2.42 (m, 4 H, 1-H/12-H of the chain), 1.35−1.23 (m, 20 H, 2-H to 11-H of the chain). − ^{13}C NMR (150.8 MHz, [D_8]toluene, 298 K): δ = 137.0 (C-1 of C_5H_4), 114.2 (C-3/C-4 of C_5H_4), 113.1 (C-2/C-5 of C_5H_4), 29.5 (C-1/C-12), 28.1, 27.7, 27.6, 27.4, 26.9 (C-2 to C-11). − The dynamic features of **3d** were examined by ^{1}H NMR spectroscopy in $CDFCl_2/CDF_2Cl$ in a temperature range between 253 K and 133 K; the 1-H,H′/12-H,H′ resonance shows the start of decoalescence at the lowest temperature reached (133 K). Since the temperature could not be lowered further in this solvent, the separated signals were not observed. − ^{1}H NMR (599.9 MHz, $CDFCl_2/CDF_2Cl$, 253 K): δ = 6.39 (pseudo-t, 4 H, 3-H, 4-H of C_5H_4), 6.19 (pseudo-t, 4 H, 2-H, 5-H of C_5H_4), 2.62 (m, 4 H, 1-H, 12-H), 1.63−1.27 (m, 20 H, 2-H to 11-H of the chain).

Olefin Polymerization Reactions: These were carried out in a toluene solution using a Büchi glass autoclave. Activation of the zirconocene dichlorides was carried out by treatment with a 10.5 w-% MAO solution in toluene, and the polymers worked up as previously described by us.[36] The ^{1}H NMR end group analysis of the polypropylene samples were carried out in 1,2,4-trichlorobenzene ([D_8]benzene lock) at 353 K. The stereochemical characterization was performed by ^{13}C NMR methyl pentade analysis.[24] Details of the polymerization experiments are compiled in Table 4.

Acknowledgments

Financial support from the Fonds der Chemischen Industrie and the Deutsche Forschungsgemeinschaft is gratefully acknowledged. We thank Dr. Christian Mück-Lichtenfeld for his help with the computational studies.

[1] Review: H.-H. Brintzinger, D. Fischer, R. Mülhaupt, B. Rieger, R. M. Waymouth, *Angew. Chem.* **1995**, *107*, 1255−1283; *Angew. Chem. Int. Ed. Engl.* **1995**, *34*, 1143−1171; see also: F. Piemontesi, I. Camurati, L. Resconi, D. Balboni, A. Sironi, M. Moret, R. Zeigler, N. Piccolravazzi, *Organometallics* **1995**, *14*, 1256−1266; H. Lee, P. J. Desrosiers, I. Guzei, A. L. Rheingold, G. Parkin, *J. Am. Chem. Soc.* **1998**, *120*, 3255−3256; J. C. Green, *Chem. Soc. Rev.* **1998**, *27*, 263−271, and references cited therein; H. G. Alt, E. Samuel, *Chem. Soc. Rev.* **1998**, *27*, 323−329.

[2] J. A. Smith, J. von Seyerl, G. Huttner, H. H. Brintzinger, *J. Organomet. Chem.* **1979**, *173*, 175−185; F. R. W. P. Wild, L.

Zsolnai, G. Huttner, H.-H. Brintzinger, *J. Organomet. Chem.* **1982**, *232*, 233−247; F. R. W. P. Wild, M. Wasiucionek, G. Huttner, H. H. Brintzinger, *J. Organomet. Chem.* **1985**, *288*, 69−77; F. Wochner, L. Zsolnai, G. Huttner, H. H. Brintzinger, *J. Organomet. Chem.* **1985**, *288*, 69−77; S. Collins, B. A. Kuntz, N. J. Taylor, D. G. Ward, *J. Organomet. Chem.* **1988**, *342*, 21−29; J. A. Ewen, R. L. Jones, A. Razavi, J. D. Ferrara, *J. Am. Chem. Soc.* **1988**, *110*, 6255−6256; P. Burger, J. Diebold, S. Gutmann, H.-U. Hund, H.-H. Brintzinger, *Organometallics* **1992**, *11*, 1319−1327; A. Razavi, J. L. Atwood, *J. Organomet. Chem.* **1996**, *520*, 115−120; G. M. Diamond, R. F. Jordan, J. L. Petersen, *J. Am. Chem. Soc.* **1996**, *118*, 8024−8033; M. Könemann, G. Erker, R. Fröhlich, S. Kotila, *Organometallics* **1997**, *16*, 2900−2908; R. L. Halterman, A. Tretyakov, M. A. Khan, *J. Organomet. Chem.* **1998**, *568*, 41−51.

[3] H. Lang, D. Seyferth, *Organometallics* **1991**, *10*, 347−349; T. K. Hollis, A. L. Rheingold, N. P. Robinson, J. Whelan, B. Bosnich, *Organometallics* **1992**, *11*, 2812−2816; R. L. Halterman, D. Combs, J. G. Kihega, M. A. Khan, *J. Organomet. Chem.* **1996**, *520*, 163−170; R. L. Halterman, D. Combs, M. A. Khan, *Organometallics* **1998**, *17*, 3900−3907; M. Ringwald, R. Stürmer, H. H. Brintzinger, *J. Am. Chem. Soc.* **1999**, *121*, 1524−1527.

[4] M. Knickmeier, G. Erker, T. Fox, *J. Am. Chem. Soc.* **1996**, *118*, 9623−9630; G. Erker, M. Aulbach, M. Knickmeier, D. Wingbermühle, C. Krüger, M. Nolte, S. Werner, *J. Am. Chem. Soc.* **1993**, *115*, 4590−4601.

[5] R. M. Waymouth, G. W. Coates, *Science* **1995**, *267*, 217−219; M. D. Bruce, G. W. Coates, E. Hauptmann, R. M. Waymouth, J. W. Ziller, *J. Am. Chem. Soc.* **1997**, *119*, 11174−11182; T. Dreier, G. Erker, R. Fröhlich, B. Wibbeling, *Organometallics* **2000**, *19*, 4095−4103.

[6] T. H. Warren, G. Erker, R. Fröhlich, B. Wibbeling, *Organometallics* **2000**, *19*, 127−134.

[7] M. Horáček, P. Štěpnička, R. Gyeped, I. Císařová, I. Tišlerová, J. Zemánek, J. Kubišta, K. Mach, *Chem. Eur. J.* **2000**, *6*, 2397−2408.

[8] G. Erker, C. Mollenkopf, M. Grehl, R. Fröhlich, C. Krüger, R. Noe, M. Riedel, *Organometallics* **1994**, *13*, 1950−1955.

[9] U. Höweler, R. Mohr, M. Knickmeier, G. Erker, *Organometallics* **1994**, *13*, 2380−2390.

[10] J. P. Perdew, *Electronic Structure of Solids '91* (Eds.: P. Ziesche, H. Eschrig), Akademie Verlag, Berlin, **1991**, p. 11; J. P. Perdew, J. A. Chevary, S. H. Vosko, K. A. Jackson, M. R. Pederson, D. J. Singh, C. Fiolhais, *Phys. Rev. B* **1992**, 46; J. P. Perdew, J. A. Chevary, S. H. Vosko, K. A. Jackson, M. R. Pederson, D. J. Singh, C. Fiolhais, *Phys. Rev. B* **1993**, 48; K. Burke, J. P. Perdew, Y. Wang, *Electronic Density Functional Theory: Recent Progress and New Directions* (Eds.: J. F. Dobson, G. Vignale, M. P. Das), Plenum, New York, **1998**; J. P. Perdew, K. Burke, Y. Wang, *Phy. Rev. B* **1996**, *54*, 16533; P. J. Stevens, J. F. Devlin, C. F. Chabalowski, M. J. Frisch, *J. Chem. Phys.* **1998**, 11623.

[11] For other applications of force-field calculations in metallocene chemistry see e.g.: A. K. Rappé, C. J. Casewit, K. S. Colwell, W. A. Goddard III, W. M. Skift, *J. Am. Chem. Soc.* **1992**, *114*, 10024−10035; J. R. Hart, A. K. Rappé, *J. Am. Chem. Soc.* **1993**, *115*, 6159−6164; H. Kawamura-Kuribayashi, N. Koga, K. Morokuma, *J. Am. Chem. Soc.* **1992**, *114*, 8687−8694; T. V. Timofeeva, J.-H. Lii, N. L. Allinger, *J. Am. Chem. Soc.* **1995**, *117*, 7452−7459; M. Toto, L. Cavallo, P. Corradini, G. Moscardi, L. Resconi, G. Guerra, *Macromolecules* **1998**, *31*, 3431−3438; D. Guo, X. Yang, L. Yang, Y. Li, T. Lin, H. Hong, Y. Hu, *J. Polymer Sci Part A: Polymer Chem.* **2000**, *38*, 2232−2238; N. Schneider, F. Schaper, K. Schmidt, R. Kirsten, A. Geyer, H. H. Brintzinger, *Organometallics* **2000**, *19*, 3597−3604; B. Bosnich, *Chem. Soc. Reviews* **1994**, *23*, 387−395; Reviews: T. R. Cundari, *J. Chem. Soc., Dalton Trans.* **1998**, 2771−2776; A. K. Rappé, W. M. Skift, C. J. Casewit, *Chem. Rev.* **2000**, *100*, 1435−1456; K. Angermund, G. Fink, V. R. Jensen, R. Kleinschmidt, *Chem. Rev.* **2000**, *100*, 1457−1470.

[12] G. Erker, K. Engel, U. Dorf, J. L. Atwood, W. E. Hunter, *Angew. Chem.* **1982**, *94*, 915−916; *Angew. Chem. Int. Ed. Engl.* **1982**, *21*, 914; U. Dorf, K. Engel, G. Erker, *Angew. Chem.* **1982**, *94*, 916−919; *Angew. Chem. Int. Ed. Engl.* **1982**, *21*, 914−915; V. Skibbe, G. Erker, *J. Organomet. Chem.* **1983**, *241*, 15−26; A. Stockis, R. Hoffmann, *J. Am. Chem. Soc.* **1980**, *102*, 2952−2962.

[13] L. Rossa, F. Vögtle, *Top. Curr. Chem.* **1983**, *113*, 1−86, and references cited therein.

[14] J. Y. Corey, X.-H. Zhu, L. Brammer, N. P. Rath, *Acta Crystallogr., Sect. C* **1995**, *51*, 565−567.

[15] C. Saldarriaga-Molina, A. Clearfield, I. Bernal, *J. Organomet. Chem.* **1974**, *80*, 79−90.

[16] A. Clearfield, D. Warner, C. Saldarriaga-Molina, R. Ropal, *Can. J. Chem.* **1975**, *53*, 1622−1629.

[17] C. S. Bajgur, W. R. Tikkanen, J. L. Petersen, *Inorg. Chem.* **1985**, *24*, 2539−2546.

[18] R. M. Shaltout, J. Y. Corey, N. P. Rath, *J. Organomet. Chem.* **1995**, *503*, 205−212.

[19] E. L. Eliel, S. H. Wilen, *Stereochemistry of Organic Compounds*, J. Wiley, New York, **1994**, p. 762−769, and references cited therein.

[20] M. L. H. Green, L.-L. Wong, A. Seela, *Organometallics* **1992**, *11*, 2660−2668, and references cited therein.

[21] J. S. Siegel, F. A. Anet, *J. Org. Chem.* **1988**, *53*, 2629−2630.

[22] G. Erker, T. Mühlenbernd, R. Benn, A. Rufińska, Y.-H. Tsay, C. Krüger, *Angew. Chem.* **1985**, *97*, 336−337; *Angew. Chem. Int. Ed. Engl.* **1985**, *24*, 321−323; R. Benn, H. Grondey, R. Nolte, G. Erker, *Organometallics* **1988**, *7*, 777−778; G. Erker, R. Nolte, G. Tainturier, A. Rheingold, *Organometallics* **1989**, *8*, 454−460; G. Erker, R. Nolte, C. Krüger, R. Schlund, R. Benn, H. Grondey, R. Mynott, *J. Organomet. Chem.* **1989**, *364*, 119−132; S. Knüppel, J.-L. Fauré, G. Erker, G. Kehr, M. Nissinen, R. Fröhlich, *Organometallics* **2000**, *19*, 1262−1268.

[23] H. Sinn, W. Kaminsky, *Adv. Organomet. Chem.* **1980**, *18*, 99−149. W. Kaminsky, K. Külper, H. H. Brintzinger, F. R. W. P. Wild, *Angew. Chem.* **1985**, *97*, 507−508; *Angew. Chem. Int. Ed. Engl.* **1985**, *24*, 507−508.

[24] Y. Inoue, Y. Itabashi, R. Chujo, Y. Doi, *Polymer* **1984**, *25*, 1640−1644; J. A. Ewen, *J. Am. Chem. Soc.* **1984**, *106*, 6355−6364, and references cited therein; M. Farina, *Top. Stereochem.* **1987**, *17*, 1−111.

[25] R. A. Howie, G. P. McQuillan, D. W. Thompson, *J. Organomet. Chem.* **1984**, *268*, 149−154; J. L. Petersen, L. F. Dahl, *J. Am. Chem. Soc.* **1975**, *97*, 6422−6433.

[26] MAXIMOBY Version 4.025, U. Höweler, Univ. Münster and CHEOPS, Altenberge, Germany.

[27] S. J. Weiner, P. A. Kollman, D. A. Case, U. C. Singh, C. Ghio, G. Alagoa, S. Profeta Jr., P. Weiner, *J. Am. Chem. Soc.* **1984**, *106*, 765; S. J. Weiner, P. A. Kollman, D. T. Nguyen, D. A. Case, *J. Comput. Chem.* **1986**, *7*, 230.

[28] MOBY Version 2.1A, U. Höweler, Univ. Münster and CHEOPS, Altenberge, Germany.

[29] P. J. Hay, W. R. Wadt, *J. Chem. Phys.* **1985**, *82*, 299−310; W. R. Wadt, P. J. Hay, *J. Chem. Phys.* **1985**, *82*, 284−298.

[30] T. M. Dunning Jr., *J. Chem. Phys.* **1971**, *55*, 716−723; T. M. Dunning Jr., *J. Chem. Phys.* **1970**, *53*, 2823−2833.

[31] L. E. Manzer, *Inorg. Synth.* **1982**, *21*, 136−140.

[32] C. F. H. Allen, J. P. Glauser, *Anal. Chem.* **1972**, *44*, 1694−1696.

[33] C. Mollenkopf, doctoral dissertation, Univ. Münster, Germany, **1993**; P. Cheng, A. Blumenstein, S. Subramanyam, *Mol. Cryst. Liq. Cryst. Sci. Technol. Sec. A.* **1995**, *269*, 1−38.

[34] J. K. Stille, L. Plummer, *J. Org. Chem.* **1961**, *26*, 4026−4029.

[35] S. Braun, H.-O. Kalinowski, S. Berger, *150 and More Basic NMR Experiments*, VCH, Weinheim, **1998**, and references cited therein.

[36] M. Dahlmann, G. Erker, K. Bergander, *J. Am. Chem. Soc.* **2000**, *122*, 7986−7998.

Received January 25, 2001
[I01033]

The 2D and 3D Compounds $[M_2bpm(dca)_4]\cdot nH_2O$ (M = Ni, Zn; bpm = bipyrimidine; dca = dicyanamide; n = 0, 1) − Structural Analysis and Magnetic Properties

Susana Martín,[a] M. Gotzone Barandika,[a] Roberto Cortés,*[a] J. I. Ruiz de Larramendi,[a] M. Karmele Urtiaga,[b] Luis Lezama,[c] M. Isabel Arriortua,[b] and Teófilo Rojo*[c]

Keywords: Magnetic properties / Structure elucidation / N ligands / Nickel / Zinc

The combined use of bpm (2,2′-bipyrimidine) and dca (dicyanamide) has led to the preparation of two compounds of general formula $[M_2bpm(dca)_4]\cdot nH_2O$. Compound **1** (M = Ni, n = 1) exhibits a 2D layered structure based on ladder-like moieties. These units, whose steps are bpm groups, extend through single dca bridges, the connection between distinct ladder-like units taking place through double dca bridges. Compound **2** (M = Zn, n = 0) consists of a 3D structure based on the same type of ladder-like moieties that are connected to another four on the plane perpendicular to the extension of the ladders.

Introduction

The design of multidimensional networks has been an important area of research in coordination chemistry. Thus, the preparation of crystalline materials exhibiting some desired structural and topological features becomes a fascinating challenge as it implies the control of the related physical and chemical properties. In this sense, the synthetic strategy has been widely confirmed to be a major factor.

Among the variety of extended frameworks reported during the last few years, there are plenty of examples that illustrate the relevance of the synthetic strategy. Since the azide pseudohalide has been one of the most used ligands, a couple of azide systems can be mentioned in this context (Scheme 1). For instance, the compound $[Mn(N_3)_2bpy]_n$ (bpy = 2,2′-bipyridine) consists of Mn chains where the Mn^{II} ions are alternatively bridged by double *end-on* (EO) and double *end-to-end* (EE) azide bridges.[1] The substitution of bpy by the tetradentate bpm (2,2′-bipyrimidine) in an M:bpm molar ratio of 2:1 induces the connection of the Mn chains resulting in the compound $[Mn_2(N_3)_4bpm]_n$. This is a 2D honeycomb-like structure where the sheets exhibit an infinite hexagonal array of Mn^{II} ions bridged by bis-chelating bpm and double EO azide-bridges.[2]

A further step in the synthetic strategy could consist of the substitution of the azide group to generate new M-bpm-L compounds (L being the new ligand). With this aim, we have selected dicyanamide (dca), as previously done by other researchers.[3] This ligand, similarly to the azide li-

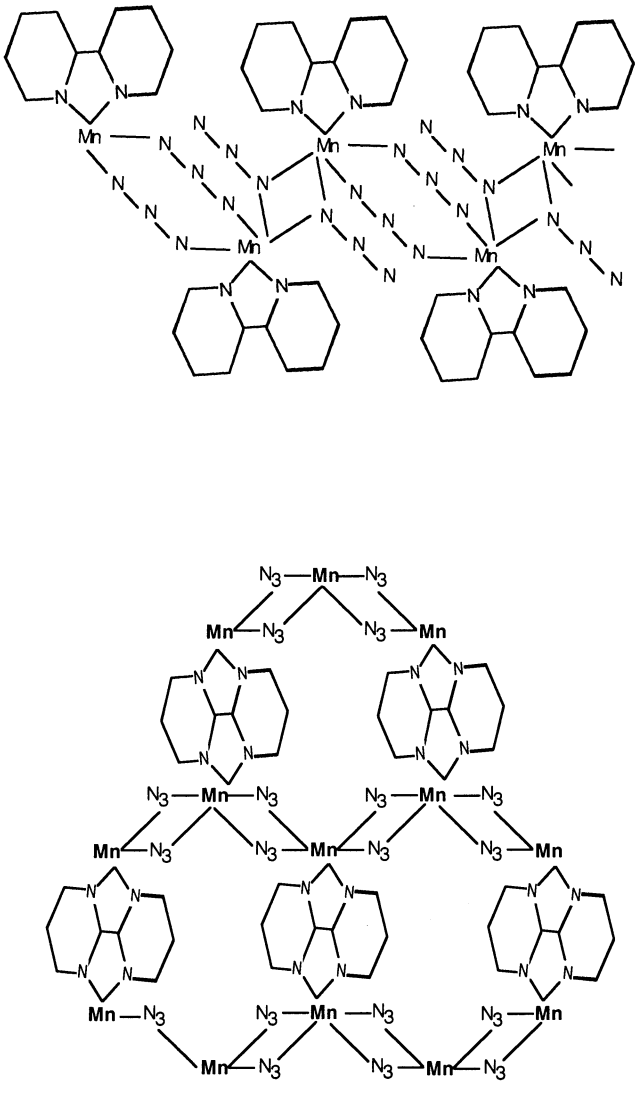

Scheme 1

[a] Departamento de Química Inorgánica, Facultad de Farmacia, Universidad del País Vasco,
Apdo. 450, Vitoria 01080, Spain
[b] Departamento de Mineralogía-Petrología, Facultad de Ciencias, Universidad del País Vasco,
Apdo. 644, Bilbao 48080, Spain
[c] Departamento de Química Inorgánica, Facultad de Ciencias, Universidad del País Vasco,
Apdo. 644, Bilbao 48080, Spain
E-mail: qiproapt@lg.ehu.es

 © WILEY-VCH Verlag GmbH, 69451 Weinheim, 2001 1434−1948/01/0808−2107 $ 17.50+.50/0

gand, exhibits several coordination modes. Thus, besides the monodentate terminal coordination,[4] bidentate,[5] tridentate[6] and even tetradentate[7] modes have been reported for dca (Scheme 2). The potential of dca for the preparation of extended frameworks is illustrated by the great deal of recent attention focussed on coordination polymers containing this ligand.[8]

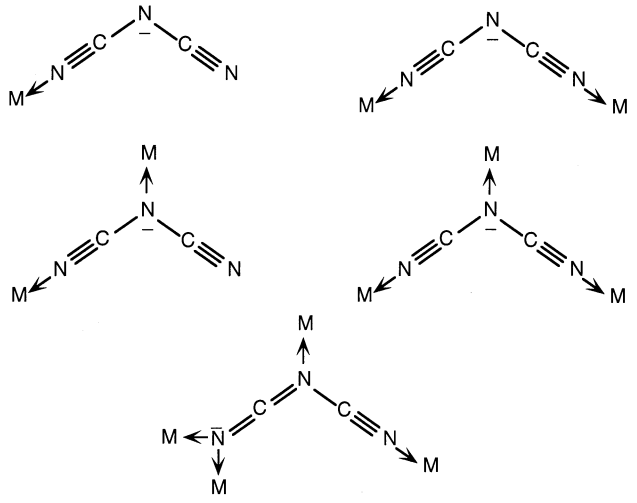

Scheme 2

Taking into account the above-mentioned aspects, two compounds of general formula $[M_2bpm(dca)_4]\cdot nH_2O$ (M = Ni, $n = 1$ for compound **1**; M = Zn, $n = 0$ for compound **2**) have been synthesised and magnetostructurally characterised. For both of them, a ladder-like moiety can be proposed as a basic structural unit whose repetition leads to a 2D array for **1** and to a 3D network for **2**.

Results and Discussion

Structural Analysis

The structural characterisation of compound **1** has been carried out by means of X-ray powder-diffraction pattern analysis on the basis of the structure of $[Co_2bpm(dca)_4]\cdot H_2O$ (**3**). This compound has been structurally characterised at 100 K by Marshall et al.[3] and at 273 K by us. Therefore, since the X-ray powder-diffraction data collection for **1** was carried out at 273 K, we have used our structural data for **3** as initial parameters for the refinement of **1**. The observed, calculated and difference X-ray diffraction pattern for **1** are displayed in Figure 1. As can readily be seen, there is a good agreement between the theoretical and experimental data. Thus, the fact that **1** and **3** exhibit the same stoichiometry and space group (*Pnma*) and similar structural parameters [a = 16.111(3) Å, b = 12.755(2) Å, c = 10.455(2) Å for **1** and a = 16.212(2) Å, b = 12.972(2) Å, c = 10.502(2) Å for **3**] clearly indicates that compounds **1** and **3** are isomorphous. This isomorphous relationship is also confirmed by the rest of the analytical techniques discussed in this work for **1**.

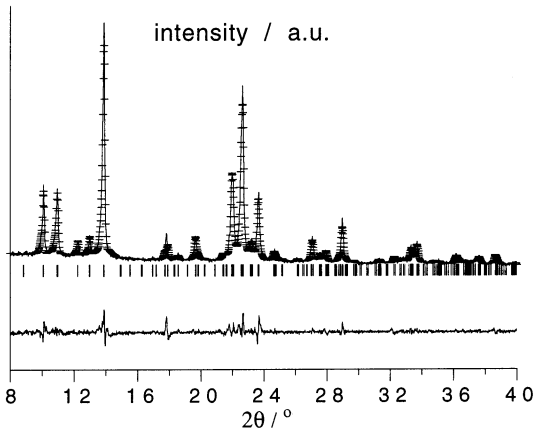

Figure 1. Observed, calculated and difference X-ray diffraction patterns for **1**

Figure 2 shows a view of the structures of **1** and **3**. As observed, they consist of layers of octahedrally coordinated metallic cations. The 2D network can be described on the basis of ladder-like moieties extending along the x direction through single dca bridges, the steps being the bpm groups. These ladders are connected through double dca bridges along the y direction. The intermetallic distance through bpm is the shortest one (5.770 Å for **3**) while the distance through the single dca bridges is the longest one (8.299 Å for **3**), with the one through double dca links being intermediate (7.202 Å for **3**). The layers are waved and are closely packed along the z direction. Additionally, there are molecules of water of crystallisation located between these layers.

Compound **2** consists of a 3D network where each Zn^{II} cation is octahedrally bonded to one bpm (through N1 and N2 atoms) and four dca ligands (two N3−C5−N4−C6−N5 groups and two N6−C7−N7−C8−N8 groups). As seen in Figure 3, the two N_{bpm} atoms occupy two of the equatorial positions. Since the bpm ligands are N,N',N'',N'''-tetradentate they allow the connection between two metallic cations. On the other hand, the four dca groups act as 1,5-bridges with the N3 and N6 atoms at the remaining equatorial positions and the N5 and N8 atoms at the axial positions. As a result each Zn^{II} cation is linked to five metallic centres: one through bpm (Zn···Zn distance is 5.895 Å) and four by dca ligands [Zn···Zn distances through the N3,N5- and N6,N8-bonded dca groups are 7.446 and 7.656 Å, respectively].

The 3D structure of **2** can also be described on the basis of covalently interconnected ladder-like moieties. Thus, as observed in Figure 4, the ladder-like moieties also consist of bpm steps. These units extend along the x direction through N3−C5−N4−C6−N5 dca groups. Each ladder unit is connected to another four through N6−C7−N7−C8−N8 dca groups along the [011] and [$\bar{0}$1] directions.

Table 1 displays the selected bond lengths and angles for **2**. As can be seen, the coordination sphere is quite distorted in relation to both distances and angles. The presence of the rigid bpm ligand accounts for the bond angles being far from the ideal values. The Zn−N8 distance deserves special

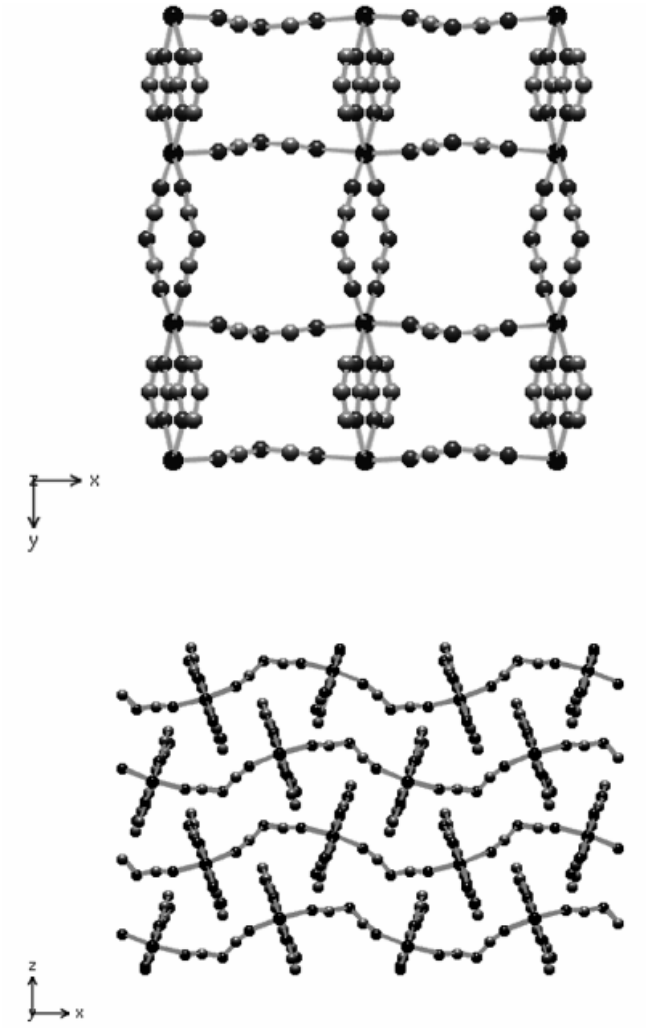

Figure 2. (top) View of the 2D structure and (bottom) the packing of the layers for **1**

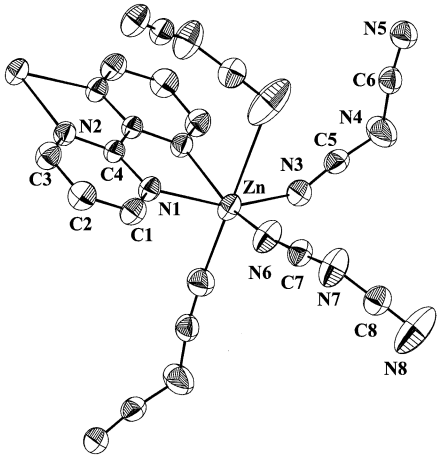

Figure 3. ORTEP view (50% probability) of the coordination environment for **2**

attention as the value of 2.8 Å clearly implies that the covalent connection between distinct ladder-like units is weak. Nevertheless, similar values have been accepted in the literature as bond lengths.[9]

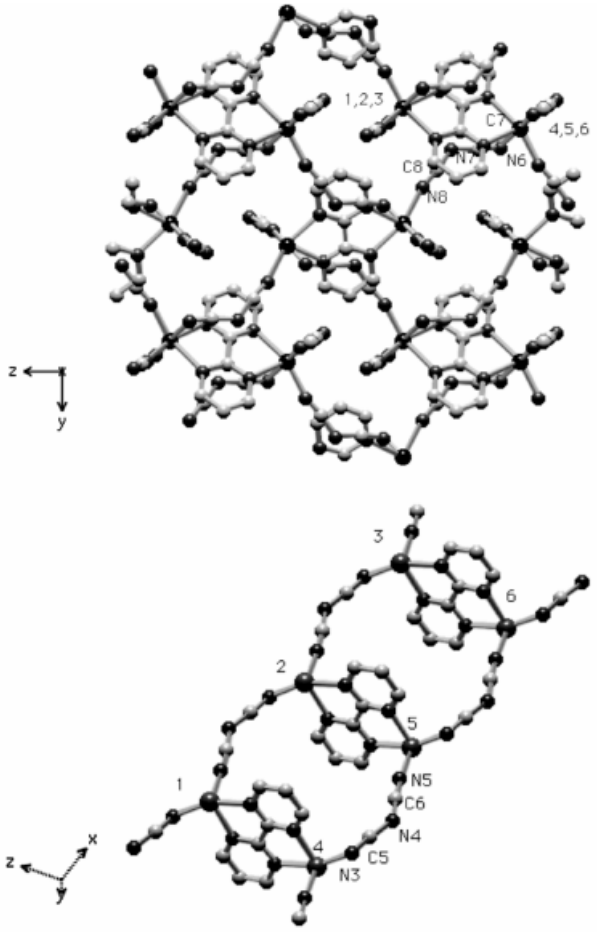

Figure 4. (Top) [011] view of the structure for **2** and (bottom) extension of the ladder-like moieties along the [100] direction

Table 1. Selected bond lengths (Å) and angles (°) for compound **2**[a]

Zn−N(1)	2.171(2)	N(5)−Zn−N(2i)	98.67(8)
Zn−N(2i)	2.258(2)	N(6)−Zn−N(3)	100.31(10)
Zn−N(3)	2.028(2)	N(6)−Zn−N(1)	92.84(8)
Zn−N(5)	2.030(2)	N(3)−Zn−N(1)	158.51(8)
Zn−N(8)	2.788(2)	N(6)−Zn−N(2i)	157.67(8)
Zn−N(6)	2.040(2)	N(3)−Zn−N(2i)	87.44(8)
N(3)−C(5)	1.149(3)	N(1)−Zn−N(2i)	74.42(6)
C(5)−N(4)	1.285(3)	C(5)−N(3)−Zn	142.07(18)
N(4)−C(6)	1.294(3)	N(3)−C(5)−N(4)	172.7(3)
C(6)−N(5ii)	1.146(3)	C(5)−N(4)−C(6)	123.5(2)
N(6)−C(7)	1.137(3)	N(5ii)−C(6)−N(4)	171.7(3)
C(7)−N(7)	1.295(3)	C(6iii)−N(5)−Zn	171.8(2)
N(7)−C(8)	1.292(3)	C(7)−N(6)−Zn	163.1(2)
C(8)−N(8)	1.127(4)	N(6)−C(7)−N(7)	172.6(3)
N(5)−Zn−N(6)	100.49(10)	C(8)−N(7)−C(7)	122.1(2)
N(5)−Zn−N(3)	100.08(9)	N(8)−C(8)−N(7)	172.8(3)
N(5)−Zn−N(1)	94.08(8)		

[a] Symmetry transformations used to generate equivalent atoms: i = $-x$, $-y$, $-z$; ii = $x-1$, y, z; iii = $x+1$, y, z.

The main difference between the structures for **1** and **2** lies in the connection between ladder-like units. Thus, while each ladder is connected to another two through double dca bridges along the *y* direction for **1**, each ladder is linked to another four through single dca bridges for **2**. This is a

consequence of the orientation of the coordination octahedra in relation to the extension of the ladder-like moiety. Thus, for **1** the axial direction of the octahedra fully coincides with the extension direction, while for **2** it does not. Obviously, this different disposition is responsible for the occurrence of a 2D array for **1** and a 3D structure for **2**.

IR and ESR spectroscopy

A summary of the most important IR bands corresponding to compounds **1** and **2**, together with their tentative assignment,[10] is displayed in Table 2. As observed, both compounds exhibit strong absorptions in the region 2315−2190 cm^{-1} that correspond to $\nu_{C\equiv N}$ modes. There are also strong bands at about 1580 cm^{-1} for both of them (with a shoulder at lower wavenumbers for **2**) that have been attributed[11] to the asymmetric doublet characteristic of ring stretching for bis-chelating bpm. The absorptions due to molecules of water of crystallisation were detected for **1** at about 3400 cm^{-1}.

Table 2. IR bands (cm^{-1}) and assignments for compounds **1** and **2**

	1	**2**
dca, ν_{sym} + ν_{asym} (C≡N)	2312i	2352i,2292i
dca, ν_{asym} (C≡N)	2257i	2265i
dca, ν_{sym} (C≡N)	2190i	2225i, 2165i
dca, ν (C−N)	1413m, 1360m	1415i, 1360i
bpm, (C=C, C=N), bis-chelating	1585m	1580i, 1565i
H_2O, crystallisation (O−H)	3410m	−

An X-band ESR spectrum at room temp. was recorded on a powdered sample of **2** doped with 1 mol % Cu (Figure 5). As observed, the signal is characteristic of an axial *g* tensor exhibiting hyperfine splitting on the parallel component which corresponds to the electronic spin−nuclear spin (^{67}Cu, $I = 3/2$) coupling. Values of $g_{\|} = 2.315$, $g_{\perp} = 2.075$ and $A_{\|} = 143 \times 10-4\,cm^{-1}$ have been determined. The sequence $g_{\|} > g_{\perp} > 2.04$ indicates a $d_{x^2-y^2}$ ground state in good agreement with the elongated octahedral topology of the $[CuN_6]$ chromophores.[12]

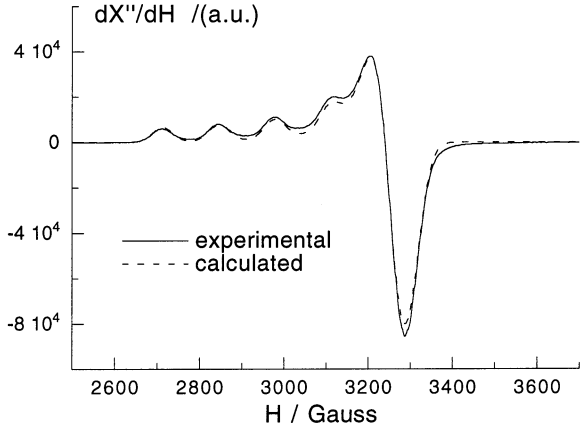

Figure 5. Experimental and calculated ESR powder spectra for $[(Zn_{0.99}Cu_{0.01})_2bpm(dca)_4]$

Magnetic Properties

The magnetic characterisation of compound **1** was carried out by measurement of the thermal variation of the magnetic susceptibility, χ_m. The experimental data, plotted as the thermal variation of the reciprocal susceptibility (χ_m^{-1}) and the product $\chi_m T$ are shown in Figure 6.

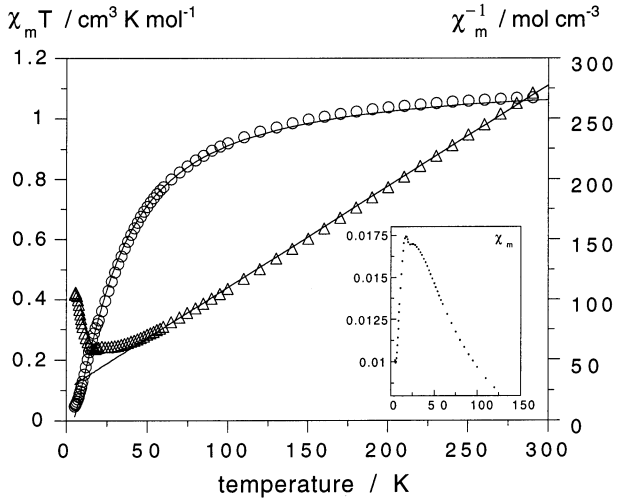

Figure 6. Thermal evolution of χ_m^{-1} and $\chi_m T$ for **1** and their corresponding theoretical curves (fit 2 for $\chi_m T$)

The χ_m values for **1** increase from 3.53×10^{-3} cm^3 mol^{-1} at room temp. up to a maximum, and afterwards decrease, tending to zero. The peak in χ_m shows two maxima (16.54×10^{-3} cm^3 mol^{-1} at 24 K and 16.95×10^{-3} cm^3 mol^{-1} at 17 K). This small anomaly, shown in the inset in Figure 6, will be discussed below. The Curie−Weiss law is followed down to 50 K with values of $C_m = 1.19$ cm^3 K mol^{-1} and $\theta = -30.75$ K. The $\chi_m T$ curve decreases continuously upon cooling from 1.07 cm^3 K mol^{-1} (per Ni atom) at room temp., tending to zero.

The magnetic results for **1** are clearly indicative of the occurrence of antiferromagnetic coupling between metallic centres. Since the dca ligand is a poor magnetic mediator,[13] these interactions should be attributed mainly to the exchange through the bpm ligand.[3,14]

In order to evaluate the antiferromagnetic interactions for **1**, Equation (1) was used first. This expression, based on the isotropic spin Hamiltonian $H = -JS_A \cdot S_B$, accounts for the molar magnetic susceptibility corresponding to a Ni^{II} dimer ($S_A = S_B = 1$).

$$\chi_m = \frac{2N\beta^2 g^2}{kT}\left[\frac{\exp(J/kT) + 5\exp(3J/kT)}{1 + 3\exp(J/kT) + 5\exp(3J/kT)}\right] \quad (1)$$

where *N* and *k* are the Avogadro and Boltzmann constants, respectively, and β is the Bohr magneton.

This model reproduces the experimental data quite accurately with values of $J = -18.3$ cm^{-1} and $g = 2.12$ (fit 1). However, as mentioned above, there is a small anomaly on the χ_m vs. *T* curve for **1** that has not been explained. This anomaly could be attributed to the occurrence of weak ex-

change through the dca bridges at low temperatures that could provoke a slight lack of compensation of the antiparallel spins. If we now consider this exchange as an interdimer molecular field,[3] the magnetic data for **1** can be interpreted by Equation (2). The best theoretical curve generated (fit 2) is displayed in Figure 6 ($J = -16.5$ cm^{-1}, $g = 2.14$ and $zJ' = -3.1$ cm^{-1}). It is worth mentioning that no significant improvement has been found compared to fit 1.

$$\chi = \frac{\chi_m}{\left(1 - \frac{2k}{Ng^2\beta^2} zJ' \chi_m\right)} \quad (2)$$

The sign and magnitude of the exchange constants J calculated for the interaction through bpm is comparable to others found in the literature. Thus, values between -14 and -11 cm^{-1} have been reported for Ni-bpm-Ni bridges.[15] The moderate efficiency of bis-chelating bpm as a magnetic coupler is explained by the strong overlap between $d_{x^2-y^2}$ magnetic orbitals (the x and y axes being the ones corresponding to the $Ni-N_{bpm}$ bonds) through the symmetry-adapted HOMO of the bpm bridge.[16] The fact that the Ni-bpm-Ni fragment is practically planar favours the overlap increasing the magnitude of the coupling.

The isomorphous Co^{II} compound (**3**) has been characterised magnetically by Marshall et al.[3] Compound **3** exhibits antiferromagnetic interactions that are mainly attributed by the authors to the dimeric exchange through bpm (as found for **1**). Unfortunately, since the attempts by Marshall et al. to model the magnetic behaviour of **3** do not lead to any J values, there is no possible comparison between the exchange constants for **1** and **3**.

Conclusion

The combined use of dca and bpm has led to the preparation of extended frameworks with two Ni^{II} and Zn^{II} atoms. The antiferromagnetic Ni^{II} compound exhibits a 2D array where ladder-like units are connected through double dca bridges. The bpm ligands are the steps in the ladder-like moieties, their extension taking place through single dca bridges. Molecules of water of crystallisation can be found between the resulting waved planes. The Zn^{II} compound is anhydrous and exhibits the same kind of ladder-like units. In this case, however, each unit is connected to another four through single dca bridges resulting in a 3D array.

Experimental Section

Synthesis: The synthesis of compound **1** was carried out by mixing an aqueous solution of $Ni(NO_3)_2\cdot 6H_20$ (0.50 mmol) and a methanolic solution of bpm (0.25 mmol). Afterwards, an aqueous solution of dca (1 mmol) was added and left to stand at room temperature. After several days, poor-quality blue crystals were obtained (45% yield, 62.57 mg). Unfortunately, further attempts to recrystallise this product did not lead to better quality crystals. The synthesis of compound **2** was performed in a similar manner with $ZnCl_2$. In this case, prismatic, yellow, X-ray quality single crystals (34% yield, 62.22 mg) were obtained.

Elemental analysis and atomic absorption results were in good agreement with the $C_8H_3N_8NiO_{0.5}$ stoichiometry for **1**, and the $C_8H_3N_8Zn$ stoichiometry for **2**.
1: calcd. C 34.4, H 1.4, N 40.2, Ni 21.0; found C 33.0, H 1.7, N 38.3, Ni 21.2.
2: calcd. C 34.7, H 1.1, N 40.5, Zn 23.6; found C 34.5, H 1.0, N 39.3, Zn 23.1.

Physical Measurements: Microanalyses were performed with a LECO CHNS-932 analyser. Analytical measurements were carried out in an ARL 3410 + ICP with a Minitorch equipment. IR spectroscopy was performed on a Nicolet 520 FTIR spectrophotometer in the 400−4000 cm^{-1} region. ESR spectroscopy was performed on powdered samples at the X-band frequency, with a Bruker ESR 300 spectrometer equipped with a standard OXFORD low-temperature device, which was calibrated by the NMR probe for the magnetic field. The frequency was measured with a Hewlett−Packard 5352B microwave frequency computer. Magnetic susceptibilities and the magnetisation of powdered samples were carried out in the temperature range 1.8−300 K at values of the magnetic field up to 10000 G, using a Quantum Design Squid magnetometer, equipped with a helium continuous-flow cryostat. The experimental susceptibilities were corrected for the diamagnetism of the constituent atoms (Pascal tables).

Crystal Structure Determination: X-ray powder diffraction data for compound **1** were collected on a PHILIPS X′PERT powder diffractometer with Cu-K_α radiation in steps of 0.02° (2θ) over the 5−60° (2θ) angular range and a fixed-time counting of 4 seconds at 25 °C. The powder diffraction patterns were indexed with the FULLPROF[16] program based on the Rietveld method[17−18]using the *Profile Matching* option. Crystallographic data and processing parameters for compound **1** are given in Table 3.

Table 3. Crystallographic data for **1**

Formula	$C_8H_3N_8NiO_{0.5}$
M	278.11
Crystal system	Orthorhombic
Space group	*Pnma*
a [Å]	16.111(3)
b [Å]	12.755(2)
c [Å]	10.455(2)
α [°]	90
β [°]	90
γ [°]	90
U [Å^3]	2148.4
Z	8
T [K]	293
λ [Å]	1.5425
R_p[a]	7.50
R_{wp}[b]	9.80
GOF[c]	2.55

[a] $R_p = 100[100(|y_o - y_c|)/|y_o|]$. − [b] $R_{wp} = [(w|y_o - y_c|^2)/(w|y_o|^2)]^{1/2}$. − [c] GOF $= [R_{wp}/R_{expected}]^2$.

X-ray measurements for **2** were carried out at room temperature on an Enraf−Nonius CAD-4 diffractometer operating in the ω/2θ scanning mode. Accurate lattice parameters were determined from a least-squares refinement of 25 well-centred reflections. Intensity data were collected in the θ range 1−30°. During data collection, two standard reflections observed periodically showed no signific-

ant variation. Corrections for Lorentz and polarisation factors were applied to the intensity values. The structure for **2** was solved by heavy-atoms Patterson methods using the program SHELXS-97[19] and refined by a full-matrix least-squares procedure on F^2 using SHELXL-97.[20] Non-hydrogen atomic scattering factors were taken from International Tables of X-ray Crystallography.[21] Crystallographic data and processing parameters for **2** are shown in Table 4.

Crystallographic data (excluding structure factors) for the structure(s) included in this paper have been deposited with the Cambridge Crystallographic Data Centre as supplementary publication no. CCDC-150936 (**2**) and -150937 (**3**). Copies of the data can be obtained free of charge on application to CCDC, 12 Union Road, Cambridge CB2 1EZ, UK [Fax: (internat.) + 44-1223/336-033; Email: deposit@ccdc.cam.ac.uk].

Table 4. Crystal data and structure refinement for compound **2**

Formula	$C_8H_3N_8Zn$
M	276.55
Crystal system	Monoclinic
Space group	$P2_1/c$
a [Å]	7.446(4)
b [Å]	11.478(4)
c [Å]	12.064(4)
α [°]	90
β [°]	107.75(2)
γ [°]	90
U [Å^3]	982.0(7)
Z	4
T [K]	293
λ [Å][a]	0.71069
ρ_{obs} [g cm^{-3}]	1.85(4)
ρ_{cal} [g cm^{-3}]	1.871
μ [mm^{-1}]	2.489
Unique data	2860
Observed data	2299
$R(R')$[b]	0.0356(0.1031)

[a] Graphite monochromated Mo-K_α radiation. – [b] $R = [||F_o| - |F_c||/|F_o|]$, $R' = \{[w(F_o^2 - F_c^2)^2]/[w(F_o^2)^2]\}^{1/2}$, where $w = 1/\sigma^2\gamma|F_o|$.

Acknowledgments

This work has been carried out with the financial support of the Universidad del País Vasco/Euskal Herriko Unibertsitatea (Grant UPV 130310-EB201/1998), Gobierno Vasco/Eusko Jaurlaritza (Project 99/53) and the Ministerio de Educación y Cultura (Project PB97–0637). S. M also thanks the Gobierno Vasco/Eusko Jaurlaritza for the doctoral fellowship associated to the project PI96/39.

[1] R. Cortés, M. Drillon, X. Solans, L. Lezama, T. Rojo, *Inorg. Chem.* **1997**, *36*, 677–683.
[2] [2a] R. Cortés, L. Lezama, J. L. Pizarro, M. I. Arriortua, T. Rojo, *Angew. Chem. Int. Ed. Engl.* **1996**, *35*, 1810–1812. – [2b] R. Cortés, M. K. Urtiaga, L. Lezama, J. L. Pizarro, M. I. Arriortua, T. Rojo, *Inorg. Chem.* **1997**, *36*, 5016–5021.
[3] S. R. Marshall, C. D. Incarvito, J. L. Manson, A. L. Rheinhold, J. S. Miller, *Inorg. Chem.* **2000**, *39*, 1969–1973.
[4] [4a] I. Potocnák, M. Dunaj-Jurco, D. Miklos, L. Jäger, *Acta Crystallogr., Sect. C* **1996**, *52*, 1653–1655. – [4b] I. Potocnák, M. Dunaj-Jurco, D. Miklos, M. Kabesová, L. Jäger, *Acta Crystallogr., Sect. C* **1995**, *51*, 600–602.
[5] [5a] Y. M. Chow, *Inorg. Chem.* **1971**, *10*, 1938–1942. – [5b] Y. M. Chow, D. Britton, *Acta Crystallogr., Sect. C* **1977**, *33*, 697–699. – [5c] D. Britton, *Acta Crystallogr., Sect. C* **1990**, *46*, 2297–2299. – [5d] J. L. Manson, C. D. Incarvito, A. L Rheinhold, J. S. Miller, *J. Chem. Soc., Dalton Trans.* **1998**, 3705–3706. – [5e] J. Mrozinski, M. Hvastijová, J. Kohout, *Polyhedron* **1991**, *11*, 2867–2871.
[6] J. L. Manson, C. R. Kmety, Q. Huang, J. W. Lynn, G. Bendele, S. Pagola, P. W. Stephens, L. M. Liable-Sands, A. L. Rheingold, A. J. Epstein, J. S. Miller, *Chem. Mater.* **1998**, *10*, 2552–2560.
[7] Y. M. Chow, D. Britton, *Acta Crystallogr., Sect. C* **1975**, *31*, 1934–1936.
[8] [8a] S. R. Batten, P. Jensen, B. Moubaraki, K. S. Murray, R. Robson, *Chem. Commun.* **1998**, 439–440. – [8b] J. L. Manson, D. W. Lee, A. L. Rheingold, J. S. Miller, *Inorg. Chem.* **1998**, *37*, 5966–5967. – [8c] J. L. Manson, C. R. Kmety, A. J. Epstein, J. S. Miller, *Inorg. Chem.* **1999**, *38*, 2552–2553. – [8d] P. Jensen, S. R. Batten, G. D. Fallon, B. Moubaraki, K. S. Murray, D. J. Price, *Chem. Commun.* **1999**, 177–178. – [8e] S. R. Batten, P. Jensen, C. J. Kepert, M. Kurmoo, B. Moubaraki, K. S. Murray, D. J. Price, *J. Chem. Soc., Dalton Trans.* **1999**, 2987–2997. – [8f] P. Jensen, S. R. Batten, G. D. Fallon, D. C. R. Hockless, B. Moubaraki, K. S. Murray, R. Robson, *J. Solid State Chem.* **1999**, *145*, 387–393. – [8g] J. L. Manson, A. M. Arif, J. S. Miller, *J. Mat. Chem.* **1999**, *9*, 979–983. – [8h] P. Jensen, S. R. Batten, B. Moubaraki, K. S. Murray, *Chem. Commun.* **2000**, 793–794. – [8i] A. Escuer, F. A. Mautner, N. Sanz, R. Vicente, *Inorg. Chem.* **2000**, *39*, 1668–1673.
[9] [9a] A. Bino, N. Cohen, *Inorg. Chim. Acta* **1992**, *210*, 11–17. – [9b] D. K. Lavallee, A. B. Kovelove, O. P. Anderson, *J. Am. Chem. Soc.* **1978**, *100*, 3025–3033.
[10] K. Nakamoto, *Infrared Spectra of Inorganic and Coordination Compounds*, John Willey & Sons, New York, **1997**.
[11] [11a] F. Berezovsky, A. A. Hajem, S. Triki, J. S. Pala, P. Molinie, *Inorg. Chim. Acta* **1999**, *248*, 8–13. – [11b] G. De Munno, M. Julve, F. Lloret, J. Faus, A. J. Caneschi, *J. Chem. Soc., Dalton Trans.* **1994**, 1175–1183.
[12] J. A. Weil, J. R. Bolton, E. Wertz, *Electron Spin Resonance, Elementary Theory and Practical Applications*, 2nd Ed., John Wiley & Sons, New York, **1994**.
[13] J. L. Manson, A. M. Arif, C. D. Incarvito, L. M. Liable-Sands, A. L. Rheingold, J. S. Miller, *J. Solid State Chem.* **1999**, *145*, 369–378.
[14] G. De Munno, G. Viau, M. Julve, F. Lloret, J. Faus, *Inorg. Chim. Acta* **1997**, *257*, 121–129.
[15] [15a] G. De Munno, M. Julve, F. Lloret, A. Derory, *J. Chem. Soc., Dalton Trans.* **1992**, 1179. – [15b] G. Brewer, E. Sinn, *Inorg. Chem.* **1985**, *24*, 4580–4585.
[16] M Julve, G. De Munno, G. Bruno, M. Verdaguer, *Inorg. Chem.* **1988**, *27*, 3160–3165.
[17] J. Rodriguez-Carvajal, FULLPROF, *Program for Rietveld Pattern Matching Analysis of Powder Patterns*, **1997**.
[18] H. M. Rietveld, *Acta Crystallogr.* **1967**, *12*, 151–152.
[19] H. M. Rietveld, *J. Appl. Cryst.* **1969**, *6*, 65–67.
[20] G. M. Sheldrick, SHELXS-97. Program for the Solution of Crystal Structures. University of Göttingen, Germany, **1997**.
[21] G. M. Sheldrick, SHELXL-97. Program for the Refinement of Crystal Structures. University of Göttingen, Germany, **1997**.
[22] *International Tables for X-ray Crystallography, Vol. IV*, Kynoch Press, Birmingham, U.K, **1974**.

Received January 19, 2001
[I01036]

Syntheses, Structures and Nonlinear Optical Properties of Ferrocenyl Complexes with Arylethenyl Substituents

José A. Mata,[a] Eduardo Peris,*[a] Rosa Llusar,[b] Santiago Uriel,[b] Marie P. Cifuentes,[c] Mark G. Humphrey,*[c] Marek Samoc,[d] and Barry Luther-Davies[d]

Keywords: Ferrocene / NLO / Bimetallic compounds / Crystal structure

The complexes (*E*)- and (*Z*)-Fe(η^5-C_5H_4CHO)(η^5-C_5H_4CH=CH–C_6H_4-4-NO_2) [**2**-(*E*) and **2**-(*Z*), respectively], (*E*)- and (*Z*)-Fe(η^5-C_5H_4CHO)(η^5-C_5H_4CH=CH–C_6H_4-4-CN) [**3**-(*E*) and **3**-(*Z*), respectively], (*E*,*E*)-, (*E*,*Z*)-, and (*Z*,*Z*)-Fe(η^5-C_5H_4CH=CHC_6H_4-4-NO_2)$_2$ [**4**-(*E*,*E*), **4**-(*E*,*Z*), and **4**-(*Z*,*Z*), respectively], (*E*,*E*)-, (*E*,*Z*)-, and (*Z*,*Z*)-Fe(η^5-C_5H_4CH=CHC_6H_4-4-CN)$_2$ [**5**-(*E*,*E*), **5**-(*E*,*Z*), and **5**-(*Z*,*Z*), respectively], and Fe(η^5-C_5H_5)(η^5-C_5H_4–(*E*)-CH=CH–4-{(η^6-C_6H_4)$Cr(CO)_3$}–(*E*)-CH=CH–η^5-C_5H_4)Fe(η^5-C_5H_5) (**7**) have been synthesized. Structural studies on **2**-(*E*), **4**-(*E*,*Z*), **5**-(*E*,*E*), Fe(η^5-C_5H_5){η^5-C_5H_4–(*E*)-CH=CH–4-C_6H_4–(*E*)-CH=CH–η^5-C_5H_4}Fe(η^5-C_5H_5) (**6**) and **7** have been performed. Electrochemical studies of **2**–**5** reveal trends in the oxidation potentials which are consistent with the more effective conjugation of the (*E*) isomers, and the better electron-accepting character of NO_2 than CN and of CHO than H. Powder SHG measurements by the Kurtz technique using fs pulses at the telecommunications wavelength of 1.3 μm reveal low responses for **4**-(*E*,*E*), **5**-(*E*,*E*), and **7**. Third-order NLO measurements by Z-scan using fs pulses at 800 nm suggest an increase in |γ| on increasing the electron-acceptor strength [when proceeding from **5**-(*E*,*Z*) to **4**-(*E*,*Z*), CN is replaced by NO_2], and on introduction of the $Cr(CO)_3$ unit, when proceeding from **6** to **7**.

Introduction

Ferrocene is a versatile building block. Its excellent thermal and photochemical stability, and combination of useful redox properties and chemical versatility, provides access to materials with potentially useful physical and chemical properties.[1–3] With the importance of ferrocene in the field of material science, there is currently great interest in the chemistry of ferrocenyl-based oligomers and ferrocenyl-containing conjugated compounds. The former contain the ferrocene building block in the repeat unit, and the latter couple ferrocene to a potentially π-delocalizable system. These complexes are of interest because of, amongst other things, their nonlinear optical (NLO) properties; the significant electron-donating strength of the ferrocenyl group has made it a good candidate for the design of chromophores with high NLO responses.

We previously reported on the syntheses, characterization, and molecular quadratic NLO behavior of ferrocene-containing conjugated compounds with pyridine, nitro, and nitrile pendant groups. This allowed us to obtain heterobimetallic complexes containing a series of electron-accepting moieties derived from $M(CO)_6$ (M = Cr, Mo, W) [Scheme 1 (a) and (b)].[4–6] Electrochemical studies together with the planar conformation of the molecular structures suggested effective electron delocalization along the conjugated chains. In a continuation of these studies, we have now synthesized a series of ferrocenyl 1,1′-bis-substituted complexes with nitro and nitrile pendant groups, whose electronic and solid-state structural properties have been studied. The results from these studies are reported herein. Similar 1,1′-bis-substituted ferrocenyl complexes with pendant pyridine groups have been reported by Lee et al., and show very interesting structural features.[7]

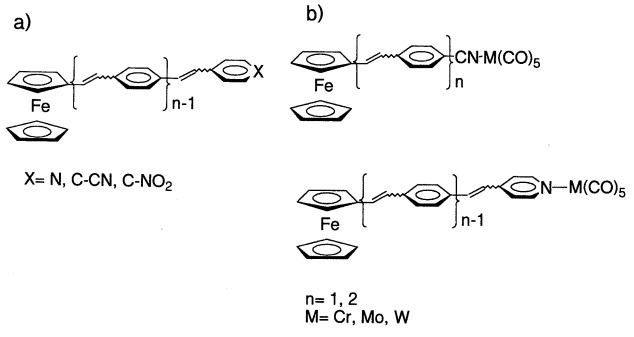

Scheme 1

We have also investigated arylethenyl-linked biferrocenes, with and without the presence of bridge arene-ligated $Cr(CO)_3$ units, the syntheses of which were reported by Müller et al.[8] while the current studies were underway. We

[a] Departamento de Química Inorgánica y Orgánica, Universitat Jaume I
Ctra. Borriol S/N, 12080 Castellón, Spain,
Fax: (internat.) +34 964/72 8214
E-mail: eperis@qio.uji.es
[b] Departamento de cc. Experimentales, Universitat Jaume I
Castellón, Spain
[c] Department of Chemistry, Australian National University
Canberra, ACT 0200, Australia
Fax: (internat.) +61 2/6125 0760
E-mail: Mark.Humphrey@anu.edu.au
[d] Australian Photonics Cooperative Research Centre, Laser Physics Centre, Research School of Physical Sciences and Engineering, Australian National University
Canberra, ACT 0200, Australia

 © WILEY-VCH Verlag GmbH, 69451 Weinheim, 2001 1434–1948/01/0808–2113 $ 17.50+.50/0

report herein a modified synthesis of the $Cr(CO)_3$-ligated complex, together with X-ray structural studies of both complexes.

Although the number of studies reporting second-order NLO responses of ferrocenyl complexes is very high, comparatively fewer studies exist in which third-order NLO responses are reported.[9] Since the effective delocalization in the molecular structures of our complexes fulfill a basic requirement for third-order NLO-active materials, we have measured and report herein on their cubic hyperpolarizabilities at 800 nm by Z-scan. While the bulk second-order susceptibilities of many ferrocenyl complexes have been reported,[10] much extant data has been obtained at wavelengths close to those of material resonances, resulting in significant resonance enhancement of the response. We therefore also report the bulk susceptibilities for these complexes by the Kurtz powder method at wavelengths remote from electronic absorption bands, thus enabling an assessment of off-resonance nonlinearity to be obtained.

Results and Discussion

Syntheses of 2−5

Based on our previous experience[4−6] we have synthesized compounds **2**−**5** by conventional Wittig and Horner−Emmons−Wadsworth methods (Scheme 2). The first step of the two-step reaction procedure afforded the bis-substituted complexes **2** and **3** with (*Z*) and (*E*) stereochemistry, together with small amounts of the bis-olefinated complexes (**4** and **5** in all their isomeric forms). Compounds **2** and **3** may be of interest in the design of new materials, since the presence of the carboxaldehyde group may provide access to a variety of functional groups. Complexes **2** and **3** undergo further olefination in the second step to yield **4** and **5** in all their isomeric forms [**4** and **5** exist as three isomers by combination of the (*E*) and (*Z*) dispositions of the vinylic group, i.e. (*E,E*), (*E,Z*) and (*Z,Z*)]. All three isomers were fully characterized for both the nitro and nitrile derivatives. Higher yields of the bis-substituted compounds **4** and **5** were obtained when performing the one-step (direct reaction) procedure. In all cases, separation of the (*E*) and (*Z*) isomers was easily achieved by column chromatography. Reaction of any of the complexes in refluxing toluene in the presence of iodine leads to the all-*E*-isomers in almost quantitative yields (see Experimental section).

Synthesis of 7

The synthesis of **6** was again based on Horner−Emmons−Wadsworth (HEW) olefinations using the corresponding phosphonate reagent. A synthesis of **7** was reported while the present studies were underway,[8] and involved olefination by HEW reaction of an η^6-coordinated carbonylchromium phenylene-bisphosphonate with ferrocenecarboxaldehyde. In the present study, η^6-coordination of the tri(carbonyl)chromium moiety to the phenylene bridging group of **6** was performed by heating compound **6** with $Cr(CO)_6$ in refluxing butyl ether (Scheme 3).

X-ray Structural Studies of 2-(*E*), 4-(*E,Z*), 5-(*E,E*), 6, and 7

The identities of **2**-(*E*) (ORTEP plots in Figures 1 and 2), **4**-(*E,Z*) (Figure 3), **5**-(*E,E*) (Figures 4 and 5), **6** (Figure 6), and **7** (Figure 7) were confirmed by single-crystal X-ray studies; crystallographic data are summarized in Table 5, and selected bond angles and distances are listed in Tables 1 and 2.

The structural studies reveal a number of interesting features. Complexes **2**-(*E*), **4**-(*E,Z*), and **5**-(*E,E*) provide the opportunity to assess the impact of π-system chain lengthening, stereochemistry, and acceptor modification on metrical parameters and crystal packing preference. In

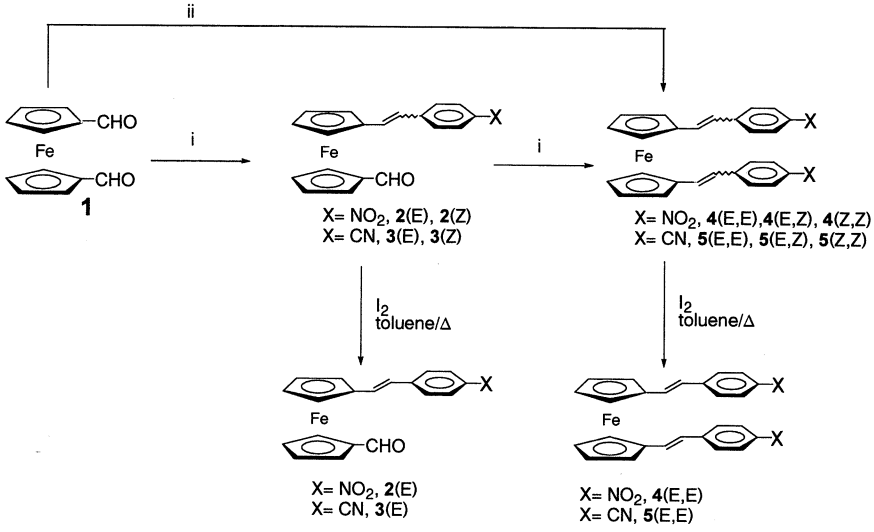

Scheme 2. Syntheses of **2**−**5**. (i) 1.5 ($PPh_3CH_2-C_6H_4$-4-NO_2)Br/KO*t*Bu or 1.5 ($PPh_3CH_2-C_6H_4$-4-CN)Br/KO*t*Bu. (ii) 3 ($PPh_3CH_2-C_6H_4$-4-NO_2)Br/KO*t*Bu, or 3 ($PPh_3CH_2-C_6H_4$-4-CN)Br/KO*t*Bu.

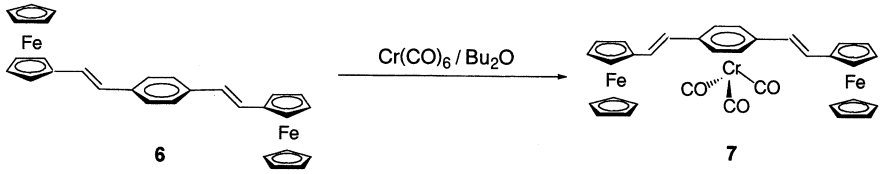

Scheme 3

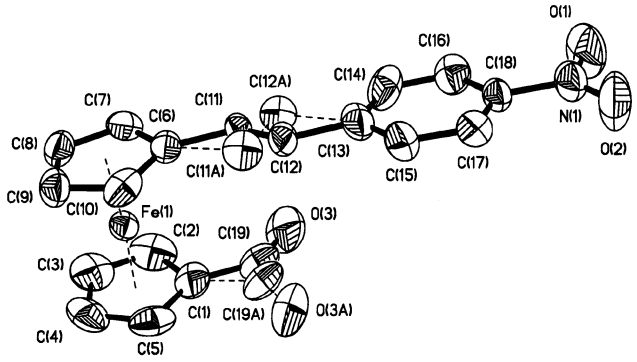

Figure 1. Molecular structure and atomic labeling scheme for **2**-(*E*), Fe(η^5-C_5H_4CHO){η^5-C_5H_4−(*E*)-CH=CHC_6H_4-4-NO_2}, with 50% anisotropic displacement ellipsoids

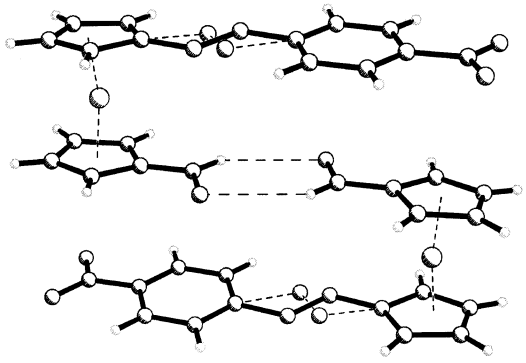

Figure 2. Crystal packing of compound **2**-(*E*) showing the hydrogen-bonding through the aldehydes of two different molecules. The distance between H···O is ca. 2.7 Å

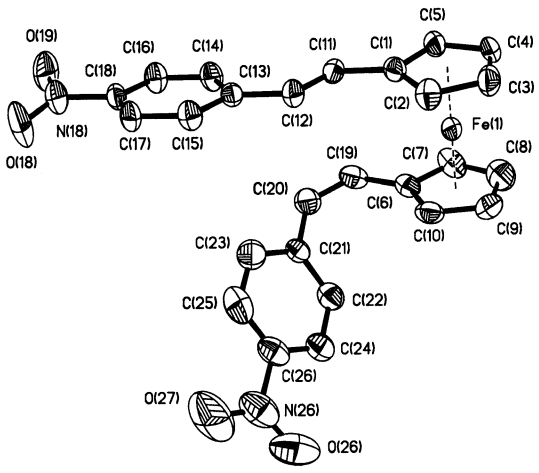

Figure 3. Molecular structure and atomic labeling scheme for **4**-(*E,Z*), Fe{η^5-C_5H_4−(*Z*)-CH=CHC_6H_4-4-NO_2}{η^5-C_5H_4−(*E*)-CH=CHC_6H_4-4-NO_2}, with 50% anisotropic displacement ellipsoids

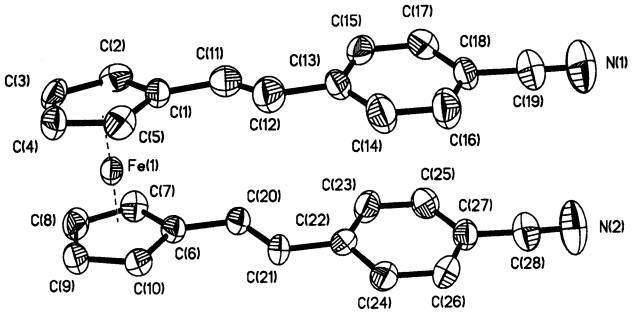

Figure 4. Molecular structure and atomic labeling scheme for **5**-(*E,E*), Fe{η^5-C_5H_4−(*E*)-CH=CHC_6H_4-4-CN}$_2$, with 50% anisotropic displacement ellipsoids

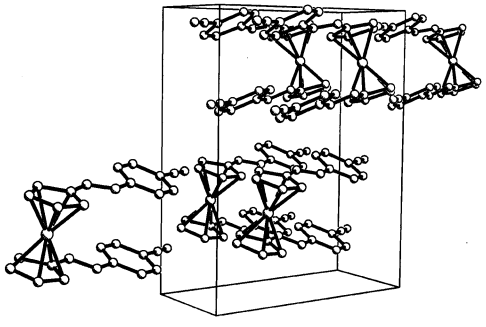

Figure 5. Cell packing diagram for **5**-(*E,E*), Fe{η^5-C_5H_4−(*E*)-CH=CHC_6H_4-4-CN}$_2$

ferrocenyl complexes, it has been reported that two molecular motions relieve steric strain:[1] (i) the rotation from an eclipsed to a staggered disposition of the two Cp rings and (ii) their tilting from a parallel disposition. For these three complexes, little tilting is observed; the two cyclopentadienyl rings are slightly tilted (dihedral angles 2.7−4.3°) with respect to each other. Compounds **2**-(*E*), **4**-(*E,Z*), and **5**-(*E,E*) show *syn* conformations with respect to the two ancillary ligands, with a perfect eclipsed disposition of the Cp rings of the ferrocene unit in **2**-(*E*) and **5**-(*E,E*).

The distances from iron to the cyclopentadienyl rings and the C−C distances within the rings in these three structures, lie in the expected range. As seen in Figures 1, 2, 3, and 4, all the molecules with (*E*) stereochemistry have an almost idealized coplanar arrangement between the ferrocenyl donor and the vinylene-phenylene functionalized fragment. The two ancillary ligands in compound **5**-(*E,E*) show intra-

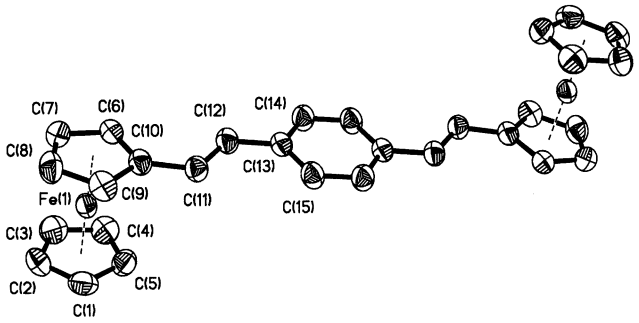

Figure 6. Molecular structure and atomic labeling scheme for **6**, Fe(η^5-C_5H_5)(η^5-C_5H_4−(*E*)-CH=CH−4-C_6H_4−(*E*)-CH=CH−η^5-C_5H_4)Fe(η^5-C_5H_5), with 50% anisotropic displacement ellipsoids

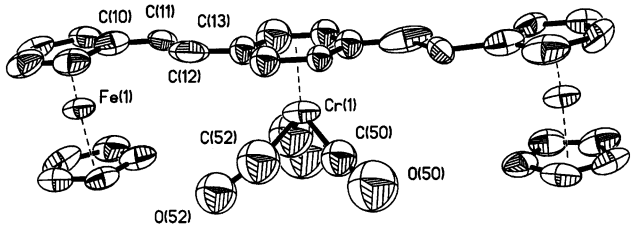

Figure 7. Molecular structure and atomic labeling scheme for **7**, Fe(η^5-C_5H_5)(η^5-C_5H_4−(*E*)-CH=CH−4-{(η^6-C_6H_4)Cr(CO)$_3$}-(*E*)-CH=CH−η^5-C_5H_4)Fe(η^5-C_5H_5) with 50% anisotropic displacement ellipsoids

Table 1. Selected bond lengths and angles for **2**-(*E*), **4**-(*E,Z*), and **5**-(*E,E*)

2-(*E*)			
N1−O1	1.216(3)	Fe1−N1 (space)	9.42
N1−O2	1.212(3)	Fe1−N1 (bonds)	11.9
C19−O3	1.188(10)		
C19A−O3A	1.135(18)		
plane Cp(1−5)−Cp(6−10)		4.28(0.21)	
plane Cp(1−5)−Ph		7.18(0.20)	
4-(*E,Z*)			
N18−O18	1.221(3)	Fe1−N18 (space)	9.41
N18−O19	1.218(4)	Fe1−N26 (space)	7.97
N26−O26	1.225(4)	Fe1−N18 (bonds)	11.90
N26−O27	1.208(4)	Fe1−N26 (bonds)	11.92
plane Cp(1−5)−Cp(6−10)		3.01(0.24)	
plane Cp(1−5)−Ph(13−18)		9.51(0.19)	
5-(*E,E*)			
C11−C20	3.44	Fe1−N1 (space)	10.46
C12−C21	3.71	Fe1−N2 (space)	10.56
C19−C28	3.89	Fe1−N1 (bonds)	13.0
N1−N2	3.92	Fe1−N2 (bonds)	13.0
plane Cp(1−5)−Cp(6−10)		2.75(0.16)	
plane Cp(1−5)−Ph(13−18)		10.93(0.16)	
plane Cp(6−10)−Ph(22−27)		7.57(0.17)	
plane Ph(13−18)−Ph(22−27)		2.30(0.13)	

Table 2. Selected bond lengths and angles for **6** and **7**

	6	**7**
Fe−C (Cp subs.)	2.047[10]	2.024[25]
Fe−C (Cp non subs.)	2.041[1]	2.022[40]
C−C (Cp subs.)	1.417 [10]	1.403[25]
C−C (Cp non subs.)	1.407[5]	1.401[8]
C(10)−C(11)	1.464(2)	1.34(2)
C(11)−C(12)	1.323(2)	1.37(3)
C(12)−C(13)	1.469(2)	1.40(3)
Cr1−C(CO)	−	1.72[9]
C(CO)−O(CO)	−	1.24[10]
Fe−Fe (space)	13.49	12.85
Fe−Fe (bonds)	17.86	16.46
Fe−Cr (space)	−	6.14
Fe−Cr (bonds)	−	8.15
C(10)−C(11)−C(12)	124.59(18)	121(2)
C(11)−C(12)−C(13)	128.02(18)	122(3)
plane Cp−Cp(subs)	1.46(16)	0.29(0.73)
plane Ph−Cp(subs)	3.37(25)	5.03(1.11)

molecular π-stacking, as can be clearly seen in Figure 4; the two ligands smoothly increase their separation from 3.44 [C(20)−C(11)] to 3.92 Å [N(1)−N(2)]. In the crystal lattice of compound **2**-(*E*), centrosymmetric dimer pairs are connected by hydrogen-bonding through the oxygen and hydrogen atoms of the aldehyde group (Figure 2). This hydrogen-bond of the type C−H···O is pervasive in crystalline organometallic transition metal complexes, especially when the C−H is of the sp^2 type.[11] In our case, the oxygen atom of the aldehyde polarizes the C−H bond enhancing its H-donor capabilities. Compound **5**-(*E,E*) crystallizes in the noncentrosymmetric space group $P2_1$. The crystal arrangement of **5**-(*E,E*) (Figure 5), despite being noncentrosymmetric, reveals an anti-parallel alignment of the molecular dipoles, therefore low second-harmonic generation (SHG) is expected for the bulk material. This canceling of the molecular dipoles has also been observed for other noncentrosymmetric ferrocenyl compounds.[12]

Compounds **6** and **7** both crystallize in the centrosymmetric space group $P2_1/c$, the inversion center for compound **6** is located in the middle of the phenyl ring. The crystallographic inversion center lies very close to the chromium atom, generating another molecule with a face to face disposition when compared with the previous one, thus resulting in disorder. The bond lengths and angles in **6** lie in the expected range,[13] with the ferrocenyl units adopting the sterically less hindered *anti* conformation. The cyclopentadienyl and phenyl rings in **6** are roughly coplanar (maximum dihedral angle 3.37°). The bond lengths and angles in **7** lie in the expected range, except the Cr−C−O angles which are significantly distorted from linearity (ca. 167°). The most significant structural feature of **7** is the *syn*/*syn* conformation adopted by the two ferrocenyl and the tri(carbonyl)chromium units. The two substituted-cyclopentadienyl rings and the phenyl group are more distorted from coplanarity (maximum dihedral angle 5.03°) than the similar rings in compound **6**.

The Fe−Cr distances in **7** are 6.1 Å (through space) and 8.2 Å (through bonds), so a direct bonding effect must be discounted. In the absence of conclusive theoretical calculations, we believe that the more sterically hindered disposition of the ligated metal units may be due to packing effects. In fact, this kind of disposition has also been observed in other related compounds.[14]

Cyclic Voltammetry

The electrochemical data obtained for complexes **2**−**5** are summarized in Table 3. In all cases, we observed the chemically reversible ferrocene/ferrocenium couple with $i_{pa}/i_{pc} = 1$. Although the peak to peak separations in all the compounds are greater than the ideal value for a fully reversible one-electron process, this difference ($E_{pc} - E_{pa}$) is similar to that measured for ferrocene under the conditions of the experiment. When compared with the previously reported ferrocenyl derivatives with one 4-nitrophenylethenyl or 4-cyanophenylethenyl substituent,[4−6] the bis-substituted complexes show a more anodic half-wave potential (ca. 100 mV), suggesting that the extra electron-accepting substituent has an important electronic effect on the ferrocenyl fragment. When comparing complexes with analogous stereochemical features, the nitro compounds **4** have a higher oxidation potential than the homologous nitrile derivatives **5**, thus confirming the better electron-accepting nature of the nitro group. The complexes with a higher degree of (*E*) stereochemistry (i.e. *E,E* > *E,Z* > *Z,Z*) possess a lower half-wave potential than those with a higher degree of (*Z*) stereochemistry (half-wave potential **4**-(*E,E*) < **4**-(*E,Z*) < **4**-(*Z,Z*) and **5**-(*E,E*) < **5**-(*E,Z*) < **5**-(*Z,Z*)]. This is in good agreement with the greater stabilization of the positive charge corresponding to the more effective conjugation of the (*E*) isomers, and indicates a higher degree of charge transfer from the metal center to the polyene backbone.[5,6,15] The aldehydes **2** and **3** possess a much higher half-wave potential than the ferrocenyl complexes with one 4-nitrophenylethenyl or 4-cyanophenylethenyl substituent,[4−6] perhaps due to the electron-accepting nature of the aldehyde group. The substitution of the aldehyde group by the corresponding conjugated ligand to give **4** and **5**, results in a shift to more cathodic potentials, probably as a consequence of the enhanced stabilization of the positive charge of the resultant ferrocenium species at the two conjugated ancillary ligands.

Literature electrochemical data suggest that biferrocene complexes similar to **6** and **7** do not show effective electronic communication between the two ferrocene moieties.[8,13] For such complexes, and homologues with pentamethylcyclopentadienyl ligands, only one peak is observed for the oxidation of the iron atoms. However, the potential for this two-electron oxidation is sensitive to modification of the bridging unit; electrochemical data for compound **7** shows that the oxidation of the iron atom is clearly influenced by the carbonyl fragment. A shift from 455 mV in compound **6** to 351 mV in **7** is consistent with oxidation of the ferrocene centers which is facilitated by incorporation of the chromium carbonyl unit.[8] In fact, one would expect that the electron-accepting nature of chromium tricarbonyl should increase the oxidation potential of the compound in contrast to what we observed. The same effect has been described by Müller for compound **7** and other related ferrocenyl-chromium tricarbonyl complexes[8] and, in fact, may be justified by the amphoteric character of $Cr(CO)_3$ proposed by the same author and his co-workers.[16]

Table 3. Electrochemical and linear optical data for complexes **2**−**5**

	λmax (nm)						
	$CHCl_3$		MeOH		THF		$E_{1/2}(\Delta E_p)$/mV
Compd.	MLCT	π-π*	MLCT	π-π*	MLCT	π-π*	(Ferrocene based)[a]
2-(*E*)	−	309	−	356	−	358	755(74)
2-(*Z*)	−	308	−	325	−	329	790(170)
3-(*E*)	−	327	−	329	−	329	775(127)
4-(*E,E*)	494	358	497	358	495	355	545(89)
4-(*E,Z*)	493	350	487	353	488	352	555(74)
4-(*Z,Z*)	481	335	−	337	481	343	585(155)
5-(*E,E*)	−	342	−	340	492	340	500(100)
5-(*E,Z*)	473	334	473	333	469	335	545(115)
5-(*Z,Z*)	−	318	−	312	−	319	565(79)
6							455
7	436[b]	306[b]					351[b]

[a] Ferrocene half-wave potential = 445(105) mV. − [b] Data taken from ref. [8].

Electronic Spectra

Table 3 contains the electronic spectroscopic data for the bis-substituted complexes **2**−**5**. In a typical electronic spectrum of substituted ferrocenyl complexes, two prominent bands are often observed in the range of 500 to 300 nm. The more energetic band (300−360 nm) is assigned to a π−π* intra-ligand transition, and the less energetic band (400−500 nm) is assigned to a metal to ligand charge-transfer band (MLCT). A weak band at higher wavelengths (about 500 nm), assigned to a *d-d* transition, is only discernible in some cases as a shoulder on the MLCT band, and is not shown in Table 3. This assignment is in accordance to the theoretical results reported by Barlow et al. (model III in ref.[17]) and to other experimental results,[5,6,12,18−23] although we are aware that some controversy about this assignment has been reported.[24] The MLCT band is influenced by the nature of the ancillary ligand, showing a hypsochromic shift on increasing the (*E*) character of the complex. The more intense π-π* band shows a similar dependence on the nature of the ligand; this is because the (*E*) stereochemistry promotes a more effective conjugation than the (*Z*) stereochemistry, thus lowering the energy of the π* orbital. Solvatochromism affords an idea of the dipole moments in the ground and in the excited states. These are related to hyperpolarizability, and therefore solvatochromism is a useful indicator for the potential for second-order NLO behavior. The bis-substituted ferrocenyl complexes show moderate solvatochromic behavior across the solvents surveyed.

Kurtz Powder Studies

Kurtz powder measurements were performed on **4**-(*E,Z*), **4**-(*Z,Z*), **4**-(*E,E*), **5**-(*E,Z*), **5**-(*E,E*), **6**, and **7**. Initial studies using ns pulses at 1.064 μm suggested the doubling of the frequency for a number of samples (green flashes were observed when the samples were irradiated), but absorption associated with the MLCT bands in these complexes rendered these results qualitative at best. A second qualitative test at the important telecommunications wavelength of 1.3 μm using fs pulses again suggested the doubling of the frequency (red flashes were observed for most complexes). A third qualitative test at 1.4 μm confirmed this result. Importantly, all complexes are transparent at both the fundamental and second-harmonic frequencies corresponding to the wavelength of 1.3 μm, so the SHG merit of these complexes was quantified against an urea standard, the results for which are summarized in Table 4.

Complexes **4**-(*E,Z*), **4**-(*Z,Z*), and **5**-(*E,Z*) showed a relatively strong emission with a significant blue component; this may be due to other NLO processes, and it masks any SHG which may be present, rendering further discussion of these complexes unwarranted. The ferrocene-containing conjugated compounds **4**-(*E,E*) and **5**-(*E,E*) both gave significant responses. Noncentrosymmetric crystal packing is a requirement for observable SHG, therefore it is worthy to note that the structural study of **5**-(*E,E*) reveals a lack of a center of symmetry in the crystal lattice. Complex **6** shows no observable SHG at 1.3 μm, in contrast to the $Cr(CO)_3$-ligated complex **7**. Both complexes crystallize in the centrosymmetric space group $P2_1/c$. The observed SHG for the centrosymmetric **7** is not unique; similar observations for $[Ru(C{=}CPhN{=}N{-}4\text{-}C_6H_4OMe)(PPh_3)_2(\eta^5\text{-}C_5H_5)]BF_4$[25] and $[(\eta^5\text{-}C_5H_5)(CO)_2Fe(\mu\text{-}CO)\{\mu\text{-}(E)\text{-}CH{=}CH{-}4\text{-}C_6H_4\text{-}NMe_2\}Fe(CO)_2(\eta\text{-}C_5H_5)]BF_4$,[26] both of which pack in centrosymmetric space groups, were assigned to effects originating in the noncentrosymmetric crystal surface, small contributions from a noncentrosymmetric phase, or minor deviations from centrosymmetry. Electron diffraction studies to resolve this ambiguity were similarly inconclusive.

The results of the present series of samples emphasize the challenges inherent in translating significant molecular nonlinearities to useful bulk susceptibilities. Thus, while $Fe(\eta^5\text{-}C_5H_5)(\eta^5\text{-}C_5H_4{-}(Z)\text{-}CH{=}CH{-}4\text{-}C_6H_4NO_2)$ is reported to give SHG with an efficiency 62 times that of urea,[19,26–28] incorporation of a further 4-nitrophenylethenyl group in proceeding to **4**-(*E,Z*) or **4**-(*Z,Z*), results in complexes for which observable SHG could not be determined unambiguously.

Third-Order NLO Studies

Third-order nonlinearities of **4**-(*Z,Z*), **5**-(*E,E*), **6**, and **7** were evaluated by the Z-scan technique at 800 nm;[29] the results of these measurements are given in Table 4. Complex **4**-(*E,E*) was insufficiently soluble, in both dichloromethane and THF, to afford useful data.

Early studies of ferrocenyl complexes by optical power limiting afforded very high nonlinearities (10^{-32} to 10^{-31} esu),[30–32] but this technique is carried out on a ns time scale, and contributions from thermal effects may exist. For structure-activity studies, it is more useful to use Z-scan with fs pulses, as in the present study. The cubic nonlinearities $|\gamma|$ of these new ferrocenyl complexes are of the same magnitude as those of related conjugated ferrocenyl complexes examined by degenerate four-wave mixing (DFWM).[33]

One advantage of Z-scan relative to DFWM is that one can readily determine the real and imaginary components of the cubic hyperpolarizabilities, (these are also listed in Table 4). We have previously used Z-scan to study the cubic hyperpolarizabilities of acetylide complexes,[34–40] for which most real components are large and negative, and imaginary components are large, indicative of significant two-photon dispersion effects. The real components of the nonlinearities γ_r for the present series of complexes are large and positive and, with the exception of **4**-(*E,Z*), the imaginary components γ_i are small; two-photon effects are therefore likely to be minor, permitting cautious comment on the effect of structural variation on cubic NLO merit. Replace-

Table 4. Linear optical and nonlinear optical response parameters for **4**-(*Z,Z*), **4**-(*E,Z*), **4**-(*E,E*), **5**-(*E,Z*), **5**-(*E,E*), **6**, and **7**

Complex	λ_{max} (nm)[a] [ε (10^4 м$^{-1}$ cm^{-1}]	SHG[b] (urea = 1)	γ_r[c] (10^{-36} esu)	γ_i[c] (10^{-36} esu)	$\lvert\gamma\rvert$ (10^{-36} esu)
$Fe\{\eta^5\text{-}C_5H_4\text{-}(E)\text{-}CH{=}CHC_6H_4\text{-}4\text{-}NO_2\}_2$ [**4**-(*E,E*)]	495 [0.47]	0.28	[e]	[e]	[e]
$Fe\{\eta^5\text{-}C_5H_4\text{-}(E)\text{-}CH{=}CHC_6H_4\text{-}4\text{-}NO_2\}$-$\{\eta^5\text{-}C_5H_4\text{-}(Z)\text{-}CH{=}CHC_6H_4\text{-}4\text{-}NO_2\}$ [**4**-(*E,Z*)]	488 [0.56]	[d]	840 ± 400	770 ± 200	1140 ± 430
$Fe\{\eta^5\text{-}C_5H_4\text{-}(Z)\text{-}CH{=}CHC_6H_4\text{-}4\text{-}NO_2\}_2$ [**4**-(*Z,Z*)]	481 [0.30]	[d]	600 ± 300	0 ± 50	600 ± 300
$Fe\{\eta^5\text{-}C_5H_4\text{-}(E)\text{-}CH{=}CHC_6H_4\text{-}4\text{-}CN\}_2$ [**5**-(*E,E*)]	492 [0.34]	0.24	280 ± 150	30 ± 20	280 ± 150
$Fe\{\eta^5\text{-}C_5H_4\text{-}(E)\text{-}CH{=}CHC_6H_4\text{-}4\text{-}CN\}$-$\{\eta^5\text{-}C_5H_4\text{-}(Z)\text{-}CH{=}CHC_6H_4\text{-}4\text{-}CN\}$ [**5**-(*E,Z*)]	469 [0.33]	[d]	310 ± 200	50 ± 30	310 ± 200
$Fe(\eta\text{-}C_5H_5)\{\eta^5\text{-}C_5H_4\text{-}(E)\text{-}CH{=}CH\text{-}4\text{-}C_6H_4\text{-}(E)\text{-}CH{=}CH\text{-}\eta^5\text{-}C_5H_4\}Fe(\eta^5\text{-}C_5H_5)$ (**6**)	457 [0.45]	[d]	640 ± 300	30 ± 20	640 ± 300
$Fe(\eta\text{-}C_5H_5)(\eta^5\text{-}C_5H_4\text{-}(E)\text{-}CH{=}CH\text{-}4\text{-}\{(\eta^6\text{-}C_6H_4)\text{-}Cr(CO)_3\}\text{-}(E)\text{-}CH{=}CH\text{-}\eta^5\text{-}C_5H_4)Fe(\eta^5\text{-}C_5H_5)$ (**7**)	455 [0.31]	0.14	850 ± 300	95 ± 30	860 ± 300

[a] All solution measurements (linear optical spectra, third-order NLO studies) in THF as solvent. All complexes are optically transparent at 1.3 μm and 800 nm. – [b] Bulk second-order responses by the Kurtz powder method at 1.3 μm. – [c] Third-order NLO measurements by Z-scan at 800 nm, referenced to the nonlinear refractive index of silica $n_2 = 3{\cdot}10^{-16}$ cm$^2{\cdot}$W^{-1}. – [d] Not determined unambiguously. – [e]Insufficiently soluble.

ment of CN by NO_2 in proceeding from **5**-(*E,Z*) to **4**-(*E,Z*), leads to a significant increase in both γ_r and $|\gamma|$; increase in acceptor-strength leads to increased quadratic nonlinearity in dipolar organometallic complexes,[10] and a similar increase in cubic nonlinearity for the present complexes on increasing acceptor-strength is not unexpected. Errors do not permit comment on the effect of bridge stereochemistry modification on γ_r and $|\gamma|$. The linked complex **6** has substantial γ_r and $|\gamma|$ values despite the absence of a molecular dipole; a large cubic nonlinearity ($\gamma = 504 \pm 52 \times 10^{-36}$ esu, as measured by DFWM at 0.60 μm) was reported for a complex with this composition in earlier work, although the bridge stereochemistry was not specified.[33] Interestingly, incorporation of the bridge-ligated $Cr(CO)_3$ unit in proceeding from **6** to **7**, results in an increase in both γ_r and $|\gamma|$. Recent studies concluded that the $Cr(CO)_3$ unit behaves as an electronically amphoteric auxochrome in chromium carbonyl arene complexes with conjugated side-chains,[16] resulting in significant quadratic nonlinearities for complexes with donor- or acceptor- substituents on the side-chain. In the present system, complex **6** has a donor-bridge-donor composition, whereas our electrochemistry studies suggest that **7** has a donor-donor-donor composition; the increase in the ease of oxidation in proceeding from **6** to **7** probably correlates with an increase in the ease of polarization of electron density, and may be responsible for the increased cubic nonlinearity.

Experimental Section

General Remarks: All reactions were carried out under a nitrogen atmosphere using standard Schlenk techniques. Solvents for synthesis and electrochemical measurements were dried and deoxygenated by standard methods before use. Chromatographic work was performed on silica gel 60 Å or neutral alumina columns.

NMR spectra were recorded on Varian Innova 300 MHz and 500 MHz spectrometers, using $CDCl_3$ as solvent unless otherwise stated. − IR spectra were recorded on a Perkin−Elmer System 2000 FT-IR using NaCl pellets. − Electronic absorption spectra were obtained on a UV-1603 Shimadzu spectrophotometer. − Elemental analyses were performed on a EA 1108 CHNS-O Carlo Erba instrument. − Cyclic voltammetry experiments were performed with a Echochemie pgstat 20 electrochemical analyzer. All measurements were carried out at room temperature with a conventional three-electrode configuration consisting of platinum working and auxiliary electrodes and a Ag/AgCl reference electrode containing aqueous 3 M KCl. The solvent used in all experiments was CH_2Cl_2, which was obtained in HPLC grade and used as received. The supporting electrolyte was 0.1 M tetra-*n*-butylammonium hexafluorophosphate, synthesized by reaction of tetra-*n*-butylammonium bromide and HPF_6, recrystallized from ethanol and dried under vacuum. $E_{1/2}$ values were determined as $(E_{p,a} + E_{p,c})/2$, where $E_{p,a}$ and $E_{p,c}$ are the anodic and cathodic peak potentials, respectively. All reported potentials are not corrected for the junction potential. − Electrospray mass spectra were recorded using a Micromass Quattro LC instrument, using CH_3CN and/or CH_3OH as the mobile phase solvent. The samples were added to give a mobile phase with an approximate concentration of 0.1 mM. This solution was injected into the spectrometer via a Rheodyne injector fitted with a 10 μL sample loop, and nitrogen was employed as a drying and nebulizing gas. − $Fe(\eta^5\text{-}C_5H_5)(\eta^5\text{-}C_5H_4\text{-}(E)\text{-}CH{=}CH\text{-}4\text{-}C_6H_4\text{-}(E)\text{-}CH{=}CH\text{-}\eta^5\text{-}C_5H_4)Fe(\eta^5\text{-}C_5H_5)$ (**6**) was synthesized by literature procedures.[41,42]

1. Preparation of (*E*)- and (*Z*)-Fe(η⁵-C₅H₄CHO)(η⁵-C₅H₄CH=CH−C₆H₄-4-NO₂) (2) and (*E*)-and (*Z*)-Fe(η⁵-C₅H₄CHO)(η⁵-C₅H₄CH=CH−C₆H₄-4-CN) (3): Potassium *tert*-butoxide (258 mg, 2.3 mmol) was added to a solution of 4-nitrobenzyltriphenylphosphonium bromide (988 mg, 2.1 mmol), or 4-cyanobenzyltriphenylphosphonium bromide (963 mg, 2.1 mmol) in THF (100 mL) at 0 °C, and the resulting suspension was allowed to warm to room temperature. After 30 min, the yellow-orange suspension indicated that the ylide was completely formed. 1,1′-Ferrocenebis(carboxaldehyde), **1** (500 mg, 2.1 mmol), was then added at 0 °C and the solution was stirred for ca. 15 h at room temperature. After removing the solvent under reduced pressure, the product was separated with a $CH_2Cl_2/H_2O/NaHCO_3$ mixture and the dichloromethane extract dried with $MgSO_4$. Purification by column chromatography on silica gel using hexane/CH_2Cl_2 (3:7) as the eluent afforded pure **2**-(*E*), **2**-(*Z*), **3**-(*E*), and **3**-(*Z*), although **3**-(*Z*) was obtained in such a low yield that only spectroscopic characterization could be achieved.

Compound 2-(*E*), Fe(η⁵-C₅H₄CHO){η⁵-C₅H₄−(*E*)-CH=CH−C₆H₄-4-NO₂}: Yield 35%. − ^{1}H NMR (500 MHz, $CDCl_3$): δ = 9.90 (s, 1 H, CHO); 8.20 (d, 2 H, $^3J_{H\text{-}H}$ = 8.4 Hz, C_6H_4); 7.56 (d, 2 H, $^3J_{H\text{-}H}$ = 8.1 Hz, C_6H_4); 6.96 (d, 1 H, $^3J_{H\text{-}H}$ = 16.2 Hz, CH=CH); 6.76 (d, 1 H, $^3J_{H\text{-}H}$ = 15.9 Hz, CH=CH); 4.78 (s, 2 H, C_5H_4); 4.62 (s, 2 H, C_5H_4); 4.58 (s, 2 H, C_5H_4); 4.46 (s, 2 H, C_5H_4). − ^{13}C NMR (500 MHz, $CDCl_3$): δ = 69.4, 71.5, 71.9, 75.0 (8 C, C_5H_4); 80.6, 84.3 (2 Cq, C_5H_4); 124.8, 126.2, 126.9, 131.2 (6 C, CH=CH and C_6H_4); 144.3, 146.9 (2 Cq, C_6H_4); 194.1 (1 C, CHO). − $C_{19}H_{15}FeNO_3$ (361.18): calcd. C 63.20, H 4.19, N 3.88; found C 63.53, H 4.27, N 3.80.

Compound 2-(*Z*), Fe(η⁵-C₅H₄CHO){η⁵-C₅H₄−(*Z*)-CH=CH−C₆H₄-4-NO₂}: Yield 17%. − ^{1}H NMR (500 MHz, $CDCl_3$): δ = 9.87 (s, 1 H, CHO); 8.14 (d, 2 H, $^3J_{H\text{-}H}$ = 8.5 Hz, C_6H_4); 7.43 (d, 2 H, $^3J_{H\text{-}H}$ = 8.0 Hz, C_6H_4); 6.55 (d, 1 H, $^3J_{H\text{-}H}$ = 12.0 Hz, CH=CH); 6.39 (d, 1 H, $^3J_{H\text{-}H}$ = 12.0 Hz, CH=CH); 4.74 (s, 2 H, C_5H_4); 4.54 (s, 2 H, C_5H_4); 4.31 (s, 2 H, C_5H_4); 4.23 (s, 2 H, C_5H_4). − ^{13}C NMR (500 MHz, $CDCl_3$): δ = 71.3, 71.4, 71.5, 75.0 (8 C, C_5H_4); 81.1, 83.0 (2 Cq, C_5H_4); 124.2, 127.4, 130.1, 130.4 (6 C, CH=CH and C_6H_4); 145.2, 147.2 (2 Cq, C_6H_4); 193.8 (1 C, CHO). − $C_{19}H_{15}FeNO_3$ (361.18): calcd. C 63.20, H 4.19, N 3.88; found C 63.01, H 4.07, N 3.79.

Compound 3-(*E*), Fe(η⁵-C₅H₄CHO){η⁵-C₅H₄−(*E*)-CH=CH−C₆H₄-4-CN}: Yield 40%. − ^{1}H NMR (500 MHz, $CDCl_3$): δ = 9.90 (s, 1 H, CHO); 7.62 (d, 2 H, $^3J_{H\text{-}H}$ = 7.5 Hz, C_6H_4); 7.52 (d, 2 H, $^3J_{H\text{-}H}$ = 8.0 Hz, C_6H_4); 6.89 (d, 1 H, $^3J_{H\text{-}H}$ = 16.0 Hz, CH=CH); 6.72 (d, 1 H, $^3J_{H\text{-}H}$ = 16.0 Hz, CH=CH); 4.79 (s, 2 H, C_5H_4); 4.60 (s, 2 H, C_5H_4); 4.58 (s, 2 H, C_5H_4); 4.44 (s, 2 H, C_5H_4). − ^{13}C NMR (500 MHz, $CDCl_3$): δ = 69.3, 71.5, 71.7, 74.9 (8 C, C_5H_4); 80.7, 84.6 (2 Cq, C_5H_4); 110.9 (1 C, CN); 126.8, 127.1, 130.1, 133.3 (6 C, CH=CH and C_6H_4); 119.8, 142.4 (2 Cq, C_6H_4); 194.2 (1 C, CHO). − $C_{20}H_{15}FeNO$ (341.19): calcd. C 70.43, H 4.43, N 4.11; found C 70.12, H 4.17, N 4.25. − Electrospray MS. Cone 60 V. *m/z* (fragment): 364 [M^+ + Na].

Compound 3-(*Z*), Fe(η⁵-C₅H₄CHO){η⁵-C₅H₄−(*Z*)-CH=CH−C₆H₄-4-CN}: ^{1}H NMR (300 MHz, $CDCl_3$): δ = 9.86 (s, 1 H, CHO); 7.56 (d, 2 H, $^3J_{H\text{-}H}$ = 8.1 Hz, C_6H_4); 7.38 (d, 2 H, $^3J_{H\text{-}H}$ = 8.4 Hz, C_6H_4); 6.50 (d, 1 H, $^3J_{H\text{-}H}$ = 12.0 Hz, CH=CH); 6.33 (d, 1 H, $^3J_{H\text{-}H}$ = 12.0 Hz, CH=CH); 4.73 (t, 2 H, $^3J_{H\text{-}H}$ = 1.8 Hz, C_5H_4);

4.54 (t, 2 H, $^3J_{H-H}$ = 1.8 Hz, C_5H_4); 4.30 (t, 2 H, $^3J_{H-H}$ = 1.8 Hz, C_5H_4); 4.22 (t, 2 H, $^3J_{H-H}$ = 1.8 Hz, C_5H_4).

2. Preparation of (*E,E*)-, (*E,Z*)-, and (*Z,Z*)-Fe{η^5-C_5H_4CH=CHC_6H_4-4-NO_2)$_2$ (4) and (*E,E*)-, (*E,Z*)-, and (*Z,Z*)-Fe{η^5-C_5H_4CH=CHC_6H_4-4-CN}$_2$ (5): These compounds were prepared by two different procedures.

(i) Potassium *tert*-butoxide (202 mg, 1.8 mmol) was added to a solution of 4-nitrobenzyltriphenylphosphonium bromide (706 mg, 1.5 mmol), or 4-cyanobenzyltriphenylphosphonium bromide (688 mg, 1.5 mmol) in THF (100 mL) at 0 °C, and the resulting suspension was allowed to warm to room temperature. After 30 min, the yellow-orange suspension indicated that the ylide was completely formed. Compound **2** or **3** (1.0 mmol) was then added at 0 °C and the solution was stirred for ca. 15 h at room temperature. After removing the solvent under reduced pressure, the product was separated with a CH_2Cl_2/H_2O/$NaHCO_3$ mixture, and the CH_2Cl_2 extract dried with $MgSO_4$. Purification by column chromatography on silica gel using hexane/CH_2Cl_2 (6:4) as the eluent afforded pure compounds **4**-(*E,Z*), **4**-(*Z,Z*), **4**-(*E,E*), **5**-(*E,Z*), **5**-(*Z,Z*), and **5**-(*E,E*).

(ii) Following the same general method described for compounds **2** and **3**, but using a threefold (3.0 mmol) excess of the phosphonium salt with 1.0 mmol Fe(η^5-$C_5H_4CHO)_2$ (**1**), afforded the complexes in higher yields.

Compound 4-(*E,Z*), Fe{η^5-C_5H_4−(*Z*)-CH=CHC_6H_4-4-NO_2}{η^5-C_5H_4−(*E*)-CH=CHC_6H_4-4-NO_2}: Yield 25%. − ^{1}H NMR (500 MHz, $CDCl_3$): δ = 8.21 (d, 2 H, $^3J_{H-H}$ = 8.5 Hz, C_6H_4); 8.07 (d, 2 H, $^3J_{H-H}$ = 8.5 Hz, C_6H_4); 7.53 (d, 2 H, $^3J_{H-H}$ = 8.5 Hz, C_6H_4); 7.38 (d, 2 H, $^3J_{H-H}$ = 8.0 Hz, C_6H_4); 6.98 (d, 1 H, $^3J_{H-H}$ = 16.0 Hz, CH=CH); 6.70 (d, 1 H, $^3J_{H-H}$ = 16.0 Hz, CH=CH); 6.40 (d, 1 H, $^3J_{H-H}$ = 11.5 Hz, CH=CH); 6.37 (d, 1 H, $^3J_{H-H}$ = 12.5 Hz, CH=CH); 4.48 (s, 2 H, C_5H_4); 4.34 (s, 2 H, C_5H_4); 4.24 (s, 2 H, C_5H_4); 4.18 (s, 2 H, C_5H_4). − ^{13}C NMR (500 MHz, $CDCl_3$): δ = 69.5, 71.4, 71.5, 72.0 (8 C, C_5H_4); 82.0, 83.5 (2 Cq, C_5H_4); 124.2, 124.9, 126.3, 126.6, 129.9, 132.0, 132.7 (12 C, CH=CH and C_6H_4); 144.8, 145.5, 146.9 (4 Cq, C_6H_4). − $C_{26}H_{20}FeN_2O_4$ (480.30): calcd. C 65.00, H 4.20, N 5.83; found C 65.12, H 4.07, N 5.89. − Electrospray MS. Cone 25 V. *m/z* (fragment): 503 [M^+ + Na].

Compound 4-(*Z,Z*), Fe{η^5-C_5H_4−(*Z*)-CH=CHC_6H_4-4-NO_2}$_2$: Yield 10%. − ^{1}H NMR (300 MHz, $CDCl_3$): δ = 8.13 (d, 4 H, $^3J_{H-H}$ = 8.7 Hz, C_6H_4); 7.46 (d, 4 H, $^3J_{H-H}$ = 8.4 Hz, C_6H_4); 6.47 (d, 2 H, $^3J_{H-H}$ = 12.0 Hz, CH=CH); 6.39 (d, 2 H, $^3J_{H-H}$ = 11.5 Hz, CH=CH); 4.20 (s, 4 H, C_5H_4); 4.10 (s, 4 H, C_5H_4). − ^{13}C NMR (300 MHz, $CDCl_3$): δ = 71.4, 71.5 (8 C, C_5H_4); 81.9 (2 Cq, C_5H_4); 124.1, 125.8, 130.0, 131.8 (12 C, CH=CH and C_6H_4); 145.5, 146.8 (4 Cq, C_6H_4). − $C_{26}H_{20}FeN_2O_4$ (480.30): calcd. C 65.00, H 4.20, N 5.83; found C 65.23, H 4.37, N 5.92. − Electrospray MS. Cone 40 V. *m/z* (fragment): 503 [M^+ + Na].

Compound 4-(*E,E*), Fe{η^5-C_5H_4−(*E*)-CH=CHC_6H_4-4-NO_2}$_2$: Yield 34%. − ^{1}H NMR (300 MHz, $CDCl_3$): δ = 8.20 (d, 4 H, $^3J_{H-H}$ = 8.7 Hz, C_6H_4); 7.56 (d, 4 H, $^3J_{H-H}$ = 8.4 Hz, C_6H_4); 7.11 (d, 2 H, $^3J_{H-H}$ = 16.2 Hz, CH=CH); 6.79 (d, 2 H, $^3J_{H-H}$ = 16.2 Hz, CH=CH); 4.62 (s, 4 H, C_5H_4); 4.49 (s, 4 H, C_5H_4). − ^{13}C NMR (300 MHz, $CDCl_3$): δ = 71.6, 72.0 (8 C, C_5H_4); 82.3 (2 Cq, C_5H_4); 124.5, 124.9, 127.0, 128.2 (12 C, CH=CH and C_6H_4); 143.5, 144.7 (4 Cq, C_6H_4). Yield 34%. − $C_{26}H_{20}FeN_2O_4$ (480.30): calcd. C 65.00, H 4.20, N 5.83; found C 64.92, H 4.32, N 5.75. − Electrospray MS. Cone 40 V. *m/z* (fragment): 503 [M^+ + Na].

Compound 5-(*E,Z*), Fe{η^5-C_5H_4−(*Z*)-CH=CHC_6H_4-4-CN}{η^5-C_5H_4−(*E*)-CH=CHC_6H_4-4-CN}: Yield 27%. − ^{1}H NMR (300 MHz, $CDCl_3$): δ = 7.62 (d, 2 H, $^3J_{H-H}$ = 8.1 Hz, C_6H_4); 7.48 (m, 4 H, C_6H_4); 7.32 (d, 2 H, $^3J_{H-H}$ = 8.4 Hz, C_6H_4); 6.91 (d, 1 H, $^3J_{H-H}$ = 15.9 Hz, CH=CH); 6.61 (d, 1 H, $^3J_{H-H}$ = 16.2 Hz, CH=CH); 6.31 (s, 2 H, CH=CH); 4.48 (s, 2 H, C_5H_4); 4.34 (s, 2 H, C_5H_4); 4.24 (s, 2 H, C_5H_4); 4.17 (s, 2 H, C_5H_4). − ^{13}C NMR (500 MHz, $CDCl_3$): δ = 69.5, 71.4, 71.7, 72.1 (8 C, C_5H_4); 82.6, 84.3 (2 Cq, C_5H_4); 110.6, 110.8 (2 C, CN); 125.5, 126.8, 129.9, 131.3, 131.5, 132.6, 133.2 (12 C, CH=CH and C_6H_4); 119.7, 119.8, 142.8, 143.4 (4 Cq, C_6H_4). − $C_{28}H_{20}FeN_2$ (440.33): calcd. C 76.42, H 4.58, N 6.36; found C 76.02, H 4.75, N 6.39. − Electrospray MS. Cone 45 V. *m/z* (fragment): 463 [M^+ + Na].

Compound 5-(*Z,Z*), Fe{η^5-C_5H_4−(*Z*)-CH=CHC_6H_4-4-CN}$_2$: Yield 10%. − ^{1}H NMR (300 MHz, $CDCl_3$): δ = 7.54 (d, 4 H, $^3J_{H-H}$ = 7.8 Hz, C_6H_4); 7.39 (d, 4 H, $^3J_{H-H}$ = 7.5 Hz, C_6H_4); 6.42 (d, 2 H, $^3J_{H-H}$ = 11.7 Hz, CH=CH); 6.32 (d, 2 H, $^3J_{H-H}$ = 11.7 Hz, CH=CH); 4.17 (s, 4 H, C_5H_4); 4.06 (s, 4 H, C_5H_4). − ^{13}C NMR (300 MHz, $CDCl_3$): δ = 71.3, 71.5 (8 C, C_5H_4); 82.1 (2 Cq, C_5H_4); 110.7 (2 C, CN); 126.2, 129.9, 131.1, 132.5 (12 C, CH=CH and C_6H_4); 119.7, 143.4 (4 Cq, C_6H_4). − $C_{28}H_{20}FeN_2$ (440.33): calcd. C 76.42, H 4.58, N 6.36; found C 76.55, H 4.26, N 6.20. − Electrospray MS. Cone 45 V. *m/z* (fragment): 463 [M^+ + Na].

Compound 5-(*E,E*), Fe{η^5-C_5H_4−(*E*)-CH=CHC_6H_4-4-CN}$_2$: Yield 36%. − ^{1}H NMR (300 MHz, $CDCl_3$): δ = 7.48 (d, 4 H, $^3J_{H-H}$ = 7.5 Hz, C_6H_4); 7.28 (d, 4 H, $^3J_{H-H}$ = 8.1 Hz, C_6H_4); 6.83 (d, 2 H, $^3J_{H-H}$ = 15.9 Hz, CH=CH); 6.53 (d, 2 H, $^3J_{H-H}$ = 15.9 Hz, CH=CH); 4.48 (s, 4 H, C_5H_4); 4.36 (s, 4 H, C_5H_4). − ^{13}C NMR (300 MHz, $CDCl_3$): δ = 69.2, 71.7 (8 C, C_5H_4); 83.8 (2 Cq, C_5H_4); 110.4 (2 C, CN); 125.4, 126.6, 130.9, 133.1 (12 C, CH=CH and C_6H_4); 119.7, 142.6 (4 Cq, C_6H_4). − $C_{28}H_{20}FeN_2$ (440.33): calcd. C 76.42, H 4.58, N 6.36; found C 76.36, H 4.63, N 6.27. − Electrospray MS. Cone 45 V. *m/z* (fragment): 463 [M^+ + Na].

3. Isomerization Reactions: Compounds **4**-(*E,Z*), **4**-(*Z,Z*), **5**-(*E,Z*), or **5**-(*Z,Z*) could be isomerized to the all-(*E*) complexes by the following method. **4**-(*E,Z*) (300 mg) (or any of the other complexes), was dissolved in 10 mL of toluene with I_2 (10 mg). The mixture was refluxed for 20 minutes, after which the solvent was eliminated by reduced pressure. The crude product was flash-chromatographed, yielding pure **4**-(*E,E*) compound. Yield 85%. Yields for **4**-(*Z,Z*), **5**-(*E,Z*), or **5**-(*Z,Z*) in the range 80−90%.

4. Preparation of Fe(η^5-C_5H_5)(η^5-C_5H_4−(*E*)-CH=CH−4-{(η^6-C_6H_4)Cr$(CO)_3$}-(*E*)-CH=CH−η^5-C_5H_4)Fe(η^5-C_5H_5) (7): $Cr(CO)_6$ (660.2 mg, 3.0 mmol) was added to a solution of compound **6** (300 mg, 0.6 mmol) in butyl ether (40 mL), and the resulting solution stirred for 15 h at 150 °C. After cooling the mixture to room temperature, the solution was filtered and the solvent removed under reduced pressure. Purification by column chromatography on alumina with CH_2Cl_2/hexane (1:1) as the eluent afforded pure **7**, yield 65%.

X-ray Diffraction Studies: Single crystals were grown by slow diffusion of hexane into concentrated CH_2Cl_2 solutions and mounted on a glass fiber in a random orientation. Data collection was performed at room temperature on a Siemens Smart CCD diffractometer using graphite monochromated Mo-K_α radiation (λ = 0.71073 Å) with a nominal crystal to detector distance of 4.0 cm. A hemisphere of data was collected based on three ω-scan runs (starting ω = −28°) at values φ = 0°, 90°, and 180° with the detector at 2θ = 28°. At each of these runs, frames (606, 435, and 230, respectively) were collected at 0.3° intervals and 20 s per frame for compound **2**-(*E*), 40 s per frame for compound **4**-(*E,Z*), 45 s per frame for compound **5**-(*E,E*), 10 s per frame for **6** and 80 s per frame for **7**. The diffraction frames were integrated using the

Table 5. Crystallographic Data

Compound	**2**-(E)	**4**-(*E*,Z)	**5**-(*E*,E)	**6**	**7**
Empirical formula	$C_{19}H_{15}FeNO_3$	$C_{26}H_{20}FeN_2O_4$	$C_{28}H_{20}FeNFeN_2$	$C_{30}H_{26}Fe_2$	$C_{33}H_{26}Fe_2CrO_3$
Molecular weight [g·mol^{-1}]	361.17	480.29	440.31	498.21	634.24
Temperature [K]	293(2)	293(2)	293(2)	293(2)	293(2)
Wavelength [Å]	0.71073	0.71073	0.71073	0.71073	0.71073
Crystal System	Monoclinic	Triclinic	Monoclinic	Monoclinic	Monoclinic
Space group	$P2_1/n$	$P\bar{1}$	$P2_1$	$P2_1/c$	$P2_1/c$
a [Å]	7.6532(5)	7.5874(17)	6.2114(4)	12.7324(4)	17.131(3)
b [Å]	7.6518(5)	10.569(2)	14.0877(8)	7.7128(2)	7.4568(13)
c [Å]	26.6880(17)	14.416(3)	12.1250(7)	11.6266(5)	10.7432(19)
α [deg.]	90	100.919(5)	90	90	90
β [deg.]	91.328(2)	103.232(5)	102.3550(10)	98.5460(10)	99.780(4)
γ [deg.]	90	101.555(6)	90	90	90
Volume [Å^3]	1562.45(18)	1068.5(4)	1036.42(11)	1129.08(7)	1352.4(4)
Z	4	2	2	2	2
Density [calcd. Mg·m^{-3}]	1.535	1.493	1.411	1.465	1.557
Absorption Coef. [mm^{-1}]	0.982	0.743	0.746	1.300	1.487
F(000)	744	496	456	516	648
Crystal Size [mm^3]	0.28×0.23×0.16	0.26×0.11×0.10	0.49×0.44×0.02	0.46×0.14×0.03	0.046×0.042×0.011
θ range [deg.]	1.53 to 30.55	1.50 to 30.59	1.72 to 30.53	1.62 to 30.85	1.21 to 24.70
Index Ranges	$-9 \le h \le 10$	$-8 \le h \le 10$	$-8 \le h \le 8$	$-18 \le h \le 17$	$-11 \le h \le 11$
	$-10 \le k \le 10$	$-15 \le k \le 14$	$-18 \le k \le 20$	$-11 \le k \le 11$	$-7 \le k \le 7$
	$-37 \le l \le 25$	$-20 \le l \le 15$	$-16 \le l \le 17$	$-16 \le l \le 16$	$-7 \le l \le 12$
Reflections Collected	12775	9110	8466	12797	4327
Independent Reflections	4766 [*R*(int.) = 0.0617]	6400 [*R*(int.) = 0.0553]	4917 [*R*(int.) = 0.0313]	3395 [*R*(int.) = 0.0439]	1353 [*R*(int.) = 0.0790]
Data/Restrains/Parameters	4766/0/245	6400/0/298	4917/1/281	3395/0/145	1353/0/182
Goodness-of-fit-on F^2	0.868	0.844	0.876	0.916	1.082
Final *R* indices [$I > 2\sigma(I)$]	*R*1=0.0454, *wR*2=0.0850	*R*1=0.0572, *wR*2=0.0943	*R*1=0.0422, *wR*2=0.0720	*R*1=0.0328, *wR*2=0.0669	*R*1=0.0699, *wR*2=0.1749
R indices (all data)	*R*1=0.1366, wR2=0.1027	*R*1=0.1679, *wR*2=0.1191	*R*1=0.0867, *wR*2=0.0805	*R*1=0.0748, *wR*2=0.0760	*R*1=0.1034, *wR*2=0.2006
ρ max, ρ min. [e Å^{-3}]	0.529, −0.261	0.758, −0.599	0.428, −0.246	0.303, −0.229	0.456, −0.507

SAINT package and corrected for absorption with SADABS.[43,44] Space group assignments are based on systematic absences, E statistics, and successful refinement of the structures. Structures were solved by direct methods with the aid of successive difference Fourier maps and were refined using the SHELXTL 5.1 software package. All non-hydrogen atoms were refined anisotropically. Hydrogen atoms were assigned to ideal positions and refined using a riding model. Data collection parameters are given in Table 5.

Kurtz Powder Studies: Samples were ungraded powders placed in the circular cavity (10 mm diameter × 0.5 mm depth) of a microscope slide with a cover slip. Powder SHG efficiencies were measured using the Kurtz technique.[45] Studies utilizing the fundamental output of a Q-switched Quanta-Ray GC-130 Nd:YAG laser (1.06 μm) were inconclusive due to material resonances at the second-harmonic frequency. The powder measurements were therefore performed at 1.3 and 1.4 μm using a Light Conversion Topas optical parametric generator pumped with a Clark MXR regenerative amplifier. This afforded approximately 150 fs pulses at a 1 kHz repetition rate which were directed onto the sample as an unfocussed beam (spot size about 5 mm; energy per pulse: up to 20 mJ). The intensity of the generated powder SHG was determined using a Coolsnap Photometric CCD camera. Measurements thus made were compared with those of a urea powder sample.

Z-scan Measurements: Z-scan measurements were performed at 800 nm using 100 fs pulses from a system consisting of a Coherent Mira Ti-sapphire laser pumped with a Coherent Innova or Coherent Verdi cw pump and a Ti-sapphire regenerative amplifier pumped with a frequency-doubled Q-switched pulsed YAG laser (Spectra Physics GCR) at 30 Hz and employing chirped pulse amplification. Tetrahydrofuran solutions were examined in a glass cell with a 0.1 cm path length. The Z-scans were recorded at three concentrations for each compound [two concentrations for **4**-(*E,E*), **4**-(*Z,Z*), and **5**-(*E,E*)] and the real and imaginary part of the nonlinear phase change determined by numerical fitting.[29] The real and imaginary part of the hyperpolarizability of the solute was then calculated assuming linear concentration dependencies of the nonlinear phase shifts. The nonlinearities and light intensities were calibrated using measurements of a 1 mm thick silica plate for which the nonlinear refractive index $n_2 = 3 \cdot 10^{-16}$ cm^2·W^{-1} was assumed.

Supplementary Data: Crystallographic data (excluding structure factors) for the structures reported in this paper have been deposited with the Cambridge Crystallographic Data Centre as supplementary publication no. CCDC-152432 for compound **2**-(*E*), CCDC-152433 for compound **4**-(*E,Z*), CCDC-152434 for compound **5**-(*E,E*), CCDC-152435 for compound **6**, and CCDC-152436 for compound **7**. Copies of the data can be obtained free of charge on application to CCDC, 12 Union Road, Cambridge CB2 1EZ, UK. [Fax: (internat.) +44−1223/336-033; E-mail: deposit@ccdc.cam.ac.uk].

Acknowledgments

We thank the DGESIC (PB98-1044), BANCAIXA (P1B98-07) and the Australian Research Council (ARC) for financial support. J. A. M. thanks the Generalitat Valenciana for a fellowship, and MGH thanks the ARC for a Senior Research Fellowship.

[1] A. Togni, T. Hayashi, *Ferrocenes: Homogeneous Catalysis-Organic Synthesis Materials-Science*, VCH Publishers, New York, NY (USA) **1995**.
[2] A. Togni, R. L. Halterman, *Metallocenes*, Wiley-VCH, Weinheim (Germany), **1998**.
[3] N. J. Long, *Metallocenes*, Blackwell Science, London, **1997**.
[4] J. Mata, S. Uriel, E. Peris, R. Llusar, S. Houbrechts, A. Persoons, *J. Organomet. Chem.* **1998**, *562*, 197.
[5] J. A. Mata, E. Falomir, R. Llusar, E. Peris, *J. Organomet. Chem.* **2000**, *616*, 80.

[6] J. A. Mata, S. Uriel, R. Llusar, E. Peris, *Organometallics* **2000**, *19*, 3797.
[7] I. S. Lee, Y. K. Chung, J. Mun, C. S. Yoon, *Organometallics* **2000**, *18*, 5080.
[8] T. J. J. Müller, *J. Organomet. Chem.* **1999**, *578*, 95.
[9] I. R. Whittall, A. M. McDonagh, M. G. Humphrey, M. Samoc, *Adv. Organomet. Chem. Vol 43*, Academic Press Inc, San Diego, **1999**, p. 349.
[10] I. R. Whittall, A. M. McDonagh, M. G. Humphrey, M. Samoc, *Adv. Organomet. Chem. Vol 42*, Academic Press Inc, San Diego, **1998**, p. 291.
[11] D. Braga, F. Grepioni, G. R. Desiraju, *Chem. Rev.* **1998**, *98*, 1375.
[12] A. Houlton, J. R. Miller, J. Silver, N. Jassim, M. J. Ahmet, T. L. Axon, D. Bloor, G. H. Cross, *Inorg. Chim. Acta* **1993**, *205*, 67.
[13] A. Hradsky, B. Bildstein, N. Schuler, H. Schottenberg, P. Jaitner, K.-H. Ongania, K. Wurst, J.-P. Launay, *Organometallics* **1997**, *16*, 392.
[14] P. A. Deck, M. J. Lane, J. L. Montgomery, C. Sebodnick, *Organometallics* **2000**, *19*, 1013.
[15] D. Naskar, S. K. Das, L. Giribabu, B. G. Maiya, S. Roy, *Organometallics* **2000**, *19*, 1464.
[16] T. J. J. Müller, A. Netz, M. Ansorge, E. Schmalzlin, C. Brauchle, K. Meerholz, *Organometallics* **1999**, *18*, 5066.
[17] S. Barlow, H. E. Bunting, C. Ringham, J. C. Green, G. U. Bublitz, S. G. Boxer, J. W. Perry, S. R. Marder, *J. Am. Chem. Soc.* **1999**, *121*, 3715.
[18] J. C. Calabrese, L.-T. Cheng, J. C. Green, S. R. Marder, W. Tam, *J. Am. Chem. Soc.* **1991**, *113*, 7227.
[19] H. E. Bunting, M. L. H. Green, S. R. Marder, M. E. Thompson, D. Bloor, P. V. Kolinsky, R. J. Jones, *Polyhedron* **1992**, *11*, 1489.
[20] J. Mata, E. Peris, I. Asselberghs, R. Van Boxel, A. Persoons, *New J. Chem.* **2001**, *25*, 299.
[21] H. Nock, H. Schottenberg, *J. Org. Chem.* **1993**, *58*, 7045.
[22] A. Houlton, N. Jasim, R. M. G. Rogerts, J. Silver, D. Cunningham, P. McArdle, T. Higgins, *J. Chem. Soc., Dalton Trans.* **1992**, 2235.
[23] V. Alain, A. Fort, M. Barzoukas, C.-T. Chen, M. Blanchard-Desce, S. R. Marder, J. W. Perry, *Inorg. Chim. Acta* **1996**, *242*, 43.
[24] D. R. Kanis, M. A. Ratner, T. J. Marks, *J. Am. Chem. Soc.* **1992**, *114*, 10338.
[25] I. R. Whittall, M. P. Cifuentes, M. J. Costigan, M. G. Humphrey, S. C. Goh, B. W. Skelton, A. H. White, *J. Organomet. Chem.* **1994**, *471,* 193.
[26] J. A. Bandy, H. E. Bunting, M.-H. García, M. L. H. Green, S. R. Marder, M. E. Thompson, D. Bloor, P. V. Kolinsky, R. J. Jones, J. W. Perry, *Polyhedron* **1992**, *11,* 1429.
[27] M. L. H. Green, S. R. Marder, M. E. Thompson, J. A. Bandy, D. Bloor, P. V. Kolinsky, R. J. Jones, *Nature* **1987**, *26*, 360.
[28] M. L. H. Greeen, J. Qin, D. O′Hare, H. E. Bunting, M. E. Thompson, S. R. Marder, K. Chatakondu, *Pure Appl. Chem.* **1989**, *61*, 817.
[29] M. Sheikh-Bahae, A. A. Said, T. Wei, D. J. Hagan, E. W. van Stryland, *IEEE J. Quant. Electr.* **1990**, 760.
[30] C. S. Winter, S. N. Oliver, J. D. Rush, *Nonlinear Optical Effects in Organic Polymers*, Kluwer, Dordrecht, **1989**.
[31] C. S. Winter, S. N. Oliver, J. D. Rush, *Optics Commun.* **1998**, *69*, 45.
[32] C. S. Winter, S. N. Oliver, J. D. Rush, *Organic Materials for Nonlinear Optics*, Royal Society of Chemistry, London, **1989**.
[33] S. Ghosal, M. Samoc, P. N. Prasad, J. J. Tufariello, *J. Phys. Chem.* **1990**, *94*, 2847.
[34] I. R. Whittall, M. G. Humphrey, M. Samoc, J. Swiatkiewicz, B. Luther-Davies, *Organometallics* **1995**, *14*, 5493.
[35] A. M. McDonagh, M. Cifuentes, I. R. Whittall, M. G. Humphrey, M. Samoc, B. Luther-Davies, D. C. R. Hockless, *J. Organomet. Chem.* **1996**, *526*, 99.
[36] I. R. Whittall, M. P. Cifuentes, M. G. Humphrey, B. Luther-Davies, M. Samoc, S. Houbrechts, A. Persoons, G. A. Heath, D. Bogsányi, *Organometallics* **1997**, *16,* 2631.
[37] I. R. Whittall, M. G. Humphrey, M. Samoc, B. Luther-Davies, *Angew. Chem. Int. Ed. Engl.* **1997**, *36*, 370.
[38] A. M. McDonagh, M. G. Humphrey, M. Samoc, B. Luther-Davies, S. Houbrechts, T. Wada, H. Sasabe, A. Persoons, *J. Am. Chem. Soc.* **1999**, *121*, 1405.
[39] A. M. McDonagh, M. G. Humphrey, M. Samoc, B. Luther-Davies, *Organometallics* **1999**, *18*, 5195.
[40] J. Vicente, M. T. Chicote, M. D. Abrisqueta, M. C. Ramírez de Arellano, P. G. Jones, M. G. Humphrey, M. P. Cifuentes, M. Samoc, B. Luther-Davies, *Organometallics* **2000**, *19*, 2968.
[41] W. H. Morrison, S. Krogsrud, D. N. Henrickson, *Inorg. Chem.* **1973**, *12*, 1998.
[42] K. R. J. Thomas, J. T. Lin, Y. S. Wen, *J. Organomet. Chem.* **1999**, *575*, 301.
[43] SAINT version 5.0, Bruker Analytical X-ray Systems, Madison, WI. G., **1998**.
[44] G. M. Sheldrick, University of Göttingen, **1996**.
[45] S. K. Kurtz, T. T. Perry, *J. Appl. Phys.* **1968**, *39*, 3798.

Received February 2, 2001
[I01069]

Reactions of Arylthiazylamides with Internal and External Fluoro Electrophiles − Formation of Products with Unusual Structures

Enno Lork,[a] Rüdiger Mews,*[a] Makhmut M. Shakirov,[b] Paul G. Watson,[a] and Andrey V. Zibarev*[b]

Keywords: Amides / Fluorine / Electrophiles / Reaction mechanisms / Pi interactions / Structure elucidation

The heteroatom reactivity of the title anions [as $(Me_2N)_3S^+$ and Cs^+ salts] toward both internal and external fluoro electrophiles has been investigated. The intramolecular nucleophilic cyclization of $[ArNSN]^-$ (as the cesium salts) bearing at least one *ortho* fluorine afforded 2,1,3-benzothiadiazoles (e.g. **2a**,**b**), whereas intermolecular condensation with polyfluorinated pyridine and naphthalene afforded Ar–N=S=N–R with R = 4-Py_F (**4**) and R = 2-Np_F (**8**). Further interaction of $[ArNSN]^-$ with **4** or **8** proceeded with the transfer of NSN units resulting in $(ArN=)_2S$ (**5**) and $[RNSN]^-$, followed by decomposition (R = 4-Py_F) to 4-Py_FNH_2 (**6**) or intramolecular cyclization (R = 2-Np_F) to the polyfluorinated thiadiazole **9**. The compounds of types **4**, **5**, **8**, and **9** have been characterized by single-crystal X-ray diffraction as having both *Z,E* and *Z,Z* configurations [**8** and **9** as molecular complexes with $C_{10}F_8$ and $(Ph–N=)_2S$ (**5e**), respectively, featuring π-stacking interactions of the arene–polyfluoroarene type]. Besides normal aryl–polyfluoroaryl interactions, the **8**·$C_{10}F_8$ complex also displays unusual polyfluoroaryl–polyfluoroaryl π-stacking.

Introduction

We recently reported the preparation, isolation, and X-ray structural characterization of $(Me_2N)_3S^+$ (TAS^+) salts of $[RNSN]^-$ anions (R = Me_3C, Me_3Si,[1] various aryl substituents[2,3]). It emerged from the X-ray data that due to the unexpectedly short terminal SN bond, these anions should be regarded as thiazylamide (**A**) rather than as sulfurdiimide (**B**) anions (Scheme 1),[1−3] in accordance with calculations at the MP2/6−31G* and B3LYP/6−311+G* levels of theory. Thus, the $[RNSN]^-$ anions belong to the rare class of compounds featuring sulfur−nitrogen triple bonds and therefore they deserve more detailed investigation.

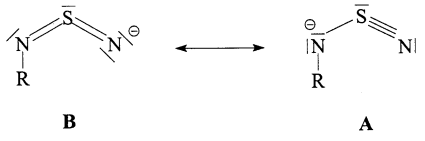

B **A**

Scheme 1

Previously, some $[RNSN]^-$ anions (R = Ar_F−X−; X = −, S) generated in situ in the form of Cs^+ salts have been shown to be involved in intramolecular nucleophilic *ortho* cyclizations, which resulted in the previously unknown and otherwise inaccessible polyfluorinated 2,1,3-benzothiadiazoles (X = −, Ar_F = 4-RC_6F_4),[4] naphtho[1,2-*c*]- and naphtho[2,3-*c*][1,2,5]thiadiazoles (X = −; Ar_F = 2-$C_{10}F_7$),[5] or 1,3,2,4-benzodithiadiazines (X = S; Ar_F = C_6F_5), depending on Ar_F and X.[6] With Ar_F = 4-Py_F and X = −; S (4-Py_F = 2,3,5,6-tetrafluoro-4-pyridinyl), however, no heterocycles could be prepared, and polyfluorinated 4-aminopyridine was the major product instead.[7] It follows from the available data[4−7] that the reactivity of these intermediate anions toward internal electrophiles (*ortho* cyclization), as well as their stability,[1−3] depends strongly on the substituents at the NSN^- moiety {whilst TAS^+ $[RNSN]^-$ salts (R = Me_3C, Me_3Si) are moderately stable at room temperature,[1] their R = Ar analogues decompose rapidly at temperatures above −20 °C[2,3]}.

The present paper provides detailed experimental information on the reactivity of $[RNSN]^-$ anions (as the TAS^+ and Cs^+ salts; R = Ar) towards both internal and external fluoro electrophiles, as well as a description of nontrivial structural features of the synthesized compounds.

Results and Discussion

Reactivity of Arylthiazylamides $[ArNSN]^-$ Towards Internal Fluoro Electrophiles

The starting point for our considerations was the isolation of salts with fluorinated anions $[Ar_FNSN]^-$,[2,3] which are probable intermediates in the CsF-induced intramolecular *ortho* cyclization of polyfluorinated sulfurdiimides $Ar_FNSNSiMe_3$ to give polyfluorinated benzo- and naphthothiadiazoles.[4,5] This approach might be extended to low-fluorinated derivatives (e.g. **1a**,**b**). When treated with CsF in boiling CH_3CN, cyclization to the well-known 2,1,3-benzothiadiazole **2a**[8] and its previously unreported 4-fluoro derivative **2b** was observed (the 5-F isomer of **2b** was prepared some time ago[9]). Our approach represents a use-

[a] Institute for Inorganic and Physical Chemistry, Bremen University,
28334 Bremen, Germany
E-mail: mews@chemie.uni-bremen.de
[b] Institute of Organic Chemistry, Russian Academy of Sciences,
630090 Novosibirsk, Russia
E-mail: zibarev@nioch.nsc.ru

 © WILEY-VCH Verlag GmbH, 69451 Weinheim, 2001 1434−1948/01/0808−2123 $ 17.50+.50/0

ful extension of the established methods for the preparation of carbocyclic-substituted derivatives of **2a**.[8]

Comparison of the ^{15}N NMR spectra of **2a** [$\delta^{15}N$ = 329.9 (t, J = 0.5 Hz)] and **2b** [$\delta^{15}N$ = 330.1 (s), 325.1 (d, J = 2.9 Hz)] allows assignment of the low-field signal of **2b** to N^1 and the high-field signal to N^3. This assignment is also consistent with the known tendency[10] for enhanced shielding of those nitrogen nuclei that are *ortho* to F in fluorinated (hetero)aromatics.

The method seems to be restricted to fluoride as a leaving group; no heterocyclic products could be obtained under the same conditions from the corresponding *ortho*-Cl- or *ortho*-O_2N-containing precursors $ArNSNSiMe_3$ **1c**,**d** [Ar = 2,6-$Cl_2C_6H_3$ (**1c**), 2-$O_2N-C_6H_4$ (**1d**)]. Only the corresponding amines $ArNH_2$ were isolated. This cyclization (Scheme 2) would require a conversion of CsF into CsCl and $CsNO_2$, respectively, which is thermodynamically unattractive and thus responsible for the lack of cyclization.

Although attempts to isolate polyfluorinated $[Ar_FNSN]^-$ anions have proved unsuccessful,[2,3] [2-$FC_6H_4NSN]^-$ (**3a**) and [2,6-$F_2C_6H_3NSN]^-$ (**3b**), the likely intermediates en route to benzothiadiazole formation (Scheme 2), have been isolated and structurally characterized in the form of TAS^+ salts.[2] Thermal decomposition of salts **3a**,**b** (Scheme 2) gave only tarry products and none of the expected thiadiazoles **2a**,**b**. This failure to isolate the expected cyclization products from the thermal decomposition of **3a**,**b** is not at variance with the formation of arylthiazylamide anions as intermediates. In the decomposition reactions of the TAS^+ salts, fluoride is an unfavorable leaving group, thus the activation barrier for this intramolecular fluoride exchange seems to exceed the stability[2,3] of the arylthiazylamide anions.

Trapping of Arylthiazylamides $[ArNSN]^-$ by External Fluoro Electrophiles

In view of the unsuccessful attempts to obtain benzothiadiazoles by intramolecular fluoride elimination from TAS^+ $[Ar_FNSN]^-$, it was expected that trapping and stabilization of the $ArNSN^-$ moiety should only be possible, if at all, with highly reactive fluoro electrophiles. Highly reactive electrophiles of this type are pentafluoropyridine and octafluoronaphthalene.[11]

It has been found that reactions of arylthiazylamide anions as their TAS^+ and Cs^+ salts with these external electrophiles afford two types of products. In the case of pentafluoropyridine, the products are the expected *N*-aryl-*N*′-(2,3,5,6-tetrafluoro-4-pyridinyl)sulfurdiimides (**4**) and the rather unexpected symmetric *N*,*N*′-bis(aryl)sulfurdiimides (**5**), as well as 4-amino-2,3,5,6-tetrafluoropyridine (**6**), depending on the Ar group and the cation (Scheme 3).

With TAS^+ salts in CH_3CN at −40 °C, it was found that the expected trapping product **4i** could only be obtained with an anion bearing a strongly electron-releasing *para*-substituent (e.g. CH_3O) on the aromatic ring. In all other such experiments, only **6** and the symmetric compounds **5**

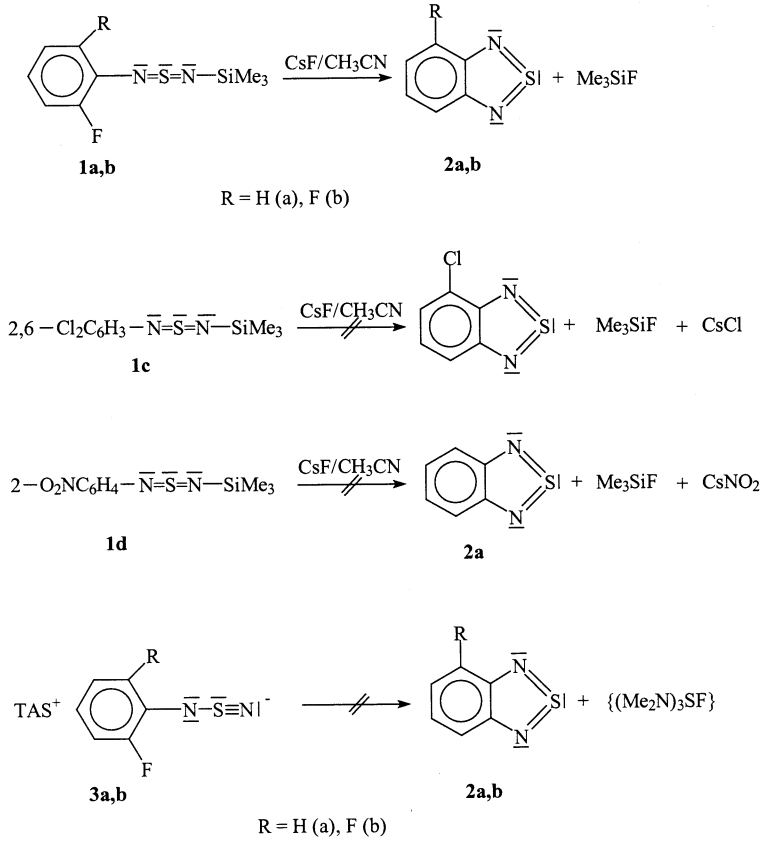

Scheme 2

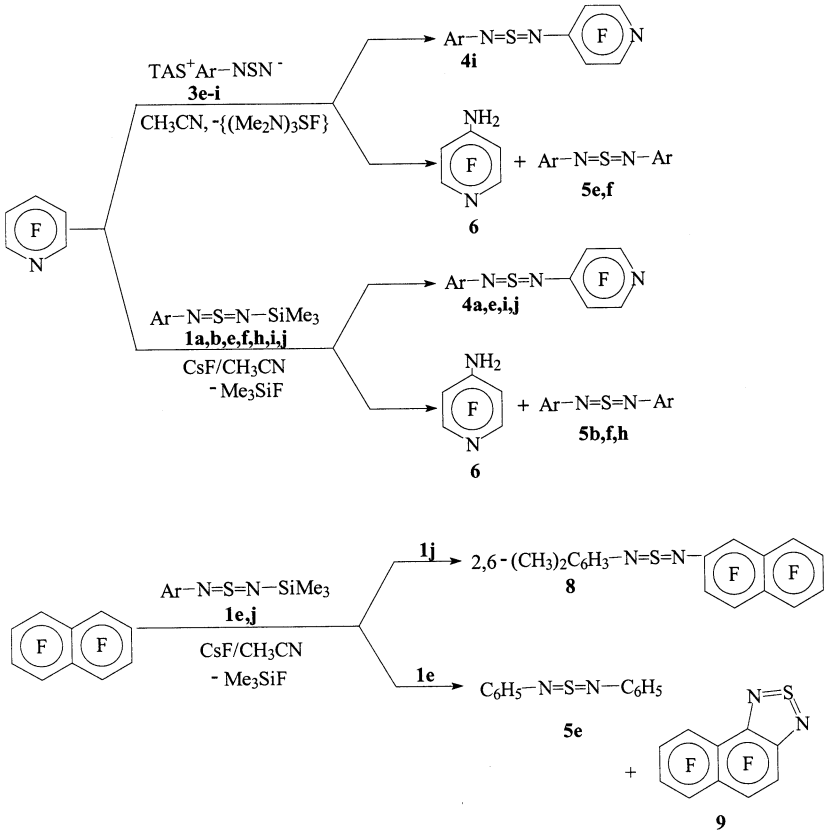

Scheme 3

were produced, except in the case of anions bearing strongly electron-withdrawing *para*-substituents (e.g. CF_3), where no products could be identified in the resulting dark tar (Scheme 3).

With Cs^+ salts in CH_3CN, the expected trapping products **4a**,**e**,**i**,**j** were obtained from the parent anion $[PhNSN]^-$ and its 2-fluoro-, 4-methoxy-, and 2,6-dimethyl-substituted derivatives, whereas amine **6** and symmetric sulfurdiimides **5b**,**f**,**h** were isolated from the reaction mixtures in all other cases (Scheme 3). With starting material **1h** (Ar = 4-$CF_3C_6H_4$), bearing a strong acceptor substituent, the latter were obtained in only trace amounts.

In the reaction of $C_{10}F_8$ with Cs^+ $[2,6\text{-}XyNSN]^-$ (2,6-Xy = 2,6-dimethylphenyl), typical octafluoronaphthalene β-substitution[11] proceeded to afford the expected *N*-(2,6-Xy)-*N*′-(2-Np_F) sulfurdiimide **8** (2-Np_F = 1,3,4,5,6,7,8-heptafluoronaphth-2-yl) (Scheme 3), which was isolated from the reaction mixture as a molecular complex **8**·$C_{10}F_8$. Complexes of this type have not been reported previously. In contrast, reaction of $C_{10}F_8$ with Cs^+ $[PhNSN]^-$ unexpectedly yielded the polyfluorinated naphtho[1,2-*c*][1,2,5]thiadiazole (**9**) and the symmetric sulfurdiimide $(PhN{=})_2S$ (**5e**) (Scheme 3), which was again isolated from the reaction mixture as a molecular complex **5e**·**9** and was of a previously unknown type.

The dichotomous reactivity of $[ArNSN]^-$ anions toward external fluoro electrophiles cannot be attributed solely to the influence of the aryl substituents since the alkylthiazylamides $[AlkNSN]^-$ [Alk = *t*Bu, adamant-1-yl (1-Ad)] show similar behaviour. Thus, the expected nonsymmetric sulfurdiimide 1-Ad−N=S=N−Py_F-4 was obtained from Cs^+ [1-AdNSN]$^-$ and pentafluoropyridine, whereas reaction of Cs^+ $[AlkNSN]^-$ (Alk = *t*Bu,1-Ad) with octafluoronaphthalene resulted in the heterocycle **9**.[12]

Thus, although the described anions have the thiazylamide structure,[2,3] they rearrange to a sulfurdiimide form in the final reaction products. In this context, it is interesting to note that the carbon analogues of the title anions, $[RNCN]^-$ (R = Me_3Si), have similar $R{-}\underline{\bar{N}}{-}C{\equiv}\bar{N}$ structures[13a] according to X-ray crystallographic data. They form $R'_2C{=}\bar{N}{-}C{\equiv}\bar{N}$ derivatives upon reaction with $R'_2C{=}O$.[14] By analogy, the initial products of the reactions of the title anions with fluoro electrophiles R_FF can be envisaged as $R_F(Ar)\bar{N}{-}\bar{S}{\equiv}\bar{N}$ undergoing intramolecular rearrangement to the more stable $R_F\bar{N}{=}\bar{S}{=}\bar{N}{-}Ar$ compounds due to the known general instability of these $R\bar{S}{\equiv}\bar{N}$ derivatives.[3] When such a rearrangement of the initial reaction products is not possible, as in the case of $R'_2C{=}\bar{N}{-}\bar{S}{\equiv}\bar{N}$ obtained from the reaction of $Cs^+Me_3Si\text{-}\underline{\bar{N}}\text{-}\underline{\bar{N}}\text{-}CR'_2$ with $R'_2C{=}O$, they are stabilized in a different manner, namely as $R'_2C{=}\bar{N}{-}\bar{N}{=}CR'_2$ compounds (R′ = various aryls).[13b]

It is quite likely that the expected trapping products **4** are formed in all cases, but that in some cases this reaction is very slow, and in the presence of an effective excess of the starting salt further interaction of the trapping product and

the salt is possible to give the symmetric $(ArN=)_2S$ (**5**) and the $[4\text{-}Py_FNSN]^-$ anion **7**. It is known that **7** does not undergo nucleophilic ring-closure even in boiling CH_3CN; it only decomposes to give the corresponding amine **6**[7] (Scheme 4). The identification of traces of $(4\text{-}Py_F)_2NH$ (**10**) in some experiments implies the participation of $[4\text{-}Py_FN\cdot^-]$ intermediates.

In the case of octafluoronaphthalene, further interaction of type **11** trapping products with the starting salt leads to the $[2\text{-}Np_FNSN]^-$ anion (Scheme 4), which, in contrast to **7**, is known to undergo highly regioselective intramolecular cyclization resulting in **9** as the major product.[5]

To the best of our knowledge, transfer of the NSN^- moiety from aromatics to polyfluoroaromatics, as depicted in Scheme 4, has not previously been observed. The driving force behind this substituent exchange is probably the well-known high electron affinity of polyfluoroaromatics.

The structures of the expected **4i,j** and **8·$C_{10}F_8$** and the unexpected **5f** and **5e·9** trapping products were confirmed by X-ray crystallographic analysis (see below). The structure of **5b**[15] had been determined previously.

Some of the synthesized compounds were also characterized by $^{14/15}N$ NMR spectroscopy. Three signals in the ^{15}N NMR spectrum of **4i** ($\delta^{15}N$ = 292.5, 278.7, and 217.8) could be assigned to Ar−N=, 4-Py_F−N=, and 4-Py_F, respectively, by comparison with the spectra of **5e** ($\delta^{14}N$ = 294),[16] **5b** (see below), other $(Ar-N=)_2S$ compounds,[17] and **6** [$\delta^{15}N$ = 212.1 (t, J = 50.0 Hz), 50.2 (t, J = 91.3 Hz)]. This assignment is also consistent with the known tendency[10] for enhanced shielding of those nitrogens that are *ortho* to F in fluorinated functional aromatics [*cf.* also **5e**[16] and **5b** ($\delta^{15}N$ = 272.1)]. The ^{15}N NMR spectrum of **8·$C_{10}F_8$** features two resonances ($\delta^{15}N$ = 312.8, 266.4), which could be assigned on the basis of similar arguments as above to 2,6-Xy−N= and 2-Np_F−N=, respectively. The ^{14}N NMR spectrum of **5e·9** shows a broad resonance ($\Delta\nu_{1/2} \approx$ 2000 Hz) with two well-defined maxima [$\delta^{14}N$ = 332 (**9**) and 301 (**5e**)], which are in very good

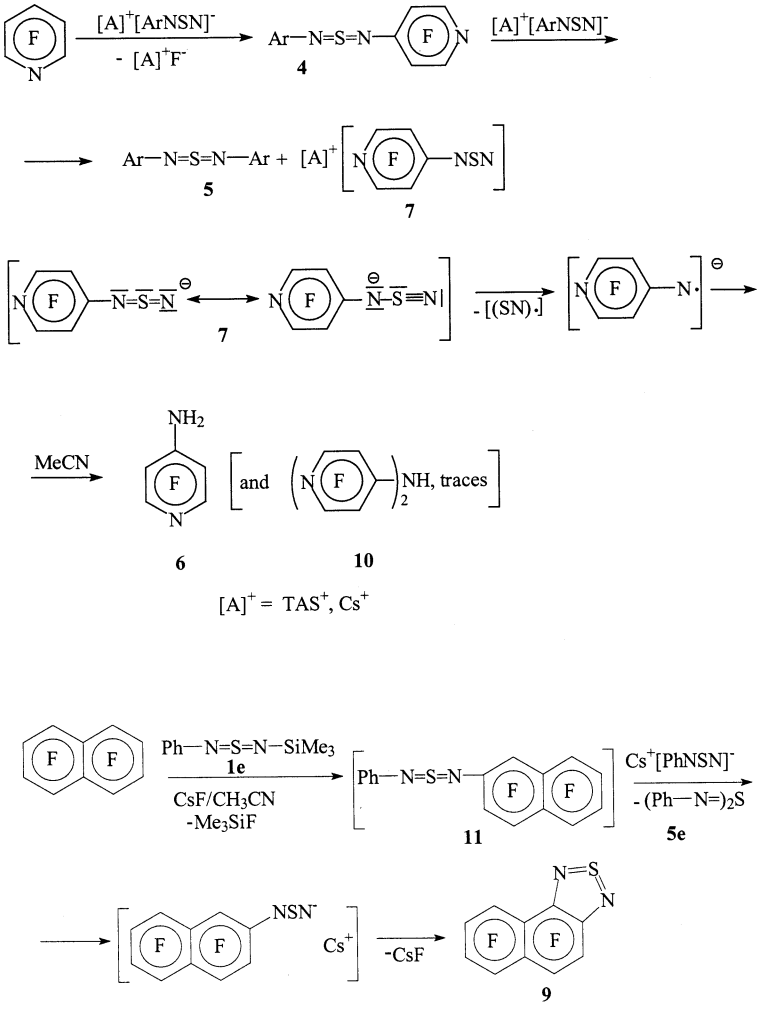

Scheme 4

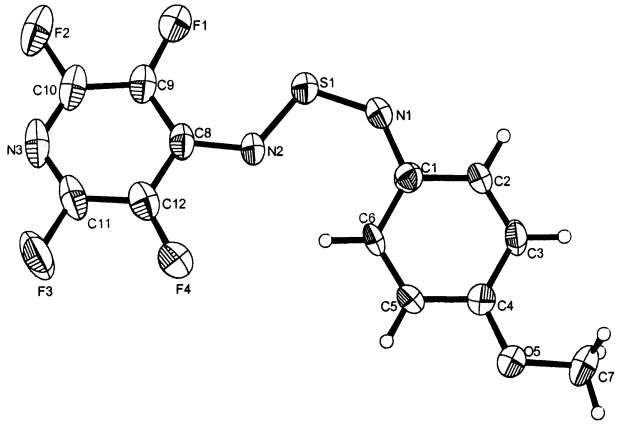

4i

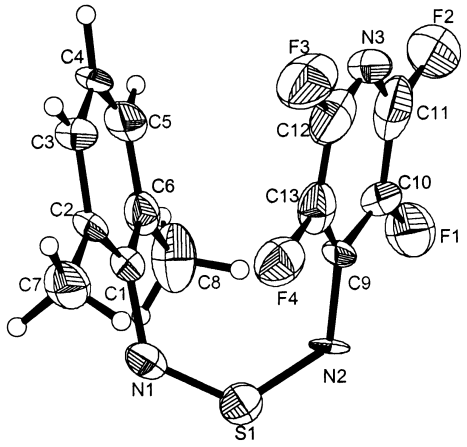

4j

Figure 1. X-ray structures of the sulfurdiimides (*Z*,*E*)-4-$CH_3O-C_6H_4-NSN-C_5F_4N$-4 (**4i**) and (*Z*,*Z*)-2,6-$(CH_3)_2C_6H_3-NSN-C_5F_4N$-4 (**4j**), selected bond lengths (pm) and angles (°): **4i:** C1−N1 138.7(6), N1−S1 153.2(4), S1−N2 156.9(4), N2−C8 138.9(6); C1−N1−S1 132.7(3), N1−S1−N2 112.3(2), S1−N2−C8 124.2(4); τ RC_6H_4/NSN 2.8(3), NSN/C_5F_4N 6.8(2); **4j:** (two independent molecules) C1−N1 142.9(5), 143.2(5); N1−S1 152.7(3), 152.9(3); S1−N2 154.3(3), 154.4(3); N2−C9 140.2(4), 139.9(5); C1−N1−S1 125.6(2), 127.0(3); N1−S1−N2 122.96(17), 123.05(17); S1−N2−C9 127.9(3), 126.5(3); τC_8H_9/NSN 68.62, 65.60; τNSN/C_5F_4N 63.46, 61.83

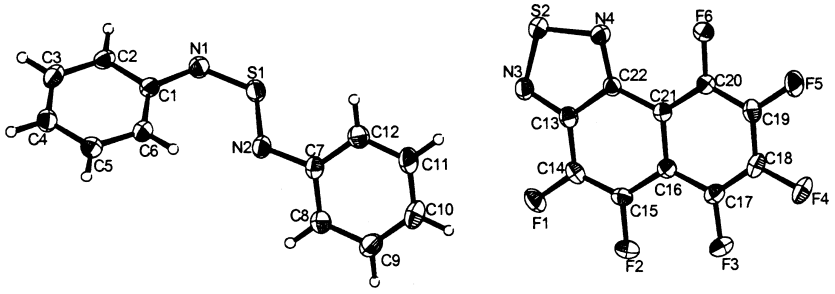

5e•9

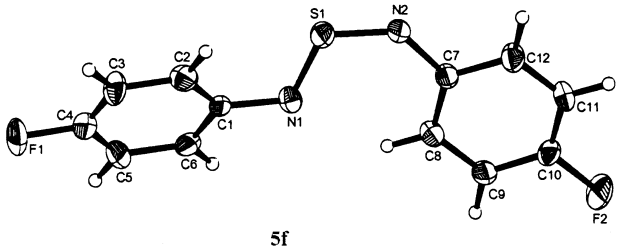

5f

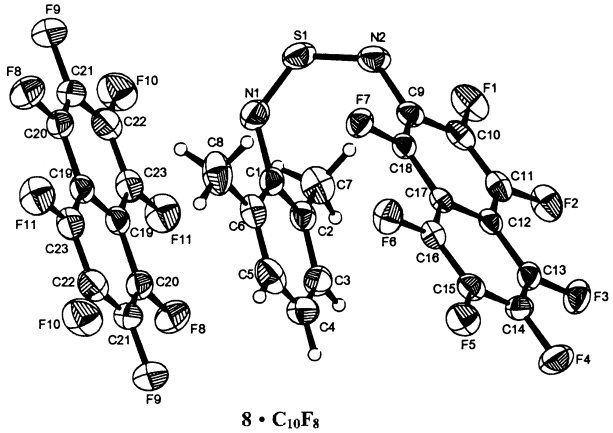

8 • $C_{10}F_8$

Figure 2. X-ray structures of $(C_6H_5N)_2S$ (**5e**)·$C_{10}F_6N_2S$ (**9**), $(4\text{-}FC_6H_4N)_2S$ (**5f**), and 2,6-$(CH_3)_2C_6H_3NSNC_{10}F_7$ (**8**)·1/2$C_{10}F_8$, selected bond lengths (pm) and angles(°): **5e·9:** C1−N1 140.5(3), N1−S1 153.5(2), S1−N2 155.3(2), N2−C7 142.5(2); C1−N1−S1 131.4(1), N1−S1−N2 116.7(1), S1−N2−C7 115.8(1), τ_1 13.1(1), τ_2 41.9(2); C13−N3 133.4(3), N3−S2 162.3(2), S2−N4 163.1(2), N4−C22 133.4(2), C22−C13 142.5(3); C13−N3−S2 105.5(1), N3−S2−N4 100.8(1), S2−N4−C22 105.9(1), N4−C22−C13 113.4(2), C22−C13−N3 114.5(2); **5f:** C1−N1 142.5(7), N1−S1 155.5(5), S1−N2 153.9(6), N2−C7 140.3(8); C1−N1−S1 116.7(4); N1−S1−N2 116.3(3), S1−N2−C7 131.8(4); τ_1 31.4(3); τ_2 7.6(4); **8**·1/2$C_{10}F_8$: C1−N1 142.5(3), N1−S1 152.2(2), S1−N2 154.4(2), N2−C9 140.4(3); C1−N1−S1 128.7(1), N1−S1−N2 123.7(1), S1−N2−C9 126.0(1); τ_1 68.2(1), τ_2 60.9(1)

agreement with the data for free **9** [$\delta^{15}N$ = 338.3 (d, J = 15.0 Hz)[5] and 325.0 (d, J = 7.0 Hz; this work)] and **5e** (see above).[16]

Structures of the Synthesized Sulfurdiimides RNSNR′

The trapping products of types **4** and **8** might be particularly interesting as ligands for coordination compounds as they possess two very different electron lone-pairs on the NSN fragments, along with a lone-pair from the tetrafluoropyridyl moiety in the case of **4**. According to X-ray crystallographic data (Figures 1 and 2, Tables 1 and 2), they adopt *Z*,*E* and *Z*,*Z* configurations in the solid state, typical of bis(aryl)sulfurdiimides.[3,15,18−23] Thus, in the crystal, compound **4i** exists as the perfectly planar *Z*,*E* isomer, whereas **4j** and **8** (in the complex with $C_{10}F_8$) exist as *Z*,*Z* isomers with the rings being essentially parallel to one another and perpendicular to the NSN plane. The bis(aryl)-sulfurdiimide parent compound **5e** (liquid in the pure state)[24] adopts the nonplanar *Z*,*E* configuration in the complex with **9**, whereas compound **5f** has an almost planar *Z*,*E* configuration. Compound **5b** (*Z*,*Z* isomer in the crystal)[15] has been structurally characterized previously.

Table 3 lists the data obtained in this work along with selected representative conformational data for previously reported bis(aryl)sulfurdiimides.[3,15,18−23] Sterically unhindered bis(aryl)sulfurdiimides adopt the *Z*,*E* configuration with the less electron-withdrawing substituent in the *Z*-position. Steric strain in this position is released by adopting a wide CNS angle (≈130°), which is 10−15° wider than that for the *E*-substituents. A further reason for the small angle in the *E*-position is the rotation of the aryl ring out of the NSN plane by 30−40°. For strongly electron-withdrawing groups (C_6F_5, C_5F_4N), this torsion angle is very small (7°), leading to an appreciable opening of the CNS angle (124−125°).

In *Z*,*E*-(2,4,6-$Br_3C_6H_2N$=)$_2$S, steric strain is released through the adoption of an almost perpendicular orientation of the aryl groups relative to the NSN plane. As pointed out previously, substitution of H by F, Br, or Me in the *o*,*o*-positions, although sterically less favoured, leads to the *Z*,*Z*-configuration.[21,22] Steric strain in these cases is released by a parallel rotation of both groups out of the NSN plane by 55−70°. In spite of this, the NSN angle in the *Z*,*Z*-configuration is 10° larger than that in the *Z*,*E* derivatives.

Notably, with planar molecular geometry in the *Z*,*E* configuration (*cf.* **4i**), the synthesized compounds satisfy the primary requirements for materials with nonlinear optical properties in that they contain donor (Ar) and acceptor (4-Py_F) fragments connected by an −N=S=N− bridge capable of π-conjugation.[25]

Table 1. Crystal and refinement data of **4i**,**j**

	4i	**4j**[a]
Empirical formula	$C_{12}H_7F_4N_3OS$	$C_{13}H_9F_4N_3S$
Molecular weight	317.27	315.29
Temperature	173(2) K	173(2) K
Wavelength	71.073 pm	71.073 pm
Crystal system	Monoclinic	Monoclinic
Space group	*C*2/*c*	$P2_1/a$
Unit cell dimensions	a = 1777.1(6) pm	a = 1447.0(4) pm
	b = 837.2(2) pm	b = 2675.6(6) pm
	c = 1710.5(4) pm	c = 1390.8(4) pm
	β = 94.53(3)°	β = 90.0°
Volume	2.537(1) nm^3	5.39(1) nm^3
Z	8	16
Density (calculated)	1.661 Mg/m^3	1.556 Mg/m^3
Absorption coefficient	0.306 mm^{-1}	0.283 mm^{-1}
F(000)	1280	2560
Crystal size/mm^3	0.6 × 0.4 × 0.2 mm^3	0.70 × 0.50 × 0.20 mm^3
θ range for data collection	2.69 to 22.50°	2.68 to 27.51°
Index ranges	$-1 \le h \le 19$	$-16 \le h \le 16$
	$-1 \le k \le 9$	$-34 \le k \le 34$
	$-18 \le l \le 18$	$-15 \le l \le 17$
Reflections collected	2080	11990
Independent reflections	1568 (R_{int} = 0.0537)	5859 (R_{int} = 0.0401)
Max. and min. transmission		0.9456 and 0.8266
Refinement method	Full-matrix least-squares on F^2	Full-matrix least-squares on F^2
Data/restraints/ parameters	1568/0/194	5859/0/387
Goodness of fit on F^2	1.002	1.014
Final R indices [$I > 2\sigma(I)$]	$R1$ = 0.0520, $wR2$ = 0.1294	$R1$ = 0.0527, $wR2$ = 0.1152
R indices (all data)	$R1$ = 0.0904, $wR2$ = 0.1522	$R1$ = 0.0900, $wR2$ = 0.1329
Absolute structure parameter	−	−
Extinction coefficient	0.0003(2)	0.00011(6)
Largest diff. peak and hole	377 and −307 e·nm^{-3}	234 and −407 e·nm^{-3}

[a] Due to the twinning by reticular merohedry, an orthorhombic intensity-weighted reciprocal lattice was chosen (with doubled cell volume) to describe the monoclinic structure.

Table 2. Crystal and refinement data for **5e·9**, **5f**, and **8**·1/2$C_{10}F_8$

	5e·9	**5f**	**8**·1/2$C_{10}F_8$
Empirical formula	$C_{12}H_{10}N_2SC_{10}F_6N_2S$	$C_{12}H_8F_2N_2S$	$C_{18}H_9F_8N_2S1/2C_{10}F_8$
Molecular weight	508.46	250.26	554.38
Temperature	173(2) K	173(2) K	173(2) K
Wavelength	71.073 pm	71.073 pm	71.073 pm
Crystal system	Monoclinic	Orthorhombic	Triclinic
Space group	$P2_1$	$Pca2/_1$	$P\bar{1}$
Unit cell dimensions	a = 612.4(1) pm b = 750.5(1) pm c = 2174.2(2) pm β = 90.83(1)°	a = 1200.8(3) pm b = 1287.8(4) pm c = 706.1(5) pm	a = 766.7(1) pm b = 1087.0(1) pm c = 1298.3(1) pm α = 83.15(1)° β = 87.35(1)° γ = 78.12(1)°
Volume	0.9992(2) nm^3	1.0919(9) nm^3	1.0510(2) nm^3
Z	2	4	2
Density (calculated)	1.690 Mg/m^3	1.522 Mg/m^3	1.752 Mg/m^3
Absorption coefficient	0.342 mm^{-1}	0.299 mm^{-1}	0.268 mm^{-1}
F(000)	512	512	552
Crystal size/mm^3	0.80 × 0.60 × 0.30 mm^3	1.2 × 0.2 × 0.1 m^3	0.80 × 0.50 × 0.50 mm^3
θ range for data collection	2.81 to 27.50°	3.16 to 27.48°	2.63 to 27.50°
Index ranges	$-7 \le h \le 7$ $-9 \le k \le 9$ $-28 \le l \le 28$	$-1 \le h \le 15$ $-1 \le k \le 16$ $-1 \le l \le 9$	$-9 \le h \le 1$ $-10 \le k \le 14$ $-16 \le l \le 16$
Reflections collected	8750	1546	5406
Independent reflections	4581 (R_{int} = 0.0392)	1299 (R_{int} = 0.0363)	4433 (R_{int} = 0.0277)
Max. and min. transmission	0.9042 and 0.7713		0.8777 and 0.8142
Refinement method	Full-matrix least-squares on F^2	Full-matrix least-squares on F^2	Full-matrix least-squares on F^2
Data/restraints/ parameters	4581/1/309	1299/1/156	4433/0/339
Goodness of fit on F^2	1.066	1.006	1.018
Final R indices [$I > 2\sigma(I)$]	$R1$ = 0.0326, $wR2$ = 0.0843	$R1$ = 0.0557, $wR2$ = 0.1269	$R1$ = 0.0418, $wR2$ = 0.1098
R indices (all data)	$R1$ = 0.0353, $wR2$ = 0.0858	$R1$ = 0.1024, $wR2$ = 0.1497	$R1$ = 0.0528, $wR2$ = 0.1176
Absolute structure parameter	−0.07(6)	0.2(3)	
Extinction coefficient	0.0052(12)	0.008(3)	0.007(14)
Largest diff. peak and hole	255 and 384 e·nm^{-3}	385 and −314 e·nm^{-3}	224 and 323 e·nm^{-3}

Table 3. Bis(aryl)sulfurdiimides Ar−N=S=N−Ar^1

Ar	Ar^1		Conf. exp. Ar Ar^1	Conf. calcd.[a] Ar Ar^1	$C_{Ar}NS$	$\tau_{Ar/NSN}$	$C_{Ar1}NS$	$\tau_{Ar^1/NSN}$	NSN	ref.
C_6H_5	C_6H_5	**5e**	*Z*,*E*	*Z*,*E*[18]	131.4	13.1	115.8	41.9	116.7	
p-C_6H_4F	*p*-C_6H_4F	**5f**	*Z*,*E*		131.8	8.7	116.7	31.4	116.3	
C_6H_5	C_6F_5		*Z*,*E*	*Z*,*E*	133.2	1.9	124.6	1.8	113.6	[22]
2,4,6-$Br_3C_6H_2$	2,4,6-Br_3CH_2		*Z*,*E*	*Z*,*E*	125.3	83.0	116.0	82.3	115.8	[21]
p-$MeOC_6H_4$	4-NC_5F_4	**4i**	*Z*,*E*		132.7	2.8	124.2	7.2	112.3	
2,6-$Me_2C_6H_3$	2,6-$Me_2C_6H_3$		*Z*,*Z*	*Z*,*Z*	127.2	32.0	131.8	37.5	127.2	[21]
2,6-$Me_2C_6H_3$	2,4,6-$Br_3C_6H_3$		*Z*,*Z*	*Z*,*Z*	132.5	64.2	130.1	67.0	126.1	[21]
					133.7	65.5	131.4	69.7	126.5	
2,6-$Me_2C_6H_3$	2-$C_{10}F_7$	**9**	*Z*,*Z*		128.7	68.2	126.0	60.9	123.7	
2,6-$Me_2C_6H_3$	4-NC_5F_4	**4j**	*Z*,*Z*		125.6	68.6	127.9	63.5	123.0	
					127.0	65.6	126.5	61.8	123.1	
2,6-$Me_2C_6H_3$	C_6F_5		*Z*,*Z*	*Z*,*Z*	129.5	63.0	128.0	67.1	123.8	[22]
C_6F_5	C_6F_5		*Z*,*Z*	*Z*,*E*	126.7	59.5	128.4	60.9	123.9	[22]
					127.7	59.2	127.4	59.7	123.2	
2,6-$F_2C_6H_3$	2,6-$F_2C_6H_3$	**5b**	*Z*,*Z*		128.5	56.5	128.5	56.4	125.2	[15]

[a] At the PM3 level of theory.[21,22]

Even more interesting than the stereochemistry of the bis(aryl)sulfurdiimides is the interaction of one of the phenyl rings of $(C_6H_5N=)_2S$ (**5e**) with the heteropolyfluoroaromatic system **9** in the solid state, as well as the interaction of 2,6-$Me_2C_6H_3N=S=NC_{10}F_7$ (**8**) with 1/2$C_{10}F_8$ (Figures 3 and 4).

It should be noted that noncovalent interactions between aromatic and polyfluoroaromatic groups[26−28] (a special

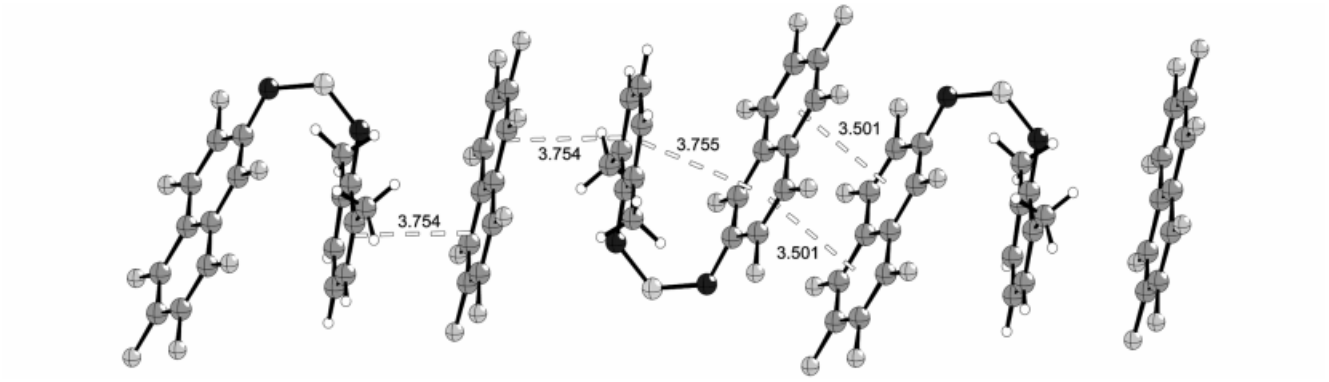

Figure 3. π-Stacking of the arene−polyfluoroarene and polyfluoroaryl−polyfluoroaryl types in the crystal of **8**·$C_{10}F_8$

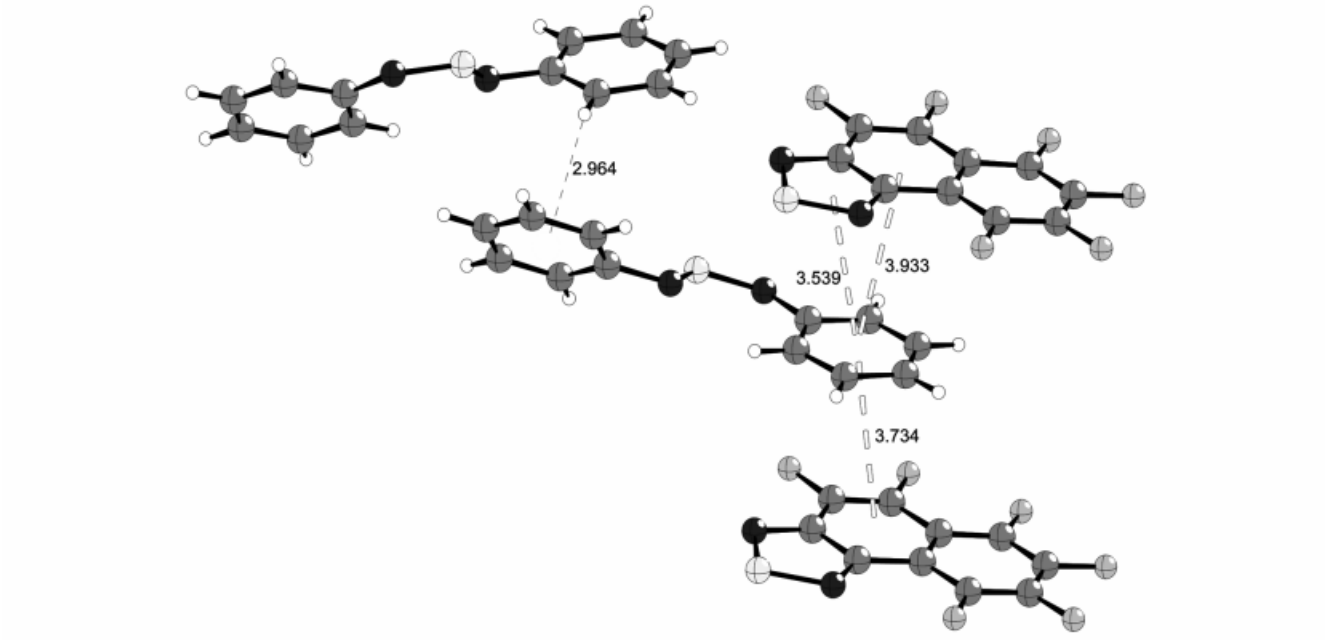

Figure 4. π-Stacking of the arene−polyfluoroarene type in the crystal of **5e**·**9**

case of noncovalent interactions between aromatic units that is known to play a significant role in determining the structures and properties of molecular assemblies in biology, supramolecular chemistry, and materials science)[29,30] have been extensively studied in recent years, leading to important new possibilities in crystal engineering for the design of advanced functional materials.[31−36] Co-crystals of benzene/hexafluorobenzene,[37,38] their (poly)substituted derivatives,[31,32,34,37,39] biphenyl/decafluorobiphenyl,[40] naphthalene/octafluoronaphthalene[41] and larger aromatic hydrocarbon/fluorocarbon,[42,43] and of decamethylferrocene/perfluorophenanthrene[44] have been produced and have been found to involve alternating 1:1 π-stacking. This face-to-face stacking arrangement is thought to be dominated by electrostatic forces,[45] in particular by large but opposite-in-sign quadrupole moments of the C_6H_6 and C_6F_6 components.[27] The electrostatic potential map of benzene reveals concentrations of negative potential above and below the molecular plane, and a ring of positive potential in the plane centred on the hydrogens; hexafluorobenzene possesses the opposite charge distribution[46] (see also ref.[31]).

Significantly, neither heterocycles (**5e**·**9**) nor markedly bent (tweezer-like) molecules (**8**·$C_{10}F_8$) have previously been found to be involved in noncovalent arene−polyfluoroarene interactions, with one probable exception in the latter case being a complex of 1,4-diiodotetrafluorobenzene with a cone-shaped 1,3-bis(pyridylmethyl)calix[4]arene.[47]

Both complexes **5e**·**9** and **8**·$C_{10}F_8$ feature face-to-face π-stacking of the arene−polyfluorene type.[26−28] Additionally, **8**·$C_{10}F_8$ shows another structural motif, namely an unprecedented π-stacking of the heptafluoronaphth-2-yl moieties with an interplanar separation of 350.1 pm (Figure 3), thus representing a new type of arene−polyfluoroarene complex. (It is noteworthy that the crystal packing of octafluoronaphthalene does not, of course, reveal any π-stacking interactions, but rather a face-to-edge orientation of neighbouring molecules[48]). The peculiarity mentioned

above is in sharp contrast to the purely electrostatic interpretation of the interactions under consideration and clearly requires further investigation, both experimentally and especially theoretically. It seems that the dispersion forces[27] (responsible, for example, for the solid-state structure of octafluoronaphthalene[48]) should also be taken into account.

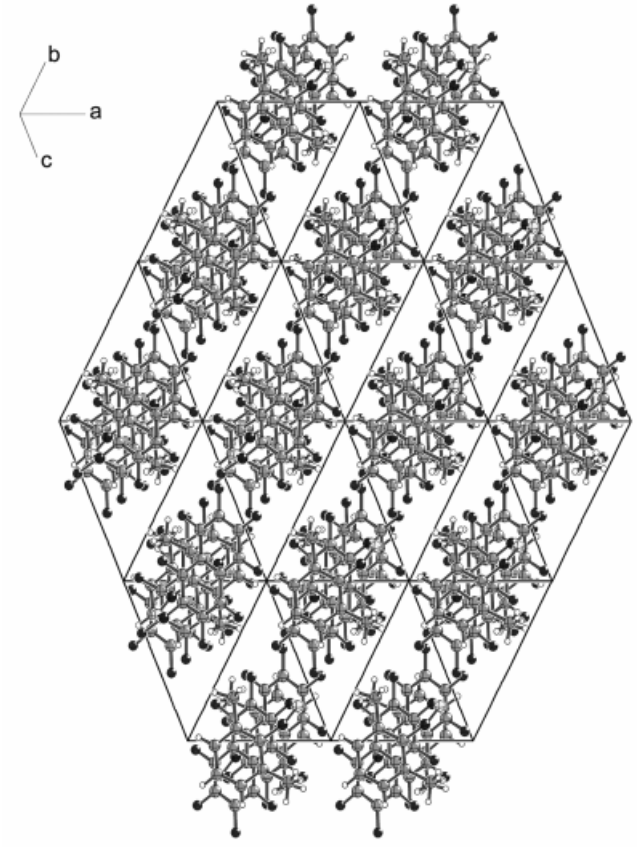

Figure 5. Crystal packing of **8**·$C_{10}F_8$

On the other hand, a 2,6-dimethylphenyl−2,6-dimethylphenyl interaction is not seen.

Within the stacks, the arene−polyfluoroarene separation is 353.9−393.3 pm for **5e·9** and 350.1−375.5 pm for **8**·$C_{10}F_8$, as compared to 377 pm for the lowest-temperature phase of the benzene/hexafluorobenzene co-crystals[38] and 368.6−377.1 pm for the naphthalene/octafluoronaphthalene co-crystals.[41]

The crystal packing of **8**·$C_{10}F_8$ and **5e·9** is depicted in Figures 5 and 6.

The alternating stacked aryl−polyfluoroaryl arrangement is concluded to be a general supramolecular motif of significant importance with regard to new developments in crystal engineering.[32] In view of the fact that **5e·9** and **8**·$C_{10}F_8$ combine π-stacked structures with the potential ability to coordinate transition metals through NSN bridges, the findings of this work can be envisaged as offering new prospects in this field.

Conclusions

The intramolecular nucleophilic cyclization of arylthiazylamides bearing at least one *ortho* fluorine offers a novel synthetic approach to 2,1,3-benzothiadiazoles. Despite some complications, the interaction of arylthiazylamides with fluoro electrophiles such as pentafluoropyridine and octafluoronaphthalene makes it possible to synthesize *N*-aryl-*N′*-(tetrafluoro-4-pyridinyl)sulfurdiimides (**4**) and *N*-aryl-*N′*-(heptafluoronaphth-2-yl)sulfurdiimides (**8**), which are not readily accessible by other means. Thus, the intramolecular nucleophilic cyclization of arylthiazylamide anions has now been expanded to intermolecular condensation. Compounds **4** and **8** represent promising ligands for coordination chemistry. With planar molecular geometries in the *Z,E* configuration (*cf.* **4i**), these compounds also satisfy

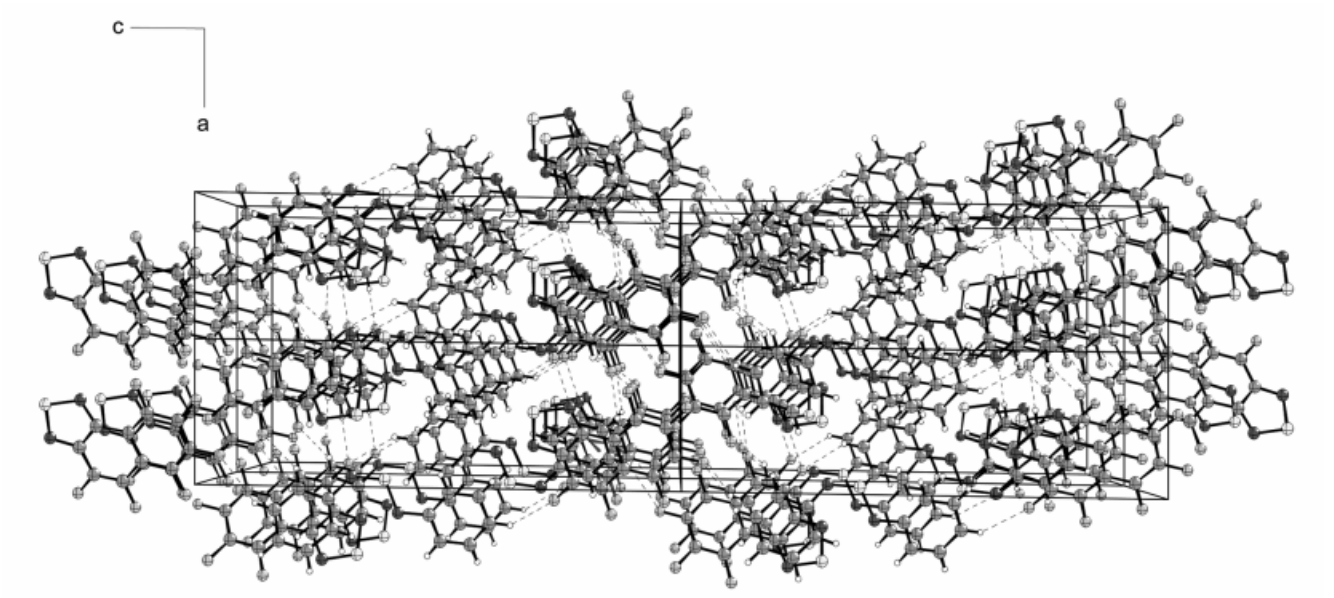

Figure 6. Crystal packing of **5e·9**

the primary requirements for materials with nonlinear optical properties as they contain donor (Ar) and acceptor (4-Py_F) fragments connected by an −N=S=N− bridge capable of π-conjugation. Complexes **5e·9** and **8**·$C_{10}F_8$ are the first examples of a heterocycle (**9**) and an essentially nonplanar tweezer-like molecule (*Z,Z*-**8**) to feature arene−polyfluoroarene π-stacking interactions. Besides typical aryl−polyfluoroaryl stacking, the crystal packing of **8**·$C_{10}F_8$ also reveals an unprecedented supramolecular motif, namely polyfluoroaryl−polyfluoroaryl π-stacking, thus making this a new type of arene−polyfluoroarene complex.

Experimental Section

General Remarks: ^{1}H and ^{19}F NMR spectra were recorded on a Bruker DPX-200 spectrometer, and ^{13}C NMR spectra on a Bruker DRX-500 spectrometer, at frequencies of 200.13, 188.28, and 125.76 MHz, respectively, with samples in $CDCl_3$ solution; chemical shifts are given with respect to TMS (^{1}H, ^{13}C) or $CFCl_3$ (^{19}F) Nitrogen NMR spectra were measured on a Bruker DRX-500 spectrometer at frequencies of 67.80 MHz (^{15}N) and 36.14 MHz (^{14}N) with samples in $CDCl_3$ solution; chemical shifts are given relative to NH_3 (liq.). − High-resolution mass spectra (EI, 70 eV) were measured with a Finnigan MAT MS 8200 mass spectrometer. − UV/Vis spectra were recorded on a Specord UV/Vis instrument with samples in heptane solution.

Crystallographic Analysis: The single-crystal X-ray structure determinations (Tables 1 and 2) were carried out on a Siemens P4 diffractometer using graphite-monochromated Mo-K_α (0.71073 Å) radiation. Refinement based on F^2; $R1 = \Sigma||F_o| - |F_c||/\Sigma|F_o|$; $wR2 = \{\Sigma[w(F_o^2 - F_c^2)^2]/\Sigma[w(F_o^2)^2]\}^{1/2}$. Programs used: SHELX-97[49] and DIAMOND.[50]

The transparent crystals were mounted on a thin glass fibre using KEL-F oil. The structures were solved by direct methods (SHELXS[49]). Subsequent least-squares refinements (SHELXL-97−2[49]) located the positions of the remaining atoms in the electron density maps. All non H-atoms were refined anisotropically.[51]

Syntheses: TASF was prepared by established methods;[52] 1-aryl-3-(trimethylsilyl)sulfurdiimides Ar−N=S=N−$SiMe_3$ (**1a**,**b**,**e**−**j**) were obtained by known procedures.[3] Tris(dimethylamino)sulfonium arylthiazylamides TAS^+ $[ArNSN]^-$ were synthesized as described previously.[2,3] Cesium fluoride was calcinated immediately prior to use. The syntheses described below were performed in dry solvents with stirring under an argon atmosphere. The reagents were added dropwise and the solvents were distilled off under reduced pressure. The compounds **2a**,[8] **6**,[53] and **5b**,**f**[54] have been reported previously. Table 4 lists the physical and analytical data for the synthesized compounds.

1-Aryl-3-(trimethylsilyl)sulfurdiimides (1c,**d):** A solution of the appropriate ArNSO[55] (60 mmol) in hexane (25 mL) was added to a suspension of $LiN(SiMe_3)_2$ (10.0 g, 60 mmol) in hexane (50 mL) at −30 °C. The temperature was raised to 20 °C over a period of 2 h, and then a solution of Me_3SiCl (6.6 g, 60 mmol) in hexane (10 mL) was added. The precipitate formed was filtered off, the solvent was distilled, and the residue was distilled in vacuo. Compounds **1c**,**d** were obtained as orange oils.

2,1,3-Benzothiadiazole (2a) and 4-Fluoro-2,1,3-benzothiadiazole (2b): A solution of the appropriate Ar−N=S=N−$SiMe_3$ (**1a**,**b**) (20 mmol) in CH_3CN (25 mL) was added to a boiling suspension of CsF (3.04 g, 20 mmol) in CH_3CN (75 mL) over a period of 30 min. After a further 30 min, the reaction mixture was allowed

Table 4. Characterization of the synthesized compounds

Compound	Yield [%]	m.p. [°C]	b.p. [°C/mm]	^{1}H NMR, δ [ppm]	^{19}F NMR, δ [ppm]	Molecular formula [MS: M^+ [*m*/*z*], measured (calculated)]
1c	50	–	80−81/0.01	7.29 (2 H), 6.94 (1 H), 0.02 (9 H)	–	$C_9H_{12}Cl_2N_2SSi$: 277.9864 (277.9868, ^{35}Cl)
1d	60	–	88−90/0.01	7.91 (1 H), 7.55 (1 H), 7.36 (1 H), 7.23 (1 H), 0.16 (9 H)	–	$C_9H_{13}N_3O_2SSi$: 255.0494 (255.0498)
2a	23	45−46	–	7.99 (2 H), 7.55 (2 H)	–	$C_6H_4N_2S$ 136.0097 (136.0095)
2b	55	29−30	–	7.51 (d, 1 H), 7.28 (ddd, 1 H), 6.97 (dd, 1 H)	−121.1 (dd)	$C_6H_3FN_2S$: 54.0006 (154.0001)
4a	48	85−86	–	7.48 (1 H), 7.17−7.12 (2 H), 6.95 (1 H)	−92.2 (2 F), −118.0 (1 F), −148.5 (2 F)	$C_{11}H_4F_5N_3S$: 305.0073 (305.0046)
4e	55	102−103	–	7.62 (2 H), 7.34 (3 H)	−92.1 (2 F), −149.6 (2 F)	$C_{11}H_5F_4N_3S$: 287.0140 (287.0140)
4i	60[a][b]	122−123	–	8.06 (2 H), 6.88 (2 H), 3.82 (3 H)	−92.1 (2 F), −150.4 (2 F)	$C_{12}H_7F_4N_3OS$: 317.0243 (317.0246)
4j	73	74−75	–	6.86 (3 H), 2.16 (6 H)	−92.8 (2 F), −149.3 (2 F)	$C_{13}H_9F_4N_3S$: 315.0450 (315.0453)
5b	40	108−109	–	6.89 (1 H), 6.62 (2 H)	−118.0	$C_{12}H_6F_4N_2S$: 286 (286)
5f	44[a] 37[b]	94−95	–	7.43 (2 H), 7.07 (2 H)	−114.9	$C_{12}H_8F_2N_2S$: 250.0371 (250.0376)
6	40−45[a] 23−25[b]	87−88	–	4.66	−94.6 (2 F), −165.5 (2 F)	$C_5H_2F_4N_2$: 166 (166)
8·$C_{10}F_8$	48	109−110	–	7.16 (2 H), 6.97 (1 H), 2.14 (6 H)	−126.3 (1 F), −142.5 (1 F), −146.8 (1 F), −147.5 (1 F), −150.3 (1 F), −155.9 (1 F), −156.6 (1 F), −146.3 (2 F), −154.8 (2 F)	$C_{18}H_9F_7N_2S$ (**8**): 418.0369 (418.0375)
5e·9	25	83−84	–	7.35−7.17	−138.1 (1 F), −143.4 (1 F), −143.9 (1 F), −147.9 (1 F), −151.5 (1 F), −153.0 (1 F)	$C_{10}F_6N_2S$ (**9**): 293.9678 (293.9686)

[a] From the Cs^+ salt. − [b] From the TAS^+ salt.

to cool to 20 °C, filtered, and the solvent was distilled off. The residue (a mixture of the target heterocycle and the corresponding $ArNH_2$, according to ^1H NMR and MS data) was redissolved in Et_2O (50 mL) and treated with 6 N hydrochloric acid (20 mL). The organic layer was separated, dried with $CaCl_2$, and the solvent was distilled off. The residue was sublimed in vacuo and then recrystallized from hexane. Compounds **2a** and **2b** were obtained as long colorless needles.

2b: ^{13}C NMR: δ = 156.0 (C^{7a}), 152.4 (C^4), 145.2 (C^{3a}), 128.7 (C^6), 116.8 (C^7), 112.0 (C^5). − UV/Vis: λ_{max} (log ε) = 307 nm (3.83) [*cf.* **2a:** 311 nm (4.15)].[56]

Under the same conditions, only the parent $ArNH_2$ compounds were obtained from **1c**,**d** (yields 50% and 65%, respectively).

Interaction of $[TAS]^+$ $[ArNSN]^-$ Salts (3e−i) with Pentafluoropyridine: *N*-(4-Methoxyphenyl)-*N*′-(2,3,5,6-tetrafluoro-4-pyridinyl)sulfurdiimide (4i), *N*,*N*′-Bis(aryl)sulfurdiimides (5e−f), and 4-Amino-2,3,5,6-tetrafluoropyridine (6): C_5F_5N (0.85 g, 5 mmol) was condensed onto a solution of $[TAS]^+$ $[ArNSN]^-$ (**3e−i**; 5 mmol) in CH_3CN (20 mL) at −196 °C by means of a vacuum line. After 16 h at −40 °C, the solvent was distilled off at the same temperature, and the residue was sublimed in vacuo and recrystallized from hexane. Compound **4i** was obtained as ruby-red crystals (single crystals suitable for X-ray structure analysis were obtained by a further recrystallization from $CHCl_3$). Compounds **5** and **6** were separated by fractional sublimation in vacuo followed by recrystallization from hexane. In the case of **3e**, compound **5e** was identified in the reaction mixture spectroscopically (^1H NMR and MS). In the case of **3g**,**h**, no products were identified.

CsF-Induced Interaction of Ar−N=S=N−SiMe$_3$ (1a,b,e,f,h−j) with Pentafluoropyridine: *N*-Aryl-*N*′-(2,3,5,6-tetrafluoro-4-pyridinyl)-sulfurdiimides (4a,e,i,j), *N*,*N*′-Bis(aryl)sulfurdiimides (5b,f,h), 4-Amino-2,3,5,6-tetrafluoropyridine (6), and Bis(2,3,5,6-tetrafluoro-4-pyridinyl)amine (10): Solutions of the appropriate Ar−N=S=N−$SiMe_3$ (**1a**,**b**,**e**,**f**,**h−j**; 5 mmol) and C_5F_5N (0.85 g, 5 mmol) in CH_3CN (5 mL aliquots) were added to a suspension of CsF in CH_3CN (25 mL) at 20 °C. After 1 h, the reaction mixture was filtered, the solvent was distilled off, and the residue was sublimed in vacuo and then recrystallized from hexane. Compounds **4a**,**e**,**i**,**j** were obtained as orange-red crystalline solids. Compounds **5b**,**f** and **6** were separated by fractional sublimation followed by recrystallization (**5b**,**f**: orange crystals; **6**: long colorless needles). In the case of **1h**, traces of **5h** and **6** were identified in the reaction residue by spectroscopic means (^1H and ^{19}F NMR, MS).

4e: UV/Vis: λ_{max} (log ε) = 412 nm (3.93) [*cf.* $(Ar-N=)_2S$].[54]

In some experiments, small amounts of compound **10** were identified alongside **6**; this could be isolated at a trace level by vacuum sublimation followed by recrystallization from hexane. **10**: Colorless crystals; m.p. 152−153 °C; ^1H NMR: δ = 8.30. − ^{19}F NMR: δ = −92.0, −153.6; these correspond to the published data.[57]

CsF-Induced Interaction of Ar−N=S=N−SiMe$_3$ (1e,j) with Octafluoronaphthalene: 4,5,6,7,8,9-Hexafluoronaphtho[1,2-*c*][1,2,5]thiadiazole (9; complex with 5e) and *N*-(2,6-Dimethylphenyl)-*N*′-(1,3,4,5,6,7,8-heptafluoronaphth-2-yl)sulfurdiimide (8; complex with $C_{10}F_8$): A solution of the appropriate Ar−N=S=N−$SiMe_3$ (**1e**,**j**) (5 mmol) and $C_{10}F_8$ (1.36 g, 5 mmol) in CH_3CN (25 mL) was added to a boiling suspension of CsF (0.76 g, 5 mmol) in MeCN (50 mL) over a period of 30 min. After a further 30 min, the reaction mixture was allowed to cool to 20 °C, the solvent was distilled off, and the residue was sublimed in vacuo and recrystallized from hexane. Compound **9** (as a complex with **5e**) was obtained as shiny orange crystals, while compound **8** (as a complex with $C_{10}F_8$) was obtained as transparent orange-red scales. Single crystals of **8**·$C_{10}F_8$ suitable for X-ray structure analysis (red prisms) were obtained by a further crystallization from $CHCl_3$.

8·$C_{10}F_8$: ^{13}C NMR: δ (2,6-Xy) = 144.2, 127.1, 125.4, 119.4, 18.2.
9·5e: ^{13}C NMR: δ (**5e**) = 145.3, 128.7, 126.7, 123.1.

Acknowledgments

The authors are grateful to Mr. Peter Brackmann for technical assistance, and to the Deutsche Forschungsgemeinschaft (Germany) and the Russian Foundation for Basic Research (Russia) for joint financial support of this work (DFG: 436 RUS 113/486/0; RFBR: 98−03−04107). A. Z. is also grateful to the Royal Society of Chemistry (U.K.) for an RSC Journals Grant for International Authors.

[1] T. Borrmann, A. V. Zibarev, E. Lork, G. Knitter, S.-J. Chen, P. G. Watson, E. Cutin, M. M. Shakirov, W.-D. Stohrer, R. Mews, *Inorg. Chem.* **2000**, *39*, 3999−4005.
[2] A. V. Zibarev, E. Lork, R. Mews, *Chem. Commun.* **1998**, 991−992.
[3] T. Borrmann, E. Lork, R. Mews, W.-D. Stohrer, P. G. Watson, A. V. Zibarev, *Chem. Eur. J.*, accepted.
[4] A. V. Zibarev, A. O. Miller, *J. Fluor. Chem.* **1990**, *50*, 359−363.
[5] I. Yu. Bagryanskaya, Yu. V. Gatilov, A. O. Miller, M. M. Shakirov, A. V. Zibarev, *Heteroatom Chem.* **1994**, *5*, 561−565.
[6] A. V. Zibarev, Yu. V. Gatilov, A. O. Miller, *Polyhedron* **1992**, *11*, 1137−1141.
[7] I. Yu. Bagryanskaya, Yu. V. Gatilov, A. Yu. Makarov, A. M. Maksimov, A. O. Miller, M. M. Shakirov, A. V. Zibarev, *Heteroatom Chem.* **1999**, *10*, 113−124.
[8] [8a] H. Ulrich, in *Methoden der Organischen Chemie (Houben-Weyl)*, vol. E8d (Ed.: E. Schaumann), Georg Thieme Verlag, Stuttgart, **1994**, pp. 170−180. − [8b] L. M. Weinstock, I. Shinkai, in *Comprehensive Heterocyclic Chemistry*, vol. 6 (Ed.: K. T. Potts), Pergamon Press, Oxford, **1984**, pp. 513−544.
[9] H. Koopman, J. J. van Daalen, J. Daams, *Weed Res.* **1967**, *7*, 200−207 (*Chem. Abstr.* **1968**, *68*, 87278x).
[10] [10a] A. V. Zibarev, I. V. Beregovaya, *Rev. Heteroatom Chem.* **1992**, *7*, 171−190. − [10b] A. V. Zibarev, M. A. Fedotov, G. G. Furin, *Izv. Akad. Nauk SSSR. Ser. Khim.* **1989**, 829−832 (in Russian; *Chem. Abstr.* **1989**, *111*, 173485a).
[11] [11a] L. S. Kobrina, *Fluor. Chem. Rev.* **1974**, *7*, 2−115. − [11b] G. M. Brooke, *J. Fluor. Chem.* **1997**, *86*, 1−76.
[12] A. V. Zibarev, R. Mews, E. Lork, *Results to be published.*
[13] [13a] R. Mews, M. Müller, *Results to be published*; M. Müller, *Diploma Thesis*, University of Bremen, Bremen, Germany, **1999**. − [13b] A. V. Zibarev, *D. Sci. Dissertation*, Institute of Organic Chemistry SB RAS, Novosibirsk, Russia, **1996**, 384pp.
[14] A. Aumüller, S. Hünig, *Angew. Chem.* **1984**, *96*, 437−438; *Liebigs Ann. Chem.* **1986**, 142−164.
[15] I. Yu. Bagryanskaya, Yu. V. Gatilov, A. V. Zibarev, *Zh. Strukt. Khim.* **1999**, *40*, 790−793 (in Russian).
[16] J. Mason, W. van Bronswijk, O. Glemser, *J. Phys. Chem.* **1978**, *82*, 463−465.
[17] W. Sicinska, L. Stefaniak, M. Witanowski, G. A. Webb, *J. Mol. Struct.* **1987**, *158*, 57−68.
[18] G. Leandri, V. Busetti, G. Valle, M. Mammi, *J. Chem. Soc. D, Chem. Commun.* **1970**, 413−414.
[19] V. Busetti, *Acta. Crystallogr., B* **1982**, *38*, 665−667.
[20] V. Busetti, G. Cevasco, G. Leandri, *Z. Kristallogr.* **1991**, *197*, 41−50.
[21] I. Yu. Bagryanskaya, Yu. V. Gatilov, M. M. Shakirov, A. V. Zibarev, *Mendeleev Commun.* **1994**, 136−137.
[22] I. Yu. Bagryanskaya, Yu. V. Gatilov, M. M. Shakirov, A. V. Zibarev, *Mendeleev Commun.* **1994**, 167−169.
[23] I. Yu. Bagryanskaya, Yu. V. Gatilov, A. V. Zibarev, *Mendeleev Commun.* **1999**, 157−158.
[24] R. Cramer, *J. Org. Chem.* **1961**, *26*, 3476−3478.
[25] N. E. Petrachenko, V. I. Vovna, A. V. Zibarev, G. G. Furin, *Zh.*

Obshch. Khim. **1993**, *63*, 1318−1324 (in Russian; *Chem. Abstr.* **1994**, *120*, 297871d).
[26] R. Filler, *Mol. Struct. Energ.* **1988**, *8*, 19−41.
[27] J. H. Williams, *Acc. Chem. Res.* **1993**, *26*, 593−598.
[28] T. Dahl, *Acta Chem. Scand.* **1994**, *48*, 95−106.
[29] C. A. Hunter, *Angew. Chem. Int. Ed. Engl.* **1993**, *32*, 1584−1586; *Chem. Soc. Rev.* **1994**, *23*, 101−109.
[30] [30a] G. R. Desiraju, *Crystal Engineering: The Design of Organic Solids*, Elsevier, New York, **1989**; *Chem. Commun.* **1997**, 1475−1482. − [30b] K. R. Seddon, M. Zaworotko, *Crystal Engineering: The Design and Application of Functional Solids*, Kluwer, Boston, MA, **1999**.
[31] M. L. Renak, G. P. Bartholomew, S. Wang, P. J. Ricatto, R. J. Lachincotte, G. S. Bazan, *J. Am. Chem. Soc.* **1999**, *121*, 7787−7799.
[32] G. W. Coates, A. R. Dunn, L. M. Henling, J. W. Ziller, E. B. Lobkovsky, R. H. Grubbs, *J. Am. Chem. Soc.* **1998**, *120*, 3641−3649.
[33] M. Weck, A. R. Dunn, K. Matsumato, G. W. Coates, E. B. Lobkovsky, R. H. Grubbs, *Angew. Chem. Int. Ed.* **1999**, *38*, 2741−2745.
[34] C. Dai, P. Nguen, T. B. Marder, A. J. Scott, W. Clegg, C. Viney, *Chem. Commun.* **1999**, 2493−2496.
[35] J. C. Collings, K. P. Roscoe, C. E. Smith, R. L. Thomas, E. G. Robins, L. M. Stimson, P. Smith, A. S. Batsanov, J. A. K. Howard, C. Dai, P. Nguen, A. J. Scott, W. Clegg, C. Viney, S. Watt, S. J. Clark, T. B. Marder, *16th International Symposium on Fluorine Chemistry* (Durham, U.K., **2000**). Book of Abstracts, C 16.
[36] R. L. Thomas, C. E. Smith, E. G. Robins, P. Smith, A. S. Batsanov, J. A. K. Howard, C. Dai, A. J. Scott, W. Clegg, S. Watt, C. Viney, T. B. Marder, *16th International Symposium on Fluorine Chemistry* (Durham, U.K., **2000**) Book of Abstracts, 1P−102.
[37] T. Dahl, *Acta Chem. Scand., Ser. A* **1988**, *A42*, 1−7.
[38] J. H. Williams, J. K. Cockcroft, A. N. Fitsch, *Angew. Chem. Int. Ed. Engl.* **1992**, *31*, 1655−1657.
[39] M. I. Bruce, M. R. Snow, E. R. T. Tiekink, *Acta Crystallogr., Sect. C* **1987**, *C43*, 1640−1641.
[40] D. G. Naae, *Acta. Crystallogr., B* **1979**, *B35*, 2765−2768.
[41] J. Potenza, D. Mastropaolo, *Acta Crystallogr., Sect. B* **1975**, *B31*, 2527−2529.
[42] J. C. Collings, K. P. Roscoe, E. G. Robins, A. S. Batsanov, J. A. K. Howard, T. B. Marder, *16th International Symposium on Fluorine Chemistry* (Durham, U.K., 2000). Book of Abstracts, 1P−104.
[43] J. C. Collings, A. S. Batsanov, J. A. K. Howard, T. B. Marder, *16th International Symposium on Fluorine Chemistry* (Durham, U.K., 2000). Book of Abstracts, 1P−103.
[44] C. M. Beck, J. Burdeniuc, R. H. Crabtree, A. L. Rheinhold, G. P. A. Yap, *Inorg. Chim. Acta* **1998**, *270*, 559−562.
[45] A. P. West, S. Mecozzi, D. A. Dougherty, *J. Phys. Org. Chem.* **1997**, *10*, 347−350.
[46] D. A. Dougherty, *Science* **1996**, *271*, 163−168.
[47] M. T. Messina, P. Metrangolo, S. Pappalardo, M. F. Parisi, T. Pilati, G. Resnati, *Chem. Eur. J.* **2000**, *6*, 3495−3500.
[48] R. Mews, E. Lork, A. V. Zibarev, results to be published.
[49] G. M. Sheldrick, *SHELX-97*, University of Göttingen, Göttingen, Germany, **1997**.
[50] *DIAMOND − Visual Crystal Structure Information System*, Crystal Impact, Bonn, Germany.
[51] Crystallographic data (excluding structure factors) for the structures reported in this paper have been deposited with the Cambridge Crystallographic Data Centre as supplementary publication nos. CCDC-154391 (**4i**), CCDC-154392 (**4j**), CCDC-154393 (**5e·9**), CCDC-153112 (**5f**), and CCDC-154394 (**8·1/2$C_{10}F_8$**). Copies of the data can be obtained free of charge on application to the CCDC, 12 Union Road, Cambridge CB2 1EZ, U.K. [Fax: (internat.) +44-1223/336-033; E-mail: deposit@ccdc.cam.ac.uk].
[52] W. J. Middleton, *Org. Synth. Coll. Vol.* **1990**, *7*, 528−530.
[53] R. E. Banks, I. F. Burgess, W. M. Cheng, R. N. Haszeldine, *J. Chem. Soc.* **1965**, 575−581.
[54] A. V. Zibarev, A. O. Miller, Yu. V. Gatilov, G. G. Furin, *Heteroatom Chem.* **1990**, *1*, 443−453.
[55] *Gmelin Handbook of Inorganic Chemistry, Sulfur-Nitrogen Compounds Part. 6*, Springer Verlag, Berlin, **1990**, pp.113−171.
[56] J. Fabian, R. Mayer, S. Bleisch, *Phosphorus Sulfur* **1979**, *7*, 61−67.
[57] I. A. Oskina, V. M. Vlasov, *Izv. Sib. Otd. Akad. Nauk SSSR. Ser. Khim. Nauk*, **1984**, 102−113 − in Russian (*Chem. Abstr.* **1984**, *101*, 2101805).

Received March 13, 2001
[I01095]

Platinum(II) and Palladium(II) Compounds Containing Chiral Thioimines

Xavier Riera,[a] Concepción López,*[a] Amparo Caubet,*[a] Virtudes Moreno,[a] Xavier Solans,[b] and Mercè Font-Bardia[b]

Keywords: Palladium / Platinum / Metallacycles / Chiral metallacycles / Cyclometallation

A comparative study of the reactivity of the optically pure thioimine: (S_C)-(−)-C_6H_5–CH=N–CH(CO_2Me)–CH_2–CH_2–SMe (**1**) versus platinum(II) and palladium(II) salts is reported. The reaction of **1** with *cis*-[$PtCl_2$(dmso)$_2$] leads to the cycloplatinated derivative (S_C,R_S)-(+)-[Pt{C_6H_4–CH=N–CH(CO_2Me)–CH_2–CH_2–SMe}Cl] (**3a**). The absolute configuration of **3a** has been established unambiguously by X-ray diffraction: orthorhombic, with a = 8.979 (4), b = 9.605(9), c = 18.205(6) Å, α = β = γ = 90.0°, space group $P2_12_12_1$. Compound **3a** contains a [6.5.6] tricyclic system generated by the fusion of a phenyl ring, a five-membered platinacycle and a six-membered chelate ring formed by the coordination of the nitrogen and sulfur to the platinum. When **1** was treated with $Na_2[PdCl_4]$ in methanol at room temperature a (7.9:1) mixture of the two diastereomers {(S_C,R_S)-**5a** and (S_C,S_S)-**5b**} of *cis*-[Pd{C_6H_5–CH=N–CH(CO_2Me)–CH_2–CH_2–SMe}Cl_2] (**5**) was formed. However, when the reaction was performed in the presence of sodium acetate, the activation of the σ($C_{sp^2,phenyl}$–H) bond took place giving the cyclopalladated complex: (S_C,R_S)-(+)-[Pd{C_6H_4–CH=N–CH(CO_2Me)–CH_2–CH_2–SMe}}Cl] (**6a**). In **6a**, the ligand acts as a monoanionic (C,N,S)$^-$ terdentate group. The study of the reactivity of **3a** and **6a** with PPh_3 is also reported.

Introduction

An important area of organometallic chemistry is that of cyclopalladated and cycloplatinated compounds.[1] Interest in such compounds has increased exponentially due to their applications in several areas.[2−12]Among the cyclometallated complexes described, those derived from optically pure N-donor ligands have attracted additional interest, since they can be used for the resolution of mono- or bidentate ligands[10−11] as well as in chiral discrimination processes.[12] As a part of a project directed towards the design of new optically pure cyclometallated complexes derived from Schiff bases of general formula: C_6H_5−CH=N−CH(R)R′ or [(η^5-C_5H_5)Fe{(η^5-C_5H_4)−CH=N−CH(R)R′}] {R = alkyl, R′ = phenyl, benzyl, or naphthyl groups}[11c,12−14] we attempted to elucidate whether the replacement of the R′ group by a pendant arm containing a prochiral atom with good donor abilities (i.e. N, O, S, or P) could determine, not only the diastereoselectivity of the coordination of the ligand to the palladium(II) or platinum(II), but also the nature of the final product formed in the cyclometallation process. The incorporation of a sulfur atom, which according to Pearsons' concept[15] is a softer base, in the backbone of the ligand may strengthen the binding to the palladium or platinum. In addition, the activation of the *ortho* σ(C−H) bond of the ligand may produce metallacycles with a (C,N,S)$^-$ terdentate group, which are uncommon in the literature.[16−17] Furthermore, optically pure platina- or palladacycles containing this sort of environment are very scarce.[18] With these aims we prepared the Schiff base: (S_C)-(−)-C_6H_5−CH=N−CH(CO_2Me)−CH_2−CH_2−SMe (**1**) (Scheme 1) and studied its reactivity towards platinum and palladium(II) salts.

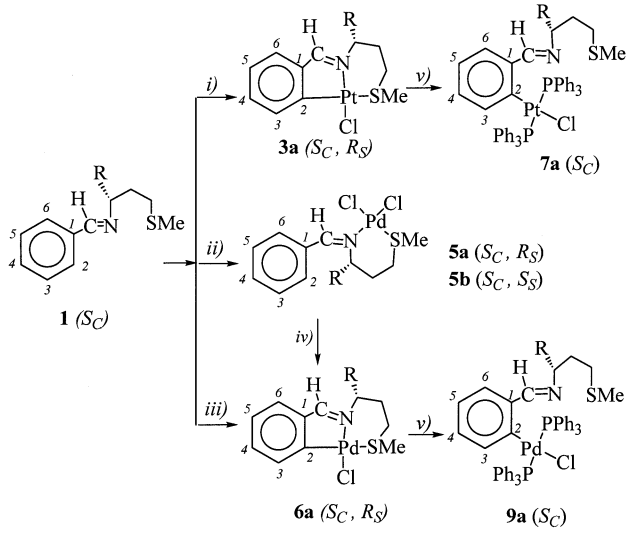

Scheme 1. R = CO_2Me. *i) cis*-[$PtCl_2$(dmso)$_2$] in refluxing methanol. *ii)* $Na_2[PdCl_4]$ in methanol at room temperature. *iii)* $Na_2[PdCl_4]$ and NaAcO in refluxing methanol. *iv)* NaAcO in refluxing methanol. *v)* PPh_3 in $CDCl_3$ at room temperature

Results and Discussion

Ligand **1** was prepared according to the general procedure described for most arylaldimines.[19] The ^{1}H and

[a] Departament de Quimica Inorgànica, Facultat de Química, Universitat de Barcelona,
Martí i Franquès 1−11, 08028-Barcelona, Spain,
Fax: (internat.) + 34-93/490-7725
E-mail: conchi.lopez@qi.ub.es
[b] Departament de Cristal·lografia, Mineralogia i Dipòsits Minerals, Facultat de Geologia,
Martí i Franquès s/n, 08028-Barcelona, Spain

 © WILEY-VCH Verlag GmbH, 69451 Weinheim, 2001 1434−1948/01/0808−2135 $ 17.50+.50/0

$^{13}C\{^1H\}$ NMR spectra of **1** (Exp. Section) suggested that only one isomer (*E*-form) was present in solution. When **1** was treated with $K_2[PtCl_4]$ at room temperature, the reaction produced a yellow solid. Its ^1H NMR spectrum was complex and three signals assigned to the imine proton were detected at $\delta \approx 9.15$, 9.26, and 8.30. The ^{195}Pt NMR spectrum showed three singlets at ca. $\delta = -3029$, -3059, and -3832 {of relative intensities: 2:0.3:3}. This indicated that the crude material contained at least three platinum(II) compounds. The position of signals at $\delta = -3029$ and -3059 was similar to those reported for: $[Pt(C_6H_5-CH=N-CH_2-CH_2-SEt)Cl_2]$,[17] $[Pt(H_2N-CH_2-CH_2-SEt)Cl_2]$,[20] and for related compounds containing a "$Pt(N,S)Cl_2$" core.[21] This result suggested that two isomers of *cis*-$[Pt\{C_6H_5-CH=N-CH(CO_2Me)-CH_2-CH_2-SMe\}Cl_2]$ may be present in solution. The chemical shift of the third signal was similar to that of $[Pt\{C_6H_4-CH=N-CH_2-CH_2-SMe\}Cl]$ (**2**),[17] $[Pt\{(\eta^5\text{-}C_5H_5)Fe[(\eta^5\text{-}C_5H_3)-CH(R)-NMe_2]\}Cl(dmso)]$,[22] and related compounds.[21,23] Unfortunately, attempts to separate the major components of the mixture by either column chromatography or fractional crystallization failed due to the formation of metallic platinum during these experiments. More satisfactory results were obtained when the reaction was carried out using *cis*-$[PtCl_2(dmso)_2]$[24] as starting material under refluxing conditions for 12 h. The slow evaporation of the solvent yielded single crystals suitable for X-ray diffraction. Elemental analyses of this material agreed with those expected for $[Pt\{C_6H_4-CH=N-CH(CO_2Me)-CH_2-CH_2-SMe\}Cl]$ (**3**). The two-dimensional heteronuclear $\{^1H\text{-}^{13}C\}$ NMR spectrum suggested that the activation of the $\sigma(C_{sp^2,phenyl}-H)$ bond had taken place. The position of the signal detected in the ^{195}Pt NMR spectrum was similar to that reported for **2**[17] and for related platinum(II) compounds with a "Pt(C,N,S,Cl)" core.[21]

Recent studies have shown that for optically pure organic imines or amines, such as: $R^1-CH=N-CH(Me)-R^2$ {R^1 = phenyl or ferrocenyl groups and R^2= phenyl or naphthyl groups} or $C_{10}H_7-CH(R^1)-NR^2R^3$ {R^1, R^2, R^3 = alkyl groups} the formation of the metallacycle through the activation of the $\sigma(C_{sp^2,aryl}-H)$ bond does not modify the absolute configuration of the stereogenic centre of the ligand.[11a,11c,25] Consequently, since **1** contains a stereogenic carbon and a prochiral sulfur atom, **3** may consist of a mixture of two diastereomers: {(S_C,R_S) or (S_C,S_S) hereinafter referred to as **3a** and **3b**}. The use of molecular models and the SPARTAN 4.0 computer program[26] indicated that in **3a**, where the $-CO_2Me$ and the Me group bound to the sulfur are on opposite sides of the coordination plane, the steric hindrance is clearly smaller than in the (S_C,S_S) isomer (**3b**). Thus, the formation of **3a** is expected to be strongly preferred to that of **3b**. ^1H and ^{13}C NMR spectra indicated that only one of the diastereomers of **3** was present in solution and its absolute configuration was determined by X-ray diffraction. An ORTEP diagram of **3a** is shown in Figure 1.

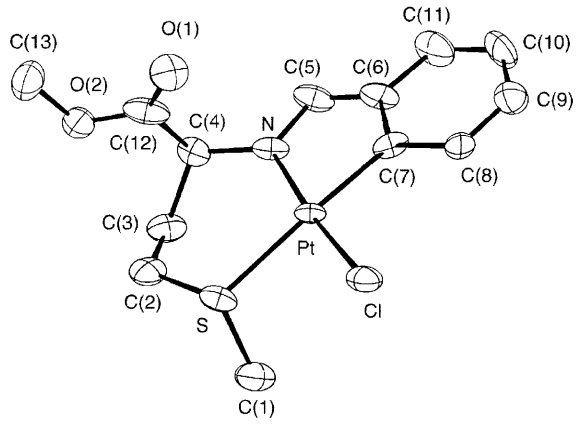

Figure 1. ORTEP diagram of the crystal structure of (S_C,R_S)−(+)−$[Pt\{C_6H_4-CH=N-CH(CO_2Me)-CH_2-CH_2-SMe\}Cl]$ (**3a**). Selected bond lengths [in Å]: Pt−N, 1.984(11); Pt−S, 2.349(3); Pt−Cl, 2.308(4); Pt−C(7), 1.954(14); N−C(5), 1.954(14). Selected bond angles [in deg.]: C(7)−Pt−Cl, 94.0(4); N−Pt−S, 99.2(3); Cl−Pt−S, 85.84(13); N−Pt−Cl, 174.8(3); Pt−N−C(5), 114.9(11); N−C(5)−C(6) 119.6(16)

The structure consists of discrete molecules of $[Pt\{C_6H_4-CH=N-CH(CO_2Me)-CH_2-CH_2-SMe\}]$ separated by van der Waals interactions. The platinum atom is bound to the chloride, the sulfur, the imine nitrogen and the *ortho*-carbon {C(7)} of the phenyl ring in a slightly distorted square-planar environment. The molecule contains a [6.5.6] tricyclic system derived from the fusion of the six-membered chelate ring, formed by the coordination of the sulfur and the nitrogen to the platinum(II), a five-membered platinacycle and the phenyl ring.

The metallacycle, which is formed by the atoms: Pt, N, C(5), C(6), and C(7), is practically planar and contains the >C=N− functional group. The >C=N− bond length is in the range described for related five-membered platinacycles derived from imines.[27] The ligand adopts the *anti*-conformation [(*E*)-form] and the phenyl ring forms an angle of 6.27° with the plane of the platinacycle.

The six-membered chelate ring formed by the platinum and the "$N-CH(CO_2Me)-CH_2-CH_2-S-$" moiety exhibits a chair-conformation in which the atoms C(3) and Pt deviate from the mean plane −0.6148 and +0.0928 Å, respectively.

The comparison of the bond lengths and angles involving the platinum(II) atom in **3a** and in **2**,[17] which contains a [6.5.5] tricyclic system, shows that in **3a** the Pt−C(7) bond length [1.954(14) Å] is clearly shorter than in **2** [2.012(8) Å]. However, this variation does not significantly affect the length of the Pt−S bond in a *trans* position [2.349(3) Å in **3a** and 2.334(10) Å in **2**]. In contrast, an increase in the size of the chelate ring [a five-membered ring in **2** and a six-membered ring in **3a**] introduces significant differences in the angles involving the pair of atoms Pt and Cl. For instance, in **2**, the angles: C−Pt−Cl and Cl−Pt−S are bigger than in **3a**. This finding, together with the higher value of

the Pt−Cl bond length in **3a** compared with **2**, suggests that the environment of the chlorine is more crowded in **3a**.

The absolute configuration of the molecule is determined by the chirality of the carbon atom (S_C) and the relative arrangement of the Me bound to the sulfur towards the $-CO_2Me$ group. In **3a**, these groups face opposite sides of the coordination plane of the palladium [the torsion angle C(1)−S−C(4)−C(12) is 166.81°]. As mentioned above, if these substituents were on the same side a strong steric hindrance would arise. This arrangement of groups on the stereogenic centres of **3a** is formally identical to that found in $[Pd_2\{(C_4H_3S)-CH=N-C(CO_2Me)-CH_2-CH_2-SMe\}_2Cl_2]$ (**4**).[18]

The comparison of the results obtained in the reaction of *cis*-$[PtCl_2(dmso)_2]$ with **1** or $C_6H_5-CH=N-CH_2-CH_2-SEt$[17] shows that cycloplatination of **1** occurs easily, leading to one of the two diastereomers. These differences may be attributed to the presence of a bulky group[28] in the proximity of the imine nitrogen.

When **1** was treated with $Na_2[PdCl_4]$ in methanol at ca. 20 °C *cis*-$[Pd\{C_6H_5-CH=N-CH(CO_2Me)-CH_2-CH_2-SMe\}Cl_2]$ (**5**) was obtained. The ^1H NMR spectrum of **5** showed two superimposed sets of signals of relative intensities 7.9:1.0, which suggested the presence of two species in solution. $^{13}C\{^1H\}$ NMR spectroscopic studies also confirmed these results. Complex **5** could also consist of different isomers which may differ in *a)* the conformation of the ligand (*E*- or *Z*-forms) and/or *b)* the chirality of the sulfur atom in the complex (R_S or S_S). Previous NMR spectroscopic studies of palladium(II) and platinum(II) compounds containing imines have shown that the chemical shift of the methinic proton indicates the conformation of the ligand.[13,17,29,30] The ^1H NMR spectrum of **5** showed two singlets assigned to the imine protons at lower fields (δ = 8.41 and 8.38) than in **1**, thus suggesting that in the two species the imine had the (*Z*) form. Consequently, the two isomers may have a different origin, which might be related to the presence of the prochiral sulfur atom in **1**. The formation of the six-membered chelate ring by coordination of the N and S atoms to the palladium(II) may produce two diastereomers [(S_C,R_S) and (S_C,S_S)]. On this basis we assumed that the complexity of the ^1H and ^{13}C NMR spectra of **5** could be due to the presence of the two diastereomers [(S_C,R_S), **5a** and (S_C,S_S), **5b**]. Attempts to separate them by crystallization or SiO_2-column chromatography failed due to the low solubility of **5**.

The use of molecular models and the SPARTAN 4.0 computer program[26] also suggested that the less hindered isomer corresponds to the (S_C,R_S) diastereomer (**5a**). Thus, we assume that the absolute configuration of the main component is (S_C,R_S).

In order to examine whether the activation of the $\sigma(C_{sp^2,phenyl}-H)$ bond of **1** could be promoted by palladium(II) salts, more drastic reaction conditions were used (i.e. refluxing methanol and reaction periods of up to 7 days). However, no evidence of the formation of any palladacycle was detected by NMR spectroscopy. Better results were obtained when the reaction was carried out under reflux in the presence of NaAcO, which yielded a bright yellow solid. Its elemental analyses agreed with those expected for the complex $[Pd\{C_6H_4-CH=N-CH(CO_2Me)-CH_2-CH_2-SMe\}Cl]$ (**6**). Its ^1H, $^{13}C\{^1H\}$, and the two dimensional heteronuclear $\{^1H$-$^{13}C\}$ NMR spectra suggested the formation of a palladacycle with a $\sigma(Pd-C_{sp^2,phenyl}-H)$ bond and the presence of only one of the two diastereomers of **6** in solution. In the view of the results obtained from the SPARTAN 4.0 program[26] and from the X-ray crystal structure of the platinum(II) analogue (see above) we assume that the absolute configuration of the isolated material is (S_C,R_S).

Compound **6a** could also be isolated by treatment of **5** with the stoichiometric amount of NaOAc in refluxing methanol. The transformation of **5** to **6a** requires the isomerization (*Z*) → (*E*) of the ligand and the formation of the $\sigma(Pd-C_{sp^2,aryl})$ bond.

Potentially terdentate chelating ligands $[N,C,X]^-$ {where X = N, P, O, or S} may adopt different binding modes and hapticities which is relevant to catalytic processes. As a first approach to explore whether the mode of binding or the hapticity of **1** could be modified under mild experimental conditions, the reactions of **3a** and **6a** with PPh_3 were studied in solution. When PPh_3 was added to a solution of **3a** {Pt:PPh_3 molar ratio equals to 1:2} in $CDCl_3$ at 20 °C, a pale yellow solution was obtained. Its ^1H and $^{13}C\{^1H\}$ NMR spectra suggested the formation of $[Pt\{C_6H_4-CH=N-CH(CO_2Me)-CH_2-CH_2-SMe\}Cl(PPh_3)_2]$ (**7a**). Its ^{195}Pt NMR spectroscopic data is consistent with the values reported for platinum(II) compounds having a *trans*-"Pt(C,Cl,P_2)" core.[31]

This result is in sharp contrast with that reported for **2**, for which the addition of large excesses of PPh_3 did not produce the cleavage of the Pt−N bond[17] and suggests a higher lability of the Pt−N bond in complex **3a**. The use of the SPARTAN 4.0 computer program[26] for the diastereomer (S_C)-$[Pt\{C_6H_4-CH=N-CH(CO_2Me)-CH_2-CH_2-SMe\}Cl(PPh_3)]$ (**8a**) reveals that the environment around the metal is very crowded and at least one of the phenyl rings of the PPh_3 ligand is very close to the atoms of the $-CO_2Me$ group. This would increase the steric hindrance and reduce the stability of the molecule which may be related to the higher proclivity of **3a** {compared with **2**} to undergo a ring-opening process. The cleavage of the Pt−N bond would permit the free rotation around the N−C* bond, leading to a larger separation between the aryl rings and the "CO_2Me" fragment.

When the reaction was performed in identical experimental conditions, but using **6a** and PPh_3, $[Pd\{C_6H_4-CH=N-CH(CO_2Me)-CH_2-CH_2-SMe\}Cl(PPh_3)_2]$ (**9a**) was formed in solution and its ^{31}P NMR spectrum suggested a *trans*- arrangement of the PPh_3 ligands.

Since the formation of **7a** and **9a** involves the cleavage of the M−S bond (in **3a** and **6a**, respectively), the absolute configuration of these derivatives is expected to be S_C.

To sum up, the results reported in this work show the importance of the presence of a bulky and electron-withdrawing group on the stereogenic carbon atom of **1** in the

diastereoselectivity of the reactions under study. The preferential formation of **5a** versus **5b** (*d.e.* = 77.5%) may be attributed to steric effects. In **5a**, where the $-CO_2Me$ group and the Me bound to the sulfur are pointing towards opposite sides of the coordination plane of the metal, the steric hindrance is clearly smaller than in **5b**. A similar argument can be used to explain the formation of the metallacycles **3a** and **6a**. These findings suggest that the absolute configuration of the stereogenic carbon in **1** induces a high degree of diastereoselectivity in the coordination of the prochiral sulfur.

Several authors have postulated that the presence of an electron-withdrawing group favours the metallation of aliphatic carbon atoms.[1,18,32] On this basis, for **1**, which contains an electron-withdrawing group[28] at the stereogenic carbon, the activation of a ($C_{sp^2,phenyl}-H$) or a ($C^*_{sp^3}-H$) bond, in principal, could be expected. However, for **1**, the metallation of the phenyl ring is strongly preferred and no evidence of the presence of the metallacycles with a $\sigma(M-C^*_{sp^3})$ bond was detected by NMR spectroscopy. These findings are in sharp contrast with those obtained in the cyclopalladation of $[(C_4H_3S)-CH=N-CH(CO_2Me)-CH_2-CH_2-SMe\}]$[18] which produced: $[Pd_2\{(C_4H_3S)-CH=N-C(CO_2Me)-CH_2-CH_2-SMe\}_2Cl_2]$ (**4**) through activation of the $\sigma(C^*_{sp^3}-H)$ bond.[18] Consequently, the results presented here reveal the importance of the group bound to the imine carbon in determining the type of the $\sigma(M-C)$ bond to be formed [$\sigma(M-C_{sp^2,aryl})$ or $\sigma(M-C^*_{sp^3})$] in the cyclometallation process. Besides that, compounds **3a** and **6a** have an additional interest since they may be potentially useful in a wide variety of processes, i.e. as chiral recognition compounds or discriminators, or as precursors for the asymmetrical synthesis of novel organic or organometallic derivatives.

Experimental Section

Materials and Synthesis: Benzaldehyde was obtained from standard sources and purified by vacuum distillation before use. (S_C)-Methionine methyl ester hydrochloride was obtained from Janssen Chimica and transformed into the free amine before use. *cis*-$[PtCl_2(dmso)_2]$ was prepared as previously described.[24] All the solvents used in this study were HPLC grade.

Elemental analyses (C, H, N, and S) were carried out at the Serveis Científico Tècnics de la Universitat de Barcelona and at the Serveis de Recursos Científics (Universitat Rovira i Virgili, Tarragona). − Infrared spectra were obtained with a Nicolet Impact 400 instrument using NaCl discs for **1** and KBr pellets for the solid samples. − ^1H and the two dimensional $\{^1H$-$^{13}C\}$ heteronuclear NMR experiments were run using a Varian VXR-500 or a Bruker Avance 500DMX instrument. The solvents and references used are specified in the characterization section of each compound. $^{13}C\{^1H\}$- and ^{195}Pt NMR spectra were recorded with a Bruker-250DXR instrument. The ^{195}Pt chemical shifts are referred to a $Na_2[PtCl_6]$ solution in D_2O as external reference. $^{31}P\{^1H\}$ NMR spectra were obtained with a Bruker-250DXR instrument using $CDCl_3$ as solvent and $P(OMe)_3$ as reference $\{\delta^{31}P[P(OMe)_3] = 140.17\}$. The chemical shifts (δ) are given in ppm and the coupling constants (*J*) in Hz. − The optical rotations were determined in CH_2Cl_2 using a Perkin−Elmer 241MC-polarimeter. − FAB^+ mass spectra were obtained with a VG-Quatro Fisions instrument using 3-nitrobenzyl alcohol as matrix.

Preparation of (S_C)-(−)-$C_6H_5-CH=N-CH(CO_2Me)-CH_2-CH_2-SMe$ (1): Benzaldehyde (304 mg, $2.86\cdot10^{-3}$ mol) was added to a solution of $H_2N-CH(CO_2Me)-CH_2-CH_2-SMe$ (467 mg, $2.86\cdot10^{-3}$ mol) in 15 mL of methanol. The mixture was refluxed for 3 h. Then, the solution was concentrated to dryness giving a whitish oil. (Yield 601 mg, 82%). − IR: ν(−CO): 1736 and ν(>C=N−): 1644 cm^{-1}. − ^1H NMR (in $CDCl_3$):[33] δ = 2.09 (s, 3 H, −SMe), 2.18−2.35 (m, 2 H, $-CH_2-$), 2.46−2.60 (m, 2 H, $-SCH_2-$), 3.75 (s, 3 H, −OMe), 4.22 (m, 1 H, >CH−), 7.43 (m, 1 H, H^4), 7.45 (m, 2 H, H^3 and H^5), 7.80 (d, 2 H, H^2 and H^6), 8.33 (s, 1 H, −CH=N−). − $^{13}C\{^1H\}$ NMR (in $CDCl_3$):[33] δ = 16.2 (−SMe), 30.2 ($-SCH_2-$), 31.9 ($-CH_2-$), 52.3 (−OMe), 71.2 (>CH−), 135.4 (C^1), 128.5 (C^2 and C^6), 128.5 (C^3 and C^5), 131.2 (C^4), 164.3 (−CH=N−), 172.1 ($>CO_2$). $[\alpha]_{24\ °C}$ (c = 0.05 g/100 mL) = −24.12.

Preparation of (S_C,R_S)-(+)-[Pt{$C_6H_4-CH=N-CH(CO_2Me)-CH_2-CH_2-SMe$}Cl] (3a): To a hot solution formed by *cis*-$[PtCl_2(dmso)_2]$ (100 mg, $2.36\cdot10^{-4}$ mol) and 20 mL of methanol, **1** (59 mg, $2.35\cdot10^{-4}$ mol) was added. The suspension was refluxed for 12 h and filtered out. Then, the filtrate was concentrated to ca. 5 mL on a rotary evaporator. The slow evaporation of the solvent at ca. 20 °C produced golden crystals, which were collected and air-dried. (Yield 92 mg, 81.0%). − $C_{13}H_{16}ClNO_2SPt$: calcd. (found) C 32.5 (32.5), H 3.3 (3.3), N 2.9 (3.0), S 6.7 (6.7). − IR: ν(−CO): 1739 cm^{-1} and ν(>C=N−): 1594 cm^{-1}. − ^1H NMR (in $CDCl_3$):[33] δ = 2.55 [s, 3 H, −SMe, ^3J(Pt−H) = 20], 2.62 and 2.79 (m, 2 H, $-SCH_2-$), 2.30 and 2.60 (m, 2 H, $-CH_2-$), 3.74 (s, 3 H, −OMe), 4.52 [m, 2 H, >CH−, ^3J(Pt−H) = 52], 7.31 (d, 1 H, H^3), 7.09 (t, 1 H, H^4), 7.28 (t, 1 H, H^5), 7.95 [d, 1 H, H^6, ^4J(Pt−H) = 39], 8.27 [s, 1 H, −CH=N−, ^3J(Pt−H) = 133]. − $^{13}C\{^1H\}$ NMR (in $CDCl_3$):[33] δ = 21.2 (Me), 27.7 ($-SCH_2$), 31.4 ($-CH_2-$), 53.3 (−OMe), 66.3 (>CH−), 143.0 (C^1), 152.1 (C^2), 128.2 (C^3), 124.3 (C^4), 133.4 (C^5), 132.2 (C^6), 181.9 (−CH=N−), 170.0 ($-CO_2$). − ^{195}Pt NMR (in $CDCl_3$): −3832. $[\alpha]_{24\ °C}$ (c = 0.1 g/100 mL) = +73.9. FAB^+(selected data): 481 $[M + H]^+$, 445 $[M - Cl]^+$.

Preparation of *cis*-[Pd{$C_6H_5-CH=N-CH(CO_2Me)-CH_2-CH_2-SMe$}$Cl_2$] (5): Ligand **1** (157 mg, $6.25\cdot10^{-4}$ mol) was dissolved in 15 mL of methanol. A solution formed by $Na_2[PdCl_4]$ (184 mg, $6.25\cdot10^{-4}$ mol) and 10 mL of methanol was then added. The mixture was stirred at ca. 20 ° C for 3 h. The solid formed was collected, washed with methanol (3·2 mL) and air-dried. (Yield 143 mg, 53.3%). − $C_{13}H_{17}Cl_2NO_2SPd$: calcd. (found) C 36.5 (36.3), H 4.0 (4.0), N 3.3 (3.1), S 7.5 (7.45). − IR: ν(−CO): 1740 cm^{-1} and ν(>C=N−) = 1624 cm^{-1}. − ^1H NMR spectroscopic data (in $CDCl_3$):[33] *Major isomer,* **5a** $\{(S_C,R_S)\}$: δ = 2.63 (s, 3 H, −SMe), 2.50 and 2.55 (m, 2 H, $-SCH_2-$), 3.40 and 3.90 (m, 2 H, $-CH_2-$), 3.88 (s, 3 H, −OMe), 4.22 (m, 1 H, >CH−), 7.69−7.82 (m, 3 H, H^3, H^4 and H^5), 8.38 (s, 1 H, −CH=N−) and 9.23 (d, 2 H, H^2 and H^6). *Minor isomer,* **5b** $\{(S_C,S_S)\}$: δ = 2.52 (s, 3 H, SMe), 2.60 and 2.45 (m, 2 H, $-SCH_2-$), 3.40 and 3.90 (m, 2 H, $-CH_2-$), 3.81 (s, 3 H, −OMe), 4.02 (m, 1 H, >CH−), 7.69 (m, 3 H, H^3, H^4 and H^5), 8.41 (s, 1 H, −CH=N−), 9.05 (d, 2 H, H^2 and H^6). − ^1H NMR spectroscopic data (in $[D_6]$DMSO):[33] *Major isomer,* **5a** $\{(S_C,R_S)\}$: δ = 2.88 (s, 3 H, −SMe), 2.96−3.11 (m, 2 H,$-SCH_2-$), 3.40−3.90 (m, 2 H, $-CH_2-$), 4.07 (s, 3 H, −OMe), 4.96 (m, 1 H, >CH−), 7.69−7.82 (m, 3 H, H^3, H^4, and H^5), 8.38 (s, 1 H, −CH=N−), 9.23 (d, 2 H, H^2 and H^6). − $^{13}C\{^1H\}$ NMR spectroscopic

data (in [D$_6$]DMSO):[33] *Major isomer,* **5a** {(S_C,R_S)}: δ = 21.1 (−SMe), 29.3 (−SCH_2−), 30.7 (−CH_2−), 53.2 (OMe), 70.5 (>CH−), 132.0 (C^1), 132.3 (C^2 and C^4), 129.2 (C^3 and C^5), 134.7 (C^4), 168.4 (−CO_2), 178.3 (−CH=N−).

Preparation of (S_C,R_S)-(+)-[Pd{C_6H_4−CH=N−CH(CO_2Me)−CH_2−CH_2−SMe}Cl] (6a): This complex was isolated by two different procedures using either compounds **1** or **5** [methods *(a)* and *(b)*, respectively] as starting materials.

Method A: A 100 mg amount ($3.98\cdot10^{-4}$ mol) of **1** was dissolved in 10 mL of methanol. $Na_2[PdCl_4]$ (117 mg, $3.98\cdot10^{-4}$ mol) and NaOAc (33 mg, $4.0\cdot10^{-4}$ mol) were then added and the mixture was refluxed for 2 h. The solid formed was removed by filtration and discarded. Slow evaporation of the filtrate produced the precipitation of a yellow solid, which was filtered out and air-dried. (Yield 87 mg, 56).

Method B: Compound **5** (98 mg, $2.28\cdot10^{-4}$ mol) was suspended in methanol (15 mL), and a solution of NaOAc (19 mg, $2.31\cdot10^{-4}$ mol) and 10 mL of methanol was added. The mixture was refluxed for 2 h and filtered out. The filtrate was allowed to evaporate at ca. 20 °C and the solid formed was collected by filtration and air-dried. (Yield 58 mg, 68%). $C_{13}H_{16}ClNO_2PdS$: calcd. (found) C 39.8 (39.8), H 4.1 (4.2), N 3.6 (3.6), S 8.2 (8.3). − IR: ν(−CO): 1736 cm^{-1} and ν(>C=N−): 1601 cm^{-1}. − ^{1}H NMR spectroscopic data (in $CDCl_3$):[33] δ = 2.51 (s, 3 H, −SMe), 2.22−2.70 (m, 2 H, −SCH_2−), 2.58−2.72 (m, 2 H, CH_2−), 3.80 (s, 3 H, −OMe), 4.42 (m, 1 H, >CH−), 8.06 (s, 1 H, −CH=N−), 7.33 (d, 1 H, H^3), 7.09 (t, 1 H, H^4), 7.21 (t, 1 H, H^5), 7.94 (t, 1 H, H^6). − ^{13}C{^{1}H} NMR spectroscopic data (in $CDCl_3$):[33] δ = 19.9 (−SMe), 27.6 (−SCH_2−), 30.4 (−CH_2−), 53.1 (−OMe), 66.6 (>CH−), 179.8 (−CH=N−), 169.2 (−CO_2), 144.0 (C^1), 160.1 (C^2), 128.2 (C^3), 124.9 (C^4), 131.6 (C^5), 134.7 (C^6). − $[\alpha]_{24\ °C}$ (c = 0.05 g/100 mL) = −51.6. − FAB$^+$(selected data): 391 $[M + H]^+$, 357 $[M - Cl]^+$.

Table 1. Crystal data and details of the refinement of the crystal structure of **3a**

Empirical formula	$C_{13}H_{16}ClNO_2PtS$
Mr	480.88
Crystal size [mm × mm × mm]	0.1 × 0.1 × 0.2
a [Å]	8.797(4)
b [Å]	9.605(9)
c [Å]	18.205(6)
α, β, γ [deg.]	90.0
V [Å^3]	1538.2(17)
Crystal System	Orthorhombic
Space group	$P2_12_12_1$
Z	4
λ [Å]	0.71069
T [K]	293(2)
$D_{calcd.}$ [Mg·m^3]	2.081
Absorption coefficient [mm^{-1}]	9.891
F(000)	912
Θ range for data collection [deg.]	from 2.57 to 29.94
Refinement method	Full-matrix least-squares on F^2
Number of collected reflections	2571
Number of independent reflections	2552 [R(int) = 0.0107]
Number of data	2526
Number of parameters	173
Goodness of fit on F^2	0.994
Final R indices [$I \geq 2\sigma(I)$]	R_1 = 0.0484, wR_2 = 0.1124
R indices (all data)	R_1 = 0.0709, wR_2 = 0.1205
Absolute structure parameter	0.00(2)
Largest difference peak and hole [eÅ^{-3}]	0.835 and −0.894

Preparation of (S_C)-[Pt{C_6H_4−CH=N−CH(CO_2Me)−CH_2−CH_2−SMe}Cl(PPh_3)$_2$] (7a): This complex was prepared on an NMR spectroscopic scale. A 10 mg ($2.05\cdot10^{-5}$ mol) amount of **3a** was dissolved in 0.7 mL of $CDCl_3$, then PPh_3 (11 mg, $4.16\cdot10^{-5}$ mol) was added. The mixture was stirred vigorously for 5 min. at ca. 20 ° C and the pale solution was characterized by NMR spectroscopies. − ^{1}H NMR spectroscopic data (in $CDCl_3$):[33] δ = 2.59 (s, 3 H, −SMe), 2.54 and 2.72 (m, 2 H, −SCH_2−), 2.61 and 2.75 (m, 2 H, −CH_2−), 3.75 (s, 3 H, −OMe), 5.72 [br., 1 H, >CH-], 6.45 [d, 1 H, H^3], 6.90 [t, 1 H, H^4], 6.58 (t, 1 H, H^5), 8.68 (s, 1 H, −CH=N−) and 7.10−7.80 (m, 31 H, H^6 and protons of PPh_3). − ^{13}C{^{1}H} NMR spectroscopic data (in $CDCl_3$):[33−35] δ = 16.6 (−SMe), 29.9 (−SCH_2−), 30.0 (−CH_2−), 57.7 (−OMe), 68.3 (>CH−), 171.4 (−CO_2), 168.6 (−CH=N−), 131.8 (C^3), 123.4 (C^4), 132.6 (C^5), 138.1 (C^6). − ^{195}Pt NMR (in $CDCl_3$): δ = −4439, ^1J(^{195}Pt-^{31}P)= 3637. − ^{31}P NMR spectroscopic data (in $CDCl_3$): δ = 13.69, ^1J(^{31}P-^{195}Pt)= 3635.

Preparation of (S_C)-[Pd{C_6H_4−CH=N−CH(CO_2Me)−CH_2−CH_2−SMe}Cl(PPh_3)$_2$] (9a): This complex was prepared according to the procedure described for **7a** but using **6a** (40 mg, $5.1\cdot10^{-5}$ mol) and PPh_3 (54 mg, $2.06\cdot10^{-5}$ mol). − ^{1}H NMR spectroscopic data (in $CDCl_3$):[33] δ = 2.09 (s, 3 H, −SMe), 2.38 and 2.48 (m, 2 H, −SCH_2−), 2.60 and 2.65 (m, 2 H, −CH_2−), 3.74 (s, 3 H, −OMe), 5.46 (m, 1 H, >CH−), 6.39 (d, 1 H, H^3), 6.90 (t, 1 H, H^4), 6.56 (t, 1 H, H^5), 8.42 (s, 1 H, −CH=N−), 7.30−8.60 (m, 31 H, H^6 and *protons* of PPh_3). − ^{13}C{^{1}H} NMR spectroscopic data (in $CDCl_3$):[33−34] δ = 15.3 (−SMe), 30.5 (−SCH_2−), 31.8 (−CH_2−), 52.4 (−OMe), 65.0 (>CH−), 171.7 (−CO_2), 177.3 (−CH=N−), 158.8 (C^1), 147.90 (C^2), 130.8 (C^3), 124.0 (C^4), 128.9 (C^5), 138.1 (C^6). − ^{31}P NMR spectroscopic data (in $CDCl_3$): δ = 28.86.

Crystallography: A prismatic crystal of **3a** was selected and mounted on an Enraf CAD4 four-circle diffractometer. Unit cell parameters were determined from automatic centering of 25 reflections in the range $12° < \Theta < 21°$ and refined by least-squares method. Intensities were collected with graphite monochromated Mo-K_α radiation, using ω/2Θ scan technique. Three reflections were measured every 2 h as orientation and intensity control, and no significant intensity decay was observed. Lorentz-polarization and absorption corrections were made. The structure was solved by Direct methods using the SHELXS97 computer program[36] and refined by full-matrix least-squares method with the SHELXL97 computer program[37] using 2526 reflections (very negative intensities were not assumed). The function minimized was $\Sigma||F_o|^2 - |F_c|^2|^2$, where $w = [\sigma^2(I) + (0.0795\ P)^2]^{-1}$ and $P = (|F_o|^2 + 2\ |F_c|^2)/3$. f, f', and f'' were obtained from the literature.[38] The chirality of the structure was defined from the Flack coefficient.[39] All the hydrogen atoms were computed and refined with an overall isotropic temperature factor using a riding model. The final R(on F) factor was 0.048 and wR(on F) = 0.112. Further details concerning the resolution and refinement of the crystal structure of **3a** are presented in Table 1. Crystallographic data (excluding structure factors) for the structure reported in this paper have been deposited with the Cambridge Crystallographic Data Centre as supplementary publication no. CCDC-152831. Copies of the data can be ob-

tained free of charge on applications to CCDC, 12 Union Road, Cambridge CB2 1EZ, UK [Fax: (internat) +44−1223/336-033; E-mail: deposit@ccdc.cam.ac.uk].

Acknowledgments

We are grateful to the Generalitat de Catalunya, Ministerio de Educación y Cultura and to the Ministerio de Ciencia y Tecnología of Spain (projects PB98-1236, BQU2000-0652, and 1999-SGR-00045) for financial support.

[1] [1a] A. D. Ryabov, *Chem. Rev.* **1990**, *90*, 403−424. − [1b] V. V. Dunina, O. A. Zalevskaya, V. M. Potatov, *Russ. Chem. Rev.* **1988**, *57*, 434−473. − [1c] I. Omae, *Coord. Chem. Rev.* **1988**, *83*, 137−169. − [1d] R. G. Newkome, W. E. Puckett, V. G. Gupta, E. Kiefer, *Chem. Rev.* **1986**, *86*, 451−489.

[2] I. Omae, *Applications of Organometallic Compounds*; John Wiley & Sons, Chichester, U. K., **1998**, chapt. 20.

[3] A. J. Klaus, *Modern Colorants: Synthesis and Structure*; **1995**; Vol. *3*, pp 1, London, U. K.

[4] [4a] P. H. Leung, K. H. Ng, Y. Li, A. J. P. White, D. J. Williams, *Chem. Commun.* **1999**, 2435−2436. − [4b] A. Bose, C. H. Saha, *J. Mol. Catal.* **1989**, *49*, 271−283. − [4c] P. K. Santra, C. H. Saha, *J. Mol. Catal.* **1987**, *39*, 279−292. − [4d] Y. Wakatsuki, H. Yamazaki, P. A. Grutsch, M. Santhanam, C. Kutal, *J. Am. Chem. Soc.* **1985**, *107*, 8153−8159.

[5] [5a] P. Espinet, M. A. Esteruelas, L. A. Oro, J. L. Serrano, E. Sola, *Coord. Chem. Rev.* **1992**, *117*, 215−274 and references therein. − [5b] M. Ghedini, A. Crispini, *Comments on Inorg. Chem.* **1999**, *21*, 53−68 and references therein.

[6] [6a] M. Maestri, D. Sandrini, V. Balzani, A. von Zelewsky, P. Jolliet, *Helv. Chim. Acta* **1988**, *71*, 135−138. − [6b] C. Cornioley-Deschel, T. Ward, A. von Zelewsky, *Helv. Chim. Acta* **1988**, *71*, 130−133. − [6c] K. A. King, P. J. Spellane, R. J. Watts, *J. Am. Chem. Soc.* **1985**, *107*, 1431−1432. − [6d] Y. Oshawa, S. Sprouse, K. A. King, M. K. de Armond, K. W. Hanck, R. J. Watts, *J. Phys. Chem.* **1987**, *91*, 1047−1054.

[7] [7a] J. Spencer, M. Pfeffer, *Advances in Metal-Organic Chemistry* **1998**, *6*, 103−144 and references therein. − [7b] M. Pfeffer, *Recl. Trav. Chim. Pays-Bas* **1990**, *109*, 567−576 and references therein. − [7c] A. D. Ryabov, *Synthesis* **1985**, 233−252 and references therein.

[8] C. Navarro-Ranninger, I. López-Solera, J. R. Masaguer, C. Alonso, *Appl. Organomet. Chem.* **1993**, *7*, 57−61.

[9] C. Navarro-Ranninger, I. López-Solera, V. M. González, J. M. Pérez, A. Alvarez-Valdés, A. Martin, P. R. Raithby, J. R. Masaguer, C. Alonso, *Inorg. Chem.* **1996**, *35*, 5181−5187.

[10] S. B. Wild, *Coord. Chem. Rev.* **1997**, *166*, 291−311 and references therein.

[11] For recent publications on optically active cyclometallated complexes see for instance: [11a] V. V. Dunina, L. G. Kuz′mina, M. Y. Rubina, Y. K. Grishin, Y. A. Veits, E. J. Kazakova, *Tetrahedron: Asymmetry* **1999**, *10*, 1483−1497 and references therein. − [11b] P. Leung, G. H. Quek, H. Lang, A. M. Liu, K. F. Mok, A. J. White, D. J. Williams, N. Rees, W. McFarlane, *J. Chem. Soc., Dalton Trans.* **1998**, 1639−1643. − [11c] M. Benito, C. López, X. Solans, M. Font-Bardía, *Tetrahedron: Asymmetry* **1998**, *9*, 4219−4238. − [11d] A. Böhm, T. Hauk, W. Beck, *Z. Naturforsch., Teil B* **1999**, *54*, 1360−1372.

[12] C. López, R. Bosque, D. Sainz, X. Solans, M. Font-Bardía, *Organometallics* **1997**, *16*, 3261−3266.

[13] [13a] C. López, J. Sales, R. Zquiak, X. Solans, *J. Chem. Soc., Dalton Trans.* **1992**, 2321−2328. − [13b] R. Bosque, C. López, J. Sales, X. Solans, M. Font-Bardía, *J. Chem. Soc., Dalton Trans.* **1994**, 735−747. − [13c] R. Bosque, M. Font-Bardía, C. López, J. Sales, J. Silver, X. Solans, *J. Chem. Soc., Dalton Trans.* **1994**, 747−752. − [13d] C. López, R. Bosque, X. Solans, M. Font-Bardía, *J. Organomet. Chem.* **1997**, *539*, 99−107. − [13e] R. Bosque, C. López, J. Sales, X. Solans, *J. Organomet. Chem.* **1994**, *483*, 61−71.

[14] C. López, R. Bosque, X. Solans, M. Font-Bardía, *Tetrahedron: Asymmetry* **1996**, *7*, 2527−30.

[15] R. G. Pearson, *J. Am. Chem. Soc.* **1963**, *85*, 3533−3539.

[16] [16a] S. Chattopadhyay, C. Sinha, P. Basu, A. Chakravorty, *Organometallics* **1991**, *10*, 1135−1139. − [16b] S. Chattopadhyay, C. Sinha, P. Basu, A. Chakravorty, *J. Organomet. Chem.* **1991**, *414*, 421−431. − [16c] C. K. Pal, S. Chattopadhyay, C. Sinha, A. Chakravorty, *J. Organomet. Chem.* **1992**, *439*, 91−99. − [16d] R. Bjhaumik, H. Biswas, P. Bandyopadhyay, *J. Organomet. Chem.* **1995**, *498*, 81−83. − [16e] R. Bhaumik, P. Bandyapadhyay, *Trans. Met. Chem.* **1996**, *21*, 187−188. − [16f] K. Kamaraj, D. Bandyopadhayay, *Organometallics* **1999**, *18*, 438−446. − [16g] P. Chattopadhyay, M. K. Nayack, S. P. Bhattacharyay, C. Sinha, *Polyhedron* **1997**, *16*, 1291−1295. − [16h] A. K. Mahapatra, D. Bandyopadhyay, P. Bandyopadhyay, A. Chakravorty, *Inorg. Chem.* **1986**, *25*, 2214−2221. − [16i] J. M. Vila, M. T. Pereira, J. M. Ortigueira, M. Graña, D. Lata, A. Suarez, J. J. Fernández, A. Fernández, M. López-Torres, A. Adams, *J. Chem. Soc., Dalton Trans.* **1999**, 4193−4201.

[17] X. Riera, A. Caubet, C. López, V. Moreno, X. Solans, M. Font-Bardía, *Organometallics* **2000**, *19*, 1384−1390.

[18] H. A. Ankersmit, P. T. Witte, H. Kooijman, M. T. Lakin, A. L. Spek, K. Goubitz, K. Vrieze, G. van Koten, *Inorg. Chem.* **1996**, *35*, 6053−6063.

[19] [19a] D. Barton, W. D. Ollis, (Eds.), *Comprenhensive Organic Chemistry: The Syntheses and Reactions of Organic Compounds*, Pergamon Press, **1979**, Vol. *1*, Exeter, U. K. − [19b] A. R. Katritzky, O. Meth-Cohn, C. W. Rees, (Eds.), *Comprenhensive Organic Functional Group Transformations*, Pergamon Press, **1995**, Vol. *1*, Cambridge, U. K.

[20] X. Riera, V. Moreno, M. Font-Bardía, X. Solans, *Polyhedron* **1998**, *18*, 65−73.

[21] P. S. Pregosin, *Coord. Chem. Rev.* **1982**, *44*, 247−291.

[22] [22a] P. R. R. Ranatunge-Bandarage, B. H. Robinson, J. Simpson, *Organometallics* **1994**, *13*, 500−510. − [22b] P. R. R. Ranatunge-Bandarage, N. W. Duffy, S. M. Johnston, B. H. Robinson, J. Simpson, *Organometallics* **1994**, *13*, 511−521.

[23] The diastereomer (S_S,R_S) of the cycloplatinated complex: [Pt{C_6H_4−CH=N−CH(CO_2Me)−CH_2−CH_2−SMe}Cl] (**3a**) has also been isolated and characterized in this work (see below), and its ^{195}Pt NMR spectrum also showed a singlet at δ = −3832 ppm. In addition, the signals observed in the ^{1}H NMR spectrum of **3a** were also coincident with one of the sets of signals observed in the crude material. These findings suggested that one of the components of the mixture was the platinacycle **3a**.

[24] J. H. Price, A. N. Williamson, R. F. Schramm, B. B. Wayland, *Inorg. Chem.* **1972**, *11*, 1280−1284.

[25] [25a] J. Albert, J. M. Cadena, J. Granell, *Tetrahedron: Asymmetry.* **1997**, *8*, 991−994. − [25b] V. V. Dunina, E. B. Golovan, *Tetrahedron: Asymmetry.* **1995**, *6*, 2747−2754. − [25c] V. V. Dunina, E. B. Golovan, A. V. Buyerich, *Tetrahedron: Asymmetry* **1995**, *6*, 2731−2746. − [25d] V. I. Sokolov, L. L. Trotiskaya, T. I. Rozhkova, *Gazz. Chim. Ital.* **1987**, *117*, 525−527.

[26] *SPARTAN, 4.0.* In Wavefunction Inc. 1840, Von Karman Av. 3370. Irvine, CA-92715, **1995**.

[27] T. H. Allen, O. Kennard, *Chem. Design Automation News* **1993**, *8*, 146−149.

[28] C. Hansch, A. Leo, D. Hoekman, *Exploring QSAR. Hydrophobic, Electronic and Steric Constants.* ACS-Prof. reference Book, **1995**, Washington D. C., U. S. A.

[29] [29a] J. Albert, M. Gómez, J. Granell, J. Sales, X. Solans, *Organometallics* **1990**, *9*, 1405−1413. − [29b] J. Albert, R. M.

Ceder, M. Gómez, J. Granell, J. Sales, *Organometallics* **1992**, *11*, 1536−1541. − [29c] Y. J. Wu, X. L. Cui, C. X. Du, W. L. Wang, R. Y. Guo, R. F. Chen, *J. Chem. Soc., Dalton Trans.* **1998**, 3727−3730.
[30] R. G. Miller, R. D. Stauffer, D. R. Fahey, D. R. Pernell, *J. Am. Chem. Soc.* **1970**, *92*, 1511−1521.
[31] [31a] M. Crespo, X. Solans, M. Font-Bardia, *J. Organomet. Chem.* **1996**, *518*, 105−113. − [31b] M. Crespo, C. Grande, A. Klein, M. Font-Bardía, X. Solans, *J. Organomet. Chem.* **1998**, *563*, 179−190.
[32] [32a] G. R. Newkome, E. G. Kiefer, Y. A. Frere, M. Onishi, V. K. Gupta, F. R. Fronczek, *Organometallics* **1986**, *5*, 348−355. − [32b] G. R. Newkome, D. K. Kohli, F. R. Fronczek, *J. Am. Chem. Soc.* **1982**, *104*, 994−998. − [32c] G. R. Newkome, T. Kawato, D. K. Kohli, W. E. Puckett, B. D. Olivier, G. Chiari, F. R. Fronczek, W. A. Deutsch, *J. Am. Chem. Soc.* **1981**, *103*, 3423−3428. − [32d] R. D. Billadeaux, F. R. Fronzeck, A. Yoneda, G. R. Newkome, *Acta Crystallogr., Sect. C* **1998**, *C54*, 1439−1441.
[33] Labelling of the atoms correspond to those shown in Scheme 1.
[34] Four additional doublets centered at ca. δ = 131, 135, 129, and 128 due to the carbon atoms of the phenyl rings of the PPh_3 ligand were also detected.
[35] The signals due to the carbons C^1 and C^2 were not detected.
[36] G. M. Sheldrick, *SHELXS. A computer program for the determination of crystal structures.* **1997**. Univ. of Göttingen, Germany.
[37] G. M. Sheldrick, *SHELXL. A computer program for the determination of crystal structures.* **1997**. Univ. of Göttingen, Germany.
[38] Kynoch Press, *International Tables of X-ray Crystallography*; **1974**; Vol. IV, pp. 99−100 and 149.
[39] H. D. Flack, *Acta Crystallogr., Sect. A* **1983**, *39*, 876−881.
Received January 3, 2001
[I01003]

Intramolecular Metal Ligand Aromatic Cation−π Interactions in Crystal Structures of Transition Metal Complexes

Miloš Milčić[a] and Snežana D. Zarić*[a]

Dedicated to Prof. M. B. Ćelap on the occasion of his 80th birthday

Keywords: Cation−π interactions / Density functional calculations / Metal complexes / Crystal structures

Cation–π interactions between ligands coordinated to a metal cation and aromatic groups have been predicted by theoretical calculations, and have been found in crystal structures of metalloproteins from the Protein Data Bank (PDB). We proposed metal ligand aromatic cation–π (MLACπ) interaction as intramolecular interactions in transition metal complexes. Searching crystal structures of transition metal complexes from the Cambridge Structural Database (CSD) reveals that there are quite a number of metal complexes, where an aromatic ring interacts with a hydrogen atom from a ligand in the same complex. The hydrogen atom is separated from the metal center by a few bonds and gains positive charge from the metal atom. In the complexes there are various metal atoms and various ligands. In the most of the complexes, the aromatic ring is separated from the metal center by two or four bonds, and interacts with the hydrogen atom of another ligand. In complexes where the aromatic ring is separated from the metal center by four or five bonds, there are examples of aromatic groups interacting with the hydrogen atom in the same ligand. By quantum chemical computations it was evaluated for the model systems of cationic cobalt(III) complexes with a charge of +1, that the energy of this intramolecular MLACπ interaction is about 4 kcal/mol.

Introduction

The cation−π interaction is considered an important non-covalent bonding force in a wide range of molecular systems.[1,2] Gas-phase studies of ion-molecule complexes established that cations bind strongly to molecules with π bonds.[2] High-level theoretical studies of ion−molecule systems have shown excellent agreement between calculated and experimental bonding energies, and have shown the geometries of the ion−molecule complexes.[3−15] The experimental and theoretical studies provide an understanding of the nature of the cation−π interaction.[1,16−18]

Cation−π interactions are important for molecular recognition in many biological systems.[1,2] Investigations on cation−π interactions in proteins show that cation−π interaction pairs contribute at least as much to protein stability and the structural motifs of a native protein as more conventional interactions. Hence, it was proposed that cation−π interactions should be considered the same way as hydrogen bonds, salt bridges, and hydrophobic effects in analyses of the stability of the native protein structure.[16,19,20]

Recently, the interaction of metal complexes as cations with π systems were investigated.[21−23] It is possible to predict cation−π interactions by quantum chemical calculations, since in theoretical work it was shown that calculated interaction energies for cation−π systems are in agreement with experimental data.[3−15] In our previous work, the interactions of π systems with the cationic metal complex $[Co(NH_3)_6]^{3+}$ were predicted by quantum chemical calculations. The bonding energies obtained with the B3LYP method for benzene, acetylene, and ethylene π complexes are 31.34 kcal/mol,[21] 18.30 kcal/mol, and 17.02 kcal/mol,[22] respectively. Since these calculations showed strong cation−π interactions, we proposed[21,22] that the cation−π interaction may exist when ligands coordinated to a metal ion can get in contact with π systems. This can be the case in metalloproteins, in metal complexes, in supramolecular structures, and when DNA and RNA interact with metal cations.

Cation−π interactions with a cationic metal complex were observed by analyzing crystal structures of DNA and RNA. It was noticed that cation−π interactions of divalent cations with the π systems of bases are important in stabilizing unstacked conformations of DNA and RNA.[24,25] Metal ligand aromatic cation−π (MLACπ) interactions in metalloproteins were discovered by searching crystal structures of metalloproteins from the Protein Data Bank (PDB).[23] These data reveal that there are quite a number of metalloproteins, where aromatic rings from phenylalanine, tyrosine, and tryptophan are close to a metal center, interacting with coordinated ligands. Among these ligands are amino acids like asparagine, aspartate, glutamate, histidine, and threonine, but also substrates like water and ethanol. These interactions play a role in stability and conformation of metalloproteins, and in some cases may also be directly involved in the mechanism of enzymatic reactions which occur at the metal center. For the enzyme superoxide dismutase, we evaluated by quantum chemical

[a] Department of Chemistry, University of Belgrade,
Studentski trg 16, P. O. B. 158, 11001 Belgrade, Yugoslavia
Fax: (internat.) + 381-11/638-785
E-mail: szaric@helix.chem.bg.ac.yu

 © WILEY-VCH Verlag GmbH, 69451 Weinheim, 2001 1434−1948/01/0808−2143 $ 17.50+.50/0

computations that Trp163 has an interaction energy of 10.09 kcal/mol with the ligands coordinated to the iron center.

We propose that intraligand MLACπ interactions, where ligands coordinated to a metal center interact with aromatic groups, exist in transition metal complexes. Intermolecular interactions between hydrogen atoms and π systems have been noticed in organometallic crystals.[24] In this work, we screened crystal structures of metal complexes in the Cambridge Structural Database (CSD) in order to find such intramolecular interactions. The structures with these interactions are described and the energy of the interactions was evaluated by quantum chemical calculations on model systems.

Results and Discussion

We have found that intramolecular MLACπ interactions, between a coordinated ligand and the aromatic ring in the

Table 1. Intramolecular metal-ligand cation−aromatic π interactions in complexes with two bonds between aromatic ring and metal center

#	Ref.	RFCODE[a]	*R* factor	Metal	X[b]	X···center of ring[c]	H···center of ring[d]	X···C[e]	H···C[f]	Y[g]
1	[27]	BZSACS	0.038	Co^{3+}	N	3.98	3.82	3.27	3.16	S
							3.35		2.83	
2	[28]	CUBXAY	0.051	Co^{3+}	N	3.39	3.54	3.22	3.00	P
							3.64		2.94	
					N	4.11	3.49	3.37	3.44	P
							4.17		2.89	
3	[29]	JORJAB	0.054	Co^{2+}	N	3.35	3.17	3.02	2.72	N
4	[30]	JUJPEJ	0.051	Cu^{2+}	N	3.92	3.22	3.36	2.82	N
5	[31]	TSACOP	0.039	Co^{3+}	N	3.79	3.45	3.12	2.96	S
							3.39		2.80	
6	[32]	TULBEH	0.051	Mn^{1+}	N	3.77	2.95	3.19	2.51	P
7	[33]	GAFKED10	0.028	Cd^{2+}	N	3.65	2.81	3.33	2.52	N
8	[34]	HELYUS	0.036	Ru^{2+}	N	3.83	3.06	3.18	2.61	S
9	[35]	PAXCAS	0.049	Mo^{4+}	N	3.89	3.13	3.07	2.43	S
10	[36]	PIRKAC	0.031	Ru^{1+}	N	3.55	3.39	3.14	2.92	P
							3.29		3.02	
11	[37]	TOJCIE	0.056	$Ru^{1/5+}$	O	3.94	3.00	3.27	2.37	P
12	[38]	VERGEE	0.048	Tc^{5+}	N	3.73	2.80	3.08	2.30	S
					N	3.72	2.80	3.04	2.25	S
13	[39]	WEFLOI	0.045	Ru^{2+}	N	4.02	3.36	3.28	2.71	Si
14	[40]	AQTPRU	0.048	Ru^{2+}	O	3.58		3.03		P
					O	2.74		3.09		P
15	[41]	KAJROC	0.027	Rh^{2+}	N	4.48	3.59	3.46	2.67	Sb
					N	4.15	3.26	3.36	2.63	Sb
16	[42]	BAXJOZ	0.034	Re^{4+}	O	3.98		3.34		P
17	[43]	CIRNUM	0.041	$Os^{2/3+}$	O	3.73		3.23		P
18	[44]	DIKMUF	0.058	Os^{2+}	O	3.64		3.14		P
					O	3.64		3.14		P
19	[45]	PEDXAX	0.056	Ir^{3+}	N	3.63	2.76	3.01	2.25	P
					N	3.71	3.05	3.09	2.64	P
							3.64		2.82	
20	[46]	PEWRUE	0.026	Re^{5+}	N	3.75		3.17		P
21	[47]	WAXGIL	0.055	Re^{3+}	N	3.53	2.69	3.14	2.48	P

[a] BZSACS, pentaammine(benzenesulfonyl)cobalt(III); CUBXAY, *cis*-(*NCS*,*NCS*),*trans*-(*P*,*P*)-bis[(2-aminoethyl)diphenylphosphanyl-*N*,*P*]di(isothiocyanato)cobalt(III); JORJAB, aniline(chloro)bis(ethylendiamine)cobalt(II); JUJPEJ, *catena*-[diamminobis{2-(*p*-aminobenzensulfonamido)-5-ethyl-1,3,4-thiadiazole-*N*,*N''*}copper(II)]; TSACOP, pentaammine(*p*-toluenesulfonyl)cobalt(III); TULBEH, tricarbonyl(hydrazine)bis(phenyl diethylphosphonite)manganese(I); GAFKED10, *catena*-[bis(μ-cyano-*C*,*N*)dicyano(μ-1,6-diaminohexane-*N*,*N*)bis(*p*-toluidine-*N*)−cadmium(II)−nickel(II)]; HELYUS, [1,2-bis(2-aminophenylthio)phenylene]dichloro(triphenylphosphane)ruthenium(II); PAXCAS, (diphenylmethylphosphane)hydrido(phenylhydrazine)tris(2,4,6-triisopropylphenylthiolato)molybdenum(IV); PIRKAC, *trans*(Ammino-bis(1,2-bis(diphenyl-phosphanyl)ethane)-phenylethynyl)-ruthenium(I); TOJCIE, dodecacarbonyl[μ_5-2-(diphenylphosphanyl)ethynylidene][μ-bis(diphenylphosphanyl)methane][1-(2-diphenylphosphanylphenyl)ethyl](μ-hydroxo)pentaruthenium; VERGEE, nitridobis(2,3,5,6-tetramethylbenzenethiolato-*S*)bis(1,1,2,2-tetramethylguanidine-*N*)technetium(V); WEFLOI, bis(benzylamino)dicarbonyl(phenyldimethylsilyl)(iodo)ruthenium(II); AQTPRU, aquadicarbonyl(hydrido)bis(triphenylphosphane)ruthenium(II); KAJROC, tris(μ-acetamidato-*N*,*O*)(μ-acetato-*O*,*O'*)bis(triphenylstibine)dirhodium(II); BAXJOZ, *trans*-trichlorobis(diethylphenylphosphane)(hydroxo)rhenium(IV); CIRNUM, 1,1,2,2,2,3,3,3,3-nonacarbonyl-1-(dimethylphenylphosphane)-1,2-(μ-hydrido)-1,2-(μ-hydroxo)triosmium; DIKMUF, (aqua)dicarbonyl(hydrido)bis(triphenylphosphane)osmium(II); PEDXAX, *trans*,*mer*-[dichlorotris(dimethylphenylphosphanyl)amino]iridium(III); PEWRUE, chloro[*N*-(*N*,*N*-diethylthiocarbamoyl)benzamidinato]bis(dimethyl- phenylphosphane)(nitrido)rhenium(V); WAXGIL, ammine(benzoyldiazenido-*N*)dichlorobis(triphenylphosphane)rhenium(III). − [b] Heavy atom to which the interacting hydrogen atom is bound. − [c] The distance [Å] between the heavy atom and the center of the aromatic ring. − [d] The distance [Å] between the interacting hydrogen and the center of the aromatic ring. − [e] The distance [Å] between the heavy atom and the closest carbon atom of the aromatic ring. − [f] The distance [Å] between the interacting hydrogen atom and the closest carbon atom of the aromatic ring. − [g] he atom between the metal atom and the aromatic ring.

same complex, can be observed in a number of crystal structures of transition metal complexes. Data about these interactions in different crystal structures are compiled in Table 1 and Table 2. The data show that there are numerous metal complexes where there is close contact between an aromatic ring and a hydrogen atom from a ligand, and that different metal ions and ligands can be involved.

In all of the observed cases where this interaction occurs, the ligand interacting with an aromatic group possesses a hydrogen atom pointing towards the aromatic ring. A partial positive charge of the ligand, induced by the metal charge, is situated on the hydrogen atom interacting with the aromatic ring. In most of the crystal structures the positions of hydrogen atoms were given, and in Table 1 and Table 2 the distances from the interacting hydrogen atom to the center of the aromatic ring and to the closest carbon atom of the aromatic ring are given. We also list the distances from the heavy atom (oxygen or nitrogen) to which the hydrogen atom is bound.

Based on the type of the ligand containing with the aromatic group, we can separate the metal complexes with MLACπ interactions into two groups. In the first group are

Table 2. Intramolecular metal-ligand cation−aromatic π interactions in complexes with several bonds between aromatic ring and metal center

#	Ref.	RFCODE[a]	*R* factor	Metal	X[b]	X···center of ring[c]	H···center of ring[d]	X···C[e]	H···C[f]
1	[48]	CEBREG	0.052	Cu^{2+}	N	4.00	3.42	3.06	2.66
2	[49]	FUCSIF	0.029	Cu^{2+}	N	3.90	3.29	2.96	2.58
3	[50]	NEFRAR	0.050	Co^{3+}	N	3.90	3.22	2.99	2.54
4	[51]	POKMAD02	0.041	Co^{3+}	N	3.75	3.08	2.90	2.56
					N	3.75	3.08	2.90	2.56
5	[52]	TONPUH	0.04	Cu^{2+}	N	3.88	2.99	2.99	2.23
6	[53]	VAFSIE	0.054	Co^{3+}	N	3.85	3.03	2.92	2.33
7	[54]	RUFKUY	0.019	Rh^{3+}	N			2.93	2.46
8	[55]	NEGREW	0.023	Re^{1+}	N	3.81	3.16	2.82	2.38
						3.55	2.87	3.29	2.51
9	[56]	DUSJIK	0.044	Ni^{3+}	N	3.27	2.21	3.46	2.54
10	[57]	DEMHAE	0.056	Ni^{2+}	N	3.55	2.87	3.29	2.62
						3.55	2.87	3.29	2.51
11	[58]	DIXHAT	0.051	Cu^{2+}	N	4.48	3.79	3.84	3.18
					N	4.53	3.84	3.84	3.18
12	[59]	GLTRCU01	0.041	Cu^{2+}	O	3.25	2.31	3.37	2.52
13	[60]	LETYCU10	0.035	Cu^{2+}	O	3.32	2.58	3.39	2.66
14	[61]	NALPIZ	0.057	Fe^{2+}	N	3.63	2.63	3.16	2.72
					N	3.63	2.63	3.16	2.29
15	[62]	NOVBAB	0.060	Ni^{2+}	O	4.06	3.28	3.53	2.76
					O	3.93	3.23	3.27	2.49
16	[63]	NUTKES	0.048	Mn^{2+}	O	3.24	2.36	3.32	2.74
					O	4.13	3.22	3.52	2.65
17	[52]	TONPOB	0.034	Cu^{2+}	O	3.17		3.31	
18	[64]	FOBTAR	0.038	Mo^{4+}	N	3.42	2.84	3.26	2.53
19	[65]	SIRCOL	0.047	Mo^{4+}	N	3.91	2.97	3.50	2.67
					N	3.91	2.97	3.50	2.67
20	[66]	ZURREJ	0.042	Cd^{2+}, Ni^{2+}	N	3.77	2.91	3.55	2.68
21	[67]	NOLQIO	0.031	Mo^{6+}	N	3.47	2.94	3.33	2.85

[a] CEBREG, (dimethyl sulfoxide)bis(L-phenylalaninato)copper(II); FUCSIF, [(*R*)-2-amino-1,1-bis(2-methoxyphenyl)-3-phenylpropanol-*N*,O])-[(*R*)-1,1-bis(2-methoxyphenyl)-3-phenyl-2-saliciylideneamino-1-propanolato-*N*,*O*,*O*′]copper(II); NEFRAR, Δ-α-[*N*,*N*′-dimethyl-*N*,*N*′-di(2-picolyl)-1*S*,2*S*-diaminocyclohexane](*S*-phenylalaninato)cobalt(III); POKMAD02, hydrogen[bis{*N*-(3-hydroxy-5-hydroxymethyl-2-methylpyridin-4-ylmethyl)-L-phenylalaninato}]cobalt(III); TONPUH, *catena*-[(μ$_3$-L-leucyl-L-phenylalaninato)copper(II)]; VAFSIE, (−)-Λ-β$_2$-[*N*,*N*′-{bis(1,1,1-trifluoro-4-imino-2-pentanonato)ethylene-*O*,*O*′,*N*,*N*′}(l-phenylalaninato-*O*,*N*)cobalt(III)]; RUFKUY, chloro[hydrotris(3,5-dimethylpyrazolyl)borato](L-tryptophanato)rhodium(III); NEGREW, octacarbonyl(μ-benzophenone hydrazinato)(μ-hydrido)dirhenium(I); DUSJIK, aqua(15-benzyl-1,13-didehydro-1,4,7,10,13-pentaazacyclohexadecane-14,16-dione-*N*,*N*′,*N*′′,*N*′′′,*N*′′′′)-nickel(III); DEMHAE, [{*cis*-bis(isothiocyanato-*N*)}bis{(*R*)-(+)-1-phenyl-1-ethylamine-*N*}bis{(*S*)-(−)-1-phenyl-1-ethylamine-*N*}-nickel(II){*cis*-bis(isothiocyanato-*N*}tetrakis{(*R*)-(+)-1-phenyl-1-ethylamine-*N*}nickel(II)]; DIXHAT, bis(μ-2-amino-2-methyl-1-propanolato-*O*,*O*,*N*)bis(2-amino-2-methyl-1-propanol-*N*,*O*)tetrakis(phenylacatato-*O*)tricopper(II); GLTRCU01, diaqua(glycyl-L-tyrosyl)-copper(II); LETYCU10, *catena*-[aqua(μ-L-leucyl-L-tyrosinato)copper(II)]; NALPIZ, amminebis[diphenylborato(dimethylglyoximato)]-pyridineiron(II); NOVBAB, (*R*,*R*)-triaqua-4,6-dibenzofurandiyl-2,2′-bis(4-phenyloxazoline)nickel(II); NUTKES, *catena*-[tetraaquabis(μ-triphenylacetato)bis(triphenylacetato)dimanganese(II)]; TONPOB, *catena*-[aqua(μ-L-leucil-D-phenylalaninato)copper(II)]; FOBTAR, (2,6-diphenylphenoxy-*O*)bis(2,6-diphenylphenoxy-*O*)(dimethylammonio)molybdenum(IV); SIRCOL, *trans*-bis(dimethylamine-*N*)tetrakis(2-phenylphenoxy-*O*)molybdenum(IV); ZURREJ, *catena*-[bis(μ-cyano)bis(μ-*p*-xylylenediamine)dicyanocadmium(II)nickel(II)]; NOLQIO, triethylammonium [*mer*-trichloro(diphenylmethylimido)(2,2-diphenylglycinato)molybdenum(VI)]. − [b] Heavy atom to which the interacting hydrogen atom is bound. − [c] The distance [Å] between the heavy atom and the center of the aromatic ring. − [d] The distance [Å] between the interacting hydrogen and the center of the aromatic ring. − [e] The distance [Å] between the heavy atom and the closest carbon atom of the aromatic ring. − [f] The distance [Å] between the interacting hydrogen atom and the closest carbon atom of the aromatic ring.

complexes where the aromatic group is bound to the atom that is coordinated to the metal ion. In this way there are only two bonds between the metal center and the aromatic group (Figure 1, a and b). In the second group are complexes where the aromatic group is separated from the metal center by several bonds (Figure 1, c, d, and e).

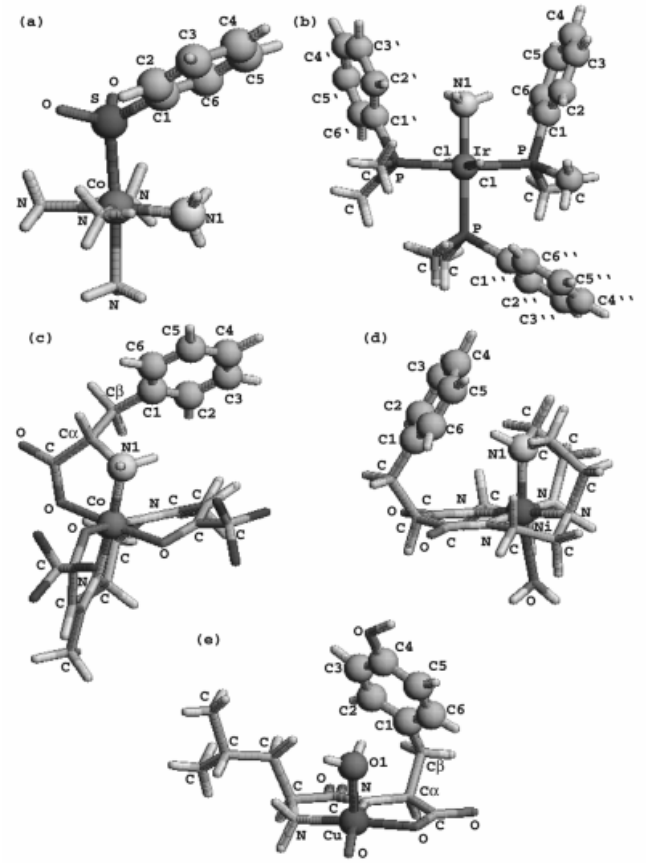

Figure 1. Structures of complexes with intramolecular MLACπ interaction; (a) BZSACS, (b) PEDXAX, (c) VAFSIE, (d) DUSJIK, (e) LETYCU10

Complexes with Two Bonds between the Aromatic Ring and the Metal Center

In these complexes, organic ligands with aromatic groups can make MLACπ interactions only if the ligand is coordinated in a *cis* position, and there is no possibility for such an interaction within the same ligand. In the structures given in Table 1 the aromatic ring is bonded to the atoms N, P, S, Si, Sb (last column in Table 1), while at the same time these atoms are coordinated to the metal ion. The carbon atom of the aromatic ring that is the closest to the interacting hydrogen atom is the one that is bonded to the heteroatom, and is the closest to the metal center (C1 in Figure 1, a). An example for this type of complex, structure BZSACS, is shown in Figure 1, a. In this complex, a cobalt ion is octahedrally coordinated by five NH_3 groups and the sulfur atom of a benzenesulfinato ligand. The phenyl ring of the benzenesulfinato ligand interacts with the hydrogen atoms of the NH_3 ligand in *cis* position. In the crystal structure there are two hydrogen atoms oriented towards the aromatic ring, with the distances to the closest carbon atom of 3.16 and 2.83 Å. The torsion angle C1−S−Co−N1 is 15.8° which is very favorable for a MLACπ interaction.

In other complexes (structures CUBXAY, TSACOP, PIRKAC, PEDXAX) there are also two hydrogen atoms of the same ligand interacting with the same aromatic ring (Table 1). In some complexes there are two MLACπ interactions in the same complex. In the structures AQTPRU, DIKMUF, PEDXAX, and WAXGIL there are two aromatic groups of two ligands interacting with the hydrogen atoms of the same ligand (Table 1). The structure of the *trans,mer*-$[IrCl_2(NH_3)(PMe_2Ph)_3]^+$ complex (PEDXAX) is shown in the Figure 1, b. Two PMe_2Ph ligands, which are in *cis* positions relative to the NH_3, have phenyl groups oriented towards NH_3. The torsion angles C1−P−Ir−N1 and C1′−P−Ir−N1 are 7.5 and 26.9°, and the N1−C1 and N1−C1′ distances are 3.01 and 3.09 Å, respectively (Table 1, column 7). In this structure there is one more MLACπ interaction, that is not listed in the Table 1, since we searched and listed only interactions where there are two bonds between the hydrogen atom and the metal center. The third interaction in this complex is the interaction of a third phenyl group with the hydrogen atom of the CH_3 group (Figure 1, b); the C1′′−H distance is 2.43 Å.

It can be expected that when the interacting hydrogen atom is separated from the metal center by more bonds it could gain less positive charge from the metal ion, resulting in a diminished interaction. However, here we are considering intramolecular interactions, and there are many steric constrains. Hence, it is not possible to observe a regular correlation between the interaction distances and the amount of positive charge on the hydrogen atom, as is possible with metalloproteins where MLACπ interactions are not as constrained by steric influences.[23] It is interesting to point out that from spectra of the *trans,mer*-$[IrCl_2(NH_3)(PMe_2Ph)_3]^+$ complex in solution, it is evident that there is rapid rotation about the Ir−P bonds,[45] which means that there are no MLACπ interactions in solution.

The structures TOJCIE, KAJROC, and CIRNUM are structures of binuclear complexes. In these three complexes the aromatic rings interact with the hydrogen atoms of the ligands in the bridge.

In the complexes listed in the Table 1 there is not much freedom for the ligands to adjust their mutual orientation. Due to steric constraints, the mutual orientation of the aromatic ring and the interacting hydrogen atom of the ligand in a *cis* position is such that the hydrogen atom and the heavy atom are close to the C1 atom of the aromatic ring, but rather far from its center (Figure 1, a). This can also be noticed by comparing the interaction distances in these complexes (Table 1) with the distances in other complexes listed in Table 2.

Complexes with Several Bonds between the Aromatic Ring and the Metal Center

The data for these complexes are shown in Table 2. In most of the structures there are four bonds between the

metal center and the aromatic ring, but there are a few exceptions. In the structures DEMHAE, NOVBAB, ZURREJ, and NOLQIO, there are three bonds between the metal center and the aromatic ring, and in structure DUSJIK there are five bonds.

In the structures with several bonds between the metal center and the aromatic ring there is a possibility for MLACπ interactions with the hydrogen atom of another ligand, but also with the hydrogen atom of the same ligand (structures 1−8 in Table 2). In the phenylalaninato complex (structure VAFSIE, Figure 1, c) there is an intraligand MLACπ interaction, where the phenyl ring interacts with the hydrogen atom bonded to the coordinated nitrogen atom. The value of the torsion angle C1−Cβ−Cα−N1 is −52.8°. Due to steric constraints, as in all other structures with intraligand MLACπ interactions, the closest carbon atom to the interacting hydrogen atom is C1 (Figure 1, c). The C1−H distance is 2.33 Å, one of the shortest C−H distances among complexes listed in Table 2. In the structure NEGREV there is a binuclear complex, and the ligand with intraligand MLACπ interaction is in the bridge, coordinated to both metal ions.

For complexes with an intraligand MLACπ interaction, the range of the interaction distances (Table 2, structures 1−8) is small compared to other complexes with such interactions (Table 1 and Table 2). For example, the C−H distances range from 2.66 to 2.23 Å, which is smaller than in other complexes in Table 1 and Table 2 (structures 10−22). The C−H and C−N distances are the shortest (Table 1 and Table 2), but distances to the center of the aromatic ring are longer than for other complexes in Table 2. The reason for the small range of distances is that in all these complexes the interactions are very similar, and in all cases there are very strong steric constraints as the aromatic group and the interacting hydrogen atom are on the same ligand. At the same time the steric constrains do not allow the hydrogen atom to be directed to the center of the ring, but it remains close to only one or two carbon atoms in the ring.

Among all structures in Table 1 and Table 2, DUSJIK is the structure with the shortest distance between the hydrogen atom and the center of the ring. It is a very special structure, where Ni^{III} is coordinated by one pentadentate ligand and a water molecule. A pentadentate ligand is coordinated with five nitrogen atoms and has a benzyl group (Figure 1, d). There are a large number of bonds between the aromatic ring and the interacting hydrogen atom, and there is a possibility for the phenyl ring to orient itself in a way that the interacting hydrogen atom is directed to the center of the aromatic ring. The distance from the hydrogen atom to the center of the ring is 2.21 Å. The authors[56] noticed an unusual orientation of the benzyl group and a very short distance between the hydrogen atom and the aromatic ring, and attributed this to π-electron donor−acceptor interactions.

Among the structures where the aromatic group is separated from the metal center by several bonds (Table 2) there are a number of structures where the aromatic ring interacts with the hydrogen atom of another ligand (structures 10−22). In the structure LETYCU10 there is a five-coordinate complex of Cu^{II} (Figure 1, e). The dipeptide L-leucyl-L-tyrosine is coordinated as a tridentate chelate; the fourth coordination site is occupied by water. The fifth ligand is the carboxyl oxygen atom of a dipeptide, coordinated to another metal atom. In this way there are chains in the crystal structure. The aromatic ring interacts with the hydrogen atom of coordinated water. In this structure the interacting hydrogen atom is closer to the center of the ring (2.58 Å) than to the carbon atom (2.66 Å) (Table 2).

The ligand with the interacting hydrogen atom is very often coordinated water (all examples in Table 2, where the heavy atom is oxygen). In other cases the interacting hydrogen atom is part of some coordinated amine. In structures NALPIZ and ZURREJ there is a simple NH_3 ligand.

In many of the structures there are two MLACπ interactions in the same complex. In some complexes there are two pairs of identical ligands making almost identical interactions, as in the structures DEMHAE, DIXHAT, and NOVBAB (Table 2). In case of NALPIZ, two phenyl groups interact with the same NH_3 ligand, and it is the only structure in this group with this type of interaction. In the structure NUTKES, the complex is binuclear. In this case, in one of the MLACπ interactions the aromatic group is of the ligand forming the bridge, in the other interaction an aromatic group of one metal ion interacts with the H_2O molecule ligated to the other metal ion. These two interactions are rather different (Table 2).

In the complexes with the aromatic ring separated from the metal center by several bonds and interacting with hydrogen atoms of another ligand (Table 2, structures 11−22) there are less steric constraints preventing the interaction of the whole aromatic ring. Here the interaction distances to the center of the ring are shorter, and at the same time the distances to the closest carbon atom are longer compared with other complexes (Table 1 and Table 2, structures 1−8).

Calculated Intramolecular MLACπ Interactions

Since the complexes in which intramolecular MLACπ interactions exist are rather large, for DFT calculations model systems with smaller ligands were used. The geometries and energies for structures with various conformations of the aromatic ring in the model systems were calculated. Based on the difference in energy for conformers with and without MLACπ interactions, the energy of the interactions was evaluated. It can be expected that the partial positive charge on interacting hydrogen atoms depends on the charge of the whole complex. By quantum chemical calculations it was shown that the MLACπ interaction is stronger if the complex is more positively charged.[68] The evaluated energy in these calculations is for the model systems of cationic complexes of Co^{III} with charge of +1.

Calculations on Complexes with Two Bonds between the Aromatic Ring and the Metal Center

A suitable model system for calculations on this type of interactions was the cobalt(III) complex $[CoCl_2(NH_3)_3$-

Table 3. Some geometrical data of optimized conformers of model systems

Structure[a]	Type of interaction	Torsion angle [°][b]	N···center of ring [Å]	H···center of ring [Å]	N···C [Å]	H···C [Å]
$[CoCl_2(NH_3)_3(C_6H_5NH_2)]^+$	ligand in *cis* position	2.6	3.638	2.721	2.965	2.269
$[CoCl(NH_3)_3Phe]^+$						
	intraligand	49.8	3.875	3.091	2.973	2.425, 2.497
	ligand in *cis* position	49.8	3.674	2.654	3.584	2.579
	intraligand	−50.8	3.859	3.112	2.964	2.439, 2.683

[a] Structures are shown in Figure 2. – [b] In case of $[CoCl_2(NH_3)_3(C_6H_5NH_2)]^+$, the torsion angle is C1−N1−Co−N2, in case of $[CoCl(NH_3)_3Phe]^+$ the torsion angle is C1−Cβ−Cα−N1.

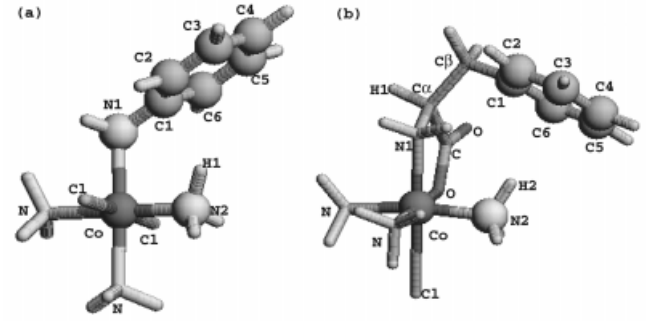

Figure 2. Geometries of model systems used for calculations of intramolecular MLACπ interactions: (a) $[CoCl_2(NH_3)_3(C_6H_5NH_2)]^+$, (b) $[CoCl(NH_3)_3Phe]^+$

$(C_6H_5NH_2)]^+$ (Figure 2, a). The coordinated aniline molecule has two NH_3 and two Cl^- ligands in *cis* positions. Optimizing the geometry for this complex always gives a structure where the aromatic ring is situated above the NH_3 group. In this structure the torsion angle C1−N1−Co−N2 (Figure 2, a) is 2.6°. One hydrogen atom of the NH_3 ligand is oriented towards the aromatic ring. The interaction distances C1···H1 and C1···N2 are 2.269 and 2.965 Å, respectively (Table 3). These distances are a little shorter than distances found in the crystal structures (Table 1). In order to find the energy of the geometry where the aromatic ring is above Cl we fixed the torsion angle C1−N1−Co−Cl to 2.6°, a value that we obtained for the torsion angle C1−N1−Co−N2 of the optimized structure. The difference in energy for structures where the aromatic ring is above the NH_3 and Cl^- ligands is 7.28 kcal/mol. In the first structure the aromatic ring has attractive interactions with the partially positively charged hydrogen atom (+0.36), in the second one it has repulsive interactions with the partially negatively charged chloro ligand (−0.22). Hence, the difference in energy is not only caused by attractive MLACπ interactions, but also by repulsive interactions. We evaluate that the energy of MLACπ interaction is about half of this difference, so it is between 3.5 and 4.0 kcal/mol.

Calculations on Complexes with Several Bonds between the Aromatic Ring and the Metal Center

In these complexes there is the possibility for the aromatic ring to interact with a hydrogen atom in the same ligand, or with the hydrogen atom in another ligand. To study both of these interactions we used the $[CoCl(NH_3)_3Phe]^+$ complex as model system (Figure 2, b). In the coordinated phenylalaninato ligand there are three possible conformations of the phenyl ring, which can be defined by the torsion angle C1−Cβ−Cα−N1 (Figure 2, b). The ideal values for this torsion angle are 60°, −60°, and 180°. Using these ideal torsion angles as a starting point for the optimization, gave optimized structures with angles of 49.8, −50.8, and −143.6°, respectively (Table 3). In the first conformer (with a torsion angle of 49.8°) there is an intraligand MLACπ interaction and a MLACπ interaction with the *cis*-NH_3 ligand. In the conformer with a torsion angle of −50.8° there is only an intraligand interaction, and in the conformer with the torsion angle of −143.6° there is no interaction. The calculated distances for intraligand MLACπ interactions (Table 3) are in the range of distances that are observed in crystal structures (Table 2, structures 1−8). In the case of the interaction of the phenyl ring with the NH_3 ligand in *cis* position, the calculated C−H distance (Table 3) is shorter than most of the C−H distances in crystal structures, while the calculated C−N distance is longer than most C−N distances in crystal structures (Table 2, structures 11−22).

The conformer with only one intraligand MLACπ interaction is more stable then the conformer without MLACπ interaction by 3.63 kcal/mol. The conformer with two MLACπ interactions is more stable by 7.61 kcal/mol. Since the distances of intraligand interactions are very similar in both conformers (Table 3), one can conclude that the energies are also similar. It means that in the conformer with the two MLACπ interactions, about 3.5 kcal/mol is stabilization for the intraligand interaction and the rest of about 4 kcal/mol is stabilization of interaction with the ligand in the *cis* position.

Conclusion

MLACπ interactions are proposed as intramolecular interactions in metal complexes. By coordination to a metal cation, ligands get positive charge, and can interact with an aromatic ring in the same complex. The Cambridge Structural Database was systematically searched to find intramolecular interactions between ligands coordinated to a metal center and aromatic rings. It turned out that this type of

interaction is ubiquitous in metal complexes. Examples were found for various metal ions and ligands. In most of the complexes there are two or four bonds between the metal center and the aromatic ring. The aromatic ring of an organic ligand can interact with a hydrogen atom of another ligand, or, in complexes where there are four or five bonds between the metal center and the aromatic ring also with hydrogen atoms of the same ligand. In this latter case, the aromatic ring can also interact with hydrogen atoms of the same ligand. The steric constraints in the complexes have an important influence on the geometry and probably the strength of intramolecular MLACπ interactions.

DFT calculations on model systems of Co^{III} complexes with a total charge of +1 have been done in order to evaluate the energy of intramolecular MLACπ interactions. Geometries and energies have been calculated for conformers with different orientations of the phenyl ring. Calculated geometric parameters of the interactions were very similar to those found in the crystal structures of complexes. By comparing the energies of conformers both with and without MLACπ interactions, we determined that the energy of interactions in these model systems is about 4 kcal/mol.

Experimental Section

Data Screening and Computational Methods: Crystal structures of metal complexes containing a phenyl ring and transition metal ions with coordinated nitrogen or oxygen atoms were extracted from the CSD. The structures of these metal complexes were screened for intramolecular cation−π interactions between ligands coordinated to the metal ion and aromatic groups using geometric criteria. We used the same criterion for distance as proposed by McFail-Isom et al.[25] for screening crystal structures of DNA for cation−π interactions between a metal ion and an aromatic base of DNA, for searching for MLACπ interactions in metalloproteins.[23] However, we did not use any restrictive criteria for the angle of the normal of the aromatic ring plane with the distance vector between the center of the aromatic ring and the metal center. Since in this case we were investigating intramolecular interactions, the aromatic ring is part of a ligand and therefore the orientation of the aromatic ring can be different. This is not the case where the aromatic group was not part of a coordinated ligand. We searched for structures, where the distance between the metal ion and the center of the aromatic ring is less than d_0 = 5.5 Å. Screening the CSD with the described criterion provided a large number of structures, where an aromatic ring is close to a metal center. We considered only structures with R factors < 0.06, and chose a number of structures where it was clear that an intramolecular MLACπ interaction between coordinated ligand and aromatic ring exists. Since it was shown that the interaction is stronger if the hydrogen atom that is interacting with the aromatic group is closer to the metal center,[23] we considered only structures where there are only two bonds between the hydrogen atom and the metal ion. − The optimized geometries and energies for the model system of the complexes with the cation−π interaction were obtained using the density functional theory (DFT) with the Becke (B3) three-parameter exchange function,[69] and the Lee−Yang−Parr (LYP) correlation functional.[70] These B3LYP calculations were carried out with the Gaussian98 program.[71] For all atoms the LANL2DZ basis sets were chosen. Recently, reliable results with DFT methods were obtained for other cation−π systems.[17][72−75] On the other hand, DFT methods also give good results for all transition metal complexes including transition metal complexes of the first row,[76−88] hence in this work the DFT method was used. − The geometries of all conformers of the model systems were fully optimized. Only in one case where the conformer was not a stationary point did we constrain the torsion angle of the aromatic ring in order to keep it in a certain position.

Acknowledgments

We would like to thank Prof. E. W. Knapp and Z. Tomić for useful discussions. M. M. was supported by a DAAD fellowship. The calculations were carried out at the computer center of the Free University of Berlin.

[1] D. A. Dougherty, *Science* **1996**, *271*, 163.
[2] J. C. Ma, D. A. Dougherty, *Chem. Rev.* **1997**, *97*, 1303.
[3] J. W. Caldwell, P. A. Kollman, *J. Am. Chem. Soc.* **1995**, *117*, 4177.
[4] R. A. Krumpf, D. A. Dougherty, *Science* **1993**, *261*, 1708.
[5] S. Mecozzi, A. P. West, Jr., D. A. Dougherty, *Proc. Natl. Acad. Sci. USA* **1996**, *93*, 10566.
[6] S. Mecozzi, A. P. West, Jr., D. A. Dougherty, *J. Am. Chem. Soc.* **1996**, *118*, 2307.
[7] P. C. Kearney, L. S. Mizoue, R. A. Kumpf, J. E. Forman, A. McCurdy, D. A. Dougherty, *J. Am. Chem. Soc.* **1993**, *115*, 9907.
[8] R. C. Dunbar, S. J. Klippenstein, J. Hrusak, D. Stocking, H. Schwarz, *J. Am. Chem. Soc.* **1996**, *118*, 5277.
[9] K. S. Kim, J. Y. Lee, S. J. Lee, T.-K. Ha, D. H. Kim, *J. Am. Chem. Soc.* **1994**, *116*, 7399.
[10] J. Y. Lee, S. J. Lee, H. S. Choi, S. J. Cho, K. S. Kim, T.-K. Ha, *Chem. Phys. Lett.* **1995**, *232*, 67.
[11] C. A. Deakyne, M. Meot-Ner (Mautner), *J. Am. Chem. Soc.* **1985**, *107*, 469.
[12] J. Mavri, J. Koller, D. Hadzi, *J. Mol. Struct. (Theochem)* **1993**, *283*, 305.
[13] H. Basch, W. J. Stevens, *J. Mol. Struct. (Theochem)* **1995**, *338*, 303.
[14] E. Cubero, F. J. Luque, M. Orozco, *Proc. Natl. Acad. Sci. USA* **1998**, *95*, 5976.
[15] W. Zhong, J. P. Gallivan, Y. Zhang, L. Li, H. A. Lester, D. A. Dougherty, *Proc. Natl. Acad. Sci. USA* **1998**, *95*, 12088.
[16] J. P. Gallivan, D. A. Dougherty, *J. Am. Chem. Soc.* **2000**, *122*, 870.
[17] J. Wouters, *J. Comput. Chem.* **2000**, *21*, 847.
[18] M. A. L. Eriksson, P. Y. Morgantini, P. A. Kollman, *J. Phys. Chem. B* **1999**, *103*, 4474.
[19] S. K. Burley, G. A. Petsko, *FEBS Lett.* **1986**, *203*, 139.
[20] J. P. Gallivan, D. A. Dougherty, *Proc. Natl. Acad. Sci. USA* **1999**, *96*, 9459.
[21] S. Zarić, *Chem. Phys. Lett.* **1999**, *311*, 77.
[22] S. Zarić, *Chem. Phys.* **2000**, *256*, 213.
[23] S. D. Zarić, D. Popović, E. W. Knapp, *Chem. Eur. J.* **2000**, *6*, 3935.
[24] D. Braga, F. Grepioni, E. Tadesco, *Organometallics* **1998**, *17*, 2669.
[25] L. McFail-Isom, X. Shui, L. D. Williams, *Biochemistry* **1998**, *37*, 17105.
[26] X. Shui, L. McFail-Isom, G. G. Hu, L. D. Williams, *Biochemistry* **1998**, *37*, 8341.
[27] R. C. Elder, M. J. Heeg, E. Deutsch, *Inorg. Chem.* **1978**, *17*, 427.
[28] M. Atoh, K. Kashiwabara, H. Ito, T. Ito, J. Fujita, *Bull. Chem. Soc. Jpn.* **1984**, *57*, 3139.
[29] R. J. Butcher, H. H. Hayden, M. M. D. Deyrup, C. B. Storm, *Acta Crystallogr., Sect. C* **1992**, *48*, 1122.

[30] V. N. Biyushkin, V. I. Gerasimov, V. A. Neverov, K. F. Belyaeva, V. N. Shafranskii, I. A. Popa, *Koord. Khim.* **1991**, *17*, 1115.
[31] R. C. Elder, M. J. Heeg, M. D. Payne, M. Trkula, E. Deutsch, *Inorg. Chem.* **1978**, *17*, 431.
[32] G. Albertin, S. Antoniutti, A. Bacchi, E. Bordignon, F. Busatto, G. Pelizzi, *Inorg. Chem.* **1997**, *36*, 1296.
[33] T. Hasegawa, T. Iwamoto, *J. Inclusion Phenom. Macrocycl. Chem.* **1988**, *6*, 143.
[34] D. Sellmann, K. Engl, T. Gottschalk-Gaudig, F. W. Heinemann, *Eur. J. Inorg. Chem.* **1999**, 333.
[35] P. B. Hitchcock, D. L. Hughes, M. J. Maguire, K. Marjani, R. L. Richards, *J. Chem. Soc., Dalton Trans.* **1997**, 4747.
[36] D. Touchard, C. Morice, V. Cadierno, P. Haquette, L. Toupet, P. H. Dixneuf, *J. Chem. Soc., Chem. Commun.* **1994**, 859.
[37] C. J. Adams, M. I. Bruce, B. W. Skelton, A. H. White, *J. Organomet. Chem.* **1996**, *513*, 255.
[38] N. de Vries, C. E. Costello, A. G. Jones, A. Davison, *Inorg. Chem.* **1990**, *29*, 1348.
[39] B. J. Rappoli, K. J. McGrath, C. F. George, J. C. Cooper, *J. Organomet. Chem.* **1993**, *450*, 85.
[40] S. M. Boniface, G. R. Clark, T. J. Collins, W. R. Roper, *J. Organomet. Chem.* **1981**, *206*, 109.
[41] S. P. Best, P. Chandley,R. J. H. Clark, S. McCarthy, M. B. Hursthouse, P. A. Bates, *J. Chem. Soc., Dalton Trans.* **1989**, 581.
[42] M. Sacerdoti, V. Bertolasi, G. Gilli, A. Duatti, *Acta Crystallogr., Sect. B* **1982**, *38*, 96.
[43] A. J. Deeming, P. J. Manning, I. P. Rothwell, M. B. Hursthouse, N. P. C. Walker, *J. Chem. Soc., Dalton Trans.* **1984**, 2039.
[44] C. Conway, R. D. W. Kemmitt, A. W. G. Platt, D. R. Russell, L. J. S. Sherry, *J. Organomet. Chem.* **1985**, *292*, 419.
[45] A. J. Deeming, S. Doherty, J. E. Marshall, J. L. Powell, A. M. Senior, *J. Chem. Soc., Dalton Trans.* **1993**, 1093.
[46] U. Abram, S. Ritter, *Inorg. Chim. Acta* **1993**, *210*, 99.
[47] J. R. Dilworth, P. Jobanputra, J. R. Miller, S. J. Parrott, Qin Chen, J. Zubieta, *Polyhedron* **1993**, *12*, 513.
[48] H. Muhonen, R. Hamalainen, *Finn. Chem. Lett.* **1983**, 120.
[49] K. Yanagi, M. Minobe, *Acta Crystallogr., Sect. C* **1987**, *43*, 2060.
[50] P. Leverett, J. Petherick, P. A. Williams, R. S. Vagg, *J. Coord. Chem.* **1996**, *37*, 195.
[51] K. Jitsukawa, K. Iwai, H. Masuda, H. Ogoshi, H. Einaga, *J. Chem. Soc., Dalton Trans.* **1997**, 3691.
[52] G. Maccarrone, G. Nardin, L. Randaccio, G. Tabbi, M. Rosi, A. Sgamellotti, E. Rizzarelli, E. Zangrando, *J. Chem. Soc., Dalton Trans.* **1996**, 3449.
[53] Y. Fujii, H. Shinohara, M. Mikuriya, S. Kida, Y. Konishi, *Bull. Chem. Soc. Jpn.* **1988**, *61*, 3511.
[54] A. Fehn, S. Mihan, K. Polborn, W. Beck, *Z. Anorg. Allg. Chem.* **1997**, *623*, 665.
[55] L. Carlucci, G. Ciani, D. W. v. Gudenberg, G. D′Alfonso, *J. Organomet. Chem.* **1997**, *534*, 233.
[56] R. Machida, E. Kimura, Y. Kushi, *Inorg. Chem.* **1986**, *25*, 3461.
[57] L. R. Nassimbeni, M. L. Niven, K. J. Zemke, *Chem. Commun.* **1985**, 1788.
[58] H. Muhonen, W. E. Hatfield, *Acta Chem. Scand., Ser. A* **1986**, *40*, 41.
[59] I. Dey, B. P. Mukhopadhyay, B. N. Das, S. Chakraborty, A. Banerjee, *J. Crystallogr. Spectrosc. Res.* **1993**, *23*, 65.
[60] D. van der Helm, S. E. Ealick, J. E. Burks, *Acta Crystallogr., Sect. B* **1975**, *31*, 1013.
[61] I. Vernik, D. V. Stynes, *Inorg. Chem.* **1996**, *35*, 6210.
[62] S. Kanemasa, Y. Oderaotoshi, H. Yamamoto, J. Tanaka, E. Wada, D. P. Curran, *J. Org. Chem.* **1997**, *62*, 6454.
[63] T. S. Yaukey, O. W. Steward, Shih-Chi Chang, *Acta Crystallogr., Sect. C* **1998**, *54*, 1081.
[64] J. L. Kerschner, P. E. Fanwick, I. P. Rothwell, *J. Am. Chem. Soc.* **1987**, *109*, 5840.
[65] M. J. Bartos, C. E. Kriley, J. S. Yu, J. L. Kerschner, P. E. Fanwick, I. P. Rothwell, *Polyhedron* **1989**, *8*, 1971.
[66] H. Yuge, Y. Noda, T. Iwamoto, *Inorg. Chem.* **1996**, *35*, 1842.
[67] V. C. Gibson, C. Redshaw, W. Clegg, M. R. J. Elsegood, *J. Chem. Soc., Dalton Trans.* **1997**, 3207.
[68] S. D. Zarić, unpublished results
[69] A. D. Becke, *J. Chem. Phys.* **1993**, *98*, 5648.
[70] C. Lee, W. Yang, R. G. Parr, *Phys. Rev. B* **1988**, *37*, 785.
[71] M. J. Frisch, G. W. Trucks, H. B. Schlegel, G. E. Scuseria, M. A. Robb, J. R. Cheeseman, V. G. Zakrzewski, J. A. Montgomery, Jr., R. E. Stratmann, J. C. Burant, S. Dapprich, J. M. Millam, A. D. Daniels, K. N. Kudin, M. C. Strain, O. Farkas, J. Tomasi, V. Barone, M. Cossi, R. Cammi, B. Mennucci, C. Pomelli, C. Adamo, S. Clifford, J. Ochterski, G. A. Petersson, P. Y. Ayala, Cui, Q., K. Morokuma, D. K. Malick, A. D. Rabuck, K. Raghavachari, J. B. Foresman, J. Cioslowski, J. V. Ortiz, B. B. Stefanov, G. Liu, A. Liashenko, P. Piskorz, I. Komaromi, R. Gomperts, R. L. Martin, D. J. Fox, T. Keith, M. A. Al-Laham, C. Y. Peng, A. Nanayakkara, C. Gonzalez, M. Challacombe, P. M. W. Gill, B. Johnson, W. Chen, M. W. Wong, J. L. Andres, C. Gonzalez, M. Head-Gordon, E. S. Replogle, J. A. Pople, *Gaussian 98, Revision A.6*, Gaussian, Inc., Pittsburgh PA, **1998**.
[72] X. J. Tan, H. L. Jiang, W. L. Zhu, K. X. Chen, R. Y. Ji, *J. Chem. Soc., Perkin Trans. 2* **1999**, 107.
[73] P. C. Miklis, R. Ditchield, T. A. Spencer, *J. Am. Chem. Soc.* **1998**, *120*, 10482.
[74] J. B. Nickolas, B. P. Hay, D. A. Dixon, *J. Phys. Chem. A* **1999**, *103*, 1394.
[75] W. L. Zhu, H. L. Jiang, C. M. Puah, X. J. Tan, K. X. Chen, Y. Cao, R. Y. Ji, *J. Chem. Soc., Perkin Trans. 2* **1999**, 2615.
[76] S. Niu, M. B. Hall, *J. Am. Chem. Soc.* **1997**, *119*, 3077.
[77] J. L. C. Thomas, M. B. Hall, *Organometallics* **1997**, *16*, 2318.
[78] S. Zarić, M. B. Hall, *J. Phys. Chem.* **1998**, *102*, 1963.
[79] J. L. C. Thomas, C. W. Jr. Bauschlicher, M. B. Hall, *J. Phys. Chem.* **1997**, *101*, 8530.
[80] D. L. Strout, S. Zarić, S. Niu, M. B. Hall, *J. Am. Chem. Soc.* **1996**, *118*, 6068.
[81] S. Niu, M. B. Hall, *J. Am. Chem. Soc.* **1998**, *120*, 6169.
[82] S. Niu, S. Zarić, D. L. Strout, C. A. Bayse, M. B. Hall, *Organometallics* **1998**, *17*, 5139.
[83] P. E. M. Siegbahn, R. H. Crabtree, *J. Am. Chem. Soc.* **1997**, *119*, 3103.
[84] D. H. Jones, A. S. Hinman, T. Ziegler, *Inorg. Chem.* **1993**, *32*, 2092.
[85] C. Rovira, P. Ballone, M. Parrinelo, *Chem. Phys. Lett.* **1997**, *271*, 247.
[86] C. Rovira, K. Kunc, J. Hutter, P. Ballone, M. Parrinelo, *Int. J. Quant. Chem.* **1998**, *69*, 31.
[87] T. Ziegler, *Can. J. Chem.* **1995**, *73*, 743.
[88] C. Rovira, K. Kunc, J. Hutter, P. Ballone, M. Parrinelo, *J. Phys. Chem. A* **1997**, *101*, 8914.

Received September 19, 2000
[I00357]

Stereoselective Interactions and Photo-Electron Transfers between Mononucleotides or DNA and the Stereoisomers of a HAT-Bridged Dinuclear Ru^{II} Complex (HAT = 1,4,5,8,9,12-hexaazatriphenylene)

André Brodkorb,[a] Andrée Kirsch-De Mesmaeker,*[a] Todd J. Rutherford,[b] and F. Richard Keene[b]

Keywords: Electron transfer / Ruthenium / DNA recognition / Molecular recognition / Stereoselectivity

The dinuclear complex $[\{Ru(phen)_2\}_2(\mu\text{-HAT})]^{4+}$ (phen = 1,10-phenanthroline, HAT = 1,4,5,8,9,12-hexaazatriphenylene), can exist in three different stereoisomeric forms: the *meso* ($\Delta\Lambda$) and *rac* diastereoisomers, the latter of which has two enantiomeric forms, namely $\Delta\Delta$ and $\Lambda\Lambda$. Each of the stereoisomers was studied in the presence of the mononucleotides guanosine 5′-monophosphate (GMP) and adenosine 5′-monophosphate (AMP), and deoxyguanosine (dG) at pH = 7 and 9. Absorption studies revealed the formation of ion pairs or aggregates between the complexes and the mononucleotides (GMP and AMP) and dG. The equilibrium constants for the formation of these species were higher for the *meso* form than for the $\Delta\Delta$ and $\Lambda\Lambda$ enantiomers. Laser flash photolysis indicated the existence of a stereoselective photo-induced electron-transfer between the guanine of GMP and the stereoisomers. Luminescence data with the purine mononucleotides also indicated the existence of an equilibrium between the free excited complex and a luminescent ion pair or an emitting aggregate between the complex and the mononucleotide. The luminescence of these species depended on the pH and on the identity of the stereoisomer. The investigated spectroscopic behaviour of the complex stereoisomers in the presence of denatured CT-DNA was also isomer-dependent, in agreement with the conclusions drawn from the data with the mononucleotides. The results of this work clearly indicate stereoselectivity of the interaction with the purine mononucleotides and denatured CT-DNA in the ground and excited state of the complex, in favour of the *meso* form in both cases.

Introduction

Ruthenium complexes involving polypyridyl ligands have been studied in numerous research contexts,[1−3] more recently as photo-probes and photo-reagents of DNA.[4−6] It was shown that the mononuclear Ru^{II} complexes with oxidising polyazaaromatic ligands are able to photo-oxidise the guanines by a direct electron transfer with formation of a reduced complex.[7,8] This charge transfer process was demonstrated by laser flash photolysis and was compared with the photo-induced electron transfer observed with guanosine 5′-monophosphate (GMP). The associated luminescence quenching by GMP could be analysed easily.

The dinuclear complex $[\{Ru(phen)_2\}_2(\mu\text{-HAT})]^{4+}$ (Figure 1) is also rather oxidising due to the bridging hexaazatriphenylene ligand HAT (the redox potential in the excited state is significantly positive, +1.04 V/SCE).[9] Therefore, like the mononuclear complexes with oxidising polyazaaromatic ligands, this species under illumination is also able to abstract an electron from a guanine molecule. However, in contrast to the situation with the mononuclear species, the first experiments with the dinuclear complex revealed the presence of aggregates with GMP, which made the quenching behaviour by GMP difficult to interpret.[10] These experiments with GMP had been performed with the nonseparated stereoisomers present after synthesis of the dinuclear complex. As the stereoisomeric mixture could be the cause of the complicated behaviour, in this work, we have carefully examined the effects of GMP and the other mononucleotides on the photophysical behaviour of each stereoisomer (viz. the $\Delta\Delta$ and $\Lambda\Lambda$ enantiomers and the *meso* form $\Delta\Lambda$, Figure 1) obtained after chromatographic separation.[11] The goal is not only to clarify the quenching behaviour, but also to investigate the possible existence of stereospecific formation of aggregates and stereospecific electron transfer process.

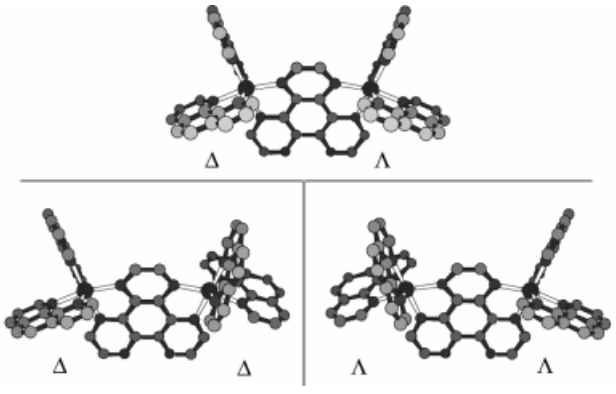

Figure 1. Chem 3D structure of the three stereoisomers $\Delta\Delta$, $\Lambda\Lambda$, and $\Delta\Lambda$ (*meso*) of the dinuclear complex $[\{Ru(phen)_2\}_2(\mu\text{-HAT})]^{4+}$

[a] Laboratoire de Chimie Organique Physique CP 160/08, Université Libre de Bruxelles,
50 avenue F. D. Roosevelt, 1050 Bruxelles, Belgium
E-mail: akirsch@ulb.ac.be
[b] School of Biomedical and Molecular Sciences, James Cook University,
Townsville, Queensland 4811, Australia

 © WILEY-VCH Verlag GmbH, 69451 Weinheim, 2001 1434−1948/01/0808−2151 $ 17.50+.50/0

Although with the mononuclear Ru^{II} compounds, understanding of the behaviour with the mononucleotides constituted a valuable help in rationalising the effect of DNA, with the dinuclear complex $[\{Ru(phen)_2\}_2(\mu\text{-HAT})]^{4+}$ the situation is again more complicated. It was indeed shown that this species does not interact with a polynucleotidic double helix (normal calf thymus DNA or synthetic polynucleotides), but interacts with denatured calf thymus DNA.[12] This behaviour was attributed to the fact that the large dinuclear complex cannot penetrate inside the DNA grooves of a normal double-stranded DNA, but can be hosted inside pockets formed by the two strands of denatured DNA separated along a certain number of bases. These deformation sites (bulges, hairpins etc.) contain more AT than GC base pairs.[13] Therefore, a correlation between a luminescence quenching of the complex by GMP and by denatured DNA, as observed previously with mononuclear complexes, is not expected. Moreover, the interaction of the complex is probably controlled by the recognition of certain uncharacterised deformation sites present in denatured DNA. This is in contrast to the situation with mononuclear species that interact inside the regular grooves of a normal DNA double helix. In spite of these limitations for the comparison of the effects of mononucleotides and DNA, we have also examined in this work, the behaviour of each stereoisomer of $[\{Ru(phen)_2\}_2(\mu\text{-HAT})]^{4+}$ with denatured DNA. The goal is to test whether there would be some stereospecific recognition in the interaction sites of this DNA and whether it would be the same as that with the mononucleotides.

Results

1. Absorption Spectroscopy in the Presence of Mononucleotides and dG

In water, the absorption spectra of the three stereoisomers of $[\{Ru(phen)_2\}_2(\mu\text{-HAT})]^{4+}$ are similar (Figure 2a, b, c). Organic solvents were avoided in this study because it was previously observed[9] that slow (photo) degradation of the complex occurred in nonaqueous environments.

As shown in Figure 2a, the addition of GMP to the *meso* form of $[\{Ru(phen)_2\}_2(\mu\text{-HAT})]^{4+}$ in aqueous solution at pH = 7 induced an important blue shift on the 570-nm absorption component of the MLCT band. AMP had a much less pronounced effect, and shifted this band slightly to the red region. CMP and TMP had no effect at all. On the other hand, as shown by the comparison of Figure 2a with b and c, the *meso* form displayed the most significant change on the addition of GMP compared with the ΛΛ and ΔΔ enantiomers (the *meso* form was also the most affected by AMP). Only the GMP and dG effects were analysed quantitatively, because the influence of AMP was too weak (even with the *meso* form) to allow a quantitative treatment.

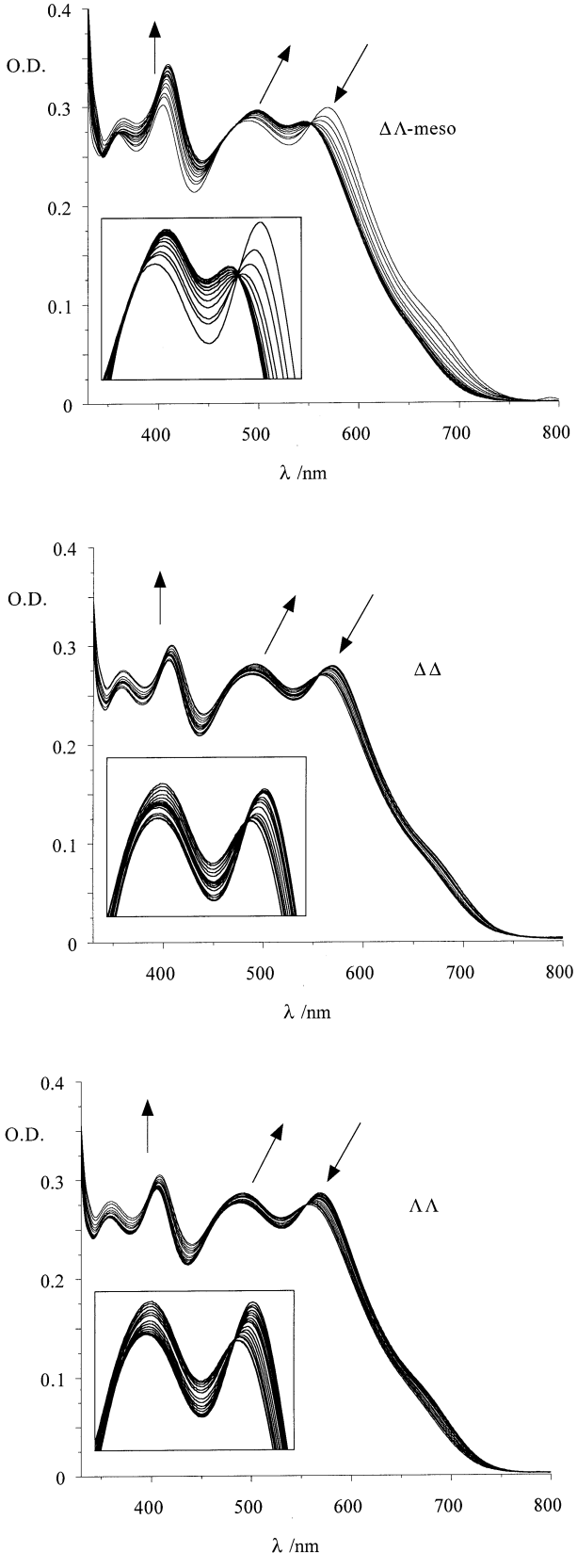

Figure 2. Absorption spectra of (a, top) *meso*-, (b, center) ΔΔ-, and (c, bottom) ΛΛ-$[\{Ru(phen)_2\}_2(\mu\text{-HAT})]^{4+}$ (5×10^{-5} M) in the presence of increasing GMP concentrations until 80 mM GMP at pH = 7 (100 mM phosphate buffer); inset: expansion of the MLCT band

Analysis of the GMP Effect at pH = 7

Examination of the spectra (Figure 2a, b, c) shows that isosbestic points were observed. This suggests that a 1:1

ground state association exists between the Ru complex and the mononucleotide, but only at lower GMP concentrations (< 80 mM). For higher GMP concentrations, the isosbestic points became diffuse and associations of higher order or different geometry probably took place.

$$[\{Ru(phen)_2\}_2(\mu\text{-HAT})]^{4+} + GMP \overset{K_{gs}}{\rightleftharpoons} \{[\{Ru(phen)_2\}_2(\mu\text{-HAT})]^{4+}\cdots GMP\}$$

The ground state association constant K_{gs} can be calculated using the Hildebrand−Benesi Equation (1)[14], where ΔA represents the difference in absorption in the absence and in the presence of mononucleotide ($\Delta A = A_0 - A_{GMP}$) at a given wavelength, and $\Delta\varepsilon$ is the difference of the molar extinction coefficients of the free and associated complex ($\Delta\varepsilon = \varepsilon_F - \varepsilon_A$).

$$\frac{1}{\Delta A} = \frac{1}{\Delta\varepsilon[Ru]} + \frac{1}{\Delta\varepsilon[Ru]K_{gs}[GMP]} \quad (1)$$

The changes of concentration of free GMP due to this equilibrium were negligible compared with the amount of added GMP (i.e. $[GMP]_0$). This was not true for the free Ru complex concentration that varied with the addition of GMP because the initial concentration (i.e. $[Ru]_0 = 5 \times 10^{-5}$ M for each stereoisomer) was much lower. When $1/\Delta A$ was plotted as a function of $1/[GMP]_0$, K_{gs} was obtained from the intercept/slope ratio (Figure 3). The corresponding values for the association constants for each stereoisomer were tentatively determined in this way. Only the value of the association constant for the *meso* form is given in Table 1, because there is no dependence with the wavelength in this case, and the variation of absorption is well measurable.

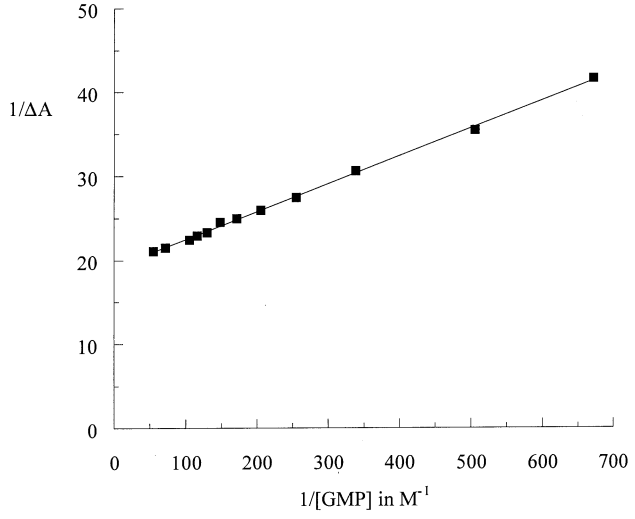

Figure 3. Hildebrand−Benesi plots for *meso*-[{Ru(phen)$_2$}$_2$(μ-HAT)]$^{4+}$ in the presence of GMP at pH = 7 (100 mM phosphate buffer) at 570 nm

Table 1. Association constants K_{gs} for the *meso* form in the presence of GMP and dG at pH = 7 and 9; estimated experimental error ca. 10%

	pH	K_{gs} [M^{-1}]
GMP	7	585
GMP	9	445
dG	7	335
dG	9	270

As shown in Figure 2b and c, the absorbance changes for the two enantiomers ΔΔ and ΛΛ were weak (the errors associated with K_{gs} thus become larger), and in addition the estimated values for the association constants varied with the wavelength of the measurement. For the ΛΛ enantiomer, the value varied from 65 M^{-1} at 570 nm to 7 M^{-1} at 405 nm. For the ΔΔ enantiomer, K_{gs} = 17 M^{-1} at 570 nm and could not be determined at 405 nm because the Hildebrand−Benesi plot was not linear in the concentration range studied. These problems reveal the presence of more than one type of aggregate complex-GMP, so that the Hildebrand−Benesi model of a 1:1 association is no longer valid for the two enantiomers.

Analysis of the GMP Effect at pH = 9

As some luminescence experiments were carried out at pH = 9 (see below), the effect of GMP on the absorption spectra of the complexes was also examined at pH = 9. The charge of GMP became more negative at pH = 9 due to further deprotonation of the phosphate group and to partial deprotonation of the guanine base.[13] The addition of GMP to a buffered solution (pH = 9) of *meso*-[{Ru(phen)$_2$}$_2$(μ-HAT)]$^{4+}$ again revealed a significant change in the absorption spectra (not shown), which was very similar to the one observed at pH = 7. The resulting calculated association constant (Table 1) is of the same order of magnitude as observed at pH = 7, at least for GMP concentrations below 25 mM. For higher GMP concentrations, deviations in the linear Hildebrand−Benesi plot appear. Again, the ΔΔ and ΛΛ enantiomers behaved differently. The K_{gs} values varied with the wavelength of measurement; for the ΛΛ enantiomer it varied from 140 M^{-1} at 570 nm to 7 M^{-1} at 405 nm, and for the ΔΔ enantiomer from 200 M^{-1} at 570 nm to a nonmeasurable value at 405 nm. This wavelength dependence again reflects the presence of more than one type of aggregate, where the Hildebrand−Benesi model is no longer valid.

Analysis of the dG Effect at pH = 7 and 9

The effect of dG on the absorption of the complexes was examined. A difference in the complex behaviour by the addition of GMP or dG is indeed possible due to the absence of the negatively charged phosphate group in dG, while the base and the chirality of the sugar component remained unchanged. The deoxyguanosine was selected instead of guanosine because of its better solubility in water,

although still limited. The titration with dG could thus be carried out only up to a concentration of 7 mM in dG.

The absorption spectrum of the *meso* form at pH = 7 was significantly changed by the presence of dG (not shown). There was a blue shift in the 570 nm band, similar to that observed with GMP at pH = 7. The association constant was smaller compared with the case for GMP at pH = 7 (Table 1). In contrast to this, the variation of absorption of the two enantiomers ΔΔ and ΛΛ with the addition of dG did not produce isosbestic points, and determination of the association constants was not possible because the Hildebrand−Benesi plots were not linear.

At pH = 9, only the *meso* form exhibited a significant change of the absorption in the presence of dG, with the appearance of an isosbestic point. The corresponding value of K_{gs} was smaller than at pH = 7 (Table 1). The treatment of the results for the enantiomers ΔΔ and ΛΛ at pH = 9 led to the same problems observed at pH = 7.

2. Steady State Emission Spectroscopy in the Presence of Mononucleotides and dG

Emission occurs from the triplet MLCT state, which corresponds to the lowest excited state of the dinuclear species (i.e. an Ru → μ-HAT ^{3}MLCT state).[9] In the absence of nucleotide no difference in the luminescence maximum was found between the *meso* compound and the two enantiomers. However, a difference of quantum yield of emission was observed with $\varphi_{meso} < \varphi_{racemic}$.[11]

Change of Emission with GMP

The addition of GMP at pH = 7 and 9 produced a significant blue shift of the emission, which followed the order *meso* (ca. 30 nm) > ΔΔ (ca. 5 nm) > ΛΛ (no shift). Because the emission maximum appeared in the region of 800 nm, where the sensitivity of the red-sensitive photomultiplier tube drastically decreases, all the spectra had to be corrected. As this correction becomes very important around 800 nm, it is difficult to give accurate values for the spectral shifts. The same problem of sensitivity has previously prevented us from determining the emission quantum yield of each stereoisomer.[11]

Emission Intensity at pH = 7

For the *meso* form, the emission intensity increased slightly with the addition of GMP at pH = 7 (30% emission increase with 80 mM GMP). Figure 4 shows the plot of I_0/I versus the GMP concentration, where I_0 represents the luminescence intensity in the absence of GMP and I in the presence of GMP. As the emission intensity I was enhanced with GMP, I_0/I decreased for the *meso* form and reached a plateau at approximately 20 mM in GMP. In contrast, the I_0/I values versus the GMP concentration for the two enantiomers at pH = 7 appear to lead to normal Stern−Volmer plots, indicating a quenching by GMP (for ΛΛ 24% and for ΔΔ 12% quenching at 80 mM GMP). However, these plots exhibit a downward curvature for increasing GMP concentrations.

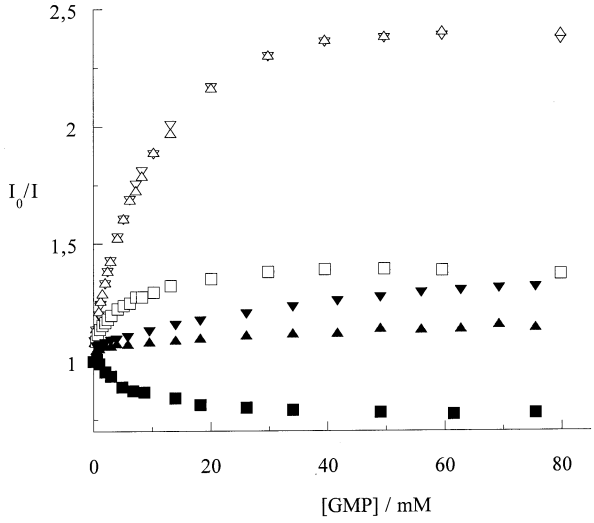

Figure 4. I_0/I vs. GMP concentration (I_0 is the emission intensity in the absence of GMP and I is the emission intensity in the presence of GMP) for the stereoisomers of $[\{Ru(phen)_2\}_2(\mu\text{-HAT})]^{4+}$ (100 mM phosphate buffer); full markers for pH = 7, open markers for pH = 9; ■ = *meso*, ▲ = ΔΔ, ▼ = ΛΛ

Emission Intensity at pH = 9

The guanine base is partially deprotonated at pH = 9. Therefore, the redox potential associated with the oxidation of the guanine of GMP is less anodic at pH = 9 than at pH = 7 (60 mV/pH unit). In agreement with this increased reducing power of the guanine at pH = 9, the excited state of $[\{Ru(phen)_2\}_2(\mu\text{-HAT})]^{4+}$ was reductively quenched more efficiently by the nucleotide base at pH = 9 than at pH = 7, following the order ΛΛ ≈ ΔΔ (58% quenching at 80 mM GMP) > *meso* (27% quenching at 80 mM GMP). Thus the emission of the *meso* form, although enhanced by GMP at pH = 7, was quenched at pH = 9 (Figure 4). The corresponding I_0/I plots versus [GMP] for the three stereoisomers at pH = 9 deviate significantly from a linear Stern−Volmer plot, and reveal a downward curvature, reaching a plateau for GMP concentrations larger than 20 mM for the *meso* form and 40 mM for the enantiomers. It is interesting to note that for the *meso* form, the I_0/I plots at pH = 9 (luminescence quenching) and at pH = 7 (luminescence enhancement) appear to be quasi-mirror images around the x axis.

Effect of dG at pH = 7

It is difficult to measure the change of luminescence of the three stereoisomers upon addition of dG at pH = 7. This is mainly due to the low concentration of dG that can be used for the titration (not higher than 7 mM). However, the slight change in the emission intensities followed the same tendency as for the titration with GMP at pH = 7. Thus, the emission of the *meso* form increased slightly,

whereas the emission of the ΔΔ and ΛΛ enantiomers decreased slightly with the addition of dG.

Effect of dG at pH = 9

As expected, the change in pH again had a significant effect on the emission. As observed with GMP, the emission of the three stereoisomers was quenched when dG was added at pH = 9, following the order ΛΛ ≈ ΔΔ (45% quenching at 7 mM dG) > *meso* (35% quenching at 7 mM dG). The Stern−Volmer plots are curved slightly downward and are very similar to the titrations with GMP at pH = 9 in the same concentration range of quencher (< 7 mM).

Effect of the other Mononucleotides at pH = 7

The presence of AMP did not significantly change either the intensity or the λ_{max} value of emission at pH = 7. Thus, no change was observed for the ΛΛ form, and a very slight intensity increase was detected for the ΔΔ and the *meso* forms. As no quenching was detected with AMP at pH = 7, no further experiments were performed at pH = 9 for a comparison of quenching efficiency. No effect of CMP and TMP was detected on the emission

3. Laser Flash Photolysis in the Presence of Mononucleotides

The existence of a photo-induced electron transfer from GMP (pH = 7) to the excited $[\{Ru(phen)_2\}_2(\mu\text{-HAT})]^{4+}$ with samples containing the three nonseparated stereoisomers has been demonstrated previously by laser flash photolysis experiments.[10] However, since each stereoisomer exhibited a different absorption and luminescence behaviour in the presence of GMP at pH = 7, laser flash photolysis experiments were carried out again in the present work with each stereoisomer separately. In each case, the differential transient absorption recorded 1 μs after the laser pulse, in the presence of 70 mM GMP, indicated the existence of a long-lived mono-reduced complex (even with the *meso* compound). The absorption transients decayed during a few hundred μs and did not reach the baseline after this decay time (Figure 5).

This absorption that remained, was attributed to the formation of a photo-product.[10] The intensity of the transient absorption (Figure 5) was too weak to perform a kinetic analysis. However, the differential transient absorption was slightly higher for the ΛΛ enantiomer than for the ΔΔ form, and the signal of the latter was somewhat higher than that of the ΔΛ (*meso*) form. Although this difference in intensity was not much larger than the error limit, it is interesting to note that it followed the same trend as observed for the luminescence quenching, i.e. ΛΛ > ΔΔ, and no quenching for the *meso* form. Although no flash photolysis experiments were performed at pH = 9, nor with dG, the existence of a photo-electron transfer can nevertheless be assumed at pH = 9 as a luminescence quenching was clearly observed at this pH for the three stereoisomers, and it was more pronounced than at pH = 7. No mono-reduced species was detected in the presence of AMP, CMP, or TMP

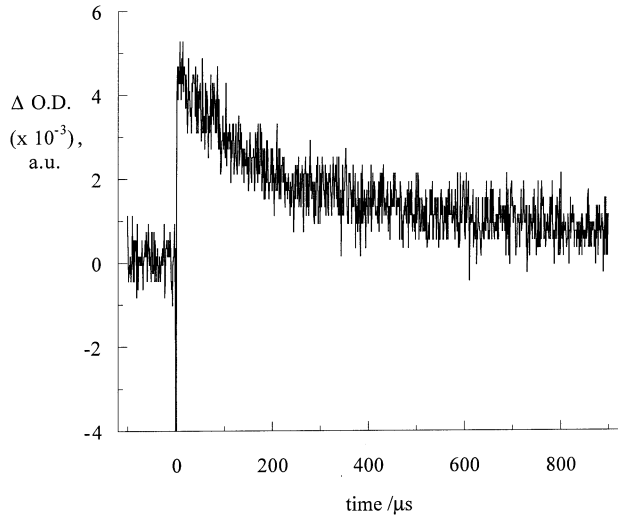

Figure 5. Laser flash photolysis; transient absorption decay for ΔΔ-$[\{Ru(phen)_2\}_2(\mu\text{-HAT})]^{4+}$ under pulsed excitation in the presence of 70 mM GMP at pH = 7 (100 mM phosphate buffer)

at pH = 7, which means that there is no electron transfer between these mononucleotides and the excited complex $[\{Ru(phen)_2\}_2(\mu\text{-HAT})]^{4+}$ under these conditions.

4. Time-Resolved Emission Spectroscopy in the Presence of Mononucleotides and dG

In the absence of mononucleotides, the excited state lifetimes in air-equilibrated buffered solutions at pH = 7 were the same (as expected) for both enantiomers ΔΔ and ΛΛ, τ_0 = 295 ± 5 ns, but it was shorter for the diastereoisomer ΔΛ-(*meso*), τ_0 = 221 ± 4 ns (Table 2). No differences in lifetimes were detected between pH = 7 and 9. Moreover, no clear measurable differences were observed in the presence of CMP or TMP.

In contrast, the luminescence decays of each stereoisomer in the presence of GMP, dG (at both pH = 7 and pH 9), and AMP (at pH = 7) were not strictly single-exponential decays (Table 2). They could be analysed according to bi-exponential decays, where the short component had a very low percentage contribution and the longer component always contributed more than 80% (normalised pre-exponential factor, see Table 2). Since laser flash photolysis experiments clearly showed that there was no electron transfer from AMP to the excited complex at pH = 7, the shorter lifetime components with AMP (Table 2) cannot be associated with a quenching process by the mononucleotide. Therefore, in this case the short component probably arises from dynamic processes, such as those associated with the equilibrium in the excited state between the free complex and the complex in aggregation with the mononucleotide. Such biphasic decays can indeed be expected when an equilibrium takes place in the same time domain as the deactivation processes to the ground state.[15] Under such conditions the lifetimes correspond to apparent lifetimes.

With GMP or dG, the short components could have the same origin because GMP and dG also form ion pairs or aggregates with the complex, as discussed above. Both long

Table 2. Luminescence lifetimes in ns for the stereoisomers in buffered solution (100 mM phosphate buffer pH = 7 and 9) under air; weighted average lifetimes[19]

[a]	*meso*	ΔΔ	ΛΛ
In buffer (pH = 7 or 9)	221 ± 4	295 ± 5	295 ± 5
GMP (a) pH = 7	**τ_{av} = 258**	**τ_{av} = 278**	**τ_{av} = 260**
	τ_1 = 275 ± 5 (91%)	τ_1 = 288 ± 5 (93%)	τ_1 = 281 ± 5 (88%)
	τ_2 = 114 ± 10 (9%)	τ_2 = 142 ± 40 (7%)	τ_2 = 100 ± 15 (12%)
GMP (a) pH = 9	**τ_{av} = 170**	**τ_{av} = 141**	**τ_{av} = 155**
	τ_1 = 192 ± 5 (84%)	τ_1 = 165 ± 5 (82%)	τ_1 = 169 ± 5 (84%)
	τ_2 = 60 ± 3 (16%)	τ_2 = 32 ± 13 (18%)	τ_2 = 79 ± 13 (16%)
dG (b) pH = 7	τ = 230 ± 0.3 (100%)	τ = 294 ± 0.5 (100%)	τ = 290 ± 0.5 (100%)
dG (b) pH = 9	τ = 146 ± 0.2 (100%)	**τ_{av} = 157**	**τ_{av} = 180**
		τ_1 = 179 ± 0.3 (86%)	τ_1 = 171 ± 3 (94%)
		τ_2 = 25 ± 3 (14%)	τ_2 = 322 ± 44 (6%)
AMP (a) pH = 7	**τ_{av} = 312**	**τ_{av} = 302**	**τ_{av} = 337**
	τ_1 = 335 ± 5 (89%)	τ_1 = 311 ± 5 (94%)	τ_1 = 333 ± 5 (91%)
	τ_2 = 111 ± 15 (11%)	τ_2 = 163 ± 35 (6%)	τ_2 = 128 ± 40 (9%)
Denat. DNA (a, c)	**τ_{av} = 494**	**τ_{av} = 431**	**τ_{av} = 392**

[a] $\tau_{av} = (\Sigma B_i\tau_i)/\Sigma B_i$ for the bi-exponential decays; $I(t) = A + B_1 \exp(-t/\tau_1) + B_2 \exp(-t/\tau_2)$ in the presence of mononucleotides, τ_1 and τ_2 are the corresponding two lifetimes components with their normalised contribution; $\alpha_j = 100\% \times B_j/\Sigma B_i$. The mononucleotide concentrations correspond to the approximate plateau value of I_0/I (Figure 4), i.e. [GMP] = 100 mM at pH = 7, [GMP] = 20 mM at pH = 9, [dG] = 7 mM (maximum concentration which can be reached) at pH = 7 and 9, [AMP] = 20 mM at pH = 7. (a): Measurements performed with the mode-locked argon pumped dye laser (see Exp. Sect.). (b): Measurements performed with the Edinburgh Instruments SPC (see Exp. Sect.). The number of counts at the decay maximum is lower for these measurements (5000 counts). The decays are therefore of poor quality so that they do not always allow the detection of a low contribution of a second decay component. (c): Weighted average lifetimes for the multi-exponential decays; 10 mM phosphate buffer pH = 7, [Nu]/[Ru] = 30 (Nu = concentration of equivalent nucleobases in denatured CT-DNA).

and short decay components varied with the GMP or dG concentration. Because of the difficulties related to the experimental measurements at 800 nm, and the resultant poor quality of the signal, and the complexity of the kinetic treatment (see Discussion), only the results for the decays corresponding to the higher nucleotide concentration (where a plateau was reached for the I_0/I plots, Figure 4) are collected in Table 2. For the sake of comparison, the weighted average lifetimes are given in Table 2 as the values of each component probably correspond to apparent lifetimes.

Effect of GMP

The weighted average lifetimes were slightly affected by the presence of 100 mM GMP at pH = 7 (Table 2). The ΔΔ and ΛΛ forms appeared to be quenched, whereas for the *meso* form the average emission lifetime increased in the presence of GMP. At pH = 9, the lifetimes of the three stereoisomers were clearly shortened by GMP in the order ΔΔ > ΛΛ > *meso*. It is interesting to note that at both pH values, the luminescence quenching was more pronounced for the enantiomers than for the *meso* form. These results are in agreement with the steady-state emission results. In order to detect a possible short-lived species in the subnanosecond time range, an additional experiment was carried out with the *meso* form in the presence of 100 mM GMP at pH = 7 in a much shorter time range. No luminescent short-lived component with a lifetime shorter than a few hundred ps could be detected under those conditions. This experiment was performed with the *meso* form because the laser flash photolysis experiments indicated the formation of a small amount of monoreduced complex, although no obvious decrease of emission intensity or of the average luminescence lifetime could be detected.

Effect of dG

As the concentration of dG did not exceed 7 mM, an effect on the lifetimes was difficult to detect. A shortening of the τ_{av} value was only clearly observed at pH = 9, and it followed the same trend as in the equivalent experiment with GMP at pH = 9.

Effect of AMP

The addition of AMP at pH = 7 significantly increased the weighted average luminescence lifetime of the excited *meso* form. There was no major effect on the average emission lifetimes of the enantiomers.

6. Absorption and Emission Spectroscopy with Denatured DNA

Absorption and emission measurements for different ratios of denatured DNA/complex at a constant complex concentration were taken, starting from a high ratio and diluting the sample step by step with a buffered stock solution of the complex (10 mM phosphate buffer). No NaCl was added in order to induce a higher binding of the complex to the DNA. In this part of the work, as explained in the introduction, only the effect of denatured CT-DNA was examined because normal double-stranded DNA had no effect,[10] even when the experiment was performed with each stereoisomer.

In the presence of denatured CT-DNA at pH = 7, the absorption spectra changed in a similar manner as observed in the presence of GMP (i.e. a hypsochromic shift), with the same trends from one isomer to the other. Thus the *meso* diastereoisomer showed the largest hypsochromic absorption shift, followed by the ΔΔ and ΛΛ forms. However, the hypsochromic shift of the 570-nm absorption band with denatured CT-DNA was not as pronounced as with GMP.

The emission intensity of the three stereoisomers increased in the presence of denatured CT-DNA (Figure 6). The *meso* form exhibited the highest increase of emission and the ΛΛ form showed the weakest enhancement (*meso* > ΔΔ > ΛΛ).

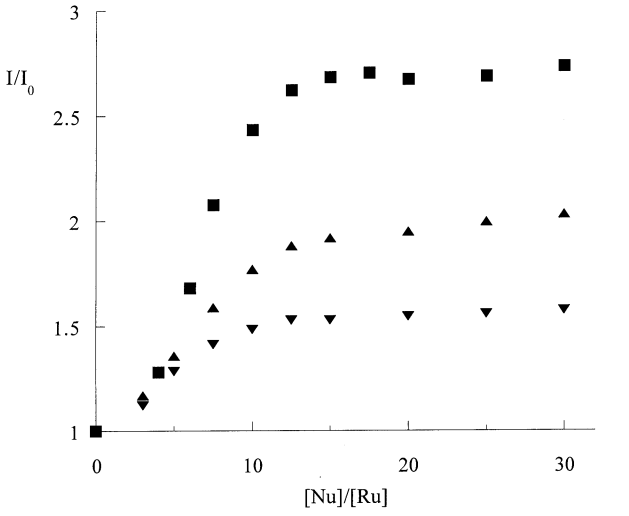

Figure 6. Steady-state emission with denatured CT-DNA (10 mM phosphate buffer pH = 7); I/I_0 vs. [Nu]/[Ru] ratio for the three stereoisomers of $[\{Ru(phen)_2\}_2(\mu\text{-HAT})]^{4+}$; I_0 is the emission intensity in the absence of denatured DNA; I is the emission intensity in the presence of denatured DNA; [Nu] is the equivalent concentration of nucleotide in the DNA; [Ru] is the concentration of Ru complex; ■ = *meso*, ▲ = ΔΔ, ▼ = ΛΛ

7. Time-Resolved Emission Measurements in the Presence of Denatured DNA

The emission decays in the presence of denatured CT-DNA at pH = 7 had to be analysed according to multi-exponential decays (Table 2). A distribution of different luminescence lifetimes can indeed be expected. In addition to different binding sites in single-stranded parts of the denatured DNA, the fact that these sites contain guanine or adenine residues also differently affects the luminescence lifetimes since a quenching or an enhancement of emission can take place. Hence, the emission lifetimes given in Table 2 are expressed as weighted average lifetimes. In the distribution of lifetimes, it is interesting to note that only the ΔΔ and ΛΛ forms displayed some short-lifetime components of 238 ± 10 ns (32%) and 209 ± 9 ns (28%), respectively. These were shorter than the luminescence lifetime of the corresponding excited free complex in solution (295 ± 5 ns). The presence of denatured DNA increased the weighted average luminescence lifetime of the three stereoisomers (Table 2). The lifetime enhancement followed the same tendency as that in the steady-state experiments, *meso* > ΔΔ > ΛΛ.

Discussion

1. Interaction with the Mononucleotides

Formation of Ion Pairs or Aggregates

Absorption spectra show that ion pairs (1 complex/1 mononucleotide) or aggregates (1 complex/> 1 mononucleotide) are formed between each stereoisomer and the purine mononucleotides (GMP and AMP). As the complex has a 4+ charge and the mononucleotides are negatively charged, this interaction could be regarded as purely electrostatic. However, this is not the case because the association constants (K_{gs}, Table 1) related to the formation of these species are not significantly different when the phosphate group of GMP is absent, such as in dG. Formation of these ion pairs or aggregates could thus be driven by a π-stacking interaction between a part of the π-aromatic system of the HAT ligand and the π system of the purine base. It is also clear in this work that the *meso* form of the dinuclear complex is more disposed than the two enantiomers ΔΔ or ΛΛ to form an ion pair at pH = 7 and 9 (K_{gs} for *meso* > ΔΔ or ΛΛ). Moreover, for the ΔΔ and ΛΛ forms, the data from the absorption change do not correspond to a 1:1 ground state association, but to aggregates. From the absorption data, it is thus concluded that stereoselectivity plays some role when the complex interacts with the purine mononucleotides.

Different Behaviour between AMP and GMP

Although both purine mononucleotides interact with the complex, AMP does not form the same types of ion pairs or aggregates as GMP. This is shown by the different change exhibited by the MLCT absorption of the complex in response to the addition of GMP or AMP (hypsochromic effect with GMP and bathochromic shift with AMP). This may be due to different conformations adopted by AMP and GMP in solution (*anti* for AMP and *syn* for GMP).[13,16] Moreover, with AMP, no photo-electron transfer from the base to the excited complex was observed by laser flash photolysis experiments. This absence of photoredox processes can be attributed to the poorer reducing power of adenine as compared with guanine (0.1 V difference). In contrast, the guanine of GMP is capable, according to the laser flash photolysis data, of producing a mono-reduced complex under visible illumination of the system "complex + GMP" at pH = 7 or 9.

Model To Explain the Different Luminescence Behaviours in the Presence of GMP

At pH = 7, although the laser flash photolysis of the complex in the presence of GMP indicated the presence of

a monoreduced complex with each of the three stereoisomers, the steady-state luminescence data showed a slight luminescence quenching by GMP only with the ΔΔ or ΛΛ enantiomers. In contrast, a slight increase of luminescence was observed for the *meso* form with increasing GMP concentrations.

The *meso* Form at pH = 7

The increasing emission of the *meso* isomer reached a plateau value at approximately 20 mM in GMP. According to the affinity constant of the *meso* form in the ground state for GMP at pH = 7 (585 M^{-1}), more than 92% of the *meso* complex would be in the form of an ion pair in the presence of 20 mM GMP. Therefore, the luminescence data could be explained by the reactions shown in Scheme 1.

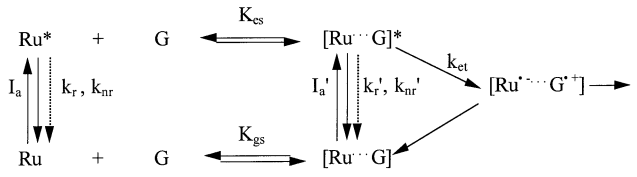

Scheme 1. Photophysical scheme; K_{gs} and K_{es} are the equilibrium constants in the ground and excited state, I_a and I'_a are the excitation rates, k_{et} is the rate of electron transfer, $k_r^{(\prime)}$ and $k_{nr}^{(\prime)}$ are the radiative and nonradiative decay rates, respectively

In this Scheme, we assume that the ion pair pumped in the excited state by irradiation corresponds to a new luminescent species. This explains the appearance of constant luminescence intensity once the equilibrium is completely shifted towards the excited ion pair. According to the data, the latter has a λ_{max} value of emission different from the free excited complex, a higher quantum yield of emission (leading under steady-state illumination to a ratio of emission intensity $I_0/I < 1$), and a longer excited-state lifetime. This lifetime, measured under pulsed illumination, is of the order of τ_{av} = 258 ns (longer than that of the free excited complex, 221 ns). Moreover, in competition with the deactivation of the excited ion pair to the ground state, this species has to lead to an electron transfer process (k_{et}) with formation of monoreduced complex as observed by laser flash photolysis.

The I_0/I curves have been simulated for the *meso* form for different values of the parameters associated with Scheme 1; i.e. the excited-state lifetime of the ion pair, keeping the value of the equilibrium constant in the excited state the same as in the ground state (i.e. 585 M^{-1}). It is concluded that this simulation does not fit with the experimental data points of Figure 4 for the *meso* form at pH = 7, although this Scheme takes into account a decrease of I_0/I with increasing GMP concentration up to a plateau value. This discrepancy can be attributed to the fact that the equilibrium constant in the excited state is not the same as in the ground state.[17,18] This is in agreement with the observation that luminescence decays were not purely mono-exponential in the presence of mononucleotides under pulsed illumination (even for the higher mononucleotide concentrations). As discussed above, this can be attributed to the dynamics of the equilibrium in the excited state, so that the excited-state lifetimes most probably correspond to apparent lifetimes.

Due to the poor experimental conditions for these measurements (long emission wavelength, low emission intensity), good accurate data for the luminescence decays cannot be obtained for all the nucleotide concentrations, and therefore we have no experimental access to the different rate constants associated with Scheme 1.

The *meso* Form at pH = 9

The data at pH = 9 for the *meso* form can also be rationalised using the same Scheme; i.e. with formation of a luminescent ion pair. The difference, compared to pH = 7, is that k_{et} from the luminescent ion pair has to be higher than at pH = 7, so that the resulting excited-state lifetime of the ion pair becomes shorter than that of the free excited complex. Consequently, the plateau value I_0/I is > 1, when the equilibrium is displaced to the right. As explained previously, a higher k_{et} can be attributed[10] to an increased driving force of the electron transfer process due to partial deprotonation of the guanine at pH = 9 (the base form of the guanine has a higher reducing power).

In conclusion, the appearance of plateau values in the I_0/I curves versus the GMP concentration at pH = 9 and 7 with the *meso* complex can be explained by formation of luminescent excited ion pairs between the *meso* form and GMP. The curves at pH = 7 and 9 appear quasi-symmetric along the abscissa for the *meso* form because the equilibrium constant values associated to Scheme 1 are indeed rather similar at both pH values.

The Enantiomers at pH = 7 and 9

The data for these forms are also in agreement with Scheme 1. The I_0/I plateau values for the two enantiomers are reached at higher GMP concentrations (> 40 mM; the plateau cannot be clearly observed at pH = 7). This is in agreement with a lower tendency of the enantiomers to form aggregates with GMP (at least in the ground state). Moreover, the I_0/I plateau values are larger than 1 (at pH = 7 and 9), and the excited-state lifetimes of the luminescent aggregates are shorter than the free excited enantiomers (for [GMP] > 40 mM, τ_{av} = 141 ns and 155 ns for each enantiomer at pH = 9, thus shorter than 295 ns observed for the free excited enantiomers). This behaviour indicates an electron transfer (k_{et}), which is faster for the ΔΔ and ΛΛ luminescent aggregates than for the emitting *meso* ion pair (pH = 7 or 9). Moreover, this electron transfer process for the enantiomer aggregates is faster at pH = 9 than at pH = 7 due to a difference in the driving force of the process, as concluded for the *meso* form.

2. Interaction with Denatured DNA

As explained in the introduction, the comparison of the effects of mononucleotides and denatured DNA is rather difficult because many other factors play a role in denatured DNA. For example the hydrophobic micro-environment of

the deformed sites in denatured DNA, where the complex interacts, increases the luminescence intensity and lifetime of the complex and influences its absorption. These factors are of course absent with the mononucleotides.

A striking similarity emerges, however, from the comparison. The most important effects in absorption and luminescence are indeed observed with the *meso* form in the presence of mononucleotides and for denatured DNA. The stereoselectivity is thus the same for these two systems. There are other qualitative similarities with the effects of the purine mononucleotides (pyrimidine mononucleotides have no effect):

1. In absorption, denatured DNA has a slight hypsochromic shift effect, similar, but less pronounced than that of GMP. This would be in agreement with resulting effects of AMP and GMP. Indeed, although AMP gives a bathochromic effect, it is less important than the hypsochromic shift with GMP.

2. In luminescence, the interaction of the two enantiomers with the guanine residues of denatured DNA should produce a lower luminescence than in solution if the behaviour was similar to that with GMP. In agreement with this, one component of the luminescence lifetimes of the enantiomers with denatured DNA is indeed shorter than that in solution. The fact that the data show a significant overall increase in both the emission intensity and weighted average lifetime, is due to the hydrophobic environment present in denatured DNA as mentioned above.

3. In addition to this hydrophobic environment, it is probable that the effect of the adenine and guanine nucleobases at pH = 7 also play a role in the emission intensity increase of the *meso* form, due to some contribution to the global emission of the luminescent ion pair, detected with the mononucleotides.

3. Conclusion

This study has shown the presence of new interesting processes in the systems "dinuclear complex plus mononucleotides" i.e. a stereoselectivity in the ion pairing and in the photo-induced electron transfer. To the best of our knowledge, this is the first time that such stereoselective processes have been evidenced. This work has also clarified the complicated behaviour observed previously with the nonresolved mixture of stereoisomers.[10]

We have shown that the formation of aggregates or ion pairs in the ground state with purine mononucleotides is stereospecific. The aggregation originated from some π-stacking interaction. The order of selectivity is: *meso* > ΔΔ, ΛΛ. This study also demonstrates from the emission data, the existence of luminescent ion pairs or aggregates with the purine mononucleotides. These species have longer or shorter excited-state lifetimes than those of the corresponding free excited isomers, depending on the stereoisomer, on GMP or AMP, and on the pH of the solution. In competition with the deactivation process to the ground state, these luminescent aggregates with GMP can lead to an electron transfer process that is faster at a same pH for the enantiomer aggregates than with the *meso* form ion pairs.

For the reasons developed in the introduction, a comparison between the systems "complex plus mononucleotides" and "complex plus denatured DNA" is not obvious. However, this study shows also a stereoselectivity in the interaction of the complex with denatured DNA, which is the same as with the purine mononucleotides, i.e. the *meso* form interacts better than the enantiomers. The origin of this same stereoselectivity could be due to the fact that the dinuclear complex hosted in sites where the DNA strands are separated, exhibits a stereoselectivity governed mainly by the nucleotidic chain and of course not by the DNA helicity which is absent in these interaction sites.

Experimental Section

Materials: The pure stereoisomers [ΔΔ, ΛΛ, (*meso*-)ΔΛ] of $[\{Ru(phen)_2\}_2(\mu\text{-HAT})]^{4+}$ were prepared by T. Rutherford et al.[11] The phosphate buffers were adjusted by mixing Na_2HPO_4 and NaH_2PO_4 (Aldrich, A.C.S. reagent) in Milli Q water. Deoxyguanosine, guanosine- and adenosine-5′-monophosphate (dG, GMP and AMP; Sigma Chemicals) were used without further purification as sodium salt. Denatured CT-DNA was prepared as described previously.[10]

Absorption and Emission Spectroscopy: All measurements were carried out at room temperature (25 °C). A 100 mM phosphate buffer at pH = 7 or 9 was used for the titrations with the mononucleotides and dG, and a 10 mM phosphate buffer at pH = 7 for the titrations with denatured DNA. − Absorption spectra were recorded with a double-beam UV/Vis spectrophotometer Perkin−Elmer Lambda 40 or an HP 8452 UV/Vis diode array. − Emission spectra were obtained using a Shimadzu RF-5001 PC spectrofluorimeter equipped with a Hamamatsu R928 red-sensitive photomultiplier tube. The samples were excited at 550 nm and corrected for a same percentage of absorbed light. Because the complexes emit in the near infrared (λ_{max} = 820 nm), which is on the edge of the response curve of the PM tube, corrections were needed. The data were therefore treated externally with a correction file, which was elaborated using a calibrated tungsten source from Edinburgh Analytical Instruments. The emission spectra were integrated to obtain the I_0/I ratios. − Emission lifetimes were determined using a mode-locked argon pumped dye laser [λ_{exc} = 550 nm, ν_0 = 400 kHz, fwhm (full width half maximum) = 80 ps] in the laboratory of Prof. De Schryver (KU Leuven, Belgium). Emission was detected by a micro-channel plate Hamamatsu R2909 Single Photon Counting unit at 800 nm. Deconvolution was achieved using home-made software with a porphyrin as a reference (τ = 15 ns). Other SPC measurements were performed with an Edinburgh Instruments FL-900 spectrofluorimeter equipped with a nitrogen-filled discharge lamp and a Peltier-cooled Hamamatsu R-928 photomultiplier tube. The emission decays were analysed with the Edinburgh Instruments software (version 3.0), based on nonlinear least-square regressions using Marquardt algorithms. − Laser flash photolysis experiments were performed in a cross beam setup using a xenon lamp as the monitoring source and the second harmonic of a pulsed Nd/YAG laser (Continuum NY 61−10, λ = 532 nm, 20 mJ per pulse). The transient signal was detected by a modified Applied Photophysics laser kinetic spectrometer equipped with a red-sensitive Hamamatsu R-928 photomultiplier tube connected to an oscilloscope HP

5248. The transient absorption signals were transferred to a PC and treated externally.

Acknowledgments

A. B. and A. K. D. are grateful to the SSTC (Service affaires Scientifiques Techniques et Culturelles, PAI-IUAP 4/11 program) and the EU (Training and Mobility of Researchers, TMR program) for financial support. The authors thank F. De Schryver and his coworkers, L. Latterini in particular, for the use of the argon pumped dye laser at the KU Leuven, Belgium. F. R. K. acknowledges the financial support of the Australian Research Council.

[1] C. A. Bignozzi, J. R. Schoonover, F. Scandola, *Molecular Level Artificial Photosynthetic Materials*, **1997**, vol. 44.
[2] T. J. Meyer, *Acc. Chem. Res.* **1989**, *22*, 163−170.
[3] V. Balzani, F. Barigelletti, L. De Cola, *Top Curr. Chem.* **1990**, *158*, 31−71.
[4] A. M. Pyle, J. K. Barton, *Prog. Inorg. Chem.* **1990**, *38*, 413.
[5] A. Kirsch-De Mesmaeker, J.-P. Lecomte, J. M. Kelly, "Photoreactions of Metal Complexes with DNA, Especially Those Involving a Primary Photo-Electron Transfer", in: *Topics in Current Chemistry: Electron Transfer II* (Eds.: J. D. Dunitz, K. Hafner, S. Ito, J.-M. Lehn, K. N. Raymond, C. W. Rees, J. Thiem, F. Vögtle), Springer Verlag, Berlin, Heidelberg, **1996**, vol. 177, pp. 25−76.
[6] C. Moucheron, A. Kirsch-De Mesmaeker, J. M. Kelly, *J. Photochem. Photobiol. B: Biology* **1997**, *40*, 91−106.
[7] J.-P. Lecomte, A. Kirsch-De Mesmaeker, J. M. Kelly, A. B. Tossi, H. Görner, *Photochem. Photobiol.* **1992**, *55*, 681−689.
[8] J.-P. Lecomte, A. Kirsch-De Mesmaeker, M. M. Feeney, J. M. Kelly, *Inorg. Chem.* **1995**, *34*, 6481−6491.
[9] L. Jacquet, A. Kirsch-De Mesmaeker, *J. Chem. Soc., Faraday Trans.* **1992**, *88*, 2471−2480.
[10] O. Van Gijte, A. Kirsch-De Mesmaeker, *J. Chem. Soc., Dalton Trans.* **1999**, 951−956.
[11] T. J. Rutherford, O. Van Gijte, A. Kirsch-De Mesmaeker, F. R. Keene, *Inorg. Chem.* **1997**, *36*, 4465−4474.
[12] Denatured calf thymus DNA contains approximately 60% of double helix and 40% of portions where the two strands are separated.
[13] W. Saenger, *Principles in Nucleic Acid Structure*; Springer-Verlag, New York, **1984**.
[14] H. A. Benesi, J. H. Hildebrand, *J. Am. Chem. Soc.* **1949**, *71*, 2703−2707.
[15] J. N. Demas, *Excited State Lifetime Measurements*, Academic Press, New York, **1983**.
[16] W. Guschlbauer, *Jerus. Symp. Quant. Chem. Biochem.* **1972**, *4*, 297−310.
[17] V. Y. Shafirovich, S. H. Courtney, N. Ya, N. E. Geacintov, *J. Am. Chem. Soc.* **1995**, *117*, 4920−4929.
[18] P. Lianos, S. Georghiou, *Photochem. Photobiol.* **1979**, *29*, 13−21.
[19] E. R. Carraway, J. N. Demas, B. A. De Graff, *Anal. Chem.* **1991**, *63*, 332−336.

Received October 18, 2000
[I00394]

Synthesis, Structure, Electrochemistry, and Magnetism of [$Mn^{III}Mn^{III}$], [$Mn^{III}Fe^{III}$] and [$Fe^{III}Fe^{III}$] Cores: Generation of Phenoxyl Radical Containing [$Fe^{III}Fe^{III}$] Species

Cláudio Nazari Verani,[a] Eberhard Bothe,[a] Dirk Burdinski,[a] Thomas Weyhermüller,[a] Ulrich Flörke,[b] and Phalguni Chaudhuri*[a]

Dedicated to Prof. H.-J. Haupt on the occasion of his 65th birthday

Keywords: N,O ligands / Electrochemistry / Manganese / Iron / Radicals / Magnetic properties

Neutral homo- and heterobinuclear complexes with the general formula [(tmtacn)M_A(salox)$_3M_B$] where M_A (Mn^{III} or Fe^{III}) is facially coordinated to the cyclic amine 1,4,7-trimethyl-1,4,7-triazacyclononane (tmtacn) and M_B (Mn^{III} or Fe^{III}) is coordinated to the azomethine nitrogens and phenolate oxygens of the bridging ligand, salicylaldoxime, thus yielding $M_AN_3O_3$ and $M_BN_3O_3$ cores. The compounds were characterized by IR, UV/Vis, mass spectrometry, Mössbauer spectroscopy, electrochemistry, and variable-temperature (2–295 K) magnetic susceptibility measurements. The molecular structures of the compounds [(tmtacn)Fe^{III}(salox)$_3$-Fe^{III}] (**3**) and [(tmtacn)Fe^{III}(*t*BuSalox)$_3Fe^{III}$] (**4**) were established by X-ray diffraction. Three oximate groups –HC=N–O bridge the metal centers with Fe···Fe separations of 3.571(1) and 3.486(1) Å for (**3**) and (**4**), respectively. Analysis of the susceptibility data yields antiferromagnetic interactions between the metal centers for the complexes $Fe^{III}Fe^{III}$ and Mn^{III}-Fe^{III}, but a ferromagnetic interaction for $Mn^{III}Mn^{III}$. The electrochemistry of all complexes was investigated in detail. For the complexes $Fe^{III}Fe^{III}$ (**3**) and (**4**) a series of reversible one-electron transfer waves leads to the formation of the cations $[Fe_2]^{1+/2+/3+}$ that are attributed to the generation of salox-based phenoxyl radicals.

Introduction

Current interest in the coordination chemistry of phenol containing ligands[1−4] is mainly due to the discovery of the widespread occurrence of tyrosinase radicals in metalloproteins, involved in oxygen-dependent enzymatic radical catalysis.[5−8] Amongst the catalytically essential redox-active amino acids, glycyl, cysteinyl, tryptophan, tyrosyl, and modified tyrosyl are the most prevalent, and tyrosine-based radical enzymes are the best characterized.

As part of an effort directed toward the development of biologically inspired homogeneous catalysis[9−11] for the aerial oxidation of organic substrates like alcohols and amines, we are investigating the synthesis and reactivity of phenolate complexes of the transition metals, together with their one-electron oxidized phenoxyl radical complexes. Such phenoxyl radical complexes, stable in the solid state, are rather rare. This scarcity is partly due to the fact that the metal−phenolate bond to a late transition metal ion should be relatively weak. For the early transition metal ions, the metal−phenolate bonding is strengthened by π-donation from the lone pair of electrons on oxygen into an empty d-orbital on the metal, but for the late transition metal ions such empty low-lying orbitals are not always available.

In another field of modern coordination chemistry there is a continuous interest in polynuclear exchange-coupled systems that are relevant to the area of both magnetic materials[12−15] and biomodeling.[5,16−18] Of special interest in this context is the rational synthesis of polynuclear complexes with desired nuclearity by reaction of mono or dinuclear complexes with different metal complexes[19] of the same or different nature, i.e. the use of metal complexes as ligands.

In this regard we have reported several series of linear complexes comprising [M_A-M_B], [$M_A-M_B-M_A$], [$M_A-M_B-M_C$], and [$M_A-M_B-M_B-M_A$] cores,[20−23] involving the end-capping amine tmtacn and several bridging oximes together with nonlinear tetranuclear [$(M_A)_2(\mu$-$O)_2(M_B)_2$] complexes containing salicylaldoxime, *salox*.[24]

Although salicylaldoxime was used as a complexing agent as early as 1930,[25] comparatively few reports on its ligating properties towards the trivalent transition metal ions have been published.[24,26−30] During the course of the preparative work involving M^{III}(saloxH)$_3$, where M = Fe^{III}, Mn^{III}, saloxH = the monoanion of salicylaldoxime H_2salox, we envisaged the possibility of preparing a series of neutral dinuclear complexes with the general formula [(tmtacn)M_A(salox)$_3M_B$], where M_A = Mn^{III} or Fe^{III}, and is facially coordinated to the cyclic amine 1,4,7-trimethyl-1,4,7-triazacyclononane, *tmtacn*, and M_B = Mn^{III} or Fe^{III} and is coordinated to the three salox units.

[a] Max-Planck-Institut für Strahlenchemie,
Stiftstrasse 34−36, 45470 Mülheim an der Ruhr, Germany
E-mail: chaudh@mpi-muelheim.mpg.de
[b] Anorganische und Analytische Chemie, Universität Gesamthochschule,
D-33098 Paderborn, Germany

 © WILEY-VCH Verlag GmbH, 69451 Weinheim, 2001 1434−1948/01/0808−2161 $ 17.50+.50/0

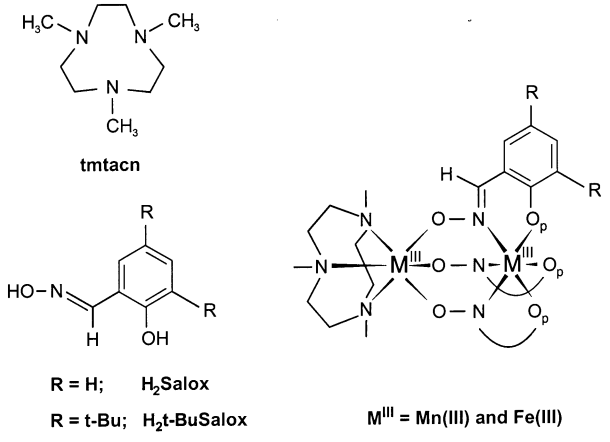

Scheme 1. Ligands and general frame of the [(*tmtacn*) M_A (*salox*)$_3$ M_B] complexes

It has been recently established by Wieghardt et al.[31] that *tert*-butyl substituents at the *ortho* and *para* positions of the phenolates facilitate one-electron oxidation to the corresponding phenoxyl radicals, because these substituents decrease the oxidation potential of the phenolates and provide enough steric bulk to suppress bimolecular decay reactions. Accordingly, we have synthesized salicylaldoxime with *tert*-butyl substituents at the *ortho* and *para* positions i.e., 4,6-di-*tert*-butyl salicylaldoxime, abbreviated *tBu-salox*, and investigated the electrochemical behavior amongst other studies, to generate the phenoxyl radical species from the parent dinuclear Fe^{III} complex. Thus, the compounds [(tmtacn)Mn^{III}(salox)$_3$$Mn^{III}$] (**1**), [(tmtacn)$Mn^{III}$(salox)$_3$$Fe^{III}$] (**2**), [(tmtacn)$Fe^{III}$(salox)$_3$$Fe^{III}$] (**3**), and [(tmtacn)$Fe^{III}$(*t*Bu-salox)$_3$$Fe^{III}$] (**4**), were synthesized and characterized by means of various spectroscopic methods. The single crystal X-ray structure determinations of (**3**) and (**4**) were also performed.

Results and Discussion

The complexes [(tmtacn)M_A(salox)$_3$$M_B$] were obtained by reaction of an appropriate metal salt with the ligand H_2salox in oxygen-free methanol, in the presence of triethylamine, followed either by the solid [Fe(tmtacn)Cl_3] or [(tmtacn)$_2$$Mn^{III}_2$(μ-O)(μ-OAc)$_2$]$^{2+}$, produced in situ, in stoichiometric equivalents. Dark microcrystalline products were collected with yields varying between 40 to 70%. Satisfactory analyses (C, H, N, Fe, Mn) were obtained. Our attempts to characterize the species produced by the reaction of salicylaldoxime with either $FeCl_3$ or "Mn^{III} acetate" are yet to be successful. However, these species are able to yield the dinuclear complexes **1**, **2**, **3**, and **4**, in the presence of a base (Et_3N) and the [M(tmtacn)]$^{3+}$ unit [M = Fe^{III} or Mn^{III}]. The function of the added base is to provide a medium needed for deprotonation of the −HC=N−OH groups present.

Since the IR spectra of complexes **1**, **2**, **3**, and **4** are quite similar, the discussion is confined to the most important vibrations of the 4000−400 cm^{-1} region in relation to the structure. The free ligands, H_2salox and 4,6-*t*Bu-H_2salox, have intense sharp absorptions at 3411 and 3438 cm^{-1}, attributed to the ν(OH) vibrations of the phenolic and enolic groups, respectively. This absorption is missing in the spectra of the dinuclear complexes, indicating that the phenolic and enolic protons are lost on chelation. The very intense band at 1619 cm^{-1} for H_2salox and a medium intense at 1609 cm^{-1} for 4,6-*t*Bu-H_2salox are assigned to the $\nu_{(C=N)}$ vibration mode. These bands shift to ca. 1592 cm^{-1} for **1**−**4**. The medium strong band at ca. 1150−1170 cm^{-1} for the free oxime ligands shifts slightly (ca. 5 cm^{-1}) to higher frequency for all dinuclear complexes and has been assigned to the $\nu_{(N=O)}$ vibration of the oxime groups. Finally, a set of intense and medium-intensity peaks between 3007 and 2864 cm^{-1} is present in both ligand 4,6-*t*Bu-H_2salox and complex **4** and reveals the presence of the *tert*-butyl groups.

Mass spectrometry in the ESI positive mode has been proved to be a very useful analytical tool for characterization of complexes **1**−**4**. Homometal complexes **1**, **3**, and **4** provide the respective molecular ion peaks with the expected isotope ratios in the ESI positive mode as the base peaks (100%), but the heterometal complex, **2** fails to provide the molecule peak as the base peak; the latter is observed at *m*/*z* = 710, and can be assigned to the ion [M + Na]$^+$.

The optical spectra of **1**, **2**, and **3** in MeCN have been measured in the 350−1200 nm wavelength range. Only one maximum is observed for each complex: for **1** at 571 nm (ε = 2820 L mol^{-1} cm^{-1}), for **2** at 501 nm (ε = 5880 L mol^{-1} cm^{-1}), and for **3** at 486 nm (ε = 7844 L mol^{-1} cm^{-1}). As these transitions are unusually intense for a high-spin Mn^{III} or Fe^{III} d-d transition, they are assigned to a phenolate-to-M^{III} [M^{III} = Fe or Mn] transition. Thus these bands can be assigned to a transition from pπ orbitals on the phenolate oxygen atoms to the dπ* orbitals on M^{III}.[32−35] The expected ligand field transitions, $^6A_1 \rightarrow {}^4T_2$ (^4G) for Fe^{III} and $^5E_g \rightarrow {}^5T_{2g}$ for Mn^{III}, which are likely to

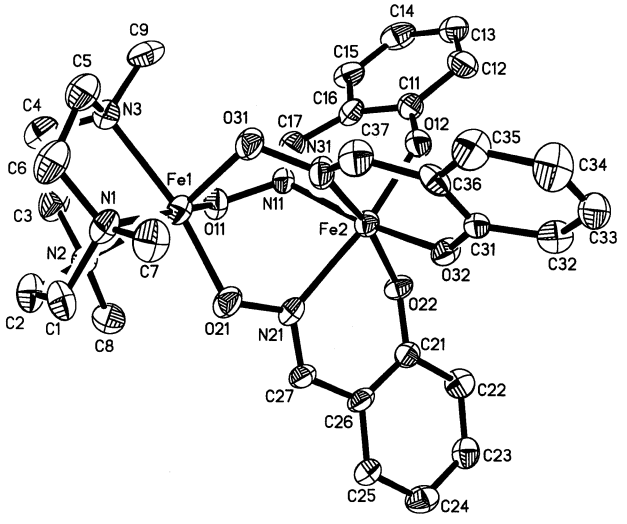

Figure 1. Molecular structure of the dinuclear $Fe^{III}Fe^{III}$ core in **3**, showing the atom-numbering scheme

occur in the 500−700 nm region, are obscured by the more intense charge transfer phenolate-to-metal (III) transition.

Molecular Structure of [(tmtacn)Fe^{III}(salox)$_3Fe^{III}$]·MeOH (3) and of [(tmtacn)Fe^{III}(*t*Bu-salox)$_3Fe^{III}$]·3.5 $CHCl_3$ (4)

The structures of the neutral complexes in crystals of **3** and **4** were determined, and as expected they are identical with respect to the coordination geometry of the Fe^{III} centers. Hence we are refraining from describing both structures in detail, and accordingly the ORTEP for **3** is shown in Figure 1. Table 1 lists selected bond lengths and angles for both **3** and **4**.

The coordination geometry of Fe(1) is distorted octahedral with three nitrogen atoms, N(1), N(2), and N(3), from the facially coordinated tridentate macrocyclic amine, and three oxygen atoms O(11), O(21), and O(31) from the bridging oximate groups. The Fe(1)−N (average 2.22 Å) and Fe(1)−O (average 1.94 Å) correspond to those of the known values[36,37] for Fe^{III} complexes with this macrocyclic amine, and are in agreement with a d^5 high-spin electron configuration of the Fe^{III}-center. A deviation from the idealized orthogonal geometry is found for the ligand tmtacn, the N−Fe(1)−N angles ranging between 78.6° and 79.3°, whereas O−Fe(1)−O angles fall between 96.1° and 99.6°. The Fe(1) is displaced by 0.10 Å from the mean basal plane comprising N(1)N(3)O(11)O(21) atoms, toward the apical oxygen atom O(31) of the oximate group. The ligand tmtacn exhibits no unexpected features.

The Fe(2) center is also six-fold coordinated. Coordination occurs facially through three phenolate oxygen atoms, O(12), O(22), and O(32), and three azomethine nitrogen atoms, N(11), N(21), and N(31), from the salox ligands. The average Fe(2)−N and Fe(2)−O bond lengths, 2.16 Å and 1.94 Å, respectively, fall within the ranges that are consid-

Table 1. Selected bond lengths [Å] and angles [°] for **3** and **4**

[(tmtacn)Fe^{III}(salox)$_3Fe^{III}$] (**3**)		[(tmtacn)Fe^{III}(4,6-*t*Bu-salox)$_3Fe^{III}$] (**4**)	
Fe(1)−N(1)	2.225(9)	Fe(1)−N(1)	2.249(2)
Fe(1)−N(2)	2.224(8)		
Fe(1)−N(3)	2.222(8)		
Fe(1)−O(11)	1.948(6)		
Fe(1)−O(21)	1.935(7)	Fe(1)−O(2)	1.930(2)
Fe(1)−O(31)	1.934(6)		
Fe(2)−N(11)	2.144(7)		
Fe(2)−N(21)	2.199(8)	Fe(2)−N(2)	2.141(2)
Fe(2)−N(31)	2.136(8)		
Fe(2)−O(12)	1.951(6)	Fe(2)−O(1)	1.931(2)
Fe(2)−O(22)	1.942(6)		
Fe(2)−O(32)	1.911(6)		
N(1)−Fe(1)−N(2)	79.3(3)		
N(2)−Fe(1)−N(3)	78.6(3)		
N(2)−Fe(1)−O(11)	85.1(3)	O(2)−Fe(1)−O(2)#2	100.16(7)
N(1)−Fe(1)−O(21)	88.1(3)	O(2)#1−Fe(1)−N(1)	93.89(8)
N(3)−Fe(1)−O(21)	166.7(3)	O(2)−Fe(1)−N(1)	85.70(8)
N(1)−Fe(1)−O(31)	95.0(3)		
N(3)−Fe(1)−O(31)	87.5(3)		
O(21)−Fe(1)−O(31)	96.9(3)	O(2)−Fe(1)−N(1)#1	163.50(8)
O(12)−Fe(2)−O(22)	95.8(3)		
O(12)−Fe(2)N(21)	168.7(3)		
O(22)−Fe(2)−N(21)	83.7(3)		
N(11)−Fe(2)−O(32)	171.9(3)	O(2)−Fe(1)−N(1)#2	93.89(8)
N(21)−Fe(2)−O(32)	98.1(3)		
N(11)−Fe(2)−N(31)	88.4(3)	N(1)−Fe(1)−N(1)#2	78.49(9)
N(21)−Fe(2)−N(31)	83.4(3)		
N(1)−Fe(1)−N(3)	79.0(3)	O(1)−Fe(2)−O(1)#2	95.78(7)
N(1)−Fe(1)−O(11)	164.3(3)		
N(3)−Fe(1)−O(11)	95.5(3)	O(1)Fe(2)−N(2)#1	83.46(7)
N(2)−Fe(1)O(21)	96.0(3)		
O(11)−Fe(1)−O(21)	96.1(3)	O(1)#2−Fe(2)−N(2)#1	171.29(8)
N(2)−Fe(1)−O(31)	165.8(3)	O(1)−Fe(2)−N(2)	92.93(8)
O(11)−Fe(1)−O(31)	99.6(3)	O(1)#1−Fe(2)−N(2)	171.30(8)
O(12)−Fe(2)−N(11)	83.6(3)		
N(11)Fe(2)−O(22)	97.3(3)	N(2)#1−Fe(2)−N(2)	87.92(8)
N(11)−Fe(2)−N(21)	85.2(3)		
O(12)−Fe(2)−O(32)	93.2(3)		
O(22)−Fe(2)−O(32)	90.4(3)		
O(12)−Fe(2)−N(31)	98.1(3)		
O(22)−Fe(2)−N(31)	165.5(3)		
O(32)−Fe(2)−N(31)	84.6(3)		

ered as normal covalent bonds for Fe^{III} centers with a d^5 high-spin electronic configuration.[29,30] The largest deviation from idealized 90° inter-bond angles is 6.3°, which occurs within the six-membered N−Fe(2)−O−C−C−C chelate rings, the N−Fe(2)−N angles ranging between 88.4° and 83.4°, whereas the O−Fe(2)−O angles fall between 90.4° and 95.8°. The Fe(2) lies practically on the best basal plane comprising N(11)N(21)O(12)O(32) atoms, and is displaced only 0.08 Å above the plane toward the apical atom O(22) of a phenolate group. Thus, the metrical parameters of the Fe(2) center in **3** are very similar in magnitude to the Fe(1) center and to those reported earlier for the FeN_3O_3 core.[37]

The binuclear skeleton is not coplanar, but is bent with a Fe(1)···Fe(2) separation of 3.570(1) Å. The dihedral angle between the planes Fe(1)N(1)N(3)O(11)O(21) and Fe(2)N(11)N(21)O(12)O(32) is 109.8°.

The deviation from octahedral symmetry for the Fe(1) and Fe(2) centers has been evaluated from the twist angle (60° for an ideal octahedral and 0° for a trigonal prismatic arrangement). The $Fe(2)N_3O_3$ core is more trigonally distorted than the $Fe(1)N_3O_3$ core. The N_3O_3 donor atoms are arranged around the Fe(2) center with a twist angle of 49.2°, whereas for the Fe(1) center the twist angle is 51.1°. In other words, the coordination polyhedron around Fe(2) is 10.8° away from the octahedral symmetry.

The N−O (average 1.38 Å) and C=N (average 1.28 Å) bond lengths and C−N−O bond angle (average 113.4°) of the bridging salicylaldoxime ligand are found to be very similar to those of other comparable structures.[38−39]

The structure determinations for **3** and **4** unambiguously show that, in both structures, the oxidation level of all iron centers is +3 with d^5 high-spin electron configuration.

Table 1 compares the important bond lengths in both salox complexes. It can be easily observed that in **3** these distances are slightly longer than those in complex **4**. This general trend can be explained by considering that the *tert*-butyl groups act in both inductive (+I) and mesomeric (+M) fashion as electron-donors. It implies that the substituted salox complex **4** provides a more electron-rich coordination environment and consequently the interaction between donor atoms (O, N) and iron is stronger, producing a small but significant shortening of the bond lengths.

Mössbauer Spectroscopy and Magnetic Susceptibility Measurements

The 3+ oxidation state and the high spin electronic configuration of the iron centers in complexes **2** and **3** were confirmed by Mössbauer spectroscopy.[40] The spectra were measured at 80 K and zero-field. They consist of asymmetrical quadrupole doublets with isomer-shifts (δ) of 0.530 mms^{-1} for **2**, 0.566 mms^{-1} and 0.451 mms^{-1} for **3**, and quadrupole splitting (ΔE_Q) of 0.350 for **2**, 0.261 and 0.175 mms^{-1} for **3**.

The Mössbauer spectra have provided us with another piece of important information. Examination of the literature values[41] for the isomer-shifts (ΔE_Q) of the Fe^{III}-center that is capped by the tmtacn ligand shows that the ΔE_Q values lie within the range 0.44 to 0.47 mms^{-1}. Thus the isomer shifts of 0.530 for **2** and 0.566 mms^{-1} for **3** are attributed to the Fe^{III} centers coordinated to the phenolate oxygen and azomethine nitrogen atoms of the salicylaldoxime ligand. This establishes that the Mn^{III} center in **2** is coordinated to the macrocyclic tmtacn ligand. In other words, the fact that the metal ions have remained associated with their different ligands originating from their respective starting materials and practically no scrambling of the ligands has occurred, are evidenced by the Mössbauer experiments.

Magnetic susceptibility data for polycrystalline samples of **1**, **2**, **3**, and **4** were collected in the temperature range 2 to 290 K and the magnetic parameters are listed in Table 2. The spin Hamiltonian $\mathbf{H} = -2\boldsymbol{J}\cdot\boldsymbol{S_1}\cdot\boldsymbol{S_2}$ with $S_1 = S_2 = 2$ for **1**, $S_1 = 2$, $S_2 = {}^5/_2$ for **2**, and $S_1 = S_2 = {}^5/_2$ for **3** and **4** is used throughout.

Table 2. Magnetochemical data for complexes **1** to **4**

Compound	J [cm^{-1}]	$g_1 = g_2$	θ [K]	PI
[(tmtacn)$\mathbf{Mn^{III}}$(salox)$_3$$\mathbf{Mn^{III}}$] (**1**)	+6.5	2.07	−0.43	–
[(tmtacn)$\mathbf{Mn^{III}}$(salox)$_3$$\mathbf{Fe^{III}}$] (**2**)	−4.8	2.03	–	0.06
[(tmtacn)$\mathbf{Fe^{III}}$ (salox)$_3$$\mathbf{Fe^{III}}$] (**3**)	−11.8	2.00	–	–
[(tmtacn)$\mathbf{Fe^{III}}$(*t*Bu-salox)$_3$$\mathbf{Fe^{III}}$] (**4**)	−12.2	2.07	–	–

The effective magnetic moment for **1** increases monotonically with decreasing temperature until a plateau is reached at 20−15 K with an μ_{eff} value of 9.11 μ_B (Figure 2). Below 15 K μ_{eff} starts to decrease reaching a value of 8.4 μ_B at 2 K. The temperature behavior of μ_{eff} for **1**, Mn^{III} Mn^{III}, is characteristic of a ferromagnetic exchange coupling between two high-spin d^4 Mn^{III} ions. The data could be fitted using the Heisenberg−Dirac−van Vleck (HDvV) model and the least-squares fitting computer program Julius-F[42] with a full-matrix diagonalization approach. The best fit was obtained with $J = +6.5$ cm^{-1}, $g = 2.07$ and $\theta = -0.43$ K and is shown in Figure 2.

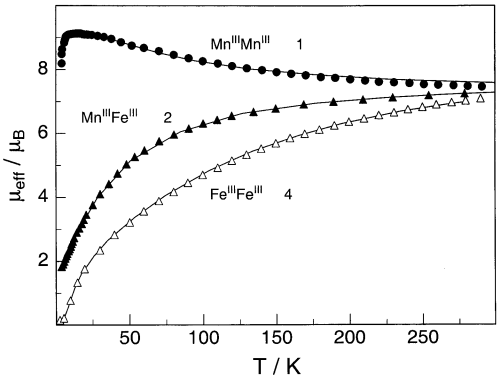

Figure 2. Plots of μ_{eff} vs. temperature for **1**, **2**, and **4**. Temperature-dependence of μ_{eff} of **3** is nearly identical to that of **4**. The solid lines represent the best fits to the spin Hamiltonian $H = -2J\cdot S_1\cdot S_2$ (see text)

For complex **2** the temperature dependence of the effective magnetic moment shows a monotonic decrease from 7.25 μ_B at 275 K to 1.85 μ_B at 4 K. This is typical of an

Table 3. Electrochemical data for complexes **1** to **4**; all potentials in Volts referred to Fc^+/Fc in CH_3CN ($E_{1/2}$ = 0.081 V)

Compound	$E_{1/2}$ (ox3)	$E_{1/2}$ (ox2)	$E_{1/2}$ (ox1)	$E_{1/2}$ (red1)	$E_{1/2}$ (red2)
[(tmtacn)**Mn^{III}**$(salox)_3$ **Mn^{III}**] (**1**)	–	0.30	−0.28	−0.86	−1.30
[(tmtacn)**Mn^{III}**$(salox)_3$ **Fe^{III}**] (**2**)	–	–	−0.19	−0.89	−1.81
[(tmtacn)**Fe^{III}** $(salox)_3$ **Fe^{III}**] (**3**)	0.97	0.77	0.41	−1.32	−1.86
[(tmtacn)**Fe^{III}**(tBu-salox)$_3$ **Fe^{III}**] (**4**)	0.89	0.47	0.31	−1.37	−2.08

antiferromagnetically coupled two-spin system with total spin ground state $S_t = {}^1/_2$ arising from $S_{Mn} = 2$ and $S_{Fe} = {}^5/_2$. Temperature independent paramagnetism (TIP) of $400 \cdot 10^{-6}$ cm^3 mol^{-1} and a monomeric impurity (6%, $S = 2$) were considered to account for the excess magnetic moment of the sample at 4 K. Fitting for the isotropic exchange yielded $J = -4.8$ cm^{-1} and $g = 2.03$ (Figure 2).

The magnetic behaviors of complexes **3** and **4** are, as expected, nearly identical, and hence they will be treated together. On lowering the temperature, the effective magnetic moments decrease monotonically for both complexes. Representative μ_{eff} values for complexes **3** and **4** (given in brackets) are 6.86 μ_B (7.09 μ_B) at 290 K, 4.68 μ_B (4.70 μ_B) at 100 K, 0.24 μ_B (0.21 μ_B) at 5 K, and 0.16 μ_B (0.15 μ_B) at 2 K, indicating a diamagnetic ground state $S_t = 0$ for both **3** and **4**. This arises from antiparallel spin coupling between two Fe^{III} centers with $S = {}^5/_2$. Simulation of the data yielded $J = -11.8$ cm^{-1}, $g_1 = g_2 = 2.00$ for **3** and $J = -12.2$ cm^{-1}, $g_1 = g_2 = 2.07$ for **4**. It was not necessary to consider terms for TIP or paramagnetic impurity in the simulation procedure. The experimental data together with the simulation for complex **4** are shown in Figure 2.

Electro- and Spectroelectrochemistry

Complexes **1**−**4** were submitted to electrochemical studies in order to characterize the nature of its redox processes. Table 3 summarizes the results, and Figure 3 and Figure 4 show representative examples of the electrochemical measurements.

The cyclic voltammogram of [(tmtacn)$Mn^{III}$$(salox)_3Mn^{III}$] (**1**) shows four consecutive reversible one-electron-transfer waves (Figure 3), which are detected with scan rates varying from 20 to 500 mVs^{-1} at +0.30 V, −0.28 V, −0.86 V, and −1.30 V versus Fc^+/Fc. The oxidation processes at +0.30 V and −0.28 V are assigned to the following equilibria shown in Equation (1).

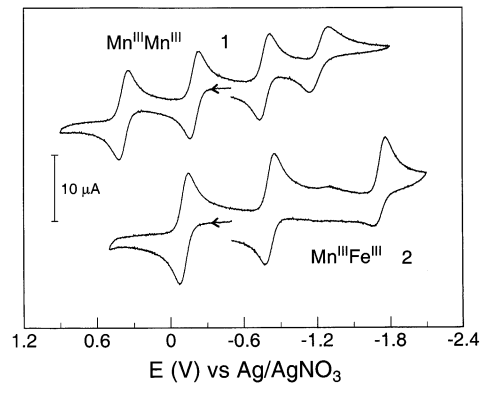

Figure 3. Cyclic voltammograms of **1** (top) and **2** (bottom) in CH_3CN (0.10 M $[(nBu_4)N]PF_6$ at a glassy carbon electrode; scan rate: 200 mV/s; complex ≈ 10^{-3} M; 298 K)

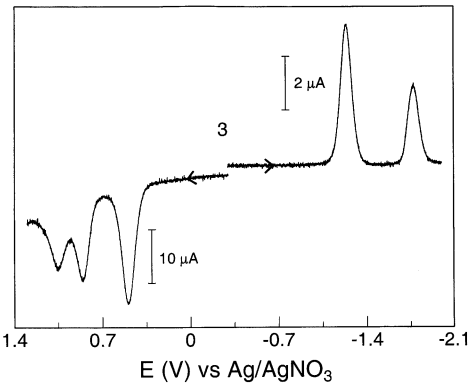

Figure 4. Square wave voltammograms for oxidation and reduction of **3** in MeCN, 0.1 M $[TBA]PF_6$. Oxidation: 0.25 mm Pt working electrode (WE), scan frequency 3000 Hz. Reduction: 2 mm GC WE, 5 Hz

$$\begin{array}{l} [(tmtacn)Mn^{III}(salox)_3Mn^{III}]^0 \\ \quad\quad \mathbf{1} \\ E_{1/2}(ox1) \quad -1e^- \downarrow\uparrow +1e^- \\ [(tmtacn)Mn^{IV}(salox)_3Mn^{III}]^+ \\ E_{1/2}(ox2) \quad -1e^- \downarrow\uparrow +1e^- \\ [(tmtacn)Mn^{IV}(salox)_3Mn^{IV}]^{2+} \end{array} \quad (1)$$

Electrochemically-reversible one-electron-transfer steps preclude any significant structural rearrangement during these oxidation processes, i.e., no change in the actual framework of the structures for all three species has occurred. The electrochemical behavior of complex **1** in the more negative potential range (−0.4 to −2.0 V vs. Ag/$AgNO_3$) can be assigned to the following redox scheme shown in Equation (2), on the basis of earlier reports.[21]

$$\begin{array}{l} [(tmtacn)Mn^{II}(salox)_3Mn^{II}]^{2-} \\ E_{1/2}(red2) \quad -1e^- \downarrow\uparrow +1e^- \\ [(tmtacn)Mn^{II}(salox)_3Mn^{III}]^- \\ E_{1/2}(red1) \quad -1e^- \downarrow\uparrow +1e^- \\ [(tmtacn)Mn^{III}(salox)_3Mn^{III}]^0 \\ \quad\quad \mathbf{1} \end{array} \quad (2)$$

The CV of **2** (Figure 3) exhibits two reversible one-electron waves at −0.19 V and −0.89 V versus Fc^+/Fc, and one quasi-reversible cathodic wave at more negative potentials that may be attributed to the reduction of iron center coordinated with phenolate and azomethine nitrogen atoms of the salicylaldoxime. Controlled-potential coulometry established a one-electron transfer process for the reversible cases. The following equilibria are thus involved during the manganese-centered electron-transfer processes (Equation 3).

$$
\begin{array}{l}
[(tmtacn)Mn^{III}(salox)_3Fe^{III}]^0 \\
\mathbf{2} \\
E_{1/2}(ox1) \quad -1e^- \downarrow\uparrow +1e^- \\
[(tmtacn)Mn^{IV}(salox)_3Fe^{III}]^+ \\
[(tmtacn)Mn^{III}(salox)_3Fe^{III}]^0 \\
\mathbf{2} \\
E_{1/2}(red1) \quad -1e^- \uparrow\downarrow +1e^- \\
[(tmtacn)Mn^{II}(salox)_3Fe^{III}]^- \\
E_{1/2}(red2) \quad -1e^- \uparrow\downarrow +1e^- \\
[(tmtacn)Mn^{II}(salox)_3Fe^{II}]^{2-}
\end{array}
\qquad (3)
$$

Complex **3** in MeCN exhibits five redox processes. The voltammetric waves of two of them, at +0.41 V and at −1.32 V versus Fc^+/Fc show reversible appearance under "standard" conditions (2 mm working electrode and scan rates of 0.05−0.5 V/s in CV and about 60 Hz in square wave voltammetry, SQW). Controlled potential coulometry at the appropriate potentials reveals that these waves originate from a one-electron oxidation and a one-electron reduction, respectively. The oxidation must be ligand-centered, and the reduction is assigned to an Fe^{III}/Fe^{II} couple. Two further (ligand-centered) oxidations at +0.77 and +0.97V and one more reduction at −1.86 V (assigned to reduction of the second iron) are detectable by SQW. The second reduction is best seen at relatively slow scan frequencies (< 10 Hz) most probably due to its slow heterogeneous electron transfer step. The two additional oxidations are detectable only at much higher frequencies (> 1000 Hz) because of rapid homogeneous following-up reactions. The results for the oxidations and reductions are displayed in Figure 4.

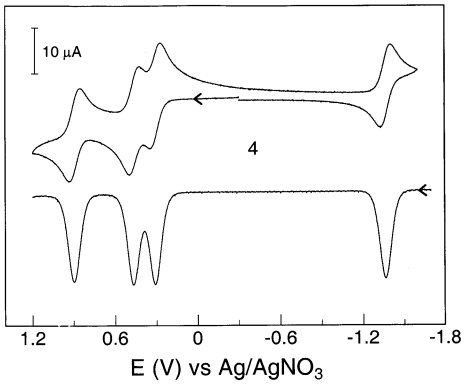

Figure 5. Square wave voltammogram (at 20 Hz) and CV (at 0.2 V/s) of **4** in MeCN, 0.1 M [TBA]PF_6

For complex **4** in MeCN, four reversible one electron waves were observed at the following potentials: +0.89, +0.47, +0.31, and −1.37 V, versus Fc^+/Fc. Additionally, an irreversible wave at $E_p^{ox} = -2.08$ V versus Fc^+/Fc is also found (Figure 5). The two reductive waves at −1.37 V and −2.08 V versus Fc^+/Fc are attributed to processes centered on the metal centers as described in Equation (4a), whereas the three oxidation waves are attributed to successive ligand-centered phenoxyl-radical formation [Equation (4b)]. The overall redox processes are given below where ($salox^\bullet$) represents a salox-based phenoxyl-radical.

reductive processes

$$
\begin{array}{l}
[(tmtacn)Fe^{II}(t\text{Bu-salox})_3Fe^{II}]^{2-} \\
E_{1/2}(red2) \quad -1e^- \downarrow\uparrow +1e^- \\
[(tmtacn)Fe^{II}(t\text{Bu-salox})_3Fe^{III}]^{1-} \\
E_{1/2}(red1) \quad -1e^- \downarrow\uparrow +1e^- \\
[(tmtacn)Fe^{III}(t\text{Bu-salox})_3Fe^{III}]^0 \\
\mathbf{4}
\end{array}
\qquad (4a)
$$

oxidative processes

$$
\begin{array}{l}
[(tmtacn)Fe^{III}(t\text{Bu-salox})_3Fe^{III}]^0 \\
\mathbf{4} \\
E_{1/2}(ox1) \quad -1e^- \downarrow\uparrow +1e^- \\
[(tmtacn)Fe^{III}(t\text{Bu-salox})_2(t\text{Bu-salox}^\bullet)Fe^{III}]^+ \\
E_{1/2}(ox2) \quad -1e^- \downarrow\uparrow +1e^- \\
[(tmtacn)Fe^{III}(t\text{Bu-salox})(t\text{Bu-salox}^\bullet)_2Fe^{III}]^{2+} \\
E_{1/2}(ox3) \quad -1e^- \downarrow\uparrow +1e^- \\
[(tmtacn)Fe^{III}(t\text{Bu-salox}^\bullet)_3Fe^{III}]^{3+}
\end{array}
\qquad (4b)
$$

Each of these waves involves a $1e^-$-transfer, as detected by coulometry at fixed potentials. Both complexes **3** and **4** contain two high spin Fe^{III} ions in an octahedral *fac*-N_3O_3 donor set, but complex **4** in MeCN exhibits two additional ligand-centered reversible oxidation processes absent in **3**, as shown in Figure 5.

Spectroelectrochemical experiments were performed intending to isolate and characterize (by EPR spectroscopy) the resulting oxidized complexes. As the electron transfer processes during coulometric measurements at appropriately fixed potentials at ambient temperature has been found to be too slow (>> $^1/_2$ h), characterization of the radical complexes by UV/Vis and EPR spectroscopy has not been possible. Lowering the temperature of the experiments was also not effective, and the measurements resulted

Table 4. Crystallographic data for **3**·MeOH and **4**·3.5 $CHCl_3$

	[(tmtacn)Fe^{III}(salox)$_3Fe^{III}$] **3**·MeOH	[(tmtacn)Fe^{III}(4,6-*t*Bu-salox)$_3Fe^{III}$] **4**·3.5 $CHCl_3$
Empirical formula	$C_{30}H_{36}Fe_2N_6O_6 \cdot CH_3OH$	$C_{54}H_{84}Fe_2N_6O_6 \cdot 3.5\ CHCl_3$
Molecular weight	720.39	1442.76
Temperature	293(2) K	100(2) K
Wavelength	0.71073 Å	0.71073 Å
Crystal system	orthorhombic	trigonal
Space group	$P2_12_12_1$	$P\bar{3}$
Unit cell dimensions	a = 12.105(5) Å	a = 17.341(2) Å α = 90°
	b = 15.655(5) Å	b = 17.341(2) Å β = 90°
	c = 17.374(7) Å	c = 13.656(2) Å γ = 120°
Volume	3292(2) Å^3	3556.3(8) Å^3
Z	4	2
Density (calculated)	1.453 Mg/m^3	1.347 Mg/m^3
Absorption coefficient	0.936 mm^{-1}	0.851 mm^{-1}
F(000)	1504	1506
Crystal size	0.40 × 0.09 × 0.08 mm^3	0.67 × 0.49 × 0.42 mm^3
Color	dark red needle	deep violet
Diffractometer used	Siemens R3m/V	Siemens SMART
θ range for data collection	2.34 to 27.56°	2.02 to 30.00°
Index ranges	$0 \le h \le 15$	$-24 \le h \le 26$
	$0 \le k \le 20$	$-21 \le k \le 26$
	$0 \le l \le 22$	$-19 \le l \le 20$
Reflections collected	4237	35066
Independent reflections	4237	6851 [R_{int} = 0.0358]
Refinement method	Full-matrix least-squares on F^2	Full-matrix least-squares on F^2
Data/restraints/parameters	4237/0/418	6617/0/266
Goodness-of-fit on F^2	0.854	1.170
Absolute structure parameter	0.02(4)	-
Final R indices [$I > 2\sigma(I)$]	$R1$ = 0.0551, $wR2$ = 0.0976	$R1$ = 0.0605, $wR2$ = 0.1378
R indices (all data)	$R1$ = 0.1363, $wR2$ = 0.1353	$R1$ = 0.0750, $wR2$ = 0.1475

in ill-defined isosbestic points. Nevertheless, the growth of peaks around 420−450 nm (ε ≈ 10580 $M^{-1}cm^{-1}$) serves as a strong indication for the radical nature of the generated complexes.

Concluding Remarks

The results summarized here for **3** and **4** suggest the generation of three ligand-centered oxidation processes, attributable to phenoxyl-radicals, rather than the formation of unusually high oxidation states at the central iron centres. On the contrary, in case of manganese, facile oxidation of metal centres rather than the ligands occurs. In contrast to the general notion that azomethine N-donor sets stabilize the 2+ oxidation state of iron centers, salicylaldoxime as a ligand with coordinated phenolato and azomethine groups enormously stabilizes 3+ oxidation state in such metal centers. This is a general feature of the phenolato iron complexes.

Experimental Section

Solvents and reagents were obtained from commercial sources and used without further purification. The synthon [Fe(tmtacn)]Cl_3[37] and the cyclic amine 1,4,7-trimethyl-1,4,7-triazacyclononane, tmtacn[43] were prepared according to previous published methods. − Infrared spectra were measured from 4000 to 400 cm^{-1} as KBr pellets at room temperature on a Perkin−Elmer FT-IR-Spectrophotometer 2000. − C, H, N, and metal content of the compounds were determined by the Microanalytical Laboratory of the Ruhr-Universität Bochum. − UV/Visible spectra of $5.0 \cdot 10^{-4}$ M solution in MeCN were recorded on a Perkin−Elmer UV/Vis Spectrophotometer Lambda 19 in the range 200−1200 nm. − Cyclic voltammetry and square wave voltammetry experiments were performed using an EG&G Potentiostat/Galvanostat 273A. A standard three-electrode-cell was employed with a glassy-carbon working electrode, a platinum-wire auxiliary electrode, and a $Ag/AgNO_3$ reference electrode. Measurements were made under an inert atmosphere at room temperature. All the potentials are referenced to Fc^+/Fc as the internal standard. − The magnetochemical measurements of the powdered samples were performed in a Quantum Design SQUID-Magnetometer MPMS in a field of 1 T. The samples were put in gelatine-capsules, and the response function was measured four times for each 32 measured temperature points. Diamagnetic contributions were estimated for each compound by making use of Pascal's constants. − Mössbauer data were recorded on alternating constant-acceleration spectrometers. The minimal experimental linewidth was 0.24 mms^{-1} full width at half maximum. The sample temperature was kept constant at 80 K either in an Oxford Variox or an Oxford Mössbauer-Spectromag cryostat. $^{57}Co/Rh$ was used as the radiation source. The measurements were carried out with solid samples containing the isotope ^{57}Fe and the isomer shifts are given relative to α-Fe at room temperature.

X-ray Crystallography: The crystallographic data of [LFe(salox)$_3$Fe] (**3**) and [LFe(*t*Bu-salox)$_3$Fe] (**4**) are summarized in Table 4.

Graphite monochromated Mo-K_α radiation (λ = 0.71073 Å) was used throughout. Intensity data were corrected for Lorentz-Polarization and absorption effects using the program SADABS.[44] The structures were solved by direct methods using SHELXTL plus.[45] The function minimized during full-matrix least-squares refinement was $\Sigma w(|F_o| - |F_c|)^2$. Hydrogen atoms attached to carbon were placed at calculated positions and refined as riding atoms with isotropic thermal parameters. All non-hydrogen atoms were refined with anisotropic thermal parameters. Crystallographic data (excluding structure factors) for the structure reported in this paper have been deposited with the Cambridge Crystallographic Data Centre as supplementary publication number CCDC-151864. Copies of the data can be obtained free of charge on application to the CCDC, 12 Union Road, Cambridge CB2 1EZ, U.K. [Fax: (internat.) + 44-1223/336-033; E-mail: deposit@ccdc.cam.uk].

Preparation of the Compounds

Salicylaldoxime (H_2salox): was prepared by heating a solution of salicylaldehyde and free hydroxylamine in EtOH for 0.5 h under reflux. The yellowish white solid obtained on cooling was recrystallized from EtOH. Purity of the sample was checked by comparing its spectroscopic properties with those of the material salicylaldoxime available on the market.

4,6-Di-*tert*-butylsalicylaldoxime (4,6-*t*Bu-H_2salox): In a round bottom flask hydroxylamine−hydrochloride (5.6 g: 80 mmol) was dissolved in 10 mL of distilled water. Simultaneously, 4,6-di-*tert*-butylsalicylaldehyde (5.0 g: 20 mmol) was dissolved in 40 mL of warm MeOH. Both solutions were mixed and heated gently for 1 h under reflux. On cooling, a white product was isolated and washed with distilled water. M.p. 130−134 °C; yield 5.10 g (96%).− $C_{15}H_{23}NO_2$ (249.4): calcd. C 72.25, H 9.30, N 5.62; found C 72.5, H 9.4, N 5.4. − ^{1}H NMR [250 MHz, $CDCl_3$, 300 K] δ/ppm = 1.28; 1.42 [2 × s, 2 × 9 H (*t*Bu)], 6.98 [s, 1 H (H−ON)], 7.09; 7.35 [2 × s, 2 × 1 H (H-Ar)], 8.22 [s, 1 H (H−O−Ar)], 10.02 [s, 1H (H−C-Ar)]. − EI-MS: m/z = 249 $[M]^+$ and 234 $[M - CH_3]^+$ (100%).

[(*tmtacn*)Mn^{III}(*salox*)$_3Mn^{III}$] (1): A solution of the cyclic amine (0.17 g; 1 mmol) in 40 mL of MeOH was treated with a sample of manganese(III) acetate (0.52 g; 2 mmol) under vigorous stirring in an atmosphere of argon. After 0.5 h the resulting red-brown solution was charged with a sample of salicylaldoxime (0.41 g; 3 mmol) and 1 mL of triethylamine. The very dark solution was heated under reflux for 1 h, followed by a filtration to get rid of some green solid, presumably, Mn(Hsalox)$_3$. The solution kept at room temperature provided deep brown (almost black) crystals. The crystals were collected by filtration and air-dried. Yield 350 mg (≈50%). − $C_{30}H_{36}Mn_2N_6O_6$ (686.5): calcd. C 52.26, H 5.26, N 12.19, Mn 15.94; found C 52.0, H 5.3, N 12.3, Mn 16.0. − MS (ESI-positive in CH_3CN): m/z = 686 $[M]^+$ (100%).

[(tmtacn)Mn^{III}(salox)$_3Fe^{III}$] (2): A solution of the cyclic amine (0.17 g; 1 mmol) in 40 mL of MeOH was treated with a sample of manganese(III) acetate (0.52 g; 2 mmol) under vigorous stirring in an atmosphere of argon. After 0.5 h the resulting red-brown solution was charged with a suspension of $FeCl_3$ (0.16 g; 1 mmol) and salicylaldoxime (0.41 g; 3 mmol) in MeOH (30 mL) containing 1 mL of triethylamine. The very dark solution was heated under reflux for 2 h and then filtered to remove any solid particles. The solution kept at room temperature provided a deep brown solid. Deep brown crystals were obtained by diffusion of n-pentane into a MeCN solution of the solid. The crystals were collected by filtration and air-dried. Yield 270 mg (≈40%). − $C_{30}H_{36}FeMnN_6O_6$ (687.4): calcd. C 52.19, H 5.28, N 12.20, Mn 7.99, Fe 8.12; found C 52.3, H 5.2, N 12.1, Mn 7.8, Fe 8.1. − MS (ESI-positive in CH_3CN): m/z = 688 $[M + H]^+$ (75%), 710 $[M + Na]^+$ (100%).

[(tmtacn)Fe^{III}(salox)$_3Fe^{III}$]·MeOH (3): $FeCl_3$ (0.16 g; 1 mmol) was added to a degassed solution of salicylaldoxime (0.41 g; 3 mmol) in dry MeOH (50 mL) containing 1 mL of triethylamine under vigorous stirring. The resulting suspension was stirred at room temperature for 1 h and then charged with a solid sample of [Fe(tmtacn)Cl_3][37] (0.33 g; 1.0 mmol) and gently heated under reflux for 1 h. The resulting dark brown solid was collected by filtration and air-dried. X-ray quality crystals as dark red needles were obtained by diffusion of MeOH into a MeCN solution of **3**. Yield 450 mg (≈62%). − $C_{31}H_{40}N_6O_7Fe_2$ (720.4): calcd. C 51.69, H 5.60, N 11.67, Fe = 15.53; found C 52.0, H 5.5, N 11.6, Fe 15.3. − MS (ESI-positive in CH_3CN): m/z = 689 (100%) $[M + H]^+$.

[(tmtacn)Fe^{III}(*t*Busalox)$_3Fe^{III}$]·3.5 $CHCl_3$ (4): [Fe(tmtacn)Cl_3] (0.33 g; 1.0 mL) was added to a degassed solution of 4,6-di-*tert*-butylsalicylaldoxime (0.75 g; 3 mmol) in MeOH (50 mL) containing 0.84 mL of triethylamine under vigorous stirring. A solid sample of $FeCl_3$ (0.16 g; 1 mmol) was added and the resulting dark-red solution was stirred for further 0.5 h under gentle reflux. The solution kept at room temperature provided a dark-red microcrystalline solid, which was collected by filtration and air-dried. Yield 710 mg (≈70%). − $C_{54}H_{84}Fe_2N_6O_6$ (1025.0): calcd. C 63.28, H 8.26, N 8.20, Fe 10.9; C 62.9, H 8.2, N 8.2, Fe 10.8. − MS (ESI-positive in CH_3CN): a single peak at m/z = 1025 (100%) $[M + H]^+$. Recrystallization from $CHCl_3$ yielded X-ray quality crystals.

Acknowledgments

The authors thank the Fonds der Chemischen Industrie and the Max-Planck-Society for financial support. C. N. V. thanks DAAD for a fellowship. Technical assistance of Mrs. H. Schucht and Mrs. P. Höfer is gratefully acknowledged. Our thanks are also due to R. Werner and W. Haase (Darmstadt) and J. Bonvoisin (Toulouse) for the preliminary susceptibility measurements.

[1] For example: J. A. Halfen, B. A. Jzdzewski, S. Mahapatra, L. M. Berreau, E. C. Wilkinson, L. Que Jr., W. B. Tolman, *J. Am. Chem. Soc.* **1997**, *119*, 8217−8227.
[2] Y. Wang, T. D. P. Stack, *J. Am. Chem. Soc.* **1996**, *118*, 13097−13098.
[3] D. Zurita, I. Gautier-Luneau, S. Menage, J. L. Pierre, E. Saint-Aman, *J. Biol. Inorg. Chem.* **1997**, *2*, 46−55.
[4] E. Bill, J. Müller, T. Weyhermüller, K. Wieghardt, *Inorg. Chem.* **1999**, *38*, 5795−5802 and references therein.
[5] R. H. Holm, E. I. Solomon, Guest Editors, *Chem. Rev.* **1996**, no. 7, *96*.
[6] *Metal Ions in Biological Systems* (Ed.: H. Sigel, A. Sigel), **1994**, Vol. 30.
[7] G. T. Babcock, M. Espe, C. Hoganson, N. Lydakis-Simantiris, J. McCracken, W. Shi, S. Styring, C. Tommas, K. Warncke, *Acta Chem. Scand.* **1997**, *51*, 533−540.
[8] J. Stubbe, W. A. van der Donk, *Chem. Rev.* **1998**, *98*, 705−762.
[9] P. Chaudhuri, M. Hess, U. Flörke, K. Wieghardt, *Angew. Chem. Int. Ed.* **1998**, *110*, 2217−2220.
[10] P. Chaudhuri, M. Hess, T. Weyhermüller, K. Wieghardt, *Angew. Chem. Int. Ed.* **1999**, *38*, 1095−1098.
[11] P. Chaudhuri, M. Hess, J. Müller, K. Hildenbrand, E. Bill, T. Weyhermüller, K. Wieghardt, *J. Am. Chem. Soc.* **1999**, *119*, 9599−9610.
[12] O. Kahn, *Molecular Magnetism*, VCH Verlagsgesellschaft: Weinheim, Germany, **1993**.
[13] *Research Frontiers in Magnetochemistry* (Ed.: C. J. O'Connor), World Scientific, Singapore, **1993**.

[14] *Magnetic Molecular Materials* (Eds.: D. Gatteschi, O. Kahn, J. S. Miller, F. Palacio), Kluwer Academic Publishers: Dordrecht, The Netherlands, **1991**.
[15] *Magneto-Structural Correlations in Exchange Coupled Systems* (Eds.: R. D. Willett, D. Gatteschi, O. Kahn), Kluwer Academic Publishers: Dordrecht, The Netherlands, **1985**.
[16] S. J. Lippard, J. M. Berg, *Principles of Bioinorganic Chemistry*, University Science Books, CF **1994**.
[17] *Bioinorganic Chemistry of Copper* (Eds.: K. D. Karlin, Z. Tyeklár), Chapman & Hall, New York **1993**.
[18] W. Kaim, B. Schwederski, *Bioanorganische Chemie*, B. G. Teubner, Stuttgart **1991**.
[19] O. Kahn, *Adv. Inorg. Chem.* **1995**, *43*, 179−259.
[20] D. Burdinski, F. Birkelbach, T. Weyhermüller, U. Flörke, H.-J. Haupt, M. Lengen, A. X. Trautwein, E. Bill, K. Wieghardt, P. Chaudhuri, *Inorg. Chem.* **1998**, *37*, 1009−1020.
[21] F. Birkelbach, U. Flörke, H.-J. Haupt, C. Butzlaff, A. X. Trautwein, K. Wieghardt, P. Chaudhuri, *Inorg. Chem.* **1998**, *37*, 2000−2008 and references therein.
[22] C. N. Verani, E. Rentschler, T. Weyhermüller, E. Bill, P. Chaudhuri, *J. Chem. Soc., Dalton Trans.* **2000**, 251−258 and references therein.
[23] C. Krebs, M. Winter, T. Weyhermüller, E. Bill, K. Wieghardt, P. Chaudhuri, *J. Chem. Soc., Chem. Commun.* **1995**, 1913−1915 and references therein.
[24] P. Chaudhuri, F. Birkelbach, M. Winter, V. Staemmler, P. Fleischhauer, W. Haase, U. Flörke, H.-J. Haupt, *J. Chem. Soc., Dalton Trans.* **1994**, 2313−2319 and references therein.
[25] F. Epharain, *Ber. Dtsch. Chem. Ges.* **1930**, *63*, 1928−1930.
[26] S. J. Rettig, A. Storr, J. Trotler, *Acta Crystallogr., Sect. C* **1992**, *48*, 1587−1590.
[27] E. Toyota, K. Umakoshi, Y. Yamamoto, *Bull. Chem. Soc. Jpn.* **1995**, *68*, 858−865.
[28] K. R. Manolov, *Russ. J. Inorg. Chem.* **1967**, *12*, 1431−1434.
[29] J. M. Thorpe, R. L. Beddoes, D. Collison, C. D. Garner, M. Helliwell, J. M. Holmes, P. A. Tasker, *Angew. Chem. Int. Ed.* **1999**, *38*, 1119−1121.
[30] E. Bill, C. Krebs, M. Winter, M. Gerdan, A. X. Trautwein, U. Flörke, H.-J. Haupt, P. Chaudhuri, *Chem. Eur. J.* **1997**, *3*, 193−201.
[31] B. Adam, E. Bill, E. Bothe, B. Goerdt, G. Haselhorst, K. Hildenbrand, A. Sokolowski, S. Steenken, T. Weyhermüller, K. Wieghardt, *Chem. Eur. J.* **1997**, *3*, 308−319.
[32] B. P. Gaber, V. Miskowski, T. G. Spiro, *J. Am. Chem. Soc.* **1974**, *96*, 6868−6873.
[33] P. Chaudhuri, M. Winter, F. Birkelbach, P. Fleischhauer, W. Haase, U. Flörke, H.-J. Haupt, *Inorg. Chem.* **1991**, *30*, 4291−4293.
[34] U. Auerbach, U. Eckert, K. Wieghardt, B. Nuber, J. Weiss, *Inorg. Chem.* **1990**, *29*, 938−944.
[35] S. K. Chandra, P. Basu, D. Ray, S. Pal, A. Chakravorty, *Inorg. Chem.* **1990**, *29*, 2423−2428.
[36] P. Chaudhuri, *Proc. Indian Acad. Sci (Chem. Sci)* **1999**, *111*, 397−411.
[37] P. Chaudhuri, M. Winter, K. Wieghardt, S. Gehring, W. Haase, B. Nuber, J. Weiss, *Inorg. Chem.* **1988**, *27*, 1564−1569.
[38] P. L. Orioli, E. C. Lingafelter, B. W. Brown, *Acta Crystallogr.* **1964**, *17*, 1113−1118.
[39] H. Saarainen, J. Korvenranta, E. Näsäkkälä, *Acta Chem. Scand., Ser. A* **1980**, *34*, 443−448 and references therein.
[40] N. N. Greenwood, T. C. Gibb, *Mössbauer Spectroscopy*, Chapman and Hall, London, **1971**.
[41] H. Hummel, Dissertation, Bochum, **1998** and references therein.
[42] F. Birkelbach, C. Krebs, V. Staemmler, Bochum, unpublished.
[43] K. Wieghardt, P. Chaudhuri, B. Nuber, J. Weiss, *Inorg. Chem.* **1982**, *21*, 3086−3090.
[44] G. M. Sheldrick, *SADABS*, University of Göttingen, **1994**.
[45] G. M. Sheldrick, *SHELXTL PLUS*, Siemens Analytical X-ray Instruments, Madison, WI, **1990**.

Received November 2, 2000
[I00417]

syn−*anti* Conversion in Octahedral Bis(β-diketonato)diorganotin(IV) Derivatives Containing Fluorinated 4-Acyl-5-pyrazolonato Donors

Claudio Pettinari,*[a] Fabio Marchetti,[a] Augusto Cingolani,[a] Asta Gindulyte,[b,c] Lou Massa,[b,c] Miriam Rossi,[d] and Francesco Caruso*[e]

Keywords: Ab initio calculations / Configuration determination / Diazo compounds / Ligand effects

Six-coordinate organotin derivatives L_2SnR_2 [L = 3-methyl-1-(4-trifluoromethylphenyl)-4-R^3-C=O-5-pyrazolonato (R^3 = CH_3, L = L^1; R^3 = C_6H_5, L = L^2; R^3 = CF_3, L = L^3; R = CH_3, *n*-C_4H_9, C_6H_5)] have been synthesized and characterized by analytical and spectroscopic (^1H, ^{13}C, ^{119}Sn, and ^{19}F NMR, IR) techniques. Partial dissociation of one ligand in chlorohydrocarbon solvents gives rise to cationic five-coordinate L-(solvent)-diorganotin(IV) complexes. The X-ray crystal structure of bis[4-benzoyl-3-methyl-1-(4-trifluoromethylphenyl)pyrazolon-5-ato]diphenyltin (**6**) shows the metal in a distorted octahedron (skewed trapezoidal bipyramidal) with the two β-diketonato donors in *syn* positions, a C–Sn–C bond angle of 165.2(2)° and two sets of tin–oxygen bonds [2.141(5) and 2.139(3) Å for Sn–O(pyrazolonato) and 2.250(4) and 2.272(5) Å for Sn–O(acyl)]. Surprisingly, the recently reported dimethyltin derivative has the *anti* configuration, in contrast to expectations based on all previous experience. Large scale Hartree–Fock (HF) and Density Functional Theory (DFT) calculated structures for the *anti* configuration of bis[4-benzoyl-3-methyl-1-(4-trifluoromethylphenyl)pyrazolon-5-ato]dimethyltin show good agreement with the experimental structure obtained from X-ray methods. The hypothetical *syn* configuration of bis[4-benzoyl-3-methyl-1-(4-trifluoromethylphenyl)pyrazolon-5-ato]dimethyltin was also studied theoretically and both methods also predict characteristic structural features, such as: (from HF) a C–Sn–C bond angle of 150.0°, Sn–O(pyrazolonato) bond lengths of 2.088 and 2.084 Å and Sn–O(acyl) bond lengths of 2.385 and 2.401 Å. Results from the *syn* calculated structures suggest that intramolecular repulsive F···F interactions contribute to the *syn*–*anti* conversion.

Introduction

Organotin compounds have varied applications, including their use as boat paint additives to prevent attack by microorganisms,[1] and as insecticides and fungicides.[2−3] They are also effective antitumor agents.[4−8] We are particularly interested in organotin derivatives of 4-acyl-5-pyrazolones because these ligands possess several sites for substitution, allowing for a systematic analysis of their effects on the subsequent biological activity. So far, only the variation at R^3 has been fully explored (Figure 1).[9−20]

Recently, we have modified the R^1 position and synthesized some organotin derivatives, with R^1 = methyl[21] (usually it is a phenyl group), that possess an increased solubility in water and alcohols, an important feature for biological applications. Since halogen-substituted anions induce stronger biological activity in their organotin derivatives, both as antitumor agents[5−8] and as insecticides,[22] and, in particular, fluorine substituents have been reported to strongly influence the antitumor activity,[23−26] we then synthesized a ligand with R^1 = *p*-CF_3-Ph (Figure 2). This chemical modification results in a ligand with a lower donating ability of the O(pyrazolonato) atom and a greater ring-electron delocalization in the crystalline compound bis[4-benzoyl-3-methyl-1-(4-trifluoromethylphenyl)pyrazolon-5-ato]dimethyltin. However, its structure rather unexpectedly has an *anti* configuration,[27] the first to be observed.

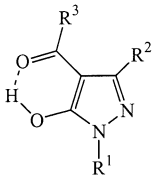

Figure 1. Proligands

Since the *anti* configuration was obtained after a seemingly subtle change in a peripheral area (substitution of a CF_3 group for a H atom in the *para* position of R^1 phenyl), we discuss the *syn*−*anti* variation after analyzing the theoretically calculated *syn* molecular structure and supporting experimental data. Large-scale ab initio calculations were performed on these metal complexes as a large number of atoms is involved.

[a] Dipartimento di Scienze Chimiche, Università degli Studi, Via S. Agostino 1, 62032 Camerino, (MC) Italy
Fax: (internat.) +39-737/637-345
E-mail: pettinar@camserv.unicam.it
[b] Department of Chemistry, Hunter College, 695 Park Avenue, New York, NY 10021, USA
[c] The Graduate School, City University of New York, 365 Fifth Avenue, New York, NY 10016, USA
[d] Vassar College, Department of Chemistry, Poughkeepsie, NY 12604−0484, USA
[e] Istituto di Strutturistica Chimica "G. Giacomello", Consiglio Nazionale delle Ricerche (CNR), CP 10, 00016, Monterotondo Stazione, (Rome) Italy
Fax: (internat.) +39 06 90672630
E-mail: francesco.caruso@mlib.cnr.it
Supporting information for this article is available on the WWW under http://www.wiley-vch.de/home/eurjoc or from the author.

 © WILEY-VCH Verlag GmbH, 69451 Weinheim, 2001 1434−1948/01/0808−2171 $ 17.50+.50/0

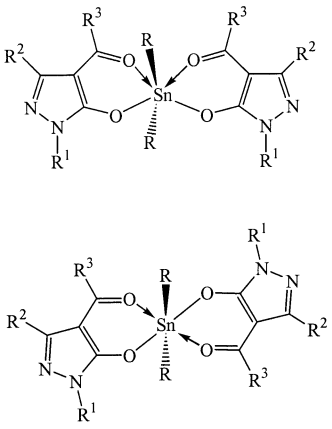

Figure 2. (top) *syn* configuration (normally observed in bis(4-acyl-5-pyrazolonato)diorganotin complexes; (bottom) *anti* configuration

A related *cis*−*trans* conversion has been reported by Gielen[28,29] and us,[11−13,17−19,21] for analogous monoorganotin(IV) β-diketonates in solution. However, in the case of diorganotin(IV) acylpyrazolonates, the *syn*−*anti* variation seems also to be feasible in the solid state, as previously demonstrated by multinuclear NMR spectroscopy and Mössbauer studies.[11,17]

Results and Discussion

We analyzed other diorganotin derivatives containing related ligands and the same R^1 (*p*-CF_3-Ph) substituent in an attempt to explain why the unexpected *anti* configuration of bis[4-benzoyl-3-methyl-1-(4-trifluoromethylphenyl)pyrazolon-5-ato]dimethyltin is the form experimentally observed (described in Exp. Sect.). Since a previous diphenyltin derivative of a related 4-acyl-5-pyrazolonato showed less octahedral deformation than usual,[17] we selected bis[4-benzoyl-3-methyl-1-(4-trifluoromethylphenyl)pyrazolon-5-ato]diphenyltin **6** from the compounds synthesized, and determined its molecular structure by X-ray diffraction methods.

Diffraction Study of $(L^2)_2SnPh_2$, 6

The crystal structure is formed from well-separated discrete molecules with no imposed crystallographic symmetry (Figure 3). The six-coordinate metal is surrounded by four O atoms from the two anionic chelating pyrazolonato ligands, and two C atoms from the phenyl groups, in a distorted octahedral arrangement so that the ligands have their equivalent arms facing one another (*syn* configuration), a geometry normally observed for bis(4-acyl-5-pyrazolonato)-diorganotin complexes. The relatively small octahedral distortion, described later in Table 1, is similar (although a bit larger) to that of another diphenyltin derivative, namely bis[4-(*p*-bromobenzoyl)-3-methyl-1-phenylpyrazolon-5-ato]-diphenyltin,[17] [C−Sn−C′ bond angle of 173.0(7)°, Sn−O1 bond length of 2.143(7) Å, Sn−O1′ bond length of 2.12(1) Å, Sn−O2 bond length of 2.223(8) Å, Sn−O2′ bond length

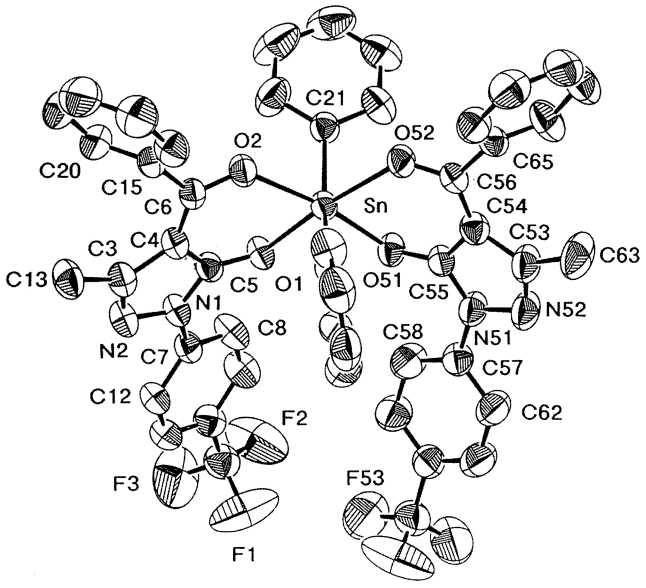

Figure 3. X-ray ORTEP drawing of bis[4-benzoyl-3-methyl-1-(4-trifluoromethylphenyl)pyrazolon-5-ato]diphenyltin **6**

of 2.26(1) Å, O1−Sn−O2 bite angle of 84.5° and O1′−Sn−O2′ bite angle of 85.1(3)°].

The dihedral angles between the pyrazole ring and its attached *p*-CF_3-Ph ring are 16.6(7)° in one ligand, and −13.6(7)° in the other ligand, whereas in the above-mentioned bis(4-*p*-bromobenzoyl-3-methyl-1-phenyl)diphenyltin structure[17] the values are 13.9° and −11.7°, respectively. This quasi co-planarity between the rings is associated with the intramolecular distances O1···H1 [2.294(7) Å] and O51···H13 [2.265(8) Å], which are shorter than the van der Waals value of 2.60 Å[30] (H1 and H13 are bound to C8 and C58, respectively); this feature is also characteristic of these compounds. A specific feature of this structure is that the sum of the equatorial bond angles is equal to 360°: all other previously reported *syn* bis(4-acyl-5-pyrazolonato)-diorganotin complexes[10−14,17−21] show the tin somewhat shifted out of the equatorial plane, which makes this value smaller than 360°.

Theoretical Calculations

The molecular structures of bis[4-benzoyl-3-methyl-1-(4-trifluoromethylphenyl)pyrazolon-5-ato]dimethyltin in both the *anti* and *syn* configurations were studied by theoretical methods. The starting coordinates for the *anti* compound were those obtained by X-ray diffraction[27] and were optimized by energy minimization with the Hartree−Fock (HF) and Density Functional Theory (DFT) methods (see Figures 4 and 5). Table 1 shows some geometrical features. There is excellent agreement with X-ray[27] data for the Sn polyhedron although HF calculates slightly shorter Sn−O bonds and slightly smaller bite angles, and, generally, DFT agrees better with the X-ray data than HF. A marked difference between HF and DFT is seen in the dihedral angle between the planar pyrazole and its attached phenyl. These values are 3.8 and −3.9° (DFT) and 24.2 and −24.3° (HF),

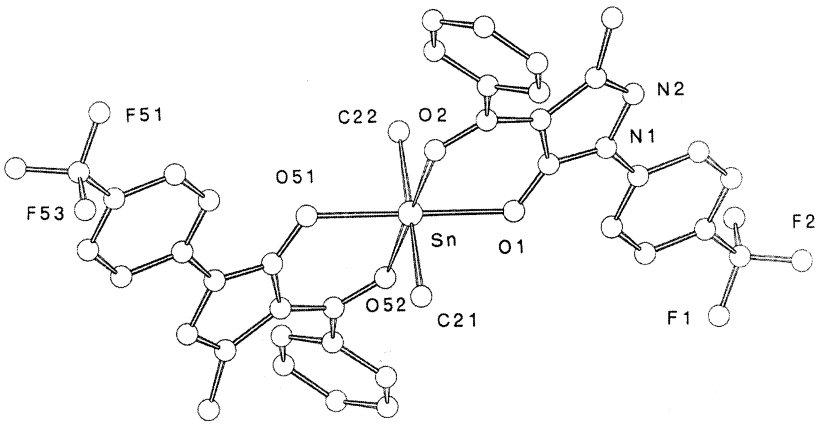

Figure 4. Bis[4-benzoyl-3-methyl-1-(4-trifluoromethylphenyl)pyrazolon-5-ato]dimethyltin (*anti* configuration) obtained by the DFT method

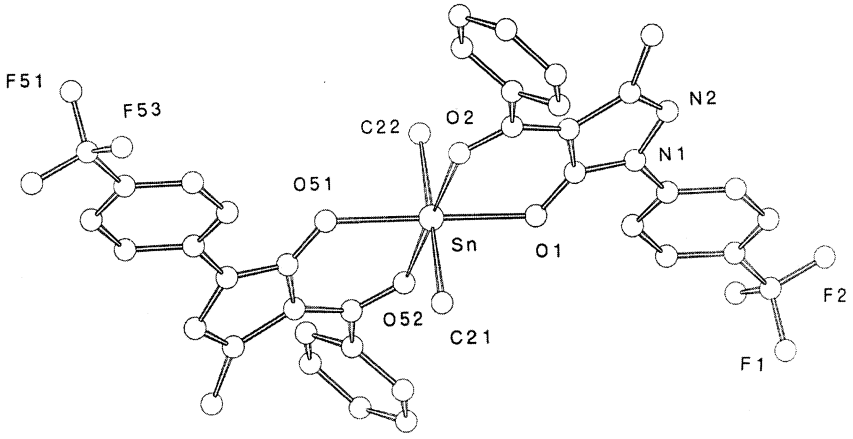

Figure 5. Bis[4-benzoyl-3-methyl-1-(4-trifluoromethylphenyl)pyrazolon-5-ato]dimethyltin (*anti* configuration) obtained by the HF method

whereas the X-ray values are 16.6 and −16.6°. In the *syn* compounds there is a tendency for these two planes to be co-planar,[19] although this dihedral angle shows a large range of values, which suggests that the energy changes as a function of dihedral angle are small, and therefore can be affected by packing and/or intramolecular forces. Moreover, this angle can differ greatly even within the same molecule: for instance, in bis[4-(*p*-bromobenzoyl)-3-methyl-1-phenylpyrazolon-5-ato]dimethyltin it is 13.7° in one ligand and −39.8° in the second ligand.[13]

Since the theoretical results agree closely with the experimental values, we then proceeded to calculate the molecular structure of the *syn* configuration with the coordinates of bis[4-benzoyl-3-methyl-1-(4-trifluoromethylphenyl)-pyrazolon-5-ato]diphenyltin **6** described above. The phenyl groups bound to tin were replaced by methyl groups and the structure was optimized as above. Selected structural parameters are also given in Table 1 and the calculated structures are shown in Figures 6 and 7.

The *syn* structures in Table 1 confirm that when methyl groups are replaced by phenyl groups a smaller octahedral distortion is induced. This was previously observed in bis(4-acylpyrazolon-5-ato)diorganotin complexes studied using X-ray diffraction methods.[17] The driving force is the electron-withdrawing effect of the Ph that attracts electron density from the tin atom and induces further ligand donation, which is provided by O2.[17] Consequently, in diphenyltin derivatives the Sn−O2 bond length is shorter than in dialkyltin derivatives. As a result, diphenyltin derivatives have similar Sn−O1 and Sn−O2 bond lengths and show less octahedral deformation, that is, the C−Sn−C′ bond angle is closer to 180°.

Table 1 shows that the polyhedron deformation in the *syn* structures (for the three methods, XR, HF, and DFT) is characterized by having Sn and its four linked O atoms in a plane [the sum of the four angles, O1−Sn−O2 (ligand 1 bite), O1′−Sn−O2′ (ligand 2 bite), O1−Sn−O1′ and O2−Sn−O2′, equals 360°]. As mentioned above, this is the first time that this feature (seen in compound **6**) has been observed for *syn*-bis(4-acyl-5-pyrazolonato)diorganotin complexes, and is confirmed theoretically.

All bis(4-acylpyrazolon-5-ato)diorganotin *syn* structures solved so far by X-ray diffraction display approximate mirror symmetry, with the mirror plane containing Sn and its two bonded C atoms. The calculated molecules are single and isolated (intermolecular forces do not exist) and, if mirror symmetry exists, should show equivalence in both bite angles, as well as the bond lengths Sn−O1 and Sn−O1′, Sn−O2 and Sn−O2′, and the angles O1−Sn−O2′ and O1′−Sn−O2. However, Table 1 shows that this is not the

Table 1. Selected geometrical parameters in bis[4-benzoyl-3-methyl-1-(4-trifluoromethylphenyl)pyrazolon-5-ato]-di-R-tin compounds obtained with different structural methods (XR = X-ray diffraction, HF = Hartree−Fock, DFT = Density Functional Theory)

Compound	**4**	**4**	**4**
R	methyl	methyl	methyl
Method	XR	HF	DFT
Configuration	*anti*	*anti*	*anti*
Sn−O1	2.214(5)	2.179	2.216
Sn−O1′	2.214(5)	2.187	2.217
Sn−O2	2.220(6)	2.216	2.233
Sn−O2′	2.220(6)	2.205	2.233
O1−Sn−O2	85.9(2)	82.4	83.9
O1′−Sn−O2′	85.9(2)	82.6	84.0
C−Sn−C′	180	179.3	180
O1−Sn−O1′	180	179.5	180
O2−Sn−O2′	180	179.5	180
O1−Sn−O2′	94.1(2)	97.0	96.0
O1′−Sn−O2	94.1(2)	98.0	96.0
Compound	**6**	[a]	[a]
R	phenyl	methyl	methyl
Method	XR	HF	DFT
Configuration	*syn*	*syn*	*syn*
Sn−O1	2.140(4)	2.088	2.149
Sn−O1′	2.141(4)	2.084	2.145
Sn−O2	2.250(3)	2.385	2.338
Sn−O2′	2.273(5)	2.401	2.331
O1−Sn−O2	83.5(1)	79.1	81.5
O1′−Sn−O2′	84.1(1)	79.1	82.0
C−Sn−C′	165.2(2)	150.0	158.4
O1−Sn−O1′	87.2(1)	82.4	83.0
O2−Sn−O2′	105.2(1)	119.7	113.7
O1−Sn−O2′	171.3(1)	160.8	164.6
O1′−Sn−O2	170.4(2)	161.0	164.2

[a] Hypothetical compound. Labels in Figure 3 are related so that O51 is O1′, O52 is O2′, N51 is N1′, etc. Distances [Å], angles [°]. Energy values for calculated structures (a.u.): HF, −2573.72811 (*anti*), −2573.73406 (*syn*); DFT, −2587.11444 (*anti*), −2587.11749 (*syn*).

case. A peripheral structural feature confirms this: the dihedral angle between the pyrazole and its attached phenyl differs in each ligand (24.4° and 8.2° for DFT and 30.6° and 25.8° for HF). These results are in contrast with the *anti* species described above where both dihedral angles obtained from DFT, HF, and X-ray methods are equal.

Further analysis of the calculated *syn* structures for bis[4-benzoyl-3-methyl-1-(4-trifluoromethylphenyl)pyrazolon-5-ato]dimethyltin in Table 1 shows good agreement with a characteristic feature observed by X-ray diffraction:[10−21] the Sn−O(pyrazolonato) bond lengths are shorter than the Sn−O(acyl) bond lengths. The variation between these sets of bond lengths using the DFT method is less than when using the HF method. This geometry was described as skewed trapezoidal bipyramidal (STB) by Kepert in a theoretical treatment.[31] The short side of the trapezoid links the two O(pyrazolonato) atoms that form the short Sn−O bonds, whereas the long side links the two O(acyl) atoms that form the long Sn−O bonds (see Figure 8).

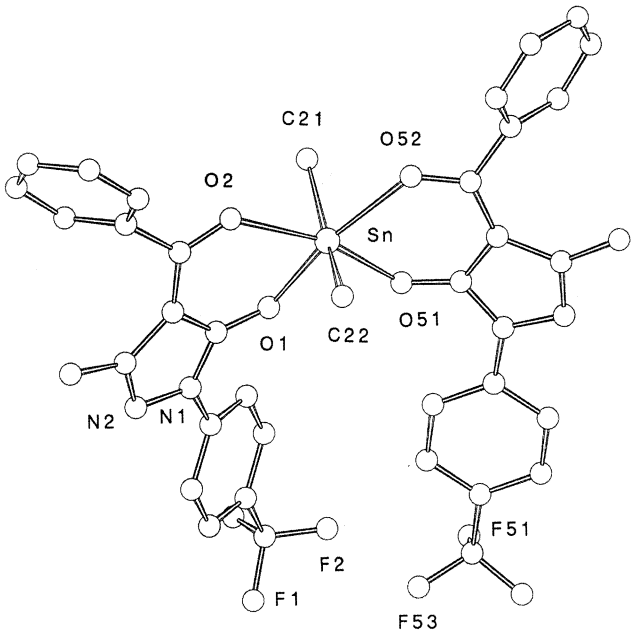

Figure 6. Bis[4-benzoyl-3-methyl-1-(4-trifluoromethylphenyl)pyrazolon-5-ato]dimethyltin (*syn* configuration) obtained by the DFT method

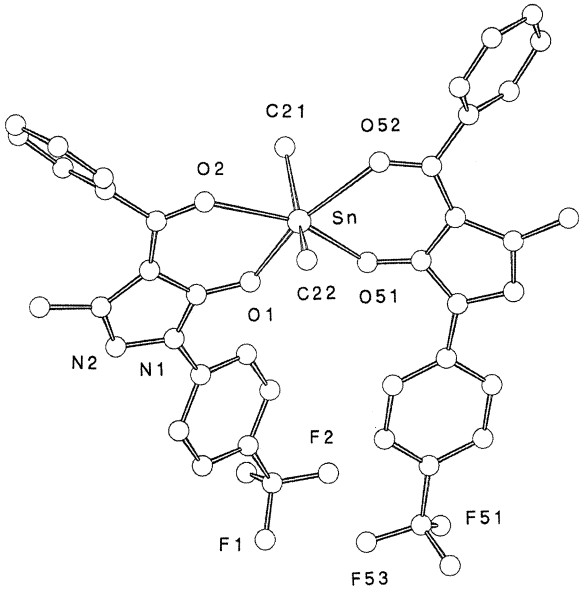

Figure 7. Bis[4-benzoyl-3-methyl-1-(4-trifluoromethylphenyl)pyrazolon-5-ato]dimethyltin (*syn* configuration) obtained by the HF method

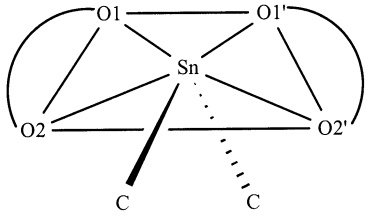

Figure 8. Skewed trapezoidal bipyramidal configuration

In the experimental *syn*-bis(4-acyl-5-pyrazolonato)-di-R-tin complexes studied so far, it is the R = alkyl substituents that induce the strongest octahedral deformation[10−14,17−21] on the geometry of these complexes. This is described by:[19]

(a) a small *trans* C−Sn−C′ angle
(b) a small O1−Sn−O1′ angle
(c) a large O2−Sn−O2′ angle.

Experimentally, when R^1 = Ph, R^2 = methyl, R^3 = Ph and R = methyl, a *syn* species is obtained,[12] whereas when R^1 = *p*-CF_3-Ph, an unexpected *anti* species results.[27] Therefore, the CF_3 group causes a "perturbation". DFT and HF methods react differently to the CF_3 "perturbation": DFT predicts a large C−Sn−C′ angle while, in contrast, HF calculates a smaller C−Sn−C′ angle. Table 1 shows markedly different (a) and (c) values for HF and DFT calculations on the hypothetical *syn*-bis[4-benzoyl-3-methyl-1-(4-trifluoromethylphenyl)pyrazolon-5-ato]dimethyltin. However, the value of O1−Sn−O1′ is similar for both DFT (83.0°) and HF (82.4°); in general, the value of O1−Sn−O1′ in bis(4-acyl-5-pyrazolonato)dialkyltin complexes (containing R^1 = Ph) is smaller. The O1−Sn−O1′ angle for both DFT and HF theoretical methods corresponds to the closest approach of the F atoms (the shortest separations are F1···F53 = 3.09 Å and F2···F53 = 3.05 Å, for HF, and F2···F53 = 2.88 Å and F2···F51 = 3.00 Å, for DFT; these distances are close to the F···F van der Waals value of 2.94 Å).[30] We see that the limiting *syn* octahedral deformation predicted by theory corresponds to an O1−Sn−O1′ angle that differs from those previously observed[19] (as mentioned above, X-ray values are smaller). We conclude that the CF_3 "perturbation" is associated with greater intramolecular R^1···R^1 steric hindrance; it is therefore not surprising that an *anti* species (that avoids such strain) is obtained. It is worthwhile to note that diorganotin STB deformation can be greatly enhanced; for instance, in the less crowded bis(*N*-benzoyl-*N*-phenylhydroxylamino)di-*n*-butyltin complex, the C−Sn−C′ bond angle is 133(9)°.[32] This also suggests that repulsion factors are responsible for the extent of deformation in the STB configuration. Moreover, Kepert's theoretical treatment is based on repulsion features[31] (in other words increasing deformation may imply stronger repulsion on the short side of the trapezoid).

The strength of repulsive F···F interactions is demonstrated by the existence of WF_6 as a gas at room temperature. The large polarization of F−W bonds makes the F atoms highly negatively charged; the WF_6 octahedrons therefore repel each other inducing an unusual gaseous state. In our case, the alternative to the sterically hindered R^1···R^1 *syn* structure is the *anti* structure. We have calculated the energy for bis[4-benzoyl-3-methyl-1-(4-trifluoromethylphenyl)pyrazolon-5-ato]dimethyltin to be slightly lower for the *syn* structure than for the *anti* structure (3.7 kcal/mol, for HF, and 1.9 kcal/mol for DFT); this feature will be addressed later.

Solution Study

Since the crystals of *anti*-bis[4-benzoyl-3-methyl-1-(4-trifluoromethylphenyl)pyrazolon-5-ato]dimethyltin **4** were obtained directly from the alcoholic reaction mixture,[27] while all the previous bis(4-acylpyrazolon-5-ato)diorganotin derivatives precipitated in such a medium (they were later recrystallized from other solvents to obtain crystals suitable for diffraction),[11−13,16−21] we decided to study the behavior of **4** and related complexes containing ligands with the same R^1 substituent, in solution.

The proligands 4-acetyl-3-methyl-1-(4-trifluoromethylphenyl)pyrazol-5-one (L^1H), 4-benzoyl-3-methyl-1-(4-trifluoromethylphenyl)pyrazol-5-one (L^2H), and 3-methyl-4-(trifluoroacetyl)-1-(4-trifluoromethylphenyl)pyrazol-5-one (L^3H) react with dichlorodiorganotin(IV) acceptors in basic methanol solution by substitution of the two chlorine atoms and yield the six-coordinate tin(IV) derivatives L_2SnR_2 **1−9** (see Scheme 1).

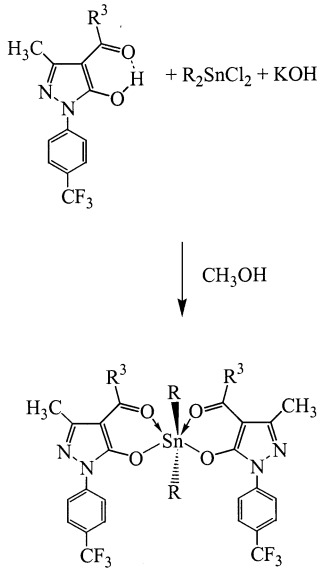

Compound	L	R^3	R
1	L^1	CH_3	CH_3
2	L^1	CH_3	Bu^n
3	L^1	CH_3	Ph
4	L^2	Ph	CH_3
5	L^2	Ph	Bu^n
6	L^2	Ph	Ph
7	L^3	CF_3	CH_3
8	L^3	CF_3	Bu^n
9	L^3	CF_3	Ph

Note: R^1 = *p*-CF_3-Ph and R^2 = CH_3 in all compounds.

Scheme 1

They are air- and moisture-stable solids, very soluble in aromatic and chlorohydrocarbons, acetone and dimethylsulfoxide (DMSO). They are partially dissociated in all these solvents with the exception of the aromatic hydrocarbons: In fact, vapor pressure osmometric molecular mass determinations of derivatives **1** and **3−5** in chloroform indicate a partial dissociation, the ratio *r* (molecular mass/formula mass) being generally in the range 0.60−0.90. Conductivity data carried out in dichloromethane seem to indicate the presence of non-ionic species. This could be due to ion-pairing effects, which result in a much lower conductivity value than that observed in DMSO. The molecular mass study on derivative $(L^2)_2SnMe_2$ **4**, shown in Figure S1 (Supporting Information, see also footnote on the first page of this article), indicates that dissociation increases with dilution. In fact, the experimental molecular mass values increase with concentration of the solution, approaching the theoretical formula mass when the concentration is higher than 0.02 m (m = mol of solute/kg of solvent). This behavior in solution is unexpected since previous studies[11−13,16−21] show an absence of conductivity for bis(4-acyl-5-pyrazolonato)diorganotin complexes, and the experimental molecular mass values in solution are typical of mononuclear non-ionic species. These results demonstrate that the CF_3 substituent in the *para* position of R^1 phenyl can influence the stability of the L_2SnR_2 species in solution.

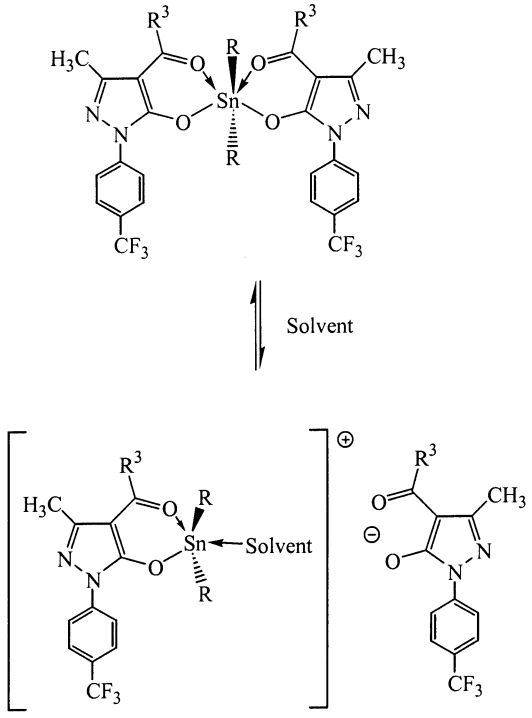

Scheme 2

Dissociation is confirmed by multinuclear NMR spectroscopic experiments. Broad resonances (compounds **1** and **2**) or three sets of signals (compounds **4** and **5**) for the ligand moiety in the ^1H NMR spectra, and two sets of signals for the $(alkyl)_2Sn$ moiety in the ^1H and ^{119}Sn NMR spectra are observed. This is in agreement with Scheme 2. We observed the same multiplicity in the ^{13}C NMR spectra. The assignments of the ^{13}C resonances of the groups bonded to tin are straightforward from the $^nJ(^{13}C\text{-}^{119/117}Sn)$ coupling constants, whereas the L carbon resonance assignments are based on the $^{13}C\text{-}^{19}F$ coupling constants. Holecek[33] and Lockhart[34] reported that $^1J(^{13}C\text{-}^{119}Sn)$ can be used to indicate the tin coordination number in diorganotin(IV) compounds. Six-coordinate dialkyl- and diaryltin(IV) complexes exhibit couplings in the range 800−1000 Hz, whereas five-coordinate complexes are in the range 500−700 Hz.[33−35] Most of the diorganotin(β-diketonates) in this work exhibit at least one signal with characteristic coupling satellites. The $^1J(^{13}C\text{-}^{119}Sn)$ coupling constants vary in the range 700−900 Hz, in accordance with a coordination number halfway between 5 and 6. These values can also be related to the size of the C−Sn−C angle, according to the equations derived by Holecek[33] and Lockhart.[34] The θ values of the studied compounds range from 145 to 157°. They are greater for L^1 and L^2 than for L^3 diorganotin(IV) derivatives. This suggests that the solid state six-coordinate structure is lost in solution in the case of L^3 complexes to generate a five-coordinate species, as also indicated by the values of the $^2J(^1H\text{-}^{119}Sn)$ coupling constants in the spectra of the dimethyl- and diphenyltin derivatives **7** and **9**, which correspond to typical five-coordinate diorganotin(IV) complexes.[33−35] However, it should be noted that the coupling constants values are determined by the metal coordination number as well as by electronic and steric factors, and we cannot exclude the occurrence of strong deformations from the octahedral structure in solution.

^{119}Sn NMR spectroscopic data further confirm the presence of different species in solution for dimethyl, di-*n*-butyl and diphenyltin(IV) derivatives of L^1 and L^2 as at least two resonances are found. The more intense is in the typical range for six-coordinate species [δ = −300 to −500 from $Sn(CH_3)_4$],[17] whereas the other is in the typical range for five-coordinate species δ = −80 to −250 from $Sn(CH_3)_4$].[33,35] The existence of species such as $[L(solvent)_xSn(CH_3)_2]^+$ (deduced from the equilibrium in Scheme 2) was confirmed by treating an acetone solution of $(L^3)_2Sn(CH_3)_2$ **7** with $AgClO_4$, yielding $[(L^3)Sn(CH_3)_2ClO_4]$ (**10**) according to Scheme 3 (see Exp. Sect.). Upon addition of a large excess of HL^1 and NEt_3 (1:1 relative molar ratio) to a $CDCl_3$ solution of **1**, the signal at δ = −100.6 disappeared, whereas that at δ = −323.9 remained unchanged.

The ^{19}F NMR spectra of the L^1 derivatives **1** and **3** have one resonance at room temperature that splits into four or five resonances at −50 °C (Figure S2), whereas the ^{19}F NMR spectra of derivatives **4−9** recorded at room temperature show several signals, in accordance with dissociation (Scheme 2).

Therefore, dissociation of a pyrazolonato anion in Scheme 2 generates ionic species, increasing the solubility in the moist alcoholic reaction mixture and allowing slow crystallization of the *anti* species **4**.

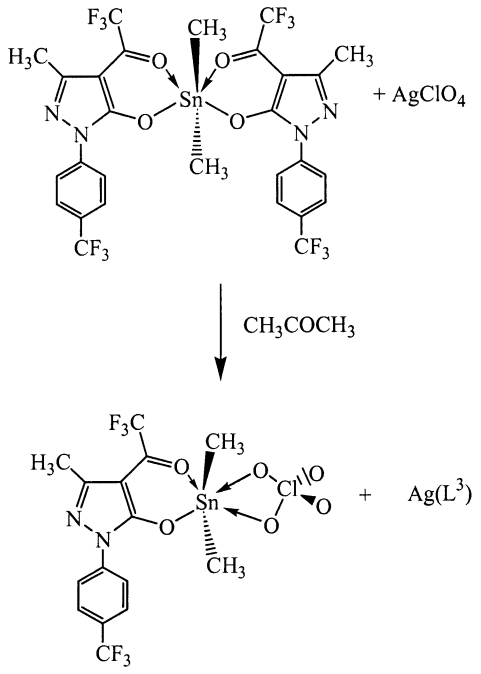

Scheme 3

Conclusion

Theoretical methods (HF and DFT) give calculated energies for the *syn* and *anti* configurations of bis[4-benzoyl-3-methyl-1-(4-trifluoromethylphenyl)pyrazolon-5-ato]dimethyltin that are almost equivalent: the energy needed for the existence of the *anti* species could easily be provided by crystallization. In addition, such an arrangement for bis[4-benzoyl-3-methyl-1-(4-trifluoromethylphenyl)pyrazolon-5-ato]dimethyltin, experimentally obtained in the solid state after crystallization from the reaction mixture, is favored by partial complex dissociation with the formation of the ionic species $[(solvent)(L)Sn(CH_3)_2]^+$ and the pyrazolonato anion (in contrast to ligands containing R^1 = Ph or methyl). Furthermore, the calculated O1−Sn−O1′ angle of the hypothetical *syn*-bis[4-benzoyl-3-methyl-1-(4-trifluoromethylphenyl)pyrazolon-5-ato]dimethyltin is wider than those of other bis(4-acyl-5-pyrazolonato)dialkyltin complexes and this is due to repulsive F···F interactions. Therefore, the *anti* species arises from the synergistic action of: a) increased solubility in the reaction mixture due to ionic separation; b) repulsion between CF_3 groups for the *syn* configuration that is avoided in the *anti* species; and c) the small energy difference between the *syn* and *anti* configurations, which can be accounted for by the crystallization process.

The *syn* configuration [clearly preferred in bis(4-acyl-5-pyrazolonato)diorganotin complexes] is observed experimentally for bis[4-benzoyl-3-methyl-1-(4-trifluoromethylphenyl)pyrazolon-5-ato]diphenyltin (**6**) The intramolecular repulsion between $R^1\cdots R^1$ groups in this less-distorted octahedral species is avoided because of the wider O1−Sn−O1′ angle than that of the calculated dimethyltin analogue.

Experimental Section

General: The organotin(IV) halides were purchased from Alfa (Karlsruhe) and Aldrich (Milwaukee) and used as received. − The samples for microanalysis were dried in vacuum to constant mass (20 °C, about 0.1 Torr). − Elemental analyses (C,H,N) were performed in house with Fisons Instruments 1108 CHNS-O Elemental Analyzer. − Molecular mass determinations (molecular mass) were performed at 40 °C with a Knauer KNA0280 vapor pressure osmometer calibrated with benzil. The solvent was Baker Analyzed Spectrophotometric grade chloroform. The results were reproducible to ±2%. − IR spectra were recorded from 4000 to 100 cm^{-1} with a Perkin−Elmer System 2000 FT-IR instrument. − ^1H, ^{19}F, ^{13}C, and ^{119}Sn NMR spectra were recorded on a VXR-300 Varian spectrometer operating at room temperature (300 MHz for ^1H, 75 MHz for ^{13}C, 282.2 MHz for ^{19}F, and 111.9 MHz for ^{119}Sn), referred to TMS (^1H and ^{13}C), $CFCl_3$ (^{19}F), and $(CH_3)_4Sn$ (^{119}Sn). The ^{119}Sn NMR experiments were carried out with a spectral width of 900 ppm. − Melting points were taken on an IA 8100 Electrothermal Instrument. − The electrical conductances (reported as Ω^{-1} cm^2 mol^{-1}) of dichloromethane, DMSO, and acetone solutions (M = mol/L) were measured with a Crison CDTM 522 conductimeter at room temperature.

Synthesis of the Donors: The donors L^1H, L^2H, and L^3H were synthesized by previously reported methods.[36]

Synthesis of the Metal Derivatives

Bis[4-acetyl-3-methyl-1-(4-trifluoromethylphenyl)pyrazolon-5-ato]-dimethyltin(IV) $(L_1)_2SnMe_2$ (1): KOH (2 mmol) and Me_2SnCl_2 (1 mmol) were added to a methanol solution (30 mL) of L^1H (2 mmol). A precipitate formed immediately. The mixture was stirred overnight and the precipitate was then filtered, washed with methanol (ca. 10 mL) and dried under reduced pressure at room temperature. The product was then recrystallized from chloroform/*n*-hexane. Yield: 86%. M.p. 230−231 °C. − $C_{26}H_{26}F_6N_4O_4Sn$: calcd. C 47.02, H 3.66, N 7.83; found C 47.34, H 3.76, N 8.02; formula mass 715; molecular mass 486 ($0.9\cdot10^{-2}$ m; r = 0.68), 529 ($1.4\cdot10^{-2}$ m; r = 0.74). − Molar conductance: Λ_M ($0.8\cdot10^{-3}$ M in CH_2Cl_2) = 0.3; Λ_M [$0.9\cdot10^{-3}$ M in $(CH_3)_2SO$] = 17.7. − IR (nujol): $\tilde{\nu}$ = 1618 s ν(C=O), 593 s ν(Sn−C), 442 s, 401 s ν(Sn−O). − ^1H NMR ($CDCl_3$): δ = 0.86 [s, $^2J(^1H\text{-}Sn)$ = 103.6, 99.6 Hz, 3 H, Sn−CH_3], 1.12 [s, $^2J(^1H\text{-}Sn)$ = 79.3 Hz, 3 H, Sn−CH_3], 2.44, 2.46 (2 br. s, 12 H, CH_3C=O and C3−CH_3), 7.55, 7.70, 8.10, 8.16 (4 d, 8 H, AA′BB′ pattern for the four protons in C_6H_4-4-CF_3). − ^{13}C NMR ($CDCl_3$, 20 °C): δ = 9.18 (s, Sn−CH_3), 9.75 (s, Sn−CH_3), 16.14 (s, 3-CH_3), 17.89 (s, 3-CH_3), 26.10 (s, CH_3CO), 28.51 (s, CH_3CO), 105.20 (s, C3), 120.4 (s, CH_{arom}), 120.9 (s, CH_{arom}), 124.4 [q, CF_3, ^1J(C−F): 271.5 Hz], 126.4 (s, CH_{arom}), 127.1 (s, CH_{arom}), 141.4 (s, C4), 141.62 (s, C4), 150.22 (s, C−N), 150.35 ($C-CF_3$), 162.92 (C5), 193.7 (C=O). − ^{19}F NMR ($CDCl_3$, 20 °C): δ = −62.9; ($CDCl_3$, −50 °C): δ = −62.1, −62.2, −62.3, −62.6. − ^{119}Sn NMR ($CDCl_3$): δ = −100.6 [1], −323.9 [2]; ^{119}Sn NMR ([D_6]benzene): δ = −324.1. − Derivatives **2−3**, **5−6**, **9**, were synthesized in a similar way.

Bis[4-acetyl-3-methyl-1-(4-trifluoromethylphenyl)pyrazolon-5-ato]di-*n*-butyltin(IV) $(L^1)_2Sn$*n*Bu_2 (2): Yield: 73%. M.p. 173−175 °C. − $C_{34}H_{38}F_6N_4O_4Sn$: calcd. C 51.02, H 4.79, N 7.01; found C 50.96, H 4.63, N 7.13; formula mass 799. Molar conductance: Λ_M ($0.3\cdot10^{-3}$ M in CH_2Cl_2) = 0.5; Λ_M [$0.6\cdot10^{-3}$ M in $(CH_3)_2SO$] = 16.3. − IR (nujol): $\tilde{\nu}$ = 1618 s ν(C=O), 604 s ν(Sn−C), 440 s, 425 s, 392 s ν(Sn−O). − ^1H NMR ($CDCl_3$): δ = 0.80 (t), 0.94 (t), 1.28 (m), 1.52 (m), 1.75 (m), (18 H, Sn−*n*Bu), 2.45, 2.48 (2 br. s, 12 H, CH_3C=O and C3−CH_3), 7.52, 7.70, 8.05, 8.17 (4 d), 8 H, AA′BB′

pattern for the four protons in C_6H_4-4-CF_3). – ^{13}C NMR ($CDCl_3$, 20 °C): δ = 13.56 (s, Sn−*n*Bu), 16.86 (s, 3-*C*H$_3$), 17.45 (s, 3-*C*H$_3$), 25.97 (s, Sn−*n*Bu) 26.36 (s, Sn−*n*Bu) 26.86 (s, Sn−*n*Bu), 27.66 (s, Sn−*n*Bu), 28.01 (s, Sn−*n*Bu) 28.03 (s, *C*H$_3$CO), 28.98 (s, Sn−*n*Bu), 29.70 [s, Sn−*n*Bu, ^1J(^{13}C-Sn) = 875 Hz], 104.87 (s, *C*3), 120.12 (s, *C*H$_{arom}$), 120.47 (s, *C*H$_{arom}$), 123.8 (q, *C*F$_3$), 125.98 (s, *C*H$_{arom}$), 126.90 (s, *C*H$_{arom}$), 141.25 (s, *C*4), 149.63 (s, C−N), 152.8 (s, C−CF$_3$), 161.9 (C5), 193.49 (C=O). – ^{19}F NMR ($CDCl_3$): δ = −62.8. – ^{119}Sn NMR ($CDCl_3$): δ = −126.1 [1], −358.2 [4].

Bis[4-acetyl-3-methyl-1-(4-trifluoromethylphenyl)pyrazolon-5-ato]-diphenyltin(IV) (L^1)$_2$SnPh$_2$ (3): Yield: 80%. M.p. 205−207 °C. – $C_{38}H_{30}F_6N_4O_4Sn$: calcd. C 54.38, H 3.60, N 6.67; found C 54.30, H 3.42, N 6.38; formula mass 839; molecular mass 658 ($1.1\cdot10^{-2}$ m; *r* = 0.78), 709 ($2.9\cdot10^{-2}$ m; *r* = 0.84). – Molar conductance: Λ_M ($0.8\cdot10^{-3}$ M in CH_2Cl_2) = 0.1; Λ_M [$0.9\cdot10^{-3}$ M in $(CH_3)_2SO$] = 13.0. – IR (nujol): $\tilde{\nu}$ = 1617 s ν(C=O), 247 m, 215 s ν(Sn−C), 455 m, 439 vs, 404 m ν(Sn−O). – ^{1}H NMR ($CDCl_3$): δ = 2.27, 2.38 (2 br. s), 2.46, 2.63 (2 s, 12 H, CH_3C=O and C3−CH_3), 7.30−7.40, 7.50−7.70, 7.90−8.24 (3 m, 18 H, AA′BB′ pattern for the four protons in C_6H_4-4-CF_3 + Sn-Ph). – ^{13}C NMR ($CDCl_3$, 20 °C): δ = 16.72, 16.86, 17.45, 17.7 (4 s, 3-*C*H$_3$), 28.01, 28.05, 28.32, 28.53 (4 s, *C*H$_3$CO), 104.7, 104.92, 104.96 (3 s, *C*3), 120.8 (s, *C*H$_{arom}$), 120.9 (s, *C*H$_{arom}$), 121.2 (s, *C*H$_{arom}$), 123.8 (q, *C*F$_3$), 126.1 (s, *C*H$_{arom}$), 126.9 (s, *C*H$_{arom}$), 128.5 [s, Sn−Ph, ^3J(^{13}C-Sn) = 54 Hz], 128.6 (s, Sn−Ph), 129.6 [s, Sn−Ph, ^4J(^{13}C-Sn) = 19 Hz], 130.1 (s, Sn−Ph), 135.7 [s, Sn−Ph, ^2J(^{13}C-Sn) = 60 Hz], 135.82 (s, Sn−Ph), 135. 9 (s, Sn−Ph), 141.3 (s, *C*4), 149.8 (s, C−N), 153.4 (s, C−CF$_3$), 162.3 (C5), 193.0 (C=O). – ^{19}F NMR ($CDCl_3$, 20 °C): δ = −62.7, −62.8; ($CDCl_3$, −50 °C): δ = −62.0, −62.1, −62.2, −62.4, −62.5. – ^{119}Sn NMR ($CDCl_3$, 20 °C): δ = −275.2 [1], −483.2 [6].

Bis[4-benzoyl-3-methyl-1-(4-trifluoromethylphenyl)pyrazolon-5-ato]-dimethyltin(IV) (L^2)$_2$SnMe$_2$ (4): This compound was reported previously;[27] additional data are: formula mass 839; molecular mass 562 ($0.6\cdot10^{-2}$ m; *r* = 0.67), 612 ($0.9\cdot10^{-2}$ m; *r* = 0.73), 647 ($1.3\cdot10^{-2}$ m; *r* = 0.77), 712 ($1.9\cdot10^{-2}$ m; *r* = 0.84), 787 ($2.5\cdot10^{-2}$ m; *r* = 0.94). – Molar conductance: Λ_M ($0.7\cdot10^{-3}$ M in CH_2Cl_2) = 0.2; Λ_M [$0.8\cdot10^{-3}$ M in $(CH_3)_2SO$] = 18.7; Λ_M [$0.9\cdot10^{-3}$ M in $(CH_3)_2CO$] = 1.3. – ^{13}C NMR ($CDCl_3$, 20 °C): δ = 9.62 [s, Sn−*C*H$_3$, ^1J(^{13}C-Sn): 900 Hz], 16.5 (s, 3-*C*H$_3$), 104.8 (s, *C*3), 120.4 (s, *C*H$_{arom}$), 120.3 (s, *C*H$_{arom}$), 124.1 [q, *C*F$_3$, ^1J(C-F): 288 Hz], 126.7 (s, *C*H$_{arom}$), 127.8 (s, *C*H$_{arom}$), 128.4 (s, *C*H$_{arom}$), 131.5 (s, *C*H$_{arom}$) 139.15(s, *C*H$_{arom}$), 141.0 (s, *C*4), 150.22 (s, C−N), 150.2 (*C*−CF$_3$), 163.49 (C5), 191.5, 193.0 (C=O). – ^{119}Sn NMR ($CDCl_3$, 20 °C): δ = −102.00 [1], −321.4 [5].

Bis[4-benzoyl-3-methyl-1-(4-trifluoromethylphenyl)pyrazolon-5-ato]-di-*n*-butyltin(IV) (L^2)$_2$Sn*n*Bu$_2$ (5): Yield: 74%. M.p. 99−102 °C. – $C_{44}H_{42}F_6N_4O_4Sn$: calcd. C 57.23, H 4.58, N 6.07; found C 57.08, H 4.72, N 5.95; formula mass 923. Molar conductance: Λ_M ($0.7\cdot10^{-3}$ M in CH_2Cl_2) = 0.4; Λ_M [$0.5\cdot10^{-3}$ M in $(CH_3)_2SO$] = 12.9. – IR (nujol): $\tilde{\nu}$ = 1616 m ν(C=O), 592 s, 513 vs ν(Sn−C), 445 sh, 434 vs, 398 vs ν(Sn−O). – ^{1}H NMR ($CDCl_3$): δ = 1.83, 1.92, 2.14 (3 s, 6 H, C3−CH_3); 0.75 (t), 0.92 (t), 1.20−1.40 (m), 1.55−1.75 (m) [18 H, Sn−C_4H_9, ^2J(^{1}H-^{119}Sn) = 104.2, ^2J(^{1}H-^{117}Sn) = 99.8 Hz], 7.46 (d), 7.50−7.70 (m), 7.75 (m), 8.10 (m), 8.22 (d) (18 H, AA′BB′ pattern for the four protons in C_6H_4-4-CF_3 and aromatic protons in the benzoyl moiety). – ^{13}C NMR ($CDCl_3$, 20 °C): δ = 13.61 (s, Sn−*n*Bu), 16.57 (s, 3-*C*H$_3$), 25.98 [s, Sn−*n*Bu, J(^{13}C-Sn = 132 Hz)], 27.09 [s, Sn−*n*Bu, J(^{13}C-Sn) = 47 Hz], 29.69 [s, Sn−*n*Bu, ^1J(^{119}Sn-^{13}C) = 875 Hz, ^1J(^{117}Sn-^{13}C) = 820 Hz], 105.02 (s, *C*3), 120.1 (s, *C*H$_{arom}$), 124.0 [q, *C*F$_3$, ^1J(C-F): 280 Hz)], 126.0 (s, *C*H$_{arom}$), 127.7 (s, *C*H$_{arom}$), 128.4 (s, *C*H$_{arom}$), 131.4 (s, *C*H$_{arom}$) 139.4 (s, *C*H$_{arom}$), 141.2 (s, *C*4), 150.2 (*C*−CF$_3$), 163.71 (C5), 191.9 (C=O). – ^{19}F NMR ($CDCl_3$, 20 °C): δ = −62.7, −62.8, −62.9. – ^{119}Sn NMR ($CDCl_3$, 20 °C): δ = −127.7 [1], −359.5 [4].

Bis[4-benzoyl-3-methyl-1-(4-trifluoromethylphenyl)pyrazolon-5-ato]-diphenyltin(IV) (L^2)$_2$SnPh$_2$ (6): Yield: 78%. M.p. 244−246 °C. – $C_{48}H_{34}F_6N_4O_4Sn$: calcd. C 59.80, H 3.56, N 5.81; found C 59.72, H 3.64, N 5.76; formula mass 963; molecular mass 732 ($0.8\cdot10^{-2}$ m; *r* = 0.76), 818 ($1.6\cdot10^{-2}$ m; *r* = 0.85). – Molar conductance: Λ_M ($0.9\cdot10^{-3}$ M in CH_2Cl_2) = 0.9; Λ_M [$0.5\cdot10^{-3}$ M in $(CH_3)_2SO$] = 12.3. – IR (nujol): $\tilde{\nu}$ = 1615 m ν(C=O), 252 vs, 249 sh ν(Sn−C), 451 vs, 417 vs, 404 s ν(Sn−O). – ^{1}H NMR ($CDCl_3$, 20 °C): δ = 1.63, 1.89 (2 br. s, 6 H, C3−CH_3), 7.30−7.60 (m), 7.75 (m), 7.98 (d), 8.08 (d), 8.27 (d) [28 H, AA′BB′ pattern for the four protons in C_6H_4-4-CF_3 + aromatic protons in the benzoyl moiety + Sn−C_6H_5, ^2J(^{1}H-Sn) = 102 Hz]. – ^{13}C NMR ($CDCl_3$, 20 °C): δ = 16.7 (s, 3-*C*H$_3$), 105.93 (s, *C*3), 120.49 (s, *C*H$_{arom}$), 120.6 (br., *C*H$_{arom}$), 124.7 [q, *C*F$_3$, ^1J(C-F): 290 Hz], 126.4 (s, *C*H$_{arom}$), 126.51 (s, *C*H$_{arom}$), 127.22 (s, *C*H$_{arom}$), 128.3 (s, *C*H$_{arom}$), 128.5 [s, Sn−Ph, ^3J(Sn-^{13}C) = 54 Hz], 128.86 (s, *C*H$_{arom}$), 129.58 [s, Sn−Ph, ^4J(Sn-^{13}C) = 18 Hz], 132.29 (s, *C*H$_{arom}$), 135.72 [s, Sn−Ph, ^2J(Sn-^{13}C) = 60 Hz], 136.33 (s, *C*H$_{arom}$), 138.69 (s, *C*H$_{arom}$), 141.00 (s, *C*4), 148.04 (s, C−N), 150.6 (*C*−CF$_3$), 165.19 (C5), 192.24 (C=O). – ^{19}F NMR ($CDCl_3$, 20 °C): δ = −62.7, −62.8. – ^{119}Sn NMR ($CDCl_3$, 20 °C): δ = −274.0 [1], −480.9 [1], −486.6 [2].

Bis[3-methyl-4-(trifluoroacetyl)-1-(4-trifluoromethylphenyl)-pyrazolon-5-ato]dimethyltin(IV) (L^3)$_2$SnMe$_2$ (7): KOH (2 mmol) and Me_2SnCl_2 (1 mmol) were added to a methanol solution (30 mL) of L^1 (2 mmol). The clear solution was stirred overnight at room temperature, and the solvent was then removed under reduced pressure, chloroform (10 mL) was added to the crude product and the mixture was filtered to separate the KCl precipitate. Light petroleum (20 mL) was then added to the filtrate and a precipitate was formed, which was filtered, washed with light petroleum (about 10 mL) and dried under reduced pressure at room temperature. This was recrystallized from dichloromethane/*n*-hexane. Yield: 65%. M.p. 149−150 °C. – $C_{28}H_{20}F_{12}N_4O_4Sn$: calcd. C 40.86, H 2.45, N 6.81; found C 40.59, H 2.65, N 6.84; formula mass 823.2. – Molar conductance: Λ_M ($0.9\cdot10^{-3}$ M in CH_2Cl_2) = 0.5; Λ_M [$0.6\cdot10^{-3}$ M in $(CH_3)_2SO$] = 27.5. – IR (nujol): $\tilde{\nu}$ = 1628 s ν(C=O), 588 s ν(Sn−C), 463 s, 437 m ν(Sn−O). – ^{1}H NMR ($CDCl_3$, 20 °C): δ = 1.00 [s, ^2J(^{1}H-Sn) = 83.8 Hz, 6 H, Sn−CH_3], 2.23 (q, 6 H, C3−CH_3), 7.68 (d), 8.04 (d) (8 H, AA′BB′ pattern for the four protons in C_6H_4-4-CF_3). – ^{13}C NMR ($CDCl_3$, 20 °C): δ = 9.5 [s, Sn-*C*H$_3$, ^1J(Sn-C) = 780 Hz], 12.4 (s, Sn-*C*H$_3$), 13.7 (s, Sn-*C*H$_3$), 15.8 (q, 3-*C*H$_3$), 17.05 (s, 3-*C*H$_3$), 101.4 (s, *C*3), 117.06 [q, *C*F$_3$, ^1J(C-F) = 284 Hz], 118.07 (s, *C*H$_{arom}$), 120.7 (s, *C*H$_{arom}$), 122.7 (s, *C*H$_{arom}$), 123.67 [q, *C*F$_3$, ^1J(C-F) = 270 Hz], 126.01 (s, *C*H$_{arom}$), 127.1 (s, *C*H$_{arom}$), 129.01 (s, *C*H$_{arom}$), 131.1 (s, *C*H$_{arom}$), (s, *C*H$_{arom}$), 140.07 (s, *C*4), 140.8 (s, *C*4), 149.00 (s, C−N), 156.89 (*C*−CF$_3$), 165.02 (C5), 170.76 (C=O). – ^{19}F NMR ($CDCl_3$, 20 °C): δ = −62.6, −75.7. – ^{19}F NMR ($CDCl_3$, −50 °C): δ = −62.0, −75.3. – ^{119}Sn NMR ($CDCl_3$, 20 °C): δ = −139.2, −140.9.

Bis[3-methyl-4-(trifluoroacetyl)-1-(4-trifluoromethylphenyl)-pyrazolon-5-ato]di-*n*-butyltin(IV) (L^3)$_2$SnBu$^n_2$ (8): This compound was obtained using the same procedure as for **7**. Yield: 45%. M.p. 98−100 °C. – $C_{34}H_{32}F_{12}N_4O_4Sn$: calcd. C 45.01, H 3.55., N 6.17; found C 44.88, H 3.68, N 6.25; formula mass 907.3. – Molar conductance: Λ_M ($0.8\cdot10^{-3}$ M in CH_2Cl_2) = 0.4; Λ_M [$0.9\cdot10^{-3}$ M in $(CH_3)_2SO$] = 19.5. – IR (nujol): $\tilde{\nu}$ = 1628 s ν(C=O), 557 s ν(Sn−C), 462 s, 407 m ν(Sn−O). – ^{1}H NMR ($CDCl_3$, 20 °C): δ = 2.63 (q), 2.44 (q), 2.40 (q) (6 H, C3−CH_3). 7.40−7.60 (m),

7.92−8.20 (m) (8 H, AA′BB′ pattern for the four protons in C_6H_4-4-CF_3), 0.95 (br. t), 1.32−1.90 (br. m) (18 H, Sn−*n*Bu). − ^{13}C NMR ($CDCl_3$, 20 °C): δ = 13.85 (s, Sn−*n*Bu), 14.02 (s, Sn−*n*Bu), 14.09 (s, Sn−*n*Bu), 16.33 (s, 3-*C*H_3), 16.44 (s, 3-*C*H_3), 17.46 (s, 3-*C*H_3), 26.35 [s, Sn−*n*Bu, J(^{13}C-Sn) = 125 Hz], 26.73 (s, Sn−*n*Bu), 26.96 (s, Sn−*n*Bu), 27.16 [s, Sn−*n*Bu, J(^{13}C-Sn) = 43 Hz], 27.52 (s, Sn−*n*Bu), 27.79 (s, Sn−*n*Bu), 30.41 [s, Sn−*n*Bu, ^1J(^{13}C-^{119}Sn) = 775 Hz, ^1J(^{13}C-^{117}Sn) = 720 Hz], 32.63 (s, Sn−*n*Bu), 32.74 (s, Sn−*n*Bu), (s, Sn−*n*Bu, 33.34 (s, Sn−*n*Bu), 102.03 (s, *C*3), 117.06 [q, *C*F_3, ^1J(^{19}F-^{13}C) = 284 Hz], 118.55 (s, *C*H_{arom}), 121.0 (s, *C*H_{arom}), 121.6 (s, *C*H_{arom}), 123.67 [q, *C*F_3, ^1J(^{19}F-^{13}C) = 270 Hz], 126.01 (s, *C*H_{arom}), 126.62 (s, *C*H_{arom}), 128.66 [q, C−*C*F_3, ^2J(^{19}F-^{13}C) = 33.5 Hz], 132.3 (s, *C*H_{arom}), 132.8 (s, *C*H_{arom}), 140.7 (s, *C*4), 141.1 (s, *C*4), 149.38 (s, *C*H_{arom}) 157.41, (s, C−N), 165.78 (s, C5), 171.28 (s, C5) 174.25 [q, C=O, ^2J(^{19}F-^{13}C) = 37.5 Hz]. − ^{19}F ($CDCl_3$, 20 °C) NMR: δ = −63.1, −63.3, −63.7, −71.8, −75.6, −76.0, −82.2, −82.4. − ^{119}Sn NMR ($CDCl_3$, 20 °C): δ = −88.5 [2], −112.3 [1], −114.9 [1], −126.2 [3], −130.2 [2], −143.2 [2], −173.7 [1].

Bis[3-methyl-4-(trifluoroacetyl)-1-(4-trifluoromethylphenyl)-pyrazolon-5-ato]diphenyltin(IV) (L^3)$_2$SnPh$_2$ (9): Yield: 72%. M.p. 254−256 °C. − $C_{38}H_{24}F_{12}N_4O_4Sn$: calcd. C 48.18, H 2.55, N 5.91; found C 47.95, H 2.70, N 5.68; formula mass 947.3. Molar conductance: Λ_M ($1.0\cdot10^{-3}$ M in CH_2Cl_2) = 0.3; Λ_M [$1.1\cdot10^{-3}$ M in $(CH_3)_2SO$] = 4.5. − IR (nujol): $\tilde{\nu}$ = 1628 s ν(C=O), 266 s, 223 vs ν(Sn−C), 449 vs, 424 s ν(Sn−O). − ^{1}H NMR ($CDCl_3$, 20 °C): δ = 2.19, 2.21, 2.30, 2.38 (4 q, 6 H, C3−CH_3), 7.12−7.62, 7.78−7.94 (2 br. m, 18 H, AA′BB′ pattern for the four protons in C_6H_4-4-CF_3 and Sn−Ph). − ^{13}C NMR ($CDCl_3$, 20 °C): δ = 15.65 (br., 3-*C*H_3), 15.93 (s, 3-*C*H_3), 17.05 (s, 3-*C*H_3), 102.0 (br., *C*3), 118.1 (s, *C*H_{arom}), 120.5 (br., *C*H_{arom} + *C*F_3), 125.86, 126.02, 126.08, 126.1 (m, *C*H_{arom} + *C*F_3 + Sn−Ph), 127.5, 128.0, 128.3, 128.5, 128.7, 128.9, 129.1 (m, *C*H_{arom} + *C*F_3 + Sn−Ph), 130.0 [s, Sn−Ph, ^4J(^{13}C-Sn) = 16 Hz], 134.6 (s, *C*H_{arom}), 135.4 (br., *C*H_{arom} + *C*F_3 + Sn−Ph), 136.2 (s, *C*H_{arom}) 140.0 (br., *C*4), 149.0 (br., *C*H_{arom}) 157.2, (br., C−N), 164.0 (m, C5). − ^{19}F ($CDCl_3$, 20 °C) NMR: δ = −63.3, −63.6, −69.3, −71.6, −76.7, −82.1. − ^{119}Sn NMR ($CDCl_3$, 20 °C): δ = −278.7 [2], −301.4 [1], −319.2 [1], −320.2 [1].

[3-Methyl-4-(trifluoroacetyl)-1-(4-trifluoromethylphenyl)pyrazolon-5-ato]dimethyltin(IV) Perchlorate [(L^3)SnMe$_2$(ClO_4)] (10): Silver perchlorate (0.104 g, 0.5 mmol) was added to a stirred acetone solution (30 mL) of [(L^3)$_2$SnMe$_2$] (0.358 g, 0.5 mmol). A colorless precipitate formed within 6 hours which was filtered and identified as Ag(L^3) by elemental analysis and IR data. Yield: 40%. M.p. <300 °C. − $C_{13}H_{10}AgF_3N_2O_2$ (391.1): calcd. C 39.92, H 2.58, N 7.16; found C 40.12, H 2.70, N 7.34. − IR (nujol): $\tilde{\nu}$ = 1646 vs ν(C=O). The clear solution was then evaporated and the pale yellow residue was washed with diethyl ether/*n*-hexane (20 mL) and shown to be compound **10**. It was recrystallized from acetone/diethyl ether. Yield: 40%, M.p. 150 °C. − $C_{15}H_{16}ClF_3O_6N_2Sn$ (531.4): calcd. C 33.90, H 3.03, N 5.27; found C 34.03, H 3.16, N 5.45. − IR (nujol): $\tilde{\nu}$ = 1621 vs ν(C=O), 1099 vs. br., 1076 vs. br., 618 s ν(ClO_4), 586 m ν(Sn−C), 440 s, 422 m ν(Sn−O). − ^{1}H NMR ($CDCl_3$, 20 °C): δ = 1.26 [^2J(^{1}H-^{119}Sn) = 105 Hz; ^2J(^{1}H-^{117}Sn) = 100 Hz, 6 H, Sn−CH_3], 2.48 (s, 3 H, C_3−CH_3), 2.63 (s, 3 H, CH_3C=O), 7.40, 7.73 (2 d, 4 H, N−$C_6H_4$$CF_3$).

X-ray Crystallographic Study: A preliminary study was performed with a Weissenberg Camera to determine cell parameters and the triclinic space group. A $P2_1$ Syntex diffractometer was used for the measurements of the cell constants and for the data collection; a set of 25 reflections (with high theta angle) was used to obtain refined cell parameters. Decay correction was applied since monitoring of three reflections (taken every 100 reflections) indicated decay, average 14.8%. Slight absorption anisotropy was found after a psi-scan (transmission factor range 0.93−1.00), and so data were corrected for absorption, as well as for Lorentz and polarization effects.[37] The molecular structure was solved using the Patterson−Fourier method using CAOS.[38]

Subsequent calculations were performed as follows: refinement based on the minimization of the function $w(|F_o| - |F_c|)^2$ with the weighting scheme $w = 1/(a + F_o + cF_o^2)$, where a and c are of the order of $2F_o$(min) and $2/F_o$(max), respectively;[39] anisotropic displacement parameters were refined for non-H atoms. After refinement convergence, H atoms were introduced at fixed positions with a C−H distance of 0.96 Å, and H isotropic displacement parameters were kept fixed until final refinement convergence was reached. Atomic scattering factors and anomalous dispersion terms were taken from the literature.[40] Chemical formula, $C_{48}H_{34}F_6N_4O_4Sn$; M_w = 963.50; crystal habitat, block; crystal size [mm], 0.40 × 0.25 × 0.15; crystal system, triclinic; space group, $P\bar{1}$ (no. 2); crystal color, colorless; a = 9.299(4), b = 16.004(7), c = 15.557(6) Å; α = 96.03(2)°, β = 95.69(2)°, γ = 112.80(2)°; V = 2098(3) Å^3; Z = 2; T = 298 K; $D_{calcd.}$ = 1.526 g/cm^3; $2\theta_{max}$ = 60°; μ = 0.698 mm^{-1} graphite monochromated wavelength, Mo-K_α; scan speed = 4 °/min; scan range = 1.3°; index range, *h*: 0/12, *k*: −22/20, *l*: −21/21; measured reflections, 12904; unique reflections, 12863; refined reflections [$F>6\sigma(F)$] = 8261; refined parameters, 568; R, R_w = 0.052, 0.068; S = 1.29; $R(F) = \Sigma||F_o| - |F_c||/\Sigma F_o$; $S = [\Sigma\{w(F_o^2 - F_c^2)^2\}/(n - p)]^{0.5}$, n = no. of data and p = no. of refined parameters.

Crystallographic data for the structure reported in this paper have been deposited with the Cambridge Crystallographic Data Centre as supplementary publication no. CCDC-149841. Copies of the data can be obtained free of charge on application to CCDC, 12 Union Road, Cambridge CB2 1EZ, UK [fax 44 123/336-033; E-mail: deposit@ccdc.cam.ac.uk].

Theoretical Study: All computations were carried out with the MULLIKEN program[41] package on an IBM/SP2 supercomputer. Hartree−Fock and MB3LYPDFT (Density Functional Theory)[42] methods were used. The basis set used with both methods was 6-31G*. For the tin atom an ECP approximation[43−51] was applied, as implemented within MULLIKEN, using a double zeta basis. The MULLIKEN default convergence criteria were used in computations of energies and geometries.

Supporting Information Available: Figure S1 (molecular mass vs. concentration of **4**), Figure S2 (^{19}F NMR spectra of **1** and **3** at −50 °C); see footnote on the first page of this article.

Acknowledgments

C. Smart (Vassar College) for helpful discussion. Financial support by Università di Camerino, CARIMA Foundation, Consiglio Nazionale delle Ricerche C.N.R. − Rome, The Research Committee at Vassar College, Camille and Henry Dreyfus Foundation Special Grant for Chemical Sciences. This research was also supported by an IBM Shared University Research (SUR) grant, a CUNY Research Award, a CUNY Collaborative award, and a NASA JOVE grant.

[1] A. M. Rouhi, *Chem. Eng. News* **1998**, *76*, 41−44.
[2] W. T. Piver, *Environ. Health Perspect.* **1973**, *4*, 61−79.
[3] G. J. M. van der Kerk, in *Organotin Compounds: New Chemistry and Applications* (Ed.: J. J. Zuckerman), American Chemical Society; Washington, DC, **1976**, p. 1−34.

[4] V. L. Narayanan, M. Nasr, K. D. Paull, in *Tin-based Antitumor Drugs* (Ed.: M. Gielen), Springer, Berlin, **1990**, p. 200−217.
[5] R. Willem, A. Bouhdid, M. Biesemans, J. C. Martins, D. de Vos, E. R. T. Tiekink, M. Gielen, *J. Organomet. Chem.* **1996**, *514*, 203−213.
[6] R. Willem, A. Bouhdid, B. Mahieu, L. Ghys, M. Biesemans, E. R. T. Tiekink, D. de Vos, M. Gielen, *J. Organomet. Chem.* **1997**, *531*, 151−158.
[7] M. Gielen, *Coord. Chem. Rev.* **1996**, *151*, 41−51.
[8] M. Gielen, M. Biesemans, D. de Vos, R. Willem, *J. Inorg. Biochem.* **2000**, *79*, 139−145.
[9] F. Bonati, L. A. Oro, M. T. Pinillos, *Polyhedron* **1985**, *4*, 357−364.
[10] S. Saxena, R. Bhora, A. K. Ray, *Inorg. Chim. Acta* **1990**, *173*, 191−194.
[11] C. Pettinari, G. Rafaiani, G. Gioia Lobbia, A. Lorenzotti, F. Bonati, B. Bovio, *J. Organomet. Chem.* **1991**, *458*, 75−92.
[12] B. Bovio, A. Cingolani, F. Marchetti, C. Pettinari, *J. Organomet. Chem.* **1993**, *458*, 39−48.
[13] C. Pettinari, F. Marchetti, D. Leonesi, M. Rossi, F. Caruso, *J. Organomet. Chem.* **1994**, *483*, 123−137.
[14] A. Jain, S. Saxena, R. Bohra, A. K. Ray, *Main Group Met. Chem.* **1995**, *18*, 139−145.
[15] M. F. Mahon, K. C. Molloy, B. A. Omotowa, M. A. Mesubi, *J. Organomet. Chem.* **1996**, *511*, 227−237.
[16] F. Marchetti, C. Pettinari, A. Cingolani, G. Gioia Lobbia, A. Cassetta, L. Barba, *J. Organomet. Chem.* **1996**, *517*, 141−154.
[17] F. Caruso, D. Leonesi, F. Marchetti, E. Rivarola, M. Rossi, V. Tomov, C. Pettinari, *J. Organomet. Chem.* **1996**, *519*, 29−44.
[18] C. Pettinari, F. Marchetti, A. Gregori, A. Cingolani, J. Tanski, M. Rossi, F. Caruso, *Inorg. Chim. Acta* **1997**, *257*, 37−48.
[19] C. Pettinari, F. Marchetti, A. Cingolani, A. Lorenzotti, E. Mundorff, M. Rossi, F. Caruso, *Inorg. Chim. Acta* **1997**, *262*, 33−46.
[20] F. Marchetti, C. Pettinari, M. Rossi, F. Caruso, *Main Group Met. Chem.* **1998**, *21*, 255−259.
[21] C. Pettinari, F. Marchetti, A. Cingolani, D. Leonesi, E. Mundorff, M. Rossi, F. Caruso, *J. Organomet. Chem.* **1998**, *557*, 187−205.
[22] B. A. Omotowa, A. M. Mesubi, *Appl. Organomet. Chem.* **1997**, *11*, 1−10.
[23] M. Gielen, A. El Khloufi, M. Biesemans, F. Kayser, R. Willem, *Appl. Organomet. Chem.* **1993**, *7*, 201−206.
[24] M. Gielen, A. El Khloufi, M. Biesemans, R. Willem, *Appl. Organomet. Chem.* **1993**, *7*, 119−125.
[25] M. Gielen, E. R. Tiekink, A. Bouhdid, D. de Vos, M. Biesemans, I. Verbruggen, R. Willem, *Appl. Organomet. Chem.* **1995**, *9*, 639−648.
[26] R. Willem, H. Dalil, M. Biesemans, J. C. Martins, M. Gielen, *Appl. Organomet. Chem.* **1999**, *13*, 605−608.
[27] F. Caruso, M. Rossi, F. Marchetti, C. Pettinari, *Organometallics* **1999**, *18*, 2398−2400.
[28] R. Willem, M. Gielen, H. Pepermans, J. Brocas, D. Fastenakel, P. Finocchiaro, *J. Am. Chem. Soc.* **1985**, *107*, 1146−1152.
[29] R. Willem, M. Gielen, H. Pepermans, K. Hallenga, A. Recca, P. Finocchiaro, *J. Am. Chem. Soc.* **1985**, *107*, 1153−1160.
[30] L. Pauling, *The Nature of the Chemical Bond*, 3rd ed., Cornell University. Ithaca, NY, **1960**; p. 260.
[31] D. L. Kepert, *Prog. Inorg. Chem.* **1977**, *23*, 1−65.
[32] V. S. Petrosyan, N. S. Yashina, T. V. Sizova, T. V. Leonova, L. A. Aslanov, A. V. Yatsenko, L. Pellerito, *Appl. Organomet. Chem.* **1994**, *8*, 11−17.
[33] J. Holecek, M. Nadvornik, K. Handzř, A. Lycka, *J. Organomet. Chem.* **1986**, *315*, 299−308.
[34] T. P. Lockhart, W. F. Manders, *Inorg. Chem.* **1986**, *25*, 892−895.
[35] P. G. Harrison, *Chemistry of Tin*, Blackie, Glasgow, **1989**; p. 60−117.
[36] F. Marchetti, C. Pettinari, A. Cingolani, L. Brocanelli, M. Rossi, F. Caruso, *J. Organomet. Chem.* **1999**, *580*, 344−353.
[37] M. P. Byrn, C. E. Strouse, *J. Am. Chem. Soc.* **1991**, *113*, 2501−2508.
[38] M. Camalli, R. Spagna, *CAOS Program: J. Appl. Cryst.* **1994**, *27*, 861−862.
[39] D. J. Cruickshank, in *Computing Methods in Crystallography* (Ed.: J. Rollet), Pergamon, Oxford, **1965**, p. 114.
[40] *International Table for X-ray Crystallography*; Kynoch, Birmingham, **1974**.
[41] *MULLIKEN* is IBM proprietary software.
[42] P. J. Stephens, F. J. Devlin, C. F. Chabalowski, M. J. Frisch, *J. Phys. Chem.* **1994**, *98*, 11623−11627. MB3LYP is very similar to B3LYP defined in this paper, except it uses the local correlation functional of Perdew and Wang (J. P. Perdew, Y. Wang, *Phys. Rev. B* **1992**, *45*, 13244−13249) instead of the Vosko, Wilk, and Nusair functional.
[43] A. D. Becke, *J. Chem. Phys.* **1993**, *98*, 5648−5652.
[44] W. J. Stevens, H. Basch, M. Krauss, *J. Chem. Phys.* **1984**, *81*, 6026−6033.
[45] W. J. Stevens, P. G. Jasien, M. Krauss, H. Basch, *Can. J. Chem.* **1992**, *70*, 612−630.
[46] T. R. Cundari, W. J. Stevens, *J. Chem. Phys.* **1993**, *98*, 5555−5565.
[47] L. F. Pacios, P. A. Christiansen, *J. Chem. Phys.* **1985**, *82*, 2664−2671.
[48] M. M. Hurley, L. F. Pacios, P. A. Christiansen, R. B. Ross, W. C. Ermler, *J. Chem. Phys.* **1986**, *84*, 6840−6853.
[49] L. A. LaJohn, P. A. Christiansen, R. B. Ross, T. Atashroo, W. C. Ermler, *J. Chem. Phys.* **1987**, *87*, 2812−2824.
[50] R. B. Ross, J. M. Powers, T. Atashroo, W. C. Ermler, L. A. LaJohn, P. A. Christiansen, *J. Chem. Phys.* **1990**, *93*, 6654−6670.
[51] W. C. Ermler, R. B. Ross, P. A. Christiansen, *Int. J. Quantum Chem.* **1991**, *40*, 829−846.

Received January 22, 2001
[I01028]

Applications of the Laddering Principle — A Two-Stage Approach to Describe Lithium Heterocarboxylates

Andrew Downard[a] and Tristram Chivers*[a]

Dedicated to the memory of the late Dr. Ron Snaith[+]

Keywords: Lithium / Carboxylate ligands / Electrostatic interactions / Cluster compounds / Ladder polymers

Since the development of the laddering principle in the mid-1980s, it has become a useful concept for describing structural features in a wide variety of organoalkali metal (particularly organolithium) and other main-group element oligomers. Here a brief account of the laddering principle is given, and a two-stage approach to understanding structural diversity is described for several lithium heterocarboxylates. "Primary laddering" describes the initial aggregation of monomeric units, whereas "secondary laddering" deals with the assembly of these primary laddered units into larger structures. Both homo- and heteromolecular clusters can be formed by these processes. In this context, several examples are discussed, with particular emphasis on the effects of solvation and heteroatoms.

1. Introduction

Our group has been concerned for some time with novel cluster structures involving alkali metal cations and polyimido anions with a central p-block element.[1] The structures of these polycyclic systems can usually be rationalized after they are known, but the goal of accurately predicting cluster geometry remains elusive. Here we outline a two-stage approach to application of the laddering principle that has proven useful for describing a range of lithium heterocarboxylates with diverse architectures. The ideas of "primary" and "secondary" laddering are explored, and several recent examples are rationalized using this binary version of the principle as a guide. While the goal of developing a complete principle with predictive validity far exceeds the scope of this Microreview, we hope that some progress towards a better comprehension of laddered structures will be possible at its conclusion.

[a] Department of Chemistry, University of Calgary,
2500 University Drive, Calgary, Alberta, Canada T2N 1N4
Fax: (internat.) +1-403/289-9488
E-mail: chivers@ucalgary.ca
[+] Pioneer of the concept of laddering in organoalkali metal chemistry

1.1. The Laddering Principle

The concept of laddering first appeared in the mid-1980s in seminal papers by Snaith and co-workers describing the formation of imidolithium hexamers.[2] These prototypical

Tristram Chivers was born in Bath, England in 1940. He received his B. Sc. in chemistry from the University of Durham (U.K.) in 1961 and his Ph. D. from the same university in 1964 working with R. D. Chambers on pentafluorophenylboron chemistry. He carried out postdoctoral studies in organometallic electrochemistry with R. E. Dessy at the University of Cincinnati (1964−65) and on inorganic ring systems with N. L. Paddock at the University of British Columbia (1967−69). From 1965 to 1967 he was a Tutorial Fellow at the University of Sussex. He joined the University of Calgary in 1969 and was promoted to Professor in 1978. The focus of his research is the chemistry of the main group elements. He is a Fellow of the Royal society of Canada (1991). Recent awards include the Alcan (1987) and E. W. R. Steacie (2001) Awards of the Canadian Society for Chemistry and the Main Group Element Chemistry award of the Royal Society of Chemistry (1993).

Andrew Downard was born in Calgary, Canada in 1974. He graduated with first class honours in Chemistry (with a minor in Philosophy) from the University of Calgary, Canada, in 1996. He obtained his Ph. D. from the same university in 2000 under the supervision of Professor T. Chivers in the area of main group element chemistry. Dr. Downard is currently an NSERC (Canada) postdoctoral fellow at the Queen's University Ionic Liquids Laboratories, Belfast, N. Ireland in the group of Professor K. Seddon.

MICROREVIEWS: This feature introduces the readers to the authors' research through a concise overview of the selected topic. Reference to important work from others in the field is included.

 © WILEY-VCH Verlag GmbH, 69451 Weinheim, 2001 1434−1948/01/0909−2193 $ 17.50+.50/0

compounds contained Li_6N_6 cores and were described as "stacked pairs of cyclic trimers" joined by Li−N bonds.[2a] The original laddering principle has been expanded and elucidated in the intervening years by the groups of Snaith and Mulvey, among many others. It is now known that laddering can give rise to many different cluster architectures depending on the steric and electronic environment of the centres involved, and on the presence/absence of coordinating solvent.

Laddering has been reviewed extensively,[3,4] and laddered aggregates are now well-known throughout main-group element chemistry. This is particularly true among organoalkali metal compounds, where a wide variety of clusters ranging from dimers to polymers has been found.[3] While the reasons for the occurrence of laddering as a structural motif are generally well understood, the method by which the principle of laddering should be applied, particularly in advance of structural characterization, is still a topic of ongoing investigation.

Here we will define laddering in the simplest case as the lateral association of E−M (E = group 15−17, M = group 1−2) units to form E_2M_2 rings. Such interactions are typically electrostatic in origin, occurring as a result of polarity within the E−M moiety, and can be considered as essentially ionic.[4] In addition to "open" ladders of various lengths, a variety of "closed" ladder clusters can also be constructed from the basic E_2M_2 dimeric unit (Figure 1). For many of these aggregates multiple descriptions apply; for example, an E_6M_6 hexamer might be called a closed six-rung ladder or a pair of stacked E_3M_3 rings. We will generally focus on the former view in order to stress the utility and consistency of the approach discussed here, although in some cases other descriptions may be more appropriate.

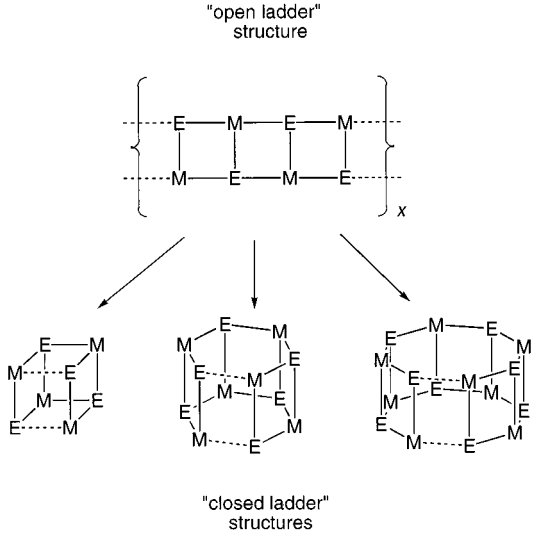

Figure 1. Open and closed E_xM_x ladder frameworks; the substituents on E have been omitted for clarity

1.2. Cisoid and Transoid Geometries

Laddered structures generally exhibit curvature, twisting, or other deviations from planarity in order to accommodate the steric demands of the substituents. The terminology to describe this effect in primary and secondary lithium amides was first introduced by Mulvey,[5] and focused on the relative orientation of substituents about the Li_2N_2 rings. We have adopted a natural extension of these terms, using *cisoid* and *transoid* to describe arrays of any three contiguous four-membered rings as well (Figure 2).[6]

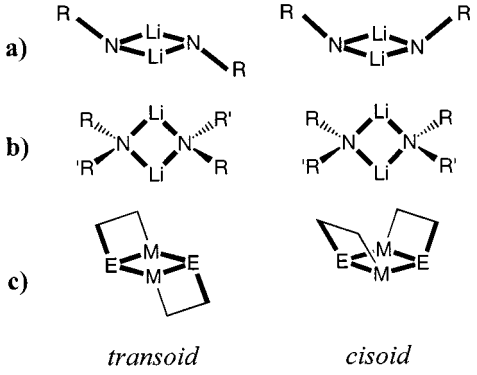

Figure 2. *Cisoid* and *transoid* orientations in: a) primary lithium amides; b) asymmetric, secondary lithium amides; c) arrays of three contiguous four-membered rings

Where laddering is limited to dimerization by bulky substituents and/or solvation, a *transoid* geometry is most often observed,[7] as would be expected on steric grounds. However, in ladders with three or more rungs there is often a preference for regions of *cisoid* geometry, either exclusively or intermixed with *transoid* regions.[5,6,8] Presumably this is because a *cisoid* geometry sometimes provides a greater separation of substituents that are two or more rungs apart than would the corresponding *transoid* arrangement. This distribution of ring conformations influences the overall topology of laddered aggregates as curving occurs to minimize van der Waals repulsions between the substituents. For example, in four-rung ladder segments, an exclusive *transoid* geometry produces a sterically crowded, repeating stair-shape, whereas an exclusive *cisoid* geometry produces a curvilinear shape (Figure 3). Since the ring conformation has a pronounced effect on the eventual outcome of laddering, any general principle describing such aggregation must take it into account.

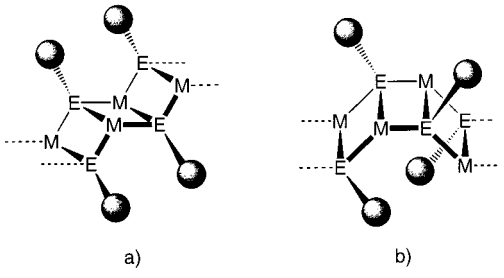

Figure 3. Alternative conformations in E_xM_x ladders with bulky substituents on E (represented by filled spheres): a) *transoid* region; b) *cisoid* region

1.3. Solvation Effects

Donor solvent molecules generally limit the oligomerization of laddered compounds in two ways: 1) by the forma-

tion of E−M bonds that are too sterically encumbered to undergo lateral association; 2) by maximizing the coordination number of the cations through solvent contacts. Solvents which are effective at limiting ladder length typically have one or more Lewis basic centres capable of forming dative bonds with cations such as lithium, sodium, magnesium, etc. Common examples include *N*,*N*,*N*′,*N*′-tetramethylethylenediamine (TMEDA), pentamethyldiethylenetriamine (PMDETA), and tetrahydrofuran (THF).

2. A Two-Stage Approach to Laddering

Snaith's original description of an imidolithium hexamer as two stacked trimers[2a] implied that the laddering principle should be somewhat hierarchical in nature. While it is true that any aggregate can be described as a collection of monomeric units, it is often more fruitful for laddered compounds to be described as being formed from slightly larger units that then associate in various ways to produce oligomers. For example, while an E_6M_6 hexamer can be thought of as six EM monomers, a more useful description might make reference to two E_3M_3 trimers associated by ring stacking, or three E_2M_2 dimers associated by laddering. In this way multiple distinct, but related, aggregation pathways may be invoked to explain the architecture of any given structure.

The purpose of this Microreview is to outline our method of describing lithium heterocarboxylates by using a two-stage approach to the laddering principle, and to show how this can be applied to other, similar, systems within the rubric of organolithium chemistry. Our methodology for rationalizing structures focuses on the use of small building blocks to construct large aggregates. As such, we have found it useful to formally separate the process of laddering into "primary" and "secondary" components as follows (Scheme 1):

Primary laddering describes the lateral association of monomeric EM fragments to produce a primary laddering unit (PLU). Such units are often homomolecular dimers, but other types of oligomers are also possible.

Secondary laddering describes the association of PLUs to form clusters. When secondary laddering does occur, the structure of the compound as a whole can often be rationalized by understanding the behaviour of PLUs as they aggregate.

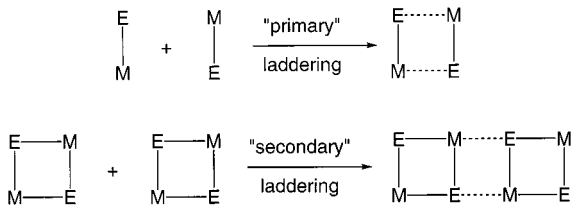

Scheme 1. Homomolecular primary and secondary laddering of E_xM_x; the substituents on E have been omitted for clarity

The hierarchical nomenclature of these principles is intentional; primary laddering processes must occur before secondary, and secondary laddering cannot occur in the absence of primary. Thus, when examining a laddered system the pertinent questions to ask are:

1) Will primary laddering occur?
2) If so, what is the resultant PLU?
3) Will secondary laddering of PLUs occur?
4) If so, what is the resultant structure?

We have found that by answering the four questions above a good conceptual understanding of laddered lithium heterocarboxylate structures can be gained, and we believe that this approach may be applicable to a wider variety of systems. In the cases discussed here the most common PLU is a dimer, as illustrated in Scheme 1. We note, however, that this need not be the case — primary laddering can, in theory, generate trimers, tetramers, etc., as well as dimers, and secondary laddering can occur with any combination of these PLUs. Thus, while the dimer will be given special attention in this account, it is not true that the dimers are the only PLUs of interest.

The idea of primary and secondary units of aggregation is well-established in other areas, most prominently supramolecular chemistry.[9] Indeed, although they are not typically discussed as such, many laddered compounds can be considered as supramolecules.[3a,10] In addition, Snaith's description of a hexamer as two stacked trimers[2a] is one of many examples where a two-stage approach to laddering is used without invoking the terminology suggested here. Thus, the novelty and value of this approach lies not in the concepts of primary and secondary aggregation themselves, but rather in developing an understanding of how this two-stage framework can be *systematically* and *consistently* applied in the specific context of laddering.

3. Two-Stage Laddering in Lithium Heterocarboxylates

Carboxylate anions $[RCO_2]^-$ are ubiquitous ligands, as are a number of other related "heterocarboxylates" $[RCXY]^-$ (X, Y = main group centre, e.g. xanthates $[(RO)CS_2]^-$, thiocarbamates $[(R_2N)COS]^-$, dithiocarboxylates $[RCS_2]^-$, etc.). Such systems can be understood as monomeric units in which a single unit of negative charge is delocalized throughout an XCY unit. While lithium heterocarboxylates are well-known as sources of anionic ligands in metathetical syntheses, we have investigated several lithium amidinates, oxoamidates, and thioamidates as probes to explore a two-stage approach to the laddering principle. Convenient access to these compounds is provided by the reaction between nucleophiles and heteroallenes [X=C=Y] (1). Use of this route to synthesize carboxylic acids from CO_2 is well-known.[11]

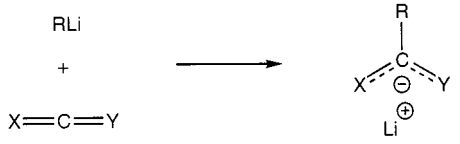

(1)

X = Y = O, carbon dioxide → carboxylate
X = Y = NR', carbodiimide → amidinate
X = NR', Y = O, isocyanate → oxoamidate
X = NR', Y = S, isothiocyanate → thioamidate

3.1. Secondary Laddering of Dimeric Primary Laddered Units

The lithium oxoamidate and thioamidate hexamers $[Li\{(nBu)CE(NtBu)\}]_6$ (**1**: E = O; **2**: E = S)[12,13] provide illustrative examples of secondary laddering employing dimeric PLUs. However, even though both structures clearly involve laddering, comparing the hexameric cores of **1** and **2** (Figure 4) highlights an interesting contrast: the two Li_6E_6 hubs are quite similar even though the ligand orientations are strikingly different.

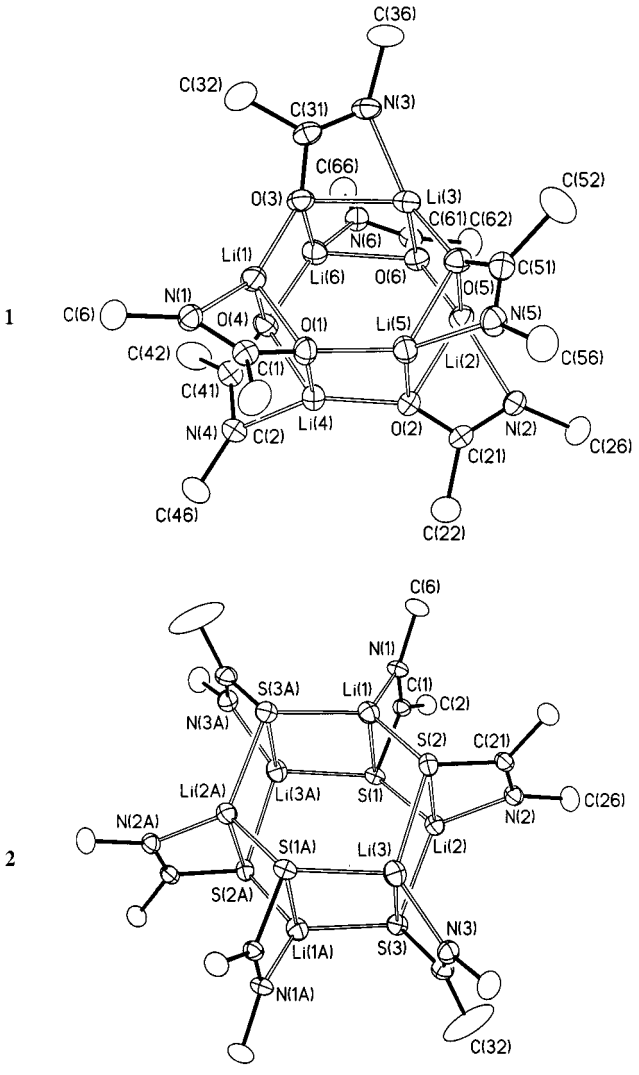

Figure 4. The cores of $[Li\{(nBu)CE(NtBu)\}]_6$ (**1**: E = O; **2**: E = S)

This phenomenon can be explained by using a two-stage approach to the laddering principle. The formation of both hexamers can be visualized as a secondary laddering (trimerization) of *cisoid*, dimeric PLUs (Scheme 2). In the case of **1**, secondary laddering occurs such that the transannular bonds of the PLU form the Li_3O_3 rings in the hexamer. In **2**, however, the transannular bonds of the PLU become the links between the two Li_3S_3 hexagonal rings of the hexameric unit. Thus, whereas **1** adopts a D_3-symmetric, trilobate conformation in the solid-state, **2** is observed to assume a D_{3d}-symmetric, paddle-wheel like shape.

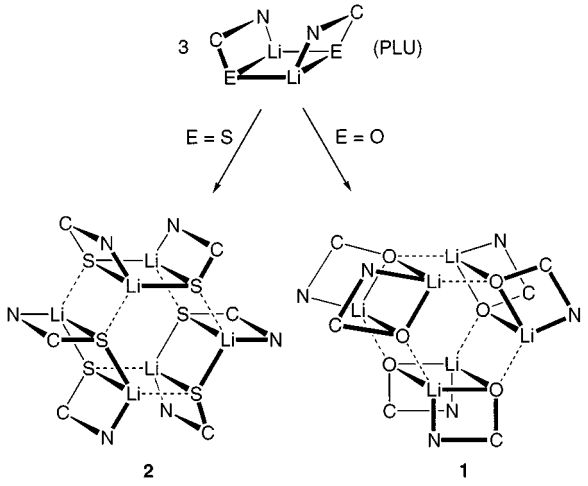

Scheme 2. Secondary laddering (trimerization) of dimeric, *cisoid* PLUs producing **1** and **2**; the dashed lines indicate bonds being formed

We attribute the difference in conformations for **1** and **2** to a heteroatom-related secondary laddering effect. The shorter Li−O (compared to Li−S) distances result in steric constraints that prevent **1** from adopting the paddle-wheel conformation, which otherwise would be preferred.[12] Some credence is lent to the notion of secondary laddering of dimeric PLUs as a mechanism of assembly for **1** and **2** by the fact that **1** adopts a conformation in which the lobes of the Li_3O_3 rings are eclipsed rather than staggered. While a staggered conformation (Figure 5) would certainly be less sterically hindered, this is not the conformation actually adopted by the hexamer. We speculate that this is because it is not accessible as an aggregate of dimers, and hence cannot be generated by the primary and secondary laddering of such dimers.

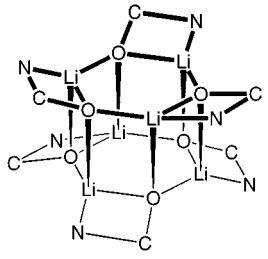

Figure 5. A possible, but unobserved, conformation for the core of $[Li\{(nBu)CO(NtBu)\}]_6$ (**1**)

A different scenario is encountered in the case of the hexameric lithiated hydroxylamine $[Li\{ON(CHPh)_2\}]_6$.[14] The situation here is somewhat similar to the ones discussed above: each lithium cation is chelated by both oxygen and nitrogen, yielding three membered [NOLi] rings. However, in the case of oxoamidates and thioamidates, the geometry at nitrogen is three-coordinate and planar (**A**), while in the lithiated hydroxylamine it is four-coordinate and pyramidal (**B**). This prevents the formation of the *cisoid* dimer **B** on steric grounds.

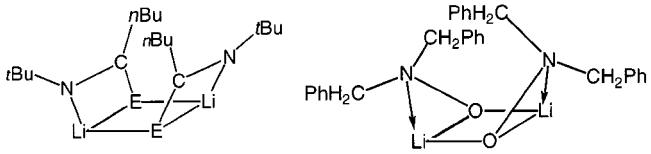

A **B**

Interestingly, the architecture adopted by $[Li\{ON(CHPh)_2\}]_6$ is a Li_6O_6 hexagonal prism with staggered $N(CHPh)_2$ lobes. This arrangement probably arises due to the stacking of trimeric rings, thus it is unsurprising that the less sterically demanding staggered conformation is preferred[14] over the eclipsed conformation of **2**. We note that this observation lends support to our hypothesis that **2** forms by the secondary laddering of dimers, since ring stacking should evidently prefer the conformation depicted in Figure 5. We note also that both the solvated and unsolvated forms of the lithium oxoamidate $[Li\{(C_6H_5)CO(NiPr)\}]_x{\cdot}n$THF (**3a**: $x = 6$, $n = 2$; **3b**: $x = 8$, $n = 0$)[15] can be generated from *cisoid*, dimeric PLUs in a manner similar to that described for **1** and **2** (Figure 6).

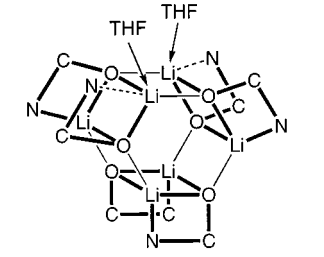

3a

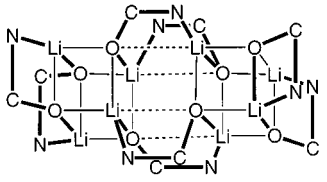

3b

Figure 6. The cores of $[Li\{(C_6H_5)CO(NiPr)\}]_x{\cdot}n$THF (**3a**: $x = 6$, $n = 2$; **3b**: $x = 8$, $n = 0$) viewed as secondary laddered aggregates of dimeric PLUs

3.2. Heteromolecular Primary and Secondary Laddering

In cases where steric constraints are preclusive, dimeric homomolecular PLUs like those discussed above may be unable to associate further. Thus, while lithium oxo- and thioamidates will readily form dimeric PLUs which then undergo secondary laddering, the same is not true of the lithium amidinate $Li[(nBu)C(NtBu)_2]$ (**4**). In this case, other, less hindered laddering units must be employed to promote secondary laddering. For example, the aggregation of **4** with Li_2O in a non-coordinating solvent yields the cluster $[Li\{(nBu)C(NtBu)_2\}]_4{\cdot}Li_2O$ (**5**).[16] In **5**, two $Li[(nBu)C(NtBu)_2]$ monomers associate laterally to give a homomolecular, dimeric PLU. Unlike **1** and **2**, the secondary laddering of these PLUs cannot occur due to steric hindrance. However, in the presence of an unhindered, incipient Li_2O fragment, heteromolecular secondary laddering involving three fragments takes place to give the aggregate **5** (Scheme 3).

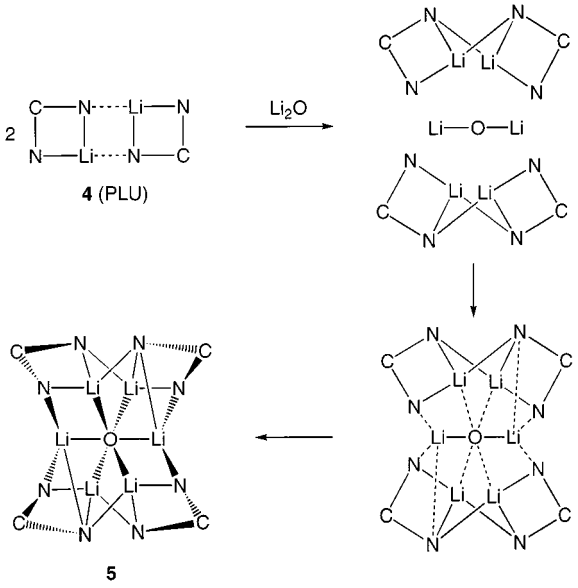

4 (PLU)

5

Scheme 3. Formation of $[Li\{(nBu)C(NtBu)_2\}]_4{\cdot}Li_2O$ (**5**) by primary and heteromolecular secondary laddering; the dashed lines indicate bonds being formed

The addition of a coordinating solvent to **4** effectively appends a substituent at lithium and causes even greater steric congestion around the monomeric unit. This apparently prevents homomolecular primary laddering. However, the presence of an unhindered fragment suitable for the promotion of primary laddering can alleviate this circumstance. Thus, the addition of LiX (X = OH, Cl, Br) to a solution of **4** in THF generates the laddered complexes $[(Li\{(nBu)C(NtBu)_2\})_2{\cdot}LiX{\cdot}THF]_2$ (**6a**, X = OH; **6b**, X = Cl; **6c**, X = Br),[6] which arise *via* heteromolecular laddering (Scheme 4). Here two $Li[(nBu)C(NtBu)_2]{\cdot}THF$ monomers and one LiX fragment associate to produce a heteromolecular PLU, which then undergoes secondary laddering (dimerization) with concomitant loss of solvent.

The topologies of **6a**−**c** are clearly a consequence of the conformation adopted by the PLUs involved. Each three-rung ladder is composed of contiguous *cisoid* and *transoid* units, an arrangement which minimizes the steric congestion and imparts a gentle undulation to the structure as a

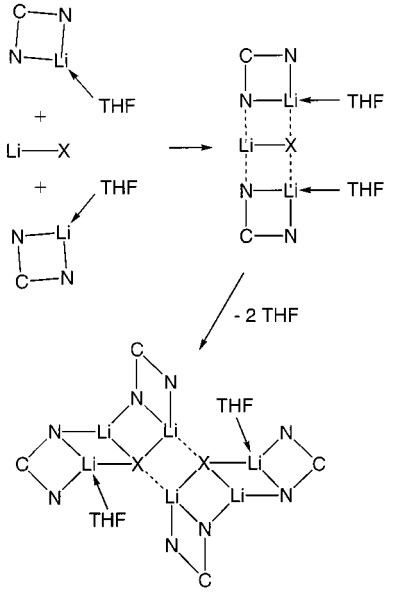

Scheme 4. Formation of $[(Li\{(nBu)C(NtBu)_2\})_2{\cdot}LiX{\cdot}THF]_2$ (**6a**, X = OH; **6b**, X = Cl; **6c**, X = Br) by heteromolecular primary and secondary laddering; the dashed lines indicate bonds being formed

whole. Secondary laddering occurs through a *transoid* $[LiX]_2$ ring. We note that this secondary laddering process does not occur when the added fragment is LiI; in that case the heteromolecular PLU $[(Li\{(nBu)C(NtBu)_2\})_2{\cdot}LiI{\cdot}2THF]$ (**7**) forms and does not associate further, probably due to the relative weakness of Li−I bonds compared to the other lithium halides.[6] Thus, solvation is preferable as a mechanism to disperse charge in this case, and no secondary laddering occurs. We note also that **7** has the same basic topology as the PLUs proposed for **6a**−**c**.

3.3. Unladdered Structures from Primary Laddered Units

The previous examples demonstrated that various PLUs can associate through secondary laddering to produce a range of molecular architectures. However, other aggregation pathways are also possible, some of which lead to unladdered, extended arrays. While it is not immediately clear that such structures should fall in the same category as their laddered counterparts, it would certainly be useful if the laddering principle could explain not only situations where laddering *does* occur, but also situations where laddering could reasonably be expected to occur but *does not*.

For lithium thioamidates at least, this is the case: use of a two-stage approach to laddering is sufficient to explain the formation of unladdered, solvated polymers in addition to the laddered structures discussed above. Originally we reasoned that replacing the bulky butyl groups in **2** by methyl groups might afford alternative secondary laddering routes resulting in higher laddered oligomers. Accordingly, the lithium thioamidates Li[MeCS(NR)] (**8**: R = *t*Bu; **9**: R = Me) were prepared. However, the crystallographic characterization of these species revealed the unladdered, solvated polymers $[Li\{MeCS(NtBu)\}{\cdot}THF]_\infty$ (**8a**) and $[Li\{MeCS(NMe)\}{\cdot}2THF]_\infty$ (**9a**).[13]

Although the connection between structures **8a** and **9a** and the laddering principle is not obvious, both polymeric forms can in fact be derived from a common dimeric PLU, which is then broken down upon solvation by THF (Scheme 5). Significantly, the putative PLUs for **8a** and **9a** are analogous to the one which undergoes secondary laddering (trimerization) to form **2**. The degradation of laddered structures upon solvation is a well-documented phenomenon in the literature, although it is usually used to explain the disassembly of higher states of oligomerization to lower oligomers.[17] Here the opposite occurs, with solvation producing polymers by opening the Li_2S_2 and LiNCS rings of laddered dimers.

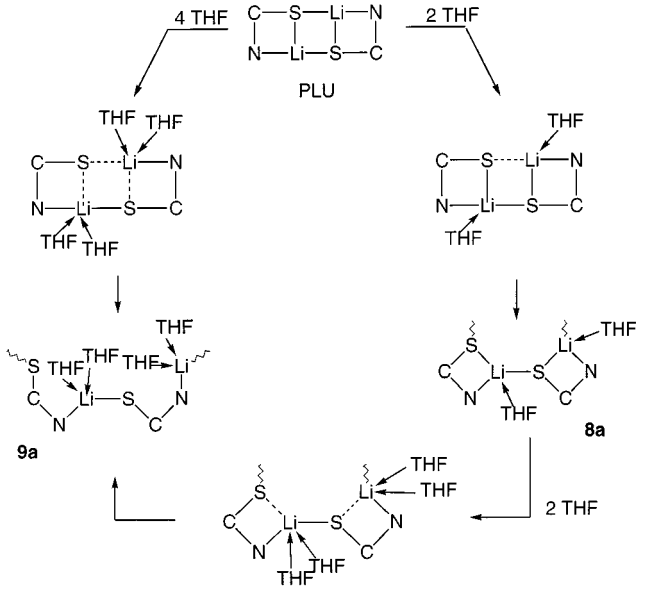

Scheme 5. Generation of $[Li\{MeCS(NR)\}{\cdot}xTHF]_\infty$ (**8a**: R = *t*Bu, *x* = 1; **9a**: R = Me, *x* = 2) from a common dimeric PLU; the dashed lines indicate bonds being broken

The polymer **8a** is produced by the solvation of both lithium centres in the dimeric PLU, leading to the rupture of one Li−S bond. The orientation adopted by **9a** is generated either from further solvation, leading to disruption of the exocyclic Li−S bonds, or directly from the dimeric PLU upon solvation of each lithium ion by two THF molecules; thus the three disparate structures **2**, **8a**, and **9a** all stem from the same primary unit. While other descriptions are certainly possible for each structure viewed independently, the use of a two-stage approach to the laddering principle affords a consistent rationale for all three structures despite their substantial differences.

The fact that **2** remains unsolvated in the solid state, even when recrystallized from THF, is of significance. We suggest that this occurs because the steric bulk of the substituents in **2** prevents solvent molecules from entering the coordination sphere of the PLU. This allows an unsolvated, oligomeric structure to form through secondary laddering. In **8a** and **9a**, smaller substituents allow solvation of the PLU; solva-

tion effectively competes with secondary laddering as a mechanism to disperse electronic charge and solvated, unladdered polymers result.

3.4. Other Examples

A two-step approach to laddering is also useful for understanding systems other than lithium heterocarboxylates. For example, the lithium arenethiolate $[\{Li[SC_6H_4\{(R)\text{-}CH(Me)NMe_2\}\text{-}2]\}]_6$ forms a hexamer[18] composed of three dimeric PLUs assembled in much the same manner as **2**. Likewise the laddered polymer $[PhCH_2SLi{\cdot}NC_6H_5]_\infty$ can be viewed as resulting from the secondary association of monosolvated dimers.[19]

An illustrative series of examples from alkali metal amide chemistry is provided by the lithium,[20] sodium,[5] and heterobimetallic lithium/sodium[5] derivatives of *tert*-butyl amide,[3e] all of which can be rationalized through primary and secondary laddering processes (Scheme 6). The unsolvated octamer $[Li(HNtBu)]_8$ (**10**) can be viewed as a secondary aggregate of dimeric, *cisoid*, homomolecular PLUs forming a closed ladder. Primary laddering in the mixed system $[LiNa(HNtBu)_2{\cdot}TMEDA]_2$ (**11**) probably forms a solvated, dimeric $[Li_2N_2]$ PLU initially, which then loses solvent upon secondary laddering with Na−N units. The final aggregate is thus centred around a *cisoid* $[Li_2N_2]$ ring, and further laddering is prevented by solvation of the outer Na−N rungs. In contrast, the solvated polymer $[\{Na(HNtBu)\}_3{\cdot}NH_2tBu]_\infty$ (**12**) arises from the unhindered secondary laddering of solvated and unsolvated dimeric PLUs. As in **10** the PLUs are all *cisoid*, but secondary laddering in **12** involving the solvated Na−N unit produces a *transoid* $[NaN]_2$ ring, probably due to the "steric intrusion"[5] of the solvent molecule.

Clearly, alternative descriptions are possible for each of the systems discussed here. For example, **10** could be viewed as an arrangement of eight monomers or two stacked tetramers rather than four laddered dimers. However, as was the case for the lithium heterocarboxylate structures discussed earlier, a two-stage approach to the laddering principle allows a diverse range of architectures to be understood using a single conceptual framework. While we feel that this is an important point in favour of using the two-stage approach consistently, we note that is not sufficient for every case, such as, for example, structures arising from the stacking of M_nE_n ($n > 2$) rings[14] as well as odd-numbered and/or asymmetric oligomers.[17g] Such cases are in the minority, however, and can generally be handled by using a similar two-stage approach wherein building blocks may be unladdered and further aggregation steps (tertiary, etc.) may need to be invoked. We have seen this in our own work, for example the lithium diazasulfite hexamers $[Li_2\{SO(NtBu)(NR)\}]_6$ (R = *t*Bu, $SiMe_3$), derived from the aggregation of three hexagonal prisms through Li_2O_2 faces (R = *t*Bu), or the dimerization of eighteen-atom cages through Li_3O_3 faces (R = $SiMe_3$).[21]

4. Polymeric Laddered Compounds

It has been accepted for some time that organolithium species that precipitate as insoluble, amorphous solids (i.e. do not crystallize easily) are probably laddered polymers. While confirmation of this hypothesis has long been anticipated for lithium amides in particular, few "unsolvated," polymeric ladder structures have been characterized to date, and in each of these cases some form of internal solvation is present. For example, 2,3,4,5-tetramethyl-1-sodiopyrrole[22]

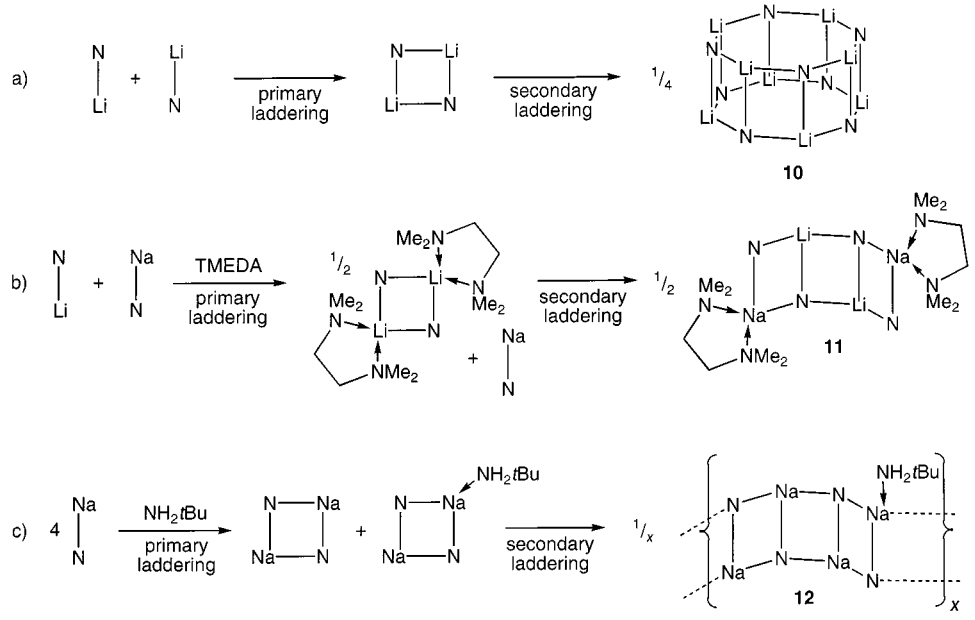

Scheme 6. Primary and secondary laddering processes leading to: a) $[Li\{HNtBu\}]_8$ (**10**); b) $[LiNa(HNtBu)_2{\cdot}TMEDA]_2$ (**11**); c) $[\{Na(HNtBu)\}_3{\cdot}NH_2tBu]_\infty$ (**12**)

and phenyllithium[23] both form ladder polymers wherein the lithium cations are coordinated by the aromatic substituents on neighbouring rungs. Likewise, monolithiated ethylenediamine $[Li\{HN(CH_2)_2NH_2\}]_\infty$ [8] consists of an infinite ladder wherein each lithium cation is chelated by both the amide and amine ends of the molecule. In fact, although a few truly unsolvated, laddered lithium amides are now known,[17b,20] none have proven to be polymeric. Conversely, although some alkali metal amide polymers have been characterized (notably $[LiN(i\text{Pr})_2]_\infty$ [24]), none have been found that are both laddered and unsolvated.

A recent survey[10] tallied only two examples of unsolvated organolithium polymers involving any laddered portions, $[LiOPh]_\infty$ [25] and $[LiC(OEt)=CH_2)]_\infty$,[26] among several solvated examples and several unsolvated, finite ladders. This demonstrates two important points: 1) that solvation does not preclude polymerization, and may even encourage it in some cases (e.g. **8a** and **9a**); and 2) that unsolvated laddered compounds, whether polymeric or not, can indeed be crystallized (i.e. they are not necessarily amorphous solids). With these observations in mind, we note that the two-stage framework presented here leaves room, and provides rationale, for a number of alternative architectures; it does not point exclusively to laddered polymers for any particular class of compounds. Given the wide diversity of laddered structures now known, we feel that this is a point in favour of this approach.

5. Conclusions and Outlook

We have tried to show briefly how a two-stage approach to the laddering principle provides a useful framework for describing and understanding laddered structures, particularly among lithium heterocarboxylates. We note also an initially unanticipated feature of this approach: it can explain unladdered systems topologically related to laddered ones. Thus, as with the lithium thioamidates **2**, **8**, and **9**, widely disparate structures can be understood in terms of a single conceptual process. Furthermore, we have shown that the nature of secondary laddered structures is strongly dependent on the behaviour of PLUs with regard to steric effects, solvation, etc. This is true for both homo- and heteromolecular aggregation. While these influences on laddering processes have been noted previously,[3] the two-stage approach discussed here affords a consistent and systematic method of gauging their effect on structure.

Finally, we anticipate that the continued development of the laddering principle may have implications outside the realm of main-group element chemistry. Recently we have seen that a process much like primary and secondary laddering (involving dimeric PLUs) can be used to explain the formation of copper(I) thioamidate oligomers.[27] Although not strictly within the rubric of laddering as defined here, the behaviour of these derivatives can evidently be understood in a similar manner. A complete investigation of this phenomenon is currently underway, and may prove germane to developing a more generally applicable laddering principle.

Acknowledgments

We thank the NSERC (Canada) for financial support and the University of Calgary for a Silver Anniversary Fellowship (A. D.).

[1] J. K. Brask, T. Chivers, *Angew. Chem. Int. Ed.* **2001**, in press.
[2] [2a] D. Barr, W. Clegg, R. E. Mulvey, R. Snaith, K. Wade, *J. Chem. Soc., Chem. Commun.* **1986**, 295−297. − [2b] D. R. Armstrong, D. Barr, W. Clegg, R. E. Mulvey, D. Reed, R. Snaith, K. Wade, *J. Chem. Soc., Chem. Commun.* **1986**, 869−870. − [2c] D. R. Armstrong, D. Barr, W. Clegg, S. M. Hodgson, R. E. Mulvey, D. Reed, R. Snaith, D. S. Wright, *J. Am. Chem. Soc.* **1989**, *111*, 4719−4727.
[3] Review articles: [3a] D. Seebach, *Angew. Chem. Int. Ed. Engl.* **1988**, *27*, 1624−1654. − [3b] K. Gregory, P. von R. Schleyer, R. Snaith, *Adv. Inorg. Chem.* **1991**, *37*, 47−142. − [3c] R. E. Mulvey, *Chem. Soc. Rev.* **1991**, *20*, 167−209. − [3d] E. Weiss, *Angew. Chem. Int. Ed. Engl.* **1993**, *32*, 1501−1523. − [3e] R. E. Mulvey, *Chem. Soc. Rev.* **1998**, 339−346.
[4] R. Snaith, D. S. Wright, in *Lithium Chemistry, A Theoretical and Experimental Overview* (Eds.: A. Sapse, P. von R. Schleyer), Wiley, New York, **1995**, p.229.
[5] W. Clegg, K. W. Henderson, L. Horsburgh, F. Mackenzie, R. E. Mulvey, *Chem. Eur. J.* **1998**, *1*, 53−56.
[6] T. Chivers, A. Downard, M. Parvez, *Inorg. Chem.* **1999**, *38*, 4347−4353.
[7] M. Beswick, D. S. Wright, in *Comprehensive Organometallic Chemistry II, Vol. 1* (Ed.: C. Housecroft), Pergamon, Oxford, **1995**, p. 9.
[8] G. Kowach, C. Warren, R. Haushalter, F. Disalvo, *Inorg. Chem.* **1998**, *37*, 156−159.
[9] For examples, see: [9a] G. Férey, *J. Solid State Chem.* **2000**, *152*, 37. − [9b] M. O′Keeffe, M Eddaoudi, H. Li, T. Reineke, O. M. Yaghi, *J. Solid State Chem.* **2000**, *152*, 3.
[10] I. Haiduc, F. T. Edelmann, *Supramolecular Inorganic Chemistry*, Wiley-VCH Verlag GmbH, Federal Republic of Germany, **1999**, ch. 6.
[11] J. March, *Advanced Organic Chemistry, Reactions, Mechanisms and Structure*, 4th ed., John Wiley and Sons, Canada, **1992**, pp. 933−934.
[12] T. Chivers, A. Downard, G. P. A. Yap, *Inorg. Chem.* **1998**, *37*, 5708−5709.
[13] T. Chivers, A. Downard, M. Parvez, *Inorg. Chem.* **1999**, *38*, 5565−5570.
[14] D. R. Armstrong, W. Clegg, S. M. Hodgson, R. Snaith, A. E. H. Wheatley, *J. Organomet. Chem.* **1998**, *550*, 233−240.
[15] [15a] C. P. Hidber, T. Maetzke, D. Seebach, *J. Am. Chem. Soc.* **1990**, *112*, 8248−8250. − [15b] T. Maetzke, D. Seebach, *Organometallics* **1990**, *9*, 3032−3037.
[16] T. Chivers, A. Downard, G. P. A. Yap, *J. Chem. Soc., Dalton Trans.* **1998**, 2603−2605.
[17] For examples, see: [17a] D. Barr, W. Clegg, L. Cowton, L. Horsburgh, F. M. Mackenzie, R. E. Mulvey, *J. Chem. Soc., Chem. Commun.* **1995**, 891−892. − [17b] W. Clegg, L. Horsburgh, F. M. Mackenzie, R. E. Mulvey, *J. Chem. Soc., Chem. Commun.* **1995**, 2011−2012. − [17c] R. v. Bülow, H. Gornitzka, T. Kottke, D. Stalke, *Chem. Commun.* **1996**, 1639−1640. − [17d] A. Kennedy, R. E. Mulvey, A. Robertson, *Chem. Commun.* **1998**, 89−90. − [17e] T. Chivers, M. Parvez, G. Schatte, *J. Organomet. Chem.* **1998**, *550*, 213−220. − [17f] W. Clegg, S. T. Liddle, R. E. Mulvey, A. Robertson, *Chem. Commun.* **1999**, 511−512. − [17g] W. Clegg, S. T. Liddle, R. E. Mulvey, A. Robertson, *Chem. Commun.* **2000**, 223−224. − [17h] W. Clegg, L. Horsburgh, S. T. Liddle, F. M. Mackenzie, R. E. Mulvey, A. Robertson, *J. Chem. Soc., Dalton Trans.* **2000**, 1225−1231.
[18] M. D. Janssen, E. Rijnberg, C. A. de Wolfe, M. P. Hogerheide, D. Kruis, H. Kooijmann, A. L. Spek, D. M. Grove, G. van Koten, *Inorg. Chem.* **1996**, *35*, 6735−6741.

[19] A. J. Banister, W. Clegg, W. R. Gill, *J. Chem. Soc., Chem. Commun.* **1987**, 850−851.
[20] N. D. R. Barnett, W. Clegg, L. Horsburgh, D. M. Lindsay, F. M. Mackenzie, R. E. Mulvey, P. G. Willard, *Chem. Commun.* **1996**, 2321−2322.
[21] [21a] J. K. Brask, T. Chivers, M. Parvez, G. Schatte, *Angew. Chem. Int. Ed. Engl.* **1997**, *36*, 1986−1988. − [21b] J. K. Brask, T. Chivers, G. Schatte, *Phosphorus, Sulfur, Silicon Relat. Elem.* **1997**, *124*, 203−212.
[22] N. Kuhn, G. Henkel, J. Kreutzberg, *Angew. Chem. Int. Ed. Engl.* **1990**, *29*, 1143−1144.
[23] R. E. Dinnebier, U. Behrens, F. Olbrich, *J. Am. Chem. Soc.* **1998**, *120*, 1430−1433.
[24] N. D. R. Barnett, R. E. Mulvey, W. Clegg, P. A. O′Neil, *J. Am. Chem. Soc.* **1991**, *113*, 8187−8188.
[25] [25a] R. E. Dinnebier, M. Pink, J. Sieler, P. W. Stephens, *Inorg. Chem.* **1997**, *36*, 3398−3401. − [25b] R. E. Dinnebier, M. Pink, J. Sieler, P. Norby, P. W. Stephens, *Inorg. Chem.* **1998**, *37*, 4996−5000.
[26] K. Sorger, W. Bauer, P. von R. Schleyer, D. Stalke, *Angew. Chem. Int. Ed. Engl.* **1995**, *34*, 1594−1596.
[27] T. Chivers, A. Downard, M. Parvez, G. Schatte, *Organometallics* **2001**, *20*, 727−733.

Received February 15, 2001
[I01059]

Cobalt(III) Complexes with Carboxamido-*N* and Sulfenato-*S* or Sulfinato-*S* Ligands Suggest that a Coordinated Sulfenate-*S* is Essential for the Catalytic Activity of Nitrile Hydratases

Laurent Heinrich,[a] Aude Mary-Verla,[a] Yun Li,[a] Jacqueline Vaissermann,[b] and Jean-Claude Chottard*[a]

Keywords: Cobalt / Nitrile hydratase / Enzyme mimics / S ligands / Catalysis

A bis(sulfenato-*S*)Co^{III} complex and its corresponding bis(sulfinato-*S*) complex were prepared. Their catalytic nitrile hydration activity was tested. Whereas the former catalyzes the hydration of CH_3CN under mild acidic conditions, the latter is inactive. A mechanism for this reaction is proposed, in relation with nitrile hydratase activity.

Introduction

Nitrile hydratases (NHases) are non-heme iron or non-corrinoid cobalt-containing enzymes that catalyze the hydration of nitriles to amides.[1] NHases are used for the industrial production of acrylamide[2] and for the removal of nitriles from waste streams.[3] Both active and inactive forms of the iron NHases have recently been characterized by X-ray diffraction and ENDOR (Electron Nuclear Double Resonance) spectroscopy. The coordination sphere of the metal centre is very unusual. For the active form of the NHase from *Rhodococcus* sp.R312, the structure at 2.65 Å resolution showed that iron is bound to three cysteinthiolates, two amido nitrogen atoms from peptide bonds of the protein main chain,[4] and an axial hydroxide or water molecule as the sixth ligand.[5] For the inactive form of the NHase from *Rhodococcus* sp.N-771, the structure at 1.7 Å resolution revealed that two of the coordinated sulfur atoms belong to sulfenic (Cys-SOH) and sulfinic (Cys-SO_2H) moieties, and one nitric oxide ligand occupies the sixth position.[6] The cysteine-sulfinate and cysteine-sulfenate ligands are assigned to the post-translational modification of former cysteines. The iron and cobalt NHases have similar metal sites, according to EXAFS data.[7] A very recent study of a Co-substituted Fe-NHase showed that the catalytic activity is correlated to the post-translational oxidation of a cysteine.[8] This oxidation of one cysteine into cysteine-sulfinate has been established by mass spectrometry, but this does not exclude the existence of a former relatively unstable cysteine-sulfenate at the enzyme active site.

All these data did not suggest a role for the sulfenato-*S* and/or sulfinato-*S* ligands in NHase catalysis. The study of relevant mimetic complexes, however, should yield clues to this question. Several mimetic Fe^{III} and Co^{III} model compounds of NHases have recently been synthesized.[9–12] Some of them have been oxidized by H_2O_2 to give the sulfinato-*S* species[10a][11a][11d] and one gave an inert η^2-sulfenato, sulfinato-*S* derivative.[12b] Only one cobalt mimetic complex has been reported to have nitrile hydratase activity.[11b] The structure of this presumably hydroxo complex $[Co(PyPS)(OH)]^{2-}$ is not known (although it is assumed to contain one pyridine, two carboxamido-*N* and one thiolato ligands in a plane, and the second thiolate in an axial position). It allowed conversion of acetonitrile into acetamide at 50 °C and pH = 9.5 (18 turnovers). This reaction probably involves the nucleophilic property of the hydroxide ligand.

We have reported the first example of the oxidation of a carboxamido-*N*, thiolato-Fe^{III} complex $[FeN_2S_3]^{2-}$ by dioxygen to give a sulfinato-*O* species $[FeN_2S_2OSO]^{2-}$ raising the question of *S*- vs. *O*-coordination to the metal.[9c] To investigate which factors could control the eventual oxidation of the bound in-plane thiolates in Co-NHases, we have synthesized a tetradentate eleven-atom ligand $H_4N_2S_2$, containing two aliphatic thiols and two aliphatic amides **1** (H_4L).[13] The derived square-planar complex $[Co^{III}L]^-$ (**2**) was characterized by X-ray diffraction.[9b] Cyanides and isocyanides were the only ligands found able to give hexacoordinated complexes upon bis-axial coordination, as shown by spectroscopic data together with an EXAFS study.[9b] Such a coordination allows oxygenation of the in-plane thiolates to take place by air or hydrogen peroxide. We have thus reported the preparation of the disulfenato compound $Na[Co(L\text{-}N_2SOSO)(t\text{BuNC})_2]$ (**3**).[9a] We now report the preparation of the corresponding disulfinato derivative $(Me_4N)[Co(L\text{-}N_2SO_2SO_2)(t\text{BuNC})_2]$ (**4**). Whereas **3** exhibits nitrile hydration catalytic activity, **4** is inactive.

Results and Discussion

The addition of 50% aq. H_2O_2 to a solution of the square-planar complex $[Co^{III}L]^-$ (**2**)[9b] in EtOH, in the

[a] Laboratoire de Chimie et Biochimie Pharmacologiques et Toxicologiques, Université René Descartes, UMR 8601 CNRS, 45 rue des Saints-Pères, 75270 Paris Cedex 06, France
E-mail: Jean-Claude.Chottard@biomedicale. univ-paris5.fr
[b] Laboratoire de Chimie Inorganique et Matériaux Moléculaires, Université Pierre et Marie Curie, ESA 7071
75252 Paris Cedex 05, France

 © WILEY-VCH Verlag GmbH, 69451 Weinheim, 2001 1434–1948/01/0909–2203 $ 17.50+.50/0

presence of excess *t*BuNC and one equivalent of Me_4NCl, gave the yellow disulfinato complex $(Me_4N)[Co(L\text{-}N_2SO_2\text{-}SO_2)(t\text{BuNC})_2]$ (**4**) (Scheme 1). Single crystals of **4** suitable for X-ray analysis were formed by slow diffusion of Et_2O into an EtOH solution in the presence of a small amount of H_2O. The X-ray structure of **4** is shown in Figure 1.

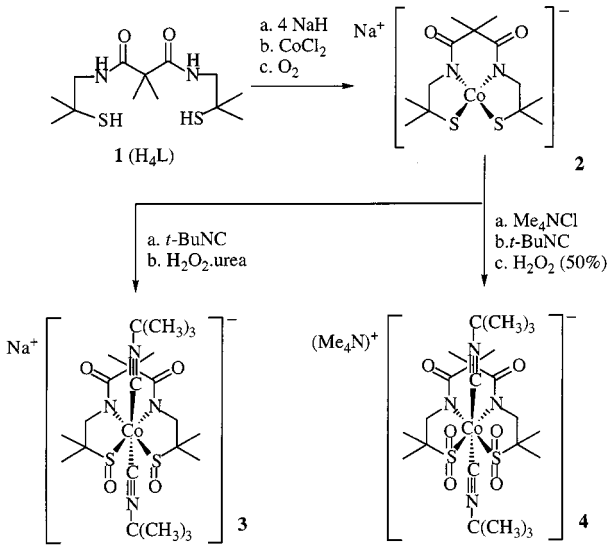

Scheme 1. Synthetic scheme for complexes **3** and **4**

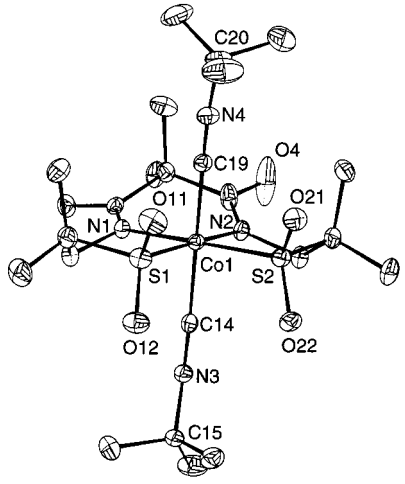

Figure 1. CAMERON representation (ellipsoid at 30% probability level) of **4**; H atoms are omitted for clarity; selected bond lengths (Å) and angles (°): Co(1)−S(1) 2.2114(9), Co(1)−S(2) 2.2255(9), Co(1)−N(1) 1.962(3), Co(1)−N(2) 1.954(3), Co(1)−C(14) 1.877(3), Co(1)−C(19) 1.867(3), C(14)−N(4) 1.149(4), C(19)−N(4) 1.143(4), S(1)−O(11) 1.449(3), S(1)−O(12) 1.470(3), S(2)−O(21) 1.452(3), S(2)−O(22) 1.472(3); S(1)−Co(1)−S(2) 95.56(4), S(1)−Co(1)−N(1) 86.87(8), N(1)−Co(1)−N(2) 90.9(1), S(1)−Co(1)−N(1) 86.87(8), S(2)−Co(1)−N(2) 86.65(8), C(14)−Co(1)−C(19) 174.7(1), Co(1)−C(19)−N(4) 175.0(3), Co(1)−C(14)−N(3) 176.5(3), C(14)−N(3)−C(15) 166.5(3), C(19)−N(4)−C(20) 173.6(3)

Compound **4** is a distorted octahedral Co^{III} complex with an N_2S_2 equatorial plane containing carboxamido-*N* and sulfinato-*S* ligands and two axial isocyanido ligands. Water molecules help to stabilize the crystal lattice through hydrogen bonding to the oxygen atoms of the sulfinato-*S* and carboxamido-*N* ligands. The presence of one Me_4N^+ cation per cobalt in the unit cell of **4** confirms the oxidation state as cobalt(III). The Co−N bond lengths are similar to those reported for carboxamido-*N* ligands in hexacoordinated Co^{III} complexes,[11] but are 0.08 Å longer than those found in the parent square-planar complex **2**.[9b] The Co−S bond lengths (2.22 Å) are similar to those reported for structurally characterized Co^{III}-sulfinato complexes.[10a,11a,11d] The Co−*C*-isocyanido bonds are 0.04 Å longer than the only reported values (1.83−1.79 Å) for Co^{III}−*C*-isocyanido cyclopentadienyl compounds.[14] The isocyanides are almost linearly coordinated to the metal, with a Co−C−N angle of 176°, a C−N−C angle of 173° and a C−N bond length of 1.14 Å, which confirms a C≡N triple bond. The IR spectrum (KBr pellet) of **4** shows the characteristic coordinated carboxamido-*N* ν_{CO} frequency at 1565 cm^{-1} and strong absorptions at 1195, 1065 cm^{-1} corresponding to the ν_{SO} stretching vibrations of coordinated *S*-sulfinates.[9b] The strong asymmetric ν_{CN} stretching frequencies of the isocyanides are increased from 2140 cm^{-1} to 2215 cm^{-1} upon coordination, indicating a higher bond order in **4** than in the free ligand, fitting the C≡N triple bond description and a prevailing σ-donor character of the isocyanide ligands rather than a potential π-acceptor contribution.

It is noteworthy that the overall geometries of $[Co(L\text{-}N_2SOSO)(t\text{BuNC})_2]^-$ (**3**) and $[Co(L\text{-}N_2SO_2SO_2)(t\text{BuNC})_2]^-$ (**4**) are very similar. The two complexes have comparable Co−N and Co−S bond lengths, but the Co−C bonds are longer in **4** than in **3** suggesting that the sulfinato (SO_2) group is a stronger-field ligand than the sulfenato (SO) group.

Yellow solutions of **4** in polar solvents (alcohols, DMSO, DMF, H_2O) are stable in air and the complex behaves as a hexacoordinated species with a diamagnetic low spin Co^{III} (Evans method). The electrospray mass spectrum exhibits a peak at m/z = 591 ($[Co(L\text{-}N_2SO_2SO_2)(t\text{BuNC})_2]^-$). The structural and spectral characteristics of **4** are similar to those of a Co^{III}-sulfinato complex reported very recently.[10a]

The testing of the hydration catalytic activity of compounds **3** and **4** was conducted in a mixture of CH_3CN/H_2O under various conditions of temperature and pH. The reaction is slow and could be followed by ^1H NMR spectroscopy using 1,3,5-trimethoxybenzene as internal reference for turnover number determination. Only **3** led to the formation of acetamide; no trace could be detected with **4**. Under alkaline conditions (aq. $NaHCO_3$, pH = 9), no conversion of CH_3CN was observed. At pH = 7 and 20 °C, acetamide was formed (2 turnovers) and **3** remained unchanged (^1H NMR spectroscopy) after 24 h. Varying the temperature did not improve the turnover number. Acidic pH = 4.8 (1 M HOAc/NaOAc buffer) at 4 °C gave the best

result (50 turnovers). Other acidic conditions (0.5 M HOAc/NaOAc buffer, pH = 4.8; 0.4 M HOAc; 0.03 M HCl; or 0.5 M H_3PO_4/KH_2PO_4 buffer, pH = 2.1) gave a less efficient reaction.

Although **3** gives a slow reaction under the conditions studied, the hydration mechanism deserves interest. At variance with the known[11b] complex $[Co(PyPS)(OH)]^{2-}$, which promotes the conversion of acetonitrile into acetamide (18 turnovers) only at 50 °C and pH = 9.5 (Tris buffer), probably through a Co^{III}-bound hydroxide ligand, **3** does not catalyze nitrile hydration in basic conditions (pH = 9). The reaction works better in mildly acidic conditions, although **3** undergoes a slow decomposition under these conditions, probably due to the protonation of the carboxamido-*N* ligands. Compound **3** has no free coordination site to allow either water or acetonitrile binding to Co^{III} and our results suggest that a general acid catalysis could be required for nitrile hydration catalyzed by **3**. The absence of catalytic activity of **4** points to a possible role of the nucleophilicity of the coordinated *S*-sulfenates in **3**. The oxygen atom of S-bound sulfenates has been shown to exhibit nucleophilic properties.[15]

When 30% $H_2{}^{18}O/H_2{}^{16}O$ was used for the hydration of acetonitrile in a 1 M HOAc/NaOAc buffer (pH = 4.8) at 4 °C for 17 h, complex **3** gave the complexes $[Co(L\text{-}N_2S^{18}OS^{16}O)(t\text{BuNC})_2]^-$ (**3a**) and $[Co(L\text{-}N_2S^{18}OS^{18}O)(t\text{BuNC})_2]^-$ (**3b**) characterized by electrospray mass spectrometry (*m*/*z* = 561, 563 respectively). This indicates that an exchange of oxygen atom occurs at the coordinated sulfenates during the hydration catalysis. That this exchange occurs during the actual hydration catalysis is demonstrated by the absence of any ^{18}O incorporation into **3** when acetonitrile is absent in exactly the same conditions.

Our observations, together with the known nucleophilic properties of coordinated *S*-sulfenates,[15] lead us to propose a tentative mechanism for the formation of complexes **3a** and **3b** during the hydration of CH_3CN catalyzed by **3** (Scheme 2). Complex **3** displays nucleophilic catalysis, assisted by general acid catalysis by the HOAc/NaOAc buffer.

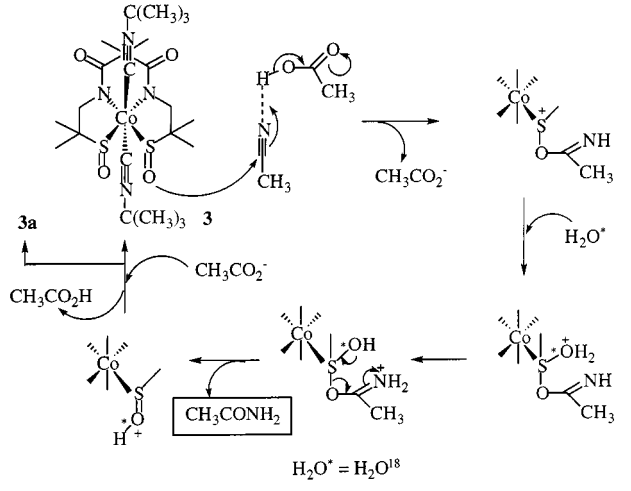

Scheme 2. Tentative mechanism for the hydration of CH_3CN catalyzed by **3**

Conclusion

This study has shown the importance of coordinated sulfenates (SO) for nitrile hydration catalysis by a carboxamido-*N* Co^{III} complex. The corresponding sulfinato (SO_2) derivative is inactive under the same conditions. Our results suggest that in the case of Fe or Co NHases, the post-translational oxidation of metal-bound cysteines into sulfenic moieties, is a crucial step for nitrile hydration. Although the hydration reaction catalyzed by **3** appears to be of low efficiency due to its intermolecular character, this situation could be overcome by a proximity reaction within the enzyme active site. The conjunction of nucleophilic and general acid catalyses might explain the enzyme uncommon route for nitrile hydration.

Experimental Section

Complex 3: This compound was prepared according to our previously reported procedure[9a] with some slight modifications. *t*BuNC (51 mg, 0.6 mmol) was added to a deep green solution of Na[CoL]·DMF (**2**)[9b] (46 mg, 0.1 mmol) in DMF (0.5 mL) and acetone (1 mL) cooled to −10 °C. The resulting pink solution was stirred for 10 min. and then solid H_2O_2·urea (56 mg, 0.6 mmol) was added. After 1 h at −10 °C, acetone (1 mL) was added and the orange precipitate was filtered, rinsed with acetone, and dried under vacuum to afford $Na[Co^{III}(L\text{-}N_2SOSO)(t\text{BuNC})_2]$·urea (**3**) (55 mg, 85%). − ^1H NMR (250 MHz, [D$_6$]DMSO): δ = 5.44 (s, 4 H, urea), 3.60 (d, *J* = 13.3 Hz, 2 H, NCH_AH_B), 3.09 (d, 2 H, NCH_AH_B), 1.39 (s, 18 H, *t*BuNC), 1.28 (s, 6 H, CH_3), 1.17 (s, 6 H, CH_3), 1.12 (s, 6 H, CH_3).

Complex 4: Me_4NCl (16 mg, 0.15 mmol) and *t*BuNC (60 mg, 0.72 mmol) were added successively to a deep green solution of Na[CoL]·DMF (**2**)[9b] (54 mg, 0.12 mmol) in degassed EtOH (1 mL) cooled to −10 °C. The resulting pink solution was stirred under Ar for 10 min. and an aq. 50% solution of H_2O_2 (310 mg, 5.44 mmol) was then added dropwise. The orange solution was stirred at −10 °C for 3 h and kept in a refrigerator overnight. The precipitate (NaCl) was filtered off and rinsed with EtOH (95%, 1 mL). Et_2O (≈ 20 mL) was added to the combined yellow solution and kept at 4 °C overnight. The resulting yellow crystals were filtered and dried under vacuum to afford $(Me_4N)[Co^{III}(L\text{-}N_2SO_2SO_2)(t\text{BuNC})_2]\cdot H_2O$ (**4**) (70 mg, 96%). − $C_{27}H_{54}CoN_5O_7S_2$ (683.81): calcd. C 47.42, H 7.96, N 10.24, S 9.38; found C 47.17, H 7.54, N 10.11, S 9.26. − UV/Vis (MeOH) [λ_{max}, nm (ε, $m^{-1}\,cm^{-1}$)]: 400 (sh), 312 (20000), 208 (13000). − IR (KBr): $\tilde{\nu}$ = 2215 (s, ν_{CN}), 1565 (s, ν_{CO}), 1195 and 1065 (s, ν_{SO}) cm^{-1}. − ^1H NMR (250 MHz, [D$_6$]DMSO): δ = 7.75 (br. s, 2 H, D_2O exchangeable, H_2O), 3.18 (s, 4 H, NCH_2), 1.39 (s, 18 H, *t*BuNC), 1.31 [s, 12 H, $(CH_3)_4N^+$], 1.27 (s, 6 H, CH_3), 1.18 (s, 12 H, CH_3). − Electrospray MS (MeOH): *m*/*z* (%) = 591 [M − Me_4N^+]$^-$.

Crystal Data for 4·H_2O: $C_{27}H_{54}CoN_5O_7S_2$, *M* = 683.81, yellow crystals, monoclinic, space group $P2_1/n$, *a* = 11.621(7), *b* = 16.845(6), *c* = 18.468(4) Å, *Z* = 4, β = 79.64(3)° *V* = 3556(3) Å^3, D_c = 1.28 g·cm^{-3}, *T* = 295 K, Mo-K_α radiation (λ = 0.71069 Å),

7606 reflections were measured, 4631 of which were used in all calculations (R_{int} = 0.02). The structure was solved by SHELXS-86[16] and refined by least-squares analysis using anisotropic thermal parameters, H atoms were introduced in calculated positions, with $F_o > 3\sigma(F_o)$, the programs CRYSTALS[17] and CAMERON[18] were used, R = 0.0479, R_W = 0.0574.

Crystallographic data (excluding structure factors) for the structure reported in this paper have been deposited with the Cambridge Crystallographic Data Centre as supplementary publication no. CCDC-161812. Copies of the data can be obtained free of charge on application to CCDC, 12 Union Road, Cambridge CB2 1EZ, UK [Fax: (internat.) +44-1223/336-033; E-mail: deposit@ccdc.cam.ac.uk].

Typical Procedure for the Catalytic Hydration of CH_3CN: A mixture of Na[Co^{III}(L-N_2SOSO)(tBuNC)$_2$]·urea (**3**) (5 mg, 0.008 mmol) and 1,3,5-trimethoxybenzene (7 mg, 0.042 mmol) in CH_3CN (0.5 mL) and a HOAc/NaOAc buffer (1 M, pH = 4.8, 0.5 mL) was stirred at 4 °C for 17 h. After lyophilization, [D_6]Me_2SO was added to the mixture and the presence of 0.144 mmol of acetamide was determined (18 turnovers) by ^{1}H NMR spectroscopy. The turnover number increases with the reaction time. 42 Turnovers and 50 turnovers were found after 3 and 6 days, respectively.

Acknowledgments

This work was supported by the European Commission TMR-NOHEMIP research network no. ERB FMRX-CT98-0174. We thank Dr. F. Gonnet (University Paris 6) for the electrospray mass spectrometry analysis.

[1] S. Nagashima, M. Nakasato, N. Dohmae, M. Tsujimura, K. Takio, M. Odaka, M. Yohda, N. Kamiya, I. Endo, *Nature Struct. Biol.* **1998**, *5*, 347−351.
[2] M. Kobayashi, T. Nagasawa, H. Yamada, *Trends Biotechnol.* **1992**, *10*, 402−408.
[3] J. M. K. Wyatt, C. J. Knowles, *Int. Biodeterior. Biodegrad.* **1995**, *35*, 227−248.
[4] W. Huang, J. Jia, J. Cumming, M. Nelson, G. Schneider, Y. Lindqvist, *Structure* **1997**, *5*, 691−699.
[5] P. E. Doan, M. J. Nelson, H. Jin, B. M. Hoffman, *J. Am. Chem. Soc.* **1996**, *118*, 7014−7015;
[6] S. Nagashima, M. Nakasato, N. Dohmae, M. Tsujimura, K. Takio, M. Odaka, M. Yohda, N. Kamiya, I. Endo, *Nature Struct. Biol.* **1998**, *5*, 347−351.
[7] B. A. Brennan, G. Alms, M. J. Nelson, L. T. Durney, R. C. Scarrow, *J. Am. Chem. Soc.* **1996**, *118*, 9194−9195.
[8] N. Masaki, H. Nakayama, M. Odaka, M. Yohda, K. Takio, I. Endo, *FEBS Letters* **2000**, *465*, 173−177.
[9] [9a] L. Heinrich, Y. Li, J. Vaisserman, J. C. Chottard, *Eur. J. Inorg. Chem.* **2001**, 1407−1409. − [9b] L. Heinrich, Y. Li, K. Provost, A. Michalowicz, J. Vaisserman, J. C. Chottard, *Inorg. Chim. Acta* **2001**, *318*, 117−126. − [9c] L. Heinrich, Y. Li, J. Vaisserman, G. Chottard, J. C. Chottard, *Angew. Chem. Int. Ed.* **1999**, *38*, 3526−3528.
[10] [10a] M. Rat, R. Alves de Sousa, J. Vaisserman, D. Mansuy, I. Artaud, *J. Inorg. Biochem.* **2001**, *in press.* − [10b] S. Chatel, M. Rat, S. Dijols, P. Leduc, J. P. Tuchagues, D. Mansuy, I. Artaud, *J. Inorg. Biochem.* **2000**, *80*, 239−246. − [10c] I. Artaud, S. Chatel, A. S. Chauvin, D. Bonnet, M. A. Kopf, P. Leduc, *Coord. Chem. Rev.* **1999**, *190*, 577−586.
[11] [11a] L. A. Tyler, J. C. Noveron, M. M. Olmstead, P. K. Mascharak, *Inorg. Chem.* **2000**, *39*, 357−362. − [11b] J. C. Noveron, M. M. Olmstead, P. K. Mascharak, *J. Am. Chem. Soc.* **1999**, *121*, 3553−3554. − [11c] J. C. Noveron, R. Herradora, M. M. Olmstead, P. K. Mascharak, *Inorg. Chim. Acta* **1999**, *285*, 269−276. − [11d] L. A. Tyler, J. C. Noveron, M. M. Olmstead, P. K. Mascharak, *Inorg. Chem.* **1999**, *38*, 616−617. − [11e] J. C. Noveron, M. M. Olmstead, P. K. Mascharak, *Inorg. Chem.* **1998**, *37*, 1138−1139.
[12] [12a] J. Shearer, I. Y. Kung, S. Lovell, W. Kaminsky, J. A. Kovacs, *J. Am. Chem. Soc.* **2001**, *123*, 463−468. − [12b] I. Kung, D. Schweitzer, J. Shearer, W. Taylor, H. L. Jackson, S. Lovell, J. A. Kovacs, *J. Am. Chem. Soc.* **2000**, *122*, 8299−8300. − [12c] J. Shearer, I. Y. Kung, S. Lovell, J. A. Kovacs, *Inorg. Chem.* **2000**, *39*, 4998−4999. − [12d] J. J. Ellison, A. Nienstedt, S. C. Shoner, D. Barnhart, J. A. Cowen, J. A. Kovacs, *J. Am. Chem. Soc.* **1998**, *120*, 5691−5700. − [12e] S. C. Shoner, D. Barnhart, J. A. Kovacs, *Inorg. Chem.* **1995**, *34*, 4517−44518. − [12f] D. Schweitzer, J. J. Ellison, S. C. Shoner, S. Lovell, J. A. Kovacs, *J. Am. Chem. Soc.* **1998**, *120*, 10996−10997.
[13] L. Heinrich, J. C. Chottard, Y. Li, *Synth. Comm.* **2001**, *31* (9), 47−57.
[14] [14a] J. Doherty, J. Fortune, A. R. Manning, F. S. Stephens, *J. Chem. Soc., Dalton Trans.* **1984**, 1111−1116. − [14b] Y. Wakatsuki, K. Aoki, H. Yamazaki, *J. Chem. Soc., Dalton Trans.* **1986**, 1193−1199.
[15] J. D. Lydon, E. Deutsch, *Inorg. Chem.* **1982**, *21*, 3180−3185.
[16] G. M. Sheldrick, *SHELXS-86, Program for Crystal Structure Solution,* University of Göttingen, **1986**.
[17] D. J. Watkin, C. K. Prout, J. R. Carruthers, P. W. Betteridge, Crystals Chemical Crystallography Laboratory, University of Oxford, *10*, **1996**.
[18] D. J. Watkin, C. K. Prout, L. J. Pearce, *CAMERON,* Crystallography Laboratory, University of Oxford, **1996**.

Received April 23, 2001
[I01144]

[μ_2-(*O*-Acylhydroxycarbene)]dicobalt Hexacarbonyls by Carbon-to-Oxygen Acyl−Acyl Coupling

Claudia Zucchi,[a] Erika Soós,[b] Vilmos Galamb,[b] Gyula Váradi,[c] László Párkányi,[d] and Gyula Pályi*[a]

Keywords: Cobalt / Carbonyl ligands / Tishchenko reaction / Acylations

The acylcobalt tetracarbonyls [RC(O)Co(CO)$_4$] (**1**) undergo self-acylation in the presence of *n*Bu$_4$NI, in toluene at room temp., to yield the dinuclear μ_2-acylhydroxycarbene-type complexes [{RC(O)}$_2$Co$_2$(CO)$_6$] (**2**). Complex **2**, with R = *t*Bu, was also characterised by X-ray diffraction.

Introduction

The acylcobalt tetracarbonyls[1] (**1**) have been identified as intermediates of industrially important C−C bond-forming reactions.[2] Since the discovery of the favourable influence of tertiary phosphanes in hydroformylation[3] several reactions of complexes **1** with nucleophiles (Lewis bases) have been studied,[1] although reactions with electrophiles have not been studied so often.[1,4] Here we report on the electrophilic reaction of the acyl oxygen of compounds **1**.

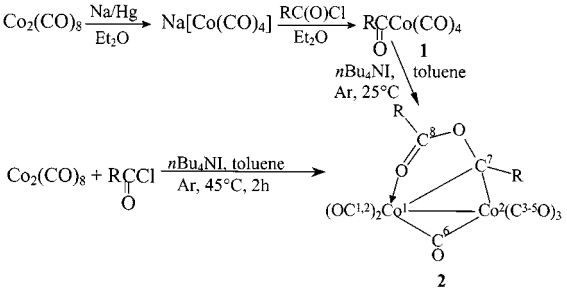

Scheme 1

Results and Discussion

We observed (Scheme 1) that the acylcobalt tetracarbonyls[1] [RC(O)Co(CO)$_4$] (**1**) undergo self-acylation (a kind of Tishchenko reaction[5]) in toluene solution in the presence of *n*Bu$_4$NI, under mild conditions, yielding the dinuclear complexes [{RC(O)}$_2$Co$_2$(CO)$_6$] (**2**). A one-pot synthesis starting from [Co$_2$(CO)$_8$], RC(O)Cl and *n*Bu$_4$NI under similar conditions was also found to give **2** as the only cobalt carbonyl. Complexes **2** were characterised by elemental analysis, IR, ^{1}H and ^{13}C NMR spectroscopy and single crystal X-ray diffraction of one representative compound (**2c**) (Figure 1).

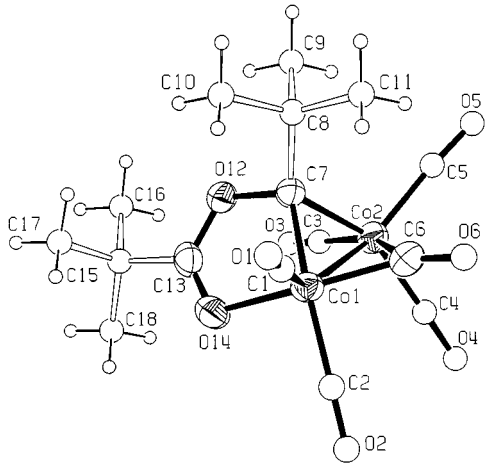

Figure 1. ORTEP drawing of the molecular structure of **2c**; selected bond lengths (pm) and angles (deg.): Co−Co 241.5(1), Co−C(O)$_t$ (av.) 180.9, Co−C(O)$_{br}$ (av.) 191.7, Co−C(7) (av.) 198.7, Co(1)−O(14) 202.6(4), Co(1)−C(13) 273.4(4), C(13)−O(14) 123.0(6), C(13)−O(12) 131.4(6), C(7)−O(12) 146.9(6); Co(1)−C(7)−Co(2) 74.8(3), Co(1)−C(6)−Co(2) 78.0(4), C(7)−O(12)−C(13) 116.6(6), C(8)−C(7)−O(12) 103.6(6)

The spectra show close analogies with other [(μ_2-L′)(μ_2-L′′)Co(CO)$_5$L′′′] complexes.[4,6] The X-ray crystal structure shows a Co$_2$(CO)$_6$ skeleton with the acylhydroxy carbene and a carbonyl ligand in bridging positions and an O-to-

[a] Department of Chemistry, University of Modena and Reggio Emilia,
Via Campi, 183, 41100 Modena, Italy
Fax: (internat.) +39-059/373-543
E-mail: palyi@unimo.it
[b] Research Group for Petrochemistry, University of Veszprém, 8200 Veszprém, Hungary
[c] Department of Pharmacology and Cell Biophysics, University of Cincinnati,
Cincinnati, OH 45267-0828, USA
[d] Central Research Institute of Chemistry, Hungarian Academy of Sciences
P.O. Box 17, 1525 Budapest, Hungary
Supporting information for this article is available on the WWW under http://www.wiley-vch.de/home/eurjic or from the author.

 © WILEY-VCH Verlag GmbH, 69451 Weinheim, 2001 1434−1948/01/0909−2207 $ 17.50+.50/0

Co coordination of the oxygen in the "acylating" acyl group. The overall structure of complexes **2** is a new type of cobalt carbonyl, showing some analogy to that of the "lactone" complexes [(μ_2-butenolide)(μ_2-CO)$Co_2(CO)_6$].[7] Such an O-to-Co coordination is a very rare phenomenon[8] with low-valent cobalt carbonyls. The relative orientation of the bridging carbonyl and the ester groups indicates a quantitative stereoselectivity of the formation of complexes **2**.[9] The preparative and structural results can be rationalized by supposing I^- coordination to (a part of) the acylcobalt carbonyls, which could increase the charge separation and thus facilitate the formation of the acyl electrophile, followed by the organization of the dinuclear structure of **2** (Scheme 2). This picture could give an insight into the mechanism of action of ionic additives in Co-catalysed CO chemistry.[10] I^- coordination to low-valent cobalt carbonyls has been documented previously.[11] The μ_2-hydroxycarbene ligand in complexes **2** might bear some relevance to the as-yet not fully explored question of the mechanism of the Fischer−Tropsch reaction.[12]

$$RC(O)Co(CO)_4 + (nBu_4N)I \rightleftharpoons (nBu_4N)[RC(O)Co(CO)_3(I)] + CO$$

$$RC(O)Co(CO)_4 + [RC(O)Co(CO)_3(I)]^- \longrightarrow \{\mu_2,O\text{-}\eta^1\text{-}[RC(O)]_2\}(\mu_2\text{-}CO)Co_2(CO)_5 + CO + I^-$$

Scheme 2

Experimental Section

All experiments were performed using standard Schlenk techniques, with carefully deoxygenated, dry gases and solvents.

Preparation of Complex 2c: Dicobalt octacarbonyl (684 mg, 2 mmol) and *n*-tetrabutylammonium iodide(960 mg, 2.6 mmol) were placed into a thermostated reaction vessel under Ar. Toluene (15 mL) was then added and the mixture was stirred for 10 min. at 25 °C. After this period *t*BuC(O)Cl (640 mg, 5.3 mmol) was added. The temperature was then raised to 45 °C and the solution was stirred for an additional 2 h. After this period the solution was left to cool to room temp., filtered, the filtrate was dried at reduced pressure (room temp.) and an oily product (1551 mg, 82%) was obtained which contained **2c** as the only cobalt carbonyl (IR). This crude product was dissolved in 3 mL *n*-hexane and the solution cooled to −78 °C to give brownish yellow [m.p. 73.5 °C (dec.)] crystals (278 mg, 15%). Occasionally the recrystallization was repeated using 0.5−1.5 mL of *n*-hexane. The product is very soluble in all solvents which did not react with **2c**, hence the low yields of crystalline product.

2c could also be prepared from 1 mmol of **1c** {obtained from $Na[Co(CO)_4]$ (195 mg, 1 mmol) and pivaloyl chloride (121 mg, 1 mmol) in 15 mL Et_2O} and pivaloyl chloride (60 mg, 0.5 mmol) in toluene (15 mL), at room temp., under Ar atmosphere after 2 h stirring. Yield: 60−70% (IR). − $C_{16}H_{18}Co_2O_8$ (456.18): calcd. C 42.13, H 3.98, Co 25.84; found C 42.3, H 4.1, Co 25.7. MW calcd. 456.18; found (m.s.) 456.

Spectroscopic Characterisation of Compounds 2 [{RC(O)}$_2$-Co$_2$(CO)$_6$] (for carbon position see Scheme 1)

2a (R = Me): IR (*n*-hexane): ν(C−O)$_t$: 2088.0 s, 2052.3 vs, 2020.4 vs, 2013.4 vs, 2006.1 s; ν(C−O)$_{br}$: 1830.1 ms; ν(C−O)$_{org.}$: 1640 w cm^{-1}. − ^{1}H NMR (400.13 MHz, C_6D_6, 300 K, TMS): δ = 1.24 [s, 3 H, C*H*$_3$-C(8)], 2.20 [s, 3 H, C*H*$_3$-C(7)]. − ^{13}C NMR (100.62 MHz, C_6D_6, 300 K, TMS): δ = 19.3 [*C*H$_3$-C(8)], 23.3 [*C*H$_3$-C(7)], 179.5 [*C*(7)], 181.5 [*C*(8)], 199.3 [(*C*O)$_2$-Co(1)], 201.0 [(*C*O)$_3$-Co(2)], 229.1 [*C*(6)].

2b (R = *i*Pr): IR (*n*-hexane): ν(C−O)$_t$: 2084.5 s, 2048.5 vs, 2016.5 vs, 2009.0 s, 2004.5 s; ν(C−O)$_{br}$: 1837.5 s; ν(C−O)$_{org.}$: 1623 w cm^{-1}. − ^{1}H NMR (400.13 MHz, C_6D_6, 300 K, TMS): δ = 1.19 [d, ^3J(H,H) = 7.60 Hz, 6 H, (C*H*$_3$)$_2$-CH-C(7)], 1.25 [d, ^3J(H,H) = 6.80 Hz, 6 H, (C*H*$_3$)$_2$-CH-C(8)], 2.26 [m, ^3J(H,H) = 6.80 Hz, 1 H, C*H*-C(8)], 2.39 [m, ^3J(H,H) = 7.60 Hz, 1 H, C*H*-C(7)]. − ^{13}C NMR (100.62 MHz, C_6D_6, 300 K, TMS): δ = 24.6, [(*C*H$_3$)$_2$-CH-C(8)] 25.0 [(C*H*$_3$)$_2$-CH-C(7)], 34.1 [*C*H-C(8)], 50.8 [*C*H-C(7)], 187.5 [*C*(8)], 198.0 [*C*(7)], 200.5 [(*C*O)$_2$-Co(1)], 201.5 [(*C*O)$_3$-Co(2)], 229.9 [*C*(6)].

2c (R = *t*Bu): IR (n-hexane): ν(C−O)$_t$: 2083.5 s, 2047.5 vs, 2014.0 vs, 2008.0 s, 2003.5 s; ν(C−O)$_{br}$: 1830.1 ms; ν(C−O)$_{org.}$: 1640 w cm^{-1}. − ^{1}H NMR (400.13 MHz, C_6D_6, 300 K, TMS): δ = 0.95 [s, 9 H, C*H*$_3$-C-C(8)] 1.23 [s, 9H C*H*$_3$-C-C(7)]. − ^{13}C NMR (100.62 MHz, C_6D_6, 300 K, TMS): δ = 27.6 [(*C*H$_3$)$_3$-C-C(8)], 31.6 [(*C*H$_3$)$_3$-C-C(7)], 39.4 [*C*-C(8)], 51.1 [*C*-C(7)], 188.9 [*C*(8)], 200.6 [(*C*O)$_2$-Co(1)], 201.8 [(*C*O)$_3$-Co(2)], 206.7 [*C*(7)], 230.0 [*C*(6)].

A full list of spectra is available as Supporting Information.

Crystal Structure of 2c: Crystal dimensions 0.30 × 0.20 × 0.15 mm, triclinic, space group $P\bar{1}$, a = 8.759(2), b = 9.305(1), c = 12.794(2) Å, α = 86.35(2), β = 88.35(4), γ = 73.12(4)°, V = 995.7(3) Å^3, Z = 2, $\rho_{calcd.}$ = 1.521 g/cm^3 μ = 13.394mm^{-1}, θ range 3.46−75.00°, F(000) = 464, 241 parameters and 12 restraints were refined for 4058 [R(int) = 0.0109] independent reflections with $I > 2\sigma(I)$ to $R1$ = 0.0915, $wR2$ = 0.1078 and GOF = 0.91.
Crystallographic data (excluding structure factors) for the structure reported in this paper have been deposited with the Cambridge Crystallographic Data Centre as supplementary publication no. CCDC-133917. Copies of the data can be obtained free of charge on application to CCDC, 12 Union Road, Cambridge CB2 1EZ, UK [Fax: (internat.) +44-1223/336-033; E-mail: deposit@ccdc.cam.ac.uk).

Acknowledgments

Financial support obtained from the Italian Ministry of University and Research (MURST ex-40%) as well as from the Hungarian Research Council (OTKA) is acknowledged. The authors acknowledge helpful discussions with Prof. L. Markó and Dr. A. Sisak (Veszprém) as well as cooperation in some of the experiments from Mr. G. Coccolini (Modena).

[1] Reviews: [1a] V. Galamb, G. Pályi, *Coord. Chem. Rev.* **1984**, *59*, 203−238. − [1b] I. Kovács, F. Ungváry, *Coord. Chem. Rev.* **1997**, *161*, 1−32.
[2] *Applied Homogeneous Catalysis with Organometallic Compounds* (Eds.: B. Cornils, W. A. Herrmann), Vol. 1−2, VCH, Weinheim, **1996**, Chapters 2.1, 3.1.8, 3.2.4, 3.2.7, 3.3.7, 3.3.9.

[3] [3a] R. D. Mullineaux (Shell), Belg. Pat., 603,820, **1961**. – [3b] L. H. Slaugh. R. D. Mullineaux (Shell), Belg. Pat., 608,408, **1961**; U. S. Pat., 3,239,569, **1966**. – [3c] L. H. Slaugh. R. D. Mullineaux, *J. Organomet. Chem.* **1968**, *13*, 469−477.
[4] A. Sisak, A. Sironi, M. Moret, C. Zucchi, F. Ghelfi, G. Pályi, *J. Chem. Soc., Chem. Commun.* **1991**, 176−178.
[5] See, for example, J. March, *Advanced Organic Chemistry*, Wiley, New York, **1985**, p. 1119, and references therein.
[6] G. Váradi, A. Vizi-Orosz, S. Vastag, G. Pályi, *J. Organomet. Chem.* **1976**, *108*, 225.
[7] [7a] I. T. Horváth, G. Pályi, L. Markó, G. Andreetti, *Inorg. Chem.* **1983**, *22*, 1049−1053. – [7b] R. Perlaki, L. Markó, G. Gervasio, E. Sappa, G. Pályi, *J. Organomet. Chem.* **1995**, *502*, 25−34.
[8] W. A. Herrmann, J. Schweizer, M. Creswick, J. Bernal, *J. Organomet. Chem.* **1979**, *165*, C17−C20.
[9] The presence of stereoisomers other than the type shown in Figure 1 can be excluded on the basis of the spectra. See also a review: G. Pályi, G. Váradi, L. Markó, in *Stereochemistry of Organometallic and Inorganic Compounds* (Ed.: I. Bernal), Elsevier, Amsterdam, **1986**. pp. 358−410.
[10] G. A. Somorjai, *Introduction to Surface Science and Catalysis*, Wiley, New York, **1994**, pp. 483−500.
[11] [11a] m. Tasi, G. Pályi, *Organometallics* **1985**, *4*, 1523−1528. – [11b] M. Röper, C. Krüger, *J. Organomet. Chem.* **1988**, *339*, 159−164. – [11c] F. Haász, T. Bartik, V. Galamb, G. Pályi, *Organometallics* **1990**, *9*, 2773−2779.
[12] [12a] F. Fischer, H. Tropsch, DE 484337, (1925/29); 524468 (1926/31). – [12b] F. Fischer, H. Tropsch, *Brennstoff-Chem.* **1926**, *7*, 97−104; *Ber. Dtsch. Chem. Ges.* **1926**, *59B*, 830−831, 832−836, 923−925. – [12c] G. Wilke, *Festschrift zum 75jährigen Bestehen des Max-Planck-Instituts für Kohlenforschung.* Mülheim, **1989**. – [12d]B. Cornils, W. A. Herrmann, M. Rasch, *Angew. Chem.* **1994**, *106*, 2219−2238; *Angew. Chem. Int. Ed. Engl.* **1994**, *33*, 2144−2163.

Received May 16, 2001
[I01172]

Macrocyclic Siloxanes with Two Exocyclic *trans*-Silanol and Two Exocyclic *trans*-Amino Functions − Stereoselective Syntheses and Structures

Reinhold Tacke,*[a] Christian Burschka,[a] Joachim Heermann,[a] Ingo Richter,[a] Brigitte Wagner,[a] and Reiner Willeke[a]

Keywords: Silicon / Macrocycles / Siloxanes / Silanols / Pentacoordination

A simple preparative method for the stereoselective synthesis of ten- and twelve-membered cyclosiloxanes with two exocyclic *trans*-silanol and two exocyclic *trans*-amino functions has been developed. Thus, treatment of trimethoxy(morpholinomethyl)silane (**5**) with two molar equivalents of $HOPh_2Si–SiPh_2OH$ and $HOPh_2Si–O–SiPh_2OH$, respectively, yielded *trans*-1,6-bis(2-hydroxy-1,1,2,2-tetraphenyldisilan-1-yloxy)-1,6-bis(morpholinomethyl)-3,3,4,4,8,8,9,9-octaphenyl-2,5,7,10-tetraoxa-1,3,4,6,8,9-hexasilacyclodecane (**6**, 10-membered ring) and *trans*-2,8-bis(3-hydroxy-1,1,3,3-tetraphenyldisiloxan-1-yloxy)-2,8-bis(morpholinomethyl)-4,4,6,6,10,10,12,12-octaphenylcyclohexasiloxane (**7**, 12-membered ring). In contrast, treatment of **5** with two molar equivalents of $HOPh_2C–CPh_2OH$ afforded (morpholiniomethyl)bis[tetraphenylethane-1,2-diolato(2−)]silicate (**3**), a zwitterionic spirocyclic λ^5*Si*-silicate. Compounds **3**, **6**·EtOAc, and **7**·PhMe were characterized by elemental analyses (C, H N), solid-state ^{29}Si VACP/MAS NMR studies, solution NMR experiments (^{1}H, ^{13}C, ^{29}Si; $CDCl_3$), and crystal structure analyses.

Introduction

Various organic *vic*-diols (e.g. 1,2-dihydroxybenzene and glycolic acid derivatives) have been used to prepare zwitterionic spirocyclic λ^5*Si*-silicates with two bidentate diolato(2−) ligands,[1] such as compounds **1** and **2**. Following the strategy applied to the syntheses of **1** and **2**, we attempted to prepare the related zwitterionic λ^5*Si*-silicates **3** and **4**.

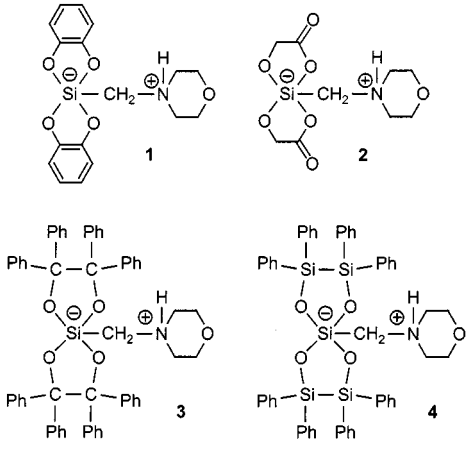

Results and Discussion

To synthesize compounds **3** and **4**, trimethoxy(morpholinomethyl)silane[2] (**5**) was treated with two molar equivalents of the respective *vic*-diol, tetraphenylethane-1,2-diol or tetraphenyldisilane-1,2-diol[3] (Scheme 1 and 2). Both reactions were performed in acetonitrile at room temperature, and compound **3** was obtained in 93% yield as a colorless crystalline solid. However, to our great surprise treatment of **5** with $HOPh_2Si−SiPh_2OH$ under the same conditions as applied to the synthesis of **3** did not yield the expected product **4**, we instead obtained the ten-membered cyclosiloxane **6**. This compound was isolated, after recrystallization from ethyl acetate, as the solvate **6**·EtOAc (yield 70%).

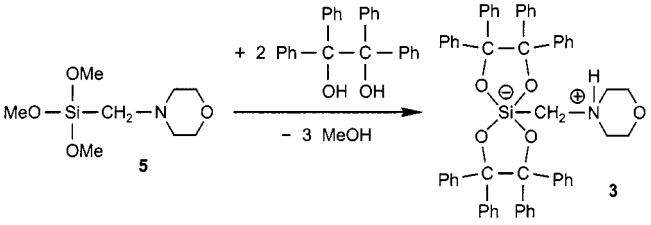

Scheme 1. Synthesis of the zwitterionic λ^5*Si*-silicate **3**

From a formal point of view, the formation of **6** could be rationalized in terms of a dimerization of **4**; however, there is no experimental evidence for this assumption. The reaction mechanism is still under investigation and it is an open question as to whether the zwitterion **4** is an intermediate in this reaction or not. Nevertheless, it appears that we have discovered an efficient stereoselective synthetic method for the preparation of macrocyclic siloxanes with two exocyclic *trans*-silanol groups and two exocyclic *trans*-amino functions. As a further example of this method, we have succeeded in synthesizing the twelve-membered cyclosiloxane **7**. This compound was obtained analogously to the synthesis of **6** by treatment of **5** with two molar equivalents of tetraphenyldisiloxane-1,3-diol[4] in acetonitrile at room

[a] Institut für Anorganische Chemie, Universität Würzburg, Am Hubland, 97074 Würzburg, Germany
Fax: (internat.) +49-931/888-4609
E-mail: r.tacke@mail.uni-wuerzburg.de

 © WILEY-VCH Verlag GmbH, 69451 Weinheim, 2001 1434−1948/01/0909−2211 $ 17.50+.50/0

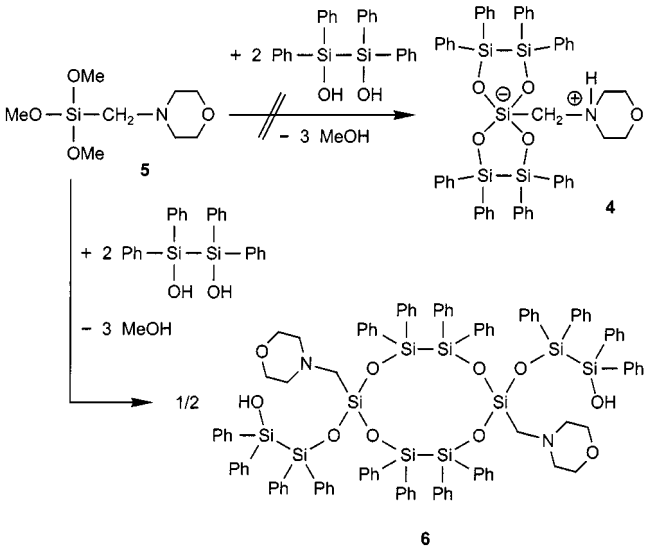

Scheme 2. Synthesis of the ten-membered cyclosiloxane **6**

temperature (Scheme 3). The product was isolated, after recrystallization from toluene/petroleum ether, as the solvate **7**·PhMe (yield 72%).

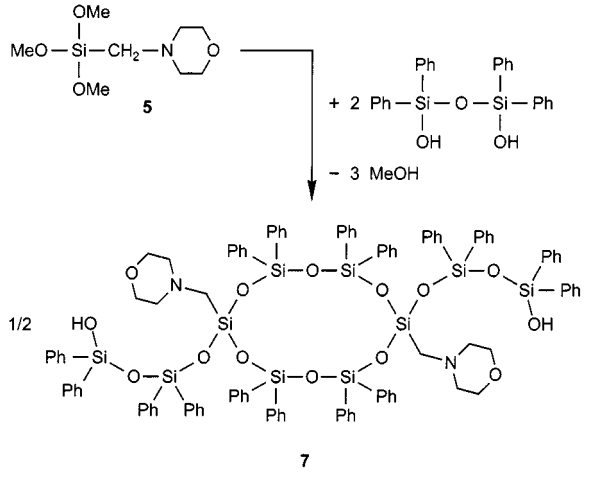

Scheme 3. Synthesis of the twelve-membered cyclosiloxane **7**

Compounds **3**, **6**·EtOAc, and **7**·PhMe were characterized by elemental analyses (C, H N), solid-state ^{29}Si VACP/MAS NMR studies, solution NMR experiments (^{1}H, ^{13}C, ^{29}Si; $CDCl_3$),[5] and crystal structure analyses.

The Si coordination polyhedron of **3** is a strongly distorted trigonal bipyramid (Berry distortion 42.3%),[6] each bidentate tetraphenylethane-1,2-diolato(2−) ligand spanning one axial and one equatorial site (Figure 1). The zwitterion forms an intramolecular N−H···O1 hydrogen bond in the crystal [N−H 0.85(3), H···O1 2.31(2), N···O1 2.746(2) Å, N−H···O1 112(2)°].[7]

Compounds **6**·EtOAc and **7**·PhMe show some common structural features (Figure 2 and 3). With respect to the positions of their silicon atoms, the ten- and twelve-membered rings adopt a chair conformation, both ring systems being characterized by a center of symmetry. The two morpholinomethyl substituents occupy axial positions, whereas the

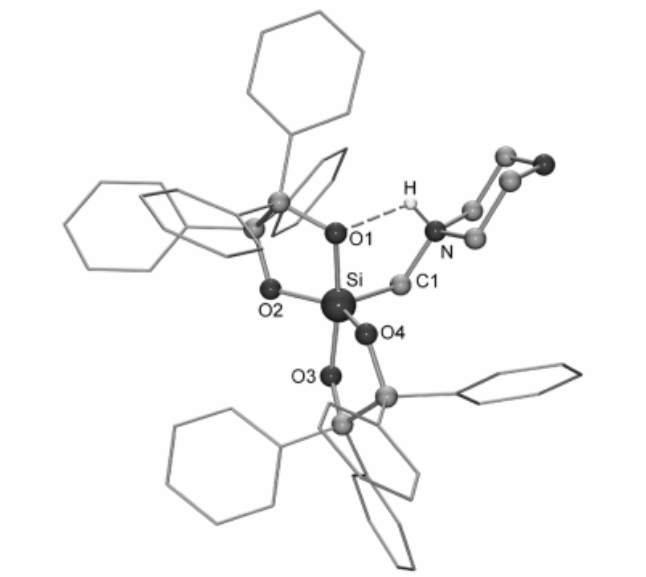

Figure 1. Molecular structure of **3** in the crystal (hydrogen atoms, except for N*H*, are omitted for clarity); selected distances [Å] and angles [°] (standard deviations in parentheses): Si−O1 1.7728(15), Si−O2 1.6992(15), Si−O3 1.7303(15), Si−O4 1.6987(15), Si−C1 1.909(2); O1−Si−O2 86.67(7), O1−Si−O3 170.44(7), O1−Si−O4 89.05(7), O1−Si−C1 94.32(8), O2−Si−O3 88.95(7), O2−Si−O4 136.82(7), O2−Si−C1 111.01(9), O3−Si−O4 88.33(7), O3−Si−C1 95.18(9), O4−Si−C1 112.15(9)

two $OPh_2Si-SiPh_2OH$ (**6**·EtOAc) or $OPh_2Si-O-SiPh_2OH$ (**7**·PhMe) groups occupy equatorial sites. Thus, each of the two pairs of identical exocyclic functional groups (two silanol and two amino moieties) are in *trans*-position to each other. The conformations present in the crystal allow the formation of intramolecular O−H···N hydrogen bonds [**6**·EtOAc: O4−H 0.8198, H···N 1.9325, O4···N 2.737(3) Å, O4−H···N 166.75°; **7**·PhMe: O4−H 0.78(7), H···N 2.02(7), O4···N 2.787(5) Å, O4−H···N 172(8)°].[7] The three Si1−O distances of **6**·EtOAc [1.6034(17)−1.6092(16) Å] and **7**·PhMe [1.603(3)−1.605(3) Å] are somewhat shorter than the other Si−O distances [**6**·EtOAc: 1.6369(16)−1.6482(18) Å; **7**·PhMe: 1.620(3)−1.635(3) Å]. The Si−O−Si angles of the ring systems amount to 157.13(11) and 164.18(12)° (**6**·EtOAc) and to 152.1(2)−153.9(2)° (**7**·PhMe). The Si−C distances are in the range 1.866(2)−1.882(2) Å (**6**·EtOAc) and 1.843(5)−1.859(5) Å (**7**·PhMe), and the Si−Si distances (**6**·EtOAc) amount to 2.3610(11) and 2.3907(11) Å.

In conclusion, contrary to the reaction of silane **5** with two molar equivalents of $HOPh_2C-CPh_2OH$ (which gives formation of the zwitterionic λ^5*Si*-silicate **3**), treatment of **5** with two molar equivalents of $HOPh_2Si-SiPh_2OH$ or $HOPh_2Si-O-SiPh_2OH$ leads to the formation of macrocyclic siloxanes. With the syntheses of compounds **6** and **7** we have discovered an efficient stereoselective synthesis of ten- and twelve-membered macrocyclic siloxanes with two exocyclic silanol and two exocyclic amino functionalities in mutual *trans*-positions. To the best of our knowledge, functionalized cyclic siloxanes of this particular formula type have not been described in the literature.[8] Due to these exocyclic functionalities, in addition to the characteristic chemical reactivity of the Si−O−Si and

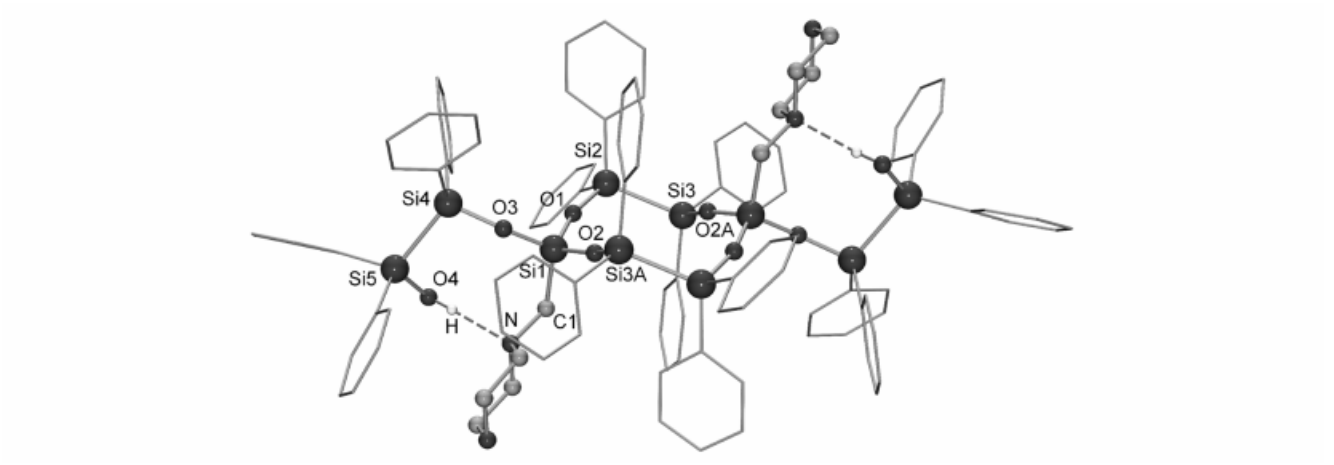

Figure 2. Molecular structure of **6** in the crystal of **6**·EtOAc (hydrogen atoms, except for O*H*, are omitted for clarity); selected distances [Å] and angles [°] (standard deviations in parentheses): Si1−O1 1.6073(16), Si1−O2 1.6092(16), Si1−O3 1.6034(17), Si1−C1 1.875(2), Si2−Si3 2.3610(11), Si2−O1 1.6448(15), Si3−O2A 1.6369(16), Si4−Si5 2.3907(11), Si4−O3 1.6482(18), Si5−O4 1.6378(17), Si−C(Ph) 1.866(2)−1.882(2); Si1−O1−Si2 157.13(11), Si1−O2−Si3A 164.18(12), Si1−O3−Si4 157.64(11), Si2−Si3−O2A 108.51(7), Si3−Si2−O1 109.68(7), Si4−Si5−O4 101.71(8), Si5−Si4−O3 104.16(7), O1−Si1−O2 108.99(9), O1−Si1−O3 109.37(9), O1−Si1−C1 109.90(10), O2−Si1−O3 110.29(9), O2−Si1−C1 105.79(9), O3−Si1−C1 112.40(10), Si−Si−C(Ph) 107.44(9)−119.51(9), O−Si−C(Ph) 105.05(10)−109.57(10), C(Ph)−Si−C(Ph) 107.81(12)−109.34(10)

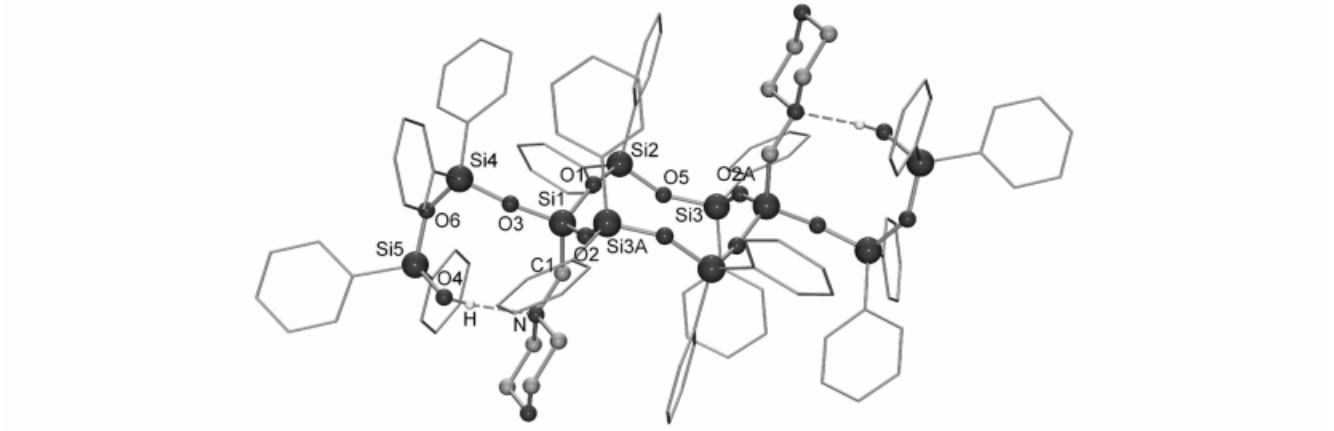

Figure 3. Molecular structure of **7** in the crystal of **7**·PhMe (hydrogen atoms, except for O*H*, are omitted for clarity); selected distances [Å] and angles [°] (standard deviations in parentheses): Si1−O1 1.603(3), Si1−O2 1.603(3), Si1−O3 1.605(3), Si1−C1 1.844(5), Si2−O1 1.628(3), Si2−O5 1.625(3), Si3−O2A 1.623(3), Si3−O5 1.620(3), Si4−O3 1.622(3), Si4−O6 1.622(3), Si5−O4 1.621(4), Si5−O6 1.635(3), Si−C(Ph) 1.843(5)−1.859(5); Si1−O1−Si2 152.1(2), Si1−O2−Si3A 153.9(2), Si1−O3−Si4 166.1(2), Si2−O5−Si3 153.8(2), Si4−O6−Si5 137.3(2), O1−Si1−O2 108.6(2), O1−Si1−O3 110.0(2), O1−Si1−C1 107.2(2), O2−Si1−O3 108.4(2), O2−Si1−C1 111.2(2), O3−Si1−C1 111.3(2), O1−Si2−O5 108.9(2), O2A−Si3−O5 110.6(2), O3−Si4−O6 109.5(2), O4−Si5−O6 111.1(2), O−Si−C(Ph) 106.3(2)−112.0(2), C(Ph)−Si−C(Ph) 110.3(2)−112.4(2)

Si−Si bonds in the ring skeletons, such compounds represent promising starting materials for the preparation of novel polymeric SiO-based materials.[9] Future studies will elucidate the synthetic potential of the title compounds.

Experimental Section

General: All syntheses were carried out under dry nitrogen. The organic solvents used were dried and purified according to standard procedures and stored under nitrogen. Melting points were determined with a DuPont Instruments differential scanning calorimeter, type Thermal-Analyzer 910. The ^{1}H, ^{13}C, and ^{29}Si solution NMR spectra were recorded at 22 °C on a Bruker DRX-300 NMR spectrometer (^{1}H: 300.1 MHz; ^{13}C: 75.5 MHz; ^{29}Si: 59.6 MHz). $CDCl_3$ was used as solvent. Chemical shifts (ppm) were determined relative to internal $CHCl_3$ (^{1}H: δ = 7.24), $CDCl_3$ (^{13}C: δ = 77.0), or external TMS (^{29}Si: δ = 0). Assignment of the ^{13}C NMR data was supported by DEPT 135 experiments. Solid-state ^{29}Si VACP/MAS NMR spectra were recorded at 22 °C on a Bruker DSX-400 NMR spectrometer with bottom layer rotors of ZrO_2 (diameter 7 mm) containing ca. 300 mg of sample [79.5 MHz; TMS as external standard (δ = 0); spinning rate: 5 kHz (**3**, **6**·EtOAc) or 7 kHz (**7**·PhMe); contact time: 5 ms; 90° ^{1}H transmitter pulse length: 3.6 μs; repetition time: 4 s].

Synthesis of (Morpholiniomethyl)bis[tetraphenylethane-1,2-diolato(2−)]silicate (3): Compound **5** (1.04 g, 4.70 mmol) was added at 20 °C to a stirred solution of tetraphenylethane-1,2-diol (3.44 g, 9.39 mmol) in acetonitrile (250 mL) and the mixture then kept un-

disturbed for 4 days at the same temperature. The resulting precipitate was isolated by filtration, washed with acetonitrile (2 × 10 mL), and dried in vacuo (0.01 Torr, 1 h) to give 3.83 g (4.46 mmol) of colorless crystals (yield 95%). M.p. 260 °C (dec.). – Due to the poor solubility of **3**, solution NMR experiments failed. – ^{29}Si VACP/MAS NMR: δ = −98.9. – $C_{57}H_{51}NO_5Si$ (858.1): calcd. C 79.78, H 5.99, N 1.63; found C 79.8, H 5.9, N 1.8.

Synthesis of *trans*-1,6-Bis(2-hydroxy-1,1,2,2-tetraphenyldisilan-1-yloxy)-1,6-bis(morpholinomethyl)-3,3,4,4,8,8,9,9-octaphenyl-2,5,7,10-tetraoxa-1,3,4,6,8,9-hexasilacyclodecane−Ethyl Acetate (6·EtOAc): Compound **5** (27.8 mg, 126 μmol) was added at 20 °C to a stirred solution of tetraphenyldisilane-1,2-diol (100 mg, 251 μmol) in acetonitrile (5 mL). Stirring was continued for 1 h and the mixture then kept undisturbed for 2 days at the same temperature. The resulting precipitate was isolated by filtration, washed with acetonitrile (2 × 1 mL), recrystallized from ethyl acetate, and dried in vacuo (0.01 Torr, 1 h) to give 85.3 mg (44.1 μmol) of colorless crystals (yield 70%). M.p. 212 °C (loss of ethyl acetate at ca. 127 °C). – ^{1}H NMR: δ = 1.25 (t, 3 H, OCH_2CH_3), 1.40 (s, 4 H, $SiCH_2N$), 1.83−2.05 (m, 8 H, CCH_2N), 2.03 [s, 3 H, $C(O)CH_3$, overlapping with the multiplet for CCH_2N], 3.29−3.42 (m, 8 H, CCH_2O), 4.10 (q, 2 H, OCH_2CH_3), 6.77−6.86, 6.87−7.01, and 7.06−7.36 (m, 80 H, SiC_6H_5), 8.3 (br. s, 2 H, SiOH). – ^{13}C NMR: δ = 14.2 (OCH_2CH_3), 21.1 [$C(O)CH_3$], 48.0 ($SiCH_2N$), 56.9 (CCH_2N), 60.4 (OCH_2CH_3), 65.6 (CCH_2O), 127.5, 127.6, 127.7, and 127.9 (C-2/C-6 or C-3/C-5, SiPh), 129.1, 129.3, 129.65, and 129.71 (C-4, SiPh), 134.6 (two non-equivalent sites, not resolved), 135.1, and 135.2 (C-2/C-6 or C-3/C-5, SiPh), 135.8, 136.2, 136.6, and 138.0 (C-1, SiPh), $CO)CH_3$ resonance not found. – ^{29}Si NMR: δ = −73.7 (SiO_3C), −17.1, −16.1, and −15.3 ($SiSiOC_2$). – ^{29}Si VACP/MAS NMR: δ = −75.6 (SiO_3C), −17.4, −15.2, −14.1, and −10.7 ($SiSiOC_2$). – $C_{110}H_{110}N_2O_{12}Si_{10}$ (1932.9): calcd. C 68.35, H 5.74, N 1.45; found C 68.6, H 5.8, N 1.5.

Synthesis of *trans*-2,8-Bis(3-hydroxy-1,1,3,3-tetraphenyldisiloxan-1-yloxy)-2,8-bis(morpholinomethyl)-4,4,6,6,10,10,12,12-octaphenylcyclohexasiloxane−Toluene (7·PhMe): Compound **5** (133 mg, 601 μmol) was added at 20 °C to a stirred solution of tetraphenyldisiloxane-1,3-diol (500 mg, 1.21 mmol) in acetonitrile (4 mL). Stirring was continued at the same temperature for 1 day, and the resulting precipitate was isolated by filtration, washed with acetonitrile (2 × 1 mL), crystallized from toluene/petroleum ether [1:1 (v/v); addition of petroleum ether (b.p. 40−60 °C) to a solution of **7** in toluene at 20 °C], and dried in vacuo (0.01 Torr, 1 h) to give 434 mg (217 μmol) of colorless crystals (yield 72%). M.p. (dec.) 169−170 °C (loss of toluene at ca. 90 °C). – ^{1}H NMR: δ = 1.38 (s, 4 H, $SiCH_2N$), 1.65−1.80 (m, 8 H, CCH_2N), 2.32 (s, 3 H, CCH_3), 3.02−3.16 (m, 8 H, CCH_2O), 6.98−7.44 (m, 85 H, SiC_6H_5, $C_6H_5CH_3$), 8.9 (br. s, 2 H, SiOH). – ^{13}C NMR: δ = 21.8 ($PhCH_3$), 47.5 ($SiCH_2N$), 57.1 (CCH_2N), 66.1 (CCH_2O), 125.3 (C-4, PhMe), 127.5, 127.6 (two non-equivalent sites, not resolved), and 127.8 (C-2/C-6 or C-3/C-5, SiPh), 128.2 and 129.0 (C-2/C-6 or C-3/C-5, PhMe), 129.6, 130.0 (two non-equivalent sites, not resolved), and 130.2 (C-4, SiPh), 133.8 and 134.1 (C-1, SiPh), 134.3 (two non-equivalent sites, not resolved), 134.5, and 134.6 (C-2/C-6 or C-3/C-5, SiPh), 134.9 (C-1, PhMe), 136.0 (C-1, SiPh), one resonance signal (C-1, SiPh) not found. – ^{29}Si NMR: δ = −77.3 (SiO_3C), −47.0, −44.4, and −37.2 ($SiSiOC_2$). – ^{29}Si VACP/MAS NMR: δ = −77.6 (SiO_3C), −48.8, −47.7, −42.9, and −35.3 ($SiSiOC_2$). – $C_{113}H_{110}N_2O_{14}Si_{10}$ (2000.9): calcd. C 67.83, H 5.54, N 1.40; found C 67.9, H 5.9, N 1.3.

Crystal Structure Analyses of 3, 6·EtOAc, and 7·PhMe: Suitable single crystals were mounted in inert oil (perfluoroalkyl ether, ABCR) on a glass fiber and then transferred to the cold nitrogen-gas stream of the diffractometer (Stoe IPDS; graphite-monochromated Mo-K_α radiation, λ = 0.71073 Å). The structures were solved by direct methods (SHELXS-97) and refined by full-matrix least-squares on F^2 with all unique reflections (SHELXL-97).[10] For the hydrogen atoms, a riding model was employed, except for the N*H* atom of **3** and O*H* atom of **7**·PhMe, which were refined freely.

Selected Data for 3: Single crystal (0.4 × 0.3 × 0.3 mm) obtained from the reaction mixture, $C_{57}H_{51}NO_5Si$, M_r = 858.08, analysis at 173(2) K, monoclinic, space group $P2_1/n$, a = 14.930(3), b = 16.257(3), c = 18.462(4) Å, β = 99.54(3)°, V = 4419.2(15) Å^3, Z = 4, $\rho_{calcd.}$ = 1.290 g cm^{-3}, μ = 0.107 mm^{-1}, $F(000)$ = 1816, $2\theta_{max}$ = 49.62°, 36433 collected reflections, 7550 unique reflections (R_{int} = 0.0682), 581 parameters, R_1 = 0.0433 [$I > 2\sigma(I)$], wR_2 (all data) = 0.1117, S = 0.889, largest difference peak and hole +0.285 and −0.447 e Å^{-3}.

Selected Data for 6·EtOAc: Single crystal (0.4 × 0.4 × 0.2 mm) obtained from ethyl acetate at 20 °C, $C_{106}H_{102}N_2O_{10}Si_{10}$·EtOAc, M_r = 1932.90, analysis at 253(2) K, triclinic, space group $P\bar{1}$, a = 14.274(2), b = 14.363(3), c = 14.459(2) Å, α = 61.057(19), β = 87.579(19), γ = 82.08(2)°, V = 2568.4(7) Å^3, Z = 1, $\rho_{calcd.}$ = 1.250 g cm^{-3}, μ = 0.189 mm^{-1}, $F(000)$ = 1020, $2\theta_{max}$ = 53.84°, 29307 collected reflections, 10267 unique reflections (R_{int} = 0.0757), 599 parameters, R_1 = 0.0457 [$I > 2\sigma(I)$], wR_2 (all data) = 0.1267, S = 0.906, largest difference peak and hole +0.692 and −0.510 e Å^{-3}. The crystal contains ethyl acetate molecules located on a center of inversion.

Selected Data for 7·PhMe: Single crystal (0.4 × 0.3 × 0.1 mm) obtained from toluene/petroleum ether at 20 °C, $C_{106}H_{102}N_2O_{14}Si_{10}$·PhMe, M_r = 2000.93, analysis at 173(2) K, triclinic, space group $P\bar{1}$, a = 13.832(2), b = 14.207(2), c = 16.989(2) Å, α = 74.54(2), β = 71.44(2), γ = 64.97(2)°, V = 2833.6(7) Å^3, Z = 1, $\rho_{calcd.}$ = 1.173 g cm^{-3}, μ = 0.175 mm^{-1}, $F(000)$ = 1054, $2\theta_{max}$ = 46.62°, 20277 collected reflections, 7726 unique reflections (R_{int} = 0.0738), 683 parameters, 581 restraints, R_1 = 0.0545 [$I > 2\sigma(I)$], wR_2 (all data) = 0.1525, S = 0.861, largest difference peak and hole +0.551 and −0.374 e Å^{-3}. The crystal contains tubes along [1 0 0] which are occupied by the toluene molecules.

Crystallographic data (excluding structure factors) for the structures reported in this paper have been deposited with the Cambridge Crystallographic Data Centre as supplementary publication nos. CCDC-158876 (**3**), CCDC-158877 (**6**·EtOAc), and CCDC-158878 (**7**·PhMe). Copies of the data can be obtained free of charge on application to CCDC, 12 Union Road, Cambridge CB2 1EZ, UK [Fax: (internat.) +44-1223/336-033; E-mail: deposit@ccdc.cam.ac.uk].

Acknowledgments

This work was supported by the Deutsche Forschungsgemeinschaft and the Fonds der Chemischen Industrie.

[1] Review dealing with zwitterionic λ^5*Si*-silicates: R. Tacke, M. Pülm, B. Wagner, *Adv. Organomet. Chem.* **1999**, *44*, 221−273.
[2] Synthesis of **5**: J. Sperlich, J. Becht, M. Mühleisen, S. A. Wagner, G. Mattern, R. Tacke, *Z. Naturforsch.* **1993**, *48b*, 1693−1706.
[3] Synthesis of tetraphenyldisilane-1,2-diol: H. J. S. Winkler, H. Gilman, *J. Org. Chem.* **1961**, *26*, 1265−1271.

[4] Synthesis of tetraphenyldisiloxane-1,3-diol: G. I. Harris, *J. Chem. Soc.* **1963**, 5978−5982.
[5] As the NMR spectra change as a function of time, freshly prepared solutions were used for these experiments.
[6] [6a] E. L. Muetterties, L. J. Guggenberger, *J. Am. Chem. Soc.* **1974**, *96*, 1748−1756. − [6b] R. R. Holmes, J. A. Deiters, *J. Am. Chem. Soc.* **1977**, *99*, 3318−3326. − [6c] The degree of distortion was calculated by using the dihedral angle method described in refs.[6a,6b] (all nine dihedral angles and the values for the reference geometry of the ideal square pyramid given in ref.[6a] were considered for this calculation).
[7] The hydrogen-bonding system was analyzed by using the program PLATON: A. L. Spek, PLATON, University of Utrecht, The Netherlands, **1998**.
[8] [8a] The existence of the ten-membered Si_6O_4 ring system of **6** (with $SiCl_2$ groups in positions 1 and 6 and with $SiMe_2$ moieties in positions 3, 4, 8, and 9) has been claimed, but no experimental data for this compound have been reported: C. Wendler, H. Reinke, H. Kelling, in *Organosilicon Chemistry IV − From Molecules to Materials* (Eds.: N. Auner, J. Weis), Wiley-VCH, Weinheim, **2000**, pp. 451−455. − [8b] The twelve-membered Si_6O_6 ring system of **7** {with SiR^1R^2 moieties [such as SiMeCl, SiMeOH, and $Si(CH=CH_2)Cl$] in positions 2 and 8 and with $SiPh_2$ moieties in positions 4, 6, 10, and 12} has been reported; however, only a few experimental data for these compounds and no information concerning their stereochemistry have been given: S. M. Meladze, O. V. Mukbaniani, L. M. Khananashvili, *J. Gen. Chem.* **1981**, *51*, 1382−1385.
[9] For example, the use of SiOH-functionalized cyclosiloxanes in the synthesis of polycyclic copolymers has already been demonstrated: [9a] O. Mukbaniani, M. Karchadze, M. Matsaberidze, V. Achelashvili, L. M. Khananashvili, N. Kvelashvili, *Intern. J. Polymeric Mater.* **1998**, *41*, 103−112. − [9b] L. M. Khananashvili, O. V. Mukbaniani, I. A. Inaridze, G. V. Porchkhidze, K. E. Koberidze, *Eur. Polym. J.* **1998**, *34*, 581−584.
[10] [10a] G. M. Sheldrick, SHELXS-97, University of Göttingen, Germany, **1997**; G. M. Sheldrick, *Acta Crystallogr., Sect. A* **1990**, *46*, 467−473. − [10b] G. M. Sheldrick, SHELXL-97, University of Göttingen, Germany, **1997**.

Received April 6, 2001
[I01125]

Synthesis of a [{Mono-*N*-(4-vinylbenzyl)-1,4,7-triazacyclononane}$_2$Hg](OTf)$_2$ Sandwich Complex, Polymerization of this Monomer with Divinylbenzene, and Hg^{2+} Ion Selectivity Studies with the Demetallated Resin[‡]

H. Christine Lo,[a,b] Hong Chen,[a,c] and Richard H. Fish*[a]

Keywords: Template synthesis / Mercury / Cations / Sandwich complexes / Polymers

We have synthesized a novel, 1,4,7-triazacyclononane (TACN)-Hg^{2+} sandwich monomer, [{mono-*N*-(4-vinylbenzyl)-1,4,7-TACN}$_2$Hg](OTf)$_2$, which was co-polymerized with the cross-linking agent divinylbenzene to form a Hg^{2+}-ion templated polymer that was demetallated (>96%) with 6 N HCl, and subsequently found to be highly selective to reintroduced Hg^{2+} ions in competition with Cd^{2+}, Ag^{+}, Pb^{2+}, Cu^{2+}, and Fe^{3+} ions at pH 2, the ionic radius and the thermodynamic parameter being more critical than imprinting.

Introduction

The elegant concept of templated polymers was introduced by Wulff and Mosbach, and further developed by Shea, among others,[1] and initially involves formation of a vinyl monomer host and a bound guest acting as a template. This vinyl monomer host-guest template complex is then polymerized with a cross-linking agent, which provides spatially regulated sites in the polymer matrix and, if possible, the continual recognition of the removable guest template in subsequent reintroduction steps (Scheme 1).

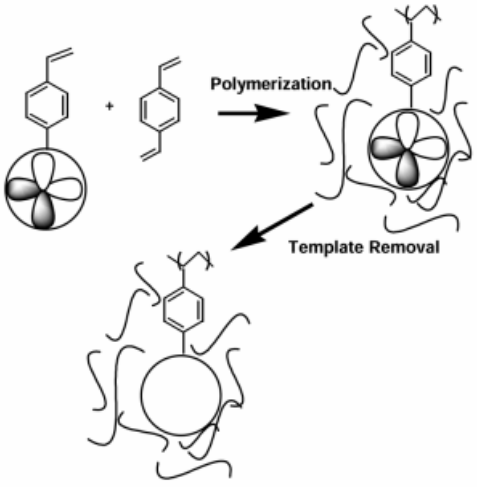

Scheme 1. The templated polymer concept

More importantly, the area of metal-ion templated polymers has received much less attention than the corresponding organic compound templated polymers.[2] Recently, we extended the metal-ion templated polymer field to a novel system that utilized the mono-*N*-(4-vinylbenzyl)TACN ligand (**1**) and found that the monomeric Zn^{2+} sandwich complex of **1**, [{mono-*N*-(4-vinylbenzyl)TACN}$_2$Zn](OTf)$_2$, could be polymerized to provide the same spatial sandwich arrangement in the polymer matrix (2:1 ratio of TACN:Zn).[3,4] Subsequent demetallation of the Zn^{2+}-templated polymer with 6 N HCl, followed by reintroduction of the Zn^{2+} ions in competition with Ni^{2+}, Co^{2+}, and Mn^{2+} at pH 4.5, maintained the ≈2:1 TACN:Zn ratio, and there-

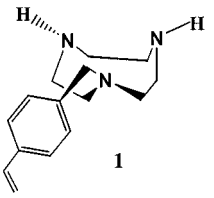

1

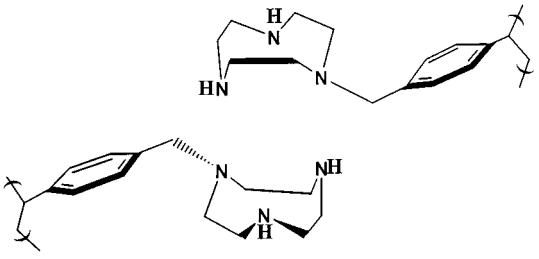

2

[‡] Metal-ion-templated Polymers, 3. − Part 2: Ref.[4]

[a] Lawrence Berkeley National Laboratory, University of California,
Berkeley, CA 94720, USA
E-mail: rhfish@lbl.gov
[b] Present address: Scripps Research Institute,
La Jolla, CA, USA
[c] Present address: Bio-Rad Laboratories,
2000 Alfred Nobel Dr., Hercules, CA 94547, USA

 © WILEY-VCH Verlag GmbH, 69451 Weinheim, 2001 1434−1948/01/0909−2217 $ 17.50+.50/0

fore *allowed us to speculate that the demetallated polymer also had a sandwich arrangement of TACN ligands, polymer* **2**, *with the distance between the polymeric TACN ligands possibly a consequence of the ionic radius of Zn (0.69 Å).*

Results and Discussion

To further determine whether this interesting result was a consequence of the ionic radius of the template metal-ion used in the original polymerization reaction, which would possibly allow selective metal-ion removal from aqueous acidic solution, we prepared the Hg^{2+} (with a larger ionic radius of 1.10 Å) templated sandwich monomer of ligand **1**, [{mono-*N*-(4-vinylbenzyl)-1,4,7-TACN}$_2$Hg](OTf)$_2$ (**3**),[3,4] [Equation (1)] in 70% yield, and polymerized it with the cross-linking agent 80% divinylbenzene (DVB) using AIBN in methanol at 75 °C (overnight in a Schlenk tube covered with aluminum foil) to provide the Hg^{2+}-templated polymer **4** [Equation (2)].

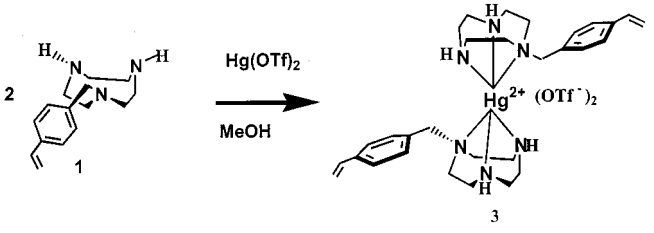

(1)

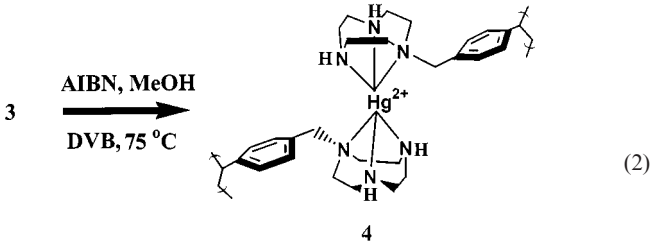

(2)

62 % Crosslinked; 8% Hg; TACN, 0.84 mmol/g
2:1 TACN: Hg ratio

After the total removal of the template Hg^{2+} ion from **4** with 6 N HCl, a demetallated bulk polymer resulted (0.35% Hg, > 96% removed), which had very high selectivity for reintroduced Hg^{2+} ions in competition with a mixture of Cd^{2+} (0.97 Å; 518:1), Pb^{2+} (1.21 Å; 259:1), Ag^{+} (1.26 Å; 1111:1), Cu^{2+} (0.72 Å; 165:1), and Fe^{3+} ions (0.53 Å; 24:1), at pH 2.0, with very high equilibrium selectivity coefficients, $K_{Hg^{2+}/M^{n+}}$, in favor of the Hg^{2+} ion (Table).[5]

Initial observations indicate that the template Hg^{2+} ion is able to compete extremely effectively with metal ions of similar or larger ionic radii, as well as with those that are smaller. However, to our total surprise, we found that the reintroduced Hg^{2+}-ion content in the bulk demetallated polymer was now *15.6% Hg*, and this provided a ratio of TACN:Hg of ~1:1, dramatically different from the Zn^{2+} demetallated polymer, which gave a ~2:1 TACN:Zn/Cu ratio upon reintroduction of Zn^{2+} or Cu^{2+} ions.[3] More importantly, we had previously verified, in a control experiment,[3] that we were *not able* to synthesize a polymer of the vinyl monomer **1** *without the metal ion template*, in order to show that this non-templated polymer lacked selectivity, in comparison to the templated polymer, for the metal ions studied. We observed soluble oligomers by FAB-MS analysis, but no insoluble polymer. We therefore concluded that the metal ions are critical for the dramatic increase in polymerization rates for the templated metal-ion complexes of vinyl monomer **1**, presumably due to an electronic effect.

Clearly, it appears that as you go to metal ions with higher ionic radii, such as Hg^{2+}, the larger distances between the TACN ligands may cause them to operate independently, as suggested in the demetallated Hg^{2+}-selective polymer formed from **4** (Table 1). It is also important to note that in the *absence* of the competing Hg^{2+} ion very small amounts of the other competitor metal ions were removed from solution with demetallated **4**. This is especially dramatic for Cu^{2+} ions (0.83%; ionic radius, 0.72 Å), which were found to be highly selective when reintroduced into the *sandwich arrangement* of polymer **2** (initially Zn templated), where it was observed that ~2% Cu^{2+} ions were removed from acidic solution (pH 2, Cu:Fe = 240:1 vs. 4:1 in Table 1; 5−8% at pH 4.5).[3] This latter result may add some

Table 1. Competitive metal-ion selectivity studies with the demetallated Hg^{2+} polymer

Metal ion[c]	In the presence of Hg^{2+} ions [$K_{Hg^{2+}/M^{n+}}$]	In the absence of Hg^{2+} ions
Hg^{2+}	15.6% (777.7 μmol/g)	–
Cd^{2+}	0.017% (1.5 μmol/g) [2.2×10^8]	not determined
Ag^{+}	0.008% (0.7 μmol/g) [9.8×10^9]	0.26% (24.1 μmol/g)
Pb^{2+}	0.063% (3.0 μmol/g) [1.6×10^8]	0.018% (0.87 μmol/g)
Cu^{2+}	0.030% (4.7 μmol/g) [6.7×10^8]	0.83% (130.6 μmol/g)
Fe^{3+}	0.18% (32.2 μmol/g) [1.9×10^7]	0.23% (41.2 μmol/g)

[a] Demetallated Hg^{2+} polymer (6 mg) and a mixture of metal ions (0.04 M each) were suspended in a stirring H_2O solution (10 mL) at room temperature for 18 h (pH = 2). The resulting polymer was washed thoroughly with H_2O and MeOH, and then dried in vacuo over P_2O_5 for 24 h. Inductive Coupled Plasma (ICP) was used for all the metal analyses. – [b] The reported numbers represent % metal ion by weight, and μmol/g of polymer (in parentheses) indicates the mol of each metal ion on the final collected polymer (per gram). – [c] The counter ion used for the selectivity studies was NO_3^-; therefore, Hg analysis for the sandwich Hg^{2+} polymer from polymerization of **3** (prior to demetallation) was back-calculated to be 8.3% instead of 7.66%, where the counter ion was OTf.

credence to the concept that the ionic radius of the template metal-ion has an effect on both the selectivity of reintroduced metal ions and on the ability of the polymeric TACN ligands to either maintain the sandwich arrangement (Zn^{2+}, Cu^{2+}) or to operate independently (Hg^{2+}).

Thus, our results suggest that the high selectivity for reintroduced Hg^{2+} ions might be better predicated on the basis of the thermodynamic stability of the complex between Hg^{2+} and the proposed polymeric arrangement of the demetallated TACN ligands, as shown in polymer **5**, as well as, to some extent, on the larger ionic radius.

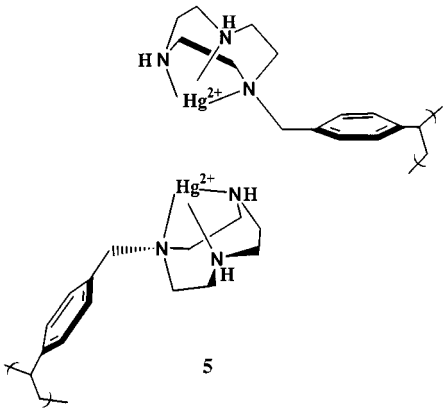

5

More importantly, as discussed, we were never able to synthesize a non-templated polymer of vinyl monomer **1** to compare to the templated polymer **2**. However, in order to overcome this dilemma, we found that simply anchoring a TACN ligand on a 6% crosslinked chloromethylated **PS-DVB** bead gave **PS-TACN** (0.7 mmol/g) with a statistical distribution of TACN ligands rather than a sandwich arrangement, which demonstrated a dramatically lower selectivity for Cu^{2+}, Co^{2+}, Ni^{2+}, Zn^{2+}, and Mn^{2+} ions, as well as a greatly diminished capacity (a ratio of 0.014!; ratio of Cu/Zn = 41:1 vs. 240:1 in polymer **2**).[4]

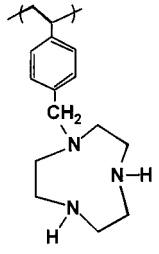

PS-TACN

In contrast, similar preliminary studies with **PS-TACN** and Hg^{2+} ions show high selectivity, as do all the polymer pendant ligands we have studied with Hg^{2+}.[5] Accordingly, the **PS-TACN** results further strengthen the concept of the spatial sandwich arrangement of TACN ligands in a templated polymer matrix being a novel method for the selectivity of metal ions of smaller ionic radius, as well as for the removal of higher capacities of those metal ions from aqueous solution, while also implicating the ionic radius in the apparent loss of the sandwich arrangement for a higher-than-expected Hg^{2+}-ion capacity. Additionally, other parameters could include the softness of the Hg^{2+} ion and its affinity for the relatively soft nitrogen atom (a thermodynamic effect with an equilibrium selectivity coefficient of $K > 10^7$), as well as the preorganized geometry of the TACN ligands in the surrounding coordination sphere.

It is interesting to note that the $[(TACN)_2Cd]^{2+}$ sandwich complex has been characterized by X-ray analysis[6] and shows Cd−N bond lengths of ~2.3 Å and a distance between the two TACN ligands of ~3.3 Å. This type of X-ray data may, in the future, provide more definitive information on the relationship between the ionic radius of the template metal-ion and the TACN:metal ratio of the reintroduced metal ions. Moreover, tying the two *N*-(4-vinylbenzyl)TACN ligands together with an appropriate sized tether might prevent the TACN ligands from operating independently with larger sized metal ions. Finally, the application of these TACN-templated polymers in environmental remediation studies, especially for highly selective Hg^{2+} ion removal from acidic waste streams containing benign metal ions such as Fe^{3+}, as well as for Hg^{2+}-ion sensor applications, will be pursued in the future.[7]

Experimental Section

***N*-(4-vinylbenzyl)-1,4,7-triazacyclononane, 1:**[8] A 50-mL 2-necked Schlenk flask equipped with a J-coiled condenser was charged with TACN (500.0 mg, 3.87 mmol), followed by the addition of EtOH (12 mL, deoxygenated), and the second neck was capped with a septum. LiOH·H_2O (35.8 mg, 0.85 mmol) in 5 mL of deoxygenated H_2O was then added in one portion to this stirring mixture through the septum. The resulting solution was slightly cloudy and was allowed to stir at 50 °C in an oil bath for 2 h, after which time the septum was replaced with an addition funnel, and 4-vinylbenzyl chloride (115.0 mg, 0.75 mmol) in 5 mL of EtOH was added dropwise to the reaction flask through this funnel under N_2. The reaction mixture was refluxed under N_2 and the course of the reaction was followed by TLC (EtOAc/MeOH = 2:3 with a drop of Et_3N). After 3 h, the reaction mixture was concentrated on a rotary evaporator to ~5 mL. About 15 mL of H_2O was added to the residue and CH_2Cl_2 (25 mL × 3) was used to extract the product. The combined CH_2Cl_2 extracts were then washed with brine (20 mL) and dried with Na_2SO_4, filtered, and the collected filtrate was concentrated on a rotary evaporator to ~10 mL. The impurity was removed by adding a small amount of pentane to the resulting CH_2Cl_2 solution until a cloudy suspension was observed. The mixture was then allowed to sit at room temperature for 15 min., and any precipitate or suspension was filtered off. The process was repeated three times until no appreciable cloudiness was observed upon the addition of pentane. The solution was then concentrated to ~ 1 mL and pentane was used to solidify the desired compound upon removing the solvent on a high vacuum line. The obtained solid was further dried in vacuo over P_2O_5 to give the title compound as a pale-yellow, foamy solid (144.2 mg, 78%). If the product did not solidify after the removal of solvent, more pentane was added to the resulting residue along with a small amount of CH_2Cl_2 and the solvent was removed on a high vacuum line. Another alternative to solidify the product was by using Et_2O instead

of pentane. The title compound (mp 58−60 °C) was hygroscopic and was kept in the freezer, and in the dark.

[{*N*-(4-vinylbenzyl)-1,4,7-triazacyclononane}$_2$Hg](OTf)$_2$, 3: Compound **1** (169.6 mg, 691.2 × 10^{-3} mmol) was placed in a 100-mL round flask, followed by the addition of MeOH (25 mL, deoxygenated). An addition funnel was then connected to the top of the flask and Hg(OTf)$_2$ (172.0 mg, 344.8 × 10^{-3} mmol) in 10 mL of MeOH (deoxygenated) was added dropwise to the reaction flask through the addition funnel over 30 min. in the dark. The flask was then covered with aluminum foil. Upon the addition of Hg(OTf)$_2$ solution, some cloudiness was observed. The reaction was allowed to stir at room temperature for 48 h, and any insoluble species were filtered off. The solvent was removed from the filtrate on a high vacuum line to give a foamy, pale-yellow solid. This solid was transferred into a N_2-filled glove box, and ~3 mL of MeOH was added to make a solution. The resulting solution was slightly cloudy, and some insoluble species were observable. A small amount of Et_2O was then added until the solution turned cloudy. The resulting mixture was allowed to sit at room temperature for 2 min., and precipitate was filtered off over a Celite bed. This process was repeated three times, and the solvent of the final filtrate was removed on a high vacuum line to yield an off-white foamy solid, which was further dried in vacuo over P_2O_5 to give the title complex in 70% (238.1 mg) yield. The title complex was found to be light sensitive, and demercuriation occured upon exposing a solution of the title complex to light and air for a long time.

^{1}H NMR (400 NMR,CD_3OD) δ = 7.47−7.30 (m, 8 H), 6.73 (dd, *J* = 10.9, 17.5, 2 H), 5.77 (d, *J* = 17.5, 2 H), 5.23 (d, *J* = 10.9, 2 H), 3.84 (s, 4 H), 3.10−2.74 (m, 24 H). − FAB/MS (*m*-nitrobenzyl alcohol) *m*/*z* (%) = 990 (1) [M^+]. − $C_{32}H_{46}F_6HgN_6S_2O_6\cdot 9H_2O\cdot 2CH_3OH$: calcd. C 33.6, H 5.98, N 6.91; found C 34.3, H 6.20, N 6.26.

Table 2. Polymerization[3] of monomer **3**

Monomer **3** (M)	Cross-linker[b]	Conv. (%)[c]	Polymer **4**[d]
0.045	DVB/EVB 0.180	40	Monomer/ Cross-linker 1:1.6

[a] Polymerization in MeOH with 0.006 M AIBN at 78 °C overnight. − [b] Contained 80% divinylbenzene (DVB) and 20% ethylvinylbenzene (EVB). − [c] Based on DVB/EVB. − [d] C 72.57, H 7.22, N 3.52, Hg 7.76; TACN:Hg ratio is 2.1:1, 7.66% Hg (ICP). TACN capacity is 0.84 mmol/g of resin.

Acknowledgments

The studies at LBNL were generously supported by the Office of Environmental Management, Office of Science and Technology, Office of Technology Systems, Efficient Separations and Processing Cross Cutting Program under the U. S. Department of Energy Contract No. DE-ACO3-76SF00098.

[1] [1a] G. Wulff, *Angew. Chem. Int. Ed. Engl.* **1995**, *34*, 1812. − [1b] G. Wulff, in *Biomimetic Polymers* (Ed.: C. G. Gebelein), Plenum Press: New York. **1990**, p. 1. − [1c] G. Wulff, in *Polymeric Reagents and Catalysts* (Ed.: W. T. Ford), ACS Symposium Series 308, American Chemical Society, Washington, **1986**, p. 186. − [1d] K. Mosbach, *Trends Biochem. Sci.* **1994**, *19*, 19 and references therein. − [1e] K. Shea, *Trends Polym. Sci.* **1994**, *2*, 166 and references therein. − [1f] *Molecular and Ionic Recognition with Imprinted Polymers* (Eds.: R. A. Bartsch and M. Maeda), ACS Symposium Series 703, American Chemical Society, Washington, DC, **1998**, and chapters and references therein.

[2] [2a] A. D. Pomgailo, V. S. Savost′yanov, *Synthesis and Polymerization of Metal- Containing Monomers*, CRC Press: Boca Raton, **1994**, p. 134 and references therein. − [2b] P. K. Dahl, F. H. Arnold, *Macromolecules* **1992**, *25*, 7051. − [2c] T. Rosatzin, L. I. Andersson, W. Simon, K. Mosbach, *J. Chem. Soc., Perkin Trans. 2* **1991**, 1261. − [2d] S. N. Gupta, D. Neckers, *J. Poly. Sci. Polym. Chem. Ed.* **1982**, *20*, 1609. − [2e] W. Kuchen, J. Schram, *Angew. Chem. Int. Ed. Engl.* **1988**, *27*, 1695. − [2f] H. Nishide, J. Deguchi, E. Tsuchida, *Chem. Lett.* **1976**, 169. − [2g] H. Nishide, E. Tsuchida, *Makromol. Chem.* **1976**, *177*, 2295. − [2h] M. Kato, H. Nishide, E. Tsuchida, T. Sasaki, *J. Polym. Sci. Polym. Chem. Ed.* **1981**, *19*, 1803. − [2i]M. Biswas, A. Mukherjee, in *Advances in Polymer Science*, Springer Verlag, Berlin Heidelberg, **1994**, vol. 115, p. 89 and references therein. − [2j] X. Zeng, G. M. Murray, *Sep. Sci. Technol.* **1996**, *31*, 2403.

[3] H. Chen, M. M. Olmstead, R. L.Albright, J. Devenyi, R. H. Fish, *Angew. Chem. Int. Ed. Engl.* **1997**, *36*, 642.

[4] R. H. Fish in ref.[1f], chapter 16, p. 238.

[5] S.-P. Huang, K.J. Franz, E. H. Arnold, J. Devenyi, R. H. Fish, *Polyhedron* **1996**, *15*, 4241.

[6] H. Strasdeit, A.-M. Duhme, M. Weber, S. Pohl, *Acta Crystallogr., Sect. C* **1992**, *48*, 437.

[7] T. F. Baumann, J. G. Reynolds, G. A. Fox, *Chem. Commun.* **1998**, 1637 and references therein.

[8] Revised synthetic procedure for **1** (see reference 3 for all analytical data for **1**, and the polymerization procedure used for the preparation of polymer **4**).

Received September 11, 2000
[I00342]

A Novel and Perfectly Aligned Crystal of a Ferrocenyl Chromophore Displaying High Quadratic Nonlinear Optical Bulk Efficiency

Jérome Chiffre,[a] Frédéric Averseng,[a] Gilbert G. A. Balavoine,[a] Jean-Claude Daran,[a] Gabriel Iftime,[a] Pascal G. Lacroix,[a] Eric Manoury,*[a] and Keitaro Nakatani[b]

Keywords: Iron / Chromophores / Nonlinear optics / Crystal engineering

The highest nonlinear optical bulk efficiency for a 2-(4-nitrophenyl)ethenylferrocene (140 times that of urea) has been achieved for ***E*-4** owing to a favourable noncentrosymmetrical packing in which all molecules are perfectly aligned (*P*1 space group).

Introduction

Molecular nonlinear optical materials has been recognised for many years as a promising field because of their potential applications in emerging photonic technologies.[1] Most efforts have been devoted to organic molecules in which electron donor/acceptors are linked through conjugated backbones. More recently organometallic molecules have attracted attention because metal complexes are capable of strong electron acceptor/donor effects depending upon the nature of the metal, its oxidation states and coordination spheres. These new characteristics may allow a subtle tuning of the NLO properties and make organometallic species very attractive.[2] In any case, two prerequisites are needed for quadratic NLO activity: first, the constituting chromophores have to possess a molecular hyperpolarizability (β) as large as possible, and secondly they must be arranged in a noncentrosymmetrical fashion. A dramatic illustration of such requirements can be found in organometallic chemistry.[3] The (*Z*)-2-(4-nitrophenyl)ethenylferrocene isomer **Z-1** has a β value of 13×10^{-30} esu, and the *E* isomer ***E*-1** possesses a larger hyperpolarizability at the molecular level ($\beta = 31 \times 10^{-30}$ esu; see Table 1). However, whereas the *Z* isomer exhibits a large second harmonic generation (SHG) efficiency in the solid state (62 times that of urea), the *E* isomer is completely inactive in the solid state due to its centrosymmetrical crystal packing.[4] We have been able to overcome this tendency for centrosymmetric crystallisation of ***E*-1** by using chiral enantiomerically pure analogues of this molecule that furnished noncentrosymmetrical crystals, sometimes with high bulk efficiencies (up to 100 times that of urea).[5] More recently, we became interested in analogues of ***E*-1** bearing substituents on the second cyclopentadienyl ring (see Scheme 1) in order to modulate crystal packing or to incorporate chromophores into polymers. In the next section we will disclose our first results with a particular emphasis on ***E*-4**, which possesses a high NLO efficiency because of a very unusual crystal packing.

Results and Discussion

To obtain our target molecules, we developed a new procedure to prepare 1,1′-disubstituted ferrocenes involving the monoacetal **2** (see Scheme 1). The free aldehyde function was used to build the first substituent. Hydrolysis of the acetal function could then furnish a new formyl group in order to build up the second substituent. During our studies, we were able to isolate compound ***E*-4** and to obtain single crystals suitable for X-ray diffraction analysis. ***E*-4** crystallises in the *P*1 space group. Each unit cell contains one single molecule (Figure 1). The crystal has no symmetry elements so all the molecules of ***E*-4** are strictly identical and absolutely parallel to each other (see Figure 2). This packing is unique and very favourable for the NLO efficiency because each chromophore will add its contribution to the overall property. The *P*1 space group is very rare for NLO active chromophores. Only few examples of such crystal packings have been disclosed, usually for merocyanine- or 4-nitrophenol-based materials.[6] However, to the best of our knowledge, only one such crystal where the NLO chromophore is alone and perfectly aligned, has already been described.[6a]

The NLO properties of these materials has been measured by a Kurtz−Perry powder test.[7] An SHG efficiency of 140 times that of urea has been recorded at 1.906 μ. This efficiency is the highest value recorded so far in this series of 2-(4-nitrophenyl)ethenylferrocenes and one of the highest for organometallic compounds in general.[2,8] The optical properties of ***E*-4** are very close to those of the related compound ***E*-1**.[9] Furthermore, the molecular hyperpolarizability β of ***E*-4** has been calculated by ZINDO (see Table1).[10] The calculated β value is only slightly higher for ***E*-4** than for ***E*-1**, so the high NLO bulk efficiency of ***E*-4**

[a] Laboratoire de Chimie de Coordination,
205 route de Narbonne, 31077 Toulouse Cedex, France,
Fax.: (internat.) +33-5/6133-3131
E-mail: manoury@lcc-toulouse.fr
[b] P.P.S.M., CNRS UA 1906, Ecole Normale Supérieure de Cachan,
Avenue du Président Wilson, 94235 Cachan Cedex, France

 © WILEY-VCH Verlag GmbH, 69451 Weinheim, 2001 1434−1948/01/0909−2221 $ 17.50+.50/0

Table 1. ZINDO calculated absorption maxima (in nm), experimental absorption maxima (in nm in an ethanol solution), oscillator strengths (*f*), dipole moment changes between ground and excited states (in D), composition of the excited state in the configuration interaction and β_0 (in 10^{-30} cm^3·esu^{-1}) for ***E*-4** and ***E*-1**

	λ_{max}(calcd.)	λ_{max}(expt.)	*f*	$\Delta\mu$	Composition of CI expansion[a]	β_0
***E*-4**	360	364	0.84	16.7	$-0.780\ \chi 70 \rightarrow 71\ -0.462\ \chi 68 \rightarrow 71$	26.3
***E*-1**	343	362	0.80	17.6	$-0.729\ \chi 56 \rightarrow 57\ -0.538\ \chi 54 \rightarrow 57$	20.9

[a] Orbital 70 and 56 are the HOMOs for ***E*-4** and ***E*-1**, respectively.

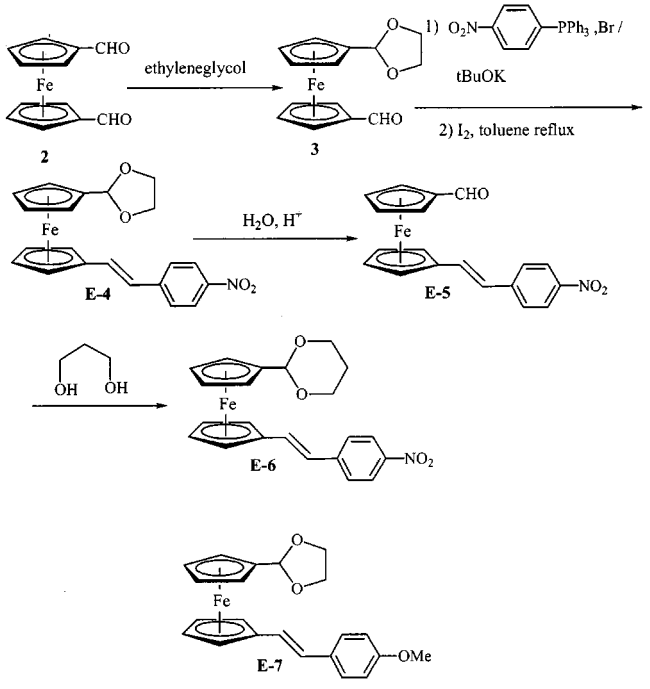

Scheme 1

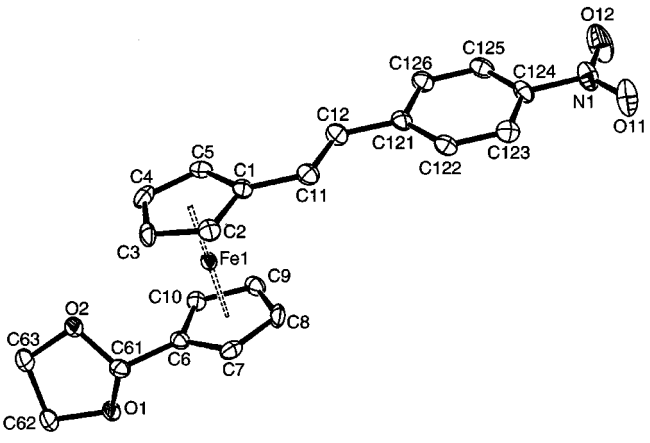

Figure 1. Molecular view of ***E*-4** with atom labelling scheme; ellipsoids represent 30% probability

crystals is probably due to the very favourable crystal packing.

The nonlinear optical properties of 2-(4-nitrophenyl)ethenylferrocenes have been extensively studied,[2] but only a few types of crystal packing for such compounds have been reported. These compounds have a clear tendency for head-to-tail crystallisation.[4,5,11] Why, then, does ***E*-4** crystallise with such a completely different packing? The still common opinion about a tendency of molecules with a large dipole moment for head-to-tail crystallisation has been ruled out by a thorough study.[12] It therefore seems clear to us that the noncentrosymmetrical crystallisation of ***E*-4** is not due to a lower dipole moment compared to ***E*-1**.[13] The crystal structure of ***E*-4** arises from infinite ribbons of molecules with short nitro−dioxane distances. A close study of the distances within the crystal reveals six relatively short H−O contacts that cannot be explained by geometrical constraints within the molecule (see Table 2 and Figure 3). These contacts may be described as C−H···O hydrogen bonds, as defined in the literature, between slightly acidic protons and oxygen acceptors.[14] Indeed, all C−O distances and all C−H···O angles fall into the expected range for such bonds (3−4 Å and 90−180°, respectively).[14b] The six short H−O contacts correspond to two unsymmetrically bifurcated interactions between one hydrogen atom and the two oxygen atoms of the nitro group, and two interactions between one hydrogen atom and only one oxygen atom of the nitro group (see Figure 3).[14d] In the absence of stronger intermolecular forces, such as OH···O hydrogen bonds, π-π stacking or donor−acceptor interactions, we believe that these C−H···O interactions are responsible for the unique crystal packing of ***E*-4**. Furthermore, this proposal is

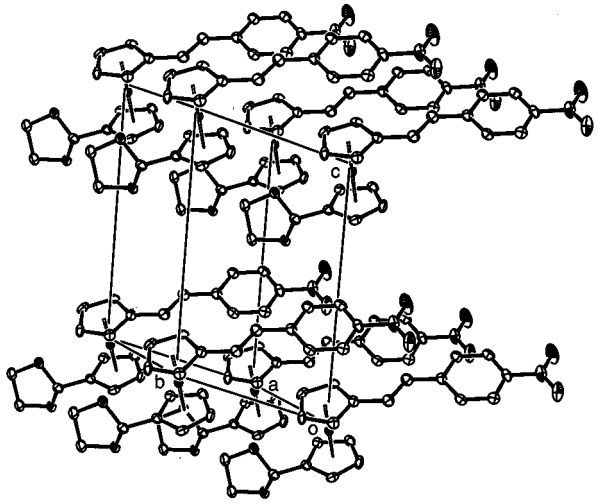

Figure 2. View of the packing in ***E*-4** showing the perfect alignment of the chromophores

Table 2. Distances and angles for C−H···O contacts

Contact[a]	O−C distance (Å)	O−H distance (Å)	O−H−C angle (°)
O(11)−H(62b)−C(62)	3.204(3)	2.99	93.7
O(11)−H(62a)−C(62)	3.204(3)	2.80	106.1
O(11)−H(63b)−C(63)	3.542(3)	3.16	105.4
O(12)−H(62b)−C(62)	3.477(3)	2.97	113.8
O(12)−H(63a)−C(63)	3.329(4)	2.90	107.9
O(12)−H(63b)−C(63)	3.329(4)	3.23	87.3

[a] The symmetry transformations used to generate the dioxane fragment [C(62), C(63), H···] are $x - 1$, $y - 2$, $z + 1$.

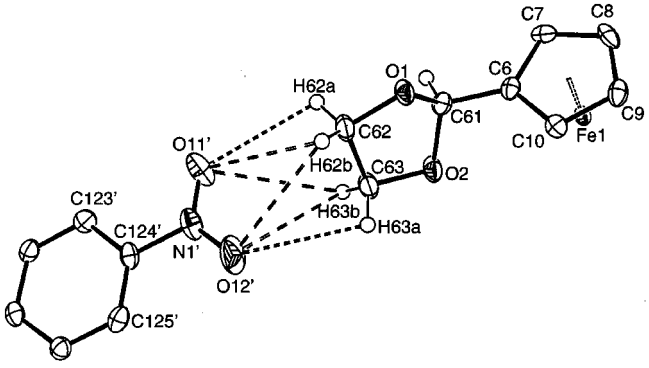

Figure 3. View showing the hydrogen interactions C−H···O between the hydrogen atoms of the dioxane moiety and the O atoms of the nitro group in ***E*-4**

strengthened by the study of a closely related molecule ***E*-7**, obtained by formally replacing the acceptor nitro group of ***E*-4** by a methoxy group. ***E*-7** lacks a good acceptor, such as a nitro group, able to form C−H···O hydrogen bonds and crystallises in the centrosymmetric space group $P2_1/c$.[15]

We also decided to study a close analogue of ***E*-4** where the five-membered dioxane ring has been replaced by the six-membered dioxolane ring, namely compound ***E*-6**. Single crystals suitable for X-ray diffraction analysis were obtained by slow diffusion of hexane into a dichloromethane solution of ***E*-6** (Figure 4). In this case, we observed a centrosymmetrical packing and, of course, no NLO bulk

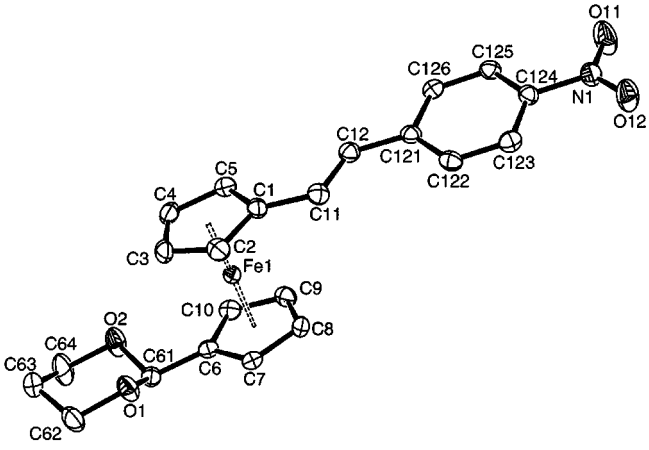

Figure 4. Molecular view of ***E*-6** with atom labelling scheme; ellipsoids represent 30% probability

efficiency. If the nitrostyryl fragments of ***E*-4** and ***E*-6** are identical within experimental errors as shown in Table 2, the relative geometry of the dioxane or dioxolane with respect to the Cp ring to which they are attached is different. The dioxane ring is twisted with respect to the Cp by a dihedral angle of 73.9°, whereas the dioxolane moiety is nearly parallel to the Cp with a dihedral angle of 13.5°. The twist observed for the dioxane in ***E*-4** allows the four hydrogens of the two CH_2 groups to form hydrogen bonds with the nitro fragment of the symmetry related molecule, as shown in Figure 3. In ***E*-6**, however, the presence of a third CH_2 group prevents the interaction of the four acidic hydrogens close to the oxygen atoms with the nitro group, the tendency for centrosymmetrical packing cannot therefore be overcome, and it packs in a more common centrosymmetrical way. However, the intermolecular packing is still stabilised by C−H···O interactions between the oxygen of the nitro group and two hydrogens H(8′) and H(9′) of the unsubstituted Cp ring of the symmetry related molecule. Such C−H···O interactions between a Cp ring of a ferrocene moiety and the O atoms of a nitro group seems to be rather common and many examples can be found in the literature.[16] These interactions lead to the head-to-tail packing of two molecules arranged around the inversion centre shown in Figure 5.

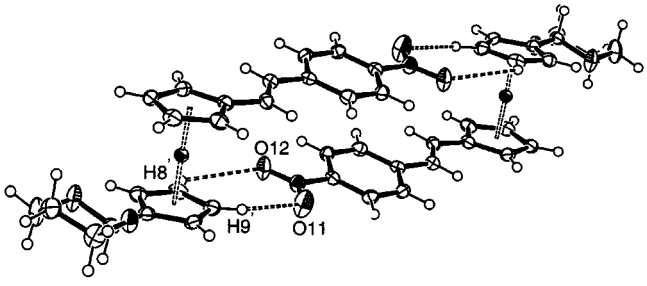

Figure 5. View showing the hydrogen interactions between the oxygen of the nitro group and some hydrogen atoms of the Cp ring in ***E*-6** [O(11)···C(9′) 3.627(3), O(11)···H(9′) 2.99 Å and O(11)···H(9′)−C(9′) 124.7(2)°; O(12)···C(8′) 3.744(3), O(12)···H(8′) 2.44 Å and O(12)···H(8′)−C(8′) 156.3(2)°]

In conclusion, we have reported a rare example of a highly efficient NLO materials (SHG efficiency 140 times the value for urea!) where the crystal contains only perfectly aligned chromophores. Furthermore, we have discovered specific interactions between a dioxane ring and a nitro group which, if they can be generalised in other systems,

might be a new and useful example of a supramolecular building block for crystal engineering.[17]

Experimental Section

All reactions were carried out in the absence of air using standard Schlenk techniques and vacuum line manipulations. Thin layer chromatography was carried out on Merck 60F254 precoated silica gel plates. Preparative flash chromatography was performed on Merck Kieselgel. Instrumentation: Bruker AM250 (^1H, ^{13}C NMR), Hewlett−Packard HP MSD 7590 (GC-MS), Stoe IPDS (X-ray). Elemental analyses were performed by the Service d'Analyse du Laboratoire de Chimie de Coordination, Toulouse (France).

1,1′-Ferrocenedicarboxaldehyde was synthesised according to ref.[18] 4-(Nitrobenzyl)triphenylphosphonium bromide was synthesised by a similar procedure to that described in ref.[19] for the synthesis of 4-(nitrobenzyl)triphenylphosphonium chloride.

2-(1′-Formylferrocenyl)-1,3-dioxolane (3): 1,1′-Ferrocenedicarboxaldehyde (5 g, 20.6 mmol) was added to a round-bottomed flask equipped with a Dean−Stark apparatus. The system was purged with argon and the red solid was dissolved in 80 mL of dry toluene. Ethylene glycol (1.15 mL, 20.6 mmol) and *p*-toluenesulfonic acid (300 mg, 1.58 mmol) were then added successively to the reaction mixture. After heating for 2 h at 170 °C, the reaction mixture was cooled back to room temp. and diluted with 100 mL of dichloromethane. Anhydrous potassium carbonate was then added and the mixture was stirred for 1 h. After filtration through celite and evaporation of the solvents, the crude materials was purified by flash chromatography on silica gel with a pentane/ether mixture (1:2, v/v) as eluent to yield 3.54 g of **3** as a brown solid (yield = 60%). − ^1H NMR ($CDCl_3$): δ = 9.90 (s, 1 H, CHO), 5.55 (s, 1 H, O−CH−O), 4.76 (t, *J* = 1.9 Hz, 2 H, Cp), 4.57 (t, *J* = 1.9 Hz, 2 H, Cp), 4.36 (t, *J* = 1.9 Hz, 2 H, Cp), 4.21 (t, *J* = 1.9 Hz, 2 H, Cp), 3.93 (m, 4 H, CH_2-CH_2). − ^{13}C NMR ($CDCl_3$): δ = 193.9 (CHO), 101.8 (O−CH−O), 86.2 (quat. Cp), 80.1 (quat. Cp), 80.0 (Cp), 73.9 (Cp), 70.4 (Cp), 69.9 (Cp), 65.4 (CH_2-CH_2). − MS (DCI, NH_3): *m*/*z* (%) = 287 (32) [M + 1]. − $C_{14}H_{14}FeO_3$ (286.11): calcd. C 58.77, H 4.93; found C 58.73, H 4.75.

(*E*)-2-[1′-(4-Nitrostyryl)ferrocenyl]-1,3-dioxolane (*E*-4): *t*BuOK (2.10 g, 18.7 mmol, 3.1 equiv.) and 50 mL of dry toluene were added to a distillation apparatus. The system was purged with argon. 4-(Nitrobenzyl)triphenylphosphonium bromide (7.20 g, 15.1 mmol, 2.5 equiv.) was then added and the mixture was warmed up to reflux. After one hour, 30 mL of toluene was removed by distillation and the solution was kept at reflux for another two hours. After cooling back to room temp., a solution of **3** (1.70 g, 5.94 mmol) dissolved in 40 mL of dry toluene was added and the solution was warmed again to reflux. 20 mL of toluene was removed by distillation over a period of one hour and the solution was kept at reflux for another two hours. After cooling to room temperature, the organic phase was extracted with dichloromethane, washed with brine, dried over sodium sulfate and the solvents evaporated under reduced pressure. The crude material was purified by flash chromatography with a pentane/ether mixture (3:1, v/v) on silica gel to yield 2.38 g of **4** (yield 99%) as a mixture of Z and *E* isomers (*Z*/*E* = 1:3).

A mixture of **4** (***Z***+***E***) (1.45 g, 3.58 mmol) and I_2 (90 mg, 0.1 equiv.) dissolved in 40 mL of dry toluene was added to a one-necked round bottomed flask equipped with a condenser. The system was purged with argon and the mixture was then refluxed for 15 minutes. After cooling back to room temperature, the mixture was extracted with dichloromethane, washed with a sodium thiosulfate solution (2 M) then with brine, dried over sodium sulfate and the solvents were evaporated. After flash chromatography on silica gel, 1.40 g (97%) of pure ***E*-4** was isolated. − ^1H NMR ($CDCl_3$): δ = 8.21 (d, *J* = 8.8 Hz, 2 H, Ph), 7.75 (d, *J* = 8.8 Hz, 2 H, Ph), 7.34 (d, AB, *J* = 16.2 Hz, 1 H, vinyl), 6.95 (d, AB, *J* = 16.2 Hz, 1 H, vinyl), 5.66 (s, 1 H, O−CH−O), 4.66 (t, *J* = 1.8 Hz, 2 H, Cp), 4.44 (t, *J* = 1.8 Hz, 2 H, Cp), 4.31 (t, *J* = 1.9 Hz, 2 H, Cp), 4.19 (t, *J* = 1.9 Hz, 2 H, Cp), 3.84−4.01 (m, 4 H, CH_2-CH_2). − ^{13}C NMR ($CDCl_3$): δ = 146.3 (quat. Ph), 145.4 (quat. Ph), 133.4 (vinyl), 126.2 (Ph), 124.4 (Ph), 124.0 (vinyl), 102.4 (O−CH−O), 86.5 (quat. Cp), 83.1 (quat. Cp), 71.0 (Cp), 69.8 (Cp), 68.7 (Cp), 68.6 (Cp), 65.3 (CH_2-CH_2). − MS (DCI, NH_3): *m*/*z* (%) = 406 (100) [M + 1]. − $C_{21}H_{19}FeNO_4$ (405.23): calcd. C 62.24, H 4.73, N 3.46; found C 61.97, H 4.34, N 3.68.

(*E*)-1′-(4-Nitrostyryl)ferrocenecarboxaldehyde (*E*-5): A solution of ***E*-4** (1.40 g) in 30 mL of dichloromethane was added to 15 mL of a solution containing 150 mg of *p*-toluenesulfonic acid monohydrate in deoxygenated water in a Schlenk tube. The mixture was stirred for 3 h at 60 °C. After cooling, the solution was diluted with diethyl ether, washed with water, dried with sodium sulfate, evaporated and purified by flash chromatography with a pentane/ether mixture (1:2, v/v) on silica gel to yield 1.10 g of pure ***E*-5** (yield 88%). − ^1H NMR ($CDCl_3$): δ = 9.88 (s, 1 H, CHO), 8.19 (d, *J* = 8.9 Hz, 2 H, Ph), 7.55 (d, *J* = 8.9 Hz, 2 H, Ph), 6.94 (d, AB, *J* = 16.3 Hz, 1 H, vinyl), 6.75 (d, AB, *J* = 16.3 Hz, 1 H, vinyl), 4.78 (t, *J* = 2.0 Hz, 2 H, Cp), 4.60 (t, *J* = 1.9 Hz, 2 H, Cp), 4.58 (t, *J* = 2.0 Hz, 2 H, Cp), 4.44 (t, *J* = 1.9 Hz, 2 H, Cp). − ^{13}C NMR ($CDCl_3$): δ = 193.5 (CHO), 146.4 (quat. Ph), 143.7 (quat. Ph), 130.6 (vinyl), 126.3 (Ph), 125.6 (Ph), 124.2 (vinyl), 83.7 (quat. Cp), 80.1 (quat. Cp), 74.3 (Cp), 71.2 (Cp), 70.8 (Cp), 68.7 (Cp). − MS (DCI, NH3): *m*/*z* (%) = 379 (100) [M + 18], 362 (32) [M + 1]. − $C_{19}H_{15}FeNO_3$ (361.18): calcd. C 63.20, H 4.20, N 3.88; found C 63.01, H 4.47, N 3.64.

(*E*)-2-[1′-(4-nitrostyryl)ferrocenyl]-1,3-dioxane (*E*-6): ***E*-5** (1.0 g, 2.64 mmol) dissolved in 30 mL of dry toluene was added to a round-bottomed flask equipped with a Dean−Stark apparatus. The system was purged with argon and 1,3-propanediol (0.265 mL, 3.66 mmol) and *p*-toluenesulfonic acid (53 mg, 0.27 mmol) were added successively to the reaction mixture. After 2 h heating at 110 °C, the reaction mixture was cooled back to room temp. and diluted with 100 mL of dichloromethane. Anhydrous potassium carbonate was then added and the mixture was stirred for 1 h. After filtration through celite and evaporation of the solvents, the crude material was purified by flash chromatography on silica gel with a pentane/ether mixture (3:1, v/v) as eluent to yield 0.85 g of ***E*-6** as a red solid (yield 79%). − ^1H NMR ($CDCl_3$): δ = 8.18 (d, *J* = 8.8 Hz, 2 H, Ph), 7.52 (d, *J* = 8.8 Hz, 2 H, Ph), 7.08 (d, AB, *J* = 16.1 Hz, 1 H, vinyl), 6.70 (d, AB, *J* = 16.1 Hz, 1 H, vinyl), 5.25 (s, 1 H, O−CH−O), 4.51 (t, *J* = 1.8 Hz, 2 H, Cp), 4.39 (t, *J* = 1.8 Hz, 2 H, Cp), 4.29 (t, *J* = 1.8 Hz, 2 H, Cp), 4.14 (m, 2 H, OCH_2), 4.11 (t, *J* = 1.8 Hz, 2 H, Cp), 3.79 (td, *J* = 12.3 Hz and 2.3 Hz, 2 H, OCH_2), 2.2−1.9 (m, 1 H, $CH_2CH_2CH_2$), 1.34 (br. d, *J* = 13 Hz, 1 H, $CH_2CH_2CH_2$). − ^{13}C NMR ($CDCl_3$): δ = 145.8 (quat. Ph), 144.4 (quat. Ph), 132.7 (vinyl), 125.8 (Ph), 124.2 (Ph), 123.4 (vinyl), 99.6 (O−CH−O), 87.1 (quat. Cp), 82.2 (quat. Cp), 70.8 (Cp), 69.2 (Cp), 68.3 (Cp), 67.7 (Cp), 67.1 (OCH_2), 25.7 ($CH_2CH_2CH_2$). − MS (DCI, NH3): *m*/*z* (%) = 420 (100) [M + 1]. − $C_{22}H_{21}FeNO_4$ (419.26): calcd. C 62.21, H 4.73, N 3.46; found C 63.24, H 4.94, N 3.10.

Table 3. Crystal data of ***E*-4** and ***E*-6**

	***E*-4**	***E*-6**
Empirical formula	$C_{21}H_{19}FeNO_4$	$C_{22}H_{21}FeNO_4$
Formula mass	405.23	419.26
Crystal shape	Box (dark red)	Flattened needle (orange red)
Crystal size, mm	0.46 × 0.32 × 0.30	0.57 × 0.12 × 0.05
Temperature, K	180(2)	180(2)
Crystal system	Triclinic	Triclinic
space group	*P*1	*P*1
a, Å	6.0102(8)	6.1214(7)
b, Å	7.0127(9)	8.5527(9)
c, Å	11.264(2)	17.532(2)
α, °	73.39(1)	93.37(1)
β, °	88.28(2)	94.66(1)
γ, °	70.17(1)	95.59(1)
U, Å^3	426.8(1)	908.4(2)
Z	1	2
ρ(calcd), g·cm^{-3}	1.576	1.533
μ(Mo-K_α), cm^{-1}	9.082	8.599
Diffractometer used	Stoe IPDS	Stoe IPDS
Radiation used	Mo-K_α (0.71073)	Mo-K_α (0.71073)
Scan mode		
Reflections measured	3148	9123
θ range, °	5.68 < θ < 24.0	2.34 < θ < 26.02
Independent reflections (R_{int})	2302(0.0461)	3353(0.0403)
Reflections used [$I > 2\sigma(I)$]	2298	2550
Refinement	*F*	*F*
R	0.0226	0.0279
R_w	0.0257	0.0322
$(\Delta/\sigma)_{max}$	0.06	0.04
$\Delta\rho_{min}/\Delta\rho_{max}$	−0.37/0.38	−0.34/0.31
Flack's parameter	0.00(1)	
GOF	1.077	1.032
No of parameters	246	254

NLO Measurements: The measurements of second harmonic generation (SHG) intensity were carried out by the Kurtz−Perry powder technique[7] with a nanosecond Nd-YAG-pulsed (10 Hz) laser operating at λ = 1.064 μm. The outcoming Stokes-shifted radiation at 1.907 μm, generated by Raman effects in a hydrogen cell, was used as the fundamental beam for second harmonic generation. The SHG signal was detected by a photomultiplier and read on an ultrafast Tektronic 7834 oscilloscope. Samples were calibrated as microcrystalline powders obtained by grinding in the range 50−80 μm and put between two glass plates. The recorded efficiencies were expressed versus that of powdered (50−80 μm) urea.

X-ray Crystallographic Study: Data for ***E*-4** and ***E*-6** were collected on a Stoe IPDS diffractometer. The final unit cell parameters were obtained by the least-squares refinement of 8000 reflections. Only statistical fluctuations were observed in the intensities monitored over the course of the data collections.

Both structures were solved by direct methods (SIR97[20]) and refined by least-squares procedures on *F*. All H atoms were introduced in the calculation in idealised positions [d(CH) = 0.96 Å] and treated as riding models with isotropic thermal parameters related to the carbon to which they are attached. Least-squares refinements were carried out by minimising the function $\Sigma w(|F_o| - |F_c|)^2$, where F_o and F_c are the observed and calculated structure factors. The absolute configuration for ***E*-4** was determined by refining the Flack enantiopole parameter.[21] The weighting scheme used in the last refinement cycles was $w = w'[1 - \{\Delta F/6\sigma(F_o)\}^2]^2$, where $w' = 1/\Sigma_1^n A_r T_r(x)$ with three coefficients A_r for the Chebyshev polynomial $A_r T_r(x)$ where x is $F_c/F_c(\max)$.[22] The models reached convergence with $R = \Sigma(||F_o| - |F_c||)/\Sigma(|F_o|)$ and $R_w = [\Sigma w(|F_o| - |F_c|)^2/\Sigma w(F_o)^2]^{1/2}$, with the values listed in Table 3.

The calculations were carried out with the CRYSTALS package programs.[22] Molecular views were produced with the help of ORTEP32.[23]

Crystallographic data (excluding structure factors) for the structures reported in this paper have been deposited with the Cambridge Crystallographic Data Centre as supplementary publication nos. CCDC-160780 (***E*-4**) and -160781 (***E*-6**). Copies of the data can be obtained free of charge on application to CCDC, 12 Union Road, Cambridge CB2 1EZ, UK [Fax: (internat.) + 44-1223/336-033; E-mail: deposit@ccdc.cam.ac.uk].

[1] [1a] J. Zyss, *Molecular Nonlinear Optics*, Academic Press, New York, **1994**. − [1b] *Nonlinear Optical Properties of Organic Materials, Proceedings of SPIE*, **1988−1994**, *Vol. 971*. − [1c] T. Verbiest, S. Houbrechts, M. Kauranen, K. Clays, A. J. Persoons, *J. Mater. Chem.* **1997**, *7*, 2175−2189.

[2] [2a] N. J. Long, *Angew. Chem. Int. Ed. Engl.* **1995**, *34*, 21−38. − [2b] I. R. Whittall, A. M. Mc Donagh, M. G. Humphrey, *Adv. Organomet. Chem.* **1998**, *42*, 291−357.

[3] M. L. H. Green, S. R. Marder, M. E. Thompson, J. A. Bandy, D. Bloor, P. V. Kolinsky, R. J. Jones, *Nature* **1987**, *330*, 360−362.
[4] J. A. Mata, E. Peris, I. Asselberghs, R. van Boxel, A. Persoons, *New J. Chem.* **2001**, *25*, 299−304.
[5] [5a] G. G. A. Balavoine, J.-C. Daran, G. Iftime, P. G. Lacroix, E. Manoury, J. A. Delaire, I. Maltey-Fanton, K. Nakatani, S. Di Bella, *Organometallics* **1999**, *18*, 21−29. − [5b] G. Iftime, G. G. A. Balavoine, J.-C. Daran, P. G. Lacroix, E. Manoury, *CR Acad. Sciences* Paris, Série IIc **2000**, *3*, 139−146.
[6] [6a] T. B. Marder, G. Lesley, Z. Yuan, H. B. Fyfe, P. Chow, G. Stringer, I. R. Jobe, N. J. Taylor, I. D. Williams, S. K. Kurtz, *ACS Symposium Series* **1991**, *455*, 605−615. [6b] F. Pan, M. S. Wong, V. Gramlich, C. Bossard, P. Günter, *J. Am. Chem. Soc.* **1996**, *118*, 6315−6316. − [6c] S. Okada, A. Masaki, H. Matsuda, H. Nakanishi, M. Kato, R. Muramatsu, M. Otsuka, *Jpn. J. Appl. Phys.* **1990**, *29*, 1112−1115; M. Muthuraman, Y. Le Fur, M. Bagieu-Beucher, R. Masse, J.-F. Nicoud, G. R. Desiraju, *J. Mater. Chem.* **1999**, *9*, 2233−2239. − [6d] Anwar, S. Okada, H. Oikawa, H. Nakanishi, *Chem. Mater.* **2000**, *12*, 1162−1170.
[7] [7a] S. K. Kurtz, T. T. Perry, *J. Appl. Phys.* **1968**, *39*, 3798−3813. [7b] J. P. Dougherty, S. K. Kurtz, *J. Appl. Cryst.* **1976**, *9*, 145−158.
[8] S. R. Marder, J. W. Perry, B. G. Tiemann, W. P. Schaefer, *Organometallics* **1991**, *10*, 1896−1901.
[9] In ethanol, λ_{max} = 364 nm (ε = 14880 $L\cdot mol^{-1}\cdot cm^{-1}$) and λ_{max} = 510 nm (ε = 3910 $L\cdot mol^{-1}\cdot cm^{-1}$) for ***E*-1**; λ_{max} = 362 nm (ε = 17250 $L\cdot mol^{-1}\cdot cm^{-1}$) and λ_{max} = 504 nm (ε = 4420 $L\cdot mol^{-1}\cdot cm^{-1}$) for ***E*-4**.
[10] For experimental details, see ref.[5a]
[11] A. Togni, G. Rihs, *Organometallics* **1993**, *12*, 3368−3372.
[12] J. K. Whitesell, R. E. Davis, L. L. Saunders, R. J. Wilson, J. P. Feagins, *J. Am. Chem. Soc.* **1991**, *113*, 3267−3270.
[13] The dipolar moment of ***E*-4** has been calculated to be 9.9 D, close to the value obtained similarly for ***E*-1** (7.6 D). For experimental details, see ref.[5a]
[14] [14a] R; Taylor, O. Kennard, *J. Am. Chem. Soc.* **1982**, *104*, 5063−5070. − [14b] G. R. Desiraju, *Acc. Chem. Res* **1991**, *24*, 290−296. − [14c] T. Steiner, *New J. Chem.* **1998**, 1099−1103. − [14d] J. M. A. Robinson, D. Philp, K. D. M. Harris, B. M. Kariuki, *New J. Chem.* **2000**, *24*, 799−806.
[15] C.-O. Turrin, J. Chiffre, D. de Montauzon, J.-C. Daran, A.-M. Caminade, E. Manoury, G. G. A. Balavoine, J.-P. Majoral, unpublished results
[16] [16a] B. J. Coe, J.-D. Foulon, T. A. Hamor, C. J. Jones, J. A. Mc Cleverty, *Acta Crystallogr., Sect. C* **1996**, *15*, 3032−3035. [16b] G. Iftime, J.-C. Daran, E. Manoury, G. G. A. Balavoine, *Organometallics* **1996**, *15*, 4808−4815.
[17] G. R. Desiraju, *Angew. Chem. Int. Ed. Engl.* **1995**, *34*, 2311−2327.
[18] G. G. A. Balavoine, G. Doisneau, T. Fillebeen-Khan, *J. Organomet. Chem.* **1991**, *412*, 381−382.
[19] R. Ketcham, D. Jamboktar, L. Martinelli, *J. Org. Chem.* **1962**, *27*, 4666−4667.
[20] A. Altomare, M. C. Burla, M. Camalli, G. Cascarano, C. Giacovazzo, A. Guagliardi, A. G. G. Moliterni, G. Polidori, R. Spagna, SIR97 − A Program for Automatic Solution of Crystal Structures by Direct Methods, *J. Appl. Cryst.* **1999**, *32*, 115−119.
[21] [21a] H. D. Flack, *Acta Crystallogr., Sect. A* **1983**, *39*, 876−881. − [21b] G. Bernardinelli, H. D. Flack, *Acta Crystallogr., Sect. A* **1985**, *41*, 500−511.
[22] D. J. Watkin, C. K. Prout, J. R. Carruthers, P. W. Betteridge, *CRYSTALS ISSUE 11*, Chemical Crystallography Laboratory, University of Oxford, Oxford, 1999.
[23] L. J. Farrugia, ORTEP3 for Windows, *J. Appl. Cryst.* **1997**, *30*, 565.

Received March 6, 2001
[I01123]

Mononuclear Thiomolybdenyl Complexes − Synthesis and Structural and Spectroscopic Characterization

Charles G. Young,*[a] Robert W. Gable,[a] Jason P. Hill,[a] and Graham N. George[b]

Keywords: Molybdenum / Sulfur / Thiomolybdenyl complexes / EPR spectroscopy / X-ray absorption spectroscopy

The first series of mononuclear thiomolybdenyl complexes, $Tp^*Mo^VSX_2$ [Tp^* = hydrotris(3,5-dimethylpyrazol-1-yl)borate, X/X_2 = anion/dianion], has been prepared. The complexes, which have been characterized by analytical, mass spectrometric, spectroscopic and X-ray crystallographic studies, provide insights into the electronic nature and chemistry of the catalytically and biologically important thiomolybdenyl unit.

Introduction

The thiomolybdenyl unit, $\{Mo^V{=}S\}^{3+}$, has been implicated in the turnover of industrial catalysts[1,2] and mononuclear, pterin-containing molybdenum enzymes such as xanthine oxidase and aldehyde oxidase.[3−6] However, mononuclear thiomolybdenyl complexes are extremely rare due to their susceptibility to redox, polynucleation, and hydrolysis reactions.[3−6] Consequently, our understanding of their chemical, structural, and spectroscopic characteristics is very limited. This stands in stark contrast to well advanced studies of molybdenyl, $\{Mo^V{=}O\}^{3+}$, complexes.[7−17] Indeed, only two mononuclear thiomolybdenyl complexes have ever been isolated and completely characterized. The first of these, $Tp^*Mo^VSCl_2$ [Tp^* = hydrotris(3,5-dimethylpyrazol-1-yl)borate], was reported by Young et al. in 1987.[18] This complex was prepared by treating Tp^*MoOCl_2 with boron sulfide and has been characterized by infrared, UV-visible, electron paramagnetic resonance (EPR), Raman, and X-ray absorption (XAS) and extended X-ray absorption fine structure (EXAFS) spectroscopy.[18−21] Crystallographic characterization of the compound has not been attempted due to the high probability of disorder of the thio and chloro ligands.[22] A number of related complexes, viz., $[Tp^*MoS(S_2PR_2)]^+$ and $[Tp'MoS(S_2PR_2)]^+$ [Tp' = hydrobis(3-isopropylpyrazol-1-yl)(5-isopropylpyrazol-1-yl)borate] have been generated in solution.[23,24] Recently, a second mononuclear thiomolybdenyl complex, $Mo^VS(N[R]Ar)_3$ {N[R]Ar = $N[C(CD_3)_2CH_3](3,5\text{-}Me_2C_6H_3)$}, was reported by Johnson et al.[25] This complex, a member of the series MoE(N[R]Ar)$_3$ (E = O, S, Se, Te), was prepared by oxidizing Mo(N[R]Ar)$_3$ with S_8 or ethylene sulfide. The MoE(N[R]Ar)$_3$ complexes exhibit rhombic EPR spectra with A_{Mo} values decreasing in the order Mo=O > Mo=S > Mo=Se > Mo=Te, consistent with increasing covalency in complexes of the heavier chalcogenides. The crystal structure of MoS(N[R]Ar)$_3$ revealed a distorted tetrahedral complex possessing a terminal thio ligand with an Mo=S distance of 2.1677(12) Å.

Synthetic access to a series of related thiomolybdenyl complexes would permit systematic spectroscopic and structural studies leading to a detailed electronic description of the $\{Mo^V{=}S\}^{3+}$ unit and insights into its vital roles in industrial and biological catalysis. We report here the synthesis and characterization of the complexes $Tp^*Mo^VSX_2$ [X = OPh, 2-(ethylthio)phenolate (etp), 2-(*n*-propyl)phenolate (pp); X_2 = benzene-1,2-diolate (cat), 4-methylbenzene-1,2-dithiolate (tdt), benzene-1,2-dithiolate (bdt)] and the crystal structures of $Tp^*MoS(etp)_2$ and $Tp^*MoS(bdt)$; the latter, features a pseudo-dithiolene co-ligand and is of direct relevance to molybdoenzyme intermediates such as the Very Rapid centre of xanthine oxidase, proposed to contain an $[Mo^VOS(dithiolene)]^-$ moiety.[3−6]

Results and Discussion

We have employed two general methods in the generation of Tp^*MoSX_2 complexes. The first, the reaction of Tp^*MoOX_2[9] with boron sulfide, is useful for the generation of species in situ (as demonstrated by EPR spectroscopy) but does not lend itself to isolation of the compounds. The second method, metathesis of Tp^*MoSCl_2[18] with salts of X^- or X_2^{2-}, permits the isolation of pure Tp^*MoSX_2 (e.g., X = OPh, etp, pp; X_2 = cat, bdt, tdt) following workup. The reactions are conveniently monitored by EPR spectroscopy, which reveals the clean replacement of Tp^*MoSCl_2 by product in reaction times of 2 to 16 h. Rapid anaerobic work-up, including volume reduction and passage through a short bed of silica, is essential to the isolation of pure products. As solids the compounds are moderately air-stable but recrystallizations and solution studies must be performed under strictly anaerobic conditions. The stability of the thiomolybdenyl complexes appears to be enhanced by the presence of very bulky *O*-donor co-ligands, such as

[a] School of Chemistry, University of Melbourne, Victoria 3010, Australia
Fax: (internat.) +61 (0)3 9347 5180
E-mail: cgyoung@unimelb.edu.au
[b] Stanford Synchrotron Radiation Laboratory, SLAC, P. O. Box 4349, MS 69, Stanford, CA 94309, U.S.A.

 © WILEY-VCH Verlag GmbH, 69451 Weinheim, 2001 1434−1948/01/0909−2227 $ 17.50+.50/0

etp and pp, or chelate ligands. The complexes have been characterized by microanalytical, mass spectrometric and spectroscopic methods. Clean electron-impact mass spectra with strong parent ions are observed for the more stable (etp, pp, cat, tdt, bdt) derivatives. The IR spectra of the complexes exhibit a single, strong ν(Mo=S) band in the range 505−490 cm^{-1}, as well as bands characteristic of Tp* and the *O*- or *S*-donor co-ligands.

The structures of Tp*MoS(etp)$_2$ and Tp*MoS(bdt) have been determined by X-ray crystallography and ORTEP diagrams are given in Figure 1 and Figure 2, respectively. The distorted octahedral complexes contain a terminal thio ligand, two monodentate *O*-donor ligands (etp) or a bidentate, dithiolenic, *S*-donor ligand (bdt), and a facial, tridentate Tp* ligand. The Mo−S(1) distances of 2.1279(10) Å and 2.1231(11) Å, respectively, are typical of Mo=S units observed in MoS(N[R]Ar)$_3$[25] and polynuclear complexes.[26] For Tp*MoS(etp)$_2$, the Mo−O(4) and Mo−O(5) distances are 1.953(2) Å and 1.951(2) Å and the associated Mo−O−C angles are 140.9(2)° and 134.4(2)°, respectively. The Mo atom lies 0.264(1) Å out of the plane of the O(4), O(5), N(21) and N(31) atoms toward the thio ligand and the S(1)−Mo−O angles are consequently opened to ca. 103°. The Mo−N(*n*1) distances are dictated by the relative *trans* influences of the co-ligands, the Mo−N(11) distance being lengthened by 0.104(6) Å relative to the other Mo−N bonds. A very similar *trans* influence of 0.105(5) Å is observed for Tp*MoO(etp)$_2$.[27] For Tp*MoS(bdt), the Mo−S(4) and Mo−S(5) distances are 2.3704(12) Å and 2.3668(12) Å, respectively, and the associated Mo−S−C angles are ca. 104.2°. The Mo atom lies 0.296(1) Å out of the plane of the S(4), S(5), N(21), and N(31) atoms and 0.592(7) Å out of the plane of the bdt ligand, toward the thio ligand. The Mo−N(11) distance is lengthened by ca. 0.2 Å relative to the other two Mo−N bonds. A comparatively large *trans* influence has also been observed for Tp*MoO(catCl$_4$) (catCl$_4$ = 1,2,3,4-tetrachlorobenzene-5,6-diolate)[12] and Tp*MoO(bdt);[13] steric interaction between bidentate ligands and the nearby 3-methyl group [C(11) in Figure 2] accounts for this lengthening as well as the discernable bend in the MoX$_2$ fragment about the E···E vector (E = O, S) (such that the benzene ring moves away from said methyl group). In the thiomolybdenyl complexes, there are no interactions between the terminal thio ligand and co-ligand sulfur atoms, the S···S distances (> 4.5 Å) being considerably larger than the van der Waals contact distance.

Related structures for the other members of the series have been established by molybdenum and sulfur K-edge XAS and EXAFS studies. MoK-edge EXAFS spectra exhibit a strong backscattering component consistent with the presence of a thiomolybdenyl unit, with Mo=S distances in the range 2.1−2.2 Å. Intense pre-edge features are seen in the S K-edge X-ray absorption spectra of the compounds (Figure 3). The most intense feature, at ca. 2466 eV, is characteristic of terminal thio ligation and is assigned to S(1s)→Mo=S π* transitions.[19] In each case, the pre-edge feature is broader than expected based on the experimental resolution and deconvolution of the band provides evidence

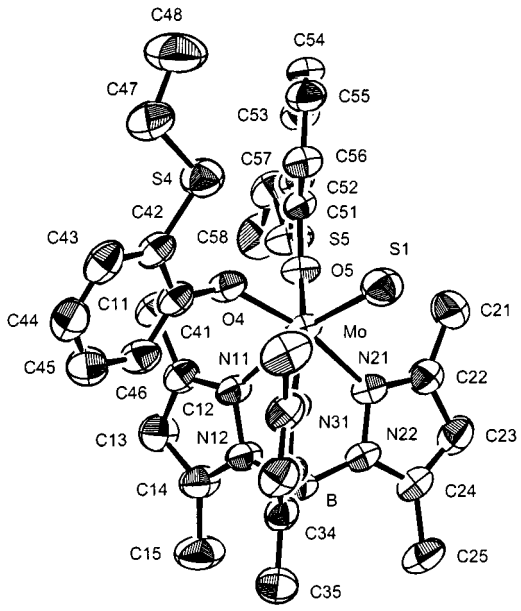

Figure 1. Molecular structure of Tp*MoS(etp)$_2$. Additional bond lengths [Å] and angles [deg]: Mo−N(11) 2.279(3), Mo−N(21) 2.174(3), Mo−N(31) 2.175(3); S(1)−Mo−O(4) 104.20(8), S(1)−Mo−O(5) 101.11(7), S(1)−Mo−N(11) 168.28(7), S(1)−Mo−N(21) 91.01(8), S(1)−Mo−N(31) 92.81(8), O(4)−Mo−O(5) 89.96(9)

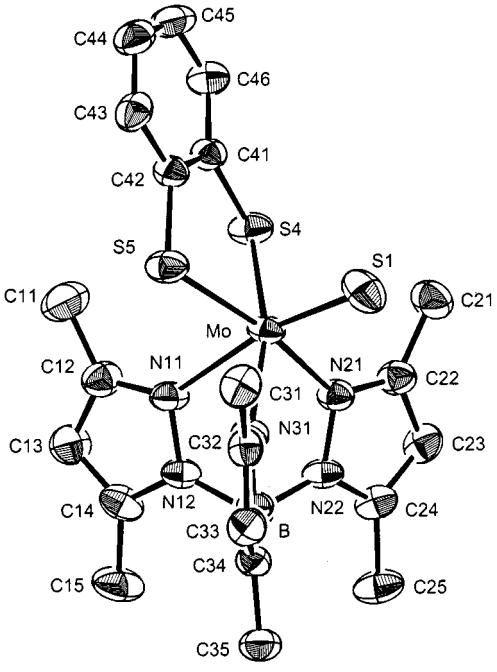

Figure 2. Molecular structure of Tp*MoS(bdt). Additional bond lengths [Å] and angles [deg]: Mo−N(11) 2.393(3), Mo−N(21) 2.201(3), Mo−N(31) 2.189(3); S(1)−Mo−S(4) 101.24(5), S(1)−Mo−S(5) 100.99(5), S(1)−Mo−N(11) 168.93(8), S(1)−Mo−N(21) 92.88(9), S(1)−Mo−N(31) 95.09(9), S(4)−Mo−S(5) 83.84(8)

for several transitions, probably to nearly degenerate Mo=S π* orbitals with S p and Mo d_{xz} and d_{yz} orbital character (*z* along Mo=S). For example, deconvolution of the spectrum of Tp*MoS(pp)$_2$ (Figure 3, a) reveals transitions at

2466.3 and 2467.0 eV. The precise origin of these and related transitions is currently under further experimental and theoretical interrogation. Similar pre-edge features are observed in the S K XAS spectra of Tp*WOSCl[28,29] and Tp^{Pr}MoOS(OPh) [Tp^{Pr} = hydrotris(3-isopropylpyrazol-1-yl)borate].[29] These complexes exhibit three distinct S K pre-edge features at energies different to those of the thiomolybdenyl complexes (around 2466.1, 2467.7 and 2469.6 eV compared to 2466 and 2469 eV for the thiomolybdenyl complexes). The feature at 2469 eV is tentatively assigned to a sulfur 1s→σ* transition associated with the Mo=S unit.

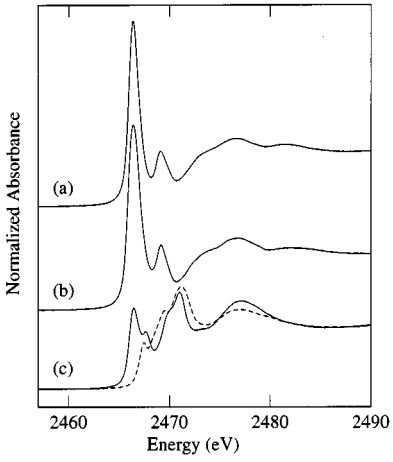

Figure 3. Selected sulfur K-edge X-ray absorption spectra of solids at 293 K. (a) Tp*MoS(pp)$_2$, (b) Tp*MoS(cat), (c) Tp*MoS(bdt), overlaid with the (dashed) spectrum of Tp*MoO(bdt)

The thiomolybdenyl complexes are EPR-active and generally exhibit highly anisotropic monoclinic frozen-glass EPR spectra (Table 1), with g_{iso} values substantially lower than their oxo analogues.[9] This results from a lowering of all the ***g*** tensor components, particularly g_3, rather than any change in the sense of the anisotropy. Very similar EPR parameters, with an unusually low g_3 and consequently high ***g*** anisotropy, characterize the three available Tp*MoS(OR)$_2$ complexes. These complexes exhibit relatively large A_{iso} values around 46×10^{-4} cm^{-1}. As a group, they also exhibit similar electronic spectra with intense LMCT absorptions in the regions 465−509 nm and 354−400 nm, and a d−d band at ca. 1300 nm (ε ca. 100 м$^{-1}$·cm^{-1}, cf. d−d band at 800 nm in oxo analogues[9,18]). Expressions for the principal ***g*** tensor components for compounds of this type have been presented;[18] the decrease in the tensor components is ascribed to a decrease in the energies of the ground to excited-state d−d transitions, most importantly $(d_{x^2-y^2})^1 \rightarrow (d_{xz})^1$ and $(d_{x^2-y^2})^1 \rightarrow (d_{yz})^1$, as a consequence of the weaker ligand field of the thio ligand. The similar A_{Mo} values for the Tp*MoSX$_2$ (X = Cl, OR) complexes implies an essentially similar ground state electronic configuration [viz., $(d_{x^2-y^2})^1$] with a similar degree of Mo−X covalency. The EPR spectrum of Tp*MoS(cat), which contains a pseudo ene-1,2-diolate moiety, differs dramatically from those of the Tp*MoS(OR)$_2$ complexes; for Tp*MoS(cat), g_1 and g_2 are very similar and g_{iso} is consequently increased compared to Tp*MoS(OR)$_2$. Similar "chelate effects" have been observed for analogous oxo complexes and may be ascribed to an increase in the energy of ground to excited-state transitions as a consequence of pπ−dπ interactions.[10] Higher g_{iso} and lower A_{iso} parameters characterize the thiolate complexes Tp*MoS(SPh)$_2$, Tp*MoS(bdt), and Tp*MoS(tdt), with the chelate complexes again exhibiting a higher g_{iso} than the non-chelated complex. The electronic spectra of Tp*MoS(cat), Tp*MoS(SPh)$_2$, and Tp*MoS(tdt) exhibit intense charge transfer bands only in accessible spectral regions; a near-IR absorption around 1300 nm is not observed. A multi-frequency EPR study of the compounds is currently underway.

Table 1. Selected EPR parameters (A values $\times 10^{-4}$ cm^{-1})

Compound	g_1	g_2	g_3	g_{iso}	Δg_i	A_{iso}
Tp*MoSCl$_2$[18]	1.941	1.921	1.919	1.928	0.022	46.8
Tp*MoS(etp)$_2$	1.961	1.914	1.864	1.909	0.097	46.6
Tp*MoS(pp)$_2$	1.956	1.909	1.858	1.902	0.098	46.6
Tp*MoS(OPh)$_2$	1.955	1.913	1.860	1.900	0.095	46.8
Tp*MoS(cat)	1.960	1.960	1.900	1.934	0.060	38.9
Tp*MoS(SPh)$_2$[a]	1.993	1.945	1.910	1.940	0.083	36.8
Tp*MoS(tdt)	2.000	1.971	1.919	1.956	0.081	36.9
Tp*MoS(bdt)	1.996	1.968	1.915	1.960	0.081	36.6

[a] Generated in situ, not isolated.

Success in derivatizing Tp*MoSCl$_2$ has provided synthetic access to a variety of thiomolybdenyl complexes of the type Tp*MoSX$_2$. These are currently the focus of systematic structural and spectroscopic, especially EPR, MCD, XAS, and EXAFS, studies aimed at elucidating the electronic structure of thiomolybdenyl and related units and understanding their roles in industrial and biological catalysis.

Experimental Section

General: All syntheses and solution studies were carried out under an atmosphere of dinitrogen using dried, deoxygenated, and distilled solvents. The method of Young et al.[18] was employed in the synthesis of Tp*MoSCl$_2$. The course of metathesis reactions were monitored using EPR spectroscopy and work-up was initiated upon complete conversion of Tp*MoSCl$_2$ to product. − Chromatographic separations and purifications were performed under dinitrogen using dried, deoxygenated solvents and Merck Art 7734 Kieselgel 60. Spectroscopic studies were carried out under strictly anaerobic conditions. − Mass spectra were obtained on a JOEL JMS-AX505H mass spectrometer. − Infrared spectra were recorded on a BIO-RAD FTS-165 FTIR spectrophotometer as pressed KBr discs. − EPR spectra were run on a Bruker ECS 106 ESR spectrometer, equipped with a flow through low temperature device, allowing frozen spectra to be recorded at approximately 120 K. The spectral parameters in Table 1 were obtained by inspection. − Electronic spectra were obtained on a Hitachi 150-20 spectrophotometer. − Microanalyses were performed by Atlantic Microlabs, Norcross, GA, USA.

Tp*MoS(etp)$_2$: 2-Ethylthiophenol (0.18 cm^3, 1.01 mmol) and triethylamine (0.15 cm^3, 1.01 mmol) were added to a stirred solution

of Tp*MoSCl$_2$ (250 mg, 0.5 mmol) in dichloromethane (30 cm^3). The solution rapidly turned a purple color, then became brown. After 4 h the volume of the solution was reduced by half and it was filtered through a bed (4−5 cm) of silica gel. The bed of silica was washed with dichloromethane (30 cm^3), then the combined filtrate and washings were reduced to a minimum volume and treated (dropwise) with methanol to precipitate the red crystalline product. Yield 150 mg (41%).

$C_{31}H_{40}BMoN_6O_2S_3$ (731.6): calcd. C 50.89, H 5.51, N 11.49, S 13.15; found C 51.06, H 5.27, N 11.69, S 13.30. − IR (KBr): $\tilde{\nu}$ = 2525, m, ν(BH); 1570, m; 1541, s, ν(CN); 1459, s; 1364, s; 1261, s; 1201, s; 1068, s; 857, s; 748, s; 693, s; 615, s; 500, s, ν(Mo=S). − Mass Spec: *m*/*z* [M − H]$^+$ 732.

Tp*MoS(bdt): 1,2-Benzenedithiol (0.1 cm^3, 0.90 mmol) and triethylamine (0.29 cm^3, 1.90 mmol) were added to a stirred solution of Tp*MoSCl$_2$ (450 mg, 0.90 mmol) in dichloromethane (30 cm^3). The solution rapidly turned a red color and after 2 h the volume of the solution was reduced to a minimum, filtered through a short bed of silica and recrystallized as described above for Tp*MoS(etp)$_2$. The yield of red crystals was 220 mg (43%). The analytical sample was purified by anaerobic column chromatography on silica gel using 3:2 dichloromethane/hexane as eluent, then recrystallized from dichloromethane/methanol.

$C_{21}H_{26}BMoN_6S_3{\cdot}0.5CH_3OH$ (581.4): calcd. C 44.41, H 4.85, N 14.45, S 16.54; found: C 44.02, H 4.77, N 14.40, S 16.49. − IR (KBr): $\tilde{\nu}$ = 2557, m, ν(BH); 1540, s, ν(CN); 1447, s; 1435, s; 1412, s; 1357, s; 1262, m; 1202, s; 1093, m; 1074, s; 1036, s; 854, m; 814, m; 790, s; 745, s; 692, m; 666, w; 647, w; 499, s, ν(Mo=S) cm^{-1}. − Mass Spec: *m*/*z* [M + H]$^+$ 568.

The other members of the series were prepared by essentially similar methods.

Crystal Structure Determination for Tp*MoS(etp)$_2$: Crystallographic data: $C_{31}H_{40}BMoN_6O_2S_3$, M = 731.65, triclinic, $P\bar{1}$, a = 10.825(2), b = 11.584(2), c = 14.428(2) Å, α = 86.735(11), β = 88.669(12), γ = 71.998(13)°, V = 1717.8(5) Å^3, d_c = 1.414 g·cm^{-3}, Z = 2. A total of 6039 unique data with 4871 reflections having $I > 2\sigma(I)$ were collected. The structure was solved by Patterson and direct methods (SHELXS-86)[30] and was refined on F^2 by a full-matrix least-squares procedure (SHELXL-97)[31] using all data. All hydrogens were included at geometrical estimates. R_1 [$I > 2\sigma(I)$] = 0.0390 and wR_2 (all data) = 0.0998. Figure 1 and Figure 2 were prepared using the program ORTEP.[32]

Crystal Structure Determination for Tp*MoS(bdt): Crystallographic data: $C_{21}H_{26}BMoN_6S_3$, M = 565.43, monoclinic, $P2_1/n$, a = 10.0296(13), b = 14.729(2), c = 16.846(2) Å, β = 95.456(10)°, V = 2477.3(6) Å^3, d_c = 1.516 g·cm^{-3}, Z = 4. A total of 4346 unique data with 2922 reflections having $I > 2\sigma(I)$ were collected and the structure was solved as described above. R_1 [$I > 2\sigma(I)$] = 0.0346 and wR_2 (all data) = 0.0967.

Crystallographic data (excluding structure factors) for the structures reported in this paper have been deposited with the Cambridge Crystallographic Data Centre as supplementary publications nos. CCDC-157193 and CCDC-157194. Copies of the data can be obtained free of charge on application to CCDC, 12 Union Road, Cambridge CB2 1EZ, UK [Fax: (internat.) +44−1223/336-033; E-mail: deposit@ccdc.cam.ac.uk].

X-ray Absorption Spectroscopy: X-ray absorption spectroscopy was carried out at the Stanford Synchrotron Radiation Laboratory with the SPEAR storage ring containing 60−100 mA at 3.0 GeV. Molybdenum K-edge spectra were collected on beamline 7−3 using a Si(220) double crystal monochromator with an upstream vertical aperture of 1 mm and a wiggler field of 1.8 T. Harmonic rejection was accomplished by detuning one monochromator crystal to approximately 60% off-peak. X-ray absorption was measured in transmittance using nitrogen-filled ionization chambers. The spectrum of molybdenum foil was collected simultaneously with that of the sample and data were calibrated with reference to the lowest energy inflection point of the standard (assumed to be 20003.9 eV). Samples were prepared in a boron nitride matrix and during data collection were maintained at a temperature of approximately 10 K using an Oxford Instruments liquid helium flow cryostat.

Sulfur K edge experiments were performed on beamline 6−2 using an Si(111) double crystal monochromator and wiggler field of 1.0 T. Harmonic rejection was accomplished by using a flat nickel coated mirror downstream of the monochromator adjusted so as to have a cutoff energy of about 4500 eV. Incident intensity was monitored using an ion chamber contained in a (flowing) helium-filled flight path. X-ray absorption was monitored by recording total electron yield and the energy scale was calibrated with reference to the lowest energy peak of the sodium thiosulfate standard ($Na_2S_2O_3{\cdot}5H_2O$) which was assumed to be 2469.2 eV. Samples were examined at ambient temperature. Peak positions in near-edge spectra were estimated by curve-fitting to a sum of pseudo-Voigt peaks using the program EDG FIT (pseudo-Voigt deconvolution).[33]

Acknowledgments

We gratefully acknowledge the financial support of the Australian Research Council and the Australian Department of Industry, Science and Technology. SSRL is funded by the Department of Energy (DOE) BES, with further support by DOE OBER and the NIH.

[1] E. G. Derouane, E. Pedersen, B. S. Clausen, Z. Gabelica, H. Topsøe, *J. Catal.* **1987**, *107*, 587−588.
[2] M. Rakowski DuBois, *Chem. Rev.* **1989**, *89*, 1−9.
[3] R. Hille, *Chem. Rev.* **1996**, *96*, 2757−2816.
[4] R. S. Pilato, E. I. Stiefel, in: *Bioinorganic Catalysis* (Ed.: J. Reedijk, E. Bouwman), Marcel Dekker, New York, **1999**, 2nd ed., p. 81−152.
[5] J. H. Enemark, C. G. Young, *Adv. Inorg. Chem.* **1993**, *40*, 1−88.
[6] C. G. Young, *J. Biol. Inorg. Chem.* **1997**, *2*, 810−816.
[7] H. B. Gray, C. R. Hare, *Inorg. Chem.* **1962**, *1*, 363−368.
[8] G. R. Hanson, A. A. Brunette, A. C. McDonell, K. S. Murray, A. G. Wedd, *J. Am. Chem. Soc.* **1981**, *103*, 1953−1959.
[9] W. E. Cleland, Jr., K. M. Barnhart, K. Yamanouchi, D. Collison, F. E. Mabbs, R. B. Ortega, J. H. Enemark, *Inorg. Chem.* **1987**, *26*, 1017−1025.
[10] C. S. J. Chang, D. Collison, F. E. Mabbs, J. H. Enemark, *Inorg. Chem.* **1990**, *29*, 2261−2267.
[11] M. D. Carducci, C. Brown, E. I. Solomon, J. H. Enemark, *J. Am. Chem. Soc.* **1994**, *116*, 11856−11868.
[12] P. Basu, M. A. Bruck, Z. Li, I. K. Dhawan, J. H. Enemark, *Inorg. Chem.* **1995**, *34*, 405−407.
[13] I. K. Dhawan, J. H. Enemark, *Inorg. Chem.* **1996**, *35*, 4873−4882.
[14] C. Balagopalakrishna, J. T. Kimbrough, T. D. Westmoreland, *Inorg. Chem.* **1996**, *35*, 7758−7768.
[15] S. Nipales, T. D. Westmoreland, *Inorg. Chem.* **1997**, *36*, 756−757.

[16] J. Swann, T. D. Westmoreland, *Inorg. Chem.* **1997**, *36*, 5348−5357.
[17] F. E. Inscore, R. McNaughton, B. L. Westcott, M. E. Helton, R. Jones, I. K. Dhawan, J. H. Enemark, M. L. Kirk, *Inorg. Chem.* **1999**, *38*, 1401−1410.
[18] C. G. Young, J. H. Enemark, D. Collison, F. E. Mabbs, *Inorg. Chem.* **1987**, *26*, 2925−2927.
[19] R. Singh, J. T. Spence, G. N. George, S. P. Cramer, *Inorg. Chem.* **1989**, *28*, 8−10.
[20] G. Backes, J. H. Enemark, T. M. Loehr, *Inorg. Chem.* **1991**, *30*, 1839−1842.
[21] D. Collison, D. R. Eardley, F. E. Mabbs, K. Rigby, M. A. Bruck, J. H. Enemark, P. A. Wexler, *J. Chem. Soc., Dalton Trans.* **1994**, 1003−1011.
[22] The structure of Tp*$MoOCl_2$ has been determined and the Cl and O atoms were found to be randomly disordered over the three sites *trans* to the N-donor atoms: G. Ferguson, B. Kaitner, F. J. Lalor, G. Roberts, *J. Chem. Res. (S)* **1982**, 6−7.
[23] L. J. Laughlin, C. G. Young, *Inorg. Chem.* **1996**, *35*, 1050−1058.
[24] C. G. Young, L. J. Laughlin, S. Colmanet, S. D. B. Scrofani, *Inorg. Chem.* **1996**, *35*, 5368−5377.
[25] A. R. Johnson, W. M. Davis, C. C. Cummins, S. Serron, S. P. Nolan, D. G. Musaev, K. Morokuma, *J. Am. Chem. Soc.* **1998**, *120*, 2071−2085.
[26] A. G. Orpen, L. Brammer, F. H. Allen, O. Kennard, D. G. Watson, R. Taylor, *J. Chem. Soc., Dalton Trans.* **1989**, S1−S83.
[27] R. W. Gable, J. P. Hill, C. G. Young, unpublished crystallographic study.
[28] A. A. Eagle, E. R. T. Tiekink, G. N. George, C. G. Young, *Inorg. Chem.* **2001**, *40*, in press.
[29] P. D. Smith, D. A. Slizys, G. N. George, C. G. Young, *J. Am. Chem. Soc.* **2000**, *122*, 2946−2947.
[30] G. M. Sheldrick, *SHELXS-86* **1986**, University of Göttingen, Germany.
[31] G. M. Sheldrick, *SHELXL-97* **1997**, University of Göttingen, Germany.
[32] C. K. Johnson, *ORTEP.* Report ORNL-5138, Oak Ridge National Laboratory, Oak Ridge, TN, **1976**.
[33] I. Pickering, G. N. George, *Inorg. Chem.* **1995**, *34*, 3142−3152.

Received January 31, 2001
[I01037]

Dinucleating Hybrid Ligands Providing a "Soft" P∩N and an Adjacent N-Rich Coordination Pocket − Controlled Synthesis of Unsymmetric Homodinuclear and Heterodinuclear Complexes

Matthias Konrad,[a] Susanne Wuthe,[a] Franc Meyer,*[a] and Elisabeth Kaifer[a]

Dedicated to Prof. Dr. Ernst-G. Jäger on the occasion of his 65th birthday

Keywords: Bridging ligands / Nickel / P,N ligands / Palladium / Bimetallic complexes

New unsymmetric dinucleating pyrazolate ligands with different chelating side arms in the 3- and 5-positions of the heterocycle have been prepared. These ligands provide a "soft" P∩N site and either an adjacent "N_3" (HL^a) or "N_2S_2" (HL^b) coordination pocket, and they have been employed to build homo- and heterobimetallic complexes featuring various types of asymmetry. Both L^a and L^b form the mixed-spin dinickel(II) chloride systems **4** and **5**, respectively, which in the former case dimerizes via Cl bridges to give a tetranuclear compound. In the heterobimetallic complex **6** the Pd^{II} is specifically housed within the P∩N compartment. All new complexes have been characterized by X-ray crystallography, and conformational and electronic coupling between the two metal ions of the dinuclear scaffolds have been analyzed.

Introduction

At present, research on di- and oligonuclear transition metal complexes is a flourishing field with major interests focused on the modeling of metallobiosites and on cooperative phenomena in catalysis and magnetism.[1−4] Among the diverse ligand frameworks designed and employed to hold two metal centers in close proximity and to induce the sought-after cooperativity, pyrazole derivatives appear particularly suited due to their well-known ability to span adjacent metal ions at a favorable distance.[5] Further control of the metal−metal separation, as well as of the steric and electronic properties of the individual metal ions can be achieved by appropriate chelating side arms attached to the 3- and 5-positions of the heterocycle. Most of these multidentate pyrazolate systems known to date are of the symmetric type,[6−11] although the individual metal ions are often assumed to play quite distinct roles in bimetallic catalysis, both in nature and in synthetic systems. The development of unsymmetrical dinucleating ligands that would give unsymmetric homobimetallic complexes, or might allow the controlled synthesis of heterobimetallic complexes is thus highly desirable.[2] However, a major obstacle to a more widespread use of such systems is their limited accessibility since, in general, the synthesis of unsymmetrical dinucleating ligands is much more arduous than the synthesis of the symmetrical analogues. Recently, we developed a versatile synthetic route which provides access to asymmetric pyrazole-based ligand matrices, providing two different coordination compartments.[11] These ligands enabled a predictable preparation of bimetallic complexes that exhibit various kinds of asymmetry. Initial emphasis was laid on the design and study of dinucleating systems that provide chemically distinct N- and S-rich donor atom sets for the two metal ions. Following the same synthetic strategy, we now report on the preparation and coordination chemistry of new compartmental type **A** ligands (Scheme 1) that comprise a bidentate P∩N binding site and an adjacent N-rich coordination pocket. Chelating P∩N ligands have been extensively used in organometallic chemistry, in particular in palladium-catalyzed reactions.[12] It is our intention in this context to tune the activity or selectivity of substrate transformations occurring at such organometallic centers by the cooperative effect of a second Lewis acidic metal ion positioned in close proximity of the active site. The present contribution lays a foundation for this goal by providing appropriate ligand frameworks that might help to preorganize the two metal ions, and by demonstrating the suitability of these new ligands for the building of heterobimetallic Pd−M complexes.

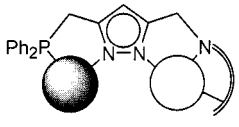

A

Scheme 1

Results and Discussion

Ligand Synthesis

The synthesis of type **A** ligands was accomplished according to the strategy developed previously (Scheme 2).[11] The unsymmetrically substituted pyrazole derivative **1** is

[a] Anorganisch-Chemisches Institut der Universität Heidelberg, Im Neuenheimer Feld 270, 69120 Heidelberg, Germany
Fax: (internat.) + 49-(0)6221/545707
E-mail: franc.meyer@urz.uni-heidelberg.de

 © WILEY-VCH Verlag GmbH, 69451 Weinheim, 2001 1434−1948/01/0909−2233 $ 17.50+.50/0

obtained by cycloaddition of ethyl diazoacetate and propynol,[13] and subsequent treatment with thionyl chloride.[11] Of the two different side arms, the diphenylphosphanyl moiety is introduced first by treating **1** with $KPPh_2$ to establish the P∩N site. The ester group in **2** is then converted into an amide function by treatment with different lithiated amines. Reduction of the resulting amide in **3a**,**b** completes the assembly of the second coordination compartment, which provides an "N_3" donor set in HL^a or an "N_2S_2" donor set in HL^b. The complexation potential of such individual P∩N,[6] "N_3"[10] and "N_2S_2"[11] sites has previously been explored to some extent in coordination compounds of related symmetric pyrazolate ligand systems.

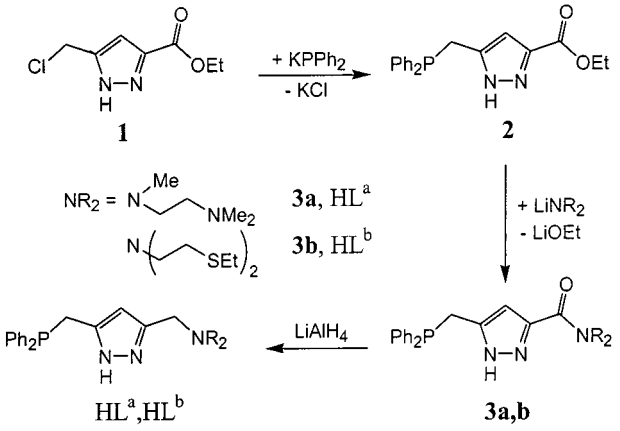

Scheme 2

Synthesis and Structural Characterization of Complexes

Homobimetallic dinickel(II) complexes of HL^a and HL^b were studied in order to provide some insight into the specific coordination behavior of the different donor sites.

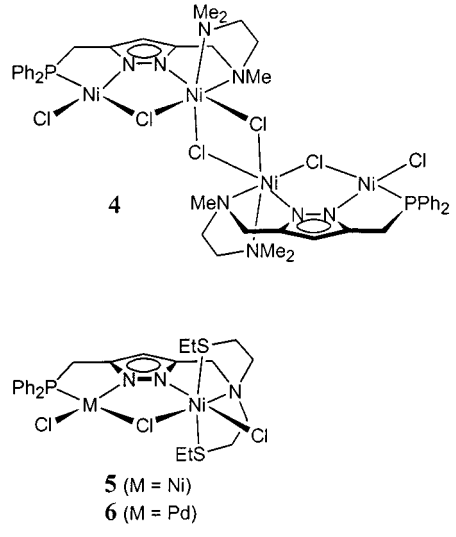

Scheme 3

Complexes $[L^aNi_2Cl_3]_2$ (**4**) and $L^bNi_2Cl_3$ (**5**) (Scheme3) were prepared by deprotonation of the pyrazole ligand with KO*t*Bu and subsequent treatment with 2 equiv. of $NiCl_2{\cdot}6H_2O$. Crystalline red material was obtained by diffusion of petroleum ether into solutions of the products in CH_2Cl_2 (**5**) or $CH_2Cl_2/CHCl_3$ (**4**), respectively. Complex **4** crystallizes in the space group *Pbcn*, while **5** crystallizes in the space group *Pc* with two independent molecules in the unit cell. The molecular structures of the complexes as determined by X-ray crystallography are depicted in Figures 1 and 2 together with selected atom distances and bond angles.

In both cases, the nickel ions are nested within their respective coordination compartments. The P∩N donor set exerts a stronger ligand field and brings about a low-spin configuration with an approximate square-planar coordination environment around its bound nickel ion [sum of the four angles around Ni1 in **4** 360.3(7)° and around Ni2 in **5** 359.9(6)°; magnetic measurements confirm the presence of only one high-spin nickel(II) ion per bimetallic entity in both **4** and **5**]. In contrast, the nickel ions in the "N_3" and "N_2S_2" sites are six-coordinate, which in the former case results from dimerization of two pyrazolate-based bimetallic moieties through a double Cl bridge to form the tetranuclear compound $[L^aNi_2Cl_3]_2$ (**4**). Similar structural motifs have also been observed for nickel chloride complexes of related symmetric pyrazolate ligand systems providing either two "N_3" or two "N_2S_2" compartments.[10,11] According to a common classification,[2a,14] **4** and **5** exhibit various kinds of asymmetry, e.g. donor atom asymmetry and coordination number asymmetry. As expected, bond lengths are generally shorter for the low-spin nickel(II) ions, which is most obvious for the asymmetrically bridging Cl2 atom within each pyrazolate-based dinuclear array: d(Ni1−Cl2) = 2.240(9) Å versus d(Ni2−Cl2) = 2.512(1) Å in **4** and d(Ni2−Cl2) = 2.255(2)/2.275(1) Å versus d(Ni1−Cl2) = 2.436(4)/2.432(8) Å in **5**. The double Cl bridges in **4** are asymmetric as well: d(Ni2−Cl3) = 2.394(5) versus d(Ni2−Cl3 A) = 2.456(7) Å. In all cases the distance between the low-spin Ni^{II} and the Cl atom *trans* to P is significantly larger than those between the low-spin Ni^{II} and the terminal Cl, because of the greater *trans* influence of the P ligand and the bridging position of the former Cl atom. A number of rather short interactions (< 3.0 Å) with C−H groups are present for all Cl ligands, which may be considered as weak hydrogen-bond interactions.[15]

Owing to the very different characteristics of their adjacent donor compartments, HL^a and HL^b appear to be well preorganized for the controlled synthesis of bimetallic complexes containing two different metal ions in distinct environments. When HL^b was first deprotonated and subsequently treated with 1 equiv. each of $PdCl_2$ and $NiCl_2{\cdot}6H_2O$ in a sequential fashion, the heterobimetallic green complex $L^bNiPdCl_3$ (**6**) was obtained in excellent yield. FAB mass spectrometry did confirm the heterodinuclear nature of the complex and did not reveal any indication of the presence of its homobimetallic analogues, i.e. of **5** or $L^bPd_2Cl_3$, thus suggesting that the complexation reaction is highly selective and that each of the different metal ions binds specifically to one of the distinct ligand compartments.

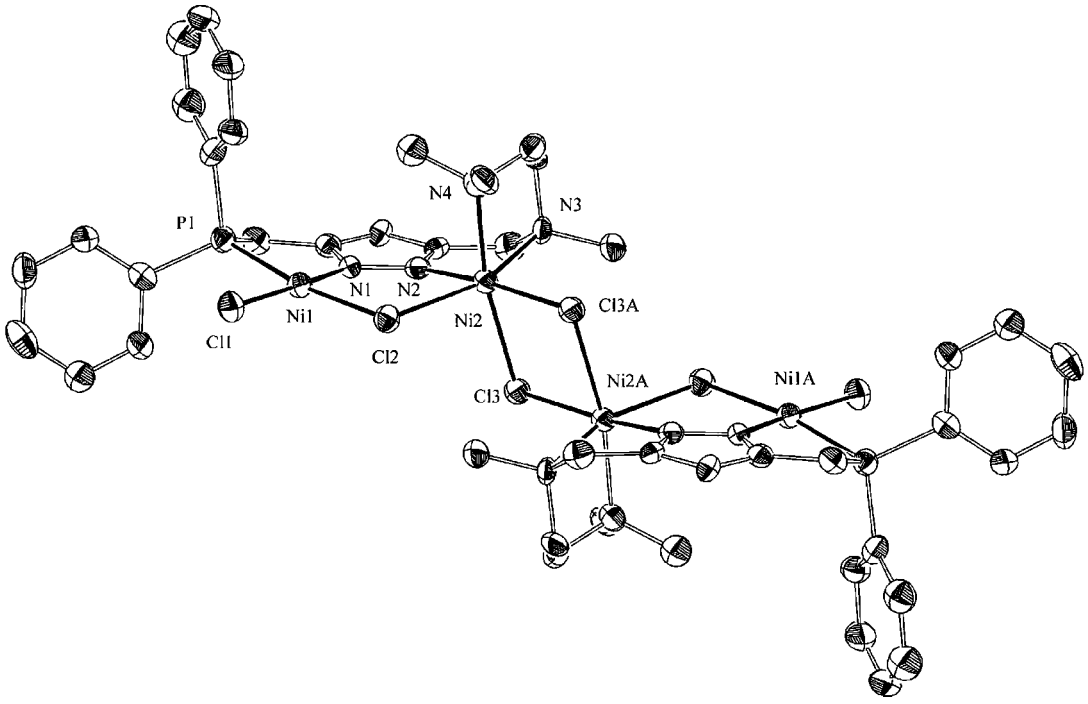

Figure 1. View of the molecular structure of **4**; in the interests of clarity all hydrogen atoms have been omitted; selected interatomic distances [Å] and bond angles [°]: Ni1−N1 1.869(2), Ni1−P1 2.155(8), Ni1−Cl1 2.171(6), Ni1−Cl2 2.240(9), Ni2−N2 1.997(2), Ni2−N3 2.200(3), Ni2−N4 2.151(2), Ni2−Cl2 2.512(3), Ni2−Cl3 2.394(5), Ni2−Cl3A 2.456(7), Ni1···Ni2 3.780(6), Ni2···Ni2A 3.705(1); Ni1−Cl2−Ni2 105.24(3), Ni2−Cl3−Ni2A 99.58(3), N1−Ni1−P1 83.06(7), P1−Ni1−Cl1 91.75(3), Cl1−Ni1−Cl2 92.76(3), Cl2−Ni1−N1 92.80(7)

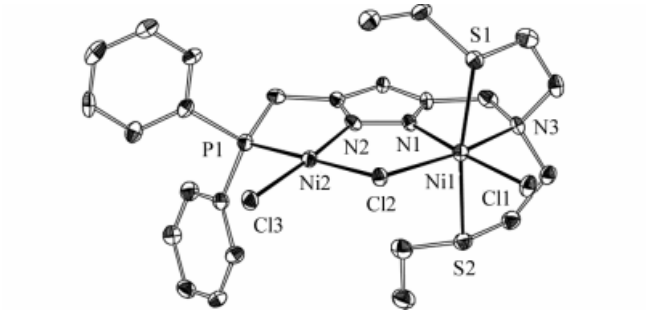

Figure 2. View of the structure of one of the two independent molecules of **5**; in the interests of clarity all hydrogen atoms have been omitted; selected interatomic distances [Å] and bond angles [°] [values for the second independent molecule in brackets]: Ni1−N1 1.958(5) [1.989(5)], Ni1−N3 2.151(5) [2.168(5)], Ni1−Cl1 2.357(2) [2.384(1)], Ni1−Cl2 2.436(4) [2.432(8)], Ni1−S1 2.473(2) [2.428(1)], Ni1−S2 2.435(1) [2.439(1)], Ni2−N2 1.857(5) [1.855(5)], Ni2−P1 2.137(2) [2.141(2)], Ni2−Cl2 2.255(2) [2.275(1)], Ni2−Cl3 2.168(1) [2.158(2)], Ni1···Ni2 3.697(5) [3.707(2)]; Ni1−Cl2−Ni2 103.9(5) [103.8(4)], N2−Ni2−P1 84.4(5) [83.6(8)], P1−Ni2−Cl3 88.6(4) [88.5(1)], Cl3−Ni2−Cl2 93.4(1) [94.4(1)], Cl2−Ni2−N2 93.4(8) [93.3(2)]

Two different types of single crystals suitable for a crystallographic analysis were obtained by layering solutions of complex **6** in CH_2Cl_2 with light petroleum ether. In one form (**6′**), the compound crystallizes in the space group *Pn* with two independent molecules in the unit cell. In the second form (**6′′**), the compound crystallizes in the space group $P2_1/n$ with two CH_2Cl_2 solvent molecules included in the crystal lattice. The overall constitution of **6** is the same in both crystal forms, but details of its molecular features are distinct, as described below. The structures of **6′′** and of one of the two independent (but similar) molecules of **6′** are depicted in Figures 3a and b together with selected atom distances and bond angles.

The bimetallic framework of **6** is closely related to the structure of its homobimetallic dinickel(II) analogue **5**. As anticipated, the palladium atom is found in an approximate square-planar environment within the P∩N pocket, while the nickel ion is located in the "N_2S_2" compartment. Geometric parameters of the Pd fragment are as expected [sum of the four angles around the Pd atom equal to 359.9(6)/360.0(6)/359.9(2)° for **6′** and **6′′**, respectively] and are comparable with the findings for a related $PdCl_2$ complex of a mononucleating pyrazolate-based P∩N ligand.[16] Geometric characteristics of the nickel ions housed in the "N_2S_2" compartments are basically identical for all cases. In particular, the Ni1("N_2S_2")−N1(pyrazole) bond lengths are found in the same range [1.965(5) − 1.991(5) Å] for **5**, **6** and for the symmetric ("N_2S_2")$_2$ complex reported previously.[11] This suggests that the choice of the second metal ion (high-spin Ni^{II} or low-spin Ni^{II}, or Pd^{II}) may only have a slight influence on the electronic properties of the six-coordinate nickel ion within the "N_2S_2" binding pocket. This is further analyzed by means of electrochemical experiments as described below.

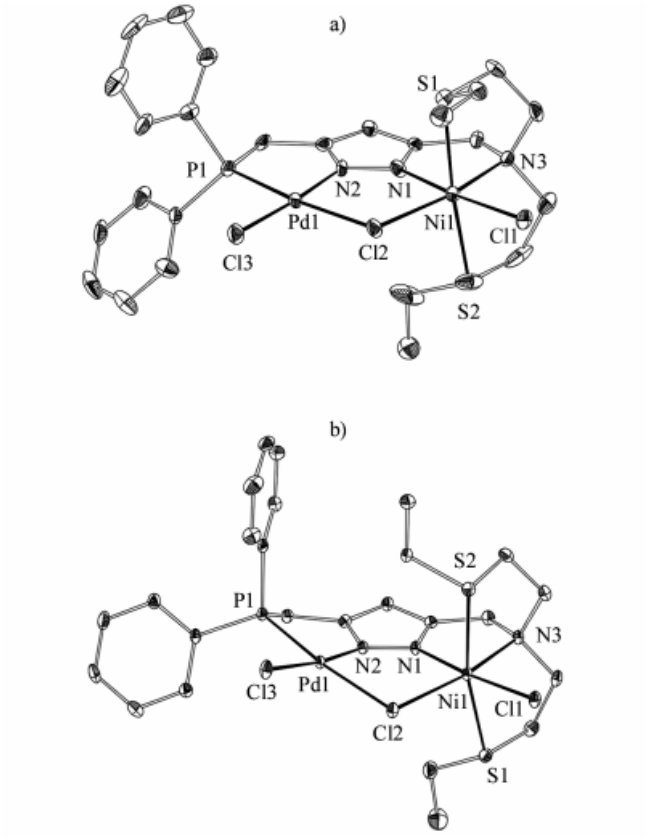

Figure 3. View of the structures of **6′** (a) (one of the two independent molecules) and **6′′** (b); in the interests of clarity all hydrogen atoms have been omitted; selected interatomic distances [Å] and bond angles [°]: **6′** [values for the second independent molecule in brackets]: Pd1−N2 1.989(7) [2.010(7)], Pd1−P1 2.219(2) [2.214(3)], Pd1−Cl2 2.395(2) [2.394(2)], Pd1−Cl3 2.299(2) [2.296(2)], Ni1−N1 1.981(6) [1.986(8)], Ni1−N3 2.166(7) [2.171(7)], Ni1−S1 2.455(2) [2.454(3)], Ni1−S2 2.397(3) [2.464(3)], Ni1−Cl1 2.366(2) [2.325(3)], Ni1−Cl2 2.452(2) [2.420(2)], Pd1···Ni1 3.808(2) [3.779(2)]; Pd1−Cl2−Ni1 103.57(8) [103.44(9)], N2−Pd1−P1 81.6(2) [81.7(2)], P1−Pd1−Cl3 94.11(8) [93.50(9)], Cl3−Pd1−Cl2 91.98(8) [93.21(9)], Cl2−Pd1−N2 92.3(2) [91.5(2)]; **6′′**: Pd1−N2 1.993(2), Pd1−P1 2.221(1), Pd1−Cl2 2.425(5), Pd1−Cl3 2.313(7), Ni1−N1 1.984(2), Ni1−N3 2.173(2), Ni1−S1 2.408(5), Ni1−S2 2.427(1), Ni1−Cl1 2.369(3), Ni1−Cl2 2.479(2), Pd1···Ni1 3.806(4); Pd1−Cl2−Ni1 101.79(3), N2−Pd1−P1 81.84(7), P1−Pd1−Cl3 92.54(3), Cl3−Pd1−Cl2 96.00(3), Cl2−Pd1−N2 89.49(7)

The most noticeable difference between the various crystalline forms of **6** is the conformation adopted by the five-membered chelate ring of the bidentate P∩N site and the resulting displacement of the P and Pd atoms out of the plane defined by the pyrazolate heterocycle. This is best visualized from a superposition of the P∩N subunits of the individual solid-state molecular structures of **6** shown in Figure 4 (one of the two independent molecules of **5** has been included as well, although the metal−ligand bond lengths are slightly shorter for Ni than for Pd). These various structures reflect individual geometric points on the pathway of interconversion between the λ and the δ conformers of the five-membered chelate ring. A trajectory of such fluxional motion has to pass through a flattened planar ring structure, which is represented by one of the two independent molecules of **6′** (see also Figure 3a). The observation of different static geometries for the P∩N chelate ring located between the limiting λ and δ conformers − which at the same time exhibit very similar geometric arrangements of the Ni("N_2S_2") coordination site − confirms that the two subunits of the bimetallic pyrazolate framework are conformationally largely decoupled. Conformational interconversion of the P∩N coordination unit is evidently facile, and each particular situation observed in the solid state should thus be mainly determined by intermolecular crystal-packing interactions.

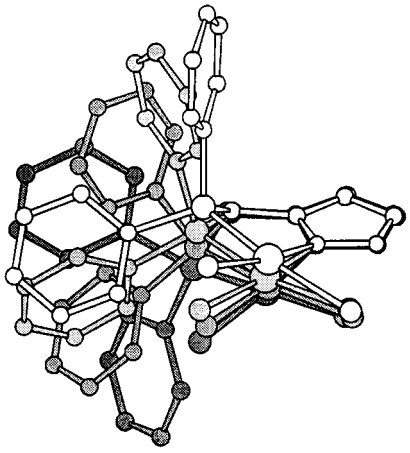

Figure 4. Overlay of the P∩N fragments of the solid-state structures of **5** (one of the two independent molecules), **6′** (both independent molecules), and **6′′**

Spectroscopy and Electrochemistry

While any comprehensive NMR-spectroscopical characterization of the complexes is hampered by their paramagnetic nature, broad low-field shifted ^{31}P NMR signals of the diamagnetic subunits are still found at δ = +241 and +257 for CD_2Cl_2 solutions of **4** and **5**, respectively. In the case of **6**, poor solubility precludes the detection of its ^{31}P NMR resonance.

The electronic absorption spectrum of **6** in CH_2Cl_2/MeCN (5:1) shows two weak bands at λ = 1100 (ν_1; ε = 26 $M^{-1}\cdot cm^{-1}$) and 620 nm (ν_2; ε = 12 $M^{-1}\cdot cm^{-1}$) that are assigned to spin-allowed transitions from $^3A_{2g}$ to $^3T_{2g}$ and $^3T_{1g}(F)$ for the six-coordinate Ni^{II}. The ν_3 band [$^3A_{2g}$ to $^3T_{1g}(P)$] expected for a near-octahedral d^8 ion[17] seems to be masked by strong high-energy absorptions extending as low as λ = 450 nm [peaks at λ = 336 nm (ε = 1710 $M^{-1}\cdot cm^{-1}$) and 301 nm (ε = 2620 $M^{-1}\cdot cm^{-1}$)]. These bands presumably correspond to intraligand and LMCT excitations. From the ν_1 band a ligand-field value of Δ_{oct} = 9090 cm^{-1} can be deduced for the nickel(II) ion in **6**. Complex **5** likewise features a low-intensity ν_1 band (λ = 1095 cm^{-1}; ε = 35 $M^{-1}\cdot cm^{-1}$), indicating Δ_{oct} = 9130 cm^{-1}. The almost identical ligand-field splitting observed for the high-spin Ni^{II} in both **5** and **6** confirms the conclusion already derived from the structural data, i.e. the choice of the second metal ion (either Pd^{II} in **6** or low-spin Ni^{II} in **5**) does not significantly alter the electronic situation at the high-spin ("N_2S_2")Ni^{II} site. Δ_{oct} for a related symmetrical dinickel(II)

complex that is composed of two identical "N_2S_2" compartments was found to be 8730 cm^{-1}.[11] An additional strong absorption for **5** at $\lambda = 498$ nm ($\varepsilon = 690$ $M^{-1}\cdot cm^{-1}$) is assigned to the square-planar low-spin Ni^{II}, presumably masking the much weaker ν_2 band. Intraligand and LMCT excitations dominate the spectrum of **5** below 350 nm, but a further d-d absorption is discernible as a shoulder at $\lambda =$ 379 nm ($\varepsilon \approx 645$ $M^{-1}\cdot cm^{-1}$).

Complexes **5** and **6** have been studied by cyclic voltammetry in CH_2Cl_2 solution (Figure 5). The dinickel(II) complex **5** undergoes a quasi-reversible oxidation at +1.00 V ($\Delta E = 162$ mV) versus the saturated calomel electrode (SCE), closely followed by further anodic processes at higher potential. The first oxidation wave at +1.00 V can be assigned to the six-coordinate nickel ion within the "N_2S_2" compartment, by comparison with the electrochemical properties of the PdNi compound **6** as well as the symmetric ("N_2S_2")$_2$dinickel(II) complex studied previously.[11] Complex **6** features a reversible oxidation at $E_{1/2} = +1.04$ V [i_{pa}/i_{pc} close to 1; $i_{pc}/v^1/_2 \approx$ const.; $\Delta E_p = 115$ mV with $\Delta E_p(Cp_2Fe/Cp_2Fe^+) = 120$ mV under the same experimental conditions] that is assigned to the formation of the $Pd^{II}Ni^{III}$ species. In this case, further oxidation processes are only observed at much higher potentials above +1.5 V. Obviously, oxidation of the nickel ion in the "N_2S_2" binding pocket is not significantly influenced by the choice of either a low-spin Ni^{II} or a Pd^{II} ion in the nearby P∩N site. This is in accordance with the above interpretation of the electronic spectra and structural features of **5** and **6**. The symmetric ("N_2S_2")$_2$dinickel(II) complex was shown to undergo a reversible first oxidation at $E_{1/2} = +0.87$ V, followed by a further oxidation process at $E_p^{ox} = +1.26$ V, indicating that Ni^{III} within the "N_2S_2" compartment is somewhat more efficiently stabilized by a second high-spin Ni^{II} ion than by an adjacent low-spin Ni^{II} (or Pd^{II}) as in **5** and **6**. Cathodic processes are irreversible for both **5** and **6**, with $E_p^{red} = -1.22$ V for the NiNi compound, and an ill-defined cyclic voltammetric response with a peak around −1.6 V for the PdNi species (all values at scan rate 200 mVs^{-1}).

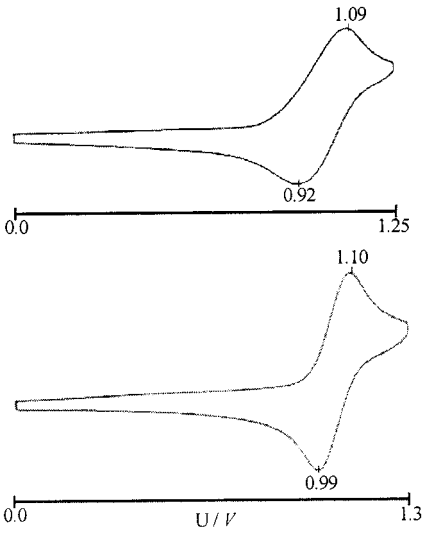

Figure 5. Cyclic voltammograms of complex **5** (top) and **6** (bottom) in CH_2Cl_2 containing 0.1 M $nBu_4N^+PF_6^-$ at a scan rate of 200 mVs^{-1}

Conclusions

New dinucleating ligands have been synthesized that feature two distinct binding pockets: a "soft" P∩N site, and either an adjacent "N_3" (HL^a) or "N_2S_2" (HL^b) compartment. These systems proved suitable for the preparation of unsymmetric bimetallic complexes in a controlled and predetermined fashion. In homobimetallic $(Ni^{II})_2$ compounds, a mixed-spin configuration is enforced by the strongly different ligand fields of the two binding pockets, while in a heterobimetallic $Ni^{II}Pd^{II}$ complex the different metal ions are selectively incorporated into their respective binding pockets, i.e. the Pd^{II} is exclusively nested in the P∩N site. Structural, spectroscopic and electrochemical features of the bimetallic systems indicate that the two coordination subunits are only moderately coupled with regard to conformational and electronic aspects. It is now hoped that these ligands will provide tailored scaffolds for the synthesis of novel bimetallic systems combining an organometallic and a Werner-type fragment in close proximity, which might enable unusual cooperative effects in metal-mediated substrate transformations.

Experimental Section

General Procedures and Methods: All manipulations were carried out under dry nitrogen by employing standard Schlenk techniques. Compound **1** was prepared as reported.[11] Solvents were dried according to established procedures, all other chemicals were used as purchased. Microanalyses: Mikroanalytische Laboratorien des Organisch-Chemischen Instituts der Universität Heidelberg. − NMR spectra: Bruker AC 200 at 200.13 (^{1}H) and 50.32 (^{13}C) MHz; solvent signal as chemical shift reference ($CDCl_3$: $\delta_H = 7.27$; $\delta_C = 77.0$). − Cyclic voltammetry: PAR equipment (potentiostat/galvanostat 273), in 0.1 M Bu_4NPF_6/CH_2Cl_2. Potentials in V on glassy carbon electrode, referenced to SCE at ambient temperature. − IR spectra: Perkin−Elmer 983G; recorded as KBr pellets. − FAB-MS spectra: Finnigan MAT 8230. − UV/Vis spectra: Perkin−Elmer Lambda 19; recorded in CH_2Cl_2 (**5**) or CH_2Cl_2/MeCN 5:1 (**6**). − Magnetic measurement: Bruker Magnet B-E 15 C8, field-controller B-H 15, Sartorius microbalance M 25 D-S. Experimental susceptibility data were corrected for the underlying diamagnetism.

Ethyl 5-[(Diphenylphosphanyl)methyl]-1*H*-pyrazole-3-carboxylate (2): A solution of diphenylphosphane (4.1 g, 22.0 mmol) in THF (100 mL) was treated with 1 equiv. of KO*t*Bu (2.5 g, 22.0 mmol). The red solution was stirred for 1 h, cooled to −70 °C and a solution of ethyl 5-(chloromethyl)pyrazole-3-carboxylate[11] (1.9 g, 10.0 mmol) in THF (50 mL) was slowly added. After warming to room temperature, the solution was left stirring overnight, then quenched with saturated NH_4Cl solution. The organic phase was dried with $MgSO_4$ and filtered. The solvent was evaporated in vacuum and the residue was redissolved in a small amount of Et_2O. The product was precipitated as a white powder by addition of light petroleum ether, filtered and dried in vacuum to yield 2.9 g

(8.5 mmol, 85%) of **2**. – ^{1}H NMR: δ = 1.33 (t, J_{HH} = 7.1 Hz, 3 H, CH_3), 3.51 (s, 2 H, PCH_2), 4.31 (q, J_{HH} = 7.1 Hz, 2 H, OCH_2), 6.51 (s, 1 H, CH^{pz}), 7.30–7.45 (m, 10 H, CH^{ar}). – ^{13}C NMR: δ = 14.0 (CH_3), 25.8 (d, $^1J_{CP}$ = 15.9 Hz, PCH_2), 60.6 (OCH_2), 107.3 (d, $^3J_{CP}$ = 5.3 Hz, $C^{pz,4}$), 128.3–132.6 (C^{ar}), 137.2 (d, $^2J_{CP}$ = 14.6 Hz, $C^{q,ar}$), 140.8 ($C^{pz,3}$), 143.4 (d, $^1J_{CP}$ = 10.9 Hz, $C^{pz,5}$), 161.5 (CO). – ^{31}P NMR: δ = –16.4. – MS (FAB*): m/z* (%) = 338 (100) [M^+], 309 (10) [M^+ – Et], 292 (12) [M^+ – OEt], 261 (9) [M^+ – Ph], 185 (100) [PPh_2^+], 183 (95) [dibenzophosphole$^+$]. – $C_{19}H_{19}N_2O_2P$ (338.35): calcd. C 67.45, H 5.66, N 8.28; found C 66.71, H 5.70, N 8.15.

***N*-[2-(Dimethylamino)ethyl]-5-[(diphenylphosphanyl)methyl]-*N*-methyl-1*H*-pyrazole-3-carboxamide (3a):** A solution of BuLi (3.4 mL, 2.5 M) in hexane was added to a solution of trimethylethylenediamine (1.8 g, 17.2 mmol) in THF (75 mL) at –70 °C. This mixture was slowly added to a solution of **2** (2.9 g, 8.6 mmol) in THF (150 mL) at –70 °C. After warming to room temperature, the solution was left stirring overnight, then quenched with saturated NH_4Cl solution and the aqueous phase extracted several times with Et_2O. The combined organic phases were dried with $MgSO_4$ and filtered. After evaporation of the solvent in vacuum, the product **3a** (2.7 g, 81%) remained as a yellow oil. – ^{1}H NMR: δ = 2.30 (s, 6 H, NMe_2), 2.57 (m, 2 H, CH_2), 3.01/3.15 (br, 3 H, NMe, *Z*/*E*), 3.44 (s, 2 H, PCH_2), 3.57 (br, 2 H, CH_2), 6.15/6.33 (br, 1 H, CH^{pz}), 7.29–7.44 (m, 10 H, CH^{ar}). – ^{13}C NMR: δ = 27.2 (br, PCH_2), 33.8/37.1 (NMe, *Z*/*E*), 46.2 (NMe_2), 45.5/49.5 (CH_2, *Z*/*E*), 56.4/57.1 (CH_2, *Z*/*E*), 106.8/107.5 ($C^{pz,4}$), 128.4–132.8 (C^{ar}), 138.0 (d, $^1J_{CP}$ = 10.7 Hz, $C^{q,ar}$), $C^{pz,3}$/$C^{pz,5}$ not observed, 162.4 (CO). – ^{31}P NMR: δ = –16.5. – MS (EI): *m/z* (%) = 395 (16) [M^+], 58 (100) [$CH_2NMe_2^+$]. – $C_{22}H_{27}N_4OP$ (394.45): calcd. C 66.99, H 6.89, N 14.20, P 7.85; found C 66.98, H 7.05, N 13.80, P 8.24.

5-[(Diphenylphosphanyl)methyl]-*N*,*N*-bis[2-(ethylsulfanyl)ethyl]-1*H*-pyrazole-3-carboxamide (3b): Compound **3b** was synthesized as described for **3a** using bis[2-(ethylsulfanyl)ethyl]amine[11] (3.3 g, 17.2 mmol). Yield (3.8 g, 91%). – ^{1}H NMR: δ = 1.25 (m, 6 H, CH_3), 2.48–2.78 (m, 8 H, SCH_2), 3.46 (s, 2 H, PCH_2), 3.64 (m, br, 2 H, NCH_2), 3.79 (m, br, 2 H, NCH_2), 6.34 (s, 1 H, C^{pz}), 7.33–7.51 (m, 10 H, CH^{ar}). – ^{13}C NMR: δ = 14.7 (CH_3), 25.8/26.2 (PCH_2/SCH_2) 28.6/30.0 (SCH_2, *Z*/*E*), 47.6/49.4 (NCH_2, *Z*/*E*), 106.8 ($C^{pz,4}$), 128.3–132.6 (C^{ar}), 137.1 (d, $^1J_{CP}$ = 14.0 Hz, $C^{q,ar}$), $C^{pz,3}$/$C^{pz,5}$ not observed, 162.4 (CO). – ^{31}P NMR: δ= –17.0. – MS (EI): *m/z* (%) = 486 (8) [M^+], 457 (87) [M^+ – Et], 397 (54) [M^+ – CH_2CH_2SEt], 293 (68) [M^+ – $N(CH_2CH_2SEt)_2$], 185 (64) [PPh_2^+], 183 (76) [dibenzophosphole$^+$], 89 (100) [$CH_2CH_2SEt^+$]. – $C_{25}H_{32}N_3OPS_2$ (485.65): calcd. C 61.83, H 6.64, N 8.65; found C 61.68, H 6.63, N 8.02.

***N*²-{5-[(Diphenylphosphanyl)methyl]-1*H*-pyrazol-3-yl}-*N*¹,*N*¹,*N*²-trimethylethane-1,2-diamine (HL^a):** A solution of **3a** (2.7 g, 6.8 mmol) in THF (100 mL) was slowly added to a suspension of $LiAlH_4$ (0.24 g, 6.8 mmol) in THF (50 mL). After stirring overnight, the mixture was refluxed for 30 min, then cooled to 0 °C and hydrolyzed by dropwise addition of H_2O (0.5 mL), NaOH (0.5 mL, 15%) and H_2O (1.5 mL). The solids were filtered off and washed several times with Et_2O. The combined organic phases were dried with $MgSO_4$ and filtered. After evaporation of the solvent in vacuum, the product HL^a (2.1 g, 81%) remained as a colorless oil. – ^{1}H NMR: δ = 2.15 (s, 6 H, NMe_2), 2.18 (s, 3 H, NMe), 2.35 (m, 4 H, CH_2), 3.42 (s, 2 H, PCH_2), 3.48 (s, 2 H, NCH_2), 5.79 (s, 1 H, CH^{pz}), 7.25–7.43 (m, 10 H, CH^{ar}). – ^{13}C NMR: δ = 27.5 (br, PCH_2), 42.7 (NMe), 45.5 (NMe_2), 53.1 (br, CH_2), 54.2 (CH_2), 57.3 (CH_2), 103.9 (d, $^3J_{CP}$ = 5.1 Hz, $C^{pz,4}$), 127.8–132.9 (C^{ar}), 138.3 (d, $^1J_{CP}$ = 14.5 Hz, $C^{ar,q}$), $C^{pz,3}$/$C^{pz,5}$ not observed. – ^{31}P NMR: δ = –16.6. – MS (EI): *m/z* (%) = 380 (7) [M^+], 322 (44) [M^+ – CH_2NMe_2], 279 (40) [M^+ – $MeNCH_2CH_2NMe_2$], 185 (45) [PPh_2^+], 183 (80) [dibenzophosphole$^+$]. – $C_{22}H_{29}N_4P$ (380.47): calcd. C 69.45, H 7.68, N 14.73; found C 68.72, H 7.78, N 12.88.

***N*-{5-[(Diphenylphosphanyl)methyl]-1*H*-pyrazol-3-yl}-*N*,*N*-bis[(2-ethylsulfanyl)ethyl]amine (HL^b):** A solution of **3b** (3.8 g, 7.8 mmol) in THF (50 mL) was slowly added to a suspension of $LiAlH_4$ (0.27 g, 7.8 mmol) in Et_2O (100 mL). After stirring overnight, the mixture was refluxed for 30 min, then cooled to 0 °C and hydrolyzed by dropwise addition of H_2O (0.6 mL), NaOH (0.6 mL, 15%) and H_2O (1.8 mL). The solids were filtered and washed several times with Et_2O. The combined organic phases were dried with $MgSO_4$ and filtered. After evaporation of the solvent in vacuum, the product HL^b (2.2 g, 59%) remained as a colorless oil. – ^{1}H NMR: δ = 1.23 (t, J_{HH} = 7.3 Hz, 6 H, CH_3), 2.44–2.74 (m, 12 H, CH_2), 3.43 (s, 2 H, PCH_2), 3.64 (s, 2 H, NCH_2), 5.85 (s, 1 H, CH^{pz}), 7.33–7.49 (m, 10 H, CH^{ar}). – ^{13}C NMR: δ = 14.6 (CH_3), 25.9 (SCH_2), 27.3 (d, $^1J_{CP}$ = 14.8 Hz, PCH_2), 29.4 (SCH_2), 49.8 (NCH_2), 53.5 (NCH_2), 103.5 (d, $^3J_{CP}$ = 5.5 Hz, $C^{pz,4}$), 128.1–132.7 (C^{ar}), 138.0 (d, $^1J_{CP}$ = 14.3 Hz, $C^{ar,q}$), 143.7 (br, $C^{pz,3/5}$). – ^{31}P NMR: δ = –16.8. – IR (film): $\tilde{\nu}$ = 3180–2863 (vs), 1950/1870/1806 (w), 1565/1476 (s), 1446/1428 (vs), 1369/1302/1262/1182 (s), 1096 (vs), 1065/1024/997/803 (s), 741/695 cm^{-1} (vs). – MS (EI): *m/z* (%) = 471 (5) [M^+], 396 (100) [M^+ – CH_2SEt], 279 (78) [M^+ – $N(CH_2CH_2SEt)_2$], 185 (13) [PPh_2^+], 183 (16) [dibenzophosphole$^+$], 89 (61) [$CH_2CH_2SEt^+$]. – $C_{25}H_{34}N_3PS_2$ (471.67): calcd. C 63.66, H 7.27, N 8.91; found C 63.43, H 7.17, N 8.44.

($L^aNi_2Cl_3$)$_2$ (4): Solutions of KO*t*Bu (0.06 g, 0.5 mmol) in EtOH (30 mL) and $NiCl_2·6H_2O$ (0.37 g, 1.0 mmol) in EtOH (15 mL) were added stepwise to a solution of HL^a (0.19 g, 0.5 mmol) in THF (50 mL) at 0 °C. After stirring for 3 h, the solvent was evaporated in vacuum. Layering a solution of the product in CH_2Cl_2/$CHCl_3$ (1:1) with light petroleum ether afforded red crystals of **4** (0.24 g, 80%). – ^{31}P NMR: δ = 241 (br). – MS (EI): *m/z* (%) = 567 (100) [$L^aNi_2Cl_2^+$], 532 (31) [$L^aNi_2Cl^+$]. – $C_{44}H_{56}Cl_6N_8Ni_4P_2$ (1206.42): calcd. C 43.81, H 4.68, N 9.29; found C 44.32, H 5.38, N 8.62.

$L^bNi_2Cl_3$ (5): KO*t*Bu (0.06 g, 0.5 mmol) and a solution of $NiCl_2·6H_2O$ (0.37 g, 1.0 mmol) in EtOH (15 mL) were added stepwise to a solution of HL^b (0.24 g, 0.5 mmol) in CH_2Cl_2 (50 mL). The red reaction mixture was stirred for 3 h. After evaporation of the solvent, the remaining solid was washed with EtOH and Et_2O. Layering a solution of the product in CH_2Cl_2 with Et_2O afforded red crystals of **5** (0.28 g, 80%). – ^{31}P NMR (CD_2Cl_2): δ = 257 (br). – IR (KBr): $\tilde{\nu}$ = 2957–2861 (vs), 1461/1447 (w), 1430 (s), 1312/1255 (w), 1102 (s), 1062/1039/736/688/536 cm^{-1} (w). – MS (FAB): *m/z* (%) = 658 (70) [M^+ – Cl], 609 (100). – UV/Vis: λ (ε [$M^{-1}·cm^{-1}$]) = 379 (645, sh), 498 (690), 1095 nm (35). – M.p. > 240 °C. – $C_{25}H_{33}Cl_3N_3Ni_2PS_2$ (694.39): calcd. C 43.24, H 4.80, N 6.05; found C 42.75, H 4.70, N 5.93.

$L^bNiPdCl_3$ (6): KO*t*Bu (0.06 g, 0.5 mmol), $NiCl_2·6H_2O$ (0.12 g, 0.5 mmol) and $PdCl_2$ (0.09 g, 0.5 mmol) were added stepwise to a solution of HL^b (0.24 g, 0.5 mmol) in CH_2Cl_2 (50 mL). The product was isolated as described for **5** to yield green crystals of **6** (0.26 g, 69%). – IR (KBr): $\tilde{\nu}$ = 3084–2835 (vs), 1445 (w), 1429 (s), 1311/1256 (w), 1100 (s), 1065/1036/690/534 cm^{-1} (w). – MS (FAB): *m/z* (%) = 706 (100) [M^+ – Cl]. – UV/Vis: λ (ε [$M^{-1}·cm^{-1}$]) = 301 (2620), 336 (1710), 620 (12), 1100 nm (26). – $C_{25}H_{33}Cl_3N_3NiPPdS_2$ (741.12): calcd. C 40.52, H 4.49, N 5.67; found C 39.73, H 4.52, N 5.57.

X-ray Crystallography: The measurements were carried out with a Nonius–Kappa CCD diffractometer using graphite-monochrom-

Table 1. Crystal data and refinement details for complexes **4**, **5**, **6′** and **6′′**

	$[L^aNi_2Cl_3]_2$ (**4**)	$L^bNi_2Cl_3$ (**5**)	$L^bNiPdCl_3$ (**6′**)	$L^bNiPdCl_3$ (**6′′**)
Empirical formula	$C_{22}H_{28}Cl_3N_4Ni_2P{\cdot}CH_2Cl_2$	$C_{25}H_{33}Cl_3N_3Ni_2PS_2$	$C_{25}H_{33}Cl_3N_3NiPPdS_2$	$C_{25}H_{33}Cl_3N_3NiPPdS_2{\cdot}2CH_2Cl_2$
M_r	644.68	694.40	742.10	911.95
Crystal size [mm]	0.35 × 0.20 × 0.20	0.30 × 0.10 × 0.10	0.10 × 0.08 × 0.08	0.40 × 0.20 × 0.08
Crystal system	orthorhombic	monoclinic	monoclinic	monoclinic
Space group	*Pbcn*	*Pc*	*Pn*	$P2_1/n$
a [Å]	26.517(5)	14.162(3)	17.233(3)	12.754(3)
b [Å]	15.302(3)	13.263(3)	8.882(2)	15.913(3)
c [Å]	14.349(3)	15.756(3)	19.312(4)	18.178(4)
β [°]	90	98.75(3)	105.38(3)	104.26(3)
V [Å^3]	5822(2)	2925(1)	2850(1)	3576(1)
$\rho_{calcd.}$ [g cm^{-3}]	1.471	1.577	1.724	1.694
Z	8	4	4	4
T [K]	200	200	200	200
μ (Mo-K_α) [mm^{-1}]	1.734	1.780	1.797	1.739
Scan mode	ω	ω	ω	ω
hkl range	±34, ±19, ±17	±16, ±16, −19 to 17	±21, ±10, ±23	±16, −20 to 15, ±23
2θ range [°]	4.2−55.0	4.0−52.2	3.7−52.0	3.4−54.8
Measured refl.	12709	34726	11867	15240
Unique refl. (R_{int})	6576 (0.036)	11259 (0.105)	9972 (0.038)	8126 (0.032)
Observed refl. $I > 2\sigma(I)$	4871	4922	7777	6285
Refined parameters	314	608	608	388
Residual electron density [eÅ^{-3}]	0.77/−0.52	0.67/−0.50	1.10/−0.78	1.06/−1.04
R1	0.037	0.041	0.061	0.036
wR2 (all data)	0.097	0.065	0.101	0.075
Goodness-of-fit	1.041	0.621	1.048	1.020

ated Mo-K_α radiation. All calculations were performed using the SHELXT PLUS software package. Structures were solved by direct methods with the SHELXS-97 and refined with the SHELXL-97 program.[18] Atomic coordinates and thermal parameters of the non-hydrogen atoms were refined in anisotropic models by full-matrix least-squares calculation based on F^2. In general the hydrogen atoms were placed at calculated positions and allowed to ride on the atoms they are attached to. Table 1 compiles the data for the structure determinations. Crystallographic data (excluding structure factors) for the structures reported in this paper have been deposited with the Cambridge Crystallographic Data Centre as supplementary publication no. CCDC-159461 (**6′**), -159462 (**5**), -159463 (**6′′**) and -159464 (**4**). Copies of the data can be obtained free of charge on application to CCDC, 12 Union Road, Cambridge CB2 1EZ, UK [Fax: (internat.) + 44-1223/336-033; E-mail: deposit@ccdc.cam.ac.uk].

Acknowledgments

We are grateful to Prof. Dr. G. Huttner for his generosity and his continuous interest in our work. The Deutsche Forschungsgemeinschaft is sincerely thanked for a Heisenberg-fellowship (to F. M.) and the Fonds der Chemischen Industrie for financial support. A donation of $PdCl_2$ by Degussa AG (Hanau) is gratefully acknowledged.

[1] [1a] S. R. Collinson, D. E. Fenton, *Coord. Chem. Rev.* **1996**, *148*, 19−40. − [1b] H. Okawa, H. Sakiyama, *Pure Appl. Chem.* **1995**, *67*, 273−280. − [1c] L. Que, jun., Y. Dong, *Acc. Chem. Res.* **1996**, *29*, 190−196. − [1d] H. Steinhagen, G. Helmchen, *Angew. Chem.* **1996**, *108*, 2489−2492; *Angew. Chem. Int. Ed. Engl.* **1996**, *35*, 2339.

[2] [2a] D. E. Fenton, H. Okawa, *Chem. Ber./Recueil* **1997**, *130*, 433−442. − [2b] H. Okawa, H. Furutachi, D. E. Fenton, *Coord. Chem. Rev.* **1998**, *174*, 51−75.

[3] [3a] D. G. McCollum, B. Bosnich, *Inorg. Chim. Acta* **1998**, *270*, 13−19. − [3b] M. Shibasaki, H. Sasai, T. Arai, T. Iida, *Pure Appl. Chem.* **1998**, *70*, 1027−1034. − [3c] E. K. van den Beuken, B. L. Feringa, *Tetrahedron* **1998**, *54*, 12985−13011.

[4] [4a] O. Kahn, *Angew. Chem.* **1985**, *97*, 837−853. − [4b] O. Kahn, *Adv. Inorg. Chem.* **1995**, *43*, 179−259.

[5] [5a] S. Trofimenko, *Progr. Inorg. Chem.* **1986**, *34*, 115−210. − [5b] A. P. Sadimenko, S. S. Basson, *Coord. Chem. Rev.* **1996**, *147*, 247−297. − [5c] G. La Monica, G. A. Ardizzoia, *Progr. Inorg. Chem.* **1997**, *46*, 151−238. − [5d] L. A. Oro, M. A. Ciriano, C. Tejel, *Pure Appl. Chem.* **1998**, *70*, 779−788.

[6] [6a] T. G. Schenck, J. M. Downes, C. R. C. Milne, P. B. Mackenzie, H. Boucher, J. Whelan, B. Bosnich, *Inorg. Chem.* **1985**, *24*, 2334−2337. − [6b] [a] T. G. Schenck, C. R. C. Milne, J. F. Sawyer, B. Bosnich, *Inorg. Chem.* **1985**, *24*, 2338−2344.

[7] [7a] J. Casabó, J. Pons, K. S. Siddiqi, F. Teixidor, E. Molins, C. Miravitlles, *J. Chem. Soc., Dalton Trans.* **1989**, 1401−1403. − [7b] T. Kamiusuki, H. Okawa, E. Kitaura, M. Koikawa, N. Matsumoto, S. Kida, H. Oshio, *J. Chem. Soc., Dalton Trans.* **1989**, 2077−2081. − [7c] T. Kamiusuki, H. Okawa, N. Matsumoto, S. Kida, *J. Chem. Soc., Dalton Trans.* **1990**, 195−198. − [7d] J. Pons, X. López, E. Benet, J. Casabó, F. Teixidor, F. J. Sánchez, *Polyhedron* **1990**, *9*, 2839−2845. − [7e] T. Kamiusuki, H. Okawa, E. Kitaura, K. Inoue, S. Kida, *Inorg. Chim. Acta* **1991**, *179*, 139−143. − [7f] J. C. Bayón, P. Esteban, G. Net, P. G. Rasmussen, K. N. Baker, C. W. Hahn, M. M. Gumz, *Inorg. Chem.* **1991**, *30*, 2572−2574. − [7g] K. Shindo, Y. Mori, K. Motoda, H. Sakiyama, N. Matsumoto, H. Okawa, *Inorg. Chem.* **1992**, *31* 4987−4990. − [7h] C. Acerete, J. M. Bueno, L. Campayo, P. Navarro, M. I. Rodriguez-Franco, A. Samat, *Tetrahedron* **1994**, *50*, 4765−4774. − [7i] M. Itoh, K. Motoda, K. Shindo, T. Kamiusuki, H. Sakiyama, N. Matsumoto, H. Okawa, *J. Chem. Soc., Dalton Trans.* **1995**, 3635−3641. − [7j] S. Baitalik, U. Flörke, K. Nag, *Inorg. Chem.* **1999**, *38*, 3296−3308.

[8] [8a] L. Behle, M. Neuburger, M. Zehnder, T. A. Kaden, *Helv. Chim. Acta* **1995**, *78*, 693−702. − [8b] H. Weller, L. Siegfried, M. Neuburger, M. Zehnder, T. A. Kaden, *Helv. Chim. Acta* **1997**, *80*, 2315−2328.

[9] [9a] F. Meyer, S. Beyreuther, K. Heinze, L. Zsolnai, *Chem.*

Ber./Recueil **1997**, *130*, 605−613. − [9b] F. Meyer, A. Jacobi, L. Zsolnai, *Chem. Ber., Recueil* **1997**, *130*, 1441−1447. − [9c] F. Meyer, K. Heinze, B. Nuber, L. Zsolnai, *J. Chem. Soc., Dalton Trans.* **1998**, 207−213.

[10] F. Meyer, U. Ruschewitz, P. Schober, B. Antelmann, L. Zsolnai, *J. Chem. Soc., Dalton Trans.* **1998**, 1181−1186.

[11] M. Konrad, F. Meyer, K. Heinze, L. Zsolnai, *J. Chem. Soc., Dalton Trans.* **1998**, 199−205.

[12] See for example: [12a] P. von Matt, A. Pfaltz, *Angew. Chem.* **1993**, *105*, 614−615; *Angew. Chem. Int. Ed. Engl.* **1993**, *32*, 556−568. − [12b] A. Togni, U. Burckhardt, V. Gramlich, P. S. Pregosin, R. Salzmann, *J. Am. Chem. Soc.* **1996**, *118*, 1031−1037. − [12c] M. Sperrle, G. Consiglio, *Chem. Ber./Recueil* **1997**, *130*, 1557−1565. − [12d] G. Helmchen, *J. Organomet. Chem.* **1999**, *576*, 203−214. − [12e] K. R. Reddy, C.-L. Chen, Y.-H. Liu, S.-M. Peng, J.-T. Chen, S.-T. Liu, *Organometallics* **1999**, *18*, 2574−2576. − [12f] B. Crociani, S. Antonaroli, G. Bandoli, L. Canovese, F. Visentin, P. Uguagliati, *Organometallics* **1999**, *18*, 1137−1147.

[13] E. Mugnaini, P. Grünanger, *Atti. Accad. Naz. Lincei, Cl. Sci. Fis. Mat. Nat., Rend.* **1953**, *14*, 958.

[14] J. H. Satcher, Jr., M. W. Droege, T. J. R. Weakley, R. T. Taylor, *Inorg. Chem.* **1995**, *34*, 3317−3328.

[15] [15a] G. Aullon, D. Bellamy, L. Brammer, E. A. Bruton, A. G. Orpen, *Chem. Commun.* **1998**, 653−654. − [15b] C. B. Aakeröy, T. A. Evans, K. R. Seddon, I. Palinko, *New J. Chem.* **1999**, 145−152.

[16] D. B. Grotjahn, D. Combs, S. Van, G. Aguirre, F. Ortega, *Inorg. Chem.* **2000**, *39*, 2080−2086.

[17] D. Nicholls, in *Comprehensive Inorganic Chemistry* (Eds.: J. C. Bailar, H. J. Emeleus, Sir R. Nyholm, A. F. Trotman-Dickenson), 1st ed., Pergamon, Oxford, **1973**, vol. 3, p. 1152 ff.

[18] [18a] G. M. Sheldrick, *SHELXL-97, Program for Crystal Structure Refinement*, Universität Göttingen, **1997**. − [18b] G. M. Sheldrick, *SHELXS-97, Program for Crystal Structure Solution*, Universität Göttingen, **1997**.

Received March 7, 2001
[I01085]

$K_2In_{12}Se_{19}$, a Complex New Structure Type Based on Icosahedral Units of Se^{2-}

Marc Schlosser,[a] Christof Reiner,[a] Hans-Jörg Deiseroth,*[a] and Lorenz Kienle[b]

Dedicated to Prof. Dr. W. Jeitschko on the occasion of his 65th birthday

Keywords: Potassium selenoindate / Crystal structure / Icosahedron / Order-disorder transition

$K_2In_{12}Se_{19}$ is a new ternary chalcogenide in the system K_2Se–In_2Se_3 (m.p. 997 K; colour: dark red) with the two components in a molar ratio of 1:6. This unusual solid shows a temperature-dependent order-disorder transition originating mainly from a dynamical disorder of In^{3+} at elevated temperatures. The average structure of the dynamically disordered phase at 673 K was analysed by means of high-temperature single-crystal X-ray data [a = 1393.18(5) pm, c = 1772.26(9) pm, Z = 3, $R\bar{3}$, hexagonal setting]. The most prominent feature of the complex solid is a partial structure of slightly distorted icosahedra formed by Se1 (central atom), Se3, and Se4. The topological arrangement of the icosahedra corresponds to a cubic close packing. A further independent partial structure enveloping the icosahedra is build up by Se2. The latter form large distorted polyhedra intermediate between icosahedra and cuboctahedra. In1, In2, and In3 occupy tetrahedral holes inside (In2) and outside the icosahedra (In1 and In3), whereas K is located in distorted octahedral holes. In2 and In3 are located in neighboured face-sharing tetrahedra showing an approximate 50% occupancy. They are alternatively occupied in the sense of a dynamical disorder ("average structure"). In1 and K are not affected directly by the disorder. Structural relations between $K_2In_{12}Se_{19}$ and an earlier published unusual quaternary indium chalcogenide are discussed.

Introduction

Close packing of tetrahedra based on three-dimensional interpenetrating icosahedra as structural units is common with intermetallic compounds,[1–4] but not with semiconducting or isolating solids, such as the one represented by the title compound.

We recently, however, published structural and NMR results[5,6] that surprisingly showed clear evidence for the importance of tetrahedral close packing also in the field of non-metallic solids. Typical examples are found among the group of filled β-manganese phases like $M_2Ga_6Te_{10}$ (M: Li, Na) or α-$RbAg_4I_5$,[7,8] both representing well-defined solids with interpenetrating icosahedral arrangements of the β-Mn type formed by the anions Te^{2-} and I^{1-}, respectively. A low percentage of tetrahedral holes (ca. 15%) is filled by the cations Ga^{3+} and Ag^+. Furthermore, Li^+, Na^+, or Rb^+ occupy a few additional non-tetrahedral holes ("metaprisms"). Another classical example for the importance of tetrahedral close packing with non-metals is represented by the family of filled Laves phases ("argyrodites"), in which the arrangement of anions (Se^{2-}, Te^{2-}, ...) is topologically identical to the arrangement of the Mg and Cu atoms in the cubic Laves phase $MgCu_2$.[9] Again, a low percentage (ca. 30%) of the tetrahedral holes is filled by cations.

The physical properties of filled Laves phases as well as of filled β-Mn phases are characterized by a high mobility of cations, primarily moving between face-sharing tetrahedra. Special aspects of the dynamical disorder of Ag^+ in γ-Ag_9AlSe_6 were recently analysed by means of an anharmonic structure refinement based on X-ray data.[10]

$K_2In_{12}Se_{19}$, the title compound of this paper, is a new crystalline solid that in contrast to the conventional oxidation numbers of its constituents (K^+, In^{3+}, Se^{2-}) is based on unconventional icosahedral subunits of Se^{2-}. It is evident that the structure is neither of the filled β-Mn nor of the filled Laves phase types. Furthermore, the structural characterization of the new solid is unexpectedly complicated by a temperature-dependent order-disorder transformation caused by a dynamical disorder of indium atoms and accompanied by the formation of a superstructure. The latter one is indicated by diffuse X-ray reflections and the occurrence of anti-phase domains at low temperatures. Combined X-ray and TEM (transmission electron microscopy) investigations, in particular concerning the complex microstructure of the anti-phase domains and the superstructure are currently in progress.[11] This paper is therefore mainly restricted to single-crystal X-ray results obtained for the dynamically disordered high-temperature structure (*average structure*) of $K_2In_{12}Se_{19}$ at 673 K. The ordering process at lower temperatures does not influence the general

[a] Anorganische Chemie, Universität Siegen,
Adolf-Reichwein-Straße, 57068 Siegen, Germany
Fax: (internat.) + 49-271/740-2555
E-mail: deiseroth@chemie.uni-siegen.de
[b] Max-Planck-Institut für Festkörperforschung,
Heisenbergstraße 1, 70569 Stuttgart, Germany
Fax: (internat.) + 49-711/689-1091
E-mail: lkienle@sim.mpi-stuttgart.mpg.de

 © WILEY-VCH Verlag GmbH, 69451 Weinheim, 2001 1434–1948/01/0909–2241 $ 17.50+.50/0

topology of the structure, but only specific aspects of the crystal chemical behaviour of selected In positions.

Results and Discussion

General

The title compound adds one further example to the small group of known normal and mixed valence alkali metal selenoindates that are summarized in Table 1.

Table 1. Summary of known alkali metal selenoindates

Formula	Structure type	Ref.
$LiInSe_2$	β-$NaFeO_2$	[16]
$NaInSe_2$	α-$NaFeO_2$	[17]
$KInSe_2$	$TlGaSe_2$	[18]
$RbInSe_2$	$TlGaSe_2$	[19]
$RbIn_7Se_9$	$CsIn_7S_9$	[19]
$CsIn_7Se_9$	$CsIn_7S_9$	[19]
$Rb_4In_2Se_5$	$Rb_4In_2S_5$	[18]
$Na_7In_3Se_8$	$Na_7In_3Se_8$	[20]
$Na_2In_6Se_{10}$	$Na_2In_6Se_{10}$	[21]

In most of these compounds (except the mixed valence ones) In^{3+} is exclusively tetrahedrally coordinated by Se^{2-} whereas the alkali metal atoms show larger coordination numbers with different coordination polyhedra. It turned out that the unsatisfactorily characterized mixed-valent indium chalcogenide $In_{\approx 2.01}X_3$ (X = S, Se, Te)[12] is structurally related to the title compound. A short discussion at the end of this chapter will refer to this relationship.

Selected X-ray data, positional and thermal parameters, as well as interatomic distances for the average structure of $K_2In_{12}Se_{19}$ at $T = 673$ K are summarized in Tables 2, 3, 4 and 5.

At a first glance, the overall structure looks rather complicated in that it shows up as a complex three-dimensional arrangement of corner-, edge-, and face-sharing $InSe_4$ tetrahedra with K atoms distributed in "isolated" distorted octahedra (Figure 1).

A typical feature of the average structure is the observed disorder for two (In2, In3) of the three crystallographically independent indium positions. Due to the extreme weakness of superstructure reflections for $T > 400$ K, but a continuously increasing occurrence of diffuse X-ray scattering upon cooling exclusively in layers *hkl*, with $l = 2n + 1$ (referring to the superstructure with a double *c* axis) (Figure 2) we assume a dynamical disorder at high temperatures. This disorder shows up in an approximate 50% occupancy of the respective positions (In2, In3, see Table 3). All other atomic positions (K, In1, Se) are fully occupied and do not show any irregularities.

The just mentioned diffuse scattering in the vicinity of Bragg positions in layers *hkl* with $l = 2n + 1$ indicates a successive ordering with respect to the atomic positions In2 and In3. The crystallographic aspects are seriously complicated by the ordering process and result in a *c* axis doubling and the associated formation of anti-phase domains.

Table 2. Selected X-ray data for the average structure of $K_2In_{12}Se_{19}$ at 673 K

Crystal data	
Empirical formula	$K_2In_{12}Se_{19}$
Molecular mass [g·mol^{-1}]	2956.28
Colour	dark red
Lattice constants [pm]	$a = 1393.18(5)$ $c = 1772.26(9)$
Volume [nm^3]	29.790(2)
Z, $\rho_{calcd.}$ [Mg·m^{-3}]	3, 4.944
Crystal system	trigonal
Space group	$R\bar{3}$ (No. 148)
Data collection	
Diffractometer	STOE IPDS, Mo-K_α, $\lambda = 71.073$ pm, oriented graphite monochromator
Crystal size [mm]	$0.25 \times 0.22 \times 0.13$
Temperature [K]	673
φ-mode	oscillation
φ-range [°], Δφ [°]	$-1 \le \varphi \le 360.2$, 0.6
$\theta_{min.}$ [°], θ_{max} [°]	2.85, 25.98
hkl range	$-17 \le h \le 17$ $-17 \le k \le 17$ $-21 \le l \le 21$
Image plate distance [mm]	70
Irradiation time/image [min]	2.2
No. of reflections, R_{int}	14538, 0.0388
No. of independent reflections	1299
Absorption coefficient [mm^{-1}]	24.446
T_{min}, T_{max}	0.0223, 0.0934
Absorption correction	numerical, crystal description with 20 faces, shape-optimised with X-SHAPE[22]
Structural analysis and refinement	
Solution method	direct methods
Refinement method	full-matrix least squares on F^2
No. of parameters	68
$F(000)$	3816
$R1$, $wR2$ [$I > 2\sigma(I)$]	0.0295, 0.0612
$R1$, $wR2$ [all reflections]	0.0346, 0.0636
Program	SHELX-97 program package[22][23]
Extinction coefficient	0.00064(3)
GooF on F^2	1.030
Largest diff. peak and hole $\Delta\rho_{max}$, $\Delta\rho_{min}$ [10^{-6} e·pm^{-3}]	1.286, −0.959

It should be noted, however, that the ordering process does *not* remarkably change the overall structure of $K_2In_{12}Se_{19}$, which is the focus of this paper. There are, however, some important changes in detail that are closely related to the shape of the diffuse reflections, to crystal chemical aspects of the local coordination of selected atoms and the *c* axis doubling.

Table 3. Atomic coordinates, Wyckoff notations, occupancies, and equivalent isotropic displacement parameters U_{eq} [10^4 pm^2] for the average structure of $K_2In_{12}Se_{19}$ (T = 673 K)

Atom	Wyck.	x	y	z	Occ.	U_{eq}
In1	18*f*	0.22511(4)	0.87381(4)	0.65031(3)	0.993(4)	0.0526(2)
In2	18*f*	0.1187(2)	0.9207(1)	−0.56729(8)	0.453(4)	0.0641(8)
In3	18*f*	0.1715(1)	0.8903(1)	−0.57746(6)	0.540(4)	0.0571(6)
Se1	3*b*	0	0	1/2	1.001(1)	0.0657(9)
Se2	18*f*	0.14670(9)	0.73275(7)	0.75552(5)	0.989(5)	0.0741(4)
Se3	18*f*	0.19098(8)	1.03551(7)	0.69218(5)	0.998(5)	0.0599(3)
Se4	18*f*	0.08455(6)	0.76690(6)	0.53700(4)	1	0.0458(3)
K	6*c*	1/3	2/3	0.8328(4)	0.96(2)	0.141(4)

In order to gain some systematic understanding for the complex structure, the discussion of its main structural aspects is divided into three parts:

– *Primary structure:* individual coordination polyhedra

– *Secondary structure:* complex icosahedral and distorted cuboctahedral units of Se^{2-} and their decoration by In^{3+} and K^+

– *Tertiary structure:* three-dimensional connection of primary and secondary structural elements

Primary Structure

Relevant aspects of the local tetrahedral coordination of In^{3+} and the distorted octahedral ("metaprismatic") coordination of K^+ in the average structure are shown in Figure 3 (a, b). Whereas In2 and In3, located in neighbouring face-sharing tetrahedra, show an approximate 50% occupancy, the In1 position is fully occupied.

A simple distance calculation immediately demonstrates that the atomic positions In2 and In3 *cannot* be occupied *simultaneously* due to an unreasonable short interatomic distance d(In2−In3) = 103 pm. This contradiction is resolved at high temperatures by assuming a dynamic exchange process between both positions, resulting in a successive ordering at lower temperatures, a picture that is

Table 4. Anisotropic displacement parameters U_{ij} [10^4 pm^2] for the average structure of $K_2In_{12}Se_{19}$

Atom	U_{11}	U_{22}	U_{33}	U_{12}	U_{13}	U_{23}
In1	0.0450(3)	0.0472(3)	0.0605(4)	0.0070(2)	0.0045(2)	0.0193(3)
In2	0.064(1)	0.0510(9)	0.0467(8)	−0.0009(6)	−0.0079(7)	0.0055(7)
In3	0.0605(9)	0.0485(7)	0.0430(6)	−0.0020(4)	0.0096(5)	0.0127(6)
Se1	0.067(1)	0.067(1)	0.063(4)	0	0	0.0336(5)
Se2	0.0931(8)	0.0483(5)	0.0464(5)	0.0026(4)	−0.0029(4)	0.0095(5)
Se3	0.0755(6)	0.0611(6)	0.0524(5)	0.0025(4)	0.0072(4)	0.0411(5)
Se4	0.0395(4)	0.0462(4)	0.0489(5)	0.0031(3)	−0.0008(3)	0.0194(3)
K	0.147(4)	0.147(4)	0.129(6)	0	0	0.074(2)

Table 5. Selected interatomic distances [pm] for the average structure of $K_2In_{12}Se_{19}$

K	−Se2	344.7(3) (3×)	Se1	−In2	268.4(3) (6×)
	−Se3	350.9(5) (3×)			
			Se2	−In1	252.7(1)
In1	−Se2	252.7(1)		−In1	253.2(1)
	−Se2	253.2(1)		−K1	344.7(3)
	−Se3	263.1(1)			
	−Se4	267.75(9)	Se3	−In2	247.8(2)
				−In1	263.1(1)
In2	−Se3	247.8(2)		−In3	263.1(2)
	−Se4	261.8(2)		−In3	263.5(2)
	−Se1	268.4(3)			
	−Se4	268.6(2)	Se4	−In3	254.1(1)
				−In3	254.4(1)
In3	−Se4	254.1(1)		−In2	261.8(2)
	−Se4	254.4(1)		−In1	267.75(9)
	−Se3	263.1(2)		−In2	268.6(2)
	−Se3	263.5(2)			
In2	−In3	103.3(2)			

		Icosahedra $(Se1)_1@(Se3/Se4)_{icos.}$
Se1	−Se4	402.35(7) (6×)
	−Se3	419.62(9) (6×)
Se3	−Se3	424.5(2) (6×)
	−Se4	426.8(1) (6×)
	−Se4	434.4(1) (6×)
	−Se4	458.8(1) (6×)
Se4	−Se4	418.08(8) (6×)

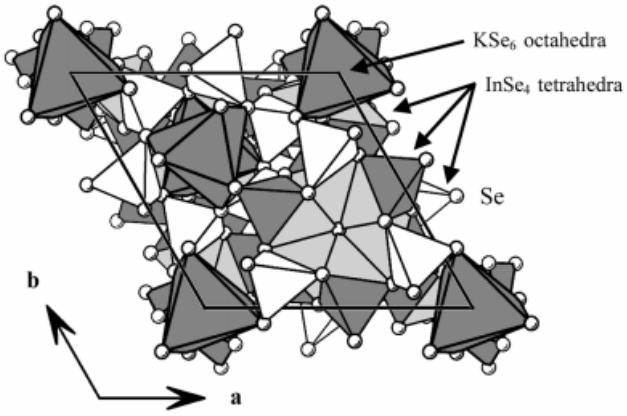

Figure 1. Projection of the average structure of $K_2In_{12}Se_{19}$ along [001] emphasising the complex arrangement of InS_4 tetrahedra and distorted KSe_6 octahedra (because of the closed polyhedra representation the In atoms inside the tetrahedra and the K atoms inside the octahedra are "invisible")

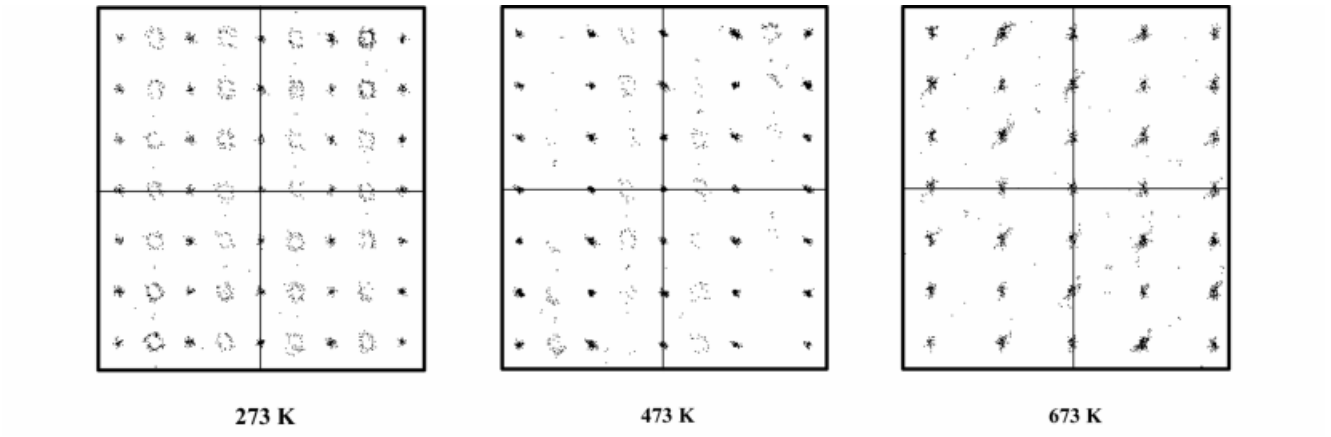

Figure 2. A temperature-dependent sequence of similar reciprocal lattice sections showing the gradual appearance of diffuse disk-shaped reflections in layers *hkl* ($l = 2n + 1$, referring to the superstructure with a double *c* axis) with decreasing temperature

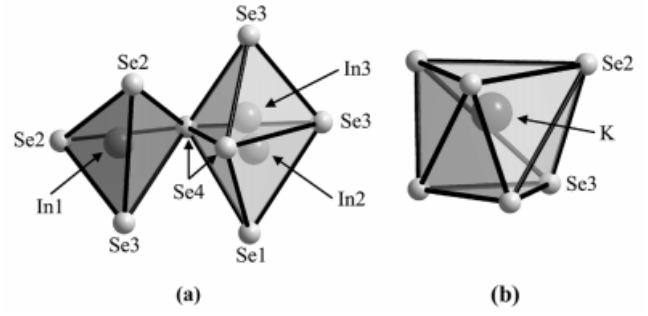

Figure 3. A comparison of the first coordination sphere polyhedra for In1, In2, In3 (a), and K (b) in the average structure of $K_2In_{12}Se_{19}$; note that In2 and In3 are not simultaneously present [$d = 103.3(2)$ pm] but represent two positions with a 50% occupancy corresponding to *one* In atom that is dynamically disordered

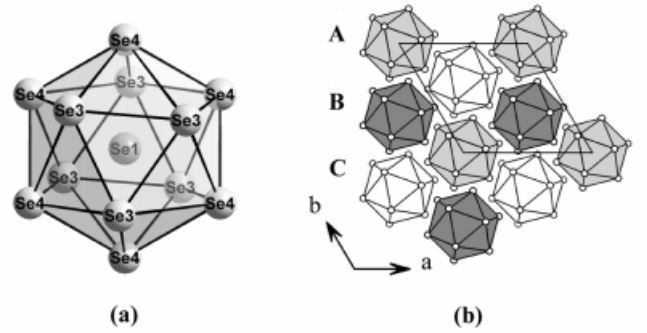

Figure 4. One icosahedral unit around Se1 formed by Se3 and Se4 (a) and a section of the three-dimensional arrangement of these units (b) representing the pattern of a cubic close packing

strongly supported by single-crystal X-ray studies at different temperatures and additional TEM investigations.

A special situation occurs for Se^{2-} for which a coordination number (CN) of 4 or 3 ($3 \times In + 1 \times K$ or $2 \times In + 1 \times K$ etc.) is usually found in similar compounds. This, however, seems to be true only in the case of Se2 and Se3 (Table 5). The seemingly unreasonable coordination numbers > 4 for Se1 and Se4 are due to the fact that both atom types are direct neighbours of the dynamically disordered In2 and In3. Obviously the type of static disorder emerging at lower temperatures is among others closely related to the attempt of the structure to reach a reasonable coordination for all Se^{2-} (CN = 3−4). Indeed, the determination of the ordered structure at low temperatures ($c_{LT} = 2 \times c_{HT}$) results in normal values for the coordination number of all Se^{2-}.[11]

Secondary Structure

Fascinating aspects of the secondary structure of $K_2In_{12}Se_{19}$ emerge upon analysing the partial structure of Se^{2-} omitting at first the In and K atoms. Figure 4 (a) shows Se1 together with Se3 and Se4 forming icosahedra of symmetry $\bar{3}$ centred by Se1. The icosahedra are made up by two types of triangles: equilateral ones formed by Se3 and non-equilateral ones formed by Se3 and Se4.

Typical interatomic distances between the central Se1 and the peripheral Se3 and Se4 are in the range of 402−420 pm. Distances between peripheral Se3 and Se4 differ somewhat more, between 418 and 459 pm (Table 5). Figure 5 (a) shows how the dynamically disordered atomic positions In2 and In3 decorate the icosahedra around Se1. As can be seen from Figure 5 (a, b), Se1 forms one apex of a tetrahedron around In2 (i.e. the central atom of the given icosahedron), whereas one apex of a tetrahedron around In3 is Se3 of a *neighbouring* icosahedron. The six In3 positions belonging to one icosahedron connect to three icosahedra *above* and to three *below* the central one, thus forming a cubic close packing of icosahedra [Figure 4 (b), Figure 5 (b)].

Figure 6 (a) shows that Se2, which does not participate in the icosahedra, forms large, strongly distorted polyhedra that encapsulate the icosahedra around Se1. They can be described as intermediate between icosahedra and cuboctahedra. The difficulties of classifying these polyhedra result from the fact that their description as cuboctahedra neglects the slight folding of the quadrilateral planes (dihedral angle: 21.5°) defined by four Se2. If one assumes the

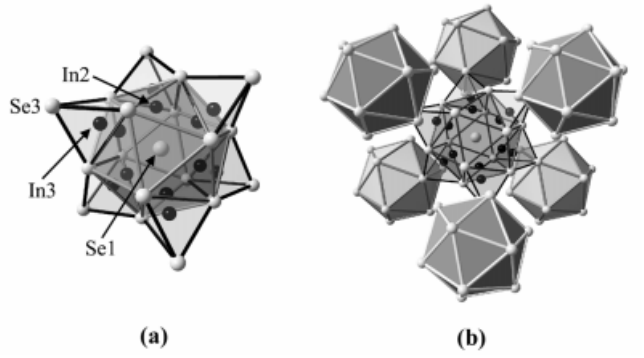

Figure 5. The decoration of the icosahedral units around Se1 by the dynamically disordered positions In2/In3 (a) and their connection to neighboured icosahedra (b)

folding line to be an additional edge, the polyhedron would better be described as an icosahedron formed by 20 strongly distorted triangular faces. Due to the just mentioned encapsulation, an endohedral unit of the type $(Se1)_1@(Se3/Se4)_{icos.}@(Se2)_{cuboct./icos.}$ can be formulated.

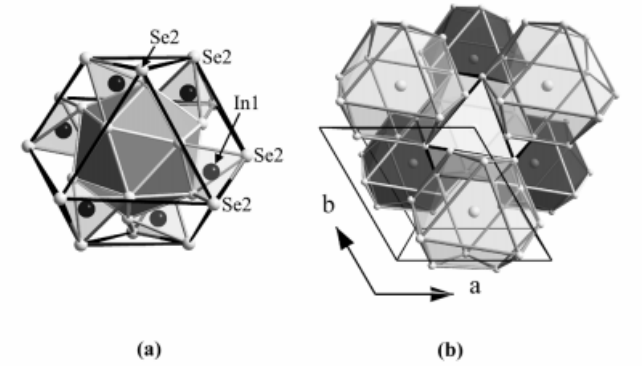

Figure 6. The large distorted cuboctahedral/icosahedral unit (see text) formed by Se2 which encapsulates the icosahedra around Se1: $Se1@(Se3,4)_{icos.}@(Se2)_{cuboct./icos.}$ and the positions of the tetrahedrally coordinated In1 in a shell between the surface of the icosahedron and the cuboctahedron/icosahedron (a); three-dimensional arrangement of the large cuboctahedra/icosahedra (b)

As Figure 6 (a) shows, atoms of the type In1 are located in tetrahedra (2 × Se2, 1 × Se3, 1 × Se4) within a shell between the surface of an icosahedron and the large surrounding cuboctahedron. The first coordination sphere of K^+ is formed by three Se3 atoms belonging to an icosahedron around Se1 and three Se2 each belonging to two *neighbouring* distorted cuboctahedra (the latter ones are not shown in Figure 7).

Tertiary Structure

As mentioned above [Figure 4 (b)], the three-dimensional arrangement of the icosahedra around Se1 corresponds to the pattern of a cubic close packing with a stacking vector parallel to [001]. Moreover, one can see from Figure 7 that the polyhedra around K are connected to somewhat smaller polyhedra along [001] that are, however, empty in $K_2In_{12}Se_{19}$. Filled and empty polyhedra form three-membered columns that connect neighbouring icosahedra along [001]. In the $In_{\approx 2.01}X_3$ phase (see below) In^{3+} is located in half of these empty polyhedra. A further consequence of the complex atomic arrangement is the fact that In2/In3 together with the icosahedra around Se1 form a three-dimensional independent substructure, which interpenetrates the arrangement of distorted cuboctahedra made up by Se2. Because Se1 atoms act as common centres also for the cuboctahedra, the topology of these endohedral units, which are connected by common edges, again corresponds to cubic-close packing [Figure 6 (b)]. Both K and In1 are cations that act as connecting links between the two partial structures.

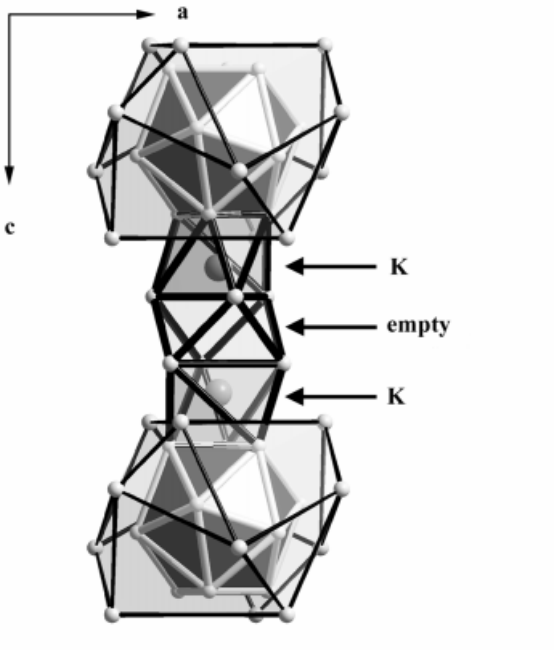

Figure 7. Section of the structure that emphasises the alternating arrangement of filled (K) and empty metaprismatic polyhedra along [001], and their connecting function between neighboured symmetrically equivalent icosahedra/distorted cuboctahedra along the same direction

Order-Disorder Transition (General Aspects)

The ordering process for In2/In3 positions at lower temperatures, which is visualised by the gradual appearance of ring shaped diffuse reflections around Bragg positions in layers *hkl* with $l = 2n + 1$ (Figure 2), and an associated doubling of the *c* axis, does not influence the above described atomic arrangement in principle (except small adjustments of the interatomic distances and angles). Face sharing between tetrahedra occupied by In atoms, however, is avoided in the ordered structure.

An important crystal chemical aspect of the ordering process is that the coordination of In2 and 3 by Se and vice versa is optimised with respect to reasonable coordination numbers for both species (see above) and with respect to interatomic distances *d*(In−In). Due to the experimentally observed doubling of the *c* axis, the ordering patterns that

do not require a *c* axis doubling can be excluded from the set of possible ordering patterns. Among the rest, there are several patterns with a non-balanced variety of short and long distances d(In−In) that can also be excluded. The remaining solution, however, leads to a structure model that inevitably produces anti-phase domains of variable size. The latter are responsible for the appearance of diffuse reflections, and reflect a complex structural frustration problem along the boundaries between adjacent anti-phase domains. Further crystallographic details of the ordered low-temperature structure, in particular with respect to results of TEM investigations, focussing on the formation of anti-phase domains are discussed in detail elsewhere.[11]

Comparison between $K_2In_{12}Se_{19}$ and the Mixed Crystal $In_{\approx 2.01}X_3$ (X = S, Se, Te)

$In_{\approx 2.01}X_3$ (X = S, Se, Te)[12] is a quaternary mixed crystal indium chalcogenide with crystallographic data closely related to those of the ordered low-temperature phase of $K_2In_{12}Se_{19}$ ($In_{\approx 2.01}X_3$: a = 1400.3 pm, c = 3522.8 pm, space group $R\bar{3}$). A closer inspection of the results published,[12] however, shows several anomalies and contradictions in particular with respect to split positions, disorder, and interatomic distances. In general, the anionic partial structure (S/Se/Te) of $In_{\approx 2.01}X_3$ and $K_2In_{12}Se_{19}$ are topologically more or less identical, although the complex secondary and tertiary structural features as described in this paper were not recognized for $In_{\approx 2.01}X_3$. In addition, there are discrepancies with respect to the positions of various cations, e.g. the positions for K atoms in $K_2In_{12}Se_{19}$ are claimed to be empty sites in $In_{\approx 2.01}X_3$. A more detailed comparison of both structures is given in ref.[13]

Conclusion

The high-temperature structure (“average structure”) of $K_2In_{12}Se_{19}$ represents a new structure type for ternary selenides, which is characterized by two interpenetrating Se substructures. One is formed by Se1, Se3, and Se4, and corresponds to a cubic close packed arrangement of centred Se_{13} icosahedra. The other one consists of a three-dimensional arrangement of large distorted polyhedra (intermediate between cuboctahedra and icosahedra), and is formed by Se2 exclusively. Both polyhedra form endohedral units of the type $(Se1)_1@(Se3/Se4)_{icos.}@(Se2)_{cuboct./icos.}$ with common centre atoms (Se1). This means that the polyhedral system formed by Se2 envelopes the icosahedra. The dynamically disordered In2/In3 positions (50% occupancy) are located inside (In2) and outside (In3) the icosahedra with the tetrahedra around In3 connecting neighbouring icosahedra. The position In1 is fully occupied, and located in tetrahedra between the outer surface of the icosahedra (Se1,Se3,Se4) and the inner surface of the distorted cuboctahedra (Se2). The K atoms occupy metaprismatic holes each connecting one neighboured icosahedron and six neighboured distorted cuboctahedra.

Experimental Section

Single crystals and homogeneous powder samples of $K_2In_{12}Se_{19}$ were prepared by heating stoichiometric mixtures of the elements in evacuated dry quartz glass ampoules. The elements were heated to 1270 K for 3 h and finally quenched in ice-cold water. After homogenisation under argon, the raw product was annealed at 950 K for 14 d, resulting in a completely homogeneous product. X-ray powder diffraction data at room temp. for the lattice refinement were determined from an X-ray powder diffraction pattern (Cu-$K_{\alpha 1}$ radiation) using a Siemens D5000 X-ray powder diffractometer. For the refinement of the lattice parameters the program package WinXPow[14] was used. All lines can be indexed with a trigonal *R*-centred cell with the hexagonal constants a = 1384.69(6) pm, c = 1758.32(9) pm. Figure 8 shows a good agreement between the measured (293 K) and calculated X-ray powder data for $K_2In_{12}Se_{19}$ (atomic parameters based on the average structure). Superstructure reflections could not be observed because of their diffuse character and weakness.

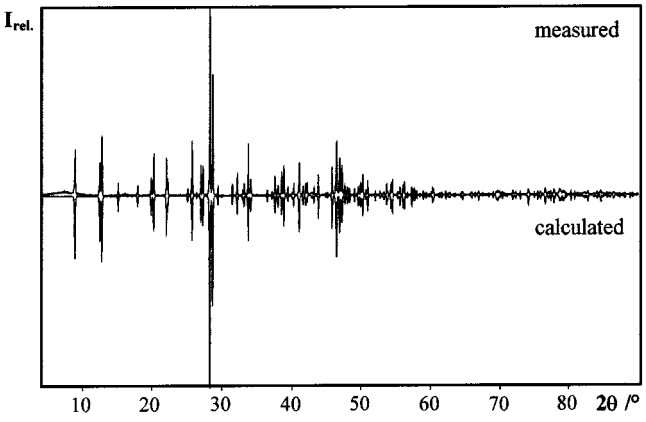

Figure 8. Comparison of experimental and calculated powder diagrams (Cu-$K_{\alpha 1}$) for $K_2In_{12}Se_{19}$ (calculation based on atomic positions for the average structure)

Well-shaped single crystals of mm size were found, both on top of the bulk product and, due to a gas-phase transport of unknown mechanism, in the colder section of the ampoule too. Powdered samples of $K_2In_{12}Se_{19}$ are reddish-brown, crystals − dependent on their thickness − dark red to black. $K_2In_{12}Se_{19}$ is not markedly air-sensitive and decomposes at 997 K. All experimental details concerning the single crystal measurement of $K_2In_{12}Se_{19}$ at 673 K are given in Table 2. The chemical composition of $K_2In_{12}Se_{19}$, especially the occurrence of K with respect to the compound $In_{\approx 2.01}X_3$, was independently proven from the X-ray results, by wavelength-dispersive analytical scanning microscopy with a CamScan microprobe CS44, equipped with a MICROSPEC WDX spectrometer. Graphics were obtained with DIAMOND 2.1.[15] Further details of the crystal-structure investigation may be obtained from the Fachinformationszentrum Karlsruhe, D-76344 Eggenstein-Leopoldshafen, Germany, on quoting the depository number CSD-411816.

Acknowledgments

The authors would like to thank the "Deutsche Forschungsgemeinschaft" and the "Fonds der Chemischen Industrie" for their continuous financial support.

[1] F. C. Frank, J. S. Kasper, *Acta Crystallogr.* **1958**, *11*, 184−191.
[2] F. C. Frank, J. S. Kasper, *Acta Crystallogr.* **1959**, *12*, 483−499.
[3] C. B. Shoemaker, D. P. Shoemaker, *Monatsh. Chem.* **1971**, *102*, 1643−1666.
[4] D. P. Shoemaker, C. B. Shoemaker, *Acta Crystallogr., Sect. B* **1986**, *42*, 3−11.
[5] H. J. Deiseroth, L. Kienle, H. Günther, M. Hartung, *Z. Anorg. Allgem. Chem.* **2000**, *626*, 302−308.
[6] L. Kienle, H. J. Deiseroth, *Z. Kristallogr.* **1998**, *213*, 569−574.
[7] S. Geller, *Science* **1967**, 310.
[8] S. Geller, *Phys. Rev.* **1976**, *B14*, 4345.
[9] B. G. Hyde, S. Andersson, in: *Inorganic Crystal Structures*, John Wiley & Sons Inc., New York, **1989**, chapter 14.
[10] E. Gaudin, H. J. Deiseroth, T. Zaiß, *Z. Kristallogr.* **2001**, *216*, 39−44.
[11] L. Kienle, to be published.
[12] C. Svensson, J. Albertsson, *J. Solid State Chem.* **1983**, *46*, 46−55.
[13] M. Schlosser, PhD thesis, University of Siegen, in progress.
[14] STOE & CIE, *WinXPow*, Darmstadt, **1999**.
[15] Crystal Impact, *DIAMOND 2.1*, Bonn, **1999**.
[16] W. Hönle, G. Kühn, H. Neumann, *Z. Anorg. Allgem. Chem.* **1986**, *543*, 161−168.
[17] R. Hoppe, W. Lidecke, F.-C. Frorath, *Z. Anorg. Allgem. Chem.* **1961**, *309*, 49−54.
[18] B. Krebs, *Angew. Chem.* **1983**, *95*, 113−134; *Angew. Chem. Int. Ed. Engl.* **1983**, *22*, 113−134.
[19] M. Schlosser, Diploma thesis, University of Siegen, **1999**.
[20] B. Eisenmann, A. Hofmann, *Z. Kristallogr.* **1991**, *197*, 159−160.
[21] L. Kienle, PhD thesis, University of Siegen **1998**.
[22] STOE & CIE, *X-SHAPE 1.02*, Darmstadt, **1997**.
[23] G. M. Sheldrick, *SHELXS-97, Program for the solution of Crystal Structures*, University of Göttingen, Germany, **1997**.
[24] G. M. Sheldrick, *SHELXL-97, Program for Structures Refinement*, University of Göttingen, Germany, **1997**.

Received January 16, 2001
[I01021]

Biomimetic Catalysis of Catechol Cleavage by O_2 in Organic Solvents − Role of Accessibility of O_2 to Fe^{III} in 2,11-Diaza[3,3](2,6)pyridinophane-Type Catalysts

Nathalie Raffard,[a] Riccardo Carina,[b] A. Jalila Simaan,[a] Joëlle Sainton,[a] Eric Rivière,[a] Luba Tchertanov,[c] Sophie Bourcier,[d] Guy Bouchoux,[d] Michel Delroisse,[b] Frédéric Banse,*[a] and Jean-Jacques Girerd*[a]

Keywords: Enzyme models / Catalysis / Iron / Oxygen / N ligands

Three new complexes, $[Fe(LN_4H_2)Cl_2]^+$, $[Fe(LN_4H_2)(Cat)]^+$, and $[Fe(LN_4H_2)(DBC)]^+$, were synthesized by using the tetradentate macrocyclic ligand LN_4H_2 (where LN_4H_2, Cat, and DBC stand for 2,11-diaza[3,3](2,6) pyridinophane, catecholate, and 3,5-di-*tert*-butylcatecholate, respectively). The structure of $[Fe(LN_4H_2)Cl_2]^+$ was determined by X-ray diffraction. It crystallizes in the monoclinic space group *C*2/*c* with $a = 9.613(1)$, $b = 11.589(1)$, $c = 14.063(2)$ Å, β=110.20(2)°, $V = 1541.9(3)$ Å^3, and $Z = 4$. These complexes were found to catalyze the oxidation of catechol groups using O_2. This was performed in various organic solvents at 20 °C. The reaction rates were measured for the stoichiometric complexes $[Fe(LN_4H_2)(Cat)]^+$ and $[Fe(LN_4H_2)(DBC)]^+$. It was found that despite the relatively high energy of the ligand-to-metal charge transfer O(DBC or Cat)→Fe^{III}, their activity was comparable to that of the fast TPA systems [TPA indicates tris(2-pyridylmethyl)amine]. The oxidation products of $DBCH_2$ have been studied. It has then been shown that the LN_4H_2 systems catalyse by means of both intra- and extradiol cleavage of catechol groups. The existence of multiple reactive pathways can account for the fast reactivity observed.

Introduction

Catechol dioxygenases catalyze the ring cleavage of catechols using O_2 without coreductants. Two sub-classes of these enzymes can be distinguished. Intradiol ones contain a trigonal bipyramidal Fe^{III} ion and catalyze the insertion of both atoms of O_2 between the OH groups [C(1) and C(2)] of the catechol. Two different mechanisms have been proposed to account for their reactivity after the chelation of a doubly deprotonated catecholate. The first one proceeds by electrophilic attack of the catechol by O_2.[1] The alternative pathway implicates the Fe^{II}−semiquinonate character of the Fe^{III}−catecholate moiety generated by the charge transfer from the chelated ring to the metal center. The spin-forbidden rule for a reaction between an organic molecule and dioxygen is bypassed, so the oxidation occurs by the attack of the biradical O_2 on the spin density acquired by the substrate ring.[2] The following steps are the same for both pathways. The O_2 moiety binds to the iron center to yield a peroxo bridge between the metal ion and the substrate. The decomposition of this intermediate then leads to the release of the product and regeneration of the active site. Extradiol catechol dioxygenases contain a square-pyramidal Fe^{II} ion and catalyze the oxidative cleavage of catechols in a different fashion: Both atoms of the dioxygen molecule are inserted between C(1) and C(6) or C(2) and C(3). Que and Ho[2] proposed a mechanism for this subclass of enzymes. The first step of the catalytic cycle involves the chelation of a monoanionic substrate followed by the binding of O_2 to Fe^{II}. The Fe^{III}−superoxo species thus formed is proposed to have nucleophilic character on the distal oxygen atom.[2] The nucleophilic oxygen atom of the superoxo species then attacks the ring at the carbon atoms C(3) or C(6), and the product is released.

Among the models described in the literature,[2,3] the vast majority show intradiol catechol dioxygenase reactivity whereas a few behave as extradiol models.[4−9] Que and coworkers have suggested that the key step for the reactivity of intradiol models resides in the charge transfer from the catecholate to Fe^{III}.[10] Among the known models in the literature, the system based on TPA[11] presents the maximum Fe^{II}−semiquinone character and shows a fast ring cleavage of the catechols in stoichiometric conditions. Koch and Krüger[12] used the LN_4Me_2 macrocyclic ligand to achieve efficient catalysis although the rate was approximately 40 times slower than the stoichiometric TPA system.

Studies of extradiol dioxygenase models are scarce. However, basic requirements such as weak steric hindrance and a vacant coordination site for O_2 on the iron center seem essential.[7,8] An analysis of the structure of $[Fe(LN_4Me_2)cat]^+$ reported by Koch and Krüger[12] revealed that the steric hindrance provided by the methyl groups of the ligand could prevent the formation of the

[a] Laboratoire de Chimie Inorganique, UMR CNRS 8613, Université Paris-Sud,
91405 Orsay, France
[b] Unilever Research, Port Sunlight Laboratory,
Port Sunlight L63 3JW, England
[c] CNRS, Institut de Chimie des Substances Naturelles, UPR 2301,
Avenue de la Terrasse, 91198 Gif/Yvette, France
[d] Laboratoire des Mécanismes Réactionnels, UMR CNRS 7651, Ecole Polytechnique,
91128 Palaiseau, France

 © WILEY-VCH Verlag GmbH, 69451 Weinheim, 2001 1434−1948/01/0909−2249 $ 17.50+.50/0

peroxo bridge between the Fe^{III} ion and the catecholate. Removing these groups appeared then a matter to favor the formation of the peroxo bridge and speed up the reaction. In the present paper, we investigate the effect of steric hindrance on the reactivity of Fe^{III}–catecholate complexes with O_2. We report the results obtained with the system based on the ligand 2,11-diaza[3,3](2,6) pyridinophane (LN_4H_2) (Scheme 1), the analog of the bulkier LN_4Me_2.

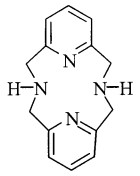

Scheme 1. Schematic representation of the ligand LN_4H_2

Results and Discussion

X-ray Crystal Structure Determination

The starting Fe^{III} complex is $[Fe(LN_4H_2)Cl_2]Cl$. Its structure has been determined. The complex cation is represented in Figure 1. Selected bond lengths and angles are listed in Table 1.

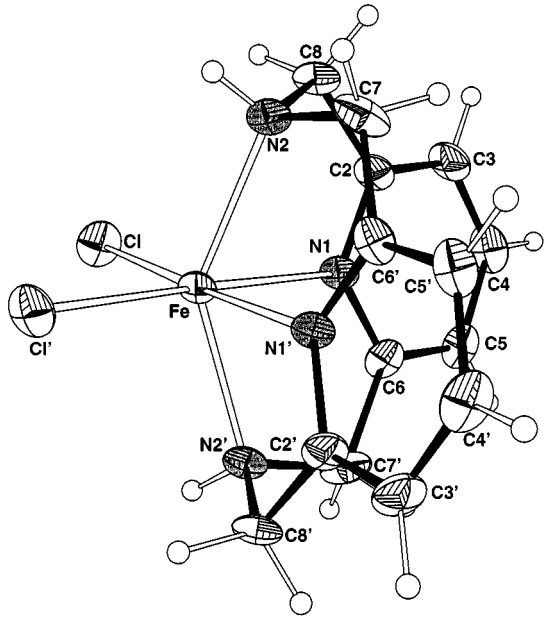

Figure 1. ORTEP plot showing the structure of $[Fe(LN_4H_2)(Cl)_2]^+$ with atom-labeling scheme; primed atoms are related to unprimed ones by symmetry elements of the molecule; displacement ellipsoids are drawn at the 50% probability level; H atoms are shown as small circles of arbitrary radii

It shows an internal C_{2v} symmetry with two mirror planes, one defined by the iron(III) and the *N*-pyridine atoms, and the other by the iron(III) and the *N*-amine atoms. As in previous studies with this macrocycle[13] or its analog LN_4Me_2,[12,14,15] the pseudo-octahedral iron ion is coordinated to the four nitrogen atoms of the ligand leaving two *cis* positions at the metal center that are occupied by two chloro groups in the present species. The ligand is folded along the $N_{amine}-N_{amine}$ axis, the pyridine moieties being nearly perpendicular to each other with a dihedral angle of 96.5(1)°. The $Fe-N_{py}$ distance of 2.09 Å and the $Fe-N_{amine}$ distance of 2.19 Å are slightly shorter than the same distances in the related high-spin $[Fe(LN_4Me_2)Cl_2]^+$ complex.[14] This surprising evolution, especially for the $Fe-N_{amine}$ distances, reflects without ambiguity the decreased steric hindrance at the metal center with LN_4H_2. The Fe–Cl distance of 2.29 Å agrees with the mean value of 2.283(4) Å calculated from other Fe^{III} complexes.[16]

Table 1. Selected bond lengths [Å] and angles [°] for $[Fe(LN_4H_2)(Cl)_2]Cl$; symmetry transformations used to generate equivalent atoms: $-x, y, -z + 1/2$

Fe–N(1)	2.094(1)
Fe–N(2)	2.189(1)
Fe–Cl	2.289(5)
N(1)′–Fe–N(1)	84.95(7)
N(1)–Fe–N(2)	77.51(5)
N(1)–Fe–N(2)′	74.99(5)
N(2)–Fe–N(2)′	142.41(7)
N(1)′–Fe–Cl	175.09(4)
N(1)–Fe–Cl	90.16(4)
N(2)–Fe–Cl	104.39(4)
N(2)′–Fe–Cl	100.83(4)
N(1)–Fe–Cl′	175.09(4)
Cl–Fe–Cl′	94.73(3)

UV/Vis Absorption Spectroscopy

The reaction of the yellow $[Fe(LN_4H_2)Cl_2]Cl$ in MeOH or CH_3CN with a catecholate immediately yielded a deep purple-blue solution. A purple-blue complex can be precipitated on addition of $NaBPh_4$. The UV/Vis spectrum of a solution of the resulting powder or of the solution obtained by mixing $[Fe(LN_4H_2)Cl_2]Cl$ and cat^{2-} shows two intense bands in the visible region. They are assigned as ligand-to-metal charge transfer (LMCT) bands from the doubly deprotonated chelating catecholate to the iron(III) ion.[10,17–19] This charge transfer generates some Fe^{II}–semiquinonate character[10] in the ground state, which is a key factor in the reactivity. The optical data of the catecholate (Cat) or 3,5-di-*tert*-butylcatecholate (DBC) complexes in MeOH or CH_3CN are given in Table 2.

As expected, the DBC species absorbs at a higher wavelength than the Cat species. This observation is consistent with the stronger electron-donating ability of the *tert*-butyl groups leading to an easier charge transfer from the DBC^{2-} to the iron ion.

The LMCT bands of these complexes can be considered as probes for the intradiol reactivity: the lower in energy the LMCT bands are, the faster the intradiol reactivity is. In comparison to other auxiliary ligands[11,20,21] or the close analog LN_4Me_2[12] the LMCT bands of our Fe^{III}–catecholate complexes lie at relatively high energies. However, other factors may be involved in the efficient oxidative cleavage of the catechols, in particular weak bulki-

Table 2. Characteristics of the LMCT bands and second-order rate constants k at 20 °C for $[Fe(LN_4H_2)(Cat)]^+$ and $[Fe(LN_4H_2)(DBC)]^+$, in MeOH and CH_3CN

	$[Fe(LN_4H_2)(Cat)]^+$			$[Fe(LN_4H_2)(DBC)]^+$		
	λ_1 [nm] (ε [$M^{-1}\cdot cm^{-1}$])	λ_2 [nm] (ε [$M^{-1}\cdot cm^{-1}$])	k [$M^{-1}\cdot s^{-1}$]	λ_1 [nm] (ε [$M^{-1}\cdot cm^{-1}$])	λ_2 [nm] (ε [$M^{-1}\cdot cm^{-1}$])	k [$M^{-1}\cdot s^{-1}$]
MeOH	497 (3040)	689 (3230)	0.027	553 (2860)	744 (3070)	8.6
CH_3CN	488 (2960)	704 (3130)	0.45	546 (3050)	753 (3280)	48

ness of the auxiliary ligand[20,22] or spin equilibrium for the iron ion.[23]

Stoichiometric Kinetic Studies

The oxidative cleavage of catechols can be monitored by UV/Vis spectroscopy by following the decay of the LMCT bands with time. This procedure is characteristic of these kinds of studies.[20,21] The complexes $[Fe(LN_4H_2)(Cat)]BPh_4$ and $[Fe(LN_4H_2)(DBC)]BPh_4$ have been dissolved in CH_3CN or MeOH in order to obtain a final concentration in iron about 10 times lower than that of O_2 ($[O_2]$ = 1.62 mM in CH_3CN[24] and $[O_2]$ = 2 mM in MeOH,[25] at 20 °C under air). The kinetic analyses were then carried out by using a pseudo-first-order law. The second-order rate constants, at 20 °C, are tabulated in Table 2. A typical evolution of the LMCT bands during the oxygenation of the catecholate complex and the kinetic analysis are shown in Figure 2.

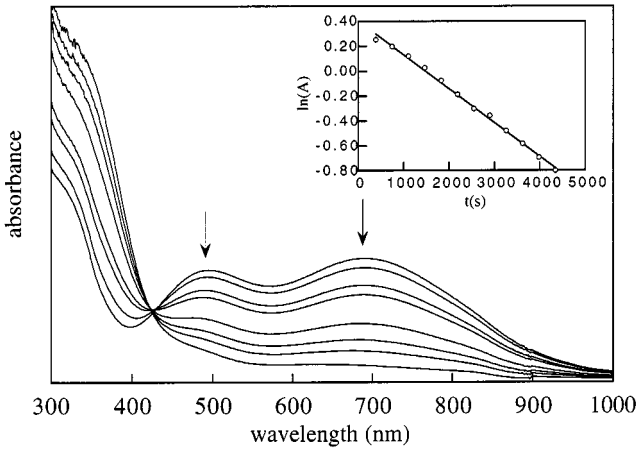

Figure 2. Evolution of the UV/Vis spectrum of $[Fe(LN_4H_2)(Cat)]^+$ in air-saturated MeOH at 20 °C; inset: plot of ln(A) vs. time

Compared to the LN_4Me_2 analog (k = 0.277 10^{-2} $M^{-1}s^{-1}$ for the substrate catecholate, and k = 0.377 $M^{-1}s^{-1}$ for the substrate di-*tert*-butylcatecholate in CH_3CN),[12] one can note a 160-fold increase and a 130-fold increase, respectively. These spectacular accelerations are certainly not attributable to electronic factors as deduced from UV/Vis spectra. Steric factors must be implicated as revealed by the structure analysis of $[Fe(LN_4H_2)Cl_2]^+$. The great accessibility of O_2 to the iron center appears then to be a very important parameter in order to perform a fast ring cleavage of the catechols. The rate constants can also be compared to that of the TPA system, the fastest intradiol catechol dioxygenase model reported so far[11]: in MeOH, the rate constants are very similar to those of TPA (10 vs. 8.6 $M^{-1}s^{-1}$).

Catalytic Catechol Dioxygenase Activity of $[Fe(LN_4H_2)Cl_2]Cl$

In a typical experiment, $[Fe(LN_4H_2)Cl_2]Cl$ was dissolved in CH_3CN, then 50 equiv. of $DBCH_2$ + 2 equiv. of NEt_3 in the same solvent were added. The reaction mixture was analyzed by Electrospray Ionization Mass Spectrometry (ESI-MS) at the end of the reaction, or by ^1H NMR spectroscopy during the course of the reaction, when the sample was prepared in CD_3CN, CD_3OD or $CDCl_3$.

Figure 3. shows the evolution, by NMR spectroscopy, of the reaction mixture in CD_3OD. The results are similar in other solvents. The excess of substrate is sufficient to avoid broadening of the peaks due to the paramagnetism of the Fe^{III} complex. The signals of the free substrate are observed at δ = 1.24, 1.37, 6.72 (d), and 6.73 (d). They disappear during the course of the reaction whereas other signals grow in intensity. The new signals correspond to three major products plus some other minor species that have not been further characterized by this technique. For the major products, the assignments have been made by comparing the spectra with those recorded in CD_3CN or in $CDCl_3$. We also referred to the complete work of Funabiki et al.[4] It appears then that muconic anhydride [the common intradiol cleavage product 3,5-di-*tert*-butyl-1-oxacyclohepta-3,5-diene-2,7-dione (**1**)] is detected at δ = 1.18, 1.27, 6.21 (d), and 6.61 (d). Two extradiol cleavage products are also detected: The first one is 3,5-di-*tert*-butyl-2-pyrone (**2**) (δ = 1.15, 1.24, 6.56, 6.58). The second one is detected at δ = 1.13, 1.16, 5.38, and 6.18. We propose that these signals correspond to the enol form of *cis*,*cis*-3,5-di-*tert*-butyl-2-hydroxymuconic semialdehyde (**3**). Indeed, its keto form has been detected unambiguously in $CDCl_3$ at δ = 1.10, 1.19, 5.28, and 9.75. These values are close to those reported by Funabiki et al.[4] It thus makes sense to propose that the more polar form of this product is stable in the more polar solvent whereas the less polar form is stabilized in the less polar solvent. The by-product 3,5-di-*tert*-butyl-1,2-benzoquinone (**6**) was not detected or only as trace amounts. Due to overlapping of the signals, the final spectrum has been

deconvoluted[26] in order to estimate intradiol versus extradiol cleavage. The results show that the oxygenation of 3,5-di-*tert*-butylcatechol by the LN_4H_2 system proceeds with an intradiol/extradiol ratio close to 1. Attempts to purify the reaction mixture by column chromatography have been unsuccessful due to the instability of the products. As a matter of fact, we cannot report a more quantitative attribution of the products.

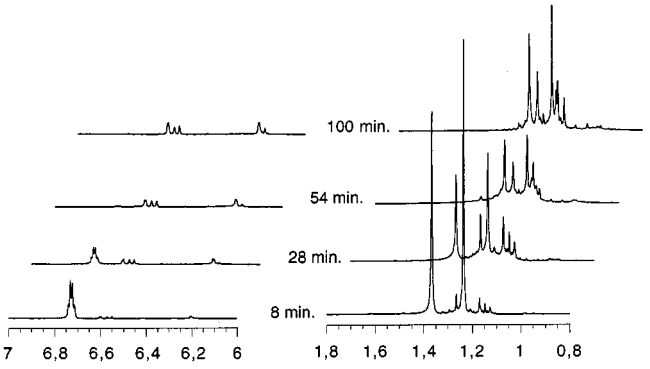

Figure 3. Progress of the reaction of $[Fe(LN_4H_2)(Cl)_2]^+$ + 50 $DBCH_2$ + 2 NEt_3 in air-saturated CD_3OD monitored by ^1H NMR spectroscopy; the peak at δ = 5.38 (see text) is omitted for clarity

The oxygenation products have also been analyzed by ESI-MS from a reaction mixture in CH_3CN. An MeOH/H_2O (0.1% formic acid) mixture has been used for the detection of some species. The 3 major products are observed at *m*/*z* = 237.2 (**1**), *m*/*z* = 209.2 (**2**) and *m*/*z* = 255.4 (**3**). Other peaks are observed; some of them can be assigned as follows: *m*/*z* = 441.6 {4′,6,6′,8-tetrakis(1,1-dimethylethyl)spiro[1,4-benzodioxin-2(3*H*),2′-[2*H*]pyran]-3-one, **4**}, *m*/*z* = 225.3 (3,5-di-*tert*-butyl-5-formyl-2-furanone, **5**) and *m*/*z* = 221.2 (**6**). The results are summarized in Scheme 2.

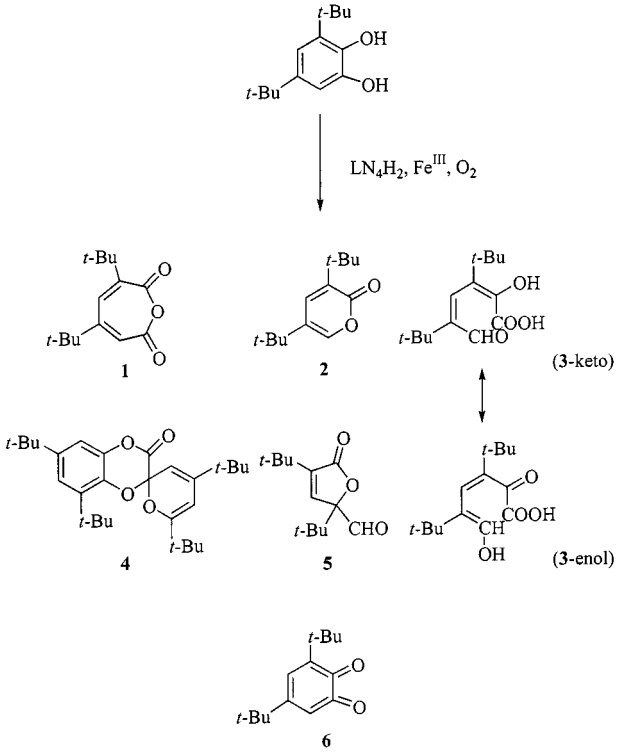

Scheme 2. Oxidation products of 3,5-di-*tert*-butylcatechol detected in this study

To the best of our knowledge, there are only two examples of structurally characterized synthetic iron complexes capable of carrying out extradiol cleavage. They are based on the tridentate ligands TACN (1,4,7-triazacyclononane)[5,7] or hydrotris(3,5-diisopropyl-1-pyrazolyl)-borate[8]. The authors evoke the necessity to dispose of several factors, namely a vacant site around the iron center for the coordination of O_2 and a moderate steric hindrance. Moreover Ito and Que[7] show that Lewis bases such as pyridines must be available in the reaction mixture. They propose that the Lewis base substitutes an oxygen atom of the substrate and thus converts it into a monodentate anion. The structure of the intermediate obtained allows the extradiol cleavage to occur.

Because of the rigidity of the 12-membered LN_4H_2 macrocycle, we never observed species with this ligand acting as tridentate. We therefore report here the first example of extradiol dioxygenase activity with a tetradentate ligand.

As revealed by UV/Vis, $[Fe(LN_4H_2)(DBC)]^+$ has some Fe^{II}–semiquinonate character which is believed to be at the origin of intradiol cleavage activity (pathway 1 in Scheme 3), as usually observed for complexes with tetradentate ligands.[10–12,20,21]

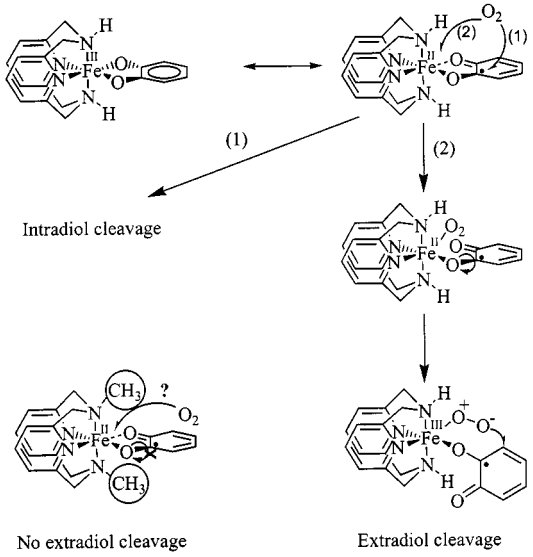

Scheme 3. Proposed mechanism for the reaction of $[Fe(LN_4H_2)(DBC)]^+$ with O_2

For the extradiol cleavage, we propose a mechanism inspired by Ito and Que[7] (see Scheme 3). In one, O_2 binds to the iron center to yield an Fe^{III}–superoxo species leading to the release of an oxygen atom of the enediolate moiety (pathway 2 in Scheme 3). The next sequence is then the ro-

tation of the substrate ring which is permitted due to the weak steric congestion on the amino groups. Finally, the oxygenation proceeds by the attack of the nucleophilic superoxide[2] at the carbon atom adjacent to the C−O group bound to the iron ion yielding extradiol cleavage of the aromatic ring.

The reason why the reactivity pattern of $[Fe(LN_4H_2)(DBC)]^+$ is clearly different from its analog LN_4Me_2 can only be related to the substituents of the macrocycles. The accessibility of the metal center is allowed with LN_4H_2 while the bulkiness of the methyl groups provides a crowded iron center in LN_4Me_2. The Fe^{III}−superoxo species responsible for the extradiol cleavage therefore cannot be obtained with the latter ligand. Moreover, the rotation of the ring catecholate should be forbidden due to the methyl groups. Consequently, the intermediate with the convenient stereospecificity for extradiol cleavage cannot be formed (see Scheme 3). Finally, we propose two reasons, related to the relative steric hindrance of the tetradentate macrocycles, to explain their different reactivity pattern.

The large rate constants observed for our catalyst may thus be due not only to the accessibility to the metal center but also to the existence of multiple reactive paths. To the best of our knowledge, no kinetic data for extradiol cleavage of catechols have been reported. At this stage we therefore cannot conclude whether one hypothesis is more valuable than the other one.

Conclusion

We isolated new Fe^{III} complexes based on the macrocyclic tetradentate ligand LN_4H_2. The structure of the chloro complex $[Fe(LN_4H_2)(Cl)_2]Cl$ has been determined. It reveals that the ligand adopts a bent conformation leaving two *cis* positions at the metal center that are occupied by two chloro ligands. The comparison of its bond lengths with the ones of the related $[Fe(LN_4Me_2)(Cl)_2]^+$ reported by Koch and Krüger bears evidence of the increased accessibility to the metal center in $[Fe(LN_4H_2)(Cl)_2]^+$.

Two other complexes with catecholate groups as exogeneous ligands have been prepared: $[Fe(LN_4H_2)(Cat)]^+$ and $[Fe(LN_4H_2)(DBC)]^+$. Their characterization by optical spectroscopy and ESI-MS are given. The reported complexes react with O_2 and the kinetics of the reaction has been measured. They show one of the fastest catechol dioxygenase reactivity ever reported for coordination compounds.

The catalysis of oxidative cleavage of $DBCH_2$ by $[Fe(LN_4H_2)(Cl)_2]Cl$ has been studied by ^1H NMR and ESI-MS. It indicates that this complex undergoes both intra- and extradiol dioxygenase activity, which is the first case reported with a tetradentate ligand, to date. The fast reactivity observed may thus be due to multiple reactive pathways. A mechanism based on the steric characteristics of the ligand is proposed to explain this tendency.

Experimental Section

General: Starting materials were purchased from Acros and were used as received. Solvents were purchased from Merck and used without purification except when indicated below. Syntheses of catecholate and 3,5-di-*tert*-butylcatecholate complexes were carried out in a glovebox equipped with an O_2/H_2O purifier (Jacomex BS531) − UV/Vis: Varian Cary 5E or Cary 300 Bio equipped with temperature controllers. − MS: VG Quattro II (Micromass, Manchester, UK) triple quadrupole electrospray mass spectrometer. Typical optimized values for the source parameters were: capillary 2.5 kV, counter electrode 0.4 kV, cone voltage 15−50 V, source temperature 80 °C. − NMR spectra were recorded with a Bruker AM250 at 20 °C, using the protonated impurity of the solvent as internal reference.

Synthesis of the Ligand: The ligand LN_4H_2 was prepared according to reported methods[27] and improved with slight modifications.

Syntheses of the Complexes

$[Fe(LN_4H_2)Cl_2]Cl$: A solution of $FeCl_3$ (54.1 mg; 0.33 mmol) in CH_3CN was added dropwise to a solution of LN_4H_2 (80 mg, 0.33 mmol) in CH_2Cl_2. The solution was refluxed for a few minutes and then allowed to cool down. A yellow powder was collected by filtration. Yield 70 mg (50%). Crystals for X-ray analysis were grown from an MeOH solution with aerial diffusion of CH_3CN. − ESI-MS m/z = 366.2 $[Fe(LN_4H_2)Cl_2]^+$. − $[Fe(LN_4H_2)Cl_2]Cl{\cdot}0.8H_2O$ $C_{14}H_{16}N_4Cl_3Fe{\cdot}0.8H_2O$ (416.9): calcd. C 40.33, H 4.25, Cl 25.51, N 13.44; found C 40.75, H 4.05, Cl 24.51, N 13.05.

$[Fe(LN_4H_2)(Cat)]BPh_4$: A solution of catechol (22 mg; 0.2 mmol) and NEt_3 (56 μL; 0.40 mmol) was added dropwise to a dry methanol solution of $[Fe(LN_4H_2)Cl_2]Cl$ prepared in the glovebox at room temperature with 48 mg of LN_4H_2 (0.2 mmol) and 32.4 mg of anhydrous $FeCl_3$ (0.2 mmol). The dark blue solution was stirred for 5 min, then 0.9 equiv. of $NaBPh_4$ (61.4 mg) in dry MeOH was added to give a dark blue microcrystalline powder. The solid was isolated by filtration, washed with MeOH and dried under vacuum. Yield 97 mg (60%). − EI-MS m/z = 404.2 $[Fe(LN_4H_2)(Cat)]^+$. − $[Fe(LN_4H_2)(Cat)]BPh_4{\cdot}1.4CH_3OH$ $C_{44}H_{40}N_4O_2BFe{\cdot}1.4CH_2OH$ (812.8): calcd. C 70.97, H 5.98, B 1.41, Fe 7.27, N 7.29; found C 70.90, H 5.53, B 1.33, Fe 7.1, N 7.43.

$[Fe(LN_4H_2)(DBC)]BPh_4$: The experimental procedure was similar to the one described for $[Fe(LN_4H_2)(Cat)]BPh_4$. Yield 120 mg (70%). − EI-MS m/z = 516.4 $[Fe(LN_4H_2)(DBC)]^+$. − $[Fe(LN_4H_2)(DBC)]BPh_4{\cdot}1.1CH_3OH$ $C_{52}H_{56}N_4O_2BFe{\cdot}1.1CH_3OH$ (869.4): calcd. C 73.23, H 6.99, B 1.24, Fe 6.41, N 6.43; found C 73.20, H 7.01, B 1.27, Fe 6.45, N 6.67.

Structure Determination: The crystal data of $[Fe(LN_4H_2)Cl_2]Cl$ and the parameters of data collection are summarized in Table 3. A flattened octahedron-shaped yellow crystal with the dimensions 0.65 × 0.40 × 0.30 mm of $[Fe(LN_4H_2)Cl_2]Cl$ was chosen for the X-ray diffraction experiment. The unit-cell and intensity data were measured with an Enraf−Nonius CAD-4 diffractometer with graphite-monochromated Mo-K_α radiation (λ = 0.71070 Å). The cell constants were obtained by least-squares procedures based upon the 2Θ values of 25 reflections measured in the ranges $18.3° < 2\Theta < 25.2°$ at ambient temperature. During data collection three control reflections were measured every 3 h; the crystal was stable, and the check reflections showed a slight decay in intensity of only 7% during the X-ray data collection. A total of 2335 reflections were collected in the range $5.6° < 2\Theta < 59.9°$

within [$-13 \le h \le 13$, $0 \le k \le 16$, $0 \le l \le 19$]. From 2249 independent reflections, 2186 were considered as observed [$I > 2\sigma(I)$]. The structure was solved by direct methods with the program Shelxs86[28] and refined by using the Shelxl93 program.[29] The drawing was prepared with OrtepII.[30] The molecular cation was located in a special crystallographic position with the iron atom at the twofold rotation axis, along with the chloride anion. The structure was refined anisotropically (non-hydrogen atoms) by full-matrix least-squares approximation based on F^2. The hydrogen atom at the secondary nitrogen atom was localized in a difference Fourier synthesis and refined isotropically. Other hydrogen atom positions were calculated by assuming geometrical positions and were included in the structural model. Final weighting scheme was $w = 1/[\sigma^2(F_o^2) + (0.0411P)^2 + 2.0320P]$, where $P = (F_o^2 + 2F_c^2)/3$. The final refinement of this model was continued until convergence when $R1 = 0.0302$ for $F^2 > 2\sigma(F^2)$ and $R_w = 0.0806$ were reached. The final difference map showed the largest residual peaks which are 0.424 and -0.641 e·Å^{-3}. The two largest peaks were found at the Fe and Cl atoms. Complete crystallographic data (excluding structure factors) for the structure reported in this paper has been deposited at the Cambridge Crystallographic Data Centre with no. CCDC-148680. Copies of the data can be obtained free of charge on application to CCDC, 12 Union Road, Cambridge CB2 1EZ, UK [Fax: (internat.) + 44-1223/336-033, E-mail: deposit@ccdc.cam.ac.uk, World Wide Web: http://www.ccdc.cam.ac.uk].

Table 3. Crystal data and structure refinement for $[Fe(LN_4H_2)(Cl)_2]Cl$

Empirical formula	$C_{14}H_{16}Cl_3Fe_1N_4$
Molecular mass	402.51
Temperature	294(2) K
Wavelength (Mo-K_α)	0.71070 Å
Crystal system	monoclinic
Space group	*C*2/*c*
a [Å]	9.613(1)
b [Å]	11.589(1)
c [Å]	14.063(2)
β [°]	110.20(2)
Volume [Å^3]	1541.9(3)
Z	4
d_x [Mg/m^3]	1.728
μ [mm^{-1}]	1.498
F(000)	820
Crystal size [mm]	0.65 × 0.40 × 0.30
Θ range [°]	2.78−29.95
Index ranges	$-13 \le h \le 13$
	$0 \le k \le 16$
	$0 \le l \le 19$
$N_{collect}$	2335
N_{indt}	2249 [*R*(int) = 0.0398]
N_{obs}	2186 [$I > 2\sigma(I)$]
$R1$ [$I > 2\sigma(I)$]	0.0302
$wR2$	0.0806
ρ_{max} [eÅ^{-3}]	0.424
ρ_{min} [eÅ^{-3}]	−0.641

[1] J. D. Lipscomb, A. M. Orville, *Met. Ions Biol. Syst.* **1992**, *28*, 285.
[2] L. Que, R. Y. N. Ho, *Chem. Rev.* **1996**, *96*, 2607.
[3] T. Funabiki, *Catalysis by Metal Complexes*, Kluwer Academic Publishers, Dordrecht/Boston/London, **1997**, p. 19.
[4] T. Funabiki, A. Mizoguchi, T. Sugimoto, S. Tada, M. Tsudi, H. Sakamoto, S. Yoshida, *J. Am. Chem. Soc.* **1986**, *108*, 2921.
[5] A. Dei, D. Gatteschi, L. Pardi, *Inorg. Chem.* **1993**, *32*, 1389.
[6] T. Funabiki, I. Yoneda, M. Ishikawa, M. Ujiie, Y. Nagai, S. Yoshida, *Chem. Commun.* **1994**, 1453.
[7] M. Ito, L. Que, *Angew. Chem. Int. Ed. Engl.* **1997**, *36*, 1342.
[8] T. Ogihara, S. Hikichi, M. Akita, Y. Moro-oka, *Inorg. Chem.* **1998**, *37*, 2614.
[9] H. Weiner, R. G. Finke, *J. Am. Chem. Soc.* **1999**, *121*, 9831.
[10] D. D. Cox, L. Que, *J. Am. Chem. Soc.* **1988**, *110*, 8085.
[11] H. G. Jang, D. D. Cox, L. Que, *J. Am. Chem. Soc.* **1991**, *113*, 9200.
[12] W. O. Koch, H. J. Krüger, *Angew. Chem. Int. Ed. Engl.* **1995**, *34*, 2671.
[13] R. Carina et al., unpublished results.
[14] W. O. Koch, V. Schünemann, M. Gerdan, A. X. Trautwein, H. J. Krüger, *Chem. Eur. J.* **1998**, *4*, 686.
[15] W. O. Koch, V. Schünemann, M. Gerdan, A. X. Trautwein, H. J. Krüger, *Chem. Eur. J.* **1998**, *4*, 1255.
[16] F. H. Allen, O. Kennard, *Chem. Design Aut. News* **1993**, *8*, 31.
[17] D. D. Cox, S. J. Benkovich, L. M. Bloom, F. C. Bradley, M. J. Nelson, L. Que, D. E. Wallick, *J. Am. Chem. Soc.* **1988**, *110*, 8085.
[18] S. Salama, J. D. Stong, J. B. Neilands, T. G. Spiro, *Biochemistry* **1978**, *17*, 3781.
[19] A. Dei, D. Gatteschi, L. Pardi, *Inorg. Chem.* **1993**, *32*, 1389.
[20] P. Mialane, L. Tchertanov, F. Banse, J. Sainton, J.-J. Girerd, *Inorg. Chem.* **2000**, *39*, 2440.
[21] M. Pascaly, M. Duda, A. Rompel, B. H. Sift, W. Meyer-Klaucke, B. Krebs, *Inorg. Chim. Acta* **1999**, *291*, 289.
[22] M. Pascaly, C. Nazikkol, F. Schweppe, A. Wiedemann, K. Zurlinden, B. Krebs, *Z. Anorg. Allg. Chem.* **2000**, *626*, 50.
[23] A. J. Simaan, M.-L. Boillot, E. Rivière, A. Boussac, J.-J. Girerd, *Angew. Chem. Int. Ed.* **2000**, *39*, 196.
[24] Value obtained by dividing by 5 the concentration under pure O_2 (8.1 mM, see for example ref.[12]).
[25] J. Tokunaga, *J. Chem. Eng. Data* **1975**, *20*, 41.
[26] The final spectrum has been deconvoluted with a sub-program of WinNMR 5.1 software, Bruker. Only the peaks attributed to the three major products have been analyzed in downfield and upfield regions. The results obtained in both regions have been compared. We made the hypothesis that the minor products were negligible.
[27] [27a]B. Alpha, E. Anklam, R. Deschenaux, J.-M. Lehn, M. Pietrakiewicz, *Helv. Chim. Acta* **1988**, *71*, 1042. − [27b] F. Bottino, M. Di Grazia, P. Finocchiaro, F. R. Fronczek, A. Mamo, S. Pappalardo, *J. Org. Chem.* **1988**, *53*, 3521.
[28] G. M.Sheldrick, *Shelxs86*, Univ. of Göttigen, Germany, **1986**.
[29] G. M. Sheldrick, *Shelxl93*, Univ. of Göttigen, Germany, **1993**.
[30] C. K. Johnson, *OrtepII*, Report ORNL-5138. Oak Ridge National Laboratory, Tennessee, USA, **1976**.

Received February 16, 2001
[I01054]

Intramolecular Hydrogen-Bonding, Cation−π, and π-Stacking Interactions Affecting *cis*/*trans* Isomerization: Hexacarbonyltungsten Derivatives of Pyridyl-Substituted Arylphosphane Ligands

Leeni Hirsivaara,*[a] Matti Haukka,[b] and Jouni Pursiainen[a]

Keywords: *cis*/*trans* Isomerism / Hydrogen bonding / Intramolecular interactions / Phosphanes / Tungsten

A series of triphenylphosphane- and diphenyl(2-pyridyl)phosphane-substituted tetracarbonyltungsten derivatives has been prepared. Attractive intramolecular interactions between the phosphane ligands have been studied in both the neutral and protonated complexes; π-stacking, hydrogen-bonding, and cation–π bonding interactions were identified and were found to have an influence on the *cis*/*trans* isomerism of the complexes. It was found that the *cis*/*trans* isomerism could be switched by protonation or deprotonation of the diphenyl(2-pyridyl)phosphane derivatives. The complexes have been characterized by ^{31}P-, ^{1}H-, and ^{13}C NMR spectroscopy, X-ray crystallography, IR spectroscopy, and mass spectrometry.

Introduction

Supramolecular complexation through hydrogen-bonding, cation−π, or π-stacking interactions is an expanding area of research in chemistry, and is of enormous potential with regard to applications in several fields of chemistry and biology.[1] For example, enzyme catalysis is typically effected by attractive interactions between the enzyme and the substrate.

In organometallic chemistry, repulsive interactions between ligands are important parameters in determining the structures and reactivities of complexes. Supramolecular attractive interactions between ligands in the coordination sphere of a single transition metal complex have not attracted such attention. There are, however, examples of intramolecular π-stacking in transition metal complexes, both interligand[2,3] and intraligand.[4−6] There have also been studies concerning interligand hydrogen bonding in biochemically interesting purine and pyrimidine complexes,[7,8] theoretical studies of interligand hydrogen bonding between nitrogen donor ligands and small ligands such as H_2O, HF, or NH_3,[9,10] and some studies concerning interligand CH−π interactions.[11,12]

The full potential of attractive interactions between the ligands of organometallic complexes has not been evaluated: Attractive interactions between the ligands or between a ligand and a substrate offer a very promising approach to organometallic catalysis. In metalloenzymes, for instance, the interactions at the active site of an enzyme−substrate complex have been regarded as ligand−ligand interactions around the metal atom, playing a vital role in enzyme catalysis.[11]

[a] Department of Chemistry, University of Oulu,
P. O. Box 3000, 90014 Oulu, Finland
Fax: (internat.) + 358-8/553-1603
E-mail: leeni.hirsivaara@oulu.fi
[b] Department of Chemistry, University of Joensuu,
P. O. Box 111, 80101 Joensuu, Finland

In this work, attractive supramolecular interactions between phosphane ligands are used to modify *cis*/*trans* isomerization in complexes of the type $[W(CO)_4LL']$. Complexes $[W(CO)_4(PPh_3)_2]$ (**1**),[13] $[W(CO)_4(py)(PPh_3)]$ (**2**), $[W(CO)_4\{P(2\text{-py})Ph_2\}_2]$ (**3**), $[W(CO)_4\{P(2\text{-pyH})^+Ph_2\}\{P(2\text{-py})Ph_2\}](ClO_4^-)$ (**4**), $[W(CO)_4\{P(2\text{-py})Ph_2\}(PPh_3)]$ (**5**), and $[W(CO)_4\{P(2\text{-pyH})^+Ph_2\}(PPh_3)](ClO_4^-)$ (**6**)[13] have been used in this study.

Results

Synthesis of the Complexes

The aim of this study was to prepare and evaluate complexes in which phosphane ligands would be able to exhibit intramolecular attractions. These interactions could be π-stacking in neutral complexes, or cation−π or hydrogen-bonding interactions in cationic complexes. Sterically similar diphenyl(2-pyridyl)phosphane $[P(2\text{-py})Ph_2]$ and triphenylphosphane (PPh_3) were chosen as ligands.

Complexes $[W(CO)_4(PPh_3)_2]$ (**1**), $[W(CO)_4(py)(PPh_3)]$ (**2**), and $[W(CO)_4\{P(2\text{-py})Ph_2\}_2]$ (**3**) were synthesized by treating $[W(CO)_4(py)_2]$ with the appropriate phosphane ligand in benzene solution at 40−45 °C overnight.[14] When the reaction was performed using PPh_3 as the ligand, a mixture of complexes **1** and **2** was obtained. When $P(2\text{-py})Ph_2$ was used as the ligand, the only isolable product from the reaction was **3**, with no trace of a derivative analogous to **2**. The complex $[W(CO)_4\{P(2\text{-py})Ph_2\}(PPh_3)]$ (**5**) was prepared from **2** by the method described above. In the case of complexes **1**, **3**, and **5**, a mixture of *cis* and *trans* isomers was produced. When these complexes were purified by column chromatography, the *cis* isomer was eluted slightly faster than the *trans* isomer, but the bands could not be completely resolved. Complexes **3** and **5** were protonated with perchloric acid in chloroform solution to give the com-

 © WILEY-VCH Verlag GmbH, 69451 Weinheim, 2001 1434−1948/01/0909−2255 $ 17.50+.50/0

pounds $[W(CO)_4\{P(2\text{-}pyH)^+Ph_2\}\{P(2\text{-}py)Ph_2\}](ClO_4^-)$ (**4**) and $[W(CO)_4\{P(2\text{-}pyH)^+Ph_2\}(PPh_3)](ClO_4^-)$ (**6**).

Solution Behavior of the Complexes

All the reported complexes were characterized by NMR spectroscopy. ^1H NMR spectroscopic data are reported in the Exp. Sect. $^{13}C\{^1H\}$ NMR data for complexes **1**−**6** are presented in Table 1. In the case of complexes forming a mixture of *cis* and *trans* isomers, where possible, the spectra of the individual isomers were measured starting from the pure isomer obtained by column chromatography. In the case of ^{13}C NMR spectroscopy, however, the time required for spectral acquisition was too long to keep the isomer

Table 1. $^{13}C\{^1H\}$ NMR spectra of compounds **1**−**6**

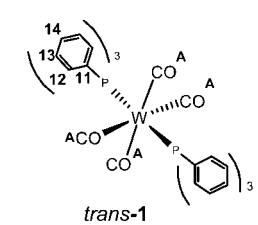

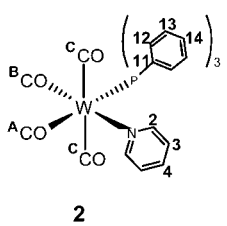

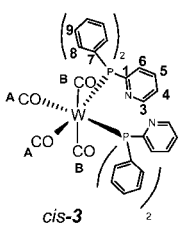

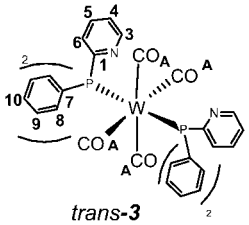

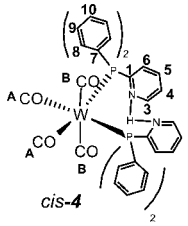

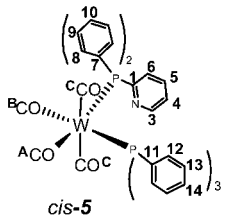

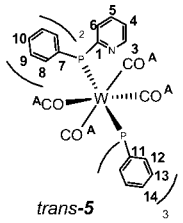

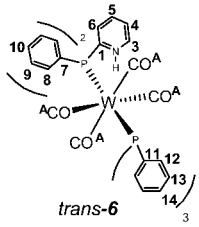

	trans-**1**[a]	*cis*-**2**	*cis*-**3**[a]	*trans*-**3**[a]	*cis*-**4**	*cis*-**5**	*trans*-**5**	*trans*-**6**
C^A (ppm)	203.68	208.69	203.03	202.95	202.03	intensity	202.95	201.78
$^2J_{CP}$ (Hz)	6.4 (t)	36.5 (d)	7.0 (t)	6.3 (t)	6.8 (t)	too low	6.3 (dd)	6.3 (dd)
C^B (ppm)	−	210.00	205.43	−	203.11	intensity	−	−
$^2J_{CP}$ (Hz)		4.9 (d)	(m)		9.9(t)	too low		
C^C (ppm)	−	204.72	−	−	−	−	−	−
$^2J_{CP}$ (Hz)		6.8 (d)						
C^1 (ppm)	−	−	161.82	162.98	156.29	158−172	158−172	157.85
$^1J_{CP}$ (Hz)			(m)	(m)	48 (d)			9.2 (d)
C^2 (ppm)	−	155.41	−	−	−	−	−	−
$^3J_{CP}$ (Hz)		1.7 (d)						
C^3 (ppm)	−	124.66	149.31	149.40	147.52	149.31	149.38	145.18
$^3J_{CP}$ (Hz)		(s)	(m)	7.3 (dd)	4.2 (dd)	16.1 (d)	15.8 (d)	6.4 (d)
C^4 (ppm)	−	135.72	122.7	122.78	126.07	122.99	122.87	126.46
$^4J_{CP}$ (Hz)		(s)	(s)	(s)	(s)	(s)	(s)	(s)
C^5 (ppm)	−	−	135.32	135.46	141.02	135.33	135.77	143.96
$^3J_{CP}$ (Hz)			(m)	3.6 (dd)	(s)	5.9 (d)	12.5 (d)	(s)
C^6 (ppm)	−	−	127.26	127.24	127.80	127.01	127.27	128.61
$^2J_{CP}$ (Hz)			(m)	11.3 (dd)	4.2 (dd)	18.0 (d)	22.0 (d)	5.7 (d)
C^7 (ppm)	−	−	135.93	137.61	134.78	137.47	137.47	134.13
$^1J_{CP}$ (Hz)			(m)	20.7 (dd)	22.0 (d)	(d)	41.1(d)	13.4 (d)
C^8 (ppm)	−	−	133.94	135.53	133.57	133.84	133.52	133.35
$^2J_{CP}$ (Hz)			5.7 (dd)	5.7 (dd)	6.3 (dd)	11.3 (d)	11.5 (d)	13.2 (d)
C^9 (ppm)	−	−	127.98	128.02	129.48	127.92	128.07	128.44
$^3J_{CP}$ (Hz)			(m)	4.8 (dd)	4.7 (dd)	9.5 (d)	9.5 (d)	9.7 (d)
C^{10} (ppm)	−	−	129.52	129.41	131.47	129.65	129.49	131.4−130.2
$^4J_{CP}$ (Hz)			(s)	(s)	(s)	2.2 (d)	1.5 (d)	
C^{11} (ppm)	137.87	134.33	−	−	−	138.00	138.00	136.44
$^1J_{CP}$ (Hz)	20.2 (dd)	36.7 (d)				(d)	40.3 (d)	43.1 (d)
C^{12} (ppm)	133.09	133.35	−	−	−	133.52	133.09	132.99
$^2J_{CP}$ (Hz)	5.9 (dd)	11.8 (d)				11.5 (d)	11.6 (d)	11.5 (d)
C^{13} (ppm)	128.07	128.32	−	−	−	127.92	128.05	128.07
$^3J_{CP}$ (Hz)	4.7 (dd)	9.2 (d)				9.5 (d)	9.5 (d)	9.5 (d)
C^{14} (ppm)	129.34	129.61	−	−	−	129.38	129.32	129.7−130.3
$^4J_{CP}$ (Hz)	(s)	1.7 (d)				1.5 (d)	1.5 (d)	

[a] Signals labeled dd appeared as triplets in the spectra.

pure during the measurements. In the case of complex **5** (Table 1), initial measurements were made on the mixture of *cis* and *trans* isomers as these could not be separated. The data obtained for the isomeric mixture were interpreted with the help of 2D HSQC spectra.

In the $^{13}C\{^1H\}$ NMR spectra of the symmetrically substituted complexes *trans*-**1**, *cis*-**3**, *trans*-**3**, and *cis*-**4**, the phosphane ligands are seen to be coupled,[15] causing the ^{13}C-^{31}P coupled resonance peaks to appear as pseudo triplets in the spectra (denoted as doublets of doublets in Table 1). In the case of unsymmetrical complexes, the spectra show normal doublets due to ^{13}C-^{31}P coupling.

$^{31}P\{^1H\}$NMR spectroscopic data for complexes **1** and **3**−**6** are presented in Table 2. The table also shows the relative amounts of the *cis* and *trans* isomers of the complexes. These equilibrium percentages were checked after the solutions had been left to stand for a week. It has been shown in previous studies that increased steric bulk of the phosphane favors the *trans* isomers, arylphosphanes showing only a very small proportion of the *cis* isomer.[14]

Table 2. ^{31}P NMR chemical shifts and proportion of *cis* isomers for complexes **1**, **3**−**6**

	$^{31}P_{cis}$ ($^1J_{WP}$/Hz)		$^{31}P_{trans}$ ($^1J_{wp}$/Hz)		% *cis*
	PPh_3	$PPyPh_2$	PPh_3	$PPyPh_2$	
1	23 (229)	−	28 (238)	−	32
3	−	26 (236)	−	30 (285)	56
4	−	28 (244)	−	34 (288)[d][d][e]	100
5	24[a]	25[a]	29 (269)[b]	30 (270)[b]	41
6	21[c]	34[c]	24 (275)[d]	38 (297)[d]	14

[a] d, $^2J_{pp}$ = 24 Hz, $^1J_{WP}$ not shown. − [b] d, $^2J_{pp}$ = 58 Hz. − [c] d, $^2J_{pp}$ = 23 Hz, $^1J_{WP}$ not shown. − [d] d, $^2J_{pp}$ = 61 Hz. − [e] Measured immediately after protonation, before disappearance of the signal.

In this study, complex $[W(CO)_4(PPh_3)_2]$ (**1**) behaved as expected, giving 32% of the *cis* isomer in $CDCl_3$ solution. On replacing one or two of the PPh_3 ligands by P(2-py)Ph_2, the amount of the *cis* isomer increased, even though the steric properties of the ligands were essentially unchanged. Thus, when one of the PPh_3 ligands was replaced by P(2-py)Ph_2 (complex **5**), the *cis* content increased to 41%, and when both of the PPh_3 ligands were replaced by P(2-py)Ph_2 (complex **3**), the *cis* content increased further to 56%. When complex **3** was protonated to give $[W(CO)_4\{P(2\text{-}pyH)^+Ph_2\}\{P(2\text{-}py)Ph_2\}](ClO_4^-)$ (**4**), the equilibrium changed entirely in favor of the *cis* form within a few hours. On protonation of complex **5** to give $[W(CO)_4\{P(2\text{-}pyH)^+Ph_2\}(PPh_3)](ClO_4^-)$ (**6**), the opposite occurred, and the equilibrium was shifted almost totally in favor of the *trans* form. These protonation reactions proved to be reversible: By adding base to a solution of **4** or **6**, the original *cis*/*trans* ratio was re-established within a few hours in the case of complex **4** or after standing overnight in the case of complex **6**.

X-ray Crystallography

Crystal structures were determined for complexes **2** and **3**. The structures of complexes **1** and **4** have been published in a preliminary communication.[13] Complex **5** did not crystallize adequately, while complex **6** decomposed upon attempted crystallization. Selected bond lengths and angles in all the structures are presented in Table 3 and Table 4. The determined crystal structures correspond to the major isomers in solution.

All the complexes were found to have a slightly distorted octahedral geometry, the angle between the ligands being widened in the *cis*-disubstituted derivatives: The angles between the phosphane ligands in diphosphane derivatives **3** and **4** were found to be 99.7 and 95.7°, respectively, while in the sterically less crowded triphenyl(2-pyridiyl)phosphane derivative **2** (Figure 1), the N−W−P angle was found to be 91.6°. Bond lengths around the metal centers reflect the relative *trans* effects of N, P and CO donors.

Complex $[W(CO)_4(PPh_3)_2]$ (**1**) crystallized in the *trans* form, as expected for a bulky phosphane ligand.[14] Complex $[W(CO)_4(py)(PPh_3)]$ (**2**, Figure 1) crystallized in the *cis* form, as found in solution. In the latter case, there is little

Table 3. Bond lengths [Å] around the metal centers in complexes **1**−**4**

	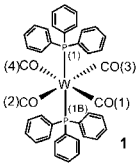 1	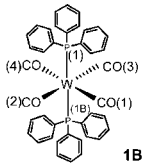 1B	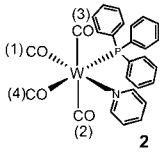 2	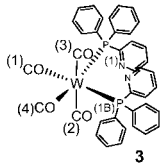 3	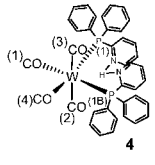 4
W–P(1)	2.4789(8)	2.4889(8)	2.5396(9)	2.5562(4)	2.5170(7)
W–P(1B)	2.4789(8)	2.4689(8)	–	2.5562(4)	2.5482(7)
W–N(1)	–	–	2.287(3)	–	–
W–C(1)	2.045(4)	2.028(3)	1.962(4)	1.9703(18)	2.000(3)
W–C(2)	2.036(2)	2.034(3)	2.026(4)	2.040(2)	2.038(3)
W–C(3)	2.036(2)	2.031(3)	2.013(4)	2.040(2)	2.041(3)
W–C(4)	2.045(4)	2.058(3)	1.994(4)	1.9703(18)	1.991(3)
C(1)–O(1)	1.141(4)	1.141(4)	1.169(5)	1.163(2)	1.142(4)
C(2)–O(2)	1.146(4)	1.137(4)	1.155(5)	1.141(2)	1.143(4)
C(3)–O(3)	1.146(4)	1.148(4)	1.154(5)	1.141(2)	1.139(4)
C(4)–O(4)	1.141(4)	1.128(4)	1.147(5)	1.163(2)	1.147(4)

Table 4. Bond angles [°] around the metal centers in complexes **1**–**4**

	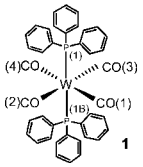 1	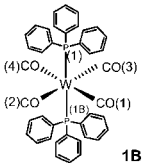 1B	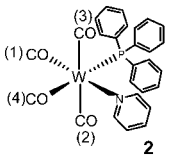 2	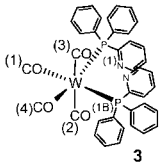 3	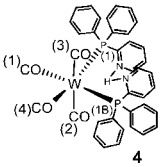 4
P(1)–W–C(1)	88.03(10)	95.16(10)	88.73(12)	90.62(5)	87.51(8)
P(1)–W–C(2)	90.66(9)	89.12(9)	90.33(11)	85.20(5)	96.90(8)
P(1)–W–C(3)	89.34(9)	90.71(9)	91.41(12)	94.96(5)	89.92(8)
P(1)–W–C(4)	91.97(10)	87.95(9)	176.85(11)	166.97(5)	170.88(9)
P(1)–W–N(1)	–	–	91.55(8)	–	–
P(1B)–W–P(1)	180.0	176.32(2)	–	99.70(2)	95.72(2)
P(1B)–W–C(1)	91.97(10)	88.32(10)	–	166.97(5)	175.44(9)
P(1B)–W–C(2)	89.34(9)	89.55(9)	–	94.96(5)	85.39(8)
P(1B)–W–C(3)	90.66(9)	90.79(9)	–	85.20(5)	93.85(7)
P(1B)–W–C(4)	88.03(10)	88.63(9)	–	90.62(5)	92.96(9)
N(1)–W–C(1)	–	–	177.83(13)	–	–
N(1)–W–C(2)	–	–	91.33(13)	–	–
N(1)–W–C(3)	–	–	90.18(15)	–	–
N(1)–W–C(4)	–	–	91.33(13)	–	–
C(1)–W–C(2)	90.45(12)	92.34(12)	90.82(15)	93.81(7)	91.04–(11)
C(1)–W–C(3)	89.55(12)	84.95(12)	87.66(17)	86.00(7)	89.36(11)
C(1)–W–C(4)	180.0(2)	175.64(13)	88.34(15)	80.40(10)	83.98(12)
C(2)–W–C(3)	180.0	177.26(12)	177.66(17)	179.75(10)	173.18(11)
C(2)–W–C(4)	89.55(12)	90.75(12)	90.89(15)	86.00(7)	86.57(12)
C(3)–W–C(4)	90.45(12)	91.97(12)	87.29(16)	93.81(7)	86.71(12)

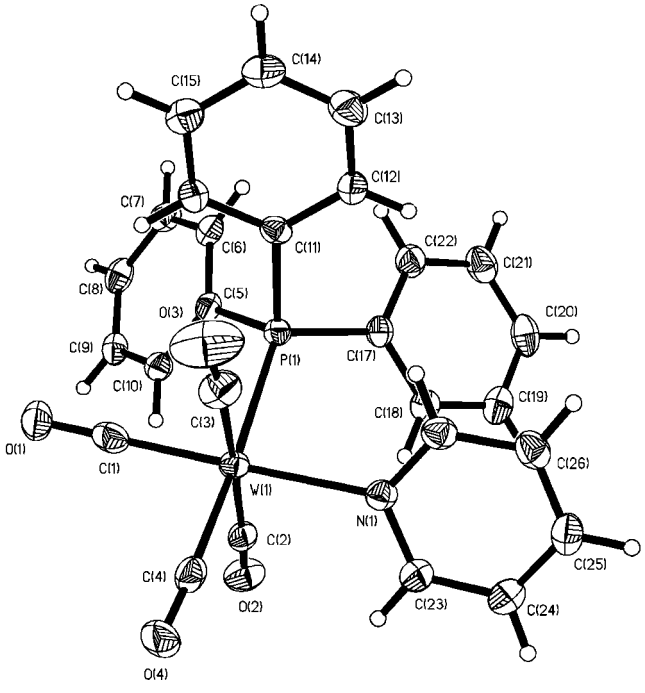

Figure 1. Crystal structure of complex $[W(CO)_4(py)(PPh_3)]$ (**2**)

steric stress to enforce adoption of the *trans* form. The complex $[W(CO)_4\{P(2\text{-py})Ph_2\}_2]$ (**3**, Figure 2) also crystallized in the *cis* form, despite being sterically similar to complex **1**. The structure of *cis*-**3** showed a face-to-face π-stacking interaction between the pyridyl rings, the distance between the centers of the rings being 3.902 Å, and the shortest distance between the atoms of the two rings being 3.527 Å, this being found between the carbon atoms directly attached to the P atom. The planes were found to be almost parallel, having a mutual angle of 7.18(7)°. This interaction is intramolecular rather than extending throughout the crystal system. The centroid–centroid distance between two π-stacked pyridine fragments is typically 3.3–3.8 Å, with contact angles usually falling between a parallel arrangement and a maximum of 40°.[16]

The protonated derivative of **3**, *cis*-$[W(CO)_4\{P(2\text{-pyH})^+Ph_2\}\{P(2\text{-py})Ph_2\}](ClO_4^-)$ (**4**, Figure 3) was found to have a structure in which the N atoms of the pyridyl rings are connected by a hydrogen bond, the distance between the two N atoms being 2.736(3) Å. Because of this hydrogen bond, the positive charge is delocalized over the two pyridine rings. Moreover, the structure of this complex also showed two cation–π bonds between the pyridinium cations and phenyl rings: One such interaction is found between the rings labeled R1 and R3, the centroid–centroid distance of the rings being 3.915 Å with an angle of 23.99°, while the other such interaction is found between the rings labeled R2 and R4, the distance between the centers of the rings being 3.918 Å with an angle of 19.17(15)°. In both cases, the closest distances between the atoms of the rings are found between the N atoms of the pyridyl rings and the C atoms of the phenyl rings directly attached to the P atom, the N1–C distance being 3.179 Å and the N2–C distance being 3.145 Å.

In addition to π-stacking, other weak interactions are also apparent in the solid state. Weak hydrogen bonding between the CO ligands and aryl hydrogen atoms is evident in all the studied complexes. This type of interaction has

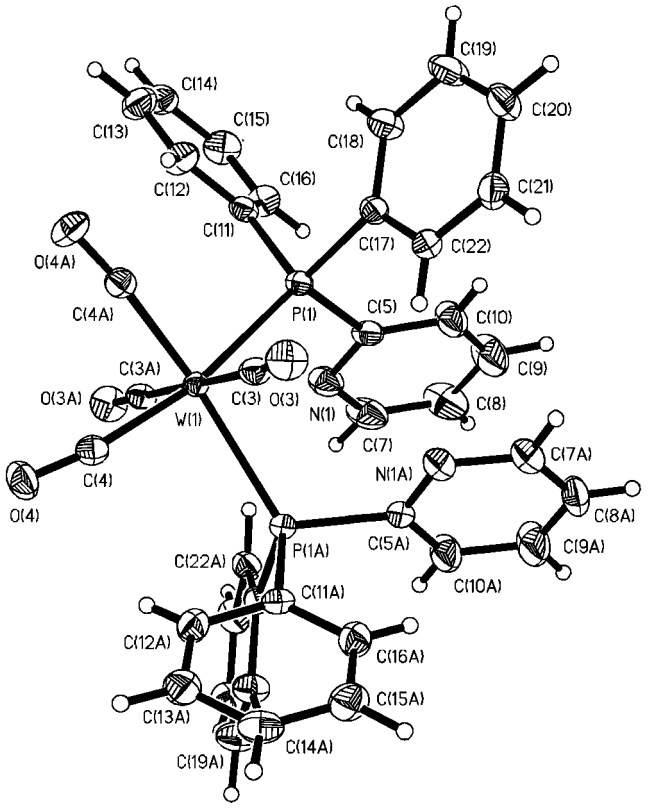

Figure 2. Crystal structure of complex *cis*-$[W(CO)_4\{P(2\text{-py})Ph_2\}_2]$ (**3**)

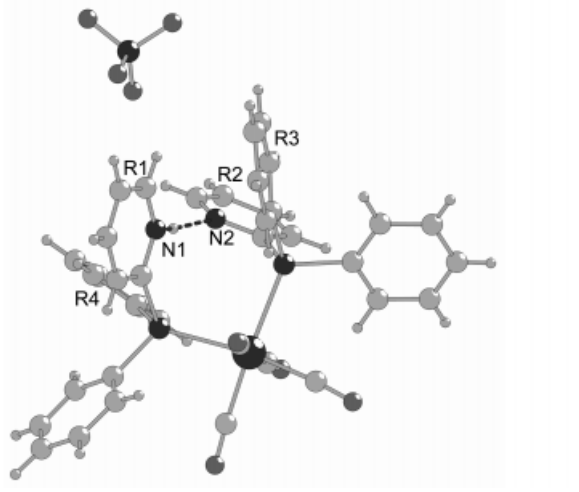

Figure 3. Structure of complex *cis*-$[W(CO)_4\{P(2\text{-pyH})^+Ph_2\}\{P(2\text{-py})Ph_2\}](ClO_4^-)$ (**4**)

been reported for several carbonyl transition metal complexes.[17] As an example of weak hydrogen bonding in complex **1**, an intermolecular C−O···H distance of 2.529 Å with a C−O···H angle of 172.6° can be seen. Similarly, complex **2** shows an intermolecular C−O···H distance of 2.453 Å with an angle of 161.2°, while complex **3** shows a C−O···H distance of 2.58 Å with a C−O···H angle of 162.4°. Complex **4** shows two C−O···H distances of 2.52 Å with angles of 157.8° and 161.9°. In all of these complexes, this hydrogen-bonding interaction is mainly seen between neighboring molecules in the solid state. These interactions are thus expected to play no significant role in the *cis*/*trans* isomerism in solution.

Discussion

In solution, attractive or repulsive interactions between the ligands have an effect on the isomerization processes. Similar interactions also occur between the ligands and, for example, solvent molecules. The net effect of these interactions, in addition to the electronic properties of the coordination, determines the final structure. In this work, we have deliberately varied the attractions between phosphane ligands in order to cause changes in the relative amounts of the *cis* and *trans* isomers (Schemes 1, 2, and 3).

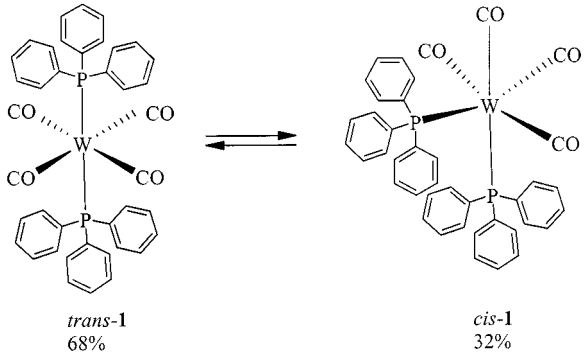

Scheme 1. Solution behavior of complex **1**

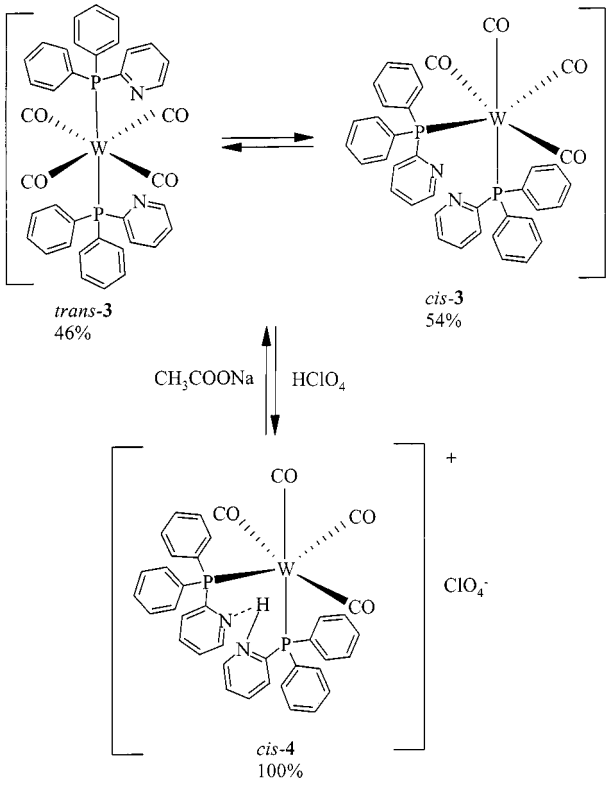

Scheme 2. Solution behavior of complexes **3** and **4**

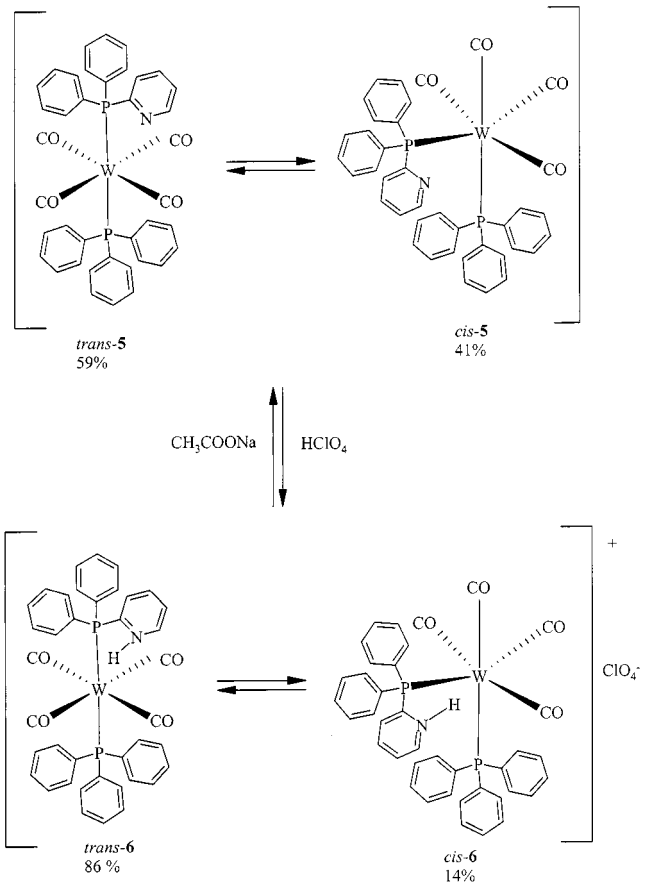

Scheme 3. Solution behavior of complexes **5** and **6**

The differences in solution behavior of the neutral complexes $[W(CO)_4(PPh_3)_2]$ (**1**), $[W(CO)_4\{P(2\text{-py})Ph_2\}_2]$ (**3**), and $[W(CO)_4(PPh_3)\{P(2\text{-py})Ph_2\}]$ (**5**) can be explained in terms of reduced repulsion between the phosphane ligands due to attractive π−π interactions: Due to the heteroatom, the pyridyl ring is more polarized than the phenyl ring, making attractive π-stacking of pyridyl rings more favorable compared to that of phenyl rings.[18] In the *cis* isomer, showing π−π interactions, the steric repulsion between the ligands is minimized and evidently not much attraction is needed between the rings to favor the *cis* form.

In the case of complex **1**, the steric repulsion between the ligands clearly favors the *trans* isomer. Complex **6** has just one pyridyl ring, which could be involved in attractive π−π interactions with one of the phenyl rings, leading to a slight increase in the *cis* content compared to complex **1**, but the *trans* conformation is still slightly preferred. In complex **3**, the *cis* conformer is favored over the *trans* conformer. In this case, the π-stacking between the pyridyl rings has been confirmed by X-ray crystallography (Figure 2).

The solvent effects are difficult to estimate, but on the grounds of the enthalpies of adduct formation for pyridine (−22 kJ/mol) and benzene (−4.9 kJ/mol) with $CHCl_3$,[19,20] and the empirical solvent polarity parameters of $CHCl_3$ (E_T^N = 0.259), pyridine (E_T^N = 0.302), and benzene (E_T^N = 0.111),[21] pyridine can be expected to show a somewhat greater attraction towards chloroform than benzene. The solvent should actually favor a higher proportion of the *trans* arrangement for complexes **3** and **5** compared to complex **1**, because in the *trans* form the pyridyl groups would maximize their solvent interactions: In the structure of **3** (Figure 2) there are fewer possibilities for solvent interactions with the pyridyl groups. In view of this, the observed isomeric ratios necessitate attractive interactions that override both the steric repulsion of bulky ligands and the solvent interactions.

When complex **3** is protonated, the resulting complex **4** is 100% in the *cis* form. We have isolated the complex $[W(CO)_4\{P(2\text{-pyH})^+Ph_2\}\{P(2\text{-py})Ph_2\}](ClO_4^-)$ (**4**) with one protonated pyridyl ring. This structure offers the possibility of intramolecular N−H···N hydrogen bonding (Figure 3). This hydrogen bond, together with the two cation−π interactions observed, explains the preference for the *cis* isomer.

When complex **5** is protonated, the resulting complex $[W(CO)_4\{P(2\text{-pyH})^+Ph_2\}(PPh_3)](ClO_4^-)$ (**6**) is predominantly (86%) in the *trans* form. Here, there is only one pyridyl ring to bear the positive charge; the possibility still exists for intramolecular cation−π interactions between the pyridinium cation and the phenyl ring, but there is no possibility of intramolecular hydrogen bonding. In this case, the repulsion between the two phosphane ligands becomes important. Additionally, there is a possibility of intermolecular interactions, such as hydrogen bonding between the pyridinium hydrogen atom and the ClO_4^- anion, which may also increase the preference for the *trans* isomer (the *trans* form is even more clearly favored than in the case of the triphenylphosphane derivative **1**). Since the relative strengths of the solvent interactions in complexes **4** and **6** should be comparable, they do not provide an explanation for the structural differences between these two complexes.

The protonation reactions have been found to be reversible; the *cis*/*trans* isomer ratio can be tuned by adjusting the pH. Phosphane complexes are used in various catalytic reactions,[22] hence the ability to control *cis*/*trans* isomerism through attractive interligand interactions opens up possibilities for controlling the mechanisms of homogeneous catalytic reactions.

Experimental Section

General Remarks: All reactions were carried out under nitrogen using standard Schlenk techniques. Synthetic procedures were modified from the method described previously.[14] Benzene (Baker, 99%) was distilled from sodium and benzophenone ketyl under nitrogen. Hexacarbonyltungsten (Aldrich), triphenylphosphane (FF Chemicals), diphenyl(2-pyridyl)phosphane (Aldrich), dichloromethane (FF Chemicals, 99.8%), and hexane (Lab Scan, 95%) were used as received. Perchloric acid (Merck, 70%) was diluted to about 26%. The starting material $[W(CO)_4(py)_2]$ was prepared according to a literature method.[23] Crystals were grown by slow evaporation of the solvents from solutions in dichloromethane/hexane, and in the case of complex **4** from a solution in dichloromethane containing some perchloric acid.

Spectroscopy: ^{1}H NMR spectra (400 MHz; TMS), ^{13}C{^{1}H} NMR spectra (100 MHz; $CDCl_3$ at δ = 77.0), two-dimensional HSQC spectra, and ^{31}P{^{1}H} NMR spectra (162 MHz; ext. stand. 85% H_3PO_4) were recorded with a Bruker DPX 400 spectrometer with samples in $CDCl_3$ (CIL, 99.8% D, 0.03% TMS). IR spectra were recorded with a Bruker IFS 66 spectrometer with samples in dichloromethane. Exact masses were measured with a Micromass LCT mass spectrometer using the ESI+ method.

X-ray Crystallography. − Crystal Data for 2: $C_{27}H_{20}NO_4PW$, M_r = 637.26, monoclinic, a = 10.1507(2), b = 20.0282(3), c = 11.6940(3) Å, β = 97.6790(10)°, 2356.07(8) Å^3, T = 120 K, space group $P2_1/n$ (no. 14), Z = 4, D_{calcd} = 1.797 g cm^{-1}, μ(Mo-$K_α$) = 5.005 mm^{-1}, 25482 reflections collected, 4709 unique (R_{int} = 0.0474). The final R_1 was 0.0235 ($I > 2σ$) and $wR_2(F^2)$ = 0.0564 ($I > 2σ$). − **Crystal Data for 3:** $C_{38}H_{28}N_2O_4P_2W$, M_r = 822.41, monoclinic, a = 13.7402(2), b = 12.6068(2), c = 19.2044(3) Å, β = 96.4360(10)°, 3305.62(9) Å^3, T = 120 K, space group $C2/c$ (no. 15), Z = 4, D_{calcd} = 1.653 g cm^{-1}, μ(Mo-$K_α$) = 3.635 mm^{-1}, 19439 reflections collected, 3622 unique (R_{int} = 0.0238). The final R_1 was 0.0147 ($I > 2σ$) and $wR_2(F^2)$ = 0.0343 ($I > 2σ$). − Data were collected with a Nonius KappaCCD diffractometer using Mo-$K_α$ radiation (λ = 0.71073 Å). For compound **2**, hydrogen atoms were constrained to ride on their parent atom (C−H = 0.95 Å, U_{iso} = 1.2·C_{eq}). In the case of **3**, hydrogen atoms were located from the difference Fourier map and were refined isotropically. Crystallographic data for the structures reported in this paper have been deposited with the Cambridge Crystallographic Data Centre as supplementary publication nos. CCDC-153439 (**2**) and -153440 (**3**). Crystallographic data for the structures reported in a preliminary communication have also been deposited. Copies of the data can be obtained free of charge on application to the CCDC, 12 Union Road, Cambridge CB2 1EZ, U.K. [Fax: (internat.) + 44-1223/336-033; E-mail: deposit@ccdc.cam.ac.uk].

[W(CO)$_4$(PPh$_3$)$_2$] (1) and [W(CO)$_4$(py)(PPh$_3$)] (2): [W(CO)$_4$(py)$_2$] (242 mg, 0.533 mmol) was suspended in benzene (40 mL). Triphenylphosphane (151 mg, 0.577 mmol) was added and the mixture was stirred for 24 h at 40−45 °C. The solvent was then evaporated and the residue was purified by column chromatography using dichloromethane/hexane (1:1) as the eluent. Two products, [W(CO)$_4$(PPh$_3$)$_2$] (**1**) (132 mg, 40%) and [W(CO)$_4$(py)(PPh$_3$)] (**2**) (132 mg, 47%) were obtained. − **1**: $C_{40}H_{30}O_4P_2W$ (820.5), calcd. C 58.56, H 3.69; found C 58.32, H 3.20. − *trans*-**1**: ^{1}H NMR: δ = 7.26−7.56 (m). − IR (CH_2Cl_2): ν(CO) = 1886 cm^{-1}. − **2:** Exact mass: m/z = 638.0754 [M$^+$ − H] (calcd. for $C_{27}H_{21}NO_4PW$: 638.0718). − ^{1}H NMR (see Table 1 for numbering scheme): δ = 8.39 (d, 2-H), 7.49 (m, 4-H), 7.36 (m, 12-H), 7.31 (m, 14-H), 7.28 (m, 13-H), 6.82 (t, 3-H). − ^{31}P{^{1}H} NMR: δ = 33 ($^1J_{PW}$ = 238 Hz). − IR (CH_2Cl_2): ν(CO) = 2011 (s), 1884 (vs), 1846 (s) cm^{-1}.

[W(CO)$_4${P(2-py)Ph$_2$}$_2$] (3): [W(CO)$_4$(py)$_2$] (225 mg, 0.495 mmol) was suspended in benzene (40 mL). Diphenyl(2-pyridyl)phosphane (261 mg, 0.991 mmol) was added and the mixture was stirred for 24 h at 40−45 °C. After evaporation of the solvent, the residue was purified by column chromatography using dichloromethane as the eluent to afford [W(CO)$_4${P(2-py)Ph$_2$}$_2$] (225 mg, 55%). Exact mass: m/z = 823.1122 [M$^+$ − H] (calcd. for $C_{38}H_{29}N_2O_4P_2W$: 823.1112). − *cis*-**3:** ^{1}H NMR (see Table 1 for numbering scheme): δ = 8.51 (d, 3-H), 7.45 (m, 8-H), 7.41 (m, 5-H), 7.30 (m, 10-H), 7.26 (m, 9-H), 7.06 (m, 4-H), 7.02 (m, 6-H). − IR (CH_2Cl_2): ν(CO) = 2018 (m), 1911 (sh), 1898 (s), 1872 (sh) cm^{-1}. − *trans*-**3:** ^{1}H NMR (see Table 1 for numbering scheme): δ = 8.78 (d, 3-H), 7.65 (m, 8-H), 7.59 (td, 5-H), 7.36 (m, 9-,10-H), 7.29 (d, 6-H), 7.15 (t, 4-H). − IR (CH_2Cl_2): ν(CO) = 1890 cm^{-1}.

[W(CO)$_4${P(2-pyH)$^+$Ph$_2$}{P(2-py)Ph$_2$}](ClO$_4^-$) (4): Perchloric acid was added to a solution of complex **3** in $CDCl_3$. The product was deprotonated with CH_3COONa solution. − *cis*-**4:** Exact mass: m/z = 823.1109 [M$^+$ − H] (calcd. for $C_{38}H_{29}N_2O_4P_2W$ 823.1112); 98.9509 [ClO_4^-] (calcd. for ClO_4 98.9485). − ^{1}H NMR (see Table 1 for numbering scheme): δ = 8.18 (dd, 3-H), 7.89 (td, 5-H), 7.48 (m, 10-H), 7.47 (m, 9-H), 7.38 (m, 4-H), 7.34 (m, 8-H), 7.23 (dd, 6-H).

[W(CO)$_4${P(2-Py)Ph$_2$}(PPh$_3$)] (5): [W(CO)$_4$(py)(PPh$_3$)] (**2**, 110 mg, 0.173 mmol), obtained in the preparation of complex **1** as described above, was dissolved in benzene (20 mL) and diphenyl(2-pyridyl)-phosphane (55 mg, 0.209 mmol) was added. The resulting solution was stirred for 24 h at 40−50 °C and then the solvent was evaporated. The product was purified by column chromatography, first with dichloromethane/hexane (1:1) as eluent until the first fraction (starting material and traces of complex **1**) eluted, and thereafter with a 1:3 mixture until the product was eluted. Exact mass: m/z = 822.1194 [M$^+$ − H] (calcd. for $C_{39}H_{30}NO_4P_2W$: 822.1160). − *cis*-**5:** ^{1}H NMR (see Table 1 for numbering scheme): δ = 8.55 (dd, 3-H), 7.59 (m, 8-H), 7.45 (m, 5-H), 7.42−7.25 (m, 10-H), 7.30−7.20 (m, 9-H, 11- to 14-H), 7.08 (m, 4-H), 6.97 (m, 6-H). − *trans*-**5:** ^{1}H NMR (see Table 1 for numbering scheme): δ = 8.80 (dd, 3-H), 7.67 (m, 8-H, 11- to 14-H), 7.59 (m, 5-H), 7.45−7.35 (m, 9-H), 7.42−7.25 (m, 10-H), 7.29 (m, 6-H), 7.16 (m, 4-H). − IR (CH_2Cl_2): ν(CO) = 1888 cm^{-1}.

[W(CO)$_4${P(2-pyH)$^+$Ph$_2$}(PPh$_3$)](ClO$_4^-$) (6): Perchloric acid was added to a solution of complex **5** in $CDCl_3$. The product **6** was deprotonated with CH_3COONa solution. The protonated complex showed a tendency to decompose if the solution was left to stand over a period of days. − *trans*-**6:** Exact mass: m/z = 822.1164 [M$^+$ − H] (calcd. for $C_{39}H_{30}NO_4P_2W$: 822.1160); 98.9510 [ClO_4^-] (calcd. for ClO_4 98.9485). − ^{1}H NMR (see Table 1 for numbering scheme): δ = 9.16 (dd, 3-H), 7.90−7.20 (m, 4- to 14-H).

Acknowledgments

Financial support from the Neste foundation is gratefully acknowledged. We thank Mrs. Päivi Joensuu for recording the mass spectra, and Mrs. Päivi Pirilä for advice in the area of solution chemistry.

[1] J. Atwood, J. Davies, D. MacNicol, F. Vögtle (Eds.), *Comprehensive Supramolecular Chemistry*, 1st ed., Elsevier, Oxford, **1996**, vol. 2.
[2] V. Albano, P. L. Bellon, V. Scatturin, *J. Chem. Soc., Chem. Commun.* **1966**, 507, 2321.
[3] R. Kroener, M. J. Heeg, E. Deutsch, *Inorg. Chem.* **1988**, *27*, 558.
[4] B. G. Jones, B. J. Chapman, *Synlett* **1997**, 439.
[5] B. J. Chapman, G. B. Jones, W. T. Pennington, *J. Chem. Crystallogr.* **1999**, *29*, 383.
[6] F. P. Fanizzi, M. Lanfranchi, G. Natile, A. Tiripicchio, *Inorg. Chem.* **1994**, *33*, 3331.
[7] T. Sorrel, T. L. A. Epps, T. J. Kistenmacher, L. G. Marzilli, *J. Am. Chem. Soc.* **1977**, *99*, 2173.
[8] D. J. Szalda, T. J. Kistenmacher, L. Marzilli, *Inorg. Chem.* **1976**, *15*, 2783−2788.
[9] E. Clot, O. Eisenstein, R. H. Crabtree, *New J. Chem.* **2001**, *25*, 66.
[10] T. W. Hambley, *Inorg. Chem.* **1988**, *27*, 1073.

[11] K. Jitsukawa, K. Iwai, H. Masuda, H. Ogoshi, H. Einaga, *J. Chem. Soc., Dalton Trans.* **1997**, 3691.
[12] H. Okawa, K. Ueda, S. Kida, *Inorg. Chem.* **1982**, *21*, 1594.
[13] L. Hirsivaara, M. Haukka, J. Pursiainen, *Inorg. Chem. Commun.* **2000**, *3*, 508.
[14] M. L. Boyles, D. V. Brown, D. A. Drake, C. K. Hostetler, C. K. Maves, J. A. Mosbo, *Inorg. Chem.* **1985**, *24*, 3126.
[15] D. A. Redfield, J. H. Nelson, L. W. Cary, *Inorg. Nucl. Chem. Lett.* **1974**, *10*, 727.
[16] C. Janiak, *J. Chem. Soc., Dalton Trans.* **2000**, 3885.
[17] D. Braga, F. Grepioni, *Acc. Chem. Res.* **1997**, *30*, 81.
[18] C. A. Hunter, J. K. M. Sanders, *J. Am. Chem. Soc.* **1990**, *112*, 5525.
[19] F. L. Slejko, R. S. Drago, *J. Am. Chem. Soc.* **1973**, *95*, 6935.
[20] L. Barta, Z. S. Kooner, L. G. Helpler, G. Roux-Desgranges, J.-P. E. Grolier, *Can. J. Chem.* **1989**, *67*, 1225.
[21] C. Reichard, *Chem. Rev.* **1994**, *94*, 2319.
[22] L. H. Pignolet (Ed.), *Homogeneous Catalysis with Metal Phosphane Complexes*, Plenum Press, New York, **1983**.
[23] C. S. Kraihanzel, F. A. Cotton, *Inorg. Chem.* **1963**, *2*, 533.
Received March 2, 2001
[I01080]

The Dioxoosmium(VI) Complex $[OsO_2(H_2biim)_2](NO_3)_2$ as Oxygen-Transfer Reagent − Synthesis and Solid-State Structure of Bis(2,2′-biimidazole)-bis(triphenylphosphane oxide)osmium(III) Nitrate

Andrei Maiboroda,[a] Gerd Rheinwald,[a] and Heinrich Lang*[a]

Dedicated to Prof. D. Sellmann on the occasion of his 60th birthday

Keywords: Coordination chemistry / Osmium / N ligands / Oxygen transfer / X-ray structure analysis

Treatment of OsO_4 (**1**) with 2,2′-biimidazole (H_2biim) (**2**) in a methanol/acetone mixture, and in the presence of nitric acid produces the novel dioxoosmium(VI) complex $[OsO_2(H_2biim)_2](NO_3)_2{\cdot}CH_3OH$ (**3**). Addition of 2 equiv. of PPh_3 (**4**) and 1 equiv. of nitric acid to **3** affords mononuclear $[Os(H_2biim)_2(O{=}PPh_3)_2](NO_3)_3$ (**5**) by a redox reaction which involves the transfer of oxygen from osmium to PPh_3. The X-ray crystal structure of **5** reveals an octahedral coordination sphere around the osmium(III) centre. This occurs as a result of the two H_2biim chelating ligands in the equatorial positions and two datively bonded phosphane oxide groups $O{=}PPh_3$ in the axial positions. Hydrogen bonds are responsible for the formation of a polymeric structure in the solid state. The latter complex reacts with KOH to form monocationic $[Os(Hbiim)_2(O{=}PPh_3)_2]NO_3$ (**6**).

Introduction

Platinum metal containing complexes with, for example, five-membered nitrogen-containing heterocycles are of considerable interest since they can be used as starting materials for the synthesis of oligo- and polymetallic species, featuring at least two different metal centres.[1,2] Representative examples of such species are the pyrazolato-bridged homobimetallic rhodium and iridium complexes $[\{Rh_2(\mu\text{-}pz)_2(I)(C{\equiv}N\textit{t}Bu)_4\}_2(\mu\text{-}I)](CF_3SO_3)$,[1b] $[M(\mu\text{-}pz)(I)(C{\equiv}N\textit{t}Bu)_2]_2$,[1b] (M = Rh, Ir) and $Ir_2(\mu\text{-}H)(\mu\text{-}pz)(N{\equiv}CMe)(P\textit{i}Pr_3)_2$[2b] (pz = pyrazolate). In these complexes, the nitrogen-containing heterocyclic π-conjugated bridging units span the corresponding transition metal centres, giving rise to a bonding situation which allows the metal atoms to communicate with each other.[1] A further common feature of oligo- or polymetallic complexes is their significantly higher activity in many homogeneous catalytic processes, e.g. hydrogenation, hydroformylation, compared with their predecessors.[2] This catalytic enhancement can be explained in terms of an intramolecular electron transfer between the corresponding transition metal centres, via the π-conjugated organic building blocks.[3] Hence, the development of the chemistry of azolato-containing transition metal complexes of platinum metals is of interest, either in homogeneous catalysis, due to cooperative and synergetic effects, or in the study of intramolecular electronic communication.

For the synthesis of osmium complexes bearing 2,2′-biimidazole chelating ligands, the hydrido(phosphane) complexes $OsH_2Cl_2(P\textit{i}Pr_3)_2$[4a] or $OsH_6(P\textit{i}Pr_3)_2$[4b] were exclusively used as the synthetic tool. Nevertheless, all complexes prepared by this method contain only one 2,2′-biimidazole chelating group. Using the 2,2′-biimidazole as the bridging unit, also some heterobimetallic complexes, such as $(P\textit{i}Pr_3)_2H_2ClOs(\mu\text{-}Hbiim)MCl(cod)$ (M = Rh, Ir; cod = cyclooctadiene)[4a] or $(P\textit{i}Pr_3)_2H_3Os(\mu\text{-}biim)Ir(cod)$[4b] could also be prepared. Our aim in the present work was to synthesise different osmium complexes, containing at least two 2,2′-biimidazole chelating ligands, so as to use these species as effective starting materials for the preparation of oligonuclear transition metal complexes, based on the central osmium fragments $[Os(biim)_2(O{=}PPh_3)_2]^-$ or $[Os(Hbiim)_2(O{=}PPh_3)_2]^+$. We thus describe the reaction of OsO_4 with H_2biim in order to synthesise neutral and/or ionic osmium complexes, which feature two 2,2′-biimidazole ligands.

Results and Discussion

Synthesis and Spectroscopic Characterisation

In an attempt to synthesise osmium complexes with H_2biim chelating ligands (H_2biim = 2,2′-biimidazole) in the equatorial positions, we chose the dioxoosmium entity as the central building block. OsO_4 (**1**) was treated with two equivalents of H_2biim (**2**), in a 1:1 methanol/acetone mixture, and in the presence of nitric acid to afford the osmium(VI) complex $[OsO_2(H_2biim)_2](NO_3)_2{\cdot}CH_3OH$ (**3**) in a 60% yield (Scheme 1).

[a] Technische Universität Chemnitz, Fakultät für Naturwissenschaften, Institut für Chemie, Lehrstuhl für Anorganische Chemie,
Straße der Nationen 62, 09111 Chemnitz, Germany
E-mail: heinrich.lang@chemie.tu-chemnitz.de

 © WILEY-VCH Verlag GmbH, 69451 Weinheim, 2001 1434−1948/01/0909−2263 $ 17.50+.50/0

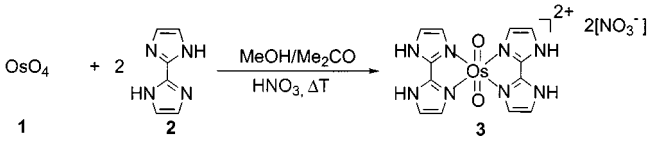

Scheme 1

After appropriate workup, mononuclear **3** was obtained as an air-stable orange solid. However, it was found that **3** is poorly soluble in all well-known organic solvents, except dimethyl sulfoxide. The spectroscopic data (IR, ^{1}H, ^{13}C{^{1}H} NMR spectroscopy) of **3**, in which a planar Os(H$_2$biim)$_2$ arrangement is present, are consistent with the formulated structure (vide supra).

In the IR spectrum of **3** an intensive absorption band at 858 cm^{-1} is found, which can be assigned to the $\nu_{a(Os=O)}$ stretching vibration of the linear O=Os=O entity.[5] Additionally, a very sharp and narrow $\nu_{(NH)}$ absorption band is observed at 3140 cm^{-1}. As is typical for noncoordinated NO_3^- counter ions, only one band arises at 1488 cm^{-1} which is due to the asymmetric $\nu_{(NO)}$ stretching vibration.[6]

In the noncoordinated state the H$_2$biim ligand gives rise to only one ^{1}H NMR resonance signal at δ = 7.1 assigned to the CH protons, whereas in mononuclear **3**, two signals at δ = 7.81 (5-, 5′-H), as well as δ = 8.45 (4-, 4′-H) are observed in a 1:1 intensity ratio. This points to the fact that the H$_2$biim entity is bonded to the osmium(VI) centre as a chelate, via the two sp^2-hybridised nitrogen atoms; the NH functionalities are located on the opposite side.

Nevertheless, due to the low solubility of **3** in [D$_6$]dimethyl sulfoxide, only the resonance signals for the carbon atoms in the 4,4′- (δ = 128.7) and the 5,5′-position (δ = 123.4) could be detected in the ^{13}C{^{1}H} NMR spectrum, which also supports the symmetrical bonding of the H$_2$biim chelates to the osmium centre.

Dimethyl sulfoxide is the only suitable solvent for **3**, despite its high boiling point and its high coordination ability. It is for this reason that we wanted to prepare complexes with similar structures which are more soluble in common organic solvents, so that we could use these complexes as starting materials in the synthesis of oligometallic transition metal complexes. Therefore, we treated complex **3** with 2 equiv. of Ph$_3$P (**4**) and 1 equiv. of HNO$_3$ in boiling tetrahydrofuran containing 10% H$_2$O. During this reaction, the oxygen atoms bonded to the osmium centre transfer to the phosphorus atom of the added PPh$_3$. The resulting phosphane oxides Ph$_3$P=O selectively bond to the osmium centre of the Os(H$_2$biim)$_2$ segment, through their oxygen atoms in a dative fashion, to produce [Os(H$_2$biim)$_2$(O=PPh$_3$)$_2$]$^{2+}$ at first. The latter osmium(II) species is the most likely intermediate, which is then oxidised by nitric acid to produce [Os(H$_2$biim)$_2$(O=PPh$_3$)$_2$](NO$_3$)$_3$ (**5**) in a 76% yield based on **3** (Scheme 2).

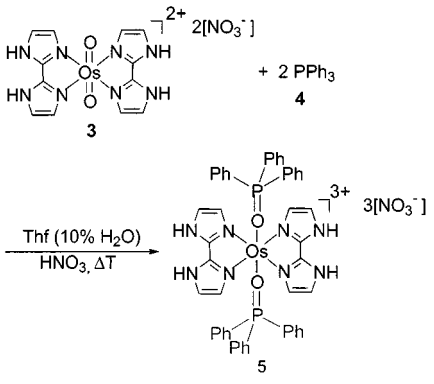

Scheme 2

Complex **5**, when compared with **3**, is significantly more soluble in common organic solvents, such as dichloromethane, methanol, or acetone. However, similar oxygen transfer reactions producing osmium(II) complexes were established earlier for the reaction of the dioxo(porphyrino)osmium(VI) complex OsO$_2$(OEP) (OEP = *o*cta*e*thyl*p*orphyrine) with triphenylphosphane.[7]

One very noticeable feature in the preparation of **3** is that on treatment of **3** with PPh$_3$ in dry tetrahydrofuran or other organic solvents like acetone or toluene, no reaction takes place. This result leads to the conclusion that this reaction is catalysed by protic species. If this is true, complex **3** should react with PPh$_3$ in protic solvents, e.g. alcohols. Hence, **3** was treated with PPh$_3$ in a methanolic medium and **5** was indeed produced, however, with an isolated yield of only 15%. This can be explained by the fact that MeOH can act as σ-donating ligand to the osmium centre, which might reduce the selectivity of the reaction of **3** with PPh$_3$ (vide supra). The need for the protic solvent for the reaction of **3** with **4** to produce **5**, indicates that the mechanism for this reaction may also include the protonation of the central O=Os=O building block, thus the oxo atoms in **3** would exchange with H$_2$O by protonation. The IR- and NMR-spectroscopic data of **5** agree with the structure found by X-ray crystal structure analysis (see below).

In the IR spectrum of **3**, a strong N−H stretching vibration is found, whereas in the IR spectrum of **5**, a broad $\nu_{(NH)}$ absorption band centred at around 3100 cm^{-1} is characteristic. The strong $\nu_{a(NO3)}$ vibration found at 1488 cm^{-1} in **3** is significantly shifted to lower frequencies in **5**, and is observed at 1384 cm^{-1}. These observations point to the formation of hydrogen bonds between the NH groups of the 2,2′-biimidazole building blocks, the oxygen atoms of the NO_3^- counter ions, the MeOH and the H$_2$O molecules.

As result of the reduction of osmium(VI) in **3** by PPh$_3$, the linear O=Os=O group in **3** is transferred to a zigzag Ph$_3$P=O→Os←O=PPh$_3$ unit in **5**. As a result, the $\nu_{a(Os=O)}$ absorption band found in the IR spectrum of **3** at 858 cm^{-1} is not present in the spectrum of **5**. Nevertheless, the disappearance of $\nu_{(Os=O)}$ is accompanied with the appearance of the P=O stretching vibrations at 1131 cm^{-1} in the IR spectrum of **5**.

In the ^{1}H NMR spectrum of **5** a multiplet between δ = 7.0 and 8.2 is observed, resulting from the superimposition of the resonance signals of the protons of the phenyl groups, as well as the protons of the 2,2′-biimidazole chelating ligands. The ^{13}C{^{1}H} NMR spectrum of **5** shows the

four resonance signals expected for the sp^2-hybridised phenyl carbon atoms of the $Ph_3P{=}O$ entities, between δ = 129 and 133. The resonance signals of the H_2biim chelating ligands are shifted to a lower field, relative to **3**, and are observed at δ = 135.1 (5,5′-position), δ = 137.9 (4,4′-position) and δ = 139.9 (2,2′-position), respectively.

$^{31}P\{^1H\}$-NMR-spectroscopic studies carried out on **5** clearly demonstrate the appearance of one resonance signal for the phosphorus atom of the triphenylphosphane oxide at δ = 36.4. Relative to the noncoordinated $Ph_3P{=}O$, the signal is shifted to a lower field by 9.4 ppm, revealing the coordination to the osmium(III) centre through the oxygen atom. Similar observations were made for other complexes featuring the P=O group, e.g. $[(\eta^5\text{-}C_5H_5)Co\{O{=}P(OR)_3\}_3]^-$ (R = Me, Ph).[8] The absorbance bands at 360 nm (ε = $3.5{\cdot}10^3$ $mol^{-1}{\cdot}dm^3{\cdot}cm^{-1}$) and 388 nm (ε = $3.5{\cdot}10^3$ $mol^{-1}{\cdot}dm^3{\cdot}cm^{-1}$) in the UV/Vis spectrum of **5** can be attributed to ligand-to-metal charge-transfer transitions.[9]

Complex **5** possesses a total of four NH functionalities, which can be easily deprotonated using KOH as a suitable base. Thus, the reaction of **5** with KOH in a molar ratio of 1:2 leads, on loss of KNO_3 and H_2O to the formation of the monocationic complex $[Os(Hbiim)_2(O{=}PPh_3)_2]NO_3$ (**6**) (Scheme 3). This reaction is accompanied by a colour change from red (**5**) to violet (**6**). After appropriate workup, **6** can be isolated in a 85% yield.

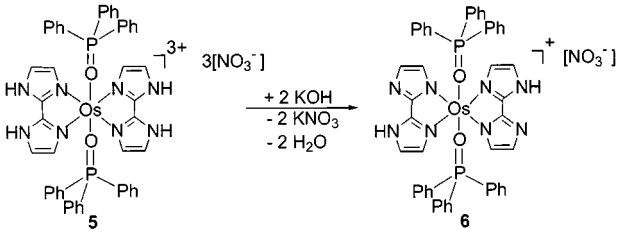

Scheme 3

A very noticeable feature in the IR spectrum of **6**, when compared with those of **3** and **5**, is the significant decrease in the intensity of the absorption bands of the NH and NO_3^- groups relative to the other vibrations observed in the spectrum. These absorptions are found at 3095 (NH) and 1386 cm^{-1} (NO_3^-), respectively. This result gives the first hint that the NH units of the 2,2′-biimidazole ligands could be at least partly metallated. This deprotonation influences the donor/acceptor properties of the 2,2′-biimidazole ligands, resulting in a change of the electronic absorbance in the UV/Vis spectrum of **6**. In contrast to **5**, the UV/Vis spectrum of **6** contains two maxima at 344 and at 541 nm, respectively.

All other spectroscopic studies carried out on **6** (^1H, $^{13}C\{^1H\}$ NMR spectroscopy) do not show a significant influence on the chemical shifts of the organic ligands when compared with **5**. However, the $^{31}P\{^1H\}$-NMR-spectroscopic studies demonstrate that on extended measurements further resonance signals appear. This can be attributed to ligand exchange reactions obtained by substitution of O=PPh_3 by solvent molecules, e.g. CD_3OD. As a result, signals with lower intensity are observed at δ = 33.7 ($Ph_3P{=}O{\rightarrow}Os{\leftarrow}DOMe$) and δ = 22.3 (*non*coordinated $Ph_3P{=}O$), next to the resonance signal at δ = 37.1 which is typical for **6**.

Electrochemical Studies

Cyclic voltammetric studies were carried out on complex **5** in dichloromethane at 25 °C and at −5 °C. The obtained voltammograms are depicted in Figure 1. However, due to the low solubility of **3** (vide supra) no electrochemical studies could be carried out on this complex for comparison. Figure 1 shows cyclic voltammograms of $[Os(H_2biim)_2(O{=}PPh_3)_2](NO_3)_3$ (**5**) in dichloromethane at 25 °C (top) and at −5 °C (bottom) (scan rate 60 mV s^{-1}).

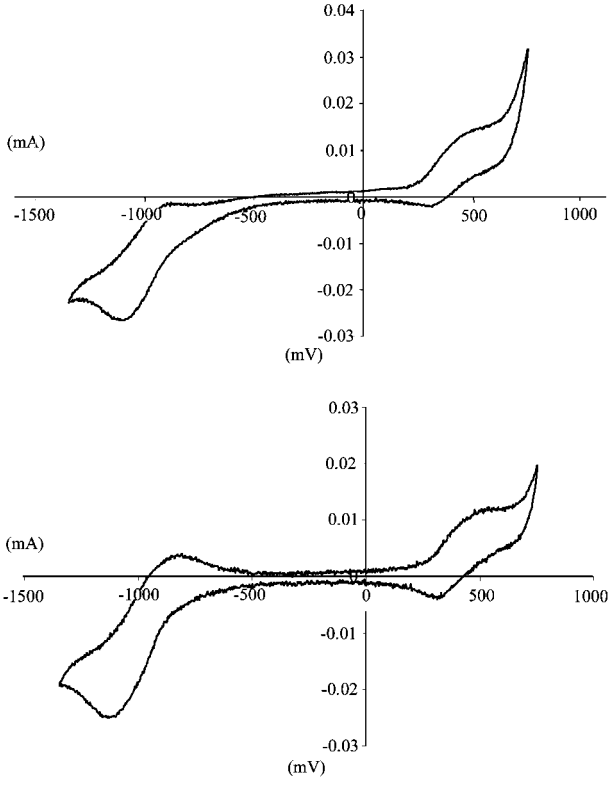

Figure 1. Cyclic voltammograms of $[Os(H_2biim)_2(O{=}PPh_3)_2](NO_3)_3$ (**5**) in dichloromethane at 25 °C (top) and at −5 °C (bottom) (scan rate 60 mV s^{-1})

It was found that both the Os^{III}/Os^{II} reduction (E_{red} = −1.09 V) and the Os^{III}/Os^{IV} oxidation processes (E_{ox} = +0.52 V) are irreversible at 25 °C. However, on lowering the temperature to −5 °C these processes are quasi-reversible. Thus, the potentials of the redox couples Os^{IV}/Os^{III} ($E_{1/2}$ = −0.97 V, ΔE = 290 mV) and Os^{IV}/Os^{V} ($E_{1/2}$ = +0.42 V, ΔE = 210 mV) could be determined. Similar observations were made for the Os^{IV} complex anion $[OsCl_5(H_2O)]^-$,[10] thus indicating that a reversible redox behaviour is seen only at low temperatures. This is a characteristic feature for some osmium complexes.[11] This can be explained by the kinetic stabilisation of the reactive intermediates e.g. the dicationic Os^{II} complex $[Os(H_2biim)_2(O{=}$

$PPh_3)_2]^{2+}$ at low temperatures. This species is produced by the electrochemical reduction of **5** and can be chemically oxidised by the NO_3^- ion. Decreasing temperatures slow down this reaction and lead to the formation of the anodic peak in the cyclic voltammogram, due to the electrochemical oxidation of the corresponding Os^{II} species.

A characteristic feature of the electrochemical behaviour of complex **6** is a significant shift of the redox potentials of the Os^{III}/Os^{IV} and Os^{III}/Os^{II} couples to a more negative value, relative to **5**. This results from a partial deprotonation of the H_2biim chelating ligands, followed by an increase in the electronic density on the appropriate osmium centre in **6**. In contrast to **5**, the shape of the cyclic voltammogram of **6** is temperature independent. Both at 25 °C and at −5 °C, the half potential of the Os^{III}/Os^{IV} redox couple is observed at +0.29 V. However, the Os^{III}/Os^{II} redox process is irreversible with $E_{red} = -1.29$ V.

Solid-State Structure of 5

Single crystals of **5**, suitable for X-ray structure analysis, were obtained by slow evaporation of a 1:1 methanol/dichloromethane solution at 25 °C. Complex **5** crystallises with two molecules of the complex, one molecule of water and half a molecule of methanol per asymmetric unit in the triclinic space group $P\bar{1}$, with $a = 10.9098(13)$, $b = 10.9726(12)$, $c = 21.330(3)$, $\alpha = 78.280(2)$, $\beta = 87.315(2)$, $\gamma = 87.992(2)°$, $V = 2496.6(5)$ Å^3 and $Z = 1$. Each of the complex molecules possesses a centre of inversion located at the osmium atom (Figure 2); the symmetry-generated atoms are indicated with the suffixes a and b. The molecular structure of **5** is shown in Figure 2. Experimental crystal data are listed in Table 3 and geometric details are presented in Table 1. Figure 2 shows a ZORTEP drawing of one complex cation $[Os(H_2biim)_2(O{=}PPh_3)_2]^{3+}$ of **5** (50% probability level; the second cation, NO_3^-, H_2O, and MeOH are omitted for clarity).

Each individual complex cation $[Os(H_2biim)_2(O{=}PPh_3)_2]^{3+}$ (Figure 2) of **5** possesses an osmium(III) centre in an octahedral environment, with two datively bonded $O{=}PPh_3$ units in the axial positions and two H_2biim chelating ligands in the equatorial positions. Complex **5** is the first example of an osmium(III) complex with two axial $O{=}PPh_3$ ligands. Similar complexes are known for osmium(II) and osmium(IV) systems, e.g. $Os(OEP)(O{=}PPh_3)_2$ (OEP = octaethylporphyrine)[7a] and $K_2[\{Os(\eta^4\text{-chba-Et})(O{=}PPh_3)_2\}_2O]$ [chba-Et = 1,2′-bis(3,5-dichloro-2-hydroxybenzaimido)ethane].[12]

The H_2biim arrangement in **5** is thereby planar (r. m. s. deviation of the fitted atoms Os1, N1 to N4, and C1 to C6 = 0.072 Å, as well as Os2, N5 to N8, and C25 to C30 = 0.085 Å). The angles around the osmium centres in the latter entity deviate from an idealised square-planar geometry [N1−Os1−N4 = 77.14(8)°, N5−Os2−N8 = 77.70(8)°], due to the formation of a five-membered OsN_2C_2 cycle. This value is typical for transition metal biimidazole complexes in which bite angels of 75.3° {$[NEt_4]$-$[Ir(COD)(PPh_3)(tcbiim)]\cdot CH_2Cl_2$ (tcbiim = tetracyanobiimidazole)}[13] and 82.78° {$[Cu_2(Me_5dien)_2(biim)][BPh_4]_2$ (Me_5dien = pentamethyldiethylentriamine)}[14] are found. A similar bite angle as observed in **5** was experimentally observed in $Ir_2(COD)_2(CH_3C{\equiv}N)$(tcbiim) (78.214°).[14] Furthermore, this N−Os−N angle induces a distortion in the other angles of the equatorial square plane (Table 1).

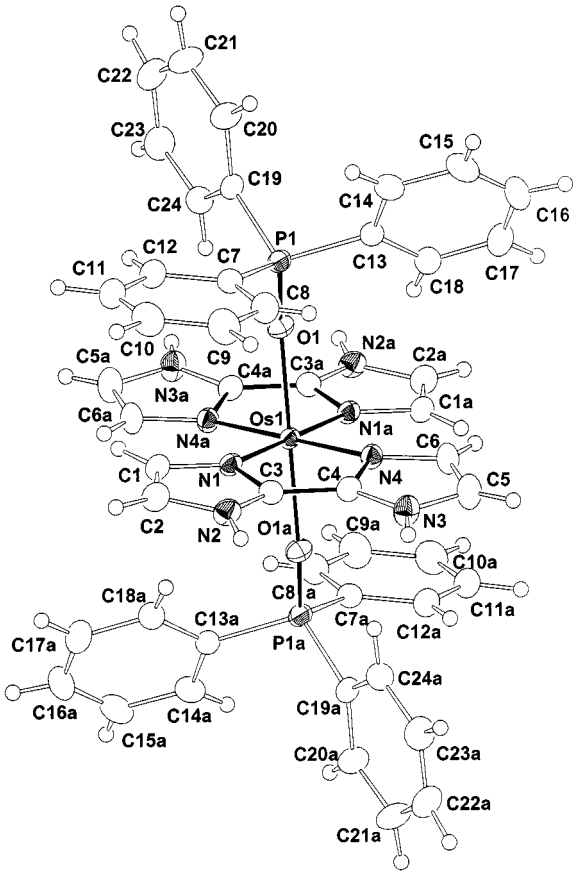

Figure 2. ZORTEP drawing of one complex cation $[Os(H_2biim)_2(O{=}PPh_3)_2]^{3+}$ of **5** (50% probability level; the second cation, NO_3^-, H_2O, and MeOH are omitted for clarity)

The two axially positioned $O{=}PPh_3$ ligands complete the octahedral coordination around the osmium atoms (for N−Os−O angles see Table 1). The Os−O−P angles of 146.53(11)° (Os1−O1−P1) and 140.16(11)° (Os2−O2−P2) are smaller than those found in $Os(OEP)(O{=}PPh_3)_2$ [154.2(5)°][7] and $K_2[\{Os(\eta^4\text{-chba-Et})(O{=}PPh_3)_2\}_2O]$ (153.0),[12] but still in the range typical for this type of arrangements. In general, M−O−P angles in $L_nM{-}O{=}PPh_3$ complexes (L_nM = transition metal fragment) range from 140 to about 180°, depending on the nature of the metal.[15]

The Os−O distances in **5** are 2.0129(16) Å (Os1−O1) and 2.0365(16) Å (Os2−O2), in between that found in $K_2[\{Os(\eta^4\text{-chba-Et})(O{=}PPh_3)_2\}_2O]$ (1.971 Å)[12] and $Os(OEP)(O{=}PPh_3)_2$ [2.036(7) Å].[7] This observation corresponds with the different ionic radii of Os^{II}, Os^{III}, and Os^{IV}.[5] The Os−N bonds, Os1−N1 [2.065(2) Å], Os1−N4 [2.072(2) Å], Os2−N5 [2.060(2) Å], and Os2−N8 [2.067(2) Å] are longer than the interatomic Os−N distances in the above-mentioned osmium complexes containing N ligands

Table 1. Selected geometrical details of $[Os(H_2biim)_2(O{=}PPh_3)_2](NO_3)_3{\cdot}H_2O{\cdot}0.5CH_3OH$ (**5**)

Bond lengths [Å][a] Molecule 1		Molecule 2	
Os1−O1	2.0129(16)	Os2−O2	2.0365(16)
Os1−N1	2.0651(19)	Os2−N5	2.060(2)
Os1−N4	2.072(2)	Os2−N8	2.067(2)
P1−O1	1.5195(17)	P2−O2	1.5224(18)
N1−C1	1.388(3)	N5−C25	1.375(3)
N2−C2	1.371(3)	N6−C26	1.372(4)
N1−C3	1.346(3)	N5−C27	1.355(3)
N2−C3	1.336(3)	N6−C27	1.329(3)
N3−C4	1.336(3)	N7−C28	1.337(3)
N3−C5	1.369(3)	N7−C29	1.373(4)
N4−C4	1.341(3)	N8−C28	1.344(3)
N4−C6	1.377(3)	N8−C30	1.379(3)
C1−C2	1.358(4)	C25−C26	1.358(4)
C3−C4	1.432(3)	C27−C28	1.432(3)
C5−C6	1.353(4)	C29−C30	1.346(4)
Bond angles [°] Molecule 1		**Molecule 2**	
O1−Os1−N1	94.13(7)	O2−Os2−N5	92.87(7)
O1−Os1−N1a	85.87(7)	O2−Os2−N5b	87.13(7)
O1−Os1−N4	97.61(7)	O2−Os2−N8	95.47(7)
O1−Os1−N4a	82.39(7)	O2−Os2−N8b	84.53(7)
N1−Os1−N4	77.14(8)	N5−Os2−N8	77.70(8)
P1−O1−Os1	146.53(11)	P2−O2−Os2	140.16(11)

[a] Symmetry transformations used to generate equivalent atoms: $a = -x + 1, -y + 1, -z$; $b = -x, -y, -z + 1$.

and triphenylphosphane oxide, but significantly shorter than those found in osmium complexes featuring the H_2biim ligand and phosphanyl groups, e.g. $[OsCl(\eta^2\text{-}H_2)(H_2biim)(P{i}C_3H_7)_2]Cl$ (2.110−2.135 Å).[4a]

Figure 3 shows the SCHAKAL-99 drawing of **5** including the hydrogen-bonding scheme (phenyl groups of the $O{=}PPh_3$ ligands are omitted for clarity). As depicted in Figure 3, complex **5** possesses a polymeric zigzag chain in the solid state, due to hydrogen bonds between the complex cations $[Os(H_2biim)_2(O{=}PPh_3)_2]^{3+}$, NO_3^-, and the neutral solvent molecules H_2O and MeOH. The corresponding interatomic distances for all specified hydrogen bonds are presented in Table 2 and are in accordance with typical bond lengths between donor and acceptor atoms forming hydrogen bonds.[16] The complex cations in **5** (Figure 3) are spanned by two different linking units: (i) NO_3^- and (ii) NO_3^- and H_2O. However, the H_2O molecule of the latter building arrangement gives rise to a further hydrogen bond with the third NO_3^- ion, which itself is hydrogen-bonded to a terminal MeOH moiety (Figure 3).

Table 2. Specified hydrogen bonds in $\mathbf{5}{\cdot}H_2O{\cdot}0.5MeOH$

Atoms[a] D	H	A	Interatomic distances [Å] D−H	H−A	D−A	Angles [°] D−H−A
N2	H1N2	O8	0.82(3)	1.98(3)	2.795(3)	173(3)
N3	H1N3	O4c	0.85(3)	1.98(3)	2.788(3)	161(3)
N6	H1N6	O6d	0.84(3)	1.90(3)	2.733(3)	171(3)
N7	H1N7	O12e	0.84(3)	1.87(4)	2.680(3)	161(3)
O12	H112	O10	0.78(4)	2.00(4)	2.767(4)	167(4)
O12	H113	O3	0.78(4)	2.12(4)	2.794(3)	145(4)
O12	H113	O6f	0.78(4)	2.50(4)	2.971(3)	120(4)
O13	H13	O9	0.84	2.15	2.918(9)	152.6

[a] D = Donor, H = Hydrogen, A = Acceptor; symmetry transformations used to generate equivalent atoms: $c = x - 1, y, z$; $d = x, y - 1, z$; $e = x - 1, y - 1, z$; $f = x + 1, y, z$.

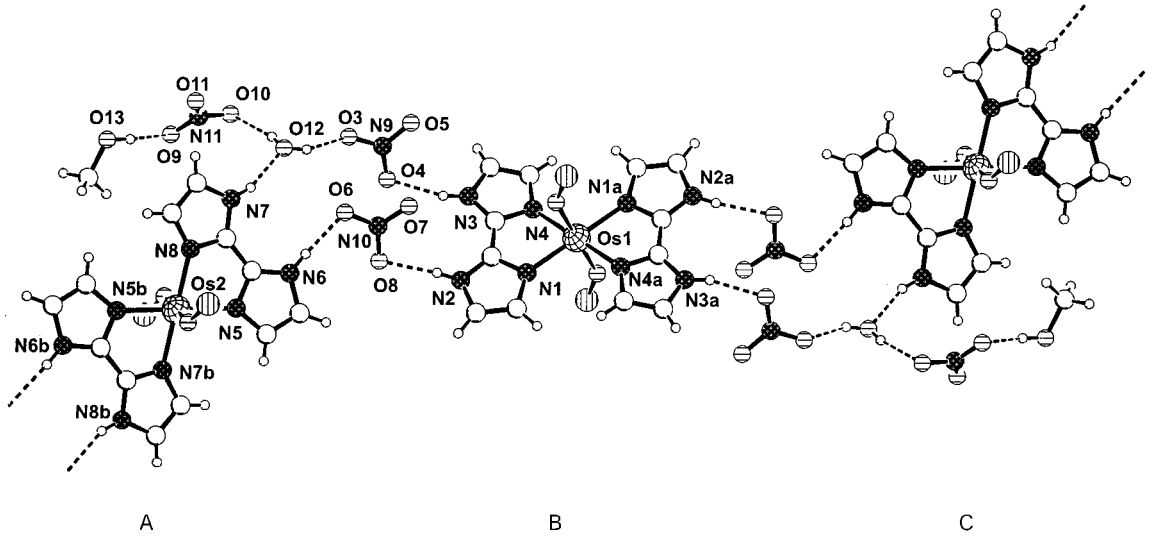

Figure 3. SCHAKAL-99 drawing of **5** including the hydrogen-bonding scheme (phenyl groups of the $O{=}PPh_3$ ligands are omitted for clarity)

Conclusions

In this study, it is shown that novel osmium complexes, featuring two 2,2′-biimidazole ligands are easily accessible. In addition, the novel dioxoosmium(VI) complex $[OsO_2(H_2biim)_2](NO_3)_2$ (**3**) is a very useful precursor for the preparation of an osmium(III) complex, $[Os(H_2bim)_2(O{=}PPh_3)_2](NO_3)_3$ (**5**), on reaction with PPh_3 in the presence of HNO_3. This reaction involves the transfer of an oxygen atom from osmium to phosphorus, and hence redox processes are typical. Furthermore, complex **5** can be deprotonated, with KOH as a suitable base, to afford monocationic $[Os(Hbiim)_2(O{=}PPh_3)_2](NO_3)$ (**6**). Complexes **5** and **6** both possess an osmium centre in an octahedral environment, as a result of the two 2,2′-biimidazole chelating ligands which are in the equatorial positions and two triphenylphosphane oxide groups in the axial positions *trans* to each other.

In future studies, the use of the latter complexes in the preparation of oligometallic complexes is of interest, since they bear with their 2,2′-biimidazole ligands coordination sites for the addition of further transition metal building blocks. These accessible complexes should provide very promising model systems for the study of electron transfer reactions and, in addition, they should be excellent catalysts in homogeneous catalysis due to the synergistic and cooperative effects of further transition metals being present.

Experimental Section

General Remarks: IR spectra were recorded with a Perkin−Elmer FT-IR spectrometer (Spectrum 1000) as KBr pellets. − UV/Vis spectra were recorded with a Perkin−Elmer Lambda 40 spectrophotometer in dichloromethane solutions and the concentrations were $8.0{\cdot}10^{-5}$ mol·dm^{-3}. − NMR spectra were recorded with a Bruker Avance 250 spectrometer, operating in the Fourier transform mode; NMR spectra were recorded at 250.131 MHz (^{1}H), 62.902 MHz (^{13}C{^{1}H}) or 101.249 MHz (^{31}P{^{1}H}, T = 303 K); chemical shifts (δ) are given in ppm with respect to $CDCl_3$ (^{1}H: δ = 7.29; ^{13}C{^{1}H}: δ = 77.5) as an internal standard. ^{31}P chemical shifts (δ) are given in ppm with respect to 85% H_3PO_4 (^{31}P: δ = 0) and $P(OMe)_3$ (δ = 139) as an external standard. − Melting (decomposition) points were determined with a Gallenkamp MFB 595 010 M melting point apparatus. − Electrochemical measurements were performed by cyclic voltammetry in dichloromethane solutions containing $[n\mathrm{Bu_4N}]PF_6$ (0.1 mol·dm^{-3}) at 25 °C and at −5 °C, using a standard three-electrode Pt−Pt−calomel cell and a Radiometer DEA 101 potentiostat. A scan rate of 60 mV·s^{-1} was used. All potentials were referenced to the ferrocene/ferrocenium FcH/Fc$^+$ couple ($E_{1/2}$ = 0.000 V). − Organic solvents (methanol, acetone, tetrahydrofuran, dichloromethane, CCl_4) were freshly distilled before use. Commercially available triphenylphosphane was used without further purification. 2,2′-Biimidazole was synthesised according to a literature procedure.[17] − Microanalyses were performed by the Laboratory of Elemental Analysis of the Technische Universität Bergakademie Freiberg.

Synthesis of $[OsO_2(H_2biim)_2](NO_3)_2{\cdot}CH_3OH$ (3): OsO_4 (**1**) (0.75 mmol, 5 mL of a 0.15 M solution), in CCl_4 was added to 40 mL of a 1:1 methanol/acetone mixture, containing H_2biim (**2**) (250 mg, 1.87 mmol) and HNO_3 (2.0 mmol) at 25 °C. The reaction mixture was heated to reflux for 4 h, and an orange product precipitated. After the reaction mixture was cooled to 25 °C, the orange precipitate was filtered, washed with 20 mL of acetone and dried in an oil-pump vacuum to afford **3**. Yield: 290 mg (0.45 mmol), 60% based on OsO_4. − M.p. gradual decomposition at T > 150 °C. − IR (KBr, cm^{-1}): $\nu_{a(Os=O)}$ 858, $\nu_{a(NO_3^-)}$ 1488, $\nu_{(NH)}$ 3140. − ^{1}H NMR ([D$_6$]DMSO): δ = 7.8 (br. s, 4 H, 5- ,5′-H/H_2biim), 8.5 (br. s, 4 H, 4- ,4′-H/H_2biim). − ^{13}C{^{1}H} NMR ([D$_6$]DMSO): δ = 123.4 (C-5, -5′/H_2bim), 128.7 (C-4, -4′/H_2biim). − Due to the low solubility of **3**, no further resonance signals could be detected. − $C_{13}H_{16}N_{10}O_9Os$ (646.54): calcd. C 24.15, H 2.50; N 21.67; found C 24.19, H 3.00, N 22.63.

Synthesis of $[Os(H_2biim)_2(O{=}PPh_3)_2](NO_3)_3{\cdot}H_2O{\cdot}0.5CH_3OH$ (5): $[OsO_2(H_2biim)_2](NO_3)_2{\cdot}CH_3OH$ (**3**) (200 mg, 0.31 mmol) was suspended in 50 mL of tetrahydrofuran (10% H_2O) containing PPh_3 (**4**) (175 mg, 0.665 mmol). The reaction mixture was heated to reflux for 3 h. HNO_3 (0.6 mL of a 0.5 M solution) was then added and the solution immediately turned from brown to red. The solution was cooled to 25 °C and filtered through a glass filter. All volatiles were then removed in an oil-pump vacuum. The remaining red residue was washed several times with 20 mL of toluene and 20 mL of dry tetrahydrofuran, and was then dried in vacuo to give a crude red product, which was crystallised from a dichloromethane/methanol mixture (4:1) at 25 °C to afford **5** as red crystals. Yield: 290 mg (0.23 mmol), 76% based on **3**. − M.p. 189 °C (dec.). − IR (KBr, cm^{-1}): $\nu_{a(NO_3)}$ 1385, $\nu_{(NH)}$ 3106, $\nu_{(P=O)}$ = 1131. − ^{1}H NMR ([D$_6$]DMSO): δ = 7.0−8.2 (m, C_6H_5, H_2biim). − ^{13}C{^{1}H} NMR ([D$_6$]DMSO): δ = 129.1 (C-*i*/C_6H_5), 130.2 (CH/C_6H_5), 131.8 (CH/C_6H_5), 133.0 (CH/C_6H_5), 135.1 (C-5, -5′/H_2biim), 137.9 (C-4, -4′/H_2biim), 139.9 (C-2, -2′/H_2bim). − ^{31}P{^{1}H} NMR ([D$_6$]DMSO): δ = 36.4. − UV/Vis (CH_2Cl_2): λ_{max} = 360 nm (ε = $3.5{\cdot}10^3$ mol^{-1}·dm^3·cm^{-1}), 388 nm (ε = $3.5{\cdot}10^3$ (mol^{-1}·dm^3·cm^{-1}). − CV (CH_2Cl_2, −5 °C): Os^{III}/Os^{II} redox couple, $E_{1/2}$ = −0.97 V (ΔE = 290 mV), Os^{III}/Os^{IV} redox couple, $E_{1/2}$ = +0.42 V (ΔE = 210 mV). − $C_{48}H_{48}N_{11}O_{12}OsP_2$ (1236.20): calcd. C 47.12, H 3.84, N 12.47; found C 47.36, H 4.19, N 12.11.

Synthesis of $[Os(Hbiim)_2(O{=}PPh_3)_2](NO_3){\cdot}2H_2O$ (6): Potassium hydroxide (30 mg, 0.53 mmol, dissolved in 5 mL of methanol) was added to a solution of $[Os(H_2bim)_2(O{=}PPh_3)_2](NO_3)_3{\cdot}H_2O{\cdot}0.5CH_3OH$ (**5**) (300 mg, 0.26 mmol) in a 4:1 dichloromethane/methanol mixture at 25 °C. The reaction mixture immediately turned from red to violet and KNO_3 subsequently precipitated. The reaction mixture was additionally stirred for 20 min and then filtered through a glass filter. From the filtrate all volatiles were removed in an oil-pump vacuum. The violet residue was washed with 10 mL of H_2O, 5 mL of acetone, and then dried in vacuo to afford **6** as a violet solid. Yield: 240 mg (0.22 mmol), 85% based on **5**. − M.p. 226 °C (dec.). − IR (KBr, cm^{-1}): $\nu_{a(NO_3)}$ 1386, $\nu_{(NH)}$ 3095, $\nu_{(P=O)}$ 1132. − ^{1}H NMR ([D$_4$]methanol): δ = 7.4−8.1 (m, C_6H_5, H_2biim). − ^{13}C{^{1}H} NMR ([D$_4$]methanol): δ = 130.5 (CH/C_6H_5), 133.4 (CH/C_6H_5), 133.6 (CH/C_6H_5), 134.6 (C-5, -5′/H_2biim), 138.6 (C-4, -4′/H_2biim), 141.3 (C-2, -2′/H_2bim). − Due to the low solubility of **6** the C-*i*/C_6H_5 resonance signal could not be detected. − ^{31}P{^{1}H} NMR ([D$_6$]DMSO): δ = 37.1. − UV/Vis (CH_2Cl_2): λ_{max} = 341 nm (ε = $4.5{\cdot}10^3$ mol^{-1}·dm^3·cm^{-1}), 541 nm (ε = $4.5{\cdot}10^2$ (mol^{-1}·dm^3·cm^{-1}). − CV (CH_2Cl_2, 25 °C): Os^{III}/Os^{II} redox couple, E_{red} = −1.29 V (irr.); Os^{III}/Os^{IV} redox couple, $E_{1/2}$ = +0.29 V (ΔE = 180 mV). − $C_{48}H_{44}N_9O_6OsP_2$ (1095.15): calcd. C 52.64, H 4.06, N 11.51; found C 52.82, H 3.89, N 12.11.

X-ray Crystallographic Study of 5: X-ray structure data (total/unique reflections: 20917/13900) were collected at 170 K with a

Bruker SMART CCD diffractometer for the red crystals of **5** (Table 3). The crystal was attached to a glass fiber with perfluoropolyalkyl ether (ABCR GmbH & Co KG, viscosity 1600 cSt.). The unit cell parameter was checked for the presence of higher lattice symmetry using PLATON.[18] Data were corrected for absorption using SADABS.[19] The structure was solved by direct methods (SHELXS-97).[20] Refinement was carried out by full-matrix least-squares techniques on F^2 (SHELXL-97/2).[20] Hydrogen atoms were located from the difference Fourier map. All hydrogen atoms were fully refined with the exception of H13, H49a, H49b, and H49c, which belong to the CH_3OH molecule and were included on their ideal positions, riding on their carrier atoms. All non-hydrogen atoms were refined anisotropically. The structural data (without structural factors) are deposited at the Cambridge Crystallographic Data Centre and can be acquired under the depositing number CCDC-152194 under the following address: CCDC, 12 Union Road, Cambridge CB2 1EZ, UK [Fax: (internat.) + 44-1223/336-033; E-mail: deposit@ccdc.cam.ac.uk].

Table 3. Crystallographic data for **5**·H_2O·0.5MeOH

Crystal shape	plate
Crystal colour	red
Crystal size [mm]	1.00 × 0.40 × 0.10
Empirical formula	$C_{97}H_{92}N_{22}O_{25}Os_2P_4$
Molecular mass	2470.21
Crystal system	triclinic
Space group	$P\bar{1}$
a [Å]	10.9098(13)
b [Å]	10.9726(13)
c [Å]	21.330(3)
α [°]	78.280(2)
β [°]	87.315(2)
γ [°]	87.992(2)
V [Å^3]	2496.6(5)
Z	1
$d_{calcd.}$ [g·cm^{-3}]	1.643
Type of diffractometer	Bruker SMART CCD
Radiation used (λ [Å])	Mo-K_α (0.71073)
Monochromator	graphite
Data collection mode	ω-scans
Linear absorption coefficient [mm^{-1}]	2.694
Temperature [K]	173(2)
Max/Min transmission	0.7744/0.1737
Number of measured reflections	20917
Number of independent reflections	13900
Unique reflections ($I \geq 2\sigma(I)$]	10155
R(int)	0.0224
Scan range	$0.98° \leq \theta \leq 30.87°$
Completeness to θ_{max}	98.3%
Index range	$-15 \leq h \leq 15$
	$-15 \leq k \leq 15$
	$-29 \leq l \leq 19$
F(000)	1240
R [$I > 2\sigma(I)$]/all[a]	0.0245/0.0388
wR^2 [$I > \sigma(I)$]/all[b]	0.0581/0.0626
Maximum δ/σ	1.444
Max./min. electron density [e·Å^{-3}]	1.176/−1.333
Reflections used for refinement	13900
Refined parameters	863
Goodness-of-fit on F^2 [c]	0.983

[a] $R = \Sigma||F_o| - |F_c||/\Sigma|F_o|$. − [b] $[\Sigma[w(F_o^2 - F_c^2)^2]/\Sigma(wF_o^4)]^{1/2}$), calcd. $w = 1/[\sigma^2(F_o^2) + (0.0339P)^2 + 0.0000P]$ where $P = (F_o^2 + 2F_c^2)/3$. − [c] $S = [\Sigma w(F_o^2 - F_c^2)2]/(n - p)^{1/2}$, n = number of reflections, p = parameters used.

Acknowledgments

This work was supported in part by the Deutsche Forschungsgemeinschaft, the Fonds der Chemischen Industrie and the Deutscher Akademischer Austauschdienst DAAD (A. M.). We also would like to thank Degussa-Hüls AG for the generous gift of OsO_4 and $OsCl_3$.

[1] [1a] L. A. Oro, E. Sola, J. A. López, F. Torres, A. Elduque, F. Lahoz, *Inorg. Chem. Commun.* **1998**, *1*, 64−67. − [1b] C. Tejel, M. A. Ciriano, J. A. López, F. J. Lahoz, L. A. Oro, *Organometallics* **1997**, *16*, 4718−4727. − [1c] P. G. Rasmussen, J. E. Anderson, O. H. Bailey, M. Tamres, J. C. Bayón, *J. Am. Chem. Soc.* **1985**, *107*, 279−281. − [1d] P. G. Rasmussen, O. H. Bailey, J. C. Bayón, W. M. Butler, *Inorg. Chem.* **1984**, *23*, 338−343.

[2] [2a] L. A. Oro, M. A. Ciriano, C. Tejel, *Pure Appl. Chem.* **1998**, *70*, 779−788. − [2b] E. Sola, V. I. Bakhmutov, F. Torres, A. Elduque, J. A. López, F. J. Lahoz, H. Werner, L. A. Oro, *Organometallics* **1998**, *17*, 683−696. − [2c] M. A. Esteruelas, M. P. Garcia, A. M. Lopez, L. A. Oro, *Organometallics* **1992**, *11*, 702−705. − [2d] M. P. Garcia, A. M. Lopez, M. A. Esteruelas, F. J. Lahoz, L. A. Oro, *J. Chem. Soc., Chem. Commun.* **1988**, 793−795.

[3] M. A. Esteruelas, M. P. García, A. M. López, L. A. Oro, *Organometallics* **1991**, *10*, 127−133.

[4] [4a] M. A. Esteruelas, F. J. Lahoz, L. A. Oro, E. Onate, N. Ruiz, *Inorg. Chem.* **1994**, *33*, 787−792. − [4b] M. A. Esteruelas, F. J. Lahoz, A. Lopez, E. Onate, L. A. Oro, N. Ruiz, E. Sola, J. Tolosa, *Inorg. Chem.* **1996**, *35*, 7811−7817.

[5] W. P. Griffith, Osmium, *Comprehensive Coordination Chemistry*, vol. 4 (Ed.: G. Wilkinson), Oxford, Pergamon Press, **1987**, p. 580−587.

[6] K. Nakamoto, *Infrared and Raman Spectra of Inorganic and Coordination Compounds*, John Wiley and Sons, Inc., NY, **1986**, p. 295−301.

[7] [7a] C. M. Che, T. F. Lai, W. C. Chung, W. P. Schaefer, H. B. Grey, *Inorg. Chem.* **1987**, *26*, 3907−3911. − [7b] C. M. Che, C. K. Poon, W. C. Chung, H. B. Grey, *Inorg. Chem.* **1985**, *24*, 1277−1278.

[8] [8a] B. Domhoever, H. Hammers, W. Klaeui, M. Pfeffer, *J. Organomet. Chem.* **1996**, *522*, 197−206. − [8b] B. Domhoever, W. Klaeui, *J. Organomet. Chem.* **1996**, *522*, 207−212. − [8c] W. Kläui, H. O. Asbah, G. Schramm, V. Englert, *Chem. Ber./Recueil* **1997**, *130*, 1223−1229.

[9] A. B. P. Lever, *Inorganic Electronic Spectroscopy*, Elsevier, Amsterdam, London, New York, **1968**, p. 225−236.

[10] A. Maiboroda, G. Rheinwald, H. Lang, *Inorg. Chem.* **2000**, *39*, 5725−5730.

[11] K. J. Taylor, L. J. Yellowlees, *Molecular Electrochemistry of Inorganic, Bioorganic and Organometallic Compounds, NATO ASI Ser., Ser. C.*, Kluwer Academic Publishers, Amsterdam, **1993**, p. 69−75.

[12] J. A. Christie, T. J. Collins, Terry E. Krafft, Bernard D. Santasiero, G. H. Spies, *J. Chem. Soc., Chem. Commun.* **1984**, 198−199.

[13] G. A. Jeffrey, H. Maluszynska, J. Mitra, *Int. J. Biol. Macromol.* **1985**, *7*, 336−348.

[14] P. G. Rasmussen, O. H. Bailey, J. C. Bayón, W. M. Butler, *Inorg. Chem.* **1984**, *23*, 338−343.

[15] M. S. Haddad, E. N. Duesler, D. N. Hendrickson, *Inorg. Chem.* **1979**, *18*, 141−148.

[16] *Comprehensive Organometallic Chemistry* (Eds. G. Wilkinson et al.), Pergamon Press, Oxford, **1982**, vol. 1−9.

[17] F. Holmes, K. M. Jones, E. G. Torrible, *J. Chem. Soc.* **1961**, 4790−4794.

[18] A. L. Spek, *Acta Crystallogr., Sect. A* **1990**, *46*, C34.

[19] Area Detector, *Absorption Corrections*, Bruker axs Inc., Madison, WI, **1996**.

[20] G. M. Sheldrick, *Shelx97, Programs for Crystal Structure Analysis (Release 97-2)*, University of Göttingen, Germany, **1997.**

Received December 8, 2000
[I00466]

$Mo^{V}_{2}O_{4}^{2+}$ Directs the Formation and Subsequent Linking of Potential Building Blocks under Different Boundary Conditions: A Related Set of Novel Cyclic Polyoxomolybdates

Achim Müller,*[a] Christoph Kuhlmann,[a] Hartmut Bögge,[a] Marc Schmidtmann,[a] Mario Baumann,[a] and Erich Krickemeyer[a]

Dedicated to Prof. Dieter Sellmann on the occasion of his 60th birthday

Keywords: Molybdenum / Polyoxometalates / Clusters / Ring structures

The synthesis and structural characterization of a novel series of deep-red mixed-valence (Mo^{VI}/Mo^{V}) compounds with nano-sized spherically shaped cluster anions containing 18, 40, or 54 Mo atoms, respectively, is reported: $Na_{10}[H_4Mo_{18}O_{56}(CH_3COO)_2] \times$ ca. 36 $H_2O \times 3$ CH_3COOH (**1**), $(NH_4)_{12}Na_{12}[Mo_{40}O_{128}] \times$ ca. 70 H_2O (**2**), $(NH_4)_{12}Na_{20}[H_4Mo_{54}O_{168}(CH_3COO)_4] \times$ ca. 64 H_2O (**3**), $Na_{32}[H_4Mo_{54}O_{168}(CH_3COO)_4] \times$ ca. 128 H_2O (**4**), and $Na_{32}[H_4Mo_{54}O_{168}(CH_3COO)_4] \times$ ca. 98 H_2O (**5**). Clusters **3**, **4**, and **5** differ in the packing of the rings in the lattice. The anions are easily formed by reduction of an acidified aqueous molybdate solution while the deliberately generated $Mo^{V}_{2}O_{4}^{2+}$ group – abundant in all clusters – has a directing influence on the formation of the preliminary building blocks. Furthermore, it is possible to control the ratio of the $\{Mo^{V}_{2}\}$ units to the Mo^{VI} centres by adjusting the specific concentration of the employed reducing agent.

Introduction

Obtaining a strategy for the formation of complex molecular systems with desired properties − constructed from simple building blocks by conservative self-assembly processes − is an ambitious endeavour in contemporary chemistry. In this context, the polyoxomolybdate system under consideration shows a variety of units (either as existing or virtual species), whose linking can be controlled by the deliberate generation of stable and transferable fragments.[1] An important step for us in this regard was, for example, the use of pentagonal $\{(Mo)Mo_5\}$-type units that allowed us not only to adjust the size of giant spherical species, but also to generate such types of molecules with practically 150 unpaired electrons at their periphery by linking these pentagonal units with Fe^{III} ($S = {}^5/_2$) centres.

A prominent feature of the chemistry of molybdenum is the formation of numerous polyoxomolybdate(VI) anions in aqueous solutions. Depending on the boundary conditions, the large number of species existing simultaneously in strongly overlapping equilibria can be considered − in this context − as an extensive library of building blocks, accessible on demand. The equilibria (the dynamics of aggregation reactions) are mostly characterized by the degree of acidity. On the other hand, the negative charge and therefore the nucleophilicity of intermediate cluster fragments can be increased by reduction, resulting in further attraction of electrophiles and thus in growth of the molecular systems.[2]

[a] Lehrstuhl für Anorganische Chemie der Universität
Postfach 100131, 33501 Bielefeld, Germany
E-mail: a.mueller@uni-bielefeld.de

Reducing an acidified aqueous solution of ammonium heptamolybdate with sodium dithionite − under conditions that favour the generation of $Mo^{V}_{2}O_{4}^{2+}$ [= $Mo^{V}_{2}O_{4}(H_2O)_6^{2+} = \{Mo^{V}_{2}\}$] units (controlled pH and redox potential), led to the simultaneous precipitation of two compounds, $(NH_4)_{12}Na_{12}[Mo_{40}O_{128}] \times$ ca. 70 H_2O (**2**) and $(NH_4)_{12}Na_{20}[H_4Mo_{54}O_{168}(CH_3COO)_4] \times$ ca. 64 H_2O (**3**), which are easily distinguishable by their different crystal shapes.[3]

Since the ratio of the red lozenge-shaped crystals of **2** relative to the red needle-shaped ones of **3** depends upon the amount of reducing agent, our challenge was thus to find suitable conditions − based on our knowledge of the different Mo^{V}/Mo^{VI} ratios in **2a** and **3a** − for obtaining both compounds in a pure form. These experiments led to the discovery of a series of related new compounds.[4]

Results and Discussion

All mentioned cluster anions were formed by stepwise growth processes, initiated and directed by the in situ generated $Mo^{V}_{2}O_{4}^{2+}$ units. (During the last decade, several other compounds containing one, two, or more $\{Mo^{V}_{2}\}$ units have been reported.[5]) The important result, however, in the context of our a priori intention, is that all the clusters with $\{Mo^{V}_{2}\}$ groups reported here are distinguishable by their $\{Mo^{V}_{2}\}/Mo^{VI}$ ratios that result from the different redox equivalents of reducing agent used and from the proton concentration or acidity of the reaction medium. Table 1 summarizes these trends and includes clusters of the type $\{Mo_{48}\}$[6] and $\{Mo_{132}\}$[7] that also contain $\{Mo^{V}_{2}\}$ building

 © WILEY-VCH Verlag GmbH, 69451 Weinheim, 2001 1434−1948/01/0909−2271 $ 17.50+.50/0

Table 1. Some properties of the cluster anions isolated from aqueous molybdate solution (pH ≈ 4) in presence of acetate; the asterisk stands in all cases for the reduced form

	Building blocks	Mo^V centres	Mo^{VI} centres	Mo^V/Mo	Charge per Mo	O/Mo
$[Mo_{40}O_{128}]^{24-}$	$\{Mo_2^*\}_4\{Mo_8\}_4$	8	32	0.20	0.60	3.2
$[H_4Mo_{54}O_{168}(CH_3COO)_4]^{32-}$	$\{Mo_2^*\}_2\{Mo_8^*\}_4\{Mo_9^*\}_2$	20	34	0.37	0.59	3.3
$[Mo_{48}O_{148}]^{28-}$ [a]	$\{Mo_2^*\}_2\{Mo_4\}_2\{Mo_9^*\}_4$	20	28	0.42	0.58	3.1
$[Mo_{116}O_{331}(CH_3COO)_{30}(H_2O)_{56}]^{46-}$ [b]	$\{Mo_2^*\}_{25}\{(Mo)Mo_5\}_{11}$	50	66	0.43	0.40	3.1
$[H_4Mo_{18}O_{56}(H_3CCOO)_2]^{10-}$ [b]	$\{Mo_9^*\}_2$	8	10	0.44	0.56	3.3
$[Mo_{132}O_{372}(H_3CCOO)_{30}(H_2O)_{72}]^{42-}$ [c]	$\{Mo_2^*\}_{30}\{(Mo)Mo_5\}_{12}$	60	72	0.45	0.32	3.3

[a] To be published. – [b] See ref.[9] – [c] See ref.[7]

blocks. Notably, at *lower* pH values, molybdenum blue species like the ring-shaped $\{Mo_{154}\}$ cluster are formed where no $\{Mo_2^V\}$ units are present.[8]

All compounds were characterized by elemental analyses [including cerimetric titration for the determination of the (formal) number of reduced centres], thermogravimetry (to determine the amount of crystal water), spectroscopy (UV/Vis, IR, Raman), and single-crystal X-ray structure analyses [including bond valence sum (BVS) calculations for the determination of the position of the H_2O ligands, as well as for the distinction between Mo^{VI} and Mo^V centres]. The crystallographic data for the diamagnetic, mixed-valence compounds $Na_{10}[H_4Mo_{18}O_{56}(CH_3COO)_2] \times$ ca. 36 $H_2O \times$ 3 CH_3COOH (**1**), $(NH_4)_{12}Na_{12}[Mo_{40}O_{128}] \times$ ca. 70 H_2O (**2**), $(NH_4)_{12}Na_{20}[H_4Mo_{54}O_{168}(CH_3COO)_4] \times$ ca. 64 H_2O (**3**), $Na_{32}[H_4Mo_{54}O_{168}(CH_3COO)_4] \times$ ca. 128 H_2O (**4**), and $Na_{32}[H_4Mo_{54}O_{168}(CH_3COO)_4] \times$ ca. 98 H_2O (**5**) are given in Tables 2 and 3.

Detailed structural information can be obtained from Figures 1–4. Figure 1 illustrates the importance of the mentioned $Mo_2^VO_4^{2+}$ dumb-bell-type "linkers" (equivalent to the $\{Mo_2^VO_{10}\}$ structural building block in the solids, which of course does not exist in solution) for the $\{Mo_{18}\}$-, $\{Mo_{40}\}$-, and $\{Mo_{54}\}$-type clusters. These units have a high formation tendency in molybdate solutions in the presence of reducing agents at pH values relevant for the present investigations.

As an example, the $\{Mo_{18}\}$ cluster anion **1a**[9] (Figures 1 and 4) reflects the tendency of even small polyoxomolybdates to adopt ring-shaped structures. The anion itself has approximately C_{2h} symmetry, and consists of two identical building blocks – denoted as *cis*-$\{Mo_9^*\}$ – each containing five Mo^{VI} centres and two $\{Mo_2^V\}$ units (the asterisk * denotes the presence of reduced centres, i.e. of $\{Mo_2^VO_{10}\}$ groups, either as $\{Mo_2^*\}$ units or as part of the $\{Mo_8^*\}$ or $\{Mo_9^*\}$ framework). These four $\{Mo_2^V\}$ units

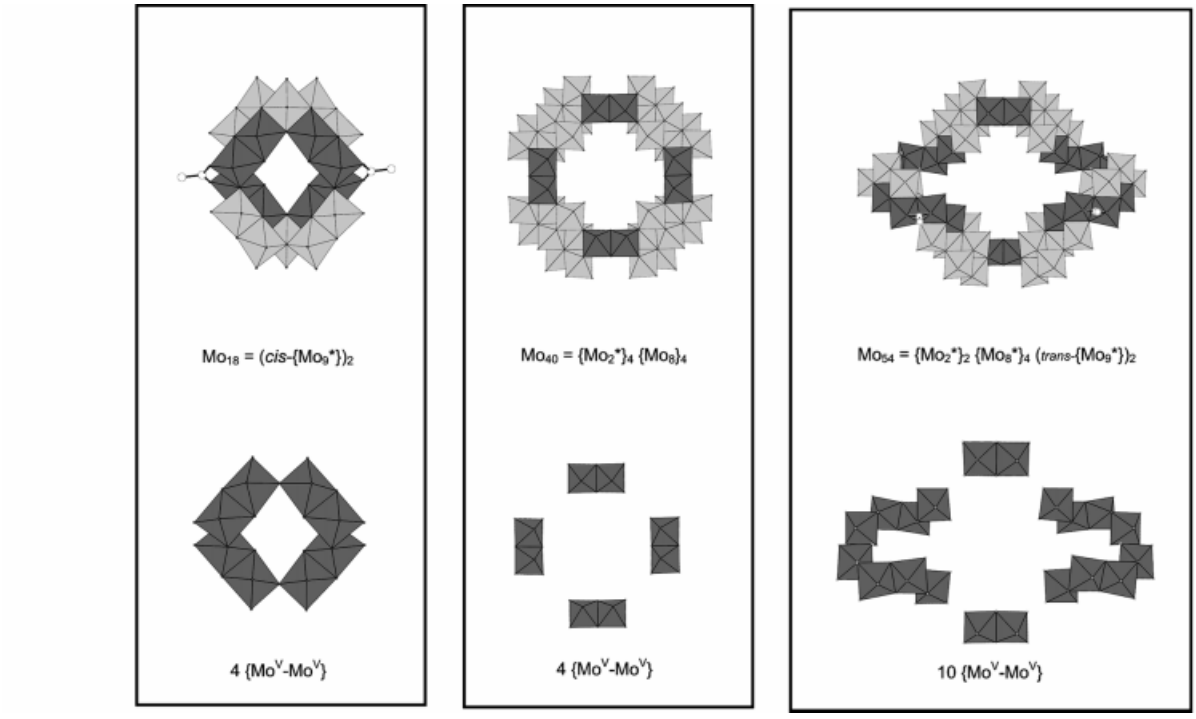

Figure 1. Polyhedral representations of the complete $\{Mo_{18}\}$ (**1a**) (left), $\{Mo_{40}\}$ (**2a**) (centre), and $\{Mo_{54}\}$ (**3a**–**5a**) (right) clusters based on the $\{Mo_2^*\}$ dumb-bells with Mo^V–Mo^V single bonds, highlighted in dark-grey (top); for clarity, the abundant $\{Mo_2^*\}$ groups are also shown separately (bottom)

form an oxomolybdenum(V) core fragment (see Figure 1, bottom) with a puckered cyclic framework comparable to that of the compound $Mo_8O_{16}(OMe)_8(PMe_3)_4$.[10] A more detailed view can be obtained from Figure 4, which also elucidates the notation *cis*- and *trans*-{Mo_9*} (occurring in the {Mo_{54}} cluster anion) regarding the different positions of the two molybdenum octahedra directed towards the central {Mo_7} moiety (note that the local symmetry of the *cis*-{Mo_9*} unit is C_s).

The polymorphic compound **2** crystallizes in two different space groups, $P2_1/m$ and *Pnma*. Its ring-shaped anions form layers that are separated by the cations. Depending on the orientation of the anions of two layers towards each other, either the monoclinic or the orthorhombic polymorph results.[11] The {Mo_{40}} anion **2a** (Figure 1) consists of 168 non-hydrogen atoms, i.e. 40 molybdenum centres (including eight Mo^V) and 128 oxygen atoms, and has approximately C_{4v} symmetry whereby eight {$Mo^{VI}O_6$ } and two {Mo^VO_6} octahedra form one {Mo_{10}} unit possessing a mirror plane. Cleaving two of the terminal octahedra of this {Mo_{10}} unit leads to an {Mo_8} framework resembling the γ-octamolybdate that was recently isolated as a main constituent of a nonamolybdate formed under a comparable proton concentration.[12] Here we prefer the alternative description: Four {Mo_2^V} groups link four {Mo_8} units (note that these units are not identical with the above-mentioned γ-octamolybdate), corresponding to the formula given above (Figure 1). Whereas in the case of **2** [containing the {Mo_{40}} (= {Mo_2*}$_4${Mo_8}$_4$) cluster anion **2a**] the {Mo_2^V} building units are not the dominating structural feature, this is actually the case for the {Mo_{54}} (= {Mo_9*}$_2$-{Mo_8*}$_4${Mo_2*}$_2$) cluster anion of **3**, **4**, and **5**, as well as for the {Mo_{18}} = {Mo_9*}$_2$ cluster anion of **1**, where all such units are directly connected (see Figures 1−4).

The crown-shaped (twisted) anion {Mo_{54}} (= {Mo_9*}$_2$ {Mo_8*}$_4${Mo_2*}$_2$, see Figure 2), abundant in compounds **3**, **4**, and **5**, consists of 238 non-hydrogen atoms, i.e. 54 molybdenum atoms (including 20 Mo^V), 176 oxygen, and eight carbon atoms, and has approximately C_{2v} symmetry (in the crystal lattice the site symmetry of the twisted anion is in all cases *i*). The formulation based on the three different building blocks ({Mo_2*}, {Mo_8*}, {Mo_9*}) − shown in Figure 2 − corresponds to the above-mentioned formula. Figures 3 and 4 show a comparison of the latter two building blocks with the two other related cluster anions **1a** and **2a**. The {Mo_8*} unit, containing six $Mo^{VI}O_6$ as well as two Mo^VO_6 octahedra, can be (formally) derived from the corresponding {Mo_8} unit of the {Mo_{40}} anion by a two-electron reduction step, i.e. by formation of an {Mo_2^V} group (Figure 3). The other building block (denoted *trans*-{Mo_9*}), present twice in the {Mo_{54}} cluster, consists of nine molybdenum−oxygen octahedra, and has approximately C_2 symmetry. Four Mo^V centres form two {Mo_2^V} units and point to opposite sites thereby enabling an interesting comparison with the *cis*-{Mo_9*} unit of the {Mo_{18}} cluster (Figure 4). Due to the different orientation of the {Mo_2^V} units towards each other (compared to the *cis*-{Mo_9*} units), the further linking of these structural building blocks is already fixed.

The {Mo_{54}} cluster anion can be "constructed" in the following way: Two of the {Mo_8*} units are linked by an {Mo_2^V} unit resulting in a super-unit of the type {Mo_8*}

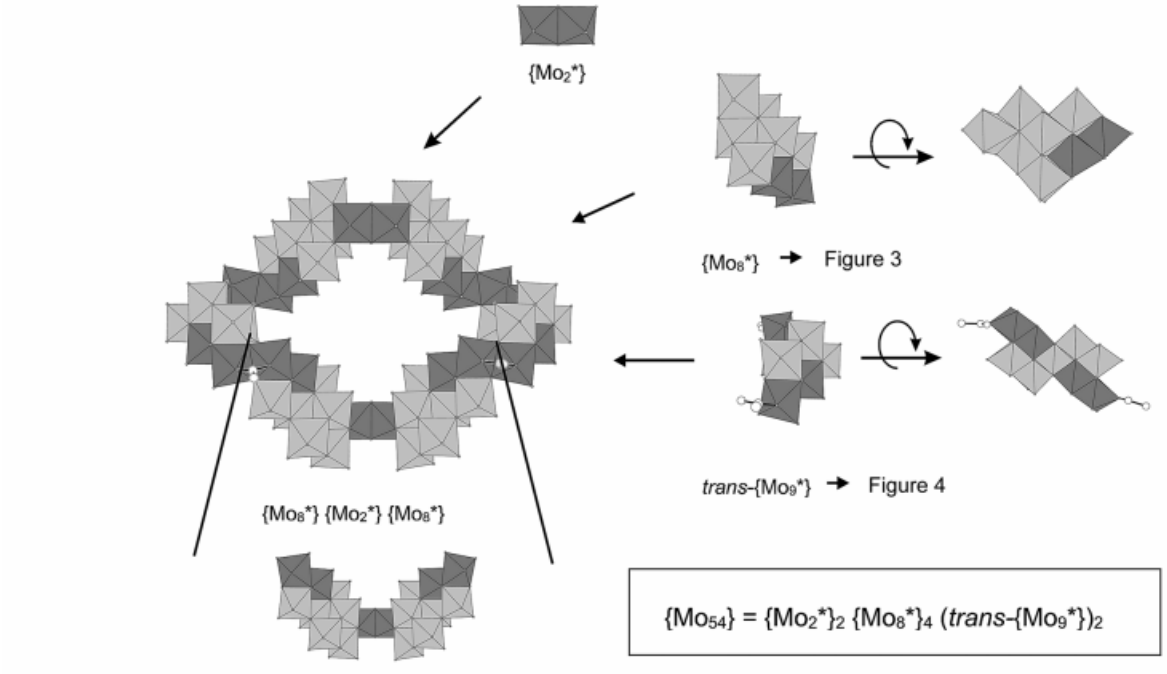

Figure 2. Polyhedral representation of the {Mo_{54}} cluster (left) and its three formal building blocks (right): {Mo_2*}, {Mo_8*}, and {Mo_9*} ({Mo_2*} = $[Mo_2^VO_4O_6]^{10-}$, {Mo_8*} = $[Mo_2^VMo_6^{VI}O_{28}]^{10-}$, and {$Mo_9$*} =$[(\mu_3\text{-}OH)_2Mo_4^VMo_5^{VI}O_{26}(CH_3COO)_2]^{10-}$); one super-unit of the type {Mo_8*}{Mo_2*}{Mo_8*} is also shown (bottom)

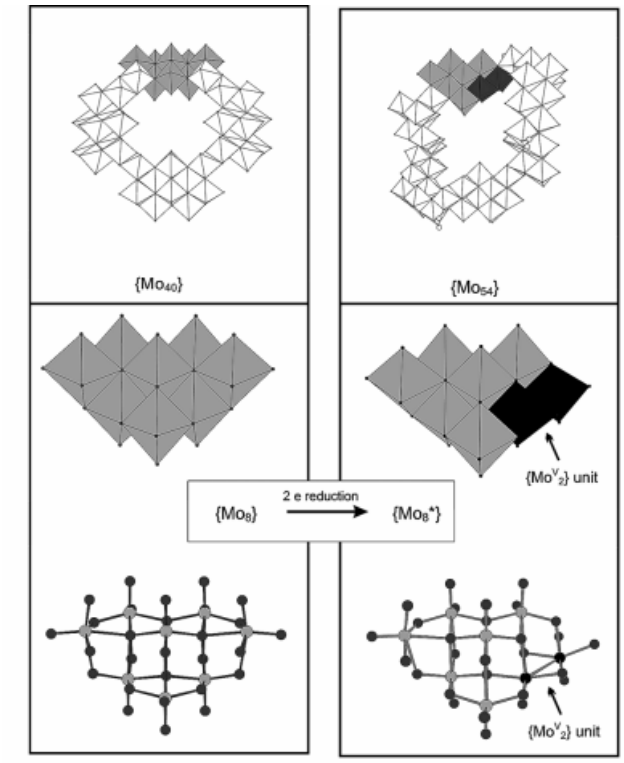

Figure 3. Structural comparison of an $\{Mo_8\}$ unit derived from $\{Mo_{40}\}$ (left) with the corresponding $\{Mo_8{*}\}$ unit (containing one $\{Mo^V{-}Mo^V\}$ type unit) of the $\{Mo_{54}\}$ (right) cluster in polyhedral representation (top) and as ball-and-stick model (bottom); ball-and-stick representation: Mo^V dark-grey, Mo^{VI} light-grey, O atoms medium grey; polyhedral representation: $\{Mo^V_2\}$ units dark-grey, $\{Mo^{VI}{}_mO_n\}$ moieties light-grey

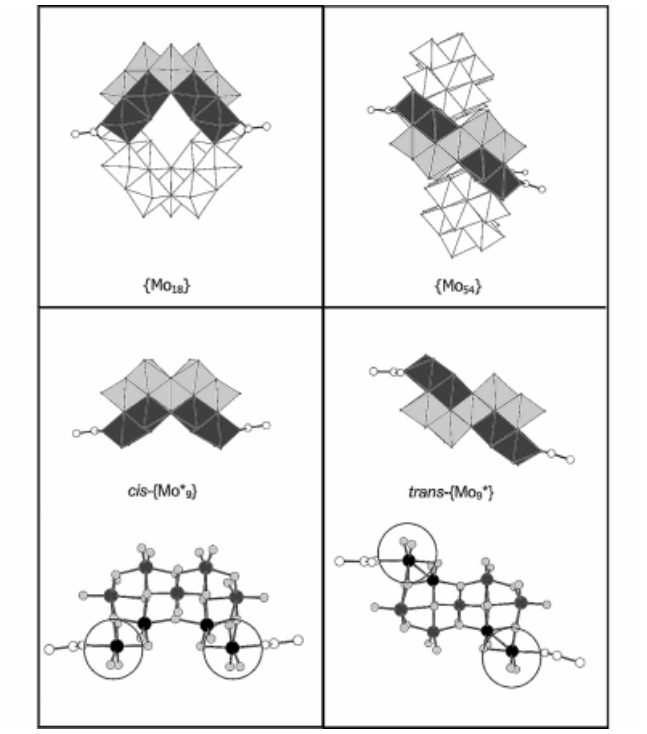

Figure 4. Structural comparison of $\{Mo_9{*}\}$ units − derived from the $\{Mo_{18}\}$ (top, left) and from the $\{Mo_{54}\}$ cluster (top, right) − in polyhedral and ball-and-stick representation; the classification of *cis* and *trans* corresponds to the position of the $\{Mo^V{-}Mo^V\}$ units relative to each other; ball-and-stick representation: Mo^V black, Mo^{VI} light-grey, O atoms medium grey; polyhedral representation: $\{Mo^V_2\}$ units dark-grey, $\{Mo^{VI}{}_mO_n\}$ moiety light-grey; the acetate ligands (carbon: open circle) are shown in both cases in ball-and-stick representation)

$\{Mo_2{*}\}\{Mo_8{*}\}$. Two of these are finally bridged at both ends through edge-sharing with the two *trans*-$\{Mo_9{*}\}$ building blocks and by an acetate ligand (Figures 2 and 4). Remarkably, the construction of the $\{Mo_{40}\}$ cluster can be described in the same way: Two super-units of the type $\{Mo_8\}\{Mo_2{*}\}\{Mo_8\}$ (i.e., the aforementioned non-reduced $\{Mo_8\}$ groups!) are linked by additional $\{Mo_2{*}\}$ groups resulting in the bowl-shaped anion.

Interestingly, it is possible to vary the packing of the cluster units by adding different reagents, e.g., acetylacetone or sodium chloride. Comparing the sodium salts of the $\{Mo_{54}\}$ compounds **4** and **5**, it is obvious that the crystal water content, and thus the unit cell volume, is reduced by ca. 1:7 through replacing sodium chloride by acetylacetone during the crystallization process. Adding other cations, e.g. ammonium leads to a further shrinking of the cell and relevant investigations are presently in progress.

Looking at the charge per Mo atom and the value $R = \Sigma O/\Sigma Mo$ for all aggregates shows values that are practically constant, except for the charge per Mo atom in case of the $\{Mo_{132}\}$ ball-type species and its derivative. A value of $R \approx 3$ is observed in many cases, and even for large aggregates like the big wheel $[(MoO_3)_{154}H_{14}]^{14-}$.

Conclusions

Our synthetic route has as its aim the deliberate synthesis of clusters based on the use of $\{Mo^V_2\}$ units under different boundary conditions. In this context, it is interesting to note that the $\{Mo^{VI}_8\}$ building block, which is important for the present preparation conditions,[13] can at least formally be reduced to the actual $\{Mo_8{*}\}$ building block containing one $\{Mo^V_2\}$ dumb-bell unit (Figure 4) and, in the presence of additional molybdenum and reducing agent, to the $\{Mo_9{*}\}$ building block. The general strategic approach to control molecular growth by conservative self-organization processes offers, in principle, a wide variety of new species that can be constructed from simple building blocks.

Experimental Section

General Techniques: All reactions were performed using 100-mL Erlenmeyer flasks where no attempts were made to exclude oxygen. All chemicals except sodium dithionite were at least of reagent grade, and were used as supplied. Note, that sodium dithionite (85% iodometrically) should be fresh and powdered prior to use. The use of aged charges, which contain more water and might be

partly decomposed, will result in lower yields and gives less crystalline materials. − Elemental analyses (C,H,N) were performed using a LECO CHN 920 analyzer. The nitrogen values were determined by the Kjeldahl method, the sodium content by flame photometry. (The error limits for the determination of the sodium and ammonium cations in **2** and **3** restrict somewhat the reliability of their quantity in the formula unit by ±1.) − Vibrational spectroscopy was carried out with a Bruker IFS66/FRA106. − The amounts of crystal water were determined thermogravimetrically with a Shimadzu TA-60WSI thermo-balance under argon. − The UV/Vis spectra were measured using either a Shimadzu UV-160A or a Beckman Acta M IV instrument (solid with cellulose as reference). The compounds are stable in dry air but decompose easily while dissolving in water.

Preparation of 1: To a solution of 7.70 g of sodium molybdate dihydrate (31.8 mmol), 50.0 g of sodium acetate trihydrate (367.4 mmol), and 5.0 g of sodium chloride (85.6 mmol) in 300 mL of H_2O, an aqueous hydrazine sulfate solution (0.1 M, 61 mL) and afterwards 75 mL of acetic acid (100%) were added. The reaction medium was heated whilst stirring for 4 d at 35 °C (slow colour change from green to brownish-green) while the volume of the solution was kept constant by adding water. The solution was subsequently cooled to room temperature and filtered. The filtrate was kept in an open beaker and the volume of the solution was reduced by slow evaporation (up to 130 mL). Crystalline **1** was filtered off after 1 week and dried with $CaCl_2$. Yield 2.0 g (30% based on Mo). − IR (KBr pellet): $\tilde{\nu}$ = 3440 (s), 3162 (s), 1636 (m) [$\delta(H_2O)$], 1541 (m), 1443 (m), 1394 (sh), 1330 (m), 1028 (w), 960 (sh), 935 (s), 898 (m), 712, 636, 565, 498, 411. − Raman (λ_e = 1064 nm, undiluted powder): $\tilde{\nu}$ = 966, 930 [ν(Mo=O)], 747, 774, 662, 574, 507, 358, 330, 286, 200, 157 cm^{-1}. − UV/Vis (cellulose): λ_{max} = ca. 260, ca. 340, ca. 395, ca. 535, ca. 1040 nm. − $C_{10}H_{94}Mo_{18}Na_{10}O_{102}$ (3803.6): calcd. C 3.16, H 2.49, Na 6.04, H_2O 17.0; found C 3.3, H 2.4, Na 8.2, H_2O 14. − Cerimetric titration: 8±1 e.

Preparation of 2. − (a) After a solution of 3.00 g of ammonium heptamolybdate tetrahydrate (2.4 mmol) in 25 mL of water was acidified with 0.8 mL of acetic acid (100%), 0.20 g of sodium dithionite (1.1 mmol) were added (colour change to deep-green). After stirring the solution for 5 min, 3.00 g of sodium chloride was dissolved and the resulting solution was allowed to stand for 4.5 h for crystallization. The precipitated red lozenge-shaped crystals were filtered off, washed with aqueous acetone (50 vol-%) and finally dried in air. Yield 0.28 g (9% based on Mo). ***Note:*** After 5 h, crystals of **3** also start to precipitate. Pure crystalline **2**, i.e. an {Mo_{54}}-free product, can be obtained by replacing acetic acid by hydrochloric acid (**2** does not contain acetate ligands!). − **(b)** After a solution of 3.00 g of ammonium heptamolybdate tetrahydrate (2.4 mmol) in 25 mL of water was acidified with 3.0 mL of hydrochloric acid (1 M), 0.20 g of sodium dithionite (1.1 mmol) was added (colour change to deep-green). After stirring the solution for 5 min, 3.00 g of sodium chloride was dissolved and the resulting solution was allowed to stand for 4.5 h for crystallization. The precipitated red lozenge-shaped crystals were filtered off, washed with aqueous acetone (50-vol%) and finally dried in air. − Yield 0.58 g (18% based on Mo). ***Note:*** Comparing the two preparation methods the total yield was higher when hydrochloric acid was used, but the crystals were less suitable for single-crystal X-ray structure analysis. − IR (KBr pellet): $\tilde{\nu}$ = 3440 (s), 3162 (s), 1617 (m) [$\delta(H_2O)$], 1400 (s) [$\delta_{as}(NH_4^+)$], 946 (s) [ν(Mo=O)], 903 (sh), 869 (s), 765 (m), 724 (s), 652 (s), 486 (m) cm^{-1}. − Raman (λ_e = 1064 nm, undiluted powder): $\tilde{\nu}$ = 965, 937 [ν(Mo=O)], 909, 989, 842, 774, 723, 489, 375, 347, 276, 203, 143 cm^{-1}. − UV/Vis (cellulose): λ_{max} = ca. 285, ca. 380 nm. − $H_{188}Mo_{40}N_{12}Na_{12}O_{198}$ (7638.9): calcd. H 2.46, N 2.20, Na 3.61, H_2O 16.5; found H 2.08, N 2.22, Na 3.8, H_2O 14 (calcd. for compound containing 70 H_2O). − Cerimetric titration: 8±1 e.

Preparation of 3. − (a) After acidifying a solution of 3.00 g of ammonium heptamolybdate tetrahydrate (2.4 mmol) and 0.5 g of sodium acetate trihydrate in 25 mL of water with 3.0 mL of hydrochloric acid (1 M), 0.30 g of sodium dithionite (1.7 mmol) was added (colour change to deep-green). After stirring for 5 min, 3.00 g of sodium chloride was added and the resulting solution was allowed to stand for crystallization for 15−18 h. The precipitated red needle-shaped crystals were filtered off, washed with acetone and finally dried in air. Yield 0.67 g (20% based on Mo). − **(b)** After a solution of 3.00 g of ammonium heptamolybdate tetrahydrate (2.4 mmol) in 25 mL of water was acidified with 0.8 mL of acetic acid (100%), 0.30 g of sodium dithionite (1.7 mmol) was added (colour change to deep-green). After stirring the solution for 5 min, 3.00 g of sodium chloride was dissolved and the resulting solution was allowed to stand for 12−15 h for crystallization. The precipitated red needle-shaped crystals were filtered off, washed with aqueous acetone (50-Vol%), and finally dried in air. − Yield 0.3 g (8% based on Mo). ***Note:*** Comparing the two preparation methods, the total yield is higher when hydrochloric acid is used (similar to compound **2**), but the crystals are less suitable for single-crystal X-ray structure analysis. − IR (KBr pellet): $\tilde{\nu}$ = 3459 (s), 1624 (m) [$\delta(H_2O)$], 1540 (m) [$\nu_{as}(COO^-)$], 1436 (sh), 1402 (s), 962 (m), 944 (m) [ν (Mo=O)], 899 (m), 860 (m), 716 (m), 660 (m), 624 (m), 490 (m) cm^{-1}. − Raman (λ_e = 1064 nm, undiluted powder): $\tilde{\nu}$ = 969, 945, 936 [ν(Mo=O)], 765, 660, 491, 380, 357, 280, 242, 204 cm^{-1}. − UV/Vis (cellulose): λ_{max} = ca. 270, ca. 325, ca. 360 nm. − $C_8H_{192}Mo_{54}N_{12}Na_{20}O_{240}$ (9938.3): calcd. C 0.97, H 1.93, N 1.68, Na 4.63, H_2O 11.6; found C 0.94, H 2.38, N 1.68, Na 4.3, H_2O 11. − Cerimetric titration: 20±1 e.

Preparation of 4: To a solution of 4.50 g of sodium molybdate dihydrate (18.6 mmol) and 1.00 g of sodium acetate trihydrate in 25 mL of water, 1.00 g of sodium dithionite (5.75 mmol) was added (colour change to deep-brown). After stirring for 5 min, the solution was acidified with 3.00 mL of hydrochloric acid (1 M), stirred for an additional 15 min and finally allowed to stand for crystallization. The red needle-shaped crystals were filtered off after 7 d, washed with acetone and subsequently dried in air. − Yield 0.37 g (10% based on Mo). − IR (KBr pellet): $\tilde{\nu}$ = 3459 (s), 1635 (m) [$\delta(H_2O)$], 1541 (m) [$\nu_{as}(COO^-)$], 1445 (m), 961 (m), 944 (m) [ν(Mo=O)], 900 (m), 861 (m), 718 (m), 667 (m), 620 (m), 491 (m) cm^{-1}. − Raman (λ_e = 1064 nm, undiluted powder): $\tilde{\nu}$ = 975, 947, 936 [ν(Mo=O)], 838, 762, 663, 509, 478, 358, 284, 243, 205 cm^{-1}. − UV/Vis (cellulose): λ_{max} = ca. 280, 320, 360 nm. − $C_8H_{272}Mo_{54}Na_{32}O_{304}$ (11150.7): calcd. C 0.86, H 2.44, Na 6.60, H_2O 20.6; found C 0.88, H 2.10, Na 6.8, H_2O 18. − Cerimetric titration: 20±1 e.

Preparation of 5: To a solution of 4.50 g of sodium molybdate dihydrate (18.6 mmol) in 25 mL of water, 2.0 mL of acetylacetone was added dropwise (colour change to yellow) followed by 1.00 g of sodium dithionite (5.75 mmol) (colour change to deep-brown). After stirring for 5 min, the reaction medium was acidified with 2.0 mL of acetic acid (100%) and stirred for an additional 15 min. After 3 d, the red needle-shaped crystals were filtered off, washed with aqueous acetone (70 vol-%) and finally dried in air. − Yield 0.33 g (10% based on Mo). − IR (KBr): $\tilde{\nu}$ = 3459 (s), 1635 (m) [$\delta(H_2O)$], 1541 (m) [$\nu_{as}(COO^-)$], 1445 (m), 961 (m), 944 (m) [ν(Mo=O)], 900 (m), 861 (m), 718 (m), 667 (m), 620 (m), 491 (m) cm^{-1}. − Raman (λ_e = 1064 nm, undiluted powder): $\tilde{\nu}$ = 974, 952,

Table 2. Crystallographic data of compounds **1** and **2**

Compound	**1** $Na_{10}[H_4Mo_{18}O_{56}(CH_3COO)_2] \times 36\ H_2O \times 3\ CH_3COOH$	$Na_{12}(NH_4)_{12}[Mo_{40}O_{128}] \times 74\ H_2O$	**2** $Na_{12}(NH_4)_{12}[Mo_{40}O_{128}] \times 70\ H_2O$
Color and shape	red	red lozenge	red lozenge
Ratio $Mo^V/\Sigma Mo$	0.44	0.25	0.25
M [g mol^{-1}]	3803.67	7711.17	7639.10
Empirical formula	$C_{10}H_{94}Mo_{18}Na_{10}O_{102}$	$H_{196}Mo_{40}N_{12}Na_{12}O_{202}$	$H_{188}Mo_{40}N_{12}Na_{12}O_{198}$
Crystal system	triclinic	monoclinic	orthorhombic
Space group	$P\bar{1}$	$P2_1/m$	$Pnma$
a [Å]	12.1293(5)	13.1752(6)	24.5144(15)
b [Å]	15.2523(6)	34.922(2)	34.940(2)
c [Å]	15.2852(6)	22.0247(10)	23.3214(14)
α [°]	114.911(1)		
β [°]	94.227(1)	101.378(1)	
γ [°]	101.647(1)		
Volume [Å^3]	2471.4(2)	9934.4(8)	19976(2)
Z	1	2	4
$\rho_{calcd.}$ [Mgm^{-3}]	2.556	2.578	2.540
μ [mm^{-1}]	2.373	2.583	2.567
Crystal size [mm^3]	0.40 × 0.22 × 0.16	0.24 × 0.20 × 0.06	0.20 × 0.10 × 0.02
2θ range	1.52 to 30.02°	0.94 to 27.01°	1.66 to 26.99°
Reflections collected	33526	58486	115056
Reflections observed	12493	16617	10726
$[I > 2\sigma(I)]$	(R_{int} = 0.0219)	(R_{int} = 0.0383)	(R_{int} = 0.1348)
Refined parameters	643	1175	1028
$R1$ $[I > 2\sigma(I)]$	0.0356	0.0490	0.0643
$wR2$ $[(I > 2\sigma(I)]$	0.0997	0.1272	0.1532
max. and min. residual electron density [eÅ^{-3}]	2.138 and −1.828	2.916 and −1.582	2.883 and −1.324

Table 3. Crystallographic data of compound **3**−**5**

Compound	**3** $Na_{20}(NH_4)_{12}[H_4Mo_{54}O_{168}(CH_3COO)_4] \times 64\ H_2O$	**4** $Na_{32}[H_4Mo_{54}O_{168}(CH_3COO)_4] \times 128\ H_2O$	**5** $Na_{32}[H_4Mo_{54}O_{168}(CH_3COO)_4] \times 98\ H_2O$
Color and shape	red needles	red needles	red needles
Ratio $Mo^V/\Sigma Mo$	0.37	0.37	0.37
M [g mol^{-1}]	9938.30	11150.70	10610.22
Empirical formula	$C_8H_{192}Mo_{54}N_{12}Na_{20}O_{240}$	$C_8H_{272}Mo_{54}Na_{32}O_{304}$	$C_8H_{212}Mo_{54}Na_{32}O_{274}$
Crystal system	triclinic	triclinic	triclinic
Space group	$P\bar{1}$	$P\bar{1}$	$P\bar{1}$
a [Å]	13.4911(10)	17.3511(7)	17.8483(5)
b [Å]	21.729(2)	20.2180(8)	18.0932(6)
c [Å]	23.149(2)	23.0180(10)	21.7368(7)
α [°]	67.827(1)	91.574(1)	84.032(1)
β [°]	76.448(1)	103.591(1)	71.598(1)
γ [°]	73.341(1)	98.215(1)	85.337(1)
Volume [Å^3]	5959.3(8)	7752.5(6)	6615.7(4)
Z	1	1	1
$\rho_{calcd.}$ [Mgm^{-3}]	2.769	2.388	2.663
μ [mm^{-1}]	2.896	2.268	2.643
Crystal size [mm^3]	0.22 × 0.06 × 0.06	0.45 × 0.20 × 0.15	0.20 × 0.14 × 0.08
2θ range	0.96 to 27.01°	1.6 to 29.99°	0.99 to 27.02°
Reflections collected	57485	104693	63938
Reflections observed	15162	31157	19328
$[I > 2\sigma(I)]$	(R_{int} = 0.0685)	(R_{int} = 0.0541)	(R_{int} = 0.0460)
Refined parameters	1337	1534	1457
$R1$ $[I > 2\sigma(I)]$	0.0596	0.0582	0.0490
$wR2$ $[(I > 2\sigma(I)]$	0.1446	0.1452	0.1289
max. and min. residual electron density [eÅ^{-3}]	3.040 and −1.924	3.027 and −1.776 eÅ^{-3}	2.825 and −2.107

936 [ν(Mo=O)], 765, 661, 491, 380, 357, 280, 242, 204, 182, 150 cm^{-1}. – UV/Vis (cellulose): λ_{max} = ca. 270, ca. 325, ca. 360 nm. – $C_8H_{212}Mo_{54}Na_{32}O_{274}$ (10610.2): calcd. C 0.90, H 2.00, Na 6.94, H_2O 16.6; found C 1.15, H 2.00, Na 6.50, H_2O 14. – Cerimetric titration: 20±1 e.

X-ray Crystallography: Crystals were taken directly from the mother liquor and mounted on a glass fibre at 183 K. In case of **3**, the crystals were first dried and then mounted for X-ray investigations. Diffraction data were collected with a Bruker AXS three-circle diffractometer with a 1 K-CCD detector. The structures were solved by direct methods using SHELXS-97 and refined by full-matrix least squares with SHELXL-93/97. All non-hydrogen atoms were refined anisotropically. The assignment of Mo^V and Mo^{VI} centres, as well as the protonation, clearly follows from bond valence sum calculations[14] and is in agreement with the charge on the cluster anions and the fact that all the Mo^V centres form dumbbell-type $\{Mo_2^V\}$ units with covalent Mo–Mo single bonds. Due to disorder, not all cations could be localized. The crystallographic data for **1** and **2** are given in Table 2, for **3**, **4**, and **5** in Table 3. Further details on the crystal structure investigation of **2** may be obtained from the Fachinformationszentrum Karlsruhe, 76344 Eggenstein-Leopoldshafen, Germany [Fax: (internat.) + 49-(0)7247/808-666; E-mail: crysdata@fiz-karlsruhe.de] on quoting the depository numbers CSD-411693 and 411694. Crystallographic data (excluding structure factors) for compounds **1** and **3–5** have been deposited with the Cambridge Crystallographic Data Centre as supplementary publication no. CCDC-156640 (**1**), -156641 (**3**), -156642 (**4**), and -156643 (**5**). Copies of the data can be obtained free of charge on application to CCDC, 12 Union Road, Cambridge CB2 1EZ, UK [Fax: (internat.) + 44-1223/336-033; E-mail: deposit@ccdc.cam.ac.uk].

Acknowledgments

This work was supported by the Deutsche Forschungsgemeinschaft and the Fonds der Chemischen Industrie.

[1] A. Müller, P. Kögerler, C. Kuhlmann, *Chem. Commun.* **1999**, 1347.
[2] A. Müller, J. Meyer, E. Krickemeyer, C. Beugholt, H. Bögge, F. Peters, M. Schmidtmann, P. Kögerler, M. J. Koop, *Chem. Eur. J.* **1998**, *4*, 1000.
[3] M. Baumann, Diploma Thesis, University of Bielefeld, **1999**.
[4] While preparing this publication, C. Lu – a former Alexander von Humboldt fellow in our group at Bielefeld – obtained the compound $Na_{32}[H_4Mo_{54}O_{168}(H_3CCOO)_4]$ × ca. 120 H_2O, using a different preparation method (similar to that of our $\{Mo_{132}\}$-type keplerate $\{Mo_{132}\}$); the structural description, in spite of the correct structure determination, is different to that described here: W. Yang, C. Lu, X. Lin, H. Zhuang, *Chem. Commun.* **2000**, 1623.
[5] H. K. Chae, W. G. Klemperer, T. A. Marquart, *Coord. Chem. Rev.* **1993**, *128*, 209.
[6] Recently, we isolated crystals of another ring-shaped polyoxomolybdate. Preliminary investigations led to the (empirical) formula $Na_{28}[Mo^V_{20}Mo^{VI}_{28}O_{148}]$. The anion is built up from the three different building blocks $\{Mo_2*\}$, $\{Mo_4\}$, and $\{Mo_9*\}$.
[7] A. Müller, E. Krickemeyer, H. Bögge, M. Schmidtmann, F. Peters, *Angew. Chem.* **1998**, *110*, 3567; *Angew. Chem. Int. Ed.* **1998**, *37*, 3360–3363. Structural and topological features can be found in the following review article: A. Müller, H. Bögge, P. Kögerler, *Struct. Bonding* **2000**, *96*, 203.
[8] A. Müller, C. Serain, *Acc. Chem. Res.* **2000**, *33*, 1.
[9] This compound was isolated and reported for the first time as a by-product of the "open" keplerate, i. e. the basket-type analogue of the spherical $\{Mo_{132}\}$-type cluster (see also ref.[7]): A. Müller, S. Polarz, S. K. Das, E. Krickemeyer, H. Bögge, M. Schmidtmann, B. Hauptfleisch, *Angew. Chem.* **1999**, *111*, 3439; *Angew. Chem. Int. Ed.* **1999**, *38*, 3241–3245. An improved synthetic method is currently under investigation. Recently, S.-W. Zhang and co-workers isolated an isostructural compound with the acetate ligands being replaced by L-alanine (G. Liu, Y.-G. Wei, J. Liu, Q. Liu, S.-W. Zhang, Y.-Q. Tang, *J. Chem. Soc., Dalton Trans.* **2000**, 1013).
[10] D. J. Darensbourg, R. L. Gray, T. Delord, *Inorg. Chim. Acta* **1985**, *98*, L39.
[11] Furthermore, we succeeded in isolating a sodium salt of **2**, revealing a fascinating solid-state structure that will be discussed elsewhere in context with the different packing of the cluster anions in the respective lattices.
[12] T. Yamase, M. Sugeta, E. Ishikawa, *Acta Crystallogr., Sect. C* **1996**, *52*, 1869. The γ-$[Mo_8O_{28}]^{4-}$ anion has been postulated to be an intermediate in the related α–β interconversion: W. G. Klemperer, W. Shum, *J. Am. Chem. Soc.* **1976**, *98*, 8291.
[13] Preliminary mass spectra (ESI) of such solutions indicate the presence of hexa-, hepta-, and octamolybdate species.
[14] I. D. Brown, in: *Structure and Bonding in Crystals*, vol. II (Eds.: M. O'Keeffe, A. Navrotsky), Academic Press, New York, **1981**, p. 1–30.

Received February 13, 2001
[I01050]

Organotellurium(IV) Derivatives of Tetraphenyldichalcogenoimidodiphosphinates − The Crystal and Molecular Structure of $[C_4H_8TeI\{Ph_2(Se)PNP(Se)Ph_2\}]$, $[C_4H_8TeI\{Ph_2(S)PNP(S)Ph_2\}]$, $[C_4H_8Te\{Ph_2(S)PNP(S)Ph_2\}_2]$, $[C_8H_8TeI\{Ph_2(S)PNP(S)Ph_2\}]$, and $[O(TeC_4H_8)_2\{Ph_2(O)PNP(O)Ph_2\}]_2[I, I_3]$ Representing a Novel Type of Ring Systems

Verónica García-Montalvo,*[a] M. Kenia Zamora-Rosete,[a] Diego Gorostieta,[a] Raymundo Cea-Olivares,[a] R. Alfredo Toscano,[a] and Simón Hernández-Ortega[a]

Keywords: Tellurium / Chalcogens / Metallacycles / Imidodiphosphinates / Crystal structure

The synthesis of the following organotellurium(IV) compounds $[C_4H_8TeI\{Ph_2(Se)PNP(Se)Ph_2\}]$ (**2**), $[C_4H_8TeI\{Ph_2(S)PNP(S)Ph_2\}]$ (**3**), $[C_8H_8TeI\{Ph_2(S)PNP(S)Ph_2\}]$ (**4**), $[C_4H_8Te\{Ph_2(S)PNP(S)Ph_2\}_2]$ (**5**), and $[O(TeC_4H_8)_2\{Ph_2(O)PNP(O)Ph_2\}]_2[I, I_3]$ (**6**) was achieved. These compounds have been characterized by microanalysis, multielement NMR and IR spectroscopy, positive ion FAB mass spectrometry and single-crystal X-ray diffraction analysis. The solid-state structures show that the coordination geometry at the tellurium center in every derivative can be described as a distorted pseudo-trigonal bipyramid, in which the lone-pair of electrons is supposed to occupy an equatorial position. The selenium and sulfur ligands exhibit an aniso-bidentate chelating coordination mode on interaction with the tellurium center. When the aniso-bonded donor atoms are included in the coordination sphere, the environment about Te becomes distorted square-pyramidal for the monochelate derivatives **2**–**4** and distorted octahedral for the bis(chelate) compound **5**. In compound **6**, two oxygen ligands act as bridges between two $C_4H_8Te–O–TeC_4H_8$ units, forming a 16-membered cationic ring. The anions, I^- and I_3^-, are located above and below the twisted ring with Te···I interactions ranging from 3.532(2) to 3.902(3) Å.

Introduction

We became interested in the chemistry of organotellurium(IV) in conjunction with our studies on the coordination chemistry of heavy main group elements with tetraphenyldichalcogenoimidodiphosphinate ligands. It became apparent that the $[Ph_2(Q)PNP(Q')Ph_2]^-$ [Q/Q′ = O/O (**1a**), S/S (**1b**), Se/Se (**1c**), O/S (**1d**), S/Se(**1e**)] ligands are ideal for studying the influence of distinct donor-atom sets and the stereochemical influence of the electron lone-pair on the geometry of main group metal complexes.[1−5] This is because they offer the opportunity to vary both the donor atoms and because of the large degree of conformational freedom observed in the variable M−Q−P angle and P−N−P conjugated systems. Some interesting and unusual examples of compounds containing these ligands are certain lanthanide complexes,[1] the quasi-ideal *trans*-octahedral organotin compounds,[2] the true square-planar $[Sn\{Ph_2(Se)PNP(Se)Ph_2\}_2]$,[3] $[Te\{Ph_2(Q)PNP(Q)Ph_2\}_2]$ (Q= S[6] and Se[7]), $[Se\{Ph_2(Q)PNP(Q)Ph_2\}_2]$ (Q= S[8] and Se[9]) complexes, and the tellurium-containing 12-membered ring, $[4\text{-}MeOC_6H_4Te\{Ph_2(S)PNP(S)Ph_2\}]_2$.[7]

We decided to synthesize new 2,2-dihydrobenzotellurophene and 1,1-tetrahydrotellurophene derivatives employing the symmetrical imidodichalcogenidephosphinates **1a**−**c** in order to study the effect of the donor atom strength on the tellurium geometry and the comparison with analogous organotellurium(IV) derivatives containing oxygen- sulfur- and selenium-based ligands such as dithio-[10−12] and monothiocarbamates,[13] dithiophosphinates,[12] dithiophosphates,[14] carboxylates,[15] $R_2(Q)PNP(Q')R_2$,[6,7,16,17] and $R_2(S)P(CH_2)_2P(S)R_2$,[17] etc.

Here we report five new organotellurium(IV) compounds, $[C_4H_8TeI\{Ph_2(Se)PNP(Se)Ph_2\}]$ (**2**), $[C_4H_8TeI\{Ph_2(S)PNP(S)Ph_2\}]$ (**3**), $[C_8H_8TeI\{Ph_2(S)PNP(S)Ph_2\}]$ (**4**), $[C_4H_8Te\{Ph_2(S)PNP(S)Ph_2\}_2]$ (**5**), and the ionic ring $[O(TeC_4H_8)_2\{Ph_2(O)PNP(O)Ph_2\}]_2[I, I_3]$ (**6**). They have been characterized by microanalysis, multielement NMR and IR spectroscopy, positive ion FAB mass spectrometry and single-crystal X-ray diffraction analysis.

Results and Discussion

The reported compounds were obtained by the reaction of $C_4H_8TeI_2$ or $C_8H_8TeI_2$ with the appropriate sodium or potassium salt of the ligands in either a twofold excess or in equimolecular amounts. The mono- or disubstituted derivatives were isolated from the selenium and sulfur ligands [RTeIL] [R = C_4H_8, C_8H_8 (**2**−**4**)] and $[C_4H_8TeL_2]$ (**5**).

[a] Instituto de Química, Universidad Nacional Autónoma de México,
Circuito Exterior, Ciudad Universitaria, México, 04510, D.F., Mexico
Fax: (internat.) + 52-5/622-4505
E-mail: vgm@servidor.unam.mx

 © WILEY-VCH Verlag GmbH, 69451 Weinheim, 2001 1434−1948/01/0909−2279 $ 17.50+.50/0

As byproducts the known Te^{II} bis(chelates), $[Te\{Ph_2(Q)PNP(Q)Ph_2\}_2]$ (Q= S[6] and Se[7]), were also obtained. By using the oxygen ligand, only the unexpected 16-membered ionic ring $[O(TeC_4H_8)_2\{Ph_2(O)PNP(O)Ph_2\}]_2^{2+}$ (**6**) was isolated. This compound is probably formed from a 1,1-oxydiiodine ditellurium compound ($[C_4H_8TeI]_2O$) in the reaction mixture as the analogous 1,1-oxydibromide[18] was isolated previously from aqueous alkali solution. The formation of **6** may be explained by the fact that the $C_4H_8TeI_2$ was added to the non-anhydrous alkali solution in which the ligand salt was synthesized. Two of the oxygen ligands could then react with the $[C_4H_8TeI]_2O$ to form the ring system. All the compounds are soluble in common organic solvents (CH_2Cl_2, $CHCl_3$, C_6H_6). However, in solution they undergo rapid exchange and reductive elimination, such as has been observed previously in many chalcogen-bonded organotellurium(IV) derivatives.[12−14,16b,16c,17] Due to the difficulty of relying on the characterization in solution, every effort was made to obtain X-ray quality crystals of each compound.

The NMR spectroscopic data presented in the Exp. Sect. were assigned based on the spectra recorded immediately after dissolution in $CDCl_3$ solution. The ^1H and ^{13}C NMR spectra show the expected methylene (and also aromatic for **4**) protons and carbon atoms from the organoyltellurium moiety, as well as the phenyl resonance from the ligands. The signal of the CH_2 group attached to the tellurium center experiences a small upfield shift relative to that of the starting materials $C_4H_8TeI_2$ and $C_8H_8TeI_2$. The peaks of the 16-membered ring are the most upfield-shifted. The peaks in the phenyl region of the spectra are similar to those found for other derivatives containing imidophosphinates, but are poorly resolved so that the phosphorus-carbon coupling was ill-defined in some cases and the *ipso*-carbon resonances are not observed in others. In all cases the spectra recorded after one day, in the case of the selenium compound after a few hours, show more signals than those of the initially dissolved compound. According to the observed chemical shifts, some of these peaks may be attributable to the $[Te\{Ph_2(Q)PNP(Q)Ph_2\}_2]$ (Q= S[6] and Se[7]) species and the free acid ligands. The ^{31}P resonances are upfield-shifted by about 15 ppm relative to the corresponding free-acid ligand for all the compounds. The signals are closer to the chemical shift of the corresponding deprotonated ligands. The ^{125}Te resonance of C_4H_8TeIL and $C_4H_8TeL_2$ are shifted downfield compared to that of $C_4H_8TeI_2$ (δ = 782 ppm). This is in contrast to the upfield shift observed for the related $C_4H_8TeI(S_2PR_2)$ (R = Me, Et)[12] and some R_2TeL_2 and R_2TeXL (L = $SOCNR_2$,[10b][10e] S_2CNR_2 [13]) species. Some other analogous derivatives also exhibit deshielded ^{125}Te resonances relative to R_2TeI_2, such as R_2TeIL (R = Me and L = S_2COR,[10c] S_2POGO[10a] with G = alkylene moieties) and R_2TeL_2 (R = *p*-$MeOC_6H_4$ and L = dimethyl- and diethyldithiocarbamates).[10d] The ^{125}Te resonance of the 16-membered ionic compound is shifted upfield compared to that of $C_4H_8TeI_2$.

The positive ion FAB mass spectra recorded immediately after dissolving the compounds in CH_2Cl_2 show low-intensity signals for the corresponding molecular ions, but rather intense peaks of fragments containing tellurium, i.e. *m*/*z* = 186 $[C_4H_8Te]^+$, 313 $[C_4H_8TeI]^+$, $[C_4H_8Te\ L]^+$ with L = **1a** (*m*/*z* = 416), **1b** (*m*/*z* = 448), and **1c** (*m*/*z* = 544). All of the observed signals exhibit the expected isotopic distribution patterns.

The infrared spectra of **2** to **6** exhibit strong absorption bands in the range of 1259 to 1219 cm^{-1} for the $\nu(P_2N)$ vibrations and two characteristic bands for phosphorus−donor atom stretching vibrations {1122 and 1095 cm^{-1} [ν(PO)] for **6**, two ν(PS) bands in the range 554−517 for **3**−**5**, and 437 [ν(PSe)] for **2**}.

Structural Description

Figure 1 shows the molecular structures and atomic labeling scheme for derivative **2**, while those of **3** and **4** are illustrated in Figure 2. The molecular structure of **5** is given in Figure 3, and that of $[O(TeC_4H_8)_2\{Ph_2(O)PNP(O)Ph_2\}][I, I_3]$ (**6**) is shown in Figure 4. Selected bond lengths and angles are summarized in Table 1.

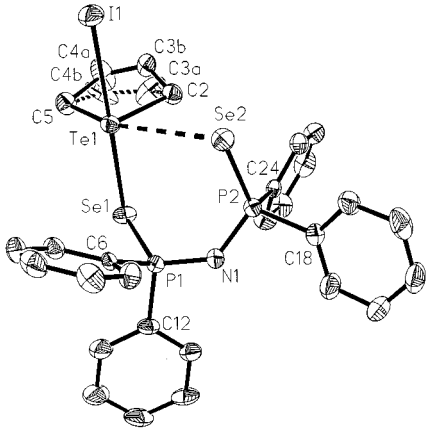

Figure 1. Molecular structure of $[C_4H_8TeI\{Ph_2(Se)PNP(Se)Ph_2\}]$ (**2**); the ellipsoids enclose a 30% probability

The coordination geometry at the tellurium center in every compound can be described as the sawhorse structure typical of tellurium(IV) compounds in which the lone-pair of electrons is supposed to occupy an equatorial position in a distorted trigonal bipyramid.[10−16c] The carbon atoms occupy the remaining equatorial positions with an average C−Te−C angle of 84.8°. The average Te−C bond length (2.135 Å) is within the range of the values observed in related organotellurium(IV) derivatives with chalcogen-containing ligands.[10−18]

In compounds containing sulfur and selenium donor atoms (**2**−**5**), the ligands display an asymmetrical chelating coordination mode on interaction with the tellurium center. This results in two sets of Te−donor atom bond lengths. The short Te−S bond lengths cover the range 2.61−2.67 Å, comparable with the values reported for related R_2TeXL structures containing analogous $R_2(Q)PNP(Q')R_2$,[6,7,16,17]

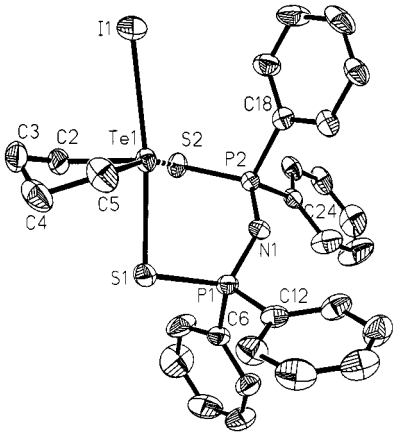

3

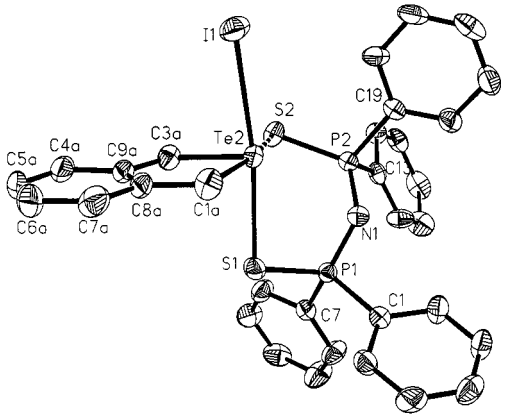

4

Figure 2. Molecular structures of $[C_4H_8TeI\{Ph_2(S)PNP(S)Ph_2\}]$ (**3**) and $[C_8H_8TeI\{Ph_2(S)PNP(S)Ph_2\}]$ (**4**); the ellipsoids enclose a 30% probability

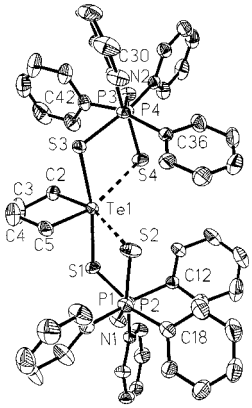

Figure 3. Molecular structures of the bis(chelate) compound $[C_4H_8Te\{Ph_2(S)PNP(S)Ph_2\}_2]$ (**5**); the ellipsoids enclose a 30% probability

and $R_2(S)P(CH_2)_2P(S)R_2$ [17] ligands. The short Te−Se bond length [2.721(1) Å] is slightly shorter than the values observed in $[Te\{R_2(Se)PNP(Se)R_2\}_2]$ [R = Ph (av.

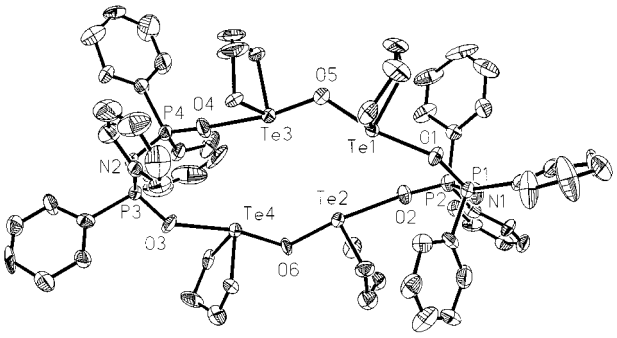

Figure 4. Molecular structure of the cation $[O(TeC_4H_8)_2\{Ph_2(O)PNP(O)Ph_2\}]_2^{2+}$; the ellipsoids enclose a 30% probability

2.797 Å)[6] and R = *i*Pr (av. 2.804 Å)[16d]]. The weakly bonded donor atoms are attached to the tellurium atom at larger Te···S distances ranging from 3.282(2) to 3.451(2) Å and at a Te···Se length of 3.4650(12) Å. The normalized Pauling partial bond orders[16c] of these longer Te···S/Se bonds are within the range of 0.16 to 0.27, that of Te···Se being 0.19. Thus, they are still compatible with their being part of the coordination sphere, and hence aniso-bonded. The S−Te−S bite angles in complexes **3**−**5** are similar to those found in the analogous $[Me_2Te\{Ph_2(S)PNP(S)Ph_2\}_2]$ and $[Me_2TeI\{Ph_2(S)PNP(S)Ph_2\}]$.[16c]

In the bis(chelate) derivative **5**, the two strongly bonded sulfur atoms occupy the axial positions, while in the mono-substituted compounds the axial sites are occupied by the iodine atom and the strongly bonded donor atom. The I−Te−Se axial angle [177.51(3)°] is considerably larger than the I−Te−S angle [171.8(1)°], while the S−Te−S axial angle is smaller [170.59(5)°]. When the aniso-bonded donor atoms are included in the coordination sphere, the environment about Te becomes distorted square-pyramidal in the mono derivatives **2**−**4** and distorted octahedral in the bis-(chelate) compound **5**.

The Te−I bond lengths of RTeIL (**2** and **4**) are similar to those in $C_4H_8TeI_2$,[12] $C_8H_8TeI_2$ [19] and related R_2TeI_x species.[20] This and the generally longer Te−S bond in compounds containing imidodiphosphinates suggest a lower *trans* influence than in analogous halodithiocarbamates, -monothiocarbamates and dithiocarbonates.[10−13,15] However, the most remarkable difference with these 1,1-dithiolate compounds is that the imidophosphinate compounds do not exhibit any intermolecular interactions.

The TeS_2P_2N chelate rings of **3** and **4** are arranged in a distorted boat conformation with the tellurium and nitrogen atoms at the apices.[21] However, the $TeSe_2P_2N$ and TeS_2P_2N rings of the remaining chelate compounds **2** and **5** exhibit a folded geometry with one phosphorus atom lying essentially within the coordination plane and with the P−N−P−Se/S plane folded by 120.2° out of the coordination plane Te1−Se1−Se2−P2 for **2**, and by 40.7° and 129.9° out of the planes Te1−S1−S2−P1 and Te1−S3−S4−P4 for **5**. The ring bond lengths are consistent with some localization of the bonding, i.e. the short

Table 1. Selected bond lengths [Å] and angles [°] for compounds **2**−**6**

	2 (Q = Se)	**3** (Q = S)	**4** (Q = S)	**5** (Q = S)		**6**
Te−Q1	2.721(1)	2.616(3)	2.622(2)	2.670(2)	Te1−O1	2.27(2)
Te···Q2	3.465(2)	3.435(3)	3.282(2)	3.300(2)	Te2−O2	2.42(2)
Te−Q3				2.643(2)	Te4−O3	2.33(2)
Te···Q4				3.451(2)	Te3−O4	2.45(2)
Te−I1	2.967(1)	2.946(1)	2.922(1)		Te1−O5	1.99(2)
Te−C2	2.149(9)	2.144(9)	2.165(8)[a]	2.152(7)	Te3−O5	1.96(2)
Te−C5	2.162(9)	2.141(1)	2.136(8)[a]	2.153(6)	Te2−O6	1.97(2)
P1−Q1	2.226(2)	2.058(3)	2.058(3)	2.060(2)	Te4−O6	2.01(2)
P2−Q2	2.121(2)	1.973(3)	1.986(3)	1.966(2)	P1−O1	1.55(2)
P3−Q3				2.056(2)	P2−O2	1.52(2)
P4−Q4				1.970(2)	P3−O3	1.51(2)
P1−N1	1.572(7)	1.571(8)	1.570(6)	1.581(5)	P4−O4	1.479(2)
P2−N1	1.614(7)	1.604(8)	1.607(6)	1.614(5)	P1−N1	1.56(2)
P3−N2				1.574(5)	P2−N1	1.61(2)
P4−N2				1.611(5)	P3−N2	1.57(2)
C2−Te−C5	84.3(4)	83.5(5)	85.9(3)[a]	84.8(3)	P4−N2	1.61(2)
C2−Te−Q1	89.9(3)	86.8(3)	84.5(2)[a]	83.7(2)	av. Te−C	2.121
C5−Te−Q1	87.4(3)	87.2(4)	86.1(2)[a]	89.3(2)	av. Te···I	3.682
C2−Te−Q3				89.7(2)	Te1−O5−Te3	127.9(9)
C5−Te−Q3				83.4(2)	Te2−O6−Te4	124.9(9)
Q1−Te···Q2	93.6(3)	81.9(3)	88.7	91.2(5)	O1−Te1−O5	166.5(7)
Q1−Te−Q3				170.59(5)	O2−Te2−O6	170.1(8)
Q3−Te···Q4				87.6(5)	O4−Te3−O5	170.7(8)
Q1−Te−I1	177.51(3)	172.73(7)	171.8(1)		O3−Te4−O6	168.3(7)
Q2···Te−I1	88.7(3)	97.3(7)	95.9		Te1−P1−O1	139.1(10)
P1−Q1−Te	99.55(7)	99.3(2)	101.6(1)	106.52(9)	Te2−P2−O2	169.8(14)
P2−Q2···Te	97.7(7)		86.30	110.40(9)	Te4−P3−O3	140.7(13)
P3−Q3−Te				108.64(7)	Te3−P4−O4	176.9(13)
P4−Q4···Te				103.80(7)	N1−P1−O1	120.5(13)
N1−P1−Q1	118.7(3)	117.4(3)	117.3(3)	117.2(2)	N1−P2−O2	120.4(12)
N1−P2−Q2	119.3(3)	119.3(3)	118.4(2)	118.3(2)	N2−P3−O3	120.5(12)
N2−P3−Q3				119.2(2)	N2−P4−O4	117.2(11)
N2−P4−Q4				119.4(2)	P1−N1−P2	131.4(17)
P1−N1−P2	132.1(5)	138.9(5)	140.1(4)	129.9(3)	P3−N1−P4	129.2(13)
P3−N1−P4				132.5(3)	I2−I3−I4	177.5(16)

[a] In molecule **4**, the C2 and C5 labels correspond to the C1a and C3a atoms, respectively.

and long bonds alternate through the six-membered ring (see Table 1).

The molecular structure of $[O(TeC_4H_8)_2\{Ph_2(O)PNP(O)Ph_2\}]_2[I, I_3]$ (**6**) is shown in Figure 4. In the 16-membered cationic ring two oxygen ligands behave as bridges between two $C_4H_8Te-O-TeC_4H_8$ units. The Te−O(ligand) bond lengths cover the range 2.273(17) to 2.453(17) Å. These bonds are slightly longer than the sum of the covalent radii,[22] and are also longer than the corresponding distances found in chelates like $[Me_2TeCl\{Ph_2(O)PNP(S)Ph_2\}]$,[16c] $[Ph_2Te(O_2CR)_2]$ (R = CH_3, CCl_3),[15b,15c] and $[C_4H_8Te(O_2CPh)_2]$.[15a] The average Te−O bond length in the $C_4H_8Te-O-TeC_4H_8$ moiety is 1.988 Å. The Te−O−P angles (av. 154.5°) are notably larger than the observed Te−S−P angles (av. 104.84°) in the complexes containing the sulfur-bridge ligand, i.e. $[4\text{-}MeOC_6H_4Te\{Ph_2(S)PNP(S)Ph_2\}]_2$ [7] and $[(4\text{-}MeOC_6H_4TeCl_3)_2\{\mu\text{-}Ph_2(S)PCH_2CH_2P(S)Ph_2\}]$.[17] The average of the axial O−Te−O angles is 168.9°, comparable with the values observed in related tellurium(IV) sawhorse structures.[10−18] The 16-membered ring adopts a twisted conformation. The two anions I^- and I_3^- are located above and below the 16-membered ring $[O(TeC_4H_8)_2\{Ph_2(O)PNP(O)Ph_2\}]_2^{2+}$ with Te···I1 and Te···I2 distances ranging from 3.532(2) to 3.902(3) Å, within the sum of the van der Waals radii (4.35 Å).[23]

Conclusion

The isolation and spectroscopic characterization of mono- and disubstituted tetrahydro- and benzodihydrotelluropheno-containing symmetric $[Ph_2(Q)PNP(Q)Ph_2]^-$ ligands was achieved despite the propensity for such species to undergo disproportionation and reductive elimination in solution. The selenium and sulfur ligands act as anisobidentate chelate ligands such as was observed previously in related organotellurium derivatives containing 1,1-dithio- or monothio ligands, carboxylates, and asymmetric $R_2(Q)PNP(Q')R_2$.[10−16] The bite angles and Te−Q bond lengths are larger than those in compounds with 1,1-ligands, so that the angles about Te are less distorted. No

intermolecular interactions involving iodine or donor atoms were observed. The employment of the oxygen ligand leads to the formation of a novel 16-membered cationic ring $[O(TeC_4H_8)_2\{Ph_2(O)PNP(O)Ph_2\}]_2^{2+}$ (**6**) in which the ligand acts as a bridge. This compound may be formed from the two ligands and the $[C_4H_8TeI]_2O$ formed in the reaction mixture.

Experimental Section

General Remarks: Chemicals of commercial grade were purchased from Aldrich and were used as supplied. The compounds $C_4H_8TeI_2$ and $C_8H_8TeI_2$ were prepared according to the methods described by Al-Rubaie et al.[24] and by Ziolo et al.[19b] The ligand salts were prepared by treatment of the free ligands with potassium ethoxide or sodium hydroxide. The FAB mass spectra were measured using a 3-nitrobenzyl alcohol support in the positive ion mode with a Jeol JMS-SX102A instrument. The ^1H (300 MHz), ^{13}C (75 MHz), ^{31}P (121 MHz), ^{77}Se (57 MHz) and ^{125}Te (94 MHz) NMR spectra were recorded in $CDCl_3$ with a Jeol Eclipse+ 300 spectrometer at room temperature using as external references TMS, 85% H_3PO_4, $TeCl_4$, and Ph_2Se_2. The IR spectra (KBr discs) were recorded with a Nicolet FT-IR Magna 750 spectrometer. Microanalyses were performed by Galbraith Laboratories, Inc., Knoxville, TN.

$[C_4H_8TeI\{Ph_2(Se)PNP(Se)Ph_2\}]$ (2): A solution of $C_4H_8TeI_2$ (0.25 g, 0.57 mmol) in dichloromethane was added to freshly prepared $K[Ph_2(Se)PNP(Se)Ph_2]$ (0.33 g, 0.57 mmol). The mixture was stirred and elemental Te precipitated almost immediately from the solution. The mixture was filtered after 10 min of stirring and the filtrate was concentrated by pumping off the solvent. A layer of *n*-hexane was allowed to diffuse slowly into the concentrated solution leading to yellow crystals of $[C_4H_8TeI\{Ph_2(Se)PNP(Se)Ph_2\}]$ (**2**) and orange-yellow crystals of $[Te\{Ph_2(Se)PNP(Se)Ph_2\}_2]$[7] [m.p. 266 °C, ref.[7] 275 °C; ^{31}P NMR ($CDCl_3$): δ = 23.6 (s) (ref.[7] δ = 24.4)]. − **2**: Yield: 0.31 g (64.6%); m.p. (dec.) 153−154 °C. −IR (KBr): $\tilde{\nu}$ =1220 cm^{-1} s [ν(PN)], 437 m [ν(PSe)]. − MS (FAB^+, $CHCl_3$): *m*/*z* = 186 [$C_4H_8{}^{130}Te^+$], 313 [$C_4H_8{}^{130}TeI^+$], 544 [$(^{80}SePPh_2)_2N^+$], 672 [$^{130}Te(^{80}SePPh_2)_2N^+$], 728 [$C_4H_8{}^{130}Te(^{80}SePPh_2)_2N^+$], 854 [$C_4H_8{}^{130}TeI(^{80}SePPh_2)_2N^+$]. − ^1H NMR ($CDCl_3$): δ = 2.16−3.0 (m, 4 H, $TeCH_2CH_2$), 3.3−3.8 (m, 4 H, $TeCH_2$) 7.37 (m, 12 H, Ph-H_{m+p}), 7.9 (m, 8 H, Ph-H_o). − ^{13}C NMR ($CDCl_3$): δ = 33.9 ($TeCH_2CH_2$), 45.34 ($TeCH_2$), 128.3 (Ph-C_m), 130.68 (Ph-C_p), 131.4−131.1 (Ph-C_o). − ^{31}P NMR ($CDCl_3$): δ = 35.5 (br. s). − ^{77}Se NMR ($CDCl_3$): δ = −146.64 (d). − ^{125}Te NMR ($CDCl_3$): δ = 797 (t). − $C_{28}H_{28}INP_2Se_2Te$ (852.9): calcd. C 39.43, H 3.31; found C39.17, H 3.19. − A similar procedure was attempted starting from $C_8H_8TeI_2$ and the ligand, however only the tellurium(II) derivative $[Te\{Ph_2(Se)PNP(Se)Ph_2\}_2]$,[7] was isolated.

$[C_4H_8TeI\{Ph_2(S)PNP(S)Ph_2\}]$ (3): This compound was synthesized by placing $C_4H_8TeI_2$ (0.5 g, 1.14 mmol), $K[Ph_2(S)PNP(S)Ph_2]$ (0.55 g, 1.14 mmol), and approximately 25 mL of dichloromethane in a flask, and stirring this mixture was stirred at room temperature for 30 min. It was then filtered and the filtrate was concentrated by pumping off all the solvent. The compounds were crystallized by allowing a layer of *n*-hexane to diffuse slowly into a concentrated solution of the remaining solid in CH_2Cl_2. Yield: 0.72 g (82.9%); m.p. (dec.) 146−147 °C. − IR (KBr): $\tilde{\nu}$ = 1216 cm^{-1} vs [ν(PN)], 544 s, 517 m [ν(PS)]. − MS (FAB^+, $CHCl_3$): *m*/*z* = 186 [$C_4H_8{}^{130}Te^+$], 448 [$(SPPh_2)_2N^+$], 578 [$^{130}Te(SPPh_2)_2N^+$], 634 [$C_4H_8{}^{130}Te(SPPh_2)_2N^+$]. −$^1H$ NMR ($CDCl_3$): δ = 2.56−2.78 (m, 4 H, $TeCH_2CH_2$), 3.3−3.6 (m, 4 H, $TeCH_2$) 7.36 (m, 12 H, Ph-$CH_{m,p}$), 7.88 (m, 8 H, Ph-CH_o). − ^{13}C NMR ($CDCl_3$): δ = 33.6 ($TeCH_2CH_2$), 46.06 ($TeCH_2$), 128.08 (Ph-C_m), 130.4 (Ph-C_p), 131.0 (Ph-C_o). − ^{31}P NMR ($CDCl_3$): δ = 45 (br. s). −^{125}Te NMR ($CDCl_3$): δ = 834.2 (t). − $C_{28}H_{28}INP_2S_2Te$ (759.11): calcd. C 44.30, H 3.72; found C43.99, H 3.60.

$[C_8H_8TeI\{Ph_2(S)PNP(S)Ph_2\}]$ (4): This compound was obtained according to the procedure described for **3** from $C_8H_8TeI_2$ (0.5 g, 1.03 mmol) and $K[Ph_2(S)PNP(S)Ph_2]$ (0.49 g, 1.03 mmol). Yield: 0.51 g (61.3%); m.p. (dec.) 127−129 °C. − IR (KBr): $\tilde{\nu}$ = 1226 cm^{-1} s [ν(PN)], 546 m, 525 s [ν(PS)]. − MS (FAB^+, $CHCl_3$): *m*/*z* = 234 [$C_8H_8{}^{130}Te^+$], 361[$C_8H_8{}^{130}TeI^+$], 448 [$(SPPh_2)_2N^+$], 682 [$C_8H_8{}^{130}Te(SPPh_2)_2N^+$]. − ^1H NMR ($CDCl_3$): δ = 4.99 (m, 4 H, $TeCH_2$), 7.14 (m, 4 H, C_6H_4), 7.35 (m, 12 H, Ph-$CH_{m,p}$), 7.9 (m, 8 H, Ph-CH_o). −^{13}C NMR ($CDCl_3$): δ = 49.92 ($TeCH_2$), 127.7 ($C_{4,7}$) 128.27 (Ph-C_m), 129.8 ($C_{5,6}$), 130.9 (Ph-C_p), 131.2 (Ph-C_o), 139.2 ($C_{3a,7a}$). −^{31}P NMR ($CDCl_3$): δ = 42.3 (br. s). − ^{125}Te NMR ($CDCl_3$): δ = 760 (m). − $C_{38}H_{28}INP_2S_2Te$ (807.16): calcd. C 47.62, H 3.50; found C47.36, H 3.37

$[C_4H_8Te\{Ph_2(S)PNP(S)Ph_2\}_2]$ (5): This compound was prepared as described for **3** from $C_4H_8TeI_2$ (0.5 g, 1.14 mmol) and $K[Ph_2(S)PNP(S)Ph_2]$ (1.10 g, 2.28 mmol). Yield: 0.86 g (69.6%); m.p. (dec.) 135−137 °C. − IR (KBr): $\tilde{\nu}$ = 1219 cm^{-1} s [ν(PN)], 554 s, 508 m [ν(PS)]. −MS (FAB^+, $CHCl_3$): *m*/*z* = 186 [$C_4H_8Te^+$], 448 [$(SPPh_2)_2N^+$], 578 [$^{130}Te(SPPh_2)_2N^+$], 634 [$C_4H_8{}^{130}Te(SPPh_2)_2N^+$]. − ^1H NMR ($CDCl_3$): δ = 2.30 (br. s, 4 H, $TeCH_2CH_2$), 3.18 (br. s, 4 H, $TeCH_2$), 7.27 (m, 12 H, P-$CH_{m,p}$), 7.88 (m, 8 H, P-CH_o). −^{13}C NMR ($CDCl_3$): δ = 33.21 ($TeCH_2CH_2$), 47.46 ($TeCH_2$), 128.2 (Ph-C_m), 130.12 (Ph-C_p), 131.3 (Ph-C_o). − ^{31}P NMR ($CDCl_3$): δ = 44.2 (br. s). − ^{125}Te NMR ($CDCl_3$): δ = 856 (m). − $C_{52}H_{48}N_2P_4S_4Te$ (1080.71): calcd. C 57.79, H 4.8; found C57.51, H 4.71

$[O(TeC_4H_8)_2\{Ph_2(O)PNP(O)Ph_2\}]_2[I, I_3]$ (6): This compound was prepared as described for **3** from $C_4H_8TeI_2$ (0.8 g, 1.83 mmol), freshly prepared $Na[Ph_2(O)PNP(O)Ph_2]$ (0.8 g, 1.83 mmol), and approximately 25 mL of ethanol. $[O(TeC_4H_8)_2\{Ph_2(O)PNP(SO)Ph_2\}]_2$ (**6**) was isolated as dark brown crystals from the bottom of the crystallization flask. Yield 0.79 g (20.5%); m.p. (dec.) 137 °C. − IR (KBr): $\tilde{\nu}$ = 1259 cm^{-1}s [ν(PN)], 1122 vs, 1095 s [ν(PO)]. − MS (FAB^+, $CHCl_3$): *m*/*z* = 416 [$(OPPh_2)_2N^+$], 602 [$C_4H_8{}^{130}Te(OPPh_2)_2N^+$], 760 [$^{130}Te_4O_6P_4N_2^+$]. − ^1H NMR ($CDCl_3$): δ = 2.21 (m, 4 H, $TeCH_2CH_2$), 2.97 (m, 4 H,$TeCH_2$), 7.26 (m, 12 H, P-$CH_{m,p}$), 7.73 (m, 8 H, P-CH_o). − ^{13}C NMR ($CDCl_3$): δ = 29.8 ($TeCH_2CH_2$), 31.27 ($TeCH_2$), 127.96 (Ph-C_m), 130.33 (Ph-C_p), 131.39 (Ph-C_o). − ^{31}P NMR ($CDCl_3$): δ = 14.3 (s). − ^{125}Te NMR ($CDCl_3$): δ = 777.2 (br. s). − $C_{64}H_{72}I_4N_2O_6P_4Te_4$ (2107.18): calcd. C 36.48, H 3.44; found C36.11, H 3.25.

X-ray Crystallographic Study: Suitable crystals were mounted on glass fibers and sealed with epoxy glue. Data were collected at room temperature on a Siemens P4/PC diffractometer with graphite-monochromated Mo-K_α radiation (λ = 0.71073). Details of the data collections and refinements are summarized in Table 2. Data were collected using the ω-scan mode (3° ≤ 2θ ≤ 50°). The intensity data (except those for **5**) were corrected for absorption (Ψ-scan). The structures were solved by direct methods using SHELXS-97[25] (for **2**, **5** and **6**) and SIR-97[26] (for **3** and **4**). They were all refined by full-matrix least-squares calculations using the program system SHELXL-97.[27] Non-hydrogen atoms were refined anisotropically. In the case of **2**, there was disorder involving atoms

Table 2. Crystallographic data for compounds **2**−**6**

	2	**3**	**4**	**5**	**6**
Empirical formula	$C_{28}H_{28}INP_2Se_2Te$	$C_{28}H_{28}INP_2S_2Te$	$C_{32}H_{28}INP_2S_2Te$	$C_{52}H_{48}N_2P_4S_4Te$	$C_{64}H_{72}I_4N_2O_6P_4Te_4$
Color; habit	yellow; prism	yellow; prism	yellow; prism	yellow; prism	purple; prism
Molecular mass	852.87	759.07	807.1	1080.64	2107.12
Crystal size [mm]	0.64 × 0.40 × 0.24	0.30 × 0.16 × 0.16	0.38 × 0.10 × 0.06	0.28 × 0.22 × 0.08	0.40 × 0.24 × 0.24
Crystal system	monoclinic	monoclinic	monoclinic	monoclinic	orthorhombic
Space group	$P2_1/c$ (no. 14)	Cc (no. 9)	$P2_1/c$ (no.14)	$P2_1/c$ (no.14)	$P2_12_12_1$ (no.19)
a [Å]	14.450(3)	10.738(5)	16.331(2)	14.890(3)	14.026(2)
b [Å]	10.126(1)	14.479(5)	8.493(2)	10.748(3)	20.924(4)
c [Å]	20.615(3)	19.604(5)	23.312(4)	32.311(7)	25.114(2)
α [°]	90	90	90	90	90
β [°]	94.74(1)	90.860(5)	91.45(2)	91.08(1)	90
γ [°]	90	90	90	90	90
Z	4	4	4	4	4
V [Å^3]	3006.1(8)	3047.6(2)	3232.4(2)	5170(2)	7376.8(2)
μ [mm^{-1}]	4.563	2.249	2.126	0.897	3.74
Transmission, max/min	0.140/0.079	0.7149/0.5579	0.8830/0.4988		0.372/0.225
Reflections collected	5499	2841	5874	9487	7117
Independent reflections	5275 (R_{int} = 0.0411)	2841 (R_{int} = 0.0)	5661 (R_{int} = 0.088)	9110 (R_{int} = 0.1084)	7117 (R_{int} = 0.0)
Number of parameters	336	317	353	568	756
$R(F_o)$[a]	0.0479	0.0328	0.0397	0.0483	0.0651
$Rw(F_o)$[b]	0.0967	0.0703	0.0736	0.0984	0.1464
Goodness-of-fit	1.026	0.930	0.831	0.847	1.062

[a] $R1 = \Sigma||F_o| - |F_c||/\Sigma|F_o|$. − [b] $wR2 = [\Sigma w(F_o^2 - F_c^2)^2/\Sigma w(F_o^2)^2]^{1/2}$.

C3 and C4 from the C_4H_8Te moiety. The best solution was obtained with occupancies of 0.53 for C4A and C3B and 0.47 for C3A and C4B. The hydrogen atoms were calculated as a riding model with fixed isotropic U. The calculated absolute structure parameter for **3** was η = 0.0033 (0.0311).[28]

Crystallographic data (excluding structure factors) for the structures reported in this paper have been deposited with the Cambridge Crystallographic Data Centre as supplementary publication nos. CCDC-153533 (**2**), -153534 (**3**), -153535 (**4**), -153536 (**5**), -153537 (**6**). Copies of the data can be obtained free of charge on application to CCDC, 12 Union Road, Cambridge CB2 1EZ, UK [Fax: (internat.) + 44-1223/336-033; E-mail: deposit@ccdc.cam.ac.uk].

Acknowledgments

We are grateful to the DGAPA-UNAM for the project grant IN15898.

[1] I. Rodríguez, C. Alvarez, J. Gómez-Lara, R. Cea-Olivares, *Lanthanide Actinide Res.* **1985− 1986**, *1*, 253−256.
[2] See, for example: C. Silvestru, I. Haiduc, R. Cea-Olivares, A. Zimbron, *Polyhedron* **1994**, *13*, 3159−3165.
[3] [3a] R. Cea-Olivares, V. García-Montalvo, J. Novosad, J. D. Woollins, A. M. Z. Slawin, G. Espinosa-Pérez, P. García y García, *Chem. Commun.* **1996**, 519−520. − [3b] V. García-Montalvo, R. Cea-Olivares, J. Novosad, J. D. Woollins, A. M. Z. Slawin, G. Espinosa-Pérez, P. García y García, *J. Chem. Soc., Dalton Trans.* **1997**, 1025−1029.
[4] V. García-Montalvo, R. Cea-Olivares, D. J. Williams, G. Espinosa-Pérez, *Inorg. Chem.* **1996**, 3948−3953.
[5] V. García-Montalvo, R. Cea-Olivares, J. Novosad, J. D. Woollins, R. A. Toscano, G. Espinosa-Pérez, *Chem. Ber.* **1996**, *129*, 919−923.
[6] S. Bjørnevåg, S. Husebye, K. Maartmann-Moe, *Acta Chem. Scand., Ser. A* **1982**, *36*, 195−202.
[7] J. Novosad, S. V. Lindeman, J. Marek, J. D. Woollins. S. Husebye, *Heteroatom Chem.* **1998**, *9*, 615−621.
[8] S. Husebye, K. Maartmann-Moe, *Acta Chem. Scand., Ser. A* **1983**, *37*, 219−225.
[9] R. Cea-Olivares, G. Canseco-Melchor, V. García-Montalvo, S. Hernández-Ortega, J. Novosad, *Eur. J. Inorg. Chem.* **1998**, 1573−1576.
[10] See, for example: [10a] J. E. Drake, L. N. Khasrou, A. G. Mislankar, R. Ratnani, *Inorg. Chem.* **1999**, *38*, 3994−4004. − [10b] J. E. Drake, J. Yang, *Inorg. Chem.* **1997**, *36*, 1890−1903. − [10c] J. E. Drake, R. J. Drake, L. N. Khasrou, R. Ratnani, *Inorg. Chem.* **1996**, *35*, 2831−2840. − [10d] J. H. E. Bailey, J. E. Drake, *Can. J. Chem.* **1993**, *71*, 42−50. − [10e] J. H. E. Bailey, J. E. Drake, *Can. J. Chem.* **1991**, *69*, 1948−1956. − [10f] S. Husebye, K. Maartmann-Moe, W. Steffenson, *Acta Chem. Scand.* **1990**, *44*, 139.
[11] [11a] D. Dakternieks, R. Di Giacomo, R. W. Gable, B. Padmanabhan, *J. Am. Soc. Chem.* **1988**, *110*, 6753−6761. − [11b] D. Dakternieks, R. Di Giacomo, R. W. Gable, B. F. Hoskins, *J. Organomet. Chem.* **1988**, *349*, 305−315. − [11c] J. O. Bogason, D. Dakternieks, S. Husebye, K. Maartmann-Moe, H. Zhu, *Phosphorus Sulfur Silicon Relat. Elem.* **1992**, *71*, 13−24. − [11d] V. García-Montalvo, R. A. Toscano, A. Badillo-Delgado, R. Cea-Olivares, *Polyhedron* **2001**, *20*, 203−208.
[12] V. García-Montalvo, A. Marcelo-Polo, R. Montoya, S. Hernández-Ortega, R. A. Toscano, R. Cea-Olivares, *J. Organomet. Chem.* **2001**, *623*, 74−80.
[13] J. E. Drake, L. N. Khasrou, A. G. Mislankar, R. Ratnani, *Inorg. Chem.* **1994**, *33*, 6154−6162.
[14] J. E. Drake, L. N. Khasrou, A. G. Mislankar, R. Ratnani, *Can. J. Chem.* **1994**, *72*, 1328−1337.
[15] [15a] P. C. Srivastava, S. Bajpai, R. J. Butcher, *J. Organomet. Chem.* **1999**, *586*, 119−124. − [15b] N. W. Alcock, W. D. Harrison, C Howes, *J. Chem. Soc., Dalton Trans.* **1984**, 1709−1716. − [15c] N. W. Alcock, J. Culver, S. M. Ross, *J. Chem. Soc., Dalton Trans.* **1992**, 1477−1484.

[16] [16a] A. Silvestru, I. Haiduc, R. A. Toscano, H. J. Breunig, *Polyhedron* **1995**, *14*, 2047−2053. − [16b] J. E. Drake, A. Silvestru, J. Yang, I. Haiduc, *Inorg. Chim. Acta* **1998**, *271*, 75−82. − [16c] J. E. Drake, R. J. Drake, A. Silvestru, J. Yang, *Can. J. Chem.* **1999**, *77*, 356−366. − [16d] D. J. Birdsall, J. Novosad, A. M. Z. Slawin, J. D. Woollins, *J. Chem. Soc., Dalton Trans.* **2000**, 435−439.

[17] J. Novosad, K. W. Törnroos, M. Necas, A. M. Z. Slawin, J. D. Woollins, S. Husebye, *Polyhedron* **1999**, *18*, 2861−2867.

[18] I. G. Morgan, F. H. Burstall, *J. Chem. Soc.* **1931**, 180−184.

[19] [19b] J. D. McCullough, C. Knobler, R. F. Ziolo, *Inorg. Chem.* **1985**, 1814−1818. − [19a]. R. F. Ziolo, W. H. H. Günther, *J. Organomet. Chem.* **1979**, *178*, 423−431.

[20] J. D. McCullough, C. Knobler, *Inorg. Chem.* **1976**, *15*, 2728−2731.

[21] [21a] N. L. Allinger, *J. Am. Chem. Soc.* **1959**, *81*, 5727−5732. − [21b] J. B. Hendrickson, *J. Am. Chem. Soc.* **1964**, *86*, 4854−4860.

[22] N. W. Alcock, *Bonding and structure principles in inorganic and organic chemistry*, Ellis Horwood, NY, **1993**, p. 195.

[23] A. Bondi, *J. Phys. Chem.* **1964**, *68*, 441−451.

[24] A. Z. Al-Rubaie, H. A. Y. Alshirayda, P. Granger, S. Chapelle, *J. Organomet. Chem.* **1985**, *287*, 321−327.

[25] G. M. Sheldrick, *SHELXS-97, Crystal Structure Solution*, version 97-1, Institut für Anorganische Chemie, Universität, Göttingen, Germany, **1997**.

[26] A. Altomare, M. C. Burla, M. Camalli, G. L. Cascarano, C. Giacovazzo, A. Guagliardi, A. G. G. Moliterni, G. Polidori, R. Spagna, *J. Appl. Crystallogr.* **1999**, *32*, 115−119.

[27] G. M. Sheldrick, *SHELXL-97, Crystal Structure Refinement*, version 97.1, Institut für Anorganische Chemie, Universität Göttingen, Germany, **1997**.

[28] H. D. Flack, *Acta Crystallogr., Sect. A* **1983**, *39*, 876−881.

Received March 9, 2001
[I01093]

Kinetics and Thermodynamics of Complex Formation between Fe^{III} and Two Synthetic Chelators of the Dicatecholspermidine Family

Jean-Michel El Hage Chahine,*[a] Anne-Marie Bauer,[a] Karin Baraldo,[a] Claude Lion,[a] Florence Ramiandrasoa,[b] and Gerhard Kunesch[b]

Keywords: Siderophores / Iron / Chelation / Drug targeting / Fast kinetics

This report deals with a kinetic and thermodynamic study of complex formation between Fe^{III} and a new series of synthetic chelators, 2,3- (FR401) and 3,4-dicatecholspermidine (FR295). For the following data, the first value concerns FR295 and the second FR401. Each ligand undergoes five acid-base dissociations, four of which involve the hydroxy groups of the catechol moieties and the final one the central ammonium group. They occur with average at pK_{2a} = 8.40 and 7.95 for the first two hydroxy groups, pK_{3a} = 12.6 and 12.20 for the two remaining hydroxy groups and pK_{1a} = 5.50 and 4.90 for the ammonium group. Complex formation with both chelators occurs rapidly in acidic media (pH < 2), resulting in the second-order complex formation rate constants k_1 = 450 M^{-1} s^{-1} and 500 M^{-1} s^{-1} and first-order complex dissociation rate constants k_{-1} = 0.82 s^{-1} and 0.28 s^{-1}. From these two elementary rates, the complex dissociation constant is determined in acidic media: $K_1 = 1.82 \cdot 10^{-3}$ M and $5.6 \cdot 10^{-4}$ M. The Fe^{III} complexes also undergo five proton dissociations with marked decreases in the catechol pK_a value: ΔpK_{1a} = 1.25 and 1.25, ΔpK_{2a} = 6.60 and 6.50, ΔpK_{3a} = 6.55 and 6.95. From ΔpK_a and K_1, the affinity of both FR295 and FR401 for Fe^{III} is determined: log β = 29 and 31 with pFe = 22 and 25. This new series of chelators is aimed for antibiotic targeting. It proved efficient in inhibiting *Plasmodium falciparum* growth and delivered iron ions to Gram-negative bacteria.

Introduction

Iron is one of the most essential elements for practically all life forms. In its most common state of oxidation, Fe^{III} is insoluble in neutral media. It is, therefore, directly unavailable for the living species.[1] Consequently, this element is solubilised and regulated in physiological media by several iron transport and acquisition systems. In microorganisms, one of the most important is constituted by siderophores.[2] Siderophores are very efficient low molecular mass iron chelators used and or synthesized when iron is required. Once in the chelate form these iron transport systems are recognized by the cell, where they are admitted across the membranes by specific paths, and iron is delivered.[3]

Synthetic chelators can be siderophore-like and, therefore, used by some cells for the acquisition of iron.[3] Considerable effort to synthesize siderophore-like and other high-efficiency iron chelators has been made in the last twenty years. Most of these molecules were synthesised for the therapy of iron-overload which can be partially eliminated by chelation.[4,5] Other approaches were investigated to use the siderophore for drug delivery inside pathogenic microorganisms.[6] Siderophores can also be effective against malaria.[7]

Most of the iron ligands in siderophores are catechols and/or hydroxamates.[1,2] A series of synthetic chelators based on a spermidine skeleton bearing catechols behaved as siderophores and as iron scavengers. They inhibited *Plasmodium falciparum* proliferation in vitro and delivered iron to several Gram-negative bacteria, thereby, promoting their growth.[8,10]

This inhibition of *Plasmodium falciparum* is of interest as malaria is still the major cause of human mortality in the tropics where an increasing prevalence of strains of *Plasmodium falciparum* resistant to chloroquine and other antimalarial drugs.[7,11] As for the siderophore activity, it opens up ideas of using these molecules for drug delivery. Indeed, with the emergence of AIDS, and the consequent increase in the number of immunodepressive patients, opportunistic diseases such as tuberculosis with new forms of resistance to antibiotics have appeared.[12] Some of these forms of resistance are mostly related to impermeability of the microorganism's membrane to the drug than to a the classical deactivating enzymes.[12] This impermeability can be overcome by delivering the drug as an antibiotic−siderophore adduct using the microorganism's iron acquisition pathway.[3,8,12,13] Macrolide antibiotics linked to catecholspermidines proved to be effective against antibiotic-resistant mycobacteria.[8,13] These promising results may lead to a new series of antibiotic carriers and antimalarial drugs based on the catecholspermidine series.

Fe^{III} is insoluble in neutral media. It can be complexed to other chelators, in physiological media in the so-called low molecular mass iron pool.[2] However, in vertebrates and some invertebrates, it is regulated by the transferrins, which possess very high affinities for the metal (> 10^{20}

[a] Institut de Topologie et de Dynamique des Systèmes, Université Paris 7 − CNRS,
1 rue Guy de la Brosse, 75005 Paris, France
Fax: (internat.) + 33-1/44276814,
E-mail: chahine@paris7.jussieu.fr
[b] Laboratoire de Chimie Bioorganique et Bioinorganique, Université Paris 11 − CNRS, Bât. 420,
91405 Orsay Cedex, France

 © WILEY-VCH Verlag GmbH, 69451 Weinheim, 2001 1434−1948/01/0909−2287 $ 17.50+.50/0

M^{-1}).[14] Therefore, in order to be competitive and to keep their iron charge, synthetic siderophores must possess extremely high affinities for Fe^{III}.[15−18] The affinity constants of natural or synthetic siderophores for iron range from 10^{20} M^{-1} to $> 10^{40}$ M^{-1}.[15−18] These extremely high affinities render any thermodynamic or kinetic analysis of complex formation with Fe^{III} difficult.[18] In this article we analyse, by the chemical relaxation approach and analytical chemistry,[14,19−21] the kinetic and thermodynamic behaviour of the siderophore-like 2,3 (FR401) and 3,4-dicatecholspermidines (FR295, Scheme 1) during complex formation with Fe^{III}.

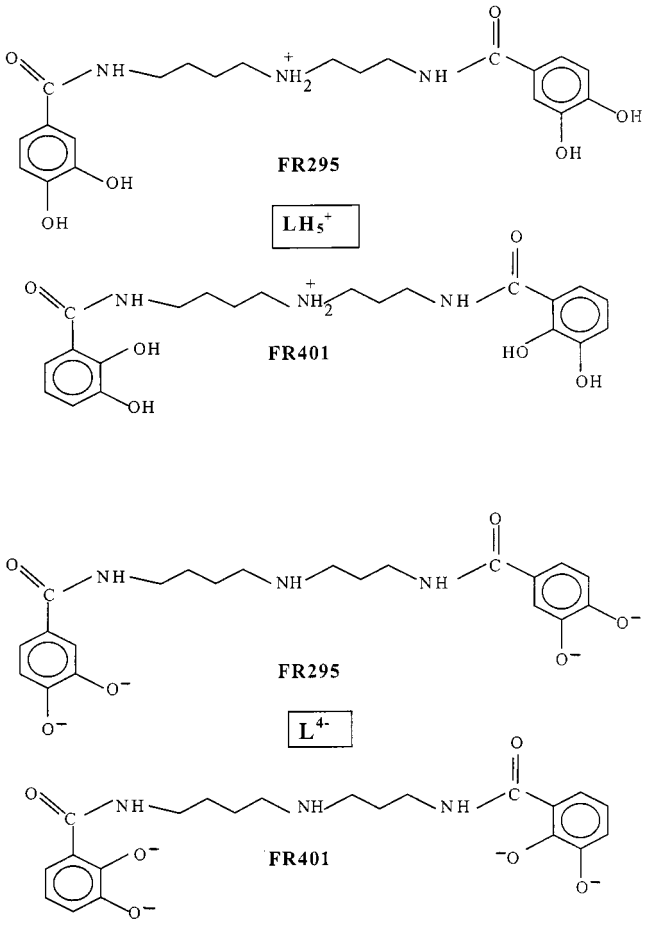

Scheme 1

Results and Discussion

All our experiments were performed at an ionic strength of μ = 0.2 in the presence of Cl^-. At pH = 2−4, the absorption spectra of both FR295 and FR401 are independent of acidity, which indicates the presence of a single prototropic species for each of them. From pH = 4 to 7, the absorption spectra vary to attain a first plateau at pH = 7−8. They vary again to attain a second plateau at pH = 9−10. From pH = 10−13, the spectra vary again to reach a third plateau in very basic media (Figures 1, 2, and 3).

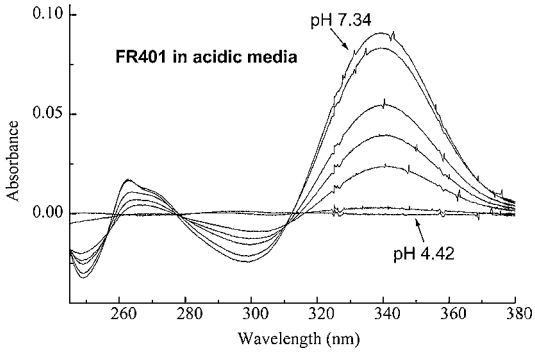

Figure 1. Differential absorption spectra of FR401 between pH = 4.42 and 7.34 with $c_0 = 4.5 \cdot 10^{-5}$ M and μ = 0.2 at 25±0.5 °C

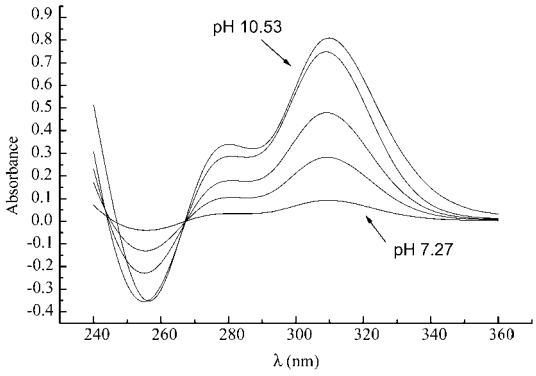

Figure 2. Differential absorption spectra of FR295 between pH = 7.27 and pH 10.53 with $c_0 = 4.5 \cdot 10^{-5}$ M and μ = 0.2 at 25±0.5 °C

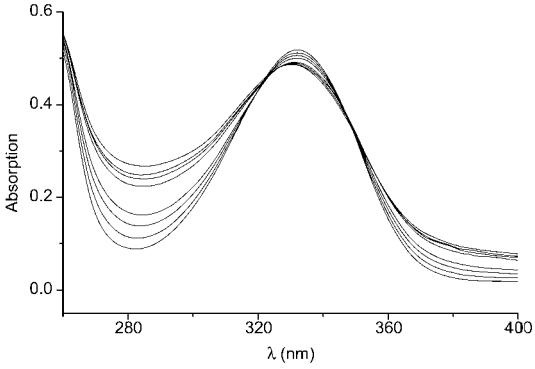

Figure 3. Absorption spectra of FR401 between pH = 10.56 and 13.15 with $c_0 = 5.0 \cdot 10^{-5}$ M and μ = 0.2 at 25 °C

When $FeCl_3$ is added to an acidic solution (pH ≈ 2) of FR295 or FR401, marked modifications in the absorption spectra of both ligands occur (Figure 4). This implies the formation of an iron(III) complex with FR295 and FR401.

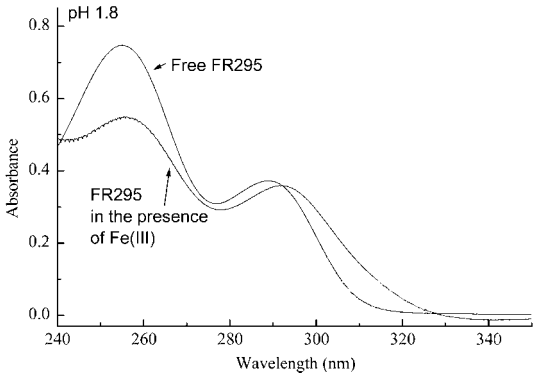

Figure 4. Absorption spectra of FR295 at pH = 1.80 in the absence and presence of 1 equiv. of $FeCl_3$ with $c_0 = c_1 = 4.5 \cdot 10^{-5}$ M and $\mu = 0.2$ at 25±0.5 °C

When the pH of solutions of FR295 and FR401 containing 1 equiv. of $FeCl_3$ are varied from acidic to basic ($2 < pH < 10$), modifications in the absorption spectra occur (Figure 5). Adding another equivalent of Fe^{III} does not have any effect on these absorption spectra and leads to the precipitation of iron hydroxide at $pH > 2.5$. All these experiments were performed under argon in order to avoid catechol oxidation and all the processes observed were reversible.

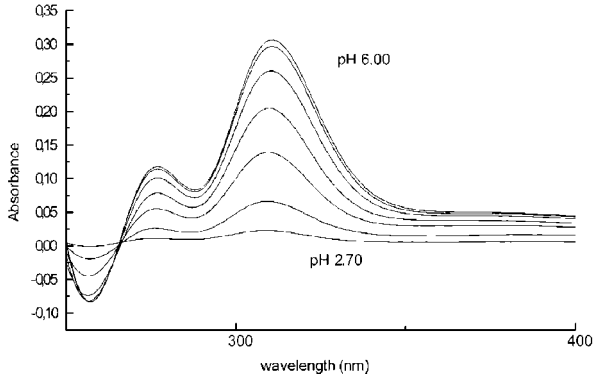

Figure 5. Differential absorption spectra of FR295 in the presence of 1 equiv. of $FeCl_3$ between pH = 2.70 and 6.00 with $c_0 = c_1$ and $\mu = 0.2$ at 25±0.5 °C

Free Ligand Proton Dissociations

The two dicatecholspermidine ligands FR401 and FR295 can exist as several prototropic species (Scheme 1).[22] When the pH of FR401 and FR295 solutions is increased, the variations in the absorption spectra of the ligands indicate the presence of one or more prototropic species in each of the 3−7, 7−9.5 and 9.5−13 pH ranges (Figures 1, 2, 3). To a first approximation, we assume that in each pH range, a ligand species can deprotonate according to Equation (1) where ion charges are not written.

$$LH_{(m-n)} + n\,H^+ \rightleftarrows LH_m \quad (1)$$

The Beer−Lambert law can be expressed in each of the pH ranges as in Equation (2) where A is the absorbance at a given wavelength, with $l = 1$ cm for all of the experiments, m is 5 in acidic media, n is the number of the protons involved in the acid-base reactions, $\varepsilon_{(m-n)}$ is the molecular extinction coefficient of the $LH_{(m-n)}$ species and ε_m is the molecular extinction coefficient of the of the LH_m species.

$$A = \{\varepsilon_{(m-n)}[LH_{(m-n)}] + \varepsilon_m[LH_m]\}l \quad (2)$$

Equation (2) can also be expressed as Equation (3)[23,24] where $\Delta A = A - A_0$, $\Delta\varepsilon = \varepsilon_{(m-n)} - \varepsilon_m$ and c_0 is the ligand concentration, with A_0 the absorbance due to the LH_m species and $\boldsymbol{K}_a = [LH_m][H^+]^n/[LH_{(m-n)}]$.

$$\Delta\varepsilon/\Delta A = 1/c_0 + [H^+]^n/(K_a c_0) \quad (3)$$

The best linear regression of the experimental $\Delta\varepsilon/\Delta A$ against $[H^+]^n$ is obtained for $n = 1$ in all of the pH ranges (Figures 6, 7, and 8 and Table 1).

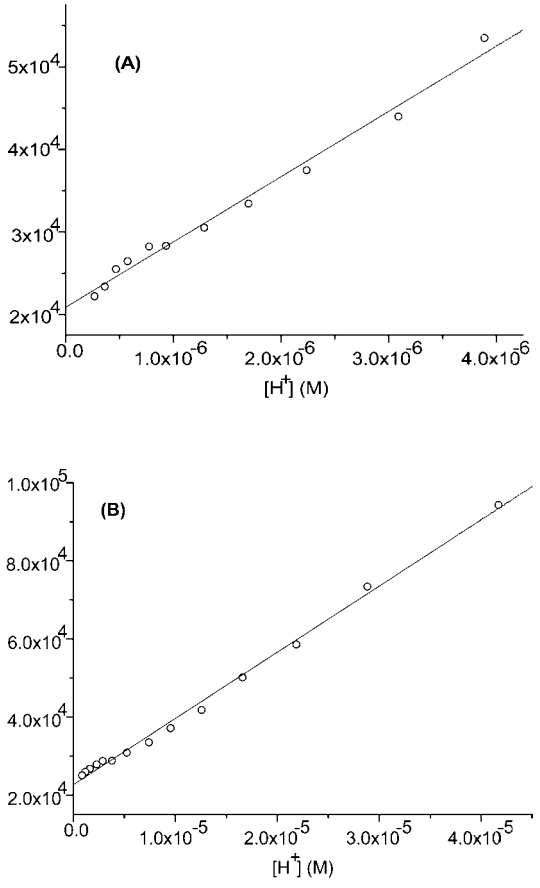

Figure 6. Plot of $\Delta\varepsilon/\Delta A$ against $[H^+]$ at pH ≤ 7: A) FR295, intercept, $(2\pm0.05)\cdot10^4$ M^{-1}; slope $(7.90\pm0.50)\cdot10^9$ M^{-2}; $r = 0.99357$; B) FR401, intercept, $(2.25\pm0.05)\cdot10^4$ M^{-1}; slope, $(1.70\pm0.05)\cdot10^9$ M^{-1}

In both ligands, there are five deprotonation sites; four proton losses can occur from the two dicatechol moieties of FR295 and FR401 and another proton loss from the central quaternary ammonium group. However, we only detected three proton dissociations, each of which seems to

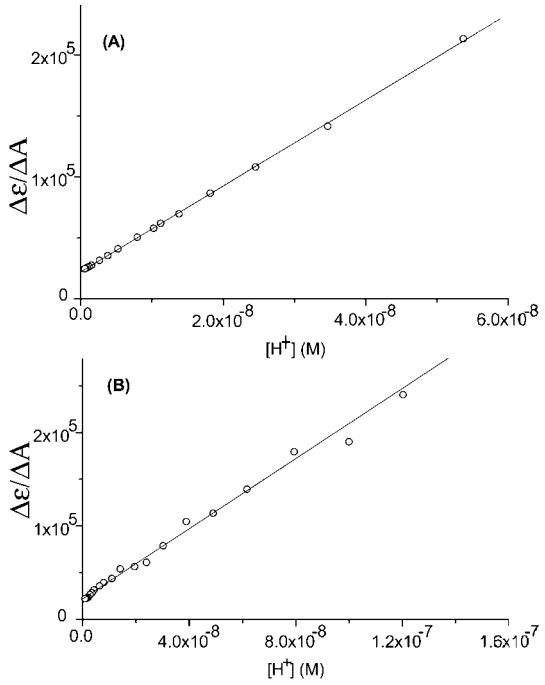

Figure 7. Plot of $\Delta\varepsilon/\Delta A$ against $[H^+]$ at 10. 50 ≥ pH ≥ 7: A) FR295, intercept, $(2.20\pm0.5)\cdot10^4$ M^{-1}; slope, $(3.50\pm0.05)\cdot10^{12}$ M^{-1}; r = 0.99983; B) FR401, intercept, $(2.20\pm0.05)\cdot10^4$ M^{-1}; slope, $(1.90\pm0.05)\cdot10^{12}$ M^{-1}

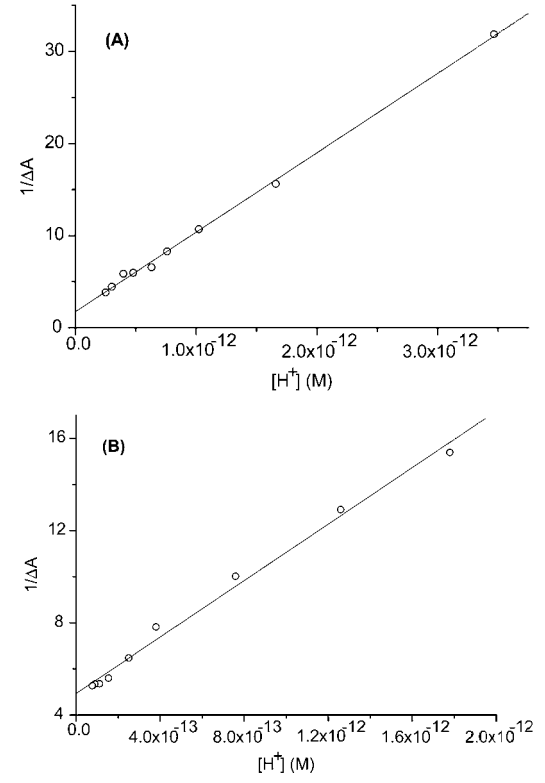

Figure 8. Plot of $1/\Delta A$ against $[H^+]$ at pH ≥ 10.50: A) FR295, intercept, 1.80±0.2; slope, $(8.60\pm0.15)\cdot10^{12}$ M^{-1}; r = 0.99912; B) FR401, intercept, 4.90±0.30; slope, $(6.20\pm0.30)\cdot10^{12}$ M^{-1}; r = 0.99569

Table 1. An approximation of the overall proton dissociation constants involved in the acid-base equilibria of FR295 and FR401

Ligand	3 < pH < 6 pK_{1a}	6 < pH <9 pK_{2a}	9 < pH < 13 pK_{3a}
FR295	5.50 ± 0.02	8.40 ± 0.02	12.60 ± 0.02
FR401	4.90 ± 0.02	7.95 ± 0.02	12.10 ± 0.02

involve a single proton transfer. Although the two dicatecholspermidine ligands are not symmetrical, in each of the ligands, the catechol moieties have the same environment and are practically identical. Therefore, these dicatechols should behave in the same way towards proton dissociation that can explain the presence of what seems to be isosbestic points in Figures 1 to 3 and 5. An isosbestic point may imply the presence of two species in the medium. Nonetheless, it cannot constitute as evidence for this presence.[25] Subsequently, we can assume that the three measured pK_a values of Table 1 can describe five proton dissociations. We can, therefore, write Equations (4) to (8) with L^{4-}, the completely deprotonated species, $K_{1a} = [LH_4][H^+]/[(LH_5)^+]$, $K_{2a} = [(LH_3)^-][H^+]/[LH_4]$, $K_{3a} = [(LH_2)^{2-}][H^+]/[(LH_3)^-]$, $K_{4a} = [(LH)^{3-}][H^+]/[(LH_2)^{2-}]$ and $K_{5a} = [L^{4-}][H^+]/[(LH)^{3-}]$.

$$LH_4 + H^+ \rightleftarrows (LH_5)^+ \quad (4)$$

$$(LH_3)^- + H^+ \rightleftarrows LH_4 \quad (5)$$

$$(LH_2)^{2-} + H^+ \rightleftarrows (LH_3)^- \quad (6)$$

$$(LH)^{3-} + H^+ \rightleftarrows (LH_2)^{2-} \quad (7)$$

$$L^{4-} + H^+ \rightleftarrows (LH)^{3-} \quad (8)$$

At pH < 9.5, three protons are involved in acid-base reactions with both ligands (Table 1) In this case the Beer−Lambert law can be expressed as in Equation (9).

$$A = \varepsilon_1[LH_5] + \varepsilon_2[LH_4] + \varepsilon_3[LH_3] + \varepsilon_4[LH_2] + \varepsilon_5[LH^{3-}] + \varepsilon_6[L^{4-}] \quad (9)$$

At 6 < pH < 9.5 $[LH_5^+]$, $[LH_4]$, $[LH_3^-]$ >> $[LH_2^{2-}]$, $[LH^{3-}]$, $[L^{4-}]$ and at pH > 9.5 $[LH_5^+]$, $[LH_4]$, $[LH_3^-]$ << $[LH_2^{2-}]$, $[LH^{3-}]$, $[L^{4-}]$. In this case, with K_{1a}, K_{2a}, K_{3a}, K_{4a}, and K_{5a} and the conservation of mass, we can write Equations (10) and (11) at 6 < pH <9.5 and pH > 9.5, respectively.

$$A = \frac{\{\varepsilon_1[H]^3 + \varepsilon_2[H]^2K_{1a} + \varepsilon_3[H]K_{1a}K_{2a} + \varepsilon_4K_{1a}K_{2a}K_{3a}\}c_0}{([H]^3 + [H]^2K_{1a} + [H]K_{1a}K_{2a} + K_{1a}K_{2a}K_{3a})} \quad (10)$$

$$A = \frac{c_0\{\varepsilon_4[H^+]^2 + \varepsilon_5[H^+]K_{4a} + \varepsilon_6 K_{4a}K_{5a}\}}{[H^+]^2 + [H^+]K_{4a} + K_{4a}K_{5a}} \quad (11)$$

Two non-linear least-squares regressions were obtained for each of the two ligands. The first two were for the data collected at pH < 9.5 [Equation (10)] and the other two for the data collected at pH > 9.5 [Equation (11)]. They gave very close $K_{2a} \approx K_{3a}$ and $K_{4a} \approx K_{5a}$ values. This implies that the values reported in Table 1 can be expressed as $pK_{2a} \approx (pK_{2a} + pK_{3a})/2$ and $pK_{3a} \approx (pK_{4a} + pK_{5a})/2$. All these pK_a values are in agreement with those reported for catechol proton dissociations. These occur in the vicinity of neutrality for one hydroxy group and at pH > 10 for the second.[22] As for the ammonium group of the spermidine, the values of the proton dissociation constant are highly dependent on the nature of the associated moieties and can vary from about 2 to more than 10.[26]

Complex Proton Dissociation

If a monocomplex is formed between Fe^{III} and FR295 or FR401, as Figure 4 seems to imply, it can also deprotonate at the catechol moieties and the central ammonium group. The variation of the absorption spectra of the two complexes seems to indicate the presence of at least three prototropic species in the pH = 3−6 area (Figure 5).

As in the case of the free ligands, we assume to a first approximation that in each pH range when at least one species deprotonates to yield the other, we can write Equation (12).

$$FeLH_{(m-n)} + nH^+ \leftrightarrows FeLH_m \quad (12)$$

As m is unknown, ion charges are not written. The Beer−Lambert law can be expressed in each of the pH ranges as Equation (13) [where A is absorbance at a given wavelength, with l = 1 cm for all our experiments; $\varepsilon'_{(m-n)}$ is the molecular extinction coefficient of the $FeLH_{(m-n)}$ species and ε''_m is the molecular extinction coefficient of the of $FeLH_m$] and Equation (14) {where $\Delta A = A - A_0$ and $\Delta\varepsilon' = \varepsilon'_{(m-n)} - \varepsilon''_m$, with A_0 the absorbance due to the LH_m species and $K_n = [FeLH_{(m-n)}][H^+]^n/[FeLH_m]$}.

$$A = \{\varepsilon'_{(m-n)}[LH_{(m-n)}] + \varepsilon''_m[LH_m]\}l \quad (13)$$

$$\Delta\varepsilon'/\Delta A = 1/c_0 + [H^+]^n/(K_n c_0) \quad (14)$$

Equation (14) is never obeyed by our experimental data. However, the plot of $1/\Delta A$ against $[H^+]$ can be roughly simulated by three lines, each of which obeys Equation (15) with $K'_{na} = [FeLH_{(m-1)}][H^+]/[FeLH_m]$, where ΔA_{n0} is the experimental differential absorption determined from the intercept of each of the three regression lines.

$$1/\Delta A = 1/\Delta A n_0 + [H^+]/\Delta A_0 K'_{na} \quad (15)$$

We, therefore, assumed that the Fe^{III} complex undergoes at least three proton losses when the pH range is ca. 2 to ca. 8 [Equations (16) to (18)].

$$FeLH_{(m-3)} + H^+ \leftrightarrows FeLH_{(m-2)} \quad (16)$$

$$FeLH_{(m-2)} + H^+ \leftrightarrows FeLH_{(m-1)} \quad (17)$$

$$FeLH_{(m-1)} + H^+ \leftrightarrows FeLH_m \quad (18)$$

In this case the Beer−Lambert relation can be expressed as Equation (19) in which, ε'_3, ε'_2, ε'_1, and ε' are the molecular extinction coefficients of species $FeLH_{(m-3)}$, $FeLH_{(m-2)}$, $FeLH_{(m-1)}$, and $FeLH_m$, respectively.

$$A = \varepsilon'_3[FeLH_{(m-3)}] + \varepsilon'_2[FeLH_{(m-2)}] + \varepsilon'_1[FeLH_{(m-1)}] + \varepsilon'[FeLH_m] \quad (19)$$

Equation (19) can be expressed as a function of c_0, $K'_{1a} = [FeLH_{(m-1)}][H^+]/[FeLH_m]$, $K'_{2a} = [FeLH_{(m-2)}][H^+]/[FeLH_{(m-1)}]$ and $K'_{3a} = [FeLH_{(m-3)}][H^+]/[FeLH_{(m-2)}]$ as in Equation (20).

$$\Delta A = \frac{(\varepsilon'_3 - \varepsilon')K_{1a}K'_{2a}K'_{3a} + (\varepsilon'_2 - \varepsilon')K'_{1a}K'_{2a}[H^+] + (\varepsilon'_1 - \varepsilon')K'_{1a}[H^+]^2}{K'_{1a}K'_{2a}K'_{3a} + K'_{1a}K'_{2a}[H^+] + K'_{1a}[H^+]^2} \times c_0 \quad (20)$$

A non-linear least-squares regression of the data against Equation (20), where $(\varepsilon'_3 - \varepsilon')$ is determined experimentally and the equilibrium constants are roughly estimated from the three lines related to Equation (15) in the three different pH ranges, gave the K'_{1a}, K'_{2a}, and K'_{3a} values with about 10 to 15% of uncertainty (Figure 9, Table 2).

Therefore, the proton dissociation constants of the FR295 and FR401 ligands are shifted from basic to acidic when the ligands are complexed by Fe^{III}. As for the free ligand, we will assume that the apparent pK_a values reported in Table 2 concern the deprotonation of the ligands engaged in the complex. Complex formation can be accompanied by the deprotonation of the ligands involved which stabilises the complex.[27−29] Catechols are very good chelators for Fe^{III} whereas amines are not.[27,29] Since the affinity of a ligand for a metal increases upon proton loss,[28] we assume that pK'_{1a} and pK'_{3a} are related to catechol deprotonation. Consequently, each of pK'_{1a} or pK'_{3a} involves two proton dissociations, whereas pK'_{2a} involves the amine single proton dissociation.

Kinetics of Complex Formation

When acidic solutions of FR295 or FR401 are mixed rapidly with a solution of $FeCl_3$, a single kinetic process is observed. It appears as an exponential increase of absorption at λ = 290 nm for each of the ligands (Figures 10 and 11). The rate of this process depends on the $FeCl_3$ concentration and the pH value for 1.5 ≤ pH ≤ 2.2. At pH > 2.2 iron hydroxides start appearing.[30]

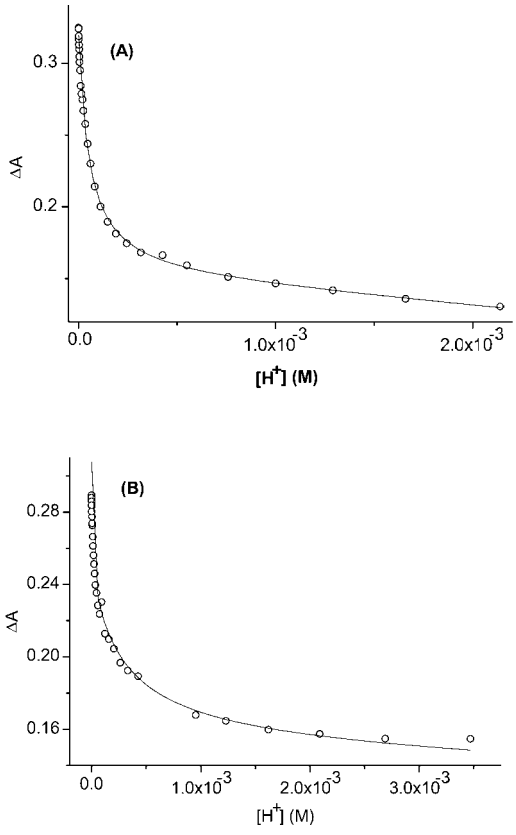

Figure 9. Plot of ΔA against $[H^+]$ at 25±0.5 °C for $c_1 = 4.5\cdot10^{-5}$ M and $\mu = 0.2$, and the non-linear least-squares regression fit according to Equation (20): A) FR295 with $K'_{1a} = (9.0\pm1.0)\cdot10^{-7}$ M, $K'_{2a} = (5.0\pm0.3)\cdot10^{-5}$ M and $K'_{3a} = (1.60\pm0.15)\cdot10^{-2}$ M; B) FR401 with $K'_{1a} = (7\pm1)\cdot10^{-6}$ M, $K'_{2a} = (2.30\pm0.30)\cdot10^{-4}$ M and $K'_{3a} = (3.5\pm0.3)\cdot10^{-2}$ M

Table 2. An approximation of the overall proton dissociation constants involved in the acid-base equilibria of the Fe^{III} monocomplexes of FR295 and FR401

Ligands	pK'_{2a} ammonium	pK'_{1a} catechol	pK'_{3a} catechol
FR295	4.25 ± 0.05	1.80 ± 0.05	6.05 ± 0.05
FR401	3.65 ± 0.05	1.50 ± 0.05	5.15 ± 0.05

In FR295 and FR401, the pK_a values of the catechol and central ammonium groups are both higher than 3 (Table 1). Subsequently, under our experimental conditions (pH ≤ 2), both chelators are in the protonated form $(LH_5)^+$ (Scheme 1). In this case, the chemical relaxation approximation will only be relevant for $c_1 \geq 2c_0$,[21] where c_1 is the analytical $FeCl_3$ concentration. The kinetic processes of Figures 10 and 11 always appear as a single exponential phenomenon that may imply the formation of a single complex. All this suggests that, because the two kinetic phenomena are pH-dependent, and because there is an excess of iron along with the detection of a single relaxation mode,[19–21,23,24,27] $(LH_5)^+$ may react with one Fe^{III} with

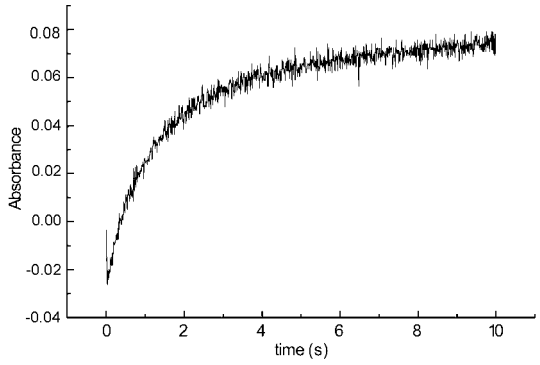

Figure 10. Exponential increase of the absorption with time at λ = 290 nm when an FR295 solution is rapidly mixed with a $FeCl_3$ solution with $c_0 = 4\cdot10^{-4}$ M, $c_1 = 5\cdot10^{-3}$ M and $\mu = 0.2$ at pH = 1.90 and 25±0.5 °C

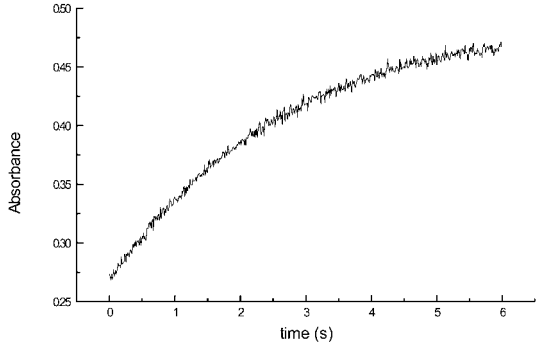

Figure 11. Exponential increase of the absorption with time at λ = 290 nm when a FR401 solution is rapidly mixed with a $FeCl_3$ solution with $c_0 = 4\cdot10^{-4}$ M, $c_1 = 3.6\cdot10^{-3}$ M and $\mu = 0.2$ at pH = 1.47 and 25±0.5 °C

the involvement of a proton transfer process. This can occur according to three possible mechanisms in which $FeLH_3^{2+}$ is the iron complex with each of the catechol moieties deprotonated on one hydroxy group and LH_3^- is the ligand species, also deprotonated on one hydroxy group.[27]

Mechanism I

$$Fe^{3+} + LH_5^+ \underset{k_{-1}}{\overset{k_1}{\rightleftarrows}} FeLH_5^{4+} \text{ (rate-limiting)} \quad (21)$$

$$Fe\,LH_{(5-n)}^{(n+2)+} + nH^+ \leftrightarrows FeLH_5^{4+} \quad (22)$$

Mechanism II

$$LH_{(5-n)}^{(n-1)-} + nH^+ \leftrightarrows LH_5^+ \quad (23)$$

$$Fe^{3+} + LH_{(5-n)}^{(n-1)-} \underset{k_{-1}}{\overset{k_2}{\rightleftarrows}} FeLH_{(5-n)}^{(n+2)+} \text{ (rate-limiting)} \quad (24)$$

Mechanism III

$$Fe^{3+} + LH_5^+ \underset{k_{-3}}{\overset{k_3}{\rightleftarrows}} FeLH_{(5-n)}^{(n+2)+} + nH^+ \quad (25)$$

A proton dissociation is usually diffusion-controlled and occurs in the μs range.[19,20,23,24] Therefore the phenomena of Figures 10 and 11 must involve rate-limiting complex formation. The reciprocal relaxation time equations associated with rate-limiting Equation (21) and Equation (24) and with Equation (25) are expressed as Equations (26) to (28) where $\boldsymbol{K}^2_{2a} = [LH_{(5-n)}{}^{(n-1)-}][H^+]^n/[LH_5{}^+]$ and $\boldsymbol{K}'^2_{1a} = [Fe LH_{(5-n)}{}^{(n+2)+}][H^+]^n/[FeLH_5{}^{4+}]$.[19,20,27]

$$\tau_1^{-1} = k_{-1}[H^+]^n/([H^+]^n + \boldsymbol{K}'_{1a}) + k_1([LH_5{}^+] + [Fe^{3+}]) \quad (26)$$

$$\tau_2^{-1} = k_{-2} + k_2([LH_5{}^+] + [Fe^{3+}])\boldsymbol{K}^2_{2a}/[H^+]^2 \quad (27)$$

$$\tau_3^{-1} = k_3([Fe^{3+}] + [LH_5{}^+]) + k_{-3}[H^+]^n \quad (28)$$

Under our experimental conditions where $c_1 \geq 2c_0$, and where $\boldsymbol{K}'_{1a}$, $[H^+] >> c_1$, c_0 and $\boldsymbol{K}_{2a}$, Equations (26), (27), and (28) can be simplified into Equations (29), (30), and (31), respectively.

$$\tau_1^{-1}(1 + \boldsymbol{K}'^2_{1a}/[H^+]^n) \approx k_{-1} + k_1(c_1 - c_0)(1 + \boldsymbol{K}'^2_{1a}/[H^+]^n) \quad (29)$$

$$\tau_2^{-1} \approx k_{-2} + k_2(c_1 - c_0)\boldsymbol{K}_{2a}{}^n/[H^+]^n \quad (30)$$

$$\tau_3^{-1} \approx k_3(c_1 - c_0) + k_{-3}[H^+]^n \quad (31)$$

Equations (30) and (31) are not obeyed by the experimental data. This eliminates Mechanisms II and III. Two good linear least-squares regressions of the experimental relaxation times against Equation (29) are obtained for FR295 and FR401 when $n = 2$ (Figures 12 and 13). From the slope and intercept of these two regression lines k_1, k_{-1} and $\boldsymbol{K}_1 = k_{-1}/k_1 = [Fe^{3+}][LH_5{}^+]/[FeLH_5{}^{4+}]$ are determined (Table 3).These rate constants are of the same order of magnitude as those reported for complex formation with Fe^{3+}.[18,27,32,33]

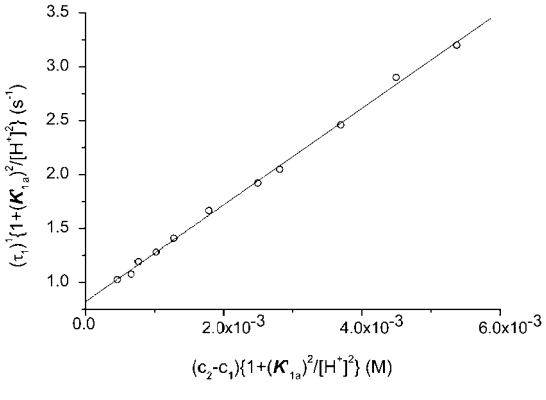

Figure 12. Plot of $\tau^{-1}(1 + \boldsymbol{K}'^2_{1a}/[H^+]^2)$ against $(c_1 - c_0)(1 + \boldsymbol{K}'^2_{1a}/[H^+]^2)$ in acidic media ($1.47 \leq pH \leq 2.20$): intercept, 0.82 ± 0.04 s^{-1}; slope, 450 ± 20 M^{-1} s^{-1}; $r = 0.99905$

If the fast formation of another complex following that of $FeLH_3{}^{2+}$ is involved in Mechanism I, to a first approximation, we can write at a fixed pH value reactions in Equations (32) and (33).

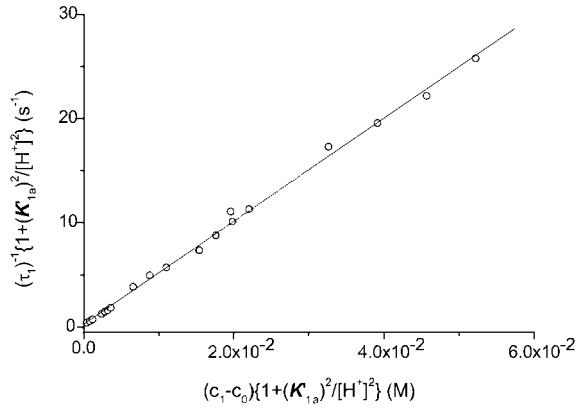

Figure 13. Plot of $\tau^{-1}(1 + \boldsymbol{K}'^2_{1a}/[H^+]^2)$ against $(c_1 - c_0)(1 + \boldsymbol{K}'^2_{1a}/[H^+]^2)$ in acidic media ($1.50 \leq pH \leq 2.20$) for FR401: intercept, 0.28 ± 0.03 s^{-1}; slope, 500 ± 20 $M^{-1} \cdot s^{-1}$; $r = 0.99849$

Table 3. The rate and equilibrium constants involved in complex formation between FR295 and FR401 with Fe ^{III} in acidic media

Ligand	k_1 [$M^{-1}s^{-1}$]	k_{-1} [s^{-1}]	$K_1 \times 10^4$ [M]	$K_1^{-1} \times 10^{-3}$ [M^{-1}]
FR295	450 ± 20	0.82 ± 0.04	18.2	0.55
FR401	500 ± 20	0.28 ± 0.03	5.6	1.80

$$Fe^{3+} + \mathcal{L} \underset{k_{-(obs)}}{\overset{k_{(obs)}}{\rightleftharpoons}} Fe\mathcal{L} \text{ (rate-limiting)} \quad (32)$$

$$Fe\mathcal{L} + L \leftrightarrows Fe\mathcal{L}_2 \quad (33)$$

In these reactions, the state of protonation of the ligand L and the complexes $Fe\mathcal{L}$ and $Fe\mathcal{L}_2$ are not known. Under our experimental conditions ($c_1 >> c_0$) with a fixed pH, the expression of the reciprocal relaxation time associated with rate limiting Equation (32) can be estimated by Equation (34) where the apparent equilibrium constant $K = [L][Fe\mathcal{L}]/[Fe\mathcal{L}_2]$.[20]

$$\tau_1^{-1} = k_{-obs}(K/[L]) + k_{obs}(c_1 - c_0) \quad (34)$$

This last equation is not obeyed by our experimental data. Furthermore, in acidic media, at $pH \approx 2$, Fe^{III} starts being present in the $FeOH^{2+}$ form [Equation (35)][31] with an equilibrium constant $K_{(FeOH)} = [H^+][FeOH^{2+}]/[Fe^{3+}] \approx 2 \cdot 10^{-3}$ M.[31]

$$FeOH^{2+} + H^+ \leftrightarrows Fe^{3+} + H_2O \quad (35)$$

If complex formation occurs between $FeOH^{2+}$, and FR401or FR295 the reciprocal relaxation time equation associated with Equation (36) will be expressed as Equation (37).[24]

$$LH_5^+ + FeOH^{2+} \underset{k_{-4}}{\overset{k_4}{\rightleftharpoons}} FeOHLH_5^{3+} \quad (36)$$

$$\tau_3^{-1} = k_{-4} + k_4\{c_1 K_{FeOH}/(K_{FeOH} + [H^+]) - c_0\} \quad (37)$$

Equation (37) is not obeyed by our experimental data. In contrast, if we take into account the presence of $FeOH^{2+}$ in the experimental medium, the reciprocal relaxation equation associated with the reaction in Equation (21) of Mechanism I will be expressed as Equation (38).

$$\tau^{-1} = k_1\{c_1[H^+]/([H^+] + K_{FeOH}) - c_0\} + k_{-1}[H^+]^n/([H^+]^n + K'_{1a}) \quad (38)$$

Under our experimental conditions ($1.4 < pH < 2$, $[FeOH^{2+}]$) Equation (38) simplifies into Equation (29). In this case, the presence of $FeOH^{2+}$ will not affect our kinetic analysis.

With dicatechols in non-hexadentate chelators such as amonabactins, more than one chelator can be engaged in complex formation with Fe^{III}.[22] Under our experimental conditions, we only detected a single 1:1 complex. This, however, does not exclude the formation of complexes with different stoichiometries (Fe_2L_3) under other experimental conditions where for instance $c_0 \leq c_1$. Moreover, as in the case of enterobactin, in FR401, the protonation of the oxygen ligand at position 2 may lead to a monosalicylate-type coordination with Fe^{III}.[34] Nevertheless, this coordination cannot occur with FR295 because it does not have a hydroxy group at position 2. Furthermore, the fact that the behaviours of both the FR401 and FR295 ligands towards complex formation are identical tends to exclude the salicylate-type coordination with FR401. In acidic media, for both FR295 and FR401, a complex is formed between Fe^{3+} and $L(H_5)^+$. This complex loses five protons from pH = 2 to 9. If we assume that, as in the case of the free ligands, the proton dissociation constants reported in Table 3 refer to two proton losses from the equivalent hydroxy groups in each of the two catechol moieties and from the central ammonium group, as shown for the free ligands, then $p\boldsymbol{K}'_{1a} = (pK_{2a} + pK'_{3a})/2$, $p\boldsymbol{K}'_{3a} = (pK'_{4a} + pK'_{5a})/2$ and $p\boldsymbol{K}'_{2a} = pK'_{1a}$ with $K'_{1a} = [(FeLH_4)^{3+}][H^+]/[(FeLH_5)^{4+}]$, $K'_{2a} = [(FeLH_3)^{2+}][H^+]/[(FeLH_4)^{3+}]$, $K'_{3a} = [(FeLH_2)^+][H^+]/[(FeLH_3)^{2+}]$, $K'_{4a} = [FeLH][H^+][(FeLH_2)^+]$ and $K'_{5a} = [(FeL)^-][H^+][FeLH]$.

$$(FeLH_4)^{3+} + H^+ \leftrightarrows (FeLH_5)^{4+} \quad (39)$$

$$(FeLH_3)^{2+} + H^+ \leftrightarrows (FeLH_4)^{3+} \quad (40)$$

$$(FeLH_2)^+ + H^+ \leftrightarrows (FeLH_3)^{2+} \quad (41)$$

$$FeLH + H^+ \leftrightarrows (FeLH_2)^+ \quad (42)$$

$$(FeL)^- + H^+ \leftrightarrows FeLH \quad (43)$$

The affinities of catechols for iron are extremely high.[16,18,22,28,29,31] We may, therefore, assume that with the analytical Fe^{III} concentration $c_1 \approx c_0$, the complexes of FR295 and FR401 are the predominant species from mildly acidic to basic media. This is always required with Fe^{III} complexes in order to avoid ferric hydroxide precipitation.

The Affinities of FR295 and FR401 for Fe^{III}

The affinity of a ligand for a metal increases upon proton loss.[28] This is manifested by the so-called chelation effect in which the apparent pK_a of the ligand engaged in the coordination with the metal decreases upon complex formation.[29]. The greater the pK_a difference (ΔpK_a) is between the free ligand proton dissociation and that of the same ligand engaged in the complex media, the higher is the affinity for the metal.[14,23,27] In Mechanism I, upon complex formation [Equation (20)], $FeLH_5^{4+}$ readily deprotonates by a diffusion-controlled acid-base dissociation to produce $FeLH_3^{2+}$ [Equation (21)]. The proton loss increases the affinities of both FR401 and FR295 for the metal by more than 12 orders of magnitude ($[Fe^{3+}][LH_3^-]/[FeLH_3^{2+}] = K_1K'_{1a}K'_{2a}/K_{1a}K_{2a}$). $FeLH_5^{4+}$ is, therefore, practically inexistent in the experimental medium. $FeLH_3^{2+}$ in turn deprotonates to finally yield FeL^- with another increase in the affinity of several orders of magnitude (Table 4). This is deduced from Equation (1) and the proton dissociation constants of the free ligand and of the complex [Equations (44) and (45)]. This yields $\log\beta$ ($-\log K$) values of Equations (29) and (31) for FR295 and FR401, respectively.

$$Fe^{3+} + L^{4-} \leftrightarrows FeL^- \quad (44)$$

$$1/\beta = K = [L^{4-}][Fe^{3+}]/[FeL^-] = K_1(K'_{1a}K'_{2a}K'_{3a}K'_{4a}K'_{5a})/(K_{1a}K_{2a}K_{3a}K_{4a}K_{5a}) \quad (45)$$

Table 4. The affinity constants and the pFe involved in complex formation between Fe^{III} and FR295 and FR401

Ligand	log β	pFe
FR295	29	22
FR401	31	25

These values are high and place both ligands in the classical range of affinities expected for dicatechols. Indeed, with monocatechols, the affinities for iron are about 37 ($\log\beta_3$) and for a tricatechol they are about 40.[16,18,22] The pH increase stabilises the complex by the consequent deprotonation of the hydroxy groups and allows it to achieve the $\log\beta$ value of 30 with the completely deprotonated ligands. An amine is not a particularly good ligand for Fe^{III}.[30] However, the pK_a we ascribed to the deprotonation of the ammonium group in the free ligand is shifted by more than 1 pK_a unit in the complex. This implies that the central

amine is also engaged in complex formation. This engagement is not, however, as strong as that observed for the catechol moieties where the ΔpK_a value exceeds 6 pK_a units implying, as expected, a very strong coordination to the metal centre.[28,29] Fe^{III} can then be considered to be coordinated to two catechol moieties and one amine group with the sixth coordination site probably occupied by water. Although we succeeded in synthesising the Fe^{III} and Ga^{III} complexes of FR401 and FR295 (Exp. Sect.), we do not yet have direct evidence to confirm such a structure. All that we can say is, that under our experimental conditions, with $c_1 \geq c_0$ a monoferric complex is formed between Fe^{III} and one FR295 or FR401 ligand and that in both cases five donor atoms seem to be engaged in the formation of this complex.

The affinities of FR295 and FR401 for iron are reported for complex formation with the fully ionised ligand L^{4-} [Equation (46)]. The FeL^- form is not the only one present in the vicinity of neutrality. Therefore, in order to have a scale of efficiency for iron chelators, Raymond et al. defined the pFe ($-\log[Fe^{3+}]$) scale. The pFe is determined for an analytical ligand concentration of 10^{-4} M and an analytical Fe^{III} concentration of 10^{-6} M at pH = 7.4, which is equivalent to that of physiological media.[15] From the different proton dissociation constants of Tables 2 and 3 and from mass conservation [Equations (46) and (47)] we can determine the analytical expression of $[Fe^{3+}]$ [Equation (48)] with $c_0 << [L] \approx c_1$.

$$c_1 = [FeL^-] + [FeLH_2^+] + [FeLH_4^+] + [Fe] \quad (46)$$

$$c_0 = [L] + [FeL^-] + [FeLH_2^+] + [FeLH_4^+] \quad (47)$$

$$[Fe^{3+}] = \frac{K\{[H^+]^5 + (K_{2a})^2[H^+]^3 + (K_{2a}K_{3a})^2[H^+] + (K_{2a}K_{3a})^2K_{1a}\}c_1}{\{[H^+]^5 + (K'_{1a})^2[H^+]^3 + (K'_{1a}K'_{3a})^2[H^+] + (K'_{1a}K'_{3a})^2K_{2a}\}c_0} \quad (48)$$

Table 4 represents the affinities of both ligands for iron and the relevant pFe. These values indicate that FR295 and FR401 can be considered as very good ligands for Fe^{III}.[15–18,22,34] This can explain their siderophore-like role with mycobacteria and their capacity to inhibit the growth of *Plasmodium falciparum* in vitro, where they probably act as iron sequestering agents depriving the medium of this element essential for the development of the microorganism.

Experimental Section

KCl (Merck Suprapur), NaOH, and HCl (Merck Titrisol), EDTA (Merck Titriplex), $FeCl_3$, sodium hydrogen carbonate (Normapur), EtOH, acetic acid (100%), DMSO, sodium acetate, sodium formate and sodium citrate (Merck), gallium nitrate (ACROS), and Hepes (Aldrich) were used without further purification. Water and glassware were prepared as described previously.[14] FR295 and FR401 were synthesized and purified according to published procedures and were kept under vacuum at −20 °C.[8,10,13]

Stock Solutions: All stock solutions were used fresh. Because of the chelator's slight solubility in aqueous media ($< 10^{-3}$ M), FR295 and FR401 were first dissolved in ethanol at 10^{-2} M. These solutions were later diluted to the 10^{-4} to 10^{-5} M range in the final buffers. The solutions at pH < 2.5 were not buffered; those at 2.5 < pH < 3.5 were buffered with formate, those at 3.5 < pH < 6 with acetate, those at 6 < pH < 8.5 with Hepes and those at pH > 8.5 with carbonate. Buffer salt concentration was $5 \cdot 10^{-2}$ M and the final pH was attained by microinjections of concentrated HCl, NaOH, or AcOH. $FeCl_3$ solutions were prepared in acidic media at pH < 2. The Fe^{III} complexes of FR401 and FR295 were prepared in acidic media by adding the required amount of $FeCl_3$ to the ligands. The pH was then gently raised to final values by microinjections of concentrated NaOH. The final ionic strength of all solutions was adjusted to 0.2 with KCl. For pH > 5, all solutions were prepared under argon in a glove bag.

pH Measurements: The pH values were measured at 25±0.5 °C with a Jenco pH-meter equipped with an "Ingold" combined microelectrode calomel/glass. Buffers used for pH standardization were of pH = 4.00, 7.00, and 10.01 (Sigma).

Spectrophotometric Measurements: Spectrophotometric measurements were performed in anaerobic conditions under argon at 25±0.5 °C with a Cary C210 or a Perkin–Elmer Lambda 2 spectrophotometer equipped with a magnetic stirring device and thermostatted cell carrier. For each set of experiments, the spectra were recorded under different pH values. The reversibility of the observed processes with $[H^+]$ was checked at the end of each series of measurements by lowering the final pH to the initial values and by comparing the final to the initial absorption spectra. Values were discarded throughout the series where there was a difference of > 3% between the spectra of identical pH values. This was done in order to avoid the risk of catechol oxidation mainly in basic media.

Stopped-Flow Measurements: Kinetic measurements were performed by mixing acidic solutions of FR401 or FR295 with solutions of $FeCl_3$ under argon in an SF 3 L Hi-Tech stopped-flow spectrophotometer equipped with a thermostatted bath (25±0.5) °C.

Mathematical Formalism and Signal Analysis: The experimental conditions were set so as to permit the use of chemical relaxation formalism.[21] All experimental signals were analysed as described elsewhere.[14] They were all pure exponentials and were dealt with as relaxation modes.[14,19–21]

Solubility of the Ligands and Synthesis of the Fe^{III} and Ga^{III} Complexes with the FR295 and FR401 Ligands: Saturated ethanol solutions of FR401 and FR295 were added to solutions of $FeCl_3$ in 50% water and ethanol. The colour of the mixture immediately turned dark and a precipitate appeared. The pH was then gently raised to neutrality, and the precipitate filtered, washed, and dried under vacuum. It was slightly soluble in DMSO, ethanol, and methanol. Electrospray mass spectrometry experiments performed on the methanolic solutions of the precipitate showed only the presence of FR401 and FR295 ligands and iron. The same experiments were repeated by mixing the same alcoholic solutions of FR295 and FR401 with solutions of gallium nitrate. The solubility of the dark precipitate was too low to allow any NMR spectroscopic measurements. Both FR295 and FR401 are scarcely soluble in purely aqueous media. Under our experimental conditions the highest concentration attained was $< 10^{-3}$ M. This concentration did not allow the use of other measurement techniques such as potentiometric p***K*** determination.

[1] B. R. Byers, J. L. Arceneaux, in: *Metal Ions in Biological Systems, Iron Transport and Storage in Micro-organisms Plants and Animals* (Eds.: A. Sigel, H. Sigel), Marcel Dekker, New York, **1998**, vol. 35, pp. 37−66.
[2] R. R. Crichton, *Inorganic Biochemistry of Iron Metabolism*, Ellis Horwood, New York, **1991**.
[3] M. J. Miller, F. Malouin, *Acc. Chem. Res.* **1993**, *26*, 241−249.
[4] R. C. Hider, J. B. Porter, S. Singh, in: *The Development of Iron Chelators for Clinical Use* (Eds.: R. J. Bergereron, G. M. Brittenham), CRC Press, Boca Raton, **1994**, pp. 353−371.
[5] N. Lowther, R. Kox, B. Faller, H. Nick, Y. Jin, T. Sergejew, Y. Hirschberg, R. Oberle,, H. Donnelly, *Pharm. Res.* **1999**, *16*, 434−440.
[6] S. Ramurthy, M. J. Miller, *J. Org. Chem.* **1996**, *61*, 4120−4124.
[7] R. C. Hider, Z. Liu, *J. Pharmacy Pharmacology* **1997**, *49*, 59.
[8] H. Poras, G. Kunesch, J. C. Barrière, A. Andremont, *J. Antibiot. (Tokyo)* **1998**, *8*, 786−794.
[9] B. Pradines, F. Ramiandrasoa, L. K. Basco, L. Bricard, G. Kunesch, J. Le Bras, *Antimicrob. Agents Chemother.* **1996**, *40*, 2094−2098.
[10] R. Reissbrodt, F. Ramiandrasoa, L. Bricard, G. Kunesch, *BioMetals* **1997**, *10*, 95−103.
[11] P. Ollario, D. Wirth, *Journal of Pharm. Pharmacol.* **1997**, *49*, 29.
[12] J. Hu, M. J. Miller, *J. Am. Chem. Soc.* **1997**, *119*, 3462−3468.
[13] S. Bosne-David, L. Bricard, F. Ramiandrasoa, A. Deroussent, G. Kunesch, A. Andremont, *Antimicrob. Agents Chemother.* **1997**, *8*, 1937−1839.
[14] F. Bou Abdallah, J.-M. El Hage Chahine, *J. Mol. Biol.* **2000**, *303*, 255−266.
[15] W. R. Harris, C. J. Carrano, K. N. Raymond, *J. Am. Chem. Soc.* **1979**, *101*, 2722−2727.
[16] M. Persmark, J. B. Neilands, *BioMetals* **1992**, *5*, 29−36.
[17] P. Baret, C. G. Béguin, C. C Boukhalfa, J. P. Laulhère, J. L. Pierre, G. Serratrice, *J. Am. Chem. Soc.* **1995**, *117*, 9760−9761.
[18] A. M. Albrecht-Gary, A. L. Crumbliss, in: *Metal Ions in Biological Systems vol. 35*, *Iron Transport and Storage in Micro-organisms Plants and Animals* (Eds.: A. Sigel, H. Sigel), Marcel Dekker, New York, **1998**, pp. 239−327.
[19] M. Eigen, L. DeMaeyer, in: *Techniques of Organic Chemistry − Investigation of Rates and Mechanism of Reactions*, part II (Eds.: S. L. Friess, E. S. Lewis, A. Weissberger), Wiley Interscience, New York, **1963**, vol. 8, pp. 895−1029.
[20] C. F. Bernasconi, *Relaxation Kinetics*, Academic Press, New York, **1976**.
[21] R. Brouillard, *J. Chem. Soc., Faraday Trans. 1* **1982**, *76*, 583−587.
[22] J. L. Telford, K. N. Raymond, *Inorg. Chem.* **1998**, *37*, 4578−4583.
[23] J. M. El Hage Chahine, J. P. Bertigny, M. A. Schwaller, *J. Chem. Soc., Perkin Trans. 2* **1989**, 629−633.
[24] J. E. Dubois, H. Fakhrayan, J. P. Doucet, J. M. El Hage Chahine, *Inorg. Chem.* **1992**, *31*, 859−859.
[25] R. Winkler-Oswatitsch, M. Eigen, *Angew. Chem. Int. Ed. Engl.* **1979**, *18*, 20−49.
[26] A. J. Geall, R. J. Taylor, M. E. Earll, M. A. W. Eaton, I. S. Blagbrough, *Bioconjugate Chem.* **2000**, *11*, 314−326.
[27] J. M. El Hage Chahine, D. Fain, *J. Chem. Soc., Dalton Trans.* **1993**, 3137−3143.
[28] R. D. Hancock, A. E. Martell, *Chem. Rev.* **1989**, *89*, 1875−1914.
[29] R. G. Wilkins, *The Study of Kinetics and Mechanism of Reactions of Transition Metal Complexes*, Allyn and Bacon, Boston, **1976**.
[30] R. G. Pearson, *J. Am. Chem. Soc.* **1963**, *85*, 3533−3539.
[31] R. M. Smith, A. E. Martell, *Critical Stability Constants*, vol. 6, Plenum Press, New York, **1989**.
[32] M. Eigen, R. G. Wilkins, *Adv. Chem. Ser. Am. Chem. Soc.* **1965**, *49*, 55−65.
[33] M. Birus, Z. Bradic, N. Kujundzic, M. Fibranic, P. C. Wilkins, R. G. Wilkins, *Inorg. Chem.* **1985**, *24*, 3980−3983.
[34] S. M. Cohen, K. N. Raymond, *Inorg. Chem.* **2000**, *39*, 3624−3631.

Received October 25, 2000
[I00407]

Concerted Development of Chiral Conformations in [(Alkyloxycarbonyl)methyl]tricarbonyl(triphenylphosphane)cobalt Complexes

Claudia Zucchi,[a] Roland Boese,[b] Kathy Alberts,[a][‡] Thomas Herbrich,[a][‡] Gergely Tóth,[c] Lajos Bencze,[c] and Gyula Pályi*[a]

Keywords: Cobalt / Carbonyl ligands / Chirality / Phosphanes

The *trans*-[(alkyloxycarbonyl)methyl]tricarbonyl(triphenylphosphane)cobalt complexes $[ROC(O)CH_2]Co(CO)_3PPh_3$ (R = Me, *n*Pr, *i*Pr, *t*Bu, and *c*Hex) have been prepared and characterized by IR, ^1H, ^{13}C, and ^{31}P NMR spectroscopy. Crystal and molecular structure determination by X-ray diffraction analysis revealed the following phases: $P\bar{1}$ (R = Me), $P2_1/n$ (R = *n*Pr), $P\bar{1}$ (R = *i*Pr), $P2_1/c$ (R = *t*Bu), $P\bar{1}$ and $P2_1/c$ (R = *c*Hex). The results show concerted development of chiral conformations (both enantiomers) in all cases.

Introduction

The generation of molecular chirality presents an attractive challenge, both from an intellectual and a preparative point of view.[1] The mechanisms for the transfer of chiral information from one reacting group or molecule to the product are of the utmost importance for the design of more efficient systems.[2] In transition metal catalysed or assisted reactions, this transfer is usually an intramolecular process.[3] Since a number of the most efficient chiral ligands used in asymmetric catalysis (e.g., BINAP) exhibit conformational chirality,[4] the development of chiral conformations[5] in transition metal complexes acting as catalysts in these reactions represents an important research goal.

As part of a program aimed at learning more about the mechanisms of intramolecular transfer of chiral information in mono-[6] and dinuclear[7] organocobalt complexes, we have undertaken a systematic preparative and structural study of the [(alkyloxycarbonyl)methyl]tricarbonyl(triphenylphosphane)cobalt complexes, $[ROC(O)CH_2]Co(CO)_3PPh_3$ (R = Me, *n*Pr, *i*Pr, *t*Bu, and *c*Hex).[8] The results obtained with these complexes are reported herein.

Results and Discussion

trans-[(Alkyloxycarbonyl)methyl]tricarbonyl(triphenylphosphane)cobalt complexes (**3**) with achiral alkyl groups in the ester fragment (Me: **a**; *n*Pr: **b**; *i*Pr: **c**; *t*Bu: **d**; *c*Hex: **e**) were prepared in three steps. These steps (Scheme 1) consisted of ion metathesis, ligand-promoted carbonylation, and subsequent thermal decarbonylation.

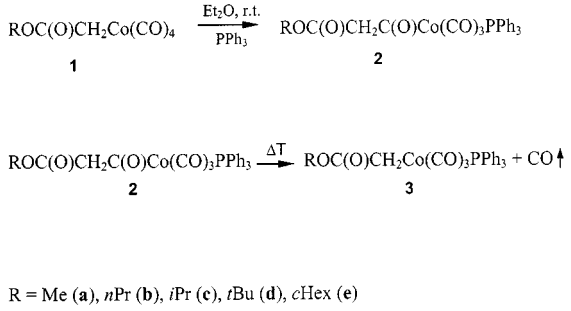

Scheme 1

The constitutions and structures of complexes **3** were established by elemental analyses, by IR and NMR spectroscopy (spectroscopic data were compared with those of previously characterized compounds of similar structure[6b,6c,8–10]), and by determination of the crystal and molecular structures of the crystalline products by X-ray diffraction analysis (Figures 1–3; Tables 1–6 in the Exp. Sect.).

The crystal structures belong to centrosymmetric space groups with two or four molecules per unit cell, respectively. The *c*Hex ester complex **3e** was obtained in two different crystal forms ($P\bar{1}$ and $P2_1/c$ phases), highlighting the fact that the conformational effects are not critically dependent on intermolecular forces but rather on intramolecular interactions. Complex **3a** contains one diethyl ether solvate

[‡] On leave from the Martin Luther University, Halle-Merseburg, Germany
[a] Department of Chemistry, University of Modena and Reggio Emilia,
Via Campi 183, 41100 Modena, Italy
E-mail: palyi@unimo.it
[b] Institute of Inorganic Chemistry, University of Essen,
Universitätstraße 5/7, 45117 Essen, Germany
[c] Müller Laboratory, Department of Organic Chemistry, University of Veszprém,
Egyetem-u. 6, 8200 Veszprém, Hungary

 © WILEY-VCH Verlag GmbH, 69451 Weinheim, 2001 1434–1948/01/0909–2297 $ 17.50+.50/0

molecule for every two molecules of the complex in the lattice of the $P\bar{1}$ phase; crystalline phases of the complexes **3b**−**e** were found to be solvate-free.

The X-ray diffraction results show that the overall molecular structure of complexes **3** (Figures 1−3) can be described in terms of approximate trigonal-bipyramidal geometry, with the two non-carbonyl ligands in the axial positions, which is a common feature of all alkyl-type [RCo-$(CO)_3$L][6b,6c,8a,9b,9c,11,12] and acyl-type [RC(O)Co$(CO)_3$L] (L = tertiary phosphane, I^-)[9b,9c,12,13] monosubstituted carbonylcobalt complexes. The molecules of complexes **3** may be regarded as being composed of three main moieties: (i) the (alkyloxycarbonyl)methyl fragment, (ii) the central (equatorial) $Co(CO)_3$ group, and (iii) the triphenylphosphane ligand (Scheme 2).

These moieties are linked by two single bonds, Co−C(H_2) and Co−P, about which rotation can occur. The C(H_2)−C(O) and P−C_{ar} bonds, rotations about which are directly related to the chiral inversions, are far away from each other with the cobalt atom and the Co−C(H_2) and Co−P bonds in between. The plane of the five heavy atoms of the ester group C−C(O)OC is oriented quasi-parallel to the plane of the $Co(CO)_3$ group (interplanar angle less than 25°). Other possible conformations of this group allowed by the rotation around the C_{sp^2}−C_{sp^3} bond are not populated. The slightly bent carbonylcobalt "plane" (consisting of seven atoms) has its concave face directed towards the ester fragment.

The σ-bond system that extends along the molecular axis is composed of two- and threefold conformational axes and adopts a highly relaxed staggered conformation throughout the molecule. The substituents at the sp^3-carbon atom (adjacent to Co), i.e. two H atoms and the ester group, are positioned above the OC−Co−CO forks (Scheme 3).

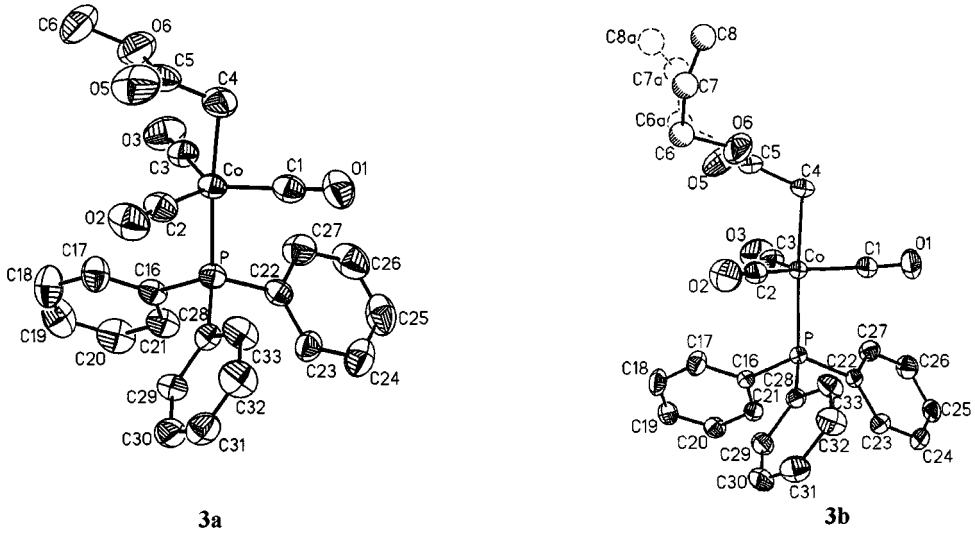

Figure 1. ORTEP drawing of the X-ray molecular structure of the complexes **3a** and **3b**, perpendicular view to the Co−P axis (one structure each)

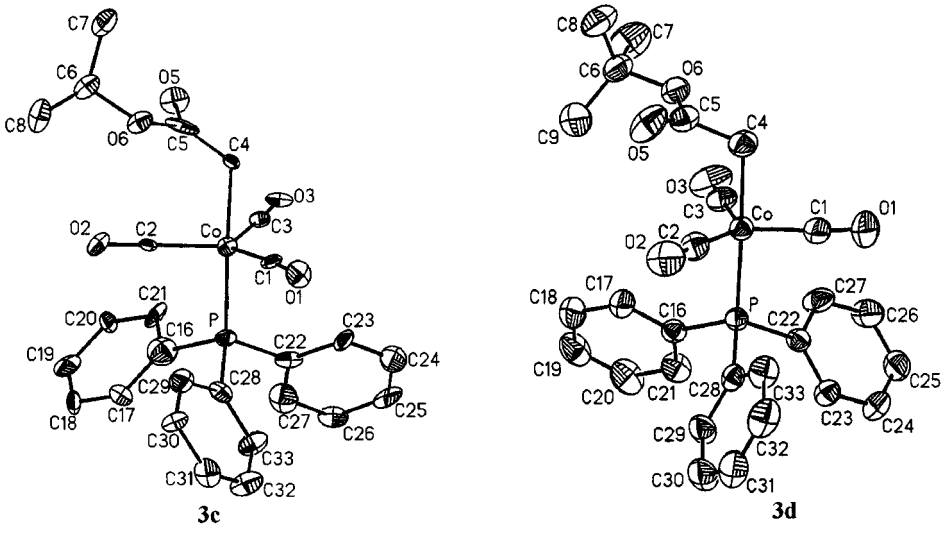

Figure 2. ORTEP drawing of the X-ray molecular structure of complexes **3c** and **3d**, perpendicular view to the Co−P axis (one structure each)

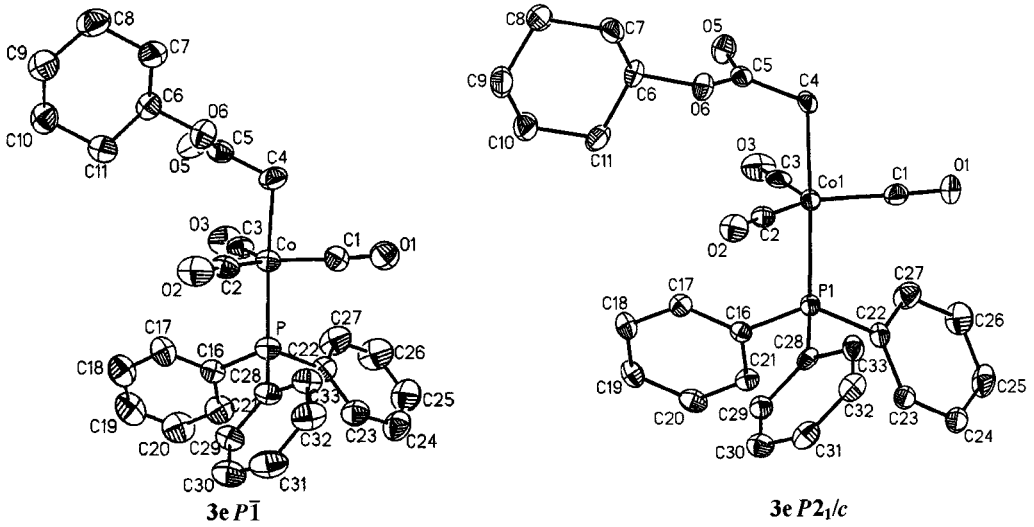

Figure 3. ORTEP alrawing of the X-ray molecular structure of complex **3a** ($P\bar{1}$ and $P2_1/c$ phases), perpendicular view to the Co−P axis (one structure each)

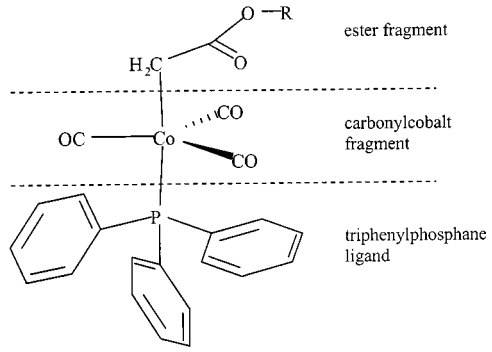

Scheme 2. Main fragments of the complexes **3**

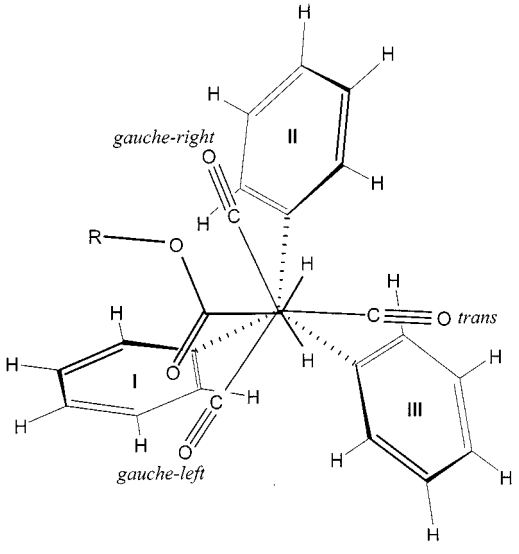

Scheme 3. Complexes **3**, view in the Co−P axis

Due to the bulkiness of the ester group, the adjacent OC−Co−CO angle is widened to release the strain, with a concomitant compression of the other angles at Co. The staggered conformation of the $Co(CO)_3-PPh_3$ rotor is manifested in the orientation of the *ortho*-H atoms of the aromatic rings towards the equatorial plane rather than in the orientations of the $P-C_{ar}$ bonds. The "natural" (as in the free ligand) propeller shape of the triphenylphosphane ligand is preserved, but the positions ($Co-P-C_{ar}-C_{ar}$ angles) of the individual phenyl rings are not identical in complexes **3a**−**e** due to the perturbation, which seems to be most pronounced at the Ph group denoted by **I** in Scheme 3. This perturbation is clearly less pronounced in the methyl ester (**3a**) and the *n*-propyl ester (**3b**) and reaches a maximum in the isopropyl derivative (**3c**). It is not so great in the *tert*-butyl ester (**3d**), for reasons which will be discussed later.

An interesting feature seen in all but one (**d**) of the complexes **3** is a relatively short intramolecular contact between an α-H atom of the ester group and the ester carbonyl oxygen atom, as illustrated for the cyclohexyl derivative **3e** in Figure 4. The distance of this intramolecular interaction is certainly within the limits for H-bonding[14,15] (2.9−3.3[14a] or even 3.6 Å[14b] between two bridged heavy atoms). The five atoms (O−C−O−C−H) define a somewhat distorted ring. The formation of such a ring cannot be observed in the case of the *t*Bu derivative (**3d**), which lacks an α-H atom on the ester group. The charge transfer to the ester carbonyl group is also reflected in a shift to higher wavenumbers of its ν(C−O) band in the solution IR spectra; complex **3d** shows the lowest-energy absorption in this series. This systematic change in the solution spectra also indicates that the ring-forming H-bond interaction remains intact in *n*-hexane solution. The formation of this H-bonded ring obviously contributes to the rigidity of the ester group.

Where the ester has two α-H atoms, the >C=O···H−C(H)R interaction leads to a differentiation of the hydrogen atoms of this $>CH_2$ group. This generates a centre of chirality at the ester α-C_{sp^3} atom of complex **3b** as well as at the corresponding position in the Et derivative

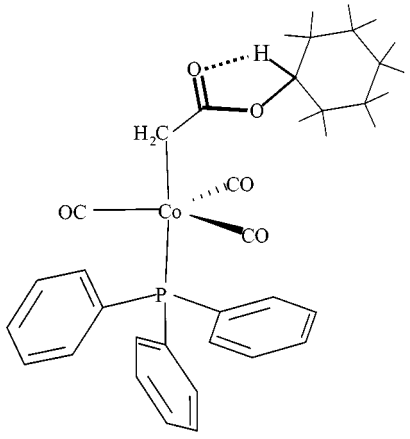

	OH (Å)	O-C(sp^3) (Å)	O-C-O-C (deg.)	C-O-C-H (deg.)
3e P-1	2.317	2.699	1.0	-21.3
3e $P2_1/c$	2.264	2.703	10.4	-11.0

Figure 4. Conformations of the ester and triphenylphosphane ligands

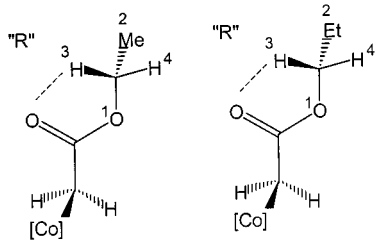

[Co] = *re*,**P**-$Co(CO)_3PPh_3$

Scheme 4. New centres of chirality generated by hydrogen bonding

(discussed elsewhere[8a,16]), as shown in Scheme 4. We were, however, unable to detect this effect in the solution phase by low-temperature ^1H NMR spectroscopy down to −80 °C in CD_2Cl_2 or to −50 °C in [D_6]acetone.

An additional "through-space" interaction could be identified between the Co atom and the ester $C_{sp}{}^2$ atom in complexes **3a**−**e**. These atoms are separated by only 292−298 pm (Table 6), which is significantly shorter than the sum of the van der Waals radii (Co−C 385 pm[17]), indicating a kind of coordinative interaction (termed "auto-solvation"[18]) between these atoms. As a result of this interaction, the carboxyl $C_{sp}{}^2$ atom becomes tetracoordinated; since it then bears four different substituents, it can adopt (*R*) and (*S*) enantiomeric configurations, as shown in Scheme 5.

Scheme 5

The overall approximate trigonal-bipyramidal geometry of complexes **3** is very important with regard to the main viewpoint of the present study: The *trans*-axial distribution of the (generally) flexible alkyl (or acyl) and phosphane ligands provides an ideal situation for the investigation of concertedness in the development of certain conformations in these ligands on the "opposite" sides of the molecule. In fact, a quantitative concertedness can be observed for the conformations of the ester fragment, with respect to the $Co(CO)_3$ moiety, and the triphenylphosphane ligand in all derivatives **3** described herein (the schematic representation

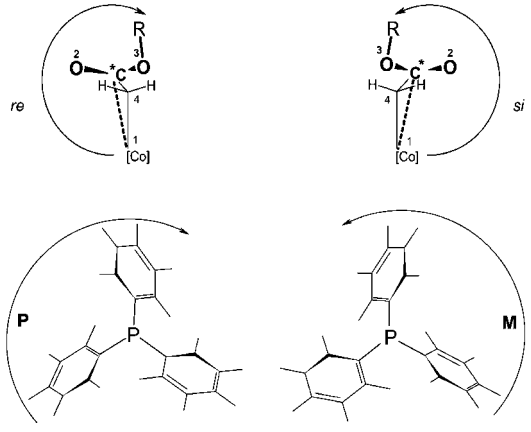

Scheme 6

Table 1. ν(C−O) bands in the FT-IR spectra of compounds **1**−**3** in *n*-hexane [cm^{-1}]

	a	**b**	**c**	**d**	**e**
1	2112 m, 2046 s, 2037 vs, 2028 vs, 1752 vw, 1721 w	2112 m, 2046 s, 2036 vs, 2027 vs, 1746 vw, 1717 w	2111 m, 2046 s, 2036 vs, 2027 vs, 1750 (sh), 1742 w, 1713 m	2111 m, 2044 s, 2035 vs, 2026 vs, 1760 (sh), 1740 m, 1708 w	2111 m, 2045 s, 2035 vs, 2027 vs, 1760 (sh), 1740 w, 1715 w
2	2050 vw, 1986 s, 1975 s, 1755 w, 1702 w	2053 w, 1987 s, 1969 s, 1747 m, 1680 m	2050 vw, 1988 s, 1978 s, 1744 w, 1704 w	−[a]	2046 w, 1984 s, 1975 s, 1740 w, 1700 w
3	2050 vw, 1985 s, 1974 s, 1712 w	2050 vw, 1985 s, 1974 s, 1709 w	2050 vw, 1984 s, 1974 s, 1704 w	2050 vw, 1984 s, 1973 s, 1700 w	2046 w, 1984 s, 1975 s, 1705 w

[a] Decomposed during measurement.

Table 2. ^{1}H NMR signals due to the CH_2 protons in complexes **1** and **3** in $CDCl_3$ (δ in ppm, *J* in Hz)

	a	**b**	**c**	**d**	**e**
1	2.19	2.19	2.19	2.18	2.19
3	2.20 ($^3J_{HP}$ = 3.34)	2.20 ($^3J_{HP}$ = 2.86)	2.20 ($^3J_{HP}$ = 2.93)	2.15 ($^3J_{HP}$ = 2.86)	2.16 ($^3J_{HP}$ = 3.10)

Table 3. ^{13}C NMR signals (^{1}H-decoupled) of the CH_2 carbon atoms in complexes **1** and **3** in $CDCl_3$ (δ in ppm, *J* in Hz)

	a	**b**	**c**	**d**	**e**
1	6.98	7.98	8.03	8.04	8.01
3	4.56 ($^3J_{CP}$ = 16.318)	5.75 ($^3J_{CP}$ = 16.518)	5.76 ($^3J_{CP}$ = 16.452)	5.85 ($^3J_{CP}$ = 16.454)	5.78 ($^3J_{CP}$ = 16.145)

Table 4. ^{31}P NMR signals (^{1}H-decoupled) of complexes **3** in $CDCl_3$ (δ in ppm)

	a	**b**	**c**	**d**	**e**
3	57.30	57.22	57.43	57.56	57.78

and the notation used for these conformations is shown in Scheme 6).

The following two important points emerged:

(i) In the solid phase, the molecules invariably show 100% concertedness in the sense that for each conformer of the ester group, there is *only one* corresponding conformer of the triphenylphosphane fragment.

Table 5. Experimental parameters relating to the X-ray diffraction measurements of complexes **3**

	a	**b**	**c**	**d**	**e** ($P\bar{1}$)	**e** ($P2_1/c$)
Empirical formula	$C_{24}H_{20}CoO_5P \cdot {}^1/_2\ C_4H_{10}O$	$C_{26}H_{24}CoO_5P$	$C_{26}H_{24}CoO_5P$	$C_{27}H_{26}CoO_5P$	$C_{29}H_{28}CoO_5P$	$C_{29}H_{28}CoO_5P$
Molecular mass	515.387	506.380	506.380	520.407	546.445	546.445
Temperature	r.t.	r.t.	125 K	r.t.	r.t.	125 K
Wavelength [Å]	0.71069	0.71069	0.71069	0.71069	0.71069	0.71069
Crystal system, space group	$P\bar{1}$	$P2_1/n$	$P\bar{1}$	$P2_1/c$	$P\bar{1}$	$P2_1/c$
Unit cell dimensions:						
a [Å]	9.838(2)	9.575(1)	9.813(4)	13.789(3)	9.625(2)	9.968(4)
b [Å]	10.175(2)	18.169(2)	10.852(4)	11.406(3)	11.349(2)	21.094(8)
c [Å]	14.201(5)	14.662(2)	12.648(5)	17.854(4)	14.368(2)	13.215(6)
α [°]	73.71(2)	90	85.70(3)	90	102.30(1)	90
β [°]	70.40(2)	104.49(1)	77.75(3)	109.27(2)	108.24(1)	104.13(3)
γ [°]	87.65(2)	90	67.43(3)	90	103.38(1)	90
Volume [Å^3]	1283.0(6)	2469.5(5)	1212.0(8)	2651.0(1)	1379.2(4)	2694.6(1.6)
Z, calculated density [Mg/m^3]	2, 1.239	4, 1.362	2, 1.384	4, 1.304	2, 1.313	4, 1.345
Absorption coefficient [mm^{-1}]	0.76	0.79	0.81	0.74	0.72	0.73
Crystal size [mm^3]	0.27×0.25×0.18	0.48×0.33×0.27	0.30×0.26×0.18	0.48×0.36×0.27	0.32×0.27×0.21	0.23×0.19×0.17
θ range for data collection	3° ≤ 2θ ≤ 47°	3° ≤ 2θ ≤ 55°	3° ≤ 2θ ≤ 45°	3° ≤ 2θ ≤ 50°	3° ≤ 2θ ≤ 45°	3° ≤ 2θ ≤ 48°
Reflections collected/unique	4429/4223	6074/5655	4861/3170	4720/4305	5027/3572	4527/4205
Absorption correction	no	no	[a]	no	no	no
Refinement method	full matrix	full matrix	full matrix	full matrix	full matrix	full matrix
Final *R* indices [$I > 2\sigma(I)$]	0.0570	0.0486	0.0375	0.0435	0.0812	0.0438
R indices (all data; R_{ω})	0.1441	0.1340	0.0991	0.1153	0.2555	0.1150
Largest diff. peak and hole [eÅ^{-3}]	0.51 and −0.27	0.55 and −0.42	0.43 and −0.25	0.46 and −0.66	0.68 and −1.00	0.55 and −0.43
Instrument	Nicolet R3M/V	Nicolet R3M/V	Nicolet R3M/V	Siemens P4	Nicolet R3M/V	Nicolet R3M/V
Program	SHELXTL-PLUS; micro VAX II	SHELXTL-PLUS; micro VAX II	SHELXTL-PLUS; micro VAX II	SHELXTL-PLUS; SGI IRIS Indigo	SHELXTL-PLUS; micro VAX II	SHELXTL-PLUS; micro VAX II

[a] Empirical, ψ-scan in the 2θ range [°]: 3 ≤ 2θ ≤ 50; min./max. transmission: 0.72/0.87; $R_{merg.}$ before/after correction: 0.054/0.044.

(ii) The above mechanism excludes 50% of the statistically possible combinations, allowing only *re*,**M** and *si*,**P** for **3a**, **3c**, and **3d**, and only *re*,**P** and *si*,**M** for **3b** and for the two phases of **3e**.

This selection rule appears to be independent of (a) the number of molecules in the unit cell ($Z = 2$ or 4 for complexes **3**), and (b) the point group (as demonstrated by the behaviour of the two different phases of complexes **3e**). Recently, we performed an exhaustive molecular mechanical and quantum chemical analysis of the ethyl ester derivative[8a,16] $EtOC(O)CH_2Co(CO)_3PPh_3$. In this study, we found that the concerted conformational changes in this complex are controlled by a clockwork-analogous mechanism, where the displacements in the ester ligand are "felt" by the phosphane by transmission through the cogwheel-like $Co(CO)_3$ moiety.[16] This mechanism is responsible for the marked reduction in the number of statistically possible isomers to the number observed experimentally. The main goal of the present study has been to explore whether this concerted development of conformations is operative for other ester derivatives, with configurationally achiral groups in the ester fragment. The six structures reported in the present paper indicate a fairly general validity of this rule.

Beyond the correlations in the development of chiral conformations in molecules **3**, a strict correlation of these chiral conformations with the "secondary" centres of chirality, identified in the crystalline phases, has been observed. The (*R*) and (*S*) enantiomers (formed by H-bonding) of the ester alkyl α-C_{sp}^3 atoms (Scheme 4) in the Et and *n*Pr derivatives are 100% correlated to the corresponding *re*,**P** and *si*,**M** conformations, respectively.

These findings will hopefully aid detailed understanding of the mechanism of the intramolecular transfer of chiral information, which is of particular importance with regard to the design of third-generation (conformational) chiral catalysts and auxiliaries. We are extending our investigations to ester derivatives containing one or more configurational chiral centre(s) in the ester group or the phosphane ligand. The findings of these studies will be reported in subsequent papers.

Experimental Section

General Remarks: Starting materials were of commercial origin, with the exception of cyclohexyl bromoacetate[19] and octacarbonyldicobalt,[20] which were prepared by published procedures. − All

Table 6. Selected bond lengths and angles in complexes **3**

	Me *re***M**/*si***P**	*n*Pr *re***P**/*si***M**	*i*Pr *re***M**/*si***P**	*t*Bu *re***M**/*si***P**	*c*Hex1 *re***P**/*si***M**	*c*Hex2 *re***P**/*si***M**
Distances [Å]						
Co−P	2.213	2.216	2.208	2.214	2.211	2.217
Co−C_{sp3}	2.089	2.084	2.090	2.076	2.064	2.090
Co−C_{sp} (*trans*)	1.767	1.777	1.788	1.791	1.703	1.793
Co−C_{sp} (*gauche*-right)	1.778	1.778	1.789	1.790	1.781	1.788
Co−C_{sp} (*gauche*-left)	1.788	1.787	1.800	1.773	1.775	1.789
C=O (ester)	1.206	1.197	1.212	1.190	1.218	1.213
C−O (ester)	1.332	1.331	1.352	1.350	1.344	1.356
C−O (*trans*)	1.138	1.137	1.145	1.132	1.187	1.143
C−O (*gauche*-right)	1.138	1.141	1.143	1.137	1.144	1.150
C−O (*gauche*-left)	1.132	1.133	1.212	1.142	1.150	1.143
Co−C_{sp2}	2.949	2.953	2.975	2.919	2.955	2.933
Angles [°]						
Co−C_{sp3}−C_{sp2}	110.8	111.6	111.9	108.9	112.8	109.4
P−Co−C_{sp3}	175.5	176.1	177.1	178.1	176.5	176.8
Co−P−C_{ar} (I)	106.0	115.2	112.5	112.9	115.5	114.4
Co−P−C_{ar} (II)	113.5	114.8	116.0	113.9	113.4	113.4
Co−P−C_{ar} (III)	114.4	114.2	113.8	116.0	113.8	116.1
C_{sp}(*g.*-right)−Co−C_{sp}(*g.*-left)	117.3	119.9	117.8	126.7	120.7	125.1
C_{sp}(*trans*)−Co−C_{sp}(*g.* right)	120.7	119.2	120.4	114.2	120.7	119.5
C_{sp}(*g.*-left)−Co−C_{sp}(*trans*)	121.3	120.2	121.3	118.7	117.9	115.1
P−Co−C_{sp} (*trans*)	92.0	92.5	92.3	95.0	92.3	94.6
P−Co−C_{sp} (*gauche*-right)	92.5	93.2	91.4	90.9	92.2	89.8
P−Co−C_{sp} (*gauche*-left)	93.2	92.5	93.7	91.5	93.3	92.0
C_{sp} (*trans*)−Co−C_{sp3}	83.5	84.6	84.9	86.9	84.3	87.1
C_{sp} (*gauche*-right)−Co−C_{sp3}	89.6	90.5	90.2	88.1	89.2	87.0
C_{sp} (*gauche*-left)−Co−C_{sp3}	89.6	86.8	87.6	87.8	88.7	89.7
Dihedral angles [°]						
Co−C_{sp3}−C_{sp2}−O_{sp3}	−91/91	−76/76	−80/80	−91/91	−76/76	−93/93
Co−P−C_{ar}−C_{ar}(**I**)	43/−43	47/−47	55/−54	36/−36	−41/41	−38/38
Co−P−C_{ar}−C_{ar}(**II**)	41/−41	46/−46	43/−43	45/−45	−48/48	−52/52
Co−P−C_{ar}−C_{ar}(**III**)	46/−46	45/−45	41/−42	36/−36	−48/48	−38/38

operations were performed using standard Schlenk techniques.[21] − IR spectra were recorded with a Bruker FT-IR IFS 113V spectrometer. − ^{1}H, ^{13}C, and ^{31}P NMR spectra were recorded with a Bruker AMX-400 instrument. − X-ray diffraction measurements were made with a Nicolet R3m/V four-circle diffractometer with Mo-K_α radiation at 298 K. Calculations were performed using the Bruker-AXS SHELXTL Vers. 5.10. Atomic scattering factors were taken from SHELXTL and ref.[22] Corrections for anomalous dispersion were made according to ref.[23] − For the preparation of the alkylcobalt complexes $[ROC(O)CH_2]Co(CO)_3PPh_3$, the procedures followed were essentially those described in ref.[8b] (Scheme 1).

Preparation of *c*HexOC(O)CH$_2$Co(CO)$_3$PPh$_3$ (3e): $Co_2(CO)_8$ (171 mg, 0.5 mmol) in Et_2O (15 mL) was reduced to $Na[Co(CO)_4]$ with Na/Hg. The resulting solution, containing 1 mmol of $Na[Co(CO)_4]$, was filtered into a Schlenk vessel under Ar and then cooled to −20 °C. Under stirring, cyclohexyl bromoacetate (221 mg, 1 mmol) was added in a single portion, which led to the immediate precipitation of white NaBr. Stirring was continued at this temperature for 4 h, in the course of which the colour of the solution gradually became more yellow and eventually turned brown. Thereafter, the solution was allowed to warm to room temperature and stirred for a further 1 h. A sample was taken (1 mL), which was analysed by IR spectroscopy in the 1600−2200 cm^{-1} range. This analysis showed the disappearance of the strong band due to $[Co(CO)_4]^-$ (at ca. 1900 cm^{-1}) and the emergence of a band system corresponding to an $RCo(CO)_4$-type complex,[9] further accompanied by an "organic" ν(C−O) absorption at ca. 1720−1710 cm^{-1}. This result indicated *c*HexOC(O)CH$_2$Co(CO)$_4$ (**1e**) to be the only carbonylcobalt species present in the reaction mixture. The solution was then filtered and to the filtrate, containing 1 mmol of complex **1e**, triphenylphosphane [P(C$_6$H$_5$)$_3$; 262 mg, 1 mmol] was added in a single portion at room temp. The resulting mixture was stirred for 3 h, in the course of which a gradual colour change from brown to light-yellow was observed. At this point, a sample (1 mL) was withdrawn and analysed by IR spectroscopy in the C−O stretching range (1600−2200 cm^{-1}); complete disappearance of the band system attributed to complex **1e** was observed, and two new band systems had emerged with an approximate intensity ratio of 1:9. The stronger band system, showing absorptions at higher wavenumbers, was attributed to the acylcobalt-type complex *c*HexOC(O)CH$_2$C(O)Co(CO)$_3$(PPh$_3$) (**2e**)[9] based on the fact that two acyl ν(C−O) bands were observed for this system. The weaker band pattern was assigned to *c*HexOC(O)CH$_2$Co(CO)$_3$(PPh$_3$) (**3e**) on the basis of comparisons with the spectra of previously characterized $ROC(O)CH_2Co(CO)_3PPh_3$ complexes.[6,8] The reaction mixture was subsequently warmed to 32 °C and stirred for a further 8 h at this temperature. After this treatment, a further sample was analysed by IR spectroscopy. This analysis showed the quantitative transformation of the acyl-type complex **2e** to the alkyl-type complex **3e**. The solvent was then evaporated at room temp. under reduced pressure. The crude product was recrystallized from Et_2O/*n*-hexane (ca. 6:1) to yield a yellow crystalline product (178 mg, 32.6%). This was characterized by elemental analyses, IR and NMR spectroscopy, and X-ray diffraction analysis. − $C_{29}H_{28}CoO_5P$ (546.445): calcd. C 63.74, H 5.16, Co 10.78, P 5.67; found C 63.9, H 5.4, Co 10.8, P 5.7. − X-ray diffraction analysis of this product revealed a $P\bar{1}$ phase (see later). The crude product obtained from an identical experiment was recrystallized from *n*-hexane. This operation yielded 168 mg (30.8%) of a yellow crystalline product, which was subsequently identified as belonging to the $P2_1/c$ phase. − Found C 63.8, H 5.3, Co 11.0, P 5.5.

Complexes 3a, 3b, 3c, and 3d: These were prepared by essentially the same procedure as described above. IR, ^{1}H, ^{13}C, and ^{31}P NMR spectroscopic data are listed in Tables 1, 2, 3, and 4. Experimental parameters relating to the X-ray diffraction measurements are shown in Table 5. Selected bond lengths and angles are collected in Table 6. Crystallographic data (excluding structure factors) for the structures reported in this paper have been deposited with the Cambridge Crystallographic Data Centre as supplementary publication no. CCDC-163127 (**3a**) -163128 (**3b**), -163129 (**3c**), -163130 (**3d**), -163131 (**3e** monoclinic), -163132 (**3e** triclinic). Copies of the data can be obtained free of charge on application to the CCDC, 12 Union Road, Cambridge CB2 1EZ, U.K. [Fax: (internat.) + 44-1223/336-033; E-mail: deposit@ccdc.cam.ac.uk].

3a: $C_{26}H_{22}CoO_{5.5}P$ [**3a**·$^1/_2(C_2H_5)_2O$] (515.387): calcd. C 60.95, H 4.33; found C 61.1, H 4.7.

3b: $C_{26}H_{24}CoO_5P$ (506.380): calcd. C 61.67, H 4.78; found C 62.1, H 5.0.

3c: $C_{26}H_{24}CoO_5P$ (506.380): calcd. C 61.67, H 4.78, Co 11.64, P 6.12; found C 61.9, H 5.1, Co 11.3, P 5.9.

3d: $C_{27}H_{26}O_5CoP$ (520.407): calcd. C 62.32, H 5.04, Co 11.32; found C 62.1, H 5.1, Co 10.8.

Acknowledgments

We acknowledge financial support of this work by the [Italian] Ministry of University and Research (MURST; 60%), the [Italian] National Research Council (CNR), and the [Hungarian] OTKA program (contract nos: T-016326 and T-035221).

[1] Reviews on theoretical problems: [1a] L. Keszthelyi, *Quart. Rev. Biophys.* **1995**, *28*, 473−507. − [1b] D. Cline, *Comments Nucl. Part. Phys.* **1997**, *22*, 131−154. − [1c] L. Markó, *Diss. Savariensis* **1998**, *24*, 1−64. − [1d] G. Pályi, C. Zucchi, L. Caglioti, in: *Advances in BioChirality* (Eds.: G. Pályi, C. Zucchi, L. Caglioti), Elsevier, Amsterdam, **1999**, pp. 3−12. − [1e] L. Keszthelyi, in: *Advances in BioChirality* (Eds.: G. Pályi, C. Zucchi, L. Caglioti), Elsevier, Amsterdam, **1999**, pp. 99−103. − Reviews on preparative aspects: [1f] J. Ojima (Ed.), *Catalytic Asymmetric Synthesis*, VCH, New York, **1993**. − [1g] H. Brunner, W. Zettlmeier, *Handbook of Enantioselective Catalysis*, vols. 1−2, VCH, Weinheim, **1993**. − [1h] R. A. Sheldon, *Chirotechnology*, M. Dekker, New York, **1993**. − [1i] S. C. Stinson, *Chem. Eng. News* **1998** (Sept. 21), 83−104; **1999** (Oct. 11), 101−120; **2000** (May 8), 59−70.

[2] P. Heimbach, T. Bartik, *An Ordering Concept on the Basis of Alternative Principles in Chemistry*, Springer, Berlin, **1990**, chapter 5.3.

[3] See, for example, almost all mechanisms discussed in: B. Cornils, W. A. Herrmann (Eds.), *Applied Homogeneous Catalysis with Organometallic Compounds*, vols. 1−2, VCH, Weinheim, **1996**.

[4] [4a] R. Noyori, *Science* **1990**, *248*, 1194−1199. − [4b] H. Takaya, T. Ohta, K. Mashima, R. Noyori, *Pure Appl. Chem.* **1990**, *62*, 1135−1138. − [4c] R. Noyori, *Acta Chem. Scand.* **1996**, *50*, 380−390.

[5] Selected references: [5a] H. Dodziuk, *Tetrahedron: Asymmetry* **1992**, *3*, 43−50. − [5b] H. Dodziuk, *Modern Conformational Analysis*, VCH, New York, **1995**. − [5c] S. E. Garner, A. G. Orpen, *J. Chem. Soc., Dalton Trans.* **1993**, 533−541. − [5d] N. Nardi, B. Bagchi, *J. Am. Chem. Soc.* **1996**, *118*, 11208−11216. − [5e] Y. Inoue, H. Tsuneishi, T. Hakushi, A. Tai, *J. Am. Chem. Soc.* **1997**, *119*, 472−478. − [5f] S. B. Prusiner, *Science* **1997**, *278*, 245−251. − [5g] M. Simonyi, *Adv. Drug Res.* **1997**, *30*, 73−110.

[6] [6a] V. Galamb, G. Pályi, M. Kajtár, *Inorg. Chim. Acta* **1981**, *55*, L113−L114. − [6b] G. Pályi, C. Zucchi, T. Bartik, T. Herbrich, C. Kriebel, R. Boese, A. Sorkau, G. Frater, *Atti Accad. Sci. Bologna, Rend. Cl. Sci. Fis.* **1992/93**, *281* [14/10], 159−167. − [6c] G. Pályi, K. Alberts, T. Bartik, R. Boese, G. Fráter, T. Herbrich, A. Herfurth, C. Kriebel, A. Sorkau, C. M. Tschoerner, C. Zucchi, *Organometallics* **1996**, *15*, 3253−3255.

[7] M. Kajtár, J. Kajtár-Miklós, G. Giacomelli, G. Gaál, G. Váradi, I. T. Horváth, C. Zucchi, G. Pályi, *Tetrahedron: Asymmetry* **1995**, *6*, 2177−2194.

[8] [8a] V. Galamb, G. Pályi, F. Cser, M. G. Furmanova, Yu. T. Struchkov, *J. Organomet. Chem.* **1981**, *209*, 183−195. − [8b] V. Galamb, G. Pályi, in: *Organometallic Syntheses* (Eds.: J. J. Eisch, R. B. King.), vol. 3, Elsevier, Amsterdam, **1986**, pp. 142−146.

[9] [9a] V. Galamb, G. Pályi, *J. Chem. Soc., Chem. Commun.* **1982**, 487−488. − [9b] V. Galamb, G. Pályi, F. Ungváry, L. Markó, R. Boese, G. Schmid, *J. Am. Chem. Soc.* **1986**, *108*, 3344−3351. − [9c] V. Galamb, G. Pályi, R. Boese, G. Schmid, *Organometallics* **1987**, *6*, 861−867. − [9d] J. Somlyai-Haász, F. Haász, V. Galamb, A. Benedetti, C. Zucchi, G. Pályi, T. Krümmling, B. Happ, T. Bartik, *J. Organomet. Chem.* **1991**, *419*, 205−217. − [9e] C. Zucchi, G. Pályi, V. Galamb, E. Sámpár-Szerencsés, L. Markó, P. Li, H. Alper, *Organometallics* **1996**, *15*, 3222−3231.

[10] Z. Nagy-Magos, G. Bor, L. Markó, *J. Organomet. Chem.* **1968**, *14*, 205−209.

[11] F. Ungváry, I. Kovács, B. Hammerschmidt, G. Cordier, *Organometallics* **1993**, *12*, 2849−2852.

[12] Reviews: [12a] V. Galamb, G. Pályi, *Coord. Chem. Rev.* **1984**, *59*, 203−238. − [12b] I. Kovács, F. Ungváry, *Coord. Chem. Rev.* **1997**, *161*, 1−32.

[13] [13a] T. Bartik, T. Krümmling, C. Krüger, L. Markó, R. Boese, G. Schmid, P. Vivarelli, G. Pályi, *J. Organomet. Chem.* **1991**, *421*, 323−333. − [13b] C. Zucchi, A. Cornia, R. Boese, E. Kleinpeter, H. Alper, G. Pályi, *J. Organomet. Chem.* **1999**, *586*, 61−69. − [13c] M. Röper, C. Krüger, *J. Organomet. Chem.* **1988**, *339*, 159−164.

[14] Reviews: [14a] J. Rebek, Jr., *Acc. Chem. Res.* **1990**, *23*, 399−404. − [14b] G. R. Desiraju, *Acc. Chem. Res.* **1991**, *24*, 290−296. − [14c] J. C. MacDonald, G. M. Whitesides, *Chem. Rev.* **1994**, 2383−2420. − [14d] G. R. Desiraju, *Angew. Chem. Int. Ed. Eng.* **1995**, *34*, 2311−2327.

[15] Some selected references on C−H···O hydrogen bonding: [15a] G. R. Desiraju, *J. Chem. Soc., Chem. Commun.* **1990**, 454−455. − [15b] J. D. Chaney, C. R. Gross, K. Folting, B. D. Santarsiero, M. D. Hollingsworth, *J. Am. Chem. Soc.* **1996**, *118*, 9432−9433. − [15c] J. L. Karle, D. Ranganathan, V. Haridas, *J. Am. Chem. Soc.* **1996**, *118*, 7128−7133. − [15d] F. H. Allen, V. J. Hoy, J. A. K. Howard, V. R. Thalladi, G. R. Desiraju, C. C. Wilson, G. J. McIntyre, *J. Am. Chem. Soc.* **1997**, *119*, 4377−3480.

[16] L. Bencze, R. Szilágyi, M. Szabó, R. Boese, C. Zucchi, G. Pályi, in: *Fundamentals of Life*, Elsevier, Paris, accepted.

[17] [17a] G. Capaccio, P. Giacomello, E. Giglio, *Acta Crystallogr., Sect. A* **1971**, *27*, 229−233. − [17b] A. I. Kitaigorodski, *Organic Chemical Crystallography*, Consultant Bureau, New York, **1961**. − [17c] F. Cser, *Acta Chim. (Budapest)* **1974**, *80*, 317−331. − [17d] N. L. Allinger, J. A. Hirsch, M. A. Miller, I. J. Tyminsky, *J. Am. Chem. Soc.* **1969**, *91*, 337−343.

[18] G. Pályi, *Transition Met. Chem.* **1977**, *2*, 273−275.

[19] From esterification of $BrCH_2C(O)Br$ with *c*HexOH. See, for example: I. T. Harrison, S. Harrison, *Compendium of Organic Synthetic Methods*, vol. 1, Wiley & Sons, New York, **1971**, p. 272.

[20] P. Szabó, L. Markó, G. Bor, *Chem. Techn. (Berlin)* **1961**, *13*, 549−550.

[21] D. F. Shriver, M. A. Drezdzon, in: *Manipulation of Air-Sensitive Compounds*, 2nd ed., Wiley, New York, **1986**.

[22] D. T. Cromer, J. B. Mann, *Acta Crystallogr., Sect. A* **1968**, *24*, 321−324.

[23] $\Delta f'$, $\Delta f''$ from: D. T. Cromer, D. Liberman, *J. Chem. Phys.* **1970**, *53*, 1891−1898.

Received November 8, 2000
[I00424]

Ruthenium-Capping of Di- and Tetraethynylbiphenyls

Berta Gómez-Lor,[a] Amelia Santos,*[a] Marta Ruiz,[a] and Antonio M. Echavarren*[b]

Keywords: Ruthenium / Vinylidene complexes / Hydrido complexes / Alkynes

The di- and tetraalkynyl biphenyls **3** and **5** have been synthesized from the tetrabromo derivative **1** by using Pd-catalyzed cross-coupling reactions. The reaction of **3** or **5** with *cis*-[$RuCl_2(dppe)_2$] (**8**) affords vinylidene ruthenium complexes, which were deprotonated with Et_3N to give the terminal σ-alkynylruthenium derivatives **9**–**12**. The reaction of **3** or **5** with [$Ru(CO)ClH(PPh_3)_3$] (**13**) gave the corresponding di-σ-alkenyl ruthenium complexes **14** and **15**.

Introduction

Carbon-rich organometallics containing rigid conjugated branches have attracted great attention, since they are potentially useful for building carbon-rich networks,[1] organometallic polymers[2] and π-conjugated polymetallic systems,[3] which can all find applications in material science. Of special interest are the σ-alkynyl complexes, since they allow electronic communication between coordinated metal centers through the C≡C bonds in the π-conjugated systems. Indeed, a number of alkynyl complexes have been designed for use in nonlinear optics[4] and as liquid crystals.[5] Polyethynylated complexes may form organometallic polymers in which the metal binds two ethynyl groups.[4b,5c,6] Polymetallic compounds with -$(C{\equiv}C)_n$- or polyethynylbenzene bridges have also been studied.[3,4b,4c,5c,7] Other di- or trimetallic alkynyl complexes have been prepared from ethynyl ferrocene.[8] Additionally, alkynyl derivatives have given rise to mixed-valence systems,[9] and organometallic macrocycles[10] have also been prepared.

The assembly of carbon-rich two- or three dimensional nanomaterials from ethynylated scaffolds has also attracted great attention.[11,12] Major achievements in this field are the preparation of tetraethynylmethane (**I**),[13] tetraethynylethene,[14] hexaethynylbenzene,[15] and π-metal complexes of tetraethynylcyclobutadiene,[16] and pentaethynylcyclopentadiene.[17] Tetraethynylallene (**II**), topologically related to the tetraalkyne **I**, still remains an elusive target. The biphenyls **III**[18] and **IV**, which display the four alkynes in a flexible elongated tetrahedral arrangement, could offer a potential alternative to **I** and **II** (Scheme 1).

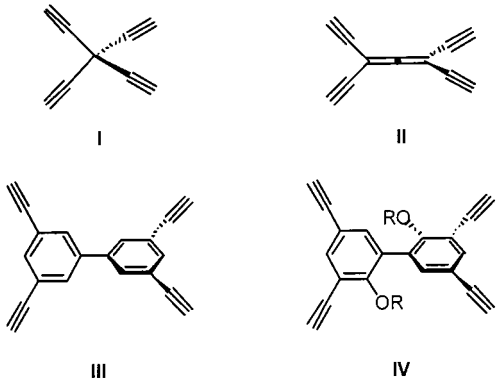

Scheme 1

Herein we report the synthesis of alkynes **3** and **5** as new potential building blocks for the construction of carbon-rich networks,[19] and their reactions with the ruthenium complexes *cis*-[$RuCl_2(dppe)_2$] (**8**) [dppe = 1,2-bis(diphenyl)-phosphanylethane] and [$Ru(CO)ClH(PPh_3)_3$] (**13**), which afford mono- and di-alkynyl and di-alkenyl ruthenium complexes, respectively, in good yields.[20]

Results and Discussion

Synthesis of Di- and Tetraalkynylbiphenyls

The synthesis of alkynes **3** and **5** was based on palladium-catalyzed transformations as the key steps. The tetrabromo diester **1** was readily obtained from 2,2′-biphenol by bromination with excess bromine in methanol at 23 °C,[21] followed by acylation with pivalic anhydride (95% overall yield). Thus, Sonogashira coupling[22] of tetrabromo dipivalate ester (**1**) with excess trimethylsilylacetylene {[$PdCl_2(PPh_3)_2$] and CuI catalysts (20 mol % each), Et_3N, 70 °C, 48 h] led to **2** (89% yield). No further coupling between **2** and trimethylsilylacetylene took place through the more hindered *o*-bromides by using this coupling procedure, even under severe conditions (Scheme 2).

[a] Instituto de Ciencia de Materiales de Madrid, CSIC,
Cantoblanco, 28049 Madrid, Spain
E-mail: amelia.santos@icmm.csic.es
[b] Departamento de Química Orgánica, Universidad Autónoma de Madrid,
Cantoblanco, 28049 Madrid, Spain
Fax: (internat.) +34-91/397-3966
E-mail: anton.echavarren@uam.es

 © WILEY-VCH Verlag GmbH, 69451 Weinheim, 2001 1434−1948/01/0909−2305 $ 17.50+.50/0

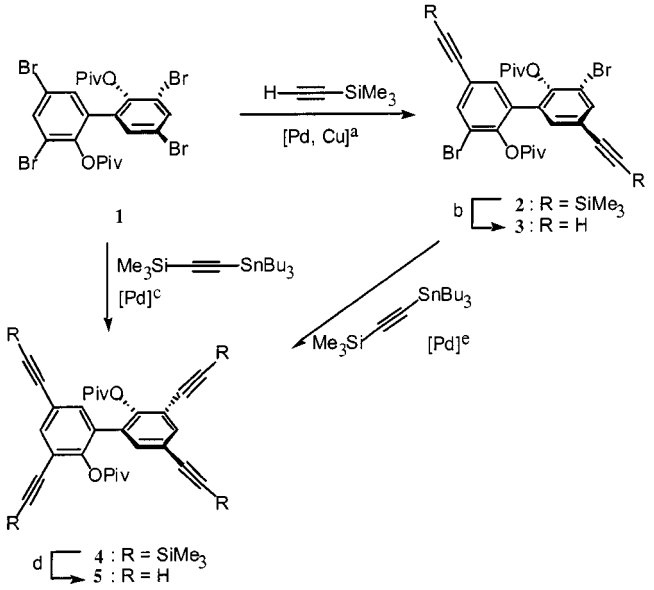

Scheme 2. a: $[PdCl_2(PPh_3)_2]$ (20 mol %), CuI (20 mol %), Et_3N, 70 °C, 48 h (89%); b: K_2CO_3, MeOH, 23 °C, 30 min. (90%); c: $[Pd(PPh_3)_4]$ (20 mol %), toluene, reflux, 4 h (90%); d: K_2CO_3, MeOH, 23 °C, 30 min. (95%); e: $[Pd(PPh_3)_4]$ (20 mol %), toluene, reflux, 4 h (92%)

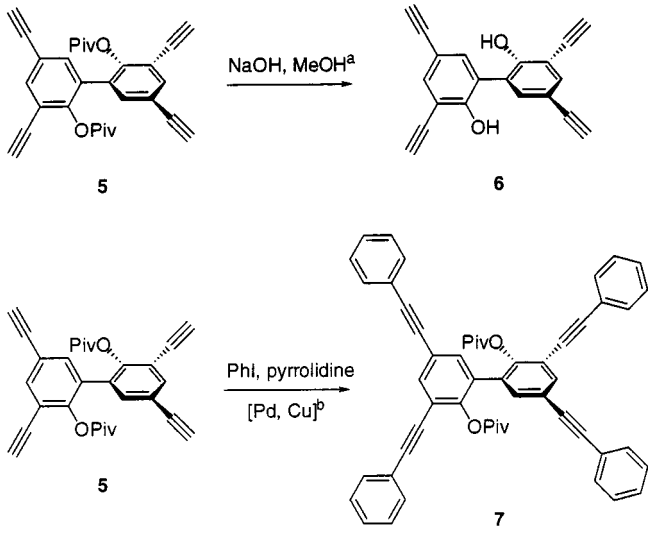

Scheme 3. a: NaOH, MeOH, 23 °C, 18 h (80%); b: $[Pd(PPh_3)_4]$ (20 mol %), CuI (20 mol %), pyrrolidine, 23 °C, 3 h (83%)

However, by using the Stille coupling[23] the four bromides could be efficiently replaced by alkynyl substituents in a single step. Thus, coupling of **1** with (trimethylsilylethynyl)-tributylstannane[24] in the presence of $[Pd(PPh_3)_4]$ as catalyst gave the tetraalkynyl derivative **4** (90% yield) as a stable colorless oil. The biphenyl **4** was also obtained by the coupling of dibromide **2** with (trimethylsilylethynyl)tributylstannane under the same conditions (92% yield). The terminal alkynes **3** and **5** could be obtained by standard deprotection of the TMS groups with K_2CO_3 in MeOH in 90 and 95% yields, respectively. The pivaloyl groups of **5** could be efficiently removed under stronger basic conditions [NaOH, MeOH, 23 °C, 18 h, 80%] to yield the biphenol **6**. This compound could undergo self-condensation by copper- or palladium-catalyzed alkyne−alkyne coupling to furnish three dimensional polymers bearing hydrophilic cavities.

While alkynes **3** and **5** are stable compounds that can be stored under ordinary conditions, alkyne **6** undergoes slow decomposition as a solid. However, it can be easily manipulated and stored in the dark without significant decomposition. The potential utility of these tetraethynylbiphenyls as tectons for the building of more complex structures relies upon their ability to couple with appropriate electrophiles. Thus, the coupling of **5** with iodobenzene (4 equiv.) afforded **7** [$Pd(PPh_3)_4$ and CuI (20 mol % each), pyrrolidine, 23 °C, 3 h, 83%; Scheme 3].

Synthesis of Ruthenium Alkynyl Complexes

The reactions of alkynes **3** and **5** with one equivalent of *cis*-$[RuCl_2(dppe)_2]$ (**8**) and two equivalents of KPF_6 in CH_2Cl_2 at room temperature for four days led to the conversion of the starting alkynes into a mixture of two ruthenium complexes. On the basis of the spectroscopic data and literature precedent,[25−27] these products were tentatively assigned as the monovinylidene and η^2-alkyne ruthenium complexes. Thus, the IR spectra show relatively intense bands in the range 1625−1630 cm^{-1}, characteristic of the vinylidene ruthenium complexes. However, the ^1H NMR spectra were complex, suggesting that isomeric (η^2-alkyne)ruthenium complexes were also present in solution. These complexes decompose readily in the presence of dissolved oxygen or water to furnish the carbonyl complex $[Ru(CO)Cl(dppe)_2]PF_6$ almost quantitatively. This ruthenium(II) complex was characterized by IR and ^1H NMR spectroscopy and by the determination of the crystal structure.[28,29] Similar transformations of vinylidene- or allenylidene complexes into their carbonyl derivatives have been reported previously.[30]

The crude mixtures containing the monovinylidene and η^2-alkyne isomers were readily deprotonated with Et_3N in CH_2Cl_2 at room temperature to give the corresponding monoalkynyl complexes **9** (72%) and **10** (74%), respectively. Similarly, reaction of **3** and **5** with two equivalents of *cis*-$[RuCl_2(dppe)_2]$ (**8**) and four equivalents of KPF_6 for seven days at room temperature, followed by deprotonation, furnished the dialkynyl ruthenium complexes **11** (72%) and **12** (85%) (Scheme 4).

Crystals of complexes **11** and **12** could be obtained, although the crystal structure determination could not be performed due to their decomposition by the X-rays. The IR spectra of all these alkynyl complexes are very similar and show very strong ν(C≡C) bands around 2050 cm^{-1}. In the ^{13}C NMR spectrum of **12** the quintet at δ = 127.9 ($^2J_{PC}$ = 16 Hz) was assigned to the alkynyl carbon which is α to Ru, thus demonstrating a *trans*-configuration of the chloro- and ethynyl ligands.

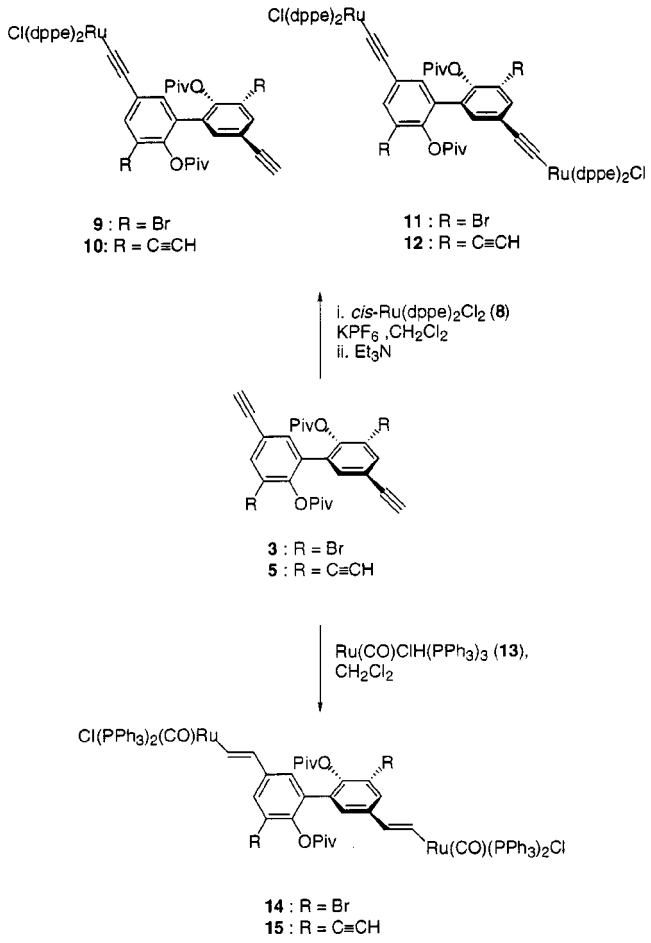

Scheme 4

A cyclic voltammetric study of complex **12** showed a single quasi-reversible redox wave for both ruthenium systems [$E_{1/2}$ versus Cp_2Fe^+/Cp_2Fe: + 0.72 V (ΔE_p = 63 mV)]. This unique oxidation wave shows that the dialkynyl complex **12** is capable of providing two electrons at the same potential and that the bridge between the ethynylated phenyl rings of the biphenyl system does not allow significant communication between the ruthenium centers.

Synthesis of Ruthenium Alkenyl Complexes

The reaction of alkynes **3** and **5** with two equivalents of [Ru(CO)HCl(PPh_3)$_3$] (**13**) in CH_2Cl_2 at room temperature gave rise to the red dialkenyl complexes **14** (92%) and **15** (91%). As expected,[31] the hydroruthenation proceeds in a cis fashion, as demonstrated by a trans $^3J(^1H\text{-}^1H)$ coupling of 13.7−14 Hz. Although the pentacoordinated Ru centers of these complexes are less sterically hindered than those of **9**−**12**, a tetrametallated derivative could not be obtained by reaction of alkyne **5** with four equivalents of hydride **13**.

Conclusions

We have described the synthesis of the di- and tetraalkynyl biphenyls **3** and **5** from the tetrabromo derivative **1** by using Pd-catalyzed cross-coupling reactions as well as their derivatization with ruthenium complexes to afford stable alkynyl and alkenyl complexes. The reaction of the terminal −C≡CH groups of **3** and **5** with *cis*-[$RuCl_2$(dppe)$_2$] (**8**), followed by deprotonation of these mixtures with Et_3N, leads to the terminal σ-alkynylruthenium derivatives. Reaction of **3** and **5** with the ruthenium hydride [Ru(CO)ClH(PPh_3)$_2$] (**13**) gave the corresponding di-σ-alkenyl complexes. The diruthenium complexes **12** and **15** bear two free terminal alkyne groups, which could be further metallated to form heterometallic complexes. Further work in this area is in progress.

Experimental Section

General: Infrared spectra were recorded at the ICMM on a Nicolet 20 SXC FT-IR spectrophotometer, using KBr disks. The NMR determinations were carried out on a Bruker AC-200 (or a Bruker AMX-300) apparatus at 23 °C. Mass spectra were performed at the SIdI (UAM), using the fast cesium-ion bombardment (liquid secondary ion mass spectrometry, LSIMS) or EI-MS techniques. Only the most significant IR frequencies and MS fragmentations are given. Elemental analyses were performed at the ICMM or SIdI (UAM). Differential thermal analysis (DTA) curves were obtained at the ICMM, using a Stanton STA 781 analyzer. All reactions were performed under a nitrogen atmosphere, using Schlenk techniques and the solvents were deoxygenated and dried by standard methods.

Cyclic voltammetric measurements were carried out at the Universidad Complutense de Madrid (Departamento de Química Inorgánica I, Facultad de Ciencias Químicas) on an Autolab apparatus equipped with a PSTA 10 potentiostat, using a three-electrode cell with platinum wire as working and auxiliary electrodes and Ag/AgCl electrode as a reference with a solution of the complex (10^{-3} mol/dm^3) in dichloromethane containing [Nbu_4][BF_4] (0.2 mol/dm^3) as the base electrolyte, at a scan rate of 200 mV s^{-1}. Values are referred to an Ag/AgCl electrode and ferrocene was used as internal standard.

The complexes [$PdCl_2(PPh_3)_2$], [$Pd(PPh_3)_4$],[32] *cis*-[$RuCl_2$(dppe)$_2$] (**8**),[33] and [RuHCl(CO)(PPh_3)$_3$] (**13**)[34] were prepared by known procedures.

3,5,3′,5′-Tetrabromobiphenyl-2,2′-diyl Dipivalate (1): A solution of 3,3′,5,5′-tetrabromo-2,2′-dihydroxybiphenyl (2.00 g, 4.0 mmol) in pyridine (50 mL) and pivalic anhydride (4.0 mL, 19.7 mmol) was heated under refluxing conditions for 2 h. After being cooled to room temperature, the mixture was diluted with water and extracted with EtOAc. The organic layer was washed with aqueous HCl (10%), dried (Na_2SO_4) and the solvent was evaporated to yield **1** (2.60 g, 97%) as a beige solid: m.p. 115 °C. − ^{1}H NMR ($CDCl_3$, 300 MHz): δ = 1.13 (s, 18 H), 7.34 (s, 2 H), 7.78 (s, 1 H), 7.79 (s, 1 H). − ^{13}C NMR ($CDCl_3$, 75.5 MHz): δ = 26.7, 39.1, 118.2, 119.00, 132.5, 132.6, 135.8, 145.5, 174.9. − EI-MS: *m*/*z* (%) = 666 (0.5) [M$^+$], 582 (5), 498 (8), 417 (4), 339 (1), 311 (3), 85 (43), 57 (100). − $C_{22}H_{22}Br_4O_4$ (670.03): calcd. C 39.44, H 3.31; found C 39.40, H 3.15.

3,3′-Dibromo-5,5′-bis(trimethylsilylethynyl)biphenyl-2,2′-diyl Dipivalate (2): A mixture of **1** (500 mg, 0.74 mmol), trimethylsilylacetylene (0.42 mL, 3 mmol), [$PdCl_2(PPh_3)_2$] (103 mg, 0.148 mmol), and CuI (56 mg, 0.30 mmol) in Et_3N (25 mL) was stirred at 23 °C

for 12 h. The mixture was diluted with CH_2Cl_2, washed with H_2O, dried and the solvents evaporated. The residue was chromatographed (hexane/EtOAc, 4:1) to give **2** as a colorless oil (466 mg, 89%). − ^{1}H NMR ($CDCl_3$, 300 MHz): δ = 0.23 (s, 9 H), 0.25 (s, 9 H), 1.12 (s, 18 H), 7.30 (s, 1 H), 7.31 (s, 1 H), 7.70 (s, 1 H), 7.71 (s, 1 H). − ^{13}C NMR ($CDCl_3$, 75.5 MHz): δ = −0.2, 26.7, 39.1, 96. 6, 102.0, 116.9, 122.4, 133.4, 131.61, 136.2, 146.2, 175.2. − EI-MS: *m*/*z* (%) = 702 (2) [M^+], 618 (14), 534 (13), 519 (5), 439 (8), 179 (7), 85 (11), 73 (12) 57 (100). − $C_{32}H_{40}Br_2O_4Si_2$ (704.64): calcd. C 54.54, H 5.72; found C 54.88, H 6.11.

3,3′-Dibromo-5,5′-diethynylbiphenyl-2,2′-diyl Dipivalate (3): A mixture of **2** (466 mg, 0.66 mmol) and K_2CO_3 (182 mg, 1.3 mmol) in a mixture of CH_2Cl_2 (2 mL), MeOH (10 mL), and H_2O (0.5 mL) was stirred at 23 °C for 30 min. The mixture was diluted with CH_2Cl_2, washed with H_2O, aqueous HCl (10%), dried (Na_2SO_4) and the solvents evaporated to yield **3** as a colorless oil (332 mg, 90%). Recrystallization (Et_2O/hexane, 1:1) gave **3** as a white solid, m.p. 121−123 °C. − IR (KBr): ṽ = 3262 s ν(≡CH), 2104 w ν(C≡C), 1748 vs ν(C=O). − ^{1}H NMR ($CDCl_3$, 300 MHz): δ = 1.11 (s, 18 H), 3.12 (s, 2 H), 7.33 (s, 1 H), 7.73 (s, 1 H), 7.74 (s, 1 H), 7.75 (s, 1 H). − ^{13}C NMR ($CDCl_3$, 75.5 MHz): δ = 26.7, 39.0, 79.2, 80.8, 117.1, 121.3, 131.6, 133.5, 136.5, 146.6, 174.7. − EI-MS: *m*/*z* (%) = 558 (0.1) [M^+], 474 (80), 389 (0.1), 309 (0.2), 231 (2), 85 (21), 57 (100). − $C_{26}H_{24}Br_2O_4$ (560.28): calcd. C 55.74, H 4.32; found C 56.58, H 4.77.

3,3′,5,5′-Tetrakis(trimethylsilylethynyl)biphenyl-2,2′-diyl Dipivalate (4): A mixture of **1** (134 mg, 0.2 mmol), [$Pd(PPh_3)_4$] (46 mg, 0.04 mmol) and (trimethylsilyl)ethynyltributylstannane (470 mg, 1.2 mmol) in toluene (10 mL) was heated under refluxing conditions for 4 h. After being cooled to room temperature, the mixture was diluted with CH_2Cl_2, washed with water and a saturated solution of KF, dried (Na_2SO_4) and the solvents evaporated. The residue was chromatographed (hexane/EtOAc, 9:1) to give **4** as a colorless oil (133 mg, 90%). − ^{1}H NMR ($CDCl_3$, 300 MHz): δ = 0.21 (s, 18 H), 0.23 (s, 18 H), 1.13 (s, 18 H), 7.30 (s, 1 H), 7.31 (s, 1 H), 7.61 (s, 1 H), 7.62 (s, 1 H). − ^{13}C NMR ($CDCl_3$, 75.5 MHz): δ = −0.2, 26.8, 38.9, 95.4, 98.7, 99.8, 102.8, 118.5, 120.9, 130.3, 134.3, 136.7, 149.2, 175.2. − EI-MS: *m*/*z* (%) = 738 (36) [M^+], 654 (100), 570 (28), 481 (4), 467 (13), 57 (25). − $C_{42}H_{58}O_4Si_4 \cdot 0.5H_2O$ (748.26): calcd. C 67.42, H 7.95; found C 67.41; 8.18.

3,3′,5,5′-Tetraethynylbiphenyl-2,2′-diyl Dipivalate (5): A mixture of **4** (139 mg, 0.118 mmol) and K_2CO_3 (33 mg, 0.24 mmol) in a mixture of CH_2Cl_2 (1 mL), MeOH (5 mL), and H_2O (0.3 mL) was stirred at 23 °C for 30 min. The mixture was diluted with CH_2Cl_2, washed with H_2O and aqueous HCl (10%), dried (Na_2SO_4) and the solvents evaporated to give **5** (77 mg, 95%) as a white solid: m.p. 125 °C. − IR (KBr): ṽ = 3306 ms, 3279 sh ν(≡CH), 2165 w, 2135 w ν(C≡C), 1750 vs ν(C=O). − ^{1}H NMR ($CDCl_3$, 300 MHz): δ = 1.11 (s, 18 H), 3.08 (s, 2 H), 3.21 (s, 2 H), 7.37 (d, *J* = 2.0 Hz, 2 H), 7.66 (d, *J* = 2.0 Hz, 2 H). − ^{13}C NMR ($CDCl_3$, 75.5 MHz): δ = 26.7, 38.9, 77.6, 78.5, 81.4, 82.6, 117.7, 120.1, 130.4, 134.8, 136.9, 150.1, 175.3. − FAB-MS: *m*/*z* (%) = 450 (15) [M^+], 366 (47), 282 (87), 253 (11), 224 (15), 85 (9), 57 (100). − $C_{30}H_{26}O_4 \cdot 0.5H_2O$ (459.53): calcd. C 78.41, H 5.92; found C 78.87, H 5.97.

2,2′-Dihydroxy-3,3′,5,5′-tetra(ethynyl)biphenyl (6): A mixture of **5** (10 mg, 0.022 mmol) and NaOH (6 mg, 0.15 mmol) in a mixture of MeOH (2 mL), and H_2O (0.1 mL) was stirred at 23 °C for 18 hours. The mixture was diluted with CH_2Cl_2, washed with H_2O and aqueous HCl (10%), dried (Na_2SO_4) and the solvents evaporated to give **6** (5 mg, 80%) as a white solid: (decomposes without melting; the DTA curve shows two exothermic peaks at 115 °C and 196 °C). − ^{1}H NMR (200 MHz, $CDCl_3$): δ = 3.01 (s, 2 H), 3.49 (2 H), 7.43 (d, *J* = 2.0 Hz, 2 H), 7.59 (d, *J* = 2.0 Hz, 2 H). − ^{13}C NMR (75 MHz, $CDCl_3$): δ = 76.7, 77.4, 82.1, 84.8, 109.9, 114.7, 123.5, 136.0, 136.2, 154.7. − EI-MS: *m*/*z* (%) = 282 (100) [M^+], 253 (23), 224 (32).

3,3′,5,5′-Tetra(phenylethynyl)biphenyl-2,2′-diyl Dipivalate (7): A mixture of **5** (41 mg, 0.1 mmol), [$Pd(PPh_3)_4$] (23 mg, 0.02 mmol), iodobenzene (60 μL, 0.53 mmol), and CuI (4 mg, 0.02 mmol) in pyrrolidine (5 mL) was stirred at 23 °C for 3 h. The mixture was diluted with CH_2Cl_2, washed with H_2O, dried and the solvents evaporated. The residue was chromatographed (hexane/EtOAc, 9:1) to give **7** as a colorless oil (62 mg, 83%). − ^{1}H NMR (200 MHz, $CDCl_3$): δ = 1.17 (s, 18 H), 7.78 (d, *J* = 2.1 Hz, 2 H), 7.39−7.27 (m, 12 H), 7.55−7.45 (m, 10 H). − ^{13}C NMR (75 MHz, $CDCl_3$): δ = 26.9, 39.1, 83.7, 87.5, 90.4, 94.2, 118.8, 121.3, 122.7, 122.8, 128.4, 128.5, 128.7, 130.8, 131.6, 131.7, 133.8, 135.9, 148.9, 175.6. − EI-MS: *m*/*z* (%) = 754 (8) [M^+], 670 (25), 586 (62), 57 (100). − HRMS calcd. for $C_{54}H_{42}O_4$: 754.3083; found 754.3054.

Synthesis of the Monosubstituted Alkynyl Complex 9: A solution of alkyne **3** (29 mg, 0.052 mmol), *cis*-[$RuCl_2$(dppe)$_2$] (**8**) (50 mg, 0.052 mmol), and KPF_6 (18.96 mg, 0.103 mmol) in CH_2Cl_2 (5 mL) was stirred for 4 days at room temperature. The intermediate vinylidene complex could be isolated by trituration with hexane as a brown-beige powder (75 mg, 88%). − IR (KBr): ṽ = 3274 w ν(≡CH), 1750 ms ν(C=O), 2110 vw ν(C≡CH), 1620 ms ν(=C=C), 836 vs ν(PF_6). − ^{1}H NMR ($CDCl_3$, 300 MHz): δ = 1.07, (s, 9 H), 1.17 (s, 9 H), 2.60−3.05 (m, 8 H), 3.11 (s, 1 H), 3.12 (br. s, 1 H), 6.85−7.55 (m, 43 H), 7.68 (br. s, 1 H) (minor signals of an η^2-alkyne complex were also observed); − $C_{78}H_{72}Br_2ClF_6O_4P_5Ru$ (1638.61): calcd. C 57.17, H 4.43; found C 57.11, H 4.48. An excess of Et_3N (0.05 mL, 0.35 mmol) was added to the brownish-yellow solution containing the vinylidene complex and the resulting solution was stirred for 1 h at 23 °C. After addition of CH_2Cl_2 (15 mL), this yellow solution was washed with water (3 ×). After the usual extractive workup, the solvent was partially evaporated. Addition of hexane led to a yellow precipitate, which was filtered off to give **9** (55 mg, 72%). − IR (KBr): ṽ = 3298 w ν(≡CH), 2110 vw ν(C≡CH), 2054 s ν(C≡C), ν(C=O). − ^{1}H NMR ($CDCl_3$, 300 MHz): δ = 1.14 (s, 9 H), 1.16 (s, 9 H), 2.66 (br. s, 8 H), 3.17 (s, 1 H), 6.22 (br. s, 1 H), 6.64 (br. s, 1 H), 6.84−7.49 (m, 33 H), 7.51 (br. s, 8 H), 7.75 (s, 1 H). − ^{31}P{^{1}H} NMR (121.5 MHz, $CDCl_3$): δ = 49.55 (s). − $C_{78}H_{71}Br_2ClO_4P_4Ru \cdot 0.5H_2O$ (1501.63): calcd. C 62.39, H 4.83; found C 62.44, H 4.89.

Formation of *trans*-[Ru(CO)Cl(dppe)$_2$]PF_6 from Biphenyl 3 and Ruthenium Complex 8: A solution of alkyne **3** (26 mg, 0.05 mmol), *cis*-[$RuCl_2$(dppe)$_2$] (**8**) (89 mg, 0.10 mmol), and KPF_6 (34 mg, 0.20 mmol) in CH_2Cl_2 (5 mL) was stirred for 7 days at 23 °C until no free alkyne was detectable by TLC. The mixture was filtered and the filtrate was partially evaporated. Addition of hexane led to precipitation of a solid, which was filtered off and washed with hexane to give a beige powder (140 mg, quantitative yield). This solid was suspended in CH_2Cl_2 (2 mL) and hexane (10 mL), and was then stirred in air at 23 °C for 3 h. The solvents were evaporated and the greenish-brown solid was triturated with Et_2O and filtered off to give a greenish-beige powder. To eliminate residual vinylidene, the crude product was dissolved in CH_2Cl_2 (5 mL) and treated with Et_3N (0.1 mL) at 23 °C. The solution was washed with water (3 ×) and, after the usual extractive workup, the residue was filtered through basic alumina. Partial evaporation of the solvent and addition of hexane gave *trans*-[Ru(CO)Cl(dppe)$_2$]PF_6 as gray-white crystals (98 mg, 59%) and the dialkynyl complex **9** (20 mg,

11%) as yellow crystals, which were separated by fractional crystallization.

***trans*-[Ru(CO)Cl(dppe)$_2$]PF$_6$:** IR (KBr): $\tilde{\nu}$ = 1946 vs ν(C=O), 837 vs ν(PF_6). − ^{1}H NMR ($CDCl_3$, 300 MHz): δ = 2.66 (m, 4 H), 2.92 (m, 4 H), 6.95−7.50 (m). − $C_{53}H_{48}ClF_6OP_5Ru$ (1106.3): calcd. C 57.54, H 4.37; found C 57.51, H 4.40.

Synthesis of the Monosubstituted Alkynyl Complex 10: Alkyne **5** (23 mg, 0.052 mmol) was treated as above to give **10** as a yellow powder (52 mg, 74%). − IR (KBr): $\tilde{\nu}$ = 3282 ms ν(≡CH), 2110 vw ν(C≡CH), 2049 s ν(C≡C), 1748 s ν(C=O). − ^{1}H NMR ($CDCl_3$, 300 MHz): δ = 1.13 (s, 9 H), 1.15 (s, 9 H), 2.67 (br. s, 8 H), 3.13 (s, 2 H), 3.21 (s, H), 6.22 (br. s, 1 H), 6.60 (br. s, 1 H), 6.89−7.10 (2m, 16 H), 7.10−7.32 (2m, 16 H), 7.37 (br. s, 1 H), 7.46 (br. s, 8 H), 7.67 (s, 1 H). − ^{31}P{^{1}H} NMR (121.5 MHz, $CDCl_3$): δ = 49.45(s). − $C_{82}H_{73}ClO_4P_4Ru{\cdot}H_2O$ (1400.89): C 70.30, H 5.40; found C 70.40, H 5.34. The intermediate vinylidene complex could be isolated as above to give a brown-beige powder: IR (KBr): $\tilde{\nu}$ = 3273 ms ν(≡CH), 2110 w ν(C≡CH), 1751 ms ν(C=O), 1628 ms ν(=C=C), 843 vs ν(PF_6). − $C_{82}H_{74}ClF_6O_4P_5Ru$ (1528.9): calcd. C 64.42, H 5.18; found C 64.75, H 5.52.

Synthesis of the Disubstituted Alkynyl Complex 11: A solution of alkyne **3** (29 mg, 0.052 mmol), *cis*-[$RuCl_2$(dppe)$_2$] (**8**) (100 mg, 0.10 mmol), and KPF_6 (38 mg, 0.21 mmol) in CH_2Cl_2 (5 mL) was stirred for 7 days at 23 °C. The mixture was filtered and the filtrate was partially evaporated. Addition of hexane led to precipitation of a solid, which was filtered off and washed with hexane to give the divinylidene complex. − IR (KBr): $\tilde{\nu}$ = 1750 ms ν (C=O), 1626 s ν (=C=C), 836 vs ν (PF_6). − $C_{130}H_{120}Br_2Cl_2F_{12}O_4P_{10}Ru_2$ (2716.9): calcd. C 57.47, H 4.45; found C 57.41, H 4.46. An excess of Et_3N (0.71 mmol, 0.1 mL) was added to the solution containing the vinylidene complex, and the resulting solution was stirred for 1 h at 23 °C. The yellow solution, after addition of CH_2Cl_2 (15 mL), was washed with water (3 ×). After the usual workup the solvent was partially evaporated. Addition of hexane led to the formation of a yellow microcrystalline powder, which was filtered off to give **11** (89 mg, 72%). − IR (KBr): $\tilde{\nu}$ = 2050 s ν(C≡C), 1750 s ν(C=O). − ^{1}H NMR ($CDCl_3$, 300 MHz): δ = 1.19 (s, 18 H), 2.66 (br. s, 16 H), 6.48 (br. s, 2 H), 6.54 (br. s, 2 H), 6.92 (m, 16 H), 7.02 (m, 20 H), 7.18 (m, 12 H), 7.29 (m, 16 H), 7.40 (m, 16 H). − ^{13}C NMR ($CDCl_3$, 50.32 MHz): δ = 26.9, 30.6 (m), 39.0, 110.7, 115.4 (br. s, Ru−C≡*C*), 127.0, 127.3 (br. s), 128.1 (quint, $^2J_{PC}$ = 16 Hz, C≡*C*−Ru), 128.9 (br. s), 131.7, 132.6, 133.9, 134.5 (br. s), 134.7, 135.8 (m), 141.5, 175.3. − ^{31}P{^{1}H} NMR (121.5 MHz, $CDCl_3$): δ = 49.90 (s). − FAB-MS: *m*/*z* (%) = 2421 (8) [M^+], 2386 (3), 2026 (59), 897 (59), 685 (6), 499 (42), 316 (56), 185 (95), 57 (100). − $C_{130}H_{122}Br_2Cl_2O_6P_8Ru_2{\cdot}2H_2O$ (2461.00): calcd. C 63.45, H 5.00; found C 63.26, H 5.17.

Synthesis of the Disubstituted Alkynyl Complex 12: An excess of Et_3N (0.1 mL, 0.71 mmol) was added to the brownish-yellow solution containing the divinylidene complex prepared from **5** (23 mg, 0.052 mmol), and the resulting solution was stirred for 1 h at 23 °C. The yellow solution, after addition of CH_2Cl_2 (15 mL), was washed with water (3 ×). After the usual extractive workup, the solvent was partially evaporated. Addition of hexane led to a yellow microcrystalline powder of the dialkynyl complex **12** (101 mg, 85%) as a yellow powder. This compound contained traces of the monoalkynyl complex **10**. A pure product was obtained by crystallization from CH_2Cl_2/hexane to yield yellow crystals, which decompose on exposure to X-ray radiation. IR (KBr): $\tilde{\nu}$ = 3282 m ν(≡CH), 2110 w ν(C≡CH), 2049 s ν(C≡C), 1748 s ν(C=O). − ^{1}H NMR ($CDCl_3$, 300 MHz): δ = 1.18 (s, 18 H), 2.66 (br. s, 16 H), 3.15 (s, 2 H), 6.48 (br. s, 2 H), 6.58 (br. s, 2 H), 6.88−7.10 (m, 34 H), 7.10−7.22 (m, 16 H), 7.36 (br. s, 32 H). − ^{13}C NMR ($CDCl_3$, 75.5 MHz): δ = 26.8, 30.6, 38.8, 79.4 (s, *C*≡CH), 80.0 (s, C≡*C*H, 111.2, 115.5 (s, Ru−C≡*C*), 126.9 (br. s), 127.3 (br. s), 127.9 (quint., $^2J_{PC}$ = 16 Hz, C≡*C*−Ru), 128.4, 128.9 (br. s), 130.5, 131.8, 133.9, 134.5 (br. s), 135.2, 135.8 (q, *J* = 22.7 Hz, dppe), 145.2, 175.5. − ^{31}P{^{1}H} NMR (121.5 MHz, $CDCl_3$): δ = 49.89 (s). − FAB-MS: *m*/*z* (%) = 2315.1 (6) [M^+], 1917 (4), 1381 (2), 957 (9), 933 (19), 897 (100), 685 (16.). − $C_{134}H_{120}Cl_2O_4P_8Ru_2{\cdot}1.5H_2O$ (2342.25): calcd. C 68.71, H 5.28; found C 68.69, H 5.30. The intermediate divinylidene could be isolated as above as a beige powder: IR (KBr): $\tilde{\nu}$ = 3285 m ν(≡CH), 2110 vw ν(C≡CH), 1757 ms ν(C=O), 1628 s ν(=C=C), 843 vs ν(PF_6). − $C_{134}H_{122}Cl_2F_{12}O_4P_{10}Ru$ (2607.2): 61.73, H 4.72; found C 62.61, H 5.15.

Synthesis of the Disubstituted Alkenyl Complex 14: A solution of [$RuHCl(CO)(PPh_3)_3$] (**13**; 80 mg, 0.084 mmol) and alkyne **3** (23.5 mg, 0.042 mmol) was stirred at 23 °C in CH_2Cl_2 (10 mL) for 30 min. The orange-red solution was concentrated and hexane was added. after cooling to 0 °C, the mixture was filtered and the filtrate was evaporated. The residue was taken up in CH_2Cl_2/Et_2O and filtered. Hexane was added to the filtrate to give a precipitate, which was filtered off to give **14** (78 mg, 92%) as an orange solid. − IR (KBr): $\tilde{\nu}$ = 1924 vs ν(C≡O), 1736 s ν(C=O). − ^{1}H NMR ($CDCl_3$, 300 MHz): δ = 0.93 (s, 18 H), 5.49 (d, $^3J_{HP}$= 13.7 Hz, 2 H), 6.35 (s, 2 H), 6.89 (s, 2 H), 7.20−7.42 (m, 36 H, Ph), 7.45−7.70 (m, 24 H, Ph), 8.38 (d, $^3J_{HP}$ = 13.7 Hz, 2 H). − $C_{100}H_{86}Br_2Cl_2O_6P_4Ru_2{\cdot}CH_2Cl_2$ (2025.43): calcd. C 59.89, H 4.38; found C 59.83, H 4.27.

Synthesis of the Disubstituted Alkenyl Complex 15: Similarly, a solution of [$RuHCl(CO)(PPh_3)_3$] (**13**; 50 mg, 0.0525 mmol) and the alkyne **5** (11.83 mg, 0.0263 mmol) was stirred at 23 °C in CH_2Cl_2 (5 mL) for 1.5 h. After partial evaporation of solvent, addition of Et_2O led to a precipitate, which was filtered off to give **15** (44 mg, 91%). − IR (KBr): $\tilde{\nu}$ = 3288 w ν(≡CH), 2110 vw ν(C≡CH), 1922 vs ν(C≡O), 1740 ν(C=O). − ^{1}H NMR ($CDCl_3$, 300 MHz): δ = 0.93 (s, 18 H), 3.11 (s, 2 H), 5.53 (d, $^3J_{HP}$ = 14.0 Hz, 2 H), 6.41 (d, *J* = 2.0 Hz, 2 H), 6.84 (d, *J* = 2.0 Hz, 2 H), 7.42−7.20 (m, 36 H), 7.70−7.45 (m, 24 H, Ph), 8.33 (dm, $^3J_{HP}$ = 14.0 Hz, 2 H); − $C_{104}H_{88}Cl_2O_6P_4Ru_2{\cdot}0.75H_2O$ (1844.26): calcd. C 67.73, H 4.89; found C 67.80, H 4.80.

Acknowledgments

We are grateful to the DGES (Projects PB97-0002-C2-01 and 02) for support of this research. We also thank the MEC for a predoctoral fellowship to M. R. and to the CAM for a postdoctoral fellowship to B. G.-L. We acknowledge Johnson Matthey PLC for a generous loan of $PdCl_2$ and $RuCl_3$.

[1] [1a] R. Faust, F. Diederich, V. Gramlich, P. Seiler, *Chem. Eur. J.* **1995**, *1*, 111−117. − [1b] U. H. F. Bunz, *Synlett* **1997**, 1117−1127.

[2] [2a] I. Manners, *Angew. Chem. Int. Ed. Engl.* **1996**, *35*, 1602−1621. − [2b] M. Altmann, V. Enkelmann, G. Lieser, U. H. F. Bunz, *Adv. Mater.* **1995**, *7*, 726−728. − [2c] M. Altmann, U. H. F. Bunz, *Angew. Chem. Int. Ed. Engl.* **1995**, *34*, 569−571. − [2d] S. J. Davies, B. F. G. Johnson, J. Lewis, P. R. Raithby, *J. Organomet. Chem.* **1991**, *414*, C51−C53. − [2e] S. J. Davies, B. F. G. Johnson, M. S. Khan, J. Lewis, *J. Chem. Soc., Chem. Commun.* **1991**, 187−188. − [2f] H. B. Fyfe, M. Mlekuz, D. Zargarian, N. J. Taylor, T. B. Marder, *J. Chem. Soc., Chem. Commun.* **1991**, 188−191.

[3] N. J. Long, A. J. Martin, F. Fabrizi di Biani, P. Zanello, *J. Chem. Soc., Dalton Trans.* **1998**, 2017−2021, and references therein.

[4] [4a] N. J. Long, Organometallics for Nonlinear Optics, Optoelectronic Properties of Inorganic Compounds, *Modern Inorganic Chemistry Series* **1999**, 107−167. − [4b] N. J. Long, *Angew. Chem. Int. Ed. Engl.* **1995**, *34*, 21−38. − [4c] A. M. Mcdonagh, M. G. Humphrey, M. Samoc, B. Luther-davies, S. Houbrechts, T. Wada, H. Sasabe, A. Persoons, *J. Am. Chem. Soc.* **1999**, *121*, 1405−1406, and references therein.

[5] [5a] J. P. Rourke, D. W. Bruce, T. B. Marder, *J. Chem. Soc., Dalton Trans.* **1995**, 317−318. − [5b] T. Kaharu, H. Matsubara, S. Takahashi, *J. Mater. Chem.* **1992**, *2*, 43−47. − [5c] S. Takahashi, Y. Takai, H. Morimoto, K. Sonogashira, *J. Chem. Soc., Chem. Commun.* **1984**, 3−5.

[6] A. Buttinelli, E. Viola, E. Antonelli, C. Lo Sterzo, *Organometallics* **1998**, *17*, 2574−2582;

[7] Selected references: [7a] T. Bartik, B. Bartik, M. Brady, R. Dembinski, J. A. Gladysz, *Angew. Chem. Int. Ed. Engl.* **1996**, *35*, 414−416. − [7b] M. Brady, W. Weng, Y. Zhou, J. W. Seyler, A. J. Amoroso, A. M. Arif, M. Böhme, G. Frenking, J. A. Gladysz, *J. Am. Chem. Soc.* **1997**, *119*, 775−788, and references therein. − [7c] V. W. Yam, V. C. Lau, K. Cheung, *Organometallics* **1996**, *15*, 1740−1744. − [7d] U. H. F. Bunz, *Angew. Chem. Int. Ed. Engl.* **1996**, *35*, 969−971. − [7e] F. Coat, C. Lapinte, *Organometallics* **1996**, *15*, 477−479. − [7f] T. Weyland, C. Lapinte, G. Frapper, M. J. Calhorda, J. F. Halet, L. Toupet, *Organometallics* **1997**, *16*, 2024−2031. − [7g] T. Weyland, K. Costuas, A. Mari, J. F. Halet, C. Lapinte, *Organometallics* **1998**, *17*, 5569−5579. − [7h] O. Lavastre, J. Plass, P. Bachmann, S. Guesmi, C. Moinet, P. H. Dixneuf, *Organometallics* **1997**, *16*, 184−189. − [7i] M. Uno, P. H. Dixneuf, *Angew. Chem. Int. Ed.* **1998**, *37*, 1714−1718. − [7j] T. Wayland, I. Ledoux, S. Brasselet, J. Zyss, C. Lapinte, *Organometallics* **2000**, *19*, 5235−5237.

[8] [8a] C. Lebreton, D. Touchard, L. Le Pichon, A. Daridor, L. Toupet, P. H. Dixneuf, *Inorg. Chim. Acta* **1998**, *272*, 188−196. − [8b] M. C. B. Colbert, J. Lewis, N. J. Long, P. R. Raithby, A. J. P. White, D. J. Williams, *J. Chem. Soc., dalton Trans.* **1997**, 99−104. − [8c] N. D. Jones, M. O. Wolf, D. M. Giaquinta, *Organometallics* **1997**, *16*, 1352−1354.

[9] [9a] M. Sato, Y. Hayashi, S. Kumakura, N. Shimizu, M. Katada, S. Kawata, *Organometallics* **1996**, *15*, 721−728. − [9b] M. I. Bruce, M. Ke, P. Low, *Chem. Commun.* **1996**, 2405−2406.

[10] K. Onitsuka, S. Yamamoto, S. Takahashi, *Angew. Chem. Int. Ed.* **1999**, *38*, 174−176.

[11] [11a] F. Diederich, in *Modern Acetylene Chemistry* (Eds.: P. J. Stang, F. Diederich), VCH, Weinheim, **1995**, Chapter 13. − [11b] F. Diederich, *Nature* **1994**, *369*, 199−207. − [11c] F. Diederich, Y. Rubin, *Angew. Chem. Int. Ed. Engl.* **1992**, *31*, 1101−1264. − [11d] J. M. Tour, *Chem. Rev.* **1996**, *96*, 537−553.

[12] Review of acetylenic coupling: P. Siemsen, R. C. Livingston, F. Diederich, *Angew. Chem. Int. Ed.* **2000**, *39*, 2633−2657.

[13] K. S. Feldman, C. M. Kraebel, M. Parvez, *J. Am. Chem. Soc.* **1993**, *115*, 3846−3847.

[14] Y. Rubin, C. B. Knobler, F. Diederich, *Angew. Chem. Int. Ed. Engl.* **1991**, *30*, 698−700.

[15] R. Diercks, J. C. Armstrong, R. Boese, K. P. C. Vollhardt, *Angew. Chem. Int. Ed. Engl.* **1986**, *25*, 268−269.

[16] Irontricarbonyl complex: U. H. F. Bunz, V. Enkelmann, *Angew. Chem. Int. Ed. Engl.* **1993**, *32*, 1653−1655.

[17] [17a] Manganesetricarbonyl complex: U. H. F. Bunz, V. Enkelmann, J. Räder, *Organometallics* **1993**, *12*, 4745−4747. − [17b] See also: N. Jux, K. Holczer, Y. Rubin, *Angew. Chem. Int. Ed. Engl.* **1996**, *35*, 1986−1990.

[18] Synthesis of 3,3′,5,5′-tetraethynylbiphenyl (**III**) and its application as a dendron: F. Morgenroth, E. Reuther, K. Müllen, *Angew. Chem. Int. Ed.* **1997**, *36*, 631−634.

[19] Preliminary communication on the synthesis of **3** and **5**: B. Gómez-Lor, A. M. Echavarren, A. Santos, *Tetrahedron Lett.* **1997**, *38*, 5347−5350.

[20] Ruthenation of 1,4-diethynylbenzene: G. Jia, W. F. Wu, R. C. Y. Yeung, H. P. Xia, *J. Organomet. Chem.* **1997**, *539*, 53−59.

[21] [21a] J. van Alphen, *Recl. Trav. Chim. Pays-Bas* **1932**, *51*, 715−725. − [21b] H. Gilman, J. Swiss, L. C. Cheney, *J. Am. Chem. Soc.* **1940**, *62*, 1963−1967.

[22] K. Sonogashira, in *Comprehensive Organic Synthesis* (Eds.: B. M. Trost, I. Fleming), Pergamon, Oxford, **1991**. Vol. 3, Chapter 2.4.

[23] [23a] J. K. Stille, *Angew. Chem. Int. Ed. Engl.* **1986**, *25*, 508−524. − [23b] V. Farina, V. Krishnamurthy, W. J. Scott, *Organic Reactions*, Wiley, New York, 1997; Vol. 50.

[24] M. W. Logue, K. Teng, *J. Org. Chem.* **1982**, *47*, 2549−2553.

[25] [25a]R. M. Bullock, *J. Chem. Soc., Chem. Commun.* **1989**, 165−167. − [25b] J. R. Lomprey, J. P. Selegue, *J. Am. Chem. Soc.* **1992**, *114*, 5518−5523. − [25c] M. A. Bennett, G. A. Heath, D. C. R. Hockles, I. Kovacik, A. C. Willis, *Organometallics* **1998**, *17*, 5867−5873. − [25d] I. de los Ríos, M. Jiménez-Tenorio, M. C. Puerta, P. Valerga, *J. Am. Chem. Soc.* **1997**, *119*, 6529−6538. − [25e] P. Nombel, N. Lugan, R. Mathieu, *J. Organomet. Chem.* **1995**, *503*, C22−C25. − [25f] M. P. Gamasa, J. Gimeno, C. González-Bernardo, J. Borge, S. García-Granda, *Organometallics* **1997**, *16*, 2483−2485. − [25g] V. Cadierno, M. P. Gamasa, J. Gimeno, E. Pérez-Carreño, S. García-Granda, *Organometallics* **1999**, *18*, 2821−2832, and references therein.

[26] [26a] V. Cadierno, J. Díez, M. P. Gamasa, J. Gimeno, E. Lastra, *Coord. Chem. Rev.* **1999**, *193−195*, 147−205. − [26b] V. Cadierno, M. P. Gamasa, J. Gimeno, *Eur. J. Inorg. Chem.* **2001**, 571−591.

[27] H. Werner, P. Bachmann, M. Laubender, O. Gevert, *Eur. J. Inorg. Chem.* **1998**, 1217−1224.

[28] M. A. Monge, E. Gutiérrez-Puebla, unpublished results.

[29] The corresponding tetrafluoroborate $[Ru(CO)Cl(dppe)_2]BF_4$ has been characterized previously: L. F. Szczepura, J. Giambra, R. F. See, H. Lawson, T. S. Janik, A. J. Jircitano, M. R. Churchill, K. J. Takeuchi, *Inorg. Chim. Acta* **1995**, *239*, 77−85.

[30] [30a] H. Werner, T. Rappert, R. Wiedemann, J. Wolf, N. Mahr, *Organometallics* **1994**, *13*, 2721−2727. − [30b] H. Katayama, F. Ozawa, *Organometallics* **1998**, *17*, 5190−5196. − [30c] C. Bianchini, M. Peruzzini, F. Zanobini, C. López, I. de los Ríos, A. Romerosa, *Chem. Commun.* **1999**, 443−444. − [30d] L. A. Oro, M. A. Ciriano, M. Campo, C. Foces-Foces, F. H. Cano, *J. Organomet. Chem.* **1985**, *289*, 117−131.

[31] M. R. Torres, A. Vegas, A. Santos, *J. Organomet. Chem.* **1986**, *309*, 169−177.

[32] F. A. Cotton, *Inorg. Synth.* **1972**, *13*, 121−123.

[33] B. Chaudret, G. Commenges, R. Poilblanc, *J. Chem. Soc., Dalton Trans.* **1984**, 1635−1639.

[34] N. Ahmed, J. J. Levison, S. D. Robinson, M. F. Uttley, *Inorg. Synth.* **1974**, *15*, 48.

Received December 20, 2000
[I00480]

Molecular Features of Co^{III} Tetra- and Pentammines Affect Their Influence on DNA Structure

Alison Rodger,*[a] Andrew Parkinson,[a] and Stephen Best[b]

Keywords: Bioinorganic chemistry / Non-covalent interactions / Coordination chemistry / Circular dichroism / UV/Vis spectroscopy

The polyamines spermine and spermidine cause a range of structural effects on DNA. $[Co(NH_3)_6]^{3+}$ is known to mimic many of these effects and we have shown previously that (+)-$[Co(en)_3]^{3+}$ and (–)-$[Co(en)_3]^{3+}$ (en = ethylenediamine) do so as well. In this paper the effects of mono- and disubstitution of the Co^{III} ammines by aqua, halo and nitro groups is explored. The overall effectiveness of the amines in conferring thermal stability on the ct-DNA proceeds in the order: spermine > (+)-$[Co(en)_3]^{3+}$ ≈ (–)-$[Co(en)_3]^{3+}$ ≈ $[Co(NH_3)_6]^{3+}$ ≈ spermidine > $[Pt(NH_3)_4]^{2+}$ > $[Co(NH_3)_5H_2O]^{3+}$ ≈ $[Co(NH_3)_5Cl]^{2+}$ ≈ $[Co(NH_3)_5Br]^{2+}$ > *cis*-$[Co(en)_2NH_3Cl]^{2+}$ > $[Co(NH_3)_5(NO_2)]^{2+}$ ≈ *trans*-$[Co(NH_3)_4(H_2O)_2]^{3+}$; whereas the B→Z transition-induction ordering is: spermine ≈ $[Co(NH_3)_6]^{3+}$ > (+)-$[Co(en)_3]^{3+}$ ≈ $[Co(NH_3)_5(H_2O)]^{3+}$ > (–)-$[Co(en)_3]^{3+}$ > $[Co(NH_3)_5Br]^{2+}$ > $[Co(NH_3)_5Cl]^{2+}$, with the other amines failing to cause the transition under the 11 mM salt concentration and temperature ramp conditions used; the DNA bending ranking is: spermine > $[Co(NH_3)_6]^{3+}$ > (+)-$[Co(en)_3]^{3+}$ > (–)-$[Co(en)_3]^{3+}$ > $[Co(NH_3)_5(H_2O)]^{3+}$ > *trans*-$[Co(NH_3)_4(H_2O)_2]^{3+}$ > spermidine, with the other 2+ amines (the aquo complexes will be 2+ at neutral pH), especially the bromo and nitro compounds, having comparatively little effect. While the presentation of NNN triangular faces is found to be important in the B→Z transition, the fact that the halo ligands are probably substituted by the DNA phosphates plays a role, especially in the DNA bending, where deep penetration of the major groove is concluded to be required. A favourable interaction between the backbone and the aquo ligands may enhance the B→Z transition.

Introduction

The two DNA-binding polycations spermidine $[H_3N(CH_2)_3NH_2(CH_2)_4NH_3]^{3+}$ and spermine $[H_3N(CH_2)_3NH_2(CH_2)_4NH_2(CH_2)_3NH_3]^{4+}$ are present in all cells.[1] The precise cellular functions of polyamines are unclear but they are known to neutralise over 40% of chromosomal DNA and to inhibit damage by reactive oxygen species,[2] radiation,[3,4] and alkylating agents.[5] Furthermore, polyamines stabilise DNA to heat and induce and stabilise A, B, Z (usually observed with alternating G-C sequences) and collapsed DNA structures.[6–8] We have recently shown that the cobalt(III) ammine complexes $[Co(NH_3)_6]^{3+}$, (+)-$[Co(en)_3]^{3+}$, and (−)-$[Co(en)_3]^{3+}$ (en = ethylenediamine) mimic different aspects of the DNA interaction of the small polyamine molecules spermidine and spermine.[8,9]

Our molecular modelling study[9] of $[Co(NH_3)_6]^{3+}$, (+)-$[Co(en)_3]^{3+}$, and (−)-$[Co(en)_3]^{3+}$ with DNA shows that these cobalt ammines do not bind in the minor groove of any sequence, and their residence times in the major groove decrease in the order spermine > $[Co(NH_3)_6]^{3+}$ > (+)-$[Co(en)_3]^{3+}$ > (−)-$[Co(en)_3]^{3+}$. In addition, while the spermine binding was found by Yuki et al. to be cooperative,[11] in analogous simulations[9] the others were found not to be. These amines all reduce the linear dichroism (LD) signal of DNA by bending calf thymus (ct) and micrococcus lysodeikticus (ml) DNAs. Since the molecules are major groove binders, we concluded that their behaviour supports the amine-major-groove bending model.[12] The comparative effectiveness of the cobalt ammines at bending DNA suggests that the presentation of a triangular NNN face to the DNA optimises the bend-causing interaction — $[Co(NH_3)^{3+}]$ has a high number of pre-formed NNN triangles, whereas spermine does not. The ethylenediamine complexes are somewhat less effective as they have fewer such faces. A similar geometric argument is required for the induction of the B→Z transition. Crystal structure data are consistent with the formation of five hydrogen bonds between $[Co(NH_3)_6]^{3+}$ and the major-groove convex surface of Z-DNA, specifically to guanine O6 and N7 and the phosphate oxygens.[13]

In order to probe the role of NNN triangular faces further, we have investigated the interaction of a set of cobalt(III) tetra- and pentaamines with DNA. In this work we have used temperature-dependent normal absorption to probe the stabilising effect of the ammines on duplex DNA; circular dichroism (CD), which depends on the asymmetric character of an absorbing chromophore, to probe ligand binding; and linear dichroism (LD) to probe the effect of the ammines on DNA length and flexibility.

[a] Department of Chemistry, University of Warwick, Coventry, CV4 7AL, UK
Fax: (internat.) +44-24/7652-4112
E-mail: a.rodger@warwick.ac.uk
[b] School of Chemistry, University of Melbourne, Parkville, 3010, Victoria, Australia

 © WILEY-VCH Verlag GmbH, 69451 Weinheim, 2001 1434–1948/01/0909–2311 $ 17.50+.50/0

Results and Discussion

ct-DNA Absorbance Temperature Dependence

The absorbance spectra of a set of substituted cobalt ammines are illustrated in Figure 1. A wavelength of 280 nm, rather than the usual 260 nm, was chosen to follow the temperature dependence of ct-DNA absorbance in the presence of these ammines (Figure 2) to minimise the ligand contribution to the changes. The DNA melting curves show unusual pre- and post-melting transitions, most of which are consistent with the temperature dependence of the free ligand (data not shown), although the negative pre-melting transitions are all enhanced in the presence of the DNA. There was no evidence of light scattering above 300 nm in either temperature-dependent absorbance (data not shown) or CD spectra (Figure 4). The ligand effects were largest for the bromine-substituted compound (a 40 μM solution had a change of −0.02 absorbance units from baseline at 60 °C), so it is likely, at least in this case, that a substitution reaction removes a ligand-to-metal charge-transfer transition and that the DNA influences the kinetics of such reactions. Whether the ligands end up covalently bound to the DNA or their aquation is catalysed is not clear from these data.

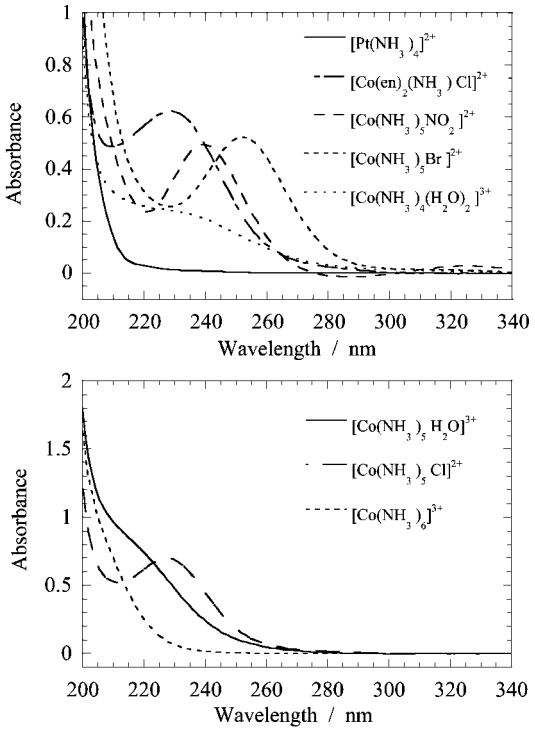

Figure 1. Normal absorption spectra of DNA binding ammines (40 μM in 10 mM NaCl and 1 mM cacodylate); $[Co(NH_3)_4(H_2O)_2]^{3+}$ is the *trans* isomer and $[Co(en)_2NH_3Cl]^{2+}$ (en = ethylenediamine) the *cis* isomer

Taking derivatives of the main hyperchromic denaturing transitions, thus assuming that the pre- and post-melting transitions could be ignored, the stabilization conferred upon the DNA by the amines is summarized in Figure 3. Substituting an amine group in $[Co(NH_3)_6]^{3+}$ by a Cl, Br, NO_2 or H_2O ligand, seriously impedes the metal complex's ability to stabilize DNA. The post-melting transition of $[Co(en)_2NH_3Cl]^{2+}$ makes it impossible to determine T_m for this system accurately after the first few ammine concentrations. The values would lie below the other halo species.

Effect of Ammines on poly[d(G-C)$_2$] Structure

The pentammine $[Co(NH_3)_5(H_2O)]^{3+}$ induces Z-form DNA as effectively as (+)-$[Co(en)_3]^{3+}$ (data not shown). $[Co(NH_3)_5Br]^{2+}$ and $[Co(NH_3)_5Cl]^{2+}$ also induce the Z-form DNA of poly[d(G-C)]$_2$ (Figure 4) to some extent. Concentrations of 20 μM spermidine,[9] *cis*-$[Co(en)_2NH_3Cl]^{2+}$, $[Pt(NH_3)_4]^{2+}$, $[Co(NH_3)_5(NO_2)]^{2+}$, and *trans*-$[Co(NH_3)_4(H_2O)_2]^{3+}$ do not promote the B→Z transition in poly[d(G-C)]$_2$ (60 μM in 10 mM NaCl) (Figure 4). The CD changes observed with these ligands, with the exception of *trans*-$[Co(NH_3)_4(H_2O)_2]^{3+}$, are the same as those induced by increasing the temperature of poly[d(G-C)$_2$].[9] $[Co(NH_3)_5(NO_2)]^{2+}$ does, however, promote the B→Z transition at 0 mM NaCl, 1 mM cacodylate buffer which is the behaviour previously observed for spermidine.[9]

LD of ct-DNA with Cobalt Tetra- and Pentaammines

Figure 5 summarises the LD of ct-DNA at 260 nm with added cobalt ammine. The initial addition of each ammine results in a small decrease in DNA orientation. We previously found that ≈20 μM spermine, ≈60 μM $[Co(NH_3)_6]^{3+}$, ≈80 μM $[Co(en)_3]^{3+}$, and 240 μM of spermidine are required to cause the LD signal to be sharply reduced. The monoaquo complex requires ≈140 μM and the diaquo complex begins to bend the DNA at ≈ 200 μM, and requires ≈400 μM to complete it.

Comparison of the Amines

The overall effectiveness of the amines in conferring thermal stability on the ct-DNA proceeds in the order:

spermine > (+)-$[Co(en)_3]^{3+}$ ≈ (−)-$[Co(en)_3]^{3+}$ ≈ $[Co(NH_3)_6]^{3+}$ ≈ spermidine > $[Pt(NH_3)_4]^{2+}$ > $[Co(NH_3)_5H_2O]^{3+}$ ≈ $[Co(NH_3)_5Cl]^{2+}$ ≈ $[Co(NH_3)_5Br]^{2+}$ > *cis*-$[Co(en)_2NH_3Cl]^{2+}$ > $[Co(NH_3)_5(NO_2)]^{2+}$ ≈ *trans*-$[Co(NH_3)_4(H_2O)_2]^{3+}$

whereas the B→Z transition induction ordering is:

spermine ≈ $[Co(NH_3)_6]^{3+}$ > (+)-$[Co(en)_3]^{3+}$ ≈ $[Co(NH_3)_5(H_2O)]^{3+}$ > (−)-$[Co(en)_3]^{3+}$ > $[Co(NH_3)_5Br]^{2+}$ > $[Co(NH_3)_5Cl]^{2+}$

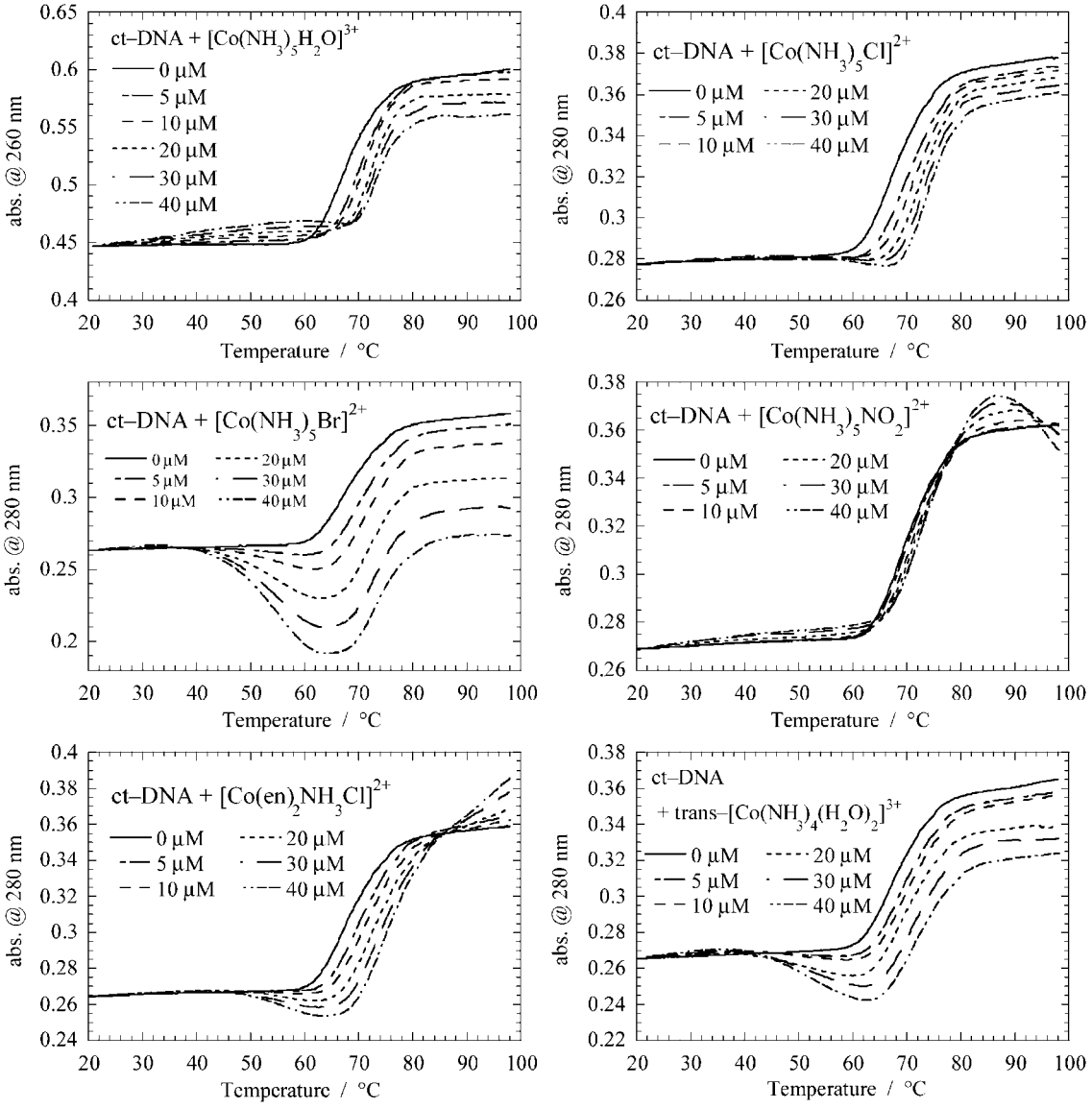

Figure 2. Absorbance versus temperature plot for ct-DNA (60 μM, 10 mM NaCl, 1 mM cacodylate) with addition of cobalt ammines at various concentrations as indicated in the figure

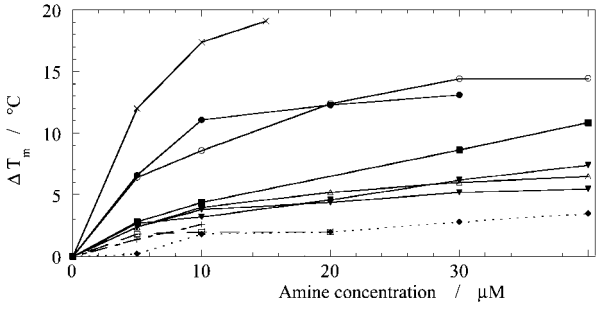

Figure 3. Summary of the change in T_m of ct-DNA (60 μM, 10 mM NaCl, 1 mM cacodylate) as a function of the amine concentration (concentrations are indicated in the figure); spermine, spermidine and $[Co(NH_3)_6]^{3+}$ data are taken from ref.[9]; the order of the melting temperature plots is, from top to bottom at 10 μM: spermine > $[Co(NH_3)_6]^{3+}$ > spermidine > $[Pt(NH_3)_4]^{2+}$ > $[Co(NH_3)_5Cl]^{2+}$ > $[Co(NH_3)_5Br]^{2+}$ > $[Co(NH_3)_5H_2O]^{3+}$ > *cis*-$[Co(en)_2NH_3Cl]^{2+}$ > $[Co(NH_3)_5(NO_2)]^{2+}$

with the other amines failing to cause the transition under the 11 mM salt concentration and temperature ramp conditions used; the DNA bending ranking is:

spermine > $[Co(NH_3)_6]^{3+}$ > (+)-$[Co(en)_3]^{3+}$ > (−)-$[Co(en)_3]^{3+}$ > $[Co(NH_3)_5(H_2O)]^{3+}$ > *trans*-$[Co(NH_3)_4(H_2O)_2]^{3+}$ > spermidine

with the other ammines having comparatively little effect. The most notable things about the above lists is that, with the exception of spermine, the ranking of the molecules varies. There is a general trend of reducing efficacy with reducing charge (the aquo complexes will be deprotonated at pH = 6.8[16]). The two enantiomers of $[Co(en)_3]^{3+}$ behave in a similar fashion, but with the possible exception of the thermal stability, where they have a very similar effect, the (−)-enantiomer affects the DNA structure less than the (+)-enantiomer. This correlates with the previous simula-

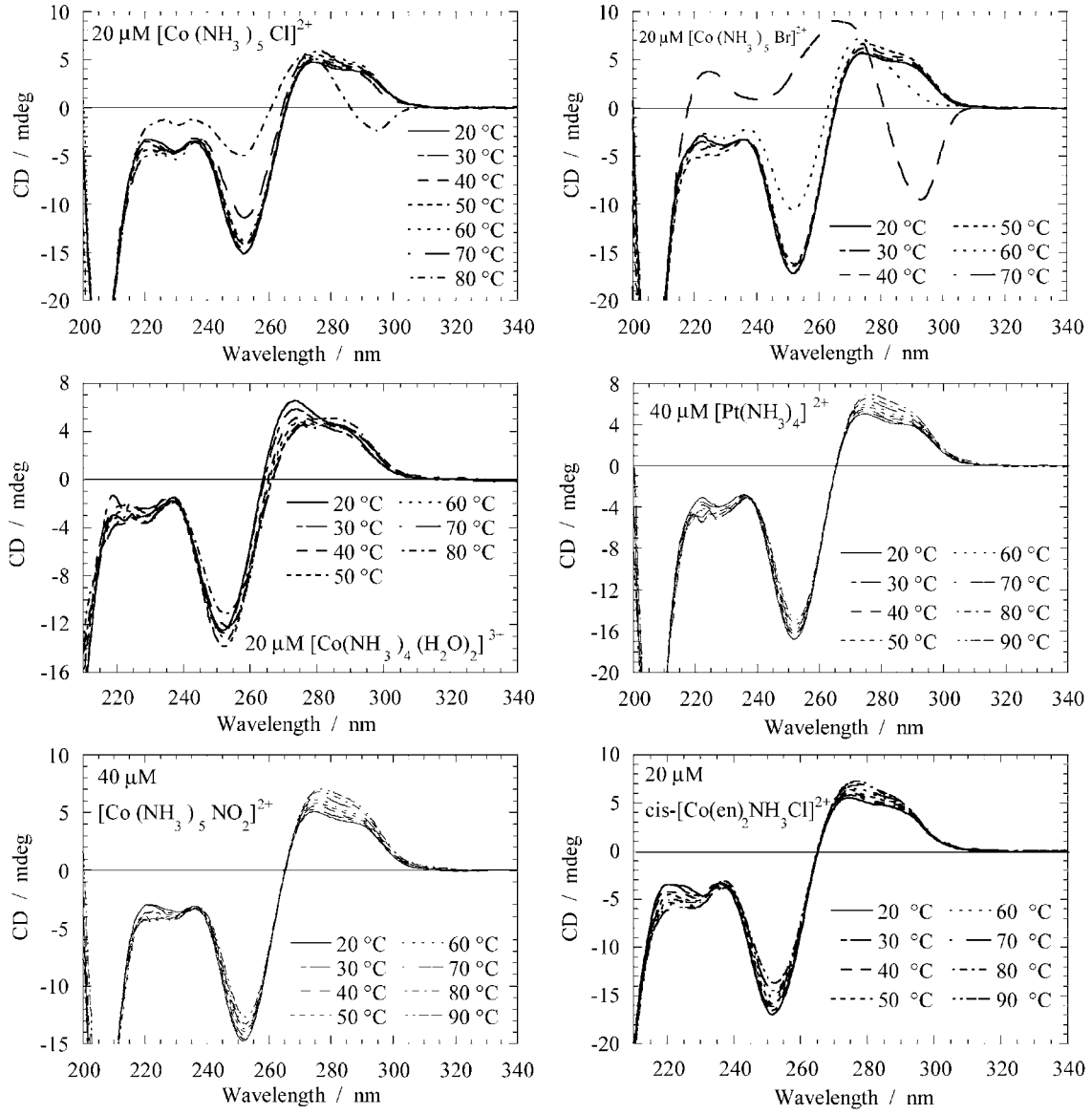

Figure 4. CD spectra of poly[d(G-C)]$_2$ (100 μM in 10 mM NaCl and 1 mM cacodylate buffer) in the presence of a fixed concentration of various amines as the temperature is raised at 4 °C/minute; amine concentration and temperatures are indicated in each figure

tion studies[8] that showed the (+)-enantiomer spending more time localised on the DNA than the (−)-enantiomer.

The DNA thermal stability gives an indication of binding strength, assuming the binding site size and binding modes are similar,[17] so we can conclude that water, halo and especially nitro substitution reduces the DNA affinity of a molecule or significantly changes the binding mode.

The changes in the absorbance of the cobalt tetra- and pentammines observed at elevated temperatures suggest that substitution reactions may be occurring (the change is not reversed upon temperature reduction). The halo-substituted complexes all lose absorbance intensity consistent with the loss of ligand (in this case the halogen ligand)-to-metal charge-transfer transitions. Strong direct cobalt−phosphate interactions have previously been observed by FTIR spectroscopy between $[Co(NH_3)_5Cl]^{2+}$ and the phosphates in ct-DNA with H-bonding interactions observed with the bases.[18] In contrast, no direct bonding was evident with $[Co(NH_3)_6]^{3+}$.[18] This was interpreted to mean that the chloro group was displaced, facilitating the direct bonding of the cobalt to the DNA backbone. Direct cobalt phosphate binding has also been observed between $[Co(NH_3)_5Cl]^{2+}$ and purine nucleotides.[19] From a DNA-charge neutralisation viewpoint these 2+ cobalt ammines thus effectively become 3+ when they loose the Cl^-; in addition they cannot be located particularly deeply in the major groove. It is reasonable to suppose that *cis*-$[Co(en)_2NH_3Cl]^{2+}$ behaves analogously but with lower affinity due to the steric hindrance of the ethylenediamines. The lower thermal stability of DNA in the presence of the

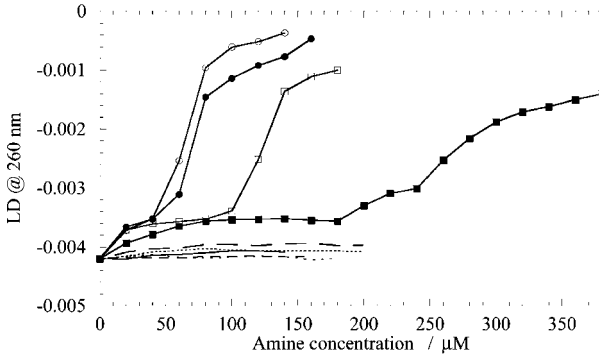

Figure 5. Summary of the LD signals of ct-DNA (60 μM in 10 mM NaCl, 1 mM cacodylate buffer) in the presence of ammines (concentration are indicated in the figure); experiment performed with the same rotation speed; order of LD plots is, from top to bottom at 50 μM: (+)-$[Co(en)_3]^{3+}$ > (−)-$[Co(en)_3]^{3+}$ > $[Co(NH_3)_5H_2O]^{3+}$ > $[Co(NH_3)_4(H_2O)_2]^{3+}$ > *cis*-$[Co(en)_2NH_3Cl]^{2+}$ > $[Pt(NH_3)_4]^{2+}$ > $[Co(NH_3)_5Cl]^{2+}$ > $[Co(NH_3)_5Br]^{2+}$ > $[Co(NH_3)_5(NO_2)]^{2+}$

halo compounds compared with $[Co(NH_3)_6]^{3+}$ may thus be deduced to correlate with a different binding site and a smaller binding affinity.

By way of contrast, the bulky negatively charged NO_2^- ligand will not have a good affinity for the backbone. Its groove binding preferences will also differ from those of an NH_3 ligand since its hydrogen bonding requirements are as an acceptor not a donor.

Conclusion

The inability of the nitro and halo compounds to bend the DNA significantly thus leads us to the conclusion that the bend-inducing binding mode requires deep penetration of the groove by hydrogen-bonding donors. In this context the low hydrogen bonding energy of $[Co(NH_3)_6]^{3+}$ compared with, for example, Mg^{2+} determined by Black and Cowan[20] is not necessarily significant — the hydrogen bonding energy just has to be large enough to position and orient the metal complex in the mode that favours DNA bending once the dominant electrostatic binding energy has assured DNA−metal complex binding.

The halo compounds creep up the ranking order for the B→Z transition, suggesting that the induction of this transition is favoured by some backbone interaction as well as groove binding. It has previously been concluded[9,10] that a triangular face of amines facing the DNA that could interact with the N7/O6 sites of intrastrand guanine bases is required to induce the B→Z transition. In agreement with this hypothesis, *trans*-$[Co(NH_3)_4(H_2O)_2]^{3+}$ and $[Pt(NH_3)_4]^{2+}$,[21] which have no triangular arrangements of amine groups, are incapable of inducing the B→Z transition (even in the absence of NaCl). Substitution of one amine on the $[Co(NH_3)_6]^{3+}$ reduces the transition induction and also reduces the number of triangular faces from 8 to 4. This is consistent with there being fewer effective binding modes to promote the B→Z transition. Neither spermidine nor the weaker binding NO_2 induces a transition in the presence of NaCl, however, they do so at 0 mM NaCl. This presumably relates to the need to reduce the competition for DNA sites from any other positively charged species. In the case of the ethylenediamine ligands, their bulk requires that an effective NNN face must not include the backbone of the ethylenediamine, so the number of NNN faces is reduced again resulting in the slip down the ranking order of the tris-ethylenediamine complexes, with the enantiomer that fits better into the major groove, according to our molecular modelling studies,[9] being able to optimise its interaction. The halo-ethylenediamine complex cannot present a triangular face to the groove while binding to the phosphates, and therefore cannot induce the transition. The mono-aquo complex ends up between the two tris-ethylenediamine enantiomers in its effectiveness, showing a balance of the number of NNN faces (which is higher for the mono-aquo complex) and DNA binding strengths (which is lower for the mono-aquo complex).

Experimental Section

Materials: Ultra pure water (18.2 MΩ) was used in all experiments. ct-DNA was purchased from Sigma/Aldrich Chemical Co. Ltd. Poly[d(G-C)]$_2$ was obtained from Pharmacia Biochemicals. All polynucleotides were dissolved in water without further purification (this required overnight stirring for ct-DNA) and kept frozen until the day of the experiment. DNA solutions were prepared by diluting in 1 mM cacodylate buffer (made up from the sodium salt of cacodylic acid, $C_2H_6AsO_2Na$, 98% purchased from Sigma/Aldrich buffered with hydrochloric acid to a pH of 6.8) with the required NaCl (>99.5% purity, Sigma/Aldrich). The concentration of DNA was determined spectroscopically using ε_{247nm} = 8400 $M^{-1}cm^{-1}$ for poly[d(G-C)]$_2$ and ε_{258nm} = 6600 $M^{-1}cm^{-1}$ for ct-DNA, expressed as the molarity of the phosphate groups.

Methods

Absorbance: Normal absorption spectra were obtained using a Cary 1E spectrometer equipped with a multicell cell changer and Peltier heating unit accessories. Rectangular quartz cuvettes with a reduced volume (4 mm width) and 1 cm path length were used for the absorbance versus temperature melting curves. The cuvettes were filled almost completely (approximately 1300 μL) and the top of the cuvette was sealed with PTFE thread seal tape to ensure no leakage occurred during heating. Samples were heated from 20−98 °C with a ramp rate of 0.1 °C/minute to eliminate any lag between the temperature of the solution and the heating block. Melting temperatures were determined by the derivative method in the Cary software with a data interval equal to the data collection interval (0.2 °C).

CD: Circular dichroism (CD), the difference in absorption of left and right circularly polarised light, was used to follow the transition of poly[d(G-C)]$_2$ into the Z-form in the presence of the ammines. Spectra were collected in 1 cm rectangular path length cuvettes using a Jasco J-715 spectropolarimeter equipped with a Peltier temperature-control device. The samples were heated from 20 °C at a ramp rate of 40 °C/hour and a CD spectrum collected every 10 °C. No equilibration time was allowed prior to the collection of the first spectrum. Since CD is uniquely sensitive to the symmetry of a system, even the achiral transition metal complexes will gain an induced signal at wavelengths where they absorb light. This be-

comes a particular issue for the brominated complex, which has significant absorbance at 260 nm (see Figure 1).

Flow LD: Linear dichroism (LD) is the difference in absorption of light linearly polarised parallel, $A_{\parallel}$, and perpendicular, $A_{\perp}$, to an orientation axis:

$$LD = A_{\parallel} - A_{\perp}$$

In this work, DNA was oriented by shear flow of the DNA sample between a fixed outer cylinder and a rotating solid quartz inner cylinder separated by a 0.5 mm wide gap.[14,15] The linearly polarised light was incident radial to the flow cell. A Jasco J-715 spectropolarimeter adapted for LD measurements was used. The LD of DNA is dominated by the $\pi-\pi^*$ transitions of the DNA bases. Thus, DNA LD probes the average orientation of the DNA bases. On a qualitative level, the LD of DNA can indicate changes in length and variations in the conformation of DNA induced by a binding drug. If the DNA is made more flexible or shortened then it will orient less effectively and the LD signal will be reduced.

Acknowledgments

The following support is gratefully acknowledged: Leverhulme Trust (AR, F/215/BC); BBSRC (AP) PhD studentship.

[1] S. Sarhan, N. Seiler, *Biol. Chem. Hoppe-Seyler* **1989**, *370*, 1279−1284.
[2] H. C. Ha, J. D. Yager, P. A. Woster, R. A. Casero, *Biochem. Biophys. Res. Commun.* **1998**, *244*, 298−303.
[3] M. Spotheim-Maurizot, Z. Ruiz, R. Sabattier, M. Charlier, *Int. J. Radiat. Biol.* **1995**, *68*, 571−577.
[4] K. D. Held, S. Awad, *Int. J. Radiat. Biol.* **1991**, *59*, 699−710.
[5] S. Rajalakshmi, P. M. Rao, D. S. R. Sarma, *Biochem. Biophys. Res. Commun.* **1978**, *81*, 936−940.
[6] H. S. Basu, L. J. Marton, *Biochem. J.* **1987**, *244*, 243−246.
[7] H. Tabor, *Biochemistry* **1962**, *1*, 496−501.
[8] A. Rodger, K. J. Sanders, M. J. Hannon, I. Meistermann, A. Parkinson, D. S. Vidler, I. S. Haworth, *Chirality* **2000**, *12*, 221−236.
[9] A. Parkinson, M. Hawken, M. Hall, K. J. Sanders, A. Rodger, *PCCP* **2000**, *2*, 5469−5478.
[10] T. J. Thomas, V. A. Bloomfield, *Biopolymers* **1984**, *23*, 1295−1306.
[11] M. Yuki, V. Grukhin, C. S. Lee, I. S. Haworth, *Arch. Biochem. Biophys.* **1996**, *325*, 39−46.
[12] I. Rozina, V. A. Bloomfield, *Biophys. J.* **1998**, *74*, 3152−3164.
[13] R. V. Gessner, G. J. Quigley, A. H. J. Wang, G. A. V. D. Marcel, J. H. V. Boom, A. Rich, *Biochemistry* **1985**, *24*, 237−240.
[14] A. Rodger, *Methods in Enzymol.* **1993**, *226*, 232−258.
[15] A. Rodger, B. Nordén, *Circular Dichroism and Linear Dichroism*, Oxford University Press (Oxford Chemistry Masters), **1997**.
[16] J. Burgess, *Ions in Solution: Basic Principles of Chemical Interactions*, Ellis Horwood Ltd. Chichester, England, **1988**.
[17] J. D. McGhee, *Biopolymers* **1976**, *15*, 1345−1375.
[18] H. A. Tajmir-Riahi, M. Naoui, R. Ahmad, *J. Biomol. Struct. Dyn.* **1993**, *11*, 83−93.
[19] H. A. Tajmir-Riahi, *J. Biomol. Struct. Dyn.* **1991**, *8*, 1169−1186.
[20] C. B. Black, J. A. Cowan, *J. Am. Chem. Soc.* **1994**, *116*, 1174−1178.
[21] A. Johnson, Y. Qu, B. V. Houten, N. Farrell, *Nucleic Acids Res.* **1992**, *20*, 1697−1703.

Received December 29, 2000
[I00486]

Ligand Effects on the Kinetics of the Reversible Binding of NO to Selected Aminocarboxylato Complexes of Iron(II) in Aqueous Solution

Thorsten Schneppensieper,[a] Alicja Wanat,[a,b] Grazyna Stochel,*[a] Sara Goldstein,[c] Dan Meyerstein,[d] and Rudi van Eldik*[a]

Keywords: Catalysts / Chelates / Iron / Kinetics / Nitrogen oxides

Rate constants for the formation and dissociation of Fe^{II}(L)NO (L = aminocarboxylato) have been determined using stopped-flow, temperature jump, flash photolysis, and pulse radiolysis techniques. For a series of ligands the formation rate constants vary between 1.6×10^6 and 2.4×10^8 M^{-1} s^{-1}, whereas the dissociation rate constants vary between 0.11 and 3.2×10^3 s^{-1} at 25 °C. These rate constants result in stability constants ($K_{NO} = k_f/k_d$) ranging from 5.0×10^2 to 1.1×10^7 M^{-1}, which are in good agreement with values of K_{NO} determined by a combined spectrophotometric and potentiometric technique. The results are discussed with reference to available literature data, and interpreted in terms of a generalized reaction mechanism.

Introduction

It has been our interest in recent years to find metal chelates for the selective and efficient binding of NO in aqueous solution, to be employed in alternative denitrification processes.[1] Metal ions can catalyse such processes and can also increase the degree of absorption of NO by direct coordination to the metal center.[2,3] The fundamental coordination chemistry involves the reversible or partially reversible binding of NO by inexpensive and highly soluble metal complexes. Aminocarboxylato complexes of iron(II) are known for their ability to bind NO rapidly,[4–7] and are therefore used to enhance the solubility of NO in aqueous solution in industrial applications, in order to remove NO from exhaust gases. Little mechanistic information is presently available on these reactions, although some scattered rate constants for these reactions and stability constants are reported in the literature.[8–20]

In a recent systematic study[1] we reported the extent to which the reversible binding of NO to aminocarboxylato complexes of iron(II) can be tuned by the selected chelate. In general, a good correlation between the oxygen sensitivity of the chelated iron(II) complex and the formation constant for the Fe^{II}(L)NO complex, i.e. the ability of chelated iron(II) to bind NO was found. This trend correlated with a decreasing reversibility of the reaction, i.e. the ability of Fe^{II}(L)NO to release NO, and an increasing tendency of Fe^{II}(L)NO to exist as Fe^{III}(L)NO^- in solution. The latter complex underwent subsequent slow decomposition, during which Fe^{III}(L) and N_2O were formed.

We have now performed systematic kinetic studies on the reaction of NO with selected Fe^{II} complexes, based on their rather unique behaviour as observed in our more general and qualitative investigation referred to above.[1] These include Fe^{II} complexes of edta, hedtra, nta, dtpa, ttha, and mida (see Table 1 for selected abbreviations). Of this series, the Fe^{II}mida and Fe^{II}edta complexes behave totally differently with respect to the binding of NO. The Fe^{II}mida complex shows almost no oxygen sensitivity, exhibits a low binding affinity for NO, and releases NO almost completely when an inert gas was passed through the solution. In contrast, Fe^{II}edta is extremely oxygen-sensitive, shows a very high binding affinity for NO, and releases NO slowly and incomplete when treated with an inert gas. Kinetic studies on the formation and dissociation reactions were performed using complementary stopped-flow, temperature jump, flash photolysis, and pulse radiolysis techniques. The results are compared to available data for some of these systems reported in the literature. Our studies provide a quantitative basis for the earlier observed trends and reveal important mechanistic information.

[a] Institute for Inorganic Chemistry, University of Erlangen-Nürnberg,
Egerlandstraße 1, 91058 Erlangen, Germany
Fax: (internat.) + 49-(0)9131/85-27387
E-mail: vaneldik@chemie.uni-erlangen.de
[b] Department of Inorganic Chemistry, Jagiellonian University, Ingardena 3, 30-060 Krakow, Poland
Fax: (internat.) + 48-12/633-5392
E-mail: stochel@chemia.uj.edu.pl
[c] Department of Physical Chemistry, The Hebrew University of Jerusalem,
Jerusalem 91904, Israel
[d] Chemistry Department, Ben-Gurion University of the Negev, Beer-Sheva, and The College of Judea and Samaria,
Ariel, Israel

Results and Discussion

Employed Kinetic Techniques

It was the purpose of this study to clarify the basic kinetics of the binding of NO to a series of aminocarboxylato complexes of iron(II). Table 2 summarizes the available kinetic and thermodynamic data on such reactions using a variety of techniques.[4] In many cases the reported rate constants were determined in an indirect manner, which re-

 © WILEY-VCH Verlag GmbH, 69451 Weinheim, 2001 1434–1948/01/0909–2317 $ 17.50+.50/0

Table 1. Summary of the chelate ligands used in this study

Structure Name (Abbreviation)
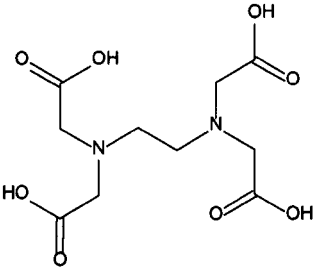 Ethylenediaminetetraacetic acid (edta)
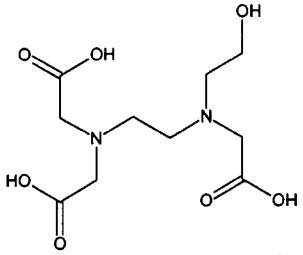 Hydroxyethylenediaminetriacetic acid (Hedtra)
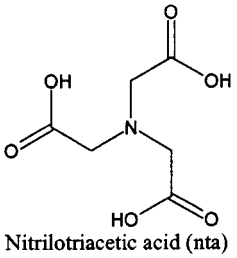 Nitrilotriacetic acid (nta)
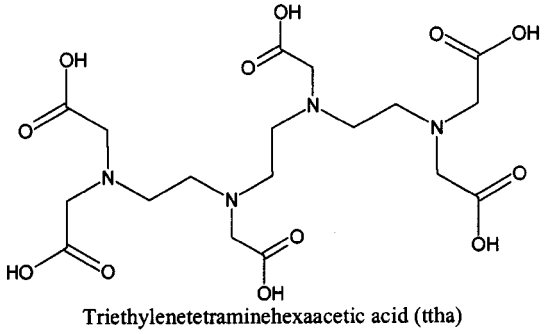 Triethylenetetraminehexaacetic acid (ttha)
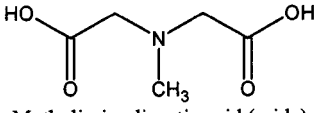 Methyliminodiacetic acid (mida)
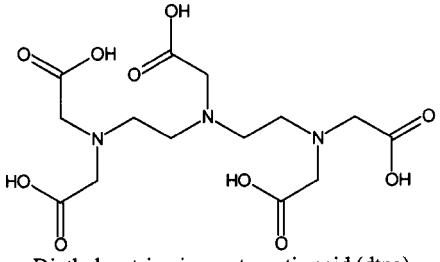 Diethylenetriaminepentaacetic acid (dtpa)

sulted in large variations in the reported data. In order to verify the earlier data and obtain data on new systems, we employed different complementary kinetic techniques (for more details see Exp. Sect.).

The binding of NO to $Fe^{II}(L)$ can be expressed by the overall reaction shown in Equation (1). Different kinetic techniques can be used to measure k_f and k_d.

$$Fe^{II}(L)(H_2O)_n + NO \underset{k_d}{\overset{k_f}{\rightleftharpoons}} Fe^{II}(L)(H_2O)_{n-1}NO + H_2O \quad (1)$$

Stopped-flow techniques can be employed to rapidly mix solutions containing the reactants if the reactions occur on the millisecond time scale. The observed rate constant in the presence of excess of $Fe^{II}(L)$ can be expressed as shown in Equation (2), from which k_f and k_d can be extracted by measuring k_{obs} as a function of $[Fe^{II}(L)]$. The ratio k_f/k_d equals the overall equilibrium constant K_{NO}, and should be in agreement with values for K_{NO} determined in other non-kinetic ways. A combination of UV/Vis spectroscopy and electrochemical detection of NO was used to determine K_{NO}, which was found to range from $(1.0 \pm 0.1) \times 10^3$ to $(1.5 \pm 0.2) \times 10^7$ M^{-1} at 25 °C for the series of complexes investigated.[1]

$$k_{obs} = k_f[Fe^{II}(L)] + k_d \quad (2)$$

In principle it is also possible to measure k_d directly, and not by the determination of an intercept according to Equation (2), by using an NO-trapping technique with the stopped-flow method. In this case $Fe^{II}(L)NO$ is treated with another complex that binds NO more strongly and rapidly than the system under investigation. Under such condition, release of NO can become the rate-limiting step, which means that k_d can be determined directly from the observed kinetic trace. Two suitable complexes for determining k_d for the release of NO from $Fe^{II}(L)NO$ are $Fe^{II}(edta)(H_2O)^{2-}$ (excluding L = edta) and $Ru^{III}(edta)H_2O^-$, both of which react rapidly (k_f is ca. 1×10^8 M^{-1} s^{-1} at pH = 5 and 25 °C)[4,21] with NO to form the corresponding nitrosyl complexes (see Scheme 1). When an excess of either of these complexes is employed, such that the release of NO, i.e. k_d, becomes the rate-limiting step, the observed rate constant becomes independent of the excess concentration employed and equals k_d.

Flash photolysis can be employed to study the kinetics of Equation (1) on a significantly faster time scale. Irradiation at 532 nm induces the release of NO, followed by relaxation kinetics to the original equilibrium position (see Scheme 2), for which the rate expression of Equation (2) applies.

A third kinetic technique employed in this study is temperature jump. This technique can be used to perturb changes in the equilibrium position for systems that exhibit a significant temperature dependence. For the observed relaxation kinetics, the first-order rate constant is given by

Table 2. Literature values of kinetic data and stability constants for the binding of NO to aminocarboxylate complexes of iron(II) in aqueous solution

Complex	pH	T [K]	k_f [M^{-1} s^{-1}]	k_d [s^{-1}]	K_{NO} [M^{-1}]	Ref.
Fe^{II}(edta)	4.6−8.0	298	1.7×10^8		1.5×10^6	[8]
	7.6	313			1.5×10^6	[8]
	3.0	311			3.5×10^6	[9]
	3.0	328			8.6×10^5	[9]
	3.0	343			3.4×10^5	[9]
	1.5−2.5	298	$(3.3 \pm 0.2) \times 10^7$			[10]
	7.0	298	$(1.2 \pm 0.1) \times 10^8$			[10]
	9.5−10	298	$(1.0 \pm 0.1) \times 10^8$			[10]
	5.1	298	$> 6.0 \times 10^7$	> 60		[2]
	6.0−8.0	308			9.9×10^6	[11]
	2.5−11.0	298	9.4×10^7		3.1×10^6	[12]
	7.0	298	1.2×10^8			[13]
	7.0	313	1.4×10^8			[13]
	7.0	333	1.4×10^8			[13]
	7.0	353	1.5×10^8			[13]
	−	288			2.2×10^6	[14]
	−	298			1.5×10^6	[14]
	−	308			7.8×10^5	[14]
	−	328			5.3×10^5	[14]
	−	348			2.5×10^5	[14]
	−	293			1.7×10^6	[15]
	−	313			3.9×10^5	[15]
	−	333			1.1×10^5	[15]
Fe^{II}(dtpa)	5.0	298	$(2.7 \pm 0.2) \times 10^5$	$< 23 \pm 11$	$> 1.2 \times 10^4$	[5]
Fe^{II}(nta)	−	295			5.9×10^5	[16]
	−	313			3.0×10^5	[16]
	−	333			1.0×10^5	[16]
	4.5−9.0	298	1.6×10^7		3.3×10^6	[12]
	5.0−7.0	298	$> 7.1 \times 10^7$	> 35	$>2 \times 10^6$	[17]
	5.5	313			$(8.7 \pm 0.2) \times 10^5$	[17]
	5.5	323			$(4.6 \pm 0.2) \times 10^5$	[17]
	5.5	333			$(2.5 \pm 0.2) \times 10^5$	[17]
	4.0−9.0	293			1.8×10^6	[18]
	4.0−9.0	313			7.7×10^5	[18]
	4.0−9.0	333			2.2×10^5	[18]
$Fe^{II}(H_2O)_6$	< 1.0	298	6.2×10^5	1.4×10^3	4.5×10^2	[19]
	2.0	298	8.7×10^5	2.3×10^3	3.8×10^2	[20]
	< 1.0	298	$(7.1 \pm 1.0) \times 10^5$	$(1.5 \pm 0.6) \times 10^3$	$(4.7 \pm 2.0) \times 10^2$	[2]

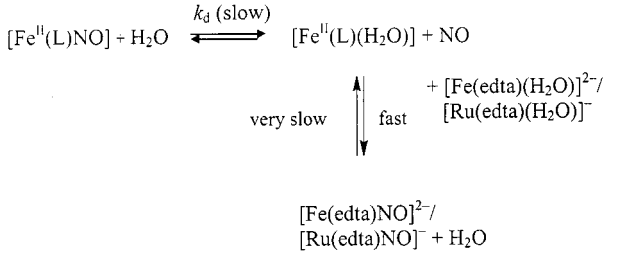

Scheme 1. Determination of k_d with the scavenger complexes $Fe^{II}(edta)(H_2O)^{2-}$ or $Ru^{III}(edta)(H_2O)^-$ for complexes of the type $Fe^{II}(L)NO$

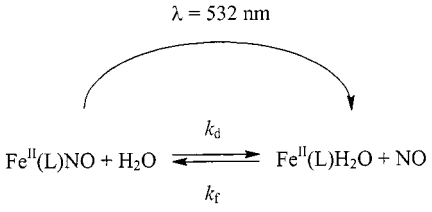

Scheme 2. NO release following irradiation at 532 nm during flash photolysis experiments

Equation (3), where $[Fe^{II}(L)H_2O]_e$ and $[NO]_e$ represent the equilibrium concentrations. According to rate law of Equation (3), measurements of k_{obs} as a function of the sum of the equilibrium concentrations should enable the determination of k_f and k_d.

$$k_{obs} = 1/\tau = k_f\{[Fe^{II}(L)(H_2O)]_e + [NO]_e\} + k_d \quad (3)$$

A fourth kinetic technique employed in this study is pulse radiolysis. The reaction of $Fe^{II}(L)$ with NO was studied by pulse-irradiation of aqueous solutions containing 2 mM $Fe^{III}(L)$, 58−170 μM NO, 1 M methanol, and either 2 mM acetate or phosphate buffer. Under these conditions, e^-_{aq} reduces $Fe^{III}(L)$ to $Fe^{II}(L)$ and $^{\cdot}OH$ is scavenged by CH_3OH to produce $^{\cdot}CH_2OH$ as shown in Equations (4) to (6). (The numbers in parenthesis are G values, which represent the

number of molecules formed per 100 eV energy absorbed by pure water.[22])

$$H_2O \xrightarrow{\gamma,\ e^-} e^-_{aq}\ (2.6),\ {}^{\cdot}OH\ (2.7),\ {}^{\cdot}H\ (0.6),\ H_2\ (0.45),\ H_2O_2\ (0.7),\ H_3O^+\ (2.6) \quad (4)$$

$$e^-_{aq} + Fe^{III}L \rightarrow Fe^{II}L \quad (5)$$

$$CH_3OH + {}^{\cdot}OH \rightarrow {}^{\cdot}CH_2OH + H_2O \quad (6)$$

The ·H radicals are only a small fraction (ca. 10%) of the total radicals formed by the radiation, and most of them are scavenged by CH_3OH to produce $^{\cdot}CH_2OH$, while the rest react with NO.[22] The reaction rate of NO with $^{\cdot}CH_2OH$ is expected to be similar to that with ethanol radical, i.e. 3×10^9 M^{-1} s^{-1},[22] most probably forming O=N−CH_2OH as the primary product, which might further react to form HO−N=CH_2. The rate constant for the reaction of $Fe^{II}L$ with NO was determined by monitoring the formation of the absorbance at 440 or 450 nm under pseudo-first-order conditions, where $[Fe^{II}L] = \text{dose} \times G_e \approx 5$ μM and $[NO] \approx [NO]_0 - \text{dose} \times G_{OH} \approx 53-165$ μM.

Data Measured for k_f and k_d

Stopped-Flow Measurements

Recently,[23] k_f was measured directly using the stopped-flow technique, in the case of $Ru^{III}(edta)H_2O^-$ to be 1×10^7 M^{-1} s^{-1} in phosphate buffer at pH = 7.4 and 7.3 °C. In order to measure such high rate constants, second-order reaction conditions and low concentrations of both reactants were selected to obtain conditions where the reaction is slower than the dead time (2−4 ms) of the stopped-flow instrument. We repeated the measurements on the $Ru^{III}(edta)H_2O^-$ system in acetate buffer at pH = 5.0 and 8 °C,[21] but surprisingly found $k_f = 1 \times 10^5$ M^{-1} s^{-1}, which is ca. 100 times slower than the literature value.[23] This apparent discrepancy could be resolved by considering that the buffer should not be present in the Ru^{III} solution, but only in the NO-containing solution prior to mixing in the stopped-flow instrument. The buffer can substitute the labile water molecule in $Ru^{III}(edta)H_2O^-$ and cause a much slower substitution reaction with NO in producing the final product $Ru^{II}(edta)(NO^+)^-$. It follows from these measurements that the literature value is valid at 8 °C, and a reasonable extrapolation to 25 °C results in $k_f \approx 1 \times 10^8$ M^{-1} s^{-1}. Similar experiments with Fe^{II}(edta) and Fe^{II}(hedtra) at low temperature and low reactant concentrations revealed that k_f for these complexes is on the limit or faster than 5×10^7 M^{-1} s^{-1} at pH = 5 and 25 °C, i.e. very similar to that reported for $Ru^{III}(edta)H_2O^-$, and could not be resolved using this kinetic technique. The high k_f values make these complexes ideal candidates for studying the reverse release of NO on complexes that bind NO less rapidly, using the trapping technique referred to above. Alternatively, an excess of such a complex can be used to study the release of NO from a complex that exhibits a similar reactivity towards NO, since the concentration ratio then determines the nature of the final product and the extent to which the rate-determining release of NO will be observed.

For the systems under the current investigation, k_f could not be determined using stopped-flow techniques, even under low temperature and concentration conditions, and therefore flash photolysis, pulse radiolysis, and temperature jump techniques were employed. However, for all the investigated systems, k_d could be measured directly using either $Ru^{III}(edta)H_2O^-$ and/or $Fe^{II}(edta)H_2O^{2-}$ to trap NO as described below.

With $Fe^{II}(edta)H_2O^{2-}$ as the NO scavenger during the release of NO from Fe^{II}(mida)NO, the absorption maximum at 444 nm, which is characteristic for Fe^{II}(mida)NO,

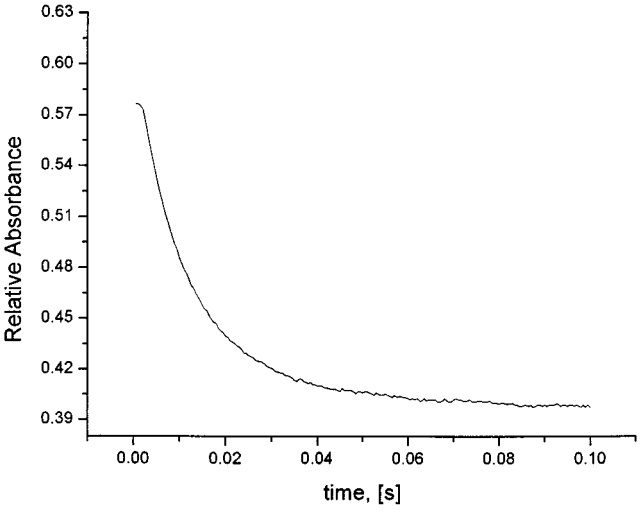

Figure 1. Typical absorbance-time plot for the release of NO from 0.25 mM $Fe^{II}(edta)NO^{2-}$, recorded with the stopped-flow instrument using 7.5 mM $Ru^{III}(edta)H_2O^-$ as a scavenger at pH = 5.0 (0.05 M NaAc), λ = 436 nm, T = 24.4 °C

Table 3. Dependence of k_d on $[Fe^{II}(edta)H_2O^{2-}]$ and $[Ru^{III}(edta)H_2O^-]$ in the presence of 0.2 M acetate buffer [pH = 5.0; I = 0.5 M ($NaClO_4$), T = 25 °C] for the release of NO from $Fe^{II}(mida)_2NO^{2-}$

1.5×10^{-3} M $Fe^{II}(mida)_2NO^{2-}$ + x M $Fe^{II}(edta)H_2O^{2-}$		2.5×10^{-3} M $Fe^{II}(mida)_2NO^{2-}$ + x M $Ru^{III}(edta)H_2O^-$	
$[Fe^{II}(edta)(H_2O)^{2-}]$ [M]	k_d [s^{-1}]	$[Ru^{III}(edta)(H_2O)^-]$ [M]	k_d [s^{-1}]
1.0×10^{-3}	55.0 ± 0.4	5.0×10^{-3}	53.0 ± 0.5
1.5×10^{-3}	60.0 ± 0.5	7.5×10^{-3}	54.0 ± 0.3
2.5×10^{-3}	57.3 ± 0.4	1.0×10^{-2}	52.5 ± 0.3

decreased in intensity while a new band at 435 nm appeared, indicating the formation of $Fe^{II}(edta)NO^{2-}$. The rate constant for NO release from $Fe^{II}(mida)NO$ was found to be 57.3 ± 0.4 s^{-1} in the presence of excess of $Fe^{II}(edta)H_2O^{2-}$ and 52.5 ± 0.3 s^{-1} in the presence of excess of $Ru^{III}(edta)H_2O^{-}$ at 25 °C. Thus, there is a good agreement between the values of k_d determined using the two different NO scavengers. In both cases the rate-limiting step is the release of NO from the nitrosyl complex.

Table 4. Dependence of k_d for the release of NO from $Fe^{II}(edta)NO^{2-}$ on $[Ru^{III}(edta)H_2O^{-}]$ in the presence of 0.2 M acetate buffer [pH = 5.0; I = 0.5 M ($NaClO_4$), T = 25 °C]

2.5×10^{-4} M $Fe(edta)^{-2}$ + x M $Ru(edta)H_2O^{-}$ $[Ru(edta)(H_2O)^{-}]$ [M]	k_d [s^{-1}]
2.5×10^{-3}	91.0 ± 0.4
5.0×10^{-3}	90.4 ± 0.6
7.5×10^{-3}	91.8 ± 0.6

The release of NO from $Fe^{II}(edta)NO^{2-}$ with $Ru^{III}(edta)H_2O^{-}$ as a scavenger was complete within 100 ms, and k_d was calculated to be 91.0 ± 0.4 s^{-1} at 25 °C. A typical stopped-flow trace for this reaction is shown in Figure 1. The decrease in the absorption at 436 nm is consistent with the reaction equilibrium presented in Scheme 1. The observed rate constants were found to be independent of the concentration of the trapping complex as shown in

Table 5. Summary of kinetic data determined during this study for the reaction of NO with aminocarboxylato complexes of iron(II) at 25 °C

Complex	pH	k_f [$M^{-1}s^{-1}$]	k_d [s^{-1}]	K_{NO} (= k_f/k_d)[a][b] [M^{-1}]	K_{NO} [M^{-1}]	Method
$Fe^{II}(edta)$	4.9	$(1.5 \pm 0.2) \times 10^8$				pulse radiolysis
	7.2	$(1.7 \pm 0.4) \times 10^8$				
	5.0	$(2.4 \pm 0.1) \times 10^8$				flash photolysis
	5.0		91.0 ± 0.4			stopped flow
				$(2.1 \pm 0.5) \times 10^6$	$(2.1 \pm 0.2) \times 10^6$	
$Fe^{II}(hedtra)$	5.6	$(3.4 \pm 0.1) \times 10^7$				pulse radiolysis
	6.9	$(3.1 \pm 0.2) \times 10^7$				
	5.0	$(6.1 \pm 0.1) \times 10^7$				flash photolysis
	5.0		4.2 ± 0.1			stopped flow
				$(1.1 \pm 0.4) \times 10^7$	$(1.5 \pm 0.2) \times 10^7$	
$Fe^{II}(nta)$	3.5	$(1.2 \pm 0.1) \times 10^7$				pulse radiolysis
	5.4	$(1.3 \pm 0.1) \times 10^7$				
	6.8	$(1.4 \pm 0.1) \times 10^7$				
	5.0	$(2.1 \pm 0.1) \times 10^7$				flash photolysis
	5.0		9.3 ± 0.2			stopped flow
				$(1.8 \pm 0.5) \times 10^6$	$(1.8 \pm 0.2) \times 10^6$	
$Fe^{II}(dtpa)$	6.8	$(2.7 \pm 0.3) \times 10^5$				pulse radiolysis
	5.0	$(1.1 \pm 0.1) \times 10^7$				flash photolysis
	5.0		5.5 ± 0.4			stopped flow
				$(2.0 \pm 0.2) \times 10^6$	$(3.0 \pm 0.3) \times 10^6$	
$Fe^{II}_2(ttha)$	5.2	$(6.5 \pm 0.7) \times 10^5$				pulse radiolysis
	5.0	$(3.5 \pm 0.1) \times 10^6$				flash photolysis
	5.0		0.11 ± 0.01			stopped flow
				$(3.1 \pm 0.3) \times 10^7$	$(3.0 \pm 1.0) \times 10^7$	
$Fe^{II}(ttha)$	5.2	$(3.0 \pm 0.7) \times 10^5$				pulse radiolysis
	5.0	$(1.0 \pm 0.1) \times 10^6$				flash photolysis
	5.0		0.39 ± 0.01			stopped flow
				$(2.6 \pm 0.2) \times 10^6$	$(4.0 \pm 0.1) \times 10^6$	
$Fe^{II}(mida)$	5.0	$(1.9 \pm 0.1) \times 10^6$				flash photolysis
	5.0	$(8.5 \pm 2.4) \times 10^5$				temperature jump
	5.0		57.3 ± 0.4			stopped flow
				$(2.1 \pm 0.6) \times 10^4$	$(9.5 \pm 0.7) \times 10^3$	
$Fe^{II}(mida)_2$	5.0	$(1.8 \pm 0.1) \times 10^6$				flash photolysis
	5.0		62.2 ± 0.6			stopped flow
				$(2.9 \pm 0.2) \times 10^4$	$(2.2 \pm 0.6) \times 10^4$	
$Fe^{II}(H_2O)_6$	5.0	$(1.6 \pm 0.1) \times 10^6$ (from slope)	$(3.2 \pm 0.7) \times 10^3$ (from intercept)			flash photolysis
	5.0		788 ± 100 (at 5 °C)			stopped flow
				$(5.0 \pm 1.4) \times 10^2$	$(1.2 \pm 0.1) \times 10^3$	

[a] The stability constants were calculated from k_f/k_d, which were obtained kinetically. – [b] Stability constants for nitrosyl complexes are based on the equilibrium between $Fe^{II}(L)_x$ and $Fe^{II}(L)_x(NO)$ complexes; the complex concentrations were measured using UV/Vis spectroscopy and the concentration of free NO in solution was determined directly with an NO electrode, from which K_{NO} was calculated.[1]

Tables 3 and 4, and therefore represent values for k_d. The results of these measurements are summarized in Table 5. The lowest k_d values were found for $Fe^{II}(ttha)NO^{4-}$ and $Fe_2^{II}(ttha)NO^{2-}$ with $k_d = 0.39 \pm 0.01$ and 0.11 ± 0.01 s^{-1} at 25 °C, respectively. The release of NO was found to be slightly faster for $Fe^{II}(hedtra)NO^-$ ($k_d = 4.2 \pm 0.1$ s^{-1}), $Fe^{II}(dtpa)NO^{3-}$ ($k_d = 5.5 \pm 0.4$ s^{-1}), and $Fe^{II}(nta)NO^-$ ($k_d = 9.3 \pm 0.2$ s^{-1}). Significantly higher rate constants were obtained for $Fe^{II}(mida)NO$ ($k_d = 57.3 \pm 0.4$ s^{-1}) and $Fe^{II}(mida)_2NO^{2-}$ ($k_d = 62.2 \pm 0.6$ s^{-1}), while the highest value was found for $Fe^{II}(edta)NO^{2-}$ ($k_d = 91.0 \pm 0.4$ s^{-1}). Kinetic data for the NO release in the case of edta, nta, and dtpa are available from the literature (see Table 2).[2,5,17] In the case of Fe^{II}(edta) the predicted literature value of $k_d > 60$ s^{-1} could be confirmed, whereas significantly lower rates were measured in the present study for nta and dtpa. The trapping technique employed enables a direct measurement of the dissociation rate constant, and in principle must give more accurate values than those obtained using indirect methods. By way of comparison, k_d for aquated iron(II) was found to be 788 ± 100 s^{-1} (at 5 °C), i.e. aquated iron(II) binds NO very weakly and releases it rapidly. Extrapolated to 25 °C, the latter value is in good agreement with the value obtained from flash photolysis experiments (see further Discussion).

Flash Photolysis Measurements

The procedure outlined in Scheme 2 was employed for all investigated systems. A typical kinetic trace is shown in Figure 2. The concentration dependence of k_{obs} resulted in linear plots, as predicted by Equation (2), for which typical examples are shown in Figures 3 and 4 for $Fe^{II}(nta)NO^-$ and $Fe^{II}(H_2O)_5NO^{2+}$, respectively. The Fe^{II}(edta) complex is the species with the highest formation rate constant, i.e. $k_f = (2.4 \pm 0.1) \times 10^8$ M^{-1} s^{-1} at 25 °C (pH = 5). This result agrees well with literature data (see Table 2), where rate constants around 1.3×10^8 M^{-1} s^{-1} at different pH values and temperatures were found. For Fe^{II}(nta), Fe^{II}(hedtra), and Fe^{II}(dtpa), k_f was found to be $(2.1 \pm 0.1) \times 10^7$, $(6.1 \pm 0.1) \times 10^7$ and $(1.1 \pm 0.1) \times 10^7$ M^{-1} s^{-1} at 25 °C, respectively. While the value for the nta system is in good agreement with data reported in the literature,[12] the obtained rate constant for the dtpa system is significantly higher than that obtained before with the temperature jump technique.[5] We believe, however, that the value measured in the present study is more reliable, since the stability constants (K_{NO}) obtained from kinetic and thermodynamic measurements are in perfect agreement with these data (see Table 5). The Fe^{II}(hedtra) complex reacts only half as fast as the edta complex, but the stability constant is more than five times higher, as a result of the NO release kinetics reported above. The k_f values for Fe_2^{II}(ttha) and Fe^{II}(ttha) are $(3.5 \pm 0.1) \times 10^6$ and $(1.0 \pm 0.1) \times 10^6$ $M^{-1}s^{-1}$ at 25 °C, respectively. The lowest k_f values were found for $Fe^{II}(mida)$ (1.9×10^6 M^{-1} s^{-1}), $Fe^{II}(mida)_2$ (1.8×10^6 M^{-1} s^{-1}) and $Fe^{II}(H_2O)_6$ (1.6×10^6 M^{-1} s^{-1}), respectively.

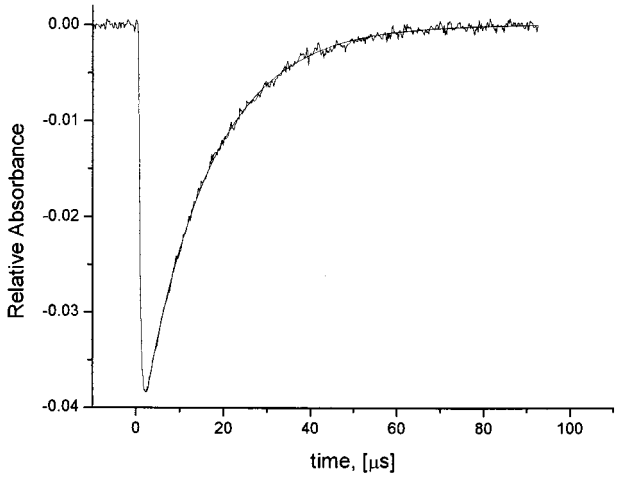

Figure 2. Typical absorbance-time plot for the reaction of Fe^{II}(nta) with NO at pH = 5.0 (0.1 M NaAc), $I = 0.5$ M ($NaClO_4$) and $T = 25$ °C; photolysis wavelength = 532 nm, detection wavelength = 439 nm

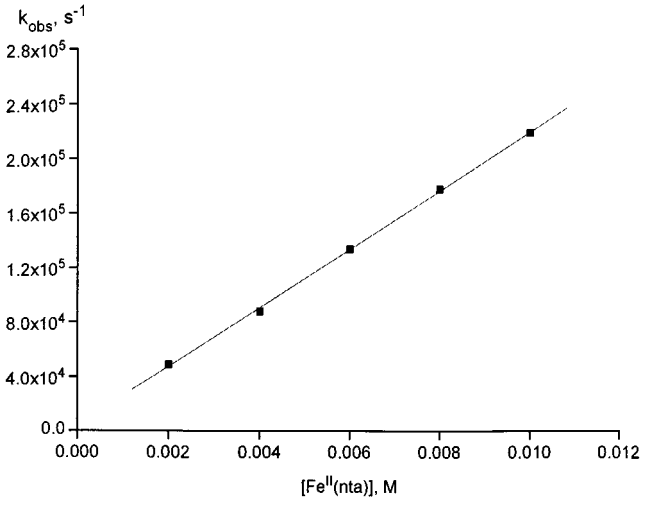

Figure 3. Plot of k_{obs} as a function of [Fe^{II}(nta)], measured at pH = 5.0 (0.2 M NaAc) and $T = 25$ °C; photolysis wavelength = 532 nm, detection wavelength = 439 nm

Pulse Radiolysis Measurements

Figure 5 presents a typical absorbance-time trace recorded for the reaction of Fe^{II}(edta) with NO using the pulse radiolysis procedure described above. Values of k_f determined with this method were slightly lower in comparison with the results obtained from the flash photolysis experiments, viz. 1.5×10^8 M^{-1} s^{-1} at pH = 4.9 for Fe^{II}(edta), 3.4×10^7 M^{-1} s^{-1} at pH = 5.6 for Fe^{II}(hedtra), and 1.3×10^7 M^{-1} s^{-1} at pH = 5.4 for Fe^{II}(nta). This difference can probably be accounted for in terms of the different temperatures at which the experiments were performed, viz. ca. 20 °C in the pulse radiolysis experiments compared to 25 °C in the flash photolysis experiments. However, in the case of

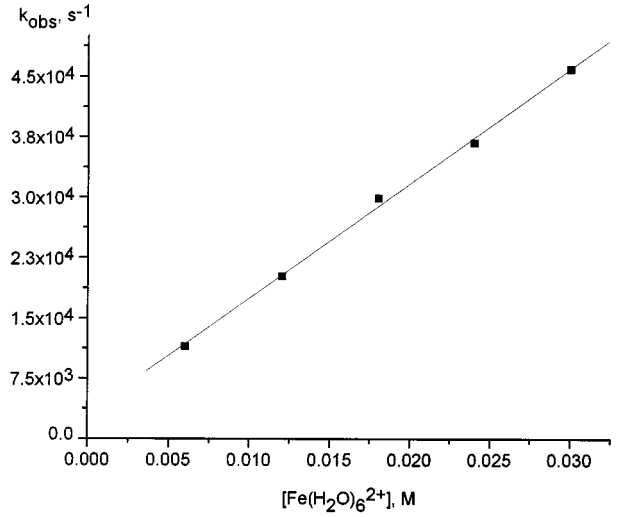

Figure 4. Plot of k_{obs} as a function of $[Fe(H_2O)_6^{2+}]$, measured at pH = 5.0 (0.2 M NaAc) and T = 25 °C; photolysis wavelength = 532 nm, detection wavelength = 451 nm

dtpa and ttha complexes (see Table 5), the values of k_f are much lower than those obtained in the flash photolysis experiments. For these systems it was not possible to perform a concentration dependence study due to the high absorbance of the 2 mM $Fe^{III}(L)$ solution. The second-order rate constant had to be calculated from a single point measured in the presence of 0.104 mM NO at 500 and 470 nm for the dtpa and ttha complexes, respectively. The absorbance changes at these wavelengths are extremely small, which further adds to the uncertainty in the rate constants. In addition, the calculated value of K_{NO} based on the rate constants from the flash photolysis experiments is in good agreement with the directly determined value. These facts lead us to conclude that the flash photolysis data probably represent the more realistic rate constants for the studied systems.

Temperature Jump Measurements

Measurements of k_f for the Fe^{II}(mida) complexes failed using pulse radiolysis. This led us to probe the temperature jump method to establish the accuracy of the data measured with the flash photolysis technique. Equilibrium mixtures of Fe^{II}(mida) and Fe^{II}(mida)NO were studied, and a typical absorbance-time trace is reported in Figure 6. A systematic concentration-dependence study according to Equation (3) (shown in Figure 7) resulted in $k_f = (8.6 \pm 0.8) \times 10^5$ M^{-1} s^{-1}, which agrees within experimental errors with the data from the flash photolysis experiments. The intercept of the line represents k_d for the release of NO, and was found to be 69 ± 50 s^{-1}. Considering the large error limits (up to 15%) usually encountered in temperature jump

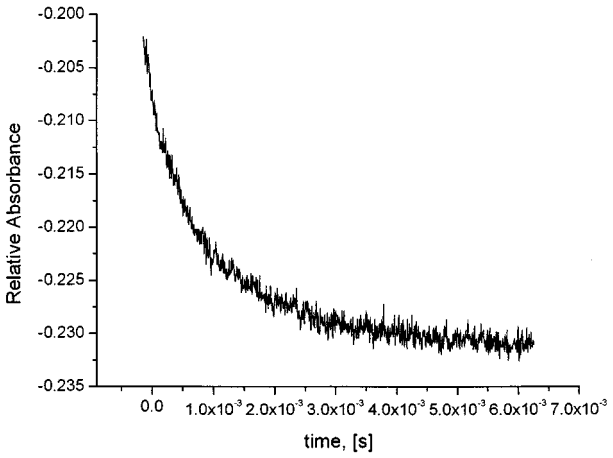

Figure 6. Typical absorbance-time trace for the reaction of Fe^{II}(mida) with NO using the temperature jump techniques; $k_{obs} = 1.08 \times 10^3$ M^{-1} s^{-1}; experimental conditions: $\lambda_{det.}$ = 444 nm, T = 25 °C, $[Fe^{II}(mida)NO] = 7.9 \times 10^{-4}$ M, $[Fe^{II}(mida)] = 1.2 \times 10^{-3}$ M, $[NO] = 5.5 \times 10^{-5}$ M, pH = 5.0 (0.1 M NaAc), I = 0.5 ($NaClO_4$)

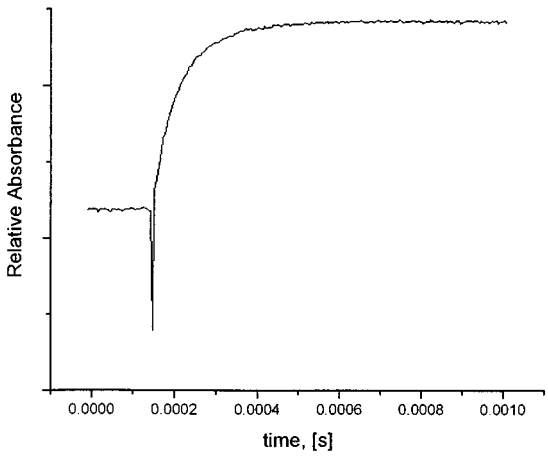

Figure 5. Typical absorbance-time trace for the reaction of $Fe^{II}(edta)H_2O^{2-}$ with NO using pulse radiolysis; the solution contained 2 mM $Fe^{III}(edta)H_2O^-$, 1 M CH_3OH, and 0.115 mM NO at pH = 7.2 (4 mM phosphate buffer), 1.5 μs pulse duration, λ = 440 nm, T = 20 °C

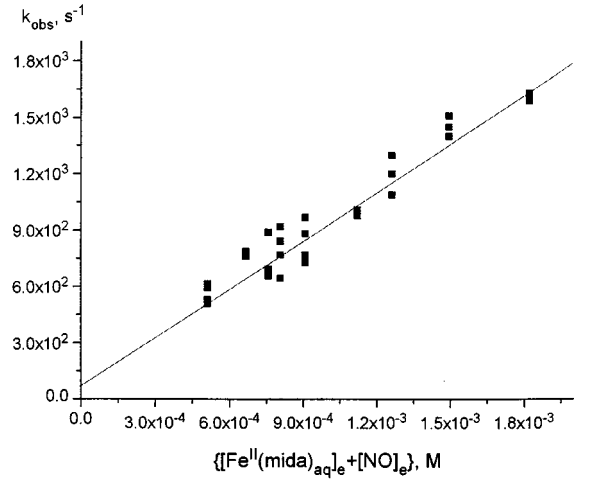

Figure 7. Plot of k_{obs} as a function of $\{[Fe^{II}(mida)_{aq}]_e + [NO]_e\}$ for the reaction of Fe^{II}(mida) with NO obtained using the temperature jump technique; experimental conditions: $\lambda_{det.}$ = 444 nm, T = 25 °C, pH = 5.0 (0.1 M NaAc), I = 0.5 ($NaClO_4$)

experiments, this value is in reasonable agreement with the more accurate one determined via stopped-flow measurements using the trapping technique.

Conclusion

Four different kinetic techniques were employed to study the binding reaction of NO to a series of aminocarboxylato complexes of iron(II). Depending on the selected system, one or more techniques could be used to determine k_f. The rate constant for the dissociation of NO could be measured successfully in all cases using the stopped-flow technique and $Fe^{II}(edta)H_2O^{2-}$ or $Ru^{III}(edta)H_2O^{-}$ as NO scavengers. As a result of its higher stability and much less oxygen sensitivity, $Ru^{III}(edta)H_2O^{-}$ appears to be more promising for practical applications as an NO scavenger than $Fe^{II}(edta)H_2O^{2-}$, although they both bind NO at approximately the same rate.

The fastest rate constant for the binding of NO was found in the case of edta, which is ca. 4 times faster than the reaction of $Fe^{II}(hedtra)H_2O$ with NO. Taking into account the 22 times faster NO release from the edta complex, the nitrosyl adduct of the hedta complex is around 5 times more stable than the edta complex at 25 °C. On this basis, we can account for the reported difference in the stability constants for these two complexes. The $Fe^{II}(nta)NO^{-}$ complex has approximately the same stability constant as the edta complex, where in this case both k_f and k_d are smaller. All other complexes have significantly lower stability constants due to their lower k_f values. On comparing the iron(II) complexes of mida and edta in terms of their application as catalysts for the exhaust gas denitrification, the reaction of $Fe^{II}(mida)$ with NO is approximately 100 times slower than the corresponding reaction with $Fe^{II}(edta)H_2O^{2-}$, which accounts for almost the same difference in the value of K_{NO}. This apparent disadvantage of the mida complex could for example be partially compensated for by longer contact time between the exhaust gas and the catalyst. In addition, the mida complex is almost oxygen-insensitive, which prevents unwanted oxidation of the chelate and allows the effective regeneration of the catalyst.

In general, a good agreement between the values of K_{NO} calculated from the kinetic data and those determined directly with the aid of the NO electrode was observed (see Table 5). The thermodynamic value furthermore assisted the selection of appropriate kinetic data in those cases where differing k_f values were found. The results in Table 5 demonstrate the large influence of the aminocarboxylato chelates on the values of the rate constant and the overall equilibrium constant. There seems to be no simple correlation between these constants and the selected donor groups or charge on the iron(II) complexes. The formation reaction must to some degree be controlled by the lability of the coordinated water molecules on the iron(II) centre, whereas the dissociation reaction is largely affected by the oxidation state of the metal centre, viz. $Fe^{II}-NO$ or $Fe^{III}-NO^{-}$ or $Fe^{I}-NO^{+}$. The distribution of charge density in the Fe−NO bond should depend on the donor properties of the selected chelate. Solomon et al.[24] have clearly shown that in the case of $Fe^{II}(edta)NO$, the Fe−NO centre has an $Fe^{III}-NO^{-}$ character.

Details on the intimate mechanism of these reactions cannot be obtained from rate constant measurements only. With the kinetic methods now well worked out to investigate these reactions, it has become possible to go a step further and to study the temperature and pressure dependence of the formation and dissociation reactions reported here. From these dependencies the activation parameters ($\Delta H^{\neq}$, $\Delta S^{\neq}$, and $\Delta V^{\neq}$) can be obtained and used to gain further insight into the intimate nature of the underlying reaction mechanisms. In addition, since it is reasonable to expect that k_f is controlled by the lability of coordinated water, the rate and activation parameters for the solvent exchange reactions on the selected iron(II) complexes should also be studied. These results and their mechanistic interpretation will be reported in a forthcoming paper.

Experimental Section

Materials and Methods

Chemicals: All chemicals were of analytical grade and were used as received. Solutions were prepared with distilled and purified water using a Milli-Q water purification system. The ligands mida and nta were supplied by Akzo Nobel. All other ligands and chemicals were purchased from Arcos Chimica, Fluka, Lancaster Synthesis, or Sigma-Aldrich with the highest available purity (at least 97%). NO gas, purchased from Messer Griesheim or Rießner Gase in a purity of at least 99.5 vol-%, was cleaned from trace amounts of higher nitrogen oxides like N_2O_3 and NO_2 by passing it through an Ascarite II column (NaOH on silica gel, Sigma-Aldrich). NO from a gas tank should not be used after six months following the date of its industrial preparation, since decomposition causes a drastic decrease in the purity of the gas. The decomposition is pressure-dependent, which led us to only use bottles filled with a maximum pressure of 20 bar, and resulted in a longer lifetime of the NO gas. All experiments were performed under strict exclusion of air oxygen. Buffer solutions were deaerated for extended periods (in general 1 min per mL solution) with pure N_2 or Ar, or in some cases using freeze-thaw cycles under vacuum, in order to completely remove the dissolved dioxygen in solution, before they were brought in contact with Fe^{II} salts or nitric oxide.

Measurements: The pH was measured using a Mettler Delta 340 pH-meter. The reference electrode was filled with NaCl instead of KCl to prevent precipitation of $KClO_4$. UV/Vis spectra were recorded with a Cary 1G UV/Vis spectrophotometer from Varian using a 1-cm quartz cuvette directly attached to a round flask with a side gas connection. The determination of the stability constants was performed as described elsewhere.[1] The concentration of free NO was determined with an ISO-NOP electrode connected to an ISO-NO Mark II nitric oxide sensor from World Precision Instruments. The NO electrode consists of a membrane-covered anode that selectively oxidizes NO to NO_3^{-} ions. The resulting current is proportional to the concentration of NO in solution. The NO electrode was calibrated daily with fresh solutions of sodium nitrite and potassium iodide according to the method suggested by the manufacturers. The calibration factor nA/μM was determined with a linear fit program.

Kinetic Measurements

Laser Flash Photolysis: Laser flash photolysis kinetic studies were carried out with the use of the LKS.60 Spectrometer from Applied Photophysics for detection and a Nd:YAG laser (SURLITE I − 10 Continuum) pump source operating in the second ($\lambda_{exc.}$ = 532 nm) harmonic (245 mJ pulses with ca. 7-ns pulse widths). Spectral changes at appropriate wavelength were monitored using a 100-W Xenon arc lamp, monochromator, and photomultiplier tube PMT − 1P22. The absorbance reading was balanced to zero before the flash, and data were recorded with a digital storage oscilloscope DSO HP 54522A and then transferred to a computer for sequential analysis. Gas-tight quartz cuvettes were used throughout this study. The rate constant for the NO uptake reaction was detected around 435 nm, where a maximum in the UV/Vis spectrum is present. A stock solution of NO was prepared in a gas-tight syringe by degassing a 0.2 M acetate buffer solution (pH = 5.0), followed by saturation with NO. Dilutions of known concentration were prepared from this saturated solution by the use of the syringe technique. Oxygen-free solutions of iron(II) complexes were synthesized and diluted to appropriate concentrations in the vacuum line.

Pulse Radiolysis: Pulse radiolysis experiments were carried out with the Varian 7715 linear accelerator with 5-MeV electrons pulses of 0.5 μs and 200 mA current. The dose per pulse was determined with the hexacyanoferrate(II) dosimeter [5 mM $K_4Fe(CN)_6$ in N_2O-saturated water] using $G\varepsilon[Fe(CN)_6^{3-}] = 6.7 \times 10^3\ M^{-1}\ cm^{-1}$ at 420 nm[25] to be 13.8 Gy. A 150-W Xe lamp produced the analysing light. Appropriate filters were used to minimize photochemistry. Irradiation was carried out in a 4-cm Spectrosil cell using three light passes. Nitric oxide solutions were prepared in gas-tight syringes by purging first the water with He to remove O_2, followed by bubbling for 30 min with NO. NO-saturated solutions (1.8 mM at 21 °C and 690 Torr)[26] were stored in syringes and subsequently diluted with He-saturated solutions to the desired concentrations by the syringe technique.

Temperature Jump: The complex formation reactions were studied using the earlier described joule-heating temperature jump apparatus (rise time ≈ 10 μs) (Messanlagen, Göttingen)[27] A temperature jump of 3 °C was applied to solutions thermostatically maintained at 22 °C during an electric discharge of ca. 20 kV. Kinetic traces for relaxation were monitored mostly at 444 nm, with at least 5, and up to 10, replicate traces being processed as reported earlier,[28,29] by emulating a transient recorder with a 486 PC equipped with a TR-PC 25-8 card from Dr. Strauss System Elektronik GmbH. After the jump, a single relaxation process was observed in each trace. The rate constant for the relaxation curve was fitted with the OLIS KINFIT program.[30]

Stopped-Flow: The kinetics of NO release from $Fe^{II}(L)NO$ were studied with a thermostated (±0.1 °C) stopped-flow spectrometer (SX-18 MV, Applied Photophysics) coupled to an online data acquisition system. At least five kinetic runs were recorded under all conditions, and the reported rate constants represent the mean values. The kinetic data were analysed with the OLIS KINFIT program.

Acknowledgments

T. S. and R. v. E. gratefully acknowledge financial support from Akzo Nobel Functional Chemicals, Paques Bio Systems, Fonds der Chemischen Industrie, and the Max-Buchner-Forschungsstiftung. Studies at the Jagiellonian University were supported by the State Committee for Scientific Research, Poland, KBN (3TO9A11515 and 1605/T09/2000/19) and the Foundation for Polish Science ("Fastkin"No. 8/97). D. M. acknowledges support from the Alexander von Humboldt Foundation.

[1] T. Schneppensieper, S. Finkler, A. Czap, R. van Eldik, M. Heus, P. Nieuwenhuizen, C. Wreesmann, W. Abma, *Eur. J. Inorg. Chem.* **2001**, 491−501.
[2] D. Littlejohn, S.-G. Chang, *J. Phys. Chem.* **1982**, *86*, 537−540.
[3] S.-G. Chang, D. Littlejohn, S. Lynn, *Environ. Prog. Technol.* **1983**, *17*, 649.
[4] J. F. Demmink, I. C. F. van Gils, A. A. C. M. Beenackers, *Ind. Eng. Chem. Res.* **1997**, *36*, 4914−4927.
[5] V. Zang, R. van Eldik, *Inorg. Chem.* **1990**, *29*, 4462−4468.
[6] S. S. Tsai, S. A. Bedell, L. H. Kirby, D. J. Zabcik, *Environ. Prog.* **1989**, *8*, 126−129.
[7] V. Zang, M. Kotowski, R. van Eldik, *Inorg. Chem.* **1988**, *27*, 3279.
[8] M. Teramoto, S. −I. Hiramine, Y. Shimada, Y. Sugimoto, H. Teranishi, *J. Chem. Eng. Jpn.* **1978**, *11*, 450−457.
[9] Y. Hishunuma, R. Kaji, H. Akimoto, F. Nakajima, T. Mori, T. Kamo, Y. Arikawa, S. Nozawa, *Bull. Chem. Soc. Jpn.* **1979**, *52*, 2863−2865.
[10] E. Sada, H. Kumazawa, I. Kudo, T. Kondo, *Ind. Eng. Chem. Proc. Des. Dev.* **1980**, *19*, 377−382.
[11] E. Sada, H. Kumazawa, Y. Takada, *Ind. Eng. Chem. Fundam.* **1984**, *23*, 60−64.
[12] W. Weisweiler, R. Blumhofer, T. Westermann, *Chem. Eng. Proc.* **1986**, *20*, 155−166.
[13] S.-M. Yih, C.-W. Lii, *Chem. Eng. Comm.* **1988**, *73*, 43−53.
[14] L. Huasheng, F. Wenchi, *Ind. Eng. Chem. Res.* **1988**, *27*, 770−774.
[15] H. Nymoen, D. van Velzen, H. Langenkamp, *Chem. Eng. Proc.* **1993**, *32*, 9−12.
[16] J. Hofele, D. van Velzen, H. Langenkamp, K. Schaber, *Chem. Eng. Proc.* **1996**, *35*, 295−300.
[17] N. Lin, D. Littlejohn, S.-G. Chang, *Ind. Chem. Proc. Des. Dev.* **1982**, 21.
[18] E. Sada, H. Kumazawa, H. Machida, *Ind. Eng. Chem. Res.* **1987**, *26*, 1468−1472.
[19] K. Kustin, I. A. Taub, E. Weinstock, *Inorg. Chem.* **1996**, *5*, 1079−1082.
[20] H. Hikita, S. Asai, H. Ishikawa, S. Hirano, *J. Chem. Eng. Jpn.* **1977**, *10*, 120−124.
[21] T. Schneppensieper, A. Wanat, G. Stochel, R. van Eldik, manuscript in preparation.
[22] A. B. Ross, W. G. Mallard, W. P. Helman, J. V. Buxton, R. E. Huie, P. Neta *NIST Standard References Database 40*, *Version 2.0*, **1994**.
[23] N. A. Davies, M. T. Wilson, E. Slade, S. P. Fricker, B. A. Murrer, N. A. Powell, G. R. Henderson, *Chem. Commun.* **1997**, 47−48.
[24] C. A. Brown, M. A. Pavlosky, T. E. Westre, Y. Zhang, B. Hedman, K. O. Hodgson, E. I. Solomon, *J. Am. Chem. Soc.* **1995**, *117*, 715−732.
[25] G. V. Buxton, C. R. Stuart, *J. Chem. Soc., Faraday Trans.* **1995**, *91*, 279.
[26] *Lange's Handbook of Chemistry*, 13th ed. (Ed.: J. A. Dean), Mc Graw-Hill, New York, p. 10.
[27] R. Doss, R. van Eldik, H. Kelm, *Rev. Sci. Instrum.* **1982**, *9*, 715.
[28] D. H. Powell, A. E. Merbach, I. Fábián, S. Schindler, R. van Eldik, *Inorg. Chem.* **1994**, *33*, 4468.
[29] H. D. Projahn, S. Schindler, R. van Eldik, *Inorg. Chem.* **1995**, *3*, 5935.
[30] OLIS KINFIT, Bogart, GA, USA.

Received January 30, 2001
[I01038]

A Facile Route to Carbonylhalogenometal Complexes (M = Rh, Ir, Ru, Pt) by Dimethylformamide Decarbonylation

Philippe Serp,[a] Marc Hernandez,[b] Brigitte Richard,[a] and Philippe Kalck*[a]

Keywords: Amides / Carbonylations / Carbonyl complexes / Rhodium

Dimethyl formamide (DMF) can be a convenient source of the carbonyl ligand in the coordination chemistry of rhodium, ruthenium, iridium, and platinum. We have undertaken a thorough study concerning the course of this reaction. In a first step, DMF-containing complexes are produced, which is usually accompanied by chloride redistribution. Then, upon refluxing, carbonyl species in the same oxidation state are obtained, presumably as a result of HCl-mediated DMF decomposition. Provided that water levels are kept low, reduction can occur to provide the complexes $[NH_2(CH_3)_2][RhCl_2(CO)_2]$, $[NH_2(CH_3)_2][RuCl_3(CO)_2(DMF)]$, $[RuCl_2(CO)_2(DMF)_2]$, and $[NH_2(CH_3)_2][IrCl_2(CO)_2]$. In the case of platinum, reduction is not effective and $[NH_2(CH_3)_2][PtCl_3(CO)]$ is obtained. No carbonylpalladium species can be synthesized in this way, the reaction producing copious amounts of colloidal metal. Adding phosphanes to these chlorocarbonyl-containing solutions allows easy, one-step syntheses of a variety of complexes.

Introduction

Because of its properties (stable, aprotic, polar, and high boiling point), DMF has been employed as a solvent in a wide variety of catalytic reactions including hydrogenations, hydroformylations, carbonylations, and syn-gas reactions.[1−17] Nevertheless, in some cases, its implication as a reactant has been observed and solvent effects that do not seem to be directly linked with its polarity have been noticed, particularly when the catalytic reaction involves carbon monoxide or further reactions with carbonyl compounds. Thus, in the course of an investigation of the ruthenium-catalyzed hydroesterification of ethylene, the results of which have been reported previously,[1,2] a strong solvent effect was noted. In this reaction, the solvent could be involved in the formation of the active species; in particular, the complex $[PPN][RuCl_3(CO)_2(DMF)]$ has been isolated after reaction of the precatalyst $[PPN][RuCl_3(CO)_3]$ with boiling DMF.[1] In the hydroformylation of formaldehyde using a rhodium catalyst of the general formula $[RhCl(CO)L_2]$ (L: tertiary phosphane ligand), a dramatic effect has been noticed when using DMF as the solvent.[3] This represents an unusual solvent dependence, particularly as the hydroformylation of alkenes can normally be carried out in almost any solvent. The authors postulated that coordination by the solvent could affect the catalyst reactivity. Recently, DMF has been shown to be a ligand of palladium and copper in the course of the oxidation of an alkene to the corresponding ketone.[4] Finally, Mitsudo et al. have developed the direct hydroamidation of alkenes by formamides using ruthenium catalysts.[5] A C−H formyl activation step is invoked in the catalytic cycle.

In the transfer hydrogenation of D-glucose carried out in DMF with $[RuCl_2(PPh_3)_3]$ as a catalyst, a deactivation of the catalyst has been observed.[6,7] At 123 °C, the starting complex was transformed into the catalytically inactive species $[RuCl_2(CO)(DMF)(PPh_3)_2]$, for which the authors assumed that a decarbonylation of the solvent had occurred to generate the carbonyl ligand. In the case of ethylene hydroesterification starting from $RuCl_3{\cdot}xH_2O$, Petit et al.[8] proposed a partial decomposition of DMF to explain the production of $[NMe_4]I$, which involves iodomethane, used to promote the reaction, and dimethylamine produced by DMF decomposition. For the decarbonylation of alkyl formates in the presence of chloride salts of osmium,[9] a positive effect of the solvent has also been noticed. In this case, a catalytic decomposition of DMF to give CO and dimethylamine was proposed; the production of the amine, which can catalyze the decarbonylation of alkyl formates, would seem to provide a good explanation of this effect since formates are usually decomposed in basic media. In this latter study, no information was given regarding the osmium species present at the end of the reaction.

Apart from the aforementioned catalytic reactions, a careful examination of the literature shows that the use of DMF as a carbonylating agent for the synthesis of organometallic compounds has not yet been systematically examined. Even though it has long been known that transition metal salts can give well-characterized carbonyl complexes,

[a] Laboratoire de Catalyse, Chimie Fine et Polymères, Ecole Nationale Supérieure d'Ingénieurs en Arts Chimiques et Technologiques,
118, route de Narbonne, 31077 Toulouse Cedex, France
Fax: (internat.) + 33-5/62885600
E-mail: pkalck@ensct.fr
[b] Department of Chemistry, University of Victoria,
P. O. Box 3065, Victoria, B.C. V8W 36V, Canada

 © WILEY-VCH Verlag GmbH, 69451 Weinheim, 2001 1434−1948/01/0909−2327 $ 17.50+.50/0

or in some cases carbonylhydrido complexes, upon treatment with alcohols, acyl halides, aldehydes, or formic acid, little is known about the decarbonylation of DMF. Rusina and Vlćek were the first to report such a reaction,[18] studying the formation of carbonyl complexes of the platinum group metals and using DMF as the CO source. Thus, the complex $[RhCl(CO)(PPh_3)_2]$ was prepared by refluxing a solution of $RhCl_3$ in DMF in the presence of triphenylphosphane. Later, Varshavskii and Cherkasova[19] prepared the acetylacetonato complex $[Rh(acac)(CO)_2]$ by two different routes. The first was similar to that employed by Rusina and Vlćek, involving a one-pot reaction of the salt and acetylacetone in boiling DMF (procedure A). The second route (procedure B) required the prior formation of carbonyl-containing rhodium intermediates obtained by heating $RhCl_3$ in DMF, which were then treated with acetylacetone to give $[Rh(acac)(CO)_2]$. The same group has proposed that in the case of $RhCl_3{\cdot}3H_2O$ and H_2PtCl_6, the $[RhCl_2(CO)_2]^-$ and $[PtCl_3(CO)]^-$ anions, respectively, are produced by DMF decarbonylation.[20] Nevertheless, no explanation was given concerning the course of the reaction.

Since these first synthetic results, other β-diketonato complexes of rhodium have been prepared according to procedure A.[21−24] Vaska's compound $[IrCl(CO)(PPh_3)_2]$ has also been prepared by this procedure.[25] The same method was used to prepare other carbonylphosphane-containing iridium complexes.[26,27] Decarbonylation of DMF has also been used for the preparation of ruthenium species containing bipyridyl ligands of the general formula $[Ru(CO)L(bipy)_2]^{n+}$ starting from $RuCl_3{\cdot}3H_2O$.[28−33] In most of these cases, procedure A is employed and very long reaction times are required. Recently, Forster et al.[34] have reported a 1-h synthesis of the complex $[RuCl(CO)(L{-}L')_2]^+$ (L−L′: pyridyltriazole) using procedure B. The 2-methylimidazole-containing complex *trans*-$[Ru(CO)(DMF)(2\text{-}MeIm)_4][CF_3SO_3]_3$ was synthesized from $[Ru(DMF)_6][CF_3SO_3]_3$ by a reaction involving abstraction of CO from DMF,[35] the required dimethylamine co-product having been detected. The decarbonylation of DMF has also been investigated with the molybdenum complex *trans*-$[Mo(N_2)_2(dppe)_2]$ [dppe: bis(diphenylphosphanyl)ethane] in refluxing benzene.[36] The products of this reaction are the complex $[Mo(CO)(DMF)(dppe)_2]$ and dimethylamine, which was detected by GLC. The authors proposed a mechanism that is exactly the reverse process of the carbonylation of amines by noble metals. The complex $[Mo(CO)(HCONEt_2)(dppe)_2]$ has been similarly prepared starting from diethylformamide. Carbon monoxide and dimethylamine have also been found as the sole products of the decomposition of DMF photocatalyzed by a ruthenium compound containing a porphyrin ligand.[37]

In the course of our investigations on noble metal catalyzed carbonylation reactions, we have undertaken a comprehensive study of the reactions of $RhCl_3{\cdot}3H_2O$, $IrCl_3{\cdot}3H_2O$, $RuCl_3{\cdot}3H_2O$, K_2PtCl_4, $PdCl_2$, and Na_2PdCl_6 with DMF and other amides. Preliminary results of our investigations of the reactions of $RhCl_3{\cdot}3H_2O$ and $IrCl_3{\cdot}3H_2O$ with DMF have already been reported.[38]

Results and Discussion

A. Reaction of $RhCl_3{\cdot}3H_2O$ with DMF

Infrared Monitoring of the Reduction and Identification of Several Intermediate Species

When $RhCl_3{\cdot}3H_2O$ is refluxed in commercially available *N*,*N*-dimethylformamide, the color of the solution changes from dark red to orange within 30 min. If the heating is continued, some metallic rhodium begins to precipitate, indicating a complete reduction of the salt. IR monitoring of the reaction shows that, after 2 min, the dark-red solution contains a carbonyl species at low concentration since a weak carbonyl band is detected at 2092 cm^{-1}. After 5 min, as the solution lightens, two new bands with the same intensity appear beside the band at 2092 cm^{-1}, one at 2063 cm^{-1} and the other at 1984 cm^{-1}. After 15 min, the band at 2092 cm^{-1} has disappeared and only the two strong bands at 2063 and 1984 cm^{-1}, characteristic of the $[RhCl_2(CO)_2]^-$ anion, are present; their intensity remains constant after 30 min of reaction.

Direct evaporation of the solvent from the final orange solution leads to the deposition of large amounts of black insoluble rhodium species along with the complex $[NH_2(CH_3)_2][RhCl_2(CO)_2]$ and the salt $[NH_2(CH_3)_2]Cl$. Alternatively, addition of one molar equivalent of $[AsPh_4]Cl$ affords $[AsPh_4][RhCl_2(CO)_2]$ in 70% yield after recrystallization of the crude product from dichloromethane/*n*-heptane (see Table 1).

In order to identify the first carbonyl intermediate species giving a ν_{CO} band at 2092 cm^{-1}, several experiments were performed that showed this compound to be $[RhCl_4(CO)(DMF)]^-$, as detailed below. A precedent for this anion is the related complex $[RhCl_4(CO)(CH_3OH)]^-$, which gives a ν_{CO} band at 2103 cm^{-1}.[39] This rhodium(III) intermediate is depicted in Scheme 1, together with all the isolated intermediates that can be proposed as being involved in the formation of $[RhCl_2(CO)_2]^-$ from $RhCl_3{\cdot}3H_2O$ through DMF decarbonylation.

In the first of the aforementioned experiments, direct FAB^- mass-spectrometric analysis of the dark-red DMF solution obtained after 2 min revealed only the presence of two main fragments, one at m/z = 245 corresponding to $[RhCl_4]^-$ and the other at m/z = 210 due to $[RhCl_3]^-$. To intercept this first intermediate, 1 mol-equiv. of $[AsPh_4]Cl$ was added to this solution, the solvent was evaporated, and the product was precipitated by adding acetone/*n*-heptane. A reddish powder was obtained, which did not show any carbonyl−rhodium band in its IR spectrum, but rather a broad CO band at 1641 cm^{-1} characteristic of coordinated DMF (free DMF: 1673 cm^{-1}). As mass-spectrometric analysis suggested that chloro-rich species were produced at an early stage of the reaction and that direct isolation of the first carbonyl compound was not possible, probably due to its low concentration and the lability of the CO ligand under our experimental conditions, we investigated the effect of an excess of chloride with regard to the stabilization of

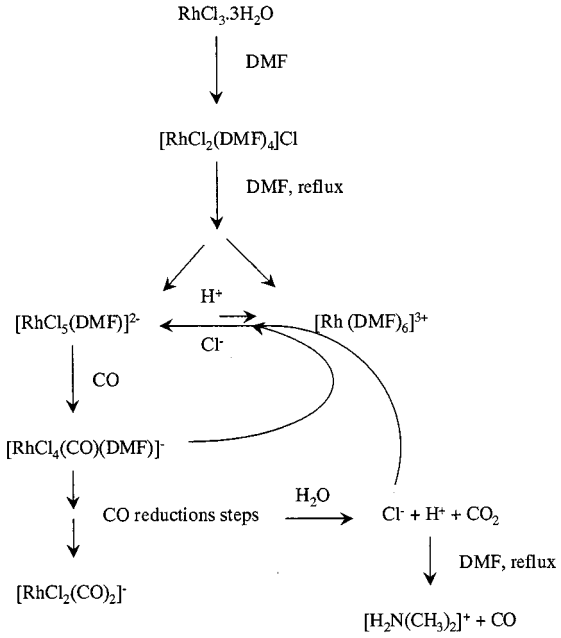

Scheme 1. General reaction pathway for the generation of $[RhCl_2(CO)_2]^-$ from $RhCl_3{\cdot}3H_2O$ and DMF

intermediate species. In the presence of 5−10 mol-equiv. of KCl, rapid precipitation of the violet complex $[NH_2(CH_3)_2]_2[RhCl_5(DMF)]$ was observed upon refluxing $RhCl_3{\cdot}3H_2O$ solutions in DMF. Further heating of the reaction mixture led to the quick re-dissolution of this species, and pure $[AsPh_4][RhCl_2(CO)_2]$ was obtained from the orange solution by adding $[AsPh_4]Cl$ after 25 min of reaction. Therefore, the presence of excess of Cl^- in the medium does not change the outcome of the reaction but allows trapping of $[NH_2(CH_3)_2]_2[RhCl_5(DMF)]$. The corresponding aqua anion $[RhCl_5(H_2O)]^{2-}$ has been reported to be the predominant chlororhodium(III) complex present in hydrochloric acid solutions of $RhCl_3{\cdot}3H_2O$.[26]

In a separate experiment, we carbonylated $[NH_2(CH_3)_2]_2[RhCl_5(DMF)]$ by bubbling CO through a solution in DMF for 15 min at 50 °C. After the addition of $[AsPh_4]Cl$ and evaporation of the solvent, an orange powder was recovered, which analyzed as $[AsPh_4]_2[RhCl_5(CO)]$ and gave a ν_{CO} band at 2081 cm^{-1} (see Table 1). The $[RhCl_5(CO)]^{2-}$ anion has previously been reported by Colton et al. as an intermediate species when $RhCl_3{\cdot}3H_2O$ is treated with hydrochloric and formic acid mixtures to produce $[RhCl_2(CO)_2]^-$.[40] Thus, upon monitoring of the reaction in the absence of CO bubbling, $[RhCl_5(CO)]^{2-}$ is not detected.

We have discovered that reaction of $[AsPh_4]_2[RhCl_5(CO)]$ with 5 equiv. of DMF in boiling chloroform allows isolation of the reddish complex $[AsPh_4][RhCl_4(CO)(DMF)]$ in good yields. This compound shows a ν_{CO} band at 2092 cm^{-1} in DMF.

As these latter anionic species contain more chlorine (five and four Cl ligands, respectively) than the starting rhodium salt, further attempts were made to identify the corresponding cationic complexes, which should presumably have a lower chlorine content. After treating $RhCl_3{\cdot}3H_2O$ with DMF at room temperature for 16 h, we isolated a cationic species that could clearly be formulated as $[RhCl_2(DMF)_4]Cl$. This complex shows one ν_{CO} band at 1639 cm^{-1} (m, broad) in its IR spectrum, which is consistent with a D_{4h} group symmetry, the four coordinated DMF ligands lying in the equatorial plane.

A second cationic complex was isolated as a blue by-product from the $RhCl_3{\cdot}3H_2O$ solution in DMF after heating with an excess of KCl. After 15 min, $[NH_2(CH_3)_2]_2[RhCl_5(DMF)]$ precipitated; after this had been filtered off, the blue species was obtained by slow crystallization from the filtrate. Positive-mode electrospray MS data of the blue material showed that no chloro ligands were present, although the assignment of the more intense peaks at m/z = 280.9, 340.8, 415.0, and 502.8 remains uncertain due to rather facile loss of the coordinated DMF. The presence of one ν_{CO} band at 1655 cm^{-1} in the IR spectrum due to the DMF ligands, and of peaks corresponding to coordinated DMF {in D_2O solution: δ = 7.80 [s, 1 H, $HCON(CH_3)_2$], 2.88 and 2.73 [s, 3 H, $HCON(CH_3)_2$]} in the ^1H NMR spectrum, leads us to propose an $[Rh(DMF)_6]^{3+}$ structure for this complex. The analogous ruthenium complex $[Ru(DMF)_6]^{n+}$ (n = 2, 3) has recently been characterized.[41] This $[Rh(DMF)_6]^{3+}$ complex, for which the counterions are light, as shown by FAB-MS (negative mode), can be formulated as $[Rh(DMF)_6]Cl_3$ and can be expected to react with an excess of Cl^- anions to afford the anionic species $[RhCl_5(DMF)]^{2-}$. The various intermediate cationic rhodium species that have been isolated are reported in Table 1.

It can be concluded from IR monitoring of the reaction and from the isolation or trapping of some of the intermediate species, that the reaction of DMF with the starting rhodium(III) salt involves a complex series of equilibria. The presence of Cl^- ions strongly affects the balance between the identified anionic and cationic species. Both the CO ligand and the $[NH_2(CH_3)_2]^+$ cation arising from DMF have been identified, but no evidence of DMF activation at the metal centre can be given.

Water- and/or HCl-Assisted DMF Activation

A further series of experiments was carried out in order to gain better insight into the parameters that affect the course of the reaction, in particular the role of Cl^- ions. Firstly, the use of commercial DMF, containing around 0.1% of water, produced $[RhCl_2(CO)_2]^-$ in 30 min as an orange solution containing a small amount of black rhodium (Table 2, Figure 1). In each experiment, $[AsPh_4]Cl$ was added and the yield of isolated $[AsPh_4][RhCl_2(CO)_2]$ was determined. In run 1 of Table 2, the yield achieved was 70%.

The addition of chloride (KCl) to the reaction medium stabilizes the system, as shown by the absence of any metallic rhodium, but no significant promoting effect on the reduction was observed (runs 2 and 3 in Table 2). Such an

Table 1. Isolated intermediate rhodium species

Product	Color	IR (ν_{CO} [cm^{-1}]) DMF[c]	KBr pellets	MS[a][b] (*m*/*z*)
$[Rh(DMF)_6]Cl_3$	blue	–	1655	502.8[a]: not assigned
$[RhCl_2(DMF)_4]Cl$	red	–	1639	465[a]: $[RhCl_2(DMF)_4]^+$
$[NH_2(CH_3)_2]_2[RhCl_5(DMF)]$	violet	–	1641	326[a]: $[RhCl_5(NH_2(CH_3)_2)]^-$
$[AsPh_4]_2[RhCl_5(CO)]$	orange	2081	2075	662.8[b]: $[AsPh_4RhCl_5]^-$
$[AsPh_4][RhCl_4(CO)(DMF)]$	reddish	2092	2085, 1637	273[a]: $[RhCl_4(CO)]^-$
$[AsPh_4][RhCl_2(CO)_2]$	yellow	2063, 1984	2054, 1975	229[a]: $[RhCl_2(CO)_2]^-$

[a] FAB. – [b] Electrospray. – [c] Free DMF: 1675 cm^{-1}.

Table 2. Influence of the addition of chloride and/or water on the reaction

(Run number) Formulation[a]	Isolated products (yield), reaction time	Solution colour and comments
(1) $RhCl_3·3H_2O$/DMF	$[AsPh_4][RhCl_2(CO)_2]$ (70%); 30 min	Orange – small amount of black rhodium
(2) $RhCl_3·3H_2O$/5 KCl/DMF	$[NH_2(CH_3)_2]_2[RhCl_5(DMF)]$; 5 min	Orange – no black rhodium
(3) $RhCl_3·3H_2O$/10 KCl/DMF	$[AsPh_4][RhCl_2(CO)_2]$ (72%); 25 min	Orange – no black rhodium
(4) $RhCl_3·3H_2O$/5 HCl/dioxane/DMF	$[AsPh_4][RhCl_2(CO)_2]$ (65%); 45 min	Orange – some black rhodium
(5) $RhCl_3·3H_2O$/10 HCl/dioxane/DMF	Reaction incomplete after 45 min	–
(6) $RhCl_3·3H_2O$/5 HCl/water/DMF	$[AsPh_4][RhCl_2(CO)_2]$ (88%); 12 min	Lemon-yellow – no black rhodium
(7) $RhCl_3·3H_2O$/10 HCl/water/DMF	–	–
(8) $RhCl_3·3H_2O$/5 H_2O/DMF	$[AsPh_4][RhCl_2(CO)_2]$ (85%); 12 min	Lemon-yellow – no black rhodium

[a] $RhCl_3·3H_2O$: 0.2 g (0.75 mmol); DMF: 5 mL; T = 160 °C; subsequent addition of $[AsPh_4]Cl$ for product isolation.

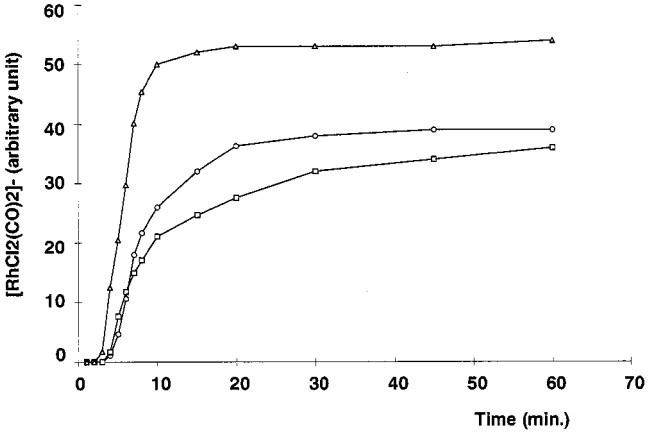

Figure 1. Intensity of the ν_{CO} band of $[RhCl_2(CO)_2]^-$ at 1984 cm^{-1} during the reaction of $RhCl_3·3H_2O$ with: (○) DMF; (□) DMF + 10 mol-equiv. of dry HCl per $RhCl_3·3H_2O$; (△) DMF + 5 mol-equiv. of H_2O per $RhCl_3·3H_2O$

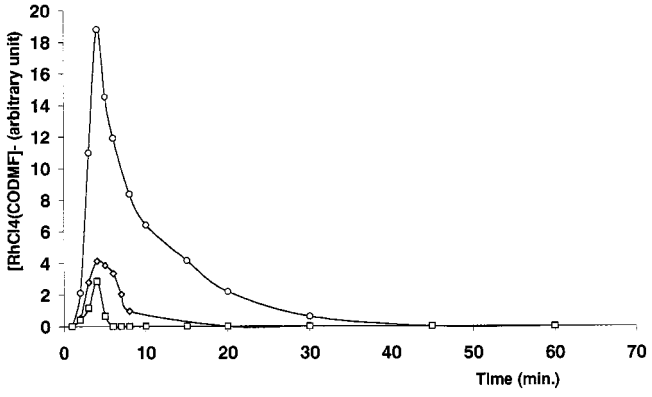

Figure 2. Intensity of the ν_{CO} band of $[RhCl_4(CO)DMF]^-$ at 2092 cm^{-1} during the reaction of $RhCl_3·3H_2O$ with: (○) DMF; (□) DMF + 10 mol-equiv. of dry HCl per $RhCl_3·3H_2O$; (◇) DMF + 5 molar equivalents of H_2O per $RhCl_3·3H_2O$

excess of chloride improved the precipitation of $[NH_2(CH_3)_2]_2[RhCl_5(DMF)]$.

The addition of 5–10 equiv. of dry HCl (5 M HCl in diethyl ether or dioxane) to the $RhCl_3·3H_2O$/DMF mixture was found to have a different and pronounced effect (runs 4 and 5 in Table 2). With 10 equiv., even after reaction for 45 min, the solution remained dark-orange with precipitation of black rhodium. Moreover, the carbonyl band at 2092 cm^{-1} persisted in the IR spectrum (Figures 1 and 2), beside the two bands due to $[RhCl_2(CO)_2]^-$, indicating that the reaction was incomplete. Precipitation of $[NH_2(CH_3)_2]Cl$, arising from DMF decomposition, was also noted. In this case, it is clear from Figure 2 that the production of $[RhCl_4(CO)(DMF)]^-$ was greatly enhanced compared to run 1, suggesting that larger quantities of CO were provided by the acid-catalyzed DMF decomposition. As the yield of $[RhCl_2(CO)_2]^-$ was lower when the concentration of $[RhCl_4(CO)(DMF)]^-$ was significant, we suggest that anhydrous HCl is rapidly neutralized by $NH(CH_3)_2$ arising from the DMF. Thus, no more carbon monoxide can be generated in the medium to maintain the reaction and more particularly the reduction. This experiment further shows that rhodium is unlikely to directly promote the DMF decomposition.

On the contrary, when aqueous solutions of HCl were used (37% in water), another phenomenon was observed; with 5–10 equiv. of acid (runs 6 and 7 in Table 2), the reaction was complete within 12 min and the solution became lemon-yellow, giving the highest yield achieved in this study

(88%). The change in color, i.e. from orange for runs 1 to 5 to lemon-yellow for runs 6 and 7, might be taken to indicate a more complete reaction, as evidenced by the higher yields of the isolated product achieved in the latter cases.

Finally, the role of water itself was examined. We have observed that by adding 5 equiv. of water per mol of rhodium, the reduction can be achieved within 12 min (Table 2, Figure 1 and Figure 2) and the yield of $[RhCl_2(CO)_2]^-$ reaches 85% with no black rhodium formation. We propose that the presence of water assists the reduction step from $[RhCl_4(CO)(DMF)]^-$ to $[RhCl_2(CO)_2]^-$ and that the addition of HCl accelerates the production of CO from DMF, as evidenced by the significant amounts of ammonium chloride detected in the medium. Formally, $COCl_2$ is eliminated in the reduction step and is rapidly hydrolyzed, but we prefer to consider the water-gas shift reaction, which produces CO_2 and H_2 from CO and H_2O. The reduction step is, in fact, the reductive elimination of HCl from the coordination sphere of the rhodium(III) species. Equation (1) shows the overall stoichiometry of several reactions. The complex $[RhI_2(CO)_2]^-$ has previously been shown to be a good catalyst of the water-gas shift reaction.[42]

$$[RhCl_4(CO)(DMF)]^- + 2\,CO + H_2O \rightarrow [RhCl_2(CO)_2]^- + 2\,HCl + CO_2 + DMF \quad (1)$$

To sum up this section on the rhodium activity, we have shown that DMF coordinates to the rhodium salt to give $[RhCl_2(DMF)_4]Cl$, disproportionation of which affords $[RhCl_5(DMF)_2]^{2-}$ and $[Rh(DMF)_6]^{3+}$. The latter species gives the former dianionic one in the presence of chloro ligands. Isolation of $[RhCl_5(DMF)]^{2-}$ with $[NH_2(CH_3)_2]^+$ as the counterion shows that, at this stage of the rhodium(III) chemistry, significant amounts of DMF have been decomposed, thus indicating the presence of an acidic medium. As commercial $RhCl_3{\cdot}3H_2O$ is obtained by evaporation of acidic aqueous solutions of rhodium trichloride, traces of HCl can be present at the beginning of the reaction. However, as no carbonyl species have been detected in the early stages, we conclude that the formation of $[RhCl_2(CO)_2]^-$ resembles an autocatalytic process, which does not involve the activation of DMF at the rhodium center.

Use of Other Amides

In order to test the generality of the reaction, we investigated the behavior of various formamides in this reductive carbonylation. At 180 °C, *N*-methylformamide gave yellow solutions containing a small amount of black material in around 1 min. In their IR spectra, such solutions showed only the two ν_{CO} bands of $[RhCl_2(CO)_2]^-$ at 2073 and 1997 cm^{-1}. The yield of $[AsPh_4][RhCl_2(CO)_2]$ was 72%. When the same reaction was performed at 140 °C, the expected product was obtained in less than 10 min without any precipitation of metallic rhodium. When a solution of $RhCl_3{\cdot}3H_2O$ in formamide was gently heated from room temperature to 120 °C (i.e., well below its boiling point of 210 °C), the ν_{CO} bands of $[NH_4][RhCl_2(CO)_2]$ were detected at 2079 and 2005 cm^{-1} above 100 °C, but the solution was dark and large quantities of black material were deposited. Using diethylformamide at 160 °C produced $[H_2NEt_2][RhCl_2(CO)_2]$ (ν_{CO} = 2060, 1981 cm^{-1}) in 30 min without any metallic precipitate. Although this reaction appeared to be quantitative on the basis of IR measurements, on a small preparative scale the yield of isolated product, usually $[AsPh_4][RhCl_2(CO)_2]$, was ca. 70%. Yields of around 85% were achieved when small quantities of water were introduced to promote the reductive carbonylation. Finally, using *N*-methylacetamide ($CH_3CONHCH_3$; m.p. 28 °C) at 180 °C, a black solution with copious precipitation of a black material was obtained in less than 5 min, and no CO stretching band could be detected in the IR spectrum of the solution.

Direct Preparation of Several Rhodium Complexes

Starting from DMF solutions containing the $[NH_2(CH_3)_2][RhCl_2(CO)_2]$ complex, we added various ligands at room temperature to produce the corresponding rhodium(I) complexes (procedure B). Direct addition of 2 equiv. of PPh_3, as reported by Varshavskii et al.,[19] $P(OPh)_3$, or tris(*m*-sulfonatophenyl)phosphane (TPPTS) furnished the corresponding $[RhCl(CO)L_2]$ square-planar complexes in high yields. Addition of 3 mol of $P(OPh)_3$ resulted in the generation of $[RhCl\{P(OPh)_3\}_3]$. The use of bis(diphenylphosphanyl)propane gave $[Rh(CO)(dppp)_2]Cl$ in 75% yield.

Substitution of the chloro ligand can also be performed. As in the case of $[Rh(acac)(CO)_2]$,[19] addition of 1,1-dimethylethanethiol afforded the corresponding bridged dinuclear complex $[Rh_2(\mu\text{-}S\textit{t}Bu)_2(CO)_4]$ in 80−85% yield. After stirring for 5 min, IR monitoring showed that the tetracarbonyl complex had been formed, and the subsequent addition of 2 equiv. of PPh_3 or TPPTS resulted in the formation of $[Rh_2(\mu\text{-}S\textit{t}Bu)_2(CO)_2(PPh_3)_2]$ or $[Rh_2(\mu\text{-}S\textit{t}Bu)_2(CO)_2(TPPTS)_2]$, respectively.

We have observed that for phosphane ligands, procedure A, in which all the reactants are introduced at the beginning, gives the same results but with much longer reaction times (2−5 h). However, no clean reaction could be achieved by adding HS*t*Bu according to procedure A. Hence, the present method allows the high-yielding preparation in a one-pot procedure of various carbonylrhodium complexes without the use of carbon monoxide gas.

B. Reaction of $IrCl_3{\cdot}3H_2O$ with DMF

An identical study has been carried out on $IrCl_3{\cdot}3H_2O$ in DMF. It is known from the literature[43] that $[IrCl_2(CO)_2]^-$ can be generated using carbon monoxide by refluxing in a high boiling point alcohol such as 2-methoxyethanol. This is presumably due to the higher stability or inertness of iridium(III) compared to rhodium(III).

In the present case, refluxing of a solution of $IrCl_3{\cdot}3H_2O$ in DMF resulted in a beige precipitate after 5 min, which rapidly redissolved on further heating. This species was isol-

ated by stopping the reaction and, after cooling, analyzed as $[NH_2(CH_3)_2]_2[IrCl_5(DMF)]$. As for rhodium, the formation of this species was favored in the presence of an excess of Cl^- ions, for instance in aqueous HCl. After reaction for 10 min, the IR spectrum of the solution showed a ν_{CO} band at 2048 cm^{-1}. The intensity of this band increased, while the color of the solution became progressively more orange. After 30 min, addition of $[AsPh_4]Cl$ to trap this intermediate species resulted in the production of $[AsPh_4][IrCl_4(CO)(DMF)]$, which was isolated as an orange precipitate in 69% yield following the addition of water. On further heating of the initial solution, the two ν_{CO} bands at 2045 and 1965 cm^{-1} intensified, which was accompanied by a concomitant decrease in the band at 2048 cm^{-1}. Heating for 15 h was required to completely transform the starting complex into $[IrCl_2(CO)_2]^-$, albeit with a large amount of black metal. Addition of $[AsPh_4]Cl$ allowed the isolation of $[AsPh_4][IrCl_2(CO)_2]$ in 10% yield.

In order to improve the reduction step from $[IrCl_4(CO)(DMF)]^-$ to $[IrCl_2(CO)_2]^-$, 5 equiv. of water were added. The reaction indeed became faster, but large amounts of the black precipitate were still present. Addition of 5 equiv. of aqueous HCl (37% in water) and heating for 60 min resulted in the clean production of $[IrCl_2(CO)_2]^-$ in 70% yield. Anhydrous HCl or larger amounts of aqueous HCl were found to have a negative effect.

This reaction was thus slower than that for rhodium. The direct isolation of $[IrCl_5(DMF)]^{2-}$ and $[IrCl_4(CO)(DMF)]^-$ indicates that the same mechanism should be operative for both metals. As for rhodium, both the CO ligand and the $[NH_2(CH_3)_2]^+$ cation arising from DMF decomposition could be identified, but again no evidence was found for DMF activation at the metal center.

Addition of 2 equiv. of PPh_3 to the solution containing $[IrCl_2(CO)_2]^-$ was found to result in the immediate formation of $[IrCl(CO)(PPh_3)_2]$. Thus, it appears that procedure B, which involves addition of the ligand after generation of the carbonylchloro anion, is faster than procedure A for generating the desired compound.

C. Reaction of $RuCl_3 \cdot 3H_2O$ with DMF

In the case of ruthenium, the reaction was found to be slower and more complex than that for rhodium. Scheme 2 depicts the various complexes detected during this study.

On heating a solution of $RuCl_3 \cdot 3H_2O$ in DMF, a ν_{CO} band was seen at 2020 cm^{-1} in the IR spectrum after 15 min, corresponding to the red species $[PPN]_2[RuCl_5(CO)]$, which was isolated following the addition of [PPN]Cl. After further heating for 25 min, five more ν_{CO} bands appeared at 2054, 2041, 1975, 1963, and 1929 cm^{-1}. The band at 2020 cm^{-1} rapidly disappeared, whereas that at 1929 cm^{-1} persisted for up to 2 h. The other four bands showed no evolution on heating for longer times. No ruthenium black was observed in the course of the reaction. In a separate experiment, reaction of $RuCl_3 \cdot 3H_2O$ with DMF in the presence of 5 equiv. of aqueous HCl allowed isolation of the green ruthenium(II) product

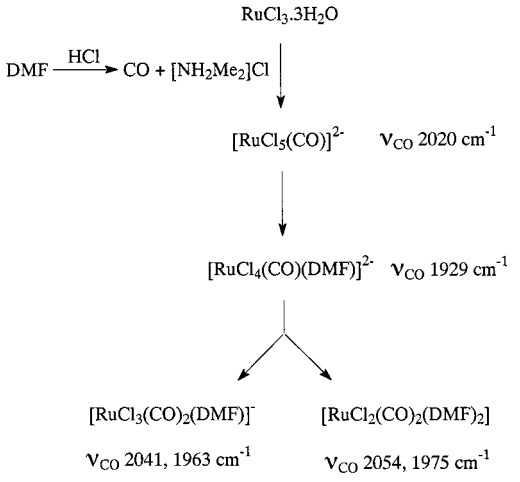

Scheme 2. General reaction pathway for the generation of $[RuCl_3(CO)_2(DMF)]^-$ and $[RuCl_2(CO)_2(DMF)_2]$ from $RuCl_3 \cdot 3H_2O$ and DMF

$[PPN]_2[RuCl_4(CO)(DMF)]$, showing ν_{CO} bands at 1929 cm^{-1} and 1638 cm^{-1} due to coordinated DMF.

We found that by adding 2.5 equiv. of dry HCl to a solution of $RuCl_3 \cdot 3H_2O$ in DMF, a single complex showing two ν_{CO} bands at 2041 and 1963 cm^{-1} was obtained after reaction for 60 min. In the course of the reaction, the two intermediates giving rise to the bands at 2020 and 1929 cm^{-1} (here shifted to 1919 cm^{-1} due to medium effect) were also transiently observed, but disappeared more quickly. The two final ν_{CO} bands at 2041 and 1963 cm^{-1} are attributable to $[RuCl_3(CO)_2(DMF)]^-$,[1] which was isolated as the PPN salt in 65% yield. Addition of larger amounts of dry HCl resulted in the production of small amounts of $[RuCl_3(CO)_3]^-$ (ν_{CO} bands at 2124, 2008 cm^{-1}), together with $[RuCl_3(CO)_2(DMF)]^-$; this can be attributed to a higher concentration of CO in the solution.

A second complex, showing ν_{CO} bands at 2054 and 1975 cm^{-1}, was isolated following the addition of [PPN]Cl to the yellow solution exhibiting the four ν_{CO} bands at 2054, 2041, 1975, and 1963 cm^{-1} (after refluxing a solution of $RuCl_3 \cdot 3H_2O$ in DMF for 2 h). The products were isolated by precipitation with water. The yellow precipitate was found to contain $[PPN][RuCl_3(CO)_2(DMF)]$ and the unknown complex. Column chromatographic separation on silica allowed isolation of the latter species as pure $[RuCl_2(CO)_2(DMF)_2]$. Scheme 2 summarizes the reaction pathway for the reductive carbonylation of $RuCl_3 \cdot 3H_2O$; it does not involve any DMF activation at the metal center.

As for rhodium and iridium, the solution containing the carbonylchloro species could be used to prepare various complexes. The complex *cis,cis,trans*-$[RuCl_2(CO)_2(PPh_3)_2]$ could be selectively obtained by adding PPh_3 to the solution containing the $[RuCl_3(CO)_2(DMF)]^-$ anion (obtained from a DMF/dry HCl mixture) at 140 °C.

D. Reactions of K_2PtCl_4, $PdCl_2$, and Na_2PdCl_6 with DMF

The reactivities of palladium and platinum salts were found to differ markedly from those of rhodium, iridium,

and ruthenium. Indeed, on refluxing $PdCl_2$ or Na_2PdCl_6 in DMF, the rapid formation of colloidal palladium suspensions was observed within 10 min. Attempts to stabilize possible carbonyl species by adding anhydrous or aqueous HCl, KCl, or even [PPN]Cl, were unsuccessful. Heating a solution of $PdCl_2$ in DMF at 100 °C for 2 h resulted in the formation of a dark solid, which was identified as $[PdCl_2(DMF)_2]$. This compound has already been prepared[44] by treating $PdCl_2$ with DMF at room temperature. However, upon dissolution in another solvent, this complex dissociates with loss of its two DMF ligands. Thus, we did not succeed in finding conditions under which a carbonylpalladium complex could be directly produced from a palladium salt through DMF decarbonylation.

As regards platinum, the refluxing of K_2PtCl_4 in DMF produced copious amounts of black metal. Neither HCl (anhydrous or aqueous) nor KCl prevented this precipitation. Nevertheless, the IR spectrum of the solution showed the presence of a weak ν_{CO} band at 2087 cm^{-1}. Thus, we added 1 equiv. of [PPN]Cl at the beginning of the reaction. Under these conditions, the carbonylplatinum(II) complex [PPN][$PtCl_3(CO)$] could be cleanly obtained without any black precipitate, albeit in a yield of just 52%.

Conclusion

Dimethylformamide, as well as diethylformamide and methylformamide, can act as convenient sources of carbon monoxide. This study has shown that, mainly for rhodium, iridium, and ruthenium, it is possible to produce carbonylhalo complexes in high yields. The presence of small amounts of water clearly assists the reduction of the commercial salts into rhodium(I), $[RhCl_2(CO)_2]^-$, iridium(I) $[IrCl_2(CO)_2]^-$, and ruthenium(II) $[RuCl_4(CO)(DMF)]^{2-}$. Presumably, the reduction proceeds through the water-gas shift reaction. As no evidence has been found for DMF activation at the metal center, an HCl-mediated decomposition of the solvent is proposed to explain the formation of CO and $[NH_2(CH_3)_2]^+$.

The good yields obtained for these carbonyl complexes show that the methodology used in this work is either an attractive one-step route for preparation of the complexes, or a means of directly obtaining the catalytic precursors in DMF solution. Such a procedure is not applicable in the case of palladium, since it leads only to deposition of the black metal, and appears to be limited for platinum, for which $[PtCl_3(CO)]^-$ is obtained in modest yield. Finally, by the direct addition of various ligands to the carbonylhalo-containing DMF solutions, as described here with a few examples, the corresponding classical complexes may be obtained in high yields according to a simplified procedure.

Experimental Section

General Remarks: All synthetic manipulations were carried out under nitrogen using standard Schlenk techniques. Dimethylformamide and the other reagents were used as received (Aldrich). − Elemental analyses were performed with a Carlo Erba EA-1110 instrument. − Infrared spectra were recorded with a Perkin−Elmer 225 spectrophotometer using a 0.1-mm cell equipped with CaF_2 windows. − NMR spectra were recorded with a Bruker AC 200 MHz instrument (^1H, ^{31}P, and ^{13}C). ^1H and ^{13}C NMR spectroscopic data were referenced to the solvent peaks, while ^{31}P NMR spectra were referenced to 85% H_3PO_4 as an external standard. Chemical shifts are expressed in ppm and coupling constants in Hz. − Mass spectrometry (FAB, Xe 100 eV, NBA matrix) was performed with a Nermag R10-10 apparatus. − Procedure B was used for all the syntheses.

Rhodium Complexes

$[NH_2(CH_3)_2]_2[RhCl_5(DMF)]$: The complex was prepared from $RhCl_3{\cdot}3H_2O$ (1.0 g, 3.8 mmol) and KCl (1.41 g, 19 mmol) in DMF (15 mL). On heating the solution under reflux (160 °C) for 15 min, it turned progressively from deep-red to dark-orange and the product precipitated as a violet powder. After cooling to room temperature, the product was collected by filtration using a Büchner funnel, washed with acetone, and dried in vacuo to give 0.255 g (15% based on $RhCl_3{\cdot}3H_2O$). − IR (KBr pellets): ν_{CO} = 1636 cm^{-1} (coordinated DMF). − ^1H NMR (D_2O): δ = 7.81 [s, 1 H, $HCON(CH_3)_2$], 2.88 and 2.73 [2 s, 2 × 3 H, $HCON(CH_3)_2$], 2.60 [s, 6 H, $NH_2(CH_3)_2$]. − $^{13}C\{^1H\}$ NMR (D_2O): δ = 165.2 [d, $HCON(CH_3)_2$, J_{Rh-C} = 17 Hz], 31.4 and 36.9 [s, $HCON(CH_3)_2$], 34.6 [s, $NH_2(CH_3)_2$]. − MS (FAB^-, H_2O): *m/z* (%) = 418 (100) $[\{NH_2(CH_3)_2\}_2\{RhCl_5[HN(CH_3)_2]\}]^-$, 383 (19) $[\{NH_2(CH_3)_2\}_2\{RhCl_4[HN(CH_3)_2]\}]^-$, 326 (26) $[RhCl_5\{HN(CH_3)_2\}]^-$, 244 (31) $[RhCl_4]^-$. − $C_7H_{23}Cl_5N_3ORh$ (445.45): calcd. C 18.87, H 5.20, N 9.43, O 3.59; found C 18.53, H 5.20, N 9.39, O 3.32.

$[AsPh_4][RhCl_4(CO)(DMF)]$: The complex was prepared from $[AsPh_4]_2[RhCl_5(CO)]$ (0.18 g, 0.179 mmol) and DMF (0.065 g, 0.895 mmol) in $CHCl_3$ (10 mL). The solution was heated under reflux for 15 min, allowed to cool, filtered, and the product was precipitated by adding *n*-heptane. It was collected by filtration using a Büchner funnel, washed with *n*-heptane, and dried in vacuo to give 0.11 g {88% based on $[AsPh_4]_2[RhCl_5(CO)]$}. − IR (KBr pellets): ν_{CO} = 2085, 1637 cm^{-1} (coordinated DMF). − ^1H NMR ($CDCl_3$): δ = 7.88 [s, 1 H, $HCON(CH_3)_2$], 2.89 and 2.75 [2 s, 2 × 3 H, $HCON(CH_3)_2$]. − MS (FAB^-, CH_3CN): *m/z* (%) = 362 (10) $[RhCl_4(DMF)]^-$, 289 (100) $[RhCl_4]^-$. − $C_{28}H_{27}AsCl_4NO_2Rh$ (729.17): calcd. C 46.12, H 3.73, N 1.92, O 4.39; found C 45.53, H 3.40, N 1.79, O 4.32.

$[RhCl_2(DMF)_4]Cl$: The complex was prepared from $RhCl_3{\cdot}3H_2O$ (0.5 g, 1.9 mmol) in DMF (15 mL). The solution was stirred at room temperature for 48 h, then filtered, and the solvent was evaporated in vacuo at 50 °C. The resulting oil was treated at room temperature with acetone to yield a brown precipitate. The final product was washed several times with acetone and dried in vacuo to give 0.105 g (11% based on $RhCl_3{\cdot}3H_2O$). − IR (KBr pellets): ν_{CO} = 1639 cm^{-1} (coordinated DMF). − ^1H NMR (D_2O): δ = 8.04 [s, 1 H, $HCON(CH_3)_2$], 2.96 and 2.78 [2 s, 2 × 3 H, $HCON(CH_3)_2$]. − $^{13}C\{^1H\}$ NMR (D_2O): δ = 168.8 [d, $HCON(CH_3)_2$, J_{Rh-C} = 19 Hz], 41.4 and 36.1 [s, $HCON(CH_3)_2$]. − MS (FAB^+, H_2O): *m/z* (%) = 465 (6) $[RhCl_2(DMF)_4]^+$, 392 (5) $[RhCl_2(DMF)_3]^+$, 356 (11.8) $[RhCl(DMF)_3]^+$, 319 (3) $[RhCl_2(DMF)_2]^+$, 248 (100) $[RhCl_2(DMF)]^+$. − $C_{12}H_{28}Cl_3N_4O_4Rh$ (501.64): calcd. C 28.73, H 5.63, N 11.17, O 12.76; found C 28.43, H 5.29, N 10.39, O 11.32.

$[AsPh_4][RhCl_2(CO)_2]$: The complex was prepared from $RhCl_3{\cdot}3H_2O$ (1.0 g, 3.8 mmol) and H_2O (0.35 mL, 19.5 mmol) in

DMF (15 mL). On heating the solution under reflux (160 °C), it turned progressively from deep-red to yellow. IR monitoring indicated the formation of the carbonylchloro anion. After 15 min, $[AsPh_4]Cl$ (1.58 g, 3.8 mmol) was added and the mixture was concentrated to a volume of 3 mL in vacuo at 100 °C. It was then allowed to cool to room temperature and ca. 6 N aq. HCl (20 mL) was added dropwise to precipitate the complex as a yellow powder. The product was collected by filtration using a Büchner funnel, washed with ca. 6 N aq. HCl (100 mL), and dried in vacuo to give 1.98 g (85% based on $RhCl_3 \cdot 3H_2O$). – IR (KBr pellets): ν_{CO} = 2054, 1975 cm^{-1}. – MS (FAB$^-$, CH_3CN): *m/z* (%) = 229 (8) $[RhCl_2(CO)_2]^-$, 201 (16) $[RhCl_2(CO)]^-$, 173 (100) $[RhCl_2]^-$. – $C_{26}H_{20}AsCl_2O_2Rh$ (613.18): calcd. C 50.93, H 3.29; found C 50.62, H 3.27.

[RhCl(CO)L$_2$] Complexes [L = PPh$_3$, P(OPh)$_3$, or TPPTS]: These three compounds were prepared from $RhCl_3 \cdot 3H_2O$ (0.3 g, 1.14 mmol) and H_2O (0.11 mmL, 6.11 mmol) in DMF (10 mL) in a closed Schlenk tube without any reflux condenser system. On heating the solution under reflux, it turned progressively from deep-red to yellow. IR monitoring of the reaction indicated the formation of the carbonylchloro anion $[RhCl_2(CO)_2]^-$. After 15 min, the mixture was cooled to room temperature and 1.95 equiv. of the appropriate phosphane was added [0.58 g of PPh_3, 0.69 g of $P(OPh)_3$ or 1.45 mg of TPPTS]. The reaction was immediate, giving a significant evolution of CO. An IR spectrum of the solution showed a single ν_{CO} band at 1977 cm^{-1} (PPh_3 complex), 2012 cm^{-1} [$P(OPh)_3$ complex], or 1982 cm^{-1} (TPPTS complex). The yellow complexes were precipitated by the addition of cold water (50 mL) [PPh_3 and $P(OPh)_3$ complexes] or ethanol (50 mL) (TPPTS complex). Collection of the products by filtration using a Büchner funnel and washing with water (150 mL) [PPh_3 and $P(OPh)_3$ complexes] or ethanol (150 mL) (TPPTS complex) afforded clean products in reproducible yields of around 80%.

[RhCl(CO)(PPh$_3$)$_2$]: IR (KBr pellets): ν_{CO} = 1960 cm^{-1} (vs). – $^{31}P\{^1H\}$ NMR ($CDCl_3$): δ = 32.5 (d, J_{Rh-P} = 125 Hz). – $C_{37}H_{30}ClOP_2Rh$ (690.95): calcd. C 64.32, H 4.38, O 2.32; found C 64.36, H 4.57, O 3.08.

[RhCl(CO){P(OPh)$_3$}$_2$]: IR (KBr pellets): ν_{CO} = 1998 cm^{-1} (vs). – $^{31}P\{^1H\}$ NMR ($CDCl_3$): δ = 113.6 (d, J_{Rh-P} = 214 Hz). – $C_{37}H_{30}ClO_7P_2Rh$ (786.95): calcd. C 56.47, H 3.84, O 14.23; found C 56.24, H 4.07, O 14.34.

[RhCl(CO)(TPPTS)$_2$]: IR (KBr pellets): ν_{CO} = 1968 cm^{-1} (vs). – $^{31}P\{^1H\}$ NMR ($CDCl_3$): δ = 34.2 (d, J_{Rh-P} = 126 Hz). – $C_{37}H_{36}ClNa_6O_{25}P_2S_6Rh$ (1411.32): calcd. C 31.49, H 2.57, O 28.34; found C 32.12, H 2.63, O 29.68.

[RhCl{P(OPh)$_3$}$_3$]: This compound was prepared by adding 3 equiv. of $P(OPh)_3$ (1.05 g, 3.42 mmol) to the aforementioned $[NH_2(CH_3)_2][RhCl_2(CO)_2]$ solution [prepared from $RhCl_3 \cdot 3H_2O$ (0.3 g, 1.14 mmol) and H_2O (0.35 mL, 19.5 mmol) in DMF (15 mL)] at room temperature. The reaction was immediate, giving a significant evolution of CO. The complex was precipitated by adding cold water (50 mL). Collection of the product by filtration using a Büchner funnel and washing with water (150 mL) afforded a clean product in reproducible yields of around 80%. – $^{31}P\{^1H\}$ NMR ($CDCl_3$): δ = 112.5 (dd, J_{Rh-PA} = 222 Hz, J_{PA-PB} = 55 Hz), 118.9 (td, J_{Rh-PB} = 281 Hz, J_{PA-PB} = 55 Hz). – $C_{54}H_{45}ClO_9P_3Rh$ (1069.23): calcd. C 60.66, H 4.24, O 13.47; found C 60.29, H 4.43, O 13.08.

[Rh(CO)(dppp)$_2$]Cl (dppp = 1,3-diphenylphosphanylpropane): This compound was prepared by adding 2 equiv. of dppp (0.94 g, 2.28 mmol) to the aforementioned $[NH_2(CH_3)_2][RhCl_2(CO)_2]$ solution [prepared from $RhCl_3 \cdot 3H_2O$ (0.3 g, 1.14 mmol) and H_2O (0.35 mL, 19.5 mmol) in DMF (15 mL)] at room temperature. The reaction was immediate, giving a significant evolution of CO. The complex was precipitated by adding cold water (50 mL). Collection of the product by filtration using a Büchner funnel and washing with water (150 mL) afforded a clean product in yields of around 70%. – IR (KBr pellets): ν_{CO} = 1930 cm^{-1}. – $^{31}P\{^1H\}$ NMR ($CDCl_3$): δ = –11.8 (td, P_{eq}, J_{Rh-Peq} = 122 Hz, $J_{Peq-Pax}$ = 30 Hz), 16.1 (td, P_{ax}, J_{Rh-Pax} = 85 Hz, $J_{Peq-Pax}$ = 30 Hz) [A_2B_2X]. – ^{31}P-^{103}Rh COSY ($CDCl_3$): δ_{Rh} = 1255. – $C_{55}H_{52}ClOP_4Rh$ (991.27): calcd. C 66.64, H 5.29, O 1.61; found C 66.42, H 4.87, O 1.84.

[Rh$_2$(μ-S*t*Bu)$_2$(CO)$_4$]: This compound was prepared by adding 10 equiv. of 1,1-dimethylethanethiol (900 μL, 11 mmol) to the aforementioned $[NH_2(CH_3)_2][RhCl_2(CO)_2]$ solution [prepared from $RhCl_3 \cdot 3H_2O$ (0.3 g, 1.14 mmol) and H_2O (0.35 mL, 19.5 mmol) in DMF (15 mL)] at room temperature. After 5 min, the IR spectrum of the solution showed four ν_{CO} bands at 2062, 2050, 1999, and 1984 cm^{-1}. The complex was precipitated by the dropwise addition of cold water (50 mL). Collection of the product by filtration using a Büchner funnel and washing with water (150 mL) afforded a clean product in 80–85% yield. – IR (KBr pellets): ν_{CO} = 2060, 2044, 2003, 1990, 1983 cm^{-1}. – $C_{12}H_{18}O_4Rh_2S_2$ (496.22): calcd. C 29.05, H 3.66, O 12.92, S 12.90; found C 28.87, H 3.77, O 12.45, S 12.56.

[Rh$_2$(μ-S*t*Bu)$_2$(CO)$_2$L$_2$] Complexes (L = PPh$_3$ or TPPTS): To the aforementioned solution of $[Rh_2(\mu\text{-}StBu)_2(CO)_4]$ in DMF (see previous synthesis), which exhibited four ν_{CO} bands at 2062, 2050, 1999, and 1984 cm^{-1}, 1 equiv. of the appropriate phosphane per mol of rhodium was added (0.3 g of PPh_3 or 0.73 g of TPPTS). An immediate evolution of CO was noticed and the reaction was complete within 5 min. The IR spectrum of the solution showed a ν_{CO} band at 1977 cm^{-1} (PPh_3 complex) or 1982 cm^{-1} (TPPTS complex). The complex was precipitated by adding cold water (50 mL) (PPh_3 complex) or ethanol (50 mL) (TPPTS complex). Collection of the product by filtration using a Büchner funnel and washing with water (150 mL) (PPh_3 complex) or ethanol (150 mL) (TPPTS complex) afforded clean products in reproducible yields of around 80%.

[Rh$_2$(μ-S*t*Bu)$_2$(CO)$_2$(PPh$_3$)$_2$]: IR (KBr pellets): ν_{CO} = 1964, 1948 cm^{-1}. – $^{31}P\{^1H\}$ NMR ($CDCl_3$): δ = 37.5 (d, J_{Rh-P} = 151 Hz). – $C_{26}H_{20}O_2P_2Rh_2S_2$ (964): calcd. C 56.91, H 5.57, O 3.30, S 6.60; found C 56.81, H 5.51, O 3.20, S 6.38.

[Rh$_2$(μ-S*t*Bu)$_2$(CO)$_2$(TPPTS·3H$_2$O)$_2$]: IR (KBr pellets): ν_{CO} = 1967 cm^{-1}. – $^{31}P\{^1H\}$ NMR (D_2O): δ = 39.7 (d, J_{Rh-P} = 152 Hz). – $C_{46}H_{54}O_{26}Na_6P_2Rh_2S_8$ (1685.14): calcd. C 32.79, H 3.23, O 24.69; found C 33.24, H 3.25, O 25.41.

Iridium Complexes

[NH$_2$(CH$_3$)$_2$]$_2$[IrCl$_5$(DMF)]: The complex was prepared from $IrCl_3 \cdot 3H_2O$ (0.5 g, 1.42 mmol) and aqueous HCl (37%, 250 μL) in DMF (5 mL). On heating the solution under reflux (160 °C), it turned progressively from deep-red to dark-orange and the product precipitated as a beige powder. After 6 min, the mixture was allowed to cool to room temperature and the product was collected by filtration using a Büchner funnel, washed with acetone, and dried in vacuo to give 0.155 g (20% based on $IrCl_3 \cdot 3H_2O$). – IR (KBr pellets): ν_{CO} = 1645 cm^{-1} (coordinated DMF). – ^1H NMR (D_2O): δ = 7.99 [s, 1 H, *H*CON(CH_3)$_2$], 3.07 and 2.98 [2 s, 2 × 3 H, HCON(C*H*$_3$)$_2$], 2.63 [s, 6 H, NH_2(C*H*$_3$)$_2$]. – $^{13}C\{^1H\}$ NMR (D_2O): δ = 174.4 [d, H*C*ON(CH_3)$_2$, J_{Rh-C} = 16 Hz], 35.8 and 40.8

[s, $HCON(CH_3)_2$], 37.4 [s, $NH_2(CH_3)_2$]. − $C_7H_{23}Cl_5IrN_3O$ (534.76): calcd. C 15.72, H 4.34, N 7.86, O 2.99; found C 15.77, H 4.23, N 7.63, O 3.60.

[AsPh$_4$][IrCl$_4$(CO)(DMF)]: The complex was prepared from $IrCl_3 \cdot 3H_2O$ (0.5 g, 1.42 mmol) in DMF (5 mL). On heating the solution under reflux (160 °C), it turned progressively from deep-red to orange. After 30 min, the heating was stopped and [AsPh$_4$]Cl (0.6 g, 1.43 mmol) was added. The mixture was concentrated to a volume of 2 mL and the pale-yellow complex was precipitated by the addition of cold water (25 mL), washed with water (50 mL), and dried in vacuo to give 302 mg (26% based on $IrCl_3 \cdot 3H_2O$). − IR (KBr pellets): ν_{CO} = 2060, 1645 cm^{-1} (coordinated DMF). − ^{1}H NMR ($CDCl_3$): δ = 8.53 [s, 1 H, $HCON(CH_3)_2$], 3.02 and 2.98 [2 s, 2 × 3 H, $HCON(CH_3)_2$]. − MS (FAB$^-$, CH_3CN): *m*/*z* (%) = 405 (100) [$IrCl_4(DMF)]^-$, 362 (12) [$IrCl_4(CO)]^-$, 337 (25) [$IrCl_4]^-$. − $C_{28}H_{27}AsCl_4IrNO_2$ (818.48): calcd. C 41.09, H 3.32, N 1.71, O 3.91; found C 40.86, H 3.33, N 1.78, O 2.75.

[AsPh$_4$][IrCl$_2$(CO)$_2$]: The complex was prepared from $IrCl_3 \cdot 3H_2O$ (0.3 g, 0.85 mmol) and HCl (0.15 mL, 37% in water) in DMF (10 mL). On heating the solution under reflux, it turned from red to orange. After 50 min, HCl (0.10 mL, 37% in water) was added and refluxing was maintained for a further 10 min. Thereafter, the solution was allowed to cool to room temperature and [AsPh$_4$]Cl (0.355 g, 0.85 mmol) was added. After evaporation of the solvent, the complex was washed with acetone/diethyl ether (1:9) to furnish 0.42 g of yellow crystals (71% based on $IrCl_3 \cdot 3H_2O$). − IR (KBr pellets): ν_{CO} = 2036, 1967 cm^{-1}. − MS (FAB$^-$, CH_3CN): *m*/*z* (%) = 319 (19) [$IrCl_2(CO)_2]^-$, 291 (100) [$IrCl_2(CO)]^-$. − $C_{26}H_{20}AsCl_2IrO_2$ (702.49): calcd. C 44.45, H 2.87, O 4.56; found C 44.62, H 2.98, O 4.34.

[IrCl(CO)(PPh$_3$)$_2$]: The complex was prepared by adding 2 equiv. of PPh_3 (0.89 g, 3.4 mmol) to the aforementioned $[NH_2(CH_3)_2][IrCl_2(CO)_2]$ solution in DMF [prepared from $IrCl_3 \cdot 3H_2O$ (0.6 g, 3.8 mmol) and HCl (0.35 mL, 37% in water) in DMF (15 mL)] at room temperature. The reaction was immediate and the IR spectrum of the solution showed a single ν_{CO} band at 1965 cm^{-1}. The lemon-yellow complex was then precipitated by adding cold water (100 mL), collected by filtration using a Büchner funnel, and washed with cold methanol (100 mL). After drying in vacuo, 1.59 g of [IrCl(CO)(PPh$_3$)$_2$] was collected (60% based on $IrCl_3 \cdot 3H_2O$). − IR (KBr pellets): ν_{CO} = 1957 cm^{-1}. − ^{31}P{^{1}H} NMR ($CDCl_3$): δ = 24.1 (s). − $C_{37}H_{30}ClIrOP_2$ (780.27): calcd. C 56.96, H 3.88, O 2.05; found C 56.62, H 4.27, O 3.34.

Ruthenium Complexes

[PPN]$_2$[RuCl$_5$(CO)]: The complex was prepared from $RuCl_3 \cdot 3H_2O$ (0.4 g, 1.53 mmol) in DMF (15 mL) in a closed Schlenk tube without any reflux condenser system. The solution was heated under reflux and IR monitoring of the reaction showed the formation of the carbonylchloro anion (ν_{CO} = 2020 cm^{-1}). After 10 min, the solution was allowed to cool and [PPN]Cl (0.88 g, 1.53 mmol) was added. After concentration of the solution in vacuo at 100 °C to a volume of 5 mL, cold water (10 mL) was added dropwise to precipitate the complex as a dark-red powder. After collection of the product by filtration using a Büchner funnel and washing with water (100 mL), the product was dried in vacuo to give 0.15 g (7% based on $RuCl_3 \cdot 3H_2O$). − IR (KBr pellets): ν_{CO} = 2008 cm^{-1}. − $C_{73}H_{60}Cl_5N_2OP_4Ru$ (1383.52): calcd. C 63.37, H 4.37, N 2.02, O 1.16; found C 63.22, H 4.33, N 2.18, O 1.55.

[PPN]$_2$[RuCl$_4$(CO)(DMF)]: The complex was prepared from $RuCl_3 \cdot 3H_2O$ (0.3 g, 1.15 mmol) and HCl (250 μL, 37% in water) in DMF (8 mL) in a closed Schlenk tube without any reflux condenser system. On heating the solution under reflux (160 °C), it turned progressively from deep-red to dark-green. After 30 min, the heating was stopped and [PPN]Cl (0.4 g, 0.7 mmol) was added. The green complex was precipitated by adding cold water (25 mL), washed with further water (50 mL), and dried in vacuo to give 0.138 g (26% based on $RuCl_3 \cdot 3H_2O$). − IR (KBr pellets): ν_{CO} = 1918, 1644 cm^{-1} (coordinated DMF). − ^{1}H NMR (CD_2Cl_2): δ = 8.61 [s, 1 H, $HCON(CH_3)_2$], 2.98 and 2.95 [2 s, 2 × 3 H, $HCON(CH_3)_2$]. − $C_{76}H_{67}Cl_4N_3O_2P_4Ru$ (1421.16): calcd. C 64.23, H 4.75, N 2.96, O 2.25; found C 64.32, H 4.52, N 2.38, O 1.86.

[PPN][RuCl$_3$(CO)$_2$(DMF)]: The complex was prepared from $RuCl_3 \cdot 3H_2O$ (0.4 g, 1.53 mmol) and anhydrous 4 M HCl in dioxane (1 mL, 4 mmol) in DMF (15 mL) in a closed Schlenk tube without any reflux condenser system. On refluxing the solution, it turned progressively from red to orange. IR monitoring indicated the formation of the carbonylchloro anion (ν_{CO} = 2042 and 1964 cm^{-1}). After 1 h, the solution was allowed to cool and [PPN]Cl (0.88 g, 1.53 mmol) was added. After concentration of the mixture in vacuo at 100 °C to a volume of 5 mL, cold water (10 mL) was added dropwise to precipitate the complex as a yellow powder. The product was collected by filtration using a Büchner funnel, washed with water (100 mL), dried in vacuo, and recrystallized from acetone/heptane to give 0.85 g of yellow crystals (64% based on $RuCl_3 \cdot 3H_2O$). − IR (KBr pellets): ν_{CO} = 2045, 1970, 1636 cm^{-1} (coordinated DMF). − ^{1}H NMR ($CDCl_3$): δ = 8.52 [s, 1 H, $HCON(CH_3)_2$], 2.91 [s, 6 H, $HCON(CH_3)_2$]. − MS (FAB$^-$, CH_3CN): *m*/*z* (%) = 300 (100) [$RuCl_3(CO)(DMF)]^-$, 280.5 (19) [$RuCl_3(DMF)]^-$, 264.8 (7) [$RuCl_3(CO)_2]^-$, 208 (31) [$RuCl_3]^-$. − $C_{41}H_{37}Cl_3N_2O_3P_2Ru$ (875.13): calcd. C 56.27, H 4.26, N 3.20, O 5.48; found C 56.62, H 4.27, N 3.05, O 5.34.

[RuCl$_2$(CO)$_2$(DMF)$_2$]: The complex was prepared from $RuCl_3 \cdot 3H_2O$ (0.4 g, 1.53 mmol) in DMF (15 mL) in a closed Schlenk tube without any reflux condenser system. On refluxing the solution, it turned progressively from red to orange. After 2 h, it was allowed to cool and [PPN]Cl (0.88 g, 1.53 mmol) was added. After concentration of the mixture in vacuo at 100 °C to a volume of 5 mL, cold water (10 mL) was added dropwise to precipitate a yellow powder. The product was collected by filtration using a Büchner funnel, washed with water (100 mL), and dried in vacuo. Chromatographic separation on a column of silica [Degussa Sipernat 22; eluent: acetone/2-propanol (20:80, v/v)] furnished the pure complex in the first fraction; yield 0.17 g (30% based on $RuCl_3 \cdot 3H_2O$). − IR ($CHCl_3$): ν_{CO} = 2073, 2009, 1652, 1645 cm^{-1} (coordinated DMF). − ^{1}H NMR ($CDCl_3$): δ = 8.28 [s, 1 H, $HCON(CH_3)_2$], 8.37 [s, 1 H, $HCON(CH_3)_2$], 3.18 [s, 3 H, $HCON(CH_3)_2$], 3.16 [s, 3 H, $HCON(CH_3)_2$], 3.06 [s, 3 H, $HCON(CH_3)_2$], 3.00 [s, 3 H, $HCON(CH_3)_2$]. − $C_8H_{14}Cl_2N_2O_4Ru$ (374.19): calcd. C 25.68, H 3.77, N 7.49, O 17.10; found C 25.58, H 3.11, N 6.92, O 16.45.

***cis*,*cis*,*trans*-[RuCl$_2$(CO)$_2$(PPh$_3$)$_2$]:** The complex was prepared by adding 2 equiv. of PPh_3 (0.8 g, 3.05 mmol) to the aforementioned $[NH_2(CH_3)_2][RuCl_3(CO)_2(DMF)]$ solution in DMF [prepared from $RuCl_3 \cdot 3H_2O$ (0.4 g, 1.53 mmol) and anhydrous HCl (1 mL, 4 mmol, 4 M in dioxane) in DMF (15 mL)] at 140 °C. The solution was maintained at this temperature until its IR spectrum showed the ν_{CO} bands at 2058 and 1994 cm^{-1} characteristic of *cis*,*cis*,*trans*-$[RuCl_2(CO)_2(PPh_3)_2]$ (1 h). The yellow solution was then allowed to cool to room temperature, and the pale-yellow complex was precipitated by adding cold water. It was collected by filtration using a Büchner funnel, washed with water (100 mL), and dried in vacuo to give 0.7 g of the title compound (64% based on $RuCl_3 \cdot 3H_2O$).

− IR (KBr pellets): ν_{CO} = 2054, 1992 cm^{-1}. − $^{31}P\{^1H\}$ NMR ($CDCl_3$): δ = 17.2 (s). − $C_{38}H_{30}Cl_2O_2P_2Ru$ (752.58): calcd. C 60.65, H 4.02, O 4.25; found C 60.85, H 4.15, O 4.94.

Palladium and Platinum Complexes

[$PdCl_2(DMF)_2$]: The complex was prepared from $PdCl_2$ (0.2 g, 1.13 mmol) in DMF (15 mL). The solution was heated for 120 min at 100 °C and then concentrated to dryness in vacuo at 50 °C. The complex (0.091 g, 25% based on $PdCl_2$) was recovered as a black powder. − IR (KBr pellets): ν_{CO} = 1656 cm^{-1} (coordinated DMF). − $C_6H_{14}Cl_2N_2O_2Pd$ (323.52): calcd. C 22.28, H 4.36, N 8.66; found C 22.50, H 3.91, N 7.90.

[PPN][$PtCl_3(CO)$]: The complex was prepared from K_2PtCl_4 (0.4 g, 0.96 mmol) and [PPN]Cl (0.554 g, 0.97 mmol) in DMF (15 mL). The solution was refluxed for 120 min and then allowed to cool to room temperature. The complex (0.438 g, 53% based on K_2PtCl_4) was recovered by precipitation with cold water and washed with further water (100 mL). − IR (KBr pellets): ν_{CO} = 2072 cm^{-1}. − $^{13}C\{^1H\}$ NMR ($CDCl_3$): δ = 150.2 (s). − $C_{37}H_{30}Cl_3NOP_2Pt$ (868.04): calcd. C 51.20, H 3.48, N 1.61; found C 51.89, H 3.77, N 2.14.

Acknowledgments

The authors are grateful to Engelhard CLAL for a generous loan of rhodium and palladium salts.

[1] N. Lugan, G. Lavigne, J. M. Soulié, S. Fabre, Ph. Kalck, J. Y. Saillard, J. F. Halet, *Organometallics* **1995**, *14*, 1712.
[2] S. Fabre, Ph. Kalck, G. Lavigne, *Angew. Chem. Int. Ed. Engl.* **1997**, *36*, 1092.
[3] A. Spencer, *J. Organomet. Chem.* **1980**, *194*, 113.
[4] T. Hosokawa, T. Nomura, S. I. Murahaschi, *J. Organomet. Chem.* **1998**, *55*, 387.
[5] T. Kondo, T. Okada, T. A. Mitsudo, *Organometallics* **1999**, *18*, 4123.
[6] S. Rajagopal, S. Vancheesan, J. Rajaram, J. C. Kuriacose, *J. Mol. Catal.* **1983**, *22*, 131.
[7] S. Rajagopal, S. Vancheesan, J. Rajaram, J. C. Kuriacose, *J. Mol. Catal.* **1983**, *22*, 137.
[8] C. Legrand, Y. Castanet, A. Mortreux, F. Petit, *J. Chem. Soc., Chem. Commun.* **1994**, 1173.
[9] C. Legrand, Y. Castanet, A. Mortreux, F. Petit, *Tetrahedron Lett.* **1992**, *33*, 3753.
[10] T. A. Mitsudo, N. Suzuki, T. Kondo, Y. Watanabe, *J. Org. Chem.* **1994**, *59*, 7759.
[11] F. Ramirez Vega, J. C. Clément, H. des Abbeyes, *Tetrahedron Lett.* **1993**, *34*, 8117.
[12] T. Hayashi, F. Abe, T. Sakakura, M. Tanaka, *J. Mol. Catal.* **1990**, *58*, 165.
[13] T. Hayashi, Z. Hui Gu, T. Sakakura, M. Tanaka, *J. Organomet. Chem.* **1988**, *352*, 373.
[14] G. Süss-Fink, G. F. Schmidt, *J. Mol. Catal.* **1987**, *42*, 361.
[15] G. Süss-Fink, J. Reiner, *J. Mol. Catal.* **1982**, *16*, 231.
[16] G. Süss-Fink, *J. Organomet. Chem.* **1980**, *193*, C20.
[17] P. Isnard, B. Denise, R. P. A. Sneeden, *J. Organomet. Chem.* **1983**, *256*, 135.
[18] A. Rusina, A. A. Vlćek, *Nature* **1965**, *206*, 295.
[19] Y. Varshavskii, T. G. Cherkasova, *Russ. J. Inorg. Chem. Int. Ed. Engl.* **1967**, *12*, 899.
[20] Y. Varshavskii, N. V. Kiseleva, T. G. Cherkasova, N. A. Busina, *J. Organomet. Chem.* **1971**, *31*, 119.
[21] E. Kwaskowska-Chec, J. J. Ziokowski, *Transition Met. Chem.* **1983**, *8*, 103.
[22] E. Kwaskowska-Chec, J. J. Ziokowski, *Transition Met. Chem.* **1991**, *16*, 212.
[23] F. Bonati, L. A. Oro, M. T. Pinillos, *Polyhedron* **1985**, *4*, 357.
[24] A. M. Trzeciak, J. J. Ziokowski, *Inorg. Chim. Acta* **1985**, *15*, 96.
[25] J. P. Collman, C. T. Sears Jr., M. Kubota, *Inorg. Synth.* **1969**, *11*, 101.
[26] R. G. Goel, W. O. Ogini, *Organometallics* **1982**, *1*, 654.
[27] R. G. Goel, R. G. Montemayor, W. O. Ogini, *J. Am. Chem. Soc.* **1978**, *100*, 3629.
[28] D. J. Cole-Hamilton, *J. Chem. Soc., Chem. Commun.* **1980**, 1213.
[29] J. M. Clear, J. M. Kelly, C. M. O'Connell, J. G. Vos, C. J. Cardin, S. R. Costa, *J. Chem. Soc., Chem. Commun.* **1980**, 750.
[30] R. F. Jones, D. J. Cole-Hamilton, *Inorg. Chim. Acta* **1981**, L3.
[31] D. Choudury, R. F. Jones, G. Smith, D. J. Cole-Hamilton, *J. Chem. Soc., Dalton Trans.* **1982**, 1143.
[32] J. M. Kelly, C. M. O'Connell, J. G. Vos, *J. Chem. Soc., Dalton Trans.* **1986**, 253.
[33] B. P. Sullivan, D. J. Salmon, T. T. Meyer, *Inorg. Chem.* **1978**, *17*, 3334.
[34] R. J. Forster, A. Boyle, J. G. Vos, R. Haze, A. J. G. Dijkhuis, R. A. G. de Graeff, J. G. Haasnoot, R. Prins, J. Rudijk, *J. Chem. Soc., Dalton Trans.* **1990**, 121.
[35] I. R. Baird, S. J. Rettig, B. R. James, K. A. Skov, *Can. J. Chem.* **1998**, *76*, 1379.
[36] T. Tatsumi, H. Tominaga, M. Hidai, Y. Uchida, *J. Organomet. Chem.* **1981**, *215*, 67.
[37] M. J. Camenzind, B. R. James, D. Dolphin, J. W. Sparapany, J. A. Ibers, *Inorg. Chem.* **1988**, *27*, 3054.
[38] Ph. Serp, M. Hernandez, Ph. Kalck, *C. R. Acad. Sci. Paris* **1999**, 267.
[39] M. J. Clear, W. P. Griffith, *J. Chem. Soc. A* **1970**, 2788.
[40] R. Colton, R. H. Farthing, J. Knapp, *Aust. J. Chem.* **1970**, *23*, 1351.
[41] R. J. Judd, R. Cao, M. Bliner, T. Armbruster, H.-B. Bürgi, A. E. Merbach, A. Ludi, *Inorg. Chem.* **1995**, *34*, 5080.
[42] C. H. Cheng, D. E. Hendriken, R. Eisenberg, *J. Am. Chem. Soc.* **1977**, *99*, 2791.
[43] D. Forster, *Inorg. Nucl. Lett.* **1969**, *5*, 433.
[44] B. B. Wayland, R. F. Schramm, *Inorg. Chem.* **1969**, *8*, 971.

Received February 5, 2001
[I01040]

Synthesis, Characterization and Ethylene Polymerization Activity of Zirconium Complexes Containing Nonsymmetric Diamido Ligands Derived from 2-Aminobenzylamine

Régis M. Gauvin,[a] Christian Lorber,*[b] Robert Choukroun,[b] Bruno Donnadieu,[b] and Jacky Kress*[a]

Keywords: Amines / Zirconium / Fluxionality / Catalysis / Olefin polymerizations

Several *N*,*N*′-bis(trialkylsilyl)-substituted diamines of the general formula [$(SiR_3)_2$-ABA]H_2 [ABA = 2-amidobenzylamido, SiR_3 = $SiMe_3$ (**1a**), $SiMePh_2$ (**1b**), $SiMe_2t$Bu (**1c**) or Si*i*Pr_3 (**1d**)], together with related compounds in which the substituents of the two nitrogen atoms are different, e.g. [($SiMePh_2$)($SiMe_3$)-ABA]H_2 (**1g**), have been synthesized. Their reaction with 2 equiv. of *n*BuLi afforded the dilithiated derivatives, which reacted with $ZrCl_4$ to yield metallaspirocyclic complexes of the type Zr[$(SiR_3)_2$-ABA]$_2$. Protonolysis of $Zr(NMe_2)_4$ with 1 equiv. of the parent diamines led to the monosubstituted complexes Zr[$(SiR_3)_2$-ABA]$(NMe_2)_2$ [SiR_3 = $SiMe_3$ (**4a**), $SiMePh_2$ (**4b**) or $SiMe_2t$Bu (**4c**)] and Zr[($SiMePh_2$)($SiMe_3$)-ABA]$(NMe_2)_2$ (**4g**) in high yield, and subsequent reaction with excess $SiMe_3Cl$ afforded the dichlorides Zr[$(SiMe_3)_2$-ABA]Cl_2 (**5a**), Zr[$(SiMe_2t$Bu$)_2$-ABA]Cl_2 (**5c**), and Zr[($SiMePh_2$)($SiMe_3$)-ABA]Cl_2 (**5g**). The X-ray crystal structure of **5c** shows that it forms dimers via two Zr–Cl bridges; moreover, a bonding interaction between the zirconium centre and the aryl *ipso*-carbon atom linked to the anilinic nitrogen atom is evident. A hydrochlorinated derivative of **5c**, Zr[$(SiMe_2t$Bu$)_2$(H)-ABA]Cl_3 (**6c**), was also analysed by X-ray diffraction and shown to exhibit analogous structural characteristics. Low-temperature NMR studies revealed all these complexes to be fluxional and permitted an insight into the molecular structures in solution. The ABA framework undergoes a rocking motion about the corresponding ZrN_2 plane, whose activation energy is between 37 and 43 kJ mol^{-1}. Compounds **3** and **5** exist as several stereoisomers that interconvert by this process. On activation with MAO, the dichloride complexes of type **5** polymerize ethylene at both room temperature and pressure to yield linear high molecular mass polyethylenes with a broad molecular mass distribution.

Introduction

The search for new olefin polymerization catalysts based on chelating diamido ligands has concentrated mostly on Group 4 transition metal complexes of symmetric ligands containing two identical amide functions.[1] However, attempts to design catalysts for the stereoselective polymerization of α-olefins with the help of such ligands has met with limited success.[2] Nonsymmetric diamido ligands containing two different amido functions are potentially of great interest in this regard, particularly if the nitrogen substituents of each amido function can be modified independently. This would help us, if polymerization of α-olefins could be obtained, to better understand the influence of electronic and steric effects of the ligands on the stereoselectivity results.

Herein, we wish to describe the synthesis of several *N*,*N*′-disubstituted 2-aminobenzylamines. This fragment affords a suitable framework for the purpose outlined. Its application resulted in the generation of a series of bis(dimethylamido)- and dichlorozirconium complexes. The fluxional behaviour ot these new complexes and their ability to catalyse the polymerization of olefins have been analysed. One of these ligands has been reported recently, together with three titanium and two zirconium complexes containing the ligand.[3]

Results and Discussion

Ligands Precursors

The *N*,*N*′-bis(trialkylsilyl)-substituted diamines [$(SiR_3)_2$-ABA]H_2 (**1a**−**1d**) were synthesized as reported for **1a**[3] by treating the dilithio salt of 2-aminobenzylamine with 2

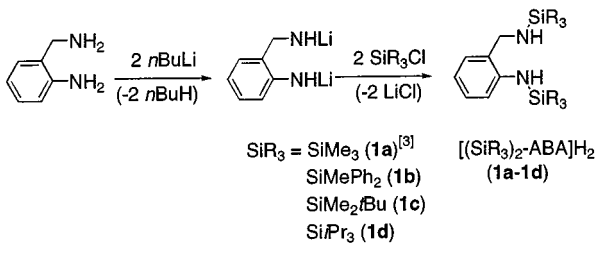

Scheme 1

[a] Laboratoire de Chimie des Métaux de Transition et de Catalyse, UMR du CNRS 7513, Institut Le Bel, Université Louis Pasteur,
4, rue Blaise Pascal, 67000 Strasbourg, France
E-mail: jkress@chimie.u-strasbg.fr
[b] Laboratoire de Chimie de Coordination, UPR du CNRS 8241, 205 route de Narbonne, 31077 Toulouse Cedex 04, France
E-mail: lorber@lcc-toulouse.fr

 © WILEY-VCH Verlag GmbH, 69451 Weinheim, 2001 1434−1948/01/0909−2337 $ 17.50+.50/0

equiv. of trialkylchorosilanes in diethyl ether (or THF for **1d**)/hexane (Scheme 1), and isolated as viscous oils (or a cream solid for **1c**) in 80−90% yield. For **1d**, 18 h of heating in THF to reflux was necessary to complete the reaction. Compound **1a**, but not the others, could also be obtained by the reaction of 2-aminobenzylamine with 2 equiv. of Me_3SiCl in the presence of triethylamine (96% yield).

Initial attempts to synthesize $[(SiR_3)(SiR'_3)$-ABA$]H_2$ derivatives possessing two different nitrogen substituents led to the diamines $[(SiMe_3)$(H)-ABA$]H_2$ (**1e**) and $[(SiMePh_2)$(H)-ABA$]H_2$ (**1f**) being obtained as yellow-orange oils (93−95% yield, Scheme 2), which contain silyl substituents located solely on the anilino nitrogen atom. These compounds tend to disproportionate into **1a**−**b** and 2-aminobenzylamine. Compound **1e** was hence contaminated (7% total amount) with **1a**, and also with $[(H)(SiMe_3)$-ABA$]H_2$, of which neither could be properly separated. On the other hand, treatment of 2-aminobenzylamine with 1 equiv. of Me_3SiCl in the presence of triethylamine preferentially introduces the substituent on the benzylamino nitrogen atom, affording $[(H)(SiMe_3)$-ABA$]H_2$, but this reaction is also unselective and leads to the formation of **1a** in almost equal proportions. Only compound $[(SiMePh_2)(SiMe_3)$-ABA$]H_2$ (**1g**) could be generated as a viscous oil from **1f** (87% isolated yield, Scheme 2). The diamines were characterized by ^1H and ^{13}C NMR spectroscopy. It is of interest to note that the benzylic protons give rise to a doublet or a triplet, whether the adjacent nitrogen atom is substituted or not. This indicates that hydrogen exchange in the benzylamino groups is slower in these compounds than in the 2-aminobenzylamine precursor, for which the corresponding coupling is not observed.

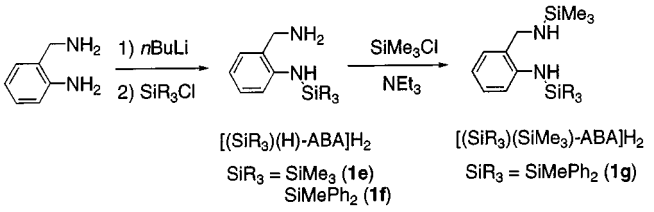

Scheme 2

The dilithiated derivatives $[(SiR_3)_2$-ABA$]Li_2$ [SiR_3 = $SiMe_3$ (**2a**), $SiMePh_2$ (**2b**), $SiMe_2tBu$ (**2c**)] or $SiiPr_3$ (**2d**)] and $[(SiMePh_2)(SiMe_3)$-ABA$]Li_2$ (**2g**) were obtained as white solids or a brown paste (**2d**) (34−95% yield) by double deprotonation of **1a**−**d** or **1g** with *n*BuLi in hexane. The observation of an AX pattern for the room-temperature ^1H NMR signal of the CH_2 groups of **2a** and **2g**, and of a broad singlet for the corresponding protons of **2b**−**d**, suggests that these compounds possess a disymmetrical aggregated structure in solution. This is confirmed by the dimeric ladder structure of **2a** in the solid state, established by X-ray diffraction.[4] The fluxional nature of these lithiated compounds was further characterized by the coalescence of the AX spectrum of **2a** into a singlet at 41 °C ($\Delta G^{\neq}$ = 61.6 kJ·mol^{-1}),[5] and by the splittting of the broad singlet of **2b** into a doublet of doublets at δ = 4.56 and 3.53 at −33 °C in $[D_8]$toluene.

Zirconium Complexes

Even when only low proportions of the dilithio reactants were used, transmetallation reactions between **2a**, **2c** or **2g** and $ZrCl_4$ led to the metallaspirocyclic complexes $Zr[(SiMe_3)_2$-ABA$]_2$ (**3a**), $Zr[(SiMe_2tBu)_2$-ABA$]_2$ (**3c**), and $Zr[(SiMePh_2)(SiMe_3)$-ABA$]_2$ (**3g**) (Scheme 3), as reported earlier for **3a**.[3] However, compounds **2b** and **2d** gave only mixtures that could not be separated. In particular, using 2 equiv. of **2g**, compound **3g** was synthesized in good yield in hot toluene and isolated as a yellow solid. Its ^1H NMR spectrum at room temperature is analogous to that of **3a**,[3] displaying an AX pattern at δ = 4.89 and 3.93 (CD_2Cl_2, ^2J = 13.4 Hz) for the two CH_2 groups, which is consistent with a tetrahedral structure of C_2 symmetry, of the type of that determined for **3a** by X-ray diffraction.[3]

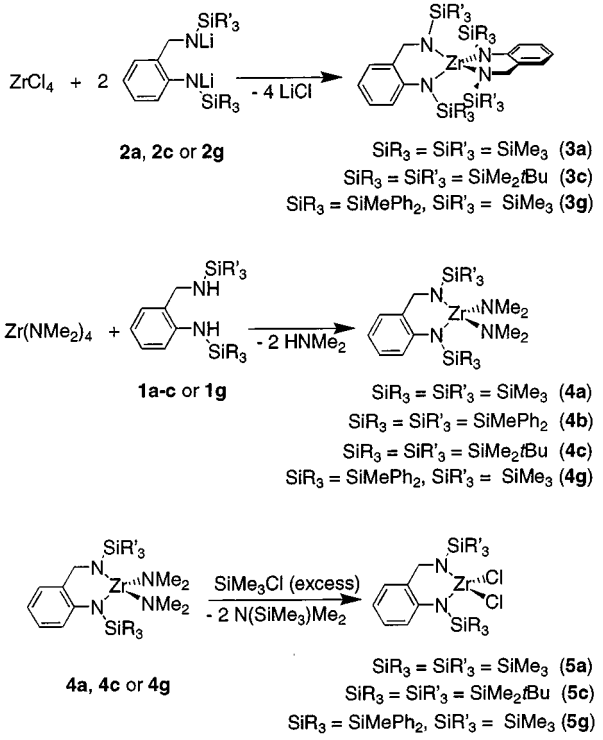

Scheme 3

The dichloride derivatives were prepared from the bis(dimethylamido) precursors. These were synthesized by protonolysis of $Zr(NMe_2)_4$ [6] with 1 equiv. of the diamines **1** (Scheme 3). Complexes $Zr[(SiMe_3)_2$-ABA$](NMe_2)_2$ (**4a**), $Zr[(SiMePh_2)_2$-ABA$](NMe_2)_2$ (**4b**), $Zr[(SiMe_2tBu)_2$-ABA$](NMe_2)_2$ (**4c**), and $Zr[(SiMePh_2)(SiMe_3)$-ABA$](NMe_2)_2$ (**4g**) were obtained in high yield (96−99%) as pale yellow to orange, viscous oils. The diamine **1d**, however, did not react with $Zr(NMe_2)_4$. The ^1H and ^{13}C NMR spectra of the four complexes, at room temperature, reveal the presence of two apparently equivalent and symmetrical NMe_2 ligands for one coordinated ABA group, the two benzylic protons

of which give rise to a singlet. The fluxional behaviour that lies at the root of these unexpected observations is specified below.

Complexes **4a**, **4c** and **4g** react with an excess of trimethylsilyl chloride to give the respective dichloride derivatives Zr[$(SiMe_3)_2$-ABA]Cl_2 (**5a**),[7] Zr[$(SiMe_2tBu)_2$-ABA]Cl_2 (**5c**), and Zr[$(SiMePh_2)(SiMe_3)$-ABA]Cl_2 (**5g**) in good yield (Scheme 3). However, the analogous reaction involving **4b** was unsuccessful. The solid pale yellow products are poorly soluble in hydrocarbons, and the singlets observed at δ = 4.72, 4.59 and 4.87 in their ^1H NMR spectra (C_6D_6, room temperature), which are assigned to their methylene groups, are indicative of a high apparent symmetry similar to that found for the amido complexes of type **4**.

Single crystals of **5c** were grown by cooling a saturated toluene/pentane solution to −20 °C and were analysed by X-ray diffraction. The molecular structure of **5c** is shown in Figure 1, and selected bond lengths and angles are listed in Table 1. The structure consists of discrete dimers that reside on an inversion centre of the space group, the association between the two monomeric units being realised via two weak zirconium−chlorine bridging interactions [Zr−Cl(2)′ = 2.706 Å]. Hence, each zirconium atom is pentacoordinate and possesses a distorted trigonal-bipyramidal coordination geometry. The benzylamido nitrogen atom and the bridging chloride ion occupy the axial sites [N(1)−Zr−Cl(2)′ = 163.7°]. The main distortion results from the acute Cl(2)−Zr−Cl(2)′ angle in the planar bridging Zr_2Cl_2 unit (75.5°), while the diamide ligand chelate angle [N(1)−Zr−N(2) = 93.1°], as well as the other bond angles around the zirconium centre, are within the usual ranges. Short Zr−N bond lengths [Zr−N(1) = 2.016 Å, Zr−N(2) = 2.012 Å] and sp^2-hybridized nitrogen atoms [the summation of bond angles is 359.0° at both N(1) and N(2)] indicate strong π-donation from the two nitrogen atoms to the electron-deficient zirconium centre. As expected, the zirconium−chlorine bond length of the bridging halide ion [Zr−Cl(2) = 2.554 Å] is longer than that of the terminal one [Zr−Cl(1) = 2.386 Å].

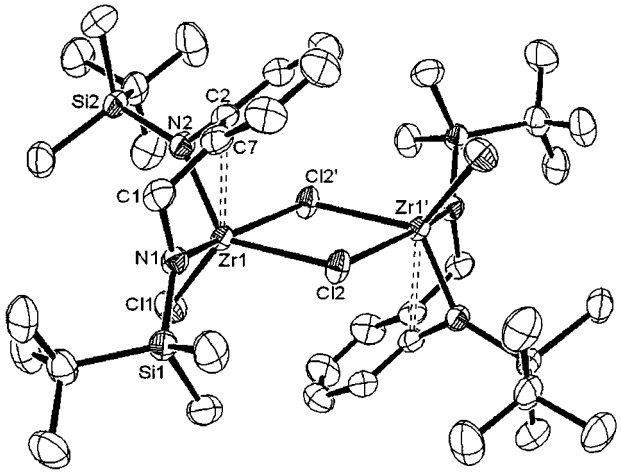

Figure 1. ORTEP view of the molecular structure of **5c** (50% probability thermal ellipsoids); hydrogen atoms are omitted for clarity; primed atoms refer to centrosymmetric equivalents

Table 1. Selected bond lengths [Å] and angles [°] for **5c**

Zr−N(1)	2.0163(17)	Zr−N(2)	2.0120(15)
Zr−C(2)	2.538(2)	Zr−Cl(1)	2.3864(8)
Zr−Cl(2)	2.5545(13)	Zr−Cl(2)′	2.7062(10)
Zr−C(1)	2.903(3)	Zr−C(7)	2.908(2)
N(1)−C(1)	1.489(2)	N(2)−C(2)	1.437(2)
C(1)−C(7)	1.510(3)	C(2)−C(7)	1.401(3)
N(2)−Zr−N(1)	93.09(7)	N(2)−Zr−Cl(1)	110.18(5)
N(2)−Zr−Cl(2)	124.92(5)	N(1)−Zr−Cl(2)	90.00(6)
Cl(1)−Zr−Cl(2)	122.18(3)	Cl(1)−Zr−Cl(2)′	90.08(3)
N(2)−Zr−Cl(2)′	89.30(6)	N(1)−Zr−Cl(2)′	163.71(5)
Cl(2)−Zr−Cl(2)′	75.51(3)	N(1)−Zr−Cl(1)	104.15(5)
N(2)−Zr−C(2)	34.43(6)	C(2)−N(2)−Zr	93.25(11)
Zr−Cl(2)−Zr′	104.49(3)		

The ligand chelate ring is severely puckered. Of particular relevance is its significant folding along the C(1)−N(2) axis (70.7°), and the correspondingly very short Zr−C(2) distance (2.537 Å). This effect, which is more pronounced than in compound **3a**,[3] and certainly contributes to an even shorter Zr−N(2) bond along with reduction of the C(2)−N(2)−Zr angle to 93.3°, is similar to that discussed for several *o*-phenylenediamido complexes.[8] It is ascribed to a bonding interaction between the zirconium centre and the aryl *ipso*-carbon atom linked to the anilinic nitrogen atom. This way of compensating electronic unsaturation at the metal centre is distinct from that found in the analogous titanium complex Ti[$(SiMe_3)_2$-ABA]Cl_2. In the latter case, an interaction between the metal centre and the benzylic methylene group, that gives rise to a significantly different ligand geometry, has been shown to occur.[3] It is similar, however, to that found in the lithium derivative **2a**.[4] The infrared spectra suggest that **5a** is also dimeric in the solid state, as revealed by the broad absorption observed at 254 cm^{-1}, assigned to zirconium−chloride bridges, but not **5g** for which an analogous band is totally absent.

By following the same crystallization procedure but, apparently, under slightly different and uncontrolled conditions, a further zirconium complex was unexpectedly crystallized in low yield from solutions of **5c**. An X-ray analysis of this compound revealed it to be Zr[$(SiMe_2tBu)_2$(H)-ABA]Cl_3 (**6c**) (i.e. the hydrochlorinated derivative of **5c**), in which the benzylamido nitrogen atom of **5c** has been protonated to afford a coordinated benzylamino function. This results in the sp^3 hybridization of this nitrogen atom [sum of angles formed by non-H atoms around N(2) = 343.2°] and in the substantial lengthening of the corresponding zirconium−nitrogen bond [Zr−N(2) = 2.388 Å]. The other structural characteristics of **6c** are similar to those of **5c**. Compound **6c** crystallizes in the same space group, and also consists of discrete centrosymmetric dimers that are associated via two chloride bridges (Figure 2, Table 2). The geometry of each monomeric unit is now a distorted octahedron, leading to somewhat different bond angles around the zirconium centre. However, the distinctive configuration of the ABA chelate ring is retained in this complex. The interaction between the zirconium centre and the anilinic *ipso*-carbon atom of the aryl ring is strengthened, as revealed by

the shorter corresponding distance [Zr−C(1) = 2.513 Å] and the more acute C(1)−N(1)−Zr angle (91.2°), suggesting that the metal centre is slightly more electron-deficient than in **5c**. It may also be noted that the chloride bridges are *trans* to the anilido function and not to the benzylamido nitrogen atom as in **5c**. As a consequence, the aryl rings are perpendicular to the Zr_2Cl_2 plane, instead of overhanging it as in **5c**.

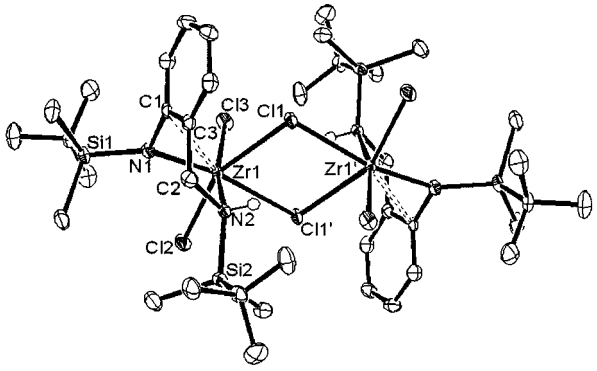

Figure 2. ORTEP view of the molecular structure of **6c** (50% probability thermal ellipsoids); hydrogen atoms are omitted for clarity, except those located on the benzylamino nitrogen atoms; primed atoms refer to centrosymmetric equivalents

Table 2. Selected bond lengths [Å] and angles [°] for **6c**

Zr−N(1)	2.030(3)	Zr−N(2)	2.388(3)
Zr−Cl(2)	2.4043(9)	Zr−Cl(3)	2.4181(10)
Zr−Cl(1)	2.6054(10)	Zr−Cl(1)′	2.6928(10)
Zr−C(2)	3.101(3)	Zr−C(3)	2.968(3)
Zr−C(1)	2.513(3)		
N(1)−Zr−N(2)	88.11(11)	Cl(2)−Zr−Cl(3)	99.05(3)
N(1)−Zr−Cl(2)	89.16(8)	N(2)−Zr−Cl(2)	95.21(7)
N(1)−Zr−Cl(3)	96.46(8)	N(2)−Zr−Cl(3)	165.07(8)
N(2)−Zr−Cl(1)	80.60(8)	Cl(2)−Zr−Cl(1)	153.00(3)
Cl(3)−Zr−Cl(1)	84.68(3)	N(1)−Zr−Cl(1)	117.15(8)
N(1)−Zr−Cl(1)′	168.84(8)	N(2)−Zr−Cl(1)′	91.16(8)
Cl(2)−Zr−Cl(1)′	79.81(3)	Cl(3)−Zr−Cl(1)′	87.05(3)
Cl(1)−Zr−Cl(1)′	73.65(3)	C(1)−N(1)−Zr	91.26(19)
Zr−Cl(1)−Zr′	106.35(3)		

Fluxionality

The apparent discrepancy between the twisted, nonplanar geometry of the ABA ligands in complexes **5c** and **6c** and the room-temperature NMR spectra of complexes **4**−**5** prompted us to examine the low-temperature ^{1}H NMR spectra of compounds **3**−**5**. Thus, it was possible to verify that the two benzylic hydrogen atoms are actually diastereotopic in all cases, but equilibrate rapidly at higher temperatures in **4**−**5** by a dynamic process that seems common to all members of the series. We suggest this process consists of the rocking motion of each ABA framework about the corresponding ZrN_2 plane, as illustrated in Scheme 4 for a monomeric tetrahedral structure. This process will interconvert the two enantiomeric configurations of the complexes if X = Y (complexes **4** and **5**, if monomeric), but not if X ≠ Y (complexes **3**).

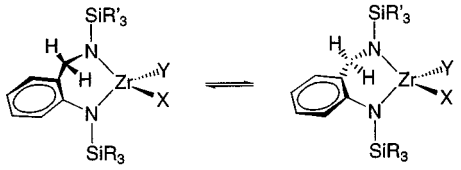

Scheme 4

Figure 3 illustrates the coalescence of the broad AB quadruplet observed at 205 K for the benzylic protons of **4a** in [D_8]toluene (δ = 4.51/4.25, ^2J = 15.4 Hz) into the singlet already mentioned above. However, the two NMe_2 ligands give rise to a lone singlet over the whole temperature range, although up to four singlets may be expected in the limiting spectrum of this complex. Compound **4b** behaves similarly, revealing a doublet of doublets at δ = 4.30/4.08 at 185 K (CD_2Cl_2, ^2J = 15.1 Hz) that coalesce into a singlet at 202 K. Moreover, two distinct NMe_2 signals are observed, in this case, at 185 K (δ = 2.73 and 1.99), as well as two resonances at δ = 7.63 and 7.55 assigned to the *ortho*-protons of the $SiMePh_2$ substituent of the anilinic nitrogen atom, and these two pairs coalesce at 211 K and 194 K, respectively. This is in agreement with the proposed monomeric structure of this molecule and the fluxionality represented on Scheme 4. Compound **4g** affords less clear-cut observations because the limiting spectrum is not reached, even at 180 K in CD_2Cl_2. However, two broad $SiMePh_2$ resonances are distinguished again at δ = 7.60 and 7.49, that coalesce at 183 K. The activation energies determined[5] for these three complexes are reported in Table 3. Clearly, they depend on both the electronic and steric properties of the trialkylsilyl substituents of the two ABA nitrogen atoms, and on the strength of the Zr−aryl interaction discussed above for **5c** and **6c**.

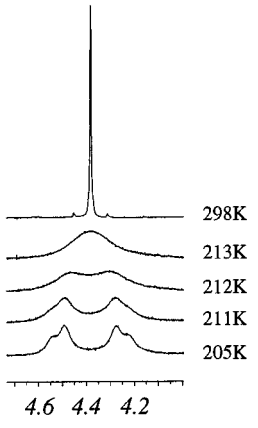

Figure 3. Variable-temperature ^{1}H NMR spectra of complex **4a** in the benzylic region ([D_8]toluene, 300 MHz)

Spirocyclic complexes of type **3** contain two ABA ligands and may therefore exist as three isomers differing in the respective configuration of these ligands. One of the isomers

Table 3. Activation energy for the ABA rocking process in complexes **4**

	4a ([D$_8$]toluene)	**4b** (CD_2Cl_2)	**4g** (CD_2Cl_2)
$\Delta G^{\neq}$ [kJ mol^{-1}]	42.4 (± 0.2)	40.3 (± 0.4)	37.5 (± 0.4)

would be nonsymmetric and the others ideally C_2-symmetric, so that the resonances of up to four nonequivalent ligands may be expected in the ^{1}H NMR limiting spectrum of each of the compounds. In full agreement with this assumption, complex **3g** at 185 K in CD_2Cl_2 exhibits four $SiMe_3$ singlets (δ = 0.06, −0.01, −0.09 and −0.20) and four Si*Me*Ph$_2$ singlets (δ = 1.03, 0.64, 0.46 and 0.22) of unequal intensity (Figure 4). The three isomers are therefore present in comparable amounts. The other regions of the spectrum are less well resolved but follow the same trend. On raising the temperature, all sets of resonances coalesce to yield the simple spectrum observed at room temperature. The complexity of the spectral changes makes the determination of the corresponding activation energies unsafe. Notwithstanding, these appear to be close to the values obtained for compounds **4** and it seems reasonable to conclude that the interconversion of the three stereoisomers occurs by the ligand rocking process of Scheme 4.

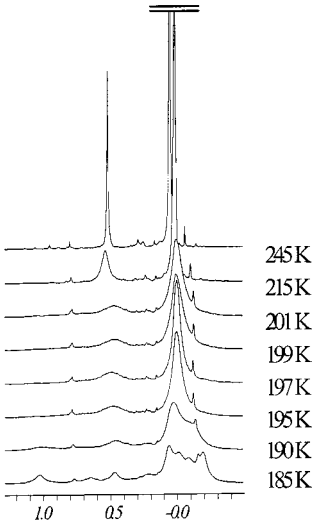

Figure 4. Variable-temperature ^{1}H NMR spectra of complex **3g** in the Si−Me region (CD_2Cl_2, 300 MHz)

Complex **3a** has been described as a single isomer in the solid state as well as in solution.[3] However, its ^{1}H NMR spectrum at 185 K in CD_2Cl_2 shows two broad singlets at δ = 0.42 and 0.07 for the $SiMe_3$ substituent of the anilinic nitrogen atom. The relative intensities of these signals, that coalesce at 195 K ($\Delta G^{\neq}$ = 38.2 ± 0.4 kJ mol^{-1}), are in the approximate ratio 3:1. Despite the fact that an analogous observation was not made for the benzylamido $SiMe_3$ substituent, nor for the benzylic protons (whose signals overlap at 185 K), this indicates that at least two of the three possible stereoisomers are present in solution, and that they interconvert at a rate which is close to that of **3g**.

The dichloride complexes **5** may remain dimeric in solution, as are **5a** and **5c** in the solid state, or they may dissociate into tetrahedral monomers. An ^{1}H NMR spectroscopic analysis of [D$_8$]toluene solutions of 5**a** and **5g** clearly favors the former, since very complicated spectra were obtained at 200 K (Figure 5). These coalesce again at a higher temperature. As for compounds **3**, the existence of the three stereoisomers expected for these dimers, and their interconversion by the ABA rocking process, are thus indicated. However, chemical exchange between the monomeric constituents of the dimers is also implied in this case, resulting in the singlet observed above 275 K for the benzylic protons, instead of the AB spin system shown by compounds **3**. The monomeric form could even be present in substantial amounts and be the origin of some of the resonances detected at 200 K. As illustrated in Figure 5, the coalescence phenomenon indeed seems to occur in two or three successive steps with slightly different rates.

On the other hand, the spectrum of **5a** in CD_2Cl_2 at 180 K is simpler and reveals only one doublet of doublets for the benzylic protons (δ = 5.42/4.33, ^2J = 16.2 Hz), that coalesces into a singlet on raising the temperature. This is analogous to the behavior of the bis(dimethylamido) derivatives **4** and may indicate the monomeric nature of **5a** in this solvent. However, it may also result from faster intermolecular exchange between the monomeric units of dimeric species, both assumptions are consistent with the more polar nature of dichloromethane with respect to toluene. From the temperature of coalescence (213 K), the activation energy of the ABA rocking motion that corresponds to this observation was calculated to be $\Delta G^{\neq}$ = 39.9 ± 0.4 kJ mol^{-1}, which is close to the values obtained for **3a** and **4a**, but markedly higher than that of the analogous titanium complex Ti[(SiMe$_3$)$_2$-ABA]Cl$_2$, for which the signal for the benzylic protons remains as a singlet at 183 K.[3] This latter observation may be correlated with the absence of any M−C$_{ipso}$ contact in the titanium complex. The importance of such interactions on the activation energies is further emphasized by the substantially higher value ($\Delta G^{\neq}$ = 51 kJ mol^{-1}) reported for a similar process involving compound [*o*-C$_6$H$_4$(NSi*i*Pr$_3$)$_2$Zr(O*t*Bu)$_2$], in which the Zr−aryl interaction in the 5-membered chelate ring is on the contrary stronger.[8]

Ethylene Polymerization

In the presence of MAO as cocatalyst, the dichloride complexes of type **5** polymerize ethylene at both room temperature and pressure, but remain inactive against α-olefins such as propylene and 1-hexene. As appears from Table 4, the ethylene polymerization activity of all compounds is low[1] and of a short life time. It is considerably inhibited at 0 °C for **5g**, but only slightly affected at 50 °C for **5a**. The resulting polyethylenes, which were separated by conventional methods, are linear (by ^{1}H NMR spectroscopy) and show a very broad molecular mass distribution, characteristic of multisite catalysts. Activation of the catalytic precursors with MAO thus appears more complicated than envisaged.[9] The molecular masses obtained with **5a** are high,

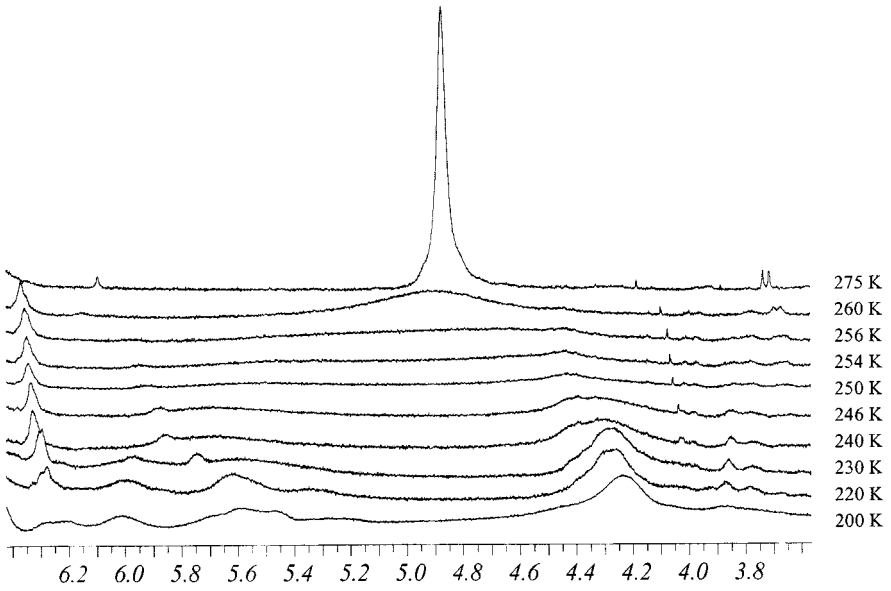

Figure 5. Variable-temperature ^{1}H NMR spectra of complex **5g** in the benzylic region ([D_8]toluene, 300 MHz)

Table 4. Ethylene polymerization results

Entry[a]	Cat. [μmol]	T [°C]	$p(C_2H_4)$ [bar]	t [h]	Yield [mg]	Activity [kg/mol bar h]	$10^{-3}M_w$[b] [g/mol]	$10^{-3}M_n$ [b] [g/mol]	M_w/M_n
1	**5a** (23.4)	25	6	3	1200	2.8	820	28.5	28.8
2	**5a** (2.34)	25	6	0.5	47	6.7			
3	**5a** (11.7)	50	6	0.25	132	7.5	insoluble		
4	**5c** (9.8)	25	1	0.17	21	13			
5	**5g** (18.1)	25	1	1	90	5.0	153	5.6	27.2
6	**5g** (18.1)	0	1	1	6	0.3			

[a] The reactions were run in toluene (10 mL) under constant ethylene pressure, using 1000 equiv. of MAO as cocatalyst (except for Entry 4: 500 equiv.). − [b] By SEC (140 °C, 1,2,4-trichlorobenzene) vs. polystyrene standards.

whereas **5g** leads to much lower values. If this difference does not result from the difference in ethylene pressure between experiments 1 and 5, it would indicate a ligand effect showing that ABA-based ligands remain bound to the zirconium centre in the catalytically active species. These catalytic systems were not further optimized.

Conclusion

We have shown that various trialkylsilyl substituents can be linked to the two nitrogen atoms of 2-aminobenzylamine, and that the chelating diamido ligands derived from these diamines can serve to stabilize a series of zirconium complexes and to modulate their properties. Structural investigations have shown that the chloride compounds form dimers, and that zirconium−aryl interactions are probably responsible for the restrained flexibility of the ligands. As expected from their low coordination numbers and high electron deficiency, these complexes catalyse the polymerization of ethylene, but unfortunately the activities remain low in all cases.

Experimental Section

General Procedures: All experiments were performed in a high-vacuum line using standard Schlenk techniques or in a dry box under N_2. Solvents were dried with Na/benzophenone ketyl (pentane, toluene, hexane, THF, ether) or P_2O_5 (dichloromethane) and distilled prior to use under nitrogen. Deuterated solvents were dried with activated 4-Å molecular sieves. Known compounds that were not commercial were prepared according to literature procedures. Methylaluminoxane (MAO) was purchased as a 10% toluene solution from Schering or Aldrich. − NMR spectra were recorded with a Bruker AC-300, AC-250 or SY-200 spectrometer at ambient probe temperature unless otherwise indicated. ^{1}H and ^{13}C chemical shifts are reported in ppm versus $SiMe_4$ and were determined by reference to the residual solvent peaks. − Elemental analyses were performed by the Service Central d'Analyse du CNRS (Vernaison), the Service Commun de Microanalyse de l'ULP (Strasbourg), or the Service d'Analyse du LCC (Toulouse). − Infrared spectra were recorded with a Perkin−Elmer 1600 FT-IR spectrometer in the 4000−200 cm^{-1} range using KBr or CsI disks. − Size Exclusion Chromatography (SEC) analyses were carried out at BP−Grangemouth with a AT7 GPC Waters 150-CV instrument in 1,2,4-trichlorobenzene at 140 °C relative to polystyrene standards. − Activation energies were calculated using the Eyring equation.[5]

[(SiMe$_3$)$_2$-ABA]H$_2$ (1a): The synthesis of this compound has been reported in the literature.[3] In an alternative method, 13.8 mL of triethylamine (99.0 mmol) was added to a vigorously stirred solution of 2-aminobenzylamine (3 g, 24.6 mmol) in 130 mL of diethyl ether at 0 °C, and 6.90 mL of chlorotrimethylsilane (54.4 mmol) was then added dropwise. The reaction mixture containing a voluminous white precipitate was stirred for 48 h at room temperature and filtered, and the filtrate was concentrated to dryness. Extraction of the residue with 20 mL of pentane and removal of the volatiles in vacuo yielded the product as a yellow oil which could be used without further purification. Short-path distillation under high vacuum, however, led to an analytically pure colorless oil (6.281 g, 96%). − ^{1}H NMR (C$_6$D$_6$, 300 MHz): δ = 7.17 (dt, 1 H, H^4 or H^5), 7.02, 6.92 (dd, 1 H, H^3 and H^6), 6.76 (dt, 1 H, H^4 or H^5), 5.30 (s, broad, 1 H, ArN*H*), 3.73 (d, ^3J = 6.8 Hz, 2 H, CH$_2$), 0.27 (s, 9 H, ArNHSi*Me*$_3$), 0.12 (t, broad, 1 H, CH$_2$N*H*), 0.00 (s, 9 H, CH$_2$NHSi*Me*$_3$). − ^{13}C NMR (C$_6$D$_6$, 75 MHz): δ = 147.83 (C^2), 129.98, 128.52, 117.66, 116.43 (C^3−C^6), 45.95 (CH$_2$), 0.43 (SiMe$_3$), −0.44 (SiMe$_3$). The C^1 signal could not be detected. − IR (neat): $\tilde{\nu}$ = 3342 (sh) and 3298 cm^{-1}, (ν_{N-H}). − C$_{13}$H$_{26}$N$_2$Si$_2$ (266.5): calcd. C 58.58, H 9.83, N 10.51; found C 58.24, H 9.68, N 10.37.

[(SiMePh$_2$)$_2$-ABA]H$_2$ (1b): 10.2 mL of a 1.6 M solution of *n*BuLi in hexane (16.4 mmol) was slowly added whilst stirring at −78 °C to a solution of 2-aminobenzylamine (1 g, 8.2 mmol) in 60 mL of diethyl ether. The yellow solution was allowed to warm to room temperature, stirred for 3 h, and cooled again to −20 °C; 3.81 g of chloro(methyl)diphenylsilane (16.4 mmol) in 20 mL of diethyl ether was then added dropwise. After stirring overnight at room temperature, the brown reaction mixture was centrifuged and the resulting orange solution was concentrated to dryness to yield 3.629 g of a yellow oil (86%) which can be recrystallized from cold pentane. − ^{1}H NMR (C$_6$D$_6$, 300 MHz): δ = 7.72 (m, 4 H, H$_o$ ArNHSiMe*Ph*$_2$), 7.43 (m, 4 H, H$_o$ CH$_2$NHSiMe*Ph*$_2$), 7.18 (m, 12 H, H$_m$ + H$_p$ SiMe*Ph*$_2$), 6.92 (m, 3 H, Ar), 6.64 (m, 1 H, Ar), 5.70 (s, broad, 1 H, ArN*H*), 3.88 (d, ^3J = 6.4 Hz, 2 H, CH$_2$), 0.80 (t, broad, 1 H, CH$_2$N*H*), 0.78 (s, 3 H, ArNHSi*Me*Ph$_2$), 0.37 (s, 3 H, CH$_2$NHSi*Me*Ph$_2$). − ^{13}C NMR (C$_6$D$_6$, 75 MHz): δ = 146.67 (C^2), 137.10, 136.86 (C$_{ipso}$ SiMe*Ph*$_2$), 135.03, 134.88 (C$_{o/m}$ SiMe*Ph*$_2$), 130.13 (Ar), 130.08, 129.74 (C$_p$ SiMe*Ph*$_2$), 128.56 (Ar), 128.43, 128.18 (C$_{o/m}$ SiMe*Ph*$_2$), 118.31, 117.52 (Ar), 46.12 (CH$_2$), −2.22 (ArNHSi*Me*Ph$_2$), −3.39 (CH$_2$NHSi*Me*Ph$_2$). The C^1 signal could not be detected. − IR (nujol mull): $\tilde{\nu}$ = 3336 and 3256 cm^{-1}, (ν_{N-H}). − C$_{33}$H$_{34}$N$_2$Si$_2$ (514.8): calcd. C 76.99, H 6.66; found C 76.34, H 6.37.

[(SiMe$_2$*t*Bu)$_2$-ABA]H$_2$ (1c): This compound was prepared in THF according to the procedure described for **1b**. After removal of the volatiles under vacuum, the reaction residue was extracted with pentane. Concentration to dryness gave the product as a cream solid which was used without further purification (85% yield). − ^{1}H NMR (C$_6$D$_6$, 250 MHz): δ = 7.15 (t, 1 H, H^4 or H^5), 7.02, 6.98 (d, 1 H, H^3 and H^6), 6.79 (t, 1 H, H^4 or H^5), 5.21 (s, broad, 1 H, ArN*H*), 3.84 (d, 2 H, CH$_2$), 1.03 (s, 9 H, *t*Bu), 0.85 (s, 9 H, *t*Bu), 0.29 (s, 6 H, ArNHSi*Me*$_2$*t*Bu), 0.01 (s, 6 H, CH$_2$NHSi*Me*$_2$*t*Bu). The CH$_2$N*H* signal was not detected, but was found at δ = 1.44 in [D$_8$]THF. − C$_{19}$H$_{38}$N$_2$Si$_2$ (322.6): calcd. C 65.07, H 10.92, N 7.99; found C 64.9, H 10.8, N 7.9.

[(Si*i*Pr$_3$)$_2$-ABA]H$_2$ (1d): This compound was prepared in THF according to the procedure described for **1b**. The chlorotriisopropylsilane was added at room temperature, and the solution was refluxed for 18 h. After concentration to dryness, the product was extracted as a brown oil with pentane (82% yield). − ^{1}H NMR (C$_6$D$_6$, 300 MHz): δ = 7.18 (dd, 1 H, H^3 or H^6), 7.12 (dt, 1 H, H^4 or H^5), 6.89 (dd, 1 H, H^3 or H^6), 6.77 (dt, 1 H, H^4 or H^5), 4.44 (s, broad, 1 H, ArN*H*), 3.92 (d, ^3J = 6.1 Hz, 2 H, CH$_2$), 1.15 (m, 42 H, Si*iPr*$_3$), 0.35 (t, broad, 1 H, CH$_2$N*H*). − ^{13}C NMR (C$_6$D$_6$, 75 MHz): δ = 147.04 (C^2), 129.47 (C^1), 129.58, 128.38, 118.10, 116.88 (C^3−C^6), 46.02 (CH$_2$), 18.72 (SiCH*Me*$_2$), 11.99 (SiC*H*Me$_2$), 11.64 (SiC*H*Me$_2$). − IR (neat): $\tilde{\nu}$ = 3361 (sh) and 3331 cm^{-1}, (ν_{N-H}). − C$_{25}$H$_{50}$N$_2$Si$_2$ (434.9): calcd. C 69.05, H 11.59, N 6.44; found C 68.66, H 11.47, N 6.35.

[(SiMe$_3$)(H)-ABA]H$_2$ (1e): To a solution of 250 mg of 2-aminobenzylamine (2.05 mmol) in 25 mL of diethyl ether at −80 °C, 1.3 mL of a 1.6 M solution of *n*BuLi in hexane (2.05 mmol) was added. A white precipitate built up rapidly. After 2 h at room temperature, the reaction mixture was cooled to −80 °C and 0.26 mL of chorotrimethylsilane (2.05 mmol) was added. The temperature was left to reach room temperature. After 12 h, filtration through Celite and concentration to dryness yielded an orange oil containing 93% of **1e** (by ^{1}H NMR). − ^{1}H NMR (C$_6$D$_6$, 300 MHz): δ = 7.17 (dt, 1 H, H^4 or H^5), 6.92 (m, 2 H, H^3 and H^6), 6.75 (dt, 1 H, H^4 or H^5), 6.10 (s, broad, 1 H, ArN*H*), 3.51 (t, ^3J = 5.8 Hz, 2 H, CH$_2$), 0.45 (t, broad, 1 H, CH$_2$N*H*$_2$), 0.28 (s, 9 H, ArNHSi*Me*$_3$).

[(SiMePh$_2$)(H)-ABA]H$_2$ (1f): This compound was prepared as a yellow viscous oil according to the procedure described for **1e** (95% yield). − ^{1}H NMR (C$_6$D$_6$, 300 MHz): δ = 7.76 (m, 4 H, H$_o$ SiMe*Ph*$_2$), 7.19 (m, 6 H, H$_m$ + H$_p$ SiMe*Ph*$_2$), 6.89 (m, 3 H, Ar), 6.83 (s, broad, 1 H, ArN*H*), 6.65 (m, 1 H, Ar), 3.53 (t, ^3J = 5.8 Hz, 2 H, CH$_2$), 0.80 (s, 3 H, ArNHSi*Me*Ph$_2$), 0.45 (t, broad, 2 H, CH$_2$N*H*$_2$). − ^{13}C NMR (C$_6$D$_6$, 75 MHz): δ = 147.97 (C^2), 137.39 (C$_{ipso}$ SiMe*Ph*$_2$), 134.96 (C$_{o/m}$ SiMe*Ph*$_2$), 129.93 (C$_p$ SiMe*Ph*$_2$), 129.82, 128.57 (Ar), 128.38 (C$_{o/m}$ SiMe*Ph*$_2$), 118.01, 117.82 (Ar), 46.73 (CH$_2$), −2.22 (ArNHSi*Me*Ph$_2$). The C^1 signal could not be detected. − C$_{20}$H$_{22}$N$_2$Si$_2$ (346.6): calcd. C 75.42, H 6.96; found C 75.77, H 7.07.

[(SiMePh$_2$)(SiMe$_3$)-ABA]H$_2$ (1g): 2.480 g of **1f** (7.8 mmol) was dissolved in 30 mL of diethyl ether at 0 °C; 1.26 mL of triethylamine (9 mmol) and 1.04 mL of chlorotrimethylsilane (9 mmol) were added successively, and the reaction mixture was left to reach room temperature. After 3 h, the white precipitate of triethylammonium chloride was filtered and the resulting solution was concentrated to dryness to yield 2.640 g of a pale yellow oil (87%). This can be used without further purification. − ^{1}H NMR (C$_6$D$_6$, 300 MHz): δ = 7.72 (m, 4 H, H$_o$ SiMe*Ph*$_2$), 7.19 (m, 6 H, H$_m$ + H$_p$ SiMe*Ph*$_2$), 7.00 (dd, 1 H, H^3 or H^6), 6.91 (m, 2 H, H^4 or H^5 and H^3 or H^6), 6.69 (dt, 1 H, H^4 or H^5), 5.98 (s, broad, 1 H, ArN*H*), 3.79 (d, ^3J = 6.6 Hz, 2 H, CH$_2$), 0.78 (s, 3 H, ArNHSi*Me*Ph$_2$), 0.18 (t, broad, 1 H, CH$_2$N*H*), −0.12 (s, 9 H, CH$_2$NHSi*Me*$_3$). − ^{13}C NMR (C$_6$D$_6$, 75 MHz): δ = 147.45 (C^2), 137.00, (C$_{ipso}$ SiMe*Ph*$_2$), 135.00, (C$_{o/m}$ SiMe*Ph*$_2$), 130.04 (C$_p$ SiMe*Ph*$_2$), 129.89, 128.52 (Ar), 128.39 (C$_{o/m}$ SiMe*Ph*$_2$), 118.14, 117.53 (Ar), 46.21 (CH$_2$), −0.73 (CH$_2$NHSi*Me*$_3$), −2.47 (ArNHSi*Me*Ph$_2$). The C^1 signal could not be detected. − IR (neat): $\tilde{\nu}$ = 3372 (sh) and 3264 cm^{-1}, (ν_{N-H}).

[(SiMe$_3$)$_2$-ABA]Li$_2$ (2a): To a solution of 1.7 g of **1a** (6.38 mmol) in 50 mL of pentane at −70 °C, 8.4 mL of a 1.6 M solution of *n*BuLi in hexane (13.4 mmol) was slowly added. After leaving overnight at room temperature, the yellow solution was concentrated to ca. 15 mL and placed at −20 °C. Large crystals could be separated after one night, and a second crop was obtained on concentrating further (1.025 g, 58%). − ^{1}H NMR (C$_6$D$_6$, 300 MHz): δ = 6.94 (dt, 1 H, H^4 or H^5), 6.84 (dd, 1 H, H^3 or H^6), 6.58 (dt, 1 H, H^4 or H^5), 6.27 (d, 1 H, H^3 or H^6), 4.39 (d, ^2J = 10.3 Hz, 1 H, C*H*H′), 3.68 (d, ^2J = 10.3 Hz, 1 H, CH*H*′), 0.22 (s, 9 H, ArNSi*Me*$_3$), 0.05 (s, 9 H, CH$_2$NSi*Me*$_3$). On heating to 330 K, the two doublets at

δ = 4.39 and 3.68 coalesce into a broad singlet at δ = 3.96 (2 H); T_c = 314 K. − ^{13}C NMR (C_6D_6, 75 MHz): δ = 157.26 (C^2), 136.53 (C^1), 131.60, 129.62, 125.83, 119.11 (C^3−C^6), 48.78 (CH_2), 2.96 ($SiMe_3$), 0.60 ($SiMe_3$). − IR (nujol mull): No absorptions above 3000 cm^{-1}.

[(SiMePh$_2$)$_2$-ABA]Li$_2$ (2b): This compound was prepared from **1b** according to the procedure described for **2a**. After 48 h of stirring at room temperature, the product was directly filtered as a white powder that was dried in vacuo (34% yield). − ^{1}H NMR (C_6D_6, 300 MHz): δ = 7.46 (m, broad, 20 H, SiMe*Ph*$_2$), 6.70 (m, 2 H, Ar), 6.67, 6.17 (m, 1 H, Ar), 4.02 (s, broad, 2 H, CH_2), 0.40 (s, 3 H, ArNSi*Me*Ph$_2$), 0.13 (s, 3 H, CH_2NSi*Me*Ph$_2$). − IR (nujol mull): No absorptions above 3000 cm^{-1}.

[(SiMe$_2$*t*Bu)$_2$-ABA]Li$_2$ (2c): This compound was prepared from **1c** according to the procedure described for **2a**. After 24 h of stirring at room temperature, the product was obtained as a thick brown oil after concentration to dryness, that eventually solidified as an off-white solid (80% yield). − ^{1}H NMR (C_6D_6, 200 MHz): δ = 7.20 (s, 1 H, H^4 or H^5), 7.05 (m, 2 H, H^3 and H^6), 6.56 (t, 1 H, H^4 or H^5), 4.37 (s, 2 H, CH_2), 1.16 (s, 9 H, *t*Bu), 1.15 (s, 9 H, *t*Bu), 0.33 (s, 6 H, ArNSi*Me*$_2$*t*Bu), 0.19 (s, 6 H, CH_2NSi*Me*$_2$*t*Bu).

[(Si*i*Pr$_3$)$_2$-ABA]Li$_2$ (2d): This compound was prepared as a viscous brown oil from **1d** according to the procedure described for **2c** (95% yield). − ^{1}H NMR (C_6D_6, 300 MHz): δ = 7.10 (m, 2 H, Ar), 6.97 (d, 1 H, H^3 or H^6), 6.70 (t, 1 H, H^4 or H^5), 4.23 (s, broad, 2 H, CH_2), 1.15 (m, 42 H, Si-*i*Pr$_3$).

[(SiMePh$_2$)(SiMe$_3$)-ABA]Li$_2$ (2g): This compound was obtained as a white powder from **1g** according to the procedure described for **2b** (45% yield). − ^{1}H NMR (C_6D_6, 300 MHz, 286 K): δ = 7.69 (d, 2 H, H_o SiMe*Ph*Ph′), 7.48 (d, 2 H, H_o SiMePh*Ph*′), 7.23 (m, 6 H, H_m + H_p SiMe*Ph*$_2$), 6.77 (dt, 1 H, H^4 or H^5), 6.60 (dd, 1 H, H^3 or H^6), 6.50 (dt, 1 H, H^4 or H^5), 6.12 (d, 1 H, H^3 or H^6), 4.56 (d, ^2J = 11.9 Hz, 1 H, C*H*H′), 3.60 (d, ^2J = 11.9 Hz, 1 H, CH*H*′), 0.48 (s, 3 H, ArNSi*Me*Ph$_2$), 0.01 (s, 9 H, CH_2NSi*Me*$_3$). − IR (nujol mull): No absorptions above 3000 cm^{-1}.

Zr[(SiMe$_2$*t*Bu)$_2$-ABA]$_2$ (3c): This compound was obtained from **2c** according to the procedure described for **3g** (52% yield). − ^{1}H NMR (C_6D_6, 200 MHz): δ = 7.16−7.00 (m, 6 H, Ar), 6.88 (d, 2 H, H^3 or H^6), 4.80 (s, broad, 2 H, C*H*H′), 4.05 (s, broad, 2 H, CH*H*′), 1.08 (s, 18 H, *t*Bu), 0.82 (s, 18 H, *t*Bu), 0.44 (s, 12 H, ArNSi*Me*$_2$*t*Bu), 0.15 (s, 12 H, CH_2NSi*Me*$_2$*t*Bu).

Zr[(SiMePh$_2$)(SiMe$_3$)-ABA]$_2$ (3g): A mixture of 25 mg of $ZrCl_4$ (0.11 mmol) and 86 mg of **2g** (0.22 mmol) in 15 mL of toluene was stirred at 80 °C for 48 h. After cooling to room temperature, the mixture was centrifuged and the clear yellow solution was concentrated to dryness to yield 71 mg of a yellow solid (76%). − ^{1}H NMR (CD_2Cl_2, 300 MHz): δ = 7.25 (m, 22 H, SiMe*Ph*$_2$ + Ar), 6.99 (m, 4 H, Ar), 6.55 (m, 2 H, Ar), 4.89 (d, ^2J = 13.4 Hz, 2 H, C*H*H′), 3.93 (d, ^2J = 13.4 Hz, 2 H, CH*H*′), 0.53 (s, 6 H, ArNSi*Me*Ph$_2$), 0.09 (s, 18 H, CH_2NSi*Me*$_3$).

Zr[(SiMe$_3$)$_2$-ABA](NMe$_2$)$_2$ (4a): To a solution of 497 mg of $Zr(NMe_2)_4$ (1.86 mmol) in 25 mL of pentane at −70 °C, a solution of 497 mg of **1a** (1.86 mmol) in 10 mL of pentane was added. After room temperature had been reached, the reaction mixture was stirred for one night. After evaporation of all volatiles under primary, and then secondary vacuum, 798 mg of a pale yellow oil (96%) was obtained. − ^{1}H NMR (C_6D_6, 300 MHz): δ = 7.14 (m, 2 H, Ar), 6.99 (d, 1 H, H^3 or H^6), 6.79 (dt, 2 H, H^4 or H^5), 4.42 (s, 2 H, CH_2), 2.84 (s, 12 H, NMe_2), 0.32 (s, 9 H, ArNSi*Me*$_3$), 0.13 (s, 9 H, CH_2NSi*Me*$_3$). − ^{13}C NMR (C_6D_6, 75 MHz): δ = 151.23 (C^2), 137.8 (C^1), 129.10, 128.23, 123.53, 120.38 (C^3−C^6), 49.71 (CH_2), 41.92 (NMe_2), 1.43 ($SiMe_3$), 0.95 ($SiMe_3$).

Zr[(SiMePh$_2$)$_2$-ABA](NMe$_2$)$_2$ (4b): This compound was prepared from **1b** according to the procedure described for **4a**. It consists of a very viscous orange oil (96% yield). − ^{1}H NMR (C_6D_6, 300 MHz): δ = 7.70 (m, 4 H, H_o SiMe*Ph*$_2$), 7.62 (m, 4 H, H_o SiMe*Ph*$_2$), 7.20 (m, 12 H, H_m + H_p SiMe*Ph*$_2$), 7.08, 6.97 (d, 1 H, H^3 and H^6), 6.95, (t, 1 H, H^4 or H^5), 6.70 (t, 1 H, H^4 or H^5), 4.61 (s, 2 H, CH_2), 2.45 (s, 12 H, NMe_2), 0.74 (s, 3 H, Si*Me*Ph$_2$), 0.65 (s, 3 H, Si*Me*Ph$_2$). − ^{13}C NMR (CD_2Cl_2, 75 MHz): δ = 151.56 (C^2), 139.13, 137.16, 136.67 (C^2 and C_{ipso} SiMe*Ph*$_2$), 135.77, 135.13 (C_o SiMe*Ph*$_2$), 130.30, 129.46 (C_p SiMe*Ph*$_2$), 128.96 (Ar), 128.20, 128.04 (C_m SiMe*Ph*$_2$), 127.79, 124.01, 119.88 (Ar), 50.42 (CH_2), 41.60 (NMe_2), −1.12 (Si*Me*Ph$_2$), −1.61 (Si*Me*Ph$_2$). The C^1 signal could not be detected.

Zr[(SiMe$_2$*t*Bu)$_2$-ABA](NMe$_2$)$_2$ (4c): This compound was prepared from **1c** according to the procedure described for **4a**, along with 5 d of stirring at room temperature in pentane, or 4 h in refluxing toluene. The product was further purified by extraction with pentane (orange oil, 99% yield). − ^{1}H NMR (C_6D_6, 250 MHz): δ = 7.20−7.09 (m, 3 H, Ar), 6.82 (t, 1 H, H^4 or H^5), 4.60 (s, broad, 2 H, CH_2), 2.80 (s, 12 H, NMe_2), 1.04 (s, 9 H, *t*Bu), 1.03 (s, 9 H, *t*Bu), 0.29 (s, 6 H, ArNSi*Me*$_2$*t*Bu), 0.16 (s, 6 H, CH_2NSi*Me*$_2$*t*Bu). − $C_{23}H_{48}N_4Si_2Zr$ (436.8): calcd. C 52.32, H 9.16, N 10.61; found C 52.29, H 9.77, N 10.73.

Zr[(SiMePh$_2$)(SiMe$_3$)-ABA](NMe$_2$)$_2$ (4g): This compound was prepared from **1g** according to the procedure described for **4a**. It consists of a yellow oil (98% yield). − ^{1}H NMR (C_6D_6, 300 MHz): δ = 7.65 (m, 4 H, H_o SiMe*Ph*$_2$), 7.14 (m, 7 H, H_m + H_p SiMe*Ph*$_2$ and H^3 or H^6), 7.06 (d, 1 H, H^3 or H^6), 6.89, 6.73 (dt, 1 H, H^4 and H^5), 4.52 (s, 2 H, CH_2), 2.63 (s, 12 H, NMe_2), 0.79 (s, 3 H, ArNSi*Me*Ph$_2$), 0.14 (s, 9 H, CH_2NSi*Me*$_3$). − ^{13}C NMR (C_6D_6, 75 MHz): δ = 152.18 (C^2), 136.96 (C_{ipso} SiMe*Ph*$_2$), 136.10, 135.96 (C^1 and C_o SiMe*Ph*$_2$), 130.27 (C_p SiMe*Ph*$_2$), 128.61 (Ar), 128.14 (C_m SiMe*Ph*$_2$), 127.85, 122.90, 119.74 (Ar), 49.14 (CH_2), 41.88 (NMe_2), 1.22 (CH_2NSi*Me*$_3$), −1.21 (ArNSi*Me*Ph$_2$). − ^{13}C NMR (CD_2Cl_2, 75 MHz): δ = 152.80 (C^2), 136.59, 136.38 (C^1 and C_{ipso} SiMe*Ph*$_2$), 135.91 (C_o SiMe*Ph*$_2$), 130.48 (C_p SiMe*Ph*$_2$), 128.32 (Ar), 128.25 (C_m SiMe*Ph*$_2$), 127.30, 122.23, 119.98 (Ar), 48.67 (CH_2), 41.95 (NMe_2), 1.04 (CH_2NSi*Me*$_3$), −1.36 (ArNSi*Me*Ph$_2$).

Zr[(SiMe$_3$)$_2$-ABA]Cl$_2$ (5a): To a solution of 830 mg of **4a** (1.9 mmol) in 40 mL of pentane at −50 °C, 2.4 mL of chlorotrimethylsilane (19 mmol) was added. After room temperature had been reached, the reaction mixture was vigorously stirred overnight. After filtration, washing of the precipitate with cold pentane (20 mL) and drying in vacuo, one obtained 622 mg of a pale yellow solid (78%). − ^{1}H NMR (C_6D_6, 300 MHz): δ = 7.00 (m, 2 H, Ar), 6.77 (m, 2 H, Ar), 4.72 (s, 2 H, CH_2), 0.43 (s, 9 H, ArNSi*Me*$_3$), 0.15 (s, 9 H, CH_2NSi*Me*$_3$). − ^{13}C NMR (C_6D_6, 75 MHz): δ = 149.81 (C^2), 132.22 (C^1), 128.72, 128.72, 122.47, 120.24 (C^3−C^6), 49.50 (CH_2), 0.56 ($SiMe_3$), 0.45 ($SiMe_3$). − IR (nujol mull): $\tilde{\nu}$ = 313 (f), 289 (m) and 254 (F, broad) cm^{-1}, (ν_{Zr-Cl}).

Zr[(SiMe$_2$*t*Bu)$_2$-ABA]Cl$_2$ (5c): This compound was prepared from **4c** according to the procedure described for **5a** and a slightly different workup. The reaction mixture was first concentrated to dryness and the solid residue extracted with small amounts of toluene. Removal of toluene and other volatiles under vacuum afforded a solid that was washed again with 2×1 mL of cold pentane and dried under vacuum (55% yield). − ^{1}H NMR (C_6D_6, 250 MHz): δ = 7.20 (m, 2 H, Ar), 7.00−6.96 (m, 2 H, Ar), 4.59 (s, 2 H, CH_2), 1.02

(s, 9 H, *t*Bu), 0.95 (s, 9 H, *t*Bu), 0.40 (s, 6 H, ArNSi*Me*$_2$*t*Bu), 0.31 (s, 6 H, CH_2NSiMe_2tBu). – $C_{19}H_{36}Cl_2N_2Si_2Zr$ (475.4): calcd. C 44.68, H 7.10, N 5.48; found C 44.45, H 6.71, N 5.24.

Zr[(SiMePh$_2$)(SiMe$_3$)-ABA]Cl$_2$ (5g): This compound was prepared from **4g** according to the procedure described for **5a**. It consists of a pale yellow solid (81% yield). – ^{1}H NMR (C_6D_6, 300 MHz): δ = 7.79 (m, 4 H, H$_o$ SiMe*Ph*$_2$), 7.15 (m, 6 H, H$_m$ + H$_p$ SiMe*Ph*$_2$), 6.93 (d, 2 H, H^3 and H^6), 6.75, 6.67 (dt, 1 H, H^4 and H^5), 4.87 (s, 2 H, CH_2), 0.92 (s, 3 H, ArNSi*Me*Ph$_2$), 0.19 (s, 9 H, CH_2NSiMe_3). – ^{13}C NMR (C_6D_6, 75 MHz): δ = 151.36 (C^2), 137.21 (C$_o$ SiMe*Ph*$_2$), 132.79 (C$_{ipso}$ SiMe*Ph*$_2$), 131.53 (C$_p$ SiMe*Ph*$_2$), 131.40 (C^1), 129.00 (C$_m$ SiMe*Ph*$_2$), 128.24, 121.87, 120.36 (Ar), 48.60 (CH_2), 0.89 (CH_2NSiMe_3), −1.52 (ArNSi*Me*Ph$_2$). – IR (nujol mull): 339 (m) and 294 (m) cm^{-1}, (ν_{Zr-Cl}).

X-ray Crystallographic Structure Determination and Refinements of 5c and 6c: Data for **5c** (and **6c**) were collected at low temperature (T = 160 K) with a Stoe Imaging Plate Diffraction System (IPDS), equipped with an Oxford Cryosystems Cryostream Cooler Device and using graphite-monochromated Mo-K_α radiation (λ = 0.71073Å). The crystal-to-detector distance was 70 (80) mm, 179 (147) exposures were obtained with 0° < φ < 250° and with the crystal rotated through 1.4° (1.7°) in φ. The final unit cell parameters were obtained by means of a least-squares refinement of a set of 5000 well-measured reflections, and a crystal decay was monitored in the course of data collection by measuring 200 reflections by image. No significant fluctuations of intensities have been observed during measurements. Structures have been solved by direct methods using SIR92,[10] and refined by least-squares procedures on F^2 with the aid of SHELXL97.[11] The atomic scattering factors were taken from International Tables for X-ray Crystallography.[12] All non-hydrogen atoms were anisotropically refined and the last cycles of refinement weighting schemes[12] were applied. All hydrogen atoms were located on a difference Fourier map and refined with a riding model, except the hydrogen atom H(2) connected to the amine group of **6c** which has been isotropically refined. For **5c** a molecule of solvent (toluene) has been located, this molecule seems to be disordered around an inversion center and has been anisotropically refined with restraints on distances and angles. Drawings of molecules are performed with the program ZORTEP[13] with 50% probability displacement ellipsoids for non-hydrogen atoms. Crystallographic data (excluding structure factors) for the structures reported in this paper have been deposited with the Cambridge Crystallographic Data Centre as supplementary publication no. CCDC-155993 (CCDC-155994). Copies of the data can be obtained free of charge on application to CCDC, 12 Union Road, Cambridge CB2 1EZ, UK [Fax: (internat.) + 44-1223/336-033; E-mail: deposit@ccdc.cam.ac.uk]. Main data for **5c** and **6c** are reported in Table 5.

Ethylene Polymerization Procedures: Polymerization experiments were performed in a 50-mL glass reactor equipped with a mechanical stirrer or in standard Schlenk-type glassware with magnetic stirring, whether ethylene pressure was 6 bar or 1 bar, respectively. The catalyst precursor was first introduced into the reactor as a toluene solution of controlled volume and concentration. The MAO solution was added at the desired temperature, before the reactor was pressurized as rapidly as possible with ethylene and the pressure, as well as vigorous stirring, maintained constant during the polymerization time. The polymerization was then quenched by pouring the reaction mixture into a 10% solution of aqueous HCl in methanol. The polymer was collected by filtration, washed several times with methanol and then acetone, dried in vacuo at 80 °C, and weighed. ^{1}H NMR and SEC analyses were carried out at 140 °C in $C_2D_2Cl_4$ or 1,2,4-trichlorobenzene respectively.

Table 5. Crystallographic data for **5c** and **6c**

	5c	**6c**
Empirical formula	$C_{19}H_{36}Cl_2N_2Si_2Zr\cdot(C_7H_8)_{0.5}$	$C_{19}H_{37}Cl_3N_2Si_2Zr$
Formula mass	556.86	547.26
Crystal system	triclinic	triclinic
Space group	$P\bar{1}$	$P\bar{1}$
a [Å]	9.107(2)	8.5483(13)
b [Å]	12.019(2)	11.7137(18)
c [Å]	14.313(3)	14.916(2)
α [°]	69.26(3)	94.373(18)
β [°]	85.54(3)	106.485(17)
γ [°]	77.10(3)	110.619(17)
V [Å^3]	1428.2(5)	1314.4
Z	2	2
$D_{calcd.}$ [g cm^{-3}]	1.295	1.383
μ(Mo-K_α) [mm^{-1}]	0.668	0.822
F(000)	582	568
2θ range [°]	3.3–52.1	2.9–48.4
d(hkl) range [Å]	12.453–0.809	14.228–0.867
Measured reflections	10410	7738
Unique reflections	3818	3581
Parameters/ restraints	309/87	258/0
Final R1	0.0201	0.0306
Final wR2	0.0514	0.0673
Goodness of fit	1.025	0.939

Acknowledgments

We thank the CNRS and the Ministère de l'Education Nationale, de la Recherche et de la Technologie for funding this work, late Prof. J. A. Osborn for his support, Dr. J. R. Blackborow (B. P. Chemicals, Grangemouth, UK) for SEC analysis, and C. Mazet (ULP, Strasbourg) for his assistance.

[1] [1a] G. J. P. Britovsek, V. C. Gibson, D. F. Wass, *Angew. Chem. Int. Ed.* **1999**, *38*, 428–447, and references therein. – [1b] C. H. Lee, Y.-H. La, J. W. Park, *Organometallics* **2000**, *19*, 344–351. – [1c] C. Lorber, B. Donnadieu, R. Choukroun, *Organometallics* **2000**, *19*, 1963–1966. – [1d] L.-C. Liang, R. R. Schrock, W. M. Davis, *Organometallics* **2000**, *19*, 2526–2531. – [1e] R. R. Schrock, A. L. Casado, J. T. Goodman, L.-C. Liang, P. J. Bonitatebus, Jr., W. M. Davis, *Organometallics* **2000**, *19*, 5325–5341.

[2] [2a] F. G. N. Cloke, T. J. Geldbach, P. B. Hitchcock, J. B. Love, *J. Organomet. Chem.* **1996**, *506*, 343–345. – [2b] B. Tsuie, D. C. Swenson, R. F. Jordan, J. L. Petersen, *Organometallics* **1997**, *16*, 1392–1400. – [2c] Y.-M. Jeon, S. J. Park, J. Heo, K. Kim, *Organometallics* **1998**, *17*, 3161–3163. – [2d] T. I. Gountchev, T. Don Tilley, *Organometallics* **1999**, *18*, 2896–2905.

[3] Y.-M. Jeon, J. Heo, W. M. Lee, T. Chang, K. Kim, *Organometallics* **1999**, *18*, 4107–4113.

[4] R. M. Gauvin, N. Kyritsakas, J. Fischer, J. Kress, *Chem. Commun.* **2000**, 965–966.

[5] H. Günther, *La Spectroscopie de RMN*, 5th ed., Masson, Paris, France, **1993**.

[6] [6a] M. F. Lappert, P. P. Power, A. R. Sanger, R. C. Srivastava, *Metal and Metalloid Amides*, Ellis Horwood, Chichester, West Sussex, **1980**. – [6b] G. Chandra, M. F. Lappert, *J. Chem. Soc. A* **1968**, 1940–1945. – [6c] J. D. Scollard, D. H. McConville, J. J. Vittal, *Organometallics* **1995**, *14*, 5478–5480.
[7] The analogous compound reported previously was described as a THF adduct.[3]
[8] K. Aoyagi, P. K. Gantzel, K. Kalai, T. Don Tilley, *Organometallics* **1996**, *15*, 923–927, and references therein.
[9] E. You-Xian Chen, T. J. Marks, *Chem. Rev.* **2000**, *100*, 1391–1434, and references therein.
[10] *SIR92 program for automatic solution of crystal structures by direct methods*: A. Altomare, G. Cascarano, G. Giacovazzo, A. Guagliardi, M. C. Burla, G. Polidori, M. Camalli, *J. Appl. Cryst.* **1994**, *27*, 435.
[11] *International Tables for X-ray Crystallography*, Kynoch Press, Birmingham, England, **1974**, vol. IV.
[12] J. R. Carruthers, D. J. Watkin, *Acta Crystallogr., Sect. A* **1979**, *35*, 698–699.
[13] L. Zolnaï, *ZORTEP, Graphical Program for X-ray Structures Analysis*, University of Heidelberg, Germany, **1998**.

Received February 21, 2001
[I01062]

New Octahedral $RuCl_2(CO)(L)[\eta^2$-(*P*,*O*)-ketophosphane] Complexes Containing One Hemilabile Ketophosphane Ligand

Bernard Demerseman[a]

Keywords: Ruthenium / Phosphanes / O ligands / Carbonyl ligands / Isomerizations

The reaction of the ketophosphanes $Ph_2PCH_2C(=O)t$Bu (**1**), $Ph_2PCMe_2C(=O)i$Pr (**1′**), or $Ph_2PCMe_2CH_2C(=O)$Me (**1′′**) with a precursor complex $RuCl_2(L)(\eta^6$-*p*-cymene) [L = PMe_3 (**a**), $PMePh_2$ (**b**), P*i*PrPh$_2$ (**c**), PPh_3 (**d**), $P(OMe)Ph_2$ (**e**), $P(OMe)_3$ (**f**)] in methanol and under carbon monoxide, provides an access to a novel family of complexes (*ttt*)-$RuCl_2(CO)(L)[\eta^2$-(*P*,*O*)-ketophosphane] (**2a–e**, **2′a**,**e**,**f**, and **2′′a**) with *trans*-chlorine and *trans*-phosphorus atoms. Further reaction with carbon monoxide or acetonitrile under thermal activation yields the *cis*,*cis*,*trans* derivatives (*cct*)-$RuCl_2(CO)_2(L)[\eta^1$-(*P*)-ketophosphane] **4a**,**b** and **4′a**, and (*cct*)-$RuCl_2(CO)(MeCN)(L)[\eta^1$-(*P*)-ketophosphane] **5a**,**b**,**d**. Complexes **2a**,**b** and **2′a** rearrange under thermal activation, or after exposure to sunlight, into the (*ctc* and *ccc*)-$RuCl_2(CO)(L)[\eta^2$-(*P*,*O*)-ketophosphane] isomers, with *cis*-chlorine and *cis*-phosphorus atoms, **6a**,**b** and **6′a**, respectively. Complexes **6a**,**b** reversibly add one molecule of carbon monoxide when forming the all-*cis* derivatives (*ccc*)-$RuCl_2(CO)_2(L)[\eta^1$-(*P*)-ketophosphane] **7a**,**b**, respectively. The removal of one chloride ligand in complexes **4a**, **4′a**, or **5a** with silver tetrafluoroborate affords the stable cationic derivatives $\{RuCl(CO)(L')(PMe_3)[\eta^2$-(*P*,*O*)-ketophosphane]$\}[BF_4]$, **8a** and **8′a** (L′ = CO) and **9a** (L′ = MeCN), respectively. Mild basic conditions are sufficient to allow the synthesis of the enolatophosphane derivatives (*ttt*)-$RuCl(CO)_2(L)[\eta^2$-(*P*,*O*)-$Ph_2PCH{=}C(t$Bu)O], **10a**,**c**,**e**, and of the analogous (*ccc*) and (*cct*) isomers, **11a**,**b** and **12a**, respectively.

Introduction

The discovery of the hemilabile behaviour of an ether−phosphane ligand,[1] in which the ether functionality coordinates at a ruthenium centre, has undoubtedly stimulated the interest of organometallic chemists with regard to functional phosphanes. The complexation of such ligands is of interest since the oxygen−metal bond is weak, thus providing facile access to coordinative unsaturation.[2,3] The series of $RuCl_2[\eta^2$-(*P*,*O*)-functional phosphane]$_2$ complexes, in which the organic function consists of an ether,[1,4−8] an ester,[9−11] or a keto group, have been largely studied.[12,13] Interestingly, their geometry is of type **I** (see Scheme 1), consisting of *trans*-chlorine, *cis* phosphorus, and *cis*-oxygen atoms, respectively. The preferred *cis* arrangement of the phosphorus atoms is unusual, as emphasised by the ability of complexes **I** to trap carbon monoxide through an irreversible process involving a *cis*-to-*trans* rearrangement of the phosphorus atoms (Scheme 1). The resulting complexes **II** exhibit a noteworthy fluxional behaviour through easy exchange between the coordinating modes of the oxygen atoms (not depicted in Scheme 1) and are able to interconvert with type-**III** complexes by reversible addition of carbon monoxide. We report herein a convenient route to new hybrid (*ttt*)-$RuCl_2(CO)(L)[\eta^2$-(*P*,*O*)-ketophosphane] complexes with *trans*-chlorine and *trans*-phosphorus atoms. They are analogous of both type-**II** and all-*trans* $RuCl_2(CO)_2L_2$ complexes, and their study will allow further comparison. Furthermore, under basic conditions they are suspected of generating coordinatively unsaturated η^2-(*P*,*O*)-enolatophosphane derivatives by a formal HCl abstraction.

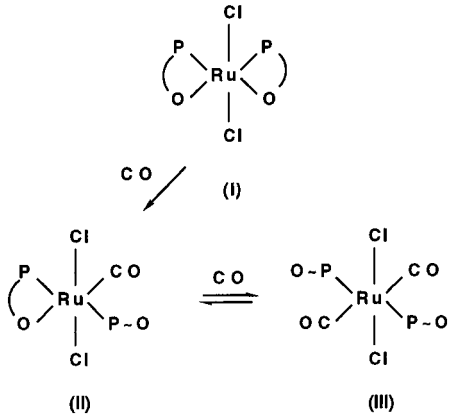

Scheme 1

Results

Synthesis of (*ttt*)-$RuCl_2(CO)(L)[\eta^2$-(*P*,*O*)-ketophosphane] Complexes 2−2′′

An equimolar mixture consisting of a precursor complex $RuCl_2(L)(\eta^6$-*p*-cymene) [L = PMe_3 (**a**), $PMePh_2$ (**b**), P*i*PrPh$_2$ (**c**), PPh_3 (**d**), $P(OMe)Ph_2$ (**e**), $P(OMe)_3$ (**f**)] and a ketophosphane [$Ph_2PCH_2C(=O)t$Bu (**1**), $Ph_2PCMe_2C(=O)i$Pr (**1′**), $Ph_2PCMe_2CH_2C(=O)$Me (**1′′**)] in methanol was stirred at ambient temperature under carbon monoxide. Subsequent workup allowed all-*trans* (based on two *trans*-

[a] Laboratoire de Chimie de Coordination et Catalyse, UMR-CNRS 6509, Campus de Beaulieu, Université de Rennes I, 35042 Rennes Cédex, France
E-mail: Bernard.Demerseman@univ-rennes1.fr

 © WILEY-VCH Verlag GmbH, 69451 Weinheim, 2001 1434−1948/01/0909−2347 $ 17.50+.50/0

chlorine and two *trans*-phosphorus atoms, respectively) complexes (*ttt*)-$RuCl_2(CO)(L)[\eta^2$-(*P*,*O*)-ketophosphane] **2a**−**e**, **2′a**,**e**,**f**, and **2′′a**, to be isolated in moderate to high yields (49−84%) as orange air-stable crystals (except for **2d**) (Scheme 2). The reaction formally consists of the substitution of a 6e-donor ligand (*p*-cymene) by one molecule of carbon monoxide and one molecule of ketophosphane acting as a 4e-donor. The generality of the reaction is not only shown by the involvement of a β- (**1**, **1′**) or a γ-ketophosphane (**1′′**), but also by the ability of the precursor complex $RuCl_2(\eta^6$-*p*-cymene)$[\eta^1$-(*P*)-$Ph_2PCH_2C(=O)t$Bu][14] in providing an alternative route to complexes of type **2**, when reacting with a ligand L such as $P(OMe)Ph_2$ and with carbon monoxide, to afford the expected derivative **2e** (see Scheme 2). The permethylated β-ketophosphane **1′** is unable to form a similar $RuCl_2(\eta^6$-*p*-cymene)$[\eta^1$-(*P*)-$Ph_2PCMe_2C(=O)i$Pr] derivative, but reacts with dimeric $[RuCl_2(\eta^6$-*p*-cymene)$]_2$ in methanol to generate a cationic species $\{RuCl(\eta^6$-*p*-cymene)$[\eta^2$-(*P*,*O*)-$Ph_2PCMe_2C(i$Pr)=O]$\}^+$, which has previously been characterised as its PF_6 salt.[14] Such solutions of $\{RuCl(\eta^6$-*p*-cymene)$[\eta^2$-(*P*,*O*)-$Ph_2PCMe_2C(i$Pr)=O]$\}$Cl in methanol may also be used to synthesise complexes **2′**. As summarised in Scheme 2, these distinct pathways leading to complexes **2**−**2′′** may be rationalised in terms of the formation of a transient cationic species $\{RuCl(\eta^6$-*p*-cymene)(L)$[\eta^1$-(*P*)-ketophosphane]$\}^+$ that will further react with carbon monoxide. Such a mechanism accounts for the requirement of methanol as the solvent, which allows a transient cleavage of one Ru−Cl bond. The reaction does not work in a solvent such as CH_2Cl_2. This strongly suggests the key role of methanol in the labilisation of the Ru−Cl bond.

The structures of complexes **2**−**2′′** were determined from a combination of elemental analysis, IR spectroscopy and ^{1}H, $^{31}P\{^1H\}$, $^{13}C\{^1H\}$, and ^{13}C NMR spectroscopy. Elemental analysis indicates the retention of two chlorine atoms per Ru atom. The IR spectra (Table 1) exhibit a very strong absorption close to 1940 cm^{-1} assigned to the carbon monoxide ligand, as well as a strong absorption close to 1640 cm^{-1} (1673 cm^{-1} for **2′′a**) indicating the coordination of the oxygen atom of the ketophosphane.[14] The $^{31}P\{^1H\}$ NMR spectra (Table 1) consist of an AB spin system and the large coupling constant values (> 300 Hz) indicate a mutual *trans* arrangement of the two phosphorus nuclei.[15] The ^{1}H and $^{13}C\{^1H\}$ NMR spectra both indicate a plane of symmetry requiring a relative *trans* arrangement of the two chloride ligands. Accordingly, the PCH_2 protons in complexes **2** and the $PCMe_2$ methyl groups in complexes **2′** and **2′′** are found to be equivalent by ^{1}H NMR spectroscopy. Furthermore, the two phenyl groups of the Ph_2P fragment are found to be equivalent by $^{13}C\{^1H\}$ NMR spectroscopy. The ^{13}C NMR resonances assigned to the C=O and C≡O carbon nuclei are close, but a simple comparison between the $^{13}C\{^1H\}$ and ^{13}C NMR spectra allows an unambiguous determination, since only the keto resonance is affected by far ^1H-^{13}C coupling.

The thermal stability of complexes **2**−**2′′** depends on the nature of the ancillary ligand L. The most stable complexes

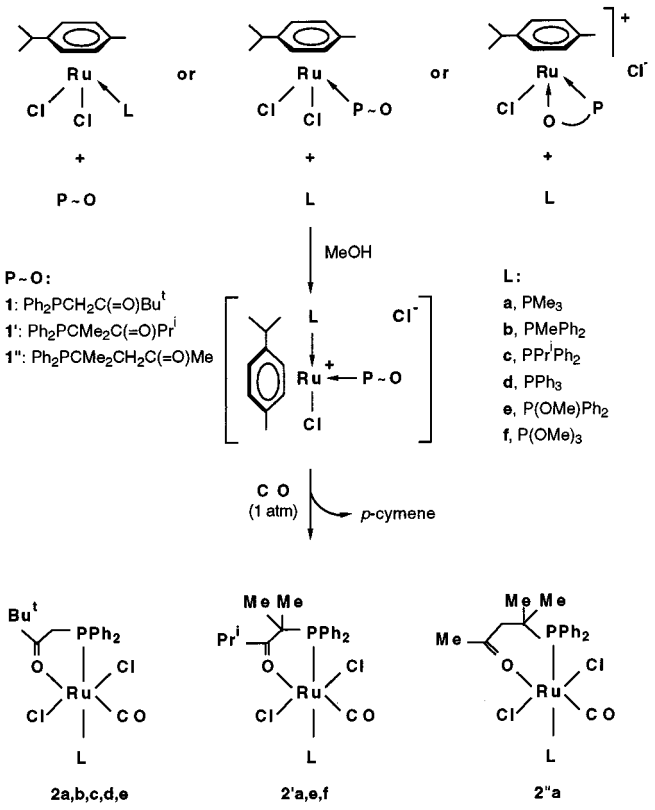

Scheme 2

are **2a**, **2′a**, and **2′′a** (in which L = PMe_3). They were unaffected when thermally treated under reflux in methanol for several hours. In contrast, **2e** [in which L = $P(OMe)Ph_2$] decomposed in hot methanol as indicated by the formation of $RuCl_2(CO)[\eta^1$-(*P*)-$Ph_2PCH_2C(=O)t$Bu][η^2-(*P*,*O*)-$Ph_2PCH_2C(t$Bu)=O].[12] This latter complex was detected by $^{31}P\{^1H\}$ NMR spectroscopy.

Reversible and Irreversible Carbon Monoxide Binding by Complexes 2−2′

The $^{31}P\{^1H\}$ NMR spectrum of a solution of **2a** (or **2b**) in CD_2Cl_2 that was kept under carbon monoxide disclosed a new species, besides the minor presence of **2a** (or **2b**). After removal of the carbon monoxide, recovery of pure **2a** (or **2b**) is indicated by the corresponding NMR spectrum. The set of $^{31}P\{^1H\}$ NMR resonances corresponding to the new species still consists of an AB spin system and large coupling constant values (> 300 Hz), thus indicating a mutual *trans* arrangement of the two phosphorus nuclei. Attempts to isolate the species failed, but such reversible carbon monoxide binding by **2a** (or **2b**) is very similar to the reversible formation of complexes **III** from complexes **II**, as depicted in Scheme 1. Therefore, the reversible formation of the all-*trans* derivatives (*ttt*)-$RuCl_2(CO)_2(L)[\eta^1$-(*P*)-$Ph_2PCH_2C(=O)t$Bu] (**3a**,**b**) may be reasonably assumed (Scheme 3). In contrast, an irreversible binding of carbon monoxide by toluene solutions of complexes **2a**,**b** and **2′a** occurs upon thermal activation (≥ 80 °C), yielding the colourless *cis*,*cis*,*trans* derivatives (*cct*)-$RuCl_2(CO)_2(L)[\eta^1$-(*P*)-

Table 1. IR and $^{31}P\{^1H\}$ NMR data of the new complexes

Compound	IR[a] ν(C≡O)	ν(C=O) or (C=CO)	$^{31}P\{^1H\}$ NMR δ(PO)	δ(L)	$^2J_{PP}$
(*ttt*)-$RuCl_2(CO)(L)[\eta^2\text{-}(P,O)$-ketophosphane)] complexes **2a**−**e**, **2′a**,**e**,**f**, **2′′a**					
2a	1948, 1929	1635, 1624	45.3	5.6	356[b]
2b	1939	1630	48.5	19.8	353[b]
2c	1946, 1938	1633, 1627	49.0	41.9	343[c]
2d	1941	1624	49.4	33.0	357[c]
2e	1942	1620	45.1	131.8	389[c]
2′a	1936	1634	65.1	4.5	344[c]
2′e	1938	1637	65.1	131.6	374[b]
2′f	1965	1637	64.0	128.4	508[c]
2′′a	1942	1673	38.2	2.5	347[c]
(*ttt*)-$RuCl_2(CO)_2(L)[\eta^1\text{-}(P)$-ketophosphane)] complexes **3a**,**b**					
3a			10.9	−4.1	269[b]
3b			13.5	10.1	272[b]
(*cct*)-$RuCl_2(CO)_2(L)[\eta^1\text{-}(P)$-ketophosphane)] complexes **4a**,**b**, **4′a**					
4a	2056, 1988	1705	16.5	−2.2	339[c]
4b	2052, 1991	1694	20.5	13.4	336[b]
4′a	2045, 1992	1699	21.8	1.0	346[c]
(*cct*)-$RuCl_2(CO)(MeCN)(L)[\eta^1\text{-}(P)$-ketophosphane)] complexes **5a**,**b**,**d**					
5a	1957	1702	23.7	−1.0	364[c]
5b	1950	1701	26.5	18.0	359[c]
5d	1966	1708	27.5	21.9	362[c]
(*ccc*)-$RuCl_2(CO)(L)[\eta^2\text{-}(P,O)$-ketophosphane)] complexes **6a**,**b**, **6′a**					
6a	1972	1624	52.7	23.1	31[c]
6a, minor isomer in solution:			63.8	16.8	24[c]
6b	1951	1632	49.6	38.3	28[b]
6b, minor isomer in solution:			60.9	34.5	22[b]
6′a	1960	1620	74.2	21.3	30[b]
(*ccc*)-$RuCl_2(CO)_2(L)[\eta^1\text{-}(P)$-ketophosphane)] complexes **7a**,**b**					
7a	2078, 1988	1706	14.8	5.6	28[c]
7a, minor isomer in solution:			28.6	−9.7	29[c]
7b	2077, 1994	1706	26.1	12.4	29[b]
7b, minor isomer in solution:			28.7	3.4	28[b]
Cationic derivatives **8a**, **8′a**, **9a**					
8a	2081, 2018	1610	41.8	2.3	291[c]
8′a	2076, 2016	1622	58.6	1.8	285[c]
9a	1987	1615	45.4	3.7	324[c]
(*ttt*)-$RuCl(CO)_2(L)[\eta^2\text{-}(P,O)$-enolatophosphane)] complexes **10a**,**c**,**e**					
10a	1989	1510	25.0	−3.8	222[c]
10c	1991	1498	26.4	36.0	219[c]
10e	2006	1505	23.8	123.8	255[c]
(*ccc*)-$RuCl(CO)_2(L)[\eta^2\text{-}(P,O)$-enolatophosphane)] complexes **11a**,**b**					
11a	2070, 1968	1498	47.0	−5.6	31[c]
11b	2065, 1980	1500	46.6	7.8	31[c]
11b, minor isomer in solution:			42.6	21.9	31[c]
(*cct*)-$RuCl(CO)(L')(L)[\eta^2\text{-}(P,O)$-enolatophosphane)] complexes **12a** (L′ = CO), **13a** (L′ = MeCN)					
12a	2034, 1977	1505	41.4	−1.1	302[c]
13a	1940	1493	43.8	0.8	333[c]

[a] $\tilde{\nu}$ in cm^{-1}. – [b] In $CDCl_3$. – [c] In CD_2Cl_2.

ketophosphane] (**4a**,**b** and **4′a**) (Scheme 3). The formation of **4a**,**b** and **4′a** involves an additional *trans*-to-*cis* rearrangement of the chloride ligands, relative to the $\eta^2\text{-}(P,O) \rightarrow \eta^1\text{-}(P)$ transformation of the coordination of the ketophosphane, therefore allowing the entrance of one carbon monoxide molecule.

The $^{31}P\{^1H\}$ NMR spectra of **4a**,**b** still consist of an AB spin system and the large coupling constant values ($^2J_{PP} >$ 300 Hz, Table 1) indicate the retention of the mutual *trans* arrangement of the two phosphorus nuclei. Both the ^1H and $^{13}C\{^1H\}$ NMR spectra of **4a**,**b** and **4′a** indicate a plane of symmetry. Their IR spectra exhibit two strong absorptions (close to 2055 and 1990 cm^{-1}) as expected for a relative *cis* arrangement of two carbonyl ligands, as well as an absorption close to 1700 cm^{-1} assigned to the uncoordinated keto functionality. A relative *cis* arrangement of the two carbonyl ligands obviously requires a relative *cis* arrangement of the two chlorine atoms.

Reversible Acetonitrile Binding by Complexes 2

A *trans*-to-*cis* rearrangement of the chloride ligands is also involved when complexes **2a**,**b**,**d** are heated under reflux in acetonitrile, yielding the lemon-yellow *cis*,*cis*,*trans* complexes (*cct*)-$RuCl_2(CO)(N{\equiv}CMe)(L)[\eta^1\text{-}(P)$-ketophos-

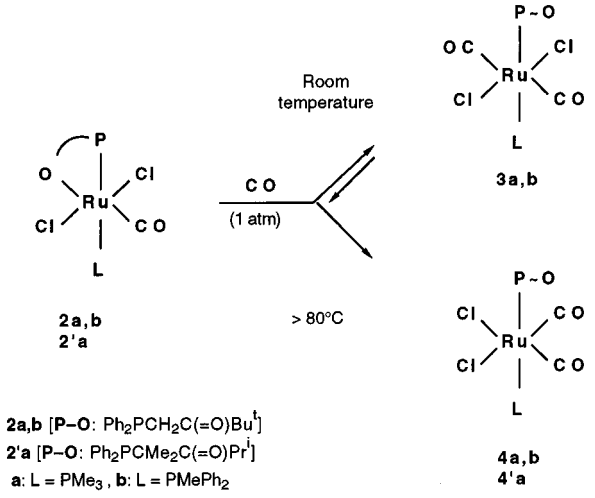

Scheme 3

phane] (**5a**,**b**,**d**) (Scheme 4). The η^2-(*P*,*O*) → η^1-(*P*) modification of the coordination of the ketophosphane allows one acetonitrile ligand to enter. The $^{31}P\{^1H\}$ NMR spectra of complexes **5a**,**b**,**d** exhibit large $^2J_{PP}$ coupling constant values, indicating a retention of the relative *trans* arrangement of the phosphorus atoms. However, their ^1H NMR spectra show the two PCH_2 protons of the ketophosphane to be diastereotopic. Their $^{13}C\{^1H\}$ NMR spectra also indicate a loss of symmetry. This lack of a plane of symmetry suggests a relative *cis* arrangement of the two chloride ligands. Complexes **5a**,**b**,**d** were found to be stable in the solid state but not in dichloromethane solutions, as monitored by ^1H and $^{31}P\{^1H\}$ NMR spectroscopy. Thus, after standing for 1 d at room temperature, an NMR-spectroscopic sample of pure **5a** in CD_2Cl_2 shows a substantial presence of free acetonitrile, as well as the recovery of **2a**. The reaction of acetonitrile with crude **2d** (L = PPh_3), that was obtained as an insoluble precipitate which retained several impurities, allows the preparation of **5d** as analytically pure yellow crystals. Furthermore, a concentrated solution of **5d** in dichloromethane deposited orange crystals of pure **2d**, merely by standing for several days. A simple substitution of the weakly bonded acetonitrile ligand by carbon monoxide (instead of the formation of **2a** or **2d**) was not observed when a solution of **5a** or **5d** in dichloromethane was kept under carbon monoxide. This result is likely to be related to the kinetically favoured formation of *trans* derivatives in such processes.[16]

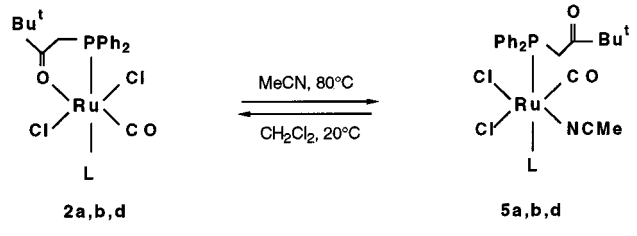

Scheme 4

Isomerisation of Complexes 2−2′

A slow reaction occurred when an orange solution of **2a** in toluene was heated at 80 °C under an inert gas, as indicated by the formation of a pale-yellow precipitate. After heating for 2 d and subsequent removal of the volatiles, the ^1H and $^{31}P\{^1H\}$ NMR analysis of the resulting material revealed a mixture consisting of a new species, **6a**, as well as unreacted **2a**, in a 2:1 ratio (Scheme 5). It is worth noting the thermal stability of complex **6a** which was successfully isolated in a 75% yield as an analytically pure precipitate after a solution of **2a** in toluene was heated under reflux. Thus, this procedure was used to synthesize **6b** starting from **2b**, while **6′a** was conveniently obtained after heating **2′a** in ethanol under reflux. The isomerisation of complexes **2a**,**b** and **2′a** into complexes **6a**,**b** and **6′a** also occurred when solutions of **2a**,**b** and **2′a** in dichloromethane were exposed to sunlight. Similar treatment of a solution of **2a** or alternatively **6a**, both led to mixtures of **2a** and **6a** in a 15:85 ratio, indicating a reversible process. This was determined by ^1H NMR spectroscopy. From the ratio it can be seen that **6a** is highly favoured. Irradiation from sunlight proved useful in synthesising **6a** and **6′a**, as detailed in the Exp. Sect. Complexes **6a**,**b** and **6′a** were characterised by elemental analysis and spectroscopic studies. The $^{31}P\{^1H\}$ NMR spectrum of **6′a** exhibits a small $^2J_{PP}$ coupling constant value (Table 1), indicating a relative *cis* arrangement of the phosphorus atoms.[15] The ^1H NMR spectrum shows two inequivalent $PCMe_2$ methyl groups. IR spectroscopy indicates the coordination of the keto functionality, and this η^2-(*P*,*O*) coordination of the ketophosphane obviously requires a relative *cis* arrangement of the corresponding oxygen and phosphorus coordinating atoms. Furthermore, the $^{13}C\{^1H\}$ NMR resonance assigned to the carbon monoxide ligand in **6′a** discloses two small $^2J_{PC}$ coupling constant values ($^2J_{PC}$ = 19.8 and 12.6 Hz), indicating a *cis* position of the carbon monoxide ligand relative to both phosphorus atoms. Therefore, only two octahedral structures, namely **A** and **B** as depicted in Scheme 5, remain conceivable. The NMR- and IR-spectroscopic study of **6a** leads to the same conclusion when some additional weak resonances are omitted. These resonances are too weak to allow further characterisation of the corresponding species; however, $^{31}P\{^1H\}$ NMR spectroscopy does show a small $^2J_{PP}$ coupling constant value. The NMR-spectroscopic study of **6b** was more informative and shows the presence of two isomers in a 3:2 ratio. These two isomers involve both a mutual *cis* arrangement of the phosphorus atoms and a *cis* arrangement of the carbon monoxide ligand relative to the phosphorus atoms, as expected for a mixture of **A** and **B**. To summarise these results, complex **6′a**, which involves the bulkiest ketophosphane **1′** and a small ligand L = PMe_3, shows only one isomer in solution, **A** or **B**. Complex **6b**, which involves the smaller ketophosphane **1** but a bulkier ligand L = $PMePh_2$, shows a mixture of **A** and **B** isomers in solution. Complex **6a**, which involves the ketophosphane **1** and L = PMe_3, will also show a mixture of **A** and **B** isomers, but one is highly favoured.

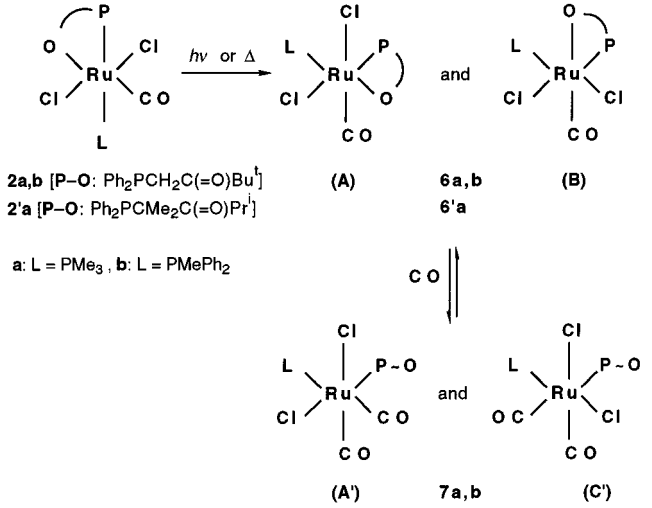

Scheme 5

Binding of Carbon Monoxide by Complexes 6−6′

Dichloromethane solutions of **6a** and **6b** were found to bind carbon monoxide (1 atm, ambient temperature) affording **7a** and **7b**, respectively (Scheme 5). Complexes **6a** and **6b** were recovered in the absence of carbon monoxide, indicating a reversible reaction. It should be noted that this process does not affect the **A/B** ratio (in **6a** and **6b**). In contrast, **6′a** irreversibly adds carbon monoxide affording the *cct* derivative **4′a**. This involves a *cis*-to-*trans* rearrangement of the phosphorus atoms. The NMR spectra of both **7a** and **7b** show a mixture of two isomers, namely **A′** and **C′** (Scheme 5). The small $^2J_{PP}$ coupling constant values (Table 1) clearly indicate the retention of the *cis* arrangement of the phosphorus atoms. The ^1H NMR spectrum shows the PCH_2 protons of the ketophosphane **1** to be inequivalent and rules out a *trans* mutual arrangement of the two chlorine atoms. The $^{13}C\{^1H\}$ NMR spectra indicate, for each molecule **A′** and **C′** that one carbon monoxide ligand is located in a *cis* position relative to the two phosphorus atoms and the second one in a *trans* P−Ru−CO arrangement.[15] Thus, only the two octahedral structures **A′** and **C′** remain conceivable. The isomeric structures **A′** and **C′** both show *cis* mutual arrangements of the two chlorine atoms and of the two carbonyl ligands, respectively, and are thus the two conceivable structures for an all-*cis*-$RuX_2(CO)_2(L)(L')$ complex. It is interesting to note that a simple substitution of the coordinated oxygen atom in **A** by an entering carbon monoxide molecule will lead to **A′**. However, a similar exchange of the coordinated oxygen atom in **B** by carbon monoxide will result in the formation of a symmetrical structure with *trans* carbon monoxide ligands, rather than **C′**. This is not experimentally detected. The stability of complexes **7a**,**b** is related to the nature of the ancillary ligand L. Complex **7a** (L = PMe_3) was found to be stable in a dichloromethane solution, or alternatively in a methanol solution, at ambient temperature and under carbon monoxide, but is converted into **4a** in hot methanol (see Exp. Sect.). In contrast, **7b** (L = $PMePh_2$) is stable in a dichloromethane solution, but is converted into **4b** on dissolution in methanol, even at ambient temperature. The straightforward formation of **4′a** on treatment of **6′a** with carbon monoxide, is indicative of the steric effect of the bulky ketophosphane **1′**, favouring a *cis*-to-*trans* rearrangement of phosphorus atoms.

Formation of Cationic Derivatives

Halide abstraction from **7a** using silver tetrafluoroborate creates an unsaturated centre that was found to trigger a *cis*-to-*trans* rearrangement of phosphorus atoms. This produces the cationic derivative **8a** in which the oxygen atom from the ketophosphane ligand completes the coordination at the ruthenium centre (Scheme 6). Complexes **4a** and **4′a** are also convenient precursors for the synthesis of such cationic derivatives, and afford the expected derivatives **8a** and **8′a**, respectively, through the removal of a chloride ligand (Scheme 6). In contrast, attempts to obtain cationic derivatives starting from a complex **2**, such as **2a**, invariably failed, even under carbon monoxide.

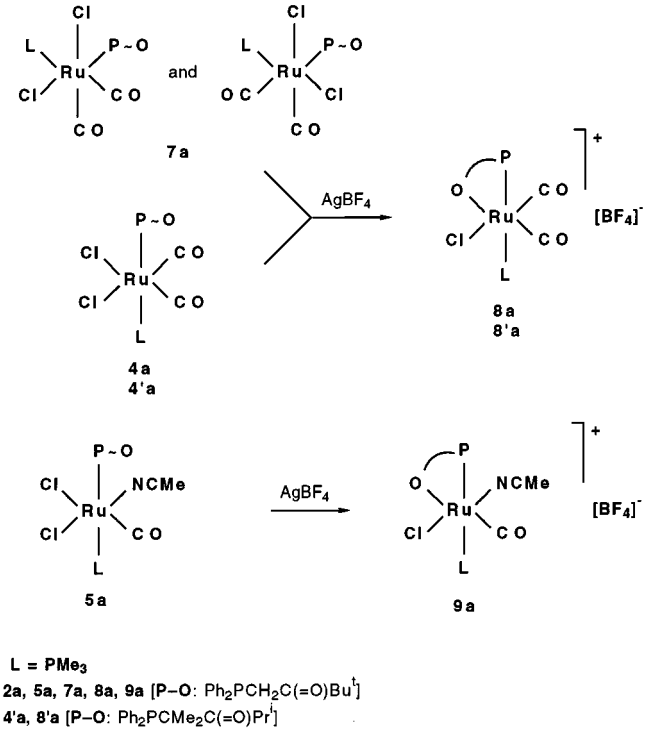

Scheme 6

The structures of complexes **8a** and **8′a** are unambiguously deduced from their $^{31}P\{^1H\}$ NMR spectra, which exhibit large $^2J_{PP}$ coupling constant values (Table 1) indicating a *trans* arrangement of the phosphorus atoms, and from their IR spectra which indicate a *cis* arrangement of the carbonyl ligands and the coordination of the keto functionality. The observation of two inequivalent PCH_2 protons by ^1H NMR spectroscopy also suggests a relative *cis* arrangement of the two carbonyl ligands. The substitution of one chloride ligand by the oxygen atom from the ketophosphane was also achieved starting from the fragile (pre-

sumably owing to its labile acetonitrile ligand) complex **5a**, which reacts with silver tetrafluoroborate to yield the more stable cationic derivative **9a** (Scheme 6).

Stereoselective Synthesis of Enolatophosphane Derivatives

Complexes **2a**,**c**,**e** were found to be rather robust under basic conditions (K_2CO_3 in dichloromethane or KOH in methanol). However, the consumption of the starting material was detected by $^{31}P\{^1H\}$ NMR spectroscopy after prolonged reaction times (several days at ambient temperature), but the observation of very numerous new resonances indicated an intractable mixture. Under such basic conditions and under carbon monoxide, a fast and selective process occurred, resulting in the formation of the enolatophosphane complexes **10a**,**c**,**e**. It is worth noting that the complexes **10a**,**c**,**e** retain an all-*trans* structure based on two *trans*-coordinating phosphorus atoms, two *trans*-carbonyl ligands and two *trans*-X-type coordinating atoms (Scheme 7). The process formally consists of the removal of one HCl molecule and the coordination of one molecule of carbon monoxide. Derivatives **6a**,**b** reacted in a similar manner and afforded the enolatophosphane derivatives **11a**,**b**, respectively, which retain a relative *cis* arrangement of the phosphorus atoms. The NMR-spectroscopic study of **11a**,**b** discloses one isomer for **11a**, but a mixture of two isomers for **11b**. These isomers involve both a relative *cis* arrangement of the phosphorus atoms and of the carbon monoxide ligands, respectively. For each structure, one carbon monoxide ligand is located in a *cis* position relative to the two phosphorus atoms, whereas the second carbon monoxide ligand is located in a *trans* position relative to a phosphorus atom, but three structures remain conceivable (vide infra). The formation of the enolatophosphane derivatives **12a** and **13a**, starting from the neutral *cct* isomer **4a** and from the cationic derivative **9a**, respectively, formally consists solely of the removal of one molecule of HCl or $H[PF_6]$ (Scheme 7), and was also found to be very stereoselective. This was monitored by $^{31}P\{^1H\}$ NMR spectroscopy.

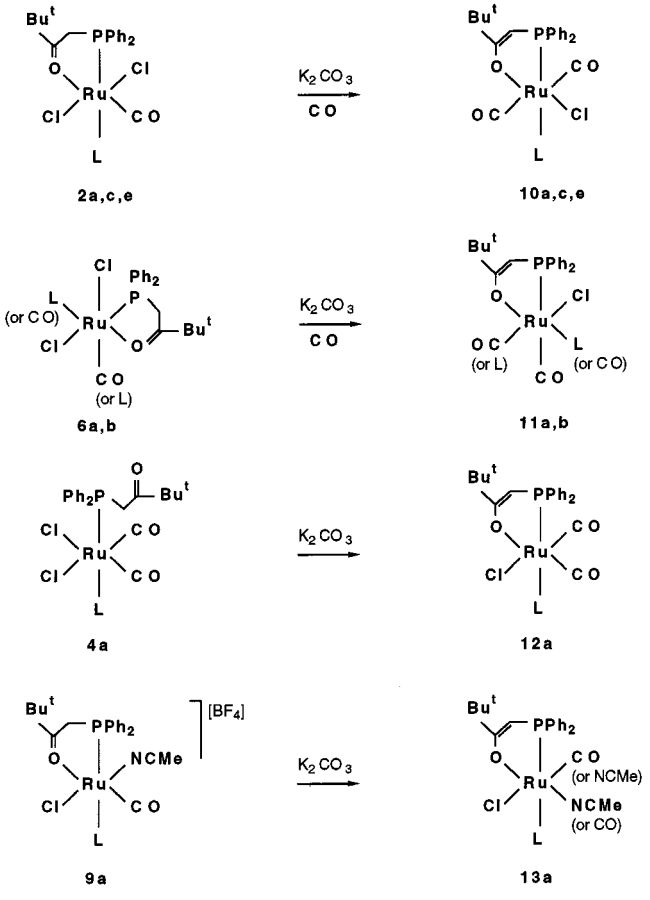

a, L = PMe_3; **b**, L = $PMePh_2$; **c**, L = PPr^iPh_2; **e**, L = $P(OMe)Ph_2$

Scheme 7

Discussion

The removal of the arene ligand from $RuCl_2(L)(\eta^6$-*p*-cymene) complexes allows the coordination of a ketophosphane along with a CO ligand, thus providing access to a new family of octahedral Ru complexes bearing two distinct phosphorus-containing ligands. The process selectively leads to all-*trans* complexes based on of two *trans*-chlorine and *trans*-phosphorus atoms. The hemilabile character of the ketophosphane ligand allows the reversible formation of new all-*trans*-$RuX_2(CO)_2L_2$-type complexes (but with distinct L ligands) by reversible uptake of carbon monoxide. Previous studies concerning $RuX_2(CO)_2L_2$ complexes have proved that all-*trans* complexes easily rearrange under thermal activation into their thermodynamically favoured *cct* isomers through a preliminary cleavage of one Ru−CO bond. The mechanism of this transformation has been thoroughly elucidated.[16] Therefore, the formation of complexes of type **4** and **5** under thermal activation and in the presence of an entering ligand such as carbon monoxide or acetonitrile might be expected, and this accounts for the recovery of complexes of type **2** from **5** by loss of acetonitrile. The behaviour of complexes **2** under thermal activation and in the absence of an entering ligand was less predictable. Whereas all-*trans*-$RuX_2(CO)_2L_2$ complexes rearrange into their *cct* isomers, complexes of type **2** selectively afford the corresponding all-*cis* isomers **6**. This observation suggests that the formation of *cct* isomers of **2** (with *cis*-chlorine and *trans*-phosphorus atoms) is disfavoured due to the requirement of a (C=)O→Ru−Cl *trans* arrangement (only O→Ru−Cl *cis* arrangements are observed in complexes **2** and **6**). In contrast, the coordination of carbon monoxide is stabilised through the *trans* effect of a chloride ligand in (*cct*)-$RuX_2(CO)_2L_2$ complexes. As depicted in Scheme 8, the transformation of complexes **2** into complexes **6** may be assumed to involve a pentacoordinated intermediate arising from the cleavage of the oxygen−ruthenium bond. Such a Berry rearrangement[17] through a dissociative pathway already accounts for the isomerisation of all-*trans*-$RuX_2(CO)_2L_2$ complexes into their all-*cis* isomers.[16]

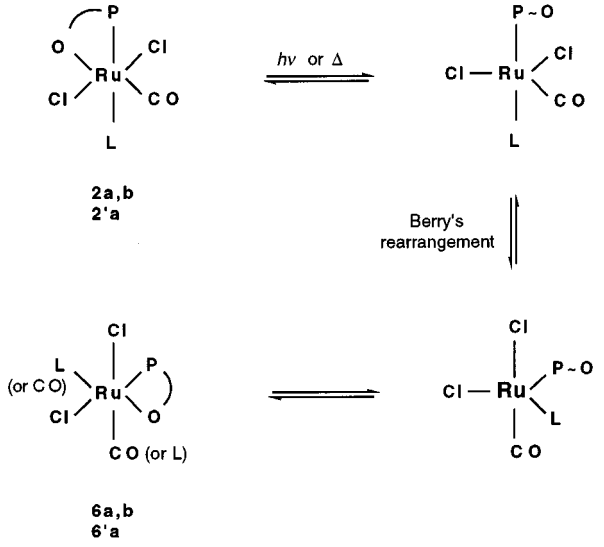

Scheme 8. Rationale accounting for the reversible isomerisation of complexes **2a**,**b** and **2′a** into complexes **6a**,**b** and **6′a**

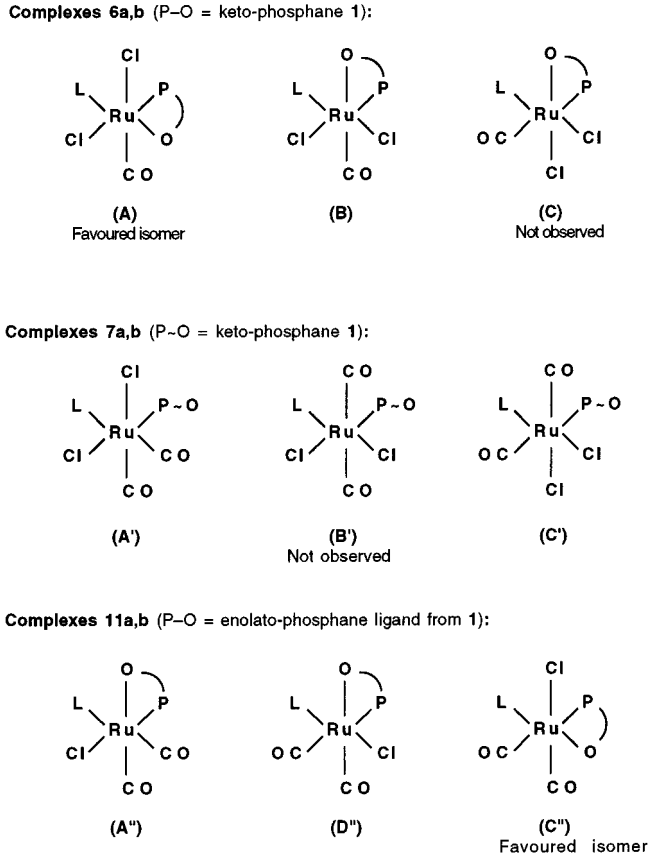

Scheme 9. Comparison between the distinct structures of complexes **6a**,**b**, **7a**,**b**, and **11a**,**b**

The formation of complexes **6** preserves the hemilabile property of the ketophosphane ligand as emphasised by the reactivity of complexes **6** towards carbon monoxide. Complexes **6a** and **6b** reversibly bind carbon monoxide to afford **7a** and **7b**, respectively. Solutions of **7a** and **7b** in dichloromethane both reveal a mixture of two all-*cis* isomers. As depicted in Scheme 9, a comparison of the structures of type **6** and **7** complexes excludes a mechanism based on the CO displacement of the weakly bound oxygen atom in complexes **6**, despite the fact that the structure **A′** of **7** may arise from **A** of **6**. The structure **C′** which is also observed in complexes **7**, is unexpected when compared with **A** and **B** of complexes **6**. The expected structure **B′** (Scheme 9) was not detected experimentally.

Moreover, the **A′**/**C′** ratio in a complex of **7** is unambiguously distinctly related to the **A**/**B** ratio in the parent complex **6**. Thus, the complete reversibility of the transformation of **6** to **7** provides further evidence for a dynamic equilibrium between **A** and **B**, and between **A′** and **C′**. The facile recovery of **6a** (or **6b**) from **7a** (or **7b**) illustrates the easy loss of carbon monoxide by **7**. However, preliminary cleavage of one Ru−CO bond in **7** (dissociative mechanism) will transiently generate a coordinatively unsaturated intermediate favouring a *cis*-to-*trans* rearrangement of the phosphorus atoms.[16] Therefore, an associative mechanism will more likely account for the retention of the all-*cis* geometry. The reversible **A** ⇄ **B** and **A′** ⇄ **C′** transformations are also easy. They may formally involve the exchange of the positions of the chlorine atom and the oxygen atom for the **A** ⇄ **B** isomerisation, and of the chlorine atom and the carbon monoxide ligand for the **A′** ⇄ **C′** isomerisation. As depicted in Scheme 10, all these reversible transformations may be achieved without any involvement of coordinatively unsaturated species. Associative pathways consisting of the transient formation of halogen-bridged dinuclear species easily account for the experimental observations. The formation of analogous dinuclear compounds by halogen-bridge formation from $RuX_2(CO)_2L_2$ complexes, which has been previously reported,[15,16] further supports such a mechanism.

The formation of the enolatophosphane derivatives **10a**,**c**,**e**, **11a**,**b**, and **12a** (Scheme 7) was found to be highly stereoselective. Preliminary coordination of the entering ligand, subsequent deprotonation of the η^1-(P)-coordinated ketophosphane and substitution of one chloride ligand by an anionic oxygen atom are the steps of a simple mechanism which account for the stereoselective formation of **10a**,**c**,**e** and **11a**,**b**. The formation of **12a** starting from **4a**, in which the ketophosphane is already η^1-(P)-coordinated, clearly provides the experimental support to such a mechanism. The formation of **13a** starting from the cationic complex **4a**, involves the simple deprotonation of the ketophosphane ligand. The NMR-spectroscopic study of **10a**,**c**,**e** allows an unambiguous structural determination. The structural determination is less accurate in the case of **11a**,**b**, but only *cis*-phosphorus and *cis*-carbonyl arrangements are observed. Thus, three structures, namely **A″**, **D″**, and **C″** (Scheme 9), remain conceivable after the examination of the NMR-spectroscopic data. Only one of them is involved in the case of **11a**, but two in the case of **11b** which reveals a mixture of two isomers. The **A″** and **D″** structures show an O−Ru−CO *trans* arrangement which may arise from **A′** and **C′** in the corresponding parent compound **7**.

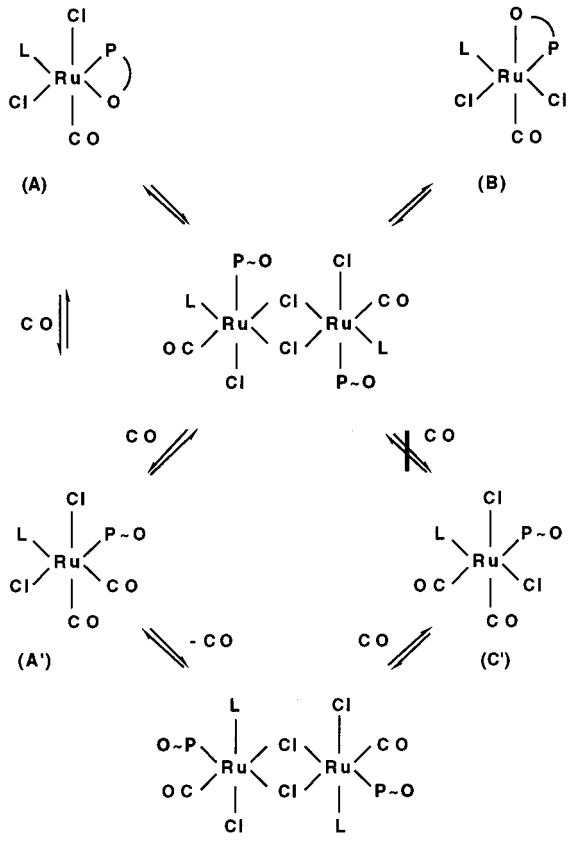

Scheme 10. Simple rationale accounting for the easy isomerisation of complexes **6a**,**b** and **7a**,**b**

Only **C**′ may lead to the third structure **C**′′, which shows a Cl−Ru−CO *trans* arrangement. It should be noted that a chloride ligand is more labile when *trans* to a phosphorus atom. Therefore, the **C**′ → **C**′′ transformation will be a favoured pathway and the observation of only one isomer when starting from **7a** will thus suggest the structure **C**′′ for **11a**. The precursor **7b** involves a bulkier ancillary ligand L = $PMePh_2$ than L = PMe_3 in **7a**. For steric reasons, a slower **C**′ → **C**′′ transformation may result and a **C**′ → **D**′′ remains highly disfavoured, however, the **A**′ → **A**′′ transformation may become more competitive. This will result in a mixture of the two isomers **C**′′ and **A**′′ in the case of **11b**. This behaviour emphasises the high stability of the Cl−Ru−CO *trans* arrangement, and therefore also suggests that the favoured isomer in complexes **6a**,**b** and **6**′**a** is **A**. The observation of isomer **B** is related to steric hindrance.

Conclusion

This study of the new family of complexes *trans*-$RuCl_2(CO)(L)[\eta^2$-(*P*,*O*)-ketophosphane] (**2**) emphasises the stability of the O→Ru bond in a *trans*-(C)=O→-Ru←(C≡O) arrangement, and the inability of the oxygen atom of the ketophosphane to coordinate *trans* to the chloride ligand. Due to this inability, the *cct* isomers of complexes **2** remain the speculative species. From this point of view, $RuCl_2(CO)(L)[\eta^2$-(*P*,*O*)-ketophosphane] complexes remarkably differ from $RuX_2(CO)_2L_2$ compounds in which the *cct* isomers are thermodynamically favoured. The cleavage of the O→Ru bond in complexes **2**, that occurs under thermal activation or sunlight irradiation, results in a true coordinatively unsaturated species which allows the formation of stable *cis*-$RuCl_2(CO)(L)[\eta^2$-(*P*,*O*)-ketophosphane] derivatives according to a Berry rearrangement. Under less drastic conditions, the substitution of the coordinated oxygen atom by an entering ligand such as carbon monoxide probably occurs through an associative mechanism, allowing the geometry to be retained. The easy deprotonation of the ketophosphane $Ph_2PCH_2C(=O)t$Bu allows the generation of $RuCl(CO)_2(L)[\eta^2$-(*P*,*O*)-enolatophosphane] derivatives, and this transformation also preserves the geometry of the corresponding precursor complexes.

Experimental Section

General: The reactions were performed using Schlenk-type techniques, but only the handling of ketophosphanes required a rigorous exclusion of oxygen. Solvents were distilled under an inert gas after drying according to conventional methods. − Elemental analyses were performed by the Service de Microanalyse du CNRS, Vernaison, France. − Infrared spectra were recorded with a Nicolet 205 FT infrared spectrometer as Nujol mulls. − NMR spectra were recorded at 297 K with an AC 300 FT Bruker instrument (^{1}H: 300.13; ^{13}C: 75.47; ^{31}P: 121.50 MHz; absolute values of coupling constants in Hz) and referenced internally to the solvent peak. The following abbreviations are used: s: singlet; d: doublet; t: triplet; t_a: apparent triplet; q_4: quadruplet; m, unresolved multiplet. − The precursor complexes $RuCl_2(L)(\eta^6$-*p*-cymene) were obtained by treating $[RuCl_2(\eta^6$-*p*-cymene)]$_2$ with a stoichiometric amount of the corresponding phosphorus derivative L.[18] The ketophosphanes $Ph_2PCH_2C(=O)t$Bu (**1**), $Ph_2PCMe_2C(=O)i$Pr (**1**′), and $Ph_2PCMe_2CH_2C(=O)$Me (**1**′′), were prepared as previously reported.[12,14]

Synthesis of Complexes 2−2′′

(*ttt*)-$RuCl_2(CO)(PMe_3)[Ph_2PCH_2C(t$Bu)=O] (2a): $RuCl_2(PMe_3)$(*p*-cymene) (13.3 g, 34.8 mmol) was added to a solution of ketophosphane **1** (9.90 g, 34.8 mmol) in methanol (200 mL). As for the preparation of the other complexes **2−2**′′, the Schlenk tube was protected from light with aluminium foil and the mixture was then stirred under carbon monoxide at room temperature. After 2 d, the resulting slurry was heated and then filtered to obtain an orange solution that deposited orange crystals on cooling. Yield 13.6 g, 70%. − ^{1}H NMR ($CDCl_3$): δ = 7.60−7.39 (m, 10 H, Ph), 4.04 (dd, 2 H, $^2J_{PH}$ = 10.1, $^4J_{PH}$ = 1.4, PCH_2), 1.70 (dd, 9 H, $^2J_{PH}$ = 10.3, $^4J_{PH}$ = 2.3, PMe_3), 1.33 (s, 9 H, *t*Bu). − ^{13}C{^{1}H} NMR (CD_2Cl_2): δ = 229.5 (dd, $^2J_{PC}$ = 8.6, $^3J_{PC}$ = 4.9, C=O), 205.8 (dd, $^2J_{PC}$ = 17.1 and 11.0, C≡O), 133.6 (d, $^3J_{PC}$ = 11.0, Ph_2P, *meta*), 131.2 (dd, $^1J_{PC}$ = 42.1, $^3J_{PC}$ = 7.3, Ph_2P, *ipso*), 131.0 (d, $^4J_{PC}$ = 2.4, Ph_2P, *para*), 128.9 (d, $^2J_{PC}$ = 9.8, Ph_2P, *ortho*), 46.3 (d, $^3J_{PC}$ = 3.5, CMe_3), 43.0 (d, $^1J_{PC}$ = 23.8, PCH_2), 27.1 (s, CMe_3), 13.8 (d, $^1J_{PC}$ = 28.9, PMe_3). − ^{13}C NMR (CD_2Cl_2, selected values): δ = 229.5 (broad, C=O), 205.8 (dd, $^2J_{PC}$ = 17.1 and 11.0, C≡O), 43.0 (td, $^1J_{HC}$ = 131, $^1J_{PC}$ = 23.8, PCH_2), 13.8 (q_4d, $^1J_{HC}$ = 130, $^1J_{PC}$ = 28.9, PMe_3). − $C_{22}H_{30}Cl_2O_2P_2Ru$ (560.4): calcd. C 47.15, H 5.40, Cl 12.65, P 11.05; found C 47.48, H 5.49, Cl 12.60, P 11.00. − Probably due to a solid-state effect, the IR absorptions (Table 1)

assigned to the carbon monoxide ligand and to the keto functionality are split.

(*ttt*)-$RuCl_2(CO)(PMePh_2)[Ph_2PCH_2C(tBu)=O]$ (2b): A mixture consisting of $RuCl_2(PMePh_2)$(*p*-cymene) (7.00 g, 13.8 mmol) and ketophosphane **1** (4.00 g, 14.1 mmol) was dissolved in dichloromethane (30 mL), and methanol (70 mL) was then added. The mixture was stirred for 3 d (under carbon monoxide) and the resulting yellow slurry was concentrated under vacuum and diethyl ether was then added. The yellow precipitate was collected by filtration and then dissolved in dichloromethane (50 mL). The solution was filtered and the orange filtrate was covered with ethanol (250 mL) in an open flask allowing natural evaporation. Orange crystals were obtained. Yield 6.40 g, 68%. – ^{1}H NMR ($CDCl_3$): δ = 7.82–7.36 (m, 20 H, Ph), 4.06 (dd, 2 H, $^2J_{PH}$ = 10.5, $^4J_{PH}$ = 1.3, PCH_2), 2.23 (dd, 3 H, $^2J_{PH}$ = 9.2, $^4J_{PH}$ = 1.9, PMe), 1.08 (s, 9 H, *t*Bu). – $C_{32}H_{34}Cl_2O_2P_2Ru$ (684.5): calcd. C 56.15, H 5.01, Cl 10.36, P 9.05; found C 56.18, H 4.92, Cl 10.31, P 9.06.

(*ttt*)-$RuCl_2(CO)(PiPrPh_2)[Ph_2PCH_2C(tBu)=O]\cdot CH_2Cl_2$ (2c): Complex **2c** was similarly obtained in a 49% yield starting from $RuCl_2(PiPrPh_2)$(*p*-cymene) and ketophosphane **1**. – ^{1}H NMR (CD_2Cl_2): δ = 7.69–7.30 (m, 20 H, Ph), 3.97 (dd, 2 H, $^2J_{PH}$ = 10.2, $^4J_{PH}$ = 0.7, PCH_2), 3.46 (m, 1 H, C*H*Me$_2$), 1.04 (dd, 6 H, $^3J_{HH}$ = 7.0, $^3J_{PH}$ = 14.8, CH*Me*$_2$), 0.87 (s, 9 H, *t*Bu). – ^{13}C{^{1}H} NMR (CD_2Cl_2): δ = 228.0 (dd, $^2J_{PC}$ = 7.1, $^4J_{PC}$ = 4.6, C=O), 206.8 (t_a, $^2J_{PC} \approx {}^2J_{P'C} \approx$ 13.4, C≡O), 135.2 (d, $^3J_{PC}$ = 8.2, Ph_2P, *meta*), 133.6 (dd, $^3J_{PC}$ = 9.9, $^5J_{PC}$ = 1.5, Ph_2P, *meta*), 131.1 (d, $^4J_{PC}$ = 2.1, Ph_2P, *para*), 130.9 (dd, $^1J_{PC}$ = 44.0, $^3J_{PC}$ = 4.4, Ph_2P, *ipso*), 130.2 (d, $^4J_{PC}$ = 1.7, Ph_2P, *para*), 130.1 (dd, $^1J_{PC}$ = 35.6, $^3J_{PC}$ = 3.3, Ph_2P, *ipso*), 128.8 (d, $^2J_{PC}$ = 9.8, Ph_2P, *ortho*), 128.1 (d, $^2J_{PC}$ = 8.8, Ph_2P, *ortho*), 45.9 (d, $^3J_{PC}$ = 2.9, *C*Me$_3$), 43.1 (d, $^1J_{PC}$ = 24.2, PCH_2), 26.8 (s, C*Me*$_3$), 22.6 (dd, $^1J_{PC}$ = 23.9, $^3J_{PC}$ = 1.8, *C*HMe$_2$), 18.1 (s, CH*Me*$_2$). – Easy loss of dichloromethane from the crystals occurs as seen by the elemental analysis results, which indicated the retention of only 0.8 CH_2Cl_2 per Ru; $C_{34}H_{38}Cl_2O_2P_2Ru\cdot$(0.8 CH_2Cl_2) (712.6 + 67.9 = 780.5): calcd. C 53.55, H 5.11, Cl 16.35, P 7.94; found C 53.56, H 5.15, Cl 16.47, P 7.95. – Probably due to a solid-state effect, the IR absorptions (Table 1) assigned to the carbon monoxide ligand and to the keto functionality are split.

(*ttt*)-$RuCl_2(CO)(PPh_3)[Ph_2PCH_2C(tBu)=O]\cdot{}^2/_3CH_2Cl_2$ (2d): A mixture was prepared starting from $RuCl_2(PPh_3)$(*p*-cymene) (9.50 g, 16.7 mmol), ketophosphane **1** (4.84 g, 17.0 mmol), dichloromethane (25 mL), and methanol (130 mL). It was stirred for 3 d. The resulting yellow precipitate was collected by filtration and washed with diethyl ether (100 mL). Yield 9.70 g, 72%. The low solubility of the compound precludes further purification.

Recovery of 2d from 5d: A solution of **5d** (4.00 g, 5.08 mmol) in dichloromethane (50 mL) was kept in the dark at room temperature. Orange crystals were collected after 10 d. Yield 1.58 g, 39%. – ^{1}H NMR (CD_2Cl_2): δ = 7.75–7.35 (m, 25 H, Ph), 4.12 (dd, 2 H, $^2J_{PH}$ = 10.7, $^4J_{PH}$ = 1.4, PCH_2), 1.11 (s, 9 H, *t*Bu). – $C_{37}H_{36}Cl_2O_2P_2Ru\cdot({}^2/_3\ CH_2Cl_2)$ (746.6 + 56.6 = 803.2): calcd. C 56.32, H 4.69, Cl 14.71, P 7.71; found C 56.06, H 4.69, Cl 15.12, P 7.33.

(*ttt*)-$RuCl_2(CO)[P(OMe)Ph_2][Ph_2PCH_2C(tBu)=O]$ (2e): Methanol (120 mL) was added to a solution consisting of $RuCl_2[Ph_2PCH_2C(=O)tBu]$(*p*-cymene)[14] (5.47 g, 9.26 mmol) and $P(OMe)Ph_2$ (3.20 mL, 16.0 mmol) in dichloromethane (60 mL). This mixture was stirred for 3 d. The resulting yellow slurry was concentrated under vacuum and diethyl ether was added. The yellow precipitate was collected by filtration and washed with diethyl ether. Yield 3.40 g, 52%. This crude product was found pure by NMR-spectroscopic analysis. Fractional crystallisation from a dichloromethane/ethanol mixture allowed the formation of orange-yellow crystals of analytical quality. – ^{1}H NMR (CD_2Cl_2): δ = 7.93–7.40 (m, 20 H, Ph), 4.07 (dd, 2 H, $^2J_{PH}$ = 10.5, $^4J_{PH}$ = 1.5, PCH_2), 3.65 (d, 3 H, $^3J_{PH}$ = 13.0, OMe), 0.99 (s, 9 H, *t*Bu). – $C_{32}H_{34}Cl_2O_3P_2Ru$ (700.5): calcd. C 54.86, H 4.89, Cl 10.12, P 8.84; found C 54.59, H 4.87, Cl 10.30, P 8.50.

(*ttt*)-$RuCl_2(CO)(PMe_3)[Ph_2PCMe_2C(iPr)=O]$ (2′a): A mixture consisting of $RuCl_2(PMe_3)$(*p*-cymene) (2.37 g, 6.20 mmol), ketophosphane **1′** (1.85 g, 6.20 mmol) and methanol (40 mL), was stirred for 2 d. The resulting yellow slurry was cooled to –20 °C and the yellow crystalline precipitate was then collected by filtration and washed with cold methanol (20 mL). Yield 3.00 g, 84%. Orange-yellow crystals were obtained by recrystallisation from hot methanol. – ^{1}H NMR (CD_2Cl_2): δ = 7.61–7.40 (m, 10 H, Ph), 3.33 (m, 1 H, C*H*Me$_2$), 1.67 (dd, 9 H, $^2J_{PH}$ = 10.4, $^4J_{PH}$ = 2.2, PMe_3), 1.54 (d, 6 H, $^3J_{PH}$ = 9.9, $PCMe_2$), 1.27 (d, 6 H, $^3J_{HH}$ = 6.6, CH*Me*$_2$). – ^{13}C{^{1}H} NMR (CD_2Cl_2): δ = 229.8 (dd, $^2J_{PC}$ = 13.2, $^3J_{PC}$ = 3.9, C=O), 205.2 (dd, $^2J_{PC}$ = 16.4 and 10.0, C≡O), 136.1 (dd, $^3J_{PC}$ = 10.3, $^5J_{PC}$ = 1.1, Ph_2P, *meta*), 131.1 (d, $^4J_{PC}$ = 2.3, Ph_2P, *para*), 128.4 (dd, $^1J_{PC}$ = 38.6, $^3J_{PC}$ = 1.7, Ph_2P, *ipso*), 128.1 (d, $^2J_{PC}$ = 9.7, Ph_2P, *ortho*), 55.3 (d, $^1J_{PC}$ = 17.2, P*C*Me$_2$), 36.9 (d, $^3J_{PC}$ = 2.9, *C*HMe$_2$), 24.4 (s, PC*Me*$_2$), 20.9 (s, CH*Me*$_2$), 13.7 (dd, $^1J_{PC}$ = 29.8, $^3J_{PC}$ = 1.5, PMe_3). – $C_{23}H_{32}Cl_2O_2P_2Ru$ (574.4): calcd. C 48.09, H 5.62, Cl 12.34, P 10.78; found C 48.10, H 5.63, Cl 12.11, P 10.93.

(*ttt*)-$RuCl_2(CO)[P(OMe)Ph_2][Ph_2PCMe_2C(iPr)=O]$ (2′e): A mixture consisting of $RuCl_2[P(OMe)Ph_2]$(*p*-cymene) (5.20 g, 9.95 mmol), ketophosphane **1′** (3.08 g, 10.3 mmol), dichloromethane (15 mL), and methanol (90 mL), was stirred for 4 d. The resulting mixture was concentrated under vacuum and diethyl ether was then added. A yellow precipitate (6.20 g) was collected by filtration and washed with diethyl ether. This solid was dissolved in dichloromethane (40 mL) and the orange solution was covered with methanol (40 mL) and diethyl ether (100 mL) to obtain orange crystals. Yield 5.15 g, 72%. – ^{1}H NMR ($CDCl_3$): δ = 7.98–7.39 (m, 20 H, Ph), 3.63 (d, 3 H, $^3J_{PH}$ = 12.9, OMe), 3.09 (m, 1 H, C*H*Me$_2$), 1.52 (d, 6 H, $^3J_{PH}$ = 9.9, $PCMe_2$), 0.80 (d, 6 H, $^3J_{HH}$ = 6.7, CH*Me*$_2$). – $C_{33}H_{36}Cl_2O_3P_2Ru$ (714.6): calcd. C 55.47, H 5.08, Cl 9.92, P 8.67; found C 55.38, H 5.06, Cl 10.12, P 8.47.

(*ttt*)-$RuCl_2(CO)[P(OMe)_3][Ph_2PCMe_2C(iPr)=O]$ (2′f): A solution obtained from $RuCl_2[P(OMe)_3]$(*p*-cymene) (4.66 g, 10.8 mmol), ketophosphane **1′** (3.23 g (10.8 mmol) and methanol (60 mL), was stirred for 7 d. The resulting orange-yellow slurry was heated to obtain an orange solution that was filtered. The filtrate was slowly cooled to –20 °C to afford orange crystals. Yield 4.10 g, 61%. – ^{1}H NMR (CD_2Cl_2): δ = 7.59–7.38 (m, 10 H, Ph), 3.86 (d, 9 H, $^3J_{PH}$ = 11.1, OMe), 3.34 (m, 1 H, C*H*Me$_2$), 1.56 (d, 6 H, $^3J_{PH}$ = 10.1, $PCMe_2$), 1.28 (d, 6 H, $^3J_{HH}$ = 6.7, CH*Me*$_2$). – ^{13}C{^{1}H} NMR (CD_2Cl_2): δ = 234.6 (dd, $^2J_{PC}$ = 12.9, $^3J_{PC}$ = 4.5, C=O), 204.0 (dd, $^2J_{PC}$ = 23.1 and 10.6, C≡O), 136.2 (dd, $^3J_{PC}$ = 9.8, $^5J_{PC}$ = 1.7, Ph_2P, *meta*), 131.3 (d, $^4J_{PC}$ = 1.9, Ph_2P, *para*), 128.1 (d, $^2J_{PC}$ = 9.9, Ph_2P, *ortho*), 127.4 (dd, $^1J_{PC}$ = 41.6, $^3J_{PC}$ = 3.2, Ph_2P, *ipso*), 54.6 (d, $^1J_{PC}$ = 18.0, P*C*Me$_2$), 53.2 [d, $^2J_{PC}$ = 3.8, $P(OMe)_3$], 36.9 (d, $^3J_{PC}$ = 2.7, *C*HMe$_2$), 24.5 (s, PC*Me*$_2$), 20.8 (s, CH*Me*$_2$). – $C_{23}H_{32}Cl_2O_5P_2Ru$ (622.4): calcd. C 44.38, H 5.18, Cl 11.39, P 9.95; found C 44.48, H 5.21, Cl 11.43, P 9.90.

(*ttt*)-$RuCl_2(CO)(PMe_3)[Ph_2PCMe_2CH_2C(Me)=O]$ (2′′a): Methanol (80 mL) was added to a mixture of $RuCl_2(PMe_3)$(*p*-cymene) (2.70 g, 7.06 mmol) and ketophosphane **1′′** (2.65 g, 9.32 mmol),

and this mixture was stirred for 2 d. The volatiles were evaporated under vacuum. The resulting solid was dissolved in dichloromethane (30 mL). The solution was filtered and methanol (50 mL) was added to the orange filtrate. The slow concentration of this solution afforded orange crystals. Yield 2.35 g, 59%. − ^{1}H NMR (CD_2Cl_2): δ = 7.84−7.30 (m, 10 H, Ph), 3.50 (d, 2 H, $^3J_{PH}$ = 20.3, CH_2), 2.50 (s, 3 H, MeCO), 1.57 (dd, 9 H, $^2J_{PH}$ = 10.2, $^4J_{PH}$ = 2.1, PMe_3), 1.30 (d, 6 H, $^3J_{PH}$ = 11.3, $PCMe_2$). − $^{13}C\{^1H\}$ NMR (CD_2Cl_2): δ = 221.7 (s, C=O), 205.7 (dd, $^2J_{PC}$ = 16.5 and 13.0, C≡O), 135.8 (d, $^3J_{PC}$ = 9.0, Ph_2P, *meta*), 133.4 (d, $^1J_{PC}$ = 38.8, Ph_2P, *ipso*), 130.1 (d, $^4J_{PC}$ = 2.2, Ph_2P, *para*), 127.7 (d, $^2J_{PC}$ = 9.3, Ph_2P, *ortho*), 52.8 (d, $^2J_{PC}$ = 6.4, CH_2), 36.2 (s, MeCO), 30.3 (dd, $^1J_{PC}$ = 12.6, $^3J_{PC}$ = 1.7, P*C*Me_2), 25.6 (s, PC*Me*$_2$), 13.2 (d, $^1J_{PC}$ = 28.8, PMe_3). − $C_{22}H_{30}Cl_2O_2P_2Ru$ (560.4): calcd. C 47.15, H 5.40, Cl 12.65, P 11.05; found C 47.35, H 5.38, Cl 12.84, P 11.00.

Reactivity of Complexes 2 towards Carbon Monoxide

(*ttt*)-$RuCl_2(CO)_2(PMe_3)[Ph_2PCH_2C(=O)tBu]$ (3a): A solution of **2a** (0.15 g) in $CDCl_3$ (2.0 mL) was stirred for 2 h under carbon monoxide. The ^{1}H NMR spectrum of the resulting solution shows a 1:4 mixture of **2a** and **3a**, but the addition of hexane to such a solution selectively led to the recovery of **2a**. − ^{1}H NMR ($CDCl_3$, available values for **3a** from such a mixture of **2a** and **3a**): δ = 4.04 (dd, 2 H, $^2J_{PH}$ = 9.4, $^4J_{PH}$ = 1.4, PCH_2), 1.69 (dd, 9 H, $^2J_{PH}$ = 10.1, $^4J_{PH}$ = 2.1, PMe_3), 1.05 (s, 9 H, *t*Bu).

(*ttt*)-$RuCl_2(CO)_2(PMePh_2)[Ph_2PCH_2C(=O)tBu]$ (3b): A solution of **2b** (0.15 g) in $CDCl_3$ (2.0 mL) was treated similarly, and the ^{1}H NMR spectrum of the resulting solution shows a ca. 1:1 mixture of **2b** and **3b**. − ^{1}H NMR ($CDCl_3$, mixture of the two complexes): δ = 7.82−7.36 (m, 20 H, Ph), ca. 4.10 (2 H, PCH_2), ca. 2.20 (m, 3 H, PMe), 1.08 and 1.05 (2 s, 9 H, *t*Bu).

(*cct*)-$RuCl_2(CO)_2(PMe_3)[Ph_2PCH_2C(=O)tBu]$ (4a): An orange solution of **2a** (1.00 g, 1.78 mmol) in hot toluene (80 °C, 40 mL) was stirred for 2 d under carbon monoxide and the resulting colourless solution was concentrated under vacuum to leave the crude product. Recrystallisation from hot methanol afforded colourless crystals of **4a**. Yield 0.79 g, 75%. − ^{1}H NMR (CD_2Cl_2): δ = 7.78−7.34 (m, 10 H, Ph), 4.28 (d, 2 H, $^2J_{PH}$ = 7.6, PCH_2), 1.60 (dd, 9 H, $^2J_{PH}$ = 10.8, $^4J_{PH}$ = 2.4, PMe_3), 0.76 (s, 9 H, *t*Bu). − $^{13}C\{^1H\}$ NMR (CD_2Cl_2): δ = 210.0 (dd, $^2J_{PC}$ = 10.0, $^4J_{PC}$ = 1.9, C=O), 193.4 (dd, $^2J_{PC}$ = 11.5 and 10.0, C≡O), 133.6 (d, $^3J_{PC}$ = 9.8, Ph_2P, *meta*), 131.2 (dd, $^1J_{PC}$ = 44.9, $^3J_{PC}$ = 1.4, Ph_2P, *ipso*), 131.1 (d, $^4J_{PC}$ = 2.3, Ph_2P, *para*), 128.5 (d, $^2J_{PC}$ = 10.0, Ph_2P, *ortho*), 46.0 (s, *C*Me_3), 31.8 (d, $^1J_{PC}$ = 25.0, PCH_2), 26.0 (s, C*Me*$_3$), 15.3 (dd, $^1J_{PC}$ = 33.3, $^3J_{PC}$ = 1.2, PMe_3). − ^{13}C NMR (CD_2Cl_2, selected values): δ = 31.8 (td, $^1J_{HC}$ = 130, $^1J_{PC}$ = 25.0, PCH_2). − $C_{23}H_{30}Cl_2O_3P_2Ru$ (588.4): calcd. C 46.95, H 5.14, Cl 12.05, P 10.53; found C 46.63, H 5.33, Cl 11.83, P 10.16.

(*cct*)-$RuCl_2(CO)_2(PMePh_2)[Ph_2PCH_2C(=O)tBu]\cdot CH_2Cl_2$ (4b): Complex **4b** was similarly obtained as colourless crystals in a 70% yield starting from **2b**. − ^{1}H NMR ($CDCl_3$): δ = 7.90−7.37 (m, 20 H, Ph), 4.50 (d, 2 H, $^2J_{PH}$ = 8.0, PCH_2), 2.30 (dd, 3 H, $^2J_{PH}$ = 10.6, $^4J_{PH}$ = 1.6, PMe), 0.79 (s, 9 H, *t*Bu). − $C_{33}H_{34}Cl_2O_3P_2Ru\cdot CH_2Cl_2$ (712.6 + 84.9 = 797.5): calcd. C 51.21, H 4.55, Cl 17.78, P 7.77; found C 51.21, H 4.64, Cl 16.98, P 7.71; the low chlorine value is attributed to an easy partial loss of CH_2Cl_2.

(*cct*)-$RuCl_2(CO)_2(PMe_3)[Ph_2PCMe_2C(=O)iPr]\cdot MeOH$ (4′a): A solution of **2′a** (3.00 g, 5.22 mmol) in hot toluene (85 °C, 60 mL) was stirred for 20 h under carbon monoxide, and the resulting colourless solution was concentrated to dryness under vacuum. Recrystallisation from hot methanol afforded colourless crystals. Yield 2.86 g, 86%. − ^{1}H NMR (CD_2Cl_2): δ = 7.87−7.28 (m, 10 H, Ph), 3.38 (s, 3 H, MeOH), 3.26 (m, 1 H, C*H*Me_2), 1.66 (dd, 9 H, $^2J_{PH}$ = 10.9, $^4J_{PH}$ = 2.4, PMe_3), 1.47 (d, 6 H, $^3J_{PH}$ = 12.9, $PCMe_2$), 1.19 (d, 6 H, $^3J_{HH}$ = 6.7, CH*Me*$_2$). − $^{13}C\{^1H\}$ NMR (CD_2Cl_2): δ = 218.0 (s, C=O), 193.9 (t_a, $^2J_{PC} \approx {}^2J_{P'C} \approx$11.3, C≡O), 136.4 (d, $^3J_{PC}$ = 7.9, Ph_2P, *meta*), 132.8 (d, $^1J_{PC}$ = 35.8, Ph_2P, *ipso*), 130.5 (d, $^4J_{PC}$ = 2.2, Ph_2P, *para*), 127.8 (d, $^2J_{PC}$ = 9.4, Ph_2P, *ortho*), 53.2 (dd, $^1J_{PC}$ = 17.2, $^3J_{PC}$ = 2.3, P*C*Me_2), 50.8 (s, MeOH), 35.7 (s, *C*HMe_2), 22.0 (s, PC*Me*$_2$), 20.7 (s, CH*Me*$_2$), 15.3 (d, $^1J_{PC}$ = 35.4, PMe_3). − $C_{24}H_{32}Cl_2O_3P_2Ru\cdot MeOH$ (602.4 + 32.0 = 634.5): calcd. C 47.33, H 5.72, Cl 11.18, P 9.76; found C 47.26, H 5.85, Cl 10.93, P 9.54.

Reactivity of Complexes 2 towards Acetonitrile

(*cct*)-$RuCl_2(CO)(MeCN)(PMe_3)[Ph_2PCH_2C(=O)tBu]$ (5a): **2a** (1.96 g, 3.50 mmol) was heated in acetonitrile (25 mL) to obtain a pale-yellow solution. On standing overnight at room temperature, lemon-yellow crystals formed. They were collected and then washed with acetonitrile (10 mL). Yield 1.75 g, 83%. − ^{1}H NMR (CD_2Cl_2): δ = 7.97−7.36 (m, 10 H, Ph), 4.40 (dd, 1 H, $^2J_{HH}$ = 17.1, $^2J_{PH}$ = 8.6, PCH_2, H_a), 4.25 (dd, 1 H, $^2J_{HH}$ = 17.0, $^2J_{PH}$ = 5.0, PCH_2, H_b), 1.64 (s, 3 H, MeCN), 1.54 (dd, 9 H, $^2J_{PH}$ = 10.3, $^4J_{PH}$ = 2.3, PMe_3), 0.74 (s, 9 H, *t*Bu). − $^{13}C\{^1H\}$ NMR (CD_2Cl_2): δ = 211.0 (dd, $^2J_{PC}$ = 10.7, $^4J_{PC}$ = 2.5, C=O), 199.5 (dd, $^2J_{PC}$ = 13.6 and 11.5, C≡O), 135.2 (d, $^3J_{PC}$ = 10.8, Ph, *meta*), 133.2 (d, $^3J_{PC}$ = 9.0, Ph, *meta*), 131.5 (d, $^1J_{PC}$ = 38.6, Ph, *ipso*), 130.9 (d, $^4J_{PC}$ = 2.7, Ph, *para*), 130.7 (d, $^1J_{PC}$ = 38.6, Ph, *ipso*), 129.6 (d, $^4J_{PC}$ = 1.8, Ph, *para*), 128.2 (d, $^2J_{PC}$ = 9.9, Ph, *ortho*), 128.0 (d, $^2J_{PC}$ = 9.0, Ph, *ortho*), 122.7 (s, Me*C*N), 45.9 (s, *C*Me_3), 31.4 (d, $^1J_{PC}$ = 19.9, PCH_2), 25.8 (s, C*Me*$_3$), 14.1 (d, $^1J_{PC}$ = 30.5, PMe_3), 3.6 (s, *Me*CN). − $C_{24}H_{33}Cl_2NO_2P_2Ru$ (601.5): calcd. C 47.93, H 5.53, Cl 11.79, N 2.33, P 10.30; found C 48.20, H 5.69, Cl 11.69, N 2.45, P 10.33.

(*cct*)-$RuCl_2(CO)(MeCN)(PMePh_2)[Ph_2PCH_2C(=O)tBu]$ (5b): Similarly, **2b** (2.12 g, 3.10 mmol) was heated in acetonitrile (30 mL) to obtain a pale-yellow solution that deposited lemon-yellow crystals. Yield 1.83 g, 81%. − ^{1}H NMR (CD_2Cl_2): δ = 8.00−7.32 (m, 20 H, Ph), 4.48 (dd, 1 H, $^2J_{HH}$ = 17.1, $^2J_{PH}$ = 8.9, PCH_2, H_a), 4.40 (dd, 1 H, $^2J_{HH}$ = 17.1, $^2J_{PH}$ = 5.8, PCH_2, H_b), 2.21 (dd, 3 H, $^2J_{PH}$ = 9.9, $^4J_{PH}$ = 1.7, PMe), 1.05 (s, 3 H, MeCN), 0.75 (s, 9 H, *t*Bu). − $^{13}C\{^1H\}$ NMR (CD_2Cl_2): δ = 210.9 (dd, $^2J_{PC}$ = 10.6, $^4J_{PC}$ = 1.7, C=O), 199.8 (t_a, $^2J_{PC} \approx {}^2J_{P'C} \approx$ 12.5, C≡O), 135.6−127.8 (m, 4 Ph groups), 122.0 (s, Me*C*N), 46.0 (s, *C*Me_3), 31.3 (d, $^1J_{PC}$ = 21.3, PCH_2), 25.8 (s, C*Me*$_3$), 12.5 (dd, $^1J_{PC}$ = 30.4, $^3J_{PC}$ = 1.4, PMe), 2.7 (s, *Me*CN). − $C_{34}H_{37}Cl_2NO_2P_2Ru$ (725.6): calcd. C 56.28, H 5.14, Cl 9.77, N 1.93, P 8.54; found C 56.16, H 5.18, Cl 9.76, N 2.12, P 8.25.

(*cct*)-$RuCl_2(CO)(MeCN)(PPh_3)[Ph_2PCH_2C(=O)tBu]$ (5d): Crude **2d** (5.05 g, ≈ 6.29 mmol) was heated in a mixture of acetonitrile (60 mL) and dichloromethane (15 mL) to obtain a pale-yellow solution. On standing overnight at room temperature, lemon-yellow crystals (3.23 g) were obtained. The concentration of the mother liquor afforded a supplementary crop of crystals. Overall yield 3.92 g, 79%. − ^{1}H NMR (CD_2Cl_2): δ = 8.03−7.33 (m, 25 H, Ph), 4.59 (dd, 1 H, $^2J_{HH}$ = 17.0, $^2J_{PH}$ = 8.4, PCH_2, H_a), 4.52 (dd, 1 H, $^2J_{HH}$ = 17.0, $^2J_{PH}$ = 6.5, PCH_2, H_b), 1.03 (s, 3 H, MeCN), 0.76 (s, 9 H, *t*Bu). − $C_{39}H_{39}Cl_2NO_2P_2Ru$ (787.7): calcd. C 59.47, H 4.99, Cl 9.00, N 1.78, P 7.86; found C 59.54, H 4.97, Cl 9.24, N 1.83, P 7.67.

Isomerisation of Complexes 2−2′

(*ccc*/*ctc*)-RuCl$_2$(CO)(PMe$_3$)[Ph$_2$PCH$_2$C(*t*Bu)=O] (6a). − Photo-Isomerisation of 2a: In a typical experiment, **2a** (2.00 g, 3.57 mmol) was dissolved in dichloromethane (50 mL) in a Schlenk flask. The flask was closed and placed behind a window where it was exposed to sunlight. After standing for two weeks (corresponding to ca. 50 h of exposure to sunlight), the solvent was removed under vacuum. The resulting solid was analysed by ^{1}H NMR spectroscopy, which indicated a 85% formation of **6a**. The solid was then dissolved in hot ethanol (60 mL) to obtain a solution that deposited pale-yellow crystals of **6a** on cooling. Yield 1.35 g, 68%. − **Thermally Induced Isomerisation of 2a:** A mixture of **2a** (2.00 g, 3.57 mmol) and toluene (30 mL) was heated under reflux for 20 h. The resulting cream-coloured precipitate was collected by filtration and dried under vacuum. Yield 1.54 g, 77%. − ^{1}H NMR (CD_2Cl_2): δ = 7.92−7.29 (m, 10 H, Ph), 4.26 (dd, 1 H, $^2J_{HH}$ = 17.9, $^2J_{PH}$ = 11.4, PCH_2, H_a), 4.09 (dd, 1 H, $^2J_{HH}$ = 17.9, $^2J_{PH}$ = 10.8, PCH_2, H_b), 1.51 (d, 9 H, $^2J_{PH}$ = 11.2, PMe_3), 1.29 (s, 9 H, *t*Bu). − $^{13}C\{^1H\}$ NMR (CD_2Cl_2): δ = 227.2 (t_a, $^2J_{PC} \approx {}^3J_{PC} \approx$ 2.0, C=O), 197.5 (dd, $^2J_{PC}$ = 19.5 and 12.8, C≡O), 134.4 (d, $^3J_{PC}$ = 10.4, Ph, *meta*), 133.9 (d, $^1J_{PC}$ = 50.1, Ph, *ipso*), 132.2 (d, $^4J_{PC}$ = 2.4, Ph, *para*), 131.7 (d, $^4J_{PC}$ = 2.4, Ph, *para*), 131.2 (d, $^2J_{PC}$ = 10.4, Ph, *ortho*), 130.2 (d, $^1J_{PC}$ = 24.4, Ph, *ipso*), 129.7 (d, $^3J_{PC}$ = 9.8, Ph, *meta*), 129.2 (d, $^2J_{PC}$ = 11.0, Ph, *ortho*), 47.2 (d, $^1J_{PC}$ = 30.5, PCH_2), 46.0 (t_a, $^3J_{PC} \approx {}^4J_{PC} \approx$ 3.0, *C*Me_3), 27.1 (s, C*Me*$_3$), 19.2 (d, $^1J_{PC}$ = 37.3, PMe_3). The second but very minor isomer was only detected by $^{31}P\{^1H\}$ NMR spectroscopy (Table 1). − $C_{22}H_{30}Cl_2O_2P_2Ru$ (560.4): calcd. C 47.15, H 5.40, Cl 12.65, P 11.05; found C 47.41, H 5.43, Cl 12.21, P 10.77.

(*ccc*/*ctc*)-RuCl$_2$(CO)(PMePh$_2$)[Ph$_2$PCH$_2$C(*t*Bu)=O] (6b). − Photo-Isomerisation of 2b: A solution of **2b** (11.3 g, 16.5 mmol) in dichloromethane (150 mL) was treated as above. After 3 weeks of exposure to sunlight, the solvents were evaporated and the remaining solid was dissolved in methanol (100 mL) to obtain a solution that slowly deposited pale-yellow crystals of **6b**. Yield 5.95 g, 53%. The mother liquor was stirred under carbon monoxide for 20 h to afford a colourless precipitate of **4b** (3.08 g, overall yield 79%, with respect to the recovery of ruthenium). − **Thermally Induced Isomerisation of 2b:** A mixture of **2b** (3.54 g, 5.17 mmol) and toluene (50 mL) was heated as above to obtain a cream-coloured precipitate. Yield 2.60 g, 73%. − ^{1}H NMR (CD_2Cl_2, asterisk-marked values for the major ca. 3:2 isomer): δ = 7.90−7.60 (m, 20 H, Ph), 4.24* and 4.32 (2 dd, 1 H, $^2J_{HH}$ = 17.9* and 18.0, $^2J_{PH}$ = 10.8* and 10.9, PCH_2, H_a), 4.15 and 4.11* (2 dd, 1 H, partially overlapped, $^2J_{PH}$ = 10.8*, PCH_2, H_b), 2.19* and 1.15 (2 d, 3 H, $^2J_{PH}$ = 10.9* and 9.5, PMe), 1.30* and 1.12 (2 s, 9 H, *t*Bu). − $^{13}C\{^1H\}$ NMR ($CDCl_3$, asterisk-marked values for the major isomer): δ = 227.4* (t_a, $^2J_{PC} \approx {}^3J_{P'C} \approx$ 1.7, C=O), 227.2 (d, $^2J_{PC}$ = 2.9, C=O), 203.9 (dd, $^2J_{PC}$ = 19.1 and 14.5, C≡O), 197.4* (dd, $^2J_{PC}$ = 19.0 and 12.9, C≡O), 137.8−127.6 (m, Ph resonances for both isomers), 48.7* (d, $^1J_{PC}$ = 31.5, PCH_2), 48.5 (d, $^1J_{PC}$ = 33.9, PCH_2), 45.6* (d, $^3J_{PC}$ = 3.4, *C*Me_3), 45.6 (d, $^3J_{PC}$ = 2.9, *C*Me_3), 27.0* (s, C*Me*$_3$), 26.7 (s, C*Me*$_3$), 17.9* (d, $^1J_{PC}$ = 36.1, PMe), 16.6 (d, $^1J_{PC}$ = 37.0, PMe). − $C_{32}H_{34}Cl_2O_2P_2Ru$ (684.5): calcd. C 56.15, H 5.01, Cl 10.36, P 9.05; found C 55.86, H 5.10, Cl 10.40, P 9.29.

(*ccc*/*ctc*)-RuCl$_2$(CO)(PMe$_3$)[Ph$_2$PCMe$_2$C(*i*Pr)=O] (6′a). − Photo-Isomerisation of 2′a: Exposure to sunlight of a solution of **2′a** (3.00 g, 5.22 mmol) in dichloromethane (50 mL) resulted in a pale-yellow solution. Toluene (150 mL) was then added and partial slow evaporation of the solvents afforded pale-yellow crystals of **6′a·toluene**. Yield 2.36 g, 68%. − **Thermally Induced Isomerisation of 2′a:** A mixture of **2′a** (4.00 g, 6.96 mmol) and ethanol (60 mL) was heated under reflux for 3 d. The resulting solution was concentrated to dryness to leave a pale-yellow solid that was identified as pure **6′a** by NMR spectroscopy and elemental analysis. − ^{1}H NMR ($CDCl_3$): δ = 8.16−7.20 (m, 10 H, Ph), 3.28 (m, 1 H, C*H*Me_2), 1.52 (d, 9 H, $^2J_{PH}$ = 11.0, PMe_3), 1.49 (d, 3 H, $^3J_{PH}$ = 9.5, PC*Me*), 1.39 (d, 3 H, $^3J_{PH}$ = 12.8, PC*Me*), 1.39 (d, 3 H, $^3J_{HH}$ = 6.8, CH*Me*), 1.32 (d, 3 H, $^3J_{HH}$ = 6.6, CH*Me*). − $^{13}C\{^1H\}$ NMR (CD_2Cl_2): δ = 232.4 (dd, $^2J_{PC}$ = 7.2, $^3J_{PC}$ = 1.8, C=O), 197.6 (dd, $^2J_{PC}$ = 19.8 and 12.6, C≡O), 136.4 (d, $^2J_{PC}$ = 9.0, Ph, *ortho*), 133.0 (d, $^1J_{PC}$ = 46.7, Ph, *ipso*), 133.0 (d, $^3J_{PC}$ = 9.0, Ph, *meta*), 132.7 (s, Ph, *para*), 131.5 (s, Ph, *para*), 129.1 (d, $^3J_{PC}$ = 10.8, Ph, *meta*), 128.7 (d, $^2J_{PC}$ = 10.8, Ph, *ortho*), 125.9 (d, $^1J_{PC}$ = 43.1, Ph, *ipso*), 58.6 (d, $^1J_{PC}$ = 25.1, P*C*Me_2), 37.1 (d, $^3J_{PC}$ = 3.6, *C*HMe_2), 24.4 (s, CH*Me*), 23.0 (s, CH*Me*), 20.7 (s, PC*Me*), 20.5 (s, PC*Me*), 18.8 (d, $^1J_{PC}$ = 37.7, PMe_3). − $C_{23}H_{32}Cl_2O_2P_2Ru$: calcd. C 48.09, H 5.62, Cl 12.34, P 10.78; found C 48.10, H 5.70, Cl 12.26, P 10.67. − $C_{23}H_{32}Cl_2O_2P_2Ru$·toluene (574.4 + 92.1 = 666.5): calcd. C 54.06, H 6.05, Cl 10.64, P 9.29; found C 53.93, H 6.13, Cl 10.67, P 9.23.

Reactivity of Complexes 6−6′ towards Carbon Monoxide

(*ccc*)-RuCl$_2$(CO)$_2$(PMe$_3$)[Ph$_2$PCH$_2$C(=O)*t*Bu] (7a): A pale-yellow solution of **6a** (2.50 g, 4.46 mmol) in dichloromethane (30 mL) was stirred for 20 h under carbon monoxide, and the resulting clear solution was covered with hexane (100 mL) under the carbon monoxide, to obtain **7a** as colourless crystals. Yield 2.28 g, 87%. Alternatively, a solution of **6a** (2.00 g, 3.57 mmol) in methanol (40 mL) was stirred for 20 h under carbon monoxide to afford **7a** (as determined by NMR and IR spectroscopy) as a white precipitate that was collected by filtration and dried. Yield 1.73 g, 82%. Attempts to recrystallise from hot methanol afforded colourless crystals, but of the *cct* isomer **4a**. − ^{1}H NMR (CD_2Cl_2, asterisk-marked values for the major 3:1 isomer): δ = 7.86−7.41 (m, 10 H, Ph), 4.72* and 4.33 (2 dd, 1 H, $^2J_{HH}$ = 17.8* and 17.3, $^2J_{PH}$ = 7.5* and 6.8, PCH_2, H_a), 4.39* and 4.02 (2 dd, 1 H, $^2J_{PH}$ = 7.5* and 9.9, PCH_2, H_b), 1.24* and 1.23 (2 d, 9 H, $^2J_{PH}$ = 10.6* and 10.3, PMe_3), 1.06 and 0.81* (2 s, 9 H, *t*Bu). − $^{13}C\{^1H\}$ NMR (CD_2Cl_2, asterisk-marked values for the major isomer): δ = 209.9* (d, $^2J_{PC}$ = 10.4, C=O), 208.7 (d, $^2J_{PC}$ = 6.1, C=O), 194.9 (dd, $^2J_{PC}$ = 15.9 and 12.2, C≡O), 194.0* (t_a, $^2J_{PC} \approx {}^2J_{P'C} \approx$ 13.4, C≡O), 190.1* (dd, $^2J_{PC}$ = 115.4 and 11.6, C≡O), 189.7 (dd, $^2J_{PC}$ = 118.4 and 11.0, C≡O), 134.3−128.5 (m, Ph resonances for both isomers), 46.1* (d, $^3J_{PC}$ = 1.8, *C*Me_3), 45.8 (d, $^3J_{PC}$ = 2.4, *C*Me_3), 36.4 (d, $^1J_{PC}$ = 35.5, PCH_2), 32.0* (d, $^1J_{PC}$ = 28.5, PCH_2), 26.7* (s, C*Me*$_3$), 26.0 (s, C*Me*$_3$), 18.9* (d, $^1J_{PC}$ = 36.0, PMe_3), 14.3 (d, $^1J_{PC}$ = 33.0, PMe_3). − $C_{23}H_{30}Cl_2O_3P_2Ru$ (588.4): calcd. C 46.95, H 5.14, Cl 12.05, P 10.53; found C 46.80, H 5.12, Cl 11.91, P 10.73.

(*ccc*)-RuCl$_2$(CO)$_2$(PMePh$_2$)[Ph$_2$PCH$_2$C(=O)*t*Bu] (7b): Complex **7b** was studied by NMR spectroscopy after a solution of **6b** in $CDCl_3$ (or CD_2Cl_2) was stirred overnight under carbon monoxide. − ^{1}H NMR ($CDCl_3$, asterisk-marked values for the major 4:1 isomer): δ = 7.80−7.13 (m, 20 H, Ph), 4.88* and 4.47 (2 dd, 1 H, $^2J_{HH}$ = 18.0* and 17.4, $^2J_{PH}$ = 6.2* and 4.8, PCH_2, H_a), 4.35* and 1.98 (2 dd, 1 H, $^2J_{PH}$ = 7.9* and 10.2, PCH_2, H_b), 2.36 and 1.35* (2 d, 3 H, $^2J_{PH}$ = 10.9 and 10.5*, PMe), 0.82* and 0.71 (2 s, 9 H, *t*Bu). − $^{13}C\{^1H\}$ NMR ($CDCl_3$, asterisk-marked values for the major isomer): δ = 209.9* (d, $^2J_{PC}$ = 10.6, C=O), 208.2 (d, $^2J_{PC}$ = 9.9, C=O), 194.4* (t_a, $^2J_{PC} \approx {}^2J_{P'C} \approx$ 12.4, C≡O), 193.6 (dd, $^2J_{PC}$ = 13.4 and 11.1, C≡O), 188.8 (dd, $^2J_{PC}$ = 117.4 and 10.8, C≡O), 187.7* (dd, $^2J_{PC}$ = 116.0 and 10.3, C≡O), 139.5−127.8 (m, Ph resonances for both isomers), 45.8* (d, $^3J_{PC}$ = 1.6, *C*Me_3), 45.6 (d, $^3J_{PC}$ = 1.3, *C*Me_3), 32.3* (d, $^1J_{PC}$ = 28.9, PCH_2), 31.3 (d, $^1J_{PC}$ = 26.8, PCH_2), 26.0 (s, C*Me*$_3$), 25.8* (s, C*Me*$_3$), 11.9 (d, $^1J_{PC}$ = 35.9,

PMe), 11.6* (d, $^1J_{PC}$ = 33.8, PMe). − The removal of the solvent from such solutions left a white solid consisting of a mixture of **7b** and **6b**, but allowing the determination of the main IR absorptions of **7b** in the solid state (Table 1).

Formation of 4b in Methanol: See synthesis of **6b**.

Reaction of 6′a with Carbon Monoxide: A solution of **6′a** in dichloromethane was stirred for 20 h under carbon monoxide and then examined by $^{31}P\{^1H\}$ NMR spectroscopy which indicated a complete conversion of **6′a** into **4′a**.

Cationic Derivatives

(*cct*)-{RuCl(CO)$_2$(PMe$_3$)[Ph$_2$PCH$_2$C(*t*Bu)=O]}(BF$_4$)·$^1/_2$CH$_2$Cl$_2$ (8a): A mixture consisting of **4a** (3.50 g, 5.95 mmol) and $AgBF_4$ (1.16 g, 5.95 mmol) in dichloromethane (60 mL) was stirred overnight. The resulting solution was decanted, then filtered and the filtrate was covered with diethyl ether (150 mL) to afford colourless crystals. Yield 3.15 g, 78%. Complex **8a** was obtained in a similar manner when starting from **6a** instead of **4a**. − ^1H NMR (CD_2Cl_2): δ = 7.84−7.33 (m, 10 H, Ph), 4.79 (ddd, 1 H, $^2J_{HH}$ = 18.7, $^2J_{PH}$ = 11.2, $^4J_{PH}$ = 2.9, PCH$_2$, H$_a$), 4.11 (dd, 1 H, $^2J_{HH}$ = 18.7, $^2J_{PH}$ = 10.9, PCH$_2$, H$_b$), 1.84 (dd, 9 H, $^2J_{PH}$ = 11.3, $^4J_{PH}$ = 2.6, PMe$_3$), 1.36 (s, 9 H, *t*Bu). − $^{13}C\{^1H\}$ NMR (CD_2Cl_2): δ = 238.0 (t$_a$, $^2J_{PC} \approx {}^3J_{P'C} \approx$ 4.9, C=O), 195.5 (dd, $^2J_{PC}$ = 13.3 and 9.0, C≡O), 190.0 (dd, $^2J_{PC}$ = 11.6 and 9.2, C≡O), 134.4 (dd, $^3J_{PC}$ = 11.7, $^5J_{PC}$ = 1.5, PhP, *meta*), 133.3 (d, $^4J_{PC}$ = 2.6, PhP, *para*), 132.7 (d, $^4J_{PC}$ = 2.3, PhP, *para*), 131.6 (d, $^1J_{PC}$ = 47.7, PhP, *ipso*), 130.9 (d, $^3J_{PC}$ = 11.4, PhP, *meta*), 130.4 (d, $^2J_{PC}$ = 10.7, PhP, *ortho*), 130.0 (d, $^2J_{PC}$ = 11.6, PhP, *ortho*), 125.2 (dd, $^1J_{PC}$ = 53.5, $^3J_{PC}$ = 2.6, PhP, *ipso*), 47.9 (d, $^3J_{PC}$ = 3.5, *C*Me$_3$), 44.0 (d, $^1J_{PC}$ = 30.5, PCH$_2$), 27.0 (s, C*Me*$_3$), 14.9 (dd, $^1J_{PC}$ = 33.9, $^3J_{PC}$ = 1.4, PMe$_3$). − $C_{23}H_{30}BClF_4O_3P_2Ru\cdot{}^1/_2CH_2Cl_2$ (639.7 + 42.6 = 682.2): calcd. C 41.37, H 4.58, Cl 10.39, P 9.08; found C 41.16, H 4.49, Cl 10.38, P 9.22.

(*cct*)-{RuCl(CO)$_2$(PMe$_3$)[Ph$_2$PCMe$_2$C(*i*Pr)=O]}(BF$_4$) (8′a): Complex **8′a** was obtained as colourless crystals in a 84% yield, as above, starting from **4′a**. − ^1H NMR (CD_2Cl_2): δ = 7.94−7.20 (m, 10 H, Ph), 3.47 (m, 1 H, C*H*Me$_2$), 1.86 (dd, 9 H, $^2J_{PH}$ = 11.3, $^4J_{PH}$ = 2.6, PMe$_3$), 1.71 (d, 3 H, $^3J_{PH}$ = 10.1, PCMe), 1.51 (d, 3 H, $^3J_{PH}$ = 12.9, PCMe), 1.41 (d, 3 H, $^3J_{HH}$ = 6.8, C*H*Me), 1.23 (d, 3 H, $^3J_{HH}$ = 6.6, C*H*Me). − $C_{24}H_{32}BClF_4O_3P_2Ru$ (653.8): calcd. C 44.09, H 4.93, Cl 5.42, P 9.48; found C 43.95, H 4.83, Cl 5.66, P 9.60.

(*cct*)-{RuCl(CO)(MeCN)(PMe$_3$)[Ph$_2$PCH$_2$C(*t*Bu)=O]}(BF$_4$) (9a): Compound **5a** (1.67 g, 2.78 mmol) was added to a cold mixture (−60 °C) of $AgBF_4$ (0.54 g, 2.78 mmol), dichloromethane (50 mL), and acetonitrile (5 mL). After stirring overnight at room temperature, the solvents were evaporated leaving a solid that was extracted with dichloromethane (20 mL). The solution was filtered and the yellow filtrate was then covered with diethyl ether (100 mL) to afford lemon-yellow crystals. Yield 1.58 g, 87%. − ^1H NMR (CD_2Cl_2): δ = 7.88−7.23 (m, 10 H, Ph), 4.62 (ddd, 1 H, $^2J_{HH}$ = 18.4, $^2J_{PH}$ = 11.0, $^4J_{PH}$ = 2.9, PCH$_2$, H$_a$), 3.82 (dd, 1 H, $^2J_{HH}$ = 18.4, $^2J_{PH}$ = 10.2, PCH$_2$, H$_b$), 1.82 (t$_a$, 3 H, $^5J_{PH} \approx {}^5J_{P'H} \approx$ 0.8, MeCN), 1.69 (dd, 9 H, $^2J_{PH}$ = 10.7, $^4J_{PH}$ = 2.5, PMe$_3$), 1.38 (s, 9 H, *t*Bu). − $^{13}C\{^1H\}$ NMR (CD_2Cl_2): δ = 234.7 (dd, $^2J_{PC}$ = 7.0, $^3J_{PC}$ = 4.6, C=O), 201.9 (dd, $^2J_{PC}$ = 14.8 and 9.8, C≡O), 135.0 (dd, $^3J_{PC}$ = 12.0, $^5J_{PC}$ = 1.8, Ph, *meta*), 132.8 (d, $^4J_{PC}$ = 2.5, Ph, *para*), 131.5 (d, $^4J_{PC}$ = 1.9, Ph, *para*), 131.1 (d, $^3J_{PC}$ = 10.8, Ph, *meta*), 130.4 (dd, $^1J_{PC}$ = 41.4, $^3J_{PC}$ = 1.5, Ph, *ipso*), 130.0 (d, $^2J_{PC}$ = 10.0, Ph, *ortho*), 129.7 (d, $^2J_{PC}$ = 10.9, Ph, *ortho*), 122.4 (s, Me*C*N), 127.0 (dd, $^1J_{PC}$ = 49.7, $^3J_{PC}$ = 2.3, Ph, *ipso*), 47.3 (d, $^3J_{PC}$ = 3.2, *C*Me$_3$), 43.0 (d, $^1J_{PC}$ = 27.0, PCH$_2$), 27.1 (s, C*Me*$_3$), 13.7 (dd, $^1J_{PC}$ = 31.3, $^3J_{PC}$ = 1.5, PMe$_3$), 3.5 (s, *Me*CN). − $C_{24}H_{33}BClF_4NO_2P_2Ru$ (652.8): calcd. C 44.16, H 5.10, Cl 5.43, N 2.15, P 9.49; found C 43.93, H 5.25, Cl 5.12, N 2.08, P 9.37.

Enolatophosphane Complexes

(*ttt*)-RuCl(CO)$_2$(PMe$_3$)[Ph$_2$PCH=C(*t*Bu)O] (10a): A mixture consisting of **2a** (3.00 g, 5.35 mmol) and K_2CO_3 (0.75 g, 5.43 mmol) in dichloromethane (30 mL) was stirred for 2 d under carbon monoxide. The resulting mixture was filtered and the yellow filtrate was concentrated leaving a crude product that was recrystallised from a mixture of benzene (10 mL) and hexane (100 mL). Lemon-yellow crystals were obtained. Yield 1.93 g, 65%. − ^1H NMR (CD_2Cl_2): δ = 7.87−7.37 (m, 10 H, Ph), 4.78 (dd, 1 H, $^2J_{PH}$ = 2.7, $^4J_{PH}$ = 1.7, PCH=), 1.66 (dd, 9 H, $^2J_{PH}$ = 9.9, $^4J_{PH}$ = 1.9, PMe$_3$), 1.11 (s, 9 H, *t*Bu). − $^{13}C\{^1H\}$ NMR (CD_2Cl_2): δ = 203.1 (dd, $^2J_{PC}$ = 16.4, $^3J_{PC}$ = 5.2, =CO), 196.6 (t$_a$, $^2J_{PC} \approx {}^2J_{P'C} \approx$ 13.9, C≡O), 139.1 (dd, $^1J_{PC}$ = 48.9, $^3J_{PC}$ = 2.1, Ph, *ipso*), 131.5 (dd, $^3J_{PC}$ = 10.5, $^5J_{PC}$ = 1.6, Ph, *meta*), 130.0 (d, $^4J_{PC}$ = 2.3, Ph, *para*), 128.7 (d, $^2J_{PC}$ = 10.1, Ph, *ortho*), 71.7 (dd, $^1J_{PC}$ = 61.5, $^3J_{PC}$ = 1.8, PCH=), 39.7 (d, $^3J_{PC}$ = 11.8, *C*Me$_3$), 29.6 (s, C*Me*$_3$), 15.6 (dd, $^1J_{PC}$ = 29.4, $^3J_{PC}$ = 1.6, PMe$_3$). − $C_{23}H_{29}ClO_3P_2Ru$ (552.0): calcd. C 50.05, H 5.30, Cl 6.42; found C 49.88, H 5.36, Cl 6.03.

(*ttt*)-RuCl(CO)$_2$(P*i*PrPh$_2$)[Ph$_2$PCH=C(*t*Bu)O]·CH$_2$Cl$_2$ (10c): A mixture consisting of **2c** (1.41 g, 1.77 mmol) and K_2CO_3 (0.30 g, 2.17 mmol) in dichloromethane (25 mL), was stirred for 20 h under carbon monoxide. The resulting mixture was filtered and the filtrate was covered with methanol to afford yellow crystals. Yield 0.81 g, 65%. − ^1H NMR (CD_2Cl_2): δ = 7.83−7.27 (m, 20 H, Ph), 4.69 (dd, 1 H, $^2J_{PH}$ = 3.2, $^4J_{PH}$ = 2.1, PCH=), 3.16 (m, 1 H, C*H*Me$_2$), 1.10 (dd, 6 H, $^3J_{HH}$ = 7.0, $^3J_{PH}$ = 15.7, CH*Me*$_2$), 1.01 (s, 9 H, *t*Bu). − $^{13}C\{^1H\}$ NMR (CD_2Cl_2): δ = 203.5 (dd, $^2J_{PC}$ = 15.7, $^4J_{PC}$ = 5.2, =CO), 196.8 (dd, $^2J_{PC}$ = 14.0 and 12.1, C≡O), 138.3 (dd, $^1J_{PC}$ = 50.4, $^3J_{PC}$ = 2.5, Ph$_2$P, *ipso*), 134.2 (d, $^3J_{PC}$ = 9.4, Ph$_2$P, *meta*), 132.1 (dd, $^1J_{PC}$ = 37.7, $^3J_{PC}$ = 1.4, Ph$_2$P, *ipso*), 131.5 (dd, $^3J_{PC}$ = 10.0, $^5J_{PC}$ = 1.2, Ph$_2$P, *meta*), 130.6 (d, $^4J_{PC}$ = 1.8, Ph$_2$P, *para*), 130.1 (d, $^4J_{PC}$ = 2.4, Ph$_2$P, *para*), 128.7 (d, $^2J_{PC}$ = 10.5, Ph$_2$P, *ortho*), 128.6 (d, $^2J_{PC}$ = 9.1, Ph$_2$P, *ortho*), 70.9 (d, $^1J_{PC}$ = 62.7, PCH=), 39.5 (d, $^3J_{PC}$ = 12.2, *C*Me$_3$), 29.7 (s, C*Me*$_3$), 24.4 (d, $^1J_{PC}$ = 22.6, *C*HMe$_2$), 17.9 (s, CH*Me*$_2$). − ^{13}C NMR (CD_2Cl_2, selected values): δ = 70.9 (dd, $^1J_{HC}$ = 164, $^1J_{PC}$ = 62.7, PCH=). − $C_{35}H_{37}ClO_3P_2Ru$ (704.1): calcd. C 59.70, H 5.30, Cl 5.03, P 8.80; found C 59.64, H 5.44, Cl 5.46, P 8.52.

(*ttt*)-RuCl(CO)$_2$[P(OMe)Ph$_2$][Ph$_2$PCH=C(*t*Bu)O]·CH$_2$Cl$_2$ (10e): A mixture consisting of **2e** (4.14 g, 5.91 mmol) and K_2CO_3 (0.82 g, 5.93 mmol) in dichloromethane (60 mL), was stirred for 3 d under carbon monoxide. The resulting mixture was filtered and the yellow filtrate was concentrated leaving a yellow solid. Yield 3.20 g, 70%. Yellow crystals were obtained after recrystallisation from dichloromethane/methanol. − ^1H NMR (CD_2Cl_2): δ = 7.83−7.30 (m, 20 H, Ph), 4.72 (t$_a$, 1 H, $^2J_{PH} \approx {}^4J_{PH} \approx$ 2.6, PCH=), 3.63 (d, 3 H, $^3J_{PH}$ = 13.3, OMe), 1.04 (s, 9 H, *t*Bu). − $C_{33}H_{33}ClO_4P_2Ru\cdot CH_2Cl_2$ (692.1 + 84.9 = 777.0): calcd. C 52.56, H 4.54, Cl 13.69, P 7.97; found C 52.16, H 4.61, Cl 12.46, P 7.92; the low chlorine value is likely to be due to to the easy loss of dichloromethane.

(*ccc*)-RuCl(CO)$_2$(PMe$_3$)[Ph$_2$PCH=C(*t*Bu)O] (11a): A mixture consisting of **6a** (3.43 g, 6.12 mmol) and K_2CO_3 (0.85 g, 6.15 mmol) in dichloromethane (40 mL), was stirred for 20 h under carbon monoxide. The resulting slurry was filtered and the filtrate was covered with toluene (30 mL) and then hexane (100 mL), to afford pale-yellow (almost colourless) crystals. Yield 2.86 g, 85%. − ^1H NMR (CD_2Cl_2): δ = 7.73−7.33 (m, 10 H, Ph), 4.74 (d, 1 H, $^2J_{PH}$ = 4.4,

PCH=), 1.27 (s, 9 H, *t*Bu), 1.06 (d, 9 H, $^2J_{PH}$ = 10.4, PMe_3). − $^{13}C\{^1H\}$ NMR (CD_2Cl_2): δ = 201.7 (d, $^2J_{PC}$ = 14.4, =CO), 199.4 (dd, $^2J_{PC}$ = 14.4 and 10.8, C≡O), 189.3 (dd, $^2J_{PC}$ = 113.1 and 10.8, C≡O), 141.1 (dd, $^1J_{PC}$ = 58.8, $^3J_{PC}$ = 2.2, Ph, *ipso*), 136.4 (dd, $^1J_{PC}$ = 56.1, $^3J_{PC}$ = 3.6, Ph, *ipso*), 131.5 (d, $^3J_{PC}$ = 9.9, Ph, *meta*), 131.1 (d, $^4J_{PC}$ = 2.7, Ph, *para*), 130.3 (d, $^2J_{PC}$ = 10.8, Ph, *ortho*), 130.3 (part of d, Ph, *para*), 129.6 (d, $^3J_{PC}$ = 10.8, Ph, *meta*), 129.1 (d, $^2J_{PC}$ = 10.8, Ph, *ortho*), 69.5 (d, $^1J_{PC}$ = 64.6, PCH=), 39.9 (d, $^3J_{PC}$ = 12.6, *C*Me_3), 29.7 (s, C*Me*$_3$), 13.3 (d, $^1J_{PC}$ = 31.4, PMe_3). − ^{13}C NMR (CD_2Cl_2, selected values): δ = 69.5 (dd, $^1J_{HC}$ = 164, $^1J_{PC}$ = 64.6, PCH=). − $C_{23}H_{29}ClO_3P_2Ru$ (552.0): calcd. C 50.05, H 5.30, Cl 6.42, P 11.22; found C 50.02, H 5.42, Cl 6.36, P 11.28.

(*ccc*)-RuCl(CO)$_2$(PMePh$_2$)[Ph$_2$PCH=C(*t*Bu)O] (11b): A mixture consisting of **6b** (2.04 g, 2.98 mmol) and K_2CO_3 (0.45 g, 3.26 mmol) in dichloromethane (40 mL), was stirred for 20 h under carbon monoxide. The resulting slurry was filtered and the filtrate was concentrated to dryness. The resulting solid was dissolved in a hot mixture of toluene (30 mL) and dichloromethane (15 mL) to obtain a clear solution that was covered with hexane (130 mL). Colourless crystals were obtained. Yield 1.69 g, 84%. − ^1H NMR (CD_2Cl_2, asterisk-marked values for the major 9:1 isomer): δ = 7.55−7.28 (m, 20 H, Ph), 4.89* and 4.84 (2 d, 1 H, $^2J_{PH}$ = 4.4* and 2.0, PCH=), 1.38* and 1.35 (2 s, 9 H, *t*Bu), 1.22 and 1.20* (2 dd, 3 H, $^2J_{PH}$ = 10.7 and 9.5*, $^4J_{PH}$ = 1.2 and 0.9*, PMe). − $^{13}C\{^1H\}$ NMR (CD_2Cl_2, asterisk-marked values for the major isomer): δ = 201.8* (d, $^2J_{PC}$ = 14.5, =CO), 199.4 (d, $^2J_{PC}$ = 17.4, =CO), 199.5 (dd, $^2J_{PC}$ = 13.7 and 10.7, C≡O), 198.5* (dd, $^2J_{PC}$ = 12.6 and 11.1, C≡O), 190.9 (dd, $^2J_{PC}$ = 105.3 and 11.4, C≡O), 189.4* (dd, $^2J_{PC}$ = 114.1 and 11.4, C≡O), 141.5−127.9 (m, Ph resonances for both isomers), 70.6* (d, $^1J_{PC}$ = 64.9, PCH=), 68.5 (d, $^1J_{PC}$ = 61.8, PCH=), 40.2* (d, $^3J_{PC}$ = 12.2, *C*Me_3), 39.7 (d, $^3J_{PC}$ = 12.2, *C*Me_3), 29.9 (s, C*Me*$_3$ for both isomers), 11.6 (dd, $^1J_{PC}$ = 23.0, $^3J_{PC}$ = 1.5, PMe), 11.2* (d, $^1J_{PC}$ = 28.2, $^3J_{PC}$ = 2.3, PMe). − $C_{33}H_{33}ClO_3P_2Ru$ (676.1): calcd. C 58.63, H 4.92, Cl 5.24, P 9.16; found C 58.35, H 4.98, Cl 5.42, P 9.33.

(*cct*)-RuCl(CO)$_2$(PMe$_3$)[Ph$_2$PCH=C(*t*Bu)O] (12a): A mixture consisting of **4a** (1.50 g, 2.20 mmol) and K_2CO_3 (0.31 g, 2.24 mmol) in dichloromethane (20 mL), was stirred for 7 d as required to complete the reaction, and then concentrated to dryness. The remaining solid was extracted with toluene (25 mL). The solution was filtered and the filtrate was covered with hexane (100 mL) to afford colourless crystals. Yield 0.90 g, 74%. − ^1H NMR (CD_2Cl_2): δ = 7.70−7.35 (m, 10 H, Ph), 4.58 (t_a, 1 H, $^2J_{PH} \approx {}^4J_{PH} \approx$ 3.0, PCH=), 1.66 (dd, 9 H, $^2J_{PH}$ = 10.6, $^4J_{PH}$ = 2.1, PMe_3), 1.20 (s, 9 H, *t*Bu). − $^{13}C\{^1H\}$ NMR (CD_2Cl_2): δ = 200.6 (dd, $^2J_{PC}$ = 18.0, $^3J_{PC}$ = 7.2, =CO), 198.2 (dd, $^2J_{PC}$ = 11.2 and 8.5, C≡O), 193.9 (t_a, $^2J_{PC} \approx {}^2J_{P'C} \approx$ 11.2, C≡O), 138.7 (d, $^1J_{PC}$ = 51.2, Ph, *ipso*), 133.6 (dd, $^1J_{PC}$ = 44.0, $^3J_{PC}$ = 3.6, Ph, *ipso*), 133.2 (dd, $^3J_{PC}$ = 9.9, $^5J_{PC}$ = 1.8, Ph, *meta*), 131.5 (dd, $^3J_{PC}$ = 10.8, $^5J_{PC}$ = 1.8, Ph, *meta*), 130.1 (d, $^4J_{PC}$ = 2.7, Ph, *para*), 130.0 (d, $^4J_{PC}$ = 2.7, Ph, *para*), 128.9 (d, $^2J_{PC}$ = 9.9, Ph, *ortho*), 128.4 (d, $^2J_{PC}$ = 10.8, Ph, *ortho*), 69.8 (dd, $^1J_{PC}$ = 61.0, $^3J_{PC}$ = 1.8, PCH=), 39.5 (d, $^3J_{PC}$ = 12.6, *C*Me_3), 29.8 (s, C*Me*$_3$), 14.8 (d, $^1J_{PC}$ = 30.4, PMe_3). − $C_{23}H_{29}ClO_3P_2Ru$ (552.0): calcd. C 50.05, H 5.30, Cl 6.42, P 11.22; found C 49.98, H 5.31, Cl 6.34, P 10.77.

(*cct*)-RuCl(CO)(MeCN)(PMe$_3$)[Ph$_2$PCH=C(*t*Bu)O] (13a): A mixture consisting of **9a** (1.00 g, 1.53 mmol) and K_2CO_3 (0.26 g, 1.90 mmol) in dichloromethane (25 mL), was stirred for 6 d and then concentrated to dryness. The remaining solid was extracted with toluene (15 mL). The solution was filtered and acetonitrile (1.0 mL) was added to the filtrate that was then covered with hexane (100 mL) to afford pale-yellow crystals. Yield 0.44 g, 50%. − ^1H NMR (CD_2Cl_2): δ = 7.80−7.29 (m, 10 H, Ph), 4.52 (dd, 1 H, $^2J_{PH}$ = 3.3, $^4J_{PH}$ = 1.1, PCH=), 1.58 (t_a, 3 H, $^5J_{PH} \approx {}^5J_{P'H} \approx$ 0.9, MeCN), 1.53 (dd, 9 H, $^2J_{PH}$ = 9.9, $^4J_{PH}$ = 2.1, PMe_3), 1.21 (s, 9 H, *t*Bu). − $C_{24}H_{32}ClNO_2P_2Ru$ (565.0): calcd. C 51.02, H 5.71, Cl 6.27, N 2.48, P 10.96; found C 51.03, H 5.78, Cl 6.14, N 2.49, P 10.84.

Acknowledgments

This work was supported by the "Centre National de la Recherche Scientifique". The author is grateful to J.-P. Guégan for NMR-technical assistance.

[1] J. C. Jeffrey, T. B. Rauchfuss, *Inorg. Chem.* **1979**, *18*, 2658−2666.
[2] A. Bader, E. Lindner, *Coord. Chem. Rev.* **1991**, *108*, 27−110.
[3] E. Lindner, S. Pautz, M. Haustein, *Coord. Chem. Rev.* **1996**, *155*, 145−162.
[4] E. Lindner, A. Möckel, H. A. Mayer, H. Kühbauch, R. Fawzi, M. Steimann, *Inorg. Chem.* **1993**, *32*, 1266−1271.
[5] E. Lindner, A. Möckel, H.A. Mayer, R. Fawzi, *Chem. Ber.* **1992**, *125*, 1363−1367.
[6] E. Lindner, A. Möckel, *Z. Naturforsch., Teil B* **1992**, *47*, 693−696.
[7] E. Lindner, B. Karle, *Chem. Ber.* **1990**, *123*, 1469−1473.
[8] E. Lindner, U. Schober, R. Fawzi, W. Hiller, U. Englert, P. Wegner, *Chem. Ber.* **1987**, *120*, 1621−1628.
[9] P. Braunstein, D. Matt, D. Nobel, S.-E. Bouaoud, B. Carluer, D. Grandjean, P. Lemoine, *J. Chem. Soc., Dalton Trans.* **1986**, 415−419.
[10] P. Braunstein, D. Matt, Y. Dusausoy, *Inorg. Chem.* **1983**, *22*, 2043−2047.
[11] H. Werner, A. Stark, M. Schulz, J. Wolf, *Organometallics* **1992**, *11*, 1126−1130.
[12] B. Demerseman, R. Le Lagadec, B. Guilbert, C. Renouard, P. Crochet, P. H. Dixneuf, *Organometallics* **1994**, *13*, 2269−2283.
[13] P. Braunstein, Y. Chauvin, J. Nähring, Y. Dusausoy, D. Bayeul, A. Tiripicchio, F. Ugozzoli, *J. Chem. Soc., Dalton Trans.* **1995**, 851−862.
[14] B. Demerseman, B. Guilbert, C. Renouard, M. Gonzalez, P. H. Dixneuf, D. Masi, C. Mealli, *Organometallics* **1993**, *12*, 3906−3917.
[15] D. W. Krassowski, J. H. Nelson, K. R. Brower, D. Hauenstein, R. A. Jacobson, *Inorg. Chem.* **1988**, *27*, 4294−4307.
[16] C. F. J. Barnard, J. A. Daniels, J. Jeffery, R. J. Mawby, *J. Chem. Soc., Dalton Trans.* **1976**, 953−961.
[17] R. S. Berry, *J. Chem. Phys.* **1960**, *32*, 933−938.
[18] H. Le Bozec, D. Touchard, P. H. Dixneuf, *Adv. Organomet. Chem.* **1989**, *29*, 163−247.

Received March 2, 2001
[I01077]

Synthesis and Structure of an Asymmetric Binuclear Phenylhydrazonato Anionic Complex of Palladium Containing a Pd−C(aryl) Bond *cis* to a Pd−N(amido) Bond

Arancha Carbayo,[a] José V. Cuevas,[a] Gabriel García-Herbosa,*[a] Santiago García-Granda,[b] and Daniel Miguel[c]

Dedicated to Professor D. Rafael Uson on the occasion of his 75th birthday

Keywords: Palladium / Hydrazones / Cyclopalladatation / Amido compounds

The synthesis and structure of a unique asymmetric folded binuclear anionic complex of palladium containing two different hydrazonato ligands and showing a Pd–N(amido) bond *cis* to a Pd–C(aryl) bond is described.

Introduction

Organometallic complexes of the platinum-group metals containing M−N(amido) bonds arranged *cis* to the M−C bond are of interest for their role as catalysts in important reactions that involve C−N bond formation, such as alkene hydroamination[1,2] and the synthesis of arylamines from aryl halides,[3] or in other processes such as hydrogenation of imines.[4,5] Non-planar binuclear complexes formed by two equivalent square-planar halves can exhibit C_2 or C_s symmetry (see Scheme 1 where M means any metal with square-planar geometry, X any atom or group of atoms bridging the two equivalent sides and A and B are different ligands). The most commonly found C_2 isomers are chiral even when formed by two equivalent moieties.

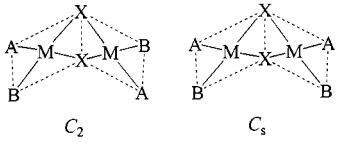

Scheme 1

Arylhydrazones are versatile ligands that provide both C−H and N−H bonds to activate. Binuclear orthopalladated phenylhydrazonato C_2 palladium(II) complexes containing Pd−C(aryl) bonds arranged *trans* to terminal Pd−N(amido) bonds have been reported, thus proving that, although rare, it is possible to obtain palladium compounds containing both bonds.[6,7] Mononuclear complexes of general formula $[PdAr(NHPh)(PMe_3)_2]$ with these two bonds in *trans* array have also been reported.[8] They were stabilized against the natural tendency of terminal Pd−N(amido) bonds to make bridges, by using P-donor ligands *cis* to the amido bond.

The stabilization of palladium compounds containing Pd−C and Pd−N(amido) bonds in a *cis* disposition has been achieved introducing the P-donor nonlabile chelating ancillary ligand DPPF [1,1′-bis(diphenylphosphanyl)ferrocene].[3] An interesting example is the recently reported mononuclear palladium hydrazonato complex $[Pd(DPPF)(Ar)(NH-N=CPh_2)]$ (Ar = *p*-tolyl); it undergoes C−N reductive elimination and plays and active role in the catalytic arylation of diphenylhydrazones.[9]

Results and Discussion

Here we report the synthesis and structural characterization of $[Bu_4N][Pd\{C_6H_4C(CH_3)=N-NHPh\}\{\mu\text{-}N(Ph)-N=C(CH_3)C_6H_4\}(\mu\text{-}Cl)PdCl]$ (**1**), an asymmetric C_1 binuclear phenylhydrazonato palladium(II) complex containing a Pd−C(aryl) bond *cis* to a Pd−N(amido) bond. It is a remarkable structure since binuclear complexes have commonly two equivalent halves and also because the *cis* arrangement of amido and aryl bonds around the palladium center is achieved without the use of P-donor ligands.

The reaction of the dimeric orthopalladated complex $[Pd\{C_6H_4C(CH_3)=N-NHPh\}(\mu\text{-}Cl)]_2$[10] with Bu_4NOH (molar ratio 1:1) in MeOH cleanly affords **1** in 79% yield. The use of an excess of Bu_4NOH (molar ratio 1:2) led to the same result indicating that the second N−H bond is difficult to deprotonate. The ^1H NMR spectrum of **1** shows two sharp singlets at δ = 2.18 and 2.24 corresponding to two methyl groups, demonstrating the presence of two nonequivalent hydrazonato ligands. A multiplet at δ = 6.28 is

[a] Departamento de Química, Facultad de Ciencias, Universidad de Burgos
09001 Burgos, Spain
E-mail: gherbosa@ubu.es
[b] Departamento de Química Física y Analítica, Facultad de Química, Universidad de Oviedo
33071 Oviedo, Spain
[c] Departamento de Química Inorgánica, Facultad de Ciencias, Universidad de Valladolid
47005 Valladolid, Spain

 © WILEY-VCH Verlag GmbH, 69451 Weinheim, 2001 1434−1948/01/0909−2361 $ 17.50+.50/0

assigned to the proton attached to C(14) and involved in a weak agostic Pd(2)−H−C(14) interaction.[11] The IR spectrum of **1** shows two C=N bands at $\tilde{\nu}$ = 1574 and 1587 cm^{-1}.

An ORTEP drawing of **1** is provided in Figure 1. The two previous examples of binuclear palladium hydrazonato complexes found in the Cambridge Crystallographic Database correspond to species with two equivalent halves and the Pd−C(aryl) bond *trans* to the Pd−N(amido) bond.[6,7] No previous examples of binuclear palladium(II) complexes containing a Pd−C bond *cis* to a Pd−N(amido) bond were found. Complex **1** consists of two square-planar units in a folded (C_1) array bridged by one chlorine atom and one hydrazonato ligand. The folding angle between the two coordination planes is 133.72(1)°. While both phenylhydrazonato ligands present in **1** are orthometallated to each palladium atom in a five-membered well-known fashion, only one phenylhydrazonato ligand is *N*-deprotonated. Thus, one of the phenylhydrazonato ligands is doubly deprotonated, at the C−H bond of the phenyl group and at the N−H bond. The other phenylhydrazonato ligand is singly deprotonated at a C−H bond of the phenyl group keeping the NH group protonated and uncoordinated. Attention has recently been paid to metal complexes containing a pendant NH group that can be considered as being in the intermediate coordination sphere, as they are neither directly bound to the metal center nor being in the outer sphere.[12] It allows selective two-point binding of other ligands such as ketones that may bond normally to the metal center and through hydrogen bond interaction to the NH group.

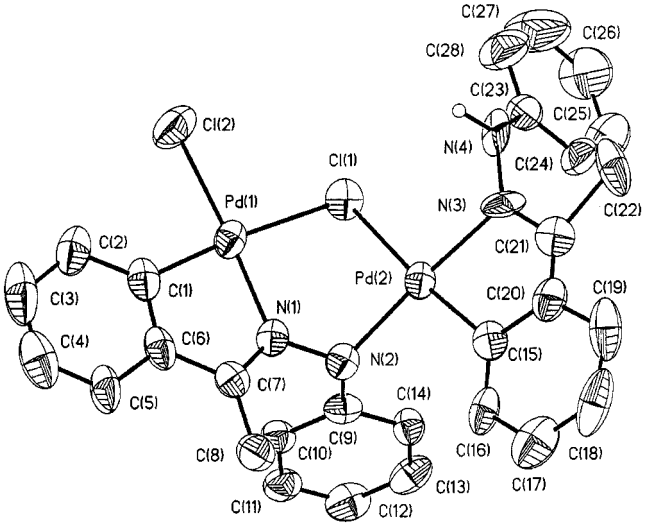

Figure 1. ORTEP drawing of **1**; hydrogen atoms are omitted for clarity; selected bond lengths [Å] and angles [°]: Pd1−Pd2 3.533(1), Pd1−C1 2.008(17), Pd1−N1 2.084(12), Pd1−Cl1 2.434(5), Pd1−Cl2 2.310(6), Pd2−C15 1.99(2), Pd2−N2 2.021(16), Pd2−N3 2.052(17), Pd2−Cl1 2.412(5), N1−N2 1.42(2), N3−N4 1.36(3); Cl2−Pd1−C1 94.0(9), C1−Pd1−N1 81.6(9), N1−Pd1−Cl1 92.8(5), Cl1−Pd1−Cl2 91.5(2), Cl1−Pd2−N2 89.3(5), N2−Pd2−C15 95.9(9), C15−Pd2−N3 79.0(9), N3−Pd2−Cl 95.9(5)

The sum of the four angles is 359.9° for Pd(1) and 360° for Pd(2). The Pd(2)−N(2) amido distance is 2.021(16) Å, similar to 2.035(9) Å which is the distance found in $[Pd(DPPF)(Ar)(NH-N=CPh_2)]$[9], a complex containing also a Pd−C(aryl) bond *cis* to a Pd−N(amido) bond. The N−N distance is noticeably different in both hydrazonato ligands. In the bridging one the N(1)−N(2) bond length is 1.42(2) Å, whereas in the other one the corresponding N(3)−N(4) distance is 1.36(3) Å. They are extreme examples of the typical N−N bond-length range in hydrazones (1.38−1.41 Å).[13]

A detailed discussion of the mechanism leading to **1** is not possible at this stage. In any case, it is clear that complex **1** is the result of the coupling of two monometallic fragments through the dashed line as shown in Scheme 2.

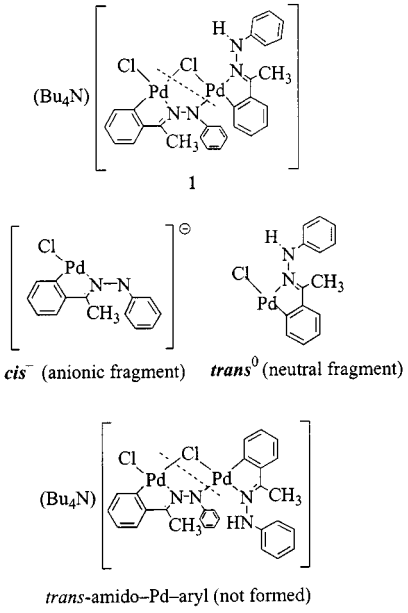

Scheme 2

The final geometry requires that the fragment containing the deprotonated nitrogen atom has a *cis* configuration of C and Cl atoms, whereas the fragment with the protonated nitrogen must bear a *trans* arrangement of Cl and C. It is likely that the reaction involves the cleavage of the symmetric parent dimer, probably by incorporation of solvent molecules (methanol) as labile ligands. Quantum chemical calculations using the PM3 model implemented in Mac-Spartan Pro indicate that for the neutral fragment the *trans* "C−Pd−Cl" array is more stable than the *cis* one by 4.174 $kcal \cdot mol^{-1}$. On the contrary, for the anionic fragment the *cis* arrangement is more stable than the *trans* one by 5.635 $kcal \cdot mol^{-1}$, this being consistent with the formation of the resulting geometry. Additionally, calculations carried out on both **1** and its *trans* amido−Pd−aryl isomer (see Scheme 2) indicate that the *cis* isomer **1** is more stable than the alternative *trans* isomer by ca. 18 $kcal \cdot mol^{-1}$. Aryl-palladium complexes tend to coordinate hard ligands in a position *trans* to the Pd−C(aryl) bond and to avoid

coordination of soft ligands. This fact has been reported as transphobia,[14,15] and is followed in *trans*-[PdAr(NHPh)(PMe_3)$_2$].[8] In complex **1** the hard N(amido) ligand arranges *cis* to the Pd−C(aryl) bond, leaving the softer ligand chloro in *trans* position to the Pd−C(aryl) bond. The alternative *trans* isomer of **1** would contain a Pd−C(aryl) bond with the harder amido ligand in *trans* position, obeing transphobia arguments, but this isomer is not formed. Further, but elusive at the moment, examples of amido−palladium−aryl complexes seems to be required to be able to say more about the factors that control the arrangement of these C and N donor ligands around the palladium center.

Interestingly, in spite of the adequate (and unusual) *cis* arrangement of the aryl and amido ligands to undergo reductive elimination reaction, complex **1** showed to be very stable when heated under reflux in acetone. Even in excess of PPh_3 the products of the reaction do not contain Pd^0 but Pd^{II} derivatives whose characterization is currently being carried out.

Experimental Section

General: ^{1}H (80 MHz) and ^{13}C (200 MHz) NMR data were collected in $CDCl_3$ solutions (298 K) using TMS as standard reference with a Bruker AC 80 and with a Varian VXR 200 spectrometer, respectively. Elemental analyses were performed by the Servicio Central de Apoyo a la Investigación of the University of Burgos (Spain).

Preparation of [Bu_4N][Pd{$C_6H_4C(CH_3)$=N−NHPh}{μ-N(Ph)−N=$C(CH_3)C_6H_4$}(μ-Cl)PdCl] (1): 200 mg (0.28 mmol) of [Pd{$C_6H_4C(CH_3)$=N−NHPh}(μ-Cl)]$_2$[10] were suspended in 50 mL of dichloromethane, and then 0.28 mL (0.28 mmol) of Bu_4NOH (1 M solution in methanol) was added. After stirring for 30 min at room temperature, the complex was completely dissolved to afford a red solution. The solution was stirred for 6 h and then it was filtered through kieselgur in order to remove any traces of solid. The filtrate was concentrated in vacuo and layering with hexane afforded a red precipitate which was collected and washed with hexane. The product was recrystallised from dichloromethane/hexane to yield 206 mg (79%) of the complex **1**. − $C_{44}H_{61}Cl_2N_5Pd_2$: calcd. C 55.99, H 6.52, N 7.42; found C 55.62, H 6.42, N 7.15. − ^{1}H NMR: δ = 0.91 [m, 12 H, ($^{\delta}CH_3)_4$N−], 1.32 [m, 16 H, (−$^{\gamma}CH_2$−$^{\beta}CH_2)_4$N−], 2.18 [s, 3 H, −C(CH_3)=N−N−Ph], 2.24 [s, 3 H, −C(CH_3)=N−N(H)−Ph], 3.13 [m, 8 H, (−$^{\alpha}CH_2)_4$N], 6.28 (m, 1 H, agostic), 6.99 (m, 14 H, aromatic), 7.65 (m, 2 H, aromatic), 7.91 (m, 1 H aromatic), 8.98 (s, 1 H, −NH−). − ^{13}C{^{1}H} NMR: δ = 13.8, 14.1, 14.2, 19.8, 24.0, 58.5, 113.0, 114.6, 115.6, 121.7, 123.0, 123.6, 124.5, 125.2, 125.6, 126.4, 127.7, 128.4, 128.6, 129.0, 130.2, 135.1, 135.7, 136.4, 144.7, 146.9, 154.8, 156.0, 157.3, 158.0, 176.5, 177.2.

X-ray Crystallographic Study: Crystals of **1** were grown from dichloromethane/hexane. Data were collected with an Enraf−Nonius CAD4 diffractometer. The structure was solved by Patterson methods, phase expansion, and subsequent Fourier maps with DIRDIF.[16] Full-matrix least-squares refinement was made with SHELX-93.[17] Perspective drawing in Figure 1 was made with PLATON.[18] $C_{44}H_{61}Cl_2N_5Pd_2$, M = 944.69, monoclinic, space group $P2_1/c$, a = 21.514(4) Å, b = 20.353(4) Å, c = 20.709(4) Å, β = 86.14(3)°, V = 9048(3) Å^3, Z = 8, D_c = 1.387 Mg/m^3, crystal size 0.26 × 0.20 × 0.17 mm, F(000) = 3896, T = 293(2) K, Mo-K_α radiation, λ = 0.71073 Å. 16378 reflections were measured, giving 8196 independent reflections after merging (R_{int} = 0.0564), with 4469 reflections having $I > 2\sigma(I)$. Two chemically equivalent but crystallographically independent anion/cation pairs were found in the asymmetric unit. The final indices [$I > 2\sigma(I)$] were $R1$ = 0.0808, $wR2$ = 0.2074. Crystallographic data (excluding structure factors) for the structure reported in this paper has been deposited with the Cambridge Crystallographic Data Center as supplementary publication no. CCDC-156983.Copies of the data can be obtained free of charge on application to CCDC, 12 Union Road, Cambridge CB2 1EZ, UK [Fax: (internat.) + 44-1223/336-033; E-mail: deposit@ccdc.cam.ac.uk].

Acknowledgments

The authors gratefully acknowledge the Spanish Dirección General de Enseñanza Superior (PB97-0470-C02, BQU2000-0219) and the Junta de Castilla y León (BU08/99) for financial support.

[1] T. E. Müller, M. Beller, *Chem. Rev.* **1998**, *98*, 675−703.
[2] H. M. Senn, P. E. Blochl, A. Togni, *J. Am. Chem. Soc.* **2000**, *122*, 4098−4107.
[3] J. F. Hartwig, *Angew. Chem. Int. Ed.* **1998**, *37*, 2046−2067.
[4] B. R. James, *Catal. Today* **1997**, *37*, 209−221.
[5] R. Dorta, P. Egli, F. Zürcher, A. Togni, *J. Am. Chem. Soc.* **1997**, *119*, 10857−10858.
[6] P. Espinet, G. García, F. J. Herrero, Y. Jeannin, M. Philoche-Levisalles, *Inorg. Chem.* **1989**, *28*, 4207−4211.
[7] P. Espinet, M. Y. Alonso, G. García-Herbosa, J. M. Ramos, Y. Jeannin, M. Philoche-Levisalles, *Inorg. Chem.* **1992**, *31*, 2501−2507.
[8] L. A. Villanueva, K. A. Abboud, J. M. Boncella, *Organometallics* **1994**, *13*, 3921−3931.
[9] J. F. Hartwig, *Angew. Chem. Int. Ed.* **1998**, 2090−2093.
[10] B. N. Cockburn, D. V. Howe, T. Keating, B. F. G. Johnson, J. Lewis, *J. Chem. Soc., Dalton Trans.* **1973**, 404−410.
[11] R. H. Crabtree, E. M. Holt, M. Lavin, S. M. Morehouse, *Inorg. Chem.* **1985**, *24*, 1986−1992.
[12] K. Gruet, R. H. Crabtree, D. H. Lee, L. Liable-Sands, A. L. Rheingold, *Organometallics* **2000**, *19*, 2228−2232.
[13] P. A. S. Smith, *Derivatives of Hydrazone and other Hydronitrogens Having N−N Bonds*, Benjamin, Reading, MA, **1983**, p.46.
[14] J. Vicente, A. Arcas, D. Bautista, P. G. Jones, *Organometallics* **1997**, *16*, 2127−2138.
[15] J. Vicente, J. A. Abad, A. D. Frankland, M. C. R. de Arellano, *Chem. Eur. J.* **1999**, *5*, 3066−3075.
[16] P. T. Beurskens, G. Admiraal, W. P. Bosman, G. Beurskens, H. M. Doesburg, S. García-Granda, R. O. Gould, J. M. M. Smits, C. Smikalla, *The DIRDIF Program System, Technical Report of the Crystallography Laboratory*, University of Nijmegen, The Netherlands, **1992**.
[17] G. M. Sheldrick, *SHELXL-93*, University of Göttingen, **1993**.
[18] A. L. Spek, *The EUCLID Package in Computational Crystallography* (Ed.: E. Sayre), Clarendon Press, Oxford, England, **1982**.

Received March 27, 2001
[I01110]

Structure−Property Dependence of the First Hyperpolarisabilities of Organometallic Merocyanines Based on the μ-Vinylcarbynediiron Acceptor and Ferrocene Donor

Tony Farrell,*[a] Anthony R. Manning,*[a] Timothy C. Murphy,[a] Timo Meyer-Friedrichsen,[b] Jürgen Heck,[b] Inge Asselberghs,[c] and André Persoons[c]

Keywords: Nonlinear optical materials / Ferrocene / Merocyanine / Hyper Rayleigh scattering / Solvatochromism / Bond-length alternation

In order to investigate the structure–property relationship of nonlinear optical materials, a series of organometallic chromophores were synthesised utilising the $[Fe_2(\eta\text{-}C_5H_5)_2(CO)_2(\mu\text{-}CO)(\mu\text{-}C\text{–})]^+$ electron-accepting moiety and the ferrocenyl group, Fc, as the electron donor. The π-linker between these two termini was systematically modified and the mutual electronic communication between them was determined using IR, NMR, and electronic absorption spectroscopy. An X-ray structure determination of $[Fe_2(\eta\text{-}C_5H_5)_2(CO)_2(\mu\text{-}CO)(\mu\text{-}C\text{–}CH{=}CH\text{–}CH{=}C(Cl)\text{–}Fc)][BF_4]$ confirmed the strong electronic interaction between the donor and the acceptor with reduced π-bridge bond-length alternation. The nonlinear optical properties of these complexes were examined using the hyper Rayleigh scattering technique. The experimental first hyperpolarisabilities are some of the highest obtained for ferrocenyl chromophores and, significantly, no enhancement was found due to two-photon absorption fluorescence. When polyene linkers $-(CH{=}CH)_n-$ are used, the values for β_0 increase with a ca. $n^{1.5}$ dependence with no sign of saturation up to $n = 4$. However, the highest values for β and β_o were obtained for linkers which contained an aromatic ring as opposed to pure polyenes and in this respect a benzene ring was more effective than a thiophene or furan. Consequently, the higher β and β_0 are not exhibited by those merocyanines with the highest values for λ_{max}. It is concluded for these compounds that a low excitation energy E_{eg} and a large transition moment M for the electronic excitation are less important than a large change in the dipole moment $\Delta\mu_{eg}$. Furthermore, a chloro substituent on the olefinic double bond proximate to the ferrocenyl group has a dramatic effect on the β and β_0 values.

Introduction

Molecular electronics is an emerging and intriguing area of research. Understanding the structure−property relationship of NLO-active chromophores is of fundamental importance if molecular architecture is to be tailored to achieve specific NLO responses. The strategy requires sequential variation of molecular parameters, full evaluation of the effects which these variations have on the ground and excited states, and then analysing the outcome on the NLO response. Organic systems have been subject to extensive studies whereby the effects of modulating such variables as spacer aromaticity, bond-length alternation, and end-group donor and acceptor strengths have been quantified.[1−7] Less work has been carried out on organometallic chromophores despite the fact that organometallic complexes are often particularly appealing because their redox states may be changed easily. However, there are now increasing numbers of ferrocenyl complexes which display interesting molecular electronic functions such as nonlinear optical (NLO) properties (including frequency doubling and tripling of incident light),[8−13] and metallocenes have been used in amperometric sensory devices[14] and liquid crystals.[15,16]

One of our approaches has been to synthesise complexes which utilise the cationic diiron moiety $[Fe_2(\eta\text{-}C_5H_5)_2(CO)_2(\mu\text{-}CO)(\mu\text{-}C-)]^+$ moiety, as an electron acceptor in molecular systems which are candidates for second harmonic generation (SHG). This end-group is particularly attractive because theoretical[17] and experimental[18−22] research has indicated that conjugation between the $Fe_2(\mu\text{-}C)$ unit and the substituted vinyl system is maintained throughout rotation about the μ-C-vinyl bond.

Hyper Rayleigh scattering (HRS) studies using 1064 nm incident light on the stilbenyldiiron series $[Fe_2(\eta\text{-}C_5H_5)_2(CO)_2(\mu\text{-}CO)(\mu\text{-}C{-}CH{=}CH{-}C_6H_4{-}CH{=}CH{-}C_6H_4{-}R)][BF_4]$ (where R = NO_2, H, OMe, NMe_2), were promising.[22] Based on these findings the objective of this work was to prepare a comparable series of merocyanines utilising the diiron cationic electron acceptor and ferrocene as the donor. It was proposed that modifications of the π-bridge between these termini by incorporating olefins and aryl or heteroaryl units as well as more subtle changes, i.e. replacing an H atom on an olefinic unit by a Cl atom along

[a] Department of Chemistry, University College Dublin, Belfield, Dublin 4, Ireland
[b] Institut für Anorganische und Angewandte Chemie, Universität Hamburg, Martin-Luther-King-Platz 6, 20146 Hamburg, Germany
[c] Laboratorium voor chemische en biologische dynamica, Katholieke Universiteit Leuven, Celestijnenlaan 200D, 3001 Leuven, Belgium

 © WILEY-VCH Verlag GmbH, 69451 Weinheim, 2001 1434−1948/01/0909−2365 $ 17.50+.50/0

the π-linker, could give systems which exhibit large second-order NLO effects and would help to clarify the criteria necessary to achieve this.[23−26]

Results and Discussion

Synthesis

Wittig condensation of terephthalaldehyde mono(diethyl acetal) with an equimolar amount of the phosphonium salt [Fc−CH_2−PPh_3][I] (**1**)[27,28] and *t*BuOK, provided the acetal Fc−CH=CH−C_6H_4−$CH(OEt)_2$ which was not isolated but immediately converted into the aldehyde Fc−CH=CH−C_6H_4−CHO (**2**) by treating with aqueous HCl (Scheme 1). Wittig condensation of **1** with 5-iodothiophene-2-carboxaldehyde[29−31] and 5-bromofuryl-2-carboxaldehyde[29,32,33] followed by lithium/halogen exchange and DMF quenching gave the heteroarylferrocenyl aldehydes Fc−CH=CH−C_4H_2S−CHO (**3**) and Fc−CH=CH−C_4H_2O−CHO (**4**).

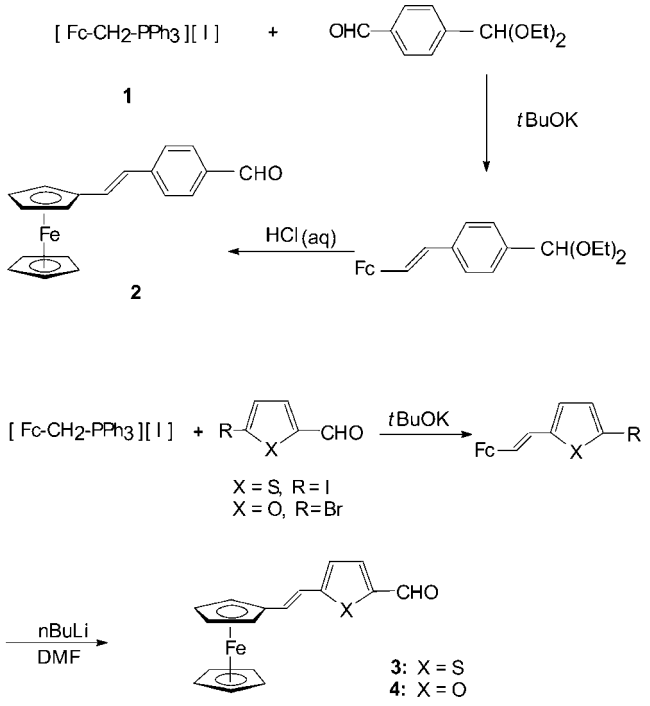

Scheme 1. Synthesis of ferrocenyl aldehydes **2−4**

Ferrocene aldehyde[34] **5** and (chlorovinyl)ferrocene aldehyde[35] **6** were prepared by known procedures while the extended [formyl(vinyl)$_n$]ferrocenes **7−9** were obtained by the method of Spangler and McCoy (Scheme 2).[36] The extended vinylthienyl aldehydes Fc−CH=CH−CH=CH−C_4H_2S−CHO (**10**) and Fc−C(Cl)=CH−CH=CH−C_4H_2S−CHO (**11**) were prepared by a Wittig−Horner−Wadsworth−Emmons procedure using diethyl [(2-bromothienyl)methyl]phosphonate[22] (Scheme 2). As before, lithium/halogen exchange followed by DMF quenching afforded **10** and **11** in high yields. All ferrocenyl aldehydes were characterised by ^{1}H NMR spectroscopy and exhibited signals, which were consistent with all-(*E*) geometries.

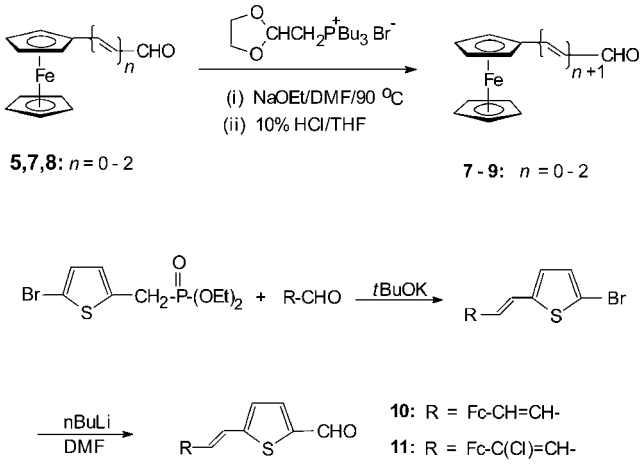

Scheme 2. Synthesis of ferrocenyl aldehydes **7−11**

When the aldehydes **2−11** were condensed with [Fe_2(η-C_5H_5)$_2$(CO)$_2$(μ-CO)(μ-C−CH_3)][BF_4][37] (**12**) in CH_2Cl_2 at 35 °C for 12 h, they gave intensely coloured reaction mixtures. The air-stable merocyanine salts [Fe_2(η-C_5H_5)$_2$(CO)$_2$(μ-CO)(μ-C−{π-linker}−Fc)][BF_4], **13−22**, were isolated by filtering the reaction mixture and layering the filtrate with diethyl ether (Scheme 3). The complexes **13−22** were fully characterized by spectroscopic and elemental analysis. However, some of the products contained solvent of crystallization that could not be removed by vacuum drying. This was confirmed by NMR spectroscopy that revealed varying amounts of CH_2Cl_2, diethyl ether and/or water. No attempt was made to quantify this solvent of crystallisation and the microanalytical data are given as found. However, the spectroscopic data are in agreement with the proposed formulae and we are confident of them.

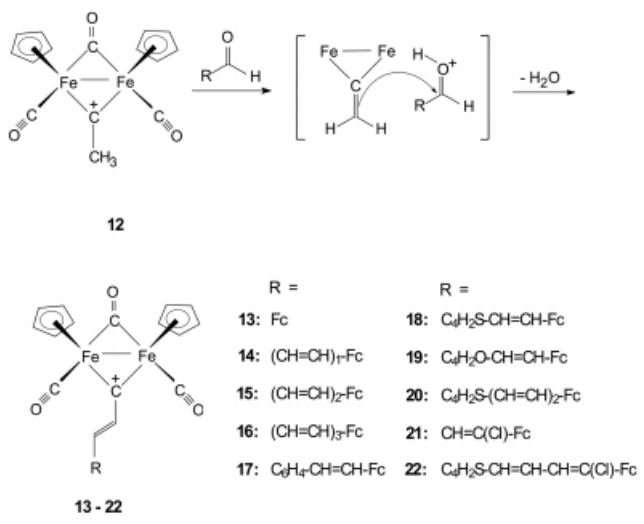

Scheme 3. Reactions of **12** with ferrocenyl aldehydes **2−11**

Crystal Structure of $[Fe_2(\eta\text{-}C_5H_5)_2(CO)_2(\mu\text{-}CO)(\mu\text{-}C{-}CH{=}CH{-}CH{=}C(Cl){-}Fc)][BF_4]$ (21)

Suitable crystals of **21** were grown from a CH_2Cl_2/OEt_2 solution and subjected to an X-ray diffraction study. Crystal data and structure refinement are given in Table 5. A perspective view of the molecule and its atom numbering is depicted in Figure 1. Selected bond lengths and angles are listed in Table 1. The $Fe_2(\eta\text{-}C_5H_5)_2(CO)_2(\mu\text{-}CO)(\mu\text{-}C)$ moiety has a *cis* structure with dimensions similar to those found in other μ-vinylcarbyne cations.[22,38,39] The −CH=CH−CH=C(Cl)− π-bridge linker displays all-(*E*) geometry with C15−C16 and C17−C18 bond lengths of 1.359(5) and 1.356(5) Å respectively, which are rather long for $C_{sp^2}-C_{sp^2}$ double bonds. Furthermore, there is a shortening of the $C_{sp^2}-C_{sp^2}$ single bonds towards the diiron terminus [C14−C15 = 1.414(5), C16−C17 = 1.424(9), and C18−C19 = 1.447(9) Å], which is evidence for the delocalisation of the positive charge into the vinylcarbyne system and particularly through the first double bond in the solid state.[19−21] This is particularly important because bond-length alternation (BLA, the difference between the average lengths of carbon−carbon single and double bonds in a merocyanine) has been established as a useful parameter in relation to NLO response.[23,40,41] A good correlation between theory and experiment led to the conclusion that optimal NLO activity is achieved when BLA = 0.03−0.05 Å. The BLA across the π-bridge of **21** is 0.07 Å, which indicates a potentially high first hyperpolarisability.

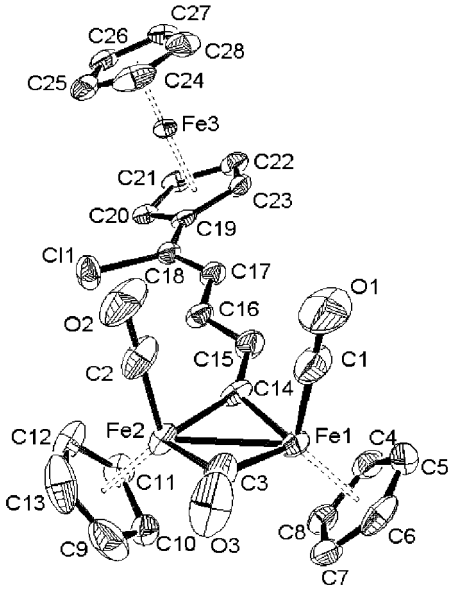

Figure 1. Molecular structure and atom labelling of $[Fe_2(\eta\text{-}C_5H_5)_2(CO)_2(\mu\text{-}CO)(\mu\text{-}C{-}CH{=}CH{-}CH{=}C(Cl){-}Fc)][BF_4]$ (**21**); 30% ellipsoids; hydrogen atoms and $[BF_4]^-$ anion omitted for clarit)

Further evidence for the π-interaction between the diiron moiety and the first double bond is the planarity of the $Fe_2(\mu\text{-}C)$ and C14−C16 units with the dihedral angle between the their best planes being only 1.5(6)°. The entire π-linker (C14−C19) is also quite planar with C17 and C14 displaying greatest deviations [+10.4(3) and −10.1(2)°, respectively] and a dihedral angle of 9.2(7)° between the best planes through C14−C16 and C17−C19. Nonetheless, the dihedral angle of 24.3(2)° between the C19−C23 (ferrocenyl $\eta\text{-}C_5H_4$) and the $Fe_2(\mu\text{-}C)$ planes suggests that the ground state (GS) electronic delocalisation within the cation is effected mainly via the π-bridge with only a limited contribution from the ferrocenyl end group.

Spectroscopy

The solution IR spectra of complexes **13−22** contain three absorption bands in the ν(CO) region (Table 2). Their relative intensities are consistent with the presence of a *cis*-$Fe_2(\eta\text{-}C_5H_5)_2(CO)_2(\mu\text{-}CO)(\mu\text{-}C)$ moiety similar to those found in other $[Fe_2(\eta\text{-}C_5H_5)_2(CO)_2(\mu\text{-}CO)(\mu\text{-}C{-}R)]^+$ complexes.[19−22,38,39] The frequencies of these bands are a good indication of the electronic coupling between the $Fe_2(\mu\text{-}C)$ electron accepting moiety and the vinylferrocenyl complex donor system. Increased electron density at the diiron terminus results in increased M→CO back donation with a concomitant shift of the ν(CO) bands to lower frequencies. The ν(CO) vibrations of the vinylcarbyne complexes **13−22** are found at lower frequencies than those of $[Fe_2(\eta\text{-}C_5H_5)_2(CO)_2(\mu\text{-}CO)\{\mu\text{-}C{-}CH{=}CHC(CH_3)_3\}][BF_4]$[19] (**23**) (2036, 2003, 1853 cm^{-1}) and at very much lower frequencies than those of $[Fe_2(\eta\text{-}C_5H_5)_2(CO)_2(\mu\text{-}CO)(\mu\text{-}C{-}CH_3)][BF_4]$[19] (**12**) (2047, 2016, 1853 cm^{-1}). They demonstrate that in the ground state (GS), (i) extension of the π-linker with polarisable olefinic units increases the positive charge at the $Fe_2(\mu\text{-}C)$ core, (ii) when aromatic groups are included in the spacer, the delocalisation of this positive charge decreases with increasing aromaticity of that group, and (iii) the CH=C(Cl)−Fc unit is a weaker donor than CH=CH−Fc.

The spectra also display the expected absorption bands due to the BF_4^- ion and some unexpectedly strong bands lying between 1450 and 1600 cm^{-1}. The intensities of the latter are comparable to those of the ν(CO) modes e.g. for **21** they are found at 1553 (4.6) and 1521 (13.1) cm^{-1} [relative intensities with ν(CO) set to 10]. As they are not present in the IR spectrum of **12**, they are attributed to the ν(C=C) and other internal vibrations of the vinylferrocenyl ligand. Their enhanced intensities is a consequence of the high degree of polarisation within the π-system of the molecule.

The ^1H NMR spectra of **13−22** are consistent with the proposed structures. In particular, the ^1H-^1H coupling constants across all the olefinic CH=CH units ($J > 13.5$ Hz), confirm an (*E*) configuration in all cases. Although the two C_5H_5 ligands of the diiron unit are formally in different environments, a single resonance is observed in the ^1H NMR spectra of all the complexes. This suggests that in all cases there is facile rotation about the μ-C−CH bond which has a low bond order and is close to a single bond. This is consistent with the X-ray data discussed above. The protons of the ferrocenyl C_5H_4 ring appear as two broad resonances downfield from the singlet due to its C_5H_5 group. The

Table 1. Selected bond lengths [pm] and angles [°] for $[Fe_2(\eta\text{-}C_5H_5)_2(CO)_2(\mu\text{-}CO)\{\mu\text{-}C-CH=CH-CH=C(Cl)-Fc\}][BF_4]$ (**21**)

Bond lengths		Bond angles	
Fe(1)−C(1)	177.5(5)	Fe(1)−[C4−C8][a]	174.8(3)
Fe(1)−C(3)	192.2(3)	Fe(2)−[C9−C13][b]	174.8(3)
Fe(1)−C(14)	184.3(5)	Fe(1)−C(3)−Fe(2)	80.8(2)
Fe(2)−C(2)	176.8(4)	Fe(1)−C(14)−Fe(2)	85.6(2)
Fe(2)−C(3)	194.9(4)	C(14)−C(15)−C(16)	122.4(4)
Fe(2)−C(14)	185.2(5)	C(15)−C(16)−C(17)	122.5(3)
Fe(1)−Fe(2)	250.9(11)	C(16)−C(17)−C(18)	120.1(5)
C(1)−O(1)	114.4(6)	C(16)−C(17)−C(22)	125.2(3)
C(2)−O(2)	114.2(5)	C(17)−C(18)−C(19)	124.7(3)
C(3)−O(3)	116.4(5)	C(17)−C(18)−Cl(1)	119.6(3)
C(14)−C(15)	141.4(5)	[Fe(1)−C(14)−Fe(2)][C(14)−C(16)]	1.5(6)
C(15)−C(16)	135.9(5)	[C(14)−C(16)][C(17)−C(19)][c]	9.2(7)
C(16)−C(17)	142.4(5)	[C(19)−C(23)][C(14)−C(19)][c]	23.1(3)
C(17)−C(18)	135.6(5)	[Fe(1)−C(14)−Fe(2)][C(19)−C(23)]	24.3(2)
C(18)−C(19)	144.7(5)		
C(18)−Cl(1)	174.0(3)		
C(20)−C(21)	138.5(8)		

[a] Center of the Cp ring C(4)−C(8). − [b] Center of Cp ring C(9)−C(13). − [c] Angle between the two planes.

Table 2. Solution IR and ^{13}C NMR spectroscopic data for the $[Fe_2(\eta\text{-}C_5H_5)_2(CO)_2(\mu\text{-}CO)\{\mu\text{-}C-(\pi\text{-linker})-Fc\}][BF_4]$ salts **13**−**22**

	π-linker	IR (cm^{-1}) [a]		^{13}C NMR (ppm)
		ν(CO)	ν(μ-CO)	μ-C
13		2024, 1993	1837	408 [b]
14		2027, 2001	1837	411 [b]
15		2028, 2000	1837	414 [b]
16		2029, 2001	1839	416 [b]
17	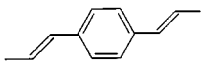	2035, 2004	1844	432 [c]
18	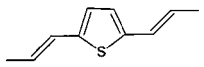	2030, 1999	1839	410 [c]
19	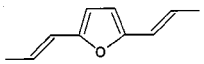	2029, 2000	1838	407 [c]
20	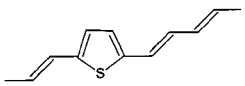	2030, 2000	1839	414 [b]
21	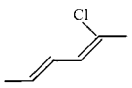	2031, 2001	1841	423 [d]
22	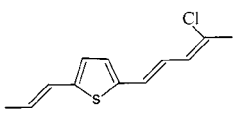	2031, 2001	1840	421 [b]

[a] CH_2Cl_2. − [b] $(CD_3)_2CO$. − [c] $CDCl_3$. − [d] CD_3CN.

chemical shift of these signals depends on the interaction between the ferrocenyl electron donor and the cationic di-iron terminus and is related to both the length and the ease of polarisation of the bridge. For example, as the π-linker in the $[Fe_2(\eta\text{-}C_5H_5)_2(CO)_2(\mu\text{-}CO)\{\mu\text{-}C-(CH=CH)_n-Fc\}]^+$ cations is extended from $n = 1$ to $n = 4$, the C_5H_4 ^1H NMR signals are shifted 0.71 ppm upfield.

The ^{13}C NMR spectra of **13**−**22** exhibit all the anticipated resonances, but the most informative are those due to the μ-C atom (δ = 408−432, Table 2). They are highly shielded relative to the μ-C signal of **12** (δ = 499), but deshielded compared with the μ-C signal of alkenylidenediiron complexes $[Fe_2(\eta\text{-}C_5H_5)_2(CO)_2(\mu\text{-}CO)(\mu\text{-}C=CH-R)]$ (δ = 270−340).[18,21,22,42−45] The greater the degree of charge delocalisation within the μ-carbyne moiety of the cation, the more pronounced is the upfield shift of this signal which will therefore depend on the length and ease of polarisation of the π-linker. The effect of π-bridge modification on the chemical shift of the μ-C resonance can be summarised as follows: (i) increasing conjugation by adding olefinic units results in a slight downfield shift, (ii) replacing a heteroaryl π-spacer by the more aromatic benzenoid unit also results in a downfield shift and (iii) replacing the CH=CH proximate to the ferrocene by a CH=C(Cl) unit produces an upfield shift. Thus the electron donating effect of the ferrocenyl group in the GS decreases with donor−acceptor separation, the presence of aromatic π-spacers and the increasing electronegativity of the bridge carbon atom α to it.

The UV/Vis spectra of **13**−**22**, like those of most ferrocenyl derivatives, exhibit two intense absorption bands in the visible region (Table 3).[8−12,46−49] Figure 2 demonstrates the effect of π-bridge extension on the absorption spectra of $[Fe_2(\eta\text{-}C_5H_5)_2(CO)_2(\mu\text{-}CO)\{\mu\text{-}C-(CH=CH)_n-Fc\}]^+$. Both bands are red-shifted with increasing polyenic chain length but this is more pronounced for the

Table 3. Optical data for the $[Fe_2(\eta\text{-}C_5H_5)_2(CO)_2(\mu\text{-}CO)\{\mu\text{-}C-(\pi\text{-linker})-Fc\}][BF_4]$ salts **13−22**

	λ_{max} [nm] (ε [$M^{-1}\cdot cm^{-1}$])				$\Delta\tilde{\nu}$[a]		β[b]	β_0[c]
	CH_2Cl_2		CH_3CN		[cm^{-1}]		[10^{-30} esu]	
	DA−CT	LL−CT	DA−CT	LL−CT	DA−CT	LL−CT		
13	655 (10 953)	428 (17 736)	634 (9 390)	421 (15 245)	−506	−388	113	36
14	734 (13 881)	484 (17 094)	698 (10 029)	471 (14 397)	−703	−570	156	74
15	775 (18 277)	541 (22 488)	717 (16 275)	508 (21 034)	−1 044	−1 201	227	120
16	813 (23 106)	582 (24 670)	720 (14 954)	521 (21 678)	−1 589	−2 012	562	313
17	705 (12 162)	512 (28 692)	616 (12 803)	480 (26 773)	−2 049	−1 302	1 106	469
18	757 (19 966)	569 (32 538)	688 (17 147)	542 (26 378)	−1 324	−875	679	343
19	747 (22 325)	577 (33 211)	683 (21 202)	551 (28 946)	−1 254	−818	352	173
20	764 (22 363)	606 (29 169)	677 (19 199)	590 (30 565)	−1 682	−448	1 195	615
21	746 (17 173)	495 (27 589)	713 (13 986)	477 (24 439)	−620	−762	459	225
22	731 (24 000)	606 (34 798)	644 (30 695)	572 (36 213)	−1 848	−981	1 424	674

[a] $\Delta\nu$ = ($\tilde{\nu}_{max}$ in CH_2Cl_2 − $\tilde{\nu}_{max}$ in CH_3CN). − [b] Measured in CH_2Cl_2 with ref. *p*-NA (β = 21.6·10^{-30} esu). − [c] Calculated from the TLM using the lower energy CT band.

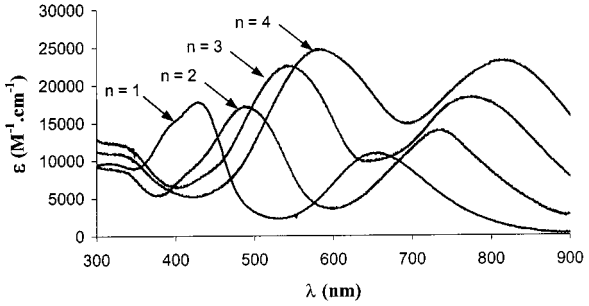

Figure 2. Effect of π-bridge extension on the absorption spectra of the $[Fe_2(\eta\text{-}C_5H_5)_2(CO)_2(\mu\text{-}CO)(\mu\text{-}C-(CH=CH)_n-Fc)][BF_4]$ salts **13−16**

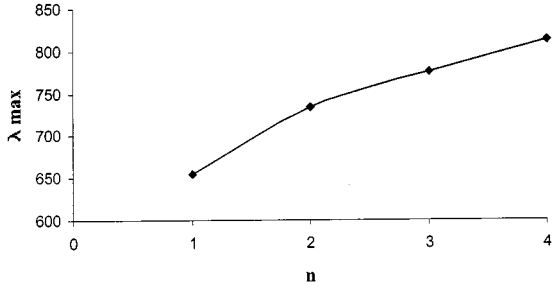

Figure 3. The variation of λ_{max} of the DA−CT absorption band of the $[Fe_2(\eta\text{-}C_5H_5)(CO)_2(\mu\text{-}CO)(\mu\text{-}C-(CH=CH)_n-Fc)][BF_4]$ salts **13−16**, with increasing *n*

higher energy band. In the case of organic donor−acceptor dyes, extending the π-linker results in the CT band moving to a limiting value known as the merocyanine limit (Figure 3).[50] Therefore we suggest that the low-energy band is probably due to a donor−acceptor transition (DA−CT) and the higher energy band to an intraligand π−π* transition (LL−CT). Many contrasting theoretical models have attempted to describe the electronic origin of these bands and their contribution to the second-order response.[51−53] Our assignments are in agreement with the most recent of these.[53]

The wavelengths of both absorption bands in the electronic spectra of **13−22** are solvent-dependent (Table 3). This is important because theoretical and experimental results suggest that the performance of NLO chromophores is optimised when there is a large difference between the dipole moments of the ground state (GS) and the excited state (ES) of the system.[54,55] and solvatochromism of the CT bands of chromophores is considered a manifestation of this change in dipole moment upon excitation.[50] In the case of **13−22** both bands are significantly blue-shifted with increasing solvent polarity (Figure 4 and Table 3). This indicates a large change in dipole moment upon excitation from a more charge-localised GS with a high dipole moment to an excited state where the positive charge is more delocalised throughout the entire molecule and the dipole moment is lower. In **13−16** the distance between donor and acceptor is increased by inserting more CH=CH units into the linker. Consequently it is not surprising that the solvatochromic shifts $\Delta\tilde{\nu}$ also increase along the same series as dipole moments are a function of charge and distance. Furthermore, when the benzene spacer in **17** is replaced by a thiophene in **18** or a furan in **19**, the charge delocalisation in the GS is increased, the dipole moment change on excitation is reduced, and so is the solvatochromic shift (Table 3). At the same time, one would expect a decrease in solvatochromism upon incorporation of heterocycles into the π-linker because of their ability to act as auxiliary donors within the bridge.[3−6,22]

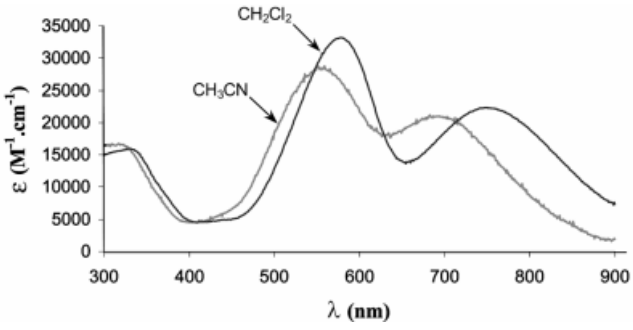

Figure 4. Solvatochromic behaviour of $[Fe_2(\eta\text{-}C_5H_5)_2(CO)_2(\mu\text{-}CO)(\mu\text{-}C-CH=CH-C_4H_2O-CH=CH-Fc)][BF_4]$ (**19**)

Another notable feature is the effect of replacing the −CH=CH− double bond proximate to the metallocene by a −CH=C(Cl)− unit. This increases the electronegativity of the ferrocenyl α-carbon atom and reduces the electron-donating capability of the ferrocenyl unit. If we consider that mesomers **A** and **B**, and to a lesser extent **C**, are the principal contributors to the GS of the diene π-bridged complexes **14** and **21** (Figure 5), then replacing X = H by X = Cl significantly reduces the stability of **C** and its contribution to the overall GS structure. Reduced charge delocalisation has the effect of raising the HOMO and we can presume that it also raises the energy of the LUMO, as mesomer **C** contributes substantially to the ES. Inspection of the spectra shows that on going from **14** to **21** there is (i) a downfield shift of the μ-C signal in the ^{13}C NMR spectrum, (ii) an increase of the frequencies of the ν(CO) modes, (iii) a red-shift of the λ_{max} of the DA−CT band, and (iv) a decrease of its solvatochromism. These observations show that the second olefinic unit contributes significantly to charge delocalisation in the GS and that perturbing it has a significant effect on the HOMO.

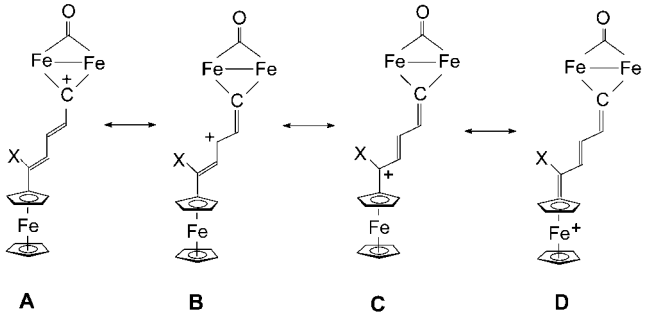

Figure 5. Four mesomeric forms of **14** and **21** (C_5H_5 and CO ligands omitted for clarity)

The same structural modification but in the extended π-bridged complexes incorporating a thienyl group, i.e. **20** and **22**, has a different effect. The IR and NMR spectroscopic data suggest that electronic communication between the termini is reduced upon incorporation of the aromatic heterocycle but that there are only minor changes in the degree to which positive charge is delocalised away from the $Fe_2(\eta\text{-}C_5H_5)_2(CO)_2(\mu\text{-}CO)(\mu\text{-}C^+)$ group. However, the electronic absorption spectra suggest that introduction of the chloro substituent affects the LUMO on going from **20** to **22** and brings about a blue-shift of the DA−CT band.

Hyperpolarisability Measurements

The NLO properties of **13−22** were evaluated by the hyper Rayleigh scattering (HRS) technique to determine their first hyperpolarisability β.[56] This technique involves detecting the incoherently scattered frequency-doubled light $I(2\omega)$ generated from a solution of the sample. Several different concentrations of solute are taken so as to eliminate possible solvent contributions, which are generally linear. The dependence of the ratio $I(2\omega)/I(\omega)^2$ from the concentration of the NLO chromophore referred against a standard leads to the β(HRS) value.

There are certainly pitfalls associated with the technique which, if unchecked, lead to overestimation of the β values. Nonetheless, it remains the easiest means of assessing the first hyperpolarisability of ionic and octupolar molecules.[57] The most common source of unreliable results is from two-photon fluorescence absorption (TPAF).[58−61] However, there are now several methods which may be used to discriminate between a true SHG signal and a TPAF-enhanced one, e.g. the use of bandpass filters[12,22] or a scanning monochromator.[62] Also, numerous techniques have been developed to avoid or abstract the TPAF contribution to β: long wavelength measurement,[63−65] time-resolved HRS,[66] high-frequency demodulation[67] and the measurement of the TPAF spectrum to abstract the fluorescence contribution to the HRS signal.[68,69]

The HRS experiments were carried out in CH_2Cl_2 solution at 1064 nm fundamental wavelength using *p*-nitroaniline (*p*NA) as an external reference. The calculated β values of the complexes **13−22** are presented in Table 3. These values are resonance-enhanced and therefore the static first hyperpolarisabilities (β_o) have been calculated using the two-level model [TLM, Equation (1)].[54,55] We have reservations about using the TLM to calculate β_o as (i) strictly speaking, it is not applicable in situations where there is significant absorption near the SHG signal (532 nm) and (ii) the relative contributions of the two transitions in metallocene chromophores are still uncertain with the latest study reporting that both transitions contribute significantly to the optical nonlinearity.[53] Nonetheless, to allow comparisons to be drawn between these complexes and the rest of the body of work on ferrocenyl systems we calculate the β_o values using the lower energy CT transition (Table 4).

$$\beta_{CT}(-2\omega,\omega,\omega) = \frac{3\Delta\mu_{eg}M^2}{(\hbar\omega)^2}\cdot\frac{\omega_{eg}^2}{\left(1-4\omega^2/\omega_{eg}^2\right)\cdot\left(\omega_{eg}^2-\omega^2\right)} \qquad (1)$$

$$\beta_0 = \frac{3\Delta\mu_{eg}M^2}{(E_{eg})^2}\cdot$$

To ensure that the calculated values are real, a check for multiphoton-induced fluorescence enhancement was undertaken using bandpass filters at λ = 400, 450, 500, 532, 560, 650, and 700 nm with a bandwidth of 10 nm as reported earlier.[22] A fluorescence signal should have a considerably broader line than the sharp HRS signal (Figure 6) and the maximum of the emission band occurs infrequently at λ/2.[62,68,69] Overall the β values obtained for this series of cationic ferrocenyl chromophores are exceptionally high, but they have been rigorously checked for TPAF and show no enhancement.

There are two points of general interest in the values of β and β_0 (Table 3). Firstly, those of the $[Fe_2(\eta\text{-}C_5H_5)_2(CO)_2(\mu\text{-}CO)\{\mu\text{-}C-(CH=CH)_n-Fc\}][BF_4]$ (**13−16**) complexes increase on lengthening the π-system with olefinic units, and a plot of log *n* against log β_o (Figure 7)

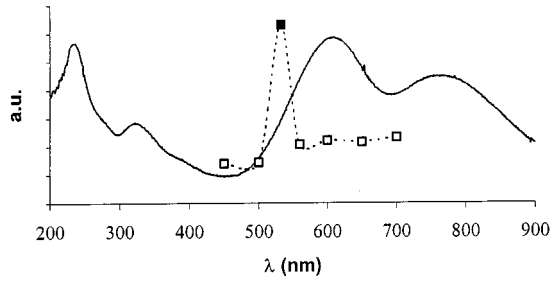

Figure 6. Absorption (full) and emission (dotted) spectra of the $[Fe_2(\eta\text{-}C_5H_5)(CO)_2(\mu\text{-}CO)\{\mu\text{-}C{-}CH{=}CH{-}C_4H_2S{-}(CH{=}CH)_2{-}Fc\}][BF_4]$ (**20**) in CH_2Cl_2; filled square is λ = 532 nm signal

shows that $\beta_o \propto n^{1.5}$. This confirms that the static first hyperpolarisability of donor−acceptor polyene systems rise sharply with the length of the conjugated path. Furthermore, there is no evidence for the "saturation" of the β_o enhancement with n increasing to 4, unlike λ_{max}, which is levelling off (Figure 3). In view of our results coupled with the linear optical data it would appear that the enhancement of β_o for these cationic merocyanines could be largely attributed to $\Delta\mu_{eg}$, and M and less on the energy of the transition E_{eg}.

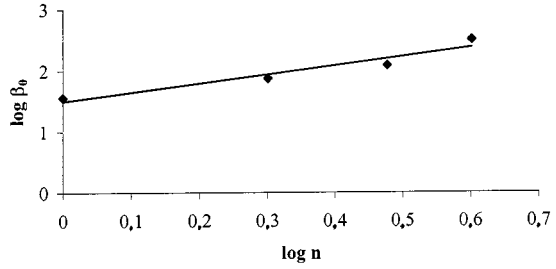

Figure 7. Conjugation length dependence of β_0 for the $[Fe_2(\eta\text{-}C_5H_5)(CO)_2(\mu\text{-}CO)\{\mu\text{-}C\text{-}(CH{=}CH)_n{-}Fc\}][BF_4]$ salts **13−16**

The second point of interest is that for the aromatically bridged $[Fe_2(\eta\text{-}C_5H_5)_2(CO)_2(\mu\text{-}CO)(\mu\text{-}C{-}CH{=}CH{-}(ring){-}CH{=}CH{-}Fc)][BF_4]$ salts the order of molecular nonlinearity decreases when the bridging aromatic ring is based on benzene (**17**) > thiophene (**18**) > furan (**19**). This result differs from those of recent studies of the second-order NLO effects in organic materials which have led to the conclusion that heterocyclic aromatic units provide better conjugation with increased first hyperpolarisabilities than do benzenoid moieties.[5−7] Albert et al. have demonstrated that the position of aromatic spacers within the conjugated system is important, and that in neutral molecules optimal NLO response is achieved by appending strong donors to electron-excessive spacers and strong acceptors to electron-deficient ones.[4] Consequently it is possible that in cationic molecules the combination of the acceptor with π-deficient aromatic groups may optimise the NLO response.

However, we are not convinced that this is the whole answer, and in seeking to explain our results we note that the TLM predicts that large, frequency-independent first hyperpolarisabilities are obtained for compounds exhibiting

− a low-energy CT transition (energy E_{eg}),

− a large transition moment M which is directly correlated to the oscillator strength i.e. the extinction coefficient ε should be large,

− a large change in dipole moment $\Delta\mu_{eg}$, which is indicated by a pronounced solvatochromism of the CT transition.

The optical data for **17−19** show that absorption band wavelengths ($1/E_{eg}$) and intensities decrease along the series **19** > **18** > **17**, whilst the solvatochromic effect $\Delta\tilde{\nu}$ and β/β_0 increase. This is consistent with the proposal that the most important factor in determining the values of β and β_0 for these compounds is the dipole moment change during the electronic transition, $\Delta\mu_{eg}$, and that a low transition energy E_{eg} and a high transition moment M is much less important. We suggest that for these compounds increasing the ring aromaticity reduces the delocalisation of the positive charge onto the ferrocenyl group and limits it to the μ-C−CH=CH moiety in the GS but not in the ES, and therebye enhances the change in dipole moment $\Delta\mu_{eg}$ on excitation. Further support is lent to this suggestion by comparing the β_o values of complexes **14** and **21**. The spectroscopic and X-ray data show that the CH=C(Cl) unit also reduces the delocalisation of the ferrocenyl electrons in the GS and as a consequence the β_0 value of **21** is very much larger than that of **14**. However, the same modification has a much reduced effect in the extended π-bridged complexes **20** and **22**, where the donor and acceptor are further apart and the conjugated linker includes a heterocyclic aromatic group.

Table 4. Previously reported β and β_o values of some organometallic merocyanines for comparison with those of **13−22**

Donor	Acceptor	π-bridge	λ_{max} [nm]	$\beta \times 10^{-30}$ [esu][a]	$\beta_0 \times 10^{-30}$ [esu][b]	Ref.
C_6H_5	$[Fe_2(\eta{-}C_5H_5)(CO)_2(\mu{-}CO)(\mu{-}C{-})]^+$	$-CH{=}CH{-}C_6H_4{-}CH{=}CH-$	513	792	43	[22]
Fc	$(\eta^5{-}C_9H_7)Ru(PPh_3)_2$	$-C{\equiv}C{-}C{\equiv}C-$	345	273	141	[70]
Fc	$(thiophene)Mn(CO)_3^+$	$-(CH{=}CH)_3-$	548	771[c]	−34	[71]
Fc	$-C(OMe){=}W(CO)_5$	$-(CH{=}CH)_4-$		960		[76]
Fc	$-C(OMe){=}W(CO)_5$	$-(CH{=}CH)_4-$		2420[d]		[76]
Fc	$Azulenylium^+$	$-CH=$	716	326	145	[77]

[a] Measured in CH_2Cl_2. − [b] Measured in THF. − [c] Measured in $MeNO_2$. − [d] Measured in CH_3CN.

There have been a number of studies of NLO-active organometallic complexes utilising the ferrocene fragment as an electron donor[71−77] and the $[Fe_2(\eta\text{-}C_5H_5)_2(CO)_2(\mu\text{-}CO)(\mu\text{-}C-)]^+$ electron-accepting moiety.[22,45] However, problems arise when comparing NLO values obtained from different techniques and solvents.[57][58] Meaningful comparisons can only be made between our complexes and others characterised using the HRS technique at 1064 nm incident radiation (Table 4). The second-order hyperpolarisabilities presented in Table 4 confirm that the combination of ferrocenyl donor with the $[Fe_2(\eta\text{-}C_5H_5)_2(CO)_2(\mu\text{-}CO)(\mu\text{-}C-)]^+$ acceptor is very effective as **13−22** have some of the highest β and β_0 values so far observed for organometallic compounds.

Conclusion

In summary, we have systematically modified the conjugation pathway of the cationic organometallic merocyanine system $[Fe_2(\eta\text{-}C_5H_5)_2(CO)_2(\mu\text{-}CO)(\mu\text{-}C-CH=CH-\{\pi\text{-linker}\}-Fc)][BF_4]$ and examined the effects on the linear and nonlinear optical properties. The results agree with some previously held tenets in that extending the π-linker with olefinic units result in a bathochromic shift of the λ_{max} and concomitantly increase the second-order NLO response. However, they do not agree with others. When aromatic spacers are included, the results suggest that the first hyperpolarisabilities are optimised when the ground state delocalisation of the ferrocenyl electrons is reduced. Better results are achieved when the more aromatic benzene unit replaces thiophene or furan moieties. It appears that for our cationic merocyanines (**13−22**) a low excitation energy E_{eg} for the electronic excitation is less important than a large change in the dipole moment $\Delta\mu_{eg}$ and a large transition moment *M*. Furthermore, the observation that the substituent on the olefinic double bond proximate to the ferrocenyl group has a dramatic effect on the β and β_0 values (cf. **14−21**) emphasises the necessity for further rigorous and systematic research to elucidate the structure−property relationship, which is so vital for the advancement of this field.

Experimental Section

Solvent Purification and Instrumentation: Dichloromethane and THF were dried by refluxing in the presence of calcium hydride and distilled prior to use. THF was further distilled from sodium/benzophenone. Acetonitrile was dried by refluxing in the presence of calcium sulfate and distilled prior to use. − Infrared spectra were recorded with a Perkin−Elmer Paragon 1000 spectrometer. Peak positions are in cm^{-1} with relative peak heights in parentheses. − UV/Vis spectra were recorded with a Perkin−Elmer Lambda 6 spectrometer. Band positions are in nm with band intensities in parentheses. − NMR spectra were recorded with a JEOL JNM-GX 270 FT spectrometer. Chemical shifts are in ppm downfield from TMS as an internal standard and in parentheses are (multiplicity, integration, coupling constants *J* in Hz) where appropriate. − Elemental analyses were carried out in the Microanalytical Laboratory, University College, Dublin.

General Procedure for the Condensation of Ferrocenyl Aldehydes 9−11 with $[Fe_2(\eta\text{-}C_5H_5)_2(CO)_2(\mu\text{-}CO)(\mu\text{-}C-CH_3)][BF_4]$ (12): Complex **12**[37] (0.25 g, 0.57 mmol) and an excess of aldehyde (1.2 equiv.) was stirred in CH_2Cl_2 (50 mL) at 35 °C for twelve hours. The reaction mixture was filtered and the product precipitated from the filtrate by carefully adding diethyl ether (25 mL) and cooling overnight.

$[Fe_2(\eta\text{-}C_5H_5)_2(CO)_2(\mu\text{-}CO)(\mu\text{-}C-CH=CH-Fc)][BF_4]$ (13): Yield 0.20 g (54%). − ^{1}H NMR [$(CD_3)_2CO$]: δ = 9.64 (d, 1 H, *J* = 14.1 Hz, μ-C−CH), 8.46 (d, 1 H, *J* = 14.1 Hz, μ-C−CH=CH), 5.55 (s, 10 H, C_5H_5), 5.42, 5.36 (C_5H_4, Fc), 4.43 (C_5H_5, Fc). − ^{13}C NMR [$(CD_3)_2CO$]: δ = 408.0 (μ-C), 257.7 (μ-CO), 209.8 (CO), 162.3, 150.9 (μ-C−CH=CH), 92.1 (C_5H_5), 80.7, 80.3, 74.5, 74.0 (Fc). − IR (CH_2Cl_2): ν(CO) 2024 (10.0), 1993 (2.7); ν(μ-CO) 1837 (5.4); ν(C=C) 1605 (2.8), 1525 (13.2), 1461 (2.3). − UV/Vis: (CH_2Cl_2): λ_{max} (ε) = 655 nm (10,953 $M^{-1}\cdot cm^{-1}$), 428 nm (17,736 $M^{-1}\cdot cm^{-1}$); (CH_3CN): λ_{max} (ε) = 634 (9,390 $M^{-1}\cdot cm^{-1}$), 421 (15,245 $M^{-1}\cdot cm^{-1}$). − $C_{26}H_{21}BF_4Fe_3O_3$ (635.8): calcd: C 49.07, H 3.30; found C 48.70, H 3.31.

$[Fe_2(\eta\text{-}C_5H_5)_2(CO)_2(\mu\text{-}CO)(\mu\text{-}C-CH=CH-CH=CH-Fc)][BF_4]$ (14): Yield 0.21 g (57%). − ^{1}H NMR [$(CD_3)_2CO$]: δ = 9.40 (d, 1 H, *J* = 13.2 Hz, μ-C−CH), 8.28 (d, 1 H, *J* = 14.1 Hz, μ-C−CH=CH−CH=CH), 8.02 (t, 1 H, μ-C−CH=CH), 7.06 (t, 1 H, μ-C−CH=CH−CH), 5.54 (s, 10 H, C_5H_5), 5.04, 4.99 (C_5H_4, Fc), 4.38 (C_5H_5, Fc). − ^{13}C NMR (CD_3CN): δ = 410.5 (μ-C), 257.2 (μ-CO), 208.8 (CO), 163.1, 156.5, 152.6, 125.3 (μ-C−CH=CH−CH=CH), 91.6 (C_5H_5), 82.1, 76.3, 72.0, 71.4 (Fc). − IR: (CH_2Cl_2): ν(CO) 2027 (10.0), 2001 (3.6); ν(μ-CO) 1837 (4.4); ν(C=C) 1605 (2.5), 1582 (5.6), 1525 (16.7). − UV/Vis: (CH_2Cl_2): λ_{max} (ε) = 734 (13,881 $M^{-1}\cdot cm^{-1}$), 484 (17,094 $M^{-1}\cdot cm^{-1}$); (CH_3CN): λ_{max} (ε) = 698 (10,029 $M^{-1}\cdot cm^{-1}$), 471 (14,397 $M^{-1}\cdot cm^{-1}$). − $C_{28}H_{23}BF_4Fe_3O_3$ (661.8): calcd. C 50.76, H 3.47; found C 46.69, H 3.82.

$[Fe_2(\eta\text{-}C_5H_5)_2(CO)_2(\mu\text{-}CO)(\mu\text{-}C-CH=CH-CH=CH-CH=CH-Fc)][BF_4]$ (15): Yield 0.27 g (67%). − ^{1}H NMR [$(CD_3)_2CO$]: δ = 9.42 (d, 1 H, *J* = 13.8 Hz, μ-C−C*H*), 7.96 (m, 2 H, μ-C−CH=CH−CH=CH−CH=CH), 7.42 (d, 1 H, *J* = 14.6 Hz, μ-C−CH=CH−CH=CH−CH=C*H*), 7.00 (t, 1 H, μ-C−CH=CH−CH=CH−CH=CH), 6.82 (t, 1 H, μ-C−CH=CH−CH−CH=CH−CH=CH), 5.55 (s, 10 H, C_5H_5), 4.90, 4.84 (C_5H_4, Fc), 4.33 (C_5H_5, Fc). − ^{13}C NMR [$(CD_3)_2CO$]: δ = 413.8 (μ-C), 257.1 (μ-CO), 209.5 (CO), 159.2, 157.3, 154.1, 151.4, 129.8, 128.4 (μ-C−CH=CH−CH=CH), 92.2 (C_5H_5), 82.3, 74.1, 71.4, 70.4 (Fc). − IR: (CH_2Cl_2): ν(CO) 2028 (10.0), 2000 (3.4); ν(μ-CO) 1837 (5.1); ν(C=C) 1603 (3.1), 1572 (5.4), 1488 (19.5). − UV/Vis: (CH_2Cl_2): λ_{max} (ε) = 775 (18,277 $M^{-1}\cdot cm^{-1}$), 541 (22,488 $M^{-1}\cdot cm^{-1}$); (CH_3CN): λ_{max} (ε) = 717 (16,275 $M^{-1}\cdot cm^{-1}$), 508 (21,034 $M^{-1}\cdot cm^{-1}$). − $C_{30}H_{25}BF_4Fe_3O_3$ (687.9): calcd. C 52.33, H 3.66; found C 52.30, H 3.92.

$[Fe_2(\eta\text{-}C_5H_5)_2(CO)_2(\mu\text{-}CO)(\mu\text{-}C-CH=CH-CH=CH-CH=CH-CH=CH-Fc)][BF_4]$ (16): Yield 0.29 g (72%). − ^{1}H NMR [$(CD_3)_2CO$]: δ = 9.42 (d, 1 H, *J* = 13.5 Hz, μ-C−C*H*), 7.93 (m, 2 H, μ-C−CH=CH−CH=CH−CH=CH−CH=CH−CH=CH), 7.14 (m, 2 H, μ-C−CH=CH−CH=CH−CH=CH−CH=CH−CH=CH), 6.77 (m, 3 H, μ-C−CH=CH−CH=CH−CH=CH−CH=CH−CH=CH), 5.55 (s, 10 H, C_5H_5), 4.74, 4.64 (C_5H_4, Fc), 4.25 (C_5H_5, Fc). − ^{13}C NMR [$(CD_3)_2CO$]: δ = 415.8 (μ-C), 256.9 (μ-CO), 209.5 (CO), 158.9, 156.3, 154.2, 158.6, 145.2, 132.0, 131.4, 127.6 (μ-C−CH=CH−CH=CH−CH=CH−CH=CH−CH=CH), 92.2 (C_5H_5), 82.8, 72.4,

70.8, 69.3 (Fc). − IR: (CH_2Cl_2): ν(CO) 2029 (10.0), 2001 (3.5); ν(μ-CO) 1839 (5.0); ν(C=C) 1606 (4.2), 1548 (6.7), 1494 (26.5). − UV/Vis: (CH_2Cl_2): λ_{max} (ε) = 813 (23,106 $M^{-1}\cdot cm^{-1}$), 582 (24,670 $M^{-1}\cdot cm^{-1}$); (CH_3CN): λ_{max} (ε) = 720 (14,954 $M^{-1}\cdot cm^{-1}$), 521 (21,678 $M^{-1}\cdot cm^{-1}$). − $C_{32}H_{27}BF_4Fe_3O_3$ (713.9): calcd. C 53.84, H 3.81; found C 53.54, H 3.71%.

[$Fe_2(\eta$-$C_5H_5)_2(CO)_2(\mu$-CO)(μ-C−CH=CH−C_6H_4−CH=CH−Fc][BF_4] (17): Yield 0.15 g (61%). − ^{1}H NMR ($CDCl_3$): δ = 9.82 (d, 1 H, *J* = 14.5 Hz, μ-C−CH), 8.11 (d, 2 H, *J* = 8.4 Hz, C_6H_4), 7.59 (hidden, μ-C−CH=CH), 7.58 (d, 2 H, *J* = 8.4 Hz, C_6H_4), 7.24 (hidden, C_6H_4−CH=CH), 6.71 (d, 1 H, *J* = 16.0 Hz, C_6H_4−CH=CH), 5.29 (s, 10 H, C_5H_5), 4.60, 4.48 (C_5H_4, Fc), 4.21 (C_5H_5, Fc). − ^{13}C NMR ($CDCl_3$): δ = 431.6 (μ-C), 255.1 (μ-CO), 207.7 (CO), 153.1, 151.7 (μ-C−CH=CH), 134.4, 127.8 133.4, 125.8 (C_6H_4−CH=CH), 132.8, 131.0 (*Cq*-C_6H_4), 92.1 (C_5H_5), 71.3, 72.1, 70.9 (Fc). − IR: (CH_2Cl_2): ν(CO) 2035 (10.0), 2004 (2.7); ν(μ-CO) 1844 (5.2); ν(C=C) 1605 (4.4), 1593 (4.6), 1556 (4.6), 1527 (11.5), 1506 (7.7), 1456 (2.8). − UV/Vis (CH_2Cl_2): λ_{max} (ε) = 705 (12,162 $M^{-1}\cdot cm^{-1}$), 512 (28,692 $M^{-1}\cdot cm^{-1}$); (CH_3CN): λ_{max} (ε) = 616 (12,803 $M^{-1}\cdot cm^{-1}$), 480 (26,773 $M^{-1}\cdot cm^{-1}$). − $C_{34}H_{27}BF_4Fe_3O_3$ (737.9): calcd. C 55.28, H 3.66; found C 53.87, H 3.85.

[$Fe_2(\eta$-$C_5H_5)_2(CO)_2(\mu$-CO)(μ-C−CH=CH−C_4H_2S−CH=CH−Fc][BF_4] (18): Yield 0.22 g (52%). − ^{1}H NMR (CD_3CN): δ = 9.24 (d, 1 H, *J* = 13.8 Hz, μ-C−CH), 8.49 (d, 1 H, *J* = 3.9 Hz, C_2H_4S), 7.95 (d, 1 H, *J* = 13.8 Hz, μ-C−CH=CH), 7.24 (d, 1 H, *J* = 15.2 Hz, C_2H_4S−CH=CH−Fc), 7.12 (d, 1 H, *J* = 3.9 Hz, C_2H_4S), 6.82 (d, 1 H, *J* = 15.2 Hz, C_2H_4S−CH=CH−Fc), 5.21 (s, 10 H, C_5H_5), 4.72, 4.64 (C_5H_4, Fc), 4.31 (C_5H_5, Fc). − ^{13}C NMR ($CDCl_3$): δ = 409.5 (μ-C), 256.9 (μ-CO), 209.4 (CO), 160.4, 138.3 (*Cq*-C_2H_4S), 149.7, 146.6, 146.3, 138.4, 123.0, 119.2 (μ-C−CH=CH; C^3, C^4-C_2H_4S; C_2H_4S−CH=CH−Fc), 92.8 (C_5H_5), 82.2, 76.2, 70.5, 69.2 (Fc). − IR: CH_2Cl_2: ν(CO) 2030 (10.0), 1999 (3.4); ν(μ-CO) 1839 (5.3); ν(C=C) 1604 (5.9), 1529 (14.9), 1493 (4.9). − UV/Vis (CH_2Cl_2): λ_{max} (ε) = 757 (19,966 $M^{-1}\cdot cm^{-1}$), 569 (32,538 $M^{-1}\cdot cm^{-1}$); (CH_3CN): λ_{max} (ε) = 688 (17,147 $M^{-1}\cdot cm^{-1}$), 542 (26,378 $M^{-1}\cdot cm^{-1}$). − $C_{32}H_{25}BF_4Fe_3O_3S$ (744.0): calcd. C 51.61, H 3.36; found C 54.85, H 3.95.

[$Fe_2(\eta$-$C_5H_5)_2(CO)_2(\mu$-CO)(μ-C−CH=CH−C_4H_2O−CH=CH−Fc)][BF_4] (19): Yield 0.23 g (55.6%). − ^{1}H NMR (CD_3CN): δ = 9.64 (d, 1 H, *J* = 13.9 Hz, μ-C−CH), 7.92 (br. s, C_2H_4O), 7.82 (d, 1 H, *J* = 15.8 Hz, C_2H_4O−CH=CH−Fc), 7.61 (d, 1 H, *J* = 13.9 Hz, μ-C−CH=CH), 6.95 (d, 1 H, *J* = 3.9 Hz, C_2H_4O), 6.87 (d, 1 H, *J* = 15.8 Hz, C_2H_4O−CH=CH−Fc), 5.39 (s, 10 H, C_5H_5), 4.79, 4.68 (C_5H_4, Fc), 4.31 (C_5H_5, Fc). − ^{13}C NMR (CD_3CN): δ = 406.8 (μ-C), 258.1 (μ-CO), 209.8 (CO), 165.9, 147.5 (*Cq*-C_2H_4O), 147.4, 141.3, 137.5, 136.1, 117.1, 113.3 (μ-C−CH=CH; C^3, C^4-C_2H_4O; C_2H_4O−CH=CH−Fc), 92.3 (C_5H_5), 82.6, 7.35, 7.45, 70.0 (Fc). − IR: CH_2Cl_2: ν(CO) 2029 (10.0), 2000 (3.3); ν(μ-CO) 1838 (5.1); ν(C=C) 1605 (7.5), 1560 (1.7), 1529 (12.7), 1493 (5.1). − UV/Vis: (CH_2Cl_2): λ_{max} (ε) = 747 (22,325 $M^{-1}\cdot cm^{-1}$), 577 (33,211 $M^{-1}\cdot cm^{-1}$); (CH_3CN): λ_{max} (ε) = 683 (21,202 $M^{-1}\cdot cm^{-1}$), 551 (28,946 $M^{-1}\cdot cm^{-1}$). − $C_{32}H_{25}BF_4Fe_3O_4$ (727.9): calcd. C 52.75, H 4.43; found C 51.48, H 3.72.

[$Fe_2(\eta$-$C_5H_5)_2(CO)_2(\mu$-CO)(μ-C−CH=CH−C_4H_2S−CH=CH−CH=CH−Fc)][BF_4] (20): Yield 0.21 g (49%). − ^{1}H NMR [$(CD_3)_2CO$]: δ = 9.75 (d, 1 H, *J* = 14.1 Hz, μ-C−CH), 8.33 (d, 1 H, *J* = 14.1 Hz, μ-C−CH=CH), 8.27 (d, 1 H, *J* = 4.2 Hz, C_2H_4S), 7.49 (d, 1 H, *J* = 4.2 Hz, C_2H_4S), 7.27 (dd, 1 H, *J* = 15.2, 10.69 Hz, C_2H_4S−CH=CH−CH=CH−Fc), 6.94 (d, 1 H, *J* = 15.2 Hz, C_2H_4S−CH=CH−CH=CH−Fc), 6.91 (d, 1 H, *J* = 15.5 Hz, C_2H_4S−CH=CH−CH=CH−Fc), 6.77 (dd, 1 H, *J* = 15.5, 10.7 Hz, C_2H_4S−CH=CH−CH=CH−Fc), 5.60 (C_5H_5), 4.67, 4.52 (C_5H_4, Fc), 4.22 (C_5H_5, Fc). − ^{13}C NMR [$(CD_3)_2CO$]: δ = 414.1 (μ-C), 255.6 (μ-CO), 208.3 (CO), 159.0, 137.8 (*Cq*-C_2H_4S), 148.7, 145.2, 144.5, 139.1, 136.9, 129.4, 126.0, 121.8 (μ-C−CH=CH; C^3, C^4-C_2H_4S; C_2H_4S−CH=CH−CH=CH−Fc), 91.2 (C_5H_5), 83.4, 70.6, 69.7, 67.7 (Fc). − IR: CH_2Cl_2: ν(CO) 2030 (10.0), 2000 (2.5); ν(μ-CO) 1839 (5.1); ν(C=C) 1604 (6.1), 1586 (3.0), 1528, (16.8), 1490 (4.0). − UV/Vis: (CH_2Cl_2): λ_{max} (ε) = 764 (22,363 $M^{-1}\cdot cm^{-1}$), 606 (29,169 $M^{-1}\cdot cm^{-1}$); (CH_3CN): λ_{max} (ε) = 677 (19,199 $M^{-1}\cdot cm^{-1}$), 590 (30,565 $M^{-1}\cdot cm^{-1}$). − $C_{34}H_{27}BF_4Fe_3O_3S$ (770.0): calcd. C 52.99, H 3.51; found C 48.93, H 3.69.

[$Fe_2(\eta$-$C_5H_5)_2(CO)_2(\mu$-CO)(μ-C−CH=CH−CH=C(Cl)−Fc)][BF_4] (21): Yield 0.25 g (61.9%). − ^{1}H NMR [$(CD_3)_2CO$]: δ = 9.29 (d, 1 H, *J* = 13.8 Hz, μ-C−CH), 7.85 (dd, 1 H, *J* = 11.5, 13.8 Hz, μ-C−CH=CH), 7.14 (d, 1 H, *J* = 11.5 Hz, μ-C−CH=CH−CH), 5.33 (s, 10 H, C_5H_5), 5.12, 5.00 (C_5H_4, Fc), 4.35 (C_5H_5, Fc). − ^{13}C NMR (CD_3CN): δ = 422.5 (μ-C), 255.6 (μ-CO), 208.6 (CO), 160.7 [μ-C−CH=CH−CH=C(Cl)], 153.2, 148.1, 121.7 (μ-C−CH=CH−CH), 92.0 (C_5H_5), 83.0, 76.0, 72.7, 70.9 (Fc). − IR: CH_2Cl_2: ν(CO) 2031 (10.0), 2001 (2.3); ν(μ-CO) 1841 (4.4); ν(C=C) 1605 (1.4), 1553 (4.6), 1521 (13.1). − UV/Vis: (CH_2Cl_2): λ_{max} (ε) = 746 (17,173 $M^{-1}\cdot cm^{-1}$), 495 (27,589 $M^{-1}\cdot cm^{-1}$); (CH_3CN): λ_{max} (ε) = 713 (13,986 $M^{-1}\cdot cm^{-1}$), 477 (24,439 $M^{-1}\cdot cm^{-1}$). − $C_{28}H_{22}BClF_4Fe_3O_3$ (696.3): calcd. C 48.24, H 3.16; found C 47.74, H 3.43.

[$Fe_2(\eta$-$C_5H_5)_2(CO)_2(\mu$-CO)(μ-C−CH=CH−C_4H_2S−CH=CH−CH=C(Cl)−Fc)][BF_4] (22): Yield 0.26 g (56.9%). − ^{1}H NMR [$(CD_3)_2CO$]: δ = 9.85 (1 H, d, *J* = 14.4 Hz, μ-C−CH), 8.34 (d, 1 H, *J* = 14.3 Hz, μ-C−CH=CH), 8.26 (d, 1 H, *J* = 3.7 Hz, C_2H_4S), 7.54 (d, 1 H, *J* = 3.7 Hz, C_2H_4S), 7.44 [dd, 1 H, *J* = 15.2, 10.7 Hz, C_2H_4S−CH=CH−CH=C(Cl)−Fc], 7.17 [d, 1 H, *J* = 15.2 Hz, C_2H_4S−CH=CH−CH=C(Cl)−Fc], 7.02 [d, 1 H, *J* = 10.7 Hz, C_2H_4S−CH=CH−CH=C(Cl)−Fc] 5.64 (C_5H_5), 4.82, 4.54 (C_5H_4, Fc), 4.26 (C_5H_5, Fc). − ^{13}C NMR ($(CD_3)_2CO$): δ = 420.8 (μ-C), 256.2 (μ-CO), 209.4 (CO), 158.2, 139.8, 139.4 [*Cq*-C_2H_4S; C_2H_4S−CH=CH−CH=C(Cl)−Fc], 150.3, 145.8, 145.2, 131.6, 131.4, 125.9, 122.1 [μ-C−CH=CH; C^3, C^4-C_2H_4S; C_2H_4S−CH=CH−CH=C(Cl)−Fc], 92.6 (C_5H_5), 84.3, 71.8, 71.2, 68.7 (Fc). − IR: CH_2Cl_2: ν(CO) 2031 (10.0), 2001 (2.3); ν(μ-CO) 1840 (5.0); ν(C=C) 1605 (1.7), 1583 (2.7), 1528 (16.6), 1490 (4.3). − UV/Vis: (CH_2Cl_2): λ_{max} (ε) = 731 (24,000 $M^{-1}\cdot cm^{-1}$), 606 (34,798 $M^{-1}\cdot cm^{-1}$); (CH_3CN): λ_{max} (ε) = 644 (30,695 $M^{-1}\cdot cm^{-1}$), 572 (36,213 $M^{-1}\cdot cm^{-1}$). − $C_{34}H_{26}BClF_4Fe_3O_3S$ (804.4): calcd. C 50.71, H 3.23; found C 49.44, H 3.50.

X-ray Structure Determination of 21: Crystals suitable for an X-ray structure analysis were obtained by diffusion of Et_2O into a CH_2Cl_2 solution of **21**. The data were collected with a four-circle Hilger & Watts diffractometer, Mo-K_α, λ = 0.71073 Å. The structure was resolved by direct methods (SHELXL-86).[78] Refinement on F^2 was carried out by full-matrix least-squares techniques (SHELXL-93).[79] All non-hydrogen atoms were refined with anisotropic thermal parameters. The hydrogen atoms were refined with a fixed isotropic thermal parameter related by a factor of 1.2 to the value of the equivalent isotropic thermal parameter of their carrier atoms. Weights were optimised in the final refinement cycles. Crystal data and structure refinement are given Table 5, whilst selected bond lengths [pm] and angles [°] are listed in Table 1. Crystallographic data (excluding structure factors) for the reported structure have been deposited with the Cambridge Crystallographic Data Centre as supplementary publication no. CCDC-149412. Copies of the data can be obtained free of charge on application

to CCDC, 12 Union Road, Cambridge CB2 1EZ, UK [Fax: (internat.) + 44 1223/336-033; E-mail: deposit@ccdc.cam.ac-uk].

Table 5. Crystal data and structure refinement for [$Fe_2(\eta$-$C_5H_5)_2(CO)_2(\mu$-CO){μ-C−CH=CH−CH=C(Cl)−Fc}][BF_4] (**21**)

Empirical formula	$C_{28}H_{22}BClF_4Fe_3O_3$
Molecular mass [g/mol]	696.27
Temperature [K]	173
λ [pm]	7.1073
Crystal system	monoclinic
Space group	*P*2/*c*
Unit cell dimensions [Å, °]	$a = 8.846(4)$
	$b = 24.087(8)$
	$c = 13.025(4)$
	$\beta = 97.90(3)$
V [Å^3]	2749.0(17)
Z	4
$\rho_{calcd.}$ [g/cm^3]	1.682
Absorption coefficient [mm^{-1}]	1.716
$F(000)$	1400
Crystal size [mm]	0.6 × 0.4 × 0.3
$\theta_{min}-\theta_{max}$ [°]	2.31−25.07
Index ranges	$-1 \le h \le 10$
	$0 \le k \le 28$
	$-15 \le l \le 15$
Collected reflections	5382
Unique reflections	4882
R_{int}	0.0245
Data [$I > 4\sigma(I)$]	4882
Parameters	361
Goodness-of-fit	1.045
$R1/wR2$ [$I > 2\sigma(I)$]	0.0390/0.0986
$R1/wR2$ (all data)	0.0489/0.1040
min./max. residual electron density [e·Å^{-3}]	−0.552, 0.612

HRS Measurements of the First Hyperpolarisabilities: Experimental setup details can be found in ref.[56] An Nd:YAG laser with a wavelength of 1064 nm was used as incident light source. All measurements were carried out in dry CH_2Cl_2 with sample concentrations of 10^{-6} to 10^{-4} M using *p*-NA as the external reference [$\beta(CH_2Cl_2) = 21.6\cdot10^{-30}$ esu[56]]. The compounds were checked for flourescence using the bandpass filter method described in ref.[22]

Acknowledgments

This work was supported by the European Community through the TMR Network Contract No. ERBFMRX-CT98-0166.

[1] D. R. Kanis, M. A. Ratner, T. J. Marks, *Chem. Revs.* **1994**, *94*, 195.
[2] L-T. Cheng, W. Tam, S. H. Stevenson, G. R. Meredith, G. Rikken, S. R. Marder, *J. Phys. Chem.* **1991**, *95*, 10631.
[3] L-T. Cheng, W. Tam, S. R. Marder, A. E. Stiegman, G. Rikken, C. W. Spangler, *J. Phys. Chem.* **1991**, *95*, 10643.
[4] I. D. L. Albert, T. J. Marks, M. A. Ratner, *J. Am. Chem. Soc.* **1997**, *119*, 6575.
[5] A. K-Y. Jen, V. Pushkara Rao, K. Y. Wong, K. J. Drost, *J. Chem. Soc., Chem. Commun.* **1993**, 90.
[6] V. Pushkara Rao, A. K-Y. Jen, K. Y. Wong, K. J. Drost, *J. Chem. Soc., Chem. Commun.* **1993**, 1118.
[7] A. K-Y. Jen, Y. Cai, P. V. Bedworth, S. R. Marder, *Adv. Mater.* **1997**, *9*, 132.
[8] S. R. Marder, J. W. Perry, B. G. Tiemann, *Organometallics* **1991**, *10*, 1896.
[9] V. Alain, M. Blanchard-Desce, C-T. Chen, S. R. Marder, A. Fort, M. Barzoukas, *Synth. Met.* **1996**, *81*, 133.
[10] C. Lambert, W. Gaschler, M. Zabel, R. Matschiner, R. Wortmann, *J. Organomet. Chem.* **1999**, *592*, 109.
[11] T. J. J. Müller, A. Netz, M. Ansorge, *Organometallics* **1999**, *18*, 5066.
[12] H. Wong, T. Meyer-Friedrichsen, T. Farrell, C. Mecker, J. Heck, *Eur. J. Inorg. Chem.* **2000**, 631 and reference [1] therein.
[13] I. R. Whitall, A. M. McDonagh, M. G. Humphrey, *Adv. Organomet. Chem.* **1998**, *42*, 291.
[14] T. Saji, I. Kinoshita, *J. Chem. Soc., Chem. Commun.* **1986**, 716.
[15] J. Malthete, J. Billard, *Mol. Cryst. Liq. Cryst.* **1976**, *34*, 117,
[16] R. Deschenaux, J. Santiago, *J. Mater. Chem.* **1993**, *3*, 219.
[17] M. B. Hall, R. F. Fenske, *Inorg. Chem.* **1972**, *11*, 768.
[18] C. P. Casey, M. S. Konings, S. R. Marder, Y. Takezawa, *J. Organomet. Chem.* **1988**, *358*, 347.
[19] C. P. Casey, M. S. Konings, S. R. Marder, *Polyhedron* **1988**, *7*, 881.
[20] C. P. Casey, M. S. Konings, S. R. Marder, *J. Organomet. Chem.* **1988**, *345*, 125.
[21] J. A. Bandy, H. E. Bunting, M-H. Garcia, M. L. H. Green, S. R. Marder, M. E. Thompson, *Polyhedron* **1992**, *12*, 1429.
[22] T. Farrell, T. Meyer-Friedrichsen, J. Heck, A. R. Manning, *Organometallics* **2000**, *19*, 3410.
[23] S. R. Marder, J. W. Perry, *Adv. Mater.* **1993**, *5*, 804.
[24] C.-T. Chen, S. R. Marder, L.-T. Cheng, *J. Chem. Soc., Chem. Commun.* **1994**, 259.
[25] S. R. Marder, D. N. Beratan, L.-T. Cheng, *Science* **1991**, *252*, 103.
[26] S. R. Marder, B. Kippelen, A. K. Jen, N. Peyghambarian, *Nature* **1997**, *388*, 845.
[27] D. Lednicer, C. R. Hauser, *Org. Synth. 40*, 31.
[28] P. L. Pauson, W. E. Watts, *J. Chem. Soc.* **1963**, 1990.
[29] T. Farrell, Ph.D. Thesis, University College Dublin, **1998**.
[30] J. M. Barker, P. R. Huddleston, M. L. Wood, *Synth. Commun.* **1975**, *5*, 65.
[31] R. Guilard, P. Fournai, M. Person, *Bull. Soc. Chim. Fr.* **1967**, *11*, 4121.
[32] R. Antonioletti, M. D'Auria, G. Piancatelli, A. Scettri, *J. Chem. Soc., Perkin Trans. 1* **1985**, 1285.
[33] D. J. Chadwick, J. Chambers, G. D. Meakins, R. L. Snowden, *J. Chem. Soc., Perkin Trans. 1* **1973**, 1766.
[34] G. D. Broadhead, J. M. Osgerby, P. L. Pauson, *J. Chem. Soc.* **1958**, 650.
[35] M. Rosenblum, N. Braun, J. Papenmeier, M. Applebaum, *J. Organomet. Chem.* **1966**, *15*, 173.
[36] C. W. Spangler, R. K. McCoy, *Synth. Commun.* **1988**, *18*, 51.
[37] M. Nitay, W. Priester, M. Rosenblum, *J. Am. Chem. Soc.* **1978**, *100*, 3620.
[38] C. P. Casey, M. S. Konings, R. E. Palermo, R. E. Colborn, *J. Am. Chem. Soc.* **1985**, *107*, 5296.
[39] M. Etienne, J. Talarmin, L. Toupet, *Organometallics* **1992**, *11*, 2058.
[40] G. Bourhill, J. L Bredas, L. T. Cheng, S. R. Marder, F. Meyers, J. W. Perry, B. G. Tiemann, *J. Am. Chem. Soc.* **1994**, *116*, 2619;
[41] S. R. Marder, L. T. Cheng, B. G. Tiemann, A. C. Friedli, M. Blanchard-Desce, J. W. Perry, J. Skindhoj, *Science* **1994**, *263*, 511.
[42] C. P. Casey, M. S. Konings, S. R. Marder, *Polyhedron* **1988**, *7*, 881.
[43] C. P. Casey, M. S. Konings, S. R. Marder, *J. Organomet. Chem.* **1988**, *345*, 125.
[44] C. P. Casey, M. S. Konings, S. R. Marder, Y. Takezawa, *J. Organomet. Chem.* **1988**, *358*, 347.
[45] J. A. Bandy, H. E. Bunting, M.-H. Garcia, M. L. H. Green, S. R. Marder, M. E. Thompson, *Polyhedron* **1992**, *12*, 1429.
[46] J. A. Campo, M. Cano, J. V. Heras, C. Lopez-Garabito, E. Pinilla, R. Torres, G. Rojo, F. Agullo-lopez, *J. Mater. Chem.* **1999**, *9*, 899.

[47] B. J. Coe, C. J. Jones, J. A. McCleverty, D. Bloor, G. Cross, *J. Organomet. Chem.* **1994**, *464*, 225.
[48] A. Houlton, J. Naseralla, R. M. G. Roberts, J. Silver, D. Cunningham, P. McArdle, T. Higgins, *J. Chem. Soc., Dalton Trans.* **1992**, 2236.
[49] S. R. Marder, J. W. Perry, B. G. Tiemann, W. P. Schaefer, *Organometallics* **1991**, *10*, 1896.
[50] C. Reichardt, *Solvents and Solvent Effects in Organic Chemistry*, 2nd ed., VCH, Weinheim, **1988**.
[51] J. C. Calabrese, L.-T. Cheng, J. C. Green, S. R. Marder, W. Tam, *J. Am. Chem. Soc.* **1991**, *113*, 7227.
[52] D. R. Kanis, M. A. Ratner, T. J. Marks, *J. Am. Chem. Soc.* **1992**, *114*, 10338.
[53] S. Barlow, B. E. Bunting, C. Ringham, J. C. Green, G. U. Bublitz, S. G. Boxer, I. W. Perry, S. R. Marder, *J. Am. Chem. Soc.* **1999**, *121*, 3715.
[54] J. L. Oudar, D. S. Chemla, *Chem. Phys.* **1977**, *66*, 2664.
[55] E. Hendrickx, K. Clays, A. Persoons, C. Dehu, J. L. Bredas, *J. Am. Chem. Soc.* **1995**, *363*, 58.
[56] K. Clays, A. Persoons, *Rev. Sci. Instrum.* **1992**, *63*, 3285.
[57] J. J. Wolff, R. Wortmann, *Adv. Phys. Org. Chem.* **1999**, 121
[58] K. Clays, E. Hendrickx, T. Verbiest, A. Persoons, *Adv. Mater.* **1998**, *10*, 643.
[59] J. J. Wolff, R. Wortmann, *J. Prakt. Chem.* **1998**, *340*, 99.
[60] S. Stadler, G. Bourhill, C. Bräuchle, *J. Phys. Chem.* **1996**, *100*, 6927.
[61] M. C. Flipse, R. De Jonge, R. H. Woudenberg, A. W. Marsman, C. A. Van Walree, L. W. Jenneskens, *Chem. Phys. Letts.* **1995**, *245*, 297.
[62] S. K. Pal, A. Krishnan, K. D. Puspendu, A. G. Samuelson, *J. Organomet. Chem.* **2000**, *604*, 248.
[63] S. Stadler, R. Dietrich, G. Bourhill, C. Bräuchle, A. Pawlik, W. Grahn, *Chem. Phys. Lett.* **1995**, *247*, 271.
[64] M. A. Pauley, C. H. Wang, *Rev. Sci. Instrum.* **1999**, *70*, 3285.
[65] S. Stadler, R. Dietrich, G. Bourhill, C. Bräuchle, *Opt. Lett.* **1996**, *21*, 251.
[66] O. F. J. Noordman, N. F. van Hulst, *Chem. Phys. Lett.* **1996**, *253*, 145.
[67] G. Olbrechts, R. Strobbe, K. Clays, A. Persoons, *Rev. Sci. Instrum.* **1998**, *69*, 2233.
[68] N. W. Song, T.-I. Kang, S. C. Jeoung, S.-J. Jeon, B. R. Cho, D. Kim, *Chem. Phys. Lett.* **1996**, *261*, 307
[69] O. K. Song, J. N. Woodford, C. H. Wang, *J. Phys. Chem. A* **1997**, *101*, 3222.
[70] V. Cadiero, S. Conejero, M. P. Camasa, J. Gimeno, I. Asselberghs, S. Houbrechts, K. Clays, A. Persoons, J. Borge, S. Garcia-Granda, *Organometallics* **1999**, *18*, 582.
[71] I. S. Lee, H. Seo, Y. K. Chung, *Organometallics* **1999**, *18*, 1091
[72] O. Briel, K. Sünkel, I. Krossing, H. Nöth, E. Schmälzlin, K. Meerholz, C. Brüuchle, W. Beck, *Eur. J. Inorg. Chem.* **1999**, 483.
[73] I. S. Lee, S. S. Lee, H. Seo, Y. K. Chung, *Inorg. Chim. Acta.* **1998**, *279*, 243.
[74] J. Mata, S. Uriel, E. Peris, R. Llusar, S. Houbrechts, A. Persoons, *J. Organomet. Chem.* **1998**, *562*, 197.
[75] E. Hendrickx, A. Persoons, S. Samson, G. R. Stephenson, *J. Organomet. Chem.* **1997**, *542*, 295.
[76] K.N. Jayaprakash, P. C. Ray, I. Matsuoka, M. M. Bhadbhade, V. G. Puranik, P. K. Das, H. Nishihara, A. Sarkar, *Organometallics* **1999**, *18*, 3851.
[77] T. Farrell, T. Meyer-Friedrichsen, M. Malessa, D. Haase, W. Saak, I. Asselberghs, K. Wostyn, K. Clays, A. Persoons, J. Heck, A. R. Manning, *J. Chem. Soc., Dalton Trans.*, in press.
[78] G. M. Sheldrick, *SHELXS-86 Program for crystal structure determination. University of Göttingen*, Germany, **1986**.
[79] G. M. Sheldrick, *SHELXL-93 Program for crystal structure refinement*. University of Göttingen, Germany, **1993**.

Received September 12, 2000
[I00341]

Interaction of Some Methylenediphosphanes with Hexafluoroacetone and Hexafluorothioacetone Dimer

Igor V. Shevchenko,*[a] Rostislav N. Mikolenko,[a] Enno Lork,[b] and Gerd-Volker Röschenthaler*[b]

Keywords: Phosphanes / Hexafluoroacetone / Hexafluorothioacetone / Ylides / Wittig reactions

The reactions of methylenediphosphanes **1a–c** with hexafluoroacetone (HFA) and hexafluorothioacetone dimer (HFTA) gave the respective carbodiphosphoranes **5a**, **5b**, **6**, **15**, and **19**. The carbodiphosphoranes **6** and **19**, with phenyl groups at phosphorus, were able to react further with C=O or C=S functions. Compound **6** added one equivalent of HFA across one of the ylidic P=C bonds to give compound **9**, a stable intermediate of the Wittig reaction. The addition of HFTA to **19** gave, unexpectedly, the isomeric compound **21**. The molecular structures of **9**, **15**, and **21** were confirmed by X-ray investigations.

Introduction

It is well-known that the reaction of hexafluoroacetone (HFA) with phosphorus(III) derivatives can lead to the formation of 1,3,2- or 1,4,2-dioxaphospholanes.[1–4] Recently we found that the interaction of HFA with the methylenediphosphanes **1a** and **1b** proceeds in a different way to yield quantitatively the carbodiphosphoranes **5a** and **5b**,[5,6] but not the expected 1,3,2-dioxaphospholanes **2a** and **2b** (Scheme 1).

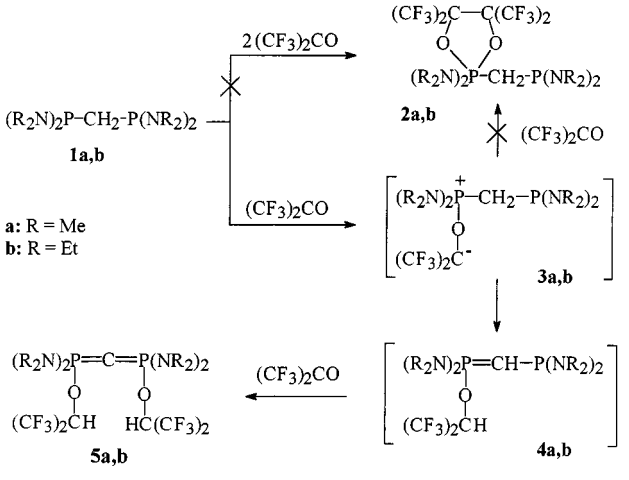

Scheme 1

The mechanism probably involves the intermediate formation of the unstable betaines **3a** and **3b**, which do not add a second molecule of hexafluoroacetone to give **2a** and **2b**, but undergo a proton migration from the $P-CH_2-P$ unit to the secondary carbon of the hexafluoroisopropoxy group forming the monoylides **4a** and **4b**. It is difficult to detect these products by NMR spectroscopy at room temperature since they react quickly with HFA to give the final products **5a** and **5b**. Thus, the presence of the methylene group with labile protons in the α-position to the phosphorus atoms is a necessary condition for this reaction.

Results and Discussion

In order to answer the question as to whether this reaction is an exception or it has more common character, we decided to use the *P*-phenyl-substituted starting material **1c** (Scheme 2).

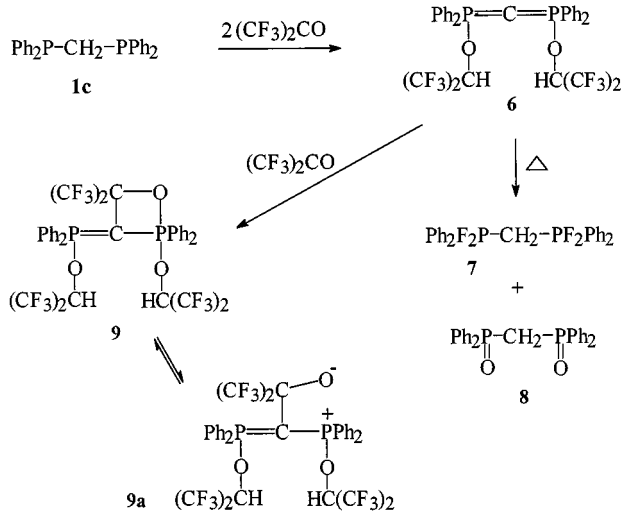

Scheme 2

[a] Institute of Bioorganic Chemistry,
Murmanskaya Str. 1, 02094 Kiev, Ukraine
Fax: (internat.) +38-44/573-2552
E-mail: ishev@bpci.kiev.ua
[b] Institute of Inorganic and Physical Chemistry,
University of Bremen, NW2 C2350
Leobener Straße, 28334 Bremen, Germany
Fax: (internat.) +49-421/218-4267
E-mail: gvr@chemie.uni-bremen.de

 © WILEY-VCH Verlag GmbH, 69451 Weinheim, 2001 1434–1948/01/0909–2377 $ 17.50+.50/0

Like compounds **1a** and **1b**, the bis(diphenylphosphanyl-methane) **1c** reacts with HFA to give the respective carbodiphosphorane **6**. After slow bubbling of gaseous HFA through a solution of **1c** in benzene at 20 °C, the ^{31}P NMR spectrum of the reaction mixture showed the presence of only compound **6** as a singlet at $\delta = 35.3$. The ^{19}F NMR spectrum displays only a doublet at $\delta = -72.45$ ($^3J_{HF} = 6.6$ Hz) confirming the equivalence of the all fluorine atoms and the presence of one proton in each $HC(CF_3)_2$ unit.

The carbodiphosphorane **6** is stable in solution at room temperature for several hours and quickly decomposes in the absence of the solvent. The decomposition of the molecule proceeds analogously to that of **5a** or **5b**, and gives methylene bis(difluorophosphorane) **7**[6] and methylenediphosphane oxide **8**. It is interesting that the formation of the dioxide **8** is not accounted for by the hydrolysis of the bisdifluorophosphorane **7**, as the reaction was carried out under anaerobic conditions. The formation of the analogous dioxide was also observed for **5a** and **5b**.[6]

Unlike compounds **5a** and **5b**, the carbodiphosphorane **6** is able to add one more equivalent of HFA across one of the ylidic P=C bonds with the formation of the cyclic product **9**, which is poorly soluble and crystallizes from the reaction mixture in good yield. It can be considered as a Wittig reaction intermediate, which are usually unstable at room temperature and cannot be isolated. Only a few compounds of this type are known. For example, an analogous addition has been observed for some other carbodiphosphoranes.[7–9] The proposed structure of compound **9** is in accordance with ^{31}P and ^1H NMR spectroscopy; the two different $HC(CF_3)_2$ groups display two characteristic multiplets at $\delta = 3.21$ and 4.36 in the ^1H NMR spectrum. However, the ^{19}F NMR spectrum displays an interesting peculiarity that may reflect the molecular structure of **9**. The two CF_3 groups connected to the four-membered ring are equivalent and display a common signal rather than the two quadruplets that we observed earlier for an analogous compound.[6] The equivalence of these CF_3 groups could be a result of the appropriate symmetry of the molecule: for example, if the plane of symmetry were to coincide with the four-membered cycle. However, the appearance of such symmetry in this molecule is very unlikely. Another explanation is that the four-membered cycle is open in solution, making the rotation of the $(CF_3)_2C$ unit possible. Looking for an answer to this question, we investigated this compound by X-ray analysis (Figure 1).

This analysis showed that the molecule does not have a plane of symmetry, which is why the equivalence of the CF_3 groups in solution can be only explained by the cleavage of one of the bonds of the four-membered ring. The ring is strained, as the C(1)−P(2)−O(1) angle is only 76° (in crystalline form), which should promote its opening. Although the C(1)−C(2) bond (152 pm) is somewhat longer then the normal $C_{sp^2}-C_{sp^3}$ bond, and is closer to normal $C_{sp^3}-C_{sp^3}$ bond lengths, its cleavage is unlikely, as this would result in the formation of the carbene structure, which, according to our previous results, should be unstable. We have already tried to obtain phosphonium-substituted carbenes, however they were very unstable and we could isolate only the products of their decomposition.[6]

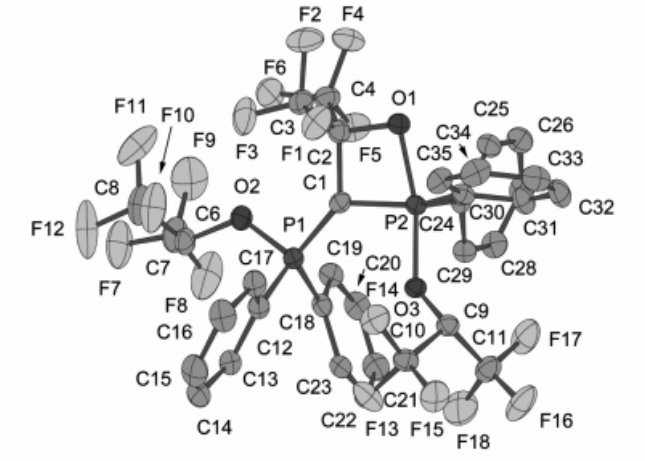

Figure 1. Perspective view and labeling scheme for the molecule **9**; selected bond lengths [pm] and angles [°]: P(1)−O(2) 162.16(19), P(1)−C(1) 170.3(3), P(1)−C(12) 179.2(3), C(1)−P(2) 175.1(3), C(1)−C(2) 151.5(4), C(2)−O(1) 141.0(3), P(2)−O(1) 178.38(19), P(2)−O(3) 177.80(18), P(2)−C(24) 182.4(3); P(1)−C(1)−P(2) 130.10(15), C(1)−P(2)−O(1) 76.00(11), C(1)−C(2)−O(1) 96.1(2), C(2)−O(1)−P(2) 94.96(15), C(2)−C(1)−P(2) 92.63(17), C(2)−C(1)−P(2)−O(1) 3.97(14)

We think that cleavage of the C(2)−O(1) bond [141.0(3) pm] is less preferable than that of the P(2)−O(1) bond, as in the latter case it would form the more stable zwitterionic structure **9a**. The reversible cleavage of the P−O bond of the intermediate oxaphosphetanes has also been postulated by other authors for the Wittig reaction mechanism.[10]

Indeed, heating compound **9** in chloroform or toluene solution at 60−100 °C led to the completion of the Wittig reaction, and gave a mixture of compounds **10**−**13** (Scheme 3), their relative amounts depending on the temperature and the solvent used. Compound **10** was not stable during the decomposition and was only detected by ^{31}P NMR spectroscopy as a singlet at $\delta = 36$. Compound **11** was isolated in low yield as a pure crystalline product. The formation of two other products **12** and **13** can be accounted for by the decomposition of the compounds **10** and **11**, in accordance with our above-mentioned conclusion about the formation of the dioxide **8**. Compound **12** showed two characteristic quadruplets for the two inequivalent CF_3 groups in the ^{19}F NMR spectra. Compound **13** was identified by comparison with a sample obtained independently.

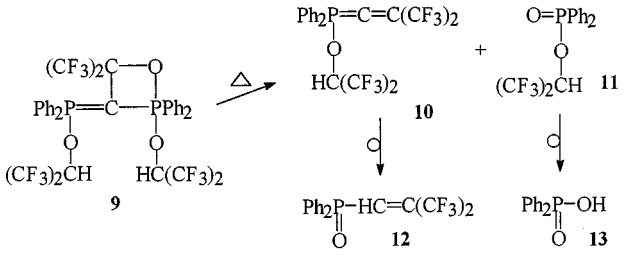

Scheme 3

Thus, the substitution of the dialkylamino groups at phosphorus in methylenediphosphanes **1a** and **1b** by phenyl groups did not change the course of the reaction with HFA.

Our further interest was directed to the reaction of methylenediphosphanes **1a**−**c** with HFTA, whose properties are somewhat different from that of HFA (e.g. it easily dimerizes, and exists as a dimer at room temperature).[11] Therefore, one could expect that the softer sulfur atom might change the course of reaction (Scheme 1). However, compound **1b** and HFTA in hexane gave the carbodiphosphorane **15** quantitatively at −40 °C (Scheme 4). The ^{31}P NMR spectrum of the reaction mixture, taken immediately after the addition of HFTA to **1b**, displayed only one intense singlet at δ = 41.22 (similar to the chemical shift value found for **5b**), indicating two magnetically equivalent phosphorus nuclei of **15**. A two-step reaction is proposed with the intermediate formation of the mono ylide **14**, which was detected in the reaction mixture by ^{31}P NMR spectroscopy as two doublets at δ = 67.4 and 74.7 ($^2J_{PP}$ = 61 Hz) when only one equivalent of HFTA was added to the starting material.

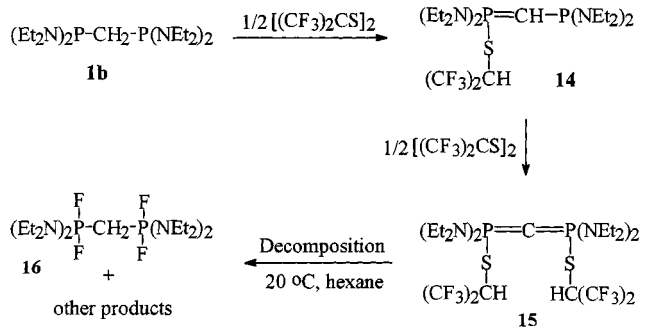

Scheme 4

The carbodiphosphorane **15** turned out to be less stable than its oxygen analog **5b**. It decomposed in hexane solution at room temperature after several hours, whereas carbodiphosphorane **5b** was stable for two days under the same conditions. The choice of hexane as a solvent is very important for this reaction as in other solvents compound **15** is not stable or its synthesis may be accompanied by the formation of by-products. The decomposition of **15** gave a complex mixture with the predominant product being methylenebis(difluorophosphorane) **16**. This product was previously isolated after the decomposition of **5b** and showed the same signal in the ^{31}P NMR spectrum of a triplet at δ = −52.2 ($^1J_{FP}$ = 728 Hz).[6]

Despite the reduced stability of carbodiphosphorane **15**, it was possible to isolate it in a crystalline form, although all our efforts to obtain crystals of the more stable oxygen derivative **5b** failed. Colorless crystals of compound **15** can be stored at −25 °C, however they turn yellow and slowly decompose at room temperature. The X-ray analysis of **15** showed the following molecular structure (Figure 2).

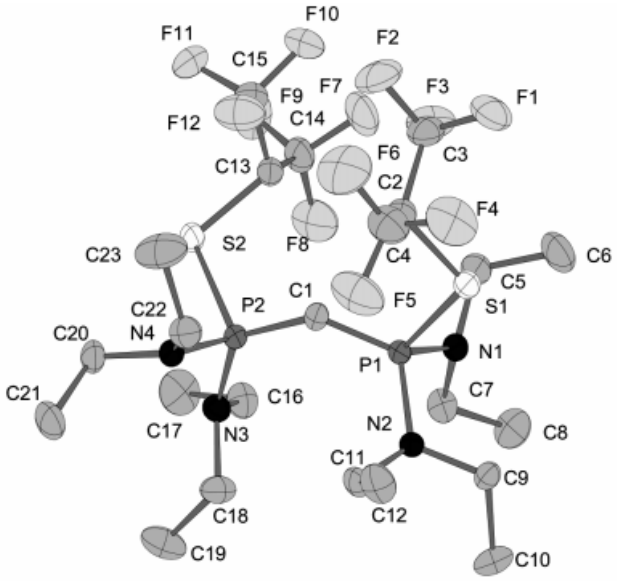

Figure 2. Perspective view and labeling scheme for the molecule **15** (H atoms are omitted for clarity); selected bond lengths [pm] and angles [°]: P(1)−N(1) 167.32(12), P(1)−C(1) 162.57(15), C(1) −P(2) 162.60(15), P(1)−S(1) 217.60(5), S(1)−C(2) 180.40(16), N(1)−C(5) 147.81(19), C(2)−C(3) 152.1(2); C(1)−P(1)−N(1) 122.84(7), C(1)−P(1)−S(1) 108.73(5), N(1)−P(1)−N(2) 101.47(6), N(1)−P(1)−S(1) 98.12(5), P(1)−C(1)−P(2) 139.52(9), P(1)−S(1)−C(2) 101.81(5)

Unlike allenes[12] and heteroallenes, in which the angle between the two double bonds is about 180°, the P=C=P angle in carbodiphosphoranes lies in the range 117−150°, depending on the structure and packing effects.[13−17] The only exception is hexa(dimethylamino)carbodiphosphorane, which has a linear structure and D_{3d} symmetry.[18] Here, the P=C=P angle of carbodiphosphorane **15** is 139.5° with a P=C bond length of 162.57 pm. Both phosphorus atoms of compound **15** have significantly distorted tetrahedral symmetry, with the largest deviation from the ideal angle being 13.3°. It is interesting that because of the low symmetry of the molecule in the solid state the ethyl groups of the diethyl substituents and CF_3 groups of the hexafluoroisopropoxy units are not equivalent. In solution, however, these groups are equivalent and have equal spectral characteristics. For example, all fluorine nuclei display a doublet at δ = −67.7 ($^3J_{HF}$ = 8.14 Hz) in the ^{19}F NMR spectra, which means that in a solution of **15** there is either a rotation or a rapid flip-flop movement around the P−C−P bonds.

The carbodiphosphorane **15**, as a strong base, reacts with acids: for example, with HCl or HBF_4 it gives the corresponding colorless salts **17** and **18** (Scheme 5). As was to be expected, the positive charge of the cation is delocalized over the P−C−P triad, resulting in the magnetic equivalence of the phosphorus nuclei. The ^{31}P NMR spectra of compounds **17** and **18** show only one singlet at δ = 62 and 68, respectively. The analogous salts have been obtained earlier for carbodiphosphoranes **5a** and **5b**, and showed the same spectroscopic data.[5] The chloride **17**, however, differs

from its oxygen derivative. After the addition of HCl to a solution of **15** in hexane compound **17** immediately precipitates from the reaction mixture as a colorless crystalline product that is insoluble in non-polar solvents. This product is stable at room temperature in the solid state. However, the dissolution of this compound leads to its transformation (slowly in [D_8]toluene and rapidly in $CDCl_3$) into another product, which shows two doublets at $\delta = 62.7$ and 71.1 ($^2J_{PP} = 42.6$ Hz) in the ^{31}P NMR spectrum. Since the analogous oxygen derivatives are stable in symmetrical form,[5] the decomposition of **17** can only be explained by the presence of sulfur atoms and by the nucleophilicity of the chlorine anion. Although the appearance of substantial amounts of by-products was not observed in the ^{31}P NMR spectra, we could not isolate the unknown product in a crystalline form and investigate it more thoroughly.

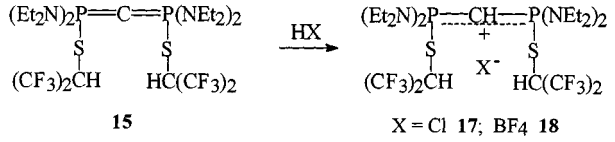

Scheme 5

In contrast to the chloride anion, the tetrafluoroborate is less nucleophilic and the corresponding salt **18** was stable and did not decompose even in boiling $CDCl_3$ solution. This compound crystallized easily allowing us to establish its structure by X-ray analysis (Figure 3).

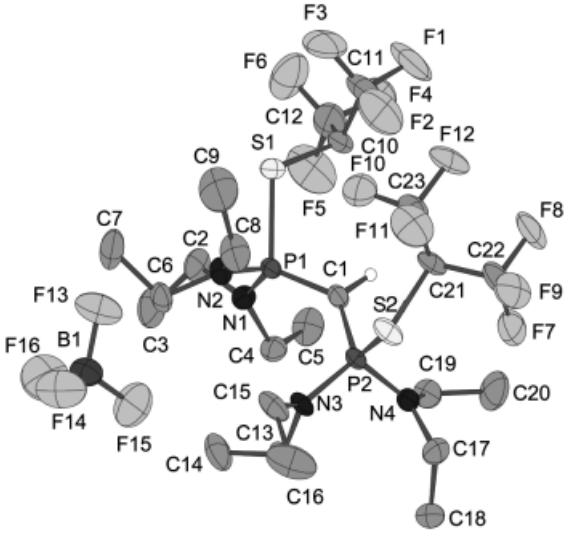

Figure 3. Perspective view and labeling scheme for the molecule **18**; selected bond lengths [pm] and angles [°]: P(1)−N(1) 163.6(3), P(1)−C(1) 169.6(4), C(1) −P(2) 169.7(4), P(1)−S(1) 212.72(14), S(1)−C(10) 182.5(4), N(1)−C(2) 148.2(5), C(10)−C(11) 152.2(6); C(1)−P(1)−N(2) 116.21(19), C(1)−P(1)−S(1) 111.42(14), N(1)−P(1)−S(1) 107.61(13), N(1)−P(1)−N(2) 108.99(17), P(1)−C(1)−P(2) 129.2(2), P(1)−S(1)−C(10) 111.86(15)

The addition of one proton to the P=C=P carbon atom of **15** leads to certain changes in the geometry of the product. As one would expect, the P−C−P angle in **18** becomes significantly narrower (129.2° versus 139.5°). The angles between the phosphorus atoms bonds become closer to those for a tetrahedral geometry. The P−C−P bond lengths of **18** are larger than those of **15** [169.6(4) versus 162.57(15) pm]. However, the other bonds at the phosphorus atoms are shorter in **18** than in **15**. The largest difference (4.9 pm) was found for the P−S bonds, which may indicate the possible participation of the sulfur atoms in delocalization of the positive charge.

The interaction of the dimer of HFTA with methylenebis(diphenylphosphane) **1c** turned out to be quite unusual. The first phase of this reaction, the addition of the two HFTA units to **1c**, does not differ from the analogous reaction with HFA and gives carbodiphosphorane **19** (Scheme 6). Unlike carbodiphosphoranes **5**, **6**, and **15**, which are relatively stable in solution at room temperature, compound **19** exists in diethyl ether solution only at −70 °C and can be detected spectroscopically only at this temperature. There is no doubt about the symmetrical structure of this compound as the ^{31}P NMR spectrum at this temperature shows only one intense singlet at $\delta = 22.5$. The oxygen derivative **6** displays similar spectroscopic data. At −40 °C the carbodiphosphorane **19** decomposes completely in solution within 30−40 min.

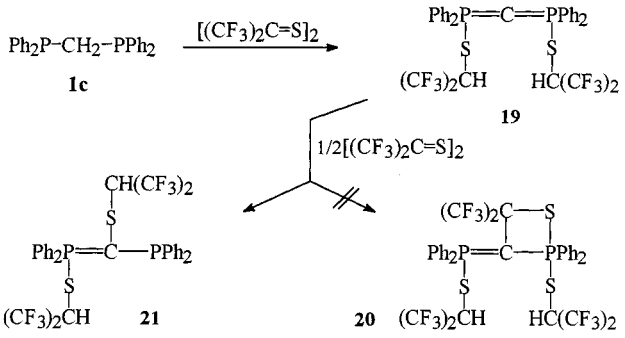

Scheme 6

In contrast to carbodiphosphorane **6**, which reacts further with HFA very slowly at room temperature, carbodiphosphorane **19** is very active and easily reacts even at low temperature (−70 °C) with HFTA. However, the character of this interaction is not quite clear. If 1.5 equivalents of the dimer of HFTA were added to the methylenediphosphane **1c** the reaction mixture only showed two doublets in the ^{31}P NMR spectrum at $\delta = 65.2$ and −4.5, with a coupling constant of 185.3 Hz. The same spectroscopic data were found for the colourless crystalline product that was isolated from the reaction mixture in good yield. We were sure that this was the cyclic product **20**, which is analogous to compound **9**. However, the ^{19}F NMR spectrum showed the presence of only two fragments of HFTA in the molecule. Beside this, the mass spectrum together with the analytical data pointed to a molecular weight of 748.56, the same as in carbodiphosphorane **19**. The X-ray analysis solved

this puzzle and gave structure **21** (Figure 4) which is the constitutional isomer of compound **19**.

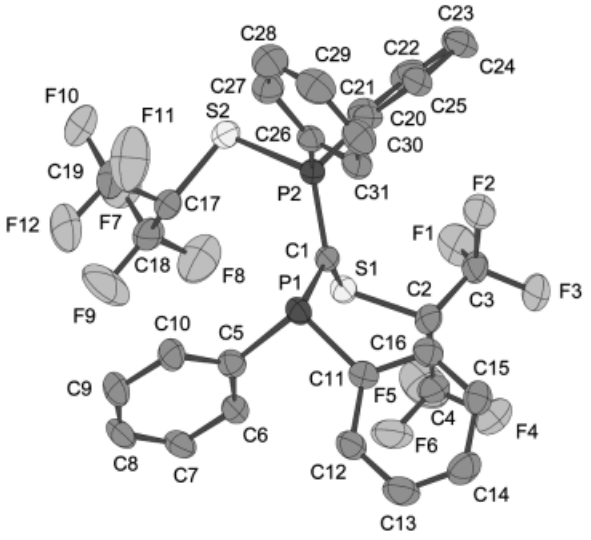

Figure 4. Perspective view and labeling scheme for the molecule **21**; selected bond lengths [pm] and angles [°]: P(1)−C(1) 181.4(5), C(1)−P(2) 170.4(5), P(2)−S(2) 215.55(19), C(1)−S(1) 176.8(5), P(1)−C(5) 183.1(5), P(2)−C(20) 181.3(5); P(1)−C(1)−P(2) 117.6(3), C(1)−P(1)−C(5) 106.2(2), P(1)−C(1)−S(1) 125.5(3), P(2)−C(1)−S(1) 113.4(3), C(1)−P(2)−S(2) 117.22(18), C(1)−P(2)−C(20) 116.0(2)

These two isomers exist independently from each other and do not interconvert. Carbodiphosphorane **19** is unstable and decomposes with the formation of a mixture of compounds that does not contain signals of the other isomer. Thus, in order to transform the symmetric carbodiphosphorane **19** into its asymmetrical isomer **21** the presence of HFTA is necessary. HFTA most likely plays a catalytic role in this process. However in this case it is not clear why the same yield of **21** cannot be obtained with only a small excess of HFTA.

It is interesting to note that the value of the $^2J_{PP}$ coupling constant of compounds containing the P−C−P system may vary in the range from less then 1 Hz to over 100 Hz. The $^2J_{PP}$ coupling constant of the compound **21** was unusually large 185 Hz. However, the largest value of this constant has been recently reported for $1\sigma^4,3\sigma^2$-diphosphaallene.[19]

Although, to the best of our knowledge, this unusual isomerization does not have direct analogies in the literature, it may be related to other migration processes observed for phosphorus compounds.[19,20]

Experimental Section

All operations were performed under nitrogen in a glove box. The solvents were dried by standard procedures. − The NMR spectra were measured with a JEOL FX-90Q, Bruker DPX 200 or Bruker AMX 360 spectrometer. The ^{1}H and ^{13}C chemical shifts are referenced to tetramethylsilane (TMS). The ^{31}P chemical shifts were measured using 85% aqueous orthophosphoric acid as an external standard. As usual, high frequency shifts are given positive signs. The digital resolutions were 0.25 Hz, 0.5 Hz, and 1.25 Hz for ^{1}H, ^{13}C, and ^{31}P NMR spectra, respectively.

Synthesis of Compound 6: A solution of methylenebis(diphenylphosphane) **1c** (30 mg, 0.078 mmol) in [D_6]benzene (0.5 mL) was placed in a tube with diameter 4−5 mm (a 5 mm NMR tube can be used) and 3.8 mL (0.172 mmol) of gaseous HFA were slowly bubbled through it at room temperature using a syringe with a thin needle. The end of the needle was placed at the bottom of the tube. The reaction mixture showed the following spectral parameters: ^{1}H NMR (89.56 MHz, C_6D_6): δ = 6.27 [br. sept., $^3J_{HF}$ = 6.58 Hz, 2 H, *H*C(CF_3)$_2$], 6.95 (m, 12 H, Ph), 7.70 (m, 8 H, Ph). − ^{19}F NMR (84.26 MHz, C_6D_6): δ = −72.46 (d, $^3J_{HF}$ = 6.58 Hz, 12 F, C*F*$_3$). − ^{31}P NMR (36.2 MHz, C_6D_6): δ = 35.3 (s, 2P).

Synthesis of Compound 9: Gaseous hexafluoroacetone (19 mL, 0.832 mmol) was condensed into a solution of methylenebis(diphenylphosphane) **1c** (100 mg, 0.260 mmol) in benzene (1 mL) in a glass tube. The tube was sealed and kept at room temperature for 3 days. According to the NMR spectroscopic data the reaction was complete in 30 h, and the rest of the time was needed for the crystallization of the product as a colorless crystals. The crystals were filtered off, washed with 0.4 mL of dichloromethane and dried in vacuo 0.05 mm. Yield 145 mg (63%), m.p. 121−124 °C. − ^{1}H NMR (89.56 MHz, $CDCl_3$): δ = 3.57 [d. sept., $^3J_{PH}$ = 10.6 Hz, $^3J_{FH}$ = 6.6 Hz, 1 H, C*H*(CF_3)$_2$], 4.72 [d. sept., $^3J_{PH}$ = 13.2 Hz, $^3J_{FH}$ = 5.6 Hz, 1 H, C*H*(CF_3)$_2$], 7.25−8.12 (m, 20 H, Ph). − ^{19}F NMR (84.26 MHz, $CDCl_3$): δ = −70.98 (d, $^3J_{FH}$ = 6.6 Hz, 6 F, CF_3), −72.26 (s, 6 F, CF_3), −74.39 (s, 6 F, CF_3). − ^{31}P NMR (36.2 MHz, $CDCl_3$): δ = −32.5 (d, $^2J_{PP}$ = 56.0 Hz), 58.8 (d, $^2J_{PP}$ = 56.0 Hz). − $C_{34}H_{22}F_{18}O_3P_2$ (882.46): calcd. C 46.28, H 2.51; found C 46.26, H 2.53.

Synthesis of Compound 11: A solution of compound **9** (100 mg, 0.113 mmol) in toluene (1 mL) was heated at 100 °C for 5 h. The solvent was removed in vacuo (0.05 mm), the remaining oil was dissolved in boiling hexane and the solution was left at 20 °C overnight. A mixture of compounds **11**−**13** with predominant content of **11** was separated, and the mother liquid was kept for two weeks at 20 °C followed by two weeks at −20 °C. Colourless crystals of **11** (7 mg, 16%) were separated from the precipitated oil and dried in vacuo. − ^{1}H NMR (89.56 MHz, $CDCl_3$): δ = 5.41 [d. sept., $^3J_{PH}$ = 12.29 Hz, $^3J_{FH}$ = 5.86 Hz, 1 H, C*H*(CF_3)$_2$], 7.35−7.95 (m, 10 H, Ph). − ^{19}F NMR (84.26 MHz, $CDCl_3$): δ = −73.96 (d, $^3J_{FH}$ = 5.86 Hz, 6 F, CF_3). − ^{13}C NMR (22.5 MHz, $CDCl_3$): δ = 68.33 [d. sept., $^2J_{PC}$ = 4.8 Hz, $^2J_{FC}$ = 35.1 Hz, 1 C, *C*H(CF_3)$_2$], 120.4 (d, $^1J_{PC}$ = 274.9 Hz, 2 C, Ph), 128.5 (d, $^2J_{PC}$ = 14.7 Hz, 4 C, Ph), 131.2 (d, $^3J_{PC}$ = 11.7 Hz, 4 C, Ph), 132.95 (d, $^4J_{PC}$ = 2.9 Hz, 2 C, Ph),. − ^{31}P NMR (36.2 MHz, $CDCl_3$): δ = 39.85 (s, 2 P). − $C_{15}H_{11}F_6OP_2$ (368.22): calcd. C 48.93, H 3.01; found C 48.21, H 3.13.

Synthesis of Compounds 12 and 13: A solution of compound **9** (150 mg, 0.170 mmol) in chloroform (1.5 mL) was heated to 60 °C for 48 h and then the solvent was removed in vacuo (0.05 mm). Crystallization of the residue from dichloromethane/hexane gave a mixture of two types of crystals for compounds **12** and **13** (24 mg), which were mechanically separated.

12: − ^{1}H NMR (89.56 MHz, $CDCl_3$): δ = 7.37 (d, $^2J_{PH}$ = 11.6 Hz, 1 H), 7.44−7.92 (m, 10 H, Ph). − ^{19}F NMR (84.26 MHz, $CDCl_3$): δ = −65.7 (q, $^4J_{FF}$ = 7.33 Hz, 3 F, CF_3), −59.1 (q, $^4J_{FF}$ = 7.33 Hz, 3 F, CF_3). − ^{31}P NMR (36.2 MHz, $CDCl_3$): δ = 17.1 (s, 2 P).

13: − ^{1}H NMR (89.56 MHz, $CDCl_3$): δ = 7.28−7.90 (m, 10 H, Ph), 8.81 (br. s, 1 H) − ^{31}P NMR (36.2 MHz, $CDCl_3$): δ = 26.5 (s, 2 P).

Synthesis of Compound 15: A solution of HFTA (50 mg, 0.137 mmol) in hexane (1.2 mL), cooled to −40 °C, was quickly added to a solution of methylenebis[bis(diethylamino)phosphane] **1b** (50 mg, 0.137 mmol) in hexane (1.2 mL) at the same temperature. The reaction mixture was stirred at −20 °C for 5 min. and then kept at this temperature for 20 min. The colorless crystalline product **16** was filtered off and dried in vacuo. Yield of the crystals 48 mg (48%). According to the ^{31}P NMR spectrum the mother liquor contained compound **15** only. − ^{1}H NMR (360.13 MHz, C_6H_{14}): δ = 1.33 (t, $^{1}J_{HH}$ = 7.1 Hz, 24 H, CH_2CH_3), 3.33 (m, 16 H, CH_2CH_3), 5.02 [sept, 2 H, $CH(CF_3)_2$]. − ^{19}F NMR (188.31 MHz, C_6H_{14}): δ = −67.7 (d, $^{3}J_{HF}$ = 8.14 Hz, 12 F, CF_3). − ^{31}P NMR (145.78 MHz, C_6H_{14}): δ = 41.4 (s, 2 P). − $C_{23}H_{42}F_{12}N_4P_2S_2$ (728.67): calcd. C 37.91, H 5.81; found C 37.57, H 5.79.

Synthesis of Compound 18: The reaction mixture of the carbodiphosphorane **15** obtained as described above was diluted with hexane (2 mL) and warmed to 20 °C. At this temperature the crystals of **15** dissolved completely. The solution was then quickly cooled to −20 °C and the equivalent amount of HBF_4 (solution in ether) was added to it. The colourless crystalline product that precipitated immediately was filtered off and dried in vacuo. Yield 98 mg (88%); after crystallization from CH_2Cl_2/diethyl ether at −25 °C the yield is 61% (68 mg). − ^{1}H NMR (360.13 MHz, $CDCl_3$): δ = 1.20 (t, $^{3}J_{HH}$ = 7.06 Hz, 24 H, NCH_2CH_3), 1.91 (t, $^{2}J_{PH}$ = 4.9 Hz, 1 H, P−CH−P), 3.27 (m, 16 H, NCH_2CH_3), 4.25 [br. sept., $^{3}J_{FH}$ = 7.1 Hz, 2 H, $HC(CF_3)_2$]. − ^{19}F NMR (188.31 MHz, $CDCl_3$): δ = −69.5 (d, $^{3}J_{HF}$ = 7.1 Hz, 12 F, CF_3), −151.2 (s, BF_4). − ^{31}P NMR (145.78 MHz, $CDCl_3$): δ = 68.2 (s, 2 P). − $C_{23}H_{43}BF_{16}N_4P_2S_2$ (816.48): calcd. C 33.83, H 5.31; found C 33.71, H 5.02.

Synthesis of Compound 21: A solution of thiohexafluoroacetone (72 mg, 0.198 mmol) in ether (2 mL) was cooled to −70 °C and quickly added to a solution of methylenebis(diphenylphosphane) **1c** (50 mg, 0.130 mmol) in ether (3 mL) at the same temperature. The reaction mixture was stirred at −70 °C for 10 min. The reaction solution was then concentrated to a volume of about 0.6 mL. Hexane (1 mL) was added and solution was kept at −25 °C for 3 days. The colourless crystalline product formed over this time was filtered off and dried in vacuo. Yield of the crystals 50 mg (50%). According to the ^{31}P NMR spectrum the mother liquid contained compound **21** only. − ^{1}H NMR (360.13 MHz, $CDCl_3$): δ = 3.20 [sept., $^{3}J_{FH}$ = 8.07 Hz, 1 H, $CH(CF_3)_2$], 4.36 [d. sept., $^{3}J_{FH}$ = 7.34 Hz, $^{3}J_{PH}$ = 1.98 Hz, 1 H, $CH(CF_3)_2$], 6.85−7.18 (m, 12 H, Ph), 7.78−8.08 (m, 8 H, Ph). − ^{19}F NMR (188.31 MHz, $CDCl_3$): δ = −66.15 (dd, $^{3}J_{HF}$ = 7.4 Hz, J_{PF} = 2.6 Hz, 6 F, CF_3), −65.75 (d, $^{3}J_{HF}$ = 7.4 Hz, 6 H, CF_3) − ^{31}P NMR (145.78 MHz, $CDCl_3$): δ = −4.5 (d, $^{2}J_{PP}$ = 185 Hz, 1 P, P−C−P), 65.2 (d, $^{2}J_{PP}$ = 185 Hz,

Table 1. Crystal data and structure refinement parameters of compounds **9**, **15**, **18**, **21**

	9	**15**	**18**	**21**
Formula	$C_{34}H_{22}F_{18}O_3P_2$	$C_{23}H_{42}F_{12}N_4P_2S_2$	$C_{23}H_{43}BF_{16}N_4P_2S_2$	$C_{31}H_{22}F_{12}P_2S_2$ x 1/2 $C_4H_{10}O$
Mol. wt.	882.46	728.67	816.48	785.57
Temperature K	173(2)	173(2)	173(2)	173(2)
Wavelength pm	71.073	71.073	71.073	71.073
Crystal size [mm]	0.6 × 0.4 × 0.3	0.8 × 0.6 × 0.5	0.6 × 0.4 × 0.3	1.0 × 0.5 × 0.3
Crystal system	Monoclinic	Monoclinic	Monoclinic	Monoclinic
Space group	*C*2/*c*	*Cc*	$P2_1/n$	$P2_1/n$
a [pm]	1826.7(5)	2162.7(2)	1151.8(3)	1675.8(4)
b [pm]	948.75(11)	1030.60(10)	1798.8(3)	1083.0(2)
c [pm]	3989.7(6)	1799.4(2)	1730.8(3)	1917.0(2)
α [°]	90	90	90	90
β [°]	6.83(1)	123.420(10)	96.14(2)	96.86(2)
γ [°]	90	90	90	90
V [nm^3]	3.3475(6)	3.3475(6)	3.5654(13)	3.4542(11)
Z	8	4	4	4
$D_{calcd.}$ [Mg/m^3]	1.716	1.446	1.521	1.501
Absorption coefficient [mm^{-1}]	0.263	0.343	0.346	0.337
2θ range [°]	2.52 to 25.00	2.71 to 27.51	2.26 to 25.00	2.55 to 22.49
F(000)	3536	1512	1680	1576
Index range	$-21 \le h \le 21$, $-1 \le k \le 11$, $-47 \le l \le 47$	$-28 \le h \le 28$, $-1 \le k \le 13$, $-23 \le l \le 18$	$-11 \le h \le 13$, $-1 \le k \le 21$, $-20 \le l \le 20$	$-18 \le h \le 1$, $-11 \le k \le 1$, $-20 \le l \le 20$
Reflections collected	13731	8241	7844	5706
Independent reflections	6012 [*R*(int) = 0.0432]	7255 [*R*(int) = 0.0161]	6235 [*R*(int) = 0.0294]	4477 [*R*(int) = 0.0471]
Completeness to θ_{max}	99.9	99.8	99.2	99.0
Max. and min. transmission	0.9251 and 0.8579	0.8472 and 0.7709	0.9033 and 0.8193	0.9056 and 0.7292
Data/Restraints/Parameter	6012/0/517	7255/2/401	6235/0/446	4477/1/462
Goodness-of-fit on F^2	1.020	1.040	1.024	1.033
Final *R* indices [$I > 2\sigma(I)$]	*R*1 = 0.0448, *wR*2 = 0.1021	*R*1 = 0.0249, *wR*2 = 0.0655	*R*1 = 0.0677, *wR*2 = 0.1687	*R*1 = 0.0544, *wR*2 = 0.1276
Largest difference peak and hole [e·Å^{-3}]	0.427 and −0.462	0.330 and −0.225	0.827 and −0.832	0.368 and −0.388 The solvent molecule is disordered.
Absolute structure parameter	−	0.44(3) The structure was refined as a merohedric twin	−	−

1 P, P−C−P). − $C_{23}H_{42}F_{12}N_4P_2S_2$ (748.57): calcd. C 49.74, H 2.96; found C 49.35, H 3.11.

X-ray Crystal Structure Determination of Compounds 9, 15, 18, and 21: All crystallographic measurements were performed at 173(2) K on a Siemens P4 diffractometer, using graphite monochromated Mo-K_α radiation (λ = 71.073 pm) and an LT2 low temperature device. The structures were solved by direct methods and refined by full-matrix least-squares on F^2 using SHELX-97 (Sheldrick, 1997). All non-hydrogen atoms were refined anisotropically and the position of the hydrogen atoms were calculated using a riding model. Crystal data, data collection and processing parameters are given in Table 1.

Crystallographic data (excluding structure factors) for the structures reported in this paper have been deposited with the Cambridge Crystallographic Data Center as supplementary publication nos. CCDC-150573 (**9**), CCDC-150574 (**15**), CCDC-150575 (**18**), and CCDC-150576 (**21**). Copies of the data can be obtained free of charge on application to CCDC, 12 Union Road, Cambridge CB2 1EZ, UK [Fax: (internat.) +44-1223/336-033; E-mail: deposit@ccdc.cam.ac.uk].

Acknowledgments

We thank the Deutsche Forschungsgemeinschaft for financial support (436 UKR 17/15/99) We are thankful to Dr. Th. Dülcks for the MS measurements and Peter Brackmann for his assistance in the X-ray structure analyses.

[1] M. Witt, K. S. Dathathreyan, H. W. Roesky, *Adv. Inorg. Chem. Radiochem.* **1986**, *30*, 223−312.
[2] R. Burgada, R. Setton, *Preparation, Properties and Reactions of Phosphoranes*, in *The Chemistry of Organophosphorus Compounds* (Ed.: F. R. Hartley), in *The Chemistry of Functional Groups*, Series ed. S. Patai, Wiley, Chichester, New York, Brisbane, Toronto, Singapore, **1994**, vol. 3; pp. 185−272.
[3] F. U. Seifert, G.-V. Röschenthaler, *J. Fluorine Chem.* **1995**, *70*, 171−174.
[4] I. Neda, C. Melnicky, A. Vollbrecht, A. Fischer, P. G. Jones, R. Schmutzler, *Z. Anorg. Allg. Chem.* **1996**, *622*, 1047−1059.
[5] I. V. Shevchenko, *Chem. Commun.* **1998**, 1203−1204.
[6] I. Shevchenko, R. Mikolenko, S. Loss, H. Grützmacher, *Eur. J. Inorg. Chem.* **1999**, 1665−1671.
[7] G. H. Birum, C. N. Matthews, *J. Org. Chem.* **1967**, *32*, 3554−3559.
[8] S. Verma, M. Athale, M. M. Bokadia, *Indian J. Chem. Sect. B* **1981**, *20*, 1096−1097.
[9] I. Shevchenko, R. Mikolenko, A. Chernega, E. Rusanov, H. Grützmacher, *Eur. J. Inorg. Chem.* **2001**, 195−199.
[10] O. I. Kolodiazhniy (Ed.), in: *Phosphorus Ylides*, Wiley-VCH; Weinheim, New York, Chichester, Brisbane, Singapore, Toronto, **1999**, pp. 497−517.
[11] W. J. Middleton, E. Howard, W. Sharkey, *J. Org. Chem.* **1965**, *30*, 1375.
[12] R. Weiss, H. Wolf, U. Schubert, T. Clark, *J. Am. Chem. Soc.* **1981**, *103*, 6142−6147.
[13] U. Schubert, Ch. Kappenstein, B. Milewski-Mahrla, H. Schmidbaur, *Chem. Ber.* **1981**, *114*, 3070−3078.
[14] H. Schmidbaur, T. Costa, B. Milewski-Mahrla, U. Schubert, *Angew. Chem.* **1980**, *92*, 557−558; *Angew. Chem. Int. Ed. Engl.* **1980**, *19*, 555−556.
[15] A. T. Vincent, P. J. Wheatley, *J. Chem. Soc., Dalton. Trans.* **1972**, 617−622.
[16] G. E. Hardy, J. I. Zink, W. C. Kaska, J. C. Baldwin, *J. Am. Chem. Soc.* **1978**, *100*, 8001−8002.
[17] E. A. V. Ebsworth, T. E. Fraser, D. W. H. Rankin, O. Gasser, H. Schmidbaur, *Chem. Ber.* **1977**, *110*, 3508−3516.
[18] R. Appel, U. Baumeister, F. Knoch, *Chem. Ber.* **1983**, *116*, 2275−2284.
[19] T. Kato, H. Gornitzka, A. Baceiredo, G. Bertrand, *Angew. Chem. Int. Ed.* **2000**, *39*, 3319−3321.
[20] H. Schmidbaur, A. Wohlleben-Hommer, *Chem. Ber.* **1979**, *112*, 510−516.

Received November 15, 2000
[I00435]

New Rhodium(I) and Iridium(I) Complexes of the Chiral 1,1′-Diphenyl-3,3′,4,4′-tetramethyl-2,2′-biphosphole Ligand − Synthesis and Applications to Catalytic Hydrogenation and Hydroformylation Reactions

Olivier Tissot,[a] Maryse Gouygou,[a] Frédéric Dallemer,[b] Jean-Claude Daran,*[a] and Gilbert G. A. Balavoine*[a]

Keywords: Chirality / Biphosphole / Rhodium / Iridium / Catalysis / Hydrogenations / Hydroformylations

A convenient method for the synthesis of new racemic Rh^I and Ir^I complexes $[M(BIPHOS)(COD)]BF_4$ have been developed from the BIPHOS ligand and $[M(COD)Cl]_2$ precursors. These complexes have been tested as catalysts for hydrogenation and hydroformylation reactions. Excellent regioselectivities in branched aldehyde (98%) have been obtained in hydroformylation with the rhodium $[Rh(BIPHOS)(COD)]BF_4$ complex. The application of this convenient method to the synthesis of enantiomerically pure $[M(BIPHOS)(COD)]BF_4$ complexes has been investigated.

Introduction

Chiral diphosphane ligands, in particular those with C_2 symmetry,[1] have proved to be powerful auxiliaries in catalytic asymmetric processes.[2] We were interested in the possibilities offered by the 1,1′-diphenyl-3,3′,4,4′-tetramethyl-2,2′-biphosphole (BIPHOS, **1**), first synthesized by Mathey et al. in 1986.[3] This diphosphane combines the axial chirality generated by the biphosphole framework with the central chirality of the phosphorus atoms. This implies the existence of six stereoisomers corresponding to three pairs of enantiomers (Figure 1). In a previous report,[4] we have shown that BIPHOS exists in solution as an equilibrium mixture of two diastereoisomers, **1a** and **1b**, because of the configurational instability of the central chirality of the phosphorus atoms and probably also because of the axial chirality. This stereolability does not exist in the solid state and the three diastereoisomers have been fully characterized by X-ray diffraction.[4] In solution in the presence of a transition metal, the equilibrium shifts to the most favorable configurations for chelating the metal $\{[a]^S_{RR}$ and $[a]^R_{SS}\}$. In this way, we have obtained numerous chiral complexes of Ni, Pd, Pt, Rh[5] and Ru,[6] as racemic mixtures. Recently, the enantiomerically pure palladium complex $[PdCl_2(BIPHOS)]$ was synthesized from the enantiomerically pure BIPHOS ligand **1** $\{[a]^S_{RR}$ or $[a]^R_{SS}\}$ obtained by spontaneous resolution upon crystallization. It proved to be active in catalytic asymmetric allylic substitution.[7]

Here, we report a convenient method for synthesizing new racemic rhodium(I) and iridium(I) complexes $[M(BIPHOS)(COD)]^+$, and their use in the catalytic hydrogenation and hydroformylation reactions. We have also investigated the synthesis of enantiomerically pure complexes $[M(BIPHOS)(COD)]^+$ from the enantiomerically pure BIPHOS ligand **1**.

[a] Laboratoire de Chimie de Coordination du CNRS,
205, Route de Narbonne, 31077 Toulouse Cedex (France)
Fax: (33) 05 61 55 30 03,
E-mail: daran@lcc-toulouse.fr; balavoin@lcc-toulouse.fr
[b] Rhodia Recherches, Centre de Recherche de Lyon,
85, Avenue des Freres Perret, BP 62, 69192 Saint-Fons Cedex (France)

Results and Discussion

Synthesis of $[M(BIPHOS)(COD)]BF_4$ Complexes in Racemic Form

In our previous work on 2,2′-biphosphole (BIPHOS), we have shown that this diphosphane is a rather good ligand for transition metals, as evidenced by the formation of bis-biphosphole complexes.[8] For example, under the conditions used with classical diphosphanes,[9] BIPHOS (1 equiv. per rhodium atom) reacted rapidly with $[Rh(COD)Cl]_2$ or $[Rh(COD)_2]BF_4$ at ambient temperature by displacement of the two labile COD ligands to afford $[Rh(BIPHOS)_2]^+$ (**2**)[5] instead of $[Rh(BIPHOS)(COD)]^+$ (**3**) (Scheme 1).

In order to prepare the monosubstituted biphosphole complex **3**, which could be an interesting catalyst precursor for hydrogenation[10] and hydroformylation,[10] we attempted to reduce the reactivity of BIPHOS towards the rhodium precursors by working at low temperature. At −78 °C with the $[Rh(COD)_2]BF_4$ precursor, the reaction proceeded rapidly in a dichloromethane solution and afforded a mixture of two complexes, **3** and **2′′**, in the ratio 75:25, which could not be separated.

When the $[Rh(COD)Cl]_2$ precursor was used under the same conditions, a new rhodium complex **4** was observed by ^{31}P NMR spectroscopy (δ = 40.65, $^1J_{P-Rh}$ = 137 Hz) at −78 °C, along with the minor complex **2′** (δ = 46.10, $^1J_{P-Rh}$ = 122 Hz). This new complex slowly disappeared when the temperature increased, leading quantitatively to complex **2′** at room temperature. Complex **4**, which appears as an intermediate in the formation of complex **2′**, might

 © WILEY-VCH Verlag GmbH, 69451 Weinheim, 2001 1434−1948/01/0909−2385 $ 17.50+.50/0

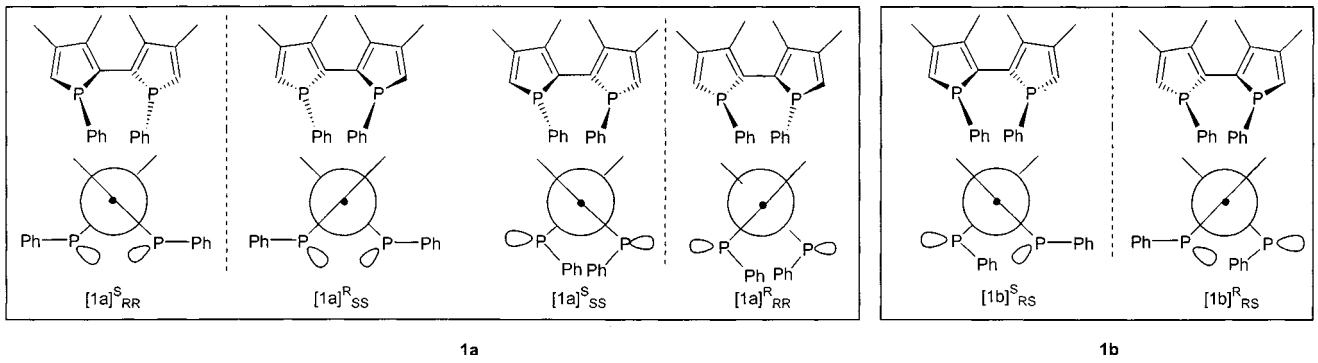

Figure 1. The different stereoisomers of BIPHOS (**1**) that possess two chiral centers and one chiral axis; each stereoisomer is also represented in a Newman projection along the axis of the C−C linking the phosphole rings; superscript refers to the axial chirality and subscript to the central chirality; the two diastereoisomers **1a** and **1b** observed in solution appear in this figure

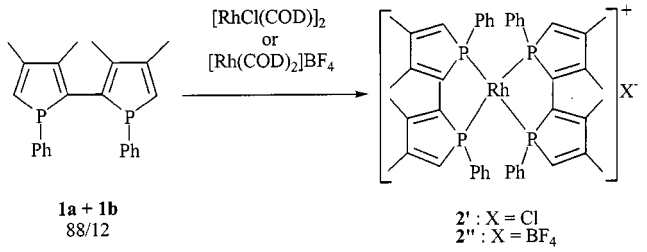

Scheme 1

be the dinuclear complex $[Rh(BIPHOS)Cl]_2$.[11] Such an intermediate might allow the preparation of the desired complex $[Rh(BIPHOS)(COD)]BF_4$ by cleavage of the μ-Rh−Cl bonds and subsequent coordination of COD at the vacant rhodium site. Indeed, $[Rh(BIPHOS)Cl]_2$, quantitatively obtained by addition of two equivalents of a dichloromethane

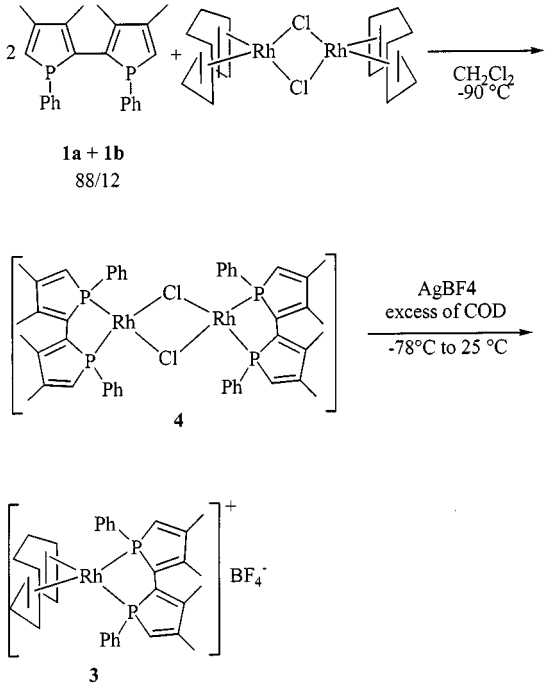

Scheme 2

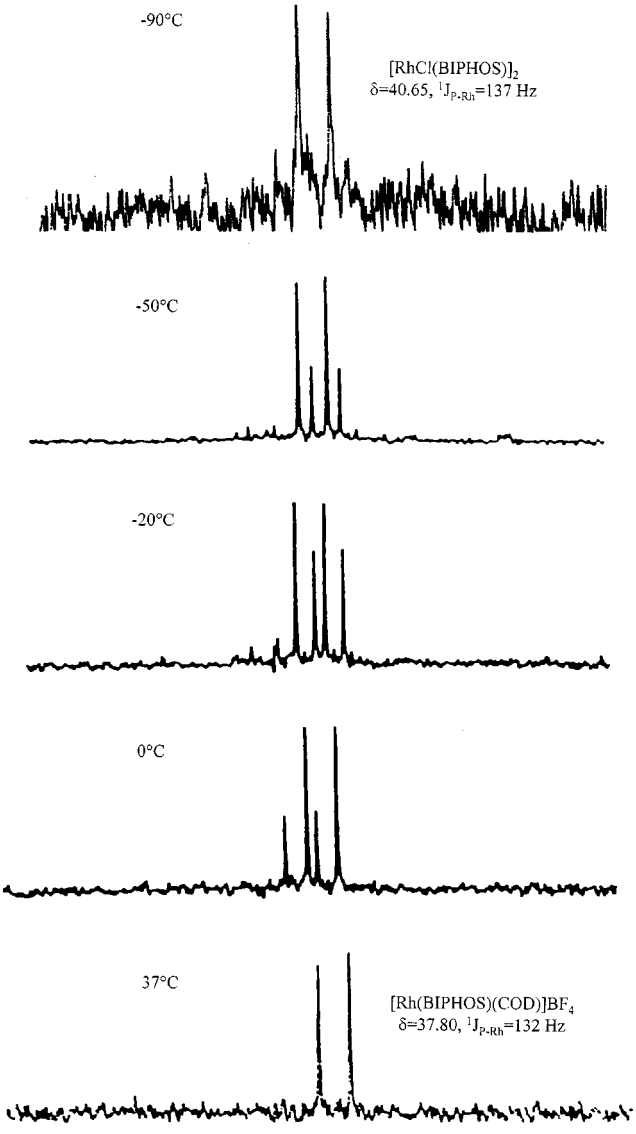

Figure 2. ^{31}P NMR studies from −90 °C to ambient temperature for the reaction of BIPHOS with $[Rh(COD)Cl]_2$

solution of BIPHOS to a dichloromethane solution of $[Rh(COD)Cl]_2$ precursor cooled to −90 °C, led to $[Rh(BIPHOS)(COD)]BF_4$ (**3**) after addition of four equivalents of $AgBF_4$ and an excess of cyclooctadiene at −78 °C (Scheme 2). This reaction was monitored by ^{31}P NMR spectroscopy from −78 °C to ambient temperature (Figure 2) showing the disappearance of complex **4** and the concomitant appearance of complex **3** (δ = 37.80, $^1J_{P-Rh}$ = 132 Hz). Complex **3** was isolated in 95% yield and characterized by multinuclear NMR spectroscopy, mass spectrometry and elemental analysis.

This method was then applied to the synthesis of an analogous iridium complex. Starting from $[Ir(COD)Cl]_2$ under similar conditions (Scheme 3), the ^{31}P NMR studies from −78 °C to ambient temperature revealed that the reaction was more complicated, since various intermediates were detected during the course of the reaction. However, the $[Ir(BIPHOS)(COD)]BF_4$ complex **5** was obtained quantitatively at room temperature, and was isolated in a pure form as a red solid, which was characterized by NMR spectroscopy, mass spectrometry and elemental analysis.

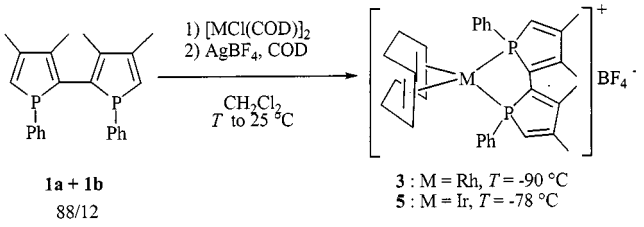

Scheme 3

Catalysis

As a preliminary evaluation of the catalytic properties, these new rhodium and iridium complexes $[M(BIPHOS)(COD)]BF_4$ were tested in hydrogenation and hydroformylation reactions. Initial hydrogenation experiments were performed with the complexes **3** and **5** as precursor catalysts in the hydrogenation of α-acetoamidocinnamic acid. The rhodium complex $[Rh(BIPHOS)(COD)]BF_4$ (**3**) shows moderate activity for this hydrogenation in MeOH, THF or CH_2Cl_2 giving complete conversion over 20 h at 25 °C under 15 atm. of H_2 (Scheme 4, Table 1). Under the same conditions, the iridium complex $[Ir(BIPHOS)(COD)]BF_4$ (**5**) proved to be inactive. At higher pressure (150 atm.), very weak conversions, in the range 6−10%, were recorded (Table 1).

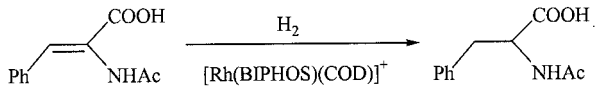

Scheme 4

Table 1. Hydrogenation of α-acetoamidocinnamic acid with $[M(BIPHOS)(COD)]BF_4$ [M = Rh (**3**) and M = Ir (**5**)][a]

Entry	Precursor	Solvent	P(Atm.)	Conv. (%)
1	**3**	MeOH	15	100
2	**3**	THF	15	100
3	**3**	CH_2Cl_2	15	100
4	**3**	Et_2O	15	45
5	**3**	CH_3CN	15	0
6	**5**	MeOH	150	10
7	**5**	THF	150	6
8	**5**	CH_2Cl_2	150	7

[a]Reaction conditions: T = 25 °C, t = 20 h, [cat]/[substrat] = 2:100.

To extend the utility of the $[Rh(BIPHOS)(COD)]BF_4$ catalyst precursor the hydroformylation of styrene was examined. The reaction was carried out at a temperature of 25 °C and a pressure of 150 atm. of CO/H_2 (1:1) (Scheme 5). High conversions of styrene were recorded, giving predominantly aldehydes with branched selectivities in CH_2Cl_2 (97%) or MeCN (98%) (Table 2). In MeOH, the regioselectivity towards the branched aldehyde regioisomer was lower, and the linear alcohol resulting from hydrogenation of the corresponding aldehyde was also formed in addition to the formyl regioisomer. Complex **4** proved to be a very regioselective catalyst in the hydroformylation of styrene.[12]

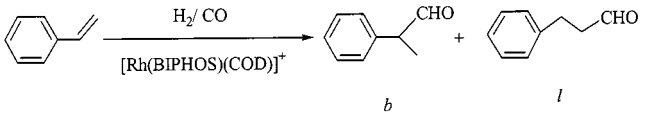

Scheme 5

Table 2. Hydroformylation of styrene with $[Rh(BIPHOS)(COD)]BF_4$ (**3**)[a]

Entry	Solvents	Conversion	br/l
1	CH_2Cl_2	55	93:7
2	MeCN	72	98:2
3	EtOH	75	–[b]
4	MeOH	88	29:71[c]

[a] Reaction conditions: T = 25 °C, t = 20 h, p(CO) = p(H_2) = 150 atm., [cat]/[substrate] = 2:100. – [b] Not determined. – [c] In this case, the linear aldehyde was transformed into corresponding alcohol.

Synthesis of $[M(BIPHOS)(COD)]BF_4$ Complexes in Optically Active Form

In order to get an insight into asymmetric catalysis, we attempted to synthesize optically pure $[M(BIPHOS)(COD)]BF_4$ complexes. The present methods developed for the synthesis of racemic $[M(BIPHOS)(COD)]BF_4$ complexes, which require low temperature conditions, should be a convenient method for the synthesis of the optically pure

complexes. Indeed, enantiomerically pure BIPHOS ligand **1** {$[a]^{S}_{RR}$ or $[a]^{R}_{SS}$} was obtained by spontaneous resolution upon crystallization;[4] it racemizes in solution above −60 °C.[4] We investigated these syntheses with large single crystals (typically 50 to 150 mg) and the purity of each crystal was checked with polarized light before being used in the reaction. Using a slightly modified procedure that involved the addition of a single crystal of BIPHOS instead of a solution of BIPHOS, the reaction did not lead to complex **3** but quantitatively afforded complex **2′′**. Upon reverse addition, two problems arose. The first problem was to obtain a complete dissolution of the crystal at low temperature before addition of the metal precursor. For that, the solubilisation of one single crystal of **1** was carried out by stirring for 16 hours at −78 °C. Then, the solution was cooled to −90 °C before adding the solution of $[M(COD)Cl]_2$ precursor. However, this caused the second problem. During the addition, the ligand was always kept in excess with respect to the metal, and the formation of $[Rh(BIPHOS)_2]^+$ (**2**) could not be avoided, hence we obtained a mixture of complexes **2′′** and **3** in a 1:1 ratio at low temperature (Scheme 6). These two complexes could not be separated, as reported above for the racemic version. However, the optical rotation observed, $[\alpha]_D$ = 172, proved that optically active complexes $[Rh(BIPHOS)_2]BF_4$ and/or $[Rh(BIPHOS)(COD)]BF_4$ had been obtained.

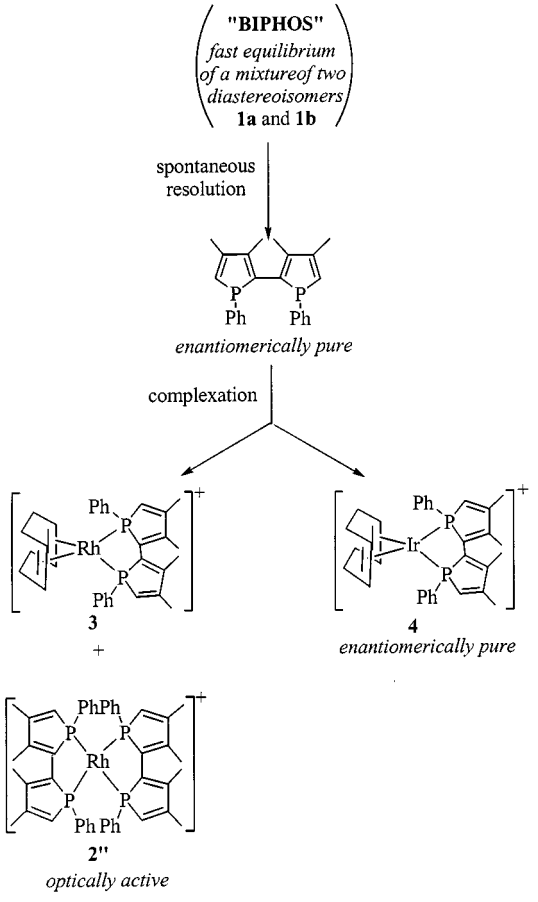

Scheme 6

In contrast to the rhodium case, we were easily able to obtain the iridium complex **5** in an optically active form. In this case, the reaction was carried out by addition of one pure single crystal of BIPHOS to a dichloromethane solution of $[Ir(COD)Cl]_2$ cooled to −78 °C, followed by treatment with $AgBF_4$ in the presence of an excess of cyclooctadiene (Scheme 6). This complex was isolated as a red solid in 95% yield with $[\alpha]_{578}$ = −95 (c = 0.02, CH_2Cl_2). The enantiomeric purity of complex **5** has not been evaluated; however, starting from different single crystals of BIPHOS, the same absolute value of [α] was obtained for complex **5**. Therefore, as in the case of the palladium complex,[7] we can consider that in dichloromethane at −78 °C, a single crystal of enantiomerically pure BIPHOS ligand reacts with $[Ir(COD)Cl]_2$ to give the enantiomerically pure complex [Ir(BIPHOS)(COD)]BF_4.

Conclusions

We have developed a convenient route for the preparation of new racemic Rh^I and Ir^I complexes [M(BIPHOS)(COD)]BF_4, and we have evaluated their catalytic properties in the hydrogenation and hydroformylation reactions. The efficiency of the rhodium complex was demonstrated in particular in hydroformylation, in which excellent regioselectivities (98%) in the branched aldehyde were obtained. In contrast, no specific efficiency was observed for the iridium complex.

This convenient synthetic method, when applied to the enantiomerically pure BIPHOS ligand, allows the synthesis of an enantiomerically pure iridium complex and an optically active mixture of the rhodium complexes **2′′** and **3**. Were are currently studying a method for the isolation of the rhodium complex in an optically pure form and hence carrying out studies of its use in asymmetric catalysis.

Experimental Section

Instrumentation: All reactions were carried under an inert atmosphere of dry argon using Schlenk glassware and vacuum line techniques. The experiments requiring H_2 or H_2/CO pressure were carried out into a stainless steel high pressure reactor by "TOP-industrie". Floodgates for gas introduction and evacuation were fixed on the lid. A glass ampoule containing the reaction mixture was inserted into the reactor and stirring and heating were external.

^{1}H, ^{13}C{^{1}H, ^{31}P} and ^{31}P {^{1}H} NMR spectra were recorded on a Bruker WMX 400 instrument operating at 400, 100 or 162 MHz, respectively, or on a Bruker AM 250 instrument operating at 250, 63 or 101 MHz, respectively. Chemical shifts are reported in parts per million (ppm) relative to Me_4Si (^{1}H and ^{13}C) or 85% H_3PO_4 (^{31}P). Mass spectra were obtained on a Mermag R10−10 instrument. Elemental analyses were performed by the "Service d′Analyse du Laboratoire de Chimie de Coordination" at Toulouse, France. Optical rotations were measured on a Perkin−Elmer 241 polarimeter.

Chemicals: BIPHOS **1**[3] and the complexes **2′**[5] and **2′′**[5] were synthesised as previously described. $[Rh(COD)Cl]_2$ precursor was purchased from Aldrich Chemical Co. $[Ir(COD)Cl]_2$ precursor was purchased from Fluka. Solvents were freshly distilled from standard drying agents.

Preparation of Complex 3. Racemic Form: BIPHOS (**1**; 82 mg, 0.22 mmol) in dichloromethane (1.5 mL) at −90 °C was quickly added to a solution of (1,5-cyclooctadiene)rhodium(I) chloride dimer (54 mg, 0.11 mmol) in dichloromethane (4 mL) at −90 °C. The mixture was stirred for 20 min. and was then rapidly warmed to −78 °C. 1,5-Cyclooctadiene (0.107 mL, 0.88 mmol) was then slowly added followed by addition of silver tetrafluoroborate (42 mg, 0.22 mmol). The reaction mixture was warmed to 25 °C within 2 hours and filtered. The solvent was removed in vacuo and the resulting red solid was washed four times with diethyl ether (5 mL). The residue was dried in vacuo giving a brown solid (139 mg, 95%). − ^{1}H NMR (CD_2Cl_2): δ = 1.70 (s, 6 H, CH_3), 2.21 (s, 6 H, CH_3), 2.12−2.54 [m, 8 H, CH_2 (COD)], 5.17 [m, 2 H, CH (COD)], 5.89 [m, 2 H, CH (COD)], 6.60 (d, $^2J_{H-P}$ = 32.6 Hz, 2 H, CH-P), 7.37−7.63 (m, 10 H, Ph). − $^{13}C\{^1H\}$ NMR (CD_2Cl_2): δ = 159.8 (s, *C*−CH_3), 145.6 (t, J_{C-P} = 14.6 Hz, *C*−CH_3), 136.8 (t, J_{C-P} = 39.3 Hz, *C*=C−CH_3), 132.9 (t, J_{C-P} = 6.2 Hz, Ph), 131.8 (s, Ph), 129.7 (t, J_{C-P} = 5.1 Hz, Ph), 120.0 (m, CH-P), 99.2 [m, CH (COD)], 98.5 [m, CH (COD)], 30.2 [s, CH_2 (COD)], 30.0 [s, CH_2 (COD)], 18.9 (t, J_{C-P} = 5.5 Hz, CH_3), 15.2 (t, J_{C-P} = 4.2 Hz, CH_3). − $^{31}P\{^1H\}$ NMR (CD_2Cl_2): δ = 37.80 (d, $^1J_{P-Rh}$ = 132.2 Hz). − FAB-MS (MNBA, CH_2Cl_2): *m/z* (%) = 585 (100) [M − BF_4]$^+$. − $C_{32}H_{36}BF_4P_2Rh$ (672.30): calcd. C 57.17, H 5.39; found C 56.82, H 5.09.

Optically Active Form: A single crystal of BIPHOS was added to dichloromethane at −78 °C and the mixture was stirred overnight. After cooling to −90 °C, a dichloromethane solution of (1,5-cyclooctadiene)rhodium(I) chloride dimer was then added to the BIPHOS solution and the resulting mixture was stirred for only 5 min. The procedure is then the same as described above. The final product was a 1:1 mixture of $[Rh(BIPHOS)_2]BF_4$ (**2′′**) and $[Rh(BIPHOS)(COD)]BF_4$ (**3**). $[\alpha]_D$ = 172 (*c* = 0.3, CH_2Cl_2).

Preparation of Complex 5. Racemic Form: BIPHOS (97 mg, 0.26 mmol) in dichloromethane (1.5 mL) at −78 °C was quickly added to a solution of(1,5-cyclooctadiene)iridium(I) chloride dimer (87 mg, 0.13 mmol) in dichloromethane (4 mL) at −78 °C. The mixture was stirred for 1 h at −78 °C. 1,5-Cyclooctadiene (0.130 mL, 1.03 mmol) was then slowly added followed by the addition of silver tetrafluoroborate (44 mg, 0.26 mmol). The reaction mixture was warmed to 25 °C within 2 hours and filtered. The solvent was removed in vacuo and the resulting purple solid was washed four times with *n*-pentane (5 mL). The residue was dried in vacuo giving a dark red solid (140 mg, 95%). − ^{1}H NMR (CD_2Cl_2): δ = 1.72 (d, $^4J_{H-H}$ = 1 Hz, 6 H, CH_3), 2.25 (s, 6 H, CH_3), 2.06−2.04 [m, 8 H, CH_2 (COD)], 4.73 [m, 2 H, CH (COD)], 5.43 [m, 2 H, CH (COD)], 6.67 (d, $^2J_{H-P}$ = 32.8 Hz, 2 H, CH-P), 7.37−7.56 (10 H, m, Ph). − $^{13}C\{^1H\}$ NMR (CD_2Cl_2): δ = 159.7 (s, *C*−CH_3), 145.8 (t, J_{C-P} = 14.6 Hz, *C*−CH_3), 136.5 (dd, J_{C-P} = 55.1 Hz, J_{C-P} = 25.8 Hz, *C*=C−CH_3), 132.4 (d, J_{C-P} = 9.7 Hz, Ph), 131.7 (s, Ph), 129.5 (d, J_{C-P} = 10.2 Hz, Ph), 120.4 (d, J_{C-P} = 44.4 Hz, CH-P), 83.2 [m, CH (COD)], 32.8 [s, CH_2 (COD)], 31.3 [s, CH_2 (COD)], 18.9 (d, J_{C-P} = 11.7 Hz, CH_3), 15.9 (t, J_{C-P} = 9.5 Hz, CH_3). − $^{31}P\{^1H\}$ NMR (CD_2Cl_2): δ = 32.78. − FAB-MS (MNBA, CH_2Cl_2): *m/z* (%) = 675 (100) [M − BF_4]$^+$. − $C_{32}H_{36}BF_4IrP_2$ (761.61): calcd. C 50.46, H 4.76; found C 49.90, H 4.66.

Optically Active Form: A single crystal of BIPHOS was added directly to a dichloromethane solution of(1,5-cyclooctadiene)iridium(I) chloride dimer at −78 °C and the resulting mixture was stirred overnight at −78 °C. The procedure was the same as described above. $[\alpha]_{578}$ = 95 (*c* = 0.02, CH_2Cl_2).

Hydrogenation Experiments: In a typical experiment, a solution of 2×10^{-2} mmol of catalyst and substrate (50 equiv.) in 2 mL of the desired solvent was transferred under argon into a 3 mL glass ampoule. It was then placed into a stainless steel autoclave and stirred for 3 h with α-acetamidocinnamic acid. The reaction vessel was then pressurized to the required H_2 pressure and stirred for the desired time. After slow venting of the reactor, the mixture containing *N*-acetylphenylalanine was filtered through silica with ethyl acetate as eluent. The conversion was measured directly by integration of the CH_3 signals in the ^{1}H NMR spectrum.

Hydroformylation Experiments: The procedure was the same as described for hydrogenation. The mixture was stirred for 1 h before the autoclave was pressurized (CO/H_2 = 1:1). The conversion rate was measured directly by integration of the C*H*O and PhC*H*CH_2 signals in the ^{1}H NMR spectrum and the branched/linear value was given by integration of the C*H*O signals (branched: δ = 9.1, linear: δ = 9.2).

Acknowledgments

We thank the Centre National de la Recherche Scientifique and Rhodia for financial support.

[1] [1a] T. P. Dang, H. B. Kagan, *J. Chem. Soc., Chem. Commun.* **1971**, 481. − [1b] J. K. Whitesell, *Chem. Rev.* **1989**, *89*, 1581−1590 and references therein.
[2] For a recent review, see: *Comprehensive Asymmetric Catalysis* (Eds. E. N. Jacobsen, A. Pfaltz, H. Yamamoto), Springer-Verlag, **1999**.
[3] F. Mercier, S. Holand, F. Mathey, *J. Organomet. Chem.* **1986**, *316*, 271−279.
[4] O. Tissot, M. Gouygou, J-C. Daran, G. G. A. Balavoine, *Chem. Commun.* **1996**, 2287−2288.
[5] M. Gouygou, O. Tissot, J.-C. Daran, G. G. A. Balavoine, *Organometallics* **1997**, *16*, 1008−1015.
[6] O. Tissot, M. Gouygou, J-C. Daran, G. G. A. Balavoine, *Organometallics* **1998**, *17*, 5927−5930.
[7] O. Tissot, M. Gouygou, F. Dallemer, J.-C. Daran, G. G. A. Balavoine, *Angew. Chem. Int. Ed.* accepted.
[8] O. Tissot, J. Hydrio, M. Gouygou, F. Dallemer, J.-C. Daran, G. G. A. Balavoine, *Tetrahedron* **2000**, *56*, 85−93.
[9] P. R. Sharp, *Comprehensive Organometallic Chemistry* (Eds.: E. W. Abel, F. G. A. Stone, G. Wilkinson), Pergamon, **1995**, p. 263.
[10] For recent references, see: *Applied Homogeneous Catalysis with Organometallic Compounds* (Eds. B. Cornils, W. A. Hermann), VCH, Weinheim, **1996**.
[11] Such bridged rhodium complexes with bidentate diphosphane are rare and difficult to isolate. See: P. S. Sheridan, F. Jardine, *Comprehensive Coordination Chemistry* (Eds. G. Wilkinson, R. D. Giollard, J. A. McCleverty), Pergamon Press, **1987**, p. 912.
[12] A branched selectivity of 95% was reported with a binaphthophosphepine-Rh(I) complex: S. Gladiali, D. Fabbri, *Chem. Ber./Recueil* **1997**, *130*, 543−554. A similar result was recently obtained with an other diphosphane, the bis(diazaphospholidine): S. Breeden, D. J. Cole-Hamilton, D. F. Foster, G. J. Schwarz, M. Wills, *Angew. Chem. Int. Ed.* **2000**, *39*, 4106−4108.

Received November 29, 2000
[I00455]

Hydrido(3-hydroxyalkynyl) Complexes as Intermediates in the Activation of Propargyl Alcohol Derivatives by [Cp*RuCl(dippe)] [Cp* = C_5Me_5, dippe = 1,2-bis(diisopropylphosphanyl)ethane]

Emilio Bustelo,[a] Manuel Jiménez-Tenorio,[a] M. Carmen Puerta,[a] and Pedro Valerga*[a]

Keywords: Sandwich complexes / Ruthenium / Isomerizations / Hydrido ligands / Allenylidene ligands

The reaction of propargyl alcohol derivatives with the complex [Cp*RuCl(dippe)] [dippe = 1,2-bis(diisopropylphosphane)ethane] and $NaBPh_4$ in MeOH yields hydrido(3-hydroxyalkynyl) compounds [Cp*Ru(H){C≡CC(OH)RR′}(dippe)][BPh_4] [R, R′ = Ph, Ph (**1a**); H, Ph (**1b**); H, Me (**1c**)]. These represent intermediates in the formation of 3-hydroxyvinylidene species [Cp*Ru{=C=CHC(OH)RR′}(dippe)][BPh_4] [R, R′ = Ph, Ph (**2a**); H, Ph (**2b**); H, Me (**2c**)], into which they irreversibly rearrange both in solution and in the solid state. Solution kinetic studies have been carried out on this isomerization process. Ulterior dehydration processes are feasible, resulting in the formation of allenylidene [Cp*Ru(=C=C=CRR′)(dippe)][BPh_4] [R, R′ = Ph, Ph (**3a**); H, Ph (**3b**)] or vinylvinylidene [Cp*Ru{=C=CHCH(=CH_2)}(dippe)][BPh_4] (**4**) species. The X-ray crystal structure of the novel secondary allenylidene complex [Cp*Ru(=C=C=CHPh)(dippe)][BPh_4] is presented.

Introduction

It is well known that coordination of terminal alkynes to metal complexes reverses the relative stabilities of acetylene and vinylidene, this being a general procedure used for the synthesis of a wide range of vinylidene complexes.[1] In the case of propargyl alcohols HC≡CC(OH)R_2, subsequent dehydration of the resulting 3-hydroxyvinylidene complex may eventually lead to allenylidene compounds.[2,3] By analogous methods, complexes containing even longer unsaturated carbon chains have been obtained.[2,4] Interest in vinylidene complexes has been partly focussed on their utility in stoichiometric or catalytic transformations of alkenes and alkynes.[5] On the other hand, how the alkyne to vinylidene tautomerization takes place is still subject of research.

As a first reasonable approach to the isomerization mechanism, one may envisage oxidative addition of the alkyne to the metal centre thereby furnishing an alkynyl(hydrido)-metal complex.[6] (Scheme 1, Pathway A). Several cases of this are known in the chemistry of Co, Rh, and Ir,[7] and it is supported by ab initio MO calculations.[8] In the case of d^6 systems (Ru^{II}, Os^{II}, Mn^{I}), however, a pathway involving oxidative addition would seem to be a thermodynamically unfavourable process,[9] and a direct 1,2-hydrogen shift in the initially formed alkyne complex would be the most plausible pathway to a vinylidene[10] (Scheme 1, Pathway B). Actually, reactions of $[CpM(PR_3)_2]^+$ (M = Fe, Ru, Os) fragments with 1-alkynes normally lead directly to vinylidene complexes $[CpM(=C=CHR)(PR_3)_2]^+$ without any observable intermediates.[1,11] In the case of the complex [CpOsCl(P*i*Pr_3)$_2$], the isomerization of the π-alkyne complex [CpOsCl(P*i*Pr_3)(η^2-HC≡CPh)] into the vinylidene derivative takes place without any evidence of the intermediacy of alkynyl(hydrido) species.[12] Its reaction with alkynes and alkynols to afford the first examples of alkynyl(hydrido)osmium(IV) complexes that do not rearrange to their vinylidene isomers has only recently been reported.[13] In the case of ruthenium, there are several examples of direct isomerization to vinylidene,[14] vinylidene/π-alkyne equilibria,[15] and vinylidene to π-alkyne isomerization,[16] for which alkynyl(hydrido) species have never been detected. The relatively recent use of basic ruthenium fragments containing η^5-C_5Me_5 and their application in the activation of terminal alkynes[17] has allowed new insights into this matter.

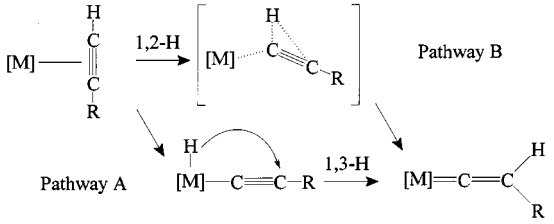

Scheme 1

Thus, study of the interaction of [Cp*RuCl(dippe)] with 1-alkynes allowed for the first time the isolation and characterization of metastable alkynyl(hydrido)ruthenium(IV) species as intermediates in the formation of the more stable vinylidene isomers.[18] These studies showed that the mechanism of this isomerization involves hydrido ligand dissociation as a proton and subsequent protonation on the β-carbon atom of the alkynyl ligand (Scheme 2).[19] It was also found that the isolation of these metastable intermediates is strongly dependent on the preparative method

[a] Departamento de Ciencia de los Materiales e Ingeniería Metalúrgica y Química Inorgánica, Facultad de Ciencias, Universidad de Cádiz,
Apartado 40, 11510 Puerto Real, Cádiz, Spain
Fax: (internat.) + 34-956/016288
E-mail: pedro.valerga@uca.es

 © WILEY-VCH Verlag GmbH, 69451 Weinheim, 2001 1434−1948/01/0909−2391 $ 17.50+.50/0

used. In the case of propargyl alcohols, which form complexes that are more soluble in the methanol used as solvent, this dependence proved to be crucial in that only 3-hydroxyvinylidene or dehydration products were isolated in the course of our earlier studies on [Cp*RuCl(dippe)].[20] A similar study has recently been carried out on the system [Cp*RuCl(PEt_3)$_2$], which contains a monodentate and sterically less demanding phosphane as a co-ligand. In this case, it was possible to detect η^2-alkynol derivatives and to monitor by $^{31}P\{^1H\}$ NMR their isomerization by two alternative pathways that are simultaneously operative at low temperature, namely direct 1,2-H shift and oxidative addition.[21] Furthermore, following an appropriate strategy, hydrido(3-hydroxyalkynyl) derivatives of the type [Cp*Ru(H){C≡CC(OH)R_2}(PEt_3)$_2$][BPh_4] were isolated and fully characterized. In view of these results, we have now re-examined the reactivity of [Cp*RuCl(dippe)] towards alkynols. As a result, we have been able to isolate new hydrido(3-hydroxyalkynyl) complexes, which have allowed us to perform further kinetic studies of the isomerization process into 3-hydroxyvinylidene species. Dehydration reactions of these compounds have led to new allenylidene and vinylvinylidene complexes, which have been fully characterized.

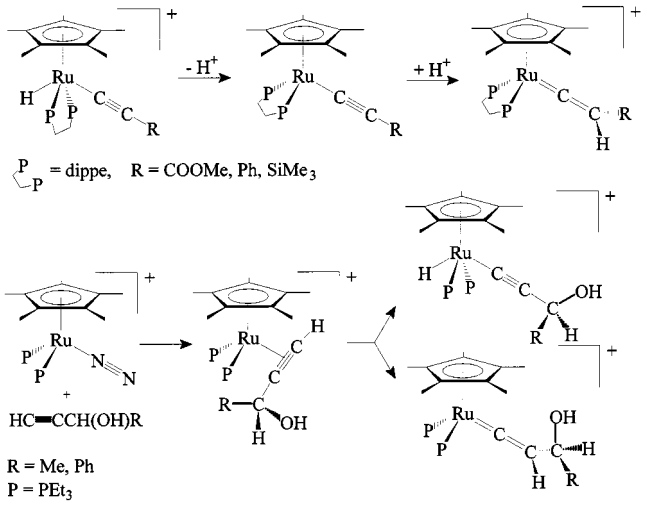

Scheme 2

Results and Discussion

The metastable complexes [Cp*Ru(H){C≡CC(OH)RR′}(dippe)][BPh_4] [R, R′ = Ph, Ph (**1a**); H, Ph (**1b**); H, Me (**1c**)] were isolated by precipitation following addition of the solid chloro complex [Cp*RuCl(dippe)] to a solution of $NaBPh_4$ and the alkyne in the minimum volume of MeOH at 0 °C. With an alkyne such as HC≡CCOOEt, the complex [Cp*Ru(H)(C≡CCOOEt)(dippe)][BPh_4] (**1d**) is easily obtained by adding $NaBPh_4$ prior to the alkyne. However, alkynols form more alcohol-soluble complexes owing to the presence of the hydroxy group. As a consequence, hydrido(3-hydroxyalkynyl) compounds can remain unnoticed due to the fact that isomerization to the vinylidene may occur to a greater or lesser extent prior to precipitation. This could only be avoided by adhering strictly to the aforementioned procedure and accounts for the fact that species analogous to compounds **1a**−**1c** were not detected in our previous work on this system. Furthermore, the reaction with HC≡C−CH_2OH yields the alkynyl(hydrido) complex only as a minor product even under these experimental conditions. Only in the case of HC≡CC(OH)Ph_2 was it possible to isolate the complex [Cp*Ru(H){C≡CC(OH)Ph_2}(dippe)][BPh_4] as a solid in pure form, uncontaminated by any of the 3-hydroxyvinylidene isomer. In the IR spectrum of compound **1a**, the ν(OH), ν(C≡C), and ν(Ru−H) bands are seen at 3578, 2100, and 2045 cm^{-1}, respectively. The $^{31}P\{^1H\}$ NMR spectrum recorded in $CDCl_3$ at 0 °C consists of a singlet at δ = 73.1, whereas in the ^1H NMR spectrum the terminal hydride ligand appears as a triplet at δ = −9.17 with a coupling constant of 30.5 Hz. Since this compound does not isomerize at 0 °C, it was possible to record the $^{13}C\{^1H\}$ NMR spectrum, which features a triplet at δ = 103.7 and a singlet at δ = 116.4, in good accord with the expected resonances for the α- and β-carbon atoms of the alkynyl ligand. In the case of the alkynols HC≡CCH(OH)R (R = Me, Ph), the corresponding hydrido(3-hydroxyalkynyl) complexes **1b** and **1c** could also be obtained in good yields, but were invariably accompanied by minor amounts of their 3-hydroxyvinylidene isomers.

The spectral properties of these complexes closely resemble those of complex **1a**. The main difference is observed in the $^{31}P\{^1H\}$ NMR spectrum of **1b** (Figure 1), where the presence of a chiral centre at the γ-carbon atom induces a magnetic nonequivalence of the phosphorus atoms, giving rise to an AB spin system at low temperatures ($^3J_{PP'}$ = 18 Hz). This pattern has also been observed in some analogous complexes such as [Cp*Ru(H){C≡CC(OH)RR′}(PEt_3)$_2$][BPh_4] (R, R′ = H, Ph; Me, Ph) ($^3J_{PP'}$ = 20−21 Hz)[21] and [CpOs(H){C≡CC(OH)MePh}(P*i*Pr_3)$_2$][PF_6] ($^3J_{PP'}$ = 23.5 Hz).[13] The pattern is

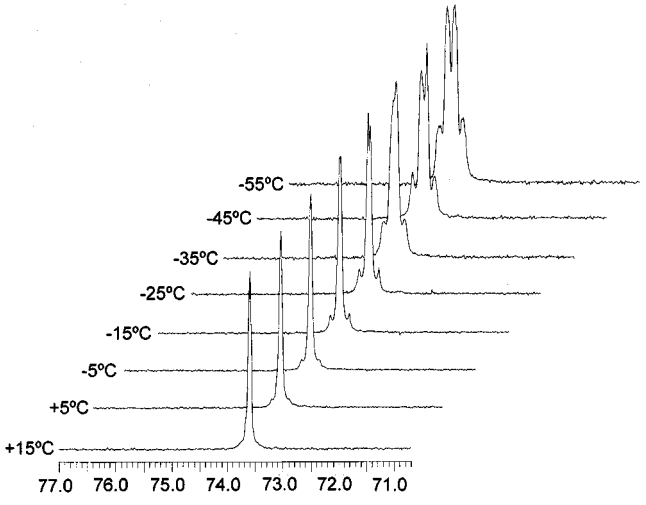

Figure 1. Stacked $^{31}P\{^1H\}$ NMR spectra illustrating the evolution of the [Cp*Ru(H){C≡CCH(OH)Ph}(dippe)][BPh_4] (**1b**) signal with temperature

temperature-dependent and the doublets coalesce to a singlet above +15 °C, most likely due to an averaging of the anisotropy of the phosphorus atom environments through rotation of the CH(OH)Ph group about the C−C bond.

Compounds **1a−1c** isomerize into the vinylidene species [Cp*Ru{=C=CHC(OH)RR′}(dippe)][BPh_4] [R, R′ = Ph, Ph (**2a**); H, Ph (**2b**); H, Me (**2c**)] both in solution and in the solid state at room temperature (see Scheme 3), as has also been reported elsewhere.[6,18,21] However, as for [Cp*RuH(C≡CCOOMe)(dippe)][BPh_4],[19] the tautomerization of **1d** into the vinylidene complex [Cp*Ru(=C=CHCOOEt)(dippe)][BPh_4] (**2d**) only occurs in solution, and not in the solid state. Orange crystalline products, identified as vinylidene complexes by IR and NMR spectroscopy, were obtained when samples of **2a−2c** were heated in the solid state for several hours at 40 °C. In contrast to the other complexes, a clean preparation of [Cp*Ru{=C=CHC(OH)Ph_2}(dippe)][BPh_4] (**2a**) by isomerization of **1a** in solution is not possible due to the fact that spontaneous dehydration ensues. The vinylidene protons of **2a** and **2d** appear as broad singlets at δ = 4.37 and 4.52 in the respective ^{1}H NMR spectra, while in the ^{13}C{^{1}H} NMR spectra, the vinylidene α-carbon atoms give triplets at δ = 338.8 and 338.7 with coupling constants of 16.1 and 14.3 Hz, respectively. In the ^{1}H NMR spectra of **2b** and **2c**, the vinylidene protons appear as doublets at δ = 4.33 and 3.98, while the protons on the γ-carbon atoms give signals at δ = 5.40 (doublet) and 4.51 (doublet of quadruplets), respectively. The ^{31}P{^{1}H} NMR spectra of **2b** (Figure 2) and **2c** at 25 °C each consist of an AB spin pattern with a coupling constant of 17.1 Hz. In these cases, the doublets are more clearly separated from each other. This suggests an increased anisotropy in the chemical environments of the phosphorus atoms of **2b** and **2c** as compared to **1b** and **1c** due to the effect of the chiral centre on the γ-carbon atom. This can be attributed to the change in hybridization from sp to sp^2 at the β-carbon atom. The doublets move closer to each other as the temperature is increased, indicating chemical shift averaging, but do not coalesce even at 45 °C. In fact, the phosphorus atoms are expected to remain magnetically nonequivalent even at the fast-exchange limit due to the presence of the chiral substituent. This is consistent with the observed pattern, which has also been reported for related compounds such as [Cp*Ru{=C=CHCH(OMe)-Me}(PMe_2Ph)$_2$][PF_6] [17a] and [(η^5-C_9H_7)Ru{=C=CHCH(OMe)Ph}(PPh_3)$_2$][PF_6].[22]

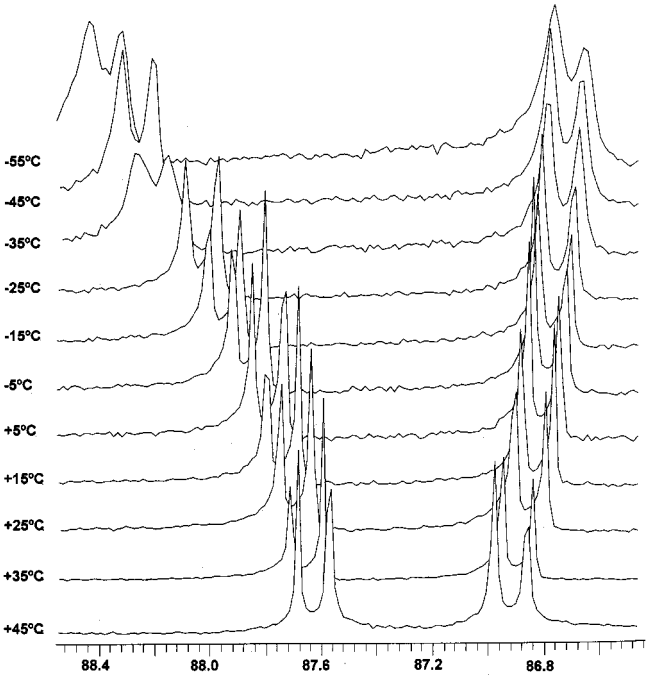

Figure 2. Stacked ^{31}P{^{1}H} NMR spectra illustrating the evolution of the [Cp*Ru{=C=CHCH(OH)Ph}(dippe)][BPh_4] (**2b**) signal with temperature

In order to establish the sequence of intermediates in the activation of alkynes and alkynols by the moiety {[Cp*Ru(dippe)]$^+$}, we first attempted to detect the intermediacy of π-alkyne complexes in the first step of the overall process. While an equilibrium between the π-alkyne and alkynyl(hydrido) species was found for the previously described [Cp*Ru(η^2-HC≡CH)(dippe)][BPh_4],[19] in the case of substituted alkynes these adducts are expected to be thermodyn-

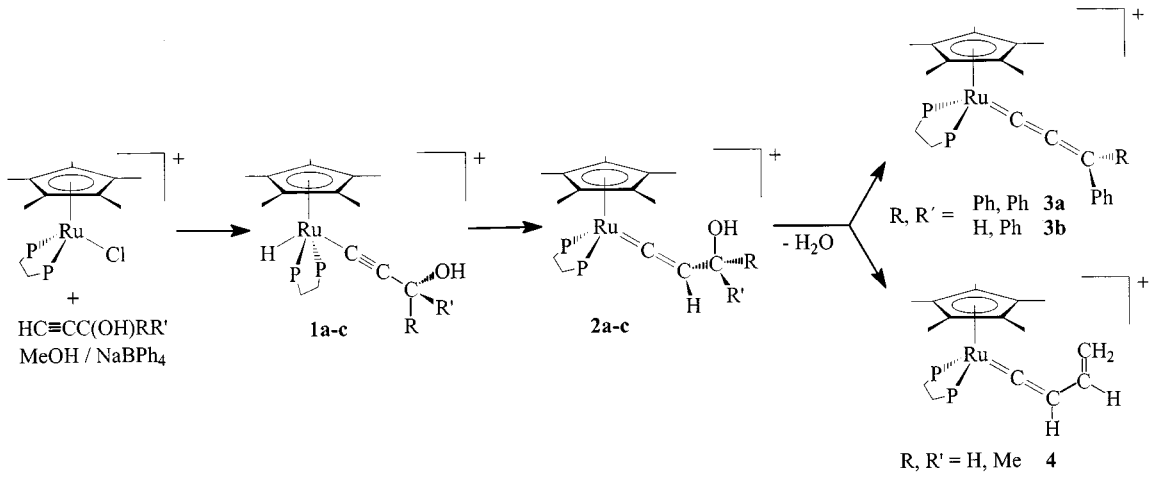

Scheme 3

amically less favourable. The substituent on the alkyne makes steric interactions with the phosphane and Cp* methyl groups much stronger when this ligand is bound to the metal centre in an η^2-fashion as compared to those in an η^1-alkynyl or -vinylidene complex.

At variance with our latest results on the system containing the moiety $\{[Cp^*Ru(PEt_3)_2]^+\}$, the reaction of alkynes with labile cationic adducts of the type $[Cp^*Ru(L)(dippe)]^+$ (L = C_2H_4, N_2)[23] at low temperature did not provide any supporting evidence for the formation of π-alkyne intermediates. Upon addition of an excess of the appropriate alkynol (or HC≡CCOOEt) to a precooled $CDCl_3$ solution of the ethylene complex $[Cp^*Ru(C_2H_4)(dippe)][BPh_4]$[23] at −40 °C, the initial resonance in the $^{31}P\{^1H\}$ NMR spectrum (one singlet at δ = 77.9) remained unchanged below −20 °C. Above this temperature, this signal irreversibly disappeared, being replaced by a single resonance attributable to the corresponding alkynyl(hydrido) species **1a−1d**. The metallic fragments $\{[Cp^*Ru(PEt_3)_2]^+\}$ and $\{[Cp^*Ru(dippe)]^+\}$ are able to activate C−H bonds in alkynes by virtue of their high basicities. This ability is enhanced for the $\{[Cp^*Ru(dippe)]^+\}$ moiety: While complexes containing PEt_3 give mixtures of alkynyl(hydrido) and vinylidene species, formed through the intermediacy of π-alkyne adducts, the analogous compounds containing dippe only form vinylidene species, according to a pathway involving the intermediacy of the alkynyl(hydrido) species. Prior coordination of the alkyne seems to favour the formation of the vinylidene isomer by a direct pathway involving a 1,2-hydrogen shift, as has been observed for $[Cp^*Ru(\eta^2\text{-}HC{\equiv}CH)(dippe)]^+$,[19] $[Cp^*Ru\{\eta^2\text{-}HC{\equiv}CCH(OH)R\}(PEt_3)_2]^+$,[21] and $[CpOsCl(\eta^2\text{-}HC{\equiv}CPh)(P\mathit{i}Pr_3)]$.[13]

The kinetics of the isomerization of complexes **1a−1d** into **2a−2d** has been studied. The temperature range in which the process takes place at measurable rates is clearly determined by the substituent on the γ-carbon atom (see Table 1). Thus, the isomerization of **1a** proceeds at measurable rates in the range 25−45 °C, whereas for **1d** it can only be observed at 10−30 °C. The stepwise substitution of the phenyl groups on the γ-carbon atom decreases the temperature range by ca. 10 °C. In all cases, the rate is first order with respect to the alkynyl(hydrido) complex. From Eyring plots, the activation parameter was determined (Table 1) to be $\Delta G^{\ddagger}_{298} \approx 21$ kcal mol^{-1} in each case. These results can be compared with those reported for cobalt complexes, i.e. $\Delta G^{\ddagger}_{298} \approx 31$ kcal mol^{-1} for $[Co(H)(C{\equiv}CPh)PP_3]^+$ [PP_3 = $P(CH_2CH_2PPh_2)_3$],[7a] and with our earlier kinetic studies on the isomerization of $[Cp^*Ru(H)(C{\equiv}CR)(dippe)]^+$ [19] (R = COOMe, Ph, $SiMe_3$), in which $\Delta G^{\ddagger}_{298}$ was estimated to be ca. 20 kcal mol^{-1}. Migration of the hydrido ligand as a proton following dissociation and subsequent protonation of the β-carbon atom has previously been proposed as the mechanism for this transformation in solution, and it is supported by sound experimental evidence.[7a,19] It is further supported in the present case by the observed solvent effect on the isomerization rate. The formation of the vinylidene complex **2d** from **1d** is subject to a strong solvent dependence: the process takes place more rapidly in acetone, in which the constant at 5 °C is $(3.16 \pm 0.16) \times 10^{-3}$ s^{-1}, whereas a comparable constant of $(3.74 \pm 0.21) \times 10^{-3}$ s^{-1} is only found at 25 °C in $CDCl_3$. The slower rate in $CDCl_3$ made this the solvent of choice for our kinetic NMR studies. In acetone, the time scale of the faster isomerization overlaps with that of the process of ethylene substitution used to obtain the alkynyl(hydrido) species in situ. Chloroform invariably contains trace amounts of HCl (DCl), which may hamper the dissociation of the hydride as a proton during the course of isomerization. Given the small quantities of acid present, it merely slows down the process, but it is known that strong acids such as HBF_4 can completely inhibit the isomerization. On the other hand, the Lewis base character of acetone possibly has the reverse effect (i.e. base catalysis), accelerating the proton transfer from the metal centre to the β-carbon atom.

As a consequence of the steric hindrance and electron-releasing ability of the $\{[Cp^*Ru(dippe)]^+\}$ moiety, its vinylidene complexes are less electrophilic and more stable towards the addition of an alcohol to the α-carbon atom, but dehydration should also be disfavoured in electron-rich complexes.[4] However, complex **2a** undergoes spontaneous

Table 1. Pseudo first order rate constants and activation parameters for alkynyl(hydrido) to vinylidene isomerization

R =	**1a → 2a** C(OH)Ph_2	**1b → 2b** CH(OH)Ph	**1c → 2c** CH(OH)Me	**1d → 2d** COOEt
T [K]	$k \times 10^{-3}$ s^{-1}	$k \times 10^{-3}$ s^{-1}	$k \times 10^{-3}$ s^{-1}	$k \times 10^{-3}$ s^{-1}
283	−	−	1.22 ± 0.03	0.6 ± 0.1
288	−	0.93 ± 0.03	2.20 ± 0.03	1.04 ± 0.08
293	−	1.91 ± 0.03	5.5 ± 0.4	1.9 ± 0.2
298	0.42 ± 0.02	3.2 ± 0.1	8.3 ± 0.4	3.7 ± 0.2
303	1.11 ± 0.03	7.4 ± 0.5	14.3 ± 0.6	6.4 ± 0.1
308	2.17 ± 0.07	10.0 ± 0.6	−	−
313	3.8 ± 0.1	−	−	−
318	5.9 ± 0.6	−	−	−
$\Delta H^{\ddagger}$ [kcal/mol]	24 ± 2	21.0 ± 1.5	21 ± 1	20 ± 1
$\Delta S^{\ddagger}$ [cal/mol K]	7 ± 6	1 ± 5	1 ± 5	−4 ± 4
$\Delta G^{\ddagger}_{298}$ [kcal/mol]	22 ± 2	21 ± 2	21 ± 2	21 ± 2

dehydration in solution, yielding the allenylidene complex [Cp*Ru(=C=C=CPh_2)(dippe)][BPh_4] (**3a**) as a dark-red solid after workup. In the case of 3-hydroxyvinylidene complexes bearing one H on the γ-carbon atom (**2b** and **2c**), complete dehydration can only be achieved by passing a solution in CH_2Cl_2 through an acidic alumina column. In the first case, the *secondary* allenylidene [Cp*Ru(=C=C=CHPh)(dippe)][BPh_4] (**3b**) is obtained as a dark-green solid (see Scheme 3). The IR absorption due to the cumulated C=C=C in **3a** and **3b** appears at 1890 and 1915 cm^{-1}, respectively, i.e. at the lower end of the usual range (1800−2100 cm^{-1}).[2] Other monosubstituted allenylidenes have been obtained by activation of secondary propargyl alcohols with the fragments $[(\eta^5\text{-}C_9H_7)Ru(PPh_3)_2]^+$ [22] and $[Ru(Ph_2PCH_2PPh_2)_2Cl]^+$.[25] In both cases, the infrared absorption is seen at higher $\tilde{\nu}$ [cm^{-1}] for monosubstituted than for disubstituted systems. Monosubstituted allenylidenes are very scarce due to their higher reactivity, and are only known in electron-rich complexes. Ongoing studies on allenylidene reactivity have confirmed that **3b** is indeed more reactive than **3a**.

In the $^{13}C\{^1H\}$ NMR spectra of compounds **3a** and **3b**, the metal-bound carbon atoms show characteristic low-field resonances (δ = 287.2 and 294.3), and the order $\delta(C^\alpha) > \delta(C^\beta) > \delta(C^\gamma)$ is found in both cases. The ^1H NMR spectrum of the allenylidene compound **3b** shows a broad singlet at δ = 9.20 due to the proton on the γ-carbon atom as the only notable feature. Slow recrystallization of **3b** from acetone/ethanol (1:2) afforded green crystals suitable for X-ray diffraction analysis, and its X-ray crystal structure was determined. An ORTEP[24] view of the cationic complex is shown in Figure 3.

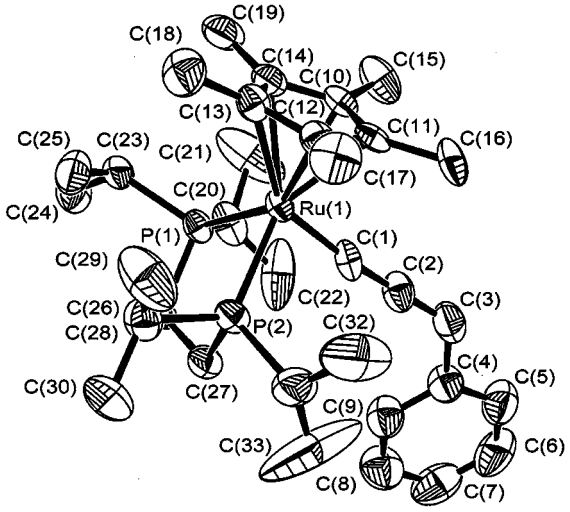

Figure 3. ORTEP view of the cation [Cp*Ru(=C=C=CHPh)(dippe)]$^+$ in compound **3b** showing the atom labelling scheme; hydrogen atoms have been omitted for clarity; selected bond lengths [Å] and angles [°]: Ru1−C10 2.266(7), Ru1−C11 2.258(6), Ru1−C12 2.294(7), Ru1−C13 2.337(7), Ru1−C14 2.329(7), Ru1−C1 1.865(8), Ru1−P1 2.3479(19), Ru1−P2 2.336(2), C1−C2 1.249(10), C2−C3 1.320(12); P1−Ru1−P2 81.99(7), Ru1−C1−C2 172.8(7), C1−C2−C3 177.5(9), C2−C3−C4 128.1(8)

The allenylidene ligand appears to be almost linearly assembled on the ruthenium centre. The bond lengths Ru(1)−C(1) = 1.865(8) Å, C(1)−C(2) = 1.249(10) Å, and C(2)−C(3) = 1.320(12) Å are consistent with a substantial contribution from the alkynyl mesomer, as is usually the case for compounds of this type. In a recent review, the normal ranges of such distances for a variety of allenylidene complexes were quoted as $Ru-C^\alpha$ = 1.84−2.00 Å, $C^\alpha-C^\beta$ = 1.18−1.27 Å, and $C^\beta-C_\gamma$ = 1.35−1.41 Å, respectively.[2] From a rapid overview, it can be concluded that electron-rich allenylidenes of this type more closely resemble the mesomeric form A, which is the usual way of representing them.

The atoms of the allenylidene ligand define a least-squares plane that forms a dihedral angle of 3.51° with the plane defined by C(1), Ru(1), and the centroid of the Cp*. This disposition has been commonly observed in other half-sandwich (allenylidene)Ru derivatives, since it appears to maximize the effectiveness of the metal−ligand π-overlap.[26] It is interesting to note that in this structure the phenyl substituent of the allenylidene ligand is oriented in an *endo* fashion, being directed away from the methyl substituents of the Cp* ring in order to minimize steric interactions. This is in contrast to the structure of the closely related derivative [CpRu(=C=C=CMePh)(dippe)][BPh_4],[20] in which the phenyl group is *exo*-oriented with respect to the Cp ligand and points away from the phosphane isopropyl groups. This example once again illustrates the effect of the differences in the steric properties of the Cp and Cp* ligands on the stereochemistry of their complexes.

Finally, dehydration of compound **2c** leads to the vinylvinylidene complex [Cp*Ru(=C=CH−CH=CH_2)(dippe)][BPh_4] (**4**) rather than to the corresponding allenylidene derivative (see Scheme 3). This is expected for 3-hydroxyvinylidene compounds bearing labile protons on their δ-carbon atoms, as a consequence of the reduced stabilization of the partial positive charge generated on the γ-carbon atom in allenylidene ligands (Scheme 4, canonical form B). The ^1H NMR spectrum of **4** exhibits four signals in the range δ = 4.4−6.2, which were assigned by two-dimensional correlation (COSY) and show an appropriate coupling pattern. The vinylidene carbon atom gives rise to a low-field triplet at δ = 347.7 in the $^{13}C\{^1H\}$ NMR spectrum.

$$[Ru]^+{=}C{=}C{=}CRR' \longleftrightarrow [Ru]{-}C{\equiv}C{-}\overset{+}{C}RR'$$

A B

Scheme 4

Our current interest is centred on the reactivity of the allenylidene complexes described in this work. Despite their electron-rich character, they are able to undergo nucleophilic attack by a series of donor molecules. The resulting species will be described in detail in a forthcoming paper.

Conclusion

It has been demonstrated that previously overlooked hydrido(3-hydroxyalkynyl)Ru^{IV} complexes of the type [Cp*

Ru(H){C≡CC(OH)RR′}(dippe)][BPh_4] are the only observable intermediates in the activation of propargyl alcohols by [Cp*RuCl(dippe)], and that they can be isolated in high yields by careful control of the reaction conditions. These species rearrange into their vinylidene tautomers according to a dissociative mechanism. The thus generated 3-hydroxyvinylidene complexes undergo dehydration yielding either allenylidene or vinylvinylidene species depending upon the substituents present at the γ-carbon atom.

Experimental Section

General Remarks: All synthetic operations were performed under dry dinitrogen or argon using conventional Schlenk techniques. Tetrahydrofuran, diethyl ether, and petroleum ether (boiling point range 40−60 °C) were distilled from the appropriate drying agents. All solvents were deoxygenated immediately prior to use. [Cp*RuCl(dippe)][27] and [Cp*Ru(η²-CH_2=CH_2)(dippe)][BPh_4][23] were prepared according to reported procedures. − IR spectra were recorded from Nujol mulls of the samples with a Perkin−Elmer FT-IR Spectrum 1000 spectrophotometer. − NMR spectra were recorded with a Varian Unity 400 MHz or a Varian Gemini 200 MHz instrument. Chemical shifts are given in parts per million relative to $SiMe_4$ (^1H and $^{13}C\{^1H\}$) or 85% H_3PO_4 ($^{31}P\{^1H\}$). In the NMR spectra, the tetraphenylborate protons and carbon atoms of all cationic compounds showed signals in the appropriate shift ranges, while in the IR spectra a band was seen at 1580 cm^{-1}. − Microanalyses were performed by the Serveis Científico-Tècnics, Universitat of Barcelona.

Preparation of Alkynyl(hydrido) Derivatives [Cp*RuH(C≡CR)(dippe)][BPh_4] [R = C(OH)Ph_2 (1a), CH(OH)Ph (1b), CH(OH)Me (1c), COOEt (1d)]: [Cp*RuCl(dippe)] (133 mg, 0.25 mmol) was added to a solution of the appropriate alkyne or alkynol (0.30 mmol) and $NaBPh_4$ (81 mg, 0.50 mmol) in MeOH (5 mL) at 0 °C (ice bath). The mixture was allowed to warm until a white microcrystalline solid precipitated, which was collected by filtration, washed with cold EtOH and petroleum ether, and stored at −20 °C. As expected for isomeric compounds, microanalytical data were identical to those for 3-hydroxyvinylidenes **2a**−**2d**. Selected spectroscopic data are as follows.

1a: Yield 226 mg (88%). − $C_{63}H_{79}BOP_2Ru$ (1026.1): calcd. C 73.7, H 7.76; found C 73.8, H 7.74. − IR (Nujol): $\tilde{\nu}$ = 3578 ν(OH), 2100 ν(C≡C), 2045 cm^{-1} ν(RuH). − ^1H NMR (400 MHz, $CDCl_3$, 273 K): δ = −9.17 (t, $^2J_{HP}$ = 30.5 Hz, 1 H, Ru−H), 1.84 [s, 15 H, $C_5(CH_3)_5$], 2.52 (br. s, 1 H, OH), 0.99−1.14 [m, 24 H, PCH(CH_3)$_2$], 1.37 and 1.63 (m, 2 H each, PCH_2), 2.12 and 3.12 (m, 2 H each, PCH), 7.30−7.36 (m, 6 H, C_6H_5), 7.47 (m, 4 H, C_6H_5). − $^{31}P\{^1H\}$ NMR (161.89 MHz, $CDCl_3$, 273 K): δ = 73.1 (s). − $^{13}C\{^1H\}$ NMR (100.58 MHz, $CDCl_3$, 273 K): δ = 10.97 [s, $C_5(CH_3)_5$], 18.17, 18.77, 19.11, and 20.69 [s, PCH(CH_3)$_2$], 21.43 (m, PCH_2), 24.89 and 27.93 (m, PCH), 75.34 (s, C^γ), 101.3 [s, $C_5(CH_3)_5$], 103.7 (t, $^2J_{CP}$ = 25.2 Hz, C^α), 116.4 (s, C^β), 126.0, 127.6, 128.2, and 145.7 (s, C_6H_5).

1b: Yield 195 mg (82%). − $C_{57}H_{75}BOP_2Ru$ (950.0): calcd. C 72.1, H 7.96; found C 72.1, H 7.90. − IR (Nujol): $\tilde{\nu}$ = 3563 ν(OH), 2106 ν(C≡C), 2062 cm^{-1} ν(RuH). − ^1H NMR (400 MHz, $CDCl_3$, 273 K): δ = −9.11 (t, $^2J_{HP}$ = 30.5 Hz, 1 H, Ru−H), 1.04−1.17 and 1.26−1.36 [m, 24 H, PCH(CH_3)$_2$], 1.82 [s, 15 H, $C_5(CH_3)_5$], 2.08 (m, 4 H, PCH_2), 2.88 and 3.01 (m, 2 H each, PCH), 3.10 (br. s, 1 H, OH), 5.45 [s, 1 H, Ru−C≡CC*H*(OH)Ph], 7.40 and 7.56 (m, 5 H, C_6H_5). − $^{31}P\{^1H\}$ NMR (161.89 MHz, $CDCl_3$, 273 K): δ = 73.7 (s).

1c: Yield 189 mg (85%). − $C_{52}H_{73}BOP_2Ru$ (888.0): calcd. C 70.3, H 8.29; found C 70.1, H 8.29. − IR (Nujol): $\tilde{\nu}$ = 3532 ν(OH), 2115 ν(C≡C), 2050 cm^{-1} ν(RuH). − ^1H NMR (400 MHz, $CDCl_3$, 273 K): δ = −9.10 (t, $^2J_{HP}$ = 31.0 Hz, 1 H, Ru−H), 0.96−1.11 and 1.16−1.21 [m, 24 H, PCH(CH_3)$_2$], 1.35 [d, $^3J_{HH}$ = 6.0 Hz, 3 H, Ru−C≡C−CH(OH)CH_3], 1.84 [s, 15 H, $C_5(CH_3)_5$], 2.08 (m, 4 H, PCH_2), 3.09 (m, 4 H, PCH), 3.43 (br. s, 1 H, OH), 4.50 [q, $^3J_{HH}$ = 6.0 Hz, 1 H, Ru−C≡C−C*H*(OH)CH_3]. − $^{31}P\{^1H\}$ NMR (161.89 MHz, $CDCl_3$, 233 K): δ = 73.20 (s).

1d: Yield 211 mg (92%). − $C_{53}H_{73}BO_2P_2Ru$ (916.0): calcd. C 69.5, H 8.03; found C 69.4, H 7.89. − IR (Nujol): $\tilde{\nu}$ = 2099 ν(C≡C), 2062 ν(RuH), 1681 cm^{-1} ν(C=O). − ^1H NMR (400 MHz, $CDCl_3$, 273 K): δ = −8.78 (t, $^2J_{HP}$ = 28.2 Hz, 1 H, Ru−H), 0.98−1.27 [m, 24 H, PCH(CH_3)$_2$], 1.19 (t, $^3J_{HH}$ = 6.8 Hz, 3 H, $COOCH_2CH_3$), 1.84 [s, 15 H, $C_5(CH_3)_5$], 1.98 and 2.07 (m, 2 H each, PCH_2), 2.90 (m, 4 H, PCH), 4.12 (q, $^3J_{HH}$ = 6.8 Hz, 2 H, $COOCH_2CH_3$). − $^{31}P\{^1H\}$ NMR (161.89 MHz, $CDCl_3$, 273 K): δ = 72.3 (s). − $^{13}C\{^1H\}$ NMR (100.58 MHz, $CDCl_3$, 273 K): δ = 10.89 [s, $C_5(CH_3)_5$], 14.37 (s, $COOCH_2CH_3$), 18.24, 18.30, 19.45, and 19.88 [s, PCH(CH_3)$_2$], 21.74 (m, PCH_2), 25.94 and 25.60 (m, PCH), 60.52 (s, $COOCH_2CH_3$), 102.0 (t, $^2J_{CP}$ = 23.0 Hz, C^α), 104.2 [s, $C_5(CH_3)_5$], 109.4 (s, C^β), 164.1 (s, *C*OOEt).

Preparation of Vinylidene Derivatives [Cp*Ru(=C=CHR)(dippe)][BPh_4] [R = C(OH)Ph_2 (2a), CH(OH)Ph (2b), CH(OH)Me (2c), COOEt (2d)]: The solid complexes **1a**−**1c** (1 mmol) were heated at 35 °C for 3 h under an inert gas, in the course of which they gradually underwent a colour change from white/yellow to orange. This corresponded to a quantitative and clean isomerization process to give the respective vinylidene isomers. Complex **2d** was obtained after stirring a solution of **1d** (916 mg, 1 mmol) in acetone for 2 h at room temperature, followed by removal of the solvent. Selected IR and NMR spectroscopic data are as follows.

2a: Yield 1026 mg (100%). − $C_{63}H_{79}BOP_2Ru$ (1026.1): calcd. C 73.7, H 7.76; found C 73.8, H 7.72. − IR (Nujol): $\tilde{\nu}$ = 3558 ν(OH), 1633 cm^{-1} ν(C=C). − ^1H NMR (400 MHz, $CDCl_3$, 298 K): δ = 0.94−1.18 [m, 24 H, PCH(CH_3)$_2$], 1.81 [s, 15 H, $C_5(CH_3)_5$], 1.73 and 1.86 (m, 2 H each, PCH_2), 2.02 and 2.23 (m, 2 H each, PCH), 2.32 (br. s, 1 H, OH), 4.37 (br. s, 1 H, Ru=C=CHR), 7.27−7.34 (m, 10 H, C_6H_5). − $^{31}P\{^1H\}$ NMR (161.89 MHz, $CDCl_3$, 298 K): δ = 83.7 (s). − $^{13}C\{^1H\}$ NMR (50.29 MHz, $CDCl_3$, 298 K): δ = 11.04 [s, $C_5(CH_3)_5$], 18.46, 18.67, 19.58, and 20.27 [s, PCH(CH_3)$_2$], 21.44 (vt, $^{1,3}J_{CP}$ = 21.5 Hz, PCH_2), 25.50 and 33.39 (m, PCH), 102.8 [s, $C_5(CH_3)_5$], 121.3 (s, C^β), 95.63 (s, C^γ), 125.4, 127.9, 128.6, and 145.5 (s, C_6H_5), 338.7 (t, $^2J_{CP}$ = 16.1 Hz, C^α).

2b: Yield 950 mg (100%). − $C_{57}H_{75}BOP_2Ru$ (950.0): calcd. C 72.1, H 7.96; found C 72.1, H 7.90. − IR (Nujol): $\tilde{\nu}$ = ν(OH) not obsd., 1643 cm^{-1} ν(C=C). − ^1H NMR (400 MHz, $CDCl_3$, 298 K): δ = 0.94−1.20 [m, 24 H, PCH(CH_3)$_2$], 1.83 [s, 15 H, $C_5(CH_3)_5$], 2.00 (m, 4 H, PCH_2), 2.11 and 2.30 (m, 2 H each, PCH), 2.57 (br. s, 1 H, OH), 4.33 [d, $^3J_{H^aH^b}$ = 9.0 Hz, 1 H, Ru=C=C*H*^{a}CH^b(OH)Ph], 5.40 [d, $^3J_{H^aH^b}$ = 9.0 Hz, 1 H, Ru=C=CH^{a}C*H*^{b}(OH)Ph], 7.28, 7.36, and 7.39 (m, 5 H, C_6H_5). − $^{31}P\{^1H\}$ NMR (161.89 MHz, $CDCl_3$, 298 K): δ = 87.7 and 86.9 (d, $^2J_{PP'}$ = 17.1 Hz). − $^{13}C\{^1H\}$ NMR (50.29 MHz, $CDCl_3$, 298 K): δ = 10.88 [s, $C_5(CH_3)_5$], 18.14, 19.18, 19.42, and 19.69 [m, PCH(CH_3)$_2$], 21.13, 25.23, and 31.74 (m, PCH and PCH_2), 66.97 (s, C^γ), 102.6 [s, $C_5(CH_3)_5$], 116.0 (s, C^β), 128.3, 128.5, 128.8, and 143.1 (s, C_6H_5), 337.4 (t, $^2J_{CP}$ = 14.3 Hz, C^α).

2c: Yield 888 mg (100%). − $C_{52}H_{73}BOP_2Ru$ (888.0): calcd. C 70.3, H 8.29; found C 70.1, H 8.28. − IR (Nujol): $\tilde{\nu}$ = ν(OH) not obsd., 1643 cm^{-1} ν(C=C). − ^1H NMR (400 MHz, $CDCl_3$, 298 K): δ = 0.94−1.99 and 1.05−1.21 [m, 24 H, PCH(CH_3)$_2$], 1.28 [d, $^3J_{H^bH^c}$ = 6.0 Hz, 3 H, Ru=C=CH^{a}CH^b(OH)CH^c_3], 1.83 [s, 15 H, $C_5(CH_3)_5$], 2.01 (m, 4 H, PCH_2), 2.14 and 2.23 (m, 2 H each, PCH), 3.23 (br. s, 1 H, OH), 3.98 (d, $^3J_{H^aH^b}$ = 9.0 Hz, 1 H, Ru=C=CH^aCH^b), 4.51 [dq, $^3J_{H^aH^b}$ = 9.0 Hz, $^3J_{H^bH^c}$ = 6.0 Hz, 1 H, Ru=C=CH^a−CH^b(OH)CH$^c_3$]. − $^{31}P\{^1H\}$ NMR (161.89 MHz, $CDCl_3$, 298 K): δ = 87.1 and 87.5 (d, $^2J_{PP'}$ = 17.1 Hz). − $^{13}C\{^1H\}$ NMR (50.29 MHz, $CDCl_3$, 298 K): δ = 10.88 [s, $C_5(CH_3)_5$], 18.22, 19.80, and 19.36 [d, PCH(CH_3)$_2$], 21.98 [s, Ru=C=CH−CH(OH)CH_3], 21.39 and 25.39 (m, PCH_2), 31.22 and 32.64 (m, PCH), 69.03 (s, C^γ), 102.7 [s, $C_5(CH_3)_5$], 115.4 (s, C^β), 337.2 (t, $^2J_{CP}$ = 14.7 Hz, C^α).

2d: Yield 916 mg (100%). − $C_{53}H_{73}BO_2P_2Ru$ (916.0): calcd. C 69.5, H 8.03; found C 69.2, H 8.00. − IR (Nujol): $\tilde{\nu}$ = 1693 ν(C=C), 1680 cm^{-1} ν(C=O). − ^1H NMR (400 MHz, $CDCl_3$, 298 K): δ = 0.88−1.00 and 1.08−1.30 [m, 24 H, PCH(CH_3)$_2$], 1.18 (t, $^3J_{HH}$ = 7.0 Hz, 3 H, $COOCH_2CH_3$), 1.84 [s, 15 H, $C_5(CH_3)_5$], 1.96 (m, 4 H, PCH_2), 2.28 and 2.85 (m, 2 H each, PCH), 4.13 (q, $^3J_{HH}$ = 7.0 Hz, 2 H, $COOCH_2CH_3$), 4.52 (br. s, 1 H, Ru=C=CH−). − $^{31}P\{^1H\}$ NMR (161.89 MHz, $CDCl_3$, 298 K): δ = 84.6 (s). − $^{13}C\{^1H\}$ NMR (50.29 MHz, $CDCl_3$, 298 K): δ = 10.85 [s, $C_5(CH_3)_5$], 14.37 (s, $COOCH_2CH_3$), 18.32, 19.50, and 19.90 [s, PCH(CH_3)$_2$], 21.89 (vt, $^{1,3}J_{CP}$ = 20.2 Hz, PCH_2), 25.20 and 32.25 (m, PCH), 60.46 (s, $COOCH_2CH_3$), 104.3 [s, $C_5(CH_3)_5$], 109.5 (s, C^β), 164.0 (s, *C*OOEt), 338.8 (t, $^2J_{CP}$ = 14.3 Hz, C^α).

Preparation of Allenylidene Complexes [Cp*Ru(=C=C=CRPh)(dippe)][BPh$_4$] [R = Ph (3a), H (3b)] and Vinylvinylidene Complex [Cp*Ru(=C=CHCH=CH$_2$)(dippe)][BPh$_4$] (4): Complex **3a** was obtained by adding the alkynol (0.30 mmol) to a solution of [Cp*RuCl(dippe)] (133 mg, 0.25 mmol) in MeOH (15 mL). After stirring the mixture for 6 h under reflux, the addition of $NaBPh_4$ (81 mg, 0.50 mmol) caused the precipitation of a dark-red solid, which was collected by filtration, washed with EtOH and petroleum ether, and dried in vacuo. The solid was recrystallized from acetone/ethanol (1:2) to give dark-red needles. Complexes **3b** and **4** were obtained by passing a solution of the corresponding 3-hydroxyvinylidene complex (0.25 mmol) in CH_2Cl_2 (1 mL) through a column of Al_2O_3 (acidic, activity grade I, height of column 10 cm) and collecting a dark-green band of **3b** and a brown band of **4**. Removal of the solvent from these fractions left solids, which were dried in vacuo and recrystallized from acetone/ethanol (1:2). Slow crystallization gave dark-green crystals of **3b**. Selected spectroscopic data are as follows:

3a: Yield 238 mg (94%). − $C_{63}H_{77}BP_2Ru$ (1008.1): calcd. C 75.1, H 7.70; found C 75.0, H 7.67. − IR (Nujol): $\tilde{\nu}$ = 1890 cm^{-1} ν(C=C=C). − ^1H NMR (400 MHz, $CDCl_3$, 298 K): δ = 0.88−0.96, 1.00−1.06, and 1.13−1.18 [m, 24 H, PCH(CH_3)$_2$], 1.84 [s, 15 H, $C_5(CH_3)_5$], 1.89 (m, 4 H, PCH_2), 1.99 and 2.17 (m, 2 H each, PCH), 7.36 (t, $^3J_{HH}$ = 8.3 Hz, 2 H, *p*-C_6H_5), 7.57 (d, $^3J_{HH}$ = 8.3 Hz, 4 H, *o*-C_6H_5), 7.59 (t, $^3J_{HH}$ = 8.3 Hz, 4 H, *m*-C_6H_5). − $^{31}P\{^1H\}$ NMR (161.89 MHz, $CDCl_3$, 298 K): δ = 87.9 (s). − $^{13}C\{^1H\}$ NMR (50.29 MHz, $CDCl_3$, 298 K): δ = 11.27 [s, $C_5(CH_3)_5$], 18.15, 19.80, and 19.43 [s, PCH(CH_3)$_3$], 21.29 (vt, $^{1,3}J_{CP}$ = 18.8 Hz, PCH_2), 25.83 and 30.79 (m, PCH), 102.7 [s, $C_5(CH_3)_5$], 128.5, 129.0, 130.5, and 144.2 (s, C_6H_5), 150.1 (s, C^γ), 214.7 (s, C^β), 287.2 (t, $^2J_{CP}$ = 17.2 Hz, C^α).

3b: Yield 170 mg (73%). − $C_{57}H_{73}BP_2Ru$ (932.0): calcd. C 73.5, H 7.89; found C 73.6, H 7.85. − IR (Nujol): $\tilde{\nu}$ = 1915 cm^{-1} ν(C=C=C). − ^1H NMR (400 MHz, CD_2Cl_2, 298 K): δ = 0.84−0.95, 1.01−1.09, and 1.13−1.18 [m, 24 H, PCH(CH_3)$_2$], 1.89 [s, 15 H, $C_5(CH_3)_5$], 1.97 (m, 4 H, PCH_2), 2.21 (m, 4 H, PCH), 7.36 (t, $^3J_{HH}$ = 8.3 Hz, 1 H, *p*-C_6H_5), 7.66 and 7.69 (m, 4 H, C_6H_5), 9.20 (br. s, 1 H, Ru=C=C=C*H*Ph). − $^{31}P\{^1H\}$ NMR (161.89 MHz, CD_2Cl_2, 298 K): δ = 88.3 (s). − $^{13}C\{^1H\}$ NMR (50.29 MHz, CD_2Cl_2, 298 K): δ = 11.36 [s, $C_5(CH_3)_5$], 18.41, 19.47, and 19.90 [s, PCH(CH_3)$_3$], 21.87 (vt, $^{1,3}J_{CP}$ = 20.1 Hz, PCH_2), 26.14 and 30.57 (m, PCH), 103.5 [s, $C_5(CH_3)_5$], 129.9, 130.4, 131.6, and 142.8 (s, C_6H_5), 139.3 (s, C^γ), 219.8 (s, C^β), 294.3 (t, $^2J_{CP}$ = 17.6 Hz, C^α).

4: Yield 163 mg (75%). − $C_{52}H_{71}BP_2Ru$ (870.0): calcd. C 71.8, H 8.23; found C 71.6, H 8.21. − IR (Nujol): $\tilde{\nu}$ = 1633 cm^{-1} ν(C=C). − ^1H NMR (400 MHz, $CDCl_3$, 298 K): δ = 0.93−1.19 [m, 24 H, PCH(CH_3)$_2$], 1.62 and 1.79 (m, 2 H each, PCH_2), 1.81 [s, 15 H, $C_5(CH_3)_5$], 1.99 and 2.16 (m, 2 H each, PCH), 4.88 (d, $^3J_{H^aH^b}$ = 17.0 Hz, 1 H, Ru=C=CH^a−CH^b = CH$^c_2$), 4.46 and 4.91 (d, $^3J_{H^bH^c}$ = 10.0 Hz, 1 H each, Ru=C=CH^a−CH^b = CH^c_2), 6.19 (dt, $^3J_{H^aH^b}$ = 17.0 Hz, $^3J_{HbHc}$ = 10.0 Hz, 1 H, Ru=C=CH^a−CH^b = CH$^c_2$). − $^{31}P\{^1H\}$ NMR (161.89 MHz, $CDCl_3$, 298 K): δ = 87.3 (s). − $^{13}C\{^1H\}$ NMR (50.29 MHz, $CDCl_3$, 298 K): δ = 11.00 [s, $C_5(CH_3)_5$], 18.35, 19.31, and 19.79 [s, PCH(CH_3)$_3$], 21.61 (vt, $^{1,3}J_{CP}$ = 18.8 Hz, PCH_2), 25.45 and 31.42 (m, PCH), 111.1 (s, C^β), 103.3 [s, $C_5(CH_3)_5$], 117.2 (s, Cδ), 121.4 (s, C^γ), 347.7 (t, $^2J_{CP}$ = 14.8 Hz, C^α).

Kinetics Studies of Alkynyl−Hydride to Vinylidene Isomerization: Solutions of the complex [Cp*Ru(η^2-H_2C=CH_2)(dippe)][BPh_4] were prepared in $CDCl_3$ under an inert gas in NMR tubes and were cooled to −80 °C in a liquid N_2/ethanol bath. An excess of the appropriate alkyne or alkynol was added and the tubes were kept at this temperature to arrest the isomerization process during transport and handling. A tube was then removed from the cooling bath and inserted into the precooled probe head of a Varian UNITY 400 spectrometer at 243 K. Once shims had been adjusted, the probe was warmed to 263 K to allow the in situ formation of the corresponding alkynyl(hydrido) complexes. After completion of this reaction, the temperature was raised to the desired level for study. The NMR temperature controller was previously calibrated against a methanol sample, the reproducibility being ± 0.5 °C. $^{31}P\{^1H\}$ NMR spectra were recorded at regular intervals for at least three half-lives using the spectrometer software for accurate time control. Peak intensities were analysed from stacked plots of the $^{31}P\{^1H\}$ NMR spectra. First-order rate constants were derived from the least-squares best-fit lines of the ln(intensity) versus time plots. The uncertainty in the isomerization rate constants represents one standard deviation (± σ) derived from the slope of the best-fit line. Uncertainties in the activation enthalpies and entropies were calculated from the uncertainties in the slope and intercept of the best-fit lines of the Eyring plots.

X-ray Structure Determination of [Cp*Ru(=C=C=CHPh)(dippe)][BPh$_4$] (3b): Empirical formula $C_{57}H_{73}BP_2Ru$, molecular mass 931.97, crystal size 0.30 × 0.30 × 0.14 mm, monoclinic, space group $P2_1/c$ (no. 14), a = 14.763(3) Å, b = 18.320(3) Å, c = 18.433(3) Å, β = 92.44(2) °, V = 4980(15) Å^3, Z = 4, $\rho_{calcd.}$ = 1.243 g cm^{-3}, T = 290(2) K, λ(Mo-$K_α$) = 0.71069 Å, graphite monochromator, μ(Mo-$K_α$) = 4.15 cm^{-1}, F(000) = 1976, transmission factor interval 0.76−1.00, scan speed (ω) 4° min^{-1}, 5.64° < 2θ < 50.12°, 7720 measured reflections, 7305 unique reflections, 4693 observed reflections [$I > 2\sigma(I)$], 550 parameters, reflection/parameter ratio 13.3. X-ray diffraction measurements were made on crystals of the appropriate size, which were mounted on a glass fibre and transferred to a Rigaku AFC6S automatic diffractometer. In each case, accurate unit cell parameters and an orientation matrix were determined by least-squares fitting from the settings of 25

high-angle reflections. Data were collected by the ω/2θ scan method. Decay was monitored by measuring three standard reflections every 100 measurements. Lorentz and polarization corrections were applied. Decay and semiempirical absorption corrections (ψ method) were also applied. The structure was solved by the Patterson method and subsequent expansion of the model using DIRDIF.[28] All calculations for data reduction and structure solution were carried out with a VAX 3520 computer at the Servicio Central de Ciencia y Tecnología de la Universidad de Cádiz, using the TEXSAN[29] software system. All hydrogen atoms were included at idealized positions and were allowed to ride on the parent carbon atoms. Full-matrix least-squares refinements were carried out by minimizing $\Sigma w(F_o^2 - F_c^2)^2$ with SHELXL-97,[30] concluding with the values $R1 = 0.0678$ and $wR2 = 0.1810$ for data having $I > 2\sigma(I)$. ORTEP[24] was used for plotting. Crystallographic data (excluding structure factors) for the structure reported in this paper have been deposited with the Cambridge Crystallographic Data Centre as supplementary publication no. CCDC-157842. Copies of the data can be obtained free of charge on application to the CCDC, 12 Union Road, Cambridge CB2 1EZ, U.K. [Fax: (internat.) + 44-1223/336-033; E-mail: deposit@ccdc.cam.ac.uk].

Acknowledgments

We wish to thank the Ministerio de Educación y Cultura of Spain (DGICYT, Project PB97-1357) and the Junta de Andalucía (PAI − FQM 0188) for financial support. We also thank Johnson Matthey plc for including us in their precious metal loan scheme, and the Royal Society of Chemistry for the award of a grant for International Authors (to M. J. T.).

[1] M. I. Bruce, *Chem. Rev.* **1991**, *91*, 197.
[2] M. I. Bruce, *Chem. Rev.* **1998**, *98*, 2798.
[3] H. Werner, *Chem. Commun.* **1997**, 903.
[4] D. Touchard, P. Dixneuf, *Coord. Chem. Rev.* **1998**, 178−180, 409.
[5] C. Bruneau, P. H. Dixneuf, *Acc. Chem. Res.* **1999**, *32*, 311; M. C. Puerta, P. Valerga, *Coord. Chem. Rev.* **1999**, *193−195*, 977−1025 and references therein.
[6] A. N. Nesmeyanov, G. G. Aleksandrov, A. B. Antonova, K. N. Anisimov, N. E. Kolobova, Y. T. Struchkov, *J. Organomet. Chem.* **1976**, *110*, C36; A. B. Antonova, N. E. Kolobova, P. V. Petrovsky, B. V. Lokshin, N. S. Obezyuk, *Organometallics* **1994**, *13*, 1089.
[7] [7a] [Co]: C. Bianchini, M. Peruzzini, A. Vacca, F. Zanobini, *Organometallics* **1991**, *10*, 3697. − [7b] [Rh]: T. Rappert, O. Nürnberg, N. Mahr, J. Wolf, H. Werner, *Organometallics* **1992**, *11*, 4156; H. Werner, M. Baum, D. Schneider, B. Windmüller, *Organometallics* **1994**, *13*, 1089. H. Werner, T. Rappert, R. Wiedemann, J. Wolf, N. Mahr, *Organometallics* **1994**, *13*, 2721; C. Bianchini, D. Masi, A. Meli, M. Peruzzini, J. A. Ramírez, A. Vacca, F. Zanobini, *Organometallics* **1989**, *8*, 2179. − [7c] [Ir]: F. J. García Alonso, A. Höhn, J. Wolf, H. Otto, H. Werner, *Angew. Chem. Int. Ed. Engl.* **1985**, *24*, 406; A. Höhn, H. Otto, M. Dziallas, H. Werner, *J. Chem. Soc., Chem. Commun.* **1987**, 852; A. Höhn, H. Werner, *J. Organomet. Chem.* **1990**, *382*, 255; H. Werner, A. Höhn, M. Schluz, *J. Chem. Soc., Dalton Trans.* **1991**, 777; H. Werner, R. W. Lass, O. Gevert, J. Wolf, *Organometallics* **1997**, *16*, 4077.
[8] Y. Wakatsuki, N. Koga, H. Werner, K. Morokuma, *J. Am. Chem. Soc.* **1997**, *119*, 360; E. Pérez-Carreño, P. Paoli, A. Ienco, C. Mealli, *Eur. J. Inorg. Chem.* **1999**, *8*, 1315.
[9] Y. Wakatsuki, N. Koga, H. Yamazaki, K. Morokuma, *J. Am. Chem. Soc.* **1994**, *116*, 8105.
[10] J. Silvestre, R. Hoffmann, *Helv. Chim. Acta* **1985**, *68*, 1461.
[11] M. I. Bruce, A. G. Swincer, *Adv. Organomet. Chem.* **1983**, *22*, 59; S. G. Davies, J. P. McNally, A. J. Smallridge, *Adv. Organomet. Chem.* **1990**, *30*, 1.
[12] M. A. Esteruelas, A. M. López, N. Ruiz, J. I. Tolosa, *Organometallics* **1997**, *16*, 4657; P. Crochet, M. A. Esteruelas, A. M. López, N. Ruiz, J. I. Tolosa, *Organometallics* **1998**, *17*, 3479.
[13] M. Baya, P. Crochet, M. A. Esteruelas, E. Gutiérrez-Puebla, A. M. López, J. Modrego, E. Oñate, N. Vela, *Organometallics* **2000**, *19*, 2585.
[14] R. M. Bullock, *J. Chem. Soc., Chem. Commun.* **1989**, 165; J. R. Lomprey, J. P. Selegue, *J. Am. Chem. Soc.* **1992**, *114*, 5518; M. Martín, O. Gevert, H. Werner, *J. Chem. Soc., Dalton Trans.* **1996**, 2275; C. Bianchini, P. Innocenti, M. Peruzzini, A. Romerosa, F. Zanobini, *Organometallics* **1996**, *15*, 272; J. Y. Shen, C. Slugovc, P. Wiede, K. Mereiter, R. Schmid, K. Kirchner, *Inorg. Chim. Acta* **1998**, *268*, 69.
[15] M. P. Gamasa, J. Gimeno, C. González-Bernardo, J. Borge, S. García-Granda, *Organometallics* **1997**, *16*, 2483; P. Nombel, N. Lugan, R. Mathieu, *J. Organomet. Chem.* **1995**, *503*, C22; C. Gemel, J. C. Huffman, K. G. Caulton, K. Mauthner, K. Kirchner, *J. Organomet. Chem.* **2000**, *593−594*, 342.
[16] C. Slugovc, V. N. Sapunov, P. Wiede, K. Mereiter, R. Schmid, K. Kirchner, *J. Chem. Soc., Dalton Trans.* **1997**, 4209; V. Cadierno, M. P. Gamasa, J. Gimeno, E. Pérez-Carreño, S. García-Granda, *Organometallics* **1999**, *18*, 2821.
[17] [17a] R. Le Lagadec, E. Román, L. Toupet, U. Müller, P. Dixneuf, *Organometallics* **1994**, *13*, 5030. − [17b] T. Braun, P. Steinert, H. Werner, *J. Organomet. Chem.* **1995**, *488*, 169; M. I. Bruce, B. C. Hall, N. N. Zaitseva, B. W. Skelton, A. H. White, *J. Chem. Soc., Dalton Trans.* **1998**, 1793.
[18] I. de los Ríos, M. Jiménez Tenorio, M. C. Puerta, P. Valerga, *J. Chem. Soc., Chem. Commun.* **1995**, 1757.
[19] I. de los Ríos, M. Jiménez Tenorio, M. C. Puerta, P. Valerga, *J. Am. Chem. Soc.* **1997**, *119*, 6529.
[20] I. de los Ríos, M. Jiménez Tenorio, M. C. Puerta, P. Valerga, *J. Organomet. Chem.* **1997**, *549*, 221.
[21] E. Bustelo, M. Jiménez Tenorio, M. C. Puerta, P. Valerga, *Organometallics* **1999**, *18*, 950; E. Bustelo, M. Jiménez Tenorio, M. C. Puerta, P. Valerga, *Organometallics* **1999**, *18*, 4563.
[22] V. Cadierno, M. P. Gamasa, J. Gimeno, M. González-Cueva, E. Lastra, J. Borge, S. García-Granda, E. Pérez-Carreño, *Organometallics* **1996**, *15*, 2137.
[23] I. de los Ríos, M. Jiménez Tenorio, J. Padilla, M. C. Puerta, P. Valerga, *Organometallics* **1996**, *15*, 4565.
[24] C. K. Johnson, *ORTEP, A Thermal Ellipsoid Plotting Program*, Oak Ridge National Laboratory, Oak Ridge, TN, **1965**.
[25] D. Touchard, N. Pirio, P. H. Dixneuf, *Organometallics* **1995**, *14*, 4920.
[26] B. E. R. Schelling, R. Hoffmann, D. L. Lichtenberger, *J. Am. Chem. Soc.* **1977**, *101*, 585.
[27] I. de los Ríos, M. Jiménez Tenorio, J. Padilla, M. C. Puerta, P. Valerga, *J. Chem. Soc., Dalton Trans.* **1996**, 377.
[28] P. T. Beurskens, *DIRDIF*, Technical Report 1984/1, Crystallography Laboratory, Toernooiveld, The Netherlands, **1984**.
[29] *TEXSAN, Single-Crystal Structure Analysis Software*, version 5.0, Molecular Structure Corp., Houston, TX, **1989**.
[30] G. M. Sheldrick, *SHELXL-97*, University of Göttingen, **1997**.

Received February 16, 2001
[I01053]

Chemistry at the Sterically Shielded Mercury Centre of the [(η^4-pp3)PtHg] Fragment

Walter Schuh,[a] Holger Kopacka,[a] Klaus Wurst,[a] and Paul Peringer*[a]

Keywords: Mercury / Platinum / Cluster compounds / Phosphanes / NMR spectroscopy

Treatment of [(η^4-pp3)PtH]OTf (pp3 = tris[2-(diphenylphosphanyl)ethyl]phosphane) with PhHgCl gave [(η^4-pp3)PtHgCl]OTf (**1a**) in good yield. The reaction of **1a** with the carbonylmetallates $[Mn(CO)_5]^-$ or $[Co(CO)_4]^-$ and TlOTf produced the linear trinuclear clusters [(η^4-pp3)PtHgMn(CO)$_5$]OTf (**2**) or [(η^4-pp3)PtHgCo(CO)$_4$]OTf (**3**), respectively. The reaction of **1a** with PR_3 and TlOTf gave [(η^4-pp3)PtHg(PR_3)](OTf)$_2$ (**4**: R = *n*Bu; **5**: R = Ph), with $Ph_2P(CH_2)_nPPh_2$ (*n* = 1, 2) or dppmSe [dppmSe = bis(diphenylphosphanyl)methane monoselenide] adducts in which the diphosphane/diphosphane monoselenide adopts a monodentate, bridging or chelating bonding mode depending on the ligand and the stoichiometry. The mercury-bound phosphane complexes extrude elemental Hg within hours or days. The new compounds were characterised by multinuclear NMR spectroscopy and, in part, by single-crystal X-ray diffraction. The NMR investigations yielded unprecedented parameters, e.g. very large ^{31}P coordination chemical shift for a monodentate phosphane or ^2J(Hg–Pt–P) couplings that were two to three times larger than Hg–P one-bond couplings within the same complex.

Introduction

Clusters containing an unsupported mercury−platinum bond tend to extrude elemental mercury.[1] The noticeable stability of the Pt−Hg bond in [(η^4-pp3)PtHgPh]OTf[2] and the closely related compound [(η^4-np3)PtHgMe](BPh$_4$)[3] (np3 = tris[2-(diphenylphosphanyl)ethyl]amine) has been attributed to the shield of the six phenyl groups of the pp3 or np3 ligand. This stimulated an investigation of the chemistry of the [(η^4-pp3)PtHg] fragment. We report here on a comfortable and high-yielding access to [(η^4-pp3)PtHgCl]OTf (**1a**), which is an appropriate compound for substitution reactions with carbonylmetallates, mono- and bidentate phosphanes, or phosphane selenides at the mercury site.

2. Results and Discussion

2.1. Syntheses and Reactions

We observed that [(η^4-pp3)PtHgPh]OTf slowly degrades in chloroform solution to give [(η^4-pp3)PtHgCl]OTf (**1a**), attributable to the presence of trace amounts of HCl in $CHCl_3$, which cleave the mercury−carbon bond and leads to the substitution of the phenyl group by chloride. This was exploited in a comfortable high-yield synthesis of **1a** by treatment of [(η^4-pp3)PtH]OTf with PhHgCl according to Scheme 1: The reaction is thought to proceed by intermediate formation of [(η^4-pp3)PtHgPh]$^+$, which is in turn acidolysed by HCl formed in stoichiometric amounts.

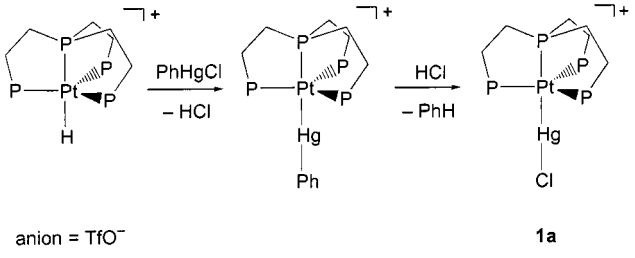

Scheme 1. Proposed synthetic pathway for **1a**

In the presence of excess chloride, **1a** slowly degrades by extrusion of elemental mercury to [(η^4-pp3)PtCl]Cl.[4] Compound **1a** is air-stable in solution and in the solid state, readily soluble in CH_2Cl_2, slightly soluble in MeOH, and was isolated as a yellow microcrystalline powder from CH_2Cl_2/toluene. Compound **1a** was characterised by ^{31}P, ^{195}Pt and ^{199}Hg NMR spectroscopy. Yellow crystals of [(η^4-pp3)PtHgCl](PF$_6$)·CH_2Cl_2 (**1b**·CH_2Cl_2), which were suitable for single-crystal X-ray diffraction, were obtained by slow diffusion of a methanolic solution of NH_4PF_6 into a CH_2Cl_2 solution of **1a**. The reaction of **1a** with the carbonylmetallates $[Mn(CO)_5]^-$ or $[Co(CO)_4]^-$ in THF and subsequent treatment with TlOTf gave the linear heterotrinuclear clusters [(η^4-pp3)PtHgMn(CO)$_5$]OTf (**2**) and [(η^4-pp3)PtHgCo(CO)$_4$]OTf (**3**) (Scheme 2). Both were characterised by multinuclear NMR and elemental analysis, **2** in addition by single-crystal X-ray diffraction. There are only three reports on complexes with a Pt−Hg−Mn or Pt−Hg−Co bond sequence in the literature,[5] the compounds were characterised by spectroscopic methods, no single crystal structure determinations had been performed.

[a] Institut für Allgemeine, Anorganische und Theoretische Chemie, Universität Innsbruck,
Innrain 52a, 6020 Innsbruck, Austria
E-mail: paul.peringer@uibk.ac.at

 © WILEY-VCH Verlag GmbH, 69451 Weinheim, 2001 1434−1948/01/0909−2399 $ 17.50+.50/0

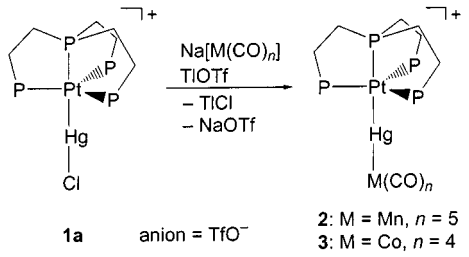

Scheme 2. Synthesis of **2** and **3**

Treatment of **1a** with the monodentate phosphanes P*n*Bu$_3$ and PPh$_3$ in the presence of TlOTf led quantitatively (according to ^{31}P NMR) to the complexes [(η^4-pp3)PtHg(PR$_3$)](OTf)$_2$ (**4**: R = *n*Bu; **5**: R = Ph) as depicted in Scheme 3.

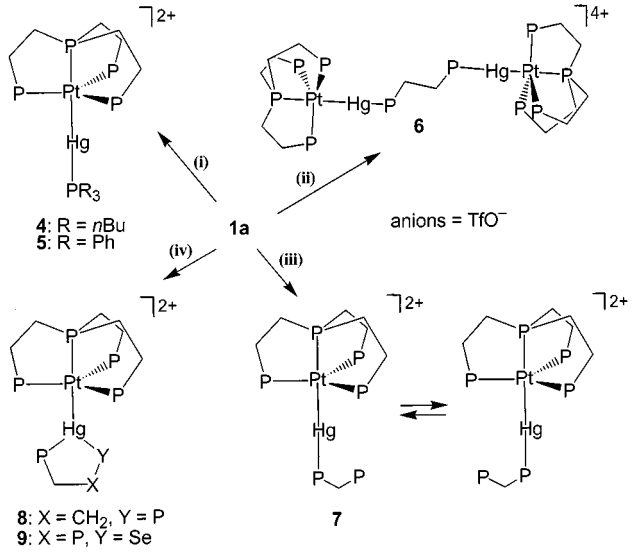

Scheme 3. (i) TlOTf/PR$_3$; (ii) TlOTf/0.5 dppe; (iii) TlOTf/dppm; (iv) TlOTf/dppe (**8**) or TlOTf/dppmSe (**9**)

Since the complexes decompose very rapidly in the presence of halides, TlOTf was used as a chloride scavenger. In the absence of phosphanes, TlOTf is not able to abstract the chloride ligand from **1a**. This was, however, accomplished by AgOTf, but the presumptive product [(η^4-pp3)PtHg](OTf)$_2$ immediately extruded elemental mercury. The phosphane complexes **4** and **5** decomposed within 1 d − in the presence of chloride or excess phosphane within hours − into elemental mercury and [(η^4-pp3)-Pt(PR$_3$)](OTf)$_2$, which were identified according to their ^{31}P NMR spectroscopic data.[6,7] Hence, **4** and **5** as well as the other phosphane derivatives described below could not be isolated in the solid state. The use of P(OMe)$_3$ or P(H)Ph$_2$ instead of PR$_3$ according to Scheme 3 immediately produced elemental mercury and the mononuclear platinum complexes [(η^4-pp3)Pt{P(H)Ph$_2$}](OTf)$_2$ or [(η^4-pp3)Pt{P(OMe)$_3$}](OTf)$_2$, respectively, identified by their ^{31}P NMR spectroscopic data.[8,9]

The products of the reaction of **1a** with 0.5 equiv. of Ph$_2$P(CH$_2$)$_n$PPh$_2$ in the presence of TlOTf depends on *n*: Whereas dppe (*n* = 2) gives the phosphane-bridged tetranuclear complex [(η^4-pp3)PtHg(μ-dppe)HgPt(η^4-pp3)]-(OTf)$_4$ (**6**) shown in Scheme 3, dppm (*n* = 1) reacts, presumably because of steric reasons, with only 0.5 equiv. of **1a** to give the complex [(η^4-pp3)PtHg(η^1-dppm)](OTf)$_2$ (**7**) containing monodentate dppm. Complex **7** shows a fluxional behaviour in solution, monitored by variable-temperature ^{31}P NMR spectroscopy (see below), which can be interpreted as an intramolecular end-over-end exchange between the mercury-bound and the free-dppm phosphorus atom. Compound **7** can be synthetised quantitatively (according to ^{31}P NMR spectroscopy) by treating **1a** with dppm in a molar ratio of 1:1 (Scheme 3).

The potential for mercury to increase its coordination number in the fragment [(η^4-pp3)PtHg] can be seen from the reaction of **1a** with dppe or dppmSe in a molar ratio of 1:1. As indicated in Scheme 3, we propose a chelate bonding mode of dppe and dppmSe (according to ^{31}P NMR spectroscopic results) in the complexes [(η^4-pp3)PtHg(η^2-dppe)](OTf)$_2$ (**8**) and [(η^4-pp3)PtHg(η^2-dppmSe)](OTf)$_2$ (**9**), resulting in a tricoordinate mercury centrer that is part of a five-membered ring system.

2.2. NMR Spectroscopy

The NMR parameters of compounds **1**−**9** are collected in Tables 1 and 2. In the Tables and the subsequent discussion, the axial phosphorus atom of the platinum-bound pp3 ligand is designated as P^a, while P^e denotes the equatorial pp3 phosphorus atoms. P^3 denotes the mercury-bound phosphorus atom(s), and all other phosphorus atoms are designated as P^4.

Table 1. NMR parameters of the compounds **1a**, **2** and **3** in CH_2Cl_2

	1a	**2**	**3**
δ(P^a)	142.5	162.9	146.6
J(P^{a}P^e)	2	5	not resolved
J(PtP^a)	2100	1977	2032
J(HgP^a)	3538	2006	2692
δ(P^e)	36.4	38.9	39.9
J(PtP^e)	2635	2889	2773
J(HgP^e)	412	251	299
δ(Pt)	−5577	−5188	−5292
J(HgPt)	11010	6200	8035
δ(Hg)	910	2017	1370

The one-bond Hg−Pt coupling of the linear bond sequence Pt−Hg−X is thought to give an estimate of the *trans* influence of the group X, as has been extensively exploited for linear P−Pt−X or P−Hg−X arrangements.[10] According to Table 1 this reveals a greater *trans* influence of the Mn(CO)$_5$ fragment compared with Co(CO)$_4$, the smallest *trans* influence in the present series is exerted by the chloride ligand. One-bond Hg−Pt couplings reported in the literature range between 37610 and 2783 Hz.[2,3,11] The size of ^{1}*J*(PtP^a) and ^{2}*J*(HgP^a) couplings of **1a**−**3** show a similar dependence on the ligand attached to the mercury centre. The diagonal P^a−Pt−Hg geometry effects very large two-bond Hg−P^a couplings. This is also true for compounds **4**−**9** (see below), and has been previously noted for

Table 2. NMR parameters of the compounds **4**−**9** in CH_2Cl_2/MeOH (4:1)

	4 (T = 0 °C)	**5** (T = −40 °C)	**6** (T = −60 °C)	**7** (T = −30 °C)	**8** (T = −40 °C)	**9**[a] (T = 20 °C)
δ(P^a)	150.5	149.3	148.1	154.0	146.5	148.2
$J(P^aP^e)$	not resolved	not resolved	not resolved	not resolved	not resolved	not resolved
$J(P^aP^3)$	191	193	196	93	100	165
$J(PtP^a)$	1961	2020	2017	2010	1997	2063
$J(HgP^a)$	2726	2869	3171	2900	3362	3539
δ(P^e)	36.9	41.2	38.7	41.0	36.2	36.0
$J(P^eP^3)$	10	9	9	not resolved	not resolved	6
$J(PtP^e)$	2672	2627	2650	2656	2678	2669
$J(HgP^e)$	307	343	352	294	373	364
δ(P^3)	87.5	87.3	84.8	33.1	36.0	55.9
$J(PtP^3)$	577	605	604	292	279	494
$J(HgP^3)$	902	1290	1484	554	1265	1248
$J(P^3P^{3\prime})/(P^3P^4)$	−	−	64	−	−	43
δ(P^4)	−	−	−	−	−	34.0

[a] **9**: δ(Se) = −203, J(HgSe) = 842, $J(SeP^4)$ = 672; δ(Pt) = −5526, δ(Hg) = 1598.

[(η⁴-pp3)PtHgPh]OTf.[2] Even larger ^2J(HgP) coupling constants have been observed in Hg−Ir clusters (3879−3822 Hz).[12]

The tetranuclear complex **6** displays an $[AM_3P]_2$ spin system, the ^{199}Hg and ^{195}Pt satellites show an $AA'M_3M'_3PP'X$ pattern. This reflects the dppe-bridged structure of **6**. The values of $^1J(HgP^3)$ are 1484−902 Hz, revealing a strong *trans* influence of the [(η⁴-pp3)Pt] moiety. There are only few reports on compounds exhibiting a M−Hg−P bond sequence (M = transition metal),[11c,13] and the ^1J(HgP) couplings in these clusters are comparatively small as well (2483−170 Hz).

Compounds **7** and **8** exhibit an AM_3P_2 spin system flanked by ^{199}Hg and ^{195}Pt satellites at temperatures given in Table 2. The bonding modes of the bidentate phosphanes dppm and dppe in these complexes are monodentate and chelating, respectively.

The dppm ligand in **7** is involved in an end-over-end exchange that is fast on the NMR time scale at −30 °C. End-over-end fluxionality is also present in other mercury−dppm complexes.[14] The slow exchange limit is not reached at −100 °C, the lowest temperature attained. However, significant broadening of the P^3 signal in comparison with the other ^{31}P resonances of **7** is observed at this temperature. All couplings involving P^3 as well as its chemical shift given in Table 2 may be considered as mean values of the parameters for the mercury-bound and the free-dppm phosphorus atom. The fluxionality at −30 °C is responsible for the relatively small values of these parameters compared with compounds **4**−**6**. The preference of the monodentate bonding mode of dppm in **7** over a chelate structure is attributed to considerable strain in four-membered Hg−dppm rings.

The structure of **8** is based on the value of the one-bond Hg−P^3 coupling of 1265 Hz, which is comparable to the couplings observed for compounds **4**−**6**. No significant broadening of the P^3 signal in comparison with the other ^{31}P resonances could be observed down to −100 °C. The relatively small values of δ(P^3), $^2J(PtP^3)$, and $^3J(P^aP^3)$ are attributed to a nonlinear Pt−Hg−P^3 geometry as a consequence of the increased coordination number at the Hg atom. This is in keeping with the data of **9**.

Compound **9** involving the potentially bidentate ligand dppmSe shows an AM_3PX spin system in the $^{31}P\{^1H\}$ NMR spectrum flanked by ^{199}Hg, ^{195}Pt, and ^{77}Se satellites. The value for Hg−P^3 coupling approximately coincides with that found for **8**, revealing an Hg−P^3 bond. The coordination of the selenium atom to the mercury centre is inferred by an Hg−Se coupling of 842 Hz compared with a range for ^1J(HgSe) couplings of 960−750 Hz.[15] The reduced value of $^1J(SeP^4)$ with respect to the free ligand is also indicative for the coordination of Se.[15] Due to the value of $^2J(PtP^3)$ (494 Hz) ranging between that found in **6**, with an essentially linear Pt−Hg−P geometry, and **8**, with a symmetrically bent Pt−Hg−P arrangement, we suppose an asymmetric coordination geometry around the Hg atom in **9**, where P^3 is shifted towards the Pt−Hg vector and Se is consequently shifted away. The magnitude of $^3J(P^aP^3)$ (165 Hz) is in agreement with this presumption. A related angular dependence for two-bond P−Hg−P coupling constants has been pointed out by Dakternieks.[16] The asymmetric bonding of P^3 and Se in **9** is thought to be caused by steric demands.

The most exciting feature of compounds **4**−**6**, **8**, and **9** is that the Hg−P^a coupling constants over two bonds are larger by a factor of two to three than the corresponding $^1J(HgP^3)$ couplings within the same molecule (compound **7** has not been considered in this context, because Hg−P one-bond couplings are not accessible due to chemical exchange). This observation implies that care should be taken for the assignment of connectivities in mercury-containing clusters on the basis of the magnitudes of Hg−P coupling constants.

Complexes **4**−**6**, for which an essentially linear Pt−Hg−P^3 arrangement is anticipated, are characterised by very large ^{31}P shifts of the mercury-coordinated phosphorus atom. The corresponding coordination shifts (Δδ) amount up to +120 ppm in compound **4**. Slightly lower

values were found for the mercury-bound phosphanes in the compounds $[L'HgMo(CO)_2L(\eta^5\text{-}C_5H_5)](BF_4)$ (L' = PPh_3, PCy_3; L = CO, diverse phosphane ligands),[13a] where the mercury atom is dicoordinated by Mo and P.

2.3. Crystallography

Yellow crystals of $[(\eta^4\text{-pp3})PtHgCl](PF_6)\cdot CH_2Cl_2$ (**1b**·CH_2Cl_2) were grown by slow diffusion of a methanolic solution of NH_4PF_6 into a CH_2Cl_2 solution of $[(\eta^4\text{-pp3})PtHgCl]OTf$. The molecular structure of the complex cation of **1b** is shown in Figure 1, selected bond lengths and angles are collected in Table 3.

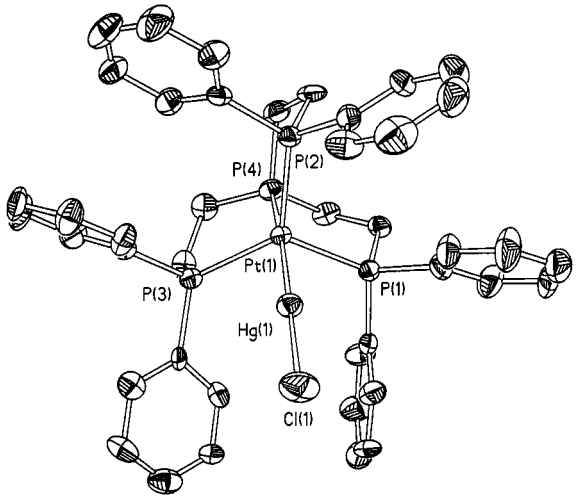

Figure 1. Molecular structure of the complex cation of **1b**·CH_2Cl_2

Table 3. Selected bond lengths [pm] and angles [°] in **1b**·CH_2Cl_2

Hg(1)−Cl(1)	237.7(2)	Cl(1)−Hg(1)−Pt(1)	174.63(7)
Hg(1)−Pt(1)	255.11(9)	P(4)−Pt(1)−Hg(1)	172.96(6)
Pt(1)−P(4)	224.3(2)	P(3)−Pt(1)−Hg(1)	89.11(6)
Pt(1)−P(3)	230.9(2)	P(1)−Pt(1)−Hg(1)	90.80(6)
Pt(1)−P(1)	233.4(2)	P(2)−Pt(1)−Hg(1)	100.98(6)
Pt(1)−P(2)	235.1(2)		

The platinum atom of the complex cation of **1b** exhibits a quasi-trigonal-bipyramidal coordination sphere with the central pp3 phosphorus atom and the mercury centre in axial positions and the three terminal pp3 phosphorus ligands in equatorial positions. The mercury atom is dicoordinated by Pt and Cl in an approximately linear manner. The Pt−Hg distance is very similar to that found in $[(\eta^4\text{-np3})PtHgMe](BPh_4)$ (253.1 pm),[3] the Hg−Cl bond length is slightly increased compared to that in $HgCl_2$ (225 pm).[17]

The Pt−Hg−Cl angle amounts to 174.63(7)° in keeping with the absence of any Hg···Cl interactions with chloride ions of other cations. This is most likely the result of the steric shielding of the phenyl groups of the pp3 ligand and/or the poor acceptor qualities of the mercury centre.

Yellow crystals of $[(\eta^4\text{-pp3})PtHgMn(CO)_5]OTf\cdot 1.5\ CH_2Cl_2$ (**2**·1.5 CH_2Cl_2) were obtained at −19 °C from a solution of **2** in MeOH/CH_2Cl_2 (1:1) saturated at room temperature. The crystals contain two crystallographically independent $[(\eta^4\text{-pp3})PtHgMn(CO)_5]OTf$ entities per asymmetric unit both possessing very similar geometries. The molecular structure of one of the crystallographically independent complex cations of **2** is shown in Figure 2, selected bond lengths and angles are collected in Table 4.

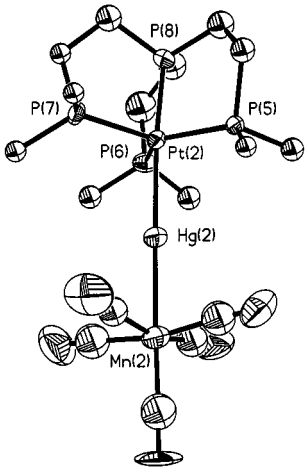

Figure 2. Molecular structure of one of the crystallographically independent complex cations in **2**·1.5 CH_2Cl_2; for clarity only the *ipso*-carbon atoms of the phenyl groups attached to the pp3 phosphorus atoms are shown

Table 4. Selected bond lengths [pm] and angles [°] in **2**·1.5CH_2Cl_2

Hg(1)−Pt(1)	260.5(2)	P(3)−Pt(1)−Hg(1)	95.0(2)
Hg(1)−Mn(1)	264.7(5)	P(1)−Pt(1)−Hg(1)	93.1(2)
Hg(2)−Pt(2)	259.0(2)	P(8)−Pt(2)−Hg(2)	175.1(2)
Hg(2)−Mn(2)	261.8(4)	P(6)−Pt(2)−Hg(2)	93.5(2)
Pt(1)−P(4)	223.6(7)	P(5)−Pt(2)−Hg(2)	89.1(2)
Pt(1)−P(2)	231.5(7)	P(7)−Pt(2)−Hg(2)	97.3(2)
Pt(1)−P(3)	233.3(7)	C(4)−Mn(1)−Hg(1)	84(2)
Pt(1)−P(1)	233.5(7)	C(1)−Mn(1)−Hg(1)	84.4(13)
Pt(2)−P(8)	224.4(7)	C(5)−Mn(1)−Hg(1)	176.4(11)
Pt(2)−P(6)	229.7(7)	C(2)−Mn(1)−Hg(1)	83.7(13)
Pt(2)−P(5)	230.5(7)	C(3)−Mn(1)−Hg(1)	84(2)
Pt(2)−P(7)	232.5(6)	C(7)−Mn(2)−Hg(2)	79.5(10)
Pt(1)−Hg(1)−Mn(1)	178.96(14)	C(8)−Mn(2)−Hg(2)	84.4(11)
Pt(2)−Hg(2)−Mn(2)	176.12(12)	C(9)−Mn(2)−Hg(2)	82.7(9)
P(4)−Pt(1)−Hg(1)	177.7(2)	C(10)−Mn(2)−Hg(2)	178.2(11)
P(2)−Pt(1)−Hg(1)	91.7(2)	C(6)−Mn(2)−Hg(2)	84.4(11)

The platinum atom of the complex cation of **2** exhibits a quasi-trigonal-bipyramidal coordination sphere, with the central pp3 phosphorus atom and Hg in axial positions and the three terminal pp3 phosphorus ligands in equatorial positions. The mercury atom is dicoordinated by Pt and Mn in an approximately linear manner, Mn showing a slightly distorted octahedral environment. The Pt−Hg distances are slightly longer than in **1b**, the Hg−Mn bond lengths are increased in comparison with the compounds $[\{\eta^2\text{-}(2\text{-}ClC_6H_4)_2N_3\}HgMn(CO)_5]$ (255.7 pm)[18] and $[Hg\{Mn(CO)_5\}_2]$ (260.8, 261.0 pm).[19]

Experimental Section

Elemental analyses were performed by the Institut für Physikalische Chemie, Universität Wien. − $^{31}P\{^1H\}$ NMR spectra were re-

corded at variable temperatures (if not otherwise stated at 20 °C) with a Bruker DPX 300 spectrometer, and were referenced against external 85% H_3PO_4. $^{199}Hg\{^1H\}$, $^{195}Pt\{^1H\}$, and $^{77}Se\{^1H\}$ NMR spectra were recorded at 20 °C with the same instrument and referenced against external 2 mmol HgO in 1 mL of 60% $HClO_4$, 1 mol/l Na_2PtCl_6 and neat $SeMe_2$, respectively. Compound [(η⁴-pp3)PtCl]Cl[4] and solutions of $Na[Mn(CO)_5]$ and $Na[Co(CO)_4]$ in THF[20] were prepared according to literature procedures, all other compounds were purchased from commercial suppliers and used without further purification. If not stated otherwise, all reactions were carried out under an inert gas in absolute solvents purified by standard procedures.

[(η⁴-pp3)PtHgCl]OTf (1a): A suspension of [(η⁴-pp3)PtCl]Cl (936.7 mg, 1 mmol) in CH_2Cl_2/MeOH 4:1 (25 mL) was treated with $NaBH_4$ (113.4 mg, 3 mmol), which was added under vigorous stirring in small portions over a period of 10 min. The resulting pale yellow solution was stirred for 1 h. The organic phase was washed four times with water (10 mL). This represents a slightly modified synthesis of [(η⁴-pp3)PtH]Cl to that reported by Brüggeller.[21] [(η⁴-pp3)PtH]Cl was then treated with a solution of TlOTf (353.4 mg, 1 mmol) in MeOH (2 mL), and [(η⁴-pp3)PtH]OTf formed by anion metathesis and precipitation of TlCl. The precipitate was separated by centrifugation, the pale yellow solution was concentrated to dryness in vacuo. The residue was redissolved in 20 mL of CH_2Cl_2, then treated with PhHgCl (313.2 mg, 1 mmol) and stirred for 24 h. After filtration, the clear yellow solution was concentrated to a volume of ca. 2 mL, then [(η⁴-pp3)PtHgCl]OTf (**1a**) was precipitated by addition of toluene (20 mL). The product was separated by centrifugation and dried in vacuo. Yield: 1.08 g (89%).

[(η⁴-pp3)PtHgCl](PF₆)·CH₂Cl₂ (1b): Yellow crystals were grown by slow diffusion of a methanolic solution of NH_4PF_6 into a CH_2Cl_2 solution of [(η⁴-pp3)PtHgCl]OTf. − $C_{43}H_{42}ClF_6HgP_5Pt{\cdot}CH_2Cl_2$ (1258.8): calcd. C 39.33, H 3.30; found C 39.05, H 3.25.

[(η⁴-pp3)PtHgMn(CO)₅]OTf (2): A solution of $Na[Mn(CO)_5]$ (0.05 mmol) in THF (0.25 mL) was added to **1a** (62.5 mg, 0.05 mmol) and stirred for 5 min. After evaporation of the solvent, the residue was redissolved in CH_2Cl_2 (0.5 mL) and treated with a solution of TlOTf (17.7 mg, 0.05 mmol) in MeOH (0.2 mL). The resulting precipitate of TlCl was removed by centrifugation and the clear orange solution was concentrated until precipitation of [(η⁴-pp3)PtHgMn(CO)₅]OTf (**2**) began. A small amount of CH_2Cl_2 was added to redissolve the precipitate and the solution left for crystallisation at −19° C for 2 d. Yield: 30 mg (43%). − $C_{48}H_{42}F_3HgMnO_8P_4PtS$ (1410.4): calcd. C 40.88, H 3.00; found C 40.47, H 2.87.

[(η⁴-pp3)PtHgCo(CO)₄]OTf (3): A solution of $Na[Co(CO)_4]$ (0.05 mmol) in THF (0.25 mL) was added to **1a** (62.5 mg, 0.05 mmol) and stirred for 5 min. After evaporation of the solvent, the residue was redissolved in CH_2Cl_2 (0.5 mL) and treated with a solution of TlOTf (17.7 mg, 0.05 mmol) in MeOH (0.2 mL). The resulting precipitate of TlCl was removed by centrifugation and the clear yellow solution washed two times with 1 mL of water. The solvent was then evaporated, the residue dissolved in CH_2Cl_2 (0.2 mL) and the product precipitated by addition of petroleum ether (60−70 °C) (2 mL). The yellow precipitate was collected by centrifugation and dried in vacuo. Yield: 52 mg (76%). − $C_{47}H_{42}CoF_3HgO_7P_4PtS$ (1386.4): calcd. C 40.72, H 3.05; found C 40.78, H 2.95.

Table 5. Crystal data and structure refinement for **1b**·CH_2Cl_2 and **2**·1.5CH_2Cl_2.

	1b·CH_2Cl_2	**2**·1.5CH_2Cl_2
Empirical formula	$C_{42}H_{42}ClF_6HgP_5Pt{\cdot}CH_2Cl_2$	$C_{48}H_{42}F_3HgMnO_8P_4PtS{\cdot}1.5CH_2Cl_2$
Molecular mass	1331.66	1537.76
Crystal system	monoclinic	monoclinic
Space group	$P2_1/n$ (no.14)	$P2_1/c$ (no.14)
Unit cell dimensions	a = 1928.8(3) pm	a = 1943.7(4) pm
	b = 1406.8(2) pm, β = 119.00(2)°	b = 3220.1(6) pm, β = 94.44(2)°
	c = 1950.5(4) pm	c = 1741.1(4) pm
Volume	4.6290(14) nm³	10.865(4) nm³
Z	4	8
Temperature	213(2) K	218(2) K
Density (calculated)	1.911 Mg/m³	1.880 Mg/m³
Absorption coefficient	6.733 mm⁻¹	5.982 mm⁻¹
F(000)	2560	5944
Color, Habit	yellow prism	yellow prism
Crystal size	0.65 × 0.35 × 0.35 mm	0.5 × 0.3 × 0.25 mm
θ range for data collection	2.53−23.00°	2.07−19.50°
Index ranges	$0 < h < 19$, $0 < k < 15$, $-20 < l < 19$	$-18 < h < 18$, $-30 < k < 0$, $0 < l < 14$
Reflections collected	6076	8512
Independent reflections	5860 (R_{int} = 0.0341)	8465 (R_{int} = 0.0645)
Reflections with $I > 2\sigma(I)$	4815	5162
Max./min. transmission	1.000/0.710	0.876/0.575
Data/restraints/parameters	5598/0/532	7260/0/793
Goodness-of-fit on F^2	1.064	1.038
Final R indices [$I > 2\sigma(I)$]	$R1$ = 0.0344, $wR2$ = 0.0757	$R1$ = 0.0613, $wR2$ = 0.1176
R indices (all data)	$R1$ = 0.0507, $wR2$ = 0.0822	$R1$ = 0.1372, $wR2$ = 0.2731
Largest diff. peak/hole	764/−1057 e·nm⁻³	1004/866 e·nm⁻³
Scan speed	variable; 7.0−35.0°/min in ω	variable; 7.0−35.0°/min in ω
Scan range (ω)	0.8°	0.75°
Weighting scheme	calcd. $w = 1/[\sigma^2(F_o^2) + (0.0417{\cdot}P)^2 + 7.0681{\cdot}P]$, where $P = (F_o^2 + 2{\cdot}F_c^2)/3$	calcd. $w = 1/[\sigma^2(F_o^2) + (0.0437{\cdot}P)^2 + 175.1567{\cdot}P]$, where $P = (F_o^2 + 2{\cdot}F_c^2)/3$

[(η^4-pp3)PtHgL](OTf)$_2$ (4: L = P*n*Bu$_3$; 5: L = PPh$_3$; 7: L = dppm; 8: L = dppe; 9: L = dppmSe): TlOTf (17.7 mg, 0.05 mmol) was dissolved in MeOH (0.1 mL) and **1a** (62.5 mg, 0.05 mmol) added with stirring to give a yellow suspension. The ligand (0.05 mmol) and CH_2Cl_2 (0.4 mL) were added and the suspension stirred for 5 min. After this, the precipitate of TlCl was separated from the yellow solution by centrifugation. All compounds rapidly decompose by extrusion of elemental mercury and could not be obtained analytically pure in the solid state.

[(η^4-pp3)PtHg(μ-dppe)HgPt(η^4-pp3)](OTf)$_4$ (6): TlOTf (17.7 mg, 0.05 mmol) was dissolved in MeOH (0.1 mL) and **1a** (62.5 mg, 0.05 mmol) added with stirring to give a yellow suspension. The ligand (0.05 mmol) and CH_2Cl_2 (0.4 mL) were added and the suspension stirred for 5 min. After this, the precipitate of TlCl was separated from the yellow solution by centrifugation. Compound **6** rapidly decomposed by extrusion of elemental mercury and could not be obtained analytically pure in the solid state.

X-ray Structure Determinations: Crystals of **1b**·CH_2Cl_2 and **2**·1.5CH_2Cl_2 were examined by similar procedures. Crystals were mounted on a glass fibre, X-ray data were collected with a Siemens P4 diffractometer using Mo-K_α radiation (λ = 71.073 pm, monochromator: highly oriented graphite crystal, ω scan). Unit cell parameters were determined from 30−41 randomly selected reflections in the range θ = 5.3−12.5°, obtained by P4 automatic routine. Every 97 reflections 3 standard reflections were measured. Data were corrected for Lorentz polarisation and absorption effects (ψ scans). The structures were solved by direct methods and subsequent difference Fourier techniques (SHELXS-86).[22] Refinement on F^2 was carried out by full-matrix least-squares techniques (SHELXL-93).[23] All non-hydrogen atoms in the structure of **1b** as well as all non-hydrogen and non-carbon atoms in the structure of **2** were refined anisotropically, the carbon atoms in structure of **2** were refined isotropically. All hydrogen atoms were placed at calculated ideal positions (riding model). Crystal data and details of structure determinations and refinements are collected in Table 5. Crystallographic data (excluding structure factors) for the structure of **1b**·CH_2Cl_2 and **2**·1.5CH_2Cl_2 have been deposited with the Cambridge Crystallographic Data Centre as supplementary publication numbers CCDC-157011 and -157010. Copies of the data can be obtained free of charge on application to CCDC, 12 Union Road, Cambridge CB21EZ, UK [Fax: (internat.) + 44-1223/336-033; E-mail: deposit@ccdc.cam.ac.uk].

Acknowledgments

Financial support by the Jubiläumsfonds der Österreichischen Nationalbank (Proj.-Nr. 7416) is gratefully acknowledged.

[1] [1a] V. I. Sokolov, O. A. Reutov, *Coord. Chem. Rev.* **1978**, *27*, 89. – [1b] V. I. Sokolov, V. V. Bashilov, O. A. Reutov, *J. Organomet. Chem.* **1975**, *97*, 299.
[2] A. Handler, P. Peringer, E. P. Müller, *J. Organomet. Chem.* **1990**, *389*, C23.
[3] C. A. Ghilardi, S. Midollini, S. Moneti, A. Orlandini, G. Scapacci, D. Dakternieks, *J. Chem. Soc., Chem. Commun.* **1989**, 1686.
[4] R. B. King, R. N. Kapoor, M. S. Saran, P. N. Kapoor, *Inorg. Chem.* **1971**, *10*, 1851.
[5] [5a] O. Rossell, M. Seco, G. Segales, S. Alvarez, *Organometallics* **1994**, *13*, 2205. – [5b] R. A. T. Gould, L. H. Pignolet, *Inorg. Chem.* **1994**, *33*, 40. – [5c] O. Rossell, M. Seco, I. Torra, *J. Chem. Soc., Dalton Trans.* **1986**, 1011.
[6] J. Schwald, *Thesis*, University of Innsbruck, **1989**, p. 61.
[7] M. Peter, P. Peringer, E. P. Müller, *J. Chem. Soc., Dalton Trans.* **1991**, 2459.
[8] A. Handler, P. Peringer, E. P. Müller, *J. Chem. Soc., Dalton Trans.* **1990**, 3725.
[9] P. Brüggeller, *Inorg. Chem.* **1987**, *26*, 4125.
[10] T. G. Appleton, H. C. Clark, L. E. Manzer, *Coord. Chem. Rev.* **1973**, *10*, 335.
[11] [11a] M. C. Janzen, M C. Jennings, R. J. Puddephatt, *Inorg. Chem.* **2001**, *40*, 1728. – [11b] L. Hao, J. Vittal, R. J. Puddephatt, *Organometallics* **1996**, *15*, 3115. – [11c] K.-H. Dahmen, D. Imhof, L. M. Venanzi, T. Gerfin, V. Gramlich, *J. Organomet. Chem.* **1995**, *486*, 37. – [11d] P. Braunstein, M. Knorr, M. Strampfer, A. Tiripicchio, F. Ugozzoli, *Organometallics* **1994**, *13*, 3038. – [11e] M. Krumm, E. Zangrando, L. Randaccio, S. Menzer, A. Danzmann, D. Holthenrich, B. Lippert, *Inorg. Chem.* **1993**, *32*, 2183. – [11f] A. Albinati, K.-H. Dahmen, F. Demartin, J. M. Forward, C. J. Longley, D. M. P. Mingos, L. M. Venanzi, *Inorg. Chem.* **1992**, *31*, 2223. – [11g] Y. K. Grishin, V. A. Roznyatovskii, Y. A. Ustynyuk, S. N. Titova, G. A. Domrachev, G. A. Razuvaev, *Polyhedron* **1983**, *2*, 895.
[12] [12a] A. L. Balch, V. J. Catalano, *Inorg. Chem.* **1992**, *31*, 2730. – [12b] P. I. van Vliet, J. Kuyper, D. Vrieze, *J. Organomet. Chem.* **1976**, *122*, 99.
[13] [13a] D. F. Mullica, S. L. Gipson, L. C. Snell, E. L. Sappenfield, D. H. Leschnitzer, *Polyhedron* **1992**, *11*, 2265. – [13b] P. Braunstein, L. Douce, M. Knorr, M. Strampfer, M. Lanfranchi, A. Tiripicchio, *J. Chem. Soc., Dalton Trans.* **1992**, 331. – [13c] M. Cano, J. A. Campo, *Polyhedron* **1991**, *10*, 2611. – [13d] A. Knoepfler-Mühlecker, W. Schuh, B. Scheffter, H. Kopacka, K. Wurst, P. Peringer, *Inorg. Chim. Acta* **2000**, *303*, 70.
[14] [14a] P. Peringer, M. Lusser, *Inorg. Chem.* **1985**, *24*, 109. – [14b] P. A. W. Dean, R. S. Srivastava, *Can. J. Chem.* **1985**, *63*, 2829.
[15] [15a] A. M. Bond, R. Colton, J. Ebner, *Inorg. Chem.* **1988**, *27*, 1697. – [15b] I. J. Colquhoun, W. McFarlane, *J. Chem. Soc., Dalton Trans.* **1981**, 658.
[16] D. Dakternieks, *Inorg. Chim. Acta* **1984**, *89*, 209.
[17] [17a] H. Braekben, W. Scholten, *Z. Kristallogr.* **1934**, *89*, 448. – [17b] D. Grdenic, *Arkiv. Kemi.* **1950**, *22*, 14.
[18] P. E. Jaitner, P. Peringer, G. Huttner, L. Zsolnai, *Transition Met. Chem.* **1981**, *6*, 86.
[19] [19a] M. L. Katcher, G. L. Simon, *Inorg. Chem.* **1972**, *11*, 1651. – [19b] W. Clegg, P. J. Wheatly, *J. Chem. Soc. A* **1971**, 3572.
[20] J. K. Ruff, W. J. Schlientz, *Inorg. Synth.* **1974**, *15*, 84.
[21] P. Brüggeller, *Inorg. Chim. Acta* **1987**, *129*, L27.
[22] G. M. Sheldrick, *SHELXS-86, Program for crystal structure solution*s, Göttingen, **1986**.
[23] G. M. Sheldrick, *SHELXL-93, Program for refinement of crystal structures*, Göttingen, **1993**.

Received February 18, 2001
[I01061]

Formation and Structure of Thulium(III) Cyclopentadienides as Products of Reactions Directed Towards the Synthesis of Thulium(II) Cyclopentadienides

Igor L. Fedushkin,*[a] Frank Girgsdies,[b] Herbert Schumann,*[b] and Mikhail N. Bochkarev[a]

Keywords: Cyclopentadienyl ligands / Ether splitting / Redox reactions / Thulium / X-ray structures

$TmI_2(THF)_2$ and $[C_5Me_5]K$ react in THF to yield the Tm^{III} complex $(C_5Me_5)_2TmI(THF)$ (**1**). The reaction of **1** with excess sodium in 1,2-dimethoxyethane (DME) leads, through Tm^{II} intermediates and a reductive splitting of DME solvent molecules, to the trisodium dithulium(III) complex $[(DME)_2Na(\mu\text{-}\eta^5\text{:}\eta^5\text{-}C_5Me_5)Tm(\eta^5\text{-}C_5Me_5)(\mu_2\text{-}OMe)_2(Na\text{-}\mu\text{-}\eta^5\text{:}\eta^5\text{-}C_5Me_5)\text{-}Na(\mu\text{-}OMe)_2Tm(\eta^5\text{-}C_5Me_5)_2]$ (**2**). Treatment of $TmI_2(THF)_2$ with $[(Me_3Si)_2C_5H_3]MgCl$ (**3**) in THF yields the dimeric Tm^{III} complex $[\{1,3\text{-}(Me_3Si)_2C_5H_3\}_2TmCl]_2$ (**4**), while $TmI_3(THF)_3$ reacts with $[C_5H_4CH_2CH_2NMe_2]K(THF)$ (**5**) to yield solvent-free $(C_5H_4CH_2CH_2NMe_2)_2TmI$ (**6**). The new Tm^{III} compounds have been characterized by elemental analysis, IR spectroscopy, and mass spectrometry. The molecular structures of **2**, **4**, **5**, and **6** have been determined by single-crystal X-ray diffraction analysis.

Introduction

We recently reported on the first molecular thulium(II) complex, $TmI_2(DME)_3$, which was prepared by reduction of TmI_3 with metallic thulium in DME.[1] Analogous organic solvent adducts of neodymium and dysprosium diiodide were obtained by high-temperature reactions (> 200 °C) of the respective metal powders with iodine in sealed glass ampoules followed by treatment of the reaction products with DME or THF.[2] The molecular lanthanide(II) diiodides characterized to date include those of samarium, europium, ytterbium, thulium, neodymium, and dysprosium. According to their standard potentials, the stability of the divalent oxidation state decreases in the order $Eu^{II} > Yb^{II} > Sm^{II} > Tm^{II} > Dy^{II} > Nd^{II}$.[3] Whereas organometallic complexes of divalent europium, ytterbium, and samarium are well known and syntheses of the first organolanthanum(II) complex, $[K(18\text{-crown-}6)(C_6H_6)_2][(Cp^{tt}{}_2La)_2(C_6H_6)]_2\text{-}C_6H_6$ (Cp^{tt} = 1,3-tBu$_2$C$_5$H$_3$),[4a] and of the first organoscandium(II) complex, $[\{(P_3C_2tBu_2)Sc\}_2(P_3C_3tBu_3)]$,[4b] have recently been reported, organometallic derivatives of divalent thulium, dysprosium, and neodymium are still unknown. Therefore, we have tried to synthesize organothulium(II) complexes, in the knowledge that they would be very reactive towards organic substrates.[5] Thulium(II) iodide promised to be a suitable starting material. However, as demonstrated by the experiments described below, we were not successful in isolating organothulium(II) complexes, but isolated some interesting new thulium(III) complexes instead. Their formation and structures are reported herein.

Results and Discussion

Malachite-green $TmI_2(THF)_2$ reacts with $[C_5Me_5]K$ (molar ratio 1:2) in THF at −30 to +20 °C; the color of the reaction mixture changes first to brownish-green and finally to light-brown. After removal of the solvent, extraction of the remaining solid with toluene, and concentration of the toluene extract, yellow needle-shaped crystals precipitate. These were found to be composed of the thulium(III) complex $(C_5Me_5)_2TmI(THF)$ (**1**) rather than the expected $(C_5Me_5)_2Tm^{II}$ compound (Scheme 1). Compound **1** melts at 285 °C without decomposition; the high relative intensities of the molecular fragment ions $[(C_5Me_5)_2TmI]^+$ (49.86%), $[(C_5Me_5)TmI]^+$ (50.27%), and $[(C_5Me_5)_2Tm]^+$ (100%) in the EI mass spectrum at 241 °C confirm its remarkable thermal stability. The IR spectrum of **1** is rather uninformative, allowing only a clear assignment of the

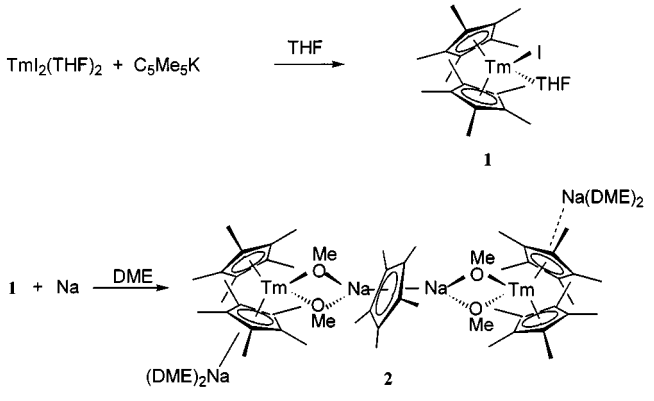

Scheme 1

[a] G. A. Razuvaev Institute of Organometallic Chemistry of the Russian Academy of Sciences,
Tropinina 49, 603950 Nizhny Novgorod GSP-445, Russia
Fax: (internat.) + 7-8312/661-497
E-mail: igorfed@imoc.sinn.ru
[b] Institut für Chemie der Technischen Universität,
Straße des 17. Juni 135, 10623 Berlin, Germany
Fax: (internat.) + 49-39/3142-2168
E-mail: schumann@chem.tu-berlin.de

 © WILEY-VCH Verlag GmbH, 69451 Weinheim, 2001 1434−1948/01/0909−2405 $ 17.50+.50/0

strong THF absorptions at 1010 and 860 cm^{-1}. We have previously observed a similar oxidation of Tm^{II} to Tm^{III} in the reaction of $TmI_2(DME)_3$ with $[Me_2Si(3\text{-}t\text{Bu-5-Me-}C_5H_3)(C_9H_6CH_2CH_2NMe_2)]Na_2$, which afforded the thulium(III) complex *ansa*-$[Me_2Si(3\text{-}t\text{Bu-5-Me-}C_5H_3)(C_9H_6CH_2CH_2NMe_2)]TmI$.[6]

In a subsequent experiment, we tried to obtain the bis(pentamethylcyclopentadienyl)thulium(II) complex by reducing compound **1** with sodium. At the start of the reaction of **1** with excess sodium in DME at 20 °C, a green coating appeared on parts of the metal surface indicating the formation of a thulium(II) species. However, this green coating disappeared very quickly and after stirring for 1 h, a light-yellow reaction mixture was obtained. Filtration and concentration of the solution afforded an oily residue, which partly redissolved in diethyl ether. From the concentrated clear ethereal solution, colorless crystals precipitated, which were found to contain thulium, but were free of iodine and melted at 68−72 °C with decomposition. The IR spectrum of these crystals shows an absorption band attributable to coordinated DME, together with a very strong, broad band at 1100 cm^{-1} indicating the presence of methoxide groups, these arising from cleavage of the DME solvent molecules. Such C−O activation has previously been observed by Lappert et al.,[7] who studied the reactions of $[1,3\text{-}(SiMe_3)_2C_5H_3]_3Nd$ and $(1,3\text{-}t\text{Bu}_2C_5H_3)_3Ce$ with lithium in DME yielding the corresponding methoxide complexes $[1,3\text{-}(Me_3Si)_2C_5H_3]_2Nd(\mu\text{-}OMe)_2Li(DME)$ and $[(1,3\text{-}t\text{Bu}_2C_5H_3)_2Ce(\mu\text{-}OMe)]_2$, respectively. The isolated crystals were characterized by single-crystal X-ray diffraction analysis. Whereas the data from a first diffraction experiment[8] implied some intrinsic contradictions, a second X-ray analysis of a crystal of the same crop afforded precise structural data, from which the formula of the compound formed in the reaction of **1** with sodium in DME could be assigned as $[(DME)_2Na(\mu\text{-}\eta^5\text{:}\eta^5\text{-}C_5Me_5)Tm(\eta^5\text{-}C_5Me_5)(\mu_2\text{-}OMe)_2(Na\text{-}\mu\text{-}\eta^5\text{:}\eta^5\text{-}C_5Me_5)Na(\mu\text{-}OMe)_2Tm(\eta^5\text{-}C_5Me_5)]$ (**2**), i.e. one containing only thulium(III) ions. The first step in the reaction is the expected reduction of **1** with the formation of green Tm^{II} species, which, because of their high reduction potential and high oxophilicity, attack DME solvent molecules with reductive splitting of MeO−C bonds and the formation of thulium(III) methoxide units. The generation of the four methoxide groups of **2** requires four electrons. Since two of the intermediately formed thulium(II) species provide only two electrons, the sodium metal must also take part in the reductive cleavage of DME. At this point, it should be noted that sodium metal does not react with DME in the absence of lanthanide compounds, not even on prolonged reflux. The organic products formed in the DME splitting process could not be identified.

From the results reported above, we conclude that the possibility of synthesizing a stable organothulium(II) compound will probably arise by the use of space-demanding substituted cyclopentadienyl ligands or of cyclopentadienyl ligands containing nitrogen as a strong donor atom in the side chain, thus stabilizing the complex by additional intramolecular metal coordination. Lappert et al.[4a] have previously demonstrated that bulky cyclopentadienyl ligands are effective in stabilizing Ln^{II} ions. Therefore, we studied the interactions of $TmI_2(THF)_2$ with $[1,3\text{-}(Me_3Si)_2C_5H_3]M$ [M = K[9] or MgCl (**3**)]. Since only intractable product mixtures were obtained using the potassium cyclopentadienide, which can only be recovered from organic media in an impure state, we turned our attention to the corresponding cyclopentadienylmagnesium chloride, $[1,3\text{-}(Me_3Si)_2C_5H_3]MgCl$ (**3**), which can be obtained from $[1,3\text{-}(Me_3Si)_2C_5H_3]K$ and $MgCl_2$ (1:1 molar ratio) in diethyl ether as a pure crystalline solid. Addition of **3** to a solution of $TmI_2(THF)_2$ in THF (2:1 molar ratio) led to the immediate formation of a highly dispersed dark-grey solid, which reacted readily with water and was found to consist of metallic magnesium formed by reduction of MgICl by intermediately formed organothulium(II) species. As a consequence, workup of the reaction mixture again afforded only an organothulium(III) derivative, the dimeric compound $[\{1,3\text{-}(Me_3Si)_2C_5H_3\}_2TmCl]_2$ (**4**) (Scheme 2). Compound **4** was isolated in 67% yield and did not melt below 280 °C. Its mass spectrum shows ion peaks of a fragment of the dimer, $[M - 2\ CH_3 - (CH_3)_3Si]_2^+$ (0.5%), of the monomeric unit $[Cp^{\#}{}_2TmCl]^+$ (8%), and of fragments predominantly formed by cleavage of Si−C bonds. The MS data indicate that the metallocene structure of **4** is thermodynamically rather stable.

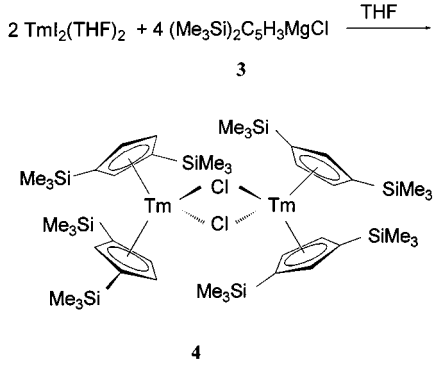

Scheme 2

The [2-(dimethylamino)ethyl]cyclopentadienyl ligand, which has already been used successfully for the synthesis of the ytterbium(II) complex $(Me_2NCH_2CH_2C_5H_4)Yb$,[10] should offer another possible means of obtaining a stable organothulium(II) complex. The corresponding potassium salt, $[Me_2NCH_2CH_2C_5H_4]K(THF)$ (**5**), was prepared from $Me_2NCH_2CH_2C_5H_5$ [11] and KH in THF according to literature methods (Scheme 3).[12] It forms long needle-shaped crystals, the structure of which we determined by X-ray diffraction analysis (Figure 3). Once again, compound **5** and $TmI_2(THF)_2$ did not react to form a Tm^{II} derivative. Indeed, in this case, workup of the reaction mixture did not even allow the isolation of a Tm^{III} complex, which we expected to be formed by oxidation of a Tm^{II} intermediate. However, the expected thulium(III) complex $(Me_2NCH_2CH_2C_5H_4)_2TmI$ (**6**) could be isolated as solvent-free colorless needles in 74% yield by treating **5** with

$TmI_3(THF)_3$ (2:1 molar ratio) in THF at 20 °C (Scheme 3). The crystals melt at 109−111 °C without decomposition. The EI mass spectrum of **6** shows no molecular ion peak at temperatures up to 220 °C. The most intense molecular fragments, $[(DoCp)_2Tm]^+$ (9%) and $[(DoCp)TmI]^+$ (4%), were detected at 158 °C (DoCp = $C_5H_4CH_2CH_2NMe_2$).

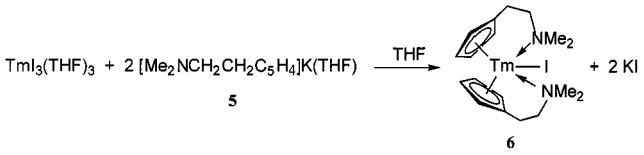

5 6

Scheme 3

Again, at the initial stage of the reaction of **6** with excess sodium in diethyl ether, the intermediate formation of a Tm^{II} compound was indicated by a light-green color of the mixture. However, this coloration disappeared within a few minutes and workup of the reaction mixture did not afford any well-defined products. This is in accordance with previously reported attempts[13] to synthesize cyclopentadienylthulium(II) complexes by reduction of the corresponding Tm^{III} compounds with alkali metals.

Molecular Structures of 2, 4, 5, and 6

Crystals suitable for single-crystal X-ray diffraction studies were obtained from diethyl ether (**2**), hexane (**4**), or THF (**5** and **6**). The crystal and structure refinement data for **2**, **4**, **5**, and **6** are listed in Table 1.

The molecule of **2** (Figure 1) contains two regions of disorder, both located around centers of symmetry. In the center of the molecule, a pentamethylcyclopentadienyl unit is statistically distributed between two symmetry-related alternative orientations. Since the centroid positions of the two orientations are different, the adjacent sodium position is split. At the ends of the molecule, the fragment $[Na(DME)_2]$ has a statistical occupancy of 50%. Due to overlap of the DME regions of neighboring molecules, at first glance the structure seems to be polymeric. However, two different DME molecules may not occupy the same space simultaneously, hence only one orientation can be realized between a given pair of molecules. Consequently, the structure consists of discrete isolated units. The picture given in Figure 1 (top) can be viewed in two ways. The open ellipsoids, together with their filled counterparts, represent the disordered parts of the structure. These atoms have crystallographic occupancies of 50%, resulting in an averaged structure corresponding to $[(DME)_2Na]_{1/2}$(μ-

Table 1. Crystal data and structure refinement for **2**, **4**, **5**, and **6**

	2	**4**	**5**	**6**
Empirical formula	$C_{62}H_{107}Na_3O_8Tm_2$	$C_{44}H_{84}Cl_2Si_8Tm_2$	$C_{13}H_{22}KNO$	$C_{18}H_{28}IN_2Tm$
M_r [g mol^{-1}]	1387.31	1246.59	247.42	568.25
Crystal system	monoclinic	monoclinic	orthorhombic	orthorhombic
Space group	$P2_1/n$	$P2_1/c$	$P2_12_12_1$	$Pcnb$
Unit cell dimensions				
a [Å]	10.1900(11)	10.694(2)	9.7254(1)	10.7653(2)
b [Å]	20.158(3)	14.429(3)	10.6654(2)	13.0419(1)
c [Å]	16.8410(19)	19.980(6)	14.0639(2)	13.5427(2)
β [°]	103.921(12)	104.35(2)	90	90
V [Å^3]	3357.7(7)	2986.8(13)	1458.78(4)	1901.39(5)
Z	2	2	4	4
$\rho_{calcd.}$ [g/cm^3]	1.372	1.386	1.127	1.985
μ [mm^{-1}]	2.692	3.227	0.347	6.289
F(000)	1428	1264	536	1088
Crystal dimensions [mm]	0.54 × 0.46 × 0.36	0.48 × 0.48 × 0.42	0.66 × 0.35 × 0.08	0.30 × 0.24 × 0.12
Data collection θ range [°]	1.60−30.00	2.10−27.46	2.40−27.50	2.42−27.50
h	−14/14	0/13	−7/12	−13/+10
k	−28/28	0/18	−13/13	−16/16
l	−18/+23	−25/25	−18/18	−17/17
Collected/unique reflections	30283/9790	7174/6812	11095/3351	13319/2188
R_{int}	0.0389	0.0748	0.0626	0.0397
Absorption correction	SADABS	none	SADABS	SADABS
Max./min. transmission	0.4278/0.2945	−	0.9774/0.3639	0.3852/0.2426
Data/restraints/parameters	9790/0/440	6802/0/265	3351/0/148	2188/0/104
Goodness-of-fit on F^2	1.051	1.054	1.019	1.075
R_1 [$I > 2\sigma(I)$]	0.0262	0.0498	0.0539	0.0260
wR_2 [$I > 2\sigma(I)$]	0.0517	0.1279	0.1181	0.0507
R_1 (all data)	0.0445	0.0583	0.0904	0.0498
wR_2 (all data)	0.0579	0.1398	0.1339	0.0591
Largest diff. peak and hole [e/Å^3]	0.689/−0.738	3.039/−2.610	0.235/−0.262	1.008/−1.067

$C_5Me_5)Tm(C_5Me_5)(\mu\text{-}OMe)_2[Na(\mu\text{-}C_5Me_5)Na]_{2/2}(\mu\text{-}OMe)_2\text{-}Tm(C_5Me_5)(\mu\text{-}C_5Me_5)[Na(DME)_2]_{1/2}$. Alternatively, ignoring the open ellipsoids and taking the filled ones as complete atoms leads to one possible structure of an actual molecule, which may be described as $[(DME)_2Na(\mu\text{-}\eta^5\text{:}\eta^5\text{-}C_5Me_5)Tm(\eta^5\text{-}C_5Me_5)(\mu_2\text{-}OMe)_2(Na\text{-}\mu\text{-}\eta^5\text{:}\eta^5\text{-}C_5Me_5)Na(\mu\text{-}OMe)_2Tm(\eta^5\text{-}C_5Me_5)_2]$ [Figure 1 (bottom)]. The relevant bond lengths and angles fall within the characteristic ranges for the various fragments.[13,14]

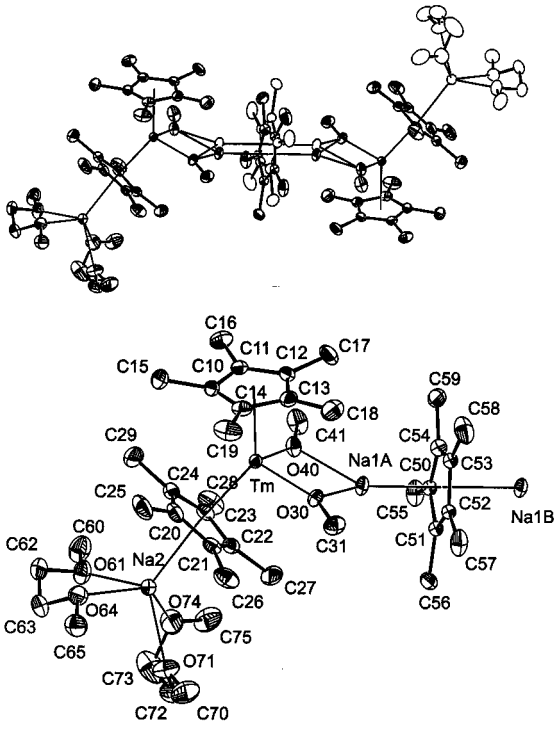

Figure 1. Molecular structure of **2** with 30% probability thermal ellipsoids: representation of a molecule including disorder (see text for details) (top); asymmetric unit showing the atom numbering scheme (bottom); all hydrogen atoms have been omitted for clarity; selected bond lengths [A] and angles [°]: Tm−Cp(1) 2.4010(14) [Tm−C 2.669(2)−2.703(3)], Tm−Cp(2) 2.4159(13) [Tm−C 2.672(3)−2.732(3)], Tm−O 2.1062(17)−2.1184(17), Na(1A)−Cp(3) 2.328(10) [Na(1A)−C 2.601(11)−2.639(12)], Na(1B)−Cp(3) 2.364(10) [Na(1B)−C 2.606(11)−2.685(11)], Na(1A)−O 2.210(11)−2.350(10), Na(1B)′−O 2.191(10)−2.331(11), Na(2)−Cp(2) 2.620(2) [Na(2)−C 2.656(3)−3.098(4)], Na(2)−O 2.370(8)−2.450(5); Cp(1)−Tm−Cp(2) 135.79(4), O(30)−Tm−O(40) 86.60(7), Cp−Tm−O 105.72(6)−106.17(6), Tm−Cp(2)−Na(2) 166.33(8), Tm−O−Na(1) 93.8(2)−99.2(3), O(30)−Na(1)−O(40) 78.8(3)−79.6(4), O−Na(1)−Cp(3) 137.2(5)−141.6(5), Na(1A)−Cp(3)−Na(1B) 179.2(3); Cp(1), Cp(2), and Cp(3) represent the centroid positions of the rings C(10)−C(14), C(20)−C(24), and C(50)−C(54), respectively; symmetry transformation (′) used to generate equivalent atoms: $1-x$, $1-y$, $1-z$

The X-ray crystal structure of $[\{1,3\text{-}(Me_3Si)_2C_5H_3\}_2TmCl]_2$ (**4**) shows this complex to be a centrosymmetric, chloro-bridged dimer (Figure 2). Compound **4** crystallizes in the monoclinic space group $P2_1/c$ with two dimers in the unit cell. The bond lengths and bond angles estimated for **4** are in the characteristic ranges for the various fragments.[13,14]

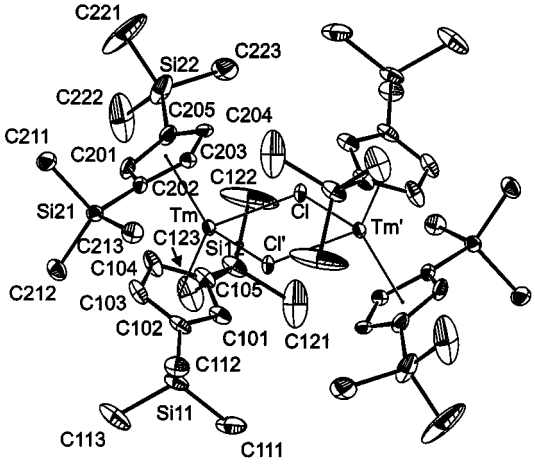

Figure 2. Molecular structure of **4** showing the atom numbering scheme (30% probability thermal ellipsoids); all hydrogen atoms have been omitted for clarity; selected bond lengths [A] and angles [°]: Tm−Cp(1) 2.314(3) [Tm−C 2.582(6)−2.642(5)], Tm−Cp(2) 2.316(3) [Tm−C 2.604(6)−2.618(5)], Tm−Cl 2.6829(15), Tm−Cl′ 2.6883(13); Cp(1)−Tm−Cp(2) 130.08(10), Cp(1)−Tm−Cl 110.60(7), Cp(1)−Tm−Cl′ 111.03(8), Cp(2)−Tm−Cl 106.82(8), Cp(2)−Tm−Cl′ 106.46(8), Cl−Tm−Cl′ 80.85(4), Tm−Cl−Tm′ 99.15(4); Cp(1) and Cp(2) represent the centroid positions of the rings C(101)−C(105) and C(201)−C(205), respectively; symmetry operation (′) used to generate equivalent atoms: $1-x$, $1-y$, $1-z$

$[Me_2NCH_2CH_2C_5H_4]K(THF)$ (**5**) (Figure 3) is polymeric and crystallizes in the chiral orthorhombic space group $P2_12_12_1$ with four formula units per unit cell. The structure consists of infinite one-dimensional chains extending parallel to the *b* axis. Each potassium atom is coordinated by one THF molecule, the C_5H_4 aromatic ring system, the nitrogen atom of the 2-(dimethylamino)ethyl side chain, and, additionally, by the C_5H_4 ring system of a neighbouring molecule. The $\mu_2\text{-}\eta^5\text{:}\eta^5$ coordination of the cyclopentadienyl moi-

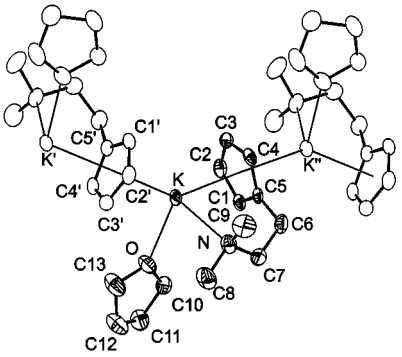

Figure 3. Section of the polymeric structure of **5** showing the atom numbering scheme (30% probability thermal ellipsoids); symmetry-equivalent atoms are represented by open ellipsoids to emphasize the asymmetric unit; all hydrogen atoms have been omitted for clarity; selected bond lengths [A] and angles [°]: K−Cp 2.8082(16) [K−C 3.007(3)−3.097(3)], K−Cp′ 2.8183(16) [K−C 3.007(3)−3.119(3)], K−N 2.867(3), K−O 2.734(3); Cp−K−Cp′ 143.23(5), O−K−N 88.01(10), Cp−K−N 85.38(7), Cp−K−O 109.43(6), Cp′−K−N 115.23(8), Cp′−K−O 101.76(6), K−Cp−K′′ 174.56(6); Cp represents the centroid position of the ring C(1)−C(5); symmetry transformations used to generate equivalent atoms: (′) $1-x$, $1/2+y$, $1/2-z$; (′′) $1-x$, $-1/2+y$, $1/2-z$

ety is characterized by only small differences in the K−C bond lengths (3.007−3.119 Å) and an almost linear K−Cp−K arrangement (174.56°).

The complex $(Me_2NCH_2CH_2C_5H_4)_2TmI$ (**6**) crystallizes in the orthorhombic space group *Pcnb*. The molecules possess a twofold rotational axis containing the thulium and iodine atoms (Figure 4). Consequently, the asymmetric unit comprises half a molecule for a total of two formula units per unit cell. In **6**, both donor atoms are intramolecularly coordinated to the thulium atom. As for other donor-functionalized bis(cyclopentadienyl)lanthanide(III) halides having a formal coordination number of 9,[15] the coordination geometry around the thulium atom is that of a distorted trigonal bipyramid with the two cyclopentadienyl rings and the iodine atom occupying the equatorial positions and the two nitrogen atoms of the cyclopentadienyl side chains in the axial positions forming an N−Tm−N angle of 157.9°. The distance from the thulium atom to the ring centers is 2.352 Å and the Tm−I and Tm−N distances of 3.014 and 2.789 Å, respectively, are within the ranges found for other thulium(III) complexes.[13,14]

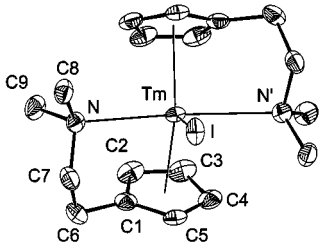

Figure 4. Molecular structure of **6** showing the atom numbering scheme (50% probability thermal ellipsoids); all hydrogen atoms have been omitted for clarity; selected bond lengths [Å] and angles [°]: Tm−Cp 2.352(2) [Tm−C 2.627(5)−2.650(4)], Tm−I 3.0145(4), Tm−N 2.789(4); I−Tm−Cp 114.27(6), I−Tm−N 78.97(8), Cp−Tm−Cp′ 131.46(8), Cp−Tm−N 90.91(11), Cp−Tm−N′ 98.12(11), N−Tm−N′ 157.94(16); Cp represents the centroid position of the ring C(1)−C(5); symmetry transformation (′) used to generate equivalent atoms: $1 - x$, $1/2 - y$, z

Conclusion

Reactions of thulium(II) iodide with cyclopentadienylpotassium or -magnesium derivatives do not yield stable cyclopentadienylthulium(II) complexes. Under the conditions used, only thulium(III) derivatives are formed. Neither the C_5Me_5 ligand nor the donor-functionalized $Me_2NCH_2CH_2C_5H_4$ or the bulky 1,3-$(Me_3Si)_2C_5H_3$ ligand are able to stabilize organothulium(II) complexes in coordinating ether solvents.

Experimental Section

General Remarks: All manipulations were carried out either in vacuo or under nitrogen using standard Schlenk techniques. The solvents used were dried with sodium/benzophenone and were condensed in vacuo prior to use. − Melting points and decomposition temperatures were determined for samples sealed in capillaries in vacuo. − Elemental analyses were performed on a Perkin−Elmer Series II CHNS/O Analyser 2400. − IR spectra were recorded with a Specord M-80 spectrometer. The samples were prepared as mulls in Nujol. − Mass spectra (EI, 70 eV) were recorded with a Varian MAT 311A spectrometer. Only characteristic fragments and highest-abundance isotope peaks are listed. Relative intensities (%) are given in parentheses. − Informative NMR spectra of the thulium(III) complexes could not be obtained due to the strong paramagnetism of thulium(III) (μ_{eff} = 7.0−7.5 B.M.). $TmI_2(THF)_5$ formed in the reaction of $TmI_3(THF)_3$ with metallic thulium in THF changes into $TmI_2(THF)_2$ upon drying at 90 °C. The detailed experimental procedure will be published elsewhere. Literature methods were used for the synthesis of $[Me_2NCH_2CH_2C_5H_4]K(THF)$ (**5**),[12] and [1,3-$(Me_3Si)_2C_5H_3$]K.[9]

$(C_5Me_5)_2TmI(THF)$ (1): To a stirred suspension of $(C_5Me_5)K$ (1.12 g, 6.42 mmol) in THF (25 mL), precooled to −30 °C, was added $TmI_2(THF)_2$ (1.84 g, 3.24 mmol). The brownish-green mixture was allowed to warm to ambient temperature over a period of 2 h and then stirred for a further 1 h. The solvent was then removed in vacuo and the remaining solid was extracted with toluene (3 × 15 mL). Concentration of the combined toluene extracts to a volume of 8−10 mL led to the deposition of **1** (0.69 g, 34%) as yellow needle-shaped crystals; m.p. 285 °C. − IR (Nujol): $\tilde{\nu}$ = 1230 (w), 1190 (m), 1010 (vs), 965 (w), 920 (m), 860 (vs), 670 cm^{-1} (w). − MS (241 °C, ^{169}Tm): *m*/*z* (%) = 565.8 (49.86) $[M - THF]^+$, 439.0 (100) $[M - THF - I]^+$, 430.8 (50.27) $[M - THF - C_5Me_5]^+$, 295.8 (43.39) $[M - THF - 2\ C_5Me_5]^+$. − μ_{eff} (295 K) = 7.7 B.M. − $C_{24}H_{38}IOTm$ (638.40): calcd. I 19.88, Tm 26.46; found I 21.02, Tm 26.54.

$[(DME)_2Na][(C_5Me_5)_2Tm(OMe)_2\{Na(C_5Me_5)Na\}(OMe)_2Tm(C_5Me_5)_2]$ (2): A mixture of $(C_5Me_5)_2TmI(THF)$ (1.61 g, 2.52 mmol) and sodium (0.3 g, 13.04 mg-atom) in DME (10 mL) was stirred for 1 h at ambient temperature. The light-yellow solution was then decanted from the excess sodium, the solvent was removed under reduced pressure, and the oily residue was dried in vacuo. Treatment of this residue with diethyl ether (15 mL) led to the precipitation of NaI. The ether solution was centrifuged and decanted from the precipitate. Within 1 d, colorless crystals of **2** had precipitated from the concentrated (5 mL) ether solution. Yield 0.51 g (29%); m.p. 68−72 °C (decomp). − IR (Nujol): $\tilde{\nu}$ = 1300 (m), 1250 (m), 1160 (m), 1100 (vs), 1030 (s), 980 (m), 920 (w), 870 cm^{-1} (s). − μ_{eff} (295 K) = 7.4 B.M. − $C_{62}H_{107}Na_3O_8Tm_2$ (1387.36): calcd. C 53.68, H 7.77, Tm 24.35; found C 53.87, H 6.41, Tm 24.77.

[1,3-$(Me_3Si)_2C_5H_3$]MgCl (3): To a stirred suspension of $MgCl_2$ (0.77 g, 8.08 mmol) in diethyl ether (50 mL), [1,3-$(Me_3Si)_2C_5H_3$]K (1.95 g, 7.84 mmol) was added. After 2 h, the mixture was filtered. The ether solution was concentrated in vacuo and the remaining waxy solid was washed with hexane (20 mL). Recrystallization of the solid from diethyl ether gave **3** (1.12 g, 53%). − MS (73 °C, ^{24}Mg): *m*/*z* (%) = 442.2 (78.31) $[Cp^{\#}{}_2Mg]^+$, 427.3 (84.16) $[Cp^{\#}{}_2Mg - CH_3]^+$, 339.1 (16.14) $[Cp^{\#}{}_2Mg - 2\ CH_3 - TMS]^+$, 268.1 (1.02) $[Cp^{\#}MgCl]^+$, 251.0 (9.76) $[Cp^{\#}{}_2Mg - 3\ CH_3 - 2\ TMS]^+$, 233.2 (9.95) $[Cp^{\#}Mg]^+$, 210.2 (5.84) $[Cp^{\#}]^+$, 195.2 (8.91) $[Cp^{\#} - CH_3]^+$, 73.0 (100) $[TMS]^+$, 59.0 (5.07) $[MgCl]^+$. − $C_{11}H_{21}ClMgSi_2$ (269.22): calcd. C 49.08, H 7.86; found C 49.44, H 8.27.

$[\{1,3\text{-}(Me_3Si)_2C_5H_3\}_2TmCl]_2$ (4): Addition of [1,3-$(Me_3Si)_2C_5H_3$]MgCl (0.84 g, 3.13 mmol) to a solution of $TmI_2(THF)_2$ (0.95 g, 1.67 mmol) in THF (40 mL) led to an immediate darkening of the reaction mixture. The solvent was removed in vacuo and the residual solid was extracted with hexane at 50 °C. The colorless

compound **4** (0.65 g, 67%) crystallized on cooling of the hexane extract; m.p. > 280 °C. − IR (Nujol): $\tilde{\nu}$ = 1440 (s), 1400 (m), 1320 (m), 1250 (vs), 1095 (vs), 985 (w), 930 (s), 845 (vs), 800 (s), 765 (s), 700 (m), 640 (m), 620 cm^{-1} (m). − MS [$Cp^{\#}$ = 1,3-$(Me_3Si)_2C_5H_3$, 207 °C, ^{169}Tm]: *m/z* (%) = 622.4 (8.22) $[M]^+$, 607.4 (100) $[M - CH_3]^+$, 587.1 (10.99) $[M - Cl]^+$, 518.9 (15.92) $[M - 2\ CH_3 - TMS]^+$, 499.2 (24.31) $[M - CH_3 - (CH_3)_3Si - Cl]^+$, 413.0 (6.45) $[M - Cp^{\#}]^+$, 397.0 (9.83) $[M - Cp^{\#} - CH_3]^+$, 210.2 (8.20) $[Cp^{\#}]^+$, 195.2 (10.92) $[Cp^{\#}\ CH_3]^+$, 73.0 (97.51) $[TMS]^+$. − μ_{eff} (295 K) = 7.2 B.M. − $C_{22}H_{42}ClSi_4Tm$ (623.30): calcd. C 42.38, H 6.79, Tm 27.19; found C 41.11, H 6.55, Tm 27.95.

$(C_5H_4CH_2CH_2NMe_2)_2TmI$ (6): To a suspension of $TmI_3(THF)_3$ (1.9 g, 2.48 mmol) in THF (35 mL) was added $(C_5H_4CH_2CH_2NMe_2)K(THF)$ (1.25 g, 5.06 mmol). The mixture was stirred for 1 h at room temperature. Evaporation of the solvent and extraction of the residual solid with toluene (3 × 10 mL) gave **6** (1.05 g, 74%) as colorless crystals; m.p. 109−111 °C. − MS (DoCp = $C_5H_4CH_2CH_2NMe_2$, 158 °C, ^{169}Tm): *m/z* (%) = 440.9 (9.09) $[M - I]^+$, 431.8 (4) $[M - DoCp]^+$, 295.7 (1.71) $[M - 2\ DoCp]^+$, 58.2 (100) $[CH_2NMe_2]^+$. − $C_{18}H_{28}IN_2Tm$ (568.27): calcd. C 38.02, H 4.97, N 4.93; found C 37.53, H 4.33, N 5.14.

Crystal Structure Determinations: Data were collected with a Siemens SMART CCD area detector diffractometer (ω scans, *T* = 173 K) for **2**, **5**, **6** or with an Enraf−Nonius CAD4 diffractometer (ω−2θ scans, *T* = 163 K) for **4**. Both diffractometers were equipped with low-temperature devices and were operated with graphite-monochromated Mo-K_α radiation (λ = 0.71073 Å). The structures were solved by direct methods using SHELXS-97[16] (**2**, **5**, **6**) or SHELXS-86[17] (**4**) and were refined against F^2 using SHELXL-97[18] (**2**, **5**, **6**) or SHELXL-93[19] (**4**). In the case of **2**, **5**, and **6**, an empirical absorption correction was applied using the program SADABS.[20] All non-hydrogen atoms were refined with anisotropic thermal parameters, except for the ring atoms of the disordered C_5Me_5 ligand in **2**. Hydrogen atoms were placed in idealized positions with fixed isotropic temperature factors (U_{iso} = 0.08 $Å^2$). Crystal and structure refinement data are given in Table 1. Crystallographic data (excluding structure factors) for the structures reported in this paper have been deposited with the Cambridge Crystallographic Data Centre as supplementary publication nos. CCDC-158695 (**2**), -158696 (**4**), -158697 (**5**), and -158698 (**6**). Copies of the data can be obtained free of charge on application to the CCDC, 12 Union Road, Cambridge CB2 1EZ, U.K. [Fax: (internat.) + 44-1223/336-033; E-mail: deposit@ccdc.cam.ac.uk].

Acknowledgments

This work was supported by the Alexander von Humboldt Stiftung, the Russian Academy of Sciences (grants for young scientists), as well as the Deutsche Forschungsgemeinschaft and the Fonds der Chemischen Industrie.

[1] M. N. Bochkarev, I. L. Fedushkin, A. A. Fagin, T. V. Petrovskaya, J. W. Ziller, R. N. R. Broomhall-Dillard, W. J. Evans, *Angew. Chem.* **1997**, *109*, 123−124; *Angew. Chem. Int. Ed. Engl.* **1997**, *36*, 133−134.

[2] M. N. Bochkarev, A. A. Fagin, *Chem. Eur. J.* **1999**, *5*, 2990−2992.

[3] [3a] G. Meyer, *Chem. Rev.* **1988**, *88*, 93−107. − [3b] A. N. Kamenskaya, *Russ. J. Inorg. Chem.* **1984**, *29*, 251−254. − [3c] R. A. Sallach, J. D. Corbett, *Inorg. Chem.* **1964**, *7*, 993−996. − [3d] N. B. Mikheev, *Russ. J. Inorg. Chem.* **1984**, *29*, 258−261.

[4] [4a] M. C. Cassani, D. J. Duncalf, M. F. Lappert, *J. Am. Chem. Soc.* **1998**, *120*, 12958−12959. − [4b] P. L. Arnold, F. G. N. Cloke, P. B. Hitchcock, J. F. Nixon, *J. Am. Chem. Soc.* **1996**, *118*, 7630−7634.

[5] [5a] W. J. Evans, N. T. Allen, *J. Am. Chem. Soc.* **2000**, *122*, 2118−2119. − [5b] M. N. Bochkarev, A. A. Fagin, I. L. Fedushkin, T. V. Petrovskaya, J. W. Ziller, R. N. R. Broomhall-Dillard, W. J. Evans, *Russ. Chem. Bull.* **1999**, *48*, 1782−1784. − [5c] I. L. Fedushkin, M. Weydert, A. A. Fagin, S. E. Nefedov, I. L. Eremenko, M. N. Bochkarev, H. Schumann, *Z. Naturforsch., Teil B* **1999**, *54*, 466−468. − [5d] M. N. Bochkarev, I. L. Fedushkin, A. A. Fagin, H. Schumann, J. Demtschuk, *Chem. Commun.* **1997**, 1783−1784.

[6] H. Schumann, F. Erbstein, D. F. Karasiak, I. L. Fedushkin, J. Demtschuk, F. Girgsdies, *Z. Anorg. Allg. Chem.* **1999**, *625*, 781−788.

[7] Yu. K. Gun'ko, P. B. Hitchcock, M. F. Lappert, *J. Organomet. Chem.* **1995**, *499*, 213−219.

[8] M. N. Bochkarev, A. A. Fagin, I. L. Fedushkin, A. A. Trifonov, E. N. Kirillov, I. L. Eremneko, S. E. Nefedov, *Mater. Sci. Forum* **1999**, *315−317*, 144−153.

[9] E. W. Abel, S. Moorhouse, *J. Organomet. Chem.* **1971**, *29*, 227−232.

[10] M. N. Bochkarev, I. L. Fedushkin, V. I. Nevodchikov, A. V. Protchenko, H. Schumann, F. Girgsdies, *Inorg. Chim. Acta* **1998**, *280*, 138−142.

[11] T. F. Wang, Y. T. Lee, J. W. Chou, C. W. Ong, *J. Organomet. Chem.* **1992**, *423*, 31−38.

[12] W. A. Herrmann, R. Anwander, F. C. Munck, W. Scherer, *Chem. Ber.* **1993**, *126*, 331−337.

[13] [13a] S. Al Juaid, Y. K. Gun'ko, P. B. Hitchcock, M. F. Lappert, S. Tian, *J. Organomet. Chem.* **1999**, *582*, 143−152. − [13b] P. B. Hitchcock, M. F. Lappert, Sh. Tian, *Organometallics* **2000**, *19*, 3420−3428.

[14] [14a] M. N. Bochkarev, L. N. Zakharov, G. S. Kalinina, *Organoderivatives of Rare Earth Elements*, Kluwer Academic Publishers, Dordrecht, **1995**. − [14b] H. Schumann, J. A. Meese-Marktscheffel, L. Esser, *Chem. Rev.* **1995**, *95*, 865−986. − [14c] W. J. Evans, Ch. A. Seibel, J. W. Ziller, *J. Am. Chem. Soc.* **1998**, *120*, 6745−6752.

[15] [15a] G. Molander, H. Schumann, E. C. E. Rosenthal, J. Demtschuk, *Organometallics* **1996**, *15*, 3817−3824. − [15b] H. Schumann, E. C. E. Rosenthal, J. Demtschuk, *Organometallics* **1998**, *17*, 5324−5333.

[16] G. M. Sheldrick, *SHELXS-97, Program for the Solution of Crystal Structures*, Universität Göttingen, **1990**.

[17] G. M. Sheldrick, *SHELXS-86, Program for the Solution of Crystal Structures*, Universität Göttingen, **1985**.

[18] G. M. Sheldrick, *SHELXL-97, Program for the Refinement of Crystal Structures*, Universität Göttingen, **1997**.

[19] G. M. Sheldrick, *SHELXL-93, Program for the Refinement of Crystal Structures*, Universität Göttingen, **1993**.

[20] G. M. Sheldrick, *SADABS, Empirical Absorption Correction Program*, Universität Göttingen, **1996.**

Received February 26, 2001
[I01065]

Trifunctional Phosphane Ligands and Their Application in the Synthesis of Novel Cage-Structured Platinacyclophanes and Trinuclear Chain-Like Platinacycles by Self-Assembly[‡]

Ekkehard Lindner,*[a] Monther Khanfar,[a] and Manfred Steimann[a]

Dedicated to Professor Dieter Sellmann on the occasion of his 60th birthday

Keywords: Cyclophanes / Platinum / P ligands / Supramolecular chemistry / Self assembly

The synthesis of the 1,3,5-tris[(diphenylphosphoryl)alkyl]-benzenes **7**–**10** succeeds by reaction of the corresponding 1,3,5-tris(bromoalkyl)benzenes **3**–**6** with ethyl diphenylphosphinite in an Arbusov-type reaction. Reduction of these phosphane oxides leads to the trifunctional phosphane ligands **11**–**14**. Their potency of self-assembly was examined by the employment of platinum(II) complex fragments. A five-component self-assembly consisting of 3 equiv. of the platinum complex $Cl_2Pt(NCPh)_2$ and 2 equiv. of the ligands **11**–**14** under high-dilution conditions led to the formation of the nanoscaled triplatinacyclophanes **1** and **15**–**17**. Polymers were formed as by-products from the reactions between **11**–**13** and $Cl_2Pt(NCPh)_2$, whereas in the case of **14** three other platinacyles **18**–**20** with a chain-like structure were formed. The structures of the metallacycles **1** and **15**–**17** as well as **18**–**20** were elucidated by $^{31}P\{^1H\}$, $^{13}C\{^1H\}$, and $^{195}Pt\{^1H\}$ NMR spectroscopic investigations.

Introduction

Supramolecular chemistry, which may be regarded as a result of modern coordination chemistry,[1] is at the frontier of molecular sciences as is shown by the fast growth of publications in this area in the last decade.[2] Cyclophanes and in particular metallacyclophanes are part of this chemistry.[3,4] They contain cavities that have the capacity to include guest molecules of different kinds.[4] The synthesis of these fascinating compounds was troublesome. However, studies in self-organization have provided a lot of interesting molecular architectures capable of being used for host−guest chemistry, such as "cyclophane boxes",[5] squares and polygons,[6] cylinders,[7] rods[8] and many others.[9] Unlike two-dimensional metallacyclophane boxes, three-dimensional multicyclic species are still rare today.[5,10]

Mono- and multidentate phosphanes are attractive ligands for the generation of complexes with a great variety of transition metal fragments.[11] Recently, van Koten et al.[12] synthesized a tetradentate ligand in which the phosphane arms are attached via methylene groups to a benzene ring in the 1,2,4,5-positions. The introduction of a symmetrically 1,3,5-trisubstituted benzene ring with at least C_3 symmetry into phosphane chemistry has advantages for the synthetic design[13] of self-assembled supramolecular molecules[14] and for chemical selectivity.[15] As it was demonstrated recently such tridentate phosphanes are suitable for assembly via three platinum atoms to give an elastic, three-dimensional molecular cage. By virtue of its size it was possible to reversibly encapsulate 1,2-dichloroethane into the triplatinacyclophane **1** (Figure 1).[16] In continuation of this work several triplatinacyclophanes were generated with different cage sizes in order to study the dependence of the number of methylene groups in the ligand system on the type of self-assembly. Due to this novel tridentate phosphane ligands are introduced in this investigation. They are based on a central benzene ring which is provided with three flexible aliphatic spacer units, each carrying a phosphane group at their ends. Such ligands can be employed in catalysis and supramolecular chemistry.

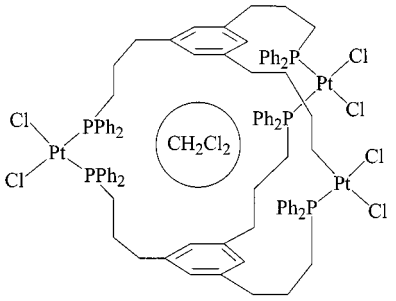

Figure 1. Inclusion of 1,2-dichloroethane into the three-dimensional triplatinacyclophane **1**

[‡] Preparation, Properties, and Reactions of Metal-Containing Heterocycles, 104. − Part 103: E. Lindner, R. Zong, K. Eichele, *Phosphorus Sulfur Silicon Relat. Elem.*, in press.

[a] Institut für Anorganische Chemie der Universität,
Auf der Morgenstelle 18, 72076 Tübingen, Germany
Fax: (internat.) + 49-(0)7071/295306
E-mail: ekkehard.lindner@uni-tuebingen.de

 © WILEY-VCH Verlag GmbH, 69451 Weinheim, 2001 1434−1948/01/0909−2411 $ 17.50+.50/0

Results and Discussion

Ligand Synthesis

For the synthesis of the target ligands **11**−**14** the 1,3,5-tris(bromoalkyl)benzenes **3**−**6** are used as starting materials. However, according to the literature 1,3,5-tris(bromopropyl)benzene (**5**) is only available in a complicated eight-step reaction sequence.[17] Therefore a much simpler access to **5** was developed. Lithiation of mesitylene with *n*BuLi/TMEDA in *n*-hexane afforded the trilithium derivative **2**. Subsequent addition of a suspension of **2** in *n*-pentane to a solution of 1,2-dibromoethane in *n*-pentane at −85 °C resulted in the formation of **5** in about 20% yield (Scheme 1).

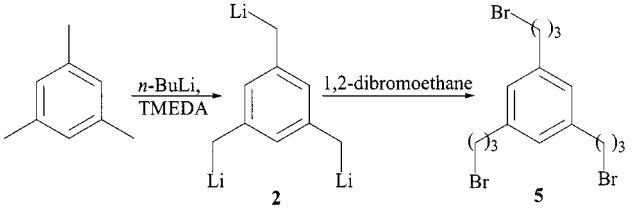

Scheme 1

Reactions of the trifunctionalized chloro- or bromoalkylbenzenes **3**−**6** with $MPPh_2$ (M = Li, Na) or $LiCH_2PPh_2$ were not successful. Also treatment of **2** with $ClPPh_2$ or $ClCH_2PPh_2$ did not result in the isolation of a defined product. Therefore a method of van Koten et al. was applied which was recently published.[12,18] According to this procedure an Arbusov reaction was carried out between **3**−**6** and $Ph_2POC_2H_5$ yielding quantitatively the phosphane oxides **7**−**10** (Scheme 2). In *o*-dichlorobenzene these phosphane oxides can easily be reduced with $HSiCl_3$ to the corresponding trifunctionalized phosphanes **11**−**14** (Scheme 2). Whereas the phosphane oxides **7**−**10** represent colorless solids with rather high melting points, which are soluble in all organic solvents of high and medium polarity, the colorless phosphanes are obtained as waxy (**11**), crystalline (**12**), or gummy products (**13**,**14**). In contrast to **7**−**10** they are not soluble in polar solvents. The composition of **7**−**14** was confirmed by FAB and EI mass spectra, showing in each case the molecular peak. The IR spectra (in KBr) of **7**−**10** display a sharp absorption between 1197 and 1225 cm^{-1} which is assigned to the P=O stretching vibration. Expectedly, in the $^{31}P\{^1H\}$ NMR spectra (in $CDCl_3$) of the phosphane oxides **7**−**10** one singlet is observed for each of them (δ = 31 to 34) which is shifted to higher fields (δ = −9 to −15) on going from **7**−**10** to the phosphanes **11**−**14**.

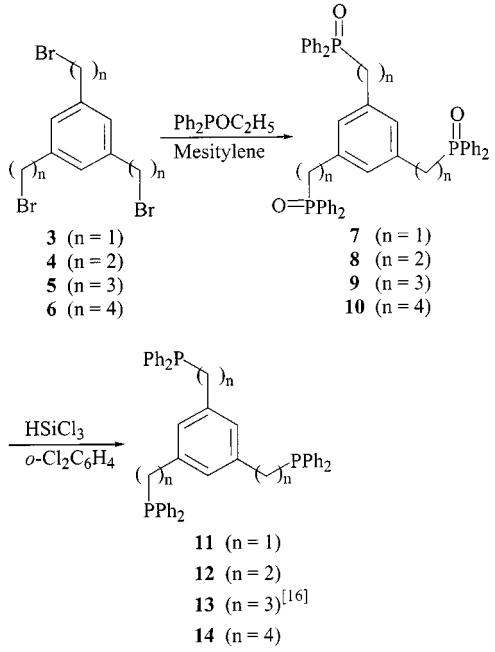

Scheme 2

Crystal Structures of 9 and 12

To obtain more detailed structural information about the trifunctional phosphane oxides and their oxygen-free analogues, X-ray structural analyses were performed on compounds **9** and **12** (Scheme 2). ORTEP drawings of their molecular structures with atom labeling are depicted in Figures 2 and 3. Although the crystal structure of **9** is of restricted quality, it can be used for a brief discussion. Because **9** has a C_3 axis of symmetry which is passing through the center of the benzene ring all three phosphane arms are equivalent. This fact gives rise to several structural implications. All distances between the phosphorus and carbon atoms of the central benzene ring are equal [5.307(5) Å] and the P1−C2, P1A−C2A, and P1B−C2B axes are bent towards the plane of the central benzene ring by an angle of 144.2(6)°. A further consequence is that the phosphorus atoms are located at the vertices of an equilateral triangle that is parallel to the benzene ring. The distance between the phosphorus atoms is 10.179(6) Å (Figure 2).

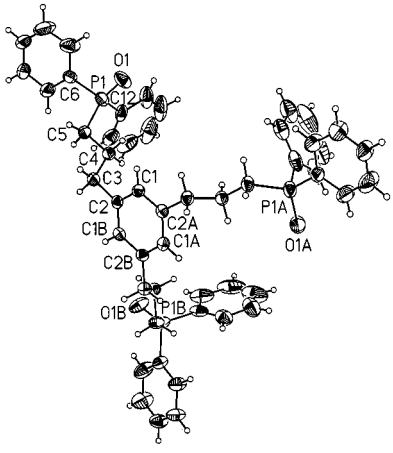

Figure 2. Molecular structure of **9** in the crystal; ORTEP plot with thermal ellipsoids at 20% probability; selected distances [Å] and angles [°]: P1−O1 1.487(4), P1−C6 1.800(5), P1−C5 1.809(4), P1−C12 1.809(8), P1−C2 5.307(5), P1−P1A = P1A−P1B = P1−P1B 10.179; C1A−C2−P1 = C1B−C2A−P1A = C1−C2B−P1B 144.2(6)

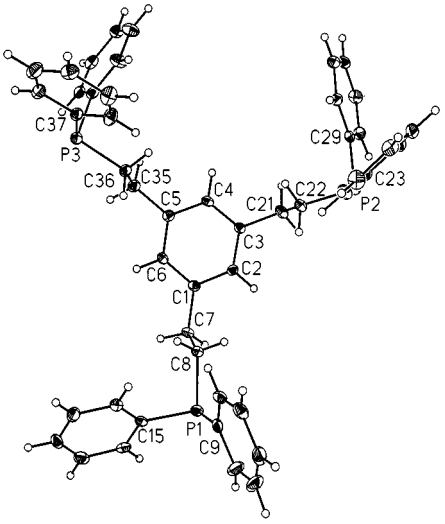

Figure 3. Molecular structure of **12** in the crystal; ORTEP plot with thermal ellipsoids at 20% probability; selected distances [Å] and angles [°]: P1−C9 1.831(7), P1−C8 1.834(5), P1−C15 1.849(5), P2−C23 1.809(6), P2−C29 1.833(5), P2−C22 1.847(5), P3−C36 1.854(5), P3−C37 1.811(7), P3−C43 1.839(5) P1−C1 4.180(3), P2−C3 4.166(3), P3−C5 4.169, P1−P2 8.672, P2−P3 9.292(4), P1−P3 9.329; C4−C1−P1 154.9(3), C6−C3−P2 157.9(4), C2−C5−P3 157.7(4)

In the structure of the phosphane **12** such a C_3 axis of symmetry is not existent. Therefore the different distances between the phosphorus atoms as well as between these and the carbon atoms of the central benzene ring are not equal (Figure 3) and the nonsymmetric triangle constituted by phosphorus atoms is not parallel to the benzene ring. The P1−C1, P2−C3 and P3−C5 axes are bent towards the plane of the benzene ring by angles of 154.9(3), 157.9(4), and 157.7(4)°, respectively.

Motifs Generated by Self-Assembly

To obtain self-assembled cyclophane structures a pre-organization of the components is a necessary prerequisite. Trifunctionalized phosphane ligands of the type **11**−**14** provide the necessary rigidity that is important for this pre-organization. For the generation of the three-dimensional platinacyclophanes **15**, **16**, and **17** the ligands **11**, **12**, and **14** were treated with $Cl_2Pt(NCPh)_2$ in dichloromethane according to the high-dilution method (Scheme 3).[19] In contrast to the platinacyclophane **1**, which was recently described,[16] the smaller cages **15** and **16** were obtained in lower yields. In particular the platinacyclophane **15** could not be isolated in pure form, since polymers and oligomers were formed as by-products, an observation which was also made by Fujita et al. with comparable nitrogen ligands.[10c] The solubility of **15** as well as these by-products is too low for separation. This property also led to the prevention of a template synthesis being performed in order to enhance the yield of **15**. Because of its better solubility **16** could be obtained as a pure compound by chromatography.

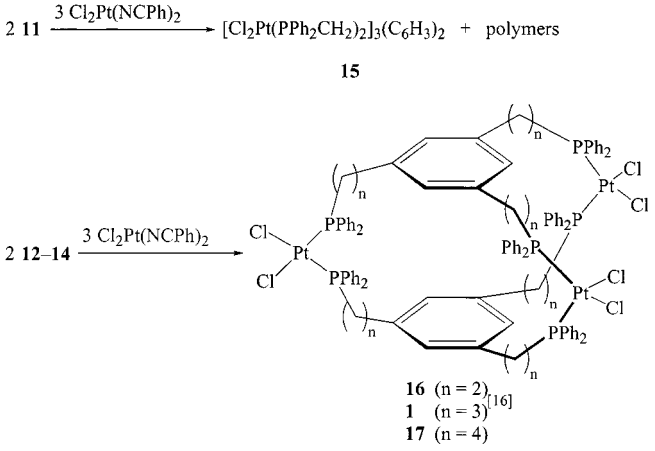

Scheme 3

Compared to **11** and **12** the behavior of ligand **14,** with four methylene units towards $Cl_2Pt(NCPh)_2$, was different. No oligomers or polymers were detected. In addition to the occurrence of the triplatinacyclophane **17** three other species **18**−**20** were isolated with increasing yields in the sequence **18** > **19** > **20** (Scheme 4). The separation of **17**−**20** was performed by column chromatography. However, **17** always contained impurities of **20**. According to their FAB mass spectra these compounds show the same molecular mass and it turned out that they are structural isomers. To optimize the yield of the triplatinacyclophane **17** the reaction between **14** and $Cl_2Pt(NCPh)_2$ was carried out at different temperatures (−70 to +40 °C) in dichloromethane. At low temperatures the yields were around 10% and decreased with increasing temperature. At 40° C the structural isomer **18** is predominant (86%) and the formation of **17** is thermodynamically unfavorable.[20] Benzene is the best solvent for the generation of **17**; it is superior to CCl_4 or $CHCl_3$.

The triplatinacyclophanes **1**, **15**−**17** and trinuclear platinacycles **18**−**20** represent colorless to pale yellow compounds that show similar solubility behavior to their corresponding ligands **11**−**14**. However, **15** is nearly insoluble in all organic solvents. The *all-trans* complex **18** transforms slowly to the *trans-cis-trans* complex **19**.

Structural information about the motifs and geometry of the platinacyles **16**−**20** is available by $^{31}P\{^1H\}$ NMR spectroscopic investigations. ^{31}P chemical shifts and $^{195}Pt-^{31}P$ coupling constants allow an unambiguous distinction between the architecture of the molecules and their stereoisomerism. Complexes with *cis* geometry show coupling constants of about 3500 Hz, whereas those with a *trans* environment reveal values of about 2500 Hz.[21] It is also well known that ^{31}P signals of *trans* isomers are shifted upfield compared to those of *cis* isomers.[21] The $^{31}P\{^1H\}$ NMR spectra of **16** and **17** each show a singlet for the six chemical equivalent phosphorus atoms at δ = 7.1 and 9.6, respectively, and a doublet for the ^{195}Pt satellites, which is typical for *cis*-PtP_2 fragments. This assignment is confirmed by $^{195}Pt\{^1H\}$ NMR spectra, which each display a triplet at δ = −4423 and −4413 with coupling constants of $^1J_{PtP}$ = 3600 and 3668 Hz, respectively. Moreover, the structure of **1** was recently confirmed by an X-ray structural analysis.[16] Because **15** was impurified by polymers and because of its low

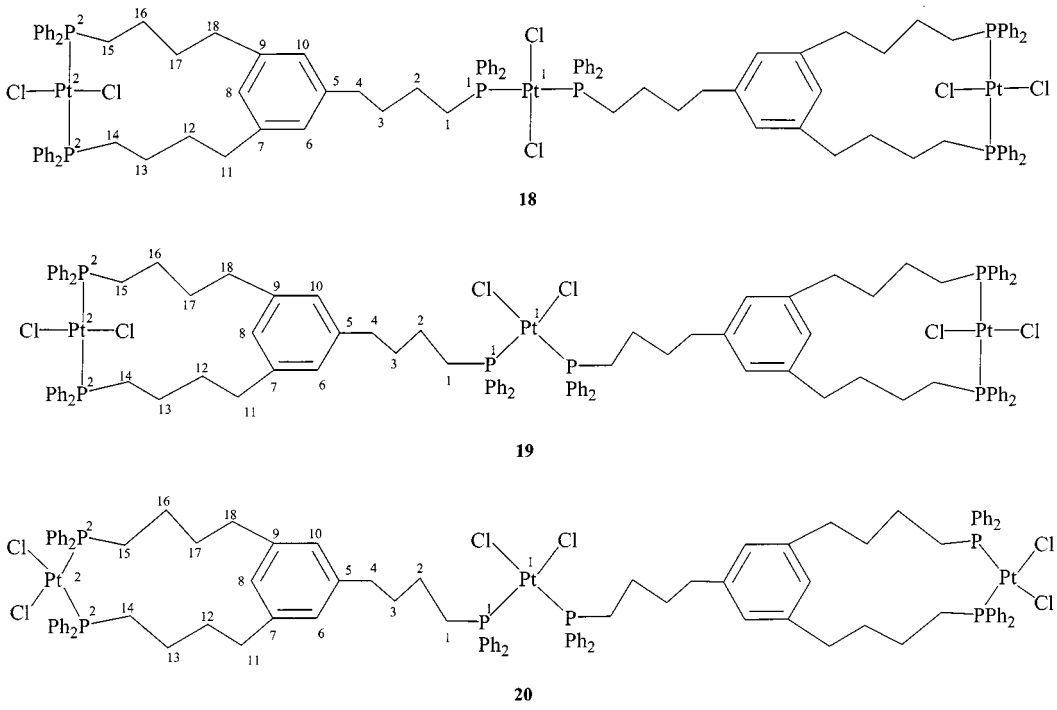

Scheme 4

solubility in all organic solvents, no exact NMR spectroscopic data were available.

In contrast to **16**, **17** (and **1**[16]) the $^{31}P\{^{1}H\}$ NMR spectra of the trinuclear platinacycles **18**−**20** show two ^{31}P singlets in a ratio of 2:1. This is a clear indication that two different ^{31}P nuclei are present. Each singlet is accompanied by a doublet as satellites that is traced back by the $^{195}Pt-^{31}P$ coupling (see Exp. Sect.). According to the chemical shifts and the size of the coupling constants, **18** is characterized by an *all-trans* structure. In the case of the metallacycle **19** the central platinum atom (Pt^1, Scheme 4) has a *cis* geometry, whereas both terminal platinum atoms (Pt^2) have a *trans* configuration. In compound **20** an *all-cis* structure was established. The fact that the terminal platinum atoms in **18**−**20** are incorporated in a cycle was confirmed by the value of the $^{195}Pt-^{31}P$ coupling constants which is higher than that of the noncyclized central platinum atom. Moreover the terminal cyclized P_2Pt moieties show higher chemical shifts than the central *trans*-P_2Pt unit. A reverse observation was made in the case of **20**.

A short discussion of the ^{1}H and $^{13}C\{^{1}H\}$ NMR spectra of the cycles **16**−**20** is with regards to the central benzene rings and the adjacent methylene groups. Only one ^{1}H signal is observed in the spectra of **16** (δ = 6.42) and **17** (δ = 6.86) for the aromatic protons. A different situation was found in the cases of **18**−**20**. Two singlets in a 2:1 ratio are assigned to H^6/H^{10} and H^8, which is in agreement with the proposed structure (Scheme 4). The methylene protons only give rise to broad unresolved signals. Two different ^{13}C resonances occur in the spectra of the cages **16** and **17** and they are ascribed to the methine (δ = 126.1) and quaternary carbon atoms [δ = 129.6 (**16**), 132.4 (**17**)] of the benzene rings. In the case of **16** the second one is split into a doublet, because of the $^{31}P-^{13}C$ coupling ($^{3}J_{PC}$ = 7 Hz). The corresponding signals for the aromatic methine and quaternary carbon atoms in the spectra of **18**−**20** are split into two peaks with an intensity of 2:1 (see Exp. Sect.). A doublet at δ = 28.6 ($^{2}J_{PC}$ = 47 Hz) in the spectrum of **16** and a singlet at δ = 35.8 in that of **17** are assigned to the methylene carbon atoms which are adjacent to the benzene rings. These resonances are split into two signals with an intensity of 2:1 in the spectra of **18**−**20**.

Conclusion

In contrast to metallacyclophanes, the chemistry of organic cyclophanes is much more developed.[3] However, within the last five to ten years several new architectures of metallacyclophanes with interesting properties have been described in the literature.[1−3,5,6] This new variant of cyclophanes is available by self-assembly of multifunctional ligands with suitable metal fragments. In the present investigation a simple strategy was introduced that allows a convenient access to trifunctional phosphanes. They are provided with a central benzene ring with three phosphane arms in a symmetrical 1,3,5-position. The distance of these phosphanes from the benzene ring is controlled by methylene functions of different length. Ligands of this type cannot be used only for the generation of metallocyclophanes, but also as the first generation of dendrimers[10b,22] and for the synthesis of catalytically active transition metal complexes.[14a] It was demonstrated that these trifunctional phosphane ligands are capable of undergoing self-assembly

with adequate platinum complex fragments. Three items are observed that affect the formation of three-dimensional platinacyclophanes: 1) the rigidity of the ligand system, 2) steric factors, and 3) intramolecular chelation. The first point is predominant in the formation of cages with a trisphosphane that contains no methylene groups between the central benzene ring and the phosphorus donors. Therefore, the system appears to be rigid and it is not possible for the phosphanes to avoid contact between each other to reduce the steric congestion caused by the phenyl substituents. Also the P-donors are too far away from a metal center to give intramolecular chelation.[10b] By the introduction of methylene groups and by increasing their number, the ligand system becomes more flexible and the phosphane moieties are able to move away from each other to minimize the interactions and hence the steric demand. This was clearly observed in the crystallization patterns of these systems from triclinic (**7**, one phosphane group is in the opposite direction of the other two[23]), via monoclinic (**12**, this report) to cubic (**9**, this report) for trifunctional phosphanes with one, two, and three methylene groups, respectively, as was shown from X-ray crystal structural analyses. However, the introduction of only one methylene group is not enough to reduce the steric hindrance, which means intermolecular chelation results in the favored formation of polymers. The flexibility of a phosphane system with four methylene bridges is accompanied by a release of the steric factor and thus enables intramolecular chelation. This is the reason that the formation of the chain-like platinacycles **18**−**20** are favored compared with that of the cage **17**. The optimum for self-assembly is obtained if the ligand contains three methylene groups.

Experimental Section

General: All synthetic reactions and manipulations were performed under dry argon using standard Schlenk techniques. *n*-Pentane and TMEDA were freshly distilled from $LiAlH_4$, dichloromethane from calcium hydride, benzene from sodium benzophenone ketyl, and mesitylene and *o*-dichlorobenzene from molecular sieves (5 Å). − Column chromatography: Activated silica gel, 0.063−0.200 mm or 0.04−0.063 (Merck); column dimensions are reported in the specific sections describing the synthesis of the compounds. − Purifications by thin layer chromatography were carried out on preparative TLC glass plates (20 × 20 cm) using silica gel 60 F254, 0.5 mm (Merck). − Elemental analysis: Elementar Vario EL analyzer. − Mass spectra: EI-MS: Finnigan TSQ 70 eV (200 °C); FD and FAB-MS: Finnigan 711A (8 kV), modified by AMD. − IR: Bruker IFS 48 FT-IR. − ^1H, $^{13}C\{^1H\}$, $^{31}P\{^1H\}$, and $^{195}Pt\{^1H\}$ NMR: Bruker DRX-250 spectrometer operating at 250.13, 62.90, 101.26, and 53.55 MHz, respectively. ^1H NMR chemical shifts were referenced with TMS as the internal standard. $^{13}C\{^1H\}$ NMR chemical shifts were calibrated against the deuterated solvent multiplet and referenced to TMS. $^{31}P\{^1H\}$ NMR chemical shifts were measured relative to external 85% H_3PO_4 with downfield values being taken as positive. $^{195}Pt\{^1H\}$ NMR chemical shifts were measured relative to external 37.5% $Na_2[PtCl_6]\cdot 6\,H_2O$. − Compounds **3**,[24] **4**,[25] **2**,[26] ethyl diphenylphosphinite,[27] $Cl_2Pt(NCPh)_2$,[28] and **14**[29] were synthesized according to the literature methods.

1,3,5-Tris(3′-bromopropyl)benzene (5): Pyrophoric **2**, prepared from *n*-butyllithium (500 mL, 15% in *n*-hexane), TMEDA (92.97 g, 800 mmol) and mesitylene (16.4 g, 136 mmol), was suspended in *n*-pentane (250 mL) and added in portions to a solution of 1,2-dibromoethane (150 g, 800 mmol) in *n*-pentane (200 mL) at −85 °C. After stirring for 2 h, the resulting mixture was allowed to warm slowly to room temperature. After neutralization, the organic phase was separated and the aqueous phase was extracted twice with CH_2Cl_2. The combined organic extracts were dried (Na_2SO_4) and the volatile materials were distilled. The residual material was subjected to column chromatography (30 × 7 cm, *n*-hexane) to afford a colorless oil. Yield 12.0 g, 20%. − ^1H NMR ($CDCl_3$): δ = 1.36 (quint, $^3J_{HH}$ = 7.0 Hz, 6 H, CH_2CH$_2$Br), 2.73 (t, $^3J_{HH}$ = 7.4 Hz, 6 H, CH_2CH$_2$CH$_2$Br), 3.40 (t, $^3J_{HH}$ = 6.6 Hz, 6 H, CH$_2$CH_2Br), 6.88 (s, 3 H, aromatic H). − $^{13}C\{^1H\}$ NMR ($CDCl_3$): δ = 33.4 (CH_2Br), 34.0 (*C*H$_2$CH$_2$Br), 34.3 (*C*H$_2$CH$_2$CH$_2$Br), 126.8 (aromatic CH), 141.2 (aromatic C). − MS (70 eV, EI, 200 °C): *m*/*z* (%) = 438 (27), 440 (92), 442 (100), 444 (27) [M^+], 363 (4), 361 (8), 359 (5) [M^+ − Br], 331 (41), 333 (69), 335 (40) [M^+ − CH_2CH_2Br].

1,3,5-Tris(diphenylphosphorylmethyl)benzene (7): A modification to the literature procedure was applied.[30] To a suspension of **3** (4.25 g, 12 mmol) in mesitylene (20 mL), Ph_2POEt (15.37 g, 67 mmol) was added. Heating of the reaction mixture to 110 °C afforded a colorless solution. After heating of the reaction mixture to 150 °C for 2 h, a white precipitate was formed. The solid was collected and crystallized from hot benzene, to afford a colorless solid. Yield 8.0 g, 93%, m.p. 210−211 °C (m.p.[30] 205−206 °C). − ^1H NMR ($CDCl_3$): δ = 3.44 (d, $^3J_{PH}$ = 13.8 Hz, 6 H, CH_2P), 6.96 (d, $^4J_{PH}$ = 1.9 Hz, 3 H, aromatic C_6H_3), 7.47−7.50 (m, 18 H, *ortho*- and *para*-P−C_6H_5), 7.59 (m, 12 H, *meta*-P−C_6H_5). − $^{13}C\{^1H\}$ NMR ($CDCl_3$): δ = 37.7 (d, $^1J_{PC}$ = 66.9, *C*H$_2$P), 123.6 (s, *tert*-C_6H_3), 128.6 (d, $^3J_{PC}$ = 12.1 Hz, *meta*-C_6H_5), 130.6 (m, *quat*-C_6H_3), 131.1 (d, $^2J_{PC}$ = 9.3 Hz, *ortho*-C_6H_5), 131.8 (s, *para*-C_6H_3), 137.4 (d, $^1J_{PC}$ = 99.6 Hz, *ipso*-C_6H_5). − $^{31}P\{^1H\}$ NMR ($CDCl_3$): δ = 30.9. − IR (KBr): $\tilde{\nu}$ = 3053, 3024 (aromatic CH), 2950, 2893 (CH_2), 1437 (P−Ph), 1198 (P=O) cm^{-1}. − MS (70 eV, EI, 200 °C): *m*/*z* (%) = 720 (1) [M^+], 596 (9) [M^+ − P(O)Ph], 519 (5) [M^+ − $P(O)Ph_2$], 201 (100) [$P(O)Ph_2^+$].

1,3,5-Tris(2′-diphenylphosphorylethyl)benzene (8): To a suspension of **4** (3.99 g, 10 mmol) in mesitylene (20 mL), Ph_2POEt (14.0 g, 61 mmol) was added. Heating of the reaction mixture to 90 °C afforded a colorless solution. The procedure continued as outlined for **7** to afford a colorless solid. Yield 7.0 g, 98%, m.p. 234−235 °C. − ^1H NMR ($CDCl_3$): δ = 2.49 (m, 6 H, CH_2P), 2.82 (m, 6 H, CH_2CH$_2$P), 6.79 (s, 3 H, C_6H_3), 7.42−7.55 (m, 18 H, *ortho*- and *para*-P−C_6H_5), 7.75 (m, 12 H, *meta*-P−C_6H_5). − $^{13}C\{^1H\}$ NMR ($CDCl_3$): δ = 27.5 (d, $^3J_{PC}$ = 2.14 Hz, *C*H$_2$CH$_2$P), 32.0 (d, $^1J_{PC}$ = 69.0, *C*H$_2$P), 126.1 (s, *tert*-C_6H_3), 128.9 (d, $^3J_{PC}$ = 11.4 Hz, *meta*-C_6H_5), 130.9 (d, $^2J_{PC}$ = 9.3 Hz, *ortho*-C_6H_5), 132.0 (d, $^4J_{PC}$ = 2.14 Hz, *para*-C_6H_5), 132.8 (d, $^1J_{PC}$ = 99.6 Hz, *ipso*-C_6H_5), 142.1 (d, $^3J_{PC}$ = 14.9 Hz, *quat*-C_6H_3). − $^{31}P\{^1H\}$ NMR ($CDCl_3$): δ = 32.7. − IR (KBr): $\tilde{\nu}$ = 3052, 3022 (aromatic CH), 2935 (CH_2), 1438 (P−Ph), 1188 (P=O) cm^{-1}. − MS (70 eV, EI, 200 °C): *m*/*z* (%) = 560 (37) [M^+ − $P(O)Ph_2$], 359 (100) [M^+ − 2P(O)Ph_2], 201 (56) [$P(O)Ph_2^+$]. − MS (FD, CH_2Cl_2, 30 °C): *m*/*z* (%) = 763 (100) [M^+]. − $C_{48}H_{45}O_3P_3$ (762.8): MS (HR, pos. FAB, NBA, 50 °C): *m*/*z* = 763.25960 [M^+]; calcd. 763.26599. − $C_{48}H_{45}O_3P_3$ (762.8): calcd. C 75.58, H 5.95; found C 75.36, H 5.82.

1,3,5-Tris[3′-(diphenylphosphoryl)propyl]benzene (9): Ph_2POEt (4.70 g, 20.4 mmol) was added to a suspension of **4** (1.50 g, 3.4 mmol) in mesitylene (20 mL). Heating of the reaction mixture

to 70 °C afforded a colorless solution. After heating of the reaction mixture to 150 °C for 4 h, the volatile materials were removed under vacuum at 90 °C. The residue was solidified after cooling. A colorless solid product was obtained upon crystallization from benzene/*n*-hexane. Yield 2.54 gm, 93%, m.p. 115 °C. – ^{1}H NMR ($CDCl_3$): δ = 1.90 (m, 6 H, CH_2P), 2.24 (m, 6 H, CH_2CH$_2$P), 2.61 (t, $^3J_{HH}$ = 7.4 Hz, 6 H, CH_2CH$_2$CH$_2$P), 6.70 (s, 3 H, C_6H_3), 7.39–7.51 (m, 18 H, *ortho*- and *para*-P–C_6H_5), 7.68 (m, 12 H, *meta*-P–C_6H_5). – ^{13}C{^{1}H} NMR ($CDCl_3$): δ = 23.0 (d, $^2J_{PC}$ = 3.4, CH$_2$*C*H$_2$CH$_2$P), 29.2 (d, $^1J_{PC}$ = 71.4 Hz, *C*H$_2$P), 37.1 (d, $^3J_{PC}$ = 14.8 Hz, *C*H$_2$CH$_2$CH$_2$P), 126.5 (s, *tert*-C_6H_3), 129.1 (d, $^3J_{PC}$ = 12.1 Hz, *meta*-C_6H_5), 130.7 (d, $^2J_{PC}$ = 8.8 Hz, *ortho*-C_6H_5), 131.8 (d, $^4J_{PC}$ = 2.7 Hz, *para*-C_6H_5), 133.0 (d, $^1J_{PC}$ = 98.4 Hz, *ipso*-C_6H_5), 141.2 (s, *quat*-C_6H_3). – ^{31}P{^{1}H} NMR ($CDCl_3$): δ = 33.8. – IR (KBr): ṽ = 3054, 3055 (CH_2), 2960, 2934 (aromatic CH), 1184 (P=O) cm^{-1}. – MS (pos. FAB, NBA, 50 °C): *m*/*z* (%) = 805 (37) [M$^+$ + H], 603 (9) [M$^+$ – P(O)Ph$_2$], 589 (15) [M$^+$ – CH$_2$P(O)Ph$_2$], 576 (2) [M$^+$ – CH$_2$CH$_2$P(O)Ph$_2$], 229 (16) [CH$_2$CH$_2$P(O)Ph$_2^+$], 215 (100) [CH$_2$P(O)Ph$_2^+$], 201 (55) [P(O)Ph$_2^+$]. – $C_{51}H_{51}O_3P_3$ (804.9). – MS (HR, pos. FAB, NBA, 50 °C): *m*/*z* = 805.31829 [M$^+$]; calcd. 805.31294. – $C_{51}H_{51}O_3P_3$ (804.9): calcd. C 76.11, H 6.39; found C 76.39, H 6.40.

1,3,5-Tris(diphenylphosphanylmethyl)benzene (11): A suspension of **3** (1.23 g, 1.7 mmol) in *o*-dichlorobenzene (10 mL) was heated in a three-necked 100-mL round-bottom flask, equipped with reflux condenser. The suspension became a clear solution at about 90 °C. The reaction mixture was further heated to 120 °C. At this temperature trichlorosilane (2.10 g, 15.5 mmol) was added dropwise through a septum. After 2 h, the reaction mixture was allowed to cool slowly to room temperature. The reaction mixture was neutralized by degassed sodium hydroxide (20%, 40 mL) which was added through a dropping funnel at –10 °C (ice/salt bath). The organic layer was separated and the aqueous layer was extracted with dichloromethane (3 × 30 mL). The combined organic extracts were dried (Na_2SO_4) filtered (P3) and dried in vacuum to give a colorless solid. Yield 1.1 g, 96%, m.p. 58 °C. – ^{1}H NMR ($CDCl_3$): δ = 3.08 (s, 6 H, CH_2P), 6.50 (s, 3 H, C_6H_3), 7.18 (s, 30 H, P–C_6H_5). – ^{13}C{^{1}H} NMR ($CDCl_3$): δ = 35.9 (d, $^1J_{PC}$ = 15.7 Hz, *C*H$_2$P), 128.4 (d, $^3J_{PC}$ = 6.4 Hz, *meta*-C_6H_5), 128.7 (s, *para*-C_6H_3), 130.7 (s, *tert*-C_6H_3), 133.0 (d, $^2J_{PC}$ = 18.5 Hz, *ortho*-C_6H_5), 137.4 (dt, $^2J_{PC}$ = 8.5 Hz, $^4J_{PC}$ = 1.4 Hz, *quat*-C_6H_3), 138.6 (d, $^1J_{PC}$ = 15.7 Hz, *quat*-C_6H_5). – ^{31}P{^{1}H} NMR ($CDCl_3$): δ = –9.4. – IR (KBr): ṽ = 3070, 3050 (aromatic CH), 2925, 2904 (CH_2), 1432 (P–Ph) cm^{-1}. – MS (70 eV, EI, 200 °C): *m*/*z* (%) = 672 (37) [M$^+$], 595 (3) [M$^+$ – Ph], 487 (37) [M$^+$ – Ph$_2$], 301 (25) [M$^+$ – 2PPh$_2$]. – $C_{45}H_{39}P_3$ (672.7): MS (HR, 70 eV, EI, 210 °C): *m*/*z* = 672.230597 [M$^+$]; calcd. 672.226445. – $C_{45}H_{39}P_3$ (672.7): calcd. C 80.35, H 5.84; found C 80.04, H 5.85.

1,3,5-Tris[(2′-diphenylphosphanyl)ethyl]benzene (12): The same procedure outlined for **11** was applied for the synthesis of **12**. A suspension of compound **8** (3.05 g, 4.0 mmol) in *o*-dichlorobenzene (10 mL) became a colorless solution at 110 °C. After reduction with trichlorosilane (4.94 g, 36.5 mmol) and work-up, a white solid was obtained. Yield 2.80 g, 98%, m.p. 108–109 °C. – ^{1}H NMR ($CDCl_3$): δ = 2.32 (m, 6 H, CH_2P), 2.66 (m, 6 H, CH_2CH$_2$P), 6.78 (s, 3 H, C_6H_3), 7.33–7.35 (m, 18 H, *ortho*- and *para*-P–C_6H_5), 7.45 (m, 12 H, *meta*-P–C_6H_5). – ^{13}C{^{1}H} NMR ($CDCl_3$): δ = 30.3 (d, $^2J_{PC}$ = 12.8 Hz, *C*H$_2$CH$_2$P), 32.3 (d, $^1J_{PC}$ = 18.5 Hz, CH$_2$P), 125.9 (s, *tert*-C_6H_3), 128.6 (d, $^3J_{PC}$ = 7.1 Hz, *meta*-C_6H_5), 128.8 (s, *para*-C_6H_5), 132.9 (d, $^2J_{PC}$ = 18.5 Hz, *ortho*-C_6H_5), 138.7 (d, $^1J_{PC}$ = 12.8 Hz, *ipso*-C_6H_5), 143.1 (d, $^3J_{PC}$ = 12.8 Hz, *quat*-C_6H_3). – ^{31}P{^{1}H} NMR ($CDCl_3$): δ = –14.3. – IR (KBr): ṽ = 3068, 3051 (aromatic CH), 2940, 2924 (CH_2), 1479 (P–Ph) cm^{-1}. – MS (70 eV, EI, 200 °C): *m*/*z* (%) = 714 (13) [M$^+$], 637 (7) [M$^+$ – Ph], 529 (27) [M$^+$ – Ph$_2$]. – $C_{48}H_{45}P_3$ (714.8): MS (HR, pos. FAB, NBA, 50 °C): *m*/*z* = 715.26919; found 715.26919. – $C_{48}H_{45}P_3$ (714.8): calcd. C 80.66, H 6.35; found C 80.56, H 6.15.

1,3,5-Tris[(3′-diphenylphosphanyl)propyl]benzene (13): The same procedure outlined for **11** was applied for the synthesis of **13**. A suspension of compound **9** (1.29 g, 1.6 mmol) in *o*-dichlorobenzene (10 mL) became a colorless solution at 80 °C. After reduction with trichlorosilane (2.0 g, 14.8 mmol) and work-up, a colorless oil was obtained. Yield 1.10 g, 91%. – ^{1}H NMR ($CDCl_3$): δ = 1.74 (m, 6 H, CH_2CH$_2$P), 2.08 (m, 6 H, CH$_2$CH_2P), 2.66 (t, $^3J_{HH}$ = 7.4 Hz, 6 H, CH_2CH$_2$CH$_2$P), 6.73 (s, 3 H, *tert*-C_6H_3), 7.33 (m, 18 H, *ortho*- and *para*-P–C_6H_5), 7.41 (m, 12 H, *meta*-P–C_6H_5). – ^{13}C{^{1}H} NMR ($CDCl_3$): δ = 27.6 (d, $^2J_{PC}$ = 6.1 Hz, *C*H$_2$CH$_2$P), 27.7 (d, $^1J_{PC}$ = 20.9 Hz, CH$_2$P), 37.2 (d, $^3J_{PC}$ = 14.2 Hz, *C*H$_2$CH$_2$CH$_2$P), 126.4 (s, *tert*-C_6H_3), 128.6 (d, $^3J_{PC}$ = 6.7 Hz, *meta*-C_6H_5), 128.9 (s, *para*-C_6H_5), 132.9 (d, $^2J_{PC}$ = 17.5 Hz, *ortho*-C_6H_5), 138.3 (d, $^1J_{PC}$ = 10.1 Hz, *ipso*-C_6H_5), 141.9 (s, *quat*-C_6H_3). – ^{31}P{^{1}H} NMR ($CDCl_3$): δ = –14.8. – MS (70 eV, EI, 200 °C): *m*/*z* (%) = 756 (53) [M$^+$], 571 (28) [M$^+$ – PPh$_2$], 557 (29) [M$^+$ – CH$_2$PPh$_2$], 543 (35) [M$^+$ – CH$_2$CH$_2$PPh$_2$], 199 (100) [CH$_2$PPh$_2$]$^+$. – MS (pos. FAB, NBA, 50 °C): *m*/*z* (%) = 757 (16) [M$^+$ + H], 571 (7) [M$^+$ – PPh$_2$], 557 (7) [M$^+$ – CH$_2$PPh$_2$], 543 (5) [M$^+$ – CH$_2$CH$_2$PPh$_2$], 199 (100) [CH$_2$PPh$_2^+$].

Preparation of the Triplatinacyclophanes 15–17 and the Trinuclear Platinacycles 18–20: Solutions of Cl_2Pt(NCPh)$_2$ (708 mg, 1.5 mmol) and the corresponding ligand (1.0 mmol) in dichloromethane (250 mL each) were simultaneously added dropwise during 36 h into stirred dichloromethane (600 mL). After the addition was complete, the reaction mixture was stirred for 24 h at room temperature. The solvent was then removed under vacuum and the resulting residue was subjected to column chromatography.

3,3,14,14,25,25-Hexachloro-2,2,4,4,13,13,15,15,24,24,26,26-dodecaphenyl-2,4,13,15,24,26-hexaphospha-3,14,25-triplatina[5$_3$]-(1,3,5)-cyclophane (15): Yield 54 mg, 5%, white solid, m.p. 273–275 °C. – ^{1}H NMR ($CDCl_3$): δ = 3.9 (br. s, CH_2P), 6.68 (s, C_6H_3), 7.31–7.65 (m, C_6H_5). – ^{31}P{^{1}H} NMR ($CDCl_3$): δ = 15.8 (t, $^1J_{PtP}$ = 2548 Hz). – IR (KBr): ṽ = 3050 (aromatic CH), 2928 (CH_2), 1435 cm^{-1} (P–Ph). – MS (neg. FAB, NBA, 50 °C): *m*/*z* = 2180 [M$^-$ + Cl]. – $C_{90}H_{78}Cl_6P_6Pt_3$ (2143.3): calcd. C 50.43, H 3.67; found C 49.98, H 3.40.

4,4,17,17,30,30-Hexachloro-3,3,5,5,16,16,18,18,29,29,31,31-dodecaphenyl-3,5,16,18,29,31-hexaphospha-4,17,30-triplatina[7$_3$]-(1,3,5)-cyclophane (16): Yield 56 mg, 15%, white solid, m.p. 241–242 °C. – ^{1}H NMR ($CDCl_3$): δ = 2.64, 2.36 (br. s, 24 H, CH_2P, CH_2CH$_2$P), 6.42 (s, 6 H, C_6H_3), 7.11–7.49 (m, 60 H, C_6H_5). – ^{13}C{^{1}H} NMR (62.90 MHz, $CDCl_3$, 25 °C): δ = 22.2 (d, $^1J_{PC}$ = 90 Hz, *C*H$_2$P), 28.6 (d, $^2J_{PC}$ = 47 Hz, *C*H$_2$CH$_2$P), 126.1(s, *tert*-C_6H_3), 128.1 (d, $^3J_{PC}$ = 20 Hz, *meta*-C_6H_5), 129.6 (m, *ipso*-C_6H_5), 129.9 (s, *para*-C_6H_5), 131.6 (d, $^2J_{PC}$ = 23 Hz, *ortho*-C_6H_5), 140.3 (m, *quat*-C_6H_3). – ^{31}P{^{1}H} NMR ($CDCl_3$): δ = 7.14 (sd, $^1J_{PtP}$ = 3600 Hz). – ^{195}Pt NMR ($CDCl_3$): δ = –4423 (t, $^1J_{PtP}$ = 3600 Hz). – IR (KBr): ṽ = 3051 (aromatic CH), 2923 (CH_2), 1434 (P–Ph) cm^{-1}. – MS (neg. FAB, NBA, 50 °C): *m*/*z* = 2262 [M$^-$ + Cl]. – $C_{96}H_{90}Cl_6P_6Pt_3$ (2227.5): calcd. C 51.76, H 4.07; found C 51.53, H 4.10.

6,6,29,29,40,40-Hexachloro-5,5,7,7,22,22,24,24,39,39,41,41-dodecaphenyl-5,7,22,24,39,41-hexaphospha-6,23,40-triplatina[11$_3$]-(1,3,5)-cyclophane (17): Yield 108 mg, 9%, colorless amorphous solid, m.p. 230 °C. – ^{1}H NMR ($CDCl_3$): δ = 1.65 (br. s, 24 H,

$CH_2CH_2CH_2P$), 2.37 (s, 12 H, CH_2P), 2.55 (s, 12 H, $CH_2CH_2CH_2CH_2P$), 6.86 (s, 6 H, *tert*-C_6H_3), 7.1−7.7 (m, 60 H, P−C_6H_5). − $^{13}C\{^1H\}$ NMR ($CDCl_3$): δ = 24.4 (s, $CH_2CH_2CH_2CH_2P$), 25.9 (d, $^2J_{PC}$ = 45 Hz, CH_2CH_2P), 32.9 (d, $^1J_{PC}$ = 16 Hz, CH_2P), 35.8 (s, $CH_2CH_2CH_2CH_2P$), 126.1 (s, *tert*-C_6H_3), 128.3 (t, $^3J_{PC}$ = 5.7 Hz, *meta*-P−C_6H_5), 131.1 (s, *para*-P−C_6H_5), 132.4 (m, *ipso*-P−C_6H_5), 133.5 (t, $^2J_{PC}$ = 6.3 Hz, *ortho*-P−C_6H_5), 143.4 (s, *quat*-C_6H_3). − $^{31}P\{^1H\}$ NMR ($CDCl_3$): δ = 9.6 (sd, $^1J_{PtP}$ = 3668 Hz). − ^{195}Pt NMR ($CDCl_3$): δ = − 4413 (t, $^1J_{PtP}$ = 3668 Hz). − IR (KBr): $\tilde{\nu}$ = 3051 (aromatic CH), 2925, 2853 (CH_2), 1435 (P−Ph) cm^{-1}. − MS (neg. FAB, NBA, 50 °C): *m/z* = 2395 [M^-]. − (pos. FAB, NBA, 50 °C): *m/z*: 2359 [M^+ − Cl]. − $C_{108}H_{114}Cl_6P_6Pt_3$ (2395.9): calcd. C 54.14, H 4.80; found C 54.40, H 4.71.1

Compound 18: Yield 60 mg, 5%, colorless amorphous solid, m.p. 158 °C. − ^1H NMR ($CDCl_3$): δ = 1.51, 1.71 (br. s, 24 H, H2,3,12,13,16,17, for labeling see Scheme 4), 2.23 (m, 4 H, H-1), 2.37 (m, 12 H, H-4,-11,-18), 2.51 (br. s, 8 H, H-14,-15), 6.65 (s, 4 H, H-6, -10), 6.98 (s, 2 H, H-8), 7.2−7.7 (m, 60 H, P−C_6H_5). − $^{13}C\{^1H\}$ NMR ($CDCl_3$): δ = 21.7 (s, C12,17), 22.0 (s, C3), 22.8 (d, $^2J_{PC}$ = 41 Hz, C2), 23.1 (d, $^2J_{PC}$ = 46 Hz, C13,16), 30.9 (t, $^1J_{PC}$ = 16 Hz, C14,15), 32.0 (t, $^1J_{PC}$ = 13 Hz, C1), 33.7 (s, C11,18), 34.4 (s, C4), 125.5 (s, C6,10), 126.0 (s, C8), 127.1 (t, $^3J_{PC}$ = 5 Hz, *meta*-P−C_6H_5), 129.3 (s, *para*-P−C_6H_5), 129.7 (m, *ipso*-P^2−C_6H_5), 129.9 (m, *ipso*-P^1−C_6H_5), 132.4 (t, $^2J_{PC}$ = 6 Hz, *ortho*-P^2−C_6H_5), 132.7 (t, $^2J_{PC}$ = 6 Hz, *ortho*-P^1−C_6H_5), 140.3 (s, C7,9), 141.2 (s, C5). − $^{31}P\{^1H\}$ NMR ($CDCl_3$): δ = 13.6 (sd, $^1J_{PtP}$ = 2534 Hz, 2P, P^1), 14.8 (sd, $^1J_{PtP}$ = 2566 Hz, 4P, P^2). − $^{195}Pt\{^1H\}$ NMR ($CDCl_3$): δ = −3973 (t, $^1J_{PtP}$ = 2566 Hz, 2Pt, Pt^2), −3960 (t, $^1J_{PtP}$ = 2534 Hz, 1Pt, Pt^1). − IR (KBr): $\tilde{\nu}$ = 3053, 3006 (aromatic CH), 2926, 2854 (CH_2), 1434 (P−Ph) cm^{-1}. − MS (neg. FAB, NBA, 50 °C): *m/z* = 2395 [M^-]. − $C_{108}H_{114}Cl_6P_6Pt_3$ (2395.9): calcd. C 54.14, H 4.80, found C 54.32, H 4.81.

Compound 19: Yield 240 mg, 20%, pale yellow amorphous solid, m.p. 171 °C. − ^1H NMR ($CDCl_3$): δ = 1.50, 1.70 (br. s, 24 H, H-2,3,12,13,16,17), 2.23 (m, 4 H, H-1), 2.37 (m,12 H, H-4,-11,-18), 2.54 (br. s, 8 H, H-14,-15), 6.60 (s, 4 H, H-6,-10), 6.98 (s, 2 H, H-8), 7.1−7.6 (m, 60 H, P−C_6H_5). − $^{13}C\{^1H\}$ NMR ($CDCl_3$): δ = 22.0 (s, C3,12,17), 23.4 (s, $^2J_{PC}$ = 37 Hz, C13,16), 23.8 (d, $^2J_{PC}$ = 38 Hz, C2), 30.9 (t, $^1J_{PC}$ = 17 Hz, C14,15), 31.6 (t, $^1J_{PC}$ = 16 Hz, C1), 33.7 (s, C11,18), 34.2 (s, C4), 125.4 (s, C6,10), 126.1 (s, C8), 127.0 (t, $^3J_{PC}$ = 5 Hz, *meta*-P−C_6H_5), 129.3 (s, *para*-P−C_6H_5), 129.7 (m, *ipso*-P^1−C_6H_5), 129.9 (m, *ipso*-P^2−C_6H_5), 132.4(t, $^2J_{PC}$ = 6 Hz, *ortho*-P−C_6H_5), 140.4 (s, C7,9), 140.9 (s, C5). −

Table 1. Crystal data, data collection and structure refinement for compounds **9** and **12**

	9	**12**
Crystal data		
Empirical formula	$C_{51}H_{51}O_3P_3$	$C_{48}H_{45}P_3$
Molecular mass	804.83	714.75
Crystal system	cubic	monoclinic
Space group	$Pa\bar{3}$	$P2_1/n$
Z	8	4
$d_{calcd.}$ [g/cm^3]	0.964	1.192
a [Å]	22.303(4)	16.112(4)
b [Å]	22.303(4)	10.602(17)
c [Å]	22.303(4)	23.607(6)
β [°]	90	99.118(14)
V *[A^3]*	11094(4)	3982(6)
μ [mm^{-1}]	0.140	0.182
F(000)	3408	1512
Data collection		
Radiation	Mo-K_α	Mo-K_α
Monochromator	graphite	graphite
Wave length [Å]	0.71073	0.71073
Crystal size [mm^3]	0.35 × 0.35 × 0.35	0.15 × 0.55 × 0.15
Temperature [K]	298(2)	293(2)
Scan mode	ω	ω
$\theta_{min/max}$ [°]	2.04/27.50	2.11/27.52
hkl range	$-1 \le h \le 28$	$-20 \le h \le 2$
	$-1 \le k \le 28$	$-13 \le k \le 13$
	$-28 \le l \le 1$	$-30 \le l \le 30$
Measured reflections	14521	20325
Independent reflections	4248 (R_{int} = 0.0680)	9147 (R_{int} = 0.1798)
Absorption correction	None	None
Refinement		
Refinement method	full-matrix least squares on F^2	full-matrix least squares on F^2
Data/restraints/parameters	4248/0/173	9147/0/461
Hydrogen treatment	calculated	calculated
Final *R* values [$I > 2\sigma(I)$]		
*R*1[a]	0.1358	0.0879
*wR*2[b]	0.3171	0.1920
$\rho_{residual}$(max/min) [e Å^{-3}]	1.060/−0.291	0.907/−0.867

[a] $R1 = ||F_o| - |F_c||/|F_o|$. − [b] $wR2 = \{ [w(F_o^2 - F_c^2)^2]/[[w(F_o^2)]\}^{1/2}$; $w = 1/[\delta^2(F_o^2) + (ap)^2 + bp]$; $p = (F_o^2 + 2F_c^2)/3$; $a = 0.0946$; $b = 8.58$; $S = \{[w(F_o^2 - F_c^2)^2]/(n - p)\}^{1/2}$.

$^{31}P\{^1H\}$ NMR ($CDCl_3$): δ = 8.7 (sd, $^1J_{PtP}$ = 3648 Hz, 2 P, P^1), 14.7 (sd, $^1J_{PtP}$ = 2565 Hz, 4 P, P^2). − ^{195}Pt NMR ($CDCl_3$): δ = −3973 (t, $^1J_{PtP}$ = 2565 Hz, 2 Pt, Pt^2), − 4410 (t, $^1J_{PtP}$ = 3648 Hz, 1 Pt, Pt^1). − IR (KBr): $\tilde{\nu}$ = 3052 (aromatic CH), 2925, 2854 (CH_2), 1434 cm^{-1} (P−Ph). − MS (neg. FAB, NBA, 50 °C): *m/z* = 2395 [M^-]. − $C_{108}H_{114}Cl_6P_6Pt_3$ (2395.9): calcd. C 54.14, H 4.80; found C 54.28, H 4.76.

Compound 20: Yield 720 mg, 60%, pale yellow amorphous solid, m.p. 191−193 °C. − ^1H NMR ($CDCl_3$): δ = 1.47, 1.85 (br. s, 24 H, H-2,-3,-12,-13,-16,-17), 2.13 (m, 8 H, H-14,-15), 2.37 (m, 4 H, H-1), 2.55 (br. s, 12 H, H-4,-11,-18), 6.82 (s, 4 H, H-6,-10), 6.92 (s, 2 H, H-8), 7.1−7.7 (m, 60 H, P−C_6H_5). − $^{13}C\{^1H\}$ NMR (62.90 MHz, $CDCl_3$, 25 °C): δ = 24.4 (s, C3), 24.6 (s, C12,17), 25.9 (d, $^2J_{PC}$ = 45 Hz, C2), 27.5 (d, $^2J_{PC}$ = 48 Hz, C13,16), 32.9 (t, $^1J_{PC}$ = 16 Hz, C14,15), 33.6 (t, $^1J_{PC}$ = 13 Hz, C1), 35.5 (s, C11,18), 36.0 (s, C4), 126.1 (s, C8), 126.6 (s, C6,10), 128.1 (t, $^3J_{PC}$ = 5 Hz, *meta*-P^2−C_6H_5), 128.3 (s, $^3J_{PC}$ = 5 Hz, *meta*-P^1−C_6H_5), 130.9 (s, *para*-P^2−C_6H_5), 131.1 (s, *para*-P^1−C_6H_5), 131.2 (m, *ipso*-P−C_6H_5), 133.1(t, $^2J_{PC}$ = 5 Hz, *ortho*-P^2−C_6H_5), 133.5 (t, $^2J_{PC}$= 5 Hz, *ortho*-P^1−C_6H_5), 141.8 (s, C7,9), 142.3 (s, C5). − $^{31}P\{^1H\}$ NMR ($CDCl_3$): δ = 6.7 (sd, $^1J_{PtP}$ = 3610 Hz, 4 P, P^2), 8.7 (sd, $^1J_{PtP}$ = 3635 Hz, 2 P, P^1). − ^{195}Pt NMR ($CDCl_3$): δ = − 4431 (t, $^1J_{PtP}$ = 3610 Hz, 2 Pt, Pt^2), − 4413 (t, $^1J_{PtP}$ = 3635 Hz, 1 Pt, Pt^1). − IR (KBr): $\tilde{\nu}$ = 3051 (aromatic CH), 2925, 2853 (CH_2), 1435 (P−Ph) cm^{-1}. − MS (neg. FAB, NBA, 50 °C): *m/z* = 2395 [M^-]. − $C_{108}H_{114}Cl_6P_6Pt_3$ (2395.9): calcd. C 54.14, H 4.80; found C 54.50, H 4.91.

X-ray Structure Determination of 9 and 12: Crystallographic data for both compounds are summarized in Table 1. Colorless single crystals were obtained from slow cooling of a benzene/*n*-hexane solution of **9** and slow diffusion of *n*-pentane into a solution of **12**, respectively. Each crystal was mounted on a glass fiber with the aid of perfluoropolyether RS 3000 and transferred to a Siemens P4 diffractometer (Mo-K_α radiation, graphite monochromator). The lattice constants for both compounds were determined by 25 precisely centered high-angle reflections and refined by least-square methods. Accurate unit cell parameters and orientation matrices were formed by least-squares refinement of setting angles of a set of well-centered reflections, which were found by a random search. Intensities were collected by the ω-scan technique. No absorption correction was made. While **12** crystallized in the monoclinic space group $P2_1/n$ (Z = 4), **9** crystallized in the cubic space group $Pa\bar{3}$ (Z = 8), and no solvent molecules were detected in the crystal lattice. The structures were solved by direct methods with ShelXTL V5.1 (NT version)[31] and refined by least squares using the same program with anisotropic thermal parameters for all non-hydrogen atoms. All hydrogen atoms were located in calculated positions (riding mode). Maximum and minimum peaks in the final difference synthesis were 1.076 and −0.275 (**9**), and 0.907 and −0.867 (**12**) e $Å^{-3}$, respectively. Crystallographic data (excluding structure factors) for the structures reported in this paper have been deposited with the Cambridge Crystallographic Data Centre as supplementary publication nos. CCDC-158457 (**9**) and -158456 (**12**). Copies of the data can be obtained free of charge on application to CCDC, 12 Union Road, Cambridge CB2 1EZ, UK [Fax: (internat.) + 44-1223/336-033; E-mail: deposit@ccdc.cam.ac.uk].

Acknowledgments

Support of this research by the Deutsche Forschungsgemeinschaft and the Fonds der Chemischen Industrie is gratefully acknowledged. Degussa AG is thanked for supplying starting materials.

[1] G. F. Swiegers, T. A. Malefetse, *Chem. Rev.* **2000**, *100*, 3483.
[2] [2a] B. Olenyuk, A. Fechtenkötter, P. J. Stang, *J. Chem. Soc., Dalton Trans.* **1998**, 1707. − [2b] L. R. MacGillivray, J. L. Atwood, *Angew. Chem.* **1999**, *111*, 1080; *Angew. Chem. Int. Ed.* **1999**, *38*, 1018. − [2c] M. Albrecht, *Angew. Chem.* **1999**, *111*, 3671; *Angew. Chem. Int. Ed.* **1999**, *38*, 3463.
[3] C. J. Jones, *Chem. Soc. Rev.* **1998**, *27*, 289.
[4] F. N. Diederich, *Cyclophanes*, *Royal Society of Chemistry Monographs in Supramolecular Chemistry* (Ed. J. F. Stoddart), Royal Society of Chemistry, Cambridge, **1991**.
[5] [5a] S. Hiraoka, M. Fujita, *J. Am. Chem. Soc.* **1999**, *121*, 10239. − [5b] F. Ibukuro, T. Kusukawa, M. Fujita, *J. Am. Chem. Soc.* **1998**, *120*, 8561. − [5c] T. Kusukawa, M. Fujita, *J. Am. Chem. Soc.* **1999**, *121*, 1397. − [5d] T. Kusukawa, M. Fujita, *Angew. Chem.* **1998**, *110*, 3327; *Angew. Chem. Int. Ed.* **1998**, *37*, 3142. − [5e] M. Fujita, S.-Y. Yu, T. Kusukawa, H. Funaki, K. Ogura, K. Yamaguchi, *Angew. Chem.* **1998**, *110*, 2192; *Angew. Chem. Int. Ed.* **1998**, *37*, 2082. − [5f] E. Leize, A. van Dorsselaer, R. Krämer, J.-M. Lehn, *J. Chem. Soc., Chem. Commun.* **1993**, 990. − [5g] C.-K. Chan, K.-K. Cheung, C.-M. Che, *Chem. Commun.* **1996**, 227. − [5h] P. J. Stang, B. Olenyuk, D. C. Muddinan, R. D. Smith, *Organometallics* **1997**, *16*, 3094. − [5i] M. Fujita, D. Ogura, M. Miyazama, H. Oka, K. Yamaguchi, K. Ogura, *Nature* **1995**, *378*, 469. − [5j] C. M. Harshorn, P. J. Steel, *Chem. Commun.* **1997**, 541. − [5k] S. Aoki, M. Shiro, E. Kimura, *J. Am. Chem. Soc.* **2000**, *122*, 570. − [5l] R. L. Paul, S. M. Couchman, J. C. Jefferey, J. A. McCleverty, Z. R. Reeves, M. D. Ward, *J. Chem. Soc., Dalton Trans.* **2000**, 845. − [5m] F. A. Cotton, L. M. Daniels, C. A. Murillo, *Chem. Commun.* **1999**, 841. − [5n] J. A. R. Navarro, E. Freisinger, B. Lippert, *Inorg. Chem.* **2000**, *39*, 2301.
[6] [6a] S. M. Woessner, J. B. Helms, Y. Shen, B. P. Sullivan, *Inorg. Chem.* **1998**, *37*, 5406. − [6b] K. D. Benkstein, J. T. Hupp, C. L. Stern, *Inorg. Chem.* **1998**, *37*, 5404. − [6c] M. Fujita, M. Aoyagi, K. Ogura, *Inorg. Chim. Acta* **1995**, *246*, 53. − [6d] S. Leininger, B. Olenyuk, P. J. Stang, *Chem. Rev.* **2000**, *100*, 853. − [6e] D. L. Caulder, K. N. Raymond, *J. Chem. Soc., Dalton Trans.* **1999**, 1185. − [6f] K. N. Raymond, *Acc. Chem. Res.* **1999**, *32*, 975. − [6g] E. Lindner, M. Mohr, C. Nachtigal, R. Fawzi, G. Henkel, *J. Organomet. Chem.* **2000**, *595*, 166. − [6h] E. Lindner, R. Veigel, K. Ortner, C. Nachtigal, M. Steimann, *Eur. J. Inorg. Chem.* **2000**, 959. − [6i] E. Lindner, I. Krebs, R. Fawzi, M. Steimann, B. Speiser, *Organometallics* **1999**, *18*, 480. − [6j] E. Lindner, M. F. Günther, H. A. Mayer, R. Fawzi, M. Steimann, *Chem. Ber./Recueil* **1997**, *130*, 1815. − [6k] E. Lindner, M. Pitsch, R. Fawzi, M. Steimann, *Chem. Ber.* **1996**, *129*, 639. − [6l] E. Lindner, R. Wassing, R. Fawzi, M. Steimann, *Angew. Chem.* **1994**, *106*, 363; *Angew. Chem. Int. Ed. Engl.* **1994**, *33*, 321. − [6m] E. Lindner, R. Wassing, R. Fawzi, M. Steimann, *Inorg. Chim. Acta* **1994**, *220*, 107.
[7] [7a] A. Marquis−Rigault, A. Dupont−Gervais, P. N. W. Baxter, A. van Dorsseler, J.-M. Lehn, *Inorg. Chem.* **1996**, *35*, 2307. − [7b] P. Baxter, J.-M. Lehn, A. Decian, J. Fischer, *Angew. Chem. Int. Ed. Engl.* **1993**, *32*, 69. − [7c] J.-M. Lehn, G. Baum, D. Fenske, *Chem. Eur. J.* **1999**, *5*, 102. − [7d] P. N. W. Baxter, J.-M. Lehn, B. O. Kneisel, G. Baum, D. Fenske, *Chem. Eur. J.* **1999**, *5*, 113. − [7e] J.-M. Lehn, *Supramolecular Chemistry*, VCH Publishers, Weinheim, Germany, **1995**. − [7f] A. M. Carcia, D. M. Bassani, J.-M. Lehn, G. Baum, D. Fenske, *Chem. Eur. J.* **1999**, *5*, 1234.
[8] [8a] F. Barrigelletti, L. Flamingni, J.-P. Collin, J.-P. Sauvage, *Chem. Commun.* **1997**, 333. − [8b] J.-P. Collin, P. Gavina, V. Heitz, J.-P. Sauvage, *Eur. J. Inorg. Chem.* **1998**, 1. − [8c] J.-P. Sauvage, J. P. Collin, J.-C. Chambron, S. Guillerez, C. Coudret, V. Balzani, F. Barigelletti, L. Decola, L. Flamigni, *Chem. Rev.* **1994**, *94*, 993.
[9] [9a] J.-C. Chambron, C. O. Dietrich−Buchecker, J.-P. Sauvage, *Comprehensive Supramolecular Chemistry*, Elsevier, London, **1996**, vol. 9. − [9b] M. Fujita, *Acc. Chem. Res.* **1999**, *32*, 53. − [9c] C. P. McArdle, M. J. Irwin, M. C. Jennings, R. J. Puddephat,

Angew. Chem. **1999**, *111*, 3571; *Angew. Chem. Int. Ed.* **1999**, *38*, 3376.
[10] [10a] M. Hong, Y. Zhao, W. Su, R. Cao, M. Fujita, Z. Zhou, A. S. C. Chan, *J. Am. Chem. Soc.* **2000**, *122*, 4819. – [10b] P. M. Van Calcar, M. M. Olmstead, A. L. Balch, *Chem. Commun.* **1996**, 2597. – [10c] M. Fujita, S. Nagao, K. Ogura, *J. Am. Chem. Soc.* **1995**, *117*, 1649.
[11] [11a] P. G. Edwards, J. S. Fleming, S. J. Coles, M. B. Hursthouse, *J. Chem. Soc., Dalton Trans.* **1997**, 3201. – [11b] P. G. Edwards, F. Ingold, S. J. Coles, M. B. Hursthouse, *Chem. Commun.* **1998**, 45.
[12] P. Steenwinkel, S. Kolmschot, R. A. Gossage, P. Dani, N. Veldman, A. L. Spek, G. van Koten, *Eur. J. Inorg. Chem.* **1998**, 477.
[13] T.-L. Ho, *Symmetry, A Basis for Synthesis Design*, Wiley, New York, **1995**.
[14] [14a] T. Beissel, R. E. Powers, K. N. Raymond, *Angew. Chem.* **1996**, *108*, 1166; *Angew. Chem. Int. Ed. Engl.* **1996**, *35*, 1084. – [14b] A. Müller, C. Beugholt, *Nature* **1996**, *383*, 296.
[15] I. Hargittai, M. Hargittai, *Symmetry Through the Eyes of a Chemist*, Plenum, New York, **1995**.
[16] E. Lindner, C. Hermann, G. Baum, D. Fenske, *Eur. J. Inorg. Chem.* **1999**, 679.
[17] Y. Yamagiwa, Y. Koreishi, S. Kiyozumi, M. Kobayashi, T. Kamikawa, M. Tsukino, H. Goi, M. Yamamoto, M. Munakata, *Bull. Chem. Soc. Jpn.* **1996**, *69*, 3317.
[18] [18a] I. P. Beletskaya, A. V. Chuchurjukin, H. P. Dijkstra, G. P. N. van Klink, G. van Koten, *Tetrahedron Lett.* **2000**, *41*, 1075. – [18b] I. P. Beletskaya, A. V. Chuchurjukin, H. P. Dijkstra, G. P. N. van Klink, G. van Koten, *Tetrahedron Lett.* **2000**, *41*, 1081.
[19] P. Knops, N. Sendhoff, H.-B. Mekelburger, F. Vögtle, *High Dilution Reactions − New Synthetic Applications: Topics in Current Chemistry* (Eds. E. Weber, F. Vögtle), Springer, Heidelberg, **1992**.
[20] X. Chi, A. J. Gurrin, R. A. Haycock, C. A. Hunter, L. D. Sarson, *J. Chem. Soc., Chem. Commun.* **1995**, 2563, and references therein.
[21] [21a] W. E. Hill, J. G. Taylor, C. P. Falshaw, T. J. King, B. Beagley, D. M. Tonge, R. G. Pritchard, C. A. McAuliffe, *J. Chem. Soc., Dalton Trans.* **1986**, 2289.[21b] W. Hill, D. M. A. Minahan, J. G. Taylor, C. A. McAufliffe, *J. Am. Chem. Soc.* **1982**, *104*, 6011. – [21c] S. O. Grim, R. L. Keiter, W. McFarlane, *Inorg. Chem.* **1967**, *6*, 1133. – [21d] W. McFarlane, *J. Chem. Soc. A* **1967**, 1922.
[22] [22a] E. Diez-Barra, J. C. Garcia-Martinez, J. Rodriguez-Lopez, *Tetrahedron Lett.* **1999**, *40*, 8181. – [22b] M. Lehmann, B. Schartel, M. Hennecke, H. Meier, *Tetrahedron* **1999**, *55*, 13377.
[23] K. M. Petrusevich, V. E. Kataev, I. I. Patsanovskii, L. V. Ermolaeva, E. A. Ishmaeva, A. V. Kataev, W. Wieczorek, K. Zygo, *Russ. J. Gen. Chem.* **1998**, *68*, 1510.
[24] R. F. Beeston, W. S. Aldridge, J. A. Treadyway, M. C. Fitzgerald, B. A. DeGraff, S. E. Stitzel, *Inorg. Chem.* **1998**, *37*, 4368.
[25] W. P. Cochrane, P. L. Pauson, T. S. Stevens, *J. Chem. Soc. C* **1968**, 630.
[26] J. Klein, A. Medlik, A. Y. Meyer, *Tetrahedron* **1976**, *32*, 51.
[27] R. Rabinowitz, J. Pellon, *J. Org. Chem.* **1961**, *26*, 4623.
[28] T. Uchiyama, Y. Toshiyasu, Y. Nakamura, T. Miwa, S. Kawaguchi, *Bull. Chem. Soc. Jpn.* **1981**, *54*, 181.
[29] E. Lindner, M. Khanfar, *Phosphorus Sulfur Silicon Relat. Elem.*, in press.
[30] G. V. Bodrin, M. I. Kabachnick, N. E. Kochetkova, T. Ya. Medved, B. F. Myasoedov, Yu. M. Polikarpov, M. K. Chmutova, *Izv. Akad. Nauk. SSSR, Ser. Khim.* **1979**, 2572; *Engl. Trans.* **1980**, 2388.
[31] G. M. Sheldrick, *SHELXTL V5.03, Program for crystal structure refinement*, University of Göttingen, Germany **1995.**

Received February 23, 2001
[I01066]

Dipyridylamine Ligands − Synthesis, Coordination Chemistry of the Group 10 Metals and Application of Nickel Complexes in Ethylene Oligomerization

Thomas Schareina,[a] Gerhard Hillebrand,[a] Hans Fuhrmann,[a] and Rhett Kempe*[a]

Keywords: N ligands / Nickel / Palladium / Polymerization / Catalysis

A great variety of 2,2′-bipyridylamines can be synthesized starting from primary amines or 2-aminopyridines (for instance, symmetrically and unsymmetrically substituted as well as chiral ligands) by palladium-catalyzed aryl amination. The reaction of such ligands with [$PdCl_2$(COD)] or [$NiBr_2$(DME)] (COD = cycloocta-1,5-diene; DME = 1,2-dimethoxyethane) led to the corresponding dichloro or dibromo complexes. The results of X-ray crystal structure analyses of selected compounds show that the ligands coordinate through the two pyridine N-atoms. Their palladium complexes have a slightly distorted planar coordination (in the case of nickel a distorted tetrahedral coordination), with N–M–N angles of 96.0(2)° (M = Ni) and 85.7° (averaged, M = Pd). The nickel complexes are highly active ethylene oligomerization catalysts if activated with $Et_3Al_2Cl_3$.

Introduction

2,2′-Bipyridylamines are accessible by sequential palladium-catalyzed aryl amination reactions starting from a primary amine[1,2] (Scheme 1, above). Such compounds have three sites where coordination to a transition metal may occur: the two pyridine moieties and the amine function. Since the amine N-atom can only bind in a strained fashion together with one or two pyridyl units, such ligands act as bidentate chelates with binding only to the pyridyls. In contrast to the classical 2,2′-bipyridine type ligand, which was described recently as the most widely used ligand,[3] six-membered rings are formed (Scheme 1, below). Recently N-ligands have received much attention,[4] as bipyridylamines might be an interesting alternative to diphosphane or diimine ligands, the latter of which has recently attracted considerable interest in regard to its combination with the group 10 metals as olefin polymerisation catalysts.[5,6] Due to the great variety of substitution patterns which can be easily established for the bipyridylamines (variation of R, R′ and R′′, Scheme 1) it may be possible to fine-tune transition metal complex reactivity. To the best of our knowledge, work on applications of bipyridylamine ligand complexes in olefin polymerization has not been published yet.[6] The coordination chemistry of the simplest member of the bipyridylamine group, the 2,2′-dipyridylamine (commercially available), has been described in detail for copper.[7] However, compounds of other transition metals such as complexes of the chromium triad,[8] of rhodium,[9] cobalt,[10] nickel,[11] palladium,[12] ruthenium,[13] and cadmium[14] are much rarer. In this article we report on the ligand synthesis and coordination chemical studies of novel bipyridylamines, as well as some applications of the synthesized nickel complexes in ethylene oligomerization.

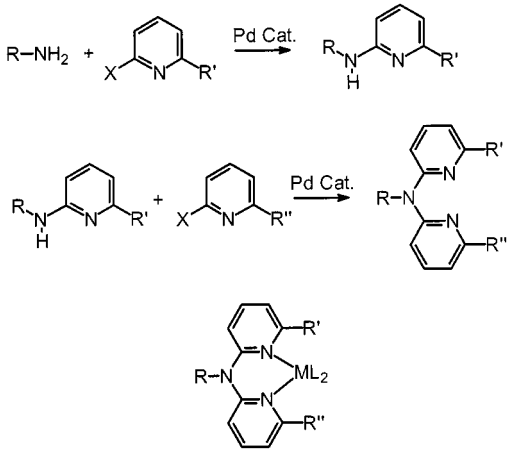

Scheme 1. Synthesis of bipyridylamines and the coordination mode of these ligands in transition metal complexes (R, R′, R′′ = alkyl, aryl substituents; X = Cl, Br; L = additional ligands)

Results and Discussion

Ligand Syntheses

Palladium-catalyzed aryl−X activation (X = I, Br or Cl) reactions are an efficient tool for the synthesis of bi- and triarylamines by C−N bond formation.[1] If 2-X-pyridines are used X can be Cl as the systems are activated, although the formation of catalyst-deactivating palladium pyridine complexes has to be avoided. In order to prevent this the palladium catalyst has to be stabilized by chelating bisphosphane ligands.[1a] Reactions of 2-aminopyridines with one or two equivalents of the corresponding 2-halopyridines and 1.25 or 2.5 equiv. of sodium-*tert*-butoxide in the presence of 1 mol % 1,3-bis(diphenylphosphanyl)propane and 0.5 mol % Pd_2dba_3 in toluene at 80 °C leads, usually after less than one hour, to a color change to yellow. After stirring for an additional 12 hours, work up with dichlorome-

[a] Institut für Organische Katalyseforschung (IfOK), Buchbinderstraße 5−6, 18055 Rostock, Germany

 © WILEY-VCH Verlag GmbH, 69451 Weinheim, 2001 1434−1948/01/0909−2421 $ 17.50+.50/0

thane, or ether, and water followed. The compounds were purified by chromatography, distillation or crystallization. Compound **1** was prepared from 2,6-diisopropylaniline, compound **2** from 2-(benzylamino)-4-methylpyridine, compound **3** from 2-(benzylamino)-6-methylpyridine, compound **4** from 2-pyridylaniline and compound **5** from (*S*)-1-phenylethylamine (Scheme 2).

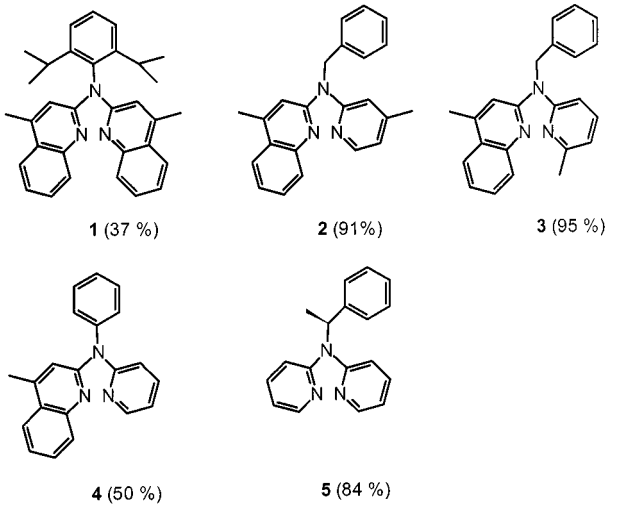

Scheme 2. The bipyridylamine ligands used, including numbering

Group 10 Metal Complex Syntheses and Structures

The reaction of **1**, **3** and **4** with [$NiBr_2$(DME)] (DME = dimethoxyethane) gave rise to blue- or purple-colored crystalline materials (Scheme 3). The structures of all the synthesized group 10 metal complexes are summarized in Scheme 4. NMR investigation of **6**, **8** and **9** gave rather broad signals indicating the existence of d^8 high-spin complexes. EPR spectra in dilute CH_2Cl_2 solutions could not be recorded either at room or at lower temperatures. Single crystals of **8** suitable for an X-ray crystal structure analysis (Figure 1) could be grown from a CH_2Cl_2 solution; crystallographic details are listed in Table 1. The coordination of the nickel center is best described as tetrahedral as observed for dibromodipyridylnickel(II) complexes[15] {dibromodipyridylnickel(II) = [$NiBr_2$(dipy)]}. The $Ni-N_{pyridine}$ bond lengths of **8** (mean = 1.99 Å) are well in accordance with those observed for (dipy)$NiBr_2$ complexes (mean = 2.00 Å). The N−Ni−N angle in **8** [96.0(2)°] is significant larger than that observed in [$NiBr_2$(dipy)] complexes (mean = 82.8°). Thus it can be concluded that the bipyridylamine-type ligands may favor tetrahedral coordination, similar to bipyridyl ligands, since the six-membered chelate is closer to the ideal tetrahedral angle, although still far from the ideal value.

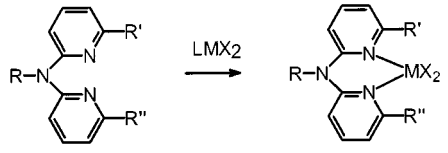

Scheme 3. Synthesis of the group 10 metal complexes (R, R′, R′′ = alkyl, aryl substituents; X = Cl, Br; L = additional ligands)

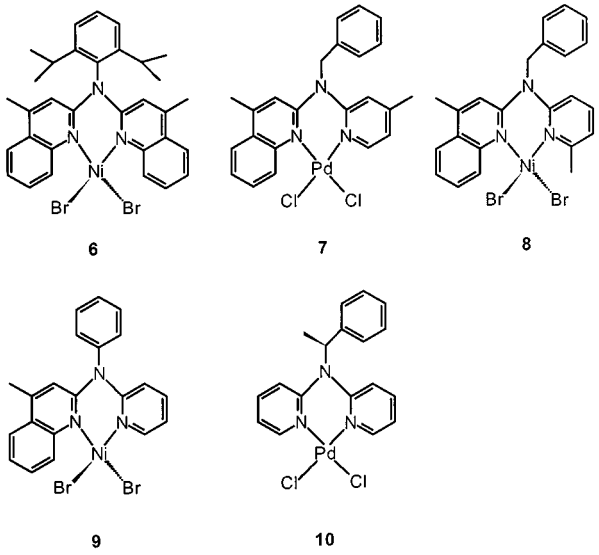

Scheme 4. Synthesized Ni and Pd complexes, including numbering

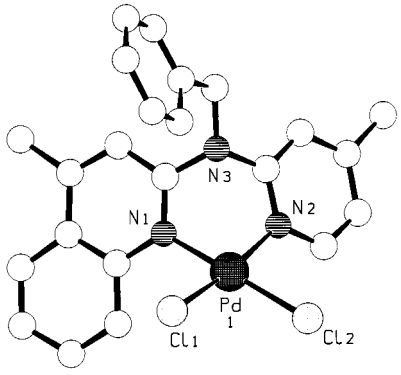

Figure 1. Molecular structure of **7**; selected bond lengths [Å] and angles [°]: N1−Pd1 2.032(3), N2−Pd1 2.012(3), Cl1−Pd1 2.3033(11), Cl2−Pd1 2.2980(10), N2−Pd1−N1 84.82(11), N2−Pd1−Cl2 91.80(8), N1−Pd1−Cl2 173.83(8), N2−Pd1−Cl1 170.54(8), N1−Pd1−Cl1 92.79(8), Cl2−Pd1−Cl1 91.36(4)

The reaction of **2** and **5** with [$PdCl_2$(COD)] (COD = cycloocta-1,5-diene) gave rise to yellow crystalline materials (Scheme 3). NMR investigation of **2** and **5** revealed a sharp single signal set suggesting the existence of monomeric diamagnetic species in solution. The X-ray crystal structure analyses of both compounds confirm these complexes to be mononuclear in the solid state as well; crystallographic details are listed in Table 1. The coordination of the palladium centers is best described as square planar, in contrast to the nickel compounds but well in agreement with what was observed previously for dipyridyldichloropalladium(II) complexes {dichlorodipyridylpalladium(II) = [$PdCl_2$(dipy)]}. A CSD[16] search for [$PdCl_2$(dipy)] complexes revealed ten hits with a mean of the Pd−N bond length of 2.029(18) and a mean of the N−Pd−N bond angle of 80.1(7)°. Similar Pd−N distances (mean = 2.02 Å) have been found in **7** and **10** (Figure 2 and 3) The N−Pd−N

Table 1. Details of the X-ray crystal structure analyses

Compound	**7**	**8**	**10**
Crystal system	triclinic	monoclinic	orthorhombic
Space group	$P\bar{1}$	$P2_1/c$	$P2_12_12_1$
a, Å	8.772(2)	9.194(2)	10.434(2)
b, Å	10.721(2)	19.609(4)	12.164(3)
c, Å	13.849(3)	12.522(3)	14.856(3)
α, deg	77.53(2)	–	–
β, deg	86.38(2)	98.75(3)	–
γ, deg	80.88(2)	–	–
V, Å^3	1255.1(5)	2231.3(9)	1885.5(7)
Z	2	4	4
Crystal size, mm	0.5 × 0.3 × 0.3	0.7 × 0.3 × 0.1	0.4 × 0.4 × 0.35
ρ_{calcd}, g cm^{-3}	1.592	1.661	1.595
μ, cm^{-1} (Mo-K_α)	1.183	4.465	1.271
T, K	200(2)	200(2)	293(2)
θ range, deg	1.97–24.13	1.95–24.22	2.39–24.29
No. of reflections	3644	6518	8678
No. of reflections unique	3644	3342	2940
No. of reflections obs. [$I > 2\sigma(I)$]	3063	2096	2854
No. of parameters	325	262	234
*wR*2 (all data)	0.073	0.119	0.090
R value [$I > 2\sigma(I)$]	0.029	0.047	0.030

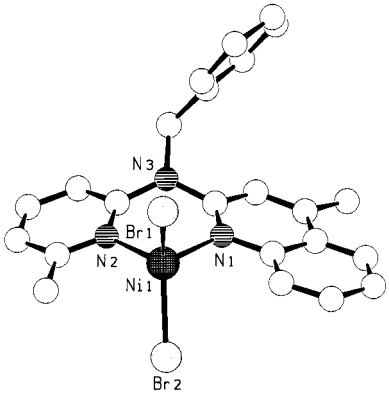

Figure 2. Molecular structure of **8**; selected bond lengths [Å] and angles [°]: N1–Ni1 1.977(5), N2–Ni1 1.997(6), Ni1–Br1 2.3699(13), Ni1–Br2 2.3898(12), N1–Ni1–N2 96.0(2), N1–Ni1–Br1 105.1(2), N2–Ni1–Br1 107.8(2), N1–Ni1–Br2105.07(15), N2–Ni1–Br2 107.5(2), Br1–Ni1–Br2 130.04(5)

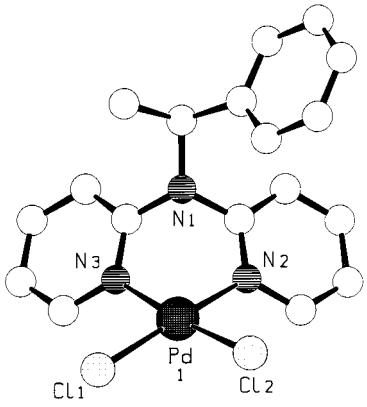

Figure 3. Molecular structure of **10**; selected bond lengths [Å] and angles [°]: N2–Pd1 2.025(4), N3–Pd1 2.020(4), Cl1–Pd1 2.2993(14), Cl2–Pd1 2.267(2), N3–Pd1–N2 86.5(2), N3–Pd1–Cl2 174.47(12), N2–Pd1–Cl2 91.23(12), N3–Pd1–Cl1 91.85(12), N2–Pd1–Cl1 175.37(13), Cl2–Pd1–Cl1 90.77(6)

bond angle (mean = 85.7°) differs by more than 5° and is even 4.5° larger than the highest value observed in known [$PdCl_2$(dipy)] complexes.

Ethylene Oligomerization Studies

Recently, considerable effort has been devoted to the synthesis of hyperbranched oligomers from inexpensive monomers such as ethylene and propene.[17] Such materials are useful in the lubricant industry as base stocks and as precursors to lubricant additives, especially since the demand for synthetic lubricants is rising.[18]

Complexes **6**, **8** and **9** were investigated with regard to catalytic applications in ethylene oligomerization after activation with chloroaluminum alkyls. The results of the oligomerization experiments are summarized in Table 2. Remarkably high activities are observed for all Ni complexes when using $Et_3Al_2Cl_3$ as a co-catalyst and CH_2Cl_2 as the solvent. All nickel complexes show a high tendency towards the formation of C4–C6 fraction products. Highly branched oligomers with a ratio of methyl protons (at δ = 0.87)/total alkyl protons (by ^{1}H NMR integration) of 0.61 were obtained for the higher boiling fraction. An important quantity of these oligomeric products were saturated, as found by GC-IR studies. A low temperature and low ethylene pressure were used due to the high activity of the systems under the described conditions.

Table 2. Oligomerization of ethylene with Ni complexes (5×10^{-6} mol_{Ni}, Al/Ni = 600, activator $Et_3Al_2Cl_3$, 200 mL of dichloromethane)

Comp.	T [°C]	p [bar]	t [min]	yield [g]	TON[a]	Products [%] C4−C6:C8−C16:>C16
6	12	1.3	60[b]	58.8	420 000	57:18:25
8	20	0.6	60[c]	85.1	608 000	68[d]:17:15
9	30	1.0	60[c]	83.6	597 000	71[d]:23:6

[a] TON = turnover number [$mol_{ethene}/mol_{catalyst}$]. − [b] Thereafter no gas uptake. − [c] Thereafter only marginal gas uptake. − [d] >90% butenes.

Conclusion

Several conclusions can be drawn from this study. Firstly, palladium-catalyzed aryl amination is an efficient tool in the preparation of a great variety of 2,2′-bipyridylamine ligands. Secondly, these compounds act as bidentate ligands to stabilize group 10 metal complexes. Thirdly, the nickel complexes are highly active ethylene oligomerization catalysts if activated with $Et_3Al_2Cl_3$.

Experimental Section

Materials and Procedures: All reagents were obtained commercially and used as supplied. Column chromatography was performed on silica gel 60 (0.063−0.200 mm) from Merck. All manipulations of air-sensitive materials were performed with rigorous exclusion of oxygen and moisture in dried Schlenk-type glassware on a dual manifold Schlenk line, interfaced to a high-vacuum line, or in an argon-filled glovebox (mBraun labmaster 130) with a high-capacity recirculator (<1.5 ppm O_2). Solvents (Aldrich) and NMR solvents (Cambridge Isotope Laboratories all 99 atom% D) were freshly distilled from sodium tetraethylaluminate.

Physical Measurements: NMR spectra were recorded on a BRUKER ARX 400 instrument with a variable temperature unit. ^1H and ^{13}C chemical shifts were referenced to the solvent resonances and reported relative to TMS. Elemental analysis were performed with a Leco CHNS-932 elemental analyzer. X-ray diffraction data were collected on a STOE-IPDS diffractometer using graphite monochromated Mo-K_α radiation. The crystals were mounted in a cold nitrogen stream. The structure was solved by direct methods (SHELXS-86)[19] and refined by full-matrix least-squares techniques against F^2 (SHELXL-93).[20] SCHAKAL was used for structure representations.

Crystallographic data (excluding structure factors) for the structures reported in this paper have been deposited with the Cambridge Crystallographic Data Centre as supplementary publication nos. CCDC-159116 (**7**), CCDC-159117 (**8**) and CCDC-159118 (**10**). Copies of the data can be obtained free of charge on application to CCDC, 12 Union Road, Cambridge CB2 1EZ, UK [Fax: (internat.) +44-1223/336-033; E-mail: deposit@ccdc.cam.ac.uk].

Synthesis of the Ligands

Synthesis of 1: 2,6-Diisopropylaniline (0.89 g, 5.0 mmol), 2-chlorolepidine (1.78 g, 10.0 mmol), 1,3-bis(diphenylphosphanyl)propane (25 mg, 6×10^{-5} mol), dipalladiumtris(benzylideneacetone) (28 mg, 3×10^{-5} mol) and sodium *tert*-butoxide (1.20 g, 12.5 mmol) were combined in a Schlenk vessel under argon. Toluene (20 mL) was then added and the mixture stirred at 80 °C for 120 h. After cooling, the resulting mixture was taken up with diethyl ether and washed twice with a saturated aqueous sodium chloride solution. The organic solution was dried over sodium sulfate and the solvent removed in a rotary evaporator. The resulting dark red oil was subjected to fast column chromatography over silica gel (eluent: petroleum ether/ethyl acetate, 10:1 v/v) to remove polar by-products. Recrystallization of the resulting semi-solid oil from *n*-hexane yielded 0.82 g (37%) of colorless needles. − ^1H (C_6D_6): δ = 7.95 (d, 2 H), 7.62 (d, 2 H), 7.45 (s, 2 H), 7.36 (m, 3 H), 7.29 (m, 2 H), 7.17 (m, 2 H), 3.57 (hept, J = 6.7 Hz, 2 H), 2.19 (s, 6 H), 1.11 (d, J = 6.7 Hz, 12 H). − ^{13}C NMR(C_6D_6): δ = 156.4, 148.7, 147.9, 144.5, 139.0, 129.3, 129.0, 125.9, 124.8, 124.2, 123.8, 116.9, 29.1, 24.1, 18.7. − $C_{32}H_{33}N_3$ (459.62): calcd. C 83.62, H 7.24, N 9.14; found C 82.98, H 7.54, N 9.26.

Synthesis of 2: 2-(Benzylamino)-4-methylpyridine (2.77 g, 14 mmol), 2-chloro-4-methyl-quinoline (2.5 g, 14.1 mmol), 1,3-bis(diphenylphosphanyl)propane (0.23 g, 0.56 mmol), dipalladiumtris(benzylideneacetone) (0.26 g, 0.28 mmol) and sodium *tert*-butoxide (4.06 g, 42.2 mmol) were combined in a Schlenk vessel under argon. Toluene (40 mL) was then added and the resulting brown mixture stirred at 70 °C for 40 h. After cooling to room temperature the solvent was evaporated in vacuo into a dry-ice-cooled trap. The resulting slurry was taken up with diethyl ether and the solution washed three times with a saturated aqueous sodium chloride solution. The organic solution was dried over magnesium sulfate, and the solvent removed on a rotary evaporator. The resulting brown oil was purified by column chromatography over silica gel (eluent: petroleum ether/ethyl acetate, 4:1 v/v). Yield: 4.38 g (91%) of a yellow oil, which didn′t solidify even after drying in vacuum and prolonged standing. − ^1H NMR (C_6D_6): δ = 8.41 (d, 1 H), 8.24 (d, 1 H), 7.83 (d, 2 H), 7.70 (dd, 1 H), 7.56 (td, 1 H), 7.31 (s, 2 H), 7.29 (s, 1 H), 7.08 (s, 1 H), 6.50 (d, 1 H), 6.06 (s, 2 H, benzyl. CH_2), 2.21 (d, J = 7.0 Hz, 3 H, Lp-CH_3), 1.91 (s, 3 H, py-CH_3). − ^{13}C NMR (C_6D_6): δ = 157.63, 155.72, 148.13, 147.90, 147.69, 143.93, 140.13, 135.64, 128.93, 128.38, 127.44, 126.37, 125.16, 123.38, 123.25, 118.83, 115.75, 115.43, 51.31, 20.29, 18.12. − $C_{23}H_{21}N_3$ (339.43): calcd. C 81.38, H 6.24, N 12.38; found C 81.32, H 6.21, N 12.15.

Synthesis of 3: 2-(Benzylamino)-6-methylpyridine (1.49 g, 7.5 mmol), 2-chloro-4-methyl-quinoline (1.33 g, 7.5 mmol), 1,3-bis(diphenylphosphanyl)propane (0.124 g, 0.30 mmol), dipalladiumtris(benzylideneacetone) (0.140 g, 0.153 mmol) and sodium *tert*-butoxide (0.96 g, 10 mmol) were combined in a Schlenk vessel under argon. Dry toluene (25 mL) was then added and the resulting brown mixture stirred at 70 °C for 40 h. After cooling, the solvent was removed on a rotary evaporator, the resulting slurry taken up with diethyl ether and the solution washed three times with a saturated aqueous sodium chloride solution. The organic solution was dried over magnesium sulfate and the solvents evaporated. The resulting brown oil was purified by fast column chromatography over silica gel (eluent: petroleum ether/ethyl acetate, 5:1 v/v). Yield: 2.42 g (7.13 mmol, 95%) of a yellow highly viscous oil, which didn′t solidify even after drying in vacuum and prolonged standing. − ^1H NMR (C_6D_6): δ = 2.00 (s, 3 H), 2.30 (s, 3 H), 5.53 (s, 2 H, benzyl. CH_2), 6.34 (d, 1 H), 6.79 (d, 1 H), 6.9 (t, 1 H), 6.95 (t, 1 H), 7.05 (m, 1 H), 7.07 (m, 1 H), 7.10 (m, 4 H), 7.33 (dt, 1 H), 7.48 (dd, 1 H), 7.59 (m, 2 H), 8.01 (m, 1 H). − ^{13}C NMR (C_6D_6): δ = 157.9, 157.4, 156.4, 148.6, 144.5, 140.9, 137.7, 129.6, 129.1, 128.2, 127.1, 125.8, 124.1, 124.0, 117.3, 116.1, 112.9, 51.8, 24.7, 18.8. −

$C_{23}H_{21}N_3$ (339.43): calcd. C 81.38, H 6.24, N 12.38; found C 81.05, H 6.00, N 12.31.

Synthesis of 4: 2-Pyridylaniline (1.702 g, 10 mmol), 2-chloro-4-methylquinoline (1.78 g, 10 mmol), 1,3-bis(diphenylphosphanyl)-propane (0.165 g, 0.40 mmol), dipalladiumtris(benzylideneacetone) (0.18 g, 0.20 mmol) and sodium *tert*-butoxide (1.35 g, 14 mmol) were combined in a Schlenk vessel under argon. Toluene (30 mL) was then added and the dark green mixture stirred at 70 °C for 54 h. Workup as for **3**, but with dichloromethane solvent. The raw product was isolated as a dark brown solid, which was recrystallized from absolute ethanol. Yield: 1.57 g (5.04 mmol, 50%) of yellow crystalline needles. – ^{1}H (C_6D_6): δ = 1.98 (d, 3 H, CH_3), 6.64 (m, 1 H), 6.93 (m, 2 H), 7.0–7.1 (m, 6 H), 7.18 (m, 2 H), 7.24 (ddd, 1 H), 7.48 (dd, 1 H), 7.89 (dd, 1 H), 8.15 (m, 1 H). – ^{13}C (C_6D_6): δ = 157.7, 156.1, 147.6, 147.2, 144.7, 143.8, 135.9, 128.7, 128.4, 128.2, 127.7, 125.1, 124.8, 123.4, 122.7, 117.2, 116.9, 116.8, 17.5. – $C_{21}H_{17}N_3$ (311.38): calcd. C 81.00, H 5.50, N 13.49, found C 81.00, H 5.74, N 13.27.

Synthesis of 5: 2-Bromopyridine (2.53 g, 16.0 mmol), (*S*)-1-phenylethylamine (0.97 g, 8.00 mmol), $Pd_2(DBA)_3$ (0.18 g, 0.20 mmol, 4 mol % Pd), 1,3-bis(diphenylphosphanyl)propane (0.16 g, 0.39 mmol), sodium *tert*-butoxide (1.34 g, 13.9 mmol) and 50 mL of toluene were combined in a Schlenk vessel. The mixture was stirred at 70 °C for 36 h. After cooling to room temperature the solvent was evaporated in vacuo into a dry-ice-cooled trap. Ether (50 mL) and water (50 mL) were added to the reaction mixture and, after separation, the organic phase was extracted twice with a saturated aqueous sodium chloride solution. The solution was dried over magnesium sulfate and the solvent removed on the rotary evaporator. Vacuum distillation at 150 °C/0.1 mbar yielded 1.85 g (84%) of a colorless oil. – ^{1}H NMR (C_6D_6): δ = 1.47 (d, *J* = 6.7 Hz, 3 H, CH_3), 4.64 (quint, *J* = 6.7 Hz, 1 H, CH), 6.08–6.12 (m, 2 H), 6.43–6.47 (m, 2 H), 7.13–7.17 (m, 2 H), 7.20–7.31 (m, 5 H), 7.80–8.00 (m, 2 H). – ^{13}C NMR (C_6D_6): δ = 24.3 (CH_3), 54.6 (CH), 107.2, 117.3, 117.9, 127.8, 128.7, 137.9, 145.2, 148.8, 156.2. – $C_{18}H_{17}N_3$ (275.35): calcd. C 78.52, H 6.22, N 15.26; found C 78.37, H 6.45, N 15.31.

Synthesis of the Metal Complexes

Synthesis of 6: [$NiBr_2$(DME)] (0.23 g, 0.74 mmol) was suspended in 5 mL dichloromethane. A solution of **1** (0.34 g, 0.76 mmol) in 5 mL dichloromethane was then added, the color of the solution changing to a deep purple. After standing overnight the solution was filtered and the grey residue washed with 10 mL of dichloromethane. 10 mL of toluene was then added to the solution and the solvents were evaporated until about 8 mL of toluene remained. After some days of standing crops of purple crystals precipitated, and these were separated and washed with 5 mL of toluene. Yield: 0.31 g (54%). – ^{1}H NMR ($CDCl_3$): δ = 12.70 (br. s), 7.25–7.40 (m), 7.13–7.22 (m), 2.98 (s), 2.37 (s), 1.46 (s), 1.16 (d). – ^{13}C NMR ($CDCl_3$): δ = 142.9, 133.6, 129.5, 128.7, 125.8, 123.4, 121.9, 116.8, 24.7. The NMR spectra obtained were rather broad due to the paramagnetism of the Ni. – $C_{39}H_{41}Br_2N_3Ni$ (**5**·toluene: 770.26): calcd. C 60.81, H 5.37, N 5.46; found C 61.17, H 5.21, N 5.42.

Synthesis of 7: Compound **2** (0.125 g, 0.37 mmol) was dissolved in 3 mL of dichloromethane and added to [$PdCl_2$(COD)] (0.105 g, 0.37 mmol, 1 equiv.) in a Schlenk vessel. After a week orange crystals separated from the solution, and these were used directly for an X-ray analysis. In a separate run, the solvent was removed with a syringe under argon, the crystals were washed twice with 1 mL portions of diethyl ether and dried in vacuum to yield 0.11 g (49%) of product. The crystals appeared to lose dichloromethane on vacuum treatment: the X-ray analysis showed dichloromethane, whereas the elemental analysis of the material from the second run showed none. – ^{1}H (CD_2Cl_2): δ = 9.37 (d, *J* = 8.4 Hz, 1 H), 8.60 (d, *J* = 7.4 Hz, 1 H), 7.90 (d, 2 H), 7.81 (m, 2 H), 7.57 (dt, *J* = 1.5, *J* = 8.4 Hz, 1 H), 7.43 (t, *J* = 7.4 Hz, 2 H), 7.31 (br. t, *J* = 7.5 Hz, 1 H), 7.16 (s, 1 H), 7.03 (m, 2 H), 5.45 (m, 2 H, N–CH_2), 2.66 (s, 3 H), 2.36 (s, 3 H). – $C_{23}H_{21}Cl_2N_3Pd$ (516.76): calcd. C 49.51, H 3.79, N 7.53; found C 49.50, H 3.81, N 7.59. – ^{13}C NMR (CD_2Cl_2): δ = 151.8, 150.3, 149.8, 144.5, 133.1, 130.1, 129.7, 128.5, 127.5, 126.8, 126.0, 125.6, 122.2, 121.8, 114.9, 113.0, 53.9, 28.7, 18.5.

Synthesis of 8: A solution of **3** (0.34 g, 1 mmol) in 10 mL of dichloromethane was added to [$NiBr_2$(DME)] (0.31 g, 1 mmol) in a Schlenk vessel, resulting in a purple solution. After 4 days at room temperature the solution was filtered and the remaining solid washed with three 5 mL portions of dichloromethane. The washings were added to the filtrate. The combined solution was layered with 15 mL of diethyl ether and kept for one week at room temperature. The solvent was then removed from the resulting purple prismatic crystals, which were washed with two 10 mL portions of diethyl ether. Yield: 0.32 g (0.57 mmol, 57%). – ^{1}H ($CDCl_3$): δ = (all broad singlets due to the paramagnetism of the Ni) 11.16 (0.3 H), 10.50 (0.8 H), 7.17 (3 H), 7.02 (1 H), 6.88 (2 H), 6.17/6.02 (4 H), 2.59 (1 H), 1.40 (1 H), 0.00 (12 H). – $C_{23}H_{21}Br_2N_3Ni$ (557.93): calcd. C 49.51, H 3.79, Br 28.64, N 7.53; found C 49.50, H 3.81, Br 28.45, N 7.59.

Synthesis of 9: [$NiBr_2$(DME)] (0.30 g, 0.9 mmol) was suspended in 5 mL of THF and a warm solution of **4** (0.28 g, 0.9 mmol) in 5 mL of THF was added in four portions with a syringe. A purple solid precipitated after 5 min. The next day, filtration yielded a purple, microcrystalline solid, which was dried in vacuo. The yield was not determined. For recrystallisation, a small amount was dissolved in 5 mL hot dichloromethane, cooled to room temperature and layered with 3 mL of diethyl ether. Again, only a microcrystalline powder was obtained.^{1}H ($CDCl_3$): δ = (all broad due to the paramagnetism of the Ni) 12.4 (br. s, 2 H), 8.8 (s, 1 H), 8.35 (d, 1 H), 7.97 (m, 2 H), 7.7 (m, 7 H), 7.54 (m, 1 H), 6.83 (br. s, 2 H), 6.65 (br. s, 5 H), 6.53 (s, 1 H), 2.67 (s, 3 H). – $C_{21}H_{17}Br_2N_3Ni$ (M_w = 529.88 g/mol): calcd. C 47.60, H 3.23, Br 30.16, N 7.93; found C 47.45, H 3.21, Br 29.39, N 7.74.

Synthesis of 10: [$PdCl_2$(COD)] (0.13 g, 0.47 mmol) was added to a solution of **5** (0.14 g, 0.50 mmol) in 30 mL of dichloromethane. The mixture was stored at –78 °C for crystallization. Filtration yielded 0.13 g (61%) of orange crystals. – ^{1}H NMR (C_6D_6): δ = 1.73 (d, *J* = 6.4 Hz, 3 H, CH_3), 5.44 (q, *J* = 6.4 Hz, 1 H, CH), 6.88–6.94 (m, 2 H), 7.15–7.19 (m, 2 H), 7.25–7.29 (m, 3 H), 7.43–7.49 (m, 1 H), 7.53–7.58 (m, 2 H), 7.78–7.85 (m, 1 H), 8.64–8.85 (m, 2 H). – ^{13}C NMR (C_6D_6): δ = 22.6 (CH_3), 59.7 (CH), 118.3, 119.0, 120.2, 120.8, 126.5, 127.3, 128.5, 138.7, 139.7, 140.2, 150.3, 151.2, 151.6, 152.5. – $C_{18}H_{17}Cl_2N_3Pd$ (452.68): calcd. C 62.14, H 5.05, N 7.51; found C 62.08, H 5.21, N 7.33.

Polymerization Studies: The oligomerization of ethylene (99.95%) was carried out in a batch process using a 1-L glass autoclave fitted with a gas inlet, dosing device, pressure gauge, and a magnetically driven and continuously regulated paddle stirrer with a hollow shaft (0 to 800 rpm). The solvent, dichloromethane, was dried by standard methods and distilled under argon. $Et_3Al_2Cl_3$ was used as supplied (Aldrich). 5×10^{-3} mmol of the Ni complexes were dissolved in 200 mL of dichloromethane and introduced under inert conditions into the autoclave. After the temperature of the mixture had been adjusted and $Et_3Al_2Cl_3$ had been added as a cocata-

lyst the oligomerization reaction started at an internal pressure as described in Table 2. After a reaction time of 1 hour the contents of the autoclave were decomposed by addition of methanolic HCl. The oligomers were analyzed by GC, GC-IR and NMR spectroscopy.

Acknowledgments

Financial support from the Deutsche Forschungsgemeinschaft (Heisenberg-Stipendium for RK), the Bundesministerium für Bildung und Forschung, the Fonds der Chemischen Industrie, the Max-Planck-Gesellschaft, the Karl-Winnacker-Stiftung, Aventis R & D GmbH, Degussa-Hüls AG, SKW Trostberg AG, Grünenthal GmbH, SynTec Wolfen GmbH and Organica Wolfen GmbH is gratefully acknowledged.

[1] [1a] S. Wagaw, S. L. Buchwald, *J. Org. Chem.* **1996**, *61*, 7240−7241. − [1b] J. F. Hartwig, *Synlett* **1996**, 329−340.
[2] J. Silberg, T. Schareina, R. Kempe, K. Wurst, M. R. Buchmeiser, *J. Organomet. Chem.* **2001**, *622*, 6−18.
[3] C. Kaes, A. Katz, M. W. Hosseini, *Chem. Rev.* **2000**, *100*, 3553−3590.
[4] A. Togni, L. M. Venanzi, *Angew. Chem.* **1994**, *106*, 517−547; *Angew. Chem. Int. Ed. Engl.* **1994**, *33*, 497−527.
[5] [5a] E. F. McCord, S. J. McLain, L. T. J. Nelson, S. D. Arthur, E. B. Coughlin, S. D. Ittel, L. K. Johnson, D. Tempel, C. M. Killian, M. Brookhart, *Macromolecules* **2001**, *34*, 362−371. − [5b] R. L. Huff, S. A. Svejda, D. J. Tempel, M. D. Leatherman, L. K. Johnson, M. Brookhart, *Polym. Prepr.* **2000**, *41*, 401−402. − [5c] A. C. Gottfried, M. Brookhart, *Macromolecules* **2001**, *34*, 1140−1142. − [5d] D. J. Tempel, L. K. Johnson, R. L. Huff, P. S. White, M. Brookhart, *J. Am. Chem. Soc.* **2000**, *122*, 6686−6700. − [5e] D. P. Gates, S. A. Svejda, E. Onate, C. M. Killian, L. K. Johnson, P. S. White, M. Brookhart, *Macromolecules* **2000**, *33*, 2320−2334. − [5f] S. A. Svejda, L. K. Johnson, M. Brookhart, *J. Am. Chem. Soc.* **1999**, *121*, 10634−10635. − [5g] S. A. Svejda, M. Brookhart, *Organometallics* **1999**, *18*, 65−74. − [5h] S. Mecking, L. K. Johnson, L. Wang, M. Brookhart, *J. Am. Chem. Soc.* **1998**, *120*, 888−899. − [5i] C. M. Killian, L. K. Johnson, M. Brookhart, *Organometallics* **1997**, *16*, 2005−2007. − [5j] C. M. Killian, D. J. Tempel, L. K. Johnson, M. Brookhart, *J. Am. Chem. Soc.* **1996**, *118*, 11664−11665. − [5k] L. K. Johnson, C. M. Killian, M. Brookhart, *J. Am. Chem. Soc.* **1995**, *117*, 6414−6415.
[6] For a recent review see: S. D. Ittel, L. K. Johnson, M. Brookhart, *Chem. Rev.* **2000**, *100*, 1169−1203.
[7] [7a] N. Ray, S. Tyagi, B. Hathaway, *J. Chem. Soc., Dalton Trans.* **1982**, 143−146. − [7b] J. S. Thompson, J. F. Whitney, *J. Am. Chem. Soc.* **1983**, *105*, 5488−5490. − [7c] J. S. Thompson, J. F. Whitney, *Inorg. Chem.* **1984**, *23*, 2813−2819.
[8] R. A. Howie, G. Izquierdo, G. P. McQuillan, *Inorg. Chim. Acta* **1983**, *72*, 165−172.
[9] L. A. Oro, M. A. Ciriano, F. Viguri, C. Foces-Foces, F. H. Cano, *Inorg. Chim. Acta* **1986**, *115*, 65−73.
[10] [10a] A. F. Williams, B. Bocquet, G. Bernardinelli, *Acta Crystallogr., Sect. C* **1987**, *43*, 883−885. − [10b] F. A. Cotton, L. M. Daniels, G. T. Jordan IV, C. A. Murillo, *J. Am. Chem. Soc.* **1997**, *119*, 10377−10381. − [10c] A. J. Blake, L. M. Gilby, S. Parsons, J. M. Rawson, D. Reed, G. A. Solan, R. E. P. Winpenny, *J. Chem. Soc., Dalton Trans.* **1996**, 3575−3581.
[11] [11a] R. W. Gable, B. F. Hoskins, G. Winter, *Inorg. Chim. Acta* **1985**, *96*, 151−159. − [11b] D. Poleti, D. R. Stojakovic, B. V. Prelesnik, L. Manojlovic-Muir, *Acta Crystallogr., Sect. C* **1990**, *46*, 399−402. − [11c] M. Maekawa, M. Munakata, T. Kuroda-Sowa, K. Hachiya, *Inorg. Chim. Acta* **1994**, *227*, 137−143.
[12] [12a] F. Sinner, M. R. Buchmeiser, R. Tessadri, M. Mupa, K. Wurst, G. K. Bonn, *J. Am. Chem. Soc.* **1998**, *129*, 2790−2797. − [12b] M. R. Buchmeiser, K. Wurst, *J. Am. Chem. Soc.* **1999**, *121*, 11101−11107.
[13] [13a] F. R. Keene, M. R. Snow, P. J. Stephenson, E. R. T. Tiekink, *Inorg. Chem.* **1988**, *27*, 2040−2045. − [13b] P. A. Anderson, G. B. Deacon, K. H. Haarmann, F. R. Keene, T. J. Meyer, D. A. Reitma, B. W. Skelton, G. F. Strouse, N. C. Thomas, J. A. Treadway, A. H. White, *Inorg. Chem.* **1995**, *34*, 6145−6157.
[14] E. A. H. Griffith, Hui-ying Li, E. L. Amma, *Inorg. Chim. Acta* **1988**, *148*, 203−208.
[15] [15a] R. J. Butcher, E. Sinn, *Inorg. Chem.* **1977**, *16*, 2334−2343. − [15b] D. W. Evans, G. R. Newkome, F. R. Fronczek, *Acta Crystallogr., Sect. C* **1990**, *46*, 490−491.
[16] Cambridge Crystallographic Database Version 5.20 October 2000.
[17] [17a] J. S. Kim, J. H. Pawlow, L. M. Wojcinski II, S. Murtuza, S. Kacker, A. Sen, *J. Am. Chem. Soc.* **1998**, *120*, 1932−1933. − [17b] H. Noss, H. Fuhrmann, R. Kempe, *Chem. Eur. J.* **2001**, *7*, 1630−1636.
[18] P. M. Morse, *Chem. Eng. News* **1998**, *76(36)*, 21−22.
[19] G. M. Sheldrick *SHELX-86: A program for crystal structure solution*, University of Göttingen, Germany, **1986**; G. M. Sheldrick, *Acta Crystallogr., Sect. A* **1990**, *46*, 467−473.
[20] G. M. Sheldrick *SHELXL-93: A program for crystal structure refinement*, University of Göttingen, Germany, **1993**.

Received March 14, 2001
[I01097]

Coordination Chemistry of Unsymmetrical Tripodal Ligands with an NNO_2 Donor Set

Christian Ochs,[a] F. Ekkehardt Hahn,*[b] and Roland Fröhlich[c]

Keywords: Tripodal ligands / Copper / Radicals / N ligands / O ligands

The synthesis of two new tripodal ligands $N(CH_2CH_2NH_2)(CH_2CH_2CH_2OH)_2$ (H_4-**1**) and N[2,3,5-C_6H_2-(OH)(SCH_3)(CH_3)]($CH_2CH_2CH_2NH_2$)($CH_2CH_2CH_2OH$) (H_4-**2**) is reported. Both tetradentate ligands contain a central tertiary nitrogen atom, as well as two OH and one NH_2 functionalized ligand arm. The tripods do not only exhibit an unsymmetrical N_2O_2 donor set, but also possess two C_3 and one C_2 chains between the central nitrogen atom and the terminal donors. On coordination of the central tertiary nitrogen atom, the ligands are capable of forming both six- and five-membered chelate rings in their metal complexes. Both ligands react with $[Cu(OAc)_2{\cdot}H_2O]_2$ to give the dinuclear copper(II) complexes $[Cu(\eta^4\text{-}\mu\text{-}O\text{-}H_3\text{-}\mathbf{1})_2Cu](PF_6)_2$ (**3**) and $[(\eta^3\text{-}H_3\text{-}\mathbf{2})Cu(\mu\text{-}OAc)_2Cu(\eta^3\text{-}H_3\text{-}\mathbf{2})]{\cdot}2CH_3CN$ (**4**·$2CH_3CN$). The molecular structures of **3** and **4**·$2CH_3CN$ have been determined by X-ray diffraction. Complex **3** contains two slightly distorted square-pyramidal ($\tau = 0.181$) copper atoms, with O-donors in the apical positions. The dinuclear complex **4**, which was synthesized to model the copper site in galactose oxidase, also shows a distorted square-pyramidal coordination geometry ($\tau = 0.205$ and $\tau = 0.101$) around both copper(II) atoms. Complex **4** contains two uncoordinated primary alcohol functionalities of the ligands. In addition, both the ligand H_4-**2** and its dinuclear copper complex $[(\eta^3\text{-}H_3\text{-}\mathbf{2})Cu(\mu\text{-}OAc)_2(\eta^3\text{-}H_3\text{-}\mathbf{2})]{\cdot}2CH_3CN$ can easily be oxidized to yield free or coordinated phenoxyl radicals, which are stable on the time scale of cyclic voltammetry.

Introduction

Redox reactions involving a transition metal ion and a redox-active amino acid side chain, e.g. tyrosine, play a key role in many biochemical processes.[1] Some years ago, Ito et al.[2] have shown that the reactive site in galactose oxidase (E.C. 1.1.3.9) GO, a copper enzyme that was isolated from the parasitic fungus *Fusarium dendroides*, contains a tyrosyl radical which is coordinated to a copper(II) center. Galactose oxidase catalyzes the stereospecific oxidation of D-galactose and various primary alcohols to the corresponding aldehydes, coupled to the simultaneous reduction of O_2 to H_2O_2 [Equation (1)].

$$RCH_2OH + O_2 \rightarrow RCH{=}O + H_2O_2 \quad (1)$$

The X-ray crystal structure analysis of the inactive form of galactose oxidase at a 1.7 Å resolution showed a mononuclear copper(II) center that is surrounded by a square-pyramidal N_2O_3 coordination environment.[2] As depicted in Figure 1, two histidine residues (His-496, His-581), one tyrosinate (Tyr-272) and one water or acetate molecule reside in the equatorial plane, while the remaining apical position is occupied by the oxygen atom of another tyrosinate ligand (Tyr-495). A unique characteristic of the copper site in galactose oxidase is that the equatorial tyrosinate residue Tyr-272 is covalently linked to a sulfur atom of the neighboring cysteine Cys-228. This leads to a lowering of the oxidation potential and significantly facilitates the formation of a tyrosyl radical from Tyr-272.[3] Furthermore, in the oxidized form of GO, antiferromagnetic coupling of the single electron in the copper(II) $d_{x^2-y^2}$ orbital with the tyrosyl radical is observed, giving a diamagnetic and EPR silent ($S = 0$) ground state of oxidized, active galactose oxidase.[4]

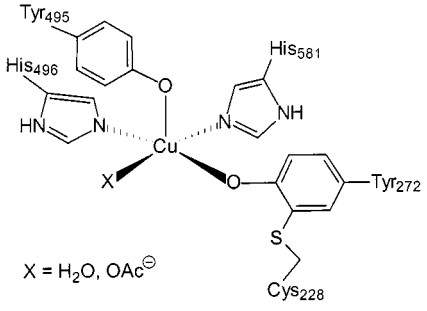

Figure 1. The active site in galactose oxidase

Several attempts have been made in the last years to mimic the geometric, spectroscopic and catalytic properties of native galactose oxidase. Functional model complexes have been presented by Tolman[5] and by Stack and coworkers.[6] Recently, Wieghardt et al.[7] described a functional model of galactose oxidase derived from a

[a] Institut für Anorganische und Analytische Chemie, Freie Universität Berlin,
Fabeckstraße 34−36, 14195 Berlin, Germany
[b] Anorganisch-Chemisches Institut, Westfälische Wilhelms-Universität Münster,
Wilhelm-Klemm-Straße 8, 48149 Münster, Germany
[c] Organisch-Chemisches Institut, Westfälische Wilhelms-Universität Münster,
Corrensstraße 40, 48149 Münster, Germany

 © WILEY-VCH Verlag GmbH, 69451 Weinheim, 2001 1434−1948/01/0909−2427 $ 17.50+.50/0

Cu^{II}−iminosemiquinone with a square-planar $[Cu(O-N-O)(NEt_3)]$ (O−N−O = dianionic ligand with one imine and two two phenolate donors) reaction center, which showed a high catalytic activity despite the lack of most structural features found at the active center of native galactose oxidase.

Various Cu^{II} complexes have been prepared in order to model the structural features of the reactive center in galactose oxidase. Mostly tripodal tetradentate ligands that contain one or two phenol and pyrazole or pyridine donor groups were used, providing an N_3O[3a,8,9] or N_2O_2[10,11] coordination environment for the copper center. Pentacoordination is normally achieved by coordination of a counterion or a solvent molecule. Unfortunately, all of the model compounds lack significant features found in the reactive site of native galactose oxidase. These features include a Cu^{II} atom coordinated in a square-pyramidal fashion which exhibits a thioether-functionalized phenoxyl donor in the equatorial plane and another O-donor in the apical position. Two more N-donors and one labile (possibly solvent molecule) O-donor in the equatorial plane should complete the overall N_2O_3 coordination environment.

If a GO model is to be built from a tetradentate tripodal ligand, certain restrictions apply. Such ligands, together with a monodentate coligand, form trigonal-bipyramidal or square-pyramidal complexes with Cu^{II}. For example $[Cu(tren)(NH_3)]^{2+}$ in the solid state is an almost perfect trigonal bipyramid.[12] A systematic study with higher homologues of tren, e.g. with ligands where methylene groups were added stepwise to the three ligand arms, revealed that the tripod with one ethyl and two propyl ligand arms $N(CH_2CH_2CH_2NH_2)_2(CH_2CH_2NH_2)$ forms a square-pyramidal Cu^{II} complex where the apical position is occupied by a donor linked to the central nitrogen atom by a propyl chain.[13] Thus, the topology of the tetradentate tripod determines both the overall geometry of the Cu^{II} complex (sqp vs. tbp), as well as the position of the donors in the complex (donor group at the end of a propyl chain in the apical position). Studies with unsymmetrical tetradentate tripods providing an N_3O donor set for Cu^{II} [8,9] gave similar results. Again, it was found that the formation of square-pyramidal Cu^{II} complexes is preferred when the ligand is capable of forming a 5,6,6-membered chelate ring sequence.[8]

These observations can be used to design ligands for the preparation of GO model compounds. Any tetradentate tripod with a central nitrogen atom capable of forming a 5,6,6-membered chelate ring sequence should give a more or less perfectly coordinated square-pyramidal Cu^{II} complex with a donor at the end of a propyl chain in the apical position.

The aliphatic tripodal ligand H_4-**1** (Figure 2) was synthesized to investigate the extent to which the above mentioned results for N_4 and N_3O ligands (control of complex geometry vs. ligand topology) are transferable to a N_2O_2 donor set. Ligand H_4-**1** should form a square-pyramidal Cu^{II} complex with one of the oxygen donors in the apical and the other in an equatorial position.

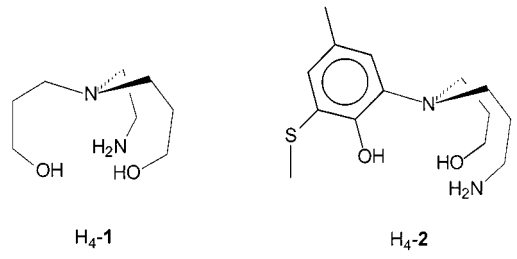

H_4-**1** H_4-**2**

Figure 2. Topology of the tripodal N_2O_2 ligands H_4-**1** and H_4-**2**

The second ligand H_4-**2** (Figure 2), providing an N_2O_2 donor set, was designed for a more accurate structural modeling of the reactive site in GO. This ligand is expected to form a square-pyramidal Cu^{II} complex with a 5,6,6-membered chelate ring sequence. The phenolate oxygen donor, linked by a C_2 chain to the central nitrogen atom, is expected to occupy an equatorial coordination site. In addition, the aromatic ring is functionalized with an *o*-(methylthio) group which in native GO is essential for the formation of a tyrosyl radical on oxidation. The mode of coordination of the two donors linked by C_3 chains to the central nitrogen atom can be elucidated by X-ray crystallography. One of them is expected to occupy an apical coordination site in a Cu^{II} complex. Overall, ligand H_2-**2** possesses an N_2O_2 donor set. It differs from N_2O_2 ligands previously reported[10,11] by possessing aliphatic amine and alcohol donor groups in the presence of an *o*-(methylthio)-functionalized phenol.

Results and Discussion

Ligand Syntheses

Our strategy for the preparation of the unsymmetrical N_2O_2 ligand H_4-**1** involves three reaction steps as depicted in Scheme 1. For the condensation of the C_3 chains to

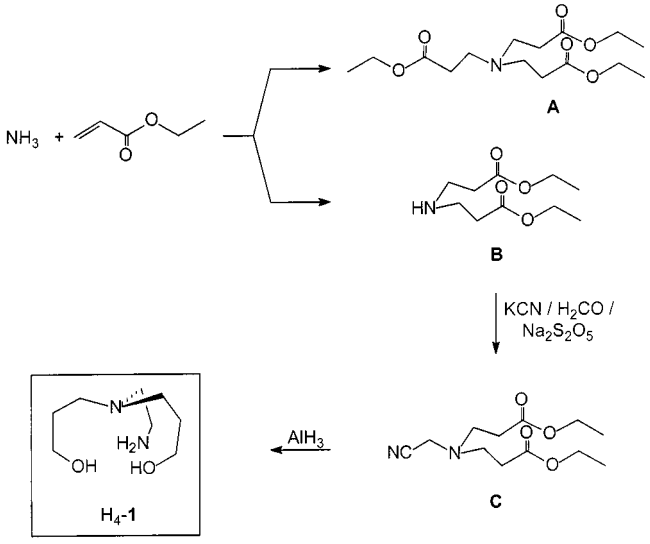

Scheme 1. Preparation of ligand H_4-**1**

ammonia, the Michael addition of ethyl acrylate had previously proved useful.[14] However, this reaction leads to a mixture of the tertiary (**A**) and secondary amines (**B**), which can be separated by distillation.[14a] Cyanomethylation of the secondary amine **B** by the Strecker synthesis according to the modification of Knoevenagel,[15] yielded the α-nitrilamine **C**. Finally, all protected donor groups were simultaneously liberated by reduction with AlH_3, which led directly to the free ligand H_4-**1**.

Ligand H_4-**1** contains one NH_2- and two OH-substituted ligand arms in addition to the central tertiary nitrogen atom. Furthermore, the ligand possesses an unsymmetrical topology with regard to the three alkyl chains, containing one C_2 and two C_3 arms. This allows for the formation of both five- and six-membered chelate rings yielding a 5,6,6 ring sequence on complex formation. Due to the flexibility and lengths of the alkyl arms, the ligand should be capable of providing an N_2O_2 coordination environment for a copper(II) ion without any steric strain.

Ligand H_4-**2** (Figure 2) was developed on the basis of simple force field calculations and molecular modeling experiments. It was assumed that a tripod, which could form a 5,6,6-chelate ring sequence, would form a square-pyramidal Cu^{II} complex with one of the C_3-linked donors in the apical position. Linking the phenol group directly to the central nitrogen atom should force the oxygen atom of this group in the equatorial position of the expected square-pyramidal complex. Taking into account the significance of the equatorial (*RS*)-substituted Tyr-272 for galactose oxidase activity, an *o*-(methylthio)phenol group was selected. In addition, the *para* position relative to the phenolic OH group was blocked by a methyl group in order to prevent dimerization when a radical intermediate is formed after one-electron oxidation. A similar N_2O_2 ligand capable of forming a 5,6,6-chelate ring sequence and possessing an *o*-(methylthio)phenol group was presented by Whittaker.[10] However, this ligand like all other tripods providing an N_2O_2 donor set and a 5,6,6-chelate ring sequence,[11] contains a phenol group connected to the central nitrogen atom in a way that the phenolic oxygen atom will be part of a six-membered chelate ring.

For the synthesis of H_4-**2**, *o*-nitro-*p*-cresol was selected as a suitable starting material. This molecule contains, at least in the protected form, all three of the desired functional groups for the construction of the aromatic part of H_4-**2**. The complete reaction sequence for the preparation of H_4-**2** is depicted in Scheme 2.

In a first reaction, the aromatic core of *o*-nitro-*p*-cresol was brominated by treatment with bromine in the presence of the Lewis acid catalyst $AlCl_3$.[16] The position *ortho* to the OH group is exclusively brominated, yielding compound **D**, due to the *ortho*- and *meta*-directing effect of the OH and the NO_2 substituents, respectively. Subsequently, **D** was deprotonated with NaOH, and the resulting phenolate was treated with (chloromethoxy)methane to give the MOM-protected derivative **E**.[17] Halogen/metal exchange of the bromine substituent, by use of phenyllithium at −105 °C resulted in the formation of a reactive aryllithium species that was not isolated.[18] This *ortho*-lithiated intermediate was quenched with dimethyl disulfide.[19] The *o*-(methylthio)-substituted compound **F** was isolated in good yield. According to a literature procedure,[20] the nitro group in **F** can be reduced quantitatively to the amine by an excess of hydrazine in the presence of Raney nickel to yield the aniline derivative **G**. Subsequently, a β-cyanoethyl group which will serve as the synthon for the 3-aminopropyl arm, was introduced by a copper(II) acetate catalyzed Michael addition of acrylonitrile to **G**. This resulted in the formation of compound **H**.[21] Finally, a C_3 chain (the precursor for the 3-hydroxypropyl arm) was added to the central nitrogen atom by acylation of **H** with β-acetoxypropionyl chloride, which was synthesized as described.[22] After chromatographic purification, amide **I** was obtained as a crystalline white solid. Reduction of **I** with AlH_3 yielded the ligand H_4-**2**. Under these conditions even the MOM-protected phenolic OH group is liberated. This is quite surprising since MOM ethers are known to be stable in basic media and are normally cleaved under acidic conditions. Ligand H_4-**2** is a sticky white solid which is slightly air-sensitive.

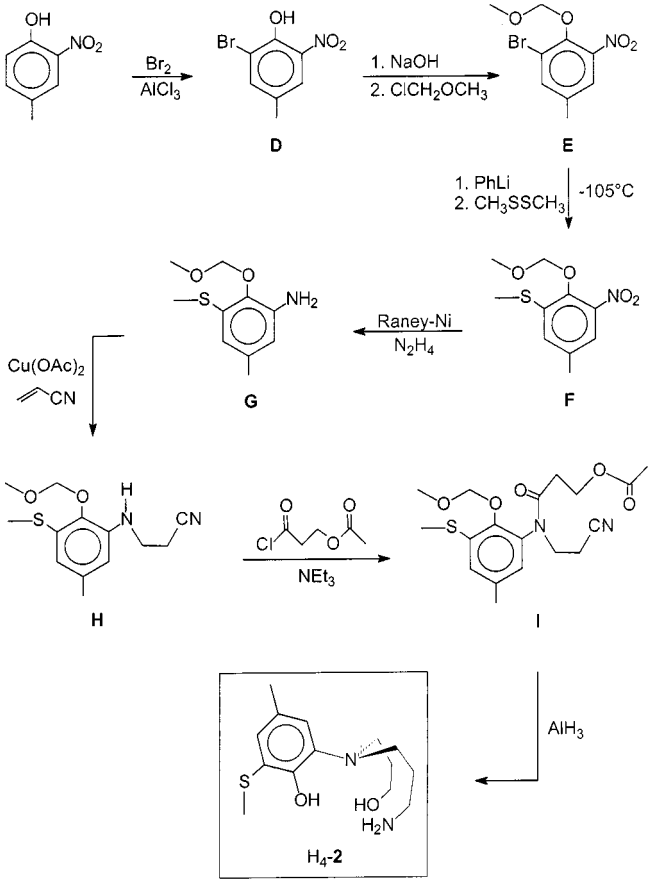

Scheme 2. Preparation of ligand H_4-**2**

Ligand H_4-**2**, like H_4-**1**, possesses an N_2O_2 donor set and an unsymmetrical topology. It is capable of forming a 5,6,6-membered chelate ring sequence and should be suitable for the preparation of square-pyramidal Cu^{II} complexes. H_4-**2** contains an *o*-(methylthio)-substituted phenol which is

directly connected to the central nitrogen atom of the ligand backbone. This is in contrast with tripodal N_2O_2 ligands published to date with regard to the modeling of the copper site in galactose oxidase. The electron-donating *o*-(methylthio) and the *p*-methyl substituents and the direct linkage of the aromatic ring to the central nitrogen atom should significantly lower the redox potential for the oxidation of this phenol group, while the substituents in the *ortho* and *para* positions relative to the OH group will prevent the formed phenoxyl radical from dimerizing.

Preparation of Copper Complexes

Freshly prepared $Cu(OH)_2$, suspended in water, reacted at 40 °C with a stoichiometric amount of ligand H_4-**1** to give a blue suspension which contained unidentified copper species (probably hydroxides). Addition of 2 equiv. of NH_4PF_6 to such a suspension yielded a deep blue solution. From this solution complex **3** crystallized over a period of 6 h (Scheme 3). The complex is air-stable and can be recrystallized from water as deep blue prisms. The reaction of $[HNEt_3]^+[H_3$-**2**$]^-$ with an equimolar amount of $[Cu(OAc)_2{\cdot}H_2O]_2$ in methanol at room temperature yielded a dark green solution. On addition of a mixture of acetonitrile and *tert*-butyl methyl ether, and on cooling to −30 °C, air-sensitive blue plates crystallized, which were identified as **4**·2CH_3CN by X-ray crystallography (Scheme 3).

Molecular Structures of 3

The X-ray crystal structure analysis shows the formation of the dinuclear complex $[Cu(\eta^4\text{-}\mu\text{-O-}H_3\text{-}\mathbf{1})_2Cu](PF_6)_2$ (**3**) from $Cu(OH)_2$ and the ligand H_4-**1**. The dication of complex **3** resides on a crystallographic inversion center in the unit cell. Each copper(II) ion is coordinated by two nitrogen atoms, one terminal propyloxy group (O1) and two μ^2-propyloxo groups (O2) (Figure 3). The bridging oxygen atom O2 is deprotonated while the monodentate oxygen atom O1 remains protonated in the complex. The charge distribution was assigned based on the presence of only two PF_6^- anions which make the complex a dication with two monodeprotonated ligands H_3-**1**$^-$. The most acidic functions of the ligand are the alcohol groups. We concluded that O2 is the deprotonated alcohol group, based on the difference in the Cu−O distances [Cu−O1 2.339(3) Å, Cu−O2 1.920(3) Å].

The coordination geometry around the copper centers is best described by the use of the τ-criterion,[23] which indicates that the coordination geometry in **3** is only slightly distorted (τ = 0.181) from square-pyramidal. Atom O1 occupies the apical position. The Cu_2O_2 core shows a significant rhombic distortion. The angle O2−Cu−O2* is 78.10(13)°, while for Cu−O2−Cu* an angle of 101.90(13)° is observed. The Cu and Cu* distance is 3.001(1) Å. The Cu−N and $Cu-O_{eq}$ bond lengths are only slightly different [Cu−N1 2.033(3), Cu−N2 1.992(4) and Cu−O2 1.920(3), Cu−O2* 1.944(3) Å], leading to an almost symmetrical bridge between the copper atoms.

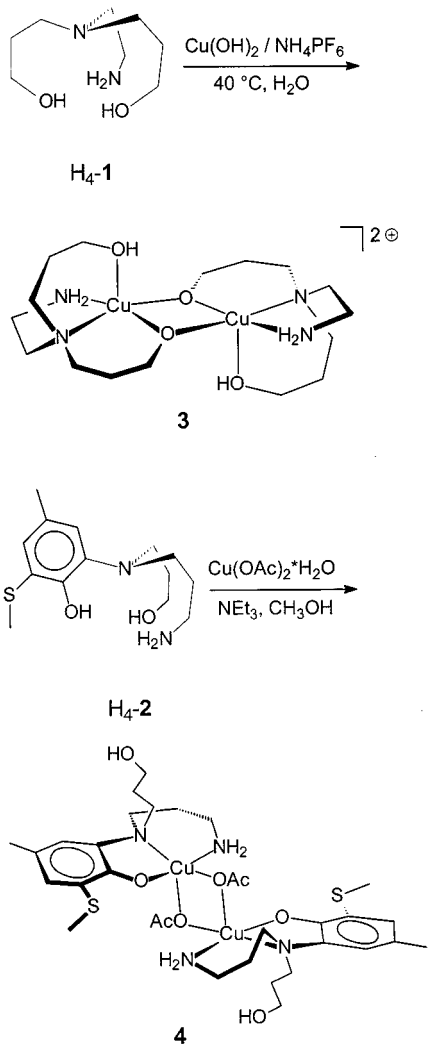

Scheme 3. Preparation of complexes **3** and **4**

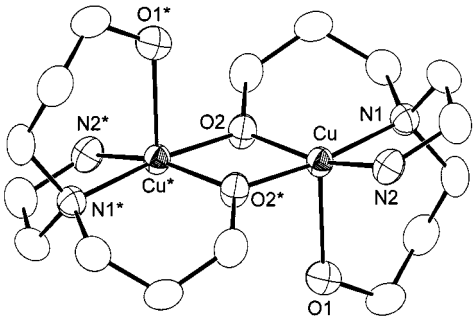

Figure 3. ORTEP plot of one complex dication of **3** (hexafluorophosphate anions are not shown); selected bond lengths [Å] and angles [°]: Cu···Cu 3.001(1), Cu−O1 2.339(3), Cu−O2 1.920(3), Cu−O2* 1.944(3), Cu−N1 2.033(3), Cu−N2 1.992(4); O1−Cu−O2 90.91(14), O1−Cu−O2* 91.77(13), O1−Cu−N1 94.74(14), O1−Cu−N2 106.3(2), O2−Cu−O2* 78.10(13), O2−Cu−N1 98.66(13), O2−Cu−N2 161.9(2), O2*−Cu−N1 172.79(14), O2*−Cu−N2 95.43(15), N1−Cu−N2 85.7(2), Cu−O2−Cu* 101.90(13)

A 5,6,6-chelate ring sequence is observed in the dication of **3**. This should and does lead to a square-pyramidal coordination geometry, with a donor atom of a six-membered

chelate ring (O1) in the apical position. In this regard, the molecular structure of **3** meets our expectations and experiences gained from related aliphatic tripodal N_4 ligand systems.[13] However, complex **3** cannot serve as a GO model compound since GO contains a mononuclear square-pyramidal copper center and not a binuclear one.

To the best of our knowledge **3** is one of two examples of a clearly square-pyramidal copper complex with an apical O-donor derived from a tripodal N_2O_2 ligand. Previously described tripodal N_2O_2 ligands with pyridyl and phenolate donors gave dinuclear copper complexes which deviate significantly from the square-pyramidal geometry, towards a trigonal-bipyramidal geometry.[10][11b] However, one tripodal N_2O_2 ligand with bulky substituents at its pyridyl and phenolate donors[11c] forms a distorted square-pyramidal mononuclear copper complex ($\tau = 0.273$) with a 5,6,6-chelate ring sequence and with an oxygen donor at the end of a C_3 chain in the apical position. These results together with the molecular structure of **3** indicate again, that the coordination geometry of copper complexes with tripodal ligands can at least partly be controlled and manipulated by the ligand topology.

Molecular Structures of 4·2CH_3CN

The X-ray structure analysis of **4**·2CH_3CN revealed that the oxygen-bridged, inversion-symmetric, dinuclear complex [(η^3-H_3-**2**)Cu(μ-OAc)$_2$Cu(η^3-H_3-**2**)]·2CH_3CN had formed (Scheme 3, Figure 4). The asymmetric unit contains two halves of the complex, which are not related by crystallographic symmetry.

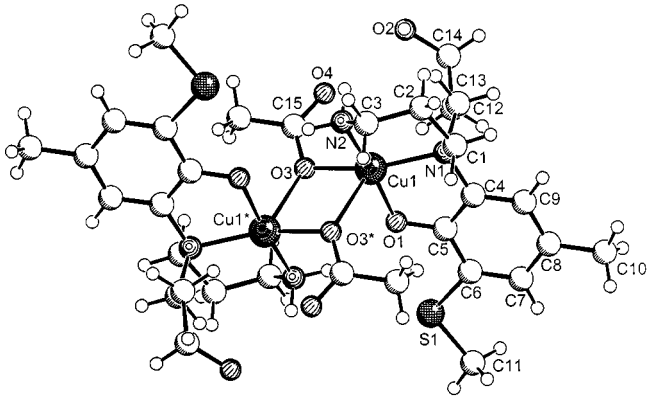

Figure 4. SCHAKAL plot of one molecule of complex **4** (the asymmetric unit contains two nearly identical halves of a molecule); selected bond lengths [A] and angles [°] for molecule A [molecule B]: Cu1···Cu1 3.2729(11) [3.2375(12)], Cu1−O1 1.916(3) [1.909(3)], Cu1−O3 1.999(3) [1.993(3)], Cu1−O3* 2.374(3) [2.529(3)], Cu1−N1 2.056(3) [2.056(4)], Cu1−N2 1.980(4) [1.970(3)]; O1−Cu1−O3 92.15(12) [92.21(12)], O1−Cu1−O3* 88.18(12) [85.33(12)], O1−Cu1−N1 86.09(13) [86.21(14)], O1−Cu1−N2 171.36(14) [169.21(14)], O3−Cu1−O3* 83.47(12) [89.36(12)], O3−Cu1−N1 159.04(14) [163.13(14)], O3−Cu1−N2 88.95(13) [88.74(14)], O3*−Cu1−N1 117.30(12) [107.23(12)], O3*−Cu1−N2 83.42(13) [83.93(13)], N1−Cu1−N2 95.91(15) [95.92(15)], Cu1−O3−Cu1* 96.53(12) [90.64(12)]

In complex **4** both copper(II) ions reside in a square-pyramidal ($\tau = 0.205$ and $\tau = 0.101$) N_2O_3 coordination environment, but in contrast to the situation in **3**, the μ^2-oxy bridges in **4** result from the bridging coordination of acetate oxygen atoms. The two acetate oxygen atoms occupy equatorial (O3) and apical (O3*) positions at the copper atom. Each Cu^{II} ion is coordinated by two nitrogen and three oxygen donors (one phenolate and two acetate oxygen atoms), while the hydroxypropyl arm (O2) of the ligand remains uncoordinated. Like in **3**, both copper atoms are coordinated in a square-pyramidal fashion, but again a dinuclear complex was obtained and hence it cannot act as an acceptable GO model compound.

The apical Cu−O bond is not exactly perpendicular to the equatorial plane which also leads to a rhombic distortion of the Cu_2O_2 core [O3−Cu−O3* 83.47(12)° and 89.36(12)°, Cu−O3−Cu* 96.53(12)° and 90.64(12)°]. For the same reason all O3*−Cu−L_{eq} angles significantly deviate from the ideal value of 90° expected for a perfect tetragonal pyramid.

The Cu−N bond lengths are almost equal, as found in **3** [Cu1−N1 2.056(3) Å and 2.056(4) Å, Cu1−N2 1.980(4) Å and 1.970(3) Å]. The Cu−O_{eq} distances [Cu−O1 1.916(3) Å and 1.909(3) Å, Cu−O3 1.999(3) Å and 1.993(3) Å] are similar. However, the separation Cu−O_{apical} is much more pronounced [Cu−O3* 2.374(3) Å and 2.529(3) Å], a behavior observed in all square-pyramidal copper complexes with an O-donor in the apical position.

Due to reasons we do not exactly know yet, and in contrast with the coordinated ligand (H_3-**1**)$^-$ in **3**, each (H_3-**2**)$^-$ ligand anion in complex **4** uses only three of the four donor groups for binding to the copper atom, while the hydroxypropyl arm is not coordinated and remains protonated. We believe that this is not exclusively due to the steric situation in **4**, but also to the low stability of the six-membered chelate ring which would have formed with the hydroxypropyl ligand arm. A similar behavior of related aliphatic tripodal ligands has been reported recently.[24] In addition it has been shown that the stability of the copper complex with the ligand trpn, which exclusively forms six-membered chelate rings is about 10^5 times lower than the stability of the corresponding tren complex that contains only five-membered chelate rings.[13b] The acetate oxygen atoms are apparently better donors than the hydroxypropyl group when competing for the coordination site at the copper center. Similar behavior has been reported for copper complexes with a tripodal ligand capable of forming a 5,6,6-chelate ring sequence, where the presence of chloride ions prevents the formation of the chelate complex, and a copper complex with chloride ligands was obtained.[11c] Table 1 lists some structural parameters for **3** and **4**.

Cyclic Voltammetry

The cyclic voltammogram of complex **3** recorded in an acetonitrile solution exhibits an irreversible oxidation potential at $E_{pa} = +1375$ mV vs. Ag/AgCl. Complex **3** is quite stable relative to to the corresponding Cu^{III} species which is highly reactive and rapidly decomposes to non-identified

Table 1. Comparison of selected structural details in complexes **3** and **4**·2CH_3CN

Complex	Cu−N_{eq} [Å]	Cu−O_{eq} [Å]	Cu−O_{ap} [Å]	τ
3	1.992(4), 2.033(3)	1.920(3), 1.944(3)	2.339(3)	0.179
4·2CH_3CN	1.980(4), 2.056(3)	1.916(3), 1.999(3)	2.374(3)	0.205, 0.101

products. Upon application of a negative potential an irreversible reduction is observed at $E_{pc} = -725$ mV vs. Ag/AgCl in acetonitrile. This corresponds to the process $Cu^{II} + e^- \rightarrow Cu^{I}$, which is followed by the dissociation of the Cu^{I} complex and disproportionation of Cu^{I} to Cu^{II} and Cu^0.

The results of the cyclic voltammetric analysis of the redox potentials of ligand H_4-**2** and complex **4** are shown in Figure 5. In the cathodic region, the free ligand H_4-**2** displays one quasireversible oxidation peak at $E = +130$ mV vs. Ag/AgCl in acetonitrile (top, solid line).

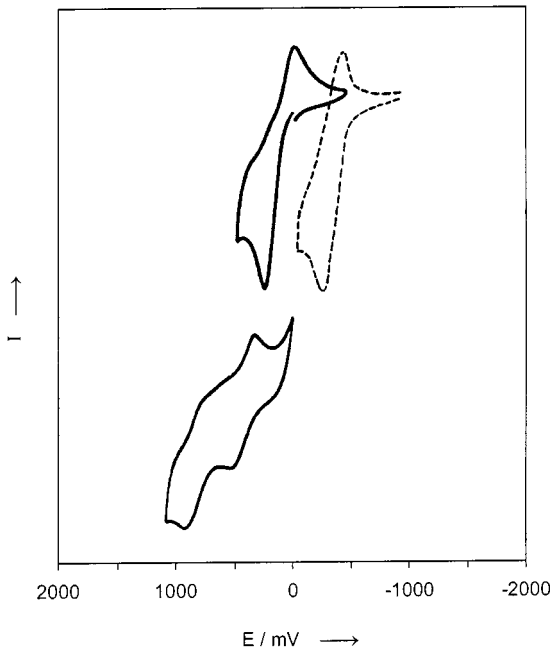

Figure 5. Cyclic voltammograms of H_4-**2** (top, solid line), $(H_3$-**2**$)^-$ (top, dashed line) and of complex **4** (bottom); *E* vs. Ag/AgCl in acetonitrile

This process corresponds to the oxidation of the phenolic moiety, leading to a phenoxyl radical which is prevented from dimerizing. The same process is observed when the phenolic OH group is deprotonated in the presence of $(n\text{Bu})_4N^+OH^-$. The oxidation potential of the phenol group is then shifted towards a more negative potential by about 440 mV than reported previously,[10,11] and is now observed as a quasireversible voltammetric response at $E = -310$ mV vs. Ag/AgCl in acetonitrile (top, dashed line). This low-potential redox step arises from the relatively facile oxidation of the electron-rich thioether and amino-substituted phenol. Recently, such stable, free phenoxyl radicals have also been shown to be essential for enzymes other than galactose oxidase, e.g. glyoxal oxidase[25] and ribonucleotide reductase[1b].

Although the oxidation of the blue dimeric copper complex **4** takes place at a somewhat higher potential than the protonated ligand H_4-**2**, **4** is also easily oxidized. A broad peak, which seems to be the result of the overlapping of two independent redox processes, is observed between 0 and +1000 mV vs. Ag/AgCl in acetonitrile (Figure 5, bottom). The oxidation of the phenolate takes place at a potential of $E^1 = +430$ mV vs. Ag/AgCl, while a second oxidation process occurs at $E^2 = +870$ mV vs. Ag/AgCl. The superimposing cyclic voltammetric responses suggest a quasireversible electron transition, which indicates that in **4** a stable phenoxyl radical is formed on oxidation. In addition, the ligand stabilizes the copper(II) state, since reduction of the complex is observed at a very low potential ($E = -1320$ mV vs. Ag/AgCl in acetonitrile; not shown in Figure 5). This reduction process is irreversible and leads to a deposit of copper(0) on the electrode surface, as concluded from a sharp anodic oxidation peak at $E_{pc} = -60$ mV during the reverse scan with the typical features of a redissolution process.[10]

Conclusion

We have prepared two novel nonsymmetric tripodal ligands which provide an N_2O_2 donor set. Both ligands are capable of coordinating to Cu^{II} to give a 5,6,6-chelate ring sequence. For this chelate ring sequence, square-pyramidal complexes with a donor linked by a C_3 chain in the apical position are expected. Ligand H_4-**1** indeed forms such a complex. However, this complex is dinuclear. With ligand H_2-**2**, we present a tripod with an *o*-amino-*o*-(methylthio)-substituted phenolate donor. This ligand also forms a square-pyramidal Cu^{II} complex, which is also dinuclear. While the dinuclear nature of complexes **3** and **4**·2CH_3CN excludes them from the acceptable mononuclear GO models, they still provide information about the ligand design for the preparation of structural GO models. Among the dinuclear complexes with an N_2O_2 donor set, **3** and **4**·2CH_3CN contain copper atoms which deviate least from the required square-pyramidal coordination geometry, as judged by the τ values of 0.181 for **3** and 0.205 and 0.101 for **4**·2CH_3CN. Thus, the 5,6,6-chelate ring sequence indeed leads to the desired square-pyramidal complexes. Finally, the unique *o*-amino-*o*-(methylthio)-substitution of the phenol donor in ligand H_4-**2** leads to a significant reduction of the redox potential for the oxidation of the free or coor-

dinated phenolate group to the corresponding phenoxyl radical, which is stabilized against dimerization by *p*-methyl substitution of the aromatic ring. Based on these observations we propose that substitution of the aliphatic OH and NH_2 donors in H_4-**2** by aromatic ones (phenol and pyridine) and sterically more bulky substituents at the phenol groups could lead to a square-planar, mononuclear Cu^{II} complex, which would serve as a satisfactory structural GO model.

Experimental Section

General Remarks: All manipulations were carried out under argon. Solvents were purified by standard methods, freshly distilled and degassed prior to use. − Infrared spectra were recorded in KBr using a Perkin−Elmer IR 983 spectrometer. − NMR spectra were recorded with a Bruker AM 250 spectrometer. − Elemental analyses (C,H,N,S) were performed with a Vario EL Elemental Analyzer. − EI and +FAB mass spectra were recorded with Finnigan MAT 112 or Finnigan MAT 711 instruments. − UV/Vis spectra were recorded with a Perkin−Elmer Lambda 9 UV/Vis/NIR spectrophotometer. − Cyclic voltammetric experiments were carried out with a Bank High Power Potentiostat Wenking HP 72 and a Bank Scan Generator Wenking Model VSG 83, using a three-electrode cell configuration (working electrode: Pt; auxiliary electrode: Pt; reference electrode: Ag/AgCl/3 M KCl; $E_{Fc/Fc+}$ = 435 mV). The experiments were performed in acetonitrile with 0.1 M tBu_4NPF_6 as the supporting electrolyte with scan rates of 100 mV/s.

Ligand Syntheses

B: 3,3′-Iminobis(ethyl propionate) **B** was prepared according to a procedure published previously.[14] − ^{1}H NMR (250 MHz, $CDCl_3$): δ = 4.12 (q, 4 H, $-OCH_2$), 2.92 (t, 4 H, NCH_2), 2.49 (t, 4 H, CH_2COO), 1.84 (s, 1 H, NH), 1.24 (t, 6 H, CH_3). − $^{13}C\{^1H\}$ NMR (62.90 MHz, $CDCl_3$): δ = 172.38 (COO), 60.15 (CH_2O), 44.68 (NCH_2), 34.52 (CH_2COO), 13.97 (CH_3).

C: Formaldehyde (2.027 g, 0.025 mol, 37% in water) was added to a solution of sodium pyrosulfite $Na_2S_2O_5$ (2.376 g, 0.0125 mol) in 10 mL of water. The reaction mixture was heated to 50 °C for a period of 45 min and then cooled to 0 °C. **B** (5.431 g, 0.025 mol) was added slowly while maintaining the temperature below 5 °C. Subsequently, the flask was allowed to warm to room temperature and the reaction mixture was stirred for 2 h. The mixture was again cooled to 0 °C and a solution of KCN (5.431 g, 0.025 mol) in 8 mL of water was added. The resulting solution was stirred overnight at room temperature. During this period an oil had separated, which was extracted with chloroform (3 × 50 mL). The organic phases were combined and dried with anhydrous $MgSO_4$. All solvents were removed in vacuo, and the residue was distilled at 115 °C ($2\cdot10^{-2}$ mbar). Yield: 5.070 g (79.1% relative to **B**) of a colorless oil. − ^{1}H NMR (250 MHz, $CDCl_3$): δ = 4.12 (q, 4 H, OCH_2), 3.64 (s, 2 H, CH_2CN), 2.90 (t, 4 H, NCH_2), 2.48 (t, 4 H, CH_2COO), 1.24 (t, 6 H, CH_3). − $^{13}C\{^1H\}$ NMR (62.90 MHz, $CDCl_3$): δ = 171.39 (COO), 114.84 (CN), 60.41 (OCH_2), 49.37 (NCH_2), 41.96 (CH_2CN), 32.85 (CH_2COO), 13.99 (CH_3).

H_4-1: All protected donor groups in **C** were liberated simultaneously by reduction with AlH_3. The AlH_3 was prepared from lithium aluminium hydride (LAH) (5.40 g, 0.143 mol) and H_2SO_4 (6.183 g, 60 mmol, 96%) in 150 mL of dry THF as described.[13a] Compound **C** (5.07 g, 19.8 mmol), dissolved in 30 mL of THF, was added dropwise to the vigorously stirred AlH_3 suspension, at room temperature. The reaction mixture was stirred for 24 h at ambient temperature, and residual AlH_3 was carefully hydrolyzed with water (8.2 mL, 0.46 mol). All solids were removed by filtration and repeatedly washed with methanol (6 × 50 mL). The organic layers were combined, all solvents removed in vacuo, and the residue was distilled at 135 °C ($2\cdot10^{-3}$ mbar). Ligand H_4-**1** was obtained as a colorless oil. Yield 2.234 g (64% relative to **C**). − ^{1}H NMR (250 MHz, $CDCl_3$): δ = 3.67 (s + t, 6 H, OH + CH_2O), 2.80 (t, 2 H, $NCH_2CH_2NH_2$), 2.58 (t, 4 H, $NCH_2CH_2CH_2$), 2.50 (t, 2 H, CH_2NH_2), 1.70 (m + s, 6 H, $CH_2CH_2CH_2$ + NH_2). − $^{13}C\{^1H\}$ NMR (62.90 MHz, $CDCl_3$): δ = 61.27 (CH_2O), 56.45 ($NCH_2CH_2NH_2$), 52.27 ($NCH_2CH_2CH_2$), 39.29 (CH_2NH_2), 28.97 ($CH_2CH_2CH_2$). − MS (EI): *m*/*z* (%) = 176 (2.55, $[M]^+$), 146 (100, $[M - H_2O]^+$), 102 (57.38), 58 (70.21). − IR (KBr): $\tilde{\nu}$ = 3343 (br. s, N−H + O−H), 2939, 2869 (s, C−H), 1593 (m, N−H), 1373 (m, O−H), 1464 (s, C−H), 1216 (m, C−N), 1063 (s, C−O).

D: Anhydrous $AlCl_3$ (18.0 g, 0.12 mol) was suspended in 50 mL of dry dichloromethane of. This mixture was treated with a solution of *o*-nitro-*p*-cresol (15.314 g, 0.1 mol) in 20 mL of dichloromethane. When the evolution of HCl had ceased, bromine (17.5 g, 0.11 mol) was added dropwise and the dark green suspension was stirred overnight at room temperature. The mixture was hydrolyzed with 10 g of ice under vigorous evolution of HCl. Subsequently, 50 mL of water and 30 mL of dichloromethane were added and the resulting suspension was mixed with 30 mL of aqueous HCl (32%). The clear orange organic layer was separated, washed twice with acidic water and dried with anhydrous $MgSO_4$. The solvent was stripped in vacuo to give 21.33 g (91%) of a yellow powder. − ^{1}H NMR (250 MHz, $CDCl_3$): δ = 11.0 (s, 1 H, OH), 7.92, 7.74 (s, 2 H, Ar-H), 2.38 (s, 3 H, CH_3). − $^{13}C\{^1H\}$ NMR (62.90 MHz, $CDCl_3$): δ = 150.09, 141.76, 132.70, 124.04, 118.94, 112.81 (Ar−C), 20.19 (CH_3).

E: The sodium salt of **D** was obtained by deprotonation of the phenolic OH group with aqueous NaOH. To achieve this **D** (11.6 g, 0.05 mol), dissolved in 24 mL of hot (70 °C) ethanol, was added to a warm solution of NaOH (2.04 g, 0.051mol) in a mixture of 24 mL of ethanol and 3.5 mL of water. Immediately a red precipitate separated, which was collected by filtration and dried in vacuo for several hours. A sample of the sodium salt of **D** (12.7 g, 0.05 mol) was suspended in 70 mL of dry THF. (Chloromethoxy)methane (MOMCl) (4.026 g, 0.05 mol) was then added dropwise to this suspension. ***Warning: (Chloromethoxy)methane (MOMCl) is known to be extremely carcinogenic!*** The mixture was refluxed for 4 h. During this period the color of the suspension changed from red to white. The reaction mixture was extracted three times with a saturated K_2CO_3 solution, and the combined organic layers were dried with anhydrous $MgSO_4$. Removal of the solvent yielded 11.95 g (86.6%) of a pale yellow powder, that was purified by recrystallization from a mixture of hexane/ether (3:1, v:v). − ^{1}H NMR (250 MHz, $CDCl_3$): δ = 7.66, 7.54 (s, 2 H, Ar-H), 5.12 (s, 2 H, OCH_2O), 3.54 (s, 3 H, OCH_3), 2.34 (s, 3 H, CH_3). − $^{13}C\{^1H\}$ NMR (62.90 MHz, $CDCl_3$): δ = 137.89, 136.05, 124.36, 119.13 (Ar−C, only 4 resonances were observed), 100.68 (OCH_2O), 58.01 (OCH_3), 20.36 (CH_3).

F: Compound **E** (16.565 g, 0.06 mol) was dissolved in 250 mL of dry THF and cooled to −105 °C with a mixture of diethyl ether/liquid nitrogen as described previously.[18b] Over a period of 30 min phenyllithium (37 mL, 0.066 mol, 1.8 M solution in hexane/ether, 70:30) was slowly added via a syringe maintaining the temperature below −100 °C. When all the phenyllithium had been added, the

red suspension was stirred for 1 h at −105 °C and subsequently quenched with dry, degassed dimethyl disulfide (11.3 mL, 0.12 mol). After 15 min, the mixture was allowed to warm to −78 °C. After stirring at this temperature for an additional 30 min, the orange suspension was carefully hydrolyzed with 15 mL of degassed water and slowly brought to 0 °C. Toluene (150 mL) was added and the total volume of the solution was reduced to 100 mL in vacuo. Ether (150 mL) was then added. The resulting organic phase was repeatedly extracted with water until the aqueous layer remained colorless. After drying with anhydrous $MgSO_4$ and removal of the solvents in vacuo, a brown oily residue was obtained. Column-chromatographic purification (SiO_2, hexane/ethyl acetate, 4:1, R_f = 0.29) yielded 10.05 g (72.3%) of an intense orange oil. − ^{1}H NMR (250 MHz, $CDCl_3$): δ = 7.30, 7.10 (s, 2 H, Ar-H), 5.02 (s, 2 H, OCH_2O), 3.50 (s, 3 H, OCH_3), 2.42 (s, 3 H, SCH_3), 2.32 (s, 3 H, CH_3). − ^{13}C{^{1}H} NMR (62.90 MHz, $CDCl_3$): δ = 144.82, 144.18, 136.14, 135.03, 130.12, 121.11 (Ar-C), 100.06 (OCH_2O), 57.88 (OCH_3), 20.80 (CH_3), 14.89 (SCH_3).

G: A solution of **F** (7.298 g, 0.03 mol) in 100 mL of methanol was cooled to 0 °C and mixed with hydrazine (6 g, 0.12 mol, 100%). After addition of three small portions of Raney nickel, it was stirred until the evolution of gas had ceased and the mixture decolorized. In order to decompose the excess hydrazine an additional portion of Raney nickel was added and the suspension was heated to reflux for 90 min. The solid metal was separated by filtration under argon, and all solvents were removed in vacuo. The oily residue obtained was dissolved in 50 mL of degassed dichloromethane and the solution was dried with anhydrous $MgSO_4$. Removal of the solvent in vacuo yielded 5.77 g (90.2%) of **G** as a yellow oil. − ^{1}H NMR (250 MHz, $CDCl_3$): δ = 6.37, 6.34 (s, 2 H, Ar-H), 5.04 (s, 2 H, OCH_2O), 3.94 (br. s, 2 H, NH_2), 3.62 (s, 3 H, OCH_3), 2.40 (s, 3 H, SCH_3), 2.24 (s, 3 H, CH_3). − ^{13}C{^{1}H} NMR (62.90 MHz, $CDCl_3$): δ = 139.80, 139.51, 135.04, 132.04, 115.88, 113.95 (Ar-C), 99.11 (OCH_2O), 57.58 (OCH_3), 21.07 (CH_3), 14.71 (SCH_3).

H: Acrylonitrile (3.188 g, 0.06 mol) and **G** (8.535 g, 0.04 mol) were mixed with the catalyst $Cu(OAc)_2 \cdot H_2O$ (0.839 g) and the polymerization inhibitor quinone (0.17 g). The mixture was heated to 110 °C and the reaction was monitored by chromatography (SiO_2, hexane/ethyl acetate, 4:1, $R_f^{\mathbf{G}}$ = 0.18, $R_f^{\mathbf{H}}$ = 0.13). The reaction was complete after 4 h, otherwise additional portions of acrylonitrile and copper catalyst had to be added. The resulting brown residue was purified by column chromatography (SiO_2, hexane/ethyl acetate). Yield 7.55 g (70.9%) of a brown crystalline solid. − ^{1}H NMR (250 MHz, $CDCl_3$): δ = 6.36, 6.25 (s, 2 H, Ar-H), 5.02 (s, 2 H, OCH_2O), 4.88 (br. s, 1 H, NH), 3.62 (s, 3 H, OCH_3), 3.50 (q, 2 H, NHC*H*$_2$), 2.62 (t, 2 H, CH_2CN), 2.40 (s, 3 H, SCH_3), 2.24 (s, 3 H, CH_3). − ^{13}C{^{1}H} NMR (62.90 MHz, $CDCl_3$): δ = 139.74, 135.36, 132.00, 118.05, 115.31 (Ar-C, only 5 resonances were observed), 108.87 (CN), 99.32 (OCH_2O), 57.71 (OCH_3), 39.56 ($NHCH_2$), 21.56 (CH_3), 18.04 (CH_2CN), 14.68 (SCH_3).

I: H (5.332 g, 20 mmol) was dissolved in a mixture of dry diethyl ether (25 mL) and chloroform (5 mL) and treated with acetoxypropionyl chloride (3.09 g, 20.5 mmol) which was synthesized according to a published procedure.[22] On reaction the mixture slightly warmed and became darker in color. After 30 min, triethylamine (2.086 g, 20.6 mmol) was added, and the solution was stirred for one additional hour at room temperature. Washing of the reaction solution with water, drying of the organic phase with anhydrous $MgSO_4$ and removal of the solvents in vacuo yielded a brown oil that was purified chromatographically (SiO_2, hexane/ethyl acetate, 1:1, $R_f^{\mathbf{I}}$ = 0.15). The product crystallized as colorless needles. Yield: 4.95 g (65%). − ^{1}H NMR (250 MHz, $CDCl_3$): δ = 6.99, 6.86 (s, 2 H, Ar-H), 5.01 (q, 2 H, OCH_2O), 4.52 + 4.41 (dd, 2 H, $NC(O)CH_2$), 4.37 + 4.30 (dd, 2 H, $NC(O)CH_2CH_2$), 3.48 (s, 3 H, OCH_3), 2.77 (q, 2 H, NCH_2), 2.60 (t, 2 H, CH_2CN), 2.46 (s, 3 H, SCH_3), 2.36 (s, 3 H, CH_3), 2.02 (s, 3 H, $C(O)CH_3$). − ^{13}C{^{1}H} NMR (62.90 MHz, $CDCl_3$): δ = 170.78 [C(O)O + C(O)N], 147.24, 135.69, 134.93, 134.24, 126.74, 126.70 (Ar-C), 117.89 (CN), 99.35 (OCH_2O), 60.32 (OCH_3), 47.51 [$NC(O)CH_2CH_2O$], 44.42 [$NC(O)CH_2$], 33.26 (NCH_2), 21.00 (Ar-CH_3), 20.88 [$C(O)CH_3$], 16.41 (CH_2CN), 14.70 (SCH_3).

H_4-2: All protected donor groups in **I** were liberated simultaneously by use of AlH_3. The AlH_3 was prepared from lithium aluminium hydride (LAH) (2.73 g, 72 mmol) and H_2SO_4 (3.065 g, 30 mmol, 96%) in 70 mL of dry THF as described.[13a] Ligand precursor **I** (3.75 g, 10 mmol), dissolved in 30 mL of THF, was added dropwise to the vigorously stirred AlH_3 suspension. The reaction mixture was stirred for 24 h at ambient temperature, residual AlH_3 was carefully hydrolyzed with water (5.4 mL, 0.3 mmol), and all solids were removed by filtration. The solid residue was repeatedly extracted with methanol under argon. All organic phases were combined and all solvents were removed in vacuo. The oily residue obtained was dissolved in a small portion of dichloromethane and this solution was filtered and dried with anhydrous $MgSO_4$. Removal of the solvent in vacuo yielded a yellow sticky oil that crystallized at −30 °C. Alternatively, addition of diethyl ether to oily H_4-**2** gave a white powder. Yield: 1.51 g (84.8%). − $C_{14}H_{24}N_2O_2S$ (284.42): calcd. C 59.12, H 8.51, N 9.85, S 11.27; found C 58.24, H 8.49, N 9.58, S 11.37. − ^{1}H NMR (250 MHz, $CDCl_3$): δ = 6.66 (s, 2 H, Ar-H), 5.64 (br. s, 4 H, Ar-OH, CH_2-OH, NH_2), 3.58 (t, 2 H, CH_2OH), 2.98 (t + t, 4 H, NCH_2), 2.84 (t, 2 H, CH_2NH_2), 2.36 (s, 3 H, SCH_3), 2.22 (s, 3 H, Ar-CH_3), 1.60 (m + m, 4 H, $CH_2CH_2CH_2$). − ^{13}C{^{1}H} NMR (62.90 MHz, $CDCl_3$): δ = 152.96, 136.99, 125.52, 124.34, 120.77, 118.36 (Ar-C), 60.95 (CH_2OH), 52.99 ($NCH_2CH_2CH_2OH$), 48.41 ($NCH_2CH_2CH_2NH_2$), 38.69 (CH_2NH_2), 29.06, 26.35 ($CH_2CH_2CH_2$), 20.95 (Ar-CH_3), 14.94 (SCH_3). − MS (EI), *m*/*z* (%) = 284 (38.79) $[M]^+$, 240 (20.22) $[M - CH_2CH_2NH_2]^+$, 196 (100), 182 (21.11), 134 (6.95). − IR (KBr): ṽ: 3504 (s, N−H), 3337 (s, O−H), 2950, 2918, 2848, 2799 (s, C−H), 1547 (m, N−H), 1448 (m, O−H), 1265 (m, C−N), 1077 (s, C−O), 830, 871 (m, C−H of a 1,2,3,5-substituted aromatic ring).

Preparation of Copper Complexes

3: For the preparation of **3** freshly precipitated $Cu(OH)_2$ (195 mg, 2 mmol) was suspended in water (10 mL) and ligand H_4-**1** (370 mg, 2.1 mmol) was added dropwise with a syringe. The blue suspension was stirred at 40 °C for 60 min, and then solid NH_4PF_6 (652 mg, 4 mmol) was added, resulting in a deep blue solution. The solution was reduced to a volume of 5 mL and cooled to 5 °C. After 24 h, deep blue crystals had formed. The crystals were collected by filtration and recrystallized from warm acetonitrile/diethyl ether. Yield 596 mg (68.9%). − $C_{16}H_{38}Cu_2F_{12}N_4O_4P_2$ (767.52): calcd. C 25.04, H 4.99, N 7.30; found C 25.09, H 5.17, N 7.46. − MS (FAB, positive ions, 3-nitrobenzyl alcohol/DMSO), *m*/*z* (%) = 475 (18.95, $[M - H]^+$), 301 (37.67, $[Cu(H_3$-**1**$) + Cu]^+$), 239 (33.19, $[$**3** $+ H]^{2+}$). − IR (KBr): ṽ: 3549, 3378, 3330 (w, O−H + N−H), 2970, 2875, 2833 (m, C−H), 1596 (m, NH_2), 1473, 1459, 1433 (m, C−H), 1065, 1046 (s, C−O); 833, 558 (s, PF_6). − UV/Vis (CH_3OH): λ_{max} [nm] (ε) = 270 (4900), 366 (2000), 585 (120).

4: H_4-**2** (62.6 mg, 0.22 mmol) was mixed with triethylamine (44.4 mg, 0.44 mmol). The mixture was added dropwise to a solution of $Cu(OAc)_2 \cdot H_2O$ (43.9 mg, 0.22 mmol) in 10 mL of methanol, resulting in the formation of a green solution. After stirring for 30 min, the solvent was removed in vacuo and the residue suspended

in acetonitrile and filtered. To the clear, deep green solution was added *tert*-butyl methyl ether. Cooling the solution to −30 °C yielded blue plate-shaped crystals. Yield 8.3 mg (4.6%) of **4**·2CH_3CN. − $C_{36}H_{58}Cu_2N_6O_8S_2$ (894.08): calcd. C 47.33, H 6.45, N 6.90, S 7.89; found C 47.48, H 6.53, N 7.09, S 8.13. − MS (FAB, positive ions, 3-nitrobenzyl alcohol/DMSO), *m/z* (%) = 409 (11.34) $[Cu_2(H_3\text{-}\mathbf{2})]^+$, 346 (18.20) $[Cu(H_3\text{-}\mathbf{2})]^+$. − UV/Vis ($CH_3OH$): λ_{max} [nm] (ε) = 310 nm (15360), 400 (sh, 220), 650 (140).

Crystal Structure Analyses: Crystallographic data for complexes **3** and **4**·2CH_3CN are presented in Table 2. Crystals of **3** are air-stable. Diffraction data were collected at room temperature with an Enraf−Nonius CAD-4 diffractometer. No absorption correction was applied. All non-hydrogen atoms were refined with anisotropic thermal parameters. Hydrogen atoms were added at geometrically idealized positions and were refined using a riding model. Complex **4**·2CH_3CN rapidly degenerates in air under loss of co-crystallized solvent. Suitable specimens were mounted at 198 K on a Nonius Kappa CCD diffractometer with a rotating anode generator. Diffraction data were collected at 198 K. An absorption correction via SORTAV was applied to the raw data ($0.85 \leq T \leq 0.99$). All other non-hydrogen atoms were refined with anisotropic thermal parameters. Hydrogen atoms were added at geometrically idealized positions and were refined using a riding model. The following programs were used: Data collection EXPRESS and COLLECT, data reduction MolEN and DENZO-SMN, absorption correction for CCD data SORTAV, structure solution SHELXS-86 and SHELXS-97, structure refinement SHELXL-97, graphical presentation ZORTEP and SCHAKAL-92. Crystallographic data (excluding structure factors) for the structures reported in this paper have been deposited with the Cambridge Crystallographic Data Centre as supplementary publication nos. CCDC-150423 and -150424 for **3** and **4**·2CH_3CN, respectively. Copies of the data can be obtained free of charge on application to CCDC, 12 Union Road, Cambridge CB2 1EZ, UK [Fax: (internat.) + 44-1223/336-033, E-mail: deposit@ccdc.cam.ac.uk].

Table 2. Summary of crystallographic data for **3** and **4**·2CH_3CN

	3	**4**·2CH_3CN
Empirical formula	$C_{16}H_{38}N_4CuF_{12}P_2O_4$	$C_{36}H_{58}N_6Cu_2O_8S_2$
M_r	767.52	894.08
T [K]	293(2)	198(2)
Crystal size [mm]	0.31×0.22×0.20	0.15×0.10×0.05
a [Å]	9.041(6)	9.978(1)
b [Å]	13.356(2)	13.433(1)
c [Å]	11.990(2)	16.398(1)
α [°]	90	97.87(1)
β [°]	98.54(3)	94.94(1)
γ [°]	90	90.36(1)
V [Å^3]	1419.8(10)	2168.7(3)
Z	2	2
Space group	$P2_1/n$ (no. 14)	$P\bar{1}$ (no. 2)
$\rho_{calcd.}$ [g cm^{-3}]	1.795	1.369
μ Mo-K_α [mm^{-1}]	1.721	1.130
Diffractometer	Enraf−Nonius CAD-4	Enraf−Nonius Kappa CCD
λ [Å]	0.71073	0.71073
2θ range [°]	$2.3 \leq 2\theta \leq 26.4$	$2.05 \leq 2\theta \leq 25.0$
Index range	$h, k, \pm l$	$\pm h, \pm k, \pm l$
Unique data	2918	7597
Observed data [$I \geq 2\sigma(I)$]	2003	5092
R	0.0414	0.0597
wR	0.0952	0.1111
No. of variables	257	735
GOF	1.050	1.022

Acknowledgments

We thank the Deutsche Forschungsgemeinschaft and the Fonds der Chemischen Industrie for financial support.

[1] [1a] J. W. Whittaker, in: *Metal Ions in Biological Systems* (Eds.: H. Sigel, A. Sigel), M. Dekker, New York **1994**, vol. 30, p. 315−359. − [1b] J. Stubbe, W. A. van der Donk, *Chem. Rev.* **1998**, *98*, 705 and references therein.

[2] [2a] N. Ito, S. E. V. Phillips, K. D. S. Yadav, P. F. Knowles, *J. Mol. Biol.* **1994**, *238*, 794. − [2b] N. Ito, S. E. V. Phillips, C. Stevens, Z. B. Ogel, M. J. McPherson, J. N. Keen, K. D. S. Yadav, P. F. Knowles, *Nature* **1991**, *350*, 87.

[3] [3a] S. Itoh, S. Takayama, R. Arakawa, A. Furuta, M. Komatsu, A. Ishida, S. Takamuku, S. Fukuzumi, *Inorg. Chem.* **1997**, *36*, 1407. − [3b] M. Ruf, C. G. Pierpont, *Angew. Chem.* **1998**, *110*, 1830; *Angew. Chem. Int. Ed.* **1998**, *37*, 1736.

[4] J. Müller, T. Weyhermüller, E. Bill, P. Hildebrandt, L. Ould-Moussa, T. Glaser, K. Wieghardt, *Angew. Chem.* **1998**, *110*, 637; *Angew. Chem. Int. Ed.* **1998**, *37*, 616.

[5] [5a] J. A. Halfen, V. G. Young, Jr., W. B. Tolman, *Angew. Chem.* **1996**, *108*, 1832; *Angew. Chem. Int. Ed. Engl.* **1996**, *35*, 1687. − [5b] J. A. Halfen, B. A. Jazdzewski, S. Mahapatra, L. M. Berreau, E. C. Wilkinson, L. Que, Jr., W. B. Tolman, *J. Am. Chem. Soc.* **1997**, *119*, 8217. − [5c] B. A. Jazdzewski, V. G. Young, Jr., W. B. Tolman, *Chem. Commun.* **1998**, 2521.

[6] [6a] Y. Wang, T. D. P. Stack, *J. Am. Chem. Soc.* **1996**, *118*, 13097. − [6b] Y. Wang, J. L. DuBois, B. Hedmann, K. O. Hodgson, T. D. P. Stack, *Science* **1998**, *279*, 537.

[7] [7a] P. Chaudhuri, M. Hess, T. Weyhermüller, K. Wieghardt, *Angew. Chem.* **1999**, *111*, 1165; *Angew. Chem. Int. Ed.* **1999**, *38*, 1095. − [7b] P. Chaudhuri, M. Hess, U. Flörke, K. Wieghardt, *Angew. Chem.* **1998**, *110*, 2340; *Angew. Chem. Int. Ed.* **1998**, *37*, 2217.

[8] H. Adams, N. A. Bailey, I. K. Campbell, D. E. Fenton, Q.-Y. He, *J. Chem. Soc., Dalton Trans.* **1996**, 2233 and references therein.

[9] M. Vaidyanathan, R. Viswanathan, M. Palaniandavar, T. Balasubramanian, P. Prabhaharan, T. P. Muthiah, *Inorg. Chem.* **1998**, *37*, 6418.

[10] M. M. Whittaker, W. R. Duncan, J. W. Whittaker, *Inorg. Chem.* **1996**, *35*, 382 and references therein.

[11] [11a] D. Zurita, C. Scheer, J.-L. Pierre, E. Saint-Aman, *J. Chem. Soc., Dalton Trans.* **1996**, 4331. − [11b] D. Zurita, I. Gauthier-Luneau, S. Ménage, J.-L. Pierre, E. Saint-Aman, *J. Biol. Inorg. Chem.* **1997**, *2*, 46. − [11c] Y. Shimazaki, S. Huth, A. Odani, O. Yamauchi, *Angew. Chem.* **2000**, *112*, 1732; *Angew. Chem. Int. Ed.* **2000**, *39*, 1666.

[12] M. Duggan, N. Ray, B. Hathaway, G. Tomlinson, P. Brint, K. Pelin, *J. Chem. Soc., Dalton Trans.* **1980**, 1342.

[13] [13a] A. M. Dittler-Klingemann, F. E. Hahn, *Inorg. Chem.* **1996**, *35*, 1996. − [13b] A. M. Dittler-Klingemann, C. Orvig, F. E. Hahn, F. Thaler, C. D. Hubbard, R. van Eldik, S. Schindler, I. Fábián, *Inorg. Chem.* **1996**, *35*, 7798. − [13c] F. Thaler, C. D. Hubbard, F. W. Heinemann, R. van Eldik, S. Schindler, I. Fábián, A. M. Dittler-Klingemann, F. E. Hahn, C. Orvig, *Inorg. Chem.* **1998**, *37*, 4022.

[14] [14a] F. E. Hahn, S. Rupprecht, *Chem. Ber.* **1991**, *124*, 481. − [14b] F. E. Hahn, S. Rupprecht, *Chem. Ber.* **1991**, *124*, 487. − [14c] B. Wolff, A. Weiss, *Angew. Chem.* **1986**, *98*, 173; *Angew. Chem. Int. Ed. Engl.* **1986**, *25*, 162.

[15] E. C. Horning (Ed.), *Org. Synth., Coll. Vol. III* **1955**, 275.

[16] L. C. Raiford, *J. Am. Chem. Soc.* **1919**, *41*, 2072.

[17] [17a] K. Brand, W. Schreber, *Ber. Dtsch. Chem. Ges.* **1942**, *75*, 156. – [17b] M. R. Agharahimi, N. A. LeBel, *J. Org. Chem.* **1995**, *60*, 1856.
[18] [18a] I. R. Hardcastle, P. Quayle, E. L. M. Ward, *Tetrahedron Lett.* **1994**, *35*, 1747. – [18b] G. Voß, H. Gerlach, *Chem. Ber.* **1989**, *122*, 1199. – [18c] G. Köbrich, P. Buck, *Chem. Ber.* **1970**, *103*, 1412.
[19] [19a] B. J. Wakefield, *Organolithium Methods*, Academic Press, London, **1990**. – [19b] L. Brandsma, H. Verkruijsse, *Preparative Polar Organometallic Chemistry*, Springer Verlag, Berlin, **1987**.
[20] S. Cabiddu, A. Maccioni, M. Secci, V. Solinas, *Gazz. Chim. Ital.* **1969**, *99*, 397.
[21] S. A. Heininger, *J. Org. Chem.* **1957**, *22*, 1213.
[22] T. L. Gresham, J. E. Jansen, F. W. Shaver, *J. Am. Chem. Soc.* **1948**, *70*, 1003.
[23] A. W. Addison, T. N. Rao, J. Reedijk, J. van Rijn, G. C. Verschoor, *J. Chem. Soc., Dalton Trans.* **1984**, 1349.
[24] C. Ochs, F. E. Hahn, R. Fröhlich, *Chem. Eur. J.* **2000**, *6*, 2193.
[25] M. M. Whittaker, P. J. Kersten, N. Nakamura, J. Sanders-Loehr, E. S. Schweizer, J. W. Whittaker, *J. Biol. Chem.* **1996**, *271*, 681.

Received October 2, 2000
[I00385]

Dinucleotide Hydrolysis Promoted by Dinuclear Zn Complexes − The Effect of the Distance between Zn Ions in the Complexes on the Hydrolysis Rate

Shun-ichi Kawahara[a] and Tadafumi Uchimaru*[a]

Keywords: Hydrolysis / Ligand effects / RNA recognition / Zinc

The rate of hydrolysis of an RNA dimer, uridylyl(3′→5′)uridine (UpU), promoted by dinuclear Zn complexes resulting from a series of ligands with differently spaced Zn ion binding sites, was examined. Although the ligands in the present study have in common two di-2-pyridylmethylamino moieties as the Zn binding sites, the activities of these ligands toward the hydrolysis were quite different. Our results suggest that the distance between metal ion coordination sites is an essential factor for the intrinsic activities of the dinuclear complexes.

Introduction

Biomimetic chemistry[1] involves the imitation of functional biomolecules, usually enzymes, by simple artificial molecules. Many studies have been carried out in this field, not only because investigations on the actions of simple artificial molecules are helpful for understanding the reaction mechanism of biomolecules, but also because biomimetic compounds have wide potential scope for medicinal and pharmaceutical applications. In particular, the design of an artificial molecule that promotes the hydrolysis of phosphodiester linkages in RNA under neutral conditions has attracted much attention, since such a molecule will provide a basic structure of anti-cancer and anti-viral drugs.

Many natural ribonucleases and ribozymes that catalyze the hydrolysis of phosphodiester bonds in RNA have metal ions in their active sites.[2] Recently, the double metal-ion mechanism has been widely accepted: the catalytic efficiency of natural nucleases is considered attributable to cooperative action of the two (or more) metal cations in the active sites.[2] Vallee et al. reported that cocatalytic motifs in the enzymes contain two or more ions, and that the distances between the ions range between 3 and 5 Å, based on the X-ray structure analyses.[2c] Our previous theoretical study supported the double metal-ion mechanism.[3] Inspired by this mechanism, several research groups have developed various dinuclear metal-ion complexes possessing high catalytic efficiency toward the hydrolysis of phosphodiester linkages.[4] The efficiency of the catalytic activity of the dinuclear complex can often be related to the distance between the two metal ions in the complex. However, very few systematic studies have been reported from this point of view. Only one exception was reported by Chapman et al.; namely, that the distance between the metals determines the selectivity of the catalysts.[4d]

We examined the rate of hydrolysis of an RNA dimer, uridylyl(3′→5′)uridine (UpU), promoted by dinuclear Zn complexes resulting from a series of ligands. Because of the lack of basicity of the uracil ring, the reaction of UpU is the simplest model of nucleotide hydrolysis. Di-2-pyridylmethylamine has a high affinity for the Zn ions: log of the binding constant (log k_{bind}) is 7.57 in 0.10 M KNO_3.[5] Our ligands have two differently distanced di-2-pyridylmethylamino groups at the benzylic positions as Zn coordination sites. Herein, we show that the efficiency of the hydrolytic activity of the Zn complexes is highly sensitive to the distance between the two Zn ions in the complexes.

Results and Discussion

Figure 1 shows the structures of the ligands used in this study. Ligands **1**−**5** have two di-2-pyridylmethylamino groups as Zn coordination sites, while ligand **6** has only one coordination site. In all the ligands, di-2-pyridylmethylamino groups are attached to the benzylic carbon atoms.

Semiempirical AM1[6] calculations suggested that the shortest distance between the two nitrogen atoms would be 4.4, 5.2, 7.7, 7.2, and 11.3 Å in **1a**, **2a**, **3a**, **4a**, and **5a**, respectively. The conformational analysis using Monte Carlo (MC) simulations was studied for bis(hydrogen dimethylammonium)dications (**1**−**5b**) as the models to confirm the distribution of the distance between the two intramolecular cations. Figure 2 shows the relationship between the distance of the two protons (horizontal axis, Å) and the energy (vertical axis, kcal/mol). The results of the conformers, which had energies within 20 kcal/mol for their most stable conformers, are shown. The order of the proton−proton distance was **1b** < **2b** < **4b** ≤ **3b** << **5b**. However, a widely spread distribution was observed in the case of **1b**, and the energy of the conformer of **1**, which has the minimum distance, was very high.

Next, the affinity of the ligands toward Zn ions was studied through competitive titration with 2-(5-bromo-2-

[a] National Institute of Advanced Industrial Science and Technology,
Tsukuba, Ibaraki 305-8565, Japan
Fax: (internat.) + 81-298/61-4487
E-mail: t-uchimaru@aist.go.jp

Supporting information for this article is available on the WWW under http://www.wiley-vch.de/home/eurjic or from the author.

 © WILEY-VCH Verlag GmbH, 69451 Weinheim, 2001 1434−1948/01/0909−2437 $ 17.50+.50/0

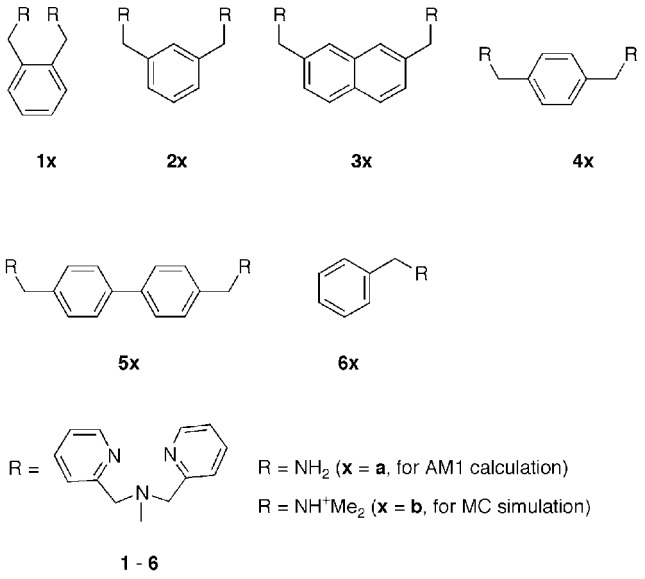

Figure 1. Structures of the ligands

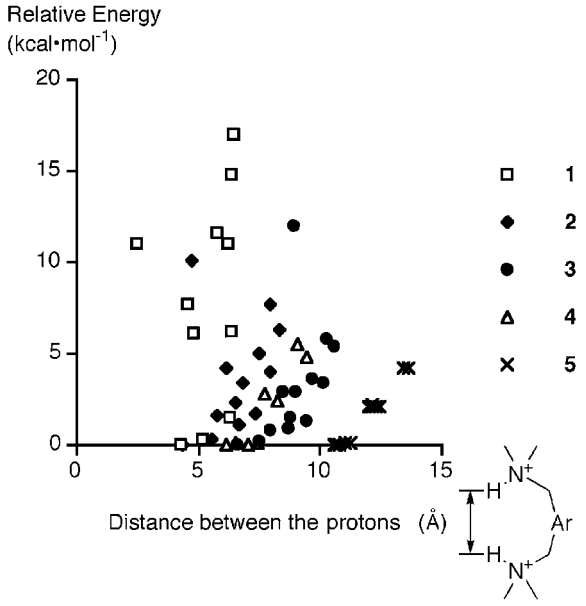

Figure 2. Relationship between the distance of the two protons (horizontal axis, Å) and the energy (vertical axis, kcal/mol)

pyridylazo)-5-[*N*-2-propyl-*N*-(3-sulfopropyl)amino]phenol (5Br-PAPS, see Supporting Information, Section 2). The titration results suggest that at least 95% of the ligands **2**−**5** in solution form a dinuclear complex under the experimental conditions in this report (typically, [Ligand] = 0.1 mM, [Zn] = 0.05 mM, see Figure 3 and Exp. Sect.). Hereafter, we refer to the dinuclear and mononuclear complexes as **L**-Zn_2 and **L**-Zn_1, respectively. We also carried out titration experiments by using Cu^{II} ion solution (see Supporting Information, Section 3). The Cu^{II} ion titration curves indicate that ligands **2**−**5** form the dinuclear Cu^{II} ion complexes and only **1** does not form a dinuclear complex. The binding affinity of the Zn ion with di-2-pyridylmethylamine is much less than that of the Cu^{II} ion (log k_{bind} = 9.31 in 0.10 M KNO_3 [5]). Additionally, from the result of the kinetics described below, it can be suggested that ligand **1** cannot form the dinuclear complex **1**-Zn_2 otherwise the amount of the dinuclear Zn ion complex of ligand **1** under the experimental conditions in this report would be considerably smaller than that of the dinuclear complex resulting from the other ligands.

We examined the rate of hydrolysis of UpU at pH 7.0 and 60 °C in the presence of the ligands. The ligands **1**−**6** showed no ability to hydrolyze UpU without Zn ions. We kept the concentration of Zn ions at 0.1 mM and measured the pseudo-first order rate constant k_{obs} under different ligand concentrations (from 0 to 0.4 mM). The values of k_{obs} are plotted against ligand concentration in Figure 3-I.[7]

The value of k_{obs} in the presence of a 0.1 mM amount of the Zn ion without any ligand was $4.0 \times 10^{-4}\ h^{-1}$. For ligands **2**, **3**, and **4**, the value of k_{obs} increased with increase of the ligand concentration, and the largest values of k_{obs} for these ligands were observed under the conditions of a concentration ratio of [Zn]/[ligand] of 2:1. Hereafter, we refer to this condition as condition A. Further increase of the concentration of these ligands resulted in a decrease of k_{obs}. These results suggest that ligands **2**, **3**, and **4** should form a considerable amount of dinuclear Zn complexes under condition A and that, compared to the Zn ion itself and the mononuclear complexes, the resulting dinuclear complexes should be more active toward the hydrolysis. The enhancement of the rate of hydrolysis for ligand **2** under condition A was the most striking: the k_{obs} found for the condition A was $1.6 \times 10^{-2}\ h^{-1}$, which was around 40 times and 4 times as large as k_{obs} measured in the absence of the ligand and that observed for the condition of [Zn]/[**2**] = 1:1 (condition B), respectively. For ligand **5**, k_{obs} gradually increased with an increase of the ligand concentration, but the enhancement of the hydrolysis rate was much less significant than for ligands **2**, **3**, and **4**. The values of k_{obs} for ligands **1** and **6** were insensitive to the ligand concentration: these ligands did not substantially affect the rate of hydrolysis.

Figure 3-II shows the difference in k_{obs} from ligand to ligand under conditions A and B. The difference in k_{obs} under condition A was much more striking than those observed under condition B. Although ligands **1**−**5** commonly have two di-2-pyridylmethylamine moieties, ligand **2** showed substantially higher activity than the other ligands.

Next, the values of k_{obs} were measured under different concentrations of the Zn ion (from 0.1 to 1.0 mM) with a constant concentration (0.1 mM) of the ligands. The values of k_{obs} are plotted against the concentration of the Zn ion ([Zn]) in Figure 3-III. Figure 3-III clearly shows again that ligand **2** enhances the rate of hydrolysis under the condition of [Zn]/[**2**] = 2:1 (condition A). We also measured k_{obs} without the ligand under the same conditions. In the absence of the ligand, although the value of k_{obs} tends to increase slightly upon increasing [Zn], the value of k_{obs} is found to be relatively insensitive to [Zn] (see Figure 3-III). For ligand **2**, however, k_{obs} increased from 1.4×10^{-3} to $1.6 \times 10^{-2}\ h^{-1}$ on going from the condition of [Zn]/[ligand] = 1:1

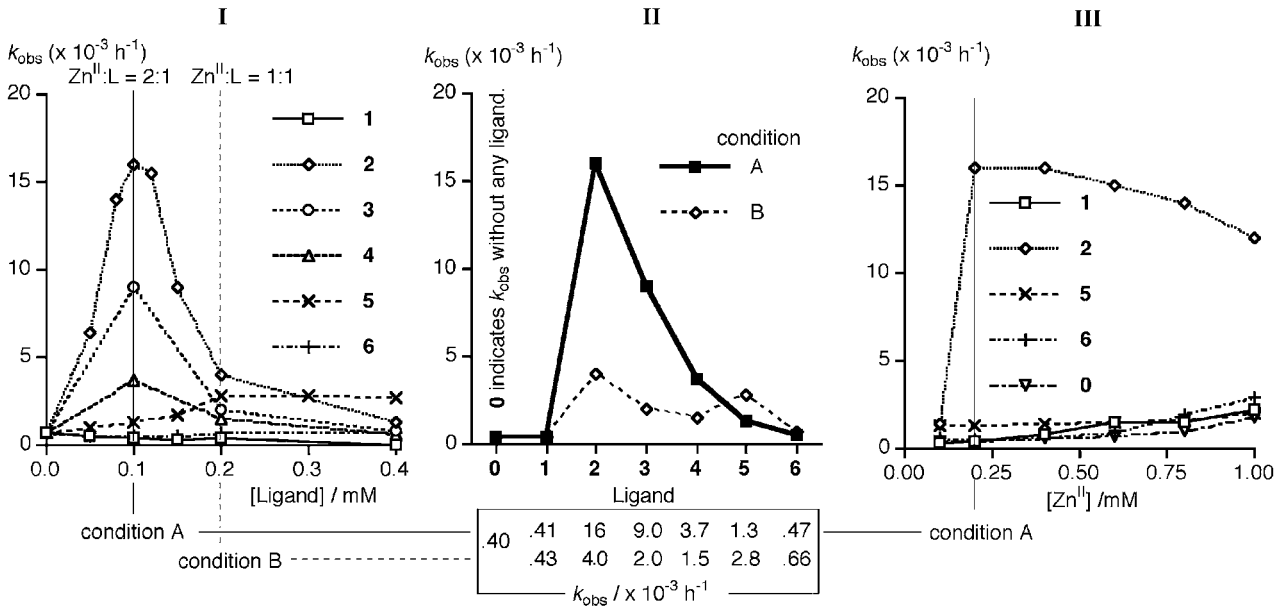

Figure 3. I) k_{obs} with various concentrations of **L** at a constant Zn ion concentration (0.2 mM); II) Relationship between k_{obs} and the backbone structure of the complexes under the conditions A and B; III) k_{obs} at a constant concentration of **L** (0.1 mM) with various Zn ion concentrations

to that of [Zn]/[ligand] = 2:1 (condition A). For ligand **2**, the value of k_{obs} decreased gradually in the presence of an excess amount of Zn ions. This finding can be interpreted as follows: Zn ions without the ligands, which have a much lower catalytic activity than that of **2**-Zn_2, interact with the substrate, and this interaction will inhibit electrostatically the approach of the dinuclear complex to the substrate. As expected from the results given in Figure 3-I, the k_{obs} values for ligands **5** and **6** were insensitive to [Zn] and these ligands showed no substantial enhancement of the rate of hydrolysis.

The binding constants of the ligands toward Zn ions and the structure of the ligands should both be related to the difference in k_{obs} values under condition A (Figure 3-II). As described above, at least 95% of the ligands form dinuclear Zn complexes under this condition. The k_{obs} values increased almost linearly with increase of [Zn] and [ligand] for both ligands **2** and **4**. This trend was observed regardless of the concentration of the dinuclear Zn complexes. We measured the rate of the hydrolysis under different concentrations of the Zn ion and ligands with the concentration ratio of [Zn]/[ligand] being kept at 2:1. As shown in Figure 4,[8] the k_{obs} value for ligand **2** was always greater than that for ligand **4**.

These results suggest that the differences in k_{obs} in Figure 3-II are attributable mainly to the difference in the structure of the ligands, and more specifically, the difference in the distance between the two metal coordination sites. The k_{obs} values under condition A in Figure 3-II are likely to be almost proportional to the intrinsic activities of the dinuclear complexes toward the hydrolysis. Ligands **2**, **3**, and **4** enhanced the hydrolysis rate under condition A and, thus, the two Zn ions in the dinuclear complexes of these

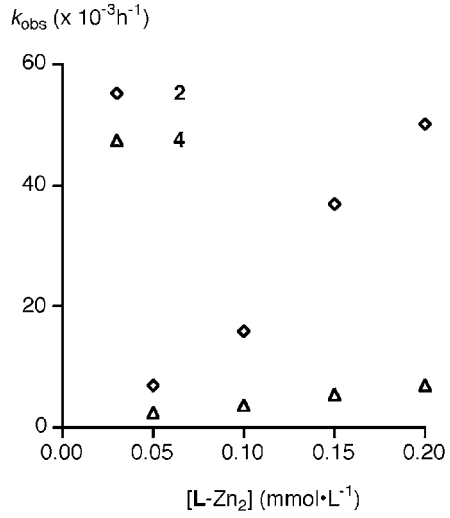

Figure 4. The k_{obs} values of **2**-Zn_2 and **4**-Zn_2 at various concentrations

ligands will act in a cooperative manner to promote the hydrolysis. According to the k_{obs} values in Figure 3-II, the intrinsic activity of the **2**-Zn_2 would be around 1.8 times and 4.3 times as large as those of **3**-Zn_2 and **4**-Zn_2, respectively. Meanwhile, ligands **1** and **5** did not enhance the hydrolysis under condition A. Formation of the dinuclear complex **1**-Zn_2 might be difficult (see above). Indeed, ligand **1** did not show enhancement of the rate of hydrolysis even under condition A. On the other hand, the two Zn ions in **5**-Zn_2 cannot act in a cooperative manner, probably because the distance between the two Zn ions is too large.

Previously, Chapman et al. examined systematically the activities of dinuclear Zn complexes toward the hydrolysis

of phosphodiesters.[4d] Their study covered a series of dinuclear complexes, with distances between the two metal ions in the binding sites similar to those for ligands **1**−**5**. They found that the dinuclear complex with a relatively large distance between the coordination sites, in which the distance between two bound metal ions would be comparable to that for ligand **5**, has the highest activity for the hydrolysis of phosphodiester, while the dinuclear complex with a short distance between the coordination sites has a higher activity for the hydrolysis of phosphomonoesters. They point out that a phosphodiester is sterically more hindered than a phosphomonoester, and that the phosphomonoester dianion is more basic than the phosphodiester monoanion. They then concluded that the phosphomonoester hydrolysis needs the two metal ions to be close, while the phosphodiester hydrolysis needs a larger separation between the two metal ions. In contrast, in the present study, ligand **2** was found to have the highest activity toward the phosphodiester hydrolysis. Obviously, a shorter distance between the two metals was preferred for the hydrolysis of phosphodiester, considering the fact that ligand **1** cannot bind two metal ions. The findings of Chapman et al. and ourselves may not seem to be in agreement with each other at first sight. However, a cyclic amine/imine structure, whose behavior of metal-ion binding will be quite different from that of the di-2-pyridylmethylamino group, was employed for the metal binding sites in their study. Consequently, their results and ours cannot be compared directly.[9] These findings show that dinuclear complexes, which have a different metal-ion binding site structure, react with the substrates in a different manner. We would like to point out that a ligand whose structure corresponds to **2** has been successfully applied as a metal coordination site for the sequence-selective hydrolysis of RNA:[4i,10] Matsuda et al. introduced the Zn ion binding site at the 5′-end of a DNA oligomer that recognizes the targeted sequence of RNA. They found that the ligand structure of **2** hydrolyzes the phosphodiester bonds in RNA at the targeted position in highly efficient manner.[4i] Xu et al. reported the X-ray structure of the phosphodiesterase (PDE4) active site.[11] They pointed out that the distance between the two ions in the active site is around 3.9 Å, and suggested that the two metal ions constitute a dinuclear motif similar to that found in other enzymes that catalyze the hydrolysis or formation of a phosphate bond. Meanwhile, our MC simulations suggested that the distance between the two ions in the dinuclear complexes resulting from ligands **1**−**5** would increase in the order **1** < **2** < **4** ≤ **3** < < **5**. For all ligands, the two metal ions would be more than 4 Å apart. However, the titration experiments showed that ligand **1** cannot form the dinuclear complex. Considering these findings, the metal complex resulting from ligand **2** (**2**-Zn_2) is likely to bear the closest resemblance to the dinuclear motif observed in enzymes: the distance between the two metal ions in **2**-Zn_2 will probably be similar to that in the dinuclear motif in PDE4. Thus, it is reasonable that **2**-Zn_2 was found to be the most efficient catalyst for the hydrolysis of UpU among the metal complexes studied in the present work.

Conclusion

We examined the activities of the ligands **1**−**6** toward the hydrolysis of UpU in the presence of Zn ions. In agreement with the double metal-ion mechanism, ligands **2**, **3**, and **4** showed the highest activity under dinuclear complex forming conditions. Interestingly, although ligands **1**−**5** have two di-2-pyridylmethylamino moieties as Zn ion binding sites in common, the activities of these ligands toward the hydrolysis are quite different. Our results suggest that the difference in the k_{obs} value for ligands **2**−**5** under the dinuclear complex forming condition (condition A) should be almost proportional to the intrinsic activity of the dinuclear complexes toward the hydrolysis, which implies that the distance between the metal ion coordination sites will be an essential factor for the intrinsic activities of the dinuclear complexes.

Experimental Section

General: Silica gel TLC and column chromatography were performed using Merck Kieselgel 60F-254 and Wakogel C-200, respectively. All NMR spectra were recorded with a Varian Gemini-300BB spectrometer. ^1H spectra were referenced to the TMS peak, and ^{13}C spectra were referenced to the $CDCl_3$ peak. IR spectra were recorded with a Jasco FT/IR-5300 instrument. Mass spectra were recorded with a Hitachi N80E instrument. HPLC purity analysis of the ligands was carried out using Luna-Si column (Phenomenex, 4.6 × 150 mm, 3 μm) using $CHCl_3$/MeOH (1:1, v/v) as an eluent. Figure 5-I in the Supporting Information shows the HPLC profiles of the free ligands. Over 99% purity was guaranteed for all ligands in the analysis.

Preparation of the Ligands: Ligand **1** was prepared by *N*-alkylation of *o*-xylylenediamine dihydrochloride,[12] in a modification of the procedure reported by Sato et al.[13] A solution of 2-(chloromethyl)-pyridinium hydrochloride (3.30 g, 20.12 mmol) and *o*-xylylenediamine dihydrochloride (1.05 g, 5.02 mmol) in water (12 mL) was added to aqueous NaOH solution (5.0 M, 12 mL). Then, hexadecyltrimethylammonium chloride (0.16 g, 0.50 mmol) and $CHCl_3$ (10 mL) were added successively to the solution. The resulting mixture was heated to reflux in $CHCl_3$ for 12 h with vigorous stirring. The precipitate was separated by filtration and the filtrate was extracted three times with $CHCl_3$ (20 mL portions). The organic layer was collected and dried over Na_2SO_4. After evaporation of the solvent, the residue was chromatographed on silica gel by elution with $CHCl_3$/MeOH (the content of MeOH was increased from 0 to 2%). The yield of the product was 44% (1.1 g).

***N*,*N*,*N*′,*N*′-Tetra-(2-pyridylmethyl)-*o*-xylylenediamine (1a):** IR(KBr): $\tilde{\nu}$ = 1591, 1570, 1473, 1433 (C=C, C=N), 1047 cm^{-1} (C−N). − ^1H NMR ($CDCl_3$): δ = 3.67 (s, 4 H, PhCH_2 × 2), 3.70 (s, 8 H, PyCH_2 × 4), 7.12−7.16 (m, 4 H, Ph), 7.18−7.65 (m, 12 H, Py^{3-5} × 4), 8.50−8.52 (m, 4 H, Py^6 × 4). − ^{13}C NMR ($CDCl_3$): δ = 55.87 (PhCH_2), 60.28 (PyCH_2), 121.97 (Py^3), 122.87 (Py^5), 126.96 ($Ph^{3\ or\ 4}$), 129.49 ($Ph^{4\ or\ 3}$), 136.52 (Py^4), 137.79 (Ph^1), 148.97 (Py^6), 159.77 (Py^2). − HRMS for $C_{32}H_{33}N_6$ $[M]^+$: calcd. 501.2767; found 501.2754.

Ligands **2**−**6** were prepared in yields of 80−95% by *N*-alkylation of 2,2′-dipyridylmethylamine with the corresponding arylmethyl-(di)bromides. A typical procedure is given for preparation of ligand

2: *m*-Xylylenedibromide (1.32 g, 5.00 mmol), di-2-pyridylmethylamine (2.00 g, 9.63 mmol), and *N*,*N*-diisopropylethylamine (1.30 g, 10.06 mmol) were dissolved in $CHCl_3$ (50 mL). After 4 h of stirring at room temperature, the resulting solution was washed once with water (25 mL) and dried over Na_2SO_4. The product was purified by silica gel chromatography with $CHCl_3$/MeOH (the content of MeOH was increased from 0 to 2%) as the eluent. The yield of the product was 95% (2.37 g).

***N*,*N*,*N*′,*N*′-Tetra-(2-pyridylmethyl)-*m*-xylylenediamine (2):** IR (neat): $\tilde{\nu}$ = 1589, 1570, 1473, 1433 (C=C, C=N), 1045 cm^{-1} (C−N). − ^{1}H NMR ($CDCl_3$): δ = 3.69 (s, 4 H, PhCH_2 × 2), 3.81 (s, 8 H, PyCH_2 × 4), 7.10−7.15 (m, 4 H, Ph), 7.27−7.65 (m, 12 H, Py$^{3-5}$ × 4), 8.50−8.52 (m, 4 H, Py^6 × 4). − ^{13}C NMR ($CDCl_3$): δ = 58.46 (Ph*C*H$_2$), 59.97 (Py*C*H$_2$), 121.91 (Py^3), 122.73 (Py^5), 127.58 (Ph^4), 128.29 (Ph$^{2\ or\ 5}$), 129.21 (Ph$^{2\ or\ 5}$), 136.40 (Py^4), 139.13 (Ph^1), 149.01 (Py^6), 159.93 (Py^2). − HRMS for $C_{32}H_{32}N_6$ $[M]^+$: calcd. 500.2688; found 500.2653.

2,7-Di(aminomethyl)-*N*,*N*,*N*′,*N*′-tetra-(2-pyridylmethyl)naphthalene (3): IR (KBr): $\tilde{\nu}$ = 1589, 1568, 1473, 1431 (C=C, C=N), 1047 cm^{-1} (C−N). − ^{1}H NMR ($CDCl_3$): δ = 3.84 (s, 4 H, PhCH_2 × 2), 3.86 (s, 8 H, PyCH_2 × 4), 7.11−7.16 (m, 4 H, Naph), 7.52−7.79 (m, 12 H, Py$^{3-5}$ × 4), 7.76 (br. s, 2 H, Naph^8), 8.51−8.53 (m, 4 H, Py^6 × 4). − ^{13}C NMR ($CDCl_3$): δ = 58.73 (Ph*C*H$_2$), 60.00 (Py*C*H$_2$), 122.03 (Py^3), 122.92 (Py^5), 126.94 (Naph^3), 127.54 (Naph$^{1\ or\ 4}$), 127.80 (Naph$^{4\ or\ 1}$), 129.21 (Ph$^{2\ or\ 5}$), 136.52 (Py^4), 136.66 (Naph$^{9\ or\ 10}$), 136.85 (Naph$^{10\ or\ 9}$), 149.10 (Py^6), 159.87 (Py^2). − HRMS for $C_{36}H_{35}N_6$ $[M + H]^+$: calcd. 551.2923; found 551.2881.

***N*,*N*,*N*′,*N*′-Tetra-(2-pyridylmethyl)-*p*-xylylenediamine (4):** IR (KBr): $\tilde{\nu}$ = 1591, 1568, 1512, 1473, 1433 (C=C, C=N), 1045 cm^{-1} (C−N). − ^{1}H NMR ($CDCl_3$): δ = 3.66 (s, 4 H, PhCH_2 × 2), 3.80 (s, 8 H, PyCH_2 × 4), 7.10−7.14 (m, 4 H, Ph), 7.27−7.65 (m, 12 H, Py$^{3-5}$ × 4), 8.50−8.51 (m, 4 H, Py^6 × 4). − ^{13}C NMR ($CDCl_3$): δ = 58.26 (Ph*C*H$_2$), 60.04 (Py*C*H$_2$), 121.99 (Py^3), 122.83 (Py^5), 128.89 (Ph^2), 136.52 (Py^4), 149.01 (Py^6), 159.97 (Py^2). − HRMS for $C_{32}H_{32}N_6$ $[M]^+$: calcd. 500.2688; found 500.2688. − $C_{32}H_{32}N_6$ (500.65): C 76.77, H 6.44, N 16.79; found C 76.58, H 6.44, N 16.73.

4,4′-Di(aminomethyl)-*N*,*N*,*N*′,*N*′-tetra-(2-pyridylmethyl)biphenyl (5): IR (neat): $\tilde{\nu}$ = 1591, 1570, 1496, 1473, 1433 (C=C, C=N), 1047 cm^{-1} (C−N). − ^{1}H NMR ($CDCl_3$): δ = 3.73 (s, 4 H, PhCH_2 × 2), 3.84 (s, 8 H, PyCH_2 × 4), 7.12−7.17 (m, 8 H, Ph), 7.27−7.70 (m, 12 H, Py$^{3-5}$ × 4), 8.52−8.54 (m, 4 H, Py^6 × 4). − ^{13}C NMR ($CDCl_3$): δ = 58.10 (Ph*C*H$_2$), 59.95 (Py*C*H$_2$), 122.00 (Py^3), 122.84 (Py^5), 126.98 (Ph$^{2\ or\ 3}$), 129.30 (Ph$^{3\ or\ 2}$), 136.51 (Py^4), 137.98 (Ph$^{1\ or\ 4}$), 139.83 (Ph$^{4\ or\ 1}$), 149.08 (Py^6), 159.86 (Py^2). − HRMS for $C_{38}H_{37}N_6$ $[M + H]^+$: calcd. 577.3080; found 577.2999.

Di-(2-pyridylmethyl)benzylamine (6): IR (neat): $\tilde{\nu}$ = 1589, 1570, 1494, 1473, 1433 (C=C, C=N), 1045 cm^{-1} (C−N). − ^{1}H NMR ($CDCl_3$): δ = 3.69 (s, 2 H, PhCH_2 × 2), 3.81 (s, 4 H, PyCH_2 × 4), 7.12−7.61 (m, 11 H, Ph, Py$^{3-5}$ × 4), 8.51−8.53 (m, 2 H, Py^6 × 2). − ^{13}C NMR ($CDCl_3$): δ = 55.46 (Ph*C*H$_2$), 59.94 (Py*C*H$_2$), 122.00 (Py^3), 122.82 (Py^5), 127.12 (Ph^4), 128.38 (Ph$^{2\ or\ 3}$), 128.91 (Ph$^{3\ or\ 2}$), 136.52 (Py^4), 139.06 (Ph^1), 149.08 (Py^6), 159.94 (Py^2). − HRMS for $C_{19}H_{19}N_3$ $[M]^+$: calcd. 289.1579; found 289.1583.

Computational Methods: All MO calculations were carried out using SPARTAN 5.11.[14] The most stable conformers of **1**−**5b** were studied in a systematic conformer search: The dihedral angle in freely rotatable bonds (two Ar−CH_2 and two CH_2−NH_2) was varied in 120° steps in the initial structures. The structures of **1**−**5b** were then optimized in an AM1 Hamiltonian. Monte Carlo simulations were carried out using Macro Model 6.0.[15] Each structure in the simulation was optimized using the Amber* force field.[16] The effect of solvation was included in the simulations by implicit treatment of solvent water with the GB/SA model.[17]

Kinetic Analysis of the UpU Hydrolysis: Reaction conditions of the UpU hydrolysis: $[UpU]_0$ = 0.02 mM in 100 mM HEPES buffer (pH = 7.0), reaction temperature = 60 °C. The reaction was monitored by reverse-phase HPLC (Phenomenex, Luna 3μ C8(2), 4.6 × 150 mm, 3 μm. Conditions: a linear gradient of 1−9% MeCN in 0.1 M aqueous $AcONH_4$ (pH = 7.0) in 8 min. at a flow of 1.0 mL·min^{-1} at 50 °C). The eluent was monitored at 258 nm by a SOMA S-310A UV/Vis detector. The pseudo-first order reaction rate constants (k_{obs}) were obtained as slopes of ln($[UpU]_0$/[UpU]) vs. time, where $[UpU]_0$ is the initial concentration of the substrate. The pseudo-first order reaction profile and its reproducibility are shown in the Supporting Information (Section 4).

Acknowledgments

The authors gratefully acknowledge financial support by the Science and Technology Agency.

[1] For example, [1a] L. A. Weiss, N. Sakai, B. Ghebremariam, *J. Am. Chem. Soc.* **1997**, *119*, 12142−12149. − [1b] B. Ghebremariam, S. Matile, *Tetrahedron Lett.* **1998**, *39*, 5335−5338. For a comprehensive review, see: [1c]J.-M. Lehn, *Supramolecular Chemistry*, VCH, Weinheim, **1995**.

[2] For example, [2a] L. S. Beese, T. A. Staitz, *EMBO J.* **1991**, *10*, 25−33. − [2b] J. F. Davies, Z. Hostmska, Z. Hostomsky, S. R. Jordan, D. A. Mathews, *Science* **1991**, *252*, 88−95. − [2c] B. L. Vallee, D. S. Auld, *Proc. Natl. Acad. Sci. U. S. A.* **1993**, *90*, 2715−2718. − [2d] T. A. Staitz, J. A. Staitz, *Proc. Natl. Acad. Sci. U. S. A.* **1993**, *90*, 6498−6502. − [2e] J. A. Piccirilli, J. S. Vyle, M. H. Caruthers, T. R. Cech, *Nature* **1993**, *361*, 85−88. − [2f] B. W. Pontius, W. B. Lott, P. H. von Hippel, *Proc. Natl. Acad. Sci. U. S. A.* **1997**, *94*, 2290−2294. For a comprehensive review see [2g] N. Sträter, W. N. Lipscomb, T. Klabunde, B. Krebs, *Angew. Chem. Int. Ed. Engl.* **1996**, *35*, 2024−2055. − [2h] D.-M. Zhou, K. Taira, *Chem. Rev.* **1998**, *98*, 991−1026.

[3] T. Uchimaru, M. Uebayasi, K. Tanabe, K. Taira, *FASEB J.* **1993**, *7*, 137−142.

[4] For example, [4a] J. R. Morrow, L. A. Butterey, V. M. Shelton, K. A. Berback, *J. Am. Chem. Soc.* **1992**, *114*, 1903−1905. − [4b] D. H. Vance, A. W. Czarnik, *J. Am. Chem. Soc.* **1993**, *115*, 12165−12166. − [4c] M. Yashiro, A. Ishikubo, M. Komiyama, *J. Chem. Soc., Chem. Commun.* **1995**, 1973−1974. − [4d] W. H. Chapman, Jr., R. Breslow, *J. Am. Chem. Soc.* **1995**, *117*, 5462−5469. − [4e] M. J. Young, J. Chin, *J. Am. Chem. Soc.* **1995**, *117*, 10577−10578. − [4f] T. Koike, M. Inoue, E. Kimura, M. Shiro, *J. Am. Chem. Soc.* **1996**, *118*, 3091−3099. − [4g] S. Liu, Z. Luo, A. D. Hamilton, *Angew. Chem.* **1997**, *109*, 2794−2796; *Angew. Chem. Int. Ed. Engl.* **1997**, *36*, 2678−2680. − [4h] S. Matsuda, A. Ishikubo, A. Kuzuya, M. Yashiro, M. Komiyama, *Angew. Chem.* **1998**, *110*, 3477−3479; *Angew. Chem. Int. Ed.* **1998**, *37*, 3284−3286. − [4i] B. N. Trawick, A. T. Daniher, J. K. Bashkin, *Chem. Rev.* **1998**, *98*, 939−960. − [4j] M. Oivanen, S. Kuusela, H. Lönnberg, *Chem. Rev.* **1998**, *98*, 961−990. − [4k] A. Blaskó, T. C. Bruice, *Acc. Chem. Res.* **1999**, *32*, 475−484. − [4l] N. H. Williams, B. Takasaki, M. Wall, J. Chin, *Acc. Chem. Res.* **1999**, *32*, 485−493. − [4m] S. Mikkola, Q. Wang, Z. Jori, M. Helkearo, H. Lönnberg, *Acta Chem. Scand.* **1999**, *53*, 453−456. − [4n] P. Ross, F. Felluga, P. Tecilla, F. Formaggio, M. Crisma, C. Toniolo, P. Scrimin, *J. Am. Chem. Soc.* **1999**, *121*, 6948−6949. − [4o] P. Molenveld, J. F. J. Engbersen, D. N. Reinhoudt, *Chem. Soc. Rev.* **2000**, *29*, 75−86. − [4p] I. O. Fritsky, R. Ott, R. Krämer, *Angew. Chem.* **2000**, *112*, 3403−3406; *Angew. Chem. Int. Ed.* **2000**, *39*, 3255−3258.

– [4q] K. Yamada, T. -I. Takahashi, H. Yamamura, S. Araki, K. Saito, M. Kawai, *Chem. Commun.* **2000**, 1315−1316.
[5] [5a] D. V. Gruenwedel, *Inorg. Chem.* **1968**, *7*, 495−501. – [5b] J. K. Romary, J. D. Barger, J. E. Bunds, *Inorg. Chem.* **1968**, *7*, 1142−1145. Hereafter, binding constants were referred to as log of the values.
[6] M. J. S. Dewer, E. G. Zoebicsh, E. E. Healy, *J. Am. Chem. Soc.* **1985**, *107*, 3902−3909.
[7] The k_{obs} values in Figures 3-I and -III are shown in the Supporting Information, section 1 (Tables 1−1 and 1−2).
[8] See Tables 1−3 in the Supporting Information, section 1, for more detail.
[9] Zepik et al. reported a set of functional molecules in which two nonmetallic cations are connected through a *m*-xylenyl backbone. They found that some molecules act as a catalyst for the UpU hydrolysis, while others act as an anticatalyst, depending on the structure of the substituents in the cationic moieties: H. H. Zepik, S. A. Benner, *J. Org. Chem.* **1999**, *64*, 8080−8083.
[10] Hattori et al. compared the efficiency of ligands **2** and **4** toward the Zn ion-promoted hydrolysis of ApA with that of *N,N,N′*,*N′*-tetrakis(2-pyridylmethyl)-2-hydroxy-1,3-diaminopropane. Ligand **2** showed higher efficiency than the others. The 72nd Annual Meeting of the Japanese Chemical Society, Tokyo (Japan), **1997**.
[11] R. X. Xu, A. M. Hassell, D. Vanderwall, M. H. Lambert, W. D. Holmes, M. A. Luther, W. J. Rocque, M. V. Milburn, Y. Zhao, H. Ke, R. T. Nolte, *Science* **2000**, *288*, 1822−1825.
[12] [12a] R. C. Brasted, T. D. O'Brien, W. L. Heino, *Inorg. Chem.* **1964**, *3*, 503−505. – [12b] S.-I. Kawahara, T. Uchimaru, *Z. Naturforsch., Teil B* **2000**, *55*, 985−987.
[13] M. Sato, Y. Mori, T. Iida, *Synthesis* **1992**, 539−540.
[14] SPARTAN 5.1.1,Wavefunction, Inc., 18401 Von Karman Ave., Ste. 370, Irvine, CA 92612 U.S.A.
[15] F. Mohamadi, N. G. J. Richards, W. C. Guita, R. Likskamp, C. Caufield, G. Chang, T. Hendrickson, W. C. Still, *J. Comput. Chem.* **1990**, *11*, 440−447.
[16] Amber* is the modified force field based on the Amber force field,[18] used in Macro Model.
[17] W. C. Still, A. Tempczk, R. C. Hawley, T. Hendrickson, *J. Am. Chem. Soc.* **1990**, *112*, 6127−6129.
[18] P. A. Kollman, *Chem. Rev.* **1993**, *19*, 2395−2417.

Received December 18, 2000
[I00477]

Nanoscopic Metal Particles − Synthetic Methods and Potential Applications

Helmut Bönnemann*[a] and Ryan M. Richards[a]

Keywords: Nanoparticles / Catalysis / Colloids / Fuel cells

Mono- and bimetallic colloidal particles have gained increasing attention in science and application throughout the last several years. In this contribution, we present a synopsis of the wet chemical syntheses of these materials and survey potential applications in catalysis and materials science. Methods for the characterization of these particles and their surfaces are not reviewed here.

Introduction

Colloidal metals − originally called gold sols − first generated interest because of their intense colors, which enabled them to be used as pigments for glass or ceramics. Nanoparticulate metal colloids are generally defined as isolable particles between 1 and 50 nm in size that are prevented from agglomerating by protecting shells. They can be redispersed in water ("hydrosols") or organic solvents ("organosols"). The number of potential applications of these colloidal particles is growing rapidly because of the unique electronic structure of the nanosized metal particles and their extremely large surface areas. A considerable body of knowledge has been accumulated on these materials over the last few decades.[1−12] Highly dispersed mono- and bimetallic colloids can be used as precursors for a new type of catalyst that is applicable both in the homogeneous and heterogeneous phases.[13−16] Besides the obvious applications in chemical catalysis, recent studies have examined the potential of nanostructured metal colloids as fuel cell catalysts.[17−20]

[a] Department of Heterogeneous Catalysis, Max Planck Institut für Kohlenforschung,
Kaiser-Wilhelm-Platz 1, 45470 Mülheim a. d. Ruhr, Germany
Fax.: (internat.) + 49-208/306-2983
E-mail: Boennemann@mpi-muelheim.mpg.de

Wet Chemical Preparations

Nanostructured metal colloids have been obtained by so-called "top-down methods", e.g. by the mechanical grinding of bulk metals and subsequent stabilization of the resulting nanosized metal particles by the addition of colloidal protecting agents.[21−22] Metal vapor techniques have provided chemists with a very versatile route for the production of a wide range of nanostructured metal colloids on a preparative laboratory scale.[23−28] The use of metal vapor techniques is, however, limited because the operation of the apparatus is demanding and it is difficult to obtain narrow particle size distributions. The "bottom-up methods" of wet chemical nanoparticle preparation rely on the chemical reduction of metal salts, electrochemical pathways, or the controlled decomposition of metastable organometallic compounds. A large variety of stabilizers, e.g. donor ligands, polymers, and surfactants, are used to control the growth of the initially formed nanoclusters and to

Prof. Dr. H. Bönnemann was born in 1939. He studied chemistry at the RWTH Aachen and began his graduate work in Mülheim in 1964 under the supervision of Nobel Laureate Prof. Karl Ziegler. He obtained his doctorate in 1967 in Aachen. In 1974, he was appointed lecturer at Aachen and obtained his Habilitation in Industrial Chemistry in 1976. After two years of industrial experience in the central research laboratories of Degussa (1978/79), he became Professor of Industrial Chemistry at the RWTH Aachen in 1981. He is currently the leader of a research group at the Max-Planck-Institute for Coal Research (Department of Heterogeneous Catalysis) in Mülheim an der Ruhr, Germany. His research fields include novel nanostructured materials, fuel cell catalysts, and organized nanometal−organic hybrid structures.

Ryan M. Richards obtained his B.Sc. degree from Michigan State University in 1994. He then obtained a Master's degree from Central Michigan University working with organometallic compounds in the laboratory of Bob Howell. From 1996 to 2000, he worked in the laboratory of Kenneth Klabunde at Kansas State University, where he conducted research on metal oxide nanoparticles. During his Ph.D. research, he spent six months as an invited scientist at the Boreskov Institute of Catalysis in Novosibirsk, Russia. After completing his Ph.D. work, he joined the research group of Helmut Bönnemann as a postdoctoral researcher at the Max-Planck-Institute für Kohlenforschung in Mülheim an der Ruhr, Germany. His research interests are nanostructured materials, fuel cell catalysts, nanoparticle−polymer hybrids.

MICROREVIEWS: This feature introduces the readers to the authors' research through a concise overview of the selected topic. Reference to important work from others in the field is included.

 © WILEY-VCH Verlag GmbH, 69451 Weinheim, 2001 1434−1948/01/1010−2455 $ 17.50+.50/0

prevent them from agglomeration. The chemical reduction of transition metal salts in the presence of stabilizing agents to generate zerovalent metal colloids in aqueous or organic media was first published in 1857 by Faraday[29] and this approach has become one of the most common and powerful synthetic methods in this field.[10,11,30] The first reproducible standard protocols for the preparation of metal colloids (e.g., for 20 nm gold by reduction of $[AuCl_4]^-$ with sodium citrate) were established by Turkevich.[1−3] He also proposed a mechanism for the stepwise formation of nanoclusters based on nucleation, growth, and agglomeration, which in essence is still valid. Data from modern analytical techniques and more recent thermodynamic and kinetic results have been used to refine this model, as illustrated in Figure 1.[31−36]

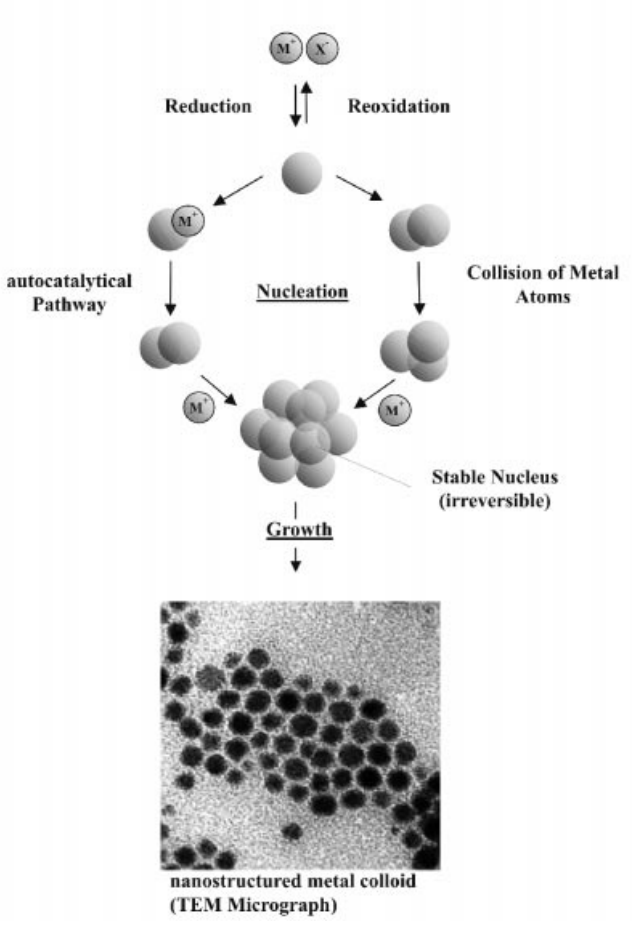

Figure 1. Formation of nanostructured metal colloids by the "salt reduction" method (adapted with permission from ref.[135])

In the embryonic stage of the nucleation, the metal salt is reduced to give zerovalent metal atoms.[31] These can collide in solution with further metal ions, metal atoms, or clusters to form an irreversible "seed" of stable metal nuclei. The diameter of the "seed" nuclei can be well below 1 nm depending on the strength of the metal−metal bonds and the difference between the redox potentials of the metal salt and the reducing agent applied.

Protective agents are necessary to stabilize nanostructured colloidal metals and to prevent agglomeration. Two basic modes of stabilization have been distinguished (Figure 2).[30]

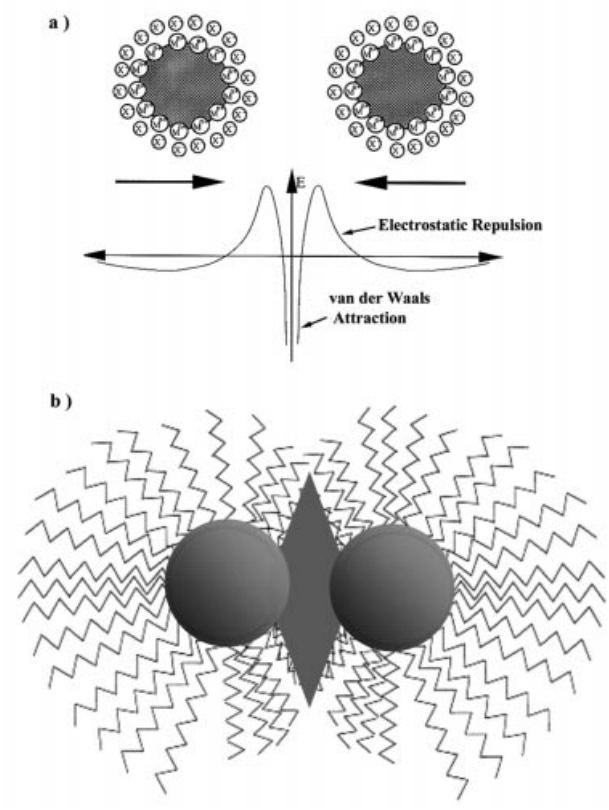

Figure 2. a) Electrostatic stabilization of nanostructured metal colloids (scheme adapted with permission from ref.[30]); b) steric stabilization of nanostructured metal colloids (scheme adapted with permission from ref.[30])

Electrostatic stabilization [see Figure 2, a)] is based on the Coulombic repulsion between the particles caused by the electrical double layer formed by ions adsorbed at the particle surface (e.g. sodium citrate) and the corresponding counterions. This is exemplified by the gold sols prepared by the reduction of $[AuCl_4]^-$ with sodium citrate.[1−3]

Steric stabilization [Figure 2, b)] is achieved by the coordination of sterically demanding organic molecules that act as protective shields on the metallic surface. In this way, nanometallic cores are separated from each other and agglomeration is prevented. The main classes of protective groups selected from the literature are: polymers[37−40] and block copolymers; P, N, and S donors (e.g. phosphanes, amines, thioethers);[6,57−82] solvents such as THF,[6,83] THF/MeOH,[84] and propylene carbonate;[85] long-chain alcohols;[41−56,86] surfactants;[6,7,9,15,16,85,87−98] and organometallics.[99−102] In general, lipophilic protective agents give metal colloids that are soluble in organic media ("organosols"), while hydrophilic agents yield water-soluble colloids ("hydrosols"). In Pd organosols, stabilized by tetra-

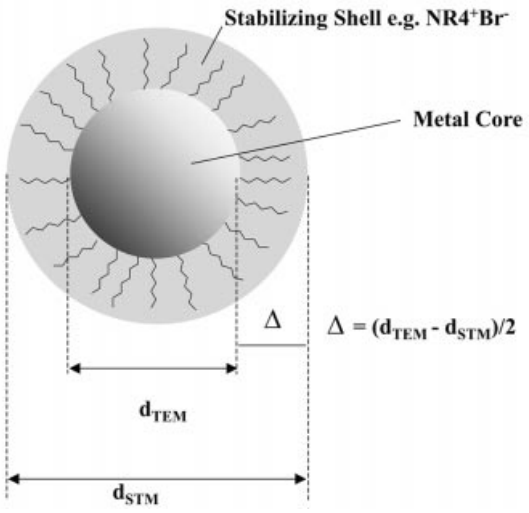

Figure 3. Differential TEM/STEM study of a Pd organosol showing that the metal core (size = d_{TEM}) is surrounded by a monolayer of the surfactant [thickness $\Delta = (d_{TEM} - d_{STM})_2$] (adapted with permission from ref.[103])

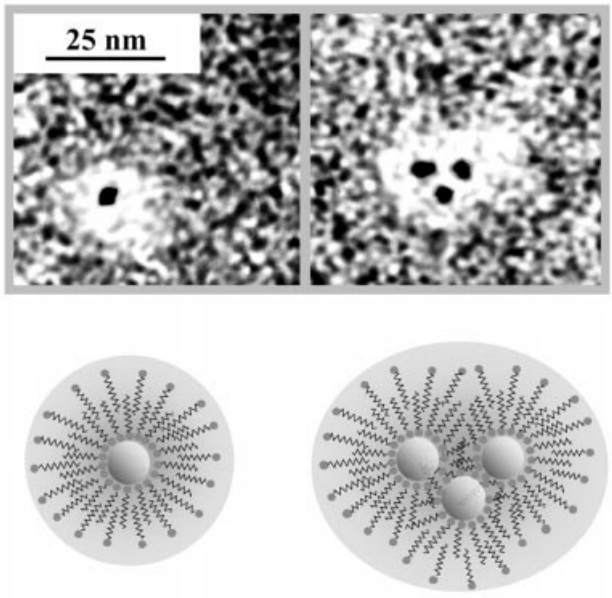

Figure 4. Top: TEM micrographs of colloidal Pt particles (single and aggregated; average core size = 2.8 nm) stabilized by carboxybetaine 12 (3−5 nm, contrasted with uranyl acetate against the carbon substrate); bottom: schematic model of the hydrosol stabilization by a double layer of the zwitterionic carboxybetaine 12 (ΛΛΛ = lipophilic alkyl chain; −o = hydrophilic, zwitterionic head group) (adapted from ref.[104])

alkylammonium halides, the metal core is protected by a monolayer of the surfactant coating (Figure 3).[103]

In contrast, metal hydrosols that are stabilized by zwitterionic surfactants capable of self-aggregation are enclosed in organic double layers. After the application of uranyl acetate as a contrasting agent, TEM micrographs show that the colloidal Pt particles (average size 2.8 nm) are surrounded by a double layer zone of the zwitterionic carboxybetaine (3−5 nm). The hydrophilic head group of the betaine interacts with the charged metal surface and the lipophilic tail is associated with the tail of a second surfactant molecule resulting in the formation a hydrophilic outer sphere (see Figure 4).[104] Pt or Pt/Au particles have been hosted in the hydrophobic holes of non-ionic surfactants, e.g. polyethylene monolaurate.[105,106]

Reducing Agents

It has been experimentally verified in the case of silver[31] that stronger reducing agents produce smaller nuclei in the "seed". These nuclei grow during the "ripening" process to yield colloidal metal particles in the size range 1−50 nm, which have a narrow size distribution. The mechanism of particle formation was assumed to involve an agglomeration of zerovalent nuclei in the "seed" or, alternatively, collisions of already formed nuclei with reduced metal atoms. Henglein[32] has monitored the stepwise reductive formation of Ag_3^+ and Ag_4^+ clusters by spectroscopic methods. His results strongly suggest that an autocatalytic pathway is involved, in which metal ions are adsorbed and successively reduced at the zerovalent cluster surface. The formation of colloidal Cu protected by cationic surfactants (NR_4^+) was investigated by in situ X-ray absorption spectroscopy, which revealed the formation of an intermediate Cu^+ state prior to nucleation of the particles.[35] It is now generally accepted that the size of the resulting metal colloid is determined by the relative rates of nucleation and particle growth, although the processes involved in nucleation and particle growth cannot be analyzed separately.

The main advantages of the salt reduction method in the liquid phase are that it is reproducible and allows colloidal nanoparticles with a narrow size distribution to be prepared on a multigram scale. The classical Faraday route, as in the reduction of $[AuCl_4]^-$ with sodium citrate for example, is still used to prepare standard 20 nm gold sols for histological staining applications.[1,107] Wet chemical reduction procedures have been applied in the last decades to successfully combine practically all transition metals with the different types of stabilizers and the whole range of chemical reducing agents. In 1981, Schmid et al. established the "diborane-as-reductant route" for the synthesis of $Au_{55}(PPh_3)_{12}Cl_6$ (1.4 nm), a full shell ("magic number") nanocluster stabilized by phosphane ligands.[57−71] Clusters of Au_{55} are uniformly formed when a stream of B_2H_6 is carefully introduced into an Au^{III} ion solution. The "diborane route" for $M_{55}L_{12}Cl_n$ nanoclusters was recently reviewed by Finke et al.[11] Bimetallic nanoclusters made accessible by this method[57−71] have been thoroughly characterized. Using silsesquioxanes, the phosphane ligands may be quantitatively exchanged in the Au_{55} nanoclusters, which causes marked changes in the physical and chemical behavior of these clusters.[71] The synthesis and general chemistry of nanosized silica-coated metal particles has been elaborated by Mulvaney.[72] The "alcohol reduction process" of Hirai and Toshima[10,37−40,323,324] is widely applicable for the preparation of colloidal precious metals stabilized by organic polymers such as poly(vinylpyrrolidone) (PVP), poly(vinyl alcohol) (PVA), and poly(methylvinyl

ether). Alcohols having α-hydrogen atoms are oxidized to the corresponding carbonyl compound (e.g. methanol to formaldehyde) during the salt reduction. The method for preparing bimetallic nanoparticles by the co-reduction of mixed ions has been evaluated in a recent review.[10] Hydrogen is an efficient reducing agent for the preparation of electrostatically stabilized metal sols and of polymer-stabilized hydrosols of Pd, Pt, Rh, and Ir.[108−112] Moiseev's "giant" palladium cluster [Figure 5, a)][73−78] and Finke's polyoxoanion- and tetrabutylammonium-stabilized transition metal nanoclusters [Figure 5, b)][11,34,113−117] were also prepared by the hydrogen reduction pathway.

The characterization of Moiseev's giant cationic palladium clusters[73−78] [Figure 5, a)] [idealized formula $Pd_{\approx 561}L_{\approx 60}(OAc)_{\approx 180}$ (L = phenanthroline, bipyridine)] and their catalytic properties have recently been reviewed by Finke et al.[11] The results of a combination of modern instrumental analysis methods applied to Finke's nanoclusters were discussed in detail in the same review.[11]

Colloidal Pt in water[2,118] was obtained using CO, formic acid, sodium formate, formaldehyde, and benzaldehyde as reductants.[119] Silanes have been found to be effective for the reductive preparation of Pt sols.[120,121] Duff, Johnson, and Baiker have successfully introduced tetrakis(hydroxymethyl)phosphonium chloride (THPC) as a reducing agent that allows the size- and morphology-selective synthesis of Ag, Cu, Pt, and Au nanoparticles from the corresponding metal salts.[122−127] Furthermore, hydrazine,[128] hydroxylamine,[129] and electrons trapped in, for example, $K^+[(crown)_2K]^-$,[130] have been applied as reductants. In addition, BH_4^- is a powerful and valuable reagent for the salt reduction method. However, a disadvantage is that transition metal borides are often found alongside the nanometallic particles.[131,132] Tetraalkylammonium hydrotriorganoborates[6,7,9,15,87−89] offer a wide range of applications in the wet chemical reduction of transition metal salts. In this case, the reductant $[BEt_3H]^-$ is combined with the stabilizing agent (e.g. NR_4^+). The surface-active NR_4^+ salts are formed immediately at the reduction center in high local concentration and prevent particle aggregation. Trialkylboron is recovered unchanged from the reaction mixture and no borides contaminate the products.

$$MX_\nu + NR_4(BEt_3H) \longrightarrow M_{colloid} + \nu\ NR_4X + \nu\ BEt_3 + \nu/2\ H_2\uparrow \quad (1)$$

M = metals of groups 6–11; X = Cl, Br; ν = 1–3; R = alkyl, C_6–C_{20}

As synthesized, the NR_4^+-stabilized "raw" metal colloids typically contain 6−12 wt-% of metal. "Purified" transition metal colloids containing ca. 70−85 wt-% of metal are obtained by work-up with ethanol or diethyl ether and subsequent reprecipitation from a solvent of different polarity (see Table 9 in ref.[6]). The pre-preparation of $[NR_4]^+[BEt_3H]^-$ can be avoided if NR_4X is coupled to the metal salt prior to the reduction step. Transition metal nanoparticles stabilized by NR_4^+ can also be obtained from NR_4X/transition metal double salts. A number of conventional reducing agents may be applied since the local concentration of the protecting group is sufficiently high for Equation (2) to hold.[7,15]

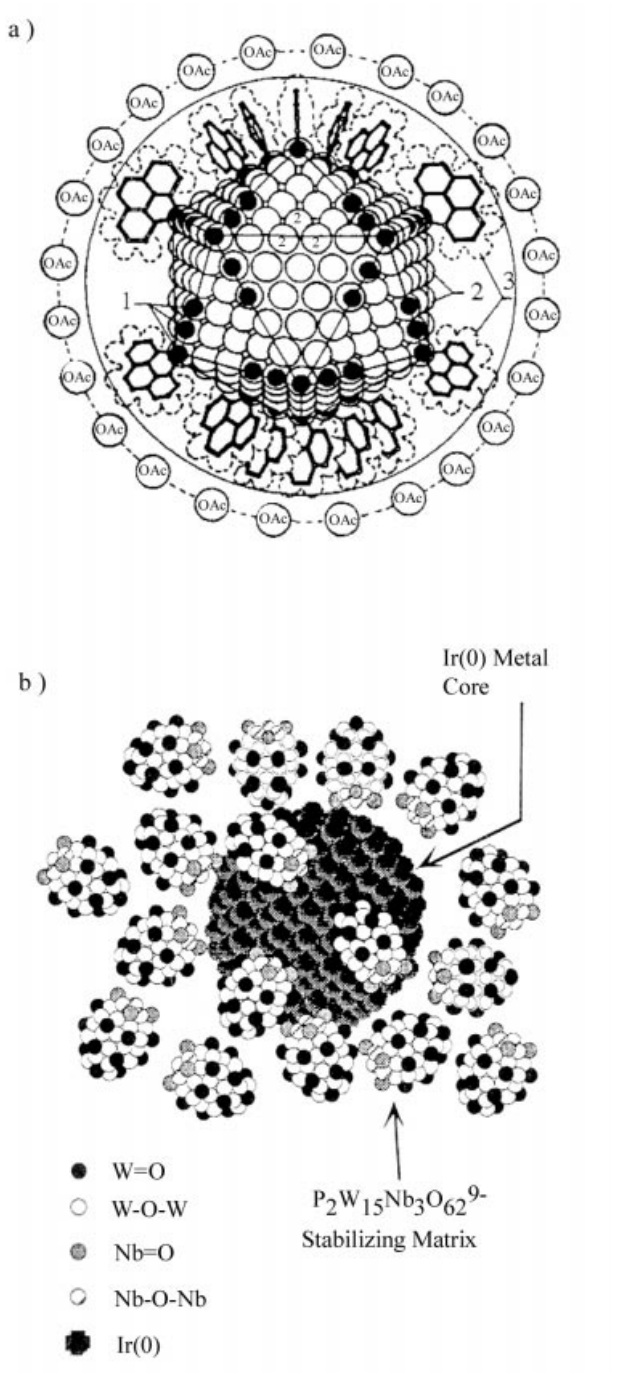

Figure 5. a) Idealized model of Moiseev's "giant palladium cluster" $Pd_{\approx 561}phen_{\approx 60}(OAc)_{\approx 180}$ (phen = phenanthroline) (adapted from ref.[73]); b) idealized model of a Finke-type Ir^0 nanocluster $P_2W_{15}Nb_3O_{62}^{9-}$ and Bu_4N^+-stabilized $Ir^0_{\approx 300}$ (adapted with permission from ref.[113])

$$(NR_4)_wMX_\nu Y_w + \nu\ Red \longrightarrow M_{colloid} + \nu\ RedX + w\ NR_4Y \quad (2)$$

M = metals; Red = H_2, HCO_2H, K, Zn, LiH, $LiBEt_3H$, $NaBEt_3H$, $KBEt_3H$; X,Y = Cl, Br; ν, w = 1–3; R = alkyl, C_6–C_{12}

Table 1. THF-stabilized organosols of early transition metals

Product	Starting material	Reducing agent	T [°C]	t [h]	Metal content [%]	Size [nm]
[Ti·0.5THF]	$TiBr_4$·2THF	$K[BEt_3H]$	room temp.	6	43.5	(< 0.8)
[Zr·0.4THF]	$ZrBr_4$·2THF	$K[BEt_3H]$	room temp.	6	42	–
[V·0.3THF]	VBr_3·3THF	$K[BEt_3H]$	room temp.	2	51	–
[Nb·0.3THF]	$NbCl_4$·2THF	$K[BEt_3H]$	room temp.	4	48	–
[Mn·0.3THF]	$MnBr_2$·2THF	$K[BEt_3H]$	50	3	70	1–2.5

In a recent review,[11] the scope and limitations of this method were evaluated. Isolable colloids of the zerovalent early transition metals stabilized only by THF have been prepared by $[BEt_3H]^-$ reduction of the preformed THF adducts of $TiBr_4$ [Equation (3)], $ZrBr_4$, VBr_3, $NbCl_4$, and $MnBr_2$. Table 1 summarizes the results. Detailed studies of [Ti·0.5 THF][83] have shown that it consists of Ti_{13} clusters in the zerovalent state, stabilized by six intact THF molecules (Figure 6).

$$x\,[TiBr_4 \cdot 2\,THF + x{\cdot}4\,K[BEt_3H] \xrightarrow{THF,\ 2\ h,\ 20\ °C} [Ti \cdot 0.5\,THF]_x + x{\cdot}4\,BEt_3 + x{\cdot}4\,KBr\downarrow + x{\cdot}4\,H_2\uparrow \quad (3)$$

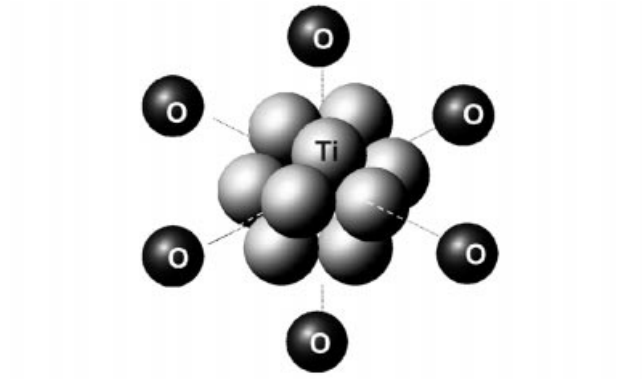

Figure 6. Ti_{13} cluster stabilized by six THF O atoms in an octahedral configuration

By analogy, [Mn·0.3THF] particles (1–2.5 nm) have been prepared[133] and their physical properties have been studied.[134] The THF in Equation (3) has been successfully replaced by tetrahydrothiophene (THT) in the case of Mn, Pd, and Pt organosols, but attempts to stabilize Ti and V in this way led to decomposition (Figure 7).[15] Figure 8 gives a survey of the $[BEt_3H]^-$ method.

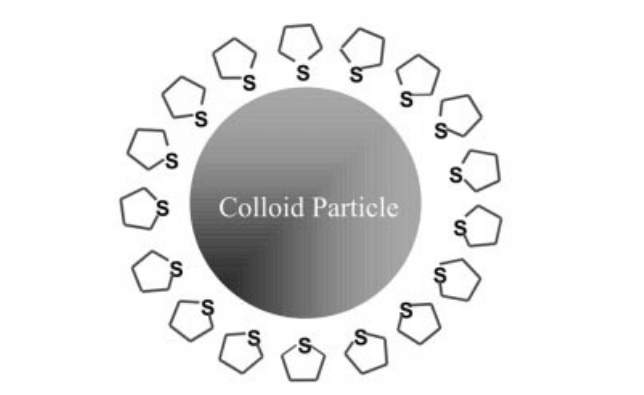

Figure 7. Organosols stabilized by tetrahydrothiophene; M = Ti, V (decomposition); M = Mn, Pd, Pt; stable colloids

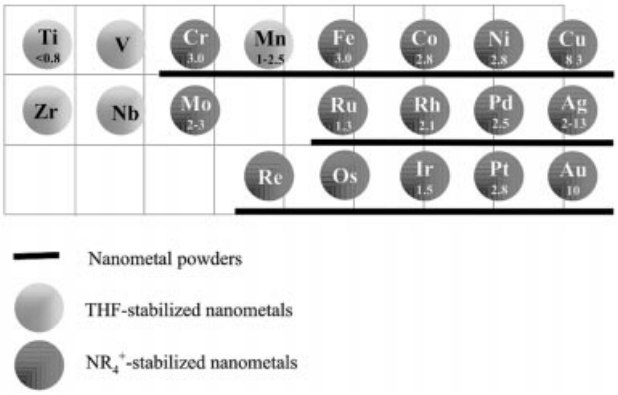

Figure 8. Nanopowders and nanostructured metal colloids accessible by the $[BEt_3H]^-$ reduction method (including the mean particle sizes obtained) (adapted with permission from ref.[7])

The advantages of the method (Figure 8) may be summarized as follows:

– The method is generally applicable to salts of metals of Groups 4–11 in the Periodic Table.
– It yields extraordinarily stable metal colloids that are easy to isolate as dry powders.
– The particle size distribution is nearly monodisperse.
– Bimetallic colloids are easily accessible by co-reduction of two different metal salts.
– The synthesis is suitable for multigram preparations and is easy to scale up.

One of the drawbacks of this method is that the particle size of the resulting sols cannot be varied by altering the reaction conditions. Highly water-soluble hydrosols, particularly those of zerovalent precious metals, were made accessible by using betaines instead of NR_4^+ salts as the protecting group in Equation (1). A wide variety of hydrophilic surfactants may be used in Equation (2).[7,15,88] Reetz and Maase have reported a new method for the size- and morphology-selective preparation of metal colloids using tetraalkylammonium carboxylates of the type $NR_4^+R'CO_2^-$ (R = octyl; R′ = alkyl, aryl, H) as both the reducing agent and the stabilizer [Equation (4)].[135–137,325]

$$M^+ + R_4N^+\ R'CO_2^- \xrightarrow{50\text{–}90\ ^\circ C} M^0(R_4NR'CO_2)_x + CO_2 + R'\text{–}R' \quad (4)$$

R = octyl, R' = alkyl, aryl, H

The resulting particle sizes were found to correlate with the electronic nature of the R′ group in the carboxylate. Electron donors produced small nanoclusters, whereas electron-withdrawing substituents R′ yielded larger particles. For example, Pd particles of size 2.2 nm were formed when $Pd(NO_3)_2$ was treated with an excess of tetra(*n*-octyl)ammonium carboxylate bearing R′ = $(CH_3)_3CCO_2^-$ (an electron-donating group) as the substituent. With R′ = $Cl_2CHCO_2^-$ (an electron-withdrawing substituent), the particle size was found to be 5.4 nm. Bimetallic colloids of the following were obtained with tetra(*n*-octyl)ammonium formate as the reductant: Pd/Pt (2.2 nm), Pd/Sn (4.4 nm), Pd/Au (3.3 nm), Pd/Rh (1.8 nm), Pt/Ru (1.7 nm), and Pd/Cu (2.2 nm). The shape of the particles was also found to depend on the reductant: With tetra(*n*-octyl)ammonium glycolate and $Pd(NO_3)_2$, a significant amount of trigonal particles was detected in the resulting Pd colloid. Organoaluminum compounds have been used for the "reductive stabilization" of mono- and bimetallic nanoparticles [see Equation (5) and Table 2].[99,100]

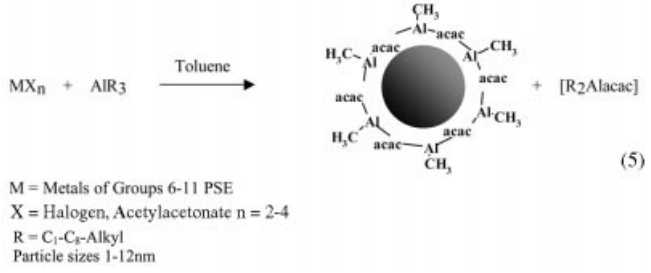

According to Equation (5), colloids of zerovalent elements of Groups 6−11 of the Periodic Table (and also of tin) may be prepared in the form of stable, isolable organosols. Available analytical data suggest that a layer of condensed organoaluminum species protects the transition metal core against aggregation, as depicted in Equation (5). However, the exact "backbone" of the colloidal organoaluminum protecting agent has not yet been completely established.

Unreacted organoaluminum groups (e.g. $Al-CH_3$, $Al-C_2H_5$) from the starting material are still present in the stabilizer and have been detected by quantitative protonolysis experiments. These active Al−C bonds have been used for a controlled protonolysis by long-chain alcohols or organic acids ("modifiers") to give Al−alkoxide groups in the stabilizer [Equation (6)].

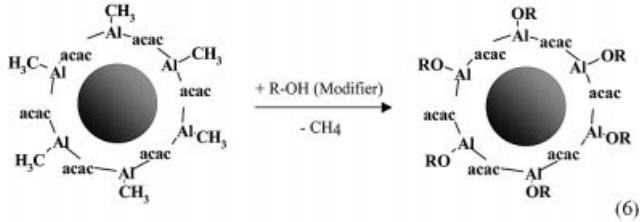

Modifiers: alcohols, carbonic acids, silanols, sugars, polyalcohols, polyvinylpyrrolidone, surfactants, silica, alumina, etc. (32).

This "modification", Equation (6), of the organoaluminum protecting shell can be used to tailor the dispersion characteristics of the original organosols. A vast spectrum of solubilities of the colloidal metals in hydrophobic and

Table 2. Mono- and bimetallic nanocolloids prepared by the organoaluminum route (see ref.[99])

Metal salt [g]	[mmol]	Reducing agent	[g]	[mmol]	Toluene [mL]	Conditions T [°C]	t [h]	Product m [g]	Metal content [wt-%]	Particle size F [nm]
$Ni(acac)_2$ 0.275	1	$Al(iBu)_3$	0.594	3	100	20	10	0.85	Ni: 13.8	2−4
$Fe(acac)_2$ 2.54	10	$Al(Me)_3$	2.1	30	100	20	3	2.4	n.d.	
$RhCl_3$ 0.77	3.1	$Al(oct)_3$	4.1	11.1	150	40	18	4.5	Rh: 8.5 Al: 6.7	2−3
Ag neodecanoate 9.3	21.5	$Al(oct)_3$	8.0	21.8	1000	20	36	17.1	Ag: 11.8 Al: 2.7	8−12
$Pt(acac)_2$ 1.15	3	$Al(Me)_3$	0.86	7.6	150	20	24	1.45	Pt: 35.8 Al: 15.4	2.5
$PtCl_2$ 0.27	1	$Al(Me)_3$	0.34	3	125	40	16	0.47	Pt: 41.1 Al: 15.2	2.0
$Pd(acac)_2$ 0.54 $Pt(acac)_2$ 0.09	1.8 0.24	$Al(Et)_3$	0.46	4	500	20	2	0.85	P: 22 Pt: 5.5 Al: 12.7	3.2
$Pt(acac)_2$ 7.86 $Ru(acac)_3$ 7.96	20 20	$Al(Me)_3$	8.64	120	400	60	21	17,1	Pt: 20.6 Ru: 10.5 Al: 19.6	1.3
$Pt(acac)_2$ 1.15 $SnCl_2$ 0.19	2.9 1	$Al(Me)_3$	0.86	12	100	60	2	1.1	Pt: 27.1 Sn: 5.2 Al: 14.4	n.d.

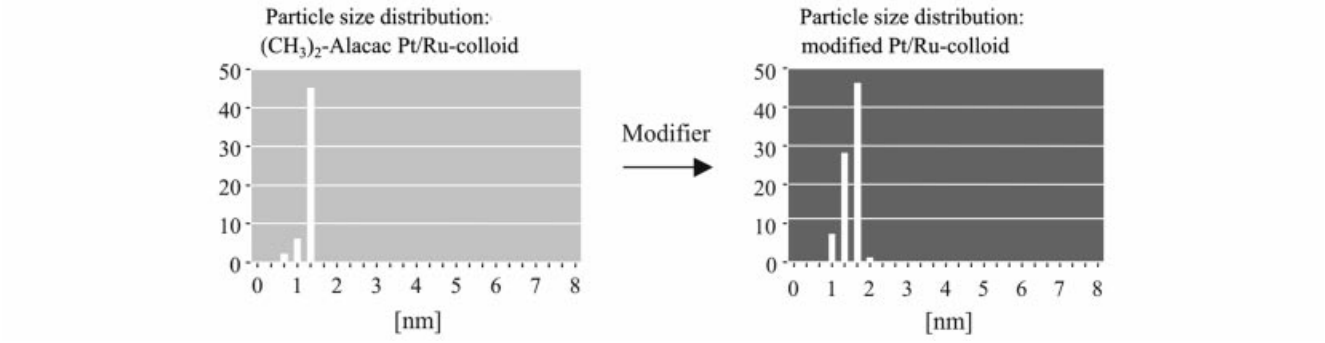

Figure 9. Size conservation of colloidal Pt/Ru particles under the hydrophilic modification of the $(CH_3)_nAl-acac$ protecting shell using polyethylene glycol/dodecyl ether

hydrophilic media (including water) has been achieved in this way. Inorganic surfaces bearing OH groups can react with the active Al−C bonds in the colloidal protecting shell, opening new possibilities for the preparation of heterogeneous catalysts. The modification process does not substantially alter the particle size of the metal core (see Figure 9).[101]

Electrochemical Synthesis

This very versatile means of preparing nanostructured mono- and bimetallic colloids has been further developed by Reetz and his group since 1994.[8,90,91] The overall process of electrochemical synthesis, Equation (7), can be divided into six elementary steps (see Figure 10).

1. Oxidative dissolution of the sacrificial M_{bulk} anode.
2. Migration of M^{n+} ions to the cathode.
3. Reductive formation of zerovalent metal atoms at the cathode.
4. Formation of metal particles by nucleation and growth.
5. Arrest of the growth process and stabilization of the particles by colloidal protecting agents, e.g., tetraalkylammonium ions.
6. Precipitation of the nanostructured metal colloids.

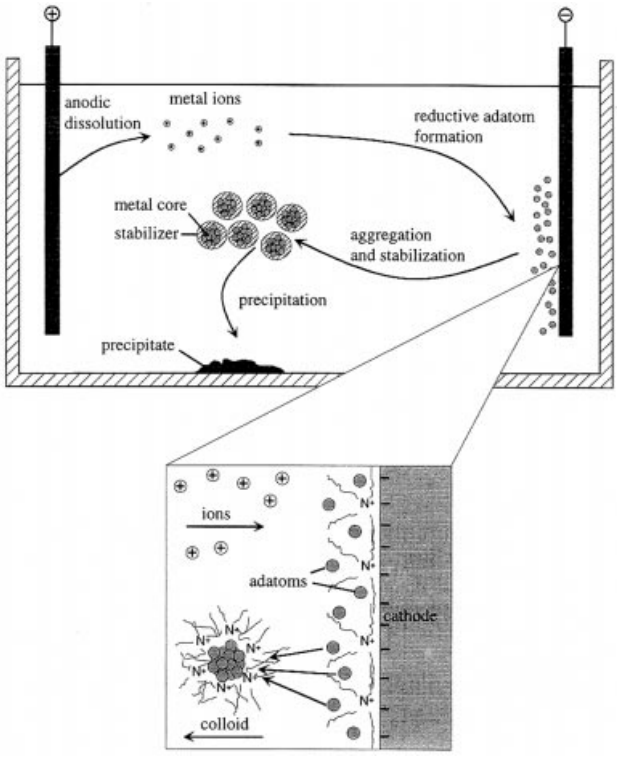

Figure 10. Electrochemical formation of $NR_4^+Cl^-$-stabilized nanometal (adapted with permission from ref.[8])

$$\begin{array}{lllll} \text{Anode:} & & M_{bulk} & \rightarrow & M^{n+} + n\,e^- \\ \text{Cathode:} & M^{n+} + n\,e^- + & \text{stabilizer} & \rightarrow & M_{coll}/\text{stabilizer} \\ \hline \text{Sum:} & M_{bulk} + & \text{stabilizer} & \rightarrow & M_{coll}/\text{stabilizer} \end{array} \quad (7)$$

Advantages of the electrochemical pathway are that contamination with by-products resulting from chemical reducing agents are avoided and that the products are easily isolated from the precipitate. Further, the electrochemical preparation allows for size-selective particle formation. Experiments using Pd as the sacrificial anode in the electrochemical cell to give $(C_8H_{17})_4N^+Br^-$-stabilized Pd^0 particles have indicated that the particle size depends on the current density applied: high current densities lead to small Pd particles (1.4 nm), whereas low current densities give larger particles (4.8 nm).[90] As was seen from a careful analysis of tetraalkylammonium-stabilized Pd and Ni by means of a combination of TEM and SAXS, the control of particle size does not have a single cause. It can be brought about by adjusting the following parameters:

– the distance between the electrodes,
– the reaction time and temperature,
– the polarity of the solvent.

Nearly monodisperse Pd^0 particles with sizes of 1–6 nm can be obtained by means of electrochemical synthesis. It was also shown that the size of NR_4^+-stabilized Ni^0 particles[92] can be adjusted at will. The electrochemical method[90–97] [Equation (7)] has been successfully applied in the preparation of a number of monometallic organosols and hydrosols, e.g. of Pd, Ni, Co, Fe, Ti, Ag, and Au, on a scale of several hundred milligrams (yields > 95%). Using the electrochemical pathway, solvent-stabilized (propylene carbonate) palladium particles (8–10 nm) have also been obtained.[85] Bimetallic nanocolloids (Pd/Ni, Fe/Co, Fe/Ni) are accessible[95] if two sacrificial M_{bulk} anodes are used in a single electrolysis cell. In the case of Pt, Rh, Ru, and Mo, which are anodically less readily soluble, the corresponding metal salts were electrochemically reduced at the cathode (see bottom part of Figure 10 and Table 3). Tetraalkylammonium acetate has been used as both the supporting electrolyte and the stabilizer in a Kolbe electrolysis at an anode [see Equation (8)].[96] By combining the electrochemical methods described in Equation (7) and Equation (8), bimetallic nanocolloids can be prepared (see Table 4).[96]

$$\begin{aligned} &\text{Cathode:} \quad Pt^{2+} + 2\,e^- \longrightarrow Pt^0 \\ &\text{Anode:} \quad 2\,CH_3CO_2^- \longrightarrow 2\,CH_3CO_2 + 2\,e^- \end{aligned} \tag{8}$$

Table 3. Electrochemical colloid synthesis

Metal Salt	*d* [nm]	EA[a]
$PtCl_2$	2.5[b]	51.21% Pt
$PtCl_2$	5.0[c]	59.71% Pt
$RhCl_3H_2O$	2.5	26.35% Rh
$RuCl_3H_2O$	3.5	38.55% Ru
$OsCl_3$	2.0	37.88% Os
$Pd(OAc)_2$	2.5	54.40% Pd
$Mo_2(OAc)_4$	5.0	36.97% Mo
$PtCl_2 + RuCl_3H_2O$	2.5	41.79% Pt + 23.63% Rh[d]

[a] Based on stabilizer-containing material. – [b] Current density: 5.00 mA/cm^2. – [c] Current density: 0.05 mA/cm^2. – [d] Pt–Ru dimetallic cluster.

Table 4. Bimetallics prepared electrochemically

Anode	Metal salt	*d* [nm]	Stoichiometry (EDX)
Sn	$PtCl_2$	3.0	$Pt_{50}Sn_{50}$
Cu	$Pd(OAc)_2$ [a]	2.5	$Cu_{44}Pd_{56}$
Pd	$PtCl_2$	3.5	$Pd_{50}Pt_{50}$

[a] Electrolyte: 0.1 M [(*n*-octyl)$_4$N]OAc/THF.

By modifying the electrochemical method, the synthesis of layered bimetallic nanocolloids (e.g. of Pt/Pd) has been achieved.[92,97] A preformed $(Oct)_4NBr$-stabilized Pt colloid core (size 3.8 nm) was electrolyzed in 0.1 M $(Oct)_4NBr$ solution in THF with Pd as the sacrificial anode (Figure 11). The preformed Pt core may be regarded as a "living-metal-polymer", on which the Pd atoms are deposited to give "onion-type" bimetallic nanoparticles (5 nm).

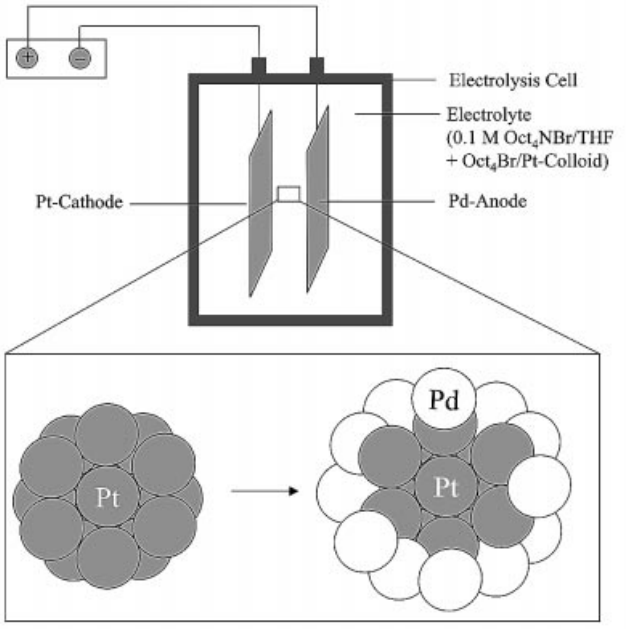

Figure 11. Modified electrolysis cell for the preparation of layered bimetallic Pt/Pd nanocolloids (adapted with permission from ref.[92])

Decomposition of Low-Valent Transition Metal Complexes

Low-valent organometallic complexes and several organic derivatives of the transition metals decompose under the action of heat, light, or ultrasound to give short-lived nucleation particles of zerovalent metals in solution, which may be stabilized by colloidal protecting agents. For example, thermolysis[138–143] leads to the rapid decomposition of carbonylcobalt complexes to give colloidal cobalt in organic solutions.[138,139] Thermolysis of labile precious metal salts in the absence of stabilizers yields colloidal Pd, Pt, and bimetallic Pd/Cu nanoparticles[140] with broad size distributions. These results were found to be greatly improved when the thermolysis was performed in the presence of stabilizing polymers, such as PVP.[141] Recently, heating in a simple household microwave oven has been proposed as a means of preparing nanosized metal particles and colloids.[142,143,326] The substrate is heated uniformly by the electromagnetic waves, leading to a more homogeneous nucleation and a shorter aggregation time. It is informative to compare the particle size of polymer-stabilized Pt colloids (spheres, 2–4 nm, narrow size distribution) prepared by dielectrical microwave heating with that of samples prepared by conventional heating under otherwise identical

Table 5. Comparison of conventional and microwave heating

No.[a]	PVP[b]	NaOH[b]	Average diameter [nm]	Standard deviation [nm]	Relative standard deviation
1	10	0	3.8	0.57	0.15
2	20	0	3.4	0.56	0.16
3	50	0	3.0	0.50	0.17
4	100	0	2.9	0.47	0.16
5	50	2	3.0	0.49	0.16
6	50	4	2.6	0.48	0.18
7	50	6	1.9	0.33	0.17
8	50	8	2.0	0.32	0.16
9	50	10	2.1	0.40	0.19
10	50	0	3.1	1.08	0.35
11	50	8	1.8	0.55	0.31
12	50	0	2.7	0.74	0.27
13	50	8	1.1	0.31	0.28

[a] Nos. 1−9 were prepared by microwave dielectric heating without stirring; nos. 10 and 11 were prepared without stirring, and nos. 12 and 13 were prepared by stirring in a heated oil bath. − [b] The data in the columns labeled PVP and NaOH refer to the molar ratios of PVP (as a monomeric unit) and NaOH to Pt.

conditions (Table 5). Sonochemical decomposition methods have been successfully developed by Suslick[144] and Gedanken[145−147] and have yielded Fe, Mo_2C, Ni, Pd, and Ag nanoparticles in various stabilizing environments.

Isolable colloidal products can be prepared in multigram amounts by the controlled chemical decomposition of zero-valent transition metal complexes by the addition of CO or H_2 in the presence of appropriate stabilizers.[79−82,148−158] Bradley and Chaudret[79−82,149−155,327−333] have demonstrated the use of low-valent transition metal olefin complexes as a very clean source for the preparation of nanostructured mono- and bimetallic colloids. Nanoparticulate colloids have also been successfully prepared in micelles, inverse micelles, and by encapsulation.[32,33][86] Although beyond the focus of this article, we should also mention that a number of nanoparticulate metal oxide systems have been successfully developed.[7,157−162]

Particle Size Control

Metal colloid sols are generally described as "monodisperse" when the particle size deviates by less than 15% from the average value. Histograms with a standard deviation σ from the mean particle size of approximately 20% are described as showing a "narrow size distribution". The kinetics of the particle nucleation from atomic units and of the subsequent growth process cannot be directly observed by physical methods. In practice, the means available to the preparative chemist for controlling the particle size are size-selective separation[43,163,164] and size-selective synthesis.[41−56,90,135−137,165−181]

The so-called *size-selective precipitation* (SPP) method was predominantly developed by Pileni.[42,334] Monodisperse silver particles (2.3 nm, σ = 15%) are precipitated from a polydisperse silver colloid solution in hexane by adding pyridine in three iterative steps. Schmid has recently reported the two-dimensional "crystallization" of truly monodisperse Au_{55} clusters.[163] Schmid has also shown that the size of nanoparticles can be limited by steric restrictions imposed by a 3D polymer network.[335] Chromatographic separation methods proved unsuccessful because the colloid was decomposed after the colloidal protecting shell had been stripped off.[135] Colfen has developed the size-selective ultra-centrifuge separation of Pt colloids.[164] However, although this elegant separation method gives truly monodisperse metal colloids, as yet it can only provide milligram-scale samples. Turkevich was the first to describe size-selective colloid synthesis.[1,2] Using the salt reduction method, he was able to vary the particle size of colloidal Pd between 0.55 and 4.5 nm. The crucial parameters were the amount of reducing agent applied and the pH of the medium. According to the literature concerning the process of nucleation and particle growth, the essential factors that control the particle size are the strength of the metal−metal bond;[40] the molar ratio of metal salt; colloidal stabilizer; and reducing agent;[1,119,126,165−182] the extent of conversion or the reaction time;[119] the applied temperature;[1,166,178] and the pressure.[166] The preparation of nearly monodisperse nanostructured metal colloids using the salt reduction pathway is well documented in the literature. In practice, however, the "control", i.e. the variation of particle sizes (and shapes), in wet chemical colloid synthesis is left to the intuition of the chemist. Recently, Pileni has also demonstrated that control of particle size and composition can be achieved using oil-in-water micelles.[336] At present, the electrochemical synthesis of Reetz and co-workers offers the most rational method for selecting the particle size. Using variable current densities and making appropriate adjustments of further key parameters, these authors have been able to obtain at will almost monodisperse samples of colloidal Pd and Ni with sizes between 1 and 6 nm.[90−97] In the thermal decomposition method, the particle size obtained depends on the heat source (see Table 5).[143] Size control has also been reported for the sonochemical decompositon method and γ-radiolysis.[183,184]

The domain of preparation methods using constrained environments offers control over the metal particle shape

by predetermining the size and morphology of the products in nanoscale reaction chambers.[41−56] The controlled temperature-induced size and shape manipulation of 2−6 nm gold particles encapsulated in alkanethiolate monolayers[54] has recently been reported. The use of near-IR laser light has led to an enormous increase in the size of thiol-passivated gold particles up to ca. 200 nm.[54] A new medium-energy ion-scattering (MEIS) simulation program has successfully been applied in analyzing the composition and average particle size of Pt/Rh/α-Al_2O_3.[55]

Applications in Catalysis

"Quasi-Homogeneous" Reactions

Lipophilic or hydrophilic nanostructured metal colloids, dissolved in the form of organosols or hydrosols, can serve as catalysts in organic solutions and in the aqueous phase, respectively. Schmid[64] has referred to these quasi-homogeneous catalytic reactions, which involve solvated metal atom dispersions (SMAD),[26] as "heterogeneous catalysis in solution". Rhodium hydrosols, dissolved in water, were shown to be effective as hydrogenation catalysts in two-phase systems, where the olefin formed the organic phase.[185] Aqueous solutions of Moiseev's giant Pd colloids [Figure 5, a)][73−78] were shown to catalyze a number of reactions in the "quasi-homogeneous" phase, namely oxidative acetoxylation reactions,[73] the oxidative carbonylation of phenol to diphenyl carbonate,[186] the hydrogen-transfer reduction of multiple bonds by formic acid,[187] the reduction of nitriles and nitroarenes, and acetal formation,[188] all with high turnover frequencies and significant lifetimes (see ref.[11]). Remarkable catalytic lifetimes for polyoxoanion- and tetrabutylammonium-stabilized transition metal nanoclusters have been reported by Finke[113−117] (see Figure 5). For example, in the catalytic hydrogenation of cyclohexene, a common test for structure-insensitive reactions, the Ir^0 nanocluster[34] showed up to 18,000 total turnovers with turnover frequencies of 3200 h^{-1}.[189] Recently, as many as 190,000 turnovers were reported in the case of the Rh^0 analogue.[190] These results are quite unprecedented. Obviously, the polyoxoanion component prevents the precious metal nanoparticles from aggregating so that the active metals have high effective surface areas.[190] A recent review[7] compares this new approach with the catalytic properties of other nanometallic systems active in the "quasi-homogeneous" phase. When nanostructured Ti colloids (3 nm), stabilized by Bu_4NBr, were used, the formation of olefins from aldehydes and ketones through McMurry-type coupling reactions was observed.[191] THF-protected Ti_{13} nanoclusters[83] were found to hydrogenate Ti and Zr sponges in the "quasi-homogeneous" phase.[192,193] Using cinchonidine-stabilized Pt colloids, the enantioselective hydrogenation of ethyl pyruvate in HOAc/MeOH solution was performed.[177] Heck and Suzuki C−C bond coupling reactions were catalyzed by $NR_4^+X^-$-stabilized Pd and Pd/Ni colloids in dimethylacetamide. The same reactions have been observed using solvent-stabilized Pd particles in propylene carbonate as the catalyst.[85,194,195] Nanosized Pd colloids generated in situ by the reduction of Pd^{II} to Pd^0 are involved in the catalysis of phosphane-free Heck and Suzuki reactions.[196] Hexagonal or quasi-two-dimensional Pd nanoparticles (*hcp* structure, 53 nm) encapsulated in graphite have also been tested as catalysts for the Heck reaction. Microphotographs confirmed that the nanoparticles were located between the spacing layers of graphite. The catalyst is very stable: Although no strong interaction is present between the nanoparticles and the carbon lattice, the particles cannot be washed out and they are still found inside the carbon lattice after the Heck reaction.[197] The [3+2] cycloaddition of methylenecyclopropane to methyl acrylate is effectively catalyzed by nanostructured nickel colloids (2.5 nm) in solution.[198] The liquid-phase hydrogenation of isomeric undecenoic acids has been shown to be selectively catalyzed by Pt colloids encapsulated in polymerized micelles.[199] Metal colloids stabilized by amphiphilic block copolymers have been used as efficient catalysts in the "quasi-homogeneous" phase.[200−203] A generally applicable synthesis of metal colloids in microemulsions, in particular of nanostructured noble metals in amphiphilic block copolymers, has been devised by Antonietti and coworkers.[200][201] Micelles incorporating nanosized metals are very stable; they undergo no significant change of their colloidal properties such as size and polydispersity and are consequently effective hydrogenation catalysts. The morphology of the metal core can be varied between a "cherry"-type and a "raspberry"-type architecture depending on the strength of the reducing agent. Block copolymer stabilized Pd "raspberry" colloids have an extraordinarily high metal surface area and no additional support is needed for catalytic applications in solution. This type of colloid catalyst combines the advantages of homogeneous and heterogeneous catalysis, i.e. the high selectivity and reactivity of homogeneous hydrogenation catalysts is coupled with the long-term stability of heterogeneous systems. Nanostructured metal colloids, stabilized with synthetic polymers,[204−208] may be regarded as artificial enzyme models. The interaction between the "polymeric fields" and the reactive substrates determines the selectivity of the colloidal nanometal catalysts. Coordinating polymers such as poly(*N*-vinyl-2-pyrrolidone) have been shown to protect nanostructured mono- and bimetallic particles having an average diameter of ca. 1−3 nm and a narrow size distribution.[346−349] The resulting materials have proved to be effective catalysts for olefin hydrogenation,[205] nitrile hydration,[206] and photoinduced electron transfer.[207] The application of dendrimer-encapsulated Pd nanoparticles to fluorous phase soluble catalysts has recently been described.[208] The scope of ligand-stabilized transition metal nanoparticles in catalysis has recently been summarized by Schmid.[68,209]

Heterogeneous Reactions

Heterogeneous catalysts are obtained by depositing preprepared nanometal colloids on supports.[2] On this basis, the so-called "precursor concept" for the manufacture of

heterogeneous metal colloid catalysts was developed in the 1990s.[6,7,9,15,87−89] As a result, so-called *egg shell* catalysts were obtained, which contain the active metal particles as a thin layer (< 250 nm) on the surface of the support. Metal colloid catalysts of this type have been successfully applied in the hydrogenation of C−C double bonds, organic carbonyl groups, unsaturated C−N bonds, and in the reduction of N−O bonds.[210] An obvious advantage of the precursor concept over the conventional salt-impregnation method is that both the size and the composition of the colloidal metal precursors may be tailored independently of the support. Furthermore, the metal particle surface may be modified by lipophilic or hydrophilic protective shells and coated by intermediate layers, e.g., of oxide. The modification of the precursor by dopants is also possible. Such catalysts are manufactured by dipping the supports into organic or aqueous media containing the dispersed precursor at ambient temperature to adsorb the pre-prepared particles. This has been demonstrated for supports such as charcoal, various oxidic support materials, and even low-surface-area materials such as sapphire, quartz, and highly oriented pyrolitic graphite (HOPG), for which no subsequent calcination is required (see Figure 12). Researchers at Degussa have demonstrated the feasibility of preparing catalysts for industrial purposes in this way.

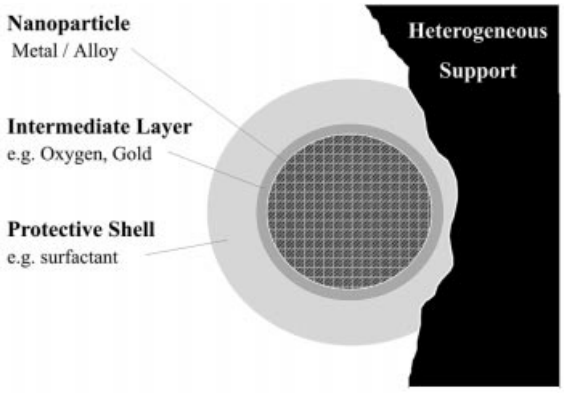

Figure 12. The precursor concept (adapted from ref.[7])

A combination of AFM, STM, and XPS[185] has been used to probe the interaction of platinum hydrosols with oxide (sapphire, quartz) and graphite single-crystal substrates (Figure 13). When dipped into aqueous Pt colloid solutions at 20 °C, the metal core is immediately adsorbed onto the support surface. The carpet-like coating formed over the particles by the protecting shell and the support surface cannot be removed from the particle surface even by repeated washing with solvents. The organic protecting shell decomposes on annealing at 280 °C and above in UHV. By monitoring the thermal degradation up to 800 °C by XPS and STM, it was shown that the Pt particles remain virtually unchanged up to ca. 800 °C, above which sintering processes take place.

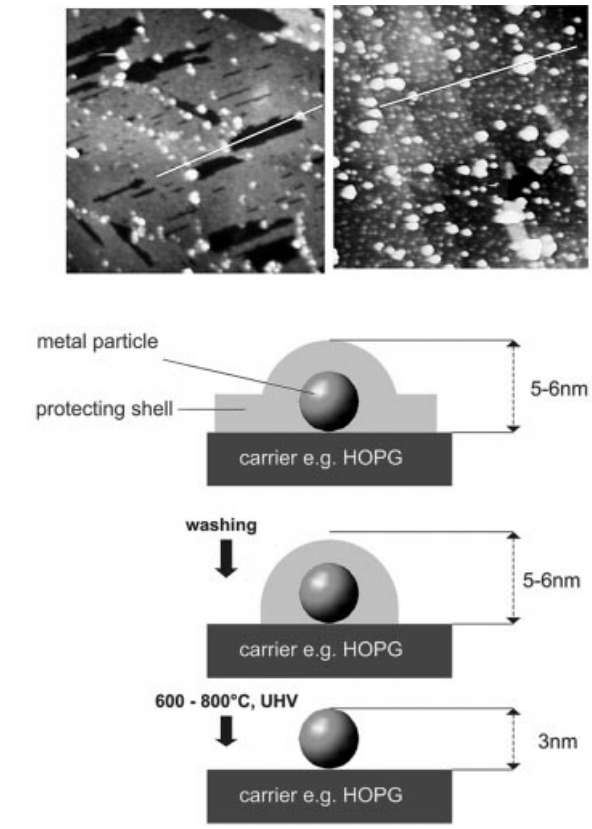

Figure 13. Top: AFM investigation of a sulfobetaine-12 stabilized Pt hydrosol (3 nm) absorbed on highly oriented pyrolytic graphite (HOPG) after dipping (left) and after additional washing (right); bottom: scheme of the Pt hydrosol adsorbtion on HOPG derived from a combined STM and XPS study (ref.[212])

Reetz et al. have used $(octyl)_4NBr$-stabilized Pd colloids (of typical size 3 nm) as precursors of so-called "*cortex catalysts*", where the active metal forms an extremely fine shell less than 10 nm thick on the support (e.g. Al_2O_3).[213] The impregnation of Al_2O_3 pellets by dispersed nanostructured metal colloids occurs with a time-dependent penetration of the support over the first 1−4 s, and is complete after 10 s [see Figure 14, a)−c)].

"*Cortex catalysts*" were reported to exhibit a threefold higher activity in olefin hydrogenation than conventionally prepared catalysts of the same metal loading (5% Pd on Al_2O_3). Schmid[64] has described phosphane-stabilized Rh_{55} nanoclusters, namely $Rh_{55}[P(t\text{Bu})_3]_{12}Cl_{20}$ and $Rh_{55}(PPh_3)_{12}Cl_{20}$, which were deposited on TiO_2. These systems were reported to catalyze the heterogeneous hydroformylation of propene with high turnover numbers giving equal amounts of *n*- and *iso*-butanal. Although the observed turnover frequencies were higher than those seen with homogeneous complex catalysts, the selectivity was found to be too low for practical applications. In the butyronitrile hydrogenation test, the activity of surfactant-stabilized colloidal rhodium (5 wt-% on charcoal) was found to surpass that of conventional salt impregnation catalysts

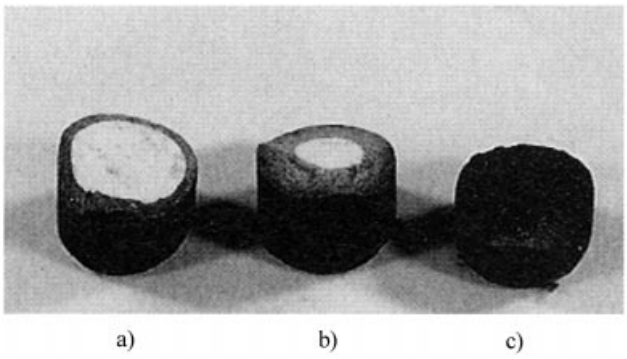

Figure 14. Heterogeneous Pd colloid catalysts of the *cortex*-type (adapted with permission from ref.[213]): a) Al_2O_3 pellets (3.2 mm) after penetration with a 0.5 M solution of $(octyl)_4NBr$-stabilized colloidal Pd in THF for 1 s, b) for 4 s, c) for 10 s

of the same metal loading. The addition of 0.2% colloidal Ti^0 to the supported noble metal[83] resulted in a significant enhancement of the activity (see Figure 15).[7]

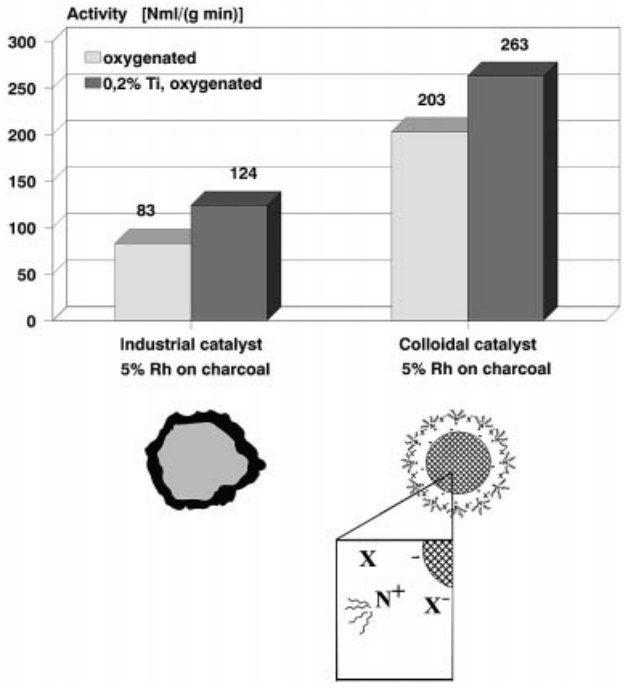

Figure 15. Activities of conventional and colloidal Rh/C catalysts, eventually doped with 2% colloidal Ti^0, compared in the butyronitrile hydrogenation test (adapted with permission from ref.[15])

The compounds used as dopants are not limited to those of the early transition metals. The addition of neodymium ions to the palladium particles was found to have a significant promoting effect on the hydrogenation of acrylic acid.[214] The selective transformation of 3,4-dichloronitrobenzene to the corresponding aniline has been selected to test pre-prepared Pt hydrosols as heterogeneous catalyst precursors (see Figure 16).[215]

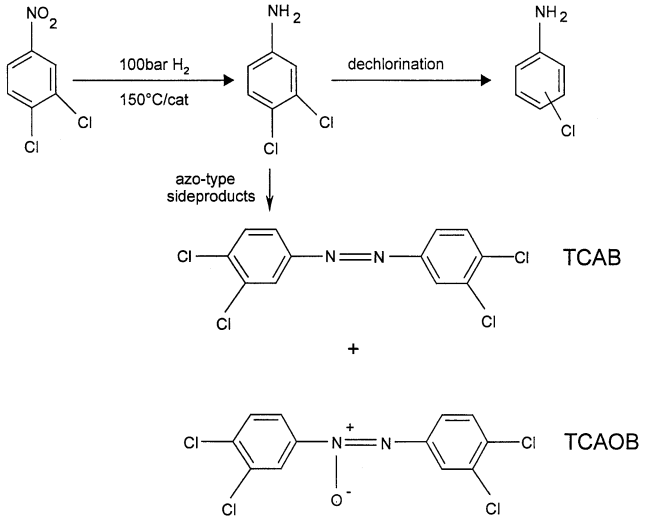

Figure 16. Reaction scheme for the hydrogenation of 3,4-dichloronitrobenzene

The performance of the colloidal catalyst system was evaluated in both batch and continuous tests and compared to that of conventional Pt/C systems. In summary, the potential of the colloidal heterogeneous catalyst stems from the fact that it is possible to tailor the properties for specific applications by the addition of specific dopants or "poisons" (such as sulfur). Further "fine tuning" of the complex process has been achieved by using the synergistic effect of bimetallic precursors (e.g. Pt/Cu). The influence of metal ions on the hydrogenation of *o*-chloronitrobenzene on platinum colloids and the effect of metal complexes on the catalytic performances of metal clusters have also been investigated.[216–218] It was found that the catalytic properties of platinum clusters for the hydrogenation of *o*-chloronitrobenzene to *o*-chloroaniline are very sensitive to the metallic cations added. Enhanced activity and selectivity was observed when Ni^{2+} ions were used as the modifier. The selectivity in the formation of *o*-chloroaniline increased from 44.7% to 66.3%, while the activity of the catalyst was almost doubled. The maximum activity and selectivity (82.9%) in the formation of *o*-chloroaniline was obtained with an Ni^{2+}/Pt molar ratio of 8:1.[216] The same authors also studied the "doping effect" of additional metal complexes on the activity and selectivity of platinum clusters in the homogeneous liquid-phase hydrogenation of cinnamaldehyde.[218] The conversion was increased from 65.5% to 78.0% by using Na_3FeF_6 as the additive, while the selectivity of cinnamic alcohol formation was increased from 17.7% to 75.0%. The addition of $Ni(bipy)_3Cl_2$ to the colloidal platinum catalyst increased the conversion to 82.1%, while the selectivity in the formation of hydrocinnamaldehyde was as high as 97.3%. By doping Rh colloid catalysts with Sn, it was found that the selectivity in the hydrogenation of cinnamic acid to cinnamic alcohol could be varied. A selectivity of 86% was achieved using a colloidal Rh/Sn (Rh/Sn = 1.5:1) catalyst on carbon.[15] Remarkably, the stabilizing surfactant was shown to modify the colloidal

metal surface and hence the catalytic properties.[215] Hanaoka et al.[219] have reported the selective photocatalytic transfer of hydrogen to 1,5-cyclooctadiene using a light transition metal modified rhodium colloid catalyst. Bulk industrial processes often rely on alloy-like bimetallic catalysts.[220−222] Here, nanostructured bimetallic colloid catalysts have provided a possibility of carrying out differential studies on the mutual influence of two different metals on the catalytic properties. The controlled co-reduction of two different metal ions has made bimetallic colloids readily accessible.[6,7,15,37−40,69,85,90−97,223] The structural characterization and some catalytic aspects of bimetallic colloids have recently been reviewed.[10] The successive reduction of different metal ions allows the homogeneous structure of bimetallic particles to be altered to one of colloidal particles having composition gradients from the core to the shell.[205,224−227] Truly layered particles consisting of, for example, a gold core plated by palladium or vice versa,[69] have also been synthesized. Bimetallic particles having a gradient metal distribution or a layered structure are most interesting for catalytic applications. In the catalytic hydrogenation of crotonic acid to give butanoic acid, a clear synergistic effect of Pt and Rh[6] was observed using bimetallic colloidal precursors ($Pt_{20}Rh_{80}$) having a gradient core/shell structure with an increase in the Rh content on going from the core to the surface of the particle (see Figure 17).[224] Toshima has discussed a similar effect in the partial hydrogenation of 1,3-cyclooctadiene with $Pt_{80}Pd_{20}$ and $Pd_{80}Au_{20}$ colloid catalysts.[10]

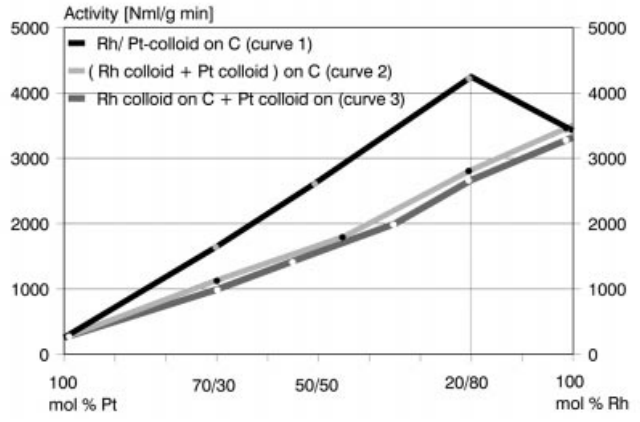

Figure 17. Activity plot of alloyed Rh/Pt/C and mixed Rh + Pt/C catalysts in the crotonic acid hydrogenation test (H_2 consumption) (adapted with permission from ref.[15])

The difference in the electronegativities of Pd and Au, together with the combination of the partially filled d band of Pd and the completely filled d band of Au, result in a novel electronic structure that may account for the catalytic behavior of gold/palladium alloys.[228−237] Fascinating prospects for the design of new catalysts have been opened up using bimetallic particles with layered structures. Schmid et al.[69] have applied the classical seed growth method[238] to synthesize layered bimetallic Au/Pd and Pd/Au colloids with sizes of 20−56 nm. The Au core is coated with Pd by the sequential reduction of gold and palladium salts with sodium citrate. The layered bimetallic colloid is stabilized by trisulfonated triphenylphosphane and sodium sulfanilate. More than 90% of the metal can be recovered in the solid state and redispersion in water is possible in high concentration. Au/Pd and Pd/Au systems on a TiO_2 support have been used in stabilized and non-stabilized forms as heterogeneous catalysts for the hydrogenation of hex-2-yne to (*Z*)-hex-2-ene. Both the palladium-plated gold seeds and the gold-plated palladium particles showed considerably increased activities compared with either pure metal. The lifetimes of the ligand-stabilized colloid catalysts are considerably enhanced by the protecting ligand shell. The influence of the electronegativity difference between Au and Pd on the activity and selectivity of the hydrosilylation reaction[239] on colloidal Pt surfaces[120,121] has been carefully investigated. In essence, the results demonstrate that the activity, selectivity, and lifetime of a metal colloid catalyst may be optimized by a defined variation of the core/shell composition in the bimetallic precursor.

Residues of the stabilizing agents that are still present on the surface of the colloidal metal precursors (1−5 wt-% metal loading on charcoal, glassy carbon, zeolites, TiO_2, Al_2O_3, $CaCO_3$, SiO_2, single-crystal oxides, or HOPG) may act as effective catalyst modifiers, controlling the selectivity and durability of the heterogeneous colloid catalysts (see Figure 13). Ligands such as phosphanes or phenanthrolines,[68] surfactants of various types[7,15] or organic "envelopes" such as polymers[199,240,241] have been found to control the regio- and enantioselectivity of heterogeneous metal colloid catalysts. In the case of the partial hydrogenation of hex-2-yne to (*Z*)-hex-2-ene, Schmid has found that even subtle changes in the chain length of the substituents of the alkyl-substituted phenanthrolines used as colloid stabilizers have a significant effect on the regioselectivity.[242] Seven- and eight-shell palladium clusters on TiO_2, protected by phenanthroline, catalyze the partial hydrogenation of hex-2-yne to (*Z*)-hex-2-ene with a selectivity of 93%. A similar selectivity was achieved using 3-(*n*-decyl)phenanthroline as the stabilizer. On substitution of the phenanthroline with *n*-butyl or *n*-heptyl groups, however, the activity drops dramatically and the subsequent isomerization or total hydrogenation of the (*Z*)-hex-2-ene is completely suppressed. Geometrical, i.e. steric, factors were proposed to explain the strong influence on the selectivity, and indeed this has been illustrated by further examples. A surfactant was found to control the selectivity in the (*Z*)-selective partial hydrogenation of 3-hexyn-1-ol giving leaf alcohol, which is a valuable fragrance [Equation (9)].[243]

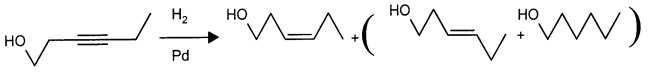

(9)

The performance in this reaction, Equation (9), of heterogeneous Pd colloid catalysts on $CaCO_3$,modified by a

number of surfactants, was compared with those of conventional Pd/C and Lindlar catalysts under optimized reaction conditions. The selectivity was found to be dependent on both the support and various promoters. The highest activity and best selectivity (98.1%) in formation of the desired (*Z*)-3-hexen-1-ol was found when a lead acetate promoted palladium colloid on $CaCO_3$, modified by the zwitterionic surfactant sulfobetaine-12 (*N*,*N*-dimethyldodecylammoniopropanesulfonate), was employed. Chemisorption measurements showed that residual amounts of the surfactant were still present on the surface of the immobilized particles. This colloid catalyst proved to be twice as active as a conventional Lindlar catalyst and gave 0.5% higher selectivity. Hydrophilic protecting shells allow improved contact between heterogenized metal colloid surfaces and substrates in aqueous media. For example, a hydrophilic ruthenium colloid catalyst on lanthanum oxide was shown to convert benzene into cyclohexene with 59% selectivity at 50% benzene conversion when suspended in an aqueous solution of sodium hydroxide.[244] Chiral molecules on the surface of the metal colloid can induce control of the enantioselectivity. In this context, a new type of enantioselective platinum sol catalyst, stabilized by the alkaloid dihydrocinchonidine, has been designed (see Figure 18).[177,245]

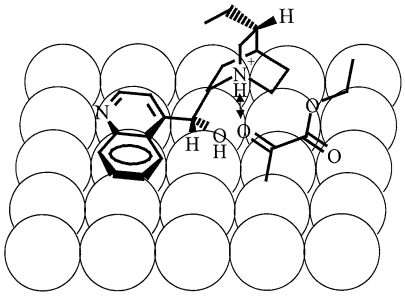

Figure 18. Enantioselective hydrogenation of ethyl pyruvate using dihydrocinchonidine-stabilized Pt colloids (adapted with permission from ref.[15])

The colloidal catalysts were prepared with different particle sizes by reducing platinum tetrachloride with formic acid in the presence of different amounts of the alkaloid. Optical yields of 75−80% *ee* were obtained in the hydrogenation of ethyl pyruvate with chirally modified Pt sols, Equation (10). These catalysts were shown to be structure-insensitive since turnover frequencies (ca. 1 s^{-1}) and enantiomeric excess proved to be independent of the particle size.

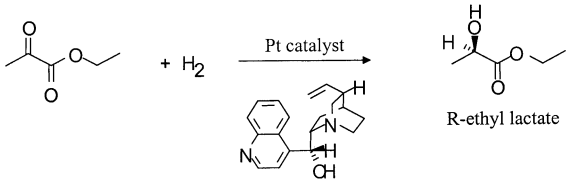

(10)

In order to evaluate the catalytic characteristics of colloidal platinum, the efficiency of Pt nanoparticles in the "quasi-homogeneous" reaction shown in Equation (10) was compared with those of supported colloids of the same charge and of a conventional heterogeneous platinum catalyst. The "quasi-homogeneous" colloidal system was found to surpass the conventional catalyst in turnover frequency by a factor of three.[245] Bradley et al.[246,247] and Liu[248,249] have studied the enantioselectivity of the reaction according to Equation (10) in the presence of polyvinylpyrrolidone as a stabilizer. In addition, Bradley[246] has observed that the presence of HCl in such Pt sols, modified by cinchona alkaloids, has a marked effect on the rate and reproducibility. The performance of the catalysts was improved in terms of both reproducibility and rate by the removal of HCl by dialysis. These "purified" colloidal catalysts can be used as reliable test systems in the screening of alternative chiral modifiers to cinchona alkaloids and for precise rate studies. In addition, a systematic variation of the reaction parameters relevant to the catalyst performance is possible without unwanted side effects. It has been shown that an excess of polyvinylpyrrolidone present on a colloidal Pt catalyst is irrelevant to the access of modifier molecules to the colloidal metal surface. However, the polymer may be adsorbed at the metal surface, thereby reducing the number of modified surface sites available for the enantioselective hydrogenation.[247] The stereoselective and enantioselective transformation of specific prochiral substrates into valuable fine chemicals can be achieved through the use of nanostructured metal colloids. The application of rational ligand control based on molecular modeling, which has been successful in homogeneous metal complex catalysis, promises similar results in heterogeneous metal colloid catalysis.

Superior lifetimes can also be expected since it is reasonable to assume, on the basis of the chemisorption results, that the "coating" on catalytically active nanometal particles, which is permeable to small molecules such as H_2 or O_2, effectively prevents contact of the metal surface with poisons. In fact, the lifetimes of the colloid catalysts are considerably longer than those of conventional precipitation catalysts. For example, the activity of a conventional Pd/C catalyst expires completely in the hydrogenation of cyclooctene to cyclooctane after 38,000 catalytic cycles per Pd atom, but the Pd colloid/C catalyst still shows a residual activity after 96,000 catalytic turnovers (Figure 19).[250]

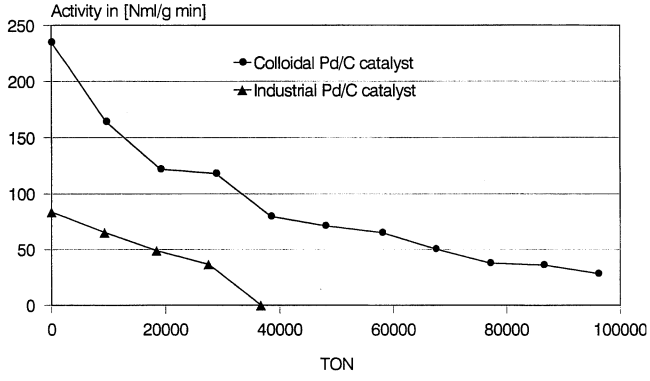

Figure 19. Durability of colloidal Pd/C catalysts in the cyclooctene hydrogenation test compared with a conventional Pd/C system (adapted with permission from ref.[15])

When surfactant-stabilized Pd/Pt precursors were supported on charcoal and promoted by bismuth, superior catalytic oxidation catalysts were obtained.[251] Compared

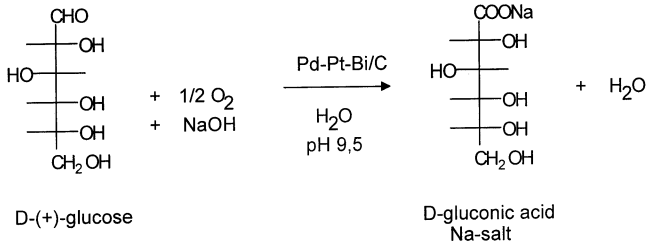

(11)

to industrial heterogeneous Pd/Pt catalysts, charcoal-supported $Pd_{88}/Pt_{12}-(oct)_4NCl$ alloy particles (1.5 to 3 nm) were found to offer an excellent activity combined with high selectivity in the oxidation of glucose to gluconic acid by molecular oxygen, see Equation (11).[251] An increased durability of the colloidal Pd/C catalysts was also observed in this case. Much greater retention of the catalytic activity was found for such a system as compared to a conventionally manufactured Pd/C catalyst after recycling both catalysts 25 times under similar conditions. Obviously, the lipophilic $(oct)_4NCl$ surfactant layer prevents the colloid particles from coagulating and being poisoned in the alkaline aqueous reaction medium. Shape-selective hydrocarbon oxidation catalysts have been described, where active Pt colloid particles are present exclusively in the pores of ultramicroscopic tungsten heteropoly compounds.[252] Phosphane-free Suzuki and Heck reactions involving iodo, bromo, or activated chloro substituents were performed using catalytic amounts of ammonium salt or poly(vinylpyrrolidone)-stabilized palladium or palladium nickel colloids [Equation (12)].[145,252]

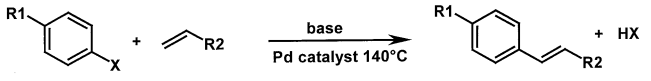

(12)

The Pd-colloid-catalyzed Heck arylation of styrene with chlorobenzene gave (*E*)-stilbene as the exclusive product. This type of C−C linkage is valuable for the production of pharmaceutical intermediates and fine chemicals. Turnover frequencies (TOF) of more than 80,000 have been achieved in the coupling of *p*-bromobenzaldehyde with butyl acrylate using poly(vinylpyrrolidone)-stabilized palladium as the catalyst.[253] Reetz has applied colloidal, water-soluble PtO_2 (i.e. a colloidal "Adams catalyst") in the immobilized form for the reductive amination of benzaldehyde by *n*-propylamine [Equation (13)].[160,161]

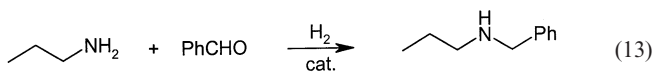

(13)

The selectivity in favor of the desired monobenzylated product was found to be > 99% and the immobilized PtO_2 was found to be four to five times more active than the commercial Adams catalysts. The PtO_2 colloid proved to be effective in the hydrogenation of carbonyl compounds and of olefins, both in solution and in immobilized form. The heterogeneous catalytic amination of aryl bromides by immobilized Pd^0 particles has recently been reported.[252] Secondary amines such as piperidine and diethylamine were used in the amination of aryl bromides. The reactions proceeded with good turnover numbers and regiocontrol. The catalysts could be reused repeatedly without loss of activity or selectivity following filtration from the reaction mixture.

A new class of heterogeneous catalyst has emerged from the incorporation of mono- and bimetallic nanocolloids in the mesopores of MCM-41 or the entrapment of pre-prepared colloidal metals in sol-gel materials.[254−256] Pre-prepared Pd colloids stabilized by phenanthroline obtained by the Schmid method[57−72] have successfully been embedded in MCM-41 mesopores (some colloid is deposited on the external surface) to give CO-oxidation catalysts.[254]

Reetz has developed a strategy for the entrapment of monodisperse nanometal colloids, e.g. R_4NX-stabilized Pd particles.[255] The nanosized particles (2−3.5 nm) are pre-prepared by electrochemical synthesis.[85,90−97] The entrapment in hydrophobic sol-gel materials occurs through the fluoride-catalyzed hydrolysis of mixtures of $CH_3Si(OCH_3)$ and $Mg(OC_2H_5)_2$. Finally, the stabilizer is extracted and the "naked" nanometallic particles are left trapped in the pores (see Figure 20).

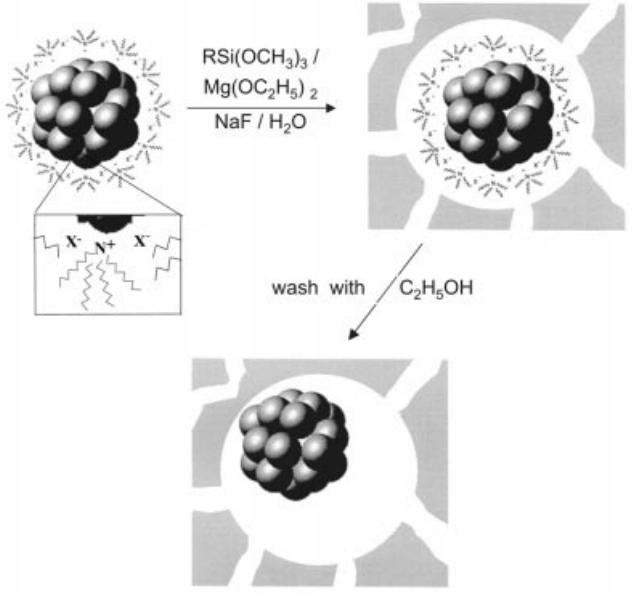

Figure 20. Incorporation of preformed metal colloids in sol−gel materials (adapted with permission from ref.[255])

Ultramicrotomic techniques in combination with shadow-casting TEM have confirmed that the Pd particles are embedded in the oxide matrix and are not fixed on the outer surface. Reetz et al.[255] have also investigated the catalytic properties of the new material. They were able to

control the hydrophobicity of the matrix by adjusting the relative amounts of the $CH_3Si(OCH_3)_3$ and $Mg(OC_2H_5)_2$ in the gel. The catalytic activity and selectivity was tested in the partial hydrogenation of COD to give cyclooctene: It was found that the activities of the new systems are governed by the specific pore volume and the hydrophobic properties of the wall. The selectivity for cyclooctene was 93% and the most active of these sol−gel-entrapped Pd catalysts exhibited a considerably higher activity than those of commercially available Pd/Al_2O_3 samples. The preparation of a fully alloyed Pd/Au colloid of 3.0 nm particle size by a modified sol−gel procedure using THF as the solvent and involving the co-reduction of Pd and Au salts with tetraalkylammonium triethylhydroborate,[6] and its subsequent embedding in silica, has been described.[256] The integrity of the incorporated Pd/Au alloy particles remained virtually unaffected. A mesoporous texture with a comparatively narrow pore distribution remained after the removal of the protecting surfactant. According to the physical characterization by a combination of techniques, the SiO_2-embedded Pd/Au colloid retains the size and structural characteristics of the colloidal metal precursor. The material exhibits excellent catalytic properties in selective hydrogenation test reactions. These few examples show that colloidal bimetallic precursors − embedded in matrices or deposited on various supports, and promoted by additives if necessary − may become of practical importance in heterogeneous catalysis.

Fuel Cell Catalysts

"Fuel cell technology" attracts a great deal of interest because it allows the direct conversion of chemical energy into electricity.[257] The catalyst systems are an integral part of the electrochemical reactor utilized in fuel cells. Among the wide-ranging applications of fuel cells are low-emission transport systems, stationary power stations, and combined heat and power sources. Classical studies were carried out in the early 1900s and major innovations and improvements have been achieved over the last few years. The first "new electric cars" are expected to be on the market around 2005, but further developments are still needed, most notably in the area of catalysts. Hydrogen fuel cell catalysts rely on pure Pt, whereas Pt alloy electrocatalysts are employed for the conversion of reformer gas or methanol into electricity. The active component in the latter cases are small Pt-containing bi- or trimetallic particles, 1−3 nm in size, which scatter X-rays as nearly perfect "single crystals". These systems offer improved efficiency and tolerance towards certain contaminants, especially CO, in the anode feed.[258−263] It was clear from patents filed in the early 1970s that finely particulate colloidal platinum sols should be the ideal precursors for the manufacture of fuel cell electrodes.[258]

This section of our microreview focuses on recent developments in catalysts for phosphoric acid fuel cells (PAFCs), proton-exchange membrane fuel cells (PEMFCs), and the aforementioned direct methanol fuel cell (DMFC). The six main types of fuel cell are described in recent reviews.[264−268] PAFCs operating at 160−220 °C use orthophosphoric acid as the electrolyte; the anode catalyst is Pt and the cathode can be, e.g., Pt/Cr/Co.[264−268] For this application, a trimetallic colloidal precursor of the composition $Pt_{50}Co_{30}Cr_{20}$ (size 3.8 nm) was prepared by the co-reduction of the appropriate metal salts.[269−271] The trimetallic particles are alloyed in an ordered *fcc* structure according to XRD analysis. The electrocatalytic performance in a standard half-cell was compared with that of an industrial standard catalyst (trimetallic crystallites of size 5.7 nm) manufactured by co-precipitation and subsequent annealing at 900 °C. The advantage of the trimetallic colloid catalyst lies in its improved durability, which is essential for PAFC applications. After 22 h, it was found that the potential had decayed by less than 10 mV.[272]

PEM fuel cells use a solid proton-conducting polymer as the electrolyte at 50−125 °C. The cathode catalyst is based on Pt alone, but because of the required tolerance to CO a combination of Pt and Ru is preferred for the anode.[258−263] Colloidal Pt/Ru catalysts are currently under widespread investigation for low-temperature (80 °C) polymer membrane fuel cells (PEMFCs).[350,351] They have also been proposed for the use in direct methanol fuel cells (DMFCs) or in PEMFCs, which are fed with CO-contaminated hydrogen produced in on-board methanol reformers. The ultimate dispersion state of the metals is essential for CO-tolerant PEMFCs, and truly alloyed Pt/Ru colloid particles less than 2 nm in size seem to fulfill these requirements.[17,18,20,258,260,273−276] Alternatively, bimetallic Pt/Ru PEM catalysts have been developed for the same purpose, where non-alloyed Pt nanoparticles of < 2 nm and Ru particles of < 1 nm are dispersed on a carbon support.[260] From the results obtained, it can be concluded that a Pt/Ru interface is essential for the CO tolerance of the catalyst, irrespective of whether the precious metals are alloyed. For the manufacture of DMFC catalysts, however, Pt/Ru nano*powders* of size 3−5 nm or thin films are used as the precursors.[261−263] For the electrocatalytic oxidation of methanol, a Pt or a Pt metal alloy catalyst has been developed, where a (phthalocyanine)Ru complex is added as a dopant to significantly enhance the catalytic effect.[271] For comparison, the electrocatalytic activity in the oxidation of CO and a CO/H_2 gas mixture (simulated reformer gas)[17] was compared with that of a bimetallic $Pt_{50}/Ru_{50}-(oct)_4NCl$ colloid prepared by the salt co-reduction method.[6][87−89] The mean particle diameter was 1.7 nm according to high-resolution transmission electron microscopy (HRTEM) [see Figure 21, a)]. The alloyed state of the particles was verified by point-resolved energy dispersive X-ray (EDX) analysis [Figure 21, b)].

Glassy carbon supported $Pt_{50}/Ru_{50}-(oct)_4NCl$ colloids were examined by CO-stripping voltammetry and the data were found to be essentially identical to those found in well-characterized bulk-alloy electrodes. The activity of the colloid in the continuous oxidation of 2% CO in H_2 at a rotating disk electrode was determined at 25 °C in 0.5 M H_2SO_4. The results led to the conclusion that these Pt/Ru colloids

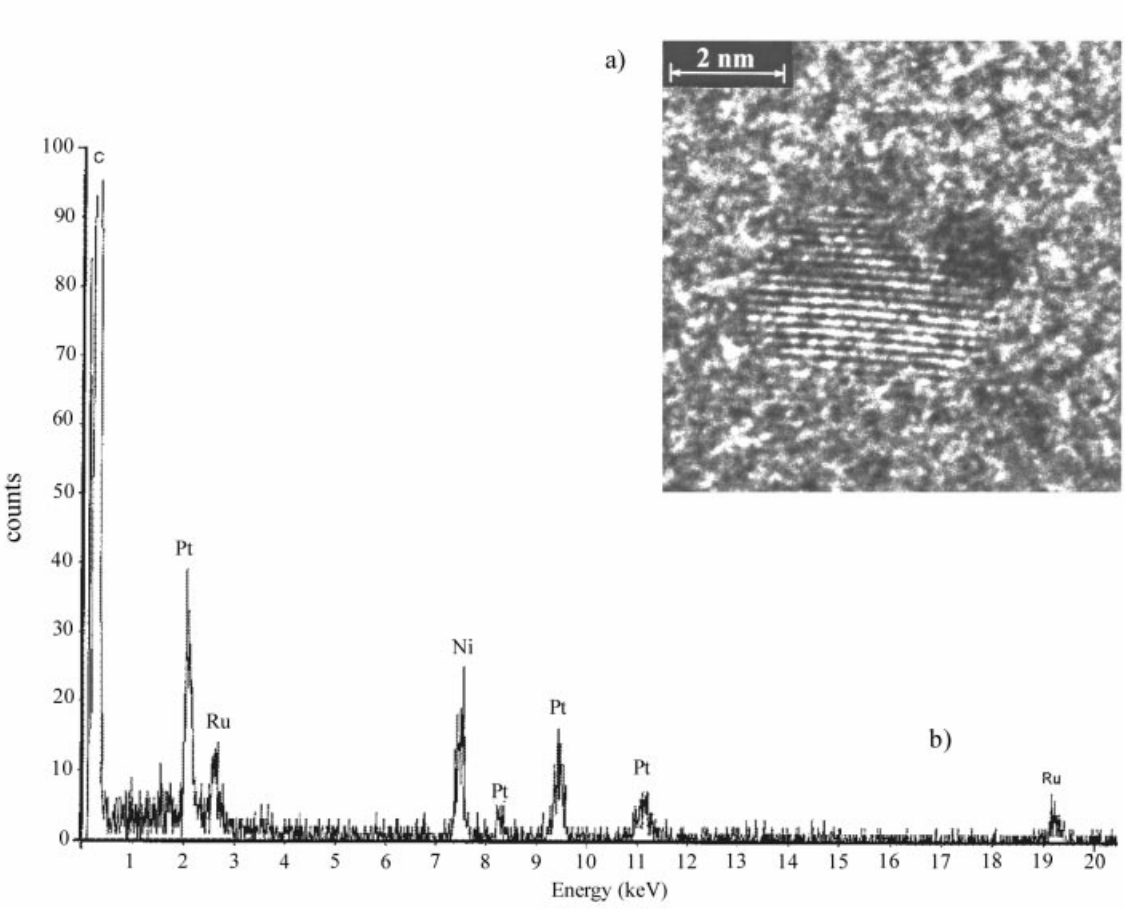

Figure 21. a) High-resolution TEM image of a single $Pt_{50}Ru_{50}$ particle (1.7 nm) (adapted from ref.[17]); b) EDX point analysis (focus 10 nm) of discrete $Pt_{50}Ru_{50}$ particles (adapted with permission from ref.[17])

are very suitable precursors for high-surface-area fuel cell catalysts.[20] XANES data were supportive of the bimetallic character of the particles. In addition, in situ XRD (by Debye function analysis) has revealed the catalytic function of the alloyed Ru in the CO oxidation: Oxide species are formed on the Ru surface at 280 °C, which slowly coalesce to form RuO_2 particles. After re-reduction, the catalyst shows a pure *hcp* ruthenium phase and larger platinum-enriched alloy particles.[277] Scanning probe microscopy (SPM) has been applied in order to characterize the real-space morphology of the electrode surfaces of supported nanostructured metal colloids on the nanometer scale.[278] Colloidal Pt_{50}/Ru_{50} precursors (< 2 nm) raise the tolerance to CO, allowing higher CO concentrations in the H_2 feed of a PEMFC without a significant drop in performance.[18−20] A selective Pt/Mo oxidation catalyst for the oxidation of H_2 in the presence of CO in fuel cells comprises Pt_xMo_y particles, where $x = 0.5-0.9$ and $y = 0.5-0.1$.[279] The colloid method was found to offer a highly suitable exploratory approach to finding improved formulations for binary and ternary anode electrocatalysts. The metals used include Pt, Ru, W, Mo, and Sn.[19] The combinatorial screening method has been successfully applied to electrocatalysts,[280] and it is an obvious step to include colloids in these experiments. As an alternative to the reductive metal colloid synthesis, the so-called "metal oxide concept" was developed, which allows the fabrication of binary and ternary colloidal metal oxides as electrocatalyst precursors [Equation (14)].[160−162]

$$PtCl_4 + RuCl_3 \xrightarrow[\text{stabilizer}]{H_2O/\text{base}} PtRuO_x \text{ colloid} \quad (14)$$

Colloidal Pt/RuO_x (1.5±0.4 nm) stabilized by a surfactant was prepared by co-hydrolysis of $PtCl_4$ and $RuCl_3$ under basic conditions. By variation of the stoichiometry of the transition metal salts, the Pt/Ru ratio in the colloids could be varied between 1:4 and 4:1. The corresponding zerovalent metal colloids were obtained by the subsequent application of H_2 to the colloidal Pt/Ru oxides (optionally in the immobilized form). Additional metals have been included in the "metal oxide concept" [Equation (14)], so as to prepare binary and ternary mixed metal oxides in colloidal form. $Pt/Ru/WO_x$ is regarded as a good pre-catalyst, especially for application in DMFCs. Main group elements such as Al have been included in multimetallic alloy systems in order to improve the durability of fuel cell catalysts. Alloys of $Pt_3AlC_{0.5}$ with Cr, Mo, or W particles of size 4−7 nm have been prepared by sequential precipitation on conducting carbon supports such as highly disperse Vulcan

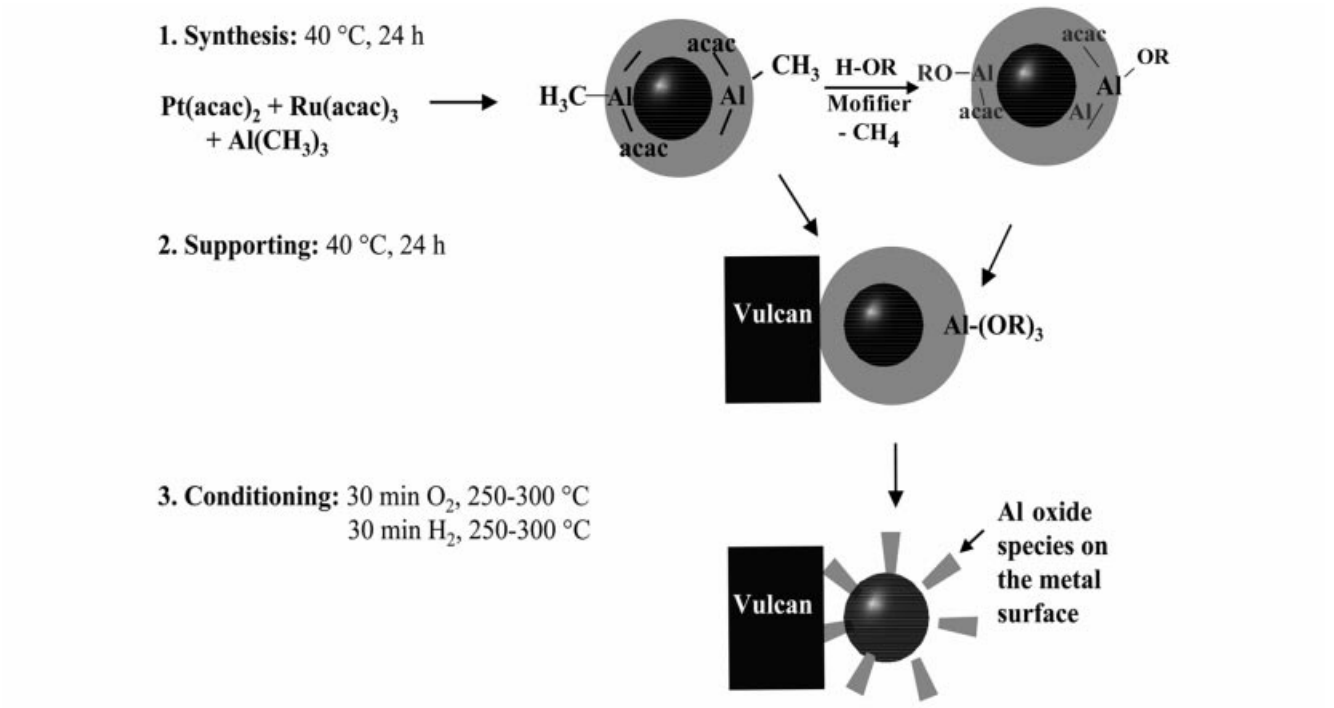

Figure 22. Scheme of the preparation of colloidal Pt/Ru/Al PEMFC anode catalysts (> 20% metal on Vulcan XC72®) by the "precursor concept"(adapted with permission from ref.[273])

XC72®.[281] Alternatively, colloidal precursors composed of Pt/Ru/Al allow the manufacture of multimetallic fuel cell catalysts (1−2 nm) having a metal loading of > 20%. The three-step catalyst preparation is summarized in Figure 22.

The colloidal Pt/Ru/Al precursor is pre-prepared by the organoaluminum route. In the absence of stabilizers, the co-reduction of organic Pt and Ru salts using $Al(CH_3)_3$ gives halogen-free, multimetallic Pt colloids, e.g. $Pt_{50}Ru_{50}$/Al (size 1.2±0.3 nm). By adjusting the stoichiometric ratio of the metal salts, the ratio of Pt to the second metal in the colloid can be adjusted. The addition of alcohols or suitable surfactants allows the dispersivity of the colloidal precursor in organic media or water to be tailored without affecting the particle size. In the second step, the Pt/Ru/Al colloid is adsorbed on high-surface-area carbon by treatment at 40 °C for 24 h. In the third step (conditioning), the dried Pt/Ru/Al Vulcan catalyst powders are exposed to O_2 and H_2 for 30 min each at 250−300 °C to completely remove the surfactants. The particle size of the Pt/Ru/Al colloid adsorbed on the support was found to be virtually unaffected by the treatment (1.3±0.4 nm) and after the thermal treatment only a moderate growth was evident (1.5±0.4 nm). The aluminum was found to be present on the Pt/Ru surface in an oxidized form. This accounts for the size-stabilization observed in the Pt/Ru particles and for the improved durability of the resulting electrocatalysts. Recently, a fuel cell for generating electric power from a liquid organic fuel ("synfuel") was described. It comprises a solid electrolyte membrane directly supporting the anode and cathode layers,

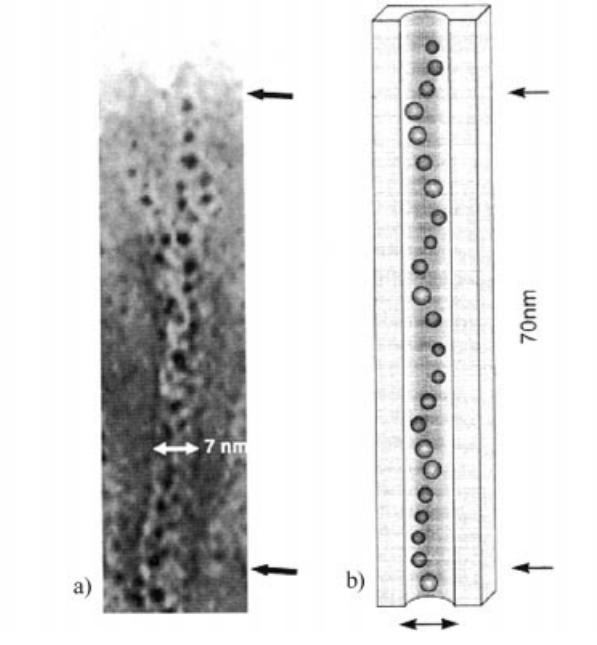

Figure 23. a) TEM image of a one-dimensional Au_{55} cluster wire in a nanoporous alumina membrane; b) schematic representation of the helical wire in a 7 nm pore (adapted with permission from ref.[277])

which contain 7−10% Pt and Ru, 70−80% perfluorovinylether sulfonic acid, and 15−20% polytetrafluoroethylene.[276] In conclusion, nanostructured metal colloids are

very promising precursors for manufacturing multimetallic fuel cell catalysts that are truly nanosized (i.e. < 2 nm) and have high metal loadings (20 wt-% of metal).

Potential Applications in Materials Science

It is expected that metal nanoparticles and their assemblies will find numerous applications in materials science. It has been demonstrated that physical properties, including magnetic, optical, melting points, specific heats, and surface reactivity are size-dependent. Quantum size effects are related to the "dimensionality" of a system in the nanometer range. "Zero-dimensional" metal particles might still comprise hundreds of atoms. One-dimensional nanoparticle arrangements (cluster wires) are of potential practical interest as semiconducting nanopaths for applications in nanoelectronics. 1D particle arrangements may be induced through the use of host templates. Using vacuum or electrophoretic methods, Schmid et al.[318−320] were able to fill the parallel channels of nanoporous alumina membranes with chains/rows of 1.4 nm gold particles giving one-dimensional "quantum wires" consisting of insulated 20−100 Au_{55} clusters in a helical array (see Figure 23). The diameter of the nanowire could be controlled by varying the pore size.

Interestingly, 1.4 nm Au particles were found to arrange themselves into a linear row when attached to single-stranded DNA oligonucleotides.[321] Driven by the technological significance associated with such architectures, the fabrication of ordered two-dimensional nanoparticle arrays has been successfully achieved by several research groups, whose work has recently been reviewed.[281][282] Planar arrays of uniform metal nanoparticles would allow the design of new "supercomputers" having a superior data storage capacity. Langmuir−Blodgett films of nanometal systems have frequently been studied in this context. Starting with nanoparticles of defined nuclearity, 2D lattices of thiolized Au_{55}, Pd_{561}, and Pd_{1415} have been prepared.[322] Recently, the first successful preparation of 2D hexagonal and cubic lattices of Au_{55} nanoparticles by self-assembly on polymer films was reported.[163] Simply dipping polyethylenimine-modified surfaces into aqueous solutions of acid-functionalized Au_{55} cluster generates the Au_{55} monolayers shown in Figure 24.

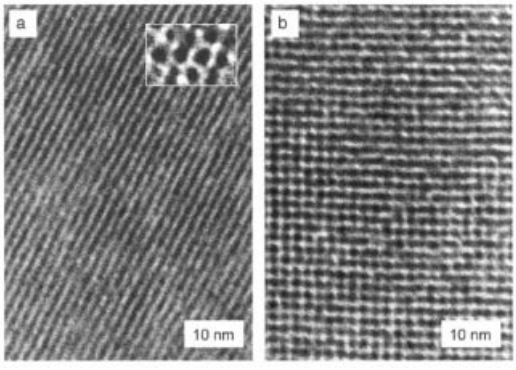

Figure 24. Au_{55} monolayers showing a hexagonal (a) and a cubic (b) structure; the insert in (a) shows single clusters in the hexagonal form (adapted with permission from ref.[163])

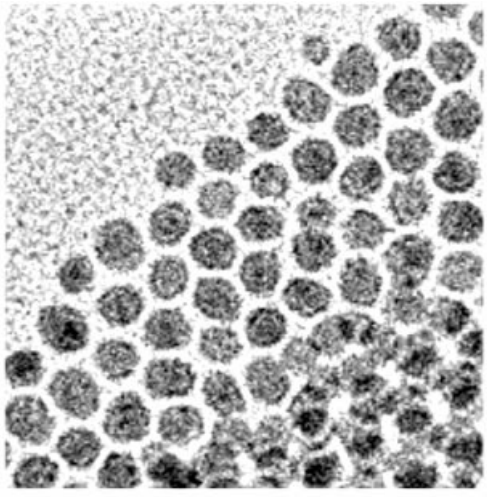

Figure 25. Pd colloid hexagonal close-packed arrangement in the first monolayer (adapted with permission from the Royal Chemical Society from ref.[291])

The interactions between the nanoparticles and the surface are obviously strong enough to prevent mechanical removal. Whereas the hexagonal form shown in Figure 24 (a) is normal for an ordered monolayer, the cubic orientation seen in Figure 24 (b) is unprecedented. Most of the work published on organized nanometal structures has been focused on gold particles and sulfur-containing groups in the various ligands.[283−288] Schiffrin et al. have achieved the self-organization of nanosized gold particles using $R_4N^+X^-$ surfactants.[289] Ramos et al. have recently reported the surfactant-mediated two-dimensional crystallization of colloidal crystals.[290] Making use of the attractive Coulomb interactions between colloids and surfactant structures offers a potential new route to the self-assembly of ordered colloidal structures. Nanostructured palladium clusters stabilized by a monomolecular coating of tetraalkylammonium halide surfactants self-assemble on carbon surfaces in an ordered manner with the formation of *hcp* structures (Figure 25).[291]

The self-organization of magnetic nanosized cobalt particles was studied by Pileni's group.[296,297] A comparison of the magnetic properties of deposited cobalt nanoparticles with those of particles dispersed in a solvent indicated a collective flip of the magnetizations of adjacent particles when they were self-assembled. Pileni et al. have recently published a number of papers concerning the self-assembly of nanoparticles and have developed a number of methods for the manipulation of these systems.[337−339] Mulvaney et al. have described two- and three-dimensional assemblies of metal core/silica shell nanoparticles in a recent review article.[298] A feature article by Balazcs[299] outlines how solid additives can be used to tailor the morphology of bin-

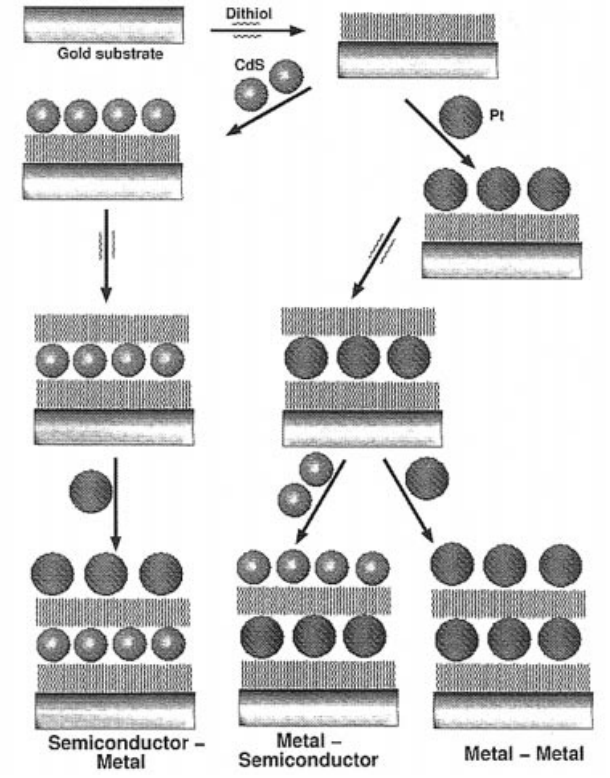

Figure 26. Three-dimensional superlattices obtained by layer-by-layer deposition of Pt particles (or CdS as a semiconductor) onto a dithiol-coated Au substrate (adapted from ref.[165])

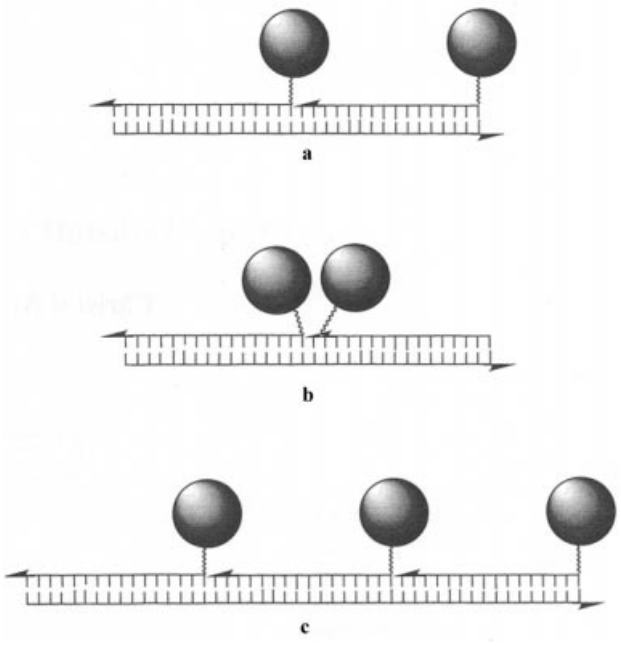

Figure 28. Self-organization of conjugates from gold particles (shaded spheres) and oligonucleotide codons to supramolecular assemblies by the addition of a template strand; derivatization of the oligonucleotides in the 3′- or 5′-position allows control over the mode of head-to-head (a) or head-to-tail (b) homodimers; the trimer (c) is formed using the complementary sequence in triplicate (adapted with permission from ref.[314])

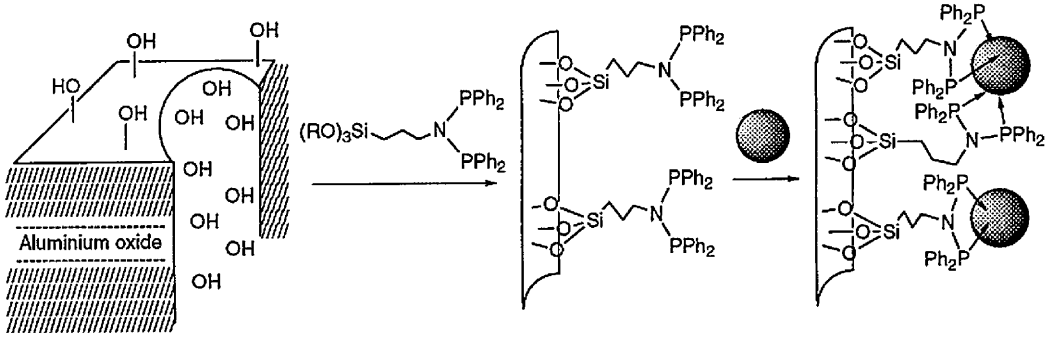

Figure 27. Functionalization of nanoporous alumina membranes and immobilization of metal colloids or clusters on the pore walls (adapted with permission from ref.[349])

ary mixtures containing nanoscopic particles and thereby control the macroscopic properties (e.g., the mechanical integrity) of composites. In addition, computer-aided design has been employed to establish how self-assembled nanostructures can be induced to form arbitrary functional arrays on surfaces.[300] Bifunctional spacer molecules such as diamines have been used in attempts to link nanoparticles three-dimensionally.[301] The multilayer deposition of particle arrays on gold has been successfully achieved by the sequential adsorption of dithiol and near-monodisperse nanometal or CdS particles (see Figure 26).

Several monometal, bimetal, and metal-semiconductor superlattices have been prepared by dipping a gold substrate into the appropriate solutions, with intermediate steps involving washing and drying.[302] The stepwise three-dimensional assembly of layered gold nanoparticles in porous silica matrices has also been reported.[303] Schmid has recently reported strategies for the anchoring of metal complexes, clusters, and colloids within nanoporous alumina (Figure 27).[349]

A different field of technological interest stems from the high spin density of nanostructured magnetic metals of the Fe, Co, Ni series.[304,305] THF-stabilized Mn^0 particles exhibiting superparamagnetism below 20 K were described as the first example of an antiferromagnetic metal colloid.[306]

New strategies utilizing DNA as a construction material for the generation of biometallic nanostructures have made it possible to develop larger "nanotechnology devices" (< 100 nm) for microelectronic photolithographic applications. DNA is regarded as a promising construction material for the selective positioning of molecular devices because of its recognition capabilities, physicochemical stability, and mechanical rigidity. Seeman was the first to propose DNA for the precise spatial arrangement of 3D networks.[307,308] Assemblies of DNA-derivatized gold colloids have recently been prepared by the DNA hybridization-based self-organization pathway and the resulting defined arrangements of nanometal particles have found applications in electronic, optical, and laser technologies.[309−313,340−345] For example, Alivisatos et al.[310] have obtained defined mono adducts from commercially available 1.4 nm gold clusters where one reactive maleimido group was attached to every particle. These were coupled with thiolated 18-mer oligonucleotides in order to add an individual "codon" sequence. When a single-stranded DNA template containing complementary codons was added, the self-assembly of nanocrystal molecules was observed (Figure 28).[310,314] This work has been the subject of recent reviews.[314−316]

Niemeyer[315] has recently reported the coupling of metal particles bearing a biotin substituent with the DNA−streptavidin hybrid. The growth of a 12 μm long, 100 nm wide conductive silver wire was achieved using a DNA molecule stretched between two gold electrodes as a template.[317] It remains to be seen how the practical applications of these materials will develop over the next few years.

[1] J. Turkevich, P. C. Stevenson, J. Hillier, *Disc. Faraday Soc.* **1951**, *11*, 55−75.
[2] J. Turkevich, G. Kim, *Science* **1970**, *169*, 873.
[3] J. Turkevich, *Gold Bull.* **1985**, *18*, 86−91.
[4] G. Schmid, in: *Aspects of Homogeneous Catalysis*, vol. 7 (Ed.: R. Ugo), Kluwer, Dordrecht, **1990**, p. 1−33.
[5] G. Schmid (Ed.), *Clusters and Colloids*, VCH, Weinheim, **1994**.
[6] H. Bönnemann, W. Brijoux, R. Brinkmann, R. Fretzen, Th. Joussen, R. Köppler, P. Neiteler, J. Richter, *J. Mol. Catal.* **1994**, *86*, 129−177.
[7] H. Bönnemann, G. Braun, W. Brijoux, R. Brinkmann, A. Schulze Tilling, K. Seevogel, K. Siepen, *J. Organomet. Chem.* **1996**, *520*, 143−162.
[8] M. T. Reetz, W. Helbig, S. A. Quaiser, in: *Active Metals* (Ed.: A. Fürstner), VCH, Weinheim, **1996**, p. 279−297.
[9] H. Bönnemann, W. Brijoux, in: *Active Metals* (Ed.: A. Fürstner), VCH, Weinheim, **1996**, p. 339−379.
[10] N. Toshima, T. Yonezawa, *New J. Chem.* **1998**, 1179−1201.
[11] J. D. Aiken III, R. G. Finke, *J. Mol. Catal. A* **1999**, *145*, 1−44.
[12] B. F. G. Johnson, *Coord. Chem. Rev.* **1999**, *190−192*, 1269−1285.
[13] G. Schmid, in: *Applied Homogeneous Catalysis with Organometallic Compounds*, vol. 2 (Eds.: B. Cornils, W. A. Herrmann), Wiley-VCH, Weinheim, **1996**, p. 636−644.
[14] W. A. Herrmann, B. Cornils, in: *Applied Homogeneous Catalysis with Organometallic Compounds*, vol. 2 (Eds.: B. Cornils, W. A. Herrmann), Wiley-VCH, Weinheim, **1996**, p. 1171−1172.
[15] H. Bönnemann, W. Brijoux, in: *Advanced Catalysts and Nanostructured Materials*, chapter 7 (Ed.: W. Moser), Academic Press, San Diego, **1996**, p. 165−196.
[16] H. Bönnemann, W. Brijoux, in: *Metal Clusters in Chemistry*, vol. 2 (Eds.: P. Braunstein, L. A. Oro, P. R. Raithby), Wiley-VCH, Weinheim, **1999**, p. 913−931.
[17] T. J. Schmidt, M. Noeske, H. A. Gasteiger, R. J. Behm, P. Britz, W. Brijoux, H. Bönnemann, *Langmuir* **1997**, *13*, 2591−2595.
[18] E. Auer, W. Behl, T. Lehmann, U. Stenke (to Degussa AG), EP 09 24 784 A1 (June 23, **1999**).
[19] M. Götz, H. Wendt, *Electrochim. Acta* **1998**, *43*, 3637−3644.
[20] T. J. Schmidt, M. Noeske, H. A. Gasteiger, R. J. Behm, P. Britz, H. Bönnemann, *J. Electrochem. Soc.* **1998**, *145*, 925−931.
[21] E. Gaffet, M. Tachikart, O. El Kedim, R. Rahouadj, *Mater. Charact.* **1996**, *36*, 185−190.
[22] A. Amulyavichus, A. Daugvila, R. Davidonis, C. Sipavichus, *Fiz. Met. Metalloved.* **1998**, *85*, 111−117.
[23] A. Schalnikoff, R. Roginsky, *Kolloid Z.* **1927**, *43*, 67−70.
[24] J. R. Blackborrow, D. Young, *Metal Vapor Synthesis*, Springer Verlag, New York, **1979**.
[25] K. J. Klabunde, *Free Atoms and Particles*, Academic Press, New York, **1980**.
[26] K. J. Klabunde, Y.-X. Li, B.-J. Tan, *Chem. Mater.* **1991**, *3*, 30−39.
[27] J. S. Bradley, in: *Clusters and Colloids* (Ed.: G. Schmid), VCH, Weinheim, **1994**, p. 477f.
[28] K. J. Klabunde, G. C. Cardenas-Trivino, in: *Active Metals* (Ed.: A. Fürstner), VCH, Weinheim, **1996**, p. 237−278.
[29] M. Faraday, *Philos. Trans. R. Soc. London* **1857**, *147*, 145−153.
[30] J. S. Bradley, in: *Clusters and Colloids* (Ed.: G. Schmid), VCH, Weinheim, **1994**, p. 469−473.
[31] T. Leisner, C. Rosche, S. Wolf, F. Granzer, L. Wöste, *Surf. Rev. Lett.* **1996**, *3*, 1105−1108.
[32] R. Tausch-Treml, A. Henglein, J. Lilie, *Ber. Bunsenges. Phys. Chem.* **1978**, *82*, 1335−1343.
[33] M. Michaelis, A. Henglein, *J. Phys. Chem.* **1992**, *96*, 4719−4724.
[34] M. A. Watzky, R. G. Finke, *J. Am. Chem. Soc.* **1997**, *119*, 10382−10400.
[35] J. Rothe, J. Hormes, H. Bönnemann, W. Brijoux, K. Siepen, *J. Am. Chem. Soc.* **1998**, *120*, 6019−6023.
[36] A. I. Kirkland, P. P. Edwards, D. A. Jefferson, D. G. Duff, *Annu. Rep. Prog. Chem., Sect. C: Phys. Chem.* **1990**, *87*, 247−305.
[37] H. Hirai, Y. Nakao, N. Toshima, K. Adachi, *Chem. Lett.* **1976**, 905.
[38] H. Hirai, Y. Nakao, N. Toshima, *Chem. Lett.* **1978**, 545.
[39] H. Hirai, Y. Nakao, N. Toshima, *J. Macromol. Sci. Chem.* **1978**, *A12*, 1117.
[40] H. Hirai, Y. Nakao, N. Toshima, *J. Macromol. Sci. Chem.* **1979**, *A13*, 727.
[41] J. Tanori, M. P. Pileni, *Langmuir* **1997**, *13*, 639−646.
[42] M. P. Pileni, *Langmuir* **1997**, *13*, 3266−3276.
[43] M. Antonietti, C. Göltner, *Angew. Chem. Int. Ed. Engl.* **1997**, *36*, 910−928.
[44] M. P. Pileni, *Supramol. Sci.* **1998**, *5*, 321−329.
[45] M. P. Pileni, *Adv. Mater.* **1998**, *10*, 259−261.
[46] M. Antonietti, *Chem.-Ing. Tech.* **1996**, *68*, 518−523.
[47] S. Förster, *Ber. Bunsenges. Phys. Chem.* **1997**, *101*, 1671−1678.
[48] J. J. Storhoff, R. C. Mucic, C. A. Mirkin, *J. Cluster Sci.* **1997**, *8*, 179−216.
[49] M. Möller, J. P. Spatz, *Curr. Opin. Colloid Interface Sci.* **1997**, *2*, 177−187.
[50] G. B. Sergeev, M. A. Petrukhina, *Prog. Solid State Chem.* **1996**, *24*, 183−211.
[51] J. P. Wilcoxon, P. Provencio, *J. Phys. Chem. B* **1999**, *103*, 9809−9812.
[52] T. Miyao, N. Toyoizumi, S. Okuda, Y. Imai, K. Tyjima, S. Naito, *Chem. Lett.* **1999**, 1125.
[53] S. T. Selvan, M. Nogami, A. Nakamura, Y. Hamanaka, *J. Non-Cryst. Solids* **1999**, *255*, 254−258.

[54] M. M. Maye, W. Theng, F. L. Leibowitz, N. K. Ly, C. J. Zhong, *Langmuir* **2000**, *16*, 490−497.
[55] Y. Niidome, A. Hori, T. Sato, S. Yamada, *Chem. Lett.* **2000**, 310.
[56] I. Konomi, S. Hyodo, T. Motohiro, *J. Catal.* **2000**, *192*, 11−17.
[57] G. Schmid, R. Pfeil, R. Boese, F. Bandermann, S. Meyer, G. H. M. Calis, J. A. W. van der Velden, *Chem. Ber.* **1981**, *114*, 3634−3642.
[58] G. Schmid, *Polyhedron* **1988**, *7*, 2321−2329.
[59] L. J. de Jongh, J. A. O. de Aguiar, H. B. Brom, G. Longoni, J. M. van Ruitenbeek, G. Schmid, H. H. A. Smit, M. P. J. van Staveren. R. C. Thiel, *Z. Phys. D: At. Mol. Clusters* **1989**, *12*, 445−450.
[60] G. Schmid, B. Morum, J. Malm, *Angew. Chem. Int. Ed. Engl.* **1989**, *28*, 778−780.
[61] G. Schmid, N. Klein, L. Korste, *Polyhedron* **1998**, *7*, 605−608.
[62] T. Tominaga, S. Tenma, H. Watanabe, U. Giebel, G. Schmid, *Chem. Lett.* **1996**, 1033.
[63] G. Schmid, *Chem. Rev.* **1992**, *92*, 1709−1727.
[64] H. A. Wicrenga, L. Soethout, I. W. Gerritsen, B. E. C. van do Leemput, H. van Kempen, G. Schmid, *Adv. Mater.* **1990**, *2*, 482.
[65] R. Houbertz, T. Feigenspan, F. Mielke, U. Memmert, U. Hartmann, U. Simon, G. Schön, G. Schmid, *Europhys. Lett.* **1994**, *28*, 641.
[66] G. Schmid, A. Lehnert, *Angew. Chem. Int. Ed. Engl.* **1989**, *28*, 780−781.
[67] G. Schmid, V. Maihack, F. Lantermann, S. Peschel, *J. Chem. Soc., Dalton Trans.* **1996**, 589−595.
[68] G. Schmid, H. West, J.-O. Malm, J.-O. Bovin, C. Grenthe, *Chem. Eur. J.* **1996**, *2*, 1099.
[69] U. Simon, R. Flesch, H. Wiggers, G. Schön, G. Schmid, *J. Mater. Chem.* **1998**, *8*, 517−518.
[70] G. Schmid, S. Peschel, *New J. Chem.* **1998**, *22*, 669−675.
[71] G. Schmid, R. Pugin, J.-O. Malm, J.-O. Bovin, *Eur. J. Inorg. Chem.* **1998**, 813−817.
[72] M. Giersig, L. M. Liz-Tarzan, T. Ung, D. Su, P. Mulvaney, *Ber. Bunsenges. Phys. Chem.* **1997**, *101*, 1617−1620.
[73] M. N. Vargaftik, V. P. Zargorodnikov, I. P. Stolarov, I. I. Moiseev, D. I. Kochubey, V. A. Likholobov, A. L. Chuvilin, K. I. Zarnaraev, *J. Mol. Catal.* **1989**, *53*, 315−349.
[74] M. N. Vargaftik, V. P. Zargorodnikov, I. P. Stolarov, I. I. Moiseev, V. A. Likholobov, D. I. Kochubey, A. L. Chuvilin, V. I. Zaikosvsky, K. I. Zamaraev, G. I. Timofeeva, *J. Chem. Soc., Chem. Commun.* **1985**, 937−939.
[75] V. V. Volkov, G. van Tendeloo, G. A. Tsirkov, N. V. Cherkashina, M. N. Vargaftik, I. I. Moiseev, V. M. Novotortsev, A. V. Kvit, A. L. Chuvilin, *J. Cryst. Growth* **1996**, *163*, 377.
[76] I. I. Moiseev, M. N. Vargaftik, V. V. Volkov, G. A. Tsirkov, N. V. Cherkashina, V. M. Novotortsev, O. G. Ellett, I. A. Petrunenka, A. L. Chuvilin, A. V. Kvit, *Mendeleev Commun.* **1995**, 87.
[77] V. Oleshko, V. Volkov, W. Jacob, M. Vargaftik, I. I. Moiseev, G. van Tendeloo, *Z. Phys. D* **1995**, *34*, 283.
[78] I. I. Moiseev, M. N. Vargaftik, T. V. Chernysheva, T. A. Stromnova, A. E. Gekhman, G. A. Tsirkov, A. M. Makhlina, *J. Mol. Catal. A: Chem.* **1996**, *108*, 77.
[79] C. Amiens, D. de Caro, B. Chaudret, J. S. Bradley, *J. Am. Chem. Soc.* **1993**, *115*, 11638−11939.
[80] D. de Caro, H. Wally, C. Amiens, B. Chaudret, *J. Chem. Soc., Chem. Commun.* **1994**, 1891−1892.
[81] A. Rodriguez, C. Amiens, B. Chaudret, M.-J. Casanove, P. Lecante, J. S. Bradley, *Chem. Mater.* **1996**, *8*, 1978−1986.
[82] M. Bardaji, O. Vidoni, A. Rodriguez, C. Amiens, B. Chaudret, M.-J. Casanove, P. Lecante, *New J. Chem.* **1997**, *21*, 1243−1249.
[83] R. Franke, J. Rothe, J. Pollmann, J. Hormes, H. Bönnemann, W. Brijoux, Th. Hindenburg, *J. Am. Chem. Soc.* **1996**, *118*, 12090−12097.
[84] O. Vidoni, K. Philippot, C. Amiens, B. Chaudret, O. Balmes, J.-O. Malm, J.-O. Bovin, F. Senocq, M.-J. Casanove, *Angew. Chem. Int. Ed.* **1999**, *38*, 3736−3738.
[85] M. T. Reetz, G. Lohmer, *Chem. Commun.* **1996**, 1921−1922.
[86] D. Mandler, I. Willner, *J. Phys. Chem.* **1987**, *91*, 3600−3605.
[87] H. Bönnemann, W. Brijoux, T. Joussen (to Studiengesellschaft Kohle mbH), U. S. Pat. 5,580,492 (August 26, **1993**).
[88] H. Bönnemann, W. Brijoux, R. Brinkmann, E. Dinjus, T. Joussen, B. Korall, *Angew. Chem. Int. Ed. Engl.* **1991**, *30*, 1344−1346.
[89] H. Bönnemann, W. Brijoux, R. Brinkmann, J. Richter (to Studiengesellschaft Kohle mbH), U. S. Pat. 849,482 (August 29, **1997**).
[90] M. T. Reetz, W. Helbig, *J. Am. Chem. Soc.* **1994**, *116*, 7401−7402.
[91] M. T. Reetz, W. Helbig, S. Quaiser (to Studiengesellschaft Kohle), U. S. Pat. 5,620,564 (Apr. 15, **1997**) and U. S. Pat. 5,925,463 (Jul. 20, **1999**).
[92] M. A. Winter, Ph.D. Thesis, Verlag Mainz, Aachen, **1998**, ISBN 3-89653-355-X.
[93] J. A. Becker, R. Schäfer, W. Festag, W. Ruland, J. H. Wendorf, J. Pebler, S. A. Quaiser, W. Helbig, M. T. Reetz, *J. Chem. Phys.* **1995**, *103*, 2520−2527.
[94] M. T. Reetz, S. A. Quaiser, C. Merk, *Chem. Ber.* **1996**, *129*, 741−743.
[95] M. T. Reetz, W. Helbig, S. A. Quaiser, *Chem. Mater.* **1995**, *7*, 2227−2228.
[96] M. T. Reetz, S. A. Quaiser, *Angew. Chem.* **1995**, *107*, 2461−2463; *Angew. Chem. Int. Ed. Engl.* **1995**, *34*, 2240.
[97] U. Kolb, S. A. Quaiser, M. Winter, M. T. Reetz, *Chem. Mater.* **1996**, *8*, 1889−1894.
[98] J. Kiwi, M. Grätzel, *J. Am. Chem. Soc.* **1979**, *101*, 7214−7217.
[99] H. Bönnemann, W. Brijoux, R. Brinkmann, U. Endruschat, W. Hofstadt, K. Angermund, *Rev. Roum. Chim.* **1999**, *44*, 1003−1010.
[100] J. Sinzig, L. J. De Jongh, H. Bönnemann, W. Brijoux, R. Köppler, *Appl. Organomet. Chem.* **1998**, *12*, 387−391.
[101] H. Bönnemann, W. Brijoux, R. Brinkmann (to Studiengesellschaft Kohle), WO 99/59713 (Nov. 25, **1999**).
[102] J. S. Bradley, E. W. Hill, M. E. Leonowicz, H. Witzke, *J. Mol. Catal.* **1987**, *41*, 59−74.
[103] M. T. Reetz, W. Helbig, S. A. Quaiser, U. Stimming, N. Breuer, R. Vogel, *Science* **1995**, *267*, 367−369.
[104] A. Schulze Tilling, Ph.D. Thesis, RWTH Aachen, **1996**.
[105] T. Yonezawa, N. Toshima, *J. Mol. Catal.* **1993**, *83*, 167−181.
[106] N. Toshima, T. Takahashi, H. Hirai, *Chem. Lett.* **1985**, 1245−1248.
[107] J. S. Bradley, in: *Clusters and Colloids* (Ed.: G. Schmid), VCH, Weinheim, **1994**, p. 471.
[108] L. D. Rampino, F. F. Nord, *J. Am. Chem. Soc.* **1941**, *63*, 2745−2749.
[109] L. D. Rampino, F. F. Nord, *J. Am. Chem. Soc.* **1941**, *63*, 3268.
[110] L. D. Rampino, F. F. Nord, *J. Am. Chem. Soc.* **1943**, *65*, 2121−2125.
[111] L. Hernandez, F. F. Nord, *J. Colloid. Sci.* **1948**, *3*, 363−375.
[112] W. P. Dunsworth, F. F. Nord, *J. Am. Chem. Soc.* **1950**, *72*, 4197−4198.
[113] Y. Lin, R. G. Finke, *J. Am. Chem. Soc.* **1994**, *116*, 8335−8353.
[114] Y. Lin, R. G. Finke, *Inorg. Chem.* **1994**, *33*, 4891−4910.
[115] T. Nagata, M. Pohl, H. Weiner, R. G. Finke, *Inorg. Chem.* **1997**, *36*, 1366.
[116] J. D. Aiken III, R. G. Finke, *J. Am. Chem. Soc.* **1998**, *120*, 9545−9554.
[117] J. D. Aiken III, R. G. Finke, *Chem. Mater.* **1999**, *11*, 1035−1047.
[118] M. R. Mucalo, R. P. Cooney, *J. Chem. Soc., Chem. Commun.* **1989**, 94−95.
[119] K. Meguro, M. Torizuka, K. Esumi, *Bull. Chem. Soc. Jpn.* **1988**, *61*, 341−345.
[120] L. N. Lewis, N. Lewis, *J. Am. Chem. Soc.* **1986**, *108*, 7228−7231.

[121] L. N. Lewis, N. Lewis, *Chem. Mater.* **1989**, *1*, 106−114.
[122] A. C. Curtis, D. G. Duff, P. P. Edwards, D. A. Jefferson, B. F. G. Johnson, A. I. Kirkland, D. E. Logan, *Angew. Chem. Int. Ed. Engl.* **1987**, *26*, 676.
[123] D. G. Duff, A. C. Curtis, P. P. Edwards, D. A. Jefferson, B. F. G. Johnson, D. E. Logan, *J. Chem. Soc., Chem. Commun.* **1987**, 1264.
[124] A. C. Curtis, D. G. Duff, P. P. Edwards, D. A. Jefferson, B. F. G. Johnson, A. I. Kirkland, A. S. Wallace, *Angew. Chem. Int. Ed. Engl.* **1988**, *27*, 1530.
[125] D. G. Duff, P. P. Edwards, J. Evans, J. T. Gauntlett, D. A. Jefferson, B. F. G. Johnson, A. I. Kirkland, D. J. Smith, *Angew. Chem. Int. Ed. Engl.* **1989**, *28*, 590.
[126] D. G. Duff, A. Baiker, P. P. Edwards, *Langmuir* **1993**, *9*, 2301−2309.
[127] W. Vogel, D. G. Duff, A. Baiker, *Langmuir* **1995**, *11*, 401−404.
[128] P. R. van Rheenen, M. J. McKelvey, W. S. Glaunsinger, *J. Solid State Chem.* **1987**, *67*, 151−169.
[129] D. G. Duff, A. Baiker, in: *Preparation of Catalysts VI* (Ed.: G. Poncelet, J. Martens, B. Delmon, P. A. Jacobs, P. Grange), Elsevier Science, Amsterdam, Netherlands, **1995**, p. 505−512.
[130] K.-L. Tsai, J. L. Dye, *Chem. Mater.* **1993**, *5*, 540−546.
[131] J. van Wonterghem, S. Mørup, C. J. W. Koch, S. W. Charles, S. Wells, *Nature* **1986**, *322*, 622.
[132] G. N. Glavee, K. J. Klabunde, C. M. Sorensen, G. C. Hadjipanayis, *Inorg. Chem.* **1993**, *32*, 474−477.
[133] R. Franke, J. Rothe, R. Becker, J. Pollmann, J. Hormes, H. Bönnemann, W. Brijoux, R. Köppler, *Adv. Mater.* **1998**, *10*, 126−131.
[134] J. Sinzig, L. J. de Jongh, H. Bönnemann, W. Brijoux, R. Köppler, *Appl. Organomet. Chem.* **1998**, *12*, 387−391.
[135] M. Maase, Ph.D. Thesis, Verlag Mainz, Aachen, **1999**, ISBN 3-89653-463-7.
[136] M. T. Reetz, M. Maase, *Adv. Mater.* **1999**, *11*, 773−777.
[137] J. S. Bradley, B. Tesche, W. Busser, M. Maase, M. T. Reetz, *J. Am. Chem. Soc.* **2000**, *122*, 4631−4636.
[138] P. H. Hess, P. H. Parker, *J. Appl. Polymer Sci.* **1966**, *10*, 1915−1927.
[139] J. R. Thomas, *J. Appl. Phys.* **1966**, *37*, 2914−2915.
[140] K. Esumi, T. Tano, K. Torigue, K. Meguro, *Chem. Mater.* **1990**, *2*, 564.
[141] J. S. Bradley, E. W. Hill, C. Klein, B. Chaudret, A. Duteil, *Chem. Mater.* **1993**, *5*, 254−256.
[142] Y. Wada, H. Kuramoto, T. Sakata, H. Mori, T. Sumida, T. Kitamura, S. Yanagida, *Chem. Lett.* **1999**, 607.
[143] W. Yu, W. Tu, H. Liu, *Langmuir* **1999**, *15*, 6−9.
[144] K. S. Suslick, T. Hyeon, M. Fang, A. Cichowlas, in: *Advanced Catalysts and Nanostructured Materials*, chapter 8 (Ed.: W. Moser), Academic Press, San Diego, **1996**, p. 197−212.
[145] A. Dhas, A. Gedanken, *J. Mater. Chem.* **1998**, *8*, 445−450.
[146] Y. Koltypin, A. Fernandez, C. Rojas, J. Campora, P. Palma, R. Prozorov, A. Gedanken, *Chem. Mater.* **1999**, *11*, 1331−1335.
[147] R. A. Salkar, P. Jeevanandam, S. T. Aruna, Y. Koltypin, A. Gedanken, *J. Mater. Chem.* **1999**, *9*, 1333−1335.
[148] F. Ciardelli, P. Pertici, *Z. Naturforsch., Teil B* **1985**, *40*, 133−140.
[149] J. S. Bradley, E. W. Hill, S. Behal, C. Klein, B. Chaudret, A. Duteil, *Chem. Mater.* **1992**, *4*, 1234−1239.
[150] A. Duteil, R. Quéau, B. Chaudret, R. Mazel, C. Roucau, J. S. Bradley, *Chem. Mater.* **1993**, *5*, 341−347.
[151] D. de Caro, V. Agelou, A. Duteil, B. Chaudret, R. Mazel, Ch. Roucau, J. S. Bradley, *New J. Chem.* **1995**, *19*, 1265−1274.
[152] F. Dassenoy, K. Philippot, T. Ould Ely, C. Amiens, P. Lecante, E. Snoeck, A. Mosset, M.-J. Casanove, B. Chaudret, *New J. Chem.* **1998**, *19*, 703−711.
[153] J. Osuna, D. de Caro, C. Amiens, B. Chaudret, E. Snoeck, M. Respaud, J.-M. Broto, A. Fert, *J. Phys. Chem.* **1996**, *100*, 14571−14574.
[154] T. Ould Ely, C. Amiens, B. Chaudret, E. Snoeck, M. Verelst, M. Respaud, J. M. Broto, *Chem. Mater.* **1999**, *11*, 526−529.
[155] J. S. Bradley, E. W. Hill, B. Chaudret, A. Duteil, *Langmuir* **1995**, *11*, 693−695.
[156] F. Dassenoy, M.-J. Casanove, P. Lecante, M. Verelst, E. Snoeck, A. Mosset, T. Ould Ely, C. Amiens, B. Chaudret, *J. Chem. Phys.* **2000**, *112*, 8137−8145.
[157] M. T. Reetz, S. Quaiser, M. Winter, J. A. Becker, R. Schaefer, U. Stimming, A. Marmann, R. Vogel, T. Konno, *Angew. Chem. Ind. Ed. Engl.* **1996**, *35*, 2092−2094.
[158] M. Verelst, T. Ould Ely, C. Amiens, E. Snoeck, P. Lecante, A. Mosset, M. Respaud, J.-M. Broto, B. Chaudret, *Chem. Mater.* **1999**, *11*, 2702−2708.
[159] C.-B. Wang, C.-T. Yeh, *J. Catal.* **1998**, *178*, 450−456.
[160] M. T. Reetz, M. Koch (to Studiengesellschaft Kohle m.b.H.), PCT/EP 99/08594 (November 9, **1999**).
[161] M. T. Reetz, M. Koch, *J. Am. Chem. Soc.* **1999**, *121*, 7933−7934.
[162] M. Koch, Ph.D. Thesis, Verlag Mainz, Aachen, **1999**, ISBN 3-89653-514-5.
[163] G. Schmid, M. Bäumle, N. Beyer, *Angew. Chem. Int. Ed.* **2000**, *39*, 182−184.
[164] H. Cölfen, T. Pauck, *Colloid Polym. Sci.* **1997**, *275*, 175−180.
[165] T. Teranishi, M. Miyake, *Chem. Mater.* **1998**, *10*, 594−600.
[166] E. Papirer, P. Horny, H. Balard, R. Anthore, C. Pepitas, A. Martinet, *J. Colloid Interface Sci.* **1983**, *94*, 220−228.
[167] T. Teranishi, M. Hosoe, M. Miyake, *Adv. Mater.* **1997**, *9*, 65−67.
[168] T. Teranishi, I. Kiyokawa, M. Miyake, *Adv. Mater.* **1998**, *10*, 596−599.
[169] K. Esumi, H. Ishizuka, S. Masayoshi, K. Meguro, T. Tano, K. Torigoe, *Langmuir* **1991**, *7*, 457−459.
[170] R. G. DiScipio, *Anal. Biochem.* **1996**, *236*, 168−170.
[171] M. A. Watzky, R. G. Finke, *Chem. Mater.* **1997**, *9*, 3083−3095.
[172] T. Yonezawa, M. Sutoh, T. Kunitake, *Chem. Lett.* **1997**, *7*, 619−620.
[173] G. Frens, *Nature* **1997**, *241*, 20−22.
[174] X. Zhai, E. Efrima, *Langmuir* **1997**, *13*, 420−425.
[175] D. V. Leff, P. C. Ohara, J. R. Heath, W. Gelbart, *J. Phys. Chem.* **1995**, *99*, 7036−7041.
[176] C. H. Chew, J. F. Deng, H. H. Huang, F. C. Loh, G. L. Loy, X. P. Ni, K. L. Tan, G. Q. Xu, *Langmuir* **1996**, *12*, 909−912.
[177] G. Braun, H. Bönnemann, *Angew. Chem. Int. Ed. Engl.* **1996**, *35*, 1992−1994.
[178] M. B. Mohamed, , Z. L. Wang, M. A. El-Sayed, *J. Phys. Chem. A* **1999**, *103*, 10255−10259.
[179] T. Teranishi, M. Miyake, *Chem. Mater.* **1999**, *11*, 3414−3416.
[180] G. W. Busser, J. G. van Ommen, J. A Lercher, in: *Advanced Catalysts and Nanostructured Materials*, chapter 7 (Ed.: W. Moser), Academic Press, San Diego, **1996**, p. 231−230.
[181] M. Antonietti, F. Gröhn, J. Hartmann, L. Bronstein, *Angew. Chem. Int. Ed. Engl.* **1997**, *36*, 2080.
[182] K. Torigoe, K. Esumi, *Langmuir* **1993**, *9*, 1664−1667.
[183] J.-S. Jeon, C.-S. Yeh, *J. Chin. Chem. Soc.* **1998**, *45*, 721−726.
[184] F. Stietz, F. Träger, *Phys. Bl.* **1999**, *55*, 57−60.
[185] C. Larpent, F. Brisse-le-Menn, H. Patin, *J. Mol. Catal.* **1991**, *65*, 35−40.
[186] I. I. Moiseev, M. N. Vargaftik, T. V. Chernysheva, T. A. Stromnova, A. E. Gekhman, G. A. Tsirkov, A. M. Makhlina, *J. Mol. Catal. A* **1996**, *108*, 77−85.
[187] I. I. Moiseev, G. A. Tsirkov, A. E. Gekhman, M. N. Vargaftik, *Mendeleev Commun.* **1997**, 1.
[188] M. N. Vargaftik, N. Y. Kozitsyna, N. V. Cherkashina, R. I. Rudyi, D. I. Kochubei, B. N. Novgorodov, I. I. Moiseev, *Kinet. Catal.* **1998**, *39*, 740−757.
[189] J. D. Aiken III, Y. Lin, R. G. Finke, *J. Mol. Catal. A* **1996**, *114*, 29−51.
[190] J. D. Aiken III, R. G. Finke, *J. Am. Chem. Soc.* **1999**, *121*, 8803−8810.
[191] M. T. Reetz, S. A. Quaiser, C. Merk, *Chem. Ber.* **1996**, *129*, 741−743.

[192] H. Bönnemann, B. Korall, *Angew. Chem. Int. Ed. Engl.* **1992**, *31*, 1490−1492.
[193] H. Bönnemann, W. Brijoux, *Nanostruct. Mater.* **1995**, *5*, 135−140.
[194] M. T. Reetz, R. Breinbauer, K. Wanninger, *Tetrahedron Lett.* **1996**, *37*, 4499−4502.
[195] M. Beller, H. Fischer, K. Kühlein, C.-P. Reisinger, W. A. Herrmann, *J. Organomet. Chem.* **1996**, *520*, 257−259.
[196] M. T. Reetz, E. Westermann, *Angew. Chem. Int. Ed.* **2000**, *39*, 165−168.
[197] J. Walter, J. Heiermann, G. Dyker, S. Hara, H. Shioyama, *J. Catal.* **2000**, *189*, 449−455.
[198] M. T. Reetz, R. Breinbauer, P. Wedemann, P. Binger, *Tetrahedron* **1998**, *54*, 1233−1240.
[199] M. Ohtaki, N. Toshima, M. Komiyama, H. Hirai, *Bull. Chem. Soc. Jpn.* **1990**, *63*, 1433−1440.
[200] M. Antonietti, E. Wenz, L. Bronstein, M. Seregina, *Adv. Mater.* **1995**, *7*, 1000−1005.
[201] M. V. Seregina. L. M. Bronstein. O. A. Platonova, D. M. Chernyshov, P. M. Valetsky, J. Hartmann, E. Wenz, M. Antonietti, *Chem. Mater.* **1997**, *9*, 923−931.
[202] S. Förster, *Ber. Bunsenges. Phys. Chem.* **1997**, *101*, 1671−1678.
[203] A. B. R. Mayer, *Mater. Sci. Eng.* **1998**, *C6*, 155−166.
[204] N. Toshima, *Supramol. Sci.* **1998**, *5*, 395−398.
[205] N. Toshima, T. Yonezawa, K. Kushihashi, *J. Chem. Soc., Faraday Trans.* **1993**, *89*, 2537.
[206] N. Toshima, Y. Wang, *Langmuir* **1994**, *10*, 4574.
[207] N. Toshima, T. Yonezawa, *Makromol. Chem. Macromol. Symp.* **1992**, *59*, 281.
[208] V. Chechik, R. M. Crooks, *J. Am. Chem. Soc.* **2000**, *122*, 1243−1244.
[209] G. Schmid, S. Emde, V. Maihack, W. Meyer-Zaika, S. Peschel, *J. Mol. Catal. A* **1996**, *107*, 95−104.
[210] A. Freund, P. Panster (to Degussa AG), EP 715 889 A2 (November 8, **1995**).
[211] G. Witek, M. Noeske, G. Mestl, S. Shaikhutdinov, R. J. Behm, *Catal. Lett.* **1996**, *37*, 35−39.
[212] S. K. Shaikhutdinov, F. A. Möller, G. Mestl, R. J. Behm, *J. Catal.* **1996**, *163*, 492−495.
[213] M. T. Reetz, S. A. Quaiser, R. Breinbauer, B. Tesche, *Angew. Chem. Int. Ed. Engl.* **1995**, *34*, 2728−2730.
[214] T. Teranishi, K. Nakata, M. Miyake, N. Toshima, *Chem. Lett.* **1996**, 277−278.
[215] H. Bönnemann, W. Wittholt, J. D. Jentsch, A. Schulze Tilling, *New J. Chem.* **1998**, *22*, 713−717.
[216] X. Yang, H. Liu, *Appl. Catal. A: General* **1997**, *164*, 197−203.
[217] W. Yu, H. Liu, X. An, X. Ma, Z. Liu, L. Qiang, *J. Mol. Catal. A* **1999**, *147*, 73−81.
[218] H. Feng, H. Liu, *J. Mol. Catal. A: Chem.* **1997**, *126*, L5−L8.
[219] T. Hanaoka, T. Matsuzaki, Y. Sugi, *J. Mol. Catal. A* **1999**, *149*, 161−167.
[220] J. H. Sinfelt, *Acc. Chem. Res.* **1987**, *20*, 134.
[221] J. H. Sinfelt, G. H. Via, F. W. Lytle, *J. Chem. Phys.* **1980**, *72*, 4832.
[222] J. H. Sinfelt, G. H. Via, F. W. Lytle, *J. Chem. Phys.* **1981**, *75*, 5527.
[223] G. Schmid, A. Lehnert, J.-O. Malm, J.-O. Bovin, *Angew. Int. Ed. Engl.* **1991**, *30*, 874−876.
[224] H. Bönnemann, W. Brijoux, J. Richter, R. Becker, J. Hormes, J. Rothe, *Z. Naturforsch., Teil B* **1995**, *50*, 333−338.
[225] L. E. Aleandri, H. Bönnemann, D. J. Jones, J. Richter, J. Roziere, *J. Mater. Chem.* **1995**, *5*, 749−752.
[226] N. Toshima, in: *Fine Particles Science and Technology* (Ed.: E. Pelizzetti), Kluwer Academic Publishers, Dordrecht, Netherlands, **1996**, p. 371−383.
[227] M. Harada, K. Asakura, N. Toshima, *J. Phys. Chem.* **1994**, *98*, 2653−2662.
[228] B. J. Joice, J. J. Rooney, P. B. Wells, G. R. Wilson, *Discuss. Faraday Soc.* **1966**, *41*, 223.
[229] J. Schwank, *Gold Bull.* **1985**, *18*, 2.
[230] W. Juszczyk, Z. Karpinski, D. Lomot, J. Pielaszek, J. W. Sobczak, *J. Catal.* **1995**, *151*, 67.
[231] A. O. Cinneide, J. K. A. Clarke, *J. Catal.* **1972**, *26*, 233.
[232] S. H. Inami. W. Wise, *J. Catal.* **1972**, *26*, 92.
[233] C. Visser, I. G. P. Zuidwijk, V. Ponec, *J. Catal.* **1974**, *35*, 407,
[234] N. Toshima, *J. Macromol. Sci.* **1990**, *A27*, 1225.
[235] A. O. Cinneide, F. G. Gault, *J. Catal.* **1975**, *37*, 311.
[236] N. Toshima, H. Harada, Y. Yamazaki, K. Asakura, *J. Phys. Chem.* **1992**, *96*, 927.
[237] H. Liu, C. Mao, S. Meng, *J. Mol. Catal.* **1992**, *74*, 275.
[238] J. B. Michel, J. T. Schwartz, in: *Catalyst Preparation Science IV* (Eds.: B. Delmon, P. Grange, P. A. Jacobs, G. Poncelet), Elsevier, New York, **1987**, p. 669−687.
[239] G. Schmid, H. West, H. Mehles, A. Lehnert, *Inorg. Chem.* **1997**, *36*, 891−895.
[240] N. Toshima, T. Takahashi, H. Hirai, *J. Macromol. Sci. Chem.* **1988**, *A25*, 669−686.
[241] M. Ohtati, M. Komiyama, H. Hirai, N. Toshima, *Macromolecules* **1991**, *24*, 5567−5572.
[242] G. Schmid, V. Maihack, F. Lantermann, S. Peschel, *J. Chem. Soc., Dalton Trans.* **1996**, 591−594.
[243] H. Bönnemann, W. Brijoux, A. Schulze Tilling, K. Siepen, *Top. Catal.* **1997**, *4*, 217−227.
[244] H. Bönnemann, P. Britz, H. Ehwald, *Chem. Tech.* **1997**, *49*, 189−192.
[245] H. Bönnemann, G. A. Braun, *Chem. Eur. J.* **1997**, *3*, 1200−1202.
[246] J. U. Köhler, J. S. Bradley, *Catal. Lett.* **1997**, *45*, 203−208.
[247] U. Köhler, J. S. Bradley, *Langmuir* **1998**, *14*, 2730−2735.
[248] X. Zuo, H. Liu, M. Liu, *Tetrahedron Lett.* **1998**, *39*, 1941−1944.
[249] X. Zuo, H. Liu, D. Guo, X. Yang, *Tetrahedron* **1999**, *55*, 7787−7804.
[250] H. Bönnemann, R. Brinkmann, P. Neiteler, *Appl. Organomet. Chem.* **1994**, *8*, 361−378.
[251] H. Bönnemann, W. Brijoux, R. Brinkmann, A. Schulze Tilling, T. Schilling, B. Tesche, K. Seevogel, R. Franke, J. Hormes, G. Köhl, J. Pollmann, J. Rothe, W. Vogel, *Inorg. Chim. Acta* **1998**, *270*, 95−110.
[252] L. Djakovitch, M. Wagner, K. Köhler, *J. Organomet. Chem.* **1999**, *592*, 225−234.
[253] J. Le Bars, U. Specht, J. S. Bradley, D. G. Blackmond, *Langmuir* **1999**, *15*, 7621−7625.
[254] G. Ihlein, B. Junges, U. Junges, F. Laeri, F. Schüth, U. Vietze, *Appl. Organomet. Chem.* **1998**, *12*, 305.
[255] M. T. Reetz, M. Dugal, *Catal. Lett.* **1999**, *58*, 207−212.
[256] H. Bönnemann, U. Endruschat, B. Tesche, A. Rufínska, C. W. Lehmann, F. E. Wagner, G. Filoti, V. Pârvulescu, V. I. Pârvulescu, *Eur. J. Inorg. Chem.* **2000**, 819−822.
[257] K. Kordesch, G. Simader, *Fuel Cells, their Applications*, VCH, Weinheim, **1996**.
[258] H. G. Petrow, R. J. Allen (to Prototech Comp.), US 4,044,193 (August 23, **1977**).
[259] G. T. Burstein, C. J. Barnett, A. R. Kucernak, K. R. Williams, *Catal. Today* **1997**, *38*, 425−437.
[260] E. Auer, A. Freund, T. Lehmann, K.-A. Starz, R. Schwarz, U. Stenke (to Degussa AG), EP 0 880 188 A2 (November 25, **1998**).
[261] M. S. Wilson, S. Gottesfeld, *J. Appl. Electrochem.* **1992**, *22*, 1−7.
[262] M. S. Wilson, X. Ren, S. Gottesfeld, *J. Electrochem. Soc.* **1996**, *143*, L12.
[263] S. C. Thomas, X. Ren, S. Gottesfeld, *J. Electrochem. Soc.* **1999**, *146*, 4354−4359.
[264] G. J. K. Acres, J. C. Frost, G. A. Hards, R. J. Potter, T. R. Ralph, D. Thompsett, G. T. Burstein, G. J. Hutchings, *Catal. Today* **1997**, *38*, 393−400.
[265] R. G. Cawthorn, *S. Afr. J. Sci.* **1999**, *95*, 481−489.
[266] Information available from "World Fuel Cell Council" e.V., Kroegerstraße 5, 60313 Frankfurt.

[267] R. F. Service, *Science* **1999**, *285*, 682−685.
[268] D. S. Cameron, *Platinum Met. Rev.* **1999**, *43*, 149−154.
[269] F. J. Luczak, D. A. Landsman (to United Technologies Corp.), US 4,613,582 (September 23, **1986**).
[270] W. Wittholt, Ph.D. Thesis, RWTH Aachen, **1997**.
[271] H. Wendt, M. Götz (to Degussa-Hüls AG), EP 0951 084 A2 (October 20, **1999**).
[272] A. Freund, J. Lang, T. Lehmann, K. A. Starz, *Cat. Today* **1996**, *27*, 279−283.
[273] H. Bönnemann, in: *Extended Abstracts of the 3rd Int. Symposium on New Materials for Electrochemical Systems* (Ed.: O. Savadogo), École Polytechnique de Montréal, Canada, **1999**, ISBN 21-553-00739-6.
[274] H. Bönnemann, R. Brinkmann, P. Britz, U. Endruschat, R. Mörtel, U. A. Paulus, G. J. Feldmeyer, T. J. Schmidt, H. A. Gasteiger, R. J. Behm, *J. New Mat. Electrochem. Syst.* **2000**, *3*, 199−206.
[275] T. Itoh, J. Sato (to N. E. Chemcat Corporation), EP 0 952 241 (October 27, **1999**).
[276] S. Narayanan, S. Surampudi, G. Halpert (to California Institute of Technology), US 5,945,231 (August 31, **1999**).
[277] W. Vogel, P. Britz, H. Bönnemann, J. Rothe, J. Hormes, *J. Phys. Chem. B* **1997**, *101*, 11029−11036.
[278] U. Stimming, R. Vogel, in: *Electrochemical Nanotechnology* (Ed.: W. J. Lorenz, W. Plieth), Wiley-VCH, Weinheim, **1998**, p. 73−86.
[279] J. R. Giallombardo, E. S. De Castro (to De Nora S. P. A.), WO 99/53557 (April 14, **1999**).
[280] E. Reddington, A. Sapienza, B. Gurau, R. Viswanathan, S. Sarangapani, E. S. Smotkin, T. E. Mallouk, *Science* **1998**, *280*, 1735−1737.
[281] A. Freund, T. Lehmann, K.-A. Starz, G. Heinz, R. Schwarz (to Degussa AG), EP 0 743 092 A1 (November 20, **1996**).
[282] S. Chen, *Adv. Mater.* **2000**, *12*, 186−189.
[283] M. Sastry, A. Gole, S. R. Sainkar, *Langmuir* **2000**, *16*, 3553−3556.
[284] T. Teranishi, M. Haga, Y. Shiozawa, M. Miyake, *J. Am. Chem. Soc.* **2000**, *122*, 4237−4238.
[285] C.-C. Hsueh, M.-T. Lee, M. S. Freund, G. S. Ferguson, *Angew. Chem. Int. Ed.* **2000**, *39*, 1228−1230.
[286] H. X. He, H. Zhang, Q. G. Li, Z. F. Liu, *Langmuir* **2000**, *16*, 3846−3851.
[287] A. K. Boal, F. Illhan, J. E. DeRouchey, T. Thurn-Albrecht, T. P. Russell, V. M. Rotello, *Nature* **2000**, *404*, 746.
[288] G. Schmid, W. Meyer-Zaika, R. Pugin, T. Sawitowski, J.-P. Majoral, A.-M. Caminade, C.-O. Turrin, *Chem. Eur. J.* **2000**, *6*, 1693.
[289] J. Fink, C. J. Kiely, D. Bethell, D. J. Schiffrin, *Chem. Mater.* **1998**, *10*, 922−926.
[290] L. Ramos, T. Lubensky, N. Dan, P. Nelson, D. Weitz, *Science* **1999**, *286*, 2325.
[291] M. Reetz, M. Winter, B. Tesche, , *Chem. Commun.* **1997**, 147−148.
[292] J. Eversole, H. Broida, *J. Appl. Phys.* **1974**, *45*, 596.
[293] N. Wada, *Jpn. J. Appl. Phys.* **1967**, *6*, 173.
[294] S. Kasukate, S. Yatsuga, R. Uyeda, *Jpn. J. Appl. Phys.* **1974**, *13*, 1714.
[295] S. Mochizuki, R. Ruppin, *J. Phys. Cond. Mater.* **1993**, *5*, 135.
[296] C. Petit, A. Taleb, M.-P. Pileni, *Adv. Mater.* **1998**, *10*, 259.
[297] C. Petit, T. Cren, D. Roditchev, W. Sacks, J. Klein, M. P. Pileni, *Adv. Mater.* **1999**, *11*, 1198.
[298] L. Marzan, P. Mulvaney, *Recent Res. Dev. Phys. Chem.* **1998**, *2*, 1−32.
[299] A. C. Balazcs, V. V. Ginzburg, F. Qiu, G. Peng, D. Jasnow, *J. Phys. Chem. B.* **2000**, *104*, 3411−3422.
[300] H. Fan, Y. Lu, A. Stump, S. T. Reed, T. Baer, R. Schunk, V. Perez-Luna, G. P. Lopez, C. J. Brinker, *Nature* **2000**, *405*, 56−60.
[301] G. Schmid, M. Bäumle, M. Geerkens, I. Heim, C. Osemann, T. Sawitowski, *Chem. Soc. Rev.* **1999**, *28*, 179−185.
[302] K. V. Sarathy, P. J. Thomas, G. U. Kulkarni, C. N. R. Rao, *J. Phys. Chem. B.* **1999**, *103*, 399.
[303] H. Fan, Y. Zhou, G. P. Lopez, *Adv. Mater.* **1997**, *9*, 728−731.
[304] J. L. Dormann, D. Fiorani (Eds.), *Magnetic Properties of Fine Particles*, North Holland, Amsterdam, **1992.**
[305] L. J. de Jongh, D. A. van Leeuwen, J. M. van Ruitenbeek, J. Sinzig, *NATO ASI Ser. C* **1996**, *484*, 615−643.
[306] L. J. de Jongh, J. Sinzig, H. Bönnemann, W. Brijoux, R. Köppler, *Appl. Organomet. Chem.* **1998**, *12*, 387−391.
[307] N. C. Seeman, *J. Theor. Biol.* **1982**, *99*, 237.
[308] B. H. Robinson, N. C. Seeman, R. C. Mucic, J. J Storhoff, *Nature* **1996**, *382*, 607.
[309] C. A. Mirkin, R. L. Letsinger, R. C. Mucic, J. J. Storhoff, *Nature* **1996**, *382*, 607−609.
[310] A. P. Alivisatos, K. P. Johnson, X. Peng, T. E. Wilson, C. J. Loweth, M. P. Bruchez, P. G. Schultz, *Nature* **1996**, *382*, 609−611.
[311] J. J. Storhoff, R. C. Mucic, C. A. Mirkin, *Chem. Rev.* **1999**, *99*, 1849−1862.
[312] J. J. Storhoff, A. A. Lazarides, R. C. Mucic, C. A. Mirkin, R. L. Letsinger, G. C. Schatz, *J. Am. Chem. Soc.* **2000**, *122*, 4640−4650.
[313] C. A. Mirkin, *Inorg. Chem.* **2000**, *39*, 2258−2272.
[314] C. M. Niemeyer, *Angew. Chem. Int. Ed. Engl.* **1997**, *36*, 585−587.
[315] C. M. Niemeyer, W. Bürger, J. Peplies, *Angew. Chem. Int. Ed.* **1998**, *37*, 2265−2268.
[316] C. M. Niemeyer, *Appl. Phys. A* **1999**, *68*, 119−124.
[317] E. Braun, Y. Eichen, U. Sivan, G. Ben-Yoseph, *Nature* **1998**, *391*, 775.
[318] G. Hornyak, M. Kröll, R. Pugin, Th. Sawitowski, G. Schmid, J.-O. Bovin, G. Karsson, H. Hofmeister, S. Hopfe, *Chem. Eur. J.* **1997**, *3*, 1951.
[319] T. Hanaoka, H.-P. Kormann, M. Kröll, T. Sawitowski, G. Schmid, *Eur. J. Inorg. Chem.* **1998**, 807−812.
[320] G. Schmid, *J. Chem. Soc., Dalton Trans.* **1998**, 1077−1082.
[321] A. P. Alivisatos, K. P. Johnson, X. Peng, T. E. Wilson, C. J. Loweth, M. P. Burchez, Jr., P. G. Schultz, *Nature* **1996**, *382*, 609.
[322] C. N. R. Rao, G. U. Kulkarni, P. J. Thomas, *Chem. Soc. Rev.* **2000**, *29*, 27−35.
[323] N. Toshima, K. Hirakawa, *Polymer J.* **1999**, *31*, 1127−1132.
[324] P. Lu, T. Teranishi, K. Asakura, M. Miyake, N. Toshima, *J. Phys. Chem. B* **1999**, *103*, 9673−9682.
[325] J. Bradley, B. Tesche, W. Busser, M. Massse, M. Reetz, *J. Am. Chem. Soc.* **2000**, *122*, 4631−4636.
[326] D. Boxall, G. Deluga, E. Kenik, W. King, C. Lukehart, *Chem. Mater.* **2001**, ASAP article.
[327] K. Soulantica, A. Maisonnat, M. Fromen, M. Casanove, P. Lecante, B. Chaudret, *Angew. Chem. Int. Ed.* **2001**, *40*, 448−451.
[328] C. Nayral, E. Viala, P. Fau, F. Senocq, J. Jumas, A. Maisonnat, B. Chaudret, *Chem. Eur. J.* **2000**, *6*, 4082−4090.
[329] S. Gomez, K. Philippot, V. Colliere, B. Chaudret, F. Senocq, P. Lecante, *Chem. Commun.* **2000**, *19*, 1945−1946.
[330] F. Dassenoy, M. Cananove, P. Lecante, M. Verelst, E. Snoeck, A. Mosset, T. Ely, C. Amiens, B. Chaudret, *J. Chem. Phys.* **2000**, *112*, 8137−8145.
[331] T. Ely, C. Pan, C. Amiens, B. Chaudret, F. Dassenoy, P. Lecante, M. Casanove, A. Mosset, M. Respaud, J. Broto, *J. Phys. Chem. B* **2000**, *104*, 695−702.
[332] C. Pan, F. Dassenoy, M. Casanove, K. Philippot, C. Amiens, P. Lecante, A. Mosset, B. Chaudret, *J. Phys. Chem. B* **1999**, *103*, 10098−10101.
[333] M. Verelst, T. Ely, C. Amiens, E. Snoeck, P. Lecante, A. Mosset, M. Respaud, J. Broto, B. Chaudret, *Chem. Mater.* **1999**, *11*, 2702−2708.
[334] M. Pileni, *Pure Appl. Chem.* **2000**, *72*, 53−65.

[335] A. Diffis, A. D'Archivio, K. Jerabek, G. Schmid, B. Corain, *Adv. Mater.* **2000**, *12*, 1909.
[336] J. Hochpied, P. Bonville, M. Pileni, *J. Phys. Chem. B* **2000**, *104*, 905−912.
[337] J. Legrand, A. Ngo, C. Petit, M. Pileni, *Adv. Mater.* **2001**, *13*, 58.
[338] A. Ngo, M. Pileni, *J. Phys. Chem. B* **2001**, *105*, 53−58.
[339] M. Maillard, L. Motte, A. Ngo, M. Pileni, *J. Phys. Chem. B* **2000**, *104*, 11871−11877.
[340] S. Park, A. Lazarides, C. Mirkin, P. Brazis, C. Kannewurf, R. Lersinger, *Angew. Chem. Int. Ed.* **2000**, *39*, 3845.
[341] T. Taton, R. Mucic, C. Mirkin, R. Letsinger, *J. Am. Chem. Soc.* **2000**, *122*, 6305−6306.
[342] R. Reynolds, C. Mirkin, R. Letsinger, *Pure Appl. Chem.* **2000**, *72*, 229−235.
[343] C. Mirkin, T. Taton, *Nature* **2000**, *405*, 626−627.
[344] J. Storhoff, A. Lazarides, R. Mucic, C. Mirkin, R. Letsinger, G. Schatz, *J. Am. Chem. Soc.* **2000**, *122*, 4640−4650.
[345] C. Mirkin, *Science* **1999**, *286*, 2095−2096.
[346] N. Toshima, *Macromol. Symp.* **2000**, *156*, 45−52.
[347] N. Toshima, *Pure Appl. Chem.* **2000**, *72*, 317−325.
[348] Y. Shiraishi, M. Nakayama, E. Takagi, T. Tominaga, N. Toshima, *Inorg. Chim. Acta* **2000**, *300*, 964−969.
[349] P. Braunstein, H. Kormann, W. Meyer-Zaika, R. Pugin, G. Schmid, *Chem. Eur. J.* **2000**, *6*, 4637−4646.
[350] U. Paulus, U. Endruschat, G. Feldmeyer, T. Schmidt, H. Bönnemann, R. Behm, *J. Catal.* **2000**, *195*, 383−393.
[351] H. Bönnemann, R. Brinkmann, P. Britz, U. Endruschat, R. Mörtel, U. Paulus, G. Geldmeyer, T. Schmidt, H. Gasteiger, R. Behm, *J. New Mat. Electrochem. Syst.* **2000**, *3*, 199−206.

Received March 6, 2001
[I0083]

Crystal Structure and Solution Behavior of the Iron(III) Complex of the Artificial Trihydroxamate Siderophore with a Tris(3-aminopropyl)amine Backbone

Kenji Matsumoto,[a] Naomi Suzuki,[a] Tomohiro Ozawa,[a] Koichiro Jitsukawa,[a] and Hideki Masuda*[a]

Keywords: Siderophores / Iron / Tripodal ligands / Hydroxamate

Tris[{3-(*N*-acetyl-*N*-hydroxy)-glycylamino}propyl]amine (TAGP) forms a 1:1 tris(hydroxamato)iron(III) complex even at a low pH(≈2), which promotes the growth of the siderophore-auxotrophic mutant *Microbacterium flavescens*.

Introduction

Microorganisms produce low molecular weight compounds called siderophores for an uptake of iron. A large number of siderophores have hydroxamates or catecholates as the iron binding site that exhibit very high affinities for iron(III), and thus form very stable iron(III) complexes.[1,2] The high stability of Fe^{III}-siderophore complexes is attributed to not only such chelating effects but also to hydrogen bonding, van der Waals interactions and the predisposition of the ligands.[3,4] Thus, the ligand backbones are quite important for the stabilization of iron(III) complexes. Many artificial tripodal siderophores have been synthesized as ferrichrome and enterobactin analogues; the synthetic siderophores possess various tripodal backbones such as follows tris(2-aminoethyl)amine (TREN),[5] triaminomethylbenzene,[6] 1,5,9-triazacyclododecane,[7] nitrilotriacetic acid,[8] and 1,1,1-tris[(2-carboxyethoxy)methyl]propane.[5] Among such tripodal backbones, TREN has been used most frequently. Recently, we have reported the synthesis of tris{2-[(*N*-acetyl-*N*-hydroxy)glycylamino]ethyl}amine (TAGE, Figure 1) as an artificial siderophore with a TREN anchor; its iron(III) complex showing an extremely high stability ($\log\beta = 28.7$).[5c] From the crystal structure of the iron(III) complex,[5c] this high stability was found to be due to the intramolecular hydrogen-bonding networks between amide hydrogens and coordinating *N*-hydroxy oxygens in the intra- and interstrands. However, tripodal anchors such as TREN have also been reported to form less-stable iron(III) complexes than the natural siderophore-iron(III) complexes, presumably due to the small size of the anchor for iron(III) chelation.[9]

Tris(3-aminopropyl)amine (TRPN), whose alkyl chains are one methylene group longer than TREN, has not been used much despite the similarities in its structure with TREN. We therefore synthesized tris{[3-(*N*-acetyl-*N*-hydroxy)glycylamino]propyl}amine (TAGP, Figure 1) as a trihydroxamate artificial siderophore with a TRPN anchor in order to examine the effect of the size. Here, we will describe the crystal structure and solution behavior of its iron(III) complex.

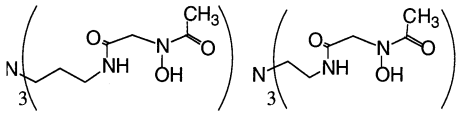

Figure 1. Ligands used in this study

Results and Discussion

As shown in Figure 2, the iron(III)-TAGP complex (**1**) was isolated as a hydrochloride salt with the tertiary amine nitrogen protonated. The quaternary amine is in the "out"

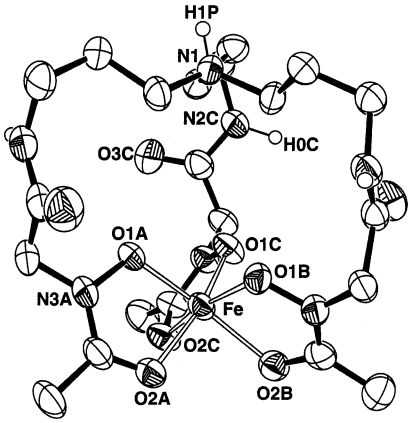

Figure 2. Crystal structure of **1**, showing the atom numbering schemes; selected bond lengths (Å) and angles (deg): Fe−O(1A) 1.971(4), Fe−O(1B) 1.992(3), Fe−O(1C) 1.967(3), Fe−O(2A) 2.036(3), Fe−O(2B) 2.081(3), Fe−O(2C) 2.041(4); O(1A)−Fe−O(2A) 79.3(1), O(1B)−Fe−O(2B) 77.6(1), O(1C)−Fe−O(2C) 78.6(1); all hydrogen atoms except for the amide and TRPN amine hydrogens and the counter anion have been omitted for clarity

[a] Department of Applied Chemistry, Faculty of Engineering, Nagoya Institute of Technology
Showa-ku, Nagoya 466-8555, Japan
Fax: (internat.) + 81-52/735-5228
E-mail: masuda@ach.nitech.ac.jp

 © WILEY-VCH Verlag GmbH, 69451 Weinheim, 2001 1434−1948/01/1010−2481 $ 17.50+.50/0

conformation, which is in contrast to many iron(III) complexes with synthetic siderophores that are in the "in" conformation.[5c−5e] The iron(III) ion has a distorted octahedral geometry with three coordinated hydroxamates, and the overall structure is twisted with a pseudo-threefold axis. This crystal structure is very similar to the calculated lowest energy conformation of the iron(III) complex of the trishydroxamate with a triscarboxylate anchor that has previously been reported by Shanzer et al.[3b]

The average bond lengths between the iron(III) atom and the coordinating *N*-hydroxyl O(1) and carbonyl O(2) atoms are 1.977(3) and 2.053(3) Å, respectively, and the average O(1)−Fe−O(2) bond angle is 78.4(1)°. The average Fe−O(2) bond length is 0.01−0.02 Å longer than those of natural and artificial trihydroxamate siderophores (2.022−2.041 Å);[2][5c] this is due to the longer Fe−O(2B) bond (0.04−0.05 Å longer than normal). The rest of the Fe−O bonds are very similar to those for other iron(III)-siderophore complexes.[2][5c] The twist angle[10] determined for **1** is 43.9°, which is comparable to the calculated value (45.7°). Considering the definition of the twist angle, these findings suggest that the configuration around the metal ion is nearly the idealized C_3 symmetry.

The distance between the iron(III) ion and the quaternary amine nitrogen in **1** is 5.205 Å, which is only slightly longer than that in Fe^{III}TAGE ($Fe\cdots N_{amine}$ = 5.139 Å). In the catechol macrobicyclic ligand-metal complexes Na_3[Fe(BCT)] and Na_3[Fe(BCTPT)],[11a] the apical N−N distance between the two TRPN caps {Na_3[Fe(BCTPT)]: 10.70 Å} is longer than that in TREN {Na_3[Fe(BCT)]: 9.76 Å}.[11b] Thus, the short distance between the iron(III) ion and the amine nitrogen in Fe^{III}TAGP may be attributed to the electrostatic interaction between the protonated amines and the hydroxamate anions. The steric restriction of the TRPN anchor may be also reduced by adopting a configuration such that the iron(III) ion is wrapped into the TAGP ligand.

The TAGP amine proton forms a hydrogen bond with a chloride ion on the pseudo-threefold axis [N(1)···Cl(1) = 3.081(4) Å]. In the crystal, the amide groups form intermolecular hydrogen bonds between the nearest neighbor molecules [N(2B)···O(1B) = 3.070(5), N(2B)···O(2A)= 3.099(5) and N(2C)···O(3B) = 3.055(6) Å] and between the complex and the water molecules [N(2A)···O(1 W) = 2.838(8) and N(2C)···O(2 W) = 3.134(7) Å]. The intramolecular hydrogen bond found in Fe^{III}TAGE,[5c] however, was not observed.

The UV/Vis spectra of iron(III)-TAGP complex measured in various pH conditions showed a characteristic absorption band corresponding to an LMCT at 425 nm, which did not show a large spectral change over a wide pH range of 2−8 (Figure 3), indicating that TAGP forms a stable tris(hydroxamato)iron(III) complex even under strongly acidic conditions. However, the iron(III)-TAGE complex exhibited the same characteristic absorption band at only pH 4−8 in aqueous solution. The difference in the formation behaviors of the iron(III) complexes with TAGP and TAGE under acidic conditions is probably due to the different conformations of the tertiary amine, "in" and "out". That is, as the tertiary amine in Fe^{III}-TAGE complex takes the "in" conformation and is protected from the outer sphere by intramolecular hydrogen bonding networks,[5c] the tertiary amine is deprotonated, which probably contributes to the formation of the stable tris(hydroxamato)-type complex. In contrast, as the tertiary amine in the Fe^{III}-TAGP complex takes the "out" conformation, the protonated tertiary amine does not affect the formation of the complex. Hence, the stable tris(hydroxamato)-type Fe^{III}-TAGP complex is formed even under acidic conditions.

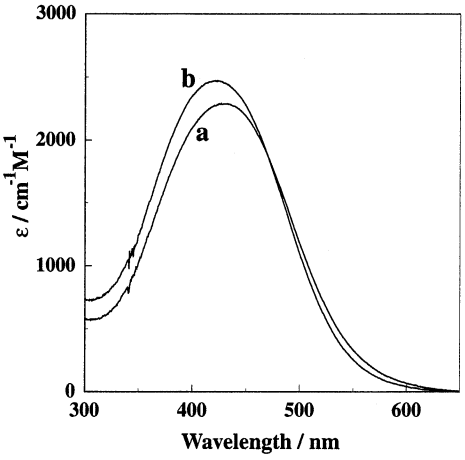

Figure 3. UV/Vis spectra of iron(III)-TAGP complexes (0.1 mM) in an aqueous solution (I = 0.1 M $NaClO_4$): (a) pH 2.0, (b) pH 7.4

The pK_a of the tertiary amine in TAGP is 7.61,[12] which is larger than that of TAGE (pK_a = 5.46), suggesting that the Fe^{III}-TAGP complex is protonated even in a neutral aqueous solution. Comparing the formation constants of the complexes, the protonated Fe^{III}-TAGP complex (log β_{111} = 30.6[12]) is more stable than the Fe^{III}-TAGE complex (log β_{110} = 28.7),[5c] and is similar to the natural siderophore ferrioxamine B (log β_{111} = 30.6).[13] These results indicate that the TRPN anchor brings about a larger stabilization of the complex than TREN, which is one of the important factors of the siderophore function. In contrast, the ferrichrome analogue with a C-terminated triscarboxylate anchor, Et-C($CH_2OCH_2CONHCH_2CONOHCH_3$)$_3$, which was previously reported by Dayan et al., forms polymeric and polynuclear complexes rather than a 1:1 Fe^{III}-ligand complex; this was explained in terms of the absence of stabilization factor such as intramolecular noncovalent interactions.[3a] In spite of the high structural similarity between our ligands and theirs, the complexation behaviors are very different. The substantial difference between the ligands is that the terminal atom of the tripodal ligand is either an amine nitrogen or an alkyl carbon. Thus, the high stability of the iron(III)-TAGP complex identified in the wide pH range of 2−8 is achieved by the electrostatic interaction between the positively charged TRPN anchor and the negatively charged aminohydoxyl oxygens.

The bioavailability of **1** was also investigated using *Microbacterium flavescens* (ATCC No. 25091), which cannot synthesize siderophores by itself. Although the growth of the strain was not observed in the siderophore-free ATCC No. 424 broth,[14] it was seen in the medium containing TAGP. This result indicates that TAGP has a siderophore function transporting an iron ion from the medium into the cell. A similar compound, TAGE, also promoted growth of the same strain under the same conditions; the difference between the TREN and TRPN anchors was not observed. However, the above-mentioned ferrichrome analogues with a C-terminated triscarboxylate anchor did not promote the growth of the siderophore-auxotrophic mutants of *Pseudomonas putida*,[3a,3c] although the strains examined are different from those which were used in this study. The microbial inactivity of these complexes is either because of the formation of polymeric and polynuclear complexes, or because the 1:1 Fe^{III}-ligand complexes, if they are formed, take a conformation that inhibits the receptor binding.[3a] As mentioned above, the substantial difference between **1** and these complexes is that the complex either has a positive charge or it does not; the former has a positive charge but the latter are neutral. Therefore, a positive charge on a complex may contribute to the promotion of biological activity.

The above findings suggest not only the availability of TRPN as an anchor in the siderophore function but also the biological implication of electrostatic interactions in the positively charged natural siderophores such as desferrioxamine B. Detailed investigations are in progress.

Experimental Section

Fe^{III}TAGP·HCl (1): The ligand TAGP was synthesized according to a modification of a previously published method.[15] The iron(III) complex of TAGP was prepared by the following method. A few drops of pyridine were added to a methanol solution containing $FeCl_3$ and TAGP in a 1:1 molar ratio.[16] Slow evaporation of the solution for a few weeks at room temperature gave a deep-red colored single crystal of **1** suitable for X-ray diffraction analysis.[17]

X-ray Crystallographic Study: Crystal data for $C_{22}H_{45}ClFeN_7O_{12}$ (molecular weight = 690.04): triclinic system with cell dimensions at 288 K of a = 11.711(7), b = 13.285(4) c = 10.974(6) Å, α = 93.04(5), β = 102.56(3), γ = 101.14(6) ° V = 1627(1) Å^3; μ(Mo-K_α) = 6.11 cm^{-1}; F(000) = 730.0; space group $P\bar{1}$ with Z = 2 and $D_{calcd.}$ = 1.41 g cm^{-3}. A selected specimen (0.56 × 0.25 × 0.19 mm.) was sealed in a thin-walled glass capillary. The unit cell parameters were derived from a least-squares refinement of 25 well-centered reflections by use of a Rigaku AFC-7R, and all diffractions were measured on a Rigaku R-AXIS-IV imaging plate area detector with graphite monochromated Mo-K_α radiation (λ = 0.71070 Å). A total of 5484 reflections with a maximum 2θ value of 51.4° were collected. The reflection data were corrected for Lorentz and polarization effects. No absorption correction was applied because of its small absorption coefficient.

The structure was solved by a combination of direct methods and Fourier techniques and refined anisotropically for non-hydrogen atoms by full-matrix least-squares calculations. Refinements were continued until all shifts were smaller than one-third of the standard deviations of the parameters involved. Atomic scattering factors and anomalous dispersion terms were taken from the literature.[18] Hydrogen atoms, which were located from the difference Fourier maps, were included for the structure factor calculation, but not refined. The final cycle of full-matrix least-squares refinement was based on 4725 observed reflections [$I > 3\sigma(I)$] and 388 variable parameters; final R and R_w values converged to 0.091 and 0.141, respectively, with the largest parameter being 0.04 times its esd. The standard deviation of an observation of unit weight was 1.28. The maximum and minimum peaks on the final difference Fourier map corresponded to 0.75 and −1.24 e/Å^3, respectively, which were detected near the metal ion. All calculations were performed using the teXan[19] crystallographic software package from the Molecular Structure Corporation.

Acknowledgments

This work was supported in part by a Grant-in-Aid for Scientific Research from the Ministry of Education, Science, Sports, and Culture of Japan (H. M.), for which we express our thanks.

[1] J. B. Neilands, *Struct. Bonding* **1984**, *58*, 1−24.
[2] B. F. Matzanke, G. Müller-Matzanke, K. N. Raymond, in *Physical Bioinorganic Chemistry Vol. 5: Iron Carriers and Iron Proteins* (Ed.: T. M. Loehr), VCH, New York, **1989**.
[3] [3a] I. Dayan, J. Libman, Y. Agi, A. Shanzer, *Inorg Chem.* **1993**, *32*, 1467−1475. − [3b] A. Shanzer, J. Libman, S. Lifson, *Pure and Appl. Chem.* **1992**, *64*, 1421−1435. − [3c] E. Jurkevitch, Y. Hadar, Y. Chen, J. Libman, A. Shanzer, *J. Bacteriol.* **1992**, *174*, 78−83.
[4] [4a] T. D. P. Stack, Z. Hou, K. N. Raymond, *J. Am. Chem. Soc.* **1993**, *115*, 6466−6467. − [4b] Z. Hou, C. J. Sunderland, T. Nishio, K. N. Raymond, *J. Am. Chem. Soc.* **1996**, *118*, 5148−5149.
[5] [5a] S. J. Rodgers, C.-W. L. Chiu, C. Y. Ng, K. N. Raymond, *Inorg. Chem.* **1987**, *26*, 1622−1625. − [5b] C. Y. Ng, S. J. Rodgers, K. N. Raymond, *Inorg. Chem.* **1989**, *28*, 2062−2066. − [5c] K. Matsumoto, T. Ozawa, K. Jitsukawa, H. Einaga, H. Masuda, *Inorg. Chem.* **2001**, *40*, 190−191. − [5d] G. Serratrice, P. Baret, H. Boukhalfa, I. Gautier-Luneau, D. Luneau, J.-L. Pierre, *Inorg. Chem.* **1999**, *38*, 840−841. − [5e] G. Xiao, D. van der Helm, R. C. Hider, P. S. Dobbin, *Inorg. Chem.* **1995**, *34*, 1268−1270.
[6] F. L. Weitl, K. N. Raymond, *J. Am. Chem. Soc.* **1979**, *101*, 2728−2731.
[7] M. A. Esteves, M. C. T. Vaz, M. L. S. Simões Gonçalves, E. Farkas, M. A. Santos, *J. Chem. Soc., Dalton Trans.* **1995**, 2565−2573.
[8] [8a] M. Akiyama, Y. Hara, H. Gunji, *Chem. Lett.* **1995**, 225−226. − [8b] Y. Hara, L. Shen, A. Tsubouchi, M. Akiyama, K. Umemoto, *Inorg. Chem.* **2000**, *39*, 5074−5082.
[9] T. B. Karpishin T. M. Dewey, K. N. Raymond, *J. Am. Chem. Soc.* **1993**, *115*, 1842−1851.
[10] The twist angle is defined by the O(N)−Fe−O(C) angle of a single hydroxamate ligand projected onto the plane perpendicular to the idealized threefold axis. The idealized twist angle is calculated by the following equation: twist angle = −73.9 + 94.1b, where b is a normalized bite and calculated from the bite angle, θ(O−Fe−O) = 2 *sin* (θ/2). See also refs. 2 and 9.
[11] [11a] BCT and BCTPT are the abbreviations for bicapped TRENCAM and bicapped TPTCAM, respectively, which are composed of three 2,3-dihydroxyterephthalic acids and two tris-

(aminoalkyl)amines. See also ref. 11b. – [11b] T. B. Karpishin, T. D. P. Stack, K. N. Raymond, *J. Am. Chem. Soc.* **1993**, *115*, 182–192.

[12] $\beta_{mlh} = [M_mL_lH_h]/[M]_m[L]_l[H]_h$ is defined as the overall formation constant for $M_mL_lH_h$ where M = metal ion, L = ligand in its deprotonated form, and H = hydrogen ion. The pK_as of TAGP ($pK_a^1 = 9.49$, $pK_a^2 = 9.18$, $pK_a^3 = 8.40$, $pK_a^4 = 7.61$) and the β_{111} of Fe^{III}-TAGP ($\log\beta_{111} = 30.6$) complex were determined by the potentiometric titration and the spectrophotometric measurement of competition reaction with EDTA according to ref. 2.

[13] G. Schwarzenbach, K. Schwarzenbach, *Helv. Chim. Acta* **1963**, *46*, 1390–1400.

[14] The siderophore-free ATCC No. 424 broth was prepared by the following method; 1 g Bacto Peptone, 1 g Yeast Extract and 0.2 g K_2HPO_4 were dissolved in 100 mL of water, and then the solution was adjusted pH to 7.4 with 1 M NaOH.

[15] [15a] T. Kolasa, A. Chimiak, *Tetrahedron* **1974**, *30*, 3591–3595. – [15b] T. Kolasa, A. Chimiak, *Tetrahedron* **1977**, *33*, 3285–3288.

[16] S. M. Cohen, M. Meyer, K. N. Raymond, *J. Am. Chem. Soc.* **1998**, *120*, 6277–6286.

[17] Crystallographic data (excluding structure factors) for the structure reported in this paper has been deposited with the Cambridge Crystallographic Data Centre as supplementary publication no. CCDC-161835. Copies of the data can be obtained free of charge on application to CCDC, 12 Union Road, Cambridge CB2 1EZ, UK [Fax: (internat.) +44-1223/336-033; E-mail: deposit@ccdc.cam.ac.uk].

[18] *International Tables for X-ray Crystallography, Vol. IV* (Eds.: J. A. Ibers, W. C. Hamilton), Kynoch Press, Birmingham, England, **1974**, Table 2.2A.

[19] teXsan: Crystal Structure Analysis Package, Molecular Structure Corporation, The Woodlands, TX (**1985** & **1992**).

Received April 19, 2001
[I01139]

Formation of Peptides at Half-Sandwich Complexes Using β- and γ-Amino Acid Esters and a Facile Dipeptide Synthesis from an *N,O*-Glycinato Half Sandwich Complex $[RuCl(NH_2CH_2CO_2)(\eta^6\text{-}C_6Me_6)]$[‡]

Katharina Haas[a] and Wolfgang Beck*[a]

Dedicated to Professor Kurt Dehnicke on the occasion of his 70th birthday

Keywords: Peptides / Amino Acids / Ruthenium / Sandwich complexes

The tripeptide ester complexes **2** and **3** are obtained from the diglycine ester complex [RuCl(*N,N′*-glyglyOMe-H$^+$)(η^6-C_6Me_6)] and the amino acid esters $H_2N(CH_2)_nCO_2Me$ (n = 2, 3). The reaction of the *N,O*-glycinato complex $[RuCl(NH_2CH_2CO_2)(\eta^6\text{-}C_6Me_6)]$ with the β-, γ- and δ-amino acid methyl esters $H_2N(CH_2)_nCO_2Me$ (n = 2,3,4) in CH_3OH and in the presence of NaOMe affords the η^3-*N,N′O*-dipeptide complexes $[Ru\{H_2N(CH_2)_nCONCH_2CO_2\}(\eta^6\text{-}C_6Me_6)]$ **5**–**7** in good yields. These complexes are also obtained in a one pot reaction from $[RuCl(\mu\text{-}Cl)(\eta^6\text{-}C_6Me_6)]_2$, glycine and the amino acid ester. The formation of small peptides at the metal represents a facile procedure which does not require either a protecting/activating group or a coupling agent.

The formation of peptides from nonactivated α-amino acid esters,[2] α-amino acids[3] or from cyclopentadienyltitanium, -zirconium and -tantalum α-aminocarboxylates[4] at the metal centres has been reported by several groups. We have shown that half-sandwich complexes of Ru, Rh and Ir promote the formation of linear oligopeptides from amino acid esters[5a] and that the continuous addition of glycine or alanine esters to [RuCl(glyglyglyOMe-H$^+$)(*p*-cymene)] leads to complexes of higher peptides.[5b] Previously we have used di- or tripeptide ester complexes and α-amino acid esters for the elongation of the peptide chain with a defined amino acid sequence. In view of the recent high interest in β-amino acids,[6] which stems from the significant developments in β-peptide chemistry by Seebach[7] and Gellman[8] and their co-workers, we wanted to see whether β- or γ-amino acid esters could be used for peptide synthesis at half-sandwich complexes. We have also found that the condensation of amino acid esters even occurs with an *N,O*-chelate glycinate complex to give dipeptide complexes.

Formation of η^3-*N,N′,N′′*-Tripeptide Ester Ruthenium Complexes with N-terminal β-Alanine and γ-Amino Valeric Acid

The η^2-*N,N′*-diglycine ester complex **1**[9] was found to insert the amino acid esters $H_2N(CH_2)_nCO_2Me$ (n = 2,3) in the presence of NaOMe giving the tripeptide complexes **2** and **3** in high yields (ca. 90%; Scheme 1). The reactions were carried out at low temperatures in order to avoid side reactions, especially cyclisation[10] of the tripeptide ester at the ruthenium centre.

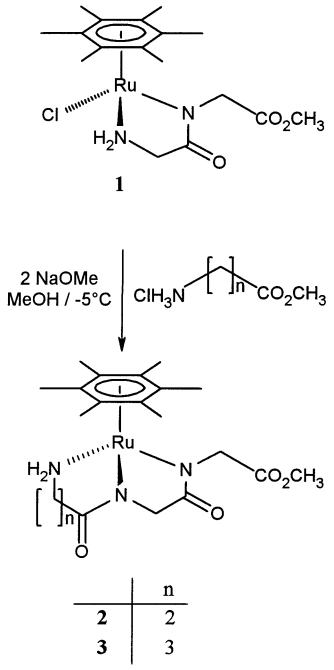

	n
2	2
3	3

Scheme 1

Compounds **2** and **3** showed the molecular ions in the FAB-MS spectra. The new complexes contain a six- or seven-membered chelate ring as well as a five-membered ring. Other examples of bis(chelate) complexes with a five- and a seven-membered ring are half-sandwich complexes of Ru, Rh and Ir with L-methionylglycinate;[11] those containing a five- and a six-membered ring are, for example,

[‡] Metal Complexes of Biologically Important Ligands, CXXXVI. – Part CXXXV: see ref.[1]

[a] Department Chemie der Ludwig-Maximilians-Universität München,
Butenandtstr. 5–13, 81377 München, Germany

 © WILEY-VCH Verlag GmbH, 69451 Weinheim, 2001 1434–1948/01/1010–2485 $ 17.50+.50/0

half-sandwich complexes of methioninate.[12] Side reactions (possibly cyclisation of the tripeptides) were observed when amino acid esters $H_2N(CH_2)_nCO_2R$ with longer carbon chains ($n > 3$) were used and the products proved not to be analytically pure.

The IR, ^1H and ^{13}C NMR spectra of **2** and **3** exhibit the expected signals (see Exp. Sect.)., and successful formation of the tripeptide at the metal is demonstrated by the appearance of only one ^{13}C NMR signal for the ester carbonyl group at $\delta = 175$.

Dipeptide Formation from [RuCl(glycinate)(η^6-C_6Me_6)] and Amino Acid Esters

The *N,O*-glycinate ruthenium complex **4**[13] is isoelectronic with the dipeptide ester complex **1** which was successfully used for the peptide synthesis at a metal centre.[5] Complexes **1** and **4** contain three facial coordination sites and a leaving group. Indeed the reaction of **4** with the hydrochlorides of the β-, γ- and δ-amino acid methyl esters $H_2N(CH_2)_nCO_2Me$ ($n = 2-4$) in MeOH at room temperature and in the presence of NaOMe affords the stable, light yellow dipeptide complexes **5**−**7** with yields of up to 97%. The yield decreases with the C-chain length of the amino acid ester (**7**: 67%). No reaction was observed with the ε-amino acid ester $H_2N(CH_2)_5CO_2Me$ and **4**.

The compounds **5**−**7** are also available in a one pot reaction from the chloro-bridged complex [RuCl(μ-Cl)(η^6-C_6Me_6)]$_2$,[14] glycine and the hydrochloride of the amino acid methyl ester in the presence of NaOMe (Scheme 2).

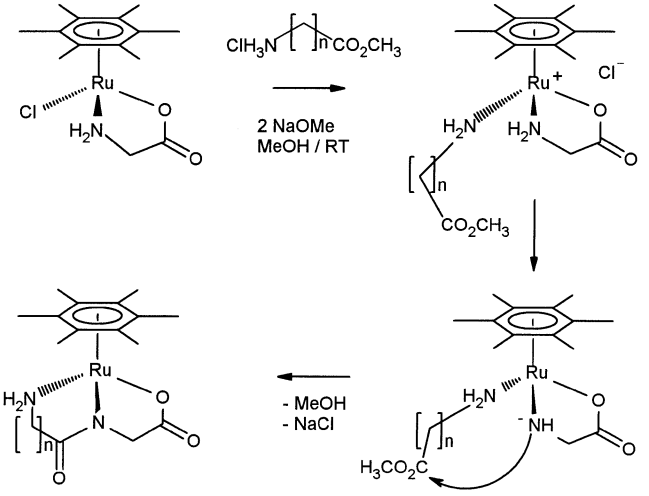

Scheme 3

Side products could not be detected. We assume a mechanism similar to that proposed by Yamada et al.[2] and Rode[3] for the Cu^{II}-catalyzed formation of peptides from α-amino acids (Scheme 3). The sterically favoured annellation of a five- and a six- or seven-membered ring may promote the formation of the bis(chelate) complexes. This reaction represents a facile peptide formation from an unprotected α-amino carboxylate which doesn't require either an activating group for the free amino acid or a coupling agent. It differs from the formation of the dipeptide esters by the reaction of cyclopentadienyltantalum(V) amino acid carboxylates with free amino acid esters, where the metal carboxylates function as "activated amino acid esters".[4] The

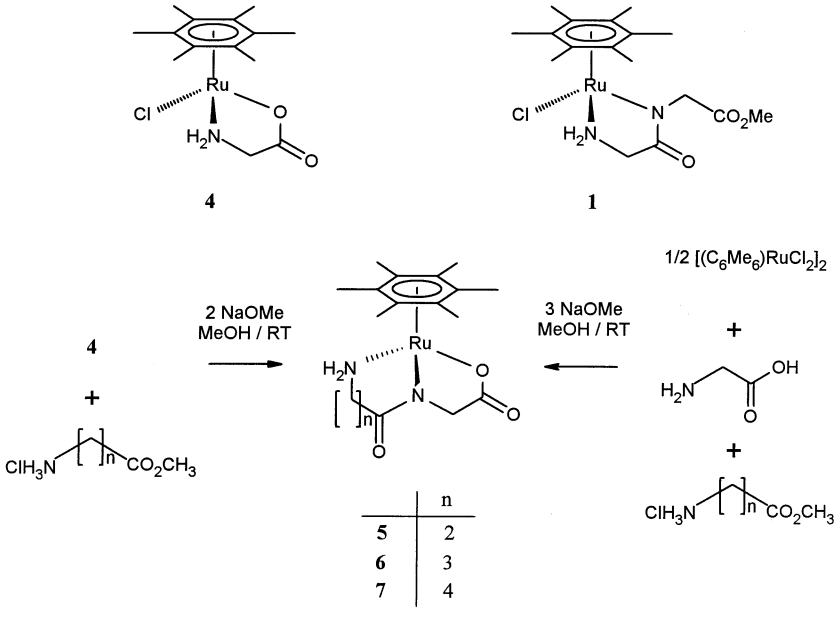

Scheme 2

possibility that in the reaction of **4** with β-, γ- and δ-amino acid esters the latter are added to the metal-activated[4] carboxylate group can be excluded, since then a dipeptide ester complex should be formed that would show IR and NMR spectroscopic data different from those of **5**−**7**; for example, a carbonyl ester absorption at 1730 cm^{-1} would be present instead of a carboxylate band at 1620 cm^{-1}.

The peptide formation can be followed from the IR spectra. Compounds **5**−**7** exhibit a strong absorption at 1541−1571 cm^{-1} for the amide group. Further characteristic bands are observed at 3200 (NH) and 1620 cm^{-1} (CO_2). In the ^1H NMR spectra sharp signals are found which point to a slow epimerization[15] at the chiral metal centre. The ^{13}C NMR spectra show the expected signals.

Experimental Section

Preparation of 2 and 3: A solution of the hydrochloride of the amino acid methyl ester (0.2 mmol) and NaOMe (0.2 mmol) in methanol (5 mL) was stirred for 10 min. at room temperature. A solution of **1**[9] (0.2 mmol) in methanol (3 mL) was then added to this mixture, followed by the dropwise addition of a solution of NaOMe (0.2 mmol) in methanol (15 mL) at −15 °C during 2−3 h. The colour of the solution changed from orange to yellow. The solvent was then removed in vacuo and the yellow, oily residue was dissolved in dichloromethane. Sodium chloride was then centrifuged off and the solution was concentrated to 2 mL. The yellow product was precipitated by addition of 50 mL of pentane, washed with more pentane and dried in vacuo.

[Ru{η³-*N*,*N*′,*N*′′-(β-ala-gly-gly-OMe)}(η⁶-C_6Me_6)] (2): Light yellow powder, yield 91%. − IR (KBr): $\tilde{\nu}$ = 3266 cm^{-1} (m), 3157 (w) [NH_2], 1732 (s) [CO_2CH_3], 1566 (vs) [Amide-I]. − ^1H NMR (400 MHz, CD_3OD): δ = 4.72 (d, ^2J = 16.8 Hz, 1 H, *H*CH), 4.58 (d, ^2J = 16.8 Hz, 1 H, HC*H*), 3.66 (s, 3 H, CO_2CH_3), 3.46 (2 d, ^2J = 16.8 Hz, 2 H, CH_2), 2.97 (m, 1 H, NH_2-CH_2−CH_2−CO), 2.78 (m, 1 H, NH_2−CH_2−CH_2−CO), 2.1−2.3 (m, 2 H, NH_2−CH_2−CH_2−CO), 2.13 [s, 18 H, $C_6(CH_3)_6$]. − ^{13}C NMR (100.5 MHz, CD_3OD): δ = 182.6, 176.1, 175.6 (*C*ONR and CO_2CH_3), 94.8 [$C_6(CH_3)_6$], 55.0, 52.9 (CH_2), 50.2 (CO_2CH_3), 39.8, 39.4 (CH_2−CH_2), 16.5 [$C_6(CH_3)_6$]. − MS (FAB+, *m*NBA): *m*/*z* (%) = 480 (5) [M + H^+], 502 (4) [M + Na^+], 538 (1) [M + H^+ + NaCl].

[Ru{η³-*N*,*N*′,*N*′′-(γ-abu-gly-gly-OMe)}(η⁶-C_6Me_6)] (3): Light yellow powder, yield 86%. − IR (KBr): $\tilde{\nu}$ = 3225 cm^{-1} (m) [NH_2], 1749 (s), 1741 (s), 1732 (s) [CO_2CH_3], 1585 (vs), 1569 (vs) [Amide-I]. − ^1H NMR (400 MHz, CD_3OD): δ = 4.38 (d, ^2J = 17.6 Hz, 1 H, *H*CH), 3.79 (d, ^2J = 17.6 Hz, 1 H, HC*H*), 3.75 (s, 3 H, CO_2CH_3), 3.22 (ddd, ^2J = 11.3, ^3J = 7.7 Hz, ^3J = 3.7 Hz, 1 H, NH_2−CH_2−CH_2−CH_2−CO), 3.10 (d, ^2J = 16.2 Hz, 1 H, *H*CH), 2.86 (dt, ^2J = 11.2, ^3J = 7.8 Hz, 1 H, NH_2−CH_2−CH_2−CH_2−CO), 2.55 (d, ^2J = 16.4 Hz, 1 H, HC*H*), 2.22−2.26 (m, 2 H, CH_2), 2.10 [s, 18 H, $C_6(CH_3)_6$], 1.95−2.10 (m, 2 H, NH_2−CH_2−CH_2−CH_2−CO). − ^{13}C NMR (100.5 MHz, CD_3OD): δ = 184.2, 182.2, 174.8 (*C*ONR and CO_2CH_3), 94.0 [$C_6(CH_3)_6$], 55.8, 55.2 (CH_2), 53.5 (CO_2CH_3), 47.1, 34.2, 24.4 (CH_2−CH_2−CH_2), 16.1 [$C_6(CH_3)_6$]. − MS (FAB+, *m*NBA): *m*/*z* (%) = 494 (7) [M + H^+], 516 (4) [M + Na^+], 552 (1) [M + H^+ + NaCl].

General Procedure for the Synthesis of 5−7 from [RuCl(glycinate)(η⁶-C_6Me_6)]: A solution of 0.3 mmol of NaOMe in methanol was added dropwise to a solution of 0.15 mmol of **4**[13] and 0.15 mmol of the hydrochloride of the amino acid methyl ester in 5 mL of dried methanol. The yellow solution was then stirred for 2 h (**5**, **6**) or 6 h (**7**) at room temperature. The solvent was removed in vacuo and the residue dissolved in 5 mL of dichloromethane containing a very small amount of methanol (ca. 0.1 mL). Sodium chloride was then centrifuged off and the solution concentrated to 2 mL. The product was precipitated with diethyl ether, washed with Et_2O and dried in vacuo.

General Procedure for the Synthesis of 5−7 from [$RuCl_2$(η⁶-C_6Me_6)]₂: A solution of 0.6 mmol of NaOMe in methanol was added to a mixture of 0.1 mmol of [$RuCl_2$(η⁶-C_6Me_6)]₂,[14] 0.2 mmol of glycine and 0.2 mmol of the hydrochloride of the amino acid methyl ester in 5 mL of methanol. Stirring for 2−6 h gave a yellow solution from which the solvent was then removed in vacuo. The residue was dissolved in 5 mL of dichloromethane containing a very small amount of methanol (ca. 0.1 mL). Sodium chloride was centrifuged off and the solution concentrated to 2 mL. The product was precipitated with diethyl ether, washed with Et_2O and dried in vacuo.

[Ru{η³-*N*,*N*′,*O*-(β-Ala-Gly-CO_2)}(η⁶-C_6Me_6)] (5): Light yellow powder, yield 97%. − IR (KBr): $\tilde{\nu}$ = 3246 cm^{-1} (m), 3150 (m) [NH_2], 1611 (vs) [CO_2Ru], 1571 (vs) [Amide-I]. − ^1H NMR (400 MHz, CD_3OD): δ = 4.59 (d, ^2J = 17.35 Hz, 1 H, *H*CH), 3.53 (d, ^2J = 17.35 Hz, 1 H, HC*H*), 2.97−2.93 (m, 2 H, CH_2−CH_2), 2.75−2.73 8m, 2 H, CH_2−CH_2), 2.16 (s, 18 H, C_6Me_6). − ^{13}C NMR (100.5 MHz, CD_3OD): δ = 183.4, 174.6 (*C*ONR and R*C*O_2Ru), 91.9 [$C_6(CH_3)_6$], 53.6 (CH_2), 48.6, 38.1 (CH_2−CH_2), 14.7 [$C_6(CH_3)_6$]. − $C_{17}H_{26}N_2O_3Ru{\cdot}H_2O$ (425.49): calcd. C 47.98, H 6.63, N 6.58; found C 47.98, H 6.46, N 6.55.

[Ru{η³-*N*,*N*′,*O*-(γ-Abu-Gly-CO_2)}(η⁶-C_6Me_6)] (6): Light yellow powder, yield 92%. − IR (KBr): $\tilde{\nu}$ = 3260 cm^{-1} (m), 3224 (m) [NH_2], 1621 (vs, br) [CO_2Ru], 1568 (vs) [Amide-I]. − ^1H NMR (400 MHz, CD_3OH): δ = 5.88 (br. t, 1 H, NH_2), 4.81 (br. m, 1 H, NH_2), 3.38 (m, 1 H, NH_2−CH_2−CH_2−CO_2), 2.99−3.11 (m, 2 H, -CH_2- + gly), 2.58−2.52 (m, 1 H, -CH_2-), 2.24−2.35 (m, 2 H, -CH_2- + gly), 2.14 (s, 18 H, C_6Me_6), 2.11−1.85 (m, 2 H, -CH_2-). − ^{13}C NMR (100.5 MHz, CD_3OD): δ = 184.9, 184.1 (*C*ONR and R*C*O_2Ru), 92.7 [$C_6(CH_3)_6$], 53.3 (CH_2), 45.3 (N−CH_2−CH_2−CH_2−CO), 34.2 (N−CH_2−CH_2−CH_2−CO), 24.5 (N−CH_2−CH_2−CH_2−CO), 16.0 [$C_6(CH_3)_6$]. − $C_{18}H_{28}N_2O_3Ru{\cdot}H_2O$ (439.49): calcd. C 49.19, H 6.88, N 6.37; found C 49.83, H 6.64, N 6.22.

[Ru{η³-*N*,*N*′,*O*-(δ-APS-Gly−CO_2-)}(C_6Me_6)] (7): Light yellow powder, yield 67%. − IR (KBr): $\tilde{\nu}$ = 3224 cm^{-1} (m) [NH_2], 1626 (vs, br) [CO_2Ru], 1541 (vs) [Amide-I]. − ^1H NMR (400 MHz, CD_3OD): δ = 3.29−3.25 (m, 2 H, CH_2), 3.05 (d, ^2J = 17.05 Hz, 1 H, *H*CH), 3.03−2.96 (m, 1 H, CH_2), 2.56 (d, ^2J = 17.35 Hz, 1 H, HC*H*), 2.31−2.25 (m, 2 H, CH_2−CH_2), 2.12 (s, 18 H, C_6Me_6), 1.82−1.80 (m, 1 H, CH_2), 1.79−1.61 (m, 1 H, CH_2), 1.50−1.41 (m, 1 H, CH_2). − ^{13}C NMR (100.5 MHz, CD_3OD): δ = 185.1, 176.8 (*C*ONR and R*C*O_2Ru), 92.3 [$C_6(CH_3)_6$], 51.2 (CH_2), 45.0 (N−CH_2−CH_2−CH_2−CH_2−CO), 33.8 (N−CH_2−CH_2−CH_2−CH_2−CO), 26.4 (N−CH_2−CH_2−CH_2−CH_2−CO), 22.8 (N−CH_2−CH_2−CH_2−CH_2−CO), 15.9 [$C_6(CH_3)_6$]. − $C_{19}H_{28}N_2O_3Ru{\cdot}H_2O$ (453.46): calcd. C 50.32, H 7.11, N 6.18; found C 50.10, H 6.66, N 5.99.

Acknowledgments

Generous support by Deutsche Forschungsgemeinschaft and Fonds der Chemischen Industrie is gratefully acknowledged. We thank Professor W. Steglich and Dr. W. Spahl, München, for mass spectra. We thank one referee for valuable comments.

[1] H. Dialer, W. Steglich, W. Beck, *Tetrahedron* **2001**, *57*, 4855−4861.

[2] [2a] D. A. Buckingham, L. G. Marzilli, A. M. Sargeson, *J. Am. Chem. Soc.* **1967**, *89*, 4539−4540; J. P. Collman, E. Kimura, *J. Am. Chem. Soc.* **1967**, *89*, 6096−6103; P. A. Sutton, D. A. Buckingham, *Acc. Chem. Res.* **1987**, *20*, 357−364; D. R. Knighton, D. R. K. Harding, M. J. Friar, W. S. Hancock, G. D. Reynolds, C. R. Clark, R. F. Tasker, D. A. Buckingham, *J. Am. Chem. Soc.* **1981**, *103*, 7025; Y. Wu, D. H. Busch, *J. Am. Chem. Soc.* **1972**, *94*, 4115−4122. For a review, see: R. J. Browne, D. A. Buckingham, C. R. Clark, P. A. Sutton, *Adv. Inorg. Chem.* **2000**, *49*, 307. − [2b] S. Yamada, S. Terashima, M. Wagatsuma, *Tetrahedron Lett.* **1970**, *18*, 1501−1504; S. Yamada, M. Wagatsuma, Y. Takeuchi, S. Terashima, *Chem. Pharm. Bull.* **1971**, *19*, 2380−2388; S. Terashima, M. Wagatsuma, S. Yamada, *Tetrahedron* **1973**, *29*, 1487−1496; M. Wagatsuma, S. Terashima, S. Yamada, *Tetrahedron* **1973**, *29*, 1497−1502; W. Hoffmüller, R. Krämer, M. Maurus, K. Polborn, W. Beck, *Z. Naturforsch.* **2000**, *55b*, 855−862.

[3] M. G. Schwendinger, B. M. Rode, *Anal. Sci.* **1989**, *5*, 411; A. H. Eder, S. Saetia, B. M. Rode, *Inorg. Chim. Acta* **1993**, *207*, 3−10; B. M. Rode, *Spectrum Wiss.* **1991**, *3*, 26; A. H. Eder, B. M. Rode, *J. Chem. Soc., Dalton Trans.* **1994**, 1125−1130; H. Le Son, Y. Suwannachot, J. Bujdak, B. M. Rode, *Inorg. Chim. Acta* **1998**, *272*, 89−94. For a review, see: B. M. Rode, Y. Suwannachot, *Coord. Chem. Rev.* **1999**, *190−192*, 1085−1099.

[4] K. Joshi, J. Bao, A. S. Goldman, J. Kohn, *J. Am. Chem. Soc.* **1992**, *114*, 6649−6652; J. Recht, B. I. Cohen, A. S. Goldman, J. Kohn, *Tetrahedron Lett.* **1990**, *31*, 7281−7284.

[5] [5a] W. Beck, R. Krämer, *Angew. Chem.* **1991**, *103*, 1492−1493; *Angew. Chem. Int. Ed. Engl.* **1991**, *30*, 1467−1469; R. Krämer, M. Maurus, K. Polborn, K. Sünkel, C. Robl, W. Beck, *Chem. Eur. J.* **1996**, *2*, 1518−1526. − [5b] W. Hoffmüller, M. Maurus, K. Severin, W. Beck, *Eur. J. Inorg. Chem.* **1998**, 729−731.

[6] E. Juaristi, D. Quintana, B. Lamatsch, D. Seebach, *J. Org. Chem.* **1991**, *56*, 2553−2557; E. Juaristi, J. Escalante, B. Lamatsch, D. Seebach, *J. Org. Chem.* **1992**, *57*, 2396−2398; D. C. Cole, *Tetrahedron* **1994**, *50*, 9517−9582.

[7] D. Seebach, M. Overhand, F. N. M. Kühnle, B. Martinoni, L. Oberer, U. Hommel, H. Widmer, *Helv. Chim. Acta* **1996**, *79*, 913−941; D. Seebach, P. E. Ciceri, M. Overhand, B. Jaun, D. Rigo, L. Oberer, U. Hommel, R. Amstutz, H. Widmer, *Helv. Chim. Acta* **1996**, *79*, 2043−2066; D. Seebach, J. L. Matthews, *Chem. Commun.* **1997**, 2015−2022; D. Seebach, K. Gademann, J. V. Schreiber, J. L. Matthews, T. Hintermann, B. Jaun, L. Oberer, U. Hommel, H. Widmer, *Helv. Chim. Acta* **1997**, *80*, 2033−2038; D. Seebach, S. Abele, K. Gademann, G. Guichard, T. Hintermann, B. Jaun, J. L. Matthews, J. V. Schreiber, L. Oberer, U. Hommel, H. Widmer, *Helv. Chim. Acta* **1998**, *81*, 932−982; X. Daura, W. F. van Gunsteren, D. Rigo, B. Jaun, D. Seebach, *Chem. Eur. J.* **1997**, *3*, 1410−1417; T. Hintermann, D. Seebach, *Synlett* **1997**, 437−438; D. Seebach, J. L. Matthews, A. Meden, T. Wessels, C. Baerlocher, L. B. McCusker, *Helv. Chim. Acta* **1997**, *80*, 173−182; T. Hintermann, D. Seebach, *Chimia* **1997**, *51*, 244; U. Koert, *Angew. Chem.* **1997**, *109*, 1922−1923; *Angew. Chem. Int. Ed. Engl.* **1997**, *36*, 1836−1837; T. Hintermann, K. Gademann, B. Jaun, D. Seebach, *Helv. Chim. Acta* **1998**, *81*, 983−1002; K. Gademann, T. Hintermann, J. V. Schreiber, *Curr. Med. Chem.* **1999**, *6*, 905−925.

[8] D. H. Appella, L. A. Christianson, I. L. Karle, D. R. Powell, S. H. Gellman, *J. Am. Chem. Soc.* **1996**, *118*, 13071−13072; D. H. Appella, L. A. Christianson, D. A. Klein, D. R. Powell, X. Huang, J. J. Barchi, Jr., S. H. Gellman, *Nature* **1997**, *387*, 381−384; B. L. Iverson, *Nature* **1997**, *385*, 113−115; S. Borman, *Chem. Eng. News* **1997**, 32−35; S. H. Gellman, *Acc. Chem. Res.* **1998**, *31*, 173−180; D. H. Appella, L. A. Christianson, D. A. Klein, M. R. Richards, D. R. Powell, S. H. Gellman, *J. Am. Chem. Soc.* **1999**, *121*, 7574−7581.

[9] R. Krämer, M. Maurus, R. Bergs, K. Polborn, K. Sünkel, B. Wagner, W. Beck, *Chem. Ber.* **1993**, *126*, 1969−1980.

[10] K. Haas, Ph. D. thesis, University of Munich **1998**.

[11] M. Prem, K. Polborn, W. Beck, *Z. Naturforsch.* **1998**, *53b*, 1501−1505.

[12] W. S. Sheldrick, E. Hauck, S. Korn, *J. Organomet. Chem.* **1994**, *467*, 283−292; W. S. Sheldrick, A. Gleichmann, *J. Organomet. Chem.* **1994**, *470*, 183−187; Y. Zhou, B. Wagner, K. Polborn, K. Sünkel, W. Beck, *Z. Naturforsch.* **1994**, *49b*, 1193−1202. For a review, see: K. Severin, R. Bergs, W. Beck, *Angew. Chem.* **1998**, *110*, 1722−1743; *Angew. Chem. Int. Ed.* **1998**, *37*, 1634−1654.

[13] D. F. Dersnah, M. C. Baird, *J. Organomet. Chem.* **1977**, *127*, C55; R. Krämer, K. Polborn, H. Wanjek, I. Zahn, W. Beck, *Chem. Ber.* **1990**, *123*, 767−778.

[14] M. A. Bennett, T.-N. Huang, T. W. Matheson, A. K. Smith, *Inorg. Synth.* **1982**, *21*, 74−78.

[15] H. Brunner, *Angew. Chem.* **1999**, *111*, 1248−1263; *Angew. Chem. Int. Ed.* **1999**, *38*, 1194−1208.

Received January 19, 2001
[I01025]

A New Cubane-Type $Ru_4(CO)_{12}(\mu_3\text{-}Se)_4$ Tetramer Tailored for Water Photooxidation Catalysis

Edgar Rupp,[a] Frank Nowak,[a] Sebastian Fiechter,*[a] Günter Reck,[b] Volker Eyert,[c] Nicolas Alonso-Vante,[d] and Helmut Tributsch[a]

Keywords: Cubanes / Ruthenium / Structure determination / Density functional calculations / Catalysts

In an effort to tailor a transition metal complex for photoinduced water splitting, a new cubane-like ruthenium chalcogenide tetramer, $Ru_4(CO)_{12}(\mu_3\text{-}Se)_4$, has been synthesized and structurally characterized by single-crystal X-ray diffraction. The orange-red compound crystallizes in the cubic space group $I\bar{4}3m$. The geometry of the Ru_4Se_4 units remains undistorted in the cubic symmetry $3m$. Such a high symmetry is exceptional among cubane-type cluster compounds. Ruthenium atoms are octahedrally coordinated by three selenium atoms and three CO groups. $Ru_4Se_4(CO)_{12}$ clusters are linked via van der Waals forces by oxygen atoms which belong to CO ligands of two different cluster units. By stacking of the cluster units along the cubic axes two weakly coupled three-dimensional frameworks are formed. First principles band structure calculations reveal the strong influence of both the C–O bonding, which leads to a large splitting into bonding and antibonding states, as well as of metal–ligand bonding. The latter gives rise to several very sharp Ru d bands of t_{2g}-like symmetry just below the valence band maximum E_v, which are expected to be useful for oxidation catalysis. While these states are bonding below –1.3 eV, they are antibonding near the edge of the valence band. For this reason, we expect a stabilization of the cubane core on depopulation of the highest occupied bands. Consequently, it is likely that a dynamic interrelation between electron transfer and crystal structure occurs.

Introduction

Photoinduced water splitting for fuel generation is a subject which over the years has received significant attention.[1] The process has been demonstrated using UV-absorbing catalysts such as TiO_2 and $SrTiO_3$, but it turned out to be very difficult to identify a catalyst which split water using visible light. The semiconducting compound RuS_2, however, photo-oxidizes water with high quantum efficiency under assistance of an electrical potential involving Ru-centerd interfacial coordination chemistry. RuS_2 has an energy gap of 1.3 eV, which is too low for water splitting, so a supporting potential is needed, for energetic reasons to provide the theoretical minimum energy (including losses) which ranges from 1.6 to 2.1 eV depending on the catalytic performance of the material concerned. Synthesizing suitable transition metal compounds with d-energy bands, separated by 2 eV, is therefore a significant challenge for solar fuel generation[2,3] and the aim of this contribution.

In the past decades numerous efforts have been made to synthesize cubane-like cluster compounds in order to elucidate the relationship between geometry and electronic configuration.[4] Our interest was stimulated by the fact that hydrogen-producing hydrogenase, e.g. from *Clostridium pasteurianum*, contains redoxable thiocubane Fe_4S_4 cores.[5] One of these cores is covalently bridged by a cysteinate thiol to an Fe_2S_2 subcluster (H-cluster).[5,6] Besides sulfur, carbonyl and cyanide ligands coordinate the iron atoms. It is thought that multi-electron transfer, for example bi-electron transfer to reduce protons to yield dihydrogen, is corroborated with the presence of d-metal centers, which can vary their oxidation state over a wide range. In the past, Chevrel-type compounds were investigated, the characteristics of which are octahedral metal cores consisting of Re, Rh−Mo, Pt−Mo, Os−Mo and Ru−Mo, respectively, linked by chalcogen and halogen atoms.[7] Light enhanced oxygen reduction was observed in $Re_6S_8Cl_2$ [8] while $Re_4Mo_2Se_8$ and $Ru_2Mo_4Se_8$ are of interest as catalysts for the reduction of molecular oxygen in acidic media.[9,10] A facile chemical synthesis route using carbonyl compounds and elemental chalcogenides to tailor novel metal clustering compounds in the form of powder was recently reported.[11] To prepare new ruthenium- and molybdenum-containing cluster compounds, which are known to be highly catalytic for many purposes, under increased pressures and temperatures, the $Ru_3(CO)_{12}$ was treated in a selenium-saturated xylene solution. Using this preparation the new compound $Ru_4(CO)_{12}(\mu_3\text{-}Se)_4$ could be obtained.

Cubane-Type Compounds

Cubane-like clusters $(ML_3)_4(\mu_3\text{-}E)_4$, which contain tetrahedral structural units of four transition metal atoms, M_4, and four main group non-metal atoms, E_4, combined to give a cubic moiety, $M_4(\mu_3\text{-}E)_4$, have been the subject of

[a] Hahn-Meitner-Institut, Abteilung Solare Energetik, Glienicker Str. 100, 14109 Berlin, Germany
E-mail: fiechter@hmi.de
[b] Bundesanstalt für Materialforschung und -prüfung, Rudower Chaussee 5, 12489 Berlin, Germany
[c] Institut für Physik, Universität Augsburg, 86135 Augsburg, Germany
[d] Université de Poitiers, Lab. Electrocatalysis, UMR CNRS 6503, 40, Avenue du Recteur Pineau, 86022 Poitiers, France

 © WILEY-VCH Verlag GmbH, 69451 Weinheim, 2001 1434−1948/01/1010−2489 $ 17.50+.50/0

numerous papers.[4,12−28] Most of the cubic clusters show a distortion from the idealized T_d symmetry to D_{2d} (with 4 short and 2 long distances or 2 short and 4 long distances) or D_2 symmetry. In a series of papers, Dahl and co-workers[12−20] have analyzed the molecular and electronic structure of Fe- and Co-based cubane-like clusters such as $[Cp_4Fe_4(\mu_3\text{-}S)_4]^n$ (n = 0 to +2),[12,13] $[Cp_4Fe_4(\mu_3\text{-}CO)_4]^n$ (n = 0, +1),[14,15] $Fe_4(CO)_{12}(\mu_3\text{-}Se)_4$,[4] $[(NO)_4Fe_4(\mu_3\text{-}S)_4]^n$ (n = 0, −1),[16,17] $(CO)_{12}Fe_4(\mu_3\text{-}S)_4$,[4] $[Cp_4Co_4(\mu_3\text{-}S)_4]^n$ (n = 0, +1),[18] $(CO)_{12}Co_4(\mu_3\text{-}Sb)_4$ [19] and $(NO)_4Co_4(\mu_3\text{-}NR)_4$.[20]

Based on molecular orbital calculations using the Fenske−Hall model[4] Dahl and co-workers have successfully explained many of the structural variations. Employing qualitative MO diagrams they suggested that for the clusters of cubane-like structures one set of four orbitals may be considered as the nonbonding lone pair localized on the four terminal ligands at low energy. There are groups of 24 orbitals corresponding to metal−Cp and metal−S bonds in $[Cp_4Fe_4(\mu_3\text{-}S)_4]^n$ (Figure 1). At higher binding energies it follows a group of 12 orbitals mainly localized on the metal atoms. These metal-based orbitals have primarily d-orbital character and are responsible for the binding to the framework of the cluster, namely the bonds between the metal atoms along the edge of the tetrahedral metal core. The 24 antibonding combinations formed by M−L and M−E interactions are located at high energies. The interaction between the 12 metal-based orbitals forms two bonding sets, one of metal−metal bonding orbitals of symmetry $a_1 + e + t_2$ and a second set of metal−metal antibonding orbitals of symmetry $t_1 + t_2$.

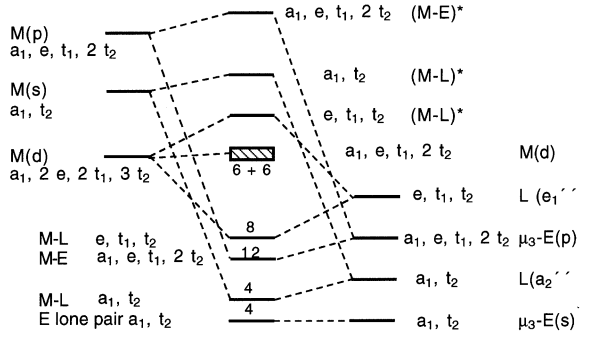

Figure 1. Qualitative energy orbital diagram of the cubane-type cluster unit $Fe_4(CO)_{12}(\mu_3\text{-}Se)_4$, inferred from molecular orbital calculations using the Fenske−Hall model (see ref.[4]); the diagram can also be used to qualitatively explain the bonding conditions in the ruthenium counterpart, investigated in this work

Lauher estimated the bonding capabilities of various transition metal clusters, based upon extended Hückel calculations on bare Rh clusters.[21] He proposed the molecular orbitals of a tetrahedral cluster to have six high-lying antibonding orbitals termed as $t_1 + t_2$ corresponding to the antibonding orbitals of metal−metal interaction of Dahl's model. Additionally, the 30 bonding cluster orbitals contain six orbitals of metal−metal interaction of symmetry $a_1 + e + t_2$ in agreement with Dahl's model. The remaining 24 bonding cluster orbitals are used for M−L and M−E bonding. The occasionally observed distortion of the metal−metal tetrahedron can be explained by an incomplete occupation of the bonding or antibonding set of metal−metal orbitals.

The Model Catalyst

In $Ru_4(CO)_{12}(\mu_3\text{-}Se)_4$, described in this paper, the 80 available valence electrons (i.e., 24 from the four d^6-Ru^{2+} atoms, 24 from the 12 CO ligands and 32 from the four bridging Se^{2-} atoms) completely fill the four lone pairs of the Se atoms, the 24 (4 + 12 + 8) bonding metal−ligand orbitals and the six bonding ($a_1 + e + t_2$) as well as the six antibonding metal−metal MOs (Figure 1). From this one would expect the tetrahedral bonds to be metal−metal nonbonding and the cubane core to be stabilized by the metal−ligand bonds. This energy level scheme nicely explains the observed distances and symmetry of cubane-like clusters with 80 valence electrons such as $(CO)_{12}Ru_4Se_4$, $Cp_4Co_4S_4$,[21] $(CO)_{12}Fe_4S_4$,[4] $(CO)_{12}Fe_4Se_4$ [4] and $(CO)_{12}Co_4Sb_4$.[19]

$Ru_4Se_4(CO)_{12}$ crystallizes in the cubic space group $I\bar{4}3m$. The coordination of the cubane-like Ru_4Se_4 core is illustrated in Figure 2 and the framework formed by the clusters in Figure 3. The ruthenium center is octahedrally coordinated by three selenium atoms and three CO groups (Figure 2). As is visible from Figure 3 the clusters are coupled by two pairs of oxygen atoms forming a common tetrahedron of 2.955 Å distance. The bonding angles Ru−Se−Ru and Se−Ru−Se are 95.05° and 84.71°. The six equivalent Ru−Ru distances amount to 3.778 Å corresponding to a nonbonding distance. The Ru−Se distance of 2.561 Å is comparable to the sum of covalent radii. The clusters are three-dimensionally interconnected via van der Waals bonds along the cubic axes and form an orthogonal framework. Due to the body-centerd Bravais lattice, a second identical framework appears diagonally translated by 1/2, 1/2, 1/2 with the origin in the center of the unit cell (Figure 2). Each oxygen atom of framework II (e.g. in cluster 3) is separated by the distance of 3.354 Å from four oxygen atoms belonging to framework I. These latter atoms show the distance to the cluster units 1 and 2, as well as the two oxygen atoms to cluster 2 and the two oxygen atoms to cluster 1 and a third cluster of framework I, not shown in Figure 4 for clarity reasons. Crystallographic data and atomic parameters are given in Tables 1 and 2. Bond lengths and angles are summarized in Table 3.

The presented structure is a highly symmetrical example of a structure with cubane-like Ru_4Se_4 cores. Such a high symmetry is exceptional among cubane-type cluster compounds and to the best of our knowledge $Ru_4Se_4(CO)_{12}$ is the first cubane-type compound of cubic symmetry described. All other known structures crystallize in lower symmetric space groups. For example in $Ru_4Se_4(CO)_{10}(Ph_2PCH_2PPh_2)$, whose cubane-like unit is closely related to our compound, the Ru−Se distances vary from

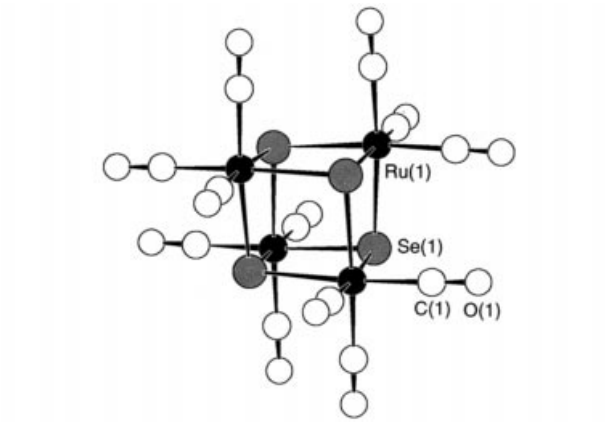

Figure 2. Cubane-type cluster unit $Ru_4(CO)_{12}(\mu_3\text{-}Se)_4$

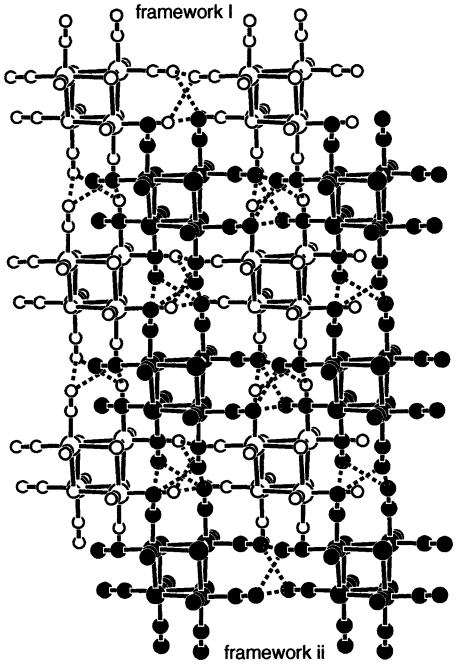

Figure 3. Arrays of cluster units of $Ru_4(CO)_{12}(\mu_3\text{-}Se)_4$ interconnected via van der Waals bonds along the cubic axes forming an orthogonal framework; due to the body-centerd Bravais lattice type, a second identical framework appears diagonally translated by 1/2, 1/2, 1/2

2.552 to 2.577Å, the inner bond angles Se−Ru−Se and Ru−Se−Ru range from 83.6 to 86.1° and from 93.4 to 96.4°. The average values (2.564 Å, 84.8° and 95°, respectively) are close to the angles and distances found in the present structure.[27]

Density Functional Calculation

The partial, i.e. orbital-projected densities of states, as determined from self-consistent calculations, are displayed in Figures 5 and 6, where we have included Ru-4d, Se-4p as well as C- and O-2p states; all other states gave only negligible contributions to the total density of states in the energy interval shown. In particular, while at lower energies there exist C- and O-2s states we find Ru-4s bands above 7 eV. In order to study the octahedral-like crystal-field splitting at the Ru sites we have separated the 4d partial DOS into its *xy*, *xz*, *yz* and $3z^2 - r^2$, $x^2 - y^2$ components, which, in an ideal octahedron, correspond to the t_{2g} and e_g or-

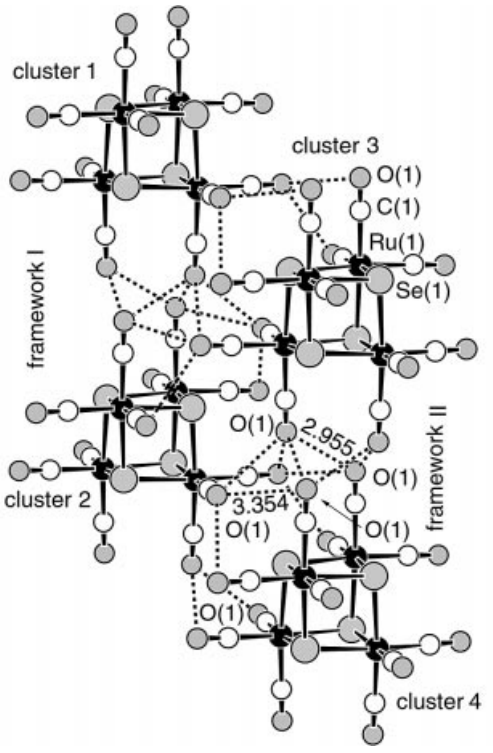

Figure 4. Section of Figure 3 showing the van der Waals bonds between cluster units of different frameworks

Table 1. Crystallographic data for $Ru_4(CO)_{12}(\mu_3\text{-}Se)_4$ (estimated standard deviations are given in parentheses)

Empirical formula	$Ru_4Se_4(CO)_{12}$
Formula mass [g mol^{-1}]	1055.42
Crystal system	cubic
Space group	$I\bar{4}3m$ (no. 217)
μ [cm^{-1}]	9.391
R values *R*1 and *wR*2	0.015, 0.046
a [Å]	10.308(1)
V [Å^3]	1095.4(2)
Temperature of data collection	25 °C
Z	2
$\rho_{calcd.}$ [g cm^{-3}]	3.200
F(000)	959

Table 2. Atomic coordinates and equivalent isotropic thermal parameters of $Ru_4(CO)_{12}(\mu_3\text{-}Se)_4$

Atom	*x*/*a*	*y*/*b*	*z*/*c*	B_{eq}
Ru	0.12958(4)	0.12958(4)	0.87042(4)	0.0203(2)
Se	0.11836(7)	0.11836(7)	0.11836(7)	0.0219(3)
C	0.1260(5)	0.1260(5)	0.6833(6)	0.0279(11)
O	0.1229(5)	0.1229(5)	0.5741(5)	0.0476(14)

Table 3. Distances and angles in $Ru_4(CO)_{12}(\mu_3\text{-}Se)_4$

Distance [Å]		Angle [°]	
Ru−Ru	3.7780(7)	Se−Ru−Se	84.71(3)
Ru−Se	2.5611(9)	Ru−Se−Ru	95.05(3)
Ru−C	1.929(6)	Ru−C−O	179.2(8)
C−O	1.127(7)		
O−O	2.955(7)		
O−O	3.354(7)		

bitals. Finally, we give the calculated partial crystal orbital overlap populations (COOP) for selected bonds in Figure 7.

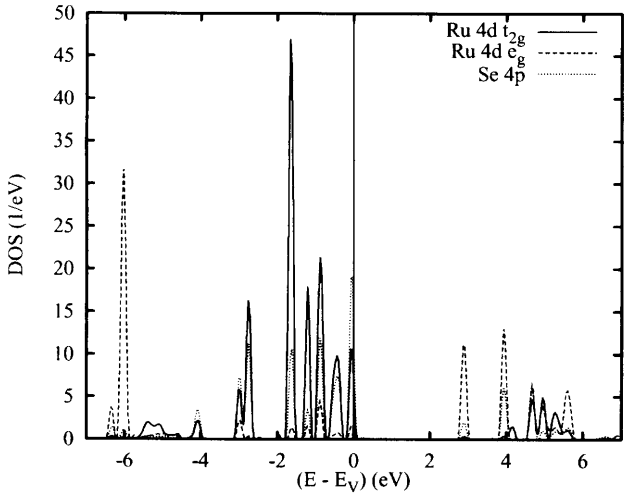

Figure 5. Partial Ru-4d-t_{2g} and -e_g as well as Se-4p densities of states; here and in the following figure energies refer to the valence band edge E_v

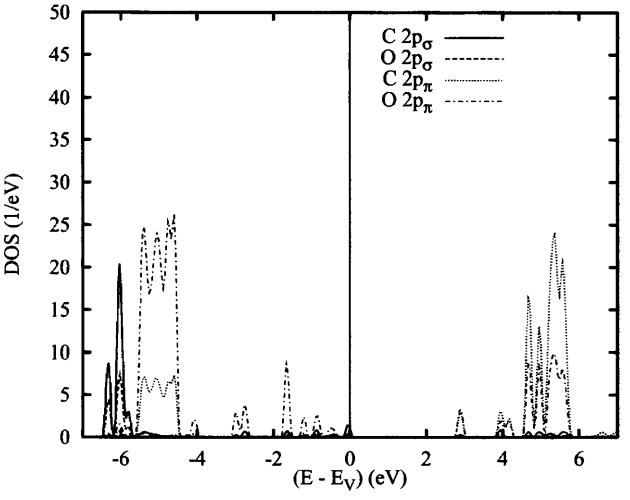

Figure 6. Partial C- and O-2p states of a single C−O pair separated into the p_π and p_σ states

In Figure 6 we display the C- and O-2p partial densities separated into their p_π and p_σ states. We observe two rather conspicuous groups of bands at ±5 eV, each separated into four sub-bands due to the small overlap of the Ru-4d states

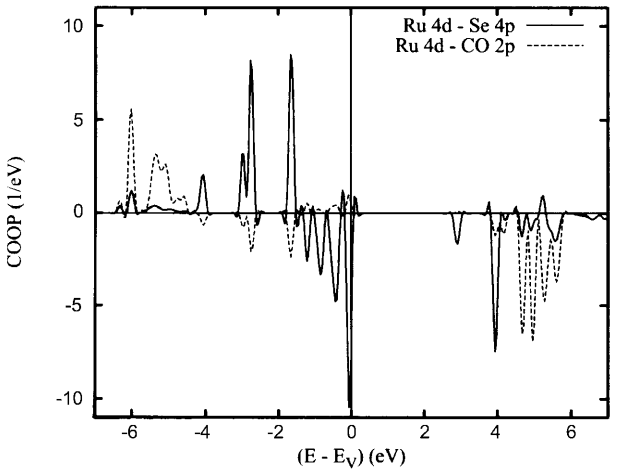

Figure 7. Partial crystal orbital overlap populations for selected bonds

with the bonding C−O orbitals as well as the low symmetry of the crystal field. According to additional analysis of the COOP, the two groups of bands at ±5 eV result from strong splitting of the C- and O-2p states into bonding and antibonding bands due to π-type overlap across the short bond of only 1.12Å. As expected, the occupied and unoccupied states have larger contributions from O and C, respectively. Since the bonding and antibonding states resulting from this π-type overlap are completely filled and empty, respectively, the C−O bonding adds the largest contribution to the stability of the compound. Furthermore, since these states are located well below and above the Fermi energy the corresponding bonds cannot be broken by simple electron transfer. This striking feature of the C−O cubane core interaction is suspected to be also relevant for the C−O terminated ferredoxins in an iron-only hydrogenase.[5]

An even larger splitting into bonding and antibonding states of about 16 eV is observed for the O- and C-2s and -$2p_\sigma$ states, where it gives rise to rather sharp peaks at about −24 and −8 eV, outside the energy range displayed in Figures 5−7. Yet, in contrast to the $2p_\pi$ bands, both these bonding and antibonding orbitals are fully occupied and thus neither contribute to the overall stability nor determine the low energy excitations of the compound. Finally, we observe a fifth group of bands derived from C- and O-2p states at approximately −6 eV below the valence band maximum. It comprises predominantly C- and O-$2p_\sigma$ as well as Ru-4d orbitals.

Bonding of Ru to its neighboring ligands is strongly influenced by the presence of two different types of ligands, namely, three selenium atoms and three C−O pairs, as well as their pseudo-octahedral coordination of the ruthenium sites. Although the particular arrangement of the ligands reduces the local symmetry at the Ru sites to C_{3v} the pseudo-octahedral coordination still allows the interpretation of the Ru-4d partial DOS in terms of its t_{2g} and e_g components as they would grow out of an ideal cubic crystal field. Whereas the t_{2g} states appear mainly in the energy

range from −4.2 eV to E_v, the e_g orbitals contribute to the sharp peaks at −6 eV as well as in the energy range from 2.8 to 6 eV above the valence band maximum. Interestingly, a finite t_{2g} partial DOS is also observed between 4.5 and 6 eV.

Due to the peculiarities of the crystal structure with two different types of ligands, selenium atoms and carbon−oxygen pairs, the ligand contributions to both the Ru-4d-t_{2g} and -e_g states change across the energy spectrum. To be specific, the occupied Ru-4d-t_{2g} states occurring in the upper part of the valence band are complemented with contributions from the Se-4p states resulting from π-type overlap. In contrast, contributions from the C−O-2p states to π-type metal−ligand bonding are rather small in this energy region. This is due to the bonding−antibonding splitting of the $2p_\pi$ states discussed above, which shifts these states to ±5 eV. As a consequence, Ru-4d-t_{2g} states, which form π bonds with the C−O-$2p_\pi$ states, are also found near ±5 eV.

A σ-type metal−ligand bonding is signalled by the ligand p contributions to the peak at approximately −6 eV as well as to the unoccupied Ru-4d-e_g dominated bands. Again, due to the special octahedral-like coordination of the metal sites by two different types of ligands the d−p overlap changes across the spectrum. While the bonding Ru-4d-e_g states overlap almost exclusively with the C−O-$2p_\sigma$ orbitals, the Ru-4d-e_g partial DOS above 2.8 eV is complemented by both Se-4p and small C−O-2p contributions. This finding is supported by the calculated COOP (Figure 7): Whereas the peak at approximately −6 eV results mainly from Ru−C−O bonding, the energy range from 2.8 to 4 eV is dominated by antibonding Ru−Se states. In conclusion, the cubane framework is predominantly stabilized by σ-type interaction between Ru and CO and π-type interactions between Ru and Se as depicted in Figure 8.

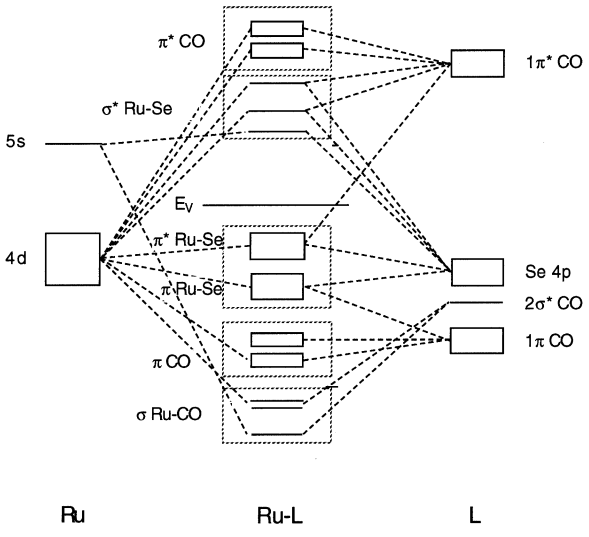

Figure 8. Qualitative energy orbital diagram of $Ru_4(CO)_{12}(\mu_3\text{-}Se)_4$

Electron-Induced Structure Dynamics

The different weighting of the ligand contributions to the Ru-4d-t_{2g} and -e_g states in the whole energy spectrum has striking consequences for the bonding properties and lays ground for the possible catalytic activity of this material. To be specific, while the metal−carbonyl bonding occurs mainly far away from the valence band edge at ±5 eV, bonding and antibonding Ru−Se states are found predominantly in the energy range from −3.2 eV to E_v. Strong bonding both within the carbonyl groups, as well as between these groups and the metal d states, shifts the corresponding states away from the gap. Furthermore, due to the rather weak π bonds both the Ru-4d−Se-4p bonding and antibonding states fall into the uppermost region of the occupied bands and give rise to the high density of states observed in this energy range. In particular, the antibonding sub-bands show up between −1.3 eV and E_v, hence, just below the Fermi energy. If these states are depopulated the Ru−Se bonds are strengthened and the cubane core that is built from penetrating coordination tetrahedra of both types of atoms will contract. In contrast, if these states are again populated, the bonding will decrease, thus causing a slight expansion of the cubane core. As a consequence, we expect substantial electron-lattice interaction, leading to a significant relationship between electron transfer and structural properties. To conclude, the presence of both strong C−O and rather weak Ru−Se bonds, which push the C−O bonding and antibonding states apart and leave room for antibonding Ru−Se states in the uppermost part of the valence band, thus provide the basis for a working mechanism for catalytic processes.

Conclusion

A new $Ru_4(CO)_{12}(\mu_3\text{-}Se)_4$ tetramer has been synthesized and characterized experimentally and theoretically. The compound fits nicely into a series of other transition metal cluster compounds possessing cubane-like cores. However, in contrast to the companion compounds, the present material crystallizes with an unusual high symmetry (space group $I\bar{4}3m$). The cluster units are weakly coupled by van der Waals interactions. In order to investigate the electronic structure we combined molecular orbital considerations and state-of-the-art band structure calculations. The theoretical results confirm the wide band gap of the material of E_g = 2.44 eV. In the cubane core Ru is pseudo-octahedrally coordinated by 3 Se and 3 CO ligands. The electronic structure of $Ru_4(CO)_{12}(\mu_3\text{-}Se)_4$ is dominated by three different types of bonds each having a characteristic strength: (i) strong π-type C−O overlap shifts the corresponding bonding and antibonding states far below and above the valence band maximum and is responsible for the overall stability of the compound; (ii) σ-type overlap of Ru-4d-e_g states with O/C-2p as well as Se-4p states as resulting from the pseudo-octahedral coordination of Ru likewise places these states at energies well below and above the edge of the valence

band; (iii) finally, rather weakly p-bonded Ru-4d-t_{2g} and Se-4p states dominate in the upper part of the valence band. The respective antibonding states are found at binding energies below 1.3 eV. As a consequence, on depopulation of these states the bonding within the cubane core will increase and the core itself will contract while repopulation will lead to a corresponding expansion. The thus expected coupling between electron and structural dynamics might support electron transfer processes and, hence, might be relevant for catalytic processes.

The prepared $Ru_4(CO)_{12}(\mu_3\text{-}Se)_4$ compound fulfils the most important theoretical criteria to act as photocatalyst for water oxidation: (i) a sufficiently large energy gap (2.44 eV) with valence states, which − as a consequence of photooxidation − are able to transfer electrons via Ru-d states; (ii) the oxidation states of ruthenium atoms in the compound can be increased to allow formation of peroxo complexes, which are able to release oxygen; (iii) the coupling between electronic and structural dynamics may favour multi-electron transfer.

However, preliminary photoelectrochemical experiments using small crystals of the synthesized complex have indicated a material property which at the moment seriously limits an application: A very high electrical resistivity was found, which has to be overcome by suitable doping techniques, by substituting ligands or by preparation of ultrathin layers.

Experimental Section

$Ru_4(CO)_{12}(\mu_3\text{-}Se)_4$: 18 mg of selenium ($2.8\cdot10^{-2}$ mmol Se_8; ALFA, powder, −325 mesh, 5N) was dissolved in 100 mL of xylene (Merck, mixture of isomers, scintillation grade) under reflux at 140 °C. Then 72.87 mg of $Ru_3(CO)_{12}$ ($1.14\cdot10^{-1}$ mmol; STREM crystalline, 99%) was added to the solution and dissolved. The solution was then brought to ambient temperature. This solution (ca. 35−40 mL) was used to fill an ampoule of Duran glass and sealed under vacuum using a water-jet pump. Further treatment was performed in a high-pressure Morey-type autoclave with a Teflon inset and a Teflon seal. The ampoule was placed in the autoclave and heated. A counterpressure was applied filling the autoclave vessel to 80 vol% with water. The autoclave was heated to 250 °C for 30 d. After cooling, the ampoule was broken and the product separated using a PTFE filter. The residue was washed with small portions of diethyl ether. Optical analysis using a light microscope revealed that besides a black powder, which was identified as elemental ruthenium by X-ray powder diffractometry, orange red crystals had been formed with a yield of 5% (4.5 mg). − Depending on the reaction time orange-red crystals up to 100 μm length grew in a black powder of Ru particles of nanometer size. This growth behaviour is very similar to the preparation of the carbidocarbonyl $Ru_6C(CO)_{17}$ described by Johnson et al.[29] and by Braga et al.[30] which could also only be obtained in a moderate yield. − The purity of the crystals and the Ru/Se ratio of unity was confirmed within an error bar of 3% by using Energy Dispersive X-ray fluorescence. The carbon monoxide content was measured thermogravimetrically and the gases released were analysed by mass spectrometry. − FTIR measurements were performed using a Bruker IFS 113v spectrometer. By means of attenuated total reflection, two strong peaks at 2079 and 2008cm^{-1} in the CO region were detected employing a micro KRS5 crystal at 45°. − To determine the energy gap of the compound an absorption measurement was performed in the range from 400 to 800 nm using a Leitz microscope. − X-ray data collection was carried out with an Enraf−Nonius CAD-4 diffractometer at 293 K using Mo-K_α (λ = 71.073pm) radiation monochromatized by a graphite crystal. Data were collected employing the 2Θ-ω scan technique in the range $3° < 2\Theta < 60°$. The total number of reflections was 936 from which 191 were independent [R_i = 0.035, 169 observed ($I > 2\sigma(I)$)]. The dimensions of the prismatic crystal were $0.12 \times 0.10 \times 0.09$ mm. The structure was solved by direct methods using SHELXS-90[31] in the space group $I23$. But an inspection of the resulting atomic coordinates showed that the higher symmetry $I\bar{4}3m$ was also fulfilled. The refinement of 23 parameters in $I\bar{4}3m$ with SHELX-97[31] converged with R_1(on F) = 0.015 and wR_2(on F^2) = 0.046. The crystallographic data (excluding structure factors) for the structure reported in this publication have been deposited with the Cambridge Crystallographic Data Centre as supplementary publication no. CCDC-155020. Copies of the data can be obtained free of charge on application to CCDC, 12 Union Road, Cambridge CB2 1EZ, UK [Fax: (internat.) + 44-1223/336-033; E-mail: deposit@ccdc.cam.ac.uk]. − In order to obtain more insight into the electronic properties of solid $Ru_4(CO)_{12}(\mu_3\text{-}Se)_4$, band structure calculations were performed as based on density functional theory and the local density approximation (LDA). In doing so, we account in an optimal balance for both the electron−lattice and the electron−electron interaction, both of which are known to strongly influence the properties of transition metal compounds. For the LDA the parametrizations by both Moruzzi, Janak and Williams as well as by Vosko, Wilk and Nusair were used without essentially any difference in the results.[32,33] As a calculational scheme we employed the augmented spherical wave (ASW) method[34] (see ref.[35] for a more recent treatment), which is one of the most efficient band structure methods in use today and offers the advantage of a minimal basis set similar to atomic orbitals. The latter fact allows, in particular, for an intuitive interpretation of the results. The basis set included Ru-5s, -5p, -4d, Se-4s, -4p as well as C- and O-2s, -2p states. Care was taken to ensure convergence of the results with respect to the completeness of the basis set as well as the fineness of the k space grid; the Brillouin zone sampling used up to 158 points within the irreducible wedge. The interpretation of the electronic properties from the calculated band structure and partial densities of states was complemented by an analysis of the crystal orbital overlap population (COOP), which allows access to the chemical bonding in more detail.[36] − In the present work we performed two different sets of calculations. In the first set we used the experimentally determined lattice constants and atomic positions. In contrast, in the second set of calculations we used a hypothetical crystal structure where the Se atoms were adjusted to positions corresponding to an ideal cubic Ru−Se core and where, hence, some degeneracies were restored. This way we were able to make closer connection to symmetry considerations employed in previous work, which were based on an ideal cubic arrangement, and thus to cross-check our results obtained for the measured crystal structure.

Acknowledgments

The authors thank Prof. Dr. K. Langer (TU Berlin) for absorption measurements and Dr. M. Hilgendorff (HMI Berlin) for FTIR measurements of the cubane phase.

[1] J. O'M. Bockris, S. U. M. Kahn, *Surface Electrochemistry*, Plenum Press, **1993**, chapters 5.16−5.18.

[2] H. M. Kühne, H. Tributsch, *J. Electroanal. Chem.* **1986**, *201*, 263−282.
[3] H. Tributsch, *Catal. Today* **1997**, *39*, 177−186.
[4] L. L. Nelson, F. Y.-K. Lo, D. Rae, L. F. Dahl, *J. Organomet. Chem.* **1982**, *225*, 309−329 and references therein; M. B. Hall, R. F. Fenske, *Inorg. Chem.* **1972**, *11*, 768−775.
[5] M. W. W. Adams, E. I. Stiefel, *Science* **1998**, *282*, 1842−1843.
[6] J. W. Peters, W. N. Lanzilotta, B. J. Lemon, *Science* **1998**, *282*, 1858.
[7] C. Fischer, N. Alonso-Vante, S. Fiechter, H. Tributsch, *J. Appl. Electrochem.* **1995**, *25*, 1004−1008.
[8] C. Fischer, N. Alonso-Vante, S. Fiechter, H. Tributsch, G. Reck, W. Schulz, *Alloys Compd.* **1992**, *178*, 305−314.
[9] W. Jaegermann, C. Pettenkofer, N. Alonso-Vante, T. Schwarzlose, H. Tributsch, *Ber. Bunsenges. Phys. Chem.* **1990**, *94*, 513−520.
[10] N. Alonso-Vante, B. Schubert, H. Tributsch, *Mater. Chem. Phys.* **1989**, *22*, 281−307.
[11] N. Alonso-Vante, *J. Chim. Phys.* **1996**, *93*, 702−710.
[12] C. H. Wei, G. R. Wilkes, P. M. Treichel, L. F. Dahl, *Inorg. Chem.* **1966**, *5*, 900−905.
[13] Trinh-Toan, B. K. Teo, J. A. Ferguson, T. J. Meyer, L. F. Dahl, *J. Am. Chem. Soc.* **1977**, *99*, 408−416.
[14] Trinh-Toan, W. P. Fehlhammer, L. F. Dahl, *J. Am. Chem. Soc.* **1972**, *94*, 3389−3397.
[15] M. A. Neumann, Trinh-Toan, L. F. Dahl, *J. Am. Chem. Soc.* **1972**, *94*, 3383−3388.
[16] C. Ting-Wah Chu, F. Yip-Kwai Lo, L. F. Dahl, *J. Am. Chem. Soc.* **1982**, *104*, 3409−3422.
[17] R. S. Gall, C. T.-W. Chu, L. F. Dahl, *J. Am. Chem. Soc.* **1974**, *96*, 4019−4023.
[18] G. L. Simon, L. F. Dahl, *J. Am. Chem. Soc.* **1973**, *95*, 2164−2174.
[19] A. S. Foust, L. F. Dahl, *J. Am. Chem. Soc.* **1970**, *92*, 7337−7341.
[20] R. S. Gall, N. G. Connelly, L. F. Dahl, *J. Am. Chem. Soc.* **1974**, *96*, 4017−4019.
[21] J. W. Lauher, *J. Am. Chem. Soc.* **1978**, *100*, 5305−5315.
[22] J. Darkwa, J. R. Lockemeyer, P. D. Boyd, T. B. Rauchfuss, A. L. Rheingold, *J. Am. Chem. Soc.* **1988**, *110*, 141−149.
[23] F. Bottomley, F. Grein, *Inorg. Chem.* **1982**, *21*, 4170−4178.
[24] J. G. Reynolds, C. L. Coyle, R. H. Holm, *J. Am. Chem. Soc.* **1980**, *102*, 4350−4355.
[25] J. A. Ferguson, T. J. Meyer, *J. Chem. Soc., Chem. Commun.* **1971**, 623−624.
[26] B. A. Averill, T. Herskovitz, R. H. Holm, J. A. Ibers, *J. Am. Chem. Soc.* **1973**, *95*, 3523−3534.
[27] D. Cauzzi, C. Graiff, M. Lanfranchi, G. Predieri, A. Tiripicchio, *J. Chem. Soc., Dalton Trans.* **1995**, 2321−2322 and references therein.
[28] C. E. Davies, J. C. Green, N. Kaltsoyannis, M. A. MacDonald, J. Qin, T. B. Rauchfuss, C. M. Redfern, G. H. Stringer, M. G. Woolhouse, *Inorg. Chem.* **1992**, *31*, 3779−3791.
[29] B. F. G. Johnson, J. Lewis, S. W. Sankey, K. Wong, *J. Organomet. Chem.* **1980**, *191*, C3−C7.
[30] D. Braga, F. Grepioni, P. L. Dyson, B. F. G. Johnson, P. Frediani, M. Bianchi, F. Piacenti, *J. Chem. Soc., Dalton Trans.* **1992**, 2565−2571.
[31] G. M. Sheldrick, *SHELX-97* and *SHELXS-90, Program for the Solution of Crystal Structures*, Universität Göttingen, Germany, **1997**.
[32] V. L. Moruzzi, J. F. Janak, A. R. Williams, *Calculated Electronic Properties of Metals*, Pergamon Press, New York, **1978**.
[33] S. H. Vosko, L. Wilk, M. Nusair, *Can. J. Phys.* **1980**, *58*, 1200−1211.
[34] A. R. Williams, J. Kübler, C. D. Gelatt, Jr., *Phys. Rev. B* **1979**, *19*, 6094−6118.
[35] V. Eyert, *Int. J. Quantum Chem.* **2000**, *77*, 1007−1031.
[36] V. Eyert, in *Density Functional Methods: Applications in Chemistry and Materials Science* (Ed.: M. Springborg), Wiley, Chichester, **1997**, pp. 233−304.

Received January 11, 2001
[I01016]

Tris(indenyl)lanthanoid Complexes (Ln = La, Pr, Nd) Containing either (*S*)-(−)-Nicotine or Two Simpler Pyridine Bases

Jingwen Guan[a,b] and R. Dieter Fischer*[a]

Keywords: Lanthanides / N ligands / Chirality

Novel examples of the complex of the type [Ln(Ind)$_3$·Nic] [Ind = indenyl; Nic = (*S*)-(–)-nicotine] with Ln = La (**2**), Pr (**3**), and Nd (**4**) have been synthesised, along with their "parent" system [LaCp$_3$·Nic] (**1**). Complexes **2**–**4** were structurally, exhaustively characterised (XRS, ^{1}H NMR spectroscopy). Attempts to prepare homologues of **3** with achiral N-bases, pyridine, α-picoline, β-picoline, 2,6-dimethylpyridine, 2,6-bis(*tert*-butyl)pyridine, 2,2′-bipyridine, and 4,4′-dimethyl-2,2′-bipyridine, were successful with only the two least bulky bases, pyridine and β-picoline, which afforded the new adducts **5** and **6**, respectively. The chiral [Ln(Ind)$_3$·Nic] adducts are virtually isostructural, although subtle but systematic conformational variations emerge from the crystal structure analyses. While the unit cells of **2**–**4** contain two epimeric diastereomers, those of **5** and **6** involve genuine optical antipodes. The chiral carbon atom of nicotine lies approximately twice as far from the metal centre than the chiral sulfur atom of the methyl tolyl sulfoxide (MTSO) ligand in the previously reported [Ln(Ind)$_3$·MTSO] systems. As a result of this, the impact of the chiral MTSO ligand, both on the molecular structure and the ^{1}H NMR spectra, is found to be notably stronger than that of (*S*)-(–)-nicotine. The comparatively weak f-f circular dichroism of **3** is also compared with that of its (*S*)-(–)-MTSO-containing congener.

Introduction

Whilst the crystal structures of a few 1:1 adducts of a tris(cyclopentadienyl)lanthanoid(III) complex and pyridine (Py), or any pyridine derivative (Py*), have already been reported,[1−3] only one corresponding indenyl complex [Ce(Ind)$_3$·Py][4] has so far been characterised, also by X-ray crystallography. Structural studies on adducts containing the *chiral* pyridine derivative (*S*)-(−)-nicotine (Nic) are yet to be reported on, although several [LnCp$_3$·Nic] systems were prepared for early spectroscopic studies.[5,6]

Our current interest in the structural details of diverse [(Ind)$_3$Ln·Py*] systems results from more recent observations in which the three bulky benzo groups of the indenyl units may be oriented in various different ways[7−9] depending on the actual bulkiness of the metal-coordinated Lewis base. Moreover, a *chiral* Lewis base L is also expected to control the chirality of the {Ln(Ind)$_3$X} fragment[7] (X is the ligand atom that is bonded to the metal centre), provided that the chiral centre of the base resides only two bonds away from the metal centre, as in chiral sulfoxides[10] and 2-methyltetrahydrofuran.[11a] In the present study, our interest will be focused on whether a chiral centre located about twice as far from the metal centre than that in the recently investigated methyl tolyl sulfoxide (MTSO) adducts,[10] would still exert any detectable configuration controlling or electronic influence. While the chiral sulfur atom of the oxygen-coordinated MTSO ligand is separated from the metal ion by only one atom, three atoms would separate the chiral carbon atom of a *nicotine* ligand (coordinated via its pyridine N atom) from the metal centre (see Figure 1). Particular attention will therefore be paid to subtle conformational details in the crystal structures, to auxiliary ^{1}H NMR signal displacement or splitting effects due to the presence of paramagnetic metal ions, and even to potential f-f circular dichroism of the central Ln^{III} ions with an incomplete 4f^q configuration. We thus wish to present an exemplary description of the employment of suitable alternative techniques, in combination with X-ray crystallography, to elucidate the influence of paramagnetic 4f^q metal ions on distinct features of the ligand sphere, and, conversely, of notably remote chirogenic centres on the 4f electrons. In addition we report on the first successful synthesis of analytically pure [Ln(Ind)$_3$·Nic] compounds (Ln = La, Pr, Nd).

Results and Discussion

Synthesis and General Properties of [La(C$_5$H$_5$)$_3$·Nic] (1)

Facile ligand exchange was found to take place, when a solution of (*S*)-(−)-nicotine in toluene was added to a suspension of [La(C$_5$H$_5$)$_3$·THF][8] in toluene. The product precipitated as a faint yellow powder which dissolves readily in CH_2Cl_2 and THF, but only moderately in benzene or toluene. In THF the reverse reaction of Equation (1) was found to occur. In the mass spectrum, both metal-containing [Cp$_n$La]$^+$ fragments with n = 3, 2, 1, 0, and smaller purely organic fragments of nicotine were observed. In the ^{139}La NMR spectrum, one relatively broad resonance at δ = −534 ($w_{1/2}$ = 979 Hz), referenced to a solution of $LaCl_3$ in

[a] Institut für Anorganische und Angewandte Chemie der Universität Hamburg,
Martin-Luther-King-Platz 6, 20146 Hamburg, Germany
Fax: (internat.) + 49-40/42838−2882
E-mail: fischer@chemie.uni-hamburg.de
[b] Department of Chemistry, University of Ottawa,
Ottawa, Ontario, Canada

 © WILEY-VCH Verlag GmbH, 69451 Weinheim, 2001 1434−1948/01/1010−2497 $ 17.50+.50/0

D_2O, appears. This compares reasonably with corresponding results for $[La(C_5H_5)_3{\cdot}THF]$ ($\delta = -558$, 450 Hz) and $[La(C_5H_5)_3{\cdot}MTSO]$ ($\delta = -563$, 390 Hz).[8,10] In the ^1H NMR spectrum of **1**, *all* the resonances for the nicotine protons were assigned in a similar manner to those in the ^1H NMR spectrum of a previously reported paramagnetic $[PrCp_3{\cdot}Nic]$ complex.[6] However, several lines in the ^1H NMR spectrum of **1** are overlapping. For the full assignment of the spectroscopic results (see Exp. Sect.), the designation of the nicotine protons is adopted as given in Figure 1. While the ^1H NMR spectrum of the paramagnetic Pr^{III} complex had already revealed that the nicotine molecule is coordinated via its pyridine N atom,[6] this particular feature is not as convincingly apparent from the spectrum of diamagnetic **1**.

$$[La(C_5H_5)_3{\cdot}THF] + \text{(S)-(-)-nicotine} \xrightarrow{\textit{toluene}} [La(C_5H_5)_3{\cdot}Nic]\ (\mathbf{1}) + THF \quad (1)$$

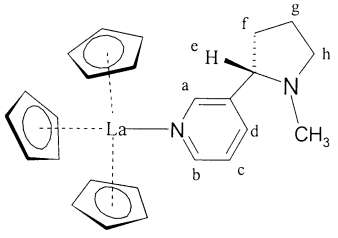

Figure 1. Schematic structure of complex **1**, including the designation of the protons on the nicotine ligand

Synthesis and General Properties of the $[Ln(Ind)_3{\cdot}Nic]$ Systems 2−4 (Ln = La, Pr, Nd)

The three nicotine adducts $[Ln(Ind)_3{\cdot}Nic]$ with Ln = La, Pr, and Nd (**2**−**4**) could be obtained similarly, by ligand exchange reactions, i.e. by adding a solution of nicotine in toluene, to a suspension of the corresponding THF adduct $[Ln(Ind)_3{\cdot}THF]$ as shown in Equation (2). Somewhat unexpectedly, all tris(indenyl) homologues of **1** resulted in viscous oils which are analytically pure. However, when the yellow-orange oil of **2** coexisted with a trace amount of toluene, the sticky syrup converted overnight into rod-like, bright yellow crystals of excellent X-ray quality. However, this simple technique was not suitable for the crystallisation of **3** and **4**. Crystals of the latter complexes could only be obtained when the viscous oils were first dissolved in small amounts of toluene, after which a large amount of hexane was slowly added. After some time, crystal-like products could be seen. Finally, the liquid phase was decanted, and the remaining solid was washed with hexane. The purified residues were redissolved in hot toluene and the temperature was lowered very slowly and steadily. Prismatic leek-green crystals of **3**, and grass-green crystals of **4**, were obtained which were of excellent quality for X-ray crystallographic studies. Toluene solutions of these crystals no longer afforded the viscous oils after the removal of the solvent.

$$[Ln(C_9H_7)_3{\cdot}THF] + \text{(S)-(-)-nicotine} \xrightarrow{\textit{toluene}} [Ln(C_9H_7)_3{\cdot}\text{(S)-nicotine}] + THF \quad (2)$$
$$Ln = La, Pr \text{ and } Nd$$

Complexes **2**−**4** are very soluble in toluene, benzene, THF, MeCN, and CH_2Cl_2, but insoluble in hexane. The nicotine adducts appear to be thermally more stable (under N_2) than their corresponding MTSO congeners.[10] In the mass spectra of all three complexes, signals corresponding to the metal-containing fragments $[Ind_nLn]^+$ with $n = 3$, 2, 1, and 0 were found. Several weaker peaks assigned to purely organic fragments such as $[Ind]^+$, $[Nic]^+$, $[C_5H_4NC_4H_7]^+$, $[C_5H_4NC_3H_5]^+$, $[C_4H_7NCH_3]^+$, etc. were observed as well. Variable-temperature ^{139}La NMR spectroscopic studies of **2** show that the signal is considerably broadened with decreasing temperature. Interestingly, this broadening effect seems to be notably more pronounced for tris(indenyl)- than for tris(cyclopentadienyl)lanthanum(III) complexes.[8] This suggests a more sensitive response of the large ^{139}La nuclear quadrupole moment on the presence of the less symmetrical (as compared with C_5H_5) indenyl ligands (see Table 1).

Table 1. Comparison of the ^{139}La NMR results (chemical shift and line width) for corresponding cyclopentadienyl and indenyl complexes $[LaCp'_3{\cdot}L]$ (Cp′= Cp or Ind)

L	Temp. [K]	δ(^{139}La) Cp	Ind	$w_{1/2}$ [Hz] Cp	Ind	Ref.
(*S*)-(−)-Nic	345	−534	−413	545	1221	
(*S*)-(−)-Nic	325	−535	−417	675	1695	
(*S*)-(−)-Nic	292	−539	−425	980	2765	
THF	320		−558		508	[8]
(*S*)-(−)-MTSO	320		−450		2480	[10]

Another interesting feature of the nicotine complexes **2**−**4** is that their melting points are quite low (**2**: 94−98; **3**: 129−132; **4**: 112−116 °C). Only the melting point of **3** compares with those of the reported $[Ln(Ind)_3{\cdot}MTSO]$ systems.[10] Possibly, the "tadpole-like" shape of a $[Ln(Ind)_3{\cdot}Nic]$ molecule, with its extended nicotine tail (vide infra), can undergo various facile conformational changes, which − with its pronounced flexibility − is likely to inhibit the arrival at a well-ordered crystalline phase.

Attempted Syntheses of Related $[Pr(Ind)_3{\cdot}Py^*]$ Adducts; Preparation and General Properties of $[Pr(Ind)_3{\cdot}Py]$ (5) and $[Pr(Ind)_3{\cdot}(3\text{-}MePy)]$ (6)

The corresponding pyridine and β-picoline adducts of complex **3** were prepared in a similar manner to complex **3** (Ln = Pr) as shown in Equation (3). In contrast to **2**−**4**, the simpler adducts **5** and **6** did not form viscous oils, but rather leek-green microcrystals formed, which could readily be recrystallised from hot toluene affording single crystals suitable for X-ray crystallography. Both compounds are reasonably soluble in toluene and benzene, but more soluble in MeCN, CH_2Cl_2, and THF. In the mass spectra, peaks of the metal-containing fragments $[Ind_nPr]^+$ with $n = 3$, 2, 1,

and the organic fragments $[Ind]^+$, $[Py]^+$, or $[MePy]^+$ were observed.

$$[Pr(Ind)_3{\cdot}THF] + Py^* \xrightarrow{toluene} [Pr(Ind)_3{\cdot}Py^*] + THF \quad (3)$$

Py^* = pyridine: **5**, 3-methylpyridine (β-picoline): **6**

^{1}H NMR spectroscopic data for the indenyl protons of **5** and **6** are included in Table 5, while the corresponding data for the protons of the Py* ligands are found in the Exp. Sect. Quite surprisingly, the chemical shifts of the H atoms next to the pyridine N atom, which are separated from the paramagnetic metal ion by one atom more than the indenyl H atoms, experience notably stronger "paramagnetic" displacements than the indenyl resonances.

Several attempts were made to vary the steric congestion of the potential ligand Py*, by changing the ring substituents and/or their positions on the pyridine fragment. Thus, the pyridine derivatives listed in Equation (4) were subjected to ligand (i.e. THF) exchange experiments, with the hope of initiating new conformational features in the final architecture of the expected complexes. However, all these preparative attempts remained unsuccessful, as the isolable leek-green, crystalline products turned out to be the starting compound $[Pr(Ind)_3{\cdot}THF]$ (as confirmed by elemental analysis, ^{1}H NMR spectroscopy, and crystal structure analysis).

$$[Pr(C_9H_7)_3{\cdot}THF] + Py^* \xrightarrow{toluene} \not\rightarrow [Pr(C_9H_7)_3{\cdot}Py^*] + THF \quad (4)$$

Py* = α-picoline, 2,6-dimethylpyridine, 2,6-bis(tert-butyl)pyridine
4,4'- dimethyl-2,2'-bipyridine and 2,2'-bipyridine

These results clearly indicate that just one methyl group in the 2-position of a pyridine molecule (i.e. α-picoline) no longer allows the indenyl ligands to adopt orientations that would provide enough space for the coordination of this pyridine derivative. This observation does not agree with recent findings in which 2-methyltetrahydrofuran (MeTHF) readily bonds to $\{Ln(\eta^5\text{-}Ind)_3\}$ fragments.[11a] Moreover, one or two of the three indenyl ligands might in principle abandon their usual η^5 coordination for a lower hapticity. This has been suggested for the recently prepared complex $[Lu(C_9H_7)_3{\cdot}3THF]$, in view of its notably higher THF content,[11b] and also for the well-documented crystalline $[LuCp_3]$ complex which has an η^1-coordinated Cp ligand.[12] The failure of α-picoline to enter the coordination sphere of a $\{Pr(Ind)_3\}$ fragment indicates that the required change from η^5 to η^1 (or η^3) coordination probably needs some auxiliary "support" to overcome the higher steric demand of the potential ligands listed in Equation (4).

Crystallographic Studies of the $[Ln(Ind)_3{\cdot}Nic]$ Complexes 2−4

Selected details of the data collection and structure refinement of **2**−**4** are listed in Table 7. Although the three complexes are virtually isostructural, their cell parameters differ significantly, suggesting at least some conformational variation (vide infra).

The C_5 fragments of the indenyl ligands are all η^5-coordinated, although the individual Ln−C distances vary considerably (Table 2). The nicotine ligand is bonded to the metal centre exclusively via its pyridine N atom. The unit cells of **2**, **3**, and **4** contain two rather similar-looking epimeric diastereomers (Figure 2). As the chiral carbon atom of the nicotine ligand lies relatively far from the metal centre, the chiral $\{Ln(Ind)_3{\cdot}N\}$ fragments for each epimeric pair behave as almost perfect mirror images. This situation strongly resembles that observed for several $[Ln(Ind)_3{\cdot}L]$ systems with an achiral L, e.g. L = THF (Ln = La or Pr),[8] L = diphenyl sulfoxide, DPSO (Ln = Nd),[10] and L = Py or β-MePy (Ln = Pr, i.e. in **5** and **6**, vide infra). Here, the unit cell of the crystal always involves both enantiomers (1:1) of a chiral $\{Ln(Ind)_3X\}$ fragment (X = either O or N). On the other hand, in the single crystals of the very closely related adducts $[Ln(Ind)_3{\cdot}L]$ with L = THF (Ln = Sm, Tm[8] and Gd[13]), and L = either (*R*)-(+)- or (*S*)-(−)-MTSO (Ln = La or Pr[10]), only one distinct $\{Ln(Ind)_3{\cdot}X\}$ enantiomer is present.

Initially, the evidence suggested that the three homologues crystallise in the centrosymmetric space group $P2_1/c$. However, after careful assessment of the systematic absence of numerous weak reflections, and along with the non-vanishing chirality of each metal complex, there is no doubt that all three homologues crystallise in the acentric and chiral space group $P2_1$. In Figure 2, the molecular structures of the three epimeric pairs of **2**, **3**, and **4** are depicted such that the orientation of their Ln1−N1−C33 and Ln2−N3−C43 vectors have been kept unchanged. While this particular view was chosen to demonstrate that large portions of each epimeric pair of molecules behave as mirror images, the two diastereomers are positioned face-to-face in the crystals of **2** and **3** (i.e. their nicotine tails turn away from each other), but back-to-back in the lattice of **4**. In all of the structures displayed in Figure 2, the methylated pyrrolidine N atom prefers just one distinct configuration. However, with respect to rotation about the ring-ring C−C bond, the two cyclic components of the nicotine ligand of **4** adopt another conformation than in **2** and **3**.

Selected bond lengths and angles of **2**, **3** and **4** are listed in Table 2. The Ln−C distances involving carbon atoms shared by the C_5 *and* C_6 units of each indenyl ligand are, as usual, significantly longer than the other Ln−C bonds of each C_5 fragment. The Ln−N distances compare well with that reported for $[Ce(C_9H_7)_3{\cdot}Py]$ [Ce−N 268.4(4) pm],[4] and are also in agreement with those in $[Nd(C_5H_5)_3{\cdot}Py]$ [266.8(5)] and in $[Sm(C_5H_5)_3{\cdot}Py]$ [265.6(3) pm].[2] Interestingly, these Ln−N distances are longer than the Ln−O distances in the corresponding $[Ln(Ind)_3{\cdot}MTSO]$ systems,[10] by about 20 pm. The Ce−N distance in $[Ce(MeC_5H_4)_3{\cdot}N(CH_2CH_2)_3CH]$ [278.6(4) pm] exceeds the aforementioned Ln−N distances by at least 10 pm.[14] Intramolecular Nd−N distances ≥ 280 pm are also reported for $[Nd(C_5H_4CH_2CH_2NMe_2)_2Cl]$ and $[Nd(C_5H_4CH_2CH_2NMe_2)_3]$[15,16] while the Nd−N(Py) distances are about 268 pm.[17]

The various molecular conformations, with respect to η^5-indenyl rotation about the individual Ln−Ct*i*5 axes (Ct15, Ct25, and Ct35 being the centres of the three C_5 fragments), of the diastereomers of crystalline **2**, **3**, and **4** may be quan-

Table 2. Selected bond lengths [pm] and angles [°] of the nicotine complexes **2**−**4**; data in italics refer to slightly more elongated Ln−C distances (see text)

	2	**3**	**4**
Bond lengths			
Ln−N(1)/(3)	265.7(6)/269.0(7)	270.8(9)/262.9(11)	265(3)/268(2)
Ln−C(101)/(201)	287.3(6)/283.6(6)	275.6(9)/286.2(11)	281(3)/274(3)
Ln−C(102)/(202)	283.1(6)/282.2(5)	278.6(11)/277.9(11)	278(2)/268(2)
Ln−C(103)/(203)	286.0(7)/289.2(6)	289.1(10)/277.7(10)	273(3)/286(2)
Ln−C(108)/(208)	*303.3(7)/303.6(7)*	*291.4(9)/299.7(10)*	*300(2)/290(3)*
Ln−C(109)/(209)	*303.1(8)/306.4(7)*	*301.8(10)/294.5(9)*	*296(2)/295(3)*
Ln−Ct(15)	266.5/267.0	260.9/260.7	258.5/255.9
Ln−C(111)/(211)	283.4(8)/289.3(7)	278.7(10)/280.1(12)	281(2)/285(3)
Ln−C(112)/(212)	284.8(9)/286.4(8)	280.0(11)/278.3(10)	272(3)/267(3)
Ln−C(113)/(213)	286.8(7)/283.0(8)	280.4(10)/281.4(10)	274(3)/280(3)
Ln−C(118)/(218)	*287.4(7)/290.0(7)*	*290.7(11)/294.8(10)*	*301(2)/303(3)*
Ln−C(119)/(219)	*288.3(7)/286.3(7)*	*292.2(11)/291.0(11)*	*287(2)/292(3)*
Ln−Ct(25)	259.3/260.5	257.2/258.7	256.1/259.1
Ln−C(121)/(221)	283.1(8)/281.9(8)	279.2(11)/276.4(11)	273(2)/267(3)
Ln−C(122)/(222)	282.8(7)/284.9(7)	278.4(10)/279.5(10)	274(3)/271(2)
Ln−C(123)/(223)	290.3(6)/291.2(7)	279.6(11)/281.5(10)	273(2)/288(2)
Ln−C(128)/(228)	*292.9(7)/290.5(6)*	*284.8(11)/280.5(11)*	*295(3)/290(2)*
Ln−C(129)/(229)	*297.5(6)/295.4(6)*	*286.7(10)/284.5(10)*	*294(3)/300(2)*
Ln−Ct(35)	262.7/262.5	253.8/254.0	255.9/256.9
Angles			
N−Ln−Ct(15)	102.1/120.7	104.5/105.3	109.3/98.3
N−Ln−Ct(25)	98.1/96.1	92.0/92.0	92.5/104.1
N−Ln−Ct(35)	97.1/98.6	100.8/100.2	98.8/94.9
Ct(15)−Ln−Ct(25)	114.4/114.0	118.2/118.0	115.9/115.8
Ct(25)−Ln−Ct(35)	117.4/117.9	117.4/117.6	120.3/116.1
Ct(35)−Ln−Ct(15)	120.6/120.6	117.0/116.9	114.8/120.7
Ct(16)−Ct(15)−Ct(35)	74.7/75.1	79.2/80.0	77.9/70.0
Ct(16)−Ct(15)−Ct(25)	133.5/133.7	126.6/126.8	130.8/125.2
Ct(26)−Ct(25)−Ct(15)	83.9/84.3	70.5/71.6	78.1/76.7
Ct(26)−Ct(25)−Ct(35)	83.4/83.1	127.0/127.2	127.4/132.2
Ct(36)−Ct(35)−Ct(25)	114.1/111.7	85.5/84.9	70.8/78.4
Ct(36)−Ct(35)−Ct(15)	89.8/90.3	84.1/83.7	125.5/127.3
Ct(16)−Ct(15)−Ln	101.5/101.2	98.4/98.7	100.2/99.7
Ct(26)−Ct(25)−Ln	92.0/91.9	96.0/96.5	98.9/101.1
Ct(36)−Ct(35)−Ln	94.7/93.7	93.2/92.7	100.6/99.5

tified by inspecting the distances of the three C_6 ring centres, Ct*i*6 (i = 1−3), from the best plane spanned by the three C_5 ring centres, Ct*i*5.[8,10] These quantities, along with the distance of the metal ion from the Ct15/Ct25/Ct35 plane, are listed in Table 3 for the complexes **2**−**7**. The second digit of the individual number of each indenyl carbon atom as found in Figure 2 (i.e. 0, 1, or 2), corresponds to the indenyl ring number *i* (1, 2, or 3) used in Table 3.

For an ideal paddlewheel-like conformation (the benzo groups are considered as "paddles"), with three *equatorially* oriented indenyl ligands, the Ct*i*6-to-plane distances should be minimal (i.e. ≤ 10 pm), whilst the ideal distance for *meridionally* oriented indenyl ligands should be ca. 220 pm.[10] The term "approximately *equatorial*" may be used for distances up to 150 pm, and the term "approximately *meridional*" may be used for distances > 150 pm. By this classification, complex **2** would have two, complex **3** one, and complex **4** no indenyl ligands of *meridional* orientation. This classification agrees well with earlier findings in which the paddlewheel-like conformation is gradually favoured as the radius of the metal ion decreases.[8,10] The opposite signs of the Ct*i*6-to-plane distances of the two meridional ligands of **2** (with i = 2 and 3) indicate that one of the two indenyl benzo groups is located *trans* to the nicotine ligand, and the other one *cis*. While the Ct*i*6-to-plane distances of the two diastereomers of **2** do not differ significantly, the corresponding data sets of **4** display more pronounced deviations. For instance, the Ct16- and Ct36-to-plane values of the two diastereomers have opposite signs. In view of these findings, the two {Nd(Ind)$_3$·N} fragments of **4** (see Figure 2), cannot even be considered as "approximate" mirror images.

Crystallographic Studies of [Pr(Ind)$_3$·Py] 5 and [Pr(Ind)$_3$·(3-MePy)] (6)

Crystals of the two complexes [Pr(Ind)$_3$·Py] (**5**) and [Pr(Ind)$_3$·3-MePy] (**6**) are orthorhombic and belong to the cubic space group *Pbca*. This can be seen in Table 8. Corresponding properties are reported for the cerium homologue [Ce(Ind)$_3$·Py] (**7**).[4] As the unit cell parameters of **5**, **6**, and **7** are similar, the three complexes are quasi-isostructural, although their molecular conformations may still

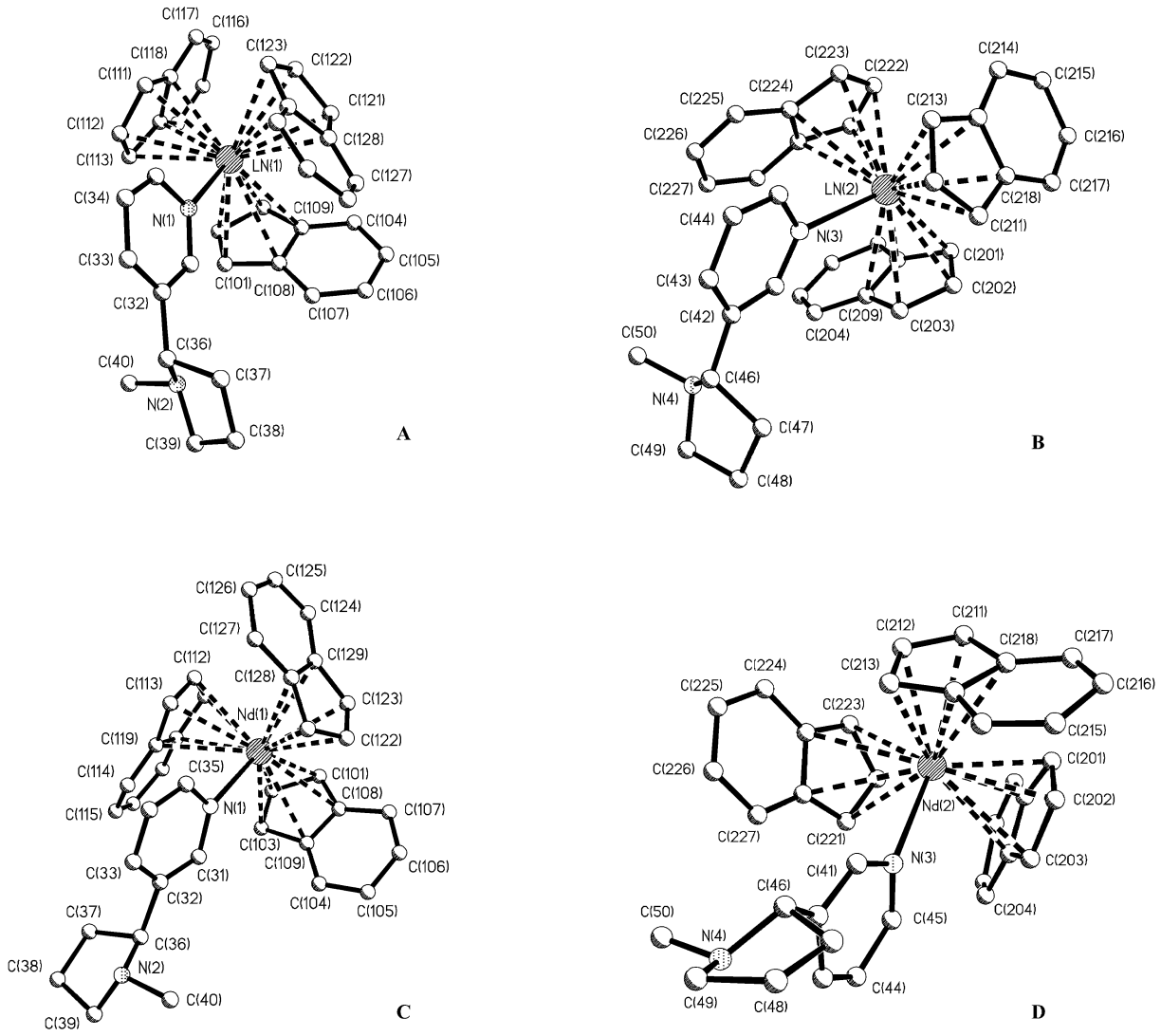

Figure 2. Molecular structure and atomic numbering scheme of the two epimeric diastereomers of **2** and **3** (**A/B**), and **4** (**C/D**), respectively; the drawings **A/B** refer to **2**, although **2** and **3** are almost isostructural; for the specific, pairwise orientation see the text

Table 3. Distances of the C_6 centers Ct*i*6 (i = 1−3), and the metal atom Ln, from the best plane spanned by the three C_5 centres, Ct*i*5, of each epimeric or racemic pair of **2**−**7** (distances in pm; a negative sign indicates the disposal of Ct*i*6 *transoid* to Py*)

Sample	Ln	Ct16	Ct26	Ct36
2 (La)	42.4/42.0	23.4/35.2	−216.4/−217.3	192.1/198.2
3 (Pr)	40.8/41.2	122.8/127.2	66.9/73.6	−218.6/−217.9
4 (Nd)	44.9/40.5	103.3/−78.1	109.6/83.1	−81.8/114.8
5 (Pr)	44.4	−107.1	113.2	113.1
6 (Pr)	50.0	153.9	152.5	88.2
7 (Ce)[4]	45.2	−106.5	113.9	114.2

vary. The molecular structures of **5** and **6** are shown in Figure 3. As the conformations of both complexes are approximately paddlewheel-like (vide supra) (Table 3), the {Ln(Ind)$_3$N} fragments are chiral. The crystal lattices of all three adducts with achiral Py* ligands involve racemic mixtures of molecules with both clockwise and anticlockwise (with respect to the Ln−N axis) oriented benzo groups.

Selected bond lengths and angles are listed in Table 4. The Pr−N distances again compare well with those of **7**[4] and with those of all other [Ln(Ind)$_3$·Py*] systems mentioned above. The Pr−C bond lengths vary between 273.8(4) and 301.8(4) pm, which is a feature also reported for **7**.[4]

Although the conformations of **5** and **6** are paddlewheel-like (like that of **4**), a closer look at the Ct*i*6-to-plane distances listed in Table 3 reveals that the data for **5** satisfactorily match with only one set of **4**. No counterpart exists for a set of three positive Ct*i*6 values (as actually found for **6**).

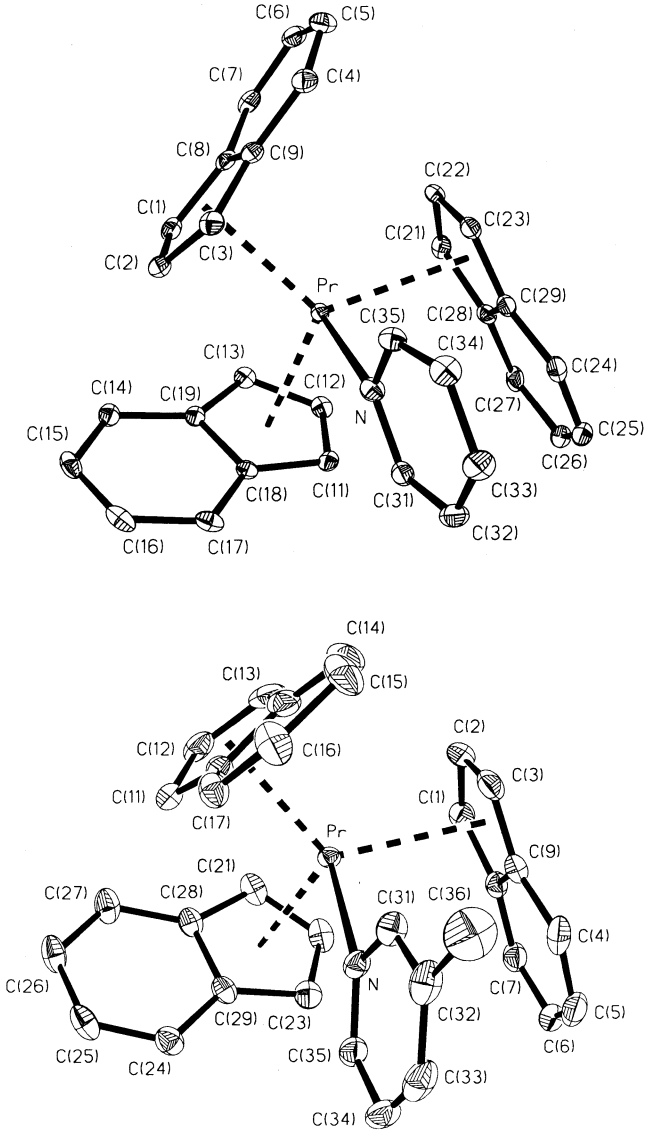

Figure 3. Molecular structure and atomic numbering scheme of the complexes **5** (top) and **6** (bottom)

Table 4. Selected bond lengths [pm] and angles [°] of **5** and **6**; data in italics refer to slightly more elongated Ln−C distances (see text)

Bond lengths	**5**	**6**	Angles	**5**	**6**
Ln−N	266.9(3)	260.8(3)	N−Ln −Ct(15)	103.8	96.2
Ln−C(1)	275.7(3)	278.7(4)	N−Ln−Ct(25)	104.1	104.3
Ln−C(2)	274.3(4)	275.2(4)	N−Ln−Ct(35)	91.8	103.1
Ln−C(3)	285.3(3)	280.0(4)	Ct(15)−Ln−Ct(25)	116.0	118.3
Ln−C(8)	*293.3(3)*	*291.7(4)*	Ct(25)−Ln−Ct(35)	118.1	114.2
Ln−C(9)	*301.0(3)*	*292.9(4)*	Ct(35)−Ln−Ct(15)	117.3	116.5
Ln−Ct(15)	259.1	256.9	Ct(16)−Ct(15)−Ct(35)	69.7	83.4
Ln−C(11)	275.1(3)	277.7(4)	Ct(26)−Ct(25)−Ct(15)	76.1	87.3
Ln−C(12)	276.4(3)	273.8(4)	Ct(36)−Ct(35)−Ct(25)	78.4	76.2
Ln−C(13)	283.9(3)	279.1(5)	Ct(16)−Ct(15)−Pr	76.1	96.4
Ln−C(18)	*289.1(3)*	*293.9(4)*	Ct(26)−Ct(25)−Pr	97.0	99.4
Ln−C(19)	*296.2(3)*	*295.2(1)*	Ct(36)−Ct(35)−Pr	98.2	99.6
Ln−Ct(25)	257.1	257.0			
Ln−C(21)	280.0(3)	285.9(4)			
Ln−C(22)	274.0(3)	275.6(5)			
Ln−C(23)	277.8(3)	277.2(5)			
Ln−C(28)	*296.8(3)*	*301.8(4)*			
Ln−C(29)	*294.9(3)*	*294.3(4)*			
Ln−Ct(35)	257.8	260.5			

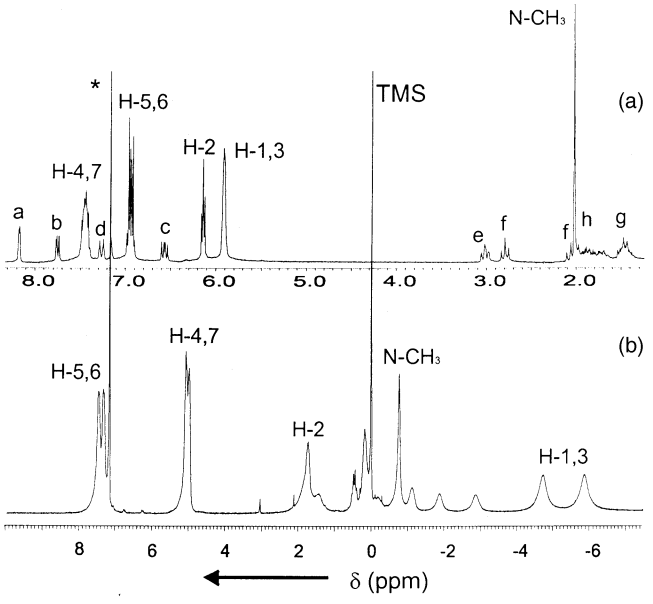

Figure 4. Room-temperature ^{1}H NMR spectra of **2** (a) and **4** (b); solvent: C_6D_6/TMS; signals of the indenyl protons are marked by asterisks; two resonances of **4** (beyond δ = −10, see Exp. Sect.) are not shown

Solution ^{1}H NMR Spectroscopy of 2, 3, and 4

The ^{1}H NMR spectrum of diamagnetic **2** (Figure 4, a) displays almost the same resonance pattern, with respect to the protons of its nicotine ligand, as the spectrum of **1** (see Exp. Sect.). The resonance pattern of the indenyl protons of **2** is consistent with the presence of three virtually equivalent C_9H_7 units. As in the case of [La(Ind)$_3$·THF],[8] no more than four multiplets (I_{rel} = 6:6:3:6) occur indicating that the six pairwise prochiral[10] C_9H_7 protons (see Figure 5) do not experience any significant diastereotopic splitting due to the relatively remote location of the chiral carbon atom of the (*S*)-(−)-nicotine ligand. In striking contrast, however, the three equivalent C_9H_7 ligands of the complex [La(Ind)$_3$·MTSO] [with either (*R*)-(+)- or (*S*)-(−)-MTSO] were found to display *seven* equally intense (I_{rel} = 3) multiplets.[7,10]

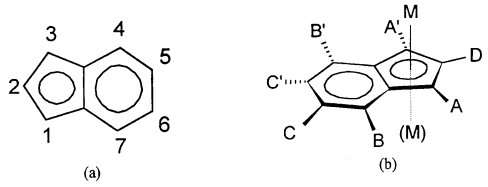

Figure 5. Conventional numbering of indenyl hydrogen atoms (a); schematic description of the prochiral nature of the atoms A/A′, B/B′ and C/C′ in an {M(η^n-indenyl)} fragment (b)

Table 5. Room-temperature chemical shifts (ppm) of the indenyl protons of various [Ln(Ind)$_3$·L] systems (solvent: C_6D_6; for the designation of the H atoms see Figure 5, a)

Ln	L	1/3-H	2-H	4/7-H	5/6-H
La	(*S*)-(−)-Nic (**2**)	5.90 (s, 6 H)	6.14 (t, 3 H)	7.46 (m,6 H)	6.94 (q,6 H)
Pr	(*S*)-(−)-Nic (**3**)	9.59 (s, 3 H); 8.79 (s, 3 H)	7.44 (s, 3 H)	8.15 (d, 3 H); 8.03 (d, 3 H)	4.19 (t, 3 H); 4.06 (t, 3 H)
Pr	Py (**5**)	10.03 (s, 6 H)	8.98 (s, 3 H)	7.88 (s, 6 H)	3.65 (s, 6 H)
Pr	3-MePy(**6**)	10.13 (s, 3 H)	7.66 (s, 3 H)	8.12 (s, 6 H)	3.68 (d, 6 H)
Pr	(*R*)-(+)-MTSO[10]	19.55 (s, 3 H); −0.52 (s, 3 H)	1.98 (s, 3 H)	10.41 (d, 3 H); 6.22 (d, 3 H)	4.95 (t, 3 H); 3.85 (t, 3 H)
Pr	DPSO[a] [10]	9.25 (s, 6 H)	4.16 (s, 3 H)	8.18 (q,6 H)	4.02 (dd,6 H)
Nd	(*S*)-(−)-Nic (**4**)	−4.73 (s, 3 H); −5.88 (s, 3 H)	1.74 (s, 3 H)[b]	7.40 (d, 6 H)[c]	5.00 (d, 6 H)[d]
Nd	(*R*)-(+)-MTSO[10]	−2.00 (s.3 H); −7.46 (s, 3 H)	6.09 (s, 3 H)	9.49 (s, 3 H); 6.10 (s, 3 H)	4.32 (s, 3 H); 3.30 (s, 3 H)
Nd	DPSO[a] [10]	−3.87 (s, 6 H)	−0.89 (s, 3 H)	7.66 (s, 6 H)	5.12 (s, 6 H)
Nd	TPPO[d] [11c]	−6.36 (s, 6 H)	−2.56 (s, 3 H)	7.27 (s, 6 H)	5.53 (s, 6 H)

[a] DPSO = diphenyl sulfoxide. − [b] With L = THF, δ(2-H) = 6.73, see ref.[8] − [c] Distance of the two components (in Hz): 480, ruling out any internuclear spin-spin coupling. − [d] TPPO = triphenylphosphane oxide (see also ref.[7]).

On the other hand, the expected diastereotopic splitting for L = (*S*)-(−)-nicotine (instead of MTSO) becomes observable in the ^{1}H NMR spectra of the *paramagnetic* homologues of **2** (i.e. of **3** and **4**) at room temperature. A survey of the relevant ^{1}H NMR spectroscopic data is given in Table 5. A detailed variable-temperature (VT) ^{1}H NMR study (between 353 and 188 K) of **3**, dissolved in [D_8]toluene, shows that the indenyl protons give rise to three singlets, two quasi-doublets and two quasi-triplets between ca. 320 and 260 K (see Figure 6, b, and Table 5). However, above room temperature (e.g. at 353 K, see Figure 6, a) the two quasi-doublets together with one of the singlets collapse to form one intense quasi-triplet, and the two initially present quasi-triplets merge to form one quasi-quadruplet. Below ca. 260 K, all residual spin-spin coupling is quenched, such that two pairs of distinct singlets appear instead of the two pairs of multiplets (Figure 6, c).

At least two different dynamic processes seem to influence the VT NMR results. Above room temperature all protons of the nicotine ligand (except those closest to the pyridine N atom, vide infra) give rise to fairly sharp singlets, or multiplets, between δ = +2 and −4 (Figure 6, a). Between ca. 300 and 250 K considerable broadening affects these signals (see Figure 6, b). On the other hand, after the recovery of these resonances to fairly sharp singlets (between δ ≈ 0 and −20), in particular two of the low-field singlets of the indenyl ligands are broadened considerably (see Figure 6, c). At the lowest accessible temperature (183 K), four of the seven indenyl resonances merge to form one broad singlet (not shown in Figure 6).

Interestingly, the chemical shifts of all indenyl resonances of **3** vary only slightly with temperature. In contrast, the α-protons of the substituted pyridine unit (see Figure 1) give rise to just one broad singlet at δ ≈ −16 at 353 K and to two broad signals at δ ≈ −65 and −75 at 188 K. This indirectly suggests that the magnetic susceptibility of the central Pr^{3+} ion of **3** should increase considerably with decreasing temperature. The singlet of the *N*-bonded methyl group of the nicotine ligand is shifted from δ = −0.85 at 353 K to δ = −8.00 at 193 K. The intermediate broadening of the nicotine resonances might be associated with the slowing down of the initially rapid (on the NMR timescale) internal motions of the nicotine molecule (e.g. the inversion of the non-planar pyrrolidine unit including that of the chiral NC_3 pyramid and/or rotation about the inter-ring C−C and N−Ln σ bonds). It should be noted that the resonances of the THF protons of the previously reported[8] adduct [Pr(Ind)$_3$·THF] show notable broadening between ca. 290 and 260 K (Figure 7), a feature which could be associated with ring inversion or restricted rotation about the O−Pr bond. Moreover, the temperature dependence of the indenyl resonances of this adduct is considerably less pronounced than that of the THF protons (Figure 8).

The unexpected broadening of the indenyl resonances of **3** below ca. 250 K most probably reflects some rapid intramolecular dynamics other than the bare rotation of each η^5-coordinated ligand about its Pr−C*ti*5 axis. We have speculated earlier[10] on periodic η^5-to-η^1 conversions affecting each of the three indenyl units equally and stereoselectively such that during this sequence of equilibria, the chiral intermediate η^1-coordinated C_5 ring carbon atom (i.e. C-1 or C-3) of each C_9H_7 ligand would maintain only one distinct configuration. Unfortunately, our present VT NMR spectroscopic study does not include results for temperatures around and below the coalescence of the dynamics, since the solvent starts crystallising below 180 K.

Most of the resonances of the indenyl protons of complex **4** (Ln = Nd) could be identified (Figure 4, b). A comparison with corresponding data for three previously reported adducts (Table 5) strongly suggests that the indenyl protons of **4** are also affected by the asymmetry of the nicotine ligand. While spin-spin coupling can be suggested as an explanation for the "doublet" character of the resonances assigned to protons in the positions 4/7 and 5/6, the assignment of the singlet at δ = 1.74 to 2-H (see Table 5) remains somewhat more uncertain. Alternatively, this signal might be assigned to the *N*-bonded methyl group of the nicotine ligand. The two equally intense signals at δ = −4.73 and −5.88 seem to be shifted too greatly by the paramagnetism of the Nd^{3+} ion, to justify the correlation of one of them

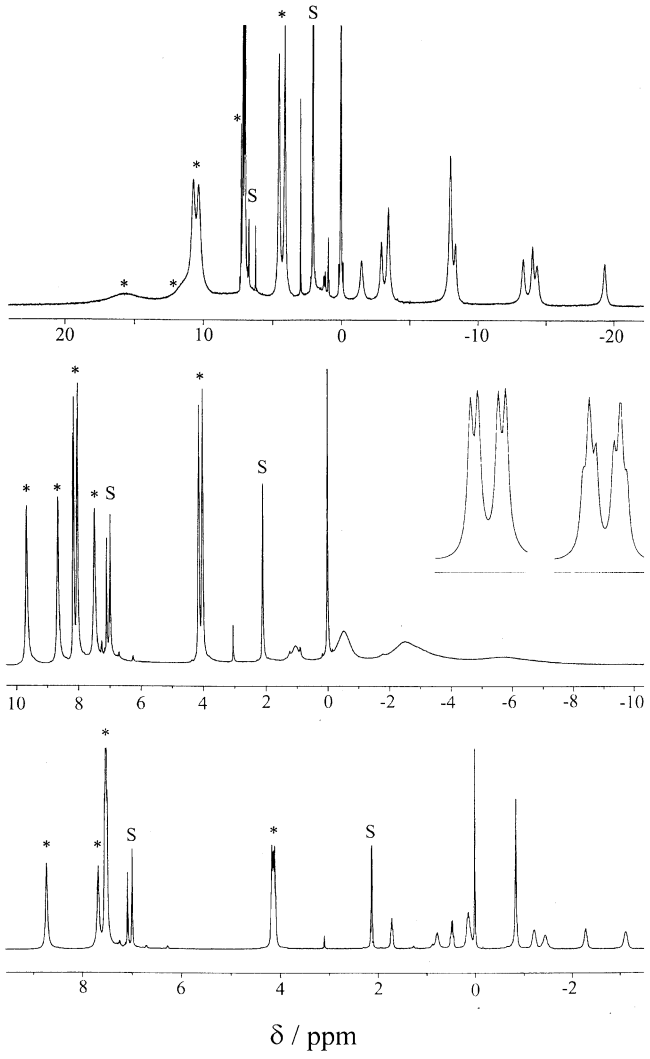

Figure 6. VT ^{1}H NMR spectra of **3** (solvent S: $CD_3C_6D_5$/TMS) at (from top to bottom) 193, 293 and 353 K; signals of the indenyl protons are marked by asterisks; the insert (for 293 K) shows the resonances of the indenyl protons 4/7-H and 5/6-H at an expanded δ scale; the spectra at 193 and 353 K do not include two additional nicotine resonances beyond δ = −20 and −4, respectively

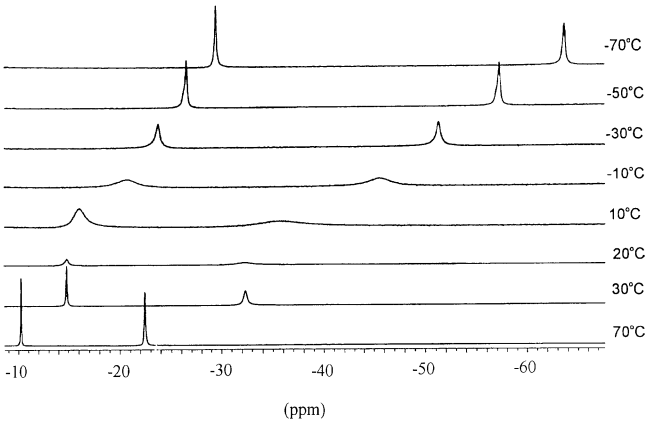

Figure 7. VT ^{1}H NMR spectra of the two THF resonances of [Pr(Ind)$_3$·THF] (solvent: $CD_3C_6D_5$)

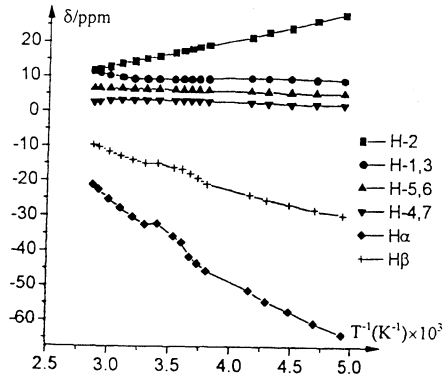

Figure 8. δ-vs-T^{-1} plots of all proton resonances of [Pr(Ind)$_3$·THF] (solvent: $CD_3C_6D_5$); the "humps" in the curves for Hα and Hβ (of THF) occur in the temperature range of pronounced line broadening (see Figure 7)

with the NCH_3 protons which are separated from the paramagnetic centre by *six* atoms. Equally far away from the metal ion are two of the CH_2 groups of the pyrrolidine unit (see Figure 1), the δ values of which should lie between δ = −2 and +2. Assuming that the signals at δ = −4.73 and −5.88 actually belong to the indenyl protons 1-H and 3-H (Figure 5, b, and Table 5), the experimentally found relative intensities of the six well-identified indenyl resonances (i.e. I_{rel} = 2 × 3, 2 × 3, 3, 3) simply require that one of the three appropriately intense signals at δ = 1.8, 0.2, or −0.8 be assigned to the proton 2-H.

f-f Circular Dichroism of 3 and 4

We have demonstrated recently that the 1:1 adducts of [Pr(Ind)$_3$] and (*R*)-(+)- and (*S*)-(−)-MTSO display, in the visible spectral range, significant circular dichroism (CD) of distinct f-f ligand-field excitations. However, the corres-

Table 6. Circular dichroism of [Pr(Ind)$_3$·(*R*)-(+)-MTSO][10] and [Pr(Ind)$_3$·(*S*)-(−)-Nic] (**3**) in the spectral range: 16100−21800 cm^{-1}

[Pr(Ind)$_3$·(*R*)-(+)-MTSO][a]		[Pr(Ind)$_3$·(*S*)-(−)-Nic][b]	
ν[c]	$10^4 \times \Delta\varepsilon_m$[d]	ν[c]	$10^4 \times \Delta\varepsilon_m$[d]
16155	−4.2		
16313	8.5		
16539	9.1		
		18677	4.8
		18890	−5.3
		19075	1.1
		19208	−1.7
		19402	2.7
19817	−30.6	19708	−2.6
		19972	−2.1
20226	16.6	20121	1.0
		20259	−1.7
20429	23.5	20429	6.8
20593	−16.9		
20781	7.4	20721	5.9
20964	−14.8	20964	−5.0
21177	1.6	21367	2.5
21758	53.7	21739	21.7

[a] $c(Pr^{3+})$ = 2.358·10^{-2} mol·L^{-1}. − [b] $c(Nd^{3+})$ = 1.298·10^{-2} mol·L^{-1} (solvent: C_6H_6). − [c] Dimension: cm^{-1}. − [d] Dimension: L·mol^{-1}·cm^{-1}.

ponding adducts involving [$PrCp_3$] and chiral MTSO were found to be practically CD-silent.[10] The new adduct [$Pr(Ind)_3$·(*S*)-(−)-Nic] (**3**) is CD-active as well, although its $|\Delta\varepsilon_m|$ values throughout are notably smaller than those reported for the MTSO adducts (see Table 6). In particular, f-f ligand excitations of **3** to states resulting from the $^1D_2$ manifold of the free Pr^{3+} ion (between ca. 16000 and 17000 cm^{-1}), which are predicted (and known) to be chiroptically less sensitive than excitations of states originating from ^3P_J manifolds with $J = 0$, 1, and 2,[18] are strictly CD-silent. The surprisingly large $\Delta\varepsilon_m$ values of both homologues around ca. 21700 cm^{-1} are probably due to an appreciable non-4f orbital admixture to the wave functions of the excited states. According to some qualitative studies (not considering the exact concentration of the dissolved sample), the neodymium homologue **4** also displays notable f-f CD. In Figure 9, the CD spectrum of **4** between 14500 and 20000 cm^{-1} is compared with the regular f-f-absorption spectrum for that spectral range.

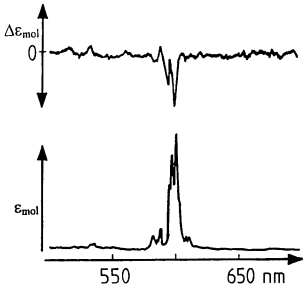

Figure 9. Absorption spectrum (bottom) and circular dichroism (top) of **4** (Ln = Nd) between 500 and 700 nm

Conclusions

According to the present study, only a relatively small selection of pyridine derivatives (Py*) is capable of occupying the vacant coordination site of an {$Ln(Ind)_3$} fragment, probably due to steric reasons. The nicotine molecule [i.e. 1-methyl-2-(3-pyridyl)pyrrolidine] *is* found to coordinate exclusively via its pyridine N atom, although *N*-methylpyrrolidine is known to combine with several {$LnCp_3$} fragments.[5] To the best of our knowledge, no crystal structure analysis of the generally liquid, free ligand has thus far been reported. The nicotine molecules coordinated in **2**, **3**, and **4** display a conformation very similar to that recently described[19] for a purely organic adduct, based upon O−H···N(Nic) hydrogen bonds.

The systematic assessment of the relevant crystallographic results for all new [$Ln(Ind)_3$·Py*] complexes supplements and confirms our earlier findings[7−10] in which the {$Ln(Ind)_3X$} fragment can adopt a large variety of mainly chiral conformations, wherein the benzo group of each indenyl ligand may be oriented either partially *meridionally* and partially *equatorially*, or all-*equatorially*. The latter situation is usually preferred as the ionic radius of the Ln^{3+} ion decreases.

By making use of the earlier described (for different types of complexes)[20] considerable amplification of the splitting of the resonance lines of initially prochiral nuclei by the auxiliary paramagnetism of Ln^{3+} ions with appropriate $4f^q$ configurations, the recognition of the remote chirality centre on the (*S*)-(−)-nicotine ligand by the indenyl protons could be readily achieved. Moreover, the 4f electrons of the ions Pr^{3+} (in **3**) and Nd^{3+} (in **4**) are capable of monitoring a chirogenic centre even more directly, such that various f-f ligand field transitions display weak, but significant circular dichroism, already at room temperature. Some very rapid (on the NMR timescale) and incompletely observable intermolecular reorganisation affecting essentially the indenyl ligands, is likely to imply a short-lived low-temperature modification of **3** involving another chirogenic centre, notably closer to the central metal ion than the dissymmetric carbon atom of the nicotine ligand.

Experimental Section

General Methods: All experimental manipulations, including sample preparation for instrumental measurements, were carried out under N_2 using vacuum-line and Schlenk techniques. The starting compound [$La(C_9H_7)_3$·THF] was prepared as described previously.[13] The nitrogen bases used were commercially available (Aldrich or Merck). − Infrared spectra were obtained with a Perkin−Elmer IR-1720 spectrometer. − ^1H NMR studies were carried out either with a Varian Gemini 200 (^1H, room temperature, solvent: [D_6]benzene) or with a Bruker AM 360 spectrometer (^1H-VT and ^{139}La-VT). Solvents for the VT studies were either [D_8]toluene (^1H) or a 3:7 mixture of [D_8]toluene and toluene and a 3:7 mixture of CD_2Cl_2 and CH_2Cl_2. ^{139}La NMR studies required the use of 10-mm NMR tubes under the following conditions: deuterium lock, SI = 4 K, TD = 8 K, SW = 71 kHz, DW = 7.0 μs, AQ =0.05s, NS = 825. A solution of either [$LaCp_3$·DMSO] in CD_2Cl_2 or of $LaCl_3$ in D_2O was used as an external standard. − Mass spectra were recorded with a Varian 3MA instrument with a spectrosystem MAT 188 (Finnigan) detector. The samples were prepared in carefully conditioned glass capillaries that could be fixed exactly on the head of the sample device, and were connected directly with the sample oven as soon as the capillary was cut off. − Optical (NIR/Vis) absorption spectra were recorded with a Cary 5E instrument, and the f-f CD spectra with a Jasco J 500 G dichrograph equipped with a DP-500 N data processor. The differential molar extinction values $\Delta\varepsilon_m$ were determined according to ref.[21]

X-ray Crystallography: Data collections were performed with a Hilger−Watts Y290 diffractometer at 153 K (Tables 7 and 8). All X-ray work was carried out with Mo-K_α radiation (λ = 70.926 pm) with the ω/2θ-scan technique. All calculations were based on SHELX-93 and SHELXTL-PLUS programme sets.[22] Heavy atoms were found from Patterson maps, and other non-hydrogen atoms were detected by Fourier techniques. Refinement was based on full-matrix least-squares techniques. Hydrogen atoms were included by use of a riding model with d(C−H) = 96 pm. $R1 = \Sigma||F_o| - |F_c||/\Sigma|F_o|$; $wR2 = [\Sigma w(F_o^2 - F_c^2)^2]/\Sigma w(F_o^2)^2]^{1/2}$; $S = [\Sigma w(F_o^2 - F_c^2)^2/\Sigma(n - P)]^{1/2}$; $P = [\max(F_o^2, 0) + 2F_c^2]/3$. Further details on the crystal structure investigations may be obtained from the Fachinformationszentrum Karlsruhe, D-76344 Eggenstein-Leopoldshafen, Germany [Fax: +49-7247/808-666; E-mail: crysdata@fiz-karlsruhe.de], on quoting the depository numbers CSD-380205 (**2**), -380204 (**3**), -380206 (**4**), -410174 (**5**), and -380201 (**6**).

Table 7. Survey of crystal data and details of data collection and refinement for the complexes **2**, **3**, and **4**; diffractometer: Hilger & Watts Y290; temperature: 153K

	2	**3**	**4**
Empirical formula	$C_{37}H_{35}LaN_2$	$C_{37}H_{35}N_2Pr$	$C_{37}H_{35}N_2Nd$
Wavelength [pm]	71.037	71.037	71.037
Space group	$P2_1$	$P2_1$	$P2_1$
a [pm]	1446.2(5)	1071.3(9)	877.1(4)
b [pm]	916.7(10)	2080(2)	2527.5(7)
c [pm]	2187(3)	1289(3)	1376(2)
β [°]	92.50(4)	91.96(11)	102.04(8)
V [nm^3]	2.896	2.871	2.984
Z	4	4	4
Density (calcd.) [gm^{-3}]	1.483	1.450	1.451
Absorption coefficient [mm^{-1}]	1.503	1.723	1.768
F(000)	1312	1280	1324
θ range for data collection [°]	2.29−30.06	2.43−25.06	2.37−27.57
h	−7 to 20	−12 to 12	−2 to 11
k	−4 to 12	−24 to 0	−5 to 32
l	−30 to 30	0 to 15	−17 to 17
Reflections collected	10633	5658	9993
Independent reflections (R_{int})	9545 (0.0199)	5248 (0.0423)	7366 (0.0460)
Data/restraints/parameters	9542/1/723	5248/1/723	7312/1/711
Goodness of fit on F^2	1.034	1.051	1.087
Final *R*1/*wR*2 indices [$I > 4\sigma(I)$]	0.0292/0.0647	0.0367/0.0974	0.0597/0.1052
*R*1/*wR*2 (all data)	0.0389/0.0694	0.0395/0.0996	0.1182/0.1421
Flack parameter	0.01(2)	0.04(3)	0.07(5)
Largest diff. peak and hole [e·nm^{-3}]	1730 and −861	1474 and −1382	479 and −744

Table 8. Summary of crystal data and details of data collection and refinements for **5** and **6**; diffractometer: Hilger & Watts (Y290); temperature: 153 K

	5	**6**
Empirical ormula	$C_{32}H_{26}NPr$	$C_{33}H_{28}NPr$
Wavelength [pm]	71.073	71.073
Space group	*Pbca*	*Pbca*
a [pm]	1376.3(3)	1163.6(4)
b [pm]	1301.5(3)	1493.7(7)
c [pm]	2631.0(5)	2940.1(13)
V [nm^3]	4.713(2)	5.110(4)
Z	8	8
Density (calcd.) [gm^{-3}]	1.594	1.506
Absorption coefficient [mm^{-1}]	2.089	1.928
F(000)	2272	2336
θ range for data collection [°]	2.29−27.54	2.32−30.15
h	−1 to 14	−2 to 16
k	−1 to 16	−2 to 21
l	−33 to 33	−2 to 41
Reflections collected	10826	10592
Independent reflections (R_{int})	4658(0.0401)	7251(0.0354)
Data/restraints/parameters	4649/0/307	7201/0/317
Goodness of fit on F^2	1.083	1.047
Final *R*1/*wR*2 indices [$I > 2\sigma(I)$]	0.0339/0.0912	0.0470/0.1175
*R*1/*wR*2 (all data)	0.0384/0.0971	0.0603/0.1455
Largest diff. peak and hole [e·nm^{-3}]	903 and −1051	2645 and −1641

Tris(cyclopentadienyl)[(*S*)-(−)-nicotine]lanthanum, [La(C_5H_5)$_3$·Nic] (1): A solution of (*S*)-(−)-nicotine (0.47 g, 2.93 mmol) in toluene (5.2 mL) was added to a suspension of [La(C_5H_5)$_3$·THF] (1.19 g, 2.93 mmol) in toluene (20 mL). After stirring (1 d) and filtration, the yellowish filtrate was concentrated and cooled to 0 °C. After washing (hexane) and drying (vacuum), the resulting precipitate was a colourless powder (yield: 1.32 g, ca. 91%; m.p. 165−170 °C). − $C_{25}H_{29}LaN_2$ (496.43): calcd. C 60.52, H 5.84, N 5.64; found C 59.67, H 5.88, N 5.84. − MS; *m*/*z*: 334, 269, 204, 162, 133, 119, 105, 83, 78 for [Cp$_n$La]$^+$ (*n* = 3, 2, 1); [nicotine]$^+$, [$C_5H_4NC_4H_7$]$^+$, [$C_5H_4NC_3H_5$]$^+$, [$C_5H_4NC_2H_3$]$^+$, [C_5H_4N]$^+$, [$C_4H_6NCH_3$]$^+$, [C_5H_5]$^+$. − ^{1}H NMR (C_6D_6/TMS, first-order as-

sessment, note that the signal assignment for the nicotine protons follows the designation chosen in Figure 1): δ = 6.13 (s, 15 H, Cp), 8.81 (s, 1 H, a), 8.30 (d, J = 5.16 Hz, b), 7.22 (d, J = 7.82 Hz, d) 6.57 (pseudo-q, 1 H, c), 2.96 (t, $J \approx$ 7.0 Hz, e) 2.68 and 1.99 (t, 1 H each, $J \approx$ 8.0 H, f) 1.95 (s, 3 H, NCH_3), 1.75, 1.39 (m, 2 H each, g/h). − ^{139}La NMR (in toluene, vide supra: see Table 1).

Tris(indenyl)[(*S*)-(−)-nicotine]lanthanum, [La(C$_9$H$_7$)$_3$·Nic] (2): A solution of (*S*)-(−)-nicotine (0.61 g, 3.76 mmol) in toluene (8.0 mL) was added at room temperature to a suspension of [La(C$_9$H$_7$)$_3$·THF] (2.09 g, 3.76 mmol) in toluene (30 mL). An almost transparent solution resulted which subsequently became turbid. The mixture was stirred overnight and finally heated to 70−80 °C. After filtration, when still warm, the solvent was removed from the yellow filtrate (in vacuo), after which a viscous yellow-orange residue was obtained. After addition of a trace amount of toluene, most of this residue converted overnight partially to yellow crystals and partially to a solid "gum". The solid product (including the crystals, some of which were suitable for X-ray studies) was washed with hexane and dried at room temperature. In total, 2.30 g (95%) of **2** was obtained. M.p. 94−98 °C. − $C_{37}H_{35}LaN_2$ (646.61): calcd. C 68.76, H 5.42, N 4.33; found C 68.51, H 5.47, N 4.45. − MS; *m*/*z*: 484, 369, 254, 115, 162, 133, 119, 84 for [Ind$_n$La]$^+$ (n = 3, 2, 1), [Ind]$^+$, [Nic]$^+$, [C$_5$H$_4$NC$_4$H$_7$]$^+$, [C$_5$H$_4$NC$_3$H$_5$]$^+$, [C$_4$H$_7$NCH$_3$]$^+$. − ^{1}H NMR (C$_6$D$_6$, TMS, first-order assessment): nicotine protons: δ = 8.17 (s, 1 H, a), 7.74 (d, J = 5.26 Hz, b), 7.26 (d, $J \approx$ 7.84 Hz, d), 6.56 (pseudo-q, $J \approx$ 5.20 and 2.62 Hz, c), 3.02 (t, $J \approx$ 8 Hz, e), 2.79 and 2.06 (t, 1 H each, $J \approx$ 8.0 Hz, f), 1.86 (m, 2 H, h), 1.49 (m, 2 H, g), 2.02 (s, 3 H, NCH_3); indenyl protons: δ = 7.46 (m, 6 H, 4,7-H), 6.94 (q, 6 H, $J \approx$ 3.0 Hz, 5,6-H), 6.14 (t, 3 H, $J \approx$ 3.30 Hz, 2-H), 5.90 (s, 6 H, 1,3-H). − ^{139}La NMR (in toluene, vide supra): see Table 1.

Tris(indenyl)[(*S*)-(−)-nicotine]praseodymium, [Pr(C$_9$H$_7$)$_3$·Nic] (3): The procedure resembled the synthesis of **2**, in that [Pr(C$_9$H$_7$)$_3$·THF] (2.64 g, 4.73 mmol) in toluene (30 mL) was treated with (*S*)-(−)-nicotine (0.77 g, 4.72 mmol) in toluene (8.5 mL). An analytically pure, yellow-green, viscous oil was obtained (yield: ≥ 85%). The oil was dissolved in a small amount of toluene, after which a large amount of hexane was added. The oil slowly converted into a yellow solid that was finally isolated and dried. Leek-green crystals suitable for an X-ray crystallographic study were obtained from a hot solution of this solid in toluene (the initially clear solution was slowly cooled down to room temperature). M.p. 129−132 °C. − $C_{37}H_{35}N_2Pr$ (648.61): calcd. C 68.54, H 5.39, N 4.32; found C 68.09, H 5.55, N 4.43. − MS; *m*/*z*: 486, 371, 256, 141, 115, 162, 133, 84 for [Ind$_n$Pr]$^+$ (n = 3, 2, 1, 0), [Ind]$^+$, [Nicotine]$^+$, [(C$_5$H$_4$N)(C$_4$H$_7$)]$^+$, [C$_4$H$_7$NCH$_3$]$^+$. − ^{1}H NMR (C$_6$D$_6$/TMS): nicotine protons a−d: δ = −32.80 (s, 1 H), −30.10 (s, 1 H), −6.74 (s, 1 H), −6.21 (s, 1 H); e−h: −5.77 (s, 1 H), −3.41 (s, 2 H), −0.75 (m, 2 + 1 H); NCH_3: δ = −2.85 (s, 3 H); indenyl protons: 1/2/3-H: δ = 9.59 (s, 3 H), 7.44 (s, 3 H), 8.79 (s, 3 H); 4/7-H: δ = 8.15 (d, 3 H, J = 7.52 Hz), 8.03 (d, 3 H, J = 7.54 Hz); 5/6-H: δ = 4.19 (t, 3 H), 4.06 (t, 3 H).

Tris(indenyl)[(*S*)-(−)-nicotine]neodymium, [Nd(C$_9$H$_7$)$_3$·Nic] (4): A procedure similar to that for the preparation of **2** was adopted, using [Nd(C$_9$H$_7$)$_3$·THF] (1.68 g, 2.99 mmol) in toluene (20 mL) and (*S*)-(−)-nicotine (0.48 g, 2.98 mmol) in toluene (5.0 mL). A red-green, analytically pure, viscous oil was obtained (1.34 g, 68.7%), which was redissolved in warm toluene. After addition of a small amount of hexane, and on slow cooling, green single crystals suitable for X-ray crystallographic studies were obtained. M.p. 112−116 °C. − $C_{37}H_{35}N_2Nd$ (651.94): calcd. C 68.20, H 5.37, N 4.29; found C 67.75, H 5.41, N 4.28. − MS; *m*/*z*: 489, 372, 259, 115, 162, 133, 84 for [Ind$_n$Nd]$^+$ (n = 3, 2, 1), [Ind]$^+$, [Nic]$^+$, [C$_5$H$_4$NC$_4$H$_7$]$^+$, [C$_4$H$_7$NCH$_3$]$^+$. − ^{1}H NMR (C$_6$D$_6$/TMS): nicotine protons: a−d: δ = −14.30 (s, 2 H), −13.40 (s, 1 H), −2.95 (s, 1 H); e−h: δ = −1.89 (s, 1 H), −1.15 (s, 1 H), 0.13 (s, 2 H), 0.42 (m, 1 H), 1.50 (br, 1 H); NCH_3: δ = −0.76 (s, 3 H); indenyl protons: δ = −5.88, −4.73 (s, 3 H each, 1,3-H), 1.74 (s, 3 H, 2-H), 7.40 (d, 6 H, 4,7-H), 5.00 (d, 6 H, 5,6-H).

Tris(indenyl)(pyridine)praseodymium, [Pr(C$_9$H$_7$)$_3$·Py] (5): The preparative procedure resembled those described before. A solution of pyridine (0.16 g, 2.07 mmol) in toluene (7 mL) was added to a suspension of [Pr(C$_9$H$_7$)$_3$·THF] (1.08 g, 1.93 mmol) in toluene (30 mL) at room temperature. After workup, 1.07 g (98%) of leek-green single crystals was collected. M.p. 199−203 °C. − $C_{32}H_{26}NPr$ (565.47): calcd. C 67.99, H 4.60, N 2.47; found C 67.17, H 4.69, N 2.49. − MS; *m*/*z*: 486, 372, 256, 141, 116, 78 for [Ind$_n$Pr]$^+$ (n = 3, 2, 1, 0), [Ind]$^+$, [Py]$^+$. − ^{1}H NMR(C$_6$D$_6$, TMS): indenyl protons: δ = 10.03 (s, 6 H, 1,3-H), 8.98 (s, 3 H, 2-H), 7.88 (s, 6 H, 5,6-H), 3.65 (s, 6 H, 4,7-H); pyridine protons: δ = −4.30 (s, 1 H, H-γ), −7.66 (s, 2 H, H-β), −33.42 (s, 2 H, H-α).

Tris(indenyl)(3-methylpyridine)praseodymium, [Pr(C$_9$H$_7$)$_3$·3-MePy] (6): As for the preparation of **5**, a solution of 3-methylpyridine (0.186 g, 2.01 mmol) in toluene (10 mL) was added to a suspension of [Pr(C$_9$H$_7$)$_3$·THF] (1.12 g, 2.06 mmol) in toluene (30 mL). 1.17 g (100%) of a crystalline product was obtained. M.p. 135−138 °C. − MS; *m*/*z*: 486, 372, 256, 116, 93, 78 for [Ind$_n$Pr]$^+$ (n = 3, 2, 1), [MePy]$^+$, [Py]$^+$. − $C_{33}H_{28}NPr$ (579.50): calcd. C 68.42, H 4.83, N 2.42; found C 68.03, H 4.94, N 2.42. − ^{1}H NMR (C$_6$D$_6$/TMS): indenyl protons: δ = 10.13 (s, 6 H, 1,3-H), 8.12 (s, 6 H, 5,6-H), 7.66 (s, 3 H, 2-H), 3.68 (d, 6 H, J = 3.30 Hz, 4,7-H); 3-methylpyridine protons: δ = −4.38 (s, 1 H, Hγ), −6.67 (s, 3 H +1 H), CH_3 + Hβ), −38.9, −30.0 (s, 1 H each, Hα)

Acknowledgments

J.-W. G. would like to express his gratitude to the Friedrich-Ebert-Stiftung (Bonn) for a fellowship. We also express our deep thanks to Mrs. S. Samba for technical assistance.

[1] E. C. Baker, K. N. Raymond, *Inorg. Chem.* **1977**, *16*, 2710−2714.
[2] G. B. Deacon, B. M. Gatehouse, S. N. Platts, D. L. Wilkinson, *Aust. J. Chem.* **1987**, *40*, 907−914.
[3] H. Breitbach, Doctoral Dissertation, Universität Hamburg, Germany **1987**, p. 42 {crystal structure of [Pr(CH$_3$C$_5$H$_4$)$_3$·γ-picoline]; Pr−N distance: 264.1(4) pm}.
[4] A. Zazzetta, A. Grew, *Acta Crystallogr., Sect. B* **1979**, *35*, 457−460.
[5] R. von Ammon, B. Kanellakopulos, R. D. Fischer, P. Laubereau, *Inorg. Nucl. Chem. Lett.* **1969**, *5*, 315−319.
[6] R. von Ammon, R. D. Fischer, *Angew. Chem.* **1972**, *84*, 737−755; *Angew. Chem. Int. Ed. Engl.* **1972**, *11*, 675−692.
[7] J. Guan, R. D. Fischer, *J. Organomet. Chem.* **1997**, *532*, 147−157.
[8] J. Guan, Q. Shen, R. D. Fischer, *J. Organomet. Chem.* **1997**, *549*, 203−212, and further references given therein. Unfortunately, in Table 5 of this paper, the δ(5/6-H) value of the complex [Nd(Ind)$_3$·THF] is missing a minus sign.
[9] J. Guan, R. D. Fischer, *J. Organomet. Chem.* **1998**, *564*, 167−177.
[10] J. Guan, J. Stehr, R. D. Fischer, *Chem. Eur. J.* **1999**, *5*, 1992−2003.
[11] J. Guan, Doctoral Dissertation, Universität Hamburg, Germany, **1998**: [11a] p. 49, [11b] p. 37, [11c] p. 141.

[12] S. H. Eggers, H. Schultze, J. Kopf, R. D. Fischer, *Angew. Chem.* **1986**, *98*, 631−632; *Angew. Chem. Int. Ed. Engl.* **1986**, *25*, 656−657.
[13] J. Xia, Z. Jin, G. Lin, W. Chen, *J. Organomet. Chem.* **1991**, *408*, 173−179.
[14] J. G. Brennan, S. D. Stults, R. A. Anderson, A. Zalkin, *Inorg. Chim. Acta* **1987**, *139*, 201−202.
[15] W. A. Herrmann, R. Anwander, F. C. Munck, W. Scherer, *Chem. Ber.* **1993**, *126*, 331−337.
[16] R. Anwander, W. A. Herrmann, F. C. Munck, W. Scherer, *J. Organomet. Chem.* **1993**, *462*, 163−174.
[17] D. M. Barnhart, D. L. Clark, J. C. Huffman, R. L. Vincent, J. G. Watkin, *Inorg. Chem.* **1993**, *32*, 4077−4083.
[18] F. S. Richardson, *Inorg. Chem.* **1980**, *19*, 2806−2812.
[19] See: K. Fukawa, S. Harada, N. Kasai, M. Toda, K. Mori, F. Toda, *Bull. Chem. Soc. Jpn.* **1989**, *62*, 2714−2716.
[20] A. Steudel, E. Siebel, R. D. Fischer, G. Paolucci, V. Lucchini, *J. Organomet. Chem.* **1998**, *556*, 229−238; A. Steudel, J. Stehr, R. D. Fischer, *J. Organomet. Chem.* **1998**, *570*, 89−96.
[21] H. B. Kagan, *Stereochemie*, Thieme, Stuttgart, **1979**; S. F. Mason, *Molecular Optical Activity and Chiral Discrimination*, Cambridge University Press, Cambridge **1982**; *Circular Dichroism. Principles and Applications* (Eds.: N. Berova, K. Nakanishi, R. W. Woody), Wiley-VCH, New York, **2000**.
[22] SHELX-86: G. M. Sheldrick, *Acta Crystallogr., Sect. A* **1990**, *46*, 467−473; G. M. Sheldrick, *Program for the Refinement of Crystal Structures*, Universität Göttingen, Germany, **1993**; G. M. Sheldrick, *SHELX-PLUS*, Release 4.21/v, Siemens Analytical X-ray Instruments, Madison, Wisconsin (USA), **1995**.

Received April 17, 2001
[I01134]

Fluorenyl and *ansa*-Dimethylsilyl*bis*(fluorenyl) Derivatives of Divalent Ytterbium and Samarium − Synthesis and Structure of the First Mixed-Ligand Ln^{II} Classic Sandwich Complex $(C_{13}H_9)(C_5Me_5)Yb(DME)$

Alexander A. Trifonov,*[a] Evgenii N. Kirillov,[a] Sebastian Dechert,[b] Herbert Schumann,*[b] and Mikhail N. Bochkarev[a]

Keywords: Lanthanides / Samarium / Cyclopentadienyl complexes / Fluorenyl complexes / *ansa*-Bis(fluorenyl) complexes / Crystal structure

Novel fluorenyl complexes of divalent ytterbium $(C_{13}H_9)_2Yb(L)_n$ [L = THF, n = 2 (**1**); L = DME, n = 1 (**2**)] have been prepared by reaction of $YbI_2(THF)_2$ with 2 equiv. of $C_{13}H_9K$ as well as by reaction of $(C_{10}H_8)Yb(THF)_2$ with fluorene in THF. Oxidation of **1** by *t*BuN=CHCH=N*t*Bu (DAD) resulted in the formation of $(C_{13}H_9)_2Yb(DAD)$ (**3**). The reaction of $\{YbI(DME)_2\}_2(\mu\text{-}C_{10}H_8)\}$ (**4**) with fluorene did not give $(C_{13}H_9)YbI(DME)$ (**5**), but the redistribution products $YbI_2(DME)$ and **2**. The first mixed-ligand sandwich complex of a divalent lanthanide metal $(C_{13}H_9)(C_5Me_5)Yb(DME)$ (**6**) was prepared in a one-pot reaction of **4** with C_5Me_5H and $C_{13}H_9K$ in DME. *ansa*-$Me_2Si(C_{13}H_8)_2Yb(THF)$ (**7**) and *ansa*-$Me_2Si(C_{13}H_8)_2Sm(THF)_4$ (**8**) were obtained by treatment of the appropriate Ln^{II} iodides with *ansa*-$Me_2Si(C_{13}H_9)_2K_2$ in THF. The molecular structures of **1** and **6** were determined by single-crystal X-ray diffraction.

Introduction

The increased attention given to the fluorenyl ligand and the extensive work in synthesis and investigation of its d-metal block complexes has been observed during the last decade. This was mainly provoked by the discovery of the high efficiency of fluorenylzirconium complexes in the stereospecific propylene polymerization.[1,2] The remarkable activity of fluorenyl-derived group-4 metallocene complexes in α-olefin polymerization was explained by the characteristics of the ligand, namely by the easy η^5-η^3-η^1 interconversion of the five-membered ring−metal bonding mode (ring slippage), providing a free site for a substrate in the metal center's coordination sphere.

The complexes with η^5- bonded aromatic carbocyclic (mainly cyclopentadienyl) ligands form the most explored class of organolanthanide compounds.[3,4] These ancillaries have proved themselves to be a suitable coordination environment of the lanthanide metal atom providing the unique reactivity of the derived hydrido and hydrocarbyl complexes in various reactions involving unsaturated substrates.[5−18] Some cyclopentadienyl derivatives of divalent lanthanides also show catalytic activity in α-olefin polymerization.[19−22]

To date the fluorenyl ligand has not been significantly involved in organolanthanide chemistry. The lanthanide fluorenyl complexes $(C_{13}H_9)_2Ce$[23] and $(C_{13}H_9)_2LnCl_2Li(THF)_2$ (Ln = La, Nd, Sm, Ho, Lu)[24,25] were described twenty years ago and are poorly characterized, but were classified by the authors as complexes with metal−ligand σ-bonds on the basis of spectroscopic data. The only fluorenyl derivative of a divalent lanthanide, $(C_{13}H_9)_2Sm(THF)_2$, was reported and structurally characterized by Evans.[26] X-ray diffraction has shown the coordination of the fluorenyl ligands in this complex to be partially distorted from η^5 towards η^3. Dramatic influence of ligation of the central atom on the fluorenyl ligand bonding mode has been found for (cyclopentadienyl)(*ansa*-fluorenyl)yttrocene complexes.[27] In *ansa*-$Me_2Si(\eta^3\text{-}C_{13}H_9)(\eta^5\text{-}Cp')YCl_2Li(OEt_2)_2$ an X-ray diffraction study revealed η^3-coordination of the central fluorenyl ring, while in the related amido derivative *ansa*-$Me_2Si(\eta^3\text{-}C_{13}H_9)(\eta^5\text{-}Cp')YN(SiMe_3)_2$, the fluorenyl ligand bonding is just partially tilted towards η^3-, but basically approaches an η^5-arrangement.

Being sterically demanding, the fluorenyl ligand is an attractive and easily available ancillary which is able to stabilize the Ln^{+2} oxidation state. This also proves that there is a well-defined environment around the metal center that allows control of reaction stereochemistry in its coordination sphere. In this paper we present the synthesis and structure investigations of novel (fluorenyl)Yb^{II} and -Sm^{II} sandwich complexes.

Results and Discussion

Two different approaches were used to synthesize the bis(fluorenyl) complex of divalent ytterbium: (i) the metathetic reaction of $YbI_2(THF)_2$ with 2 equiv. of $C_{13}H_9K$ in THF, which resulted in the formation of $(C_{13}H_9)_2Yb(THF)_2$ (**1**) in 72% yield, and (ii) by protolytic substitution of the naphthalene ligand in $(C_{10}H_8)Yb(THF)_2$[28] (**3**) by fluorene which also afforded **1** in reasonable yields. Although in the

[a] G. A. Razuvaev Institute of Organometallic Chemistry of Russian Academiy of Sciences,
Tropinina 49, 603950 Nizhny Novgorod GSP-445, Russia
Fax: (internat.) + 7-8312/661-497
E-mail: trif@imoc.sinn.ru
[b] Institut für Chemie der Technischen Universität,
Straße des 17. Juni 135, 10623 Berlin, Germany
Fax: (internat.) + 49-30/314-22168
E-mail: schumann@chem.tu-berlin.de

 © WILEY-VCH Verlag GmbH, 69451 Weinheim, 2001 1434−1948/01/1010−2509 $ 17.50+.50/0

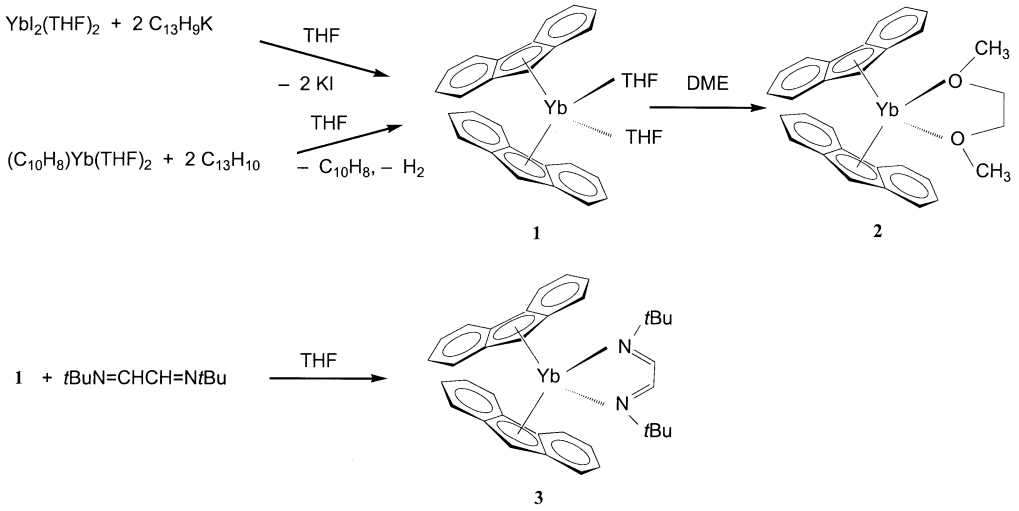

Scheme 1

latter method the yield is somewhat lower, this allows the avoidance of the tedious procedure of KI separation (Scheme 1).

Bis(fluorenyl)bis(tetrahydrofuran)ytterbium(II) (**1**) is isolated after recrystallization from hot toluene/THF mixtures (30:1) in the form of ruby-red crystals, extremely sensitive towards moisture and air. It is soluble in THF, DME, and pyridine, moderately soluble in toluene and insoluble in aliphatic hydrocarbons. Recrystallization from DME produces $(C_{13}H_9)_2Yb(DME)$ (**2**) as deep yellow crystals, which show a slightly lower solubility in the solvents mentioned above compared to **1**. Both complexes **1** and **2** are diamagnetic corresponding to the Yb^{2+} oxidation state;[29] they were characterized by means of ^1H and ^{13}C NMR and IR spectroscopy as well as by elemental analysis, and an X-ray structural analysis was also performed on **1**.

Compound **1** can easily be oxidized by *t*BuN=CHCH=N*t*Bu (DAD) in THF solution forming the corresponding (diazabutadiene)Yb^{III} derivative **3** as deep green crystals after recrystallization from hexane with nearly quantitative yield. It is very soluble in THF and toluene and moderately soluble in hexane. The magnetic moment of **3** (4.8 BM, 293 K) corresponds well to the values normally observed for complexes of trivalent ytterbium. For **3** as for other diazabutadiene derivatives of Yb^{III} [30,31] no signals of DAD radical anions were observed by ESR spectroscopy.

Heteroleptic sandwich complexes bearing different carbocyclic ligands are of essential practical interest since selection of ligands could be a useful tool for fine-tuning steric and electronic properties of the metal atom's environment. It is known from the literature,[4] that lanthanide mixed-ligand systems are predisposed to ligand redistribution, which favours the formation of homoleptic derivatives. To date, mixed ligand Ln^{II} classic sandwich complexes having two different π-donor carbocyclic ligands, are unknown. Heteroleptic Ln^{II} derivatives, in general, still remain rare. Recently, Evans described the synthesis and X-ray structure of $[Cp^*Yb(THF)]_2(\mu\text{-}\eta^8\text{:}\eta^8\text{-}C_8H_8)$, a binuclear (cyclooctatetraenyl)(pentamethylcyclopentadienyl) triple-decker complex.[32] Some (aryloxy)(cyclopentadienyl),[33,34] linked (η^6-carboranyl)(cyclopentadienyl),[35] linked (alkoxy)(cyclopentadienyl),[36–38] and (cyclopentadienyl)(pyrazolylborato) derivatives[39] have also been reported.

Our first attempts to obtain a starting material for heteroleptic fluorenyllanthanide complexes failed. Splitting of the naphthalene-bridged dinuclear complex $[(DME)_2(I)Yb(\mu\text{-}C_{10}H_8)Yb(I)(DME)_2]$ (**4**) by fluorene in DME did not yield the expected heteroleptic dimethoxyethane complex of fluorenylytterbium(II)iodide (**5**); the dis-

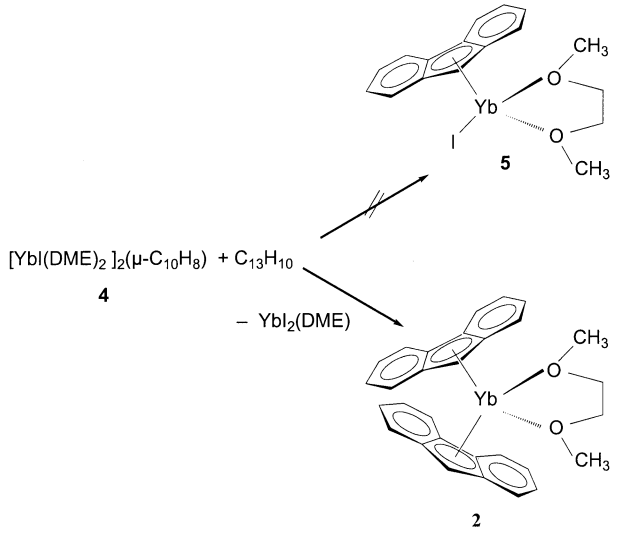

Scheme 2

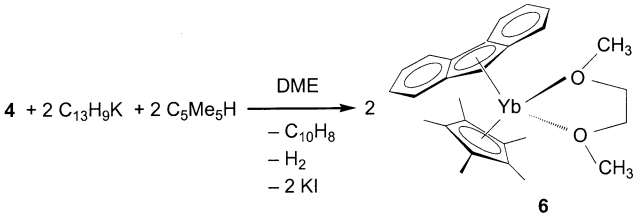

Scheme 3

mutation products $YbI_2(DME)_2$ and **2** could be isolated instead (Scheme 2). The second experiment, the consecutive "one-pot" treatment of **4** with C_5Me_5H and $C_{13}H_9K$ in DME was successful. Ligand redistribution was avoided and $(C_{13}H_9)(C_5Me_5)Yb(DME)$ (**6**) crystallized in 46% yield as diamagnetic deep-green crystals from toluene (Scheme 3).

Compound **6** is stable at room temperature in the solid state as well as in benzene, toluene and DME, but not in THF. Thus, the ^1H NMR spectrum of **6** in [D$_6$]benzene shows a singlet signal at $\delta = 2.06$ due to the CH_3 protons of the pentamethylcyclopentadienyl ligand and a set of signals typical for the fluorenide anion[40,41] in the aromatic region. The proton signals of the CH_3O groups of the DME ligand appear as a broad multiplet, significantly high-field shifted, while the signals for the CH_2 protons keep their normal position. The high-field shift of the methyl proton signals of DME can be attributed either to the influence of coordination to the Yb^{II} ion or to the influence of the ring current of the coordinated fluorenyl ligand. In contrast, the ^1H NMR spectrum of **6**, on dissolving the compound in [D$_8$]THF, immediately shows two singlet signals for the Cp* protons at $\delta = 1.82$ and 1.87 (with the ratio 3:8 which does not change within 100 h) and a complex set of signals in the region between $\delta = 6.12$ and 7.93 for the protons of the fluorenyl ligand. The reason for this may be a dismutation reaction forming partly the symmetric products $(C_{13}H_9)_2Yb(THF)_2$ (**1**) and $(C_5Me_5)_2Yb(THF)_2$ in THF solution. This could be shown in the case of other lanthanoidocene derivatives, which undergo a facile transfer of η^5-bonded cyclopentadienyl ligands.[42–44] Neither **1** nor $Cp^*_2Yb(THF)_2$ could be isolated from the reaction mixture in a pure state.

With respect to catalytic activity, the *ansa*-bis(cyclopentadienyl) and *ansa*-bis(indenyl) framework provides a considerable opening of the metal coordination sphere in lanthanidocene complexes which facilitates the substrates access to the metal centers, improving its electronic properties as well as the configuration of its frontier orbitals.[7,45–47] The *ansa*-bis(fluorenyl) ancillary ligation is supposed to combine advantages of design of the metal atom environment peculiar to the *ansa* system and flexibility of coordination of the fluorenyl ligand. Therefore *ansa*-bis(fluorenyl) derivatives of Sm^{II} and Yb^{II} should be promising catalysts for olefin polymerization.

The *ansa*-bis(fluorenyl)lanthanide(II) complexes $Me_2Si(C_{13}H_8)_2Yb(THF)$ (**7**) and $Me_2Si(C_{13}H_8)_2Sm(THF)_4$ (**8**) were obtained in more than 70% yield as red and brown solids from the reaction of $YbI_2(THF)_2$ and $SmI_2(THF)_2$, respectively, with $Me_2Si(C_{13}H_8)_2K_2$ in THF (Scheme 4). Both complexes are only slightly soluble in THF and DME. All attempts to obtain single crystals useable for X-ray structure investigations, failed. They could be characterized by ^1H, ^{13}C NMR, IR spectroscopy, and elemental analysis. The IR spectrum of **7** only shows bands for coordinated THF molecules (860 and 1020 cm^{-1}), whereas that of **8** presents bands in the range of coordinated (860 and 1040 cm^{-1}) and noncoordinated THF (910 and 1070 cm^{-1}).

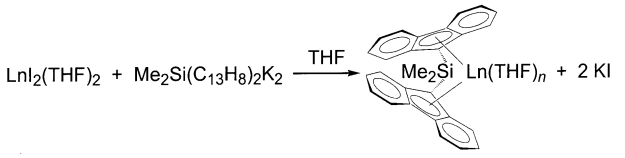

7: $n = 1$, Ln = Yb; **8**: $n = 4$, Ln = Sm

Scheme 4

Molecular Structure of 1 and 6

Compound **1** crystallizes with two crystallographically independent molecules in the asymmetric unit (Figure 1). **1** was found to be an eight-coordinate complex having a bent sandwich structure with bond angles of $(C_{13}H_9)_{Cent}-Yb-(C_{13}H_9)_{Cent}$ = 125.58(11) and

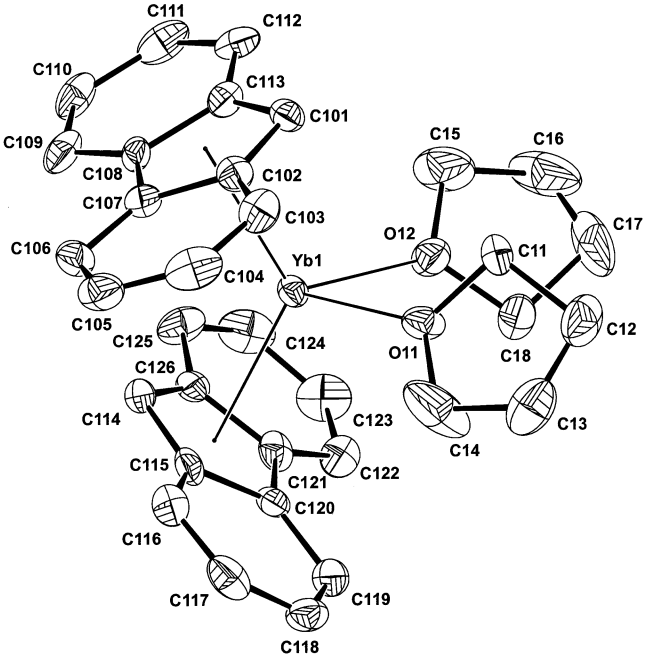

Figure 1. ORTEP[48] drawing and numbering scheme of the molecular structure of **1** with thermal ellipsoids drawn at the 50% probability level; only one of the two crystallographically independent molecules is shown; hydrogen atoms are omitted; selected bond lengths [Å] and angles [°] [Cg(1) and Cg(2) are defined by the ring atoms C(101), C(102), C(107), C(108), C(113) and C(114), C(115), C(120), C(121), C(126); Cg(3) and Cg(4) were defined by the ring atoms C(201), C(202), C(207), C(208), C(213) and C(214), C(215), C(220), C(221), C(226)]: Yb(1)–Cg(1) 2.503(3) [Yb(2)–Cg(3) 2.513(3)], Yb(1)–Cg(2) 2.512(4) [Yb(2)–Cg(4) 2.518(3)], Yb(1)–O(11) 2.389(5) [Yb(2)–O(21) 2.403(5)], Yb(1)–O(12) 2.398(5) [Yb(2)–O(22) 2.409(5)], Yb(1)–C(101) 2.663(7) [Yb(2)–C(201) 2.672(7)], Yb(1)–C(102) 2.756(7) [Yb(2)–C(202) 2.732(7)], Yb(1)–C(107) 2.852(7) [Yb(2)–C(207) 2.857(7)], Yb(1)–C(108) 2.867(6) [Yb(2)–C(208) 2.898(7)], Yb(1)–C(113) 2.774(7) [Yb(2)–C(213) 2.798(7)], Yb(1)–C(114) 2.626(7) [Yb(2)–C(214) 2.622(6)], Yb(1)–C(115) 2.780(7) [Yb(2)–C(215) 2.786(7)], Yb(1)–C(120) 2.952(7) [Yb(2)–C(220) 2.951(7)], Yb(1)–C(121) 2.893(7) [Yb(2)–C(221) 2.908(7)], Yb(1)–C(126) 2.696(7) [Yb(2)–C(226) 2.702(7)]; Cg(1)–Yb(1)–Cg(2) 125.58(11) [Cg(3)–Yb(2)–Cg(4) 124.87(10)], Cg(1)–Yb(1)–O(11) 104.63(15) [Cg(3)–Yb(2)–O(21) 106.21(15)], Cg(1)–Yb(1)–O(12) 118.14(15) [Cg(3)–Yb(2)–O(22) 116.44(15)], Cg(2)–Yb(1)–O(11) 115.40(15) [Cg(4)–Yb(2)–O(21) 114.32(15)], Cg(2)–Yb(1)–O(12) 105.25(2) [Cg(4)–Yb(2)–O(22) 106.22(15)], O(11)–Yb(1)–O(12) 78.37(18) [O(21)–Yb(2)–O(22) 80.14(18)]; ring slippage [Å]: Cg(1) 0.233, Cg(2) 0.384, Cg(3) 0.253, Cg(4) 0.392

124.87(10)°, respectively. The distances $(C_{13}H_9)_{Cent}-Yb$ are 2.503(3), 2.513(3), 2.512(4), and 2.518(3) Å for both molecules, however substantial scattering in $Yb-C_{Flu}$ bond lengths is observed for both ligands. Analysis of the bond situation reveals shorter distances between the ytterbium ion and three carbon atoms [C(113)−C(101)−C(102), C(115)−C(114)−C(126) and C(213)−C(201)−C(202), C(215)−C(214)−C(226)], while two Yb−C distances [C(107)−C(108), C(120)−C(121) and C(207)−C(208), C(220)−C(221)] are somewhat longer compared to the average value (2.78 Å). The deviation of the Yb−C distances in the range of 0.25 Å for one five-membered ring and 0.38 Å for the second one suggests a partial tilting of the fluorenyl ligand toward η^3-fashion as it has already been observed for $(C_{13}H_9)_2Sm(THF)_2$[26] and $Me_2Si(\eta^3\text{-}C_{13}H_9)(\eta^5\text{-}Cp')YN(SiMe_3)_2$.[27] It should be mentioned that in the case of the samarium analogue a significant deviation of the Sm−C distances occurs only in one of the fluorenyl ligands, while in **1** for both of them. This interesting structural feature obviously arises from the smaller radius of the Yb^{2+} ion and a consequent steric hindrance and repulsion of the bulky fluorenyl ligands.

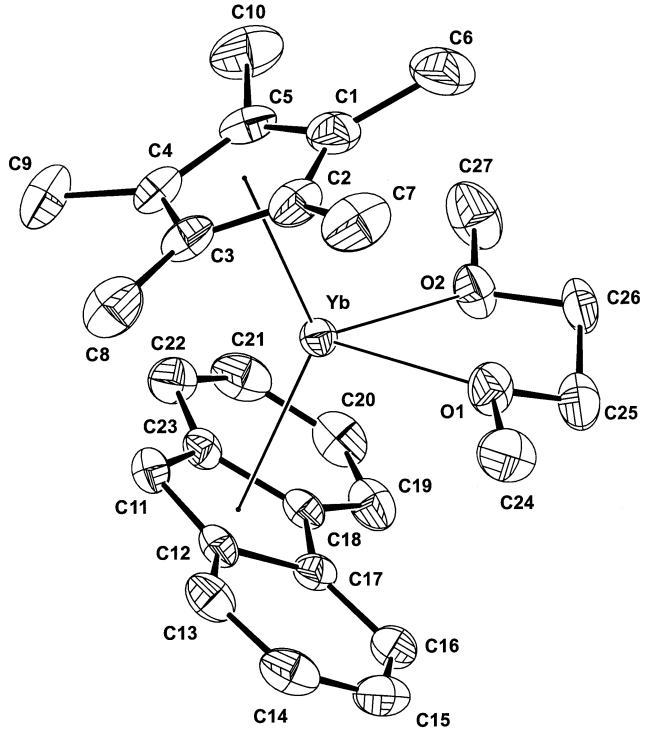

Figure 2. ORTEP[48] drawing and numbering scheme of the molecular structure of **6** with thermal ellipsoids drawn at the 50% probability level; hydrogen atoms are omitted; selected bond lengths [Å] and angles [°] [Cg(1) and Cg(2) were defined by the ring atoms C(1)−C(5) and C(11), C(12), C(17), C(18), C(23)]: Yb−Cg(1) 2.392(2), Yb−Cg(2) 2.505(2), Yb−O(1) 2.415(4), Yb−O(2) 2.440(3), Yb−C(1) 2.673(5), Yb−C(2) 2.663(5), Yb−C(3) 2.671(5), Yb−C(4) 2.695(5), Yb−C(5) 2.698(5), Yb−C(11) 2.661(4), Yb−C(12) 2.782(5), Yb−C(17) 2.915(5), Yb−C(18) 2.857(5), Yb−C(23) 2.710(4); Cg(1)−Yb−O(2) 112.73(10), Cg(2)−Yb−O(1) 107.23(9), Cg(1)−Yb−Cg(2) 134.86(8), Cg(1)−Yb−O(1) 110.07(10), Cg(2)−Yb−O(2) 104.14(9), O(1)−Yb−O(2) 68.05(12); ring slippage [Å]: Cg(1) 0.059, Cg(2) 0.286

The single-crystal X-ray structure determination of **6** shows a bent sandwich complex of divalent ytterbium with coordination number 8 (Figure 2). The $Yb-Cp^*_{Cent}$ bond length is 2.392(2) Å, and $Yb-(C_{13}H_9)_{Cent}$ = 2.505(2) Å, which is close to the value obtained for **1**. The difference of five bond lengths between the ytterbium ion and the carbon atoms of the central five-membered ring of the fluorenyl ligand (0.254 Å) indicates a partial distortion toward an η^3 coordination, while the Cp* ligand is η^5-bonded. The bond angle $Cp^*_{Cent}-Yb-(C_{13}H_9)_{Cent}$ [134.86(8)°] is significantly larger than the angle $(C_{13}H_9)_{Cent}-Yb-(C_{13}H_9)_{Cent}$ in **1** [125.58(11)/124.87(10)°] and is consistent with the higher steric demand of the Cp* ligand vs. $C_{13}H_9$.

Experimental Section

General Remarks: All experiments were performed in evacuated tubes, using standard Schlenk techniques with rigorous exclusion of traces of moisture and air. THF, DME, diethyl ether, toluene, and hexane were purified by distillation from sodium/benzophenone ketyl and were condensed under vacuum prior to use. Fluorene and pentamethylcyclopentadiene were commercially available and used as received. $YbI_2(THF)_2$,[3] $(C_{10}H_8)Yb(THF)_2$,[28] $(\mu\text{-}C_{10}H_8)[YbI(DME)_2]_2$ (**4**),[49] and $Me_2Si(C_{13}H_9)_2$[50] were prepared according to literature procedures. − IR spectra were recorded as Nujol mulls with a Specord M80 spectrophotometer, NMR spectra with a Bruker DPX200 spectrometer in [D_6]benzene or [D_8]THF at 298 K, chemical shifts for ^1H and ^{13}C NMR spectra were referenced internally using the residual solvent resonances and reported relative to TMS. − Magnetic susceptibility measurements were carried out according to the published procedure.[51]

$(C_{13}H_9)_2Yb(THF)_2$ (1). − a) To a solution of $C_{13}H_9K$ (2.21 g, 10.84 mmol) in THF (40 mL), $YbI_2(THF)_2$ (3.09 g, 5.42 mmol) was added slowly at 0 °C under rigorous stirring. The reaction mixture was allowed to warm up to room temperature and was stirred overnight. After filtration, THF was removed under vacuum and the resulting crude product was recrystallized from THF/toluene (1:30) to yield 2.52 g (72%) of **1**. − IR (Nujol): $\tilde{\nu}$ = 3020 (m), 1590 (m), 1320 (m), 1200 (m), 1090 (w), 1030 (s), 990 (w), 925 (w), 825 (m), 750 (s), 720 (s), 700 (s) cm^{-1}. − ^1H NMR (200 MHz, [D_8]THF): δ = 5.63 (s, 2 H, aryl-C^9), 6.76 [t, ^3J(H,H) = 14.4 Hz, 4 H, aryl-H^7], 7.04 [t, ^3J(H,H) = 14.6 Hz, 4 H, aryl-H^6], 7.44 [d, ^3J(H,H) = 8 Hz, 4 H, aryl-H^8], 7.93 [^3J(H,H) = 8 Hz, 4 H, aryl-H^5]. − ^{13}C NMR (50.3 MHz, [D_8]THF): δ = 113.8, 118.3, 119.8, 120.5, 122.3, 126.5, 133.7. − $C_{34}H_{34}O_2Yb$ (647.7): calcd. C 63.05, H 5.29, Yb 26.72; found C 62.76, H 4.87, Yb 26.92. − **b)** To a suspension of $(C_{10}H_8)Yb(THF)_2$ (2.13 g, 4.78 mmol) in THF (30 mL) was added fluorene (1.58 g, 9.56 mmol). The reaction mixture was heated to 60 °C for 8 h, filtered and THF was removed under vacuum. Recrystallization of the crude product from THF/toluene (1:30) yielded 2.06 g (64%) of **1**.

$(C_{13}H_9)_2Yb(DME)$ (2). − a) Compound **2** was obtained by recrystallization of **1** from DME as fine yellow crystals. − IR (Nujol): $\tilde{\nu}$ = 3020 (m), 1590 (m), 1320 (m), 1200 (m), 1090 (m), 1050 (s), 990 (w), 925 (w), 750 (s), 720 (s), 700 (s) cm^{-1}. − ^1H NMR (200 MHz, [D_8]THF): δ = 3.24 (s, 6 H, CH_3), 3.48 (s, 4 H, CH_2), 5.70 (s, 2 H, aryl-C^9), 6.72 [t, ^3J(H,H) = 14 Hz, 4 H, aryl-H^7], 7.00 [t, ^3J(H,H) = 14.2 Hz, 4 H, aryl-H^6], 7.50 [d, ^3J(H,H) = 8.8 Hz, 4 H, aryl-H^8], 8.00 [d, ^3J(H,H) = 8.2 Hz, 4 H, aryl-H^5]. − ^{13}C NMR (50.3 MHz, [D_8]THF): δ = 36.8, 83.0, 113.9, 118.2, 120.0, 120.4, 122.3, 126.5,

133.5. − $C_{30}H_{28}O_2Yb$ (594.1): calcd. C 60.59, H 4.71, Yb 29.28; found C 60.33, H 4.29, Yb 29.18. − **b)** To a suspension of [Yb-I(DME)$_2$]$_2$(μ-$C_{10}H_8$) (**4**) (2.11 g, 1.94 mmol) in DME (30 mL) was added a solution of fluorene (0.64 g, 3.88 mmol) in DME (10 mL) at room temperature and stirred for 12 h. The resulting yellowish-brown solution was separated from a precipitate of off-white crystals of YbI_2(DME) (0.82 g, 82%) by filtration, concentrated and cooled to 0 °C. Evaporation of DME yielded 0.64 g (56%) of **2**. IR and ^{1}H NMR spectra are identical to the spectra of **2** formed in the reaction pathway a).

($C_{13}H_9$)$_2$Yb(*t*BuN=CHCH=N*t*Bu) (3): To a solution of **1** (0.87 g, 1.34 mmol) in THF (15 mL), was added a solution of *t*BuN=CHCH=N*t*Bu (0.23 g, 1.36 mmol) in THF (2 mL) at room temperature. The red solution was stirred for 2 h, THF was removed in vacuo and the resulting greenish-brown solid was recrystallized from hexane yielding 0.88 g (98%) of deep-green crystals of **3**. − IR (Nujol): $\tilde{\nu}$ = 3160 (m), 2710 (w), 2280 (m), 1620 (m), 1300 (m), 1260 (s), 1200 (s), 995 (m), 900 (m), 790 (s), 720 (s) cm^{-1}. − $C_{36}H_{38}N_2Yb$ (672.2): calcd. C 64.26, H 5.70, Yb 25.87; found C 63.99, H 5.63, Yb 25.29.

($C_{13}H_9$)(C_5Me_5)Yb(DME) (6): To a suspension of **4** (2.70 g, 2.48 mmol) in DME (35 mL), was added a solution of C_5Me_5H (0.77 g, 4.96 mmol) in DME (5 mL) at room temperature. The reaction mixture was stirred at 60 °C for 18 h, $C_{13}H_9K$ (1.01 g, 4.96 mmol) in DME (10 mL) was added and the resulting suspension was stirred overnight at room temperature. The green solution was filtered, DME was removed in vacuo and the resulting solid was extracted with toluene. Recrystallization from toluene yielded 1.28 g (46%) of yellow crystals of **6**. − IR (Nujol): $\tilde{\nu}$ = 3050 (m), 1590 (m), 1320 (s), 1210 (s), 1110 (m), 1090 (s), 1050 (m), 890 (s), 750 (s), 720 (s), 700 (s) cm^{-1}. − ^{1}H NMR (200 MHz, [D$_6$]benzene): δ = 2.06 (s, 15 H, CH_3), 2.16 (m, 6 H, OCH_3), 3.49 [s(br), 4 H, CH_2O], 6.66 (s, 1 H, aryl-H), 6.94 [t, ^3J(H,H) = 14.6 Hz, 2 H, aryl-H], 7.65 [t, ^3J(H,H) = 14.6 Hz, 2 H, aryl-H], 7.86 [d, ^3J(H,H) = 8 Hz, 2 H, aryl-H], 7.97 [d, ^3J(H,H) = 7.8 Hz, 2 H, aryl-H]. − ^{13}C NMR (50.3 MHz, [D$_6$]benzene): δ = 11.1, 36.7, 82.9, 112.1, 114.1, 118.5, 120.0, 120.6, 122.9, 125.1, 126.8. − $C_{27}H_{34}O_2Yb$ (563.6): calcd. C 57.54, H 6.08, Yb 30.70; found C 57.14, H 5.77, Yb 30.58.

[$Me_2Si(C_{13}H_8)_2$]K_2: To a solution of $Me_2Si(C_{13}H_9)_2$ (1.20 g, 3.10 mmol) in THF (30 mL) was slowly added a solution of $C_{10}H_8K$, obtained from K (0.24 g, 6.20 mmol) and $C_{10}H_8$ (0.80 g, 6.25 mmol) in THF (30 mL) at room temperature while stirring. The reaction mixture was stirred for another 8 h and the solvent was removed in vacuo. The resulting residue was extracted with hexane (3 × 30 mL) to remove $C_{10}H_8$ and was dried in vacuo (80 °C, 3 h) to give 1.32 g (92%) of [$Me_2Si(C_{13}H_8)_2$]K_2 as a dark red solid. − IR (Nujol): $\tilde{\nu}$ = 3050 (m), 1550 (w), 1320 (m), 1290 (m), 1275 (m), 1240 (m), 1150 (m), 1130 (w), 1080 (w), 1005 (m), 990 (w), 970 (w), 875 (m), 830 (w), 820 (m), 805 (s), 755 (s), 740 (s), 715 (s), 690 (m), 630 (w) cm^{-1}. − ^{1}H NMR (200 MHz, [D$_8$]THF): δ = 6.5−8.2 (m, 16 H, Ar), 0.03 (s, 6 H, CH_3). − ^{13}C NMR (50.3 MHz, [D$_8$]THF): δ = 1.6, 116.5, 119.7, 124.9, 126.5, 127.9, 129.0, 142.0. − $C_{28}H_{22}K_2Si$ (464.1): calcd. C 72.40, H 4.78, K 16.79; found C 69.90, H 4.95, K 16.70.

$Me_2Si(C_{13}H_8)_2$Yb(THF) (7): To a solution of [$Me_2Si(C_{13}H_8)_2$]K_2 (1.43 g, 3.09 mmol) in THF (30 mL) was slowly added a solution of $YbI_2(THF)_2$ (1.76 g, 3.09 mmol) in THF (10 mL) at room temperature, and the reaction mixture was stirred for 20 h. The solution was concentrated in vacuo. Slow diffusion of toluene into the resulting solution produced red diamagnetic crystals of **7** (1.46 g, 75%). − IR (Nujol): $\tilde{\nu}$ = 3050 (m), 1600 (w), 1570 (w), 1330 (m), 1290 (m), 1275 (m), 1245 (m), 1200 (m), 1155 (m), 1130 (w), 1020 (m), 980 (w), 960 (s), 860 (m), 840 (m), 830 (m), 810 (s), 760 (s), 745 (s), 720 (s) cm^{-1}. − ^{1}H NMR (200 MHz, [D$_8$]THF): δ = 6.7−8.1 (m, 16 H, Ar), 0.034 (s, 6 H, CH_3). − ^{13}C NMR (50.3 MHz, [D$_8$]THF): δ = 1.7, 116.5, 119.7, 124.7, 126.5, 127.9, 128.7, 142.0. − $C_{32}H_{30}OSiYb$ (631.7): calcd. C 60.84, H 4.79, Yb 27.39; found C 59.96, H 5.03, Yb 27.20.

$Me_2Si(C_{13}H_8)_2Sm(THF)_4$ (8): To a solution of [$Me_2Si(C_{13}H_8)_2$]K_2 (2.38 g, 5.14 mmol) in THF (20 mL), was added a solution of $SmI_2(THF)_2$ (2.82 g, 5.14 mmol) in THF (30 mL) under rigorous stirring at room temperature and the reaction mixture was stirred for 20 h. The solution was concentrated in vacuo and filtered from the precipitated KI. Slow diffusion of toluene into the resulting solution produced brown crystals of **8** (3.61 g, 85%). μ_{eff} = 3.6 BM (298 K). − IR (Nujol): $\tilde{\nu}$ = 3050 (m), 1600 (m), 1570 (m), 1330 (s), 1290 (s), 1280 (s), 1240 (m), 1200 (m), 1155 (m), 1120 (m), 1070 (s), 1040 (s), 965 (m), 910 (m), 860 (m), 840 (m), 830 (m), 820 (m), 800 (m), 760 (s), 735 (s), 730 (s) cm^{-1}. − $C_{44}H_{54}O_4SiSm$ (825.4): calcd. C 64.03, H 6.59, Sm 18.22; found C 63.87, H 6.23, Sm 18.22.

X-ray Structure Determination of 1 and 6: Crystals suitable for single-crystal X-ray diffraction were obtained from toluene. The crystal and structure refinement data are listed in Table 1. Data were collected with a Siemens SMART CCD diffractometer (graphite monochromator, Mo-K_α radiation, λ = 0.71073 Å) with area detector by use of ω scans at 173 K. The structures were solved by direct methods using SHELXS-97[52] and refined on F^2 using all reflections with SHELXL-97.[53] All non-hydrogen atoms were

Table 1. Crystal data and structure refinement for **1** and **6**

	1	**6**
Empirical formula	$C_{34}H_{34}O_2Yb$	$C_{27}H_{34}O_2Yb$
M_r [g·mol^{-1}]	647.65	563.58
Crystal system	triclinic	orthorhombic
Space group	$P\bar{1}$ (No. 2)	*Pbca* (No. 61)
Unit cell dimensions		
a [Å]	10.8261(1)	17.2533(2)
b [Å]	13.2109(2)	15.4878(2)
c [Å]	19.5494(2)	18.1545(1)
α [°]	84.106(1)	90
β [°]	77.256(1)	90
γ [°]	89.855(1)	90
V [Å^3]	2712.13(6)	4851.17(9)
Z	4	8
$\rho_{calcd.}$ [g/cm^3]	1.586	1.543
μ(Mo-K_α) [mm^{-1}]	3.477	3.875
F(000)	1296	2256
Crystal dimensions [mm]	0.36×0.10×0.10	0.48×0.34×0.16
θ [°]	1.07 → 27.50	2.09 → 27.50
Index ranges		
h	−13 → 14	−22 → 18
k	−9 → 17	−20 → 19
l	−25 → 24	−23 → 23
Reflections collected	20830	34936
Independent reflections	12317 [*R*(int) = 0.0607]	5559 [*R*(int) = 0.0793]
Reflections with $I > 2\sigma(I)$	7031	3970
Max./min. transmission	0.7744/0.5613	0.6392/0.3417
Goodness-of-fit on F^2	0.916	1.052
Final *R* indices [$I > 2\sigma(I)$]	R_1 = 0.0472, wR_2 = 0.0784	R_1 = 0.0392, wR_2 = 0.0700
R indices (all data)	R_1 = 0.1073, wR_2 = 0.0987	R_1 = 0.0705, wR_2 = 0.0804
Larg. diff. peak/hole [e/Å^3]	1.095/−1.389	1.097/−0.888

refined anisotropically. The hydrogen atoms were placed in calculated positions and assigned to an isotropic displacement parameter of 0.08 Å^2.The idealized methyl groups were allowed to rotate about their X−C bond. SADABS[54] was used to perform area-detector scaling and absorption corrections. The maximum and minimum transmission factors are summarized in Table 1. The PLATON[55] program was used for the geometric analysis of the structures. Crystallographic data (excluding structure factors) for the structures reported in this paper have been deposited with the Cambridge Crystallographic Data Centre as supplementary publication nos. CCDC-162390 (**1**) and -162391 (**6**). Copies of the data can be obtained free of charge on application to CCDC, 12 Union Road, Cambridge CB2 1EZ, UK [Fax: (internat.) + 44-1223/336-033; E-mail: deposit@ccdc.cam.ac.uk].

Acknowledgments

This work was supported by the Russian Foundation for Basis Research (RFBR Grant No. 99-03-32905), the Fonds der Chemischen Industrie and the Deutsche Forschungsgemeinschaft.

[1] H. G. Alt, E. Samuel, *Chem. Soc. Rev.* **1998**, *27*, 323−329.
[2] H. G. Alt, A. Köppl, *Chem. Rev.* **2000**, *100*, 1205−1221.
[3] M. N. Bochkarev, L. N. Zakharov, C. S. Kalinina, *Organoderivatives of Rare Earth Elements*, Kluwer Academic Publishers, Dordrecht, **1995**.
[4] H. Schumann, J. A. Meese-Marktscheffel, L. Esser, *Chem. Rev.* **1995**, *95*, 865−986.
[5] M. Ephritikhine, *Chem. Rev.* **1997**, *97*, 2193−2242.
[6] H. Yasuda, H. Tamai, *Progr. Polym. Sci.* **1993**, *18*, 1097−1139.
[7] [7a] G. Jeske, H. Lauke, H. Mauermann, P. N. Swepston, H. Schumann, T. J. Marks, *J. Am. Chem. Soc.* **1985**, *107*, 8091−8103. − [7b] G. Jeske, L. E. Schock, P. N. Swepston, H. Schumann, T. J. Marks, *J. Am. Chem. Soc.* **1985**, *107*, 8103−8110. − [7c] G. Jeske, H. Lauke, H. Mauermann, H. Schumann, T. J. Marks, *J. Am. Chem. Soc.* **1985**, *107*, 8111−8118.
[8] M. A. Giardello, V. P. Conticello, L. Brard, M. R. Gagné, T. J. Marks, *J. Am. Chem. Soc.* **1994**, *116*, 10241−10254.
[9] P. F. Fu, L. Brard, Y. W. Li, T. J. Marks, *J. Am. Chem. Soc.* **1995**, *117*, 7157−7168.
[10] Y. Obora, T. Ohta, C. L. Stern, T. J. Marks, *J. Am. Chem. Soc.* **1997**, *119*, 3745−3755.
[11] C. M. Haar, C. L. Stern, T. J. Marks, *Organometallics* **1996**, *15*, 1765−1784.
[12] H. Schumann, M. R. Keitsch, J. Demtschuk, G. A. Molander, *J. Organomet. Chem.* **1999**, *582*, 70−82.
[13] Y. W. Lee, T. J. Marks, *J. Am. Chem. Soc.* **1998**, *120*, 1757−1771.
[14] G. A. Molander, E. D. Dowdy, B. C. Noll, *Organometallics* **1998**, *17*, 3754−3758.
[15] G. A. Molander, P. J. Nichols, *J. Org. Chem.* **1996**, *61*, 6040−6043.
[16] G. A. Molander, W. H. Retsch, *J. Am. Chem. Soc.* **1997**, *119*, 8817−8825.
[17] G. A. Molander, J. Winterfeld, *J. Organomet. Chem.* **1996**, *524*, 275−279.
[18] M. R. Bürgstein, H. Berberich, P. W. Roesky, *Organometallics* **1998**, *17*, 1452−1454.
[19] W. J. Evans, I. Bloom, W. E. Hunter, J. L. Atwood, *J. Am. Chem. Soc.* **1981**, *103*, 6507−6508.
[20] H. Yasuda, E. Ihara, *Tetrahedron* **1995**, *51*, 4563−4570.
[21] E. Ihara, M. Nodono, K. Katsura, Y. Adachi, H. Yasuda, M. Yamagashira, H. Hashimoto, N. Kanehisa, Y. Kai, *Organometallics* **1998**, *17*, 3945−3956.
[22] A. V. Khvostov, A. I. Sizov, B. M. Bulychev, S. Ya. Knyajanski, V. K. Belsky, *J. Organomet. Chem.* **1998**, *559*, 97−105.
[23] B. L. Kalsotra, R. K. Multani, B. D. Jain, *Curr. Sci.* **1972**, *41*, 155−159.
[24] L. F. Rybakova, A. B. Sigalov, O. P. Syutkina, E. N. Egorova, I. P. Beletskaya, *Izv. Akad. Nauk SSSR, Ser. Khim.* **1981**, 2415−2418.
[25] A. B. Sigalov, L. F. Rybakova, O. P. Syutkina, R. L. Shifrina, Yu. S. Bogachev, I. L. Zhuravleva, I. P. Beletskaya, *Izv. Akad. Nauk SSSR, Ser. Khim.* **1983**, 918−922.
[26] W. J. Evans; T. S. Gummersheimer, T. J. Boyle, J. W. Ziller, *Organometallics* **1994**, *13*, 1281−1284.
[27] M. H. Lee, J. W. Hwang, Y. Kim, J. Kim, Y. Han, Y. Do, *Organometallics* **1999**, *18*, 5124−5129.
[28] M. N. Bochkarev, A. A. Trifonov, E. A. Fedorova, N. S. Emelyanova, T. A. Basalgina, G. S. Kalinina, G. A. Razuvaev, *J. Organomet. Chem.* **1989**, *372*, 217−224.
[29] W. J. Evans, M. A. Hozbor, *J. Organomet. Chem.* **1987**, *326*, 299−306.
[30] M. N. Bochkarev, A. A. Trifonov, F. G. N. Cloke, C. I. Dalby, P. T. Matsunaga, R. A. Andersen, H. Schumann, J. Loebel, H. Hemling, *J. Organomet. Chem.* **1995**, *486*, 177−182.
[31] A. A. Trifonov, E. N. Kirillov, M. N. Bochkarev, H. Schumann, S. Mühle, *Russ. Chem. Bull.* **1999**, *48*, 382−384.
[32] W. J. Evans, M. A. Johnston, R. D. Clark, J. W. Ziller, *J. Chem. Soc., Dalton Trans.* **2000**, 1609−1612.
[33] Z. Hou, A. Fujita, T. Yoshimura, A. Jesorka, Y. Zhang, H. Yamazaki, Y. Wakatsuki, *Inorg. Chem.* **1996**, *35*, 7190−7195.
[34] Z. Hou, Y. Zhang, T. Yoshimura, Y. Wakatsuki, *Organometallics* **1997**, *16*, 2963−2970.
[35] Z. Xie, S. Wang, Z. Y. Zhou, T. C. W. Mak, *Organometallics* **1998**, *17*, 1907−1909.
[36] A. A. Trifonov, F. Ferri, J. Collin, *J. Organomet. Chem.* **1999**, *582*, 211−217.
[37] A. A. Trifonov, E. N. Kirillov, A. Fischer, F. T. Edelmann, M. N. Bochkarev, *Chem. Commun.* **1999**, 2203−2204.
[38] A. A. Trifonov, E. N. Kirillov, Ya. A. Kurskii, M. N. Bochkarev, *Russ. Chem. Bull.* **2000**, *49*, 744−746.
[39] G. M. Ferrence, R. McDonald, M. Morisette, J. Takats, *J. Organomet. Chem.* **2000**, *596*, 95−101.
[40] J. B. Grutzner, J. M. Lawlor, L. M. Jackman, *J. Am. Chem. Soc.* **1972**, *94*, 2306−2315.
[41] J. B. Stothers, C. T. Tan, N. K. Wilson, *Org. Magn. Resonance* **1977**, *9*, 408−413.
[42] T. Akhnouk, J. Müller, K. Qiao, X. F. Li, R. D. Fischer, *J. Organomet. Chem.* **1991**, *408*, 47−59.
[43] D. Stern, M. Sabat, T. J. Marks, *J. Am. Chem. Soc.* **1990**, *112*, 9558−9575.
[44] G. Desurmont, Y. Li, H. Yasuda, T. Maruo, N. Kanehisa, Y. Kai, *Organometallics* **2000**, *19*, 1811−1813.
[45] C. M. Fendrick, E. A. Mintz, L. D. Schertz, T. J. Marks, V. W. Day, *Organometallics* **1984**, *3*, 819−821.
[46] C. M. Fendrick, L. D. Schertz, V. W. Day, T. J. Marks, *Organometallics* **1988**, *7*, 1828−1838.
[47] K. Tatsumi, A. Nakamura, P. Hofmann, R. Hoffmann, K. G. Moloy, T. J. Marks, *J. Am. Chem. Soc.* **1986**, *108*, 4467−4476.
[48] L. Zsolnai, H. Pritzkow, *ZORTEP ORTEP Program for PC*, Universität Heidelberg, **1994**.
[49] M. N. Bochkarev, I. L. Fedushkin, R. B. Larichev, *Russ. Chem. Bull.* **1996**, *45*, 2443−2445.
[50] C. Eaborn, R. A. Shaw, *J. Chem. Soc.* **1955**, 1420−1425.
[51] A. V. Protchenko, M. N. Bochkarev, *Pribory i technika experimenta*, Nauka, Moscow **1990**, vol. 1, p. 194−198.
[52] G. M. Sheldrick, *SHELXS-97 Program for the Solution of Crystal Structures*, Universität Göttingen, **1990**.
[53] G. M. Sheldrick, *SHELXL-97 Program for the Refinement of Crystal Structures*, Universität Göttingen, **1997**.
[54] G. M. Sheldrick, *SADBAS Program for Empirical Absorption Correction of Area Detector Data*, Universität Göttingen, **1996**.
[55] A. L. Spek, *PLATON A Multipurpose Crystallographic Tool*, University of Utrecht, **2000**.

Received April 23, 2001
[I01140]

Crystal Engineering of 2-D and 3-D Multiporphyrin Architectures − The Versatile Topologies of Tetracarboxyphenylporphyrin-Based Materials

Yael Diskin-Posner,[a] Goutam Kumar Patra,[a] and Israel Goldberg*[a]

Keywords: Crystal engineering / Supramolecular chemistry / Porphyrinoids / Network solids

This study explores diverse crystal engineering concepts in the formulation of a series of new porphyrin-based supramolecular arrays, utilizing tetrakis(4-carboxyphenyl)porphyrin as an effective building block. Different modes of the supramolecular assembly are demonstrated. They include: (a) self-assembly of the porphyrin units into extended networks through multiple hydrogen bonding, (b) intermolecular coordination assisted by external sodium ion auxiliaries which link between the carboxylic/carboxylate groups of several units, (c) formation of coordination polymers with the aid of bidentate ligands as bridges between the metal centers of the porphyrin molecules, and (d) various combination motifs of concerted hydrogen bonding and coordination features. The resulting multiporphyrin architectures obtained in this study illustrate the expression of several motifs (synthons) of noncovalent interaction in the construction of network solids, which can be potentially useful in the design of new porphyrin-based materials with attractive properties.

Introduction

Supramolecular chemistry provides effective means for the formulation of a large variety of extended multiporphyrin architectures in solution as well as in the solid state by noncovalent forces.[1−3] The significance of such systems lies in their potential use as molecular sensing and delivery systems, charge and energy transport devices, and redox catalysts.[1] In recent years there has been a widespread interest in the design of complex porphyrin-based arrays in order to model light-harvesting systems or to construct novel solid-state receptors and microporous materials (zeolite mimics). In the latter context, we have introduced the tetrakis(carboxyphenyl)porphyrin moiety (TCPP, Scheme 1) as a uniquely versatile building block (tecton) in our efforts to crystal-engineer network solids.[4] This was followed by a demonstration that these building blocks can also be utilized effectively in the construction of molecular sieves and organic zeolite analogues.[5] The square-shaped TCPP is a robust tecton unit that can be assembled into rigid high-order structures in different ways through diverse interaction motifs (synthons). In the equatorial directions, the peripheral carboxylic functions (oriented roughly perpendicular to the porphyrin plane) provide self-complementary binding sites for a simultaneous association of every TCPP building block to several neighboring species.[4b][5b] The array of multiple hydrogen bonds that may form in such cases provides sufficient enthalpic driving force to overcome solvation and negative entropy effects and stabilize open network arrangements. The formation of other kinds of multiporphyrin arrays can be facilitated by the use of metal ion auxiliaries that prefer high coordination environments and may readily coordinate several carboxylic moieties at the same time.[4a] The preferred coordination geometries of these auxiliaries have a dominant influence on the topology of the formed supramolecular assembly (e.g., layered vs. diamondoid, and interpenetrating or grid-type networks). The additional positive charge introduced to the structure by the metal ions can be easily balanced by a single or multiple deprotonation of TCPP, without the need to incorporate additional anions (which is often the case in hybrid inorganic/organic coordination polymers).[6] This is a particularly useful feature of the TCPP framework, as the presence of external anionic species may hamper the construction of open architectures. The insertion of metal ions with high affinities for five- or six-coordinate environments into the porphyrin core (e.g., Zn^{II} or Mn^{III}, as opposed to Cu^{II}, which is usually four coordinate and not effective in axial coordination) provides another programming element for effective supramolecular design.[5a,7] These metal ions may allow additional coordination to other species in the axial direction (i.e., perpendicular to the porphyrin plane). A concerted expression of suitable molecular recognition algorithms along the lateral and axial directions in the same material represents the most desirable approach to the construction of multiporphyrin architectures with a high structural integrity.[8] The square-planar geometry of the porphyrin macrocycle, the directionality of *meso*-substituted carboxylic recognition groups of TCPP, and the coordination properties of the metal ions involved should provide effective means for inducing extended noncovalent connectivity in the design of supramolecular multiporphyrin arrays. This diversity of the TCPP building block is demonstrated by the preparation and structural characterization of four new MTCPP-based (M = Mn^{III}, Zn^{II}) materials (Scheme 1) which provide representative examples of characteristic 2-D and 3-D supramolecular assembly modes of the metalated porphyrin moiety. The considerable complexity associated with steering

[a] School of Chemistry, Sackler Faculty of Exact Sciences, Tel Aviv University
69978 Ramat Aviv, Tel Aviv, Israel
Fax: (internat.) + 972-3/640-9293
E-mail: goldberg@post.tau.ac.il

 © WILEY-VCH Verlag GmbH, 69451 Weinheim, 2001 1434−1948/01/1010−2515 $ 17.50+.50/0

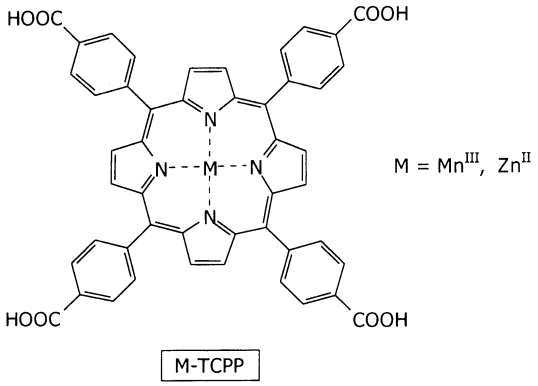

Scheme 1. The TCPP building block

the construction of stable high-order network structures of large organic species (such as the porphyrins in question) by noncovalent forces makes the current effort quite a challenging one.

Results and Discussion

Organic carboxylic acids tend to form supramolecular arrays in crystalline solids by interconnecting through hydrogen bonds into a wide variety of extended networks. These interaction motifs may consist either of the cyclic dimeric $(COOH)_2$ synthons, or of linear polymeric aggregates.[9] Although the hydrogen bonding interactions when considered alone are relatively weak (ca. 10−15 kJ/mol for a single dicarboxylic H bond involving uncharged species),[10] their cooperative effect appears to be sufficient to stabilize low-density supramolecular arrangements even in organic solids.[11] We have applied this concept to porphyrin supramolecular chemistry and demonstrated several formulations of interpenetrating as well as nonpenetrating hollow network architectures through self-complementary hydrogen bonding, without the use of external auxiliaries.[4b][4c] This includes the formation of two-dimensional arrays with either large interporphyrin voids (16 × 21 Å) or considerably smaller cavities (8.5 × 11 Å), depending on the size and nature of the template used. In the present study we describe a series of new MTCPP-based (Scheme 1) structures **1**−**4** of diverse architectures (their detailed composition is given in the Exp. Sect.). The following discussion focuses primarily on the unique features of the *supramolecular* assembly in these compounds; selected coordination and hydrogen bond lengths are summarized in Table 1.

Compound **1** (the ethyl benzoate solvate of the $Mn^{III}TCPP{\cdot}MeOH{\cdot}H_2O$ six-coordinate complex) provides a characteristic example in which multiple hydrogen bonds between the carboxylic functions positioned on the periphery of the square-shaped $Mn^{III}TCPP$ framework provide the main supramolecular organizing force of the observed assembly. Figure 1a illustrates the structure of the 2-D porphyrin β-networks formed in this case. It is directed by effective chain-polymeric-type hydrogen bonding between the carboxylic groups of adjacent molecules. These networks are anionic, as the extra positive charge of the trivalent manganese cation in the porphyrin core is balanced by the abstraction of one proton from the TCPP moiety. This is in line with the observed distribution of C−O distances in the carboxylic functions (1.22 and 1.31 Å for −COOH, and 1.24 and 1.28 Å for $-COO^-$, residues), as well as with the observed hydrogen bonding interactions ($OH\cdots O^-$ = 2.54−2.58 Å within the layer and OH···O = 2.72−2.78 Å between layers; see below). The networked supramolecular motif thus formed contains open spaces between the connecting units (Figure 1a). Only the larger voids are large enough (with van der Waals widths of about 7.0 Å) to host two molecules of the ethyl benzoate crystallization solvent oriented edge-on. The individual building blocks contain additional sites with hydrogen-bonding capacity, as the manganese cation has a high affinity for oxygen ligands and an octahedral coordination (the metalloporphyrin core is planar in such a case). Thus, under the applied conditions of crystallization the metal ion binds one water and one methanol molecule as axial ligands, which may then link further to other species. The porphyrin layers stack in the crystal in an offset manner, in which the porphyrin cores of one layer are positioned above the carboxylic sites of another layer (Figure 1b). This allows the axial water and methanol ligands (as proton donors) to approach the carboxylic groups to form interlayer hydrogen bonds. (Our efforts to cross-link between the overlapping H-bonded layers by a bidentate axial ligand that will coordinate on both sides to the Mn centers have not been successful as yet). In the observed arrangement, the ethyl benzoate molecules positioned within the inter-porphyrin voids of one layer perch on the smaller cavities (which are too small to fully accommodate a molecular species), thus yielding a rather

Table 1. Selected coordination and hydrogen bond lengths (related to diffraction measurements at 110 K)

Compound	**1**[a]	**2**[b]	**3**[b]	**4**[b]
M−N(pyrrole) bond length range [Å]	2.011−2.021	2.010−2.065	2.055−2.067	2.042−2.044
M's coordination number, and type of axial ligands	6, OH	4	5, OH	6, :N(pyr)
M's deviation from the N_4(corrole) plane [Å]	0.021	0.007	0.271	0.000
M−X(axial ligand) bond lengths [Å]	2.214, 2.246	−	2.141	2.694, 2.694
Sodium−porphyrin Na···O coordination distances [Å]	−	2.322−2.353	2.254−2.435	−
Porphyrin ligand/solvent COOH···X hydrogen bond length range [Å]	2.72−2.78[c]	2.56−2.68[d]	2.71−2.76[e]	2.68−2.79[f]
Interporphyrin hydrogen bond length range [Å]	2.54−2.58[g]	3.06[h]	2.51−2.58[g]	2.45[g]

[a] M = Mn^{III}. − [b] M = Zn^{II}. − [c] X = OH. − [d] X = COO^-. − [e] X = OH or :N. − [f] X = H_2O. − [g] COOH···$^-$OOC. − [h] COOH···COOH.

tight crystal packing of the layered porphyrin−ethyl benzoate arrays. The formulation of closely related structures has been achieved by using anionic Zn^{II}TCPP building blocks and M^+−18-crown-6 (M = Na, K) templates.[4b]

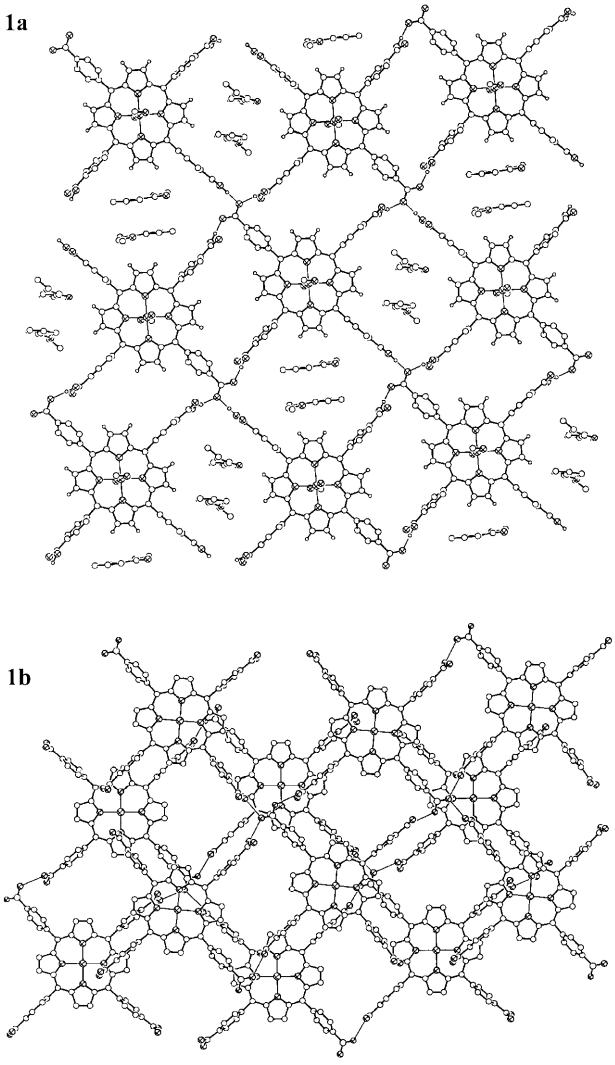

Figure 1. Intermolecular organization in **1**: (a) open layered arrays of the Mn^{III}TCPP building blocks, tessellated by chain-polymeric-type hydrogen bonding; the van der Waals width of the large inter-porphyrin enclosures that accommodate the solvent species is about 7.0 Å; (b) an offset stacking of two adjacent layers, approximately at 4.2 Å; the water and methanol axial ligands are omitted for clarity; the Mn, N and O atoms are denoted by crossed circles

Compound **2** (the ethyl benzoate solvate of the 1:1 Zn^{II}TCPP sodium benzoate complex) represents a supramolecular assembly process assisted by external sodium ion auxiliaries. As shown in Figure 2a, crystallization of Zn^{II}-TCPP in the presence of NaCl, ethyl benzoate and benzoic acid leads to the formation of 2-D multiporphyrin arrays sustained by the metal ions. In this arrangement every cation is coordinated (at 2.32−2.35 Å) to the carboxylic groups of four surrounding carboxylic moieties, forming a roughly square-planar mononuclear $Na^+(COOH)_4$ synthon (Scheme 2), and its positive charge is balanced by a neighboring molecule of deprotonated benzoic acid ($Na^+\cdots O^-$ 2.24 Å). The latter also serves as an excellent proton acceptor in hydrogen bonding interactions with the carboxylic groups ($O^-\cdots HO$ 2.56−2.68 Å) of the four converging porphyrins. The resulting supramolecular arrangement has a wavy layer structure, which consists of two differently oriented porphyrin moieties related to each other by a monoclinic twofold axis, and represents a rather robust coordination polymer in two dimensions. The absence of axial ligands on the porphyrin core in this case allows for a close stacking of the porphyrin layers (with a small offset) in the normal direction (Figure 2b). It is characterized by an average interlayer distance of 4.3 Å between the overlapping segments, as commonly observed in layered tetraarylporphyrin structures.[12] The observed architecture contains small (approximately 5 Å wide) channels which propagate through the layers along the *a* axis of the crystal, and are accommodated by molecules of the ethyl benzoate solvent. The four-coordinate metal ion in the center of the porphyrin has no role in the organization mechanism of the observed pattern. It is not surprising, therefore, that isomorphously structured coordination polymers have been obtained recently from the free-base TCPP building blocks when subjected to similar preparative conditions.[4a]

The large size and the aromatic nature of the porphyrin framework reveals a high propensity for strong dispersive attractions between the roughly flat molecular surfaces of these units (i.e., when it is not obstructed by axially ligating species). This fundamental property of the porphyrin−porphyrin interaction is well reflected in the commonly observed layered organization of the porphyrin moieties at a narrow distance range of 4−5 Å.[12,13] Its dominating role in crystals suggests, however, yet another tool for fine-tuning the supramolecular arrangement. This involves the incorporation of rigid, flat, aromatic residues of appropriate size as effective "van der Waals spacers" between the porphyrin units. We have demonstrated previously the validity of this idea in 2-D and 3-D hydrogen-bonded networks based on the tetrakis(4-hydroxyphenyl)-porphyrin unit and spaced by aromatic intermediates.[14] A similar modification of the interlayer organization by the insertion of an aromatic spacer was obtained in compound **3** (the ethyl benzoate solvate of a 2:1 adduct of $MeOH\cdot Zn^{II}TCPP^-\cdot Na^+$ and 2,7-diazapyrene) by treating Zn^{II}TCPP with a large and rigid aromatic framework such as 2,7-diazapyrene (Scheme 3) in the presence of NaCl. The latter was also used to effect inter-porphyrin coordination in the lateral directions by the sodium ion auxiliaries.

The formation of **3** is associated with the deprotonation of one carboxylic substituent of the porphyrin molecule to balance the charge of the sodium cation. Moreover, the assembly of the anionic porphyrin arrays by sodium ions in this case is via a binuclear $[(Na^+)_2(-COO^-)_2(-COOH)_4]$ synthon (centered on inversion), with two carboxylic groups bridging between the two cations (Scheme 2). The Na···O coordination distances lie within the range 2.25−2.44 Å, while the distance between the two sodium nuclei is 3.42 Å. The Zn^{II}TCPP units are now five-coordinate, revealing a

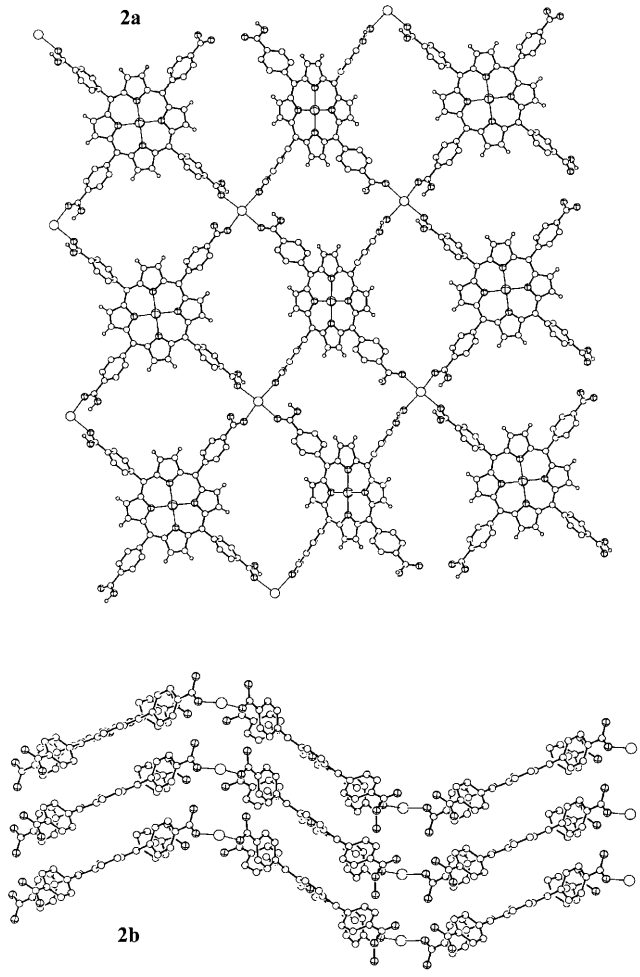

Figure 2. Interporphyrin networking and stacking in **2**: (a) two-dimensional layered arrays of the Zn^{II}TCPP building blocks sustained by metal ion auxiliaries (denoted by large open circles); every cation is strongly coordinated to the carboxylic functions of four different porphyrin units [forming an $Na^{+}(COOH)_4$ interaction synthon] and to the benzoate anion; molecules of the ethyl benzoate solvent are located, and diffused, within the interporphyrin cavities; the latter combine into straight channels in (b) the tightly stacked arrangement of the wavy multiporphyrin layers, at 4.3 Å intervals, along the *a* direction of the unit cell; the benzoate anion and the solvent species are omitted for clarity

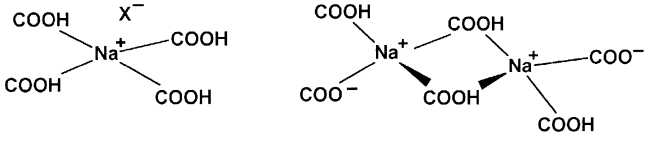

Scheme 2. The mononuclear and binuclear sodium−polycarboxyl synthons in **2** (left) and **3** (right); every carboxylic or carboxylate group shown is part of a different Zn^{II}TCPP unit

domed conformation with the zinc ion slightly displaced from the porphyrin plane (0.27 Å above the N_4 plane), and bearing a methanol species as an axial ligand. The diazapyrene spacer (also located on inversion) is inserted between, and aligned parallel to, the concave surfaces of two inverted

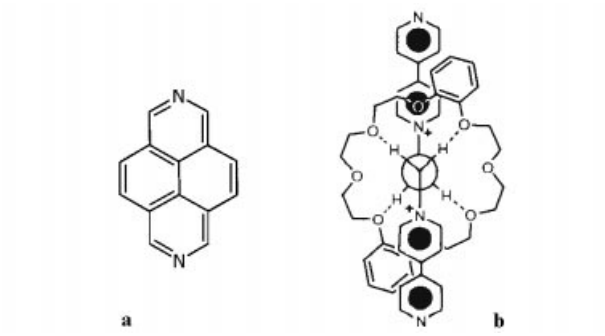

Scheme 3. The 2,7-diazapyrene (left), and [2]pseudorotaxane (right) ligands

porphyrin species. The mean separation distance of the former from the N_4 planes of the latter is 3.4 Å. The sodium ion auxiliaries link the enclosing porphyrin moieties on opposite sides, locking the diazapyrene inside a "sandwich"-type trimeric cluster (Figure 3a). A single dinuclear sodium carboxylic/carboxylate synthon interconnects two neighboring trimers displaced along the *a*+*c* axis of the crystal (parallel to the porphyrin plane), and two additional trimers displaced along a nearly perpendicular *a*+2*b*+*c* direction (Figure 3b,c). This gives rise to the formation of an extended coordination polymer, as every porphyrin unit takes part in three different coordination sites of this type. Adjacent trimers are further connected to each other sideways (along *a*+*b*) by hydrogen bonding. The N sites of the sandwiched diazapyrene entity act as good acceptors for the carboxylic groups of neighboring porphyrin moieties (OH···N 2.76 Å). In addition, the axial methanol ligands oriented perpendicularly to the porphyrin surface (roughly along *a*−*c*) provide proton-accepting sites for hydrogen bonds from other species located above and below (OH···O 2.71 Å). The concerted coordination polymerization and directional hydrogen bonding (all potential sites for intermolecular binding are utilized almost to capacity) yield a uniquely structured single framework lattice in which all porphyrin, diazapyrene and sodium components are interconnected to each other in three dimensions (Figure 3b,c). The resulting lattice is perforated by straight, ca. 4.5 Å wide, channels which are filled in this structure by diffused molecules of the ethyl benzoate solvent (three molecules of solvent per one porphyrin unit).

It should be pointed out that the different modes of interporphyrin coordination through the sodium ions in **2** and **3** occurred spontaneously, and could not be predicted or controlled. Yet, this and our previous[4a][5a] studies confirm that alkali metal auxiliaries readily induce the formation of TCPP-based coordination polymers. Evidently, the dominant nature of these ion-pairing interactions in **3** prevents the diazapyrenes from aligning perpendicular to the porphyrin plane and thus from acting as bridging ligands between adjacent porphyrin macrocycles.

Another variant of simultaneous coordination polymerization and hydrogen bonding is represented by compound **4**

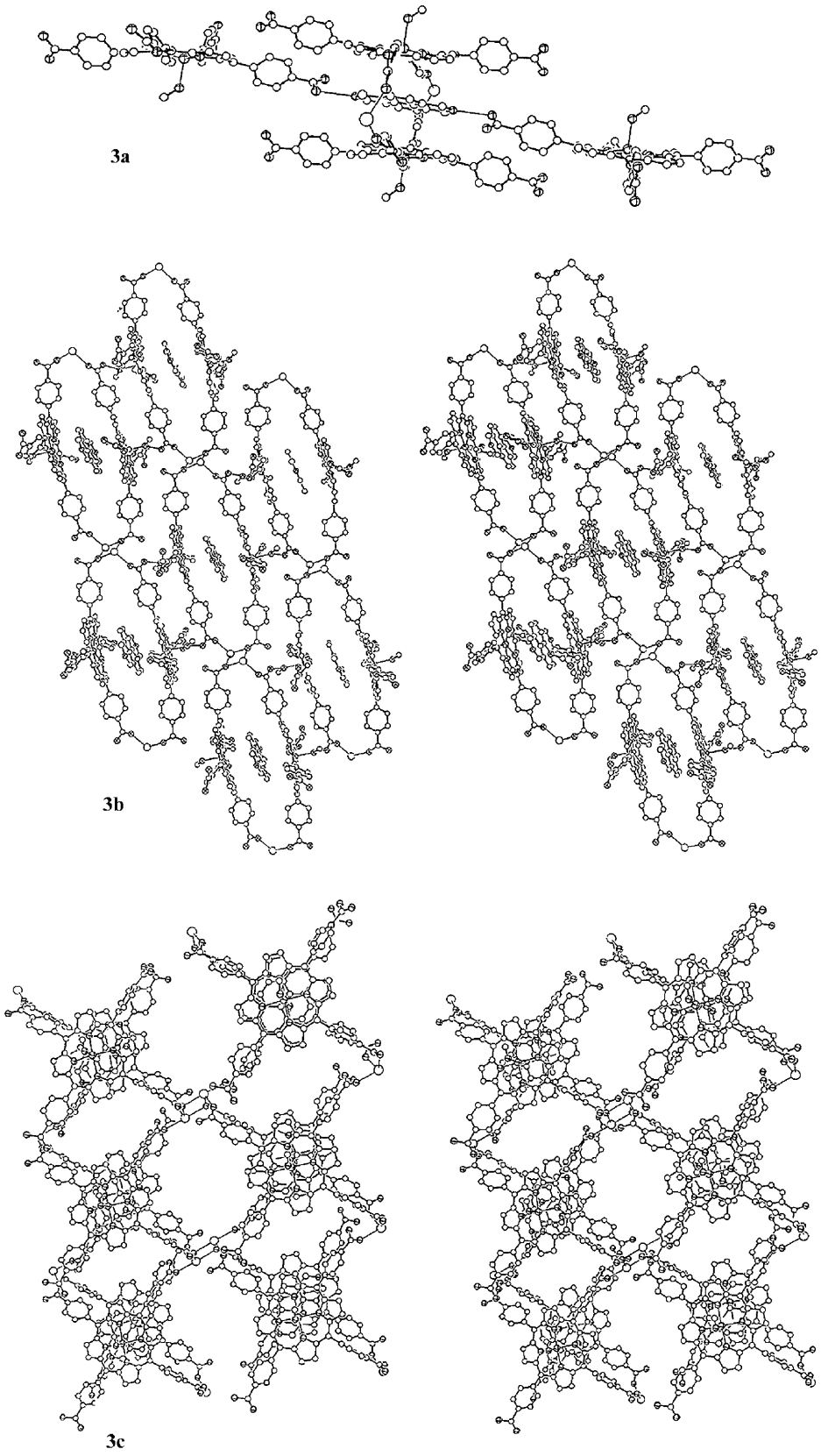

Figure 3. The complex intermolecular binding in **3**: (a) the 2,7-diazapyrene spacer held between four surrounding porphyrin units (by π−π stacking at 3.4 Å, as well as by hydrogen bonding) and two sodium cations (shown as large open circles); (b) stereoview of the structure parallel to the plane of the aromatic fragments, showing the concerted coordination and hydrogen bonding in a direction perpendicular to the porphyrin plane; (c) stereoview of the structure approximately down the open channels (the solvent molecules accommodated therein are omitted for clarity), showing interporphyrin coordination through the sodium ion auxiliaries in the equatorial direction

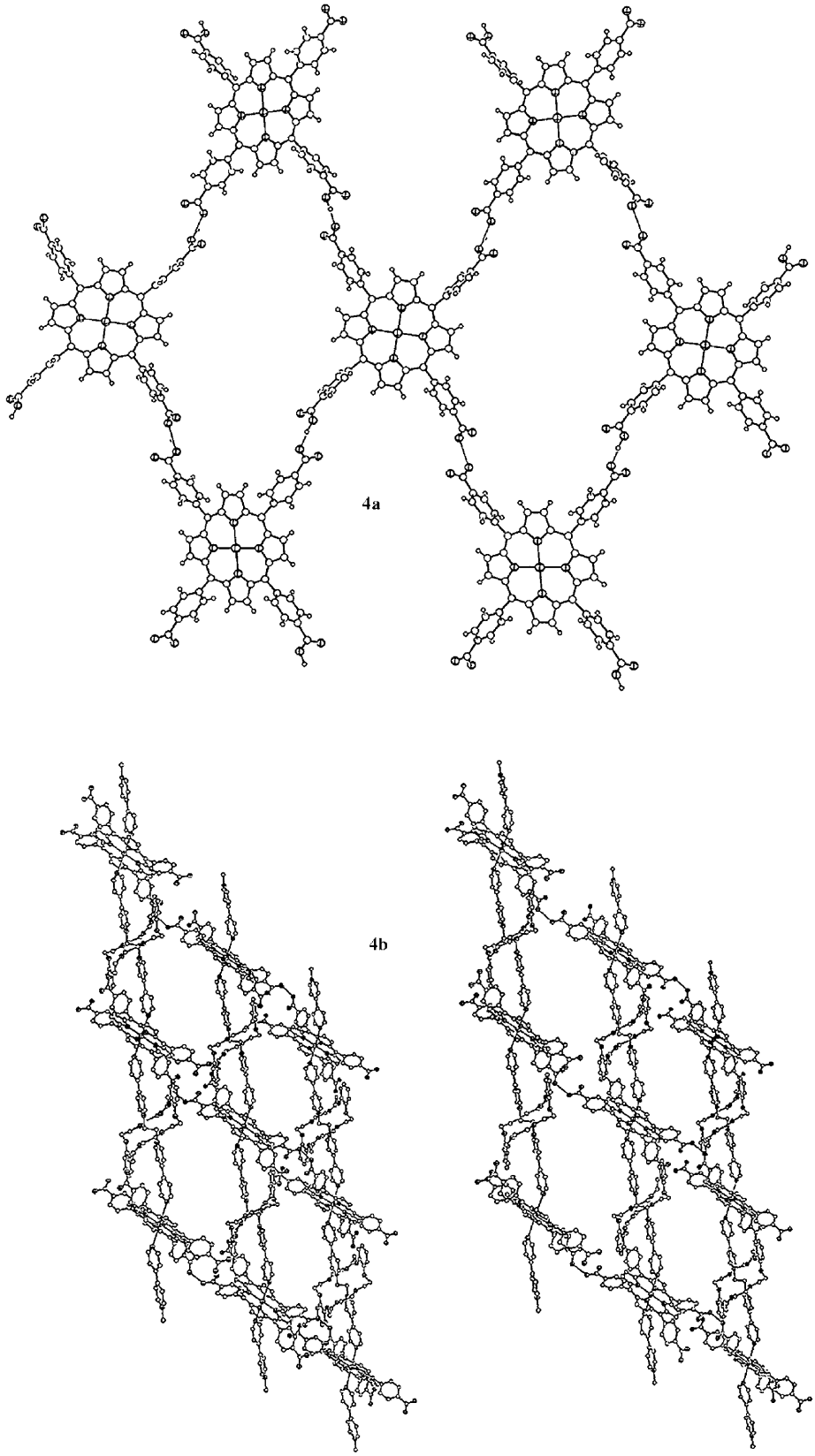

Figure 4. (a) β-Molecular networks of the Zn^{II}TCPP units in **4**; every porphyrin hydrogen atom bonds to four neighboring units and to four additional molecules of water; the van der Waals width of the interporphyrin voids is about 12 Å; (b) stereoscopic illustration of the linear coordination polymers in **4** and the cross-linking between them by interporphyring hydrogen bonds; the Zn, N and O atoms in the porphyrin and ligand moieties are denoted by dark circles

[the crystalline hydrate of the 1:1 complex between $Zn^{II}TCPP^{2-}$ and 1,2-bis(4,4′-bipyridinio)ethane−dibenzo-24-crown-8]. This involves coordination through the metal ion in the porphyrin center of $Zn^{II}TCPP$ without resorting to external auxiliaries. Indeed, earlier studies confirm that Zn^{II} may adopt a six-coordinate environment in the presence of pyridyl-type ligands, and that linear multiporphyrin oligomers and polymers may be obtained in solution as well as in the solid state with bridging bidentate ligands of this type.[7a,15] They have also indicated that a deprotonated TCPP is a better building block for the formation of robust anionic networks than the neutral unit.[7] These observations guided us to choose a cationic bidentate ligand for this synthesis. The [2]pseudorotaxane dication 1,2-bis(4,4′-bipyridinium)ethane−dibenzo-24-crown-8 (Scheme 3), which has been used in the synthesis of other supramolecular systems,[16,17] was assumed to be a perfect candidate to this aim. It is a linear doubly charged species containing a pyridyl fragments at both ends. The macrocyclic crown ring threaded on the molecular axle adds bulkiness and limits the conformational flexibility of the system. Figure 4b illustrates the structure of the anticipated polyrotaxane coordination polymer that forms. Along the linear polymer the pyridyl N atoms coordinate from both sides to the zinc ions in the porphyrin core at 2.691 Å, the Zn−N(pyridyl) bond forming an angle of about 78° with the porphyrin plane. Simultaneously, the deprotonated porphyrin units (located on crystallographic inversion) associate into continuous open networks through cooperative hydrogen bonding between their carboxylic/carboxylate groups (Figure 4a). Each of the latter is involved in one hydrogen bond to another porphyrin species (at OH···O^- 2.451 Å) and another H bond to an external molecule of water (at OH···O 2.679 and 2.789 Å). Every $Zn^{II}TCPP$ unit in this net is linked to four neighboring molecules at the corners of the square framework. The spacing between the molecular surfaces of adjacent units located across the width of the interporphyrin voids is about 12.0 Å. In the absence of a suitable template to fill such a large void space, the linear coordination polymers that propagate in a direction roughly perpendicular to the porphyrin plane interpenetrate through the hydrogen-bonded porphyrin networks. The [2]pseudorotaxane ligands that are embedded within a given layer, link to porphyrin units of neighboring layers located above and below. The resulting structure consists, therefore, of interlocked multiporphyrin β-molecular networks and linear [2]pseudorotaxane coordination polymers. The single-framework lattice is not porous in this case, as the crown-ether macrocycle framework threaded on the ligand molecular axle fills effectively the space available within the layered porphyrin arrays.

The above examples demonstrate useful synthetic tools that can be successfully applied in diverse combinations for the crystal engineering of porphyrin-based network solids. The metalated TCPP building block was found to be particularly attractive for this aim, as it allows the tessellation of multiporphyrin arrays in various ways, including through extensive hydrogen bonding, inter-coordination through external metal ion auxiliaries, and coordination polymerization assisted by bipyridyl-type axial ligands bridging between core metal ions of adjacent porphyrin units. The concerted utilization of coordination (of either type) and hydrogen bonding features yields network molecular solids with fascinating 3-D architectures. It is noteworthy that these formulations are directed primarily by specific noncovalent intermolecular interactions, and not by virtue of dispersion forces as is commonly observed in molecular crystals. Many of the multiporphyrin lattices obtained in this way contain channels accessible to other species that are not part of the supramolecular framework, providing useful models of microporous solids that may bear structural and functional resemblance to the inorganic zeolites. A priori prediction of the actual crystal structure that may form from solution in a particular case (and the detailed stoichiometric content of the interacting components in it) is still beyond reach, as many other factors are involved in the crystallization process (e.g., solubility problems, kinetic vs. thermodynamic control of crystal growth, composition and chemical reactivity of the crystallization environment, etc.). However, the above studies provide useful examples for an effective synthesis of supramolecular arrays with multidimensional architectures, and demonstrate effective tools for the solid-state synthesis of 2-D and 3-D multiporphyrin assemblies. They add to our previous reports on porphyrin-based molecular sieves and zeolite analogues with tunable architectures, and together represent an important step towards the programmed formulation of new molecular materials with useful properties.

Experimental Section

Materials: $Zn^{II}TCPP$ ($C_{48}H_{28}N_4O_8Zn$) and $Mn^{III}TCPP{\cdot}Cl$ ($C_{48}H_{28}N_4O_8MnCl$) were purchased from Porphyrin Systems GbR, and used as received. The dibenzo-24-crown-8, common solvents and other starting materials were purchased from Aldrich and used as received.

Preparative Procedures: The porphyrin phase used for the crystallizations was obtained by dissolving the commercial $Zn^{II}TCPP$ or $Mn^{III}TCPP{\cdot}Cl$ materials in hot wet methanol. Ethyl benzoate was found to be an effective crystallization solvent for obtaining X-ray quality crystals of compounds **1−3** by filling the voids in the open multiporphyrin lattices that formed. A series of different experiments is reported below to illustrate the versatile inter-porphyrin binding modes possible in these materials: (a) crystallization of TCPP networks without resorting to external ligands or metal ion auxiliaries, (b) reaction of the tetrakis(carboxy)porphyrin with sodium ion auxiliaries to effect lateral inter-coordination, also in the presence of a large aromatic spacer, and (c) crystallization of these building bocks with [2]pseudorotaxane dication (Scheme 3) as an effective bridging ligand between the porphyrin centers. They yielded four new supramolecular materials.

Compound 1 [($C_{48}H_{27}N_4O_8Mn$)·(CH_3OH)·(H_2O)·1.5($C_9H_{10}O_2$)]: A methanol solution (2 mL) of $Mn^{III}TCPP{\cdot}Cl$ (8.8 mg, 0.01 mmol) was heated to boiling (expelling HCl), and 0.2 mL of ethyl benzoate was added. The resulting solution was allowed to stand in ambient air until large, dark-red crystals were formed (ca. 2 mg).

Compound 2 [$(C_{48}H_{28}N_4O_8Zn)\cdot(C_9H_{10}O_2)\cdot Na^+\cdot(C_7H_5O_2)^-$]: A methanol solution (2 mL) of Zn^{II}TCPP (8.6 mg, 0.01 mmol) was heated to boiling in the presence of sodium chloride (one grain), and 0.1 mL of ethyl benzoate was added. This procedure was associated with partial degradation of the ethyl benzoate to benzoic acid and expulsion of HCl. The resulting solution was allowed to stand in ambient air, until a mixture of a small number of dark red crystals with mostly polycrystalline material was deposited in the reaction test tube.

Compound 3 [$(C_{48}H_{27}N_4O_8Zn)^-\cdot Na^+\cdot(CH_3OH)\cdot 0.5(C_{14}H_8N_2)\cdot 3(C_9H_{10}O_2)$]: 2,7-Diazapyrene (4.0 mg, 0.02 mmol) was added to a methanol solution (2 mL) of Zn^{II}TCPP (8.6 mg, 0.01 mmol), the mixture heated to boiling in the presence of sodium chloride, and 0.2 mL of ethyl benzoate added. In this case the preparative procedure was associated with deprotonation of the porphyrin molecule and expulsion of HCl. The resulting solution was allowed to stand in ambient air until dark red crystals were formed after a few days in relatively high yield (ca. 3 mg).

Compound 4 [$(C_{48}H_{26}N_4O_8Zn)^{2-}\cdot(C_{22}H_{20}N_4)^{2+}\cdot(C_{24}H_{32}O_8)\cdot 4(H_2O)$]: The 1,2-bis(4,4′-bipyridinio)ethane dibromide was synthesized first according to a known literature procedure and confirmed by NMR, UV and MS spectroscopy.[16] Then, a 1:4 mixture of this ligand (4 mg, 0.008 mmol) and dibenzo-24-crown-8 (15 mg, 0.033 mmol) was dissolved in chloroform (1.5 mL), and allowed to stand in air for a few days to yield a [2]pseudorotaxane (Scheme 3) in which the ligand is inserted in the crown ether ring (its formation was monitored by ^{1}H NMR spectroscopy).[17] In the next step, a methanolic solution (2 mL) of Zn^{II}TCPP (8.6 mg, 0.01 mmol) was carefully layered over the chloroform phase and allowed to stand. Slow diffusion produced numerous dark-red prisms of the composite crystals of compound **4** layered on the walls of the test tube.

Due to the small preparative scale (see above), the high content of volatile solvents in these crystals, and presence of metal ions therein, it was difficult to obtain reliable elemental analytical data. However, all the obtained crystalline compounds were unequivocally characterized by crystallographic techniques.

X-ray Crystallography: All diffraction measurements were carried out with a Nonius Kappa CCD diffractometer using graphite-monochromated Mo-K_α radiation (λ = 0.7107 Å). The crystalline samples of the analyzed compounds were covered with a thin layer of light oil and cooled to 110 K in order to minimize structural disorder and thermal motion effects, and increase the precision of the results. This allowed us to locate most of the hydrogen atoms of the porphyrin network in residual electron-density maps. The structures were solved using direct methods (SHELXS-97 and SIR-92) and refined by full-matrix least squares on F^2 (SHELXL-97).[18] Hydrogen atoms were refined using a riding model with fixed thermal parameters [U_{ij} = 1.2 U_{ij} (equiv.) for the atom to which they are bonded].

1: $(C_{48}H_{27}N_4O_8Mn)\cdot(CH_3OH)\cdot(H_2O)\cdot 1.5(C_9H_{10}O_2)$, M = 1118.0, monoclinic, space group $P2_1/c$, a = 11.5160(1), b = 22.2430(2), c = 21.8340(2) Å, β = 97.95(1)°, V = 5539.05(9) Å^3, T = 110(2) K, Z = 4, $D_{calcd.}$ = 1.341 g·cm^{-3}, μ(Mo-K_α) = 0.31 mm^{-1}, 12828 unique reflections to $2\theta_{max}$ = 55.7°, R_1 = 0.068 for 9747 observations with $I > 2\sigma(I)$, R_1 = 0.097 (wR_2 = 0.214) for all unique data.

2: $(C_{48}H_{28}N_4O_8Zn)\cdot 3(C_9H_{10}O_2)\cdot Na^+\cdot(C_7H_5O_2)^-$, M = 1448.7, monoclinic, space group $P2_1$, a = 9.9730(2), b = 32.1410(6), c = 11.2750(2) Å, β = 110.80(1)°, V = 3378.5(1) Å^3, T = 110(2) K, Z = 2, $D_{calcd.}$ = 1.424 g·cm^{-3}, μ(Mo-K_α) = 0.45 mm^{-1}, 6052 unique reflections to $2\theta_{max}$ = 50.8°, R_1 = 0.057 for 4761 observations with $I > 2\sigma(I)$, R_1 = 0.079 (wR_2 = 0.157) for all unique data. The structure is a racemic twin.

3: $(C_{48}H_{27}N_4O_8Zn)^-\cdot Na^+\cdot(CH_3OH)\cdot 0.5(C_{14}H_8N_2)\cdot 3(C_9H_{10}O_2)$, M = 1460.8, triclinic, space group $P\bar{1}$, a = 13.7460(2), b = 15.5400(2), c = 18.2670(4) Å, α = 108.422(1), β = 93.223(1), γ = 108.670(1)°, V = 3453.1(1) Å^3, T = 110(2) K, Z = 2, $D_{calcd.}$ = 1.405 g·cm^{-3}, μ(Mo-K_α) = 0.44 mm^{-1}, 12717 unique reflections to $2\theta_{max}$ = 52.0°. Conventional refinement converged at R_1 = 0.095 for 8205 observations with $I > 2\sigma(I)$, R_1 = 0.141 (wR_2 = 0.279) for all unique data. It indicated severe disorder of the three ethyl benzoate solvent molecules within the interporphyrin voids of the crystal lattice, which could not be modeled with an adequate precision. Subtraction of their contribution to the diffraction pattern by the Bypass[19] procedure resulted in a considerably improved convergence of the main supramolecular framework at R_1 = 0.065 for 8205 observations with $I > 2\sigma(I)$, R_1 = 0.099 (wR_2 = 0.185) for 12717 unique data.

4: $(C_{48}H_{26}N_4O_8Zn)^{2-}\cdot(C_{22}H_{20}N_4)^{2+}\cdot(C_{24}H_{32}O_8)\cdot 4(H_2O)$, M = 1713.1, monoclinic, space group $P2_1/n$, a = 8.070(1), b = 23.570(1), c = 22.314(1) Å, β = 98.68(1)°, V = 4195.7(2) Å^3, T = 110(2) K, Z = 2, $D_{calcd.}$ = 1.356 g·cm^{-3}, μ(Mo-K_α) = 0.37 mm^{-1}, 7181 unique reflections to $2\theta_{max}$ = 50.8°. Conventional refinement converged at R_1 = 0.105 for 4823 observations with $I > 2\sigma(I)$, R_1 = 0.147 (wR_2 = 0.323) for all unique data. It indicated a low data-to-parameters ratio and severe disorder of the crown ether species, the atomic positions of which could thus be assigned with isotropic U only and determined with low precision.

Despite the considerable disorder in structures **3** and **4**, the supramolecular framework structures could be reliably determined. The observed covalent and coordination bond lengths and angles in the ordered fragments conform to normally observed values in related porphyrin compounds, as documented in the literature. This includes also clear distinction in most cases between C−O bond lengths in a carboxylic residue (one short, near 1.2 Å, and one long, near 1.3 Å), and in a carboxylate anion (roughly equal bond lengths usually within 1.24−1.27 Å), as well as between distances of carboxyl−carboxyl, and carboxyl−carboxylate hydrogen bonding interactions.[4b,10]

Crystallographic data (excluding structure factors) for the structures reported in this paper have been deposited with the Cambridge Crystallographic Data Center as supplementary publication nos. CCDC-160614 (**1**), -160615 (**2**), -160616 (**3**) and -160617 (**4**). Copies can be obtained free of charge on the application to CCDC, 12 Union Road, Cambridge CB2 1EZ, UK [Fax: (internat.) + 44-1223/336-033; E-mail: deposit@ccdc.cam.ac.uk).

Acknowledgments

This research was supported in part by The Israel Science Foundation founded by the Israel Academy of Sciences & Humanities, as well as by Grant No. 1999082 from the United States-Israel Binational Science Foundation (BSF), Jerusalem, Israel.

[1] For recent reviews on the noncovalent assembly of porphyrin arrays and their potential applications see: [1a] J.-C. Chambron, V. Heitz, J.-P. Sauvage, *The Porphyrin Handbook*, Academic Press, Orlando, FL, **2000**, vol. 6, chapter 40, p. 1−42. − [1b] J.-H. Chou, H. S. Nalwa, M. E. Kosal, N. A. Rakow, K. S. Sus-

lick, *The Porphyrin Handbook*, Academic Press, Orlando, FL, **2000**, vol. 6, chapter 41, p. 43−132.
[2] [2a] C. M. Drain, X. Shi, T. Milic, F. Nifiatis, *Chem. Commun.* **2001**, 287−288. − [2b] C. M. Drain, F. Nifiatis, A. Vasenko, J. D. Batteas, *Angew. Chem. Int. Ed.* **1998**, *37*, 2344−2347. − [2c] P. J. Stang, J. Fan, B. Olenyuk, *Chem. Commun.* **1997**, 1453−1454.
[3] I. Goldberg, *Chem. Eur. J.* **2000**, *6*, 3863−3870, and references therein.
[4] [4a] Y. Diskin-Posner, S. Dahal, I. Goldberg, *Chem. Commun.* **2000**, 585−586. − [4b] Y. Diskin-Posner, R. Krishna Kumar, I. Goldberg, *New J. Chem.* **1999**, *23*, 885−890. − [4c] P. Dastidar, Z. Stein, I. Goldberg, C. E. Strouse, *Supramol. Chem.* **1996**, *7*, 257−270.
[5] [5a] Y. Diskin-Posner, S. Dahal, I. Goldberg, *Angew. Chem. Int. Ed.* **2000**, *39*, 1288−1292. − [5b] Y. Diskin-Posner, I. Goldberg, *Chem. Commun.* **1999**, 1961−1962.
[6] C. B. Aakeröy, A. M. Beatty, K. R. Lorimer, *J. Chem. Soc., Dalton Trans.* **2000**, 3869−3872.
[7] [7a] H. Krupitsky, Z. Stein, I. Goldberg, C. E. Strouse, *J. Incl. Phenom.* **1994**, *18*, 177−192. − [7b] K.-J. Lin, *Angew. Chem. Int. Ed.* **1999**, *38*, 2730−2732
[8] R. Krishna Kumar, S. Balasubramanian, I. Goldberg, *Chem. Commun.* **1998**, 1435−1436.
[9] [9a] G. M. Frankenbach, M. C. Etter, *Chem. Mater.* **1992**, *4*, 272−278. − [9b] L. Leiserowitz, *Acta Crystallogr., Sect. B* **1976**, *32*, 775−802.
[10] G. A. Jeffrey, *An Introduction to Hydrogen Bonding*, Oxford University Press, New York, **1997**.
[11] P. Brunet, M. Simard, J. D. West, *J. Am. Chem. Soc.* **1997**, *119*, 2737−2738.
[12] R. Krishna Kumar, S. Balasubramanian, I. Goldberg, *Inorg. Chem.* **1998**, *37*, 541−552, and references therein.
[13] M. P. Byrn, C. J. Curtis, Y. Hsiou, S. I. Khan, P. A. Sawin, S. K. Tendick, A. Terzis, C. E. Strouse, *J. Am. Chem. Soc.* **1993**, *115*, 9480−9497.
[14] I. Goldberg, H. Krupitsky, Z. Stein, Y. Hsiou, C. E. Strouse, *Supramol. Chem.* **1995**, *4*, 203−221.
[15] [15a] A. D. Shukla, P. C. Dave, E. Suresh, A. Das, P. Dastidar, *J. Chem. Soc., Dalton Trans.* **2000**, 4459−4463. − [15b] E. B. Fleischer, A. M. Shachter, *Inorg. Chem.* **1991**, *30*, 3763−3769.
[16] M. I. Attalla, N. S. McAlpine, L. A. Summers, *Z. Naturforsch., Teil B* **1984**, *39*, 74−78.
[17] [17a] K. Chichak, M. C. Walsh, N. R. Branda, *Chem. Commun.* **2000**, 847−848. − [17b] S. J. Loeb, J. A. Wisner, *Chem. Commun.* **1998**, 2757−2758.
[18] [18a] SIR-92: A. Altomare, M.C. Burla, M. Camalli, M. Cascarano, C. Giacovazzo, A. Guagliardi, G. Polidori, *J. Appl. Crystallogr.* **1994**, *27*, 435. − [18b] SHELXS-97: G. M. Sheldrick, *Acta Crystallogr., Sect. A* **1990**, *46*, 467−473, − [18c] G. M. Sheldrick, *SHELXL-97, Program Suite for the Solution and Refinement of Crystal Structures from Diffraction Data*, University of Göttingen, Germany, **1997**.
[19] [19a] P. Van der Sluis, A. L. Spek, *Acta Crystallogr., Sect. A* **1990**, *46*, 194−201. − [19b] A. L. Spek, *Acta Crystallogr., Sect. A* **1990**, *46*, C34. The "Bypass" method referred to therein is widely used in crystallographic analysis of compounds containing substantial amounts of disordered solvent which cannot be located precisely from diffraction data.

Received May 10, 2001
[I01164]

The Coordination Chemistry of *cis*-3,4-Diaminopyrrolidine and Related Polyamines[‡]

Dirk Kuppert,[a] Jürgen Sander,[a] Christian Roth,[a] Michael Wörle,[b] Thomas Weyhermüller,[c] Guido J. Reiss,[d] Uwe Schilde,[e] Iris Müller,[f] and Kaspar Hegetschweiler*[a]

Keywords: Chelates / N ligands / Ligand design / Stability constants / Coordination modes

cis-3,4-Diaminopyrrolidine (*cis*-dap), *trans*-3,4-diaminopyrrolidine (*trans*-dap), *cis*-1,2-cyclopentanediamine (*cis*-cptn), and *trans*-1,2-cyclopentanediamine (*trans*-cptn) have been prepared in multigram quantities. The complexation of these ligands and of 3-aminopyrrolidine (ampy) with Ni^{II}, Cu^{II}, Zn^{II}, and Cd^{II} has been studied in solution by means of potentiometric and spectrophotometric titrations. The complexes of the triamines *cis*-dap and *trans*-dap show a pronounced tendency to form protonated species such as $[M^{II}(HL)]^{3+}$, $[M^{II}(HL)_2]^{4+}$, and $[M^{II}(HL)L]^{3+}$, indicative of a bidentate coordination mode of the ligand L. The UV/Vis spectra of the corresponding Cu^{II} complexes further confirmed bidentate coordination with *trans*-CuN_4 geometry. The overall stabilities of the bis complexes $[ML_2]^{2+}$ decrease in the order *cis*-cptn > *cis*-dap > *trans*-cptn > ampy > *trans*-dap. The considerably lower stabilities of the ampy complexes as compared to the corresponding *cis*-dap complexes indicate metal binding to the two primary amino groups of the latter ligand. This was supported by molecular mechanics calculations (Cu^{II} and Co^{III} complexes) and confirmed by single-crystal X-ray diffraction studies of $[Pt(Hcis\text{-}dap)Cl_4]Cl\cdot H_2O$, $[Pd(Hcis\text{-}dap)_2](ClO_4)_4\cdot 2H_2O$, and $[Cu(Hcis\text{-}dap)_2(OH_2)_2](SO_4)_2\cdot 3.5H_2O$ – $2x\ H^+ + x\ Cu^{2+}$ with $0.01 \le x \le 0.11$. For the diamine ligands, coordination through the two exocyclic amino groups or through one exocyclic and one endocyclic amino group was established from the X-ray structure analyses of $[Ni(cis\text{-}cptn)_2](ClO_4)_2$ and $[Cu(3R\text{-}ampy)(3S\text{-}ampy)](ClO_4)_2$, respectively. The crystal structure determination of $[Co(cis\text{-}dap)(tach)][ZnCl_4]Cl\cdot C_2H_5OH$ (tach = *cis*-1,3,5-cyclohexanetriamine) revealed tridentate, facial coordination of *cis*-dap in this particular complex. However, the structural parameters of the $[Co(cis\text{-}dap)(tach)]^{3+}$ moiety indicate significant strain for this coordination mode. The coordinating properties of the ligand *cis*-dap are compared with those of other aliphatic and alicyclic triamines.

Introduction

Structure–stability correlations are a subject of continuing interest in coordination chemistry, and the dependence of complex stability on the individual structural properties of a ligand has been extensively discussed.[1] In this respect, cyclic polyamines that are restricted to a facial coordination (Scheme 1) are of particular interest because their rigidity considerably reduces the number of possible solution structures as compared to their open-chain analogues. Ligands based on the 1,4,7-triazacyclononane or all-*cis*-cyclohexane-1,3,5-triamine backbone are well established in the literature.[2,3] However, until recently, intermediate members of this series, such as *cis*-3,5-diaminopiperidine (dapi) or *cis*-3,4-diaminopyrrolidine (*cis*-dap), had not been investigated to any great extent. Crystal structures of Pd^{II}(dapi) complexes have been reported by Schwarzenbach,[4] and we recently published a comprehensive study of the complexation of dapi with a variety of metal cations.[5] The metal-binding properties of the related triamine *cis*-3,4-diaminopyrrolidine (*cis*-dap) have not yet been described. We have developed an efficient procedure for the preparation of *cis*-dap and wish to report herein its coordination chemistry both in aqueous solution and in the solid state. Additionally, some related cyclic di- and triamine ligands with a five-membered ring structure have also been studied (Scheme 2).

Results

Synthesis of the Ligands

The only hitherto known synthesis of *cis*-3,4-diaminopyrrolidine involves a complicated multi-step procedure and gives only unsatisfactory yields.[6] We have developed a new and efficient synthetic route that has allowed facile

[‡] Facially Coordinating Cyclic Triamines, 2. – Part 1: Ref.[5]
[a] Anorganische Chemie, Universität des Saarlandes, Postfach 151150, 66041 Saarbrücken, Germany
Fax: (internat.) + 49-(0)681/302-2663
E-mail: hegetschweiler@mx.uni-saarland.de
[b] Laboratorium für Anorganische Chemie, ETH-Zentrum, 8092 Zürich, Switzerland
[c] Max-Planck-Institut für Strahlenchemie, Stiftstraße 34–36, 45470 Mühlheim an der Ruhr, Germany
[d] Institut für Anorganische Chemie und Strukturchemie, Heinrich-Heine-Universität Düsseldorf, Universitätsstraße 1, 40225 Düsseldorf, Germany
[e] Institut für Anorganische Chemie und Didaktik der Chemie, Universität Potsdam, Karl-Liebknecht-Straße 24–25, 14476 Golm, Germany
[f] Institut für Analytische Chemie, Ruhr-Universität, 44780 Bochum, Germany
Supporting information for this article is available on the WWW under http://www.eurjic.com or from the author.

 © WILEY-VCH Verlag GmbH, 69451 Weinheim, 2001 1434–1948/01/1010–2525 $ 17.50+.50/0

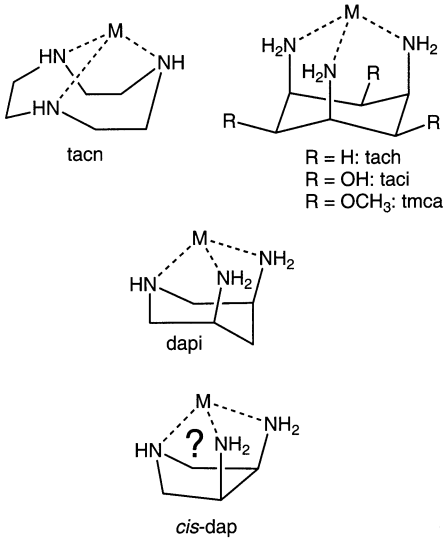

Scheme 1

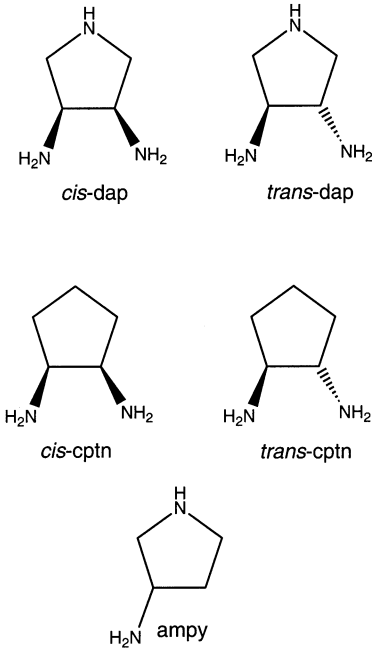

Scheme 2. Structures of the ligands and their abbreviations

preparation of this triamine in multigram quantities. Our procedure starts with 3-pyrroline, the amino group of which is protected by acetylation. The carbon−carbon double bond is then stereoselectively *cis*-dihydroxylated with OsO_4 to give 1-acetyl-*cis*-3,4-pyrrolidinediol. Subsequent conversion of the two hydroxy groups into amino groups is achieved through the corresponding diazide. After removal of the protecting acetyl group, the desired *cis*-3,4-diaminopyrrolidine can be isolated in excellent yield as the trihydrochloride salt. The *cis* configuration of the product was established by a single-crystal X-ray diffraction analysis (Figure 1, top). The corresponding chiral *trans* isomer was hitherto unknown and only some 1-substituted derivatives have been described.[7,8] We prepared this ligand from the *N*-benzylimide derivative of tartaric acid, which was again converted into the corresponding diazide. Subsequent hydrogenation resulted in reduction of the azido groups and in the removal of the benzyl group. The *trans* (3*R*,4*R*) configuration was again confirmed by a single-crystal X-ray diffraction analysis (Figure 1, bottom). The puckering parameters $Q = 0.405(2)$ Å, $\varphi = 83.0(4)°$ and $Q = 0.357(3)$ Å, $\varphi = 238.3(4)°$ for the pyrrolidine rings of H_3*cis*-dap^{3+} and H_3*trans*-dap^{3+} are indicative of a half-chair conformation with a slight twist towards an envelope form.[9] As expected, the N···N distance between the two primary amino groups in *trans*-dap is somewhat longer (3.28 Å) than that in *cis*-dap (3.00 Å).

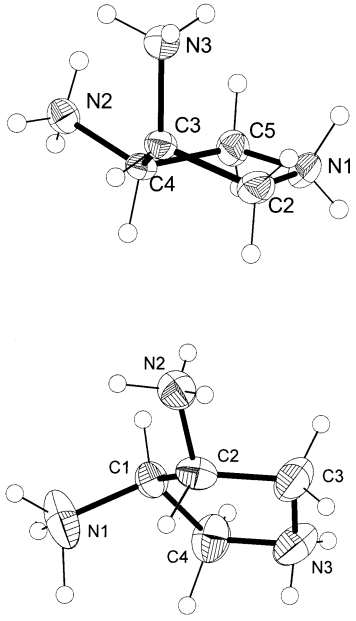

Figure 1. Molecular structures of the triply protonated triamines H_3*cis*-dap^{3+} (top) and H_3*trans*-dap^{3+} (bottom) showing the atom numbering scheme; thermal ellipsoids are drawn at a 50% probability level; hydrogen atoms are shown as spheres of arbitrary size; range of bond lengths [Å]: C−C 1.520(3)−1.533(3), C−N 1.478(3)−1.510(3); selected angles for H_3*cis*-dap^{3+} [°]: C2−C3−C4 100.93(16), N3−C3−C4 114.11(16), N2−C4−C3 116.80(17)

The structurally related diamines *cis*-1,2-cyclopentanediamine (*cis*-cptn) and *trans*-1,2-cyclopentanediamine (*trans*-cptn) were analogously prepared via the diazides using the corresponding cyclopentanediols as starting materials.[10−12] The chiral *trans*-cptn was obtained as a racemate. The two diastereomers can readily be distinguished by ^{1}H NMR spectroscopy. The *cis* isomer has C_s symmetry and shows four resonances due to the three methylene groups, whereas the chiral *trans* isomer exhibits C_2 symmetry showing only three signals for these six protons. The diamine 3-aminopyrrolidine (ampy) is commercially available and was again used as a racemate. A single-crystal X-ray diffraction analysis of H_2ampy$(ClO_4)_2$ has recently been published.[13]

Protonation Constants

The acidity constants of the protonated amines are listed in Table 1. For the two pairs of diastereomers H_3*cis*-dap^{3+}/H_3*trans*-dap^{3+} and H_2*cis*-cptn^{2+}/H_2*trans*-cptn^{2+}, the *cis* isomers of the fully protonated forms are slightly stronger acids. The triamines have different basic sites (primary and secondary amino groups) and this leads to different tautomers for species with an intermediate degree of protonation. In the case of *cis*-dap, the equilibria between these different microspecies were elucidated by ^{1}H NMR titration (Figure 2). An NOESY experiment allowed the unambiguous assignment of the two diastereotopic protons of the methylene groups. Only one proton (3-H) showed a significant NOE with the adjacent 1-H proton. The observed pH dependence of the chemical shifts could be reproduced using pK_a values of 2.15, 6.21, and 9.78 for the macrospecies H_x*cis*-dap^{x+} (Figure 2; $3 \geq x \geq 1$). These values (D_2O, 28 °C, no inert electrolyte) are in good agreement with the pK_a values obtained from the potentiometric measurements. As

Table 1. Protonation constants for the cyclic di- and triamine ligands (25 °C) at ionic strengths (I) of 0.1 mol dm^{-3} (KCl) and 1.0 mol dm^{-3} (KNO_3) as indicated

[a]	log K_1		log K_2		log K_3	
I [mol dm^{-3}]	0.1	1.0	0.1	1.0	0.1	1.0
ampy	10.39	10.66	6.82	7.20	–	–
cis-cptn	9.74	–	6.13	–	–	–
trans-cptn	9.92	–	7.22	–	–	–
cis-dap	9.66	9.90	6.25	6.63	2.42	2.96
trans-dap	9.58	9.80	6.34	6.72	3.67	4.19

[a] $K_i = [H_iL] \times [H]^{-1} \times [H_{i-1}L]^{-1}$; estimated standard deviations < 0.01.

described previously,[5] the deshielding of the (C−)H protons by protonation of a nearby basic site in a cyclic polyamine can be modeled using a limited set of deshielding constants. For the monoprotonated H*cis*-dap$^+$, such calcula-

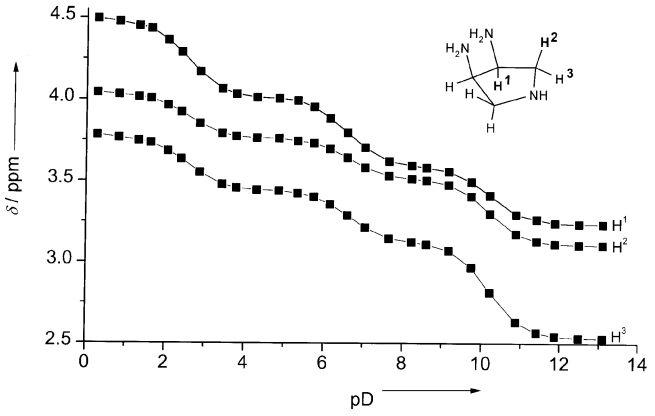

Figure 2. pD dependence of the ^{1}H NMR resonances of *cis*-dap; squares correspond to the experimental values; the lines are calculated (minimization of $[\delta_{obs} - \delta_{calcd.}]^2$) assuming a rapid equilibrium between the species H_x*cis*-dap^{x+} ($1 \leq x \leq 3$)

tions indicated that the two microspecies with a protonated primary amino group or a protonated secondary ring nitrogen atom are present in proportions of 57% and 43%, respectively. This ratio corresponds closely to a statistical distribution of the proton over the three basic sites. A different result is obtained for the doubly protonated H_2*cis*-dap^{2+}, for which the tautomer with a free primary amino group clearly predominates (75%). This result can be explained in terms of a simple electrostatic model (maximal separation of the two positive charges).

Metal Complex Formation

The coordination behavior of the polyamines in dilute aqueous solution (25 °C) was studied by means of pH-metric titration experiments. Formation constants of Ni^{II}, Cu^{II}, and Cd^{II} complexes were determined for ampy, *cis*-cptn, and *cis*-dap. Additionally, the complexation of *cis*-dap with Zn^{II} was studied. For the ligands *trans*-cptn and *trans*-dap, our study was confined to complexation with Cu^{II}. All formation constants are summarized in Tables 2 and 3. The measurements with Ni^{II}, Cu^{II}, and Zn^{II} were performed in 0.1 mol dm^{-3} KCl. Due to the relatively high affinity of Cd^{II} for Cl^-, these experiments were performed in 0.1 mol dm^{-3} KNO_3.[5]

Table 2. Formation constants of metal complexes with the triamine ligands (25 °C, 0.1 mol dm^{-3} KCl or KNO_3)

	Cu^{2+}		Ni^{2+}	Zn^{2+}	Cd^{2+}[a]
	cis-dap	*trans*-dap	*cis*-dap	*cis*-dap	*cis*-dap
log β_{xyz}[b] x,y,z					
1,1,0	–	–	6.41(1)	4.93(2)	4.44(2)
1,1,1	16.8(1)	14.68(1)	14.14(2)	12.68(2)	12.33(1)
1,2,2	32.38(2)	28.40(2)	27.06(2)	–	–
1,2,1	25.27(1)	21.59(2)	19.37(3)	–	–
1,2,0	17.53(1)	14.05(2)	11.24(2)	8.89(2)	7.90(2)
1,3,0	–	–	13.7(1)	–	–
1,2,−1	–	–	–	−0.38(2)	–

[a] Cd^{2+}: 0.1 mol dm^{-3} KNO_3; all other metal ions: 0.1 mol dm^{-3} KCl. – [b] $\beta_{xyz} = [M_xL_yH_z] \times [M]^{-x} \times [L]^{-y} \times [H]^{-z}$; estimated standard deviations (in parentheses) were calculated with HYPERQUAD[36] and multiplied by a factor of three.

The results indicate that the two triamines *cis*-dap and *trans*-dap show a pronounced tendency to form protonated complexes of the compositions $[M(HL)]^{3+}$ and $[M(HL)_2]^{4+}$ in acidic solution (Figure 3). In the presence of excess ligand, the main species formed are the bis(complexes) $[ML_2H_x]^{(2+x)+}$. The formation of a tris(chelate) $[ML_3]^{2+}$ was only verified in the case of Ni^{II}. [Ni(*cis*-dap)$_3$]$^{2+}$ was seen as a minor species at the end of a titration using an excess of the ligand. In the experiments with total Ni/total *cis*-dap = 1:2, formation of [Ni(*cis*-dap)(H*cis*-dap)]$^{3+}$ and [Ni(*cis*-dap)]$^{2+}$ was observed in the same pH range, and a fixed value of β_{ML}, as obtained from an independent 1:1 titration, was used in the evaluation to avoid mutual influ-

Table 3. Formation constants for metal complexes with the diamine ligands (25 °C, 0.1 mol dm^{-3} KCl or KNO_3)

	Cu^{2+}			Ni^{2+}		Cd^{2+}[a]	
log β_{xyz}[b] x,y,z	ampy	*cis*-cptn	*trans*-cptn	ampy	*cis*-cptn	ampy	*cis*-cptn
1,1,0	8.24(1)	10.59(1)	8.58(1)	4.1(1)	7.02(1)	3.4(2)	5.20(1)
1,2,0	15.01(1)	19.75(1)	15.81(1)	8.1(1)	12.70(1)		9.52(1)
1,3,0					15.98(4)		
1,2,−1			8.97(3)			−2.1(1)	

[a] Cd^{2+}: 0.1 mol dm^{-3} KNO_3; all other metal ions: 0.1 mol dm^{-3} KCl. – [b] $\beta_{xyz} = [M_xL_yH_z] \times [M]^{-x} \times [L]^{-y} \times [H]^{-z}$; estimated standard deviations (in parentheses) were calculated with HYPERQUAD[36] and multiplied by a factor of three.

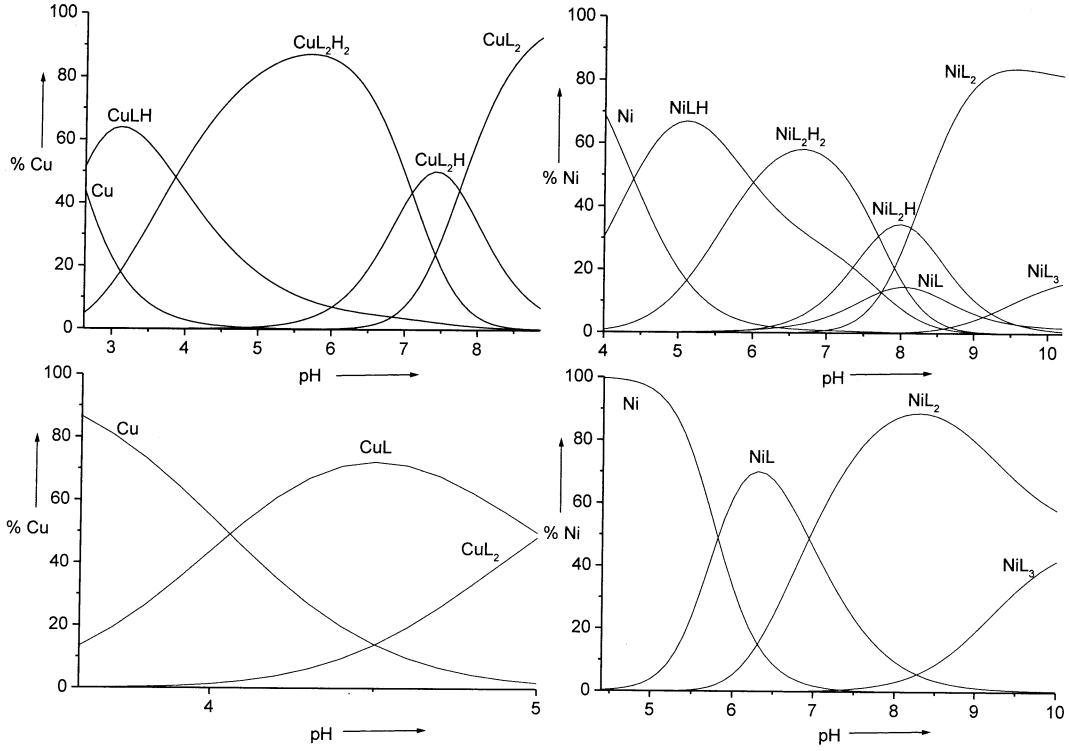

Figure 3. Species distribution plots for an equilibrated aqueous solution with a total metal ion (Ni, Cu) concentration of 10^{-3} mol dm^{-3} and a total ligand (L) concentration of 2×10^{-3} mol dm^{-3} (Cu) or 3×10^{-3} mol dm^{-3} (Ni); L = *cis*-dap (top), L = *cis*-cptn (bottom); only metal-containing species are shown; the equilibrium constants listed in Tables 2 and 3 were used for the calculations

ence (correlation effects) of the two formation constants. In the case of Cu^{II}, the unprotonated $[CuL]^{2+}$ complex was not observed.

As expected, the diamines ampy, *cis*-cptn, and *trans*-cptn do not form any protonated metal complexes and the titration curves could be evaluated simply in terms of $[ML]^{2+}$ and $[ML_2]^{2+}$ formation. In the case of *cis*-cptn and Ni^{II}, the formation of a complex of composition $[ML_3]^{2+}$ was additionally established. The complexation of Ni^{II} and Cd^{II} by ampy is rather weak and was only observed at pH > 8. To avoid precipitation of solid metal hydroxides, a large excess of ampy had to be used.

UV/Vis data of Ni^{II}- and Cu^{II}(amine) complexes provide a useful tool for assigning the structures of the different solution species.[14,15] The d-d transitions of Ni^{II} complexes with saturated amines are of rather low intensity ($\varepsilon \leq 10$) and hence rather concentrated solutions (0.1 M) had to be used. Under these conditions, both $[Ni(cis\text{-dap})_2]^{2+}$ and $[Ni(Hcis\text{-dap})_2]^{4+}$ form blue solutions, with $^3A_{2g}$-$^3T_{1g}(F)$ transitions at 571 and 577 nm, respectively. These values are consistent with an NiN_4O_2 chromophore and the minor shift upon deprotonation clearly indicates that incorporation of an additional nitrogen atom into the chromophore does not occur to any significant extent. We can therefore exclude both tridentate coordination and a bridging mode with the secondary nitrogen atom coordinated to an adjacent Ni^{II} center. In contrast to *cis*-dap, $[Ni(cis\text{-cptn})_2]^{2+}$ forms a bright-yellow solution (λ_{max} = 444 nm), indicative

of a diamagnetic complex.[10] It is noteworthy that the slightly less basic *cis*-dap does not form such a low-spin bis(complex). In the presence of excess *cis*-dap (Ni/L > 1:3), purple solutions with λ_{max} = 553 nm are observed. The considerable shift to shorter wavelengths is indicative of a tris(chelate) structure with an NiN_6 chromophore. Such an $[Ni(cis\text{-dap})_3]^{2+}$ complex had already been noted as a minor species in the aforementioned titration experiments. Since the significantly higher ligand concentration (0.3 mol dm^{-3}) favors complexation, the tris complex becomes the predominant species at pH > 10.

In aqueous solution, the d-d transitions of Cu^{II}(amine) complexes appear unresolved as a broad single band in the range 500−750 nm.[15] The intensity of this band is an order of magnitude higher than that seen for the corresponding Ni^{II} complexes, and this allowed the recording of solution spectra with a total Cu^{II} concentration of just 0.01−0.02 mol dm^{-3}. Measurements were made at an ionic strength of 1 mol dm^{-3} KNO_3 and were carried out in conjunction with an additional series of potentiometric titrations (Figure 4). These data allowed the determination of the stability constants by two independent methods. The agreement found was generally good (Table 4). Additionally, the measurements could be used for the calculation of spectra for each individual species (Figure 4, b). It is well established that for a tetragonally distorted geometry (C_{4v} or D_{4h}), successive replacement of the four water ligands by nitrogen donors in the equatorial plane results in a continuous shift of λ_{max} to shorter wavelengths, whereas substitution of the loosely bound axial water ligands results in a red shift (the "pentaammine effect").[16,17] $[Cu(H\textit{cis}\text{-dap})_2]^{4+}$, $[Cu(H\textit{cis}\text{-dap})(\textit{cis}\text{-dap})]^{3+}$, and $[Cu(\textit{cis}\text{-dap})_2]^{2+}$ were all found to exhibit absorbance maxima at 552−567 nm, indicative of a *trans*-CuN_4 chromophore. Similarly, the λ_{max} values of 560 nm (*trans*-dap), 550 nm (ampy), and 545 nm (*cis*-cptn)[18] indicate *trans*-CuN_4 geometries with one or two weakly bound water molecules at the apices in the corresponding bis complexes $[CuL_2]^{2+}$. The 1:1 complexes $[Cu(H\textit{cis}\text{-dap})]^{3+}$ (λ_{max} = 688 nm) and $[Cu(ampy)]^{2+}$ (λ_{max} = 668 nm) exhibit absorbance maxima at considerably longer wavelengths, as expected for *cis*-CuN_2 coordination.[14]

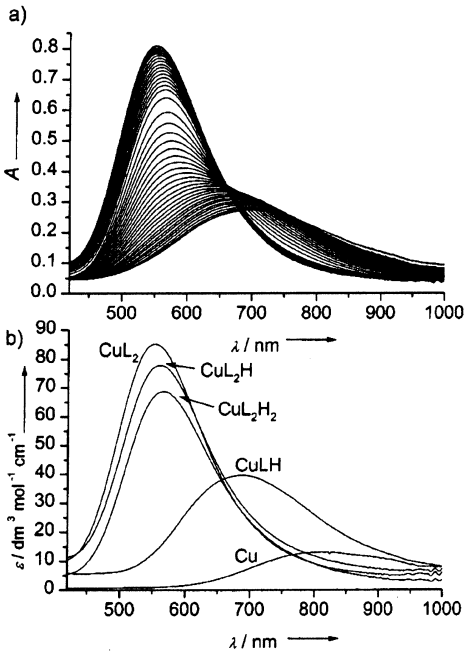

Figure 4. Spectral changes for the Cu^{II}(*cis*-dap) system during a titration experiment with total Cu = 10^{-2} mol dm^{-3} and total L = 2×10^{-2} mol dm^{-3} (a); the calculated spectra for the individual species (b)

Table 4. Comparison of formation constants of Cu^{II} complexes derived from either potentiometric (pot) or spectrophotometric (spec) titrations (25 °C, 1 mol dm^{-3} KNO_3) estimated standard deviations are given in parentheses

	pot[a]	spec[a]
log β_{xyz}[b]		
x,*y*,*z*		
ampy		
1,1,0	8.54(1)	8.53(1)
1,2,0	15.68(1)	15.65(2)
cis-dap		
1,1,1	17.64(2)	17.84(4)
1,2,0	18.41(2)	18.9(3)
1,2,1	26.62(2)	26.9(1)
1,2,2	34.23(2)	34.45(5)
trans-dap		
1,1,1	15.42(2)	15.63(3)
1,2,0	14.78(1)	14.9(2)
1,2,1	22.69(1)	22.93(9)
1,2,2	29.99(1)	30.27(5)

[a] Potentiometry: calculated with HYPERQUAD;[36] spectrophotometry: calculated with SPECFIT;[37] the obtained standard deviations are multiplied by a factor of three. − [b] $\beta_{xyz} = [M_xL_yH_z] \times [M]^{-x} \times [L]^{-y} \times [H]^{-z}$.

Structural Characterization of the Metal Complexes

In $[Pt(H\textit{cis}\text{-dap})Cl_4]Cl{\cdot}H_2O$, the ligand *cis*-dap coordinates to the Pt^{IV} center in a bidentate fashion through the two primary amino groups. The remaining secondary amino group of the pyrrolidine ring is protonated (Figure 5). The octahedral low-spin geometry of the Pt^{IV} center is completed by the coordination of four chloride ions. The positive charge of the complex cation is balanced by an additional chloride counterion. Considering the positions of the cations (A), represented by their centers of gravity, and of the counterions (B), the resulting AB-type packing can be described as a stack of layers consisting of fused six-membered rings with an alternating A−B−A−B−A−B sequence. The layers are oriented perpendicular to the *b* axis. This packing is related to the GeS structure,[19] although in GeS the six-membered Ge_3S_3 rings have a chair conformation, whereas in $[Pt(H\textit{cis}\text{-dap})Cl_4]Cl{\cdot}H_2O$ the A_3B_3 rings have a distorted boat conformation. In both cases, the nonisometric packing can be explained simply in terms of the nonisotropic shape of the cations. In $[Pt(H\textit{cis}\text{-dap})Cl_4]Cl{\cdot}H_2O$, the anions and cations within a layer are connected through N−H···Cl^- hydrogen bonds and the dif-

ferent layers are interconnected by N−H···O···H−N bridges between the coordinated amino groups and water molecules. The $[Pt(H\textit{cis}\text{-dap})Cl_4]^+$ complex cation is completely asymmetric as a consequence of the puckered conformation of the five-membered chelate ring. However, the NMR-spectroscopic data (two signals in the $^{13}C\{^1H\}$ NMR and three signals in the ^1H NMR spectrum) indicate the expected rapid ring inversion with average C_s symmetry for the complex in solution.

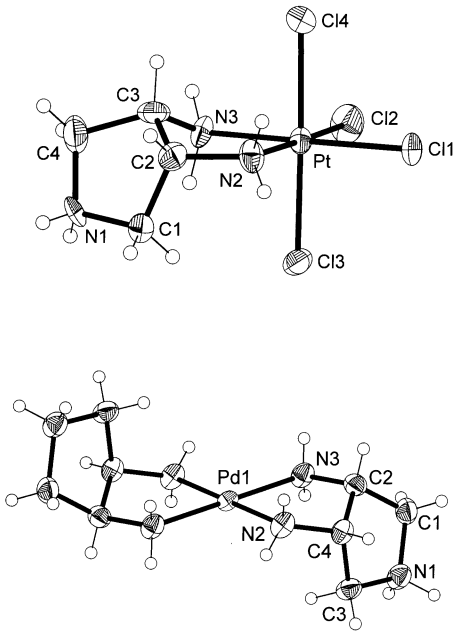

Figure 5. Molecular structures of $[Pt(H\textit{cis}\text{-dap})Cl_4]^+$ (top) and $[Pd(H\textit{cis}\text{-dap})_2]^{4+}$ (bottom); thermal ellipsoids are drawn at a 50% probability level; hydrogen atoms are shown as spheres of arbitrary size; selected bond lengths [Å] and angles [°]: (a) Pt−N2 2.075(10), Pt−N3 2.007(9), Pt−Cl1 2.333(3), Pt−Cl2 2.311(3), Pt−Cl3 2.322(3), Pt−Cl4 2.313(3), N2−Pt−N3 83.8(5); (b) Pd−N2 2.035(2), Pd−N3 2.039(2), N2−Pd−N3 83.86(9), N2−Pd−N3A 96.14(9)

A similar bidentate coordination of the protonated H*cis*-dap$^+$ ligand is observed for $[Pd(H\textit{cis}\text{-dap})_2](ClO_4)_4\cdot H_2O$ (Figure 5). The crystal structure of this compound can be described as a packing of neutral $\{[Pd(H\textit{cis}\text{-dap})_2](ClO_4)_4\}$ aggregates that are hydrogen-bonded through NH−H···OH−H···$OClO_3$···H−NH and NH−H···$OClO_3$···H−NH bridges. The Pd^{II} atom resides on a center of inversion and exhibits the well-known square-planar PdN_4 geometry (λδ conformation for the two five-membered chelate rings). The pyrrolidine rings are located at opposite sides of the PdN_4 plane and thus adopt a *transoid* orientation. A related structure with protonated endocyclic nitrogen atoms in a *transoid* geometry has been reported by Schwarzenbach et al. for the Pd complex of *cis*-3,5-diaminopiperidine (dapi).[4] These authors performed a potentiometric study to determine the acidity constants of the noncoordinating ammonium groups of $[Pd(Hdapi)_2]^{4+}$; an unusually slow equilibration was noted, which was discussed in terms of a slow rearrangement of the ligands (a change from the *transoid* to the *cisoid* form in the course of deprotonation). The required breaking and reforming of Pd^{II}−N bonds was invoked to account for the slow reaction rate. In our experiments, we found a related steady shift of pH for a freshly prepared 0.1 mol dm^{-3} aqueous solution of $[Pd(H\textit{cis}\text{-dap})_2](ClO_4)_4$. However, this shift proved to be very slow (5 mV per 24 h) and the data set of a rapid titration could be evaluated in terms of a simple two-step deprotonation with pK_a values of 6.27(1) and 7.04(1).

With Cu^{II}, a solid sample of composition $[Cu(H\textit{cis}\text{-dap})_2(OH_2)_2](SO_4)_2\cdot 3.5H_2O$ was obtained. This compound contains two crystallographically independent $[Cu(H\textit{cis}\text{-dap})_2(OH_2)_2]^{4+}$ cations (Figure 6). Cu1 is located on a twofold axis and its five-membered chelate rings thus have a λλ or δδ conformation, whereas Cu2 resides on a center of inversion with a λδ conformation of the rings. Again, the Cu centers are exclusively bound to the primary amino groups of the H*cis*-dap$^+$ ligands (square-planar $Cu^{II}N_4$ geometry with an average Cu−N bond length of 2.02 Å). The coordination sphere is completed by two loosely bound water ligands in the axial positions (average Cu−O bond length: 2.48 Å), giving the well-known tetragonally distorted CuN_4O_2 octahedron. The noncoordinating ring nitrogen atoms are protonated and the pyrrolidine rings are arranged in a *transoid* manner, akin to that described above for the Pd complex. Deprotonation of $[Cu(H\textit{cis}\text{-dap})_2(OH_2)_2]^{4+}$ could occur either at the noncoordinating ring nitrogen atoms or at the water ligands (with the formation of hydroxo complexes). In the first case, the liberation of an additional amino group would generate a potentially tridentate ligand. The additional amino group could either coordinate in a tripodal intramolecular fashion or intermolecularly as a bridging ligand to an adjacent metal center. The crystal structure of $[Cu(H\textit{cis}\text{-dap})_2(OH_2)_2](SO_4)_2\cdot 3.5H_2O$ provided evidence that the latter mode is observed with Cu^{II}. Close inspection of the difference Fourier map revealed a residual peak at $x = 3/4$, $y = 1/4$, $z = 0.2736$ with an electron density of 1.6 e/Å^3. This peak is located on a twofold axis in a cavity formed by the noncoordinating ammonium groups of two complex cations, two sulfate counterions, and a water molecule. The distances to the nearest atoms are 2 × 1.96 Å (O22 & O22A), 2.00 Å (O60), 2 × 2.19 Å (N1 & N1A). Further studies of additional specimens showed considerable variation in the intensity of this peak. Although the cell parameters and atom positions were almost the same for all the samples under investigation, the intensity of this peak corresponded to an electron density of up to 12.6 eÅ^{-3}. Based on the chemical composition of the mother liquor, the charge balance, and the distances to the five nearest neighboring atoms, we interpret this peak in terms of some additional incorporation of Cu^{II}, which is bound to the two pyrrolidine nitrogen atoms with the abstraction of two protons (Scheme 3). In fact, it became clear that this compound has a nonstoichiometric (berthollide) composition, for which the correct formula would be $[Cu(H\textit{cis}\text{-dap})_2(OH_2)_2](SO_4)_2\cdot 3.5\ H_2O - 2x\ H^+ + x\ Cu^{2+}$. In this study, the data for $x = 0.005$, 0.08, and 0.11 are reported. Although the cavity appears to

have an almost ideal size for accommodating Cu^{II}, some minor structural rearrangements are evidently required for the uptake of an additional Cu^{II} ion. This is indicated by a disorder that is found for those samples containing a large amount of additional Cu. This disorder is manifested in strong anisotropy of the displacement parameters for the atoms of the outer part of the pyrrolidine rings and the observation of two partially occupied positions for one of the oxygen atoms of the sulfate residue (Figure 6). The additional Cu^{II} center has trigonal-bipyramidal coordination with the two pyrrolidine nitrogen atoms in the axial positions and two sulfate ions and a water molecule in the equatorial positions. This additional Cu^{II} center interconnects two mononuclear $[Cu(H\textit{cis}\text{-dap})_2(OH_2)_2]^{4+}$ cations giving a trinuclear $[(H\textit{cis}\text{-dap})Cu(OH_2)_2(\mu\text{-}\textit{cis}\text{-dap})Cu(OH_2)(SO_4)_2(\mu\text{-}\textit{cis}\text{-dap})Cu(H\textit{cis}\text{-dap})(OH_2)_2]^{4+}$ entity. The observation of such trinuclear species nicely illustrates the ability of the neutral *cis*-dap molecule to participate in bridging interactions, and we regard this ligand as an interesting building block for the construction of coordination polymers.

A complex featuring a tridentate coordination mode of *cis*-dap, with all the nitrogen atoms of the ligand bound to the same metal center, could be obtained in the form of the heteroleptic $[Co^{III}(\textit{cis}\text{-dap})(tach)]^{3+}$. Attempts to prepare a homoleptic complex $[Co(\textit{cis}\text{-dap})_2]^{3+}$ by aerial oxidation of a solution of Co^{II} and *cis*-dap failed and the use of Co^{III} precursors such as $K_3[Co(CO_3)_3]$ or *trans*-$[CoCl_2(py)_4]Cl$ led to unresolved reaction mixtures. $[Co(\textit{cis}\text{-dap})(tach)]^{3+}$ was prepared from $[Co(tach)Cl_3]$, in which the relatively labile Cl^- ligands define a set of leaving groups having the required preformed facial geometry. The resulting mononuclear Co^{III} complex was crystallized as a chloride tetrachlorozincate salt. Its hexaamine geometry exhibits some rather unusual features. Bond lengths and angles for the Co(tach) moiety all fall within the expected ranges (Figure 7), whereas the $Co^{III}-N$ bonds in the Co(*cis*-dap) moiety are remarkably long. This is particularly true for the secondary nitrogen atom, which has a Co−N distance of 2.068(5) Å. The puckering parameters [$Q = 0.601(4)$ Å and $\varphi = 0.8(4)°$] for the pyrrolidine ring correspond to an almost ideal envelope conformation. This conformation implies an eclipsed orientation of the two CH protons with a torsional angle of only 8.7°, a rather short (N−)H···H(−N) separation of 2.24 Å for the primary amino groups, and a significantly elongated C7−C8 bond (1.60 Å). Owing to the rather long

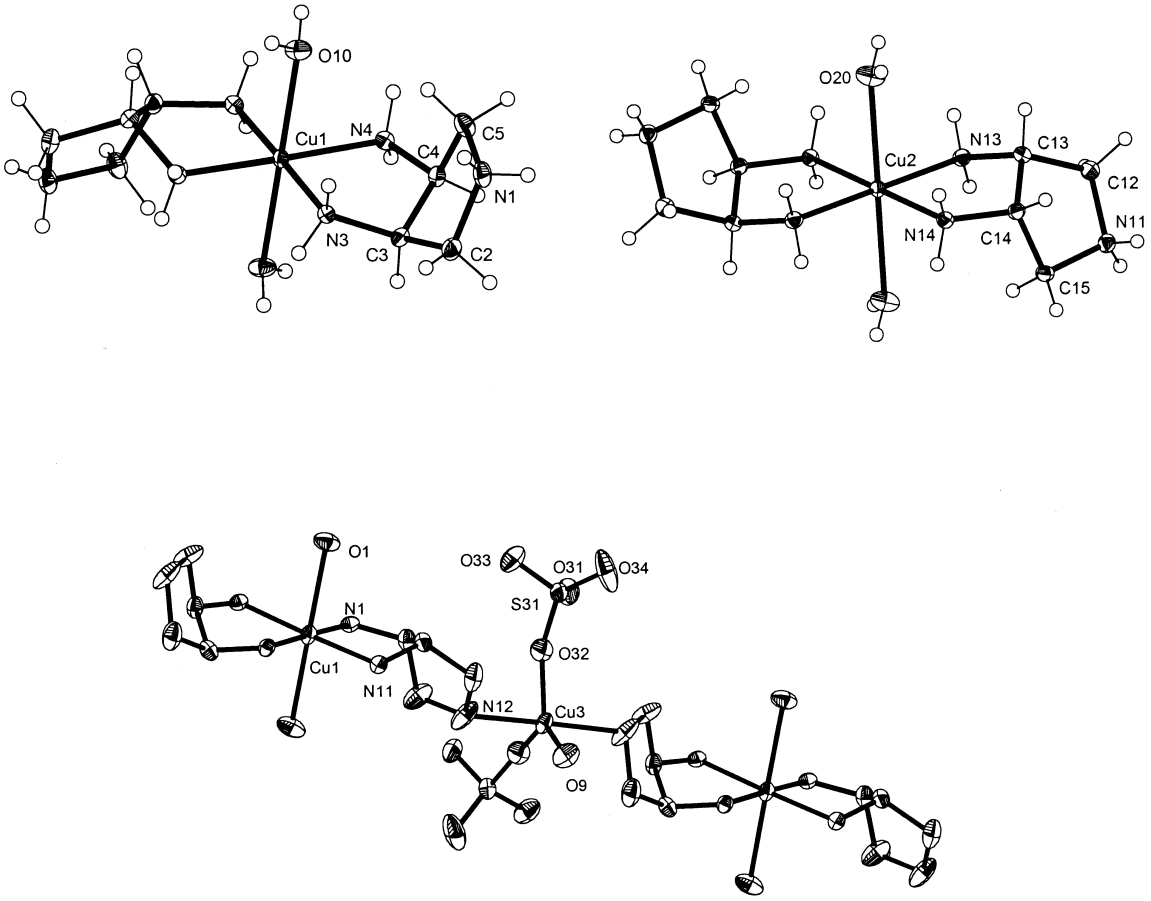

Figure 6. Structural representations of $[Cu(H\textit{cis}\text{-dap})_2(OH_2)_2](SO_4)_2{\cdot}3.5H_2O - 2x\ H^+ + x\ Cu^{2+}$: the two $[Cu(H\textit{cis}\text{-dap})_2(OH_2)_2]^{4+}$ cations for $x < 0.01$ (top); hydrogen atoms are shown as spheres of arbitrary size; selected bond lengths [Å] and angles [°]: Cu1−N3 2.0174(13), Cu1−N4 2.0271(13), Cu1−O10 2.4660(12), Cu2−N13 2.0144(13), Cu2−N14 2.0186(13), Cu2−O20 2.4985(13), N3−Cu1−N4 84.40(5), N13−Cu2−N14 84.73(5); view of the trimer with the partially occupied Cu3 position ($x = 0.11$) (bottom); hydrogen atoms are omitted for clarity; in the absence of Cu3 the ring nitrogen atom N12 is protonated, forming a hydrogen bond to the SO_4^{2-} counterion (O32); only one of the two positions of the disordered O32 is shown; thermal ellipsoids are drawn at a 50% probability level

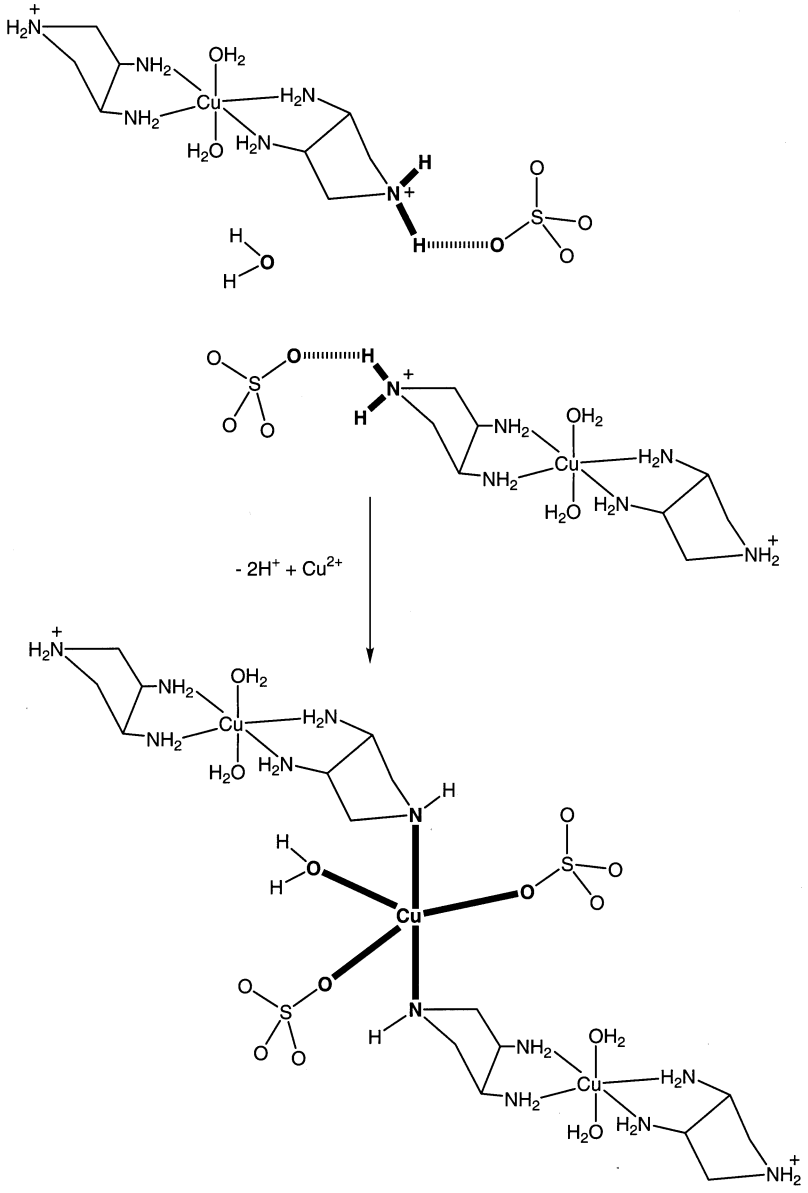

Scheme 3

$Co^{III}-N$ bonds in the Co(*cis*-dap) moiety, a decrease in ligand field and an increased tendency to form the corresponding Co^{II} complex could be expected.[20] However, [Co(*cis*-dap)(tach)]$^{3+}$ exhibits the usual yellow color with absorbance maxima at 351 and 475 nm, as expected for a normal Co^{III}(hexaamine) chromophore.[21] Cyclic voltammetry revealed quasi-reversible redox behavior with a redox potential of −0.21 V (versus NHE). Compared to the range usually observed for Co^{III}(hexaamine) complexes (0.3−0.5 V versus NHE), the potential of [Co(*cis*-dap)(tach)]$^{2/3+}$ indicates only a minor degree of stabilization of the Co^{II} species.[5,20,21]

The diamine ligands *cis*-cyclopentane-1,2-diamine (*cis*-cptn) and 3-aminopyrrolidine (ampy) have been included in this investigation as structural models for a coordination of a metal cation to either two exocyclic nitrogen donors or to one exocyclic and one endocyclic nitrogen donor, respectively. Toftlund et al. have previously reported the preparation of the yellow, diamagnetic complex [Ni(*cis*-cptn)$_2$]$^{2+}$.[10] We have crystallized this species as [Ni(*cis*-cptn)$_2$](ClO$_4$)$_2$ and report its crystal structure (Figure 8). As expected for a diamagnetic complex, the Ni center has a square-planar NiN_4 geometry with an average Ni−N bond length of 1.92 Å. Again, the two cyclopentane rings have a *transoid* arrangement with respect to the NiN_4 plane. [Cu(ampy)$_2$]$^{2+}$, which has also been crystallized as its perchlorate salt (Figure 8), represents an example of a structure where both endo- and exocyclic nitrogen donors are used for metal binding.[22−24] The ligand was used as a racemate and the crystal structure of [Cu(3*R*-ampy)(3*S*-ampy)](ClO$_4$)$_2$ showed the incorporation of both enantiomers in one complex entity. The Cu^{II} center has square-planar

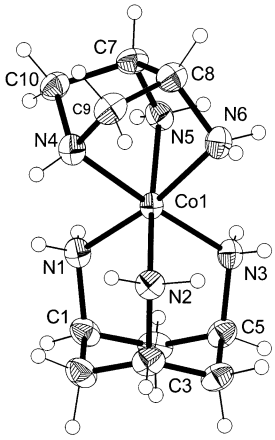

Figure 7. Molecular structure of $[Co(cis\text{-dap})(tach)]^{3+}$; thermal ellipsoids are drawn at a 50% probability level; hydrogen atoms are shown as spheres of arbitrary size; selected bond lengths [A] and angles [°]: Co−N2 1.958(6), Co−N3 1.964(5), Co−N1 1.966(4), Co−N6 1.975(4), Co−N5 2.001(7), Co−N4 2.068(5), C7−C8 1.598(5); the other C−C bonds range from 1.518(6) to 1.532(5); N6−Co−N5 76.27(15), N5−Co1−N4 85.2(3), N6−Co1−N4 84.4(2); intraligand N−Co−N angles in the Co(tach) moiety range from 89.4(3) to 92.40(14)

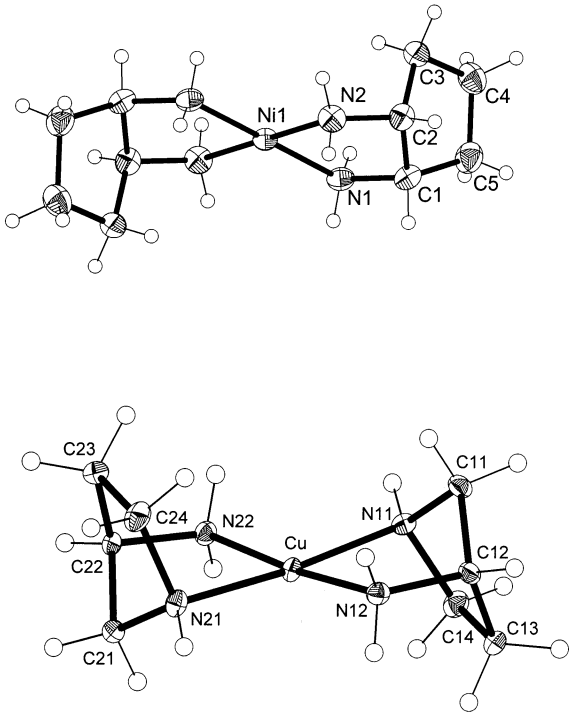

Figure 8. Molecular structures of $[Ni(cis\text{-cptn})_2]^{2+}$ (top) and $[Cu(3R\text{-ampy})(3S\text{-ampy})]^{2+}$ (bottom); thermal ellipsoids are drawn at a 30% probability level; hydrogen atoms are shown as spheres of arbitrary size; selected bond lengths [A] and angles [°]: Ni−N1 1.928(3), Ni−N2 1.916(3), N2−Ni−N1 86.01(14); Cu−N11 2.027(4), Cu−N12 2.013(4), Cu−N21 2.027(4), Cu−N22 2.010(4), N22−Cu−N12 174.4(2), N12−Cu−N11 95.91(17), N21−Cu−N11 174.8(3), N22−Cu−N11 95.91(17), N12−Cu−N21 98.18(16), N22−Cu−N21 82.44(17)

CuN_4 geometry with a very weak interaction with one of the ClO_4^- counterions. The two endocyclic and the two exocyclic nitrogen donors each have a *trans* orientation. Each Cu(ampy) fragment can be regarded as a metalla derivative of norbornane. By analogy with the structure of this hydrocarbon,[25] the geometry at the bridging methylene groups deviates significantly from a tetrahedral arrangement (N−C−C angles: 98.9° and 97.6°) and, compared to the corresponding *cis*-cptn system, the M(ampy) structure appears to be considerably strained.

Discussion

Equilibria in Aqueous Solution

A comparison of the protonation constants of *cis*-dap, *trans*-dap, *cis*-cptn, *trans*-cptn, ampy, and related amines (Table 5) indicates some characteristic trends. Compared to related monoamines such as cyclopentylamine ($pK_a = 10.6$) or pyrrolidine ($pK_a = 11.2$),[26] the triamines *cis*-dap and *trans*-dap are weaker bases. On statistical grounds, the presence of three basic sites should increase the overall basicity; however, it seems that the electron-withdrawing influence of additional amino groups outweighs this effect. In contrast to the monoamine analogues, the ^1H NMR titration did not show a significant difference for the intrinsic basicities of the primary and secondary amino groups in *cis*-dap[5] and it appears that the different behavior of the individual diastereomers is based on steric rather than electronic effects. The cyclopentane or pyrrolidine frameworks give rise to particularly rigid molecules and the different basicities of the diastereomers can simply be explained in terms of electrostatic repulsion. In H_2*trans*-$cptn^{2+}$, the two amonio groups adopt a staggered (antiperiplanar) conformation and the relevant pK_a values of H_2*trans*-$cptn^{2+}$ are in close agreement with those of the open-chained H_2en^{2+} (en = ethane-1,2-diamine): the difference $pK_1 - pK_2 = \Delta pK$ is 2.70 for H_2*trans*-$cptn^{2+}$ and 2.80 for H_2en^{2+}. In H_2*cis*-$cptn^{2+}$, the interatomic distance between the two positive charges is shorter and consequently ΔpK_a for this isomer is increased to 3.60. Analogously, the acidity constants of monoprotonated H*cis*-dap^+ and H*trans*-dap^+ are in close agreement, whereas those of the triply protonated forms differ considerably with the *cis* isomer being the stronger acid.

Analysis of the formation constants together with the spectroscopic properties of *cis*-dap complexes in aqueous solution points to a bidentate rather than a tridentate coordination mode for this ligand:

(i) Ni^{II} forms a tris(chelate) with an NiN_6 chromophore, whereas the λ_{max} values of the two bis(complexes) $[Ni(cis\text{-dap})_2]^{2+}$ and $[Ni(Hcis\text{-dap})_2]^{4+}$ are both indicative of an NiN_4 chromophore.[14] Clearly, deprotonation of the ammonium groups is not followed by metal binding, and a third ligand is required to achieve hexaamine formation. Similarly, the bis(complexes) $[CuH_xL_2]^{(2+x)+}$ ($0 \le x \le 2$, L = *cis*-dap, *trans*-dap; and $x = 0$, L = *cis*-cptn) all show a characteristic band in their visible spectra with an absorption maximum at 550−570 nm (Table 6). These values are

Table 5. Comparison of protonation (log K_i) and complex formation constants (log β_2) for some selected polyamines

Polyamine[a]	log K_3[b]	H^+ log K_2	log K_1	Cu^{II} log β_2[c]	Ni^{II} logβ_2
Triamines					
cis-dap	2.4	6.3	9.7	17.5	11.2
trans-dap[d]	3.7	6.3	9.6	14.1	–
trap	3.6	7.9	9.6	19.6	17.4
tmca	5.2	6.9	9.3	23.6	25.9
dapi	4.2	7.6	9.5	20.1	21.2
Diamines					
cis-cptn		6.1	9.7	19.8	12.7
trans-cptn[e]		7.2	9.9	15.8	–
cis-chxn		6.3	9.7	20.0	13.8
trans-chxn[e]		6.6	9.8	21.1	14.3
ampy[e]		6.8	10.4	15.0	8.1
en		7.1	9.9	19.6	13.4

[a] Abbreviation of ligands and references: *cis*-dap = *cis*-3,4-diaminopyrrolidine; *trans*-dap = *trans*-diaminopyrrolidine; trap = 1,2,3-propanetriamine;[27] tmca = all-*cis*-2,4,6-trimethoxycyclohexane-1,3,5-triamine;[28] dapi = *cis*-3,5-piperidinediamine;[5] *cis*-cptn = *cis*-cyclopentane-1,2-diamine; *trans*-cptn = *trans*-cyclopentane-1,2-diamine; *cis*-chxn = *cis*-cyclohexane-1,2-diamine;[26] *trans*-chxn = *trans*-cyclohexane-1,2-diamine;[26] ampy = 3-aminopyrrolidine; en = ethane-1,2-diamine[26]. – [b] $K_i = [H_iL] \times [H]^{-1} \times [H_{i-1}L]^{-1}$. – [c] $\beta_2 = [ML_2] \times [M]^{-1} \times [L]^{-2}$. – [d] (3*R*,4*R*) enantiomer. – [e] Racemate.

Table 6. UV/Vis data for Ni^{II}- [$^3A_{2g}$-$^3T_{1g}(F)$ transition] and Cu^{II}-(amine) complexes in aqueous solution (25 °C)

Complex	λ_{max} [nm]	ε
$[Cu(Hcis\text{-dap})]^{3+}$	688	40
$[Cu(cis\text{-dap})_2]^{2+}$	552	86
$[Cu(cis\text{-dap})(Hcis\text{-dap})]^{3+}$	566	69
$[Cu(Hcis\text{-dap})_2]^{4+}$	561	78
$[Cu(trans\text{-dap})_2]^{2+}$	560	140
$[Cu(ampy)]^{2+}$	668	64
$[Cu(ampy)_2]^{2+}$	550	142
$[Cu(cptn)_2]^{2+}$	545	92
$[Ni(cis\text{-dap})_2]^{2+}$	571	8
$[Ni(Hcis\text{-dap})_2]^{4+}$	577	6
$[Ni(cis\text{-dap})_3]^{2+}$	553	10

indicative of a *trans* (square-planar) CuN_4 chromophore with additional loosely bound water molecules at the apices.[14] It is well known that the coordination of an additional *nitrogen* donor in an apical position would lead to a significant red shift (pentaammine effect).[16] The close similarity of the spectral properties of the differently protonated species again indicates that deprotonation at the third nitrogen atom does not result in a significant rearrangement of the chromophore.

(ii) Compared to other tridentate cyclic triamines such as 3,5-diaminopiperidine (dapi) or all-*cis*-2,4,6-trimethoxycyclohexane-1,3,5-triamine (tmca), the formation constants for $[M(cis\text{-dap})_2]^{2+}$ are remarkably low (Table 5). The formation constants of $[M(cis\text{-dap})]^{2+}$ are about one order of magnitude lower than those of $[M(en)]^{2+}$. For the 1:2 complexes, this effect is doubled.

(iii) As a consequence of the Jahn–Teller distortion, triamine ligands that are restricted to a tripodal, facial coordination usually show a characteristic inversion of the Irving–Williams series with higher stability for Ni^{II} than for Cu^{II}. For *cis*-dap, however, no such inversion is observed. As shown in Figure 9, the stabilities of the *cis*-dap complexes fall in the expected range based on the linear free-energy relationship of log β_{Ni} vs. log β_{Cu} for "normal" open-chained polyamines.

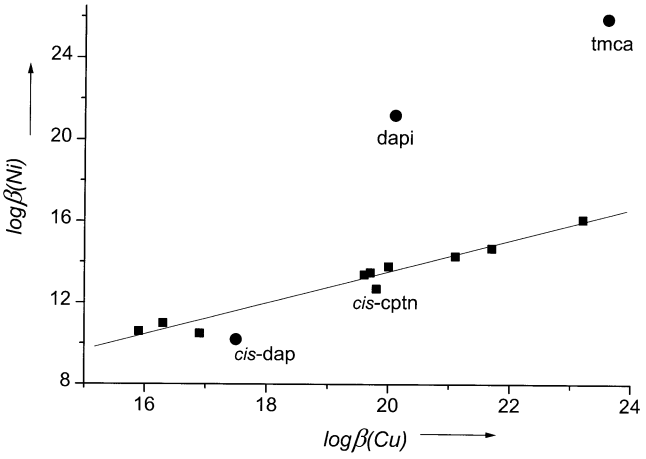

Figure 9. Comparison of formation constants for Cu^{II}- and Ni^{II}(amine) complexes; the linear free-energy relationship (squares) for selected diamines (log β_2), triamines $H_2N-(CH_2)_x-NH-(CH_2)_y-NH_2$ (log β_1), and tetraamines $H_2N-(CH_2)_x-NH-(CH_2)_y-NH-(CH_2)_z-NH_2$ (log β_1) is $\log \beta_{Ni} = 0.77 \times \log \beta_{Cu} - 1.84$; this is compared with log β_2 values of the potentially tripodal ligands *cis*-dap, dapi, and tmca (circles); the data are from refs.[5,25,27] and from this work (Tables 2 and 3)

(iv) All the *cis*-dap complexes show a pronounced tendency to form protonated species $[M^z(HL)]^{(z+1)+}$, $[M^z(HL)_2]^{(z+2)+}$, and $[M^z(HL)L]^{(z+1)+}$. $[Pt(Hcis\text{-dap})Cl_4]^+$, $[Pd(Hcis\text{-dap})_2]^{4+}$, and $[Cu(Hcis\text{-dap})_2(OH_2)_2]^{4+}$ are representative examples that have been structurally characterized by single-crystal X-ray diffraction analysis. For the divalent metal cations (M = Ni, Cu, Zn, Cd), the pK_a values for deprotonation of the partially protonated complexes fall in the range 7.1–8.1, indicating only a slight decrease in the basicity of *cis*-dap upon coordination. This effect would be incompatible with a significant interaction between the third amino group and the metal cation. It is also noteworthy that the pK_a values of $[Cu(HL)_2]^{4+}$ are very similar for L = *cis*-dap and L = *trans*-dap (7.1, 7.7 versus 6.8, 7.5, respectively). The *trans* isomer is even slightly more acidic. Since tridentate coordination of *trans*-dap can be ruled out on steric grounds, the even higher basicity of $[Cu(cis\text{-dap})_2]^{2+}$ would again be inconsistent with a significant interaction between the third nitrogen atom and the metal cation.

The arguments listed as (i)–(iv) clearly show that tridentate coordination of *cis*-dap is not observed in labile solution species. Additionally, monodentate coordination of any of

the studied ligands can also be excluded. Although some of the bis(complexes), particularly $[M(ampy)_2]^{2+}$ (M = Ni, Cu, Cd) and $[Cu(trans\text{-}dap)_2]^{2+}$, show rather low stabilities, their formation constants are still considerably higher than those for monodentate amines such as NH_3 or CH_3NH_2. Moreover, not only *cis*-dap but all the other ligands as well give rise to a visible spectrum for $[CuL_2]^{2+}$ that is indicative of a *trans*-CuN_4 chromophore.

The solid-state structures of $[Pt(Hcis\text{-}dap)Cl_4]^+$, $[Pd(Hcis\text{-}dap)_2]^{4+}$, and $[Cu(Hcis\text{-}dap)_2(OH_2)_2]^{4+}$ reveal exclusive coordination of the metal cation to the two primary amino groups. Although the potentiometric measurements do not of course allow a direct structural assignment, comparison of *cis*-dap with the model diamines provided ample evidence for a similar binding to the exocyclic nitrogen atoms in solution: Metal complexes of ampy are generally less stable than the corresponding *cis*-cptn complexes. Clearly, coordination to the two exocyclic donors is preferred. Molecular mechanics calculations on $[Cu(cis\text{-}dap)(OH_2)_4]^{2+}$ also showed that coordination to the two primary amino groups would be favored by about 9.3 kJ mol^{-1}. For $[Cu(cis\text{-}cptn)]^{2+}$ and $[Cu(ampy)]^{2+}$ the difference in stability ($\Delta\log\beta_1$) is 2.4, corresponding to a difference in free enthalpy of 13.5 kJ mol^{-1}.

Comparison of the metal complex stabilities of the different ligands investigated in this study reveals the order *cis*-cptn > *cis*-dap > *trans*-cptn > ampy > *trans*-dap. Regarding $[Cu(HL)]^{3+}$ formation, the formation constant of the *trans*-dap complex is lowered by about two orders of magnitude compared with that of the *cis*-dap derivative, and for the bis(complexes) $[Cu(HL)_2]^{4+}$, $[Cu(HL)L]^{3+}$, and $[CuL_2]^{2+}$ the decrease in stability is about four orders of magnitude. Similar effects are observed for *trans*-cptn and *cis*-cptn. The *cis*-cyclopentane-1,2-diamine structure is clearly favorable with regard to metal binding. This is in contrast to the cyclohexane-1,2-diamine structure, for which the *trans* isomer has been reported to be more stable.[26] The formation constants of the *cis*-cptn complexes are in close agreement with those reported for the corresponding en complexes. Evidently, the *cis*-cyclopentane-1,2-diamine framework does not provide any stabilization in terms of pre-organization of the donor groups. Again, this is in contrast to the cyclohexanediamines, where significantly increased stability is observed for the *trans*-cyclohexane-1,2-diamine. Since *cis*-cptn and *cis*-dap have related structures, the reduced ability of the latter to bind metal cations must be interpreted in terms of a lower nucleophilicity of the donor groups, caused by the electron-withdrawing effect of the endocyclic nitrogen atom. Consequently, the higher ligand field of *cis*-cptn is able to generate a low-spin electron configuration for $[Ni(cis\text{-}cptn)_2]^{2+}$, whereas $[Ni(cis\text{-}dap)_2]^{2+}$ is high spin. Similar considerations are applicable for the *trans*-cptn and *trans*-dap systems. The observed decrease in metal complex stability in the above series can thus be rationalized in terms of a combination of steric (a) and electronic (b) effects:

(a) For the five-membered ring frame, a steady decrease in metal complex stability is observed for the following geometries: two exocyclic nitrogen atoms in a *cis* arrangement > two exocyclic nitrogen atoms in a *trans* arrangement > one endocyclic and one exocyclic nitrogen atom.

(b) Since all the ligands coordinate in a bidentate fashion, the presence of an additional nitrogen atom reduces the nucleophilicity of the donor groups and, consequently, the triamines are generally weaker ligands than the corresponding diamines.

Although in terms of absolute stability, the metal binding ability of the triamines is lower, the opposite behavior is observed in neutral and acidic solutions. This is based upon the ability of the dap complexes to bind additional protons, which is, of course, not possible for the diamines. In terms of conditional stability,[29] *cis*-dap is a rather efficient complexing agent for Cu^{II} in acidic solution and is clearly superior to any of the known aliphatic or alicyclic diamines. It is in fact a remarkable property of this ligand that it is capable of significant complexation even under acidic conditions, such as at pH = 2.5 (Figure 3).

Structural Aspects of the Metal Complexes

Although the coordination behavior of *cis*-dap in labile complexes must be regarded as being mainly bidentate, in principal a facial tridentate coordination is possible, as exemplified by the inert Co^{III} complex $[Co(cis\text{-}dap)(tach)]^{3+}$. However, the structural parameters for this complex, particularly the long Co−N bonds, clearly reveal a severely strained structure. We were unable to model this particular $Co^{III}N_6$ geometry with a commercially available MM program.[30,31] It seems that a nonharmonic description of the Co^{III}−N bond would be required, which was not implemented by the force field used. In a complex with bidentate coordination, the noncoordinating endocyclic nitrogen atom can either accept a proton or bind to an additional metal center. The first possibility has been discussed extensively for solid-state and solution species in the previous section. Although we do not have any experimental evidence that the latter possibility is realized in aqueous solution, the crystal structure of $[Cu(Hcis\text{-}dap)_2(OH_2)_2](SO_4)_2{\cdot}3.5H_2O - 2x\ H^+ + x\ Cu^{2+}$, with its nonstoichiometric composition ($0.01 \le x \le 0.11$) shows that multiple binding of metal cations to a *cis*-dap molecule is at least possible in the solid state. It is noteworthy that *cis*-dap is structurally related to the open-chained propane-1,2,3-triamine (trap): The trap molecule can be regarded as a substructure of *cis*-dap. However, the open-chained trap is conformationally flexible whereas *cis*-dap is rigid, thus representing a model of the triamine with a locked conformation. Interestingly, the coordination behavior of these two ligands towards Cu^{II} is similar. The ligand trap, by analogy with *cis*-dap, forms similar protonated Cu complexes in acidic solution, and a bridging mode with bidentate and monodentate coordination has been established from the crystal structure of $[Cu(trap)_2]Cl_2$.[27] However, it appears that the locked conformation is not optimal for metal binding: The trap complexes are generally more stable than the corresponding *cis*-dap analogues. Moreover, with other metal cations such as Ni^{II}, the flexibility of trap allows tridentate coordination, which

is not accessible for *cis*-dap. Analogously, the structure of *trans*-dap represents another conformation of trap that is even more disfavored for metal binding.

Another interesting aspect is the comparison of the three cyclic triamine ligands tach, dapi, and *cis*-dap (Scheme 1). The ligand tach shows a very pronounced preference for facial tridentate coordination, giving an adamantane-like structure with all six-membered chelate rings. Attempts to enforce a bidentate coordination mode failed. Reaction with Pt^{II} resulted in oxidation to Pt^{IV} with a concomitant facial coordination of tach.[32] On the other hand, *cis*-dap shows a strong preference for bidentate coordination. A facial, tridentate coordination mode comprising exclusively five-membered chelate rings is severely strained. Such an [M(*cis*-dap)] structure can formally be derived from the [M(tach)] moiety by the removal of one CH_2 and one CH group. The [M(dapi)] structure contains one six-membered and two five-membered chelate rings, in analogy to noradamantane. As a true intermediate in this series, dapi predominantly coordinates in a tridentate mode. However, bidentate coordination is possible, as has been observed for Pd^{II}.[4]

Conclusion

The basic coordination mode of the cyclic triamine *cis*-3,4-diaminopyrrolidine is a bidentate coordination through the two exocyclic amino groups. This mode has been established in a variety of solid-state structures. The potentiometric data and the spectroscopic properties of *cis*-dap complexes have also provided evidence for this coordination mode in aqueous solution. The noncoordinated endocyclic nitrogen atom represents a comparatively strong basic site, and as such it is readily protonated. A facial, tridentate coordination mode results in a highly strained structure, as shown for the inert $[Co(\textit{cis}\text{-dap})(tach)]^{3+}$. The formation of such strained species is not trivial and requires specific synthetic strategies. Alternatively, coordination of *cis*-dap to two different metal cations is possible. In this mode, one metal cation is bound through the primary amino groups, whereas the other is coordinated to the endocyclic nitrogen donor. The coordination behavior of *cis*-dap is in marked contrast to that of other cyclic triamine ligands such as *cis*-3,5-diaminopiperidine or all-*cis*-cyclohexane-1,3,5-triamine, where bidentate coordination or a bridging mode are of minor importance or even unknown.

Experimental Section

Safety Notes: Organic polyazides and perchlorate salts of metal complexes with organic ligands are potentially explosive. The organic polyazides should only be handled in dilute solutions and should not be isolated as pure substances. The perchlorate salts should only be isolated in small quantities and should not be dried at elevated temperatures.

Instrumentation: ^1H and $^{13}C\{^1H\}$ NMR spectra were measured in D_2O, $CDCl_3$, CD_3CN, or [D_6]acetone at 28 °C with a Bruker DRX 500 MHz NMR spectrometer (resonance frequencies: 500.13 MHz for ^1H and 125.9 MHz for $^{13}C\{^1H\}$). Chemical shifts are given relative to [D_4]sodium (trimethylsilyl)propionate (D_2O) or tetramethylsilane (all other solvents) as internal standards ($\delta = 0$). pD values (corrected)[5] were determined with a glass electrode. The ^1H NMR titration experiment on *cis*-dap was performed and evaluated as reported previously for dapi.[5] – UV/Vis spectra of the Ni^{II} complexes were measured with a Uvikon 941 spectrophotometer (H_2O; 25 ± 3 °C). – Cyclic voltammograms were recorded as described previously (BAS C2 cell, BAS 100B/W2 potentiostat, Au working electrode, Pt counter electrode, Ag/AgCl reference electrode, ambient temperature).[5] – C,H,N analyses were performed by H. Feuerhake (Universität des Saarlandes).

Materials: Unless otherwise stated, all chemicals used for the synthetic work were commercially available products of reagent-grade quality. For the potentiometric and spectrophotometric titrations, metal salts of highest available quality (> 99.95%) were used. 3-Pyrroline[33] and (3*S*,4*S*)-1-benzyl-3,4-pyrrolidinediyl bis(methanesulfonate)[34] were prepared as described in the literature. [Co(tach)$(NO_3)_3$] was obtained from [Co(tach)Cl_3].[35] Dowex 50 W-X2 (100–200 mesh, H^+ form) and Dowex 2-X8 (50–100 mesh, Cl^- form) were purchased from Fluka. The anion resin was converted into the OH^- form using dilute aqueous NaOH.[5]

1-Acetyl-3-pyrroline: To an ice-cooled solution of 3-pyrroline (4.00 g, 57.88 mmol) in MeOH (50 mL), acetic anhydride (23.64 g, 231.56 mmol) was added dropwise. The clear solution was then stirred for 30 min at room temperature, cooled in an ice bath once more, and made alkaline with 2 M aq. NaOH. After extraction with dichloromethane (3 × 100 mL), the combined organic phases were dried with Na_2SO_4 and concentrated to dryness. The oily residue was sublimed (10^{-2} mbar, 40 °C) to yield 1-acetyl-3-pyrroline as white crystals (6.07 g, 94%). – C_6H_9NO (111.1): calcd. C 64.84, H 8.16, N 12.60; found C 64.92, H 8.41, N 12.51. – ^1H NMR ($CDCl_3$): $\delta = 2.08$ (s, 3 H), 4.25 (m, 4 H), 5.81 (m, 1 H), 5.88 (m, 1 H). – $^{13}C\{^1H\}$ NMR ($CDCl_3$): $\delta = 22.1$ (CH_3), 52.8 (CH_2), 54.2 (CH_2), 125.0 (CH), 126.5 (CH), 169.1 (C).

1-Acetyl-*cis*-3,4-pyrrolidinediol: 1-Acetyl-3-pyrroline (8.93 g, 80.35 mmol) and 4-methylmorpholine 4-oxide monohydrate (12.99 g, 96.11 mmol) were dissolved in acetone/H_2O (1:1, v/v; 160 mL). A solution of OsO_4 (2.5% in *tert*-butyl alcohol; 1 mL) was added and the pale-yellow solution was stirred for 24 h. $Na_2S_2O_5$ (1.5 g) was then added and the mixture was stirred for a further 1 h. It was then acidified to pH = 2 with 50% H_2SO_4 and extracted with CH_2Cl_2 (3 × 100 mL). The aqueous layer was diluted to a total volume of 1000 mL with H_2O and was sorbed onto Dowex 50 W-X2. The resin was washed with H_2O until neutral and the collected eluent was sorbed onto Dowex 2-X8. This second column was rinsed with H_2O and the neutral eluent was concentrated to dryness yielding the diol as a colorless oil, which solidified after drying in vacuo (10.55 g, 90%). – $C_6H_{11}NO_3$ (145.2): calcd. C 49.65, H 7.64, N 9.65; found C 49.65, H 7.84, N 9.64. – ^1H NMR (D_2O): $\delta = 2.05$ (s, 3 H), 3.36 (dd, $J = 4.5$, 12.5 Hz, 1 H), 3.47 (dd, $J = 5.5$, 11.5 Hz, 1 H), 3.61 (dd, $J = 5.5$, 12.5 Hz, 1 H), 3.78 (dd, $J = 6.0$, 11.0 Hz, 1 H), 4.31 (m, 1 H), 4.35 (m, 1 H). – $^{13}C\{^1H\}$ NMR (D_2O): $\delta = 23.8$ (CH_3), 52.6 (CH_2), 54.2 (CH_2), 72.7 (CH), 73.5 (CH), 176.1 (C).

(3*S,4*R**)-1-Acetyl-3,4-pyrrolidinediyl Bis(methanesulfonate):** 1-Acetyl-*cis*-3,4-pyrrolidinediol (4.00 g, 27.56 mmol) was dissolved in dry pyridine (150 mL) and the resulting solution was cooled to –10 °C (ice/NaCl). Methanesulfonyl chloride (4.67 mL, 60.10 mmol) was added dropwise with stirring. The ice bath was removed and

the mixture was stirred for 1 h at room temperature. The suspension was then poured into Et_2O (1000 mL) and the resulting mixture was left to stand for 2 d at 4 °C. The Et_2O was decanted and the remaining white solid was redissolved in hot acetone (150 mL). This solution was subjected to flash chromatography (silica gel/acetone) and the eluate was concentrated to dryness. Yield 7.50 g (90%) of a white solid. − $C_8H_{15}NO_7S_2$ (301.3): calcd. C 31.89, H 5.02, N 4.65; found C 31.80, H 5.01, N 4.60. − ^{1}H NMR ([D$_6$]acetone): δ = 2.01 (s, 3 H), 3.26 (s, 3 H), 3.27 (s, 3 H), 3.62 (dd, *J* = 5.5, 10.0 Hz, 1 H), 3.74 (dd, *J* = 6.0, 11.0 Hz, 1 H), 3.83 (dd. *J* = 5.0, 10.0 Hz), 4.07 (dd, *J* = 6.0, 11.0 Hz, 1 H), 5.38 (m, 1 H), 5.43 (m, 1 H). − ^{13}C{^{1}H} NMR ([D$_6$]acetone): δ = 21.8 (CH_3), 38.5 (CH_3), 38.6 (CH_3), 48.8 (CH_2), 49.9 (CH_3), 77.1 (CH), 77.3 (CH), 169.4 (C).

1-Acetyl-*cis*-3,4-diaminopyrrolidine: A stirred mixture of (3*S**,4*R**)-1-acetyl-3,4-pyrrolidinediyl bis(methanesulfonate) (7.50 g, 24.89 mmol) and NaN_3 (8.10 g, 124.60 mmol) in dry DMF (200 mL) was heated at 100 °C for 4 h. The white solid formed was filtered off and washed with dry DMF (2 × 50 mL). To the dark-red solution was added 10% Pd/C (500 mg) and the suspension was immediately transferred to an autoclave for hydrogenation. A small sample was extracted from the reaction mixture with Et_2O for NMR characterization of the diazide. This sample was set aside, the Et_2O was evaporated, and the oily residue was redissolved in CD_3CN. − ^{1}H NMR (CD_3CN): δ = 1.91 (s, 3 H), 3.28 (dd, *J* = 5.0, 12.5 Hz, 1 H), 3.38 (dd, *J* = 5.5, 11.0 Hz, 1 H), 3.56 (dd, *J* = 5.0, 12.5 Hz, 1 H), 3.77 (dd, *J* = 6.0, 10.5 Hz, 1 H), 4.38 (m, 1 H), 4.43 (m, 1 H). − ^{13}C{^{1}H} NMR (CD_3CN): δ = 22.2 (CH_3), 49.0 (CH_2), 50.3 (CH_2), 62.0 (CH), 63.0 (CH), 171.6 (C). − The main portion of the reaction mixture was hydrogenated with vigorous stirring (room temp., 4 bar) for 12 h and then the mixture was filtered. The clear filtrate was acidified to pH = 2 with 3 M HCl, diluted to a total volume of 1000 mL with H_2O, and sorbed onto Dowex 50 W-X2. The column was washed with H_2O and 0.5 M HCl. Elution with 3 M HCl gave a yellow fraction, which was concentrated to dryness. ^{1}H NMR spectroscopy indicated mainly the formation of 1-acetyl-*cis*-3,4-diaminopyrrolidine (ca. 95%) besides some *cis*-3,4-diaminopyrrolidine (5.00 g of crude product). − ^{1}H NMR of the main component (D_2O; pD < 2): δ = 2.12 (s, 3 H), 3.74 (dd, *J* = 5.5, 13.0 Hz, 1 H), 3.87 (dd, *J* = 6.0, 12.0 Hz, 1 H), 3.94 (dd, *J* = 6.5, 13.0 Hz, 1 H), 4.16 (dd, *J* = 6.5, 12.0 Hz, 1 H), 4.35 (m, 1 H), 4.40 (m, 1 H); (D_2O; pD > 12): δ = 2.06 (s, 3 H), 3.25 (dd, *J* = 5.0, 12.0 Hz, 1 H), 3.35 (dd, *J* = 6.0, 11.0 Hz, 1 H), 3.47 (m, 1 H), 3.51 (m, 1 H), 3.59 (dd, *J* = 6.5, 12.5 Hz, 1 H), 3.76 (dd, *J* = 6.5, 11.0 Hz, 1 H). − ^{13}C{^{1}H} NMR for 1-acetyl-*cis*-3,4-diaminopyrrolidine (D_2O; pD < 2): δ = 24.1 (CH_3), 49.6 (CH_2), 51.0 (CH_2), 52.4 (CH), 53.3 (CH), 176.1 (C); (D_2O; pD > 12): δ = 23.8 (CH_3), 53.5 (CH_2), 54.6 (CH), 55.2 (CH_2), 55.6 (CH), 175.8 (C).

***cis*-3,4-Diaminopyrrolidine:** The crude 1-acetyl-*cis*-3,4-diaminopyrrolidine (7.40 g) was dissolved in 3 M HCl (150 mL) and the solution was heated to 100 °C for 1 h. It was then diluted to a total volume of 2000 mL with H_2O and sorbed onto Dowex 50 W-X2. The column was eluted with H_2O, 0.5 M HCl, and 3 M HCl. The last fraction was collected and concentrated to dryness. The white solid obtained was redissolved in H_2O (50 mL) and reprecipitated with conc. HCl (100 mL). The product was washed with EtOH and Et_2O and dried in air yielding *cis*-dap·3HCl·H_2O (5.37 g, 69%). − $C_4H_{16}Cl_3N_3O$ (228.5): calcd. C 21.02, H 7.06, N 18.39; found C 20.99, H 6.97, N 18.37. − ^{1}H NMR (D_2O; pD < 2): δ = 3.71 (m, 2 H), 3.99 (m, 2 H), 4.41 (m, 2 H); (D_2O; pD > 12): δ = 2.53 (m, 2 H), 3.11 (m, 2 H), 3.23 (m, 2 H). − ^{13}C{^{1}H} NMR (D_2O; pD < 2): δ = 49.4 (CH_2), 52.5 (CH); (D_2O; pD > 12): δ = 53.9 (CH_2), 56.2 (CH). − Single crystals were grown from an aqueous solution by slow evaporation of the water; *cis*-dap·3HNO_3·H_2O was prepared by deprotonation of *cis*-dap·3HCl·H_2O (1.00 g, 4.38 mmol) on Dowex 2-X8 (OH^- form). The alkaline fraction was concentrated to dryness and the residual oil was redissolved in MeOH (50 mL). The resulting solution was acidified with 3 equiv. of HNO_3 (3 M in H_2O) and left to stand at 4 °C for 14 h. The precipitate obtained was collected by filtration and dried in air. Yield 1.12 g (83%). − $C_4H_{16}N_6O_{10}$ (308.2): calcd. C 15.59, H 5.23, N 27.27; found C 15.71, H 5.26, N 26.95.

[Pd(H*cis*-dap)$_2$](ClO$_4$)$_4$·H$_2$O: A mixture of *cis*-dap·3HCl·H_2O (0.40 g, 1.75 mmol) and $PdCl_2$ (0.16 g, 0.87 mmol) in H_2O (50 mL) was refluxed for 3 h and the clear yellow solution was sorbed onto Dowex 2-X8 (OH^- form). The column was washed with H_2O until a neutral eluent was obtained. The combined alkaline fractions were acidified with 70% $HClO_4$ and the solvents were carefully evaporated under reduced pressure until a volume of 5 mL remained. Conc. $HClO_4$ (5 mL) was added and the solution was set aside at room temperature for 2 d. Slightly yellow crystals precipitated. These were collected by filtration and washed with EtOH and Et_2O (0.52 g, 82%). − $C_8H_{26}Cl_4N_6O_{17}Pd$ (726.6): calcd. C 13.22, H 3.61, N 11.57; found C 13.33, H 3.51, N 11.54. − ^{1}H NMR (D_2O; pD < 2): δ = 3.64 (m, 4 H), 3.82 (m, 4 H), 3.95 (m, 4 H); (D_2O; pD > 12): δ = 3.02 (m, 4 H), 3.28 (m, 4 H), 3.60 (m, 4 H). − ^{13}C{^{1}H} NMR (D_2O; pD < 2): δ = 50.8 (CH_2), 50.9 (CH_2), 62.4 (CH), 62.5 (CH); (D_2O; pD > 12): δ = 52.5 (CH_2), 52.6 (CH_2), 63.9 (CH), 64.0 (CH). − UV/Vis: λ_{max} (ε) = 290 (347). − Crystals were grown by slow evaporation of the water from an aqueous solution of [Pd(H*cis*-dap)$_2$](ClO$_4$)$_4$ that had been acidified with a few drops of $HClO_4$.

[Pt(H*cis*-dap)Cl$_4$]Cl·H$_2$O: *cis*-dap·3HCl·H_2O (250 mg, 1.09 mmol) was dissolved in H_2O (10 mL) and deprotonated using Dowex 2-X8 (OH^- form). The resulting solution was then concentrated to dryness under reduced pressure. The oily residue was redissolved in dry EtOH (5 mL) and this solution was cooled to 0 °C. A solution of H_2PtCl_6·$6H_2O$ (283 mg, 0.55 mmol) in dry EtOH (10 mL) was then added dropwise, which led to the deposition of a yellow precipitate. The suspension was stirred for 2 h at 65 °C. The solid was then collected by filtration, recrystallized from hot H_2O (3 mL) and conc. HCl (20 mL), and washed with EtOH and Et_2O. Yellow powder (150 mg, 55%). − $C_4H_{14}Cl_5N_3OPt$ (492.5): calcd. C 9.75, H 2.87, N 8.53; found C 10.16, H 2.89, N 8.68. − ^{1}H NMR (D_2O; pD < 2): δ = 3.96 (m, 4 H), 4.38 (m, 2 H). − ^{13}C{^{1}H} NMR (D_2O; pD < 2): δ = 48.9 (CH_2), 66.2 (CH).

[Cu(H*cis*-dap)$_2$(OH$_2$)$_2$](SO$_4$)·3.5H$_2$O: *cis*-dap·3HCl·H_2O (250 mg, 1.09 mmol) was dissolved in H_2O (10 mL) and deprotonated using Dowex 2-X8 (OH^- form). The resulting solution was concentrated to dryness under reduced pressure and the oily residue was redissolved in MeOH (50 mL). A solution of $CuSO_4$·$5H_2O$ (272 mg, 1.09 mmol) in H_2O (5 mL) was added, which led to the deposition of a blue precipitate. The suspension was diluted with H_2O (10 mL) and refluxed for 1 h. The insoluble solid was then removed by filtration. MeOH was added dropwise to the deep-blue solution until it became turbid. Single crystals were grown by heating the suspension until the precipitate redissolved and then allowing it to slowly cool to room temperature. − $C_8H_{35}CuN_6O_{13.5}S_2$ (559.1): calcd. C 17.19, H 6.31, N 15.03; found C 17.00, H 6.19, N 14.89.

[Co(*cis*-dap)(tach)]Cl$_3$·1.5H$_2$O: *cis*-dap·3HCl·H_2O (241 mg, 1.05 mmol) was dissolved in H_2O (10 mL) and deprotonated using Dowex 2-X8 (OH^- form). The resulting solution was concentrated to dryness under reduced pressure and the oily residue was redis-

solved in dry MeOH (50 mL). This solution was added dropwise to a purple solution of [Co(tach)$(NO_3)_3$] (3.16 mmol) in dry MeOH. The mixture was refluxed for 14 h and then concentrated to dryness. The brownish residue was suspended in H_2O (30 mL) and the suspension was acidified with 3 M HCl and heated to boiling for a few minutes. Insoluble components were removed by filtration. The orange-red filtrate was diluted to a volume of 500 mL with H_2O and sorbed onto Dowex 50 W-X2. The column was eluted with 0.5 M HCl to give a pink fraction, which was discarded. Further elution with 3 M HCl gave an orange fraction, which was concentrated to dryness. Recrystallization from 6 M HCl yielded 65 mg (14%) of the trichloride salt. – $C_{10}H_{29}CoCl_3N_6O_{1.5}$ (422.7): calcd. C 28.42, H 6.92, N 19.88; found C 28.41, H 6.68, N 19.75. – ^{1}H NMR (D_2O): δ = 1.88 (m, 3 H), 2.14 (m, 3 H), 2.60 (d, J = 11.0 Hz, 2 H), 2.79 (d, J = 11.0 Hz, 2 H), 2.84 (s, 1 H), 3.09 (s, 2 H), 3.78 (s, 2 H). – ^{13}C{^{1}H} NMR: δ = 33.6 (CH_2), 33.7 (CH_2), 42.4 (CH), 42.7 (CH), 59.3 (CH), 62.6 (CH_2). – UV/Vis: λ_{max} (ε) = 351 (142), 475 (102). – CV: E = −210 mV. – Crystals of the chloride tetrachlorozincate salt suitable for X-ray diffraction analysis were grown by layering a solution of [Co(*cis*-dap)(tach)]Cl_3 and $ZnCl_2$ in conc. HCl with EtOH at 4 °C.

***trans*-(3*R*,4*R*)-Diaminopyrrolidine:** A mixture of (3*S*,4*S*)-1-benzyl-3,4-pyrrolidinediyl bis(methanesulfonate) (11.9 g, 34.06 mmol) and NaN_3 (5.2 g, 80.00 mmol) in dry DMF (150 mL) was stirred at 100 °C for 4 h. After cooling to room temperature, the white solid was filtered off and the resulting solution was subjected to hydrogenation in a two-step procedure. (1) Reduction of the diazide: The solution was transferred into an autoclave and hydrogenated for 12 h at 4 bar in the presence of 10% Pd/C (500 mg) under vigorous stirring. The catalyst was removed by filtration. The filtrate was acidified with 3 M HCl and concentrated to dryness. The brownish residue was redissolved in H_2O (250 mL) and sorbed onto Dowex 50 W-X2. The column was washed with H_2O and eluted with HCl (0.5 M, 3.0 M, 6.0 M; 500 mL each). The latter two fractions were combined and concentrated to dryness. (2) Cleavage of the benzyl group: The product was taken up in a mixture of MeOH (100 mL), H_2O (50 mL), and acetic acid (20 mL) and the suspension was again hydrogenated in an autoclave for 12 h at 4 bar in the presence of 10% Pd/C (400 mg). The catalyst was removed and the clear solution was concentrated to dryness. The solid was then suspended in refluxing conc. HCl (100 mL) and small portions of H_2O were added until complete dissolution. After cooling to room temperature, the product was precipitated by adding EtOH (50 mL), collected by filtration, washed with EtOH and Et_2O, and dried in vacuo. White crystals of the composition *trans*-(3*R*,4*R*)-dap·3HCl·0.25H_2O were obtained (3.32 g, 45%). – $C_4H_{14.5}Cl_3N_3O_{0.25}$ (215.0): calcd. C 22.34, H 6.80, N 19.54; found C 22.25, H 6.82, N 19.54. – ^{1}H NMR (D_2O; pD < 2): δ = 3.70 (dd, J = 8.0, 10.0 Hz, 2 H), 4.12 (dd, J = 7.0, 10.0 Hz, 2 H), 4.42 (m, 2 H); (D_2O; pD > 12): δ = 2.53 (dd, J = 5.0, 10.0 Hz, 2 H), 3.02 (m, 2 H), 3.15 (dd, J = 6.0, 10.0 Hz, 2 H). – ^{13}C{^{1}H} NMR (D_2O; pD < 2): δ = 50.0 (CH_2), 54.6 (CH); (D_2O; pD > 12): δ = 54.9 (CH_2), 62.1 (CH). – Single crystals of *trans*-(3*R*,4*R*)-dap·3HCl·0.5H_2O were grown from an aqueous solution by slow evaporation of the water.

(1*S,2*R**)-1,2-Cyclopentanediyl Bis(methanesulfonate):** A solution of *cis*-1,2-cyclopentanediol (2.50 g, 24.48 mmol) in dry pyridine (50 mL) was cooled to 0 °C in an ice/NaCl bath. Methanesulfonyl chloride (3.89 mL, 50.00 mmol) was then added dropwise. A white precipitate appeared. The ice bath was removed and the solution was stirred at room temperature for 1 h and then cooled to 0 °C once more. Excess pyridine was neutralized by the addition of 3 M HCl (200 mL) in small portions whilst stirring. The product precipitated as a white solid, which was collected by filtration, washed with H_2O, and dried in vacuo (5.23 g, 83%). – $C_7H_{14}O_6S_2$ (258.31): calcd. C 32.55, H 5.46; found C 32.42, H 5.31. – ^{1}H NMR ($CDCl_3$): δ = 1.67–1.73 (m, 1 H), 1.98–2.12 (m, 5 H), 3.10 (s, 6 H), 5.00 (m, 2 H). – ^{13}C{^{1}H} NMR ($CDCl_3$): δ = 18.3 (CH_2), 28.4 (CH_2), 38.5 (CH_3), 80.5 (CH).

***cis*-1,2-Diaminocyclopentane:** A mixture of (1*S**,2*R**)-1,2-cyclopentanediyl bis(methanesulfonate) (4.49 g, 17.38 mmol) and NaN_3 (3.40 g, 53.30 mmol) was heated at 100 °C whilst stirring in dry DMF (100 mL) for 4 h and then stirred for an additional 12 h at room temperature. H_2O (100 mL) was then added and the mixture was extracted with Et_2O (4 × 100 mL). The combined ethereal phases were washed with H_2O (100 mL) and dried with Na_2SO_4. A small sample (5 mL) was set aside until the ether evaporated, and the oily residue was dissolved in $CDCl_3$ for NMR characterization of the diazide. – ^{1}H NMR ($CDCl_3$): δ = 1.60–1.68 (m, 1 H), 1.76–1.94 (m, 5 H), 3.80 (m, 2 H). – ^{13}C{^{1}H} NMR ($CDCl_3$): δ = 19.9 (CH_2), 27.9 (CH_2), 64.4 (CH). – The main portion of the ethereal solution was concentrated under reduced pressure to a volume of 200 mL and then diluted with EtOH (150 mL). This solution was transferred to an autoclave and hydrogenated for 26 h at 4 bar under vigorous stirring in the presence of 10% Pd/C (300 mg). The resulting suspension was heated to boiling for a few minutes and the catalyst was removed by filtration. The clear filtrate was concentrated under reduced pressure to a volume of 150 mL. Conc. HCl was added portionwise until the product precipitated (white needles). The solid was collected by filtration, washed with EtOH, and equilibrated in air, yielding *cis*-cptn·2HCl·0.5H_2O (1.57 g; 50% based on the amount of methanesulfonate). – $C_5H_{15}Cl_2N_2O_{0.5}$ (182.1): calcd. C 32.98, H 8.30, N 15.38; found C 33.00, H 8.30, N 15.35. – ^{1}H NMR (D_2O; pD < 2): δ = 1.80–1.93 (m, 3 H), 1.94–2.00 (m, 1 H), 2.23 (m, 2 H), 3.92 (m, 2 H); (D_2O; pD > 12): δ = 1.38 (m, 2 H), 1.52 (m, 1 H), 1.70 (m, 1 H), 1.86 (m, 2 H), 3.07 (m, 2 H). – ^{13}C{^{1}H} NMR (D_2O; pD < 2): δ = 21.7 (CH_2), 29.8 (CH_2), 55.6 (CH); (D_2O; pD > 12): δ = 22.7 (CH_2), 33.7 (CH_2), 57.3 (CH).

[Ni(*cis*-cptn)$_2$](ClO_4)$_2$: *cis*-cptn·2HCl·0.5H_2O (200 mg, 0.99 mmol) was dissolved in H_2O (10 mL) and deprotonated using Dowex 2-X8 (OH^- form). The resulting solution was concentrated to dryness under reduced pressure and the oily residue was redissolved in dry MeOH (100 mL). A solution of $Ni(ClO_4)_2$·6H_2O (183 mg, 0.50 mmol) in dry MeOH (25 mL) was added. The resulting yellow solution was stored at 4 °C for 14 h. Yellow crystals suitable for X-ray diffraction studies precipitated. These were collected by filtration and dried in air (227 mg, 85%). – $C_{10}H_{24}Cl_2N_4NiO_8$ (457.9): calcd. C 26.23, H 5.28, N 12.24; found C 26.24, H 5.26, N 12.21. – UV/Vis: λ_{max} (ε) = 357 (8.8), 444 (8.3), 574 (5.3).

(1*R,2*R**)-1,2-Cyclopentanediyl Bis(methanesulfonate):** Racemic *trans*-1,2-cyclopentanediol (1.86 g, 18.21 mmol) was converted into the bis(methanesulfonate) as described above for the *cis* isomer. Yield 2.71 g (58%). – $C_7H_{14}O_6S_2$ (258.3): calcd. C 32.55, H 5.46; found C 32.46, H 5.19. – ^{1}H NMR ($CDCl_3$): δ = 1.87 (quint, J = 7.0 Hz, 2 H), 1.91–1.97 (m, 2 H), 2.22 (m, 2 H), 3.07 (s, 6 H), 5.08 (m, 2 H). – ^{13}C{^{1}H} NMR ($CDCl_3$): δ = 20.9 (CH_2), 30.5 (CH_2), 38.4 (CH_3), 84.8 (CH).

***trans*-1,2-Diaminocyclopentane:** A mixture of (1*R**,2*R**)-1,2-cyclopentanediyl bis(methanesulfonate) (2.71 g, 10.49 mmol) and NaN_3 (2.05 g, 31.53 mmol) in dry DMF (100 mL) was allowed to react and then hydrogenated as described above for the *cis* isomer. The catalyst was removed by filtration, and the filtrate was acidified

with 3 M HCl and concentrated to dryness. The residue was redissolved in H_2O (1000 mL) and sorbed onto Dowex 50 W-X2. The column was eluted with H_2O and aqueous HCl (0.5 M and 3.0 M; 500 mL each). The last fraction was concentrated to dryness and the residual white solid was dried in vacuo (1.13 g, 62%). − $C_5H_{14}Cl_2N_2$ (173.1): calcd. C 34.70, H 8.15, N 16.18; found C 34.73, H 8.03, N 16.09. − ^{1}H NMR (D_2O; pD < 2): δ = 1.83 (m, 2 H), 1.89 (quint, J = 7.0 Hz, 2 H), 2.32 (m, 2 H), 3.81 (m, 2 H); (D_2O; pD > 12): δ = 1.32 (m, 2 H), 1.64 (quint, J = 8.0 Hz, 2 H), 1.95 (m, 2 H), 2.77 (m, 2 H). − ^{13}C{^{1}H} NMR (D_2O; pD < 2): δ = 24.5 (CH_2), 32.5 (CH_2), 58.0 (CH); (D_2O; pD > 12): δ = 22.8 (CH_2), 34.9 (CH_2), 62.4 (CH).

[Cu(3*R*-ampy)(3*S*-ampy)](ClO$_4$)$_2$: Racemic ampy·2HCl (1.75 g, 11.19 mmol) was dissolved in H_2O (10 mL) and deprotonated using Dowex 2-X8 (OH^- form). The resulting solution was concentrated to dryness under reduced pressure and the oily residue was redissolved in dry EtOH (50 mL). A solution of $Cu(ClO_4)_2·6H_2O$ (1.85 g, 4.99 mmol) in dry EtOH (25 mL) was added dropwise. The blue precipitate was collected by filtration, washed with Et_2O, and dried in air (1.75 g, 81%). − $C_8H_{20}Cl_2CuN_4O_8$ (434.7): calcd. C 22.10, H 4.64, N 12.89; found C 21.76, H 4.56, N 12.81. − UV/Vis: λ_{max} (ε) = 554 (127). − Single crystals were grown by slow cooling of a hot saturated solution of $[Cu(ampy)_2](ClO_4)_2$ in MeOH.

Potentiometric Measurements: Potentiometric titrations were carried out with a Metrohm 713 pH/mV meter and a Metrohm combined glass electrode with an internal Ag/AgCl reference.[5,14] The sample solutions were titrated with 0.1 M or 1.0 M KOH using a Metrohm 665 piston burette. Addition of the titrant and the pH meter reading were controlled using an in-house computer program and a PC. The ionic strength of each 50-mL sample solution was 0.1 mol dm^{-3} KCl, 0.1 mol dm^{-3} KNO_3, or 1.0 mol dm^{-3} KNO_3 and the stability of the electrode was checked by calibration titrations prior to and after each measurement. All titrations were performed at 25.0 °C under nitrogen (scrubbed with an aqueous solution of the inert electrolyte). To determine the pK_a values of the ligands, several alkalimetric titrations were carried out with analytically pure samples of the corresponding hydrochlorides. Test solutions for the titration experiments were prepared using the solid hydrochlorides (*cis*-dap·3HCl, *cis*-cptn·2HCl, *trans*-cptn·2HCl) or a stock solution (ampy·2HCl), standardized aqueous stock solutions of the metal chlorides (Cu, Ni, Zn), or solid $Cd(NO_3)_2·4H_2O$. Complete equilibration was ensured by performing acidimetric back titrations (with 0.1 mol dm^{-3} HCl or 0.1 mol dm^{-3} HNO_3). The data were only considered reliable when no significant hysteresis was observed.

Spectrophotometric Titrations: The titrations were carried out as described in the previous section (50 mL sample solution, 0.01−0.02 mol dm^{-3} total Cu, 1 mol dm^{-3} KNO_3, 25.0 ± 0.1 °C). Additionally, the titration cell was equipped with an immersion probe (HELLMA), which was connected to a diode-array spectrophotometer (J & M, TIDAS-UV/NIR/100−1). An in-house computer program was used to control the addition of the titrant (1 mol dm^{-3} KOH). This program allowed a sample spectrum to be recorded prior to each addition of an aliquot of the titrant.

Calculation of the Equilibrium Constants: All equilibrium constants were calculated as concentration constants and pH was defined as −log [H^+]. The pK_a values of the ligands and the formation constants of the complexes were calculated using the computer program HYPERQUAD.[36] All equilibrium constants were evaluated with fixed values for the total concentrations of the reactants and for pK_w (13.78 for μ = 0.1 mol dm^{-3}, 13.71 for μ = 1.0 mol dm^{-3}).[26] For the refinement of the formation constants of the metal complexes, fixed values were used for the protonation con-

Table 7. Crystallographic data for H$_3$*cis*-dapCl$_3$·H$_2$O and H$_3$*trans*-dapCl$_3$·0.5H$_2$O

Compound	H$_3$*cis*-dapCl$_3$·H$_2$O	H$_3$*trans*-dapCl$_3$·0.5H$_2$O
Empirical formula	$C_4H_{16}Cl_3N_3O$	$C_4H_{14}Cl_3N_3O_{0.5}$
Molecular mass	228.55	218.53
Temperature [K]	293(2)	293(2)
Crystal system	monoclinic	orthorhombic
Space group	$P2_1$	$P2_12_12$
a [Å]	6.3903(7)	12.476(2)
b [Å]	11.4227(13)	12.783(3)
c [Å]	7.4879(9)	6.4860(10)
β [°]	114.969(7)	90.00
V [Å^3]	495.49(10)	1034.4(3)
Z	2	4
$D_{calcd.}$ [g cm^{-3}]	1.532	1.403
μ [mm^{-1}]	0.880	0.837
F[000]	240	456
Crystal size [mm]	0.30 × 0.35 × 0.20	0.50 × 0.45 × 0.35
θ min. and max.	5.51 to 27.50	2.28 to 24.02
Data set	−8/8; −14/14; −9/9	−14/14; −13/13; −7/7
Transmission, min. and max.	not measured	not measured
Total data, unique data	4510, 2261	6274, 1493
Reflections with $I > 2\sigma(I)$	2048	1483
Parameters/restraints	149/9	152
R_1, wR_2 [$I > 2\sigma(I)$]	0.0266, 0.0527	0.0251, 0.0696
R_1, wR_2 (all data)	0.0332, 0.0542	0.0253, 0.0698
Largest peak/hole [e/Å^3]	0.224 and −0.204	0.454 and −0.149
Max. shift/error	0.006	0.005

Table 8. Crystallographic data for $[Pd(H\textit{cis}\text{-dap})_2](ClO_4)_4\cdot 2H_2O$, $[Pt(H\textit{cis}\text{-dap})Cl_4]Cl\cdot H_2O$, $[Co(\textit{cis}\text{-dap})(tach)][ZnCl_4]Cl\cdot C_2H_5OH$, $[Ni(\textit{cis}\text{-cptn})_2](ClO_4)_2$, and $[Cu(ampy)_2](ClO_4)_2$

Compound	$[Pd(H\textit{cis}\text{-dap})_2](ClO_4)_4\cdot 2H_2O$	$[Pt(H\textit{cis}\text{-dap})Cl_4]Cl\cdot H_2O$	$[Co(\textit{cis}\text{-dap})(tach)][ZnCl_4]Cl\cdot EtOH$	$[Ni(\textit{cis}\text{-cptn})_2](ClO_4)_2$	$[Cu(ampy)_2](ClO_4)_2$
Empirical formula	$C_8H_{28}Cl_4N_6O_{18}Pd$	$C_4H_{14}Cl_5N_3OPt$	$C_{12}H_{32}Cl_5CoN_6OZn$	$C_{10}H_{24}Cl_2N_4NiO_8$	$C_8H_{20}Cl_2CuN_4O_8$
Molecular mass	744.56	492.52	577.99	457.94	434.72
Temperature [K]	293(2)	298(2)	233(2)	293(2)	213(2)
Crystal system	monoclinic	orthorhombic	monoclinic	monoclinic	monoclinic
Space group	$P2_1/c$	$Pc2_1b$	$P2_1/c$	$C2/c$	$P2_1$
a [Å]	9.8381(15)	7.984(3)	8.0147(12)	22.450(4)	8.633(3)
b [Å]	12.6413(19)	11.210(3)	18.527(3)	7.605(2)	10.789(3)
c [Å]	9.9609(15)	14.271(5)	15.440(2)	12.016(2)	8.850(4)
β [°]	104.93(3)	90.00	93.5(5)	116.68(3)	110.41(4)
V [Å^3]	1197.0(3)	1277.3(7)	2288.3(6)	1833.1(7)	772.5(5)
Z	2	4	4	4	2
$D_{calcd.}$ [g cm^{-3}]	2.066	2.561	1.678	1.659	1.869
μ [mm^{-1}]	1.317	12.006	2.372	1.395	1.807
F[000]	752	920	1184	952	446
Crystal size [mm]	0.76 × 0.34 × 0.31	0.46 × 0.46 × 0.27	0.46 × 0.10 × 0.10	0.50 × 0.45 × 0.30	0.65 × 0.63 × 0.04
Transm. coeff.	0.4342, 0.6855	0.0139, 0.0578	0.4084, 0.7974	not measured	0.445, 1.000
θ min. and max.	2.14 to 33.08	1.81 to 30.00	1.72 to 28.33	2.86 to 25.82	2.84 to 25.00
Data set	−15/10; −18/15; −14/14	−11/11; −15/15; −20/20	−10/7; −23/24; −20/20	−27/27; −8/8; −14/14	−8/10; −7/12; −8/10
Total data, unique data	12170, 4107	4326, 2260	19108, 5691	6637, 1672	1880, 1587
Reflns. with $I > 2\sigma(I)$	3295	2043	3725	1161	1554
Parameters/restraints	225/2	146/2	343/0	194/0	208/1
R_1, wR_2 [$I > 2\sigma(I)$]	0.0389, 0.1078	0.0419, 0.1088	0.0450, 0.0980	0.0423, 0.0947	0.0375, 0.0933
R_1, wR_2 (all data)	0.0508, 0.1153	0.0465, 0.1127	0.0785, 0.1076	0.0652, 0.1023	0.0386, 0.0940
Max. peak/hole [e/Å^3]	1.308/−0.914	1.998/−2.092	0.829/−1.233	0.430/−0.458	0.571/−0.836
Max. shift/error	0.014	0.000	0.008	0.000	0.000

Table 9. Crystallographic data for $[Cu(H\textit{cis}\text{-dap})_2(OH_2)_2](SO_4)_2\cdot 3.5H_2O - 2x\ H^+ + x\ Cu^{2+}$

Compound	$x < 0.01$	$x = 0.08$	$x = 0.11$
Empirical formula	$C_8H_{35}CuN_6O_{13.5}S_2$	$C_8H_{34.84}Cu_{1.08}N_6O_{13.5}S_2$	$C_8H_{34.78}Cu_{1.11}N_6O_{13.5}S_2$
Molecular mass	559.08	563.99	565.54
Temperature [K]	100(2)	293(2)	293(2)
Crystal system	orthorhombic	orthorhombic	orthorhombic
Space group	*Pccn*	*Pccn*	*Pccn*
a [Å]	24.635(2)	24.670(5)	24.703(5)
b [Å]	13.1027(12)	13.110(3)	13.115(3)
c [Å]	13.4177(12)	13.417(3)	13.479(3)
V [Å^3]	4331.0(7)	4339.4(16)	4366.9(17)
Z	8	8	8
$D_{calcd.}$ [g cm^{-3}]	1.715	1.727	1.720
μ [mm^{-1}]	1.277	1.353	1.366
F[000]	2353	2369	2375
Crystal size [mm]	0.58 × 0.48 × 0.16	0.3 × 0.25 × 0.1	0.25 × 0.20 × 0.10
Transm. coeff.	0.485, 0.753	not measured	not measured
θ min. and max.	1.76 to 33.00	1.65 to 24.02	2.32 to 26.04
Data set	−22/37; −20/19; −20/18	0/28; 0/15; 0/15	−28/29; −16/16; −16/16
Total data, unique data	44850, 8148	3407, 3407	32097, 4157
Reflns. with $I > 2\sigma(I)$	6386	2854	2484
Parameters/restraints	323/61	284/0	284/0
R_1, wR_2 [$I > 2\sigma(I)$]	0.0356, 0.0839	0.0546, 0.1446	0.0694, 0.1164
R_1, wR_2 (all data)	0.0535, 0.0918	0.0662, 0.1567	0.1325, 0.1514
Max. peak/hole [e/Å^3]	1.578/−0.371	0.603/−1.508	0.810/−0.464
Max. shift/error	0.001	0.000	0.000

stants of the ligands, as obtained from the pK_a determinations. The spectrophotometric measurements were evaluated using the computer program SPECFIT.[37,38] The spectrum of free Cu^{2+} was measured separately and was not refined. The free ligands and their protonation products were considered as colorless.

Crystal Structure Determination:[39] X-ray diffraction data were collected with the following diffractometers: STOE IPDS [protonated ligands, Ni complex, Cu(*cis*-dap) complexes with $x = 0.08$, 0.11], STOE STADI-4 (Pt complex), Nonius Kappa-CCD [Cu(*cis*-dap) complex with $x < 0.01$], Siemens SMART PLATFORM (Co complex, Pd complex), Siemens P4 four-circle diffractometer [Cu(ampy) complex]. The crystallographic data are compiled in Tables 7, 8 and 9. Graphite-monochromated Mo-K_α radiation (λ = 0.71073 Å) was used throughout. Low-temperature measurements at 233(2), 213(2), and 100(2) K were performed on the Co complex, the Cu(ampy) complex, and the Cu(*cis*-dap) complex with $x <$ 0.01, respectively. The data for all the other compounds were collected at ambient temperature. Standard reflections were monitored during the data collections. The standard reflections of the Pt complex and $[Cu(ampy)_2](ClO_4)_2$ decreased by 6.2% and 2%, respectively, during the measurements, and decay corrections were applied accordingly. All data sets were corrected for Lorentz and polarization effects. Absorption corrections were applied to the data for the Cu(*cis*-dap) complex with $x < 0.01$ (face-indexed numerical), the Pt complex (empirical with ψ-scans), the Cu(ampy) complex (empirical with DIFABS), and the Co and Pd complexes (empirical with SADABS). The structure of the Pt complex was solved by the heavy atom method; all other structures were solved by direct methods.[40] All structures were refined by full-matrix least-squares techniques[41] against F^2. One of the SO_4^{2-} counterions of the Cu(*cis*-dap) complex with $x > 0.01$ proved to be disordered. These anions exhibited two split positions for one of the oxygen atoms, which were refined with occupancies of 50% each. Non-hydrogen atoms were refined with anisotropic displacement parameters, except for the disordered oxygen positions (O32A, O32B) of the SO_4^{2-} counterions. In general, the positions of the hydrogen atoms were calculated (riding model with $U_{iso} = 1.2 \times U_{eq}$ of the bonded heavy atom), with the exception of the H_2O hydrogen atoms of H$_3$*trans*-dapCl$_3$·0.5H$_2$O, [Pt(H*cis*-dap)Cl$_4$]Cl·H$_2$O, and the Cu(*cis*-dap) complex with $x = 0.08$ and $x = 0.11$, which were not considered. All other hydrogen atoms of H$_3$*trans*-dapCl$_3$·0.5H$_2$O, all H(−N) and H(−O) hydrogen atoms of H$_3$*cis*-dapCl$_3$·H$_2$O, all hydrogen atoms of the Ni and Pd complexes (including H_2O), and the hydrogen atoms of the cation $[Co(cis\text{-dap})(tach)]^{3+}$, together with the OH hydrogen atom of EtOH, were located and refined with variable isotropic displacement parameters. The H(−N) atoms of the coordinated amino groups of [Pt(H*cis*-dap)Cl$_4$]Cl·H$_2$O were placed in calculated positions and were refined with $U_{iso} = 1.2 \times U_{eq}$. The positions of the hydrogen atoms of the noncoordinating ammonium groups and of all the H_2O molecules of the Cu(*cis*-dap) complex with $x = 0.005$ were located and refined isotropically with common bond lengths (0.775 ± 0.005 Å for H−O and 0.855 ± 0.005 Å for H−N). The small amount of additional Cu in this particular specimen (1.5 eÅ^{-3}, $x < 0.01$) was not considered in the refinement. The structures of H$_3$*cis*-dapCl$_3$·H$_2$O, H$_3$*trans*-dapCl$_3$·0.5H$_2$O, and [Pt(H*cis*-dap)Cl$_4$]Cl·H$_2$O were solved and refined in polar space groups. Their absolute structure parameters were refined to values of −0.03(6), −0.01(9), and −0.041(14), respectively.[42] The structure of $[Cu(ampy)_2](ClO_4)_2$ proved to be a racemic twin.

Molecular Modeling Calculations: Molecular modeling calculations were carried out using the commercially available program MOMEC97.[30]

Acknowledgments

We thank Anton Zaschka, Dr. Anja Zimmer, Dr. Volker Huch, Prof. Dr. Michael Veith (all Saarbrücken) and Dr. Peter Osvath (Melbourne) for valuable help and fruitful suggestions. The structure of $[Cu(cis\text{-cptn})_2](ClO_4)_2$ [18] was solved and refined by Manuela Winter (Bochum). Financial support from the Studienstiftung des Deutschen Volkes (D. K.) and the Fonds der Chemischen Industrie (K. H.) is gratefully acknowledged.

[1] A. E. Martell, R. D. Hancock, *Metal Complexes in Aqueous Solutions*, Plenum Press, New York, **1996**.
[2] P. Chaudhuri, K. Wieghardt, *Prog. Inorg. Chem.* **1987**, *35*, 329.
[3] K. Hegetschweiler, *Chem. Soc. Rev.* **1999**, *28*, 239.
[4] H. Manohar, D. Schwarzenbach, W. Iff, G. Schwarzenbach, *J. Coord. Chem.* **1979**, *8*, 213.
[5] J. W. Pauly, J. Sander, D. Kuppert, M. Winter, G. J. Reiß, F. Zürcher, R. Hoffmann, T. F. Fässler, K. Hegetschweiler, *Chem. Eur. J.* **2000**, *6*, 2830.
[6] H. C. Wormser, *J. Pharm. Sci.* **1969**, *58*, 1038.
[7] D. R. Reddy, E. R. Thornton, *J. Chem. Soc., Chem. Commun.* **1992**, 172.
[8] J. Skarzewski, A. Gupta, *Tetrahedron: Asymmetry* **1997**, *8*, 1861.
[9] D. Cremer, J. A. Pople, *J. Am. Chem. Soc.* **1975**, *97*, 1354.
[10] H. Toftlund, E. Pedersen, *Acta Chem. Scand.* **1972**, *26*, 4019.
[11] G. W. H. Potter, M. W. Coleman, A. M. Monro, *J. Heterocycl. Chem.* **1975**, *12*, 611.
[12] S. Ongeri, D. J. Aitken, H.-P. Husson, *Synth. Commun.* **2000**, *30*, 2593.
[13] D. Kuppert, C. Roth, J. Sander, K. Hegetschweiler, *Z. Kristallogr. NCS* **2001**, *216*, 111.
[14] A. Zimmer, D. Kuppert, T. Weyhermüller, I. Müller, K. Hegetschweiler, *Chem. Eur. J.* **2001**, *7*, 917.
[15] E. Prenesti, P. G. Daniele, M. Prencipe, G. Ostacoli, *Polyhedron* **1999**, *18*, 3233.
[16] J. Bjerrum, B. V. Agarwala, *Acta Chem. Scand., Ser. A* **1980**, *34*, 475.
[17] B. J. Hathaway, *J. Chem. Soc., Dalton Trans.* **1972**, 1196.
[18] A low-quality single-crystal X-ray diffraction study of $[Cu(cis\text{-cptn})_2](ClO_4)_2$ confirmed the square-planar (*trans*) CuN_4 geometry: $P\bar{1}$, a = 5.999(1) Å, b = 7.758(2) Å, c = 9.751(3) Å, α = 81.67(2)°, β = 86.83(3)°, γ = 82.71(2)°, $Z = 1$ for $C_{10}H_{24}Cl_2CuN_4O_8$, $R = 0.089$ for 1138 observed reflections [$I > 2\sigma(I)$] and 116 parameters, $wR_2 = 0.210$ for all 1534 unique reflections. The average Cu−N bond length is 2.00 Å.
[19] A. F. Wells, *Structural Inorganic Chemistry*, 5th ed., Clarendon Press, Oxford, **1984**.
[20] P. Comba, A. F. Sickmüller, *Inorg. Chem.* **1997**, *36*, 4500.
[21] P. Hendry, A. Ludi, *Adv. Inorg. Chem.* **1990**, *35*, 117.
[22] P. D. Newman, M. B. Hursthouse, K. M. Abdul Malik, *J. Chem. Soc., Dalton Trans.* **1999**, 599.
[23] C. J. Andres, P. H. Lee, T. H. Nguyen, A. I. Meyers, *J. Org. Chem.* **1995**, *60*, 3189.
[24] A. Corruble, J.-Y. Valnot, J. Maddaluno, Y. Prigent, D. Davoust, P. Duhamel, *J. Am. Chem. Soc.* **1997**, *119*, 10042.
[25] L. Doms, L. Van den Enden, H. J. Geise, C. Van Alsenoy, *J. Am. Chem. Soc.* **1983**, *105*, 158.
[26] R. M. Smith, A. E. Martell, R. J. Motekaitis, *Critically Selected Stability Constants of Metal Complexes*, NIST Standard Reference Database 46, Version 5.0, USA, **1998**.
[27] A. Zimmer, I. Müller, G. J. Reiß, A. Caneschi, D. Gatteschi, K. Hegetschweiler, *Eur. J. Inorg. Chem.* **1998**, 2079.
[28] M. Weber, D. Kuppert, K. Hegetschweiler, V. Gramlich, *Inorg. Chem.* **1999**, *38*, 859.
[29] A. Ringbom, *J. Chem. Educ.* **1958**, *35*, 282.
[30] P. Comba, T. W. Hambley, N. Okon, G. Lauer, *MOMEC: A*

Molecular Modeling Package for Inorganic Compounds, Heidelberg, **1997**.
[31] P. Comba, A. F. Sickmüller, *Angew. Chem.* **1997**, *109*, 2089; *Angew. Chem. Int. Ed. Engl.* **1997**, *36*, 2006.
[32] J. E. Sarneski, A. T. McPhail, K. D. Onan, L. E. Erickson, C. N. Reilley, *J. Am. Chem. Soc.* **1977**, *99*, 7376.
[33] J. S. Warmus, G. J. Dilley, A. I. Meyers, *J. Org. Chem.* **1993**, *58*, 270.
[34] U. Nagel, E. Kinzel, J. Andrade, G. Perscher, *Chem. Ber.* **1986**, *119*, 3326.
[35] L. Hausherr-Primo, K. Hegetschweiler, H. Rüegger, L. Odier, R. D. Hancock, H. W. Schmalle, V. Gramlich, *J. Chem. Soc., Dalton Trans.* **1994**, 1689.
[36] P. Gans, A. Sabatini, A. Vacca, *Talanta* **1996**, *43*, 1739.
[37] R. A. Binstead, B. Jung, A. D. Zuberbühler, *SPECFIT/32 Version 3.0, Spectrum Software Associates*, Marlborough, MA 01752, USA, **2000**.
[38] H. Gampp, M. Maeder, C. J. Meyer, A. D. Zuberbühler, *Talanta* **1985**, *32*, 95.
[39] Crystallographic data (excluding structure factors) for H_3*cis*-dap$Cl_3[H_2O$, H_3*trans*-dap$Cl_3 \cdot 0.5H_2O$, [Pt(H*cis*-dap)Cl_4]$Cl \cdot H_2O$, [Pd(H*cis*-dap)$_2$]$(ClO_4)_4 \cdot 2H_2O$, [Co(*cis*-dap)(tach)]-[$ZnCl_4$]$Cl \cdot$EtOH, [Cu(ampy)$_2$]$(ClO_4)_2$, and [Cu(H*cis*-dap)$_2(OH_2)_2](SO_4)_2 \cdot 3.5H_2O - 2x\ H^+ + x\ Cu^{2+}$ (x = 0, 0.08, 0.11) have been deposited with the Cambridge Crystallographic Data Centre as supplementary publication nos. CCDC-161100 to -161109. Copies of the data can be obtained free of charge on application to the CCDC, 12 Union Road, Cambridge CB2 1EZ, U.K. [Fax: (internat.) + 44-1223/336-033; E-mail: deposit@ccdc.cam.ac.uk].
[40] G. M. Sheldrick, *SHELXS-97, Program for Crystal Structure Solution*, Göttingen, **1990**.
[41] G. M. Sheldrick, *SHELXL-97, Program for Crystal Structure Refinement*, Göttingen, **1997**.
[42] H. D. Flack, *Acta Crystallogr., Sect. A* **1983**, *39*, 876.
Received May 9, 2001
[I01165]

An ab initio MO Study of the Gas-Phase Reactions 2 $SF_2 \rightarrow FS-SF_3 \rightarrow S=SF_4$ − Molecular Structures, Reaction Enthalpies and Activation Energies[‡]

Yana Steudel,[a] Ralf Steudel,*[b] Ming Wah Wong,[c] and Dieter Lentz[a]

Keywords: Sulfur fluorides / Structures / Reaction mechanisms / Dimerizations / Ab initio calculations / 1,2-Shift / Transition states

High level ab initio MO calculations at the G3(MP2) level of theory were employed to study the molecular structures of SF_2, $FSSF_3$, and SSF_4, as well as the dimerization of gaseous SF_2 to $FSSF_3$ and the isomerization of $FSSF_3$ to SSF_4. The dimerization of SF_2 was calculated to be an exothermic process ($\Delta H°_{298}$ = −77 kJ·mol^{-1}) with an activation enthalpy ($\Delta H^{\neq}_{298}$) of 65 kJ·mol^{-1}. The transition state of the dimerization reaction is characterized by a bridging fluorine atom that undergoes a 1,2-shift, and a weak sulfur-sulfur single bond. The calculated lowest-energy structure of $FSSF_3$ (**2a**) is in excellent agreement with the experimentally derived structure, with the –SF group in an equatorial position of the distorted pseudo-trigonal-bipyramid at the central sulfur atom. A significantly less stable $FSSF_3$ conformer **2b**, 76 kJ·mol^{-1} higher in energy, has the –SF group in an axial position. Unimolecular rearrangement of $FSSF_3$ (**2a**) to the trigonal-bipyramidal SSF_4 (**3**), by a 1,2-fluorine shift (**TS2**), is endothermic by 37 kJ·mol^{-1} and is inhibited by a large activation barrier of 267 kJ·mol^{-1}. SSF_4 is predicted to be an observable species in the gas phase. Calculated infrared spectra of **2a** and **3** are also reported.

Introduction

Sulfur forms at least eight binary fluorides representing all seven oxidation numbers between 0 and +6:[1]

SF_2 SF_4 SF_6 $S=SF_2$ $FS=SF$
$FS-SF_3$ $FS-S-SF_3$ F_5S-SF_5

In addition, preparation of the chain-like difluorotrisulfane (S_3F_2) and difluorotetrasulfane (S_4F_2) have been reported.[2] While SF_4 and SF_6 are industrial products,[3] the other fluorides are too unstable, toxic, and/or reactive for any large scale production and application. However, these compounds are intermediates in the preparation of the higher sulfur fluorides and are therefore of fundamental interest.

Disproportionation reactions are a characteristic feature in the chemistry of all of the above mentioned species except for SF_4, S_2F_{10}, and SF_6. One of the most intriguing disproportionation reactions is the reversible dimerization of SF_2 to form S_2F_4, which was first observed by Seel et al.[4]

$$2\,SF_2 \rightleftarrows FS-SF_3 \quad (1)$$

In this reaction, a sulfur−sulfur bond is formed by combination of two atoms that must be positively charged because of the large difference in electronegativity between fluorine and sulfur. Willner et al. managed to determine the reaction enthalpy [$\Delta H°_{298}(1)$ = 69±2 kJ·mol^{-1}] despite enormous experimental difficulties, and observed that the reaction rate depends on the nature of the walls of the container.[5] The authors also noted that the equilibrium is established only partly because of the irreversible side reaction shown in Equation (2).

$$SF_2 + FS-SF_3 \rightarrow S=SF_2 + SF_4 \quad (2)$$

Subsequently, another side reaction according to Equation (3) was discovered: $FS-S-SF_3$ is formed when SF_2 and $S=SF_2$ are condensed together.[6]

$$SF_2 + S=SF_2 \rightarrow FS-S-SF_3 \quad (3)$$

The structure of SF_2 has been determined by microwave spectroscopy. The internuclear distances were obtained as 158.7 pm and the bond angle as 98.5° (C_{2v} symmetry).[7] SF_2 is rather unstable and can therefore only be studied in dilute vapour or using matrix isolation at low temperature. Because of reactions in Equation (1) and Equation (2), the formation of SF_2 is usually accompanied by S_2F_2 and S_2F_4. The latter compound is a colourless liquid, which is best prepared by fluorination of elemental sulfur or carbonyl sulfide followed by fractional distillation of the product mixture.[8] This reaction primarily yields gaseous SF_2 that dimerizes to S_2F_4 on condensation. The structure of S_2F_4 was investigated by electron diffraction (ED), microwave spectroscopy (MW), and ab initio MO calculations at the HF level.[9] The instability of the compound, the possible existence of several conformers and by-products, and the

[‡] Sulfur Compounds, 217. Presented at the 15th Winter Fluorine Conference, St. Petersburg, Florida, USA, 14−19 January, **2001**. − Part 216: K. Hassenberg, J. Pickardt, R. Steudel, *Organometallics* **2000**, *19*, 5244−5246.

[a] Institut für Chemie, Freie Universität Berlin, 14195 Berlin, Germany
[b] Institut für Chemie, Sekr. C2, Technische Universität Berlin, 10623 Berlin, Germany
Fax: (internat.) +49 (0)30/3142 6519
E-mail: steudel@schwefel.chem.tu-berlin.de
[c] Department of Chemistry, National University of Singapore Kent Ridge, Singapore 119260
Fax: (internat.) +65 7791691
E-mail: chmwmw@nus.edu.sg

 © WILEY-VCH Verlag GmbH, 69451 Weinheim, 2001 1434−1948/01/1010−2543 $ 17.50+.50/0

low symmetry of the molecule resulting in twelve independent geometrical parameters, made the structural analysis using a single experimental method impossible. This molecule was even termed "recalcitrant".[9] The geometry derived from the combination of ED and MW data using force constants computed at HF level is shown in Figure 1.

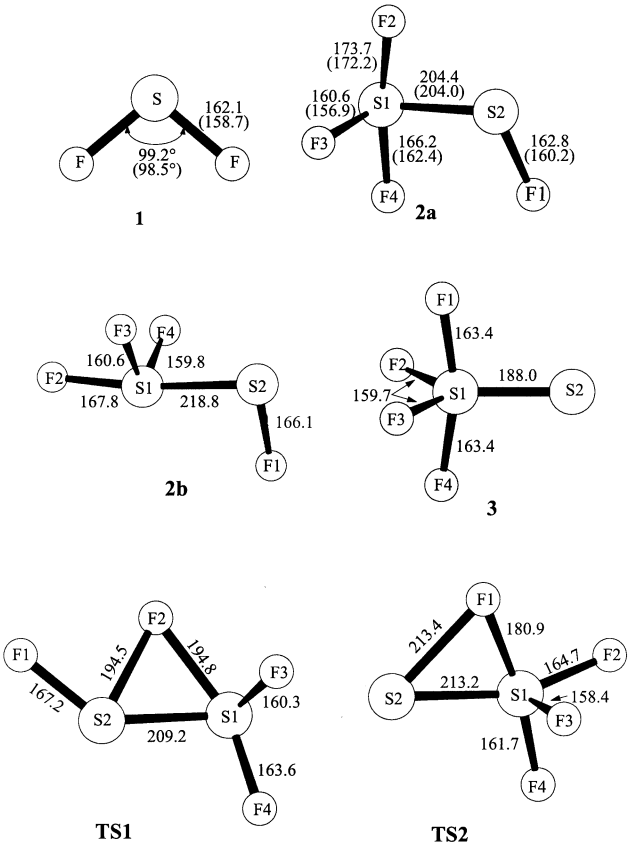

Figure 1. Calculated equilibrium structures of sulfur fluorides SF_2 (**1**), $FSSF_3$ (two conformers, **2a** and **2b**) and SSF_4 (**3**), and the transition states **TS1** and **TS2**. Internuclear distances in pm; experimental values of **1** and **2a** in parentheses. Bond angles and torsion angles are given in Table 1

There are various possible conformations of 1,2-difluorodisulfane-1,1-difluoride ($FSSF_3$). They can be considered as derivatives of the pseudo-trigonal-bipyramidal SF_4 molecule in which one equatorial (*e*) fluorine atom has been substituted by an −SF group. For the gas-phase structure of $FSSF_3$, the F_eSSF torsion angle was determined as 95° and the axial (*a*) F_aSF_a bond angle as 167.0°.[9] The ^{19}F NMR spectrum of liquid $FSSF_3$ recorded at −80° C shows signals for four non-equivalent fluorine atoms.[8] The same holds for gaseous $FSSF_3$ at ambient temperature,[10] in sharp contrast to SF_4 which undergoes rapid pseudo-rotation with an activation enthalpy of only 47 kJ·mol^{-1} at 298 K.[11]

No experimental evidence for the existence of other isomers of S_2F_4, such as $F_2S{=}SF_2$ and $S{=}SF_4$, has so far been reported in the literature. However, these species were investigated by ab initio MO calculations. Oberhammer et al. reported that $S{=}SF_4$ dissociated into SF_4 and S on attempts to optimize its geometry at the HF/3-3-21 level, although the oxygen derivative $O{=}SF_4$ is a well-known compound.[9] The same authors found that the hypothetical molecule $F_2S{=}SF_2$ corresponds to a minimum on the PES, but it lies 440 kJ·mol^{-1} above $FS{-}SF_3$ (HF/3-3-21 level).[9]

In this work, we report high level ab initio MO calculations on the structures and relative stabilities of SF_2, $FS{-}SF_3$, $S{=}SF_4$, and $F_2S{=}SF_2$. In addition, we examine the reaction profiles of the dimerization reaction of SF_2 and the rearrangement $FS{-}SF_3 \rightarrow S{=}SF_4$.

Computational Methods

Standard ab initio MO calculations were performed using the Gaussian 98 series of programs.[12] The energies of various equilibrium structures and transition states were examined using the G3(MP2) level of theory.[13] In brief, the G3(MP2) method is a composite procedure that aims at providing an accurate approximation to the high level of theory at QCISD(T)/GTMP2LARGE//MP2(full)/6-31G(d),

Table 1. Calculated bond angles and torsional angles of SF_2 (**1**), $FSSF_3$ (**2a** and **2b**), SSF_4 (**3**), the transition states (**TS1** and **TS2**), and the experimental data of **2a**

parameter	**2a** (calc)[a]	**2a** (expt)	**2b**[a]	**3** (C_{2v})[a]	**TS1**[a]	**TS2**[a]
α(FSF)	86.7 (F2S1F3)		85.7 (F2S1F3)	85.3 (F1S1F2)	79.7 (F1S2F2)	96.6 (F1S1F2)
	88.6 (F3S1F4)		87.2 (F2S1F4)	106.9 (F2S1F3)	87.0 (F2S1F3)	88.8 (F1S1F3)
	164.9 (F2S1F4)	167.0	101.7 (F3S1F4)	164.2 (F1S1F4)	93.1 (F3S1F4)	170.5 (F1S1F4)
						92.9 (F2S1F4)
						90.4 (F2S1F3)
						91.9 (F3S1F4)
α(FSS)	103.9 (F1S2S1)	105.9	87.1 (F1S2S1)	97.9 (F1S1S2)	137.2 (F1S2S1)	65.0 (F1S1S2)
	74.9 (F2S1S2)	76.0	171.6 (F2S1S2)	126.5 (F2S1S2)	105.1 (F3S1S2)	158.7 (F2S1S2)
	107.4 (F3S1S2)	104.9	86.1 (F3S1S2)		100.4 (F4S1S2)	99.3 (F3S1S2)
	92.8 (F4S2S1)	92.2	92.3 (F4S1S2)			105.5 (F4S1S2)
τ(FSSF)	178.3 (F1SSF2)		173.4 (F1SSF2)		2.4 (F1S2S1F2)	
	96.6 (F1SSF3)		158.5 (F1SSF3)		78.7 (F1S1S2F3)	
	7.3 (F1SSF4)	95±4	-99.9 (F1SSF4)		174.9 (F1S2S1F4)	
					172.5 (F2S1S2F4)	

[a] MP2(full)/6-31G* values (in degrees).

with the incorporation of the zero-point energy and higher level corrections. This level of theory is usually within ± 6 kJ·mol^{-1} of accurate experimental values.[13] Charge density analysis, at the MP2/6-31G* level, was performed using the natural bond orbital (NBO) approach.[14] Unless otherwise noted, all relative energies reported in this publication are given as $\Delta H°_{298}$ and correspond to the G3(MP2) level, while all structural parameters were obtained at the MP2(full)/6-31G* level.

Results and Discussion

Structures and Relative Stabilities

The calculated structures of all investigated molecules are shown in Figure 1, and further geometrical details are given in Table 1.

The experimental structure of SF_2 (**1**) is well reproduced by our calculations, although the calculated sulfur-fluorine distances are slightly shorter than the experimental values (see Figure 1). The sulfur atom bears an atomic charge (NBO) of +1.04 units. In the case of $FS-SF_3$, two conformers were located on the potential energy hypersurface. These conformers can be interconverted by pseudo-rotation, i.e. exchange of one equatorial for one axial ligand. As expected, the more stable isomer (**2a**) has the −SF group in an equatorial position and both axial positions occupied by fluorine as the most electronegative atoms in the molecule. In contrast, the less stable form (**2b**) has one axial position occupied by the −SF group. The total and relative energies of these species are given in Table 2.

Conformer **2a** was predicted to be more stable than **2b** by 76 kJ·mol^{-1}. This finding is in agreement with the observed structure of S_2F_4, which corresponds to **2a**. A comparison of the calculated and experimental structures of **2a** shows an excellent agreement for the SS bond length (within 0.4 pm), while the calculated SF bonds are 1.5−3.8 pm longer than the experimentally derived values. The bond angles agree within 3°. Only one torsional angle was reported for the experimental structure [τ(F3−S−S−F1) = 95±4°], in excellent accord with the calculated value (96.6°). The atoms F1−S−S−F4 are almost coplanar (τ = 7.3°). Interestingly, the S−F4 bond (166.2 pm) is significantly shorter than the other axial bond S−F2 (173.7 pm), although one would expect the opposite trend due to the repulsion between the atoms F4 and F1. Atoms F1 and F2 have a practically ideal *trans* position (τ = 178.3°).

The less stable $FS-SF_3$ conformer **2b** is also of C_1 symmetry, although the structure is just slightly distorted from a C_{2v} symmetry. In comparison with the structure of **2a**, the most remarkable differences are the rather long SS bond (218.8 pm) and the F2−S−S−F1 torsion angle of 173.4°. This places the atom F1 on the same side as one usually expects to find the "axial lone pair" at the sulfur atom in this pseudo-trigonal-bipyramidal geometry (Figure 1). These two structural features are probably the main reasons for the lower stability of **2b**. As in the case of **2a**, the axial SF bond (167.8 pm) of **2b** is longer than the two equatorial bonds (159.8 and 160.6 pm). The higher stability of **2a** compared to **2b** is in line with the valence shell electron pair repulsion (VSEPR) model,[15] which predicts that the conformer with the most electronegative substituents in the *axial* positions of a trigonal bipyramid is the most stable one.

A second isomer of S_2F_4, namely thiothionyltetrafluoride $S=SF_4$ (**3**), has a distorted trigonal-bipyramidal structure of C_{2v} symmetry. This derivative of hexavalent sulfur is 37 kJ·mol^{-1} less stable than **2a**, but surprisingly 39 kJ·mol^{-1} more stable than **2b**. The structure of **3** is very similar to that of the oxygen analogue, thionyltetrafluoride $O=SF_4$.[16] All SF bond lengths and bond angles show normal values. The SS bond length of 188.0 pm may be compared with those in the S_2 molecule (189.2 pm), S=S=O (188.2 pm), $S=SF_2$ (186.0 pm), and FS=SF (188.8 pm), which are considered as double bonds on the basis of their bond strength.[17] It is customary to indicate this strength by the symbol S=S, although it is not claimed that there exists a π bond in addition to the σ bond. In the case of **3**, the relatively short SS bond length may be attributed to the significant π interaction between the *d* orbital of S1 and *p* orbital of S2. The plausible description as a "semipolar" S^+S^- bond is only partly supported by the calculated atomic charges of SSF_4, which are given in Table 3. The NBO atomic charges of the central sulfur atoms (S1) in **2a**, **2b**, and **3** are +1.7, +1.8, and +2.4, respectively, while the terminal sulfur atom of **3** bears a rather small negative charge of −0.3 units. The dipole moment of **3** is 0.14 D, while **2a** has a dipole moment of 0.97 D.

Table 2. Total energies (in Hartrees), zero-point energies (ZPE, in kJ·mol^{-1}), and relative enthalpies (in kJ·mol^{-1}) of the sulfur fluorides SF_2, S_2F_4, SSF_4, and the transition states **TS1** and **TS2**

Species	Total energy[a]	ZPE[b]	$H°_{298} - H°_0$[a]	$\Delta H°_{298}$[a]	$\Delta G°_{298}$[a]
SF_2 (**1**)	−597.21504	13.4	11.3	76.7[c]	23.2[c]
$FS-SF_3$ (**2a**)	−1194.45819	37.8	19.6	0.0	0.0
$FS-SF_3$ (**2b**)	−1194.42973	36.5	20.7	75.8	71.0
$S=SF_4$ (**3**)	−1194.44320	43.7	17.6	37.3	43.4
TS1	−1194.40401	33.2	19.4	142.0	141.9
TS2	−1194.35631	34.6	19.4	267.3	266.0

[a] G3(MP2) level. − [b] HF/6-31G* values. − [c] Data for 2 mol SF_2 with respect to **2a**.

Table 3. Calculated NBO atomic charges and dipole moments (μ, Debyes) of the S_2F_4 isomers **2a**, **2b**, and **3**, and the transition states **TS1** and **TS2**

Atom	$FSSF_3$ (**2a**)	$FSSF_3$ (**2b**)	SSF_4 (**3**)	**TS1**	**TS2**
NBO atomic charges[a]					
S1	+1.68	+1.84	+2.40	+1.52	+2.13
S2	+0.58	+0.32	−0.30	+0.73	+0.07
F1	−0.51	−0.53	−0.55	−0.55	−0.60
F2	−0.64	−0.61	−0.49	−0.64	−0.54
F3	−0.51	−0.52	−0.49	−0.50	−0.50
F4	−0.60	−0.51	−0.55	−0.57	−0.56
dipole moments[a]					
μ	0.97	0.56	0.14	2.43	1.05

[a] MP2/6-31G* level.

In contrast to the earlier findings,[16] we were unable to locate any stable equilibrium structure for the hypothetical isomer $F_2S{=}SF_2$, both on the HF/6-31G* and MP2/6-31G* levels of theory. It collapses to a weakly-bound SF_2 dimer upon geometry optimization (without symmetry constraints). The optimized C_{2h} structure has a short SS distance, but it corresponds to a second-order saddle point on the S_2F_4 potential energy surface.

Reaction Enthalpies and Transition States

As seen in Table 1, the calculated enthalpy of the dimerization reaction of Equation (1) is -77 kJ·mol^{-1}, slightly larger than the experimental value[5] of -69 ± 2 kJ·mol^{-1} which is probably less accurate due to the difficulties mentioned in the Introduction. The dimerization reaction proceeds by an interaction between the positively charged sulfur atom of one molecule and one of the negatively charged fluorine atoms of a neighbouring molecule, while the internuclear SS distance simultaneously decreases. In other words, the process occurs via an SS bond formation and a simultaneous 1,2-fluorine shift, which is readily reflected in the transition state **TS1** (Figure 1): the S1, F2, and S2 atoms form an almost symmetrical (C_{2v}) triangle with SF distances of 194.5 and 194.8 pm and an SS separation of 209.2 pm. The latter value corresponds approximately to a single bond.[17] The F1−S2−S1−F2 atoms are almost coplanar (τ = 2.4°) while the F1−S−S−F3 and F1−S−S−F4 torsion angles are 78.7° and 174.9°, respectively.

The calculated activation enthalpy of 65 kJ·mol^{-1} ($\Delta H^{\neq}_{298}$) for the dimerization of SF_2 suggests that this equilibrium is unlikely to be rapidly established at room temperature (see Figure 2). In fact, it has been observed that the reaction rate depends on the surface of the container,[5] which may act as a catalyst. Since **TS1** has a larger dipole moment (2.43 D; Table 3) than **2a** (0.97 D), polar surface sites may support its formation. The calculated activation enthalpy for the dissociation of $FSSF_3$, i.e. the reverse of reaction of Equation (1), is 142 kJ·mol^{-1}. The observed activation enthalpies $\Delta H^{\neq}_{298}$ (12.5 and 52 kJ·mol^{-1} in two experiments) are much lower, obviously because of the surface catalysis mentioned above.[5]

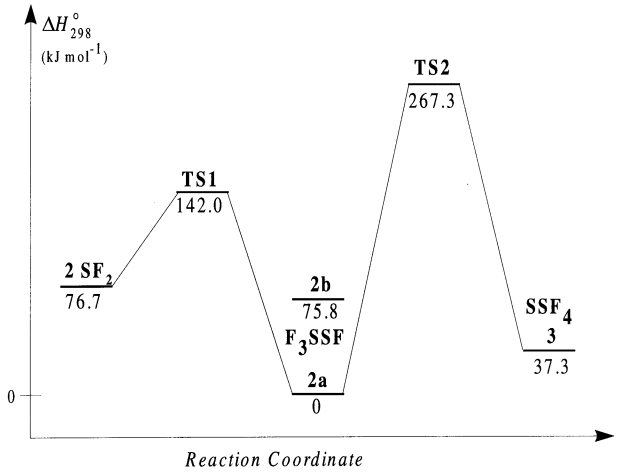

Figure 2. Schematic energy level diagram for the dimerization of SF_2 to $FSSF_3$ (**2a**) via transition state **TS1**, and for the isomerization of $FSSF_3$ (**2a**) to SSF_4 (**3**) via **TS2**. Calculated relative energy of the less stable conformer of $FSSF_3$ (**2b**) is also included

In the industrial production of SF_6 from elemental sulfur and fluorine, which is a highly exothermic process, the formation of SF_2 as an intermediate is very likely. Its exothermic dimerization to $FSSF_3$ explains the formation of the extremely toxic side-product S_2F_{10}; this species has the connectivity $F_5S{-}SF_5$ and is likely to originate from $FS{-}SF_3$ by partial fluorination.

The unimolecular isomerization of $FS{-}SF_3$ (**2a**) to $S{=}SF_4$ (**3**), by a 1,2-fluorine shift via transition state **TS2**, requires an activation enthalpy $\Delta H^{\neq}_{298}$ of 267 kJ·mol^{-1}. This means that **3** is protected by an energy barrier of 230 kJ·mol^{-1} against rearrangement back to **2a** (Figure 2). Thus we predict that species **3** is experimentally accessible, presumably in a matrix isolation experiment. The calculated vibrational wavenumbers of **3** are given below. The structure of the transition state **TS2** for the interconversion of **2a** and **3** (Figure 1) is of C_1 symmetry with a fluorine atom (F1) bridging the SS bond in an asymmetrical manner. This SS bond (213.2 pm) is longer than a typical single bond (205 pm)[17] and the bridging SF distances of 180.9 and 213.4 pm are also significantly longer than SF single bonds (160 pm). The other three SF bonds are of normal single bond lengths.

We have also computed the thermodynamic data of the formation of SSF_2 + SF_4 from SF_2 + $FSSF_3$, i.e. for reaction of Equation (2). The calculated reaction enthalpy is -6 kJ·mol^{-1} ($\Delta H°_{298}$) at the G3(MP2) level.

Harmonic Fundamental Vibrations

The calculated wavenumbers of the harmonic fundamental vibrations of $FSSF_3$ and SSF_4 were calculated at the MP2/6-311+G(2d) level of theory and are given in Table 4 together with the reported infrared absorptions[8] of $FSSF_3$.

Table 4. Fundamental harmonic vibrations [MP2/6-311+G(2d) level] of $FSSF_3$ (**2a**) and SSF_4 (**3**), and observed infrared spectrum of **2a**. Wavenumbers in cm^{-1} and absolute infrared intensities in km mol^{-1} (given in parentheses). Calculated wavenumbers were scaled by 1.05. Notation used: *e* equatorial, *a* axial, *t* terminal, ν stretching (ν_a asymmetric and ν_s symmetric), δ bending, ρ rocking, ω wagging, and τ for torsion

	F_tSSF_3 (C_1)		SSF_4 (C_{2v})	
experiment	calculated	assignment	calculated	assignment
825 vs	829 (198)	$\nu(SF_t)$	a_1: 918 (476)	ν(SS)
805 vs	805 (219)	$\nu(SF_e)$	b_1: 856 (175)	$\nu_a(SF_a)$
675 vs	681 (265)	$\nu(SF_a)$	b_2: 773 (383)	$\nu_a(SF_e)$
620 s	635 (604)	ν(SS)	a_1: 674 (0.6)	$\nu_s(SF_a) + \nu_s(SF_e) + \nu$(SS)
524 m	531 (27)	$\nu(SF_a)$	a_1: 598 (11)	$\nu_s(SF_e) + \nu_s(SF_a) + \nu$(SS)
462 vw	458 (6)	$\delta(F_eSF_a)$	b_2: 547 (18)	$\omega(F_aSF_a)$
412 w	412 (15)	$\delta(F_aSF_e)$	a_2: 536 (0)	$\delta(F_aSF_a) + \delta(F_eSF_e)$
350 w	344 (12)	$\delta(F_aSS)$	a_1: 502 (25)	$\delta(F_eSF_e) + \delta(F_aSF_a)$
	273 (3)	$\delta(F_tSS)$	b_1: 494 (5)	$\omega(F_eSF_e)$
	224 (4)	$\delta(F_aSS)$	b_2: 376 (0.6)	$\rho(F_eSF_e)$
	211 (6)	$\tau(F_tSSF_e)$	b_1: 220 (0)	$\rho(F_aSF_a)$
	136 (0.1)	$\tau(F_tSSF_a)$	a_1: 193 (0.5)	$\delta(F_aSF_a) + \delta(F_eSFF_e)$

The wavenumbers were scaled by a factor of 1.05, which was obtained by a linear least square fit to the experimental wavenumbers listed in the Table 4. There is a very good agreement between observed and calculated wavenumbers and infrared intensities of **2a**. The assignments of several normal modes are only approximate since there is a strong coupling between some fundamentals due to the low symmetry of the molecule. The same holds for the SS stretching mode and the symmetric stretching vibration of the equatorial SF_2 group in SSF_4 (**3**); these two fundamentals belong to the same symmetry class A_1.

Summary

We have shown that the molecular structure of $FSSF_3$ derived from microwave spectroscopy, electron diffraction data, and HF calculations[9] is essentially correct. For the first time, the energy differences between several S_2F_4 isomers were calculated at a high level of theory. The dimerization of SF_2, producing $FSSF_3$, proceeds via a triangular transition state that corresponds to a combination of a new SS bond formation and a 1,2-fluorine shift. The isomerization of $FSSF_3$ to SSF_4 proceeds via a 1,2-fluorine shift. Both reactions are calculated to have rather high activation barriers. With such a high barrier, the hypothetical SSF_4 molecule, which is metastable towards unimolecular rearrangement to the more stable $FSSF_3$, should be an observable species in the gas phase.

Acknowledgments

This work was supported by the Deutsche Forschungsgemeinschaft, the Konrad-Zuse-Zentrum für Informationstechnik Berlin, the Deutscher Akademischer Austauschdienst and the National University of Singapore.

[1] Reviews on sulfur fluorides: [1a] M. Schmidt, W. Siebert, in: *Comprehensive Inorganic Chemistry*, Vol. 2 (Eds.: J. C. Bailar, H. J. Emeléus, R. Nyholm, A. F. Trotman-Dickenson), Pergamon, Oxford, **1973**, p. 795−933. − [1b] F. Seel, *Adv. Inorg. Chem. Radiochem.* **1974**, *16*, 297−333. − [1c] H. L. Roberts, in: *Inorganic Sulfur Chemistry* (Ed.: G. Nickless), Elsevier, Amsterdam, **1968**, p.419. − [1d] S. P. von Halasz, O. Glemser, in: *Sulfur in Organic and Inorganic Chemistry* (Ed.: A. Senning), Vol. 1, Dekker, New York, **1971**, p. 209. − [1e] *Gmelins Handbuch der Anorganischen Chemie, Schwefel B3*, Springer, Berlin, **1963**, p. 1698. − [1f] *Gmelin Handbuch der Anorganischen Chemie, Schwefel, Ergänzungsband 2*, Springer, Berlin, **1978**, p. 3. For F_3SSSF see ref.[6]

[2] [2a] F. Seel, R. Budenz, W. Gombler, H. Seiter, *Z. Anorg. Allg. Chem.* **1971**, *380*, 262. − [2b] K.-P. Wanczek, C. Bliefert, R. Budenz, *Z. Naturforsch., Teil A* **1975**, *30*, 1156.

[3] *Ullmann's Encyclopedia of Industrial Chemistry, Vol. A11*, VCH, Weinheim, **1988**, p. 337.

[4] [4a] F. Seel, R. Budenz, W. Gombler, *Chem. Ber.* **1970**, *103*, 1701. − [4b] F. Seel, R. Budenz, K.-P. Wanczek, *Chem. Ber.* **1970**, *103*, 3946.

[5] W. Gombler, A. Haas, H. Willner, *Z. Anorg. Allg. Chem.* **1980**, *469*, 135−148.

[6] H. Willner, *Z. Anorg. Allg. Chem.* **1984**, *514*, 171−178.

[7] [7a] Y. Endo, S. Saito, E. Hirota, *J. Mol. Spectrosc.* **1979**, *77*, 222. See also: [7b] D. R. Johnson, F. X. Powell, *Science* **1969**, *164*, 950. − [7c] W. H. Kirchhoff, D. R. Johnson, F. X. Powell, *J. Mol. Spectrosc.* **1973**, *48*, 157.

[8] A. Haas, H. Willner, *Z. Anorg. Allg. Chem.* **1980**, *462*, 57−60.

[9] M. V. Carlowitz, H. Oberhammer, H. Willner, J. E. Boggs, *J. Mol. Struct.* **1983**, *100*, 161.

[10] W. Gombler, J. Schaebs, H. Willner, *Inorg. Chem.* **1990**, *29*, 2697−2698.

[11] A. N. Taha, N. S. True, C. B. LeMaster, C. L. LeMaster, S. M. Neugebauer-Crawford, *J. Phys. Chem. A* **2000**, *104*, 3341−3348.

[12] *Gaussian 98 (Revision A.7)*, M. J. Frisch, G. W. Trucks, H. B. Schlegel, G. E. Scuseria, M. A. Robb, J. R. Cheeseman, V. G. Zakrzewski, J. A. Montgomery, R. E. Stratmann, J. C. Burant, S. Dapprich, J. M. Millam, A. D. Daniels, K. N. Kudin, M. C. Strain, O. Farkas, J. Tomasi, V. Barone, M. Cossi, R. Cammi,

B. Mennucci, C. Pomelli, C. Adamo, S. Clifford, J. Ochterski, G. A. Petersson, P. Y. Ayala, Q. Cui, K. Morokuma, D. K. Malick, A. D. Rabuck, K. Raghavachari, J. B. Foresman, J. Cioslowski, J. V. Ortiz, B. B. Stefanov, G. Liu, A. Liashenko, P. Piskorz, I. Komaromi, R. Gomperts, R. L. Martin, D. J. Fox, T. Keith, M. A. Al-Laham, C. Y. Peng, A. Nanayakkara, C. Gonzalez, M. Challacombe, P. M. W. Gill, B. G. Johnson, W. Chen, M. W. Wong, J. L. Andres, M. Head-Gordon, E. S. Replogle, J. A. Pople, Gaussian, Inc., Pittsburgh, PA, **1998**.

[13] L. A. Curtiss, P. C. Redfern, K. Raghavachari, V. Rassolov, J. A. Pople, *J. Chem. Phys.* **1999**, *110*, 4703−4709.

[14] A. E. Reed, L. A. Curtiss, F. Weinhold, *Chem. Rev.* **1988**, *88*, 899.

[15] [15a] R. J. Gillespie, E. A. Robinson, *Angew. Chem.* **1996**, *108*, 539−560; *Angew. Chem. Int. Ed. Engl.* **1996**, *35*, 477−494. − [15b] R. Steudel, *Chemie der Nichtmetalle*, 2. Aufl., deGruyter, Berlin **1998**, p. 74−85.

[16] G. Gundersen, K. Hedberg, *J. Chem. Phys.* **1969**, *68*, 3548.

[17] For a review on the properties of sulfur−sulfur bonds see: R. Steudel, *Angew. Chem.* **1975**, *87*, 683−692; *Angew. Chem. Int. Ed. Engl.* **1975**, *14*, 655−664.

Received March 21, 2001
[I01092]

Molecular and Electronic Structure of (2,2′-Bidipyrrinato)nickel(II) Complexes

Martin Bröring,*[a] Carsten D. Brandt,[a] Johann Lex,[b] Hans-Ulrich Humpf,[c] Jordi Bley-Escrich,[d] and Jean-Paul Gisselbrecht[d]

Keywords: Porphyrinoids / Nitrogen ligands / Nickel / Helical structures / Electrochemistry

Nickel complexes of eight differently substituted 2,2′-bidipyrrins have been prepared and fully characterized. The X-ray analyses of three of these complexes revealed helical chiral molecules. Despite the tetrahedral deviation from the square-planar coordination geometry at the metal centres, all compounds were found to be diamagnetic in nature. For (3,3′,4,4′,8,8′,9,9′-octaethyl-10,10′-dimethyl-6,6′-diphenyl-2,2′-bidipyrrinato)nickel, a separation into the enantiomers by chiral MPLC could be achieved, and the first CD spectra of enantiomerically pure tetrapyrrole helicates are reported. An electrochemical study of the new complexes allowed a first insight into the electronic structure of (2,2′-bidipyrrinato)nickel(II), disclosing a rather high energy HOMO and metal–ligand interaction similar to that observed in metalloporphyrins.

Introduction

2,2′-Bidipyrrins constitute fully conjugated, open-chain tetrapyrroles, which serve as dianionic ligands in coordination compounds. Although known for 40 years, little work was performed towards an understanding of the coordinating properties of 2,2′-bidipyrrins, and their use as ligands has been very limited so far. The first 2,2′-bidipyrrins were obtained by Johnson et al. as the respective palladium(II) complexes by a coupling reaction of α,ω-dibromodipyrrins, using 3% palladium oxide on strontium carbonate as the reagent.[1] Only little later did the first free-base ligands as well as some nickel(II) and copper(II) chelates become accessible through a simple demetalation/remetalation protocol.[2,3] The tendency of the employed metal ions Ni^{II}, Pd^{II}, and Cu^{II} to bind to dianionic tetrapyrrole ligands in a square-planar fashion, and the UV/Vis-spectroscopic features observed led to the assignment of these compounds to the metalloporphyrin-like structure **1**. The first X-ray analysis of a metallobidipyrrin was reported in late 1998 by Dolphin et al.[4] Their study of a zinc complex revealed the M_2L_2 complex **2** and proved that 2,2′-bidipyrrin ligands are well suited for adopting different conformations in coordination compounds (Scheme 1). This behaviour, however, has been found earlier in a small number of other bile-pigment analogue complexes.[5,6] We recently showed, that 2,2′-bidipyrrins are in fact sufficiently flexible to stabilise even cluster fragments.[7]

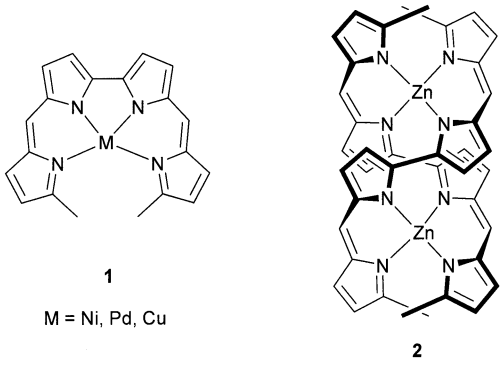

Scheme 1. Known coordination modes of 2,2′-bidipyrrin ligands

Our interest in these ligands arose from the fact, that 2,2′-bidipyrrins contain a dianionic N_4 coordination site, rather than the trianionic one found in most other bile-pigment analogues.[8] In addition to this favourable similarity with the porphyrin ligand, 2,2′-bidipyrrins are easily prepared in substantial amounts,[9] and metal complexes like **1** can be expected to display helical chiral geometries like those of other metalated bilenes.[10–18] As part of our ongoing efforts to establish helical metallo-2,2′-bidipyrrins as chiral analogues of catalytically active metalloporphyrins,[19] the determination of chirality in these complexes and investigations towards the stability of the anticipated, but never proven helical arrangement are of vital importance. This paper reports molecular and electronic features of a set of eight (2,2′-bidipyrrinato)nickel complexes **11–18** with different substituents in the *meso* positions.

Results and Discussion

Synthesis and Characterization

The syntheses of (2,2′-bidipyrrinato)nickel complexes was achieved by stirring a solution of the respective ligands

[a] Institut für Anorganische Chemie, Universität Würzburg, Am Hubland, 97074 Würzburg, Germany
E-mail: martin.broering@mail.uni-wuerzburg.de
[b] Institut für Organische Chemie, Universität Köln, Greinstraße 4, 50939 Köln, Germany
[c] Institut für Pharmazie und Lebensmittelchemie, Universität Würzburg, Am Hubland, 97074 Würzburg, Germany
[d] UMR 7512 C.N.R.S., Université Louis Pasteur, 4 rue Blaise Pascal, 67000 Strasbourg, France

 © WILEY-VCH Verlag GmbH, 69451 Weinheim, 2001 1434–1948/01/1010–2549 $ 17.50+.50/0

3−10 [9] and excess nickel(II) acetate tetrahydrate in a 1:1 mixture of dichloromethane and methanol at ambient temperature for 30 min (Scheme 2). Following extractive workup and recrystallization from dichloromethane/methanol, the pure chelates **11−18** are obtained in good to excellent yields (86−94%).

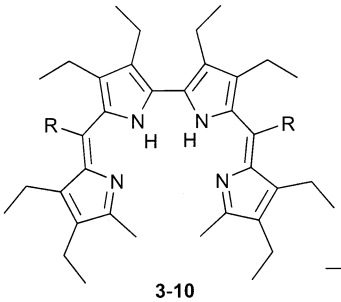

R	free base	Ni complex
H	3	11
p-$H_3COC_6H_4$	4	12
p-$H_3CC_6H_4$	5	13
Ph	6	14
p-ClC_6H_4	7	15
Ph/*p*-$O_2NC_6H_4$	8	16
p-NCC_6H_4	9	17
p-$O_2NC_6H_4$	10	18

Scheme 2. Synthesis of (2,2′-bidipyrrinato)nickel(II) complexes **11−18**

All compounds gave satisfactory elemental analyses and were further characterized by mass spectra (see Exp. Sect.). The ^{1}H-NMR-spectroscopic investigation of **12−18** revealed unsymmetric aryl groups as shown for the dinitro derivative **18** (Figure 1), in that the AA′BB′ system of the respective protons of the free-base ligand is split into four distinct groups of signals for the nickel complex. This observation can be interpreted in terms of a helical conformation of the new complexes. An accompanying diastereotopic splitting of the ethyl CH_2 groups, however, could not be detected, since the steric overcrowding of substituents in the periphery leads to hindered rotation with concomitant line broadening. This line broadening is so severe in the ^{13}C NMR spectra, that only incomplete sets of signals could be detected for **12−18**. Despite a tetrahedral distortion from the square-planar environment of the nickel(II) centre, all the complexes **11−18** are found to be low-spin and therefore are diamagnetic in nature. This finding is further supported by the result of variable-temperature NMR-spectroscopic studies conducted on **13**, showing sharp signals for all alkyl groups above 80 °C.

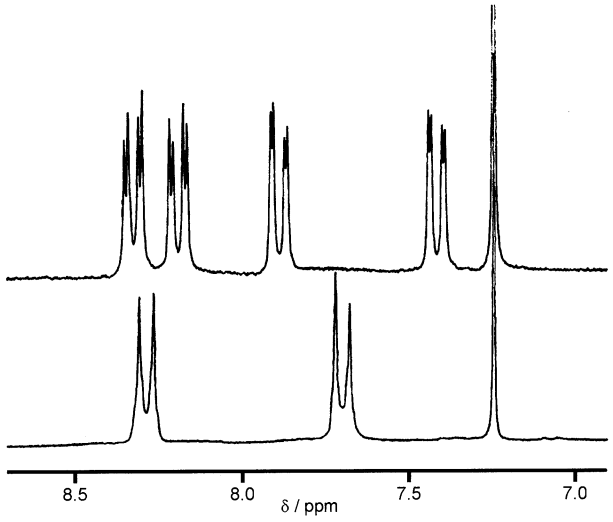

Figure 1. Aromatic regions of the ^{1}H NMR spectra of **10** (bottom) and **18** (top; 200 MHz, $CDCl_3$)

The fact, that the signal of the *meso* protons in **11** is detected $\Delta\delta = 0.62$ upfield with respect to the free base **3**, parallels the observations made in the porphyrin series ($\Delta\delta = 0.41$ for octaethylporphyrin and the respective nickel complex)[20] and gives a first indication, that the metal−ligand interactions are of a similar type in both cases. In agreement with this, the UV/Vis spectra of **11−18** and (porphyrinato)nickel complexes[21] show a somewhat related pattern with strong absorptions at 430 nm and several small ones between 500 and 900 nm (see Exp. Sect.). The red shift observed for **11−18** with respect to (porphyrinato)nickel complexes might be explained either in terms of a strained, nonplanar structure like in dodecasubstituted porphyrins,[22] and/or in a loss of symmetry, a scenario precedented by the absorption patterns of chlorins and bacteriochlorins.[23,24]

X-ray Analyses

The complexes **11**, **14**, and **16** were analysed by X-ray diffraction (Table 1). Crystals were grown in all cases by slow concentration of dichloromethane/*n*-hexane solutions. The pronounced helical structure of (2,2′-bidipyrrinato)-nickel complexes, which was already concluded from the NMR spectra, is the most striking feature of these complexes (**11**: Figure 2; **14**: Figure 3; **16**: Figure 4). The overlapping terminal methyl groups are located as close as 3.34 Å (**11**), 3.15 Å (**14**), and 3.66 Å (**16**) above each other, accounting for a certain degree of strain in these subunits. This strain has to be overcome by strong metal−nitrogen bonds. If the metal−nitrogen bonds are weak, the ligand will rather bind in an open, nonstrained fashion, as was demonstrated recently by Dolphin et al. on zinc complex **2**.[4]

The Ni−N bond lengths are also indicative of this strain, in that the nitrogen donors from the bipyrrolic units are bound more tightly [**11**: 1.8451(15) and 1.8498(14) Å; **14**:

Table 1. Selected bond lengths, distances [Å] and angles [°] for **11**, **14**, and **16**

	11	**14**	**16**
Ni−N(1)	1.9088(15)	1.889(2)	1.865(3)
Ni−N(2)	1.8451(15)	1.834(2)	1.840(3)
Ni−N(3)	1.8498(14)	1.834(2)	1.835(3)
Ni−N(4)	1.9068(15)	1.885(2)	1.893(3)
N(1)−C(1)	1.341(2)	1.342(3)	1.344(4)
N(1)−C(4)	1.409(2)	1.421(3)	1.431(5)
N(2)−C(6)	1.371(2)	1.374(3)	1.365(5)
N(2)−C(9)	1.349(2)	1.361(3)	1.362(4)
N(3)−C(10)	1.353(2)	1.356(3)	1.365(4)
N(3)−C(13)	1.373(2)	1.375(3)	1.362(5)
N(4)−C(15)	1.409(2)	1.418(3)	1.391(5)
N(4)−C(18)	1.340(2)	1.340(3)	1.350(4)
C(1)−C(2)	1.432(3)	1.424(4)	1.423(5)
C(2)−C(3)	1.372(3)	1.370(4)	1.399(5)
C(3)−C(4)	1.432(3)	1.461(4)	1.446(5)
C(4)−C(5)	1.380(3)	1.393(4)	1.413(5)
C(5)−C(6)	1.391(3)	1.419(4)	1.417(5)
C(6)−C(7)	1.426(3)	1.434(4)	1.433(4)
C(7)−C(8)	1.386(3)	1.393(4)	1.387(5)
C(8)−C(9)	1.428(3)	1.416(4)	1.423(5)
C(9)−C(10)	1.457(3)	1.456(4)	1.455(5)
C(10)−C(11)	1.425(3)	1.415(4)	1.412(5)
C(11)−C(12)	1.382(3)	1.395(4)	1.398(5)
C(12)−C(13)	1.430(3)	1.445(4)	1.444(4)
C(13)−C(14)	1.386(3)	1.417(4)	1.436(4)
C(14)−C(15)	1.383(3)	1.391(4)	1.410(5)
C(15)−C(16)	1.435(3)	1.454(4)	1.463(4)
C(16)−C(17)	1.365(3)	1.381(4)	1.360(5)
C(17)−C(18)	1.427(3)	1.426(4)	1.437(5)
$C_{term}\cdots C_{term}$	3.34	3.15	3.66
N(1)−Ni−N(2)	90.39(7)	90.03(10)	90.68(13)
N(1)−Ni−N(3)	161.72(7)	163.81(10)	164.77(13)
N(1)−Ni−N(4)	101.76(7)	100.67(10)	100.11(12)
N(2)−Ni−N(3)	80.72(7)	83.03(10)	83.03(13)
N(2)−Ni−N(4)	163.08(7)	164.10(10)	162.37(13)
N(3)−Ni−N(4)	90.55(6)	89.37(10)	89.53(12)
N(2)−C(9)−C(10)	109.57(15)	110.8(2)	111.2(3)
N(3)−C(10)−C(9)	109.99(15)	111.0(2)	110.6(3)
C(4)−C(5)−C(6)	125.45(18)	124.3(2)	124.5(4)
C(13)−C(14)−C(15)	125.33(17)	124.0(3)	123.2(3)

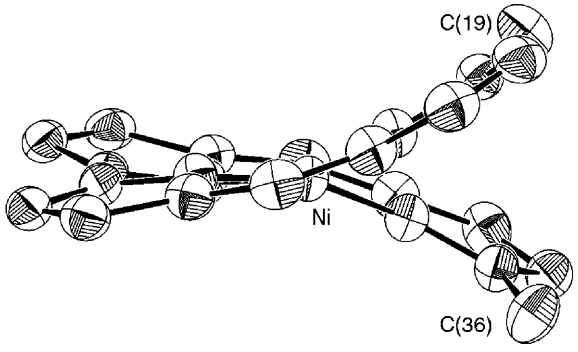

Figure 2. ORTEP plot of the molecular structure of **11** (side view)

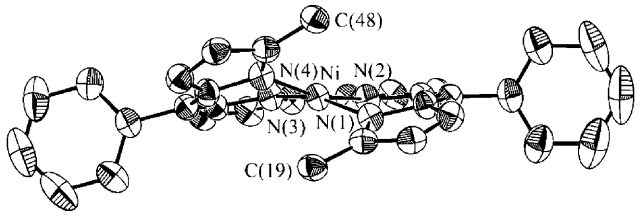

Figure 3. ORTEP plot of the molecular structure of **14** (front view)

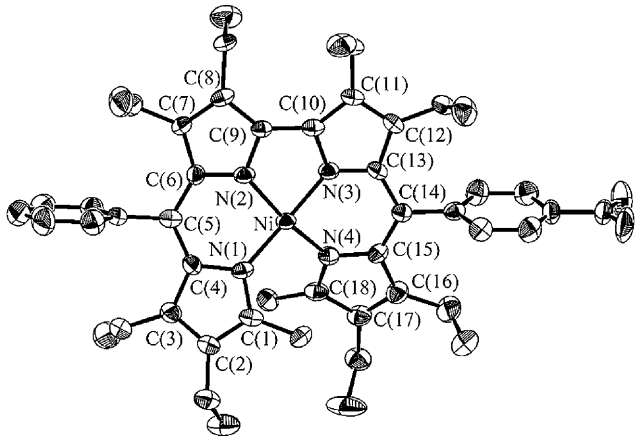

Figure 4. ORTEP plot of the molecular structure of **16** (top view)

1.834(2) and 1.834(2) Å; **16**: 1.835(3) and 1.840(3) Å] than those of the terminal C_4N rings [**11**: 1.9068(15) and 1.9088(15) Å; **14**: 1.885(2) and 1.889(2) Å; **16**: 1.865(3) and 1.893(3) Å]. All these bond lengths are shorter than those found for (porphyrinato)nickel complexes (1.90−1.96 Å), but still normal for low-spin Ni^{II}−N bonds. As a consequence of the helical ligand geometry the nickel coordination spheres show a tetrahedral distortion from planarity [angle between the planes {N(2),N(3),Ni} and {N(1),N(4),Ni} for **11**: 19.9°; for **14**: 18.8°; for **16**: 19.7°].

The steric influence of the additional peripheral aryl substituents in **14** and **16** results in reduced $C_\alpha-C_{meso}-C_\alpha$ angles [for **11**: 125.45(18)° and 125.33(17)°; for **14**: 124.3(2)° and 124.0(3)°; for **16**: 124.5(4)° and 123.2(3)°], and therefore induces a more pronounced overlap of the terminal methyl groups. Due to the open-chain character of 2,2′-bidipyrrins, the ligand framework appears to be sufficiently flexible to overcome steric encumbrance by *in-plane* distortions, and does not parallel the *out-of-plane* twisting modes, which are characteristic for dodecasubstituted porphyrins and their metal chelates.[22] The perpendicular arrangement of the aryl groups in **14** and **16** inhibits a strong electronic communication between the π-systems of the aryl rings and the tetrapyrrole moiety, so that only a small influence of the different substituents of **12**−**18** on the metal centre may be expected. Therefore, the rather distorted framework of the unsymmetrically substituted complex **16** should be addressed to crystal packing effects rather than to the electronic influence of the additional NO_2 functionality.

It is a typical bond-length characteristic of metalloporphyrins, that the $C_\beta-C_\beta$ bonds within the five-membered rings are shorter than the respective $C_\alpha-C_\beta$ bonds.[25,26] This very same characteristic can be claimed for the (bidipyrrinato)nickel complexes **11**, **14**, and **16**, accounting for a large degree of π-electron delocalization within these compounds. In contrast to this similarity, the $C_\alpha-N-C_\alpha$ moieties of the terminal C_4N rings are found to be non-symmetric (**11**: 1.34 Å/1.41 Å; **14**: 1.34 Å/1.42 Å; **16**: 1.34 and 1.35

Å/1.39 and 1.43 Å) and indicate a partial azafulvene character in these substructures.

Enantioseparation of 14

Although the helical chirality of bile-pigment analogue complexes was recognized early in the history of this branch of porphyrin chemistry, no enantiomerically pure compound has hitherto been published. In one instance, Smith and co-workers conducted an NMR-spectroscopic study on a (*meso*-oxobiladienato)nickel(II) complex bearing diastereotopic side chains, and reported a high racemisation barrier of at least 80 kJ mol^{-1}.[27,28] In a different approach, Mizutani et al. attempted to use the helicity of a zinc complex of a biliverdin derivative for the diastereoselective binding of amino acids and found, that upon addition of enantiomerically pure amines one of the helicates builds up, which is in accordance with a rather low helix inversion barrier.[29−31] Since the literature was not conclusive about the stability of the helical coordination geometry of open-chain metallotetrapyrroles we decided to separate (2,2′-bidipyrrinato)nickel complexes into the enantiomers and study them independently.

Our initial attempts to separate the isomers of **11**−**18** on an analytical Pirkle column disclosed that this is in fact possible for all aryl-substituted derivatives **12**−**18**, but not for **11**. Obviously, the interaction of the aryl moieties with the chiral stationary phase is the key to separation. Compound **14** showed the most promising solubility properties of the compounds studied and was therefore chosen for a preparative separation. Using a Pirkle column and 2% acetone in *n*-hexane as the mobile phase, an 85% enrichment was achieved; due to the rather low solubility, however, only 1.3 mg of material could be resolved at a time. Enantiopure complexes were obtained by fractionated crystallisation of the enriched material collected from several runs with dichloromethane/*n*-hexane, from which the racemate crystallises more readily. The optical purity of the helicates was proven by analytical chiral MPLC to be $> 97\%$.

The CD spectra of **14′** and **14′′**, recorded in dichloromethane ($c \approx 10^{-5}$ M), show a pattern similar to that known for biliverdin and its derivatives (Figure 5).[32,33] From the sign of the Cotton effect of the major band at 432 nm, the first eluted enantiomer **14′** can be assigned the *M* helical, and the other, **14′′**, the *P* helical isomer. This assignment is further supported by the recent findings by Vogel et al., who reported the same relationship between the sign of the Cotton effect and the helicity of the ligand for a (cyclooctaphyrinato)dipalladium.[34] The fact, that the maxima of the major CD and UV/Vis absorptions are found at the same wavelength (432 nm), is indicative of a strong electronic coupling, i.e. π-conjugation of both dipyrrin units in **14**, and is also found for biliverdin and other one-chromophore systems. For bilirubin-like tetrapyrroles, on the other hand, in which the dipyrrolic subunits are separated electronically by a CH_2 bridge, the two-chromophore arrangement leads to a bisignate CD signal within the major UV/Vis absorption, caused by exiton coupling of the independent subchromophores.[35,36]

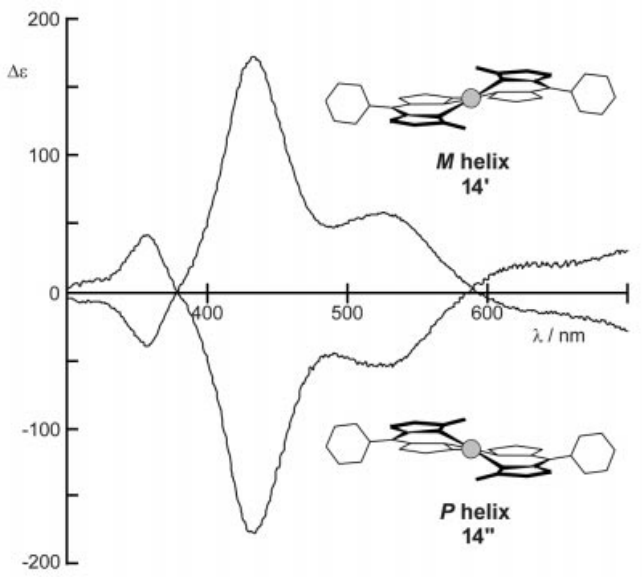

Figure 5. CD spectra of **14′** and **14′′** (CH_2Cl_2, $c \approx 10^{-5}$ M, 1 cm cell)

The stability of **14′** towards helix inversion was studied by prolonged heating of the complex in different solvents and determining the degree of racemisation by analytical chiral MPLC. Astonishingly, racemization was not ob-

Table 2. Electrochemical data for **3** and nickel complexes **11**−**18**

Compound (R)[a]	Red.2	Red.1	p-$O_2NC_6H_4$[b]	Ox.1	Ox.2	HLG[c]	2σ≅[d]
3	n.d.[e]	−1.82		−0.02	0.37	1.80	
11	−2.35	−1.71		−0.18	0.31	1.53	
12 (p-$MeOC_6H_4$)	−2.40	−1.77		−0.16	0.33	1.61	−0.536
13 (p-MeC_6H_4)	−2.40	−1.76		−0.15	0.35	1.61	−0.340
14 (Ph)	−2.36	−1.75		−0.13	0.36	1.62	0
15 (p-ClC_6H_4)	−2.30	−1.69		−0.10	0.38	1.59	0.454
16 (Ph/p-$O_2NC_6H_4$)	n.d.	−1.71	−1.44	−0.08	0.40	1.63	0.778
17 (p-NCC_6H_4)	−2.14[f]	−1.63		−0.07	0.41	1.56	1.32
18 (p-$O_2NC_6H_4$)	n.d.	−1.63	−1.46	−0.05	0.44	1.58	1.556

[a] Measured on a platinum electrode in PhCN solution with 0.1 M nBu_4NPF_6. Values are given in V relative to the Fc/Fc^+ couple. − [b] Reversible two-electron reduction of the nitrophenyl substituents. − [c] HOMO−LUMO gap (= $E_{Ox.1} - E_{Red.1}$). − [d] σ values taken from ref.[37] − [e] n.d. = not determined. − [f] Quasi-reversible electron transfer.

served in any instance, and even after 14 h in molten naphthalene at 218 °C only the starting enantiomer could be detected. This result is in accordance with the one reported earlier by Smith and co-workers.[27,28] Despite the fact, that the small size of the low-spin d^8-nickel(II) ion and its strong binding to the ligand certainly supports the helix to a large extent, this extreme resistance against inversion processes suggests, that other metallo-2,2′-bidipyrrins will behave in a similar fashion.

Electrochemistry

In order to gain insight into the electronic structure of (bidipyrrinato)nickel complexes an electrochemical investigation was undertaken on the complexes **11**−**18**. Table 2 summarises the conditions and observed redox potentials for these as well as for the free-base ligand **3**.

All metallated compounds gave well-defined CVs, in which they undergo two reversible one-electron oxidations at rather low potentials. In reduction, the first step is reversible and well resolved (with exception of the nitrophenyl-substituted derivatives **16** and **18**), whereas the second step occurs close to the electrolytic discharge. The nitrophenyl derivatives **16** and **18** display a specific redox behaviour. The waves at −1.44 V (**16**) and −1.46 V (**18**) vs. Fc/Fc^+ involve one and two electrons, respectively, and correspond to the reduction of the nitrophenyl units, which act as independent redox centres. As no data on the redox behaviour of porphyrins bearing nitrophenyl substituents on the *meso* positions could be found in the literature, 4,4′-dinitrobiphenyl was used as a reference. This compound showed a similar two-electron wave at −1.49 V. The redox characteristics of the free-base ligand **3** obviously deviate severely from those of the metallated species (Table 2). This behaviour is most probably due to the open conformation of **3**.

When plotting the redox potentials of **12**−**18** versus the Hammett constants of the phenyl substituents σ, straight lines were obtained in agreement with the previously reported potential evolution for different tetraarylporphyrins (Figure 6). In our case, the observed slopes were equal to 52 and 47 mV for the first and second oxidation, respectively, whereas the slope for the first reduction equals 71 mV. These values also parallel the above-mentioned findings in the porphyrin series.[37] This linear evolution of the redox potentials with the substituents is a good indication of ligand-centred electron transfers as metal-centred electron transfers are less sensitive to substituent effects. Further spectroelectrochemical and EPR studies towards the electronic structure of one- and two-electron-oxidized (2,2′-bidipyrrinato)nickel(II) complexes are currently under investigation.

Comparing the electrochemical behaviour of **11** (NiOEBDP) and (octaethylporphyrinato)nickel(II) (NiOEP), a striking similarity appears in the LUMO energy levels of both compounds, while the HOMO of **11** is raised by 0.58 V with respect to NiOEP. The difference thus occurring in the HOMO−LUMO gaps of these complexes (Figure 7) corresponds qualitatively with the UV/Vis-spectroscopic observation, that the maximum of the longest-wavelength

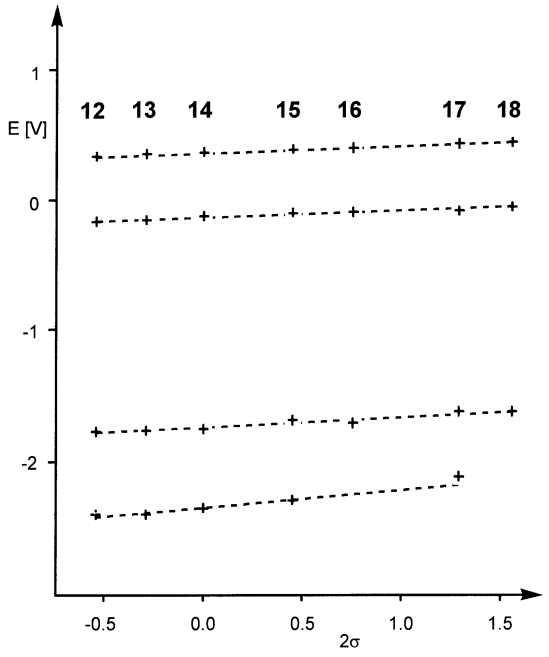

Figure 6. Evolution of redox potentials of **12**−**18** with Hammett constants σ

band is detected to be red-shifted from 551 nm in NiOEP to 863 nm in **11**.

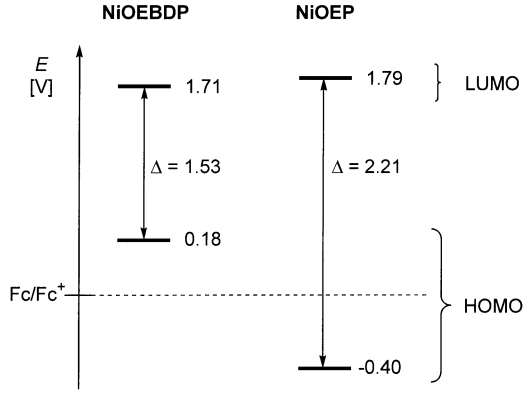

Figure 7. HOMO and LUMO energy levels of (2,2′-bidipyrrinato)nickel(II) (**9**) (NiOEBDP) and (octaethylporphyrinato)nickel(II) (NiOEP) as derived from electrochemical data

Conclusion

Our studies on the (2,2′-bidipyrrinato)nickel complexes **11**−**18** revealed complexes related to (porphyrinato)nickel complexes with respect to both, structural and electronic properties. Both ligands serve as dianionic N_4 chelates when interacting with the divalent nickel ion and produce low-spin, (distorted) square-planar coordination compounds. However, 2,2′-bidipyrrinato complexes show some special features due to their build-up as open-chain tetrapyrroles, of which the pronounced and stable helical conformation and the high-energy HOMO are the most obvious.

An interpretation of the differences found mainly in the electronic structures of (2,2′-bidipyrrinato)nickel(II) com-

plexes and (porphyrinato)nickel(II) complexes is not trivial at all, since the latter contain an aromatic 22π system, while the open-chain analogues constitute non-aromatic 20π-electron compounds without aromatic stabilisation. From the point of view of ligand electronics, any comparison of these differing classes must therefore fail, and it is quite surprising, that the spectral and structural features of (2,2′-bidipyrrinato)nickel complexes match so well with those obtained on aromatic (porphyrinato)nickel variants like chlorins, bacteriochlorins,[23,24] or overcrowded porphyrins.[22] Well-established interpretation schemes like energetic contributions through a strained, nonplanar structure and/or loss of symmetry do, when applied to these open-chain nickel(II) complexes, in fact, result in a useful description of the observed properties. While electronically the differences between the 2,2′-bidipyrrin and the porphyrin ligand are obvious, the influence on the central nickel(II) ion is too small to be detected by the applied methods. Two dipyrrin units arranged in a way as to form a (distorted) square-planar, dianionic N_4 chelate ligand thus appear sufficient to mimic at least some of the coordination chemistry of aromatic, porphyrinoid ligands.

The data presented here for a group of model complexes suggests, that helical chiral metallo-2,2′-bidipyrrins might well have the potential to serve as valuable porphyrinoid catalysts in enantioselective transformations. We are currently exploring this possibility.

Experimental Section

Solvents for chromatography were HPLC grade. All reagents and solvents were purchased from commercial sources and used as received. − NMR spectra were obtained in $CDCl_3$ solutions with a Bruker AC 200 spectrometer. Chemical shifts (δ) are given in ppm relative to residual protio solvent resonances (^{1}H spectra) or to chloroform (^{13}C). − Mass spectra (EI, 70 eV or FAB) were recorded with a Finnigan 90 MAT instrument; *m*/*z* alues are given for the most abundant isotopes only. − Melting points were measured by DTA with a Thermoanalyzer DuPont 9000. − Elemental analyses (C, H N) were performed at the microanalytical laboratory of the Institut für Anorganische Chemie, Universität Würzburg. − UV/Vis spectra were obtained in dichloromethane solution ($c \approx 10^{-4}$ mol l^{-1}) with a Hitachi U-3200 spectrophotometer. − Chiral MPLC was performed on Pirkle-type columns (D-phenylglycine on spherical silica gel; analytical: 25 cm × 4.6 mm, particle size 5 μ; preparative: 50 cm × 21.1 mm, particle size 10 μ), using a Latek P402 chromatographic system, and the fractions were detected by single-point UV absorption at 400 nm. − CD spectra were recorded as dichloromethane solutions in a 1-cm cell with a Jasco J 600 CD spectrometer. − Cyclic voltammetry was carried out in benzonitrile containing *n*Bu_4NPF_6 as supporting electrolyte (0.1 M). Benzonitrile (Aldrich) was dried with anhydrous $CaCl_2$ for 2 d, and further distilled from P_2O_5 under reduced pressure of argon. *n*Bu_4NPF_6 (Fluka, electrochemical grade) was dried under vacuum at 65 °C. Before use, the 0.1 M solution of *n*Bu_4NPF_6 in benzonitrile was purified in a glove box on activated neutral alumina (Merck). The measurements were carried out in the glove box using a classical three-electrode cell. The working electrode was a platinum disk (diameter 2 mm), the pseudo reference electrode and the counter electrode being platinum wires. All potentials are given against the ferrocene/ferrocenium couple used as internal standard. The cell was connected to an EG&G PAR potentiostat (Model 273) interfaced with a PC.

Preparation of the Nickel Complexes

(2,2′-Bidipyrrinato)nickel Complexes 11−18. − General Procedure: 0.1 mmol of 2,2′-bidipyrrin **3−10** and 566 mg (2 mmol) nickel(II) acetate tetrahydrate were stirred in a mixture of 30 mL of methanol and 30 mL of dichloromethane for 30 min (colour change from deep blue to brownish green). The reaction mixture was extracted twice with 100 mL of water, dried with sodium sulfate, and the solvent was removed in vacuo. Recrystallization from dichloromethane/methanol yielded the title compounds as violet crystals.

[3,3′,4,4′,8,8′,9,9′-Octaethyl-10,10′-dimethyl-2,2′-bi(dipyrrinato)]nickel (11): Yield 548 mg (92%); m.p. 257 °C. − ^{1}H NMR (200 MHz, $CDCl_3$): δ = 0.81 (t, 6 H, ^3J = 7.5 Hz, 2 × CH_3), 0.99 (t, 6 H, ^3J = 7.5 Hz, 2 × CH_3), 1.01 (t, 6 H, ^3J = 7.5 Hz, 2 × CH_3), 1.05 (t, 6 H, ^3J = 7.5 Hz, 2 × CH_3), 1.99 (q, ^3J = 7.5 Hz, 4 H, 2 × CH_2CH_3), 2.31−2.16 (m, 12 H, 6 × CH_2CH_3), 2.32 (s, 6 H, terminal CH_3), 6.04 (s, 2 H, H_{meso}). − ^{13}C NMR (50.3 MHz, $CDCl_3$): δ = 14.1, 16.7, 17.1, 17.2, 17.4, 17.5, 17.6, 17.8, 18.2, 119.5, 127.8, 130.9, 132.9, 136.9, 140.4, 148.2, 151.5, 168.8. − UV/Vis (dichloromethane): λ_{max} (ε) = 306 (21200), 353 (21100), 432 (80700), 535 (17800), 609 sh (13300), 864 nm (5600 mol^{-1} dm^3 cm^{-1}). − MS (70 eV, EI): *m*/*z* = 594 [M$^+$], 297 [M^{2+}]. − $C_{36}H_{48}N_4Ni$ (595.49): calcd. C 72.61, H 8.12, N 9.41; found C 72.50, H 7.84, N 9.28.

Crystallographic Data for 11: $C_{36}H_{48}N_4Ni$, violet cubes obtained by slow concentration of a CH_2Cl_2/*n*-hexane solution, crystal size: 0.25 × 0.20 × 0.20 mm, monoclinic, space group $P2_1/c$, a = 12.867(1), b = 20.140(1), c = 13.270(1) Å, β = 110.42(1)°, V = 3222.7(4) Å^3, $\rho_{calcd.}$ = 1.227 g cm^{-3}, Z = 4, $2\theta_{max}$ = 54°, Mo-K_α radiation, λ = 0.71073 Å, scan mode: φ/ω-scans, T = 293(2) K, 24167 measured, 6701 independent reflections, 5457 reflections observed for $I > 2\sigma(I)$, μ = 0.632 mm^{-1}, solved with direct methods (MolEN, Enraf−Nonius), refined with full-matrix least squares on F^2 (SHELXL-97, G. Sheldrick, University of Göttingen), 563 parameters, H atoms refined with isotropic temperature factors. R = 0.0361, wR = 0.0906, residual electron density ρ = 0.338/−0.198 e Å^{-3}. Crystallographic data (excluding structure factors) for the structure reported have been deposited with the Cambridge Crystallographic Data Centre as supplementary publication no. CCDC-153981. Copies of the data can be obtained free of charge on application to CCDC, 12 Union Road, Cambridge CB2 1EZ, UK [Fax: (internat.) + 44-1223/336-033; E-mail: deposit@ccdc.cam.ac.uk].

[6,6′-Bis(*p*-anisyl)-3,3′,4,4′,8,8′,9,9′-octaethyl-10,10′-dimethyl-2,2′-bidipyrrinato]nickel (12): Yield 759 mg (94%); m.p. 263 °C. − ^{1}H NMR (200 MHz, $CDCl_3$): δ = 0.60 (t, 6 H, ^3J = 7.5 Hz, 2 × CH_3), 0.62 (t, 6 H, ^3J = 7.5 Hz, 2 × CH_3), 0.80 (t, 6 H, ^3J = 7.5 Hz, 2 × CH_3), 0.97 (t, 6 H, ^3J = 7.5 Hz, 2 × CH_3), 1.13 (m, 4 H, 2 × CH_2CH_3), 1.49 (br.s, 4 H, 2 × CH_2CH_3), 2.1, 2.27 (2 × br.s, 14 H, terminal CH_3 and 4 × CH_2CH_3), 3.85 (s, 6 H, OCH_3), 6.82 (d, ^3J = 8.4 Hz, 2 H, H_{aryl}), 6.92 (d, ^3J = 8.4 Hz, 2 H, H_{aryl}), 7.07 (d, ^3J = 8.4 Hz, 2 H, H_{aryl}), 7.53 (d, H ^3J = 8.4 Hz, H_{aryl}). − ^{13}C NMR (50.3 MHz, $CDCl_3$): δ = 14.3, 16.8, 17.4, 18.0, 18.5, 19.3, 55.3, 112.7, 113.0, 129.5, 129.8, 130.6, 130.7, 132.7, 142.6, 151.1, 159.4. − UV/Vis (dichloromethane): λ_{max} (ε) = 308 (26700), 354 (21200), 432 (79800), 532 (18100), 613 sh (13700), 859 nm (5900 mol^{-1} dm^3 cm^{-1}). − MS (FAB): *m*/*z* = 806 [M$^+$]. − $C_{50}H_{60}N_4NiO_2$ (807.73): calcd. C 74.35, H 7.49, N 6.94; found C 73.99, H 7.38, N 6.70.

[3,3′,4,4′,8,8′,9,9′-Octaethyl-10,10′-dimethyl-6,6′-bis(*p*-tolyl)-2,2′-bidipyrrinato]nickel (13): Yield 683 mg (88%); m.p. > 300 °C. − ^{1}H NMR (200 MHz, $CDCl_3$): δ = 0.59 (t, 6 H, ^3J = 7.5 Hz, 2 × CH_3), 0.60 (t, 6 H, ^3J = 7.5 Hz, 2 × CH_3), 0.80 (t, 6 H, ^3J = 7.5 Hz, 2 × CH_3), 0.97 (t, 6 H, ^3J = 7.5 Hz, 2 × CH_3), 1.11 (m, 4 H, 2 × CH_2CH$_3$), 1.45 (br.s, 4 H, 2 × CH_2CH$_3$), 2.2 (m, 14 H, terminal CH_3 and 4 × CH_2CH$_3$), 2.40 (s, 6 H, ArCH_3), 7.06 (m, 4 H, H_{aryl}), 7.19 (d, ^3J = 7.6 Hz, 2 H, H_{aryl}), 7.51 (d, ^3J = 7.6 Hz, 2 H, H_{aryl}). − ^{13}C NMR (50.3 MHz, $CDCl_3$): δ = 14.4, 16.7, 16.9, 17.4, 17.7, 18.0, 18.5, 19.3, 21.4, 128.1, 129.5, 132.6, 134.4, 137.6, 142.5, 151.0, 168.1. − UV/Vis (dichloromethane): λ_{max} (ε) = 307 (26100), 353 (20800), 434 (78200), 534 (17700), 613 sh (13500), 863 nm (5700 mol^{-1} dm^3 cm^{-1}). − MS (FAB): *m*/*z* = 774 [M$^+$]. − $C_{50}H_{60}N_4Ni$ (775.73): calcd. C 77.42, H 7.80, N 7.22; found C 77.11, H 7.91, N 7.02.

[3,3′,4,4′,8,8′,9,9′-Octaethyl-10,10′-dimethyl-6,6′-diphenyl-2,2′-bidipyrrinato]nickel (14): Yield 658 mg (88%); m.p. 292 °C. − ^{1}H NMR (200 MHz, $CDCl_3$): δ = 0.58 (t, 6 H, ^3J = 7.5 Hz, 2 × CH_3), 0.59 (t, 6 H, ^3J = 7.5 Hz, 2 × CH_3), 0.80 (t, 6 H, ^3J = 7.5 Hz, 2 × CH_3), 0.98 (t, 6 H, ^3J = 7.5 Hz, 2 × CH_3), 0.94−1.54 (m, 8 H, 4 × CH_2CH$_3$), 1.96, 2.26 (2 × br.s, 14 H, terminal CH_3 and 4 × CH_2CH$_3$), 7.16−7.66 (m, 10 H, H_{phenyl}). − ^{13}C NMR (50.3 MHz, $CDCl_3$): δ = 14.4, 16.6, 16.8, 17.3, 17.4, 17.8, 18.0, 18.4, 19.2, 127.3, 127.4, 128.0, 129.6, 129.7, 132.8, 137.5, 142.5. − UV/Vis (dichloromethane): λ_{max} (ε) = 308 (26400), 354 (21000), 433 (79000), 535 (17900), 611 sh (13600), 863 nm (5800 mol^{-1} dm^3 cm^{-1}). − MS (70 eV, EI): *m*/*z* = 746 [M$^+$], 373 (M^{2+}). − $C_{48}H_{56}N_4Ni$ (747.68): calcd. C 77.11, H 7.55, N 7.49; found C 76.88, H 7.29, N 7.39. − Enantioseparation was effected at 10 bar (flow rate 800 mL h^{-1}); elution times: 72.4 min (F1) and 77.0 min (F2). − CD (dichloromethane): λ_{max} (Δε) (**14′**) = 357 (−39.68), 432 (172.97), 527 nm (58.06 l mol^{-1} cm^{-1}); (**14′′**) = 357 (42.02), 432 (−175.71), 527 nm (−54.16 l mol^{-1} cm^{-1}).

Crystallographic Data for 14: $C_{48}H_{56}N_4Ni$, blue-violet needles obtained by slow concentration of a CH_2Cl_2/*n*-hexane solution, crystal size: 0.25 × 0.15 × 0.10 mm, monoclinic, space group $P2_1/n$, *a* = 14.272(1), *b* = 11.529(1), *c* = 25.195(1) Å, β = 93.41(1)°, *V* = 4138.3(5) Å^3, $\rho_{calcd.}$ = 1.200 g cm^{-3}, *Z* = 4, $2\theta_{max}$ = 54°, Mo-K_α radiation, λ = 0.71073 Å, scan mode: φ/ω-scans, *T* = 293(2) K, 28093 measured, 8845 independent reflections, 5818 reflections observed for $I > 2\sigma(I)$, μ = 0.506 mm^{-1}, solved with direct methods (MolEN, Enraf−Nonius), refined with full-matrix least squares on F^2 (SHELXL-97, G. Sheldrick, University of Göttingen), 703 parameters, H atoms refined with isotropic temperature factors. *R* = 0.0577, *wR* = 0.0972, residual electron density ρ = 0.278/−0.232 e Å^{-3}. Crystallographic data (excluding structure factors) for the structure reported have been deposited with the Cambridge Crystallographic Data Centre as supplementary publication no. CCDC-153982. Copies of the data can be obtained free of charge on application to CCDC, 12 Union Road, Cambridge CB2 1EZ, UK [Fax: (internat.) + 44-1223/336-033; E-mail: deposit@ccdc.cam.ac.uk].

[6,6′-Bis(*p*-chlorophenyl)-3,3′,4,4′,8,8′,9,9′-octaethyl-10,10′-dimethyl-2,2′-bidipyrrinato]nickel (15): Yield 759 mg (93%); m.p. > 300 °C. − ^{1}H NMR (200 MHz, $CDCl_3$): δ = 0.60 (t, 6 H, ^3J = 7.5 Hz, 2 × CH_3), 0.61 (t, 6 H, ^3J = 7.5 Hz, 2 × CH_3), 0.80 (t, 6 H, ^3J = 7.5 Hz, 2 × CH_3), 0.97 (t, 6 H, ^3J = 7.5 Hz, 2 × CH_3), 1.11 (m, 4 H, 2 × CH_2CH$_3$), 1.48 (m, 4 H, 2 × CH_2CH$_3$), 2.0, 2.25 (2 × br.s, 14 H, terminal CH_3 and 4 × CH_2CH$_3$), 7.13 (dd, 2 H, ^3J = 8.0 Hz, H_{aryl}), 7.28 (dd, 2 H, ^3J = 8.0 Hz, H_{aryl}), 7.40 (dd, 2 H, ^3J = 8.0 Hz, H_{aryl}), 7.60 (dd, 2 H, ^3J = 8.0 Hz, H_{aryl}). − ^{13}C NMR (50.3 MHz, $CDCl_3$): δ = 14.3, 16.6, 16.9, 17.3, 17.5, 17.8, 18.0, 18.5, 19.3, 127.8, 129.9, 131.0, 132.5, 133.1, 134.0, 134.9, 135.9, 138.7, 142.5, 150.9, 168.8. − UV/Vis (dichloromethane): λ_{max} (ε) = 310 (26900), 352 (21400), 433 (81100), 535 (18300), 610 sh (13900), 863 nm (6000 mol^{-1} dm^3 cm^{-1}). − MS (FAB): *m*/*z* = 814 [M$^+$]. − $C_{48}H_{54}Cl_2N_4Ni$ (816.58): calcd. C 70.60, H 6.67, N 6.86; found C 70.29, H 6.65, N 6.68.

[3,3′,4,4′,8,8′,9,9′-Octaethyl-10,10′-dimethyl-6-(*p*-nitrophenyl)-6′-phenyl-2,2′-bidipyrrinato]nickel (16): Yield 680 mg (86%); m.p. 241 °C (decomp.). − ^{1}H NMR (200 MHz, CD_2Cl_2): δ = 0.61 (t, 6 H, ^3J = 7.5 Hz, 2 × CH_3), 0.63 (t, 6 H, ^3J = 7.5 Hz, 2 × CH_3), 0.83 (t, 6 H, ^3J = 7.5 Hz, 2 × CH_3), 0.99 (t, 6 H, ^3J = 7.5 Hz, 2 × CH_3), 1.0−1.6 (m, 8 H, 4 × CH_2CH$_3$), 2.0, 2.31 (2 × br.s, 14 H, terminal CH_3 and 4 × CH_2CH$_3$), 7.17−8.38 (m, 9 H, H_{aryl}). − ^{13}C NMR (50.3 MHz, CD_2Cl_2): δ = 14.5, 16.8, 17.0, 17.1, 17.4, 17.5, 17.8, 18.3, 18.4, 18.8, 19.0, 19.7, 19.8, 123.2, 123.4, 128.0, 128.1, 128.6, 130.0, 130.1, 130.3, 130.5, 131.7, 132.1, 133.2, 134.0, 134.2, 134.8, 136.0, 137.6, 137.7, 141.0, 142.5, 142.8, 145.2, 148.3, 150.8, 151.0, 152.3, 152.4, 170.1. − UV/Vis (dichloromethane): λ_{max} (ε) = 311 (27700), 357 (20200), 434 (77100), 533 (16600), 619 sh (14600), 860 nm (4900 mol^{-1} dm^3 cm^{-1}). − MS (FAB): *m*/*z* = 791 [M$^+$]. − $C_{48}H_{55}N_5NiO_2$ (792.68): calcd. C 72.73, H 6.99, N 8.84; found C 72.70, H 6.93, N 8.57.

Crystallographic Data for 16: $C_{48}H_{55}N_5NiO_2$, dark violet cubes obtained by slow concentration of a CH_2Cl_2/*n*-hexane solution, crystal size: 0.10 × 0.10 × 0.10 mm, triclinic, space group $P\bar{1}$ *a* = 12.911(3), *b* = 13.442(3), *c* = 14.264(3) Å, α = 108.85(3), β = 105.43(3), γ = 106.38°, *V* = 2103.8(7) Å^3, $\rho_{calcd.}$ = 1.251 g cm^{-3}, *Z* = 2, $2\theta_{max}$ = 50°, Mo-K_α radiation, λ = 0.71073 Å, scan mode: φ-scans, *T* = 173(2) K, 22070 measured, 6950 independent reflections, 3924 reflections observed for $I > 2\sigma(I)$, μ = 0.506 mm^{-1}, solved with direct methods (SHELXS-97, G. Sheldrick, University of Göttingen), refined with full-matrix least squares on F^2 (SHELXL-97, G. Sheldrick, University of Göttingen), 542 parameters, H atoms refined with isotropic temperature factors. *R* = 0.0487, *wR* = 0.0920, residual electron density ρ = 0.371/−0.355 e Å^{-3}. Crystallographic data (excluding structure factors) for the structure reported have been deposited with the Cambridge Crystallographic Data Centre as supplementary publication no. CCDC-161005. Copies of the data can be obtained free of charge on application to CCDC, 12 Union Road, Cambridge CB2 1EZ, UK [Fax: (internat.) + 44-1223/336-033; E-mail: deposit@ccdc.cam.ac.uk].

[6,6′-Bis(*p*-cyanophenyl)-3,3′,4,4′,8,8′,9,9′-octaethyl-10,10′-dimethyl-2,2′-bidipyrrinato]nickel (17): Yield 724 mg (91%); m.p. 224 °C (decomp.). − ^{1}H NMR (200 MHz, CD_2Cl_2): δ = 0.60 (t, 6 H, ^3J = 7.5 Hz, 2 × CH_3), 0.62 (t, 6 H, ^3J = 7.5 Hz, 2 × CH_3), 0.83 (t, 6 H, ^3J = 7.5 Hz, 2 × CH_3), 1.02 (t, 6 H, ^3J = 7.5 Hz, 2 × CH_3), 1.0−1.5 (m, 8 H, 4 × CH_2CH$_3$), 2.0, 2.28 (2 × br.s, 14 H, terminal CH_3 and 4 × CH_2CH$_3$), 7.38 (d, ^3J = 8.1 Hz, 2 H, H_{aryl}), 7.66 (d, ^3J = 8.1 Hz, 2 H, H_{aryl}), 7.79 (d, ^3J = 8.1 Hz, 2 H, H_{aryl}), 7.87 (d, ^3J = 8.1 Hz, 2 H, H_{aryl}); δ = ^{13}C NMR (50.3 MHz, CD_2Cl_2): δ = 14.5, 16.9, 17.1, 17.4, 17.8, 18.3, 18.4, 18.9, 19.8, 112.7, 119.2, 130.6, 131.1, 131.4, 131.9, 132.1, 132.3, 134.4, 135.2, 138.3, 142.8, 151.6, 151.7, 170.6. − UV/Vis (dichloromethane): λ_{max} (ε) = 312 (28900), 353 (21000), 435 (79900), 534 (17700), 613 sh (14500), 861 nm (5700 mol^{-1} dm^3 cm^{-1}). − MS (FAB): *m*/*z* = 796 [M$^+$]. − $C_{50}H_{54}N_6Ni$ (797.70): calcd. C 75.29, H 6.82, N 10.54; found C 74.95, H 6.63, N 10.26.

[3,3′,4,4′,8,8′,9,9′-Octaethyl-10,10′-dimethyl-6,6′-bis(*p*-nitrophenyl)-2,2′-bidipyrrinato]nickel (18): Yield 729 mg (87%); m.p. > 300 °C. − ^{1}H NMR (200 MHz, $CDCl_3$): δ = 0.58 (t, 6 H, ^3J =

7.5 Hz, 2 × CH_3), 0.59 (t, 6 H, ^3J = 7.5 Hz, 2 × CH_3), 0.80 (t, 6 H, ^3J = 7.5 Hz, 2 × CH_3), 0.97 (t, 6 H, ^3J = 7.5 Hz, 2 × CH_3), 1.0−1.5 (m, 8 H, 4 × CH_2CH$_3$), 2.0, 2.26 (2 × br.s, 14 H, terminal CH_3 and 4 × CH_2CH$_3$), 7.41 (d, ^3J = 8.2 Hz, 2 H, H_{aryl}), 7.88 (d, ^3J = 8.2 Hz, 2 H, H_{aryl}), 8.19 (d, ^3J = 8.2 Hz, 2 H, H_{aryl}), 8.32 (d, ^3J = 8.2 Hz, 2 H, H_{aryl}). − ^{13}C NMR (50.3 MHz, $CDCl_3$): δ = 14.2, 16.5, 16.9, 17.2, 17.4, 17.9, 18.0, 18.6, 19.4, 122.7, 130.5, 130.9, 131.2, 133.6, 134.3, 137.2, 142.3, 144.7, 147.8, 150.7, 152.2, 169.7. − UV/Vis (dichloromethane): λ_{max} (ε) = 314 (29900), 354 (21100), 434 (79200), 534 (17900), 615 sh (13500), 862 nm (5800 mol^{-1} dm^3 cm^{-1}). − MS (FAB): *m/z* = 836 [M$^+$]. − $C_{48}H_{54}N_6NiO_4$ (837.68): calcd. C 68.82, H 6.50, N 10.03; found C 68.45, H 6.33, N 9.69.

Acknowledgments

This work was funded by the Deutsche Forschungsgemeinschaft (Emmy−Noether-Programm) and by the Centre National de la Recherche Scientifique (C.N.R.S). We thank Professor H. Werner (Würzburg) and Professor A. Berkessel (Köln) for their support.

[1] A. W. Johnson, R. Price, *J. Chem. Soc.* **1960**, 1649−1653.
[2] A. W. Johnson, I. T. Kay, R. Rodrigo, *J. Chem. Soc.* **1963**, 2336−2342.
[3] D. Dolphin, R. L. N. Harris, J. L. Huppatz, A. W. Johnson, I. T. Kay, J. Leng, *J. Chem. Soc. C* **1966**, 98−106.
[4] Y. Zhang, A. Thompson, S. J. Rettig, D. Dolphin, *J. Am. Chem. Soc.* **1998**, *120*, 13537−13538.
[5] G. Struckmeier, U. Thewalt, J.-H. Fuhrhop, *J. Am. Chem. Soc.* **1976**, *98*, 278−279.
[6] W. S. Sheldrick, J. Engel, *J. Chem. Soc., Chem. Commun.* **1980**, 5−6.
[7] M. Bröring, A. Pfister, K. Ilg, *Chem. Commun.* **2000**, 1407−1408.
[8] H. Falk, *The Chemistry of Linear Oligopyrrols and Bile Pigments*, Springer, Wien, **1989**.
[9] M. Bröring, *Synthesis* **2000**, 1291−1294.
[10] M. Dobler, J. D. Dunitz, *Helv. Chim. Acta* **1971**, *54*, 90−98.
[11] M. Currie, J. D. Dunitz, *Helv. Chim. Acta* **1971**, *54*, 98−112.
[12] J. V. Bonfiglio, R. Bonnett, M. B. Hursthouse, K. M. Abdul Malik, *J. Chem. Soc., Chem. Commun.* **1977**, 83−84.
[13] J. V. Bonfiglio, R. Bonnett, D. G. Buckley, D. Hamzetash, M. B. Hursthouse, K. M. Abdul Malik, A. F. McDonagh, J. Trotter, *Tetrahedron* **1983**, *39*, 1865−1874.
[14] A. L. Balch, M. Mazzanti, B. C. Noll, M. M. Olmstead, *J. Am. Chem. Soc.* **1993**, *115*, 12206−12207.
[15] A. L. Balch, M. Mazzanti, B. C. Noll, M. M. Olmstead, *J. Am. Chem. Soc.* **1994**, *116*, 9114−9122.
[16] S. Attar, A. L. Balch, P. M. Van Calcar, K. Winkler, *J. Am. Chem. Soc.* **1997**, *119*, 3317−3323.
[17] R. Koerner, M. M. Olmstead, A. Ozarowski, S. L. Phillips, R. M. Van Calcar, K. Winkler, A. L. Balch, *J. Am. Chem. Soc.* **1998**, *120*, 1274−1284.
[18] P. A. Lord, M. M. Olmstead, A. L. Balch, *Inorg. Chem.* **2000**, *39*, 1128−1134.
[19] *The Porphyrin Handbook*, vol. 4 (Eds.: K. M. Kadish, K. M. Smith, R. Guilard), Academic, San Diego, CA, **2000**.
[20] C. J. Medforth in *The Porphyrin Handbook*, vol. 5 (Eds.: K. M. Kadish, K. M. Smith, R. Guilard), Academic, San Diego, CA, **2000**, chapter 35, pp. 1−80.
[21] D. L. Cullen, E. F. Meyer, *J. Am. Chem. Soc.* **1974**, *96*, 2095−2102.
[22] M. O. Senge in *The Porphyrin Handbook*, vol. 1 (Eds.: K. M. Kadish, K. M. Smith, R. Guilard), Academic, San Diego, CA, **2000**, chapter 6, pp. 239−347.
[23] G. Peychal-Heiling, G. S. Wilson, *Anal. Chem.* **1971**, *43*, 550−556.
[24] D. Chang, T. Malinski, A. Ulman, K.M. Kadish, *Inorg. Chem.* **1984**, *23*, 817−824.
[25] C. W. Bird, G. W. H. Cheeseman in *Comprehensive Heterocyclic Chemistry*, vol. 4 (Eds.: A. R. Katritzky, C. W. Rees), Pergamon Press, Oxford, **1984**, p. 4.
[26] K. M. Smith in *Comprehensive Heterocyclic Chemistry*, vol. 4 (Eds.: A. R. Katritzky, C. W. Rees), Pergamon Press, Oxford, **1984**, p. 386.
[27] R. G. Khoury, L. Jaquinod, K. M. Smith, *Tetrahedron* **1998**, *54*, 2339−2346.
[28] R. G. Khoury, M. O. Senge, J. E. Colchester, K. M. Smith, *J. Chem. Soc., Dalton Trans.* **1996**, 3937−3950.
[29] T. Mizutani, S. Yagi, A. Honmaru, H. Ogoshi, *J. Am. Chem. Soc.* **1996**, *118*, 5318−5319.
[30] T. Mizutani, S. Yagi, T. Morinaga, T. Nomura, T. Takagishi, S. Kitagawa, H. Ogoshi, *J. Am. Chem. Soc.* **1999**, *121*, 754−759.
[31] T. Mizutani, N. Sakai, S. Yagi, T. Takagishi, S. Kitagawa, H. Ogoshi, *J. Am. Chem. Soc.* **2000**, *122*, 748−749.
[32] G. Blauer, G. Wagnière, *J. Am. Chem. Soc.* **1975**, *97*, 1949−1954.
[33] G. Wagnière, G. Blauer, *J. Am. Chem. Soc.* **1976**, *98*, 7806−7810.
[34] A. Werner, M. Michels, L. Zander, J. Lex, E. Vogel, *Angew. Chem. Int. Ed.* **1999**, *38*, 3650−3653.
[35] N. Harada, K. Nakanishi, *Circular Dichroic Spectroscopy − Exiton Coupling in Organic Stereochemistry*, University Science Books, Mill Valley, CA, **1983**.
[36] K. Nakanishi, N. Berova in *Circular Dichroism − Principles and Applications* (Eds.: K. Nakanishi, N. Berova, R. W. Woody) ,VCH Publishers, Inc., New York, **1994**, p. 361.
[37] K. M. Kadish, M. M. Morrison, *J. Am. Chem. Soc.* **1976**, *98*, 3326−3328.

Received April 5, 2001
[I01120]

Alkynyl Substitution and Linkage in Cobaltacarborane Sandwich Complexes[‡]

Dennis Malaba,[a][‡‡] Michal Sabat,[a] and Russell N. Grimes*[a]

Keywords: Carboranes / Alkyne complexes / Metallacarboranes / Cobalt / Palladium

Linkage of $Cp^*Co(Et_2C_2B_3H_5)$ sandwich units by alkynyl and diethynylphenylene connectors was explored by the synthesis of two classes of complexes in which the linking groups are attached to the Cp^* ligands and to the carborane rings, respectively. Thus, the complex *nido*-(η^5-C_5Me_4–C≡CH)$Co(Et_2C_2B_3H_5)$ (**6**) was prepared and converted in 87% yield to the novel 1,4-diethynylphenylene-linked bis(metallacarborane) 1,4-[*nido*-$(Et_2C_2B_3H_5)Co(\eta^5$-C_5Me_4–C≡C)]$_2C_6H_4$ (**7**), which was characterized by multinuclear NMR and mass spectra and X-ray crystallography. CuI-promoted coupling of **6** with $(MeCN)_2PdCl_2$ in excess diethylamine was employed to prepare a palladium derivative, *nido*-$(Et_2C_2B_3H_5)Co(C_5Me_4)$–C≡C–$Pd(NHEt_2)_2Cl$ (**10**). Complexes of the second type, in which the organic linker is attached directly to the carborane ring, were obtained by synthesis of a *B*-ethynylcobaltacarborane, *nido*-Cp^*Co-$[Et_2C_2B_3H_3(C{\equiv}CH)(C{\equiv}CSiMe_3)]$ (**15**), which was then coupled with 1,4-diiodobenzene to generate the bis(cobaltacarborane) 1,4-[*nido*-$Cp^*CoEt_2C_2B_3H_3(C{\equiv}CSiMe_3)(C{\equiv}C)]_2$-$C_6H_4$ (**16**) in 87% yield.

Introduction

Small metallacarborane units are versatile building blocks for the design and construction of organometallic frameworks in which metal centers are bound into stable environments;[2] typically, these are sufficiently robust to allow oxidation, reduction, and functionalization without disintegration of the system.[3] Examples include multidecker stacks,[4] arene-centered polymetallacarboranes,[5] and linked clusters.[6] Of particular interest are molecular arrays designed to promote electron delocalization between the metal centers. Such systems in general have two basic features: the presence of unpaired electrons, which can be introduced via paramagnetic metals, and connecting units that facilitate metal-to-metal electron transport. Unsaturated organic groups such as alkynes are prime candidates, and alkyne-linked organometallics are currently a subject of considerable interest as potential "molecular wires".[7] In the boron cluster area, Hawthorne and co-workers have synthesized ethynyl-linked rigid-rod derivatives of *p*-carborane ($1,12\text{-}C_2B_{10}H_{12}$) by Pd-catalyzed coupling.[7n] Here we report the development of preparative routes to alkyne-linked bis(metallacarborane) systems and their application to the synthesis of two types of target compounds in which the connectors are attached to the Cp* ligands and the carborane rings, respectively.

Results and Discussion

The synthon (η^5-C_5Me_4−C≡CH)$Co(Et_2C_2B_3H_5)$ (**6**) was prepared in several steps, starting with lithiation of 1-tetramethylcyclopentadienyl-2-trimethylsilylacetylene (**1**)[8] to generate **2** (Scheme 1), which reacted with $CoCl_2$ to give a green solution of the presumed dimer **3**. Treatment of this solution with the $Et_2C_2B_4H_5^-$ ion in THF gave the red-brown complex (C_5Me_4−C≡$CSiMe_3$)$Co(Et_2C_2B_4H_4)$ (**4**), which was isolated in 32% yield and decapped with TMEDA and water to afford *nido*-(η^5-C_5Me_4−C≡C−$SiMe_3$)$Co(Et_2C_2B_3H_5)$ (**5**) as a yellow solid. Desilylation of **5** with tetrabutylammonium fluoride in THF produced yellow **6** in 82% yield. Pd/Cu-catalyzed C−C coupling[7b,7c] with 1,4-diiodobenzene was effected by reaction of **6** with bis(benzonitrile)palladium(II) chloride, copper(I) iodide, triphenylphosphane, and diethylamine, which upon workup and chromatography on silica gave the diethynyl-linked dicobalt target complex 1,4-[*nido*-$(Et_2C_2B_3H_5)Co(\eta^5\text{-}C_5Me_4{-}C{\equiv}C)]_2C_6H_4$ (**7**), isolated as a yellow-brown solid in 87% yield. A minor product (4%) was tentatively identified from its proton NMR and mass spectra as the diethynyl-linked species [*nido*-$(Et_2C_2B_3H_5)Co(\eta^5$-C_5Me_4−C≡C)]$_2$ (**8**).

Complex **7** was fully characterized by multinuclear NMR and mass spectra and X-ray crystallography, which established the centrosymmetric geometry depicted in Scheme 1 and Figure 1. To our knowledge, the only prior example of a structurally characterized complex in which two metallacarborane units are linked by an alkynyl-containing chain is [Cp*$Co(Et_2C_2B_4H_3\text{-}7\text{-})]C_2$, whose C≡C group is attached to the apical boron atoms.[6a] Compound **7** is the first structurally characterized diethynylphenylene-linked metallacarborane complex, and some features are worth noting. As can be seen in Figure 1, the chain C1R1−C4−C5−C6---C6*−C5*−C4*−C1R1* forms an approximately linear ar-

[‡] Organotransition-Metal Metallacarboranes, 58. − Part 57: Ref.[1a]

[a] Department of Chemistry, University of Virginia, Charlottesville, VA 22901, USA
Fax: (internat.) + 1-804/924-3710
E-mail: RNG@virginia.edu
[‡‡] Current address: Department of Polymer Science, University of Akron, Akron, Ohio 44325, USA

 © WILEY-VCH Verlag GmbH, 69451 Weinheim, 2001 1434−1948/01/1010−2557 $ 17.50+.50/0

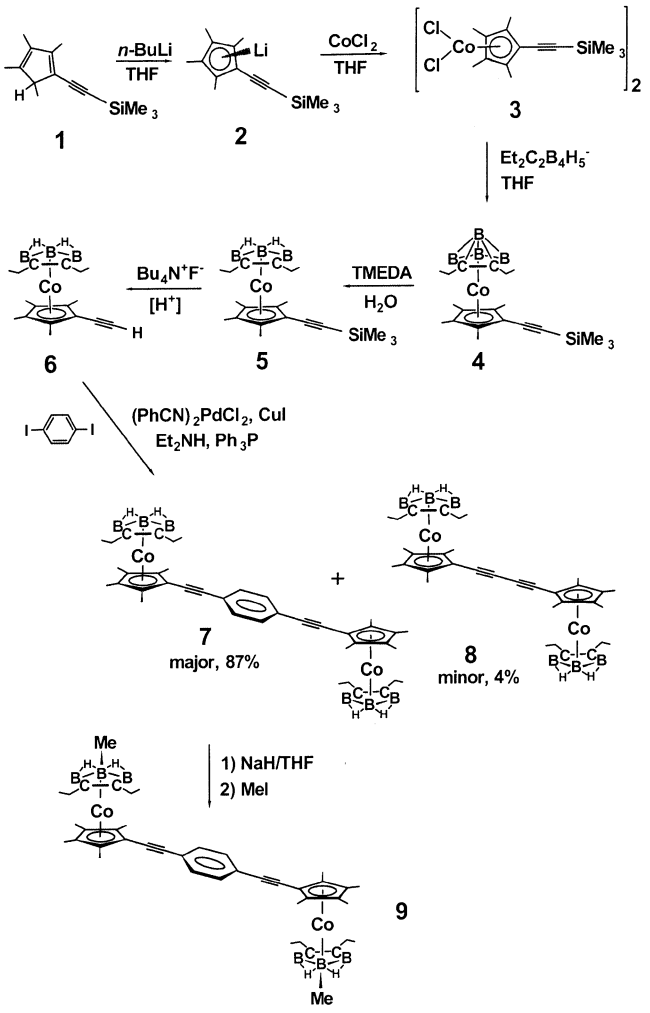

Scheme 1. B = BH, B

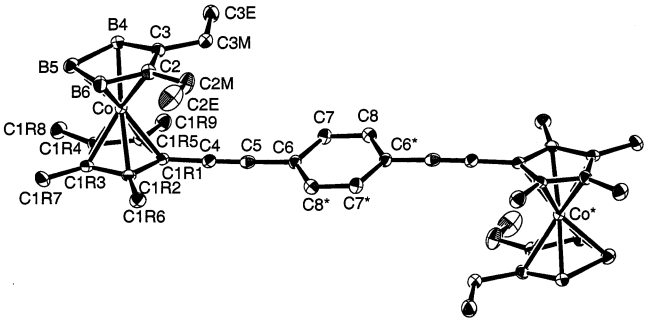

Figure 1. Molecular structure of **7** with 30% thermal ellipsoids (hydrogen atoms omitted for clarity); selected distances [Å]: C1R1−C4 1.424(7), C4−C5 1.185(7), C5−C6 1.454(7), C6−C7 1.394(7), C6−C8* 1.401(7), Co−C_5 plane 1.661, Co−C_2B_3 plane 1.508; the benzene ring subtends a dihedral angle of 13.1° with the C_5 ring plane

ray, but the phenylene ring is tilted 13° out of the plane defined by the C_5 rings. The C_2B_3 ring is not quite parallel with the C_5 plane (dihedral angle 9°) and the Co atom is closer to the carborane ring (1.508 Å) than the C_5 ring (1.66 Å), both values being typical of small cobaltacarboranes.[2−4] The short C4−C5 distance [1.185(7) Å] is within the normal range for C≡C bonds in alkynyl-linked dimetallic complexes,[9] although it is slightly shorter than that found in the previously mentioned [Cp*Co($Et_2C_2B_4H_3$−**7**−]$_2C_2$ [1.205(12) Å].[6a]

Since **7** is a bifunctional complex having two open carborane ligands available for bridge-deprotonation and η^5-coordination to metal ions,[1a] it is expected to be a useful synthon for the construction of long-chain metallacarborane oligomers or polymers containing [(C_5Me_4)Co($Et_2C_2B_3H_3$)]$_2$Co tetradecker sandwich units. This may be accomplished by removal of BHB bridging protons from both C_2B_3 end rings and stacking with transition metal ions, as was demonstrated earlier in the synthesis of phenylene- and fulvalene-bridged "staircase" oligomers.[10] It has been found, however, that such metal stacking reactions require modification of the electron population in the C_2B_3 end rings by introduction of methyl groups or halogen atoms.[3c,4,10] Accordingly, **7** was deprotonated and treated with methyl iodide to generate the *B,B′*-dimethyl derivative **9** (Scheme 1).

In an attempt to prepare the palladium-connected bis(cobaltacarborane) complex **10a** (Scheme 2), **6** was treated with bis(acetonitrile)palladium(II) chloride, copper(I) iodide, and diethylamine. However, the main product, isolated in 87% yield as a red-brown solid and characterized spectroscopically, was the mono(cobaltacarboranyl) species ($Et_2C_2B_3H_5$)Co(C_5Me_4)−C≡C−Pd($NHEt_2$)$_2$Cl (**10**). An accompanying low-yield side product was tentatively identified from its mass spectrum as [($Et_2C_2B_3H_5$)Co(C_5Me_4)−C≡C]$_2$Pd($NHEt_2$)$_2$ (**11**, Scheme 2).

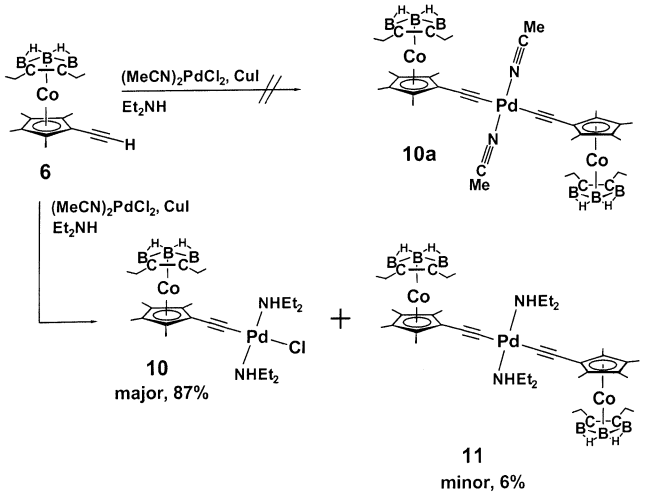

Scheme 2. B = BH, B

An alternative approach to the preparation of alkynyl-linked Cp*Co($Et_2C_2B_3H_5$) units involves attachment of the organic chain to the carborane ring rather than the Cp* group as in the preceding chemistry. Scheme 3 shows the

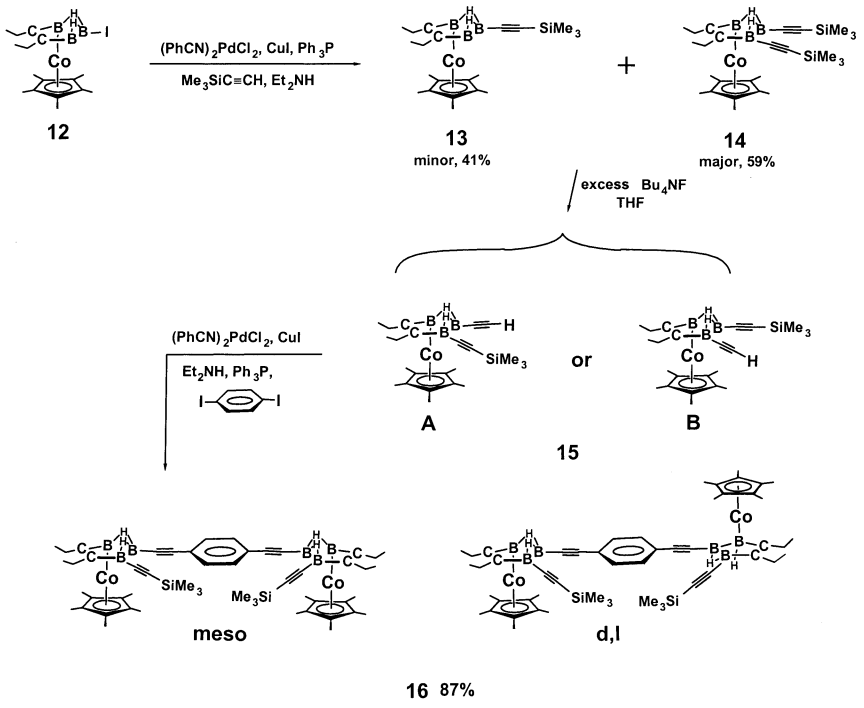

Scheme 3. B = BH, B

exploration of this idea employing as starting material the 5-iodo complex **12**,[11] which reacted with trimethylsilyl acetylene in the presence of palladium and copper reagents to produce the mono- and bis(*B*-silylethynyl) complexes **13** and **14**. The disubstituted product **14** probably formed by partial *B*-chlorination of **12** with $(PhCN)_2PdCl_2$, a process we have observed in earlier work.[12]

Treatment of **14** with excess fluoride ion removed only one trimethylsilyl group to give a single product, formulated as $Cp^*Co[Et_2C_2B_3H_3(C{\equiv}CH)(C{\equiv}CSiMe_3)]$ (**15**), whose spectroscopic data do not distinguish between the structures **A** and **B** depicted in Scheme 3. In a procedure analogous to the synthesis of **7** and **8** described above, Pd/Cu-catalyzed alkyne linkage was carried out on **15** to produce yellow 1,4-$\{nido\text{-}Cp^*Co[Et_2C_2B_3H_3(C{\equiv}CSiMe_3)(C{\equiv}C)]\}_2$-$C_6H_4$ (**16**), which was isolated in 87% yield together with a yellow minor product whose mass spectrum is consistent with the diethynyl-linked dimer $\{nido\text{-}Cp^*Co[Et_2C_2B_3H_3(C{\equiv}CSiMe_3)(C{\equiv}C)]\}_2$. Although **16** is assumed to form in solution as a mixture of the nonchiral (*meso*) and chiral forms (Scheme 3),[13] the differences in proton NMR signals of these isomers are not detectable in our spectra. Compound **16** is multifunctional, having two $-C{\equiv}CSiMe_3$ groups that are convertible to $-C{\equiv}CH$ for use in subsequent metal-catalyzed linkage, as well as two C_2B_3 end rings that are available for deprotonation and multidecker stacking (vide supra).

Conclusion

This work combines small-metallacarborane synthetic chemistry with approaches that have been developed elsewhere for preparing alkynyl-linked organometallic complexes, to generate novel alkyne-connected bis(metallacarborane) systems that are designed as building-blocks for the assembly of multimetallic extended systems. For convenience and ease of compound characterization by NMR spectroscopy, the target compounds selected in the current study are diamagnetic systems incorporating Co^{III}, which should be readily convertible by redox or electrochemistry to paramagnetic complexes; the nature and extent of electron delocalization in such systems[3] are a prime focus of interest in our laboratory. Investigations in this area are continuing and will be reported in due course.

Experimental Section

Materials and Procedures: Unless otherwise stated, all reactions were performed under dry nitrogen, maintained by standard glove box and Schlenk techniques. Workup of products was generally carried out in air using benchtop techniques. Solvents were distilled from appropriate drying agents under an inert gas. $C_5Me_4H(C{\equiv}CSiMe_3)$ (**1**) was prepared according to a literature method.[8] The carborane $Et_2C_2B_4H_6$ was prepared on a multigram scale by the reaction of B_5H_9 and 3-hexyne in diethyl ether solution, in a modification[14] of the literature method.[15] – ^1H, ^{11}B, and ^{13}C NMR spectra were obtained at 25 °C at 300, 115.8, and 75.5 MHz, respectively.

$(C_5Me_4\text{-}C{\equiv}CSiMe_3)Co(Et_2C_2B_4H_4)$ (4): A sample of $C_5Me_4H(C{\equiv}CSiMe_3)$ (**1**; 2.20 g, 10.1 mmol) was placed in a 100-mL Schlenk flask, 50 mL of dry THF was added, and the solution was cooled to 0 °C in an ice bath. Addition of *n*-butyllithium in hexanes (6.40 mL, 1.54 M, 10.0 mmol) produced a bright yellow

solution of Li[$C_5Me_4(C{\equiv}CSiMe_3)$] (**2**), which was warmed to room temperature and stirred for 1 h, after which it was slowly added via cannula to a 250-mL Schlenk flask containing $CoCl_2$ (1.31 g, 10.1 mmol) and 100 mL of dry THF. The reaction mixture was stirred at room temperature for 1 h, producing a dark green solution of the complex $[C_5Me_4(C{\equiv}CSiMe_3)CoCl]_2$ (**3**). A solution containing 10.0 mmol of $Na^+[Et_2C_2B_4H_5]^-$ was prepared by injecting the neutral carborane (1.32 g, 10.1 mmol) into a suspension of excess (0.40 g) dry NaH (previously washed twice with hexane) in 20 mL of dry THF. Stirring was continued until bubbling ceased, the suspension was allowed to settle for 30 min, and the solution was transferred to the stirred solution of **3** by slow cannula filtration. The reaction mixture was stirred at room temperature overnight, forming a reddish-brown solution from which the volatiles were removed, leaving a dark brown solid. The product was extracted with CH_2Cl_2 and then passed through a plug (3 cm) of silica gel using CH_2Cl_2 as the eluent. Solvent removal gave a reddish-brown oil which solidified on standing to yield 1.30 g (32%) of **4**. − ^{1}H NMR ($CDCl_3$): δ = 2.62 (m, 2 H, CH_2), 2.26 (m, 2 H, CH_2), 1.89 (s, 6 H, C_5Me_4), 1.87 (s, 6 H, C_5Me_4), 1.23 (t, 6 H, Et CH_3), 0.27 (s, 9 H, $SiMe_3$). − ^{13}C NMR ($CDCl_3$): δ = 99.2 (C≡C), 97.4 (C≡C), 93.7 (C_5Me_4), 92.0 (C_5Me_4), 77.7 (C_5Me_4), 21.0 (Et CH_2), 14.7 (Et CH_3), 11.0 (C_5Me_4), 10.4 (C_5Me_4), −0.1 ($SiMe_3$). − CI^+ MS (CH_4): *m*/*z* (%) = 407 (100) $[M + 1]^+$.

***nido*-(η^5-C_5Me_4−C≡C−$SiMe_3$)Co($Et_2C_2B_3H_5$) (5) and (η^5-C_5Me_4−C≡CH)Co($Et_2C_2B_3H_5$) (6):** To a solution of 0.900 g (2.22 mmol) of **4** in 15 mL of TMEDA were added a few drops of water, and the mixture was stirred at room temperature for 3 h in air. The solvent was removed in vacuo and the product was taken up in hexane and purified by flashing through a 12-cm column of silica gel with hexane as the eluent. Removal of the solvent gave a yellowish-brown oil which on standing gave 0.755 g (86%) of yellow solid **5**. − ^{13}C NMR ($CDCl_3$): δ = 99.2 (C≡C), 98.2 (C≡C), 96.1 (C_5Me_4), 93.8 (C_5Me_4), 80.3 (C_5Me_4), 22.1 (Et CH_2), 17.1 (Et CH_3), 11.3 (C_5Me_4), 11.0 (C_5Me_4), 0.6 ($SiMe_3$). − Compound **5** (0.755 g, 1.91 mmol) was dissolved in 30 mL of dry THF and the resulting solution was cooled to 0 °C. A solution of Bu_4NF (1.0 mL, 1.0 M in THF) was added dropwise and the reaction mixture was stirred at 0 °C for 1 h in air, warmed to room temperature, and stirred for 30 min. The solvent was removed using a rotary evaporator and the product was subsequently taken up in CH_2Cl_2 and placed on a 12-cm column of silica gel and eluted with hexanes, giving a yellow solution. The solvent was removed in vacuo leaving a yellowish-brown oil which solidified on standing to afford 0.504 g (82%) of yellow **6**. − ^{1}H NMR ($CDCl_3$): δ = 3.05 (s, 1 H, C≡CH), 2.12 (m, 2 H, CH_2), 1.98 (m, 2 H, CH_2), 1.87 (s, 6 H, C_5Me_4), 1.85 (s, 6 H, C_5Me_4), 1.11 (t, 6 H, Et CH_3), −5.86 (broad s, 2 H, BHB). − ^{13}C NMR ($CDCl_3$): δ = 96.2 (*C*≡*C*), 94.0 (*C*≡*C*), 80.6 (C_5Me_4), 79.1 (C_5Me_4), 22.4 (Et CH_2), 17.2 (Et CH_3), 11.1 (C_5Me_4), 11.0 (C_5Me_4). − ^{11}B NMR (C_6D_6): δ = 3.9 (d, 2 B, J_{BH} = 158 Hz), 6.8 (d, 1 B, J_{BH} = 98 Hz). − CI^+ MS (CH_4): *m*/*z* (%) = 324 (100) $[M^+]$.

1,4-[*nido*-($Et_2C_2B_3H_5$)Co(η^5-C_5Me_4−C≡C)]$_2C_6H_4$ (7) and [*nido*-($Et_2C_2B_3H_5$)Co(C_5Me_4−C≡C)]$_2$ (8): Compound **6** (0.445 g, 1.37 mmol), diiodobenzene (0.277 g, 0.687 mmol), bis(benzonitrile-)palladium (II) chloride (0.0132 g, 0.0344 mmol), copper(I) iodide (0.0131 g, 0.0687 mmol), and triphenylphosphane (0.018 g, 0.0687 mmol) were placed in a Schlenk flask, vacuum-degassed and placed under N_2. Ca. 50 mL of dry diethylamine (freshly distilled from CaH_2) was added via cannula and the reaction mixture was stirred at room temperature for 36 h. The solvent was removed under vacuum and the resulting crude product was chromatographed on silica gel with CH_2Cl_2/hexane (1:5). The first product to elute was **7**, which was obtained as a yellow-brown solid (0.43 g, 87%) upon solvent removal. Recrystallization of **7** from CH_2Cl_2/hexane gave crystals suitable for X-ray analysis. − ^{1}H NMR ($CDCl_3$): δ = 7.46 (s, 4 H, C_6H_4), 2.14 (m, 4 H, Et CH_2), 2.03 (m, 4 H, Et CH_2), 1.95 (s, 12 H, C_5Me_4), 1.87 (s, 12 H, C_5Me_4), 1.12 (t, 12 H, Et CH_3), −5.86 (broad s, 4 H, BHB). − ^{13}C NMR ($CDCl_3$): δ = 131.0 (C_6H_4), 122.8 (C_6H_4), 95.0 (C_5Me_4), 93.3 (C_5Me_4), 91.8 (C_5Me_4), 84.7 (C≡C), 79.2 (C≡C), 21.8 (Et CH_2), 16.4 (Et CH_3), 10.5 (C_5Me_4). − ^{11}B {^{1}H} NMR (C_6D_6): δ = 4.0 (s, 2 B), 6.8 (s, 1 B). − CI^+ MS (CH_4): *m*/*z* (%) = 722 (100) $[M^+]$. − The second compound eluted was **8**, which was isolated as a yellow−brown solid (ca. 20 mg, 4%) upon solvent removal. Attempts to recrystallize **8** were unsuccessful and resulted in decomposition of the product. − ^{1}H NMR ($CDCl_3$): δ = 2.15 (m, 4 H, Et CH_2), 2.05 (m, 4 H, Et CH_2), 1.92 (s, 12 H, C_5Me_4), 1.87 (s, 12 H, C_5Me_4), 1.15 (t, 12 H, Et CH_3), −5.85 (broad s, 4 H, BHB). − CI^+ MS (CH_4): *m*/*z* (%) = 647 (100) $[M + 1]^+$.

X-ray Crystallographic Study of 7: $C_{40}H_{58}B_6Co_2$ (721.62); monoclinic space group $P2_1/n$ (no. 14); a = 9.139(3), b = 16.423(5), c = 12.841(5) Å, β = 93.78(3)°, V = 1923(1) Å^3, Z = 2, $d_{calcd.}$ = 1.246 g/cm^3; μ(Mo-K_α) = 8.90 cm^{-1}. Data were collected with a Rigaku AFC6S diffractometer using graphite-monochromated Mo-K_α radiation (λ = 0.71069 Å) at −120 °C, employing an orange needle crystal having approximate dimensions of 0.28 × 0.24 × 0.48 mm mounted on a glass fiber. The ω-2θ scan technique was employed to a maximum 2θ value of 46°. Of 2978 measured reflections, 2782 were independent (R_{int} = 0.041, R_w = 0.065), 217 parameters, R = 0.047 [for reflections with $I > 3\sigma(I)$], max./min residual electron density 1.10/−0.049 e·Å^{-3}. The data were corrected for absorption, with transmission factors ranging from 0.93 to 1.00. The structure was solved by direct methods.[16] The final cycle of full-matrix least-squares refinement was based on 1875 observed reflections [$I > 3\sigma(I)$]. Hydrogen atoms were included but not refined. Neutral atom scattering factors were taken from Cromer and Waber.[17] All calculations were performed using the teXsan crystallographic software package of Molecular Structure Corporation.[18] Crystallographic data (excluding structure factors) have been deposited with the Cambridge Crystallographic Data Centre as supplementary publication no. CCDC-160497. Copies of the data can be obtained free of charge on application to CCDC, 12 Union Road, Cambridge CB21EZ, UK [Fax: (internat.) + 44-1223/336-033; E-mail: deposit@ccdc.cam.ac.uk].

***nido*-[($Et_2C_2B_3H_4Me$)Co(C_5Me_4-C≡C)]$_2C_6H_4$ (9):** Compound **7** (0.549 g, 0.761 mmol) was dissolved in 50 mL of dry THF and the solution was cooled to −78 °C using a dry ice/acetone bath. A solution of $(Me_3Si)_2NLi$ (1.70 mL, 2.2 mmol, 1.0 M in THF) was added dropwise producing a yellowish-brown precipitate. Upon warming to room temperature the precipitate dissolved and the resulting solution was stirred at room temperature for 1 h. Methyl iodide (0.216 g, 1.522 mmol) was added dropwise via a syringe and stirred at room temperature for 3 h. The solvent was removed in vacuo and the product was extracted with a small amount of CH_2Cl_2 which was then passed through a plug of silica gel. Removal of solvent gave yellow solid **9** (0.450 g, 80%). − ^{1}H NMR ($CDCl_3$): δ = 7.46 (s, 4 H, C_6H_4), 2.20 (m, 4 H, Et CH_2), 2.00 (m, 4 H, Et CH_2), 1.95 (s, 12 H, C_5Me_4), 1.81 (s, 12 H, C_5Me_4), 1.26 (s, 6 H, B-Me), 1.10 (t, 12 H, Et CH_3), −5.13 (broad s, 4 H, BHB). − CI^+ MS (CH_4): *m*/*z* (%) = 750 (100) $[M^+]$.

***nido*-($Et_2C_2B_3H_5$)Co(C_5Me_4)−C≡C−Pd(Et_2NH)$_2$Cl (10) and [*nido*-($Et_2C_2B_3H_5$)Co(C_5Me_4−C≡C)]$_2$Pd(Et_2NH)$_2$ (11):** Com-

pound **6** (0.292 g, 0.902 mmol), bis(acetonitrile)palladium (II) chloride (0.122 g, 0.902 mmol), and copper(I) iodide (8 mg, 0.025 mmol) were place in a Schlenk flask and an excess of Et_2NH was added. The reaction mixture was stirred at room temperature for 17 h, following which the solvent was removed in a rotary evaporator, and the crude product was flash-chromatographed on silica gel and eluted with hexanes. The first product eluted was **10**, isolated as a red-brown solid (0.480 g, 87%) upon solvent removal. The second product, eluted with CH_2Cl_2/hexane (1:1), was red-brown solid **11** (ca. 30 mg, 6%). − **10**: ^{1}H NMR ($CDCl_3$): δ = 3.32 (broad s, 2 H, NH), 3.17 (m, 4 H, amine CH_2), 2.66 (m, 4 H, amine CH_2), 2.13 (m, 2 H, carborane CH_2), 2.00 (m, 2 H, carborane CH_2), 1.81 (s, 6 H, C_5Me_4), 1.80 (s, 6 H, C_5Me_4), 1.60 (t, 12 H, amine CH_3), 1.24 (t, 6 H, carborane CH_3), −6.00 (broad s, 2 H, BHB). − ^{13}C NMR ($CDCl_3$): δ = 95.8 (C_5Me_4), 94.2 (C_5Me_4), 91.9 (C_5Me_4), 86.5 (C≡C), 84.9 (C≡C), 49.6 (NCH_2), 21.8 (Et CH_2), 16.9 (Et CH_3), 15.5 (NCH_3), 10.9 (C_5Me_4), 10.6 (C_5Me_4). − ^{11}B NMR (C_6D_6): δ = −6.0 (broad s, 3 B). − CI^+ MS (CH_4): *m/z* (%) = 611 (100) [M^+]. − **11**: CI^+ MS (CH_4): *m/z* (%) = 899 (100) [M + 1]$^+$.

***nido*-Cp*Co($Et_2C_2B_3H_4$−C≡$CSiMe_3$) (13) and *nido*-Cp*Co-[$Et_2C_2B_3H_3$(C≡$CSiMe_3$)$_2$] (14):** Compound **12** (0.900 g, 2.05 mmol), bis(benzonitrile)palladium(II) chloride (0.039 g, 0.102 mmol), copper(I) iodide (0.019 g, 0.102 mmol), and triphenylphosphane (0.054 g, 0.205 mmol) were placed in a Schlenk flask, vacuum-degassed and placed under an inert gas. About 100 mL of dry diethylamine was added via cannula. Excess trimethylsilylacetylene (0.50 g, 5.09 mmol, 1.1 mmol.) was added via a syringe and the reaction mixture was stirred at room temperature for 36 h. The solvent was removed under vacuum and the resulting crude product was subjected to column chromatography on silica gel [elution with CH_2Cl_2/hexane (1:5)] The first product to elute was **13**, which was obtained as a yellow solid (0.34 g, 41%) upon solvent removal. Yield. − ^{1}H NMR ($CDCl_3$): 2.14 (m, 2 H, Et CH_2), 1.91 (m, 2 H, Et CH_2), 1.77 (s, 15 H, Cp* Me), 1.08 (t, 6 H, Et CH_3), 0.20 (s, 9 H, $SiMe_3$), −5.16 (br, 2 H, B-H-B). − CI^+ MS (CH_4): *m/z* (%) = 410 (100) [M^+]. − The second compound to elute was yellow solid **14** (0.60 g, 58%). − ^{1}H NMR ($CDCl_3$) 2.11 (m, 2 H, Et CH_2), 1.90 (m 2 H, Et CH_2), 1.76 (s 15 H, Cp* Me), 1.10 (t, 6 H, Et CH_3), 0.23 (s, 9 H, $SiMe_3$), 0.16 (s, 9 H, $SiMe_3$), −4.70 (br, 2 H, B-H-B). − CI^+ MS (CH_4): *m/z* (%) = 507 (100) [M + 1]$^+$.

***nido*-Cp*Co[$Et_2C_2B_3H_3$(C≡CH)(C≡$CSiMe_3$)] (15):** Compound **14** (0.300 g, 0.593 mmol) was dissolved in 10 mL of dry THF and the solution was cooled to 0 °C. A solution of Bu_4NF (1.0 mL, 1.0 M in THF) was added dropwise and the reaction mixture was stirred at 0 °C in air for 1 h. The mixture was warmed to room temperature and stirred for 30 min. The solvent was removed using a rotary evaporator and the product was subsequently taken up in CH_2Cl_2, placed on a 12-cm column of silica gel, and eluted with hexanes affording a yellow solution. The solvent was removed in vacuo, leaving yellow solid **15** (0.206 g, 80%). − ^{1}H NMR ($CDCl_3$): δ = 3.45 (s, 1 H, C≡CH) 2.10 (m, 2 H, Et CH_2), 1.91 (m, 2 H, Et CH_2), 1.71 (s, 15 H, Cp* Me), 1.10 (t, 6 H, Et CH_3), 0.18 (s, 9 H, $SiMe_3$), −4.70 (br, 2 H, B-H-B). − CI^+ MS (CH_4): *m/z* (%) = 435 (1009 [M + 1]$^+$.

1,4-[*nido*-Cp*$CoEt_2C_2B_3H_3$(C≡$CSiMe_3$)(C≡C)]$_2C_6H_4$ (16): Compound **15** (0.200 g, 0.461 mmol), diiodobenzene (0.076 g, 0.231 mmol), bis(benzonitrile)palladium(II) chloride (0.009 g, 0.023 mmol), copper(I) iodide (0.0044 g, 0.023 mmol), and triphenylphosphane (0.012 g, 0.0461 mmol) were placed in a Schlenk flask, vacuum-degassed and placed under an inert gas. About 50 mL of dry diethylamine (freshly distilled from CaH_2) was added via cannula and the reaction mixture was stirred at room temperature for 36 h. The solvent was removed under vacuum and the resulting crude product was column chromatograped on silica gel [elution with CH_2Cl_2/hexane (1:5)]. The first product to elute was **16**, obtained as a yellow solid (0.19 g, 87%) upon solvent removal. − ^{1}H NMR ($CDCl_3$): 7.49 (s, 4 H, C_6H_4), 2.14 (m, 4 H, Et CH_2), 1.93 (m, 4 H, Et CH_2), 1.72 (s, 30 H, Cp*), 1.13 (t, 12 H, Et CH_3), 0.23 (s, 18 H, $SiMe_3$), −4.62 (br, 2 H, B-H-B). − CI^+ MS (CH_4): *m/z* (%) = 946 (100), [M + 4]$^+$. − The second compound to elute was tentatively identified from its mass spectrum as *nido*-[(C_5Me_5)$CoEt_2C_2B_3H_3$−(C≡$CSiMe_3$)(C≡C)]$_2$. − CI^+ MS (CH_4): *m/z* (%) = 870 (100) [M + 4]$^+$.

Acknowledgments

Funding from the National Science Foundation (Grants No. CHE 9322490 and CHE 9980708) is gratefully acknowledged. We thank J. Monte Russell and Barbara Gilmore for assistance in some of the syntheses and spectroscopy.

[1] [1a] H.-J. Schanz, M. Sabat, R. N. Grimes, *Angew. Chem. Int. Ed.* **2001**, *40*, 2705. − [1b] For part 56, see: M. Bluhm, H. Pritzkow, W. Siebert, R. N. Grimes, *Angew. Chem.* **2000**, *112*, 4736; *Angew. Chem. Int. Ed.* **2000**, *39*, 4562.

[2] [2a] R. N. Grimes, in: *Advances in Boron Chemistry* (Ed.: W. Siebert), Royal Society of Chemistry, **1997**, p. 321−332, and references therein. − [2b] N. S. Hosmane, in: *Contemporary Boron Chemistry* (Eds.: M. Davidson, A. K. Hughes, T. B. Marder, K. Wade), Royal Society of Chemistry, **2000**, p. 299, and references therein.

[3] [3a] T. T. Chin, R. N. Grimes, W. E. Geiger, *Inorg. Chem.* **1999**, *38*, 93. − [3b] R. N. Grimes, *J. Organomet. Chem.* **1999**, *581*, 1. − [3c]R. N. Grimes, in: *Contemporary Boron Chemistry* (Eds.: M. Davidson, A. K. Hughes, T. B. Marder, K. Wade), Royal Society of Chemistry, **2000**, p. 283.

[4] R. N. Grimes, in: *The Borane-Carborane-Carbocation Continuum* (Ed.: J. Casanova), Wiley Interscience, **1998**, chapter 13, p. 307−329, and references therein.

[5] M. Bluhm, H. Pritzkow, W. Siebert, R. N. Grimes, *Angew. Chem.* **2000**, *112*, 4736; *Angew. Chem. Int. Ed.* **2000**, *39*, 4562.

[6] [6a] M. A. Curtis, T. Müller, V. Beez, H. Pritzkow, W. Siebert, R. N. Grimes, *Inorg. Chem.* **1997**, *36*, 3602. − [6b] X. Wang, M. Sabat, R. N. Grimes, *Organometallics* **1995**, *14*, 4668.

[7] Selected recent references: [7a] S. L. Stang, F. Paul, C. Lapinte, *Organometallics* **2000**, *19*, 1035. − [7b] A. Harriman, R. Ziessel, *Chem. Commun.* **1996**, 1707. − [7c] O. Lavastre, M. Even, P. H. Dixneuf, A. Pacreau, J. P. Vairon, *Organometallics* **1996**, *15*, 1530. − [7d] F. Coat, C. LaPinte, *Organometallics* **1996**, *15*, 477. − [7e] M. Brady, W. Weng, J. A. Gladysz, *J. Chem. Soc., Chem. Commun.* **1994**, 2655. − [7f] N. D. Jones, M. O. Wolf, D. M. Giaquinta, *Organometallics* **1997**, *16*, 1352. − [7g] T. Weyland, C. Lapinte, G. Frapper, M. J. Calhorda, J.-F. Halet, L. Toupet, *Organometallics* **1997**, *16*, 2024. − [7h] M. Akita, M.-C. Chung, A. Sakurai, S. Sugimoto, M. Terada, M. Tanaka, Y. Moro-oka, *Organometallics* **1997**, *16*, 4882. − [7i] H. Schimanke, R. Gleiter, *Organometallics* **1998**, *17*, 275. − [7j] H. Fink, N. J. Long, A. J. Martin, G. Opromolla, A. J. P. White, D. J. Williams, P. Zanello, *Organometallics* **1997**, *16*, 2646. − [7k] N. J. Long, A. J. Martin, F. Fabrizi de Biani, P. Zanello, *J. Chem. Soc., Dalton Trans.* **1998**, 2017. − [7l] F. Coat, M.-A. Guillevic, L. Toupet, F. Paul, C. Lapinte, *Organometallics* **1997**, *16*, 5988. − [7m] A.

Mayr, M. P. Y. Yu, V. W-W. Yam, *J. Am. Chem. Soc.* **1999**, *121*, 1760. – [7n] W. Jiang, D. E. Harwell, M. D. Mortimer, C. B. Knobler, M. F. Hawthorne, *Inorg. Chem.* **1996**, *35*, 4355. – [7o] W. E. Meyer, A. J. Amoroso, C. R. Horn, M. Jaeger, J. A. Gladysz, *Organometallics* **2001**, *20*, 1115.

[8] J. K. Pudelski, M. R. Callstrom, *Organometallics* **1994**, *13*, 3095.

[9] N. D. Jones, M. O. Wolf, D. M. Giaquinta, *Organometallics* **1997**, *16*, 1352.

[10] X. Meng, M. Sabat, R. N. Grimes, *J. Am. Chem. Soc.* **1993**, *115*, 6143.

[11] K. W. Piepgrass, K. E. Stockman, M. Sabat, R. N. Grimes, *Organometallics* **1992**, *11*, 2404.

[12] B. A. Gilmore, J. M. Russell, R. N. Grimes, unpublished observations.

[13] This is true regardless of whether the structure of **15** is **A** or **B**; here we arbitrarily show **16** as linked via the middle boron atoms on the carborane rings.

[14] K. E. Stockman, Ph.D. Dissertation, University of Virginia, **1995**.

[15] R.B. Maynard,.L. Borodinsky, R. N. Grimes, *Inorg. Synth.* **1983**, *22*, 211.

[16] *SIR92*: M.C. Burla, M. Camalli, G. Cascarano, C. Giacovazzo, G. Polidori, R. Spagna, D. Viterbo, *J. Appl. Crystallogr.* **1989**, *22*, 389.

[17] D. T. Cromer, J. T. Waber, *International Tables for X-ray Crystallography*, The Kynoch Press, Birmingham, England, **1974**, vol. IV, Table 2.2 A.

[18] *teXsan*: Crystal Structure Analysis Package, Molecular Structure Corporation, **1985** and **1992**.

Received April 5, 2001
[I01127]

Metalated 1,3-Azaphospholes: *1H*-1,3-Benzazaphosphole and 1,3-Benzazaphospholide Tungsten(0) and Tungsten(II) Complexes

Joachim Heinicke,*[a] Anushka Surana,[a] Normen Peulecke,[a] Raj Kumar Bansal,[b] Alexander Murso,[c] and Dietmar Stalke[c]

Keywords: Phosphorus heterocycles / Tungsten / Metalation

2-*tert*-Butyl-1*H*-1,3-benzazaphosphole (**1a**) reacts with *t*BuLi without addition to the P=C bond to form a lithium benzazaphospholide that affords the η^1-(benzazaphospholide-*P*)tungsten(II) complex **2** upon reaction with [CpW(CO)$_3$Cl]. It is sensitive to alcoholysis and to air oxidation yielding **1a** and the *P*-oxo-benzazaphospholide complex **3**, respectively. The (1,3-benzazaphosphole)pentacarbonyltungsten complex **4**, obtained from **1b** and [W(CO)$_5$(THF)], reacts preferentially with *t*BuLi by lithiation of the NH function and is attacked by [CpW(CO)$_3$Cl] at phosphorus to give the mixed valence bimetallic tungsten(II)-tungsten(0) benzazaphospholide complex **5**. A side product, (3-*tert*-butyl-2-methyl-1,3-benzazaphosphole)pentacarbonyltungsten (**6**), is attributed to side-reaction where *t*BuLi adds to the P=C bond in **4**. The composition of the products was determined from X-ray structure analysis of **3** and spectroscopic data.

Introduction

Phospholide[1−4] and pyrrolide[3−6] complexes have attracted considerable interest in the past years, and some di- and triazaphosphol(id)e complexes have also been reported.[7] Azaphospholide complexes, analogues of pyrrolide or of diphospholide complexes, as well as 1,3-benzazaphospholide complexes are, however, still unknown. The recent discovery of a convenient synthetic access to 2-substituted 1*H*-1,3-benzazaphospholes[8] prompted us to fill this gap partly and to explore the reactivity and use of these very stable but under-investigated phosphaaromatic heterocycles as ligands.[8−11] The only 1,3-benzazaphosphole complex reported to date is pentacarbonyl-η^1-(2-phenyl-1,3-benzazaphosphole-*P*)chromium.[10] Lithiation of 2-phenylbenzazaphosphole by Et$_2$NLi has also been described,[10] although the lithium benzazaphospholide was not isolated and separated from the secondary amine, which is preferentially attacked by electrophiles other than alkyl halides. We report here on an alternative metalation procedure avoiding this problem and the synthesis of the first 1,3-benzazaphosphole and 1,3-benzazaphospholide tungsten complexes.

[a] Institut für Chemie und Biochemie, Ernst-Moritz-Arndt-Universität Greifswald,
Soldmannstraße 16, 17487 Greifswald, Germany,
Fax: (internat.) +49-3834/86-4319
E-mail: heinicke@uni-greifswald.de
[b] Department of Chemistry, University of Rajasthan,
Jaipur 302 004, India,
[c] Institut für Anorganische Chemie, Universität Würzburg,
Am Hubland, 97074 Würzburg, Germany,
Fax: (internat.) +49-931/888-4619
E-mail: dstalke@chemie.uni-wuerzburg.de

Results and Discussion

Synthesis

Whilst 1*H*-1,3-benzazaphospholes and *n*BuLi produce mixtures of addition and metalation products, a selective monolithiation of the NH function is achieved by treatment of **1a** with one equivalent of *t*BuLi in ether or THF at low temperature. Like ambident anions formed by the metalation of pyridylphosphanes,[12] the resulting lithium 1,3-benzazaphospholide **Li-1a** can be used directly for the synthesis of complexes as exemplified by the reaction with [CpW(CO)$_3$Cl] (Scheme 1). **Li-1a** reacts selectively at phosphorus to give the dark red-brown benzazaphospholide tungsten complex **2**. It is slightly soluble in hexane and readily soluble in more polar solvents like toluene or ethers. Like related Cp(CO)$_3$W-phospholide[13−15] or Cp(CO)$_3$W-phosphide[16] complexes, **2** is a very reactive compound. Although less sensitive towards hydrolysis than the extremely reactive *N*-silyl- or *P*-stannyl-benzazaphospholes,[17] the P−W bond of **2** is cleaved readily by OH/OD reagents, as shown by the addition of CD$_3$OD to yield **1b**. The latter is also formed on heating **2** to 80 °C in toluene for one day, whereas related but more stable Cp(CO)$_3$W complexes with non-anellated phospholide ligands form tungsten-bridged complexes.[15] Compound **2** is also sensitive to air oxidation. Crystallization of a sample oxidized in THF gave single crystals of the toluene monosolvate of the *P*-oxo-benzazaphospholide tungsten complex **3**, from toluene/hexane, which allowed an X-ray crystal structure analysis (Figure 1).

The (1,3-benzazaphosphole)pentacarbonyltungsten complex **4**, obtained from **1b** and [W(CO)$_5$(THF)], can be lithiated in an analogous manner with *tert*-butyllithium and trapped with [CpW(CO)$_3$Cl]. The formation of the mixed valence bimetallic complex **5**, with zero- and two-valent

 © WILEY-VCH Verlag GmbH, 69451 Weinheim, 2001 1434−1948/01/1010−2563 $ 17.50+.50/0

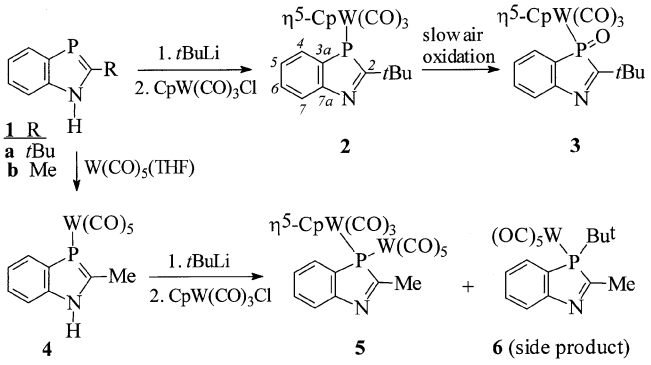

Scheme 1

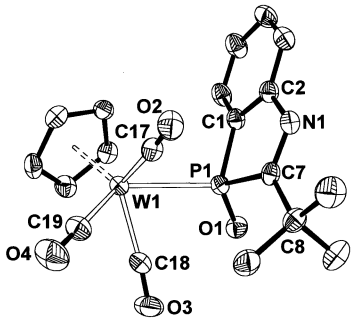

Figure 1. Solid state structure of **3** (anisotropic displacement parameters drawn at 50% probability level, hydrogen atoms and toluene omitted for clarity); selected bond lengths [Å] and angles[°]: W1−P1 2.5591(7), W−C(O) 1.989(3) − 2.005(3), W−C(Cp) 2.314(3) − 2.361(3), P1−O1 1.507(2); W1−P1−O1 116.91(8), O1−P1−C1 114.18(12), O1−P1−C7 113.32(12), W1−P1−C1 107.79(9), W1−P1−C7 113.12(8), P1−W1−C17 78.03(8), P1−W1−C18 73.43(8), C17−W1−C19 76.77(12), C19−W1−C18 77.28(12); for ring parameters see Table 1

tungsten bound at the phosphorus atom, shows that the blockage of the phosphorus lone electron pair does not favor an attack at nitrogen, but that the lithiated pentacarbonyl tungsten complex **Li·4** also prefers substitution at the softer nucleophilic site. The lithiation itself proceeds less selectively, as seen from the occurrence of **6**. It is assumed that **6** is formed by the addition of *t*BuLi to the P=C double bond of **4** followed by reaction with [$CpW(CO)_3Cl$] and elimination of [$CpW(CO)_3H$]. In the crude product the ratio **5**:**6** was found to be ca. 2:1.

Structure

The ^1H, ^{13}C and ^{31}P NMR chemical shifts and coupling patterns, the observance of molecular ions in the mass spectrum and satisfactory elemental analysis give evidence for the structures of **2**, **4** and **5**. Like related $Cp(CO)_3W$-phospholide complexes,[15] compound **2** ($\delta = -102.4$, $^1J_{P-W} = 50.1$ Hz) reveals a strong up-field coordination shift $\Delta\delta$(**2**−**Li·1a**) = −159 and a very small one-bond P−W coupling constant. The acyclic [$Cp(CO)_3W-PPh_2$] ($\delta = -63.3$, $^1J_{P-W} = 52$ Hz)[16] exhibits a similar low P−W coupling constant, but a much smaller upfield coordination shift relative to the corresponding alkali metal phosphides (Ph_2PLi: $\delta = -21.4$[18]). The larger upfield coordination shift in the formal 6π- or 10π-heterocyclic phosphido complexes with the same ML_n fragment reflects a larger increase in the electron density at phosphorus and may be attributed to a reduced ability of the π-electrons at phosphorus to take part in cyclodelocalization; it may also be supported by a more effective back donation compared to that in $Ph_2P-W(CO)_3Cp$ or in the $W^0(CO)_5$-benzazaphosphole complex **4**. The ^{13}C nuclei of the five-membered ring and of C-5 to C-7 are markedly deshielded by the complexation, $\Delta\delta$(**2**−**1a**) ≈ 20 (C-2), 12 (C-3a, C-7, C-7a) and 7 (C-5, C-6), whilst the one-bond P−C couplings show different trends, $^1J_{P-C2}$ increases from 57 Hz in **1a** to 61.8 Hz in **2**, and $^1J_{P-C3a}$ decreases from 41 to 14 Hz. The chemical shift values are significantly closer to those of 3*H*-1,3-benzazaphospholes[17,19,20] than to those of **1** although the one-bond coupling constants of **2** are significantly larger than in the 3*H*-isomers. These findings imply that the nature of **2** is in-between that of the aromatic 1*H*- and the non-aromatic 3*H*-3-alkyl-1,3-benzazaphospholes,[21−23] although probably closer to the latter. For the related phospholide $CpW(CO)_3$ complexes a similar situation was deduced from the X-ray crystal structure analysis.[15] The compounds were classified from the structural standpoint as halfway between phospholes with pyramidal P and localized π-bonds and phospholes with planar P and delocalized π-bonds.

In the oxidation product **3** the framework of **2** is preserved (Figure 1) but the transition to four-coordinate phosphorus consolidates a non-aromatic, 3*H*-indole-like π-system. The lack of cyclodelocalization becomes evident by comparison of selected bond lengths and angles of the five-membered ring in **3** and the corresponding parameters of its phosphaaromatic precursor **1a**[17] (Table 1). Within the P−C−N fragment the P−C bond is considerably widened and becomes longer than the P−C(aryl) bond, whilst the C−N bond is shortened. The smaller N1−C7 bond and the approximation of the C1−C2−N angle in **3** to an ideal sp^2 geometry at the expense of the C2−C1−P angle reflects the strengthening of a coplanar *N*-phenyl-azomethine π-system. In the acyclic metallaphosphane oxide [$oTol_2P(O)-W(CO)_3Cp$],[16b] the P1−W1 distances of the two independent molecules in the unit cell are slightly longer [2.571(8), 2.589(9) Å] than in **3**, although shorter than the sum of the covalent radii (2.65 Å),[24] and the P−O bonds (double bond character) are slightly shorter [1.46(2), 1.49(2) Å]. The W−P−O angle is larger in **3** due to the small C−P−C angle within the five-membered ring.

The known compound η^1-(2-phenyl-1,3-benzazaphosphole-*P*)pentacarbonylchromium exhibits a very low positive complexation shift ($\Delta\delta = 4.4$) and classifies 1*H*-1,3-benzazaphospholes as weak donors.[10] The tungsten pentacarbonyl complex **4** even displays a negative coordination shift ($\Delta\delta = -35.0$). The upfield shift of the tungsten relative to the related chromium complex reflects the typical core-effect in transition metal phosphane complexes[25] and is also observed for related (phosphaindolizine)metallapentacarbonyls (M = Cr, Mo, W).[26] The one bond $^{31}P-^{183}W$ coupling constant is much larger than in **2**, **5** and **6** and

Table 1. Comparison of selected structure data of **3** and corresponding data of **1a**[17]

Bond length [Å], angle [°]	**3**	**1a**
P1−C1	1.817(3)	1.793(3)
P1−C7	1.882(3)	1.712(4)
N1−C7	1.290(3)	1.374(4)
N1−C2	1.430(3)	1.380(4)
C1−C2	1.404(4)	1.389(4)
C7−C8	1.522(4)	1.514(4)
P1−C7−N1	113.43(19)	112.3(2)
C1−P1−C7	87.88(12)	90.1(2)
C2−N1−C7	112.6(2)	115.1(3)
C1−C2−N1	117.1(2)	111.9(3)
C2−C1−P1	108.27(19)	110.7(2)

similar to that in pentacarbonyltungsten complexes of less-basic triorganophosphanes.[25] The effect of the complexation on the 1*H*-1,3-benzazaphosphole π-system is rather small and limited mainly to the carbon atoms adjacent to phosphorus. C-2 and C-3a of **4** are shifted by $\Delta\delta \approx 7$ in the ^{13}C NMR spectrum and display much lower P−C coupling constants. For C-4 and the methyl carbon in the β-position to the phosphorus this trend is much smaller, and the other nuclei show no marked influence. In the tungsten complexes **5** and **6**, however, the cyclodelocalization seems to be lost. Both, the tungsten(II)- and the 3-*tert*-butyl-substituted 1,3-benzazaphosphole tungsten pentacarbonyl species, exhibit the signals of the ^{13}C nuclei C-5 to C-7a at significantly lower field than in **1** or **4**, in regions typical for 3-alkyl-1,3-benzazaphospholes.[17,19,20] The phosphido-character of the benzazaphospholide ligand is markedly reduced by complexation with $W(CO)_5$ as indicated by the less-negative phosphorus resonance of **5** relative to **2** ($\Delta\delta$ = 26.4) and the increased $^1J_{P-W}{}^{II}$ coupling constant, whereas $^1J_{P-W}{}^0$ is smaller than in **4** and **6** due to the higher donor strength of the benzazaphospholide relative to the 1*H*- and 3*H*-1,3-benzazaphospholes.

Conclusion

The aim of this work was to investigate the metalation of 1*H*-1,3-benzazaphospholes and to present novel 1,3-benzazaphospholide complexes as P−C homologues of indolides. It was shown that 1*H*-1,3-benzazaphospholes and tungsten pentacarbonyl complexes, represented by **1a** and **4**, may be lithiated by *t*BuLi selectively or preferentially at the NH function. The resulting ambident 1,3-benzazaphospholide anions react with the $[CpW(CO)_3Cl]$ exclusively at the softer nucleophilic site and furnish the η^1-*P*-coordinated tungsten(II) complex **2** and the mixed valence bimetallic tungsten(II)-tungsten(0) species **5**. The benzazaphospholide complexes are sensitive to hydrolysis and oxidation. A crystal structure analysis of the benzazaphospholide oxide complex **3** (toluene monosolvate) gave evidence of the molecular composition and, by comparing the bond lengths with those of **1a**, of a non-aromatic, 3*H*-indole-like π-system. The P-tetracoordinated di-tungsten complex **5** and the side product **6**, a 3-alkyl-benzazaphosphole $W(CO)_5$ complex, reveal ^{13}C NMR spectroscopic data which likewise are in accordance with a non-aromatic nature. Compound **2** is a borderline case: its carbon chemical shifts resemble those of 3*H*-1,3-benzazaphospholes whilst the magnitude of the $^1J_{P-C2}$ coupling constant is significantly larger. Only the electronic structure of the neutral benzazaphosphole $W(CO)_5$ complex **4** is similar to that in the phosphaaromatic heterocycles **1**.

Experimental Section

General: All manipulations were carried out under an atmosphere of dry argon using standard Schlenk and cannula techniques. Ether, THF and hydrocarbons were refluxed over sodium/benzophenone and distilled prior to use. C_6D_6 and $[D_8]$THF were dried with sodium or $LiAlH_4$ and recondensed. NMR spectra were recorded on a multinuclear FT NMR spectrometer Bruker Model ARX300 at 300.1 (^1H), 75.5 (^{13}C), and 121.5 (^{31}P) MHz. The ^1H, ^{13}C and ^{31}P chemical shifts are δ values relative to Me_4Si or H_3PO_4 (85%); coupling constants are quoted in Hz. IR spectra were measured on a Perkin−Elmer Model system 2000 and mass spectra on a single-focussing mass spectrometer AMD40 (Intectra). Melting points were determined in sealed capillaries under argon and are uncorrected. Elemental analyses were carried out using an elemental analyzer LECO Model CHNS-932 with standard combustion conditions (carbon combustion sometimes incomplete) and handling of the samples in air.

Materials: Compounds **1a** and **1b** were synthesized as reported recently;[8] $[W(CO)_5(THF)]$ and $[CpW(CO)_3Cl]$ were obtained by known procedures.[27] Other materials were used as purchased unless stated otherwise.

η^5-(2-*tert*-Butyl-1,3-benzazaphosphol-3-yl-*P*)(η^5-cyclopentadienyl)-tricarbonyltungsten (2): A solution of **1a** (290.6 mg, 1.52 mmol) in ether was cooled to −78 °C and lithiated with an equimolar amount of *t*BuLi dissolved in pentane (^{31}P NMR in $[D_8]$THF: δ = 56.6). After 30 min. a solution of $[CpW(CO)_3Cl]$ (560 mg, 1.52 mmol) in ether was added (−78 °C) affording a red brown mixture. This was allowed to warm to room temperature and stirred for one day. The precipitate was then removed, and the solvent was evaporated in vacuo. The residue was crystallized from hot toluene affording 614 mg (77%) of red solid **2**, slightly contaminated by **1a**. It is insoluble in hexane, m.p. 80−83 °C. − ^1H NMR ($[D_8]$THF): δ = 1.41 (d, $^4J_{P-H}$ = 0.6, 9 H, CMe_3), 5.34 (s, 5 H, Cp), 7.08 ("t"dd, ^3J = 7.5, $^4J_{P-H}$ = 3.3, ^4J = 1.2, 1 H, H-5), 7.22 (m, ^3J = 7.4, 7.7, $^4J \approx {}^5J_{P-H} \approx 1$, 1 H, H-6), 7.75 (br. d, ^3J = 7.7 Hz, 1 H) and 7.78 (d, ^3J = 8.1, 1 H) (H-4 and H-7). − $^{13}C\{^1H\}$ NMR ($[D_8]$THF): δ = 32.2 (d, ^3J = 5.6, C*Me*$_3$), 40.7 (d, ^2J = 20.3, *C*Me$_3$), 94.3 (Cp), 123.8 (d, ^3J = 6, C-5), 124.7 (C-7), 126.3 (C-6), 127.1 (d, ^2J = 20, C-4), 150.3 (d, ^1J = 14, C-3a), 155.5 (d, ^2J = 9, C-7a), 209.3 (d, ^1J = 62, C-2), 214.9, 218.3, 233.4 (3 CO). − $^{31}P\{^1H\}$ NMR ($[D_8]$THF): δ = −102.4 ($^1J_{P-W}$ = 50.1). − EI-MS (70 eV): *m*/*z* (%) = 523 (23) [M^+ (^{184}W)], 480 (27), 455 (44), 196 (72), 184 (93), 28 (100). − $C_{19}H_{18}NO_3PW$ (523.17): calcd. C 43.62, H 3.47, N 2.68; found C 40.52, H 3.50, N 2.47.

η^5-(2-*tert*-Butyl-3-oxo-1,3-benzazaphosphol-3-yl-*P*)(η^5-cyclopentadienyl)tricarbonyltungsten Toluene Monosolvate (3): A small amount of **2** dissolved in THF was oxidized by allowing slow diffusion of air into the Schlenk tube. Since addition of hexane failed

to give a precipitate the solvent was removed in vacuum and replaced by toluene. On addition of hexane small, pale-yellow single crystals of the toluene monosolvate **3** deposited at +4 °C within 3 days (yield not determined). The crystal and molecular structure was determined by X-ray diffraction (Table 1, Figure 1). – ^{1}H NMR (C_6D_6): δ = 1.71 (s, 9 H, CMe_3), 2.11 (s, 3 H, toluene), 4.60 (s, 5 H, Cp), 6.93 (ddd, ^3J = 7.1, J_{P-H} = 3.6, ^4J = 1.3, 1 H, 4- or 7-H), 6.97–7.13 (m, toluene), 7.05 and 7.40 (both "t"m, $^3J \approx$ 6, 7, 5- and 6-H, partially superimposed by C_6D_6 side band), 7.65 (ddd, ca. ^3J = 7.2, J = 2, 1, 1 H, 7- or 4-H). – ^{31}P{^{1}H} NMR ([D_8]THF): δ = 61.3 ($^1J_{P-W}$ = 135).

η^1-(2-Methyl-1*H*-1,3-benzazaphosphole-*P*)pentacarbonyltungsten (4): A solution of [W(CO)$_5$(THF)], prepared by irradiation of [W(CO)$_6$] (2.324 g, 6.60 mmol) in THF (300 mL; 145 mL of CO evolved), was added to a solution of **1b** (0.984 g, 6.60 mmol) in THF (5 mL). After one day at room temperature the solvent and volatile tungsten complexes were removed in vacuo and the residue fractionally extracted with hexane yielding in the later fractions 1.272 g (41%) of orange **4**, m.p. 122–124 °C. – ^{1}H NMR ($CDCl_3$): δ = 2.73 (d, $^3J_{P-H}$ = 17.8, 3 H, Me), 7.23 ("t"dd, $^3J \approx$ 7.6, 8, $^4J_{P-H}$ = 3.8, ^4J = 0.9, 1 H, H-5), 7.36 ("tt", $^3J \approx$ 7.6, $^5J_{P-H} \approx$ $^4J \approx$ 1.2, 1 H, H-6), 7.52 (d, ^3J = 8.6, 1 H, H-7), 7.87 ("t", $^3J \approx$ $^3J_{P-H} \approx$ 7.8, 1 H, H-4), 9.60 (br, 1 H, NH). – ^{1}H NMR (C_6D_6): δ = 2.04 (d, $^3J_{P-H}$ = 18, 3 H, Me), 6.98 (br. d, ^3J = 8.3, 1 H, H-7), 7.06 (dddd, ^3J = 7.0, 8.0, $^4J_{P-H}$ = 2.8, ^4J = 1.0, 1 H, H-5), 7.20 ("tt", ^3J = 8.3, 7.0, $^5J_{P-H} \approx$ $^4J \approx$ 1.3, 1 H, H-6), 7.98 ("t" br., $^3J \approx$ $^3J_{P-H} \approx$ 7, 8, 1 H, H-4). – ^{13}C{^{1}H} NMR ($CDCl_3$): δ = 15.8 (d, ^2J = 15.0, Me), 114.3 (d, ^3J = 3.2, C-7), 121.4 (d, ^3J = 14.0, C-5), 125.8 (d, ^4J = 3.5, C-6), 126.5 (d, ^2J = 13.5, C-4), 136.3 (d, ^1J = 21.9, C-3a), 141.9 (s, C-7a), 167.6 (d, ^1J = 30.8, C-2), 194.6 (d sat, ^2J = 8.5, $^1J_{C-W}$= 124, 4 CO), 199.8 (d, ^2J = 29.1, 1 CO). – ^{31}P{^{1}H} NMR ($CDCl_3$): δ = 36.7 (sat, $^1J_{P-W}$ = 242.6). – IR (Nujol): $\tilde{\nu}$ = 3405 m (NH), 2071 m, 1981 vs, 1946 vs, 1880 s (CO) cm^{-1}. – EI-MS (70 eV): *m*/*z* (%; data for ^{184}W) = 473 (80) [M$^+$], 445 (4), 417 (64) [M$^+$ – 2CO], 389 (68) [M$^+$ – 3CO], 361 (41) [M$^+$ – 4CO], 333 (62) [M$^+$ – 5CO], 149 (100) [**1b**$^+$], 148 (98). – $C_{13}H_8NO_5PW$ (473.02): calcd. C 33.01, H 1.70, N 2.96; found C 33.20, H 2.11, N 2.60.

η^1-{2-Methyl-3-[(η^5-cyclopentadienyl)tricarbonyltungsten]-1,3-benzazaphosphole-*P*}pentacarbonyltungsten (5) and η^1-(3-*tert*-Butyl-2-methyl-1,3-benzazaphosphole-*P*)pentacarbonyltungsten (6): [CpW(CO)$_3$Cl] (277 mg, 0.754 mmol) was added at –70 °C to a solution prepared from **4** (358 mg, 0.757 mmol) in ether (10 mL) and *t*BuLi in pentane (0.45 mL, 0.754 mmol) as described above. The mixture was allowed to stir at room temperature for 3 days. Then it was filtered and washed with ether. Removal of the solvent in vacuo afforded a mixture of **5** and **6** in a molar ratio of ca. 2:1 (based on ^{1}H integral ratio of the CH_3 signals) along with a small amount of unchanged **4**. Fractional crystallization with hexane and then with toluene gave 300 mg (49%) of **5** (from toluene) and 80 mg (20%) of **6** (from hexane) as red solids. Compound **6** was impure and identified by it's characteristic NMR spectroscopic data.

5: ^{1}H NMR ([D_8]THF): δ = 2.72 (d, ^3J = 7.4, 3 H, Me), 5.20 (d, J = 2.0, 5 H, Cp), 7.27–7.35 (m, 1 H H-5), 7.37 ("t", $^3J \approx$ 7.3, 1 H, H-6), 7.78 (d, ^3J = 7.6, 1 H, H-7), 7.85 (dd, ^3J = 6.7, $^3J_{P-H}$ = 5, 1 H, H-4). – ^{13}C{^{1}H} NMR ([D_8]THF): δ = 20.1 (d, ^2J = 28.8, Me), 94.9 (s, Cp), 124.7 (d, ^2J = 2.0, C-7), 126.7 (d, ^3J = 8.2, C-5), 127.3 (d, ^2J = 14.1, C-4), 129.9 (d, ^4J = 1.2, C-6), 148.4 (d, ^1J = 28.7, C-3a), 152.5 (d, ^2J = 16.6, C-7a), 193.1 (d, ^1J = 15.3, C-2), 198.6 (d, sat, ^2J = 5.4, $^1J_{C-W}$ = 126, 4 CO), 200.6 (d, ^2J = 18.3, 1 CO), 216.9 (d, ^2J = 17.7, 1 CO), 217.6 (d, ^2J = 18.2, 1 CO), 219.9 (d, ^2J = 5.5, 1 CO). – ^{31}P{^{1}H} NMR ([D_8]THF): δ = – 76.1 (sat, $^1J_{P-W}$ = 180.8, 90.8). – EI-MS (70 eV, 240 °C): *m*/*z* = 804 (34), [M$^+$ – 1 (^{184}W)], 776 (20), 749 (12) [M$^+$ – 2CO], 721 (32) [M$^+$ – 3CO], 683 (54) [M$^+$ – 2CO-Cp], 665 (100) [M$^+$ – 5CO], 645 (41), 625 (62), 604 (48), 396 (61), 341 (62), 309 (50), 149 (65). – $C_{21}H_{12}NO_8PW_2$ (804.77): calcd. C 31.34, H 1.50, N 1.74; found C 29.00, H 1.76, N 1.64.

6 (hexane): ^{1}H NMR ([D_8]THF): δ = 1.19 (d, ^3J = 16.1, 9 H, CMe_3), 2.63 (d, ^3J = 6.8 Hz, 3 H, Me), 7.41–7.45 (m, 1 H, H5), 7.54 ("tt", $^3J \approx$ 7.4, 7.8, $^4J \approx$ $^5J_{P-H} \approx$ 1.2, 1 H, H-6), 7.70–7.75 (m, 2 H, H-4, H-7). – ^{13}C{^{1}H} NMR ([D_8]THF): δ = 21.7 (d, ^2J = 15, Me), 124.7 (d, ^2J = 4, C-7), 127.8 (d, ^3J = 8.4, C-5), 130.2 (d, ^2J = 13.3, C-4), 132.5 (br., C-6), 133.5 (d, ^1J = 48.2, C-3a), 156.8 (d, ^2J = 16, C-7a), 181.3 (br., uncertain due to low intensity, C-2). – ^{31}P{^{1}H} NMR ([D_8]THF): δ = 50.8 (sat, $^1J_{P-W}$ = 216.4).

Crystal Data and Structure Determination for 3: The data set was collected at low temperature using an oil-coated shock-cooled crystal[28] on a Bruker APEX-CCD diffractometer equipped with Mo-K_α (λ = 71.073 pm) radiation and a low temperature device at 173(2) K. The structure was solved by Patterson methods (SHELXS-NT 97)[29] and refined by full-matrix least-squares methods against F^2 (SHELXL-NT 97).[30] R values defined as $R1 = \Sigma||F_o| - |F_c||/\Sigma|F_o|$, $wR2 = [\Sigma w(F_o^2 - F_c^2)^2/\Sigma w(F_o^2)^2]^{0.5}$, $w = [\sigma^2(F_o^2) + (g_1P)^2 + g_2P]^{-1}$, $P = 1/3[\max(F_o^2,0) + 2F_c^2]$. SADABS 2.0 was employed as the program for empirical absorption correction.[31]

3: $C_{26}H_{26}NO_4PW$, M = 631.30, monoclinic, space group $P2_1/n$, a = 11.3819(3), b = 10.4653(3), c = 21.1456(6) Å, β = 104.5600(10)°, V = 2.43787(12) nm^3, Z = 4, $\rho_{cal.}$ = 1.720 Mg/m^3, μ = 4.836 mm^{-1}, F(000) = 1240. 41621 reflections measured, 6055 unique, R(int) = 0.0383, $wR2$(all data) = 0.0545, $R1[I > 2\sigma(I)]$ = 0.0230, g_1 = 0.0301, g_2 = 0.8837 for 5742 data, 228 restraints and 363 parameters. In addition to the tungsten complex the unit cell contains a non-coordinating disordered toluene molecule. The occupancy factors of the solvent molecule refined to 0.788 and 0.272. The toluene molecule was assigned ideal positions and refined using ADP restraints. All non-hydrogen atoms were refined anisotropically. The hydrogen atoms of the cyclopentadienyl ligand were taken from the difference Fourier map and refined freely, all other hydrogen atoms were geometrically idealized and refined using a riding model. Selected bond lengths and angles of **3** can be found in Table 1.

Crystallographic data for the structure of **3** has been deposited with the Cambridge Crystallographic Data Centre as supplementary publication no. CCDC-161162. Copies of the data can be obtained free of charge on application to CCDC, 12 Union Road, Cambridge CB2 1EZ, UK [Fax: (internat.) +44-1223/336-033, E-mail: deposit@ccdc.cam.ac.uk].

Acknowledgments

This work was generously supported by the Deutsche Forschungsgemeinschaft and the Fonds der Chemischen Industrie. We thank B. Witt and Dr. M. K. Kindermann for NMR studies.

[1] J. F. Nixon, *Chem. Rev.* **1988**, *88*, 1327–1362.
[2] F. Mathey, *Coord. Chem. Rev.* **1994**, *137*, 1–52.
[3] K. B. Dillon, F. Mathey, J. F. Nixon, *Phosphorus: The Carbon Copy*, Wiley, New York, **1998**.
[4] A. P. Sadimenko, A. D. Garnovskii, N. Retta, *Coord. Chem. Rev.* **1993**, *127*, 237–318.
[5] C. Janiak, N. Kuhn, *Adv. Nitrogen Heterocycl.* **1996**, *2*, 179–210.

[6] M. O. Senge, *Angew. Chem. Int. Ed.* **1996**, *35*, 1923−1925.
[7] [7a] A. Schmidpeter, in *Comprehensive Heterocyclic Chemistry-II* (Eds.: A. R. Katritzky, C. W. Rees, E. F. V. Scriven), Pergamon, Oxford, **1996**, Vol. *3*, p. 709, 715; Vol. *4*, p. 771. − [7b] R. K. Bansal, K. Karaghiosoff, A. Schmidpeter, *Tetrahedron* **1994**, *50*, 7675−7745.
[8] [8a] R. K. Bansal, N. Gupta, J. Heinicke, G. N. Nikonov, F. Saguitova, D. C. Sharma, *Synthesis* **1999**, *2*, 264−269. − [8b] J. Heinicke, N. Gupta, A. Surana, N. Peulecke, B. Witt, K. Steinhauser, R. K. Bansal, P. G. Jones, manuscript in preparation.
[9] K. Issleib, R. Vollmer, H. Oehme, H. Meyer, *Tetrahedron Lett.* **1978**, 441−444.
[10] K. Issleib, R. Vollmer, *Z. Anorg. Allg. Chem.* **1981**, *481*, 22−32.
[11] J. Heinicke, A. Tzschach, *Tetrahedron Lett.* **1982**, *23*, 3643−3646.
[12] [12a] M. Pfeiffer, T. Stey, H. Jehle, B. Knüpfel, W. Malisch, V. Chandrasekhar, D. Stalke, *Chem. Commun.* **2001**, 337−338. − [12b] A. Steiner, D. Stalke, *Organometallics* **1995**, *14*, 2422−2429.
[13] E. H. Braye, K. K. Joshi, *Bull. Soc. Chim. Belg.* **1971**, *80*, 651−653.
[14] E. W. Abel, C. Towers, *J. Chem. Soc., Dalton Trans.* **1979**, 814−819.
[15] F. Mercier, L. Ricard, F. Mathey, *Organometallics* **1993**, *12*, 98−103.
[16] [16a] W. Malisch, R. Maisch, *J. Organomet. Chem.* **1981**, *220*, C1−C6. − [16b] W. Malisch, K. Hindahl, K. Grün, W. Adam, F. Prechtl, W. S. Scheldrick, *J. Organomet. Chem.* **1996**, *509*, 209−214.
[17] A. Surana, S. Singh, R. K. Bansal, N. Peulecke, A. Spannenberg, J. Heinicke, *J. Organomet. Chem.* in press.
[18] R. A. Bartlett, M. M. Olmstead, P. P. Power, G. A. Sigel, *Inorg. Chem.* **1987**, *26*, 1941−1946.
[19] J. Heinicke, *J. Organomet. Chem.* **1989**, *364*, C17−C21.
[20] H. M. Walborsky, P. Ronman, *J. Org. Chem.* **1978**, *43*, 731−734.
[21] L. Nyulászi, G. Csonka, J. Réffy, T. Veszprémi, J. Heinicke, *J. Organomet. Chem.* **1989**, *373*, 49−55.
[22] L. Nyulászi, G. Csonka, J. Réffy, T. Veszprémi, J. Heinicke, *J. Organomet. Chem.* **1989**, *373*, 57−61.
[23] [23a] L. Nyulászi, T. Veszprémi, *J. Mol. Struct.* **1995**, *347*, 57−72. − [23b] L. Nyulászi, T. Veszprémi, *Phosphorus Sulfur Silicon* **1996**, *109/110*, 109−112.
[24] L. Pauling, *Die Natur der Chemischen Bindung*, VCH, Weinheim, **1962**.
[25] P. S. Pregosin, R. W. Kunz, *^{31}P and ^{13}C NMR of Transition Metal Phosphine Complexes*, in *NMR: Basic Principles and Progress Series* (Eds.: D. Diel, E. Fluck, R. Kosfeld), Springer, Berlin Heidelberg New York, **1979**, pp. 54, 99.
[26] N. Gupta, C. B. Jain, J. Heinicke, R. K. Bansal, P. G. Jones, *Eur. J. Inorg. Chem.* **1998**, 1079−1086.
[27] [27a] H. L. Krauss, in *Synthetic Methods of Organometallic and Inorganic Chemistry* (Ed.: W. A. Herrmann), Thieme, Stuttgart, **1996**, Vol. 1, (vol. Eds.: W. A. Herrmann, A. Salzer), p. 117. − [27b] C. E. Zybill, in *Synthetic Methods of Organometallic and Inorganic Chemistry* (Ed.: W. A. Herrmann), Thieme, Stuttgart, **1997**, Vol. 8, (vol. Ed.: W. A. Herrmann), p. 103.
[28] D. Stalke, *Chem. Soc. Rev.* **1998**, *27*, 171−178.
[29] G. M. Sheldrick, *Acta Crystallogr., Sect. A* **1990**, *46*, 467−473.
[30] G. M. Sheldrick, SHELXL-NT 97, *Program for Crystal Structure Refinement*, Göttingen, **1997**.
[31] G. M. Sheldrick, SADABS 2.0, Program for absorption correction, Göttingen **1999**.

Received April 2001
[I01130]

Metal Complexes with Nitronyl Nitroxide Substituted Phenolate Ligands Providing New Magnetic Exchange Interaction Pathways − Synthesis, Structures, Magnetic Dilution Studies, and Ab Initio Calculations

Ulrich Schatzschneider,[a] Thomas Weyhermüller,[a] and Eva Rentschler*[a]

Keywords: Radicals / Nitronyl nitroxides / Copper / Nickel / Magnetic properties / Density functional calculations

The synthesis and magnetic properties of seven new nitronyl nitroxide substituted phenolates with chelating amine groups are reported. Copper(II) and nickel(II) complexes prepared with these ligands are structurally and magnetically characterized, showing exchange interactions between the metal and the radical ligands through the phenolate oxygen. Magnetically diluted samples are prepared by embedding the compounds in a poly(vinyl chloride) film to suppress intermolecular exchange interactions. This method is used for the first time in a quantitative way to separate intra- and intermolecular exchange interactions in radical-metal systems. The experimentally determined ground states are further confirmed by DFT calculations.

Introduction

In the preparation of molecular magnetic materials, transition metal complexes with organic radical ligands have found widespread interest in recent years. Research has focused on the nitronyl nitroxide family of radicals[1] since they are stable and easy to functionalize. A wide variety of transition metal complexes have been prepared with these ligands, most of them involving metal coordination to the NO groups. Since nitronyl nitroxide radicals are poor electron-donor ligands, the use of strongly electron-withdrawing coligands at the metal, like hexafluoroacetylacetonate, is required. The steric demand of these coligands restricts the dimensionality of the resulting metal-radical compounds. A large number of ring systems and infinite chain compounds have been prepared by this strategy,[2−4] but few showed ferromagnetic ordering at low temperatures due to small interchain interactions.[5−8] Only in the very last years has work been published in which the sterically demanding coligands are avoided. Functionalized nitronyl nitroxide radicals with electron-donating substituents like 2-pyridine, 2,2′-bipyridine, imidazole, benzimidazole, or 1,2,4-triazole were prepared.[9−22] In all cases the nitronyl nitroxide is in an *ortho* position to the aromatic nitrogen atom of the substituent and one NO group coordinates to the transition metal ion to form a chelate ring. This usually leads to small, discrete molecules, although some 1D- and 2D-systems were reported with imidazole-substituted nitronyl nitroxide ligands.[15,18] As we are interested in the magnetochemistry of spin systems of higher dimensionality, we were surprised that very few compounds are published in which the nitronyl nitroxide radicals are bound to transition metal ions by additional functional groups in the *para* position of the aromatic ring.[23−30] Even less work has been published in which a remarkable spin-exchange interaction between the unpaired electron of the nitronyl nitroxide and an open-shell transition metal ion, mediated by the functional group, is reported.[23,26,30] In order to try and work out a synthetic strategy to build up higher dimensional networks of radicals and transition metal ions in which the NO moiety and the functional group bind to different metal ions, we were prompted to use the phenolate group as a promising substituent. Although some nitronyl nitroxide

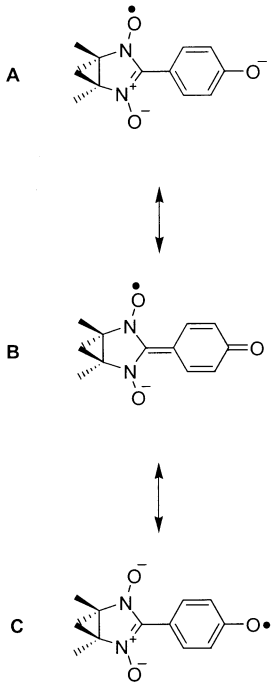

Scheme 1. Mesomeric structures of nitronyl nitroxide substituted phenolates indicating possible delocalization of the unpaired electron from the NO groups to the phenolic oxygen

[a] Max-Planck-Institut für Strahlenchemie,
Stiftstraße 34−36, 45470 Mülheim an der Ruhr, Germany
Fax: (internat.) +49-208/306-3951
E-mail: rentsch@mpi-muelheim.mpg.de

Supporting information for this article is available on the WWW under http://www.eurjic.com or from the author.

 © WILEY-VCH Verlag GmbH, 69451 Weinheim, 2001 1434−1948/01/1010−2569 $ 17.50+.50/0

substituted phenols have been prepared in an approach to form purely organic ferromagnets,[31−37] their use as ligands for transition metals has not been explored. Since phenolates are fairly basic, a strong coordination towards metal ions is possible. Moreover, a delocalization pathway of the unpaired electron from the nitronyl nitroxide moiety onto the phenolic oxygen atom can be formulated (Scheme 1), leading to a spin-exchange interaction between the radical and a coordinated metal center.

We have synthesized a family of substituted nitronyl nitroxides with a phenolate group in the *para* position of the phenyl ring and an amine substituent in the *meta* position as an additional anchoring group (Scheme 2). This eliminates the need for coligands and leaves both the NO groups, as well as unoccupied coordination sites on the metal center, free for interconnection through bridging metal centers M′ or coligands L (Scheme 3a and 3b). In addition, oxidation of the phenolate group to a phenoxyl radical might lead to triplet radical ligands allowing the preparation of metal complexes in higher spin states (Scheme 3c). In this contribution, the synthesis and magnetic properties of seven new nitronyl nitroxide radicals are described. Copper(II) and nickel(II) compounds were prepared with these ligands. Their structural, magnetic, and electrochemical properties are reported here together with the results of density functional calculations. A method for the magnetic dilution of organic radicals as well as nitronyl nitroxide-metal complexes is quantified and applied to magnetic susceptibility measurements and EPR spectroscopy.

Results and Discussion

Synthesis

The nitronyl nitroxides **1**−**6** (see Scheme 2) were prepared by an aromatic Mannich reaction from 4-hydroxybenzaldehyde or vaniline, formaldehyde, and a secondary amine, followed by coupling of the resulting aldehyde with 2,3-bis(hydroxylamino)-2,3-dimethylbutane and oxidation, as described by Ullman et al.[38] In the cases of the piperidine- and piperazine-substituted compounds **3**−**6** the yields of the Mannich reaction were higher when the intermediate *N*-(alkoxymethyl)amines were prepared and purified separately. For the bis-nitronyl nitroxide ligand **7**, a different approach utilizing the reaction between 3-chloromethyl-4-hydroxybenzaldehyde and a secondary amine was employed to prevent the formation of polymeric by-products. This synthetic strategy allows the introduction of a wide variety of chelating amine substituents to accommodate different metal-binding preferences. The copper(II) and nickel(II) complexes **8**−**10** prepared with the nitronyl nitroxide ligands **1** and **3** precipitated upon the addition of anhydrous metal chlorides to a solution of the deprotonated ligand in dry methanol and can be separated from cocrystallized sodium chloride by simple recrystallization.

Magnetism and Crystal Structure of the Ligands

The magnetic properties of purely organic nitronyl nitroxide radicals are interesting in their own right, since the

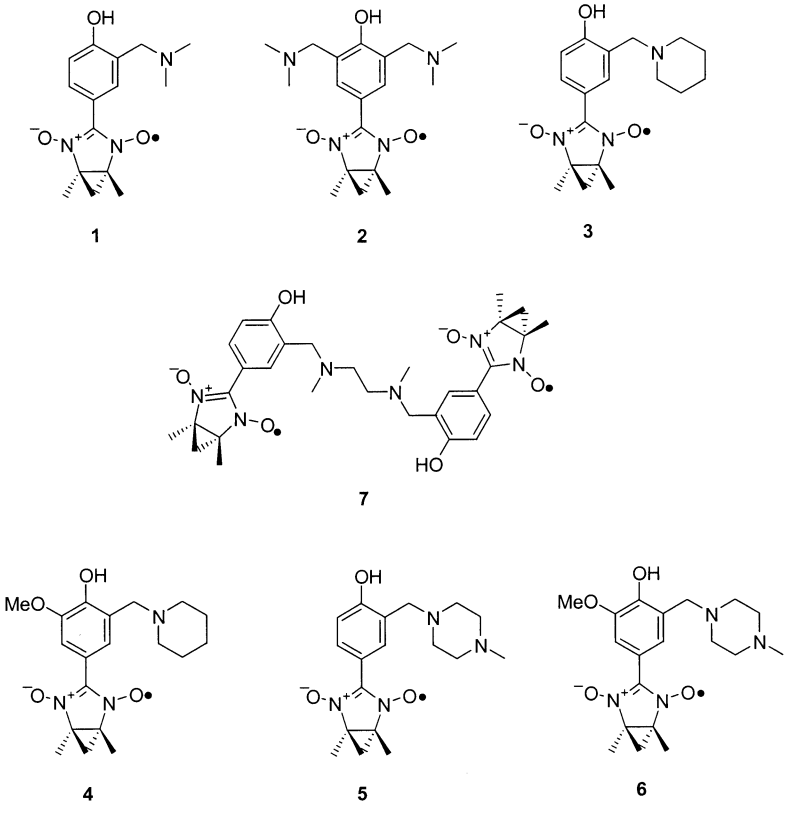

Scheme 2. Prepared nitronyl nitroxide ligands **1** to **7**

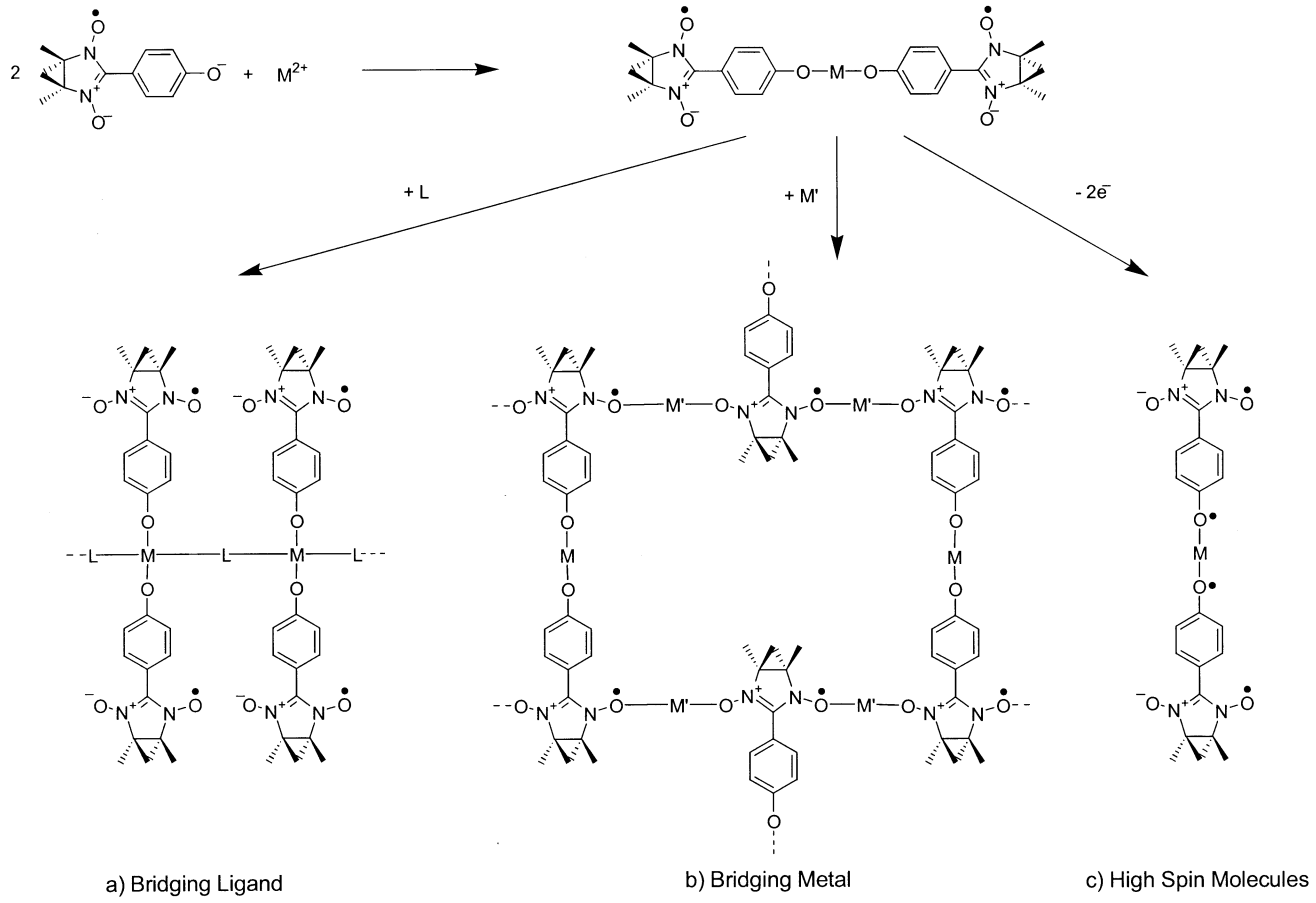

Scheme 3. Substituted nitronyl nitroxides as building blocks for high-dimensional metal-radical assemblies by: a) bridging ligands, b) bridging metals, and c) high-spin molecules

β-phase of 4-nitrophenyl nitronyl nitroxide was the first organic ferromagnet reported.[39] Therefore, we measured the temperature dependence of the magnetic moment for compounds **1**−**7**. The susceptibility follows the Curie−Weiss law over the whole temperature range from room temperature down to 4 K with θ-Weiss constants of −0.56, −0.54, −2.00, −0.84, −0.96, and +0.58 K for **1**, **2**, **3**, **5**, **6**, and **7**, respectively. An exception is found for compound **4**, where the temperature dependence of the magnetic susceptibility clearly indicates a fairly strong overall antiferromagnetic exchange interaction of the radicals. As shown in Figure 1, the $\chi_M T$ product decreases from 0.34 emu·K·mol^{-1} at room temperature, steadily with decreasing temperature, to 0.02 emu·K·mol^{-1} at 4 K. To elucidate the intermolecular exchange interaction pathways operating in this system, and for uses as a reference guide for structural changes induced in the ligands when coordinated to transition metals, we determined the crystal structures of **1**, **3**, **4**, and **7**. The crystallographic data and details of the refinement procedures are collected in Table 1. All intramolecular bond lengths and angles of the five-membered rings are as expected and comparable to other substituted nitronyl nitroxides (see Tables S1 and S2 in the supporting information). The NO bond lengths of 1.275(5)−1.288(5) Å indicate delocalization of the unpaired electron over both NO groups. The molecular structure of **4** is depicted in Figure 2. As shown in Figure 3, the molecules are arranged in alternating chains along the *x* axes with remarkably short intermolecular contacts involving both NO groups of the nitronyl nitroxide. The distance O4···O4A is shortest (3.46 Å), although O1···O1A and N1···O1A are only slightly longer (3.69 Å

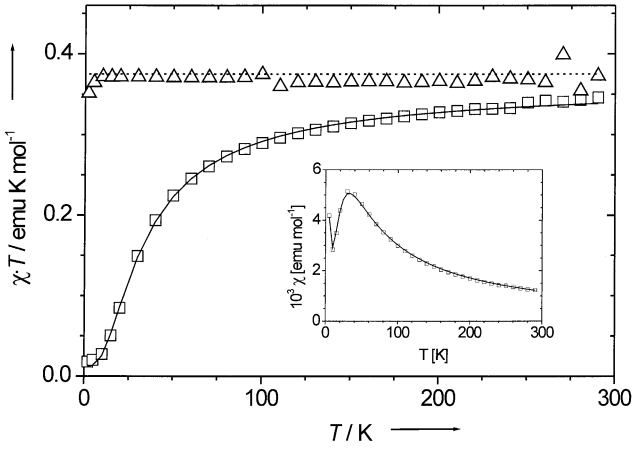

Figure 1. Temperature dependence of the magnetic susceptibility for **4** in the form of the $\chi_M T$ product versus T curve for the polycrystalline powder (□), polymer embedded sample (Δ) and theoretical curve for the dimer model (−); inset: temperature dependence of the magnetic susceptibility of **4** (□) and theoretical curve for the Heisenberg alternating linear chain model (−)

Table 1. Summary of the crystal structure data collection and refinement for **1**, **3**, **3a**, **4** and **7**

	1	**3**	**3a**	**4**	**7**
Chem formula	$C_{16}H_{24}N_3O_3$	$C_{19}H_{28}N_3O_3$	$C_{19}H_{28}N_3O_3$	$C_{20}H_{30}N_3O_4$	$C_{32}H_{46}N_6O_6$
Fw	306.38	346.44	346.44	376.47	610.75
Space group	$P2_1/c$	$P\bar{1}$	$Pbca$	$P\bar{1}$	$P2_1/c$
a, Å	7.167(3)	11.3931(9)	10.1839(8)	10.0751(8)	17.580(4)
b, Å	11.142(5)	12.1913(11)	11.4709(8)	10.6168(10)	9.974(2)
c, Å	20.610(9)	14.206(2)	31.870(2)	10.7897(10)	9.385(2)
α, deg	90	81.47(2)	90	88.019(12)	90
β, deg	94.49(3)	83.35(2)	90	65.673(12)	101.47(3)
γ, deg	90	71.82(2)	90	72.943(12)	90
V, Å	1640.8(12)	1848.8(3)	3723.0(5)	1000.4(2)	1612.7(14)
Z	4	4	8	2	4
T, K	100(2)	100(2)	100(2)	100(2)	100(2)
ρ calcd, g cm^{-3}	1.240	1.245	1.236	1.250	1.258
μ(Mo-K_α), cm^{-1}	0.87	0.85	0.84	0.87	0.90
Diffractometer used	Nonius Kappa-CCD	Siemens SMART	Nonius Kappa-CCD	Siemens SMART	Siemens SMART
Refl. Collected	6120	17868	38347	10169	16137
Unique refl. [$I > 2\sigma(I)$]	2123/1552	9761/5718	4221/3144	5689/3712	1725/1246
No. parameters	200	461	234	250	200
$2\Theta_{max}$, deg	44.98	60.00	54.80	62.00	42.00
$R1$[a] [$I > 2\sigma(I)$]	0.0750	0.0490	0.0431	0.0494	0.1501
$wR2$[b] [$I > 2\sigma(I)$]	0.1715	0.0928	0.1046	0.1080	0.4481

[a] $R1 = \Sigma||F_o| - |F_c||/\Sigma|F_o|$. – [b] $wR2 = [\Sigma[w(F_o^2 - F_c^2)^2]/\Sigma[w(F_o^2)^2]]^{1/2}$ where $w = 1/\sigma^2(F_o^2) + (aP)^2 + bP$, $P = (F_o^2 + 2F_c^2)/3$.

and 3.53 Å, respectively). The N1O1 groups are aligned antiparallel with angles N1−O1−N1A and O1−N1−O1A close to 90°, the two NO vectors thus forming a rectangle. The spin-carrying π*-orbitals are located in this plane with a distance between the NO vectors of 3.42 Å. A large overlap is therefore possible,[40,41] resulting in the observed strong antiferromagnetic exchange interaction.

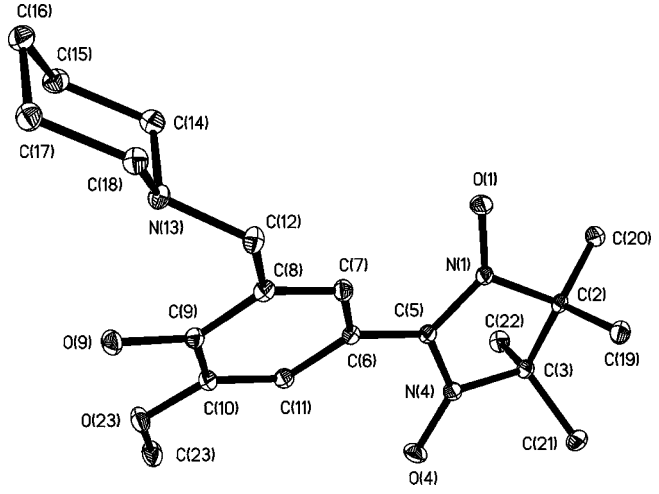

Figure 2. Molecular structure of **4**; ellipsoids are drawn at the 50% probability level

The magnetic susceptibility data can be interpreted in terms of two different models. First, assuming a dimer model with next-nearest neighbor interactions, the experimental data could be simulated applying the Heisenberg−Dirac−Van Vleck Hamiltonian [Equation (1)].

$$\hat{H} = -2J\hat{S}_1 \cdot \hat{S}_2 \quad (1)$$

The expression of magnetic susceptibility is given by Equation (2):

$$\chi_M = \frac{2N\beta^2 g^2}{3k(T-\Theta)}\left(1+\frac{1}{3\exp(-2J/kT)}\right)(1-\rho)+\left(\frac{N\beta^2 g^2}{2kT}\right)\rho \quad (2)$$

where N, g, β, k, T, Θ and ρ have their usual meanings. A least-squares fit to the magnetic susceptibility data gives the values $g = 2.00$ (fixed), $J = -21.47$ cm^{-1}, $\Theta = -4.42$ K, and $\rho = 0.066$ with $R = 1.14 \cdot 10^{-4}$ (Figure 1).

Alternatively, it was possible to fit the data according to the Heisenberg alternating chain model, with the appropriate Hamiltonian shown in Equation (3):

$$\hat{H} = -2J\sum_{i=1}^{n/2}[\hat{S}_{2i} \cdot \hat{S}_{2i-1} + \alpha\hat{S}_{2i} \cdot \hat{S}_{2i+1}] \quad (3)$$

where J and αJ are the two interaction parameters and α is the alternation parameter. The parameters $A-F$ in the expression for the magnetic susceptibility were calculated according to Hatfield et al. [Equation (4)]:[42]

$$\chi_m = \frac{N\beta^2 g^2}{kT}\frac{A+Bx+Cx^2}{1+Dx+Ex^2+Fx^3}(1-\rho)+\left(\frac{N\beta^2 g^2}{2kT}\right)\rho \quad (4)$$

with $x = |J|/(kT)$. The fit to data (inset in Figure 1) gave the parameters $g = 2.00$ (fixed), $|J| = 19.91$ cm^{-1}, $\alpha = 0.3$, and $\rho = 0.031$ with $R = 2.65 \cdot 10^{-4}$, which are in fairly good

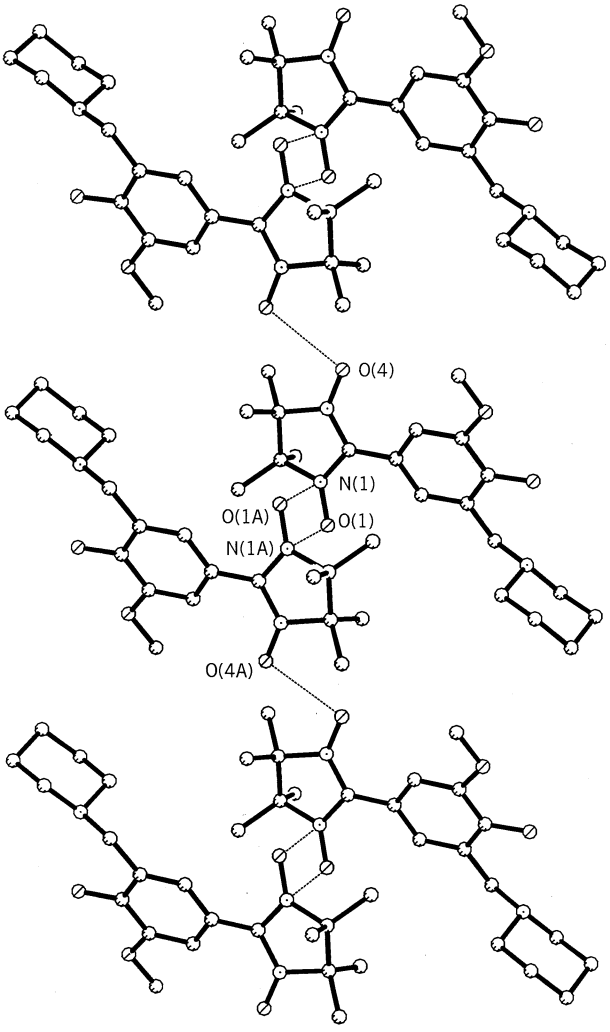

Figure 3. Molecular packing of **4** showing the intermolecular contacts between adjacent nitronyl nitroxide radicals

agreement with the parameters obtained with the previous model.

Magnetic Dilution

Since all the interactions are intermolecular in nature, compound **4** is an ideal candidate to improve a method of magnetic dilution in order to separate inter- and intramolecular exchange interactions. This experiment is essential in order to be able to analyze the transition metal complexes, in which intramolecular exchange interactions are small and have to be separated from intermolecular ones. For a pure organic radical like compound **4**, one expects to end up with an overall temperature dependence of the magnetic susceptibility of a simple paramagnet if it is possible to eliminate all intermolecular interactions. Compound **4** was therefore embedded in a poly(vinyl chloride) matrix of precisely determined weight. No chemical modification occurs during this process as proved by IR and UV/Vis spectroscopic measurements on the polymer films. The spectra obtained were identical for both the KBr disc and solution, except for additional IR bands resulting from vibrations of the polymer matrix. The diamagnetic correction for the poly(vinyl chloride) film was determined in a separate run of susceptibility measurement and subtracted from the χ_V probe measurement. The result for compound **4** is shown in Figure 1. As expected, the $\chi_M T$ product was found to be close to the theoretical value of 0.375 emu·K·mol^{-1} over the whole temperature range. The method can also be applied to EPR spectroscopy. The low temperature EPR spectrum of **4** embedded in a poly(vinyl chloride) film is depicted in Figure 4 and was found to be identical to that measured on a frozen solution. It shows the typical signal of a nitronyl nitroxide in a solid matrix[43] and was simulated with $g_1 = 2.0105$, $g_2 = 2.0120$, $g_3 = 2.0030$, $A_{11} = A_{22} = -4.5$ G, $A_{33} = 19.5$ G, and a line-width of 6 G. The anisotropy of the low temperature spectrum is in accordance with theory. Defining the local coordinates of the molecule so that the z axis is perpendicular to the O−N−C−N−O plane, we observe the smallest deviation from the Landé factor for the g value in the z direction. Contributions from the admixing of excited states into the ground state through spin-orbit coupling are negligible since the energy of the σ→σ* excitation is far too high in energy. In the xy plane, however, σ→π and π→π* excitations are more favorable which, as a result, lead to deviations from g_e for g_x and g_y. For the anisotropic hyperfine coupling constant we observe the largest value for the A_z tensor, since the spin density is highest in the p_z orbitals and the interaction of the nuclear spin with the magnetic field is most pronounced.

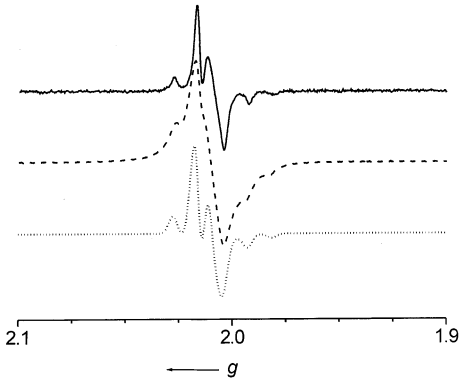

Figure 4. X-band EPR spectrum of **4** at 10 K of: a) a frozen methanol solution (microwave frequency 9.4371 GHz; power 196.7 nW; modulation amplitude 3.1 G; solid line), b) a polymer embedded sample (microwave frequency 9.443 GHz; power 1.0 μW; modulation amplitude 5.0 G; dashed line), and c) the simulated spectrum (dotted line, see text for parameters)

Crystal Structures of the Coordination Compounds 8, 9, and 11

Crystals suitable for an X-ray structure determination could be grown from acetonitrile or dichloromethane for compounds **8**, **9**, and **11**. The crystallographic data and details of the refinement procedures are collected in Table 2. Important bond lengths and angles are given in Tables 3 and 4. The molecules show the desired coordination of the

Table 2. Summary of the crystal structure data collection and refinement for **8**, **9**, and **11**

	8	**9**	**11**
Chem formula	$C_{38}H_{54}CuN_6O_6$	$C_{32}H_{46}CuN_6O_6{\cdot}H_2O{\cdot}2CH_3CN$	$C_{32}H_{46}N_6NiO_6$
Fw	754.41	774.41	669.46
space group	$P2_12_12_1$	$P2_1/c$	$Pbca$
a, Å	10.7647(8)	25.725(2)	12.7575(8)
b, Å	12.3029(9)	8.9606(4)	9.1507(12)
c, Å	28.715(2)	16.9301(8)	27.293(3)
α, deg	90	90	90
β, deg	90	97.60(1)	90
γ, deg	90	90	90
V, Å^3	3802.9(5)	3868.3(4)	3186.2(6)
Z	4	4	4
T, K	100(2)	100(2)	100(2)
ρ calcd, g cm^{-3}	1.318	1.330	1.396
μ(Mo-K_α), mm^{-1}	0.627	0.622	0.663
Diffractometer used	Siemens SMART	Nonius Kappa-CCD	Nonius Kappa-CCD
Refl. Collected	34570	36467	30911
Unique refl./[$I > 2\sigma(I)$]	8933/6601	8761/6165	6031/3748
No. parameters	468	489	211
$2\Theta_{max}$, deg	56.0	54.96	66.28
$R1$[a] [$I > 2\sigma(I)$]	0.0486	0.0442	0.0422
$wR2$[b] [$I > 2\sigma(I)$]	0.0885	0.1097	0.0973

[a] $R1 = \Sigma||F_o| - |F_c||/\Sigma|F_o|$. – [b] $wR2 = [\Sigma[w(F_o^2 - F_c^2)^2]/\Sigma[w(F_o^2)^2]]^{1/2}$ where $w = 1/\sigma^2(F_o^2) + (aP)^2 + bP$, $P = (F_o^2 + 2F_c^2)/3$.

metal through the peripheral N,O donor set of the ligand without the participation of the nitronyl nitroxide groups. The coordination geometry at the metal and the supramolecular arrangement of the molecules is mainly affected by the steric demand of the ligand.

Bis[2-(piperidin-1-ylmethyl)-4-NIT-phenolato]copper(II) (8)

In this compound, the bulky piperidine side-arm forces the copper(II) into a tetragonally compressed tetrahedral coordination (Figure 5). Although the complex possesses no center of symmetry, the Cu−O bond lengths are almost identical [1.905(2) and 1.900(2) Å] as are the Cu−N distances, [2.041(2) and 2.039(2) Å]. The N−Cu−N and O−Cu−O angles of 157.06(9)° and 149.92(10)°, respectively, show a strong distortion of the tetrahedron towards a square-planar environment. The O−Cu−N angles are all close to 90° ranging from 91.16(9)−96.45(10)°. The phenolate rings show a small deviation from a benzoid to a quinoidal structure, with the two *ortho-meta* bonds [1.371(4)−1.386(4) Å] slightly shorter than the other four C−C bonds [1.405(4)−1.417(4) Å]. This is attributable to a contribution of the quinoidal form **B** to the electronic structure of the ligands (Scheme 1). A similar distortion was also found in a manganese complex with a bridging, nitronyl nitroxide substituted benzoic acid.[29] The nitronyl nitroxide groups exhibit the usual characteristics with NO bond lengths of 1.285(3)−1.295(3) Å, indicating the delocalization of the unpaired electron over both NO groups. The torsion angles between the phenolate rings and the ONCNO planes are rather small at 3.8° and 17.4°. The C9−O9−Cu1 and C39−O39−Cu1 angles α are 123.0° and 124.6°, respectively, as expected for an sp^2-hybridized oxygen atom. The planes of the phenolate rings and the coordination mean plane of the copper are twisted, enclosing torsion angles β of 34.9° and 43.5°, respectively. The piperidine groups are in a chair conformation and oriented almost perpendicular to the coordination mean plane of the copper. There are no intermolecular contacts involving the NO groups below 4.7 Å. The shortest intermolecular distances are found between O1 and C2A as well as C3A at 3.88 and 3.94 Å ($x - 0.5$, $0.5 - y$, $1 - z$), respectively. The shortest Cu···Cu distance is 6.43 Å ($1 - x$, $y - 0.5$, $1.5 - z$) between copper atoms forming a zigzag chain along the y-axis.

Aqua[bis(2-dimethylaminomethyl-4-NIT-phenolato)]-copper(II) (9)

The copper(II) complex **9** with the smaller dimethylamino ligand forms a distorted square-pyramidal complex with an additional water molecule in the apical position (Figure 6). The base plane of the pyramid is formed by an N_2O_2 donor set with Cu−N distances of 2.073(2) and 2.080(2) Å, and Cu−O distances of 1.930(2) and 1.902(2) Å. The N−Cu−N angle is 176.02(7)°, while the O9−Cu1−O29 angle is more bent [156.25(7)°]. The N−Cu−O angles at the base of the pyramid are in the range 85.13(7)−93.27(7)°, with the copper lying 0.223 Å above the base plane. The distance of the apical oxygen O10 to Cu1 is longer [2.293(2) Å], and the O10−Cu−N/O angles are 91.35(7)−105.31(7)°. As in compounds **8** and **11**, the phenolate rings are slightly distorted towards a quinoidal structure with the *ortho-meta* bonds slightly shorter [1.368(3) to 1.390(3) Å] than the other four C−C bonds [1.403(3) to 1.415(3) Å]. The bond lengths and angles within the nitronyl nitroxide groups are in the normal range, with N−O distances of 1.280(2)−1.296(2) Å. The torsion angles between the ONCNO planes and the phenolate rings are 19.0° and 19.4°. The

Table 3. Selected bond lengths (Å) for **8**, **9** and **11**

$[(3)_2Cu]^0$ **8**		$[(1)_2(H_2O)Cu]^0$ **9**		$[(1)_2Ni]^0$ **11**	
Cu(1)−O(39)	1.900(2)	Cu(1)−O(29)	1.902(2)	Ni(1)−O(9)	1.8600(10)
Cu(1)−O(9)	1.905(2)	Cu(1)−O(9)	1.930(2)	Ni(1)N(13)	1.9783(13)
Cu(1)−N(43)	2.039(2)	Cu(1)−N(13)	2.073(2)	N(1)−O(1)	1.283(2)
Cu(1)−N(13)	2.041(2)	Cu(1)−N(33)	2.080(2)	N(4)−O(4)	1.2871(14)
O(1)−N(1)	1.295(3)	Cu(1)−O(10)	2.293(2)	N(1)−C(5)	1.364(2)
O(4)−N(4)	1.285(3)	O(1)−N(1)	1.294(2)	N(4)−C(5)	1.357(2)
N(1)−C(5)	1.358(4)	O(4)−N(4)	1.280(2)	N(1)−C(2)	1.498(2)
N(4)−C(5)	1.356(4)	N(1)−C(5)	1.346(2)	N(4)−C(3)	1.508(2)
N(1)−C(2)	1.505(4)	N(4)−C(5)	1.366(3)	C(2)−C(3)	1.548(2)
N(4)−C(3)	1.500(4)	N(1)−C(2)	1.501(3)	C(5)−C(6)	1.456(2)
C(2)−C(3)	1.546(5)	N(4)−C(3)	1.505(3)	C(6)−C(7)	1.408(2)
C(5)−C(6)	1.451(4)	C(2)−C(3)	1.550(3)	C(7)−C(8)	1.381(2)
C(6)−C(7)	1.408(4)	C(5)−C(6)	1.457(3)	C(8)−C(9)	1.410(2)
C(7)−C(8)	1.386(4)	C(6)−C(7)	1.406(3)	C(9)−C(10)	1.408(2)
C(8)−C(9)	1.417(4)	C(7)−C(8)	1.382(3)	C(10)−C(11)	1.381(2)
C(9)−C(10)	1.420(4)	C(8)−C(9)	1.419(3)	C(11)−C(6)	1.405(2)
C(10)−C(11)	1.371(4)	C(9)−C(10)	1.415(3)	C(9)−O(9)	1.326(2)
C(11)−C(6)	1.405(4)	C(10)−C(11)	1.381(3)		
C(9)−O(9)	1.315(4)	C(11)−C(6)	1.415(3)		
N(31)−O(31)	1.291(3)	C(9)−O(9)	1.317(3)		
N(34)−O(34)	1.285(4)	O(21)−N(21)	1.296(2)		
N(31)−C(35)	1.355(4)	O(24)−N(24)	1.281(2)		
N(34)−C(35)	1.353(4)	N(21)−C(25)	1.344(3)		
N(31)−C(32)	1.502(4)	N(24)−C(25)	1.367(3)		
N(34)−C(33)	1.489(4)	N(21)−C(22)	1.504(3)		
C(32)−C(33)	1.551(4)	N(24)−C(23)	1.506(3)		
C(35)−C(36)	1.453(5)	C(22)−C(23)	1.547(3)		
C(36)−C(37)	1.407(4)	C(25)−C(26)	1.458(3)		
C(37)−C(38)	1.380(5)	C(26)−C(27)	1.403(3)		
C(38)−C(39)	1.408(4)	C(27)−C(28)	1.390(3)		
C(39)−C(40)	1.410(5)	C(28)−C(29)	1.414(3)		
C(40)−C(41)	1.379(5)	C(29)−C(30)	1.406(3)		
C(41)−C(36)	1.410(5)	C(30)−C(31)	1.368(3)		
C(39)−O(39)	1.325(4)	C(31)−C(26)	1.407(3)		
		C(29)−O(29)	1.320(3)		

Table 4. Selected bond and dihedral angles (°) for **8**, **9**, and **11**

$[(3)_2Cu]^0$ **8**		$[(1)_2(H_2O)Cu]^0$ **9**		$[(1)_2Ni]^0$ **11**	
O(39)Cu(1)O(9)	149.92(10)	O(29)Cu(1)O(9)	156.25(7)	O(9)Ni(1)N(13)	93.57(5)
O(39)Cu(1)N(43)	96.45(10)	O(29)Cu(1)N(13)	85.13(7)	C(9)O(9)Ni(1)	125.91(10)
O(9)Cu(1)N(43)	91.86(10)	O(9)Cu(1)N(13)	93.27	C(2)N(1)C(5)	111.65(11)
C(9)O(9)Cu(1)	123.0(2)	N(13)Cu(1)N(33)	176.02(7)	C(3)N(4)C(5)	112.21(11)
C(39)O(39)Cu(1)	124.6(2)	O(29)Cu(1)O(10)	105.31(7)	N(1)C(5)N(4)	107.38(12)
N(43)Cu(1)N(13)	157.06(9)	O(9)Cu(1)O(10)	98.42(6)		
C(2)N(1)C(5)	112.7(3)	N(13)Cu(1)O(10)	91.63(7)		
C(3)N(4)C(5)	112.4(2)	N(33)Cu(1)O(10)	91.35(7)		
N(1)C(5)N(4)	107.0(3)	C(9)O(9)Cu(1)	125.43(14)		
C(32)N(31)C(35)	112.6(3)	C(29)O(29)Cu(1)	131.8(2)		
C(33)N(34)C(35)	113.7(3)	C(2)N(1)C(5)	112.8(2)		
N(31)C(35)N(34)	106.6(3)	C(3)N(4)C(5)	111.9(2)		
		N(1)C(5)N(4)	107.4(2)		
		C(22)N(21)C(25)	112.4(2)		
		C(23)N(24)C(25)	111.6(2)		
		N(21)C(25)N(24)	107.3(2)		
N(1)C(5)N(4)−C(7)C(8)C(10)C(11)	3.8	N(1)C(5)N(4)−C(7)C(8)C(10)C(11)	19.0	N(1)C(5)N(4)−C(7)C(8)C(10)C(11)	18.6
N(31)C(35)N(34)−C(37)C(38)C(40)C(41)	17.4	N(21)C(25)N(24)−C(27)C(28)C(30)C(31)	19.4		
C(7)C(8)C(10)C(11)−O(9)N(13)O(39)N(43)	34.9	C(7)C(8)C(10)C(11)−O(9)N(13)O(29)N(33)	40.1	C(7)C(8)C(10)C(11)−(9)N(13)O(9′)N(13)	30.2
C(37)C(38)C(40)C(41)−O(9)N(13)O(39)N(43)	43.5	C(27)C(28)C(30)C(31)−O(9)N(13)O(29)N(33)	22.6		

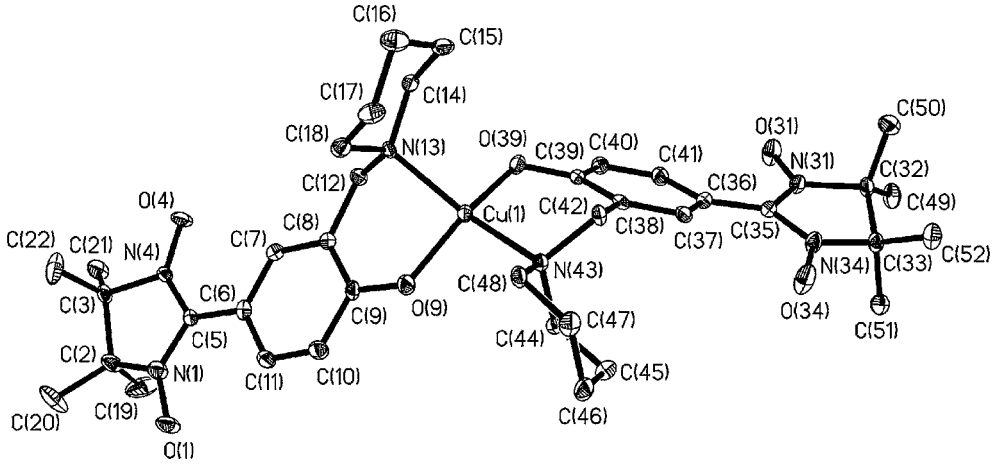

Figure 5. Molecular structure of **8**; ellipsoids are drawn at the 50% probability level

C(phenolate)−O−Cu angles α are 131.8° and 125.4°, while the torsion angles β between the coordination plane of the copper and the phenolate rings are 40.1° and 22.6°, the latter being significantly smaller than in complexes **8** and **11**. The apical water molecule is connected through hydrogen bonds to the nitronyl nitroxide groups of two adjacent molecules. The first hydrogen bond links O10 and O1A with a distance of 2.76 Å, forming a chain along the *y* axis (Figure 7). The second hydrogen bond links O10 with O21B over a distance of 2.72 Å, forming a zigzag chain along the *z* axis; these two hydrogen bonding interactions together result in a 2D network in the *yz* plane. There are additional short intermolecular contacts between adjacent nitronyl nitroxide groups, one between O24 and O24C ($-x$, $3 - y$, $-1 - z$) of two nitronyl nitroxides in a tail-to-tail arrangement, with a distance of 3.89 Å, and another one between O21 and O1D with a distance of 3.64 Å (x, $2.5 - y$, $0.5 + z$), forming another zigzag chain in the *z* direction.

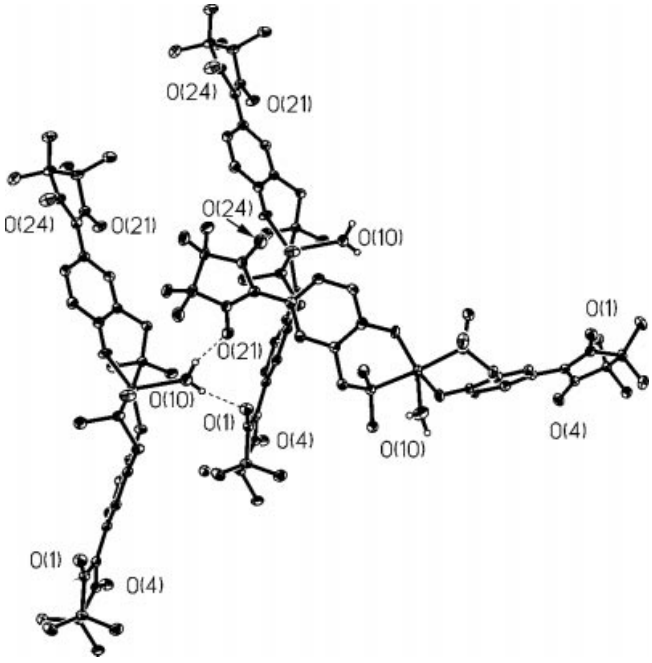

Figure 7. Crystal structure of **9**, showing the hydrogen bonds between the apical water molecule and the adjacent NO groups

Bis(2-dimethylaminomethyl-4-NIT-phenolato)nickel(II) (11)

With the smaller dimethylamino-ligand and nickel(II) one obtains a square-planar complex (Figure 8). The metal

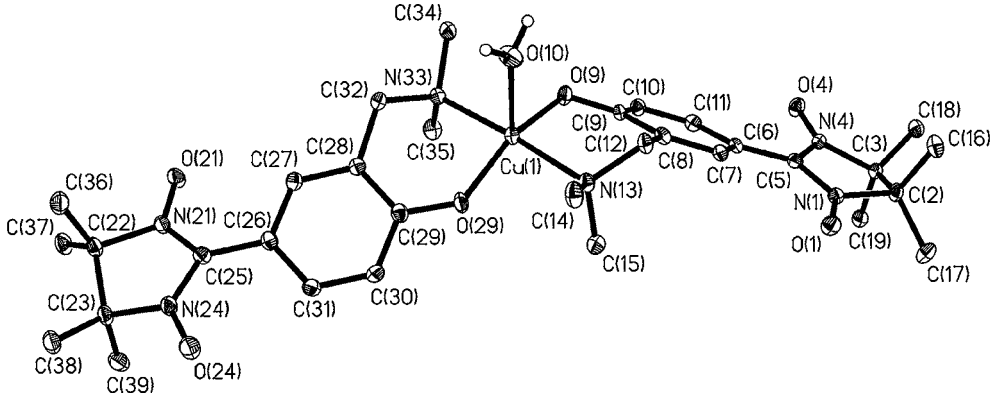

Figure 6. Molecular structure of **9**; ellipsoids are drawn at the 50% probability level

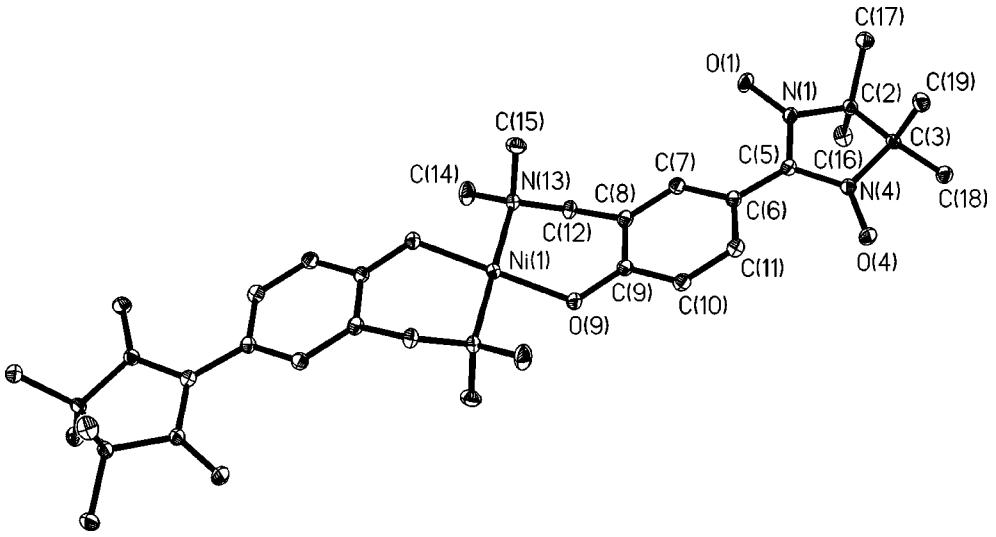

Figure 8. Molecular structure of **11**; ellipsoids are drawn at the 50% probability level

ion is located on an inversion center. The Ni−O distance is 1.86(1) Å and the Ni−N distance is 1.978(1) Å with an O−Ni−N angle of 93.57(3)°. The phenolate ring shows the same deviation from the benzoid structure as in the copper complexes **8** and **9** with both *ortho-meta* bond lengths at 1.381(2) Å, while the other carbon−carbon bond lengths are in the range 1.405(2)−1.410(2) Å. The bond lengths and angles within the nitronyl nitroxide group are in the expected range with N−O distances of 1.283(2) and 1.2871(14) Å. The torsion angle between the ONCNO plane and the phenolate ring is 18.6°. The angle α at the phenolate oxygen (C−O−Ni) is 125.9° — similar to that of the copper compound **8** — while the torsion angle β between the coordination mean plane of the nickel and the phenolate is 30.2°. Compound **11** forms an interesting 1D chain structure. Each oxygen atom O1 of the nitronyl nitroxide group points towards a nickel center of a neighboring complex with an O1···Ni1A distance of 4.33 Å, which is in turn connected in the same way, through O1A, to the Ni1 of the first complex, forming a molecular rectangle with the nickel atoms sitting in the two opposite corners. The diagonal distance between the Ni centers is 9.15 Å. Each rectangle shares the corners with its two neighbors, forming a chain of rectangles along the *y* axis (Figure 9). The chains are isolated from each other, with the shortest interchain distance being 4.19 Å between an O4 and the C3B of neighboring nitronyl nitroxide groups ($-x$, $y - 0.5$, $0.5 - z$).

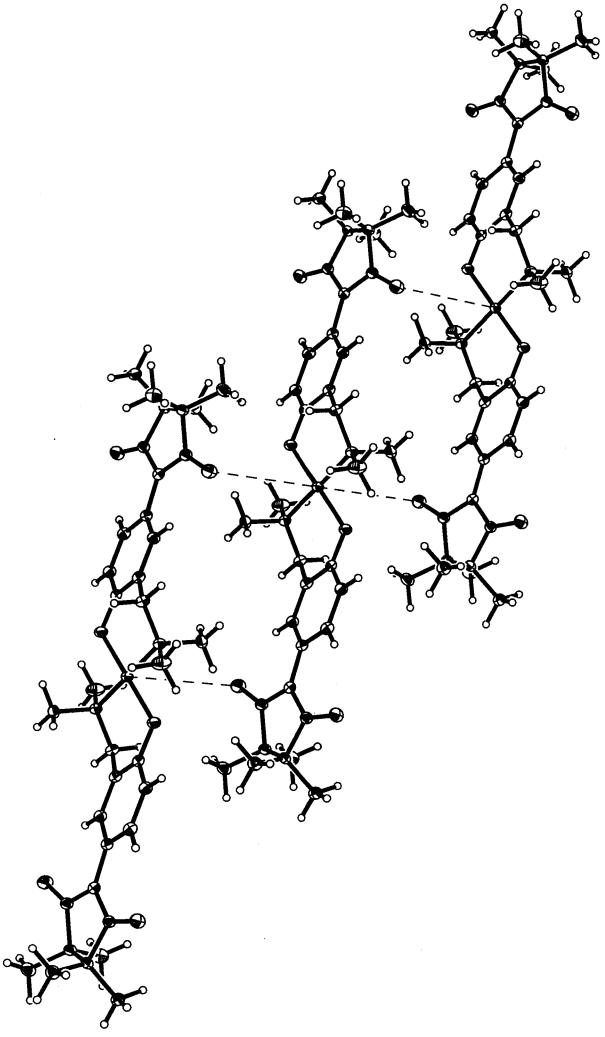

Figure 9. Crystal structure of **11**; dashed lines indicate the Ni1−O1A distances of 4.33 Å

Magnetic Properties of the Coordination Compounds

The temperature dependence of the molar magnetic susceptibility χ_M was measured in the 2−290 K range on polycrystalline samples of complexes **8**−**11**. Since nitronyl nitroxides often show considerable intermolecular exchange interactions due to close contacts between adjacent spin-carrying NO groups, it was crucial to this study to be able to differentiate between intra- and intermolecular exchange

interaction pathways. With the purely organic radical **4**, we were able to show that embedding the substance in a poly(vinyl chloride) film is a very efficient method of preparing magnetically diluted samples. No chemical modification occurs during this process. We could also apply this method to the transition metal complexes.

Bis[2-(piperidin-1-ylmethyl)-4-NIT-phenolato]copper(II) (8)

At room temperature, the value of the $\chi_M T$ product for the polycrystalline sample is 1.17 emu·K·mol^{-1}, which corresponds to that calculated for copper(II) and two nitronyl nitroxide radicals (1.125 emu·K·mol^{-1}). With decreasing temperature, $\chi_M T$ decreases continuously, reaching 0.40 emu·K·mol^{-1} at 2 K, close to the value of 0.375 emu·K·mol^{-1} expected for an isolated unpaired electron (Figure 10).

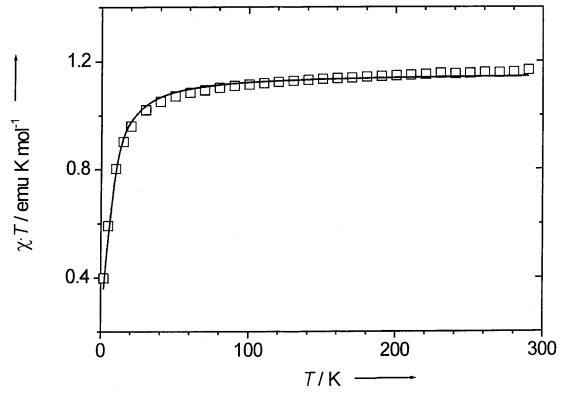

Figure 10. Temperature dependence of the product of the molar magnetic susceptibility with temperature ($\chi_M T$) for **8**; the solid line represents the best fit calculated data (see text for parameters)

The susceptibility was fitted to the Heisenberg–Dirac–Van Vleck Hamiltonian [Equation (5)]:

$$\hat{H} = -2J\left(\hat{S}_{NIT1}\hat{S}_M + \hat{S}_{NIT2}\hat{S}_M\right) \quad (5)$$

assuming the coupling between the two nitronyl nitroxides to be zero because of the large distance. The best result was obtained with the parameters $J = -2.90$ cm^{-1}, $g_{NIT} = 2.00$ (fixed), $g_{Cu} = 2.05$, and $R = 2.15 \times 10^{-4}$. In accordance with the presence of isolated molecules as seen in the solid state structure, measurements on polymer-embedded samples also showed antiferromagnetic coupling.

Aqua[bis(2-dimethylaminomethyl-4-NIT-phenolato)]copper(II) (9)

At room temperature, $\chi_M T$ has a value of 1.16 emu·K·mol^{-1}, which is close to that expected for three uncoupled $S = 1/2$ spins (1.125 emu·K·mol^{-1}). The $\chi_M T$ product decreases to 0.21 emu·K·mol^{-1} at 2 K (Figure 11). We fitted the magnetic data to the HDVV Hamiltonian [Equation (5)]. The best result was obtained with $J = -2.88$ cm^{-1}, $g_{NIT} = 2.00$ (fixed), $g_{Cu} = 2.11$ and $R = 6.11 \times 10^{-4}$. Compound **9** has a 2D network structure with several possible intra- and intermolecular exchange interaction pathways. To gain insight into the intramolecular exchange interactions in operation, we performed additional magnetic measurements on a magnetically diluted sample of **9** embedded in a poly(vinyl chloride) matrix. Here the compound shows an entirely different behavior. The room temperature value of $\chi_M T$ is 1.09 emu·K·mol^{-1}, slightly lower than expected for three uncoupled $S = 1/2$ spins (1.125 emu·K·mol^{-1}). Decreasing the temperature causes $\chi_M T$ to increase, reaching a maximum of 1.33 emu·K·mol^{-1} at 10 K. On further lowering of the temperature, the $\chi_M T$ value decreases to reach 1.13 emu·K·mol^{-1} at the lowest attainable temperature of 2 K (Figure 11). We could simulate the data down to very low temperature values satisfactorily with the values $J = +2.65$ cm^{-1}, $g_{NIT} = 2.00$ (fixed), $g_{Cu} = 2.07$, and $R = 7.24 \times 10^{-3}$. This shows that in the case of **9**, intramolecular ferromagnetic interactions are operative which are masked by the intermolecular interactions in the polycrystalline sample.

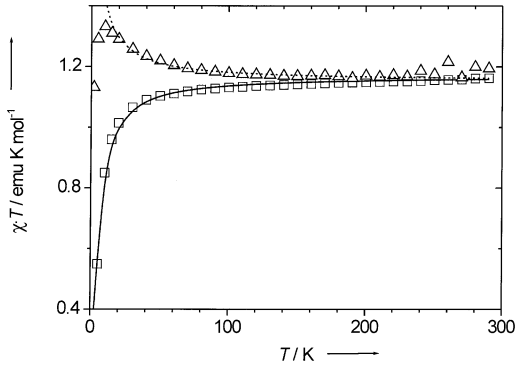

Figure 11. Temperature dependence of $\chi_M T$ for **9** as a powdered sample (□) and embedded in a poly(vinyl chloride) film (Δ); the solid and dashed lines represent the best fit calculated data (see text)

Bis(methanol)bis(2-dimethylaminomethyl-4-NIT-phenolato)nickel(II) (10)

The value of $\chi_M T$ at 290 K (1.83 emu·K·mol^{-1}) is as expected for an $S = 1$ of Ni^{II} in octahedral coordination with $g > 2$ and two nitronyl nitroxide radical ligands. When lowering the temperature, $\chi_M T$ decreases steadily to 0.81 emu·K·mol^{-1} at 2 K (Figure 12). The data were fitted to

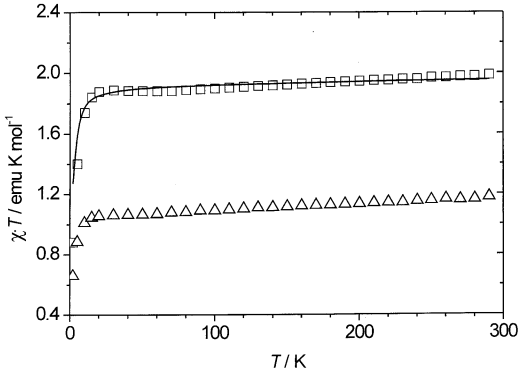

Figure 12. Temperature dependence of $\chi_M T$ for **10** (□) and **11** (Δ); the solid line represents the best fit calculated data (see text for parameters)

Equation (5) yielding $J = -0.40\ cm^{-1}$, $g_{NIT} = 2.00$ (fixed), $g_{Ni} = 2.16$ and $R = 1.99 \times 10^{-3}$. A polymer-embedded sample shows similar behavior, suggesting the presence of isolated molecules in the powdered samples.

Bis(2-dimethylaminomethyl-4-NIT-phenolato)nickel(II) (11)

The $\chi_M T$ product has a value of 1.18 emu·K·mol^{-1} at room temperature and decreases to 1.06 emu·K·mol^{-1} with decreasing temperature (Figure 12). This value is much higher than the value of 0.75 emu·K·mol^{-1} expected for two uncoupled nitronyl nitroxide ligands and an $S = 0$ for Ni^{II} in square-planar coordination, and significantly lower than the value calculated for an $S = 1$ plus two $S = 1/2$ radical spins as in **10**. However, it is very close to the value of 1.00 emu·K·mol^{-1} for an $S = 1$ state arising from a ferromagnetic coupling between the two nitronyl nitroxide ligands. Given the large distance between the two radical moieties of 13.81 Å (taken between C5 and C5′ related to each other by an inversion center), this is a surprising result, but was further confirmed by EPR spectroscopy and ab initio calculations.

Structural Correlation

In the structurally characterized copper complexes **8** and **9**, the sign of the exchange coupling constant can be related to the C(phenolate)−O−M angle α (with α = 180° denoting a linear arrangement) and the torsion angle β between the coordination mean plane at the metal center and the plane of the phenolate ligand, with β = 0° if the two planes are coplanar. In a tetrahedral environment of the copper(II) ion, its magnetic d_{xy} orbital is orthogonal to the spin-carrying p_z of the phenolate oxygen for β = 0°, irrespective of the size of α. However, with twisted planes and β > 0°, decreasing α from 180° enlarges the overlap, resulting in antiferromagnetic coupling (Figure 13). Only in the case of both α → 90° and β → 90°, the coupling becomes ferromagnetic again. In square-pyramidal coordination geometry at the copper(II), the magnetic $d_{x^2-y^2}$ orbital is also orthogonal to p_z for β = 0°, irrespective of α. In contrast to the d_{xy} orbital, the coupling stays antiferromagnetic when decreasing α for β values greater than 0°. At the intermediate values of α = 123.0° to 131.8° observed in compounds **8** and **9**, the sign of the coupling is therefore determined by the torsion angle β for both magnetic d_{xy} and $d_{x^2-y^2}$ orbitals. A ferromagnetic interaction should be observed for small angles, switching to antiferromagnetic upon increasing β. These simple considerations agree well with the experimental findings. Compound **8** with larger β angles (34.9° and 43.5°) shows an antiferromagnetic coupling, while compound **9**, in accordance with its one small value for β of 22.6°, exhibits an intramolecular ferromagnetic interaction between the metal and the nitronyl nitroxide radical ligands.

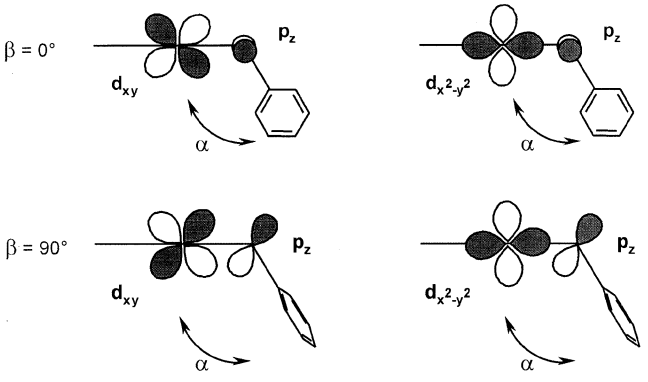

Figure 13. Depiction of the spatial arrangement of the orbitals relevant to the magnetic exchange interaction

EPR Spectroscopy

The X-band EPR spectra of **8**−**11** were measured as powders and in frozen solution at low temperature. Powdered samples of **8** show a broad isotropic signal at $g = 2.02$ with a line-width of 240 G. The spectra in frozen acetonitrile or chloroform solutions are dominated by the anisotropic signal of the nitronyl nitroxide group[43] at $g = 2.00$ with an additional broad tail between $g = 2.03$ to 2.20, better visible in the integrated spectrum. No signal clearly assignable to a copper(II) ion is observed. This is in accordance with an antiferromagnetic coupling between the copper(II) and the radical ligands, as determined from the susceptibility measurement. The spectrum measured on a polymer-embedded sample of **8** is identical to that obtained in frozen solution. The copper complex **9** in the powder has an isotropic signal centered at $g = 2.04$ with a line-width of 90 G. In frozen solution, the signal of the strongly coupled system shown in Figure 14a is observed. A quantitative evaluation of the signal intensity is not hampered by saturation, and comparison with a Cu^{II} standard shows that it accounts exactly for three electrons. In accordance with the intramolecular ferromagnetic coupling between the nitronyl nitroxide radicals and the copper(II) as seen in the susceptibility measurement on magnetically diluted samples, one observes a half-field signal at $g = 4.15$ (inset in Figure 14a). The spectrum obtained on a polymer-embedded sample of **9** is identical to that of the frozen solution. The EPR of **10**, in powder and frozen solution, is identical to that of the free protonated ligand and no signal indicative of a Ni^{II} ion is observed. The powder EPR of the nickel(II) complex **11** is shown in Figure 15. In addition to the small, intense signal at $g = 2.01$ with a line-width of only 20 G, two additional features occur that belong to an $S = 1$ system and that could be simulated assuming a zero-field splitting of $D = 0.0098\ cm^{-1}$, confirming the ferromagnetic coupling between the two radical ligands, although no half-field signal was observed.

Electrochemical Properties

We investigated the electrochemistry of the coordinated nitronyl nitroxide substituted phenolates by cyclic voltammetry, square-wave voltammetry, and spectro-electrochemistry to see if the coordinated ligands can be oxidized to singlet or triplet nitronyl nitroxide-phenoxyl diradicals, possibly leading to molecules in higher spin states (Scheme 2c).

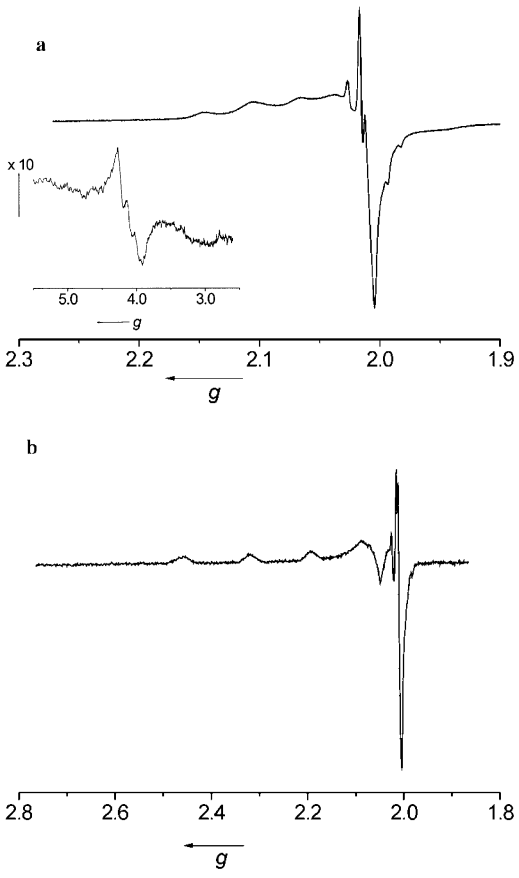

Figure 14. X-Band EPR of **9** at 60 K: a) before oxidation, with the inset showing the half-field signal, and b) after oxidation by two electrons

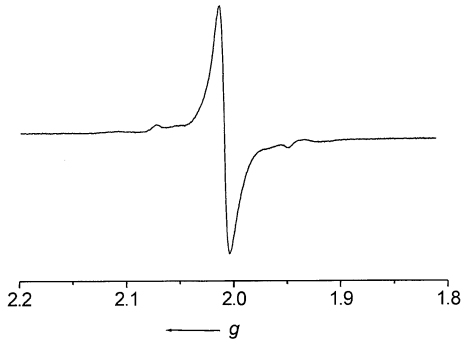

Figure 15. X-Band EPR of a powdered sample of **11** at 10 K

Compounds **8**−**10** undergo at least two oxidations in the range of 100−300 mV vs. ferrocenium/ferrocene (Fc^+/Fc), accompanied by an additional oxidative step depending on ligand, metal, and coordination geometry. The relevant data is collected in Table 5.

Compound **8** is simultaneously oxidized by three electrons at +228 mV vs. Fc^+/Fc. The most evident spectral change is the disappearance of the phenolate n→π* band at 298 nm and the simultaneous appearance of a new intense band at 412 nm, whose maximum shifts to a lower wavelength during the course of the oxidation (Figure 16a); after the complete removal of three electrons it appears at

Table 5. Half-wave potentials for **8**−**10** in mV vs. Fc^+/Fc at 100 mV/s, measured in acetonitrile solution (2×10^{-4} mol/L) containing 0.1 mol/L $TBAPF_6$

Compound	$E^{0,0/+1}$	ΔE_p
$[(3)_2Cu]^0$ **8**	+228	89
$[(1)_2(H_2O)Cu]^0$ **9**	+178	76
$[(1)_2Ni]^0$ **10**	+103	[a]
	+202	[a]
	+249	[a]
	+290	[a]

[a] Not resolved in CV.

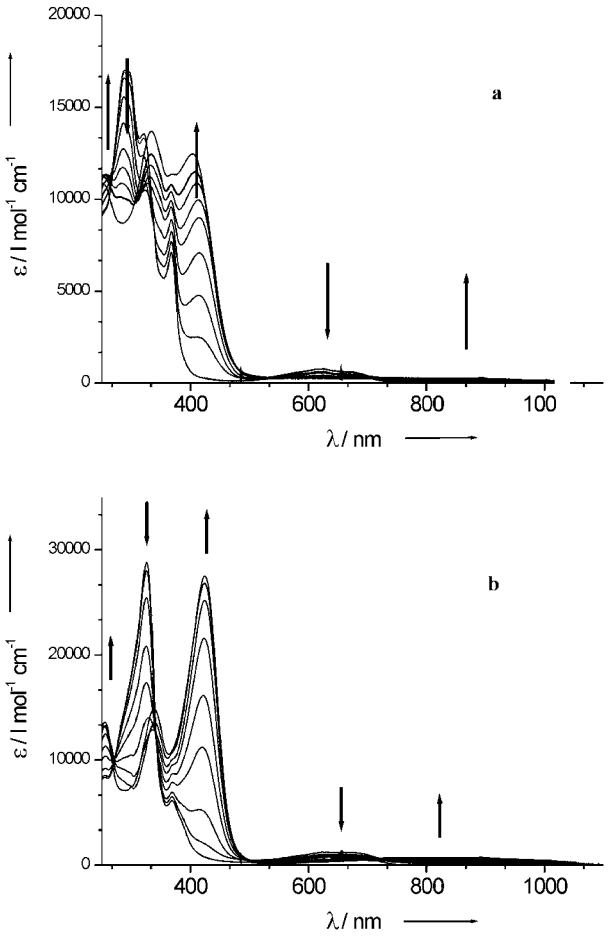

Figure 16. Spectral changes upon oxidation of: a) **8** and b) **9** in acetonitrile solution at +597 mV vs. Fc^+/Fc at −25 °C

404 nm. In addition, the n→π* band of the nitronyl nitroxide group at 615 nm decreases in intensity. In the EPR spectrum of the oxidized form, the overall signal intensity decreases without the appearance of new features. A quantitative evaluation is not possible due to signal saturation even at the lowest microwave power in the concentration range required for coulometry. These results can be interpreted as a concerted oxidation of both nitronyl nitroxide groups to diamagnetic nitrosonium cations plus the oxidation of one phenolate to a phenoxyl radical. Phenoxyl rad-

icals show similar spectral patterns and are known to be strongly coupled to coordinated copper ions.[44,45] The copper compound **9** is reversibly oxidized by two electrons at +178 mV vs. Fc^+/Fc. In the UV/Vis spectrum, this is accompanied by the appearance of a very strong band at 424 nm with isosbestic points at 270, 340, 500, and 714 nm. The phenolate n→π* band at 326 nm as well as the n→π* absorption of the nitronyl nitroxide group at 633 nm vanish, as in **8** (Figure 16b). The EPR of the oxidized species is dominated by the axial signal typical of a copper(II) atom in a square-planar coordination environment, as depicted in Figure 14b, with $g_\perp = 2.04$, $g_\parallel = 2.255$, $A_\perp = 40$ G, and $A_\parallel = 180$ G. Its intensity accounts for exactly one electron. No signals attributable to triplet radical ligands were observed. To gain further insight into the electronic structure of the oxidized product, resonance Raman (RR) spectroscopic measurements were performed on this compound. To prevent decomposition of the oxidized species, which is unstable at room temperature, the spectra were measured at 138 K on frozen solutions using an excitation wavelength of 413 nm coincident with the strong absorption of the oxidized product. Three prominent bands were observed at 1435, 1515, and 1602 cm^{-1}, respectively (Figure 17). The latter two occur at positions similar to those reported for phenoxyl-metal compounds.[46,47] According to the literature, they are assigned to ν_{7a} and ν_{8a} modes having C−O stretching and $C_{ortho}-C_{meta}$ double bond character, arising from a quinoidal mesomeric structure. The strong band at 1435 cm^{-1} is absent in the RR spectra of reported phenoxyl-metal complexes and is thought to originate from modes of the nitronyl nitroxide group. To gain evidence for this assumption, the vibrational spectrum of NIT-H was calculated by DFT (see Exp. Sect. for details on the computational procedures used). The simplest nitronyl nitroxide was chosen as a model since the whole ligand is too large to be treated theoretically and we assumed the modes of the phenolate and nitronyl nitroxide groups to be only weakly coupled. The calculated frequency of the symmetric stretching mode involving both NO groups is 1448 cm^{-1} when employing an appropriate scaling factor,[46] close to the band at 1435 cm^{-1} in the experimental spectrum. The theoretically determined frequency of the asymmetric stretching mode of the NO groups is 1484 cm^{-1}. A weak vibration is observed close to this value at 1467 cm^{-1}. These results indicate that two mesomeric structures − **D** with a nitrosonium-quinone formulation, and **E** with a nitronyl nitroxide-phenoxyl structure (Scheme 4) − contribute equally to the electronic structure of the coordinated, oxidized ligands. Although a triplet ground state was reported for a free nitronyl nitroxide-phenoxyl diradical,[48−50] which we could also confirm by theoretical calculations, no evidence for triplet or sextet signals was found here in the EPR spectrum. The quinoidal structure **D** is probably stabilized upon coordination, leading to an $S = 0$ ground state for the oxidized ligand.

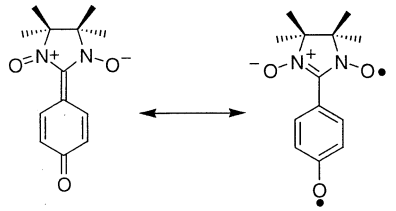

Scheme 4. Mesomeric structures of an oxidized nitronyl nitroxide radical

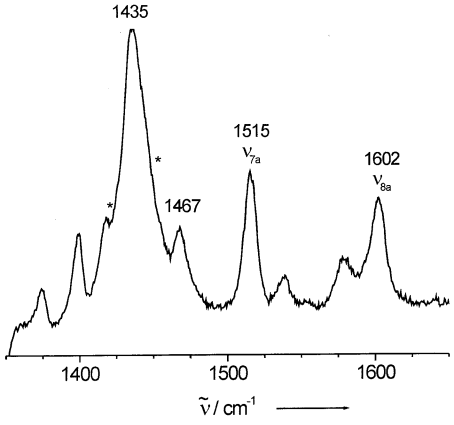

Figure 17. Resonance Raman spectrum of **9** oxidized by two electrons in frozen acetonitrile solution at 138 K (excitation wavelength 413 nm); the stars denote peaks attributed to solvent and/or supporting electrolyte

Density Functional Calculations

Density functional methods have recently been shown to give a good description of the electronic structure of nitronyl nitroxide radicals and at least a semi-quantitative picture of the spin-density distribution when compared with neutron diffraction data.[51−53] Combined with the broken symmetry approach as proposed by Noodleman,[54] they allow the theoretical determination of the exchange coupling constant in a wide variety of bimetallic compounds and diradicals to a good degree of accuracy.[55−60] To get a first idea of the exchange interaction pathways operative in our nitronyl nitroxide-metal complexes, we calculated the spin density distribution of the deprotonated nitronyl nitroxide **1** with the geometry taken from the crystal structure (see Exp. Sect. for details on computational procedures used). The HOMO (α83) is delocalized over both the five- and six-membered rings, with contributions from the phenolic oxygen and the lone pair of the amine nitrogen (Figure 18a), although the SOMO (α80) was found to be entirely localized on the ONCNO group (Figure 18b). This is also reflected in the spin density map (Figure 18c and Table 6), which shows only a minor contribution at the phenolic oxygen atom resulting from configuration interaction, and is in accordance with very recent calculations of the spin-density distribution in a large variety of structurally characterized substituted nitronyl nitroxides, which also showed localization of the unpaired electron on the ONCNO group.[61] The electronic structure of **1** is therefore

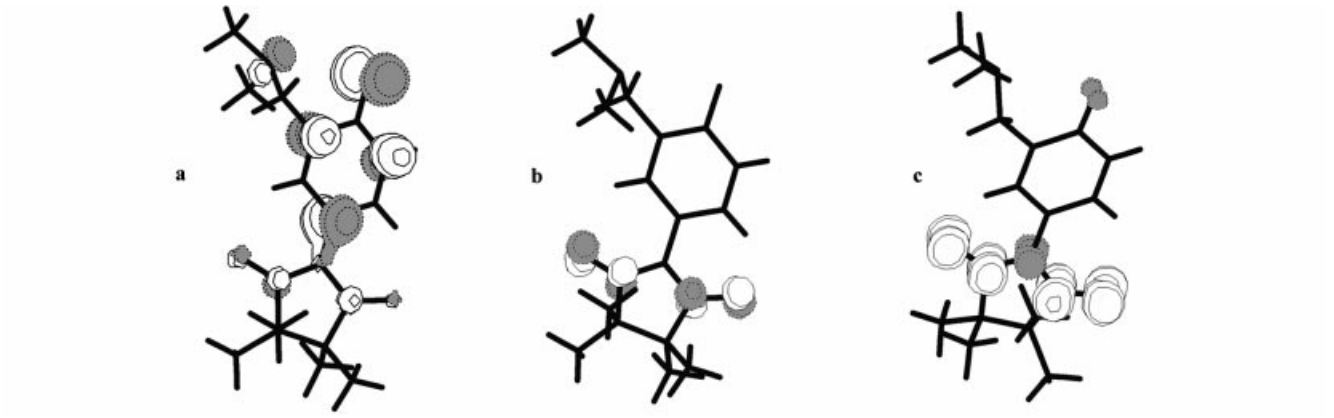

Figure 18. a) HOMO (α83) of deprotonated **1**, showing the contribution from the p_z of the phenolic oxygen, b) SOMO (α80) of deprotonated **1**, and c) spin density distribution

Table 6. Atomic spin densities of deprotonated **1** calculated at the B3LYP level; the numbering scheme is analogous to that used in Figure 2

N(1)	0.281	C(8)	−0.010
O(1)	0.365	C(9)	−0.002
C(2)	−0.017	O(9)	−0.042
C(3)	−0.013	C(10)	−0.009
N(4)	0.247	C(11)	−0.012
O(4)	0.321	C(19)	0.003
C(5)	−0.145	C(20)	0.000
C(6)	0.012	C(21)	0.018
C(7)	−0.013	C(22)	0.002

best described by the mesomeric structure **A** with little contribution from the phenoxyl form **C** (Scheme 1). This is in accordance with the observed weaker exchange interaction in the nitronyl nitroxide-metal complexes reported here, relative to published phenoxyl-metal complexes, which show a substantial spin density at the phenoxyl oxygen and in which the metal is therefore strongly coupled to the radical.[62,63]

To further substantiate the electronic ground states as determined by EPR and magnetic susceptibility measurements, we carried out broken symmetry DFT calculations at the B3LYP level on models of the copper complexes **8** and **9**, in which one of the nitronyl nitroxide groups was replaced by a hydrogen atom, to determine the energies of the triplet and singlet states. Since it has been shown that contamination from higher spin states is not significant in density functionals,[64−67] no spin projection was used and the exchange coupling parameter J was directly calculated from Equation (6):

$$J = E_{BS} - E_T \quad (6)$$

For copper models **8′** and **8′′**, referring to the different torsion angles of 3° and 17° between the five- and six-membered rings, a singlet ground state was found in accordance with the experimental data, with J calculated to be -13.0 cm^{-1} and -5.6 cm^{-1}, respectively. The triplet state was found to be lower in energy in model compound **9′** with J calculated as $+9.8$ cm^{-1}, thus confirming the intramolecular ferromagnetic coupling as observed in the magnetically diluted sample of this compound (just one calculation was done since the torsion angles on both ligands are almost equal in **9**).

For the nickel complex **11**, the calculation yielded a triplet ground state with $J = +64.0$ cm^{-1} in accordance with the EPR and susceptibility measurements. This large ferromagnetic coupling is rather surprising given the distance of 13.81 Å between the two radicals. It is thought to be mediated by the empty $d_{x^2-y^2}$ orbital of the Ni^{II} in a square-planar coordination. To gain further insight into the mechanism in operation, the corresponding zinc compound **$(1)_2$Zn**, which could not be obtained in pure form and characterized, was geometry optimized and the exchange-coupling constant calculated. With a completely filled 3d-shell, J was found to be zero within the accuracy of the calculation, thereby confirming the contribution of the empty metal $d_{x^2-y^2}$ orbital to the exchange-coupling pathway in **11**.

Conclusion

Nitronyl nitroxide substituted phenolate ligands with an additional chelating amine group were synthesized and provided the expected tight binding of transition metal ions at the periphery of the ligand without the participation of the NO groups. Four metal complexes of these ligands with copper(II) and nickel(II) were isolated and characterized. Their coordination geometry and supramolecular arrangement is controlled by the steric demand of the ligand, the preference of the metal ion for a certain geometry and the presence of coligands. The bulky piperidine group of ligand **3** forces copper(II) into a distorted tetrahedral coordination. No nickel(II) complexes could be obtained with this ligand. In addition, the large extent of the piperidine substituent prevented close intermolecular contacts between the molecular units, resulting in discrete molecules. The

smaller ligand **1** resulted in a planar arrangement of the N_2O_2 donor set of the two ligands in both its copper(II) and nickel(II) complexes, with coligands completing the preferred coordination number of the metal. With the smaller dimethylamino group, the molecular units are interconnected, forming 1D- and 2D-arrangements. The unpaired spin on the nitronyl nitroxide groups is coupled to the metal through the phenolic oxygen, as shown by susceptibility measurements and EPR spectroscopy. The intermolecular exchange interactions could be suppressed by embedding the compounds in a poly(vinyl chloride) film. The method was first tested and quantified on the free organic radical **4**, which shows strong intermolecular exchange interactions, and then successfully applied to the transition metal complexes. Both EPR and magnetic susceptibility measurements could be performed on magnetically diluted samples prepared this way, introducing it as a suitable method to investigate systems in which intra- and intermolecular exchange interactions of equal magnitude are operative. A structural relationship was found between the sign of the exchange coupling and the degree of torsion between the coordination mean plane of the metal center and the plane of the phenolate ligands. Density functional theory calculations further confirmed the experimentally determined electronic ground states. The obtained complexes will be used as synthons for supramolecular assemblies by both interconnection of the NO groups with Lewis acidic metal ions or replacement of the solvent molecules by bridging coligands.

Experimental Section

General: All reagents were purchased from commercial sources and used as received. Solvents were purified and dried by standard methods. Reactions were carried out under an atmosphere of argon where necessary. Elemental analyses were carried out by H. Kolbe, Mikroanalytisches Laboratorium, Mülheim an der Ruhr. Infrared spectra were recorded on a Perkin−Elmer FT-IR 2000. UV/Vis spectra were recorded on a Perkin−Elmer Lambda 19 spectrometer or a Hewlett Packard 8452A diode array spectrometer. EI mass spectra were measured on a Finnigan MAT 8200 instrument, and ESI mass spectra on a Finnigan MAT 95 instrument. Susceptibility measurements were performed on polycrystalline powders or polymer films on a Quantum Design MPMS SQUID magnetometer in the temperature range 2−295 K. Magnetically diluted samples were prepared by slowly evaporating a solution of poly(vinyl chloride) containing 5 wt. % of the compound under investigation in dichloromethane. The diamagnetic contribution of the polymer was determined in a separate run. EPR spectra were recorded as polycrystalline powders, in frozen solution, or on the polymer films used in the magnetic susceptibility measurements with a Bruker ESP 300 spectrometer with a Bruker ER041 XK-D microwave bridge and an Oxford Instruments cryostat model 910. Cyclic voltammograms and square-wave voltammograms were obtained with a three-electrode cell and an EG&G Princeton Applied Research 273A potentiostat. An $Ag/AgNO_3$ (0.01 mM) reference electrode, a glassy carbon disc working electrode and a Pt wire counter electrode were used. Acetonitrile solutions (10^{-4} M) contained 0.1 mol/L $(n\text{Bu})_4NPF_6$ as supporting electrolyte. Ferrocene was added as an internal standard after each measurement, its ΔE being +100 mV under these conditions. The coulometric measurements were performed at −25 °C with the same setup, and the spectral changes during oxidation were followed with a Hewlett Packard 8452A diode array spectrometer. EPR spectroscopic measurements on the oxidized species were performed on samples removed with a syringe under argon and immediately frozen in liquid nitrogen. RR spectra were obtained with the 413 nm excitation of a krypton ion laser (Coherent Innova 302) using a spectrograph (ISA U1000) equipped with a liquid nitrogen cooled CCD detector (Jobin Yvon). The spectral slit width was 5.6 cm^{-1}, and the wavenumber increment was 0.53 cm^{-1}. The sample holder was placed in a cryostat (Cryovac) at 138 K to prevent sample degradation and the scattered light collected in a 135° scattering geometry.

Preparation of the Nitronyl Nitroxide Radicals: The nitronyl nitroxide radicals were prepared from their aldehyde precursors (see Supporting Information) according to a literature procedure.[38] For **1**, **2**, **4**, **5**, and **6**, benzene was used as solvent for the coupling of the aldehyde with 2,3-bis(hydroxylamino)-2,3-dimethylbutane. Chloroform was used as solvent for **3** and tetrahydrofuran for **7**. Oxidation to the radical was carried out with lead(IV) oxide for **1**−**3** and with sodium periodate for **4**−**7**. All radicals were purified by preparative HPLC on a Phenomenex Luna-5-PhenylHexyl column with methanol/aqueous ammonium acetate as the eluent. After extraction from the buffer with chloroform, they were obtained as blue solids by crystallization from toluene for **1**, **2**, **5**−**7** and from diethyl ether for **3** and **4**.

3-Dimethylaminomethyl-4-hydroxyphenyl-NIT (1): Yield (after HPLC): 1.09 g (55%). − IR (KBr disc): $\tilde{\nu}$ = 2990, 2957, 2831, 2784, 1654, 1598, 1483, 1416, 1384, 1364, 1350, 1298, 1282, 1218, 1141, 1111, 1019, 826, 542 cm^{-1}. − EI-MS: *m*/*z* = 306 [M^+], 261, 176, 84, 69, 58, 44. − UV/Vis (MeOH): λ_{max} (ε) = 287 (12413), 317 (7926), 365 (4247), 615 nm (672 $L{\cdot}mol^{-1}{\cdot}cm^{-1}$). − EPR (solid, 60 K, 9.4391 GHz): g_{iso} = 2.0095. − EPR ($CHCl_3$, 80 K, 9.4374 GHz): g_x = 2.0105, g_y = 2.0130, g_z = 2.0040, $A_{xx} = A_{yy}$ = −4.5 G, A_{zz} = 19.5 G. − $C_{16}H_{24}N_3O_3$ (306.38): calcd. C 62.72, H 7.90, N 13.71; found C 62.65, H 7.88, N 13.92.

3,5-Bis(dimethylaminomethyl)-4-hydroxyphenyl-NIT (2): Yield (after HPLC): 1.71 g (37%). − IR (KBr disc): $\tilde{\nu}$ = 2989, 2947, 2851, 2829, 2811, 2753, 1603, 1459, 1413, 1386, 1369, 1349, 1296, 1121, 1045, 1032, 844, 813, 541, 449 cm^{-1}. − EI-MS: *m*/*z* = 363 [M^+], 346, 318, 301, 275, 187, 147, 84, 69, 44. − UV/Vis ($CHCl_3$): λ_{max} (ε) = 290 (15304), 372 (5789), 621 (952), 663 nm (783 $L{\cdot}mol^{-1}{\cdot}cm^{-1}$). − EPR ($CHCl_3$, 80 K, 9.4382 GHz): g_x = 2.0105, g_y = 2.0130, g_z = 2.0040; $A_{xx} = A_{yy}$ = −4.5 G, A_{zz} = 19.5 G. − $C_{19}H_{31}N_4O_3$ (363.48): calcd. C 62.78, H 8.60, N 15.41; found C 63.10, H 8.55, N 15.25.

4-Hydroxy-3-(piperidin-1-ylmethyl)phenyl-NIT (3): Yield (after HPLC): 1.22 g (47%). − IR (KBr disc): $\tilde{\nu}$ = 3449, 2989, 2938, 2855, 2814, 1483, 1452, 1384, 1352, 1281, 1113, 827, 755, 540 cm^{-1}. − EI-MS: *m*/*z* = 346 [M^+], 329, 261, 216, 84, 69, 56, 41. − UV/Vis ($CHCl_3$): λ_{max} (ε) = 371 (5604), 623 nm (742 $L{\cdot}mol^{-1}{\cdot}cm^{-1}$). − EPR ($CHCl_3$, 9.646 GHz, 295 K): Quintet, g_{iso} = 2.0085, A_N = 7.60 G. − EPR ($CHCl_3$, 9.646 GHz, 10 K): g_x = 2.0120, g_y = 2.0105, g_z = 2.0030, $A_{xx} = A_{yy}$ = −4.5 G, A_{zz} = 19.5 G. − EPR ($CHCl_3$, 33.916 GHz, 293 K): g_x = 2.0062, g_y = 2.0062, g_z = 2.0010. − $C_{19}H_{28}N_3O_3$ (346.45): calcd. C 65.87, H 8.15, N 12.12; found C 65.96, H 8.11, N 12.06.

4-Hydroxy-3-methoxy-5-(piperidin-1-ylmethyl)phenyl-NIT (4): Yield (after HPLC): 0.33 g (8%). − IR (KBr disc): $\tilde{\nu}$ = 3440, 2938, 1478, 1413, 1385, 1356, 1308, 1129, 1089, 1038, 858, 714, 543 cm^{-1}. −

EI-MS: *m/z* = 376 [M$^+$], 291, 246, 162, 84, 69, 41. − UV/Vis ($CHCl_3$): λ_{max} (ε) = 298 (15976), 370sh (4704), 629 nm (948 L·mol^{-1}·cm^{-1}). − EPR ($CHCl_3$, 9.464 GHz, 10 K): g_x = 2.012, g_y = 2.0105, g_z = 2.004, $A_{xx} = A_{yy}$ = −4.5 G, A_{zz} = 19.5 G. − $C_{20}H_{30}N_3O_4$ (376.48): calcd. C 63.81, H 8.03, N 11.16; found C 63.69, H 8.10, N 11.04.

4-Hydroxy-3-(4-methylpiperazin-1-ylmethyl)phenyl-NIT (5): Yield (after HPLC): 0.13 g (28%). − IR (KBr disc): $\tilde{\nu}$ = 3481, 2956, 2795, 1446, 1350, 1291, 1260, 1137, 1111, 803, 540 cm^{-1}. − EI-MS: *m/z* = 361 [M$^+$], 344, 261, 231, 99, 84, 56, 44. − UV/Vis ($CHCl_3$): λ_{max} (ε) = 288 (16719), 326 (6087), 372 (8156), 620 nm (968 L·mol^{-1}·cm^{-1}). − EPR ($CHCl_3$, 9.438 GHz, 10 K): g_x = 2.0120, g_y = 2.0110, g_z = 2.0040, $A_{xx} = A_{yy}$ = −4.50 G, A_{zz} = 19.5 G. − $C_{19}H_{29}N_4O_3$·1.5 H_2O (388.49): calcd. C 58.74, H 8.30, N 14.42; found C 59.25, H 8.51, N 13.81.

4-Hydroxy-5-methoxy-3-(4-methylpiperazin-1-ylmethyl)phenyl-NIT (6): Yield (after HPLC): 0.68 g (51%). − IR (KBr disc): $\tilde{\nu}$ = 3449, 2984, 2941, 2825, 1458, 1388, 1359, 1303, 1122, 1082, 1009, 782 cm^{-1}. − EI-MS: *m/z* = 391 [M$^+$], 374, 357, 291, 261, 190, 162, 99, 84, 69, 58, 43. − UV/Vis ($CHCl_3$): λ_{max} (ε) = 296 (17360), 339 (9103), 368 (5647), 627 nm (1061 L·mol^{-1}·cm^{-1}). − EPR ($CHCl_3$, 9.437 GHz, 10 K): g_z = 2.0120, g_y = 2.0110, g_z = 2.0040, $A_{xx} = A_{yy}$ = −4.50 G, A_{zz} = 19.5 G. − $C_{20}H_{31}N_4O_4$ (391.49): calcd. C 61.36, H 7.98, N 14.31; found C 61.48, H 7.85, N 14.39.

***N,N′*-Bis(2-hydroxy-5-NIT-benzyl)-*N,N′*-dimethylethan-1,2-diamine (7):** Yield (after HPLC): 0.08 g (5%). − IR (KBr disc): $\tilde{\nu}$ = 2988, 1607, 1484, 1411, 1383, 1349, 1274, 1107, 1025, 831, 620, 541, 448 cm^{-1}. − ESI$^+$MS (CH_2Cl_2): *m/z* = 596 [M − 15 + H], 611 [M + H], 633 [M + Na], 1191 [2M + H]. − UV/Vis ($CHCl_3$): λ_{max} (ε) = 287 (75877), 371 (17879), 619 nm (971 L·mol^{-1}·cm^{-1}). − EPR ($CHCl_3$, 80 K, 9.4372 GHz): g_x = 2.0105, g_y = 2.0130, g_z = 2.0045, $A_{xx} = A_{yy}$ = −4.5 G, A_{zz} = 19.5 G. − $C_{32}H_{46}N_6O_6$ (610.76): calcd. C 62.93, H 7.59, N 13.76; found C 63.11, H 7.68, N 13.58.

Preparation of Metal Complexes 8−11: The ligand (1.3 mmol) was dissolved in dry methanol (8 mL) under argon and deprotonated by addition of a fresh 1.2 M solution of sodium methanolate (1.6 mL; prepared by addition of a calculated quantity of sodium metal to dry methanol), resulting in a color change from deep blue to deep green. The anhydrous metal chloride (0.7 mmol) was then dissolved in dry methanol (8 mL) under argon and added dropwise to the solution of the deprotonated ligand over a period of 30 min. A crystalline precipitate began to form almost immediately. After complete addition this was collected by suction, washed with dry methanol, ether, and pentane before being dried in air. Recrystallization from the indicated solvents yielded the complexes in analytically pure form. Single crystals were grown from acetonitrile for **8** and **9**, while **11** was obtained in crystalline form by slow evaporation of a dichloromethane solution layered with ether.

Bis[2-(piperidin-1-ylmethyl)-4-NIT-phenolato]copper(II) (8): Yield: 0.60 g (99%). − IR (KBr disc): $\tilde{\nu}$ = 2922, 2854, 1599, 1470, 1408, 1382, 1357, 1309, 1260, 1117, 829, 636, 453 cm^{-1}. − ESI$^+$MS (MeOH): *m/z* = 754 [M + H], 776 [M + Na]. − UV/Vis ($CHCl_3$): λ_{max} (ε) = 298 (26500), 329 (25400), 372 (10280), 634 nm (2410 L·mol^{-1}·cm^{-1}). − $C_{38}H_{54}CuN_6O_6$ (754.43): calcd. C 60.50, H 7.21, N 11.14, Cu 8.42; found C 59.88, H 7.14, N 11.12, Cu 8.32.

Aqua[bis(2-dimethylaminomethyl-4-NIT-phenolato)]copper(II) (9): Yield: 0.39 g (73%). − IR (KBr disc): $\tilde{\nu}$ = 3416, 2983, 2923, 1599, 1473, 1408, 1381, 1348, 1323, 1301, 1117, 999, 823, 633, 541, 454 cm^{-1}. − ESI$^+$MS (MeCN): *m/z* = 674 [M − H_2O + H], 696 [M − H_2O + Na]. − UV/Vis ($CHCl_3$): λ_{max} (ε) = 329 (54620), 375 (10180), 633 (2550), 678 nm (2550 L·mol^{-1}·cm^{-1}). − $C_{32}H_{48}CuN_6O_7$ (692.32): calcd. C 55.52, H 6.99, N 12.14, Cu 9.18; found C 54.04, H 6.84, N 11.77, Cu 9.23.

Bis(methanol)bis(2-dimethylaminomethyl-4-NIT-phenolato)-nickel(II) (10): Yield: 0.32 g (87%). − IR (KBr disc): $\tilde{\nu}$ = 1595, 1484, 1471, 1410, 1376, 1333, 1297, 1118, 829, 628, 445, 453 cm^{-1}. − ESI$^+$MS (MeOH): *m/z* = 669 [M + H], 691 [M + Na]. − UV/Vis ($CHCl_3$): λ_{max} (ε) = 299 (23140), 371 (9200), 628 nm (1570 L·mol^{-1}·cm^{-1}). − $C_{34}H_{54}N_6NiO_8$ (733.53): calcd. C 55.67, H 7.42, N 11.46, Ni 8.00; found C 54.80, H 6.83, N 11.45, Ni 7.46.

Computational Details: The hybrid B3LYP method, as implemented in Gaussian 98,[68] was used in the calculation of the spin-density distribution and the energies, mixing the exact Hartree−Fock exchange with Becke′s expression for the exchange[69] and the Lee−Yang−Parr correlation functional.[70,71] A double-ζ quality basis set (Lanl2DZ) was employed throughout.[72−75] Because of the small energy differences, a tight convergence criterion with the limit set to 10^{-8} and the ultrafine grid were used. The vibrational spectrum of NIT-H was calculated with a cc-pVDZ basis set[76−78] and the BP86-functional.[79,80]

X-ray Crystallographic Collection and Refinement of the Structures: Dark blue single crystals of **1**, **3**, **3a**, **4**, **7**, **8**, **9**, and **11** were coated with perfluoropolyether, picked up with a glass fiber, and mounted on a diffractometer equipped with a nitrogen cold stream operating at 100 K. Graphite monochromated Mo-K_α radiation (λ = 0.71073 Å) was used throughout. The crystallographic data of the compounds and the diffractometer types used are listed in Tables 1 and 2. Cell constants were obtained from a least-squares fit of the diffraction angles of several thousand strong reflections. Intensity data were corrected for Lorentz and polarization effects. The crystal faces of **4** were determined and the face-indexed correction routine embedded in SHELTXL[81] was used to correct for absorption. The intensity data of **8** were collected on a Siemens Smart CCD diffractometer system and the program SADABS[82] was used to correct for absorption. An absorption correction was carried out for the data set of **9**, for which the program MulScanAbs[83] was used. The Siemens SHELXTL[81] software package was used for solution, refinement, and artwork of the structures, and the neutral-atom scattering factors of the program were used. All structures were solved and refined by direct methods and difference Fourier techniques. Non-hydrogen atoms were refined anisotropically and hydrogen atoms were placed at their calculated positions and refined as riding atoms with isotropic displacement parameters.
Crystallographic data (excluding structure factors) for the structures reported in this paper have been deposited with the Cambridge Crystallographic Data Centre as supplementary publications nos. CCDC-149525, -149526, -149527, -149528, -157121, -157122, and -157123 for structures **1**, **3**, **3a**, **4**, **8**, **9**, and **11**, respectively. Copies of the data can be obtained free of charge on application to CCDC, 12 Union Road, Cambridge, CB2 1EZ, UK [Fax: (internat.) +44−1223/336−033; E-mail: deposit@ccdc.cam.ac.uk].

Supporting Information (see footnote on page 1)**:** Synthetic procedures for preparation of the nitronyl nitroxide precursors and figures showing the molecular structure and crystal packing of compounds **1**, **3**, **3a**, and **7** (13 pages**)**.

Acknowledgments

This work was supported by a grant from the Deutsche Forschungsgemeinschaft (DFG). Thanks go to Prof. Dr. Karl Wieg-

hardt for giving us access to all laboratory facilities. We gratefully acknowledge Manuela Trinoga for HPLC purification of the nitronyl nitroxides and Matthias Pickavé for technical assistance in their preparation. We are also grateful to Petra Höfer and Dr. Eberhard Bothe for help with the spectro-electrochemistry and to Dr. Susanne Döpner and Prof. Dr. Peter Hildebrandt for the RR spectroscopic measurements. E.R. would like to thank the Ministry of Education and Science of the Land Nordrhein-Westfalen for a Lise Meitner fellowship.

---

[1] NIT = nitronyl nitroxide = 4,4,5,5-tetramethyl-4,5-dihydro-1*H*-imidazol-1-yloxyl-3-oxide.

[2] A. Caneschi, D. Gatteschi, P. Rey, *Prog. Inorg. Chem.* **1991**, *39*, 331−429.
[3] D. Gatteschi, P. Rey, in *Magnetic Properties of Organic Materials, Vol. 1* (Ed.: P. M. Lahti), Dekker, New York, **1999**, pp. 601−627.
[4] P. Rey, D. Luneau, in *Supramolecular Engineering of Synthetic Metallic Materials, Vol. 1* (Ed.: J. Veciana), Kluwer, Dordrecht, **1999**, pp. 145−174.
[5] A. Caneschi, D. Gatteschi, J. P. Renard, P. Rey, R. Sessoli, *Inorg. Chem.* **1989**, *28*, 2940−2944.
[6] A. Caneschi, D. Gatteschi, J. P. Renard, P. Rey, R. Sessoli, *Inorg. Chem.* **1989**, *28*, 3314−3319.
[7] A. Caneschi, D. Gatteschi, J. P. Renard, P. Rey, R. Sessoli, *J. Am. Chem. Soc.* **1989**, *111*, 785−786.
[8] H. O. Stumpf, L. Ouahab, Y. Pei, D. Grandjean, O. Kahn, *Science* **1993**, *261*, 447−449.
[9] H. Kumada, A. Sakane, N. Koga, H. Iwamura, *J. Chem. Soc., Dalton Trans.* **2000**, 911−914.
[10] C. Stroh, R. Ziessel, *Tetrahedron Lett.* **1999**, *40*, 4543−4546.
[11] D. Luneau, J. Laugier, G. Ulrich, R. Ziessel, P. Legoll, M. Drillon, *Chem. Commun.* **1994**, 741−742.
[12] G. Ulrich, R. Ziessel, D. Luneau, P. Rey, *Tetrahedron Lett.* **1994**, *35*, 1211−1218.
[13] F. M. Romero, D. Luneau, R. Ziessel, *Chem. Commun.* **1998**, 551−552.
[14] D. Luneau, F. M. Romero, R. Ziessel, *Inorg. Chem.* **1998**, *37*, 5078−5087.
[15] K. Fegy, D. Luneau, T. Ohm, C. Paulsen, P. Rey, *Angew. Chem.* **1998**, *110*, 1331−1335; *Angew. Chem. Int. Ed.* **1998**, *37*, 1270−1273.
[16] T. Yoshida, S. Kaizaki, *Inorg. Chem.* **1999**, *38*, 1054−1058.
[17] R. Ziessel, G. UIrich, R. C. Lawson, L. Echegoyen, *J. Mater. Chem.* **1999**, *9*, 1435−1448.
[18] K. Fegy, D. Luneau, E. Belorizky, M. Novac, J.-L. Tholence, C. Paulsen, T. Ohm, P. Rey, *Inorg. Chem.* **1998**, *37*, 4524−4532.
[19] K. Fegy, N. Sanz, D. Luneau, E. Belorizky, P. Rey, *Inorg. Chem.* **1998**, *37*, 4518−4523.
[20] J.-P. Sutter, M. L. Kahn, S. Golhen, L. Ouahab, O. Kahn, *Chem. Eur. J.* **1998**, *4*, 571−576.
[21] G. Francese, F. M. Romero, A. Neels, H. Stoeckli-Evans, S. Decurtins, *Inorg. Chem.* **2000**, *39*, 2087−2095.
[22] M. L. Kahn, J.-P. Sutter, S. Gohlen, P. Guionneau, L. Ouahab, O. Kahn, D. Chasseau, *J. Am. Chem. Soc.* **2000**, *122*, 3413−3421.
[23] A. Caneschi, F. Ferraro, D. Gatteschi, P. Rey, R. Sessoli, *Inorg. Chem.* **1990**, *29*, 4217−4223.
[24] I. Dasna, S. Golhen, L. Ouahab, O. Pena, J. Guillevic, M. Fettouhi, *J. Chem. Soc., Dalton Trans.* **2000**, 129−132.
[25] Y.-H. Chung, H.-H. Wei, G.-H. Lee, Y. Wang, *Inorg. Chim. Acta* **1999**, *293*, 30−36.
[26] M. Fettouhi, M. Khaled, A. Waheed, S. Golhen, L. Ouahab, J.-P. Sutter, O. Kahn, *Inorg. Chem.* **1999**, *38*, 3967−3971.
[27] C. Rancurel, J.-P. Sutter, T. Le Hoerff, L. Ouahab, O. Kahn, *New J. Chem.* **1999**, 1333−1335.
[28] A. Caneschi, D. Gatteschi, R. Sessoli, *Inorg. Chem.* **1993**, *32*, 4612−4616.
[29] N. C. Schiødt, F. Fabrizi de Biani, A. Caneschi, D. Gatteschi, *Inorg. Chim. Acta* **1996**, *248*, 139−146.
[30] D. A. Shultz, S. H. Bodnar, K. E. Vostrikova, J. W. Kampf, *Inorg. Chem.* **2000**, *39*, 6091−6093.
[31] J. Cirujeda, O. Jürgens, J. Vidal-Gancedo, C. Rovira, P. Turek, J. Veciana, *Mol. Cryst. Liq. Cryst.* **1997**, *305*, 367−384.
[32] J. Veciana, J. Cirujeda, C. Rovira, J. Vidal-Gancedo, *Adv. Mater.* **1995**, *7*, 221−225.
[33] J. Cirujeda, L. E. Ochando, J. M. Amigo, C. Rovira, J. Rius, J. Veciana, *Angew. Chem.* **1995**, *107*, 99−102; *Angew. Chem. Int. Ed. Engl.* **1995**, *34*, 55−57.
[34] E. Hernandez, M. Mas, E. Molins, C. Rovira, J. Veciana, *Angew. Chem.* **1993**, *105*, 919−921; *Angew. Chem. Int. Ed. Engl.* **1993**, *32*, 882−884.
[35] M. Matsushita, A. Izuoka, T. Sugawara, T. Kobayashi, N. Wada, N. Takeda, M. Ishikawa, *J. Am. Chem. Soc.* **1997**, *119*, 4369−4379.
[36] O. Jürgens, J. Cirujeda, M. Mas, I. Mata, A. Cabrero, J. Vidal-Gancedo, C. Rovira, E. Molins, J. Veciana, *J. Mater. Chem.* **1997**, *7*, 1723−1730.
[37] S. Hase, D. Shiomi, K. Sato, T. Takui, *J. Mater. Chem.* **2001**, *11*, 756−760.
[38] E. F. Ullmann, J. H. Osiecki, D. G. B. Boocock, R. Darcy, *J. Am. Chem. Soc.* **1972**, *94*, 7049−7059.
[39] M. Tamura, Y. Nakazawa, D. Shiomei, K. Nozawa, Y. Hosokoshi, M. Ishikawa, M. Takahashi, M. Kinoshita, *Chem. Phys. Lett.* **1991**, *186*, 401−404.
[40] K. Yamaguchi, M. Okumura, M. Nakano, *Chem. Phys. Lett.* **1992**, *191*, 237−244.
[41] A. Caneschi, D. Gatteschi, E. Rentschler, R. Sessoli, *Gazz. Chim. It.* **1995**, *125*, 283−286.
[42] J. W. Hall, W. E. Marsh, R. Weller, W. E. Hatfield, *Inorg. Chem.* **1981**, *20*, 1033−1037.
[43] J. A. D′Anna, J. H. Wharton, *J. Chem. Phys.* **1970**, *53*, 4047−4052.
[44] E. Bill, J. Müller, T. Weyhermüller, K. Wieghardt, *Inorg. Chem.* **1999**, *38*, 5795−5802.
[45] J. Müller, T. Weyhermüller, E. Bill, P. Hildebrandt, K. Hildenbrand, K. Wieghardt, *J. Inorg. Biochem.* **1999**, *74*, 241−241.
[46] R. Schnepf, A. Sokolowski, J. Müller, V. Bachler, K. Wieghardt, P. Hildebrandt, *J. Am. Chem. Soc.* **1998**, *120*, 2352−2364.
[47] A. Sokolowski, J. Müller, T. Weyhermüller, R. Schnepf, P. Hildebrandt, K. Hildenbrand, E. Bothe, K. Wieghardt, *J. Am. Chem. Soc.* **1997**, *119*, 8889−8900.
[48] K. Ishiguro, M. Ozaki, Y. Kamekura, N. Sekine, Y. Sawaki, *Mol. Cryst. Liq. Cryst.* **1997**, *306*, 75−80.
[49] K. Ishiguro, M. Ozaki, N. Sekine, Y. Sawaki, *J. Am. Chem. Soc.* **1997**, *119*, 3625−3626.
[50] K. Ishiguro, Y. Kamekura, Y. Sawaki, *Mol. Cryst. Liq. Cryst.* **1993**, *233*, 113−118.
[51] Y. Pontillon, A. Grand, T. Ishida, E. Leliévre-Berna, T. Nogami, E. Ressouche, J. Schweizer, *J. Mater. Chem.* **2000**, *10*, 1539−1546.
[52] Y. Pontillon, A. Caneschi, D. Gatteschi, A. Grand, E. Ressouche, R. Sessoli, J. Schweizer, *Chem. Eur. J.* **1999**, *5*, 3616−3624.
[53] A. Zheludev, V. Barone, M. Bonnet, B. Delley, A. Grandl, E. Ressouche, P. Rey, R. Subra, J. Schweizer, *J. Am. Chem. Soc.* **1994**, *116*, 2019−2027.
[54] L. Noodleman, D. A. Case, *Adv. Inorg. Chem.* **1992**, *38*, 423−470.
[55] E. Ruiz, J. Cano, S. Alvarez, P. Alemany, *J. Am. Chem. Soc.* **1998**, *120*, 11122−11129.
[56] E. Ruiz, P. Alemany, S. Alvarez, J. Cano, *J. Am. Chem. Soc.* **1997**, *119*, 1297−1303.
[57] J. Cano, A. Rodriguez-Fortea, P. Alemany, S. Alvarez, E. Ruiz, *Chem. Eur. J.* **2000**, *6*, 327−333.
[58] J. Cano, P. Alemany, S. Alvarez, M. Verdaguer, E. Ruiz, *Chem. Eur. J.* **1998**, *4*, 476−484.
[59] V. Barone, A. Bencini, A. di Matteo, *J. Am. Chem. Soc.* **1997**, *119*, 10831−10837.

[60] A. Rodríguez-Fortea, P. Alemany, S. Alvarez, E. Ruiz, *Chem. Eur. J.* **2001**, *7*, 627−637.
[61] M. Deumal, P. Lafuente, F. Mota, J. J. Novoa, *Synth. Met.* **2001**, accepted.
[62] J. Müller, A. Kikuchi, E. Bill, T. Weyhermüller, P. Hildenbrand, L. Ould-Moussa, K. Wieghardt, *Inorg. Chim. Acta* **2000**, *297*, 265−277.
[63] B. Adam, E. Bill, E. Bothe, B. Goerdt, G. Haselhorst, K. Hildenbrand, A. Sokolowski, S. Steenken, T. Weyhermüller, K. Wieghardt, *Chem. Eur. J.* **1997**, *3*, 308−309.
[64] J. Gräfenstein, A. M. Hjerpe, E. Kraka, D. Cremer, *J. Phys. Chem. A* **2000**, *104*, 1748−1761.
[65] J. P. Perdew, A. Savin, K. Burke, *Phys. Rev. B* **1995**, *51*, 4531−4541.
[66] J. M. Wittbrodt, H. B. Schlegel, *J. Chem. Phys.* **1996**, *105*, 6574−6577.
[67] J. P. Perdew, M. Ernzerhof, K. Burke, A. Savin, *Int. J. Quant. Chem.* **1997**, *1997*, 197−205.
[68] Gaussian 98, Revision A.7, M. J. Frisch, G. W. Trucks, H. B. Schlegel, G. E. Scuseria, M. A. Robb, J. R. Cheeseman, V. G. Zakrzewski, J. A. Montgomery, Jr., R. E. Stratmann, J. C. Burant, S. Dapprich, J. M. Millam, A. D. Daniels, K. N. Kudin, M. C. Strain, O. Farkas, J. Tomasi, V. Barone, M. Cossi, R. Cammi, B. Mennucci, C. Pomelli, C. Adamo, S. Clifford, J. Ochterski, G. A. Petersson, P. Y. Ayala, Q. Cui, K. Morokuma, D. K. Malick, A. D. Rabuck, K. Raghavachari, J. B. Foresman, J. Cioslowski, J. V. Ortiz, A. G. Baboul, B. B. Stefanov, G. Liu, A. Liashenko, P. Piskorz, I. Komaromi, R. Gomperts, R. L. Martin, D. J. Fox, T. Keith, M. A. Al-Laham, C. Y. Peng, A. Nanayakkara, M. Challacombe, P. M. W. Gill, B. Johnson, W. Chen, M. W. Wong, J. L. Andres, C. Gonzalez, M. Head-Gordon, E. S. Replogle, and J. A. Pople, Gaussian, Inc., Pittsburgh PA, **1998**.
[69] A. D. Becke, *J. Chem. Phys.* **1993**, *98*, 5648−5652.
[70] C. Lee, W. Yang, R. G. Parr, *Phys. Rev. B* **1988**, *37*, 785−789.
[71] B. Miehlich, A. Savin, H. Stoll, H. Preuss, *Chem. Phys. Lett.* **1989**, *157*, 200−206.
[72] T. H. Dunning, P. J. Hay, in *Modern Theoretical Chemistry*, Plenum Press, New York, **1976**, pp. 1−28.
[73] P. J. Hay, W. R. Wadt, *J. Chem. Phys.* **1985**, *82*, 270−283.
[74] P. J. Hay, W. R. Wadt, *J. Chem. Phys.* **1985**, *82*, 299−310.
[75] W. R. Wadt, P. J. Hay, *J. Chem. Phys.* **1985**, *82*, 284−298.
[76] T. H. Dunning, *J. Chem. Phys.* **1989**, *90*, 1007−1023.
[77] R. A. Kendall, T. H. Dunning, R. J. Harrison, *J. Chem. Phys.* **1992**, *96*, 6796−6805.
[78] D. E. Woon, T. H. Dunning, *J. Chem. Phys.* **1993**, *98*, 1358−1371.
[79] J. P. Perdew, *Phys. Rev. B* **1986**, *33*, 8822−8824.
[80] A. D. Becke, *Phys. Rev. A* **1988**, *38*, 3098−3100.
[81] SHELXTL V.5, Siemens Analytical X-ray Instruments, Inc. **1994**.
[82] SADABS, G. M. Sheldrick, Universität Göttingen, Germany, **1994**.
[83] MulScanAbs, Platon99 program suite, A. L. Spek, University of Utrecht, Netherlands.

Received May 11, 2001
[I01168]

P−H-Functionalized 2-(Phosphanyl)ethanethiols, Their Titanocene Derivatives $[Cp_2Ti(SCH_2CH_2PHR)_2]$ (R = Ph, 2,4,6-$Me_3C_6H_2$, 2,4,6-$iPr_3C_6H_2$) and Reaction of $[Cp_2Ti(SCH_2CH_2PHPh)_2]$ with $[Cu(CH_3CN)_4]BF_4$

Satyajeet Chaudhury,[a] Steffen Blaurock,[a] and Evamarie Hey-Hawkins*[a]

Dedicated to Prof. M. Herberhold on the occasion of his 65th birthday

Keywords: P−H-Functionalized 2-(phosphanyl)ethanethiols / Titanium / Metallocenes / Bis(phosphanylethanethiolates) / Copper

The P–H-functionalized 2-(phosphanyl)ethanethiols $RHPCH_2CH_2SH$ [R = Ph (**1**), 2,4,6-$Me_3C_6H_2$ (Mes) (**2**), 2,4,6-$iPr_3C_6H_2$ (Tipp) (**3**)] were prepared by ring cleavage of ethylene sulfide with LiPHR, followed by hydrolytic workup and distillation. **1**–**3** react with $[Cp_2TiCl_2]$ in the presence of excess NEt_3 to yield a diastereomeric mixture (ratio ca. 1:1) of *rac*- and *meso*-$[Cp_2Ti(SCH_2CH_2PHR)_2]$ [R = Ph (**4**), Mes (**5**), Tipp (**6**)]. **6** is not obtained in pure form. Compound **4** reacts with $[Cu(CH_3CN)_4]BF_4$ to yield $[Cu\{P,P'\text{-}PHPhCH_2CH_2\text{-}SB(FH)SCH_2CH_2PPh(B\text{–}P)\}_2]BF_4$ (**7**). **1**–**7** were characterized spectroscopically. **7** exhibits dynamic behavior in solution, as shown by ^{31}P NMR spectroscopy. Crystal structure determinations were carried out on **5** and **7**. In **5**, both diastereomers cocrystallize in the asymmetric unit. Although the cation of **7** has six chiral centers, only the (R_P,R_P,R_P,R_P,R_B,R_B)/(S_P,S_P,S_P,S_P,S_B,S_B) diastereomer is present in the solid state.

Introduction

While tertiary phosphanyl alcohols have been known and employed as ligands in the synthesis of transition metal complexes with catalytic properties for a long time,[1] the synthetic potential of primary[2] and secondary[3] phosphanyl alcohols has only recently been recognized. The corresponding tertiary,[4−9] secondary[4,10,11] and primary[12] phosphanylalkanethiols have received comparatively less attention. The lack of investigations in this area reflects the paucity of commercially available primary phosphanes, the synthesis of which often requires tedious procedures.[13] Catalytic reactions have been reported in which the transition metal center bears a neutral bidentate P,S ligand, such as the chiral phosphanylalkyl thioether $PR_2CH_2CHR'SR''$ (R, R′, R″ = alkyl or aryl).[8] However, these are rare due to the possibility of metal poisoning by sulfur.

While several transition metal complexes with tertiary phosphanylalkanethiolato ligands[4,6,7,14−28] are known, mainly late "soft" transition metal complexes bearing primary (Ni, Pd, Pt,[12] Co, Rh[29]) or secondary phosphanylalkanethiolato ligands (Ni,[4,30] Pd, Pt,[30] Co,[4,30,31] Cu,[30] Rh[31]) have been described**.** Here, the phosphanylalkanethiolato ligand acts as a monoanionic bidentate S,P-chelating ligand. In main-group metal chemistry, group-14 metal derivatives $Me_2M(P,S\text{-}SCH_2CH_2PPh)$ (M = Si,[11] Sn,[11,32] Ge[11,33]) and $Sn\{S,P,S\text{-}SCH_2CH_2P(Ph)CH_2CH_2S\}$[34] are known. Only a small number of early transition metal complexes is known.[7,35,36] However, the use of mixed P,S ligands appears attractive for several reasons. Group-4 and other early transition metals have well-established thiolato complexes which can be employed in catalytic processes,[37] while the late transition and coinage metals form stable phosphane complexes which can also be used in catalysis.[38] Thus, the possibility of bridging two different metal centers by using ligands with mixed donor atoms appears feasible and could conceivably result in metal−metal interaction[7] and complexes with new and unique reactivity patterns. To date, only a few heterobimetallic complexes in which a phosphanylalkanethiolato ligand bridges an early and a late transition metal center are known, namely, $[Cp_2Ti(SCH_2CH_2CH_2PPh_2)_2Rh]^+$ or $[Cp_2Ti(SCH_2CH_2CH_2PPh_2)_2Rh]^0$,[7] $[Cp_2Ti(SCH_2CH_2CH_2PPh_2)_2Ni]$,[39] $[Cp_2Ti(SCH_2CH_2CH_2PPh_2)_2Ni(CO)_2]$,[39] $[Cp_2Ti(SCH_2CH_2CH_2PPh_2)_2Pd]^{2+}$,[39] and $[Cp_2Ti(SCH_2CH_2PPh_2)_2Cu]^+$.[35] Several homodi-[26,40−44] and -trinuclear[16,30,39,45] complexes and heterobimetallic bi-[46,47] and trinuclear[39−41] complexes, in which the P,S ligand bridges two late transition metal centers (Fe, Ni, Co, Pd, Pt, Cu, Ag) have also been reported. Some of these complexes have been structurally characterized.

We now report on the synthesis and spectroscopic studies of the soft-soft P−H-functionalized 2-(phosphanyl)ethanethiols $RHPCH_2CH_2SH$ [R = Ph (**1**), 2,4,6-$Me_3C_6H_2$ (Mes) (**2**), 2,4,6-$iPr_3C_6H_2$ (Tipp) (**3**)]. The synthesis of **1** from NaPHPh and ethylene sulfide in liquid ammonia, followed by hydrolysis with hydrochloric acid was reported by Issleib et al. in 1967.[4] However, characterization of the product was limited to elemental analysis and IR-spectroscopic studies.

[a] Institut für Anorganische Chemie der Universität Leipzig, Johannisallee 29, 04103 Leipzig, Germany

 © WILEY-VCH Verlag GmbH, 69451 Weinheim, 2001 1434−1948/01/1010−2587 $ 17.50+.50/0

Results and Discussion

Synthesis and Characterization of the 2-(Phosphanyl)ethanethiols $RHPCH_2CH_2SH$ [R = Ph (1), Mes (2), Tipp (3)]

The P−H-functionalized 2-(phosphanyl)ethanethiols $RHPCH_2CH_2SH$ [R = Ph (**1**), Mes (**2**), Tipp (**3**)] were prepared by nucleophilic ring cleavage of ethylene sulfide with the lithium phosphanides LiPHR, prepared in situ from RPH_2 and BuLi, followed by hydrolytic workup and distillation (Scheme 1). A stoichiometric amount of ethylene sulfide had to be employed to prevent further reaction to $RP(CH_2CH_2SH)_2$.[6] **1**−**3** were obtained in good yields and gave satisfactory elemental analyses. They are readily oxidized by air. At room temperature, the 2-(phosphanyl)-ethanethiols are colorless oils that solidify at −30 °C.

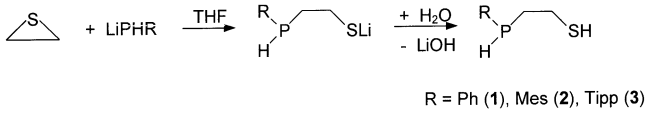

Scheme 1

The 2-(phosphanyl)ethanethiols **1**−**3** were characterized spectroscopically (^1H, ^{31}P, ^{13}C NMR spectroscopy; MS; and IR spectroscopy). A comparison of the ^1H, ^{31}P and ^{13}C data for **1**−**3** is given in Table 1. In the proton-coupled ^{31}P NMR spectra, **1**−**3** give rise to doublets, and the signals of **1** are downfield relative to those of **2** and **3** (**1** < **2** < **3**; Table 1).

In the ^1H NMR spectra, the S−H proton gives rise to a triplet (**1** and **2**) or multiplet (**3**) at δ = 1.2−1.3 ($^3J_{H-H}$ = 7.8 Hz). The methylene protons of the $HPCH_2CH_2SH$ fragment appear as complex multiplets due to $^1H-^1H$ and $^1H-^{31}P$ coupling. The P−H signal is a doublet of doublets of doublets (**1** and **2**) or a doublet of triplets (**3**) at δ ≈ 4.0−4.3 ($^1J_{P-H}$ = 209−217, $^3J_{H-H}$ = 7−9 Hz). In the ^{13}C NMR spectra, the $P-CH_2$ and $S-CH_2$ groups give rise to doublets at δ = 24.4−24.8 (P−C, $^1J_{C-P}$ = 7.1 and 7.8 Hz for **1** and **2**, 12.6 Hz for **3**) and δ = 27.7 −30.4 (P−C−*C*−S, $^2J_{C-P}$ ca. 15.8−17.0 Hz). For all compounds, molecular ion peaks were observed in the mass spectra. In the IR spectra, the S−H stretching band is observed around 2560 cm^{-1}, and ν(P−H) is found in the 2280 to 2340 cm^{-1} region (cf. ref.[4]).

Synthesis and Characterization of *rac*- and *meso*-$[Cp_2Ti(SCH_2CH_2PHR)_2]$ [R = Ph (4), Mes (5), Tipp (6)]

The P−H-functionalized 2-(phosphanyl)ethanethiols **1**−**3** react with $[Cp_2TiCl_2]$ in the presence of excess triethylamine to give the disubstituted products $[Cp_2Ti(SCH_2CH_2PHR)_2]$ [R = Ph (**4**), Mes (**5**), Tipp (**6**)], and $(NEt_3H)Cl$ (Scheme 2). In the $^{31}P\{^1H\}$ NMR spectra (Table 2), two singlets of equal intensity are present, in accordance with the presence of two diastereomers due to the chiral center at the phosphorus atom. Separation of the diastereomers was not achieved, even after repeated recrystallization. The chemical shifts of the 2-(phosphanyl)ethanethiols and of the titanium complexes are similar, the latter exhibiting a downfield shift of only δ ≈ 2.5. This indicates no Ti−P interaction in solution. In complexes in which the phosphanylalkanethiolato ligand acts as bidentate ligand, a downfield shift of δ ≈ 80 is observed in the ^{31}P NMR

Table 1. NMR-spectroscopic data for compounds **1**−**3**

	$PhPHCH_2CH_2SH$ (**1**)	$MesPHCH_2CH_2SH$ (**2**)	$TippPHCH_2CH_2SH$ (**3**)
^1H	1.31 (t, 1 H, $^3J_{H-H}$ = 7.8, SH)	1.21 (t, 1 H, $^3J_{H-H}$ = 7.8, SH)	1.19 (br, s, 6 H, CH_3 in *o*-*i*Pr)
δ/ppm, *J*/Hz	1.69 (m, 1 H, $P-CH_2$)	1.59 (m, 1 H, $P-CH_2$)	1.21 (br, s, 6 H, CH_3 in *o*-*i*Pr)
	1.83 (m, 1 H, $P-CH_2$)	1.83 (m, 1 H, $P-CH_2$)	1.28 (br, s, 3 H, CH_3 in *p*-*i*Pr)
	2.27 (m, 2 H, $S-CH_2$)	2.08 (s, 3 H, *p*-CH_3 in Mes)	1.30 (br, s, 3 H, CH_3 in *p*-*i*Pr)
	4.04 (d/d/d, 1 H, $^1J_{P-H}$ = 209.6,	2.24 (m, 2 H, $S-CH_2$)	1.25−1.30 (m, 1 H, SH)
	$^3J_{H-H}$ = 8.8, PH)	2.31 (s, 6 H, *o*-CH_3 in Mes)	1.72 (m, 1 H, $P-CH_2$)
	7.06 (d, 1 H, $^3J_{H-H}$ = 4.0, *p*-H in Ph)	4.24 (d/d/d, 1 H, $^1J_{P-H}$ = 216.5,	1.97 (m, 1 H, $P-CH_2$)
	7.26 (m, 4 H, *o*- and *m*-H in Ph)	$^3J_{H-H}$ = 8.5, PH)	2.31 (m, 2 H, $S-CH_2$)
		6.71 (s, 2 H, *m*-H in Mes)	2.75 (sept, 1 H, CH in *p*-*i*Pr, $^3J_{H-H}$ = 6.9)
			3.71 (sept, 2 H, CH in *o*-*i*Pr, $^3J_{H-H}$ = 6.5)
			4.13 (d/t, 1 H, $^1J_{P-H}$ = 216.5, $^3J_{H-H}$ = 7.1, PH)
			7.12 (s, 2 H, *m*-H in Tipp)
^{31}P	−54.0 (d, $^1J_{P-H}$ = 210.2, PH)	−88.8 (d, $^1J_{P-H}$ = 216.5, PH)	-97.1 (d, $^1J_{P-H}$ = 215.4, PH)
δ/ppm, *J*/Hz			
^{13}C[a]	24.58 (d, $^1J_{C-P}$ = 7.1, $P-CH_2$)	21.67 (s, *p*-CH_3 in Mes)	24.48 (d, $^1J_{P-C}$ = 12.6, $P-CH_2$)
δ/ppm, *J*/Hz	29.30 (d, $^2J_{C-P}$ = 15.9, $S-CH_2$	23.83 (d, $^3J_{P-C}$ = 10.9, *o*-CH_3 in Mes)	24.77 (d, $^3J_{P-C}$ = 4.7, CH_3 in *o*-*i*Pr)
	129.08 (s, *ipso*-C in Ph)	24.80 (d, $^1J_{P-C}$ = 7.8, $P-CH_2$)	25.09 (s, CH_3 in *o*-*i*Pr)
	129.43 (d, $^3J_{P-C}$ = 5.5, *m*-C in Ph)	27.73 (d, $^2J_{P-C}$ = 17.0, $S-CH_2$)	25.72 (s, CH_3 in *p*-*i*Pr)
	134.51 (d, $^2J_{P-C}$ = 15.4, *o*-C in Ph)	130.07 (d, $^3J_{P-C}$ = 2.8, *m*-C in Mes)	30.04 (d, $^2J_{P-C}$ = 15.8, $S-CH_2$)
	135.4 (d, $^4J_{P-C}$ = 11.9, *p*-C in Ph)	138.66 (s, *p*-C in Mes)	33.70 (d, $^3J_{P-C}$ = 13.7, CH in *o*-*i*Pr)
		142.45 (d, $^2J_{P-C}$ = 20.8, *o*-C in Mes)	35.39 (s, CH in *p*-*i*Pr)
			122.42 (d, $^3J_{P-C}$ = 3.0, *m*-C in Tipp)
			150.68 (s, *p*-C in Tipp)
			153.91 (d, $^2J_{P-C}$ = 11.1, *o*-C in Tipp)

[a] *ipso*-C signal of Ph (for **1**), Mes (for **2**) and Tipp (for **3**) obscured by solvent or not observed.

Table 2. NMR-spectroscopic data for compounds **4**−**6**

	$[Cp_2Ti(SCH_2CH_2PHPh)_2]$ (**4**)	$[Cp_2Ti(SCH_2CH_2PHMes)_2]$ (**5**)	$[Cp_2Ti(SCH_2CH_2PHTipp)_2]$ (**6**)[a]
^1H	1.98 (m, 2 H, P−CH_2)	1.87 (m, 2 H, P−CH_2)	[a]
δ/ppm, *J*/Hz	2.09 (m, 2 H, P−CH_2)	2.10 (s, 2 H + 6 H, P−CH_2	
	3.24 (m, 4 H, S−CH_2)	and *p*-CH_3 in Mes)	
	4.32 (d/t, 2 H, $^1J_{P-H}$ = 208.0,	2.52 (m, 12 H, *o*-CH_3 in Mes)	
	$^3J_{H-H}$ = 7.0, PH)	3.23 (m, 4 H, S−CH_2)	
	5.62 (s, 10 H, Cp)	4.51 (d, br, 2 H, $^1J_{P-H}$ = 215, PH)	
	7.09 (m, 6 H, *o*- and *p*-H in Ph)	5.59 (s, 10 H, Cp)	
	7.46 (t, 4 H, $^3J_{H-H}$ = 6.8, *m*-H in Ph)	6.80 (s, 4 H, *m*-H in Mes)	
^{31}P	−51.64 (d/t, $^1J_{P-H}$ = 207, $^3J_{P-H}$ = 5, PH)	−86.14 (d, $^1J_{P-H}$ = 215, PH)	−94.8 (d, $^1J_{P-H}$ = 203, PH)
δ/ppm, *J*/Hz	−51.67 (d/t, $^1J_{P-H}$ = 207, $^3J_{P-H}$ = 5, PH)	−86.30 (d, $^1J_{P-H}$ = 215, PH)	−94.9 (d, $^1J_{P-H}$ = 203, PH)
	(ratio ca. 1:1)	(ratio 1:1)	(ratio 4:3)
^{13}C	27.84 (br, t, P−CH_2)	21.72 (s, CH_3 in Mes)	[a]
δ/ppm, *J*/Hz	44.22 (t, $^1J_{C-H}$ = 139, S−CH_2)	23.6 (br, P−CH_2)	
	111.93 (d/t, $^1J_{C-H}$ = 176 Hz, J_{C-H} = 5.8 Hz, Cp)	44.87 (S−CH_2)	
	126.33 (d, $^1J_{C-H}$ = 161, *m*-C in Ph)	111.84 (Cp)	
	129.20 (*o*-C in Ph)[b]	130.09 (*m*-C in Mes)	
	134.71 (d, $^1J_{C-H}$ = 146, *p*-C in Ph)	138.43 (*p*-C in Mes)	
	138 (br. s, *ipso*-C in Ph)	142.6 (br, *o*-C in Mes) [c]	

[a] Impurity of $TippPHCH_2CH_2SH$ present; therefore the ^1H and ^{13}C NMR spectroscopic data could not be unambiguously assigned. − [b] Obscured by solvent signal. − [c] *ipso*-C signal obscured by solvent signal.

spectrum.[12] In the ^{13}C NMR spectra of **4** and **5**, the signal of the S−CH_2 group is shifted downfield by ca. 19 ppm relative to the free ligand.

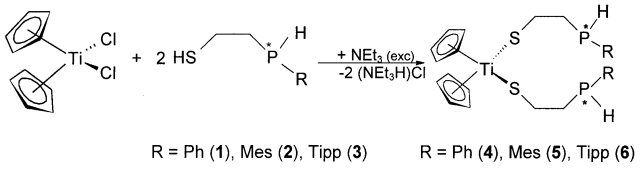

Scheme 2

For **4** and **6**, separation of the titanium complex and the 2-(phosphanyl)ethanethiol could not be achieved by column chromatography or recrystallization. When the purple oil was heated to ca. 46 °C at 10^{-3} Torr (**4**) or ca. 113 °C at 10^{-3} Torr (**6**), the 2-(phosphanyl)ethanethiol could be distilled off, but decomposition of the titanium complex also occurred.

The related Ti complexes $[Cp_2Ti(SCH_2CH_2CH_2PPh_2)_2]$[7] and $[Cp_2Ti(SCH_2CH_2PPh_2)_2]$[35] were obtained in a similar way, as a purple solid and a viscous purple oil that could not be crystallized, respectively. The difference in chemical shifts [$\Delta\delta^{31}P$(complex − ligand) = 1.3 or 0.9 ppm] is comparable to that observed for **4**−**6** relative to **1**−**3**.

Molecular Structure of $[Cp_2Ti(SCH_2CH_2PHMes)_2]$ (5)

Dark purple crystals of **5** were obtained from a saturated hexane solution at room temperature. **5** crystallizes in the centrosymmetric triclinic space group $P\bar{1}$ with four molecules in the unit cell. Both diastereomers, *rac*- and *meso*-$[Cp_2Ti(SCH_2CH_2PHMes)_2]$, are present in the asymmetric unit (Figure 1, Table 3). Cocrystallization of the two diastereomers would appear to be the major reason for the failure to separate them by fractional crystallization. Both diastereomers have similar bond lengths and bond angles.

The titanium atom is coordinated in a pseudotetrahedral fashion by two Cp rings and the S atoms of 2-(phosphanyl)-ethanethiolato ligands. The Ti−S bond lengths of 2.3699(7) to 2.4155(7) Å [average 2.3925(7) Å] and the S−Ti−S bond angles of 96.04(2) and 96.09(3)° are slightly larger than those of the related complex $[Cp_2Ti(SCH_2CH_2CH_2PPh_2)_2]$ [Ti−S 2.378(6), 2.384(6) Å, S−Ti−S 93.3(2)°].[7] One of the C−S−Ti bond angles in **5** is large [C(11)−S(1)−Ti(1) 114.6(1); C(43)−S(3)−Ti(2) 114.70(9)°], and the other is smaller, by ca. 5 to 7° [C(22)−S(2)−Ti(1) 109.08(8); C(54)−S(4)−Ti(2) 107.63(8)°]. This suggests some degree of backbonding from S(1) and S(3) to Ti, which are also involved in the shorter Ti−S bonds [Ti(1)−S(1) 2.3899(6); Ti(2)−S(3) 2.3699(7) Å]. In $[Cp_2Ti(SCH_2CH_2CH_2PPh_2)_2]$, the C−S−Ti bond angles are similar, 109.7(6) and 110.0(6)°.[7] In the titanocene dithiolato complexes, $[Cp^R_2Ti(SR')_2]$[48] (Cp^R = Cp, R′ = Me,[49] Et,[50] *t*Bu,[51] Ph;[52] Cp^R = $C_5H_4SiMe_3$, R′ = C_6F_5 [53]) and $[Cp^*_2Ti(SH)_2]$ (Cp^* = C_5Me_5),[54] the Ti−S bond lengths range from 2.387(3) (R′ = Et) to 2.438(2) Å (R′ = C_6F_5), and the S−Ti−S angles from 93.6(1) (R′ = Me) to 100.6(1)° (R′ = C_6F_5). The values observed for **5** fall inside this range. In titanocene complexes with chelating S,S ligands, the S−Ti−S angles are smaller (ca. 83°) due to the geometric requirements.[48,51,55,56]

The related heterobimetallic complexes $[Cp_2Ti(SCH_2CH_2CH_2PPh_2)_2Rh]^+$ [Ti−S 2.409(3), 2.438(3) Å],[7] $[Cp_2Ti(SCH_2CH_2CH_2PPh_2)_2Ni]$ [Ti−S 2.484(5), 2.483(5) Å],[39] $[Cp_2Ti(SCH_2CH_2CH_2PPh_2)_2Ni(CO)_2]$ [Ti−S 2.398(2), 2.398(4) Å],[39] and $[Cp_2Ti(SCH_2CH_2PPh_2)_2Cu]^+$ [Ti−S 2.465(2), 2.484(3) Å][35] have been structurally characterized. Here, the Ti−S bonds are longer when the S atom is also bonded to a second transition metal.

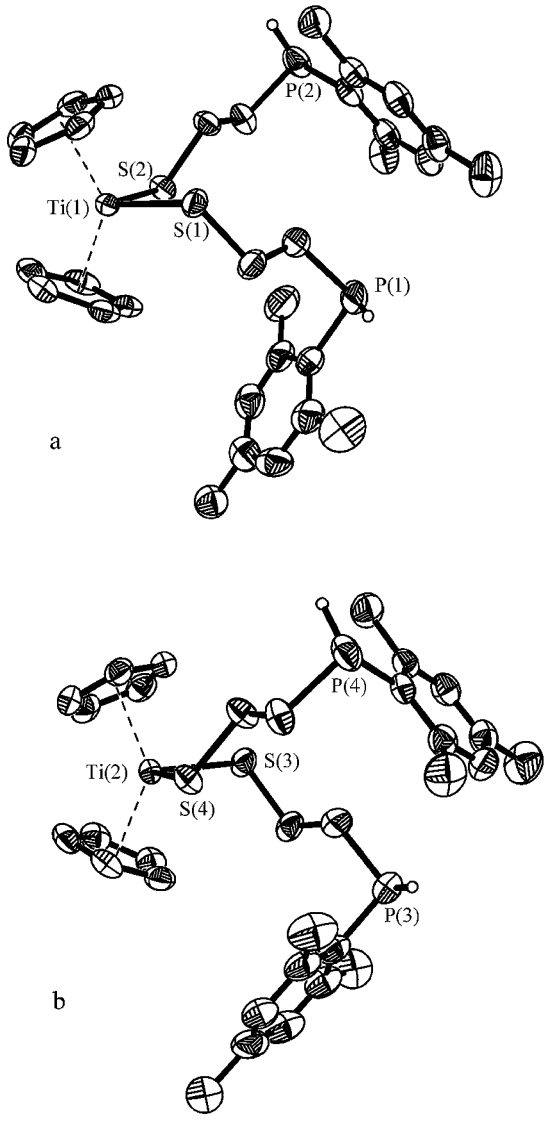

Figure 1. Molecular structure of $[Cp_2Ti(SCH_2CH_2PHMes)_2]$ (**5**) showing the atom numbering scheme employed (ORTEP, 50% probability, SHELXTL PLUS; XP);[70] a) *rac* isomer; b) *meso* isomer; hydrogen atoms (other than P−H) are omitted for clarity

Other related mononuclear transition metal complexes with S,P chelating phosphanylalkanethiolato ligands which have been structurally characterized include $[MoX(S,P\text{-}SCH_2CH_2PPh_2)_2]^{n+}$ ($n = 0$, X = O;[18] $n = 1$, X = Cp[36]), $[Re(SCH_2Ph)(S,P\text{-}SCH_2CH_2PPh_2)_2]$,[22] $[Tc(S,P\text{-}SC_6H_4PPh_2)_3]$,[14] $[Tc(S,P\text{-}SCH_2CH_2PPh_2)_2(S\text{-}SCH_2CH_2POPh_2)]$,[15] $[FeCl(CO)(PPh_3)(S,P\text{-}SC\{(t\text{Bu})(SCOMe)\}CH_2PPh_2)]$,[21] $[Fe\{\eta^2\text{-}C(OMe)S\}P(OMe)_3(S,P\text{-}SC(t\text{Bu})=CHPPh_2)]$,[24] $[Ir(H)(S,P\text{-}SCH_2CH_2PPh_2)(S,P\text{-}HSCH_2CH_2PPh_2)(CO)]^+$,[17] $[Ni(S,P\text{-}SCH_2CH_2PR_2)_2]$ (R = Me,[23] Ph[25]). Complexes with tri-, tetra- or hexadentate phosphanylalkanethiolato ligands which also have been studied are $[Mo\{S,P,S\text{-}(SCH_2CH_2)_2PPh\}_2]$,[6] $[Ni\{S,S,P,P\text{-}SCH_2CH_2P(Ph)CH_2CH_2CH_2P(Ph)CH_2CH_2S\}]$,[20] and $[Os\{P,P,S,S,S,S\text{-}P(CH_2CH_2S)(CH_2CH_2SSCH_2CH_2)_2P(CH_2CH_2S)\}]$.[9]

P,S ligands without a carbon spacer between P and S are present in thiophosphoryltitanocene complexes such as $[Cp'_2Ti\{\eta^2\text{-}S,S\text{-}SP(S)(R)P(S)(R)S\}]$ and $[Cp'_2Ti\{\eta^2\text{-}S,S\text{-}S_2P(S)R\}]$ ($Cp' = C_5H_4Me$, R = p-$OMeC_6H_4$),[57] in the (phosphane sulfide)titanocene compounds $[Cp_2Ti(SPCy_2)_2]$ and $[Cp_2Ti\{\eta^2\text{-}S,S\text{-}S_2PCy_2\}]$[58] and in the inorganic titanium(IV) complexes $[TiCl_2\{\eta^2\text{-}S,S\text{-}S_2PEt_2\}_2]$.[59] In $[Cp'_2Ti\{\eta^2\text{-}S,S\text{-}S_2P(S)R\}]$ [2.4898(8), 2.4639(8) Å],[57] $[Cp_2Ti\{\eta^2\text{-}S,S\text{-}S_2PCy_2\}]$ [2.586(4) and 2.611(5) Å],[58] and $[TiCl_2\{\eta^2\text{-}S,S\text{-}S_2PEt_2\}_2]$ [2.503(3) and 2.442(3) Å],[59] which contain chelating P,S ligands, the Ti−S bond lengths are in the range of dinuclear complexes in which the S atom of the thiolato substituent is bonded to two metal atoms. In the complex $[Cp_2Ti(SPCy_2)_2]$, with a nonchelating S,P ligand, the Ti−S bond lengths [2.420(3), 2.427(3) Å][58] are in the range observed for **5**.

Reaction of $[Cu(CH_3CN)_4]BF_4$ with $[Cp_2Ti(SCH_2CH_2PHPh)_2]$ (4) − Molecular Structure of $[Cu\{P,P'\text{-}PHPhCH_2CH_2SB(FH)SCH_2CH_2PPh(B-P)\}_2]BF_4$ (7)

When **4** was treated with $[Cu(CH_3CN)_4]BF_4$ we expected the formation of the heterodinuclear complex $[Cp_2Ti(SCH_2CH_2PHPh)_2Cu]BF_4$, analogous to the formation of the green-black complex $[Cp_2Ti(SCH_2CH_2PPh_2)_2Cu]BF_4$ (obtained in 55% yield).[35] However, although the experiment was carried out in exactly the same way as that leading to the heterodinuclear Ti−Cu complex, we were unable to isolate a heterodinuclear complex. Instead, we observed the formation of a Cu^I complex, $[Cu\{P,P'\text{-}PHPhCH_2CH_2SB(FH)SCH_2CH_2PPh(B-P)\}_2]BF_4$ (**7**), in a low yield. Apparently this was formed in a complex reaction in which ligand exchange between the BF_4^- anion and the titanium complex occurred with the formation of $[PHPhCH_2CH_2SB(F_2)SCH_2CH_2PHPh]^-$, followed by the substitution of one fluoride atom by the phosphanyl group with the transfer of the P−H proton to the remaining fluoride, to give the cyclized ligand $PHPhCH_2CH_2SB(FH)SCH_2CH_2PPh(B-P)$. Coordination of this bis(phosphane) ligand to Cu^I gives the cation $[Cu\{P,P'\text{-}PHPhCH_2CH_2SB(FH)SCH_2CH_2PPh(B-P)\}_2]^+$ (**7**) (Scheme 3). Elimination of HX from the adducts $R_2BX-PHR'_2$, with the formation of B−P single bonds, has been observed before.[60]

The participation of the BF_4^- anion in the reaction was rather unexpected and, to the best of our knowledge, is unprecedented. The only reaction reported involving BF_4^- is that with difluorophosphoric acid (HPO_2F_2) in $P_2O_3F_4$ to give $HB(PO_2F_2)_4$.[61] In addition, Stephan et al. were able to synthesize the heterodinuclear complexes $[Cp_2Ti(SCH_2CH_2CH_2PPh_2)_2Rh]^+$ [7] and $[Cp_2Ti(SCH_2CH_2PPh_2)_2Cu]^+$ [35] in ca. 60% yield starting from the corresponding BF_4^- salts of $[Rh(NBD)_2]^+$ (NBD = norbornadiene) and $[Cu(CH_3CN)_4]^+$. However, when $[Ni(CH_3CN)_4](BF_4)_2$ was treated with $[Cp_2Ti(SCH_2CH_2CH_2PPh_2)_2]$, the trinuclear Ni complex $[Ni\{(SCH_2CH_2PPh_2)_2Ni\}_2]^{2+}$ was obtained in a 75% yield due to ligand exchange.[39] Other heterodinuclear complexes with phosphanylalkanethiolato bridges are $[Ni(\mu\text{-}SCH_2CH_2PPh_2)_2Mo(CO)_4]$,[47] accessible from $[Ni(S,P\text{-}SCH_2CH_2PPh_2)_2]$ and $[Mo(CO)_4(NBD)]$, and $[Pt\{\mu$-

Table 3. Selected bond lengths [Å] and angles [°] in **5** (CEN = center of the corresponding cyclopentadienyl ring)

Molecule 1		Molecule 2	
Ti(1)−S(1)	2.3899(6)	Ti(2)−S(3)	2.3699(7)
Ti(1)−S(2)	2.3945(7)	Ti(2)−S(4)	2.4155(7)
S(1)−C(11)	1.827(3)	S(3)−C(43)	1.825(3)
S(2)−C(22)	1.821(2)	S(4)−C(54)	1.819(2)
P(1)−C(13)	1.832(3)	P(3)−C(45)	1.830(3)
P(1)−C(12)	1.855(3)	P(3)−C(44)	1.859(3)
P(1)−H(1P)	1.33(5)	P(3)−H(3P)	1.25(4)
P(2)−C(24)	1.838(2)	P(4)−C(56)	1.842(2)
P(2)−C(23)	1.858(3)	P(4)−C(55)	1.850(3)
P(2)−H(2P)	1.22(4)	P(4)−H(4P)	1.34(5)
C(11)−C(12)	1.490(4)	C(43)−C(44)	1.492(4)
C(22)−C(23)	1.515(3)	C(54)−C(55)	1.513(3)
Ti(1)−C(Cp)	2.356(2) to 2.413(3)	Ti(2)−C(Cp)	2.372(3) to 2.417(2)
C(Cp)−C(Cp)	1.380(4) to 1.407(4)	C(Cp)−C(Cp)	1.380(4) to 1.407(4)
S(1)−Ti(1)−S(2)	96.04(2)	S(3)−Ti(2)−S(4)	96.09(3)
CEN(1)−Ti(1)−CEN(2)	132.6(1)	CEN(3)−Ti(2)−CEN(4)	132.6(1)
C(11)−S(1)−Ti(1)	114.6(1)	C(43)−S(3)−Ti(2)	114.70(9)
C(22)−S(2)−Ti(1)	109.08(8)	C(54)−S(4)−Ti(2)	107.63(8)
C(13)−P(1)−C(12)	102.9(1)	C(45)−P(3)−C(44)	101.0(1)
C(13)−P(1)−H(1P)	98(2)	C(45)−P(3)−H(3P)	102(2)
C(12)−P(1)−H(1P)	94(2)	C(44)−P(3)−H(3P)	103(2)
C(24)−P(2)−C(23)	100.7(1)	C(56)−P(4)−C(55)	100.7(1)
C(24)−P(2)−H(2P)	107(2)	C(56)−P(4)−H(4P)	102(2)
C(23)−P(2)−H(2P)	103(2)	C(55)−P(4)−H(4P)	106(2)
C(12)−C(11)−S(1)	111.7(2)	C(44)−C(43)−S(3)	112.0(2)
C(11)−C(12)−P(1)	115.8(2)	C(43)−C(44)−P(3)	113.9(2)
C(18)−C(13)−P(1)	122.0(2)	C(50)−C(45)−P(3)	120.8(2)
C(14)−C(13)−P(1)	119.2(2)	C(46)−C(45)−P(3)	121.1(2)
C(23)−C(22)−S(2)	110.0(2)	C(55)−C(54)−S(4)	111.6(2)
C(22)−C(23)−P(2)	112.9(2)	C(54)−C(55)−P(4)	112.9(2)
C(25)−C(24)−P(2)	119.4(2)	C(61)−C(56)−P(4)	119.7(2)
C(29)−C(24)−P(2)	121.5(2)	C(57)−C(56)−P(4)	121.3(2)

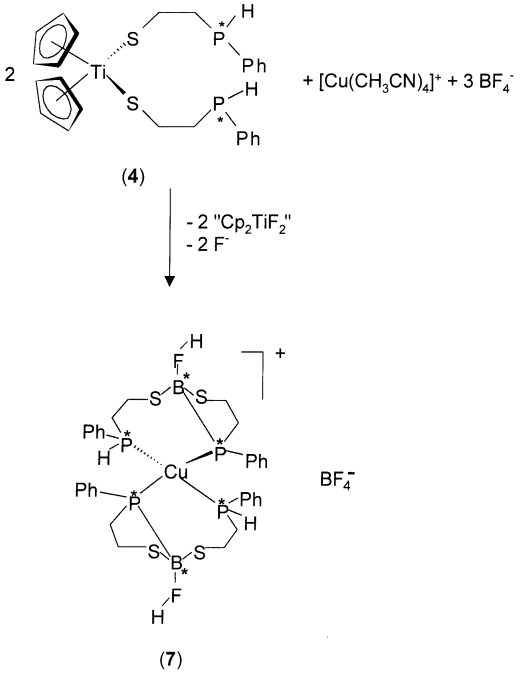

Scheme 3

$SCH_2CH_2PEt_2)_2Ag\}]_\infty(NO_3)_\infty$,[46] which is obtained from $[Pt(S,P\text{-}SCH_2CH_2PEt_2)_2]$ and $AgNO_3$.

At room temperature, two broad sets of signals are observed at $\delta \approx -32$ and $\delta \approx -43$ in the ^{31}P NMR spectrum of **7.** The absence of a signal in the EPR spectrum indicates the presence of Cu^I. The signals at $\delta \approx -43$ show further proton coupling and are thus assigned to the PHPh groups. In **7**, there are six chiral centers present (two boron and four phosphorus atoms), and hence numerous diastereomers (2^6 enantiomers) can be formed resulting in the observation of a large number of signals in the appropriate region of the NMR spectrum. Additionally, (phosphane)Cu^I complexes exhibit dynamic behavior in solution, and Cu has a quadrupole moment, hence broad signals are usually observed in the ^{31}P NMR spectra.

Only one singlet at $\delta = -0.97$ is observed in the ^{11}B NMR spectrum of **7** in $CDCl_3$. This is assigned to the BF_4^- anion by comparison with the starting material, $[Cu(CH_3CN)_4]BF_4$.[62] Apparently, the signal for the boron atom of the bis(phosphane) ligand is too broad to be observed, and this is probably due to the quadrupole moment of boron, the observed dynamic behavior, and the presence of several possible diastereomers in solution.

7 crystallizes in the monoclinic space group $P2_1/n$ with four formula units in the unit cell. One molecule of CH_2Cl_2

is present in the asymmetric unit. The BF_4^- anion is highly disordered. Although the cation of **7** has six chiral centers (two boron and four phosphorus atoms) and numerous diastereomers are observed in solution, there is only one diastereomer present in the solid state. In this diastereomer, all six chiral centers have either (*R*) or (*S*) configuration (Figure 2, Table 4). The two enantiomers are related by a crystallographic center of inversion in the centrosymmetric space group $P2_1/n$. To the best of our knowledge, this is the first structurally characterized chiral bis(diphosphane)copper(I) complex.

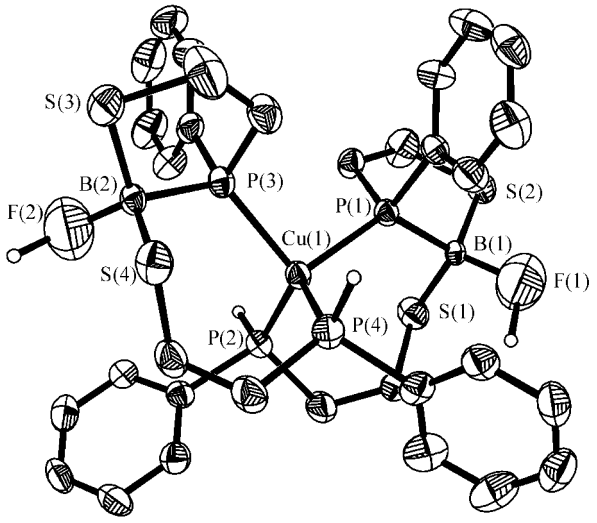

Figure 2. Molecular structure of $(R_P,R_P,R_P,R_P,R_B,R_B)$/$(S_P,S_P,S_P,S_P,S_B,S_B)$-[Cu{*P*,*P*′-$PHPhCH_2CH_2SB(FH)SCH_2CH_2PPh(B-P)$}$_2$]$BF_4$ (**7**) showing the atom numbering scheme employed (ORTEP, 50% probability, SHELXTL PLUS; XP);[70] only the cation is shown; hydrogen atoms (other than P−H or F−H) are omitted for clarity

In **7**, the copper(I) center is coordinated in a distorted tetrahedral fashion to four P atoms of two neutral chelating bis(phosphane) ligands, $PHPhCH_2CH_2SB(FH)SCH_2CH_2PPh(B-P)$. The Cu−P bond lengths of the secondary phosphane groups [Cu(1)−P(2) 2.268(1), Cu(1)−P(4) 2.276(1) Å] in **7** are slightly smaller than those of the other two phosphane ligands [Cu(1)−P(1) 2.287(1), Cu(1)−P(3) 2.295(1) Å]. The P−Cu−P bond angles of the chelating phosphanes are large [P(4)−Cu(1)−P(1) 115.26(5), P(2)−Cu(1)−P(3) 116.90(5)°], as is the P(2)−Cu(1)−P(4) bond angle [117.44(5)°]. The other P−Cu−P angles range from 101.15(4) to 104.00(4)°.

Several (tetraphosphane)copper(I) [63] and bis(diphosphane) complexes[64] have been structurally characterized (Table 5). The Cu−P bond lengths are comparable with those of **7**, while the P−Cu−P bite angle of the chelating phosphanes is dependent on the ring size. Thus, five-membered rings exhibit P−Cu−P bond angles ranging from 88.3(1) to 90.9(1)°, while these angles are larger in $[Cu(PPh_2CH_2CH_2CH_2PPh_2)_2]X$, which has a six-membered ring [X = ClO_4: 94.56(9), 96.94(9)°;[64c] BF_4: 97.66(5), 98.22(5)°[64a]]. In **7**, which has a seven-membered ring [the largest chelate ring reported for structurally characterized bis(diphosphane)Cu^I complexes to date], the bite angles of 115.26(5), 116.90(5)° are the largest observed so far. Dinuclear Cu^I complexes with bridging bis(phosphane) ligands are generally formed when the chain length of the bis(phosphane) increases to six $[PPh_2CH_2(CH_2)_2CH_2PPh_2]$ or eight atoms $[PPh_2CH_2(CH_2)_4CH_2PPh_2]$.[64c]

The bis(phosphane) ligands in **7** contain P−B bonds, presumably formed by elimination of HF. The P−B bond lengths of 1.872(4) and 1.877(5) Å agree well with those of other phosphanidoboranes of the general formula $R_2B-PR'_2$.[60] In **7**, the B−S bond lengths of 1.817(4) [S(2)−B(1)], 1.844(5) [S(1)−B(1)], 1.821(5) [S(3)−B(2)] and 1.840(5) Å [S(4)−B(2)] are in the range observed for thioboranes.[65]

Table 4. Selected bond lengths [Å] and bond angles [°] of **7**

Cu(1)−P(1)	2.287(1)	Cu(1)−P(2)	2.268(1)
Cu(1)−P(3)	2.295(1)	Cu(1)−P(4)	2.276(1)
P(1)−B(1)	1.872(4)	P(3)−B(2)	1.877(5)
P(1)−C(1)	1.823(5)	P(1)−C(7)	1.826(5)
P(2)−C(9)	1.824(4)	P(2)−C(15)	1.843(5)
P(2)−H(2P)	1.31(5)	P(4)−H(4P)	1.48(5)
P(3)−C(17)	1.830(5)	P(3)−C(23)	1.839(5)
P(4)−C(25)	1.830(5)	P(4)−C(31)	1.850(5)
S(1)−C(16)	1.820(5)	S(2)−C(8)	1.804(6)
S(1)−B(1)	1.844(5)	S(2)−B(1)	1.817(4)
S(3)−C(24)	1.823(7)	S(4)−C(32)	1.830(6)
S(3)−B(2)	1.821(5)	S(4)−B(2)	1.840(5)
B(1)−F(1)	1.538(7)	B(2)−F(2)	1.546(7)
F(1)−H(1F)	1.43(6)	F(2)−H(2F)	1.30(6)
C(7)−C(8)	1.526(7)	C(15)−C(16)	1.507(7)
C(23)−C(24)	1.518(8)	C(31)−C(32)	1.514(7)
P(2)−Cu(1)−P(4)	117.44(5)	P(2)−Cu(1)−P(1)	104.00(4)
P(4)−Cu(1)−P(1)	115.26(5)	P(2)−Cu(1)−P(3)	116.90(5)
P(4)−Cu(1)−P(3)	101.36(5)	P(1)−Cu(1)−P(3)	101.15(4)
C(1)−P(1)−C(7)	106.8(2)	C(1)−P(1)−B(1)	104.0(2)
C(7)−P(1)−B(1)	95.1(2)	C(1)−P(1)−Cu(1)	112.90(1)
C(7)−P(1)−Cu(1)	111.0(2)	B(1)−P(1)−Cu(1)	124.6(2)
C(9)−P(2)−C(15)	102.2(2)	C(9)−P(2)−Cu(1)	122.4(2)
C(15)−P(2)−Cu(1)	114.6(2)	C(9)−P(2)−H(2P)	93(2)
C(15)−P(2)−H(2P)	104(2)	Cu(1)−P(2)−H(2P)	117(2)
C(17)−P(3)−C(23)	104.8(3)	C(17)−P(3)−B(2)	103.6(2)
C(23)−P(3)−B(2)	95.7(2)	C(17)−P(3)−Cu(1)	116.3(2)
C(23)−P(3)−Cu(1)	112.6(2)	B(2)−P(3)−Cu(1)	121.0(2)
C(25)−P(4)−C(31)	105.8(2)	C(25)−P(4)−Cu(1)	121.5(2)
C(31)−P(4)−Cu(1)	113.9(2)	C(25)−P(4)−H(4P)	94(2)
C(31)−P(4)−H(4P)	103(2)	Cu(1)−P(4)−H(4P)	116(2)
C(16)−S(1)−B(1)	104.2(2)	C(8)−S(2)−B(1)	98.4(2)
B(2)−S(3)−C(24)	97.2(3)	C(32)−S(4)−B(2)	105.4(2)
F(1)−B(1)−S(2)	108.4(3)	F(1)−B(1)−S(1)	113.2(3)
S(2)−B(1)−S(1)	105.0(2)	F(1)−B(1)−P(1)	117.0(3)
S(2)−B(1)−P(1)	105.2(2)	S(1)−B(1)−P(1)	107.2(2)
F(2)−B(2)−S(3)	109.5(3)	F(2)−B(2)−S(4)	113.5(3)
S(3)−B(2)−S(4)	104.6(2)	F(2)−B(2)−P(3)	114.5(3)
S(3)−B(2)−P(3)	104.9(2)	S(4)−B(2)−P(3)	109.1(2)
B(1)−F(1)−H(1F)	115(2)	B(2)−F(2)−H(2F)	111(3)
C(2)−C(1)−P(1)	118.7(4)	C(6)−C(1)−P(1)	123.5(4)
C(8)−C(7)−P(1)	113.4(4)	C(7)−C(8)−S(2)	112.0(4)
C(10)−C(9)−P(2)	121.8(4)	C(14)−C(9)−P(2)	120.5(4)
C(16)−C(15)−P(2)	114.0(4)	C(15)−C(16)−S(1)	112.4(4)
C(22)−C(17)−P(3)	118.1(4)	C(18)−C(17)−P(3)	124.1(4)
C(24)−C(23)−P(3)	112.9(4)	C(23)−C(24)−S(3)	112.5(4)
C(26)−C(25)−P(4)	121.2(4)	C(30)−C(25)−P(4)	119.3(4)
C(32)−C(31)−P(4)	110.6(4)	C(31)−C(32)−S(4)	111.6(4)

Table 5. Comparison of Cu−P bond lengths and P−Cu−P bond angles in **7** and related bis(diphosphane)copper(I) complexes

Complex	Cu−P [Å]	P−Cu−P bite angle [°]	Ref.
7	2.287(1), 2.268(1), 2.295(1), 2.276(1)	115.26(5), 116.90(5)	this work
$[Cu(PPh_2CH_2CH_2PPh_2)_2]$	2.320(4), 2.305(4)	88.3(1), 88.6(1)	[64h]
$[Cu(Mes)_2]$			
$[Cu(PPh_2CH_2CH_2PPh_2)_2]_2$	2.285	89.6	[64g]
$[Cu_6Fe_4(CO)_{16}]$			
$[Cu(PPh_2CH_2CH_2PPh_2)_2]ClO_4$	2.259(2), 2.301(2), 2.300(2), 2.270(2)	90.34(7), 90.58(7)	[64a]
$[Cu(PMe_2CH_2CH_2PMe_2)_2]$	2.248(3), 2.250(3),	90.9(1)	[64f]
$[Cu\{Co(CO)_4\}_2]$	2.254(3), 2.248(3)		
$[Cu(PMe_2CH_2CH_2PMe_2)_2][CpTi(SCH_2CH_2S)_2]$	2.286(6), 2.280(7), 2.293(7), 2.277(7)	90.5(2)	[64d]
$[CuL^1_2]PF_6$ [a]	2.305(1), 2.324(1), 2.322(1), 2.320(1)	91.68(4), 91.26(4)	[64b]
$[Cu(PPh_2CH{=}CHPPh_2)_2]PF_6$	2.276(2), 2.288(2), 2.289(2), 2.287(2)	89.69(7), 89.90(7)	[64e]
$[Cu(PPh_2CH_2CH_2CH_2PPh_2)_2]ClO_4$	2.316(3), 2.312(3) 2.311(3), 2.330(2)	94.56(9), 96.94(9)	[64c]
$[Cu(PPh_2CH_2CH_2CH_2PPh_2)_2]BF_4$	2.303(1), 2.298(1) 2.296(1), 2.317(1)	97.66(5), 98.22(5)	[64a]

[a] L^1 = 2,3-bis(diphenylphosphanyl)maleic anhydride

We are presently further investigating the potential of **1**−**3** as thiolato- and/or phosphanido ligands in transition metal chemistry.

Experimental Section

General: All experiments were carried out under purified dry argon. Solvents were dried and freshly distilled under argon. − NMR spectra: Avance DRX 400 (Bruker), standards: ^1H NMR (400 MHz): trace amounts of protonated solvent, C_6D_6; ^{13}C NMR (100.6 MHz): internal solvent; ^{31}P NMR (162 MHz): external 85% H_3PO_4. − The IR spectra were recorded as KBr mulls with a Perkin−Elmer FT-IR spectrometer System 2000 in the range 350−4000 cm^{-1}. − The mass spectra were recorded with a Sektorfeldgerät AMD 402 (AMD Intectra GmbH; EI, 70 eV). − The melting points were determined in sealed capillaries under argon and are uncorrected. RPH_2 (R = Ph,[66] Mes,[67] Tipp[13]), and $[Cu(CH_3CN)_4]BF_4$ [68] were prepared according to literature procedures. $[Cp_2TiCl_2]$ and ethylene sulfide are commercially available (Aldrich).

Preparation of 2-(Phenylphosphanyl)ethanethiol (1): $PhPH_2$ (5 mL, 45 mmol) was dissolved in degassed THF (250 mL) and cooled to −70 °C. BuLi (30.7 mL of a 1.48 M solution, 45 mmol) in hexane was added dropwise over 30 min. The color of the solution changed to turbid orange. After stirring for 1 h at room temp., the solution was cooled again to −70 °C, and ethylene sulfide (3 mL, 49.9 mmol) was added slowly. The color of the solution became clear yellow. After stirring for 30 min at room temp., about 2 mL of degassed water was added. The solution turned turbid white due to the formation of LiOH, which was filtered off. The solvent was then evaporated, and the colorless viscous residue distilled to give **1** (5.4 g, 70%, b.p. 46 °C/10^{-3} Torr; ref.[4]: b.p. 135−137 °C/10 Torr). − EI MS: *m*/*z* (%) = 170 (57) [M^+], 142 (14) [$M^+ - 2\ CH_2$], 137 (82) [M^+ − SH], 109 (100) [$PHPh^+$], and fragments thereof. − IR [cm^{-1}]: $\tilde{\nu}$ = 2564 m (νSH; ref.[4]: 2560 cm^{-1}), 2285 vs (νPH; ref.[4]: 2290 cm^{-1}). − $C_8H_{11}PS$ (170.2): calcd. C 56.45, H 6.51, S 18.8; found C 55.00, H 6.59, S 17.6.

Preparation of 2-(Mesitylphosphanyl)ethanethiol (2): $MesPH_2$ (4.88 g, 32 mmol) was dissolved in degassed THF (250 mL), and the solution cooled to −70 °C. BuLi (22 mL of a 1.48 M solution, 32.6 mmol) in hexane was added dropwise over 30 min. The color of the solution changed to turbid orange. After stirring for 1 h at room temp., the solution was cooled again to −70 °C, and ethylene sulfide (2 mL, 33.2 mmol) was added slowly. The color of the solution became clear yellow. After stirring for 30 min at room temp., about 0.8 mL of degassed water was added. The solution turned turbid white due to the formation of LiOH, which was filtered off. The solvent was then evaporated, and the colorless viscous residue distilled to give **2** (4.3 g, 63%, b.p. 100 °C/$10^{-2.5}$ Torr). − EI MS: *m*/*z* (%) = 212 (84) [M^+], 208 (8) [$M^+ - 2\ H_2$], 179 (47) [M^+ − SH], 151 (73) [$PHMes^+$], and fragments thereof. − IR [cm^{-1}]: $\tilde{\nu}$ = 2560 m (νSH), 2334 vs (νPH). − $C_{11}H_{17}PS$ (212.3): calcd. C 62.23, H 8.67; found C 61.9, H 8.21.

Preparation of 2-(Triisopropylphenylphosphanyl)ethanethiol (3): $TippPH_2$ (5.18 g, 22 mmol) was dissolved in degassed THF (250 mL), and the solution cooled to −70 °C. BuLi (18.7 mL of a 1.17 M solution, 22 mmol) in hexane was added dropwise over a period of 30 min. The color of the solution changed to yellow, and LiPHTipp precipitated from the solution. This was isolated by filtration (3 g, 57.2%, confirmed by ^{31}P NMR[13]). LiPHTipp (2 g, 8.35 mmol) was then dissolved in THF (200 mL), and the solution cooled to −70 °C. Ethylene sulfide (0.5 mL, 8.39 mmol) was added slowly. The color of the solution became light yellow. After stirring for 30 min at room temp., about 0.2 mL of degassed water was added, and the solution turned turbid white due to the formation of LiOH, which was filtered off. The solvent was then evaporated, and the colorless viscous residue distilled to give **3** (2.1 g, 83%, b.p. 113 °C/10^{-3} Torr). − EI MS: *m*/*z* (%) = 296 (19) [M^+], 263 (100) [M^+ − SH], 235 (17) [$PHTipp^+$], and fragments thereof. − $C_{17}H_{29}PS$ (296.4): calcd. C 68.88, H 9.86; found C 69.30, H 9.96.

Preparation of $[Cp_2Ti(SCH_2CH_2PHPh)_2]$ (4): $PhPHCH_2CH_2SH$ (0.60 g, 3.5 mmol) was added to a solution of $[Cp_2TiCl_2]$ (0.35 g, 1.4 mmol) in THF (25 mL). A solution of triethylamine (0.9 mL, 6.4 mmol) in THF (25 mL) was added dropwise over 30 min. The solution was stirred for 24 h during which its color changed from red to purple. $(Et_3NH)Cl$ was removed by filtration, and the solvent was removed from the filtrate in vacuum. The oily residue was washed three times with 10 mL of hexane, then recrystallized from toluene/hexane to give **4** as a viscous oil. Yield: 0.65 g (90%). NMR spectra showed that there is a minor impurity of **1** present which could not be eliminated by recrystallization or heating to ca. 46 °C at 10^{-3} Torr (decomp. of **4** occurred). − EI MS: *m*/*z* (%) = 347 (9) [$M^+ - SCH_2CH_2PHPh$], 109 (52) [$PHPh^+$], and fragments thereof. − IR [cm^{-1}]: $\tilde{\nu}$ = 2281 vs (νPH).

Preparation of $[Cp_2Ti(SCH_2CH_2PHMes)_2]$ (5): $MesPHCH_2CH_2SH$ (1.1 g, 5.1 mmol) was added to a solution of $[Cp_2TiCl_2]$ (0.59 g, 2.3 mmol) in THF (25 mL). A solution of triethylamine (1.0 mL, 7.1 mmol) in THF (25 mL) was added dropwise over 30 min. The solution was stirred for 24 h during which its color changed from red to purple. $(Et_3NH)Cl$ was separated by filtration. The solvent was removed from the filtrate in vacuum. The oily residue was dissolved in 25 mL hexane and filtered. At room temperature, crystals of **5** formed. Yield: 0.45 g (32%), m.p. 105−108 °C. − EI MS: *m*/*z* (%) = 600 (2) [M^+], 389 (17) [$M^+ - SCH_2CH_2PHMes$], 212 (57) [$HSCH_2CH_2PHMes^+$], 178 (32) [Cp_2Ti^+], 152 (58) [PH_2Mes^+], 119 (100) [Mes^+], and fragments thereof. − $C_{32}H_{42}P_2S_2Ti$ (600.62): calcd. C 63.99, H 7.05, S 10.68; found C 63.9, H 6.57, S 10.5.

Preparation of $[Cp_2Ti(SCH_2CH_2PHTipp)_2]$ (6). $TippPHCH_2CH_2SH$ (1.03 g, 3.4 mmol) was added to a solution of $[Cp_2TiCl_2]$ (0.39 g, 1.5 mmol) in THF (25 mL). A solution of triethylamine (1.0 mL, 7.1 mmol) in THF (25 mL) was added dropwise over 30 min. The solution was stirred for 24 h during which its color changed from red to purple. $(Et_3NH)Cl$ was separated by filtration. The solvent was removed from the filtrate in vacuum. The oily residue was dissolved in 25 mL hexane and filtered. The resulting oily residue was recrystallized repeatedly from hexane. However, the NMR spectra showed the presence of an impurity of **3**, which could not be eliminated by recrystallization or heating to ca. 113 °C at 10^{-3} Torr (decomp. of **6** occurred).

Reaction of $[Cu(CH_3CN)_4BF_4]$ with $[Cp_2Ti(SCH_2CH_2PHPh)_2]$ (4): A solution of **4** (0.18 g, 0.35 mmol) in acetonitrile (20 mL) was added dropwise to a solution of $[Cu(CH_3CN)_4]BF_4$ (0.11 g, 0.35 mmol) in acetonitrile (10 mL). The solution was stirred overnight, after which it was concentrated under vacuum, and diethyl ether was added. A brownish solid precipitated. This was isolated, dissolved in CH_2Cl_2, layered with hexane and then connected to another flask containing toluene. Some yellow crystals formed over a black residue. The yellow crystals were isolated.

Data Collection and Structural Refinement of 5 and 7: Crystallographic data are given in Table 6. Data [λ(Mo-K_α) = 0.71073 Å] were collected with a Siemens CCD (SMART) diffractometer. All observed reflections were used for the determination of the unit cell parameters. Empirical absorption correction with SADABS.[69] The structures were solved by direct methods (SHELXTL PLUS[70]). Restrictions for **5**: Zr, S, P, and C atoms anisotropic; restrictions for **7**: Cu, P, B, F, S, and C atoms anisotropic; H atoms located by difference maps and refined isotropically. Crystallographic data (excluding structure factors) for the structures reported in this paper have been deposited with the Cambridge Crystallographic Data Centre (**5**: CCDC-159594; **7**: CCDC-159593). Copies of the data can be obtained free of charge on application to CCDC, 12 Union Road, Cambridge, CB2 1EZ, UK [Fax: (internat.) + 1223/336-033; E-mail: deposit@ccdc.cam.ac.uk].

Table 6. Crystal data and structure refinement for **5** and **7**

	5	**7**
Empirical formula	$C_{32}H_{42}P_2S_2Ti$	$C_{32}H_{40}B_3CuF_6P_4S_4{\cdot}CH_2Cl_2$
M_r	600.62	971.66
Temperature [K]	220(2)	220(2)
Crystal system	triclinic	monoclinic
Space group	$P\bar{1}$	$P2_1/n$
a [Å]	12.9752(2)	10.7405(2)
b [Å]	15.5545(2)	20.1003(5)
c [Å]	17.2252(1)	20.3827(6)
α [°]	65.836(1)	90
β [°]	89.180(1)	97.289(1)
γ [°]	84.942(1)	90
V [Å^3]	3158.57(7)	4364.8(2)
Z	4[a]	4
$\rho_{calcd.}$ [Mg m^{-3}]	1.263	1.479
F(000)	1272	1984
Crystal size [mm]	0.50 × 0.40 × 0.20	0.50 × 0.40 × 0.30
Abs. coeff. [mm^{-1}]	0.524	1.012
$2\Theta_{max}$ [°]	56.0	55.1
Refl. collected	18002	23877
Independent reflections	12971	9090
R_{int}	0.0354	0.0412
Parameters	955	683
R [$I > 2\sigma(I)$]	0.0398	0.0566
*wR*2 (all data)	0.0951	0.1740
$(\Delta/\rho)_{min.}$ [e·Å^{-3}]	0.373	0.993
$(\Delta/\rho)_{max.}$ [e·Å^{-3}]	−0.359	−0.833

[a] Both diastereomers are present in the asymmetric unit.

Acknowledgments

S. C. thanks the Department of Science and Technology (DST) Delhi, India, for financial support (BOYSCAST).

[1] [1a] W. Keim, *Angew. Chem.* **1990**, *102*, 251. – [1b] C. A. Willoughby, R. R. Duff, W. M. Davis, S. L. Buchwald, *Organometallics* **1996**, *15*, 472.
[2] J. Heinicke, *Trends Organomet. Chem.* **1994**, *1*, 307; J. Heinicke, I. Kovacs, L. Nyulaszi, *Chem. Ber.* **1991**, *124*, 493.
[3] [3a] J. Heinicke, U. Jux, R. Kadyrov, M. He, *Heteroatom Chem.* **1997**, *8*, 383. – [3b] J. Heinicke, M. He, R. Kadyrov, P. G. Jones, *Heteroatom Chem.* **1998**, *9*, 183.
[4] G. Schwarzenbach, *Chem. Zvesti* **1965**, *19*, 200.
[5] K. Issleib, F. Ungváry, *Z. Naturforsch., Teil B* **1967**, *22*, 1238.
[6] P. J. Blower, J. R. Dilworth, G. J. Leigh, B. D. Neaves, F. B. Normanton, J. Hutchinson, J. A. Zubieta, *J. Chem. Soc., Dalton Trans.* **1985**, 2647.
[7] G. S. White, D. W. Stephan, *Organometallics* **1987**, *6*, 2169.
[8] E. Hauptman, P. J. Fagan, W. Marshall, *Organometallics* **1999**, *18*, 2061 and ref. cited therein.
[9] J. R. Dilworth, Y. Zheng, J. R. Miller, *J. Chem. Soc., Dalton Trans.* **1992**, 1757.
[10] K. Issleib, K.-D. Franze, *J. Prakt. Chem.* **1973**, *315*, 471.
[11] J. D. Andriamizaka, J. Escudié, C. Couret, J. Satgé, *Phosphorus Sulfur* **1982**, *12*, 279.
[12] K. Issleib, W. Gans, *Z. Anorg. Allg. Chem.* **1981**, *475*, 116.
[13] S. Kurz, PhD thesis, University of Leipzig, **1995**.
[14] C. Bolzati, F. Refosco, F. Tisato, G. Bandoli, A. Dolmella, *Inorg. Chim. Acta* **1992**, *201*, 7.
[15] F. Tisato, F. Refosco, G. Bandoli, C. Bolzati, A. Moresco, *J. Chem. Soc., Dalton Trans.* **1994**, 1453.
[16] E. Pfeiffer, M. L. Pasquier, W. Marty, *Helv. Chim. Acta* **1984**, *67*, 654.
[17] D. W. Stephan, *Inorg. Chem.* **1984**, *23*, 2207.
[18] J. Chatt, J. R. Dilworth, J. A. Schmutz, J. A. Zubieta, *J. Chem. Soc., Dalton Trans.* **1979**, 1595.
[19] G. Doyle, *J. Organomet. Chem.* **1975**, *101*, 85.
[20] R. Schmelcer, D. Schwarzenbach, *Cryst. Struct. Commun.* **1981**, *10*, 1317.
[21] A. Samb, B. Demerseman, P. H. Dixneuf, C. Mealli, *Organometallics* **1988**, *7*, 26.
[22] T. Maina, A. Pecorale, A. Dolmella, G. Bandali, U. Mazzi, *J. Chem. Soc., Dalton Trans.* **1994**, 2437.
[23] M. Kita, T. Yamamoto, K. Kashiwabara, J. Fujita, *Bull. Chem. Soc. Jpn.* **1992**, *65*, 2272.
[24] [24a] A. J. Carty, F. Hartstock, N. J. Taylor, H. Le Bozec, P. Robert, P. H. Dixneuf, *J. Chem. Soc., Chem. Commun.* **1980**, 361. – [24b] P. Robert, H. Le Bozec, P. H. Dixneuf, F. Hartstock, N. J. Taylor, A. J. Carty, *Organometallics* **1982**, *1*, 1148.
[25] Y.-M. Hsiao, S. S. Chojnacki, P. Hinton, J. H. Reibenspies. M. Y. Darensbourg, *Organometallics* **1993**, *12*, 870.
[26] W. Marty, G. Schwarzenbach, *Chimia* **1970**, *24*, 431.
[27] M. Savignac, P. Cadiot, F. Mathey, *Inorg. Chim. Acta* **1980**, *45*, L43.
[28] V. Korner, G. Huttner, L. Zsolnai, M. Buchner, A. Jacobi, D. Gunauer, *Chem. Ber.* **1996**, *129*, 1587.
[29] K. Issleib, W. Gans, *Z. Anorg. Allg. Chem.* **1982**, *491*, 163.
[30] K. Issleib, D. Wienbeck, *Z. Anorg. Allg. Chem.* **1978**, *440*, 5.
[31] K. Issleib, D. Wienbeck, *Z. Anorg. Allg. Chem.* **1978**, *440*, 237.
[32] C. Couret, J. D. Andriamizaka, J. Escudié, J. Satgé, *J. Organomet. Chem.* **1981**, *208*, C3.
[33] C. Couret, J. Satgé, J. D. Andriamizaka, J. Escudié, *J. Organomet. Chem.* **1978**, *157*, C35.
[34] U. Baumeister, H. Hartung, K. Jurgschat, A. Tzschach, *J. Organomet. Chem.* **1986**, *304*, 107.
[35] G. S. White, D. W. Stephan, *Inorg. Chem.* **1985**, *24*, 1499.
[36] D. Morales, R. Poli, P. Richard, J. Andrieu, E. Collange, *J. Chem. Soc., Dalton Trans.* **1999**, 867.
[37] Review on transition metal complexes with thiolato ligands: P. J. Blower, J. R. Dilworth, *Coord. Chem. Rev.* **1987**, *76*, 121. Review on transition metal complexes with thioether ligands: S. G. Murray, F. R. Hartley, *Chem. Rev.* **1981**, *81*, 365.
[38] [38a] B. R. James, *Adv. Organomet. Chem.* **1979**, *17*, 319. – [38b] J. L. Speier, *Adv. Organomet. Chem.* **1979**, *17*, 407.
[39] G. S. White, D. W. Stephan, *Organometallics* **1988**, *7*, 903.
[40] K. Aurivillius, G.-I. Bertinsson, *Acta Crystallogr., Sect. B* **1982**, *38*, 1295.
[41] W. S. Crane, H. Beall, *Inorg. Chim. Acta* **1978**, *31*, L469.
[42] P.-H. Leung, S.-Y. Siah, A. J. P. White, D. J. Williams, *J. Chem. Soc., Dalton Trans.* **1998**, 893.
[43] F. Mathey, M.-B. Comarmond, D. Moras, *Chem. Commun.* **1979**, 417.
[44] G. Reinhard, R. Solteck, G. Huttner, A. Barth, O. Walter, L. Zsolnai, *Chem. Ber.* **1996**, *129*, 97.
[45] A. Togni, G. Rihs, R. E. Blumer, *Organometallics* **1992**, *11*, 613.
[46] P. Strickler, *Helv. Chim. Acta* **1969**, *52*, 270.
[47] S. S. Chojnacki, Y.-M. Hsiao, M. Y. Darensbourg, J. H. Reibenspies, *Inorg. Chem.* **1993**, *32*, 3573.
[48] For a recent review see: D. W. Stephan, T. T. Nadasdi, *Coord. Chem. Rev.* **1996**, *147*, 147.
[49] [49a] M. A. A. F. de C. T. Carrondo, G. A. Jeffrey, *Acta Crystallogr., Sect. C* **1983**, *39*, 42. – [49b] T. A. Wark, D. W. Stephan, *Organometallics* **1989**, *8*, 2836.
[50] M. J. Calhorda, M. A. A. F. de C. T. Carrondo, A. R. Dias, C. F. Frazão, M. B. Hursthouse, J. A. M. Simões, C. Teixeira, *Inorg. Chem.* **1988**, *27*, 2513.
[51] F. Senocq, N. Viguier, A. Gleizes, *Eur. J. Solid State Inorg. Chem.* **1996**, *33*, 1185.
[52] E. G. Muller, S. F. Watkins, L. F. Dahl, *J. Organomet. Chem.* **1976**, *111*, 73.
[53] E. Delgado, E. Hernández, A. Hedayat, J. Tornero, R. Torres, *J. Organomet. Chem.* **1994**, *466*, 119.
[54] F. Bottomley, D. F. Drummond, G. O. Egharevba, P. S. White, *Organometallics* **1986**, *5*, 1620.
[55] A. Kutoglu, *Acta Crystallogr., Sect. B* **1973**, *29*, 2891.
[56] P. R. Stafford, T. B. Rauchfuss, A. K. Verma, S. R. Wilson, *J. Organomet. Chem.* **1996**, *526*, 203.
[57] G. A. Zank, T. B. Rauchfuss, *Organometallics* **1984**, *3*, 1191.
[58] L. Gelmini, D. W. Stephan, *Organometallics* **1987**, *6*, 1515.
[59] W. Kuchen, A. Mamsch, D. Mootz, M. Steffen, *Z. Anorg. Allg. Chem.* **1981**, *472*, 133.
[60] Review: P. P. Power, *Angew. Chem.* **1990**, *102*, 527; *Angew. Chem. Int. Ed. Engl.* **1990**, *29*, 481.
[61] M. F. A. Dove, R. C. Hibbert, N. Logan, *J. Chem. Soc., Dalton Trans.* **1984**, 2719.
[62] For comparison: NMR-spectroscopic data of $[Cu(CH_3CN)_4]BF_4$ in $CDCl_3$: ^1H: $\delta = 2.11$ (s). – ^{11}B: $\delta = -1.07$ (s, not broad, no B–F coupling is observed). – ^{19}F: $\delta = 54.82, 54.87$ (s, ratio ca. 3:1).
[63] [63a] Kai-Ming Chi, J. Farkas, M. J. Hampden-Smith, T. T. Kodas, E. N. Duesler, *J. Chem. Soc., Dalton Trans.* **1992**, 3111. – [63b] R. Fuchs, P. Klüfers, *Z. Naturforsch., Teil B* **1991**, *46*, 507. – [63c] G. A. Bowmaker, P. C. Healy, L. M. Engelhardt, J. D. Kildea, B. W. Skelton, A. H. White, *Aust. J. Chem.* **1990**, *43*, 1697. – [63d] D. F. Dempsey, G. S. Girolami, *Organometallics* **1988**, *7*, 1208. – [63e] L. M. Engelhardt, C. Pakawatchai, A. H. White, P. C. Healy, *J. Chem. Soc., Dalton Trans.* **1985**, 125. – [63f] I. V. Kourkine, S. V. Maslennikov, R. Ditchfield, D. S. Glueck, G. P. A. Yap, L. M. Liable-Sands, A. L. Rheingold, *Inorg. Chem.* **1996**, *35*, 6708.
[64] [64a] P. Comba, C. Katsichtis, B. Nuber, H. Pritzkow, *Eur. J. Inorg. Chem.* **1999**, 777. – [64b] J. S. Lewis, S. L. Heath, A. K. Powell, J. Zweit, P. J. Blower, *J. Chem. Soc., Dalton Trans.* **1997**, 855. – [64c] S. Kitagawa, M. Kondo, S. Kawata, S. Wada, M. Maekawa, M. Munakata, *Inorg. Chem.* **1995**, *34*, 1455. – [64d] T. T. Nadasdi, D. W. Stephan, *Inorg. Chem.* **1994**, *33*, 1532. – [64e] S. J. Berners-Price, L. A. Colquhoun, P. C. Healy, K. A. Byriel, J. V. Hanna, *J. Chem. Soc., Dalton Trans.* **1992**, 3357. – [64f] D. J. Darensbourg, Chi-Shan Chao, J. H. Reibenspies,

C. J. Bischoff, *Inorg. Chem.* **1990**, *29*, 2153. – [64g] G. Doyle, K. A. Eriksen, D. Van Engen, *J. Am. Chem. Soc.* **1985**, *107*, 7914. – [64h] P. Leoni, M. Pasquali, C. A. Ghilardi, *Chem. Commun.* **1983**, 240. – [64i] A. Camus, N. Marsich, G. Nardin, L. Randaccio, *Transition Met. Chem.* **1976**, *1*, 205.

[65] [65a] W. Clegg, M. R. J. Elsegood, F. J. Lawlor, N. C. Norman, N. L. Pickett, E. G. Robins, A. J. Scott, P. Nguyen, N. J. Taylor, T. B. Marder, *Inorg. Chem.* **1998**, *37*, 5289. – [65b] W. Clegg, C. Dai, F. J. Lawlor, T. B. Marder, P. Nguyen, N. C. Norman, N. L. Pickett, W. P. Power, A. J. Scott, *J. Chem. Soc., Dalton Trans.* **1997**, 839. – [65c] M. Ito, N. Tokitoh, R. Okazaki, *Organometallics* **1997**, *16*, 4314. – [65d] R. Wehmschulte, K. Ruhlandt-Senge, M. M. Olmstead, M. A. Petrie, P. P. Power, *J. Chem. Soc., Dalton Trans.* **1994**, 2113. – [65e] H. Nöth, H. Pommerening, R. Staudigl, *Z. Naturforsch., Teil B* **1988**, *43*, 501. – [65f] M. Noltemeyer, G. M. Sheldrick, C. Habben, A. Meller, *Z. Naturforsch., Teil B* **1983**, *38*, 1182. – [65g] H. Nöth, K. Niedenzu, *Chem. Ber.* **1983**, *116*, 1132. – [65h] H. Nöth, R. Staudigl, W. Storch, *Chem. Ber.* **1981**, *114*, 3024.

[66] W. Kuchen, H. Buchwald, *Chem. Ber.* **1958**, *91*, 2296.

[67] S. Kurz, PhD thesis, University of Leipzig, **1995**. Synthesis according to the procedure given for (2,4,6-*t*$Bu_3C_6H_2$)PH_2 in: A. H. Cowley, N. C. Norman, M. Pakulski, *Inorg. Synth.* **1990**, *27*, 235.

[68] G. J. Kubas, *Inorg. Synth.* **1979**, *19*, 90.

[69] G. M. Sheldrick, *SADABS – a Program for Empirical Absorption Correction*, Göttingen, **1998**.

[70] *SHELXTL PLUS*, Siemens Analyt. X-ray Inst. Inc., **1990**: XS: *Program for Crystal Structure Solution*; XL: *Program for Crystal Structure Determination*; XP: *Interactiv Molecular Graphics.*

Received March 2, 2001
[I01079]

Calix[6]arene-Based N_3-Donors − A Versatile Supramolecular System with Tunable Electronic and Steric Properties − Study on the Formation of Tetrahedral Dicationic Zinc Complexes in a Biomimetic Environment

Olivier Sénèque,[a] Yannick Rondelez,[a] Loïc Le Clainche,[a] Claude Inisan,[a] Marie-Noëlle Rager,[b] Michel Giorgi,[c] and Olivia Reinaud*[a]

Keywords: Calixarenes / Zinc / *N* ligands / Bioinorganic chemistry / Coordination chemistry

Novel tridentate *N*-ligands containing tertiary amines, pyrazoles, or benzimidazole groups were synthesized from *t*Bu-calix[6]arene. Together with the previously described pyridine and imidazole-based ligands, they form a large family of biomimetic ligands ($X_6Me_3N_3$) with different electronic and steric properties. Their capacity at stabilizing a tetrahedral Zn dicationic center in acetonitrile was investigated. Tertiary amines were too basic and sterically hindered, leading to precipitation of $Zn(OH)_2$. The resulting protonated ligand was, in one case, structurally characterized by X-ray analysis. Ligands with pyrazole, benzimidazole and imidazole donors, all formed a stable Zn complex under stoichiometric conditions in acetonitrile. An ^1H NMR spectroscopic study together with X-ray crystallography showed that the metal ion is coordinated to the three nitrogen arms with MeCN as a fourth ligand included in the calixarene conic pocket. These complexes provide new but rare examples of stable dicationic tetrahedral Zn species. The calixarene functionalized by three pyridine groups, on the other hand, did not appear to be a good ligand, which stands in contrast with its remarkable ability at stabilizing copper(I). Finally, these *funnel complexes* are chiral due to their helical shape. In solution, both enantiomers are in equilibrium. However, sterically hindered *N*-donors increased the enantiomerization barrier above 16 kcal/mol.

Introduction

Zinc enzymes constitute an important class of metalloproteins. These are ubiquitous and play a fundamental role in living systems. They are mainly involved in hydrolytic processes but also catalyze hydride transfer reactions. Zn^{2+} is usually maintained in the active site through its coordination to three amino acid residues, either His, Cys, Asp, or Glu. In mononuclear zinc enzymes that have been structurally characterized, the most recurrent binding site is tris-histidine. Indeed this N_3 core has been found in snake venom proteases, matrix metalloproteases, collagenases, deaminases, β-lactamase, carbonic anhydrase, and a carboxypeptidase.[1] Model chemistry is a fundamental tool for understanding these important biological systems. To mimic the role of a tris(imidazole) core, the most widely used N_3-ligands[2,3] are macrocyclic triamines,[4] anionic tris(pyrazolyl)borates,[5−7] or neutral tris(imidazolyl)methane and -phosphane.[8] Although the steric hindrance at each synthetic core can be tuned through the introduction of appropriate substituents, their electronic properties can hardly be modulated (particularly through the change of the *N*-donor).

In the present paper, we report on a calix[6]arene-based system that not only preorganizes a binding site for the metal center but also provides a cavity next to it. This system is highly versatile since it allows the tuning of both the steric hindrance and the electronic properties due to the *N*-donor set. Here, we first describe the synthesis of a series of novel calix[6]arene-based N_3-ligands. They offer a wide variety of potential binding sites, either tertiary or aromatic amines, with various steric encumbrance. We then report on their relative ability at stabilizing a metal ion in a biomimetic environment. We previously described the first members of this family with pyridine-based Cu^I [9,10] and imidazole-based Zn^{II} complexes.[11] These so-called *funnel complexes* present a hydrophobic cavity that wraps around the free coordination site of the metal ion, thereby acting like a selective molecular funnel for small exogenous ligands and mimicking the enzyme pocket. Here, we focus on the binding part of these supramolecular systems and compare the ability of the various *N*-donors at stabilizing a tetrahedral Zn^{2+} ion.

Results and Discussion

Synthesis of Ligands

The calix[6]arene-based N_3-ligands $X_6Me_3N_3$ were synthesized in two steps starting from *t*Bu-calix[6]arene

[a] Laboratoire de Chimie et Biochimie Pharmacologiques et Toxicologiques, CNRS UMR 8601, Université René Descartes, 45 rue des Saints Pères, 75270 Paris Cedex 06, France
Fax: (internat.) +33-1-42862183
E-mail: reinaud@biomedicale.univ-paris5.fr
[b] Service de RMN, CNRS UMR 7576, E.N.S.C.P., 11 rue Pierre et Marie Curie, 75231 Paris Cedex 05, France
[c] Laboratoire de Cristallochimie, CNRS UMR 6517, Centre scientifique Saint-Jérôme, Av. Escadrille Normandie-Niemen, 13397 Marseille Cedex 20, France

 © WILEY-VCH Verlag GmbH, 69451 Weinheim, 2001 1434−1948/01/1010−2597 $ 17.50+.50/0

(X_6H_6).[12] The latter was first converted into its 1,3,5-trimethyl ether derivative ($X_6Me_3H_3$),[13] then treated with various alkyl chlorides in a THF/DMF mixture in the presence of excess NaH. The products $X_6Me_3N_3$ were obtained in good yields from $X_6Me_3H_3$ (ca. 80%). They constitute a very large family of tridentate ligands, presenting various *N*-donors: pyrrolidine (Pyr), dimethylamine (Dmema), pyrazole Pyz, 3,5-dimethylpyrazole (DMPyz), benzimidazole (Bzim), imidazole (Imme), and pyridine (Pic). All of them show good solubility in chlorinated solvents and are almost insoluble in acetonitrile (Scheme 1).

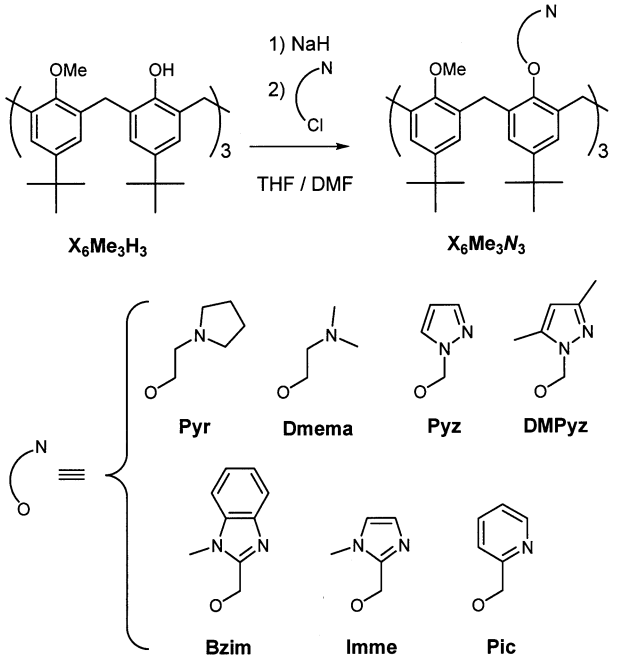

Scheme 1. Synthesis of the calix[6]arene-based N_3-ligands $X_6Me_3N_3$

Crystal Structures of $X_6Me_3Pyz_3$ and $[X_6Me_3Pyr_3.H_3](ClO_4)_3$

Two of these molecules were characterized by X-ray diffraction analysis. The molecular structures of ligand **$X_6Me_3Pyz_3$** and of the perchlorate salt of the ligand **$X_6Me_3Pyr_3$** are displayed in Figure 1 and 2, respectively. Both calix[6]arene structures stand in a flattened C_3-symmetrical cone conformation. The smallest *O*-substituents, the methoxy groups, point toward the inside of the cavity, close to the C_3 axis with the related *t*Bu groups lying in the *out*-position. The nitrogenous arms, which are the largest *O*-substituents, are projected outwards whereas the corresponding *t*Bu groups lie in the *in*-position. Figure 2 shows the regular head to head stacking of the protonated ligands forming a sandwich around a layer of perchlorates anions.

NMR Study of the Ligands

The $X_6Me_3N_3$ ligands underwent NMR spectroscopic analysis. In agreement with the X-ray structure of $X_6Me_3Pyz_3$, all of them displayed, at 298 K in $CDCl_3$, ^1H NMR spectroscopic profiles typical of a major cone conformer.

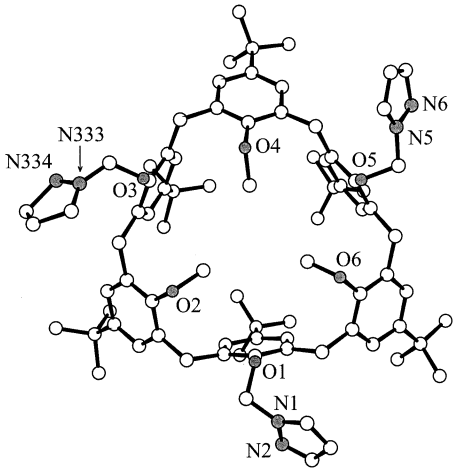

Figure 1. X-ray structure of $X_6Me_3Pyz_3$. Hydrogen atoms and solvent of crystallization were omitted for clarity. Only one out of the two isomers is shown (see Exp. Sect.)

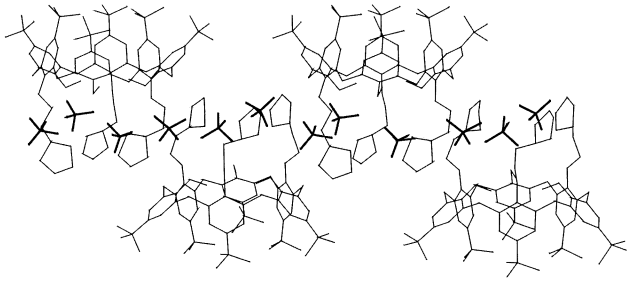

Figure 2. X-ray structure of $[X_6Me_3Pyr_3.H_3](ClO_4)_3$. Hydrogen atoms and solvent of crystallization were omitted for clarity

The high-field shift of the methoxy protons (δ_{OMe} = 2.14−2.33) attested to their partial inclusion in the calixarene π-basic cavity. It is well-known that calix[6]arenes are highly mobile molecules since interconversion processes between multiple conformers can occur via rotation through the annulus of both the *O*-alkyl and the *t*Bu groups.[14] Indeed, compounds $X_6Me_3Pyz_3$ and $X_6Me_3Dmema_3$ showed broad resonances with two large singlets for their bridging methylene protons, which is indicative of the beginning of a coalescence process at room temperature (Figure 2). In contrast, spectra of all others were sharp and well defined, with two doublets for the $ArCH_2Ar$ methylene protons. This indicated that the cone−cone interconversion was slower than the NMR timescale. In the specific case of compounds with the more sterically encumbered nitrogen arms (*N* = Pyr, DMPyz, and Bzim) a minor conformer was clearly detected at room temperature as six extra well-defined doublets for the bridging methylene groups were observed. This minor isomer probably corresponds to the 1,2,3-alternate conformer that was identified in the case of the closely related calix[6]arenes.[15] Hence, the comparative $ArCH_2Ar$ areas of the ^1H NMR spectra (displayed in Figure 3) are a good probe for the evaluation of calix[6]arene mobility.[16] A qualitative classification according to a decreasing mobility of the molecules can be made: $X_6Me_3Pyz_3$ and $X_6Me_3Dmema_3$ > $X_6Me_3Imme_3$ and $X_6Me_3Pic_3$ > $X_6Me_3Pyr_3$,

$X_6Me_3DMPyz_3$, and $X_6Me_3Bzim_3$. This indeed corresponds to an increasing steric encumbrance of the nitrogenous arms, that slows down their rotation through the annulus of the calix[6]arene.

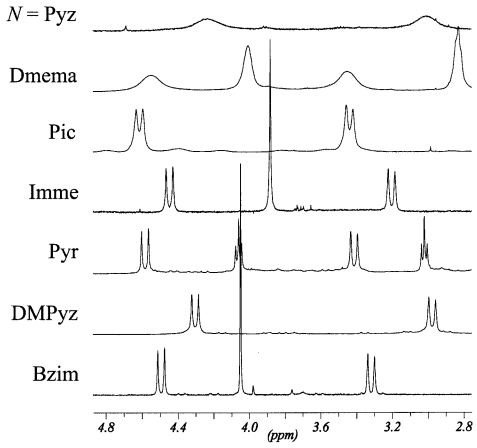

Figure 3. $ArCH_2Ar$ regions of the ^1H NMR spectra (400 MHz) of ligands $X_6Me_3N_3$ at 298 K in $CDCl_3$

Reaction with Zinc(II)

Compounds $X_6Me_3N_3$ were treated in acetonitrile with a stoichiometric quantity of $Zn(H_2O)_6(ClO_4)_2$ and the products were submitted for NMR spectroscopic analyses in CD_3CN.[17] In the case of ligands containing tertiary amine moieties ($X_6Me_3Dmema_3$ and $X_6Me_3Pyr_3$), the ^1H NMR spectra of the isolated compounds together with elemental analyses indicated the presence of three chlorine atoms per ligand which was due to the perchlorate salt of the tris-protonated ligands $[X_6Me_3N_3{\cdot}H_3](ClO_4)_3$ (N = Pyr and Dmema). Confirmation of these assignments was obtained by comparison with the authentic samples prepared with $HClO_4$. From these first results, it appears that the strong basicity of the tertiary amines-based ligands $X_6Me_3Pyr_3$ and $X_6Me_3Dmema_3$ together with the high steric hindrance at the nitrogen atoms, disfavors the formation of stable complexes and rather lead to their protonation with concomitant precipitation of $Zn(OH)_2$.

In contrast to these tertiary amine-based systems, calixarenes that have been functionalized with either pyrazole (Pyz and DMPyz), imidazole (Imme) or benzimidazole (Bzim) groups led to products with a 1:1 ligand/Zn ratio. One of them, $[Zn(X_6Me_3Imme_3)(CH_3CN)](ClO_4)_2$, was structurally characterized by X-ray analysis.

Crystal Structure of $[Zn(X_6Me_3Imme_3)(CH_3CN)](ClO_4)_2$

Single crystals were obtained by slow diffusion of Et_2O into a $CHCl_3/CH_3CN$ solution of $[Zn(X_6Me_3Imme_3)(CH_3CN)](ClO_4)_2$. The structure, displayed in Figure 4, shows a tetrahedral zinc center coordinated to all three imidazole arms and to an acetonitrile molecule. The latter is situated inside the calixarene cavity, along the C_3 axis. The calixarene is constrained in a flattened cone conformation with all OMe groups projected away from the cavity. The anisole *t*Bu groups are now in the *in*-position and the others are *out*. The average $Zn-N_{Im}$ bond length (1.973 Å) and the zinc−nitrile distance (2.008 Å) are particularly short, in accordance with the highly acidic nature of a tetrahedral zinc dication.[18] Finally, as previously observed for all other X-ray characterized *funnel complexes*, the coordinating arms (here the imidazole groups) form a chiral helix around the metal center and both enantiomers are present in the lattice.

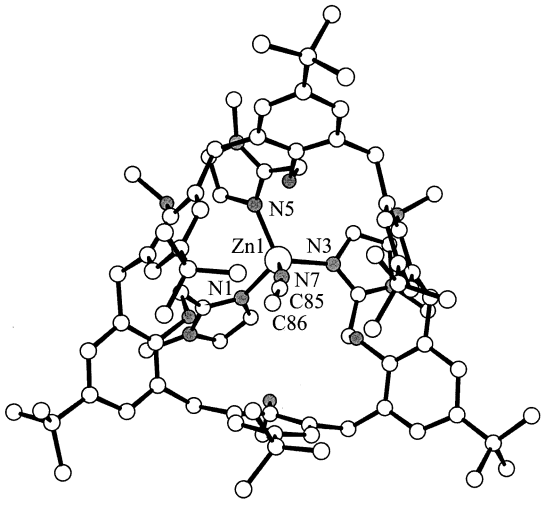

Figure 4. Crystal structure of complex $[Zn(X_6Me_3Imme_3)(CH_3CN)](ClO_4)_2$. Hydrogen atoms, counterions and solvent of crystallization were omitted for clarity. Selected bond lengths [Å] and angles [°]: Zn1−N1 1.956(9), Zn1−N3 1.993(10), Zn1−N5 1.972(9), Zn1−N7 2.008(11), N7−C85 1.132(15), N1−Zn1−N3 111.8(4), N1−Zn1−N5 110.5(4), N3−Zn1−N5 115.9(4), N1−Zn1−N7 106.3(4), N3−Zn1−N7 107.0(4), N5−Zn1−N7 104.4(4), Zn1−N7−C85 173.4(9), N7−C85−C86 174.2(2)

NMR Study of Zinc Complexes $[Zn(X_6Me_3N_3)(MeCN)](ClO_4)_2$

The Zn complexes obtained with ligands $X_6Me_3N_3$ (N = Pyz, DMPyz, Imme, Bzim) were analyzed by ^1H NMR spectroscopy in acetonitrile. Upon dissolution in CD_3CN, one equivalent of free CH_3CN was released, indicating that the isolated products possessed an acetonitrile molecule coordinated to the zinc ion.[19] In the case of $X_6Me_3Bzim_3$, the exchange process was slow enough to allow the observation of a vanishing resonance at $\delta = -0.80$.[20] This indeed corresponded to the coordinated protio-acetonitrile and its high-field shift attested to its location inside the calixarene π-basic cavity.

All NMR profiles displayed in Figure 5 are sharp and characteristic of a calix[6]arene in a C_3-symmetrical cone conformation. The methoxy protons are downfield shifted compared to the free ligand ($\delta = 3.6$ instead of ca. $\delta = 2.3$[21]). This is indicative of the change in the calixarene conformation due to the Zn^{II} coordination. The small rim of the cone is now closed up by the three nitrogen arms, which are linked together by the metal ion, thereby projecting the OMe groups outwards. An acetonitrile molecule (here the solvent) completes the coordination sphere of the

tetrahedral metal ion and fills in the empty space offered by the cavity (Scheme 2).[22] HMQC and HMBC experiments showed that the *t*Bu groups connected to the anisole present the higher shift (ca. $\delta = 0.8$ compared to $\delta = 1.4$ for the other *t*Bu) and form a gate at the entrance of the hydrophobic pocket. Hence, the calixarene adopts the same conformation in CD_3CN solution as the one depicted by the X-ray structure shown in Figure 4. Interestingly, this conformation is the opposite of that observed[10] for the related copper(I) complex $[Cu(X_6Me_3Pic_3)(CH_3CH_2CN)]^+$. As it does not seem to be ligand dependent, this different behavior may be attributed to the nature of the coordinated metal ion, and more precisely to its charge. Indeed, in the zinc conformation, the cone is flatter than in the copper(I) conformation and the metal cation gets closer to the basic oxygen of the phenoxyl moieties (3.8 vs. 4.1 Å).

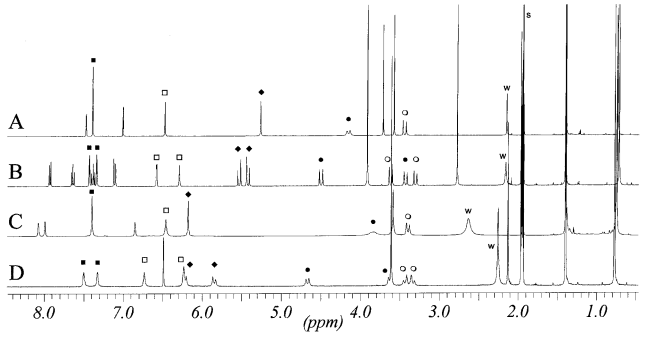

Figure 5. ^1H NMR spectra (400 MHz) of complexes $[Zn(X_6Me_3N_3)(CD_3CN)](ClO_4)_2$ at 298 K in CD_3CN. **A**: *N* = Imme, **B**: *N* = Bzim, **C**: *N* = Pyz, **D**: *N* = DMPyz. H_{Ar}: ■ and □; OCH_2: ◆; $ArCH_{ax}CH_{eq}Ar$: ●; $ArCH_{ax}CH_{eq}Ar$: ○. Solvent and water are labeled "s" and "w", respectively

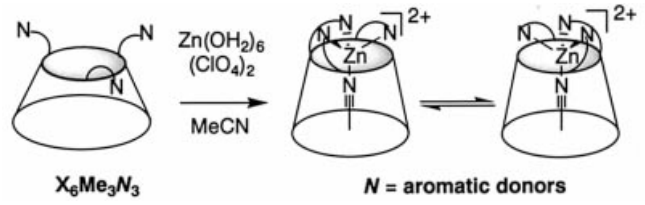

Scheme 2. Formation of "Zn-funnel complexes"

Lastly, no compound of defined stoichiometry could be isolated through the reaction of one molar equivalent of zinc perchlorate with the pyridine-based ligand $X_6Me_3Pic_3$. The ^1H NMR spectrum of the crude product presented broad signals and was hardly interpretable. However, the addition of an excess of $Zn(H_2O)_6(ClO_4)_2$ directly into an NMR tube containing ligand $X_6Me_3Pic_3$ resulted in a sharp C_3 symmetrical spectrum, which was not that of $[X_6Me_3Pic_3{\cdot}H_3](ClO_4)_3$. The down-field shift of the OMe and pyridine resonances compared to the free ligand were indicative of the formation of the complex, $[Zn(X_6Me_3Pic_3)(CD_3CN)](ClO_4)_2$, with the same conformation as the other above described Zn complexes. However, the equilibrium constant for its formation in acetonitrile is probably weak, as an excess of zinc salt was needed for its NMR characterization. This stands in contrast with the very stable tetrahedral Cu^I complexes that were obtained with the same ligand $X_6Me_3Pic_3$.[9,10]

The Zn Complexes are Chiral

As observed in the crystal structure, each complex exists as a pair of enantiomers due to its helical structure. In solution, these enantiomers are in conformational equilibrium as depicted in Scheme 2. However, the diastereotopic protons could be differentiated by ^1H NMR spectroscopy at various temperatures, depending on the ligand. The calixarene aromatic protons appeared as two pairs of singlets of equal intensity. The OCH_2 and the bridging methylene ($Ar-CH_{eq}$ and $Ar-CH_{ax}$) groups were represented by one and two pairs of doublets, respectively. Interestingly, whereas with *N* = Pyz and Imme a low temperature study was required to observe the coalescence processes, for complexes based on $X_6Me_3DMPyz_3$ and $X_6Me_3Bzim_3$, the splitting of the resonances was observed above 298 K. This different behavior may be related to the steric hindrance next to the heart of the helix, i.e. the metal center. With *N* = DMPyz and Bzim there is an extra substituent in α-position of the coordinating nitrogen atoms: a methyl group on the pyrazole when *N* = DMPyz (to be compared with Pyz) and an aromatic CH from the benzimidazole for *N* = Bzim (to compare with the imidazole from Imme). Saturation transfer experiments, however, unambiguously demonstrated that the chemical exchange still occurs for these complexes. An estimation of the enantiomerization barriers, calculated from the variable temperature experiments,[23] is given in Table 1.

Table 1. Estimation of the enantiomerization barriers for the helical complexes $[Zn(X_6Me_3N_3)(MeCN)](ClO_4)_2$

N-donor	Imme	Bzim	Pyz	DMPyz
$\Delta G^{\neq}$ (kcal·mol^{-1})[a]	< 12[b]	> 17[c]	< 12[b]	16.0 (0.2)[d]

[a] $\Delta G^{\neq}$ was determined from the relationship[23] $k_c = \sqrt{(2.22)}\ (\delta\upsilon^2 + 6J^2_{AB})$. – [b] T_c for protons Ar-αCH$_{ax}$ were 278 and 258 K, respectively. However, the whole coalescence processes could not be observed. Therefore, only lower limits for the Δυ values were obtained. – [c] Only the beginning of the first coalescence process could be observed. Hence, T_c for OCH_2 was estimated to be just above 338 K. – [d] The diastereotopic protons Ar-αCHeq, ArH, and OCH_2 coalesced at T_c = 325, 328, and 338 K, respectively. Variation of the calculated $\Delta G^{\neq}$ values over this range of temperature was not significant.

Such a behavior was also observed for some copper(I) complexes, but only at low temperature.[9,24] These zinc complexes represent the first examples where the diastereotopic protons are differentiated above room temperature. Lastly, the more flattened helical structure of Zn^{II} complexes compared to the $(X_6Me_3Pic_3)$-based Cu^I complexes is reflected by a larger splitting of the diastereotopic proton resonances. All these observations are very promising for chiral recognition and we are currently working on this aspect.

Conclusion

We have here described the synthesis of novel calix[6]arene-based N_3-ligands and studied the comparative ability of the whole series to stabilize a tetrahedral zinc dication in a biomimetic neutral environment. We previously described the first examples of such model compounds with the imidazole-based ligand. The present study shows that benzimidazole and pyrazole are also appropriate *N*-donors for the stabilization of such complexes. Indeed, stable tetrahedral Zn complexes of general formula $[Zn(X_6Me_3N_3)(MeCN)](ClO_4)_2$ were obtained in acetonitrile. The calixarene structure is constrained in a flattened cone conformation, thereby providing a hydrophobic cavity that envelops the exogeneous ligand, MeCN. The calixarene presenting three pyridine groups, however, did not give rise to a well-defined complex under stoichiometric conditions. Hence, pyridine appeared to be a *N*-donor not good enough for the stabilization of tetrahedral dicationic zinc complexes. This stands in contrast with its good capacity at stabilizing Cu^I and may be related to its relative softness. Calixarenes presenting tertiary amine groups did not behave as ligands, but rather acted as bases leading to the formation of zinc hydroxide.[25] Lastly, as revealed by X-ray and NMR analyses, complexes $[Zn(X_6Me_3N_3)(MeCN)](ClO_4)_2$ exist as a pair of helical enantiomers that are in conformational equilibrium in solution. Increasing the steric hindrance at the level of the coordinating atoms, however, considerably slowed the enantiomerization process. We are actively exploring the recognition and catalytic properties of these promising supramolecular biomimetic systems.

Experimental Section

Materials and Methods: All solvents and reagents were obtained commercially. DMF was stored over 4-Å molecular sieves under argon. THF and acetonitrile were distilled under argon over sodium/benzophenone and P_2O_5, respectively. − ^1H and ^{13}C NMR spectra were recorded on Bruker Avance 400 and Bruker AC 200 spectrometers. ^1H and ^{13}C resonances corresponding to anisole moieties are noted as ^{1} (e.g. tBu^1, ArH^1, C^1_{Ar}) and the others are noted as ^{2}. They were assigned with HMBC and HMQC experiments. − IR spectra were recorded on a Perkin−Elmer 783 spectrometer. − Elemental analyses were performed at the Institut de Chimie des Substances Naturelles, France. − 1-Chloromethylpyrazole hydrochloride (PyzCl·HCl) and 1-chloromethyl-3,5-dimethylpyrazole hydrochloride (DMPyzCl·HCl) were obtained from the corresponding alcohols.[26] (2-Chloroethyl)dimethylamine hydrochloride (DmemaCl·HCl) and 1-(2-chloroethyl)pyrrolidine hydrochloride (PyrCl·HCl) were obtained commercially. 2-Chloromethyl-1-methylbenzymidazole (BzimCl) was synthesized through the reaction of *N*-methylphenylen-1,2-diamine with chloroacetic acid in 4 N HCl.[27]

Safety Note: ***Caution!*** Although we have not encountered any problems, it is noted that perchlorate salts of metal complexes with organic ligands are potentially explosive and should be handled only in small quantities with appropriate precautions.

5,11,17,23,29,35-Hexa-*tert*-butyl-37,39,41-trimethoxy-38,40,42-tris[(1-pyrazolyl)methoxy]calix[6]arene ($X_6Me_3Pyz_3$): Under an argon atmosphere, a solution of 5,11,23,29,35-Hexa-*tert*-butyl-37,39,41-trimethoxycalix[6]aren-38,40,42-triol ($X_6Me_3H_3$) (1.0 g, 0.99 mmol) in dry THF (20 mL) was introduced into a flask containing NaH (60% in oil, washed with pentane; 1.18 g, 29.5 mmol), dry THF (20 mL), and DMF (10 mL). The mixture was stirred for 20 minutes and 1-chloromethylpyrazole hydrochloride (PyzCl·HCl) (1.50 g, 9.85 mmol) was added over a period of 10 minutes. After 3 hours on refluxing, the solvents were concentrated under reduced pressure to a quarter of the volume and water (150 mL) was poured into the solution. The resulting precipitate was collected by filtration and dried under vacuum. The crude product was washed with pentane and filtration led to $X_6Me_3Pyz_3$ as a white solid (800 mg). The filtrate was evaporated. The residue was recrystallized from MeOH/pentane to yield $X_6Me_3Pyz_3$ as a white solid (242 mg). For elemental analyses, a sample was filtered through silica gel (CH_2Cl_2/MeOH 95:5 as eluent) and dried overnight under vacuum (0.1 Torr, 50 °C). − Yield: 83%. − M.p. 265 °C (decomp.). − ^1H NMR (400 MHz, $CDCl_3$): δ = 0.82 (s, 27 H, tBu^2), 1.33 (s, 27 H, tBu^1), 2.22 (s, 9 H, OCH_3), 3.01 (br. s, 6 H, Ar-αCH$_{eq}$), 4.23 (br. s, 6 H, Ar-αCH$_{ax}$), 5.83 (s, 6 H, Pz-αCH$_2$), 6.31 (s, 3 H, PzH), 6.64 (s, 6 H, ArH^2), 7.13 (s, 6 H, ArH^1), 7.56 (s, 6 H, PzH). − ^{13}C NMR (100 MHz, $CDCl_3$): δ = 28.8 (Ar-αCH$_2$), 30.2 [C(*C*H$_3$)$_3$], 30.7 [C(*C*H$_3$)$_3$], 33.1 [*C*(CH$_3$)$_3$], 33.3 [*C*(CH$_3$)$_3$], 59.0 (OCH_3), 80.8 (Pz-αCH$_2$), 106.4 ($C_{Pz}H$), 123.1 ($C_{Ar}H$), 126.8 ($C_{Ar}H$), 129.6 ($C_{Pz}H$), 132.1 (C_{Ar}-CH$_2$), 132.7 (C_{Ar}-CH$_2$), 139.8 ($C_{Pz}H$), 144.9 (C_{Ar}), 146.6 (C_{Ar}), 149.0 ($C_{Ar}O$), 153.4 ($C_{Ar}O$). − IR (KBr): $\tilde{\nu}$ = 3480 (H_2O), 1522 (C=N), 1440, 1417, 1395, 1365 cm^{-1}. − $C_{81}H_{102}N_6O_6\cdot H_2O$ (1273.75): calcd. C 76.38, H 8.23, N 6.60; found C 76.23, H 8.01, N 7.01.

5,11,17,23,29,35-Hexa-*tert*-butyl-37,39,41-trimethoxy-38,40,42-tris[(3,5-dimethyl-1-pyrazolyl)methoxy]calix[6]arene ($X_6Me_3DMPyz_3$) was synthesized from $X_6Me_3H_3$ (1.0 g, 0.99 mmol) following the procedure described for $X_6Me_3Pyz_3$ with NaH (60% in oil, 1.18 g, 29.5 mmol) and 1-chloromethyl-3,5-dimethylpyrazole hydrochloride (DMPyzCl·HCl) (1.07 g, 5.91 mmol). The crude product was recrystallized from THF/H_2O and dried for four hours under vacuum (0.1 Torr, 60 °C) to afford pure $X_6Me_3DMPyz_3$ (1.11 g). − Yield: 84%. − M.p. 150 °C (decomp.). − ^1H NMR (400 MHz, $CDCl_3$): δ = 0.76 (s, 27 H, tBu^2), 1.38 (s, 27 H, tBu^1), 2.15 (s, 9 H, OCH_3), 2.19 (s, 9 H, Pz-CH$_3$), 2.27 (s, 9 H, Pz-CH$_3$), 2.98 (d, J = 15.2 Hz, 6 H, Ar-αCH$_{eq}$), 4.30 (d, J = 15.2 Hz, 6 H, Ar-αCH$_{ax}$), 5.73 (s, 6 H, Pz-αCH$_2$), 5.86 (s, 3 H, PzH), 6.58 (s, 6 H, ArH^2), 7.17 (s, 6 H, ArH^1). − ^{13}C NMR (50 MHz, $CDCl_3$): δ = 10.6 (Pz-CH$_3$), 13.3 (Pz-CH$_3$), 29.1 (Ar-αCH$_2$), 30.9 [C(*C*H$_3$)$_3$], 31.4 [C(*C*H$_3$)$_3$], 34.0 [*C*(CH$_3$)$_3$], 34.9 [*C*(CH$_3$)$_3$], 59.8 (OCH_3), 78.9 (Pz-αCH$_2$), 106.8 (PzH), 123.3 ($C_{Ar}H$), 127.7 ($C_{Ar}H$), 132.9 (C_{Ar}-CH$_2$), 133.4 (C_{Ar}-CH$_2$), 140.2 ($C_{Pz}CH_3$), 145.5 (C_{Ar}), 146.1 ($C_{Ar}H$), 148.3 ($C_{Pz}CH_3$), 149.7 ($C_{Ar}O$), 154.2 ($C_{Ar}O$). − IR (KBr): $\tilde{\nu}$ = 3480 (H_2O), 1569 (C=N), 1486, 1468, 1440, 1422, 1397, 1365, 1290 cm^{-1}. − $C_{87}H_{114}N_6O_6\cdot 4H_2O$ (1411.95): calcd. C 74.00, H 8.64, N 5.94; found C 74.05, H 8.42, N 5.65.

5,11,17,23,29,35-Hexa-*tert*-butyl-37,39,41-trimethoxy-38,40,42-tris[2-(*N*,*N*-dimethylamino)ethoxy]calix[6]arene ($X_6Me_3Dmema_3$) was synthesized from $X_6Me_3H_3$ (1.0 g, 0.99 mmol) following the procedure described for $X_6Me_3Pyz_3$ with NaH (60% in oil, 1.18 g, 29.5 mmol) and (2-chloroethyl)dimethylamine hydrochloride (DmemaCl·HCl) (1.42 g, 9.85 mmol). The crude product was recrystallized from THF/H_2O and dried for four hours under vacuum (0.1 Torr, 60 °C) to afford pure $X_6Me_3Dmema_3$ (1.04 g). − Yield: 86%. − M.p. 185 °C (decomp.). − ^1H NMR (400 MHz, $CDCl_3$): δ = 0.82 (s, 27 H, tBu^2), 1.38 (s, 27 H, tBu^1), 2.20 (s, 9 H, OCH_3), 2.36 (s, 18 H, NCH_3), 2.83 (br. s, 6 H, NCH_2), 3.45 (br. s,

6 H, Ar-αCH$_{eq}$), 4.00 (br. s, 6 H, OCH$_2$), 4.55 (br. s, 6 H, Ar-αCH$_{ax}$), 6.67 (s, 6 H, ArH^2), 7.27 (s, 6 H, ArH^1). − ^{13}C NMR (50 MHz, CDCl$_3$): δ = 29.2 (Ar-αCH$_2$), 30.3 [C(*C*H$_3$)$_3$], 30.8 [C(*C*H$_3$)$_3$], 33.1 [*C*(CH$_3$)$_3$], 33.4 [*C*(CH$_3$)$_3$], 45.3 (NCH$_3$), 58.2 (NCH$_2$), 59.2 (OCH$_3$), 70.0 (OCH$_2$), 122.8 (C$_{Ar}$H), 127.0 (C$_{Ar}$H), 132.3 (*C*$_{Ar}$-CH$_2$), 132.7 (*C*$_{Ar}$-CH$_2$), 144.7 (C$_{Ar}$), 144.8 (C$_{Ar}$), 151.2 (C$_{Ar}$O), 153.6 (C$_{Ar}$O). − IR (KBr): ṽ = 3560, 3480 (H$_2$O), 1485, 1470, 1460, 1440, 1417, 1395, 1365 cm^{-1}. − $C_{81}H_{117}N_3O_6{\cdot}H_2O$ (1246.85): calcd. C 78.03, H 9.62, N 3.37; found C 77.77, H 9.58, N 3.06.

5,11,17,23,29,35-Hexa-*tert*-butyl-37,39,41-trimethoxy-38,40,42-tris[2-(pyrrolidinyl)ethoxy]calix[6]arene ($X_6Me_3Pyr_3$) was synthesized from $X_6Me_3H_3$ (1.0 g, 0.99 mmol) following the procedure described for $X_6Me_3Pyz_3$ with NaH (60% in oil, 1.18 g, 29.5 mmol) and 1-(2-chloroethyl)pyrrolidine hydrochloride (PyrCl·HCl) (1.68 g, 9.85 mmol). The crude product was recrystallized from CHCl$_3$/CH$_3$CN and dried overnight under vacuum (0.1 Torr, 60 °C) to afford pure $X_6Me_3Pyr_3$ (1.03 g). − Yield: 80%. − M.p. >230 °C (decomp.). − ^{1}H NMR (400 MHz, CDCl$_3$): δ = 0.77 (s, 27 H, *t*Bu^2), 1.39 (s, 27 H, *t*Bu^1), 1.80 (br. s, 12 H, NCH$_2$C*H*$_2$), 2.19 (s, 9 H, OCH$_3$), 2.66 (br. s, 12 H, NC*H*$_2$CH$_2$), 3.02 (t, *J* = 6.4 Hz, 6 H, OCH$_2$C*H*$_2$N), 3.41 (d, *J* = 15.1 Hz, 6 H, Ar-αCH$_{eq}$), 4.06 (t, *J* = 6.4 Hz, 6 H, OC*H*$_2$CH$_2$N), 4.58 (d, *J* = 15.1 Hz, 6 H, Ar-αCH$_{ax}$), 6.64 (s, 6 H, ArH^2), 7.28 (s, 6 H, ArH^1). − ^{13}C NMR (50 MHz, CDCl$_3$): δ = 23.6 (NCH$_2$*C*H$_2$), 29.7 (Ar-αCH$_2$), 31.1 [C(*C*H$_3$)$_3$], 31.4 [C(*C*H$_3$)$_3$], 33.9 [*C*(CH$_3$)$_3$], 34.2 [*C*(CH$_3$)$_3$], 54.7 (N*C*H$_2$CH$_2$), 55.9 (OCH$_2$*C*H$_2$N), 60.1 (OCH$_3$), 71.7 (O*C*H$_2$CH$_2$N), 123.4 (C$_{Ar}$H), 128.0 (C$_{Ar}$H), 133.2 (*C*$_{Ar}$-CH$_2$), 133.6 (*C*$_{Ar}$-CH$_2$), 145.5 (C$_{ar}$), 145.8 (C$_{Ar}$), 151.8 (C$_{Ar}$O), 154.4 (C$_{Ar}$O). − IR (KBr): ṽ = 3490 (H$_2$O), 1482, 1460, 1438, 1418, 1395, 1363.1290, 1245 cm^{-1}. − $C_{87}H_{123}N_3O_6{\cdot}5H_2O$ (1397.02): calcd. C 74.79, H 9.52, N 3.00; found C 74.76, H 9.29, N 2.68.

5,11,17,23,29,35-Hexa-*tert*-butyl-37,39,41-trimethoxy-38,40,42-tris[(1-methyl-2-benzimidazolyl)methoxy]calix[6]arene ($X_6Me_3Bzim_3$) was synthesized from $X_6Me_3H_3$ (0.80 g, 0.79 mmol) following the procedure described for $X_6Me_3Pyz_3$ with NaH (60% in oil, 0.94 g, 23.7 mmol) and 2-chloromethyl-1-methylbenzimidazole hydrochloride (BzimCl·HCl) (0.84 g, 4.72 mmol). The crude product was recrystallized from CH$_2$Cl$_2$/CH$_3$CN to afford $X_6Me_3Bzim_3$ (1.06 g). − Yield: 86%. − M.p. 276 °C (decomp.). − ^{1}H NMR (400 MHz, CDCl$_3$): δ = 0.79 (s, 27 H, *t*Bu^2), 1.34 (s, 27 H, *t*Bu^1), 2.16 (s, 9 H, OCH$_3$), 3.31 (d, *J* = 15.0 Hz, 6 H, Ar-αCH$_{eq}$), 4.05 (s, 9 H, NCH$_3$), 4.49 (d, *J* = 15.0 Hz, 6 H, Ar-αCH$_{ax}$), 5.22 (s, 6 H, Bz-αCH$_2$), 6.65 (s, 6 H, ArH^2), 7.20 (s, 6 H, ArH^1), 7.26 (t, *J* = 7.7 Hz, 1 H, BzH), 7.31 (t, *J* = 7.7 Hz, 1 H, BzH), 7.38 (d, *J* = 7.7 Hz, 1 H, BzH), 7.74 (t, *J* = 7.7 Hz, 1 H, BzH). − ^{13}C NMR (50 MHz, CDCl$_3$): δ = 29.3 (Ar-αCH$_2$), 29.5 (NCH$_3$), 30.4 [C(*C*H$_3$)$_3$], 30.5 [C(*C*H$_3$)$_3$], 33.9 [*C*(CH$_3$)$_3$], 34.1 [*C*(CH$_3$)$_3$], 60.0 (OCH$_3$), 67.8 (Bz-αCH$_2$), 109.4 (C$_{Bz}$H), 120.0 (C$_{Bz}$H), 122.1 (C$_{Bz}$H), 123.0 (C$_{Bz}$H), 123.8 (C$_{Ar}$H), 127.9 (C$_{Ar}$H), 132.7 (C$_{Ar}$), 133.3 (C$_{Ar}$) 136.1 (C$_{Bz}$), 142.2 (C$_{Bz}$), 145.9 (C$_{Ar}$), 146.4 (C$_{Ar}$), 149.9 (C$_{Bz}$), 151.3 (C$_{Ar}$O), 154.1 (C$_{Ar}$O). − IR (KBr): ṽ = 1525 (sh, C=N), 1485, 1465, 1419, 1408, 1365, 1290, 1242 cm^{-1}. − $C_{96}H_{114}N_6O_6{\cdot}CH_2Cl_2{\cdot}0.5MeCN$ (1553.42): calcd. C 75.77, H 7.62, N 5.86; found C 75.85, H 7.53, N 5.76 (presence of solvent molecules was confirmed by ^{1}H NMR analysis).

5,11,17,23,29,35-Hexa-*tert*-butyl-37,39,41-trimethoxy-38,40,42-tris[(1-methyl-2-imidazolyl)methoxy]calix[6]arene ($X_6Me_3Imme_3$) was previously described.[11] We report here the ^{13}C NMR spectroscopic data (50 MHz, CDCl$_3$): δ = 29.5 (Ar-αCH$_2$), 31.2 [C(*C*^{2}H$_3$)$_3$], 31.7 [C(*C*^{1}H$_3$)$_3$], 33.5 (NCH$_3$), 34.1 [*C*^{2}(CH$_3$)$_3$], 34.3 [*C*^{1}(CH$_3$)$_3$], 60.2 (OCH$_3$), 66.9 (Im-αCH$_2$), 122.4 (C$_{Im}$H), 123.8 (C$^2_{Ar}$H), 127.9 (C$_{Im}$H), 128.2 (C$^1_{Ar}$H), 133.0 (*C*$_{Ar}$-CH$_2$), 133.7 (*C*$_{Ar}$-CH$_2$), 144.4 (C$_{Im}$), 146.0 (C$^2_{Ar}$), 146.3 (C$^1_{Ar}$), 151.4 (C$^2_{Ar}$O), 154.4 (C$^1_{Ar}$O).

5,11,17,23,29,35-Hexa-*tert*-butyl-37,39,41-trimethoxy-38,40,42-tris[(2-pyridinyl)methoxy]calix[6]arene ($X_6Me_3Pic_3$) was previously described.[9] We report here the ^{13}C NMR spectroscopic data (50 MHz, CDCl$_3$): δ = 29.7 (Ar-αCH$_2$), 31.2 [C(*C*H$_3$)$_3$], 31.6 [C(*C*H$_3$)$_3$], 34.0 [*C*(CH$_3$)$_3$], 34.2 [*C*(CH$_3$)$_3$], 60.2 (OCH$_3$), 74.9 (Py-αCH$_2$), 121.5 (C$_{Py}$H), 122.4 (C$_{Py}$H), 123.7 (C$_{Ar}$H), 128.0 (C$_{Ar}$H), 133.0 (*C*$_{Ar}$-CH$_2$), 133.7 (*C*$_{Ar}$-CH$_2$), 136.9 (C$_{Py}$H), 145.8 (C$_{Ar}$), 146.1 (C$_{Ar}$), 148.8 (C$_{Py}$H), 151.4 (C$_{Ar}$O), 154.4 (C$_{Ar}$O), 158.0 (C$_{Py}$).

$[X_6Me_3Pic_3{\cdot}H_3]^{3+}(ClO_4^-)_3$: A mixture of 70% aq. HClO$_4$ (0.1 mL) and MeOH (0.3 mL) was added to a solution of $X_6Me_3Pic_3$ (10 mg, 0.008 mmol) in CHCl$_3$ (2 mL). Precipitation with Et$_2$O gave a white solid. − Yield: 100%. − ^{1}H NMR (200 MHz, CD$_3$CN): δ = 0.89 (s, 27 H, *t*Bu), 1.32 (s, 27 H, *t*Bu), 2.60 (s, 9 H, OCH$_3$), 3.60 (br. s, 6 H, Ar-αCH$_{eq}$), 4.25 (br. s, 6 H, Ar-αCH$_{ax}$), 5.41 (s, 6 H, Py-αCH$_2$), 6.83 (s, 6 H, ArH), 7.33 (s, 6 H, ArH), 8.02 (t, *J* = 6.8 Hz, 3 H, PyH), 8.11 (d, *J* = 8.0 Hz, 3 H, PyH), 8.61 (t, *J* = 8.0 Hz, 3 H, PyH), 8.83 (t, *J* = 6.8 Hz, 3 H, PyH), 13.7 (br. s, 3 H, NH). − $C_{87}H_{108}Cl_3N_3O_{18}{\cdot}3H_2O$ (1644.20): calcd. C 63.55, H 6.99, N 2.56; found C 63.47, H 6.95, N 2.56.

$[X_6Me_3Dmema_3{\cdot}H_3]^{3+}(ClO_4^-)_3$ can be prepared either by the procedure described above for $[X_6Me_3Pic_3{\cdot}H_3]^{3+}(ClO_4^-)_3$ or by reaction of $X_6Me_3Dmema_3$ with $Zn(H_2O)_6(ClO_4)_2$. Under an argon atmosphere, CH$_3$CN (3 mL) was added into a flask containing $Zn(H_2O)_6(ClO_4)_2$ (29.8 mg, 0.080 mmol) and $X_6Me_3Dmema_3$ (98.3 mg, 0.080 mmol). The mixture was stirred for 3 hours, filtered through celite and concentrated to a sixth of the volume, leading to a white precipitate, which was separated by centrifugation, washed with MeOH (0.5 mL). Recrystallization in CH$_3$CN/Et$_2$O gave a white solid (57.5 mg). − Yield: 47%. − ^{1}H NMR (200 MHz, CD$_3$CN): δ = 0.85 (s, 27 H, *t*Bu), 1.36 (s, 27 H, *t*Bu), 2.25 (s, 9 H, OCH$_3$), 2.96 (s, 18 H, NCH$_3$), 3.51 (br. s, 6 H, NCH$_2$), 3.60 (br. s, 6 H, Ar-αCH$_{eq}$), 4.09 (br. s, 6 H, OCH$_2$), 4.40 (br. s, 6 H, Ar-αCH$_{ax}$), 6.76 (s, 6 H, ArH), 7.36 (s, 6 H, ArH). − $C_{80}H_{120}Cl_3N_3O_{18}$ (1530.19): calcd. C 63.58, H 7.90, N 2.75, Cl 6.95; found C 62.95, H 7.82, N 2.56, Cl 7.22.

$[X_6Me_3Pyr_3{\cdot}H_3]^{3+}(ClO_4^-)_3$ can be prepared either by the procedure described above for $[X_6Me_3Pic_3{\cdot}H_3]^{3+}(ClO_4^-)_3$ or by reaction of $X_6Me_3Pyr_3$ with $Zn(H_2O)_6(ClO_4)_2$. Under an argon atmosphere, CH$_3$CN (3 mL) was added into a flask containing $Zn(H_2O)_6(ClO_4)_2$ (21.7 mg, 0.058 mmol) and $X_6Me_3Pyr_3$ (76.1 mg, 0.058 mmol). The mixture was stirred for 3 hours, filtered through celite and concentrated to the third of the volume. Addition of Et$_2$O gave a white precipitate, which was separated by centrifugation and washed with Et$_2$O (43.3 mg). − Yield: 46%. − ^{1}H NMR (200 MHz, CD$_3$CN): δ = 0.80 (s, 27 H, *t*Bu), 1.39 (s, 27 H, *t*Bu), 2.12 (br. s, 12 H, NCH$_2$C*H*$_2$), 2.20 (s, 9 H, OCH$_3$), 3.4−3.8 (m, 24 H, NC*H*$_2$CH$_2$ + OCH$_2$C*H*$_2$N + Ar-αCH$_{eq}$), 4.17 (br. t, 6 H, OC*H*$_2$CH$_2$N), 4.45 (br. d, 6 H, Ar-αCH$_{ax}$), 6.70 (s, 6 H, ArH), 7.39 (s, 6 H, ArH). − $C_{87}H_{126}Cl_3N_3O_{18}{\cdot}H_2O$ (1626.31): calcd. C 64.25, H 7.93, N 2.58, Cl 6.54; found C 63.27, H 7.81, N 2.59, Cl 7.21.

$[Zn(X_6Me_3Bzim_3)(CH_3CN)](ClO_4)_2$: Under an argon atmosphere, CH$_3$CN (3 mL) was added into a flask containing $Zn(H_2O)_6(ClO_4)_2$ (32.9 mg, 0.088 mmol) and $X_6Me_3Bzim_3$ (128 mg, 0.088 mmol). The mixture was stirred for 3 hours, filtered through celite, and concentrated to a sixth of the volume, leading to a white precipitate, which was separated by centrifugation, washed with CH$_3$CN (0.1 mL) and dried under vacuum to yield a white solid (114 mg). − Yield: 72%. − M.p. 282 °C (decomp.). − ^{1}H NMR (400 MHz, CD$_3$CN): δ = 0.71 (s, 27 H, *t*Bu^1), 1.39 (s, 27 H, *t*Bu^2),

1.96 (s, 3 H, free CH_3CN), 2.77 (s, 9 H, OCH_3), 3.31 (d, J = 15.6 Hz, 3 H, Ar-αCH$_{eq}$), 3.42 (d, J = 15.2 Hz, 3 H, Ar-αCH$_{ax}$), 3.61 (d, J = 15.6 Hz, 3 H, Ar-αCH$_{eq}$), 3.91 (s, 9 H, NCH_3), 4.49 (d, J = 15.2 Hz, 3 H, Ar-αCH$_{ax}$), 5.48 (AB, J = 14.5 Hz, Δυ = 42.2 Hz, 6 H, Bz-αCH_2), 6.29 (d, J = 2.4 Hz, 3 H, ArH^1), 6.58 (d, J = 2.4 Hz, 3 H, ArH^1), 7.11 (d, J = 8.2 Hz, 3 H, BzH), 7.33 (d, J = 2.3 Hz, 3 H, ArH^2), 7.38 (t, J = 8.2 Hz, 3 H, BzH), 7.43 (d, J = 2.3 Hz, 3 H, ArH^2), 7.64 (t, J = 8.2 Hz, 3 H, BzH), 7.93 (d, J = 8.2 Hz, 3 H, BzH). − ^{13}C NMR (100 MHz, $CDCl_3$): δ = 29.7 (Ar-αCH$_{eq}$), 31.3 (Ar-αCH$_{ax}$), 31.5 [C(C^1H_3)$_3$], 31.7 [C(C^2H_3)$_3$], 32.9 (NCH_3), 34.6 [C^1(CH_3)$_3$], 35.0 [C^2(CH_3)$_3$], 60.0 (OCH_3), 65.1 (Bz-αCH_2), 113.6 ($C_{Bz}H$), 118.8 ($C_{Bz}H$), 122.7 ($C^1_{Ar}H$), 124.0 ($C^1_{Ar}H$), 126.4 ($C_{Bz}H$), 126.6 ($C_{Bz}H$), 129.6 ($C^2_{Ar}H$), 130.0 ($C^2_{Ar}H$), 132.3 (C_{Ar}-CH_2), 133.2 (C_{Ar}-CH_2), 133.7 (C_{Ar}-CH_2), 134.0 (C_{Ar}-CH_2), 135.9 (C_{Bz}), 139.5 (C_{Bz}), 146.6 (C^1_{Ar}), 148.5 (C^2_{Ar}), 153.0 ($C^1_{Ar}O$), 154.2 (C_{Bz}) 154.5 ($C^2_{Ar}O$). − IR (KBr): $\tilde{\nu}$ = 3490 (H_2O), 3420 (sh, H_2O), 1515 (sh, C=N), 1488, 1467, 1419, 1365, 1299, 1265, 1242, 1102 (ClO_4^-), 624 (ClO_4^-) cm^{-1}. − $C_{98}H_{117}Cl_2N_7O_{14}Zn{\cdot}3H_2O$ (1807.36): calcd. C 65.13, H 6.86, N 5.42; found C 65.03, H 6.76, N 5.31.

[Zn($X_6Me_3DMPyz_3$)(CH_3CN)](ClO_4)$_2$: Under an argon atmosphere, CH_3CN (3 mL) was added into a flask containing Zn(H_2O-)$_6$(ClO_4)$_2$ (35.6 mg, 0.096 mmol) and $X_6Me_3DMPyz_3$ (128 mg, 0.096 mmol). The mixture was stirred overnight, filtered through celite. Addition of Et_2O (5 mL) led to a yellow precipitate, which was separated by centrifugation. Recrystallization in CH_3CN/Et_2O yielded a white solid (77 mg). − Yield: 47%. − M.p. 256 °C (decomp.). − ^{1}H NMR (400 MHz, CD_3CN): δ = 0.77 (s, 27 H, tBu^1), 1.40 (s, 27 H, tBu^2), 1.95 (s, 9 H, $PzCH_3$), 1.96 (s, 3 H, free CH_3CN), 2.12 (s, 9 H, $PzCH_3$), 3.38 (AB, J = 15.8 Hz, Δν = 36 Hz, 6 H, Ar-αCH$_{eq}$), 3.61 (s, 9 H, OCH_3), 3.63 (d, J = 15.2 Hz, 3 H, Ar-αCH$_{ax}$), 4.66 (d, J = 15.2 Hz, 3 H, Ar-αCH$_{ax}$), 6.03 (AB, J = 14.1 Hz, Δν = 147 Hz, 6 H, Pz-αCH_2), 6.23 (s, 3 H, ArH^1), 6.49 (s, 3 H, PzH), 6.73 (s, 3 H, ArH^1), 7.33 (s, 3 H, ArH^2), 7.50 (s, 3 H, ArH^2). − ^{13}C NMR (100 MHz, $CDCl_3$): δ = 11.6 (Pz-CH_3), 13.3 (Pz-CH_3), 29.8 (Ar-αCH$_{eq}$), 31.5 [C(C^1H_3)$_3$], 31.6 (Ar-αCH$_{ax}$), 31.7 [C(C^2H_3)$_3$], 34.0 [C^1(CH_3)$_3$], 34.9 [C^2(CH_3)$_3$], 61.1 (OCH_3), 79.3 (Pz-αCH_2), 111.3 (PzH), 123.0 ($C_{Ar}H^1$), 124.6 ($C_{Ar}H^1$), 129.8 ($C_{Ar}H^2$), 129.9 (br, C_{Ar}-CH_2), 133.3 (br, C_{Ar}-CH_2), 133.9 (br, C_{Ar}-CH_2), 146.9 (C_{Ar}), 148.9 ($C_{Pz}CH_3$), 149.4 ($C_{Ar}H$), 153.1 ($C^2_{Ar}O$), 153.5 ($C^1_{Ar}O$), 154.9 ($C_{Pz}CH_3$). − IR (KBr): $\tilde{\nu}$ = 3460 (H_2O), 1560 (C=N), 1486, 1468, 1440, 1420, 1392, 1365, 1300, 1110 (ClO_4^-), 623 (ClO_4^-) cm^{-1}. − $C_{89}H_{117}Cl_2N_7O_{14}Zn{\cdot}4H_2O$ (1717.28): calcd. C 62.25, H 7.34, N 5.71; found C 61.92, H 7.13, N 5.51.

[Zn($X_6Me_3Pyz_3$)(H_2O)](ClO_4)$_2$: Under an argon atmosphere, CH_3CN (3 mL) was added into a flask containing Zn(H_2O)$_6$-(ClO_4)$_2$ (45.5 mg, 0.122 mmol) and $X_6Me_3Pyz_3$ (154 mg, 0.122 mmol). The mixture was stirred overnight and then evaporated under vacuum to give a white solid. − Yield: 100%. − M.p. 258 °C (decomp.). − IR (KBr): $\tilde{\nu}$ = 3500 (H_2O), 1526 (C=N), 1485, 1468, 1417, 1398, 1365, 1120 (ClO_4^-), 625 (ClO_4^-) cm^{-1}. − $C_{81}H_{104}Cl_2N_6O_{15}Zn{\cdot}4H_2O$ (1610.08): calcd. C 60.42, H 7.01, N 5.22; found C 60.37, H 6.52, N 4.97.

[Zn($X_6Me_3Pyz_3$)(CD_3CN)](ClO_4)$_2$ was obtained by dissolving [Zn($X_6Me_3Pyz_3$)(OH_2)](ClO_4)$_2$ in the NMR tube containing CD_3CN. − ^{1}H NMR (400 MHz, CD_3CN): δ = 0.75 (s, 27 H, tBu^1), 1.39 (s, 27 H, tBu^2), 3.40 (d, J = 15.4 Hz, 6 H, Ar-αCH$_{eq}$), 3.59 (s, 9 H, OCH_3), 3.84 (br. s, 6 H, Ar-αCH$_{ax}$), 6.18 (s, 6 H, Pz-αCH_2), 6.46 (s, 6 H, ArH^1), 6.85 (t, J = 2.3 Hz, 3 H, PzH), 7.40 (s, 6 H, ArH^2), 7.99 (d, J = 2.3 Hz, 3 H, PzH), 8.08 (d, J = 2.3 Hz, 3 H, PzH). − ^{13}C NMR (100 MHz, $CDCl_3$): δ = 30.5 (Ar-αCH_2), 31.5 [C(C^1H_3)$_3$], 31.7 [C(C^2H_3)$_3$], 34.6 [C^1(CH_3)$_3$], 35.1 [C^2(CH_3)$_3$], 60.8 (OCH_3), 82.9 (Pz-αCH_2), 109.9 ($C_{Pz}H$), 123.7 ($C^1_{Ar}H$), 129.6 ($C^2_{Ar}H$), 133.3 (C_{Ar}-CH_2), 133.5 (C_{Ar}-CH_2), 138.1 ($C_{Pz}H$), 146.2 ($C_{Pz}H$), 146.7 (C^1_{Ar}), 149.0 (C^2_{Ar}), 153.1 ($C^2_{Ar}O$), 153.5 ($C^1_{Ar}O$).

[Zn($X_6Me_3Imme_3$)(CD_3CN)](ClO_4)$_2$ was obtained by dissolving the previously described[11] [Zn($X_6Me_3Imme_3$)(OH_2)](ClO_4)$_2$ in the

Table 2. Crystallographic data

Compound	$X_6Me_3Pyz_3$	[$X_6Me_3Pyr_3{\cdot}H_3$](ClO_4)$_3$	[Zn($X_6Me_3Imme_3$)(CH_3CN)](ClO_4)$_2$
Empirical formula	$C_{185}H_{208}N_{13}O_{13}$	$C_{190}H_{292}Cl_6N_6O_{40}$	$C_{176}H_{232}Cl_{36}N_{12}O_{12}Zn_2$
M	2581.44	3513.00	4114.92
Crystal system	triclinic	monoclinic	monoclinic
Space group	$P\bar{1}$	$P2_1/c$	Cc
a [Å]	14.6920(5)	20.431(1)	16.6180(2)
b [Å]	16.5900(6)	39.929(1)	28.8930(7)
c [Å]	19.1340(7)	25.772(1)	48.0280(1)
α [°]	73.508(1)		
β [°]	73.222(1)	107.835(1)	98.060(1)
γ [°]	66.769(1)		
V [Å^3]	4025.8(8)	20014(1)	22832.6(8)
Z	1	4	8
D_c [g·cm^{-3}]	1.06	1.16	2.39
Crystal colour	colorless	colorless	colorless
Crystal size [mm^3]	0.4 × 0.3 × 0.05	0.4 × 0.3 × 0.1	0.4 × 0.3 × 0.1
μ(Mo-K_α) [cm^{-1}]	0.67	13.57	13.6
Number of unique data	14840	8490	11547
Number of parameters refined	1825	2291	2424
Number used in refinement	14840	8490	11547
$R[F^2 > 4\sigma F^2]$	0.087	0.101	0.088
wR	0.236[a]	0.263[b]	0.252[c]
Goodness of fit	1.012	1.189	1.365
Residual Fourier [e·Å^{-3}]	−0.295; 0.678	−0.325; 0.072	0.648; 0.848

[a] $w = 1/[\sigma^2(F_o^2) + (0.1764P)^2 + 2.5989P]$ where $P = (F_o^2 + 2F_c^2)/3$. − [b] $w = 1/[\sigma^2(F_o^2) + (0.123P)^2 + 155.5258P]$ where $P = (F_o^2 + 2F_c^2)/3$. − [c] $w = 1/[\sigma^2(F_o^2) + (0.2P)^2]$ where $P = (F_o^2 + 2F_c^2)/3$.

NMR tube containing CD_3CN. – ^1H NMR (400 MHz, CD_3CN): δ = 0.74 (s, 27 H, tBu^1), 1.40 (s, 27 H, tBu^2), 3.45 (d, J = 15.0 Hz, 6 H, Ar-αCH_{eq}), 3.58 (s, 9 H, OCH_3), 3.72 (s, 9 H, NCH_3), 4.16 (d, J = 15.0 Hz, 6 H, Ar-αCH_{ax}), 5.27 (s, 6 H, Im-αCH_2), 6.47 (s, 6 H, ArH^1), 7.00 (d, J = 1.5 Hz, 3 H, ImH), 7.39 (s, 6 H, ArH^2), 7.49 (d, J = 1.5 Hz, 3 H, ImH). – ^{13}C NMR (100 MHz, $CDCl_3$): δ = 30.5 (Ar-αCH_2), 31.5 [$C(C^1H_3)_3$], 31.8 [$C(C^2H_3)_3$], 34.6 [$C^1(CH_3)_3$], 34.9 [$C^2(CH_3)_3$], 35.2 (NCH_3), 60.8 (OCH_3), 64.8 (Im-αCH_2), 123.5 ($C^1_{Ar}H$), 124.7 ($C_{Im}H$), 128.2 ($C_{Im}H$), 129.6 ($C^2_{Ar}H$), 133.0 (C_{Ar}-CH_2), 133.5 (C_{Ar}-CH_2), 146.3 (C^1_{Ar}), 148.0 (C^2_{Ar}), 148.4 (C_{Im}), 153.4 ($C^1_{Ar}O$), 155.2 ($C^2_{Ar}O$).

Crystal Structure Determinations:[28] Diffraction data were measured on a Nonius KappaCCD diffractometer. Structures were solved by direct methods and refined using the program SHELXL97.[29] In all cases, the crystals were very sensitive to desolvation. Data are listed in Table 2.

$X_6Me_3Pyz_3$: Crystals were obtained by slow evaporation of a solution of ligand in a $CHCl_3/CH_3OH/CH_3CN$ mixture. The two ligands of the asymmetric unit co-crystallized with a CH_3CN solvate and one molecule of methanol. Interestingly, a mixture of two conformations could be determined from these molecules: one conformer corresponds to a ligand in which one pyrazole moiety is in the same relative orientation as the other two, with a methanol solvate inserted between the two molecules of the asymmetric unit; the second conformer corresponds to a ligand in which the same pyrazole is in a reverse orientation relative to the others, without methanol co-crystallized. The multiplicity of the disordered pyrazole arm and of the MeOH molecule was found to be equal to 0.5.

$[X_6Me_3Pyr_3{\cdot}H_3](ClO_4)_3$: Single crystals were grown by slow diffusion of Et_2O into an acetonitrile solution of the perchlorate salt. Each ligand co-crystallized with two molecules of Et_2O, and three ClO_4^- counterions. A static disorder could be determined for one pyrrolidine moiety in each molecule of the asymmetric unit, and they were split into two sites of equal multiplicity of 0.5. Due to the low data to parameter ratio, the structure was refined as two anisotropic blocs of parameters of roughly equal size, including some overlapping between them.

$[Zn(X_6Me_3Imme_3)(CH_3CN)](ClO_4)_2$: Single crystals were obtained by slow diffusion of Et_2O into a $CHCl_3/CH_3CN$ solution of the complex. The complex co-crystallized with some amount of $CHCl_3$ solvate, most of these molecules being characterized without ambiguity. However, two fragments were not well identified and correspond probably to disordered solvate. Due to the low data to parameter ratio, the structure was refined as two anisotropic blocs of parameters of roughly equal size, including some overlapping between them.

[1] W. N. Lipscomb, N. Sträter, *Chem. Rev.* **1996**, *96*, 2375–2433.
[2] G. Parkin, *Chem. Commun.* **2000**, 1971–1985.
[3] Calix[4]arenes have been used as platform for the preorganization of zinc binding sites in polynuclear Zn enzyme models, see: P. Molenveld, J. F. J. Engbersen, D. N. Reinhoudt, *Chem. Soc. Rev.* **2000**, *29*, 75–86.
[4] K. Kimura, *Acc. Chem. Res.* **2001**, *34*, 171–179.
[5] C. Bergquist, G. Parkin, *J. Am. Chem. Soc.* **1999**, *121*, 6322–6323.
[6] M. Ruf, H. Vahrenkamp, *Inorg. Chem.* **1996**, *35*, 6571–6578.
[7] R. Alsfasser, S. Trofimenko, A. Looney, G. Parkin, H. Vahrenkamp, *Inorg. Chem.* **1991**, *30*, 4098–4100.
[8] C. Kimblin, W. E. Allen, G. J. Parkin, *Chem. Soc. Chem. Commun.* **1995**, 1813–1814.
[9] S. Blanchard, M.-N. Rager, A. F. Duprat, O. Reinaud, *New J. Chem.* **1998**, 1143–1146.
[10] S. Blanchard, L. Le Clainche, M.-N. Rager, B. Chansou, J.-P. Tuchagues, A. F. Duprat, Y. Le Mest, O. Reinaud, *Angew. Chem. Int. Ed.* **1998**, *37*, 2732–2735.
[11] O. Sénèque, M.-N. Rager, M. Giorgi, O. Reinaud, *J. Am. Chem. Soc.* **2000**, *122*, 6183–6189.
[12] C. D. Gutsche, B. Dhawan, M. Leonis, D. Stewart, *Org. Syn.* **1990**, *68*, 238–242.
[13] R. G. Janssen, W. Verboom, D. N. Reinhoudt, A. Casnati, M. Freriks, A. Pochini, F. Uggozoli, R. Ungaro, P. M. Nieto, M. Carramolino, F. Cuevas, P. Prados, J. de Mendoza, *Synthesis* **1993**, 380–385.
[14] C. D. Gutsche, *Calixarenes Revisited, Monographs in Supramolecular Chemistry*, (Ed.: J. F. Stoddart), The Royal Society of Chemistry, Cambridge, **1998**.
[15] J. P. M. van Duynhoven, R. G. Janssen, W. Verboom, S. M. Franken, A. Casnati, A. Pochini, R. Ungaro, J. de Mendoza, P. M. Nieto, P. Prados, D. N. Reinhoudt, *J. Am. Chem. Soc.* **1994**, *116*, 5814–5822.
[16] S. Kanamathareddy, C. D. Gutsche, *J. Org. Chem.* **1994**, *59*, 3871–3879.
[17] Reaction of $X_6Me_3Imme_3$ with $Zn(H_2O)_6(ClO_4)_2$ in THF was described in ref. [11]. $[Zn(X_6Me_3Imme_3)(MeCN)](ClO_4)_2$ was directly obtained by dissolving the aqua complex $[Zn(X_6Me_3Imme_3)(H_2O)](ClO_4)_2$ in CD_3CN.
[18] This average $Zn-N_{Im}$ bond length is slightly shorter and the zinc-nitrile distance slightly longer than those reported for the parent propionitrile adduct (1.996 Å and 1.985 Å, respectively), see ref.[11] This is in accordance with the lower donor ability of MeCN compared to EtCN.
[19] Except for $[Zn(X_6Me_3Pyz_3)(MeCN)](ClO_4)_2$, which was too soluble to be crystallized out of an acetonitrile solution.
[20] Under millimolar conditions, the half-life time was ca. 5 minutes. Kinetic and mechanistic studies on the exchange process are under investigation.
[21] In the case of $[Zn(X_6Me_3Bzim_3)(MeCN)](ClO_4)_2$ an unusual up-field shift for the OMe resonance is observed. A Dreiding model in fact showed that these methoxy groups are situated in the anisotropic cone of the aromatic benzimidazole moieties.
[22] Similar NMR profiles were obtained when the complexes were dissolved in $CDCl_3$ in the presence of CH_3CN, with a broad resonance at δ = –0.7. This confirmed the presence of a coordinating acetonitrile molecule inside the aromatic cavity in solution; see ref. [11].
[23] J. Sandström, *Dynamic NMR spectroscopy*, Academic Press, London, **1982**.
[24] Y. Rondelez, O. Sénèque, M.-N. Rager, A. Duprat, O. Reinaud, *Chem. Eur. J.* **2000**, *6*, 4218–4226.
[25] The ability of these N-donors to act as a zinc ligand indeed does not follow their basicity, which increases in the order pyrazole < pyridine < benzimidazole ≈ imidazole < tertiary amines. The p*K*a values of the conjugate acids (BH^+) of pyrazole, pyridine, imidazole, and aliphatic amines are 2.5, 5.3, 7.0, and 9–11, respectively.
[26] S. Julia, C. Martinez-Martorell, J. Elguero, *Heterocycles* **1986**, *24*, 2233–2237.
[27] H. Skolink, J. G. Miller, A. R. Day, *J. Am. Chem. Soc.* **1943**, *65*, 1865–1856.
[28] Crystallographic data for the structures reported in this paper have been deposited with the Cambridge Crystallographic Data Center as supplementary publication no. CCDC-158190 (for $X_6Me_3Pyz_3$), CCDC-158191 {for $[Zn(X_6Me_3Imme_3)(CH_3CN)](ClO_4)_2$} and CCDC-158192 (for $X_6Me_3Pyr_3$). Copies of the data can be obtained free of charge on application to CCDC, 12 Union Road, Cambridge CB2 1EZ, UK (Fax: (internat.) + 44-1223/336-033; E-mail: deposit@ccdc. ac. uk).
[29] G. M. Sheldrick, *SHELXL97*, Program for the refinement of crystal structures, Univ. of Göttingen, Germany, **1997**.

Received March 30, 2001
[I01116]

Synthesis, X-ray Crystal Structure, and Stability of Novel Trialkylalane−Triorganylbismuthane Adducts

Andreas Kuczkowski,[a] Stephan Schulz,*[a] and Martin Nieger[a]

Dedicated to Prof. Dr. Wolfgang W. Schoeller on the occasion of his 60th birthday

Keywords: Main group elements / Donor−acceptor systems / Aluminum / Bismuth

Reactions of trialkylalanes AlR_3 (R = Me, Et, *t*Bu) and triorganylbismuthanes BiR'_3 (R′ = *i*Pr, $SiMe_3$) were performed and the products investigated both in solution and in the solid state. $Et_3Al–Bi(SiMe_3)_3$ (**2**), $tBu_3Al–Bi(SiMe_3)_3$ (**3**), and $tBu_3Al–Bi(iPr)_3$ (**6**) are stable Lewis acid–base adducts in pure form while only **3** and **6** are adducts in solution. Their dissociation enthalpies, as determined by temperature-dependent NMR spectroscopy, were estimated to 6.3 (**3**) and 6.9 kcal/mol (**6**). In contrast, $Me_3Al–Bi(SiMe_3)_3$ (**1**), $Et_3Al–Bi(SiMe_3)_3$ (**2**), $Me_3Al–Bi(iPr)_3$ (**4**), and $Et_3Al–Bi(iPr)_3$ (**5**) are fully dissociated in solution. Compounds **1**–**6** were characterized by multinuclear NMR spectroscopy (^1H, ^{13}C), mass spectrometry, and elemental analysis. In addition, the crystal structures of **2** and **6** were determined by single-crystal X-ray diffraction. Compounds **2** and **6** are the first structurally characterized alane–triorganylbismuthane Lewis acid–base adducts.

Introduction

Group-13 trialkyl compounds generally tend to form adducts with Lewis bases by utilizing their vacant p-valence orbital.[1] This basic reaction, in particular toward group-15 compounds, has been widely studied, not only due to the interesting structural features that have been discovered during the last decades, but also to the potential application of so-formed Lewis acid−base adducts to serve as single source precursors for the preparation of the corresponding binary III−V materials by CVD processes. Both the influence of the central group-13 and -15 element as well as the role of the substituents on the adduct stability, which usually is expressed by their dissociation energy, has been studied experimentally and theoretically.[2] As generally accepted, the Lewis basicity of triorganyl pnicogenides R'_3E decreases with increasing atomic number of the central pnicogenide E. Consequently, amine and phosphane adducts of a constant Lewis acid R_3M (M = B, Al, Ga, In) are much more stable than stibane and bismuthane adducts. Experimental studies strongly support these findings. While numerous adducts of boranes (BR_3) and alanes (AlR_3) (R = halogen, H or Me) with amines (R_3N) and phosphanes (R_3P) have been prepared and structurally characterized, adducts with the higher homologues of group 15, such as stibanes (R_3Sb)[3] and bismuthanes (R_3Bi), have been studied to a far lesser extend. Coates described in the early 1950s the reaction of $GaMe_3$ with trimethyl pnicogenides EMe_3 (E = N, P, As, Sb, and Bi)[4] and experimentally verified the steadily decreasing Lewis basicity of EMe_3 toward $GaMe_3$ with increasing atomic number. This tendency reaches its maximum at Me_3Bi, which did not react with Me_3Ga. The decrease of the Lewis basicity results from the increased s-character of the *lone pair*. Detailed investigations show two significant steps within the decrease of the basicity: Arsanes AsR_3 exhibit a much lower basicity than phosphanes PR_3 due to the post transition metal effect (d-contraction) and bismuthanes BiR_3 are less basic than stibanes SbR_3 both due to the lanthanoid contraction (inert pair effect) and to relativistic effects.[5]

We and others have focused on the coordination chemistry of the heavier group-15 elements during the last few years, leading to the synthesis and structural characterization of several group-13−stibane adducts.[6] Very recently, we reported on the synthesis and structural characterization of the first stable trialkylgallane−triorganylbismuthane adducts.[7]

In an attempt to expand these studies to other group-13 elements and to gain further insights into the structural properties of adducts containing a group-13−Bi linkage, we studied reactions of trialkylalanes with triorganylbismuthanes. Herein, we describe the synthesis and structural characterization of trialkylalane−bismuthane adducts. In addition, temperature-dependent NMR studies were performed to estimate the stability of these adducts in solution.

Results and Discussion

Equimolar amounts of pure trialkylalanes R_3Al (R = Me, Et, *t*Bu) and triorganylbismuthanes R'_3Bi (R′ = $SiMe_3$, *i*Pr) were combined in a glovebox. While tBu_3Al immediately formed white solids with both bismuthanes, clearly indicating the formation of the adducts

[a] Institut für Anorganische Chemie der Universität Bonn, Gerhard-Domagk-Straße 1, 53121 Bonn, Germany
Fax: (internat.) + 49-(0)228/73-5327
E-mail: sschulz@uni-bonn.de

 © WILEY-VCH Verlag GmbH, 69451 Weinheim, 2001 1434−1948/01/1010−2605 $ 17.50+.50/0

tBu$_3$Al−Bi(SiMe$_3$)$_3$ (**3**) and tBu$_3$Al−Bi(iPr)$_3$ (**6**), analogous reactions of Me$_3$Al yielded colorless liquids Me$_3$Al/Bi(SiMe$_3$)$_3$ (**1**) and Me$_3$Al/Bi(iPr)$_3$ (**4**). Et$_3$Al, however, reacted with Bi(SiMe$_3$)$_3$ to give the solid adduct Et$_3$Al−Bi(SiMe$_3$)$_3$ (**2**), while the combination with iPr$_3$Bi led to a colorless liquid [Et$_3$Al/Bi(iPr)$_3$ (**5**)].

$$R_3Al + R'_3Bi \longrightarrow R_3Al{-}BiR'_3$$
$$R = Me, Et, tBu; R' = SiMe_3, iPr$$

Pure **1**−**6** have been characterized by elemental analysis. In addition, mass spectra were recorded in the electron impact (EI) mode at 10 eV to obtain further information about the stability of the adducts in the gas phase. However, the peaks with the highest mass observed for **1**−**6** correspond to the respective trialkylalane and triorganylbismuthane fragments. The adduct molecular ion peak was never detected.

The adduct formation is obvious in case of the solid products **2**, **3**, and **6**, while it is questionable for the liquid reaction products **1**, **4**, and **5**, which could merely be simple 1:1 mixtures in pure form. Since gas phase measurements could not be performed due to the lack of suitable instrumentation, it was not possible for us to distinguish between these two possible forms. However, to the best of our knowledge, **2**, **3**, and **6** are the first stable Lewis acid−base adducts in pure form.

1−**6** have also been consequently investigated in solution by ^{1}H and ^{13}C NMR spectroscopy. ^{1}H NMR spectra of **1**−**6** show signals due to the organic groups almost at the same chemical shift as the starting compounds.[8]

Table 1. Selected ^{1}H and ^{13}C NMR shifts and Δ(H) and Δ(C) values of the trialkylalanes and the adducts **1**−**6** as obtained from solutions in C$_6$D$_6$

Compound	δ = ^{1}H[a]	δ = ^{13}C[b]	Δ(H)[c]	Δ(C)[d]
Me$_3$Al	−0.36	−6.8	−	−
Et$_3$Al	0.31	0.9	−	−
tBu$_3$Al	1.08	21.1	−	−
Me$_3$Al−Bi(SiMe$_3$)$_3$ (**1**)	−0.35	−6.7	0.01	0.1
Et$_3$Al−Bi(SiMe$_3$)$_3$ (**2**)	0.31	0.9	0	0
tBu$_3$Al−Bi(SiMe$_3$)$_3$ (**3**)	1.08	21.1	0	0
Me$_3$Al−Bi(iPr)$_3$ (**4**)	−0.36	−6.9	0	0.1
Et$_3$Al−Bi(iPr)$_3$ (**5**)	0.30	0.9	0.01	0
tBu$_3$Al−Bi(iPr)$_3$ (**6**)	1.10	21.1	0.02	0

[a] Me$_3$Al and Et$_3$Al: δ = ^{1}H(α-H); tBu$_3$Al: δ = ^{1}H(β-H). − [b] δ = ^{13}C(α-C). − [c] Me$_3$Al and Et$_3$Al: Δ(H) = δ(α-H)$_{adduct}$ − δ(α-H)$_{trialkylalane}$; tBu$_3$Al: Δ(H) = δ(β-H)$_{adduct}$ − δ(β-H)$_{trialkylalane}$. − [d] Δ(C) = δ(α-C)$_{adduct}$ − δ(α-C)$_{trialkylalane}$.

This is in contrast to the corresponding alane−stibane adducts[6b,6d] and to alane−phosphane adducts,[9] which show resonances typically shifted to lower field (ligands bound to Al) and higher field (ligands bound to P and Sb), respectively. These results strongly indicate **1**−**6** to be at least extensively dissociated in solution at ambient temperature. Unfortunately, we were not able to study the degree of dissociation by cryoscopic molecular mass determination, due to the extreme sensitivity of **1**−**6** in solution toward traces of oxygen and water. Therefore, temperature-dependent NMR studies were performed. These clearly proved the products of the reaction of Bi(iPr)$_3$ and Bi(SiMe$_3$)$_3$ with Me$_3$Al (**1**, **4**) and Et$_3$Al (**2**, **5**) to be fully dissociated in solution. While at ambient temperature the ^{1}H NMR spectra only show one resonance due to the Al−Me and Al−Et groups, at −70 °C two resonances of the Me and Et groups of relative intensities of 1:2 were observed. This clearly show the presence of (Me$_3$Al)$_2$ and (Et$_3$Al)$_2$ dimers (terminal and bridging substituents), eliminating the possibility for the presence of the desired adduct in solution. The two resonances coalesce between −25 and −40 °C. In contrast, the tBu$_3$Al−BiR$_3$ adducts **3** and **6** are not fully dissociated in solution. This was also demonstrated by temperature-dependent ^{1}H NMR spectroscopy. The dissociation enthalpy of the adducts R$_3$Bi−Al(tBu)$_3$ (R = SiMe$_3$, iRr) may be derived from the temperature dependence of the equilibrium constant K_{eq}, with Equations (1) and (2).

$$tBu_3Al + Bi(R)_3 \underset{}{\overset{K_{eq}}{\rightleftharpoons}} R_3Bi{-}Al(tBu)_3 \quad (1)$$

$$\ln K_{eq} = \frac{-\Delta H_D}{R}\left(\frac{1}{T}\right) + \frac{\Delta S_D}{R} \quad (2)$$

The equilibrium constant can be expressed in terms of the mol fraction of the alane present as free tBu$_3$Al and the total initial concentration, [total], with Equation (3).

$$K_{eq} = \frac{[\text{total}]\cdot(\chi_{free})^2}{(1-\chi_{free})} \quad (3)$$

Since the time-dependent ^{1}H NMR spectra only show a single resonance due to the Al(tBu) group over the complete temperature range, and assuming the ^{1}H NMR shift of the Al(tBu) group to be directly proportional to the mol fraction of the total species present as free tBu$_3$Al, χ_{free} may be calculated by the ^{1}H NMR chemical shift of Al(tBu) at a given temperature with Equation (5); δ_{free} is the chemical shift of the uncomplexed tBu$_3$Al and δ_{sample} is obtained directly from the sample. The "real" chemical shift of the adduct (fully coordinated species) is given by δ_{coord}. This was estimated by addition of a fivefold excess of the corresponding bismuthane R$_3$Bi to tBu$_3$Al, which was then measured at −70 °C, assuming tBu$_3$Al to be fully coordinated under these conditions.[10]

$$\chi_{free} = \frac{\delta_{sample} - \delta_{coord}}{\delta_{free} - \delta_{coord}} \quad (4)$$

Table 2. Temperature-dependent ^{1}H NMR chemical shifts and thermodynamic data of **3** and **6** in [D_8]toluene

tBu$_3$Al−Bi(SiMe$_3$)$_3$ (**3**)

T [K]	$1/T$	$\delta_{exp.}$ [ppm][a]	χ_{free}	K_{eq}	ln K
303	3.30 10^{-3}	1.32	0.606	3.72 10^{-2}	−3.29
263	3.80 10^{-3}	1.41	0.352	7.65 10^{-3}	−4.87
243	4.12 10^{-3}	1.45	0.239	3.02 10^{-3}	−5.80
223	4.48 10^{-3}	1.49	0.141	9.24E-04	−6.99
203	4.93 10^{-3}	1.51	0.070	2.13E-04	−8.45
δ_{coord} [ppm]	δ_{free} [ppm]	Concentration		ΔH [kJ/mol]	ΔS [J/Kmol]
1.53	1.18	0.04 M		26.3	59.6

tBu$_3$Al−Bi(iPr)$_3$ (**6**)

T [K]	$1/T$	$\delta_{exp.}$ [ppm][a]	χ_{free}	K_{eq}	ln K
303	3.30 10^{-3}	1.21	0.90	3.24 10^{-1}	−1.13
263	3.80 10^{-3}	1.26	0.70	6.53 10^{-2}	−2.73
243	4.12 10^{-3}	1.31	0.48	1.77 10^{-2}	−4.03
223	4.48 10^{-3}	1.36	0.30	5.14 10^{-3}	−5.27
203	4.93 10^{-3}	1.39	0.16	1.22 10^{-3}	−6.71
δ_{coord} [ppm]	δ_{free} [ppm]	Concentration		ΔH [kJ/mol]	ΔS [J/Kmol]
1.43	1.18	0.04 M		28.9	86.2

[a] β-H resonance of tBu$_3$Al.

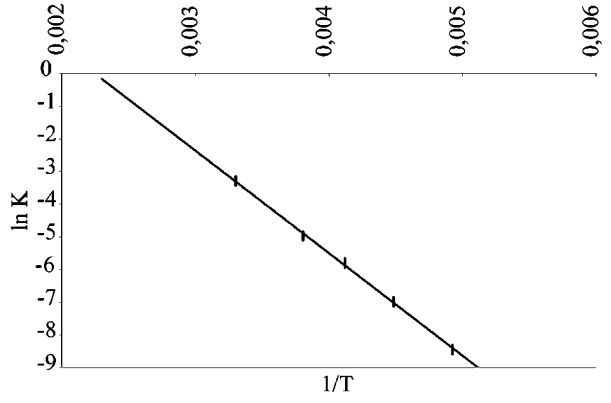

Figure 1. Temperature dependence of the equilibrium constant K_{eq} for the dissociation of **3** (R = 0.999)

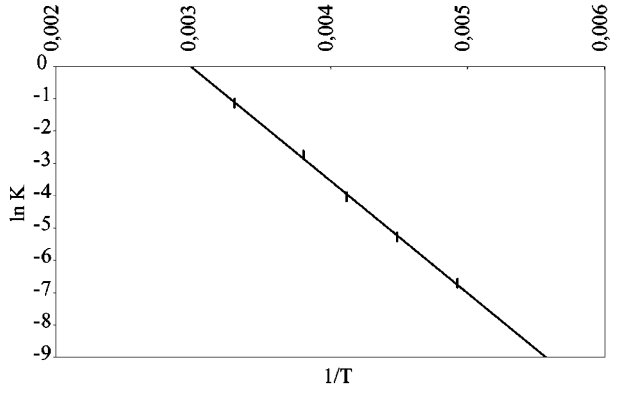

Figure 2. Temperature dependence of the equilibrium constant K_{eq} for the dissociation of **6** (R = 0.998)

The dissociation enthalpies of **3** and **6** were calculated to 26.3 kJ/mol (6.3 kcal/mol) and 28.9 kJ/mol (6.9 kcal/mol), respectively, indicating the interaction between tBu$_3$Al and the bismuthanes to be weak in solution. The ΔS values of 59.6 kJ/mol (14.2 kcal/mol) and 86.2 kJ/mol (20.6 kcal/mol) are very large and positive, as is typical for a dissociative process. However, the absolute values are erroneous due to several potential sources of errors, in particular the values for the "real" adducts. A small variation in these so-calculated values of only δ = 0.01 would lead to ΔH values which differ by about ± 2 kJ/mol.

The results obtained from temperature-dependent ^{1}H NMR spectroscopy prove the dimerization of Me$_3$Al and Et$_3$Al to be thermodynamically more favored in solution compared to the formation of a bismuthane adduct. Therefore, the preparative key for the synthesis of stable alane−bismuthane adducts in solution seems to be the use of trialkylalanes, which do not dimerize. In addition, bismuthanes containing sterically bulky and electropositive substituents, which increase the Lewis basicity due to steric (partial rehybridization of the lone pair leading to a higher p-character) and electronic reasons (+I effect of the substituents), lead to more stable adducts.[11] Repulsive interactions between the ligands of the Lewis base and acid, which play an important role for the stability of borane− and alane−amine adducts,[12] seem to be less important due to the bigger central pnicogen atom, leading to reduced steric interactions.

However, the results obtained in solution do not necessarily mean that Me$_3$Al and Et$_3$Al cannot form stable adducts with bismuthanes in general. This is obvious for the reaction product of Et$_3$Al and Bi(SiMe$_3$)$_3$, which is a solid, indicating the formation of the adduct Et$_3$Al−Bi(SiMe$_3$)$_3$ (**2**). Unfortunately, the reactions of Me$_3$Al with both bismuthanes and of Et$_3$Al with Bi(iPr)$_3$ led to liquid products. Whether these compounds are adducts or only mixtures of

the starting compounds could not be determined conclusively.

X-ray quality single crystals of $Et_3Al-Bi(SiMe_3)_3$ (**2**) and $(tBu)_3Al-Bi(iPr)_3$ (**6**) were grown from solutions in pentane at −30 °C. Figures 3 and 4 show the solid-state structures of **2** and **6.**

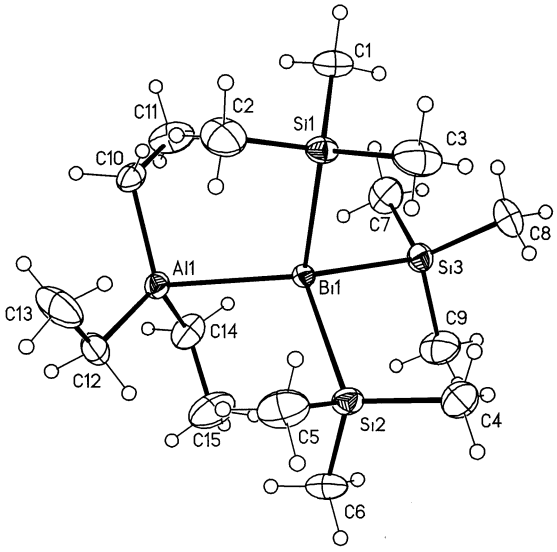

Figure 3. ORTEP diagram (50% probability ellipsoids) showing the solid-state structure and atom-numbering scheme for $Et_3Al-Bi(SiMe_3)_3$ (**2**); selected bond lengths [Å] and angles [°]: Al1−Bi1 2.921(2), Al1−C10 1.989(6), Al1−C12 1.973(5), Al1−C14 1.972(5), Bi1−Si1 2.634(2), Bi1−Si2 2.628(2), Bi1−Si3 2.635(2); C10−Al1−C12 116.0(2), C10−Al1−C14 117.3(2), C12−Al1−C14 117.5(3), Si1−Bi1−Si2 103.2(1), Si1−Bi1−Si3 100.5(1), Si2−Bi1−Si3 101.9(1)

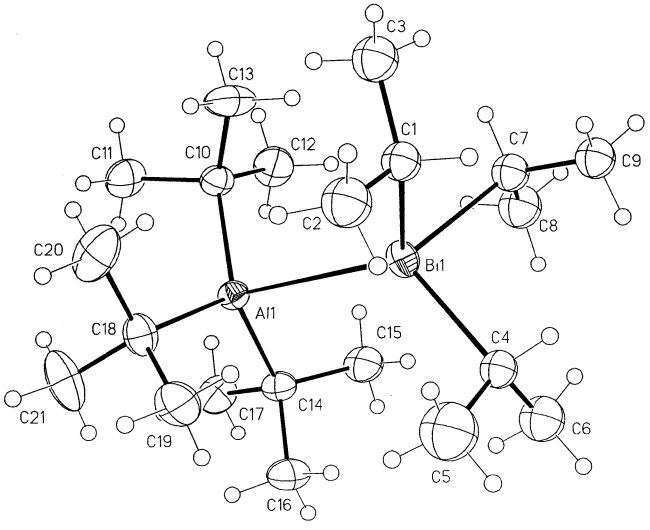

Figure 4. ORTEP diagram (50% probability ellipsoids) showing the solid-state structure and atom-numbering scheme for $tBu_3Al-Bi(iPr)_3$ (**6**); selected bond lengths [Å] and angles [°]: Al1−Bi1 308.8(2), Al1−C10 2.014(5), Al1−C14 2.014(5), Al1−C18 2.025(5), Bi1−C1 2.313(5), Bi1−C4 2.246(5), Bi1−C7 2.326(5); C10−Al1−C14 117.4(2), C10−Al1−C18 116.7(2), C14−Al1−C18 116.3(2), C1−Bi1−C4 95.8(2), C1−Bi1−C7 93.1(2), C4−Bi1−C7 97.6(2); only one orientation of the disordered *i*Pr groups is shown; in addition, only the data of the major compound are included in the tables

The Al and Bi atoms in **2** and **6** reside in distorted tetrahedral environments with their substituents adopting a staggered conformation relative to one another. The same was observed for the corresponding gallane−bismuthane adducts $Et_3Ga-Bi(SiMe_3)_3$ and $(tBu)_3Ga-Bi(iPr)_3$,[7] and alane−stibane adducts $Et_3Al-Sb(SiMe_3)_3$ [6b] and $(tBu)_3Al-Sb(iPr)_3$ [6d] The Al−Bi bond lengths of 2.921(2) Å in **2** and 3.088(1) Å in **6** are significantly elongated compared to the sum of the covalent radii of 2.75 Å (Al: 1.25 Å; Bi: 1.50 Å).[13] $[Me_2AlBi(SiMe_3)_2]_3$, (dmap)$Al(Me_2)Bi(SiMe_3)_2$ and (dmap)$Al(Et_2)Bi(SiMe_3)_2$ [dmap = 4-(dimethylamino)pyridine], so far the only structurally characterized organometallic compounds containing Al−Bi σ-bonds, also show significantly shorter Al−Bi distances [2.774 Å (average),[14] 2.755(2) Å and 2.750(2) Å[7]]. In particular the Al−Bi distance observed in **6** is very long. However, the Al−Bi bond lengths in **2** and **6** are shorter than the Ga−Bi distances found in the analogously substituted gallane−bismuthane adducts $Et_3Ga-Bi(SiMe_3)_3$ [2.966(1) Å] and $(tBu)_3Ga-Bi(iPr)_3$ [3.135(1) Å], respectively.[7] These findings agree with the decreased Lewis acidity of the gallanes compared to the alanes, leading to weaker acid−base interactions. As was found for the gallane−bismuthane adducts, the lower Lewis basicity of the triorganylbismuthanes R_3Bi compared to the corresponding triorganylstibanes R_3Sb can be observed by comparison of **2** and **6** with the analogously substituted alane−stibane adducts $Et_3Al-Sb(SiMe_3)_3$ and $(tBu)_3Al-Sb(iPr)_3$, showing Al−Sb bond lengths of 2.841(1) and 2.927(1) Å, respectively. In particular the difference of 16 pm for the $(tBu)_3Al-E(iPr)_3$ adducts [E = Sb: 2.927(1) Å, Bi: 3.088(1) Å] is significantly increased relative to the difference of the covalent radii (Sb: 1.41 Å, Bi: 1.50 Å[13]). The lower basicity of the bismuthanes in relation to the corresponding stibanes is also indicated by the smaller Si−Bi−Si and C−Bi−C angles (sum of the bond angles: 305.7° for **2** and 286.4° for **6**) compared to the Si−Sb−Si and C−Sb−C angles (sum of the bond angles: Si−Sb−Si = 310.8°; C−Sb−C = 301.5°), which might express the degree of hybridization, and therefore the Lewis basicity of the pnicogenides. The same tendency was found for trihydrides EH_3 and triorganyl pnicogenides ER_3 (R = Me, Ph). The H−E−H and C−E−C angles steadily decrease from almost tetrahedral (amines) to 90° (bismuthanes), indicating a significant increase in s-character of the *lone pair*.[15]

Haaland[2a][2b] and Frenking et al.[2e] demonstrated for borane and alane adducts, that the adduct formation between a group-13 trialkyl compound and an amine or a phosphane leads to a decrease of the C−M−C bond angle (from 120° towards tetrahedral) and an increase of the M−C bond length (M = B, Al). According to this model, a smaller C−M−C angle and a longer M−C bond within analogously substituted group-13/15 adducts indicate a weakening of the adduct. According to this model, the slightly larger C−Al−C bond angles in **2** and **6** (sum of the bond angles: 350.8° for **2** and 350.4° for **6**) compared to those of the stibane adducts [$Et_3Al-Sb(SiMe_3)_3$ 347.3°, $(tBu)_3Al-Sb(iPr)_3$ 346.9°] and the shorter Al−C bonds [av-

erage values: 1.978 Å (**2**), 2.019 Å (**6**); $Et_3Al-Sb(SiMe_3)_3$ = 1.984 Å, $(tBu)_3Al-Sb(iPr)_3$, = 2.030 Å] also demonstrate **2** and **6** to be weaker adducts than the corresponding stibane adducts. This is in agreement with the generally accepted decreasing donor capacity of triorganyl pnicogenides with increasing atomic number of the central group-15 element.[16]

Experimental Section

General Remarks: All manipulations were performed in a glovebox under N_2, or by standard Schlenk techniques. Me_3Al and Et_3Al were commercially available from Aldrich and used as received, while tBu_3Al,[17] $Bi(SiMe_3)_3$,[18] and $Bi(iPr)_3$ [19] were prepared by literature methods. − ^1H and $^{13}C\{^1H\}$ spectra were recorded using a Bruker AMX 300 spectrometer and are referenced to internal C_6D_5H (δ^1H = 7.154; $\delta^{13}C$ = 128.0), while low-temperature NMR spectra are referenced to internal [D_8]toluene (δ^1H = 7.20). − Melting points were measured in sealed capillaries and are not corrected. − Elemental analyses were performed at the Mikroanalytisches Labor der Universität Bonn.

General Experimental Procedure: Pure R_3Al (2 mmol) and R_3Bi (2 mmol) were combined in the glovebox in 10-mL flasks. $Bi(SiMe_3)_3$ immediately formed a white solid with Et_3Al and tBu_3Al, while the same occurred between $Bi(iPr)_3$ and tBu_3Al, indicating the formation of the adducts $Et_3Al-Bi(SiMe_3)_3$ (**2**), $tBu_3Al-Bi(SiMe_3)_3$ (**3**), and $tBu_3Al-Bi(iPr)_3$ (**6**). In contrast, the products of the reaction of both bismuthanes with Me_3Al and of $Bi(iPr)_3$ with Et_3Al stayed liquid at ambient temperature. Compounds **2**, **3**, and **6** were dissolved in pentane (5 mL) and stored at −30 °C, resulting in the formation of colorless crystals in almost quantitative yield. Compounds **1**, **4**, and **5** were characterized without further purification.

$Me_3Al/Bi(SiMe_3)_3$ (1): Yield 1.00 g (100%). − $C_{12}H_{36}AlBiSi_3$ (502.21): calcd. C 28.70, H 7.23, found C 28.13 H 6.99. − ^1H NMR (300 MHz, C_6D_5H, 25 °C): δ = − 0.35 (s, 3 H, MeAl), 0.65 (s, 9 H, $SiMe_3$). − $^{13}C\{^1H\}$ NMR (80 MHz, C_6D_5H, 25 °C): δ = − 6.7 (MeAl), 6.5 ($SiMe_3$). − Temperature-dependent ^1H NMR spectra (300 MHz, [D_8]toluene); 303 K: δ = − 0.25 (s, 9 H, MeAl), 0.75 (s, 27 H, $SiMe_3$); 263 K: δ = − 0.27 [s (broad), 3 H, MeAl], 0.74 (s, 9 H, $SiMe_3$). 243 K, δ = − 0.34 [s (very broad), 9 H, MeAl], 0.74 (s, 27 H, $SiMe_3$). 223 K, δ = − 0.49 [s (broad), 6 H, MeAl], 0.10 [s (very broad), 3 H, MeAl], 0.73 (s, 27 H, $SiMe_3$); 203 K: δ = − 0.49 [s (broad), 3 H, MeAl], 0.07 [s (broad), 6 H, MeAl], 0.73 (s, 27 H, $SiMe_3$).

$Et_3Al-Bi(SiMe_3)_3$ (2): Yield 0.98 g (90%). M.p. 50−51 °C. − $C_{15}H_{42}AlBiSi_3$ (542.72): calcd. C 33.20, H 7.80; found C 32.83, H 7.63. − ^1H NMR (300 MHz. C_6D_5H, 25 °C): δ = 0.31 (q, $^3J_{HH}$ = 8.1 Hz, 2 H, $MeCH_2Al$), 0.64 (s, 9 H, $SiMe_3$), 1.18 (t, $^3J_{HH}$ = 8.1 Hz, 3 H, $MeCH_2Al$). − $^{13}C\{^1H\}$ NMR (80 MHz, C_6D_5H, 25 °C): δ = 2.0 ($MeCH_2Al$), 6.3 ($SiMe_3$), 9.5 ($MeCH_2Al$). − Temperature-dependent ^1H NMR spectra (300 MHz, [D_8]toluene); 303 K: δ = 0.39 (q, $^3J_{HH}$ = 8.1 Hz, 6 H, $MeCH_2Al$), 0.75 (s, 27 H, $SiMe_3$), 1.27 (t, $^3J_{HH}$ = 8.1 Hz, 9 H, $MeCH_2Al$); 263 K: δ = 0.44 ["q" (broad), 6 H, $MeCH_2Al$], 0.72 (s, 27 H, $SiMe_3$), 1.34 ["t" (broad), 9 H, $MeCH_2Al$]. 243 K, δ = 0.44 [s (broad), 6 H, $MeCH_2Al$], 0.70 (s, 27 H, $SiMe_3$), 1.34 [s (broad), 9 H, $MeCH_2Al$]; 223 K: δ = 0.68 (s, 27 H, $SiMe_3$), 1.42 [s (very broad), 9 H, $MeCH_2Al$]; 203 K: δ = 0.17 [s (very broad), 2 H, $MeCH_2Al$], 0.66 (s, 27 H, $SiMe_3$), 0.98 [s (very broad), 4 H, $MeCH_2Al$], 1.30 [s (very broad), 3 H, $MeCH_2Al$], 1.61 [s (very broad), 6 H, $MeCH_2Al$].

$tBu_3Al-Bi(SiMe_3)_3$ (3): Yield 1.15 g (92%). M.p. 41 °C. − $C_{21}H_{54}AlBiSi_3$ (626.82): calcd. C 40.20, H 8.62; found C 39.84, H 8.49. − ^1H NMR (300 MHz. C_6D_5H, 25 °C): δ = 0.64 (s, 9 H, $SiMe_3$), 1.08 (s, 9 H, *t*Bu). − $^{13}C\{^1H\}$ NMR (80 MHz, C_6D_5H, 25 °C): δ = 6.3 ($SiMe_3$), 21.1 (Me_3CAl), 32.5 (Me_3CAl). − Temperature-dependent ^1H NMR spectra (300 MHz, [D_8]toluene); 303 K: δ = 0.74 (s, 27 H, $SiMe_3$), 1.32 (s, 27 H, *t*Bu); 263 K: δ = 0.69 (s, 27 H, $SiMe_3$), 1.41 (s, 27 H, *t*Bu); 243 K: δ = 0.66 (s, 27 H, $SiMe_3$), 1.45 (s, 27 H, *t*Bu). 223 K, δ = 0.63 (s, 27 H, $SiMe_3$), 1.49 (s, 27 H, *t*Bu); 203 K: δ = 0.58 (s, 27 H, $SiMe_3$), 1.51 (s, 27 H, *t*Bu). $tBu_3Al-Bi(SiMe_3)_3$ (1:5; 203 K, [D_8]toluene): δ = 1.53. tBu_3Al (298 K, [D_8]toluene): δ = 1.18.

$Me_3Al/Bi(iPr)_3$ (4): Yield 0.82 g (100%). − $C_{12}H_{30}AlBi$ (410.33): calcd. C 35.13, H 7.37; found C 34.98, H 7.29. − H NMR (300 MHz, C_6D_5H, 25 °C): δ = −0.36 (s, 3 H, MeAl), 1.82 (d, $^3J_{HH}$ = 7.4 Hz, 6 H, Me_2CHBi), 2.15 (sept, $^3J_{HH}$ = 7.4 Hz, 1 H, Me_2CHBi). − $^{13}C\{^1H\}$ NMR (80 MHz, C_6D_5H, 25 °C): δ = −6.9 (MeAl), 23.9 (Me_2CHBi), 29.1 (Me_2CHBi). − Temperature-dependent ^1H NMR spectra (300 MHz, [D_8]toluene); 303 K: δ = − 0.26 (s, 9 H, MeAl), 1.92 (d, $^3J_{HH}$ = 7.2 Hz, 18 H, Me_2CHBi), 2.22 (sept, $^3J_{HH}$ = 7.2 Hz, 3 H, Me_2CHBi). 263 K, δ = − 0.27 [s (broad), 9 H, MeAl], 1.99 (d, $^3J_{HH}$ = 7.2 Hz, 18 H, Me_2CHBi), 2.20 (sept, $^3J_{HH}$ = 7.2 Hz, 3 H, Me_2CHBi); 243 K: δ = − 0.38 [s (very broad), 9 H, MeAl], 1.89 (d, $^3J_{HH}$ = 7.2 Hz, 18 H, Me_2CHBi), 2.19 (sept, $^3J_{HH}$ = 7.2 Hz, 3 H, Me_2CHBi). 223 K, δ = − 0.50 [s (broad), 3 H, MeAl], 0.12 [s (very broad), 6 H, MeAl], 1.89 (d, $^3J_{HH}$ = 7.2 Hz, 18 H, Me_2CHBi), 2.18 (sept, $^3J_{HH}$ = 7.2 Hz, 3 H, Me_2CHBi); 203 K: δ = − 0.49 (s, 3 H, MeAl), 0.07 (s, 6 H, MeAl), 1.88 (d, $^3J_{HH}$ = 7.2 Hz, 18 H, Me_2CHBi), 2.16 (sept, $^3J_{HH}$ = 7.2 Hz, 3 H, Me_2CHBi).

$Et_3Al/Bi(iPr)_3$ (5): Yield 0.90 g (100%). − $C_{15}H_{36}AlBi$ (452.42): calcd. C 39.82, H 8.02; found C 39.67, H 7.99. − ^1H NMR (300 MHz, C_6D_5H, 25 °C): δ = 0.30 (q, $^3J_{HH}$ = 7.9 Hz, 2 H, $MeCH_2Al$), 1.10 (t, $^3J_{HH}$ = 7.9 Hz, 3 H, $MeCH_2Al$), 1.82 (d, $^3J_{HH}$ = 7.4 Hz, 6 H, Me_2CHBi), 2.15 (sept, $^3J_{HH}$ = 7.4 Hz, 1 H, Me_2CHBi). − $^{13}C\{^1H\}$ NMR (80 MHz, C_6D_5H, 25 °C): δ = 0.9 ($MeCH_2Al$), 9.1 ($MeCH_2Al$), 23.9 (Me_2CHBi), 29.2 (Me_2CHBi). − Temperature-dependent ^1H NMR spectra (300 MHz, [D_8]toluene); 303 K: δ = 0.38 (q, $^3J_{HH}$ = 7.9 Hz, 6 H, $MeCH_2Al$), 1.21 (t, $^3J_{HH}$ = 7.9 Hz, 9 H, $MeCH_2Al$), 1.92 (d, $^3J_{HH}$ = 7.4 Hz, 18 H, Me_2CHBi), 2.23 (sept, $^3J_{HH}$ = 7.4 Hz, 3 H, Me_2CHBi); 263 K: δ = 0.37 ["s" (broad), 6 H, $MeCH_2Al$], 1.19 ("t", $^3J_{HH}$ = 8.1 Hz, 9 H, $MeCH_2Al$), 1.90 (d, $^3J_{HH}$ = 7.2 Hz, 18 H, Me_2CHBi), 2.20 (sept, $^3J_{HH}$ = 7.2 Hz, 3 H, Me_2CHBi); 243 K: δ = 1.19 ["s" (very broad), 9 H, $MeCH_2Al$], 1.89 (d, $^3J_{HH}$ = 7.2 Hz, 18 H, Me_2CHBi), 2.19 (sept, $^3J_{HH}$ = 7.2 Hz, 3 H, Me_2CHBi); 223 K: δ = 0.19 [s (very broad), 2 H, $MeCH_2Al$], 1.26 [s (broad), 9 H, $MeCH_2Al$], 1.89 (d, $^3J_{HH}$ = 7.2 Hz, 18 H, Me_2CHBi), 2.18 (sept, $^3J_{HH}$ = 7.2 Hz, 3 H, Me_2CHBi). 203 K, δ = 0.18 [s (broad), 2 H, $MeCH_2Al$], 0.73 [s (broad), 4 H, $MeCH_2Al$], 0.99 [s (broad), 3 H, $MeCH_2Al$], 1.29 ["t" (broad), 9 H, $MeCH_2Al$], 1.88 (d, $^3J_{HH}$ = 7.2 Hz, 18 H, Me_2CHBi), 2.17 (sept, $^3J_{HH}$ = 7.2 Hz, 3 H, Me_2CHBi).

$tBu_3Al-Bi(iPr)_3$ (6): Yield 1.01 g (94%). M.p. 44−46 °C. − $C_{21}H_{48}AlBi$ (536.55): calcd. C 47.01, H 9.02; found C 46.96, H 8.55. − ^1H NMR (300 MHz, C_6D_5H, 25 °C): δ = 1.10 (s, 9 H, *t*Bu), 1.82 (d, $^3J_{HH}$ = 7.2 Hz, 6 H, Me_2CHBi), 2.16 (sept, $^3J_{HH}$ = 7.4 Hz, 1 H, Me_2CHBi). − $^{13}C\{^1H\}$ NMR (80 MHz, C_6D_5H, 25 °C): δ = 21.1 (Me_3CAl), 23.9 (Me_2CHBi), 30.9 (Me_2CHBi), 32.3

Table 3. Crystallographic data and measurements for $Et_3Al-Bi(SiMe_3)_3$ (**2**) and $tBu_3Al-Bi(iPr)_3$ (**6**)

	2	**6**
Empirical formula	$C_{15}H_{42}AlBiSi_3$	$C_{21}H_{48}AlBi$
Molecular mass	542.72	536.55
Crystal system	monoclinic	triclinic
Space group	$P2_1/c$ (No. 14)	$P\bar{1}$ (No. 2)
a [Å]	15.0063(6)	8.9756(3)
b [Å]	10.0800(4)	10.1879(4)
c [Å]	17.0467(6)	14.9615(4)
α [°]	90	85.063(2)
β [°]	91.624(2)	89.830(2)
γ [°]	90	67.926(2)
V [Å^3]	2577.51(17)	1262.49(7)
Z	4	2
Radiation (λ [Å])	Mo-K_α (0.71073)	Mo-K_α (0.71073)
μ [mm^{-1}]	7.008	7.018
T [K]	123(2)	123(2)
$D_{calcd.}$ [g cm^{-3}]	1.399	1.411
crystal dimensions (mm)	0.30 × 0.20 × 0.10	0.15 × 0.10 × 0.05
$2\theta_{max}$ [°]	50.0	50.0
No. of reflections	20387	19044
No. of nonequiv. reflections	4525	4440
R_{merg}	0.095	0.091
No. of parameters refined/restraints	181/0	191/253
$R1$[a]; $wR2$[b]	0.031, 0.079	0.027, 0.062
Goodness of fit[c]	1.051	1.057
Final max/min. Δρ [e·Å^{-3}]	2.991/−1.864	1.238/−1.094

[a] $R1 = \Sigma(||F_o| - |F_c||)/\Sigma|F_o|$ [for $I > 2\sigma(I)$]. − [b] $wR2 = \{\Sigma[w(F_o^2 - F_c^2)^2]/\Sigma[w(F_o^2)^2]\}^{1/2}$. − [c] Goodness of fit $= \{\Sigma[w(|F_o^2| - |F_c^2|)^2]/(N_{observns.} - N_{params.})\}^{1/2}$.

(Me_3CAl). − Temperature-dependent ^1H NMR spectra (300 MHz, [D$_8$]toluene); 303 K: δ = 1.21 (s, 9 H, *t*Bu), 1.91 (d, $^3J_{HH}$ = 7.2 Hz, 6 H, Me_2CHBi), 2.24 (sept, $^3J_{HH}$ = 7.2 Hz, 1 H, Me_2CHBi); 263 K: δ = 1.26 (s, 9 H, *t*Bu), 1.84 (d, $^3J_{HH}$ = 7.4 Hz, 6 H, Me_2CHBi), 2.29 (sept, $^3J_{HH}$ = 7.4 Hz, 1 H, Me_2CHBi). 243 K, δ = 1.31 (s, 9 H, *t*Bu), 1.77 (d, $^3J_{HH}$ = 7.2 Hz, 6 H, Me_2CHBi), 2.30 (sept, $^3J_{HH}$ = 7.2 Hz, 1 H, Me_2CHBi); 223 K: δ = 1.36 (s, 9 H, *t*Bu), 1.71 (d, $^3J_{HH}$ = 7.3 Hz, 6 H, Me_2CHBi), 2.27 (sept, $^3J_{HH}$ = 7.3 Hz, 1 H, Me_2CHBi); 203 K: δ = 1.39 (s, 9 H, *t*Bu), 1.67 (d, $^3J_{HH}$ = 7.1 Hz, 6 H, Me_2CHBi), 2.23 (sept, $^3J_{HH}$ = 7.1 Hz, 1 H, Me_2CHBi); $tBu_3Al-Bi(iPr)_3$ (1:5; 203 K, [D$_8$]toluene): δ = 1.43 (s, 9 H, *t*Bu), 1.84 (d, $^3J_{HH}$ = 7.4 Hz, 6 H, Me_2CHBi), 2.15 (sept, $^3J_{HH}$ = 7.4 Hz, 1 H, Me_2CHBi); tBu_3Al (298 K, [D$_8$]toluene): δ = 1.18.

X-ray Structure Solution and Refinement: Crystallographic data for **2** and **6** are summarized in Table 3. The ORTEP diagrams of the solid state structures including selected bond lengths and angles of **2** and **6** are shown in Figures 3 and 4. Data were collected with a Nonius Kappa CCD diffractometer. The structures of **2** and **6** were solved by Patterson methods (SHELXS-97)[20] and refined by full-matrix least squares on F^2 (SHELXL-97).[21] All non-hydrogen atoms were refined anisotropically and hydrogen atoms by a riding model. The *i*Pr groups in **6** are disordered (58:42). Empirical absorption corrections were applied. The crystallographic data of **2** and **6** (excluding structure factors) have been deposited with the Cambridge Crystallographic Data Centre as supplementary publication no. CCDC-158549 (**2**) and -158550 (**6**). Copies of the data can be obtained free of charge on application to CCDC, 12 Union Road, Cambridge, CB21EZ [Fax: (internat.) + 44-1223/336-033; E-mail: deposit@ccdc.cam.ac.uk].

Acknowledgments

S. S. would like to thank the Deutsche Forschungsgemeinschaft (DFG) for a Fellowship award. Generous financial support was given by the DFG, the Fonds der Chemischen Industrie, the Bundesministerium für Bildung, Wissenschaft, Forschung und Technologie (BMBF), and Prof. E. Niecke, Universität Bonn.

[1] This reaction was initially studied by Gay-Lussac almost 200 years ago, who synthesized the first compound of this type, $F_3B{\cdot}NH_3$: J. L. Gay-Lussac, J. L. Thenard, *Mem. Phys. Chim. Soc. d'Arcueil* **1809**, *2*, 210; citation in: V. Jonas, G. Frenking, *J. Chem. Soc., Chem. Commun.* **1994**, 1489.

[2] See the following and the references therein: [2a] A. Haaland, *Angew. Chem.* **1989**, *101*, 1017. − [2b] A. Haaland in *Coordination Chemistry of Aluminum* (Ed.: G. H. Robinson), VCH Verlagsgesellschaft, Weinheim, **1993**. − [2c] M. G. Gardiner, C. L. Raston, *Coord. Chem. Rev.* **1997**, *166*, 1. − [2d] J. M. Brunel, B. Faure, M. Maffei, *Coord. Chem. Rev.* **1998**, *178−180*, 665. − [2e] V. Jonas, G. Frenking, M. T. Reetz, *J. Am. Chem. Soc.* **1994**, *116*, 8741. − [2f] A. Y. Timoshkin, A. V. Suvorov, H. F. Bettinger, H. F. Schaefer III, *J. Am. Chem. Soc.* **1999**, *121*, 5687).

[3] Investigations concerning the synthesis (no structural reports) of group-13−stibine adducts were performed by: [3a] F. Hewitt, A. K. Holliday, *J. Chem. Soc.* **1953**, 530. − [3b] M. L. Denniston, D. R. Martin, *J. Inorg. Nucl. Chem.* **1974**, *36*, 2175. − [3c] D. C. Mente, J. L. Mills, R. E. Mitchell, *Inorg. Chem.* **1975**, *14*, 123. − [3d] D. C. Mente, J. L. Mills, *Inorg. Chem.* **1975**, *14*, 1802. − [3e] Y. Takashi, I. Aishima, *J. Organomet. Chem.* **1967**, *8*, 209. − [3f] D. B. Patterson, A. Carnevale, *J. Chem. Phys.* **1973**, *59*, 6464. − [3g] V. G. Tsvetkov, B. I. Kozyrkin, K. K.

Fukin, R. F. Galiallina, *Zh. Obshch. Khim.* **1977**, *47*, 2155. − [3h] B. G. Gribov, B. I. Kozyrkin, E. N. Zorina, *Dokl. Akad. Nauk SSSR* **1972**, *204*, 350. − [3i] E. N. Zorina, B. G. Gribov, B. I Kozyrkin, L. N. Bogdanova, *Sb. Nauchn. Tr. Probl. Mikroelektron.* **1974**, *19*, 148; *Chem. Abstr.* **1975**, *83*, 1571347m. − [3j] V. G. Tsvetkov, N. V. Novoselova, B. G. Gribov, *Tr. Khim. Tekhnol.* **1972**, *65*; *Chem. Abstr.* **1973**, *79*, 77865z. − [3k] T. P. Whaley, V. Norman, *U. S. Patent* **1963**, 3,071,493; *Chem. Abstr.* **1963**, *58*, 4235.

[4] G. E. Coates, *J. Chem. Soc.* **1951**, 2003.

[5] K. C. H. Lange, T. M. Klapötke in *The Chemistry of Functional Groups: The Chemistry of Organic Arsenic, Antimony and Bismuth Compounds*, J. Wiley and Sons, New York, **1994**, p. 322 ff.

[6] [6a] S. Schulz, M. Nieger, *J. Organomet. Chem.* **1998**, *570*, 275. − [6b] S. Schulz, M. Nieger, *Organometallics* **1999**, *18*, 315. − [6c] S. Schulz, M. Nieger, *J. Chem. Soc., Dalton Trans.* **2000**, 639. − [6d] S. Schulz, A. Kuczkowski, M. Nieger, *J. Organomet. Chem.* **2000**, *604*, 202. − [6e] M. S. Lube, R. L. Wells, P. S. White, *J. Chem. Soc., Dalton Trans.* **1997**, 285. − [6f] R. A. Baldwin, E. E. Foos, R. L. Wells, P. S. White, A. L. Rheingold G. P. A. Yap, *Organometallics* **1996**, *15*, 5035. − [6g] R. L. Wells, E. E. Foos, P. S. White, A. L. Rheingold, L. M. Liable-Sands, *Organometallics* **1997**, *16*, 4771.

[7] A. Kuczkowski, F. Thomas, S. Schulz, M. Nieger, *Organometallics* **2000**, *19*, 5758.

[8] The chemical shifts of Me_3Al and Et_3Al, which were obtained at ambient temperature, have to be interpreted cautiously because they display an equilibrium of terminal and bridging shifts for the Al−Me and Al−Et groups, since Me_3Al and Et_3Al are both dimeric in solution. In contrast, tBu$_3$Al is monomeric in solution.

[9] See for example: A. R. Barron, *J. Chem. Soc., Dalton Trans.* **1988**, 3047.

[10] M. B. Power, J. R. Nash, M. D. Healy, A. R. Barron, *Organometallics* **1992**, *11*, 1830.

[11] In contrast, the reaction of Me_3Bi with tBu$_3$Al gave no stable adduct; S. Schulz, unpublished result.

[12] For example, this was observed for trimethylborane adducts with NH_3, NH_2Me, $NHMe_2$ and NMe_3. The Lewis basicity increases in the following order: $NH_3 < NH_2Me < NHMe_2 < NMe_3$. However, the dissociation enthalpies as obtained from the gas phase take the following order: $Me_3B{-}NH_3 < Me_3B{-}NH_2Me = Me_3B{-}NMe_3 < Me_3B{-}NHMe_2$. Due to reduced steric interactions, Me_2NH forms a more stable adduct with BMe_3 than the electronically stronger Lewis base NMe_3. An analogous tendency was observed for the corresponding $AlMe_3$ adducts: E. N. Guryanova, I. P. Goldstein, I. P. Romm, *The Donor−Acceptor Bond*, John Wiley & Sons, New York, **1975**.

[13] A. F Holleman, E. Wiberg in *Lehrbuch der Anorganischen Chemie*, 101st ed., Walter de Gruyter, Berlin, **1995**, p. 1838ff.

[14] S. Schulz, M. Nieger, *Angew. Chem.* **1999**, *111*, 1020; *Angew. Chem. Int. Ed. Engl.* **1999**, *38*, 967.

[15] For a detailed review dealing with this problem see: W. Kutzelnigg, *Angew. Chem.* **1984**, *96*, 262−286; *Angew. Chem. Int. Ed. Engl.* **1984**, 23, 272.

[16] However, contrary results were reported by Carty and Lappert, who synthesized a series of chromium complexes of the type $(OC)_5Cr(EPh_3)$ (E = P, As, Sb, Bi). They observed an *increase* in the M−E bond order with increasing atomic number of the central pnicogenide: A. J. Carty, N. J. Taylor, A. W. Coleman, M. F. Lappert, *J. Chem. Soc., Chem. Commun.* **1979**, 639.

[17] H. Lehmkuhl, O. Olbrysch, H. Nehl, *Justus Liebigs Ann. Chem.* **1973**, 708.

[18] G. Becker, M. Rößler, *Z. Naturforsch., Teil B* **1982**, *37*, 91.

[19] S. Samaan, *Methoden Org. Chem. (Houben Weyl)*, "Metallorganische Verbindungen des Arsens, Antimons und Bismuts", 4th ed., Thieme Verlag, Stuttgart, **1978**.

[20] *SHELXS-97, Program for Structure Solution*: G. M. Sheldrick, *Acta Crystallogr., Sect. A* **1990**, *46*, 467.

[21] G. M. Sheldrick, *SHELXL-97, Program for Crystal Structure Refinement*, Universität Göttingen, **1997**.

Received April 11, 2001
[I01131]

The Photochemistry of $[CpMo(CO)_3(\eta^1\text{-}C_3H_5)]$ in Frozen Gas Matrices at 10 K and the Behaviour of $[CpMo(CO)_2(\eta^3\text{-}C_3H_5)]$ Isomers in Different Media

Christian Limberg,*[a] Anthony J. Downs,[b] Tim M. Greene,[b] and Tobias Wistuba[a]

Keywords: Photochemistry / Matrix isolation / Molybdenum / Allyl ligands

On photolysis of $[CpMo(CO)_3(\eta^1\text{-}C_3H_5)]$ in solid inert matrices at low temperature, one CO molecule is eliminated yielding the *exo* and *endo* isomers of $[CpMo(CO)_2(\eta^3\text{-}C_3H_5)]$ in almost 1:1 proportions, although the fraction of the *exo* conformer is increased by prolonged broad-band UV irradiation. If gaseous $[CpMo(CO)_2(\eta^3\text{-}C_3H_5)]$ is isolated in an Ar matrix the proportions of the two conformers are again about 1:1, indicating that they possess almost equal energies, as confirmed by DFT calculations (B3LYP/SDD). This situation changes in a solvent environment, where increasing the polarity of the solvent favours the *exo* isomer, as indicated by the ratios *exo*/*endo* = 1.7:1 (pentane or cyclohexane), 3.0:1 (benzene) and 3.3:1 (CH_2Cl_2) determined by IR and NMR measurements. Such a finding is consistent with the results of DFT calculations, which reveal that the *exo* isomer is more polar.

Introduction

The dynamics of allylmolybdenum moieties have relevance not only to the formation of new C−C bonds by way of nucleophilic attack on the coordinated allyl groups,[1] but also to catalytic processes involving olefin functionalisation. One example is the oxidation of propene in the presence of a heterogeneous molybdenum oxide catalyst, a process which is believed to proceed by the trapping of allyl radicals by Mo atoms on the catalyst surface; the resulting allyl-Mo fragments are thought subsequently to undergo several shift and rearrangement reactions, finally yielding acrolein.[2] Interest in the mechanisms of this and other reactions involving allylmolybdenum fragments initiated the present investigation of the photolytic behaviour of $[CpMo(CO)_3(\eta^1\text{-}C_3H_5)]$ (**1**)[3] in solid inert matrices at low temperatures.

The matrix photochemistry of the analogous tungsten compound $[CpW(CO)_3(\eta^1\text{-}C_3H_5)]$ has already been examined by Rest et al.[4] They found evidence for photodecarbonylation yielding products displaying two pairs of bands in the ν(CO) region of the IR spectrum. The bands were assigned to a mixture of $[CpW(CO)_2(C_3H_5)]$ isomers involving either an η^1- or an η^3-coordinated allyl group and formed in accordance with the reaction sequence set out in Figure 1. In the light of these intriguing results, it was hoped to shed more light on the fate of $[CpM(CO)_2(\eta^1\text{-}C_3H_5)]$ intermediates (M = Cr, Mo, W) generated through photodecarbonylation by investigation of the corresponding molybdenum compound. These new spectroscopic studies were to be supported by quantum mechanical calculations focussed on the proposed products of the changes.

[a] Universität Heidelberg, Anorganisch-Chemisches Institut
Im Neuenheimer Feld 270, 69120 Heidelberg, Germany
Fax: (internat.) +49-6221/545-707
E-mail: Limberg@sun0.urz.uni-heidelberg.de
[b] Inorganic Chemistry Laboratory, University of Oxford, South Parks Road, Oxford OX1 3QR, U.K.

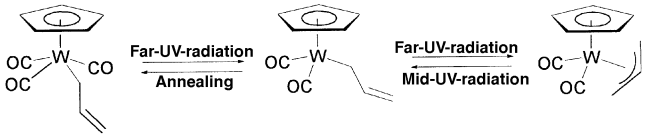

Figure 1. Proposed photochemistry of $[CpW(CO)_3(\eta^1\text{-}C_3H_5)]$ in solid CH_4, Ar, N_2, or CO matrices[4]

Results and Discussion

Photolysis of 1 in Low Temperature Matrices

The vapour of **1** was co-condensed with an excess of argon on a CsI window at 10 K. The IR spectrum of the resulting matrix showed three (matrix-split) bands in the ν(CO) region characteristic of the molecule $[CpMo(CO)_3(\eta^1\text{-}C_3H_5)]$ [Figure 2(a)]. Photolysis of the matrix with light having wavelengths near 369 or 313 nm or with broad-band UV light resulted in the quantitative decomposition of the starting material and gave rise to two pairs of bands (which will subsequently be referred to as "doublets") of almost equal intensity in the ν(CO) region of the IR spectrum (one at 1966/1891 cm^{-1} and the other at 1974/1907 cm^{-1}), together with a band near 2140 cm^{-1} due to free CO. The results are thus very similar to those observed previously in the case of the tungsten compound.[4] Furthermore, as with the tungsten system, prolonged photolysis caused one set of bands to grow somewhat in intensity at the expense of the other set. This immediately prompted the impression that molybdenum follows tungsten in the formation of two species of the type $[CpM(CO)_2(C_3H_5)]$ (M = Mo or W) with η^1- and η^3-coordinated allyl groups, respectively. It seems very surprising, however, that photolysis of both the molybdenum and tungsten compounds gives rise to 16- and 18-electron species $[CpM(CO)_2(C_3H_5)]$ in almost equal proportions, when the

 © WILEY-VCH Verlag GmbH, 69451 Weinheim, 2001 1434−1948/01/1010−2613 $ 17.50+.50/0

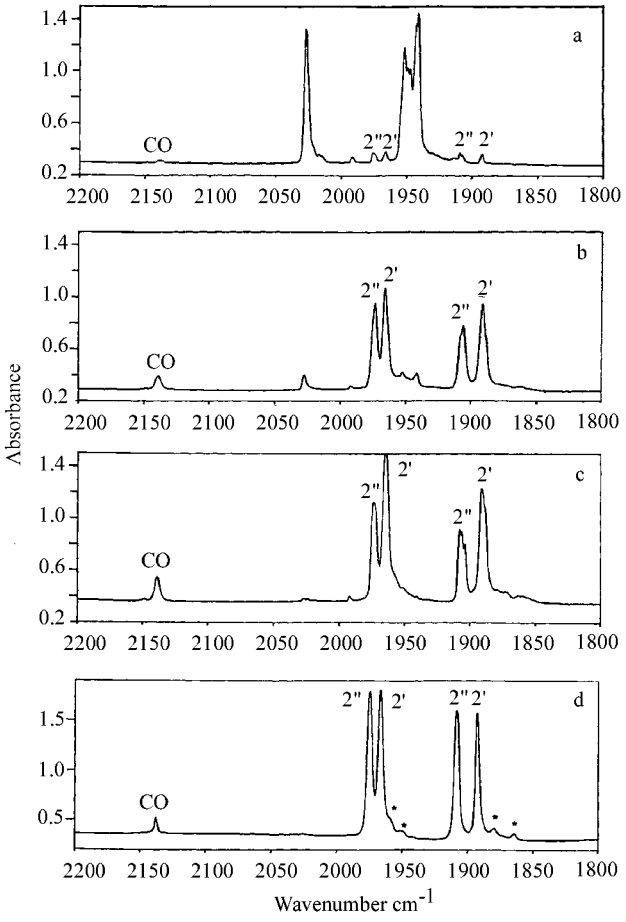

Figure 2. IR absorption spectrum in the region 2200−1800 cm^{-1} displayed by a solid Ar matrix containing [$CpMo(CO)_3(\eta^1\text{-}C_3H_5)$] at 10 K (a); showing the effects of photolysis with broad-band UV radiation for 10 min (b); and of prolonged photolysis (c); trace (d) shows the spectrum of [$CpMo(CO)_2(\eta^3\text{-}C_3H_5)$] isolated in an Ar matrix at 10 K; bands marked with an asterisk arise from [$CpMo(^{12}CO)(^{13}CO)(\eta^3\text{-}C_3H_5)$] present in natural abundance

16-electron compound is likely to be much less stable than the 18-electron one.

In order to shed more light on this finding, the compound [$CpMo(CO)_2(\eta^3\text{-}C_3H_5)$] (**2**)[3] was isolated in an argon matrix [Figure 2(d), Table 1]. Although this material contains only η^3-allyl groups, the IR spectrum of the matrix-isolated vapour showed the same two sets of doublets as did the spectrum of the matrix after photolysis of **1**. Moreover, the two doublet absorptions exhibited by the IR spectrum of **2** were observed to be almost exactly equal in intensity. It seems unlikely that [$CpMo(CO)_2(\eta^3\text{-}C_3H_5)$] rearranges in the gas phase *en route* to the cold window to the 16-electron compound [$CpMo(CO)_2(\eta^1\text{-}C_3H_5)$], with which it then co-exists in equilibrium. This finding is therefore at odds with an assignment of one of the doublets to a 16-electron compound of Mo or W, and accordingly the real origin of the extra bands has still to be unravelled.

One possible explanation for the observation of a multiplet instead of a single band is so-called "matrix splitting" caused by the residence of trapped species in different matrix sites.[5] However, the doublet splitting observed for **2** isolated in an argon matrix would be rather large (8 and 16 cm^{-1}), and the possibility of matrix splitting can be more or less excluded by the results of experiments with different matrices, for example Kr, CH_4 and CO, in which **2** continued to show two ν(CO) doublets of roughly equal intensity. Changing the matrix normally alters or eliminates any splitting that depends on the character of the solid host. Therefore the two doublets must belong to different dicarbonyl isomers, both bearing η^3-bonded allyl ligands. These are designated **2′** and **2′′** in the following text.

Table 1. IR spectrum of a solid Ar matrix doped with [$CpMo(CO)_2(\eta^3\text{-}C_3H_5)$] (**2**) at ca. 10 K in the region 2400−650 cm^{-1}

Wavenumber (cm^{-1})	likely assignment
1974	ν(CO)/**2′′**
1966	ν(CO)/**2′**
1907	ν(CO)/**2′′**
1891	ν(CO)/**2′**
1490	$\delta(CH_2)_{as}$/allyl
1462	$\delta(CH_2)_s$/allyl
1432	ν(CC)/Cp
1422	ν(CC)/Cp
1228	π(CH)/allyl
1015	β(CH)/Cp
1011	β(CH)/Cp
889	$\rho_w(CH_2)_s$/allyl
885	α(CH)/Cp
808	γ(CH)/Cp
803	γ(CH)/Cp
745	?

Dynamic Behaviour of 2 in Solution

High- and low-temperature NMR studies had suggested previously[6] that **2** enters into a conformational equilibrium in solution. There are two conformers, which can be interconverted by *formal* rotation of the η^3-allyl group [**2A** (allyl rotation angle θ = 180°) and **2B** (θ = 0°) in Figure 3]. Apart from a simple rotation of the allyl group, there are in general four possible mechanisms that might explain the dynamic behaviour of allyl groups bound to metal centres:[6−9]

(i) The olefin rotation mechanism involves an intermediate with the C^1 and C^2 atoms of the allyl group remaining bonded to the metal while rotation proceeds around the C^2-C^3 axis.

(ii) Alternatively, the C^1 and C^3 atoms in the intermediate can remain coordinated while C^2 flips from one side to the other.

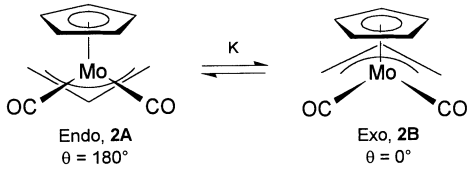

Figure 3. Conformational isomers of [$CpMo(CO)_2(\eta^3\text{-}C_3H_5)$] (**2**) in solution and their allyl rotation angle θ relative to the carbonyl ligands

(iii) In the π-σ-π mechanism, the intermediate contains an η^1-bonded allyl group which can freely rotate around the C^1-C^2 axis.
(iv) There is also the possibility that the isomers are interconverted by a kind of pseudorotation reflecting the non-rigidity of the parent ligand-metal framework.

Mechanism (iii) is commonly accepted to operate, for instance, for compounds of the type [CpMoI(NO)(η^3-C_3H_5)],[10,11] while NMR spectroscopic investigations[6] led Faller et al. to propose mechanism (iv) for **2**. The ^{1}H NMR spectra of the two individual conformers of **2** (in solution in [D_6]benzene) can be observed independently as broad signals at ambient temperatures, the relative intensities of the signals implying an equilibrium constant *K* of 3.0 at 5 °C. The two sets of resonances coalesce at 86 °C. Whatever mechanism is responsible for the isomerisation, the change is slow on the NMR timescale, with an activation barrier estimated to be 51.5 kJ/mol.[6] Compound **2** crystallises from solution with the η^3-allyl ligand in the preferred *exo* conformation (isomer **2B**).[10] Thus, the *endo*-*exo* equilibrium adjusts the solution concentrations as the *exo*-form crystallises. It follows that evaporation of the solvent affords only the *exo* conformer **2B**. Previous reports of the IR spectrum of **2** in solution referred to the presence of two doublets in the ν(CO) region,[12] and these too have been rationalised on the assumption of a conformational equilibrium between **2A** and **2B**.[13,14]

Isomerism of 2 in Low Temperature Matrices and Quantum Mechanical Calculations

Bearing all these findings in mind, it is tempting to identify the species **2′** and **2′′** observed after quenching the vapour of **2** with a large excess of matrix gas at 10 K with the two conformers **2B** and **2A**, respectively. According to the NMR results for solutions, **2A** and **2B** must then be present in the gas phase. To test this conclusion, further experiments were performed.

Rest et al. have reported that the three species present after photolysis of matrices containing [CpW(CO)$_3$(η^1-C_3H_5)] (see Figure 1) are all interconvertible, so that, for instance, the photolysis of the W(CO)$_2$ compounds regenerated the W(CO)$_3$ compound.[4,15] When **2** was isolated in a solid carbon monoxide matrix, however, it could not be converted into **1** either by photolysis with light of various wavelengths or by annealing, indicating that the η^3-allyl ligand is resistant to changing the mode of its ligation {unlike the one in [Co(CO)$_3$(η^3-C_3H_5)], which reacts to give [Co(CO)$_4$(η^1-C_3H_5)] in the presence of CO on photolysis}.[15b] On the other hand, compound **1** could be converted quantitatively into **2** in a carbon monoxide matrix by photolysis with broad-band UV light for 1 h. The CO ejection thus seems to be followed by a very rapid, irreversible η^1-η^3 ligation change, as suggested previously for [Re(CO)$_5$(η^1-C_7H_7)].[15d]

In all the matrices studied, the proportions of **2′** and **2′′** could be varied by broad-band UV photolysis, the ν(CO) bands at 1966 and 1891 cm^{-1} belonging to **2′** increasing at the expense of those at 1974 and 1907 cm^{-1} belonging to **2′′**.

These results may be summarised as follows: UV photolysis of **1** isolated in an Ar matrix results in the loss of one CO ligand, possibly to produce first the 16-electron product [CpMo(CO)$_2$(η^1-C_3H_5)] **2C** (see Figure 4), which is not observed since it isomerises rapidly to give the two (η^3-C_3H_5)Mo conformers **2′** and **2′′** in almost equal proportions. The two different sets of ν(CO) bands characterising **2′** and **2′′** are also observed, again with roughly equal intensity, after quenching the vapour of **2** initially at room temperature with a large excess of matrix gas at 10 K. Compounds **2′** and **2′′** must therefore also be present in the vapour of **2**.

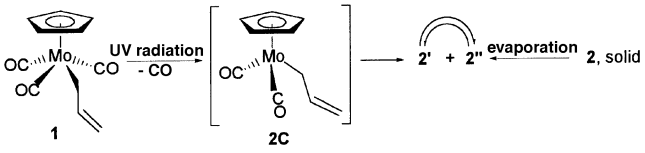

Figure 4. Proposed mechanism for the photochemistry of **1** in low temperature matrices

If energy is conveyed to such a matrix in the form of UV light (photolysis), isomer interconversion proceeds and the proportions of the two forms change in favour of what seems to be the more stable species **2′**. It has to be emphasised at this stage that the rigidity of the solid matrices at 10 K does not allow the system to reach the equilibrium state that might be anticipated for this temperature. If a π-σ-π mechanism was in operation, it would involve an intermediate **2C**. On photo-inducement of the isomerisation, however, even in the presence of an excess of CO, such an intermediate **2C** cannot revert to **1**, since the experimental results show that this is highly photolabile. The experimental results are unable therefore to argue for or against such a mechanism. On the other hand, it is possible that photoexcitation raises an electron from the low-lying HOMO (the Mo-allyl π-bonding orbital[16]) to the LUMO (the Mo-allyl π-antibonding orbital[16]). This would weaken the Mo-allyl π-bond, while the σ bond remains intact, and the allyl ligand would then be able to rotate more freely, whereas the barrier to this change is too large to be overcome by modest thermal activation of the electronic ground state.[17] A photo-isomerisation process, which has been observed previously for matrix-isolated metal *carbene* complexes,[18] is similar to the one found for **2** in that occupation of an antibonding orbital in the photo-excited state there allows free rotation around a bond, which is a rigid multiple bond in the ground state.

There is no reason therefore to question the identification of **2′** and **2′′** with **2B** and **2A**, respectively, and in order to obtain more information about these species, we set out to calculate their structures on the basis of density functional theory (B3LYP/SDD). The optimised geometries are shown

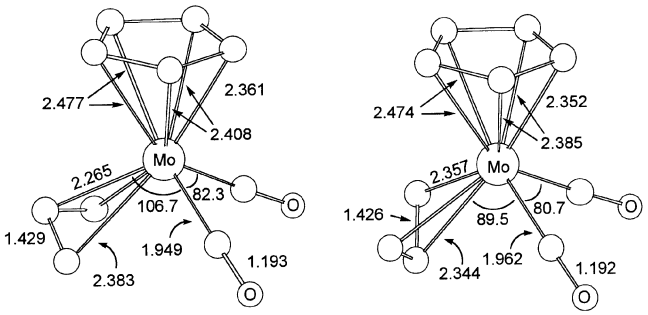

Figure 5. Structures of **2A** and **2B** as optimized by DFT calculations (B3LYP/SDD); for comparison, selected bond lengths and angles found[10] in the crystal structure of **2B** are: Mo−C_{meso} 2.236(4), Mo−C_t 2.359, Mo−CO 1.951(3), Mo−C_{Cp} 2.321(4)-2.348(6) Å; OC−Mo−CO 82.5(2), OC−Mo−C_{meso} 105.0(1)°

in Figure 5, which thus provides for the first time structural information about the *endo* conformer **2A**. The results obtained for the *exo* conformer **2B** can on the other hand be compared directly with the solid state structure.[10] As can be seen, the deviations are not unreasonable considering that theory predicts the geometry of the molecule in the gas phase, while intermolecular interactions and packing forces influence the solid state structure. Regarding the vibrational frequencies calculated for the two species, it turns out that **2B**, which had been found to be more stable in solution,[6] is indeed predicted to show a ν(CO) doublet at lower frequencies as compared with the corresponding features of **2A**. This matches the finding that the low frequency doublet observed in the matrix experiments also belongs to the more stable species **2′**. The calculations also indicate that the IR intensities of the ν(CO) modes of **2A** are very similar to those of **2B**.

It should be noted, though, that according to the NMR measurements we performed with CD_2Cl_2 as the solvent the ratio **2B/2A** (i.e. *K* in Figure 3) amounts to ca. 3.3:1 (in line with the value of $K = 3.0$ derived from previous results for a benzene solution at 5 °C[6]). At first sight, this might appear to clash with the almost equal proportions of **2′** and **2′′** implied by the nearly equal intensity of the two sets of carbonyl bands observed in the IR spectrum of **2** after matrix isolation of its vapour (see Figure 2d). Such a 1:1 intensity ratio has previously been reported for the IR spectrum of **2** in cyclohexane solution,[12−14] with the inference (based on the assumption of very similar extinction coefficients) that the equilibrium constant *K* is close to 1 at room temperature.[14] The rather large differences between *K* as deduced from the ν(CO) bands in the IR and *K* as deduced from the ^{1}H NMR spectrum were ascribed to solvent effects,[14] since different solvents had been used for the two sets of measurements [the splitting of the ν(CO) bands can be resolved only for solutions in non-polar solvents]. In order to check this explanation, we recorded a ^{1}H NMR spectrum of **2** in [D_{12}]cyclohexane solution and so concluded that $K = 1.7$ and not 1.0 at 15 °C! Careful reinvestigation of the IR spectrum of **2** in cyclohexane and pentane solutions then revealed that the *exo* bands (unlike those in the matrix spectra) are much broader than the *endo* bands (see Figure 6), and *integration* of the band areas (as opposed to

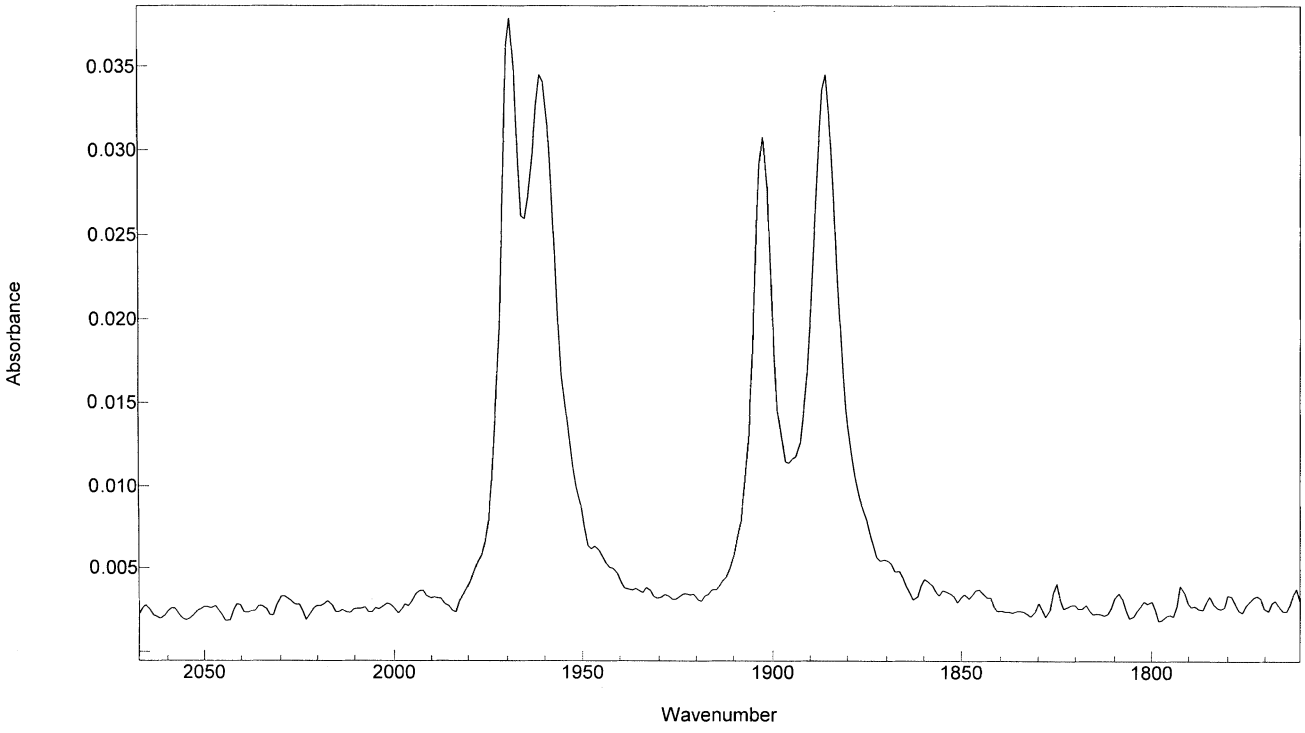

Figure 6. The IR spectrum of a pentane solution of **2** at room temperature (2 cm^{-1} resolution)

simple absorbance measurements) does indeed give a value of K close to 1.7.

In conclusion, the observation of a 1:1 intensity ratio for the bands belonging to **2′** and **2′′** (which will be referred to as **2B** and **2A** from now on) after vapour deposition of **2** in a solid matrix at low temperature indicates that the conformers have almost equal energies in the absence of any solvent, but differ quite significantly in energy when dissolved in a polar solvent like CD_2Cl_2. As the polarity of the supporting medium decreases, so the energy difference ΔE(**2A**−**2B**) decreases, until with the vapour at ambient temperatures it becomes so small that the thermal populations of the two forms are almost equal.[19] These conclusions are well supported by the results of the DFT calculations (B3LYP/SDD). For the optimum geometries depicted in Figure 5, which of course represent gas phase structures, ΔE(**2A**−**2B**) was calculated to amount to only 1.4 kJ mol^{-1}. Furthermore, the calculations indicate that **2B** is more polar (5.08 D) than **2A** (4.34 D), so that **2B** is inevitably favoured by a polar solvent environment.

In summary, there would seem to be little doubt that **2′** and **2′′** are the conformers **2B** and **2A**, respectively. In the light of these findings and those of Bitterwolf et al.,[17] it is very likely that Rest et al. were mistaken in their interpretation of the matrix photochemistry of the analogous tungsten system, which probably merits reinvestigation. Furthermore, we have shown: (i) that the different polarities of the *endo* and *exo* conformers cause the position of the equilibrium between them to be a sensitive function of solvation, and (ii) that the conformers can be interconverted by photoexcitation.

Experimental Section

Matrix samples were formed on a CsI window held at ca. 10 K with the aid of an Air Products CS 202 Displex unit (a two-stage, closed cycle helium refrigerator) enclosed by an evacuated shroud, or alternatively by the use of a liquid helium cryostat. The temperature of the window could be varied continuously between ca. 10 and 150 K by means of a resistive heating wire wound around the cold stage of the Displex refrigerator. Temperatures were measured with a chromel vs. iron-doped gold thermocouple or with a hydrogen vapour bulb. The matrix carrier gases used were Ar, N_2, Kr and CO (B.O.C., Research grade). Samples (held at 0 °C) were deposited continuously, typically over a period of 2 hours, the rate of deposition of the material to be isolated being regulated by its own low volatility. Photolysis experiments made use of an Oriel 500-W medium pressure mercury arc. A water filter was employed to minimise the intensity of IR radiation incident upon the matrix during photolysis. In addition, absorption or Balzer's interference filters provided the means of selecting photolysis radiation confined to a predetermined range of wavelengths.

$[CpMo(CO)_2(\eta^3\text{-}C_3H_5)]$ and $[CpMo(CO)_3(\eta^1\text{-}C_3H_5)]$ were prepared according to literature procedures.[3] IR spectra were recorded with a Bruker IFS 66 FTIR spectrometer. ^{1}H and ^{13}C NMR spectra of solutions were recorded using a Bruker AC 200 instrument operating at 200 MHz (^{1}H).

Density Functional Theory calculations were carried out with the Gaussian/DFT series of programs.[20] The B3LYP formulation of density functional theory was used employing the basis set SDD.[20] Harmonic vibrational frequencies and infrared intensities were predicted at these levels by numerical second derivatives using analytically calculated first derivatives.

Acknowledgments

We are grateful to the *Deutsche Forschungsgemeinschaft*, the *Fonds der Chemischen Industrie*, the *Otto-Röhm-Gedächtnisstiftung* and the *Karl-Winnacker-Stiftung* for financial support in the form of a Heisenberg-Stipendium (C.L.) and other funding, and to the EPSRC for the funding of a Research Assistantship (T.M.G.) and of cryogenic and spectroscopic equipment.

[1] B. J. Brisdon, D. W. Brown, C. R. Willis, *Polyhedron* **1986**, *5*, 439−443; B. M. Trost, M. Lautens, *J. Am. Chem. Soc.* **1982**, *104*, 5543−5545; R. H. Yu, J. S. McCallum, L. S. Liebeskind, *Organometallics* **1994**, *13*, 1476−1486, and references cited therein.

[2] R. K. Grasselli, J. D. Burrington, *Adv. Catal.* **1981**, *30*, 133−163; G. W. Keulks, L. D. Krenzke, T. M. Notermann, *Adv. Catal.* **1978**, *27*, 183−225; R. K. Grasselli, J. D. Burrington, *Ind. Engl. Chem. Prod. Res. Dev.* **1984**, *23*, 393−404.

[3] M. Cousins, M. L. H. Green, *J. Chem. Soc.* **1963**, 889−894.

[4] R. B. Hitam, K. A. Mahmoud, A. J. Rest, *J. Organomet. Chem.* **1985**, *291*, 321−333.

[5] H. Schnöckel, S. Schunck, *Chemie in unserer Zeit* **1987**, *21*, 73−81; M. J. Almond, A. J. Downs, *Spectroscopy of Matrix Isolated Species* (Eds.: R. J. H. Clark, R. E. Hester), *Advances in Spectroscopy*, Vol. 17, Wiley, Chichester, **1989**; I. R. Dunkin, *Matrix-Isolation Techniques: A Practical Approach*, Oxford Press, New York, **1998**.

[6] J. W. Faller, M. J. Incorvia, *Inorg. Chem.* **1968**, *7*, 840−842.

[7] R. B. Jordan, *Mechanismen anorganischer und metallorganischer Reaktionen* (Eds.: C. Elschenbroich, F. Hensel, H. Hopf), Teubner, Stuttgart, **1994**, p. 118.

[8] B. E. Mann, *Comprehensive Organometallic Chemistry* (Eds.: G. Wilkinson, F. G. A. Stone, E. W. Abel), Pergamon Press, Oxford, **1982**, Vol. 3, p. 89.

[9] F. P. Pruchnik, *Organometallic Chemistry of the Transition Elements*, Plenum Press, New York, **1990**, p. 444.

[10] J. W. Faller, D. F. Chodosh, D. Katahira, *J. Organomet. Chem.* **1980**, *187*, 227−231.

[11] J. W. Faller, Y. Shvo, K. Chao, H. H. Murray, *J. Organomet. Chem.* **1982**, *226*, 251−275.

[12] R. B. King, *Inorg. Chem.* **1966**, *5*, 2242−2243.

[13] A. Davison, W. C. Rode, *Inorg. Chem.* **1967**, *6*, 2124−2125.

[14] J. W. Faller, Chin-Chun Chen, M. J. Mattina, A. Jakubowski, *J. Organomet. Chem.* **1973**, *52*, 361−386.

[15] There is a lot of literature available where evidence has been provided that η^n-(polyene)$M(CO)_m$ complexes can be converted photolytically into η^{n+2}-(polyene)$M(CO)_{m-1}$ compounds (plus free CO) and also for the reverse type of reactivity. See for instance: [15a] R. B. Hitam, K. A. Mahmoud, A. J. Rest, *Coord. Chem. Rev.* **1984**, *55*, 1−29. − [15b] A. J. Rest, D. J. Taylor, *J. Chem. Soc., Dalton Trans.* **1983**, 1291−1298. − [15c] O. Crichton, A. J. Rest, D. J. Taylor, *J. Chem. Soc., Dalton Trans.* **1980**, 167−173. − [15d] A. K. Campen, R. Narayanaswamy, A. J. Rest, *J. Chem. Soc., Dalton Trans.* **1990**, 823−832.

[16] B. E. R. Schilling, R. Hoffmann, J. W. Faller, *J. Am. Chem. Soc.* **1979**, *101*, 592−598; B. E. R. Schilling, R. Hoffmann, D. L. Lichtenberger, *J. Am. Chem. Soc.* **1979**, *101*, 585−591; R. W. Fish, W. P. Giering, D. Marten, M. Rosenblum, *J. Organomet. Chem.* **1976**, *105*, 101−118.

[17] T. E. Bitterwolf, J. T. Bays, B. Scallorn, C. A. Weiss, M. W. George, I. G. Virrels, J. C. Linehan, C. R. Yonker, *Eur. J. Inorg. Chem.* **2001**, 2619−2624, following paper.
[18] P. C. Servaas, D. J. Stufkens, A. Oskam, *J. Organomet. Chem.* **1990**, *390*, 61−71.
[19] Bearing in mind the shortness of the time the molecules of **2** spend in the gas phase after vaporisation from the solid until they are frozen out in Ar, we are bound to draw the following conclusions about the solid sample. If it consisted solely of **2B**, as suggested by a single crystal X-ray analysis after recrystallisation of **2** from organic solvents, and if moreover the isomerisation barrier between **2A** and **2B** really amounted to 51.5 $kJmol^{-1}$ as determined in benzene solution, the time the molecules would require to reach thermal equilibrium of the two forms would certainly be much longer than the time actually available to them. This means either that the isomerisation barrier almost vanishes in the gas phase or — more likely — that the solid, having been collected in the vessel by condensation of gaseous **2**, already contained both isomers in almost equal proportions. The second possibility is difficult to prove, however, since it has not been possible to resolve the distinct carbonyl bands of the two isomers in the vibrational spectra of solid samples.
[20] Gaussian 98, Revision A.6, M. J. Frisch, G. W. Trucks, H. B. Schlegel, G. E. Scuseria, M. A. Robb, J. R. Cheeseman, V. G. Zakrzewski, J. A. Montgomery, Jr., R. E. Stratmann, J. C. Burant, S. Dapprich, J. M. Millam, A. D. Daniels, K. N. Kudin, M. C. Strain, O. Farkas, J. Tomasi, V. Barone, M. Cossi, R. Cammi, B. Mennucci, C. Pomelli, C. Adamo, S. Clifford, J. Ochterski, G. A. Petersson, P. Y. Ayala, Q. Cui, K. Morokuma, D. K. Malick, A. D. Rabuck, K. Raghavachari, J. B. Foresman, J. Cioslowski, J. V. Ortiz, B. B. Stefanov, G. Liu, A. Liashenko, P. Piskorz, I. Komaromi, R. Gomperts, R. L. Martin, D. J. Fox, T. Keith, M. A. Al-Laham, C. Y. Peng, A. Nanayakkara, C. Gonzalez, M. Challacombe, P. M. W. Gill, B. Johnson, W. Chen, M. W. Wong, J. L. Andres, M. Head-Gordon, E. S. Replogle, and J. A. Pople, Gaussian, Inc., Pittsburgh PA, **1998**.

Received February 14, 2001
[I01051]

Organic Matrix and Solution Photochemical Studies of (Allyl)dicarbonyl(cyclopentadienyl)molybdenum Compounds

Thomas E. Bitterwolf,*[a] J. Timothy Bays,[a] Bruce Scallorn,[a] Callie Ann Weiss,[a] Michael W. George,[b] Ian G. Virrels,[b] John C. Linehan,[c] and Clement R. Yonker[c]

Keywords: Photochemistry / Matrix isolation / Molybdenum / Allyl ligands

Photolysis of fresh samples of the η^3-allyl compounds $[(\eta^5\text{-}C_5H_5)Mo(CO)_2(\eta^3\text{-}C_3H_5)]$ or $[(\eta^5\text{-}C_5H_5)Mo(CO)_2(\eta^3\text{-}C_3H_4CH_3)]$ in a Nujol matrix at ca. 90 K at a wavelength greater than 400 nm was found by IR spectroscopy to cause conversion of the *endo* rotamer to the *exo* rotamer. Photolysis of *exo* enriched samples of $[(\eta^5\text{-}C_5H_5)Mo(CO)_2(\eta^3\text{-}C_3H_5)]$ at wavelengths of between 360 and 400 nm reversed the photoconversion leading to an *exo* to *endo* conversion. At higher energies photochemical CO loss was also observed. In the case of the 2-methylallyl derivative, a photoproduct believed to be $[(\eta^5\text{-}C_5H_5)Mo(H)(CO)(\eta^4\text{-}C_4H_6)]$ was observed along with CO loss. Time-resolved IR studies of the flash photolysis of $[(\eta^5\text{-}C_5H_5)Mo(CO)_2(\eta^3\text{-}C_3H_5)]$ in *n*-heptane confirm both *endo* to *exo* rotamer conversion and CO loss. Under these conditions, the species formed after CO loss is probably $[(\eta^5\text{-}C_5H_5)Mo(CO)(n\text{-heptane})(\eta^3\text{-}C_3H_5)]$. When $[(\eta^5\text{-}C_5H_5)Mo(CO)_2(\eta^3\text{-}C_3H_5)]$ was dissolved in supercritical ethylene and photolyzed, $[(\eta^5\text{-}C_5H_5)Mo(CO)(C_2H_4)(\eta^3\text{-}C_3H_5)]$ was formed. A mechanism involving two distinct excited states is proposed to account for the photoreversible *endo*/*exo* transformations.

Introduction

In 1963 Cousins and Green[1] reported the synthesis of $[(\eta^5\text{-}C_5H_5)Mo(CO)_3(\eta^1\text{-}C_3H_5)]$ (**1**) and $[(\eta^5\text{-}C_5H_5)Mo(CO)_2(\eta^3\text{-}C_3H_5)]$ (**2**) by reaction of $[(\eta^5\text{-}C_5H_5)Mo(CO)_3]^-$ with allyl chloride. Compound **2** could also be efficiently formed from **1** by photolysis with ultraviolet radiation. Several years after the initial discovery, King noted that **2** appeared to exist in solution as two species.[2] Davidson,[3] Faller[4] and their co-workers correctly established the structures of the two conformers to be the *endo* and *exo* rotamers shown in Figure 1 with an *exo*/*endo* ratio of 3:1 in benzene. Introduction of a methyl group into the 2-position on the allyl group in **3** reverses the orientational preference so that the *endo* rotamer becomes strongly favored. Curiously absent in this early literature were comments concerning thermal or photochemical substitution of the carbonyl groups in **2** or **3**.

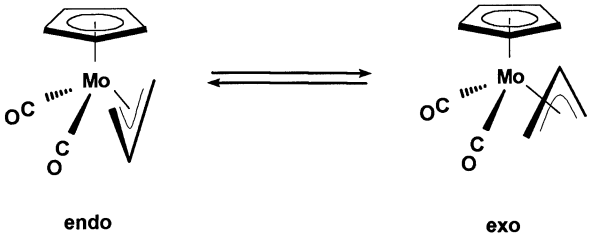

Figure 1. *endo*/*exo* equilibrium of $[(\eta^5\text{-}C_5H_5)Mo(CO)_2(\eta^3\text{-}C_3H_5)]$

[a] Department of Chemistry, University of Idaho
Moscow, ID 83844-2343, USA
E-mail: bitterte@uidaho.edu
[b] Department of Chemistry, University of Nottingham
Nottingham NG7 2RD, UK
[c] Chemical Sciences Department, Pacific Northwest National Laboratory,
P. O. Box 999, Richland, WA 99352, USA

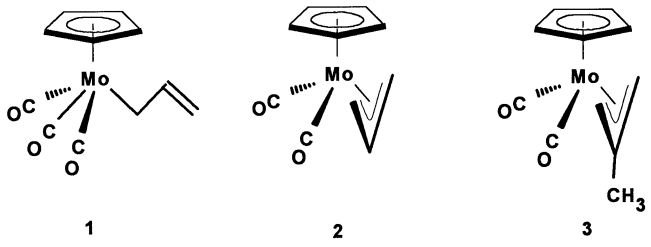

As part of our ongoing studies on the photochemistry of organometallic compounds, we have examined the photolysis of **1**, **2**, and **3** in Nujol and 2-methyltetrahydrofuran (MeTHF) glass matrices at 90 K. These studies have revealed a previously unknown photochemically driven rotation of the η^3-allyl group, as well as other haptotropic transformations. Time-resolved IR studies and photochemical reactions in supercritical ethylene have been carried out to provide additional evidence for the observed intermediates. We have previously reported Nujol matrix studies of molybdenum and chromium compounds in which a pendant η^3-cyclopentenyl ring was attached to the cyclopentadienyl ring.[5] A brief study of the photochemistry of the tungsten analog of **1** in a methane matrix has been reported by Rest.[6] The results of the present study along with those of Limberg et al.[7] on the photolysis of **1** in a frozen argon matrix reported in this issue, shed new light on the interpretation of the earlier spectroscopic data.

Results and Discussion

Organic Matrix Photochemistry

Compounds **1, 2** and **3** were prepared by standard literature procedures.[8] Nujol matrix studies were carried out us-

 © WILEY-VCH Verlag GmbH, 69451 Weinheim, 2001 1434−1948/01/1010−2619 $ 17.50+.50/0

ing a cryostat developed by Rest and procedures as previously described.[9] MeTHF glass matrix studies were carried out using a Specac Model 21525 Variable Temperature Cell.

The electronic spectrum of **2** has a strong absorption band below 290 nm that is probably associated with a metal-to-ligand charge-transfer band. A medium intensity band is observed at 345 nm with a shoulder at about 400 nm. At high concentrations of **2**, a tail of these visible bands can be seen to extend as high as 600 nm.

A Nujol solution of **2** was frozen to ca. 90 K and the IR spectrum recorded as shown in Figure 2a. IR data for all compounds are presented in Table 1. IR bands for both the *endo* (1964 and 1896 cm^{-1}) and *exo* (1955 and 1879 cm^{-1}) rotamers were found to be in an approximate 1:2 ratio. Photolysis of fresh samples at a wavelength greater than 360 nm was found by difference IR spectra to result in depletion of the *endo* rotamer bands and growth of the *exo* rotamer bands (Figure 2b). No other photochemical products were observed for photolysis at wavelengths greater than 400 nm even upon extended photolysis. When the *exo*-enriched samples formed at $\lambda_{irr} > 400$ nm were photolyzed at a wavelength between 360 and 400 nm, we were surprised to find a reversal of the photoisomerization, with conversion of the *exo* form to the *endo* form (Figure 2c). Photolysis of a fresh sample of **2** ($\lambda_{irr} = 360 \pm 10$ nm) for 3 h (Figure 2d) showed *endo* depletion and *exo* growth, and, in addition, produced a small band at 2132 cm^{-1} and a broad feature at 1843 cm^{-1}. The sample was annealed to ca. 153 K and then returned to ca. 77 K to record the IR spectrum. Under these conditions the bands at 2131 and 1843 cm^{-1} decreased while the bands of **2** increased, with the *exo* rotamer being substantially favored over the *endo* rotamer.

To further clarify the photochemical behavior of **2**, the compound was taken up in MeTHF and the solution frozen to 90 K. In this matrix the *exo* rotamer is strongly favored over the *endo* rotamer. The symmetric stretch of the *endo* isomer is detectable only as a slight asymmetry of the higher energy carbonyl stretching band, while the asymmetric *endo* band is observed as a shoulder on the lower energy band (Figure 3a). The carbonyl bands are strongly shifted (21−30 cm^{-1}) to lower energy in MeTHF relative to Nujol. Photolysis ($\lambda_{irr} = 450 \pm 70$ nm) resulted in bleaching of the *endo* rotamer bands at 1943 and 1864 cm^{-1} and growth of the *exo* rotamer bands at 1935 and 1851 cm^{-1} (Figure 3b). This process was reversed when the irradiation energy was increased ($\lambda_{irr} = 400 \pm 70$ nm) (Figure 3c). The small shifts of these band positions in the spectra in Figure 3 are subtraction artifacts. Higher energy photolysis ($330 < \lambda_{irr} < 400$ nm) resulted in the bands of both the *endo* and *exo* rotamers being bleached, with growth of new bands at 2031, 1816, 1789, 1744 and 1600 cm^{-1} (Figure 4a). Back photolysis of this sample ($\lambda_{irr} > 400$ nm) caused the bands at 1744 and 1600 cm^{-1} to decrease simultaneously while the bands at 1816 and 1789 cm^{-1} grew (Figure 4b). The 1789 cm^{-1} band was very weak compared to the 1816 cm^{-1} band. An *endo* to *exo* transformation was also observed upon this irradiation. It should be noted that there was no increase or decrease of the free CO band (2131 cm^{-1}) upon back photolysis.

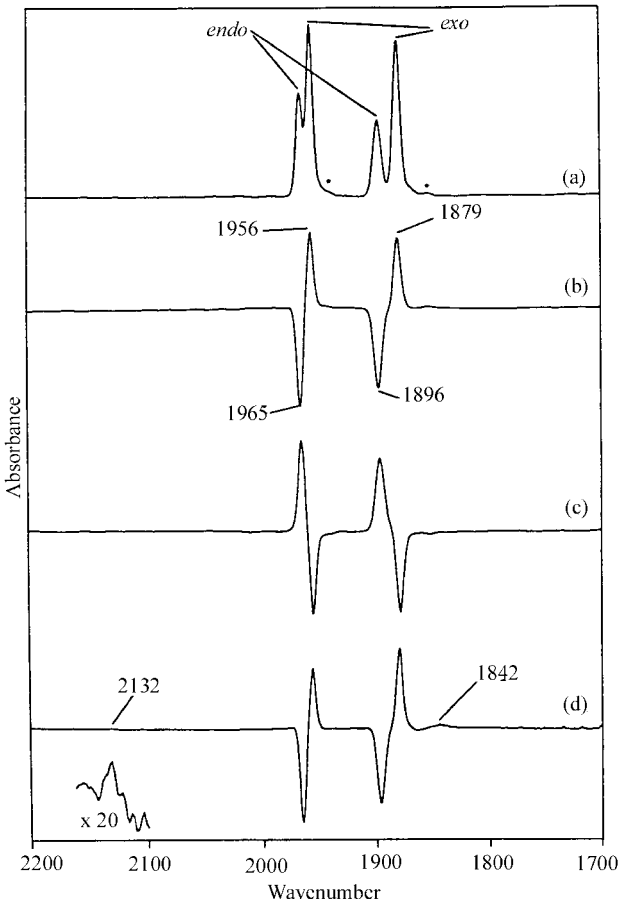

Figure 2. IR spectra of **2** isolated in a Nujol matrix: (a) starting material, ca. 90 K; (b) difference spectrum, 150 min. irradiation ($400 \text{ nm} < \lambda < 470$ nm) minus starting material; (c) difference spectrum, 30 min. irradiation ($360 \text{ nm} < \lambda < 450$ nm) minus 150 min. irradiation ($400 \text{ nm} < \lambda < 470$ nm); (d) difference spectrum, 90 min. irradiation ($350 \text{ nm} < \lambda < 370$ nm) minus starting material; bands marked with an asterisk arise from natural abundance ^{13}CO

Compound **1** is well-known to form **2** upon photolysis. In order to further clarify the photochemical behavior of these allyl complexes, a Nujol solution of **1** contaminated with about 10% **2** was prepared. At ca. 90 K, **1** has three terminal carbonyl stretching bands at 2020, 1942, and 1931 cm^{-1}, as expected for a molecule with C_s symmetry, and a weak band at 1609 cm^{-1} associated with the unbound olefin. After photolysis ($\lambda_{irr} = 500 \pm 70$ nm) for 30 min., an IR difference spectrum demonstrated that **1** is efficiently decarbonylated ("free" CO band at 2132 cm^{-1}) and converted into both rotamers of **2** in approximately equal proportions. It is not possible to establish whether **1** preferentially forms the *endo* isomer, which then undergoes subsequent photoconversion into the *exo* isomer, or whether both *endo* and *exo* isomers are actually formed upon CO loss. Under these conditions there was no evidence for the presumed $[Mo(CO)_2(\eta^1\text{-}C_3H_5)(\eta^5\text{-}C_5H_5)]$ intermediate. Again, these results parallel those observed by Limberg in a frozen Ar matrix.[7]

Table 1. Carbonyl stretching frequencies (cm^{-1}) of allyl derivatives and their photofragments

Species	Nujol R = H, **2**	MeTHF R = H, **2**	Nujol R = CH_3, **3**
endo-[(η^5-C_5H_5)Mo(CO)$_2$(η^3-C_3H_4R)]	1965, 1896	1941, 1864	1960, 1888
exo-[(η^5-C_5H_5)Mo(CO)$_2$(η^3-C_3H_4R)]	1956, 1879	1935, 1850	1955, 1878
[(η^5-C_5H_5)Mo(CO)(η^3-C_3H_5)]	1842		
[(η^5-C_5H_5)Mo(CO)(MeTHF)(η^3-C_3H_5)][a]		1816	
[(η^5-C_5H_5)Mo(CO)(MeTHF)(η^3-C_3H_5)][b]		1789	
[(η^5-C_5H_5)Mo(CO)(MeTHF)$_2$(η^1-C_3H_5)][c]		1745	
endo-[(η^5-C_5H_5)Mo(CO)(η^3-C_3H_4R)]			1868
exo-[(η^5-C_5H_5)Mo(CO)(η^3-C_3H_4R)]			1843
[(η^5-C_5H_5)Mo(CO)(H)(η^4-C_4H_6)]			1936

[a] Major rotamer. – [b] Minor rotamer. – [c] Free olefin band at 1600 cm^{-1}.

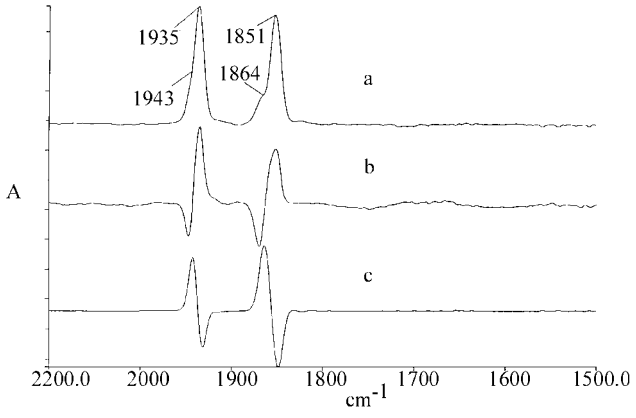

Figure 3. IR spectra of **2** isolated in a 2-methyltetrahydrofuran matrix: (a) starting material, ca. 90 K; (b) difference spectrum, 10 min. irradiation (λ_{irr} = 450 ± 70 nm) minus starting material; (c) difference spectrum, 10 min. irradiation (λ_{irr} = 400 ± 70 nm) minus 10 min. irradiation (λ_{irr} = 450 ± 70 nm); the broad features around 1700 cm^{-1} are due to trace frost buildup on the cell windows

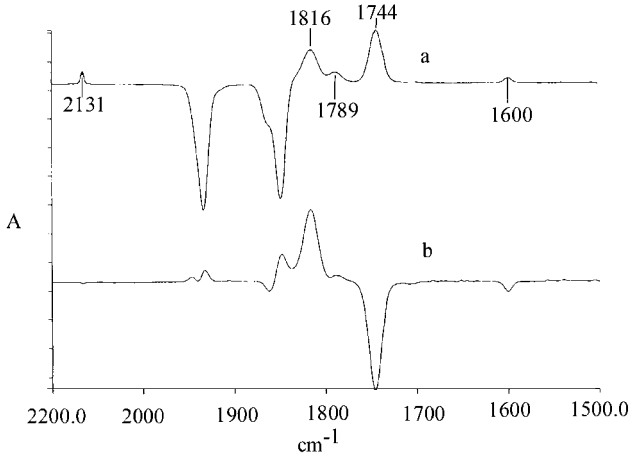

Figure 4. IR spectrum of **2** isolated in a 2-methyltetrahydrofuran matrix: (a) difference spectrum, 10 min. irradiation (330 nm < λ_{irr} < 400 nm) minus 10 min. irradiation (λ_{irr} = 400 α 70 nm); (b) difference spectrum 10 min. irradiation (λ_{irr} > 400 nm) minus 10 min. irradiation (330 nm < λ_{irr} < 400 nm)

Our interpretation of the observed photochemical transformations in Nujol and MeTHF is presented in Scheme 1. As also observed by Limberg in a frozen Ar matrix,[7] the major feature of the photolysis of **2** at longer wavelengths is the photochemical interconversion of the *endo* to the *exo* rotamers. At high energy a species formed by CO loss is observed at 1842 cm^{-1} that we assign as [Mo(CO)(η^3-C_3H_5)(η^5-C_5H_5)].

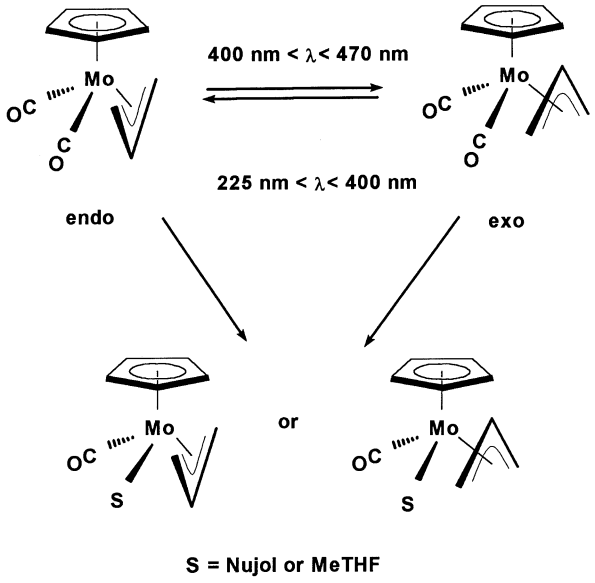

Scheme 1. Proposed photochemical transformations of [(η^5-C_5H_5)Mo(CO)$_2$(η^3-C_3H_5)]

The donor matrix solvent MeTHF has no effect on either the low energy conversion of the *endo* rotamer to the *exo* rotamer, or on the higher energy photochemical reverse of this reaction. There was no evidence for formation of [Mo(CO)$_2$(MeTHF)(η^1-C_3H_5)(η^5-C_5H_5)] under these conditions.

High energy photolysis (λ_{irr} = 330−400 nm) forms three new monocarbonyl species as well as free CO. Back photolysis bleaches the bands at 1744 and 1600 cm^{-1} and causes the bands at 1816 and 1789 cm^{-1} to grow, with no apparent gain or loss of CO. The band at 1600 cm^{-1}, consistent with a dangling η^1-allyl group, and the single, low energy carbonyl band at 1744 cm^{-1} suggest that this species is probably [Mo(CO)(MeTHF)$_2$(η^1-C_3H_5)(η^5-C_5H_5)]. Back photolysis ejects an MeTHF ligand to reform the *exo* and *endo* rotamers of [Mo(CO)(MeTHF)(η^3-C_3H_5)(η^5-C_5H_5)].

The absence of bands that might be attributable to [Mo(CO)$_2$(MeTHF)(η^1-C_3H_5)(η^5-C_5H_5)] makes it impossible to establish whether such a species is an intermediate in the formation of the observed MeTHF complexed photoproducts. The ease with which [Mo(CO)(MeTHF)$_2$(η^1-C_3H_5)(η^5-C_5H_5)] is converted into [Mo(CO)(MeTHF)(η^3-C_3H_5)(η^5-C_5H_5)] suggests that [Mo(CO)$_2$(MeTHF)(η^1-C_3H_5)(η^5-C_5H_5)] might be equally sensitive to photoreversal. Rest and co-workers have reported that [Co(CO)$_3$(η^3-C_3H_5)] undergoes photolysis in a frozen CO matrix to give [Co(CO)$_4$(η^1-C_3H_5)].[10]

Compound **3** exists almost exclusively in the *endo* form at room temperature and in Nujol at 90 K (Figure 5a), with bands at 1961 and 1888 cm^{-1}. Photolysis of **3** at long wavelengths (λ_{irr} = 450 ± 70 nm) results in a decrease of the bands associated with the *endo* rotamer and growth of new bands at 1955 and 1878 cm^{-1} which are assigned to the thermodynamically unfavorable, and previously unobserved, *exo* rotamer (Figure 5b). No bands at 2132 ± 2 cm^{-1} associated with "free" carbon monoxide were observed at these wavelengths. Photolysis of an *exo*-enriched sample (330 nm < λ_{irr} < 470 nm) (Figure 5c) results in depletion of the bands of the *exo* rotamer and growth of bands at 2131, 1961 (*endo*), 1936, 1888 (*endo*), 1866, and 1843 cm^{-1}. Continued photolysis at these wavelengths resulted in depletion of the bands of both the *exo* and *endo* rotamers and growth of the new bands. Further photolysis of this sample at high energy (270 < λ_{irr} < 290 nm) resulted in depletion of the band at 1936 cm^{-1} and those of the *endo* rotamer, and growth of the bands at 2131, 1866 and 1844 cm^{-1}. Careful wavelength-selective photolysis established that the *exo* rotamer was associated with the species with a single band at 1842 cm^{-1}, while the *endo* rotamer was associated with the species having a single band at 1866 cm^{-1}. Both of these new species were converted photochemically into the species with a single band at 1936 cm^{-1}. Upon annealing to ca. 133 K, the bands at 1866 and 1841 cm^{-1} decreased while the bands of the *endo* rotamer and the band at 1936 cm^{-1} grew in.

As found for **2**, long wavelength photolysis of **3** results in conversion of the *endo* rotamer to the *exo* rotamer, while photolysis at higher energy of a sample enriched in the *exo* isomer reforms the *endo* isomer. For **3**, photolysis at slightly higher energy is also found to stimulate carbon monoxide loss with the *endo* rotamer giving rise to a monocarbonyl species with an IR band at 1866 cm^{-1} and the *exo* rotamer producing a similar species with an IR band at 1844 cm^{-1}. Both monocarbonyl species give rise to a third monocarbonyl species with a single band 1936 cm^{-1}. We propose that the species initially formed by CO loss are the *endo* and *exo* isomers of [Mo(CO)(η^5-C_5H_5)(η^3-C_4H_7)] in which the orientation of the allyl group is retained. These species in turn undergo oxidative addition of the electron-deficient molybdenum into a C−H bond of the 2-methyl group to yield a trimethylenemethane ligand. The resulting compound, [Mo(CO)(H)(η^5-C_5H_5)(η^4-C_4H_6)], would be analogous to [Mo(CO)(CH_3)(η^5-C_5Me_5)(η^4-C_4H_6)] for which the carbon monoxide stretching frequency is reported to be 1925 cm^{-1}.[11] We have reported a similar hydride shift in the photolysis of [Mo(CO)$_2${η^5,η^3-$C_5H_4C(CH_3)_2C_5H_6$}] giving a species believed to be [Mo(CO)$_2$(H){η^5,η^4-$C_5H_4C(CH_3)_2C_5H_5$}] with a carbonyl band at 1917 cm^{-1}.[12] These reactions are functionally identical to a beta-hydride transfer such as those observed by Rest for [M(CO)$_3$(C_2H_5)(η^5-C_5H_5)], where M = Mo or W.[13] Upon photolysis both the 16-electron intermediate [M(CO)$_2$(C_2H_5)(η^5-C_5H_5)] and the ethene, hydride species [M(CO)$_2$(H)(η^2-C_2H_4)(η^5-C_5H_5)], were observed. Metal hydride bands are often weak, thus our inability to locate such a band in these spectra is not surprising. A summary of the proposed photochemical transformations for **3** is presented in Scheme 2.

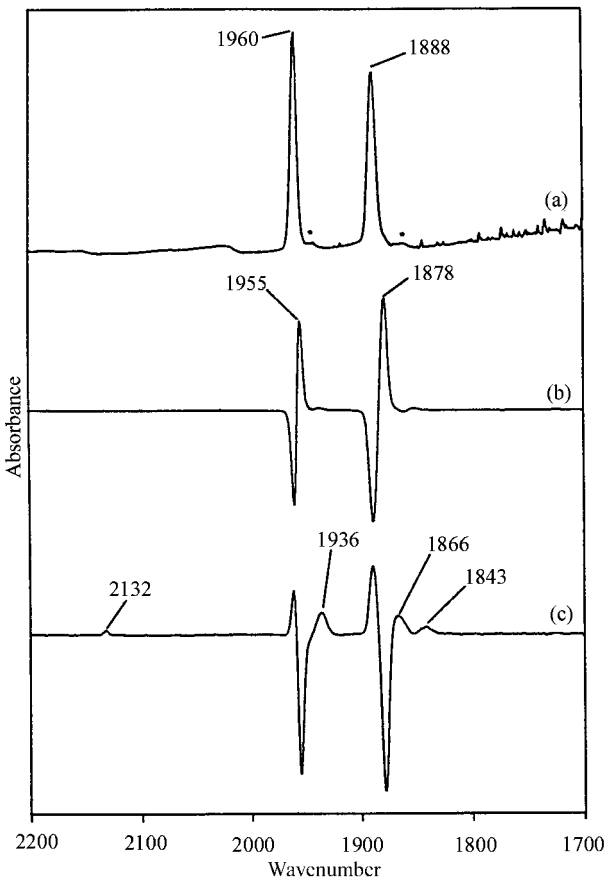

Figure 5. IR spectra of **3** isolated in a Nujol matrix: (a) starting material, ca. 90 K; (b) difference spectrum, 30 min. irradiation (380 nm < λ < 520 nm) minus starting material; (c) difference spectrum, 30 min. irradiation (330 nm < λ < 470 nm) minus 60 min. irradiation (380 nm < λ < 520 nm); the bands marked with an asterisk arise from natural abundance ^{13}CO

Time-Resolved IR Studies

In order to further clarify the intermediates in these processes, time-resolved IR (TRIR) photochemical studies of **2** in *n*-heptane were carried out at room temperature. A 355 nm laser flash was employed to initiate the chemistry. Flash photolysis at this energy results in both CO loss to form the solvated intermediate [(η^5-C_5H_5)Mo(CO)(*n*-heptane)(η^3-C_3H_5)], which has a single IR band at 1851 cm^{-1},

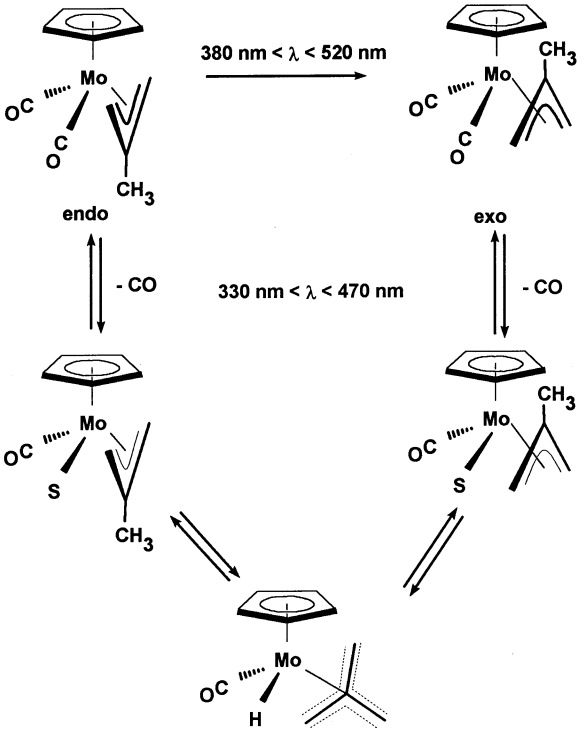

Scheme 2. Proposed photochemical transformations of $[(\eta^5\text{-}C_5H_5)Mo(CO)_2(\eta^3\text{-}C_3H_4CH_3)]$

and *endo* to *exo* photoisomerization. The observed IR band at 1851 cm^{-1} is completely consistent with our observation of the equivalent Nujol-solvated species at 1842 cm^{-1}. The rate of reaction of $[(\eta^5\text{-}C_5H_5)Mo(CO)(n\text{-heptane})(\eta^3\text{-}C_3H_5)]$ with CO was linear with [CO] and a second order rate constant, $k_2 = 1.5 \times 10^7$ $M^{-1}s^{-1}$, was obtained.

Photoisomerization of the *endo* rotamer to the *exo* rotamer under argon was observed. The *exo* species decays, with $k_{obs} = 2 \times 10^5$ s^{-1}, but does not appear to reform the *endo* species. The fate of this species is not clear at this time and additional work will be performed to clarify these observations.

Supercritical Ethene Studies

Compound **2** was found to be soluble in supercritical ethylene at 170 atm. and 40 °C with approximately equal concentrations of the *endo* and *exo* rotamers. Photolysis of this solution with an unfiltered high pressure Hg/Xe lamp (45 min.) resulted in bleaching of the bands associated with **2** and growth of a new band at 1918 cm^{-1}. A small band at 2032 cm^{-1} attributable to free CO was also observed. It is believed that the species being formed in this case is $[(\eta^5\text{-}C_5H_5)Mo(CO)(\eta^2\text{-ethene})(\eta^3\text{-}C_3H_5)]$. No effort was made to recover this compound.

Discussion

An explanation of the photochemistry of **2** and **3** must take into account the observed wavelength dependence of the *endo* to *exo* transformation. It is reasonable to postulate the existence of two distinct photochemical mechanisms, one operating at low energy ($\lambda_{irr} > 400$ nm) and a second at higher energy ($\lambda_{irr} < 400$ nm). The high-energy transformation may have its origins in the same excited state responsible for CO loss.

Molecular orbital analyses of $[(\eta^5\text{-}C_5H_5)Mo(CO)_2(\eta^3\text{-}C_3H_5)]$ have been conducted by Hoffmann[14,15] and Rosenblum[16] and their co-workers. The relevant molecular orbitals are illustrated in Figure 6. The allyl π orbital interacts with the s and p_z orbitals of the metal fragment, while the non-bonding allyl orbital (n) interacts with the a" level. The metal-based orbitals 1a′ and 2a′ are effectively non-bonding and are the highest occupied molecular orbitals, while the LUMO is the antibonding combination of the n allyl orbital and the a" (a" − n). The MO analysis is supported by ultraviolet photoelectron spectral studies,[17] in which the six observed bands were assigned to: I_1 and I_2 (metal d orbitals, 1a′ and 2a′), I_3 (allyl π HOMO, n + a"), I_4 and I_5 (cyclopentadienyl orbitals) and I_6 (second allyl π orbital, π + s + p_z).

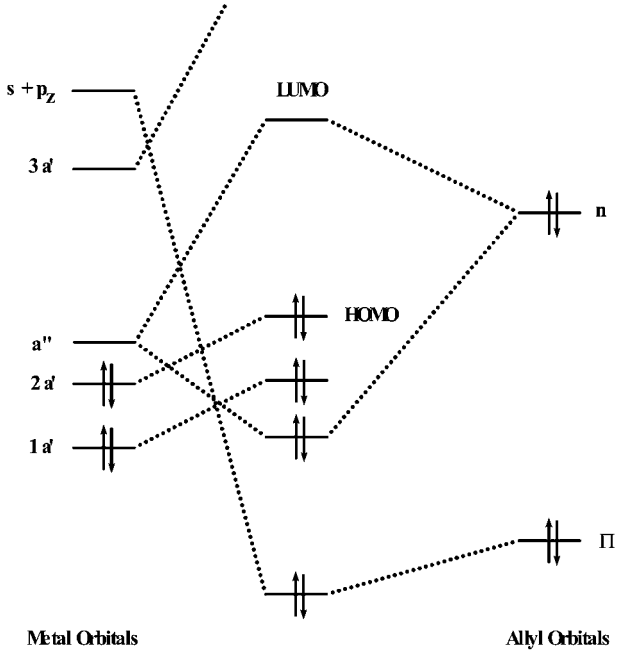

Figure 6. Molecular Orbital diagram for $[(\eta^5\text{-}C_5H_5)Mo(CO)_2(\eta^3\text{-}C_3H_5)]$ based on the previous work of Hoffmann[11,12] and Rosenblum[13]

Hoffmann has argued that *endo* to *exo* exchange observed by NMR spectroscopy should not involve simple rotation of the allyl fragment since such a rotation brings the allyl non-bonding orbitals into an orientation where the bonding with the metal is lost. However, the photochemical promotion of a 1a′ or 2a′ d electron to the LUMO level weakens this interaction permitting rotation about the symmetric allyl π − metal (π + s + p_z) orbital. Such a process is functionally identical to that which results in *cis* to *trans* olefin photoisomerization in organic chemistry. We assign the shoulder at 400 nm to the 1a′, 2a′ → a" − n transition. The band at 345 nm is assigned to the d → d transition (1a′, 2a′ → 3a′), while higher energy bands are assigned to

metal-to-ligand charge transfers. The wavelength selectivity of the filters used in this study are not sufficiently narrow to distinguish with certainty whether the excitations leading to *exo* to *endo* transformations and carbonyl loss are associated with the band at 345 nm or with the tails of the higher energy bands.

The mechanism of the higher energy *exo* to *endo* transformations is not entirely clear. The concurrent appearance of species formed by CO loss indicates that sufficient energy may available for an $\eta^3 \rightarrow \eta^1 \rightarrow \eta^3$ sequence, even though no η^1 species was observed in either Nujol or in the donor solvent MeTHF. We have, however, observed an analogous transformation in the case of $[Mo(CO)_2\{\eta^5,\eta^3\text{-}C_5H_4\text{-}C(CH_3)_2\text{-}C_5H_6\}]$ in which a pendant cyclopentenyl group is connected to the cyclopentadienyl ring by an isopropyl link. Matrix isolation studies have established that low energy photolysis results in an $\eta^3 \rightarrow \eta^1$ opening, and higher energy photolysis results in loss of CO. The comparative ease in stimulating the hapticity change in the case of this pendant allyl is attributed to the relief of strain in the open form.[5]

Our work and that of Limberg et al.[7] require a reinterpretation of the observations reported by Rest et al.[6] on the gas matrix photolysis of $[W(\eta^5\text{-}C_5H_5)(CO)_3(\eta^1\text{-}C_3H_5)]$. These workers observed loss of CO and the appearance of four bands attributable to metal carbonyl species. Continued photolysis resulted in the decrease of one pair of these new bands and growth of the second pair. Reexamination of the reported spectra in light of the present work strongly suggest that the four bands that arise upon photolysis are due to the *endo* and *exo* rotamers of $[W(\eta^5\text{-}C_5H_5)(CO)_2(\eta^3\text{-}C_3H_5)]$, and that the subsequent growth of one pair of these bands at the expense of the second is identical to the behavior of the molybdenum analogue reported herein.

Experimental Section

Compounds **1**, **2**, and **3** were prepared by standard literature procedures.[8]

Nujol matrix studies were carried out using a glass cryostat designed by Dr. A. J. Rest of the University of Southampton (UK). This apparatus and experimental procedures have been described previously.[9] Nujol solutions were prepared by dissolving 1−2 mg of sample in Nujol at room temperature. All samples were centrifuged to remove particulates and eliminate the possibility of having microcrystals in the photolysis sample. MTHF glass matrices were carried out using a Specac Model 21525 variable temperature cell with a sample temperature of ca. 90 K.

Photolyses were carried out at ca. 90 K using a 350 watt high pressure mercury lamp. A water filter was used to remove IR radiation from the beam and optical filters were used to carry out wavelength selective photochemistry. In some cases, the photolyzed sample was annealed to permit the Nujol glass to soften and allow either recombination or rearrangement reactions. The temperature of the sample during the annealing steps was monitored by a thermocouple mounted on the sample cell. All spectra are recorded at 4 cm^{-1} resolution.

Time-resolved IR studies were carried out at the University of Nottingham employing a pulsed Nd:YAG laser (Quanta-Ray GCR-12, ca. 7 ns, 355 nm) to initiate photochemical reactions. A continuous wave IR diode laser (Mütek MDS 1100) was used to monitor the transient IR absorptions. Details of the apparatus and procedures have been reported.[18]

Photolyses in supercritical ethene were conducted using a high pressure cell with diamond IR windows and a sapphire window for photolysis. Photolyses were carried out using a high pressure Hg/Xe lamp.

Acknowledgments

This work was supported by the Research Corporation and the Director, Office of Science, Office of Basic Energy Sciences, Chemical Sciences Division of the U. S. Department of Energy under contract DE-AC0676RLO 1830.

[1] M. Cousins, M. L. H. Green, *J. Chem. Soc.* **1963**, 889−894.
[2] R. B. King, *Inorg. Chem.* **1966**, *5*, 2242−2243.
[3] A. Davidson, W. C. Rode, *Inorg. Chem.* **1967**, *6*, 2124−2125.
[4] [4a] J. W. Faller, M. J. Incorvia, *Inorg. Chem.* **1968**, *7*, 840−842. − [4b] J. W. Faller, A. J. Jakubowski, *J. Organomet. Chem.* **1971**, *31*, C75−C78. − [4c] J. W. Faller, D. F. Chodosh, D. J. Katahira, *J. Organomet. Chem.* **1980**, *187*, 227−231.
[5] T. E. Bitterwolf, A. A. Saygh, J. T. Bays, B. Scallorn, C. Weiss, A. L. Rheingold, L. Liable-Sands, J. E. Shade, *J. Organomet. Chem.* **1999**, *583*, 152−161.
[6] R. B. Hitam, K. A. Mahmoud, A. J. Rest, *J. Organomet. Chem.* **1985**, *291*, 321−333.
[7] C. Limberg, A. J. Downs, T. M. Greene, T. Wistuba, *Eur. J. Inorg. Chem.* **2001**, 2613−2618, preceding paper.
[8] [8a] D. H. Gibson, W.-L. Hsu, D.-S. Lin, *J. Organomet. Chem.* **1979**, *172*, C7−C12. − [8b] R. G. Hayter, *J. Organomet. Chem.* **1968**, *13*, 1−3. − [8c] W. E. Vanarsdale, J. K. Kochi, *J. Organomet. Chem.* **1986**, *317*, 215−232.
[9] T. E. Bitterwolf, K. A. Lott, A. J. Rest, J. Mascetti, *J. Organomet. Chem.* **1991**, *419*, 113−126.
[10] A. J. Rest, D. J. Taylor, *J. Chem. Soc., Dalton Trans.* **1983**, 1291−1298.
[11] C. G. Kreiter, G. Wendt, W. S. Sheldrick, *J. Organomet. Chem.* **1987**, *333*, 47−59.
[12] T. E. Bitterwolf, A. A. Saygh, J. T. Bays, C. A. Weiss, W. B. Scallorn, J. E. Shade, A. L. Rheingold, L. Liable-Sands, *J. Organomet. Chem.* **1999**, *583*, 152−161.
[13] [13a] K. A. Mahmoud, A. J. Rest, H. G. Alt, M. E. Eichner, B. M. Jansen, *J. Chem. Soc., Dalton Trans.* **1984**, 175−186. − [13b] R. J. Kazlauskas, M. S. Wrighton, *J. Am. Chem. Soc.* **1982**, *104*, 6005−6015. − [13c] R. J. Kazlauskas, M. S. Wrighton, *J. Am. Chem. Soc.* **1980**, *102*, 1727−1730.
[14] B. E. R. Schilling, R. Hoffmann, J. W. Faller, *J. Am. Chem. Soc.* **1979**, *101*, 592−598.
[15] B. E. R. Schilling, R. Hoffmann, D. L. Lichtenberger, *J. Am. Chem. Soc.* **1979**, *101*, 585−591.
[16] R. W. Fish, W. P. Giering, D. Marten, M. Rosenblum, *J. Organomet. Chem.* **1976**, *105*, 101−118.
[17] S. D. Worley, D. H. Gibson, W.-L. Hsu, *Inorg. Chem.* **1981**, *20*, 1327−1328.
[18] M. W. George, M. Poliakoff, J. J. Turner, *Analyst* **1994**, 551−560.

Received February 28, 2001
[I01073]

Self-Assembly of Tetranuclear Iron(II) Compounds by a Combination of Rod- and Clamp-Shaped Bridging Units

Volker Jacob,[a] Susanne Mann,[a] Gottfried Huttner,*[a] Olaf Walter,[b] Laszlo Zsolnai,[a] Elisabeth Kaifer,[a] Peter Rutsch,[a] Peter Kircher,[a] and Eckhard Bill[c]

Dedicated to Prof. Marianne Baudler on the occasion of her 80th birthday

Keywords: Self-assembly / Tetranuclear compounds / Iron(II) complexes / *tripod* ligand / Cyanides / Dicyanomethanides

Dicyanomethanides, $[RC(CN)_2]^-$ (**1**$^-$), are bridging ligands with an angular clamp-type shape. In the *tripod*/iron(II) system, [*tripod* = $CH_3C(CH_2PPh_2)_3$], they form binuclear species with three of the clamp-type ligands bridging two iron centers. An appropriate stoichiometric mixture of the *tripod* ligand, iron(II) salts and the dicyanomethanide ligand leads to the exclusive formation of [*tripod*Fe{μ-NC–C(R)–CN}$_3$-Fe*tripod*]$^+$ (**3**$^+$). Altogether, seven constituent groups arrange themselves in this type of aggregate. The process of self-aggregation is distinctly modified by the presence of cyanide ions that may act as linear rod-type bridging ligands. Equimolar mixtures of *tripod*, iron(II) salts, dicyanomethanide ligands and cyanide form tetranuclear aggregates [{*tripod*Fe}$_3$(μ-NC–C(R)–CN}$_3${μ-CN}$_3$FeX]$^+$ (**5**$^+$). In these species, the iron centers form a trigonal-pyramidal arrangement with three octahedrally coordinated *low-spin tripod*iron(II) entities in the basal plane and a tetrahedrally coordinated *high-spin* iron(II) at the apex. The iron centers in the basal plane are connected by μ^2-bridging dicyanomethanide ligands. The apical iron center is coordinated by the N-termini of three cyano ligands, which complete the octahedral coordination of the basal *low-spin* iron(II) centers. The fourth, external ligand X at the tetrahedrally coordinated *high-spin* iron(II) apex can be varied, but in most cases it is found to be a terminally coordinated dicyanomethanide entity. Without counting this variable ligand X, thirteen constituent groups of four different types selectively aggregate to form the cage compounds **5**$^+$. While the dinuclear compounds **3**$^+$ are diamagnetic, the tetranuclear species **5**$^+$ have magnetic moments close to the *spin-only* value of $\mu_{s.o.}$ = 4.9 μ_B, for tetrahedral *high-spin* iron(II). The Mössbauer spectra are in agreement with the description of **5**$^+$ above, which contain three *low-spin tripod*iron(II) entities and one *high-spin* iron(II) center. The synthesis, spectroscopic data, cyclic voltammetric data, Mössbauer data and X-ray analytical data for a series of compounds of types **3**$^+$ and **5**$^+$ are presented in this paper.

Introduction

The templates *tripod*iron(II) [*tripod* = $CH_3C(CH_2PPh_2)_3$] may serve as building blocks for supramolecular aggregates. With dinitriles such as NC−CH=CH−CN, they form tetranuclear cages [(*tripod*Fe)$_4${μ-NC−CH=CH−CN}$_6$-BF_4]$^{7+}$ in which the *tripod*iron(II) entities serve to bind three nitrile functionalities at each corner of an overall tetrahedral cage, which encloses an anion in its cavity.[1] Nitrile functionalities are ideal for engaging in this type of a supramolecular aggregation process, since the binding of RCN ligands to *tripod*iron(II) templates is reversible and flexible.[2] Reversibility of metal−ligand binding is an essential prerequisite for the controlled formation of coordination oligomers.[3−7] Based on the above reasoning, the reactivity of *tripod*iron(II) templates with anionic geminal dinitriles $[RC(CN)_2]^-$ was analyzed. Neutral geminal dinitriles have been found to promote dinuclear aggregation giving [(*tripod*Fe)$_2${μ-NC−X−CN}$_3$]$^{4+}$ [X = $C(CR_2)$, $(CH_2)_2$, $(CH_2)_3$, *o*-C_6H_4].[8] Anionic dinitriles were expected to show stronger metal−ligand-bonding, which might possibly allow for the construction and stability of aggregates of higher nuclearity. A series of dinuclear and tetranuclear aggregates derived from *tripod*iron(II) and $[RC(CN)_2]^-$ is described in this paper.

Results and Discussion

Dinuclear Compounds

The anionic geminal dinitriles **1a**$^-$−**f**$^-$ [9−16] were examined with regard to their propensity to selectively form co-

	R
1a$^-$	-S(O)$_2$CH$_3$
1b$^-$	-C(O)CH$_3$
1c$^-$	-C(O)$_2$CH$_3$
1d$^-$	-CH(CN)$_2$
1e$^-$	-C(O)CN
1f$^-$	-NO

Scheme 1. Dicyanomethanide derived ligands

[a] Anorganisch-Chemisches Institut der Universität Heidelberg
Im Neuenheimer Feld 270, 69120 Heidelberg, Germany
Fax: (internat.) + 49-(0)6221/545707
E-mail: g.huttner@indi.aci.uni-heidelberg.de
[b] Institut für Technische Chemie, Bereich Chemisch-Physikalische Verfahren (ITC-CPV), Forschungszentrum Karlsruhe
P. O. Box 3640, 76021 Karlsruhe, Germany
[c] Max-Planck-Institut für Strahlenchemie,
P. O. Box 101365, 45413 Mülheim/Ruhr, Germany

 © WILEY-VCH Verlag GmbH, 69451 Weinheim, 2001 1434−1948/01/1010−2625 $ 17.50+.50/0

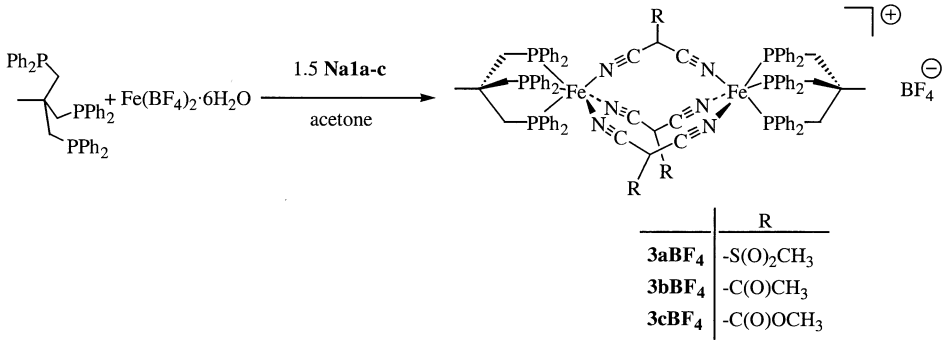

Scheme 2. Synthesis of the dinuclear compounds **3aBF$_4$**, **3bBF$_4$** and **3cBF$_4$**

ordination oligomers with *tripod*iron(II) templates (Scheme 1).

The sodium-salts of **1a**−**c**$^-$ were added to an acetone solution containing equivalent amounts of $Fe^{II}aq(BF_4)_2$ and *tripod*, in a molar ratio of 3:2 [ligand/iron(II) salt] (Scheme 2). The pale yellow solutions immediately turned red on addition of the ligands. Workup by filtration and crystallization yielded the BF_4^- salts of **3a**−**c**$^+$ as red microcrystalline solids.

Elemental analyses and mass spectra agree with the assigned constitution in each case. Coordination of the nitrile groups is evident from the observed pattern of the ν_{CN} vibrations, which are shifted to higher energies relative to the free ligands in each case (Table 2).

^{31}P NMR spectra (Table 1) show the presence of only one type of coordinated phosphorus for **3aBF$_4$**. For **3bBF$_4$**, a complicated pattern of ^{31}P NMR resonances is observed, which has not been analyzed in detail. This pattern does not change its phenotype for the temperature range 203−303 K. A rationale for this observation may be found in the assumption that the $CH_3C(O)$ substituents are not free to rotate. Conjugation within the acetyldicyanomethanido ligands will force these groups to lie within the $C(CN)_2$ planes. For the free ligand this coplanarity is evident by the observation of two ^{13}C NMR signals for the CN carbon atoms (δ = 123.9 and 121.8). One of these signals must be due to a carbon atom on the oxygen side of the acetyl substituent, and the other signal to the nitrile carbon atom at the methyl side. If the acetyl groups are in the same plane as the $C(CN)_2$ ligand entity in the coordination compound as well, and if the symmetry of the $Fe(NCCCN)_3Fe$ core is D_{3h}, there are two possible diastereomers. The statistical probability of the formation of the diastereomer, which has all three CO groups pointing to only one iron atom, is just

Table 1. ^{1}H{^{31}P}-, ^{31}P- and ^{13}C-NMR-spectroscopic data of **3BF$_4$** and **4BF$_4$** (CD_2Cl_2)

	3aBF$_4$	**3bBF$_4$**	**3cBF$_4$**	**3dBF$_4$**	**4BF$_4$**
^{1}H{^{31}P} NMR:					
tripod-CH_3	1.65 s, 6 H	1.67 s, 6 H	1.62 s, 6 H	1.79 s, 6 H	1.60 s, 6 H
tripod-CH_2	2.45 s, 12 H	2.50 s, 12 H	2.42 s, 12 H	2.55 s, 12 H	2.32 s, 12 H
ligand[a]	2.62 s, 9 H	1.52 s, 9 H	3.37 s, 9 H	2.88 s, 3 H	−
CH_{arom}	7.2−7.5 m, 60 H	7.2−7.5 m, 60 H	7.1−7.6 m, 60 H	7.2−7.8 m, 60 H	7.1−7.8 m, 60 H
^{13}C{^{1}H} NMR:					
tripod-CH_2	32.3 m	32.8 m	32.8 m	32.7 m	32.7 m
tripod-C_q	36.5 s	36.7 s	36.6 s	36.8 s	36.6 s
tripod-CH_3	37.4 m	37.6 m	37.5 m	37.0 m	37.6 m
C_{arom}	129.4−133.6	129.2−132.6	129.0−132.6	129−132.5	128.6−132.5
$C_{q,arom}$	134−136 m	134−136 m	134−136 m	135.2 dd	135.5 dd
CN[b]	−[c]	134.9[d] 135.6[d]	134.3[d] 135.0[d]	135.5 s (FeNC)	124.8 s
ligand-C_q [b]	51.7 s	−[c]	39.3 s	25.9 s	−
ligand-C[b]	47.6 s (CH_3)	191.8 s (CO) 27.6 s (CH_3)	168.8 s (COO) 51.0 s (CH_3)	113.8 s (CN) 22.3 s (CH)	−
^{31}P{^{1}H} NMR:					
PPh_2	34.8 s	31.5−39.0 m	35.4 br	38.2 s	38.8 s

[a] The ^{1}H-NMR resonances of the sodium salts of the ligands are found at δ = 2.88 (**Na1a**, [D$_6$]acetone), 1.86 (**Na1b**, [D$_6$]DMSO) and 3.51 (**Na1c**, [D$_6$]acetone). The resonance of H_2TCNE, **H1d** (CD_3NO_2), is found at δ = 5.16. − [b] The ^{13}C-NMR resonances of the sodium salts of the ligands are found at δ = 42.2 (C_q), 46.3 (CH_3) and 120.4 (CN) (**Na1a**, [D$_6$]DMSO); 26.4 (CH_3) , 47.9 (C_q), 123.9 and 121.8 (CN) and 191.0 (CO) (**Na1b**, [D$_6$]DMSO); 32.3 (C_q), 51.0 (CH_3), 123.1 and 122.0 (CN) and 168.8 (COO) (**Na1c**, [D$_6$]acetone); 119.4 s (**Na2**, [D$_6$]DMSO). The resonances of H_2TCNE, **H1d**, (CD_3NO_2) are found at δ = 26.1 (CH) and 109.1 (CN). − [c] Signal not observed. − [d] These signals interfere with signals for aromatic carbons of the *tripod* ligand.

one third of the probability of the formation of the other diastereomer, which has two CO groups pointing in the direction of one iron atom and the remaining CO group arranged in the opposite direction. In the less probable isomer all three phosphorus nuclei at each iron center are equivalent, such that a single resonance would be expected for each of the two chemically different *tripod*iron entities. In the other isomer there are two different types of phosphorus nuclei at each *tripod*iron entity, such that a doublet and a triplet resonance would be expected for each of the two different *tripod*iron entities. PP-COSY spectra show four different types of *tripod*iron entities. Due to the small differences in the chemical shifts (δ = 31.5−39) and the large coupling constants ($^2J_{PP}$ = 60 Hz), the spectrum is more complicated and has not been analyzed completely, but its general appearance is in agreement with the above hypothesis.

The ^{31}P NMR spectrum of **3cBF$_4$** shows one broad unresolved signal only, with no significant change in appearance in the temperature range from 203−303 K. With regard to the orientation of the MeOC(O) substituents relative to the coordination scaffolding, the situation is the same as discussed for **3bBF$_4$**, i.e. at least two diastereomers are expected. The coplanarity of the C(O)OR substituent with the $C(CN)_2$ part of the ligand is again evident for the free ligand from its ^{13}C NMR spectrum, which shows two different signals for the nitrile carbon atoms (δ = 123.1 and 122.0). However, in comparison with the situation in **3bBF$_4$**, the electronic differentiation between the two sides of the substituents is smaller for the methoxycarbonyl group than for the acetyl substituent. The differentiation of the chemical environment of the *tripod*iron entities by the orientation of these groups will hence be smaller for **3cBF$_4$** than for **3bBF$_4$**. This means, that the ^{31}P NMR pattern, which could still be partly resolved for **3bBF$_4$**, is no longer resolved for **3cBF$_4$** such that one broad signal is all that can be seen.

The reaction of $Fe^{II}aq(BF_4)_2$ and *tripod* with **H1d**[14] in acetone leads to the dinuclear compound **3dBF$_4$**, under spontaneous deprotonation of **H1d**.[17] Short reaction times allow for the isolation of the BF_4^- salt of **3d**$^+$ as a red microcrystalline compound, in yields of about 50% (Scheme 3).

The analytical data are in agreement with the assigned constitution (Tables 1 and 2). The ^{31}P NMR spectra (Table 1) show one sharp singlet resonance as expected for two chemically equivalent *tripod*iron(II) units. The ^{1}H NMR resonance of the dicyanomethyl substituent is found at δ = 2.88 (**3dBF$_4$**, CD_2Cl_2). With the proton signal of the neutral ligand lying at δ = 5.16 (**H1d**, CD_3NO_2), the coordination shift is remarkably high.

Sodium dicyanamide, **Na2**, also reacts in the typical way yielding the dinuclear compound **4BF$_4$** as a red violet microcrystalline material (90%) (Scheme 4).

The analytical data (Table 2) and NMR spectra (Table 1) are in agreement with the assigned constitution. The ^{13}C NMR signals of the nitrile groups shift from δ = 119.4 (**Na2**, [D$_6$]DMSO) to δ = 124.8 (**4BF$_4$**, CD_2Cl_2), on coordination (Table 1).

Crystals suitable for X-ray analysis could be grown for three compounds of the series **3BF$_4$** (**3aBF$_4$**, **3bBF$_4$**, **3dBF$_4$**). Structural analysis revealed the same principal type of coordination for all three compounds. Therefore, only the structure of **3b**$^+$ is shown in Figure 1. The structural data for all three compounds are presented (Exp. Sect., Table 5).

The $Fe(NCCCN)_3Fe$ core shows an approximate C_3 symmetry in each case (Figure 1). The distances between the iron centers are almost the same in the three compounds [Fe···Fe 692 pm (**3a**$^+$), 680 pm (**3b**$^+$), 687 pm (**3d**$^+$)]. They are determined by the geometry of the NCCCN bridging entity, which is the same in all three compounds. With almost ideal octahedral coordination at the iron centers, ligand geometry does not allow for strictly linear Fe−N−C arrangements (Figure 1). Throughout the series of the three compounds Fe−N−C angles are in the range of 157−169°. The substituents at the $C(CN)_2$ ligand constituent show no pπ−pπ conjugation with the $C(CN)_2$ unit in **3a**$^+$ and **3d**$^+$, whereas the acetyl substituent in **3b**$^+$ definitely does so. The corresponding C−C distances are only 143.7 pm in **3b**$^+$, while they are 150 pm in **3d**$^+$. This π conjugation seen in **3b**$^+$ is also evident from the strict coplanarity of all nonhydrogen atoms of each ligand in **3b**$^+$. The relevant torsion angles are around 0° and 180°, ±5°. The interpretation of the spectroscopic data for **3bBF$_4$** as given above (Table 1 and 2), is in full accord with the observed structure of **3b**$^+$, which conforms to the statistically preferred isomer with regard to the rotational position of the acetyl groups (Figure 1).

All compounds **3BF$_4$** and **4BF$_4$** show reversible one-electron oxidations to the mixed-valent Fe^{II}/Fe^{III} species. Oxidation occurs at around 1000 mV vs. SCE, with a slight variation depending on the specific type of ligand (Table 4). The lowest oxidation potential is observed for **4BF$_4$** ($E_{1/2}$ = 910 mV vs. SCE), oxidation is most difficult for **3aBF$_4$** ($E_{1/2}$ = 1120 mV vs. SCE) with its electron-withdrawing

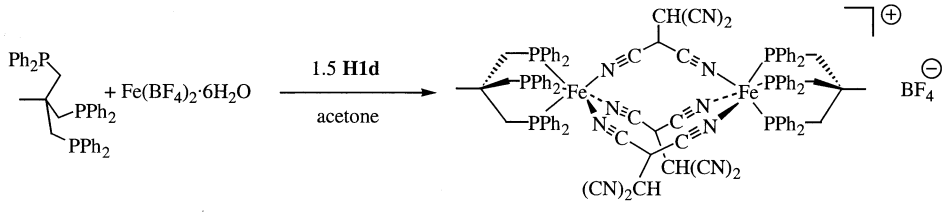

3dBF$_4$

Scheme 3. Synthesis of the dinuclear compound **3dBF$_4$**

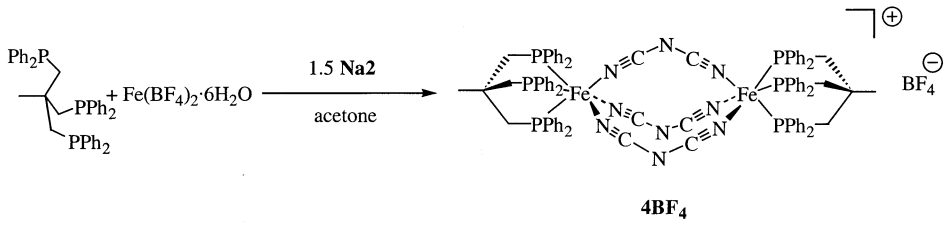

4BF$_4$

Scheme 4. Synthesis of the dinuclear compound **4BF$_4$**

Table 2. Analytical and spectroscopic data of the dinuclear compounds **3BF$_4$** and **4BF$_4$**

No.	Formula (M [g/mol])	MS m/z (%)	[Fragment]	HR-MS m/z	$M^+_{calcd.}$ M^+_{found}	C, H, N, P (calcd.) C, H, N, P (found)	IR (CsI) $\tilde{\nu}$ [cm^{-1}] ν_{CN}	$\nu_{XO,\ XO2}$
3aBF$_4$	$C_{94}H_{87}BF_4Fe_2N_6O_6S_3P_6$	1790(11)	$[M]^+$	–	–	60.12, 4.67, 4.48, 9.90	2218 sh	1323 s
	(1877.3)	823(80)	[*tripod*Fe**1a**]$^+$	–	–	59.09, 5.09, 4.30, 9.53	2200s	1137 s
3bBF$_4$	$C_{97}H_{87}BF_4Fe_2N_6O_3P_6$	1680(7)	$[M]^+$	–	–	65.86, 4.96, 4.75, 10.50	2226 sh	1628 s
	(1769.1)	1057(21)	[M − *tripod*]$^+$	–	–	65.24, 5.14, 4.80, 10.39	2204 s	1607 s
3cBF$_4$	$C_{97}H_{87}BF_4Fe_2N_6O_6P_6$	1730(11)	$[M]^+$	1729.3804	1730.3794	64.08, 4.83, 4.63, 10.23	2232 sh	1685 s
	(1817.1)	–	–	1729.3820	1730.3846	63.41, 5.10, 4.51, 10.02	2208 s	–
3dBF$_4$	$C_{100}H_{81}BF_4Fe_2N_{12}P_6$	1748(7)	$[M]^+$	–	–	65.45, 4.45, 9.16	2218 sh	–
	(1835.2)	706(100)	[*tripod*FeCN]$^+$	–	–	65.05, 4.57, 9.03	2178 vs	–
4BF$_4$	$C_{88}H_{78}BF_4Fe_2N_9P_6$	–	–	1558.3555	1559.3542	64.20, 4.78, 7.66	2298 s	–
	(1646.0)	–	–	1558.3512	1559.3538	63.45, 4.97, 7.78	2207 vs	–

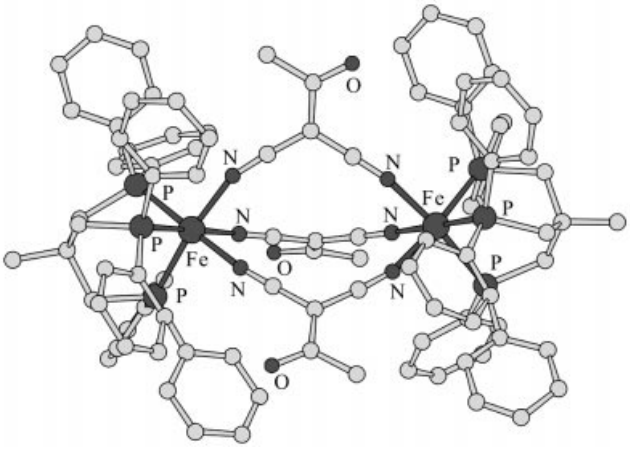

Figure 1. Crystal structure of the cation **3b$^+$**; selected bond lengths [pm] and angles [°]: Fe−P 224.3(2) to 227.9(2), Fe−N 196.8(6) to 199.0(7), C−N 112(1) to 117(1), C_{CN}−C 139(1) to 142(1), C_{CO}−C 143(1) to 144(1), C_{Me}−C_{CO} 147(1) to 151(1), C−O 123(1) to 126(1); P−Fe−P 86.7(1) to 91.0(1), N−Fe−N 82.1(2) to 84.3(2), Fe−N−C 159.3(5) to 168.9(6), N−C−C 176(1) to 179(1), C_{CN}−C−C_{CN} 114.2(6) to 116.8(6)

sulfonylmethyl substituents. A second reversible one-electron oxidation step is observed for all compounds except **3dBF$_4$** (Table 4). The separation between the first and second one-electron oxidation potential, $E_{1/2}{}^1 - E_{1/2}{}^2$, is approximately 300 mV throughout.

Tetranuclear compounds

The above results show that geminal anionic dinitriles tend to form dinuclear compounds with *tripod*iron(II) units. This cannot be a consequence of the anionic charge on the ligands, since neutral dinitriles show the same preference of forming dinuclear, triply bridged diiron compounds. Therefore, it must be a consequence of the geometry of the bridging ligands. In these dicyanomethanide derivatives, the two nitrile groups are separated by just one linker atom, thus spanning an angle between 109 and 120°. The geometry of these ligands thus differs distinctly from the one in fumaric dinitrile, where the nitrile groups are separated by two spacer atoms such that the nitrile groups are parallel to each other. Thus, with fumaric dinitrile as a bridging ligand, the ligand − including the linker entity − and the metal centers bound to it are roughly colinear (Scheme 5 **A**). However, with dicyanomethanide-type ligands, the bridging ligand and the two metal centers bound to it arrange themselves in a roughly triangular shape with the space segment along the line connecting the metals centers being empty (Scheme 5 **B**).

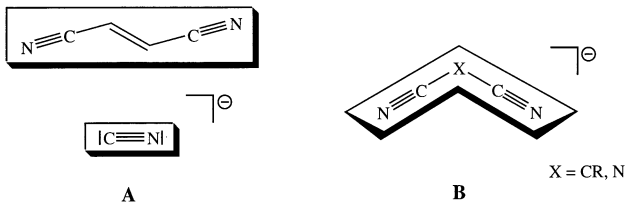

Scheme 5. Linear rod-type and triangular clamp-type bridging ligands

The main geometric difference between these two types of ligands is that fumaric dinitrile behaves as a rod-like building block, while dicyanomethanide derivatives and their analogues serve as a kind of "triangular clamp". This corresponds to the difference in behavior of these building blocks if they are used to construct oligonuclear metal com-

pounds by a self-organized process. With a linear rod-type ligand, only one ligand fits between two metal centers. With ligands forming triangular clamp-like arrangements, there is no such restriction and up to three ligands can easily be arranged to form a triply bridged dinuclear compound (e.g. **3BF$_4$** and **4BF$_4$**).

If the goal is to achieve higher nuclearity in self-arrangement processes, linear rod-type ligands would hence be the proper choice since three such ligands fixed in a monodentate way to one metal center can never ligate to another one with their other end. In fact, under conditions similar to the ones used for the preparation of compounds of the type **3BF$_4$** and **4BF$_4$** (this work), or [*tripod*Fe{μ-NC−C(CR$_2$)−CN}$_3$Fe*tripod*]$^{4+}$,[8] fumaric dinitrile yields a tetranuclear compound [(*tripod*Fe)$_4${μ-NC−CH=CH−CN}$_6$BF$_4$]$^{7+}$ [1] with a tetrahedral arrangement of the metal atoms. The opposite tendency of dicyanomethanide-derived ligands to result in triply bridged dinuclear compounds, might then be overcome in a self-organization process in which both linear rod-type ligands and triangular clamp-type species are used. This hypothesis was tested by repeating the reaction leading to **3BF$_4$** and **4BF$_4$** in the presence of varying amounts of cyanide as a linear rod-type linker (Scheme 5 **A**). It was found that tetranuclear compounds **5BF$_4$** are in fact formed with the appropriate molar ratio (Scheme 6).

When the sodium salt of **1a**$^-$ is added to a mixture of Fe^{II}aq(BF$_4$)$_2$ and *tripod* in dichloromethane/ethanol (1:1), a color change from pale yellow to red immediately occurs and up to this point the appearance of the reaction mixture is very similar to that observed in the preparation of **3a**$^+$. Solid sodium cyanide is added to this mixture. A gradual color change from red to orange-red is observed over a period of 10 h. On concentration, an orange-red material precipitates, which is purified by dissolution in dichloromethane, filtration and crystallization from dichloromethane/ethanol. Analysis of the orange microcrystalline product shows that it is **5aBF$_4$**. The ν_{CN} IR spectra show a prominent long-wavelength band at 2106 cm^{-1} (CsI) (Table 3), which is assigned to the vibration of a μ^2-bridging cyanide ligand.[18] In dichloromethane, this band is found to split into two components, which is assigned to the symmetric (A_1, 2111 cm^{-1}) and asymmetric (E, 2105 cm^{-1}) vibrations of the locally C_3-symmetric Fe(NC)$_3$ unit. This assignment is corroborated by the observation that a band at around this wavelength is present in the IR spectra of all compounds of the type **5BF$_4$**, while it is absent in the IR spectra of compounds of the type **3BF$_4$** which do not contain a bridging cyanide ligand. The ν_{CN} bands, which are characteristic of the bridging dicyanomethanide ligands in **3BF$_4$**, are found at shorter wavelengths in the range of 2180−2230 cm^{-1} (Table 2). In the tetranuclear compounds **5BF$_4$**, vibrations in the same range are hence assigned to μ^2-bridging dicyanomethanide ligands (Table 3). For **5aBF$_4$**, these bands are found at 2216 and 2184 cm^{-1}. A shoulder at 2166 cm^{-1} indicates the presence of a terminally coordinated dicyanomethanide ligand.[19,20] The shoulder observed in the CsI phase, appears as a separate band in the dichloromethane phase at 2163 cm^{-1} (Table 3). A band at this frequency (2165 ± 10 cm^{-1}) is observed for all compounds (**5aBF$_4$**, **5bBF$_4$**, **5cBF$_4$**, **6BF$_4$**) which have a geminal dinitrile coordinated as the terminal ligand to the apical iron center (Table 3). FAB$^+$ mass spectra show the signal for the parent molecular ion **5a**$^+$ at *m*/*z* = 2748. Fragments corresponding to the consecutive loss of *tripod* ligands (*m*/*z* = 2123 [M$^+$ − *tripod*], 1498 [M$^+$ − 2*tripod*]) are also observed. The Mössbauer spectrum of **5aBF$_4$** shows a pattern with four absorbance maxima, which is clearly a convolution of two doublets. One of these is centered at δ = 0.272 mm/s, with a quadrupole splitting of *q* = 0.743 mm/s. The other one occurs at δ = 0.935 mm/s, with a quadrupole splitting of *q* = 3.184 mm/s. The intensity ratio between these two signals is 3:1, corresponding to the presence of the two different types of iron centers in this ratio (Figure 2).

The observed shifts and quadrupole splittings are in agreement with the assigned structure of **5aBF$_4$**; the signal

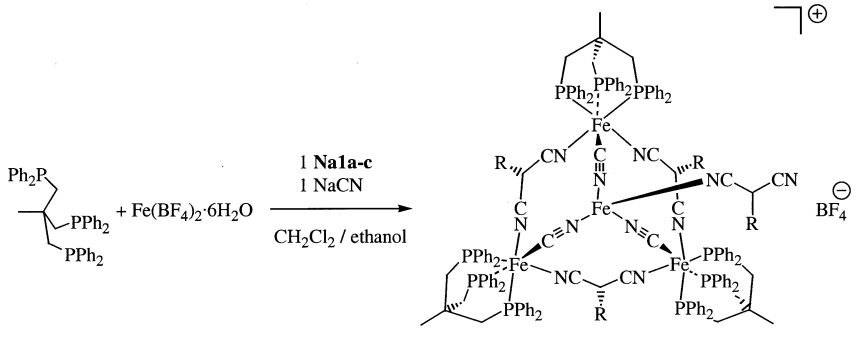

	R
5aBF$_4$	-S(O)$_2$CH$_3$
5bBF$_4$	-C(O)CH$_3$
5cBF$_4$	-C(O)OCH$_3$

Scheme 6. Synthesis of the tetranuclear compounds **5aBF$_4$**, **5bBF$_4$** and **5cBF$_4$**

Table 3. Analytical and spectroscopic data of the tetranuclear compounds **5BF$_4$** and **6BF$_4$**

No.	Formula (M [g/mol])	MS[a] m/z (%)	Magn. moment [μ_B][b][c][d]	C, H, N, P (calcd.) C, H, N, P (found)	^{57}Fe Mössbauer δ (q) [mm/s] (80 K)	IR $\tilde{\nu}$ [cm^{-1}] ν_{CN} CsI	CH_2Cl_2
5aBF$_4$	$C_{142}H_{129}BF_4Fe_4N_{11}O_8P_9S_4$	2748(4)	5.3[b]	60.16, 4.59, 5.44, 9.83	0.272 (0.743) (3 $Fe_{oct,ls}$)	2216 w; 2184 vs	2219 w; 2208 w
	(2834.9)	2123(2)	5.25[d]	59.58, 4.80, 6.02, 9.34	0.935 (3.184) (1 $Fe_{tet,hs}$)	2166 s, sh	2186 s; 2163 s
		1498(8)				2106 s	2111 m; 2105 s
5bBF$_4$	$C_{146}H_{129}BF_4Fe_4N_{11}O_4P_9$	2603(3)	4.8[c]	65.17, 4.83, 5.73	–	2218 m, 2184 vs	2205 w
	(2690.7)	1979(9)	5.2[d]	65.10, 5.25, 6.52	–		2179 s; 2166 s
		1354(10)				2105 s	2110 w, sh; 2106 m
5cBF$_4$	$C_{146}H_{129}BF_4Fe_4N_{11}O_8P_9$	2668(8)	5.2,[b] 5.5[c]	63.63, 4.72, 5.59, 10.12	–	2221 m; 2189 vs	2226 w; 2208 w
	(2754.7)	2043(8)	5.3[d]	62.96, 4.84, 5.58, 9.96	–	2172 s, sh	2191 s; 2170 s
		1418(13)				2106 s	2111 m, sh; 2107 s
5dBF$_4$	$C_{145}H_{120}BF_4Fe_4N_{16}P_9$	2589(2)	5.2[b]	65.09, 4.52, 8.38, 10.42	–	2208 m; 2165 vs	2208 w; 2164 vs
	(2675.6)	–	5.4[d]	64.43, 4.65, 8.76, 9.97	–		–
		–				2110 s	2107 s
5eBF$_4$	$C_{146}H_{117}BF_4Fe_4N_{15}O_4P_9$	2648(2)	5.3[c]	64.13, 4.31, 7.68, 10.19	–	2219 s, br	2220 w; 2194 m
	(2734.6)	–	5.5[d]	63.21, 4.53, 7.48, 10.00	–	2194 s	–
		–				2106 s	2115 s
5fBF$_4$	$C_{135}H_{117}BClF_4Fe_4N_{12}O_3P_9$	2493(4)	5.5[e]	61.85, 4.58, 6.89[e]	–	2229 w; 2213 m	–
	(2579.9)	1867(2)	5.2[d]	61.89, 4.66, 7.30	–		–
		–				2111 s	–
6BF$_4$	$C_{134}H_{117}BF_4Fe_4N_{15}P_9$	2439(15)	5.6,[b] 5.2[c]	63.70, 4.67, 8.32, 11.03	0.291 (0.788) (3 $Fe_{oct,ls}$)	2302 s; 2205 vs	–
	(2526.5)	1814(45)	5.1[d]	63.07, 4.98, 8.04, 10.82	1.006 (2.672) (1 $Fe_{tet,hs}$)	2168 vs	–
		1190(80)				2104 s	–

[a] Percentage values relate to the intensity of the signal for [*tripod*FeCN]$^+$ (m/z = 706) defined as 100 %; m/z-values are given for: M^+, [M-*tripod*]$^+$ and [M-2*tripod*]$^+$. – [b] Faraday method. – [c] Gouy method. – [d] Evans method. – [e] Elemental analysis calculated for **5fBF$_4$**·CH_3NO_2.

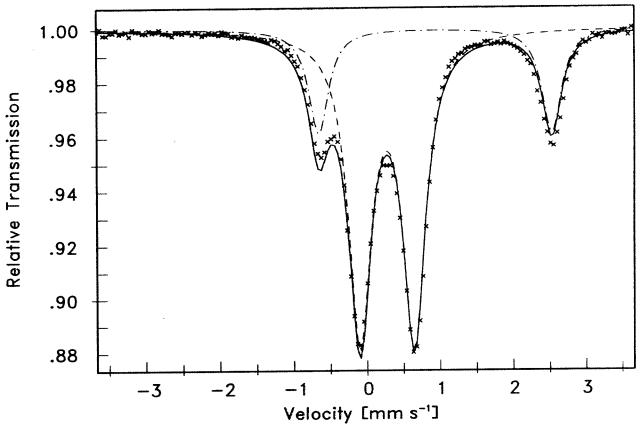

Figure 2. ^{57}Fe Mössbauer spectrum of **5aBF$_4$** (80 K)

of relative intensity 3 corresponds to three *low-spin* iron(II) units i.e. to the *tripod*iron(II) groups, each of which is coordinated to two bridging dicyanomethanide ligands and one bridging cyanide group. For comparative purposes, the Mössbauer spectrum of the tetranuclear compound [(*tripod*Fe)$_4${μ-NC−CH=CH−CN}$_6$BF$_4$](BF$_4$)$_7$,[1] which contains four *low-spin tripod*iron(II) units each coordinated to three nitrile bridging ligands, was measured. One doublet (δ = 0.363 mm/s; q = 0.255 mm/s) is observed for this compound. Shift and quadrupole splitting agree with the corresponding values of the signals assigned to *low-spin tripod*iron(II) in **5aBF$_4$**. The assignment of a *C*-coordinated μ-CN ligand to this entity, is inferred from a comparison of its Mössbauer signal with the Mössbauer data obtained for [*tripod*Fe{μ-CN}{μ-NCC(COOEt)CHC(COOEt)CN}$_2$-Fe*tripod*]BF$_4$,[21] in which one *tripod*Fe(NCR)$_2$ entity is coordinated to the carbon end of the bridging cyanide ligand and the other is coordinated to the nitrogen atom of the same ligand. One of the two observed doublets corresponds almost exactly to the doublet observed for [(*tripod*Fe)$_4${μ-NC−CH=CH−CN}$_6$BF$_4$](BF$_4$)$_7$ with three *N*-coordinated nitrile ligands; the other is characterized by the parameters (δ = 0.341 mm/s; q = 0.688 mm/s), which are very similar to those characterizing the Mössbauer data of the *tripod*iron(II) entity in **5aBF$_4$**. This is taken as a strong indication for the *C*-coordination of the cyano groups to the *tripod*iron(II) entities in **5aBF$_4$**. The magnetic moment observed for **5aBF$_4$** (μ = 5.3 μ_B, Table 3) corresponds closely to the *spin-only* value ($\mu_{s.o.}$ = 4.9 μ_B) for a tetrahedral *high-spin* iron(II) center. The Mössbauer data for this type of iron compound are in a range [$(FeCl_4)^{2-}$: δ = 1.0 mm/s; q = 2.55 mm/s[22−24]] which indicates that the apical iron(II) center with its three *N*-coordinated cyano ligands and one terminal nitrile ligand has a *high-spin* electron configuration.

The same type of reaction, as has been explicitly described for **Na1a** leading to **5aBF$_4$**, occurs if **Na1b** and **Na1c** are used as the dinitrile components, hence leading to **5bBF$_4$** and **5cBF$_4$** respectively (Scheme 6). The spectroscopic and magnetic properties of **5bBF$_4$** and **5cBF$_4$** (Table 3) are very similar to those discussed in detail for **5aBF$_4$**. Microanalyses are also in agreement with the formulae given (Table 3).

A definite proof of the structure of compounds $\mathbf{5BF_4}$ comes from the X-ray analysis of $\mathbf{5aBF_4}$. Suitable single crystals of $\mathbf{5aBF_4}\cdot 1.5\ CH_3NO_2\cdot 2.2\ C_4H_8O_2$ could be grown from nitromethane solutions of $\mathbf{5aBF_4}$, by slow vapor phase diffusion of ethyl acetate at room temperature (Figure 3).

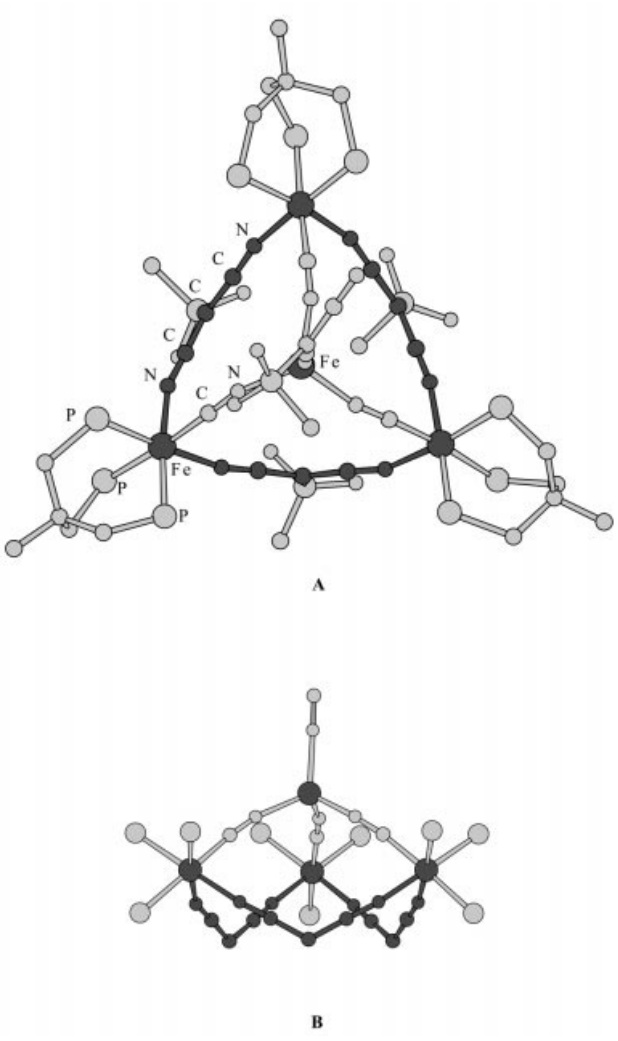

Figure 3. Two views of the cation $\mathbf{5a^+}$; for the sake of clarity only part of the ligand periphery is shown; Fe_{oct}= octahedrally coordinated iron(II); Fe_{tet}= tetrahedrally coordinated iron(II); selected bond lengths [pm] and angles [°]: $Fe_{oct}-P_{\mathit{cis}CN}$ 224.9(2) to 226.7(2), $Fe_{oct}-P_{\mathit{trans}CN}$ 231.7(2) to 232.6(2), $Fe_{oct}-N$ 196.0(7) to 200.5(7), $Fe_{oct}-C_{CN}$ 191(1) to 193(1), $Fe_{tet}-N_{CN}$ 199.2(6) to 201.1(7), $Fe_{tet}-N$ 204.3(7), $C_{CN}-N_{CN}$ 115(1) to 118(1), C−N 113(1) to 117(1), $C-C_{CN}$ 139(1) to 144(1); P−Fe−P 85.1(1) to 91.3(1), P−Fe−C 91.8(3) to 94.0(3), 174.4(3) to 177.6(3), P−Fe−N 90.1(3) to 98.2(3), $N-Fe_{oct}-N$ 83.8(3) to 84.7(3), $N_{CN}-Fe_{tet}-N_{CN}$ 104.1(2) to 107.6(2), $N_{CN}-Fe_{tet}-N$ 110.0(3) to 116.1(3), $Fe_{oct}-C_{CN}-N_{CN}$ 173(1) to 175(1), $Fe_{tet}-N_{CN}-C_{CN}$ 165(1) to 167(1)

The cation $\mathbf{5a^+}$ consists of a triangle spanned by three *tripod*iron(II) units, which are linked by three bridging (methylsulfonyl)dicyanomethanide ligands (Figure 3 **A**). Five coordination sites of the octahedrally coordinated *tripod*iron(II) centers (Fe_{oct}) are thus used to form the bonds within this triangle and to the *tripod* ligands. In each case the sixth position is occupied by a *C*-bonded cyano ligand. The N-termini of these three cyano ligands coordinate to the apical iron center, which has a tetrahedral coordination (Fe_{tet}), with the fourth position being occupied by a terminal (methylsulfonyl)dicyanomethanide ligand, which is coordinated by one nitrile functionality (Figure 3 **A**). The angles around Fe_{oct} are close to the ideal values of a coordination octahedron, although individual deviations of up to 8° (Figure 3) indicate some strain within the cage as a whole. The assumption that the μ-CN groups are *C*-bonded to the *tripod*iron(II) entities, which had been inferred from Mössbauer analysis, is corroborated by the observation that with this assignment of atom types to the bridging cyano groups, reasonable temperature factors are obtained for both carbon and nitrogen during such a refinement. Another argument in favor of this hypothesis comes from the observation that the Fe−P distances involving phosphorus atoms *trans* to the cyano ligands are some 6 pm longer than the remaining Fe−P distances, which involve phosphorus atoms which are *trans* to the organic nitrile groups (Figure 3). In addition, the Fe−C bonds are distinctly shorter than the Fe−N bonds for all three basal iron centers. The $Fe_{oct}-C_{CN}-N_{CN}$-groups are only slightly bent, while the angles $Fe_{tet}-N_{CN}-C_{CN}$ deviate from 180° to a larger extent (Figure 3). The distances $Fe_{tet}-N_{CN}$ are around 200 pm. The $Fe_{tet}-N$ distance to the terminal ligand is 204 pm. The $Fe_{tet}-N$ bonds, radiating from the tetrahedrally coordinated apical *high-spin* iron center, are definitely longer than those involving the basal, octahedrally coordinated, *low-spin* iron centers. The observed $Fe_{tet}-N$ distances (Figure 3) are in agreement with the observed values for other tetrahedrally coordinated *high-spin* iron(II) species.[25] When $\mathbf{1e^-}$ and $\mathbf{1f^-}$ are used as the dicyanomethanide components in the synthesis of $\mathbf{5BF_4}$, the reaction proceeds in a similar way (Scheme 7).

The resulting compounds $\mathbf{5eBF_4}$ and $\mathbf{5fBF_4}$ are less soluble than $\mathbf{5aBF_4}$, $\mathbf{5bBF_4}$ and $\mathbf{5cBF_4}$. They are obtained as red precipitates from the reaction solutions. These precipitates are dissolved in nitromethane for purification. After filtration through silica gel, pure samples of $\mathbf{5eBF_4}$ and $\mathbf{5fBF_4}$ are obtained from these solutions by crystallization. Cubic crystals are obtained by vapor phase diffusion of diethyl ether into nitromethane solutions of $\mathbf{5eBF_4}$ and $\mathbf{5fBF_4}$. Both compounds crystallize in the cubic space group $P\bar{4}3n$. In both cases the structures are strongly affected by disorder problems. There are positions within the crystals that are occupied by solvent molecules with varying degrees of disorder. There is also disorder with respect to the apical ligand of the tetrahedrally coordinated iron center, which is confined by crystallographic symmetry to lie on a crystallographic C_3 axis. This disorder cannot be completely resolved, neither for $\mathbf{5eBF_4}$, nor for $\mathbf{5fBF_4}$. The best solution for $\mathbf{5e^+}$ is obtained by assigning a fluoride ligand to this position. For $\mathbf{5f^+}$ a chloride ligand gives the most satisfactory result. The overall geometry of the framework of the tetrahedral cage in $\mathbf{5e^+}$, including the *tripod* ligands, is determined by structure analysis without any doubt. The only problem with regard to assigning individual atoms to the otherwise well-defined positions, remains for the μ-CN groups. The best solution is obtained if the CN groups are

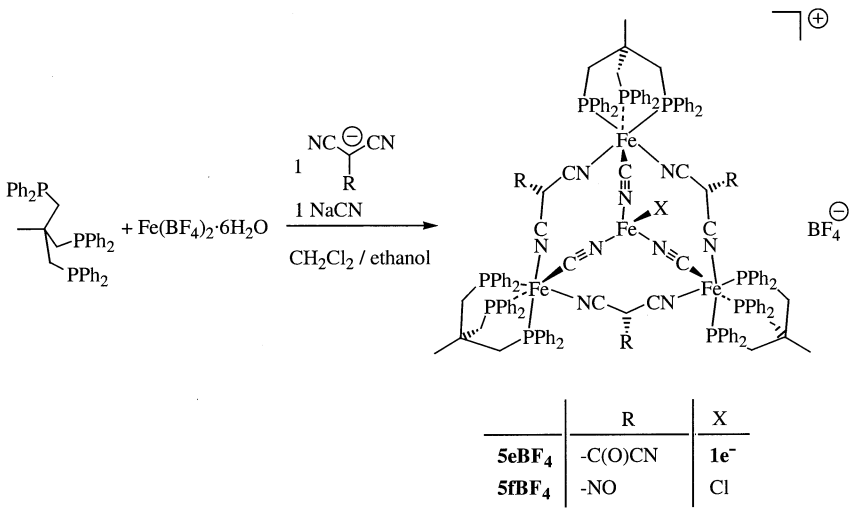

	R	X
5eBF$_4$	-C(O)CN	**1e$^-$**
5fBF$_4$	-NO	Cl

Scheme 7. Synthesis of the tetranuclear compounds **5eBF$_4$** and **5fBF$_4$**

oriented as described for **5a**$^+$. For **5f** $^+$ the overall cage structure is similarly well defined. Here however, the C(NO) linkers joining the coordinated nitrile groups of the bridging dicyanomethanide ligands show disorder, indicating that the symmetry of the η^2-coordination of this ligand does not conform exactly to the crystallographically imposed C_3 symmetry. In view of their inaccuracy in quantitative detail and their close similarity in the overall structure of the cage and the coordination environments, individual data are not discussed here. However, the structural data have been deposited. It appears that the fact that **5aBF$_4$** contains a large C_s-symmetric organic ligand in the apical position is responsible for effectively breaking the *pseudo* symmetry of the crystals. As a result, its structure could be solved without major interference by disorder problems, the only compound in the series of compounds **5BF$_4$**. The lower crystal symmetry of **5aBF$_4$** ($P2_1/n$) as compared with **5eBF$_4$** and **5fBF$_4$** (and also with **5dBF$_4$**, see below) is already macroscopically apparent by looking at the shape of the crystals. The crystals of **5aBF$_4$** form parallelepipeds, whilst those of the others form cubes or hexagonal plates.

A problem associated with compounds **5BF$_4$** is that they undergo easy exchange of their apical ligand. Thus, structure analysis showed that in the crystal specimen analyzed, **5e**$^+$ has an apical ligand with the diffraction power of a fluoride or a hydroxy group. It definitely shows that the molecule in the crystal does not contain a ligand such as **1e**$^-$ or a chloride ion in the apical position. On the other hand, FAB$^+$ mass spectrometry (Table 3) of the bulk crystalline material clarifies that the parent molecular ions observed in the gas phase do not contain either F^- or OH^-. Three types of parent ions are observed, together with their daughter ion $[(tripod\text{Fe})_3\{\mu\text{-NC}-\text{C[C(O)CN]}-\text{CN}\}_3\{\mu\text{-CN}\}_3\text{Fe}]^+$ (m/z = 2530). The mass differences between these three types of parent ions and the daughter ions are 35, 118 and 166, respectively. These mass differences are interpreted as being due to the loss of three different types of apical ligands; chloride, tricyanoethenolate (**1e**$^-$) and pentacyanopropenide ($C_8N_5^-$). Elemental analysis of the bulk material of **5eBF$_4$** shows that **1e**$^-$ is the apical ligand in the original sample (Table 3). It appears that the different processes of handling the probes during FAB$^+$ mass spectrometry, as well as during crystal growth, causes the exchange of the apical ligand. The fluoride ion (crystal structure) may have been incorporated whilst **5eBF$_4$** was in solution for several days which is necessary in order to obtain crystals. The only explanation for the observed incorporation of the chloride ion is an exchange during the processing steps where dichloromethane was used as a solvent. The presence of a pentacyanopropenide ion as an apical ligand, which is seen by mass spectrometry, can be explained by the tendency of polycyano-substituted C_2 entities to form this anion under various conditions.[15] Small peaks attributed to the exchange of the apical ligand by pentacyanopropenide are also observed for **5aBF$_4$**, **5cBF$_4$** and **5fBF$_4$**. The peak corresponding to the molecular ion **5e**$^+$ has a lower intensity than the peaks observed for the chloride and pentacyanopropenide derivative. These two latter molecular ions show daughter ions at m/z = 1940 and 2071, respectively, which correspond to the loss of one *tripod* ligand. This is consistent with the observation that **5a**, **5b**$^+$ and **5c**$^+$, as well as **6**$^+$, show prominent peaks which can be attributed to the loss of one or two *tripod* ligands from their parent ions (Table 3). The mass spectrum of **5fBF$_4$** shows a strong signal for the parent ion with the chloride ion as the apical ligand. This is consistent with the result from the X-ray analysis of **5fBF$_4$**. In addition, the mass spectrum of **5fBF$_4$** shows a molecular ion which corresponds to the exchange of the apical chloride ligand by **1f**$^-$ [m/z (%) = 2552 (8)], and a peak which corresponds to the exchange by pentacyanopropenide [m/z (%) = 2624 (3)]. The ease of exchange of the apical ligands as observed in the mass-spectrometric analyses, and the tendency to include solvent molecules as seen by the X-ray analyses, is mirrored by the microanalytical data (Table 3), which are, in some cases, not as accurate as could be expected. The magnetic moments

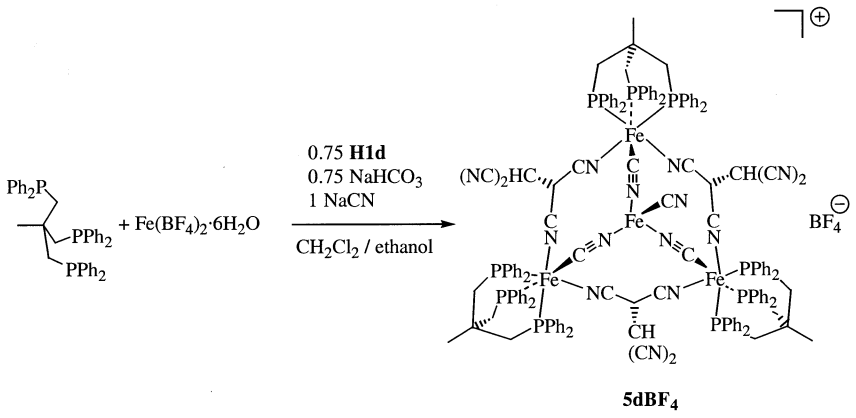

Scheme 8. Synthesis of the tetranuclear compound **5dBF$_4$** according to method **A**

of **5eBF$_4$** and **5fBF$_4$** are around the value of $\mu_{s.o.} = 4.9\ \mu_B$, as expected for a *high-spin* tetrahedral d^6 species (Table 3). It is known that with iron(II) as the d^6 center, spin−orbit coupling tends to result in moments slightly higher than the *spin-only* values.[26] The IR data of **5eBF$_4$** and **5fBF$_4$** (Table 3) are in agreement with the formulae given; the ν_{CN} bands compare well with the ones discussed for **5aBF$_4$**, **5bBF$_4$** and **5cBF$_4$**.

The reaction of $Fe^{II}aq(BF_4)_2$ and *tripod* in dichloromethane/ethanol (1:1) with 1,1,2,2-tetracyanoethane, **H1d**, produces **5dBF$_4$** on addition of stoichiometric amounts of sodium cyanide and sodium bicarbonate (method **A**) (Scheme 8). The initial pale yellow color of the $Fe^{II}aq(BF_4)_2$/*tripod* mixture immediately turns red on addition of **H1d**. No further color change is observed when sodium cyanide and sodium bicarbonate are added to the solution. However, over a period of 10 h the color of the solution changes to black, while an orange-brown precipitate forms. This precipitate is dissolved in nitromethane and purified by filtration and crystallization from nitromethane/dichloromethane/diethyl ether giving **5dBF$_4$** (40%).

An alternative synthesis of **5dBF$_4$** consists of heating **3dBF$_4$** to reflux in dichloromethane/ethanol (1:1) for 10 h (method **B**) (Scheme 9). The initial red color (**3dBF$_4$**) gradually changes to a dark red-brown. Purification by chromatography and crystallization yields **5dBF$_4$** (40%).

Yet another procedure for the synthesis of **5d$^+$** consists of the reaction of a mixture of *tripod* and $FeCl_2$ in dichloromethane/ethanol (1:1) with NaTCNE [27,28] (method **C**) (Scheme 10). On addition of NaTCNE, the solution becomes very dark which is characteristic of solutions of NaTCNE. Over a period of 10 h at room temperature, an orange-red precipitate forms, which is purified by crystallization giving **5dPF$_6$** (55%).

The cyanide ligands in **5d$^+$** must result from a partial disintegration of the TCNE-type precursors in the last two procedures **B** and **C**.

Crystals of **5dBF$_4$** have been obtained from batches produced in routes **B** and **C**. In an independent method, principally according to method **C** but by adding tetrafluoroborate as the counterion, another batch was produced from which crystals could also be obtained. The problem encountered with the structure analyses of these three different types of crystals is very similar to the one already discussed with regard to the structure analyses of **5eBF$_4$** and **5fBF$_4$**. All three types of crystals belong to highly symmetric space groups ($P\bar{4}3n$ and $P31c$), that impose crystallographic trigonal symmetry onto the tetranuclear cations. This symmetry does not correspond to the true molecular symmetry, since the $C(CN)_2H$ groups show disorder around their $C-C(CN)_2H$ bond. In addition, as already observed for **5eBF$_4$** and **5fBF$_4$**, the apical ligands of the tetrahedrally co-

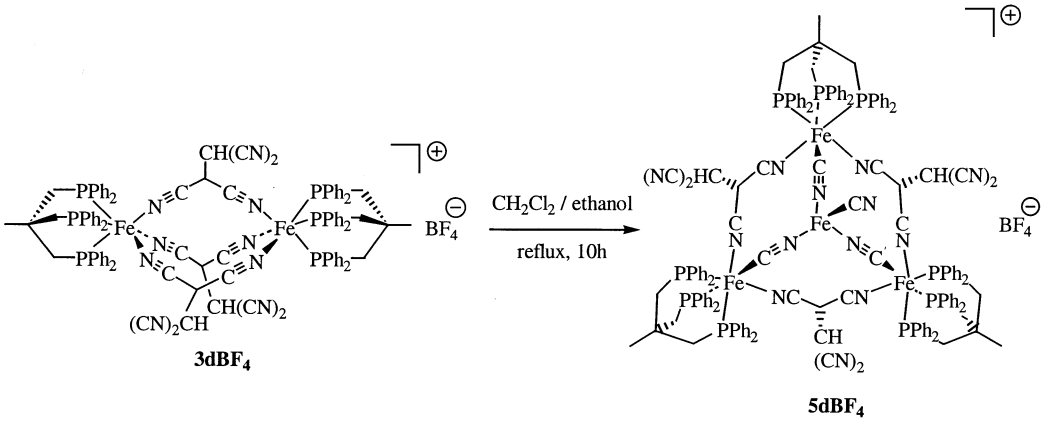

Scheme 9. Synthesis of the tetranuclear compound **5dBF$_4$** according to method **B**

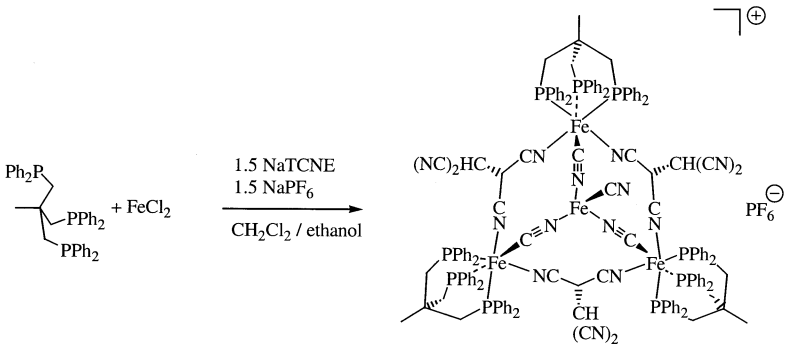

5dPF$_6$

Scheme 10. Synthesis of the tetranuclear compound **5dPF$_6$** according to method **C**

ordinated iron centers can be easily exchanged. In the crystals obtained by method **C** with hexafluorophosphate as the counterion, a chloride ion is in the apical position. The crystals produced by the same method, but with tetrafluoroborate as the counterion, are found to have cyanide as the apical ligand. In these crystals, there is not only rotational disorder of the $C(CN)_2H$ groups, but also a strong indication for the presence of $C(CN)H_2$ groups instead of $C(CN)_2H$ entities. With this assignment, the structure can be refined to an agreement factor of $R_1 = 8.7\%$ (Table 7). The quality of the individual geometric parameters is nevertheless low, due to the many disordered solvent molecules involved. The crystals produced according to method **B** are found to contain F^- or OH^- as the apical ligand. The organic bridging groups show the same type of disorder as discussed above, with the best solution being obtained by describing the rotationally disordered substituent as the $C(CN)H_2$ group. While all these structure analyses unequivocally prove the persistence of a [(*tripod*Fe)$_3${μ-NC−C(R)−CN}$_3${μ-CN}$_3$Fe−X] core, they cannot definitely elucidate the nature of R and X. FAB^+ mass spectra are more conclusive with regard to the nature of R in the bulk materials. The molecular ions are consistent with R = $C(CN)_2H$. Satellite peaks are found for R = $C(CN)H_2$. This indicates that the bulk material contains R = $C(CN)_2H$, as well as R = $C(CN)H_2$ as the substituent at the $RC(CN)_2$ bridging unit. Mass spectra are less conclusive with respect to the nature of the apical ligand X. In all spectra there is a prominent peak for the parent ion with X = CN^-. However, there are peaks for X = F^-/OH^-, Cl^-, CNO^- and $C_8N_5^-$ as well. The situation is thus very similar to the one described for **5eBF$_4$** and **5fBF$_4$**, and the final answer must be obtained from elemental analysis. Considering all combinations of possible constituents, the most satisfactory agreement is X = CN^- (Table 3). The magnetic moment of **5dBF$_4$** is in the range observed for the other compounds **5BF$_4$** (Table 3). The bridging cyano ligands are evident from their IR absorptions, as are the $RC(CN)_2$ building blocks (Table 3).

The reaction of $Fe^{II}aq(BF_4)_2$ and *tripod* in dichloromethane/ethanol (1:1) with sodium dicyanamide, **Na2**, and sodium cyanide gives **6BF$_4$** in a procedure very similar to the one used for the preparation of compounds **5BF$_4$** (Scheme 11). **6BF$_4$** is obtained as a red precipitate, which is purified by crystallization giving a red crystalline material. Although none of the many analyzed crystals gave good diffraction patterns so as to allow X-ray analysis, the spectroscopic and analytical data (Table 3) clearly prove that **6**$^+$ has a framework analogous to the one which characterizes the series of cations **5**$^+$. The magnetic moment and the infrared data (Table 3) support the above statement. The IR spectra show ν_{CN} bands that are characteristic of the dicyanamide ligand and the Fe(μ-NC)$_3$ group. The FAB^+ mass spectrum shows prominent peaks for the molecular

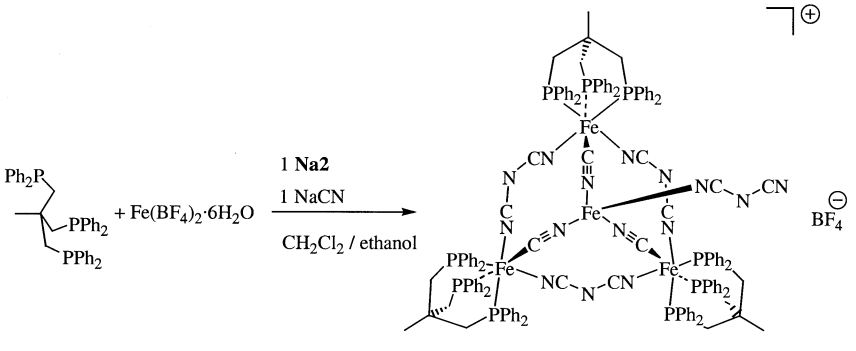

6BF$_4$

Scheme 11. Synthesis of the tetranuclear compound **6BF$_4$**

Table 4. UV/Vis and cyclic voltammetric data of compounds **3BF$_4$**, **4BF$_4$**, **5BF$_4$** and **6BF$_4$**

No.	UV (CH_2Cl_2)		CV (CH_2Cl_2, SCE)			No.	UV (CH_2Cl_2)		CV (CH_2Cl_2, SCE)	
	λ [cm^{-1}]	(ε [$M^{-1}cm^{-1}$])	$E_{1/2}$ [mV]	(ΔE)	K_C [a]		λ [cm^{-1}]	(ε [$M^{-1}cm^{-1}$])	$E_{1/2}$ [mV]	(ΔE)
3aBF$_4$	19600	(1900)	1120	(110)	$10^{4.7}$	**5aBF$_4$**	19800	(800)	1045	(110)
	24300	(1100)	1400	(116)			23000	(2200)		
							27900 sh	(6300)		
3bBF$_4$	19700	(2300)	1058	(105)	$10^{4.6}$	**5bBF$_4$**	19600	(1200)	990	(155)
	24500	(1000)	1328	(115)			22400	(2600)		
							27700 sh	(8300)		
3cBF$_4$	19700	(2100)	1000	(120)	$10^{5.4}$	**5cBF$_4$**	19600	(1300)	948	(115)
	24400	(800)	1320	(115)			22800	(2900)		
							27700 sh	(10000)		
3dBF$_4$	19500	(2200)	1020	(101)	–	**5dBF$_4$**	19400	(1500)	1000	(130)
	23900	(1300)					23000	(3500)		
							27000 sh	(9500)		
						5eBF$_4$	19800	(2100)	873	(150)
							22400	(2800)		
							27800 sh	(11000)		
						5fBF$_4$	19600	(3000)	1140	(80)
							22600	(7500)	(CH_3CN)	
							28400 sh	(16000)		
4BF$_4$	19100	(2100)	910	(113)	$10^{4.4}$	**6BF$_4$**	19500	(1800)	886	(112)
	24200	(900)	1150	(108)			22200	(2200)	1120	(140)
							28500 sh	(6200)		

[a] Equilibrium constants K_C of the comproportionation reaction (Scheme 12) calculated by: $K_C = \exp(\Delta E_{1/2}/25.69)$; $\Delta E_{1/2}$ in mV.

ion **6**$^+$ and for the daughter ions derived from the consecutive loss of two *tripod* ligands. The Mössbauer spectrum of **6BF$_4$** shows a signature which is very similar to the one observed for **5aBF$_4$** (Table 3). It demonstrates the presence of *high-spin* iron(II) and *low-spin* iron(II) in a ratio of 1:3. The microanalytical data are in full accord with the assigned formula.

Electrochemistry and UV/Vis Spectra

All compounds **3BF$_4$** to **6BF$_4$** undergo at least one one-electron oxidation. For the binuclear compounds **3BF$_4$**, the corresponding potentials are between $E_{1/2}$ = 910 mV (**4BF$_4$**) and 1120 mV (**3aBF$_4$**) (Table 4).

A second one-electron oxidation step is observed between $E_{1/2}$ = 1150 mV (**4BF$_4$**) and 1400 mV (**3aBF$_4$**) (Table 4). This second step is reversible for all binuclear compounds except **3dBF$_4$**, for which an irreversible electron transfer at E_{pa} = 1430 mV is observed. The observation of two distinctly different one-electron oxidation steps demonstrates that the iron centers take notice of each other. The distance between the two iron centers is around 700 pm (Figure 1) and the iron centers are joined by five-atom linkers. Both these facts are in favor of the stability of a mixed-valence Fe^{II}/Fe^{III} species. The equilibrium constant K_C for the comproportionation reaction (Scheme 12), as deduced from the oxidation potentials, is in fact rather high throughout (Table 4).[29] With a value of around 10^5, it characterizes the Fe^{II}/Fe^{III} complexes as class III mixed-valent species.[30]

$$M\sim\sim M + M^{ox}\sim\sim M^{ox} \underset{}{\overset{K_C}{\rightleftharpoons}} 2\ M\sim\sim M^{ox}$$

Scheme 12. Comproportionation equilibrium for mixed-valent dinuclear complexes

This means, that the iron centers and the ligands form a conjugated system together.[31,32]

The tetranuclear compounds **5BF$_4$** show only one reversible one-electron oxidation. A second reversible oxidation is observed for **6BF$_4$**, with its dicyanamide ligands (Table 4). Within each pair of compounds **3BF$_4$** and **5BF$_4$** (**4BF$_4$** and **6BF$_4$**), the first one-electron oxidation step occurs at similar potentials (Table 4), with a tendency of compounds **5BF$_4$** to be somewhat easier to oxidize than the corresponding compounds **3BF$_4$**. The similarity of the oxidation potentials of **3BF$_4$** and **5BF$_4$** shows that the oxidation of **5BF$_4$** is not centered at its *high-spin* iron(II) center.

The UV/Vis spectra of the different compounds **3BF$_4$** are rather similar (Figure 4). Bands occur at $\lambda \approx$ 19500 and 24000 cm^{-1} (Figure 4, Table 4). A similar pattern is observed for [*tripod*$Fe^{II}(NCMe)_3]^{2+}$ [33] (λ = 20500 and 26000 cm^{-1}), which has three organonitrile groups coordinated to a *tripod*iron(II) entity and is a *low-spin* compound, as are compounds **3BF$_4$**. Therefore, it is assumed that the bands observed for **3BF$_4$** correspond to the spectral signature of *low-spin tripod*$Fe^{II}(NCR)_3$ entities. Within the series of compounds **3BF$_4$** there is a slight shift of the relevant absorption energies (Table 4).

Compounds **5BF$_4$** and **6BF$_4$** show similar absorption patterns through their whole series. The bands at $\lambda \approx$ 19500 and 23000 cm^{-1} (Figure 4, Table 4) are typical for *low-spin tripod*$Fe^{II}L_3$ compounds. In the case of **5BF$_4$** and **6BF$_4$**, two of these ligands are nitrile groups from the organic bridging ligand, the third ligand is a cyano group acting as a bridging ligand to bind a tetrahedral *high-spin* iron(II) center. There is no indication in the spectra of **5BF$_4$** and **6BF$_4$** of any significant contribution from this *high-spin*

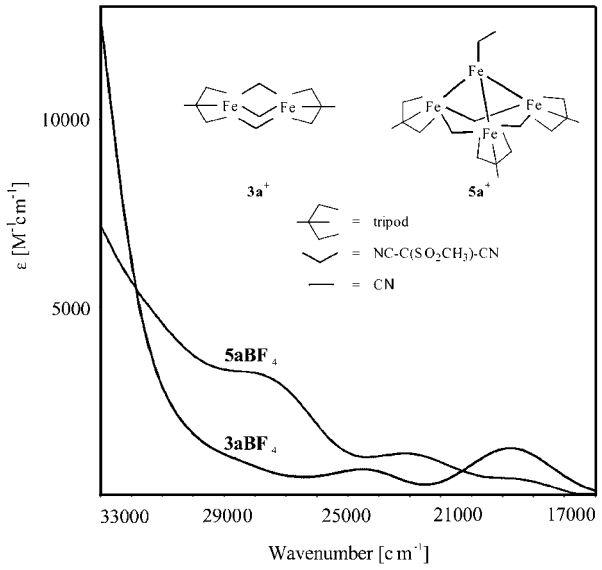

Figure 4. UV/Vis spectra of **3aBF$_4$** and **5aBF$_4$**

iron(II) center occurring in the long-wavelength range of the spectra (Figure 4, Table 4).

Conclusion

The *tripod* ligands, $Fe^{II}aq(BF_4)_2$ and dinitrile constituents engage in a self-assembly process to produce binuclear $[tripodFe\{\mu\text{-}NC-C(R)-CN\}_3Fetripod]^+$ or − in the presence of cyanide − tetranuclear compounds $[(tripodFe)_3\{\mu\text{-}NC-C(R)-CN\}_3\{\mu\text{-}CN\}_3Fe-X]^+$, exclusively. The self-organization process, which exclusively leads to $[tripodFe\{\mu\text{-}NC-C(R)-CN\}_3Fetripod]^+$ with the angular clamp-type ligands $[NC-C(R)-CN]^-$, may be switched to the exclusive formation of tetrahedral aggregates $[(tripodFe)_3\{\mu\text{-}NC-C(R)-CN\}_3\{\mu\text{-}CN\}_3Fe-X]^+$ by the interference of the linear rod-type ligand cyanide. The tetranuclear compounds $[(tripodFe)_3\{\mu\text{-}NC-C(R)-CN\}_3\{\mu\text{-}CN\}_3Fe-X]^+$ contain three *low-spin* $tripodFe^{II}L_3$ units and one tetrahedral *high-spin* iron(II) entity in one supramolecular aggregate.

The electrochemistry shows that compounds $[tripodFe\{\mu\text{-}NC-C(R)-CN\}_3Fetripod]^+$ form mixed-valent Fe^{II}/Fe^{III}-species of type III. They are stable against disproportionation into Fe^{II}/Fe^{II}- and Fe^{III}/Fe^{III}-species.

Experimental Section

General: All manipulations were carried out under argon by means of standard Schlenk techniques. All solvents were dried by standard methods [34] and distilled under argon. Silica gel and Kieselgur, used for filtration operations and chromatography, were degassed at 1 mbar for 24 h and saturated with argon. The compounds *tripod*,[35,36] $Fe(BF_4)_2{\cdot}6H_2O$,[37] (methylsulfonyl)malononitrile hydrochloride,[9] 1,1,2,2-tetracyanoethane,[14] NaTCNE,[27] tetramethylammonium tricyanethenolate[15] and sodium nitrosodicyanmethanide[16] were prepared in accordance to, or by adaptation of, literature procedures. All other chemicals were obtained from commercial suppliers and used without further purification. − NMR: Bruker Avance DPX200 spectrometer at 200.13 MHz (^{1}H), 50.323 MHz (^{13}C), 81.014 MHz (^{31}P); T = 303 K; chemical shifts (δ) in ppm with respect to CD_2Cl_2 (^{1}H: δ = 5.32; ^{13}C: δ = 53.5), [D$_6$]acetone (^{1}H: δ = 2.05; ^{13}C: δ = 20.8, 206.1) or [D$_6$]DMSO, (^{1}H: δ = 2.50; ^{13}C: δ = 39.4) as internal standards; ^{31}P chemical shifts (δ) in ppm with respect to 85% H_3PO_4 (^{31}P: δ = 0) as external standard; CD_2Cl_2, [D$_6$]acetone and [D$_6$]DMSO used, for NMR-spectroscopic measurements, were degassed by three successive "freeze-pump-thaw" cycles and dried over 4-Å molecular sieves. − Magnetic measurements: Faraday method: electromagnet B-E 1 C-8 and controller unit B-H 15 (Bruker); M 25 D-S balance (Sartorius). Gouy method: Sherwood Scientific Magnetic Susceptibility Balance (Johnson & Matthey). Evans method: Bruker Avance DPX200 spectrometer at 200.13 MHz (^{1}H); solvent: CD_2Cl_2; standard: DPPH (diphenylpikrylhydrazyl); T = 303 K. − IR: Biorad Excalibur spectralphotometer FTS 3000 [CsI discs or solutions (CaF_2 windows)]. − UV/Vis spectra: Perkin−Elmer UV/Vis spectralphotometer Lambda 9; ca.10^{-3} M solutions in CH_2Cl_2. − MS: Finnigan MAT 8320, VG ZAB 2F; FAB (Xenon; matrix: 4-nitrobenzyl alcohol). − Cyclic voltammetry: EG&G Princeton Applied Research model 273; potentials in mV versus SCE at a glassy carbon electrode at 25 °C; solutions of compounds: ca.10^{-3} M in 0.1 M Bu_4NPF_6 in CH_3CN or CH_2Cl_2. − Elemental analyses: Microanalytical Laboratory of the Organisch-Chemisches Institut, Universität Heidelberg.

Preparation of the Compounds

Na[NCC(R)CN] [Na1: R = SO_2CH_3 (Na1a), $COCH_3$ (Na1b), CO_2CH_3 (Na1c)]:[10,12,13] **Na1a** was synthesized from the hydrochloride of (methylsulfonyl)malononitrile (279 mg; 1.54 mmol) by reaction with a slight excess of sodium bicarbonate (267 mg; 3.18 mmol) in water.[9] After drying the reaction mixture and filtering with 5 mL acetone, the product was isolated by precipitation with excess diethyl ether. 187 mg (73%) of a white solid was obtained after isolation and drying in vacuo. − $C_4H_3N_2NaO_2S$ (166.1): calcd. C 28.92, H 1.82, N 16.86; found C 29.23, H 2.56, N 16.88. − ^{1}H NMR ([D$_6$]acetone): δ = 2.88 (s). − ^{13}C NMR ([D$_6$]DMSO): δ = 42.2 (s, NC*C*CN), 46.3 (s, CH_3), 120.4 (s, CN). − IR (CsI): $\tilde{\nu}$ = 2187 m, 2160 s (CN); 1295 vs, 1137 vs (SO_2) cm^{-1}. − **Na1b** was prepared by dropwise addition of acetyl chloride (5.3 g; 68 mmol) to an ice-cooled solution of malononitrile (4.5 g; 68 mmol) in 10 mL of THF and sodium hydroxide (5.2 g; 130 mmol) in 10 mL of water. A light brown suspension formed, which was filtered after warming to room temperature. The precipitate was washed twice with 2 mL of ice-cold water, dried in vacuo and recrystallized from ethyl acetate/ethanol (20:1; 100 mL) yielding 6.4 g (65%) of a white powder. For elemental analysis the product was recrystallized from acetone/diethyl ether and dried in vacuo. − $C_5H_3N_2NaO$ (130.1): calcd. C 46.17, H 2.32, N 21.54; found C 46.25, H 2.52, N 21.36. − ^{1}H NMR ([D$_6$]DMSO): δ = 1.86 (s). − ^{13}C NMR ([D$_6$]DMSO): δ = 26.4 (s, CH_3); 47.9 (s, NC*C*CN); 121.8 (s, CN); 123.9 (s, CN); 191.0 (s, CO). − **IR** (CsI): $\tilde{\nu}$ = 2219 vs, 2193 vs, 2184 s,sh (CN); 1572 vs. (CO) cm^{-1}.− **Na1c** was prepared by dropwise addition of a mixture of methyl chloroformate (7.8 g; 82 mmol) and malononitrile (5.1 g; 77 mmol) in 10 mL of THF, to an ice-cooled solution of sodium hydroxide (6.2 g; 154 mmol) in 15 mL of water. A white suspension formed, which was filtered after warming to room temperature. The white precipitate was washed twice with 3 mL of ice-cold water, dried in vacuo and recrystallized from ethyl acetate (100 mL) yielding 6.0 g (48%) of light yellow needle-type crystals. − $C_5H_3N_2NaO_2$ (146.1): calcd.

C 41.11, H 2.07, N 19.18; found C 41.08, H 2.34, N 19.07. − ^{1}H NMR ([D$_6$]acetone): δ = 3.51 (s). − ^{13}C NMR ([D$_6$]acetone): δ = 32.3 (s, NC*C*CN); 51.0 (s, CH_3); 122.0 (s, CN); 123.1 (s, CN); 172.7 (s, COO). − IR (CsI): $\tilde{\nu}$ = 2216 vs, 2184 s (CN); 1648 vs, br (CO) cm^{-1}.

[(*tripod*Fe)$_2${μ-NCC(R)CN}$_3$]BF$_4$ [3BF$_4$: R = SO_2CH_3 (3aBF$_4$), $COCH_3$ (3bBF$_4$), CO_2CH_3 (3cBF$_4$)] and [(*tripod*Fe)$_2${μ-NCNCN}$_3$]BF$_4$ (4BF$_4$): Na1a, **Na1a**, **Na1c** or **Na2** (1.5 mmol) was added as a solid, in one portion, to a solution of Fe^{II}aq(BF$_4$)$_2$ (338 mg, 1 mmol) and *tripod* (625 mg, 1 mmol) in acetone. An immediate color change from pale yellow to red was observed. After stirring for 1 h at room temperature, the solvent was evaporated. The red residue was washed once with diethyl ether and dried in vacuo. Filtration with dichloromethane through 1 cm of Kieselgur and concentration of the red filtrate yielded the products as red to violet microcrystalline solids. For purification, the products were recrystallized. Yields and solvents of crystallization: **3aBF$_4$** [74% (acetone/diethyl ether)], **3bBF$_4$** [70% (dichloromethane/ethanol)], **3cBF$_4$** [78% (acetone/diethyl ether)], **4BF$_4$** [59% (dichloromethane/ethanol)]. For further analytical and spectroscopic data of the compounds see Tables 1, 2 and 4.

[(*tripod*Fe)$_2${μ-NCC[CH(CN)$_2$]CN}$_3$]BF$_4$ (3dBF$_4$): Solid **H1d** (1.5 mmol) was added in one portion to a solution of Fe^{II}aq(BF$_4$)$_2$ (338 mg, 1 mmol) and *tripod* (625 mg, 1 mmol) in 15 mL of acetone. An immediate color change from pale yellow to violet red was observed. After stirring for 5 min at room temperature, a red solid precipitated. This precipitate was isolated by filtration. After dissolving the precipitate in dichloromethane, filtration and evaporation of the dichloromethane gave **3dBF$_4$** as a red-violet microcrystalline solid (460 mg, 48%). Crystals for X-ray diffraction studies were grown by layering a concentrated solution of **3dBF$_4$** in dichloromethane with acetone at −20 °C. For analytical data of **3dBF$_4$** see Tables 1, 2 and 4.

[(*tripod*Fe)$_3${μ-NCC(R)CN}$_3${μ-CN}$_3$Fe−NCC(R)CN]BF$_4$ [5BF$_4$: R = SO_2CH_3 (5aBF$_4$), $COCH_3$ (5bBF$_4$), CO_2CH_3 (5cBF$_4$)] and [(*tripod*Fe)$_3${μ-NCNCN}$_3${μ-CN}$_3$Fe−NCNCN]BF$_4$ (6BF$_4$): Na1a, **Na1a**, **Na1c** or **Na2** (1 mmol) and sodium cyanide (49 mg, 1 mmol) were added, in one portion, to a solution of Fe^{II}aq(BF$_4$)$_2$ (338 mg, 1 mmol) and *tripod* (625 mg, 1 mmol) in dichloromethane/ethanol (1:1; 40 mL). An immediate color change from pale yellow to red was observed. After stirring for 10 h at room temperature the color had changed to orange-red. After stirring for an additional period of 10 h, the resulting turbid orange to red solution was concentrated in vacuo to a volume of 10 mL and filtered. The orange to red precipitate was washed with ethanol and diethyl ether and dried in vacuo. Filtration with dichloromethane through 1 cm of Kieselgur and concentration of the red filtrate yielded the products as orange to red solids. The products were recrystallized from dichloromethane/ethanol yielding the compounds as orange to red crystallized solids. Yields: **5aBF$_4$** (50%), **5bBF$_4$** (38%), **5cBF$_4$** (51%), **6BF$_4$** (46%). For analytical and spectroscopic data of compounds **5aBF$_4$**, **5bBF$_4$**, **5cBF$_4$** and **6BF$_4$** see Tables 3 and 4.

Table 5. Crystallographic data of compounds **3aBF$_4$**, **3bBF$_4$** and **3dBF$_4$**

Compound	**3aBF$_4$**	**3bBF$_4$** [a]	**3dBF$_4$** [b]
Solvate	·0.6 CH_3NO_2·1 $C_4H_8O_2$	·2.5 CH_2Cl_2·1 C_2H_5OH	·0.8 C_3H_6O
Empirical formula (without solvate)	$C_{94}H_{87}BF_4Fe_2N_6O_6P_6S_3$	$C_{97}H_{87}BF_4Fe_2N_6O_3P_6$	$C_{100}H_{81}BF_4Fe_2N_{12}P_6$
Molecular mass [g/mol]	1877.3	1769.1	1835.2
Crystal size [mm]	0.20×0.10×0.05	0.02×0.02×0.03	0.25×0.25×0.25
Crystal system	triclinic	monoclinic	orthorhombic
Space group	$P\bar{1}$	$P2_1/a$	$P2_12_12$
a [pm]	1305.8(3)	1478.5(3)	2045.0(4)
b [pm]	2001.9(4)	4317.2(9)	2088.3(4)
c [pm]	2077.8(4)	1624.2(3)	1313.2(3)
α [°]	110.36(3)	90	90
β [°]	93.77(3)	95.89(3)	90
γ [°]	93.73(3)	90	90
V [10^{6}pm^3]	5058.50	10312.00	5608.10
Z	2	4	2
d_x [g·cm^{-3}]	1.355	1.309	1.114
T [K]	200	200	263
Scan range	3.1° ≤ 2θ ≤ 50.0°	2.5° ≤ 2θ ≤ 54.0°	3.7° ≤ 2θ ≤ 50.0°
Method	ω-scan, Δω =1.0°	ω-scan, Δω =1.0°	ω-scan, Δω =1.0°
Scan speed	25 s/frame	10 s/frame	5 s/frame
No. of measured rflns.	79811	40321	50449
No. of unique rflns.	17826	22346	9890
No. of observed rflns.	10433	13337	7862
Observation criterion	$I \geq 2\sigma$	$I \geq 2\sigma$	$I \geq 2\sigma$
No. of param. refined	998	1156	609
Resid. el. dens. [10^{-6} e·pm^{-3}]	2.18	1.79	0.68
R_1/R_w (%) (refinement on F^2)	7.6/21.9	12.0/39.1	6.7/21.6

[a] The quality of the analysis achieved for **3bBF$_4$** is reduced by the fact, that the crystal contains solvent molecules in disordered arrangements. In addition, there is suspicion, that there is some rotational disorder of the acetyl substituents, which could, however, not be resolved by the split-atom technique. The rotational position, which at least dominates by far is shown in Figure 1. − [b] The solution of the structure of **3dBF$_4$** is as well affected by disorder problems. **3dBF$_4$** is bound to have crystallographic C_2 symmetry, such that there is disorder for the C(CN)$_2$H group, whose central carbon atom lies at the C_2 axis. The disorder was not completely resolved.

Table 6. Crystallographic data of compounds **5aBF$_4$**, **5eBF$_4$** and **5fBF$_4$**

Compound	**5aBF$_4$** [a]	**5eBF$_4$** [b]	**5fBF$_4$** [c]
Solvate	·1.5 CH_3NO_2·2.2 $C_4H_8O_2$	·1.5 CH_3NO_2·1.5 $C_4H_{10}O$	·0.75 H_2O
Empirical formula (without solvate)	$C_{142}H_{129}BF_4Fe_4N_{11}O_8P_9S_4$	$C_{141}H_{117}BF_5Fe_4N_{12}O_3P_9$	$C_{135}H_{117}BClF_4Fe_4N_{12}O_3P_9$
Molecular mass [g/mol]	2834.9	2635.5	2579.9
Crystal size [mm]	0.02×0.02×0.02	0.01×0.01×0.01	0.20×0.20×0.20
Crystal system	monoclinic	cubic	cubic
Space group	$P2_1/n$	$P\bar{4}3n$	$P\bar{4}3n$
a [pm]	1697.22(3)	3308.5(4)	3327.2(4)
b [pm]	3619.06(5)	3308.5(4)	3327.2(4)
c [pm]	2746.04(1)	3308.5(4)	3327.2(4)
α [°]	90	90	90
β [°]	96.851(1)	90	90
γ [°]	90	90	90
V [10^6pm^3]	16746.70	36215.00	36833.00
Z	4	8	8
d_x [g·cm^{-3}]	1.302	1.033	0.934
T [K]	200	253	260
Scan range	2.3° ≤ 2θ ≤ 56.6°	2.5° ≤ 2θ ≤ 52.7°	2.4° ≤ 2θ ≤ 48.0°
Method	ω-scan, Δω =1.0°	ω-scan, Δω =1.0°	ω-scan, Δω =1.0°
Scan speed	10 s/frame	10 s/frame	20 s/frame
No. of measured rflns.	167031	24764	21708
No. of unique rflns.	40222	12384	9659
No. of observed rflns.	17384	5497	6182
Observation criterion	$I \geq 2\sigma$	$I \geq 2\sigma$	$I \geq 2\sigma$
No. of param. refined	1838	552	505
Resid. el. dens. [10^{-6} e·pm^{-3}]	1.82	1.59	1.05
R_1/R_w (%) (refinement on F^2)	11.6/32.1	10.2/34.2	11.1/34.1

[a] The data for X-ray analysis of **5aBF$_4$** were collected with a Siemens SMART 1000-CCD diffractometer. Lorentz, polarisation and absorption correction (Siemens Area Detector Absorption Correction, Siemens) were carried out. – [b] The structure is affected by disorder. The apical ligand is fluoride in the analyzed sample instead of **1e**$^-$, which is present in the bulk (Table 3). – [c] Disorder of solvate and rotational disorder of the substituents of the bridging ligands.

[(*tripod*Fe)$_3${μ-NCC[C(O)CN]CN}$_3${μ-CN}$_3$Fe–NCC-[C(O)CN]CN]BF$_4$ (5eBF$_4$) and [(*tripod*Fe)$_3${μ-NCC(NO)CN}$_3${μ-CN}$_3$Fe–Cl]BF$_4$ (5fBF$_4$): [N(CH$_3$)$_4$]1e and **Na1f** (1 mmol) and sodium cyanide (49 mg, 1 mmol) were added in one portion to a solution of $Fe^{II}aq(BF_4)_2$ (338 mg, 1 mmol) and *tripod* (625 mg, 1 mmol) in dichloromethane/ethanol (1:1; 40 mL). An immediate color change from pale yellow to violet red was observed. After stirring for 10 h at room temperature, a red precipitate had formed. Stirring for an additional period of 10 h, followed by isolation of the red precipitate, filtration with nitromethane through 1 cm of silica gel (ICN Biomedicals, 32–63 μm, 60 Å) and evaporation of the solvent, yielded the products in the form of red solids. Yields: **5eBF$_4$** (67%), **5fBF$_4$** (62%). For purification, the products were crystallized by vapor phase diffusion of diethyl ether into dilute nitromethane solutions. For analytical data of compounds **5eBF$_4$** and **5fBF$_4$** see Tables 3 and 4.

[(*tripod*Fe)$_3${μ-NCC[CH(CN)$_2$]CN}$_3${μ-CN}$_3$FeCN]BF$_4$ (5dBF$_4$) and [(*tripod*Fe)$_3${μ-NCC[CH(CN)$_2$]CN}$_3${μ-CN}$_3$FeCN]PF$_6$ (5dPF$_6$). – Method A: H1d (98 mg, 0.75 mmol), sodium bicarbonate (64 mg, 0.80 mmol) and sodium cyanide (49 mg, 1 mmol) were added in one portion to a solution of $Fe^{II}aq(BF_4)_2$ (338 mg, 1 mmol) and *tripod* (625 mg, 1 mmol) in dichloromethane/ethanol (1:1; 40 mL). An immediate change of color from pale yellow to violet red was observed. After stirring for 10 h at room temperature, an orange red precipitate had formed. Stirring for an additional period of 10 h, followed by isolation of the red precipitate, filtration with nitromethane through 1 cm of Kieselgel (ICN Biomedicals, 32–63 μm, 60 Å) and concentration of the filtrate, yielded **5dBF$_4$** in the form of an orange-brown microcrystalline solid (250 mg, 37%). For purification, the product was recrystallized by vapor phase diffusion of diethyl ether into a concentrated nitromethane/dichloromethane solution of the crude product in an almost quantitative yield. – **Method B:** A solution of **3dBF$_4$** (1700 mg, 0.93 mmol) in dichloromethane/ethanol (1:1; 70 mL) was heated to reflux. After heating for 2 h, the color of the reaction mixture had changed from violet-red to dark-brown. After 10 h of heating, the ν_{CN} absorptions of **3dBF$_4$** had completely disappeared. The mixture was cooled to room temperature, the solvent was evaporated in vacuo and the residue was purified by chromatography on silica gel (ICN Biomedicals, 32–63 μm, 60 Å). Gradually changing the solvent polarity from dichloromethane to dichloromethane/nitromethane (1:1) **5dBF$_4$** was eluted as a brown-red band. After drying in vacuo, 850 mg (70%) **5dBF$_4$** was obtained as a brown solid. Further purification by recrystallization from dichloromethane/ethanol yielded 510 mg (41%) of violet-red hexagonal and cube-shaped crystals of **5dBF$_4$**. – **Method C:** A solution of NaTCNE (227 mg, 1.5 mmol) and sodium hexafluorophosphate (218 mg, 1.3 mmol) in 30 mL of ethanol was added to a suspension of $FeCl_2$ (338 mg, 1 mmol) and *tripod* (625 mg, 1 mmol) in 30 mL of dichloromethane. Stirring of the dark solution for 20 h at room temperature resulted in the formation of a brown-red precipitate, which was isolated, extracted with nitromethane and filtered through 1 cm of silica gel (ICN Biomedicals, 32–63 μm, 60 Å). Evaporation of the solvent from the filtrate left 455 mg (68%) **5dPF$_6$** as a brown solid. For purification, this product was recrystallized by vapor phase diffusion of diethyl ether into a concentrated nitromethane/dichloromethane solution of the crude product giving 370 mg (55%) of violet cube-shaped

Table 7. Crystallographic data of compounds **5dBF$_4$** and **5dPF$_6$** with ligands derived from TCNE

Compound	**5dBF$_4$** [a]	**5dBF$_4$** [b]	**5dPF$_6$** [b] [c]
Solvate	·1.5 H_2O·1.5 C_2H_5OH	·2.1 CH_2Cl_2·4.5 H_2O	·1.5 CH_3NO_2·1.5 C_2H_5OH
Empirical formula (without solvate)	$C_{143}H_{122}BF_4Fe_4N_{14}P_9$	$C_{141}H_{124}BF_4Fe_4N_{12}OP_9$	$C_{141}H_{123}ClF_6Fe_4N_{12}P_{10}$
Molecular mass [g/mol]	2625.6	2591.6	2668.2
Crystal size [mm]	0.20×0.25×0.20	0.40×0.30×0.20	0.30×0.30×0.30
Crystal system	cubic	hexagonal	trigonal
Space group	$P\bar{4}3n$	$P31c$	$P31c$
a [pm]	3278.8(3)	1909.3(3)	1911.8(3)
b [pm]	3278.8(3)	1909.3(3)	1911.8(3)
c [pm]	3278.8(3)	2418.5(5)	2434.5(2)
α [°]	90	90	90
β [°]	90	90	90
γ [°]	90	120	120
V [10^6pm^3]	35247.6(58)	7635.00	7705.9(18)
Z	8	2	2
d_x [g·cm^{-3}]	1.013	1.231	1.218
T [K]	293	200	200
Scan range	2.8° ≤ 2θ ≤ 46.5°	3.0° ≤ 2θ ≤ 52. 0°	2.5° ≤ 2θ ≤ 50.1°
Method	ω-scan, Δω =1.0°	ω-scan, Δω =1.0°	ω-scan, Δω =0.54°
Scan speed	10 s/frame	10 s/frame	12°/min
No. of measured rflns.	16198	26051	9130
No. of unique rflns.	8469	9514	4777
No. of observed rflns.	6370	8091	3344
Observation criterion	$I \geq 2\sigma$	$I \geq 2\sigma$	$I \geq 2\sigma$
No. of param. refined	590	541	420
Resid. el. dens. [10^{-6} e·pm^{-3}]	1.13	1.48	2.07
R_1/R_w (%) (refinement on F^2)	8.7/25.3	8.0/23.4	10.9/25.5

[a] The counterion BF_4^- is replaced by CN^- in about 50 % of the molecules within the crystal. The $CH(CN)_2$ substituent is exchanged by a CH_2CN group in 65 % of the molecules. – [b] The substituents at the bridging dicyanomethanide units are found to be CH_2CN groups. – [c] Data for **5dPF$_6$** were collected with a Siemens (Nicolet synthex) R3m/V diffractometer.

crystals of **5dPF$_6$**. Analytical and spectroscopic data of compound **5dBF$_4$** are listed in Tables 3 and 4.

X-ray Crystallographic Study: Suitable crystals were taken directly out of the mother liquor, immersed in perfluorinated polyether oil and fixed to a glass capillary. The measurements were carried out with a Nonius-Kappa CCD diffractometer (low-temperature unit, graphite-monochromated Mo-K_α radiation), unless stated otherwise. The data were processed by the standard Nonius software.[38] All calculations were performed using the SHELX software package. Structures were solved by direct methods with the program SHELXS-97[39] and refined with the program SHELXL-97.[40] Graphical handling of the structural data during solution and refinement was performed with XPMA.[41] Atomic coordinates and anisotropic thermal parameters of the non-hydrogen atoms were refined by full-matrix least-squares calculations. Data for the structure determinations are compiled in Tables 5, 6 and 7. Figures 1 and 3 were prepared using WinRay-32 [42] and WinRay-GL.[43] Crystallographic data (excluding structure factors) for the structures reported in this paper have been deposited with the Cambridge Crystallographic Data Centre as supplementary publication nos. CCDC-156047 to -156055. Copies of the data can be obtained free of charge on application to CCDC, 12 Union Road, Cambridge CB2 1EZ, UK [Fax: (internat.) + 44-1223/336-033; E-mail: deposit@ccdc.cam.ac.uk].

Acknowledgments

We are indebted to the Deutsche Forschungsgemeinschaft and the Fonds der Chemischen Industrie for financial support. The unselfish cooperation of Dr. J. Groß and co-workers of the mass spectrometry department and the workers of the microanalytical laboratory of the Organisch-Chemisches Institut der Universität Heidelberg is gratefully acknowledged. We are indebted to Mr. D. Günauer for the cyclic voltammetric measurements.

[1] S. Mann, G. Huttner, L. Zsolnai, K. Heinze, *Angew. Chem.* **1996**, *108*, 2983; *Angew. Chem. Int. Ed. Engl.* **1996**, *35*, 2808.
[2] H. Heidel, J. Scherer, A. Asam, G. Huttner, O. Walter, L. Zsolnai, *Chem. Ber.* **1995**, *128*, 293.
[3] J.-M. Lehn *Supramolecular Chemistry – Concepts and Perspectives*, VCH, Weinheim, **1995**.
[4] D. L. Caulder, K. N. Raymond, *J. Chem. Soc., Dalton Trans.* **1999**, 1185.
[5] M. Fujita, *Struct. Bond.* **2000**, *96*, 177.
[6] R. W. Saalfrank, E. Uller, B. Demleitner, I. Berndt, *Struct. Bond.* **2000**, *96*, 149.
[7] B. Olenyuk, A. Fechtenkötter, P. J. Stang, *J. Chem. Soc., Dalton Trans.* **1998**, 1707.
[8] S. Mann, G. Huttner, L. Zsolnai, K. Heinze, V. Jacob, B. Antelmann, A. Driess, B. Schiemenz, *Z. Naturforsch., Teil B* **2000**, *55*, 638.
[9] J. P. Fleury, B. Libis, *Bull. Soc. Chim. Fr.* **1966**, 1966.
[10] R. Dijkstra, H. J. Backer, *Recl. Trav. Chim. Pays-Bas* **1954**, *73*, 569.
[11] H. Köhler, K. Rassmi, H. Skirl, *Z. Allg. Anorg. Chem.* **1985**, *529*, 173.
[12] F. Arndt, H. Scholz, E. Frobel, *Justus Liebigs Ann. Chem.* **1936**, *521*, 95.
[13] J. A. Elvidge, P. N. Judson, A. Percival, R. Shah, *J. Chem. Soc., Perkin Trans. 1* **1983**, 1741.

[14] W. J. Middleton, R. E. Heckert, E. L. Little, C. G. Krespan, *J. Am. Chem. Soc.* **1958**, *80*, 2783.
[15] W. J. Middleton, E. L. Little, D. D. Coffman, V. A. Engelhardt, *J. Am. Chem. Soc.* **1958**, *80*, 2795.
[16] H. Köhler, G. Lux, *Inorg. Nucl. Chem. Lett.* **1968**, *4*, 133.
[17] The anion derived from **H1d** upon monodeprotonation has been studied: O. E. Nasakin, E. G. Nikolaev, P. B. Terent'ev, V. D. Sheludyakov, *J. Org. Chem. USSR (Engl. Transl.)* **1987**, *23*, 597.
[18] A. G. Sharpe *The Chemistry of Cyano Complexes of the Transition Metals*, Academic Press, New York, **1976**.
[19] L. Jäger, B. Freude, A. Krug, H. Hartung, *J. Organomet. Chem.* **1994**, *467*, 163.
[20]]L. Jäger, B. Freude, R. Skirl, H. Köhler, *Z. Allg. Anorg. Chem.* **1993**, *619*, 711.
[21] V. Jacob, G. Huttner, E. Kaifer, P. Kircher, *Z. Naturforsch.*, in press
[22] T. C. Gibb, N. N. Greenwood, *J. Chem. Soc.* **1965**, 6989.
[23] P. R. Edwards, C. E. Johnson, R. J. P. Williams, *J. Chem. Phys.* **1967**, *47*, 2074.
[24] G. M. Bancroft, J. M. Dubery, *J. Chem. Phys.* **1969**, *50*, 2264.
[25] F. A. Cotton, C. A. Murillo, D. F. Timmons, *Polyhedron* **1999**, *18*, 423.
[26] R. S. Drago *Physical Methods in Inorganic Chemistry*, 2ed., Saunders, Philadelphia, **1992**.
[27] O. W. Webster, W. Mahler, R. E. Benson, *J. Org. Chem.* **1960**, *25*, 1470.
[28] O. W. Webster, W. Mahler, R. E. Benson, *J. Am. Chem. Soc.* **1962**, *84*, 3678.
[29] C. Creutz, *Prog. Inorg. Chem.* **1983**, *30*, 1.
[30] J. E. Sutton, P. M. Sutton, H. Taube, *Inorg. Chem.* **1979**, *18*, 1017.
[31] H. Krenzien, H. Taube, *J. Am. Chem. Soc.* **1976**, *98*, 6379.
[32] H. Krenzien, H. Taube, *Inorg. Chem.* **1982**, *21*, 4001.
[33] A. Asam, B. Janssen, G. Huttner, L. Zsolnai, O. Walter, *Z. Naturforsch., Teil B* **1993**, *48*, 1707.
[34] *Organikum*, Deutscher Verlag der Wissenschaften, Berlin, **1990**,
[35] W. Hewertson, H. R. Watson, *J. Chem. Soc.* **1962**, 1490.
[36] A. Muth, O. Walter, G. Huttner, A. Asam, L. Zsolnai, C. Emmerich, *Z. Naturforsch., Teil B* **1994**, *49*, 149.
[37] H. Funk, F. Binder, *Z. Anorg. Allg. Chem.* **1926**, *155*, 327.
[38] *DENZO-SMN*, Data processing software, Nonius **1998**; http://www.nonius.com
[39] G. M. Sheldrick, *SHELXS-97*, Program for Crystal Structure Solution, University of Göttingen, **1997**; http://shelx. uni-ac. gwdg. de/shelx/index. html
[40] G. M. Sheldrick, *SHELXL-97*, Program for Crystal Structure Refinement, University of Göttingen, **1997**; http://shelx. uni-ac. gwdg. de/shelx/index. html
[41] L. Zsolnai, G. Huttner, *XPMA*, University of Heidelberg, **1994**; http://www.uni-heidelberg.de/institute/fak12/AC/huttner/htmlsoftware. html
[42] R. Soltek, G. Huttner, *WinRay-32*, University of Heidelberg, **1998**; http://www.uni-heidelberg.de/institute/fak12/AC/huttner/htmlsoftware.html
[43] R. Soltek, G. Huttner, *WinRay-GL*, University of Heidelberg, **2000**; http://www.uni-heidelberg.de/institute/fak12/AC/huttner/htmlsoftware.html.

Received February 16, 2001
[I01056]

Mixed-Ligand Copper(II) Complexes with the Rigid Bidentate Bis(*N*-arylimino)acenaphthene Ligand: Synthesis, Spectroscopic-, and X-ray Structural Characterization

Adriana Paulovicova,[a] Usama El-Ayaan,[a,b] Koichi Shibayama,[c] Takeharu Morita,[c] and Yutaka Fukuda*[a]

Keywords: N ligands / Copper / X-ray crystal structures / Magnetic properties

Reported are the synthesis, characterization, and crystal structures of two mixed-ligand copper(II) complexes containing bis[*N*-(2,6-diisopropylphenyl)imino]acenaphthene (*o,o′*-*i*$Pr_2C_6H_3$-BIAN). In both complexes, namely [Cu(AcOH)(*o,o′*-*i*$Pr_2C_6H_3$-BIAN)Cl_2] (**1**) and [Cu(acac)(AcOH)(*o,o′*-*i*$Pr_2C_6H_3$-BIAN)](ClO_4) (**2**) (acac = acetylacetonate and AcOH = acetic acid), the copper ions are in a distorted square-pyramidal coordination environment with an acetic acid molecule in each apical position. The two imine nitrogen atoms of *o,o′*-*i*$Pr_2C_6H_3$-BIAN occupy the basal plane with the two chloride atoms and the two oxygen atoms of acac in complexes **1** and **2**, respectively. Complex formation results in certain structural changes inside the rigid N–N ligand. Such changes led to an increased planarity of the *o,o′*-*i*$Pr_2C_6H_3$-BIAN backbone, and produced a nearly perpendicular angle between the naphthalene and the aromatic imine planes. In complex **2**, the more perpendicular arrangement of the *o,o′*-diisopropylphenyl groups shielding the copper centre was structurally allowed by the elongation of one of the metal-to-ligand bonds and by the relatively larger N–Cu–N bite angle. Also discussed are IR, magnetic, and UV/Vis measurements.

Introduction

During the last decade there has been an increased interest in the use of bidentate and tridentate ligands in catalysis.[1−4] Recently, special attention has focused on the catalytic reactivity of late transition metals, for example, rhodium, palladium, and platinum, and their complexation with rigid bidentate ligands[5−9] such as bis(*N*-arylimino)acenaphthene (Ar-BIAN), which was first introduced by van Asselt and Elsevier in the early 1990s.[10] It has been shown that such metal systems containing Ar-BIAN are efficient catalysts in, for example, the homogeneous catalytic hydrogenation of alkynes,[11] in catalytic multi-component C−C coupling reactions,[10,12] and as models for co-polymerization or as catalysts in polymerization of alkenes.[13,14]

These (Ar-BIAN) ligands contain two conjugated imine functions, but they differ markedly from the commonly used diimine ligands such as 2,2′-bipyridine (bpy) and 1,10-phenanthroline (phen). Firstly, the presence of two exocyclic imines, that are not part of the heteroaromatic ring system, is expected to lead to better σ-donating and π-accepting properties as compared to bpy and phen.[15−17] This property allows (Ar-BIAN) ligands to stabilize both the higher and lower oxidation states of the coordinated metal ions. Secondly, the rigidity of the acenaphthene backbone forces the imine *N*-atoms to remain in a fixed *cis* orientation, favouring the chelating coordination to a metal centre. Despite all the effort that has been put into the chemistry of rigid bidentate nitrogen ligands, there is a lack of available structural data. This is probably caused by the difficulties in growing single crystals for X-ray determination.

Our current interest is focused on the structural accommodation of bulky derivatives of 1,10-phenanthroline around the copper ion.[18] Therefore, we thought it would be reasonable to investigate coordination possibilities of such a huge, rigid ligand, namely bis[*N*-(2,6-diisopropylphenyl)imino]acenaphthene (*o,o′*-*i*$Pr_2C_6H_3$-BIAN) (Figure 1) when imposed on a copper centre. In this paper, we describe the isolation and full characterization, including X-ray structures, of two novel mixed-ligand copper(II) complexes, namely [Cu(AcOH)(*o,o′*-*i*$Pr_2C_6H_3$-BIAN)Cl_2] (**1**), and [Cu(acac)(AcOH)(*o,o′*-*i*$Pr_2C_6H_3$−BIAN)](ClO_4) (**2**).

[a] Department of Chemistry, Faculty of Science, Ochanomizu University, 2-1-1 Otsuka,
Bunkyo-ku, Tokyo 112-8610, Japan
Fax: (internat.) + 81-3/5978-5137
E-mail: fukuda@cc.ocha.ac.jp
[b] Department of Chemistry, Faculty of Science, Mansoura University,
Mansoura 35516, Egypt
E-mail: usama@cc.ocha.ac.jp
[c] Sekisui Chemical Co., Ltd., 2-1 Hyakuyama, Shimamoto-cho, Mishima-gun,
Osaka 618-8589, Japan

Results and Discussion

Crystal-Structure Analysis of Complexes 1 and 2

[Cu(AcOH)(*o,o′*-*i*$Pr_2C_6H_3$-BIAN)Cl_2] (1)

An ORTEP plot (30% thermal ellipsoids) showing the atomic-numbering scheme employed is given in Figure 2. This complex contains a distorted square-pyramidal cop-

 © WILEY-VCH Verlag GmbH, 69451 Weinheim, 2001 1434−1948/01/1010−2641 $ 17.50+.50/0

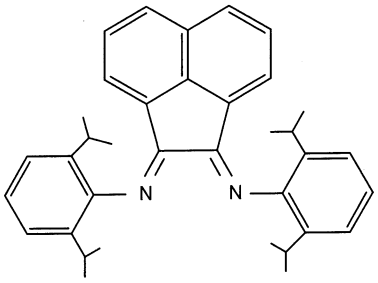

Figure 1. The structure of *o,o′*-*i*$Pr_2C_6H_3$-BIAN

per(II) moiety with two imine nitrogen atoms and two chloride atoms occupying the basal plane, as well as an acetic acid molecule in the apical site. This acetic acid ligand has the relatively longer bond length of 2.467(3) Å compared to those of the basal plane. X-ray analysis of complex **1** indicates that the imine C=N bonds N(1)−C(1) and N(2)−C(5) of 1.284(3) and 1.286(3) Å, respectively, are slightly longer than the standard N(sp^2)=C(sp^2) double bond (1.27 Å).[19] This is simply due to the coordination to the copper(II) centre. Upon coordination, a lowering of the strain in the naphthalene backbone occurs, which is indicated by the C(1)−C(5) bond shortening to 1.500(3) Å as compared to the corresponding bond length of 1.535(3) Å in case of free bis(*p*-tolylimino)acenaphthene (*p*-Tol-BIAN).[15] Torsion angels N(1)−C(1)−C(5)−N(2) of −0.3(3)° and C(2)−C(1)−C(5)−C(4) of −0.4(3)° reflect a planarity of the bis(imino)acenaphthene moiety. Angles between the planes of the naphthalene and aromatic N substituents are close to perpendicular (84°), and in good agreement with the corresponding angles of (84°) in [Pd(Me)Cl(*o,o′*-*i*$Pr_2C_6H_3$-BIAN)][15] and (85°) in [Pd(*o,o′*-*i*$Pr_2C_6H_3$-BIAN)(MA)][20] (MA = maleic anhydride), but larger than in [Pd(*p,p′*-$Me_2C_6H_3$-BIAN)(MA)][21] of (55°) and the free *p*-Tol-BIAN ligand of (61°). This must certainly be ascribed to the presence of *o*-isopropyl substituents rather than to the coordination to the metal ion.

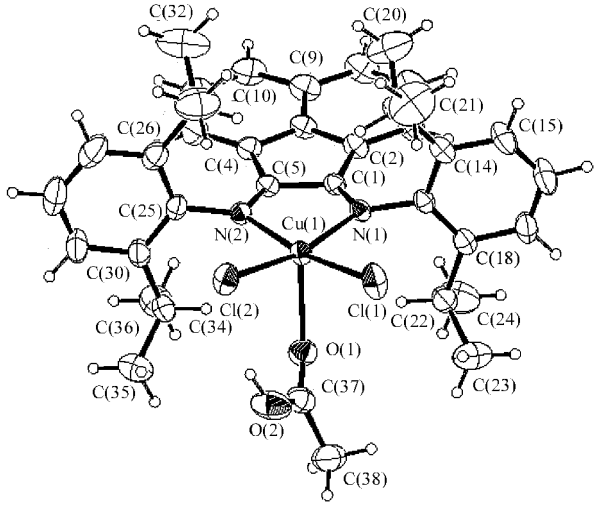

Figure 2. An ORTEP view of [Cu(AcOH)(*o,o′*-*i*$Pr_2C_6H_3$-BIAN)Cl_2] (**1**)

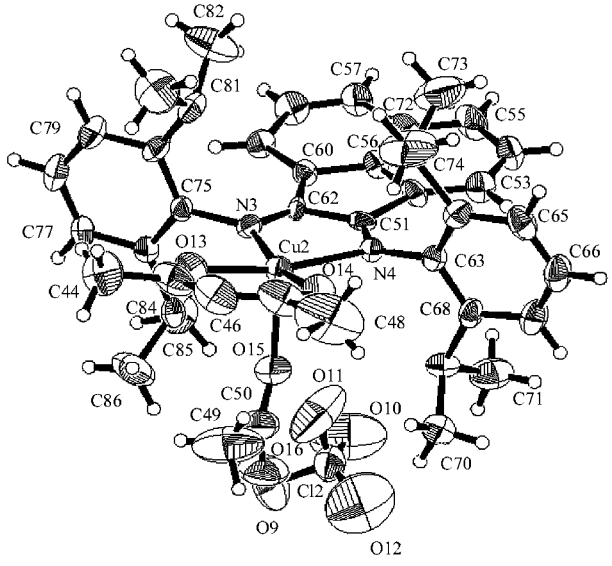

Figure 3. An ORTEP view of [Cu(acac)(AcOH)(*o,o′*-*i*$Pr_2C_6H_3$-BIAN)]·(ClO_4) (**2**)

[Cu(acac)(AcOH)(*o,o′*-*i*$Pr_2C_6H_3$-BIAN)]·(ClO_4) (2)

An ORTEP plot (30% thermal ellipsoids) showing the atomic-numbering scheme employed is given in Figure 3. The monodentate acetic acid, the bidentate acac, and (N−N) ligands coordinate to Cu^{II} to form a slightly-distorted square-pyramidal coordination geometry. Its basal plane contains two oxygen atoms of acac and two imine nitrogen atoms of *o,o′*-*i*$Pr_2C_6H_3$-BIAN, while the monodentate acetic acid is accommodated in the apical position. Selected bond lengths and angles of both complex **1** and **2** are given in Table 1.

The crystallographic asymmetry of complex **2** is clearly reflected by the different imine (N−C) bond lengths: N(3)−C(62) is 1.286(3) Å and N(4)−C(51) is 1.359(2) Å. A comparison with complex **1** shows a more planar bis(imino)acenaphthene skeleton as confirmed by the smaller torsion angles [N(3)−C(62)−C(51)−N(4) = 0.1(2)° and C(60)−C(62)−C(51)−C(52) = 0.3(2)°] and the rather shorter C(62)−C(51) bond length of 1.433(2) Å.

The *o,o′*-diisopropylphenyl groups are bent towards the naphthalene backbone, away from the copper centre, with nearly perpendicular angles between the planes of naphthalene and the aromatic imine. This approximately perpendicular arrangement of the *o,o′*-diisopropylphenyl groups in complex **2** shields the copper centre more effectively above and below the coordination plane. This extra shielding makes it difficult to accommodate the (acac) ligand within the basal plane. This problem is perfectly solved by the appropriate structural changes inside the *o,o′*-*i*$Pr_2C_6H_3$-BIAN ligand, namely by the elongation of N(4)−C(51) to 1.359(2) Å, and the larger bite angle N(3)−Cu(2)−N(4) of 82°, as compared to the corresponding angle of 80° in case of **1**. There is also a shortening of the C(62)−C(51) bond to 1.433(2) Å. Consequently, all these changes within the *o,o′*-

Table 1. Selected bond lengths [Å], angles [°], and torsion angles [°] for complexes **1** and **2**

1		**2**	
Cu(1)−N(1)	2.0561(19)	Cu(2)−N(3)	2.0153(14)
Cu(1)−N(2)	2.084(2)	Cu(2)−N(4)	2.0755(13)
Cu(1)−Cl(1)	2.2213(8)	Cu(2)−O(13)	1.8924(17)
Cu(1)−Cl(2)	2.2453(7)	Cu(2)−O(14)	1.8982(16)
Cu(1)−O(1)	2.467(3)	Cu(2)−O(5)	2.2721(13)
N(1)−C(1)	1.284(3)	N(3)−C(62)	1.286(2)
N(1)−C(13)	1.442(3)	N(3)−C(75)	1.480(2)
N(2)−C(5)	1.286(3)	N(4)−C(51)	1.359(2)
N(2)−C(25)	1.450(3)	N(4)−C(63)	1.422(2)
C(1)−C(5)	1.500(3)	C(62)−C(51)	1.433(2)
C(1)−C(2)	1.455(3)	C(62)−C(60)	1.442(2)
C(5)−C(4)	1.469(3)	C(51)−C(52)	1.505(2)
N(1)−Cu(1)−N(2)	80.36(8)	N(3)−Cu(2)−N(4)	81.81(5)
Cl(1)−Cu(1)−Cl(2)	95.58(3)	O(13)−Cu(2)−O(14)	94.87(7)
N(1)−Cu(1)−Cl(1)	91.30(6)	N(3)−Cu(2)−O(13)	90.98(7)
N(2)−Cu(1)−Cl(2)	91.63(6)	N(4)−Cu(2)−O(14)	90.42(6)
N(1)−Cu(1)−O(1)	95.4(1)	N(3)−Cu(2)−O(15)	93.36(7)
N(2)−Cu(1)−O(1)	94.6(1)	N(4)−Cu(2)−O(15)	94.33(7)
Cu(1)−N(1)−C(1)	112.92(15)	Cu(2)−N(3)−C(62)	114.96(11)
Cu(1)−N(1)−Cl(13)	129.00(15)	Cu(2)−N(3)−C(75)	129.14(11)
Cu(1)−N(2)−C(5)	112.27(17)	Cu(2)−N(4)−C(51)	107.03(11)
Cu(1)−N(2)−C(25)	127.41(16)	Cu(2)−N(4)−C(63)	128.17(10)
C(5)−N(2)−C(25)	119.8(2)	C(51)−N(4)−C(63)	124.59(14)
C(1)−N(1)−C(13)	117.66(19)	C(75)−N(3)−C(62)	115.78(14)
		O(13)−Cu(2)−O(15)	95.20(8)
		O(14)−Cu(2)−O(15)	97.83(9)
C(18)−C(13)−N(1)−C(1)	92.1(4)	C(76)−C(75)−N(3)−C(62)	86.7(2)
C(30)−C(25)−N(2)−C(5)	−98.5(4)	C(68)−C(63)−N(4)−C(51)	−87.0(2)
C(14)−C(13)−N(1)−C(1)	−87.8(4)	C(80)−C(75)−N(3)−C(62)	−94.60(19)
C(26)−C(25)−N(2)−C(5)	83.8(4)	C(64)−C(63)−N(4)−C(51)	92.6(2)
C(1)−C(2)−C(3)−C(4)	−0.2(3)	C(62)−C(60)−C(61)−C(52)	0.95(19)
C(2)−C(3)−C(4)−C(5)	−0.1(3)	C(51)−C(52)−C(61)−C(60)	−0.67(17)
N(1)−C(1)−C(5)−N(2)	−0.3(3)	N(3)−C(62)−C(51)−N(4)	0.1(2)
C(2)−C(1)−C(5)−C(4)	−0.4(3)	C(60)−C(62)−C(51)−C(52)	0.3(2)

i$Pr_2C_6H_3$-BIAN ligand led to one relatively long Cu(2)−N(4) distance of 2.0755(13) Å compared to the [Cu(2)−N(3) distance of 2.0153(14) Å]. Complex **2** with the structural index parameter value, τ, of 2.6% shows a more regular square-pyramidal geometry than complex **1** with a τ equal to 4.5%. According to Addison et al.,[22] τ should have a value of 0% for a perfect square-pyramid and 100% for a perfect trigonal pyramidal structure: $\tau = \{(\theta - \varphi)/60\} \times 100$, where θ and φ are the largest and the second largest basal angles, respectively.

The Cu−O(acac) distances, namely Cu(2)−O(13) = 1.8924(17) Å and Cu(2)−O(14) = 1.8982(16) Å, and the bite angle O(13)−Cu(2)−O(14) of 94.87(7)° are similar to the corresponding distances and bite angles observed in other mixed ligand copper(II) complexes containing the acac ligand.[18,23,24]

It is reasonable to make a structural comparison of complex **2** with the [Cu(acac)(dmph)(NO_3)] complex[18] (dmph = 2,9-dimethyl-1,10-phenanthroline). Namely, in the former complex, the two isopropylphenyl moieties allow only a planar coordination of the diimine, while in the latter, the methyl substituents that are in the same diimine plane prevent both N donors from occupying the basal plane together with the acac ligand (Figure 4).

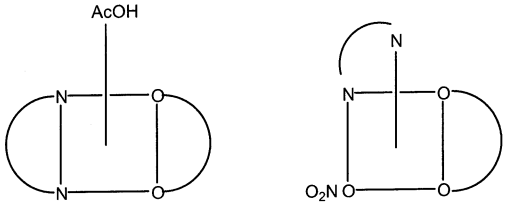

Figure 4. Schematic structures of complex **2** and [Cu(acac)(dmph)(NO_3)]

IR and UV/Vis Spectroscopy

Infrared spectroscopic data for the free *o,o′*-*i*$Pr_2C_6H_3$-BIAN ligand and both complexes **1** and **2** are listed in Table 2. Formation of the free *o,o′*-*i*$Pr_2C_6H_3$-BIAN ligand can be determined from the IR spectroscopy where only C=N stretching vibrations were observed in the 1642−1671 cm^{-1} range and no C=O stretching vibrations of the starting diketones in the 1700−1800 cm^{-1} region. The bands

assigned to ν(C=N) are shifted to lower wavenumbers in the complex formation indicating, the coordination of both diimine nitrogen atoms of *o,o′*-*i*$Pr_2C_6H_3$-BIAN ligand to the copper(II) ion. Strong bands observed in the 1695 and 1705 cm^{-1} regions for complex **1** and **2**, respectively, indicate the coordination of an acetic acid molecule.

Table 2. IR spectra (cm^{-1}) of *o,o′*-*i*$Pr_2C_6H_3$-BIAN ligand and complexes **1** and **2**

Compound	ν(C=N)	ν(ClO_4^-)	ν(AcOH)
o,o′-*i*$Pr_2C_6H_3$-BIAN	1671, 1652, 1642	–	–
Complex **1**	1661, 1635	–	1695
Complex **2**	1668, 1640	1110, 622	1705

IR spectra of complex **2** show two peaks, 1570 and 1519 cm^{-1}, that can be assigned to ν(C=O) and ν(C=C) of the acac ligands, respectively, consistent with those observed for [Cu(acac)$_2$].[25] The strong band observed at 1110 cm^{-1} (antisymmetric stretch) and the sharp band at 622 cm^{-1} (antisymmetric bend), suggest uncoordinated perchlorate anions[26] in agreement with the X-ray structure of **2**.

Solid-state room-temperature electronic spectra of **1** and **2** exhibit a broad d-d band at 700 and 625 nm, respectively, typical for square-pyramidal copper(II) complexes.[27−29] Another band appeared in the visible spectral region, 558 and 545 nm, of complexes **1** and **2**, respectively, assigned to the MLCT transitions from copper(II) to the π* orbitals of *o,o′*-*i*$Pr_2C_6H_3$-BIAN. This shift to much longer wavelength than those of other diimine ligands can be explained on the basis that the *o,o′*-*i*$Pr_2C_6H_3$-BIAN ligand provides π* orbitals at rather low energies[17,30,31] that results in the increased overlap with the metal d orbitals. Consequently, this results in a stronger π-bonding interaction accompanied by a red-shift of the MLCT transition. Electrochemical studies[32] on the π-acceptor properties of the bis(arylimino) acenaphthene reveal a much larger positive potential than those of other diimine ligands confirming the larger π-acceptor strength of bis(arylimino)acenaphthene.

Absorption spectra of both complexes show various bands below 420 nm that can be assigned to intraligand transitions of the free diimine ligand, which absorbs in the same spectral region. Electronic spectra were also recorded in solution using a variety of solvents (DCE, THF, toluene, and chloroform). All solution spectra of both complexes **1** and **2** are very similar to the corresponding solid-state spectra.

Conclusion

From the X-ray structure analysis of both copper(II) complexes **1** and **2** we can conclude that the two diisopropylphenyl moieties on the imine nitrogens of the *o,o′*-*i*$Pr_2C_6H_3$-BIAN ligand are flexible and show no conjugation with the naphthalene-diimine backbone. We have shown the difference in the coordination behaviour of this ligand when bound to the copper(II) ion. In complex **1**, a common equal-in-length bidentate coordination of *o,o′*-*i*$Pr_2C_6H_3$-BIAN was observed. In complex **2**, the pronounced shielding effect introduced by the *o,o′*-diisopropylphenyl groups, resulting from the more perpendicular arrangement, was identified by the relatively longer (Cu−N) bond, and by the respective changes inside the *o,o′*-*i*$Pr_2C_6H_3$-BIAN ligand. UV/Vis absorption spectra of both complexes indicate a strong π-back-bonding and a smaller HOMO−LUMO energy gap.

Experimental Section

Materials and Instrumentation: All chemicals were purchased from the Wako Pure Chemical Industries Ltd., and used without further purification.

Elemental analyses (C, H, N) were performed on a PE 2400 Series II CHNS/O Analyzer. − Electronic spectra were recorded on a UV-3100PC Shimadzu spectrophotometer using 10 mm quartz cells at room temperature. Powder reflectance spectra were obtained using the same instrument equipped with an integrating sphere and using $BaSO_4$ as a reference. − Infrared spectra were recorded on a Perkin−Elmer FT-IR Spectrometer Spectrum 2000 in a KBr pellet and as a Nujol mull in the 4000−370 cm^{-1} spectral range. − Magnetic susceptibilities were measured at room temperature on a Shimadzu MB-100 Torsion Magnetometer. Diamagnetic corrections were considered by using Pascal's constants.[33] − Thermogravimetric measurements were performed on a DTG-50 Shimadzu instrument. − ^1H and ^{13}C NMR spectra were run on a JEOL JNM LA 300 WB spectrometer at 300.40 and 75.45 MHz, respectively, using a 5 mm probe head. CD_2Cl_2 and $CDCl_3$ were used as a solvent. Chemical shifts are given in ppm relative to the internal TMS standard. The typical pulse width was 6.25 μs for ^1H and 4.25 μs for ^{13}C measurements. Assignment of the ^{13}C signals based on ref.[15] was confirmed by off-resonance decoupled and DEPT-135 measurements.

Synthesis of [*N*-(2,6-Diisopropylphenyl)imino]acenaphthene: This ligand was prepared using a method different to that published by Asselt, Elsevier et al.[15] Acenaphthenequinone (1.35 g, 7.4 mmol) in 65 mL of acetonitrile was heated under reflux (80 °C) for 30 min. Then 12 mL of acetic acid was added and heating was continued until the acenaphthenequinone had completely dissolved. To this hot solution, 3 mL (16 mmol) of 2,6-diisopropylaniline was added directly and the solution was heated under reflux for a further 1.5 h. It was then cooled to room temperature and the solid filtered off to give a yellow product that was washed with hexane and air-dried. Yield 3.15 g (85%). − $C_{36}H_{40}N_2$ (500.7): calcd. C 86.35, H 8.05, N 5.60; found. C 85.85, H 8.03, N 5.34%. − ^1H NMR ($CDCl_3$, 300.40 MHz, 24 °C): δ = (0.97 d, 15-H), 1.23 (d, 16-H), 3.03 (sept, 14-H), 6.63 (d, 3-H), 7.26 (s, 12-H, 11-H, 10-H), 7.36 (pst, 4-H), 7.88 (d, 5-H). − ^{13}C NMR (CD_2Cl_2, 300.40 MHz, 25.4 °C): δ = 23.1 (C-16), 23.2 (C-15), 29.1 (C-14), 123.5 (C-11), 123.9 (C-10, C-12), 124.6 (C-3), 128.3 (C-4), 129.2 (C-5), 130.0 (C-2), 131.6 (C-6), 135.5 (C-9, C-13), 141.2 (C-7), 148.0 (C-8), 161.1 (C-1).

Synthesis of [Cu(AcOH)(*o,o′*-*i*$Pr_2C_6H_3$-BIAN)Cl_2] (1): Bis[*N*-(2,6-diisopropylphenyl)imino]acenaphthene, *o,o′*-*i*$Pr_2C_6H_3$-BIAN, (0.35 g, 0.7 mmol) was dissolved in a small amount of chloroform (99%). A mixture of chloroform/acetic acid (15 mL, the 2:1 ratio) was then added, and the solution was heated for 10 min at 60 °C. Subsequently, a methanolic solution (7 mL) of $CuCl_2 \cdot 2H_2O$ (0.12 g, 0.7 mmol) was added dropwise to the *o,o′*-*i*$Pr_2C_6H_3$-BIAN solu-

tion. This mixture was then stirred for 2 h at room temperature. After 2 days of slow evaporation in air, dark-green prism-shaped crystals formed and were suitable for the single X-ray measurement. Yield 0.39 g (80%). − $C_{38}H_{44}Cl_2CuN_2O_2$ (695.20): calcd. C 65.65, H 6.38, N 4.03; found. C 66.30, H 6.35, N 3.95%. μ_{eff}: 2.0 B.M. (19 °C).

Synthesis of [Cu(acac)(AcOH)(*o,o′*-*i*$Pr_2C_6H_3$-BIAN)]·(ClO_4) (2): Two preparation methods were used.

Method A: To a suspension of 0.26 g (0.7 mmol) of $Cu(ClO_4)_2·6H_2O$ and 0.35 g (0.7 mmol) of *o,o′*-*i*$Pr_2C_6H_3$-BIAN in 15 mL of AcOH, 0.07 mL (0.7 mmol) of acetylacetonate was added directly and the mixture was stirred at room temperature. After 3 hours the microcrystalline product precipitated from the dark green solution. This solid was filtered, washed with cyclohexane and dried in air. The yield of the green micro-crystals was 0.48 g (82%). − $C_{43}H_{51}ClCuN_2O_8$ (822.86): calcd. C 62.76, H 6.25, N 3.41; found C 62.55, H 6.33, N 3.58%. μ_{eff}: 1.7 B.M. (24 °C).

Method B: (The same amounts were used as in method A). Acetylacetonate was added directly to a methanolic solution (5 mL) of $Cu(ClO_4)_2·6H_2O$. This mixture was stirred (while heating) for 10 min. A hot 2:1 chloroform/acetic acid solution (10:5 mL) of *o,o′*-*i*$Pr_2C_6H_3$-BIAN was then added. The resulting clear (i.e. no solid) green solution was stirred for 1 h and left to stand in air. After 3 days, needle-shaped and prism-shaped crystals appeared, both of which were suitable for X-ray measurements. Data were collected from a needle-shaped single crystal. − Elem. anal. found: C 61.82, H 6.26, N 3.36%.

Table 3. Crystal data, data collection, and structure refinement for complexes **1** and **2**

	1	**2**
Crystal data		
Formula	$C_{38}H_{44}Cl_2CuN_2O_2$	$C_{43}H_{51}ClCuN_2O_8$
Molecular mass	695.23	822.84
Crystal system	Orthorhombic	Orthorhombic
Space group	*P*21 21 21	*Pba*2
a [Å]	12.1400(6)	21.7710(2)
b [Å]	13.2140(6)	21.7780(3)
c [Å]	23.1620(5)	18.66700(10)
α, β, χ [°]	90.00	90.00
V [Å^3]	3715.6(3)	8850.56(15)
Z	4	8
$D_{calcd.}$ [g·cm^{-3}]	1.326	1.363
μ [cm^{-1}]	13.19	6.12
Crystal size [mm]	0.35×0.25×0.13	0.50×0.45×0.25
Data collection		
Temperature [K]	298	293
θ range [°]	1.08−27.98	1.09−27.46
Radiation	Mo-K_α (Mon), 0.71073 Å	Mo-K_α (Mon), 0.71069 Å
Scan mode	Image Plate	ω
Data set	$-15 \le h \le 16$; $-17 \le k \le 17$; $-29 \le l \le 29$	$-28 \le h \le 19$; $-28 \le k \le 27$; $-24 \le l \le 23$
Total data	8650	59497
Unique data	8630	19854
Observed data	7836 [$I > 2.00\sigma(I)$]	13207 [$I > 2.00\sigma(I)$]
Refinement		
Refined parameters	407	1014
Final *R*, w*R*	0.0476, 0.1365	0.0608, 0.1552

X-ray Structure Determination of 1 and 2: Crystallographic data for both complexes are summarized in Table 3. Single crystals of **1** and **2** were obtained directly from a chloroform/acetic acid solution. Crystal data for complex **1** were collected (Mo-K_α radiation, graphite monochromator) with a Mac Science DIP2030 K diffractometer. While for complex **2**, a SMART/RA CCD diffractometer was used. Accurate unit cell parameters and orientation matrices were determined by a least-squares refinement of setting angles of a set of well-centred reflections. An Image Plate for **1** and ω scan method for **2** were used. In both cases, the initial structure was solved by SIR92[34] and refined by least-squares methods based on F^2 using SHELXL-97.[35] Thermal ellipsoids (30% probability) and molecular plots were drawn using the maXus (MacScience) and ORTEP programs, for **1** and **2**, respectively. Absorption corrections were applied by multiscan (T_{min}/T_{max} of 0.691:0.740) for **1** and SADABS[36] (T_{min}/T_{max} of 0.829:1.000) for **2**. All non-hydrogen atoms were refined anisotropically. Hydrogen atoms were added at calculated positions and refined while riding on their respective carrier atoms using three common isotropic thermal motion parameters (constrained for **1**, and mixed treatment for **2**).

Since the space groups of both complexes are polar, it was necessary to use the Flack absolute structure parameter,[37] which refined to $x = 0.056(13)$ in **1** and to $x = 0.00$ in **2**. There were two independent molecules in the asymmetric unit of complex **2**. The crystallographic data for both structures reported in this paper have been deposited at the Cambridge Crystallographic Data Centre as supplementary publication numbers CCDC-158181 and CCDC-158307 for **1** and **2**, respectively. Copies of the data can be obtained free of charge on application to CCDC, 12 Union Road, Cambridge CB2 1EZ, UK [Fax: (internat.) + 44-1223/336-033; E-mail: deposit@ccdc.cam.ac.uk].

Acknowledgments

This work was partly supported by a Grand-in-Aid (Scientific Research No. 11304046) from the Ministry of Education, Science, Culture and Sports of Japan. Usama El-Ayaan thanks the Ochanomizu University for supporting his stay in Japan. Authors are grateful to Prof. Yuji Ohashi and Ms. Champika Vithana, Tokyo Institute of Technology, for their help with the X-ray structure determinations.

[1] C. Botteghi, G. Chelucci, G. Chessa, G. Delogu, S. Gladiali, F. Soccolini, *J. Organomet. Chem.* **1986**, *304*, 217−225.
[2] M. E. Wright, S. A. Svejda, M.-J. Jin, M. A. Peterson, *Organometallics* **1990**, *9*, 136−146.
[3] H. Nishiyama, M. Kondo, T. Nakamura, K. Itoh, *Organometallics* **1991**, *10*, 500−508.
[4] U. Leutenegger, G. Umbricht, C. Fahrni, P. von Matt, A. Pfaltz, *Tetrahedron* **1992**, *48*, 2143−2156.
[5] J. H. Groen, C. J. Elsevier, K. Vrieze, W. J. J. Smeets, A. L. Spek, *Organometallics* **1996**, *15*, 3445−3455.
[6] J. H. Groen, J. G. P. Delis, P. W. N. M. van Leeuwen, K. Vrieze, *Organometallics* **1997**, *16*, 68−77.
[7] J. G. P. Delis, J. H. Groen, K. Vrieze, P. W. N. M. van Leeuwen, N. Veldman, A. L. Spek, *Organometallics* **1997**, *16*, 551−562.
[8] J. H. Groen, M. J. M. Vlaar, P. W. N. M. van Leeuwen, K. Vrieze, H. Kooijman, A. L. Spek, *J. Organomet. Chem.* **1998**, *551*, 67−79.
[9] R. A. Klein, P. Witte, R. van Belzen, J. Fraanje, K. Goubitz, M. Numan, H. Schenk, J. M. Ernsting, C. J. Elsevier, *Eur. J. Inorg. Chem.* **1998**, 319−330.

[10] R. van Asselt, C. J. Elsevier, *Organometallics* **1992**, *11*, 1999−2001.
[11] M. W. van Laren, C. J. Elsevier, *Angew. Chem. Int. Ed.* **1999**, *38*, 3715−3717.
[12] R. van Belzen, H. Hoffmann, C. J. Elsevier, *Angew. Chem. Int. Ed. Engl.* **1997**, *36*, 1743−1745.
[13] R. van Asselt, E. E. C. G. Gielens, R. E. Rülke, K. Vrieze, C. J. Elsevier, *J. Am. Chem. Soc.* **1994**, *116*, 977−985.
[14] L. K. Johnson, C. M. Kilian, M. Brookhart, *J. Am. Chem. Soc.* **1995**, *117*, 6414−6415.
[15] R. van Asselt, C. J. Elsevier, W. J. J. Smeets, A. L. Spek, R. Benedix, *Recl. Trav. Pays-Bas* **1994**, *113*, 88−98.
[16] K. J. Cavell, D. J. Stufkens, K. Vrieze, *Inorg. Chim. Acta* **1980**, *47*, 67−76.
[17] J. Reinhold, R. Benedix, P. Birner, H. Hennig, *Inorg. Chim. Acta* **1979**, *33*, 209−231.
[18] A. Paulovicova, U. El-Ayaan, Y. Fukuda, *Inorg. Chim. Acta*, in press.
[19] M. Burke-Laing, M. Laing, *Acta. Crystallogr., Sect. B* **1976**, *32*, 3216−3224.
[20] R. van Asselt, C. J. Elsevier, W. J. J. Smeets, A. L. Spek, *Inorg. Chem.* **1994**, *33*, 1521−1531.
[21] H. Kooijman, A. L. Spek, R. van Belzen, C. J. Elsever, *Acta Crystallogr., Sect. C* **1997**, *53*, 1593−1596
[22] A. W. Addison, T. N. Rao, J. Reedijk, J. van Rijn, G. C. Verschoor, *J. Chem. Soc. Dalton Trans.* **1984**, 1349−1356.
[23] C.-C. Su, S.-P. Wu, C.-Y. Wu, T.-Y. Chang, *Polyhedron* **1995**, *14*, 267−275.
[24] N. A. Bailey, D. E. Fenton, M. V. Fracklin, M. Hall, *J. Chem. Soc., Dalton Trans.* **1980**, 984−990.
[25] K. Nakamoto, *Infrared and Raman Spectra of Inorganic and Coordination Compounds*, fourth ed., Wiley-Interscience, New York, **1986**.
[26] P. Chaudhuri, M. Winter, U. Flörke, H.-J. Haupt, *Inorg. Chim. Acta* **1995**, *232*, 125−130.
[27] L. P. Battaglia, A. C. Bonamartini, S. Ianelli, M. A. Zoroddu, G. Sanna, *J. Chem. Soc. Faraday Trans.* **1991**, *87*, 3863−3867.
[28] H. Adams, N. A. Bailey, I. K. Campbell, D. E. Fenton, Q.-Y. He, *J. Chem. Soc. Dalton Trans.* **1996**, 2233−2237.
[29] M. M. Whittaker, W. R. Duncan, J. W. Whittaker, *Inorg. Chem.* **1996**, *35*, 382−386.
[30] A. J. Lees, *Chem. Rev.* **1987**, *87*, 711−743.
[31] D. J. Stufkens, *Coord. Chem. Rev.* **1990**, *104*, 39−112.
[32] G. Knör, M. Leirer, T. E. Keyes, J. G. Vos, A. Vogler, *Eur. J. Inorg. Chem.* **2000**, 749−751.
[33] E. König, *Magnetic Properties of Coordination and Organo-Metallic Transition Metal Compounds*, Springer-Verlag, Berlin, **1966**
[34] A. Altomare, G. Cascarano, C. Giacovazzo, A. Guagliardi, M. C. Burla, G. Polidori, M. Camalli, *J. Appl. Crystallogr.* **1994**, *27*, 435.
[35] *SHELXL-97*, *Program for the Refinement of Crystal Structures*, **1997**, G. M. Sheldrick, Univ. of Göttingen, Germany.
[36] *SADABS Program*, **1996**, G. M. Sheldrick, Univ. of Göttingen, Germany.
[37] H. D. Flack, *Acta Crystallogr., Sect. A* **1983**, *39*, 876−881.

Received February 26, 2001
[I01064]

Copper(II)-Promoted Chemical Transformations of 3-Substituted 5-(2′-Pyridyl)-1,4-benzodiazepin-2-one Derivatives. Crystal Structures and Spectroscopic Characterisation of Metal Complexes

Aleksandar Višnjevac,[a] Ljerka Tušek-Božić,[a] Maja Majerić-Elenkov,[a] Vitomir Šunjić,[a] and Biserka Kojić-Prodić*[a]

Keywords: N ligands / Racemization / Oxygenations / Ring contractions / Copper / IR spectroscopy

Enantiomerically pure 7-bromo-1,3-dihydro-3-hydroxymethyl-1-methyl-5-(2′-pyridyl)-2*H*-1,4-benzodiazepin-2-one, (+)-**1**, affords the dichloro adduct **3**, [$CuCl_2$(**1**)], when treated with a solution of $CuCl_2 \cdot 2H_2O$ in ethanol. Complex **3** is isolated as a racemic compound. The replacement of one chlorine atom with DMSO gives complex **4**, [CuCl(**1**-H)(DMSO)]. The C(3)-oxygenated product appears as a racemic *N,N,O*-tridentate ligand in the square-pyramidal complex **5**. Oxidative ring contraction of (+)-**1** yields 6-bromo-4-ethoxy-1,4-dihydro-1-methyl-4-(2′-pyridyl)-1,3-quinazoline, which acts as an *N,N*-bidentate ligand in the tetrahedral complex **6**. Reaction of 3-acetoxymethyl-7-bromo-1,3-dihydro-1-methyl-5-(2′-pyridyl)-2*H*-1,4-benzodiazepin-2-one, (±)-**2**, with $CuCl_2 \cdot 2H_2O$, affords the square-pyramidal complex **7**, [$CuCl_2$(**2**)]. In this complex the lactam oxygen atom of a neighbouring molecule binds to the fifth coordination site, hence forming an infinite chain of connected polyhedra in the crystal. Oxidative ring contraction of **2** leads to 6-bromo-1,4-dihydro-4-hydroxy-1-methyl-4-(2′pyridyl)-1,3-quinazoline, which acts as an *N,N*-bidentate ligand in the centrosymmetric binuclear five-coordinate Cu^{II} complex **8**. In this complex the di-μ-chloro bridges are asymmetrical: one Cl atom is in an apical position [Cu–Cl, 2.820 (7) Å], whereas the other is in an equatorial position [Cu–Cl, 2.252 (5) Å]. The complexes are characterised by IR spectroscopy and X-ray structure analysis. Mechanisms of racemisation, oxygenation and ring contraction are discussed.

Introduction

The tranquilising and sedative-hypnotic activity of 1,4-benzodiazepines prompted chemists to investigate their complexation properties with transition metals,[1−3] in an attempt to prepare even more potent drugs. Among the first isolated was $Cu^{II}Cl_2$(diazepam)$_2$ (diazepam known as Valium®), with a square-planar geometry around Cu^{II}.[4] To the best of our knowledge, few crystal structures of 1,4-benzodiazepine complexes are known so far.[5,6] Generally, it has been of practical interest to design ligands which can enforce specific metal coordinations of suitable geometry and electronic properties which lead to desired catalytically active coordination compounds. Such complexes can also serve as good models for studying the activity of metalloenzymes.[7,8] Thus, it was interesting to examine the chelation properties of 5-substituted 1,4-benzodiazepin-2-one ligands, and to study the substitution effect at the stereogenic centre (C3) on metal complexation.[9,10] In our previous studies we investigated the use of metal complexes of C(3)-substituted 5-phenyl- and 5-pyridyl-1,4-benzodiazepin-2-ones in non-catalytic, catalytic, and biocatalytic reactions.[9−16] We have already reported on the oxidative C(3)-acetoxylation of the 5-pyridyl-1,4-benzodiazepine derivative to the 3-acetoxy derivative promoted by a mixed reagent [$Pb^{IV}(AcO)_4$]/I_2.[17] In vitro metal-catalysed C(3)-oxygenation of 1,4-benzodiazepin-2-ones has been unprecedented. However, the stereochemistry of an analogous in vivo process, which is catalysed by cytochrome P450, has already been described in detail.[18−20]

In this work we report on the preparation and characterisation of Cu^{II} complexes with ligands (+)-**1** and (±)-**2** (Scheme 1), which have undergone oxygenation at C(3) and a ring contraction. The mechanism for ligand transformations in the presence of the copper ion is explained (Scheme 2). The understanding of the mechanism is based upon the structure of the initial components and the isolated complexes. This mechanism is strongly supported in similar transformations of (5-phenyl)-1,4-benzodiazepin-2-ones already reported.[21−25]

Results and Discussion

Preparation of the Complexes

The reactions of benzodiazepine ligands (+)-**1** and (±)-**2** with $CuCl_2$ dihydrate in ethanol have yielded various types of complexes as presented in Scheme 1. It was observed that both ligands (+)-**1** and (±)-**2** initially formed the dichloro adduct (±)-**3** and (±)-**7**, respectively. Recrystallisation of (±)-**3** in ethanol at room temperature gave a mixture of the complexes (±)-**5** and (±)-**6**. Heating (±)-**7** in a mixture of ethanol and acetonitrile afforded the complex (±)-**8**. The green dichloro adduct (**3**), containing ligands bonded through two α-diimine nitrogens, a hydroxymethyl oxygen and two chlorine atoms, was isolated immediately after its formation, i.e. after about 5 minutes of stirring the reactants

[a] Rudjer Bošković Institute,
P. O. B. 180, 10002 Zagreb, Croatia
E-mail: kojic@rudjer.irb.hr

 © WILEY-VCH Verlag GmbH, 69451 Weinheim, 2001 1434−1948/01/1010−2647 $ 17.50+.50/0

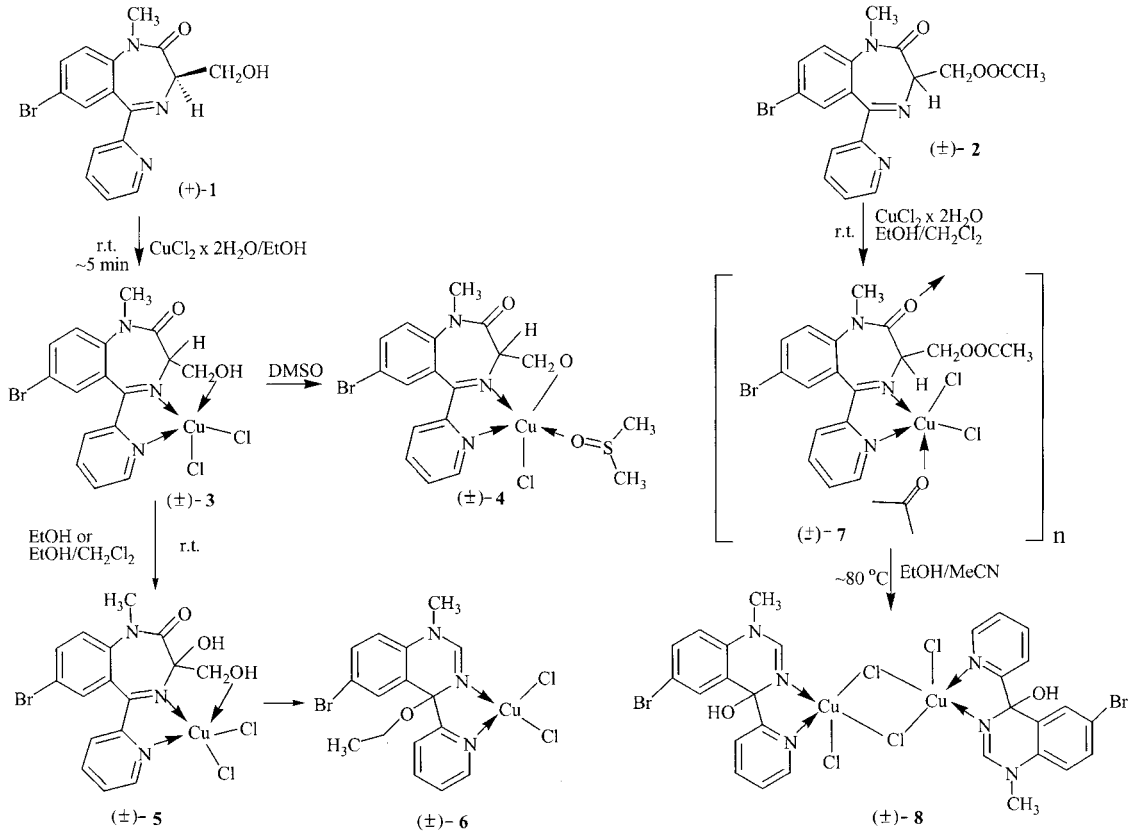

Scheme 1. Chemical diagrams of ligands and copper(II) complexes

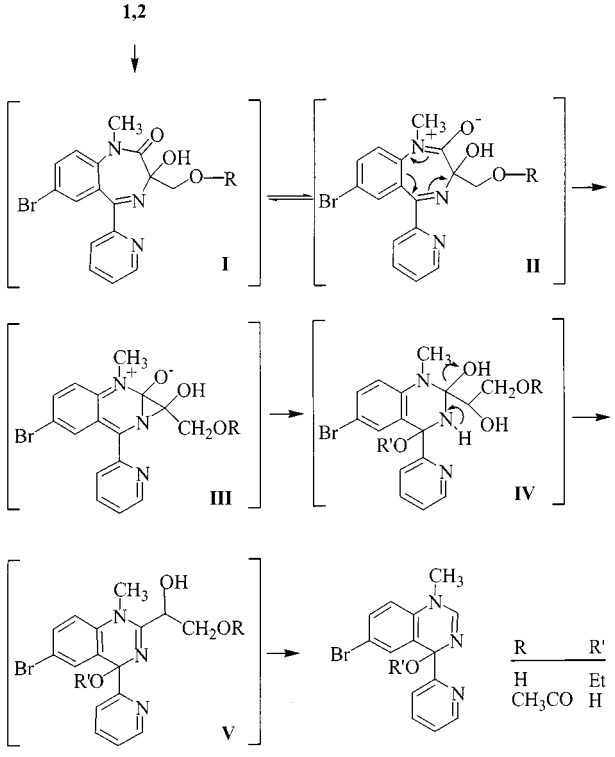

Scheme 2. Possible transition states on the route of chemical modifications of **1** and **2** to 1,3-quinazolines in the presence of Cu^{II}

in absolute ethanol at room temperature. Prolonged stirring caused the slow dissolution of this complex and the formation of a mixture of complexes; a green square-pyramidal complex **5**, dichloro-[7-bromo-1,3-dihydro-3-hydroxy-3-hydroxymethyl-1-methyl-5-(2′-pyridyl)-2*H*-1,4-benzodiazepin-2-one-*N*,*N*,*O*]copper(II) and a black tetrahedral complex **6**, dichloro-[6-bromo-4-ethoxy-1,4-dihydro-1-methyl-4-(2′-pyridyl)-1,3-quinazoline-*N*,*N*]copper(II). Recrystallisation of the complex **3** from DMSO yielded a reddish-brown complex **4**, in which one chlorine atom is replaced by a DMSO molecule (coordinated via an oxygen atom). The reaction of ligand **2** with $CuCl_2$ in a mixture of ethanol and dichloromethane, without an inert atmosphere, gave a green dichloro adduct **7**, which is insoluble in pure ethanol. Complex **7** dissolved on heating a mixture of ethanol and acetonitrile. The benzodiazepine ligand **2** was converted into the 1,3-quinazoline derivative in an ethanol and acetonitrile mixture, which then formed a dark-brown chloro-bridged dinuclear complex **8**, di-μ-chloro-bis[6-bromo-1,4-dihydro-4-hydroxy-1-methyl-4-(2′-pyridyl)-1,3-quinazoline-*N*,*N*]dichlorodicopper(II). Ligand (+)-**1** undergoes a Cu^{II} catalysed oxygenation at C(3), which is detected in the complex **5**. The amide-imide enolate equilibrium (Scheme 2, **I** ⇄ **II**) of 3-hydroxy benzodiazepine derivatives, presumably proceeds pericyclic ring-contraction leading to a tricyclic intermediate **III**, which after nucleophilic attack by an alcohol or water molecule undergoes opening of the cyclopropane ring and rearomatisation to

IV. This intermediate easily eliminates a molecule of water to form **V**, in which oxidative carbon-carbon bond splitting affords the 4-substituted 1,3-quinazoline derivatives found in the complexes **6** and **8**. Since racemisation has not been observed with C(3)-alkyl-5-pyridyl-1,4-benzodiazepines in the presence of Cu^{I} or Cu^{II} ions,[16] the racemisation and formation of complexes **5** and **6** reveal a key role of the C(3)−CH_2OH 'arm' in these processes. They probably comprise the coordination of Cu^{II}, and thus the activation of the C(3)−H bond for racemisation and oxygen insertion. However, under an inert N_2 atmosphere, similar chiral 1,4-benzodiazepines and Cu^{II} ions act catalytically in a cyclopropanation reaction, without oxygenation of the ligand.[16] The role of the Cu^{II} ion as an oxidising agent in biological and chemical catalytic systems has been repeatedly described; at the active site of galactose oxidase, the Cu^{II} ion oxidises primary alcohols to aldehydes.[21,22] Cu^{II} complexes containing *N,N*- and *N,O*-bidentate ligands proved effective in the chiral variant of Bayer−Villiger-type metal-catalysed oxidation of ketones to lactones with molecular oxygen.[23] Racemisation of (+)-**1** is a result of enolisation, since it was observed during C(3) enantiomerisation of 3-carbethoxy-1,4-benzodiazepines.[24] Ring contraction of a 1,4-benzodiazepin-2-one system has been repeatedly observed, either under acidic,[24] basic,[25] or thermal[25] conditions. A pericyclic process has already been postulated in the key ring contraction step.[24] Ring contraction is followed by substitution at the benzylic cation and elimination of the 2C fragment from the C(2) position in 1,4-dihydro-1,3-quinazoline ring, as already observed in similar substrates.[24,25]

The Crystal Structures

Both ligands **1** and **2** are chiral molecules and were used in the preparation of complexes (+)-**1** and (±)-**2**. In separate experiments we proved that enantiomerically pure compounds undergo fast racemisation in an ethanol solution and in the presence of Cu^{II} ions. Thus, during the preparation of the Cu^{II} complexes, racemic compounds were obtained from both homochiral (**1**) and racemic (**2**) ligands. Crystals of all the complexes and the ligand **2** (Scheme 1) crystallise in the centrosymmetric space groups (details given in the Experimental section, X-ray structure analysis, Tables 2 and 3). This indicates that on complexation the configurational stability of the C(3) stereogenic centre is lowered, presumably by the Cu^{II}-promoted enolisation. The Cu^{II} ion enhances the C(3)-acidity during complexation and promotes the above enolisation, which results in the racemisation of the optically active structures. In the crystal structure of **2** (Figure 1), the molecule appears in a *boat*

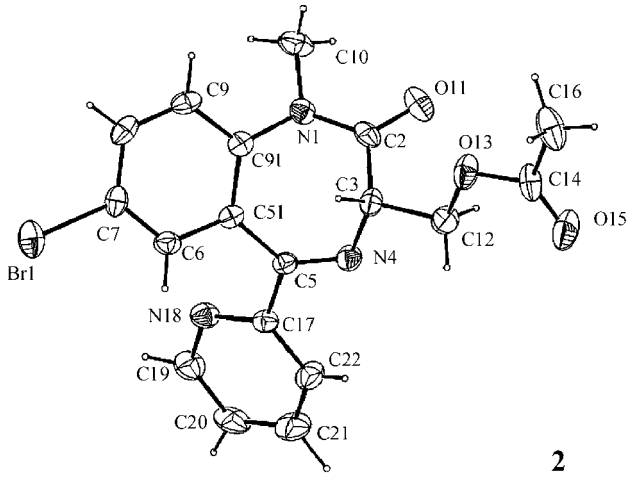

Figure 1. The ORTEP drawing of the ligand (±)-**2**; thermal ellipsoids are scaled at the 30% probability level

Table 1. Bond lengths [Å] and angles [°] in Cu^{II} coordination spheres of the benzodiazepine (**4**, **5**, **7**) and quinazoline (**6**, **8**) complexes

Bond/Angle	**4**	**5**	**7**	Bond/Angle	**6**	**8**
Cu−Cl1	2.235(3)	2.206(5)	2.237(3)	Cu−Cl1	2.257(2)	2.282(7)
Cu−Cl2	−	2.518(5)	2.222(5)	Cu−Cl2	2.236(2)	2.252(5)
Cu−N4	1.972(6)	1.93(1)	2.05(1)	Cu−Cl1[a]	−	2.820(7)
Cu−N_{Py}	1.994(6)	1.99(1)	2.02(1)	Cu−N3	1.984(4)	1.98(2)
Cu−O	1.981(6)	2.01(1)	2.27(1)	Cu−N_{Py}	2.032(5)	2.04(2)
Cu−O_{DMSO}	2.259(5)	−	−			
N_{py}−Cu−N4	79.3(2)	81.4(5)	78.9(5)	N_{py}−Cu−N3	78.7(2)	79.2(7)
N_{py}−Cu−Cl1	97.7(2)	97.3(4)	93.1(4)	N_{py}−Cu−Cl1	169.5(1)	169.7(5)
N_{py}−Cu−O_{DMSO}	93.5(2)	−	−	N_{py}−Cu−Cl2	94.0(2)	95.1(5)
N_{py}−Cu−Cl2	−	98.6(4)	162.4(4)	N3−Cu−Cl1	92.6(1)	91.8(6)
N4−Cu−Cl1	161.4(2)	165.3(4)	171.7(4)	N3−Cu−Cl2	162.4(1)	158.4(6)
N4−Cu− O_{DMSO}	95.8(2)	−	−	Cl1−Cu−Cl2	96.05(1)	95.0(2)
N4−Cu−Cl2	−	92.4(4)	94.7(4)	N_{py}−Cu− Cl1[a]	−	86.5(6)
Cl1−Cu−O_{DMSO}	102.8(2)	−	−	N3−Cu− Cl1[a]	−	99.8(5)
Cl1−Cu−Cl2	−	102.3(2)	92.2(2)	Cl1−Cu− Cl1[a]	−	90.4(2)
N_{py}−Cu−O	161.2(2)	155.2(5)	92.9(5)	Cl2−Cu− Cl1[a]	−	100.7(2)
N4−Cu−O	83.0(2)	78.4(5)	84.2(5)			
Cl1−Cu−O	97.2(2)	97.3(4)	98.7(3)			
O_{DMSO}−Cu−O	94.4(2)	−	−			
Cl2−Cu−O	−	97.7(4)	102.9(3)			

[a] $-x, -y, -z$.

conformation which is preserved in the crystal structure of its complex **7** and also in the complexes **4** and **5**. In spite of numerous efforts, crystallisation of ligand **1** and its complex **3** failed to produce good quality crystals needed for X-ray structure analysis.

Complexation with Cu^{II} ions resulted in structural changes of the ligands as was unambiguously proven by the X-ray structure analysis of the isolated complexes. The coordination geometries of the complexes are given in Table 1. The crystal structures of the complexes **5** (Figure 2) and **7** (Figure 3) reveal a distorted square-pyramidal Cu^{II} coordination. The five coordination sites are occupied by two chlorine atoms, azomethine and pyridine nitrogen atoms in both complexes, and by the hydroxymethyl oxygen in **5** and the lactam oxygen of the neighbouring molecule in **7**. Thus, in the crystal structure of **7** the coordination polyhedra are connected through a common corner into an infinite chain (Figure 3) running along the *b* axis.

In order to prove the mode of coordination of the ligand (+)-**1** in the complex **3**, it was recrystallised from DMSO, yielding the complex **4**. The crystal structure of **4** reveals

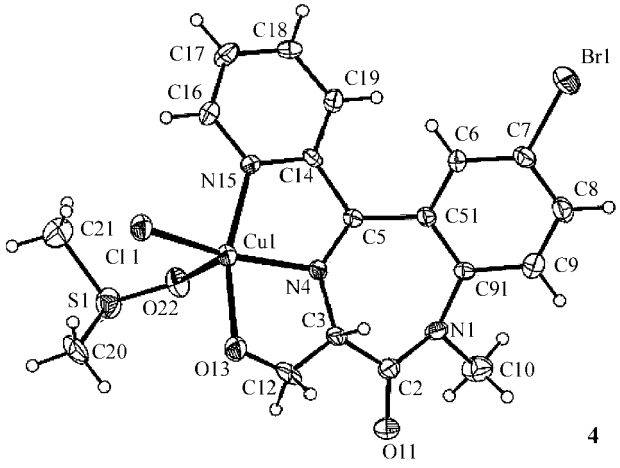

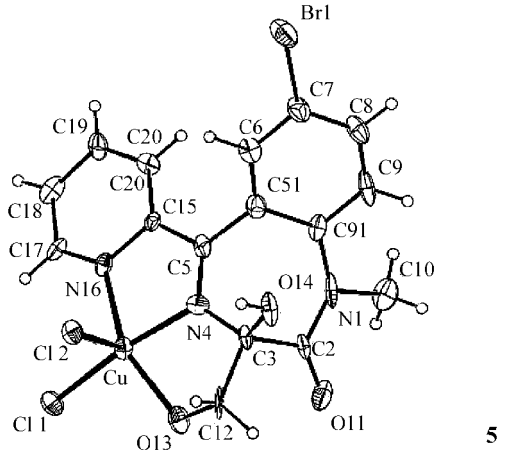

Figure 2. The ORTEP drawings of the five-coordinated chloro-{[7-bromo-1,3-dihydro-1-methyl-3-oxomethyl-5-(2′-pyridyl)-2*H*-1,4-benzodiazepin-2-one-*N*,*N*](dimethylsulfoxide)}copper(II) (**4**) and dichloro-[7-bromo-1,3-dihydro-3-hydroxy-3-hydroxymethyl-1-methyl-5-(2′-pyridyl)-2*H*-1,4-benzodiazepin-2-one-*N*,*N*,*O*]copper-(II) (**5**). Thermal ellipsoids are scaled at the 30% probability level

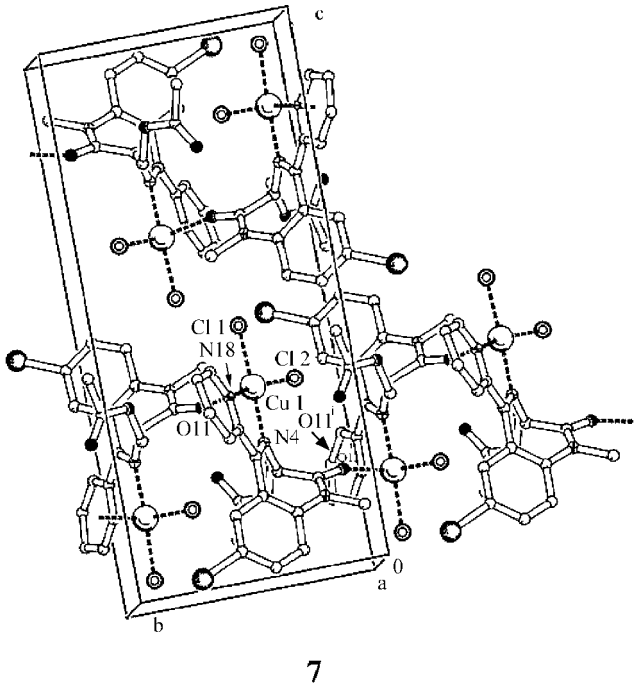

Figure 3. An infinite chain with the five-coordinated Cu^{II} coordination polyhedra of dichloro-[3-acetoxymethyl-7-bromo-1,3-dihydro-1-methyl-5-(2′-pyridyl)-2*H*-1,4-benzodiazepin-2-one-*N*,*N*,*O*]-copper(II) (**7**), connected through a common corner occupied by a lactam oxygen $O11^{i}$ of 1,4-benzodiazepine ligand running along the crystallographic axis *b*. The symmetry operation *i* is defined as $0.5 + x$, $0.5 + y$, $0.5 - z$

that the five coordination sites are occupied by the deprotonated hydroxymethyl oxygen, both nitrogen atoms of the azomethine and pyridine moieties, the chlorine atom, and the oxygen atom of a DMSO molecule (Figure 2).

The crystal structure analysis of complexes **6** and **8** reveal the ring contraction of 5-(2′-pyridyl)-1,4-benzodiazepin-2-one of **1** and **2**, respectively, into the 1,4-dihydro-1,3-quinazoline derivatives (Scheme 1, Scheme 2 and Figure 4). The tetrahedral coordination in **6** involves two nitrogens of the 1,4-dihydro-4-pyridyl-1,3-quinazoline derivative and two chlorine atoms. However, the ring contraction of ligand **2**, detected in **8**, was accompanied by the formation of the centrosymmetric dinuclear Cu^{II} complex with di-μ-chloro bridges. The Cu−Cl bond lengths are 2.252 (5) and 2.820 (7) Å (Table 1), and the Cu···Cu distance is 3.62 Å. The apical chlorine atom with the Cu^{II}−Cl distance of 2.820 (7) Å is part of a bridging system. The asymmetrical bond lengths are common in Cu^{II} binuclear species.[26−28] Such a species, with a distant ligand, might be considered as a stable transition state formed on conversion from a four to five, or vice versa, coordination complex. The third terminal chlorine atom, which completes the five-coordination, has a Cu−Cl bond length of 2.282 (7) Å.

In the crystal structures of **4** and **5**, the benzodiazepine ligands act as ***N,N,O***-tridentate ligands whereas the 1,4-dihydro-1,3-quinazoline ligand acts as an *N,N*-bidentate ligand. Both types of ligands introduce considerable distortions of the Cu^{II}-coordination polyhedra. Bite angles of these chelating ligands are in the range of 78.7(2) to 81.4(5)°

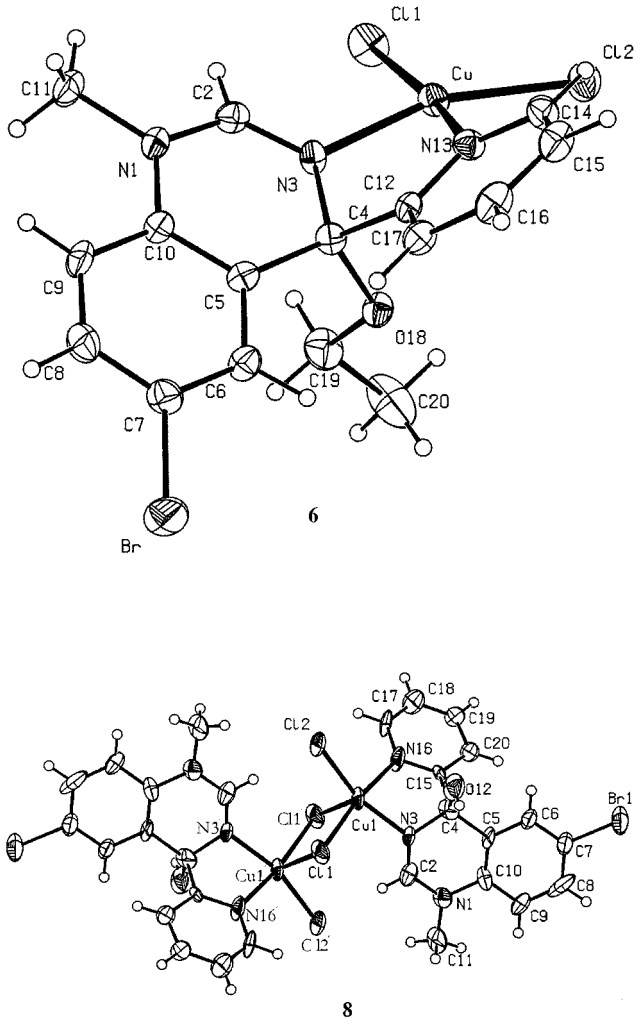

Figure 4. The ORTEP drawings of dichloro-[6-bromo-4-ethoxy-1,4-dihydro-1-methyl-4-(2′-pyridyl)-1,3-quinazoline-*N,N*]copper(II) (**6**) and di-μ-chloro-bis[6-bromo-1,4-dihydro-4-hydroxy-1-methyl-4-(2′-pyridyl)-1,3-quinazoline-*N,N*]dichlorodicopper(II) (**8**). Thermal ellipsoids are scaled at the 30% probability level

(Table 1). The atoms in the equatorial positions, as well as the Cu^{II} atom, of the square-pyramidal geometry are not coplanar (in the structures studied deviations are larger than 0.1 Å). The only exception is the structure of **5**, where deviations from the equatorial plane range from 0.012 (4) to 0.018 (9) Å.

Infrared Spectra

The IR spectra of the complexes provide some structural information of these compounds, whereas the ^1H NMR spectra show broad and badly resolved signals of little diagnostic value. When comparing the spectroscopic data of complexes with those of the free ligands,[16] the greatest changes may be noticed in the range 1750−1500 cm^{-1}. In this region bands arising from the stretching modes of the azomethine and pyridine C=N groups, as well as those from the lactam and acetate C=O, and the aromatic C=C vibrations, occur.[13,29,30] A very strong band at 1675 cm^{-1} and three weak bands at 1611, 1588, and 1562 cm^{-1} are characteristic of the free ligand (+)-**1**. On coordination of both nitrogen atoms, most of these bands in complexes **3** and **5** shift slightly to higher frequencies, and the intensity of the lower frequency bands increases. This behaviour is associated with a general π-electronic redistribution by metallation. The OH stretching mode over the 3000 cm^{-1} region is not informative due to the presence of the crystalline solvent. The spectra of the acetoxy derivative of **2** and its complex **7**, show a more complicated spectral pattern due to the strong absorptions of the acetate group. The transformation of ligand **1** to the 1,3-quinazoline derivative in complex **6** is supported by the absence of the lactam carbonyl band at 1675 cm^{-1}, as well as by the appearance of the very strong absorption at 1267 cm^{-1} due to the ν_{as}(C−O−C) vibration of the 4-substituted ethoxy group.

The far-IR spectra of the complexes show a number of bands in the 400−200 cm^{-1} region, where stretching modes of the metal-ligand vibrations occur. The low symmetry of the present complexes, particularly that of the [*N,N,O*] chelates **3**, **5**, and **7**, does not allow the characterisation of the copper-specific vibrations. In complexes **3** and **5**, a broad band around 325 cm^{-1} with a few shoulders on the lower frequency side, as well as absorption at 276 cm^{-1}, could be assigned to the ν(Cu−Cl) and ν(Cu−N) vibrations. The metal-halogen/nitrogen stretching frequency is observed over a wide range. This may be due to the variation in the two Cu−Cl and Cu−N bonds in the structure of the complex(Table 1). On the other hand coupled Cu−Cl and Cu−N bands could also be expected. The band at 364 cm^{-1} may be assigned to the ν(Cu−O) vibration, since it was found that ν(Cu−O) > ν(Cu−N) for this kind of metal complex.[31,32] The situation is more complicated in complex **7**, where the internal deformation modes of the acetate ligand also falls into the same spectral region as the metal-ligand vibrations.

Conclusion

Generally, the understanding of the structural and catalytic properties of copper complexes contributes to a better understanding of the catalytic reactions and functions of copper containing enzymes. We focused on the use of substituted 1,4-benzodiazepin-2-ones as the complexing agents for Cu^{II}. An unexpected reactivity of the 5-pyridyl-1,4-benzodiazepin-2-one derivatives (+)-**1** and (±)-**2** in the presence of Cu^{II} ions in ethanol was observed. Both starting compounds can coordinate through two oxygen atoms (hydroxy/acetoxy and lactam) and two nitrogen atoms (azomethine and pyridine) to Cu^{II}. Coordination through specific functional groups of the ligands used, and the electronic properties of the copper ions favour racemisation, (in complex **3**), oxygenation (in complex **5**) and ring contraction leading to the 1,4-dihydro-1,3-quinazoline derivatives (complexes **6** and **8**). The study presented suggests that 5-pyridyl-1,4-benzodiazepin-2-one chiral ligands in metal complexes, which are used as catalysts in enantioselective reactions, have to be employed with great caution.

Experimental Section

Materials and Instrumentation: (+)-7-Bromo-1,3-dihydro-3-hydroxymethyl-1-methyl-5-(2′-pyridyl)-2*H*-1,4-benzodiazepin-2-one, (+)-**1**, was prepared by lipase-catalysed kinetic resolution[16], whereas *rac*-3-acetoxymethyl-7-bromo-2,3-dihydro-1-methyl-5-(2′-pyridyl)-2*H*-1,4-benzodiazepin-2-one, (±)-**2**, was prepared according to the reported method.[15] All other reagents and solvents were of analytical grade and were used without purification. − FTIR spectra were recorded on a Perkin−Elmer 2000 spectrophotometer using KBr (4000−400 cm^{-1}) and polyethylene (400−200 cm^{-1}) pellets. − Elemental analyses were performed with a Perkin−Elmer Elemental Analyser E-2400 Series 2 (CHN) and thermogravimetric analyses with a Cahn RG electromicrobalance in an air atmosphere.

Preparation of Complexes 3 and 4: A solution of (+)-**1** (0.080 g, 0.22 mmol) in absolute EtOH (2 mL) was added dropwise to a stirred solution of $CuCl_2·2H_2O$ (0.038 g, 0.22 mmol) in absolute EtOH (3.0 mL) at ambient temperature, whereupon the colour of the reaction mixture changed to brown. After ca. 5 minutes the stirred solution became green again, and a green precipitate was observed. The precipitate was immediately separated by filtration, washed with cold absolute EtOH and the hygroscopic solid stored overnight under vacuum at ambient temperature. Elemental and thermogravimetric analyses indicated the formation of complex **3** as a trihydrate (yield 0.055 g, 46%). − $C_{16}H_{14}BrCl_2CuN_3O_2·3H_2O$ (548.95): calcd. C 35.00, H 3.67, N 7.69, H_2O 9.84; found C 34.80, H 3.08, N 7.30, H_2O 9.29. − IR (KBr): $\tilde{\nu}$ = 3420 m br [ν(OH], 1684 vs br [ν(C=O)], 1635 m, 1629 m, 1596 m and 1559 w-m [δ(HOH), ν(C=N), ν(C=C)], 1486 m, 1469 m, 1446 m, 1402 m, 1340 s, 1301 w, 1253 m, 1123 m, 1106 m, 1035 w, 1024 m, 972 w, 925 w, 890 w, 831 m, 800 m, 756 w-m, 741 w, 725 w, 673 m, 649 w cm^{-1}. − IR (polyethylene): $\tilde{\nu}$ = 364 w, 322 w-m br, 300 sh, 288 sh and 275 w cm^{-1}. Recrystallisation of complex **3** from DMSO gave reddish-brown single crystals of complex **4**.

Preparation of Complexes 5 and 6: Recrystallisation of complex **3**, either from absolute EtOH or a mixture of absolute EtOH and CH_2Cl_2, afforded a mixture of green (complex **5**) and black (complex **6**) crystals, both suitable for X-ray structural analysis. The solutions were subjected to slow solvent evaporation in a desiccator over silica gel. A small amount of the mixture of complexes **5** and **6** was also gradually formed from the mother solution (ethanol), after the preparation and isolation of complex **3**. Complexes were separated by hand under a microscope. Complex **5**: − IR (KBr): $\tilde{\nu}$ = 3300 w [ν(OH], 1688 vs [ν(C=O)], 1626 m, 1596 m, and 1560 w [δ(HOH), ν(C=N), ν(C=C)], 1487 m, 1468 m, 1445 m, 1399 m, 1332 s, 1303 w, 1252 m-s, 1146 m, 1100 s, 1070 m, 1026s, 1008 w-m, 989 w, 891 w, 848 w-m, 822 m, 793 m, 754 w, 684 m, 659 w, 650 w cm^{-1}. − IR (polyethylene): $\tilde{\nu}$ = 364 w, 324 w-m br, 300 sh, 286 sh, 276 w cm^{-1}. Complex **6**: − IR (KBr): $\tilde{\nu}$ = 1629s, 1595m-s, 1553m-s, 1503vs [ν(C=N), ν(C=C)], 1458 m-s, 1439 w-m, 1425 w, 1391 m, 1328 m, 1297 s, 1267 vs, 1245 m, 1202 w-m, 1175 w, 1117 w-m, 1092 w, 1039 w, 1024 m, 1001 m, 965 w, 916 w, 861 m, 825 m, 788 m, 754 w-m, 731w, 655 w-m, 643 w, 619 w cm^{-1}. − IR (polyethylene): $\tilde{\nu}$ = 340 w, 314 w, 301 w, 290 sh, 280 w cm^{-1}.

Table 2. Crystallographic data, crystallisation details, structure solution, and refinement of compounds **2**, **4**, and **5**

Compound	**2**	**4**	**5**
Formula	$C_{18}H_{16}BrN_3O_3$	$C_{18}H_{19}BrCl_2CuN_3O_3S \times 0.125\ H_2O$	$C_{16}H_{14}BrCl_2CuN_3O_3 \times 0.25\ C_2H_5OH$
M_r	402.25	536.33	510.66
Crystal system	monoclinic	monoclinic	monoclinic
Space group	*C*2/*c*	*C*2/*c*	$P2_1/n$
a [Å]	19.07(1)	10.250(3)	8.348(2)
b [Å]	7.461(3)	20.333(4)	15.030(6)
c [Å]	25.366(8)	20.036(2)	17.243(7)
α [°]	90.00	90.00	90.00
β [°]	105.32(4)	93.23(2)	91.52(4)
γ [°]	90.00	90.00	90.00
V [Å^3]	3481(3)	4169(1)	2163(1)
Z	8	8	4
D_x [Mg·m^{-3}]	1.542	1.715	1.568
Colour	colourless	reddish-brown	green
Crystallization solvent(s)	diisopropyl ether, dichloromethane, 1:1	DMSO	absolute ethanol
Temp. of crystallization	293(1) K	293 (1) K	293(1)K, dessicator
θ range [°]for cell det.	13.57−37.38	3.98−10.09	13.37−45.90
μ [mm^{-1}]	2.38	3.22	3.12
Temp. during data collection [K]	293(2)	293(2)	100(7)
Absorption correction	ψ-scan	ψ-scan	no correction
Total data collected	7852	4484	4719
Unique data	3526	4236	4387
Observed data [$I > 2\sigma(I)$]	1357	1474	1641
θ_{max} [°]	26.32	26.30	26.32
Range of *h*, *k*, *l*	−23.0; 0.9; −31.31;	−12.12; −25.0; 0.24;	−10.10; 0.18; 0, 21;
Intensity decay [%]	0.2	0.9	1.1
R_1 [$F_o > 4\sigma(F_o)$]	0.0453	0.0551	0.1146
wR_2 (F^2), all data	0.1297	0.1472	0.3267
S	0.911	0.917	1.417
No. of parameters	290	260	240
Δρ [e·Å^{-3}]	0.40, −0.46	0.53, −0.99	1.84, −2.36

Table 3. Crystallographic data, crystallisation details, structure solution, and refinement of compounds **6**, **7**, and **8**

Compound	**6**	**7**	**8**
Formula	$C_{16}H_{16}BrCl_2CuN_3O$	$C_{18}H_{16}BrCl_2CuN_3O_3$	$C_{14}H_{12}BrCl_2CuN_3O \times 0.5\ H_2O$
M_r	480.68	536.70	452.62
Crystal system	monoclinic	monoclinic	triclinic
Space group	$P2_1/n$	$P2_1/n$	$P\bar{1}$
a [Å]	10.073(2)	10.815	9.69(1)
b [Å]	13.027(3)	9.072	9.797(4)
c [Å]	14.020(3)	19.985	10.63(2)
α [°]	90.00	90.00	70.82(5)
β [°]	105.71(1)	98.64	61.93(9)
γ [°]	90.00	90.00	86.32(6)
V [Å^3]	1770.8(7)	1939(2)	836(2)
Z	4	4	2
D_x [Mg·m^{-3}]	1.803	1.841	1.796(1)
Colour	black	green	brown
Crystallization solvent(s)	absolute ethanol	acetonitrile	acetonitrile
Temp. of crystallization	293(1)K, dessicator	277.15 K	277.15 K
θ range [°]for cell det.	13.20−52.63	9.62−47.17	5.10−20.78
μ [mm^{-1}]	3.80	3.49	3.95
Temp. during data collection [K]	293(2)	100(7)	293(2)
Absorption correction	ψ-scan	ψ-scan	ψ-scan
Total data collected	5780	4332	3588
Unique data	5358	3949	3380
Observed data [$I > 2\sigma(I)$]	2104	1245	848
θ_{max} [°]	30.44	26.32	26.32
Range of h, k, l	−14, 14; 0, 18; 0, 20;	−13.13; 0.11; 0, 25;	0.12; −12.12; −13.13;
Intensity decay [%]	−0.7	−1.4	−0.2
R_1 [$F_o > 4\sigma(F_o)$]	0.0572	0.0768	0.0769
wR_2 (F^2), all data	0.1650	0.2347	0.2697
S	0.907	0.944	0.892
No. of parameters	235	207	205
Δρ [e·Å^{-3}]	0.69, −0.86	1.46, −1.62	0.72, −0.97

Preparation of Complexes 7 and 8: A solution of **2** (0.080 g, 0.20 mmol) in a 1:1 mixture of absolute EtOH and CH_2Cl_2 (5 mL) was added dropwise to a stirred solution of $CuCl_2{\cdot}2H_2O$ (0.034 g, 0.20 mmol) in the same solvent mixture (5 mL). After complete addition, the reaction mixture was continuously stirred for 1 h at ambient temperature, and the green precipitate formed was filtered off, washed with cold CH_2Cl_2 and dried under vacuum (yield 0.103 g, 96%). Green single crystals of complex **7** were obtained from MeCN on cooling at 4 °C. − $C_{18}H_{16}BrCl_2CuN_3O_3$ (536.70): calcd. C 40.28, H 3.01, N 7.83; found C 39.83, H 3.14, N 7.60. − IR (KBr): $\tilde{\nu}$ = 1750 vs and 1727 vs [ν(C=O) acetate], 1686 vs br [ν(C=O) lactam, ν_{as}(COO)], 1589 s, 1568 m, and 1557 m [ν(C=N), ν(C=C)], 1480 m, 1470 m-s, 1429 m, 1404 m, 1389 w, 1369 m, 1340 m, 1261 s, 1250 s, 1187 w, 1119 m-s, 1107 m-s, 1050 m, 1038 m, 1023 m, 980 w, 955 w, 888 w, 876 w, 835 m, 802 m, 782 w, 760 m, 743 w, 714 w, 677 m, 647 w-m, 605 w cm^{-1}. − IR (polyethylene): $\tilde{\nu}$ = 338 m, 315 m br, 294 m-s, 276 m cm^{-1}. Recrystallisation of complex **7** from a hot mixture of MeCN and absolute EtOH yielded a mixture of complex **7** (predominantly) and dark-brown single crystals of complex **8**, which were separated manually under a microscope.

X-ray Structure Analysis: Suitable single crystals were obtained by slow evaporation from different solvents; solvents used and crystallisation temperatures are listed in Table 2 and Table 3, which also summarises crystal data, experimental details of data collections and refinements. Intensities were measured on an Enraf−Nonius CAD4 diffractometer, with graphite monochromated Mo-K_α radiation, wavelength 0.71083 Å, using ω/2θ scan technique. For the compounds **5** and **7** data collections were at 100 K, whereas the others were performed at 293(±2) K. During data collections there were no significant variations in intensities of the three control reflections, which were measured every 120 minutes. The data were corrected for Lorentz and polarisation effects.[33] The absorption correction was based on a ψ-scan of seven reflections. Structures were solved using the package SIR97[34] and refined by the package SHELXL97.[35] The crystal quality of **5** was rather poor and in spite of low-temperature data the final R [for $F_o > 4\sigma$ (F_o)] was 0.1146. However, electron density maps unambiguously revealed the molecular structure of the complex. Molecular geometry calculations and illustrations of the crystal packing were prepared by PLATON98.[36] Plots of the molecules with thermal ellipsoids scaled at the probability level 30% were prepared by ORTEP.[37] Atomic scattering factors were those included in SHELXL97. The H-atom coordinates were calculated geometrically and refined using the SHELX97 riding model.

Crystallographic data for the structures reported in this paper have been deposited with the Cambridge Crystallographic Data Centre as supplementary publication nos. CCDC-158707 (**2**), CCDC-158708 (**4**), CCDC-158709 (**5**), CCDC-158710 (**6**), CCDC-158711 (**7**) and CCDC-158712 (**8**). Copies of the data can be obtained free of charge on application to CCDC, 12 Union Road, Cambridge CB2 1EZ, UK [Fax: (internat.) +44−1223/336-033; E-mail: deposit@ccdc.cam.ac.uk].

Acknowledgments

This work was supported by grants 00980607, 00980608, and 00980701 from the Ministry of Science and Technology of Croatia.

[1] A. Benedetti, C. Preti, G. Tosi, *J. Mol. Struct.* **1984**, *116*, 397−409.
[2] C. Preti, G. Tosi, *J. Coord. Chem.* **1979**, *8*, 223−229.
[3] A. Marchi, L. Marvelli, R. Rossi, V. Bertolasi, V. Ferretti, *Inorg. Chim. Acta* **1998**, *272*, 267−273 and the references therein.
[4] A. Mosset, J. P. Tuchagues, J. J. Bonnet, R. Haran, P. Sharrock, *Inorg. Chem.* **1980**, *19*, 290−294.
[5] G. Minghetti, A. Zucca, M. A. Cinellu, S. Stoccoro, M. Manassero, M. Sansoni, *J. Organomet. Chem.* **1998**, *553*, 405−415 and the references therein.
[6] S. Stoccoro, M. A. Cinellu, A. Zucca, G. Minghetti, *Inorg. Chim. Acta* **1994**, *215*, 17−26.
[7] P. Comba, *Enforced Coordination Geometries-Preorganisation, Catalysis and Beyond*, in: *Chemistry at the Beginning of the Third Millennium: Molecular Design, Suppramolecules, Nanotechnology and Beyond* (Eds.: L. Fabbrizzi, A. Poggi), Springer, Berlin, **1999**, 49−65.
[8] W. Kaim, J. Rall, *Angew. Chem. Int. Ed. Engl.* **1996**, *35*, 43−60.
[9] P. Čudić, B. Klaić, Z. Raza, D. Šepac, V. Šunjić, *Tetrahedron* **1991**, *47*, 5295−5308.
[10] B. Klaić, Z. Raza, R. Marčec, V. Vinković, V. Šunjić, *Spectrosc. Lett.* **1995**, *28*, 683−697.
[11] E. Decorte, R. Toso, A. Sega, V. Šunjić, Ž. Ružić-Toroš, B. Kojić-Prodić, *Helv. Chim. Acta* **1981**, *64*, 1145−1149.
[12] R. Marčec, Z. Raza, V. Šunjić, *J. Mol. Catal.* **1991**, *69*, 25−31.
[13] V. Vinković, Z. Raza, V. Šunjić, *Spectrosc. Lett.* **1994**, *27*, 269−279.
[14] A. Avdagić, A. Lesac, Z. Majer, M. Hollosi, V. Šunjić, *Helv. Chim. Acta* **1998**, *81*, 1567−1582.
[15] A. Avdagić, V. Šunjić, *Helv. Chim. Acta* **1998**, *81*, 85−92.
[16] M. Majerić-Elenkov, unpublished results; Ph. D. Thesis, in preparation.
[17] T. Kovač, B. Belin, T. Fajdiga, V. Šunjić, *J. Heterocycl. Chem.* **1980**, *17*, 59−62.
[18] H. J. Roth, A. Kleeman, T. Besswenger, *Pharmaceutical Chemistry*, Vol. 1, Wiley, New York, **1997**.
[19] M. Corbella, P. Gariboldi, C. Jommi, A. Forgione, F. Marcucci, E. Musini, P. Martelli, F. Mauri, *J. Chem. Soc., Chem. Commun.* **1973**, 721−722.
[20] D. Kolbah, N. Blažević, M. Hannoun, F. Kajfež, T. Kovač, S. Rendić, V. Šunjić, *Helv. Chim. Acta* **1977**, *60*, 265−283.
[21] J. W. Whittaker, *Met. Ions Biol. Syst.* **1994**, *30*, 315−318.
[22] Y. Shimazaki, S. Huth, A. Odani, O. Yamauchi, *Angew. Chem. Int. Ed.* **2000**, *39*, 1666−1669.
[23] C. Bolm, G. Schlingloff, K. Weickhardt, *Angew. Chem. Int. Ed. Engl.* **1994**, *33*, 1848−1849.
[24] A. V. Šunjić, V. Šunjić, R. Dejanović, A. Palković, L. Klasinc, F. Kajfež, *Tetrahedron Lett.* **1976**, 4493−4496.
[25] M. Kaname, T. Tsuchiya, H. Sashida, *Heterocycles* **1991**, *50*, 2407−2413.
[26] O. Q. Gonzalez, *Acta Crystallogr., Sect. C* **1993**, *49*, 1589−1591.
[27] A. M. Atria, *Acta Crystallogr., Sect. C* **1994**, *50*, 864−866.
[28] M. Barz, E. Herdtweck, W. R. Thiel, *Angew. Chem. Int. Ed.* **1998**, *37*, 2262−2265.
[29] M. Campos-Vallette, K. Figueroa, R. O. LaTorre, G. Diaz Fleming, J. Costamagna, J. C. Canales, M. Rey-Lafon, J. Derouault, *Vib. Spectrosc.* **1993**, *6*, 25−35.
[30] K. Nakamoto, *Infrared and Raman Spectra of Inorganic and Coordination Compounds, Part B: Applications in Coordination, Organometallic, and Bioinorganic Chemistry*; 5th edition, Willey-Interscience, **1997**, pp. 24 and 59.
[31] C. A. Kavounis, C. Tsiamis, C. J. Cardin, Y. Zubavichus, *Polyhedron* **1996**, *15*, 385−390.
[32] D. A. Thornton, *Coord. Chem. Rev.* **1990**, *104*, 251−295.
[33] L. Spek, *HELENA*, *Program for Data Reduction*, University of Utrecht, Utrecht, The Netherlands, **1993**.
[34] A. Altomare[1], G. Cascarano[1], C. Giacovazzo[1], A. Guagliardi[1], A. G. G. Moliterni[1], M. C. Burla[2], G. Polidori[2], M. Camalli[3], R. Spagna[3], *SIR 97: A Package for Crystal Structure Solution by Direct Methods and Refinement*; ([1]: Istituto di Ricerca per lo Sviluppo di Metodologie Cristallografiche, Bari, [2]: Dipartimento di Scienze della Terra, Perugia, [3]: Istituto di Strutturistica Chimica "G. Giacomello", Roma, Italy, **1997)**.
[35] G. M. Sheldrick, *SHELX97: Program for the Refinement of Crystal Structures*, Universität Göttingen, Germany, **1997**.
[36] L. Spek, *PLATON98: A Multipurpose Crystallographic Tool*, 120398 Version, University of Utrecht, Utrecht, The Netherlands, **1998**.
[37] C. K. Johnson: *ORTEPII*, Report ORNL-5138, Oak Ride National Laboratory, Tennessee, SAD, **1976**.

Received February 28, 2001
[I01074]

Synthesis and Structure of Heterobimetallic Compounds with a Single Thiolato-Bridged Ligand

Md. Munkir Hossain,[a] Hsiu-Mei Lin,[a] and Shin-Guang Shyu*[a]

Keywords: Tungsten / Molybdenum / S ligands / Bridging ligands

Reactions between $CpFe(CO)_2SPh$ and $M(CO)_5THF$ (M = Cr, Mo, and W) in a mixture of benzene and THF at room temperature afforded compounds of the type $CpFe(CO)_2(\mu\text{-}SPh)M(CO)_5$ (**1**) [M = Cr (**1a**), Mo (**1b**), and W (**1c**)] in high yield. However, migration of the thiolato ligand occurred during reactions between $CpM(CO)_xSPh$ (M = Fe, x = 2; M = Mo and W, x = 3) and $Fe_2(CO)_9$ forming compounds $[Fe(\mu\text{-}SPh)(CO)_3]_2$ and $[CpM(CO)_x]_2$ (M = Fe, x = 2; M = Mo and W, x = 3). Single-crystal X-ray diffraction analyses reveal that **1c** is a single thiolato-bridged hererobimetallic compound without a metal–metal bond. Metal–metal bond formation in compounds **1** by decarbonylation under thermal or photolytic condition was not observed. Reactions between compounds **1** and PPh_3 produced $CpFe(CO)_2SPh$ and $PPh_3M(CO)_5$ (M = Cr, Mo, and W) by M–S bond cleavage in **1**.

Introduction

Recent investigations of the chemical properties of phosphido-bridged bimetallic complexes have revealed several interesting cooperative effects between metals in these bimetallic complexes.[1] The dative metal−metal bond between metals can activate the substitution of the carbonyl ligands [1b−1f] and transfer the substitution site from one metal to the other.[1e] Interestingly, having a similar dative metal−metal bond, sulfido-bridged $CpW(CO)_2(\mu\text{-}SMe)W(CO)_5$(*W*−*W*) and phosphido-bridged $CpW(CO)_2(\mu\text{-}PPh_2)W(CO)_5$(*W*−*W*) complexes behave differently on substitution towards phosphanes. Thus, reaction between $CpW(CO)_2(\mu\text{-}SMe)W(CO)_5$(*W*−*W*) and phosphanes formed $CpW(PR_3)(CO)_2(\mu\text{-}SMe)W(CO)_5$ [2] while its phosphido-bridged analogue $CpW(CO)_2(\mu\text{-}PPh_2)W(CO)_5$(*W*−*W*) gave $CpW(CO)_2(\mu\text{-}PPh_2)W(PR_3)(CO)_4$(*W*−*W*).[1c] In addition, compounds with thiols as a ligand are significantly related to catalysts and biological activity.[3−8] Many of them are bimetallic complexes.[3,4,5a,6,7] As thiols having strong bridging abilities in coordination, enormous numbers of bimetallic compounds containing $(\mu\text{-}SR)_2$ bridges are reported.[9] For complexes with only one (μ-SR) bridge, only a small number of heterobimetallic compounds, without a metal−metal bond, have been synthesized.[10,11] Thus, evaluation of the influence of the thiolate ligands in the chemical behavior of bimetallic complexes could be valuable in order to compare those with phosphido-bridged analogues.

In continuing our interest in the search for cooperative effects in phosphido-bridged heterobimetallic compounds, we attempted to synthesize thiolato-bridged heterobimetallic compounds with and without metal−metal bonds. Herein, we report the synthesis and characterization of single thiolato-bridged heterobimetallic compounds $CpFe(CO)_2(\mu\text{-}SPh)M(CO)_5$ (M = Cr, Mo, and W). Removal of CO to form their metal−metal-bonded analogues $CpFe(CO)(\mu\text{-}SPh)M(CO)_5$(*Fe*−*M*) (M = Cr, Mo, and W) was unsuccessful. The M−S bond cleavage in compounds **1** by PPh_3 as well as thiolato ligand transfer from the metallothiolates $CpM(CO)_xSPh$ (M = Fe, x = 2; M = Mo and W, x = 3) to $Fe_2(CO)_9$ to form $[Fe(\mu\text{-}SPh)(CO)_3]_2$ at ambient temperature is also described.

Results and Discussion

Synthesis of Compound 1 and Structure of 1c

Stirring of a benzene solution of $CpFe(CO)_2SPh$ with a THF solution of $M(CO)_5THF$ (M = Cr, Mo, and W) at room temperature afforded compounds **1a**, **1b**, and **1c** in high yield [Equation (1)]. The compound $[W(\mu\text{-}SPh)(CO)_4]_2$ [12] was also obtained in trace amounts during isolation of compound **1c**. Compounds **1a**, **1b**, and **1c** can also be prepared in good yield by using $M(NBD)(CO)_4$ (NBD = norbornadiene; M = Cr, Mo, and W)[13] instead of $M(CO)_5THF$, but formation of the heterobimetallic compounds is comparatively slow. They are reddish-orange solids, soluble in common organic solvents, and are air-stable.

$$CpFe(CO)_2SPh + M(CO)_5THF \rightarrow CpFe(CO)_2(\mu\text{-}SPh)M(CO)_5 + THF \quad (1)$$

M = Cr (**1a**), Mo (**1b**), W (**1c**)

Single-crystal X-ray diffraction analysis of compound **1c** revealed that two independent molecules crystallized in the asymmetric unit cell. The independent two molecules are crystallographically nonidentical, where they are distinguished by the chirality of the S atom. The molecular struc-

[a] Institute of Chemistry, Academia Sinica, Taipei, Taiwan 11529, Republic of China

 © WILEY-VCH Verlag GmbH, 69451 Weinheim, 2001 1434−1948/01/1010−2655 $ 17.50+.50/0

tures are shown in Figures 1 and 2. Selected bond lengths and bond angles are listed in Table 1.

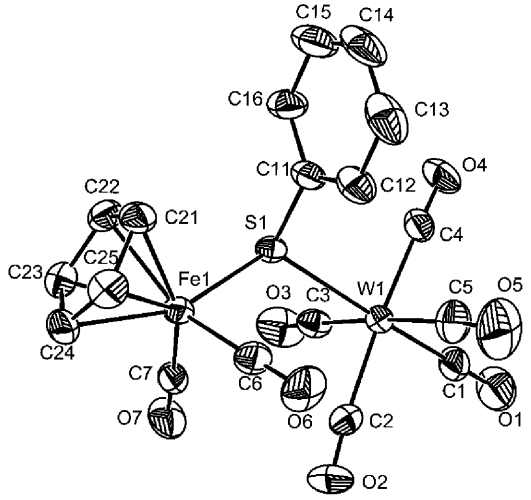

Figure 1. ORTEP drawing of **1c** (molecule 1); hydrogen atoms are omitted

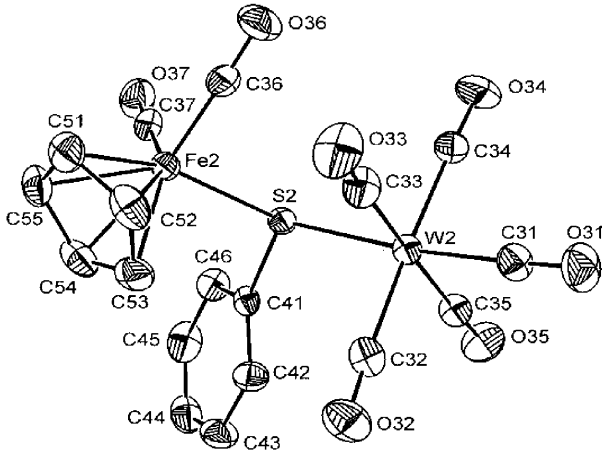

Figure 2. ORTEP drawing of **1c** (molecule 2); hydrogen atoms are omitted

There is no metal−metal bond present in any of the molecules as the bond lengths Fe1−W1 [4.2236(9) Å] and Fe2−W2 [4.1987(8) Å] are longer than the sum the covalent radii of the metal atoms. The tungsten atom has a distorted octahedral geometry, coordinated to five carbonyl groups and a bridging thiolato ligand. The W1−C1 [1.952(7) Å] and W2−C31 [1.959(5) Å] distances *trans* to the bridging thiolato ligand are shorter than the four equatorial W−C distances 2.036(7) Å (av.) and 2.039(6) Å (av.), respectively. This indicates that the thiolato ligand is a better σ-donor but a poorer π-acceptor compared to the CO ligand. The bond lengths Fe1−S1 [2.3007(15) Å], Fe2−S2 [2.3166(14) Å], W1−S1 [2.5772(13) Å], and W2−S2 [2.5865(12) Å] are comparable to the reported values.[10a] The bond angles W1−S1−Fe1 [119.86(5)°] and W2−S2−Fe2 [117.71(5)°] are also within the range of other reported M−S−M bond angles.[10a,11]

Table 1. Selected bond lengths [Å] and bond angles [°] in compound **1c**.

Molecule 1		Molecule 2	
Bond lengths			
Fe1W1	4.2236(9)	Fe2W2	4.1987(9)
W1−S1	2.5772(13)	W2−S2	2.5865(12)
W1−C1	1.952(7)	W2−C31	1.959(5)
W1−C2	2.025(6)	W2−C32	2.021(6)
W1−C3	2.027(6)	W2−C33	2.030(6)
W1−C4	2.045(6)	W2−C34	2.046(6)
W1−C5	2.047(7)	W2−C35	2.060(5)
Fe1−S1	2.3007(15)	Fe2−S2	2.3166(14)
Fe1−C6	1.766(6)	Fe2−C36	1.770(6)
Fe1−C7	1.784(6)	Fe2−C37	1.778(6)
Fe1−C21	2.103(6)	Fe2−C51	2.094(6)
Fe1−C22	2.106(5)	Fe2−C52	2.110(6)
Fe1−C23	2.109(5)	Fe2−C53	2.112(5)
Fe1−C24	2.089(5)	Fe2−C54	2.096(5)
Fe1−C25	2.101(6)	Fe2−C55	2.091(5)
S1−C11	1.781(5)	S2−C41	1.790(5)
C1−O1	1.152(9)	C31−031	1.154(7)
C2−O2	1.139(8)	C32−032	1.140(7)
C3−O3	1.134(8)	C33−033	1.135(7)
C4−O4	1.133(8)	C34−034	1.131(7)
C5−O5	1.139(9)	C35−035	1.128(7)
C6−O6	1.133(7)	C36−036	1.142(7)
C7−O7	1.130(8)	C37−037	1.134(7)
Bond angles			
W1−S1−Fe1	119.86(5)	W2−S2−Fe2	117.71(5)
W1−S1−C11	109.52(19)	W2−S2−C41	115.14(16)
Fe1−S1−C11	106.44(18)	Fe2−S2−C41	104.24(15)
S1−W1−C1	172.77(24)	S2−W2−C31	173.68(16)
S1−W1−C2	97.05(18)	S2−W2−C32	98.72(15)
S1−W1−C3	85.78(17)	S2−W2−C33	94.46(6)
S1−W1−C4	87.11(17)	S2−W2−C34	84.29(15)
S1−W1−C5	97.07(21)	S2−W2−C35	89.02 (14)
C1−W1−C2	87.4(3)	C31−W2−C32	87.58(22)
C1−W1−C3	88.5(3)	C31−W2−C33	86.21(23)
C1−W1−C4	89.5(3)	C31−W2−C34	89.41(22)
C1−W1−C5	88.8(3)	C31−W2−C35	90.39(22)
C2−W1−C3	90.03(25)	C32−W2−C33	88.46(24)
C2−W1−C4	175.83(24)	C32−W2−C34	176.99(21)
C2−W1−C5	87.4(3)	C32−W2−C35	90.53(21)
C3−W1−C4	90.67(24)	C33−W2−C34	91.37(24)
C3−W1−C5	176.4(3)	C33−W2−C35	176.49(21)
C4−W1−C5	91.7(3)	C34−W2−C35	89.47(21)
C6−Fe1−C7	95.2(3)	C36−Fe2−C37	92.1(3)
S1−Fe1−C6	90.22(19)	S2−Fe2−C36	89.77(17)
S1−Fe1−C7	90.56(19)	S2−Fe2−C37	89.48(17)

Thiolato Ligand Transfer from $CpM(CO)_xSPh$ (M = Fe, $x = 2$; M = Mo and W, $x = 3$) to $Fe(CO)_4$ by $Fe_2(CO)_9$

The reaction between $Fe_2(CO)_9$ and $CpFe(CO)_2SPh$ in THF at room temperature leads to the formation of $[CpFe(CO)(\mu\text{-}CO)]_2$ [14] and $[Fe(\mu\text{-}SPh)(CO)_3]_2$ [15] in good yield. Metallothiolates of the type $CpM(CO)_3SPh$ (M = Mo and W) also react with $Fe_2(CO)_9$ in a similar way and give the compounds $[Fe(\mu\text{-}SPh)(CO)_3]_2$ and their respective dimers $Cp_2M_2(CO)_6$ (M = Mo and W).[16,17] The above

transformation indicates that instead of obtaining any bimetallic compound like those of compounds **1,** the thiolato ligand is transferred from the CpM unit to the $Fe(CO)_4$ moiety during the reaction by M−S bond cleavage. The exact mechanism is not clear but it is believed to proceed via an associative pathway forming a bimetallic intermediate with the bridging thiolato ligand (Scheme 1).[18,19]

$$Fe_2(CO)_9 + THF \rightarrow Fe(CO)_4THF + Fe(CO)_5 \quad (a)$$

$$Fe(CO)_4THF + CpFe(CO)_2SPh \rightarrow CpFe(CO)_2(\mu\text{-}SPh)Fe(CO)_4 + THF \quad (b)$$

$$CpFe(CO)_2(\mu\text{-}SPh)Fe(CO)_4 \rightarrow CpFe(CO)_2 + Fe(CO)_4SPh \quad (c)$$

$$2CpFe(CO)_2 \rightarrow [CpFe(\mu\text{-}CO)(CO)]_2 \quad (d)$$

$$2Fe(CO)_4SPh \rightarrow [Fe(\mu\text{-}SPh)(CO)_3]_2 + 2CO \quad (e)$$

Scheme 1

$Fe_2(CO)_9$ can exist in THF solution as $Fe(CO)_4THF$ [Scheme 1, (a)].[20] Then $Fe(CO)_4THF$ can easily release the solvent molecule during the reaction, and the resultant reactive fragment $Fe(CO)_4$ coordinates to the sulfur lone pair of $CpFe(CO)_2SPh$ to generate the bimetallic intermediate $CpFe(CO)_2(\mu\text{-}SPh)Fe(CO)_4$ [Scheme 1, (b)].[18,19] It is then fragmented to $CpFe(CO)_2$ and $Fe(CO)_4SPh$ units by cleavage of the CpFe−S bond [Scheme 1, (c)]. Compound $[Fe(\mu\text{-}SPh)(CO)_3]_2$ is then formed by decarbonylation and dimerization of $Fe(CO)_4SPh$ according to Scheme1, (e).[21] Thiolato ligand transfer and formation of $[Fe(\mu\text{-}SPh)(CO)_3]_2$ in the case of $CpM(CO)_3SPh$ (M = Mo and W) is most likely to follow similar reaction paths.

Thiolato ligand transfer is reported for a few cases, these are the early to late transition metals such as titanium to cobalt,[22] rhodium,[23] or platinum.[18] It is due to the hard and soft mismatching of coordination between the titanium and thiolato ligand.[18] Thiolato ligand transfer from late to late transition metals is rare, but when it does occur it is between two different metals and under thermal conditions.[24] Thus, thiolate ligand transfer from iron to iron at ambient temperature in the above reaction is notable.

Reactivities of Compound 1

Reactions of compounds **1** with PPh_3 generate $CpFe(CO)_2SPh$ and $M(CO)_5PPh_3$ (M = Cr, Mo, and W).[25] This indicates that substitution of the metallothiolate with phosphane occurs on the W center in compounds **1**. It also suggests that PPh_3 is not only a stronger Lewis base, but also π-acceptor, in contrast to $CpFe(CO)_2SPh$. Interestingly, the reaction of $CpW(CO)_3(\mu\text{-}SMe)W(CO)_5$ and $CpW(CO)_3(\mu\text{-}SPh)W(CO)_5$ with hexafluorobut-2-yne produced $CpW(CO)(\eta^2\text{-}CF_3C_2CF_3)(\mu\text{-}SMe)W(CO)_5$ and $CpW(CO)(\eta^2\text{-}CF_3C_2CF_3)(SPh)$, respectively.[10a] In addition, the CO on Fe in $CpFe(CO)_2(\mu\text{-}PPh_2)W(CO)_5$ can be replaced by PMe_3 to produce $CpFe(CO)(PMe_3)(\mu\text{-}PPh_2)W(CO)_5$ under mild conditions.[1e] This indicates that the carbonyl ligands on the CpM moieties in these two compounds are labile towards substitution.

Under thermolytic or photolytic conditions, the CO ligand cannot be removed from compounds **1** to form $CpFe(CO)(\mu\text{-}SPh)M(CO)_5$(*Fe−M*) (M = Cr, Mo, and W). Instead, decomposition of the complex was observed. This indicates that the CO ligand on Fe cannot be substituted by the M−Fe bond formation under the reaction conditions. This observation is consistent with the results of the reaction between compounds **1** and phosphane discussed in the previous paragraph.

Conclusions

Reactions between $CpFe(CO)_2SPh$ and $M(CO)_5THF$ (M = Cr, Mo, and W) or $M(CO)_4(NDB)$ (M = Cr, Mo, and W) produce $CpFe(CO)_2(\mu\text{-}SPh)M(CO)_5$ (M = Cr, Mo, and W) in good yield. However, reactions of metallothiolates $CpFe(CO)_2SPh$ and $CpM(CO)_3SPh$ (M = Mo and W) with $Fe_2(CO)_9$ resulted in the transfer of SR from metallothiolates to $Fe_2(CO)_9$ to produce $[Fe(\mu\text{-}SPh)(CO)_3]_2$. Attempts to remove CO from $CpFe(CO)_2(\mu\text{-}SPh)M(CO)_5$ (M = Cr, Mo, and W) to form the metal−metal-bonded $CpFe(CO)(\mu\text{-}SPh)M(CO)_5$(*Fe−M*) were unsuccessful. The fact that the carbonyl ligands are inert towards substitution by the metal−metal dative-bond formation is proposed as a reason. Replacement of the metallothiolate moiety $CpFe(CO)_2SPh$ from $CpFe(CO)_2(\mu\text{-}SPh)M(CO)_5$ (M = Cr, Mo, and W) by PPh_3 and formation of $M(CO)_5(PPh_3)$ supports the above argument.

Experimental Section

General Procedures: All reactions and other manipulations were performed using standard Schlenk techniques under nitrogen at ambient temperature. Commercially available chemicals were purchased and used without further purification. All solvents were dried and distilled immediately prior to use. The compounds $CpFe(CO)_2SPh$,[26] $M(NBD)(CO)_4$ (M = Cr, Mo, and W),[13] and $CpM(CO)_3SPh$ (M = Cr, Mo, and W)[27] were prepared according to the reported procedures. − A 450-W Hanovia medium-pressure quartz mercury lamp (Ace-Glass) and a pyrex Schlenk tube, used as a reaction vessel, were used in the photoreactions. − Infrared spectra were recorded with a Perkin−Elmer 882 infrared spectrophotometer. − The ^1H NMR spectra were recorded with a Bruker Ac-200 spectrometer. − Electron impact (EI) and fast-atom bombardment (FAB) mass spectra were recorded with a VG 70−2505 or a JEOL JMS-HX 100 mass spectrometer. − Microanalyses were performed using a Perkin−Elmer 2400 CHN analyzer.

Synthesis of Compounds 1: To a benzene solution (50 mL) of $CpFe(CO)_2SPh$ (0.50 g, 1.75 mmol), a THF solution (250 mL) of $M(CO)_5THF$ (M = Cr, Mo, and W) [prepared by photolysis of $M(CO)_6$ (2.0 mmol)] was added, and the solution was stirred for 0.5 h at room temperature. The reaction mixture was concentrated to dryness. The residue was dissolved in dichloromethane/hexane (1:10) and then filtered using Celite. The filtrate was concentrated

to10 mL and subjected to silica gel chromatography using dichloromethane/hexane (1:2) as the eluent. The reddish-orange bands were collected and dried. Compounds **1** were recrystallized from the mixture of dichloromethane and hexane in high yield. − **Compound 1a:** Yield 0.66 g (79%). − $C_{18}H_{10}CrFeO_7S$ (477.89): calcd. C 45.19, H 2.09; found C 45.09, H 2.08. − IR (hexane, νCO): $\tilde{\nu}$ = 2064 m, 2039 s, 2005 s, 1988 w, 1937 vs, 1915 vs cm^{-1}. − ^1H NMR (CD_3COCD_3): δ = 7.40−7.249 (m, 5 H, C_6H_5), 5.20 (s, 5 H, C_5H_5). − MS (FAB): *m*/*z* = 478 [M^+], 450 [M^+ − CO], 422 [M^+ − 2 CO], 366 [M^+ − 4 CO], 282 [M^+ − 7 CO]. − **Compound 1b:** Yield 0.467 g (51%). − $C_{18}H_{10}FeMoO_7S$ (523.85): calcd. C 41.38, H 1.92; found C 41.46, H 2.11. − IR (hexane, νCO): $\tilde{\nu}$ = 2072m, 2041 s, 2006 s, 1989 m, 1942 vs, 1933 sh. 1916 vs cm^{-1}. − ^1H NMR (CD_3COCD_3): δ = 7.52−7.159 (m, 5 H, C_6H_5), 5.30 (s, 5 H, C_5H_5). − MS (FAB): *m*/*z* = 524 [M^+], 468 [M^+ − 2 CO], 412 [M^+ − 4 CO], 356 [M^+ − 6 CO], 328 [M^+ − 7 CO]. − **Compound 1c:** Yield 0.789 g (74%). − $C_{18}H_{10}FeO_7SW$ (610.02): calcd. C 35.41, H 1.64; found C 35.48, H 1.83. − IR (hexane, νCO): $\tilde{\nu}$ = 2068 m, 2041 s, 2006 s, 1981 m, 1965 w, 1933 vs, 1912 vs cm^{-1}. − ^1H NMR (CD_3COCD_3): δ = 7.62−7.299 (m, 5 H, C_6H_5), 5.23 (s, 5 H, C_5H_5). − MS (FAB): *m*/*z* = 610 [M^+], 554 [M^+ − 2 CO], 526 [M^+ − 3 CO], 470 [M^+ − 5 CO], 442 [M^+ − 6 CO], 414 [M^+ − 7CO].

Synthesis of Compounds 1 from M(NBD)(CO)$_4$ (M = Cr, Mo, and W; NBD = Norbornadiene): To a solid mixture of $CpFe(CO)_2SPh$ (0.5 g, 1.75 mmol) and M(NBD)(CO)$_4$ (2.5 mmol) (M = Cr, Mo, and W) 50 mL of THF was added and stirred for 2 d at room temperature. The resulting reaction mixture was concentrated to dryness. The residue was dissolved in dichloromethane and filtered through Celite. The filtrate was concentrated to 5 mL and subjected to chromatography on a silica gel column using dichloromethane/hexane (1:3) as the eluent. The reddish-orange bands were collected and dried. Recrystallization of the residues from a mixture of dichloromethane and hexane afforded compounds **1**. Yield 0.594 g (71%) (**1a**), 0.449 g (49%) (**1b**), 0.715 g (67%) (**1c**).

Reactions of CpM(CO)$_x$SPh (M = Fe, *x* = 2; M = Mo and W, *x* = 3) with Fe$_2$(CO)$_9$: To a THF (50 mL) solution of $CpM(CO)_xSPh$ (M = Fe, *x* = 2; M = Mo and W, *x* = 3) (0.5 mmol) $Fe_2(CO)_9$ (0.728 g, 2.0 mmol) was added and stirred for 2 d at room temperature. The reaction mixture was concentrated to dryness. The residue was dissolved in dichloromethane and filtered through Celite. The filtrate was concentrated to 5 mL. Silica gel chromatography of each filtrate using dichloromethane/hexane (1:3) as the eluent gave the dimers $[CpM(CO)_x]_2$ (M = Fe, *x* = 2; M = Mo and W, *x* = 3) and [Fe(μ-SPh)(CO)$_3$]$_2$ (**A**).[15] Yield 0.041 g (23%) ([FeCp(μ-CO)(CO)]$_2$),[14] 0.102 g (41%) (**A**); 0.046 g (19%) ([CpMo(CO)$_3$]$_2$),[16] 0.117 g (47%) (**A**); 0.070 g (21%) ([CpW(CO)$_3$]$_2$),[17] 0.112 g (45%) (**A**).

Reactions of CpFe(CO)$_2$(μ-SPh)M(CO)$_5$ (M = Cr, Mo, and W) with PPh$_3$: To a THF solution of $CpFe(CO)_2(\mu\text{-}SPh)M(CO)_5$ (0.5 mmol) [M = Cr (0.240 g), Mo (0.264 g) and W (0.305 g)] PPh_3 (0.262 g, 1.0 mmol) was added and the mixture stirred for 2 d at room temperature. The reaction mixture was concentrated to dryness. The residue was dissolved and then filtered through Celite. The filtrate was concentrated to 5 mL and subjected to chromatography on a silica gel column using dichloromethane and hexane as the eluent. The compounds $M(CO)_5PPh_3$ (M = Cr, Mo, and W)[25] and $CpFe(CO)_2SPh$ (B) were obtained by removing solvents from the first pale yellow band and the third reddish-orange band, respectively. The second reddish-orange band is unchanged starting materials $CpFe(CO)_2(\mu\text{-}SPh)M(CO)_5$ (M = Cr, Mo, and W). Yield 0.045 g (19%) [$CpFe(CO)_2(\mu\text{-}SPh)Cr(CO)_5$], 0.129 g (69%) [$Cr(CO)_5PPh_3$], 0.085 g (73%) (**B**); 0.062 g (24%) [$CpFe(CO)_2(\mu\text{-}SPh)Mo(CO)_5$], 0.134 g (71%) [$Mo(CO)_5PPh_3$] 0.083 g, (77%) (**B**); 0.095 g (29%) [$CpFe(CO)_2(\mu\text{-}SPh)W(CO)_5$] 0.159 g (79%) [$W(CO)_5PPh_3$], 0.079 g (81%) (**B**). Yields of the products are calculated based on that of the reacted $CpFe(CO)_2(\mu\text{-}SPh)M(CO)_5$.

Crystal Structure Determination of Compound 1c: Single crystals of compound **1c** were grown by slow vapor diffusion of hexane into a dichloromethane solution of **1c** at 0 °C. A lath yellow crystal (0.25 × 0.18 × 0.34 mm) was mounted on a glass fiber for data collection using Mo-K_α radiation of an Enraf−Nonius CAD4 diffractometer at room temperature. Detailed data collection parameters are given in Table 2. Cell parameters were refined from 25 reflections with the 2θ range 20−36°. Three standard reflections were monitored every hour throughout the data collection. The variation was within 6%. Lorentz and polarization corrections were applied. A semiempirical absorption correction was applied based on azimuthal scans of three reflections. The structure was solved by direct methods. The atomic and isotropic thermal parameters for all hydrogen atoms were fixed. Structure refinement was performed by using the NRCSDP[28] program and a VAX workstation machine. Crystallographic data (excluding structure factors) for the structure reported in this paper have been deposited with the Cambridge Crystallographic Data Centre as supplementary publication no. CCDC-158994. Copies of the data can be obtained free of charge on application to CCDC, 12 Union Road, Cambridge CB2 IEZ, UK [Fax: (internat.) + 44-1223/336-033; E-mail: deposit@ccdc.cam.ac.uk].

Table 2. Summary of crystal data for compound **1c**

Empirical formula	$C_{18}H_{10}FeO_7SW$
Formula mass	610.02
Space group	$P\bar{1}$
a [Å]	9.1039(13)
b [Å]	14.1232(15)
c [Å]	16.3126(16)
α [°]	92.586(8)
β [°]	100.8470(10)
γ [°]	103.909(10)
V [Å^3]	1990.5(4)
ρ(calcd.) [Mg·m^{-3}]	2.036
Z	4
Crystal dimensions [mm]	0.25 × 0.18 × 0.34
Temperature	room temperature
λ(Mo-K_α) [Å]	0.70930
2θ range [°]	50.0
Scan type	ω
No. of reflections	7044
No. of observed reflections	5617 [> 2.5σ(*I*)]
No. of parameters refined	506
R	0.025
R_w	0.028
GoF	1.31
D_{map} min., max. [e/ Å^3]	−1.080, 1.200

Acknowledgments

We are grateful to the National Science Council of the Republic of China and Academia Sinica for financial support of this work.

[1] [1a] R. Regragui, P. H. Dixneuf, N. J. Taylor, A. J. Carty, *Organometallics* **1986**, *5*, 1−8. − [1b] S.-G. Shyu, J.-Y. Hsu, P.-J. Lin, W.-J. Wu, S.-M. Peng, G.-H. Lee, Y.-S. Wen, *Organometallics* **1994**, *13*, 1699−1710 − [1c] S.-G. Shyu, W.-J. Wu, Y.-S. Wen, S.-M. Peng, G.-H. Lee, *J. Organomet. Chem.* **1995**, *489*, 113−122. − [1d] S.-G. Shyu, S.-M. Hsiao, K.-J. Lin, H.-M. Gau,

Organometallics **1995**, *14*, 4300−4307. − [1e] S.-G. Shyu, P.-J. Lin, K.-J. Lin, M.-C. Chang, Y.-S. Wen, *Organometallics* **1995**, *14*, 2253−2264. − [1f] S.-M. Hsiao, S.-G. Shyu, *Organometallics* **1998**, *17*, 1151−1154.[1g] P. Braunstein, M. Knoor, G. Reinhard, U. Schubert, T. Stahrfeldt, *Chem. Eur. J.* **2000**, *6*, 4265−4278. − [1h] P. Oudt, M. M. Kubicki, C. Moise, *Organometallics* **1994**, *13*, 4278−4284. − [1i] W. C. Mercer, R. R. Whittle, E. W. Burkhardt, G. L. Geoffory, *Organometallics* **1984**, *4*, 68−74. − [1j] J. Powell, J. F. Sawyer, M. V. R. Stainer, *Inorg. Chem.* **1989**, *28*, 4461−4470.

[2] J. L. LeQuèré, F. Y. Pètillon, J. E. Guerchais, Lj. Monojlovic-Muir, K. W. Muir, D. W. A. Sharp, *J. Organomet. Chem.* **1983**, *249*, 127−135.

[3] E. I. Koffi-Sokpa, D. T. Calfee, B. R. T. Allred, J. L. Davis, E. K. Haub, A. K. Rich, A. Porter, M. S. Mashuta, J. F. Richardson, M. E. Noble, *Inorg. Chem.* **1999**, *38*, 802−813.

[4] [4a] M. R. DuBois, *Chem. Rev.* **1989**, *89*, 1−9. − [4b] J. J. Garcia, B. E. Mann, N. A. Adams, N. A. Bailey, P. Maitlis, *J. Am. Chem. Soc.* **1995**, *117*, 2179−2186.

[5] [5a] P. Kalck, J. M. Frances, P. M. Pfister, T. G. Southern, A. Thorens, *J. Chem. Soc., Chem. Commun.* **1983**, 510−511. − [5b] R. Davis, J. W. Epton, T. G. Southern, *J. Mol. Catal.* **1992**, *77*, 159−163.

[6] [6a] Y. Nishibayashi, I. Wakiji, M. Hidia, *J. Am. Chem. Soc.* **2000**, *122*, 11019−11020. − [6b] J-P. Qu, D. Masui, Y. Ishii, M. Hadia, *Chem. Lett.* **1998**, 1003−1004. − [6c] Y. Nishibayshi, M. Yamanashi, I. Wakiji, M. Hidia, *Angew. Chem. Int. Ed.* **2000**, *39*, 2909−29011.

[7] Y. Takagi, H. Matsuzaka, Y. Ishii, M. Hidia, *Organometallics* **1997**, *16*, 4445−4452 and references therein.

[8] [8a] E. I. Steifel, *Prog. Inorg. Chem.* **1977**, *22*, 8−21. − [8b] K. Kustin, I. G. Macara, *Comments Inorg. Chem.* **1982**, *2*, 1−22.

[9] [9a] D. W. Stephan, T. T. Nadaski, *Coord. Chem. Rev.* **1996**, *147*, 147−208. − [9b] P. J. Blower, J. R. Dilwarth, *Coord. Chem. Rev.* **1987**, *76*, 121−185.

[10] [10a] J. E. Guerchais, J. L. LeQuèré, F. Y. Pètillon, Lj. Monojlovic-Muir, K. W. Muir, D. W. A. Sharp, *J. Chem. Soc., Dalton Trans.* **1982**, 283−289. − [10b] W. Ehrl, H. Vahrenkamp, *Chem. Ber.* **1972**, *105*, 1471−1485.

[11] R. Usön, M. A. Usön, S. Herrero, L. Rello, *Inorg. Chem.* **1998**, *37*, 4473−4476.

[12] C. R. Lucas, M. J. Newlands, E. J. Gabl, F. L. Lee, *Can. J. Chem.* **1987**, *65*, 898−902.

[13] [13a] M. A. Bennett, L. Pratt, G. Wilkinson, *J. Chem. Soc.* **1961**, 2037−2044. − [13b] R. B. King, A. Fronzaglia, *Inorg. Chem.* **1966**, *5*, 1837−1846.

[14] [14a] A. R. Manning, *J. Chem. Soc. A* **1968**, 1319−1324. − [14b] R. B. King, *Organometallic Synthesis*, Academic Press New York, **1965**, vol. 1, p. 114−115.

[15] S. F. A. Kettle, L. E. Orgel, *J. Chem. Soc.* **1960**, 3890−3891.

[16] G. Wilkinson, *J. Am. Chem. Soc.* **1954**, *76*, 209−211.

[17] D. J. Parker, M. H. B. Stiddard, *J. Chem. Soc. A* **1970**, 480−490

[18] K. Osakada, T. Kawaguchi, T. Yamamoto, *Organometallics* **1995**, *14*, 4542−4548.

[19] [19a] K. Osakada, K. Hataya, T. Yamamoto, *Bull. Chem. Soc. Jpn.* **1998**, *71*, 2853−2858. − [19b] W. F. Liaw, Y. C. Horng, D. S. Ou, C. Y. Ching, G. H. Lee, S. M. Peng, *J. Am. Chem. Soc.* **1997**, *119*, 9299−9300.

[20] F. A. Cotton, *Prog. Inorg. Chem.* **1976**, *21*, 1−10.

[21] N. S Nametkin, V. D. Tyurin, M. A. Kukina, *J. Organomet. Chem.* **1978**, *149*, 355−370.

[22] A. Shaver, S. Morris, R. Turrin, V. W. Day, *Inorg. Chem.* **1990**, *29*, 3622−3623.

[23] T. A. Wark, D. W. Stephan, *Can. J. Chem.* **1990**, *68*, 565−569.

[24] S.-W. Lu, N. Okura, T. Yoshida, S. Otsuka, *J. Am. Chem. Soc.* **1983**, *105*, 7470−7471.

[25] [25a] T. A. Magee, C. N. Matthews, T. S Wang, J. H. Wotiz, *J. Am. Chem. Soc.* **1961**, *83*, 3200−3203. − [25b] S. O. Grim, D. A. Wheatland, W. McFarlane, *J. Am. Chem. Soc.* **1967**, *89*. 5573−5577.

[26] M. Ahmad, R. Bruce, G. R. Knox, *J. Organomet. Chem.* **1966**, *6*, 1−10.

[27] [27a] D. D. Watkins Jr., T. A. George, *J. Organomet. Chem.* **1975**, *102*, 71−77. − [27b] R. Havlin, G. R. Knox, *Z. Naturforsch., Teil B* **1966**, *21*, 1108−1109.

[28] E. J. Gape, Y. Le Page, J.-P. Charland, F. L. Lee, P. S. White, *J. Appl. Crystallogr.* **1989**, *22*, 384−393.

Received March 5, 2001
[I01081]

Facile Synthesis and Ambident Coordination of Cyclohexylbis-(2-pyridyl)phosphane: Novel Dinuclear Complexes of Cu^{+1}, Ag^{+1}, and Co^{+2} Ions

Matthias Driess,*[a] Felix Franke,[a] and Klaus Merz[a]

Keywords: Phosphanes / Cross-coupling / Copper / Silver / N ligands

The title compound cyclohexylbis(2-pyridyl)phosphane (**1**) was synthesized by a Pd^0-catalyzed cross-coupling reaction from 2-bromopyridine and cyclohexylphosphane in 98% yield. Compound **1** formed colorless crystals that were moderately air-stable. It reacted, in CH_3CN, with CuOTf (OTf = OSO_2CF_3), $AgBF_4$, and $Co(BF_4)_2$ to form the complexes $[Cu_2\{CyP(2\text{-}Py)_2\}_2(NCCH_3)_2](OTf)_2$ (**2**), $[Ag_2\{CyP(2\text{-}Py)_2\}_2(NCCH_3)_2](BF_4)_2$ (**3**), and $[Co_2\{CyP(2\text{-}Py)_2\}_2(NCCH_3)_2](BF_4)_4$ (**4**), respectively. In these complexes, the pyridylphosphane ligands coordinate to two metal centers in a head-to-tail fashion involving both the P and the N atoms simultaneously. The compounds represent the first structurally characterized examples of dimeric dinuclear pyridylphosphane complexes showing the *P*,*N*,*N*′ coordination. Reactions of **1** with other salts containing Cu^{+1} and Co^{+2} centers and coordinating anions resulted in different coordination modes. Thus, CuI reacted with **1** to form the complex $[Cu_2\{CyP(2\text{-}Py)_2\}_2I_2]$ (**5**) with both coordinated P and N donor centers and a terminal iodide. In contrast, the reaction of **1** with $CoCl_2$ afforded the mononuclear complex $[Co\{CyP(2\text{-}Py)_2\}Cl_2]$ (**6**) in which only the pyridyl N atoms and the chlorine ligands were coordinated to the metal center. X-ray analyses of the compounds **1**, **2**, **3**, **5**, and **6** are reported.

Introduction

Since 2-pyridylphosphanes can act as monodentate (*P*-coordinated), bidentate (*P*,*N*- or *N*,*N*′-chelating or *P*,*N*-bridging), or tridentate (*P*,*N*,*N*′-chelating or *N*,*N*′,*N*′′′-chelating) ligands with both hard (N) and soft (P) donor centers, they have been a topic of interest in the last 30 years.[1,2] Scheme 1 shows the various possible coordination modes for pyridylphosphanes **A**−**H**. All displayed modes have been described, except the coordination mode **H**.

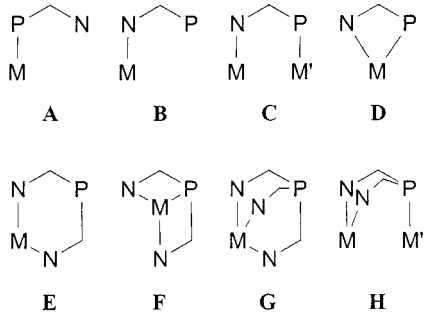

Scheme 1. Some possible coordination modes **A**−**H** for pyridylphosphanes toward metal centers

Apart from the interesting structural features, pyridylphosphane metal complexes have been shown to act as good catalysts for reactions like the carbonylation of alkynes to form methacrylate,[3] showing surprisingly high turnover rates combined with an excellent product selectivity.

In contrast to the extensive use of diphenyl-2-pyridylphosphane[4] and its derivatives,[5] and the numerous complexes described with tris(2-pyridyl)phosphane,[6] the knowledge of bis-2-pyridylphosphanes is scarce.[7,8] Only recently, Ag^{+1} and Au^{+1} complexes of 1,2-bis(dipyridylphosphanyl)-ethane have been shown to provide a promising approach in cancer research for their potent and selective antitumor activity.[9]

Usually, the synthesis of 2-pyridylphosphanes is achieved by the reaction of the 2-lithium pyridine with the appropriate chlorophosphane at very low temperatures (less than −90 °C). In searching for a convenient and more selective way of synthesizing pyridylphosphanes with varying alkyl substituents we have found that the reaction of cyclohexylphosphane with 2-bromopyridine in acetonitrile in a Pd^0-catalysed cross-coupling reaction[10] furnished cyclohexyl(2-pyridyl)phosphane (**1**) in 98% yield. This reaction type, which resembles the Stille coupling reaction,[11] has been extended to phosphanes without silyl or stannyl groups by Stelzer et al., and tolerates a number of functional groups that limit the versatility of the lithium pyridyl method.[12] Reactions of cyclohexylbis(2-pyridyl)phosphane (**1**) in acetonitrile with different Cu^{+1}, Ag^{+1}, and Co^{+2} salts containing weakly coordinating anions ($CF_3OSO_2^-$, BF_4^-) furnished the dinuclear complexes **2**, **3**, and **4**, respectively. In these complexes, the pyridylphosphane ligands coordinate in a head-to-tail bridging mode involving both the P and the N donor centers. To the best of our knowledge, these are the first structurally characterized complexes of (2-pyridyl)phosphanes that represent the coordination mode **H** (Scheme 1). CuI with the stronger coordinating iodide anion reacted with **1** to form the isostructural complex **5**, while $CoCl_2$ lead to the mononuclear complex **6**, which represents the coordination mode **E**, involving only the pyridyl

[a] Lehrstuhl für Anorganische Chemie I, Molekül- und Koordinationschemie, Ruhr-Universität Bochum,
44780 Bochum, Germany
E-mail: matthias.driess@ac1.ruhr-uni-bochum.de

 © WILEY-VCH Verlag GmbH, 69451 Weinheim, 2001 1434−1948/01/1010−2661 $ 17.50+.50/0

N atoms and the two chlorine atoms as donor centers toward the Co atom.

Results and Discussion

Synthesis of Cyclohexylbis(2-pyridyl)phosphane (1)

If cyclohexylphosphane is allowed to react with two molar equivalents 2-bromopyridine and triethylamine in the presence of catalytic amounts of tetrakis(triphenylphosphane)palladium(0) in acetonitrile for 24 hours, the desired cyclohexylbis(2-pyridyl)phosphane (**1**) is formed in 98% yield. The reaction can easily be monitored by ^{31}P-NMR spectroscopy, and proceeds stepwise via cyclohexyl-2-pyridylphosphane as the initial product. The latter can be identified by its diagnostic ^{31}P NMR signal ($\delta = -26.8$, $^1J_{PH} = 212.6$ Hz).

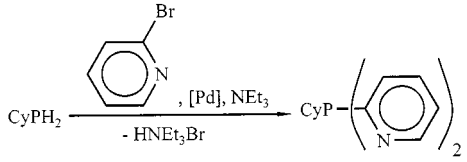

1 : Cy = C_6H_{11}

This type of Pd-catalyzed cross-coupling reaction has been described previously by Stelzer et al.,[10] and resembles the Stille coupling reaction.[11] The synthesis of **1** is the first example in which a primary aliphatic phosphane and 2-bromopyridine have been successfully coupled. The mechanism of the reaction involves the oxidative addition of 2-bromopyridine to the palladium catalyst, followed by the substitution of one triphenylphosphane ligand by cyclohexylphosphane or cyclohexyl-2-pyridylphosphane, respectively. Finally, the product is formed through a P−C bond formation in a reductive-elimination step (Scheme 2).[12]

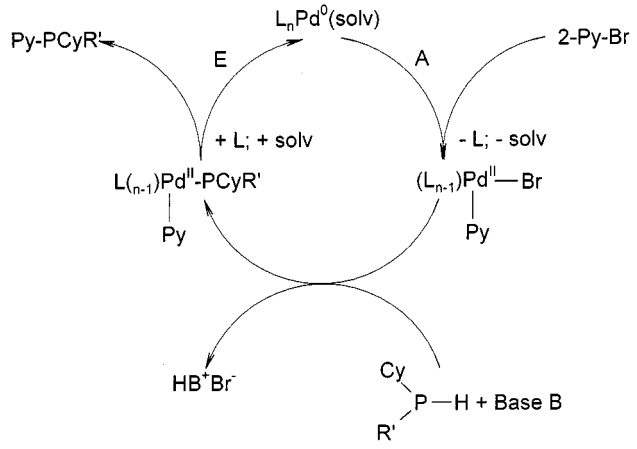

Scheme 2. Proposed mechanism for the Pd^0-catalyzed synthesis of **1** based on previous results, starting from $CyPH_2$, 2-bromopyridine, and a Base. R′ = H, L = PPh_3, solv = solvent

Compound **1** forms colorless, fairly air-stable crystals that are soluble in most organic solvents. The ^{31}P NMR spectrum of **1** in C_6D_6 shows a singlet at $\delta = -3.2$, similar to the values observed for tris(2-pyridyl)phosphane ($\delta = -1.3$), phenylbis(2-pyridyl)phosphane ($\delta = -2.9$), and diphenyl(2-pyridyl)phosphane ($\delta = -1.9$).[13]

Crystal Structure of 1

Crystals of **1** suitable for an X-ray diffraction analysis were obtained from solutions in hexane. A view of its molecular structure is shown in Figure 1 and the crystallographic details are given in the Experim. Section.

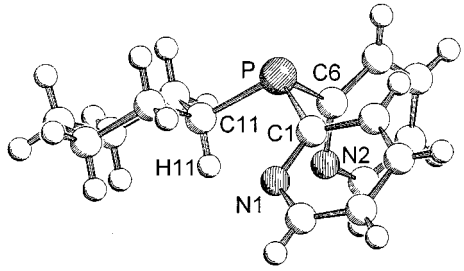

Figure 1. Molecular structure of cyclohexylbis(2-pyridyl)phosphane **1**. Selected distances [Å] and angles [°]: P1−C11 1.847(4), P1−C6 1.851(4), P1−C1 1.854(5), C11−P−C6 101.6(1), C11−P−C1 101.4(1), C6−P−C1 97.6(1)

The P−C distance of 1.847(4) Å in **1** is similar to those in tris(2-pyridyl)phosphane (1.83 Å and 1.82 Å). As expected, the P atom has a pyramidal coordination, with the sum of bond angles at phosphorus of 300.6°. The latter value is only slightly smaller than that in tris(2-pyridyl)phosphane (305.6°).

While the C11−P−C6 and the C11−P−C1 angles [101.6(1) and 101.4(1)°] are practically identical to the corresponding angles in tris(2-pyridyl)phosphane, the C6−P1−C1 angle of 97.6(1)° is notably smaller. The N centers are directed away from the lone pair at the P atom. A similar orientation is also found for two pyridyl groups in tris(2-pyridyl)phosphane, while the third pyridyl substituent in the latter compound is rotated away from the other two.[14]

Coordination Reactions of 1 with Cu^{+1}, Ag^{+1}, and Co^{+2} Salts

Treatment of acetonitrile solutions of $Cu(O_3SCF_3)$, $AgBF_4$, and $Co(BF_4)_2$ with **1** at room temperature affords the dinuclear complexes **2**, **3**, and **4**, respectively. All three complexes form colorless (**2**, **3**) or pink (**4**) crystals from acetonitrile solution and are practically insoluble in other common solvents.

A ligand exchange of acetonitrile by other solvent molecules, as has been found in similar complexes,[15,16] could therefore not be achieved. The ^{31}P-NMR spectra show singlet signals at $\delta = 0.2$ for **2** and at $\delta = 23.6$ for **3**, thus confirming the coordination of the phosphorus atom by a downfield shift with respect to the value for the "free" ligand **1**. These values compare well with those in similar Cu and Ag complexes with bridging pyridylphosphanes, as observed in $[Cu_2(\mu\text{-}Ph_2P\text{-}Py)_3CH_3CN]^{2+}$ ($\delta = 5.45$)[15] and $[Ag_2(Ph_2P-Py)_2]^{2+}$ ($\delta = 25.7$), respectively.[17]

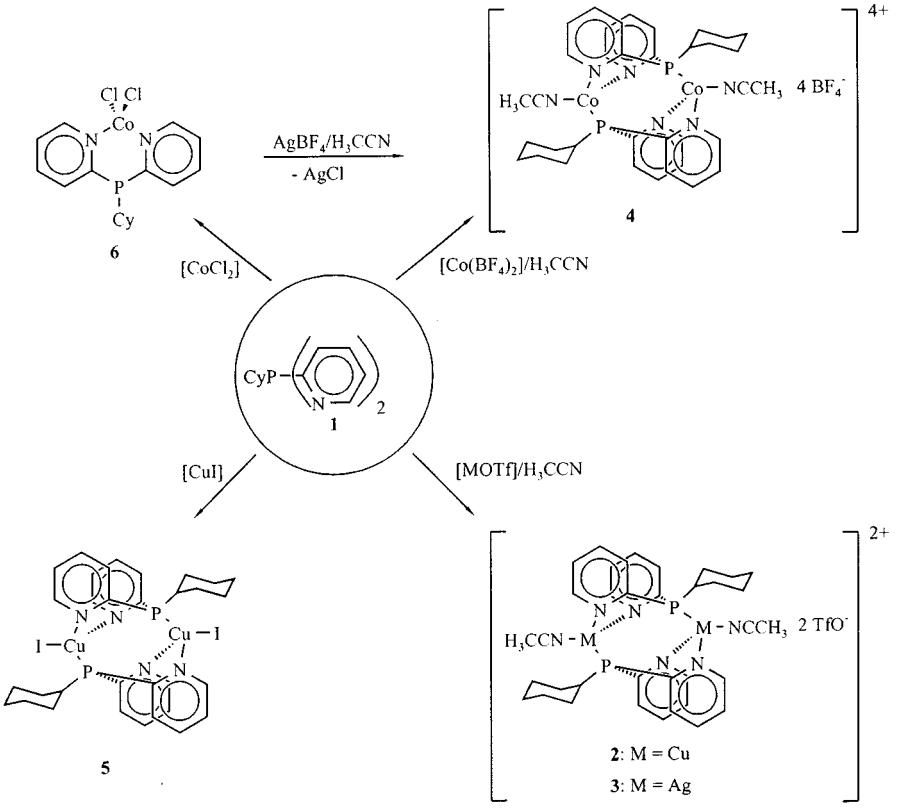

In order to investigate the influence of the anion on the coordination mode, and also to overcome the poor solubility properties of the ion pairs **2**, **3**, and **4**, CuI was allowed to react with **1** in THF at 50 °C. Yellow crystals of **5** precipitated as the desired product from the reaction mixture. Compound **5** turned out to be well soluble in THF, CH_2Cl_2, $CHCl_3$, and acetone. Its ^{31}P-NMR spectrum reveals a singlet at $\delta = 1.5$, very similar to that chemical shift observed for **2**. The crystal structure, which is described below, indeed shows that **5** is isostructural with the cation in **2**, except that the terminal acetonitrile ligands were replaced by iodine ions.

In contrast, the reaction of $CoCl_2$ with **1** yielded the complex **6** in good yields, which implies a different coordination mode of the dipyridylphosphane **1**, involving only the pyridyl N donor atoms and the Cl ligands as donor centers. As expected for a Co^{+2} complex, **6** is paramagnetic and unlike the other complexes, which are rather sensitive to air and water, is indefinitely resistant in air and moisture. It is soluble in most organic solvents and reacts with two equiv. of $AgBF_4$ in acetonitrile giving the separated ion pair **4** and AgCl.

Crystal Structures of 2, 3, and 4

The molecular structures of **2** and **3** are shown in Figure 2 and 3, while experimental details of the X-ray analyses are described in the Experim. Section and in Table 2. In all three complexes, the metal centers are held together in close proximity by the two bridging ligands that coordinate in a head-to-tail fashion and resemble the dimeric form of the coordination mode **H**, according to Scheme 1. In addition, both metal centers bear an acetonitrile ligand to achieve a distorted tetrahedral coordination sphere. Espinet et al. have merely described several dipyridylphosphane Mo^0 complexes for one of which the *P*,*N*,*N*′-coordination mode **F** was postulated, but crystallographic evidence could not be achieved.[18]

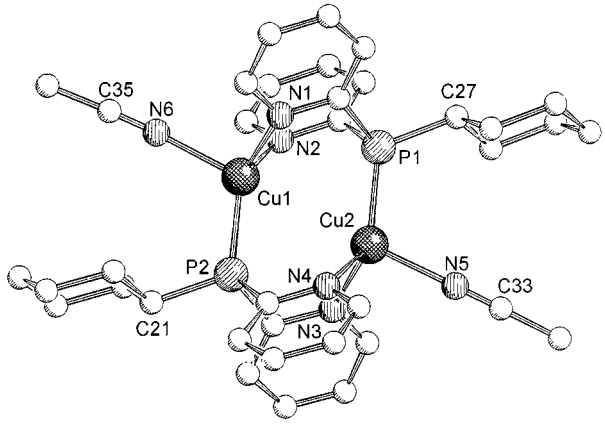

Figure 2. Molecular structure of the dication in **2**. For the sake of clarity, the H atoms have been omitted. Selected distances [A] and angles [°]: Cu2···Cu1 3.225(2), Cu−N(Py, average) 2.077(3), Cu−N (acetonitrile, average) 2.093(3), Cu1−P2 2.202(1), Cu2−P1 2.186(1); N2−Cu1−N1 94.2(1), N2−Cu1−P2 123.7(1), N1−Cu1−P2 126.2(1), N3−Cu2−N4 90.7(1), N3−Cu2−P1 125.2(1), N4−Cu2−P1 127.9(1), Cu2−N5−C33 171.0(4), Cu1−N6−C35 171.5(4)

In **2**, the copper centers are surrounded, in a distorted tetrahedral geometry, by one phosphorus and three nitro-

gen donors. The Cu centers lie about 48 pm outside of the P,N,N′-plane. The N(Py)−Cu−N(Py) bond angles of 90.7(1) and 94.2(1)°, respectively, are considerably smaller than those of the P−Cu−N(Py) angles, which vary between 123.7(1) and 127.9(1)°, respectively. Such a difference has also been observed in the $[Cu_2(\mu\text{-dppy})_3(CH_3CN)]^{2+}$ ion [dppy = diphenyl(2-pyridyl)phosphane],[15] in which one Cu center is also coordinated in a distorted tetrahedral arrangement. However, the differences between the N(Py)−Cu−N(Py)- and the P−Cu−N(Py) angles, respectively, are less significant in the latter complex, due to stronger geometric constraints in the ligand backbone in **2** than in dppy in $[Cu_2(\mu\text{-dppy})_3(CH_3CN)]^{2+}$. The Cu···Cu distance of 3.225(2) Å is larger than the respective distance in $[Cu_2(\mu\text{-dppy})_3(CH_3CN)]^{2+}$ (2.72 Å), in which one Cu center is tetrahedral and the other trigonal-planar coordinated.[19] It is, however, shorter than in $[Cu_2(dppy)_2(CH_3CN)_2]^{2+}$ (3.58 Å) with both Cu atoms being trigonal coordinated.[19] The value is also considerably shorter than in $[Cu_2(\mu\text{-}Ph_2PCH_2PPh_2)_2(CH_3CN)_4]^{2+}$ (3.75 Å),[20] in which both Cu centers are surrounded by four donor atoms. The close proximity between the Cu atoms in **2** compared with that in $[Cu_2(\mu\text{-}Ph_2PCH_2PPh_2)_2(CH_3CN)_4]^{2+}$ probably reflects the higher ring strain induced by the relatively rigid threefold coordination within the ligand backbone rather than suggesting attractive intermetallic interactions. According to Figure 3, the dinuclear Ag complex **3** adopts the same core structure as **2**. However, the tetrahedral coordination geometry around the Ag centers is even more distorted than that in **2** with P−Ag−N(Py) angles varying between 126.6(1) and 135.2(1)°, while the N(Py)−Ag−N(Py) angles are 86.7(2) and 87.4(2)°, respectively.

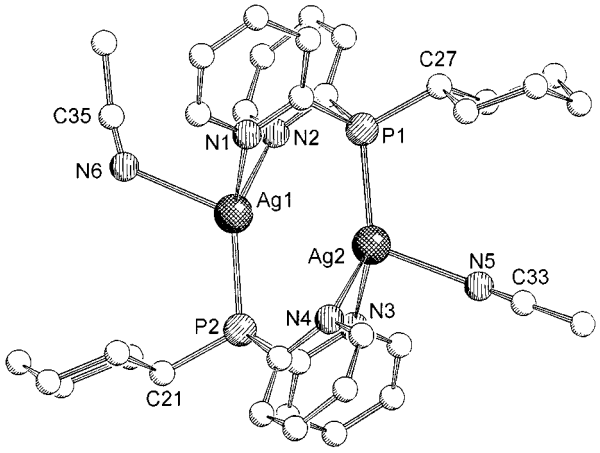

Figure 3. Molecular structure of the dication in **3**. For the sake of clarity, the H atoms have been omitted. Selected distances [Å] and angles [°]: Ag1···Ag2 2.932(4), Ag−N(Py, average) 2.397(5), Ag1−N6 2.466(7), Ag2−N5 2.373(6), Ag1−P2 2.390(1), Ag2−P1 2.383(2); N2−Ag1−N1 86.7(2), N1−Ag1−P2 129.5(1), N2−Ag1−P2 134.6(1), N3−Ag2−N4 87.4(2), N3−Ag2−P1 135.2(1), N4−Ag2−P1 126.6(1), Ag1−N6−C35 125.9(7), Ag2−N5−C33 158.9(5)

The Ag···Ag distance of 2.932(4) Å is shorter than that in other complexes with bridging pyridylphosphanes like $[Ag_2(Ph_2P\text{-}Py)_2](NO_3)_2$ (3.14 Å),[21] $[Ag_2(\eta^1\text{-}Ph_2P\text{-}Py)(\mu\text{-}Ph_2P\text{-}Py)_2](ClO_4)_2$ (3.07 Å),[17] $[Ag_2(Ph_2P\text{-}Py)_3]Cl_2$ (3.08 Å),[22] and $[Ag_2(\mu\text{-}L)_2(CH_3CN)_2](ClO_4)_2$ [L = 2-(diphenylphosphanyl)-6-(pyrazol-1-yl)pyridine] (2.96 Å).[23]

Surprisingly, the Ag···Ag distance in **3** is smaller than the Cu···Cu distance in **2**, and the same is true for the homologous complexes $[Ag_2(\mu\text{-}L)_2(CH_3CN)_2](ClO_4)_2$ and $[Cu_2(\mu\text{-}L)_2(CH_3CN)_2](ClO_4)_2$ [L = 2-(diphenylphosphanyl)-6-(pyrazol-1-yl)pyridine].[23,24] This observation may indicate attractive interactions between the Ag centers due to a larger contribution of relativistic effects. However, in the case of bridging ligands, it is difficult to distinguish between ligand-induced effects (strain) and true "metallophilic" d^{10}-d^{10} dispersion-type interactions.[25] It is also noteworthy that one of the acetonitrile molecules is coordinated to the Ag center with an Ag−N−C angle of 125.9(7)°, while the other Ag−N−C moiety adopts an angle of 158.9(5)°. A similar small Cu−N−C bond angle of 129.2° has also been observed in the case of the Cu(+1) complex [Cu(acac)(phen)(CH_3CN)](ClO_4) (acac = acetylacetonate; phen = 1,10-phenanthroline),[26] but **3** represents the first Ag^{+1} acetonitrile complexes with an Ag−N−C angle < 140° (Table 1).

Table 1. Comparison of Ag−N bond length and the Ag−N−C angle in different Ag(+1)-acetonitrile complexes

AgNC[a]	Ag−N[b]	compound	ref.
174.5	2.08	$[Ag\{CF(CF_3)_2\}(NCCH_3)]$	[30]
156.2	2.11	$[Ag_3L^1(NCCH_3)_3]$[c]	[31]
178.8	2.14	$[Rh_6C(CO)_{15}\{Ag(NCCH_3)_2\}_2]$	[32]
165.3	2.25	$[Ag(NCCH_3)_4]^+$	[33]
162.0	2.27	$[Ag_2L^2(NCCH_3)_2](BF_4)_2$[d]	[34]
146.1	2.27	$[Ag\{NCCH_3)_2\text{-}\{\mu_4\text{-}3,6\text{-}(Ph_2P)_2Pyr\}]_n$[e]	[23]
162.7	2.28	$[AgL^3(NCCH_3)_2]$ (SbF_5)[f]	[35]
152.5	2.28	$[AgL^3(NCCH_3)_2]$ (SbF_5)[f]	[23]
158.9	2.37	**3**, this work	
156.0	2.41	$[Ag\{\mu_2\text{-}2\text{-}(Ph_2P)\text{-}6\text{-}(Pyz)Py\}_2\text{-}(NCCH_3)]_2(ClO_4)_2$[g]	[23]
140.7	2.42	$[\{\mu_2\text{-}2,6\text{-}(Ph_2P)_2Py\}\text{-}Ag(NCCH_3)_2]$	[36]
125.9	2.47	**3**, this work	

[a] Ag−N−C angle at the coordinated CH_3CN (°). − [b] Bond length (Å). − [c] L^1 = μ_3-6,13,20-trimethoxycalix(3)pyridine. − [d] L^2 = μ_2-1,11-(1,2)Ph-3,6,9,13,16,19-hexathiacycloicosaphane. − [e] Pyr = pyridazine. − [f] L^3 = μ_2-3,7-di-*tert*-butyl-2,8-dioxa-5-aza-1-phosphabicyclo(3.3.0)octa-2,4,6-triene. − [g] Pyz = pyrazole

It has been proposed that the M−N−C angle of the acetonitrile ligand corresponds well with the M−N(acetonitrile) distance in such a way that longer M−N bonds imply a smaller M−N−C angle, thereby representing a rather early stage of acetonitrile coordination.[15] This trend is supported by the respective data of CH_3CN−Ag^{+1} complexes that are summarized in Table 1. However, the $[AgL^3(NCCH_3)_2]$ cation [L^3 = μ_2-3,7-di-*tert*-butyl-2,8-dioxa-5-aza-1-phosphabicyclo(3.3.0)octa-2,4,6-triene] is an exception, revealing two different Ag−N−C angles (Δ = 10°), and at the same time, equidistant Ag−N

bonds (2.28 Å).[32] Quantitative correlation of the Ag^{+1} complexes seems very difficult because a clear distinction between electronic effects, steric influences, and possible packing effects cannot be made. Nonetheless, the relatively small Ag−N−C angle of 125.6(1) at one Ag center and the much shorter Ag···Ag distance in **3** [2.932(4) Å] are consistent with the presence of metallophilic Ag(donor)−Ag(acceptor) interactions. This is because its Cu-homologue **2** is apparently different, possessing a much longer M···M distance of 3.225(2) Å and both acetonitrile ligands are inconspicuously coordinated to the Cu^{+1} centers [averaged Cu−N−C angle 171.2(4)°].

The paramagnetic dicobalt complex **4** shows basically the same core-structure as **2** and **3**. According to a preliminary X-ray structure analysis of moderate crystals of **4**, which crystallizes in the monoclinic space group $P2_1/c$ [$R1$ = 0.1319, $wR2$ (all data) = 0.3397], the Co···Co distance of 2.976(5) Å is larger than that in other dinuclear complexes like $[Co^{I}Co^{0}(\mu\text{-}Ph_2PPy)_2(\mu\text{-}CO)(CO)Cl]$[27,34] and $[Co^{0}_{2}(\mu\text{-}Ph_2PPy)(\eta^2\text{-}\mu\text{-}HC{\equiv}CSiMe_3)]$.[28,35] The latter complexes imply Co−Co bonds due to short intermetallic distances and electron deficiency. In the acetylene complex, the observed diamagnetism, shown by a ^{31}P-NMR spectrum, provides further proof of an antiferromagnetic coupling of the unpaired electrons at the Co centers. This is, however, not the case in **4**, which is reluctant to undergo direct- or ligand-induced coupling of the d^7-Co centers even at 15 K. This was proven by temperature-dependent magnetic susceptibility measurements and fitting of the observed data with the calculated values. The effective magnetic moment of η_{eff} = 5.5 B.M. at room temperature seems relatively large in comparison to mononuclear tetrahedral Co^{+2} complexes that show η_{eff} values in the range between 4.3 and 5.2 B.M. However, larger values can be expected due to the different nature of the ligands and their ligand fields.[36,37] In line with that, simulations of the magnetic moment of high-spin Co^{+2} ions in a tetrahedral ligand field revealed the η_{eff} value of 4.82 B.M., which can be increased using appropriate ligands. The results suggest that spin-spin coupling between the Co^{+2} ions in **4** is negligible.

Crystal Structure of 5

Crystals of **5** suitable for an X-ray diffraction analysis were obtained by recrystallization in CH_2Cl_2. Its structure is shown in Figure 4. As expected, the structure of **5** is identical with that of **2**, but in place of the terminal acetonitrile ligands, iodine ions are coordinated to the Cu centers of **5**. This can be explained by the superior coordinating ability of the iodine ions compared to the triflate anion. The Cu···Cu distance of 3.333(3) Å is ca. 0.1 Å longer than that in **2**, and the tetrahedral coordination geometry of the Cu centers is notably distorted. The two N(Py)−Cu−N(Py) angles of 93.9(2) and 100.8(2)° are considerably different from the corresponding values in **2** [90.7(1) and 94.2(1)°]. Several attempts to exchange the iodine atoms at copper by organo substituents, through reaction of **5** with MeLi, BuLi, and lithium phenylacetylide, did not lead to any isolable product.

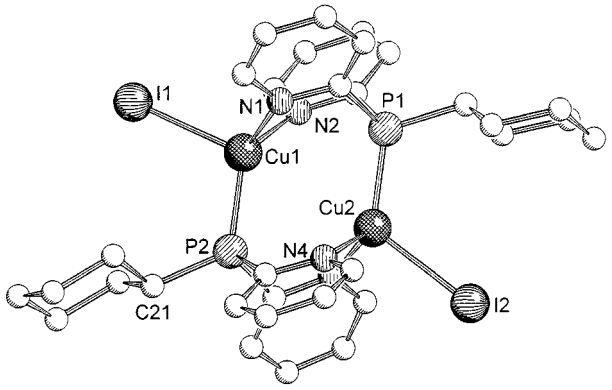

Figure 4. Molecular structure of **5**. For the sake of clarity, the H atoms have been omitted. Selected distances [Å] and angles [°]: Cu1···Cu2 3.333(3), Cu1−I1 2.7201(8), Cu2−I2 2.6978(8), Cu−N(Py, average) 2.052(4), Cu1−P2 2.189(2), Cu2−P1 2.218(2); N2−Cu1−N1 100.8(2), N2−Cu1−P2 114.6(1), N1−Cu1−P2 122.5(1), N3−Cu2−N4 93.9(2), N3−Cu2−P1 116.6(1), N4−Cu2−P1 127.5(1)

Crystal Structure of 6

The $CoCl_2$ complex **6** affords dark-blue crystals that could be recrystallized in most organic solvents. According to its X-ray diffraction analysis, the ligand **1** adopts a different coordination mode in the mononuclear complex than in the dimeric acetonitrile complex **4**, which is also apparent from their different color. Crystallographic details for **6** are summarized in Table 2 and Figure 5 shows a model of its crystal structure. In **6**, both N donor atoms of the ligand coordinate to the Co^{+2} center, affording a distorted tetrahedral N_2Cl_2 coordination geometry around the Co atom, while the P atom is only a spectator, bridging center. The ligand and the metal form a six-membered CoN_2C_2P ring that prefers the thermodynamically favorable chair conformation. As expected, the structure is similar to that of $[Co(N,N'\text{-}PhPPy_2)Cl_2]$.[38] The Co−N distances are identical with those in other Co(+2) dipyridyl complexes like

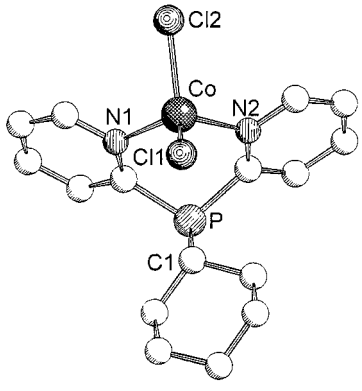

Figure 5. Molecular structure of **6**. For the sake of clarity, the H atoms have been omitted. Selected distances [Å] and angles [°]: Co−Cl1 2.213(1), Co−Cl2 2.222(1), Co−N1 2.034(3), Co−N2 2.028(3); Cl1−Co−Cl2 113.34(5), N1−Co−N2 99.5(1), N1−Co−Cl1 115.18(8), N2−Co−Cl1 116.32(8)

[Co(4-vinylpyridine)$_2$Cl$_2$][29,39] and [Co(4-methyl pyridine)$_2$Cl$_2$], respectively.[40] The tetrahedral coordination geometry at the Co(+2) center is somewhat more distorted than in the latter because of the phosphane linkage between the pyridyl rings in the *meta* positions. The N−Co−N angle of 99.5° in **6**, especially, shows a considerable deviation from the ideal tetrahedral angle. An even smaller N−Co−N angle of 94.8° is observed in [Co(*N*,*N*′-PhPPy$_2$)Cl$_2$].[38]

Conclusion

We reported here on an economical and at the same time facile synthesis of (cyclohexyl)bis(2-pyridyl)phosphane (**1**). The formation of its new complexes **2**−**5** proves the existence of the missing *P*,*N*,*N*′-coordination mode **H** for dipyridylphosphanes. Apparently, this coordination mode supports the formation of dinuclear complexes. The metals in **2**−**5** are in close proximity, which in general permits intermetallic interactions influenced by the terminal ligands at the metal center. The formation of the mononuclear Co complex **6** illustrates the directing influence of the hardness of the anion and its coordination ability on the coordination properties of the metal toward the chelate ligand **1**. Further investigations to synthesize related water-soluble dinuclear complexes and to probe their use in metal-assisted organic synthesis are in progress.

Experimental Section

All reactions and manipulations were carried out under an atmosphere of dry argon using standard Schlenk techniques unless otherwise stated. Solvents and reagents were dried by standard methods and distilled prior to use. − The ^{31}P- and ^{1}H-NMR spectra were measured on a Bruker Avance 250 spectrometer at 250 MHz (^{1}H) and 101.3 MHz (^{31}P), respectively. Chemical shifts are given in ppm relative to respective standards. External standards for ^{1}H NMR: $SiMe_4$; ^{31}P NMR: H_3PO_4 (85% aq. solution). − Elemental analyses were performed on an Elementar VarioEL microanalyser.

Synthesis of CyP(2-Py)$_2$ (1): A solution of 1.0 g (8.6 mmol) of cyclohexylphosphane, 2.7 g (17.2 mmol) of 2-bromopyridine, 1.8 g (17.8 mmol) of triethylamine, and ca. 0.1 g of tetrakis(triphenylphosphanyl)palladium(0) in 20 mL of acetonitrile were degassed thoroughly in a Schlenk tube and sealed under vacuum. The reaction mixture was heated under reflux for 36 h, monitoring the progress of the reaction by ^{31}P-NMR spectroscopy. Then the solvent was evaporated in vacuo at 25 °C and the residue was taken up with 30 mL of hexane. The triethylammonium bromide was then filtered off and washed with two 5 mL portions of hexane. The filtrates were combined and the solvent removed in vacuo. Distillation gave the crude product that was recrystallized in hexane at −20 °C and dried in vacuo to give 2.25 g (8.4 mmol, 98%) of the colorless crystalline product. − ^{31}P NMR: δ = 3.2 (s). − ^{1}H NMR: δ = 1.2−2.2 [m, 10 H, C*H*(C*H*$_2$)$_5$], 3.2 [m, 1H, C*H*(CH$_2$)$_5$], 6.7 (m, 2 H, Py), 7.1 (m, 2 H, Py), 7.5 (m, 2 H, Py), 8.6 (m, 2 H, Py). − MS (EI, 70 eV): *m*/*z* (%) = 270 (35) [M$^+$], 193 ([M − C$_6$H$_4$N]$^+$, 80), 187 ([M − C$_6$H$_{11}$]$^+$, 100), 109 ([M − C$_6$H$_{11}$-C$_6$H$_4$N], 75). − HR-MS: calcd. *m*/*z* = 270.1283 for C$_{16}$H$_{19}$N$_2$P, found 270.1281.

Synthesis of {Cu$_2$[CyP(2-Py)$_2$]$_2$(NCCH$_3$)$_2$}(OTf)$_2$ (2): A solution of 0.33 g (0.7 mmol) of (CuOTf)$_2$·C$_6$H$_6$ in 10 mL of acetonitrile was allowed to react with 0.35 g (1.3 mmol) of **1** in 5 mL of acetonitrile at room temperature. After stirring the mixture overnight, a white precipitate formed that was recrystallized in acetonitrile to afford slightly yellowish crystals in 79% yield (1.0 g). − ^{31}P NMR: δ = 0.2 (s); elemental analysis calcd. (%): calcd. C 43.55, H 4.23, N 8.02; found (%) C 43.05, H 4.18, N 7.90.

Synthesis of {Ag$_2$[CyP(2-Py)$_2$]$_2$(NCCH$_3$)$_2$}(BF$_4$)$_2$ (3): To 0.20 g (1.0 mmol) of $AgBF_4$ in 10 mL of acetonitrile a solution of 0.30 g (1.0 mmol) of **1** in 5 mL of acetonitrile was added at room temperature. After stirring the mixture overnight, a white precipitate was formed that was recrystallized in acetonitrile to form colorless crystals in 85% yield (0.86 g). − ^{31}P NMR: δ = 0.2 (s); elemental analysis calcd. (%): calcd. C 42.72, H 4.38, N 8.30; found (%) C 43.21, H 4.35, N 8.35.

Synthesis of {Co$_2$[CyP(2-Py)$_2$]$_2$(NCCH$_3$)$_2$}(BF$_4$)$_4$ (4): A blue solution of 0.26 g (1.0 mmol) of $CoCl_2$ in 20 mL of CH_3CN was added to 0.40 g (2.0 mmol) of $AgBF_4$ at room temperature, from which the color of the solution turned pink and AgCl precipitated. The latter was filtered off and the clear filtrate allowed to react with 0.30 g (1.0 mmol) of **1** in 10 mL of CH_3CN at room temperature. After stirring the pink solution for 12 h, the reaction mixture was reduced to 2 mL in vacuo and stored at −25 °C. The product precipitated in the form of pink crystals in 58% yield (0.34 g, 0.58 mmol). Elemental analysis of the mono-solvate with CH_3CN, calcd. (%): calcd. C 39.77, H 3.95, N 7.74; found (%): C 39.36, H 4.19, N 7.51.

Synthesis of {Cu$_2$[CyP(2-Py)$_2$]$_2$I$_2$} (5): CuI (0.70 g, 3.7 mmol) was dissolved in 120 mL of THF at 50 °C and a solution of 0.99 g (3.7 mmol) of **1** in 30 mL of THF was added with vigorous stirring. The reaction mixture turned yellow and standing of the solution at room temperature yielded, after 3 d, 1.75 g (1.64 mmol, 89%) of the product in the form of yellow crystals. − ^{31}P NMR ($CDCl_3$): δ = 1.5 (s, *w*1/2 = 22.8 Hz). − ^{1}H NMR ($CDCl_3$): δ = 1.2−2.2 [m, 20 H, CH(C*H*$_2$)$_5$], 3.1 [m, 2 H, *CH*(CH$_2$)$_5$], 7.5 (m, 4 H, Py), 7.8 (m, 8 H, Py), 9.1 (m, 4 H, Py); elemental analysis (solvate with two molecules THF) calcd. (%): calcd. C 45.08, H 5.12, N 5.26; found (%) C 44.14, H 5.10, N 5.36.

Synthesis of {Co[CyP(2-Py$_2$]Cl$_2$] (6): $CoCl_2$ (0.13 g, 1.0 mmol) was dissolved in 20 mL of CH_3CN at room temperature. To this deep-blue mixture a solution of **1** (0.27 g, 1.0 mmol) in 10 mL of CH_3CN was added, and the reaction mixture was stirred for 12 hours. Solvent was removed in vacuo to leave 5 mL of a dark-blue solution from which **6** crystallized in the form of dark-blue crystals. Yield: 0.37 g (0.93 mmol, 93%). − MS (EI, 70 eV): *m*/*z* (%) = 399 ([M]$^+$, 0.5), 364 ([M − Cl]$^+$, 3), 327 ([M − 2Cl]$^+$, 10), 270 ([CyPPy$_2$]$^+$, 80), 193 ([CyPPy$_2$-C$_6$H$_4$N]$^+$, 82), 187 ([CyPPy$_2$-C$_6$H$_{11}$]$^+$, 100), 109 ([CyPPy$_2$ -C$_6$H$_{11}$-C$_6$H$_4$N], 78); elemental analysis calcd. (%): calcd. C 48.03, H 4.79, N 7.00; found (%): calcd. C 47.80, H 5.22, N 6.99.

X-ray Structural Determinations: The intensities were measured with a Bruker-axs-SMART diffractometer (Mo-K_α radiation, λ = 0.7170 Å, ω scan). The structures were solved by direct methods (SHELXS97), and refined against F^2 with all measured reflections (SHELXL97). All non-hydrogen atoms were refined anisotropically and the hydrogen atoms were introduced in calculated positions. Other experimental details are summarized in Table 2.

Crystallographic data (excluding structure factors) for the structures reported in this paper have been deposited with the Cambridge Crystallographic Data Center as supplementary

Table 2. Experimental data of the X-ray analyses

	1	**2**	**3**	**5**	**6**
empirical formula	$C_{16}H_{19}N_2P$	$C_{38}H_{44}Cu_2F_6N_6O_6P_2S_2$	$C_{36}H_{44}Ag_2B_2F_8N_6P_2$	$C_{32}H_{38}Cu_2I_2N_4P_2$	$C_{16}H_{19}Cl_2CoN_2P$
molecular mass	270.30	1654.01	1012.07	921.526	400.13
temperature [K]	203(2)	203(2)	203(2)	203(2)	203
crystal system	monoclinic	triclinic	monoclinic	orthorhombic	monoclinic
space group	*Pn*	$P\bar{1}$	$P2_1/c$	*Pbca*	$P2_1/c$
unit cell dimensions [Å, °]	a = 8.776(2)	a = 9.667(2)	a = 11.170(4)	a = 17.473(8)	a = 8.997(4)
	b = 10.057(2)	b = 15.321(4)	b = 10.083(3)	b = 20.397(2)	b = 14.310(6)
	c = 9.193(2)	c = 25.610(6)	c = 38.18(1)	c = 21.314(6)	c = 13.967(6)
	α = 90	α = 81.904(5)	α = 90	α = 90.00	α = 90.00
	β = 115.45(3)	β = 84.210(4)	β = 90.478(1)	β = 90.00	β = 97.16(1)
	γ = 90	γ = 72.204(5)	γ = 90	γ = 90.00	γ = 90.00
volume [Å^3]	732.8(3)	3569.0(1)	4301(2)	7596.8	1784.2(1)
Z	2	2	4	8	4
calcd. density [Mg/m^3]	1.225	1.539	1.536	1.756	1.490
crystal size [mm]	0.3 × 0.3 × 0.5	0.2 × 0.2 × 0.1	0.2 × 0.2 × 0.3	0.2 × 0.2 × 0.3	0.3 × 0.3 × 0.5
Θ range [°]	2.68 to 25.11	1.61 to 25.17	2.10 to 25.09		2.05 to 25.11
reflections collected	3619	18765	20385	40105	9210
independent reflections	2090	12478	7552	4875	3172
parameters	172	897	507	406	275
$R1[I > 2\sigma(I)]$[a]	R = 0.0610	R = 0.0502	R = 0.0552	$R1$ = 0.0410	$R1$ = 0.0374
$wR2$(all data)[b]	$wR2$ = 0.1680	$wR2$ = 0.1424	$wR2$ = 0.1162	$wR2$ = 0.1098	$wR2$ = 0.0843

[a] $R = (\Sigma(|F_o| - |F_c|)/\Sigma|F_c|)$. – [b] $wR2 = \{\Sigma[w(|F_o|^2 - |F_c|^2)^2]/\Sigma[w(|F_c|^2)^2]\}^{1/2}$.

publication numbers CCDC-159133 (**1**), 159134 (**2**), 159135 (**3**), 159136 (**5**), and 159137 (**6**). Copies of the data can be obtained free of charge on application to CCDC, 12 Union Road, Cambridge CB2 1EZ, UK [Fax: (internat.) + 44(1223)336-033; E-mail: deposit@ccdc.cam.ac.uk].

Acknowledgments

We thank the Deutsche Forschungsgemeinschaft, the Fonds der Chemischen Industrie, and the Ministerium für Wissenschaft, Schule und Weiterbildung, Nordrhein-Westfalen (Germany), for the support.

[1] Review: P. Espinet, K. Soulantica, *Coord. Chem. Rev.* **1999**, *193–195*, 499–556.
[2] Review: G. R. Newcome, *Chem. Rev.* **1993**, *93*, 2067–2089 and ref. cited therein.
[3] P. Arnoldy, E. Drent, P. H. M. Budelzaar, *J. Organomet. Chem.* **1993**, *455*, 247–253.
[4] H. Cheng, Z. Z. Zang, *Coord. Chem. Rev.* **1996**, *147*, 1–39.
[5] J. S. Field, R. J. Haines, B. Warwick, M. M. Zulu, *Polyhedron* **1996**, *15*, 3741–3748.
[6] T. Astley, M. A. Hitchman, F. R. Keene, E. R. T. Tiekink, *J. Chem. Soc. Dalton Trans.* **1996**, 1845–1851 and ref. cited therein.
[7] [7a]M. G. Ehrlich, F. R. Fronczek, S. F. Watkins, G. R. Newcome, D. C. Hager, *Acta Crystallogr., Sect. C* **1984**, *40*, 78–80. – [7b] J. A. Casares, P. Espinet, R. Hernando, G. Iturbe, F. Villafañe, *Inorg. Chem.* **1997**, *36*, 44–49. – [7c] P. Espinet, R. Hernando, G. Iturbe, F. Villafañe, A. G. Orpen, I. Pascual, *Eur. J. Inorg. Chem.* **2000**, 1031–1038.
[8] B. R. James, A. M. Joshi, S. J. Rettig, R. P. Schutte, *Inorg. Chem.* **1997**, *36*, 5809–5817.
[9] S. J. Berners-Price, R. J. Bowen, P. Galettis, P. C. Healy, M. J. McKeage, *Coord. Chem. Rev.* **1999**, *185–186*, 823–836.
[10] O. Herd, A. Hessler, M. Hingst, P. Machnitzki, O. Stelzer, M. Tepper, *Catalysis Today* **1998**, *42*, 413–420.
[11] J. K. Stille, S. E. Tunney, *J. Org. Chem.* **1987**, *52*, 748–753.
[12] O. Herd, A. Hessler, M. Hingst, P. Machnitzki, O. Stelzer, *J. Organomet. Chem.* **1996**, *522*, 69–76.
[13] H. Schmidbaur, Y. Inoguchi, *Z. Naturforsch., Teil B* **1980**, *35*, 1329–1334.
[14] F. R. Keene, M. R. Snow, R. T. Tiekink, *Acta Crystallogr., Sect. C* **1988**, *44*, 757–758.
[15] M. P. Gamasa, J. Gimeno, E. Lastra, M. Lanfranchi, A. Tiripicchio, *J. Chem. Soc. Dalton Trans.* **1989**, 1499–1506.
[16] J. S. Field, R. J. Haines, C. J. Parry, S. H. Sookraj, *Polyhedron* **1993**, *12*, 2425–2428.
[17] A. Del Zotto, E. Zangrando, *Inorg. Chim. Acta* **1998**, *277*, 111–117.
[18] P. Espinet, P. Gómez-Elipe, F. Villafañe, *J. Organomet. Chem.* **1993**, *450*, 145–150.
[19] S. Kitagawa, M. Maekawa, M. Munakata, T. Yonezawa, *Bull. Chem. Soc. Jpn.* **1991**, *64*, 2286–2288.
[20] J. Díez, M. P. Gamasa, J. Gimeno, A. Tiripicchio, M. Tiripicchio Camellini, *J. Chem. Soc. Dalton Trans.* **1987**, 1275–1278.
[21] M. S. Huang, H. F. Liu, W. Liu, P. Zhang, L. X. Zhen, *J. Xiamen Univ. (Nat. Sci)* **1992**, *31*, 57–60.
[22] N. W. Alcock, K. F. Mok, P. Moore, P. A. Lampe, *J. Chem. Soc. Dalton Trans.* **1982**, 207–210.
[23] S. Kuang, T. C. W. Mak, Q. Wang, Z. Zhang, *J. Chem. Soc., Dalton Trans.* **1998**, 2927–2929.
[24] S. Kuang, T. C. W. Mak, Q. Wang, Z. Zhang, *J. Chem. Soc., Dalton Trans.* **1998**, 1115–1119.
[25] P. Pyykkö, *Chem. Rev.* **1997**, *97*, 597–636.
[26] C.-C. Su, S.-P. Wu, C.-Y. Wu, T.-Y. Chang, *Polyhedron* **1994**, *14*, 267–275.
[27] Z.-Z. Zhang, H.-K. Wang, Z. Xi, X.-K. Yao, R.-J. Wang, *J. Organomet. Chem.* **1989**, *376*, 5359–5360.
[28] S. Kuang, T. C. W. Mak, Q. Wang, Z. Zhang, *Chem. Commun.* **1998**, 434–440.
[29] A. Fumagalli, S. Martinengo, V. G. Albano, D. J. Braga, *Chem. Soc., Dalton Trans.* **1988**, 1237–1247.
[30] A. Blaschette, P. G. Jones, T. Hamann, M. Naveke, D. Schomburg, H. K. Cammenga, M. Epple, I. Steppuhn, *Z. Anorg. Allg. Chem.* **1993**, *619*, 912–922.
[31] B. De Groot, S. J. Loeb, G. K. H. Shimizu, *Inorg. Chem.* **1994**, *33*, 2663–2667.

[32] A. J. Arduengo III, H. V. R. Das, J. C. Calabrese, *Inorg. Chem.* **1991**, *30*, 4880−4882.
[33] S. Kuang, T. C. W. Mak, Q. Wang, Z. Zhang, *Chem. Commun.* **1998**, 581−582.
[34] Z.-Z. Zhang, H.-K. Wang, Z. Xi, X.-K. Yao, R.-J. Wang, *J. Organomet. Chem.* **1989**, *376*, 123−131.
[35] R.-E. Chang, Y.-C. Chang, F.-E. Hong, F.-L. Liao, C.-C. Lin, S.-L. Wang, *J. Organomet. Chem.* **1999**, *588*, 160−166.
[36] A. Weiss, H. Witte, *Magnetochemie − Grundlagen und Anwendungen*, Verlag Chemie, Weinheim, **1972**.
[37] H. Lueken, *Magnetochemie − Eine Einführung in Theorie und Anwendung*, Teubner-Verlag, Stuttgart, Leipzig, **1999**.
[38] M. G. Ehrlich, F. R. Fronczek, S. F. Watkins, G. R. Newkome, D. C. Hager, *Acta Crystallogr., Sect. C* **1984**, *40*, 78−80.
[39] L. J. Admiraal, G. Gafner, *J. Chem. Soc., Chem. Commun.* **1968**, 1221−1222.
[40] J. R. Allan, C. L. Jones, L. Sawyer, *J. Inorg. Nucl. Chem.* **1981**, *43*, 2707−2711.

Received March 8, 2001
[I01090]

First Example of Supported Microwave-Assisted Synthesis of New Chiral Bipyridines and a Terpyridine − Use in Asymmetric Cyclopropanation

Frédéric Pezet,[a] Isabelle Sasaki,*[a] Jean-Claude Daran,[a] Jérôme Hydrio,[a] Hassan Aït-Haddou,*[b] and Gilbert Balavoine[a]

Keywords: N ligands / Asymmetric catalysis / Cyclopropanation / Copper / Zinc

We present herein the first alumina-supported synthesis of chiral bipyridines and of a chiral C2-symmetric terpyridine conducted under microwave irradiation, and our preliminary results from copper-mediated enantioselective cyclopropanation with this terpyridine. Reaction yields were excellent and enantioselectivities of up to 87% were observed. Moreover, with *trans*-β-methylstyrene, a remarkable diastereoselectivity (ratio *trans*/*cis* = 7:93) was observed.

Introduction

Nitrogen-containing ligands for asymmetric homogeneous and heterogeneous catalysis have been highly developed.[1] Enantioselective reactions of olefins and diazoacetates catalyzed by a variety of metal complexes are also well known.[2,3] *N,N*-donor ligands led to remarkable *ee* values with copper complexes of bis-oxazolines[4,5] and semicorrins.[6] Chiral bipyridines were used for the first time by Katsuki[7,8] and very recently, Kwong and Lee[9] reported good enantioselective cyclopropanation with chiral C_2-symmetric terpyridine ligands.[10,11] Herein, we report a convenient synthesis of new chiral bi- and terpyridine ligands derived from the Kröhnke's method,[12] by using solvent-free microwave irradiation. Although microwave irradiation has been used for Suzuki coupling reactions of heterocycles,[13] to the best of our knowledge this is the first utilisation of microwave irradiation to form pyridyl rings. We also report the preparation and the characterisation of the corresponding Cu^{II} and Zn^{II} complexes, and the preliminary results of the catalytic activities of the terpyridine copper complex in asymmetric cyclopropanation.

Results and Discussion

Synthesis of polypyridine ligands usually requires a Stille coupling[14] or a Krönke reaction.[12] We used the latter, and carried out the preparation of the ligands in an expedient three-step synthesis: (−)-β-Pinene [(−)-**1**] was ozonolized to produce enantiomerically pure (+)-nopinone [(+)-**2**],[15,16] which was converted into the corresponding Mannich base **3** with the ratio 92:8 (determined by ^{1}H NMR) in favour of the (1*R*,3*R*,5*R*) diastereoisomer (Scheme 1). Condensation of the mixture of the two diastereoisomers of **3** with one equivalent of **4**[17] or **5**, or with half an equivalent of **6** under

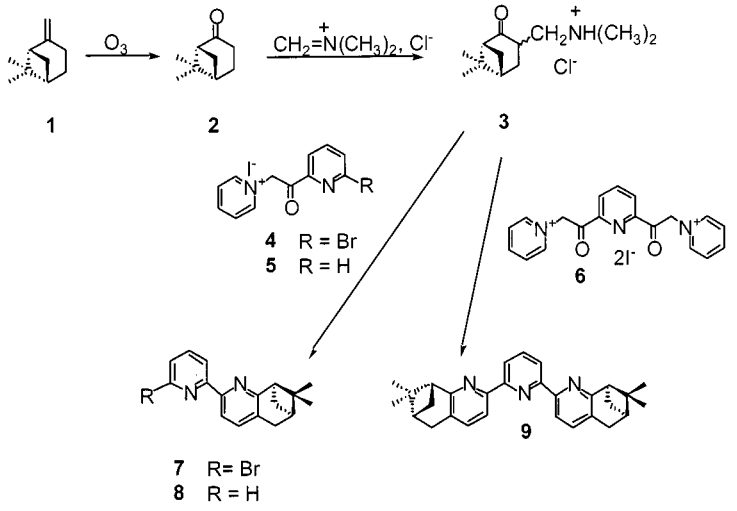

Scheme 1. Synthesis of the polypyridyl ligands

[a] Laboratoire de Chimie de Coordination, CNRS, UPR 8241, 205, route de Narbonne, 31077 Toulouse, France
Fax: (internat.) + 33-5/6155-3003
E-mail: sasaki@lcc-toulouse.fr
[b] University of Texas at Austin, Department of Chemistry and Biochemistry,
Austin, Texas, USA

 © WILEY-VCH Verlag GmbH, 69451 Weinheim, 2001 1434−1948/01/1010−2669 $ 17.50+.50/0

the usual conditions (AcOH or formamide, NH_4OAc, 100 °C) led to **7**, **8**, or **9**, respectively, in very low yields (traces).

The polar solvents used for this reaction absorb microwaves very efficiently,[18] so we decided to carry out Kröhnke's synthesis under microwave irradiation. The yields increased to 10% (130 W, 5−15 min.), but the high temperatures decomposed most of the reactants or intermediates. In order to decrease the temperature dramatically, we tested solvent-free alumina-supported reaction conditions under microwave irradiation.[19] The alumina was mixed with ammonium acetate as an ammonia source. We expected that the strong affinity between alumina and salt reactants would provide a cleaner chemical conversion into the intermediate 1,5-diketone. Indeed, the microwave irradiation of this solvent-free mixture at 260 W for a few minutes led to the expected ligands **7**, **8**,[20] and **9** with good yields (45%, 50%, and 33%, respectively). Thus, the microwave irradiation eliminated the necessity of heating the reaction under reflux in the aggressive solvent (AcOH) that is required under the standard procedure, and the reaction time was reduced from approximately 4 hours to only a few minutes. Ligand **7** is particularly interesting for further study as it is a key product for the synthesis of polypyridines (by homocoupling to C2-symmetrical chiral quaterpyridines, or, after heterocoupling, to non-symmetrical chiral quaterpyridines).

Crystals suitable for X-ray crystallography were obtained by slow evaporation of a solution of **9** in chloroform. The molecular structure of **9**, as determined by X-ray analysis, is shown with its atom labelling scheme in Figure 1. Important bond lengths and bond angles are given in Table 1.

The main part of the molecule is roughly planar with the largest deviation being 0.211 Å at C(25). However, the external pyridine rings are slightly twisted with respect to the central one, resulting in dihedral angles of 10.95° and 6.32° for rings 2 and 3, respectively. Consequently, the C atoms of the pinene fragment are not symmetrically distributed with respect to the main plane of the terpyridine fragment, C(243) and C(343) being twisted away from it by 1.622 Å and −0.712 Å, whereas C(245) and C(345) are located −0.468 Å and 1.428 Å on each side of this plane. As observed in the related dipineno-[4,5:4′′,5′′]-fused 2,2′:6′,2′′-terpyridine[11] and in other terpyridine systems,[21] the nitrogen atoms are in the trans position with respect to each other in order to minimise the interactions between the nitrogen lone pairs.

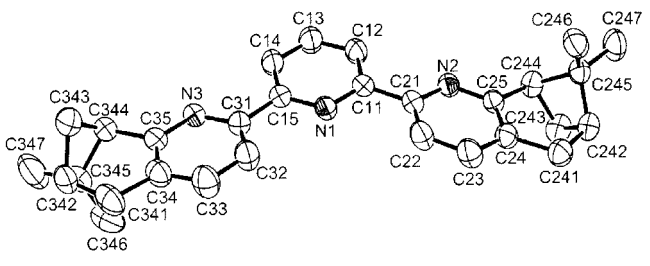

Figure 1. Molecular view of **9** with atom labelling scheme; ellipsoids represent 30% probability

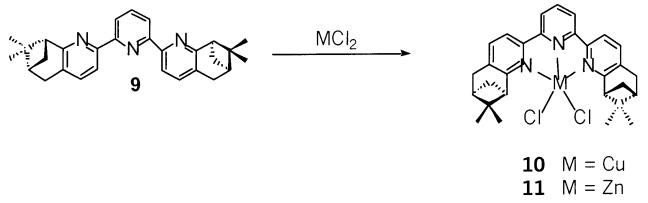

Scheme 2. Synthesis of the complexes

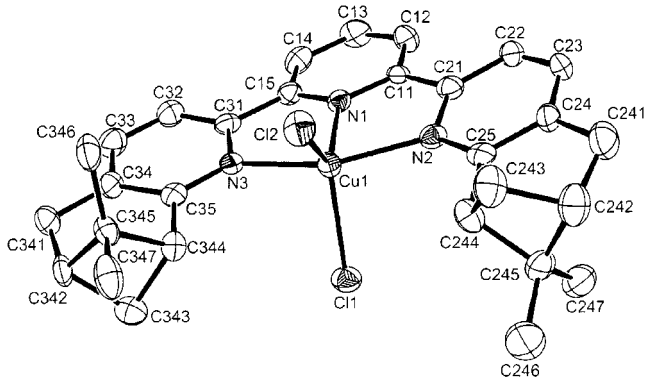

Figure 2. Molecular view of complex **10** with atom labelling scheme; ellipsoids are drawn at 30% probability

In order to investigate the coordination chemistry of this new terpyridine **9**, its copper complex was synthesised. Heating ligand **9** with $CuCl_2{\cdot}H_2O$ in EtOH for 3 hours under reflux resulted in the formation of **10** (Scheme 2). Crystals suitable for X-ray crystallography were obtained by recrystallization from dichloromethane/ether. The zinc complex **11** was also synthesised by reacting ligand **9** with $ZnCl_2$ in refluxing THF for 3 hours. Crystals suitable for X-ray crystallography were obtained by recrystallization from dichloromethane/ether. As the two complexes **10** and **11** are isostructural, only the copper one is shown, along with its atom labelling scheme, in Figure 2. Selected bond lengths and bond angles are given in Table 2.

In both complexes, the metal atom is surrounded by the three nitrogens of the terpyridine ligand and the two chlorine atoms in a distorted trigonal bipyramidal geometry (Table 2). The axial positions are occupied by two nitrogen atoms N(2) and N(3) [N(2)−Cu−N(3) = 157.2(2)° and 150.9(1)° for the Cu and Zn complexes, respectively]. The equatorial plane is made up of the two chlorine atoms and the nitrogen N(1) of the terpyridine moiety. The two M−Cl bonds are identical within experimental errors [M−Cl(1)= 2.317(1), 2.250(1) Å and M−Cl(2) = 2.314(1), 2.258(1) Å for the Cu and Zn complexes, respectively]. Although such a geometry has been observed for related five-coordinate $ZnCl_2$ species,[22] it is unusual for five-coordinate $CuCl_2$ complexes, which normally prefer square pyramidal conformations.[23] However, a similar pseudo trigonal-bipyramidal geometry has been observed in [Cu(terpy)X_2] (X= Br, I, NCS) complexes.[24] The occurrence of a trigonal bipyramidal geometry might be related to the presence of the bulky pinene substituents.

Table 1. Selected bond lengths [Å] and angles [°] for **9**, **10**, **and 11**

9		**10**		**11**	
N(1)−C(11)	1.340(3)	Cu(1)−N(1)	1.974(4)	Zn(1)−N(1)	2.074(3)
N(1)−C(15)	1.344(2)	Cu(1)−N(2)	2.074(4)	Zn(1)−N(2)	2.217(3)
N(2)−C(25)	1.336(2)	Cu(1)−N(3)	2.081(4)	Zn(1)−N(3)	2.218(3)
N(2)−C(21)	1.353(3)	Cu(1)−Cl(1)	2.3169(12)	Zn(1)−Cl(1)	2.2505(9)
N(3)−C(35)	1.341(3)	Cu(1)−Cl(2)	2.3136(13)	Zn(1)−Cl(2)	2.2580(9)
N(3)−C(31)	1.346(3)	N(1)−C(11)	1.333(5)	N(1)−C(11)	1.337(4)
C(11)−C(12)	1.379(3)	N(1)−C(15)	1.334(6)	N(1)−C(15)	1.341(5)
C(11)−C(21)	1.482(3)	N(2)−C(25)	1.340(6)	N(2)−C(25)	1.337(4)
C(12)−C(13)	1.374(3)	N(2)−C(21)	1.367(6)	N(2)−C(21)	1.357(4)
C(13)−C(14)	1.371(3)	N(3)−C(35)	1.348(6)	N(3)−C(35)	1.327(5)
C(14)−C(15)	1.382(3)	N(3)−C(31)	1.364(5)	N(3)−C(31)	1.356(5)
C(15)−C(31)	1.480(3)	N(1)−Cu(1)−N(2)	78.50(16)	N(1)−Zn(1)−N(2)	75.25(10)
C(21)−C(22)	1.378(3)	N(1)−Cu(1)−N(3)	78.80(16)	N(1)−Zn(1)−N(3)	75.62(11)
C(22)−C(23)	1.376(3)	N(2)−Cu(1)−N(3)	157.24(15)	N(2)−Zn(1)−N(3)	150.86(11)
C(23)−C(24)	1.381(3)	N(1)−Cu(1)−Cl(1)	118.63(11)	N(1)−Zn(1)−Cl(1)	118.78(8)
C(24)−C(25)	1.392(3)	N(2)−Cu(1)−Cl(1)	97.57(11)	N(2)−Zn(1)−Cl(1)	98.19(8)
C(31)−C(32)	1.378(3)	N(3)−Cu(1)−Cl(1)	94.68(9)	N(3)−Zn(1)−Cl(1)	95.35(7)
C(32)−C(33)	1.386(3)	N(1)−Cu(1)−Cl(2)	122.68(11)	N(1)−Zn(1)−Cl(2)	117.41(8)
C(33)−C(34)	1.370(3)	N(2)−Cu(1)−Cl(2)	93.72(11)	N(2)−Zn(1)−Cl(2)	95.61(8)
C(34)−C(35)	1.390(3)	N(3)−Cu(1)−Cl(2)	97.11(10)	N(3)−Zn(1)−Cl(2)	98.06(7)
C(11)−N(1)−C(15)	118.6(2)	Cl(1)−Cu(1)−Cl(2)	118.68(5)	Cl(1)−Zn(1)−Cl(2)	123.81(4)
C(25)−N(2)−C(21)	117.8(2)	C(11)−N(1)−C(15)	121.1(4)	C(11)−N(1)−C(15)	120.8(3)
C(35)−N(3)−C(31)	117.3(2)	C(11)−N(1)−Cu(1)	119.5(3)	C(11)−N(1)−Zn(1)	119.3(2)
N(1)−C(11)−C(12)	122.4(2)	C(15)−N(1)−Cu(1)	119.1(3)	C(15)−N(1)−Zn(1)	119.5(2)
N(1)−C(11)−C(21)	116.0(2)	C(25)−N(2)−C(21)	118.1(4)	C(25)−N(2)−C(21)	118.5(3)
C(12)−C(11)−C(21)	121.6(2)	C(25)−N(2)−Cu(1)	127.4(3)	C(25)−N(2)−Zn(1)	126.8(2)
C(13)−C(12)−C(11)	118.6(2)	C(21)−N(2)−Cu(1)	113.7(3)	C(21)−N(2)−Zn(1)	114.5(2)
C(14)−C(13)−C(12)	119.7(3)	C(35)−N(3)−C(31)	118.0(4)	C(35)−N(3)−C(31)	119.2(3)
C(13)−C(14)−C(15)	119.1(2)	C(35)−N(3)−Cu(1)	128.0(3)	C(35)−N(3)−Zn(1)	125.7(2)
N(1)−C(15)−C(14)	121.7(2)	C(31)−N(3)−Cu(1)	113.9(3)	C(31)−N(3)−Zn(1)	113.6(2)
N(1)−C(15)−C(31)	116.1(2)				
C(14)−C(15)−C(31)	122.17(19)				
N(2)−C(21)−C(22)	122.0(2)				
N(2)−C(21)−C(11)	115.9(2)				
C(22)−C(21)−C(11)	122.11(19)				
C(23)−C(22)−C(21)	119.4(2)				
C(22)−C(23)−C(24)	119.6(2)				

Table 2. Crystallographic data

	9	**10**	**11**
Formula	$C_{29}H_{31}N_3$	$C_{29}H_{31}Cl_2N_3Cu$	$C_{29}H_{31}Cl_2N_3Zn$
Fw (g)	421.6	556.01	557.84
Temperature, K	293 (2)	180 (2)	180 (2)
Crystal system	Monoclinic	Trigonal	Trigonal
Space group	$P2_1$	$P6_1$	$P6_1$
a, Å	13.0610 (11)	10.3549 (8)	10.4288 (4)
b, Å	6.3367 (8)	10.3549 (8)	10.4288 (4)
c, Å	15.5512 (14)	42.080 (4)	42.213 (2)
α, °	90.0	90.0	90.0
β, °	113.64 (9)	90.0	90.0
γ, °	90.0	120.0	120.0
U/Å^3	1179.1 (2)	3907.5 (6)	3976.0 (3)
Z	2	6	6
ρ (calcd.), g,cm^{-3}	1.187	1.418	1.398
μ (Mo-K_α), cm^{-1}	0.698	10.67	11.51
θ range, °	$2.68 < \theta < 26.13$	$2.27 < \theta < 20.95$	$2.25 < 2\theta < 20.96$
Reflections measured	11778	11611	14569
Independent reflections (R_{int})	4509 (0.0586)	2680 (0.0565)	2805 (0.0468)
Data/restraints/parameters	4509/1/293	2680/1/320	2805/1/320
*R*1, w*R*2 [$I > 2\sigma(I)$]	0.0372, 0.0693	0.0274, 0.0405	0.0256, 0.0536
*R*1, w*R*2 (all data)	0.0921, 0.0848	0.0398, 0.0429	0.0293, 0.0552
$(\Delta/\sigma)_{max}$	0.001	0.001	0.001
$\Delta\rho_{min}/\Delta\rho_{max}$	−0.13/0.11	−0.21/0.22	−0.16/0.16
GOF	0.881	0.922	1.023

Owing to some hydrogen interactions occurring between the H attached to carbon C(12) and Cl(1)[20] [C−H···Cl: C−H = 0.95 Å, C···Cl = 3.501(5) Å, H···Cl = 2.568(1) Å, C−H···Cl= 167.6(1)°] the packing in the cell displays a right-handed helix arrangement of the complexes around the 6_1 axes (Figure 3). Such an arrangement explains the long *c* axes relative to *a* and *b*. The crystallisation in this space group is certainly induced by the shape and the (*R*,*R*) configuration of the terpyridine ligand.

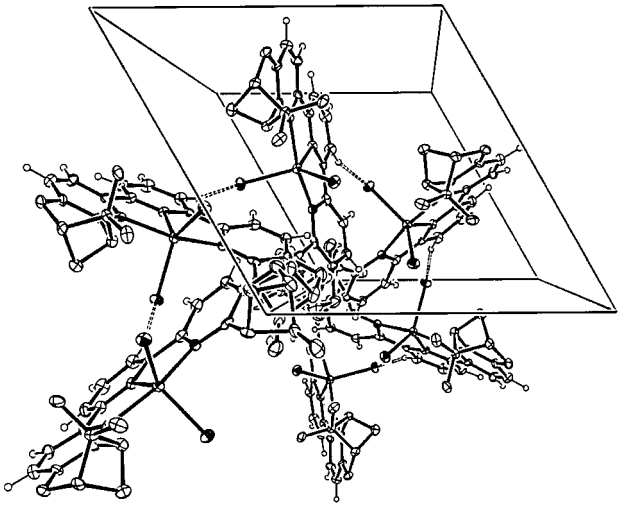

Figure 3. View along the 0 0 1 axis showing the right handed helix packing of the complexes around the 6_1 axes

To explore the catalytic potential of the copper terpyridine we examined the well-investigated cyclopropanation of various olefins with ethyl diazoacetate (Scheme 3). This commercially available diazoester, which is neither chiral nor a bulky reactant, has a very poor effect on the asymmetric induction, and allows one to evaluate the inherent capacity of the terpyridine to be a chiral controller. The reactions were carried out in the presence of 2mol % copper(II)triflate (2 mol % chiral ligand) in dichloromethane at ambient temperature. The use of other solvents such as toluene or THF led to much lower catalytic efficiency. The complex was found to be an efficient catalyst, converting alkenes and ethyldiazoacetate to optically active cyclopropanes (Table 3). Reaction of the mono-substituted olefins showed excellent yields of chiral cyclopropanes with good *trans*-selectivity, but moderate levels of enantioselectivity (6−66% *ee*) were observed. When ethyl diazoacetate was changed for the bulkier commercially available trimethylsilyldiazomethane, the diastereoselectivity increased slightly to a *trans*/*cis* ratio of 90:10, which has been observed with other copper catalysts.[7,8,25] Styrene derivatives bearing electron-donating groups showed lower enantioselectivity than those with electron-withdrawing groups, but higher reactivity (shorter reaction time). This result indicates that the active catalyst species is a strong electrophilic carbene copper complex.

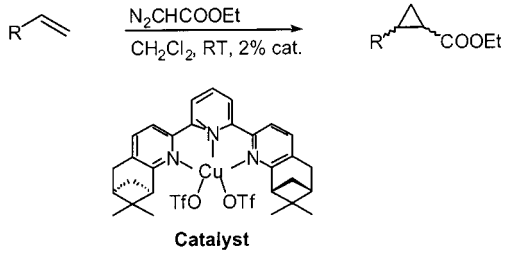

Scheme 3. Cyclopropanation of olefins

Table 3. Catalytic asymmetric cyclopropanation with ethyl diazoacetate and chiral copper (II)terpyridine complex

Alkene	Time [h]	Ligand	Yield (%)	*trans*/*cis* ratio	e.e. *trans*	e.e. *cis*
	16	4	95	83/17 [a]	24 [b] (1*S*/2*S*)	54 [b] (1*S*/2*R*)
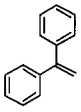	16	4	91	–	74 [c] (*S*)	
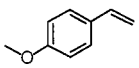	8	4	99	69/31 [a]	25 [b] N.D.	29 [b] N.D.
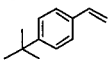	16	4	96	66/34 [a]	40 [f] N.D.	6 [f] N.D.
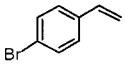	24	4	86	77/23 [a]	52 [f] N.D.	41 [f] N.D.
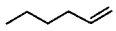	16	4	82	78/22 [e]	41 [f] N.D.	66 [f] N.D.
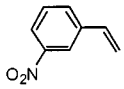	36	4	74	64/36 [g]	23 [h] N.D.	12 [h] N.D.
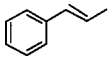	16	4	98	7/93 [a,d]	9 [h] (1*S*/2*S*/3*S*)	65 [h] (1*S*/2*R*/3*R*)
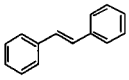	24	4	90		87 [c] N.D.	
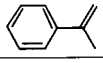	16	4	87	88/12	64 [h] N.D.	72 [h] N.D.

[a] GC. − [b] HPLC chiral column Pharmachir 7C (hexane/2-propanol 99:1 flow: 0.7 mL/min). − [c] Determined by ^{1}H NMR spectroscopy with Eu (hfc)$_3$. − [d] Major diastereoisomer: ethyl *trans*-3-methyl-*cis*-2-phenyl cyclopropanecarboxylate; minor diastereoisomer: ethyl *trans*-3-methyl-*trans*-2-phenylcyclopropanecarboxylate. − [e] Determined by ^{1}H NMR integration of methylene ($COOCH_2CH_3$). − [f] GC analytic chiral column Supelco-120 (oven temperature 120 °C to 200 °C **0.5** °C/min). − [g] Determined by ^{1}H NMR integration of the cyclopropyl protons. − [h] Determined by chiral GC after transesterification with (−)-menthol (99% *ee*). N.D.: absolute configuration not determined

Based on the results and the sense of asymmetric induction, the metal carbenoid attack could be compared to the model previously reported by Pfaltz for *N,N*-bidentate ligands,[6] and by Kwong for *N,N,N*-tridentate ligands.[9] Using 1,1′- or 1,2-disubstituted olefins led to better results, showing that the steric interaction between the ligand and these olefins increased with respect to monosubstituted ones. For instance, a good *ee* of up to 87% was observed

with *trans*-stilbene. In contrast to the other substrates, *trans*-β-methylstyrene showed a remarkable reversed *cis*-selectivity, as already observed by Katsuki[8] with chiral bipyridine. The ratio *cis*/*trans* = 93:7 is of the same order as the results described by Nishiyama[26] with hydroxymethyl derivative of pybox and (+)-menthyl diazoacetate.

Conclusion

We have successfully synthesised new chiral ligands by microwave irradiation. The copper complex of the terpyridine derivative is an active catalyst for cyclopropanation and *ee*s up to 87% were observed. Cyclopropanation of *trans*-β-methylstyrene showed a very high *cis*-selectivity with ethyl diazoacetate. Further studies on other disubstituted olefins are under investigation.

Experimental Section

General: All reactions were carried out under an inert argon atmosphere. Chemicals were of reagent-grade quality and were obtained commercially. NMR spectra were recorded with a Bruker AM-250 (250 MHz) or AMX-400 (400 MHz) spectrometer for ^1H and ^{13}C and chemical shifts are reported in ppm downfield from Me_4Si in $CDCl_3$ or in CD_2Cl_2. All melting points are uncorrected and were measured on a SMP1 Stuart Scientific melting point apparatus. CI mass spectra and FAB mass spectra (*m*-nitrobenzyl alcohol matrix) were recorded with a quadrupolar Nermag R10−10H instrument. Optical rotations were measured on a Perkin−Elmer 241 polarimeter. Elemental analyses were performed by LCC (Laboratoire de Chimie de Coordination) Microanalytical Service. Column chromatography purifications were performed with Merck aluminum oxide (70−230 mesh ASTM), deactivated with 8% water. (+)-Nopinone was obtained from ozonolysis of (−)-β-pinene.[15]

Mannich Base of the Nopinone 3: *N*,*N*-dimethylmethyleneiminium chloride (6.8 g) was added to nopinone (**2**; 9 g) in 135 mL of dry acetonitrile. After stirring at room temperature for four days the white precipitate was filtered off and rinsed with acetonitrile. The filtrate was concentrated and more of the product was recovered (9.1 g, 60% yield). − M.p. 188 °C − ^1H NMR ($CDCl_3$): δ = 12.12 (m, 1 H), 3.5 (dd, ^2J = 12.8, ^3J = 3.6 Hz, 1 H), 3.23 (dd, ^2J = 12.8, ^3J = 10.0 Hz, 1 H), 2.92 (s, 6 H), 2.87 (m, 1 H), 2.66 (m, 2 H), 2.54 (m, ^2J = 14.0, ^3J = 2.4 Hz, 1 H), 2.34 (m sept, ^3J = 2.8 Hz, 1 H), 2.23 (ddd, ^2J = 14.0, ^3J = 3.6, ^3J = 3.6 Hz, 1 H), 1.34 (s, 3 H), 1.29 (d, ^2J = 10.8 Hz, 1 H), 0.94 (s, 3 H). − ^{13}CNMR ($CDCl_3$): δ = 211.9, 64.0, 58.4, 41.0, 40.7, 40.4, 29.7, 27.1, 26.2, 22.9. − MS (DCI, NH_3): *m*/*z* (%) = 196 (100), 197 (15). − $C_{12}H_{24}ClNO_2$·0.25H_2O: calcd. C 61.01, H 10.16, N 5.93; found C 60.92, H 9.23, N 6.01.

General Procedure for the Synthesis of Ligands 7 to 9 Under Microwave Irradiation: The aluminium oxide was prepared by mixing 10 g of aluminium oxide 90, 5 g of ammonium acetate, and 1 mL of AcOH in a mortar.

Freshly prepared aluminium oxide (3 g) was then added to a solution of **3** (1 mmol) and the pyridinium salt (1 mmol) in MeOH (30 mL). The solvent was evaporated and the resulting mixture was irradiated in the microwave oven for 4 min. at 260 W. After cooling, the ligand was extracted with CH_2Cl_2 and purified by column chromatography on aluminium oxide (eluent: 3% AcOEt in pentane)

Ligand 7: Following the above procedure with **4**, and the usual workup, gave **7** (0.142 g, 43%). − $[\alpha]_D^{20}$ = + 23.0 (*c* = 1, CH_2Cl_2). − M.p. 122 °C. − ^1H NMR ($CDCl_3$): δ = 8.33 (dd, ^3J = 7.5, ^4J = 1.0 Hz, 1 H), 8.15 (d, ^3J = 7.5 Hz, 1 H), 7. 60 (t, ^3J = 7.5 Hz, 1 H), 7.51 (d, ^3J = 7.5 Hz, 1 H), 7.41 (dd, ^3J = 7.5, ^4J = 1.0 Hz, 1 H), 3.04 (t, ^3J = 5.5 Hz, 1 H), 2.97 (d, ^3J = 2.5 Hz, 2 H,), 2.73 (td, ^2J = 9.5, ^3J = 5.5 Hz, 1 H), 2.33 (m sept, ^3J = 2.8 Hz, 1 H), 1.43 (s, 3 H), 1.32 (d, ^2J = 9.5 Hz, 1 H), 0.67 (s, 3 H). − ^{13}C NMR ($CDCl_3$): δ = 165.9, 158.0, 150.3, 141.3, 139.0, 135.9, 131.4, 127.2, 119.5, 119.2, 50.5, 40.0, 39.2, 31.3, 30.8, 26.0, 21.2. − MS (DCI, NH_3): *m*/*z* (%) = 317 (98), 319 (100) $[MH^+]$. − $C_{17}H_{17}BrN_2$ (329.24): calcd. C 62.02, H 5.20, N 8.51; found C 62.12, H 4.99, N 8.34.

Ligand 8: Following the above procedure with **5**, and the usual workup, gave **8** (0.125 g, 50%). − $[\alpha]_D^{20}$ = + 17.6 (*c* = 1, CH_2Cl_2). − M.p. 84 °C. − ^1H NMR ($CDCl_3$): δ = 8.61 (ddd, ^3J = 4.8, ^4J = 1.4 Hz, ^5J = 0.7 Hz, 1 H), 8.34 (d, ^3J = 8.0 Hz, 1 H), 8.12 (d, ^3J = 7.8 Hz, 1 H), 7.76 (dt, ^3J = 7.8, ^4J = 1.8 Hz, 1 H), 7.53 (d, ^3J = 7.8 Hz, 1 H), 7.19 (ddd, ^3J = 8.5, ^3J = 4.8 Hz, ^4J = 1.1 Hz, 1 H), 3.08 (dd, ^3J = 5.6, ^3J = 5.6 Hz, 1 H), 2.98 (d, ^3J = 2.5 Hz, 2 H), 2.74 (td, ^2J = 9.7, ^3J = 5.9 Hz, 1 H), 2.34 (m sept, ^3J = 2.8 Hz, 1 H), 1.43 (s, 3 H), 1.34 (d, ^2J = 9.7 Hz, 1 H), 0.69 (s, 3 H). − ^{13}C NMR ($CDCl_3$): δ = 165.9, 156.7,152.0, 149.1, 136.7, 135.9, 130.6, 123.0, 120.9, 118.7, 50.5, 40.0, 39.2, 31.3, 30.8, 26.0, 21.2. − MS (DCI, NH_3): *m*/*z* (%) = 251 $[MH]^+$. − $C_{17}H_{18}N_2$ (250.34): calcd. C 81.56, H 7.15, N 11.19; found C 81.59, H 7.13, N 11.15.

Ligand 9: Following the above procedure with half an equivalent of **6**, and the usual workup, gave **9** (0.080 g, 38%) − $[\alpha]_D^{20}$ = − 8.4 (*c* = 1, CH_2Cl_2). − M.p. 255 °C. − ^1H NMR ($CDCl_3$): δ = 8.38 (d, ^3J = 3.8 Hz, 2 H), 8.35 (d, ^3J = 3.8 Hz, 2 H), 7.86 (t, ^3J = 7.8 Hz, 1 H), 7.56 (d, ^3J = 7.8 Hz, 2 H), 3.09 (dd, ^3J = 5.6, ^3J = 5.6 Hz, 2 H), 2.99 (d, ^3J = 2.5 Hz, 4 H), 2.74 (td, ^2J = 9.7, ^3J = 5.9 Hz, 2 H), 2.35 (m sept, ^3J = 2.8 Hz, 2 H), 1.44 (s, 6 H), 1.35 (d, ^2J = 9.7 Hz, 2 H), 0.70 (s, 6 H). − ^{13}C NMR ($CDCl_3$): δ = 165.7, 155.7, 152.3, 137.6, 135.9, 130.5, 120.2, 118.8, 50.5, 40.1, 39.2, 31.3, 30.9, 26.0, 21.3. − MS (DCI, NH_3): *m*/*z* (%) = 422 $[MH]^+$. − $C_{29}H_{31}N_3$ (421.58): calcd. C 82.11, H 7.63, N 10.26; found C 82.51, H 7.28, N 9.55.

Synthesis of Copper Complex 10: Complex **10** was synthesized by mixing ligand **9** (0.1 mmol) and copper(II) chloride dihydrate (0.05 mmol) in absolute EtOH (6 mL). The mixture was heated under reflux for 3 hours and the precipitate then collected. The green-yellow complex crystallised by slow diffusion of ether into a solution of **10** in dichloromethane (16 mg, 58% yield). − Positive ion FAB-MS: *m*/*z* = 519 $[M - Cl]^+$, 484 $[M - 2Cl]^+$.

Synthesis of Zinc Complex 11: Complex **11** was synthesised by adding ligand **9** (0.1 mmol) in THF (20 mL) to a stirred solution of zinc(II) chloride (0.1 mmol) in THF (10 mL). The mixture was then heated under reflux for 3 hours. After cooling, the solvent was evaporated and the white solid was recrystallized from a mixture of dichloromethane and ether (38 mg, 70% yield). − ^1H NMR (CD_2Cl_2): δ = 8.16 (m, 3 H), 7.98 (d, ^3J = 7.9 Hz, 2 H), 7.73 (d, ^3J = 7.9 Hz, 2 H), 4.25 (dd, ^3J = 5.5, ^3J = 5.5 Hz, 2 H), 3.10 (d, ^3J = 2.5 Hz, 4 H), 2.89 (m, 2 H), 2.39 (m sept, ^3J = 2.8 Hz, 2 H), 1.55 (s, 6 H), 1.41 (d, ^2J = 10.1 Hz, 2 H), 0.76 (s, 6 H). − ^{13}C NMR (CD_2Cl_2): δ = 169.1, 151.5, 144.1, 142.4, 138.4, 136.6, 121.4, 119.5, 49.6, 40.2, 39.9, 32.5, 30.8, 26.3, 21.8. − Positive ion FAB-MS: *m*/*z* = 520 $[M - Cl]^+$, 484 $[M - 2Cl]^+$.

X-ray Crystallographic Study: Suitable crystals of ligand **9** were grown by slow evaporation of a chloroform solution. Suitable crystals of complexes **10** and **11** were grown by dissolving each of them in dichloromethane and allowing diethyl ether to diffuse into the solution. Data for **9**, **10**, and **11** were collected on a Stoe IPDS diffractometer. The final unit cell parameters were obtained by the least-squares refinement of 8000 reflections. Only statistical fluctuations were observed in the intensity monitors over the course of the data collections.

All the structures were solved by direct methods (SIR97[27]) and refined by least-squares procedures on F^2. All H atoms were introduced in calculated idealised positions [d(CH) = 0.96 Å] and treated as riding models with isotropic thermal parameters related to the carbon to which they are attached. Least-squares refinements were carried out by minimising the function $\Sigma w(F_o^2 - F_c^2)^2$, where F_o and F_c are the observed and calculated structure factors. The absolute structure for **10** and absolute configuration for **11** were determined by refining the Flack enantiopole parameter.[28] The weighting scheme used in the last refinement cycles was $w = 1/[\sigma^2(F_o^2) + (aP)^2 + bP]$, where $P = (F_o^2 + 2F_c^2)/3$ Models reached convergence with $R = \Sigma (||F_o| - |F_c||)/\Sigma(|F_o|)$ and $wR2 = \{\Sigma w(F_o^2 - F_c^2)^2/\Sigma w (F_o^2)^2\}^{1/2}$ with the values listed in Table 2. The calculations were carried out using the SHELXL-97 program[29] running on a PC. Molecular views were realised with the help of ORTEP32.[30] Crystallographic data (excluding structure factors) for the structure(s) included in this paper have been deposited with the Cambridge Crystallographic Data Centre as supplementary publication no. CCDC-158858 (**9**), -158859 (**10**) and -158860 (**11**). Copies of the data can be obtained free of charge on application to CCDC, 12 Union Road, Cambridge CB2 1EZ, UK [Fax: (internat.) + 44-1223/336-033; E-mail: deposit@ccdc.cam.ac.uk].

Procedure for Copper-Catalysed Cyclopropanation: A solution of 0.2 mmol of ligand and 0.2 mmol of $Cu(OTf)_2$ in dichloromethane (2 mL) under argon was stirred for 2 hours at room temperature. The alkene (4 mmol) and the ethyl diazoacetate (0.2 mmol) were then added and the mixture was stirred for 30 min. The reduction of Cu^{II} to Cu^{I} could also be activated by gentle heating of the solution (the colour of the solution changing from green to reddish). Slow addition of 2 mL of a 0.5 mM solution of the diazo compound in CH_2Cl_2 was carried out over a period of 3 hours, using a syringe pump. The mixture was allowed to stir overnight at room temperature then worked up by removing the solvent and purifying the crude product by column chromatography (pentane/ethyl acetate). All isolated cyclopropanes were known compounds and were characterised by ^1H and ^{13}C NMR spectroscopy, and mass spectrometry.

Acknowledgments

We are grateful for financial support by the Centre National de la Recherche Scientifique (CNRS) and for a doctoral fellowship for F.P. by the Ministère de l'Education Nationale, de la Recherche et de la Technologie. We also wish to thank Y. Coppel for recording NMR spectra of compound **3** on the 400 MHz spectrometer.

[1] F. Fache, E. Schulz, M. L. Tommasino, M. Lemaire, *Chem. Rev.* **2000**, *100*, 2159−2232.
[2] A. Pfaltz, in *Comprehensive Asymmetric Catalysis* II (Eds.: E. N. Jacobsen, A. Pfaltz, H. Yamamoto), Springer Verlag, **1999** p. 513.
[3] M. P. Doyle, M. N. Protopopova, *Tetrahedron* **1998**, *54*, 7919−7946.
[4] D. A. Evans, K. A. Woerpel, M. H. Hinmann, M. M. Faul, *J. Am. Chem. Soc.* **1991**, *113*, 726−728.
[5] R. E. Lowenthal, A. Abiko, S. Masumune, *Tetrahedron Lett.* **1990**, *31*, 6005−6008.
[6] H. Frischi, U. Leutenneger, A. Pfaltz, *Helv. Chim. Acta* **1988**, *71*, 1553−1565.
[7] K. Ito, S. Tabuchi, T. Katsuki, *Synlett* **1992**, 575−577.
[8] K. Ito, T. Katsuki, *Synlett* **1993**, 638−640.
[9] H. L. Kwong, W. S. Lee, *Tetrahedron: Asymmetry* **2000**, *11*, 2299−2308.
[10] D. Lötscher, S. Rupprecht, H. Stoeckli-Evans, A. Von Zelewsky, *Tetrahedron: Asymmetry* **2000**, *11*, 4341−4357.
[11] M. Ziegler, V. Monney, H. Stoeckli-Evans, A. Von Zelewsky, I. Sasaki, G. Dupic, J.-C. Daran, G. G. A Balavoine, *J. Chem. Soc., Dalton Trans.* **1999**, 667−675.
[12] F. Kröhnke, *Synthesis* **1976**, 1−24.
[13] D. Villemin, M. J. Gomez-Escalonilla, J. F. Saint-Clair, *Tetrahedron Lett.* **2001**, *42*, 635−637.
[14] D. J. Càrdenas, J. P. Sauvage, *Synlett* **1996**, 916−918.
[15] H. C. Brown, S. A. Weissman, P. T. Perumal, U. P. Dhokte, *J. Org. Chem.* **1990**, *55*, 1217−1223.
[16] The *ee* of the isolated nopinone is superior to 98% {optical rotation $[\alpha]_D^{25} = 39.8$ ($c = 4.0$, MeOH), ref.:[15] $[\alpha]_D = 40.5$ ($c = 4.0$, MeOH)}
[17] G. R. Newkome, D. C. Hager, G. E. Kiefer, *J. Org. Chem.* **1986**, *51*, 850−853.
[18] H. M. S. Kingston, S. J. Haswell, in *Microwave-enhanced Chemistry*, ACS Monograph, **1998**.
[19] A. Y. Usyatinsky, Y. L. Khmelnitsky, *Tetrahedron Lett.* **2000**, *41*, 5031−5034.
[20] Very recently, another synthesis of ligand **8** was described via the preparation of the enone: A. V. Malkov, I. R. Baxendale, M. Bella, V. Langer, J. Fawcett, D. R. Russell, D. J. Mansfield, M. Valko, P. Kocovsky, *Organometallics* **2001**, *20*, 673−690.
[21] E. Bejan, H. Ait Haddou, J.-C. Daran, G. G. A. Balavoine, *Synthesis* **1996**, *8*, 1013−1018.
[22] [22a] M. Vlasse, T. Rojo, D. Beltran-Porter, *Acta Crystallogr., Sect. C* **1983**, *39*, 560−563. − [22b] H. Kooijman, A. L. Spek, A. Mulder, K. J. C. van Bommel, W. Verboom, D. N. Reinhoudt, *private communication.*
[23] [23a] W. Henke, S. Kremer, D. Reinen, *Inorg. Chem.* **1983**, *22*, 2858−2863. − [23b] A. Angeloff, J.-C. Daran, J. Bernadou, B. Meunier, *Eur. J. Inorg. Chem.* **2000**, 1985−1996.
[24] [24a] M. I. Arriortua, J. L. Mesa, T. Rojo, T. Debaerdemaeker, D. Beltran-Porter, H. Stratemeier, D. Reinen, *Inorg. Chem.* **1988**, *27*, 2976−2981. − [24b] A. Kutoglu, R. Allmann, J.-V. Folgado, M. Atanasov, D. Reinen, *Z. Naturforsch., Teil B* **1991**, *46*, 1193−1199.
[25] [25a] C. Bolm, M. Zender, D. Bur, *Angew. Chem. Int. Ed. Engl.* **1990**, *29*, 205−207. − [25b] K. Ito, T. Katsuki, *Tetrahedron Lett.* **1993**, *34*, 2661−2664.
[26] S. Isawa, F. Takezawa, Y. Tuchiya, H. Nishiyama, *Chem. Commun.* **2001**, 59−60.
[27] A. Altomare, M. C. Burla, M. Camalli, G. L. Cascarano, C. Giacovazzo, A. Guagliardi, A. G. G. Moliterni, G. Polidori, R. Spagn, SIR97 a program for automatic solution of crystal structures by direct methods, *J. Appl. Cryst.* **1999**, *32*, 115−119.
[28] [28a] H. D. Flack, *Acta Crystallogr., Sect. A* **1983**, *39*, 876−881. − [28b] G. Bernardinelli, H. D. Flack, *Acta Crystallogr., Sect. A* **1985**, *41*, 500−511.
[29] G. M. Sheldrick, SHELXL-97 *a program for crystal structure refinement*, University of Göttingen, Germany, **1997**.
[30] L. J. Farrugia, ORTEP3 for Windows, *J. Appl. Cryst.* **1997**, *30*, 565.

Received March 7, 2001
[I01091]

Kinetics of the Oxidative Addition of *ortho*-Substituted Aryl Halides to Palladium(0) Complexes

Mouad Alami,[a] Christian Amatore,*[b] Samia Bensalem,[b,c] Abdelharim Choukchou-Brahim,[c] and Anny Jutand*[b]

Keywords: Palladium / Oxidative addition / Kinetics / P ligands / P, P ligands

The rate constant of the oxidative addition of *ortho*-substituted aryl halides, *o*-ZCH_2–C_6H_4–X [X = I, Br; Z = OMe, NEt_2, $N(CH_2)_5$] to $Pd^0(PPh_3)_4$ or to Pd^0(dba)(dppp) generated from $Pd^0(dba)_2$ and 1 equiv. of dppp is determined. The oxidative addition is slower for *ortho*-substituted aryl halides than for the corresponding nonsubstituted or *meta*-substituted aryl halides. The *ortho* substituents investigated here do not participate in the oxidative addition by a preliminary complexation of the active $Pd^0(PPh_3)_2$ or Pd^0(dppp) complex. The observed decelerating effect induced by the *ortho* substituents is due to steric hindrance and electronic donor effects and is less important for aryl bromides than for aryl iodides; *ortho*-substituted aryl iodides remain more reactive than *ortho*-substituted aryl bromides for both ligands PPh_3 and dppp. The *cis*-(*o*-ZCH_2–C_6H_4)PdX(dppp) complexes are formed in the oxidative addition whereas an equilibrium takes place between *trans*-(*o*-ZCH_2–C_6H_4)$PdX(PPh_3)_2$ and (*o*-ZCH_2–C_6H_4)$PdX(PPh_3)$(*Z*–*Pd*) complexes.

Introduction

Dimeric *ortho*-palladated complexes **1** are synthesized by reaction of a Pd^{II} salt and a substituted arene, in which the substituent may be a ligand for the Pd^{II} centers [Equation (1)].[1–7] This reaction is regarded as a preliminary complexation of the Pd^{II} salt by the substituent of the arene, followed by an intramolecular electrophilic aromatic substitution of the Pd^{II} center.[8] When the coordinated atom Z (Z = N, O) is linked to the arene through one atom (C or N) the resulting five-membered palladated complexes **1** are quite stable.[1–7] Monomeric complexes **2** and **3** are generated from dimeric complexes **1** by addition of 1 or 2 equiv. of L per Pd, respectively [Equation (2)];[9,10] *ortho*-palladated complexes **1** are also generated by an oxidative addition of an *ortho*-substituted aryl halide to a Pd^0 complex, $Pd^0(dba)_2$ [Equation (3)], with subsequent formation of complexes **2** and **3** after addition of a ligand [Equation (2)].[9–10]

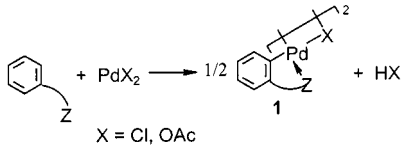

(1)

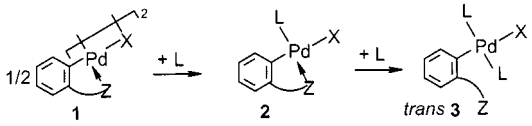

(2)

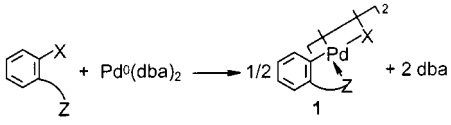

(3)

A recent paper[11] reports the synthesis of phosphane-bis(ligated) complexes **3** by oxidative addition of aryl bromides, substituted in the *ortho* position by CHO or C(O)Me, to Pd^0 complexes ligated by PPh_3 [Equation (4)]. Phosphane-monoligated complexes **2** are formed in the case of a bulky ligand L = P(*o*-tolyl)$_3$ and a C(O)Me substituent, which is able to coordinate the Pd^{II} center by the O atom.

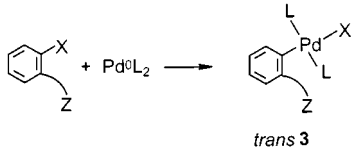

(4)

Whereas reactions of *ortho*-substituted aryl halides with nucleophiles (alkynes,[12,13] alkenes,[13,14] organometallic reagents[6,15]) are catalyzed by Pd^0 complexes, reactions involving substituted arenes cannot be catalyzed by Pd^{II} complexes able to activate the initial substituted arene, unless the Pd^0 complex generated in the last step[4,7,16] is oxidized back to a Pd^{II} complex. To the best of our knowledge, the recycling of the Pd^{II} catalyst by oxidation has not yet been realized.[7]

[a] Laboratoire de Chimie Thérapeutique BIOCIS, Faculté de Pharmacie,
Rue Jean-Baptiste Clément, 92296 Chatenay Malabry, France
[b] Ecole Normale Supérieure, Département de Chimie, UMR CNRS 8640
24 Rue Lhomond, 75231 Paris Cedex 5, France
Fax: (internat.) + 33-1/44323325
E-mail: amatore@ens.fr
Anny.Jutand@ens.fr
[c] Université de Tlemcen, Faculté des Sciences, Département de Chimie,
B. P. 119, 13000 Tlemcen, Algérie

 © WILEY-VCH Verlag GmbH, 69451 Weinheim, 2001 1434–1948/01/1010–2675 $ 17.50+.50/0

Pd^0-catalyzed cross-coupling reactions of nucleophiles with *ortho*-substituted aryl halides are usually slower than with the corresponding nonsubstituted or *para*/*meta*-substituted aryl halides.[6,15] The three main steps involved in the catalytic cycle (oxidative addition, transmetallation, and reductive elimination) may be affected by the *ortho* substitution of the aryl derivatives,[15] due to steric hindrance around the metal center and to electronic effects consecutive to potential intramolecular complexation of the substituent for the metal centers. Nonsubstituted or *para*/*meta*-substituted aryl iodides are usually more reactive than the corresponding aryl bromides.[6,15] This is rationalized by considering that the oxidative addition becomes rate-determining when considering aryl bromides, which indeed are less reactive with Pd^0 complexes than aryl iodides in oxidative additions.[17,18] In the case of *ortho*-substituted aryl halides, the situation is much more complex in the sense that the *ortho* substituent may induce a steric hindrance, which is expected to slow down the oxidative addition. However, *ortho*-substituted aryl bromides become globally less bulky than *ortho*-substituted aryl iodides due to the smaller size of the Br atom compared to that of the I atom. On the other hand, the Pd^0L_2 (L = phosphane) complex, active in the oxidative addition step, is usually present at low concentration because it is involved in an endergonic equilibrium with a major but unreactive Pd^0L_2L' complex (L = phosphane, L′ = phosphane[19] or dba[20]). A preliminary complexation of the active Pd^0L_2 complex by the *ortho* substituents of the aryl halides should result in an intramolecular oxidative addition step with a consequently faster overall reaction.

These antagonist effects prompted us to investigate the kinetics of the oxidative addition of *ortho*-substituted aryl iodides and bromides with Pd^0 complexes ligated by a monodentate ligand as in $Pd^0(PPh_3)_4$ or by a bidentate ligand as in Pd^0(dba)(dppp). The latter was generated by treating $Pd^0(dba)_2$ with 1 equiv. of dppp [dppp = $Ph_2P-(CH_2)_3-PPh_2$].[21,22] The *ortho* substituents are either $-CH_2-NR_2$ or $-CH_2-OR$ groups so that potentially five-membered palladated complexes might be generated.

Results and Discussion

Characterization of the (Aryl)palladium(II) Complexes Formed in the Oxidative Addition of *ortho*-Substituted Aryl Iodides and Bromides to Palladium(0) Complexes

Before discussing kinetic data on the comparative reactivity of *ortho*-substituted aryl iodides and bromides with Pd^0 complexes, the (aryl)palladium(II) complexes formed in the

Table 1. (Aryl)palladium(II) complexes generated in the oxidative addition of ArX (X = I, Br) to $Pd(PPh_3)_4$ or to {$Pd(dba)_2$ + 1 equiv. dppp} in toluene

Entry	ArX	ArPdI(PPh_3)$_2$ *trans*	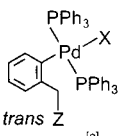	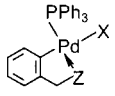	ArPdI(dppp) *cis*	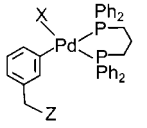	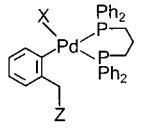
		δ_P, ppm [a]	δ_P, ppm [a]	δ_P, ppm [a]	δ_P, ppm [a]	δ_P, ppm [a]	δ_P, ppm [a]
1	PhI	22.9 (s)			–8.0 (d, *J* = 53Hz)[b] 13.1 (d, *J* = 53Hz)[b]		
2	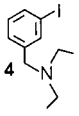 **4**	22.7 (s) *m*–**4a**				–10.3 (d, *J* = 52Hz) 10.9 (d, *J* = 52Hz) *m*–**4c**	
3	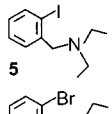 **5**		22.6 (s) **5a**	41.1 (s)[c] **5b** [traces][d]			–9.4 (d, *J* = 54 Hz) 9.4 (d, *J* = 54 Hz) **5c**
4	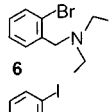 **6**		22.0 (s) **6a**	41.6 (s)[c] **6b** [traces][d]			–
5	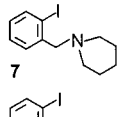 **7**		21.7 (s) **7a** [33 %][e]	41.7 (s)[e] **7b** [31 %][d,e]			–
6	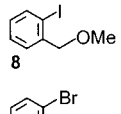 **8**		22.2 (s) **8a**	n.o.[f] **8b**			–10.4 (d, *J* = 57Hz) 9.3 (d, *J* = 57Hz) **8c**
7	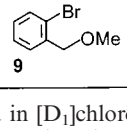 **9**		22.2 (s) **9a**	n.o.[f] **9b**			–9.6 (d, *J* = 51Hz) 12.3 (d, *J* = 51Hz) **9c**

[a] Determined in [D_1]chloroform vs. H_3PO_4 as an external standard at 293 K. – [b] *cis*-PhPdI(dppp).[36] – [c] A minor singlet for PPh_3 at δ = −5.1 was also observed. – [d] Data in square brackets are indicative of the relative integration of the ^{31}P NMR signals. – [e] A broad singlet for PPh_3 at δ = −5.2 was also observed, integrating for 32%. – [f] n.o.: not observed.

oxidative addition were first characterized. The reactions were performed by treating the aryl halides (in large excess) with either $Pd^0(PPh_3)_4$ or with a mixture $Pd^0(dba)_2$ + 1 equiv. of dppp in toluene. The complexes were isolated and characterized by ^{31}P NMR spectroscopy (Table 1).

The oxidative addition of PhI or the *meta*-substituted aryl iodide **4** to $Pd^0(PPh_3)_4$ gave the expected *trans*-$PhPdI(PPh_3)_2$ and *meta*-**4a** complexes, respectively as unique complexes. (Table 1, Entries 1,2). The *ortho*-substituted aryl iodide **5** and bromide **6** gave a major complex **5a** and **6a**, respectively, characterized by a narrow singlet at $\delta \approx 22$ in the ^{31}P NMR spectra (Table 1, Entries 3,4), which is indicative of two equivalent PPh_3 moieties ligated to the Pd^{II} center.[11] The two PPh_3 groups are in a *trans* position, in agreement with the recently published X-ray structure of a related complex with X = Br and CHO as the *ortho* substituent.[11] The complex is slightly distorted square-planar. The two triphenylphosphane ligands (δ = 23.2) are in a *trans* position, and are magnetically equivalent because the plane of the *ortho*-substituted aryl group is perpendicular to the plane of P, Pd, P, and Br.

In both cases, besides a minor signal for PPh_3 at $\delta = -5$, another minor narrow singlet was detected at $\delta \approx 41$ and assigned to complexes **5b** and **6b** (Table 1). In these complexes the Pd^{II} center is ligated by only one PPh_3, the fourth coordination site being occupied by the amine substituent. Indeed, the singlets at δ = 41.1 and 41.7 disappeared after addition of PPh_3, which is evidence of an equilibrium between the complexes **5a/5b** or **6a/6b** and PPh_3 [Equation (5)]. Moreover, the values of δ = 41.1 and 41.6 assigned to **5b** and **6b**, respectively, are very similar to those reported for related cyclopalladated complexes where the Pd^{II} center is ligated by only one PPh_3.[11,23]

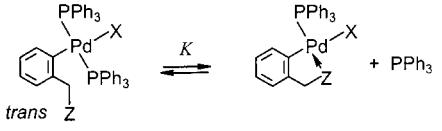

(5)

This is also in agreement with literature results, which report that phosphane-bis(ligated) (aryl)palladium(II) complexes are formed after addition of a second ligand to phosphane-monoligated complexes [Equation (2)].[9,10]

Stronger evidence for the equilibrium [Equation (5)] was provided upon treating the aryl iodide **7** with $Pd^0(PPh_3)_4$. Indeed, three broad signals ($\Delta\nu_{1/2}$ = 152 Hz) of very similar integration were observed in the ^{31}P NMR spectrum at δ = 41.7, 21.7, and −5.2, and these were assigned to complexes **7b**, **7a**, and PPh_3, respectively (Table 1, Entry 5). Addition of PPh_3 shifted the equilibrium [Equation (5)] towards its left-hand side, and complex **7a** was then observed as the major complex. The equilibrium constant *K* between **7a**, **7b**, and PPh_3 [Equation (5)] was estimated from the ^{31}P NMR spectroscopic data to K/c_0 = 0.6 (in $CDCl_3$ at 25 °C for $c_0 \approx$ 20 mM). The oxidative addition of aryl halides **8** or **9**, substituted in *ortho* position by a $-CH_2-OMe$ group, to $Pd^0(PPh_3)_4$ generated the phosphane-bis(ligated) complexes **8a** or **9a**, respectively (Table 1, Entries 6,7).

The oxidative addition of *ortho*-substituted aryl iodides or bromides to the Pd^0 complex generated from $Pd^0(dba)_2$ + 1 equiv. of dppp always gave the corresponding *cis*-ArPdX(dppp) complexes without any intramolecular coordination by the *ortho* substituent (Table 1, last column). In all cases, the ^{31}P NMR spectrum exhibited two doublets caused by the coupling of two nonequivalent P atoms ligated to the Pd^{II} center in a *cis* position. Moreover, the observed chemical shifts were very similar to those of the complexes generated by oxidative addition of PhI or *meta*-substituted phenyl iodide **4** (Table 1, Entries 1 and 2, last column), in which no internal coordination by the substituent may occur, by construction.

Therefore, in almost every case, the oxidative addition generates a major *trans*-(aryl)palladium(II) complex ligated by two phosphane ligands, without any intramolecular coordination of the *ortho* substituent. It is only with a monophosphane ligand (PPh_3) that an intramolecular complexation of the substituent may occur (Table 2, Entry 5),

Table 2. Comparative reactivity of ArX (X = I, Br) in their oxidative addition to $Pd^0(PPh_3)_4$ and to [$Pd^0(dba)_2$ + 1 equiv. of dppp] in DMF

Entry	ArX	T (°C)	$Pd^0(PPh_3)_4$	$Pd^0(dba)_2$ + 1 dppp
			k_{app} (M^{-1} s^{-1})	k_{app} (M^{-1} s^{-1})
1	PhI	25	25	–
2	PhI	40	–	1.9×10^{-3}
3	PhBr	25	1.5×10^{-3}	–
4	PhBr	40	10^{-2}	1.7×10^{-4}
5	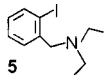 **5**	25	7.0	–
6	**5**	40	–	1.4×10^{-3}
7	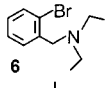 **6**	40	3.2×10^{-3}	–
8	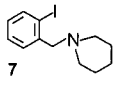 **7**	25	0.8	–
9	**7**	40	–	1.4×10^{-3}
10	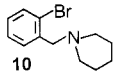 **10**	40	3.6×10^{-3}	–
11	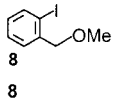 **8**	25	1.8	–
12	**8**	40	–	8.5×10^{-4}
13	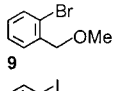 **9**	40	2.6×10^{-3}	–
14	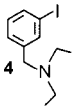 **4**	25	29	–

involving decomplexation of one PPh_3 through an endergonic equilibrium [Equation (5)]. This does not occur with the bidentate ligand dppp considered here because the decomplexation of one phosphorus atom of a bidentate P,P ligand possessing a small bite angle is not favored.[24]

Comparative Reactivity of *ortho*-Substituted Aryl Iodides and Bromides in Their Oxidative Addition to Palladium(0) Complexes in DMF

Oxidative Addition to $Pd^0(PPh_3)_4$

The mechanism of the oxidative addition of aryl halides to $Pd^0(PPh_3)_4$ is now well established and proceeds according to Scheme 1 (S = solvent).[19,25] The kinetics of the oxidative addition was monitored by amperometry performed at a rotating disk electrode, polarized at +0.3 V vs. SCE, on the plateau of the oxidation wave of $Pd^0(PPh_3)_3$ (c_0 = 2 mM in DMF containing nBu$_4$NBF$_4$, 0.3 M). The decay of the oxidation current intensity, proportional to the Pd^0 concentration, was recorded versus time, after addition of the aryl halide in excess.[25]

$$Pd^0(PPh_3)_4 \rightleftharpoons Pd^0(PPh_3)_3 + PPh_3$$

$$Pd^0(PPh_3)_3 \overset{K_0}{\rightleftharpoons} SPd^0(PPh_3)_2 + PPh_3$$

$$SPd^0(PPh_3)_2 + ArX \xrightarrow{k} ArPdX(PPh_3)_2$$

Overall reaction:

$$Pd^0(PPh_3)_4 + ArX \xrightarrow{k_{app}} ArPdX(PPh_3)_2 + 2PPh_3 \quad (6)$$

Scheme 1. Mechanism of the oxidative addition of aryl halides to $Pd^0(PPh_3)_4$; S = solvent

The plot of $2\ln(i/i_0) + 1 - i/i_0 = 2\ln([Pd^0]/[Pd^0]_0) + 1 - [Pd^0]/[Pd^0]_0$ versus time was linear (Figure 1) (i: oxidation current intensity at t; i_0: initial oxidation current intensity).

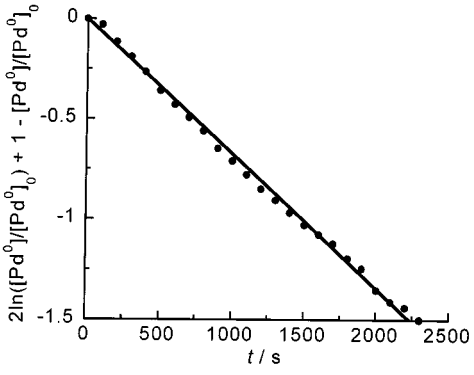

Figure 1. Oxidative addition of the aryl bromide **6** [0.2 M in DMF containing nBu$_4$NBF$_4$ 0.3 M)] to $Pd^0(PPh_3)_4$ (2 mM) at 40 °C, monitored by amperometry at a rotating gold disk electrode (i.d. 2 mm, ω = 105 rad·s^{-1}) polarized at + 0.35 V; plot of $2\ln(i/i_0) + 1 - i/i_0 = 2\ln([Pd^0]/[Pd^0]_0) + 1 - [Pd^0]/[Pd^0]_0$ versus time (i: oxidation current intensity at t; i_0: initial oxidation current intensity) [see Equation (7)]

Note that the kinetic law [Equation (7)] is not strictly logarithmic due to the PPh_3 release during the reaction (Scheme 1).[25]

$$2\ln([Pd^0]/[Pd^0]_0) + 1 - [Pd^0]/[Pd^0]_0 = -kK_0[ArX]t/c_0 = -k_{app}[ArX]t \quad (7)$$

The apparent rate constant k_{app} of the overall oxidative addition [Equation (6)] was determined from the slope of the regression lines [Equation (7), Figure 1]. From the results gathered in Table 2, one observes the following order of reactivity: ArI >> ArBr, for identical *ortho* substituents, even when considering that the experimental temperature was generally lower for ArI (25 °C) than for ArBr (40 °C). This is consistent with the higher reactivity of nonsubstituted (Table 2, Entries 1−4) or *para*/*meta*-substituted aryl iodides when compared to the related aryl bromides as observed by Fitton and Rick.[17]

In the aryl iodides series (Scheme 2), the *meta* substitution does not significantly affect the rate of the oxidative addition. This rules out a preliminary complexation of the active $Pd^0(PPh_3)_2$ by the substituent, which would have affected the rate of the oxidative addition by decreasing the active $Pd^0(PPh_3)_2$ concentration. The *ortho* substitution slows down the oxidative addition. Since no precomplexation of the $Pd^0(PPh_3)_2$ complex by the *ortho* substituent occurs before the oxidative addition step, the mechanism of the oxidative addition (Scheme 1) is still valid. The decelerating effect is then rationalized by the cumulative influence of steric hindrance and electron-donating property of the substituent efficient in the *ortho* position, which both decrease the reaction rate. Electron-donating groups are indeed known to slow down oxidative additions of aryl derivatives to $Pd^0(PPh_3)_4$ complexes.[17−19] However, although the $-CH_2-OMe$ substituent is less electron-donating and less bulky than $-CH_2-NEt_2$, the corresponding aryl iodide is significantly less reactive, a fact which is difficult to rationalize. Some stabilization may occur in the transition state en route to the Pd^{II} center.

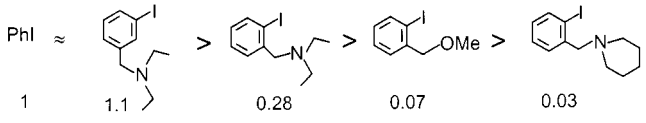

Scheme 2. Relative reactivity of aryl iodides in their oxidative addition to $Pd^0(PPh_3)_4$ at 25 °C

In the aryl bromides series (Scheme 3), the decelerating effect of the *ortho* substituent is less important than the corresponding one in the aryl iodide series (Scheme 2). This is consistent with the smaller size of the Br atom compared to that of the I atom, which globally decreases the steric constraint imposed by an *ortho* substituent in the aryl bromide compared to that in the corresponding aryl iodide.

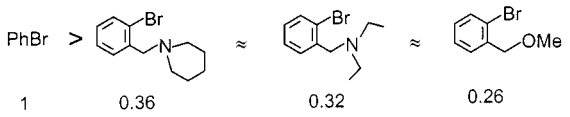

Scheme 3. Relative reactivity of aryl bromides in their oxidative addition to $Pd^0(PPh_3)_4$ at 40 °C

Oxidative Addition to $Pd^0(dba)_2$ + 1 equiv. of dppp

As already reported, a major complex $Pd^0(dba)(P,P)$ is formed from $Pd^0(dba)_2$ and 1 equiv. of bidentate P,P ligands.[21,22] The mechanism of the oxidative addition of aryl halides has been established for P,P ligands (Scheme 4). The most reactive complex is the minor complex $SPd^0(P,P)$ but the major complex $Pd^0(dba)(P,P)$ is also reactive ($k_1 > k_0$).[22]

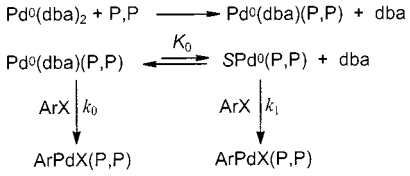

Scheme 4. Mechanism of the oxidative addition of aryl halides to the Pd^0 complexes generated from $Pd^0(dba)_2$ and 1 equiv. of bidentate P,P ligand.

In DMF, the formation of the major complex $Pd^0(dba)(dppp)$ from $Pd^0(dba)_2$ and 1 equiv. of dppp is a slow reaction because of the formation of the intermediate complex $Pd^0(dppp)_2$.[22] Therefore, the reactivity of aryl iodides or bromides in oxidative addition to $Pd^0(dba)(dppp)$ was investigated at least 90 min after mixing $Pd^0(dba)_2$ (2 mM in DMF) and dppp (2 mM) at room temperature, to ensure the total formation of $Pd^0(dba)(dppp)$. The apparent rate constant k_{app} of the overall oxidative addition [Equation (8)] was determined as explained above for $Pd^0(PPh_3)_4$, except that the rotating disk electrode was polarized at +0.7 V vs. SCE because $Pd^0(dba)(dppp)$ is less easily oxidized than $Pd^0(PPh_3)_3$.

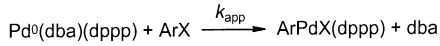

(8)

The reactions were considerably slower compared to that of $Pd^0(PPh_3)_4$. They were then performed at 40 °C even for aryl iodides (Table 2). It has already been observed that $Pd^0(PPh_3)_4$ is generally considerably more reactive than $Pd^0(dba)_2$ + 1 equiv. of P,P,[20,22] despite the fact that P,P ligands are usually more basic and possess a smaller P−Pd−P angle than PPh_3. This arises from the fact that the concentration of $SPd^0(PPh_3)_2$ in the equilibrium with $Pd^0(PPh_3)_3$ (Scheme 1) is higher than that of $SPd^0(P,P)$ in the equilibrium with $Pd^0(dba)(P,P)$ (Scheme 4).[20]

As observed above for $Pd^0(PPh_3)_4$, PhI is more reactive than PhBr (Table 2, Entries 2, 4). The kinetics of the oxidative addition was only investigated for *ortho*-substituted aryl iodides, because reactions with *ortho*-substituted aryl bromides were too slow, even in the presence of ArBr in very large excess. The concomitant decomposition of the Pd^0 complex could not be excluded. In the aryl iodides series (Scheme 5), the *ortho* substitution slows down the oxidative addition, but the decelerating effect is less important than that observed with $Pd^0(PPh_3)_4$ (Scheme 2).

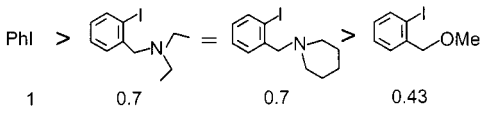

Scheme 5. Relative reactivity of aryl iodides in their oxidative addition to the Pd^0 complexes generated in the mixture $Pd^0(dba)_2$ and dppp at 40 °C

Conclusion

Determination of the rate constant of the oxidative addition of *ortho*-substituted aryl halides *o*-$ZCH_2-C_6H_4-X$ [X = I, Br; Z = OMe, NEt_2, $N(CH_2)_5$] with $Pd^0(PPh_3)_4$ or with the Pd^0 complexes generated from $Pd^0(dba)_2$ and 1 equiv. of dppp shows that the oxidative addition is slower for *ortho*-substituted aryl halides than for the corresponding nonsubstituted or *meta*-substituted aryl halides. This means that the *ortho* substituents do not participate in the oxidative addition by a preliminary complexation of the active $Pd^0(PPh_3)_2$ or Pd^0(dppp) complex. Oxygen and nitrogen ligands are indeed poor ligands for Pd^0 centers, unless they are involved in a bidentate complexation as for P,O or P,N ligands.[26] The observed decelerating effect induced by the *ortho* substituent is due to steric hindrance and electronic effects caused by the electron-donor properties of the substituents. These effects are less important for *ortho*-substituted aryl bromides than for *ortho*-substituted aryl iodides. Considering the same substituent, *ortho*-substituted aryl iodides remain more reactive than *ortho*-substituted aryl bromides, whatever the ligand. No inversion of reactivity occurs in the oxidative addition due to the *ortho* substitution. Were an inversion of reactivity observed in a Pd-catalyzed cross-coupling reaction, it should then arise at the level of the transmetallation step, which follows the oxidative addition. This probably lies at the origin of the inversion of reactivity observed in the palladium-catalyzed coupling of organomanganese derivatives with aryl halides, for which *ortho*-substituted aryl iodides were found to be less reactive than *ortho*-substituted aryl bromides.[27]

In this respect, it is worth to emphasize that an equilibrium results between *trans*-(*o*-$ZCH_2-C_6H_4$)$PdX(PPh_3)_2$ complexes formed in the oxidative addition and (*o*-$ZCH_2-C_6H_4$)$PdX(PPh_3)$(*Z*−*Pd*) exhibiting an intramolecular complexation of the *ortho* substituent. Nitrogen ligands are indeed good ligands for Pd^{II} centers, and the intramolecular character of the complexation enhances this effect. The latter complex might be involved in reactions with nucleophiles (transmetallation step). The *cis*-(*o*-$ZCH_2-C_6H_4$)PdX(dppp) complexes are formed when the Pd^0 is ligated by a bidentate ligand such as dppp. The bidentate character of this P,P ligand with a small bite angle

makes the intramolecular complexation by the *ortho* substituent less probable.

Experimental Section

General: All experiments were performed using standard Schlenk techniques under argon. − DMF was distilled from calcium hydride under vacuum. Toluene was distilled from sodium. − Iodo- and bromobenzene were commercial (Acros) and used after filtration through alumina. The dppp was commercial (Aldrich) and used without purification. $Pd(PPh_3)_4$,[28] $Pd(dba)_2$,[29] and $PhPdI(PPh_3)_2$ [17] were synthesized according to published procedures, as well as compounds **5**,[30,31] **6**,[32] **7**,[31] **8**,[33] **9**,[34] and **10**.[32] − ^{31}P NMR spectra were recorded with a Bruker spectrometer (162 MHz) using H_3PO_4 as an external reference, ^1H NMR spectra with a Bruker spectrometer (250 MHz) using TMS as an internal reference.

Diethyl(3-iodobenzyl)amine (4): Synthesis according to a published procedure[32] by treating 3-iodobenzyl bromide with diethylamine in anhydrous diethyl ether at room temperature. − ^1H NMR (250 MHz, $CDCl_3$): δ = 0.86 (t, *J* = 7.0 Hz, 6 H, CH_3), 2.33 (q, *J* = 7.0 Hz, 4 H, CH_2-CH_3), 3.31 (s, 2 H, CH_2-N), 6.83 (t, *J* = 7.7 Hz, 1 H, 5-*H*), 7.13 (d, *J* = 7.7 Hz, 1 H, 6-*H*), 7.37 (d, *J* = 7.7 Hz, 1 H, 4-*H*), 7.57 (s, 1 H, 2-*H*).

General Procedure for the Oxidative Addition: Complexes *m*-**4a**, **5a**, **6a**, **7a**, **8a**, and **9a** were synthesized according to a Fitton procedure.[17] In a Schlenk flask containing a solution of the aryl halide (from $4\cdot10^{-3}$ mol for the aryl iodides **4**, **5**, **7**, and **8** to 0.05 mol for the aryl bromides **6** and **9**) in 5 mL of degassed toluene was added 0.58 g ($0.5\cdot10^{-3}$ mol) of $Pd(PPh_3)_4$. The solution was kept overnight at room temperature for aryl iodides and heated during 4 h for aryl bromides. After filtration, the toluene was removed under vacuum, and the crude mixture was triturated with diethyl ether to eliminate the excess phosphane and aryl halide. The solid complexes were then characterized by ^{31}P NMR spectroscopy (Table 1).

(*o*-$CH_3OCH_2-C_6H_4$)PdI(PPh_3)$_2$ (8a): ^1H NMR (250 MHz, $CDCl_3$): δ = 2.85 (s, 3 H, OCH_3), 4.14 (s, 2 H, CH_2), 6.18 (t, *J* = 7.0 Hz, 1 H, 5-*H*), 6.35 (d, *J* = 7.0 Hz, 1 H, 3-*H*), 6.45 (t, *J* = 7.0 Hz, 1 H, 4-*H*), 6.74 (d, *J* = 7.0 Hz, 1 H, 6-*H*), 7.1−7.4 (m, 30 H, *H* of PPh_3).

Complexes *m*-**4c**, **5c**, **8c**, and **9c** were synthesized according to an adapted version of the Herrmann procedure.[35] In a Schlenk flask, containing a solution of 0.28 g ($0.5\cdot10^{-3}$ mol) of $Pd(dba)_2$ in 5 mL of degassed toluene, was added 0.21 g ($0.5\cdot10^{-3}$ mol) of dppp. After 2 h, 0.05 mol of the aryl halide was added. The solution was heated during 4 h for aryl iodides **4**, **5**, **8** and 6 h for the aryl bromide **9**. After filtration, the toluene was removed under vacuum, and the crude mixture was triturated with diethyl ether to eliminate the excess aryl halide. The pale-yellow complexes were then crystallized from chloroform/petroleum ether and characterized by ^{31}P NMR spectroscopy (Table 1).

Electrochemical Set-up for Amperometry and Kinetic Measurements of the Oxidative Addition: Electrochemical experiments were carried out in a three-electrode cell connected to a Schlenk line. The cell was equipped with a double envelope to maintain a constant temperature (Lauda RC20 thermostat). The working electrode consisted of a gold disk (i.d. 2 mm, Tacussel EDI 65109). The counter electrode was a platinum wire of ca. 1 cm^2 apparent surface area. The reference was a saturated calomel electrode separated from the solution by a bridge filled with a solution of nBu_4NBF_4 (0.3 mol dm^{-3}) in 3 mL of DMF. 15 mL of DMF containing the same concentration of supporting electrolyte was poured into the cell followed by 34 mg ($0.03\cdot10^{-3}$ mol) of $Pd(PPh_3)_4$. The kinetic measurements were performed using the rotating gold disk electrode with an angular velocity of 105 rad s^{-1} (Tacussel controvit). The potential of the rotating disk electrode was set at +0.35 V on the oxidation plateau wave of $Pd^0(PPh_3)_4$. The suitable amount of the aryl halide was added and the decay of the oxidation current was then monitored as a function of time. − In other experiments, 17 mg ($0.03\cdot10^{-3}$ mol) of $Pd(dba)_2$ was added, followed by 12 mg ($0.03\cdot10^{-3}$ mol) of dppp. After 2 h, the potential of the rotating disk electrode was set at +0.70 V on the oxidation plateau wave of Pd^0(dba)(dppp). The decay of the oxidation current was monitored as a function of time after addition of the suitable amount of the aryl halide.

Acknowledgments

This work has been supported in part by the Centre National de la Recherche Scientifique (CNRS, UMR 8640 "PASTEUR") and the Ministère de la Recherche (Ecole Normale Supérieure).

[1] J. Dehand, M. Pfeffer, *Coord. Chem. Rev.* **1976**, *18*, 327−352.
[2] M. I. Bruce, *Angew. Chem. Int. Ed. Engl.* **1977**, *16*, 76−86.
[3] I. Omae, *Chem. Rev.* **1979**, *79*, 287−321.
[4] A. D. Rybov, *Synthesis* **1985**, 233−252.
[5] G. R. Newkome, W. E. Puckatt, V. K. Gupta, G. E. Kiefer, *Chem. Rev.* **1986**, *86*, 451−489.
[6] S. Tsuji, *Palladium Reagents and Catalysis*, John Wiley & Sons, Chichester, **1995**.
[7] M. Pfeffer, *Pure & Appl. Chem.* **1992**, *64*, 335−342.
[8] A. C. Cope, E. C. Friedrich, *J. Am. Chem. Soc.* **1968**, *90*, 909−913.
[9] P. W. Clark, S. F. Dyke, *J. Organomet. Chem.* **1983**, *259*, C17−C19.
[10] P. W. Clark, S. F. Dyke, *J. Organomet. Chem.* **1985**, *281*, 389−396.
[11] J. Vicente, J.-A. Abad, E. Martinez-Viviente, M. C. Ramirez de Arellano, *Organometallics* **2000**, *19*, 752−760.
[12] N. Beydoum, M. Pfeffer, *Synthesis* **1990**, 729−731.
[13] B. J. Soderberg, "Transition Metal Alkyl Complexes: Oxidative Addition and Insertion" in *Comprehensive Organometallic Chemistry II*, Elsevier, Oxford, New York, Tokyo, **1995**, vol. *12*, p. 241−299.
[14] R. C. Larock, N. Berrios-Peña, K. Narayanan, *J. Org. Chem.* **1990**, *55*, 3447−3450.
[15] V. Farina, "Transition Metal Alkyl Complexes: Oxidative Addition and Transmetallation" in *Comprehensive Organometallic Chemistry II*, Elsevier, Oxford, New York, Tokyo, **1995**, vol. *12*, p. 161−240.
[16] F. Maassanari, M. Pfeffer, G. Le Borgne, *Organometallics* **1987**, *6*, 2029−2043.
[17] P. Fitton, E. A. Rick, *J. Organomet. Chem.* **1971**, *28*, 287−291.
[18] A. Jutand, A. Mosleh, *Organometallics* **1995**, *14*, 1810−1817.
[19] J. F. Fauvarque, F. Pflüger, M. Troupel, *J. Organomet. Chem.* **1981**, *208*, 419−427.
[20] C. Amatore, A. Jutand, *Coord. Chem. Rev.* **1998**, *178−180*, 511−528.
[21] W. A. Herrmann, W. R. Thiel, C. Bromer, K. Ölefe, T. Priermeier, W. Scherer, *J. Organomet. Chem.* **1993**, *46*, 51−60.
[22] C. Amatore, G. Broeker, A. Jutand, F. Khalil, *J. Am. Chem. Soc.* **1997**, *119*, 5176−5185.

[23] J. Vicente, I. Saura-Llamas, M. G. Palin, P. G. Jones, M. C. Ramirez de Arellano, *Organometallics* **1997**, *16*, 826−833.
[24] For some examples of *ortho*-palladated complexes where two Pd^{II} moieties are bonded through a diphosphane ligand possessing a large bite angle, see: J. M. Vila, M. Gayoso, A. Fernandez, N. A. Bailey, H. Adams, *J. Organomet. Chem.* **1993**, *448*, 233−239.
[25] C. Amatore, A. Jutand, F. Khalil, M. A. M′Barki, L. Mottier, *Organometallics* **1993**, *12*, 3168−3178.
[26] Even in such cases, we have reported that the oxidative addition proceeds from a Pd^0 only ligated by the P atom after cleavage of the Pd^0−N bond, see: C. Amatore, A. Fuxa, A. Jutand, *Chem. Eur. J.* **2000**, *6*, 1474−1482.
[27] E. Riguet, M. Alami, G. Cahiez, *J. Organomet. Chem.* **2001**, *624*, 376−379.
[28] D. T. Rosevear, F. G. H. Stone, *J. Chem. Soc. A* **1968**, 164−167.
[29] M. F. Rettig, P. M. Maitlis, *Inorg. Synth.* **1977**, *17*, 134−137.
[30] M. Murakami, M. Hayashi, Y. Ito, *J. Org. Chem.* **1992**, *57*, 793−794.
[31] L. Williams, S. E. Booth, K. Undheim, *Tetrahedron* **1994**, *50*, 13697−13708.
[32] N. B. Mehta, J. Z. Strelitz, *J. Org. Chem.* **1962**, *27*, 4412−4415.
[33] L. J. Andrews, L. J. Spears, R. M. Keefer, *J. Am. Chem. Soc.* **1964**, *86*, 687−690.
[34] J. Epsztajn, A. Jozwiak, A. Szczesniak, *J. Chem. Soc., Perkin Trans. 1* **1998**, *50*, 2563−2565.
[35] W. A. Herrmann, C. Bromer, T. Priermeier, K. Ölefe, *J. Organomet. Chem.* **1994**, *481*, 97−108
[36] M. Ludwig, S. Strömberg, M. Swensson, B. Akermark, *Organometallics* **1999**, *18*, 970−991.

Received March 26, 2001
[I01111]

Bis[(3,5-dimethyl-1-pyrazolyl)methyl]ethylamine − A Versatile Ligand for Complexation in Rh^I Cationic Complexes

René Mathieu,*[a] Glòria Esquius,[a,b] Noël Lugan,[a] Josefina Pons,[b] and Josep Ros*[b]

Keywords: Rhodium / Aminopyrazole / Hemilabile ligands / Cationic complexes

The bis[(3,5-dimethyl-1-pyrazolyl)methyl]ethylamine ligand (**1**) reacts with $[Rh(COD)(THF)_2][BF_4]$ leading to $[Rh(COD)(\mathbf{1})][BF_4]$ ($[\mathbf{2}][BF_4]$) in which **1** is κ^3 bonded in the solid state. Because of the steric bulk of 1,5-cyclooctadiene, it prefers the κ^2 mode of bonding in solution. Substitution of 1,5-cyclooctadiene by carbon monoxide generates $[\mathbf{3}][BF_4]$ in which **1** is κ^3 bonded in solution and solid state. Variable temperature NMR spectroscopic studies give evidence of a $\kappa^3 \rightleftarrows \kappa^2$ equilibrium in solution. $[\mathbf{3}][BF_4]$ is easily decarbonylated to $[Rh(CO)(\mathbf{1})][BF_4]$ $[\mathbf{4}][BF_4]$ in which **1** is κ^3 bonded; however on bubbling carbon monoxide through, $[\mathbf{3}][BF_4]$ is regenerated. The single-crystal X-ray structures of $[\mathbf{2}][BF_4]$, $[\mathbf{3}][BPh_4]$, and $[\mathbf{4}][BPh_4]$ are reported.

Introduction

The readily available pyrazolyl group has allowed the construction of various bi- or polydentate ligands, thus furnishing metal complexes of varying coordination geometry and nuclearity.[1−4] One of the reasons for this success arises from the ability to change the nature, number, and position of substituents in the pyrazole ring, thus allowing a fine tuning of the reactivity of the metal centre to which they are bound. For instance, the most well-developed ligands, the poly(pyrazolyl)borates and their complexes, have found interesting applications in catalysis and bioinorganic chemistry.[1,5−8]

The bonding properties of another family of pyrazole-based chelating ligands, the pyrazole derivatives of simple amines, are also well documented.[4,9,10] They are considered to be hard donor ligands, and the studies of their bonding properties have focussed on cations in high oxidation states, essentially to provide routes to a variety of bioinorganic model systems, or to evaluate their extracting properties. Prompted by the increasing success in catalysis of complexes containing amino ligands,[11−13] it was thought interesting to probe the bonding properties of aminopyrazoles toward soft cations, such as Rh^I. In contrast to the well studied tris(pyrazolyl)borate/Rh^I systems,[14−16] these ligands contain two types of donating centres with different degrees of hardness which might be expected to exhibit different types of behaviour toward the soft Rh^I centre.

We here describe the interactions of a typical aminopyrazole, bis[(3,5-dimethyl-1-pyrazolyl)methyl]ethylamine (**1**) towards a series of cationic Rh^I complexes.

Results and Discussion

Bis[(3,5-dimethyl-1-pyrazolyl)methyl]ethylamine (**1**) reacts with $[Rh(COD)(THF)_2][BF_4]$ − generated in situ from the reaction of $[Rh(COD)Cl]_2$ and $AgBF_4$ in THF − to give the complex $[Rh(COD)(\mathbf{1})][BF_4]$ ($[\mathbf{2}][BF_4]$) in 90% yield. At room temperature, the proton NMR spectrum of $[\mathbf{2}]^+$ shows the presence of two isomers $[\mathbf{2a}]^+$ and $[\mathbf{2b}]^+$ in a 2:1 ratio. The most salient feature of the spectra, and the most significant for probing structural differences, is provided by the NEt resonances, where the ethyl group resonances of the minor isomer are more deshielded than those of $[\mathbf{2a}]^+$. This observation suggests that in $[\mathbf{2b}]^+$ the nitrogen of the amine group is bonded to rhodium, and that the two isomers differ in their coordination to rhodium, which can be either the κ^2 or κ^3 type.

To clarify this point, $[\mathbf{2}][BF_4]$ was structurally characterised by X-ray crystallography. The complex crystallises with three independent ion pairs per unit cell. The three cations of $[\mathbf{2}]^+$ present the same geometry, with the respective distances and angles being equal within experimental errors. A view of one of the three independent cations (cation A) appears as Figure 1; selected bond length and angle data are provided in Table 1. In the solid state, only isomer $[\mathbf{2b}]^+$ is observed. The nitrogen of the amino group N3 is 2.513(7) Å from Rh1; it is longer than the other two Rh−N distances but smaller than the sum of van der Waals radii (3.4 Å). The pyrazolyl-nitrogen to Rh distances are slightly different but are in the range found for hydridotris(pyrazolyl)borate rhodium complexes.[15,16] The N4−Rh1 bond is significantly longer than the N1−Rh1 bond, and this is certainly the consequence of the steric crowding around rhodium as there are no electronic reasons to justify this differ-

[a] Laboratoire de Chimie de Coordination du CNRS,
205 Route de Narbonne, 31077 Toulouse Cedex4, France
Fax: (internat.) +30−5 61 55 30 03
E-mail: mathieu@lcc-toulouse.fr
[b] Departament de Quimica, Universitat Autònoma de Barcelona,
08193 Bellaterra, Cerdanyola, Spain
Fax: (internat.) +34−93/58 13 101
E-mail: josep.ros@uab.es

 © WILEY-VCH Verlag GmbH, 69451 Weinheim, 2001 1434−1948/01/1010−2683 $ 17.50+.50/0

ence. This is evident if we consider the positioning of the 1,5-cyclooctadiene ligand. The atoms C15, C18, N1, and N4 lie in a plane, which is usually[16] defined by the pyrazolyl nitrogen atoms and the middle of the olefinic carbon-carbon bonds. The rhodium atom lies 0.1 Å out of that coordination plane. The position of the cyclooctadiene undoubtedly results from steric crowding attributable to the amino group. Indeed C7 is nearer to C18 carbon than to C15, and lengthening of the Rh1−N4 distance minimises the steric crowding of the ethyl group. Likewise, the C18−Rh1−N4 angle is 10° wider than that of the C15−Rh1−N1 angle. If we consider the pyrazolyl planes, the angle between the mean plane defined by the N4 pyrazolyl ring and the Rh−N4 vector is more acute (142.8°) than the angle between the Rh−N1 vector and the mean plane of the N1 pyrazolyl ring (163.9°). Because of the strain induced by the methylene bridges, the N1−Rh1−N3 and N4−Rh1−N3 angles are around 73°.

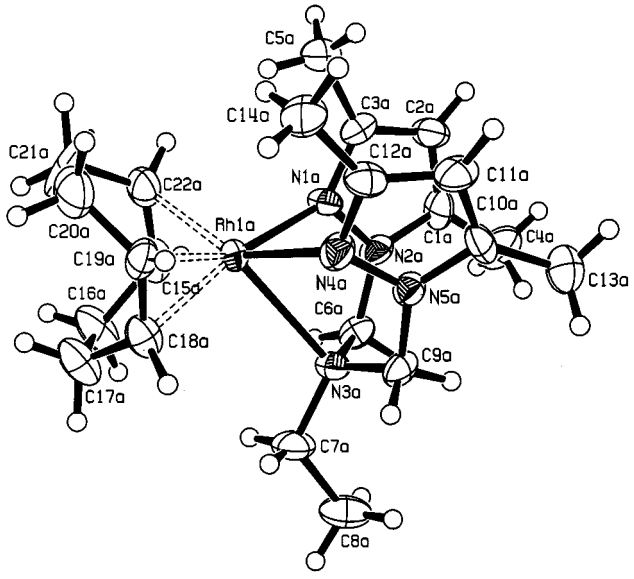

Figure 1. Structure of the cation $[\mathbf{2}]^+$ showing the numbering scheme; ellipsoids are drawn at the 50% probability level

To check whether the solid-state structure is maintained in solution, some crystals were dissolved in deuterated dichloromethane at −70 °C, and the solution was examined by ^{1}H NMR spectroscopy at this temperature. Initially, $[\mathbf{2b}]^+$ is the major component, but the concentration of $[\mathbf{2a}]^+$ slowly increases. When the temperature is raised to 20 °C, the previously observed 2:1 ratio of the isomers $[\mathbf{2a}]^+$/$[\mathbf{2b}]^+$ is rapidly restored, demonstrating the operation of a thermodynamic equilibrium which favours the less sterically encumbered isomer $[\mathbf{2a}]^+$, as summarised in Scheme 1.

We note that, as previously observed by several of the present authors, the reaction of **1** with $[Rh(COD)Cl]_2$ leads to $[Rh(COD)(\mathbf{1})]^+[Rh(COD)Cl_2]^-$.[17] However, in contrast to $[\mathbf{2}]^+$, the cationic part of this latter complex is characterised by broad ^{1}H NMR peaks assignable to ligand **1**, supporting the author's earlier hypothesis concerning the existence of an equilibrium in solution between the ionic

Table 1. Selected bond lengths [Å] and angles [°] for compounds $[\mathbf{2}][BF_4]$, $[\mathbf{3}][BPh_4]$, and $[\mathbf{4}][BPh_4]$

	$[\mathbf{2}][BF_4]$	$[\mathbf{3}][BPh_4]$	$[\mathbf{4}][BPh_4]$
C15−C22	1.403(15)		
C15−Rh1	2.091(10)		
C18−C19	1.384(14)		
C18−Rh1	2.102(10)		
C19−Rh1	2.106(9)		
C22−Rh1	2.091(10)		
N1−Rh1	2.115(7)	2.081(6)	2.015(3)
N3−Rh1	2.513(7)	2.566(5)	2.120(2)
N4−Rh1	2.216(8)	2.107(5)	2.022(3)
C15−Rh1		1.803(9)	1.809(4)
C16−Rh1		1.800(10)	
C6−N3−C9	113.4(8)	111.0(5)	111.8(2)
C6−N3−C7	111.2(8)	109.0(5)	113.2(2)
C9−N3−C7	112.2(8)	114.7(5)	113.1(2)
C6−N3−Rh1	99.7(5)	100.1(4)	105.3(2)
C9−N3−Rh1	106.9(6)	106.7(4)	103.9(2)
C7−N3−Rh1	112.8(6)	114.3(4)	108.7(2)
C15−Rh1−C18	82.6(4)		
C15−Rh1−C19	97.5(4)		
C22−Rh1−C19	81.3(4)		
C15−Rh1−N1	92.6(4)		
C22−Rh1−N1	92.4(3)		
C18−Rh1−N1	166.7(4)		
C19−Rh1−N1	154.9(4)		
C15−Rh1−N4	173.3(4)		
C22−Rh1−N4	143.9(4)		
C18−Rh1−N4	102.2(4)		
C19−Rh1−N4	89.1(3)		
N1−Rh1−N4	81.7(3)	90.4(2)	161.9(1)
C15−Rh1−N3	101.3(4)		
C22−Rh1−N3	138.3(4)		
C18−Rh1−N3	95.8(3)		
C19−Rh1−N3	126.8(3)		
N1−Rh1−N3	72.9(3)	71.7(2)	81.4(1)
N4−Rh1−N3	73.8(3)	72.4(2)	80.5(1)
C15−Rh1−N3		116.9	179.3(2)
C16−Rh1−N3		115.0(3)	
C15−Rh1−N4		89.3(3)	99.3(1)
C15−Rh1−C16		90.0(4)	
C16−Rh1−N1		89.3(3)	
C15−Rh1−N1			98.8(1)

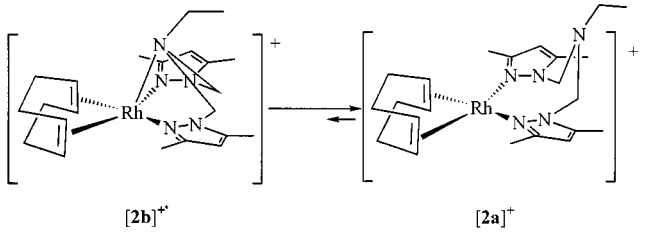

Scheme 1

form and a neutral one [Rh(COD)Cl][μ,η^2−(**1**)]-[Rh(COD)Cl].

In order to evaluate the influence of the 1,5-cyclooctadiene on the bonding capabilities of **1**, we replaced the diene by carbon monoxide. Bubbling carbon monoxide into a solution of $[\mathbf{2}]^+$ in dichloromethane at room temperature

produces $[Rh(CO)_2(\mathbf{1})][BF_4]$ ($[\mathbf{3}][BF_4]$) which can be isolated as a yellow solid in a nearly quantitative yield. The infrared spectrum in the νCO region shows two strong absorption bands at 2080 and 2011 cm^{-1}, and two weak peaks at 2100 and 2038 cm^{-1}, suggesting the presence of two complexes. This is corroborated by the ^1H NMR spectrum that, analogously to $[\mathbf{2a}]^+$ and $[\mathbf{2b}]^+$, exhibits ethyl resonances for two isomers $[\mathbf{3a}]^+$ and $[\mathbf{3b}]^+$, in the ratio 1:10. However, in contrast to $[\mathbf{2}]^+$, it is the isomer $[\mathbf{3b}]^+$, with the more deshielded ethyl resonances, that is the major compound in solution. For this complex, the methylene protons appear as a broad AB spectrum indicating the existence of a fluxional process in solution. As for $[\mathbf{2}]^+$, the NMR spectroscopic data reveals that there are two isomers where the aminopyrazole ligand can be κ^2 $[\mathbf{3a}]^+$ or κ^3 $[\mathbf{3b}]^+$ bonded. This is corroborated by the infrared data which shows that the minor isomer $[\mathbf{3a}]^+$ exhibits CO absorption at high frequencies, as expected for a 16 valence electron isomer compared to an 18 electron complex. To confirm this hypothesis an X-ray structure determination was undertaken on $[Rh(CO)_2(\mathbf{1})][BPh_4]$ ($[\mathbf{3}][BPh_4]$) obtained by metathesis with $NaBPh_4$, which was easier to crystallise than $[\mathbf{3}][BF_4]$.

Figure 2 depicts cation $[\mathbf{3}]^+$ and salient bond length and angle data are collected in Table 1. The cation has a distorted square pyramid geometry, in which the square plane is defined by the atoms C15, C16, N1, and N4, and the rhodium atom is out of that plane by 0.15 Å. As a consequence of the steric strain imposed by the methylene bridges, the N3 nitrogen atom is not perpendicular to this plane. The Rh−N3 bond is slightly longer than in $[\mathbf{2b}]^+$, but N3 remains within the bonding distance of rhodium. Thus, in the solid state, the structure corresponds to the major isomer $[\mathbf{3b}]^+$ observed in solution. The reduction of the steric crowding around rhodium induced by the replacement of 1,5-cyclooctadiene by two CO molecules is particularly evident if we consider the N1−Rh−N4 angle, which is 81.7(3)° in $[\mathbf{2b}]^+$ and 90.4(2)° in $[\mathbf{3b}]^+$. For the same reasons the Rh−N1 and Rh−N4 bond lengths are, as expected, equal within experimental error.

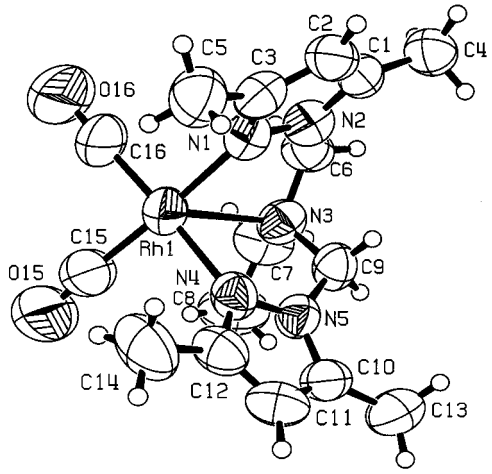

Figure 2. Structure of the cation $[\mathbf{3}]^+$ showing the numbering scheme; ellipsoids are drawn at the 30% probability level

As mentioned above, we observed a broad ^1H NMR AB spectrum for the methylene groups of the isomer $[\mathbf{3b}]^+$, indicating fluxional behaviour in solution for this complex. For this reason we have carried out a variable-temperature ^1H NMR spectroscopic study on the mixture of $[\mathbf{3a}]^+$ and $[\mathbf{3b}]^+$ in $(CD_3)_2CO$ solution. For the $[\mathbf{3a}]^+$ spectrum no significant changes were observed during this study. At 253 K the methylene hydrogens of $[\mathbf{3b}]^+$ appear as a narrow AB spectrum, but lowering the temperature to 193 K induces no other significant changes, except for a slight broadening of the *N*-ethyl resonances. Raising the temperature to 333 K brings about coalescence of the AB spectrum to a broad singlet. (The solvent and the thermal stability of the complex did not allow acquisition of spectra above this temperature.) This corresponds to a $\Delta G^{\ddagger}$ value of ca. 70 $kJ \cdot mol^{-1}$, a value consistent with the mechanism proposed in Scheme 2 which implies an inversion of configuration of the nitrogen atom.[18] The initial step is the decoordination of N3, followed by inversion at the nitrogen atom, and subsequent coordination of N3 on the other face of the square plane.

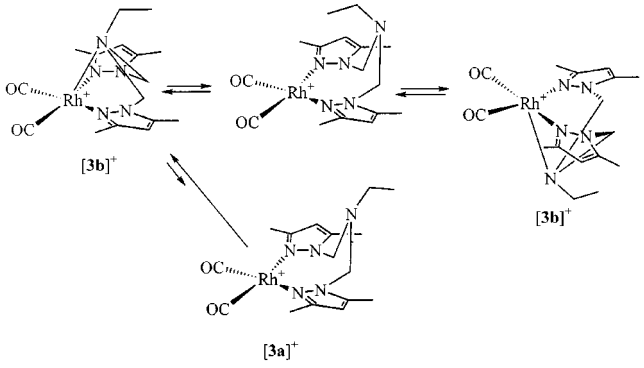

Scheme 2

During the workup of $[\mathbf{3}]^+$, and especially after the evaporation of its solutions under vacuum, we observed the formation, in small quantities, of a new product characterised by a ν(CO) absorption at 1997 cm^{-1} in the infrared spectrum. This implies a decarbonylation of $[\mathbf{3}]^+$ and, indeed, refluxing a THF solution of $[\mathbf{3}]^+$ induces the nearly quantitative formation of the new complex $[Rh(CO)(\mathbf{1})][BF_4]$ ($[\mathbf{4}][BF_4]$) possessing a ν(CO) absorption at 1997 cm^{-1}. Bubbling carbon monoxide through a solution of $[\mathbf{4}]^+$ regenerates $[\mathbf{3}]^+$ immediately (Scheme 3).

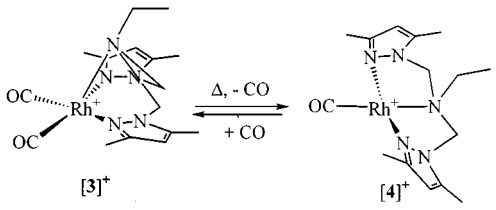

Scheme 3

The ^{1}H NMR spectrum of $[\mathbf{4}]^+$ shows only the resonances of the coordinated ligand **1**. The solid-state structure of $[\mathbf{4}]^+$ was established by X-ray crystallography on the tetraphenylborate salt $[Rh(CO)(\mathbf{1})][BPh_4]$ ($[\mathbf{4}][BPh_4]$). A view of $[\mathbf{4}]^+$ is shown in Figure 3 and bond lengths and angles of interest are gathered in Table 1. The cation is square-planar, with the atoms N1, N3, N4, and C15 defining the plane, and the rhodium atom lying 0.02 Å above it. The Rh−N3 bond is longer than the other two Rh−N bonds, a consequence of the *trans* influence of the carbonyl ligand and of the different hybridisation of the nitrogen atom. Owing to the steric strain induced by the methylene bridges, the N1−Rh−N3 and the N3−Rh−N4 angles are less than 90°.

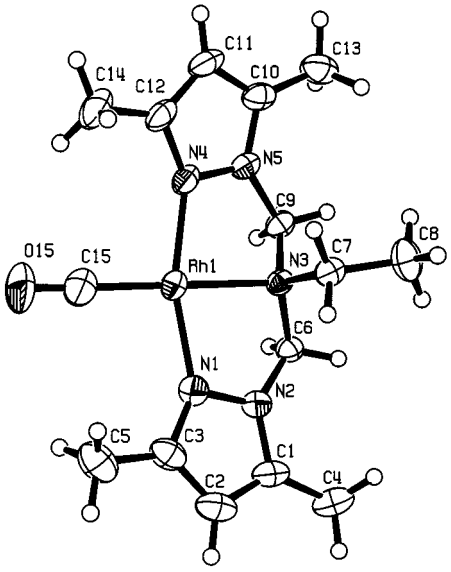

Figure 3. Structure of the cation $[\mathbf{4}]^+$ showing the numbering scheme; ellipsoids are drawn at the 50% probability level

All these structures reveal that **1** is a very flexible ligand that can accommodate, depending on the other ligands around rhodium, either a square-pyramidal geometry in a *fac* configuration or a square planar geometry in a *mer* configuration. Moreover, examination of the structures of other known complexes of bis[(3,5-dimethyl-1-pyrazolyl)methyl]-phenyl or ethylamine with Co^{II},[19,20] Ni^{II},[21] Cu^{I},[22] or Cu^{II},[19] salts shows that the most acute [81.7(3)°] N−M−N angles for the pyrazole ligands have been observed, in our case, with Rh^{I}. The smallest angle observed in the other complexes is 112.5° for the bis[(3,5-dimethyl-1-pyrazolyl)-methyl]phenylamine κ^3 bonded to the $Co(NO_3)_2$ salt[20] in a structure intermediate between a distorted trigonal bipyramid and a square pyramid. This shows that, for this family of ligands, the two pyrazolyl groups can equally adopt *cis*-positions in a square plane. In the other extreme of their bonding capabilities, i.e. in a *trans* configuration, 162° seems to be the maximum value these ligands can accommodate: 161.9(1)° for the N−M−N angle in $[\mathbf{4}]^+$ and 161.3° in an octahedral complex with the $Ni(NO_3)_2$ salt.[21]

Conclusion

This study provides further evidence of the flexibility of the ligand **1** which adapts its bonding mode to various electronic and steric situations around rhodium(I). For instance, for $[\mathbf{2}]^+$ to compensate the steric bulk of the cyclooctadiene ligand it prefers the κ^2 mode of bonding in solution. In the solid state, it adopts the κ^3 mode of bonding but minimises the steric bulk in the square plane by small variations of the length of the Rh−N (pyrazole) bonds. In the absence of steric strain, it adopts a κ^3 mode of bonding either in a *fac* (complex $[\mathbf{3}]^+$) or a *mer* (complex $[\mathbf{4}]^+$) configuration.

Experimental Section

General Remarks: All reactions were performed under a nitrogen atmosphere with the use of standard Schlenk techniques. Tetrahydrofuran and diethyl ether, used for the synthesis, were distilled under nitrogen from sodium benzophenone ketyl just before use. Other solvents were purified following the standard procedures and stored under nitrogen. − NMR spectra were recorded on Bruker AC 200, AC 250, or AMX 400 instruments. All chemical shift values are given in ppm and are referenced with respect to residual protons in the solvent for proton spectra, to solvent signals for ^{13}C spectra. − Elemental analyses were performed in our laboratory on a Perkin−Elmer 2400 CHN analyser. − The bis[(3,5-dimethyl-1-pyrazolyl)methyl]ethylamine[9] and $[Rh(COD)Cl]_2$[23] have been prepared according to published procedures.

Synthesis of [Rh(COD)(1)][BF$_4$] ([2][BF$_4$]): To a solution of 0.079 g (0.16 mmol) of $[Rh(COD)Cl]_2$ in 20 mL of THF was added 0.062 g (0.32 mmol) of $AgBF_4$ and the solution was stirred for half an hour at room temperature. The orange solution turned yellow and AgCl precipitated. The solution was then filtered through a pad of Celite and 0.084 g (0.32 mmol) of **1** was then added. After stirring for an hour, the solution was evaporated to dryness and the residue was crystallised in a dichloromethane/ether mixture to give 0.160 g (90%) of $[\mathbf{2}][BF_4]$ as yellow crystals. − $C_{22}H_{35}BF_4N_5Rh$ (559.3): C 47.24, H 6.32, N 12.52; found C 47.11, H 6.11, N 12.51. Isomer $[\mathbf{2a}]^+$: ^{1}H NMR ($CDCl_3$ solution, 250 MHz) δ = 6.58 (d, ^2J = 15.4 Hz, 2 H, CH_2N), 5.79 (s, 2 H, C*H* pyrazole), 5.42 (d, ^2J = 15.4 Hz, 2 H, pyrazole CH_2N), 3.99 (b, 4 H, C*H* cod), 2.76 (q, ^3J = 7.1 Hz, 2 H, CH_2CH$_3$), 2.68 (b, 4 H, CHH_{exo} cod), 2.61 (s, 6 H, CCH_3), 2.56 (b, 4 H, CHH_{endo} cod), 2.25 (s, 6 H, CCH_3), 0.64 (t, ^3J = 7.1 Hz, 3 H, CH$_2$CH_3). − ^{13}C{^{1}H} NMR ($CDCl_3$ solution, 50 MHz) δ: 150.8−137.3 (*C*CH$_3$), 107.5 (*C*H pyrazole), 85.2−83.6 (m, =*C*H cod), 69.4 (*C*H$_2$N), 44.8 (*C*H$_2$CH$_3$), 30.8−30.2 (*C*H$_2$ cod), 15.6−10.6 (CH$_2$*C*H$_3$, C*C*H$_3$). Isomer $[\mathbf{2b}]^+$: ^{1}H NMR ($CDCl_3$ solution, 250 MHz) δ = 5.68 (s, 2 H, C*H* pyrazole), 4.96 (d, ^2J = 12.2 Hz, 2 H, CH_2N), 4.87 (d, ^2J = 12.2 Hz, 2 H, CH_2N), 4.14 (q, ^3J = 7.2 Hz, 2 H, CH_2CH$_3$), 3.75 (b, 4 H, =C*H* cod), 2.68 (b, 4 H, CHH_{exo} cod), 2.60 (s, 6 H, CCH_3), 2.56 (b, 4 H, CHH_{endo} cod), 2.17 (s, 6 H, CCH_3), 1.56 (t, ^3J = 7.2 Hz, 3 H, CH$_2$CH_3);. − ^{13}C{^{1}H} NMR ($CDCl_3$ solution, 50 MHz)150.8−137.3 (*C*CH$_3$), 107.6 (*C*H pyrazole), 85.2−83.6 (m, =*C*H cod), 65.5 (*C*H$_2$N), 52.5 (*C*H$_2$CH$_3$), 30.8−30.2 (*C*H$_2$ cod), 15.6−10.6 (CH$_2$*C*H$_3$, C*C*H$_3$).

Synthesis of [Rh(CO)$_2$(1)][BF$_4$] ([3][BF$_4$]): Carbon monoxide was bubbled for 1 h through a solution of 0.168 g of $[\mathbf{2}][BF_4]$ dissolved in 20 mL of dichloromethane. The solution was then evaporated to dryness in vacuum leaving 0.124 g (80%) of **3** as a yellow powder.

− IR (CH_2Cl_2 solution) ν(CO): 2100 (w), 2080 (s), 2038 (w), 2011 (s) cm^{-1}. Isomer [**3a**]$^+$: ^1H NMR δ = 6.28 (s, 2 H, C*H*), 5.23 (AB system, ^2J = 11.7 Hz, 4 H, CH_2N), 3.79 (q, ^3J = 7.2 Hz, 2 H, CH_2CH$_3$), 2.64 (s, 6 H, CCH_3), 2.45 (s, 6 H, CCH_3), 1.61 (t, ^3J = 7.2 Hz, 3 H, CH$_2$CH_3); Isomer [**3b**]$^+$: ^1H NMR (CD_3)$_2$CO solution, 250 MHz) δ = 6.29 (s, 2 H, C*H*), 5.59 (broad AB system, ^2J = 11.8 Hz, 4 H, CH_2N), 3.16 (q, ^3J = 7.3 Hz, 2 H, CH_2CH$_3$), 2.58 (s, 6 H, CCH_3), 2.35 (s, 6 H, CCH_3), 1.17 (t, ^3J = 7.3 Hz, 3 H, CH$_2$CH_3). − $^{13}C\{^1H\}$ NMR ($CDCl_3$ solution, 63 MHz) δ = 185 (d, ^1J = 69.0 Hz, *C*O), 151.7 (*C*CH$_3$), 144.7 (*C*CH$_3$), 108.1 (*C*H), 65.7 (*C*H$_2$N), 50.3 (*C*H$_2$CH$_3$), 16.1, 13.9.11.2 (2 C*C*H$_3$ + CH$_2$*C*H$_3$).

Synthesis of [Rh(CO)$_2$(1)][BPh$_4$] ([3][BPh$_4$]): To a solution of 0.135 g (0.32 mmol) of [**3**][BF_4] in 10 mL of methanol was added 0.110 g (0.32 mmol) of $NaBPh_4$ and the solution was stirred for 1 h. A yellow precipitate appeared which was filtered and dried under vacuum. It was recrystallised in a dichloromethane/methanol mixture under a CO atmosphere. $C_{40}H_{43}BN_5O_2Rh$ (739.5): C 64.97, H 5.86, N 9.47; found C 64.52, H 6.01, N 9.20.

Synthesis of [Rh(CO)(1)][BF$_4$] ([4][BF$_4$]): A solution of 0.12 g of [**3**][BF_4] in 20 mL of THF was refluxed for 2 h. The solvent was evaporated to dryness in vacuum leaving 0.1 g of a yellow solid. − IR (CH_2Cl_2 solution) ν(CO): 1997 cm^{-1}. − ^1H NMR ($CDCl_3$ solution, 200 MHz) δ = 5.95 (s, 2 H, C*H*), 5.28 (AB system, ^2J = 12.1 Hz, 4 H, CH_2N), 2.93 (q, ^3J = 7.4 Hz, 2 H, CH_2CH$_3$), 2.37 (s, 6 H, CCH_3), 2.18 (s, 6 H, CCH_3), 0.98 (t, ^3J = 7.4 Hz, 3 H, CH$_2$CH_3). − $^{13}C\{^1H\}$ NMR ($CDCl_3$ solution, 50 MHz) δ = 188.3 (d, ^1J = 78.0 Hz, *C*O), 152.7 (*C*CH$_3$), 142.7 (*C*CH$_3$), 107.3 (*C*H), 68.7 (*C*H$_2$N), 51.6 (*C*H$_2$CH$_3$), 14.5−11.8, 11 (CH$_2$*C*H$_3$ + 2 C*C*H$_3$).

Synthesis of [Rh(CO)(1)][BPh$_4$] ([4][BPh$_4$]): To a solution of 0.1 g of [**4**][BF_4] in 10 mL of methanol was added 0.110 g (0.32 mmol) of $NaBPh_4$ and the solution was stirred for 1 h. A yellow precipitate appeared which was filtered and dried under vacuum. It was recrystallised in a dichloromethane/methanol mixture. $C_{39}H_{43}BN_5ORh$ (711.5): C 65.82, H 6.10, N 9.84; found C 65.67, H 5.79, N 9.63.

X-ray Crystallographic Study: Crystals of [**2**][BF_4], [**3**][BPh_4], and [**4**][BPh_4] suitable for X-ray diffraction were obtained through recrystallisation from a dichloromethane/ether mixture for [**2**][BF_4] and dichloromethane/methanol mixture for [**3**][BPh_4], and [**4**][BPh_4]. Data were collected on an STOE IPDS diffractometer at 160 K [**2**][BF_4] and [**4**][BPh_4], and at 298 K [**3**][BPh_4]. Full crystallographic data for the three complexes are gathered in Table 2. All calculations were performed on a PC-compatible computer using the WinGX system.[24] The structures were solved using the SIR92 program,[25] which revealed in each instance the position of most of the non-hydrogen atoms. All remaining non-hydrogen atoms were located by the usual combination of full-matrix least-squares refinement and difference electron density syntheses by using the SHELXS97 program.[26] Phenyl ring within the tetraphenylborate counter anion in the structure of [**4**][BPh_4] have been refined as rigid groups (D_{6h} symmetry; C−C = 1.39 Å; C−H = 0.93 Å). Atomic scattering factors were taken from the usual tabulations.[27] Anomalous dispersion terms for Rh were included in F_c.[28] All non-hydrogen atoms were allowed to vibrate anisotropically. All

Table 2. Crystal data for [**2**][BF_4], [**3**][BPh_4], and [**4**][BPh_4]

compound	[**2**][BF_4]	[**3**][BPh_4]	[**4**][BPh_4]
empirical formula	$C_{66}H_{105}B_3F_{12}N_{15}Rh_3$	$C_{41}H_{45}BCl_2N_5O_2Rh$	$C_{39}H_{43}BN_5ORh$
molecular mass, g	1677.81	824.44	711.50
temperature, K	160(2)	298(2)	160(2)
wavelength, Å	0.71073		
crystal system	triclinic	monoclinic	triclinic
space group	$P\bar{1}$ (#2)	$P2_1/c$ (#14)	$P\bar{1}$ (#2)
a, Å	11.958(2)	10.562(1)	10.335(1)
b, Å	15.218(2)	13.757(1)	11.549(1)
c, Å	20.010(3)	28.379(3)	15.208(2)
α, deg	85.76(2)		80.38(1)
β, deg	81.15(2)	95.93(1)	87.04(1)
γ, deg	88.24(2)		84.89(1)
volume, Å^3	3587.3(8)	4101.6(7)	1781.3(3)
Z	2	4	2
$D_{calcd.}$, g.cm^{-3}	1.553	1.335	1.327
μ, mm^{-1}	0.765	0.587	0.517
F(000)	1728	1704	740
θ range, deg	2.07−25.99	2.07−26.23	2.56−26.16
index ranges	$-14 \le h \le 14$	$-12 \le h \le 13$	$-12 \le h \le 12$
	$-18 \le k \le 18$	$-16 \le k \le 16$	$-14 \le k \le 14$
	$-24 \le l \le 24$	$-34 \le l \le 35$	$-18 \le l \le 18$
reflections collected	35478	28064	17761
independent reflections	13042 [*R*(int) = 0.0332]	7859 [*R*(int) = 0.0791]	6528 [*R*(int) = 0.0286]
completeness to θ_{max},%	92.5	95.2	90.9
refinement method	full-matrix least-squares on F^2		
data/restraints/parameters	13042/0/902	7859/0/474	6479/0/491
g.o.f. on F^2	0.823	0.856	1.043
$R[I > 2\text{sigma}(I)]$	0.0251	0.0577	0.0404
$R[I > 2\text{sigma}(I)]$	0.0687	0.1475	0.1012
R(all data)	0.0895	0.1529,	0.0466,
R(all data)	0.0909	0.2072	0.1052
residual electron density e·Å^{-3}	0.424 and −0.501	0.373 and −0.622 e	0.836 and −0.654

the hydrogen atoms were set in an idealised position (R_3CH, C−H = 0.96 Å; R_2CH_2 = 0.97 Å; $C(sp^2)$−H = 0.93 Å; U_{iso} 1.2 times greater than the U_{eq} of the carbon atom to which the hydrogen atom is attached) and held fixed during refinements. Crystallographic data (excluding structure factors) for the structures reported in this paper have been deposited with the Cambridge Crystallographic Data Centre as supplementary publication n° CCDC 16295, CCDC 16296, CCDC 16297. Copies of the data can be obtained free of charge on application to CCDC, 12 Union Road, Cambridge CB2 1EZ, UK; Fax: (internat.) +44−1223/336-033; E-mail: deposit@ccdc.cam.ac.uk.

Acknowledgments

We thank Professor Michael J. McGlinchey for improving the manuscript and for fruitful discussions. Support by the CNRS and the Ministerio de Educacion y Cultura of Spain (Projects PB96-1146 and BQU200-0238 and grant to G. E.) are gratefully acknowledged.

[1] S. Trofimenko, *Scorpionates: The coordination chemistry of polypyrazolylborate ligands.* Imperial College Press, London, **1999.**
[2] S. Trofimenko, *Prog. Inorg. Chem.* **1986**, *34*, 115−210.
[3] P. K. Byers, A. J. Canty, R. T. Honeyman, *Adv. Organomet. Chem.* **1992**, *34*, 1−65.
[4] R. Mukherjee, *Coord. Chem. Rev.* **2000**, *203*, 151−218.
[5] N. Kitajima, W. B. Tolman, *Prog. Inorg. Chem.* **1995**, *43*, 419−531.
[6] M. Etienne, *Coord. Chem. Rev.* **1996**, *156*, 201−236.
[7] G. Parkin, *Adv. Inorg. Chem.* **1995**, *42*, 291−393.
[8] G. Parkin, *Chem. Commun.* **2000**, 1971−1985.
[9] W. L. Driessen, *Recl. Trav. Chim. Pays-Bas* **1982**, *101*, 441.
[10] H. L. Blonk, W. L. Driessen, J. Reedijk, *J. Chem. Soc., Dalton Trans.* **1985**, 1699−1705.
[11] [11a] A. Togni, L. M. Venanzi, *Angew. Chem.* **1994**, *106*, 517ff.; *Angew. Chem. Int. Ed. Engl.* **1994**, *31*, 497−526.[11b] F. Fache, E. Schulz, M. Lorraine Tommasino, M. Lemaire, *Chem. Rev.* **2000**, *100*, 2159−2231.
[12] T. Ohkuma, D. Ishii, H. Takeno, R. Noyori, *J. Am. Chem. Soc.* **2000**, *122*, 6510−6511.
[13] K. Abdur-Rashid, A. J. Lough, R. H. Morris, *Organometallics* **2000**, *19*, 2655−2657.
[14] M. Akita, M. Hashimoto, S. Hikichi, Y. Moro-oka, *Organometallics* **2000**, *19*, 3744−3747 and references therein.
[15] D. Sanz, M. D. Santa Maria, R. M. Claramunt, M. Cano, J. V. Heras, J. A. Campo, F. A. Ruiz, E. Pinilla, A. Monge, *J. Organomet. Chem.* **1996**, *526*, 341−350.
[16] See for instance: M. Akita, K. Ohta, Y. Takahashi, S. Hikichi, Y. Moro-oka, *Organometallics* **1997**, *16*, 4121−4128.
[17] G. Esquius, J. Pons, R. Yáñez, J. Ros, *J. Organomet. Chem.* **2001**, *619*, 14−23.
[18] H. Günther, *NMR Spectroscopy*, John Wiley &Sons, **1980.**
[19] H. L. Blonk, W. L. Driessen, J. Reedijk, *J. Chem. Soc., Dalton Trans.* **1985**, 1699−1705.
[20] K. Locher, H. L. Blonk, W. L. Driessen, J. Reedijk, *Acta Crystallogr., Sect. C* **1987**, *43*, 651−653.
[21] J. W. F. M. Schoonhoven, W. L. Driessen, J. Reedijk, G. C. Verschoor, *J. Chem. Soc., Dalton Trans.* **1984**, 1053−1058.
[22] Y. C. M. Pennings, W. L. Driessen, J. Reedijk, *Acta Crystallogr., Sect. C* **1988**, *44*, 2095−2097.
[23] G. Giordano, R. H. Crabtree, *Inorg. Synthesis* **1990**, *28*, 88−90.
[24] L. J. Farrugia, *J. Appl. Crystallogr.* **1999**, *32*, 837.
[25] A. Altomare, G. Cascarano, C. Giacovazzo, A. Guagliardi, *J. Appl. Crystallogr.* **1993**, *26*, 343.
[26] G. M. Sheldrick, *SHELXS97*, *SHELXL97*, *CIFTAB − Programs for Crystal Structure Analysis (Release 97−2)*, Institüt für Anorganische Chemie der Universität, Tammanstraße 4, 3400 Göttingen, Germany (**1998**).
[27] [27a] D. T. Cromer, J. T. Waber, *International Tables for X-ray Crystallography*; Kynoch Press: Birmingham, England, vol. 4, **1974**, Table 22B. − [27b] R. F. Stewart, E. R. Davidson, W. T. Simpson, *J. Chem. Phys.* **1965**, *42*, 3175. − [27c] T. Hahn, Ed., *International Tables for Crystallography, Volume A*, Kluwer Academic Publishers, Dordrecht, The Netherlands (**1995**).
[28] D. T. Cromer, J. T. Waber, *International Tables for X-ray Crystallography*, Kynoch Press: Birmingham, England, vol. 4, **1975**, Table 2.3.1.

Received April 6, 2001
[I01124]

Solid-State and Solution Structures of a Series of [(HBPz$_3^{Me2}$)Rh(CO)(PR$_3$)] and [(HBPz$_3^{Me2,4Cl}$)Rh(CO)(PR$_3$)] Complexes

François Malbosc,[a] Valérie Chauby,[a] Carole Serra-Le Berre,[a] Michel Etienne,[b] Jean-Claude Daran,[b] and Philippe Kalck*[a]

Keywords: Pyrazolylborato ligands / Rhodium / IR spectroscopy / Square-planar complexes / Fluxional behavior

Addition of 1 equiv. of a phosphane or phosphite ligand to the κ^3-bonded [Tp^{Me2}Rh(CO)$_2$] and [Tp^{Me2,4Cl}Rh(CO)$_2$] dicarbonyl precursors gives the monosubstituted complexes [TpRh(CO)L]. The X-ray crystal structures show that the three complexes [Tp^{Me2}Rh(CO)(PMe$_3$)], [Tp^{Me2}Rh(CO)(PMePh$_2$)], and [Tp^{Me2,4Cl}Rh(CO)(PMePh$_2$)] adopt square-planar geometries. The X-ray crystal structure of [Tp^{Me2}Rh(CO){P(OPh)$_3$}] is consistent with an interaction between the dangling pyrazolyl group and the rhodium centre, the Rh–N distance being 2.762(3) Å. Analysis of ν(BH) and ν(CO) stretching frequencies shows that all the phosphane-containing complexes are square planar in solution as well as in the solid state. According to infrared analyses, the phosphite complexes [Tp^{Me2,4Cl}Rh(CO){P(OPh)$_3$}] and [Tp^{Me2,4Cl}Rh(CO){P(OMe)$_3$}] adopt a pentacoordinated geometry both in the solid state and in solution. However, the infrared data for [Tp^{Me2}Rh(CO){P(OPh)$_3$}] and [Tp^{Me2}Rh(CO){P(OMe)$_3$}] indicate that the Tp^{Me2} ligand is in a κ^3 coordination mode in the solid state, as already evidenced by the X-ray crystal structure, but in a κ^2 mode in solution. We also describe an exchange phenomenon between dangling and coordinated pyrazolyl groups, as studied by NMR.

Introduction

Since the first report of pyrazolylborato ligands by Trofimenko in 1966,[1] hydrotris(pyrazolyl)borates have been extensively used as σ donor ligands in a wide variety of transition metal complexes.[2] They can provide stable complexes, e.g. by replacing the isoelectronic cyclopentadienyl and pentamethylcyclopentadienyl ligands, and offer greater flexibility. Indeed, these ligands can adopt various modes of coordination ranging from the ubiquitous κ^3 and κ^2 forms to the less common κ^1 coordination mode.[3,4] Even rarer is their recently recognized ability to act as counterions (i.e., a κ^0 form)[5] in transition metal salts. Venanzi and co-workers have studied the geometry adopted in solution by complexes of the type [{HB(3R,4R′,5R"-pyrazolyl)$_3$}Ir(η^4-C$_8$H$_{12}$)], or, using the nomenclature of Trofimenko,[2] of the type [Tp$^{3R,4R',5R''}$Ir(COD)].[6] In its κ^2 coordination mode, the ligand can have the non-coordinated pyrazolyl group either far from the iridium centre or dangling in such a position that the κ^3 mode can readily be achieved, as depicted in Scheme 1.

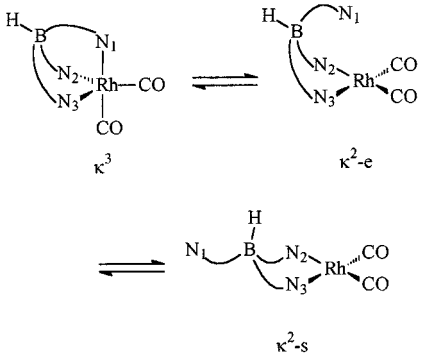

Scheme 1. The three coordination modes of Tp (adapted from ref.[3])

Electronic and steric effects of each pyrazolyl group play an important role in determining the equilibrium between the three different forms κ^2-e (the pyrazolyl in a pseudo-equatorial position), κ^2-s (scorpionate[6]), and κ^3. The nature of the substituent in the 3-position, i.e. adjacent to the potentially coordinating nitrogen atom, exerts a strong influence on this equilibrium. More specifically, steric hindrance between an R substituent in the 3-position and the hydrogen atoms of the two double bonds of the cyclooctadiene ligand in [Tp$^{3R,4R',5R''}$Ir(C$_8$H$_{12}$)] plays an important role.[6] Venanzi and co-workers,[6] as well as Akita, Moro-oka et al. for related [Tp^{iPr}Rh(diene)] complexes,[7] have used the wavenumber of the ν(BH) stretching vibration to assign a κ^2 or a κ^3 bonding mode for the Tp ligand. When ν(BH) is near to 2470 cm^{-1}, a square-planar complex in a κ^2 mode is observed, whereas a ν(BH) band at around 2540 cm^{-1} is indicative of a trigonal-bipyramidal structure with a κ^3 coordination mode.[7]

This class of complexes has become of particular interest since Ghosh and Graham demonstrated that [Tp^{Me2}Rh(CO)$_2$] photochemically activates one C–H bond of benzene or cyclohexane to afford the corresponding hydrido phenyl or cyclohexyl rhodium complexes.[8] This latter complex reacts with methane to afford

[a] Laboratoire de Catalyse, Chimie Fine et Polymères, ENSCT, 118 route de Narbonne, 31077 Toulouse Cedex, France
[b] Laboratoire de Chimie de Coordination du CNRS, 205 route de Narbonne, 31062 Toulouse Cedex, France

 © WILEY-VCH Verlag GmbH, 69451 Weinheim, 2001 1434–1948/01/1010–2689 $ 17.50+.50/0

[Tp^{Me2}Rh(CO)(H)(CH_3)]. The mechanism of this photochemically induced C−H bond activation has been studied by Purwoko and Lees,[9] as well as by Bergman and coworkers.[10] The process is believed to involve a sequence of elimination of a CO ligand, coordination of the C−H bond in an η^2 mode, a change from κ^3 to κ^2 bonding of the Tp^{Me2} ligand to the rhodium, and finally oxidative addition of the alkane.[7] The observation of the intermediate [(κ^2-Tp^{Me2})Rh(CO)(η^2-RH)] has prompted us to report the preparation of a series of [Tp′Rh(CO)(PR_3)] complexes, which were designed to have a more nucleophilic centre with a view to enhancing their C−H activating ability. The present paper deals with the preparation and characterization of [Tp^{Me2}Rh(CO)L] and [$Tp^{Me2,4Cl}$Rh(CO)L] (L = phosphane, phosphite) complexes. We have performed a detailed study of their solid-state and solution structures, as probed by infrared and NMR spectroscopies, and by X-ray crystal structure determinations. While this project was in progress,[11] the synthesis of [Tp^{Me2}Rh(CO)(PPh_3)] was published.[12] Several [Tp^{Me2}Rh(CO)(PR_3)] complexes have been described in the Ph.D. thesis of C. K. Ghosh.[13]

Results and Discussion

Preparation of [Tp^{Me2}Rh(CO)(PR_3)] and [$Tp^{Me2,4Cl}$Rh(CO)(PR_3)] Complexes

Addition of one equivalent of a phosphane or a phosphite ligand PR_3 to [Tp^{Me2}Rh(CO)$_2$] (**1**) or [$Tp^{Me2,4Cl}$Rh(CO)$_2$] (**2**) at room temperature results in the substitution of one CO ligand to afford the corresponding [TpRh(CO)(PR_3)] complexes as shown in Equations (1) and (2).

$$[Tp^{Me2}Rh(CO)_2] + PR_3 \longrightarrow [Tp^{Me2}Rh(CO)(PR_3)] + CO \quad (1)$$

1

PR_3 = PMe_3: **3**; PMe_2Ph: **4**; $PMePh_2$: **5**; PPh_3: **6**; $P(OMe)_3$: **7**; $P(OPh)_3$: **8**

$$[Tp^{Me2,4Cl}Rh(CO)_2] + PR_3 \longrightarrow [Tp^{Me2,4Cl}Rh(CO)(PR_3)] + CO \quad (2)$$

2

PR_3 = PCy_3: **9**; PMe_3: **10**; PMe_2Ph: **11**; $PMePh_2$: **12**; PPh_3: **13**; $P(OMe)_3$: **14**; $P(OPh)_3$: **15**; $P(OiPr)_3$: **16**

The rate of this reaction is determined by the nature of the ligand. The more basic but sterically hindered tricyclohexylphosphane PCy_3 reacts with **2** within about 1 h to give **9**. The ligands PMe_3, PMe_2Ph, $PMePh_2$, and even $P(OMe)_3$ react within a few minutes, as monitored by infrared spectroscopy. The syntheses of **8**, **15**, and **16**, containing the less basic ligands $P(OPh)_3$ and $P(OiPr)_3$, require several hours. According to infrared data, these substitution reactions are quantitative and isolated yields are high (> 85%). In the case of complex **11**, PMe_2Ph in dichloromethane has to be added slowly at room temperature to avoid formation of the disubstituted complex [κ^1-$Tp^{Me2,4Cl}$Rh(CO)(PMe_2Ph)$_2$].[4] **11** can then be recrystallized at low temperature, leaving **2** and the bis-adduct in solution. All the complexes have been fully characterized by infrared, ^{1}H, and ^{31}P NMR, and in some cases by ^{13}C and ^{103}Rh NMR. The solid-state structures of **3**, **5**, **8**, and **12** have been confirmed by X-ray analyses.

Molecular Structures of the Complexes 3, 5, 8, and 12

X-ray crystal structures have been obtained for four complexes, two of which (**3** and **12**) have been described in brief in previous reports.[4,11] Salient data are presented in Table 1.

Table 1. Salient distances [Å] and angles [°] (SP = square plane) in complexes with PR_3: **3**, **5**, **8**, and **12**

	PMe_3: **3**	$P(OPh)_3$: **8**	$PMePh_2$: **5**	$PMePh_2$: **12**
Rh−C1	1.797(4)	1.802(4)	1.818(4)	1.810(2)
Rh−P1	2.2447(9)	2.1794(9)	2.2503(9)	2.258(5)
Rh−N1	2.113(3)	2.110(3)	2.097(3)	2.0923(15)
Rh−N3	2.101(3)	2.097(3)	2.095(3)	2.0911(16)
Rh−N5	3.632(3)	2.762(3)	3.661(4)	3.800(2)
Pz_3−SP angle	55.05	78.91	52.12	48.05
N6−B1−H1	109.9	111.7(20)	115.5(22)	113.3(14)

We first focus on the structures of **5** and **12**, which have the same $PMePh_2$ phosphane ligand. Both complexes show the same square-planar environment (see Figure 1 for **5** and Figure 2 for **12**), with two pyrazolyl groups bonded to the rhodium metal centre and the third one in a dangling position. The Rh−N5 distances of 3.661(4) and 3.800(2) Å in **5** and **12**, respectively, preclude any bonding interaction between these atoms. The difference between these distances is due to the rotation of the free pyrazolyl group, since the angle between the pyrazolyl and the square plane varies from 52.12° to 48.05°. The Rh−N1, Rh−N3, and Rh−P1 distances can be considered as being the same in these complexes. Within each complex, the Rh−N distances to the coordinated pyrazolyl groups, Rh−N1 and Rh−N3, are equal, irrespective of the ligand in the *trans* position (i.e. CO or $PMePh_2$). As usual, the ν(CO) stretching frequencies are more sensitive to the electronic modifications of the metal centre than the Rh−C, C−O, and Rh−O distances for the CO ligands. Indeed, the four Rh−O1 bond lengths for **3**, **5**, **8**, and **12** are 2.949 [ν(CO) = 1961 cm^{-1}], 2.954 (1984 cm^{-1}), 3.099 (1975 cm^{-1}), and 2.910 Å (1996 cm^{-1}), respectively. A square-planar environment is also found for **3** (Figure 3), and the Rh−N1 and Rh−N3 bond lengths are identical within experimental error.

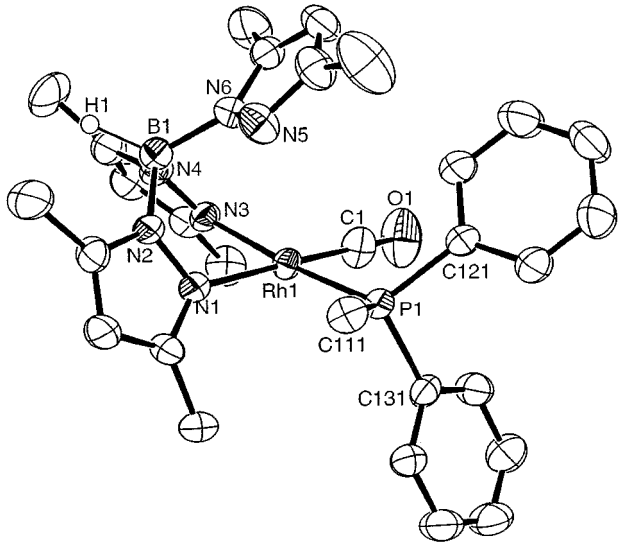

Figure 1. Molecular view of complex **5**; ellipsoids are drawn at a 30% probability level

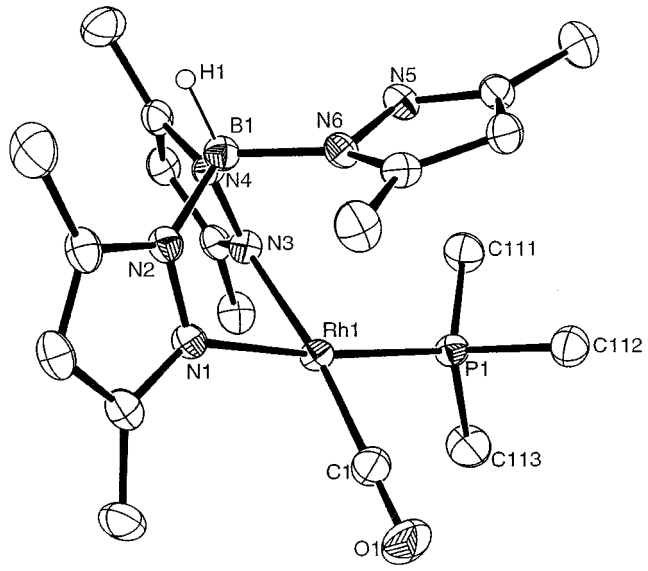

Figure 3. Molecular view of complex **3**; ellipsoids are drawn at a 30% probability level

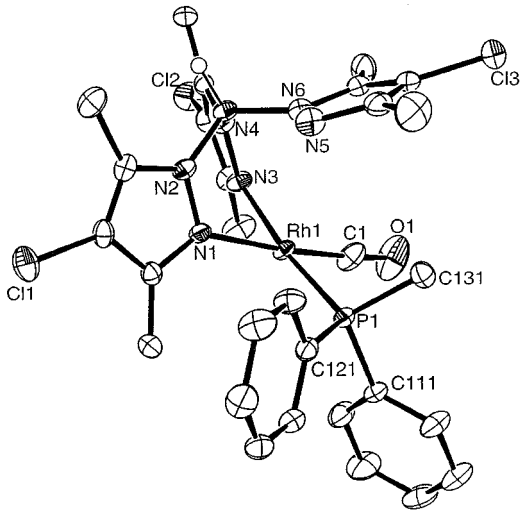

Figure 2. Molecular view of complex **12**; ellipsoids are drawn at a 30% probability level

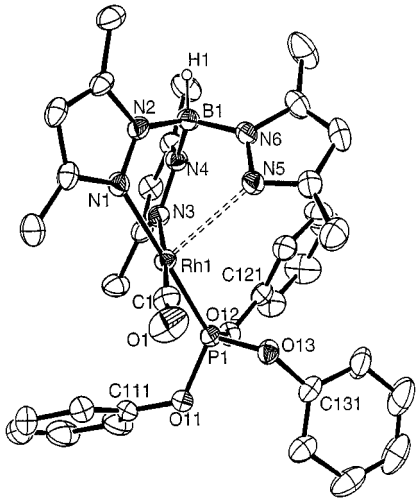

Figure 4. Molecular view of complex **8**; ellipsoids are drawn at a 30% probability level

Complex [Tp^{Me2}Rh(CO){P(OPh)$_3$}], **8**, has also been analysed by X-ray crystallography, in view of its unexpected infrared spectra (vide infra). The geometry about the rhodium is again square-planar (Figure 4). The most notable feature is an Rh−P1 distance of 2.1794(9) Å, which is significantly shorter than the Rh−P1 distances observed with PMe_3 in **3** (2.245 Å) or with $PMePh_2$ in **5** and **12** (2.250 Å and 2.258 Å, respectively). This is consistent with the better π-accepting properties of a phosphite as compared to a phosphane. A further feature deserves comment. The Rh−N5 distance is 2.762(3) Å, longer than that of a true coordination bond (ca. 2.1 Å), but shorter than the sum of the van der Waals radii (3.3 Å). Such a distance is thus consistent with an Rh−N5 interaction. Recently, Connelly et al. reported the X-ray structure of [Tp^{Me2}Rh(CO)(PPh$_3$)], which has a square-planar geometry with Tp^{Me2} adopting a κ^2 coordination mode.[12] One-electron oxidation results in the formation of [Tp^{Me2}Rh(CO)(PPh$_3$)]$^+$, X-ray analysis of which showed it to contain a κ^3-Tp^{Me2}. The rhodium(II) centre is then in a square-pyramidal environment, with the axial Rh−N5 bond length being 2.224(2) Å as opposed to 2.091(2) Å and 2.093(2) Å for the two other rhodium−nitrogen distances. Thus, the P(OPh)$_3$-containing complex **8** shows a lengthening of ca. 0.5 Å when compared to the rhodium(II) complex. Overall, we conclude that a κ^3 coordination mode is favoured by a decrease in the electron density at the metal centre.

Infrared Study of Complexes 3−15

Previous studies have shown that the ν(BH) stretching frequency offers a reliable means of ascertaining the coordination mode of tris(pyrazolyl)borato ligands.[6,7] Particularly

interesting are the absolute values of the ν(BH) frequencies determined by Moro-oka et al., which are ca. 2470 cm^{-1} for κ^2 coordination and 2540 cm^{-1} for κ^3 coordination.[7] The measured ν(BH) values for all the complexes are presented in Tables 2 and 3. Spectra were obtained from samples in both KBr and CH_2Cl_2. For the complexes bearing more basic phosphanes, i.e. those with PR_3 = PMe_3, PMe_2Ph, $PMePh_2$, and PPh_3 (**3−6** and **9−13**), the ν(BH) values are near to 2480 cm^{-1} and 2485 cm^{-1} in the solid state and in solution, respectively, irrespective of the Tp′ ligand. Figure 5 shows a plot of ν(BH) in CH_2Cl_2 as a function of the basicity of the phosphorus ligand on the Derencsényi scale;[14] ν(BH) is seen to be independent of the phosphane basicity, i.e. it is only weakly sensitive to the electron density at the metal centre. Thus, complexes **3−6** and **9−13** consistently show square-planar geometries, with Tp^{Me2} and $Tp^{Me2,4Cl}$ adopting the κ^2 coordination mode. The diagnostic criterion of Moro-oka et al., as established for [Tp^{Me2}Rh(diene)], is also valid here.

Table 2. ν(BH) and ν(CO) stretching frequencies for the complexes [Tp^{Me2}Rh(CO)(PR_3)] in KBr dispersions and in CH_2Cl_2 solutions

[Tp^{Me2}Rh(CO)(PR_3)]	ν(BH) [cm^{-1}] CH_2Cl_2	KBr	ν(CO) [cm^{-1}] CH_2Cl_2	KBr
$P(OPh)_3$	2479	2518	2009	1984
$P(OMe)_3$	2477	2508	1996	1963
PPh_3	2472	2468	1978	1965
$PMePh_2$	2476	2463	1979	1975
PMe_2Ph	2473	2464	1973	1968
PMe_3	2470	2443	1969	1961

Table 3. ν(BH) and ν(CO) stretching frequencies for the complexes [$Tp^{Me2,4Cl}$Rh(CO)(PR_3)] in KBr dispersions and in CH_2Cl_2 solutions

[$Tp^{Me2,4Cl}$Rh(CO)(PR_3)]	ν(BH) [cm^{-1}] CH_2Cl_2	KBr	ν(CO) [cm^{-1}] CH_2Cl_2	KBr
$P(OPh)_3$	2554	2542	2010	2004
$P(OiPr)_3$	2483	2469	1995	1996
$P(OMe)_3$	2553	2536	2002	1998
PPh_3	2482	2477	1984	1988
$PMePh_2$	2486	2477	1985	1996
PMe_2Ph	2485	2482	1981	1978
PMe_3	2484	2477	1973	1963
PCy_3	2483	2483	1973	1977

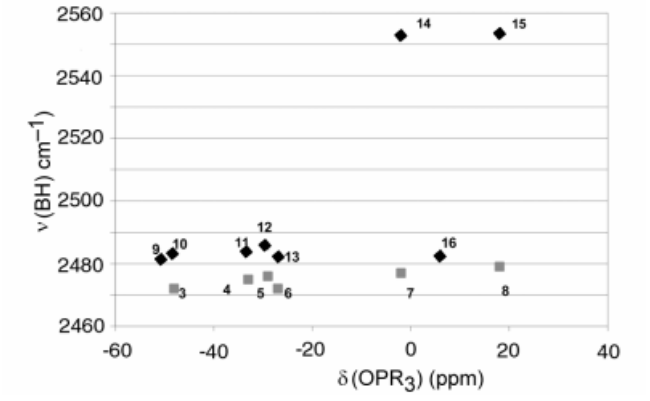

Figure 5. The ν(BH) values for complexes **3−16** in CH_2Cl_2 solution plotted as a function of phosphane basicity on the Derencsényi scale

The situation is slightly more subtle when the less basic phosphite ligands are considered. For complexes **14** and **15**, the ν(BH) values (Table 3 and Figure 5) suggest that the coordination mode of the $Tp^{Me2,4Cl}$ ligand is κ^3. Hence, although we have been unable to obtain X-ray quality crystals to confirm the proposal, complexes **14** and **15** would seem to exhibit a pentacoordinated geometry. Interestingly, for the Tp^{Me2}-based complexes **7** and **8**, which contain the same $P(OMe)_3$ and $P(OPh)_3$ phosphite ligands, the ν(BH) frequencies are only consistent with a κ^2 coordination mode in CH_2Cl_2 solution (2477 and 2479 cm^{-1}, respectively). In contrast, data obtained in KBr suggest that a κ^3 mode is preferred in the solid state (2508 and 2518 cm^{-1} for **7** and **8**, respectively). This is reminiscent of the weaker interaction between the third pyrazolyl group and the rhodium centre revealed by the X-ray crystal structure of **8** (vide supra). Consequently, the Tp^{Me2} ligand is not in a genuine κ^3 coordination mode in **8**, but the position of the third pyrazolyl substituent induces a geometry around the boron atom that results in a ν(BH) band at around 2510 cm^{-1}.

As a further representative of the phosphite family in the [$Tp^{Me2,4Cl}$Rh(CO)(PR_3)] complexes, we have introduced $P(OiPr)_3$, the basicity of which is intermediate between those of $P(OMe)_3$ and PPh_3. Table 3 and Figure 5 unambiguously show that the environment in complex **16** is square-planar, from which we conclude that the steric hindrance induced by the phosphite ligand is sufficiently strong to compensate the decrease in electron density at the metal centre that would favour the approach of the third pyrazolyl group.

The ν(CO) stretching frequencies were measured both in solution and in the solid state for all the complexes (Tables 2 and 3). Figure 6 shows a plot of ν(CO) as a function of the basicity of the PR_3 ligand (CH_2Cl_2 solution). The points representing those complexes having a κ^2-bonded Tp^{Me2} ligand lie on a straight line with a correlation coefficient of 0.98. As usual, the ν(CO) frequencies reliably reflect the electron density at Rh as the basicity of the ligand is varied.

For complexes **9−16**, the situation is less straightforward. A straight line can clearly be seen in Figure 6 for complexes **9−13** and **16**, which exhibit a κ^2 coordination mode in solution. This is in agreement with the conclusions drawn from the analysis of the ν(BH) frequencies. However, the ν(CO) values for complexes **14** and **15** lie at higher frequencies. The corresponding points in the plot do not fall on the previous straight line, but the line plotted between these two points is parallel to the first one. Thus, Figure 6 shows the monotonous variations in the electron density in [κ^2-$Tp^{Me2,4Cl}$Rh(CO)(PR_3)] (lower line) and [κ^3-$Tp^{Me2,4Cl}$Rh(CO){$P(OR)_3$}] (upper line). It is important to note that we might have expected a decrease in the ν(CO) stretching frequency due to the coordination of the third pyrazolyl group, i.e. a line in the plot lower than the κ^2

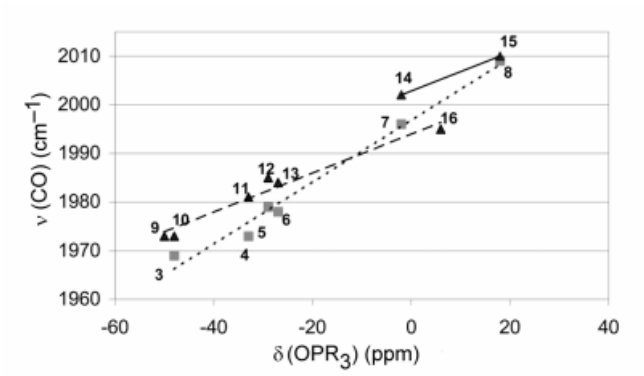

Figure 6. The ν(CO) frequencies for complexes **3**−**16** in CH_2Cl_2 solution plotted as a function of phosphane basicity on the Derencsényi scale

straight line. In fact, this coordination leads to a pentacoordinated geometry, in which the CO force constant is no longer comparable to that for a square-planar geometry.

NMR Studies; Fluxionality of Complexes 3−15

Most of the complexes have been studied by ^{1}H, ^{13}C, ^{31}P, and ^{103}Rh NMR, and in some cases at variable temperature as they are fluxional. We were particularly interested in the PMe_2Ph-containing complex **4** since, in its square-planar environment and with the third pyrazolyl group in a dangling position, as a result of which the plane of symmetry is lost, two diastereotopic methyl groups are to be expected. However, the ^{1}H NMR spectrum recorded at room temperature (Figure 7) features a doublet due to the Me groups of the PMe_2Ph ligand (J_{PH} = 9 Hz) and two singlets at δ = 2.15 and 2.21 due to the Tp^{Me2} methyl substituents. At 183 K (Figure 8), the signal due to the phosphane methyl protons is broader, two methyl groups of a pyrazolyl group give rise to signals at δ = 2.32 and 2.75, while the four remaining Tp^{Me2} methyls give rise to two signals at δ = 1.88 (broad) and 2.05. Thus, the NMR spectra show a non-rigidity for this complex, although the slow-exchange limit was not reached.

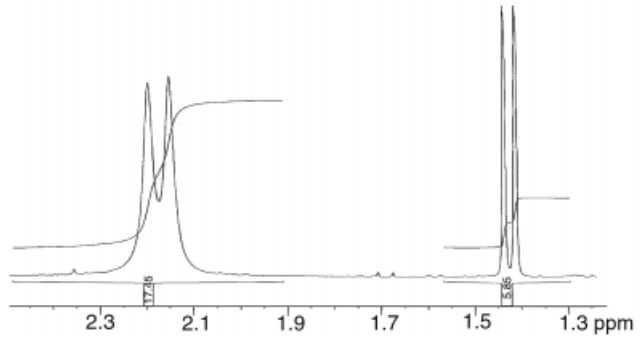

Figure 7. ^{1}H NMR spectrum of complex **4** at 293 K

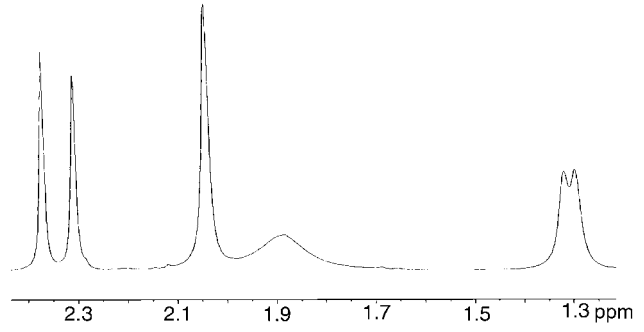

Figure 8. ^{1}H NMR spectrum of complex **4** at 183 K

In order to assign the signals in a situation in which the stereochemical non-rigidity of the complex would be avoided, we protonated **4** with 1 equiv. of HBF_4, a reaction yielding [{κ^2-HB(Pz^{Me2})$_2$(HPz^{Me2})}Rh(CO)(PMe$_2$Ph)][BF$_4$] (**4H$^+$**).[15] The infrared spectrum of **4H$^+$** in KBr shows ν(CO) and ν(BH) bands at 1987 and 2502 cm^{-1}, respectively, close to those of **4** (1968 and 2464 cm^{-1}). Direct protonation at the rhodium centre would have led to a shift in the position of the ν(CO) band of between 50 and 100 cm^{-1}. No ν(Rh−H) band was observed. These data are consistent with a square-planar environment for the rhodium atom and a κ^2 coordination mode for the Tp^{Me2} ligand. No spectroscopic evidence for a hydrido ligand was found, but a ^{1}H NMR signal at δ = 11.84 is consistent with the presence of an NH group. Thus, protonation of **4** occurs on the free pyrazolyl arm as expected. The methyl region of the ^{1}H NMR spectrum shown in Figure 9 confirms the absence of a symmetry plane in **4H$^+$**. The two methyls of PMe_2Ph are diastereotopic and six Tp^{Me2} methyl signals are observed. An Rh−H coupling (1.6 Hz) is apparent from the higher field doublet. With the aid of {^{1}H,^{1}H}, {^{1}H,^{13}C} HMQC, and HMBC measurements and {^{1}H,^{1}H} NOESY experiments, all the ^{1}H NMR signals have been assigned, as shown in Figure 10. It is worth noting that the two lower field methyl peaks at δ = 2.38 and 2.48 are attributable to the 3-Me and 5-Me groups of the pyrazolyl group *trans* to the CO ligand, respectively. Moreover, there is no exchange between the two pyrazolyl groups bonded to rhodium.

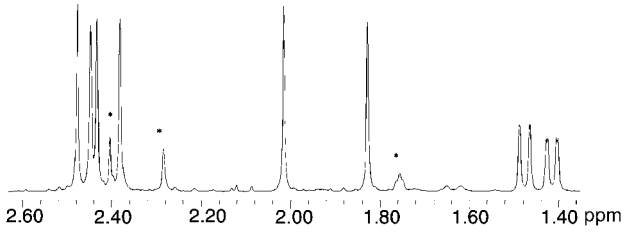

Figure 9. ^{1}H NMR spectrum of complex **4H$^+$**; *peaks attributable to the starting material **4**

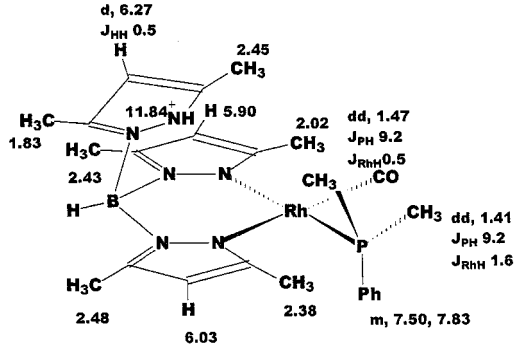

Figure 10. ^{1}H NMR signal assignments for complex **4H$^+$**

Study of the Exchange Phenomenon in 4

For complex **4** at 183 K (Figure 8), the two methyl proton signals observed at δ = 2.32 and 2.75 are assigned to the pyrazolyl *trans* to the CO ligand, these chemical shifts being very close to those of the pyrazolyl ligand *trans* to CO in **4H**$^+$. Hence, the methyl signal at δ = 1.88 is attributable to the dangling pyrazolyl, while that at δ = 2.05 is due to the pyrazolyl *trans* to the phosphane. The exchange rate for the former is slightly higher than the rate corresponding to the coalescence temperature. At low temperature, the latter pyrazolyl methyl groups undergo exchange with a low activation energy. Since the pyrazolyl *trans* to CO is not involved in the exchange phenomenon, we propose a square-pyramidal transition state, as shown in Figure 11. In a trigonal-bipyramidal transition state, the apical pyrazolyl group would exchange at the same rate with either of the two equatorial groups. When the temperature is raised, the third pyrazolyl *trans* to CO is also exchanged, so that the fast-exchange limit is reached at room temperature.

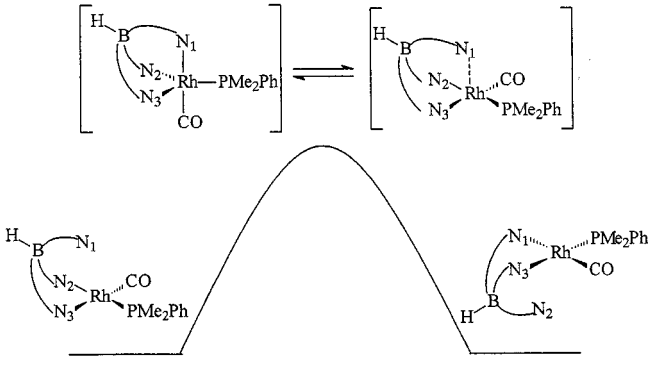

Figure 11. Proposed transition-state geometry for the exchange phenomenon between two square-planar isomers of **4**

This study shows that in a square-planar complex the pendant pyrazolyl group readily coordinates. Decoordination of the pyrazolyl *trans* to PMe_2Ph then provides the free pyrazolyl, as indicated in Figure 11. This phenomenon places the free pyrazolyl group either above or below the plane, such that the magnetic environments of the two methyl groups of PMe_2Ph become identical on the NMR time scale.[10]

The same exchange phenomenon has been observed for $[Tp^{Me2}Rh(CO)(PMe_3)]$,[11] $[Tp^{Me2,4Cl}Rh(CO)(PMePh_2)]$, and $[Tp^{Me2}Rh(CO)(PMePh_2)]$. For $[Tp^{Me2}Rh(CO)\{P(OPh)_3\}]$, however, the three pyrazolyl groups are still in fast exchange at 183 K. This is reminiscent of the results of the X-ray diffraction analysis, where the pendant pyrazolyl group and the rhodium centre were found to be in close proximity, and is consistent with the proposed geometry of the transition state and a low activation energy for the exchange between the square-planar isomers.

Conclusion

The complexes $[Tp^{Me2}Rh(CO)(PR_3)]$ and $[Tp^{Me2,4Cl}Rh(CO)(PR_3)]$ can readily be prepared by addition of one equivalent of the appropriate phosphane ligand to $[Tp^{Me2}Rh(CO)_2]$ and $[Tp^{Me2,4Cl}Rh(CO)_2]$, respectively. As shown by the X-ray crystal structures of four complexes and by an infrared study in the solid state and in solution, these complexes adopt a square-planar structure. In the case of a phosphite ligand, the dangling pyrazolyl group resides near the rhodium. The bonding mode is then intermediate between κ^2 and κ^3. NMR studies have shown a fluxional behaviour for all the $[Tp'Rh(CO)(PR_3)]$ complexes indicating that the more stable geometries are square-planar and that the transition state is close to square-pyramidal. Similar complexes have been prepared by Jones et al. with isocyanide ligands, while Carmona et al. have prepared iridium complexes with the general formula $[Tp'Ir(C_2H_4)(L)]$.[16,17]

Experimental Section

General Remarks: All experiments were carried out under argon. Reactions were performed using standard Schlenk techniques. Solvents were HPLC quality and were distilled under dinitrogen, toluene from sodium/benzophenone and dichloromethane from $CaSO_4$. They were frozen and degassed in vacuo, and were stored over molecular sieves under argon. Pentane was purified according to the method of Perrin and Armarego,[18] distilled from CaH_2 under argon, frozen, and degassed in vacuo. Commercial phosphites and phosphanes were used without purification. − NMR spectra were recorded with Bruker AC 200, WM 250, or AMX 400 spectrometers. − A Perkin−Elmer 1710 FT-IR spectrometer was used to record the infrared spectra. Solid samples were analysed in KBr and liquid samples were analysed between CaF_2 windows (vs: very strong, s: strong, m: medium, w: weak, vw: very weak, sh: shoulder). − X-ray analyses were performed with Enraf-Nonius CAD 4 or STOE IPDS diffractometers.

$HPz^{Me2,4Cl}$: This material[19] was prepared by the slow addition of hydrazine hydrate (20 mL, 412 mmol) to 3-chloro-2,4-pentanedione (49 mL, 411 mmol) in ethanol (600 mL) at 80 °C. The mixture was stirred for 3 h at 80 °C. After evaporation of the ethanol, the product was dissolved in CH_2Cl_2. The resulting solution was stirred with a small amount of $MgSO_4$ for 2 h and then filtered through Celite. The solvent was evaporated until crystallization commenced and then hexane (300 mL) was added. The solution was kept at 0 °C, whereupon white crystals were deposited. The crystals were washed with hexane (3 × 20 mL) at 0 °C and were then sublimed at 110 °C to yield 48.2 g (90%) of $HPz^{Me2,4Cl}$. − ^{1}H NMR ($CDCl_3$, 25 °C): δ = 2.24 (s, 6 H, CH_3). − IR (KBr): $\tilde{\nu}$ = 1588 cm^{-1} [ν(C=N)].

$KHBPz_3^{Me2,4Cl}$: This ligand[20] was prepared by the addition of 3,5-dimethyl-4-chloropyrazole (40.0 g, 307.2 mmol) to potassium tetrahydroborate (3.686 g, 68 mmol). The mixture was slowly heated to 120 °C. When the evolution of hydrogen had subsided, the temperature was raised to 220 °C. The reaction was seen to be complete when hydrogen evolution had ceased. Then, toluene (20 mL) was quickly added to avoid agglomeration of the product. The solution was concentrated to three-quarters of its original volume and then hexane (50 mL) was added. The resulting solution was kept at 0 °C. White crystals were deposited, which were washed with hexane (3 × 30 mL) at 0 °C. The crystals were freed of excess $HPz^{Me2,4Cl}$ by sublimation to yield 27.11 g (90%) of $KHBPz_3^{Me2,4Cl}$. − ^{1}H NMR ($CDCl_3$, 25 °C): δ = 2.00 [s, 9 H, $CH_3(Pz^{Me2,4Cl})$], 2.14 [s, 9

H, CH_3(Pz^{Me2,4Cl})]. − IR (KBr): $\tilde{\nu}$ = 2468 cm^{-1} [ν(BH)], 1541 cm^{-1} [ν(C=N)].

KHBPz$_3^{Me2}$: This ligand[21] was prepared by the addition of 3,5-dimethylpyrazole (15.0 g, 117.2 mmol) to potassium tetrahydroborate (1.405 g, 28 mmol). The mixture was slowly heated to 110 °C. When the evolution of hydrogen had subsided, the temperature was increased to 190 °C. The reaction was seen to be complete when the hydrogen evolution had ceased. Then, toluene (20 mL) was quickly added to avoid agglomeration of the product. The solution was concentrated to three-quarters of its original volume and then hexane (50 mL) was added. The resulting solution was kept at 0 °C. White crystals were deposited, which were washed with hexane (3 × 30 mL) at 0 °C. The crystals were freed of excess HPz^{Me2} by sublimation to yield 8.47 g (85%) of KHBPz$_3^{Me2}$. − ^{1}H NMR (CDCl$_3$, 25 °C): δ = 2.00 [s, 9 H, CH_3(Pz^{Me2})], 2.14 [s, 9 H, CH_3(Pz^{Me2})]. − IR (KBr): $\tilde{\nu}$ = 2438 cm^{-1} [ν(BH)], 1538 cm^{-1} [ν(C=N)].

[Rh(μ-Cl)(CO)$_2$]$_2$: This complex was prepared by bubbling CO through a solution of RhCl$_3$·3H$_2$O (3.0 g, 11.4 mmol) in methanol (100 mL) at 65 °C for 20 h. The methanol was then slowly evaporated by passing nitrogen through the solution. Red crystals were obtained, which were sublimed in vacuo at 50 °C to yield 4.21 g (95%) of the product. − IR (KBr): $\tilde{\nu}$ = 2102 m, 2082 s, 2020 s cm^{-1} [ν(CO)].

[Tp^{Me2}Rh(CO)$_2$] (1): Compound **1** was prepared by adding KHBPz$_3^{Me2}$ (1.89 g, 4.15 mmol) to a solution of [Rh(μ-Cl)(CO)$_2$]$_2$ (1.0 g, 2.57 mmol) in CH_2Cl_2 (60 mL). The mixture was stirred for 4 h, in the course of which it turned from yellow-orange to brown. The reaction was monitored by infrared spectroscopy. KCl formed during the reaction was filtered off and washed with CH_2Cl_2. The combined filtrate and washings were concentrated in vacuo, yielding 1.9 g (90%) of **1** as a yellow-orange solid. − ^{1}H NMR (C_6D_6, 25 °C): δ = 2.31, 2.37 [s, 6 H, CH_3(Pz^{Me2})], 5.77 [s, 3 H, CH(Pz^{Me2})]. − IR (KBr): $\tilde{\nu}$ = 2512 [ν(BH)], 2054 s, 1973 s cm^{-1} [ν(CO)]. − UV/Vis (pentane): λ_{max} = 355 nm.

[Tp^{Me2,4Cl}Rh(CO)$_2$] (2): Addition of solid KHBPz$_3^{Me2,4Cl}$ (2.26 g, 5.15 mmol) to a yellow-orange solution of [Rh(μ-Cl)(CO)$_2$]$_2$ (1.00 g, 2.57 mmol) in CH_2Cl_2 (60 mL) yielded a brown slurry after 4 h. The progress of the reaction was monitored by IR. The solution was then filtered and the removed solid was washed with CH_2Cl_2. The combined filtrate and washings were concentrated in vacuo, yielding 1.3 g (90%) of **2** as a yellow-orange solid. − ^{1}H NMR (C_6D_6, 25 °C): δ = 2.12, 2.41 [s, 6 H, CH_3(Pz^{Me2,4Cl})]. − IR (KBr): $\tilde{\nu}$ = 2544 [ν(BH)], 2088 w, 2059 s, 2020 w, 1984 s cm^{-1} [ν(CO)]. − UV/Vis (pentane): λ_{max} = 361 nm.

[Tp^{Me2}Rh(CO)(PMe$_3$)] (3): Complex **3** was prepared by adding PMe$_3$ (0.96 mL, 0.96 mmol, 1 M in toluene) to a solution of [Tp^{Me2}Rh(CO)$_2$] (0.4 g, 0.88 mmol) in CH_2Cl_2 (20 mL). The reaction was immediate, as indicated by a ν(CO) band at 1969 cm^{-1} in the IR spectrum. The solvent was then evaporated and the residue was washed with hexane at 0 °C and dried in vacuo at 40 °C for 6 h to yield 0.36 g (85%) of **3**. − ^{1}H NMR (C_6D_6, 25 °C): δ = 0.91 (d, 9 H, PMe$_3$, $^2J_{P-H}$ = 3 Hz), 1.75 [s, 9 H, CH_3(Pz^{Me2})], 2.15 [s, 9 H, CH_3(Pz^{Me2})]. − ^{31}P NMR (C_6D_6, 25 °C): δ = 5.02 (d, 1 P, $^1J_{Rh-P}$ = 145 Hz). − IR (KBr): $\tilde{\nu}$ = 2443 [ν(BH)], 1961 cm^{-1} [ν(CO)].

[Tp^{Me2}Rh(CO)(PMe$_2$Ph)] (4): Complex **4** was prepared by adding PMe$_2$Ph (62.4 μL, 0.44 mmol) to a solution of [Tp^{Me2}Rh(CO)$_2$] (0.20 g, 0.44 mmol) in CH_2Cl_2 (15 mL). The reaction was immediate, as shown by a ν(CO) band at 1973 cm^{-1} in the IR spectrum. The solvent was evaporated and the product was washed at 45 °C for 6 h, yielding 0.21 g (80%) of **4**. − ^{1}H NMR (C_6D_6, 25 °C): δ = 1.43 (d, 6 H, PMe$_2$, $^2J_{P-H}$ = 9 Hz), 2.15 [s, 9 H, CH_3(Pz^{Me2})], 2.21 [s, 9 H, CH_3(Pz^{Me2})], 5.83 [s, 3 H, CH(pz)], 7.82 (m, 5 H, PPh). − ^{31}P NMR (C_6D_6, 25 °C): δ = 20.13 (d, 1 P, $^1J_{Rh-P}$ = 151 Hz). − IR (KBr): $\tilde{\nu}$ = 2464 [ν(BH)], 1968 cm^{-1} [ν(CO)]. − $C_{24}H_{33}BN_6OPRh$ (566.3): calcd. C 50.91, H 5.87, N 14.84; found C 50.31, H 5.96, N 14.62.

[Tp^{Me2}Rh(CO)(PMePh$_2$)] (5): Complex **5** was prepared by adding PMePh$_2$ (89.7 μL, 0.48 mmol) to a solution of [Tp^{Me2}Rh(CO)$_2$] (0.20 g, 0.44 mmol) in CH_2Cl_2 (20 mL). The reaction was complete within 15 min, as shown by IR [ν(CO) = 1979 cm^{-1}]. The solution was filtered and the filtrate was concentrated to dryness. Crystallization of the residue from toluene/heptane at −18 °C yielded 0.23 g (85%) of yellow crystals of **5**. − ^{1}H NMR (C_6D_6, 25 °C): δ = 1.60 (dd, 3 H, P*Me*Ph$_2$, $^2J_{P-H}$ = 10, $^3J_{Rh-H}$ = 1 Hz), 2.05 [s, 9 H, CH_3(Pz^{Me2})], 2.32 [s, 9 H, CH_3(Pz^{Me2})], 5.71 [s, 3 H, CH(Pz^{Me2})], 7.42 (m, 10 H, PPh$_2$). − ^{31}P NMR (C_6D_6, 25 °C): δ = 30.60 (d, 1 P, $^1J_{Rh-P}$ = 155 Hz). − IR (KBr): $\tilde{\nu}$ = 2463 [ν(BH)], 1975 cm^{-1} [ν(CO)]. − UV/Vis (pentane): λ_{max} = 357 nm. − $C_{29}H_{35}BN_6OPRh$ (628.3): calcd. C 55.44, H 5.61, N 13.37; found C 52.40, H 5.16, N 12.34.

[Tp^{Me2}Rh(CO)(PPh$_3$)] (6): Complex **6** was prepared by adding solid PPh$_3$ (0.16 g, 0.48 mmol) to a solution of [Tp^{Me2}Rh(CO)$_2$] (0.20 g, 0.44 mmol) in CH_2Cl_2 (15 mL). The reaction was monitored by IR and was seen to be complete after 2 h [ν(CO) = 1978 cm^{-1}]. The solution was then filtered and the filtrate was concentrated to dryness. Crystallization of the residue from toluene/heptane at −18 °C yielded 0.24 g (80%) of yellow crystals of **6**. − ^{1}H NMR (C_6D_6, 25 °C): δ = 1.75 [s, 9 H, CH_3(Pz^{Me2})], 2.15 [s, 9 H, CH_3(Pz^{Me2})], 5.70 [s, 3 H, CH(Pz^{Me2})], 7.3 (m, 15 H, PPh$_3$). − ^{31}P NMR (C_6D_6, 25 °C): δ = 42.86 (d, 1 P, $^1J_{Rh-P}$ = 161 Hz). − IR (KBr): $\tilde{\nu}$ = 2468 [ν(BH)], 1965 cm^{-1} [ν(CO)]. − $C_{34}H_{37}BN_6OPRh$ (690.4): calcd. C 59.15, H 5.40, N 12.17; found C 59.48, H 5.47, N 11.90.

[Tp^{Me2}Rh(CO){P(OMe)$_3$}] (7): Complex **7** was prepared by adding P(OMe)$_3$ (52 μL, 0.44 mmol) to a solution of [Tp^{Me2}Rh(CO)$_2$] (0.20 g, 0.44 mmol) in CH_2Cl_2 (15 mL). The reaction was immediate, as shown by IR [ν(CO) = 1996 cm^{-1}]. The solvent was evaporated and the residue was washed with hexane at 0 °C and dried in vacuo to yield 0.19 g (85%) of **7**. − ^{1}H NMR (C_6D_6, 25 °C): δ = 1.92 [s, 9 H, CH_3(OMe$_3$)], 1.75 [s, 9 H, CH_3(Pz^{Me2})], 2.15 [s, 9 H, CH_3(Pz^{Me2})]. − ^{31}P NMR (C_6D_6, 25 °C): δ = 142.8 (d, 1 P, $^1J_{Rh-P}$ = 266 Hz). − IR (KBr): $\tilde{\nu}$ = 2508 [ν(BH)], 1963 cm^{-1} [ν(CO)].

[Tp^{Me2}Rh(CO){P(OPh)$_3$}] (8): Complex **8** was prepared by adding P(OPh)$_3$ (253 μL, 0.96 mmol) to a solution of [Tp^{Me2}Rh(CO)$_2$] (0.40 g, 0.87 mmol) in CH_2Cl_2 (20 mL). The reaction was complete within 2 h, as shown by IR [ν(CO) = 2009 cm^{-1}]. The solvent was then evaporated and the residue was washed with hexane at 0 °C and dried in vacuo at 45 °C for 6 h to yield 0.21 g (80%) of **8**. − ^{1}H NMR (C_6D_6, 25 °C): δ = 2.23 [s, 9 H, CH_3(Pz^{Me2})], 2.28 [s, 9 H, CH_3(Pz^{Me2})], 5.70 [s, 3 H, CH(Pz^{Me2})], 7.20 [m, 15 H, P(OPh)$_3$]. − ^{31}P NMR (C_6D_6, 25 °C): δ = 126.40 (d, 1 P, $^1J_{Rh-P}$ = 279 Hz). − IR (KBr): $\tilde{\nu}$ = 2518 [ν(BH)], 1984 cm^{-1} [ν(CO)]. − $C_{34}H_{37}BN_6O_4PRh$ (738.4): calcd. C 55.91, H 5.05, N 10.05; found C 55.30, H 5.04, N 11.38.

[Tp^{Me2,4Cl}Rh(CO)(PCy$_3$)] (9): Complex **9** was prepared by adding solid PCy$_3$ (0.16 g, 0.58 mmol) to a solution of [Tp^{Me2,4Cl}Rh(CO)$_2$] (0.30 g, 0.54 mmol) in toluene (30 mL). The mixture was stirred for

4 h. The solvent was then evaporated in vacuo and the yellow residue was washed three times with hexane at 0 °C and dried in vacuo to yield 0.39 g of **9**. − ^{1}H NMR (C_6D_6, 25 °C): δ = 1.75 (m, 33 H, PCy_3), 2.15 [s, 9 H, $CH_3(Pz^{Me2,4Cl})$], 2.30 [s, 9 H, $CH_3(Pz^{Me2,4Cl})$]. − ^{31}P NMR (C_6D_6, 25 °C): δ = 47.70 (d, $^2J_{Rh-P}$ = 152 Hz). − IR (KBr): $\tilde{\nu}$ = 2477 [ν(BH)], 1963 cm^{-1} [ν(CO)]. − UV/Vis (pentane): λ_{max} = 350 nm.

[Tp^{Me2,4Cl}Rh(CO)(PMe$_3$)] (10): Complex **10** was prepared by adding PMe_3 (0.4 mmol, 0.4 mL of a 1 M solution in toluene) to a solution of [Tp^{Me2,4Cl}Rh(CO)$_2$] (0.20 g, 0.37 mmol) in pentane (30 mL). The orange solution immediately turned yellow. The pentane was evaporated in vacuo to leave 0.20 g of **10** as a yellow solid. − ^{1}H NMR (C_6D_6, 25 °C): δ = 0.87 (d, 9 H, PMe_3, $^2J_{P-H}$ = 3 Hz), 2.09 [s, 9 H, $CH_3(Pz^{Me2,4Cl})$], 2.21 [s, 9 H, $CH_3(Pz^{Me2,4Cl})$]. − ^{31}P NMR (C_6D_6, 25 °C): δ = −9.66 (d, $^1J_{P-H}$ = 116 Hz). − IR (KBr): $\tilde{\nu}$ = 2477 [ν(BH)], 1963 cm^{-1} [ν(CO)]. − UV/Vis (pentane): λ_{max} = 350 nm.

[Tp^{Me2,4Cl}Rh(CO)(PMePh$_2$)] (12): Complex **12** was prepared by adding $PMePh_2$ (74 μL, 0.40 mmol) to a solution of [Tp^{Me2,4Cl}Rh(CO)$_2$] (0.20 g, 0.36 mmol) in pentane (30 mL) at 0 °C. A yellow solid was immediately precipitated, which was collected by filtration and dried in vacuo to afford a yellow powder. This powder was washed three times with hexane at 0 °C and dried in vacuo yielding 0.25 g of **12**. − ^{1}H NMR (C_6D_6, 25 °C): δ = 1.56 (dd, 3 H, P*Me*Ph$_2$, $^2J_{P-H}$ = 9, $^3J_{Rh-H}$ = 1 Hz), 2.09 [s, 9 H, $CH_3(Pz^{Me2,4Cl})$], 2.12 [s, 9 H, $CH_3(Pz^{Me2,4Cl})$], 7.08 (m, 10 H, PMe*Ph*$_2$). − ^{31}P NMR (C_6D_6, 25 °C): δ = 27.38 (d, 1 P, $^1J_{Rh-P}$ = 157 Hz). − IR (KBr): $\tilde{\nu}$ = 2477 [ν(BH)], 1996 cm^{-1} [ν(CO)]. − UV/Vis (pentane): λ_{max} = 352 nm.

[Tp^{Me2,4Cl}Rh(CO)(PPh$_3$)] (13): Complex **13** was prepared by adding solid PPh_3 (0.95 g, 0.36 mmol) to a solution of [Tp^{Me2,4Cl}Rh(CO)$_2$] (0.20 g, 0.36 mmol) in toluene (25 mL). The reaction was complete within 2 h. The solvent was then evaporated in vacuo yielding 0.25 g of a yellow solid. − ^{1}H NMR (C_6D_6, 25 °C): δ = 1.75 [s, 9 H, $CH_3(Pz^{Me2,4Cl})$], 2.15 [s, 9 H, $CH_3(Pz^{Me2,4Cl})$], 7.3 (m, 15 H, PPh_3). − ^{31}P NMR (C_6D_6, 25 °C): δ = 42.86 (d, 1 P, $^1J_{Rh-P}$ = 161 Hz). − ^{13}C{^{1}H} NMR (C_6D_6, 25 °C): δ = 9.86, 11.81 [s, $CH_3(Pz^{Me2,4Cl})$], 107.52 [s, $CH(Pz^{Me2,4Cl})$], 129.66 [s, $C(Pz^{Me2,4Cl})$], 127.60 (d, J_{P-C} = 10 Hz, PPh_3), 133.6 (d, J_{PC} = 12 Hz, PPh). − IR (KBr): $\tilde{\nu}$ = 2477 [ν(BH)], 1988 cm^{-1} [ν(CO)].

[Tp^{Me2,4Cl}Rh(CO){P(OMe)$_3$}] (14): Complex **14** was prepared by adding $P(OMe)_3$ (0.077 mL, 0.03 mmol) to a solution of [Tp^{Me2,4Cl}Rh(CO)$_2$] (0.15 g, 0.27 mmol) in CH_2Cl_2 (20 mL). The reaction was complete within 1 h (IR monitoring). The solvent was then evaporated to leave a yellow powder, which was washed three times with hexane at 0 °C and dried in vacuo to yield 0.16 g of **14**. − ^{1}H NMR (C_6D_6, 25 °C): δ = 1.80 [s, 9 H, $(OCH_3)_3$], 2.05 [s, 9 H, $CH_3(Pz^{Me2,4Cl})$], 2.41 [s, 9 H, $CH_3(Pz^{Me2,4Cl})$]. − ^{31}P NMR (C_6D_6, 25 °C): δ = 142.24 (d, 1 P, $^1J_{Rh-P}$ = 262 Hz). − IR (KBr): $\tilde{\nu}$ = 2536 [ν(BH)], 1998 cm^{-1} [ν(CO)].

[Tp^{Me2,4Cl}Rh(CO){P(OPh)$_3$}] (15): Complex **15** was prepared by adding $P(OPh)_3$ (0.155 g, 0.591 mmol) to a solution of [Tp^{Me2,4Cl}Rh(CO)$_2$] (0.30 g, 0.54 mmol) in CH_2Cl_2 (30 mL). The reaction mixture was stirred for 4 h. The CH_2Cl_2 was then evaporated to leave a yellow powder, which was washed three times with hexane at 0 °C and dried in vacuo yielding 0.39 g of **15**. − ^{1}H NMR (C_6D_6, 25 °C): δ = 2.06 [s, 9 H, $CH_3(Pz^{Me2,4Cl})$], 2.37 [s, 9 H, $CH_3(Pz^{Me2,4Cl})$], 7.04 [m, 15 H, $P(OPh)_3$]. − ^{31}P NMR (C_6D_6, 25 °C): δ = 123.05 (d, 1 P, $^1J_{Rh-P}$ = 279 Hz). − IR (KBr): $\tilde{\nu}$ = 2494 [ν(BH)], 2007 cm^{-1} [ν(CO)]. − UV/Vis (pentane): λ_{max} = 345 nm

[Tp^{Me2,4Cl}Rh(CO){P(O*i*Pr)$_3$}] (16): Complex **16** was prepared by adding $P(OiPr)_3$ (0.145 mL, 0.59 mmol) to a solution of [Tp^{Me2,4Cl}Rh(CO)$_2$] (0.30 g, 0.54 mmol) in CH_2Cl_2 (30 mL). The volatiles were evaporated to leave a yellow powder, which was washed three times with hexane at 0 °C and dried in vacuo yielding 0.36 g of **16**. − ^{1}H NMR (C_6D_6, 25 °C): δ = 1.10 [d, 6 H, $OCH(CH_3)_2$, $^3J_{H-H}$ = 6 Hz], 2.09 [s, 9 H, $CH_3(Pz^{Me2,4Cl})$], 2.37 [s, 9 H, $CH_3(Pz^{Me2,4Cl})$], 4.51 [m, 1 H, $OCH(CH_3)_2$]. − ^{31}P NMR (C_6D_6, 25 °C): δ = 126.53 (d, 1 P, $^1J_{Rh-P}$ = 243 Hz). − IR (KBr): $\tilde{\nu}$ = 2469 [ν(BH)], 1996 cm^{-1} [ν(CO)].

[{κ^2-HB(Pz^{Me2})$_2$(HPz^{Me2})}Rh(CO)(PMe$_2$Ph)]$^+$[BF$_4$]$^-$ (4H$^+$): Complex **4H$^+$** was prepared by adding HBF_4 (25 μL, 54% in diethyl ether) to a solution of [Tp^{Me2}Rh(CO)(PMe$_2$Ph)] (0.10 g, 0.18 mmol) in diethyl ether (10 mL) at −78 °C. The solution was stirred for 15 min at this temperature and was then allowed to slowly warm to 25 °C, whereupon a white product precipitated. This solid was collected by filtration, washed with diethyl ether, and dried in vacuo yielding 0.08 g of **4H$^+$**. − ^{1}H NMR (C_6D_6, 25 °C): δ = 1.41 [dd, 3 H, J_{P-H} = 9, J_{Rh-H} = 1.6 Hz, (P*Me*$_2$Ph)], 1.47 (dd, 3 H, J_{P-H} = 9, J_{Rh-H} = 0.5 Hz, P*Me*$_2$Ph), 1.83, 2.02, 2.38, 2.43, 2.45, 2.48 [s, 3 H, *Me*(Pz^{Me2})], 7.50 (m, 5 H, PPh). − ^{31}P NMR (C_6D_6, 25 °C): δ = 15.86 (d, J_{Rh-P} = 151 Hz). − IR (KBr): $\tilde{\nu}$ = 2502 [ν(BH)], 1987 cm^{-1} [ν(CO)].

X-ray Crystal Structure Determinations: For compound **5**, data were collected at room temperature with a STOE IPDS diffractometer equipped with a graphite-oriented monochromator using Mo-K_α radiation (λ = 0.71073 Å). The final unit cell parameters were obtained by the least-squares refinement of 5000 reflections. An Enraf-Nonius CAD4F diffractometer was used for the data collection of compound **8**. For both compounds, only statistical fluctuations were observed in the intensities of standard reflections monitored throughout the course of the data collections. The structures were solved by direct methods (SIR-97)[22] and refined by least-squares methods on *F*. All H atoms attached to carbon were introduced in calculated positions [*d*(CH) = 0.96 Å] and their atomic coordinates were recalculated after each cycle. They were given isotropic thermal parameters 20% higher than those of the carbon to which they were attached. H atoms attached to boron were located by difference Fourier syntheses and their atomic and isotropic thermal parameters were refined. The absolute configuration of **5** was determined by careful examination of the sensitive reflections and refinement of Flack's enantiopole parameter.[23] Least-squares refinements were carried out by minimizing the function $\Sigma w(|F_o| - |F_c|)$, where F_o and F_c are the observed and calculated structure factors. The weighting scheme used in the final refinement cycles was $w = w'[1 - \{\Delta F/6\sigma(F_o)\}^2]^2$; here, $w' = 1/\Sigma \cong_1^n A_r T_r(x)$ with three coefficients A_r for the Chebyshev polynomial $A_r T_r(x)$, where $x = F_c/F_c(\max)$.[24] Models reached convergence with $R = \Sigma(||F_o| - |F_c||)/\Sigma(|F_o|)$ and $R_w = [\Sigma w(|F_o| - |F_c|)^2/\Sigma w(F_o)^2]^{1/2}$, giving the values listed in Table 4. The calculations were carried out with the CRYSTALS program package[25] run on a PC. Graphical representations were generated using ORTEP.[26] Crystallographic data (excluding structure factors) for the structures reported in this paper have been deposited with the Cambridge Crystallographic Data Centre as supplementary publication nos. CCDC-149636 (**5**) and -149637 (**8**). Copies of the data can be obtained free of charge on application to the CCDC, 12 Union Road, Cambridge CB2 1EZ, U.K. [Fax: (internat.) + 44-1223/336-033; E-mail: deposit@ccdc.cam.ac.uk].

Table 4. Crystal data

	5	**8**
empirical formula	$C_{29}H_{35}BN_6OPRhCH_2Cl_2$	$C_{34}H_{37}BN_6O_4PRh$
formula mass	713.26	738.40
crystal system	orthorhombic	triclinic
space group	$P2_1ca$	$P\bar{1}$
a, Å	14.222(3)	10.673(1)
b, Å	14.673(2)	12.239(2)
c, Å	15.991(7)	13.805(2)
α, °	90.0	87.43(1)
β, °	90.0	87.44(1)
γ, °	90.0	77.57(1)
V, Å^3	3337(2)	1758.1(4)
Z	4	2
ρ (calcd.) g·cm^{-3}	1.420	1.395
2θ range, °	$3 < 2\theta < 50$	$2.9 < 2\theta < 48.4$
no. of reflns. collected	6134	13956
no. of unique reflns. (R_{int})	5868 (0.020)	5189 (0.038)
reflections used	4659 [$I > 2\sigma(I)$]	4152 [$I > 2\sigma(I)$]
R, R_w	0.0271, 0.0319	0.0355, 0.0423
GoF	1.043	1.064
Flack's parameter	0.01(2)	
Variable parameters	385	429

Acknowledgments

We thank the group Electrochimie de la Direction des Etudes et Recherches of Electricité de France for financial support of part of this study and for a fellowship to V. C. We gratefully acknowledge Engelhardt-Comptoir-Lyon-Alemand-Louyot for a loan of rhodium. G. Commenges, F. Lacassin, and Y. Coppel are thanked for carrying out NMR experiments with the 400-MHz NMR spectrometer.

[1] S. Trofimenko, *J. Am. Chem. Soc.* **1966**, *88*, 1842.
[2] S. Trofimenko, *Chem. Rev.* **1993**, *93*, 943.
[3] C. Gemel, R. John, C. Slugovc, K. Mereiter, R. Schmid, K. Kirchner, *J. Chem. Soc., Dalton Trans.* **2000**, *15*, 2607.
[4] F. Malbosc, Ph. Kalck, J.-C. Daran, M. Etienne, *J. Chem. Soc., Dalton Trans.* **1999**, 271.
[5] M. Paneque, S. Sirol, M. Trujillo, E. Gutiérnez-Publa, M. Angeles Monge, E. Carmona, *Angew. Chem. Int. Ed.* **2000**, *39*, 218.
[6] U. E. Bucher, A. Currao, R. Nesper, H. Rügger, L. M. Venanzi, E. Younger, *Inorg. Chem.* **1995**, *34*, 66.
[7] M. Akita, K. Ohta, Y. Takahashi, S. Hikichi, Y. Moro-oka, *Organometallics* **1997**, *16*, 4121.
[8] C. K. Ghosh, W. A. G. Graham, *J. Am. Chem. Soc.* **1987**, *109*, 4726.
[9] A. A. Purwoko, A. J. Lees, *Inorg. Chem.* **1996**, *35*, 675.
[10] S. E. Bronsberg, H. Yang, M. C. Asplund, T. Lian, B. K. McNamara, K. T. Kotz, J. S. Yeston, M. Wilkens, H. Frei, R. G. Bergman, C. B. Harris, *Science* **1997**, *278*, 260.
[11] V. Chauby, C. Serra-Le Berre, Ph. Kalck, J.-C. Daran, G. Commenges, *Inorg. Chem.* **1996**, *35*, 6354.
[12] N. G. Connelly, D. J. H. Emslie, B. Metz, A. G. Orpen, M. J. Quayle, *Chem. Commun.* **1996**, 2289.
[13] C. K. Ghosh, Ph.D. Dissertation, University of Alberta, Canada, **1988**. In the absence of an X-ray crystal structure of **4** and of an analysis of the ν_{BH} bands, Ghosh proposed that the exchange phenomenon occurs between two isomeric trigonal bipyramids having a plane of symmetry.
[14] T. T. Derencsényi, *Inorg. Chem.* **1981**, *20*, 665.
[15] R. G. Bull, C. K. Ghosh, J. K. Hoyano, A. D. MacMaster, W. A. G. Graham, *Chem. Commun.* **1989**, 341.
[16] W. D. Jones, *Activation of Unreactive Bonds and Organic Synthesis*, Springer, Berlin, **1999**, vol. 3, p. 9−46.
[17] E. Gutiévrez, S. A. Hudson, A. Monge, E. Carmona, *J. Chem. Soc., Dalton. Trans.* **1992**, 2651.
[18] D. D. Perrin, W. L. F. Armarego, D. R. Perrin, *Purification of Laboratory Chemicals*, Pergamon Press, Oxford, **1980**.
[19] K. v. Auvers, K. Bäht, *J. Prakt. Chem.* **1927**, *116*, 65.
[20] F. J. Lalor, T. J. Desmond, G. M. Cotter, C. A. Shanahan, G. Ferguson, M. Pervez, B. Ruhl, *J. Chem. Soc., Dalton. Trans.* **1995**, 1709.
[21] S. Trofimenko, *J. Am. Chem. Soc.* **1967**, *89*, 3170.
[22] A. Altomare, M. C. Burla, M. Camalli, G. L. Cascarano, C. Giacovazzo, A. Guagliardi, A. G. G. Moliterni, G. Polidori, R. Spagni, *J. Appl. Crystallogr.* **1999**, *32*, 115−119.
[23] [23a] H. D. Flack, *Acta Crystallogr., Sect. A* **1983**, *39*, 876−881. − [23b] G. Bernardinelli, H. D. Flack, *Acta Crystallogr., Sect. A* **1985**, *41*, 500−511.
[24] E. Prince, *Mathematical Techniques in Crystallography*, Springer-Verlag, Berlin, **1982**.
[25] D. J. Watkin, C. K. Prout, J. R. Carruthers, P. W. Betteridge, *CRYSTALS Issue 11*, Chemical Crystallography Laboratory, University of Oxford, Oxford, **1999**.
[26] M. N. Burnett, C. K. Johnson, *ORTEP III, Report ORNL-6895*, Oak Ridge National Laboratory, Oak Ridge, Tennessee, **1996**.

Received December 11, 2000
[I00468]

Improved Preparations of Molybdenum Coordination Compounds from Tetrachlorobis(diethyl ether)molybdenum(IV)

François Stoffelbach,[a] Dirk Saurenz,[a] and Rinaldo Poli*[a]

Keywords: Reduction / Molybdenum / Halides / Synthetic methods

The reduction of $MoCl_5$ with metallic tin in diethyl ether provides a rapid and convenient entry to $[MoCl_4(OEt_2)_2]$ This compound can be transformed easily and in high yields into a variety of other useful synthons. The loss of ether in the solid state affords a new and reactive form of $MoCl_4$. Treatment with THF, PMe_3 or Li*O*t*Bu affords $[MoCl_4(THF)_2]$, $[MoCl_4(PMe_3)_3]$ or $[Mo(O\,t\,Bu)_4]$ in high isolated yields. Treatment with metallic tin in THF affords $[MoCl_3(THF)_3]$ All of these reactions can be carried out under simple experimental conditions and represent significant improvements relative to previously reported syntheses of the same compounds.

Introduction

The element molybdenum displays a very rich chemistry in low, intermediate and high oxidation states. Research with this metal is intense in the organometallic/catalysis, coordination, bioinorganic, cluster, and solid state/materials fields. However, all this activity stems from a very limited amount of commercially available Mo-containing starting materials, the most convenient ones being elemental Mo, $Mo(CO)_6$, MoS_2, MoO_3 and $MoCl_5$. Some transformations require long, multiple-step procedures, resulting in a considerable investment of time and, perhaps more importantly, in considerable product losses due to the compounding of imperfect reaction yields. The improvement of known synthetic methods and the search for alternative procedures allowing a reduction of reaction times, the simplification of isolation and purification procedures, and an increase of overall yields are continuous goals of the synthetic chemist.

The situation is perhaps best illustrated by the example of $[MoCl_3(THF)_3]$, a useful intermediate for a wide variety of inorganic synthetic applications. Following the first reported preparation by a carbonyl route,[1] the compound was subsequently obtained by a reductive procedure starting from $MoCl_5$. This pentachloride compound is a strong Lewis acid and also a powerful oxidant and its direct reduction in THF is complicated by the acid-catalysed ring opening polymerization of THF, a problem which is circumvented by using other solvents. The most commonly employed synthetic procedure (Scheme 1) starts with the interaction of $MoCl_5$ with a nitrile RCN to afford $[MoCl_4(RCN)_2]$, followed by replacement of the nitrile with THF and final reduction to the Mo^{III} product. A variety of improvements of this procedure have been published over the years including three reports in Inorganic Synthesis, replacing propionitrile with acetonitrile, zinc with tin as the reducing agent, and modifying the reaction conditions and product separation procedures.[2–7] Nevertheless, this three-step procedure remains rather long and requires, in our hands, isolation of both $[MoCl_4(MeCN)_2]$ and $[MoCl_4(THF)_2]$ intermediates in order to obtain a product of sufficient quality. With individual step yields of 63–86%, the overall yield from $MoCl_5$ is 46% at best with a time investment of more than two days. Another variation on the same theme (Scheme 1) is the reduction of $[MoCl_4(MeCN)_2]$ to $[MoCl_3(MeCN)_3]$, followed by solvent exchange.[8] A direct and rapid one-step, high-yield (85%) procedure has been published more recently, but this requires the use of Ph_2SiH_2 as a reducing agent and a controlled, slow addition of the $MoCl_5$ solid to the silane-containing THF solution.[9] A reverse addition of the silane to $MoCl_5$ is possible only in pentane as solvent, prolonging the reaction time to 48 h.

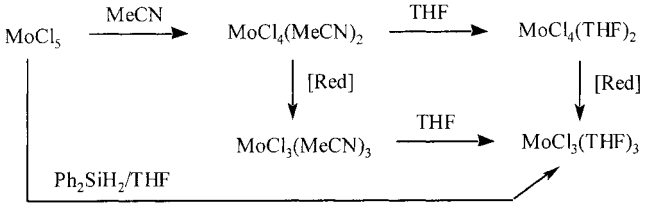

Scheme 1

Our continued interest in the coordination and organometallic chemistry of middle-valent molybdenum continuously pushes us to improve the preparative procedures of our required synthetic intermediates. Our attention has been attracted by $[MoCl_4(OEt_2)_2]$, whose high yield synthesis was reported a few years ago from $MoCl_5$ and either norbornene[10] or allyltrimethylsilane[11] as reducing agents. However, only a limited use of this compound in sub-

[a] Laboratoire de Synthèse et d'Electrosynthèse Organométalliques, Faculté des Sciences "Gabriel", Université de Bourgogne,
6 Boulevard Gabriel, 21000 Dijon, France
Fax: (internat.) + 33-03/8039-3720
E-mail: Rinaldo.Poli@u-bourgogne.fr

 © WILEY-VCH Verlag GmbH, 69451 Weinheim, 2001 1434–1948/01/1010–2699 $ 17.50+.50/0

sequent synthetic work was described. In this contribution, we shall show that $[MoCl_4(OEt_2)_2]$ can also be conveniently prepared by tin reduction of $MoCl_5$, and that it is a versatile intermediate for the preparation of a variety of other molybdenum compounds. In particular, $[MoCl_3(THF)_3]$ is now accessible in a half-day, two-step, single-flask procedure (no isolation of intermediates is required) in greater than 80% overall yields from $MoCl_5$ and the common reagents ether, THF, and metallic tin.

Results and Discussion

While the high Lewis acidity of $MoCl_5$ makes this compound incompatible with the THF solvent, causing its cationic ring-opening polymerization, non-cyclic ethers do not suffer from this decomposition pathway. Ethereal solutions of $MoCl_5$ are stable and are rapidly reduced by metallic tin to yield a fine, orange, crystalline powder of $[MoCl_4(OEt_2)_2]$ [Equation (1)]. The reaction is fast but controlled at room temperature, and is usually complete within 0.5 h as evident from the visual appearance of the powdery orange precipitate. No wild exothermic behavior has been observed during this reductive process, which therefore does not require any special precautions. In addition, the tin chloride co-product is ether-soluble while $[MoCl_4(OEt_2)_2]$ is only sparingly soluble. Therefore, the Mo^{IV} product is easily purified by washing with ether with only minimal product loss. The yields of this preparation are consistently greater than 80% for quantities of product greater than a gram. These yields and the product purity are comparable with those of the previously reported syntheses, which used more exotic reducing agents such as allyltrimethylsilane or norbornene.[10,11] It should be noted that a possible by-product, $[MoOCl_3(Et_2O)_2]$,[12] may form when wet ether and/or partially hydrolyzed $MoCl_5$ starting compound are employed. This compound, however, is green and soluble in ether,[10] while the $[MoCl_4(Et_2O)_2]$ product is orange and sparingly soluble. Thus, minor impurities of the molybdenyl species may be easily eliminated. In our work, we found no evidence for the formation of this by-product.

$$2\ MoCl_5 + Sn \xrightarrow{Et_2O} 2\ MoCl_4(OEt_2)_2 + SnCl_2 \quad (1)$$

We have not investigated in detail the nature of the oxidized tin product. The literature reports that $SnCl_2$ is capable of reducing $[MoCl_4(THF)_2]$ in THF to afford $[MoCl_3(THF)_3]$ and $[SnCl_4(THF)_2]$.[9] Metallic tin is equally capable of carrying out the same reduction and to even over-reduce the metal below the +3 level. In ether, however, any further reduction by Sn (which may be used in excess) must be extremely slow since we found no NMR evidence for the formation of Mo^{III}, after isolation of the solid material and exchange with THF (vide infra). On the basis of this observation, we assume that $SnCl_2$ is probably also a poorer reductant in ether than in THF. Thus, the tin/ether combination seems ideal, giving rise to a rapid, controlled and selective reduction.

Although $[MoCl_4(OEt_2)_2]$ is only sparingly soluble in ether, it is readily soluble in aromatic hydrocarbons. In this respect, it resembles its sulfur congener $[MoCl_4(SEt_2)_2]$.[13] Besides elemental analysis and IR, no additional characterization was shown in the previous reports. The magnetic moment ($\mu_{eff} = 2.33\ \mu_B$) is significantly lower than the spin-only value for two unpaired electrons because of the expected spin-orbit coupling for the triplet ground state derived from the pseudo-t_{2g}^2 configuration. This value is in the range observed for other $[MoCl_4L_2]$ complexes (L = THF, MeCN, PPh_3, etc.), namely 2.2−2.5 μ_B.[14] The ^1H NMR spectrum in C_6D_6 shows only one resonance for the methyl and one for the methylene protons. These resonances are broad as may be expected for a paramagnetic complex. However, they are not significantly contact-shifted from the position of free ether (cf. the highly shifted resonances of the bis-THF adduct, vide infra, or those of the sulfur congener $[MoCl_4(SEt_2)_2]$[13]). We attribute this behavior to the rapid dissociation equilibrium of Equation (2), as proposed previously.[10] Thus, the broad lines would be the time-averaged signals of the methylene and methyl protons of the diamagnetic free ether and the paramagnetic complexes, at the fast exchange limit. In comparison with the related bis-SEt_2 complex, the NMR spectrum shows that diethyl ether is a much more labile ligand than the sulfur congener, as might be expected.

$$MoCl_4(OEt_2)_2 \rightleftharpoons MoCl_4(OEt_2) + Et_2O \quad (2)$$

The only available crystal structure for a $[Mo^{IV}X_4L_2]$ complex with monodentate ligands appears to be that of $[MoCl_4(SEt_2)_2]$ which is trans.[13] $[MoCl_4(CH_3OCH_2CH_2OCH_3)]$ has a cis arrangement enforced by the chelating dimethoxyethane ligand.[15] For this reason, it is likely that $[MoCl_4(OEt_2)_2]$ also adopts a trans configuration. Most related Mo^{III} anions $[Mo^{III}X_4L_2]^-$ also adopt a trans arrangement,[16−18] although examples having a cis configuration are also known.[19,20] In spite of numerous attempts under a variety of conditions, we have not been able to grow single crystals of this compound.

The synthetic utility of $[MoCl_4(OEt_2)_2]$ has been investigated in some detail and the results are summarized in Scheme 2. Because of the facile ether loss shown by the NMR study above, it is best to use a freshly prepared sample for the purpose of further synthetic applications. Heating the isolated $[MoCl_4(OEt_2)_2]$ solid under vacuum leads to the complete loss of the ether ligands at a relatively low temperature, leaving amorphous (by X-ray powder diffraction) $MoCl_4$. Darkening of the solid already occurs at about 55 °C, while at 80 °C the powder is totally black. Samples of ether-free $MoCl_4$ have been obtained by operating at temperatures up to 130 °C. This procedure is considerably more practical and time efficient than the literature preparations (see below) and leads to a more chemically reactive material.

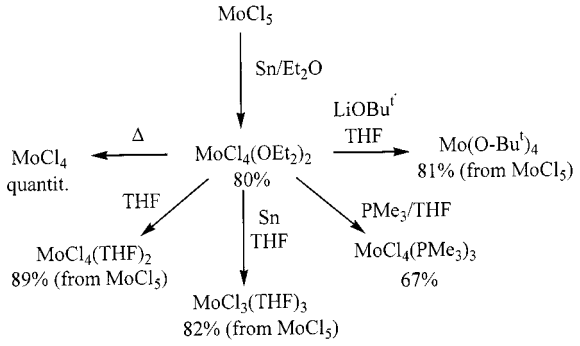

Scheme 2

Three different crystalline forms of $MoCl_4$ have been described in the literature, namely α-$MoCl_4$,[21] β-$MoCl_4$,[22,23] and γ-$MoCl_4$.[24] The α form was obtained from $MoCl_5$ by reflux with tetrachloroethylene in carbon tetrachloride; a reflux time shorter than two days is said to leave unchanged pentachloride.[21] The β form was obtained by comproportionation of $MoCl_5$ and $MoCl_3$ in a temperature gradient,[22] while the γ form was prepared by heating a mixture of MoO_2 and carbon with a nitrogen stream saturated with CCl_4 vapors.[24] The observed magnetic moment of 1.6 μ_B for our amorphous $MoCl_4$ does not compare with any of those reported for the three crystalline phases (i.e. 0.85 μ_B for α-$MoCl_4$,[21] 2.31−2.54 μ_B for β-$MoCl_4$,[22] and 1.91 μ_B for γ-$MoCl_4$ [24]), although it is closest to that of the γ phase. An additional and significant difference is observed in the temperature behavior. A disproportionation process occurs at temperatures above 140 °C to generate $MoCl_5$ and $MoCl_3$. This process is also observed for the β phase, but only at about 288 °C.[24] On the other hand, the γ phase was shown to transform at ca. 140 °C into the α phase, which in turn converts into the β phase at ca. 240 °C. Our evidence for the disproportionation of amorphous $MoCl_4$ at 140 °C is clear: volatile $MoCl_5$ sublimes and the solid residue transforms into a reddish material which is no longer soluble in ethanol, indicating the formation of lower chlorides. Furthermore, the signals of $MoCl_3$ in this material have been detected by powder X-ray diffraction. On the basis of this evidence, it seems obvious that amorphous $MoCl_4$ is a labile and reactive form, leading directly to the thermodynamic mixture of Mo^{III} and Mo^{V} chlorides at relatively low temperature, while the crystalline α, β and γ phases are more inert.

The lability of amorphous $MoCl_4$ is further shown by its high chemical reactivity. Addition of THF leads to the rapid and exothermic formation of $[MoCl_4(THF)_2]$, and treatment of the resulting mixture with other reagents (for instance, Li*O*t*Bu*) affords the expected Mo^{IV} products in excellent yields (vide infra). The conversion of $MoCl_4$ to the bis-THF adduct is quantitative and is best accomplished by addition of THF to a pentane suspension of the tetrachloride, in order to evacuate the reaction heat.

$[MoCl_4(THF)_2]$, however, is more conveniently obtained by direct substitution of the ether in $[MoCl_4(OEt_2)_2]$, which may be obtained in situ from $MoCl_5$ (overall 89% isolated yields). This route appears to give a cleaner $[MoCl_4(THF)_2]$ product relative to the previously described synthesis from $[MoCl_4(MeCN)_2]$. It is possible that the ligand-exchange equilibrium is further shifted toward the bis-THF product when the less coordinating Et_2O ligand is bonded to the metal center. As for the bis-Et_2O analogue, no NMR spectroscopic data seem to be available in the literature for $[MoCl_4(THF)_2]$. The NMR spectrum in $CDCl_3$ shows highly shifted (12.5 and −32.8 ppm) but relatively sharp ($w_{1/2}$ = 12 and 15 Hz, respectively) resonances, indicating the presence of a single isomer in solution. These chemical shifts compare relatively well with those of the bis-thioether complex $[MoCl_4(SEt_2)_2]$.[13] As for the bis-Et_2O analogue, we were unable to grow single crystals of this compound. Substitution of the ether in $[MoCl_4(OEt_2)_2]$ with PMe_3 leads to the previously reported compound $[MoCl_4(PMe_3)_3]$.[25]

Besides substitution reactions of the ether ligand, the chlorides can also be easily replaced. This metathesis process provides a convenient entry to the tetrakis(*tert*-butoxy) derivative $[Mo(O\mathit{t}Bu)_4]$. The previous synthesis of this compound involves metathesis from $[Mo(NMe_2)_4]$,[26] a compound that is available only in low yields from $MoCl_5$.[27] After its first report, this compound does not appear to have been used for further investigations, possibly because of the laborious and low-yield synthetic procedure. It is now available, however, in a practical half-day procedure in greater than 80% yields from $MoCl_5$. As such, it may constitute a new useful synthon for Mo^{IV} chemistry. Previous physical characterization of $[Mo(O\mathit{t}Bu)_4]$ comprised IR, UV/Visible and mass spectra, and magnetic susceptibility. The compound was reported as having an intermediate magnetic moment between those expected for a magnetically diluted compound with two unpaired electrons and a diamagnetic compound (μ_{eff} = 1.38 μ_B in toluene or 1.37−1.40 μ_B in the solid state).[26] In our hands, the compound is diamagnetic by solid-state magnetic susceptibility and by NMR and EPR spectroscopy. In this respect, it appears perfectly homologous to the corresponding thiolato derivative $[Mo(S\mathit{t}Bu)_4]$.[28] Other MoX_4 compounds with π-donor X ligands, namely $[Mo(NMe_2)_4]$,[29] $[Mo(2\text{-}MeC_6H_4)_4]$,[30] and other mixed amido-phosphido derivatives[31] are mononuclear and diamagnetic, while compounds with π-neutral X ligands such as $[Mo(2\text{-}MeC_6H_4)_4]$[32] and $[Mo(norbornyl)_4]$[33] are paramagnetic with two unpaired electrons.

When $[MoCl_4(OEt_2)_2]$ was exposed to THF in the presence of metallic tin, a smooth reduction to $[MoCl_3(THF)_3]$ occurred. This is not surprising as the transformation of $[MoCl_4(OEt_2)_2]$ to $[MoCl_4(THF)_2]$ in a THF slurry has been established above, and the reduction of the latter to $[MoCl_3(THF)_3]$ by tin in THF is a well-established process. However, we found that this reaction gives excellent results without the need to isolate either the $[MoCl_4(OEt_2)_2]$ product after the first reductive step or the second $[MoCl_4(THF)_2]$ intermediate. Thus, it suffices to use enough tin reagent to reduce Mo^{V} to Mo^{III} and to replace

the solvent after completion of the first reduction step, in order to achieve a convenient high-yield synthesis of $[MoCl_3(THF)_3]$, in half a day, from $MoCl_5$.

Conclusion

In conclusion, we have developed a new, simple and time-efficient preparation of $[MoCl_4(OEt_2)_2]$, and demonstrated its synthetic utility with the improved preparation of a few key materials such as $[MoCl_4(THF)_2]$, $[MoCl_3(THF)_3]$, $[Mo(O\mathit{t}Bu)_4]$, and a new and reactive form of $MoCl_4$.

Experimental Section

General: All manipulations were carried out under an atmosphere of dry and oxygen-free argon with standard Schlenk techniques. Solvents were dried and deoxygenated by refluxing over suitable reagents (THF and ether over sodium benzophenone ketyl, toluene over sodium) and distilled under argon before use. ^1H NMR measurements were carried out on a Bruker AC 200 spectrometer. The peak positions are reported with positive shifts in ppm downfield of TMS as calculated from residual solvent peaks. The magnetic susceptibility measurements were carried out with a Johnson−Matthey magnetic balance, which operates by a modified Gouy method. The molar susceptibilities for the calculation of the magnetic moments were corrected for the diamagnetism of the ligands by using Pascal's constants. Elemental analyses were performed with a Fisons EA 1108 apparatus. $MoCl_5$, PMe_3 (1 M in THF) and Sn (fine grains, 20 mesh) were purchased from Aldrich Chemical Co. and used as received.

Synthesis of $[MoCl_4(Et_2O)_2]$: $MoCl_5$ (1.20 g, 4.39 mmol) and coarse tin powder (1.04 g, 8.76 mmol) were suspended in 30 mL of Et_2O at room temperature. The mixture was then stirred for 30 min. to form an orange solution and orange solid. The latter was separated mechanically from the excess tin taking advantage of the large difference in density between the two solids. Under gentle stirring with a magnetic stirring bar, the metallic tin remained at the bottom of the flask and the supernatant suspension of the $[MoCl_4(Et_2O)_2]$ product was transferred into a new flask through a medium size (G15) cannula. The product was then collected by filtration, washed with Et_2O (5 × 5 mL) and dried under vacuum. Yield: 1.36 g, 80%. The compound has a marked tendency to lose diethyl ether (see Results and Discussion) and samples dried without special precautions systematically gave low C,H analyses; a freshly prepared sample which was dried at −20 °C gave a correct analysis ($C_8H_{20}Cl_4MoO_2$: calcd. C 24.89, H 5.22; found C 25.31, H 5.23). The IR spectrum (Nujol mull) is identical with that reported in the literature.[11] ^1H NMR (C_6D_6, 25 °C): δ = 1.1 (broad, $w_{1/2}$ = 23 Hz, CH_3) ca. 3.5 ppm (broad, $w_{1/2}$ = 200 Hz, CH_2). μ_{eff} = 2.33 μ_B (diamagnetic correction: $\chi = -196.22 \cdot 10^{-6}$ c.g.s. units).

Synthesis of $MoCl_4$: In a typical reaction, orange $[MoCl_4(Et_2O)_2]$ was placed in a dry, air-free Schlenk tube and slowly heated under vacuum in an oil bath. First darkening occurred at about 55 °C. At 80 °C the powder was totally black. The yield of $MoCl_4$ produced is quantitative. Two experiments, carried out at 120° for 5 h and at 130° for 2 h gave materials with the same properties. Elemental analysis of the black material confirmed the absence of C and H. μ_{eff} = 1.60 μ_B and 1.61 μ_B, respectively (diamagnetic correction: $\chi = -80.4 \cdot 10^{-6}$ c.g.s. units). The product dissolves completely in ethanol. When the reaction temperature is raised above 140 °C, sublimation of $MoCl_5$ is observed and the resulting reddish solid residue ($MoCl_3$) is no longer soluble in ethanol. This decomposition process is also observed for isolated $MoCl_4$ in vacuum and under an argon atmosphere in a sealed ampoule.

Synthesis of $[MoCl_4(THF)_2]$. (a) From Isolated $[MoCl_4(Et_2O)_2]$: Compound $[MoCl_4(Et_2O)_2]$ (1.26 g, ca. 3.26 mmol) was suspended in 15 mL of THF. The mixture was then stirred for 3 h at room temperature to form an orange-yellow solid. The supernatant liquid was decanted off and the solid was washed with THF (10 mL), then ether (10 mL), and finally dried under vacuum. Yield: 0.99 g (79%). − $C_8H_{16}Cl_4MoO_2$ (381.96): calcd. C 25.16, H 4.22; found C 24.99, H 4.76. − ^1H NMR ($CDCl_3$, 25 °C): δ = 12.5 ($w_{1/2}$ = 12 Hz), −32.8 ($w_{1/2}$ = 15 Hz) (intensity ratio: 1.1).

(b) From $MoCl_5$: $MoCl_5$ (1.156 g, 4.23 mmol) and coarse tin powder (1 g, 8.42 mmol) were suspended in 20 mL of Et_2O at room temperature. The mixture was stirred for 30 min. to form $[MoCl_4(Et_2O)_2]$. Then, the excess metallic tin was eliminated by transferring the supernatant suspension of $[MoCl_4(Et_2O)_2]$ into a new flask through a medium-sized cannula. The solid was washed with Et_2O (3 × 10 mL) and 20 mL of THF was subsequently added. The mixture was then stirred for 3 h at room temperature to form an orange-yellow solid. The supernatant liquid was then decanted off and the residue was washed with 10 mL of THF and then with 10 mL of ether, and finally dried under vacuum. Yield: 1.438 g, 89%. The color and ^1H NMR spectrum of this material are identical with the analyzed product obtained as described in the previous section.

(c) From $MoCl_4$: Black $MoCl_4$ (553 mg, 2.33 mmol) was suspended in 5 mL of pentane. After addition of 5 mL THF on top of the pentane layer the mixture was allowed to stir for two minutes. The reaction occurred very rapidly to produce an orange precipitate. The colorless supernatant liquid was removed by cannula and the residue was dried in vacuo leaving 890 mg of $[MoCl_4(THF)_2]$ (quantitative yield).

Synthesis of $[MoCl_3(THF)_3]$: $MoCl_5$ (3.18 g, 11.64 mmol) and coarse tin powder (2.77 g, 23.33 mmol) were suspended in 30 mL of Et_2O. The mixture was then stirred for 30 min. at room temperature to form an orange solution and orange solid. The supernatant liquid was decanted off and 30 mL of THF was added. The mixture was then stirred for 3 h at room temperature. The pale orange-brown crystalline product $[MoCl_3(THF)_3]$ was separated from excess tin as described above for the synthesis of $[MoCl_4(Et_2O)_2]$. The product was then washed with Et_2O (2 × 15 mL) and dried under vacuum. Yield: 3.99 g, 82%. − $C_{12}H_{24}Cl_3MoO_3$ (418.62): calcd. C 34.43, H 5.78; found C 34.04, H 5.51. The ^1H NMR properties of this material correspond with those previously described for $[MoCl_3(THF)_3]$.[34]

Synthesis of $[MoCl_4(PMe_3)_3]$: A THF solution of PMe_3 (1 M, 8 mL, 8 mmol) was slowly added to a magnetically stirred suspension of $[MoCl_4(Et_2O)_2]$ (0.96 g, ca. 2.5 mmol) in THF (10 mL). The orange suspension rapidly transformed into a deep violet suspension. The mixture was stirred for 4 h at room temperature, then the supernatant liquid was decanted off and the solid was washed with THF (2 × 5 mL) and dried under vacuum. Yield: 0.78 g, 67%. − $C_9H_{27}Cl_4MoP_3$ (465.99): calcd. C 23.20, H 5.84; found C 23.04, H 5.62. The ^1H NMR spectrum [broad band at δ = −17 ($w_{1/2}$ = 130 Hz) in $CDCl_3$ at 25 °C] corresponds to that reported in the literature.[25]

Synthesis of $[Mo(O\mathit{t}Bu)_4]$. (a) From $MoCl_4$: THF (15 mL) was added to 330 mg (1.39 mmol) of black $MoCl_4$ causing a slight warm-

ing and precipitation of the orange THF adduct. The suspension was cooled in an ice bath and a 1 M LiO*t*Bu solution in THF/hexane (5.55 mL, 5.55 mmol) was added with a syringe. The reaction mixture was stirred for one hour at 0 °C, then slowly warmed to room temperature and stirred overnight to complete the reaction. The THF was removed in vacuo from the dark brown solution. The brown solid was extracted with 20 mL of pentane, then with 10 mL of CH_2Cl_2. After filtration, the combined extracts were evaporated in vacuo to dryness, leaving crude $[Mo(OtBu)_4]$ as a brown solid (540 mg, quantitative yield). The product can be recrystallized in low yields (ca. 25%) from cold pentane. – $C_{16}H_{36}MoO_4$ (388.40): calcd. C 49.48, H 9.34; found C 49.58, H 9.29. – ^{1}H NMR: δ =1.55 (s) in C_6D_6, 1.66 (s) in $C_6D_5CD_3$ and 1.12 (s) in $[D_6]$acetone. All these solutions are EPR-silent, but a strong signal rapidly develops upon exposure to air. $\mu_{eff} = 0.72\ \mu_B$ (diamagnetic correction: $\chi = -219.92 \cdot 10^{-6}$ c.g.s. units).

(b) From $[MoCl_4(Et_2O)_2]$: $[MoCl_4(Et_2O)_2]$ was obtained in situ from $MoCl_5$ (3.06 g, 11.2 mmol) and tin as described above. After separation from the excess tin and the ether, it was suspended in 40 mL of THF and the suspension was cooled in an ice bath. After addition of LiO*t*Bu (40 mL of a 1 M solution in THF/hexane, 40 mmol) the reaction mixture was stirred at 0 °C for 2 h, then slowly warmed to room temperature and stirred overnight to complete the reaction. Removal of the solvent in vacuo left a brown residue which was extracted with 35 mL of CH_2Cl_2 and filtered. After total removal of the solvent in vacuo, a gummy brown-black residue was left which became an almost black powdery solid over a period of two days. The yield of crude $[Mo(OtBu)_4]$ was 3.517 g (81% from $MoCl_5$).

Acknowledgments

We are grateful to the CNRS for funding and for a student fellowship (BDI) to FS. DS thanks the Conseil Régional de Bourgogne for a postdoctoral fellowship.

[1] A. D. Westland, N. Muriithi, *Inorg. Chem.* **1972**, *11*, 2971–2975.
[2] M. W. Anker, J. Chatt, G. J. Leigh, A. G. Wedd, *J. Chem. Soc., Dalton Trans.* **1975**, 2639–2645.
[3] J. R. Dilworth, R. L. Richards, *Inorg. Synth.* **1980**, *20*, 119–127.
[4] J. R. Dilworth, J. A. Zubieta, *J. Chem. Soc., Dalton Trans.* **1983**, 397–398.
[5] J. R. Dilworth, J. Zubieta, *Inorg. Synth.* **1986**, *24*, 193.
[6] J. R. Dilworth, R. L. Richards, *Inorg. Synth.* **1990**, *28*, 33–37.
[7] R. Poli, J. C. Gordon, *Inorg. Chem.* **1991**, *30*, 4550–4554.
[8] S.-Y. Roh, J. W. Bruno, *Inorg. Chem.* **1986**, *25*, 3105–3106.
[9] D. Zeng, M. J. Hampden-Smith, *Polyhedron* **1992**, *20*, 2585–2589.
[10] L. Castellani, M. C. Gallazzi, *Trans. Met. Chem.* **1985**, *10*, 194–195.
[11] C. Persson, C. Andersson, *Inorg. Chim. Acta* **1993**, *203*, 235–238.
[12] W. Wardlaw, H. W. Webb, *J. Chem. Soc.* **1930**, 2100–2106.
[13] P. Dierkes, G. Frenzen, S. Wocadlo, W. Massa, S. Berger, J. Pebler, K. Dehnicke, *Z. Naturforsch.* **1995**, *50b*, 159–167.
[14] B. N. Figgis, J. Lewis, *Prog. Inorg. Chem.* **1964**, *6*, 37–239.
[15] E. Hey-Hawkins, H. G. Von Schnering, *Z. Naturforsch., Teil B* **1991**, *46*, 307–314.
[16] A. Hills, G. J. Leigh, J. Hutchinson, J. A. Zubieta, *J. Chem. Soc., Dalton Trans.* **1985**, 1069–1071.
[17] J. V. Brencic, B. Ceh, I. Leban, *Z. Anorg. Allg. Chem.* **1986**, *538*, 212–220.
[18] F. A. Cotton, K. Vidyasagar, *Polyhedron* **1995**, *14*, 3077–3085.
[19] J. V. Brencic, I. Leban, B. Modec, *Z. Anorg. Allg. Chem.* **1994**, *620*, 950–954.
[20] J. V. Brencic, I. Leban, B. Modec, *Polyhedron* **1994**, *13*, 3171–3176.
[21] D. L. Kepert, R. Mandyczewsky, *Inorg. Chem.* **1968**, *7*, 2091–2093.
[22] H. Schäfer, H.-G. v. Schnering, J. Tillack, F. Kuhnen, H. Wöhrle, H. Baumann, *Z. Anorg. Allg. Chem.* **1967**, *353*, 281–310.
[23] U. Müller, *Angew. Chem. Int. Ed. Engl.* **1981**, *20*, 692–693.
[24] A. D. Westland, V. Uzelac, *Inorg. Chim. Acta* **1977**, *23*, L37–L39.
[25] R. D. Rogers, E. Carmona, A. Galindo, J. L. Atwood, L. G. Canada, *J. Organomet. Chem.* **1984**, *277*, 403–415.
[26] M. H. Chisholm, W. W. Reichert, P. Thornton, *J. Am. Chem. Soc.* **1978**, *100*, 2744–2748.
[27] D. C. Bradley, M. H. Chisholm, *J. Chem. Soc. (A)* **1971**, 2741–2744.
[28] S. Otsuka, M. Kamata, K. Hirotsu, T. Higuchi, *J. Am. Chem. Soc.* **1981**, *103*, 3011–3014.
[29] M. H. Chisholm, F. A. Cotton, M. W. Extine, *Inorg. Chem.* **1978**, *17*, 1329–1332.
[30] R. T. Baker, P. J. Krusic, T. H. Tulip, J. C. Calabrese, S. S. Wreford, *J. Am. Chem. Soc.* **1983**, *105*, 6763–6765.
[31] M. H. Chisholm, C. E. Hammond, J. C. Huffman, *Polyhedron* **1989**, *8*, 1419–1423.
[32] J. Arnold, G. Wilkinson, B. Hussain, M. B. Hursthouse, *J. Chem. Soc., Dalton Trans.* **1989**, 2149–2153.
[33] R. M. Kolodziej, R. R. Schrock, W. R. Davis, *Inorg. Chem.* **1988**, *27*, 3253–3255.
[34] R. Poli, H. D. Mui, *J. Am. Chem. Soc.* **1990**, *112*, 2446–2448.

Received April 5, 2001
[I01121]

Dinuclear Cobalt(II) Complexes of an Acyclic Phenol-Based Dinucleating Ligand with Four Methoxyethyl Chelating Arms − First Magnetic Analyses in an Axially Distorted Octahedral Field

Hiroshi Sakiyama,* Rie Ito, Hitoshi Kumagai, Katsuya Inoue, Masatomi Sakamoto, Yuzo Nishida, and Mikio Yamasaki

Eur. J. Inorg. Chem. **2001**, 2027−2032

In the paper, we used the effective spin s when the magnetic exchange was considered, thus we should have used (5/3)$\boldsymbol{s}$ instead of $\boldsymbol{S}$. At this stage the Hamiltonian will be $\boldsymbol{H} = -(3/2)\kappa\ \lambda\ \boldsymbol{L}\cdot\boldsymbol{S} + \beta[-(3/2)\kappa\ \boldsymbol{L} + g_e\boldsymbol{S}]\cdot\mathrm{H} - (25/9)\ J\ \boldsymbol{s}_1\cdot\boldsymbol{s}_2$, and the magnetic susceptibility equation will be as follows:

$$\chi_A = \frac{\chi_z + 2\chi_x}{3}$$

$$\chi_{z(x)} = N\frac{\sum_{n=\pm1}\left(\frac{E^{(1)}_{z(x),n}}{kT}\right)^2 - 2E^{(2)}_{z(x),n}\exp\left[\frac{-E^{(0)}_n + \frac{25J}{36}}{kT}\right] + \sum_{n\neq\pm1}\left(\frac{E^{(1)}_{z(x),n}}{kT}\right)^2 - 2E^{(2)}_{z(x),n}\exp\left[\frac{-E^{(0)}_n}{kT}\right]}{\frac{1}{4}\sum_{n=\pm1}\exp\left[\frac{-E^{(0)}_n - \frac{75J}{36}}{kT}\right] + \frac{3}{4}\sum_{n=\pm1}\exp\left[\frac{-E^{(0)}_n + \frac{25J}{36}}{kT}\right] + \sum_{n\neq\pm1}\exp\left[\frac{-E^{(0)}_n}{kT}\right]}$$

Magnetic parameters were calculated based on the equation set, and Table 3 should be changed as shown below.

Table 3. Magnetic data for complexes **1** and **2**

Complex	κ	λ/cm^{-1}	Δ/cm^{-1}	J/cm^{-1}	g_z	g_x	D/cm^{-1}	$R(\chi_A)/10^{-3}$	$R(\mu_{eff})/10^{-4}$
1	0.98	−134	749	−0.55	2.18	4.99	120	0.12	0.89
2	0.84	−138	440	−0.70	2.45	4.84	144	1.7	1.6

Corrected supporting information is available on the WWW under http://www.eurjic.com or from the author.

H. Sakiyama
[I00420 C]

 © WILEY-VCH Verlag GmbH, 69451 Weinheim, 2001 1434−1948/01/1010−2705 $ 17.50+.50/0

On the Mechanism of the Hydroxycarbonylation of Styrene with Palladium Systems

Inmaculada del Río,[a] Carmen Claver,*[a] and Piet W. N. M. van Leeuwen[b]

Keywords: Carbonylation / Palladium / Reaction mechanisms / Regioselective catalysis / P ligands

We present a review concerning the mechanism involved in the hydroxycarbonylation of styrene. We discuss the intermediates proposed in the literature, the effect of the acidic medium, the reactivity and kinetics, as well as the results of theoretical calculations on hydroxycarbonylation and related reactions. We have performed an in situ high-pressure NMR study to obtain more insight into the mechanisms that control the regioselectivity and have assessed how this is affected by the phosphorus ligand and the catalyst precursor. We observed palladium hydride and palladium acyl species and we suggest a catalytic cycle involving palladium hydride, palladium alkyl, and palladium acyl intermediates.

Introduction

Transition-metal-catalysed transformations of alkenes play a major role in synthesizing products of industrial importance. The catalytic routes are a safer and more selective alternative to conventional methods involving stoichiometric organic syntheses that lead to considerable amounts of by-products.[1]

Particularly useful are reaction sequences in which an alkene is inserted into a metal hydride and then CO is inserted to form new C−C bonds. Some of the most successful reactions, such as hydroformylation, alkoxycarbonylation, and hydroxycarbonylation, belong to this class of reaction (Scheme 1). In general, carbonylations are important processes since they lead to the production of oxygenated products from petrochemical hydrocarbons.

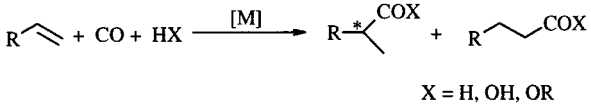

Scheme 1. General scheme for catalysed carbonylation reactions

Among the carbonylation reactions, hydroformylation using Co^{I} or Rh^{I} is now the largest industrial application of homogeneous catalysis by transition metal complexes for producing aldehydes and alcohols.[2,3] In hydroformylation chemistry, much progress has been made in recent years in

[a] Departament de Química Física i Inorgànica, Universitat Rovira i Virgili,
Pl. Imperial Tarraco 1, 43005 Tarragona, Spain
Fax: (internat.) +34-977/559-563
E-mail: claver@quimica.urv.es
[b] Institute of Molecular Chemistry,
Nieuwe Achtergracht 166, 1018 WV Amsterdam, The Netherlands
Fax: (internat.) +31-20/525-6456
E-mail: pwnm@anorg.chem.uva.nl

Inmaculada del Río (left) received her Ph.D. in 2000 from the University Rovira i Virgili working on mechanistic aspects of hydroformylation and hydroxycarbonylation reactions.

Carmen Claver (right) is Professor of Inorganic Chemistry at the University Rovira i Virgili in Tarragona (Spain), a position she has held since 1991. She received her Ph.D. in 1978 from the University of Zaragoza (Spain) working in the field of organometallic chemistry with Prof. Luis A. Oro. Her present research is focused on fundamental aspects of homogeneous catalysis with transition metals, especially in asymmetric catalysis.

Piet W. N. M. van Leeuwen is Professor of Homogeneous Catalysis at the University of Amsterdam, a position he has held since 1989. He has spent much of his career at Shell Research in Amsterdam working in the area of homogeneous catalysis and organometallic chemistry. His present research is aimed at the development of novel transition metal homogeneous catalysts, using the full range of available tools and techniques.

MICROREVIEWS: This feature introduces the readers to the authors' research through a concise overview of the selected topic. Reference to important work from others in the field is included.

 © WILEY-VCH Verlag GmbH, 69451 Weinheim, 2001 1434−1948/01/1111−2719 $ 17.50+.50/0

controlling the regioselectivity and understanding the mechanism of the process.[4]

Palladium systems have been used as catalysts in many carbonylation reactions, and their use in hydroxycarbonylation and alkoxycarbonylation reactions has been widely studied.[5] They have also been used as catalysts in many other carbonyl-based processes of industrial interest. The hydroxycarbonylation of butadiene, the dicarboxylation of alkenes, the carbonylation of alkenes, the carbonylation of benzyl and aryl halides, and oxidative carbonylations have recently been reviewed.[6]

In the palladium-catalysed reactions, products such as alcohols, aldehydes, ketones, and oligoketones can be prepared by modifying the palladium complexes with different phosphorus ligands. The selective formation of ketones by the carbonylation of higher alkenes using Pd^{II} complexes has been reported.[7,8]

A major breakthrough regarding the activity of this type of catalyst was the discovery that palladium complexes modified with *cis*-diphosphanes can be used in the alternating copolymerization of ethene or propene with carbon monoxide. This is another Pd^{II}-catalysed process that has attracted the interest of industry in the last two decades.[9]

In hydroxycarbonylation, alkoxycarbonylation, and the amidocarbonylation of alkenes, the use of a palladium carbonylation catalyst to synthesize propionic and other acids has been widely studied. The catalysts were mainly designed for the carbonylation of alkenes in the presence of alcohols in order to prepare carboxylic esters, but were also found to work well in the synthesis of carboxylic acids and anhydrides.[10]

It seems appropriate to distinguish between aliphatic alkenes and functionalized vinylic substrates, including vinyl aromatics. The carbonylation of vinyl aromatics is important for the synthesis of 2-phenylpropionic acids/esters, a class of non-steroidal anti-inflammatory drugs.[11] Also, the linear products, i.e. 3-phenylpropionic acid and its esters, have found application as speciality chemicals. In view of the synthetic importance of the preparation of phenylpropionic acids, styrene was selected as a model substrate for use in carbonylation studies.

The palladium-catalysed hydroxycarbonylation of alkenes has attracted considerable interest in recent years as a means of obtaining carboxylic acids. In general, in acidic media, palladium salts in the presence of mono- or bidentate phosphanes afford mixtures of linear and branched acids (Scheme 2).[6]

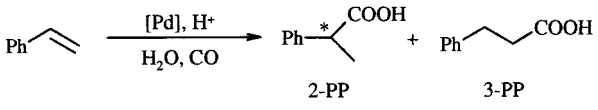

Scheme 2. Hydroxycarbonylation of styrene with palladium salts in acidic medium

This reaction has a number of associated problems, the most important of which is that metallic Pd^0 forms if the palladium species is not sufficiently well stabilized. Secondly, it is difficult to perform the reaction in an enantioselective fashion since the use of *cis*-chelate ligands provides linear acids. Also, because of the absence of a suitable nuclear spin on palladium, the characterization of its phosphane complexes in situ is more difficult than that of the corresponding rhodium or platinum complexes.

Although reports on the hydroxycarbonylation reaction with palladium systems have been published and several aspects of the mechanism have been discussed in the last few years, a review summarising the results and findings concerning the mechanism of this reaction is still lacking.

The related alkoxycarbonylation reaction has been studied in much greater detail[12–16] and two mechanisms have been suggested (Scheme 3).[17–21] One starts the cycle with a hydrido-metal complex.[19] In this cycle, an alkene inserts into a Pd–H bond, and then migratory insertion of CO into an alkyl–metal bond produces an acyl–metal complex. Alcoholysis of the acyl–metal species regenerates the palladium hydride and yields the ester. In the second mechanism, the crucial intermediate is an alkoxycarbonyl–metal complex.[20] Here, the insertion of the alkene into a Pd–carbon bond of the alkoxycarbonylmetal species is followed by alcoholysis to produce the ester and the alkoxymetal complex. The insertion of CO into the alkoxymetal species regenerates the alkoxycarbonylmetal complex.

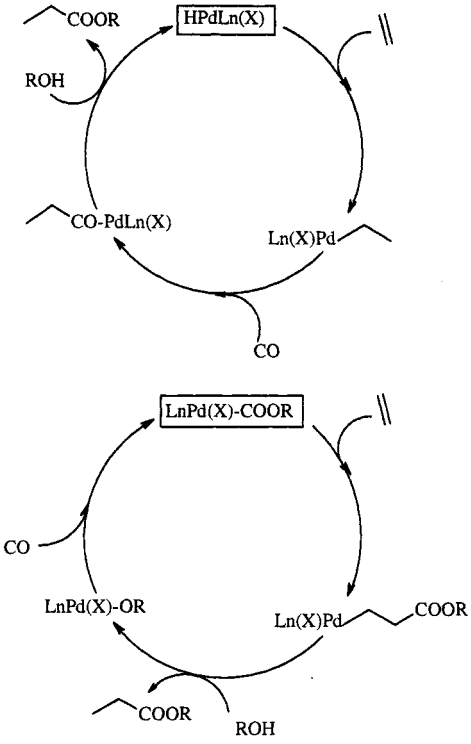

Scheme 3. Mechanisms proposed for the alkoxycarbonylation of alkenes

Most researchers currently agree that the hydrido mechanism is more common than the alkoxycarbonyl path in the alkoxycarbonylation of alkenes with palladium systems. However, alkoxycarbonyl complexes may be plausible intermediates in carbonylation reactions of alcohols or in the

formation of succinates and polyketone diesters with metals such as Co, Rh, or Pd.[7] The unifying mechanistic theme of these diverse reactions may be the generation of an alkoxycarbonylmetal intermediate, M−COOR.[20] Moreover, palladium alkoxycarbonyl complexes can produce the palladium hydride species in situ after insertion of the alkene and β-elimination of the unsaturated ester (Scheme 4), as was shown by Otsuka.[22]

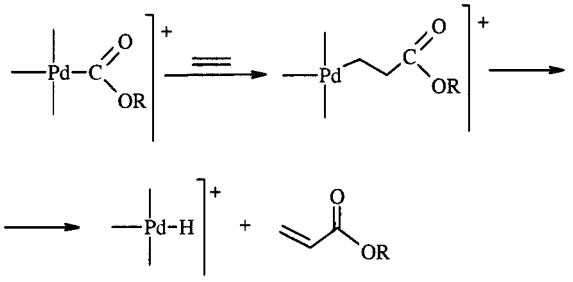

Scheme 4. Formation of Pd-hydride species from Pd-methoxycarbonyl species

The regioselectivity in the hydroxycarbonylation of styrene with palladium precursor systems under appropriate reaction conditions was controlled by modifying the auxiliary phosphorus ligand.[23] When monophosphanes are used as ligands, the major product is 2-phenylpropanoic acid with practically total regioselectivity. In contrast, the use of diphosphanes as auxiliary ligands switches the regioselectivity in favour of the linear product. Moreover, the activity and regioselectivity in the hydroxycarbonylation of styrene are both sensitive to the nature of the counteranion of the acid. The regioselectivities obtained for mono- and diphosphanes are generally strongly dependent on the nature of the anion.[24] In spite of several studies of the regioselectivity of the reaction, a satisfactory explanation for the regioselectivity is not yet available.

The aim of this Microreview is to provide a systematic overview of the mechanistic aspects and kinetic studies that have been published, as well as to provide some insight into the regioselectivity by means of a mechanistic study. We have performed in situ high-pressure NMR studies to obtain information about the resting state of the catalyst depending on the reaction conditions, the catalyst precursor, and the phosphorus ligands. Finally, we have compared the results of these studies with those of the catalytic experiments in order to arrive at a proposal for a catalytic cycle.

Reactivity and Characterization of the Palladium Species Involved in the Hydroxycarbonylation Reaction

The reactivity of Pd−H species towards the coordination and insertion of the substrate, as well as the subsequent coordination and insertion of carbon monoxide to form the palladium acyl species, have been studied for stoichiometric as well as catalytic alkoxycarbonylation reactions. Not all of these experiments, however, have been performed under the same conditions as the hydroxycarbonylation reaction; they are nevertheless useful for discussing the hydroxycarbonylation mechanism. Similarly, studies of the reactivity of Pd^0 species towards CO or phosphanes or acids are of interest to us. We will start the discussion with Pd^0 complexes.

Pd^0 carbonyl phosphane complexes are believed to be intermediates in the palladium-catalysed hydroxycarbonylation of alkenes, although they do not necessarily participate in the catalytic cycle (vide infra). $[Pd(CO)(PPh_3)_3]$ was isolated from the reaction mixture that arose from the hydroxycarbonylation of cyclohexene with $[PdCl_2(PPh_3)_2]$ as the precursor. This complex was also prepared by the direct reaction of $[Pd(PPh_3)_4]$ with CO in benzene. For the $[Pd(CO)(PPh_3)_3]$ complex, ^{31}P and ^{13}C NMR spectra suggest a rapid dissociation of PPh_3 at room temperature and a tetrahedral structure in solution at −70 °C.[25] $[Pd(CO)(PPh_3)_3]$ proved to be inactive in the hydroxycarbonylation of alkenes, like $[Pd(PPh_3)_4]$. However, the addition of traces of hydrochloric acid promoted the formation, under carbon monoxide pressure, of a catalytically active system.[26]

The Pd^0 complexes can be produced from mixtures of Pd^{II} complexes with phosphanes. Thus, stable Pd^0 complexes were generated in situ from the cationic Pd^{II} complex $[Pd(PPh_3)_2](BF_4)_2$ when water and triphenylphosphane were present in solution. Triphenylphosphane was able to reduce the Pd^{II} metal centre to Pd^0, and was itself oxidized to triphenylphosphane oxide. This reduction was performed on a Pd^{II} complex in which the palladium ion was most likely ligated by a hydroxy group.[27]

The reduction of Pd^{II} to Pd^0 has also been investigated in the presence of both monodentate PPh_3 and bidentate dppp [1,3-bis(diphenylphosphanyl)propane]. ^{31}P NMR measurements showed that triphenylphosphane can reduce $Pd(OAc)_2$ to Pd^0 in toluene. Bidentate dppp is mainly responsible for the reduction in DMF, which results in dppp hemioxide and dppp dioxide. Both mono- and bidentate coordination of dppp in intermediate species were proposed on the basis of in situ NMR studies.[28]

The key intermediates, namely palladium hydride, palladium alkyl, and palladium acyl, were detected and characterized by ^1H, ^{13}C, and ^{31}P NMR spectroscopy for the homogeneous water-gas shift reaction and for the carbonylation of ethene to diethyl ketone catalysed by the $Pd(OAc)_2$/PPh_3/CF_3COOH/H_2O system. The key palladium intermediate in both catalytic reactions was the hydride complex $[Pd(H)(PPh_3)_3]^+$. This cationic palladium hydride complex $[Pd(H)(PPh_3)_3]^+$ was formed by the oxidative addition of H^+ when the Pd^0 phosphane complex $[Pd(PPh_3)_4]$ was dissolved in an aqueous CF_3COOH solution. When the experiments were carried out starting with a Pd^{II} complex, it was shown that this complex was first reduced by CO (Scheme 5), giving CO_2 in the rate-determining step of the water-gas shift reaction.[8] Treating a solution of the hydride complex with CO at 25 °C resulted in a rapid rearrangement of a PdH^+ (a Pd^{II} species) and a Pd^0 species into the cationic dinuclear complex $[Pd_2(PPh_3)_4(\mu\text{-}H)(\mu\text{-}CO)]^+$.

When a solution of the hydride complex was treated with ethene at −25 °C, a palladium alkyl complex formulated as $[Pd(Et)(PPh_3)_2]^+$ was formed. Similarly, exposure of a solution of the hydride complex to a CO/C_2H_4 (3:1) gas mixture at 25 °C led to a rapid, quantitative formation of the palladium propionyl complex *trans*-$[Pd\{C(O)Et\}(PPh_3)_2]^+$.[8] The cationic hydride, ethyl, and propionyl palladium complexes are relatively stable as a result of the polar solvent and the non-coordinating anion.

$$PdL_2X_2 + CO + H_2O \xrightarrow[\text{slow}]{-CO_2,\ -HX} PdL_n(H)X$$

$$PdL_n(H)X \underset{\text{fast}}{\rightleftharpoons} L_4Pd^0 + HX$$

Scheme 5. Formation of palladium hydride species in the presence of CO and water

A similar involvement of palladium hydride, palladium alkyl, and palladium acyl complexes as intermediates in the catalytic cycle of the palladium-catalysed hydroxycarbonylation of alkenes was demonstrated for the analogous reaction in the aqueous phase. When a solution of $Pd(OAc)_2$ and tppts (tppts = trisulfonated triphenylphosphane) in aqueous trifluoroacetic acid was placed under a CO atmosphere, the cationic hydride $[Pd(H)(tppts)_3]^+$ was formed by reduction of the Pd^{II} complex with CO and H_2O to $[Pd(tppts)_3]$ and subsequent protonation in the acidic medium. The reaction of the hydride complex with ethene produced an equilibrium mixture of two new compounds, $[Pd(Et)(tppts)_3]^+$ and $[Pd(Et)(tppts)_2]^+$. The fourth coordination site in the latter is presumably occupied by a solvent molecule. The mixture of the palladium alkyl complexes reacted readily with CO to afford *trans*-$[Pd\{C(O)Et\}(tppts)_2]^+$ (Scheme 6).[29] Once again, the stability of the cationic intermediates may be attributed to the ionic medium and the non-coordinating nature of the anion, which is even enhanced by the aqueous solvent. The authors showed that in the stoichiometric reaction the hydrolysis of the acyl species giving propionic acid is the slowest step in the sequence.

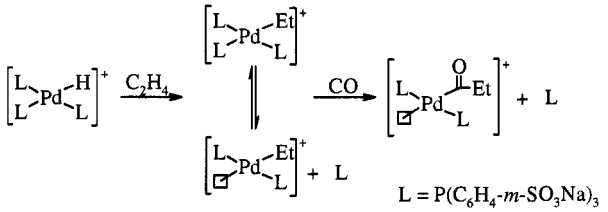

Scheme 6. The stepwise aqueous-phase hydroxycarbonylation of ethene

The intermediates involved in the palladium-catalysed methoxycarbonylation of ethene have also been characterized. The complex [Pd(L−L)(dba)] [L−L = 1,2-$(CH_2PtBu_2)_2C_6H_4$] reacts with HBF_4 or CF_3SO_3H in MeOH to produce a new compound that can be formulated as either the neutral complex [Pd(L−L)HX] or the solvated cation [Pd(L−L)H(MeOH)]X. This hydride complex reacts immediately with ethene at room temperature to form the cationic species [Pd(L−L)Et(MeOH)]X. On adding one equivalent of CO to the alkyl complex, the species [Pd(L−L){C(O)Et}(MeOH)]X is formed. Subsequent addition of a trace of MeOH to the solution leads to an immediate reaction regenerating the palladium hydride complex and forming EtCOOMe. It should be noted that the palladium hydride complex is stable even in the presence of oxidants (benzoquinone or oxygen) under these conditions. There was no evidence for the formation of any methoxycarbonyl complex.[30] For other systems, the formation of methoxycarbonyl palladium species is a well-documented process.[31,32] It should be noted, however, that the formation of methoxycarbonyl complexes under these conditions requires anhydrous conditions; in the presence of traces of water a hydroxycarbonyl-palladium species form, which rapidly loses carbon dioxide to give palladium hydride.[33] Thus, in the presence of water, hydride species will invariably be formed, which will initiate the catalytic cycle. This side reaction was efficiently suppressed by the addition of trimethyl orthoformate, which, under acidic conditions, transforms water into methanol.[34]

In the case of styrene, the mechanism of the methoxycarbonylation using $[Pd(OTs)_2(PPh_3)_2]$ formed in situ from $Pd(OAc)_2$, PPh_3, and TsOH in methanol has been investigated by isolating and characterising the intermediates. From the reaction mixtures, palladium hydridocarbonyl and palladium acyl complexes were isolated, and, accordingly, a palladium hydride mechanism has been proposed. Following exposure of the catalyst precursor system $Pd(OAc)_2$/$4PPh_3$/10HOTs to CO at 75 °C for 30 min., the complex $[Pd(H)CO(PPh_3)_2](OTs)$ was characterized. When the methoxycarbonylation was performed with $PdCl_2$ as the catalyst precursor, the acyl complex *trans*-$[PdCl(COCH_2CH_2Ph)(PPh_3)_2]$ was isolated.[35] The observation and isolation of the hydride, alkyl, and acetyl palladium species is, of course, strongly suggestive that they form part of the productive catalytic cycle; nonetheless, kinetic measurements are desirable to obtain further proof.

Palladium Hydride Complexes

Palladium hydrides are of special interest due to their exceptional relevance to catalysis. Indeed, several hydrido complexes of palladium have been proposed as key intermediates in a number of palladium-catalysed reactions.[36−38] Also, the study of palladium hydride species has been the subject of some interesting reports and reviews.[39,40] However, the reactivity of palladium hydrido complexes has still not been adequately explored. Despite the exceptionally high affinity of palladium metal for hydrogen,[41] soluble molecular hydrides of palladium are rather unstable and in many cases they cannot be isolated but only generated and characterized in solution at low temperature. The stability of analogous hydrides increases dramatically on going from palladium to platinum; for instance, $[Pt(H)Cl(PPh_3)_2]$ is stable to air and moisture and has been fully characterized.[42]

Over the last few years, the chemistry of palladium hydrides has developed significantly and a number of neutral and cationic hydrido complexes of palladium have been prepared and characterized by a variety of techniques. In fact, all known general methods for synthesising transition metal hydrides can be used to prepare palladium hydride complexes.[40]

Neutral palladium hydride complexes of the type $[PdHCl(PPh_3)_2]$ can be synthesized by oxidative addition of strong acids, as in the oxidative addition of HCl to Pd^0 complexes such as $[Pd(CO)(PPh_3)_3]$ or $[Pd(PPh_3)_4]$.[43] Related hydride complexes have been synthesized using other monophosphanes such as PEt_3,[44,45] PCy_3,[43] and PBu_3.[46] The nature of the phosphane is important, since the more basic phosphanes stabilize the product of the oxidative addition, i.e. the hydride complex.

The cationic hydrido complexes of palladium can be prepared by several methods, for example by replacing an anionic ligand in neutral palladium hydrides with a neutral ligand,[47] or by the protonation of zero-valent palladium complexes.[45,48] There have been reports of the formation of palladium cationic hydrides with H_2O, CH_3CN, or other coordinated solvents.[49−51]

With diphosphane ligands, the hydride complexes of palladium *cis*-[PdHCl(P−P)] are apparently highly unstable and numerous attempts to synthesize such species have failed; instead, cationic dinuclear complexes of palladium $[(P-P)_2Pd_2(\mu\text{-}H)(\mu\text{-}CO)]^+$ are readily formed during carbonylation reactions (vide supra and Scheme 7). These dinuclear complexes have been isolated and characterized, and their reactivity towards alkenes under CO atmosphere has been studied. Apparently, it is important to stabilize the systems with CO and to create a bridging instead of a terminal hydride *trans* to the phosphane.[52−54]

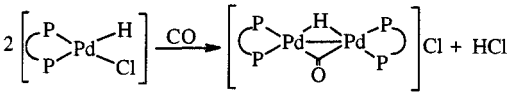

Scheme 7. Formation of the dinuclear $[(P-P)_2Pd_2(\mu\text{-}H)(\mu\text{-}CO)]^+$ in the reaction of [(P−P)PdHCl] under a CO atmosphere

The fact that palladium hydride species are stabilized under CO pressure can favour the catalysis through the intermediacy of a palladium hydride species. Moreover, it is interesting that in the alkoxycarbonylation of alkenes catalysed by a $[PdCl_2(PPh_3)_2]/PPh_3$ system, the catalytic activity is higher in the presence of molecular hydrogen. This is most likely attributable to the formation of a Pd−H intermediate through the heterolytic splitting of H_2. This represents an alternative pathway for the formation of the initial hydride species. This route does not require the reduction of Pd^{II} prior to oxidative addition of H^+. The occurrence of heterolytic splitting of hydrogen rather than oxidative addition is further substantiated by the fact that no aldehyde has been detected in the reaction products.[8,55−57] The latter reaction would require oxidative addition of dihydrogen to a palladium(II) acyl species.

Palladium Alkyl Complexes

Palladium alkyl derivatives have also been synthesized and characterized, especially the benzyl derivatives, which are stabilized as η^3-benzylic species. Since one of the most interesting palladium−styrene intermediates is the palladium η^3-benzylic species, it is useful to discuss species of this type.

The benzyl palladium complexes *trans*-$[Pd(CH_2Ph)Cl(PPh_3)_2]$ have been synthesized by the oxidative addition of benzyl chloride to Pd^0 complexes such as $[Pd(PPh_3)_4]$.[58] However, these complexes proved to be unstable and the dinuclear complex $[Pd_2(CH_2Ph)_2(PPh_3)_2(\mu\text{-}Cl)_2]$ was formed.[59] Other palladium alkyl derivatives have been obtained by adding halogenated hydrocarbons to a suspension of $[Pd(PPh_3)_4]$.[60,61]

The structures of the arylpalladium complexes of the type *trans*-$[Pd(Ph)X(PPh_3)_2]$ (X = F, Cl, Br, I) were studied by single-crystal X-ray diffraction analysis and the relative affinities of the halide anions for the metal centre were studied using ^{31}P NMR spectroscopy.[62]

Palladium η^3-benzyl complexes have also been prepared by the insertion of styrene into the Pd−Me bond of the solvated cation [PdMe(L−L)S]. This η^3-coordination of the benzyl ligand has been elucidated by X-ray structure determination and NMR spectroscopy. NMR studies showed that the palladium η^3-benzyl complexes undergo two dynamic processes in solution, namely η^3-η^1 coordination of the benzyl group, and ligand exchange of coordination sites.[63] Kinetic and isotopic labelling experiments have been employed to determine the mechanism of this benzyl exchange reaction (Scheme 8).[64] These complexes are highly prone to β-hydride elimination.[33]

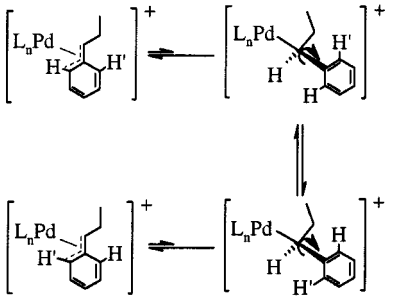

Scheme 8. An η^3-η^1-η^3 rearrangement mechanism that accounts for the observed exchange of the *ortho* hydrogens in $[(phen)Pd\{\eta^3\text{-}CH(CH_2CH_3)Ph\}]^+$

Palladium Acyl Complexes

Since the 1970s, a key question has been the involvement of either acylpalladium or alkoxycarbonylpalladium species in the reaction cycle. In the 1970s, supporting evidence for both mechanisms was put forward.[18,20] A comparative study of the reactivity and catalytic activity in the alkoxycarbonylation of alkenes using the isolated palladium acyl complex $[PdCl(COR)(PPh_3)_2]$ (R = Et, *n*-Hex) (a key inter-

mediate in the palladium hydride mechanism) and the palladium methoxycarbonyl complex [PdCl(COOMe)(PPh_3)$_2$] (an active species in the alkoxycarbonyl mechanism) was carried out by Cavinato and Toniolo.[19] With regard to the reactivity, the palladium acyl complex was found to react with an alkanol R′OH in the presence of added PPh_3 to yield the ester RCOOR′ and a mixture of [$PdCl_2(PPh_3)_2$] and [Pd(PPh_3)$_{3,4}$]. This was considered to be the slowest step of the hydride mechanism. When the isolated methoxycarbonyl complex [PdCl(COOMe)(PPh_3)$_2$] was treated with 1-hexene in methanol, under nitrogen and in the absence of carbon monoxide, the ester was not formed and the starting complex was recovered almost quantitatively, thus confirming that the step presumed to be the slowest in this cycle was indeed very slow. As regards the catalytic activity of these complexes, use of the acyl palladium complex as the catalyst precursor in the alkoxycarbonylation of ethene yielded almost stoichiometric amounts of the ester. When [PdCl(COOMe)(PPh_3)$_2$] was used as the catalyst precursor in the alkoxycarbonylation of 1-hexene in methanol, in the absence of added PPh_3 and in the presence of NEt_3 or carboxylate anions (to favour the formation of the methoxycarbonyl complex), no catalytic activity was seen and the precursor was recovered in the form of Pd^0-carbonylphosphane complexes. Only after prolonged reaction times was some of the methoxycarbonyl complex observed.[19]

Other acyl species of palladium have been synthesized and characterized. White crystals of *trans*-[Pd(CO*n*Pr)Cl(PPh_3)$_2$] were isolated in 70% yield after allowing the solution obtained following the alkoxycarbonylation of propene to stand for several hours at room temperature. This complex was found to be active in the alkoxycarbonylation of propene.[65] In situ IR spectroscopic studies were performed during the hydroxycarbonylation of ethene with [$PdCl_2(PPh_3)_2$], by which the intermediate species [Pd(COEt)Cl(PPh_3)$_2$] was observed. A mechanism involving Pd−H active species has been proposed.[66]

In favour of the participation of alkoxycarbonylpalladium species, the following two observations may be mentioned. The cationic complexes [(P−P)PdC(O)OCH_3(PPh_3)]$^+$ (P−P = dppe, dppp, dppb) undergo slow insertion of reactive alkenes such as norbornadiene.[33] The formation of diester[67][68] and diester end-group polyketones indicates that, under anhydrous conditions, cationic species may allow the insertion of alkenes into alkoxycarbonylpalladium species.[69]

As regards diphosphanes, the insertion of CO was studied for both neutral palladium chlorides and ionic triflate complexes containing the bidentate phosphanes dppe, dppp, dppb, and dppf.[70] Half-life times for the neutral complexes were between 18 and 36 min at 235 K and 25 bar of CO and the rates decreased in the order dppb > dppp > dppf >> dppe (170 min at 305 K). The ionic complexes were found to react with rates one or two orders of magnitude higher, even though acetonitrile was used as the solvent. Thus, carbon monoxide insertion should indeed be a fast step in the hydroxycarbonylation cycle.

High-pressure NMR spectroscopy was also used to follow the synthesis of the chiral ionic square-planar [Pd(Me)CO(BDPP)]BF_4 compound [BDPP = (2*S*,4*S*)-2,4-bis(diphenylphosphanyl)pentane], an intermediate in CO insertion into the Pd−Me bond. This compound was formed in situ by the reaction of the solvated [Pd(Me)S(BDPP)]BF_4 with ^{13}CO and in a high-pressure NMR tube. Concomitant with the decomposition of [Pd(Me)CO(BDPP)]BF_4, the complex [Pd(COMe)CO(BDPP)]BF_4 was formed and CO insertion was followed by the coordination of another CO ligand. This reaction was found to be completely reversible at room temperature. Several experiments were carried out to investigate whether the methyl(carbonyl) complex was also an intermediate in the formation of the methoxycarbonyl compound [Pd(Me)(COOMe)(BDPP)], but this compound could not be obtained in this way (Scheme 9).[71] [Pd(Me)(COOMe)(BDPP)] has been reported previously as the product of insertion of CO into [Pd(Me)(OMe)(BDPP)] at low temperatures.[72] Low temperatures are imperative as otherwise β-hydride elimination would take place. Interestingly, insertion takes place in the Pd−O bond rather than the Pd−C bond, as has been reported previously for platinum.[73] There are no indications that this reaction is relevant to alkoxycarbonylation since in cationic alkyl palladium species the insertion of CO into the palladium alkyl bond is very fast.[70]

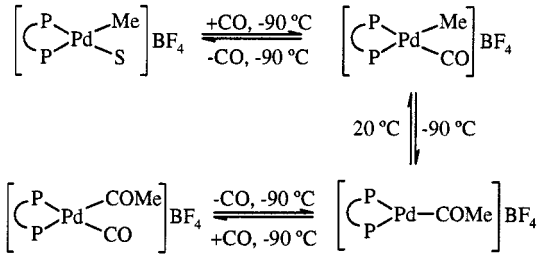

Scheme 9. Formation of palladium acyl complexes with diphosphane ligands under CO

Phosphorus-nitrogen ligands have been used for the study of the insertion of carbon monoxide into both ionic and neutral complexes.[74] In such complexes, the preferred structures have the methyl and acetyl groups *cis* to the phosphane ligand, as one would expect according to the *trans* influence. As a result, the insertion reaction for such P−N ligands is slower than those for either P−P or N−N ligands, because, in the first instance, migration leads to a less-stable isomer with the acetyl group *trans* to phosphorus. The details of such migration reactions in dissymmetric P−P* ligand complexes have been reported previously.[75][76]

A similar study has been performed concerning the reactivity of a cationic complex [(P,N)Pd(Me)(CO)]$^+$ towards CO and norbornene. Luinstra showed that in the presence of both an alkene and CO, the *trans* effect could be advantageously used to give faster reactions in some instances.[77] The same effect was reported by Mul et al.[78] This effect of ligand equilibria seems most relevant to polyketone synthesis, but similar effects can be envisaged for hydroxycar-

bonylation, casting some doubts on the rate measurements of stepwise stoichiometric reactions.

Benzylpalladium and (phenylacetyl)palladium complexes with two PMe_3 or PPh_3 ligands or a dppe ligand have been prepared as models for studying the mechanisms of carbonylation reactions by which benzyl halides are converted into singly and doubly carbonylated products.[58] The monodentate ligands give rise to *trans*-benzyl$PdX(L)_2$ structures containing η^1-benzyl fragments. When non-coordinating anions are used, η^3-benzyl species are formed. Insertion of CO is a fast and reversible process. Examination of the reactions of the (phenylacetyl)palladium complexes with secondary amines and alcohols provided evidence for the operation of different types of mechanisms leading to amides and esters. Amide formation proceeds more rapidly when more basic amines are used. The amines coordinate first to the palladium, and then attack the acyl moiety, which is assisted by another molecule of base. Ester formation proceeds more rapidly when more acidic alcohols are used. It was suggested that after coordination to palladium the alcohols are deprotonated by the base, and then the oxygen attacks the acyl carbon atom. In cationic diphosphane acylpalladium complexes, in the absence of base, the order of reactivity is $H_2O > MeOH > EtOH > 2\text{-PrOH}$, showing that the more acidic species react more rapidly.[79]

Effect of the Acidic Medium on Hydroxycarbonylation

The effect of the counteranion involved in the catalytic system has been studied, although its role is not yet fully understood. In the carbonylation of aliphatic and functionalized alkenes by cationic palladium complexes in the presence of hydrogen to give alcohols, aldehydes, ketones, or oligoketones, a selectivity control by the neutral ligand and anion was found. Non-coordinating anions primarily produce oligoketones, and increasing anion coordination strength shifts the selectivity towards aldehydes and alcohols.[7] For the latter, the heterolytic cleavage of hydrogen assisted by the more basic anions was proposed.

The regioselectivity of the alkoxycarbonylation of 1-arylethanols catalysed by Pd/acid systems is highly sensitive to the nature of the counteranion of the acid. Chloride anions favour branched products while weakly coordinating tetrafluoroborate and sulfonate anions favour linear products; the latter also enhance product yields.[80]

In the regioselective synthesis of ibuprofen by the $PdCl_2$/PPh_3/HCl-catalysed hydroxycarbonylation of 1-(4-isobutylphenyl)ethanol, the rate and selectivity of the reaction proved to be dependent on the concentration and nature of the halide ion used. It has been reported that hydrochloric acid plays a dual role in this reaction, firstly providing a proton, which promotes the dehydration of the alcohol, and secondly providing a chloride ion, which promotes the carbonylation step.[81]

In the asymmetric alkoxycarbonylation of alkenes catalysed by chiral palladium bis(dibenzophosphole) complexes, halide salts, such as LiCl or bis(triphenylphosphane)iminium chloride, and hydrogen at low pressure, were found to dramatically increase the extent of conversion without significantly decreasing the optical yield. Palladium species coordinated by halide are thought to prevent the aggregation of reduced palladium species.[82] In the asymmetric alkoxycarbonylation of styrene with palladium catalysts, both the degree of conversion and the asymmetric induction were found to be very low when acids such as MeCOOH, HCOOH, HCl, HBr, etc. were used instead of CF_3COOH.[83]

Finally, studies on the effect of the counteranion on the hydroxycarbonylation reaction have been performed. The effect of mineral acids as additives in the hydroxycarbonylation of 4-methylstyrene with $PdCl_2$/$CuCl_2$/PPh_3 has been studied. Efficient hydroxycarbonylation was only achieved after a halogen compound had been added; the addition of HCl improved the reaction rate significantly. This improvement was due to the effect of chloride ions rather than protons, as was proved by adding either other acids or other chloride salts.[84] Some reports have shown that the hydroxycarbonylation reaction also takes place if water is used instead of acid.[85,86]

In the course of a study on the use of palladium systems in the hydroxycarbonylation of styrene, we also explored how the counteranion of the acid affects this reaction when the Pd bears monophosphane and diphosphane ligands. To prevent the palladium precursor from introducing counteranions, we chose to perform a series of experiments using the catalyst precursor $[Pd_2(dba)_3]$ in the presence of acids. We showed that activity and regioselectivity in the hydroxycarbonylation of styrene are sensitive to the nature of the counteranion of the acid. The regioselectivities obtained for monophosphanes and diphosphanes (branched and linear, respectively) can be changed by judicious choice of the counteranion. When a monophosphane such as PPh_3 was used as the ligand, coordinating anions such as halides were found to favour the formation of branched acids. However, weakly coordinating anions such as sulfonic acids were found to favour the formation of linear acids. On the other hand, the regioselectivity for the systems formed with the diphosphane dppb in the presence of Br^- and I^- was found not to favour the linear acid as other diphosphanes do.[23] It has been suggested that the diphosphane could be monocoordinated depending on the nature of the counteranion, but it might also suggest that dinuclear species with the diphosphane bridging between two different palladium centres are formed (Scheme 10).[70,74] A similar behaviour

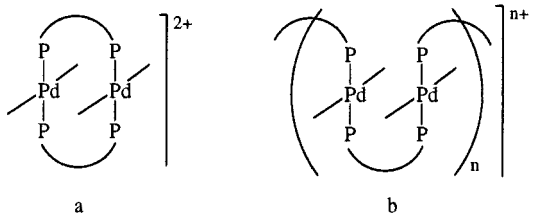

Scheme 10. Dimeric and oligomeric palladium complexes with diphosphane ligands

has recently been reported in Pd-diphosphane systems used in carbonylation processes, where differences in catalytic activity and selectivity can be rationalized in terms of monodentate coordination of the diphosphane.[87,88]

Regioselectivity in the Palladium-Catalysed Carbonylation Reactions

In spite of the reported studies, which have compared systems showing opposite regioselectivities in the palladium-catalysed alkoxycarbonylation and hydroxycarbonylation reactions, the issue of regioselectivity is still far from understood.

Since the 1970s, regioselectivity in the alkoxycarbonylation of alkenes has been shown to depend on the nature of the phosphorus ligand. Pd/monophosphane catalytic systems produce mainly the branched ester, whereas Pd/diphosphane systems produce mainly the linear one.[89,90]

In 1976, Sugi and Bando reported an interesting study of the ethoxycarbonylation of styrene with carbon monoxide and ethanol in the presence of diphosphane palladium complexes [$PdCl_2\{Ph_2P(CH_2)_nPPh_2\}$] ($n$ = 1−6, 10).[91] When diphosphanes with n = 3, 4, 5 were used, ethyl 3-phenylpropionate was obtained in significant amounts. With dppe, n = 2, however, no conversion was found. Phosphanes with n = 1, 6, 10 gave ethyl 2-phenylpropionate as the predominant isomer, in the same way as monodentate phosphanes do. The conversion increased with n, but proved to be highest for monodentate phosphanes. These results were rationalized in terms of the stability of the chelate ring under the reaction conditions, assuming the formation of monophosphane complexes for ligands with high n, similar to those with the monophosphane ligands. The current explanation is based on *cis* complexes for bidentate ligands of lower n, and *trans* complexes for ligands having higher n and monodentate ligands, at least for the resting states of the catalysts. The highest selectivity in favour of the branched ester (99.5%) was obtained using PBu_3.[91]

In several studies, monophosphanes and diphosphanes have been used together. In the asymmetric alkoxycarbonylation of α-methylstyrene using the Pd/DIOP system, the addition of PPh_3 was found to increase the amount of the branched ester.[92] In the hydroxycarbonylation of alkenes, PPh_3 was added to the $Pd(OAc)_2$/dppb system; this improved the yield without significantly affecting the product distribution.[93]

In some cases, a co-catalyst was added to the Pd/phosphane system, as in the hydroxycarbonylation of 1-heptene with [$HPdCl(PPh_3)_2$]/$SnCl_2$[94] and [$PdCl_2(PPh_3)_2$]/$Co_2(CO)_8$,[95] the hydroxycarbonylation of styrene with the [$PdCl_2(PPh_3)_2$]/$Co_2(CO)_8$ system,[96] and alkoxycarbonylation with the [$PdCl_2L_2$]/$SnCl_2$ or $GeCl_2$ systems (L = monophosphane).[48,55] In general, the co-catalyst increased the regioselectivity in favour of the linear product and decreased the rate of the reaction. In the asymmetric alkoxycarbonylation of styrene with the precursor $PdCl_2$ and chiral diphosphanes, the addition of $CuCl_2$ as a co-catalyst favoured the formation of the branched ester in good yield and with high enantiomeric excess.[97] In this case, however, the rigid structure of the iditol-derived ligand might have led to a non-chelating coordination, this being responsible for the high chiral induction. Monodentate coordination would be consistent with the high regioselectivity obtained in favour of the branched product.[98] A role of the MCl_2 salts that is frequently overlooked is that they may act as "chloride acceptors", thus assisting in the formation of weakly coordinating anions.

Interestingly, regioselectivity is seen to depend on the nature of the substrate. With aliphatic alkenes, the differences in isomeric composition are not as great as they are with vinyl arenes.[88] This can be explained in terms of π-benzylic stabilization of styrene in the styrylpalladium fragment obtained after insertion.[52,53] The steric bulk of the substrate is also important, as illustrated by the hydroxycarbonylation of simple and functionalized alkenes with $Pd(OAc)_2$/dppb/HCOOH. Control of the regioselectivity of the reaction depends in part on the effective bulk of the substituent group on the alkene; more hindered alkenes produce higher yields of the linear acid.[99] No pronounced influence of the electronic effects of the substrate on regioselectivity has been found in the alkoxycarbonylation and hydroxycarbonylation of 3,3,3-trifluoropropene and pentafluorostyrene catalysed by phosphane-palladium systems. When monophosphanes were used as ligands, the major product was the branched one, whereas when diphosphanes were used it was the linear one.[100] Thus, the fluoroalkenes follow the normal trend, although a higher preference for branched ones might have been expected.

Regioselectivity is often explained in terms of the following two mechanisms: (1) when styrene inserts into a metal−acyl bond, branched products are formed, and (2) when it inserts into a metal hydride, linear products are formed.[93][101] The regioselectivity of styrene insertion has been studied for the palladium-catalysed oligomerization of styrene and carbon monoxide. With diphosphanes, the insertion of the first styrene into the palladium hydride complex leads to the formation of a linear palladium alkyl species. This can be attributed to steric hindrance between the phenyl group of the styrene and the phosphane coordinated to the palladium centre. Insertion of styrene into the acyl palladium intermediate gives a branched insertion product.[100]

According to this interpretation, the different regioselectivities have a steric origin. In the first step, the hydride attacks the α-carbon of styrene, but the acyl species formed after insertion of CO attacks the styrene molecule at the β-carbon atom, as in our reaction (Scheme 11).[33] While this has proved to be correct for cationic complexes that act as polymerization or oligomerization catalysts, for hydroxycarbonylation this has yet to be confirmed (vide infra).

We have previously reported a systematic study into how palladium precursor systems and the phosphorus ligand affect the hydroxycarbonylation of styrene. Monophosphanes and diphosphanes behave differently when used as ligands in this reaction. Using monophosphanes, only Pd^{II} pre-

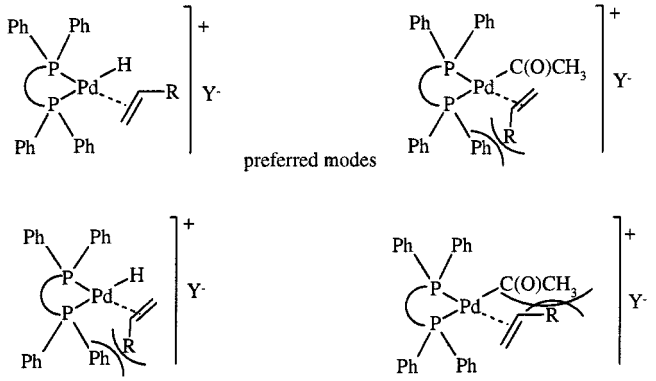

Scheme 11. Effect of steric hindrance on the stereochemistry of insertion of an alkene into a Pd−H bond and a Pd−C(O)CH_3 bond

cursors containing chloride give reasonable activity. When diphosphanes are used as auxiliary ligands, the results obtained with Pd^0 and Pd^{II} precursors are similar. As far as regioselectivity is concerned, the branched acid is the major product with monophosphanes, while the linear acid is the major product with diphosphanes. Also, monophosphanes afford much faster catalysts. It has been suggested that different intermediates are involved in the catalytic cycle for monophosphanes and diphosphanes; the association/dissociation of counteranions and phosphanes may account for the differences between the two systems.[23]

Studies of the Mechanism of Palladium-Catalysed Carbonylations

The understanding of a catalytic process requires a combination of several techniques, such as kinetic studies, deuteration experiments, determination of the intermediates, and theoretical studies. Here, we review significant studies of hydroxycarbonylation or related reactions that have contributed to the understanding of the palladium hydroxycarbonylation mechanism.

In several instances in the literature, no experimental support is presented for proposed catalytic cycles, and it should be borne in mind that these proposals are often speculative and include at best circumstantial evidence. In general, in catalytic alkene carbonylation reactions involving palladium species, a palladium hydride is proposed as the species that starts the cycle. Subsequently, coordination and insertion of the substrate occurs, which is followed by the coordination and insertion of carbon monoxide, which leads to the proposed palladium intermediates (Scheme 3).[102]

A mechanism has also been proposed for the Pd^{II} acetate/oxalic acid systems used in the presence of a chelating phosphorus ligand in the hydroxycarbonylation of alkenes. The system consisting of oxalic acid in 1,2-dimethoxyethane (DME) allows relatively mild conditions and gives high regioselectivity in favour of the linear acid when 1,4-bis(diphenylphosphanyl)butane, dppb, is used.[97] A catalytic cycle was proposed for the hydroxycarbonylation reaction starting with a $[Pd(OAc)_2(dppb)(CO)]$ complex that reacts with two equivalents of oxalic acid to afford an ionic complex $[Pd(H)CO(dppb)]^+$. For subsequent steps, palladium alkyl and palladium acyl intermediates are proposed. Finally, the linear acid is formed by decarbonylation (Scheme 12).[103]

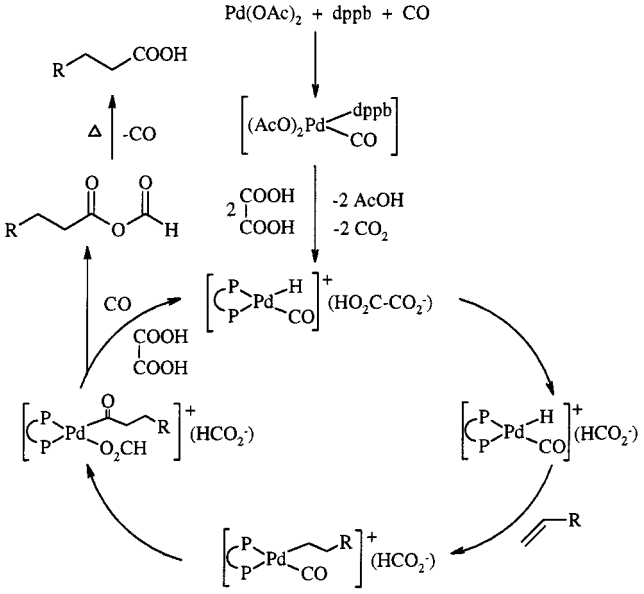

Scheme 12. Catalytic cycle proposed for the hydroxycarbonylation of alkenes with the $Pd(OAc)_2$/dppb/$H_2C_2O_4$ system

Kinetic Studies

A number of studies on the kinetics of the hydroxycarbonylation reaction with palladium systems have been reported.[104−106] These generally focus on how the carbon monoxide pressure, the concentration of styrene, the palladium precursor, the phosphane ligands, and water affect the activity and regioselectivity of the reaction.

The kinetics and mechanism of styrene hydroxycarbonylation catalysed by the complex $[PdCl_2(PPh_3)_2]$ have been reported. When water was added to the catalytic system up to $[H_2O]$ = 2 M, the rate of formation of the linear acid increased. Higher CO pressures were found to favour the formation of the branched acid. This can be attributed to the formation of species containing coordinated CO as a result of displacement of the bulkier PPh_3 ligand.[103] The rates of linear and branched acid formation both show a linear dependence on the concentration of the catalyst. Triphenylphosphane decreases the rate of formation of the branched acid more than that of the linear one; the inhibiting effect of PPh_3 is enhanced by increasing $[H_2O]$. As the styrene content increases, the rate of formation of the linear acid remains virtually constant, while the rate of formation of the branched acid increases markedly.[105] These relationships are consistent with the hydride mechanism, which involves four routes for the formation of phenylpropionic acids and three types of catalyst precursors $[Pd(H)Cl(CO)_n(PPh_3)_{2-n}]$ (n = 0−2) in equilibrium, depending on the CO pressure and the concentration of the

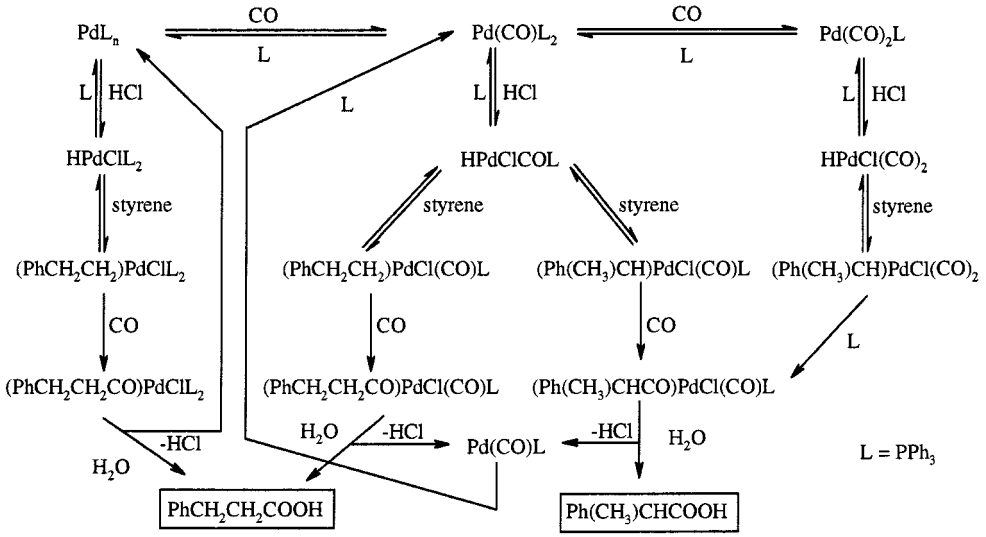

Scheme 13. Proposed mechanism for the hydroxycarbonylation of styrene with the $[PdCl_2(PPh_3)_2]/PPh_3$ system, involving $[Pd(H)Cl(CO)_n(PPh_3)_{2-n}]$ ($n = 0-2$) species

ligand. The regioselectivity of the intermediates with respect to 3-phenylpropionic acid drops from 100 to 0% as n increases from 0 to 2 (Scheme 13).[105]

More recently, a kinetic study of how the addition of $SnCl_2$ to the $[PdCl_2(PPh_3)_2]/PPh_3$ system affects the hydroxycarbonylation of styrene has been reported.[106] Adding an equimolar amount of $SnCl_2$ to $[PdCl_2(PPh_3)_2]$ increases the selectivity in favour of the linear acid from 30 to 70%, which stems from an increase in the rate of formation of this product. Kinetic and spectroscopic data were used to explain the effect of $SnCl_2$. It was proposed that it involves the displacement of CO ligands from Pd^{II}-containing intermediates by the π-acceptor $SnCl_3^-$, and leads to a higher concentration of phosphane hydride complexes that selectively afford the linear acid (Scheme 13).[107]

A kinetic study of the hydroxycarbonylation of 1-heptene catalysed by $[PdCl_2(PPh_3)_2]/PPh_3$ complexes has also been reported. The rates of formation of the acids increased as the carbon monoxide pressure was increased and as the water concentration was increased up to $[H_2O] = 2$ M. The same mechanism as that for styrene was suggested (Scheme 13).[107]

The kinetics of the alkoxycarbonylation of styrene have been studied using the $Pd(OAc)_2/PPh_3/TsOH$ catalyst system. The reaction was found to be first order with respect to the catalyst concentration and zero order with respect to styrene up to 3.8 mol·dm^{-3}. At high concentrations of styrene (3.8−6.7 mol·dm^{-3}), the rate increased significantly. Water was found to promote the alkoxycarbonylation of styrene, although beyond $9.2 \cdot 10^{-2}$ mol·dm^{-3} this effect was negligible. The rate increased when P_{CO} was below 3.4 MPa, but was not affected by higher partial pressures. A rate equation was proposed and the kinetic parameters were evaluated. A reaction mechanism involving palladium hydride, palladium alkyl, and palladium acyl species as intermediates has been proposed.[108]

In the $Pd(OAc)_2$/tppts-catalysed aqueous-phase hydroxycarbonylation of ethene, kinetic studies have shown that the conversion of a palladium acyl to a palladium hydride complex is a rate-determining, pseudo first-order reaction.[29]

Deuterium Labelling Experiments

Deuterium labelling has provided important information about the pathways that are operative in several catalytic reactions. A detailed investigation of the alkoxycarbonylation of styrene has been performed at various temperatures and conversions with the $[PdCl_2(PPh_3)_2]/SnCl_2$ system using labelled species, the content and distribution of deuterium in which was determined by mass spectral analysis and NMR (^1H, ^2H, ^{13}C) techniques. The large number of labelled species observed supports the assumption that the hydrido (Pd−H) route is the mechanism followed by this system. Significant deuteration of the unconverted styrene and the ester isomers formed was found in the alkoxycarbonylation of styrene with EtOD at low temperature (60 °C). Under more severe conditions, oligodeuterated species were formed in a less selective manner. The presence of deuterium in the unconverted alkene confirms the reversibility of the reaction (alkyl−metal intermediates readily undergo β-hydride elimination) and suggests that dissociation of the palladium alkyl intermediate occurred. Reversible alkene insertion/β-hydride elimination prior to carbonylation was deemed responsible for the incorporation of multiple deuterium atoms.[109]

A comparative study of the regioselectivity in styrene and α-methylstyrene alkoxycarbonylation in the presence of $[PdCl_2(PPh_3)_2]$ and $[PdCl_2(PPh_3)_2]/SnCl_2$ catalyst precursors has been reported. When styrene was transformed with $[PdCl_2(PPh_3)_2]/SnCl_2$ as the precursor, the linear ethyl 3-phenylpropanoate was the major product. The formation of both the linear and branched palladium alkyls was reversible, so that deuterium labelling occurred at all carbon

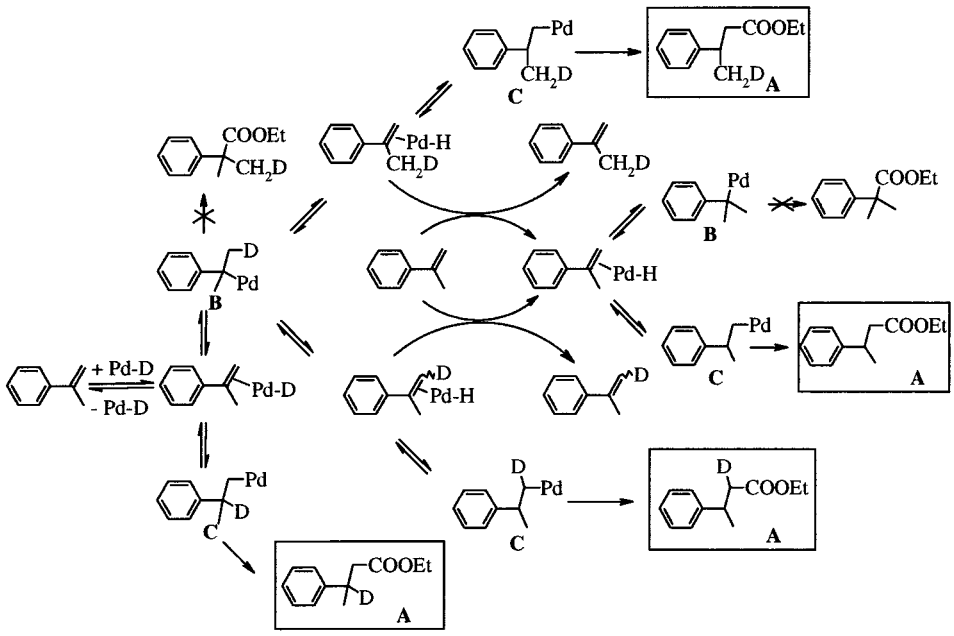

Scheme 14. Pathways for deuteration of α-methylstyrene and the derived deuterated isomeric esters

atoms of the side chains of the substrate and esters. In the absence of $SnCl_2$, the branched ethyl 2-phenylpropanoate was formed regioselectively and no deuterium was found adjacent to the phenyl rings. These results show that the routes leading to the linear metal-alkyls must be blocked.

When α-methylstyrene was used as the starting material, ethyl 3-phenylbutanoate (A) was predominantly obtained with both catalytic systems and there was no significant difference in the deuterium distributions obtained with the $[PdCl_2(PPh_3)_2]$ and $[PdCl_2(PPh_3)_2]/SnCl_2$ systems (Scheme 14). For the first time, this provides evidence for the formation of tertiary palladium alkyl species (B) with α-methylstyrene. These tertiary palladium alkyl species (B), although favoured over their primary counterparts (C), overwhelmingly underwent β-hydride elimination and, probably due to steric hindrance, the branched ester was not formed. Therefore, these intermediates undergo a slow migration of CO versus β-elimination. These results show that the different behaviour of primary, secondary, and tertiary palladium alkyl intermediates under alkoxycarbonylation conditions may account for the different regioselectivities.[110]

In the hydroxycarbonylation of styrene, the addition of $SnCl_2$ to the $[PdCl_2(PPh_3)_2]$ system also increases the selectivity in favour of the linear acid from 30 to 70%. Kinetic and spectroscopic data seem to indicate that this occurs through the displacement of a CO ligand from Pd^{II}-containing intermediates by the π-acceptor $SnCl_3^-$, as discussed above (Scheme 15).[104]

Scheme 15 shows that in systems containing chloride, when $X = Cl^-$, deuterium exchange occurs only at the β-position of the vinyl group; i.e. the rate of decomposition of species B (4) is higher than the rate of its carbonylation (6). The decomposition of species A (3) did not occur under the experimental conditions. Therefore, styrene insertion

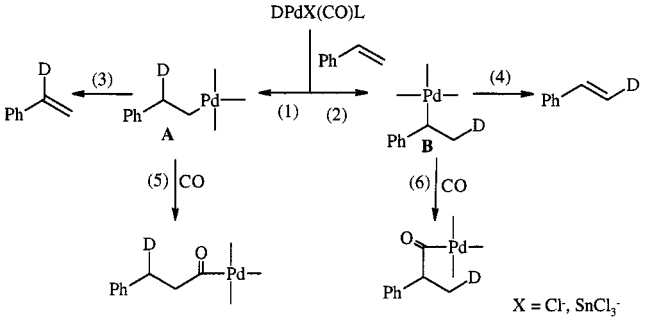

Scheme 15. Study of the regioselectivity in the hydroxycarbonylation of styrene with deuterium labels

into a Pd−H bond was considered to be an equilibrium step in route (2) and an irreversible step in route (1). In the presence of $SnCl_2$, extensive deuterium exchange occurs at both the α and β positions; i.e. the rates of steps (3) and (4) become similar. This is consistent with the data on the ability of the $SnCl_3^-$ moiety to assist the β-elimination of hydrogen from hydrocarbon groups in transition metal complexes[111,112] and allowed the authors to suggest that the formation of an intermediate of type A according to route (1) with $X = SnCl_3^-$ is an equilibrium step (Scheme 15).[106]

These studies prove that β-elimination takes place in the carbonylation reaction with the palladium catalyst. This was previously demonstrated for hydroformylation with a rhodium catalyst by means of deuterium labelling experiments.[113,114] However, the occurrence of β-elimination had already been deduced for other systems. In the hydroxycarbonylation of 1-octene with Pd/monophosphane systems at temperatures above 150 °C, dehydratocarbonylation was observed, this being the inverse reaction of hydroxycarbonylation. The acids formed reverted to the alkene, carbon

monoxide, and water. Both the forward and reverse reactions proceeded with appreciable rates.[85]

Recently, deuterium labelling experiments have been used in the hydroxycarbonylation of acenaphthylene with the $[PdCl_2(MeCN)_2]$ system in the presence of monophosphanes with different electronic properties. Deuteriocarboxylation of this substrate is, owing to the structure of the product, useful for determining the diastereoselectivity of the *cis*-addition of Pd−D to the alkene.[115]

Theoretical Studies

In an attempt to ascertain whether palladium hydride species or palladium alkoxycarbonyl species are the key intermediates in the Pd^{II}-catalysed alkoxycarbonylation of ethene, ab initio calculations were carried out to provide information on the transition state barriers of the elementary steps. The palladium hydride species was shown to be preferable to the palladium alkoxycarbonyl species as the key intermediate.[19] However, comparison of different routes remains a difficult task in view of the present state of the art. It can merely be concluded that the calculations are consistent with the experiments in that there is no prohibitive barrier for either route.[21]

In situ High-Pressure NMR Experiments

We have performed in situ high-pressure NMR studies of the hydroxycarbonylation of styrene using several palladium systems in order to obtain insight into the mechanisms that control the regioselectivity and the effects of the phosphorus ligand and the catalyst precursor. Similar in situ HPNMR studies have been performed for the rhodium hydroformylation[116,117] and palladium copolymerization reactions.[118] In particular, in the case of rhodium hydroformylation, this approach proved very useful for determining the intermediate species involved in the catalytic cycle.

In this study, the HPNMR spectroscopic investigations were carried out using $Pd(OAc)_2$ and $[PdCl_2(PhCN)_2]$ as palladium precursors, which were modified with PPh_3 as a monophosphane or dppb as a diphosphane [dppb = 1,4-bis(diphenylphosphanyl)butane]. $H_2C_2O_4$ was used as the acid under CO atmosphere with $[D_8]$THF as the solvent. The system was stirred under pressure to favour the diffusion of the gas. The experimental conditions were chosen according to previous hydroxycarbonylation catalytic experiments.[23,24]

The System $Pd(OAc)_2/PPh_3/H_2C_2O_4$

HPNMR experiments were carried out at 30 bar CO and molar ratios of P/Pd = 4 and H^+/Pd = 25 with the $Pd(OAc)_2/PPh_3/H_2C_2O_4$ system. The system was heated to 100 °C to allow the catalytic species to form. The $^{31}P\{^1H\}$ NMR spectrum of the solution showed a sharp singlet at δ = 14.4. The resonance of the oxidized phosphane was observed at δ = 32. At room temperature, the same solution exhibited a broad signal at δ = 15.0, together with the signal of the oxidized phosphane. When the temperature was lowered to −60 °C, the signal shifted downfield to δ = 23.6; a second signal of low intensity simultaneously appeared at δ = −5.0, which was assigned to the free PPh_3 ligand. Despite the acidic medium, no hydride signal was observed in the ^1H NMR spectra (Figure 1; Table 1).

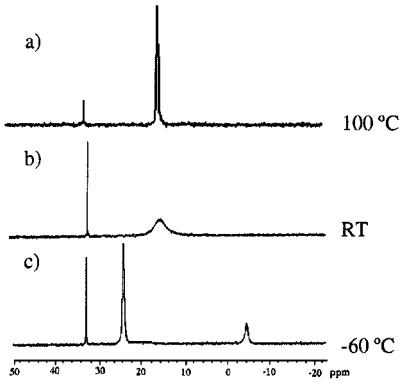

Figure 1. $^{31}P\{^1H\}$ NMR spectra for the reaction of $Pd(OAc)_2$ with PPh_3 under hydroxycarbonylation conditions at different temperatures: (a) 100 °C, (b) room temp., (c) −60 °C

In agreement with previously reported NMR spectroscopic data,[25] this behaviour may be rationalized in terms of ligand dissociation and a rapid ligand exchange according to an equilibrium between $[PdCO(PPh_3)_3]$ and $[PdCO(PPh_3)_2] + PPh_3$. At low temperatures, $[PdCO(PPh_3)_3]$ and free PPh_3 are observed.[27,28]

The HPNMR tube was then depressurized at room temperature and styrene (0.05 mL) was added under nitrogen (substrate/Pd = 4). The $^{31}P\{^1H\}$ NMR spectrum seen at 30 bar CO and room temperature remained unchanged. The temperature was then increased to 100 °C so as to reach carbonylation conditions. The formation of the acids was observed in the ^1H NMR spectrum, indicating the occurrence of hydroxycarbonylation. The major acid was the branched one, as reported previously for palladium systems with monophosphane ligands.[23] Simultaneously, the species observed in the $^{31}P\{^1H\}$ NMR spectra were those that had previously been observed when no substrate was added at these temperatures (Figure 1). When the system was cooled to −60 °C, decoalescence occurred in the same way as when there was no substrate. No hydride species were observed in the ^1H NMR spectra in the course of the experiment.

The System $[PdCl_2(PhCN)_2]/PPh_3/H_2C_2O_4$

Similar HPNMR experiments were performed for $[PdCl_2(PhCN)_2]/PPh_3/H_2C_2O_4$ at 30 and 10 bar CO, P/Pd = 4, and H^+/Pd = 25. The $^{31}P\{^1H\}$ NMR spectrum of the solution at 30 bar CO and 100 °C showed four broad signals: the signal of the oxidized monophosphane at δ = 33, two minor signals at δ = 24.5 and 22.9, and a major singlet at δ = 6.7. A broad hydride signal was observed in the ^1H NMR spectrum at δ = −13. At room temperature, the $^{31}P\{^1H\}$ NMR spectrum showed four sharp singlets at δ =

Table 1. NMR spectroscopic data for the [Pd]/PPh_3/$H_2C_2O_4$ systems under hydroxycarbonylation conditions

Complex	$\delta^{31}P\{^1H\}$ (ppm)	δ^1H (ppm)	Ref.
PPh_3[a]	−5	–	–
oxidized PPh_3[a]	32	–	–
$[PdCO(PPh_3)_3]$	23.6 (−70 °C)	–	[25]
$[Pd(PPh_3)_3]$[a]	24.9	–	–
cis/*trans*-$[PdCl_2(PPh_3)_2]$[a]	23.0, 22.8	–	–
$[Pd(H)Cl(PPh_3)_2]$	23.0 (−70 °C)	−13 (H)	[43−46]
$[PdCl(PPh_3)_2(COCH_2CH_2Ph)]$	20.6	1.4; 2.2 (CH_2)	[35]
$[PdCl(PPh_3)_2\{COCH(CH_3)Ph\}]$	19.8	0.8 (CH_3); 2.8 (CH)	[35]

[a] NMR spectroscopic data from experimental results.

32.2, 24.9, 23.0, and 22.8 and a broad signal at δ = 6.8. When the system was cooled to −70 °C, the broad signal was shifted downfield to δ = 23 and a new signal appeared at δ = −6; this was assigned to free PPh_3. No hydride signal was observed in the ^1H NMR spectrum either at room temperature or at −70 °C (Figure 2; Table 1).

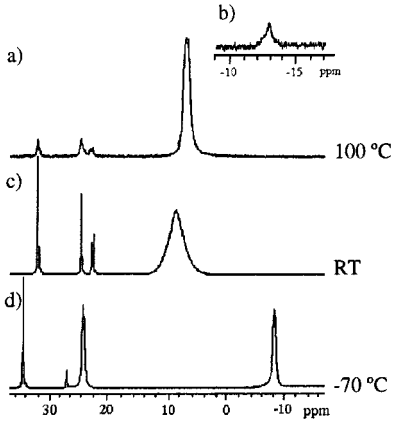

Figure 2. $^{31}P\{^1H\}$ and ^1H NMR spectra for the reaction of $[PdCl_2(PhCN)_2]$ with PPh_3 under hydroxycarbonylation conditions at different temperatures: (a) $^{31}P\{^1H\}$ NMR spectrum at 100 °C; (b) ^1H NMR spectrum at 100 °C; (c) $^{31}P\{^1H\}$ NMR spectrum at room temp.; (d) $^{31}P\{^1H\}$ NMR spectrum at −70 °C

As previously shown for the $Pd(OAc)_2/PPh_3$ system, a fast ligand exchange occurs at room temperature as well as at higher temperatures. However, the integrals of the phosphorus signals were different from those with the $Pd(OAc)_2/PPh_3$ system (Figure 1). These integrals may be indicative of the presence of a palladium complex with two monophosphanes coordinated as the $[Pd(H)Cl(PPh_3)_2]$ species.[43−46] These coordinated monophosphanes were responsible for the signal at δ = 23 in the $^{31}P\{^1H\}$ NMR spectrum and the corresponding hydride signal was observed at δ = −13 in the ^1H NMR spectrum. This hydride species is only observed at temperatures at or above 100 °C and under CO pressure.

The minor sharp singlets observed at room temperature at δ = 24.9 were attributed to the formation of $[Pd(PPh_3)_3]$ and those at δ = 23.0 and 22.8 to *cis*/*trans*-$[PdCl_2(PPh_3)_2]$. These complexes have previously been prepared in our laboratory for NMR assignment.

After cooling and depressurizing the HPNMR tube, styrene was added under nitrogen (substrate/Pd = 4). The solution was then pressurized with 30 bar CO and in the room temperature $^{31}P\{^1H\}$ NMR spectrum six sharp signals were observed at δ = 32.2 (oxidized monophosphane), 25.0, 23.1, 22.8, 20.6, and 19.8, together with a broad signal at δ = 0 (Figure 3, a). The singlets at δ = 25.0, 23.1, and 22.8 were assigned to the species previously observed in the absence of styrene, namely $[Pd(PPh_3)_3]$ and $[PdCl_2(PPh_3)_2]$. Two new singlets appeared at δ = 20.6 and 19.8 after the substrate was added, which were attributed to the palladium acyl complexes $[PdCl(PPh_3)_2(COCH_2CH_2Ph)]$ and $[PdCl(PPh_3)_2\{COCH(CH_3)Ph\}]$ (Table 1).[35] In the ^1H NMR spectrum, these palladium acyl complexes give rise to signals at δ = 1.4 and 2.2 due to the CH_2 of the linear isomer and at δ = 0.8 and 2.8 due to the CH_3 and CH of the branched acyl species, respectively. The major species was the linear palladium acyl species.

The broad signal observed at δ = 0 in the $^{31}P\{^1H\}$ NMR spectrum may be attributed to the species $[Pd(H)Cl(PPh_3)_2]$ that was previously observed in the absence of styrene at δ = 6.8 (Figure 2, c), despite there being no hydride signal in the ^1H NMR spectrum (Figure 3, a).

When the temperature was increased to 50 °C and 100 °C, hydroxycarbonylation was observed and in the $^{31}P\{^1H\}$ NMR spectrum the palladium acyl signals became broader (Figure 3, b,c). An exchange of PPh_3 between the palladium hydride and the palladium acyl species was observed.

The $^{31}P\{^1H\}$ NMR spectrum recorded after 24 hours was unchanged (Figure 3, d) and the ^1H NMR spectrum showed only 60% conversion to the acids with 64% regioselectivity in favour of the branched acid. When the temperature was increased to 120 °C (Figure 3, e), the rate of the reaction increased considerably and there was a faster phosphorus exchange between the palladium hydride and the palladium acyl species. After a few minutes, conversion reached 92% and the regioselectivity decreased to just 51% in favour of the branched acid. A dependence of the regioselectivity on the temperature was observed.

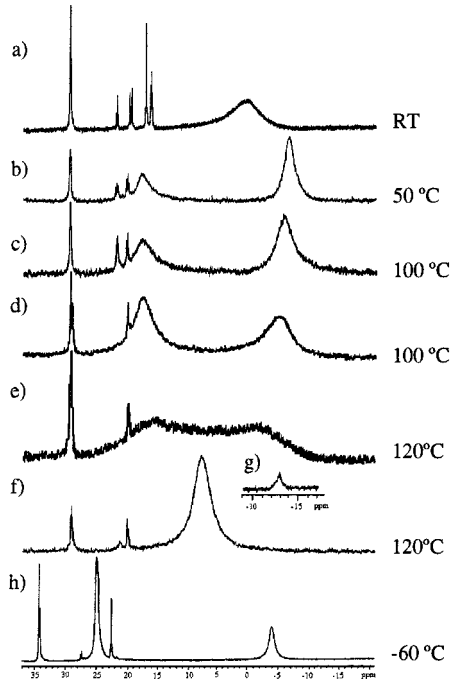

Figure 3. $^{31}P\{^1H\}$ and ^1H NMR spectra for the reaction of $[PdCl_2(PhCN)_2]$ with PPh_3 in the hydroxycarbonylation of styrene at different temperatures: (a) $^{31}P\{^1H\}$ NMR spectrum at room temp.; (b) $^{31}P\{^1H\}$ NMR spectrum at 50 °C; (c) $^{31}P\{^1H\}$ NMR spectrum at 100 °C; (d) $^{31}P\{^1H\}$ NMR spectrum after 1 day at 100 °C; (e) $^{31}P\{^1H\}$ NMR spectrum at 120 °C; (f) $^{31}P\{^1H\}$ NMR spectrum after 30 min at 120 °C; (g) ^1H NMR spectrum after 30 min at 120 °C; (h) $^{31}P\{^1H\}$ NMR spectrum at −60 °C

After 30 min, the hydroxycarbonylation was seen to be complete since the styrene and the palladium acyl complexes were no longer observed. A new hydride signal appeared at $\delta = -13$ (Figure 3, g). This signal was not observed in the course of the hydroxycarbonylation, possibly because it was below the detection level. The $^{31}P\{^1H\}$ NMR spectrum (Figure 3, f) was similar to that in the absence of styrene (Figure 2, a). Oxidized PPh_3, giving a signal at $\delta = 32$, and minor species such as $[Pd(PPh_3)_3]$ ($\delta = 25$) and $[PdCl_2(PPh_3)_2]$ ($\delta = 24$) were observed.

The solution was then cooled to −60 °C and, as previously observed in the absence of styrene (Figure 2, d), a broad signal appeared in the $^{31}P\{^1H\}$ NMR spectrum at $\delta = 24$ due to the complex $[Pd(H)Cl(PPh_3)_2]$, along with a signal due to the free phosphane at $\delta = -4$ (Figure 3, h).

To confirm the presence of the acyl species, we performed an experiment with the same $[PdCl_2(PPh_3)_2]/PPh_3/H_2C_2O_4$ system at 11 bar using a mixture of CO and ^{13}CO (10:1). Before the styrene was added, the species present were the same as those seen at 30 bar CO (Figure 2). After the addition of styrene at room temperature, the carbonyl signals of the palladium acyl complexes were observed in the ^{13}C NMR spectrum at $\delta = 234$ and 232. The temperature was then increased to 100 °C so as to reach hydroxycarbonylation conditions. This pressure favoured the formation of the linear acid and the ^1H NMR spectrum showed the presence of the hydride ($\delta = -13$) and the palladium acyl species.

During the hydroxycarbonylation, the temperature was lowered to −90 °C in an attempt to freeze out the intermediates of the reaction. The $^{31}P\{^1H\}$ spectrum was the same as that recorded without styrene (Figure 2, d; Figure 3, h), featuring signals due to the acyl complexes at $\delta = 19$ and 20. The temperature was then increased to 120 °C and at the end of the reaction the major product was the linear acid.

In conclusion, in the Pd/monophosphane systems, the palladium hydride species was only observed at high temperatures in the presence of carbon monoxide. Chloride ions favour the formation of this species. No hydrides were observed with the $Pd(OAc)_2/PPh_3$ system. With the $[PdCl_2(PhCN)_2]/PPh_3$ system at 30 bar CO, palladium acyl complexes were observed during the hydroxycarbonylation. At lower CO pressures, palladium hydride and palladium acyl species were observed. Similarly, the regioselectivity of the system was found to be dependent on the temperature and pressure; high temperatures and low pressures favoured the linear acid.

The System $Pd(OAc)_2/dppb/H_2C_2O_4$

Similar HPNMR experiments were performed with the $Pd(OAc)_2/dppb/H_2C_2O_4$ system at 60 and 20 bar CO, P/Pd = 4, and $H^+/Pd = 25$. At 60 bar CO, the system was heated to 120 °C to form the active species. The $^{31}P\{^1H\}$ NMR spectrum of the solution showed two broad signals at $\delta = 16$ and −6. Two resonances, corresponding to the oxidized diphosphane, were present at $\delta = 37$. A sharp hydride signal was seen in the ^1H NMR spectrum at $\delta = -5.6$. The $^{31}P\{^1H\}$ NMR spectrum of the same solution at room temperature showed a minor signal at $\delta = 27$ and a broad signal at $\delta = 14$, along with two signals due to the oxidized phosphane. On cooling to −70 °C, three broad signals were observed at $\delta = 27$, 16, and −14, the last of which was assigned to free dppb (Figure 4; Table 2).

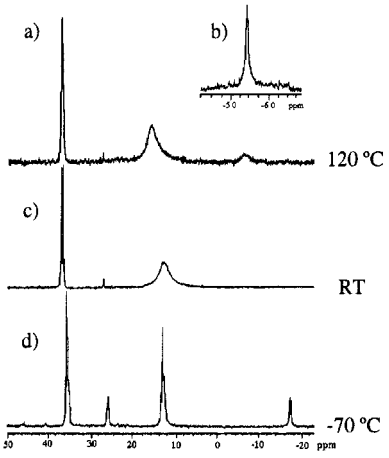

Figure 4. $^{31}P\{^1H\}$ and ^1H NMR spectra for the reaction of $Pd(OAc)_2$ with dppb under hydroxycarbonylation conditions at different temperatures: (a) $^{31}P\{^1H\}$ NMR spectrum at 120 °C; (b) ^1H NMR spectrum at 120 °C; (c) $^{31}P\{^1H\}$ NMR spectrum at room temp.; (d) $^{31}P\{^1H\}$ NMR spectrum at −70 °C

Table 2. NMR spectroscopic data for the [Pd]/dppb/$H_2C_2O_4$ systems under hydroxycarbonylation conditions

Complex	$\delta^{31}P\{^1H\}$ (ppm)	δ^1H (ppm)	Ref.
dppb[a]	−14	–	–
oxidized dppb[a]	37	–	–
[Pd(dppb)$_2$]	27 (−70 °C)	–	[119]
[Pd(OAc)$_2$dppb]	16 (−70 °C)	–	[28]
[(dppb)$_2$Pd$_2$(μ-H)(μ-CO)]OAc	23	−6.4 (μ-H)	[52,53]
[PdCl$_2$dppb][a]	28	–	–

[a] NMR spectroscopic data from experimental results.

These spectra may be explained in terms of ligand dissociation and a rapid ligand exchange at high temperatures. The signal at δ = 27 may be attributed to the complex [Pd(dppb)$_2$],[119] and that at δ = 16 to the species [Pd(OAc)$_2$dppb].[28] These species can undergo exchange of free dppb at high temperatures, thereby accounting for the broad signal at δ = 16. There may also be a dinuclear species with two bridging chelate diphosphanes coordinated to two palladium centres, with a hydride and carbon monoxide or acetate in a *trans* arrangement (Scheme 10, a). One of the two signals at δ = 37 can be attributed to monooxidized monocoordinated diphosphane. The species [Pd(P−P)(P−P=O)] or [Pd(OAc)$_2$(P−P=O)] may be formed, as has previously been suggested for the reduction of Pd^{II} species to Pd^0 as a means of initiating the catalytic cycle.[28] The sharp signal in the ^1H NMR spectrum at high temperatures did not show the expected large coupling constant for a hydride and a *trans* phosphorus atom (about 180 Hz). Therefore, the palladium hydride species did not have a hydride and the phosphane in a mutual *trans* arrangement. This species may correspond to the previously proposed dinuclear species.

The HPNMR tube was then depressurized at room temperature and styrene was added under nitrogen (substrate/Pd = 4). The $^{31}P\{^1H\}$ NMR spectrum at 60 bar CO and room temperature remained unchanged. The temperature was then increased to 120 °C so as to reach carbonylation conditions, and the formation of acids was observed in the ^1H NMR spectrum during the hydroxycarbonylation. As was previously reported for palladium systems with diphosphane ligands, the major product was the linear acid.[23] The species observed in the $^{31}P\{^1H\}$ NMR spectrum of the same solution were those that had previously been observed when no substrate was added at these temperatures (Figure 4). Furthermore, when the system was cooled to −70 °C, the behaviour was the same as that when no substrate was added. The hydride species was observed in the ^1H NMR spectrum only at high temperatures under carbon monoxide pressure. No palladium acyl species were observed.

An experiment was performed with the same system Pd(OAc)$_2$/dppb/$H_2C_2O_4$ at 20 bar CO with 1 bar of ^{13}CO. Prior to the addition of styrene, the species seen in the $^{31}P\{^1H\}$ NMR were the same as those seen at 60 bar CO (Figure 4) at the different temperatures, with only a minor singlet appearing at δ = 23. In the ^1H NMR spectrum, the sharp hydride signal was also present at δ = −5.6 and another minor broad signal was present at δ = −6.4. This palladium hydride signal and the $^{31}P\{^1H\}$ singlet at δ = 23 may be attributed to the dinuclear palladium species [(dppb)$_2$Pd$_2$(μ-H)(μ-CO)]OAc.[52,53]

When styrene was added and the system was heated to 120 °C, the $^{31}P\{^1H\}$ and ^1H NMR spectra were unchanged. In the ^{13}C NMR spectrum, however, a broad carbonyl signal due to a palladium acyl complex appeared at δ = 234. During the hydroxycarbonylation, formation of the linear acid was seen to be preferred. The system was cooled to −70 °C and the $^{31}P\{^1H\}$ NMR spectrum recorded at this temperature was the same as that when no styrene was added (Figure 4, d). The temperature was then increased to 120 °C once more and the reaction went to completion giving mainly the linear acid.

The System [PdCl$_2$(PhCN)$_2$]/dppb/$H_2C_2O_4$

Similar HPNMR experiments were performed with the [PdCl$_2$(PhCN)$_2$]/dppb/$H_2C_2O_4$ system at 60 bar CO, P/Pd = 4, and H^+/Pd = 25. The $^{31}P\{^1H\}$ NMR spectrum of the solution at 120 °C showed only free and oxidized dppb and a small signal due to the sparingly soluble [PdCl$_2$dppb] complex at δ = 28. When styrene was added to the system, no activity was observed. After one week, a small broad signal had appeared at δ = 16 in the room temperature $^{31}P\{^1H\}$ NMR spectrum. This signal was similar to that for the Pd(OAc)$_2$ system (Figure 4, c), where a small amount of the linear acid was observed. This may explain the fact that the [PdCl$_2$(PhCN)$_2$]/dppb system requires high pressures and temperatures in the catalytic experiments.

In conclusion, for the Pd(OAc)$_2$/dppb system palladium hydride species have been observed at high temperatures in the presence of carbon monoxide. On the other hand, monophosphane systems need chloride ions to stabilize the hydride species. At 20 bar CO, an acyl complex and the hydride species were observed by ^{13}C NMR spectroscopy. In the presence of palladium species, the occurrence of monooxidized, monocoordinated diphosphanes cannot be discarded, but the regioselectivity has invariably been found to favour the linear acid. The fact that some enantiomeric excess was seen with chiral diphosphanes means that some diphosphane remained coordinated as a chelate.[23]

Discussion of the Catalytic Cycle

The key questions to be answered concerning the catalytic cycle, focussing on the hydroxycarbonylation of styrene, are:

− Is the starting point a palladium hydride or a palladium alkoxycarbonyl species?

− How does the regioselectivity relate to the ligand, anion, and solvents?

Of the two proposed mechanisms, most researchers agree that the hydride mechanism is more common than the alkoxycarbonyl path in the alkoxycarbonylation of alkenes

with palladium systems. However, the involvement of alkoxycarbonyl species cannot be discarded as they are stable intermediates.[20] We must distinguish between hydroxycarbonylation and alkoxycarbonylation, as these reactions may have different characteristics. The prevailing mechanism for methoxycarbonylation is the hydride mechanism, but firm evidence has been presented for the occurrence of the methoxycarbonyl species as well. As examples, we mention double methoxycarbonylation leading to succinates,[67,68] the formation of methyl methacrylate from propyne,[120] and the formation of diesters during polyketone formation.[69] In two of these cases there is no choice, and the methoxycarbonyl species is the putative starting point. On the other hand, as pointed out by Sperrle and Consiglio,[121] it is difficult to present direct experimental evidence for either mechanism for the reactions producing monoesters or acids. For the very fast methoxycarbonylation of propene in methanol using alkyl diphosphanes, it was suggested[122,123] that palladium hydrido species were the starting points of the catalytic cycle as they were observed besides alkyl and alkanoyl species in separate NMR spectroscopy studies. Similar results have been reported[29] for the hydroxycarbonylation of propene in water using palladium complexes of tppts. However convincing it might seem though, it should be borne in mind that, strictly speaking, this remains circumstantial evidence. As we will discuss below, even kinetic measurements may not necessarily lead to clear-cut experimental evidence.

In the present study, like previous authors, we have observed palladium hydride intermediates and palladium acyl intermediates in the HPNMR experiments. The presence of hydroxycarbonyl species (or alkoxycarbonyl species[122,123]) below the detection limit responsible for the activity of the system is less likely because previous reactivity studies have shown that the alkoxycarbonyl species is less reactive than the hydride species.[16,87] This brings us to an important difference between alkoxycarbonylation and hydroxycarbonylation. The latter involves the PdCOOH fragment, which is highly unstable and rapidly degrades to palladium hydride and carbon dioxide. In the presence of oxidizing agents, divalent palladium dominates during the methoxycarbonylation, which leads to methoxycarbonyl species as the initiating group, provided that the system is anhydrous.[33,123] Tooze et al. reported an exception to this, a hydride being central to the catalytic cycle in the presence of an oxidizing agent, but it was not explicitly mentioned that this system was anhydrous. In the presence of water, the hydroxycarbonyl palladium species forms and hence palladium hydride will start the sequence.[16,122,123]

There are many other ways by which the palladium hydride species can be formed: (a) by β-elimination from the [PdCH(Ph)CH_2COOH] intermediate,[21] (b) by the formation of diacids, i.e. double carbonylation (the absence of minute amounts of these by-products in our experiments, as previously reported in catalytic experiments,[23] is incompatible with the presence of metal−carboxylic acid intermediates), (c) by reduction of phosphanes, (d) by addition of H_2, and (e) by β-elimination from [PdOCH_2R] species.[9,121] The deuterium exchange between the alkene and ROD found during the alkoxy- and hydroxycarbonylation[106,109,110] can only occur through reversible alkene insertion into a Pd−D bond, which strongly supports a reaction mechanism involving this step as well. The reversibility has implications for the regio- or enantioselectivity, as we will see below.

The regioselectivity and stereoselectivity have previously been discussed by Consiglio.[101,121] From the regioselectivity, it was concluded that the insertion of styrene into a metal−acyl bond leads to branched products, while its insertion into a metal hydride leads to linear products.[94,101,112] It is tempting to apply this finding to hydrocarboxylation as well. For the present systems, this is not the case as both the monodentate ligand systems, leading to mainly branched acid, and the bidentate ligand based systems, leading to mainly linear acid, imply insertions of styrene into a palladium hydride fragment. It has been argued[121] that insertion into a palladium hydride causes less steric constraints than insertion into a palladium alkoxycarbonyl species, and thus a lower stereospecificity can be obtained for the former. Indeed, high enantioselectivities were obtained in the formation of succinate.[67] This would make stereoselective hydroxycarbonylation difficult to accomplish. On the other hand, insertion of styrene into a palladium hydride bond may bring the aryl substituent in close proximity to a *cis* ligand, if this were a bulky and/or chiral ligand. We have previously reasoned that this steric interaction would stimulate the formation of linear products, which indeed seems to be the case for *cis* bidentate phosphane catalysts. A second problem arises from the reversibility of the insertion reactions. Alkene insertion is reversible, but so may be the insertion of carbon monoxide. If this were so, and the nucleophilic attack of water on the acyl group were to play a role in determining the overall rate, the selectivities under Curtin−Hammett conditions would be determined by all the rates and concentrations. In other words, the selectivities are determined by the differences in the overall final barriers. This may explain the low enantioselectivities obtained in many instances. It also complicates the discussion of the regioselectivity, as one pathway may involve complete equilibration while another may not.

Insertion reactions of alkenes and carbon monoxide using cationic palladium catalysts in alcohols and water may give rates of tens of thousands of turnovers per hour at 100 °C or even below.[29,87] The oxalic acid based systems are several orders of magnitude slower, for which there may be a number of reasons. Firstly, sites may be blocked by coordinating anions or by excess phosphanes. Secondly, low concentrations of alkenes may be found, especially in biphasic reactions.[29] Thirdly, palladium may be present in a state other than the required PdH^+ species, for example as Pd^0 species or as inactive dimers. Populating resting states of the latter two types diminishes the reactivity of the system, as we reported above. Stable palladium hydrides are obtained when two phosphanes occupy *cis* positions with respect to the hydride. We found that monophosphanes do indeed provide the fastest catalysts and the diphosphanes

provide much slower catalysts in the oxalic acid system.[23] In line with this, bidentate phosphanes having wide bite angles, which can also form *trans* complexes, give the most effective catalysts amongst the group of bidentate ligands.[23] Alkylphosphanes should give more stable hydride species as well, but in this system they show no activity and other side reactions must be followed, such as phosphonium salt formation perhaps.

Strong acids and polar media shift the equilibrium (Scheme 5) between Pd^0 and PdH^+ to the right. Indeed, high activities can be obtained[29,102] in water when soluble alkenes such as ethene and propene are used, but naturally this is not the case for styrene. Non-coordinating anions (i.e. the conjugate bases of strong acids) are also preferred in order to enhance coordination of alkenes and CO. Nevertheless, chloride has often been found to give the best results,[40] which may perhaps be ascribed to the higher stability of palladium hydrides when chloride anions are present. Acidic systems have an intrinsic drawback. If the nucleophilic attack on the acyl-palladium species is indeed rate determining, the strongest nucleophile present is water itself rather than the more nucleophilic hydroxide. This may be compared the very fast reaction of acyl palladium species and methoxy anions observed by Tóth.[16]

In an attempt to bring together the previously discussed reports and our in situ HPNMR study, we have summarized the catalytic cycle for the hydroxycarbonylation of styrene in Scheme 16.

A pre-equilibrium between different Pd^0 species bearing phosphane and carbon monoxide ligands is proposed; the stabilities of these species depend on the nature of the acidic medium and the phosphorus ligands, as demonstrated in the HPNMR spectra of the $Pd(OAc)_2/PPh_3/H_2C_2O_4$ system (Figure 1). This Pd^0 species can be formed by the methods discussed above, by oxidation of the phosphane,[27,28] or in the presence of CO and H_2O.[8,29] Because the acid used (AcOH) is not very strong, little hydride will be formed.

The insertion of styrene into the palladium hydride bond leads to two alkyl isomers, which can interconvert through β-elimination. Previous catalytic experiments,[85] kinetic studies,[106] and deuterium labelling methods[109,110] have demonstrated the occurrence of this β-elimination reaction.

For the branched palladium alkyl intermediate, stabilization through the formation of π-benzylic species[53,63] must also be taken into account. Thus, the regioselectivity may not yet be determined at this stage. The alkyl-alkanoyl equilibrium may reside on the side of the alkyl species, particularly for those π-benzylic species for which the insertion may be relatively slow, as has also been found for allyl palladium species.[124] The palladium acyl intermediates are formed by the insertion of carbon monoxide into the palladium−alkyl bond. The equilibrium between the palladium hydride species and palladium acyl species proposed in this catalytic cycle is in agreement with the reversibility of the CO insertion in the palladium alkyl bond, which was also verified by catalytic experiments.[71,77] Equilibration may even extend all the way between Pd^0 species and palladium acyl intermediates during hydroxycarbonylation (Scheme 17). Depending on the conditions, it seems likely that linear alkyl formation is irreversible whereas branched alkyl formation is reversible, even further down to alkanoyl formation. At least the trend will be in this direction.

Indeed, in the hydroxycarbonylation of styrene, kinetic and deuterium labelling studies have demonstrated that for the branched alkyl intermediate β-elimination is faster than

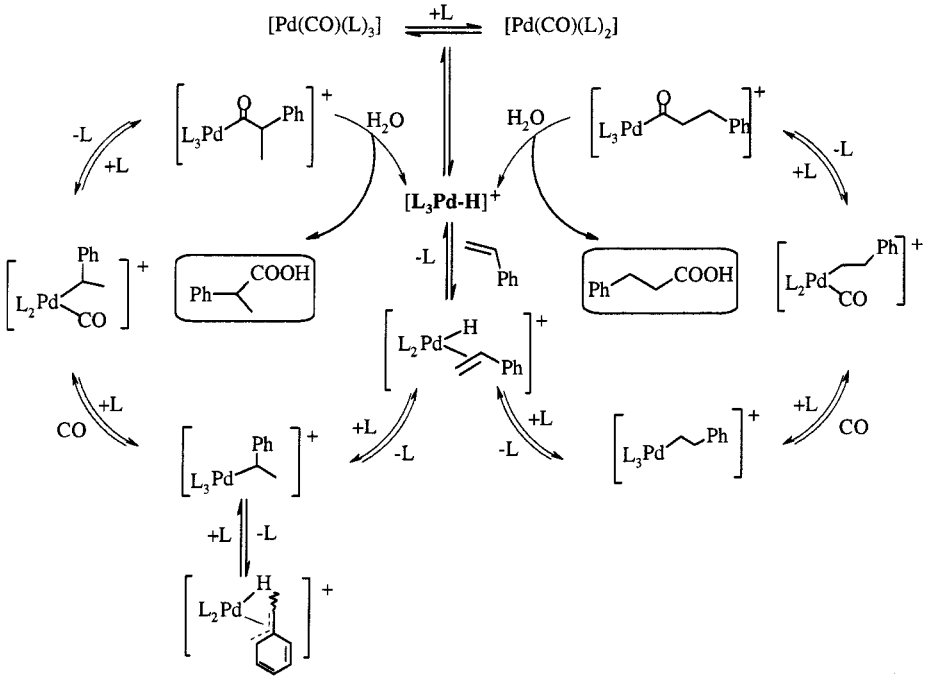

Scheme 16. Proposed catalytic cycle for the hydroxycarbonylation of styrene

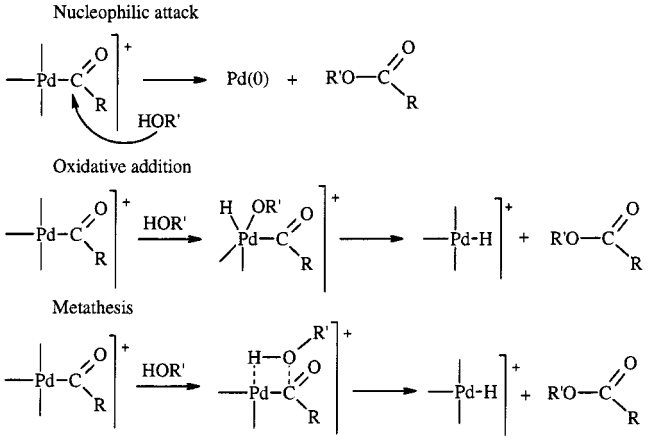

Scheme 17. Different proposals for the final step in the palladium carbonylation reactions

CO insertion, but that for the linear alkyl intermediate carbonylation is faster than β-elimination.[106,109,110]

In the HPNMR experiments using ^{31}P as the probe, we could not establish whether or not equilibration was operative all the way from the hydride to the alkanoyl, because exchange of the phosphane ligand probe between the free and complexed species proved to be the fastest reaction, thus prohibiting the observation of exchange of CO or styrene. Phosphane exchange occurs on the NMR time scale and if reversible insertions were to have rates of only a few percent of that of this exchange, they would still be faster than the overall catalytic process.

We consider next the regioselectivity. The HPNMR experiments and the previously described kinetic studies[104,105,108] have shown that regioselectivity is dependent on the pressure and temperature. High temperatures and low CO pressures favour formation of the linear acid as these conditions favour β-elimination from the stabilized π-benzylic species to give the linear palladium alkyl species.

Previously, we have offered a tentative explanation for the different regioselectivities of monophosphanes and diphosphanes. The reason for the high degree of linearity achieved with diphosphane catalysts is not the higher temperatures used. Catalytic experiments performed under identical conditions (20 bar CO, 150 °C, and P/Pd ratio = 4) with PPh_3 as the monophosphane led to a branched/linear ratio of 73:27, while the ratio was 28:72 for the diphosphane dppb.[23] We surmise that *cis*-coordinated diphosphanes versus *trans*-coordinated monophosphanes could be the key to regioselectivity control. In a *cis*-diphosphane complex, a strong interaction between the moieties on the phosphane and the aryl group of styrene leads to the formation of linear alkyl-palladium species. Reversibility plays an important role and we still have insufficient knowledge about this. Branched alkanoyl species are probably slightly more stable than linear ones, but nucleophilic attack on the latter may be faster and thus the regioselectivity under Curtin−Hammett conditions is hard to predict.

Complexes containing fewer phosphanes coordinated to the palladium form more of the branched acid.[104,105] Similarly, more hindered alkenes afford the linear acid.[99] In conclusion, the regioselectivity remains an extremely delicate issue. It is still difficult to predict given the complex kinetics involved, with rates depending on the pressure, temperature, counteranion, and phosphorus ligand.

Finally, the mechanism of the last step is not so clear and is often neglected. For the palladium carbonylation reactions, nucleophilic attack of $R'O^-$ would generally lead to Pd^0 and H^+, with oxidative addition occurring as the next step. Alternatively, the oxidative addition of R′OH to Pd^{II}, in other words a sort of α-bond metathesis, may be considered (Scheme 17).

All evidence for the recently published, fast catalyst points to the fact that the hydrolysis step is rate determining. For the many systems mentioned above, the rates vary by many orders of magnitude. On the one hand, this may be due to the intrinsic effects of the ligands, anions, and solvents on the rate, but on the other hand it may also be due to the effects these factors have on the resting states, including those outside of the catalytic cycle. Monodentate ligands give the fastest reactions.

Polyketone catalysis employing a variety of *cis*-chelating bidentate ligands shows that insertion reactions are fast (several thousands of insertions per hour), while termination at 80−100 °C occurs only several times per hour. The latter depends on the time that the growing chain end exists as an alkyl or an acyl species, but at high CO pressures appreciable amounts of acyl palladium chain ends are present.[78] Thus, an acyl species *trans* to a phosphane ligand reacts relatively slowly[79] with water or an alcohol as the nucleophile, whereas insertion reactions are fast. In monophosphane systems, the group *trans* to acyl is a solvent molecule and in this case insertion reactions are slower and the acyl group is more susceptible to nucleophilic attack due to the smaller *trans* influence.

Conclusion

The reports that we have reviewed herein have shown that the hydroxycarbonylation reaction involves a palladium hydride mechanism and that palladium hydride, palladium alkyl, and palladium acyl are the intermediates of this reaction.

Previous kinetic and deuterium labelling studies proved the involvement of a β-elimination reaction. We have now performed in situ HPNMR experiments on different systems. Pd^0, palladium hydride, and palladium acyl species were observed during the hydroxycarbonylation reaction. We propose an equilibrium between the Pd^0 and the palladium acyl species in a catalytic cycle.

Control of the regioselectivity of the hydroxycarbonylation has proved to be dependent on the phosphorus ligand, the counteranion, the pressure, and the temperature. The regioselectivity remains a complicated issue and equilibration between several intermediates seems likely to play a major role, except in the case of diphosphane systems, where steric hindrance leads to predominantly irreversible, linear alkyl formation.

Acknowledgments

We thank the Spanish Ministerio de Educación y Ciencia for financial support (DGES PB-97-0407-C05-01) and the Generalitat de Catalunya (CIRIT) for awarding a research grant (to I. del Río). We thank Ramon Guerrero and J. Chris Slootweg for their helpful contributions.

[1] R. A. Sheldon, *Organic Synthesis − Past, Present and Future*, *Chem. Ind.* **1992**, 903−906.
[2] P. W. N. M. van Leeuwen, G. van Koten, in *Catalysis: An Integrated Approach* (Eds.: R. A. van Santen, P. W. N. M. van Leeuwen, J. A. Moulijn, B. A. Averill), Elsevier, Amsterdam, **1999**, 2nd edition, chapter 6.2.
[3] M. Beller, B. Cornils, C. D. Frohning, C. W. Kohlpaintner, *J. Mol. Catal.* **1995**, *104*, 17−85.
[4] P. W. N. M. van Leeuwen, C. Claver, *Recent Advances in Rhodium-Catalyzed Hydroformylation*, Kluwer Academic Publishers, CMC series vol. 22, Dordrecht, **2000**.
[5] B. E. Ali, H. Alper, in: *Transition Metals for Organic Synthesis* (Eds.: M. Beller, C. Bolm), Willey-VCH, Weinheim, **1998**, chapter 2.2.
[6] A. Höhn, in: *Applied Homogeneous Catalysis with Organometallic Compounds* (Eds.: B. Cornils, W. A. Herrmann), VCH, Weinheim, **1996**.
[7] E. Drent, P. H. M. Budzelaar, *J. Organomet. Chem.* **2000**, *593−594*, 211−225.
[8] V. N. Zudin, V. D. Chinakov, V. M. Nekipelov, V. A. Rogov, V. A. Likholobov, Y. I. Yermakov, *J. Mol. Catal.* **1989**, *52*, 27−43.
[9] E. Drent, P. H. M. Budzelaar, *Chem. Rev.* **1996**, *96*, 663−681.
[10] [10a] E. Drent (Shell), EP 55 857, **1981**. − [10b] E. Drent, L. Petrus, S. A. J. van Langen (Shell), EP 282 142, **1988**.
[11] [11a] C. Botteghi, S. Paganelli, A. Schionato, M. Marchetti, *Chirality* **1991**, *3*, 355−369. − [11b] J.-P. Rieu, A. Boucherle, H. Cousse, G. Mouzin, *Tetrahedron* **1986**, *42*, 4095−4131.
[12] C. W. Lee, H. Alper, *J. Org. Chem.* **1995**, *60*, 250−252.
[13] K. Nozaki, M. L. Kantam, T. Horiuchi, H. Takaya, *J. Mol. Catal.* **1997**, *118*, 247−253.
[14] S. Oi, M. Nomura, T. Aiko, Y. Inoue, *J. Mol. Catal.* **1997**, *115*, 289−295.
[15] D. Zim, R. F. de Souza, J. Dupont, A. L. Monteiro, *Tetrahedron Lett.* **1998**, *39*, 7071−7074.
[16] W. Clegg, G. R. Eastham, M. R. J. Elsegood, R. P. Tooze, X. L. Wang, K. Whiston, *Chem. Commun.* **1999**, 1877−1878.
[17] R. F. Heck, *J. Am. Chem. Soc.* **1972**, *94*, 2712−2716.
[18] J. Knifton, *J. Org. Chem.* **1976**, *41*, 793−797.
[19] G. Cavinato, L. Toniolo, *J. Organomet. Chem.* **1990**, *398*, 187.
[20] D. Milstein, *Acc. Chem. Res.* **1988**, *21*, 428−434.
[21] M. Kawana, S. Nakamura, E. Watanabe, H. Urata, *J. Organomet. Chem.* **1997**, *542*, 185−189.
[22] S. Otsuka, A. Nakamura, T. Yoshida, M. Naruto, K. Ataka, *J. Am. Chem. Soc.* **1973**, *95*, 3180−3188.
[23] I. del Río, N. Ruiz, C. Claver, L. A. van der Veen, P. W. N. M. van Leeuwen, *J. Mol. Catal.* **2000**, *161*, 39−48.
[24] I. del Río, N. Ruiz, C. Claver, *Inorg. Chem. Commun.* **2000**, *3*, 166−168.
[25] F. Morandini, G. Consiglio, F. Wenzinger, *Helv. Chim. Acta* **1979**, *62*, 59−61.
[26] K. Bittler, N. V. Kutepow, D. Neubauer, H. Reis, *Angew. Chem.* **1968**, *80*, 329−335.
[27] [27a] C. Amatore, A. Jutand, M. J. Medeiros, *New J. Chem.* **1996**, *20*, 1143−1148. − [27b] C. Amatore, E. Carré, A. Jutand, M. A. M'Barki, *Organometallics* **1995**, *14*, 1818−1826. − [27c] F. Ozawa, A. Kubo, T. Hayashi, *Chem. Lett.* **1992**, 2177−2180.
[28] Z. Csákai, R. Skoda-Földes, L. Kollár, *Inorg. Chim. Acta* **1999**, *286*, 93−97.
[29] G. Verspui, I. I. Moiseev, R. A. Sheldon, *J. Organomet. Chem.* **1999**, *586*, 196−199.
[30] G. R. Eastham, B. T. Heaton, J. A. Iggo, R. P. Tooze, R. Whyman, S. Zacchini, *Chem. Commun.* **2000**, 609−610.
[31] D. Milstein, *J. Chem. Soc., Chem. Commun.* **1986**, 817−818.
[32] K. Y. J. Kim, K. Osakada, K. Sugita, T. Yamamoto, A. Yamamoto, *Organometallics* **1988**, *7*, 2182−2188.
[33] G. P. C. M. Dekker, C. J. Elsevier, K. Vrieze, P. W. N. M. van Leeuwen, C. F. Roobeek, *J. Organomet. Chem.* **1992**, *430*, 357−372.
[34] P. W. N. M. van Leeuwen, W. L. Groeneveld, *Inorg. Nucl. Chem. Lett.* **1967**, *3*, 145−146.
[35] A. Seayad, S. Jayasree, K. Damodaran, L. Toniolo, R. V. Chaudhari, *J. Organomet. Chem.* **2000**, *601*, 100−107.
[36] P. M. Maitlis, *The Organic Chemistry of Palladium*, Academic Press, New York, **1971**, vols. 1 and 2.
[37] J. Tsuji, *Organic Synthesis with Palladium Compounds*, Springer-Verlag, New York, **1980**.
[38] R. F. Heck, *Palladium Reagents in Organic Synthesis*, Academic Press, New York, **1985**.
[39] B. M. Trost, *Chem. Eur. J.* **1998**, *4*, 2405−2412.
[40] V. V. Grushin, *Chem. Rev.* **1996**, *96*, 2011−2033.
[41] F. A. Lewis, *Platinum Met. Rev.* **1994**, *38*, 112.
[42] J. C. Bailar, H. Itatani, *Inorg. Chem.* **1965**, *4*, 1618−1620.
[43] K. Kudo, M. Hidal, T. Murayama, Y. Uchida, *Chem. Commun.* **1970**, 1701−1702.
[44] M. L. Scheneider, H. M. M. Shearer, *J. Chem. Soc., Dalton Trans.* **1973**, 354−356.
[45] R. F. Jones, J. R. Fisher, D. J. Cole-Hamilton, *J. Chem. Soc., Dalton Trans.* **1981**, 2550−2555.
[46] J. Grévin, P. Kalck, *J. Organomet. Chem.* **1994**, *476*, C23−C24.
[47] M. L. H. Green, H. Munakata, *J. Chem. Soc., Chem. Commun.* **1971**, 549.
[48] V. N. Zudin, V. D. Chinakov, V. M. Nekipelov, V. A. Likholobov, Y. I. Yermakov, *J. Organomet. Chem.* **1985**, *289*, 425−430.
[49] D. Braga, P. Sabatino, C. Bugno, P. Leoni, M. Pasquali, *J. Organomet. Chem.* **1987**, *334*, C46−C48.
[50] M. Sommovigo, M. Pasquali, P. Leoni, P. Sabatino, D. Braga, *J. Organomet. Chem.* **1991**, *418*, 119−126.
[51] P. Leoni, M. Sommovigo, M. Pasquali, S. Midollini, D. Braga, P. Sabatino, *Organometallics* **1991**, *10*, 1038−1044.
[52] I. Tóth, C. J. Elsevier, *Organometallics* **1994**, *13*, 2118−2122.
[53] M. Portnoy, D. Milstein, *Organometallics* **1994**, *13*, 600−609.
[54] P. J. Perez, J. C. Calabrese, E. Bunel, *Organometallics* **2001**, *20*, 337−345.
[55] J. Knifton, *J. Org. Chem.* **1976**, *41*, 2885−2890.
[56] G. Cavinato, L. Toniolo, C. Botteghi, S. Gladiali, *J. Organomet. Chem.* **1982**, *229*, 93−100.
[57] G. Cavinato, L. Toniolo, C. Botteghi, *J. Mol. Catal.* **1985**, *32*, 211.
[58] Y-S. Lin, A. Yamamoto, *Organometallics* **1998**, *17*, 3466−3478.
[59] P. Fitton, J. E. McKeon, B. C. Ream, *Chem. Commun.* **1969**, 370−371.
[60] P. Fitton, M. P. Johnson, J. E. McKeon, *Chem. Commun.* **1968**, 6−7.
[61] A. C. Albéniz, N. M. Catalina, P. Espinet, R. Redón, *Organometallics* **1999**, *18*, 5571−5576.
[62] J. P. Flemming, M. C. Pilon, O. Y. Borbulevitch, M. Y. Antipin, V. V. Grushin, *Inorg. Chim. Acta* **1998**, *280*, 87−98.
[63] G. Gatti, J. A. López, C. Mealli, A. Muso, *J. Organomet. Chem.* **1994**, *483*, 77−89.
[64] F. C. Rix, M. Brookhart, P. S. White, *J. Am. Chem. Soc.* **1996**, *118*, 2436−2448.
[65] B. Bardi, A. Del Pra, A. M. Piazzesi, L. Toniolo, *Inorg. Chim. Acta* **1979**, *35*, L345−L346.
[66] Y. G. Noskov, M. I. Terekhova, E. S. Petrov, *Kinet. Katal.* **1993**, *34*, 1001−1004.
[67] S. C. A. Nefkens, M. Sperrle, G. Consiglio, *Angew. Chem. Int. Ed. Engl.* **1993**, *32*, 1719−1720.
[68] C. Bianchini, G. Mantovani, A. Meli, W. Oberhauser, P. Brügeller, T. Stampfl, *J. Chem. Soc., Dalton Trans.* **2001**, 690−698.
[69] E. Drent, J. A. M. van Broekhoven, M. J. Doyle, *J. Organomet. Chem.* **1991**, *417*, 235−251.

[70] G. P. C. M. Dekker, C. J. Elsevier, K. Vrieze, P. W. N. M. van Leeuwen, *Organometallics* **1992**, *11*, 1598−1603.
[71] I. Tóth, C. J. Elsevier, *J. Am. Chem. Soc.* **1993**, *115*, 10388−10389.
[72] I. Tóth, C. J. Elsevier, *Chem. Commun.* **1993**, 529−531.
[73] H. E. Bryndza, J. C. Calabrese, M. Marsi, D. C. Roe, W. Tam, J. E. Bercaw, *J. Am. Chem. Soc.* **1986**, *108*, 4805−4813.
[74] G. P. C. M. Dekker, A. Buijs, C. J. Elsevier, K. Vrieze, P. W. N. M. van Leeuwen, W. J. J. Smeets, A. L. Spek, Y. F. Wang, C. H. Stam, *Organometallics* **1992**, *11*, 1937−1948.
[75] P. W. N. M. van Leeuwen, C. F. Roobeek, H. van der Heiden, *J. Am. Chem. Soc.* **1994**, *116*, 12117−12118.
[76] P. W. N. M. van Leeuwen, C. F. Roobeek, *Recl. Trav. Chim. Pays-Bas* **1995**, *114*, 73−75.
[77] G. A. Luinstra, P. H. P. Brinkmann, *Organometallics* **1998**, *17*, 5160−5165.
[78] W. P. Mul, H. Oosterbeek, G. A. Beitel, G.-J. Kramer, E. Drent, *Angew. Chem. Int. Ed.* **2000**, *39*, 1848−1851.
[79] M. A. Zuideveld, P. C. J. Kamer, P. W. N. M. van Leeuwen (to be published).
[80] M. C. Bonnet, A. L. Monteiro, I. Tkatchenko, *J. Mol. Catal.* **1999**, *143*, 131−136.
[81] E. J. Jang, K. H. Lee, J. S. Lee, Y. G. Kim, *J. Mol. Catal.* **1999**, *138*, 25−36.
[82] T. Hayashi, M. Tanaka, I. Ogata, *J. Mol. Catal.* **1984**, *26*, 17−30.
[83] G. Cometti, G. P. Chiusoli, *J. Organomet. Chem.* **1982**, *236*, C31−C32.
[84] J.-Y. Yoon, E. J. Jang, K. H. Lee, J. S. Lee, *J. Mol. Catal.* **1997**, *118*, 181−187.
[85] D. M. Fenton, *J. Org. Chem.* **1973**, *38*, 3192−3198.
[86] D. Kruis, N. Ruiz, M. D. Janssen, J. Boersma, C. Claver, G. van Koten, *Inorg. Chem. Commun.* **1998**, *1*, 295−298.
[87] W. Clegg, G. R. Eastham, M. R. Elsegood, R. P. Tooze, X. L. Wang, K. Whiston, *Chem. Commun.* **1999**, 1877−1878.
[88] J. G. Knight, S. Doherty, A. Harriman, E. G. Robins, M. Betham, G. R. Eastham, R. P. Tooze, M. R. J. Elsegood, P. Champkin, W. Clegg, *Organometallics* **2000**, *19*, 4957−4967.
[89] G. Consiglio, M. Marchetti, *Chimia* **1976**, *30*, 26−27.
[90] G. Consiglio, S. C. A. Nefkens, C. Pisano, F. Wenzinger, *Helv. Chim. Acta* **1991**, *74*, 323−325.
[91] Y. Sugi, K. Bando, *Chem. Lett.* **1976**, 727−730.
[92] G. Consiglio, *J. Organomet. Chem.* **1977**, *132*, C26−C28.
[93] B. E. Ali, H. Alper, *J. Mol. Catal.* **1993**, *80*, 377−381.
[94] M. I. Terekhova, E. S. Petrov, *J. Gen. Chem. USSR* **1985**, *55*, 842−843.
[95] M. I. Terekhova, T. E. Kron, Y. G. Noskov, E. S. Petrov, *Neftekhimiya* **1996**, *36*, 330−335.
[96] Y. V. Tel'Naya, Y. G. Noskov, E. S. Petrov, *Zh. Obshch. Khim.* **1995**, *65*, 1391−1392.
[97] H. Zhou, J. Hou, J. Cheng, S. Lu, H. Fu, H. Wang, *J. Organomet. Chem.* **1997**, *543*, 227−228.
[98] B.-H. Xie, C.-G. Xia, S.-J. Lu, K. J. Chen, Y. Kou, Y.-Q. Yin, *Tetrahedron Lett.* **1998**, 7365−7368.
[99] B. E. Ali, H. Alper, *J. Mol. Catal.* **1992**, *77*, 7−13.
[100] T. Fuchikami, K. Ohishi, I. Ojima, *J. Org. Chem.* **1983**, *48*, 3803−3807.
[101] C. Pisano, A. Mezzetti, G. Consiglio, *Organometallics* **1992**, *11*, 20−22.
[102] S. Tilloy, E. Monflier, F. Bertoux, Y. Castanet, A. Mortreux, *New J. Chem.* **1997**, *21*, 529−531.
[103] B. E. Ali, H. Alper, *J. Mol. Catal.* **1993**, *80*, 377−381.
[104] Y. G. Noskov, E. S. Petrov, *Kinet. Catal.* **1993**, *34*, 902−908.
[105] Y. G. Noskov, E. S. Petrov, *Kinet. Catal.* **1994**, *35*, 672−677.
[106] Y. G. Noskov, E. S. Petrov, *Kinet. Catal.* **1997**, *38*, 520−526.
[107] T. A. Kron, Y. G. Noskov, M. I. Terekhova, T. S. Petrov, *Zh. Fiz. Chim.* **1996**, *70*, 82−86.
[108] A. Seayad, A. A. Kelkar, R. V. Chaudhari, L. Toniolo, *Ind. Eng. Chem. Res.* **1998**, *37*, 2180−2187.
[109] C. Benedek, G. Szalontai, A. Gömöry, S. Tõrös, B. Heil, *J. Organomet. Chem.* **1999**, *579*, 147−155.
[110] C. Benedek, S. Tõrös, B. Heil, *J. Organomet. Chem.* **1999**, *586*, 85−93.
[111] I. Cipres, J. Jenck, P. Kalck, *J. Mol. Catal.* **1990**, *58*, 387−392.
[112] M. Gómez, G. Muller, D. Sainz, *Organometallics* **1991**, *10*, 4036−4045.
[113] R. Lazzaroni, R. Settambolo, A. Raffaelli, S. Pucci, G. Vitulli, *J. Organomet. Chem.* **1988**, *339*, 357−365.
[114] R. Lazzaroni, A. Raffaelli, R. Settambolo, S. Bertozzi, G. Vitulli, *J. Mol. Catal.* **1989**, *50*, 1−9.
[115] J. Real, E. Prat, S. González-Cabello, M. Pagès, A. Polo, *Organometallics* **2000**, *19*, 4715−4719.
[116] C. Bianchini, H. M. Lee, A. Meli, F. Vizza, *Organometallics* **2000**, *19*, 849−853.
[117] I. del Río, O. Pàmies, P. W. N. M. van Leeuwen, C. Claver, *J. Organomet. Chem.* **2000**, *608*, 115−121.
[118] K. Nozaki, T. Hiyama, S. Kacker, I. T. Horváth, *Organometallics* **2000**, *19*, 2031−2035.
[119] C. Amatore, G. Broeker, A. Jutand, F. Khalil, *J. Am. Chem. Soc.* **1997**, *119*, 5176−5185.
[120] J. Keijsper, P. Arnoldy, M. J. Doyle, *Recl. Trav. Chim. Pays-Bas* **1996**, *115*, 248−255.
[121] M. Sperrle, G. Consiglio, *Chem. Ber./Recueil* **1997**, *130*, 1557−1565.
[122] R. Eastham, B. T. Heaton, J. A. Iggo, R. P. Tooze, R. Whyman, S. Zacchini, *Chem. Commun.* **2000**, 609−610.
[123] R. P. Tooze, K. Whiston, A. P. Malyan, M. J. T. Taylor, N. W. Wilson, *J. Chem. Soc., Dalton Trans.* **2000**, 3441−3444.
[124] R. J. van Haaren, H. Oevering, G. P. F. van Strijdonck, P. C. J. Kamer, P. W. N. M. van Leeuwen (to be published).

Received March 20, 2001
[I01103]

Rational Design of Open-Framework Coordination Solids − Synthesis and Structure of $[Co_5(OH)_2\{1,2,4,5\text{-}(O_2C)_4C_6H_2\}_2(H_2O)_4]\cdot xH_2O$

Siegfried O. H. Gutschke,[a] Daniel J. Price,[b] Annie K. Powell,[a] and Paul T. Wood*[c]

Keywords: Synthesis design / Cobalt / Carboxylate ligands / Mesoporous materials

A strategy for preparing open-framework coordination solids by hydrothermal synthesis has been developed and tested by the synthesis of a new porous cobalt carboxylate which can be dehydrated by heating to give a material with coordinatively unsaturated metal ions.

A number of groups are developing methods for synthesising open framework materials incorporating transition metals. These strategies include methods which aim to modify premade materials[1−8] as well as ones designed to construct the framework with the transition metal already incorporated.[9−19] Amongst the first class are syntheses in which the transition metal is substituted into a preformed zeolite,[1−3] or a metal complex is encapsulated within zeolite channels (ship-in-a-bottle catalysts)[4−7] and chemical modification of mesoporous (e.g. MCM-41) materials.[8] The second class includes the synthesis of molybdenum and vanadium phosphates,[9,10] zeolite-like cobalt (alumino) phosphate networks[11] and metal-organic coordination frameworks.[12−20] It is hoped that these materials will have the stability of zeolites with enhanced catalytic activity.

Our recent synthesis[20] of $[Co_3(OH)_2(C_4O_4)\cdot 3H_2O]$ has shown that microporous transition-metal-containing species can be produced based on metal hydroxide structural members joined together by anionic ligands. These materials can be viewed as being made up from assemblies of tubes with rectangular or diamond-shaped cross sections in which the ligands are the walls of the tube and the metal hydroxide chains form the corners. From the isolation of this material we postulated that the formation of open framework materials could be encouraged by a number a factors and we have now illustrated the usefulness of this theory by the preparation of the title compounds.

The factors which are important in the rational synthesis of open framework coordination solids relate to both the types of structural members (i.e. ligands) which can be used and also the way in which the voids can be stabilised during synthesis. The ligand should be capable of forming part of the metal hydroxide backbone and it should have a central portion which will act as part of the channel wall (Figure 1). Therefore we should be able to control the dimensions of the channel by choosing ligands with different distances between the donor groups. The channel structure can be stabilised by filling the lacunae with water molecules held in place by hydrogen bonds, particularly to bridging hydroxide ligands but also to coordinated water. The formation of species containing bridging hydroxide ligands is therefore encouraged by the use of high pH conditions for these reactions.

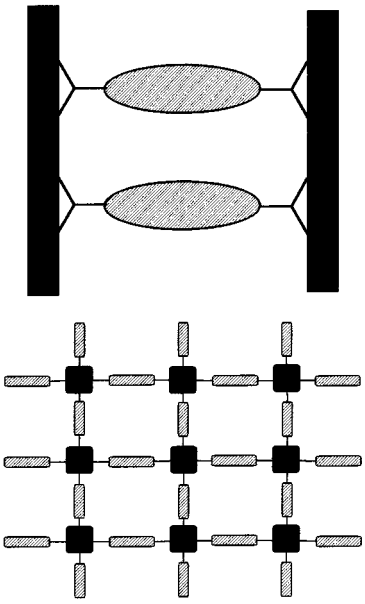

Figure 1. Schematic view of the construction of open-framework materials; black areas represent metal-oxo strips, shaded areas represent ligand "spacer" regions

The structure[21] (Figure 2) of the title compound is built around a $Co_5(\mu_3\text{-}OH)_2$ "bow-tie" cluster in which two metal triangles have a common vertex. Each triangle has a μ_3-OH at its centre and is held together by 1,3-bridging carboxylates around the periphery in a manner similar to the well-known $[M_3(O)(O_2CR)_6L_3]$ compounds. The two carboxylate functions responsible for the Co(1)−Co(2) and

[a] Institut für Anorganische Chemie der Universität, 76128 Karlsruhe, Germany
[b] Department of Chemistry, University of Southampton, Highfield, Southampton, SO17 1BJ, UK
[c] University Chemical Laboratory, Lensfield Rd, Cambridge, CB2 1EW, UK

 © WILEY-VCH Verlag GmbH, 69451 Weinheim, 2001 1434−1948/01/1111−2739 $ 17.50+.50/0

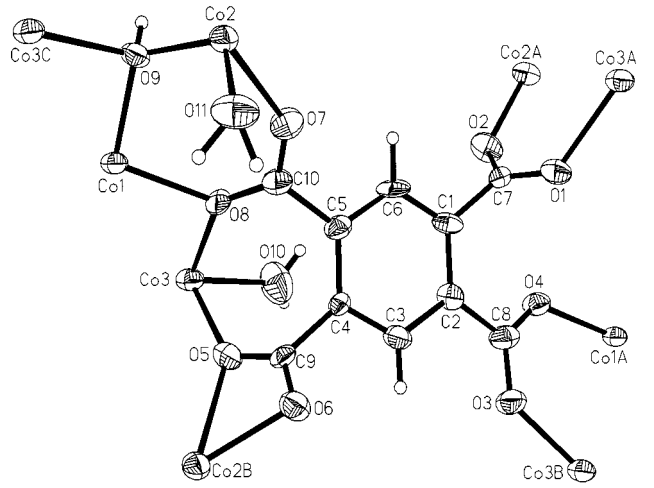

Figure 2. View of the ligand with all the metal atoms coordinated to it; selected bond lengths: Co1−O4 2.065(6), Co1−O9 2.085(5), Co1−O8 2.133(6), Co2−O9 2.013(6), Co2−O11 2.065(7), Co2−O2 2.076(6), Co2−O7 2.108(6), Co2−O6 2.136(6), Co2−O5 2.361(6), Co3−O3 2.016(6), Co3−O5 2.070(7), Co3−O1 2.083(6), Co3−O9 2.098(6), Co3−O8 2.132(5), Co3−O10 2.202(7) Å; selected bond angles: O4−Co1−O9 88.0(2), O4−Co1−O9′ 92.0(2), O4−Co1−O8 90.4(2), O4−Co1−O8′ 89.6(2), O9−Co1−O8′ 99.0(2), O9−Co1−O8 81.0(2), O9−Co2−O11 117.0(3), O9−Co2−O2 99.0(3), O11−Co2−O2 85.9(3), O9−Co2−O7 96.5(3), O11−Co2−O7 85.2(3), O2−Co2−O7 164.4(3), O9−Co2−O6 143.4(2), O11−Co2−O6 99.5(3), O2−Co2−O6 85.4(2), O7−Co2−O6 83.4(2), O9−Co2−O5 86.2(2), O11−Co2−O5 156.8(3), O2−Co2−O5 89.6(2), O7−Co2−O5 93.5(2), O6−Co2−O5 57.4(2), O3−Co3−O5 170.1(3), O3−Co3−O1 97.5(3), O5−Co3−O1 89.0(3), O3−Co3−O9 89.6(3), O5−Co3−O9 97.3(2), O1−Co3−O9 95.8(2), O3−Co3−O8 89.7(3), O5−Co3−O8 84.4(2), O1−Co3−O8 172.0(2), O9−Co3−O8 80.7(2), O3−Co3−O10 81.1(3), O5−Co3−O10 92.3(3), O1−Co3−O10 82.9(3), O9−Co3−O10 170.3(3), O8−Co3−O10 101.8(2), Co3−O5−Co2 143.2(3), Co3−O8−Co1 94.4(2), Co2−O9−Co1 118.5(3), Co2−O9−Co3 117.1(3), Co1−O9−Co3 96.9(2)°

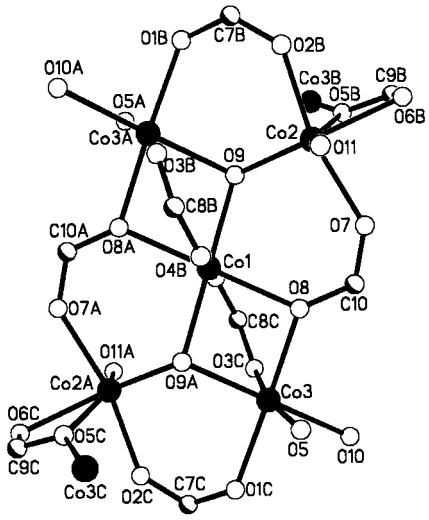

Figure 3. One of the $CO_5(OH)_2$ clusters with associated carboxylate groups; cobalt atoms from neighbouring clusters (Co3B and Co3C) have also been included

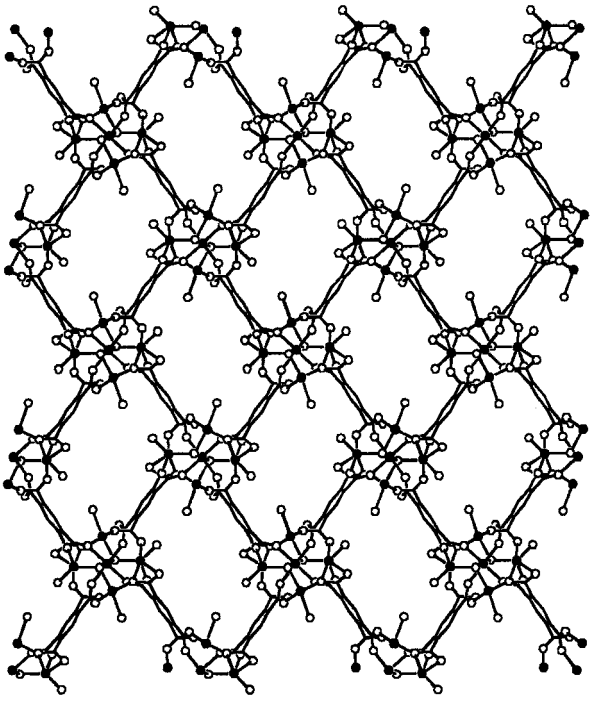

Figure 4. Packing diagram parallel to [100] with the non-coordinated water molecules omitted

Co(2)−Co(3) bridges lie close to the Co_3 plane whilst the third, Co(1)−Co(3), lies perpendicular to it. There is a further 1,1-carboxylate bridge between Co(1) and Co(3) which is common to the two fused triangles. The different types of bridging between metal atoms leads to triangles which are close to isosceles. The two edges with only OCO bridges are similar in length whereas the edge with two single-atom bridges is significantly shorter. The three crystallographically distinct metal atoms within each triangle have significantly different coordination environments. The ligand lacks any symmetry, two carboxylates on one side are 1,3-bridging and the other two acid groups together bridge four metals in a more complex arrangement. The Co_5 units are joined to adjacent clusters by four 1,1-carboxylate bridges to form a metal hydroxide-carboxylate backbone (Figure 3) running along the crystallographic *a* axis. The metal hydroxide-carboxylate rods are connected to one another by the ligand to form channels with an approximately rectangular cross-section (Figure 4). The dimensions of the rectangle are defined by the crystallographic *b* and *c* axes i.e. 16.5 × 14.6 Å. Allowing for the van der Waals radius of carbon this gives maximum dimensions of the channel of approximately 13 × 11 Å. A calculation using the PLATON[22] suite of programs shows that the framework occupies only 54.4% of the volume of the unit cell and therefore 45.6% is available for occupation by water. This compares with a free volume of 36.6% for $[Co_3(OH)_2(C_4O_4)_2{\cdot}3H_2O]$ showing that the use of larger spacer ligands not only leads to larger cavities but also to a cavity occupying a greater proportion of the material's volume. There is significant encroachment of the metal backbone into the channels, particularly for the water ligands O(10) and O(11), which hydrogen bond to some of the water molecules within the channels. There are five crystallographically distinct sites within the channels giving a maximum of 10 equivalents of

water for each Co_5 unit. At room temperature the thermal parameters of the oxygen atoms suggest that most of these sites are not fully occupied. Refinement of the X-ray data was most successful using a model which has 7.5 molecules of lattice water per Co_5 unit giving a total of 11.5 molecules of water (coordinated plus uncoordinated) per formula unit. This is in reasonable agreement with calculations using the "Squeeze" subroutine in PLATON which gives a value of 171 electrons per unit cell which corresponds to 8.5 molecules of lattice water and a total of 12.5 molecules per formula unit.

TGA studies show a gradual loss of 18% of the original mass from just above room temperature to 130 °C corresponding to 10.8 mol of water per formula unit. This suggests loss of at least half of the coordinated water, producing coordinatively unsaturated cobalt ions lining the channels which are then available as catalytic sites. The change in coordination number of cobalt is confirmed by a distinct colour change from red to blue on dehydration. The dehydrated material does not give good powder diffraction patterns showing that crystallinity is lost; however the connectivity of the lattice is maintained. When the compound is re-exposed to the atmosphere the colour change is reversed very rapidly to give a material with an IR spectrum identical to the original material and an X-ray powder diffraction pattern consistent with the single crystal structure.

In conclusion we have shown that this is a sound strategy for preparing open-framework solids and we are now applying it to other systems.

Experimental Section

Sodium hydroxide (100 mg, 2.5 mmol) was dissolved in H_2O (6 mL). A 4 mL portion of this solution was added to a solution of $CoCl_2{\cdot}6H_2O$ (250 mg, 1.9 mmol) in H_2O (2 mL) to give a blue precipitate of cobalt hydroxide. Solid 1,2,4,5-$(HO_2C)_4C_6H_2$ (100 mg, 0.4 mmol) was added to the remaining 2 mL of alkali solution. The two slurries were combined to give a molar ratio metal:ligand:base of 8:3:19 and a pH of 8.5. The mixture was placed in a 23 mL Teflon-lined autoclave and heated to 190 °C for 48 hours. The reaction vessel was cooled over a period of 4 hours and the product isolated by filtration and purified by repeated cycles of treatment of an aqueous slurry in an ultrasonic bath followed by decanting.

$[Co_5(OH)_2\{1,2,4,5\text{-}(O_2C)_4C_6H_2\}_2(H_2O)_4]{\cdot}xH_2O$ was obtained as red needles in a yield of 85 mg (39% based on ligand). – $C_{20}H_{34}Co_5O_{32}$: calcd. C 22.2, H 3.2; found C 21.7, H 2.7. Isostructural materials containing nickel (green microcrystalline powder) and zinc (colourless crystals) may also be prepared in the same way.

Acknowledgments

We wish to thank Dr Gavin Whittaker of Edinburgh University for recording the TGA data and EPSRC and the Nuffield Foundation for support.

[1] J. L. Lobree, A. W. Aylor, J. A. Reimer, A. T. Bell, *J. Catal.* **1999**, *181*, 189–204.
[2] Z. Li, M. Flytzani-Stephanopoulos, *J. Catal.* **1999**, *182*, 313–327.
[3] G. J. Millar, A. Canning, G. Rose, B. Wood, L. Trewartha, I. D. R. Mackinnon, *J. Catal.* **1999**, *183*, 169–181.
[4] N. Herron, *Inorg. Chem.* **1986**, *25*, 4714–4717.
[5] P.-P. Knops-Gerrits, D. De Vos, F. Thibault-Starzyk, P. A. Jacobs, *Nature* **1994**, *369*, 543–546.
[6] R. F. Parton, I. F. J. Vankelecom, M. J. A. Casselman, C. P. Bezoukhanova, J. B. Uytterhoeven, P. A. Jacobs, *Nature* **1994**, *370*, 541–544.
[7] K. J. Balkus, M. Eissa, R. Levado, *J. Am. Chem. Soc.* **1995**, *117*, 10753–10754.
[8] T. Maschmeyer, F. Rey, G. Sankar, J. M. Thomas, *Nature* **1995**, *378*, 159–162.
[9] R. C. Haushalter, L. A. Mundi, *Chem. Mater.* **1992**, *4*, 31–48.
[10] M. Cavellec, J. M. Grenèche, G. Férey, *Microporous Mesoporous Mater.* **1998**, *20*, 45–52.
[11] J. S. Chen, R. H. Jones, S. Natarajan, M. B. Hursthouse, J. M. Thomas, *Angew. Chem. Int. Ed. Engl.* **1994**, *33*, 639–640; P. Y. Feng, X. H. Bu, G. D. Stucky, *Nature* **1997**, *388*, 735–741.
[12] O. M. Yaghi, G. Li, H. Li, *Nature* **1995**, *378*, 703–706.
[13] A. Distler, S. C. Sevov, *Chem. Commun.* **1998**, 959–960.
[14] R. Kuhlman, G. L. Schimek, J. W. Kolis, *Inorg. Chem.* **1999**, *38*, 194–196.
[15] D. M. L. Goodgame, D. A. Gratchvogel, D. J. Williams, *Angew. Chem. Int. Ed.* **1999**, *38*, 153–156.
[16] B. E. Abrahams, P. A. Jackson, R. Robson, *Angew. Chem. Int. Ed.* **1998**, *37*, 2656–2659.
[17] S. S. Y. Chui, S. M. F. Lo, J. P. H. Charmant, A. G. Orpen, I. D. Williams, *Science* **1999**, *283*, 1148–1150.
[18] C. Livage, C. Egger, G. Férey, *Chem. Mater.* **1999**, *11*, 1546–1550.
[19] C. Janiak, *Angew. Chem. Int. Ed. Engl.* **1997**, *36*, 1431–1434.
[20] S. O. H. Gutschke, M. Molinier, A. K. Powell, P. T. Wood, *Angew. Chem. Int. Ed. Engl.* **1997**, *36*, 991–992.
[21] *Crystal data for* $C_{20}H_{46}Co_5O_{32}$, M = 1032.06, monoclinic, $P2_1/n$, a = 7.452(4), b = 16.472(6), c = 14.586(5) Å, β = 95.46(4) °, V = 1782(1) Å^3, Z = 2, D_c = 1.923 g cm^{-3}, F(000) = 1032, μ = 2.385 mm^{-1}, T = 293(2) K, crystal dimensions 0.15 × 0.08 × 0.07 mm. Data were collected on a Rigaku R-axis IIC image plate diffractometer equipped with a rotating anode X-ray source using graphite-monochromated Mo-K_α radiation (λ = 0.71073 Å). 5352 independent reflections were scaled using the Denzo-Scalepack suite of programs to give 2801 which were unique (R_{int} = 0.089). The structure was solved by direct methods and refined using full-matrix least-squares on F^2 to give *R1* = 0.0572 for $F > 4\sigma(F)$ and *wR2* = 0.1582, S = 0.926 for all data.
Crystallographic data (excluding structure factors) for the structure(s) reported in this paper have been deposited with the Cambridge Crystallographic Data Centre as supplementary publication no. CCDC-157236. Copies of the data can be obtained free of charge on application to CCDC, 12 Union Road, Cambridge CB2 1EZ, UK [Fax: (internat.) +44-1223/336-033; E-mail: deposit@ccdc.cam.ac.uk].
[22] A. L. Spek, *Acta Crystallogr., Sect. A* **1990**, *46*, C34.

Received May 16, 2001
[I01173]

[^{1}H, ^{15}N] NMR Studies of the Platination of Phosphorothioate Nucleotides – Monofunctional Sulfur Adducts versus Macrochelation

Nicole A. Kratochwil,[a] John A. Parkinson,[a] Cheryl Sacht,[a][‡] Piedad del Socorro Murdoch,[a] Tom Brown,[b] and Peter J. Sadler*[a]

Keywords: Chelates / Drug research / Nucleotides / Sulfur / Platinum

cis-[$PtI_2(^{15}NH_3)_2$] reacts rapidly with guanosine-5′-*O*-(2-thiodiphosphate) (GDP-β-S) to form a macrochelate in which Pt bridges the phosphorothioate S and guanine N7 atoms. Phosphorothioate(α-S)-containing self-complementary decamer oligonucleotides give rise to relatively long lived S-bound monofunctional adducts, the fate of which is sequence dependent.

Platinum complexes are now widely used in cancer chemotherapy.[1,2] In order to reduce toxic side effects it would be advantageous to target Pt to specific DNA base sequences on specific genes. Such a strategy is currently being explored by Lippert, Leng et. al.[3] using oligonucleotides labelled with *trans*-Pt^{II} diam(m)ine complexes, which subsequently cross-link guanine bases on the two strands. Since Pt^{II} drugs are known to have a high affinity for sulfur ligands[4] an alternative strategy might involve antisense or antigene recognition of the target gene using phosphorothioate-labelled oligonucleotides.[5–8] Phosphorothioate nucleotides are already of much clinical interest in view of their activity against HIV, for example.[9] One of our own interests is in targeting photoactivatable prodrugs to specific sites on DNA for potential photodynamic therapy.[10,11]

In the present work, we have studied the pathways and products from reactions of ^{15}N-labelled *cis*-[$PtI_2(^{15}NH_3)_2$] with the phosphorothioate guanosine-5′-*O*-(2-thiodiphosphate) [GDP-β-S, Chart 1] and three decamer oligonucleotides by NMR spectroscopy.

GDP-β-S was chosen for the study because of its ready availability. The oligonucleotides possess the self-complementary sequence 5′-TATGGCCATA-3′ (**I**) containing one phosphorothioate group either between the GG sequence 5′-TAT**GsG**CCATA-3′, **Is**, or between the CC sequence 5′-TATGG**CsC**ATA-3′, **IIs**. For comparison we also investigated the reaction of the diiodo Pt^{II} complex with the unmodified decamer **I**. Iodoplatinum complexes are also of interest because of their potential photoreactivity.[10,11]

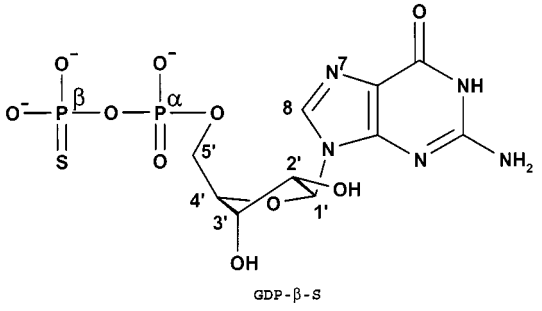

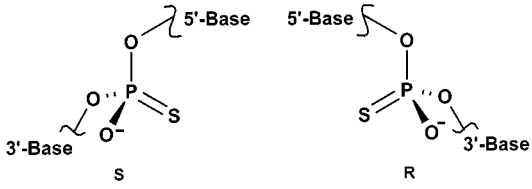

Reactions of *cis*-[$PtI_2(^{15}NH_3)_2$] (0.8 mM) with guanosine-5′-*O*-(2-thiodiphosphate) [GDP-β-S] in a 1:1 molar ratio were investigated by ^{1}H NMR spectroscopy at pH 6.94 and 310 K for a period of 24 h. Within minutes, the ^{1}H NMR signals for *cis*-[$PtI_2(^{15}NH_3)_2$] and H8 of GDP-β-S decreased in intensity. After 5 h the reaction was finished and one major product was formed, giving rise to a singlet at δ = 8.99, which was assigned to H8 of Pt-bound GDP-β-S. A high-frequency shift for the H8 resonance of 5′-GMP is typical of metal coordination to the N7 of 5′-GMP (free 5′-GMP: δ = 8.17; Pt-bound 5′-GMP: δ = 8.52). The large high-frequency shift of 0.82 ppm observed for the H8 resonance is notable. The doublet for H1′ shifted to higher frequency from δ = 5.93 to 6.06 and the ^3J(H1′-H2′) coupling constant was dramatically reduced from 6.05 to 2.75 Hz. This suggested a major change in the sugar conformation. The signal for H2′, however, shifted to low fre-

[‡] Dr. C. Sacht is a visiting scientist from Rhodes University, South Africa.
[a] Department of Chemistry, University of Edinburgh
West Mains Road, Edinburgh EH9 3JJ, UK
Fax: (internat.) +44-131/650-6452
E-mail: p.j.sadler@ed.ac.uk
[b] Biological and Medical Sciences Building, University of Southampton,
Boldrewood Bassett Crescent East, Southampton SO16 7PX, UK
Supporting information for this article is available on the WWW under http://www.wiley-vch.de/home/eurjic or from the author.

 © WILEY-VCH Verlag GmbH, 69451 Weinheim, 2001 1434–1948/01/1111–2743 $ 17.50+.50/0

quency from δ = 4.84 to 4.52. The assignments of the sugar proton resonances were confirmed by homonuclear ^{1}H-^{1}H-{^{15}N}-DQF-COSY NMR spectroscopy (Table S1 in the Supporting Information). The 2D [^{1}H, ^{15}N] HSQC NMR spectrum of the final product showed the presence of two cross-peaks with ^{15}N/^{1}H shifts of δ = −67.85/4.18 and −46.35/4.00, compatible with NH_3 *trans* to N and S, respectively, in square-planar Pt^{II} complexes.[12] The 1D ^{1}H-{^{15}N} NOE NMR difference spectrum of this product showed that irradiation of H8 increased the signal intensity of H3′ by ca. 5% and H2′ by ca. 4%, which suggested that the flexible sugar ring of free GDP-β-S changed to a more rigid structure with a C3′-endo sugar geometry in the Pt-bound GDP-β-S product. A model that is consistent with all of these observations is shown in Figure 1.

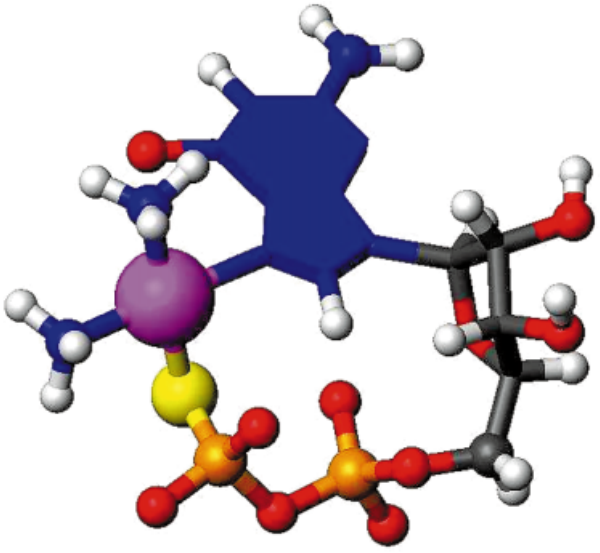

Figure 1. Model of the macrochelate complex *cis*-[$Pt(NH_3)_2$(GDP-β-S)-*N7,S*], the major adduct from the reaction of *cis*-[$PtI_2(NH_3)_2$] with the phosphorothioate GDP-β-S as deduced from NMR spectroscopic data; the macrochelate is formed by Pt binding to the S and N7 atoms of GDP-β-S

The model contains a square-planar *cis*-{$Pt(NH_3)_2$}$^{2+}$ centre bound to *N*7 and the S of GDP-β-S, thereby forming a 13-membered macrochelate ring. The composition was confirmed by ESI-MS analysis of the product of the reaction between *cis*-[$PtI_2(^{15}NH_3)_2$] and GDP-β-S (1:1 molar ratio, 100 μM) after 4 h incubation at 295 K. The negative ion electrospray mass spectrum of the product showed a cluster of ions related to the isotopic distribution of Pt, P and N at *m*/*z* = 687.1 associated with the molecular ion [$Pt(^{15}NH_3)_2C_{10}H_{12}N_5O_{10}P_2S]^-$ (calcd. 687.0) (Figure S1 in the Supporting Information), which corresponds to the macrochelate [$Pt(^{15}NH_3)_2$(GDP-β-S)*S,N*7].

Studies were also carried out to investigate the course of the reactions of *cis*-[$PtI_2(^{15}NH_3)_2$] with oligonucleotide duplexes containing a phosphorothioate group. The self-complementary oligonucleotides **I**, **Is** and **IIs** were shown to exist as duplexes in solution by the presence of imino-proton ^{1}H NMR resonances between δ = 12.00 and δ = 14.00. Reactions of *cis*-[$PtI_2(^{15}NH_3)_2$] (0.5 mM) with **Is** or **IIs** duplexes in a 1:1 molar ratio were studied by 2D [^{1}H, ^{15}N] HSQC NMR spectroscopy in 10 mM KH_2PO_4, 100 mM $KClO_4$, at pH 6.1 and 310 K for a period of 24 h. In this case the sulfur is located on the α-phosphate in contrast to the β-phosphate in GDP-β-S.

For the reactions with **Is**, the ^{15}N/^{1}H cross-peak at δ = −52.12/3.99 of *cis*-[$PtI_2(^{15}NH_3)_2$] in the 2D [^{1}H, ^{15}N] HSQC NMR spectrum had already disappeared after 4 h and four new major cross-peaks were observed (Figure 2). These peaks had ^{15}N/^{1}H chemical shifts of δ = −54.92/4.07 (**1**) and δ = −54.33/4.04 (**2**) consistent with NH_3 *trans* to I in square-planar Pt^{II} complexes, and δ = −45.97/4.24 (**3**) and δ = −46.05/4.22 (**4**), which are characteristic of NH_3 *trans* to S.[12] The intensities of cross-peaks **1**/**3** and **2**/**4** increased simultaneously and were comparable at all times, suggesting that they were due to the formation of two diastereomeric mono-iodo, mono-sulfur Pt^{II} oligonucleotide adducts, {$Pt(^{15}NH_3)_2$}-**Is**A and {$Pt(^{15}NH_3)_2$}-**Is**B, respectively. Interestingly, the cross-peaks for {$Pt(^{15}NH_3)_2$}-**Is**A, **1**/**3**, were about twice as intense as the cross-peaks **2**/**4** for {$Pt(^{15}NH_3)_2$}-**Is**B, indicating that {$Pt(^{15}NH_3)_2$}-**Is**A is the favoured product.

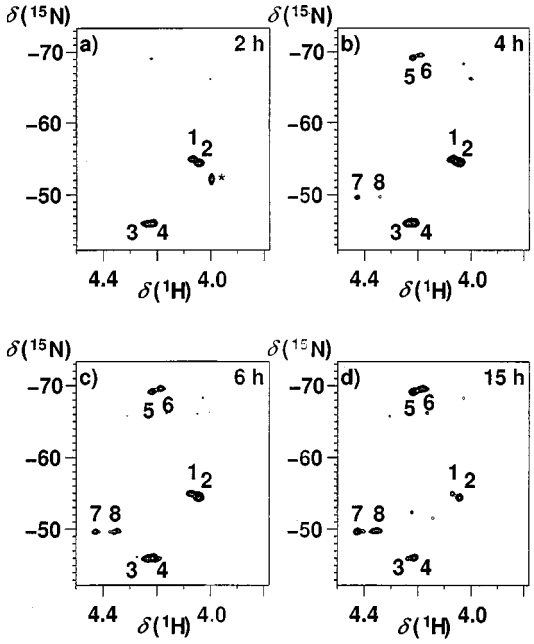

Figure 2. 2D [^{1}H, ^{15}N] HSQC NMR spectra showing the time course of the reaction between *cis*-[$PtI_2(^{15}NH_3)_2$] and **Is** at 310 K, pH 6.1: a) after 2 h; b) after 4 h; c) after 6 h; d) after 15 h; the cross-peak corresponding to the starting material is highlighted by an asterisk in a)

After 6 h, the intensities of peaks **1**/**3** and **2**/**4** decreased by ca. 27% and four new cross-peaks appeared, with intensities equivalent to the loss for signals **1**/**3** and **2**/**4**. The ^{15}N/^{1}H chemical shifts of δ = −68.98/4.22 (**5**) and δ = −69.45/4.19 (**6**) are consistent with NH_3 *trans* to N in Pt^{II} complexes, and those of the other two cross-peaks of δ = −49.69/4.43 (**7**) and δ = −49.80/4.35 (**8**) are compatible with NH_3 *trans* to S (Table S2 in the Supporting Information). These observations suggest that the mono-Pt adduct

with Pt^{II} bound to S is converted into a bifunctional-Pt adduct in which *cis*-$\{Pt(^{15}NH_3)_2\}^{2+}$ is bound to the phosphorothioate S and to N7 of a guanine base. Interestingly, the mono-iodo, mono-S Pt adducts (cross-peaks **1/3** and **2/4**) were still observable after several days, and are therefore long-lived.

We also studied the above reaction of *cis*-$[PtI_2(^{15}NH_3)_2]$ with **Is** by ^{31}P NMR spectroscopy. Oligonucleotide **Is** gave rise to two close ^{31}P NMR peaks at $\delta = 54.948$ and 54.446 due to the presence of two diastereomers (chiral P). These resonances decreased in intensity after the addition of the diiodo Pt^{II} complex, and a broad new multiplet appeared at $\delta = 41.06$. The large, low-frequency shift of the phosphorothioate ^{31}P resonance ($\delta = -13.8$) can be attributed to the direct coordination of P=S to Pt, as observed previously.[13,14] Any ^{195}Pt satellites appeared to be broadened beyond detection (by chemical shift anisotropy). The ^{31}P NMR chemical shifts of the resonances for the phosphate ^{31}P atoms of **Is** were little affected by the binding of Pt to the oligonucleotide.

The 2D [^{1}H, ^{15}N] HSQC NMR cross-peak for *cis*-$[PtI_2(^{15}NH_3)_2]$ had almost disappeared within 2 h of reaction with the oligonucleotide **IIs**, which contains the phosphorothioate group between the two cytosine residues (Figure S2 in the Supporting Information). Four new cross-peaks, **9/10** and **11/12** were then observed (^{15}N/^{1}H chemical shifts listed in Table S3 in the Supporting Information). The ^{15}N/^{1}H shifts of cross-peaks **9/10** and **11/12**) were similar to the intermediates giving rise to cross-peaks **1/3** and **2/4** in the reaction of *cis*-$[PtI_2(^{15}NH_3)_2]$ with **Is**. This suggested that two diastereomeric mono-iodo, mono-sulfur Pt^{II} adducts are also formed from **IIs** in a 2:1 (**9/10:11/12)** ratio. Surprisingly, the intermediates giving **9/10** and **11/12** for **IIs** were not as long-lived as they were during the reaction with **Is**. In particular the intermediate with cross-peaks **11/12** was short-lived compared to that with cross-peaks **9/10**. The rate of further reactions of these intermediates therefore appears to depend on the chirality at P. Cross-peaks **11** and **12** had disappeared completely after 12 h. After 8 h, five cross-peaks with ^{15}N/^{1}H shifts consistent with NH_3 *trans* to S (peaks **13**−**17**) and five cross-peaks with ^{15}N/^{1}H shifts consistent with NH_3 *trans* to N (peaks **18**−**22**; Table S3 in the Supporting Information) appeared simultaneously. This suggests that **9/10** and **11/12** undergo further reactions to form bifunctional Pt adducts in which *cis*-$\{Pt(^{15}NH_3)_2\}^{2+}$ is bound to S of the phosphorothioate and N from a base. After 12 h, two further species (cross-peaks **23**−**26**) were observed. These cross-peaks had similar ^{15}N chemical shifts to those for the products from the reaction of **Is**, indicating that *cis*-$\{Pt(^{15}NH_3)_2\}^{2+}$ is also bound to N and S. In all, about seven products appeared to form in this reaction, all of which were stable for 24 h (Table S3 in the Supporting Information) and contain Pt coordinated to S/N of the oligonucleotide. Over a longer period of time, it might be expected that some loss of coordinated NH_3 *trans* to S could occur.

For comparison, we followed the reaction of *cis*-$[PtI_2(^{15}NH_3)_2]$ with the unmodified oligonucleotide duplex **I** by 2D [^{1}H, ^{15}N] HSQC NMR spectroscopy (Figure S3 in the Supporting Information). After 10 h, three cross-peaks with similar ^{15}N/^{1}H shifts of $\delta = -68.19/4.50$, $-67.93/4.57$ and $-68.24/4.52$ were observed, consistent with NH_3 *trans* to N. This suggested that a bifunctional adduct was formed in which *cis*-$\{Pt(^{15}NH_3)_2\}^{2+}$ was bound to the N7 atoms of the two adjacent guanine bases. This is consistent with reported observations for *cis*-$\{Pt(^{15}NH_3)_2\}^{2+}$ binding to similar oligonucleotides.[15,16]

cis-$[PtI_2(^{15}NH_3)_2]$ reacts relatively rapidly with nucleotide phosphorothioates, initially at sulfur. In the case of the mononucleotide GDP-β-S, further reaction to form the S,N7 macrochelate was relatively rapid, whereas for the oligonucleotide **Is**, the *S*-bound monofunctional adducts were very long lived. Such macrochelation by Pt in phosphorothioate oligonucleotide duplexes appears to be at least partially stereoselective. Molecular modelling studies (Figure S4 in the Supporting Information) support the proposal of chelate formation by the duplex. Studies of the platination of phosphorothioate nucleotides have been reported previously,[8,13,14] but our work appears to provide the first evidence for Pt-S,N7 macrochelation. NMR evidence for O,N7 macrochelation has been reported for unmodified mono- and oligo-nucleotides.[17−19] The reaction pathways for phosphorothioate oligonucleotides appear to be highly dependent on the position of the sulfur atom. Our finding that monofunctional adducts of phosphorothioate oligonucleotides have considerable stability suggests that this might be a useful approach for the introduction of photo-active Pt−I centres into DNA and for antisense strategies.

Experimental Section

Materials: Guanosine-5′-*O*-(2-thiodiphosphate), GDP-β-S, was purchased from Aldrich and used without further purification. The oligonucleotides 5′-d(TATGGCCATA)-3′, **I**, 5′-d(TAT**Gs**G**C**CATA)-3′, **Is** and 5′-d(TATGG**Cs**CATA)-3′, **IIs**, were supplied by Oswel. *cis*-$[PtI_2(^{15}NH_3)_2]$ was synthesised according to previously described procedures[10] and was fully characterised by elemental analysis, NMR spectroscopy and FAB-MS.

ESI-MS: Atmospheric pressure ionization (API) negative ion electrospray mass spectrometry (ESI-MS) was performed using a Platform II mass spectrometer (Micromass, Manchester, UK). The mass spectra were obtained by injecting samples (concentration 100 μM in water) using an infusion pump with a flow rate of 0.48 mL/h. A source temperature of 65 °C and a drying gas flow rate of 450 $L \cdot h^{-1}$ were found to be suitable parameters for analysis. A potential of −3.17 kV was applied to the probe capillary and a cone voltage of −20 V over 100−1000 Da was used. The quadrupole was scanned at 100 $amu \cdot s^{-1}$. The acquisition and deconvolution of data were performed on a Mass Lynx (version 2.3) for Windows NT data system using the maximum entropy (MaxEnt) software algorithm. The mass accuracy of all measurements was within 0.1 *m/z* units.

NMR Spectroscopy: NMR spectroscopic data were acquired using a 500 MHz Bruker DMX NMR spectrometer according to previously described methods.[15] Typically 2D [^{1}H, ^{15}N] HSQC NMR spectra were acquired over a ^{1}H frequency width of 2 kHz and a

^{15}N frequency width of 3.55 kHz centred at δ = −55 relative to external $^{15}NH_4Cl$. 16 transients were acquired into 1024 data points for each of 256 t_1 increments. The total experiment time was typically 2 h for the acquisition of each 2D [^{1}H, ^{15}N] HSQC NMR spectroscopic data set. This was extended to 4 h (32 transients per t_1 increment) at later reaction times. $^{31}P\{^1H\}$ NMR spectra were acquired with 4096 transients over a frequency width of 50 kHz into 41662 data points (acquisition time 0.413 s). All NMR spectroscopic data were processed using Xwin-NMR version 2.0 (Bruker Ltd.).

pH Measurements: pH Measurements were made using a Corning 145 pH meter equipped with an Aldrich micro-combination electrode calibrated with Aldrich buffer solutions of pH 4, 7 and 10. Values of pH were adjusted with 1 M $HClO_4$ or NaOH as appropriate.

Acknowledgments

We are grateful to the EC for a Marie Curie Fellowship for N. A. K. and the Royal Society of Chemistry for a travel award for C. S. This research was supported by the EPSRC, BBSRC, Wolfson Foundation, Royal Society and EC COST D8/D20.

[1] J. Reedijk, *Chem. Commun.* **1996**, 801−806.
[2] E. R. Jamieson, S. J. Lippard, *Chem. Rev.* **1999**, *99*, 2467−2498.
[3] B. Lippert, M. Leng, in *Topics in Biological Inorganic Chemistry Volume 1* (Eds.: M. J. Clarke, P. J. Sadler), Springer-Velag, Berlin, **1999**, pp. 117−142.
[4] J. Reedijk, *Chem. Rev.* **1999**, *99*, 2499−2510.
[5] K. G. Strothcamp, S. J. Lippard, *Proc. Natl. Acad. Sci. USA* **1976**, *73*, 2536−2540.
[6] D. J. Szalda, F. Eckstein, H. Sternbach, S. J. Lippard, *J. Inorg. Biochem.* **1979**, *11*, 279−282.
[7] B. C. F. Chu, L. E. Orgel, *Nucleic Acids Res.* **1990**, *18*, 5163−5171.
[8] E. S. Gruff, L. E. Orgel, *Nucleic Acids Res.* **1991**, *19*, 6849−6854.
[9] J. O. Ojwang, *Antimicrob. Agents Chemother.* **1995**, *39*, 2426−2435.
[10] N. A. Kratochwil, M. Zabel, K. J. Range, P. J. Bednarski, *J. Med. Chem.* **1996**, *39*, 2499−2507
[11] N. A. Kratochwil, J. A. Parkinson, P. J. Bednarski, P. J. Sadler, *Angew. Chem. Int. Ed.* **1999**, *38*, 1460−1463.
[12] Y. Chen, Z. Guo, P. J. Sadler, in *Cisplatin − chemistry and biochemistry of a leading anticancer drug* (Ed.: B. Lippert), Wiley-VCH, Weinheim, **1999**.
[13] S. K. C. Elmroth, S. J. Lippard, *J. Am. Chem. Soc.* **1994**, *116*, 3633−3634.
[14] L. L. Slavin, E. H. Cox, R. N. Bose, *Bioconjugate Chem.* **1994**, *5*, 316−320.
[15] J. A. Parkinson, Y. Chen, P. del Socorro Murdoch, Z. Guo, S. J. Berners-Price, T. Brown, P. J. Sadler, *Chem. Eur. J.* **2000**, *6*, 3636−3644.
[16] F. Reeder, Z. J. Guo, P. del Socorro Murdoch, A. Corazza, T. W. Hambley, S. J. Berners-Price, J.-C. Chottard, P. J. Sadler, *Eur. J. Biochem.* **1997**, *249*, 370−382.
[17] M. D. Reily, L. G. Marzilli, *J. Am. Chem. Soc.* **1986**, *108*, 8299−8300.
[18] M. D. Reily, T. W. Hambley, L. G. Marzilli, *J. Am. Chem. Soc.* **1988**, *110*, 2999−3007.
[19] J. Kozelka, G. Barre, *Chem. Eur. J.* **1997**, *3*, 1405−1409.

Received June 26, 2001
[I01239]

Synthesis and Chemistry of the 16-Electron Osmium Complex [OsBr(η^5-C_5Me_5)(P*i*Pr$_3$)]

Paul B. Glaser[a] and T. Don Tilley*[a]

Keywords: Osmium / Cyclopentadienyl ligands / Oxidative addition / Coordinative unsaturation

The isolable 16-electron half-sandwich Os complex [OsBr(η^5-C_5Me_5)(P*i*Pr$_3$)] has been synthesized and structurally characterized. This unsaturated complex binds N_2 reversibly at low temperature as determined by IR and multinuclear NMR spectroscopy. The reactions of the title complex with CO, H_2, $PhSiH_3$, and its thermolysis in C_6H_6 are reported.

The stable 16-electron complexes [RuClCp*(PR$_3$)] (Cp* = η^5-C_5Me_5; R = *i*Pr, Cy) were reported in 1988.[1] These complexes, prepared by addition of the appropriate phosphane in one step from the tetrameric ruthenium species [RuClCp*]$_4$,[2] have proven to be valuable starting materials for the synthesis of various silyl,[3] silene,[4] and metallacyclic[5] complexes. Analogous 16-electron complexes of osmium are also expected to be useful synthons, but they have yet to be reported. The synthesis of coordinatively unsaturated [OsXCp*(PR$_3$)] species would seem to require a method other than that used to prepare the related ruthenium complexes, as the osmium analog of [RuClCp*]$_4$ is not known. However, Esteruelas and co-workers have recently reported[6] the preparation of an 18-electron complex, [OsClCp(P*i*Pr$_3$)$_2$], which dissociates a phosphane ligand in solution to form an unsaturated species that activates E−H bonds (E = C, Si, Ge, Sn).[7,8]

Addition of two equiv. of triisopropylphosphane to a stirred CH_2Cl_2 solution of [$Os_2Br_4Cp^*_2$][9] effected a rapid color change from dark brown to black-cherry red. Removal of all volatile components of the mixture, washing with ether, and drying under vacuum afforded a pale pink-red solid which was soluble in toluene and dichloromethane. Three broad, featureless resonances spread over a range of greater than 30 ppm in the ^{1}H NMR spectrum (CD_2Cl_2, room temperature) were consistent with a paramagnetic 17-electron complex formulated as [OsBr$_2$Cp*(P*i*Pr$_3$)] (**1**); however, a CH_2Cl_2 solution of **1** gave no detectable EPR signal at room temperature, and only below 100 K was an extremely broad signal (with no detectable hyperfine coupling) observed. A Signer molecular weight determination[10,11] (room temperature, CH_2Cl_2 solution) confirmed the monomeric nature of the complex in solution.

Treatment of a THF solution of **1** with a stoichiometric amount of 0.3% Na/Hg amalgam resulted in a striking color change from red-black to purple. Removal of all volatile materials and recrystallization from pentane at −78 °C provided dendritic, translucent, red-orange crystals. Upon isolation and warming to room temperature, these crystals became purple and opaque. Repeated attempts to obtain X-ray diffraction data on these purple crystals failed. However, multinuclear NMR spectroscopy and combustion analysis allowed characterization of this compound as the 16-electron species [OsBrCp*(P*i*Pr$_3$)] (**2**).

To characterize the origin of the temperature-dependent color change associated with **2**, a [D_8]toluene solution of **2** was cooled to −78 °C under an atmosphere of nitrogen. This resulted in a color change from purple to red-orange. Variable temperature NMR spectroscopy experiments with **2** in [D_8]toluene under N_2 revealed disappearance of the ^{31}P{^{1}H} resonance for **2** as the temperature was lowered, and the appearance of two resonances at δ = 8.71 and 8.10. After this sample was thoroughly degassed with a series of freeze-pump-thaw cycles, cooling to −78 °C did not afford a color change. The NMR spectroscopic properties of this degassed sample were essentially invariant from room temperature to −80 °C. On the basis of these observations, it was postulated that **2** reversibly binds N_2 at low temperature to give the terminal and bridging dinitrogen complexes **3** and **4**, respectively. The appearance of a relatively strong band at 2074 cm^{-1} in the low-temperature solution IR spectrum acquired under an N_2 atmosphere confirmed the presence of the end-on bound N_2 species **3**.[12] This diagnostic band did not appear when the solution was cooled under an argon atmosphere. When a sample of **2** in [D_8]toluene was cooled and sealed under an atmosphere of $^{15}N_2$, three resonances were observed in the ^{15}N NMR spectrum at low temperature, consistent with both terminal binding (δ = −47.9 and −112.4) and a bridged structure (δ = −133).[13,14] The ^{31}P{^{1}H} resonances associated with these structures also exhibited coupling to ^{15}N.

Concentration and cooling of a diethyl ether solution of **2** under argon afforded large purple-black crystals suitable for an X-ray diffraction study. The solid-state structure of **2** is shown in Figure 1. The Cp*(centroid)−P−Os−Br unit is planar within experimental error and there is no evidence for agostic C−H interactions or close intermolecular contacts. It is noteworthy that samples of **2** obtained by recrystallization under N_2 had a completely different morphology to those crystallized under argon.

[a] Department of Chemistry, University of California at Berkeley
Berkeley, California 94720-1460, USA
Fax: (internat.) +1-510/642-8940
E-mail: tdtilley@socrates.berkeley.edu

 © WILEY-VCH Verlag GmbH, 69451 Weinheim, 2001 1434−1948/01/1111−2747 $ 17.50+.50/0

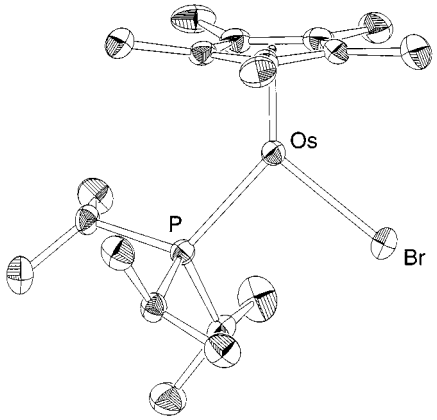

Figure 1. ORTEP diagram of **2** with 50% probability ellipsoids; hydrogens have been removed for clarity; selected bond lengths and angles (Cp^* = C_5Me_5 centroid): Os–Br 2.4785(6) Å, Os–P 2.349(2) Å, Os–Cp* 1.7898(2) Å, Br–Os–P 93.52(4)°, P–Os–Cp* 137.13(4)°, Br–Os–Cp* 129.34(2)°

Exposure of a stirred pentane solution of **2** to an atmosphere of CO resulted in a rapid color change from purple to yellow. The resulting compound, [OsBrCp*(CO)(P*i*Pr$_3$)] (**5**), exhibited a CO stretching frequency of 1896 cm^{-1} (Nujol mull). This value compares to 1908 cm^{-1} for the closely related ruthenium complex [RuClCp*(CO)(P*i*Pr$_3$)][1] and is consistent with the more basic nature of the osmium center. Coordination of CO to the osmium center destroys the effective C_s symmetry of **2**, as indicated by NMR spectroscopy. Thus, the methyl groups of the triisopropylphosphane ligand in **5** are inequivalent in the ^{1}H NMR spectrum, appearing as two virtual quadruplets integrating to nine protons each.

Compound **2** reacted under an atmosphere of hydrogen in pentane solution, as indicated by a rapid color change of the solution from purple to yellow. The ^{1}H NMR spectrum of a C_6D_6 solution of the resulting pale yellow product contained a new doublet at $\delta = -10.7$ consistent with oxidative addition of dihydrogen to the Os center to give a product formulated as [OsH$_2$BrCp*(P*i*Pr$_3$)] (**6**). $T_{1(min)}$ measurements made by the null method revealed a value of 475 ms at −81 °C for the two hydrides of **6**, demonstrating that they are "classical" in nature. The ^{1}H NMR spectrum of **6** exhibited only one set of peaks for the isopropyl methyl groups, consistent with a *trans* disposition for the hydride ligands in a "four-legged piano stool" complex. A *cis* geometry for the hydride ligands would render the isopropyl methyl groups diastereotopic and can therefore be ruled out. It is interesting to note that [RuClCp*(PR$_3$)] complexes do not react with H_2 under comparable conditions.[1]

In an experiment intended to probe the thermal stability of **2**, an NMR tube fitted with a PTFE valve was charged with a benzene solution of **2** and heated in an oil bath at 80 °C. Colorless crystals were deposited on the bottom of the tube after a few days. Although insoluble in aliphatic hydrocarbons and benzene, the crystals were soluble in CD_2Cl_2 and were determined to be the arene complex [OsCp*(η^6-C_6H_6)]Br (**7**) by ^{1}H and ^{13}C{^{1}H} NMR spectroscopy. The formation of this species presumably involves thermal dissociation of the phosphane ligand from the osmium center followed by coordination of the arene solvent to the metal center with displacement of the halide substituent. Characterization of **7** as an arene complex is supported by a comparison with the related species [RuCp*(η^6-toluene)]Cl which has been synthesized and fully characterized in these laboratories by crystallographic and spectroscopic techniques.[15]

The reaction of **2** with 1 equiv. of PhSiH$_3$ in pentane caused an immediate color change from purple to yellow. The resulting compound, [Os(H)(Br)Cp*(SiH$_2$Ph)(P*i*Pr$_3$)] (**8**), was isolated as a yellow microcrystalline solid from pentane. The ^{1}H NMR spectrum includes two resonances at $\delta = 6.60$ and 4.71 for the diastereotopic silicon-bound protons. The stereochemistry of **8** depicted in Scheme 1 was assigned based on comparison to similar ruthenium complexes[1,4] and the structurally characterized analogue [Os(H)(Br)Cp*(SiHPh$_2$)(P*i*Pr$_3$)].[11]

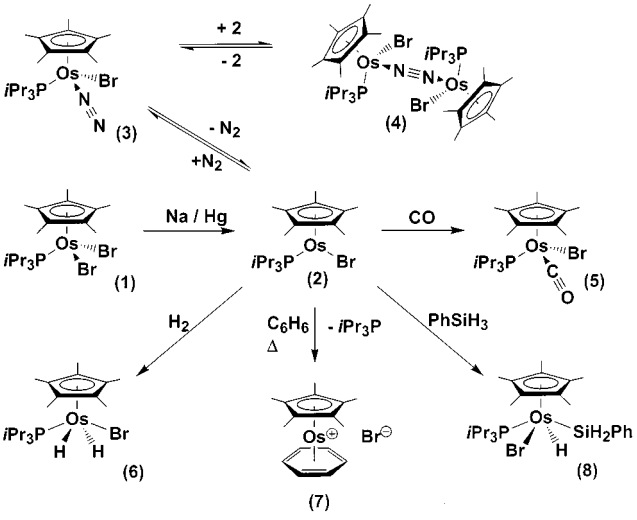

Scheme 1

We are currently probing the utility of **2** as a synthon in osmium chemistry, especially its use in generating unsaturated metal–ligand interactions. We believe that the isolable nature of **2** makes it an ideal starting material for a series of studies involving the electron rich OsCp*(R$_3$P)$^+$ fragment.

Experimental Section

All solvents were distilled under N_2 from appropriate drying agents and stored in PTFE-valved flasks. Synthetic manipulations were performed under an atmosphere of purified N_2 or argon using standard Schlenk techniques. P*i*Pr$_3$ was obtained from Strem Chemicals, Inc. and was used as received. CO was obtained from Mattheson Gas and used without further purification. [Os$_2$Br$_4$Cp*$_2$] was prepared by the published method.[8] PhSiH$_3$ was made by the reduction of PhSiCl$_3$ with LiAlH$_4$ in ether and purified by fractional distillation under N_2. ^{1}H (500.1 MHz), ^{13}C{^{1}H} (124.7 MHz), ^{31}P{^{1}H} (202.4 MHz), ^{29}Si{^{1}H} (99.3 MHz), and ^{15}N{^{1}H} (50.7 MHz) NMR spectra were ac-

quired on a Bruker DRX-500 spectrometer equipped with a BBI probe. Spectra were recorded at room temperature in C_6D_6 unless otherwise noted and were referenced to protic impurities in the deuterated solvent for ^1H, solvent peaks for ^{13}C, $SiMe_4$ for ^{29}Si, neat $MeNO_2$ for ^{15}N, and 85% H_3PO_4 for ^{31}P. Elemental analyses were performed by the University of California, Berkeley College of Chemistry Microanalytical Facility. IR absorptions are reported in units of cm^{-1} and were recorded with a Mattson Infinity 60 MI FTIR spectrometer as Nujol mulls for room temperature measurements and with an ASI React-IR apparatus for low-temperature measurements.

[$OsBr_2Cp^*(P\mathit{i}Pr_3)$] (1): A stirred CH_2Cl_2 solution of [$Os_2Br_4Cp^*_2$] (1.23 g, 1.27 mmol) was treated with 2.1 equiv. of neat $P\mathit{i}Pr_3$ at room temperature. The solution was stirred for 60 minutes, by which time it turned from brown to deep black-red. All volatile components of the mixture were removed in vacuo, and the resulting black-red solid was washed with Et_2O at 0 °C (2 × 20 mL) and dried in vacuo to give a red-pink powder. 1.36 g (83%) isolated, m.p. 205−210 °C. ^1H NMR (CD_2Cl_2): δ = −2.26 [fwhh 205 Hz, 18 H, PCH($\mathit{CH_3}$)$_2$], 6.6 [fwhh 420 Hz, 3 H, PCH(CH_3)$_2$], 23.9 [fwhh 350 Hz, 15 H, $C_5\mathit{Me_5}$). − μ_{eff} = 1.37 B.M (Evans' method,[16] CH_2Cl_2, room temperature.) Solution molecular weight (CH_2Cl_2, Signer method) 580 (645 ideal). − $C_{19}H_{36}Br_2OsP$ (645.48): calcd. C 35.35, H 5.62; found, C, 35.19, H 5.76.

[$OsBrCp^*(P\mathit{i}Pr_3)$] (2): A solution of **1** (4.1 g, 6.36 mmol) in THF was added to a flask containing a stirred Na/Hg amalgam (0.3% Na, 1 equiv.) and THF at room temperature. The solution became violet after a few minutes of vigorous stirring, and a white precipitate formed. The reaction mixture was allowed to settle after approximately 60 minutes. The supernatant was filtered away from the amalgam and precipitated solids, then was pumped dry to give a black-purple solid. Extracting the solid with pentane (5 × 20 mL) gave a purple solution, which afforded red-orange crystals of the dinitrogen adduct after concentrated cooling to −78 °C under N_2. 2.3 g (64%) isolated, m.p. 132−136 °C. X-ray quality crystals were grown from a concentrated diethyl ether solution of **2** under argon at −78 °C. ^1H NMR: δ = 1.15−1.09 [vq, 18 H, PCH($\mathit{CH_3}$)$_2$], 1.45 (s, 15 H, $C_5\mathit{Me_5}$), 2.54 [m, 3 H PCH(CH_3)$_2$]. − $^{13}C\{^1H\}$ NMR: δ = 13.4 ($C_5\mathit{Me_5}$), 20.5 [PCH($\mathit{CH_3}$)$_2$], 25.7 [d, $^1J_{PC}$ = 24.3 Hz, PCH(CH_3)$_2$], 72.8 ($\mathit{C_5}Me_5$). − $^{31}P\{^1H\}$ NMR: δ = 42.63. − $^{15}N\{^1H\}$ NMR (220 K): δ = −47.0. − $C_{19}H_{36}BrOsP$ (565.57): calcd. C 40.35, H 6.42; found C 40.45, H 6.10.

[$OsBrCp^*(^{15}N_2)(P\mathit{i}Pr_3)$] (3-$^{15}N_2$) and [$OsBrCp^*(P\mathit{i}Pr_3)]_2(\mu\text{-}\eta^1\text{:}\eta^1\text{-}^{15}N_2$) (4-$^{15}N_2$): A [$D_8$]toluene solution of **2** in a 5 mm O.D. PTFE-valved NMR tube was degassed by several freeze-pump-thaw cycles, exposed to 2 atm. of $^{15}N_2$ (Aldrich, 98%), and slowly cooled to −78 °C. The tube was then sealed and carefully brought to room temperature. $^{15}N\{^1H\}$ NMR spectra were recorded as the sample was cooled in the spectrometer. At 220 K, resonances assignable to **3**-$^{15}N_2$ [δ = −72.4 (dd, $^2J_{NP}$ = 2.5 Hz, $^1J_{NN}$ = 4.5 Hz, Os−NN), −47.9 (d, $^1J_{NN}$ = 5 Hz, Os−NN)] and **4**-$^{15}N_2$ [δ = −133.6 (d, $^2J_{NP}$ = 2.0 Hz)] were observed. − $^{31}P\{^1H\}$ NMR: (220 K): **4**-$^{15}N_2$ δ = 8.10 (d, $^2J_{NP}$ = 2.0 Hz); **3**-$^{15}N_2$ δ = 8.71 (d, $^2J_{NP}$ = 2.5 Hz).

[$OsBrCp^*(CO)(P\mathit{i}Pr_3)$] (5): A flask containing a stirred pentane solution of 125 mg of **2** (0.220 mmol) was briefly evacuated, and then filled with an atmosphere of CO. The solution changed color from purple to yellow-orange within 20 seconds at room temperature. The solution was filtered, concentrated, and cooled to −78 °C, affording a crop of well-formed orange crystals of **5**. 97 mg (75%) isolated, m.p. 209−212 °C. ^1H NMR: δ = 0.96−1.00 [vq, 9 H, PCH($\mathit{CH_3}$)$_2$], 1.29−1.24 [vq, 9 H, PCH($\mathit{CH_3}$)$_2$], 1.63 (s, 15 H, $C_5\mathit{Me_5}$), 2.30 [m, 3 H, PCH(CH_3)$_2$]. − $^{13}C\{^1H\}$ NMR: δ = 10.4 ($C_5\mathit{Me_5}$), 19.6 [d, $^2J_{PC}$ = 23 Hz, PCH($\mathit{CH_3}$)$_2$], 20.8 [PCH($\mathit{CH_3}$)$_2$], 27.2 [d, $^1J_{PC}$ = 27 Hz, PCH(CH_3)$_2$], 92.2 (d, J_{PC} = 2 Hz, $C_5\mathit{Me_5}$), 190.1 (d, $^1J_{PC}$ = 12 Hz, Os−CO). − $^{31}P\{^1H\}$ NMR: δ = 16.3. − IR: ν_{CO} = 1896 s. − $C_{20}H_{36}BrOOsP$ (593.58): calcd. C 40.47, H 6.11; found C 40.51, H 6.01.

[$OsH_2BrCp^*(P\mathit{i}Pr_3)$] (6): A flask containing a stirred pentane solution of 100 mg (0.176 mmol) of **2** was briefly evacuated, and then filled with an atmosphere of H_2. The solution changed color from purple to very pale yellow within 50 seconds at room temperature. The solution was filtered, concentrated and cooled to −78 °C, affording solid **6** as feathery, pale yellow crystals. 62 mg (62%) isolated, m.p. 152 °C (color change) 172 °C melting complete. ^1H NMR: δ = −10.7 [d, 2 H, $^2J_{PH}$ = 34.8 Hz, Os−H; $T_{1(ambient\ T)}$ = 1.73 s, $T_{1(min)}$ = 475 ms, CD_2Cl_2, −81 °C), 1.12−1.03 [vq, 18 H, PCH($\mathit{CH_3}$)$_2$], 1.80 (s, 15 H, $C_5\mathit{Me_5}$), 2.07 [m, 3 H, PCH(CH_3)$_2$]. − $^{13}C\{^1H\}$ NMR: δ = 11.3 ($\mathit{C_5}Me_5$), 19.2 [PCH($\mathit{CH_3}$)$_2$], 28.2 [d, $^1J_{PC}$ = 31 Hz, PCH(CH_3)$_2$], 90.2 ($C_5\mathit{Me_5}$). − $^{31}P\{^1H\}$ NMR: δ = 42.63. − IR: ν_{SiH} = 2105 ws, 2042 s. − $C_{19}H_{38}BrOsP$ (567.59): calcd. C 40.35, H 6.42; found C 40.45, H 6.10.

[$OsCp^*(\eta^6\text{-}C_6H_6)$]Br (7): A 5 mm O.D. PTFE-valved NMR tube was charged with a C_6H_6 solution of **2**, degassed, sealed, and immersed in an oil bath maintained at approximately 80 °C. After 1 week, several crystals were deposited at the bottom of the tube. The crystals were removed from the tube inside the drybox, washed with a little pentane at ambient temperature and dried. ^1H NMR: δ = 2.19 (15 H, $C_5\mathit{Me_5}$), 5.90 (6 H, $C_6\mathit{H_6}$). − $^{13}C\{^1H\}$ NMR: δ = 11.7 ($C_5\mathit{Me_5}$), 78.1 ($\mathit{C_5}Me_5$), 94.4 ($\mathit{C_6}H_6$). Compound **7** was not prepared on a large enough scale to facilitate further characterization.

[$Os(H)(Br)Cp^*(SiH_2Ph)(P\mathit{i}Pr_3)$] (8): A stirred pentane solution of **2** (202 mg, 0.356 mmol) was treated with 1.1 equiv. of $PhSiH_3$ dissolved in pentane. The solution immediately changed color from purple to yellow. The solution was filtered, concentrated, and cooled to −78 °C, affording a crop of polycrystalline **8**. 195 mg (81%) isolated, m.p. 163−165 °C. ^1H NMR: δ = 8.16 (d, 2 H, *o*-Ph), 7.33 (t, 2 H, *m*-Ph), 7.21 (t, 1 H, *p*-Ph), 6.60 (d, $^1J_{SiH}$ = 189 Hz, $^2J_{HH}$ = 4 Hz, 1 H, SiH), 4.71 (vq, $^1J_{SiH}$ = 182 Hz, 1 H, SiH), 2.49 [m, 3 H, PCH(CH_3)$_2$], 1.52 (s, 15 H, $C_5\mathit{Me_5}$), 1.04−1.08 [vq, 9 H, PCH($\mathit{CH_3}$)$_2$], 0.97−1.00 [vq, 9 H, PCH($\mathit{CH_3}$)$_2$], −14.8 (d, 1 H, $^2J_{PH}$ = 32 Hz, Os−H). − $^{13}C\{^1H\}$ NMR: δ = 143.39, 136.42, 127.53, 93.9 (d, $^2J_{PC}$ = 2.1 Hz, $\mathit{C_5}Me_5$), 28.04 [d, $^1J_{PC}$ = 26.7 Hz, PCH(CH_3)$_2$], 20.50 [PCH($\mathit{CH_3}$)$_2$], 19.79 [d, $^2J_{PC}$ = 3 Hz, PCH($\mathit{CH_3}$)$_2$], 10.35 ($C_5\mathit{Me_5}$). − $^{31}P\{^1H\}$ NMR: δ = 8.98. − $^{29}Si\{^1H\}$ NMR: δ = −26.0 (d, $^2J_{PSi}$ = 17 Hz). − IR: ν_{SiH} = 2061 s, 2081 s. − $C_{19}H_{38}BrOsP$ (567.59): calcd. C 44.56, H 6.58; found C 44.66, H 6.66.

X-ray Crystallographic Study: Data were collected on a Siemens SMART system using Mo-K_α graphite monochromated radiation. Structure solution and refinement was performed with the TeXsan software package.[17] $C_{19}H_{36}BrOsP$ mol. weight 565.57, purple block, cryst. size 0.35 × 0.12 × 0.20 mm, a = 16.1302(2), b = 15.5831(2), c = 16.7732(3) Å, α = β = γ = 90°, V = 4216.09(9) Å^3, orthorhombic, *Pbca*, Z = 8, $d_{calcd.}$ = 1.782 Mg m^{-3}, F_{000} = 2208.00, index ranges: $0 < h < 19$, $-17 < k < 17$, $-20 < l < 20$; 2Θ range 3.5−45.0°, T = −115 °C; refl. collected: 19152; refl. unique: 4124; R_{int} = 0.055, no. variables: 199, GOOF = 0.62, R = 0.019, R_w = 0.020, R_{all} = 0.052. Largest residual peak/hole = 0.080/−0.39 e/Å^3.

Crystallographic data (excluding structure factors) for the structure reported in this paper have been deposited with the Cambridge Crystallographic Data Centre as supplementary publication

no. CCDC-158416. Copies of the data can be obtained free of charge on application to CCDC, 12 Union Road, Cambridge CB2 1EZ, UK [Fax: (internat.) +44-1223/336-033; E-mail: deposit@ccdc.cam.ac.uk].

Acknowledgments

We gratefully acknowledge Dr. Wayne Leukens of the Lawrence Berkeley National Laboratory for EPR assistance. This work was funded by the National Science Foundation.

[1] B. K. Campion, R. H. Heyn, T. D. Tilley, *J. Chem. Soc., Chem. Commun.* **1988**, 278−280.
[2] P. J Fagan, W. S. Mahoney, J. C. Calabrese, I. D. Williams, *Organometallics* **1990**, *9*, 1843−1852.
[3] B. K. Campion, R. H. Heyn, T. D. Tilley, *J. Am. Chem. Soc.* **1988**, *110*, 7558−7560.
[4] B. K. Campion, R. H. Heyn, T. D. Tilley, *Organometallics* **1990**, *9*, 1106−1112.
[5] B. K. Campion, R. H. Heyn, T. D. Tilley, *J. Chem. Soc., Chem. Commun.* **1992**, 1201−1203.
[6] M. A. Esteruelas, A. V. Gómez, A. M. López, L. A. Oro, *Organometallics* **1996**, *15*, 878−881.
[7] M. A. Esteruelas, A. M. López, N. Ruiz, J. I. Tolosa, *Organometallics* **1997**, *16*, 4657−4667.
[8] M. Baya, P. Crochet, M. A. Esteruelas, E. Gutiérrez-Puebla, N. Ruiz, *Organometallics* **1999**, *18* 5034−5043.
[9] C. L. Gross, S. R. Wilson, G. S. Girolami, *J. Am. Chem. Soc.* **1994**, *116*, 10294−10295.
[10] R. Signer, *Justus Liebigs Ann. Chem.* **1930**, *478*, 246−266.
[11] R. W. Zoellner, *J. Chem. Ed.* **1990**, *67*, 714−715.
[12] J. Chatt, G. J. Leigh, R. L. Richards, *J. Chem. Soc* **1970**, 2243−2246.
[13] S. Donovan-Mtunzi, R. L. Richards, J. Mason, *J. Chem. Soc., Dalton Trans.* **1984**, 469−474.
[14] J. Mason, *Chem. Rev.* **1981**, *81*, 205−227.
[15] P. B. Glaser, T. D. Tilley, unpublished results.
[16] D. F. Evans, *J. Chem. Soc.* **1959**, 2003−2005.
[17] TeXsan for Windows version 1.06: Crystal Structure Analysis Package, Molecular Structure Corporation, The Woodlands, TX (**1997−99**).

Received April 23, 2001
[I01142]

New Types of Complexes Based on Re_4 Chalcocyanide Clusters − Syntheses and Crystal Structures of $[Ni(NH_3)_5]_2[Re_4Te_4(CN)_{12}]\cdot 3.4H_2O$ and $[Cd(NH_3)_5][Cd(NH_3)_3][Re_4Te_4(CN)_{12}]\cdot 4H_2O$

Yuri V. Mironov,[a] Oliver Oeckler,[b] Arndt Simon,*[b] and Vladimir E. Fedorov[a]

Keywords: Rhenium / Clusters / Transition metals / Solid-state structures

Two new tetrahedral rhenium chalcocyanide cluster compounds $[Ni(NH_3)_5]_2[Re_4Te_4(CN)_{12}]\cdot 3.4H_2O$ (**1**) and $[Cd(NH_3)_5][Cd(NH_3)_3][Re_4Te_4(CN)_{12}]\cdot 4H_2O$ (**2**), exhibiting molecular (**1**) and chain-like polymeric structures (**2**), have been synthesized by treatment of the salt-like cluster compound $K_4Re_4Te_4(CN)_{12}\cdot 5H_2O$ with solutions of nickel acetate and cadmium sulfate, respectively, in aqueous ammonia. Both compounds have been characterized by single-crystal X-ray diffraction analysis. Compound **1** crystallizes in the monoclinic space group $P2_1/c$ [a = 19.572(3), b = 14.849(2), c = 23.576(3) Å, β = 145.97(1)°, Z = 4, V = 3834.4(9) Å^3], while compound **2** crystallizes in the triclinic space group $P\bar{1}$ [a = 12.726(2), b = 13.408(2), c = 13.918(2) Å, α = 111.31(2), β = 116.77(2), γ = 90.17(2)°, Z = 2, V = 1935.3(5) Å^3].

Introduction

The chemistry of transition metal chalcocyanide cluster compounds, existing as either discrete or interconnected clusters, has been extensively developed in recent years.[1−14] One of the most interesting features of CN ligands is their ability to form cyano-bridged complexes with transition metals. In the past few years, many such complexes incorporating cluster chalcocyanide anions have been obtained, most of them based on the cluster anions $[Re_6Q_8(CN)_6]^{4-}$ (Q = S, Se) with an octahedral core.[9−14] In these polymeric compounds, all or some of the CN^- ligands may be bridging, thus allowing the formation of structures of different dimensionalities, i.e. 1D, 2D, or 3D. In recent publications,[6,15] we have reported the syntheses of the layered compound $[Cu_4(\mu_3\text{-}OH)_4][Re_4Te_4(CN)_{12}]$, obtained at pH ≈ 7, and three 3D-polymeric compounds $Mn_2[Re_4Se_4(CN)_{12}]\cdot 6H_2O$, $Cd_2[Re_4Te_4(CN)_{12}]\cdot 6H_2O$, and $Cu_2[Re_4Te_4(CN)_{12}]\cdot 4H_2O$, obtained at pH ≈ 1−5. We have now extended our studies to aqueous ammonia. Our findings demonstrate the significant dependence of the nature of the product on the reaction conditions used. In the present work, we have prepared one molecular complex $[Ni(NH_3)_5]_2[Re_4Te_4(CN)_{12}]\cdot 3.4H_2O$ (**1**) and one chain-like complex $[Cd(NH_3)_5][Cd(NH_3)_3][Re_4Te_4(CN)_{12}]\cdot 4H_2O$ (**2**). Compound **1** contains only terminal $[Ni(NH_3)_5]^{2+}$ cations, while compound **2** contains both bridging $[Cd(NH_3)_3]^{2+}$ and terminal $[Cd(NH_3)_5]^{2+}$ cations.

[a] Institute of Inorganic Chemistry of the Russian Academy of Sciences,
pr. Lavrentyeva 3, 630090 Novosibirsk, Russia
[b] Max-Planck-Institut für Festkörperforschung,
Heisenbergstraße 1, 70569 Stuttgart, Germany

Results

The treatment of $K_4Re_4Te_4(CN)_{12}$ with transition metal salts in aqueous solution leads to the formation of cyano-bridged cluster complexes, in which the transition metal atom may be coordinated by one, two, or three N atoms of CN ligands of the cluster anion $[Re_4Te_4(CN)_{12}]^{4-}$. In our earlier investigations in this area, it became clear that the preparation of single crystals of such complexes requires a very slow diffusion of the starting components. Mixing of aqueous solutions usually results only in powders, the structures of which are often different from those of the compounds obtained by slow diffusion. In the studied reactions, the transition metal adducts are aquo complexes $[M(H_2O)_6]^{n+}$. The M−(OH_2) bonds in these complexes are weaker than M−(NC) bonds and hence ligand exchange occurs.

We now extend our investigations in this area to complexes of the transition metals with ammonia. In the adduct complexes $[M(NH_3)_6]^{n+}$, the metal−ligand bonds are stronger than those in aquo complexes. Thermodynamic as well as kinetic factors may affect both the compositions of the products and the rates of their formation. Indeed, we have obtained some new types of Re_4 cluster complexes with transition metals starting from ammine complexes. Here we present two new cluster compounds with transition metals, namely $[Ni(NH_3)_5]_2[Re_4Te_4(CN)_{12}]\cdot 3.4H_2O$ (**1**) and $[Cd(NH_3)_5][Cd(NH_3)_3][Re_4Te_4(CN)_{12}]\cdot 4H_2O$ (**2**). Both compounds were prepared under similar conditions by treating an aqueous solution of $K_4Re_4Te_4(CN)_{12}$ with the ammine complexes of the corresponding transition metals.

The structures of both complexes were solved by single-crystal X-ray analysis. Both compounds contain the $[Re_4Te_4(CN)_{12}]^{4-}$ cluster anion, the structure of which is similar to that found in other complexes containing this anion. It contains an $[Re_4Te_4]$ cubane-like core formed from an almost regular tetrahedron of Re atoms in oxidation

 © WILEY-VCH Verlag GmbH, 69451 Weinheim, 2001 1434−1948/01/1111−2751 $ 17.50+.50/0

state IV with all triangular faces symmetrically capped by μ_3-Te ligands. The Re−Re bond lengths are in the ranges 2.8540(6)−2.8767(7) Å (**1**) and 2.8676(14)−2.8775(11) Å (**2**), the Re−Te bond lengths are in the ranges 2.6230(8)−2.6469(8) Å (**1**) and 2.6224(14)−2.6454(14) Å (**2**), and the Re−C distances are 2.09(1)−2.13(1) Å (**1**) and 2.03(2)−2.08(2) Å (**2**), respectively.

In the molecular structure of compound **1**, two $[Ni(NH_3)_5]^{2+}$ cations are coordinated to the N atoms of CN ligands of the $[Re_4Te_4(CN)_{12}]^{4-}$ anion (Figure 1). Each Ni atom is coordinated by the five N atoms of the NH_3 ligands with Ni−N distances ranging from 2.081(9) to 2.150(9) Å, and by one N atom from a CN ligand of the cluster with Ni−N distances of 2.067(8) and 2.097(8) Å. Interestingly, both cations are coordinated to the same Re atom. This is the first example of a chalcocyanide complex with a transition metal that exhibits a discrete molecular structure.

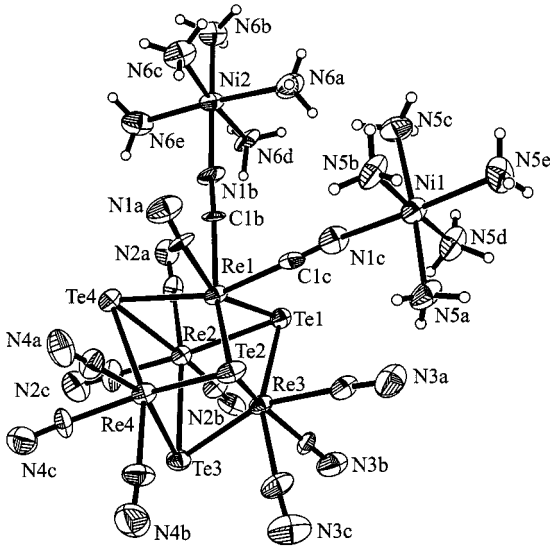

Figure 1. Crystal structure of $[Ni(NH_3)_5]_2[Re_4Te_4(CN)_{12}]\cdot 3.4H_2O$; thermal ellipsoids are drawn at a 75% probability level

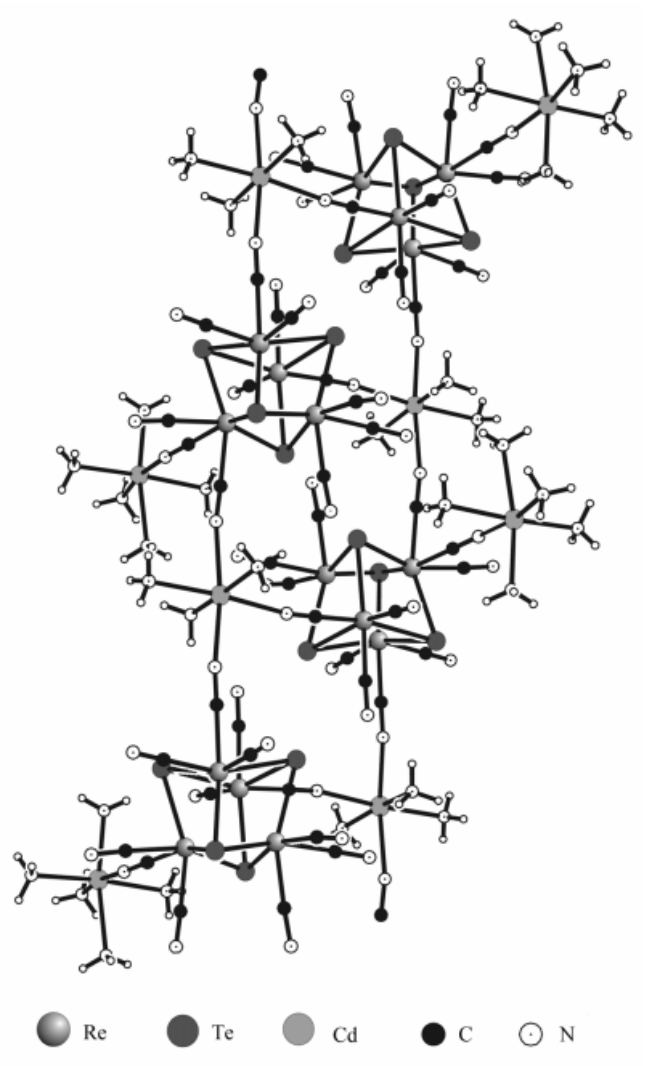

Figure 2. A fragment of the crystal structure of $[Cd(NH_3)_5][Cd(NH_3)_3][Re_4Te_4(CN)_{12}]\cdot 4H_2O$

The second compound $[Cd(NH_3)_5][Cd(NH_3)_3][Re_4Te_4(CN)_{12}]$ (**2**) contains two types of cations, namely terminal $[Cd(NH_3)_5]^{2+}$ and bridging $[Cd(NH_3)_3]^{2+}$ cations (Figure 2). The Cd atom of each $[Cd(NH_3)_5]^{2+}$ cation is coordinated by the five N atoms of the NH_3 ligands [Cd−N distances in the range 2.29(3)−2.47(4) Å] and one N atom of a CN ligand of the cluster. The Cd−N distance [2.43(3) Å] is similar to the Ni−N distance found in the Ni salt. The Cd atom of each bridging $[Cd(NH_3)_3]^{2+}$ cation is coordinated by the three N atoms of the NH_3 ligands with Cd−N distances ranging from 2.25(2) to 2.39(2) Å, and by three N atoms of CN ligands of different clusters with Cd−N distances in the range 2.36(2)−2.42(2) Å, thereby forming a chain-like structure. Each $[Re_4Te_4(CN)_{12}]^{4-}$ anion is coordinated by one terminal $[Cd(NH_3)_5]^{2+}$ group.

In the infrared spectra, two bands at 2169 and 2133 cm^{-1} (compound **1**), or at 2163 and 2133 cm^{-1} (compound **2**), can be assigned to the bridging and terminal CN groups, respectively. For both complexes, four additional bands are seen, due to coordinated ammonia molecules. Two of these, at 3345 and 1615 cm^{-1} (compound **1**) and 3340 and 1605 cm^{-1} (compound **2**), coincide with vibrations of water.

Comparison of the interaction of aqueous solutions of $[Re_4Te_4(CN)_{12}]^{4-}$ cluster anions with transition metal aquo $[M(OH_2)_6]^{2+}$ and ammine $[M(NH_3)_6]^{2+}$ complexes demonstrates that the formation of cyano-bridged complexes is dependent on the strength of the M−X (X = OH_2, NH_3, NC) bonds. In the case of aquo complexes, the weaker M−OH_2 bonds can be cleaved under formation of the thermodynamically more favourable M−NC bonds. As a result, polymeric complexes are formed, often with the maximum number of M−NC bonds. Starting from the ammine complexes $[M(NH_3)_6]^{2+}$, we observed the formation of the molecular complex **1** with only one substituted NH_3 ligand, and of the chain-like complex **2** with two types of cations, namely $[Cd(NH_3)_5]^{2+}$, from which one NH_3 molecule has been substituted, and $[Cd(NH_3)_3]^{2+}$, from which three NH_3 molecules have been substituted. This difference between these two compounds may have a kinetic origin. Under similar conditions, compound **1** is formed within 24 h, whereas

compound **2** only forms within 48 h. The compounds described herein may possibly represent the first and second steps in the formation of cyano-bridged polymeric complexes.

Experimental Section

General: All experimental manipulations were performed in air. $K_4Re_4Te_4(CN)_{12}\cdot 5H_2O$ was prepared by the reaction of $Re_4Te_4(TeCl_2)_4Cl_8$ with KCN.[5] All other reagents were used as received from commercial sources. − FT-IR: Bruker IFS-85. − Elemental analyses: Carlo Erba 1106.

$[Ni(NH_3)_5]_2[Re_4Te_4(CN)_{12}]\cdot 3.4H_2O$ (1): A solution of $Ni(CH_3COO)_2$ (20 mg) in concentrated aqueous ammonia (3 mL) was mixed with a solution of $K_4Re_4Te_4(CN)_{12}\cdot 5H_2O$ (10 mg) in water (2 mL). At ambient temperature, the resulting solution was transferred to a crystallizing dish, which was then covered by a watch glass. After 24 h, black crystals had formed, which were collected by filtration and dried on filter paper. Yield: 10 mg (95%). − $C_{12}H_{30}N_{22}Ni_2Re_4Te_4\cdot 3H_2O$ (1909.19): calcd. C 7.55, H 1.90, N 16.14; found C 7.22, H 1.41, N 15.54; the solvent content probably varies to a certain extent. − IR (KBr): $\tilde{\nu}$ = 3345 (m), 2169 (w), 2133 (s), 1615 (m), 1219 (m), 667 cm^{-1} (m). − μ_{eff} = 2.96 μ_B (298 K), 2.80 μ_B (78 K).

$[Cd(NH_3)_5][Cd(NH_3)_3][Re_4Te_4(CN)_{12}]\cdot 4H_2O$ (2): A solution of $CdSO_4\cdot 8H_2O$ (20 mg) in concentrated aqueous ammonia (3 mL) was mixed with a solution of $K_4Re_4Te_4(CN)_{12}\cdot 5H_2O$ (10 mg) in water (2 mL). At ambient temperature, the resulting solution was transferred to a crystallizing dish, which was then covered by a watch glass. After 2 days, black crystals of **2** had formed, which were collected by filtration and dried on filter paper. Yield: 10 mg (91%). − $C_{12}H_{32}Cd_2N_{20}O_4Re_4Te_4$ (2000.58): calcd. C 7.20, H 1.61, N 14.00; found C 7.26, H 0.88, N 13.65. − IR (KBr): $\tilde{\nu}$ = 3340 (w), 2163 (m), 2133 (s), 1605 (m), 1204 (m), 612 cm^{-1} (m).

X-ray Structural Analyses: Stoe IPDS diffractometer, graphite monochromator, Mo-K_α radiation (λ = 0.71073 Å); the SHELX-97 program package[16] was used for structure solution by direct methods and for refinement by full-matrix least-squares techniques.[17]

$[Ni(NH_3)_5]_2[Re_4Te_4(CN)_{12}]\cdot 3.4H_2O$ (1): M_r = 1918, monoclinic, space group $P2_1/c$, a = 19.572(3), b = 14.849(2), c = 23.576(3) Å, β = 145.97(1)°, V = 3834.4(9) $Å^3$, Z = 4, $D_{calcd.}$ = 3.32 $g\cdot cm^{-3}$, μ = 16.58 mm^{-1}, T = 93(2) K. Crystal size 0.18 × 0.07 × 0.01 mm; $2\theta_{max}$ = 53° ($-25 \le h \le 25$, $-17 \le k \le 17$, $-30 \le l \le 30$), 8390 symmetry-independent reflections from 52895 collected reflections (R_{int} = 0.078); max./min. transmission: 0.83/0.28; 439 parameters refined; $R1$ = 0.0333, $wR2$ = 0.0655 [$I > 2\sigma(I)$]; $R1$ = 0.0624, $wR2$ = 0.0737 (all reflections), GoF = 0.932; $\Delta\rho_{max}$ = 1.84 $e\cdot Å^{-3}$, $\Delta\rho_{min}$ = −1.57 $e\cdot Å^{-3}$.

$[Cd(NH_3)_5][Cd(NH_3)_3][Re_4Te_4(CN)_{12}]\cdot 4H_2O$ (2): M_r = 2000.58, triclinic, space group $P\bar{1}$, a = 12.726(2), b = 13.408(2), c = 13.918(2) Å, α = 111.31(2), β = 116.77(2), γ = 90.17(2)°, V = 1935.3(5) $Å^3$, Z = 2, $D_{calcd.}$ = 3.433 $g\cdot cm^{-3}$, μ = 16.543 mm^{-1}, T = 293(2) K. Crystal size 0.20 × 0.15 × 0.11 mm; $2\theta_{max}$ = 50° ($-15 \le h \le 15$, $-15 \le k \le 15$, $-16 \le l \le 16$), 5626 symmetry-independent reflections from 18453 collected reflections (R_{int} = 0.089); max./min. transmission: 0.288, 0.937; 423 parameters refined; $R1$ = 0.0634, $wR2$ = 0.1677 [$I > 2\sigma(I)$]; $R1$ = 0.0742, $wR2$ = 0.1753 (all reflections), GoF = 1.052; $\Delta\rho_{max}$ = 3.57 $e\cdot Å^{-3}$, $\Delta\rho_{min}$ = −2.12 $e\cdot Å^{-3}$.

Acknowledgments

This work was supported by the Russian Foundation for Basic Research, grant no. 99-03-32789.

[1] V. P. Fedin, I. V. Kalinina, D. G. Samsonenko, Y. V. Mironov, M. N. Sokolov, S. V. Tkachev, A. V. Virovets, N. V. Podberezskaya, M. R. J. Elsegood, W. Clegg, A. G. Sykes, *Inorg. Chem.* **1999**, *38*, 1956−1965.
[2] V. P. Fedin, I. V. Kalinina, A. V. Virovets, N. V. Podberezskaya, I. S. Neretin, Y. L. Slovokhotov, *Chem. Commun.* **1998**, 2579−2580.
[3] M. Laing, P. M. Kiernan, W. P. Griffith, *J. Chem. Soc., Chem. Commun.* **1977**, 221−222.
[4] Yu. V. Mironov, T. E. Albrecht-Schmitt, J. A. Ibers, *Z. Krist. NCS* **1997**, *212*, 308.
[5] Yu. V. Mironov, A. V. Virovets, V. E. Fedorov, *J. Struct. Chem. (Engl. Transl.)* **1999**, *40*, 313−316.
[6] Yu. V. Mironov, A. V. Virovets, S. B. Artemkina, V. E. Fedorov, *Angew. Chem. Int. Ed.* **1998**, *37*, 2507−2509.
[7] Yu. V. Mironov, J. A. Cody, T. A. Albrecht-Schmitt, J. A. Ibers, *J. Am. Chem. Soc.* **1997**, *119*, 493−498.
[8] A. Slougui, Yu. V. Mironov, A. Perrin, V. E. Fedorov, *Croat. Chem. Acta* **1995**, *68*, 885−890.
[9] Yu. V. Mironov, A. V. Virovets, V. E. Fedorov, N. V. Podberezskaya, O. V. Shishkin, Y. T. Struchkov, *Polyhedron* **1995**, *14*, 3171−3173.
[10] N. G. Naumov, A. V. Virovets, S. B. Artemkina, V. E. Fedorov, *Angew. Chem. Int. Ed.* **1998**, *37*, 1943−1945
[11] N. G. Naumov, S. B. Artemkina, A. V. Virovets, V. E. Fedorov, *Solid State Sci,* **1999**, *1*, 463−472.
[12] L. G. Beauvais, M. P. Shores, J. R. Long, *Chem. Mater.* **1998**, *10*, 3783−3786.
[13] M. P. Shores, L. G. Beauvais, J. R. Long, *J. Am. Chem. Soc.* **1999**, *121*, 775−779.
[14] M. P. Shores, L. G. Beauvais, J. R. Long, *Inorg. Chem.* **1999**, *38*, 1648−1649.
[15] Yu. V. Mironov, A. V. Virovets, W. S. Sheldrick, V. E. Fedorov, *Polyhedron*, in press.
[16] G. M. Sheldrick, *SHELX-97*, University of Göttingen, **1997**.
[17] Crystallographic data (excluding structure factors) for the structures reported in this paper have been deposited with the Cambridge Crystallographic Data Centre. Copies of the data (depository numbers CCDC-158006 for **1**, -158005 for **2**) may be obtained free of charge on application to CCDC, 12 Union Road, Cambridge CB2 1EZ, U.K. [Fax: (internat.) + 44-1223/336-033; E-mail: deposit@ccdc.cam.ac.uk].

Received March 12, 2001
[I01094]

Derivatives of Bis(2,2′-bipyridyl)dicyanoiron(II) with Long Alkyl Chains – Versatile Solvatochromic Probes that Form Metalloaggregates in Water-Rich Media

Paula Gameiro,*[a] Eulália Pereira,[a] Paula Garcia,[a] Sónia Breia,[a] John Burgess,[b] and Baltazar de Castro[a]

Keywords: Aggregation / Iron / Surfactants / Solvatochromism

We report on the preparation, characterisation, and solvatochromic behaviour of four new $[FeL_2(CN)_2]$ complexes, where L is the ligand 4,4′-diisobutyl-2,2′-bipyridine, 4,4′-di-*n*-pentyl-2,2′-bipyridine, 4,4′-di-*n*-heptyl-2,2′-bipyridíne, or 4-*n*-heptyl-4′-methyl-2,2′-bipyridine. The solvatochromic properties of these complexes show that the hydrophobicity imposed by the alkyl chains controls the response of the complexes towards the solvent, and that they are ideal to use as solvation probes in heterogeneous/organised media. An interesting result emerging from this work is the demonstration of the self-aggregating properties of the complexes *cis*-$[Fe(Pe_2bpy)_2(CN)_2]$, *cis*-$[Fe(He_2bpy)_2(CN)_2]$, and *cis*-$[Fe(Hebpy)_2(CN)_2]$ which are, without doubt, metallosurfactants.

Introduction

Iron(II) cyanide complexes such as *cis*-$[FeL_2(CN)_2]$, with L = 2,2′-bipyridyl, *o*-phenanthroline, or one of various Schiff base diimines, are strongly solvatochromic.[1–3] This property makes them suitable for the monitoring of their local solvation environment, not only in pure solvents, but also in binary media where they are used to assess preferential solvation and to study possible synergic solvation effects.[4,5] By varying the nature of the diimine, it is possible to control the hydrophilicity or lipophilicity of the complex. They have also been used to probe solvation in organised aqueous media, such as micelles and microemulsions.[6–9]

These inorganic complexes can complement E_T dyes, the most widely used organic solvatochromic polarity probes, since most of these dyes are not very soluble in water and are not ideal for investigating solvation in water-rich binary aqueous solvent mixtures.[10] Since systematic changes in the electrostatic/hydrophobic properties of the probes are necessary to investigate solvation in a wide range of solvents, metal complexes have proved to be particularly versatile. These metal complexes can be tuned by varying the inner coordination sphere of the metal centre while maintaining (or not) the overall charge of the probe molecule, or by appending aliphatic chains to the ligands and retaining the inner coordination sphere of the metal centre. As a result, the electrostatic or hydrophobic interactions of the complexes can be varied. This approach allows the construction of a set of solvation probes that may be used to analyse the relative importance of electrostatic/hydrophobic interactions in binary aqueous media, and also in organised media.

The most common inorganic solvatochromic probes, *cis*-$[FeL_2(CN)_2]$, with L = 2,2′-bipyridyl or 1,10-phenanthroline, are soluble in water and other protic solvents, but sparingly soluble or insoluble in nonpolar solvents. On the other hand, iron(II) complexes with lipophilic Schiff base diimines are soluble in some nonpolar solvents, and are much less sensitive to solvent polarity than those with 2,2′-bipyridyl and 1,10-phenanthroline.[3] The use of substituted 2,2′-bipyridyl ligands, containing one or two hydrophobic chains of varying length, seems a good route to isolate the changes in the inner coordination sphere of the metal centre from the changes in the hydrophobicity of the complexes. These compounds with substituted 2,2′-bipyridyl ligands combine the sensitivity of the bipyridyldicyanoiron(II) complex and the solubility of Schiff base diimines in nonpolar solvents.

In a recent paper we reported on the solvatochromic properties of the complex *cis*-$[Fe(PeMebpy)_2(CN)_2]$, where PeMebpy is bis(4-methyl-4′-*n*-pentyl-2,2′-bipyridyl).[12] This complex represents the first example of a solvatochromic compound which is soluble in water and in *n*-alkanes, and which is as sensitive to its solvent environment as the parent complex *cis*-$[Fe(bpy)_2(CN)_2]$. The solvatochromic behaviour of this complex has shown that attaching aliphatic chains to 2,2′-bipyridyl can lead to the development of versatile inorganic solvatochromic indicators for a wide range of solvent media.

In this paper we report on the preparation, characterisation and solvatochromic behaviour of four new $[FeL_2(CN)_2]$ complexes, where L is the ligand Bu_2bpy, Pe_2bpy, Hp_2bpy, or HpMebpy (Scheme 1).

Their solvatochromism was studied in pure solvents and in mixed solvents (water/methanol, water/acetonitrile, and

[a] CEQUP/Departamento de Química, Faculdade de Ciências, Universidade do Porto,
4169-007 Porto, Portugal
E-mail: agsantos@fc.up.pt
[b] Department of Chemistry, University of Leicester, Leicester LE1 7RH, UK

 © WILEY-VCH Verlag GmbH, 69451 Weinheim, 2001 1434–1948/01/1111–2755 $ 17.50+.50/0

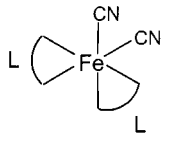

L =

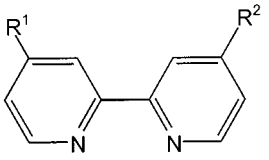

Compound		
1	$R^1 = R^2 = i\text{-}C_4H_9$:	Bu_2bpy
2	$R^1 = R^2 = n\text{-}C_5H_{11}$:	Pe_2bpy
3	$R^1 = R^2 = n\text{-}C_7H_{15}$:	Hp_2bpy
4	$R^1 = CH_3$, $R^2 = n\text{-}C_7H_{15}$:	HpMebpy
5	$R^1 = CH_3$, $R^2 = n\text{-}C_5H_{11}$:	PeMebpy

Scheme 1

water/acetone). Their solvatochromic characteristics are compared with those of the Reichardt dyes (E_T scale), as well as with those of *cis*-[Fe(bpy)$_2$(CN)$_2$], which is the most common solvatochromic inorganic probe, and of *cis*-[Fe(PeMebpy)$_2$(CN)$_2$], which is the first solvatochromic inorganic probe to be soluble in water and *n*-alkanes.

The results obtained demonstrated that complexes **1**−**4** combine the sensitivity of the bipyridyldicyanoiron(II) complexes with the solubility of the analogous, but less sensitive, complexes of Schiff base diimines in nonpolar solvents. On the other hand, the response of complexes **2**−**4** to solvent polarity in nonpolar solvents was found to be completely different from that observed for the Reichardt dyes. Finally, in water-rich media, it must be stressed that the hydrophobicity imposed by the alkyl tails clearly controls the response of the complexes to solvent polarity, and thus gives access to the synthesis of complexes for probing solvation in heterogeneous/organised solvent media.

An interesting result of complexes **2**−**4** is that they form metalloaggregates in the water-rich region of the mixed solvents used. The water content at which aggregation starts is dependent on the length and number of the alkyl chains.

Results and Discussion

Solutions of complexes **1**−**4** are violet in polar solvents, but blue in nonpolar solvents. The solvatochromic properties of these complexes were studied by visible spectrophotometry in several pure solvents, ranging from water to paraffins, and in the following mixed solvents: water/methanol, water/acetonitrile and water/acetone. The electronic absorption spectra of all complexes are identical to that reported for *cis*-[Fe(bpy)$_2$(CN)$_2$],[13] and the solvatochromic behaviour presented in this work is based on the wavenumber of the maximum absorption of the lowest-energy metal-to-ligand charge-transfer band, $\tilde{\nu}_{max}$(MLCT).

Solvatochromic Behaviour in Water and in Non-Aqueous Solvents

Table 1 includes the values of $\tilde{\nu}_{max}$(MLCT), in water and in a wide range of non-aqueous solvents, for each complex, and the values of the Reichardt parameter E_T,[14,15] and of Gutmann's acceptor number (*AN*),[16] for the solvents used. Solvatochromic data in water are restricted to *cis*-[Fe(*i*Bu$_2$-bpy)$_2$(CN)$_2$], the only complex that is water-soluble.

Comparison of solvent sensitivity of the *cis*-[FeL$_2$(CN)$_2$] complexes prepared in this work (**1**−**4**) with that of *cis*-[Fe(bpy)$_2$(CN)$_2$], the inorganic species whose solvatochromic behaviour has been most extensively studied, can be made by plotting their $\tilde{\nu}_{max}$(MLCT) values against those of *cis*-[Fe(bpy)$_2$(CN)$_2$], for solvents in which they are soluble. These plots gave straight lines, with correlation coefficients higher than 0.99±0.02, and with slopes close to unity (the average for complexes **1**−**4** is 1.05±0.05). Thus, it is possible to conclude that these complexes are as sensitive as *cis*-[Fe(bpy)$_2$(CN)$_2$] to the solvent environment, and that they also extend the range of solvents in which they can be used as probes. However, since *cis*-[Fe(bpy)$_2$(CN)$_2$] is not soluble in nonpolar solvents, it is of interest to note that a comparison of plots of $\tilde{\nu}_{max}$(MLCT) values for complexes **1**−**4** against those of the similar complex *cis*-[Fe(MePebpy)$_2$(CN)$_2$], which is soluble in solvents ranging from water to paraffins,[12] reveals that they have the same sensitivity, within experimental error (average slope: 1.00±0.02). All these results indicate that alkyl chains appended to 2,2′-bipyridine allow for a fine tuning of complex solubility, without changing the solvatochromic sensitivity of the "*cis*-[Fe(bpy)$_2$(CN)$_2$]" moiety.

It is also important to assess the solvatochromic response of complexes **1**−**4** against the E_T scale, the most widely used for empirical measurements of solvent polarity. The plots of $\tilde{\nu}_{max}$(MLCT) for similar inorganic complexes versus the solvent E_T values found in the literature typically exhibit two correlation lines, which correspond to hydroxylic and non-hydroxylic solvents.[1,17,18] Such plots for complexes **1**−**4** exhibit roughly the same behaviour, but with a novel feature: a third correlation line is observed for nonpolar solvents. This feature is absent from the plots reported in the literature, since the complexes were not soluble in nonpolar solvents. This effect is observed more clearly for the more hydrophobic complexes **3** and **4**. Figure 1 shows such a plot for *cis*-[Fe(Hp$_2$bpy)$_2$(CN)$_2$].

A comparison with Gutmann's acceptor number *AN*[16,19] (another empirical solvent polarity scale) was also carried out. For complexes **1**−**4**, plots of $\tilde{\nu}_{max}$(MLCT) against *AN* values, for all polar solvents for which this value is available, show one reasonable correlation line (average correlation coefficient: 0.90±0.05). However, as with the comparison of $\tilde{\nu}_{max}$(MLCT) with E_T data, a different line is also obtained for nonpolar solvents.

Before suggesting a possible explanation for the difference in behaviour of complexes **1**−**4** with that of the Reichardt dyes, it is important to recall that Reichardt defines solvent polarity as "the overall solvation capability of sol-

Table 1. Wavenumber of the maximum absorption ($\tilde{\nu}_{max}$/cm^{-1}) for the lowest-energy MLCT band for complexes **1**−**4**

Solvent	No.	E_T[a]	AN[b]	$\tilde{\nu}_{max}$ bpy[c]	$\tilde{\nu}_{max}$ **1**	$\tilde{\nu}_{max}$ **2**	$\tilde{\nu}_{max}$ **3**	$\tilde{\nu}_{max}$ **4**
Water	1	63.1	54.8	19194	19342	[d]	[d]	[d]
2,2,2-Trifluoroethanol	2	59.8	[e]	18975	19084	19084	19048	19120
Methanol	3	55.4	41.5	18018	17986	18083	18149	18051
Diethylene glycol	4	53.8	[e]	17668	17762	17668	17575	17730
Ethanol	5	51.9	37.1	17606	17606	17637	17637	17857
1-Propanol	6	50.7	33.7	17483	17483	17483	17544	17483
1-Butanol	7	49.7	32.2	17422	17483	17331	17301	17391
Acetylacetone	8	49.2	[e]	16367	16529	16447	16447	16502
1-Hexanol	9	48.8	[e]	17212	17271	17301	17271	17331
2-Propanol	10	48.4	33.5	17301	17271	17271	17212	17271
1-Octanol	11	48.1	30.4	17241	17271	17422	17422	17361
Nitromethane	12	46.3	20.5	16892	17094	17065	17065	17065
Acetonitrile	13	45.6	18.9	16611	16474	16474	16420	16502
Dimethyl sulfoxide	14	45.1	19.3	16207	16207	16234	16234	16234
tert-Butyl alcohol	15	43.3	27.1	16807	16779	16667	16694	16722
Dimethylformamide	16	43.2	16	16181	15949	16000	15974	15974
Acetone	17	42.2	12.5	15974	16000	15873	15773	15848
Nitrobenzene	18	41.2	14.8	16051	16129	16077	16129	16129
2-Pentanone	19	41.1	63.3	16420	16447	16420	16393	16340
Dichloromethane	20	40.7	20.4	16287	16340	16340	16340	16420
Acetophenone	21	40.6	15	16000	16051	16077	16129	16051
Pyridine	22	40.5	14.2	15898	15823	15848	15848	15848
Cyclohexanone	23	39.8	18	16077	15625	15798	15773	15699
Isobutylmethylacetone	24	39.4	[e]	16026	16026	16129	16077	15949
Chloroform	25	39.1	23.1	16474	16474	16502	16502	16502
Ethylacetate	26	38.1	9.3	[d]	15723	15773	15723	15723
Tetrahydrofuran	27	37.4	8	[d]	15129	15060	15083	15152
Chlorobenzene	28	36.8	11.9	15974	15848	15748	15898	15798
Diethyl ether	29	34.5	3.9	[d]	[d]	15337	15291	[d]
Toluene	30	33.9	6.8	[d]	15385	15456	15408	15432
Tetrachloromethane	31	32.4	8.6	[d]	[d]	15848	15723	15674
n-Pentane	32	31.1	[e]	[d]	[d]	15848	15924	[d]
n-Heptane	33	31	[e]	[d]	[d]	[d]	16077	15848
n-Hexane	34	30.8	0	[d]	[d]	[d]	15873	15748

[a] E_T values are in kcal mol^{-1}. − [b] AN = acceptor number. − [c] $\tilde{\nu}_{max}$ for the lowest energy MLCT band for [Fe(CN)$_2$(bpy)$_2$] cm^{-1}. − [d] Not soluble. − [e] Not determined.

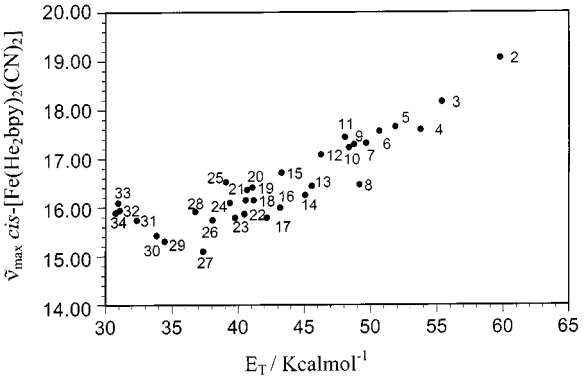

Figure 1. Wavenumber of the maximum absorption ($\tilde{\nu}_{max}$/10^3 cm^{-1}) for the lowest-energy MLCT band of *cis*-[Fe(Hp$_2$bpy)$_2$(CN)$_2$], plotted versus Reichardt E_T values; the numbering of the points corresponds to the numbering of solvents in Table 1

vents, which in turn depends on the action of all possible, non-specific and specific intermolecular interactions between solute ions or molecules and solvent molecules".[15,20] From this definition it is clear that the solvatochromic band of the Reichardt dyes (the lowest-energy charge-transfer absorption band) is not related to properties of the solvent considered as a non-structured continuum.

As the response of complexes **2**−**4**, and **5** correlates in a different manner with the E_T values, they must be responding to a different solvent property, probably to a physical property of the solvent considered as non-structured continuum. In fact a reasonable correlation is obtained when $\tilde{\nu}_{max}$(MLCT) is plotted against the dipole moment of the nonpolar solvents (correlation coefficient = 0.92).

Solvatochromic Behaviour in Binary Aqueous Solvent Mixtures

The solvatochromic behaviour of complexes **1**−**4** was also studied in three binary solvents; water/methanol, water/acetone, and water/acetonitrile. The first co-solvent is protic, and although the other two are non-protic, acetonitrile is also known as a protogenic solvent since a strongly basic solute induces the formation of hydrogen bonds with the hydrogen atoms from the methyl group adjacent to the CN group.[19]

For complexes **1**−**4** in the three binary aqueous mixtures, $\tilde{\nu}_{max}$(MLCT) data can be divided into two sets. The behaviour of the complex *cis*-[Fe(*i*Bu$_2$bpy)$_2$(CN)$_2$] (**1**) is practically identical to that of *cis*-[Fe(PeMebpy)$_2$(CN)$_2$], and is similar to that observed for other inorganic iron(II) diimine cyanide complexes.[4,12,21] However, for complexes **2**−**4**, which have longer alkyl chains attached to the 2,2′-bipyridine moiety, the $\tilde{\nu}_{max}$(MLCT) dependence on solvent composition for regions of high water content is completely different. The $\tilde{\nu}_{max}$(MLCT) values become independent of solvent composition. This unexpected result is, to the best of our knowledge, unparalleled in the literature for diimine-iron(II) cyanide complexes.

cis-[Fe(iBu$_2$bpy)$_2$(CN)$_2$] (1)

In water/methanol, plots of $\tilde{\nu}_{max}$(MLCT) against volume content (v/v) of methanol are linear, which indicates similar solvation by water and methanol in the full composition range. Analogous plots for acetone and acetonitrile as the co-solvents indicate strong preferential hydration in acetonitrile or acetone-rich media, but similar solvation by water and co-solvent in water-rich media (Figure 2). A comparable behaviour is observed for *cis*-[Fe(bpy)$_2$(CN)$_2$] in the first two solvent mixtures, but in water/acetone preferential solvation by water occurs over the full composition range, as has been reported in the literature.[4]

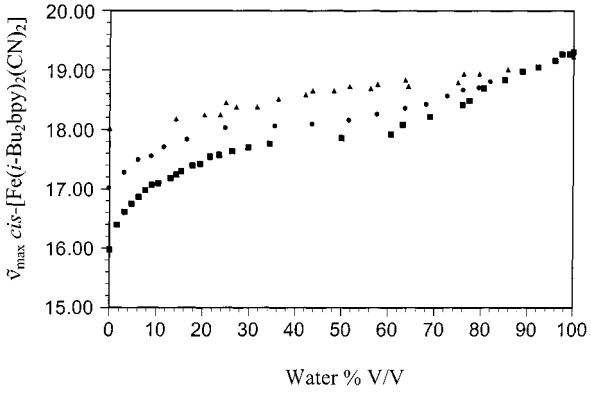

Figure 2. Wavenumber of the maximum absorption ($\tilde{\nu}_{max}/10^3$ cm^{-1}) for the lowest-energy MLCT band of *cis*-[Fe(*i*Bu$_2$bpy)$_2$(CN)$_2$] in methanol (▲), acetonitrile (●) and acetone (■) solvent mixtures

It is also of interest to compare the results for complex **1** and *cis*-[Fe(bpy)$_2$(CN)$_2$] with those for *cis*-[Fe(PeMebpy)$_2$(CN)$_2$].[12] In water/methanol and water/acetonitrile mixtures all these complexes exhibit the behaviour described above for **1**: (a) similar solvation by water and methanol in the full composition range; (b) preferential solvation by water in acetonitrile-rich media and similar solvation by water and acetonitrile in water-rich media. However, in the acetone-rich region of the water/acetone media all complexes exhibit preferential solvation by water, but for regions of high water content they exhibit different solvatochromic properties; *cis*-[Fe(bpy)$_2$(CN)$_2$] is preferentially solvated by water, *cis*-[Fe(PeMebpy)$_2$(CN)$_2$] by acetone and *cis*-[Fe(*i*Bu$_2$bpy)$_2$(CN)$_2$] is similarly solvated by water and acetone (Figure 3). These different solvatochromic characteristics must be related not only to solvent polarity, but also to differences between the hydrophobicity of the complexes (see below).

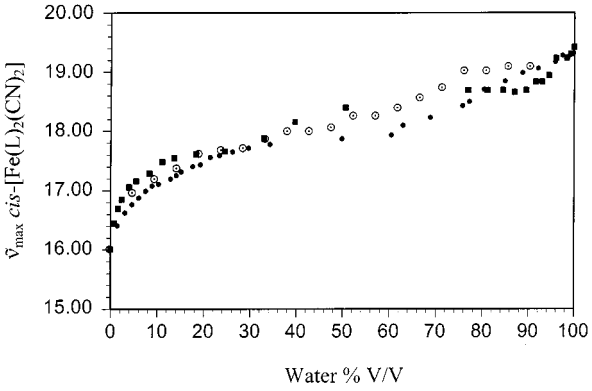

Figure 3. Wavenumber of the maximum absorption ($\tilde{\nu}_{max}/10^3$ cm^{-1}) for the lowest-energy MLCT band of *cis*-[Fe(*i*Bu$_2$bpy)$_2$(CN)$_2$] (●), *cis*-[Fe(PeMebpy)$_2$(CN)$_2$] (■) and *cis*-[Fe(bpy)$_2$(CN)$_2$] (⊙) in water/acetone mixtures; composition 0−100% H_2O, by volume before mixing, at 298 K

A plot of $\tilde{\nu}_{max}$(MLCT) of complex **1** against $\tilde{\nu}_{max}$-(MLCT) of *cis*-[Fe(bpy)$_2$(CN)$_2$] in water/acetone and water/acetonitrile mixtures is linear with a slope of 0.93±0.05. This indicates that both complexes have comparable sensitivities for these mixtures. In contrast, the slope in water/methanol is 0.78±0.05, an indication that complex **1** is less sensitive in methanol/water than *cis*-[Fe(bpy)$_2$(CN)$_2$]. This behaviour, which has already been found for *cis*-[Fe(PeMebpy)$_2$(CN)$_2$], indicates that the hydrophobicity, imparted by the presence of the aliphatic chains, renders the complexes less sensitive to small changes in the composition of a mixture of two very polar solvents.

Finally, a comparison with the Reichardt E_T scale can be made, as the E_T values are known for mixtures of water with methanol, acetone, or acetonitrile as the co-solvent.[21−23] When values of $\tilde{\nu}_{max}$(MLCT) were plotted against E_T, for all mixed solvents, linear correlations were obtained (average correlation coefficient: 0.98). This trend suggests that complex **1** is similarly affected by the mixed solvent components as is the organic betaine, upon whose spectra the E_T scale is based.

Complexes with Longer Alkyl Chains − *cis*-[Fe(Pe$_2$bpy)$_2$-(CN)$_2$] (2), *cis*-[Fe(Hp$_2$bpy)$_2$(CN)$_2$] (3), and *cis*-[Fe(HeMebpy)$_2$(CN)$_2$] (4)

Plots of $\tilde{\nu}_{max}$(MLCT) against water content for complexes **2**−**4** can be divided into two regions, co-solvent-rich and water-rich media (Figure 4).

In the co-solvent-rich region, all complexes exhibit a behaviour analogous to that of *cis*-[Fe(PeMebpy)$_2$(CN)$_2$], *cis*-[Fe(*i*Bu$_2$bpy)$_2$(CN)$_2$], and *cis*-[Fe(bpy)$_2$(CN)$_2$]: similar solvation by water and methanol in water/methanol, and preferential solvation by water in water/acetone and water/acetonitrile. Plots of $\tilde{\nu}_{max}$(MLCT) for complexes **2**−**4** versus $\tilde{\nu}_{max}$(MLCT) of *cis*-[Fe(bpy)$_2$(CN)$_2$] are linear, with an average slope of 1.02±0.05 in water/acetone and water/acetonitrile, but with a slope of 0.78±0.05 in water/methanol.

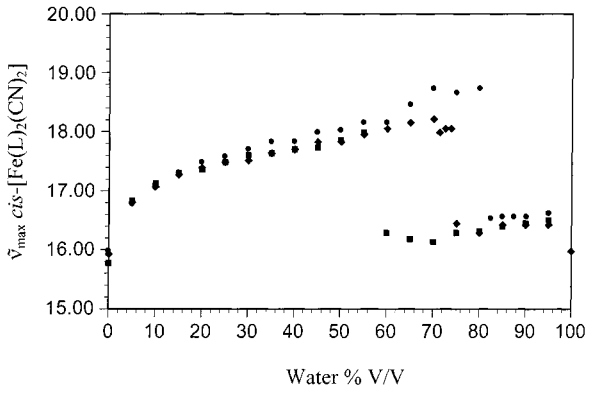

Figure 4. Wavenumber of the maximum absorption ($\tilde{\nu}_{max}/10^3$ cm^{-1}) for the lowest-energy MLCT band of *cis*-[Fe(Pe$_2$bpy)$_2$(CN)$_2$] (♦), *cis*-[Fe(Hp$_2$bpy)$_2$(CN)$_2$] (■), and *cis*-[Fe(HpMebpy)$_2$(CN)$_2$] (•) in water/acetone mixtures; composition 0−100% H_2O, by volume before mixing, at 298 K

This indicates less sensitivity to solvent polarity in this latter mixture. This situation is identical to that found for *cis*-[Fe(PeMebpy)$_2$(CN)$_2$] and *cis*-[Fe(*i*Bu$_2$bpy)$_2$(CN)$_2$] in water/methanol, and must reflect the reduced ability of hydrophobic complexes to discriminate between very polar complexes.

However, in regions of high water content and for all co-solvents, the solvatochromic behaviour of complexes **2**−**4** is completely different. An unexpected and abrupt bathochromic shift in $\tilde{\nu}_{max}$(MLCT) to the same final value of $\tilde{\nu}_{max}$(MLCT) for each complex is observed at a specific co-solvent volume content. This shift implies that nonpolar molecules must surround the complexes, since the final value of $\tilde{\nu}_{max}$(MLCT) is very similar to that observed in pure non-protic solvents. This is a very strange occurrence since the complexes are in water-rich media. This abrupt change in $\tilde{\nu}_{max}$(MLCT) is not only dependent on the complex, but also on the co-solvent (Table 2). The volume fraction of water at which the abrupt change occurs is: (a) for each complex roughly the same for acetonitrile and acetone as the co-solvents, and lower for methanol, and (b) increases in the order *cis*-[Fe(HpMebpy)$_2$(CN)$_2$] > *cis*-[Fe(Pe$_2$bpy)$_2$(CN)$_2$] > *cis*-[Fe(Hp$_2$bpy)$_2$(CN)$_2$]. For water contents above this critical value, the resulting solutions are blue and show a slight turbidity; however, the scattering does not prevent the observation of the lowest-energy MLCT band. Obviously, complexes **2**−**4** can only be used as probes for water concentrations smaller than that at which the abrupt change in $\tilde{\nu}_{max}$(MLCT) occurs, and in this region their sensitivity is similar to that of other bipyridyldicyanoiron(II) complexes.

Metalloaggregate Formation

A possible explanation for the anomalous solvatochromic behaviour of complexes **2**−**4** can be given by the formation of aggregates. These complexes have hydrophobic tails that not only have a reasonably strong affinity for themselves, but are also segregated from the polar liquid, largely due to the hydrogen bonding between the polar molecules. These factors lead to an exclusion of water molecules from the immediate environment of the complexes which sense a non-protic environment.

Solutions of complexes **2**−**4** (concentration ca. $1.5\cdot10^{-5}$ M) have been prepared in water/co-solvent mixtures with a water mol fraction higher than that at which the abrupt change in $\tilde{\nu}_{max}$(MLCT) occurs. Light-scattering analysis of these mixtures showed the existence of aggregates with a mean diameter of 1000±250 nm, and with very large polydispersion (1.00).

This observation supports the assumption that the abrupt change in $\tilde{\nu}_{max}$(MLCT) may be ascribed to the formation of metalloaggregates in regions of high water content. Formation is clearly solvent-dependent, and in the more polar water/methanol mixtures it occurs at a lower water content than in the less polar mixtures with acetone or acetonitrile (Figure 4). This is an expected result since the tails of the complexes render the monomers less soluble in the more polar mixtures. Obviously, the alkyl chains markedly control complex hydrophobicity, and the ease of formation of metalloaggregates is related to the size and number of the aliphatic chains. For complex **4**, which has four chains with seven carbon atoms, aggregation starts at a smaller water content than that for complex **2**, which has four alkyl chains with five carbon atoms each. Finally, the monomers of complex **3**, which have only two alkyl chains with seven carbon atoms each, are more soluble in water-rich media than either complex **2** or **4**.

Concluding Remarks

The complexes prepared in this work have been shown to be solvatochromic probes as sensitive to solvent polarity as [Fe(bpy)$_2$(CN)$_2$], the most studied inorganic probe, but with the added advantage of being soluble in a wider range of solvents. The hydrophilic-lipophilic balance, which in turn depends on the length of the alkyl chain, controls their solvation behaviour; short chains make the complexes insoluble in nonpolar solvents, whereas long chains render them insoluble in water. The complex [Fe(PeMebpy)$_2$(CN)$_2$], already reported in the literature, is still the only complex of this type with a hydrophilic-lipophilic balance that makes it soluble in both water and in *n*-alkanes.[12] The use of

Table 2. Water molar percent at which there is an abrupt change in the wavenumber of the maximum absorption

Solvent	[Fe(Pe$_2$bpy)$_2$(CN)$_2$]	[Fe(He$_2$bpy)$_2$(CN)$_2$]	[Fe(Hebpy)$_2$(CN)$_2$]
Acetone	92%	85%	95%
Acetonitrile	89%	84%	95%
Methanol	77%	70%	90%

iron(II) complexes with substituted 2,2′-bipyridyl ligands, which contain one or two hydrophobic chains of varying length, as solvatochromic probes combines the sensitivity of the bipyridyldicyanoiron(II) complexes with the solubility of the analogous, but less sensitive, complexes of Schiff base diimines in nonpolar solvents.

In binary mixtures the results obtained show that in co-solvent rich media, all new complexes exhibit similar behaviour: in acetone and acetonitrile, they are as sensitive as $[Fe(bpy)_2(CN)_2]$ to hydration, but less sensitive in methanol to changes in solvent polarity. In water-rich media, the hydrophobicity imposed by the alkyl tails clearly controls the behaviour of the complexes. With these new complexes we have begun the construction of a good basic set of solvation probes that seem to be ideal for the analysis of the relative importance of electrostatic/hydrophobic interactions in binary aqueous media. These complexes are very versatile solvation probes and may well prove to be valuable in assessing solvent polarity in a variety of novel heterogeneous/organised solvent media.

Finally, an interesting result emerging from this work is the demonstration of the self-aggregating properties of the complexes *cis*-$[Fe(Pe_2bpy)_2(CN)_2]$, *cis*-$[Fe(He_2bpy)_2(CN)_2]$, and *cis*-$[Fe(Hebpy)_2(CN)_2]$ which are, without doubt, metallosurfactants. Surfactants containing transition metal ions have only recently begun to be investigated. The use of a transition metal ion in the head-group permits the incorporation of useful properties such as colour, paramagnetism, variable charge, and pH sensitivity. Moreover, as transition metal complexes possess a wide range of reactivity, such as redox behaviour and catalytic activity, they can provide a good method of localising this kind of activity at interfaces.

Experimental Section

Instrumentation: Elemental analyses (C, H N) were performed by the Micro Analytical Laboratory, Department of Chemistry, University of Manchester (UK). No elemental analyses were performed for the complexes since compounds with cyanides always give unreliable results. − IE and FAB mass spectra at "Unidade de Espectrometria de Masas, Facultad de Química, Universidade de Santiago de Compostela" (Spain), using 3-nitrobenzyl alcohol (NBA) as the matrix. − ^{1}H NMR spectra were recorded with a Bruker AC 200 at 200 MHz (298 K). Chemical shifts are reported in ppm referred to TMS, used as an internal standard. − UV/Vis spectra were recorded in the 800−200 nm range with a Unicam UV-2, at room temperature, using quartz cells with 1 cm optical path. Light-scattering measurements were performed with a Malvern Instruments ZetaSizer 5000, using the 633-nm line of a He-Ne 5-mW laser.

Solvents and Reagents: All solvents were from Merck and all chemicals from Aldrich, except for 4,4′-dimethyl-2,2′-bipyridyl and the *n*-bromoalkanes which were from Fluka; all were used as received.

Ligand Synthesis

4,4′-Diisobutyl-2,2′-bipyridine (*i*Bu$_2$bpy): The ligand was prepared according to a published procedure[24] with 4,4′-dimethylbipyridine (Me_2bpy; 5.0 g; 27 mmol) and 2-bromopropane (7.7 ml; 82 mmol). All other reagents and solvents were used in the amounts described for the synthesis of the symmetric bipyridine derivatives.[24] Purification by chromatography on silica gel 60 (70−230 mesh ASTM) using 1,4-dioxane as the eluent afforded a pale yellow oil (yield: 58%, 4.20 g). − ^{1}H NMR (200 MHz, $CDCl_3$, 25 °C, TMS): δ = 0.91 (t, 3 H), 1.36 (m, 2 H), 1.70 (m, 4 H), 2.44 (s, 3 H), 2.69 (t, 2 H), 7.13 (m, 2 H), 8.22 (s, 2 H), 8.54 (m, 2 H). − $C_{18}H_{24}N_2$ (268.4): C 80.55, H 9.01, N 10.44; found C 80.55, H 9.01, N 10.38.

4,4′-Di-*n*-pentyl-2,2′-bipyridine (Pe$_2$bpy): A procedure similar to that described above was applied using 1-bromobutane (8.8 ml; 82 mmol). Purification by basic alumina column chromatography (3 × 20 cm, activity grade 1) using dichloromethane as the eluent, followed by chromatography of the appropriate fraction on silica gel (3 × 20 cm, 230−400 mesh) with a gradient starting with 10% up to 40% diethyl ether in petroleum ether, afforded the pure compound as a pale yellow oil (yield: 60.0%, 4.80 g). − ^{1}H NMR (300 MHz, $CDCl_3$, 25 °C, TMS): δ = 0.78−0.88 (m, 6 H, 2 × -CH_3), 1.25−1.34 [m, 8 H, 2 × -$(CH_2)_2$-CH_3], 1.60−1.67 (m, 4 H, 2 × Ar-CH_2-CH_2), 2.63 (t, $J_{H,H}$ = 7.79 Hz, 4 H, 2 × Ar-CH_2-), 7.06 (dd, $J_{H,H}$ = 4.99, 1.28 Hz, 2 H, 2 × Ar-5-H), 8.30 (s, 2 H, 2 × Ar-3-H), 8.55 (d, $J_{H,H}$ = 5.02 Hz, 2 H, 2 × Ar-6-H). − ^{13}C NMR (300 MHz, $CDCl_3$): δ = 13.5 (2 × -CH_3), 34.9 (2 × Ar-CH_2), 120.7, 123.3 (Ar-C3, Ar-C5), 148.4 (Ar-C4), 152.1 (Ar-C6), 155.6 (Ar-C2). − MS (70 eV, EI): *m*/*z* (%) = 296 (9) [$M^{+\cdot}$]. − $C_{20}H_{28}N_2$ (296.5): C 81.03, H 9.52, N 9.45; found C 80.92, H 9.81, N 9.58.

4,4′-Di-*n*-heptyl-2,2′-bipyridine (Hp$_2$bpy): A similar procedure was applied using 1-bromohexane (11.5 ml; 81.9 mmol). Purification by column chromatography (3 × 35 cm) with dichloromethane as the eluent afforded a white powder that was further purified by recrystallisation from ethanol (yield: 66.1%, 6.28 g), m.p. = 32−34 °C. − ^{1}H NMR (300 MHz, $CDCl_3$, 25 °C, TMS): δ = 0.88 (t, *J* = 6.81 Hz, 6 H, 2 × -CH_3), 1.24−1.37 [m, 16 H, 2 × -$(CH_2)_4$-CH_3], 1.66−1.72 (m, 4 H, 2 × ArCH_2-CH_2), 2.69 (t, $J_{H,H}$ = 7.80 Hz, 4 H, 2 × Ar-CH_2), 7.13 (dd, $J_{H,H'}$ = 5.0, 1.64 Hz, 2 H, 2 × Ar-5-H), 8.22, 8.23 (s, 2 H, 2 × Ar-3-H), 8.56 (d, $J_{H,H}$ = 5.13 Hz, 2 H, 2 × Ar-6-H). − ^{13}C NMR (300 MHz, $CDCl_3$): δ = 14.1 (2 × -CH_3), 35.5 (2 × Ar-CH_2), 121.3, 123.9 (2 × Ar-C3, 2 × Ar-C5), 148.9 (Ar-C4), 152.9 (Ar-C6), 156.1 (Ar-C2). − MS (70 eV, EI): *m*/*z* (%) = 352 (14) [$M^{+\cdot}$]. − $C_{24}H_{36}N_2$ (352): C 81.76, H 10.29, N 7.94; found C 81.66, H 10.39, N 8.26.

4-*n*-Heptyl-4′-methyl-2,2′-bipyridine (HpMebpy): 4,4′-Dimethylbipyridine (5.0 g; 27 mmol) and 1-bromohexane (11.5 ml; 81.9 mmol) were used. All other reagents and solvents were used in the amounts described for the synthesis of the asymmetric bipyridine derivatives.[24] Purification of the cream solid obtained was performed by recrystallisation from ethanol (yield: 32.0%, 2.32 g), m.p. 36−38 °C. − ^{1}H NMR (200 MHz, $CDCl_3$, 25 °C, TMS): δ = 0.84−0.91 (m, 6 H, 2 × -CH_3), 1.27−1.33 [m, 8 H, 2 × -$(CH_2)_4$-CH_3], 1.65−1.79 (m, 2 H, 2 × ArCH_2-CH_2), 2.44 (s, 3 H, Ar-CH_3), 2.69 (t, $J_{H,H}$ = 8.0 Hz, 2 H, Ar-CH_2), 7.13 (d, $J_{H,H}$ = 5.0 Hz, 2 H, 2 × Ar-5-H), 8.22 (s, 2 H, 2 × Ar-3-H), 8.54 (d, $J_{H,H}$ = 4.8, 2 H, 2 × Ar-6-H). − ^{13}C NMR (200 MHz, $CDCl_3$): δ = 14.0 (-CH_3), 31.7 (Ar-CH_3), 35.51 (Ar-CH_2), 121.3, 122.0, 123.9, 124.6(2 × Ar-C5, 2 × Ar-5), 148.0, 148.9 (2 × Ar-C4), 152.9 (Ar-C6), 156.1 (Ar-C2). − MS (70 eV, EI): *m*/*z* (%) = 268 (10) [$M^{+\cdot}$]. − $C_{18}H_{24}N_2$ (268.4): C 80.55, H 9.01, N 10.44; found C 79.95, H 9.04, N 10.99.

Synthesis of Iron(II) Complexes

***cis*-Dicyanobis(4,4′-diisobutyl-2,2′-bipyridine)iron(II) [Fe(*i*Bu$_2$bpy)$_2$(CN)$_2$]:** The complex was prepared by Schilt's method,[13] with mi-

nor modifications. A stoichiometric amount of $(NH_4)_2$-$FeSO_4 \cdot 6H_2O$ in water (5 mL) was added to a solution of *i*Bu_2bpy (0.371 g; 1.38 mmol) in refluxing methanol (25 mL). After full development of the characteristic red colour, a stoichiometric amount of KCN was added. On standing at room temperature, a blue solid formed which was washed with petroleum ether (10 × 20 mL) and recrystallised from a mixture of 1:5 v/v dichloromethane/petroleum ether (yield: 74.7%, 0.22 g), m.p. > 300 °C. − ^{1}H NMR (300 MHz, $CDCl_3$, 25 °C, TMS). δ = 0.85−0.97 (m, 6 H, 2 × -CH_3), 1.27−1.43 [m, 8 H, 2 × -$(CH_2)_2$-CH_3], 1.57−1.76 (m, 4 H, 2 × Ar-CH_2-CH_2-), 2.61, 2.77 (t, $J_{H,H}$ = 7.79, $J_{H,H}$ = 7.76 Hz, 4 H, 2 × Ar-CH_2-), 6.86, 7.20 (dd, $J_{H,H}$ = 5.71, 1.28 Hz, $J_{H,H}$ = 5.76, 1.27 Hz, 2 H, 2 × Ar-5-H), 7.12, 9.81 (d, $J_{H,H}$ = 5.75 Hz, $J_{H,H}$ = 5.80 Hz, 2 H, 2 × Ar-6-H), 7.82 (s, 2 H, 2 × Ar-3-H). − ^{13}C NMR (200 MHz, $CDCl_3$): δ = 14.0 (2 × -CH_3), 35.28 (2 × Ar-CH_2), 121.1, 125.0 (Ar-C5, Ar-C3), 150.1, 158.3 (2 × Ar-C6), 151.2, 151.4 (2 × Ar-C4), 157.7, 161.6 (2 × Ar-C2). − MS (10 keV, FAB+): *m*/*z* (%) = 700 (5) [$M^{+\cdot}$], 674 (44) [M^+ − CN], 648 (29) [M^+ − $(CN)_2$].

***cis*-Dicyanobis(4,4′-di-*n*-pentyl-2,2′-bipyridine)iron(II) [Fe(Pe_2bpy)$_2$-$(CN)_2$]:** A similar procedure was followed using Pe_2bpy (1.35 g; 4.57 mmol). The blue solid formed was washed with petroleum ether (10 × 20 cm^3) and recrystallised from a mixture of 2:10 v/v dichloromethane/petroleum ether (yield: 74.7%, 0.80 g), m.p. > 300 °C. − ^{1}HNMR (300 MHz, $CDCl_3$, 25 °C, TMS). δ = 0.85−0.97 (m, 6 H, 2 × -CH_3), 1.27−1.43 [m, 8 H, 2 × -$(CH_2)_2$-CH_3], 1.57−1.76 (m, 4 H, 2 × Ar-CH_2-CH_2-), 2.61, 2.77 (t, $J_{H,H}$ = 7.79, $J_{H,H}$ = 7.76 Hz, 4 H, 2 × Ar-CH_2-), 6.86, 7.20 (dd, $J_{H,H}$ = 5.71, 1.28 Hz, $J_{H,H}$ = 5.76, 1.27 Hz, 2 H, 2 × Ar-5-H), 7.12, 9.81 (d, $J_{H,H}$ = 5.75 Hz, $J_{H,H}$ = 5.80 Hz, 2 H, 2 × Ar-6-H), 7.82 (s, 2 H, 2 × Ar-3-H). − ^{13}C NMR (200 MHz, $CDCl_3$): δ = 14.0 (2 × -CH_3), 35.28 (2 × Ar-CH_2), 121.1, 125 (Ar-C5, Ar-C3), 150.1, 158.3 (2 × Ar-C6), 151.2, 151.4 (2 × Ar-C4), 157.7, 161.6 (2 × Ar-C2). − MS (10 keV, FAB+): *m*/*z* (%) = 700 (5) [$M^{+\cdot}$], 674 (44) [M^+ − CN], 648 (29) [M^+ − $(CN)_2$].

***cis*-Dicyanobis(4,4′-diheptyl-2,2′-bipyridine)iron(II) [Fe(Hp_2bpy)$_2$-$(CN)_2$]:** A similar procedure was applied using Hp_2bpy (1.00 g; 2.84 mmol). Recrystallisation of the product from a mixture of 1:50 v/v dichloromethane/petroleum ether, afforded a dark blue solid (yield: 63.3%, 0.49 g), m.p. > 300 °C. − ^{1}H NMR (300 MHz, $CDCl_3$, 25 °C, TMS): δ = 0.84−0.94 (m, 6 H, 2 × -CH_3), 1.19−1.40 [m, 16 H, 2 × -$(CH_2)_4$-CH_3], 1.59−1.75 (m, 4 H, 2 × $ArCH_2$-CH_2), 2.61, 2.77 (t, $J_{H,H}$ = 7.77, $J_{H,H}$ = 7.77 Hz, 4 H, 2 × $ArCH_2$), 6.86, 7.21 (d, $J_{H,H}$ = 5.19, $J_{H,H}$ = 4.89 Hz, 2 H, 2 × Ar-5-H), 7.12, 9.81 (d, $J_{H,H'}$ = 5.76 Hz, $J_{H,H}$ = 5.8 Hz, 2 H, 2 × Ar-6-H), 7.80, 7.81 (s, 2 H, 2 × Ar-3-H). − ^{13}C NMR (200 MHz, $CDCl_3$): δ = 14.10 (2 × CH_3), 35.32 (2 × $ArCH_2$), 121.2, 125.2 (Ar-C3, Ar-C5), 150.1, 158.4 (2 × Ar-C6), 151.2, 151.4 (2 × Ar-C4), 157.8, 161.6 (2 × Ar-C2). − MS (10 keV, FAB^+): *m*/*z* (%) = 812 (6) [$M^{+\cdot}$], 786 (50) [M^+ − CN], 760 (30) [M^+ − $(CN)_2$].

***cis*-Dicyanobis(4-*n*-heptyl-4′-methyl-2,2′-bipyridine)iron(II) [Fe(HpMebpy)$_2$$(CN)_2$]:** A similar procedure was applied using HpMebpy (0.912 g; 3.40 mmol). The dark blue solid was purified twice by column chromatography (3 × 20 cm, silica gel 230−400 mesh) using a gradient of acetone/methanol as the eluent. The complex was further purified by recrystallisation from acetone/ethanol (yield 24.7%, 0.18 g), m.p. > 300 °C. − ^{1}H NMR (200 MHz, $CDCl_3$, 25 °C, TMS): δ = 0.83−0.91 (m, 3 H, -CH_3), 1.20−1.36 [m, 8 H, -$(CH_2)_4$-CH_3], 1.52−1.61 (m, 2 H, $ArCH_2$-CH_2), 2.35−2.37 (m. 2 H, Ar-CH_2), 2.53 (s, 3 H, $ArCH_3$), 6.84, 7.19 (d, $J_{H,H}$ = 6.0 Hz, $J_{H,H}$ = 5.6 Hz, 2 H, 2 × Ar-5-H), 7.10, 9.77 (t, $J_{H,H}$ = 6.6 Hz, $J_{H,H}$ = 5.8 Hz, 2 H, 2 × Ar-6-H), 7.83, 7.88 (s, 2 H, 2 × Ar-3-H). − ^{13}C NMR (200 MHz, $CDCl_3$): δ = 14.0 (-CH_3), 31.6 (Ar-CH_3), 35.23 (Ar-CH_2), 121.3, 122.15, 125.28, 126.31(2 × Ar-C5, 2 × Ar-C3), 146.0, 151.6(2 × Ar-C4), 150.0, 158.3 (2 × Ar-C6), 157.6, 162.0 (2 × Ar-C2). − MS (10 keV, FAB^+): *m*/*z* (%) = 644 (3) [$M^{+\cdot}$], 618(32) [M^+ − CN], 592(24) [M^+ − $(CN)_2$].

Acknowledgments

Partial financial support for this work was provided by "Fundação para a Ciência e Tecnologia" (FCT, Lisboa). P. G. thanks FCT for a fellowship.

[1] J. Burguess, *Spectrochim. Acta* **1970**, *26A*, 1369; J. Burguess, *Spectrochim. Acta* **1970**, *26A*, 1957−1962.
[2] H. Kobayashi, B. V. Agarwala, Y. Kaizu, *Bull. Chem. Soc. Jpn.* **1975**, *48*, 465−468.
[3] M. Kotowski, R. Van Eldik, R. B. Ali, J. Burgess, S. Radulovic, *Inorg. Chim. Acta* **1987**, *131*, 225−228.
[4] J. Burgess, S. F. N. Morton, *J. Chem. Soc., Dalton Trans.* **1972**, 1712−1714.
[5] J. Burgess, M. V. Twigg, *J. Chem. Soc., Dalton Trans.* **1974**, 2032−2036.
[6] H. Elias, H. T. Macholdt, K. J. Wannowius, M. J. Blandamer, J. Burgess, B. C. Clark, *Inorg. Chem.* **1986**, *25*, 3048−3053.
[7] M. J. Blandamer, J. Burgess, B. Shraydeh, *J. Chem. Soc., Faraday Trans.* **1993**, *89*, 531−533.
[8] J. Burgess, R. C. Lane, K. Singh, B. Castro, P. Gameiro, *J. Chem. Soc., Faraday Trans.* **1994**, *90*, 3071−3075.
[9] S. Ahmed, J. Burgess, G. Capper, N. C. Fellowes, M. S. Patel, *Polyhedron* **1993**, *12*, 1145−1148.
[10] C. Laurence, P. Nicolet, C. Reichardt, *Bull. Soc. Chim. Fr.* **1987**, 125−130.
[11] A. Al-Alousy, J. Burgess, *Inorg. Chim. Acta* **1990**, *169*, 167−170.
[12] P. Gameiro, A. Maia, E. Pereira, B. Castro, J. Burgess, *Trans. Met. Chem.* **2000**, *25*, 283−286.
[13] A. A. Schilt, *J. Am. Chem. Soc.* **1960**, *82*, 3000−3005.
[14] K. Dimroth, C. Reichardt, T. Siepmann, F. Bohlmann, *Justus Liebigs Ann. Chem.* **1963**, *661*, 1- 37
[15] C. Reichardt, *Chem. Rev.* **1994**, 2319−2358.
[16] V. Gutmann, *The Donor-Acceptor Approach to Molecular Interactions*, Plenum, New York, **1978**, pp. 29−33.
[17] J. Burgess, J. G. Chambers, R. I. Haines, *Trans. Met. Chem.* **1981**, *6*, 145−151.
[18] E. E. A. Abu-Gharib, J. Burgess, *Trans. Met. Chem.* **1983**, *18*, 625−628.
[19] Y. Marcus, *The Properties of Solvents*, John Wiley & Sons, Chichester, **1998**, pp. 140−155.
[20] J. L. M. Abboud, R. Notario, *Pure Appl. Chem.* **1999**, *71*, 645−718.
[21] H. E. Toma, M. S. Takasugi, *J. Sol. Chem.* **1983**, *12*, 547−561.
[22] J. G. Dawber, J. Ward, R. A. Williams, *J. Chem. Soc., Faraday Trans. 1* **1988**, *84*, 713−727.
[23] R. D. Skwierczynski, K. A. Connors, *J. Chem. Soc., Perkin Trans. 2* **1994**, 467−472.
[24] C. G. Griggs, D. J. H. Smith, *J. Chem. Soc., Perkin Trans. 1* **1982**, 3041−3043.

Received May 30, 2001
[I01198]

Structural and Electronic Properties of Neutral Phosphoniobenzo[*c*]phospholides

Stefan Häp,[a] Laszlo Szarvas,[a] Martin Nieger,[a] and Dietrich Gudat*[a]

Keywords: Phosphorus / Phosphorus heterocycles / Electronic structure / Conjugation / Zwitterions

The neutral monophosphoniobenzo[*c*]phospholides **2** and **3** were selectively prepared by reduction of bis(triphenylphosphonio)benzophospholide chloride **1**[Cl]. Compound **3** was further converted into the borane adduct **6** and the thioxophosphorane **7**. All products were characterised by spectroscopic methods and X-ray diffraction. The most notable features of the molecular structures are the significantly different distances of the two P–C bonds adjacent to the two-coordinate phosphorus atom (P2–C1 175.0–176.6, P2–C3 171.7–173.5 pm), and a short exocyclic C–P(phosphonio) bond (C1–P1 172.5–173.7 pm) relative to cationic derivatives such as **1**. Structure comparisons revealed further variations in the bond lengths, which can be related to the changes in the inductive electron-withdrawing power of the substituents in the 3-position of the fused ring system. Computational studies of monophosphoniobenzophospholides, as well as the corresponding anions with no phosphonio substituents, and cations with two phosphonio substituents, allowed for the interpretation of the special properties of the neutral species in terms of a partial π-bond localisation. This, in terms of a VB picture, is equivalent to the prominence of a single resonance structure that can best be described as an ylide-substituted cyclic phosphaalkene. The analysis of these results allows important predictions for the chemical properties of these compounds.

Introduction

Bis(phosphonio)benzo[*c*]phospholide [bis(phosphonio)-2-phosphaindenide] cations such as **1**[1] exhibit a very special bonding situation that has been described in terms of a benzophospholide anion with a delocalised heteronaphthalenic 10π-electron system, and two positively charged phosphonio substituents.[2,3] Although electron delocalisation over the phosphonio groups and the π-electron system is low,[2,4] the electrostatic influence of the substituents still induces a marked reduction in nucleophilicity relative to the anionic phospholide derivatives, and polarises the π-electron distribution in the ring.[2–4] As a consequence of these effects, bis(phosphonio)benzophospholides display a very balanced nucleophilic and electrophilic reactivity, which is the primary reason for their remarkable stability towards solvolysis and addition reactions,[1,3,5] and their preference to coordinate to transition metal atoms through the phosphorus lone-pair[3,6] rather than the π-electron system as most other phospholide-type ligands.[7]

In the course of the investigation of the chemical properties of bis(phosphonio)benzophospholides, we established that reduction of **1** gives easy access to both neutral, zwitterionic phosphoniobenzophospholides **2**, **3**, and phosphanylbenzophospholide anions **4** (see Scheme 1).[8] Although a structural study of the carbonylnickel complex **5** revealed that the endocyclic bond lengths and angles are very similar to those of cation **1**,[8] one can expect that an increasing electrostatic polarisation by positively charged substituents should induce a concomitant modification of the π-electron distribution in the fused ring system. This view is, in principle, supported by the results of a comparative theoretical study of the parent benzo[*c*]phospholide anion and the corresponding bis(phosphonio)-substituted cation.[2] However, a concise investigation with regard to this issue is still lacking.

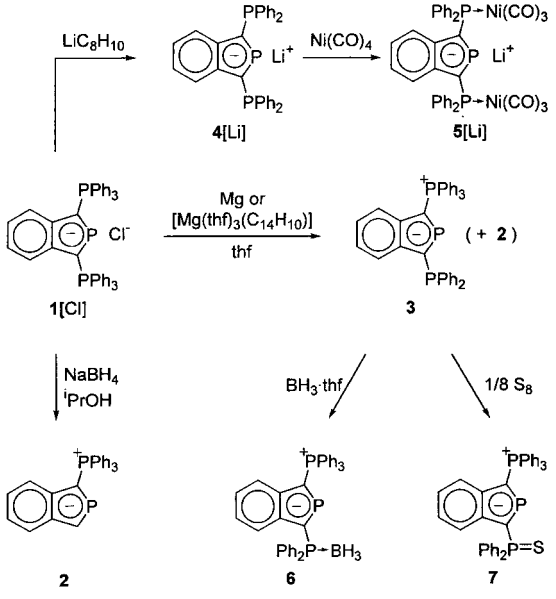

Scheme 1

In the present work we present a combined experimental and computational study of the molecular and electronic structures of the neutral 1-(triphenylphosphonio)enzo[*c*]-

[a] Anorganisch Chemisches Institut der Universität Bonn, Gerhard-Domagk-Straße 1, 53121 Bonn, Germany
Fax: (internat.) + 49-(0)228/73-5327
E-mail: dgudat@uni-bonn.de
Supporting information for this article is available on the WWW under http://www.eurjic-com or from the author.

 © WILEY-VCH Verlag GmbH, 69451 Weinheim, 2001 1434–1948/01/1111–2763 $ 17.50+.50/0

phospholides **2** and **3**, the borane adduct **6**, and the thioxophosphorane derivative **7** (Scheme 1). The studied compounds were selected for two main reasons. Firstly, comparison of the bonding situation in **2** and **3** with that in the "symmetrically" substituted ions **1** and **4**, should allow us to see if the polarisation by a *single* charged phosphonio moiety leads to an imbalance in the π-electron distribution, which may result in partial bond localisation. Secondly, comparison of the bonding situation in **3** with that in the borane adduct **6**, thioxophosphorane **7**, and the phosphonium salt **1** should allow for the monitoring of the differential effects which accompany the increasing local positive charge on the phosphorus atom of the substituent in the 3-position. The understanding of both effects is considered important for an improved understanding of the chemical properties of the studied benzo[*c*]phospholide derivatives, and, in particular, of their behaviour in complexation reactions. The latter issue is of special interest in light of the fact that aromatic phosphorus heterocycles have gained recent attention as ligands in catalysis, because of their unusual electronic properties.[9]

Results and Discussion

Syntheses and Spectroscopic Investigations

3-Diphenylphosphanyl-1-triphenylphosphoniobenzo[*c*]-phospholide (**3**) was prepared as described previously,[8] by reduction of bis(triphenylphosphonio)benzo[*c*]phospholide chloride (**1**[Cl]) with active magnesium, which was generated by the decomposition of [Mg(THF)$_3$(anthracene)][10] in boiling toluene (Scheme 1). Further investigation of this reaction revealed that direct use of Mg/anthracene as a reducing agent gave slightly lower yields of the product, but required less effort for the preparation of the reagent and shorter induction times. 1-Triphenylphosphoniobenzo[*c*]-phospholide (**2**) was formed as a by-product in all the reactions, but could not be isolated as it decomposed during the workup procedure. However, the specific formation of compound **2** was observed when the reduction of **1**[Cl] was carried out with $NaBH_4$ in 2-propanol.[11] Under these conditions the product precipitated from the reaction mixture. It was easily separated from the formed PPh_3 and borate salts by filtration, and was isolated in good yield after recrystallisation from THF/*i*PrOH.

Having shown that quaternisation of the phosphane functionality in **3** with alkyl halides provides easy access to various side-chain-functionalised bis(phosphonio)benzo[*c*]-phospholide cations,[6] we anticipated that this compound should similarly undergo other typical phosphane reactions such as oxidation or formation of adducts with Lewis acids. In agreement with this assumption, treatment of **2** with equimolar amounts of borane−THF or sulfur afforded quantitative yields (based on ^{31}P NMR spectroscopic investigation of the reaction mixtures) of the corresponding borane adduct **6** and thioxophosphorane **7**, respectively. Use of excess reagents or prolonged reaction times gave no evidence for the quaternisation of the endocyclic phosphorus atom, and both products were isolated in good yields after evaporation of the volatiles and recrystallisation from THF/hexane.

The isolated zwitterionic phosphoniobenzophospholides are bright yellow to colourless solids, which are reasonably stable towards air and moisture. All products are readily soluble in polar aprotic solvents (CH_2Cl_2, MeCN, THF), very sparingly soluble in toluene, and insoluble in hexane.

The purities and identities of all compounds were unequivocally established by analytical and multinuclear (^{1}H, ^{11}B, ^{13}C, ^{31}P) NMR spectroscopic data. The ^{31}P{^{1}H} NMR spectra display characteristic AMX (**3**, **6**, **7**) or AX patterns (**2**) (Table 1). The chemical shifts of the exocyclic phosphorus nuclei fall in the expected ranges associated with the different types of functionalities. The resonance of the endocyclic phosphorus atom in **2** appears more upfield than that in **3**, whereas the corresponding resonances in **6**, **7** are more downfield and exhibit similar chemical shifts as the bis(methyldiphenylphosphonio)benzo[*c*]phospholide cation ($\delta^{31}P = 229.0$[8]). Besides the resonances of the C_6H_5 groups, the ^{1}H NMR spectra of all the compounds display the expected ABCD patterns for the protons of the benzophospholide moiety. For **2**, the signal assigned to 3-H is buried under other resonances in the aromatic region; however, it can clearly be seen in a two-dimensional ^{1}H,^{31}P-HMQC spectrum. The ^{1}H and ^{11}B NMR spectra of **6** show the expected broad multiplets assigned to the BH_3 moiety. The ^{13}C NMR spectra of all zwitterionic benzophospholides reveal close similarities with those of the bis(phosphonio)-substituted cations.[1−4,6] However, major differences are observed predominantly for the resonances of the two carbon atoms adjacent to the endocyclic phosphorus atom (cf. Table 1). In comparison with **1**, the signals of the

Table 1. ^{31}P and selected ^{13}C NMR spectroscopic data of zwitterionic phosphoniobenzo[*c*]phospholides; phosphorus atoms are denoted as P1, P2, and P3, and carbon atoms as C1 and C3 in agreement with the numbering scheme given in Figure 1

	δ^{31}P	$J_{P,P}$ [Hz]	δ^{13}C	$J_{P,C}$ [Hz]
2	190.2 (P2) 15.1 (P1)	87.7	86.4 (C1) 138.3 (C3)	102.8 ($J_{P1,C}$), 54.8 ($J_{P2,C}$) 36.8 ($J_{P2,C}$), 13.5 ($J_{P1,C}$)
3	218.4 (P2) 14.7 (P1) −21.4 (P3)	82.4 ($J_{P1,P2}$) 97.2 ($J_{P2,P3}$)	92.8 (C1) 143.2 (C3)	99.0 ($J_{P1,C}$), 59.9 ($J_{P2,C}$), 12.0 ($J_{P3,C}$) 53.6 ($J_{P2,C}$), 14.1, 11.9
6	230.8 (P2) 15.5 (P1) 9.4 (P3)	86.1 ($J_{P2,P3}$) 88.4 ($J_{P1,P2}$)	98.3 (C1) 144.8 (C3)	98.6 ($J_{P1,C}$), 58.1 ($J_{P2,C}$), 11.6 ($J_{P3,C}$) 11.7, 9.4
7	228.3 (P2) 16.1 (P1) 35.0 (P3)	88.4 ($J_{P2,P3}$) 88.7 ($J_{P1,P2}$)	98.4 (C1) 135.7 (C3)	97.5 ($J_{P1,C}$), 58.8 ($J_{P2,C}$), 14.1 ($J_{P3,C}$) 88.1 ($J_{P3,C}$), 59.1 ($J_{P2,C}$), 13.2 ($J_{P1,C}$)

C-1 atoms adjacent to the exocyclic Ph_3P moiety are shifted upfield by about 10−20 ppm and approach the typical values observed for stable phosphonium ylides,[12] whereas the resonances of the C-3 atoms are deshielded by about 25−35 ppm and are similar to the chemical shifts for phosphinines.[12] On the whole, although the average chemical shift of both resonances (δ = 112.4−121.5) changes little relative to that of the cation **1** (δ = 109.0[1]), their large difference provides the first evidence for a marked polarisation of the π-electrons.

The UV/Vis spectra of the neutral benzo[*c*]phospholides display four major absorption bands whose positions and intensities are similar to those of the cation **1**[13] (Table 2). All observed electronic transitions display the characteristically high extinction coefficients of π−π* transitions and are much stronger than π−σ* transitions which are typical for ylides.[14] The two bands between 235 and 265 nm are assigned to π−π* transitions within the peripheral phenyl rings of the Ph_2P and Ph_3P^+ moieties, and the two bands at the lowest wavelengths are assigned to transitions of the benzophospholide chromophore. Absorption bands assigned to n−π* transitions are not observed and are presumably obscured by the much more intense π−π* transitions. The position of the energetically lowest absorption is comparable with those in 2-phosphanaphthalenes.[15] Examination

Table 2. UV/Vis data (in CH_2Cl_2) of the zwitterionic phosphoniobenzophospholides **2**, **3**, **6**, **7**, and the salt **1**[Cl] (from ref.[13])

	λ_{max} [nm] ($\varepsilon_{max}/10^3$ [l·mol^{-1}·cm^{-1}])			
1[Cl]	227 (52)	260 (16)	338 (11)	353 (13)
2	239 (33)	258 (31)	314 (17)	354 (12)
3	236 (47)	251 (45)	330 (sh)	372 (16)
6	241 (45)	263 (26)	334 (11)	359 (13)
7	238 (46)	254 (45)	336 (16)	361 (21)

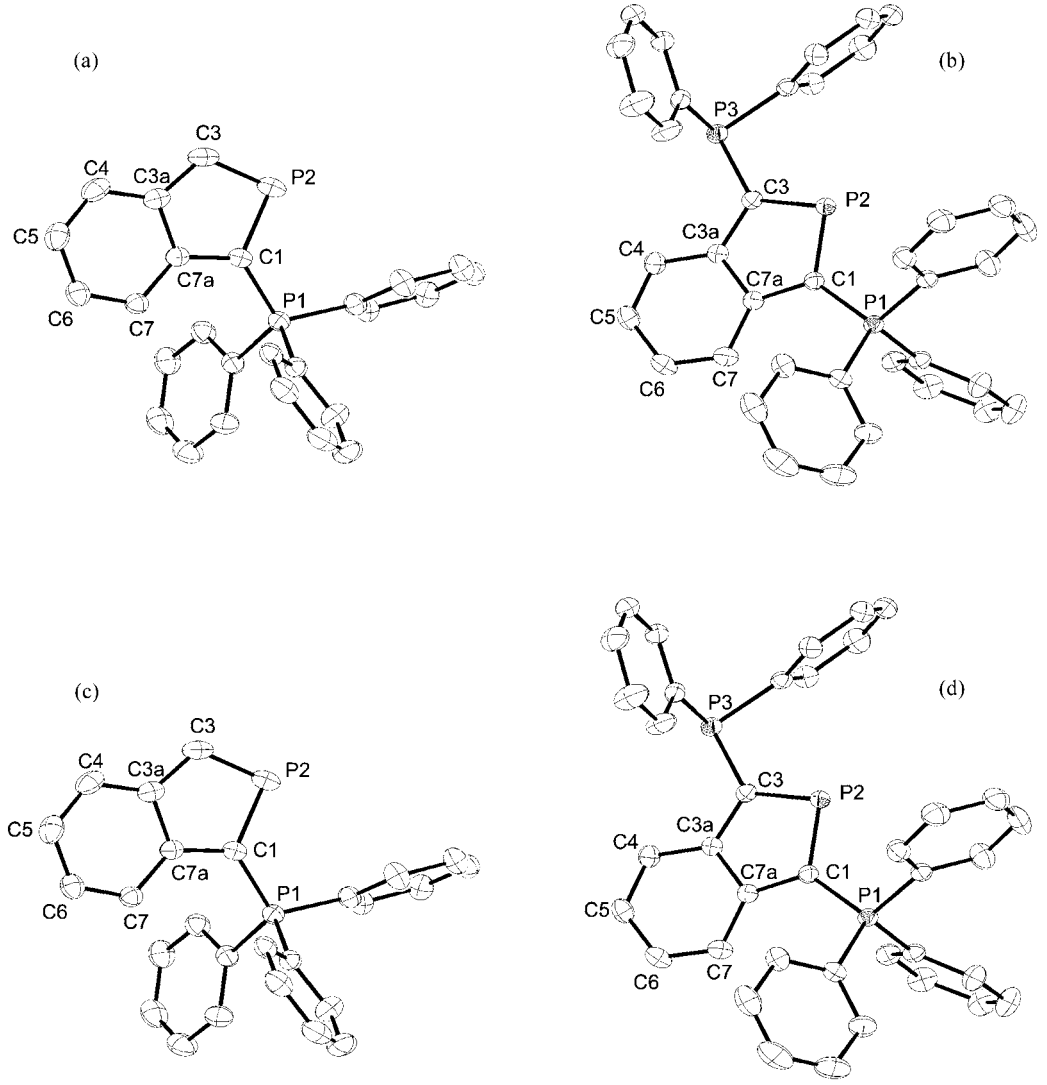

Figure 1. ORTEP-style view of the molecular structures of **2** (a), **3** (b), **6** (c), and **7** (d) with thermal ellipsoids drawn at the 50% level; hydrogen atoms are omitted for clarity, selected bond lengths are given in Table 3; in order to obtain a unique scheme, the crystallographic numbering was changed and a numbering scheme consistent with IUPAC rules used for the ring atoms; exocyclic phosphorus atoms are labelled as P1 (phosphonio group in the 1-position of the ring) and P3 (substituent in the 3-position of the ring)

of the spectra of the 3-substituted neutral compounds **3**, **6**, **7** and the cation **1**, reveals a continuous blue-shift of the energetically lowest absorption band with increasing electron-withdrawing power of the substituent in the 3-position, and an opposite trend for the second lowest absorption band.

Crystal Structure Studies

Suitable single crystals of **2**, **6**, and **7** were grown by slow evaporation of saturated THF solutions. Single crystals of **3** were obtained by cooling a saturated solution in toluene to −30 °C. The molecular structures are shown in Figure 1, and selected bond lengths are given in Table 3. The corresponding data of the cation **1**[16] and the anionic complex **5**[8] were included for comparison.

The results of the X-ray structure analyses reveal that the benzophospholide moieties in compounds **2** and **3** are planar, whereas in **6** and **7** the atoms in the benzene unit are slightly twisted around the long axis of the fused ring system. The origin of this distortion presumably arises from crystal packing effects; this effect is not considered significant and therefore will not be discussed further. The exocyclic phosphorus atoms in all compounds are located in the ring planes. The phenyl substituents at the exocyclic P2 and P3 atoms in **3** display a staggered conformation when observed along the P2−P3 axis, and those in **6** and **7** are eclipsed. As in the cation **1**,[16] the endocyclic phosphorus atom is always confined between two phenyl rings so that the P−B and P−S bonds (in **6** and **7**), or the hypothetical axis of the lone-pair (in **3**) at the exocyclic P3 atom, form angles of approx. 60−70° with the ring plane.

The lengths of all C−C bonds in the benzophospholide moiety (136−144 pm) lie in a range which is typical for aromatic systems and match those of corresponding bonds in indoles and indolyl anions.[17] Endocyclic and exocyclic P−C distances in the zwitterions **2**, **3**, **6** and **7** are similar to those in the ions **1** and **5**,[8,16] and are intermediate between pure single and double bond lengths. Comparison of the C1−P2 and P2−C3 bond lengths in the same molecule reveals the former to be significantly longer than the latter in all zwitterions. The effect is largest for **2** [Δr_{P-C} = 4.9(3) pm] and decreases continuously for **3** [Δr_{P-C} = 3.3(3) pm] and **6**, **7** [$\Delta r_{P-C} \approx$ 1.9(4) pm]. This effect is not observed in **1** and **5**, which have identical substituents at the C1 and C3 atoms, and in "asymmetric" bis(phosphonio)benzophospholides[6] with two different phosphonio groups. No similar asymmetry of the C−C bonds on opposite sides of the ring system is observed in any compound.

Comparison of corresponding bond lengths and angles in the fused rings of the disubstituted compounds **1**, **3** and **5**−**7** reveals that the C−C bonds and all bond angles are indistinguishable within experimental error. Insignificant variations were also found for the P2−C3 and the exocyclic P1−C1 bonds, whereas the C1−P2 bond lengths increase slightly but systematically in the series **3** < **6** ≈ **7** < **1**. The endocyclic P2−C3, C1−C7a, and C3−C3a bonds in the monosubstituted zwitterion **2** are shorter than the corresponding bonds in **3** by approx. 1 pm. A similar shortening is also observed for the exocyclic P1−C1 bond, and might suggest a slight increase in the ylidic nature of the phosphonio group. However, it must be noted that although the discussed differences and trends are significant when compared with the estimated standard deviations, it cannot be ruled out that these differences may have arisen from crystal packing effects or other intermolecular interactions (cf. the bond length differences between crystallographically independent molecules of **5** which are of similar magnitude). A further interpretation of these effects is thus, in our opinion, only meaningful when linked with the results of computational studies (see below).

The more pronounced variation of the C3−P3 distances in the studied zwitterions is easily explained in terms of the different substitution patterns at the P3 atom. Both the P3−B bond in **6** [193.15(19) pm] and the P3−S bond in **7** [196.90(7) pm] are longer than those in the corresponding triphenylphosphane derivatives (P−B in Ph_3P-BH_3 190.1 pm,[18] P−S in $Ph_3P{=}S$ 195.2 pm[19]), and lie near the upper limit of the known expected ranges for borane adducts and

Table 3. Selected bond lengths [pm] in the zwitterionic phosphoniobenzophospholides **2**, **3**, **6**, **7**, the cation of the salt **1**[CpW(CO)$_3$] (data taken from ref.[16]), and the anion of the salt **5**[Li(THF)$_4$] (data taken from ref.[8]); the atom numbering scheme is identical to the one given in Figure 1

	1	**2**	**3**	**5**[a]	**6**	**7**
C1−P2	172.8(4)	176.62(11)	176.23(13)	173.2(4) 174.7(4)	174.99(17)	175.40(19)
P2−C3	172.9(4)	171.71(14)	172.93(12)	1.736(4) 174.4(4)	173.23(16)	173.53(19)
C3−C3a	144.1(6)	142.09(17)	143.38(18)	144.0(5) 143.1(5)	143.6(2)	143.7(3)
C3a−C4	140.2(6)	141.46(18)	141.82(17)	141.3(5) 140.0(5)	141.0(2)	141.4(3)
C4−C5	136.3(7)	137.7(2)	137.56(19)	137.2(5) 138.0(5)	136.9(2)	137.0(3)
C5−C6	139.1(8)	140.36(18)	140.7(2)	139.9(6) 140.1(5)	140.2(2)	140.0(3)
C6−C7	138.0(8)	137.51(16)	137.66(19)	136.7(5) 137.1(5)	137.7(2)	137.4(3)
C7−C7a	139.8(6)	141.26(15)	141.58(18)	141.6(5) 141.6(5)	141.5(2)	141.0(3)
C7a−C1	144.9(6)	142.95(15)	143.93(17)	144.1(5) 142.3(5)	143.7(2)	143.7(3)
C3a−C7a	142.3(6)	143.02(15)	143.06(17)	143.2(5) 144.0(5)	143.0(2)	142.5(3)
P1−C1	174.7(4)	172.55(11)	173.47(12)	178.9(4) 177.7(4)	173.51(16)	173.65(19)
P3−C3	174.9(4)	−	180.92(13)	178.0(4) 177.4(4)	178.24(16)	177.42(19)

[a] The given values refer to two crystallographically independent molecules per unit cell.

sulfides of tertiary phosphanes (P−B 192.2±2.7, P−S 195.4±0.5 pm[17]). This suggests a comparatively low nucleophilicity of the exocyclic phosphane moiety in the studied molecules.

Computational Studies

In order to carry out a meaningful discussion of the changes in structure and bonding in the studied phosphoniobenzophospholides, and to gain a reliable basis for the interpretation of rather small structural distortions, we performed a comprehensive computational study using the B3LYP density functional method,[20] employed in the GAUSSIAN 98[21] suite of programs. To minimise computation times, the calculations were performed on the model compounds **1-H**−**4-H**, **6-H**, **7-H**, in which all peripheral phenyl rings of **1**−**4**, **6**, **7** had been replaced by hydrogen atoms, and any interaction of ionic species with the appropriate counter-ion was neglected.[22] The molecular structures of all compounds were obtained from energy optimisations at the B3LYP/6-31+g* level, and were shown to be local minima on the energy hypersurface by means of vibrational analyses. The results revealed that in the most stable conformers of compounds **3-H**, **6-H**, and **7-H**, the P−X axes of the PH_2X units (X = BH_3, S, lone-pair) form an angle of approx. 60° with the ring plane. This is in agreement with the experimentally observed conformations of **3**, **6**, **7** and implies a molecular C_1 symmetry. The molecular structures of **1-H** and **4-H** display C_{2v} symmetry, in agreement with the results of earlier computational studies of **1-H** at a different theoretical level,[2] and with the experimentally observed conformations of **1**[16] and complex **5**.[8] As the molecular structures of **3-H**, **6-H**, **5-H**, and **7-H** allow no clear-cut separation between orbitals of σ- and π-symmetry, we re-optimised the structures of these species under the constraint of C_s symmetry. The resulting molecular structures are local minima on the energy hypersurface whose energies (at the B3LYP/6-31+g* + ZPE level, see Table 4) and metric parameters (apart from the different torsion angles of the PH_2X groups) do not differ significantly from those of the C_1-symmetric conformers. Relevant structural parameters of the "symmetric" (C_s or C_{2v}) conformers, together with π-orbital populations and Wiberg bond indices (WBI), which were computed from NBO population analyses,[23] are given in Figure 2.[24] For further discussion we will refer only to the properties of the "symmetric" conformers.

Comparison of the computed bond lengths in the model compounds with the experimental data of **1**−**3**, **6**, and **7** shows a close agreement for all endocyclic C−C bonds and P1−C9 bonds (using the same numbering scheme as in Figure 1). The differences in the bond lengths are less than 1 pm. The computed lengths of the endocyclic C1−P2 bonds are generally about 3 pm longer than the experimental values, and those of the exocyclic C1−P1 bonds are shorter by the same amount. However, the variation of the individual computed bond lengths in different molecules reproduces the same trends that have been found in the experimental studies. This finding strongly suggests that the small structural variations detected reflect real differences in the electronic structures, rather than being a result of intermolecular interactions in the crystal.

Table 4. Computed absolute energies (at the B3LYP/6-31+g* level), zero-point energies, molecular point groups, and relative energies of different conformers (at the B3LYP/6-31+g* + zpe level) for the model compounds **1-H**−**4-H**, **5-H**, **6-H**

	E [a.u.]	ZPE [kJ/mol]	Symmetry	E^{rel} [kJ/mol]
1-H	−1334.6269	396.7	C_{2v}	0.0
2-H	−992.3217	344.6	C_s	0.0
3-H	−1334.2684	366.4	C_s	0.0
	−1334.2677	365.7	C_1	−1.1
4-H	−1333.7776	336.4	C_{2v}	0.0
	−1333.7735	335.2	C_2	9.7
6-H	−1360.9254	450.2	C_s	0.0
	−1360.9245	450.1	C_1	−0.2
7-H	−1732.4745	375.5	C_s	0.0
	−1732.4757	376.0	C_1	2.7

The results of NBO population analyses (cf. Figure 2b) reveal that the total π-electron population in the atoms of the annulated rings (9.75−9.86 electrons) is close to the theoretical value of 10 in all compounds. The small electron loss is attributed to weak hyperconjugation with antibonding P−H orbitals in the peripheral substituents (see below), and is almost independent of the substituent pattern. Inspection of individual atomic π-orbital population indicates a shift of π-electron density from the P2 phosphorus atoms and the remote C5/C6 carbon atoms in the six-membered ring, towards the C1/C3 carbon atoms. This shift increases with the total positive charge and, for **2-H**, **3-H**, **5-H**, and **6-H**, with the electron-withdrawing capability of the substituent on C3. In the neutral compounds, the π-electron density accumulates predominantly at the C1 atom adjacent to the strongly electron-withdrawing PH_3^+ moiety, thus introducing further pronounced "asymmetry" in the π-electron distribution. This effect is weakened in the series **2-H** > **3-H** > **5-H** ≈ **6-H**, by the growing electron-withdrawing effect of the C-9 substituents.

Inspection of the Wiberg bond indices reveals that the bond orders in the six-membered ring are essentially independent of the substituents in the 1- and 3-positions (Figure 2c). Beginning with the symmetrically substituted ions, both the C1−P2/P2−C3 and the C1−C7a/C3−C3a bond orders in the five-membered ring of the anion **4-H** are higher than those in the cation **1-H**, whereas the opposite trend is found for the C3a−C3a bonds. Interestingly, these variations result in appropriate changes in bond lengths only in the case of the C−C bonds; presumably, lower covalent P−C bond orders in **1-H** are counterbalanced by a larger electrostatic polarisation. For the betaines **2-H**, **3-H**, **6-H**, and **7-H**, the uneven distribution of π-electrons between C1 and C3 coincides with a concomitant polarisation of the P−C bond orders. The P2−C3 bonds display WBIs between 1.37 and 1.49, which are in the range between those of phosphinine (1.38) and methylenephosphane (1.94), and indicate pronounced double-bond char-

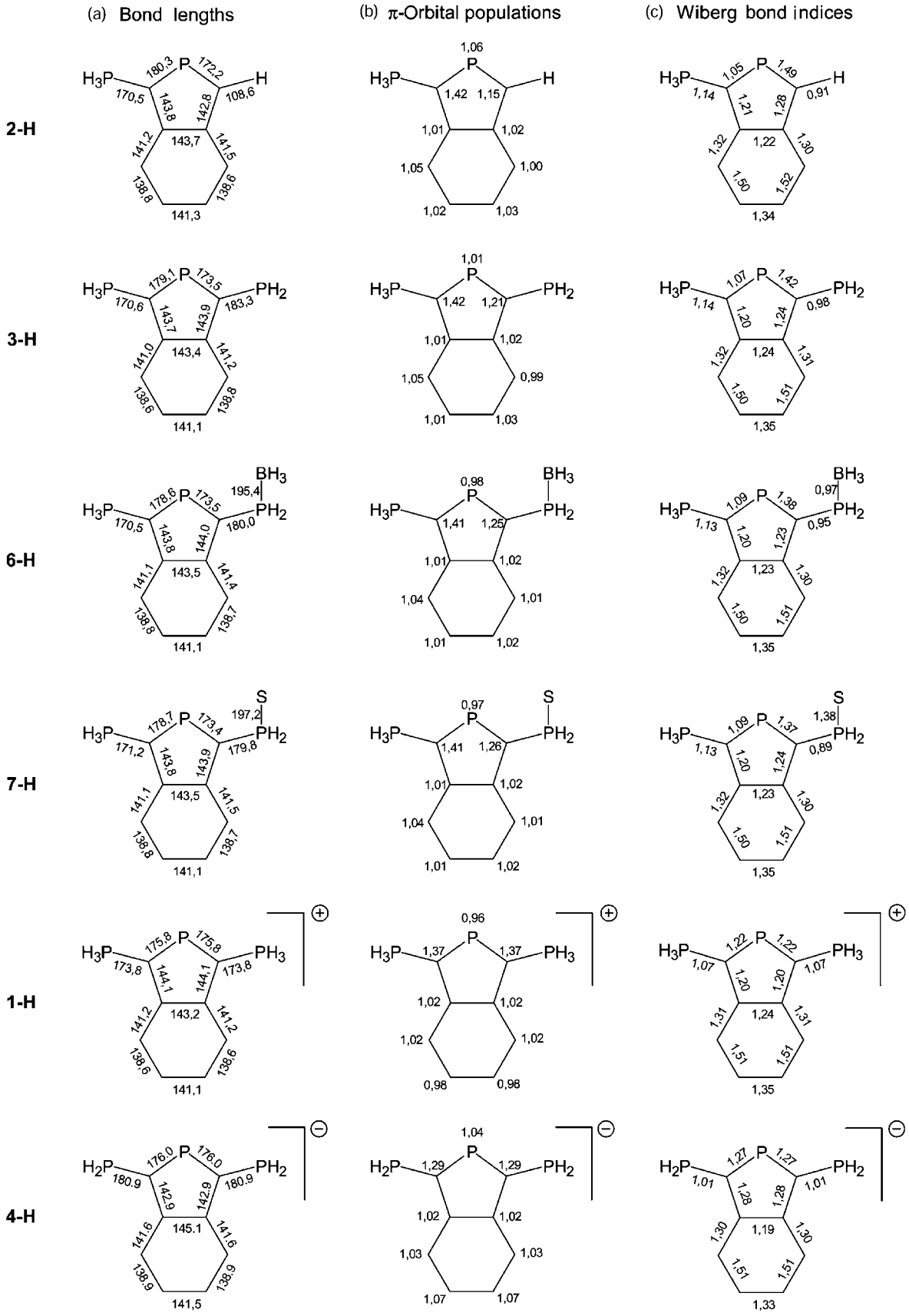

Figure 2. (a) Computed bond lengths, (b) π-orbital populations, and (c) Wiberg bond indices for the model compounds **1-H**−**4-H**, **5-H**, **6-H**; distances were obtained from energy-optimised molecular structures computed at the B3LYP/6-31+g* level, and orbital populations and bond indices from NBO population analyses[23] at the B3LYP/6-31 g*//B3LYP/6-31+g* level of theory

acter. The adjacent C1−P2 bonds display lower bond orders (WBI = 1.05−1.09), whose values nonetheless still exceed those of pure single bonds (cf. 0.98−1.01 for the exocyclic C3−P3 bonds in **2-H** and **4-H**). A less pronounced weakening of the bond (see Figure 2c) is also noted for the C1−C7a bond as compared with the C3−C3a bonds. The differences in the bond indices within each pair of P−C and C−C bonds in a single compound decreases slightly with increasing electron-withdrawing character of the substituent at C3. The higher WBIs for the exocyclic C1−P1(phosphonio) bonds in betaines (1.14) relative to the symmetrical ions **1-H** (1.07) and **4-H** (1.01), suggest a more pronounced ylide character of this bond. The exocyclic C3−P3 bonds (WBI = 0.89−0.98) are single bonds.

In the frame of a VB picture, a consistent interpretation of the changes in the bonding situation in the studied benzophospholide systems can be given in terms of a superposition of the canonical structures shown in Scheme 2. The results of the NBO analyses suggest that the dominating resonance structures in the cation **1-H** are **A**, **A′**, whose weightings are equal due to symmetry reasons.[2] For the betaines **2-H**, **3-H**, **6-H**, and **7-H**, the dominant canonical structure is **A**, even though the results of the perturbational analysis of the Fock matrix and the residual delocalisation of NLMOs suggest that the contribution of **A′** increases slightly with the growing electron-withdrawing capability of the substituent Y. The contribution of the canonical structure **B** is greater in these compounds than in the cation **I**−**H**. For the anion **4-H**, the NBO analysis suggests that the contribution of resonance structures **A**, **A′** (with H_2P instead of H_3P^+) decreases relative to that of the remaining alternatives **B**−**D**. This effect reflects a more efficient π-delocalisation along the ring perimeter and a shift of the excess charge in the π-system towards the P2 and C5, C6 atoms. The dominance of the 1,2-dipolar canonical structures **A** (and **A′**) in the phosphonio-substituted species can be understood since the charge separation is smallest. It also emphasises the fact that the shift in π-electron distributions between species with different overall charge can be understood mainly by electrostatics as the charges are in close proximity to each other.[25]

In light of the discussed results it can be concluded that all studied benzophospholides may be described as delocalised 10π-electron systems, which formally involve the interaction of a benzene (6π) and a phosphaallylic (4π) fragment.[2] The conjugation between both units (as expressed by increasing contributions of the canonical structures **B**−**C′** in Scheme 2) increases when the sum of the positive charges on the substituents decreases, and is thus most pronounced in the genuine anion **4-H**. Furthermore, substitution by a single positively charged substituent at the C2 atom in **2-H**, **3-H**, **6-H**, **7-H** lifts the degeneracy between canonical structures **A** and **A′**. The resulting essentially single resonance structure (**A**) brings a "phosphaalkene−benzylidene ylide" structure to the fore, and is equivalent to a partial π-electron localisation.

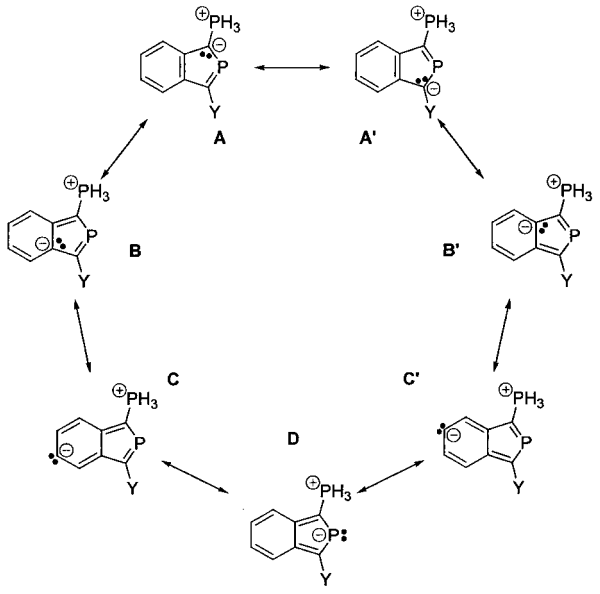

Scheme 2

With regard to the recent interest in the use of benzophospholide systems as ligands,[3,6,11] a short account of the nature and energies of frontier orbitals is of interest; this should allow some predictions on the coordination behaviour of these compounds to be made. The energies of selected molecular orbitals are listed in Table 5. As in the cation **1-H**, both HOMOs and LUMOs in the betaines **2-H**, **3-H**, **6-H**, and **7-H** have a′′ symmetry, and can be described as the 5π and 6π* orbitals of a heteronaphthalenic 10π-electron system.[2] The highest a′-type orbital in **2-H** and **6-H** lies approx. 2 eV below the HOMO and is assigned to a non-bonding pair of electrons centred at the endocyclic P1 phosphorus atom. In **3-H** and **7-H**, this orbital is best described as a "lone-pair" centred at the exocyclic P3 phosphorus or sulfur atoms, respectively. The energies of the phosphorus "lone-pair" orbitals in **2-H** and **6-H** (−7.3 to −7.5 eV) are similar to those calculated for phosphinine (−7.3 eV) or PH_3 (−7.5 eV) at the same level of theory. As expected, the energies of both occupied and unoccupied orbitals are stabilised with increasing overall positive charge of the system, but the HOMO−LUMO gap in all compounds remains essentially unchanged. Even if this finding allows a qualitative rationalisation of the observed similarity of the lowest π−π*-transition energies, a more detailed interpretation of the electronic spectra is not feasible in the frame of this simple one-electron model. Based on the computed orbital energies it can be predicted that the donor capability of benzo[*c*]phospholide ligands will decrease and their π-acceptor capability will increase with the number of positively charged phosphonio groups, whereas further modifications within the substituents will play a minor role. Furthermore, coordination of a transition metal via a phosphorus lone-pair in **3-H** and **4-H** should take place at the exocyclic three-coordinate rather than the endocyclic two-coordinate phosphorus atom, which is in agreement with

Table 5. Computed energies [eV] and symmetry descriptors (in parentheses) for selected orbitals (at B3LYP/6-31+g* level, see ref.[24]) and their differences in the "symmetric" conformers of **1-H**−**7-H**

	1-H (C_{2v})	**2-H** (C_s)	**3-H** (C_s)	**4-H** (C_{2v})	**6-H** (C_s)	**7-H** (C_s)
ε(LUMO)	−5.34 (b_1)	−1.15 (a″)	−1.40 (a″)	2.45 (b_1)	−1.76 (a″)	−1.76 (a″)
ε(HOMO)	−9.37 (a_2)	−5.26 (a″)	−5.47 (a″)	−1.47 (a_2)	−5.87 (a″)	−5.74 (a″)
ε(HOMO − 1)	−9.51 (b_1)	−5.63 (a″)	−5.80 (a″)	−1.92 (b_1)	−6.15 (a″)	−5.95 (a″)
ε(l.p.)[a]	−11.54 (a_1)	−7.31 (a′)	−6.66 (a′)[b]	−3.27 (a_1)[c]	−7.50 (a″)	−5.88 (a′)[d]
ε(LUMO) − ε(HOMO)	4.03	4.12	4.07	3.92	4.11	3.98

[a] Highest orbital of a_1 (a') symmetry. − [b] Assignment to non-bonding orbital centred at P-3. − [c] Symmetric linear combination of non-bonding orbitals centred at all three phosphorus atoms. − [d] Assignment to non-bonding orbital centred at S.

the observed formation of the nickel complex **5** starting from **4**.[8]

Conclusion

Our experimental and computational investigations have shown that the π-electron structures of neutral monophosphoniobenzo[*c*]phospholides are closely related to those of both bis(phosphonio)-substituted cations and genuine benzo[*c*]phospholide anions. However, on the other hand they have also highlighted characteristic deviations, which can be associated with the effects of π-electron polarisation by the charged phosphonio groups. Two major trends emerge from the results: (a) an increasing number of phosphonio substituents in the five-membered ring reduces π-conjugation between the fused rings; (b) a single phosphonio substituent in the 1-position of the fused ring system acts as a π-electron "trap" and induces a strong concentration of π-electron density on the adjacent ring carbon atom, and a concomitant π-bond localisation. Differential tuning of this effect is achieved by varying the inductive electron-withdrawing power of a substituent in the 3-position. With regard to the concomitant increase in ylidic character of the P(phosphonio)−C bond, the π-bond localisation brings a phosphaalkene ylide type of structure to the fore, which is most pronounced in **2**. Interestingly, a careful comparison of the computational results revealed that the observed variations in the bonding situation were only in part reflected in appropriate structural changes, thus emphasising that great care has to be taken during attempts to interpret the bonding situation exclusively on the basis of structural parameters.

The computational results further allow a number of predictions on the chemical properties of phosphoniobenzophospholides to be made. A comparison of frontier orbital energies suggests that the neutral species should behave as better σ/π-donors and weaker π-acceptors than cation **1**, which is in agreement with the conclusions drawn from a recent preliminary study of the complex chemistry of **2**.[11] In contrast to **2**, which binds a $Cr(CO)_5$ fragment via the endocyclic two-coordinate phosphorus atom,[11] complexation of **3** to a 16e-metal complex fragment is expected to occur at the exocyclic phosphane moiety, as in the anion **4**.[8] More importantly, the π-bond localisation in neutral phosphoniobenzophospholides towards a phosphaalkene−benzylidene ylide electronic structure, suggests that these compounds should also display an increased susceptibility towards addition [such as addition of reactive E−H bonds which have been found to occur for less reactive bis(phosphonio)-substituted cations[5]], or even cycloaddition reactions at the P−C double bond, or Wittig reactions at the ylide moiety. Investigations aiming at the verification of these reaction schemes for **2**, where the largest degree of π-bond localisation is observed, are currently in progress.

Experimental Section

General Remarks: NMR spectra were recorded at 30 °C with a Bruker AMX 300 spectrometer (300.13, 121.50, 96.3 and 75.46 MHz for ^1H, ^{31}P, ^{11}B and ^{13}C). Chemical shifts are referred to external TMS (^1H, ^{13}C), $Et_2O{\cdot}BF_3$ or 85% H_3PO_4. The atoms of the benzophospholide moiety are denoted C-1 to C-7a, 4-H to 7-H, and P-1 to P-3, using the numbering scheme given in Figure 1; carbon atoms of the phenyl groups by C_{para}, C_{meta} etc. − UV/Vis spectra: Kontron Uvikon 860. − FAB-MS: Kratos Concept 1 H, Xe-FAB. − Elemental analysis: Heraeus CHNO-Rapid.

3-(Diphenylphosphanyl)-1-(triphenylphosphonio)benzo[*c*]phospholide (3): 1,3-Bis(triphenylphosphonio)benzo[*c*]phospholide chloride (**1**[Cl]) (8.6 g, 12.5 mmol) and magnesium/anthracene·3THF (10.0 g, 24 mmol) were suspended in 50 mL of THF. The mixture was stirred for 8 h, filtered, and water-saturated Et_2O was added to the dark red solution until it turned yellow-orange. The mixture was filtered once more, the filtrate concentrated to dryness, and the orange residue suspended in a mixture of 20 mL of dry Et_2O and 50 mL of DME. Addition of 50 mL of MeOH gave the crude product as a yellow solid. Residual anthracene was removed by extraction with boiling hexane, and recrystallisation from DME/MeOH finally afforded 1.5 g (47%) of **2**, m.p. 179 °C. − Analytical and spectroscopic data are identical to those published in ref.[8]

1-(Triphenylphosphonio)benzo[*c*]phospholide (2): Solid $NaBH_4$ (2.5 g, 66 mmol) was added to a stirred suspension of **1**[Cl] (13.75 g, 19.9 mmol) in 150 mL of 2-propanol. It was stirred for 12 h until no starting material (^{31}P NMR control) was left. The mixture was then filtered, the precipitate washed three times with 2-propanol, and the filtrate concentrated to dryness. The yellow solid residue was extracted with 100 mL of THF and insoluble $NaBH_4$ was filtered off. After concentration of the filtrate in vacuum to a total

volume of 30−40 mL, 2-propanol was added until the precipitation of solid material started (approx. 20−30 mL). Cooling of the solution to 4 °C gave bright yellow crystals of **3**; yield 4.94 g (63%). − ^{1}H NMR ($CDCl_3$): δ = 6.71−7.63 (m, 4 H, 4-H to 7-H), 7.42−7.84 (m, 15 H, C_6H_5), 8.20 (dd, $^2J_{H,P-2}$ = 42.3 Hz, $^4J_{H,P-1}$ = 6.6 Hz, 1 H, 3-H). − $^{13}C\{^1H\}$ NMR ($CDCl_3$): δ = 86.4 (dd, $^1J_{P-2,C}$ = 54.8 Hz, $^1J_{P-1,C}$ = 102.8 Hz, C-1), 118.1 (d, $J_{P,C}$ = 0.9 Hz, C-6/5), 119.1 (d, $J_{P,C}$ = 3.9 Hz, C-5/6), 119.6 (d, $J_{P,C}$ = 4.1 Hz, C-7/4), 121.3 (dd, $J_{P,C}$ = 9.0, 1.1 Hz, C-4/7), 125.6 (dd, $^1J_{P-1,C}$ = 89.5 Hz, $^3J_{P-2,C}$ = 2.2 Hz, C_{ipso}), 129.5 (d, $^3J_{P-1,C}$ = 12.3 Hz, C_{meta}), 133.9 (dd, $^2J_{P-1,C}$ = 10.2 Hz, $^4J_{P-2,C}$ = 1.4 Hz, C_{ortho}), 134.6 (d, $^4J_{P-1,C}$ = 2.9 Hz, C_{para}), 138.3 (dd, $^1J_{P-2,C}$ = 36.8 Hz, $^3J_{P-1,C}$ = 13.5 Hz, C-3), 142.4 (dd, $J_{P,C}$ = 9.5, 2.0 Hz, C-3/3a, 145.2 (dd, $J_{P,C}$ = 17.6, 9.5 Hz, C-3/3a). − FAB-MS: *m*/*z* (%) = 394 (100) $[M]^+$ − $C_{26}H_{20}P_2$ (394.39): calcd. C 79.18, H 5.11; found C 78.17, H 5.88.

3-[(Diphenylphosphanyl)borane]-1-(triphenylphosphonio)benzo[*c*]-phospholide (6): Compound **2** (0.4 g, 0.69 mmol) was dissolved in 10 mL of THF. After 0.7 mL of a 1 M solution of BH_3·THF in THF had been added, the mixture was stirred for 10 min and then concentrated to dryness. The yellowish residue was recrystallised from THF/hexane; yield 0.41 g (100%), m.p. 227 °C. − ^{1}H NMR ($CDCl_3$): δ = 6.70−7.00 (m, 4 H, 4-H to 7-H), 7.20−8.50 (m, 25 H, C_6H_5). − $^{11}B\{^1H\}$ NMR ($CDCl_3$): δ = −28.5 (s, broad). − $^{13}C\{^1H\}$ NMR ($CDCl_3$): δ = 98.3 (ddd, $^1J_{P-2,C}$ = 58.1 Hz, $^1J_{P-1,C}$ = 98.6 Hz, $^3J_{P-3,C}$ = 11.6 Hz, C-1), 119.5 (s, C-6/5), 120.1 (s, C-5/6), 120.7 (d, $J_{P,C}$ = 3.8 Hz, C-7/4), 122.4 (d, $J_{P,C}$ = 3.9 Hz, C-4/7), 124.8 [d, $^1J_{P-1,C}$ = 89.8 Hz, $C_{ipso}(PPh_3)$], 128.6 [d, $^3J_{P-3,C}$ = 9.9 Hz, $C_{meta}(PPh_2)$], 129.7 [d, $^3J_{P-1,C}$ = 12.4 Hz, $C_{meta}(PPh_3)$], 130.5 [d, $^4J_{P-3,C}$ = 1.9 Hz, $C_{para}(PPh_2)$], 132.7 [d, $^1J_{P-3,C}$ = 4.4 Hz, $C_{ipso}(PPh_2)$], 133.4 [d, $^2J_{P-3,C}$ = 9.5 Hz, $C_{ortho}(PPh_2)$], 133.7 [d, $^4J_{P-1,C}$ = 2.7 Hz, $C_{para}(PPh_3)$], 134.4 [d, $^2J_{P-1,C}$ = 10.3 Hz, $C_{ortho}(PPh_3)$], 144.8 (dd, $^1J_{P-3,C}$ = 9.4 Hz, $^1J_{P-2,C}$ = 11.7 Hz, C-3), 145.6 (m, C-3a/7a). − FAB-MS: *m*/*z* (%) = 592 (20) $[M]^+$, 578 (100) $[M - BH_3]^+$ − $C_{38}H_{32}BP_3$ (592.40): calcd. C 77.05, H 5.44; found C 78.07, H 5.24.

3-(Diphenylthioxophosphoranyl)-1-(triphenylphosphonio)benzo[*c*]-phospholide (7): Compound **2** (0.5 g, 0.86 mmol) and sulphur (30 mg, 0.94 mmol) were dissolved in 10 mL of THF, and the resulting solution was stirred for 12 h. Subsequent addition of 20 mL of hexane produced a precipitate which was collected by filtration, washed with 5 mL of Et_2O/hexane (1:1), and dried in vacuum to give 0.46 g (87%) of a colourless solid, m.p. > 280 °C. − ^{1}H NMR ($CDCl_3$): δ = 6.70−6.93 (m, 4 H, 4-H to 7-H), 7.25−7.97 (m, 25 H, C_6H_5). − $^{13}C\{^1H\}$ NMR ($CDCl_3$): δ = 98.4 (ddd, $^1J_{P-2,C}$ = 58.8 Hz, $^1J_{P-1,C}$ = 97.5 Hz, $^3J_{P-3,C}$ = 14.1 Hz, C-1), 119.8 (s, C-6/5), 120.3 (d, $J_{P,C}$ = 1.7 Hz, C-5/6), 120.5 (d, $J_{P,C}$ = 3.6 Hz, C-7/4), 122.8 (d, $J_{P,C}$ = 4.4 Hz, C-4/7), 124.7 [d, $^1J_{P-1,C}$ = 89.7 Hz, $C_{ipso}(PPh_3)$], 128.3 [d, $^3J_{P-3,C}$ = 12.4 Hz, $C_{meta}(PPh_2)$], 129.6 [d, $^3J_{P-1,C}$ = 12.4 Hz, $C_{meta}(PPh_3)$], 130.8 [d, $^4J_{P-3,C}$ = 2.9 Hz, $C_{para}(PPh_2)$], 132.8 [d, $^2J_{P-3,C}$ = 10.1 Hz, $C_{ortho}(PPh_2)$], 133.6 [d, $^4J_{P-1,C}$ = 2.9 Hz, $C_{para}(PPh_3)$], 135.7 (ddd, $^1J_{P-2,C}$ = 59.1 Hz, $^3J_{P-1,C}$ = 13.2 Hz, $^1J_{P-3,C}$ = 88.1 Hz, C-3), 134.5 [d, $^2J_{P-1,C}$ = 10.3 Hz, $C_{ortho}(PPh_3)$], 136.3 [d, $^1J_{P-3,C}$ = 85.5 Hz, $C_{ipso}(PPh_2)$], 144.7 (m, C-3a/7a). − FAB-MS: *m*/*z* (%) = 611 (100) $[M]^+$ − $C_{38}H_{29}P_3S$ (610.63): calcd. C 74.75, H 4.79 S 5.25; found C 74.12, H 5.00 S 5.16.

Computational Studies: DFT calculations (B3LYP[20]) were carried out using the Gaussian 98 program package[21] with a 6-31 g* basis set which was augmented by one diffuse function for all ring atoms and the exocyclic halogen atoms [6-31(+)g* as implemented in the Gaussian package]. Harmonic vibrational frequencies and zero-

Table 6. Crystallographic data, and details for the structure solution and refinement of **2**, **3**, **6**, **7**

	2	**3**	**6**	**7**
Empirical formula	$C_{26}H_{20}P_2$	$C_{38}H_{29}P_3$	$C_{38}H_{32}BP_3$	$C_{38}H_{29}P_3S$
M_r	394.4	578.5	592.4	610.6
Crystal dimensions [mm]	0.50 × 0.30 × 0.25	0.30 × 0.25 × 0.20	0.35 × 0.30 × 0.25	0.25 × 0.10 × 0.05
Crystal system	monoclinic	triclinic	monoclinic	monoclinic
Space group	$P2_1/n$ (No. 14)	$P\bar{1}$ (No. 2)	$P2_1/n$ (No. 14)	$P2_1/n$ (No. 14)
a [Å]	10.6443(2)	9.2453(2)	10.6833(4)	10.4063(3)
b [Å]	15.0593(3)	11.6227(3)	18.7364(7)	18.7623(6)
c [Å]	12.8699(2)	14.7589(3)	16.2374(8)	16.1564(5)
α [°]	90	84.819(2)	90	90
β [°]	91.498(1)	89.160(2)	102.224(2)	98.960(2)
γ [°]	90	69.255(2)	90	90
V [Å^3]	2062.28(6)	1476.79(6)	3176.5(2)	3115.98(17)
Z	4	2	4	4
ρ [g·cm^{-3}]	1.27	1.30	1.24	1.30
μ [mm^{-1}]	0.22	0.23	0.21	0.29
F(000)	824	604	1240	1272
$2\theta_{max}$ [°]	56.6	56.6	50.0	50.0
	$-13 \le h \le 13$	$-12 \le h \le 12$	$-12 \le h \le 12$	$-12 \le h \le 12$
	$-20 \le k \le 20$	$-15 \le k \le 15$	$-22 \le k \le 17$	$-22 \le k \le 22$
	$-17 \le l \le 17$	$-19 \le l \le 19$	$-19 \le l \le 16$	$-19 \le l \le 19$
No. of measured data	60523	30935	20057	46091
No. of unique data	5092	7088	5590	5482
R_{int}	0.030	0.032	0.037	0.059
Absorption correction	none	none	none	none
No. parameters/restraints	253/0	370/0	381/0	379/0
R [for $I > 2\sigma(I)$]	0.032	0.033	0.033	0.035
*wR*2 (all data)	0.088	0.093	0.088	0.081
Max./min. diff. peak [e·Å^{-3}]	0.31/−0.29	0.35−/0.42	0.29/−0.31	0.26/−0.32

point vibrational energies (ZPE) were calculated at the same level. All structures reported here are minima on the potential energy surface (only positive eigenvalues of the Hessian matrix). Population analyses were carried out with the NBO module[23] included in the Gaussian 98 package. Due to problems with the handling of diffuse basis functions which occurred for some molecules in the NBO module, all population analyses were carried out using 6-31 g* wave functions with the molecular structures obtained at the 6-31(+)g* level. Comparison of the results of NBO analyses using both a 6-31 g* or a full 6-31(+)g* wave function was feasible for **2** and showed no significant differences between both approaches.

X-ray Crystallographic Study: Crystal structure determinations were carried out for **2**, **3**, **6**, **7**. All data were collected with a Nonius Kappa CCD diffractometer at −150 °C using Mo-K_α radiation (λ = 0.71073 Å). The structures were solved by direct methods (SHELXS-97[26]). The non-hydrogen atoms were refined anisotropically, H atoms were refined using a riding model [full-matrix least-squares refinement on F^2 (SHELXL-97[27])]. Details of data collection and refinement are given in Table 6. A complete list of bond lengths and angles, thermal parameters, and positions of hydrogen atoms is available as Supporting Information. Crystallographic data (excluding structure factors) for the structures reported in this paper have been deposited with the Cambridge Crystallographic Data Centre as supplementary publications no. CCDC-161501 (**2**), -161502 (**3**), -161503 (**6**), -161504 (**7**). Copies of the data can be obtained free of charge on application to CCDC, 12 Union Road, Cambridge CB2 1EZ, UK [Fax: (internat.) + 44-1223/336-033; E-mail: deposit@ccdc.cam.ac.uk].

Acknowledgments

Financial support by the Deutsche Forschungsgemeinschaft is gratefully acknowledged.

[1] A. Schmidpeter, M. Thiele, *Angew. Chem.* **1991**, *103*, 333; *Angew. Chem. Int. Ed. Engl.* **1991**, *30*, 308.
[2] D. Gudat, V. Bajorat, M. Nieger, *Bull. Chim. Soc. Fr.* **1995**, *132*, 280.
[3] D. Gudat, *Coord. Chem. Rev.* **1997**, *173*, 71.
[4] D. Gudat, M. Schrott, V. Bajorat, M. Nieger, *Phosphorus Sulfur Silicon* **1996**, *109−110*, 125.
[5] A. W. Holderberg, G. Schröder, D. Gudat, H.-P. Schrödel, A. Schmidpeter, *Tetrahedron.* **2000**, *56*, 57.
[6] D. Gudat, S. Häp, M. Nieger, *Z. Anorg. Allg. Chem.*, in press.
[7] See: K. B. Dillon, F. Mathey, J. F. Nixon, *Phosphorus: The Carbon Copy*, John Wiley, Chichester, **1998**, and references therein.
[8] D. Gudat, V. Bajorat, S. Häp, M. Nieger, G. Schröder, *Eur. J. Inorg. Chem.* **1999**, 1169.
[9] B. Breit, *J. Mol. Catal. A* **1999**, *143*, 143.
[10] B. Bogdanovic, in *Synthetic Methods of Organometallic and Inorganic Chemistry* (Ed.: W. A. Hermann), Georg Thieme Verlag, Stuttgart, **1996**, vol. 1, p. 46.
[11] See for a preliminary account: D. Gudat, S. Häp, L. Szarvas, M. Nieger, *Chem. Commun.* **2000**, 1637.
[12] See: J. Tebby, *CRC Handbook of Phosphorus-31 Nuclear Magnetic Resonance Data*, CRC Press, Boca Raton, **1991**.
[13] D. Gudat, M. Schrott, V. Bajorat, M. Nieger, *Phosphorus Sulfur Silicon* **1996**, *109−110*, 125.
[14] S. O. Grim, J. H. Ambrus, *J. Org. Chem.* **1968**, *33*, 2993.
[15] H. G. de Graaf, J. Dubbledam, H. Vermeer, F. Bickelhaupt, *Tetrahedron Lett.* **1973**, *9*, 2397.
[16] D. Gudat, M. Nieger, M. Schrott, *Chem. Ber.* **1995**, *128*, 259.
[17] B. F. Allen, O. Kennard, D. G. Watson, L. Brammer, A. G. Orpen, R. Taylor, in *International Tables for Crystallography* (Ed.: A. J. C. Wilson), Kluwer Academic Publishers, Dordrecht, **1992**, vol. C, p. 685pp.
[18] J. C. Huffman, W. A. Skupinski, K. G. Caulton, *Cryst. Struct. Commun.* **1982**, *11*, 1435.
[19] P. W. Codding, K. A. Kerr, *Acta Crystallogr., Sect. B* **1978**, *34*, 3785.
[20] A. D. Becke, *J. Chem. Phys.* **1993**, *93*, 5648.
[21] M. J. Frisch, G. W. Trucks, H. B. Schlegel, G. E. Scuseria, M. A. Robb, J. R. Cheeseman, V. G. Zakrzewski, J. A. Montgomery, R. E. Stratmann, J. C. Burant, S. Dapprich, J. M. Millam, A. D. Daniels, K. N. Kudin, M. C. Strain, O. Farkas, J. Tomasi, V. Barone, M. Cossi, R. Cammi, B. Mennucci, C. Pomelli, C. Adamo, S. Clifford, J. Ochterski, G. A. Petersson, P. Y. Ayala, Q. Cui, K. Morokuma, D. K. Malick, A. D. Rabuck, K. Raghavachari, J. B. Foresman, J. Cioslowski, J. V. Ortiz, B. B. Stefanov, G. Liu, A. Liashenko, P. Piskorz, I. Komaromi, R. Gomperts, R. L. Martin, D. J. Fox, T. Keith, M. A. Al-Laham, C. Y. Peng, A. Nanayakkara, C. Gonzalez, M. Challacombe, P. M. W. Gill, B. G. Johnson, W. Chen, M. W. Wong, J. L. Andres, M. Head-Gordon, E. S. Replogle, J. A. Pople, *Gaussian 98 (Rev. A.7)*, Gaussian, Inc., Pittsburgh, PA, **1998**.
[22] Neglection of counter-ions appeared justified considering that for both **1** and **5** experimental evidence suggested the absence of such interactions in both solution and the solid state; see refs.[8,16]
[23] [23a] J. P. Foster, F. Weinhold, *J. Am. Chem. Soc.* **1980**, *102*, 7211. − [23b] A. E. Reed, F. Weinhold, *J. Chem. Phys.* **1985**, *83*, 1736. − [23c] J. F. Carpenter, F. J. Weinhold, *J. Mol. Struct. (Theochem)* **1988**, *169*, 41.
[24] It should be noted that the calculated orbitals are Kohn−Sham orbitals. As such, these are strongly dependent on the chosen functional but may still be used for a qualitative interpretation of chemical phenomena, as has been discussed by the groups of Baerends and Hoffmann: [24a] E. J. Baerends, O. V. Gritsenko, *J. Phys. Chem.* **1997**, *101*, 5383. − [24b] R. Stowasser, R. Hoffman, *J. Am. Chem. Soc.* **1999**, *121*, 3414.
[25] Involvement of a continuous model treatment to the computed gas-phase structures revealed that the π-population are not affected by solvation effects. This suggests that the rating of the canonical contributions should be similar in the gas phase and in solution or the solid state.
[26] *SHELXS-97*: G. M. Sheldrick, *Acta Crystallogr., Sect. A* **1990**, *46*, 467.
[27] *SHELXL-97*: G. M. Sheldrick, University of Göttingen, **1997**.

Received April 9, 2001
[I01128]

First Crystallographic Investigation of Complexes of *cis*-VO_2^+, *cis*-MoO_2^{2+}, and *trans*-UO_2^{2+} Species with Schiff-Base Molecules Derived from 4,6-*O*-Ethylidene-β-D-glucopyranosylamine

Ajay K. Sah,[a] Chebrolu P. Rao,*[a] Pauli K. Saarenketo,[b] Elina K. Wegelius,[b] Erkki Kolehmainen,[b] and Kari Rissanen[b]

Dedicated to Professor Animesh Chakravorty, IACS, Calcutta, on the occasion of his 65th birthday

Keywords: Vanadium / Molybdenum / Uranium / Schiff bases / Structure elucidation

The interaction of Schiff-base ligands derived from 4,6-*O*-ethylidene-β-D-glucopyranosylamine with *cis*-VO_2^+, *cis*-MoO_2^{2+}, and *trans*-UO_2^{2+} species have been studied by isolating and characterizing the corresponding products. The structures of one complex of each type of species have been established by single-crystal X-ray diffraction analysis. In all the complexes, the saccharide moiety adopts a chair conformation and has a β-anomeric form. A gradual increase in coordination number (5, 6, and 7) and a gradual variation in the geometry (distorted trigonal-bipyramidal, distorted octahedral, and pentagonal-bipyramidal) are observed on going from the complexes of *cis*-VO_2^+ (mononuclear) to *cis*-MoO_2^{2+} (mononuclear) to *trans*-UO_2^{2+} (dinuclear). A variation in the binding mode of the ligand towards these dioxometal species is also observed. Intermolecular interactions of the type O–H···O, C–H···O, and N–H···O present in the lattices of these complexes lead to the formation of interesting structures.

Introduction

About two-thirds of the carbon in the biosphere is present in various forms of carbohydrates.[1] Carbohydrates not only act as the major source of energy for living beings, but also as building blocks for the formation of polysaccharides, nucleic acids, and antibiotics. The coexistence of saccharides and metal ions was established in the context of biological systems.[2] Although the metal ion−saccharide interactions were recognized long ago, the early literature was mainly concerned with solution studies, primarily with metal ions of the alkali and alkaline earth groups and of main group elements, as well as their adducts.[3] Only during the past decade have such interactions been delineated in the case of transition metal ions by isolation and characterization of the products.[4] In order to improve the binding affinities towards metal ions, as well as to isolate the metal ion−saccharide products in crystalline form, new strategies for saccharide modification have been developed. One such attempt of ours in this context recently resulted in the synthesis and characterization of complexes of *N*-(*o*-carboxyphenyl)-4,6-*O*-ethylidene-β-D-glucopyranosylamine with alkali and alkaline earth metal ions and the crystal structure of its potassium complex.[5] In this new strategy, the study of metal−saccharide interactions is attempted using the products of condensation of 4,6-*O*-ethylidene-β-D-glucopyranosylamine with salicylaldehyde and its derivatives as ligands suitable for metal ion binding. The results of these efforts are reported herein. Thus, the present studies are in continuation of our ongoing interest in establishing the interaction of OH-containing ligands with oxometal ion species, such as *cis*-VO_2^+, *cis*-MoO_2^{2+}, and *trans*-UO_2^{2+}. Studies of such oxometal ion species are also important with regard to the stereochemical preferences in binding to these new types of saccharide−Schiff-base ligands.

Therefore, we report herein the synthesis, characterization, and crystal structure determination of *cis*-VO_2^+, *cis*-MoO_2^{2+}, and *trans*-UO_2^{2+} metal ion complexes with salicylidene Schiff-base ligands derived from a glycosylamine, 4,6-*O*-ethylidene-β-D-glucopyranosylamine. The products have been characterized on the basis of their FT-IR- and NMR-spectroscopic data, FAB mass spectra, and single-crystal X-ray structural data. To the best of our knowledge, the three crystal structures of the saccharide−Schiff-base complexes of *cis*-VO_2^+, *cis*-MoO_2^{2+}, and *trans*-UO_2^{2+} reported herein are the first of their kind.

[a] Bioinorganic Laboratory, Department of Chemistry, Indian Institute of Technology Bombay,
Powai, Mumbai 400 076, India
Fax: (internat.) + 91-22/572-3480
E-mail: cprao@chem.iitb.ac.in
[b] Department of Chemistry, University of Jyväskylä,
40351 Jyväskylä, Finland
Supporting information for this article is available on the WWW under http://www.eurjic.com or from the author.

Results and Discussion

The ligands derived from 4,6-*O*-ethylidene-β-D-glucopyranosylamine and their complexes with dioxometal species of V, Mo, and U are shown in Scheme 1. While the reactions of *cis*-MoO_2^{2+} and *trans*-UO_2^{2+} gave the products in

 © WILEY-VCH Verlag GmbH, 69451 Weinheim, 2001 1434−1948/01/1111−2773 $ 17.50+.50/0

high yields, those with *cis*-VO_2^+ resulted in rather low yields. This is attributable to the formation of a second product in the case of the vanadium reactions, which could not be isolated in pure form. Evidence for this was provided by UV/Vis studies. The products with V and Mo were found to be mononuclear, while those with U were dinuclear. All exhibited a 1:1 metal-to-ligand ratio.

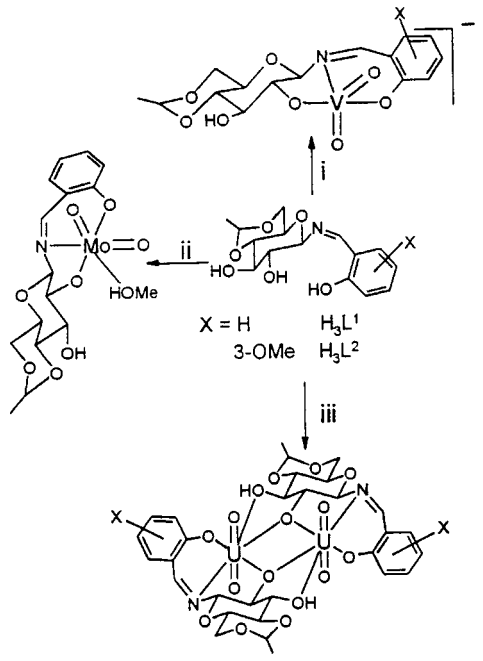

Scheme 1. Syntheses of the *cis*-VO_2^+, *cis*-MoO_2^{2+}, and *trans*-UO_2^{2+} complexes in methanol using the ligands $\mathbf{H_3L^1}$ and $\mathbf{H_3L^2}$: (i) $VO(acac)_2$, (ii) *cis*-$MoO_2(acac)_2$, and (iii) *trans*- $UO_2(OAc)_2{\cdot}2H_2O$

FT-IR

Comparison of the FT-IR spectra of all the complexes with those of their precursor ligands supported the formation of the respective complexes through the observation of substantial spectral changes. Characteristic vibrational bands corresponding to the M=O groups are observed for all the complexes. The ligand exhibits two distinct bands in the ν_{OH} region, whereas only one broad signal is observed for the corresponding complexes, indicating the loss of some hydroxy protons during complexation. This conclusion was further supported by the ^{1}H NMR spectra as well as by the crystal structure determinations. The ν_{OH} is generally shifted to higher frequencies by about 100 cm^{-1} for the uranium complexes as compared to the position of this band for their vanadium and molybdenum counterparts; this can be attributed to the fact that 3-OH is involved in metal ion binding in the former, whereas it is free in the latter.

^{1}H NMR

The spectra of all the complexes are indicative of the presence of a single anomeric form. However, upon addition of a small amount of D_2O to the respective solutions, spectral peaks corresponding to a second anomer appear with time. Upon complexation, only a single hydroxy proton signal remains in the alkyloxy region, indicating the loss of the phenolic and one of the alcoholic protons. The signals of the skeletal protons of the saccharide moiety are subject to an overall downfield shift upon complexation, this shift being more pronounced in the case of the uranium complex as compared to the vanadium and molybdenum complexes. Thus, the downfield shift of the signals of the skeletal protons is in the order *trans*-UO_2^{2+}complex >> *cis*-MoO_2^{2+} complex > *cis*-VO_2^+ complex. This may be attributed to the additional involvement of 3-OH (in addition to 2-OH) in the complexation in the case of the UO_2^{2+} species. The same trend was observed for the the HC=N and 1-H proton signals of the complexes. The $J_{C1\text{-}H}$ values were found to be 8.79 and 7.69 Hz for $VO_2(HL^1)$ and $VO_2(HL^2)$, respectively, supporting the presence of the saccharide moiety in the β-anomeric form.[16] The β-anomeric form of the saccharide moiety was unequivocally established on the basis of the crystal structures of the three complexes.

FAB MS

FAB MS studies supported the mononuclear nature of the V^V and Mo^{VI} complexes and the dinuclear nature of the U^{VI} complexes through exhibiting molecular ion peaks. Furthermore, the spectra of the vanadium complexes revealed the formation of the monooxo dinuclear species shown in Figure 1.

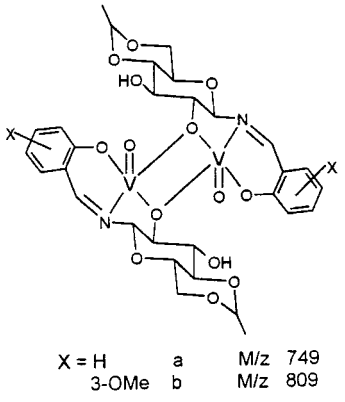

Figure 1. The dimeric species of monooxo V^V identified in the mass spectra

UV/Vis

Electronic spectra of all the complexes were recorded using freshly prepared solutions in DMSO at concentrations of 10^{-2} and 10^{-4} M; the corresponding spectra are shown in Figure 2. While the complexes of molybdenum and uranium (Figures 2b, 2c) proved to be stable in DMSO solution even after 36 h, those of vanadium underwent some cleavage and some free ligand was liberated (Figure 2a). An additional band was observed at 530−540 nm in the spectra, indicating the formation of some new oxovanadium species.

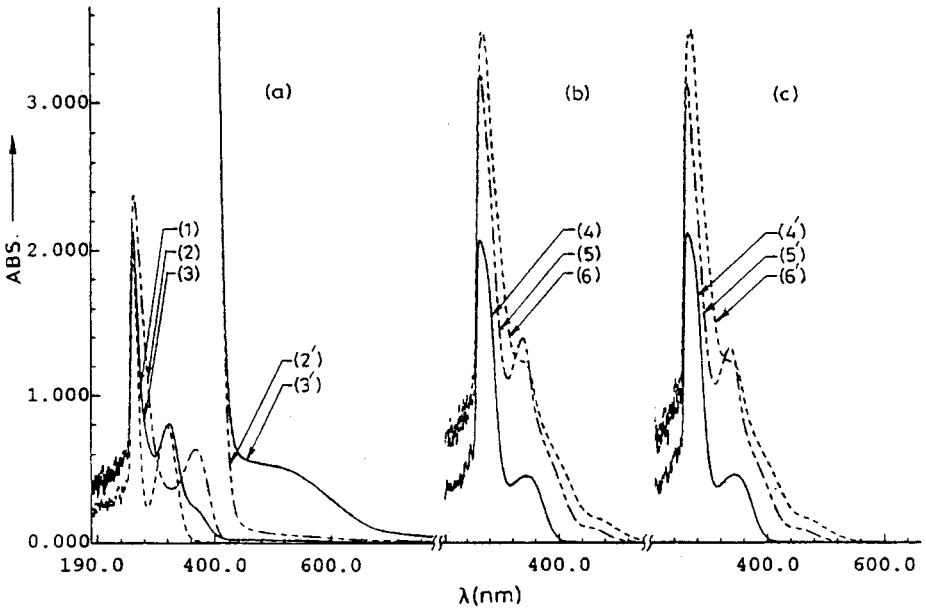

Figure 2. UV/Vis absorption spectra in DMSO: (a) spectrum (1) corresponds to H_3L^1, spectra (2, 2′) correspond to a freshly prepared solution of *cis*-$VO_2(HL^1)$, and spectra (3, 3′) correspond to the same complex analysed 36 h after dissolution; (b) and (c) spectra (4, 5, 6) correspond to freshly prepared solutions of the *cis*-$[MoO_2(HL^1)]$, *trans*-$[\{UO_2(HL^1)\}_2]$, and *trans*-$[\{UO_2(HL^1)\}_2]$ complexes, respectively, while spectra (4′, 5′, 6′) correspond to the same solutions after 36 h

Optical Rotation

The mononuclear complexes of *cis*-VO_2^+ and *cis*-MoO_2^{2+} showed a substantial change in specific rotation as compared with the specific rotations of the corresponding ligands.

Molecular and Crystal Structure of $VO_2(HL^1)$

Slow evaporation of the solvent from a concentrated methanolic solution of the complex resulted in single crystals in the monoclinic system. The crystal structure revealed the presence of a *cis*-dioxo mononuclear V^V complex, which is rather rare in vanadium−saccharide chemistry. Earlier reports dealt with either dioxo dinuclear homoleptic[7,8] or monooxo complexes of mixed ligands.[9] In the complex **$VO_2(HL^1)$**, the saccharide derivative is bound as a tridentate dianionic ligand, where 2-OH of the saccharide moiety extends coordination in its deprotonated form resulting in an ONO core, and where the other two ligations are extended by the salicylidene moiety. This results in the formation of one five- and one six-membered chelate. In order to compensate for the negative charge present on the complex, a dimethylammonium cation is present in the crystal lattice. Thus, the dioxo-V^V center exhibits a distorted trigonal-bipyramidal geometry (the *trans* angle is 156.8°), with both the oxo groups and the imine nitrogen donors occupying the basal plane. The basal plane accommodates the vanadium center without any deviation. An ORTEP view of the complex is shown in Figure 3, while crystallographic data are given in Table 1 and some selected bond lengths and angles are given in Table 2. All the metric data are well within the expected ranges and are consistent with the reported values for similar coordinations.[10] In the complex, the saccharide and aromatic moieties are arranged in a *trans* geometry with respect to the C=N bond. The dihedral angles of the saccharide moiety revealed a β-anomeric form, as was also indicated by the proton NMR study. In the solid state, both the six-membered rings of the saccharide moiety, i.e. the pyranose and the 4,6-protected part, were found to adopt a chair conformation.

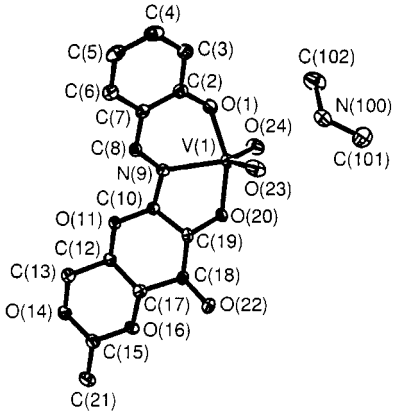

Figure 3. Molecular structure of **$[VO_2(HL^1)](Me_2NH_2)$**; thermal ellipsoids are drawn at a 50% probability level using ORTEP

Each NH group of the dimethylammonium ion is involved in one strong hydrogen bond interaction. One of the N−H bonds exhibits an additional weak interaction. These N−H protons are accepted by the oxo groups of the vanadium center (V=O) and 2-O of the saccharide moiety; 3-OH of the saccharide moiety acts as a hydrogen donor towards a second V=O group, exhibiting a strong O−H···O interaction.

Table 1. Summary of crystallographic data and parameters for $[VO_2(HL^1)](Me_2NH_2)$, $[MoO_2(HL^1)(MeOH)]MeOH$, and $[\{UO_2(HL^2)\}_2](EtOH)_2(H_2O)_2$

	$[VO_2(HL^1)](Me_2NH_2)$	$[MoO_2(HL^1)\ (MeOH)]MeOH$	$[\{UO_2(HL^2)\}_2](EtOH)_2(H_2O)_2$
Empirical formula	$C_{17}H_{25}N_2O_8V$	$C_{17}H_{25}MoNO_{10}$	$C_{36}H_{54}N_2O_{22}U_2$
Molecular mass	436.33	499.32	1342.87
T [K]	173(2)	173(2)	173(2)
Crystal system	orthorhombic	orthorhombic	hexagonal
Space group	$P2_12_12_1$	$P2_12_12_1$	$P6_2$
Cell constants			
a [Å]	6.4505(2)	7.156(1)	18.224(1)
b [Å]	10.0618(3)	14.202(1)	18.224(1)
c [Å]	29.7295(11)	19.325(1)	11.843(1)
γ [°]	–	–	120
V [Å^3]	1929.6(1)	1964.0(3)	3406.3(4)
Z	4	4	3
D [Mg/m^3]	1.502	1.689	1.964
Max./min. transmission	0.9460, 0.8495	0.8397, 0.6311	0.3760, 0.3379
Total reflections	7060	9744	18574
Unique reflections	3348 (R_{int} = 0.0318)	3400 (R_{int} = 0.0194)	3565 (R_{int} = 0.0548)
Parameters	265	273	263
Final R [$I > 2\sigma(I)$]	0.0328	0.0180	0.0463
R_w	0.0677	0.0490	0.0944

Table 2. Selected bond lengths [Å] and angles [°] for **$[VO_2(HL^1)](Me_2NH_2)$**

V(1)−O(23)	1.617(2)	V(1)−O(24)	1.626(2)
V(1)−O(20)	1.915(2)	V(1)−O(1)	1.930(2)
V(1)−N(9)	2.166(2)	O(1)−C(2)	1.314(3)
C(2)−C(7)	1.408(4)	C(7)−C(8)	1.419(4)
C(8)−N(9)	1.283(3)	N(9)−C(10)	1.448(3)
C(10)−O(11)	1.411(3)	C(10−C(19)	1.520(3)
O(11)−C(12)	1.411(3)	C(12)−C(17)	1.533(3)
C(17)−C(18)	1.519(3)	C(18)−O(22)	1.415(3)
C(18)−C(19)	1.514(3)	C(19)−O(20)	1.412(3)
O(23)−V(1)−O(24)	110.0(1)	O(23)−V(1)−O(20)	98.4(1)
O(23)−V(1)−O(1)	96.9(1)	O(23)−V(1)−N(9)	119.4(1)
O(24)−V(1)−O(20)	95.8(1)	O(24)−V(1)−O(1)	95.4(1)
O(24)−V(1)−N(9)	130.6(1)	O(20)−V(1)−O(1)	156.8(1)
O(20)−V(1)−N(9)	77.7(1)	O(1)−V(1)−N(9)	79.5(1)
V(1)−O(1)−C(2)	134.8(2)	O(1)−C(2)−C(7)	122.8(2)
C(2)−C(7)−C(8)	120.4(2)	C(7)−C(8)−N(9)	124.0(2)
C(8)−N(9)−V(1)	129.8(2)	C(8)−N(9)−C(10)	120.3(2)
N(9)−C(10)−C(19)	103.6(2)	N(9)−C(10)−O(11)	113.1(2)
C(10)−O(11)−C(12)	106.8(2)	O(11)−C(12)−C(17)	111.0(2)
C(12)−C(17)−C(18)	111.5(2)	C(17)−C(18)−O(22)	107.8(2)
C(17)−C(18)−C(19)	107.6(2)	O(22)−C(18)−C(19)	112.7(2)
C(18)−C(19)−O(20)	114.3(2)	C(18)−C(19)−C(10)	112.6(2)
C(10)−C(19)−O(20)	103.6(2)	C(19)−O(20)−V(1)	114.5(1)
C(10)−N(9)−V(1)	109.3(2)		

In addition, there are at least five C−H···O-type intermolecular interactions, for which the metric data are well within the ranges reported for such interactions in the literature.[11] The CH groups in these arise from phenyl, 3-H of saccharide, and both the methyl groups of the countercation. The acceptor oxygen atoms for these interactions are ether oxygen atoms, 2- and 3-O of the saccharide moiety, the phenolic oxygen atom, and V=O. Thus, in the lattice, each molecule is connected to four other neighbouring molecules through weak interactions, thereby forming a three-dimensional network.

Molecular and Crystal Structures of $MoO_2(HL^1)$

Slow diffusion of methanol into a concentrated solution of the complex in DMSO resulted in single crystals in the monoclinic space group. Even in this case, the ligand moiety acts as a tridentate dianion bound to a *cis*-MoO_2 unit, giving rise to one five- and one six-membered chelate, similar to the situation observed in the case of the vanadium complex. The sixth coordination site is occupied by MeOH and an additional MeOH molecule is present in the lattice. Both the molybdenum mixed-ligand complexes reported in the literature were derived from the simple protected saccharide 1,2:5,6-di-*O*-isopropylidene-D-glucofuranose.[12,13] While the complex reported by Floriani was *cis*-dioxo−Mo^{VI}, that reported by McCleverty was non-oxo−Mo^{VI}; in both the cases the saccharide acts as a monodentate ligand. To the best of our knowledge, the present structure is the first example of one in which a saccharide-based Schiff-base ligand is complexed with oxo−Mo^{VI} that has been established by single-crystal X-ray diffraction analysis. An ORTEP view of the complex is shown in Figure 4 and some selected bond lengths and bond angles are given in Table 3. All the values are consistent with earlier reports for similar coordination.[14] The crystallographic studies clearly indicate a highly distorted octahedral geometry around the molybdenum center, with the saccharide derivative binding meridionally and the metal ion deviating from the mean plane formed by O1 (phenolic), N9 (imine), O17 (saccharide 2-O), and O30 (Mo=O) by 0.305(1) Å. The *trans* angles range from 150.9(1) to 167.2(1)° and all the other angles from 75 to 107°. The remaining binding features are similar to those of the *cis*-VO_2^+ structure reported herein. The crystal structure of the Mo complex also revealed the presence of the

β-anomeric form of the saccharide moiety based on the dihedral angles. Both the six-membered rings of the saccharide moiety were found to adopt a chair conformation.

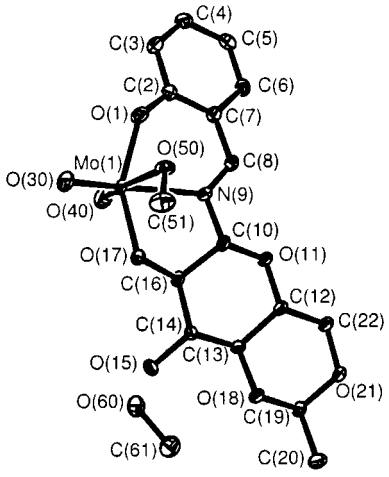

Figure 4. Molecular structure of **[MoO_2(HL^1)(MeOH)]MeOH**; thermal ellipsoids are drawn at a 50% probability level using ORTEP

Table 3. Selected bond lengths [Å] and angles [°] for **[MoO_2(HL^1)(MeOH)]MeOH**

Mo(1)−O(30)	1.704(1)	Mo(1)−O(40)	1.700(2)
Mo(1)−O(17)	1.944(1)	Mo(1)−O(1)	1.958(2)
Mo(1)−O(50)	2.368(2)	Mo(1)−N(9)	2.292(2)
O(1)−C(2)	1.343(3)	C(2)−C(7)	1.420(3)
C(7)−C(8)	1.448(3)	C(8)−N(9)	1.280(3)
N(9)−C(10)	1.444(2)	C(10)−C(16)	1.519(3)
C(10)−O(11)	1.418(2)	O(11)−C(12)	1.437(2)
C(12)−C(13)	1.528(3)	C(13)−O(18)	1.436(2)
C(13)−C(14)	1.523(3)	C(14)−O(15)	1.420(2)
C(14)−C(16)	1.527(2)	C(16)−O(17)	1.418(2)
O(40)−Mo(1)−O(30)	107.1(1)	O(40)−Mo(1)−O(17)	98.2(1)
O(40)−Mo(1)−O(1)	96.4(1)	O(40)−Mo(1)−O(50)	167.2(1)
O(40)−Mo(1)−N(9)	91.5(1)	O(30)−Mo(1)−O(17)	98.5(1)
O(30)−Mo(1)−O(1)	101.2(1)	O(30)−Mo(1)−O(50)	85.5(1)
O(30)−Mo(1)−N(9)	161.2(1)	O(17)−Mo(1)−O(1)	150.9(1)
O(17)−Mo(1)−O(50)	82.0(1)	O(17)−Mo(1)−N(9)	75.5(1)
O(1)−Mo(1)−O(50)	78.3(1)	O(1)−Mo(1)−N(9)	79.0(1)
O(50)−Mo(1)−N(9)	76.1(1)	Mo(1)−O(1)−C(2)	132.2(1)
O(1)−C(2)−C(7)	122.7(2)	C(2)−C(7)−C(8)	122.3(2)
C(7)−C(8)−N(9)	123.2(2)	C(8)−N(9)−Mo(1)	128.1(1)
C(8)−N(9)−C(10)	122.3(2)	N(9)−C(10)−O(11)	112.9(2)
N(9)−C(10)−C(16)	104.8(2)	Mo(1)−N(9)−C(10)	109.4(1)
C(16)−C(10)−O(11)	112.6(2)	C(10)−O(11)−C(12)	107.2(1)
O(11)−C(12)−C(13)	110.5(2)	C(12)−C(13)−O(18)	108.0(2)
O(18)−C(13)−C(14)	110.1(2)	C(12)−C(13)−C(14)	110.7(2)
C(13)−C(14)−O(15)	109.7(2)	C(13)−C(14)−C(16)	105.9(2)
O(15)−C(14)−C(16)	111.1(2)	C(14)−C(16)−O(17)	112.2(2)
C(16)−O(17)−Mo(1)	115.6(1)	C(14)−C(16)−C(10)	110.7(2)
O(17)−C(16)−C(10)	106.1(2)		

As a result of the extensive intermolecular involvement of both the free and bound MeOH units in the molybdenum compound, the lattice exhibits a layered structure (Figure 5), in which extended motifs, having intermolecular O−H···O and C−H···O-type interactions, are present. Both the lattice CH_3OH and 3-OH of the saccharide moiety connect the molecules present in the lattice through intermolecular O−H···O-type interactions, where the OH groups of both these moieties are involved in two such interactions by acting as both hydrogen donors and hydrogen acceptors. Thus, in effect, the molecules in the lattice are connected through zig-zag-type O−H···O interactions, as shown in Figure 6a. Similarly, the bound methanol unit is also involved in two intermolecular H-bonds, one O−H···O-type and one C−H···O-type interaction, acting as a hydrogen donor in both cases. The acceptors in these two cases are Mo=O and 6-O of the saccharide. The (metal-bound methanol)C−H···O=Mo-type interaction results in the formation of a linear chain of complex units connecting the layers, as shown in Figure 6b. Perpendicular to this chain, Ar−C−H···O=Mo type interactions extend by a connection of the molecules present in each layer, as shown in Figure 6c. Thus, the lattice consists of layers of molybdenum compounds, these being connected through extensive H-bond interactions. Furthermore, in each layer, the molecules are interconnected through H-bond interactions.

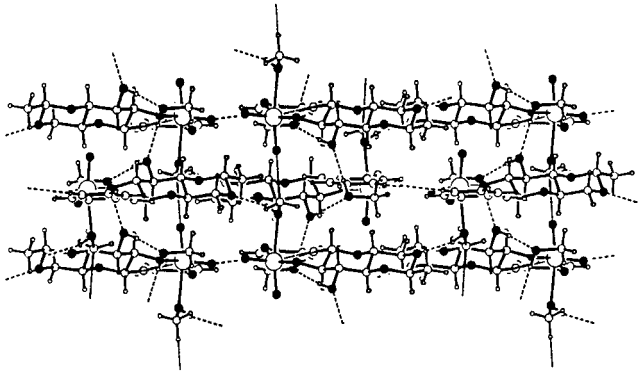

Figure 5. Layers of molecules in the lattice of the complex **[MoO_2(HL^1)(MeOH)]MeOH**; H-bond interactions are shown by dashed lines; large, open circles: metal ions; filled circles: oxygen atoms; circles with a line: nitrogen atoms

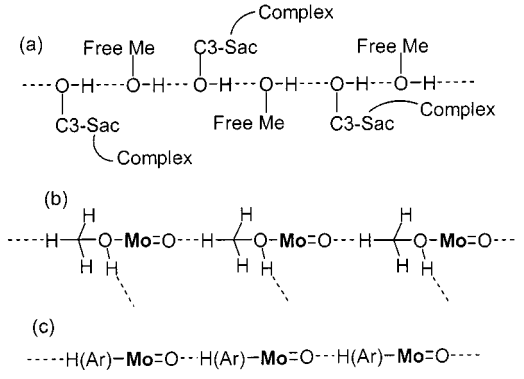

Figure 6. Weak interaction motifs present in the crystal lattice of the molybdenum complex, as determined from single-crystal X-ray diffraction analysis

Molecular and Crystal Structures of $[UO_2(HL^2)]_2$

Slow diffusion of a methanol/ethanol mixture into a concentrated solution of the complex in dichloromethane resulted in single crystals of the hexagonal system. A structural study of the product showed it to be a dinuclear *trans*-dioxo−U^{VI} complex, unlike the mononuclear complexes observed with *cis*-VO_2^+ and *cis*-MoO_2^{2+}. This is the only complex in which both the available hydroxy groups of the saccharide moiety, 2-OH and 3-OH, are involved in metal ion binding; 2-OH of the saccharide binds in its deprotonated form (2-O^-) and bridges the two metal centers giving rise to a four-membered U_2O_2 rhomb, whereas 3-OH binds to the metal ion without losing its proton. Thus, the ligand exhibits tetradentate binding plus one bridging interaction. Nevertheless, the metal-to-ligand ratio was found to be 1:1 in this complex as well. An ORTEP view of the complex is shown in Figure 7; selected bond lengths and bond angles are given in Table 4. All the values are consistent with earlier reports for a similar coordination.[15] The U_2O_2 rhomb exhibits a center of symmetry and has distances of 2.327 and 2.386 Å and angles of 113.5° and 64.9°. In addition, each asymmetric unit cell includes an ethanol and a water molecule. Even in this case, the C=N bond exhibits *trans* geometry and the saccharide moiety adopts the β-anomeric form. Both the six-membered rings of the saccharide moiety are found to adopt a chair conformation. In this complex, the *trans*-dioxo−uranium center exhibits a pentagonal-bipyramidal geometry, with the uranium ion showing almost no deviation from the basal plane [0.026(6) Å]. Thus, the *trans*-dioxo geometry of U^{VI} influences the binding characteristics of the saccharide−Schiff-base ligand.

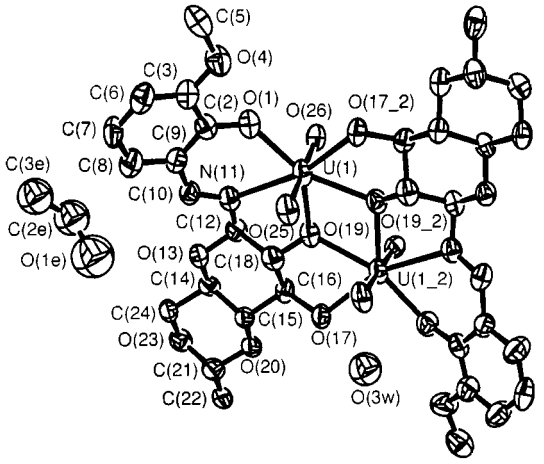

Figure 7. Molecular structure of $[\{UO_2(HL^2)\}_2](EtOH)_2(H_2O)_2$; thermal ellipsoids are drawn at a 40% probability level using ORTEP

Table 4. Selected bond lengths [Å] and angles [°] for $[\{UO_2(HL^2)\}_2](EtOH)_2(H_2O)_2$

U(1)−O(26)	1.752(16)	U(1)−O(25)	1.810(15)
U(1)−O(1)	2.235(8)	U(1)−O(19)	2.330(8)
U(1)−O(19_2)	2.404(8)	U(1)−O(17_2)	2.528(8)
U(1)−N(11)	2.571(9)	U(1)−U(1_2)	3.942(1)
O(1)−C(2)	1.337(14)	C(2)−C(9)	1.416(17)
C(9)−C(10)	1.480(18)	C(10)−N(11)	1.290(15)
N(11)−C(12)	1.452(15)	C(12)−O(13)	1.422(13)
C(12)−C(18)	1.494(17)	O(13)−C(14)	1.451(14)
C(14)−C(15)	1.527(16)	C(15)−C(16)	1.532(17)
C(16)−O(17)	1.466(14)	C(16)−C(18)	1.551(18)
C(18)−O(19)	1.386(14)		
O(26)−U(1)−O(25)	179.3(6)	O(26)−U(1)−O(1)	88.5(4)
O(26)−U(1)−O(19)	90.3(4)	O(26)−U(1)−O(19_2)	88.0(4)
O(26)−U(1)−O(17_2)	92.0(3)	O(26)−U(1)−N(11)	94.0(3)
O(25)−U(1)−O(1)	90.9(4)	O(25)−U(1)−O(19)	90.2(4)
O(25)−U(1)−O(19_2)	92.6(4)	O(25)−U(1)−O(17_2)	87.9(4)
O(25)−U(1)−N(11)	85.8(3)	O(1)−U(1)−O(19)	138.1(3)
O(1)−U(1)−O(19_2)	155.9(3)	O(1)−U(1)−O(17_2)	89.6(3)
O(1)−U(1)−N(11)	71.6(3)	O(19)−U(1)−O(19_2)	65.7(3)
O(19)−U(1)−O(17_2)	132.3(3)	O(19)−U(1)−N(11)	66.7(3)
O(19_2)−U(1)−O(17_2)	66.8(3)	O(19_2)−U(1)−N(11)	132.4(3)
O(17_2)−U(1)−N(11)	160.1(3)	U(1)−O(19)−U(1_2)	112.7(3)
C(2)−O(1)−U(1)	136.1(8)	O(1)−C(2)−C(9)	122.5(12)
N(11)−C(10)−C(9)	125.1(12)	C(10)−N(11)−C(12)	118.4(10)
O(13)−C(12)−N(11)	113.8(10)	N(11)−C(12)−C(18)	104.8(10)
C(12)−O(13)−C(14)	109.9(9)	O(13)−C(14)−C(15)	111.7(9)
O(13)−C(14)−C(24)	108.1(10)	C(15)−C(14)−C(24)	108.9(9)
O(20)−C(15)−C(14)	109.0(9)	O(20)−C(15)−C(16)	111.5(10)
C(14)−C(15)−C(16)	106.7(9)	O(17)−C(16)−C(15)	113.7(10)
O(17)−C(16)−C(18)	106.5(9)	C(15)−C(16)−C(18)	106.6(9)
O(19)−C(18)−C(16)	107.8(10)	O(19)−C(18)−C(12)	112.0(11)
C(12)−C(18)−C(16)	110.5(10)		

The *trans*-UO_2^{2+} complex crystallizes with a free ethanol and a water molecule; these do not exhibit any extended interactions, showing only discrete H-bond interactions. While the water molecule in the lattice acts as an acceptor for one O−H···O and one C−H···O interaction, the ethanol molecule acts as donor for such interactions. Thus, in the lattice, the water molecule interacts with both the ethanol molecule and 3-OH of the saccharide moiety, while the ethanol molecule is connected to 5-O of the saccharide moiety within the same molecule. In addition, the lattice contains four other C−H···O-type intermolecular interactions, which are responsible for the formation of a layer-type structure. The donors for such interactions are 4-, 5-, and 6-H of the saccharide moiety and the methoxy C−H of the salicylidene moiety, while the acceptors are 4-, 3-OH, U=O, and the phenolic O, respectively, of the neighbouring molecules in the lattice. The layer-type structure that results from these interactions is shown in Figure 8.

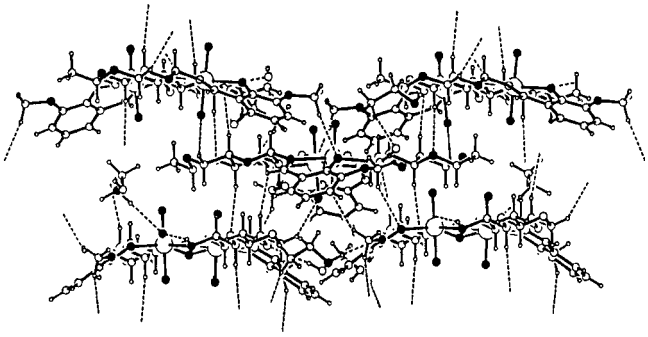

Figure 8. Layers of molecules in the lattice of the complex **[{UO_2(HL^2)}$_2$](EtOH)$_2$(H_2O)$_2$**; H-bond interactions are shown by dashed lines; large, open circles: metal ions; filled circles: oxygen atoms; circles with a line: nitrogen atoms

Conclusions

Saccharide−Schiff-base complexes of *cis*-VO_2^+, *cis*-MoO_2^{2+}, and *trans*-UO_2^{2+} have been synthesized and characterized using various analytical and spectroscopic techniques, as well as by single-crystal X-ray diffraction analysis. The NMR spectra of freshly prepared solutions in [D_6]DMSO show the saccharide moiety to be in the β-anomeric form. With *cis*-dioxo−metal ions, the ligand is tridentate, whereas with *trans*-dioxo ions it shows tetradentate coordination with an additional bridging interaction. A dianion results due to the loss of a phenolic as well as an alcoholic (2-OH of saccharide) proton. In the *trans*-UO_2^{2+} complex, 2-O^- of the saccharide moiety bridges the two uranyl centers, resulting in a dinuclear complex exhibiting a U_2O_2 rhomb, whereas 3-OH is involved in coordination without losing its proton. Metal ion binding results in the formation of one six- and two five-membered chelates. X-ray diffraction studies of the metal ion complexes revealed an increase in coordination number around the metal ion from 5 to 6 to 7 on going from *cis*-VO_2^+ to *cis*-MoO_2^{2+} to *trans*-UO_2^{2+}, corresponding to trigonal-bipyramidal, octahedral, and pentagonal-bipyramidal geometries, respectively. The dimeric structure seen in the case of the UO_2^{2+} ion complex may be attributed to the large size of the uranyl ion as well as the *trans* orientation of the oxo groups. In all the complexes, the saccharide unit adopts a chair conformation. In the lattice, weak interactions of the type O−H···O, N−H···O, and C−H···O were found to number 9, 5, and 7 for the vanadium, molybdenum, and uranium complexes, respectively. Some important features of these complexes are compared in Figure 9. As a result of these interactions, the molybdenum and uranium complexes exhibit interesting layer-type lattice structures, while the vanadium complex exhibits a three-dimensional network of hydrogen bonds. Thus, both the molecular and lattice features differ on going from *cis*-VO_2^+ to *cis*-MoO_2^{2+} to *trans*-UO_2^{2+} species, as demonstrated in this work by using saccharide-based Schiff-base ligands.

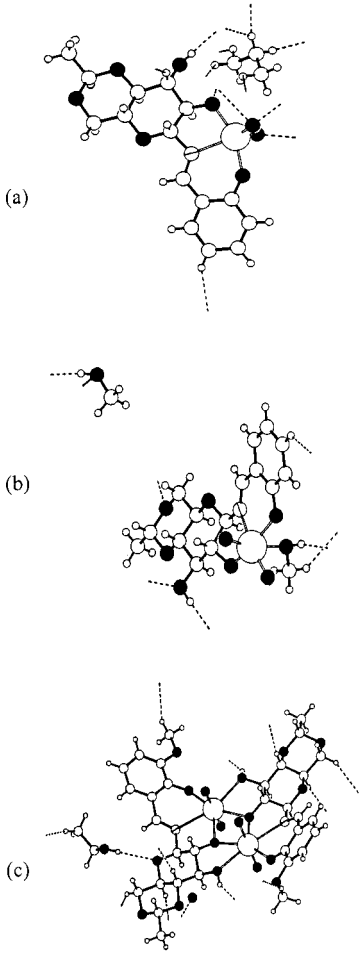

Figure 9. Coordination unit and H-bond interactions extended from each unit, as obtained from the crystal structures of (a) **[VO_2(HL^1)](Me$_2$NH_2)**, (b) **[MoO_2(HL^1)(MeOH)]MeOH**, and (c) **[{UO_2(HL^2)}$_2$](EtOH)$_2$(H_2O)$_2$**; donor/acceptor centers of H-bond interactions are indicated by dashed lines; large, open circles: metal ions; filled circles: oxygen atoms; circles with a line: nitrogen atoms

Experimental Section

General Remarks: Uranyl acetate was procured from BDH, England; the other precursors $[VO(acac)_2$ [16] and $MoO_2(acac)_2$ [17]] and 4,6-*O*-ethylidene-α-D-glucopyranose[5] and its 1-NH_2 derivative were synthesized according to reported procedures.[18] The glycosylamines $\mathbf{H_3L^1}$ and $\mathbf{H_3L^2}$ were synthesized by the condensation of 4,6-*O*-ethylidene-β-D-glucopyranosylamine with salicylaldehyde or 3-methoxysalicylaldehyde in a 1:1 ratio in ethanol, and were used after recrystallization. The solvents were procured from local sources and were purified and dried immediately prior to use. Microanalyses were carried out with a Carlo−Erba elemental analyser. − FT-IR spectra were recorded with a Nicolet Impact 400 spectrometer with samples in KBr. − UV/Vis absorption spectra were recorded with a Shimadzu UV2101PC spectrophotometer. − ^{1}H NMR spectra were recorded with Bruker Avance DRX 500 or Varian XL-300 spectrometers with samples in [D$_6$]DMSO. − FAB mass spectra were recorded with a JEOL SX 102/DA-600 mass spectrometer/data system using argon/xenon (6 kV, 10 mA) as the FAB gas and *m*-nitrobenzyl alcohol as the matrix. The accelerating voltage was 10 kV and the spectra were recorded at room temperature. − Optical rotations were measured with a JASCO model DIP-370 digital polarimeter. The abbreviations Sac, Prot, and Ar are used in the spectral assignments to denote saccharide, protecting, and aromatic groups, respectively. The ligands used and the complexes reported in this paper are shown in Scheme 1.

$[VO_2(HL^1)](Me_2NH_2)$: To a solution of $\mathbf{H_3L^1}$ (0.62 g, 2.01 mmol) in methanol (10 mL) containing dimethylamine, $VO(acac)_2$ (0.53 g, 2.00 mmol) was added and the reaction mixture was stirred at room temperature. After 10 h, oxygen was bubbled through it for 2 h and the resulting solid product was collected by filtration. The residue was washed with a small quantity of cold methanol and then with diethyl ether, and then dried in vacuo. Yield: 0.35 g (40%). − $C_{17}H_{25}N_2O_8V$ (436.33): calcd. C 46.80, H 5.77, N 6.42; found C 46.70, H 5.89, N 5.98. − ^{1}H NMR ([D$_6$]DMSO): δ = 8.50 (s, 1 H, HC=N), 7.46 (d, 1 H, ArH), 7.30 (t, 1 H, ArH), 6.67 (m, 2 H, ArH), 5.15 (br., 1 H, Sac OH), 4.75 (q, 1 H, Prot CH), 4.51 (d, 1 H, Sac 1-H), 4.18 (m, 1 H, Sac 5-H), 3.33−3.75 (m, 5 H, Sac H), 2.57 (s, 6 H, amine CH_3), 1.26 (d, 3 H, Prot CH_3). − FAB MS: *m*/*z* (%) = 391 [M + H$^+$] (95).

$[VO_2(HL^2)](Me_2NH_2)$: This compound was prepared by adopting the procedure described for **$[VO_2(HL^1)](Me_2NH_2)$**, but using $\mathbf{H_3L^2}$ (0.34 g, 1.00 mmol) and $VO(acac)_2$ (0.26 g, 0.98 mmol) in methanol (12 mL) containing dimethylamine. Yield: 0.08 g (17%). − $C_{18}H_{27}N_2O_9V$ (466.36): calcd. C 46.36, H 5.84, N 6.01; found C 46.20, H 5.56, N 6.15. − ^{1}H NMR ([D$_6$]DMSO): δ = 8.48 (s, 1 H, HC=N), 7.06 (d, 1 H, ArH), 6.93 (d, 1 H, ArH), 6.58 (t, 1 H, ArH), 5.32 (br., 1 H, Sac OH), 4.75 (q, 1 H, Prot CH), 4.51 (d, 1 H, Sac 1-H), 4.18 (m, 1 H, Sac 5-H), 3.73 (s, 3 H, $ArOCH_3$), 3.00−3.70 (m, 5 H, Sac H), 2.58 (s, 6 H, amine CH_3), 1.26 (d, 3 H, Prot CH_3). − FAB MS: *m*/*z* (%) = 418 [M − 2 H$^+$] (90).

$[MoO_2(HL^1)(H_2O)]$: To a solution of $\mathbf{H_3L^1}$ (0.62 g, 2.01 mmol) in methanol (30 mL), $MoO_2(acac)_2$ (0.65 g, 1.99 mmol) was added and the reaction mixture was stirred at room temperature for 13 h. The resulting solid product was collected by filtration, washed first with methanol and then with diethyl ether, and dried in vacuo. Yield: 0.65 g (72%). − $C_{15}H_{19}MoNO_9$ (453.25): calcd. C 39.75, H 4.22, N 3.09; found C 40.51, H 3.97, N 2.57. − ^{1}H NMR ([D$_6$]DMSO): δ = 8.55 (s, 1 H, HC=N), 7.75 (d, 1 H, ArH), 7.50 (dt, 1 H, ArH), 6.97 (t, 1 H, ArH), 6.92 (d, 1 H, ArH), 5.61 (d, 1 H, Sac OH), 4.75 (m, 2 H, Prot CH and Sac 1-H), 4.19 (m, 1 H, Sac 5-H), 3.30−3.80 (m, 5 H, Sac H), 1.27 (d, 3 H, Prot CH_3). − FAB MS: *m*/*z* (%) = 438 [M + 3 H$^+$] (40).

$[\{UO_2(HL^1)\}_2]$: This complex was prepared by adopting the procedure described for **$MoO_2(HL^1)$**, but using $\mathbf{H_3L^1}$ (0.93 g, 3.01 mmol) and $UO_2(OAc)_2{\cdot}2H_2O$ (1.27 g, 2.99 mmol) in methanol (40 mL). Yield: 1.05 g (57%). − $C_{30}H_{42}N_2O_{20}U_2$ (1226.72): calcd. C 29.37, H 3.45, N 2.28; found C 29.76, H 3.18, N 2.46. − ^{1}H NMR ([D$_6$]DMSO): δ = 9.05 (s, 1 H, HC=N), 7.50 (m, 2 H, ArH), 6.96 (d, 1 H, ArH), 6.61 (t, 1 H, ArH), 5.23 (m, 3 H, Sac OH, Sac 1-H, and Sac 3-H), 4.80 (q, 1 H, Prot CH), 4.26 (m, 1 H, Sac 5-H), 3.79 (m, 2 H, Sac H), 3.29 (m, 2 H, Sac H), 1.31 (d, 3 H, Prot CH_3). − FAB MS: *m*/*z* (%) = 1155 [M + H$^+$] (82).

$[\{UO_2(HL^2)\}_2]$: This complex was prepared by a procedure similar to that adopted for **$MoO_2(HL^1)$**, but using $\mathbf{H_3L^2}$ (1.02 g, 3.01 mmol) and $UO_2(OAc)_2{\cdot}2H_2O$ (1.27 g, 2.99 mmol) in methanol (40 mL). Yield: 1.40 g (73%). − $C_{32}H_{46}N_2O_{22}U_2$ (1286.77): calcd. C 29.86, H 3.61, N 2.17; found C 29.61, H 3.41, N 2.56. − ^{1}H NMR ([D$_6$]DMSO): δ = 9.02 (s, 1 H, HC=N), 7.13 (m, 2 H, ArH), 6.53 (t, 1 H, ArH), 5.22 (m, 3 H, Sac OH, Sac 1-H, and Sac 3-H), 4.80 (q, 1 H, Prot CH), 4.26 (m, 1 H, Sac 5-H), 3.94 (s, 3 H, $ArOCH_3$), 3.74 (m, 3 H, Sac H), 3.10−3.50 (m, 1 H, Sac H), 1.31 (d, 3 H, Prot CH_3). − FAB MS: *m*/*z* (%) = 1214 [M$^+$] (92).

X-ray Crystallography: Standard procedures were used for mounting the crystals. The diffraction data were collected with a Nonius Kappa CCD diffractometer in the φ scan + ω scan mode using Mo-K_α radiation. Single crystals of **$[VO_2(HL^1)](Me_2NH_2)$**, **$[MoO_2(HL^1)(MeOH)]MeOH$**, and **$[\{UO_2(HL^2)\}_2](EtOH)_2(H_2O)_2$** were obtained. The data were corrected for absorption by empirical methods. The structures were solved using the SHELXS-97 program package and refined using SHELXL-97.[19] The diagrams were generated using ORTEP III[20] and PLUTON-98.[21] Full-matrix least-squares refinement with anisotropic thermal parameters was used for all non-hydrogen atoms. The hydrogen atoms were treated as riding atoms with fixed thermal parameters. Other details of the data collection and structure refinement are presented in Table 1. Crystallographic data (excluding structure factors) for the structures reported in this paper have been deposited with the Cambridge Crystallographic Data Centre as supplementary publication no. CCDC-162681 for **$[VO_2(HL^1)](Me_2NH_2)$**, -162679 for **$[MoO_2(HL^1)(MeOH)]MeOH$**, -162680 for **$[\{UO_2(HL^2)\}_2](EtOH)_2(H_2O)_2$**. Copies of the data can be obtained free of charge on application to CCDC, 12 Union Road, Cambridge CB2 1EZ, UK [Fax: (internat.) + 44-1223/336-033; E-mail: deposit@ccdc.cam.ac.uk].

Acknowledgments

C. P. R. acknowledges financial support from the Council of Scientific and Industrial Research, the Department of Science and Technology, and the Board of Research in Nuclear Sciences of the Department of Atomic Energy. We thank the RSIC, CDRI Lucknow for mass spectral measurements, and Mr. R. Kuppinen for some experimental help.

[1] M. L. Sinnott, *Chem. Rev.* **1990**, *90*, 1171−1202.
[2] [2a] R. W. Gracy, E. A. Noltmann, *J. Biol. Chem.* **1968**, *243*, 5410−5419. − [2b] R. L. Root, J. R. Durrwachter, C.-H. Wong, *J. Am. Chem. Soc.* **1985**, *107*, 2997−2999. − [2c] J. Jenkins, J. Janin, F. Rey, M. Chiadmi, H. V. Tilbeurgh, I. Lasters, M. D. Maeyer, D. V. Belle, S. J. Wodak, M. Lauwereys, P. Stanssens, N. T. Mrabet, J. Snauwaert, G. Matthyssens, A.-M. Lambeir, *Biochemistry* **1992**, *31*, 5449−5458.

[3] J. A. Rendleman Jr., *Adv. Carbohydr. Chem.* **1966**, *21*, 209−271.
[4] [4a] U. Piarulli, C. Floriani, *Prog. Inorg. Chem.* **1997**, *45*, 393−429. − [4b] S. Yano, *Coord. Chem. Rev.* **1988**, *92*, 113−156. − [4c] S. Yano, K. Ohtsuka, in *Metal Ions in Biological Systems* (Eds.: H. Sigel, A. Sigel), Marcel Dekker, New York, **1996**, vol. 32, p. 27−60. − [4d] D. M. Whitfield, S. Stojkovski, B. Sarkar, *Coord. Chem. Rev.* **1993**, *122*, 171−225. − [4e] R. P. Bandwar, C. P. Rao, *Curr. Sci.* **1997**, *72*, 788−796. − [4f] Y. E. Alekseev, A. D. Garnovskii, Y. A. Zhdanov, *Russ. Chem. Rev.* **1998**, *67*, 649−669. − [4g] B. Gyurcsik, L. Nagy, *Coord. Chem. Rev.* **2000**, *203*, 81−149, and references therein.
[5] A. K. Sah, C. P. Rao, P. K. Saarenketo, E. K. Wegelius, K. Rissanen, E. Kolehmainen, *J. Chem. Soc., Dalton Trans.* **2000**, 3681−3687.
[6] R. M. Silverstein, G. C. Bassler, T. C. Morrill, *Spectrometric Identification of Organic Compounds*, 5th ed., John Wiley, New York, **1991**, p. 221−221.
[7] S. J. Angus-Dunne, R. J. Batchelar, A. S. Tracy, F. W. B. Einstein, *J. Am. Chem. Soc.* **1995**, *117*, 5292−5296.
[8] B. Zhang, S. Zhang, K. Wang, *J. Chem. Soc., Dalton Trans.* **1996**, 3257−3263.
[9] K. K. Rajak, S. P. Rath, S. Mondal, A. Chakravorty, *Inorg. Chem.* **1999**, *38*, 3283−3289.
[10] [10a] G. Asgedom, A. Sreedhara, J. Kivikoski, J. Valkonen, C. P. Rao, *J. Chem. Soc., Dalton Trans.* **1995**, 2459−2466. − [10b] G. Asgedom, A. Sreedhara, J. Kivikoski, J. Valkonen, E. Kolehmainen, C. P. Rao, *Inorg. Chem.* **1996**, *35*, 5674−5683.
[11] G. R. Desiraju, T. Steiner, *The Weak Hydrogen Bond in Structural Chemistry and Biology*, Oxford Science Publications, Oxford, **1999**, p. 29−121.
[12] A. Wlodarczyk, S. S. Kurek, M. A. J. Moss, M. S. Tolley, A. S. Batsanov, J. A. K. Howard, J. A. McCleverty, *J. Chem. Soc., Dalton Trans.* **1993**, 2027−2036.
[13] U. Piarulli, D. N. Williams, C. Floriani, G. Gervasio, D. Viterbo, *J. Chem. Soc., Dalton Trans.* **1995**, 3329−3334.
[14] [14a] C. P. Rao, A. Sreedhara, P. V. Rao, M. B. Verghese, K. Rissanen, E. Kolehmainen, N. K. Lokanath, M. A. Sridhar, J. S. Prasad, *J. Chem. Soc., Dalton Trans.* **1998**, 2383−2393.
[15] [15a] P. V. Rao, C. P. Rao, A. Sreedhara, E. K. Wegelius, K. Rissanen, E. Kolehmainen, *J. Chem. Soc., Dalton Trans.* **2000**, 1213−1218. − [15b] P. Thuéry, M. Nierlich, J. Vicens, B. Masci, *J. Chem. Soc., Dalton Trans.* **2001**, 867−874.
[16] R. A. Rowe, M. M. Jones, *Inorg. Synth.* **1957**, *5*, 113−115.
[17] M. C. Chakravorti, D. Bandyopadhyay, *Inorg. Synth.* **1992**, *29*, 129−134.
[18] K. Linek, J. Alfoldi, M. Durindova, *Chem. Pap.* **1993**, *47*, 247−250.
[19] G. M. Sheldrick, *SHELX-97 − Programs for Crystal Structure Analysis (Release 97−2)*, Institüt für Anorganische Chemie der Universität, Tammannstrasse 4, Göttingen, Germany, **1998**.
[20] M. N. Burnett, C. K. Johnson, *ORTEP III*, Report ORNL-6895, Oak Ridge National Laboratory, Oak Ridge, TN, **1996**.
[21] A. L. Spek, *Acta Crystallogr., Sect. A* **1990**, *46*, C34.

Received April 23, 2001
[I01141]

Synthesis of Oligometallic Compounds from *tripod*Iron(II) Species Using Cyano Bridging Ligands − Electronic Coupling of Two Metal Termini Through Metal Dicyano and Diisocyano Entities

Volker Jacob,[a] Gottfried Huttner,*[a] Elisabeth Kaifer,[a] Peter Kircher,[a] and Peter Rutsch[a]

Dedicated to Professor Henri Brunner on the occasion of his 66th birthday

Keywords: Cyanides / Cyclic voltammetry / Tripod ligands / Iron

Organometallic monocyanometalates $[M–CN]^-$ (**1**$^-$) [M = $Cr(CO)_5$ **1a**$^-$, $Cr(\eta^6\text{-}CF_3C_6H_5)(CO)_2$ **1b**$^-$, $Mn(\eta^5\text{-}CH_3C_5H_4)(CO)_2$ **1c**$^-$] produce tetrametallic (**2**$^-$) and trimetallic (**3**) aggregates upon reaction with *tripod* and iron(II) salts [*tripod* = $CH_3C(CH_2PPh_2)_3$]. The tetranuclear compound [*tripod*Fe{NC–M}$_3$]$^-$ (**2**$^-$) [M = $Cr(CO)_5$] or the trinuclear species [*tripod*Fe(CO){NC–M}$_2$] (**3**) [M = $Cr(CO)_5$ **3a**, $Cr(\eta^6\text{-}CF_3C_6H_5)(CO)_2$ **3b**, $Mn(\eta^5\text{-}CH_3C_5H_4)(CO)_2$ **3c**] can be selectively formed by following the appropriate reaction protocols. Organometallic dicyanometalates $[NC–M'–CN]^-$ (**4**$^-$) [M′ = $Mn(CO)_4$ **4a**$^-$, CpFe(CO) **4b**$^-$, CpCo(CN) **4c**$^-$] react in a similar manner to give pentanuclear species [*tripod*Fe{NC–M′–CN}$_3$Fe*tripod*]$^+$ (**5**$^+$). – In compounds **2**$^-$ and **3**, two easily oxidizable organometallic groups are linked through a *tripod*Fe$(NC)_2$ unit, while in **5**$^+$ two *tripod*iron(II) entities are linked through a less readily oxidizable M′$(CN)_2$ unit. For both types of compound, at least two distinct reversible oxidations are observed by cyclic voltammetry. The potentials at which these oxidations occur are characteristic of the terminal groups in each case. The potentials of the two consecutive oxidation steps are separated by between 150 and 350 mV. The oxidation products of compounds **2**$^-$, **3**, and **5**$^+$ can hence be classified as class III mixed-valence species with comproportionation constants K_C of between 10^2 and 10^6. The extent of electronic coupling mediated by the M′$(CN)_2$ or M′$(NC)_2$ bridging entities is thus similar to that mediated by $[RC(CN)_2]^-$ bridging ligands in otherwise analogous compounds, for which K_C values of around 10^4 are observed. All the aforementioned compounds have been characterized by analytical and spectroscopic techniques, including cyclic voltammetry and UV/Vis spectroscopy. In addition, X-ray crystallographic data are reported for **2**$^-$, **3a**, **3b**, **3c**, and **5a**$^+$.

Introduction

Dinitrile ligands are efficient building blocks for the synthesis of oligonuclear coordination compounds.[1] Anionic geminal dinitrile ligands [$RC(CN)_2^-$, $N(CN)_2^-$] have been found to lead to efficient electronic coupling between the terminal metal centers in the corresponding M−NC−X−CN−M arrangements.[2] It would appear that the nature of the linking unit X has little influence on the efficiency of this coupling, since the separation between the first and second oxidation potentials of the corresponding compounds is relatively constant, irrespective of the nature of X.[2] Even the replacement of RC^- by N^- as X does not greatly affect this separation.[2] The distance between the two metal centers in compounds of the type M−NC−X−CN−M (X = RC^-, N^-) is around 700 pm, which is rather similar to the distance between two metal centers linked by *cis*-dicyano complexes M′$(CN)_2$.[3] Compounds of this type have been extensively studied by Vahrenkamp,[4] who showed that these inorganic bridging ligands are quite effective in mediating electronic coupling between the two terminal metal centers in an M−(μ-CN)−M′−(μ-CN)−M arrangement.

As the efficiency of electronic coupling is easily measured by cyclic voltammetry, and since the electrochemical behavior of dinuclear *tripod*iron compounds [*tripod* = $CH_3C(CH_2PPh_2)_3$] in which the two iron centers are linked through X$(CN)_2$ entities [X = RC^-, N^-] is well known,[2] it was tempting to synthesize *tripod*iron derivatives having the two iron(II) centers linked by M′$(CN)_2$ bridging units (Scheme 1, **A**). We report herein the synthesis of such compounds (**5**$^+$) and the measurement of their degree of electronic coupling. Moreover, *tripod*iron(II) templates may also serve to address the same type of problem in an inverted version. Compounds of the type [*tripod*FeL{NC−M}$_2$] contain the *tripod*Fe^{II}L unit in a central position (Scheme 1, **B**).

In these compounds, the terminal metal centers are bridged by a CN−Fe−NC ligand entity. Cyclic voltammetry of such compounds should reveal the ability of this type of linker to electronically couple the two terminal metal centers. The synthesis of such compounds (**2**$^-$ and **3**; Scheme 2) and the efficiency of electronic coupling through the *tripod*Fe$(NC)_2$ linker are described herein.

[a] Anorganisch-Chemisches Institut der Universität Heidelberg, Im Neuenheimer Feld 270, 69120 Heidelberg, Germany
Fax: (internat.) + 49-6221/545-707
E-mail: g.huttner@indi.aci.uni-heidelberg.de

 © WILEY-VCH Verlag GmbH, 69451 Weinheim, 2001 1434−1948/01/1111−2783 $ 17.50+.50/0

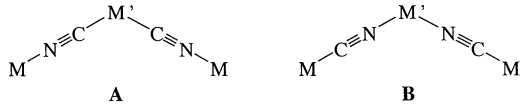

M = *tripod*Fe(II)
M'= e. g. CpCo(III)CN

M = e. g. Cr(0)(CO)$_5$
M'= *tripod*Fe(II)

Scheme 1. Two types of inorganic groups linking two metal centers M

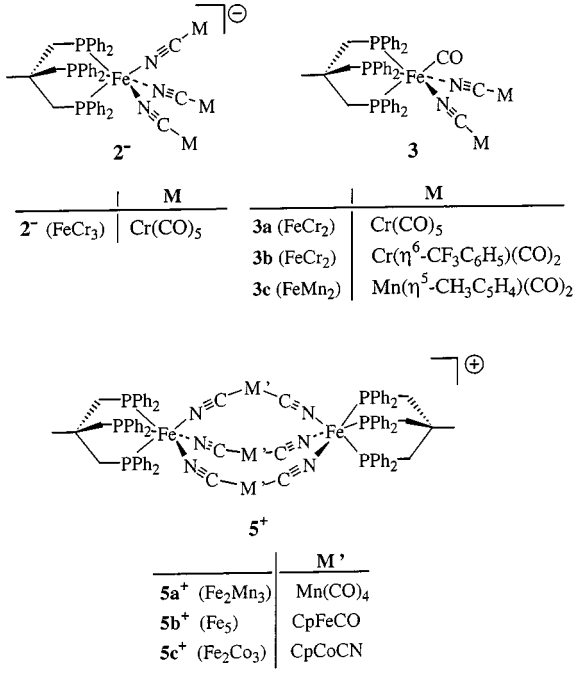

	M
2$^-$ ($FeCr_3$)	$Cr(CO)_5$

	M
3a ($FeCr_2$)	$Cr(CO)_5$
3b ($FeCr_2$)	$Cr(\eta^6\text{-}CF_3C_6H_5)(CO)_2$
3c ($FeMn_2$)	$Mn(\eta^5\text{-}CH_3C_5H_4)(CO)_2$

	M'
5a$^+$ (Fe_2Mn_3)	$Mn(CO)_4$
5b$^+$ (Fe_5)	CpFeCO
5c$^+$ (Fe_2Co_3)	CpCoCN

Scheme 2. The *tripod*iron compounds described in this paper

Results and Discussion

It has been shown that the N-termini of nitrile groups in organometallic cyano compounds are quite nucleophilic.[5] The nucleophilicity of metal-bonded cyano groups has been known since the early days of organic chemistry.[6] This appears to be a general property of anionic coordination compounds containing cyano ligands and has been amply demonstrated for species of type **1**$^-$ by their reactions with main-group-[7] or transition-metal-centered[8] electrophiles. Compounds **1a**$^-$ and **1c**$^-$ (Scheme 3) are easily accessible as their sodium or potassium salts by published procedures.[9]

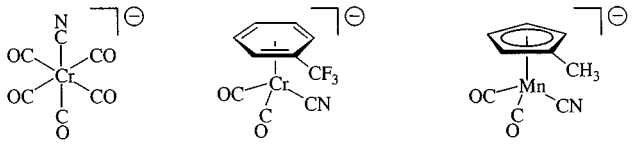

Scheme 3. Organometallic monocyanometalate ligands **1**$^-$

Compound **1b**$^-$ could be obtained by irradiation of the parent (arene)tricarbonyl species[10] in methanol in the presence of excess potassium cyanide[11] as its intensely orange-colored potassium salt. Its composition was unequivocally confirmed by its analytical and spectroscopic data (see Exp. Sect.).

K1b shows an irreversible oxidation wave in its cyclic voltammogram at $E_{pa} = -100$ mV (CH_3CN, vs. SCE). It is thus easily oxidized and is similar in this respect to **Na1a**.[12a] No data are available for **K1c** itself, but the parent compound $Na[CpMn(CO)_2CN]$ is reversibly oxidized at 40 mV vs. SCE[4][12b] and the oxidation potential of **1c**$^-$ can be expected to be of the same order. All compounds **1**$^-$ are thus oxidized at much lower potentials than the *tripod*iron(II) entity in a coligand environment of nitrile groups. The oxidation of $[tripodFe(CH_3CN)_3]^{2+}$ occurs at 1400 mV (CH_3CN, vs. SCE)[13] and oxidation of this entity in the dinuclear compounds $[tripodFe\{\mu\text{-}NC\text{-}C(R)\text{-}CN\}_3Fetripod]^+$ requires a minimum of 900 mV vs. SCE.[2c] This combination of facts makes compounds **1**$^-$ ideal ligands for testing the electronic coupling properties of a *tripod*$Fe(NC)_2$ unit linking two redox-active metal centers (Scheme 1, **B**).

The reaction of equimolar amounts of *tripod* and $FeCl_2$ with three equivalents of **Na1a** in acetone gives a red solution, from which, after cation exchange with PPNCl and crystallization, **PPN2**·0.75 CH_2Cl_2 is obtained in the form of red needle-shaped crystals (Scheme 4).

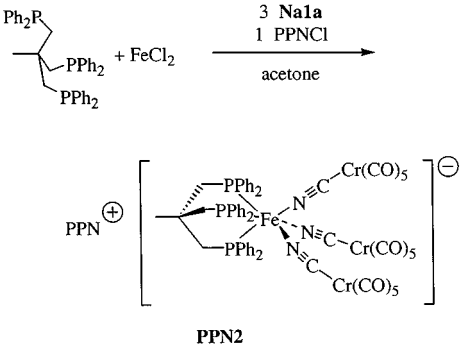

Scheme 4. Synthesis of **PPN2**

The constitution of the tetranuclear anion **2**$^-$ was unequivocally proven by the spectroscopic and analytical data of **PPN2** (Table 2). The signals of the axial and equatorial carbonyl groups as well as of the nitrile groups are clearly resolved in the ^{13}C NMR spectrum of **PPN2** (Table 3), while its infrared spectrum shows weak bands attributable to ν_{CN} absorptions at 2126 cm^{-1} and 2135 cm^{-1}. The ν_{CO} band pattern (Table 2) is consistent with the presence of $Cr(CO)_5$ groups, although the pattern is somewhat more complicated than that generally observed for $LCr(CO)_5$ compounds with undisturbed local C_{4v} symmetry. This indicates some deviation of these groups from this local symmetry in the tetranuclear anion. The structure of **PPN2**·0.75 CH_2Cl_2, as determined by single-crystal X-ray analysis (Figure 1; Tables 1 and 8), shows an overall close to C_3-symmetric arrangement for the anion **2**$^-$. The rotational

positions of the phenyl groups, as well as those of the $Cr(CO)_5$ entities, are close to this idealized symmetry (Table 1; torsion angles τ, φ, and χ).

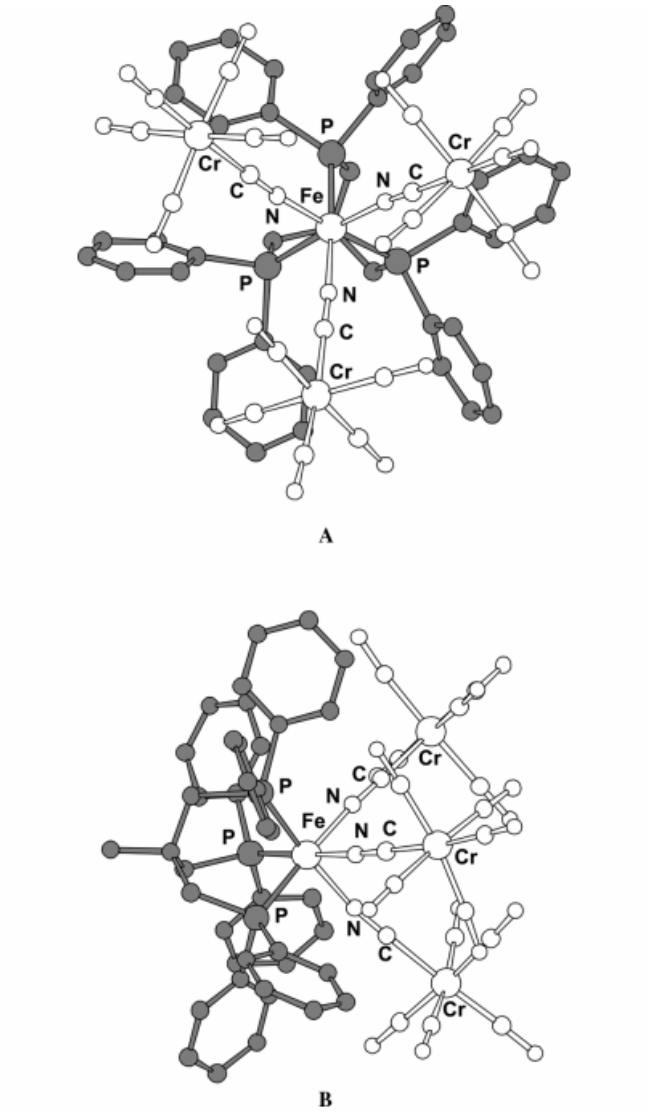

Figure 1. Two views of the structure of the tetranuclear anion **2**$^-$

Short O···H contacts are seen between some of the equatorial carbonyl groups and the protons of the phenyl rings. Each pentacarbonylchromium group is involved in at least one such contact with H···O distances in the range 260−300 pm (Table 1). Even though this is not indicative of hydrogen bonding, it shows that the *tripod*iron entity and the $Cr(CO)_5$ groups are in steric interference with one another. Disturbance of the local C_{4v} symmetry of the $Cr(CO)_5$ groups, as inferred from the IR-spectroscopic data, is thus consistent with the observed structure.

When equimolar mixtures of *tripod* and $FeCl_2$ in acetone are treated with 2 equiv. of either **Na1a**, **K1b**, or **K1c**, orange-red solutions result. On bubbling CO through these solutions, they undergo a color change to orange-brown.

The trinuclear compounds **3** were isolated as red-brown crystalline materials in yields of around 80%. The identities

Table 1. Bond lengths and angles in the tetranuclear anion **2**$^-$

Fe−P	225.3(2)−226.0(2)[a]	τ_1 [b]	35.5(4)
Fe−N	195.6(5)−197.7(5)	τ_2	32.6(4)
Cr−C_{CN}	203.5(7)−207.2(7)	τ_3	32.1(5)
Cr−$C_{CO,ax}$	185.1(7)−186.8(6)		
Cr−$C_{CO,eq}$	188.9(7)−192.7(8)	φ_a [c] [d]	−36.4 to −68.5
		φ_b	−13.7 to −19.9
Fe−N−C	170.2(4)−176.2(5)		
Cr−C−N	177.6(5)−178.8(5)	χ_1 [e]	−67/23
P−Fe−P	84.7(2)−87.3(2)		−156/112
N−Fe−N	87.4(1)−91.1(6)	χ_2	−71/21
O···H[f]	262		−163/108
	266	χ_3	−51/37
	277		−147/120

[a] The values in parentheses are standard deviations in units of the last decimal listed. − [b] τ denotes the torsion angles Fe−P−C−C within the chelate cage. − [c] The suffixes a and b refer to the two classes of aryl groups, which would be equivalent under exact C_3 symmetry (Figure 1, **A**). − [d] φ designates a torsion angle $C_{ortho}-C_{ipso}-P-Hz$, where Hz is the end point of a vector vertical to the plane spanned by the three phosphorus nuclei and fixed to one phosphorus center, pointing in the direction of the observer with respect to Figure 1, **A**. − [e] χ denotes the torsional arrangement of the $Cr(CO)_5$ groups. It is defined as the torsion angle $Hx-Fe-Cr-O_{CO,eq}$, where Hx is the end point of a vector radiating from the iron center along the idealized C_3 axis in a direction away from the observer with respect to Figure 1, **A**. − [f] Shortest distance between a carbonyl oxygen atom of any of the three pentacarbonylchromium units and a hydrogen atom of a *tripod* phenyl substituent.

of the compounds **3a**, **3b** ($FeCr_2$), and **3c** ($FeMn_2$) (Scheme 5) were unequivocally established from their spectroscopic data (Tables 2 and 3) and X-ray analyses (Tables 4 and 8; Figure 2).

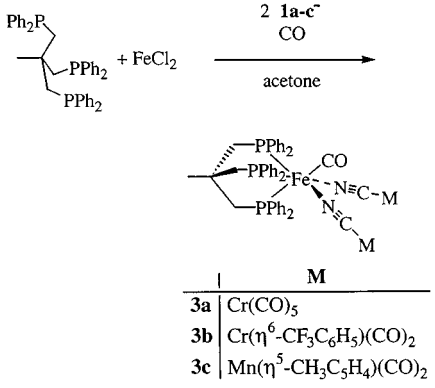

Scheme 5. Synthesis of compounds **3**

The infrared spectra of compounds **3** each feature a band at around 2030 cm^{-1} (Table 2), attributable to the iron-bonded carbonyl group. The ν_{CN} vibrations are observed as one band envelope at around 2100 cm^{-1}. The ν_{CO} vibrations of the $Cr(CO)_5$ groups in **3a** produce the expected pattern (Table 2). The CO groups of the $Cr(\eta^6\text{-}CF_3C_6H_5)(CO)_2$ entities in **3b** give rise to two bands of equal intensity, as do those of the $Mn(\eta^5\text{-}CH_3C_5H_4)(CO)_2$ entities in the $FeMn_2$ compound **3c** (Table 2). The ^{31}P NMR spectra of compounds **3** each show a doublet of higher intensity and a

Table 2. Spectroscopic and analytical data for compounds **PPN2** and **3**

No.	Formula (M [g/mol])	$C_{calcd.}$, $H_{calcd.}$, $N_{calcd.}$, $P_{calcd.}$ C_{found}, H_{found}, N_{found}, P_{found}	MS (FAB) *m/z* [fragment]	IR (CH_2Cl_2): $\tilde{\nu}$ [cm^{-1}] ν_{CN}	ν_{CO}		Yield (%)
PPN2	$C_{95}H_{69}Cr_3FeN_4O_{15}P_5$	60.91, 3.71, 2.99, 8.27	−1336 [*tripod*Fe(**1a**)$_3$]$^-$	2135 w	2062 m	1920 vs	52
	(1873.3)	60.97, 3.93, 2.99, 8.10		2126 vw	1938 vs	1887 vs	
3a	$C_{54}H_{39}Cr_2FeN_2O_{11}P_3$	56.66, 3.43, 2.45, 8.12	–	2123 w	2061 m	1937 vs	80
	(1144.5)	56.63, 3.91, 2.43, 8.00			2030 m	1923 vs	
3b	$C_{62}H_{49}Cr_2F_6FeN_2O_5P_3$	59.08, 3.85, 2.19, 7.25	+ 960 [*tripod*Fe**1b**]$^+$	2087 m	2024 w	1907 vs	84
	(1268.8)	58.80, 3.97, 2.25, 7.21				1844 vs	
3c	$C_{60}H_{53}FeMn_2N_2O_5P_3$	63.17, 4.68, 2.46	–	2089 m	2022 w	1917 vs	83
	(1140.7)	61.73, 4.79, 3.32				1851 vs	

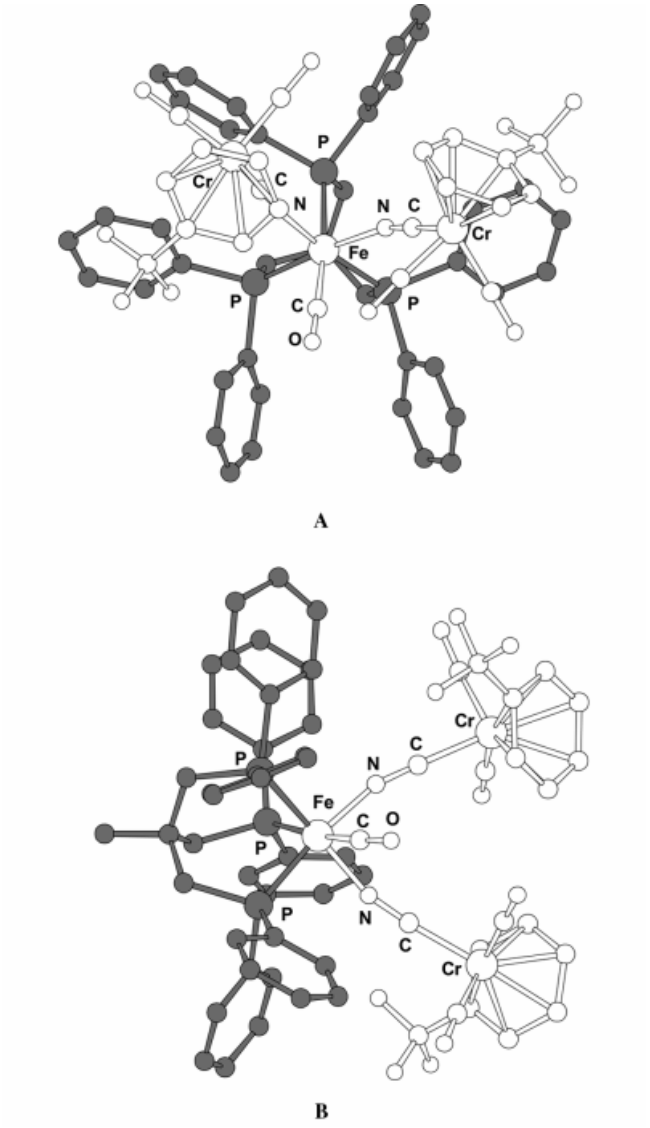

Figure 2. Two views of the structure of complex **3b**

triplet of lower intensity (Table 3). This is consistent with the static idealized octahedral coordination geometry around the iron centers, with two phosphorus nuclei lying *trans* to the nitrile ligands and the third being *trans* to the iron-bonded carbonyl group (Scheme 5, Figure 2). The coupling between these two types of phosphorus nuclei is $^2J_{PP} \approx 70$ Hz in each case (Table 3). The C_s symmetry of the coordination polyhedron around the iron center is corroborated by the ^{1}H NMR spectroscopic data of compounds **3**; two types of methylene groups are observed for the tripodal framework in the $^1H\{^{31}P\}$ NMR spectra of compounds **3** (Table 3). While the signal with a relative intensity of *two* would be expected to be a singlet, the other one with the observed relative intensity of *four* might be expected to show a more complicated pattern due to the diastereotopicity of the relevant methylene protons. However, the differentiation between these two types of protons is evidently too small to be observable with the resolution of our experiment and only an apparent singlet signal is observed for these protons (Table 3). The ^{13}C NMR spectra of the trinuclear complexes **3** show signals due to the iron-bonded carbonyl group, the carbonyl groups bonded to the chromium ($FeCr_2$ compounds **3a** and **3b**) or manganese centers ($FeMn_2$ compound **3c**), and the bridging cyanide groups (Table 3).

The presence of the (η^6-$CF_3C_6H_5$) moieties in **3b** is evident from their NMR signature. The ^{1}H NMR signals observed for this group in the spectrum of the potassium salt **K1b** are also observed in that of **3b**, with only very slight shift differences (Table 3). The ^{13}C NMR spectrum of **3b** shows signals due to the $CF_3C_6H_5$ ligands in the same spectral region as observed for **K1b**. In the ^{13}C NMR spectrum of **3b**, the CF_3 groups give rise to a quadruplet, which is partly obscured by the group of signals due to the *tripod* aryl carbon atoms. The arene carbon atoms of the $CF_3C_6H_5$ ligands, giving one signal each for the *ipso*, *ortho*, *meta*, and *para* carbon atoms in the spectrum of **K1b**, appear in part as pairs of signals in the spectrum of **3b** (Table 3). The reason for this side differentiation is not clear. It appears improbable that the two Cr(η^6-$CF_3C_6H_5$)$(CO)_2$ units would be fixed in **3b** such as to have different time-averaged chemical environments. A loss of the C_s symmetry of the environment due to the chirality of the {*tripod*Fe(CO)−NC−(η^6-$CF_3C_6H_5$)Cr$(CO)_2$} residue would appear to offer a more probable explanation.

The presence of the π-bonded $CH_3C_5H_4$ group in the $FeMn_2$ compound **3c** is evident from its characteristic ^{1}H NMR signals (Table 3). The methyl substituent gives rise to a signal at δ = 2.0, while the C_5H_4 fragment gives a partly

Table 3. NMR-spectroscopic data for compounds **PPN2** and **3**

	PPN2	**3a**	**3b**	**3c**
$^1H\{^{31}P\}$ NMR				
tripod-CH_3	1.37 s, 3 H	1.64 s, 3 H	1.61 s, 3 H	1.61 s, 3 H
tripod-CH_2	2.19 s, 6 H	2.35 s, 4 H	2.29 s, 4 H	2.30 s, 4 H
		2.75 s, 2 H	2.68 s, 2 H	2.67 s, 2 H
ligand[a]	–		4.7–5.2 m, 10 H	1.98 s, 3 H
				4.3–4.6 m, 8 H
CH_{arom}	7.1–7.7 m, 30 H	6.9–7.9 m, 30 H	7.0–7.9 m, 30 H	7.0–8.1 m, 30 H
$^{13}C\{^1H\}$ NMR				
tripod-CH_3	38.0 q	37.7 q	37.8 q	38.0 m
tripod-CH_2	33.9 m	30.9 m	30.6 m	31.0 m
		32.8 m	33.3 m	33.5 m
tripod-C_q	36.5 s	36.5 br	36.4 m	36.7 br
tripod-C_{arom}	132–135 m	128–134.5 m	128–134 m	128–135 m
tripod-$C_{q,arom}$	137–138 m	135.5–137.5 m	136–138 m	136–138 m
ligand-C[b]	–	–	126.0 q (CF_3)	14.7 (CH_3)
			($^1J_{CF}$ = 270 Hz)	
ligand-C_{arom}	–	–	90.0 s (*p*)	82 br
			88.4 q (*i*)	
			($^2J_{CF}$ = 35 Hz)	
			86.3 s/85.9 s (*m*)	
			85.2 m/84.1 m (*o*)[c]	
CN	172.1 s	182.8 s	195.4 s	191 br
ligand-CO	222.2 s	220.6 s	239.7 s	235 br
	218.0 s	217.3 s	239.8 s	
Fe-CO	–	213.5 dt	214.5 dt	216 m
		($^2J_{CPcis}$ = 20 Hz)	($^2J_{CPcis}$ = 20 Hz)	
		($^2J_{CPtrans}$ = 50 Hz)	($^2J_{CPtrans}$ = 50 Hz)	
$^{31}P\{^1H\}$ NMR				
tripod-PPh_2	37.5 s	36.5 d, 2 P	36.1 d, 2 P	36.0 d, 2 P
		10.7 t, 1 P	9.0 t, 1 P	8.2 t, 1 P
		($^2J_{PPcis}$ = 68 Hz)	($^2J_{PPcis}$ = 69 Hz)	($^2J_{PPcis}$ = 68 Hz)

[a] The ^1H NMR resonances of the ligands are found at δ = 4.5–5.1 (**K1b**, $[D_6]$acetone) and δ = 4.4 (C_5H_4), 1.9 (CH_3) (**K1c**, $[D_6]$acetone)[9b,12b]. – [b] The ^{13}C NMR resonances of the ligands are found at δ = 221.5, 218.5 (CO) and 153.8 (CN) (**Na1a**, CD_3CN)[12]; δ = 241.3 (s, CO), 168.0 (s, CN), 126.4 (q, CF_3; $^1J_{FC}$ = 270 Hz), 89.6 (s, C_{ar}), 86.5 (q, C_{ipso}; $^2J_{FC}$ = 35 Hz), 86.3 (s, C_{ar}), 84.3 (s, C_{ar}) (**K1b**, $[D_6]$acetone). – [c] The signals are split due to $^3J_{CF}$ coupling.

resolved multiplet. In the spectrum of **K1c**, the expected A_2B_2 multiplet is unresolved,[12b] as is often observed for compounds of this type. The form of this signal seen for **3c**, like that observed for **3b**, is suggestive of side differentiation induced by the prochirality of the compound. The structures of the trinuclear complexes **3** have been elucidated by X-ray crystallography (Tables 4 and 8). The basic molecular arrangement is the same in all three compounds, hence only the representative structure of **3b** is shown in Figure 2. The coordination around the iron center is idealized octahedral with the *tripod* ligand occupying one face of the octahedron. The organometallic ligands are consequently in a mutually *cis* arrangement with the coordination octahedron being completed by the iron-bonded carbonyl ligand (Figure 2).

All three organometallic ligands have at least two mutually *cis*-carbonyl groups that are also *cis* to the cyano bridging group. These carbonyl groups show roughly the same orientation with respect to the *tripod*iron(II) entity in all three cases (Table 4). The torsion angles χ defined by the rotational position of the carbonyl groups around an Fe–M axis [M = Cr (**3a** and **3b**), Mn (**3c**)] with respect to the idealized trigonal axis of the *tripod*iron entity are very similar for these four groups in the three compounds **3**. This means that three of the carbonyl groups of the pentacarbonylmetal entities in **3a** are formally replaced by η^6-arene units ($FeCr_2$ compound **3b**) or η^5-cyclopentadienyl units ($FeMn_2$ compound **3c**) without a significant change in the position of the two remaining carbonyl groups. These carbonyl groups, like those in $\mathbf{2}^-$, show short contacts to some of the phenyl protons of the *tripod* entity (Table 4). Geometrically, these contacts are again rather similar for all three compounds. Thus, the rotational positions of the aryl groups (Figure 2) of the *tripod*iron entity are also rather similar for all three species (Table 4). Overall, in fact, the crystals of **3a**, **3b** ($FeCr_2$), and **3c** ($FeMn_2$) are isotypic (Table 8). The Fe–P bond lengths are in the normal range, with the bonds to the phosphorus atom *trans* to the carbonyl groups being longer than the other two Fe–P bonds (Table 4). The Fe–N bond lengths are in the range 195.7(3)–198.5(4) pm (Table 4) and are distinctly longer than the $Fe-C_{CO}$ bonds [179.5(5)–180.5(2) pm] in each case. The Fe–N–C entities deviate from linearity, as is generally observed for *tripod*iron(II) nitrile compounds.[1,2,13] The deviation is smaller in **3a** than in **3b** or **3c** (Table 4), reflecting the lower symmetry of the organometallic termini

Table 4. Bond lengths and angles in the trinuclear complexes **3**

	3a	**3b**	**3c**
Fe−P_{cisCO}	228.9(1)/226.2(1)[a]	227.0(1)/225.8(1)	226.6(1)/224.8(1)
Fe−$P_{transCO}$	230.2(1)	230.3(1)	229.9(1)
Fe−N	196.3(3)/195.8(3)	198.2(2)/195.9(2)	198.5(4)/195.7(4)
Fe−C	180.1(4)	180.5(2)	179.5(5)
M−C_{CN}[b]	204.2(3)/203.7(4)	199.9(2)/199.0(2)	191.5(5)/190.0(5)
C−N	115.2(4)/115.3(4)	116.1(3)	115.5(6)/116.4(6)
M−C_{CO}	185.8(3)/185.7(4) (*ax*)	−	−
	188.8(4)−192.2(4) (*eq*)	183.7(3)−184.7(3)	173.4(4)−176.6(4)
M−MP[c]	−	166.8/167.2	177.3/177.3
Fe−N−C	169.9(3)/169.1(3)	164.2(2)/157.1(2)	165.1(4)/158.5(4)
M−C−N	179.0(3)/176.4(3)	177.8(2)/175.2(2)	177.9(4)/177.5(4)
P−Fe−P	86.83(4)−90.77(4)	87.00(3)−91.28(3)	86.74(4)−90.88(4)
N−Fe−N	84.2(1)	84.1(1)	84.5(1)
O···H[d]	271/288	262/284	276/297
F···H[e]	−	265/292	−
τ_1 [f]	26.8(3)	26.7(2)	26.4(3)
τ_2	16.2(3)	19.0(2)	16.8(4)
τ_3	29.7(3)	33.4(2)	30.9(3)
φ_1 [g]	−61.6	−62.4	−58.7
φ_2	−37.9	−27.9	−27.9
φ_3	+22.6	+24.1	+25.6
φ_4	+36.6	+39.0	+38.7
φ_5	+21.9	+15.4	+18.4
φ_6	−5.3	−9.4	−6.6
χ_a [h]	−156	−146	−154
χ_b	−69	−65	−63
χ_c	−72	−80	−80
χ_d	+18	+10	+16

[a] The values in parentheses are standard deviations in units of the last decimal listed. − [b] M = Cr (**3a**, **3b**), Mn (**3c**). − [c] MP is the center of the π-coordinated cyclic ligand in the organometallic units of complexes **3b** and **3c**. − [d] Shortest distances between a carbonyl oxygen atom of each of the two carbonylmetal moieties and a hydrogen atom of a *tripod* phenyl substituent. − [e] Shortest distances between a fluorine atom and a hydrogen atom of a *tripod* phenyl substituent. − [f] τ denotes the torsion angles Fe−P−C−C within the chelate cages. − [g] φ designates the torsion angles C_{ortho}−C_{ipso}−P−Hz, where Hz is the endpoint of a vector vertical to the plane spanned by the three phosphorus nuclei and fixed to one phosphorus center, pointing in the direction of the observer with respect to Figure 2, **A**. − [h] χ = Hx−Fe−M−O_{CO} denotes the torsion angle Hx−Fe−M−$O_{CO,eq}$, where Hx is the endpoint of a vector radiating from the iron center along the idealized C_3 axis in a direction away from the observer with respect to Figure 2, **A**.

in the latter compounds. The geometries of the organometallic termini themselves are unremarkable (Table 4).

While compounds $\mathbf{2}^-$ ($FeCr_3$) and **3** ($FeCr_2$, $FeMn_2$) contain organometallic groups linked by a *tripod*-iron−diisocyano group (Scheme 1, **B**), the reaction of *tripod*iron(II) entities with organometallic dinitriles should lead to compounds containing two *tripod*iron(II) entities linked by a metal−dinitrile species (Scheme 1, **A**). Quite a number of anionic organometallic dinitriles are known and some of them have been shown to be suitable building blocks for the construction of oligometallic cage compounds.[3b,3c,14] The dicyanometalates $\mathbf{4}^-$ (Scheme 6) are obtained by standard procedures.[15]

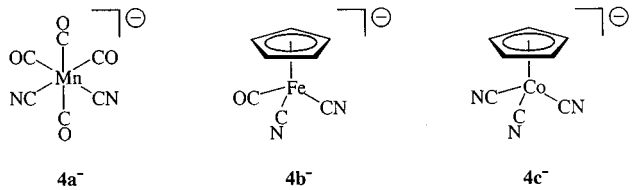

4a⁻ **4b⁻** **4c⁻**

Scheme 6. Dicyanometalate ligands $\mathbf{4}^-$

When an equimolar solution of *tripod* and $FeCl_2$ in acetone is treated with an equimolar amount of **K4a**, the initially faintly yellow solution immediately turns red. Whereas we had hoped to obtain a tetrametal square with two *tripod*FeL entities and two $Mn(CO)_4$ constituents at its corners by applying this stoichiometry, compound $\mathbf{5a}^+$ (Scheme 7) was obtained as the only characterizable product in very low yield (see Exp. Sect.).

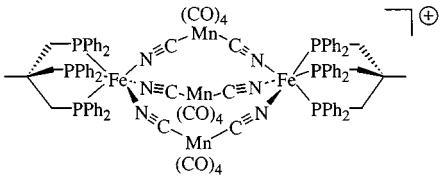

$\mathbf{5a}^+$

Scheme 7. The constitution of the pentanuclear cation $\mathbf{5a}^+$

$\mathbf{5a}^+$ was identified by X-ray crystallography of its $FeCl_4^-$ salt, which was serendipitously found to crystallize. $\mathbf{5a}^+$ is a pentanuclear Fe_2Mn_3 compound[16] composed of two *tripod*iron(II) entities, which are bridged by the *cis*-dicyano-

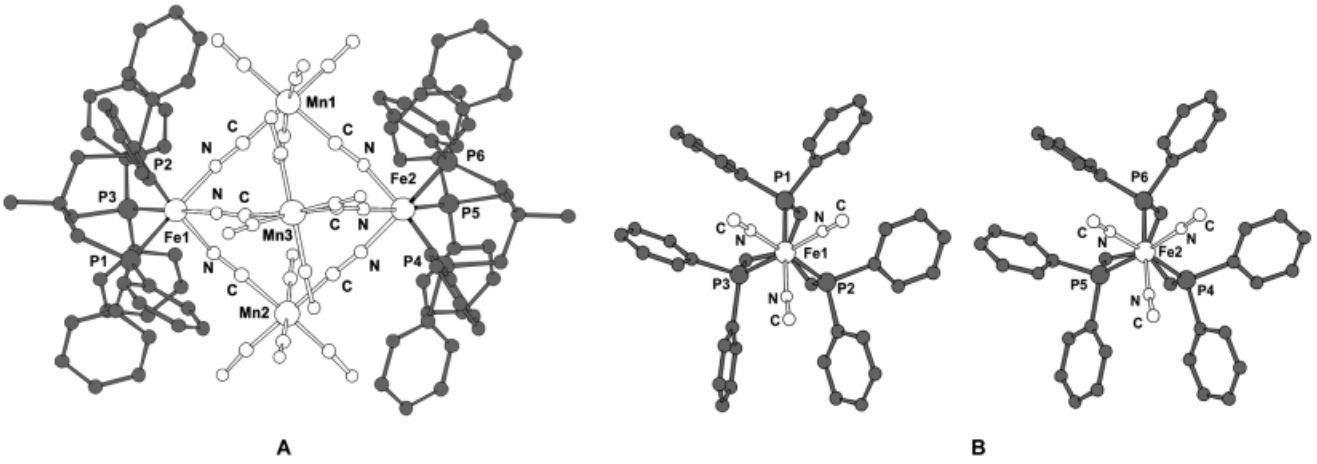

Figure 3. Structure determination of **5aFeCl$_4$**: **A**: view of the pentanuclear cation **5a**$^+$; **B**: standardized view of the two *tripod*iron(II) centers

manganese parts of three (tetracarbonyl)dicyanomanganese bridging units (Figure 3).

5a$^+$ has approximate C_2 symmetry (C_2 axis along the bisector of Fe1−Mn3−Fe2 in Figure 3, **A**). This symmetry is not imposed by crystal symmetry, but is evident from inspection of Figure 3, **A**, as well as from the values of the geometric parameters, pairs of which should be equal under this symmetry (Table 5).

Table 5. Bond lengths and angles in the pentanuclear cation **5a**$^+$

Fe−P	226.1(2)−228.4(2)[a]	Fe···Mn	507−511
Fe−N	195.1(7)−197.5(7)	τ_1[b]	40.4(6)/43.0(6)
Mn−C_{CN}	198(1)−201(1)	τ_2	27.7(7)/31.7(7)
Mn−$C_{CO,cis}$	186(1)−188(1)	τ_3	26.3(6)/28.2(6)
Mn−$C_{CO,trans}$	182(1)−185(1)	φ_I[c]	+1.5/−2.0
Fe−N−C	168.6(6)−173.2(7)	φ_{II}	−25.8/−30.0
Mn−C−N	172.2(7)−177.3(7)	φ_{III}	−61.6/−53.7
P−Fe−P	85.8(1)−91.4(1)	φ_{IV}	−43.2/−42.8
N−Fe−N	83.8(3)−85.5(3)	φ_V	+9.6/−34.5
C−N	114(1)−116(1)	φ_{VI}	−16.3/−28.0

[a] The values in parentheses are standard deviations in units of the last decimal listed. − [b] The τ values refer to the torsion angles Fe−P−C−C within the chelate cages; they are arranged in pairs to reflect the approximate C_2 symmetry of the cation **5a**$^+$. − [c] φ describes the torsion of the phenyl rings of the *tripod*iron entities. The torsion relates to the rotation around the corresponding P−C_{ipso} axis with the idealized trigonal axis of the *tripod*iron fragment as the reference axis. The first value φ_I describes the rotation of the phenyl group at P1, which points towards the observer in Figure 3, **A**, with the companion phenyl group at P6 again pointing towards the observer. Starting from this phenyl group at P1, the six pairs of values φ_I−φ_{VI} are listed in a counterclockwise sequence, when looking at Fe1 from the location of Fe2 (Figure 3, **A** and **B**).

Thus, even the torsion angles φ describing the orientation of the phenyl groups at the two *tripod*iron entities, as well as the twist angles τ describing the skew of the chelate cage, are in good pairwise agreement (Figure 3, **B**; Table 5). The Fe−N−C angles deviate from linearity in a systematic way. If, as initially expected, only two sites at each *tripod*iron entity were to be coordinated by the cyano groups of two (tetracarbonyl)dicyanomanganate units, a strain-free square arrangement with linear Fe−N−C groups would result, with the vacant coordination site at each *tripod*iron entity being perpendicular to the plane of this square. These coordination sites have to be brought into an arrangement that allows them to be spanned by the additional $Mn(CN)_2$ unit. This induces some strain in the scaffolding, which results in a bending of the Fe−N−C angles. As is well known, these angles are rather tolerant to this type of deformation (Figure 3; Table 5).

In view of the fact that pentanuclear compounds such as the Fe_2Mn_3 complex **5a**$^+$ are formed even under stoichiometric conditions, which should favor the formation of square tetranuclear aggregates, the stoichiometry was changed to *tripod*/Fe^{II}/$M'(CN)_2^-$ = 2:2:3. According to this protocol, the pentanuclear compounds **5bBF$_4$** (Fe_5) and **5cBF$_4$** (Fe_2Co_3) were prepared (Scheme 8).

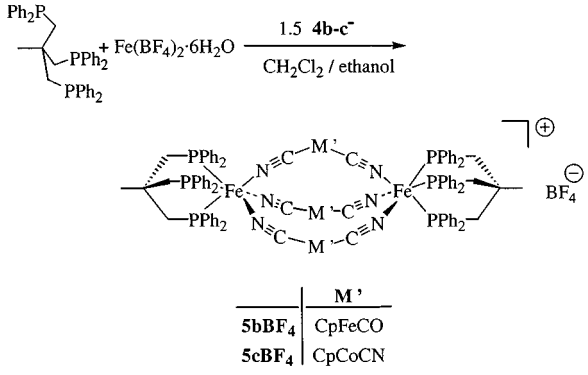

Scheme 8. Synthesis of **5bBF$_4$** and **5cBF$_4$**

Upon work-up of the respective reaction mixtures, microcrystalline red powders were obtained, which were shown by NMR spectroscopy to contain different diastereomers. With **5b**$^+$ (Fe_5), the reaction product showed four signals in the cyclopentadienyl region of the ^{1}H NMR spectrum. By repeated recrystallization, a product was obtained that showed one of these Cp peaks with 95% of the total intens-

ity. The cyclopentadienyl resonance of the crude product is clearly composed of two sets of signals, one being a sharp singlet at $\delta = 4.1$ and the other one being composed of three signals of equal intensity (see Exp. Sect.).

The intensity ratio of these two sets of signals is initially 2:1, whereas it becomes 19:1 following the recrystallization process. These observations may be explained as follows: There are two possible basic arrangements for the mutual orientation of the Cp groups in a compound of type **5b**$^+$ (Fe_5). One of them conforms to the constitutional C_3 symmetry (Scheme 9, **A**), while in the other this symmetry is lost (Scheme 9, **B**). There are six different possibilities for creating this unsymmetrical type of arrangement (Scheme 9, **B**), whereas there are only two possibilities for generating a C_3-symmetric arrangement (Scheme 9, **A**). The statistical probability of formation of the C_3-symmetric species is hence 0.25. The C_3-symmetric species will give rise to just one single Cp resonance, while for the unsymmetrical species three Cp signals of equal intensity can be expected. This is indeed what is observed in the ^{1}H NMR spectrum of crude **5b**$^+$. The ratio of the symmetrical to the unsymmetrical diastereomers is initially 2:1, which is quite different from the ratio expected on statistical grounds. This suggests that the C_3-symmetric product is formed under considerable diastereoselective control. Crystallization enriches the sample in the symmetrical product (Scheme 9, **A**), which is present to an extent of 95% after three recrystallizations.

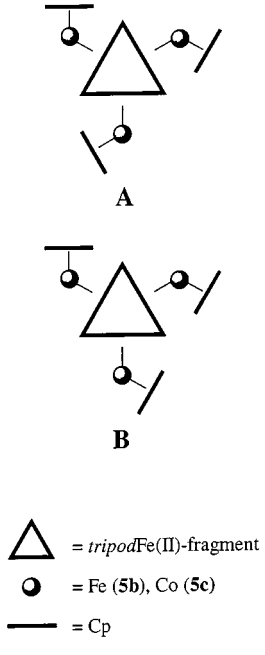

Scheme 9. Diastereomers of **5b**$^+$ and **5c**$^+$

Diastereoselectivity is also observed in the formation of **5c**$^+$ (Fe_2Co_3). In this case, the C_3-symmetric isomer is isolated as the sole product in 40% yield after just one recrystallization step. **5cBF$_4$** (Scheme 9, **A**) shows only one sharp Cp signal at $\delta = 4.7$ in its ^{1}H{^{31}P} NMR spectrum. The protons of the methylene groups of the *tripod* ligands are diastereotopic and give rise to a doublet-of-doublets signal in the ^{1}H{^{31}P} NMR spectrum (see Exp. Sect.). Likewise, the phenyl groups of the PPh_2 donors of the *tripod* ligands are diastereotopic. The ^{13}C NMR signals fall into two well-separated groups, consisting of a multiplet due to the *ortho*, *meta*, and *para* carbon atoms and a well-resolved signal due to the *ipso* carbon atoms (see Exp. Sect.). The pentanuclear structure of **5**$^+$ was unequivocally established from these findings, as were the structures of **5a**$^+$ (Fe_2Mn_3), **5b**$^+$ (Fe_5), and **5c**$^+$ (Fe_2Co_3) by the aforementioned combination of analytical methods.

The FAB$^+$ mass spectra show peaks due to the molecular ion **5**$^+$ in each case, accompanied by peaks originating from [**5** − *tripod*]$^+$ (Table 6). The infrared spectrum of **5a**$^+$ (Table 6) shows the presence of the organometallic $(CO)_4Mn(CN)_2$ building blocks through the characteristic patterns of its ν_{CO} and ν_{CN} bands, which are similar to those seen for **K4a**. Although the ν_{CO} absorptions are seen at wavelengths similar to those found for **K4a**, they show a somewhat more complicated structure than in the case of this starting material (Table 6). This observation may be similarly explained as previously proposed for the pair of compounds **Na1a** and **PPN2** ($FeCr_3$). **5bBF$_4$** shows ν_{CN} bands at 2140 cm^{-1} and 2106 cm^{-1}, positions not dissimilar from those of the bands reported for **K4b**.[17] The ν_{CO} band of **5bBF$_4$** is observed at 1961 cm^{-1}, and is thus shifted to higher energies relative to the ν_{CO} absorption of **K4b**. The (cyclopentadienyl)tricyanocobalt(III) units of **5cBF$_4$** (Fe_2Co_3) give rise to a band at 2168 cm^{-1}, which is broader and more intense than a second band at 2126 cm^{-1}. This latter band is attributed to the ν_{CN} vibrations of the terminally bonded cyano ligands, while the former is interpreted as being the envelope of the two ν_{CN} vibrations of the bridging cyano groups.

Electrochemistry and UV/Vis Spectroscopy

All compounds **PPN2**, **3**, and **5BF$_4$** contain the *tripod*iron(II) entity coordinated to at least two nitrile functions. A band at $\lambda \approx 20000$ cm^{-1} appears to be characteristic of iron(II) compounds of this type (Table 7). Irrespective of whether the nitrile functions originate from bridging cyano groups or from organic nitriles, this is a constant signature for all [*tripod*Fe^{II}(NCR)$_3$]$^{n+}$ species and obviously for all [*tripod*Fe^{II}(NCR)$_2$L]$^{n+}$ species as well. The energy of this transition is fairly constant for all compounds of this type.[2,13] A band at shorter wavelengths at $\lambda \approx 25000$ cm^{-1} is somewhat more variable with respect to its energy and extinction coefficient (Table 7), but also appears to be characteristic of compounds containing a *tripod*Fe^{II}(NCR)$_3$ or a *tripod*Fe^{II}(NCR)$_2$L (**3a**) moiety.[2,13] Based on the intensities of the relevant bands, the underlying electronic transitions must involve some charge-transfer character. At the short wavelength side, a band is present at $\lambda \approx 30000$ cm^{-1}, although it is not always observable as it may be obscured by the steep rise of shorter wavelength bands. A band in this position has also been observed for other *tripod*-Fe^{II}(NCR)$_2$L compounds.[2,13]

Table 6. Spectroscopic and analytical data of compounds **5aFeCl$_4$**, **5bBF$_4$**, and **5cBF$_4$**

No.	Formula (M [g/mol])	MS *m/z*	[Frag.]	$C_{calcd.}$, $H_{calcd.}$, $N_{calcd.}$ C_{found}, H_{found}, N_{found}	IR (CsI): $\tilde{\nu}$ [cm^{-1}][a] ν_{CN}	ν_{CO}
5aFeCl$_4$	$C_{100}H_{78}Cl_4Fe_3Mn_3N_6O_{12}P_6$	2018	$[M]^+$	54.21, 3.55, 3.79	2155 w	2091 m
	(2215.8)	1680	$[M - 12\ CO]^+$	53.30, 4.45, 3.59		2005 vs, 1987 vs
5bBF$_4$	$C_{106}H_{93}BF_4Fe_5N_6O_3P_6$	1963	$[M]^+$	62.07, 4.57, 4.10	2140 s	1961 vs
	(2050.8)	1339	$[M - tripod]^+$	61.72, 4.65, 4.25	2106 m	
5cBF$_4$	$C_{106}H_{93}BCo_3F_4Fe_2N_9P_6$	1966	$[M]^+$	61.97, 4.56, 6.14	2168 s	–
	(2054.1)	1342	$[M - tripod]^+$	60.55, 4.76, 6.07	2126 m	–

[a] IR absorptions of the potassium salts of the organometallic ligands [cm^{-1}]: 2145 w, 2103 vw, 2030 vs, 1952 vs[15a] (**K4a**); 2094, 2088, 1949[17] (**K4b**); 2130 s, 2124 vs, 2120 vs[15c] (**K4c**).

Table 7. Cyclovoltammetric and UV/Vis-spectroscopic data of compounds **PPN2**, **3**, and **5BF$_4$**; reference data for dinuclear compounds with dicyanamido- (**A$^+$**) and dicyanmethanido-bridged (**B$^+$**) dinuclear *tripod*iron(II) complexes (Scheme 11)[2c]

No.	CV $E^1_{1/2}$ [mV]	$E^2_{1/2}$ [mV]	$\Delta E_{1/2}$ [mV]	K_C [a]	$\delta\Delta G_{298}$ [b] [kJ/mol]	UV λ [cm^{-1}] (ε [M^{-1}cm^{-1}])			Bridging unit
2$^-$	425[c]	780	355	$1\cdot10^6$ [d]	34	30200 (11000)	≈ 27000[e]	20100 (820)	−CN−Fe^{II}−NC−
2	780[f]	900	120	$1\cdot10^2$	12	–	–	–	−CN−Fe^{II}−NC−
3a	825[f]	993	168	$6\cdot10^2$	16	30000 (6000)	24700 (1600)	19800 (1000)	−CN−Fe^{II}−NC−
3b	88[f]	252	164	$6\cdot10^2$	16	–	–	–	−CN−Fe^{II}−NC−
5b$^+$	652[g]	865[g]	213	$4\cdot10^3$	21	31900 (5000)	25400 (1100)	19900 (1000)	−NC−Fe^{II}−CN−
5c$^+$	939[g]	1084[g]	145	$3\cdot10^2$	14	–[e]	26000 (5000)	19900 (1800)	−NC−Co^{III}−CN−
A$^+$	910[g]	1150[g]	240	$1\cdot10^4$	23	–[e]	24200 (900)	19100 (2100)	−NC−N$^-$−CN−
B$^+$	1120[g]	1400[g]	280	$5\cdot10^4$	27	–[e]	24300 (1100)	19600 (1900)	−NC−C(R)$^-$−CN−

[a] Equilibrium constants K_C for the comproportionation reaction (Scheme 10) calculated from $K_C = \exp\{\Delta E_{1/2}/25.69\}$; $\Delta E_{1/2}$ in mV. – [b] $\delta\Delta G_{298}$ calculated from the differences $\Delta E_{1/2}$ between the oxidation potentials of the first and second oxidation steps. – [c] The negative charge of **2$^-$** leads to a value for the first oxidation potential about 400 mV lower than that observed for **3a**. – [d] The extent of electronic coupling is greatest for the negatively charged complex **2$^-$**. – [e] Band is obscured by the steep rise of shorter wavelength bands. – [f] The $Cr(CO)_5CN$ groups of **2$^-$** and **3a** are less easily oxidized than the $Cr(CF_3C_6H_5)(CO)_2CN$ group of **3b**: E_{pa}{K[Cr(η^6-$CF_3C_6H_5$)(CO)$_2$CN], **K1b**} = −100 mV (vs. SCE, CH_3CN), $E_{1/2}${Na[Cr(CO)$_5$CN], **Na1a**} = +690 mV (vs. SCE; reversible, CH_3CN).[12] – [g] The oxidation potentials of the dinuclear compounds increase with the estimated electronegativity of the central atom (right column) in the bridging moieties.

Cyclic voltammetry shows a minimum of two reversible one-electron oxidation steps for compounds **PPN2**, **3**, and **5BF$_4$**. Compounds **PPN2** ($FeCr_3$) and **3** ($FeCr_2$) contain a *tripod*Fe^{II}L entity at the bridging position between two organometallic cyano compounds. [*tripod*Fe^{II}(NCMe)$_3$]$^{2+}$ [13] is only oxidized at 1400 mV (CH_3CN; reversible vs. SCE), while the organometallic nitriles bonded to this bridging group in **3** are more easily oxidized [$E_{1/2}${Na[(CO)$_5$CrCN]; **Na1a**} = +690 mV (CH_3CN; reversible vs. SCE);[12] E_{pa}{K[(η^6-$CF_3C_6H_5$)Cr(CO)$_2$CN]; **K1b**} = −100 mV (CH_3CN; vs. SCE; see Exp. Sect.)]. The oxidation waves observed for **3a** and **3b** (Table 7) are thus in the characteristic range for the one-electron oxidations of the terminal groups. Compared to the corresponding alkali metal salts, the oxidation potentials of the iron-coordinated organometallic nitriles are shifted to higher potentials by around 200 mV (Table 7), as would be expected for the oxidation of a neutral compound compared with the oxidation of an anion. The appearance of two well-separated one-electron oxidation steps for **3a** and **3b** implies electronic conjugation between the two organometallic termini. Purely electrostatic coupling cannot account for the difference in $\Delta E_{1/2}$ of around 165 mV observed between these two cases[18] (Table 7) for two centers about 600 pm apart as they are in **3**.

The comproportionation constant (Scheme 10) for the reaction is 6×10^2 for both $FeCr_2$ compounds **3a** and **3b** (Table 7). It is thus in a range characteristic of class III mixed-valence compounds[19] and may be taken as proof of

$$M\sim\sim M + M^{ox}\sim\sim M^{ox} \overset{K_C}{\rightleftharpoons} 2\ M\sim\sim M^{ox}$$

Scheme 10. Comproportionation equilibrium

a conjugative interaction between the termini through the *tripod*Fe(NC)$_2$ linking groups.

Compound **PPN2** ($FeCr_3$) undergoes three reversible one-electron oxidation steps, which is consistent with its composition. The three $Cr(CO)_5CN$ entities are oxidized in a stepwise manner $2^- \rightarrow 2$, $2 \rightarrow 2^+$, and $2^+ \rightarrow 2^{2+}$ (Table 7). Oxidation of the first $Cr(CO)_5CN$ entity occurs at $E^1_{1/2} = 425$ mV and is thus about 400 mV easier to oxidize than with the corresponding neutral $FeCr_2$ species **3a**. The second and third one-electron oxidation steps are found at $E^2_{1/2} = 780$ mV and $E^3_{1/2} = 900$ mV and are thus in a range well below the potential needed for the oxidation of *tripod*$Fe^{II}(NCR)_3$ entities.[13] The occurrence of three one-electron oxidation steps in the observed range leaves no doubt that the individual oxidations occur at the organometallic termini. Here again, the separation between the oxidation potentials can only be explained by assuming electronic conjugation between the organometallic termini through the *tripod*Fe(NC)$_3$ linker. The comproportionation constant deduced from the first two oxidation steps of **2**$^-$ ($K_c = 10^6$) is the largest for the series of compounds analyzed (Table 7). The comproportionation constant deduced from the second and third oxidation potentials is still $K_c = 10^2$ (Table 7). Both constants are characteristic of conjugated systems, and it appears that increasing the negative charge of the molecule tends to increase conjugation.

Compounds **5bBF$_4$** (Fe_5) and **5cBF$_4$** (Fe_2Co_3) contain two *tripod*iron(II) termini coupled through organometallic dicyano linkers M′(CN)$_2$. Two reversible one-electron oxidation steps are observed for these compounds (Table 7). The oxidation potentials are well below that observed for [*tripod*Fe(NCMe)$_3$]$^{2+}$, as would be expected for a reduction of the charge of a compound containing two [*tripod*Fe(NCR)$_3$]$^{2+}$ entities by three units in **5**$^+$. The separation between the oxidation potentials is again rather large and the comproportionation constants indicate strong conjugation between the *tripod*iron(II) termini through the organometallic dicyanometalate bridges. Thus, in all examples of **2**$^-$, **3**, and **5**$^+$, the mixed-valence species are definitely of type III.[19]

A comparison can now be made between the conjugation capacities of dicyanometalate bridges and main-group-based anionic dicyano bridges. Several compounds containing two *tripod*iron(II) entities coupled by dicyanamido or dicyanomethanido ligands are known[2] (Scheme 11; **A**$^+$, **B**$^+$). Their electrochemical properties are very similar to those observed for **5b**$^+$ and **5c**$^+$ (Table 7). The relevant comproportionation constants resulting from conjugation through the organic linkers are $K_C \approx 10^4$ and are thus not significantly different from the values observed with either organometallic dicyanometalate or *tripod*$Fe^{II}(CN)_2$ linking groups. It appears that the HOMO of such compounds does not have a large orbital coefficient at the central atom of the bridging group, be it a main-group element or a transition metal. In each case studied, this central group is far more difficult to oxidize than the termini.

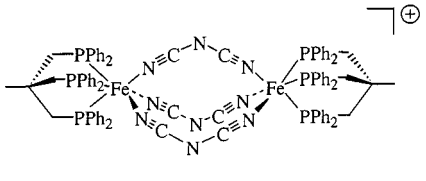

A$^+$

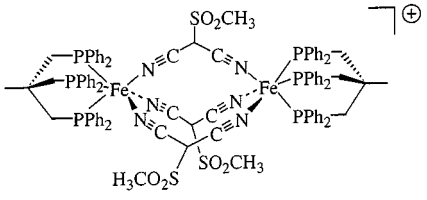

B$^+$

Scheme 11. Dinuclear *tripod*iron(II) complexes **A**$^+$ and **B**$^+$ (Table 7)

Conclusion

With monocyanometalates [M−CN]$^-$ (**1**$^-$), the *tripod*iron(II) template selectively forms tetranuclear species [*tripod*Fe{NC−M}$_3$]$^-$ (**2**$^-$) or trinuclear entities [*tripod*Fe(CO){NC−M}$_2$] (**3**) under the appropriate stoichiometric control. Dicyanometalates [M′(CN)$_2$]$^-$ (**4**$^-$) form pentanuclear compounds [*tripod*Fe{NC−M′−CN}$_3$-Fe-*tripod*]$^+$ (**5**$^+$). The organometallic termini M in compounds **2**$^-$ and **3** [e.g. $Cr(CO)_5$] are more easily oxidizable than the *tripod*iron(II) entity. Cyclic voltammetry reveals stepwise one-electron oxidation of these termini with potential differences characteristic of conjugative coupling between them. In compounds **5**$^+$, with M′ being CpFe(CO) (**5b**$^+$) or CpCo(CN) (**5c**$^+$), the *tripod*iron(II) entities are more easily oxidized than the organometallic bridging units. Cyclic voltammetry shows two well-separated, reversible, one-electron oxidation steps, which is consistent with strong conjugative coupling of the iron centers through the organometallic M′(CN)$_2$ linkers. It has been observed that the coupling efficiency of M′(CN)$_2^-$ is similar to that of [RC(CN)$_2$]$^-$ in structurally analogous compounds.

Experimental Section

General Remarks: All manipulations were carried out under argon by means of standard Schlenk techniques. All solvents were dried by standard methods[20] and distilled under argon. Silica gel and kieselguhr used for filtrations and chromatography were degassed at 1 mbar for 24 h and saturated with argon. The compounds **Na1a**,[9] **K1c**,[9] *tripod*,[21] **K4a**,[15a] **K4b**,[15b] **K4c**,[15c] and $Fe(BF_4)_2 \cdot 6H_2O$[22] were prepared according to or by adaptation of literature procedures. All other chemicals were obtained from commercial suppliers and were used without further purification. − NMR: Bruker Avance DPX200 spectrometer operating at 200.13 MHz (^{1}H), 50.323 MHz (^{13}C), 81.014 MHz (^{31}P); T = 303 K; chemical shifts (δ) in ppm with respect to CD_2Cl_2 (^{1}H: δ = 5.32; ^{13}C: δ = 53.5), [D$_6$]acetone (^{1}H: δ = 2.05; ^{13}C: δ = 20.8,

206.1), or [D$_6$]DMSO (^{1}H: δ = 2.50; ^{13}C: δ = 39.4) as internal standards; ^{31}P chemical shifts (δ) in ppm with respect to 85% H_3PO_4 (^{31}P: δ = 0) as an external standard; CD_2Cl_2, [D$_6$]acetone, and [D$_6$]DMSO used for NMR-spectroscopic measurements were degassed by three successive freeze-pump-thaw cycles and dried with 4 Å molecular sieves. − IR: Biorad Excalibur FTS 3000 spectrophotometer (samples in CsI discs or as solutions between CaF_2 windows). − UV/Vis spectra: Perkin−Elmer Lambda 9 UV/Vis spectrophotometer; ca. 10^{-3} M solutions in CH_2Cl_2. − MS: Finnigan MAT 8320 operated in FAB mode (xenon; matrix: 4-nitrobenzyl alcohol). − Cyclic voltammetry: EG&G Princeton Applied Research model 273 potentiostat; potentials in mV versus SCE at a glassy carbon electrode at 25 °C; sample solutions: ca. 10^{-3} M in 0.1 M Bu_4NPF_6 in CH_3CN or CH_2Cl_2. − Elemental analyses: Microanalytical Laboratory of the Organisch-Chemisches Institut, Universität Heidelberg.

Potassium [Dicarbonyl(cyano)(η^6-trifluoromethylbenzene)chromate(0)] (K1b): Tricarbonyl(η^6-trifluoromethylbenzene)chromium (1.72 g, 6.1 mmol) and potassium cyanide (1.14 g, 17.5 mmol) were dissolved in methanol (200 mL) in an irradiation vessel. The vessel was cooled to 0 °C and the solution was irradiated for 3 h with UV light from a high-pressure mercury lamp (Hanau TQ 150). After allowing the dark-brown reaction mixture to warm to room temperature, it was filtered and the filtrate was concentrated to dryness. The residue was washed with diethyl ether (100 mL) and filtered through 5 cm of kieselguhr with tetrahydrofuran (100 mL). Evaporation of the solvent from the orange-red filtrate and subsequent crystallization of the residue from acetone/petroleum ether (boiling range 40−60 °C) yielded **K1b** as a microcrystalline solid with an intense orange color (900 mg, 46%). − $C_{10}H_5CrF_3KNO_2$ (319.2): calcd. C 37.62, H 1.58, N 4.39; found C 36.93, H 1.89, N 4.48. − ^{1}H NMR ([D$_6$]acetone): δ = 4.5−5.1 (m). − ^{13}C NMR ([D$_6$]acetone): δ = 241.3 (s, CO), 168.0 (s, CN), 126.4 (q, CF_3, $^1J_{FC}$ = 270 Hz), 89.6 (s, C_{ar}), 86.5 (q, $C_{ar}CF_3$, $^2J_{FC}$ = 35 Hz), 86.3 (s, C_{ar}), 84.3 (s, C_{ar}). − IR (CH_3OH): $\tilde{\nu}$ = 2041 w, br (CN), 1910 s, 1856 s (CO). − MS (FAB$^-$): *m*/*z* = 280.0 [M]$^-$. − CV (CH_3CN, SCE): E_{pa} = −100 mV (irrev. ox.).

PPN[*tripod*Fe{NC−Cr(CO)$_5$}$_3$] (PPN2): To a solution of $FeCl_2$ (0.29 mmol, 34 mg) and *tripod* (0.29 mmol, 184 mg) in acetone, a solution of **Na1a** (216 mg, 0.90 mmol) in acetone was added dropwise by means of a syringe. An immediate color change from pale-yellow to red was observed. After the addition of bis(triphenylphosphanyl)iminium chloride (PPNCl; 176 mg, 0.31 mmol), the reaction mixture was concentrated to dryness in vacuo. The red residue was redissolved in dichloromethane (20 mL) and the resulting red solution was stirred for 2 h at room temperature to complete the cation exchange. Filtration through 3 cm of kieselguhr gave a red solution, which was concentrated to a volume of 5 mL and layered with ethanol (20 mL). **PPN2**·0.75 CH_2Cl_2 was obtained as red needle-shaped crystals (280 mg, 52%). For analytical and spectroscopic data of **PPN2**, see Tables 2 and 3.

[*tripod*Fe(CO){NC−M}$_2$] (3); M = Cr(CO)$_5$ (3a), Cr(η^6-CF$_3$C$_6$H$_5$)(CO)$_2$ (3b), Mn(η^5-CH$_3$C$_5$H$_4$)(CO)$_2$ (3c): To a solution of $FeCl_2$ (0.65 mmol, 34 mg) and *tripod* (0.65 mmol, 184 mg) in acetone, a solution of the alkali metal salt **Na1a** (**3a**), **K1b** (**3b**), or **K1c** (**3c**) (1.30 mmol) in acetone was added dropwise by means of a syringe. An immediate color change from pale-yellow to orange-red was observed. After bubbling carbon monoxide through the reaction mixture for 5 min, the turbid brown solution was concentrated to dryness in vacuo leaving a brown-red solid residue. This was redissolved in dichloromethane and the resulting solution was filtered through 3 cm of kieselguhr. The products were isolated in the form of brown microcrystalline powders by addition of petroleum ether (boiling range 40−60 °C) to the concentrated brown-red filtrates. Crystals of **3a**, **3b**, and **3c** suitable for X-ray analyses were grown by layering dilute solutions in acetone with petroleum ether (boiling range 40−60 °C) at room temperature. For analytical and spectroscopic data of compounds **3a**, **3b**, and **3c**, see Tables 2 and 3.

[(*tripod*Fe)$_2${NC−M′−CN}$_3$]BF$_4$ (5BF$_4$); M′ = Fe(η^5-C$_5$H$_5$)(CO) (5bBF$_4$), Co(η^5-C$_5$H$_5$)(CN) (5cBF$_4$): To a solution of $Fe^{II}aq(BF_4)_2$ (1.0 mmol, 338 mg) and *tripod* (1.0 mmol, 625 mg) in dichloromethane/ethanol (1:1, 40 mL), the potassium salt of the appropriate ligand, **K4b** (**5bBF$_4$**) or **K4c** (**5cBF$_4$**) (1.5 mmol), was added as a solid in a single portion. A color change from pale-yellow to red was observed. After stirring for 1 h at room temperature, the reaction mixture was concentrated in vacuo. The red residue was filtered through 1 cm of kieselguhr with dichloromethane. Evaporation of the solvent from the red filtrate and subsequent washing of the residue with diethyl ether left a red microcrystalline solid. The C_3-symmetric isomers (Scheme 9, **A**) of the pentanuclear complexes were purified by recrystallization from dichloromethane/ethanol. Yields: **5bBF$_4$**: 42% (crude product), ca. 10% (symmetric isomer of **5bBF$_4$**, three recrystallizations); **5cBF$_4$**: 67% (crude product), 40% (symmetric isomer of **5cBF$_4$**, one recrystallization).

5bBF$_4$: ^{1}H{^{31}P} NMR (CD_2Cl_2): δ = 1.53 (s, CH_3), 2.00−2.35 (m, CH_2), 4.10 (s, C_5H_5), 6.9−7.8 (m, H_{ar}). − ^{31}P NMR (CD_2Cl_2): δ = 37.4 (s). − The unsymmetrical isomer of **5bBF$_4$** was not isolated in pure form. Its Cp resonances were seen as singlets at δ = 4.14, 4.04, and 3.86 in the ^{1}H{^{31}P} NMR spectrum of the crude product.

5cBF$_4$: ^{1}H{^{31}P} NMR (CD_2Cl_2): δ = 1.43 (s, CH_3), 2.0−2.4 (m, CH_2), 4.7 (s, C_5H_5), 7.0−7.8 (m, H_{ar}). − ^{31}P NMR (CD_2Cl_2): δ = 39.1 (s). − ^{13}C NMR ([D$_6$]DMSO): δ = 138.6 (dd, PC_{ar}), 136.9 (dd, PC_{ar}), 134.5−128.0 (m, C_{ar}), 133.7 (s, Co−CN−Fe), 117.9 (s, Co−CN), 88.9 (s, C_5H_5), 37.6 (m, CH_3), 36.4 (m, C_q), 32.8 (m, CH_3). − For further analytical and spectroscopic data of compounds **5bBF$_4$** and **5cBF$_4$**, see Tables 6 and 7.

Crystals of compound **5aFeCl$_4$** suitable for an X-ray crystallographic structure determination were obtained in very low yield (15 mg) from the reaction of $FeCl_2$ (135 mg, 1.07 mmol), *tripod* (680 mg, 1.09 mmol), and potassium tetracarbonyl(dicyano)manganate(I) (280 mg, 1.08 mmol) in acetone. After concentrating the reaction solution to dryness and filtration of the residue through 1 cm of kieselguhr with dichloromethane, the red filtrate was concentrated to dryness. Red parallelepiped-shaped crystals of **5aFeCl$_4$** were grown by vapor diffusion of diethyl ether into a solution of the crude product in tetrahydrofuran/ethanol at room temperature. − ^{1}H{^{31}P} NMR (CD_2Cl_2): δ = 1.5 (br. s, CH_3), 2.3 (br. m, CH_2), 7.0−7.8 (m, H_{arom}); all signals are broad because of the paramagnetism of the $FeCl_4^-$ anion. − ^{31}P NMR (CD_2Cl_2): δ = 32.7 (s). − For further analytical and spectroscopic data, see Tables 5, 6, and 7.

Salts of **5a$^+$** with counteranions other than tetrachloroferrate(III) could not be obtained in analytically pure form, neither by the procedure described above for **5bBF$_4$** and **5cBF$_4$** nor under strictly anhydrous conditions. This is mainly due to problems associated with the purification of these compounds, which could not be effected by means of crystallization and chromatography.

X-ray Crystallographic Studies: Suitable crystals were taken directly from the mother liquor, immersed in perfluorinated polyether oil, and fixed to a glass capillary. Data were collected with a Nonius−Kappa CCD diffractometer (low-temperature unit, graph-

Table 8. Crystallographic data for compounds **PPN2**, **3**, and **5aFeCl$_4$**

Compound		**PPN2**	**3a**	**3b**	**3c**	**5aFeCl$_4$**
Solvate		0.75 CH_2Cl_2	–	–	–	0.4 THF ·0.5 Et_2O
Empirical formula (without solvate)		$C_{95}H_{69}Cr_3FeN_4O_{15}P_5$	$C_{54}H_{39}Cr_2FeN_2O_{11}P_3$	$C_{62}H_{49}Cr_2F_6FeN_2O_5P_3$	$C_{60}H_{53}FeMn_2N_2O_5P_3$	$C_{100}H_{78}Cl_4Fe_3Mn_3N_6O_{12}P_6$
Molecular mass [g/mol]		1873.3	1144.5	1268.8	1140.7	2215.8
Crystal size [mm]		0.30×0.10×0.05	0.10×0.15×0.15	0.15×0.25×0.12	0.15×0.20×0.20	0.25×0.10×0.03
Crystal system		monoclinic	monoclinic	monoclinic	monoclinic	monoclinic
Space group		$P2_1$	$P2_1/n$	$P2_1/n$	$P2_1/n$	$P2_1/n$
Lattice constants:	*a* [pm]	1438.3(3)	1342.9(3)	1308.5(3)	1307.3(3)	2076.5(4)
	b [pm]	1449.1(3)	2255.0(5)	2252.5(5)	2211.1(4)	2459.7(5)
	c [pm]	2198.7(4)	1717.8(3)	1863.7(4)	1802.4(4)	2250.3(5)
	α [°]	90	90	90	90	90
	β [°]	95.31(3)	92.01(3)	91.12(3)	90.42(3)	114.64(3)
	γ [°]	90	90	90	90	90
V [10^6·pm^3]		4563.00	5198.70	5492.00	5209.80	10447.00
Z		2	4	4	4	4
d_x [g·cm^{-3}]		1.410	1.462	1.535	1.454	1.455
T [K]		200	200	200	200	200
Scan range		3.4° ≤ 2θ ≤ 52.0°	3.0° ≤ 2θ ≤ 52.1°	2.8° ≤ 2θ ≤ 52.1°	2.9° ≤ 2θ ≤ 52.0°	3.5° ≤ 2θ ≤ 50.0°
Method		ω-Scan, Δω =2.0°	ω-Scan, Δω =1.0°	ω-Scan, Δω =1.0°	ω-Scan, Δω =1.0°	ω-Scan, Δω =1.0°
Scan speed		18 s/frame	10 s/frame	10 s/frame	10 s/frame	30 s/frame
No. of measured reflections		70626	71226	89959	84087	162573
No. of unique reflections		17826	10221	10815	10254	18392
No. of observed reflections		11825	5734	8611	7205	9339
Observation criterion		$I \geq 2\sigma$	$I \geq 2\sigma$	$I \geq 2\sigma$	$I \geq 2\sigma$	$I \geq 2\sigma$
No. of params. refined		987	662	734	525	1155
Resid. el. density [10^{-6} e·pm^{-3}]		0.91	0.53	0.40	1.52	1.41
R_1/R_w [%] (refinement on F^2)		6.0/13.1	5.2/8.7	3.5/8.5	6.2/16.7	7.9/22.9

ite-monochromated Mo-K_α radiation). The data were processed by the standard Nonius software.[23] All calculations were performed using the SHELX software package. Structures were solved by direct methods using the program SHELXS-97[24] and refined using the program SHELXL-97.[24] Graphical handling of the structural data during solution and refinement was performed with XPMA.[25] Atomic coordinates and anisotropic thermal parameters of the non-hydrogen atoms were refined by full-matrix least-squares calculations. Data relating to the structure determinations are compiled in Table 8. Figures 1, 2, and 3 were generated using WinRay-32 and WinRay-GL.[26] Crystallographic data (excluding structure factors) for the structures reported in this paper have been deposited with the Cambridge Crystallographic Data Centre as supplementary publication nos. CCDC-156056 to -156060. Copies of the data can be obtained free of charge on application to the CCDC, 12 Union Road, Cambridge CB2 1EZ, U.K. [Fax: (internat.) + 44-1223/336-033; E-mail: deposit@ccdc.cam.ac.uk].

Acknowledgments

We are indebted to the Deutsche Forschungsgemeinschaft and the Fonds der Chemischen Industrie for financial support. We are very grateful to Mr. D. Günauer for performing the cyclic voltammetric measurements. The scientific assistance of Dr. J. Groß and coworkers of the mass spectrometry department and the help of the microanalytical laboratory of the Organisch-Chemisches Institut der Universität Heidelberg are gratefully acknowledged.

[1] [1a] S. Mann, G. Huttner, L. Zsolnai, K. Heinze, *Angew. Chem.* **1996**, *108*, 2983; *Angew. Chem. Int. Ed. Engl.* **1996**, *35*, 2808. – [1b] S. Mann, G. Huttner, L. Zsolnai, K. Heinze, V. Jacob, B. Antelmann, A. Driess, B. Schiemenz, *Z. Naturforsch., Teil B* **2000**, *55*, 638.

[2] [2a] H. Krentzien, H. Taube, *Inorg. Chem.* **1982**, *21*, 4001. – [2b] H. Krentzien, H. Taube, *J. Am. Chem. Soc.* **1976**, *98*, 6379. – [2c] V. Jacob, S. Mann, G. Huttner, L. Zsolnai, O. Walter, E. Kaifer, P. Rutsch, P. Kircher, E. Bill, manuscript in preparation.

[3] [3a] N. Zhu, H. Vahrenkamp, *J. Organomet. Chem.* **1999**, *573*, 67; G. N. Richardson, H. Vahrenkamp, *J. Organomet. Chem.* **2000**, *593–594*, 44; A. Geiß, H. Vahrenkamp, *Inorg. Chem.* **2000**, *39*, 4029; A. Geiß, M. J. Kolm, C. Janiak, H. Vahrenkamp, *Inorg. Chem.* **2000**, *39*, 4037; G. N. Richardson, U. Brand, H. Vahrenkamp, *Inorg. Chem.* **1999**, *38*, 3070. – [3b] D. J. Darensbourg, W.-Z. Lee, M. J. Adams, D. L. Larkins, J. H. Reibenspies, *Inorg. Chem.* **1999**, *38*, 1378. – [3c] S. Bordoni, L. Busetto, P. Colucci, A. Palazzi, V. Zanotti, *J. Organomet. Chem.* **1997**, *545–546*, 117.

[4] N. Zhu, H. Vahrenkamp, *Chem. Ber./Recueil* **1997**, *130*, 1241; H. Vahrenkamp, A. Geiß, G. N. Richardson, *J. Chem. Soc., Dalton Trans.* **1997**, 3643.

[5] W. P. Fehlhammer, M. Fritz, *Chem. Rev.* **1993**, *93*, 1243.

[6] A. Gautier, *Justus Liebigs Ann. Chem.* **1867**, *142*, 289; A. W. Hofmann, *Justus Liebigs Ann. Chem.* **1867**, *144*, 115.

[7] [7a] K. R. Dunbar, R. A. Heintz, *Prog. Inorg. Chem.* **1997**, *45*, 283.[7b] R. B. King, *Inorg. Chem.* **1967**, *6*, 25. – [7c] E. Bär, W. P. Fehlhammer, D. K. Breitinger, J. Mink, *Inorg. Chim. Acta* **1984**, *82*, L17.

[8] [8a] M. Fritz, D. Rieger, E. Bär, G. Beck, J. Fuchs, G. Holzmann, W.-P. Fehlhammer, *Inorg. Chim. Acta* **1992**, *198–200*, 513. – [8b] P. Braunstein, D. Cauzzi, D. Kelly, M. Lanfranchi, A. Tiripicchio, *Inorg. Chem.* **1993**, *32*, 3373.

[9] [9a] R. B. King, *Inorg. Chem.* **1967**, *6*, 25 (**1a**$^-$). – [9b] J. A. Dineen, P. L. Pauson, *J. Organomet. Chem.* **1974**, *71*, 91–96 (**1c**$^-$).

[10] F. Bringewski, G. Huttner, W. Imhof, L. Zsolnai, *J. Organomet. Chem.* **1992**, *439*, 33.

[11] [11a] E. O. Fischer, R. J. J. Schneider, *J. Organomet. Chem.* **1968**, *12*, P27. – [11b] A. A. Ismail, I. S. Butler, G. Jaouen, *Inorg. Synth.* **1989**, *26*, 31 (**1b**$^-$).
[12] [12a] F. E. Kühn, I. S. Gonçalves, A. D. Lopes, J. P. Lopes, C. C. Romão, W. Wachter, J. Mink, L. Hajba, A. J. Parola, F. Pina, J. Sotomayor, *Eur. J. Inorg. Chem.* **1999**, 295 (**1a**$^-$). – [12b] B. Oswald, A. K. Powell, F. Rashwan, J. Heinze, H. Vahrenkamp, *Chem. Ber.* **1990**, *123*, 243 (**1c**$^-$).
[13] A. Asam, B. Janssen, G. Huttner, L. Zsolnai, O. Walter, *Z. Naturforsch., Teil B* **1993**, *48*, 1707.
[14] [14a] K. K. Klausmeyer, T. B. Rauchfuss, S. R. Wilson, *Angew. Chem.* **1998**, *110*, 1808; *Angew. Chem. Int. Ed.* **1998**, *37*, 1694. – [14b] K. K. Klausmeyer, S. R. Wilson, T. B. Rauchfuss, *J. Am. Chem. Soc.* **1999**, *121*, 2705. – [14c] S. M. Contakes, K. K. Klausmeyer, R. M. Milberg, S. R. Wilson, T. B. Rauchfuss, *Organometallics* **1998**, *17*, 3633.
[15] [15a] W. Hieber, W. Schropp Jr., *Z. Naturforsch., Teil B* **1959**, *14*, 460; R. J. Angelici, *Inorg. Chem.* **1964**, *3*, 1099; M. F. Farona, L. M. Frazee, N. J. Bremer, *J. Organomet. Chem.* **1969**, *19*, 225 (**4a**$^-$); Y. Tang, J. Sun, J. Chen, *Organometallics* **1998**, *18*, 86. – [15b] C. E. Coffey, *J. Inorg. Nucl. Chem.* **1963**, *25*, 179 (**4b**$^-$). – [15c] J. A. Dineen, P. L. Pauson, *J. Organomet. Chem.* **1974**, *71*, 77 (**4c**$^-$).
[16] Examples of pentanuclear complexes with similar geometry: [16a] K. Van Langenberg, S. R. Batten, K. J. Berry, D. C. R. Hockless, B. Moubaraki, K. S. Murray, *Inorg. Chem.* **1997**, *36*, 5006. – [16b] K. E. Vostrikova, D. Luneau, W. Wernsdorfer, P. Rey, M. Verdaguer, *J. Am. Chem. Soc.* **2000**, *122*, 1490.
[17] C.-H. Lai, W.-Z. Lee, M. L. Miller. J. H. Reibenspies, D. J. Darensbourg, M. Y. Darensbourg, *J. Am. Chem. Soc.* **1998**, *120*, 10103 (**4b**$^-$).
[18] J. E. Sutton, P. M. Sutton, H. Taube, *Inorg. Chem.* **1979**, *18*, 1017.
[19] C. Creutz, *Prog. Inorg. Chem.* **1983**, *30*, 1.
[20] *Organikum*, Deutscher Verlag der Wissenschaften, Berlin, **1990.**
[21] [21a] W. Hewertson, H. R. Watson, *J. Chem. Soc.* **1962**, 1490. – [21b] A. Muth, O. Walter, G. Huttner, A. Asam, L. Zsolnai, C. Emmerich, *Z. Naturforsch., Teil B* **1994**, *48*, 149.
[22] H. Funk, F. Binder, *Z. Anorg. Allg. Chem.* **1926**, *155*, 327.
[23] *DENZO-SMN*, Data processing software, Nonius, **1998**; http://www.nonius.com
[24] G. M. Sheldrick, *SHELXS-97*, *Program for Crystal Structure Solution*, University of Göttingen, **1997**; G. M. Sheldrick, *SHELXL-97, Program for Crystal Structure Refinement*, University of Göttingen, **1997**; http://shelx.uni-ac.gwdg.de/shelx/index.html.
[25] L. Zsolnai, G. Huttner, *XPMA*, University of Heidelberg, **1994**; http://www.uni-heidelberg.de/institute/fak12/AC/huttner/htmlsoftware.html
[26] R. Soltek, G. Huttner, *WinRay-32*, University of Heidelberg, **1998**; R. Soltek, G. Huttner, *WinRay-GL*, University of Heidelberg, **2000**; http://www.uni-heidelberg.de/institute/fak12/AC/huttner/htmlsoftware.html

Received February 19, 2001
[I01058]

Anion Conformation and Physical Properties in BETS Salts with the Nitroprusside Anion and its Related Ruthenium Halide (X = Cl, Br) Mononitrosyl Complexes: θ-$(BETS)_4[Fe(CN)_5NO]$, $(BETS)_2[RuBr_5NO]$, and $(BETS)_2[RuCl_5NO]$

Maria-Elena Sanchez,[a] Marie-Liesse Doublet,[b] Christophe Faulmann,[a] Isabelle Malfant,*[a] Patrick Cassoux,[a] Lyudmila A. Kushch,[c] and Eduard B. Yagubskii[c]

Keywords: Sulfur heterocycles / Ruthenium / Halides / Conducting materials / Electronic structure

θ-$(BETS)_4[Fe(CN)_5NO]$ (**1**), $(BETS)_2[RuBr_5NO]$ (**2**), and $(BETS)_2[RuCl_5NO]$ (**3**) [BETS = bis(ethylenedithio)tetraselenafulvalene] have been prepared by electrocrystallisation of BETS using $[Fe(CN)_5NO]^{2-}$ or $[RuX_5NO]^{2-}$, X = Cl or Br, as supporting electrolytes and 1,1,2-TCE/ethanol (10 vol%) for **1**, nitrobenzene/1,2-DCE (40 vol%)/ethanol (10 vol%) for **2**, and benzonitrile/ethanol (10%) solutions for **3** as solvents. Compound **1** exhibits a metallic behaviour down to 40 K, **2** behaves as a semiconductor and **3** as an insulator. The crystal structures of **1**, **2**, and **3** were determined by X-ray diffraction methods. BETS molecules in **1** crystallised in a θ-type mode. By contrast, the crystal structures of **2** and **3** show a packing of BETS molecules consisting of slipped, stacked $(BETS)_2$ dimers. The dimerisation is much stronger in **3** than in **2**. The physical behaviours of the three phases were investigated by means of molecular and band structure calculations and are shown to be directly related to the $[MX_5NO]$ (M = Fe, X = CN; M = Ru, X = Cl, Br) structural conformations.

Introduction

A recent new development in the research on molecular conductors concerns the possibility of creating solids in which conductivity (or superconductivity) coexists with other physical phenomena. This novel class of multifunctional materials should provide a unique opportunity to study the competition and mutual influence of, and better still a possible interplay between two properties in the same crystal lattice. Until recently, attention along this line has been primarily directed towards magnetic conductors.[1]

A parallel approach involving conducting radical cation salts with photochromic anions has been explored even more recently. The interest in the synthesis and characterisation of new molecular conductors containing photochromic anions is to analyse the influence of the electronic excitation of the anions over the conducting (superconducting) electrons. For example, one can imagine the design of a photochromic molecular conductor (or even a superconductor) in which the conducting properties can be tuned by light. In this context, the use of the photochromic nitroprusside $[Fe(CN)_5NO]^{2-}$ anion and related mononitrosyl transition-metal complexes as counter-anions in radical cation salts of BEDT-TTF [BEDT-TTF = bis(ethylenedithio)tetrathiafulvalene] and its analogues has been contemplated.[2,3] These anions are highly interesting because they possess extremely long-living metastable excited states at low temperatures that can be generated by laser irradiation.[4] Two-dimensional salts in which BEDT-TTF or its oxygen-substituted analogue BEDO-TTF [BEDO-TTF = bis(ethylenedioxy)tetrathiafulvalene] is associated with the $[Fe(CN)_5NO]^{2-}$ anion have been already reported, as well as salts with the TTF molecule.[2]

The BETS molecule [BETS = bis(ethylenedithio)tetraselenafulvalene] is a modification of BEDT-TTF obtained by substituting selenium for sulfur in the central tetrathiafulvalene fragment (Figure 1).[5] A strikingly large number of metal-like and superconducting BETS-based salts have been recently reported.[6] Thus, BETS-based conducting salts incorporating photochromic anions also seem to be promising candidate systems for the preparation of photochromic conductors and superconductors.[3]

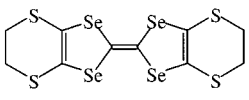

Figure 1. Atomic scheme for BETS

We report here on the preparation, the crystal and electronic structures, and the solid state properties of three phases namely, θ-$(BETS)_4[Fe(CN)_5NO]$ (**1**), $(BETS)_2[RuBr_5NO]$ (**2**), and $(BETS)_2[RuCl_5NO]$ (**3**), obtained when using the appropriate $[Fe(CN)_5NO]^{2-}$, $[RuBr_5NO]^{2-}$, $[RuCl_5NO]^{2-}$ anions.

[a] Laboratoire de Chimie de Coordination, CNRS, 205 route de Narbonne, 31077 Toulouse cedex, France
[b] Laboratoire de Structure et Dynamique des Systèmes Moléculaires et Solides USTL II, Place E. Bataillon, 34095 Montpellier cedex 5, France
[c] Institute of Problems of Chemical Physics in Chernogolovka, Russian Academy of Sciences, Chernogolovka, 142432 Russia

 © WILEY-VCH Verlag GmbH, 69451 Weinheim, 2001 1434–1948/01/1111–2797 $ 17.50+.50/0

Results and Discussion

Synthesis and Electrical Properties

Three different phases are obtained when the BETS molecule is associated with the $[Fe(CN)_5NO]^{2-}$ anion and its substituted mononitrosylruthenium halide $[RuX_5NO]^{2-}$ (X = Cl or Br) complexes. All these phases have been obtained electrochemically and characterised by X-ray structure determination and energy-dispersive X-ray spectrometry (EDS).[3b]

The different molecular arrangements of **1**, **2**, and **3** lead to different physical behaviours. The single-crystal room-temperature conductivity of **1** is 0.01 $S\cdot cm^{-1}$. As depicted in Figure 2, the temperature-dependent resistance shows a weakly metallic behaviour down to ca. 40 K ($\sigma_{40\,K}$ = 0.07 $S\cdot cm^{-1}$). Below this temperature, the compound undergoes a metal-to-semiconductor phase transition. By contrast, **2** is a semiconductor (0.2 $S\cdot cm^{-1}$) with a very small activation energy (E_a = 0.03 eV), whereas **3** behaves as an insulator, its resistivity at room temperature being larger than $4\cdot10^3$ $\Omega\cdot cm$.

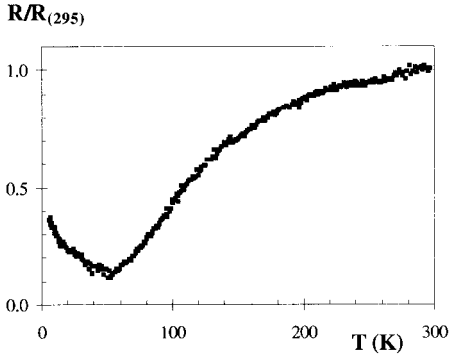

Figure 2. Temperature dependence of the resistance in **1**

X-ray Structure of 1, 2, and 3

θ-(BETS)$_4$[Fe(CN)$_5$NO] (1)

The asymmetric unit contains half a BETS molecule lying on a centre of inversion and 1/8 $[Fe(CN)_5NO]$ entity lying on a twofold rotation axis. The complete determination of the anion has not been possible because of a strong disorder: Two Fe atoms [Fe(1) and Fe(2)] are located at about 2 Å from each other along the twofold axis. This leads to a very low electronic density for the C, N, and O atoms whose positions could not be determined. Only one crown of electron density is evidenced from the Fourier map, which leads to the representation of the anion shown in Figure 3, a. A similar, not resolved disorder of the nitroprusside anion has also been observed in (BEDO-TTF)$_4$[Fe(CN)$_5$NO].[2c]

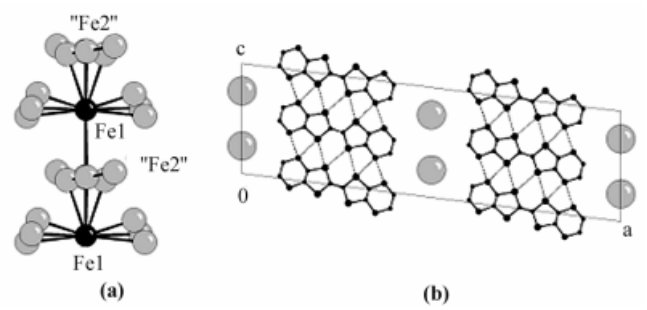

Figure 3. Cameron view of the anion in **1** along the *b* axis (a); projection in the *ac* plane of the cationic layer of **1** (b); the grey circles represent the electronic densities of the nitroprusside anion, H atoms are omitted for clarity

The crystal structure of **1** consists of sheets of adjacent columns in the *bc* plane alternating with layer of anions along the *a* direction (Figure 3, b). Two equivalent $(BETS)_2$ layers occur in the unit cell. Within each layer, the BETS molecules stack in a θ-type mode (Figure 4).[7] They form chains of parallel BETS molecules, running along the *b* direction and connected to adjacent chains through short chalcogen···chalcogen contacts (Table 1). The dihedral

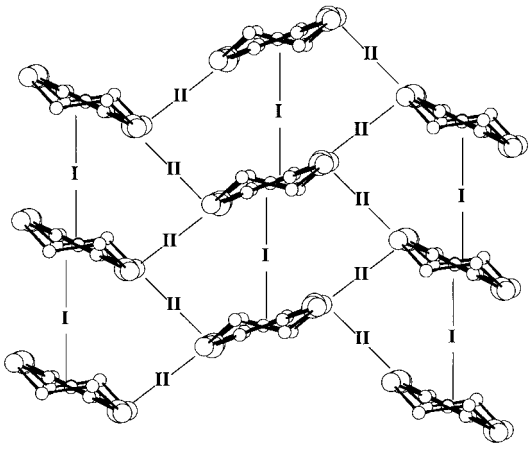

Figure 4. Projection of the cationic layer of **1** along the BETS central C=C bond, H atoms are omitted for clarity

Table 1. Se···Se distances smaller than 4.2 Å and absolute values of the $\beta_{HOMO\text{-}HOMO}$ interaction energies [eV] for the different BETS−BETS interactions in **1**, **2**, and **3** [see Figures 4, 5 (a), and 7 (a) for labelling of **1**, **2**, and **3**, respectively]

	Se ··· Se [Å]	$\beta_{HOMO\text{-}HOMO}$ [eV]
3	3.479(1) (× 2)[a]	β_{intra} = 1.274
	3.596(1) (× 2)[a]	
	4.145(1) (× 2)[b]	β_{inter} = 0.316
2	3.513(5)[c]	β_{intra} = 0.623
	3.890(5)[d], 3.994(5)[d]	β_{inter} = 0.323
1	4.072(1) (× 2)[e], 4.178(1) (× 2)[e]	β_I = 0.158
	3.734(2) (× 4)[f], 3.792(2) (× 4)[g],	β_{II} = 0.094
	3.813(2) (× 4)[h]	

[a] Symmetry operations: $1-x, -y, 1-z$. [b] $2-x, -y, 1-z$. [c] x, y, z. [d] $1+x, y, z$. [e] $x, -1+y, z$. [f] $x, -y, -0.5+z$. [g] $x, 1-y, -0.5+z$. [h] $0.5-x, -0.5+y, 2.5-z$.

angle between two BETS molecules belonging to adjacent chains is 133.82°.

$(BETS)_2[RuBr_5NO]$ (2)

The asymmetric unit contains two BETS molecules and one $[RuBr_5NO]$ entity. As shown in Figure 5, the packing consists of chains of dimerised BETS molecules (the distance between the averaged planes of two BETS molecules belonging to one dimer is 0.512 Å shorter than the distance between two dimeric entities) stacking along the *a* direction with Se···Se and Se···S contacts shorter than the van der Waals distances (Figure 5, a). The crystal structure of **2** can be described as a pseudo-hexagonal columnar architecture made of short intra- and intermolecular chalcogen···chalcogen contacts. The anionic complexes are located in the centre of each hexagon and repeat infinitely along the *a* direction (Figure 5, b).

In this phase, the anionic complex is pseudo-octahedral with averaged Ru−Br distances of 2.466(7) Å and

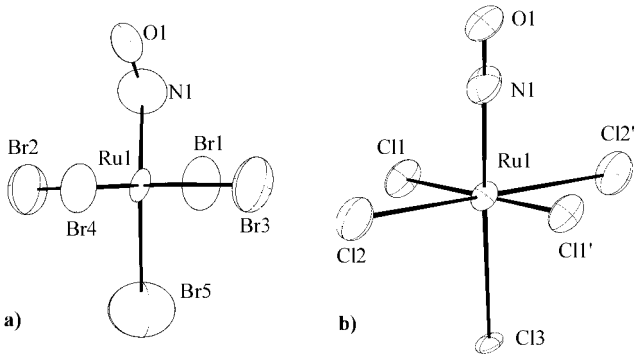

Figure 6. Cameron view of the anionic part in **2** (a) and **3** (b)

Br−Ru−Br angles close to 90° for the planar (Ru1Br1Br2Br3Br4) entity. The Ru−Br5 apical bond is almost perpendicular to the $Ru(Br)_4$ plane (89.20°). On the other hand, the Ru−N−O angle is 160.0(5)° (Figure 6, a). As already studied, this non-linearity can be connected with

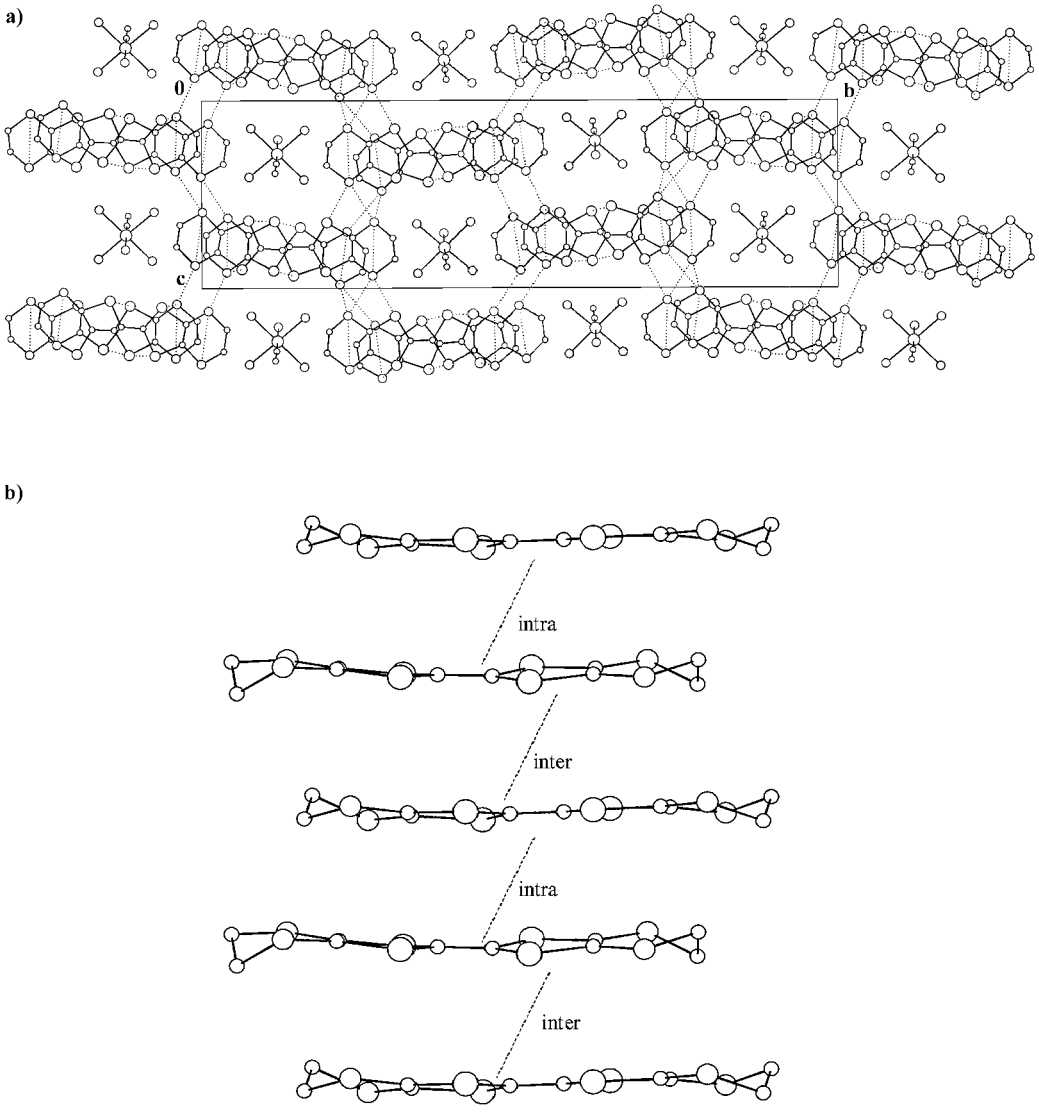

Figure 5. Projection in the *bc* plane of **2** (a); chain of BETS molecules along the *a* axis (b); H atoms are omitted for clarity

the formal charge on the nitrosyl ligand.[8] This will be discussed later in the discussion of the electronic structure.

$(BETS)_2[RuCl_5NO]$ (3)

The asymmetric unit contains one BETS molecule and half a $[RuCl_5NO]$ entity lying on a centre of inversion. Due to this special position, the nitrosyl ligand and the Cl(3) atom have an occupancy of 0.5 and are equally distributed on both sides of the Ru atom. The BETS molecule adopts a chair conformation, as shown in Figure 7, a. The crystal structure of **3** consists of chains of strongly slipped dimerised BETS molecules (built from two eclipsed BETS molecules connected through short Se···Se contacts, Table 1) stacking along the *a* direction and alternating with the anion along the *b* direction. Several chalcogen···chalcogen contacts shorter than the van der Waals distances occur between dimers belonging to the adjacent stacks (Figure 7, b). Thus, the structure can be regarded as sheets in the $(01\bar{1})$ plane of interconnected chains of isolated BETS dimers separated by $RuCl_5NO$ anions along the $[01\bar{1}]$ direction.

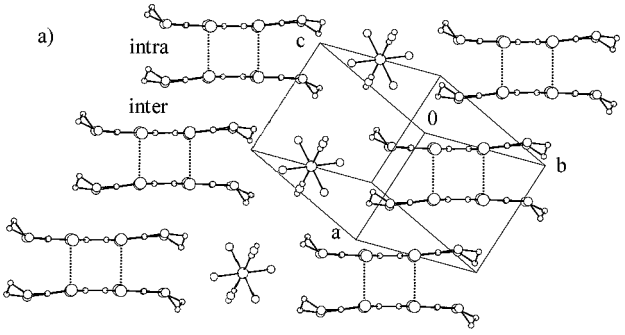

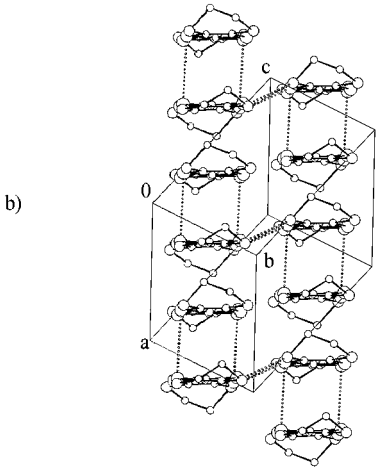

Figure 7. Projection in the $(01\bar{1})$ plane of **3** (a); projection of the cationic layer of **3** along the BETS central C=C bond (b); H atoms are omitted for clarity

As in **2**, the anionic complex presents a pseudo-octahedral configuration with averaged equatorial Ru−Cl distances of 2.381(2) Å and angles between Ru, Cl atoms, and NO ligand close to 90°. Contrary to **2**, Ru−N−O is almost linear [178.0(3)°] (Figure 6, b). This linearity will be discussed in the next part and compared to the bent conformation of $RuBr_5NO$ in **2**.

Electronic Structure of 1, 2, and 3

$(BETS)_2[RuX_5NO]$ (X = Br, Cl) (2, 3)

The intermolecular interaction energies calculated between the highest occupied molecular orbital (HOMO) of two adjacent BETS molecules are reported in Table 1. They confirm that **2** and **3** are characterised by strongly dimerised BETS chains running along the *a* direction of the crystal lattice, all inter-chain interactions being smaller by at least one order of magnitude. It is in agreement with the non-metallic properties of the BETS layers in **2** and **3**.

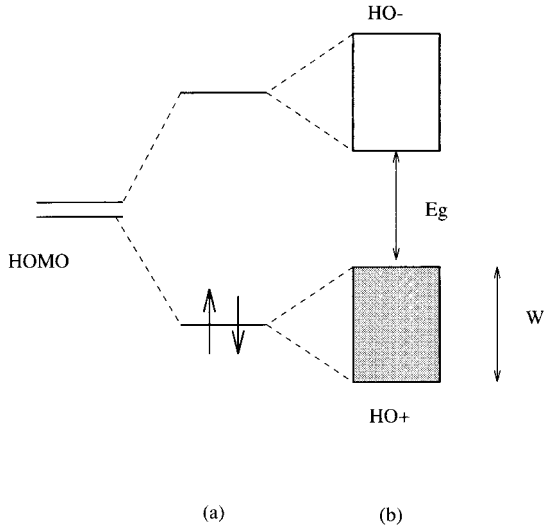

Figure 8. Qualitative electronic band structure of a strongly dimerised one-dimensional molecular solid; (a) and (b) correspond to the dimer and solid electronic structures, respectively; W and E_g stand for the bandwidths and the energy band gap, respectively

As depicted in Figure 8, the band structure of a dimerised chain consists of a fully occupied low-lying band (HO^+) and an empty high-lying band (HO^-). These two bands originate from the molecular orbitals $\Psi \cong^{+}_{HOMO}$ and $\Psi \cong^{-}_{HOMO}$ of the dimer, i.e. from the symmetric and the antisymmetric linear combinations between the HOMOs of the two interacting monomers.

The HO^+ and HO^- bandwidths (W) as well as the energy gap (E_g) between these two bands are governed by the inter-dimer and the intra-dimer interaction energies, namely β_{inter} and β_{intra}. In the case of **2** and **3**, the strong dimerisation observed in the BETS layers results in rather high band gaps ($E_g \approx 0.6$ eV for **2** and $E_g \approx 1.2$ eV for **3**) and small bandwidths, supporting their non-metallic behaviours.

However, whereas a large band gap is in agreement with the insulating behaviour of **3**, it is not consistent with the very small experimental activation energy $E_a = 0.03$ eV determined for **2**. To understand this discrepancy between experimental and theoretical results, it may be useful to pay

closer attention to the electronic structure of the anions, from which the following explanation may be proposed.

As previously mentioned, the main difference between the $[RuBr_5NO]^{2-}$ and the $[RuCl_5NO]^{2-}$ anions concerns the Ru−N−O angle α (see Figure 5). Whereas NO is linearly bonded to the ruthenium metal centre for X = Cl [α = 178.0(3)°], it is bent with an angle α = 160.0(5)° for X = Br. The subtle π-electron transfers occurring between the ruthenium atom and a bent or a linear NO ligand are well known and have been shown to depend on the nature of the ancillary ligands.[8] In particular, it has been shown that the Ru−N−O angle can be correlated to the π-donor character of the remaining ligands through a three-centre four-electron interaction, and that the nitrosyl formal charge can thus be treated as negative NO^- for a bent NO (α = 120°) and positive NO^+ for a linear one.[8] As a consequence, different Ru−N−O angles may result in different formal oxidation states for the transition metal atom. It is therefore tempting to associate the bending angle observed in the $(BETS)_2[RuBr_5NO]$ salt with a more pronounced π-donor character of Br^- compared to that of Cl^-. However, the nature of X (X = Cl or Br) does not seem to be the only factor that governs the nitrosyl conformation. Indeed, the Ru−N−O bending angles in $K_2[RuBr_5NO]$ and $K_2[RuCl_5NO]$ are nearly equivalent [α = 174.4(1)° for X = Br and α = 176.7(5)° for X = Cl].[9] Thus, the different bending angles in **2** and **3** raise the possibility that the BETS layers may interact with the anions, at the very least in **2**.

Considering further the Ru−N−O bending angles reported in the $(BETS)_2[RuBr_5NO]$ (X = Cl, Br) salts, a positive NO^+ may be conceived for X = Cl (α = 178°) and an intermediate charge between NO^+ and NO^- for X = Br (α = 160°). This would result in different oxidation states for the transition metal in the two compounds. Whereas for X = Cl, the $[Ru^{II}Cl_5^{5-}NO^+]^{2-}$ formal electron count is fully consistent with the insulating properties of a strongly dimerised $(BETS)_2^{2+}$ cationic layer, it may be envisioned that for X = Br some of the electron density missing around the transition metal (Ru^{+n}; $n > 2$) is retained by the cationic layers.

This hypothesis leads to the presence of some few electrons in the weakly dispersive HO^- band of the BETS layers, and is consistent with the very small activation energy experimentally measured for **2**. Hence, the different physical properties of $(BETS)_2[RuCl_5NO]$ and $(BETS)_2[RuBr_5NO]$ are proposed to originate from different BETS−RuX_5NO interactions, leading to different BETS→RuX_5NO electron transfers and therefore to different Ru oxidation states. EPR measurements are in progress to obtain more insight along this line. It should be noticed, however, that preliminary results have already shown a large and asymmetric signal centred at $g = 2.037$ for **2**, and no EPR signal for **3**. Such a large signal for **2** is unlikely to be the signature of isolated $BETS^+$ radicals, but is in turn consistent with our hypothesis of a Ru^{n+} ($n > 2$) oxidation state in the $(BETS)_2[RuBr_5NO]$ salt.

$(BETS)_4[Fe(CN)_5NO]$ (1)

Unlike Cl^- and Br^-, CN^- is a strong π-acceptor ligand. Consequently, the metal-like molecular orbitals of a $[Fe(CN)_5NO]$ pseudo-octahedron are expected to be less occupied, for an equivalent NO bending angle, than in the analogous $[RuX_5NO]$ (X = Cl, Br) complexes. The nitrosyl ligand most likely adopts a linear conformation to compensate (at least partially) for the lack of electron density around the transition metal centre. This seems to be corroborated by the strong disorder reported for the $[Fe(CN)_5NO]$ anions, since X-ray diffraction techniques often encounter difficulties in distinguishing close atoms such as C, N and O. Hence, to stabilise an Fe^{II} formal oxidation state,[10] the anions of **1** should require a larger electron density from the BETS layers than in the other Ru-based phases, in agreement with the 4:1 stoichiometry observed for that salt.

Since no accurate information on the anionic layers is available, the electron transfer cannot be accurately determined here. The electronic band structure and the Fermi surfaces associated with different oxidation states of the $(BETS)_2^{\rho+}$ ($\rho = 1, {}^3/_2$) cationic slabs are presented in Figure 9. Although $BETS^{+1/2}$ corresponds to the usual oxidation state found in BETS-based metal-like salts, it appeared interesting to check whether a larger oxidation state ($BETS^{+3/4}$) could alter the Fermi surface of the salt.

The electronic structures of Figure 9 are very similar to those previously reported for the homologous θ-type BETS phase associated with $[Cu_2Cl_6]^{2-}$ anions.[11] According to the topology of the intermolecular interactions (see Table 1), the Fermi surface associated with ρ = 1 exhibits a two-dimensional character (2D). This is consistent with the observed metallic behaviour of **1** at room temperature but cannot explain the first-order phase transition observed

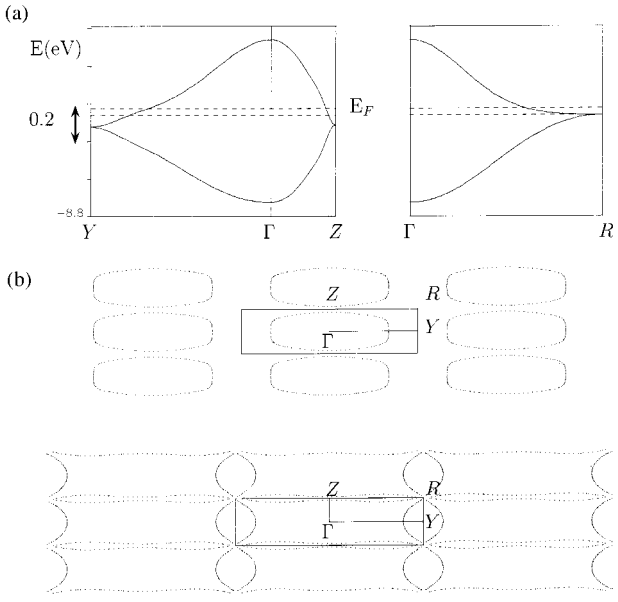

Figure 9. Electronic band structure of **1** (a), the dotted lines refer to the Fermi levels for ρ = 1 and ρ = ${}^3/_2$; Fermi surfaces of one $(BETS)_2^{\rho+}$ layer of **1** (b) for ρ = 1 (top) and ρ = ${}^3/_2$ (bottom); Γ, Y, Z and R correspond to the wave vectors (0,0), (b*/2,0), (0,c*/2) and (b*/2,c*/2), respectively

around 40 K, since such a 2D character of the Fermi surface would suggest a stable metallic state for this compound down to low temperatures. Should a larger electron transfer ($\rho = {}^{3}/_{2}$) be considered, then the Fermi level would approach the two degenerated HOMOs (see Figure 9, a).

As already suggested in a previous work,[11b] slight changes in the donor slab could occur at low temperature due to a modification of the donor−acceptor interactions. Such structural changes could be responsible for the change in the resistivity behaviour around 40 K. Let us note, however, that among all presently known BETS and BEDT-TTF cation radical based organic conductors, it is not rare that a first-order phase transition cannot be rationalised in terms of electronic instabilities of the Fermi surface. In a very recent work,[12] Canadell et al. suggested that the first-order phase transition observed in the κ-$(BETS)_2C(CN)_3$ salt mainly involves the anionic slabs and that the electronic structure of the donor slabs is only slightly altered by the transition. To obtain more insights into the mechanism of the transition observed for **1**, low-temperature X-ray investigations as well as magnetoresistance measurements could be of interest. The former may help in determining which of the cationic or/and anionic slabs is affected by the transition, and the latter may allow us to properly determine the electron transfer occurring from the donor slabs to the $[Fe(CN)_5NO]$ species, for this charge transfer is directly related to the area of the 2D Fermi surface.

Conclusions

The use of the nitroprusside $[Fe(CN)_5NO]^{2-}$ anion and its related mononitrosylruthenium halide complexes $[RuX_5NO]^{2-}$ (X = Cl, Br) in the preparation of BETS-based salts led to a number of different phases with different stoichiometries, **1**, **2**, and **3**. These various phases exhibit different interesting structures and properties. Compound **1** exhibits a metallic behaviour down to 40 K where it undergoes a first-order metal-to-semiconductor phase transition. Compound **2** is a small activated semiconductor ($E_a = 0.03$ eV) and **3** is an insulator. Molecular and band structure calculations have been carried out to rationalise the physical properties of the three salts. The results suggest a direct role of the anionic slabs on the electronic properties of the BETS layers. The different physical behaviours of **2** and **3**, corresponding to the same 2:1 stoichiometry, have been correlated to the conformation of the $[RuX_5NO]$ (X = Cl, Br) species. Depending on the Ru−N−O bending angle, different oxidation states are expected for the ruthenium atom and therefore different electron transfers from the BETS layers to the $[RuX_5NO]$ species. When NO is linearly bonded to the transition metal centre, the stabilisation of an $[Ru^{II}Cl_5NO^+]^{2-}$ anion dictates an integral oxidation state for the BETS molecules, in agreement with the insulating behaviour of **3**. When NO bends, a formal intermediate charge between NO^+ and NO^- may be considered, yielding an Ru^{n+} ($n > 2$) oxidation state. The lack of electron density around the transition metal centre is thus proposed to be retained by the BETS layers, in agreement with the small activation energy of **2**. Due to the 2D character of the $(BETS)_2^{1+}$ Fermi surface calculated for **1**, it is likely that the phase transition occurring in this compound mainly involves the anionic slabs. Nevertheless, low-temperature crystallographic data are required to check whether the donor slabs are, or are not affected by the phase transition.

In conclusion, this work has revealed possible relationships between the anion conformation and the physical properties of **1**, **2**, and **3**. We have shown that the presence of the radical cation salts affects the geometry of the nitroprusside anion and its related mononitrosylruthenium halide complexes $[RuX_5NO]^{2-}$ (X = Cl, Br). Further studies are currently in progress to investigate the photochromic properties of these systems, including DSC measurements to detect the existence of long-lived metastable states in the nitrosyl complexes, and Mössbauer experiments as well as conductivity measurements under irradiation.

Experimental Section

Syntheses: $(PPh_4)_2[Fe(CN)_5NO]$ was obtained by reaction of $Na_2[Fe(CN)_5NO]$ (Aldrich) with $(Ph_4P)Cl$ in water. $K_2[RuX_5NO]$ (X = Cl or Br) were synthesised according to the method of Mercer.[13] $(NH_4)_2[RuBr_5NO]$ was obtained by reaction of $K_2[RuBr_5NO]$ and NH_4Cl. − Crystals of **1** were obtained by electrocrystallisation from BETS solutions in 1,1,2-trichloroethane/ethanol (10 vol%) at 50 °C. $(Ph_4P)_2[Fe(CN)_5NO]$ was used as supporting electrolyte. The donor ($4\cdot10^{-4}$ M) and the electrolyte ($3\cdot10^{-3}$ M) were introduced into the different compartments of an H-shaped electrochemical cell. Oxidation of the donor was performed electrochemically (constant current density, $i = 0.5$ μA·cm^{-2}). Within 5 d, black crystals of **1** (thick blocks) grew on the anode, together with some few other diamond- and hexagonal-plate-shaped phases. − Crystals of **2** and **3** were obtained by using the same general procedure adding 18-crown-6 ($4\cdot10^{-3}$ M for **2** and $7\cdot10^{-3}$ M for **3**, respectively) with concentrations of the donor of $3\cdot10^{-4}$ M for **2** and $6\cdot10^{-4}$ M for **3**, respectively. $(NH_4)_2[RuBr_5NO]$ ($2\cdot10^{-3}$ M) and $K_2[RuCl_5NO]$ ($7\cdot10^{-3}$ M) were used as supporting electrolytes in nitrobenzene/1,2-dichloroethane (40 vol%)/ethanol (10%) for **2** and in benzonitrile/ethanol (10%) solutions for **3**. Crystals of **2** grew on the anode within 20 d (50 °C, $i = 0.5$ μA·cm^{-2}) while crystals of **3** (38 °C, $i = 1.5$ μA·cm^{-2}) grew within one month. − Conductivity measurements were performed using the standard four-probe method between room temperature and 4 K. Electrical contacts were achieved by mounting crystals on a Motorola printed circuit and gluing four gold wires on the sample with gold paint.

X-ray Crystallographic Studies: The experimental details and crystal data are listed in Table 2. The structures were solved using direct methods (SHELXS 97)[14] (**1** at 160 K, **2** at 160 K, and **3** at 193 K) and refined using full-matrix least squares on F^2. The calculations were carried out with the CRYSTALS[15] and WINGX[16] package programs running on a PC. The drawings of the molecular structures were obtained with the help of CAMERON.[17] The atomic scattering factors were taken from the International Tables for X-ray Crystallography.[18] Crystallographic data (excluding structure factors) for the structures reported in this paper have been deposited with the Cambridge Crystallographic Data Centre as supplementary publication no. CCDC-158312 (**1**), -158313 (**2**), -158314 (**3**). Copies of the data can be obtained free of charge on applica-

Table 2. Crystal data for **1**, **2**, and **3**

	θ-(BETS)$_4$[Fe(CN)$_5$NO] (**1**)	(BETS)$_2$[RuBr$_5$NO] (**2**)	(BETS)$_2$[RuCl$_5$NO] (**3**)
Empirical formula	$C_{45}H_{32}FeN_6OS_{16}Se_{16}$	$C_{20}H_{16}Br_5NORuS_8Se_8$	$C_{20}H_{16}Cl_5NORuS_8Se_8$
M	2504.92	1675.16	1452.90
Crystal system, space group	monoclinic, $C2/c$	monoclinic, $P2_1/c$	triclinic, $P\bar{1}$
a [Å]	40.259(8)	7.480(1)	8.858(2)
b [Å]	4.1768(7)	41.065(4)	10.367(2)
c [Å]	11.599(2)	12.514(1)	11.351(2)
α [°]	90	90	110.52(1)
β [°]	97.23(2)	105.00(1)	97.46(1)
γ [°]	90	90	105.46(2)
V [Å^3]	1934.9(6)	3713.0	911.7(3)
Z	1	4	1
$d_{calcd.}$ [g·cm^{-3}]	2.15	3.03	2.65
F(000)	1178	3124	680
μ(Mo-K_α) [cm^{-1}]	81.87	141.2	92.64
Data collection			
Temperature [K]	160	160	193
Diffractometer	Stoe IPDS	Stoe IPDS	Bruker Smart CCD
Scan mode	Φ	Φ	Φ and ω
Scan range Φ [°]	$0 < \Phi < 250$	$0 < \Phi < 250$	Φ = 0, 90, 180 with $-28 < \omega < 152$
No. of collected reflns.	5841	12560	14536
No. of unique reflns.	1251	2683	14536
No. of reflns. used	1013 [$I > 2\sigma(I)$]	2683 [$I > 2\sigma(I)$]	10347 [$I > 2\sigma(I)$]
R	0.082	0.0845	0.0588
wR_2	0.223	0.2674	0.1524
No. of parameters	87	397	223

tion to CCDC, 12 Union Road, Cambridge CB2 1EZ, UK [Fax: (internat.) + 44-1223/336-033; E-mail: deposit@ccdc.cam.ac.uk].

Band-Structure Calculations: The electronic band structures of the cationic layers were investigated using full tight-binding calculations based upon the effective one-electron Hamiltonian of the extended Hückel model.[19] The off-diagonal matrix elements of the Hamiltonian β_{ij} were calculated according to the modified Wolfsberg−Helmholz formula.[20] All valence electrons were explicitly treated in the calculations and the basis set, consisting in double-ζ Slater-type orbitals for C, S, Se and single-ζ Slater-type orbitals for H were taken from previous work.[11b]

Acknowledgments

The authors thank Dr. H. Gornitzka for recording data of **3**, D. Berail from Motorola Company for supplying printed circuits for conductivity measurements. M. E. S. V. thanks the CONACYT and the Instituto Tecnológico y de Estudios Superiores de Monterrey, Campus Ciudad de México for a postdoctoral grant. Support from CNRS and the Foundation for Basic Research, through an International Program for Scientific Cooperation (PICS), is gratefully acknowledged.

[1] [1a] M. Kurmoo, A. W. Graham, P. Day, S. J. Coles, M. B. Hursthouse, J. L. Caulfield, J. Singleton, F. L. Pratt, W. Hayes, L. Ducasse, P. Guionneau, *J. Am. Chem. Soc.* **1995**, *117*, 12209−12217. − [1b] P. Day, *C. R. Acad. Sci. Paris, série IIc* **1999**, *2*, 675−684, and references therein. − [1c] L. Brossard, R. Clerac, C. Coulon, M. Tokumoto, T. Ziman, D. K. Petrov, V. N. Laukhin, M. J. Naughton, A. Audouard, F. Goze, A. Kobayashi, H. Kobayashi, P. Cassoux, *Eur. Phys. J. B1* **1998**, 439−452, and references therein. − [1d] H. Kobayashi, A. Kobayashi, P. Cassoux, *Chem. Soc. Rev.* **2000**, *29*, 325−333. − [1e] E. Coronado, J. R. Galan-Mascaros, C. J. Gomez-Garcia, V. Laukhin, *Nature* **2000**, 447−449.

[2] [2a] L. Kushch, L. Buravov, V. Tkacheva, E. Yagubskii, L. Zorina, S. Khasanov, R. Shibaeva, *Synth. Met.* **1999**, *102*, 1646−1649. − [2b] M. Gener, E. Canadell, S. S. Khasanov, L. V. Zorina, R. P. Shibaeva, L. A. Kushch, E. B. Yagubskii, *Solid State Commun.* **1999**, *111*, 329−333. − [2c] L. V. Zorina, S. S. Khasanov, R. P. Shibaeva, M. Gener, R. Rousseau, E. Canadell, L. A. Kushch, E. B. Yagubskii, O. O. Drozdova, K. Yakushi, *J. Mater. Chem.* **2000**, *10*, 2017−2023. − [2d] M. Clemente-Leon, E. Coronado, J. R. Galan-Mascaros, C. Gimenez-Saiz, C. J. Gomes-Garcia, J. M. Fabre, *Synth. Met.* **1999**, *103*, 2279−2282 − [2e] M. Clemente-Leon, E. Coronado, J. R. Galan-Mascaros, C. J. Gomez-Garcia, E. Canadell, *Inorg. Chem.* **2000**, *39*, 5394−5397.

[3] [3a] P. Cassoux, C. Faulmann, B. Garreau de Bonneval, I. Malfant, S. Aonuma, M. E. Sanchez, *Synth. Met.*, in the press. − [3b] T. Courcet, Doctoral thesis. Université Paul Sabatier, Toulouse, France, **1999**.

[4] [4a] T. Woike, W. Krasser, P. Bechthold, S. Haussühl, *Phys. Rev. Lett.* **1984**, *53*, 1767−1770. − [4b] H. Zöllner, T. Woike, W. Krasser, S. Haussühl, *Z. Kristallogr.* **1989**, *188*, 139−153. − [4c] T. Woike, S. Haussühl, *Solid State Commun.* **1993**, *86*, 333−337. − [4d] M. R. Pressprich, M. A. White, V. Vekhter, P. Coppens, *J. Am. Chem. Soc.* **1994**, *116*, 5233−5238. − [4e] M. D. Carducci, M. R. Pressprich, P. Coppens, *J. Am. Chem. Soc.* **1997**, *119*, 2669−2678.

[5] [5a] R. Kato, H. Kobayashi, A. Kobayashi, *Synth. Met.* **1991**, *41−43*, 2093−2096. − [5b] T. Courcet, I. Malfant, P. Cassoux, *New J. Chem.* **1998**, 585−589.

[6] H. Kobayashi, H. Tomita, T. Naito, A. Kobayashi, F. Sakai, T. Watanabe, P. Cassoux, *J. Am. Chem. Soc.* **1996**, *118*, 368−377.

[7] The symbol θ designates a characteristic and specific type of crystal packing often encountered in BEDT-TTF radical salts; see: J. M. Williams, J. R. Ferraro, R. J. Thorn, K. D. Carlson, U. Geiser, H. H. Wang, A. M. Kini, M. H. Whangbo, *Organic*

Superconductors (including fullerenes), Prentice-Hall, Inc., Englewood Cliffs, New Jersey 07632, **1992**.

[8] M. Ogasawara, D. Huang, W. E. Streib, J. C. Huffman, N. Gallego-Planas, F. Maseras, O. Eisenstein, K. G. Caulton, *J. Am. Chem. Soc.* **1997**, *119*, 8642−8651.

[9] [9a] J. T. Veal, D. J. Hodgson, *Inorg. Chem.* **1972**, *11*, 1420−1424. − [9b] Y. N. Mikhailov, A. S. Kanishcheva, A. A. Svetlov, *Zh. Neorg. Khim.* **1989**, *34*, 2803−2806.

[10] Indeed, the Fe^{II} oxidation state is indicated by preliminary Mössbauer experiments: A. Bousseksou, personal communication.

[11] [11a] A. Kobayashi, A. Sato, E. Arai, H. Kobayashi, C. Faulmann, N. Kushch, P. Cassoux, *Solid State Commun.* **1997**, *6*, 371−374. − [11b] I. Malfant, T. Courcet, C. Faulmann, P. Cassoux, H. Gornitzka, F. Granier, M.-L. Doublet, P. Guionneau, J. A. K. Howard, N. D. Kushch, A. Kobayashi, *C. R. Acad. Sci.* **2001**, *4*, 149−160.

[12] B. Z. Narymbetov, E. Canadell, T. Togonidze, S. S. Khasanov, L. V. Zorina, R. P. Shibaeva, H. Kobayashi, *J. Mater. Chem.* **2001**, *11*, 332−336.

[13] E. E. Mercer, W. M. Campbell, R. M. Wallace, *Inorg. Chem.* **1963**, *3*, 1018−1024.

[14] G. M. Sheldrick, *SHELX97 − Programs for Crystal Structure Analysis* (Release 97-2), Institut für Anorganische Chemie der Universität, Tammanstrasse 4, Göttingen, Germany, **1998**.

[15] D. J. Watkin, C. K. Prout, J. R. Carruthers, P. W. Betteridge, *CRYSTALS*, issue 10, Chemical Crystallography Laboratory, University of Oxford, Oxford, England, **1996**.

[16] *WINGX*, Main Reference; L. J. Farrugia, *J. Appl. Crystallogr.* **1999**, *32*, 837−838.

[17] D. J. Watkin, C. K. Prout, L. J. Pearce, *CAMERON*, Chemical Crystallography Laboratory, University of Oxford, Oxford, England, **1996**.

[18] D. T. Cromer, J. T. Waber, *International Tables for X-ray Crystallography*, Kynoch Press, Birmingham, **1974**, vol. 4.

[19] R. Hoffmann, *Chem. Phys.* **1963**, *39*, 1397−1412.

[20] [20a] J. H. Ammeter, H. B. Bürgi, J. Thibeault, R. Hoffmann, *J. Am. Chem. Soc.* **1978**, *100*, 3686−3692. − [20b] M. H. Whangbo, R. Hoffmann, *J. Am. Chem. Soc.* **1978**, *100*, 6093−6098.

Received March 1, 2001
[I01075]

The First Observation and Structural Characterization of (Formamide)platinum(IV) Complexes

Nadezhda A. Bokach,[a] Stanislav I. Selivanov,[a] Vadim Yu. Kukushkin,*[a] Matti Haukka,[b] M. Fátima C. Guedes da Silva,[c,d] and Armando J. L. Pombeiro*[c]

Keywords: O ligands / N ligands / Platinum / Nitrile complexes / Structure elucidation

The reaction of *trans*-$[PtCl_4(EtCN)_2]$ and two equivalents of the formamides RR′NCHO (R/R′ = Me/Me, Me/H, *t*Bu/H) in CH_2Cl_2 led to the formation of the compounds *cis*-$[PtCl_4\{(O=)CHNRR'\}_2]$, two of which (R/R′ = Me/H, *t*Bu/H) were characterized by X-ray single-crystal diffractometry, as well as by elemental analysis, FAB$^+$-MS, and IR, ^{1}H, ^{13}C and ^{195}Pt NMR spectroscopy (including NOE, HMQC and INEPT experiments). The X-ray structures and IR spectroscopic data indicate the coordination of the formamides through the O atom and significant contribution of the bipolar structure $^-$O–C(H)=$^+$NHR in the resonance hybrid of the ligands. The complexes *cis*-$[PtCl_4\{(O=)CHNRR'\}_2]$ represent the first example of (formamide)Pt^{IV} species and also a rare case of platinum(IV) complexes with neutral O-donor ligands.

Introduction

Complexes containing weak donor ligands are essential as synthons for synthetic studies and as efficient homogeneous catalysts.[1] In recent years they have become a subject of paramount importance for the construction of multi homo- and heterometallic systems[2] with application in materials science.[3,4] Ideally, the complexes with weak donor ligands utilized in these branches of chemistry must be soluble, readily available and contain ligands which are easily replaced.[1]

As far as platinum complexes are concerned, an approach for developing compounds with weak donors includes the generation of complexes with antisymbiotic soft platinum centers and hard donor ligands, which interact only poorly and thus the weakly bound donors can be replaced by better ligands.[1,5–7] Complexes of both Pt^{II} and Pt^{IV} with *anionic* monodentate hard O-donors, for example $MeCO_2^-$, NO_2^-, NO_3^-, OH^-, SO_4^{2-}, or bidentate *anionic* hard O,O- or O,N-donors, for example carboxamidates and acetylacetonates, are common.[5] In contrast, platinum species with *neutral* O-donors are quite scarce due to the soft character of the metal centers. Moreover, if platinum(II) complexes with ligated H_2O,[5] ROH,[8] $R_2S{=}O$,[9,10] THF[11] or O-bonded formamides and amides[12] are rare, to the best of our knowledge compounds of platinum(IV) containing *neutral* O-donors are even more scarce. Indeed, apart from (aqua)Pt^{IV} [13] species only acetone[14] and (2-pyridyldiphenylphosphane oxide)platinum(IV) complexes[15] with a Pt–O interaction are known. We report herein the first representatives of O-bonded formamide-based platinum(IV) complexes and their X-ray structural characterization.

[a] Department of Chemistry, St. Petersburg State University, 198904 Stary Petergof, Russian Federation
E-mail: kukushkin@VK2100.spb.edu
[b] Department of Chemistry, P. O. Box 111, 80101, Joensuu, Finland
E-mail: Matti.Haukka@Joensuu.Fi
[c] Centro de Química Estrutural, Complexo I, Instituto Superior Técnico, Av. Rovisco Pais, 1049–001 Lisbon, Portugal
Fax: (internat.) + 351-21/846-4455
E-mail: pombeiro@ist.utl.pt
[d] Universidade Lusófona de Humanidades e Tecnologias, Campo Grande 376, 1749-024 Lisbon, Portugal
E-mail: fatima.guedes@ist.utl.pt

Results and Discussion

Our interest in the preparation of (formamide)Pt^{IV} complexes was twofold. First, this work was performed within the framework of an on-going project devoted to the search for new starting materials for platinum chemistry,[10,16] and second, we hoped to prepare new materials for the extension of our previous work on nucleophilic additions to ligands bearing double[17] and triple bonds.[2,18–20]

The reaction between *trans*-$[PtCl_4(EtCN)_2]$ and the formamides RR′NCHO in dichloromethane led to the formation of isomerically and analytically pure *cis*-$[PtCl_4\{(O=)CHNRR'\}_2]$ (R/R′ = Me/Me, Me/H, *t*Bu/H) isolated from the reaction mixture in moderate yields (ca. 40%; Scheme 1).

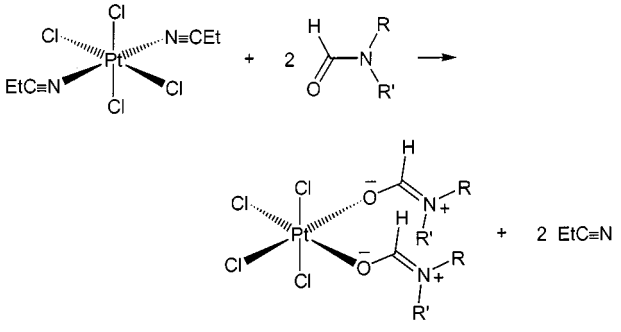

Scheme 1

 © WILEY-VCH Verlag GmbH, 69451 Weinheim, 2001 1434–1948/01/1111–2805 $ 17.50+.50/0

More *cis*-[$PtCl_4${(O=)CHNRR′}$_2$] can be obtained by the addition of diethyl ether to the filtrate, although in all three cases the solids isolated in this way were contaminated with other products which are formed, in particular, by a facile platinum(IV)-mediated hydrolysis, in the presence of traces of water to give amide[21] and ammonia species,[20,22] of the highly reactive starting nitrile complex. We also anticipate that some admixtures may be derived from the coupling of nitriles and the amines HNRR′, the latter being formed from the uncontrolled degradation of formamides, which is a well-known reaction. It is also worthwhile to mention that an attempt to perform a similar reaction between *trans*-[$PtCl_4(EtCN)_2$] and the unsubstituted formamide H_2NCHO failed due to the formation of a mixture of highly soluble products.

The structures of *cis*-[$PtCl_4${(O=)CHNHR}$_2$] (R = Me, *t*Bu) were determined by X-ray single-crystal diffraction. The coordination polyhedra of the complexes are slightly distorted octahedra (Figure 1 and 2) and the two formamide species are mutually *cis*.

An inspection of the bond lengths in the formamide ligands shows that coordination results in an increased contribution of the bipolar structure $^-O-C(H)=^+NHR$ in the resonance hybrid of the ligand, as previously observed for (dimethylformamide)Pt^{II} complexes.[11] Indeed, the C−O bond lengths [1.258(5) Å for R = Me and av. 1.271 Å for R = *t*Bu, Table 1 and 2] are longer than the C=O bond in amides (1.234 Å[24]) or in aldehydes (1.192 Å[24]), while the C−N bond [1.309(6) Å for R = Me and av. 1.305 Å for R = *t*Bu, Table 1 and 2] is shorter than that in the free amides (1.334 Å[24]).

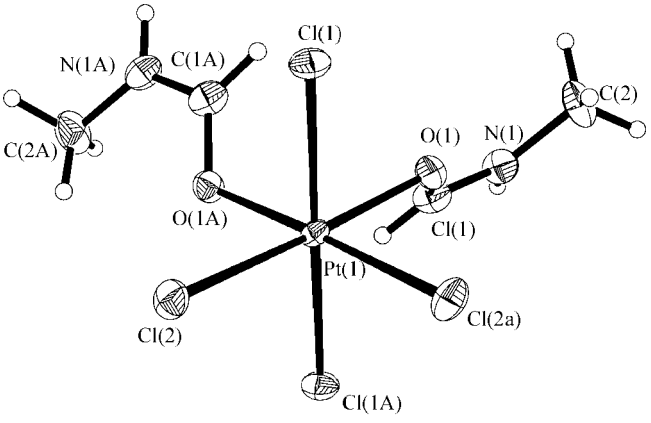

Figure 1. PLATON[23] drawing of *cis*-[$PtCl_4${(O=)CHNHMe}$_2$] with atomic numbering scheme

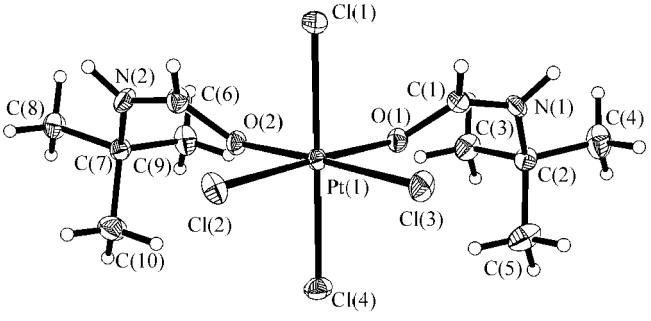

Figure 2. PLATON[23] drawing of *cis*-[$PtCl_4${(O=)CHNH*t*Bu}$_2$] with atomic numbering scheme

Table 1. Bond lengths [Å] and angles [°] for *cis*-[$PtCl_4${(O=)-CHNHMe}$_2$]

Pt−O(1)	2.057(3)	O(1)−C(1)	1.258(5)
Pt−Cl(2)	2.2788(10)	N(1)−C(1)	1.309(6)
Pt−Cl(1)	2.3106(11)	N(1)−C(2)	1.434(7)
O(1)#1−Pt−O(1)[a]	91.53(16)	Cl(2)−Pt−Cl(1)#1	90.60(4)
O(1)−Pt−Cl(2)	177.23(8)	Cl(1)−Pt−Cl(1)#1	178.81(5)
O(1)−Pt−Cl(2)#1	88.24(9)	Cl(2)−Pt−Cl(2)#1	92.11(5)
O(1)−Pt−Cl(1)	87.02(9)	C(1)−O(1)−Pt	120.2(3)
Cl(2)−Pt−Cl(1)	90.23(4)	C(1)−N(1)−C(2)	126.2(4)
O(1)−Pt−Cl(1)#1	92.15(9)	O(1)−C(1)−N(1)	120.5(5)

[a] Symmetry transformations used to generate equivalent atoms #1: $-x + 3/2$, $-y + 1$, z.

Table 2. Bond lengths [Å] and angles [°] for *cis*-[$PtCl_4${(O=)-CHNH*t*Bu}$_2$].

C(1)−O(1)	1.274(3)	C(1)−N(1)	1.300(3)
C(2)−N(1)	1.496(3)	C(2)−C(5)	1.515(3)
C(2)−C(4)	1.517(3)	C(2)−C(3)	1.526(3)
C(6)−O(2)	1.267(3)	C(6)−N(2)	1.309(3)
C(7)−N(2)	1.490(3)	C(7)−C(9)	1.517(3)
C(7)−C(10)	1.522(3)	C(7)−C(8)	1.524(3)
O(1)−Pt	2.045(2)	O(2)−Pt	2.0406(13)
Cl(1)−Pt	2.3123(5)	Cl(2)−Pt	2.2781(5)
Cl(3)−Pt	2.2783(5)	Cl(4)−Pt	2.3134(5)
O(1)−C(1)−N(1)	122.4(2)	N(1)−C(2)−C(5)	108.3(3)
N(1)−C(2)−C(4)	105.6(2)	C(5)−C(2)−C(4)	111.1(2)
N(1)−C(2)−C(3)	109.9(2)	C(5)−C(2)−C(3)	111.5(2)
C(4)−C(2)−C(3)	110.3(2)	O(2)−C(6)−N(2)	121.6(2)
N(2)−C(7)−C(9)	110.3(2)	N(2)−C(7)−C(10)	108.3(3)
C(9)−C(7)−C(10)	111.3(2)	N(2)−C(7)−C(8)	106.2(3)
C(9)−C(7)−C(8)	110.00(2)	C(10)−C(7)−C(8)	110.5(2)
C(1)−N(1)−C(2)	127.5(2)	C(6)−N(2)−C(7)	127.2(2)
C(1)−O(1)−Pt	119.55(13)	C(6)−O(2)−Pt	121.06(14)
O(2)−Pt−O(1)	87.67(6)	O(2)−Pt−Cl(2)	90.69(4)
O(1)−Pt−Cl(2)	177.03(5)	O(2)−Pt−Cl(3)	175.73(4)
O(1)−Pt−Cl(3)	89.47(4)	Cl(2)−Pt−Cl(3)	92.02(2)
O(2)−Pt−Cl(1)	91.92(5)	O(1)−Pt−Cl(1)	91.85(5)
Cl(2)−Pt−Cl(1)	90.69(2)	Cl(3)−Pt−Cl(1)	91.34(2)
O(2)−Pt−Cl(4)	85.84(5)	O(1)−Pt−Cl(4)	86.35(5)
Cl(2)−Pt−Cl(4)	91.06(2)	Cl(3)−Pt−Cl(4)	90.82(2)
Cl(1)−Pt−Cl(4)	177.18(2)		

In the IR spectra, the decrease of ν(C=O) by ca. 30−50 cm^{-1} with respect to the free ligands (see Exp. Sect.) also indicates[25] a coordination through the O atom and the contribution of the bipolar structure. It should be noted that the *cis*-geometry of the formamide compounds seems to be unusual for platinum(IV) chemistry, where in the vast majority of cases the substitution of the ligands in starting materials with a *trans* configuration gives rise to the appropriate *trans* products. Moreover, it has been reported that octahedral complexes of metals in a high oxidation state trend to isomerize from *cis* to *trans* irrespective of the nature of the ligated species.[26] In *cis*-[$PtCl_4${(O=)CHNHR}$_2$] (R = Me, *t*Bu), however, the formamides shorten the Pt−Cl

(*trans* to O) bonds [av. 2.28 Å] substantially relative to those *trans* to Cl [av. 2.31 Å]. Perhaps the *trans* Pt−O bonds do not stabilize each other to the same extent and this might be a reason for the formation of the complexes in the *cis* configuration.

The ^{1}H NMR spectra of the monoalkyl complexes *cis*-[$PtCl_4${(O=)CHNHR}$_2$] (R = Me, *t*Bu) display a =CH proton doublet resonance due to indirect coupling with the NH protons (proved by a double resonance ^{1}H{NH} experiment) with typical ^{195}Pt satellites. In both cases, NOE difference experiments showed a strong through-space interaction between the CH and NH protons of the ligated species, thus indicating the dominance of their *E*-conformation in solution. The positions of the signals in the ^{195}Pt NMR spectra of these complexes are in the normal range for other platinum(IV) compounds.

The complexes *cis*-[$PtCl_4${(O=)CHNRR′}$_2$] represent the first example of (formamide)Pt^{IV} species and also a rare case of platinum(IV) complexes with neutral O-donor ligands. Useful properties of these complexes are their good solubilities (*cis*-[$PtCl_4${(O=)CHNMe_2}$_2$], however, has a low solubility) in a number of organic solvents and also the solubility of *cis*-[$PtCl_4${(O=)CHNHMe}$_2$] in water, and these features indicate that the formamide complexes can be used for synthesis in a homogeneous liquid phase. In conclusion, it is worthwhile to mention that the (formamide)platinum(IV) complexes may be important as precursors for further synthetic work by substitution, or by addition of nucleophiles to the O=C double bond activated by the quadruply charged platinum(IV) ion; these studies are underway in our group. We hope that the useful properties of these (formamide)platinum(IV) complexes, combined with their facile synthesis, will extend the range of reactions possible in synthetic platinum(IV) chemistry.

Experimental Section

Materials and Instrumentation: The formamides were obtained from Aldrich and used as received. *trans*-[$PtCl_4(EtCN)_2$] was prepared according to a published method.[2,18] C, H and N elemental analyses were carried out by the Microanalytical Service of the Instituto Superior Técnico. Positive-ion FAB mass spectra were obtained on a Trio 2000 instrument by bombarding 3-nitrobenzyl alcohol (NBA) matrices of the samples with 8 keV (ca. 1.28×10^{15} J) Xe atoms. Mass calibration for data system acquisition was achieved using CsI. Infrared spectra (4000−400 cm^{-1}) were recorded on a BIO-RAD FTS 3000MX instrument in KBr pellets. All NMR spectra were recorded at ambient temperature on a Varian UNITY 300 [299.95, 75.42 and 64.48 MHz for ^{1}H, ^{13}C and ^{195}Pt NMR, respectively] and/or Bruker DPX−300 [300.13 and 75.47 MHz for ^{1}H and ^{13}C NMR, respectively]. An irradiating field power of 30 Hz for selective decoupling from the NH proton in double resonance experiment and a presaturation time of 1.0 s were used in the NOE-difference experiments. ^{1}H and ^{13}C chemical shifts are given relative to DMSO (δ = 2.50 and 39.5, respectively). ^{195}Pt chemical shifts are given relative to $Na_2[PtCl_6]$ ($K_2[PtCl_4]$, δ = −1630, as a standard) and the half-height line width is given in parentheses. No other sets of signals, besides those indicated below, were observed in the NMR spectra measured in [D_6]DMSO; in addition, the complexes were recovered intact from [D_6]DMSO solutions after the measurements by addition of diethyl ether, thus indicating the absence of any substitution reaction in [D_6]DMSO. This is consistent with the weak donor properties of Me_2SO towards a platinum(IV) center,[27] even though it is a good ligand for the platinum(II) ion.[28]

The inverse detection HMQC method with the BIRD sequence during the preparation period[29] was used to determine the heteronuclear spin-spin coupling constants J^{195}_{Pt}-$^{13}_{C}$. HMQC spectra were measured with a 128 × 1024 data matrix size with 256 scans per t_1 value (the delay for the creation of anti-phase magnetization was 3.5 ms and the relaxation delay was 1.0 s) and broadband ^{13}C decoupling with GARP-1[30] was applied during the acquisition (^{13}C: 90° pulse of 60 ms). The data were zero-filled in the t_1 dimension and a sine-bell filter was applied in both dimensions before the Fourier transformation. The J^1_H-$^{13}_C$ coupling constants and ^{13}C chemical shifts were obtained from the INEPT and DEPT-135 spectra.

Synthesis and Characterization. General Procedure: A solution of the formamide (0.14 mmol) in CH_2Cl_2 (0.5 mL) was added to solid *trans*-[$PtCl_4(EtCN)_2$] (0.03 g, 0.07 mmol) and the reaction mixture was heated at 35 °C for 1−2 h, whereupon crystals started to form. At this point the mixture was cooled to 15−17 °C and left to stand at this temperature for 2 days. The dark-orange crystals were filtered off, washed with three 2-mL portions of CH_2Cl_2 and dried in air at room temperature. Yields were ca. 40%.

***cis*-[$PtCl_4${(O=)CHNHMe}$_2$]:** $C_4H_{10}Cl_4N_2O_2Pt$ (455.04): calcd. C 10.58, H 2.22, N 6.16; found C 10.92, H 2.14, N 5.90. − FAB$^+$-MS: *m*/*z* = 451 [M − 3H]$^+$. − TLC on Merck 60 F_{254} SiO_2 plates: R_f = 0.64 (eluent Me_2CO/CH_2Cl_2, 1:1). − IR (KBr; selected bands): $\tilde{\nu}$ = 3347 m ν(N−H), 1638 s ν(C=O) cm^{-1} [in the free ligand ν(C=O) is found at 1668 cm^{-1}]. − ^{1}H NMR ([D_6]DMSO): δ = 2.90 (s, 3 H, Me), 8.10 (d, with ^{195}Pt-satellites on each line, J_{PtH} = 22.1 Hz, J_{HH} = 5.3 Hz, 1 H, =CH), 10.20 (br. s, 1 H, NH). − ^{13}C{^{1}H} NMR ([D_6]DMSO): δ = 32.0 (CH_3) and 173.0 ($^1J_{CH}$ = 204 Hz, $^2J_{PtC}$ = 2 Hz, =CH). − ^{195}Pt NMR ([D_6]DMSO): δ = −381 (150 Hz).

***cis*-[$PtCl_4${(O=)CHN*t*Bu}$_2$]:** $C_{10}H_{22}Cl_4N_2O_2Pt$ (539.20): calcd. C 22.28, H 4.11, N 5.20; found C 22.38, H 4.11, N 5.07. − FAB$^+$-MS: *m*/*z* = 561 [M + Na]$^+$, 539 [M]$^+$, 503 [M − Cl]$^+$, 468 [M − 2Cl]$^+$. − TLC on Merck 60 F_{254} SiO_2 plates: R_f = 0.73 (eluent Me_2CO/CH_2Cl_2, 1:1). − IR (KBr; selected bands): $\tilde{\nu}$ = 3291 m ν(N−H), 1616 s ν(C=O) cm^{-1} [in the free ligand ν(C=O) is found at 1663 cm^{-1}]. − ^{1}H NMR ([D_6]DMSO): δ = 1.34 (d, $^3J_{HH}$ = 4.8 Hz, 9 H, Me), 7.82 (d, with ^{195}Pt-satellites on each line, J_{PtH} = 23.9 Hz, J_{HH} = 4.6 Hz, 1 H, =CH), 10.26 (br. s, 1 H, NH). − ^{13}C{^{1}H} NMR ([D_6]DMSO): δ = 27.7 (CH_3), 53.7 (*t*-C), 166.9 ($^2J_{PtH}$ = 2 Hz, $^1J_{CH}$ = 204 Hz, =CH). − ^{195}Pt NMR ([D_6]DMSO): δ = −372 (150 Hz).

[$PtCl_4${(O=)CHNMe_2}$_2$]: $C_6H_{14}Cl_4N_2O_2Pt$ (483.09): calcd. C 15.03, H 2.92, N 5.85; found C 15.07, H 3.16, N 5.66. − FAB$^+$-MS: *m*/*z* = 482 [M − H]$^+$. − TLC on Merck 60 F_{254} SiO_2 plates: R_f = 0.51 (eluent Me_2CO/CH_2Cl_2, 1:1). − IR (KBr; selected bands): $\tilde{\nu}$ = 3065 w, 3005 w, and 2960 mw ν(C−H), 1638 s ν(C=O) cm^{-1} [in the free ligand ν(C=O) is found at 1687 cm^{-1} in CCl_4 [25]]. − ^{1}H NMR ([D_6]DMSO): δ = 3.07 and 3.31 (s, 3 H each, Me), 8.12 (s + d, J_{PtH} = 21.2 Hz, 1 H, =CH). The solubility of the compound is insufficient to measure ^{13}C{^{1}H} and ^{195}Pt NMR spectra even at high accumulation times.

X-ray Structure Determination: X-ray diffraction data were collected with a Nonius KappaCCD diffractometer using Mo-K_α radi-

ation (λ = 0.71073 Å). The Denzo and Scalepack[31] programs were used for cell refinements and data reduction. The structures of *cis*-[$PtCl_4${(O=)CHNHMe}$_2$] (**1**) and *cis*-[$PtCl_4${(O=)CHNH*t*Bu}$_2$] (**2**) were solved by direct methods using SIR97[32] and SHELXS-97[33] programs, respectively, with the WinGX[34] graphical user interface. The structure refinements were carried out with SHELXL-97.[35] A multi-scan absorption correction, based on equivalent reflections (XPERP in SHELXTL v5.1),[36] was applied to the data of both structure **1** (T_{max}/T_{min} 0.3812/0.2199) and structure **2** (T_{max}/T_{min} 0.2921/0.2100). In both structures the hydrogen atoms were constrained to ride on their parent atom. Selected bond lengths and angles are given in Table 1 and 2 and crystallographic data is summarized in Table 3. The crystal structures are shown in Figure 1 and 2.

Table 3. Crystallographic data for *cis*-[$PtCl_4${(O=)CHNHMe}$_2$] (**1**) and *cis*-[$PtCl_4${(O=)CHNH*t*Bu}$_2$] (**2**)

	1	**2**
Empirical formula	$C_4H_{10}Cl_4N_2O_2Pt$	$C_{10}H_{22}Cl_4N_2O_2Pt$
Fw	455.03	539.19
Temp, *K*	120	120
λ, Å	0.71073	0.71073
Crystal system	Orthorhombic	Orthorhombic
Space group	*Pcca* (No. 54)	$P2_12_12_1$ (No. 19)
a, Å	12.1606(4)	10.0686(1)
b, Å	7.1754(2)	11.7214(2)
c, Å	13.3051(4)	15.2529(2)
V, Å^3	1160.97(6)	1800.12(4)
Z	4	4
ρ_{calcd}, g/cm^3	2.603	1.990
μ(Mo-K_α), mm^{-1}	12.978	8.387
R_1 [a]	0.0241	0.0114
wR_2 [b]	0.0601	0.0268

[a] $[I > 2\sigma(I)]$; $R_1 = \Sigma||F_o| - |F_c||/\Sigma|F_o|$. – [b] $wR_2 = \{\Sigma[w(F_o^2 - F_c^2)^2]/\Sigma[w(F_o^2)^2]\}^{1/2}$.

Crystallographic data (excluding structure factors) for the structures reported in this paper have been deposited to the Cambridge Crystallographic Data Centre as supplementary publication nos. CCDC-159079 and -159080. Copies of the data can be obtained free of charge on application to CCDC, 12 Union Road, Cambridge CB2 1EZ, U. K. [Fax: (internat.) + 44-1223/336-033; E-mail: deposit@ccdc.cam.ac.uk].

Acknowledgments

N.A.B. expresses gratitude to the International Science Foundation (Soros Foundation) and also to the Centro de Química Estrutural, Complexo I, Instituto Superior Técnico, Portugal, for fellowships. V. Yu. K. thanks the PRAXIS XXI programme (grant BCC16428/98) for a grant. A.J.L.P. is indebted to the FCT (Foundation for Science and Tecnology) and the PRAXIS XXI programme for financial support. We thank Dr. D. A. Garnovskii for valuable comments on the manuscript.

[1] J. A. Davies, C. M. Hockensmith, V. Yu. Kukushkin, Yu. N. Kukushkin, *Synthetic Coordination Chemistry: Principles and Practice*, World Scientific, Singapore-New Jersey, **1996**, p. 58 and references therein; J. J. Rack, P. K. Hurlburt, P. J. Kellett, J. S. Luck, O. P. Anderson, S. H. Strauss, *Inorg. Chim. Acta* **1996**, *242*, 71.

[2] V. Yu. Kukushkin, T. B. Pakhomova, N. A. Bokach, G. Wagner, M. L. Kuznetsov, M. Galanski, A. J. L. Pombeiro, *Inorg. Chem.* **2000**, *39*, 216 and references therein.

[3] For recent experimental work see: W. E. Buschmann, J. Ensling, P. Gütlich, J. S. Miller, *Chem. Eur. J.* **1999**, *5*, 3019; W. E. Buschmann, J. S. Miller, *Inorg. Chem.* **2000**, *39*, 2411.

[4] For a recent review see: A. D. Garnovskii, A. P. Sadimenko, A. I. Uraev, I. S. Vasilchenko, D. A. Garnovskii, *Russ. J. Coord. Chem.* **2000**, *26*, 311.

[5] S. Cotton, *Chemistry of Precious Metals*, Chapman & Hall: London, **1997**, 460 pp.

[6] F. R. Hartley, *The Chemistry of Platinum and Palladium*, Applied Science Publishers: London, **1973**, p. 544; F. R. Hartley (Ed.), *Chemistry of the Platinum Group Metals*, Amsterdam, Elsevier, **1991**.

[7] S. E. Livingstone, in *Comprehensive Inorganic Chemistry* (Eds.: J. C. Bailar, H. J. Emelius, R. S. Nyholm and A. F. Trotman-Dickenson), Oxford, Pergamon, **1973**, vol. 3, p. 1274.

[8] K. Siegmann, P. S. Pregosin, L. M. Venanzi, *Organometallics* **1989**, *8*, 2659.

[9] L. I. Elding, Å. Oskarsson, *Inorg. Chim Acta* **1987**, *130*, 209.

[10] V. Yu. Kukushkin, A. J. L. Pombeiro, C. M. P. Ferreira, L. I. Elding, *Inorg. Synth.*, accepted for publication.

[11] E. Delgado, B. Donnadieu, E. Hernandez, E. Lalinde, N. Mansilla, M. T. Moreno, *J. Organomet. Chem.* **1999**, *592*, 283; I. Ara, L. R. Falvello, S. Fernandez, J. Fornies, E. Lalinde, A. Martin, M. T. Moreno, *Organometallics* **1997**, *16*, 5923; I. Ara, L. R. Falvello, J. Fornies, E. Lalinde, A. Martin, F. Martinez, M. T. Moreno, *Organometallics* **1997**, *16*, 5392; R. Uson, J. Fornies, M. A. Uson, M. Tomas, M. A. Ibanez, *J. Chem. Soc., Dalton Trans.* **1994**, 401; J. Fornies, E. Lalinde, A. Martin, M. T. Moreno, *J. Chem. Soc., Dalton Trans.* **1994**, 135.

[12] R. M. Roat, S. Yolles, A. L. Rheingold, *Inorg. Chem.* **1986**, *25*, 3102; G. Bandoli, G. Trovo, A. Dolmella, B. Longato, *Inorg. Chem.* **1992**, *31*, 45; F. D. Rochon, P. C. Kong, R. Melanson, *Can. J. Chem.* **1980**, *58*, 97; R. Cini, F. P. Intini, L. Maresca, C. Pacifico, G. Natile, *Eur. J. Inorg. Chem.* **1998**, 1305.

[13] J.-G. Uttecht, W. Preetz, *Z. Naturforsch., Teil B* **1998**, *53*, 569; H. Junicke, C. Bruhn, R. Kluge, A. S. Serianni, D. Steinborn, *J. Am. Chem. Soc.* **1999**, *121*, 6232; F. Lianza, A. Albinati, B. Lippert, *Inorg. Chim. Acta* **1997**, *255*, 313; D. Steinborn, O. Gravenhorst, C. Bruhn, D. Miklos, M. Dunaj-Jurco, A. Kolbe, *Z. Anorg. Allg. Chem.* **1997**, *623*, 1954; A. J. Canty, S. D. Fritsche, Hong Jin, R. T. Honeyman, B. W. Skelton, A. H. White, *J. Organomet. Chem.* **1996**, *510*, 281; O. Renn, B. Lippert, A. Albinati, F. Lianza, *Inorg. Chim. Acta* **1993**, *211*, 177.

[14] H. Junicke, C. Bruhn, D. Strohl, R. Kluge, D. Steinborn, *Inorg. Chem.* **1998**, *37*, 4603.

[15] F. E. Wood, M. M. Olmstead, J. P. Farr, A. L. Balch, *Inorg. Chim. Acta* **1985**, *97*, 77.

[16] L. I. Elding, Å. Oskarsson, V. Yu. Kukushkin, *Inorg. Synth.* **1997**, *31*, 276; V. Yu. Kukushkin, Å. Oskarsson, L. I. Elding, *Inorg. Synth.* **1997**, *31*, 279; V. Yu. Kukushkin, Å. Oskarsson, L. I. Elding, N. Farrell, *Inorg. Synth.* **1998**, *32*, 141; V. Yu. Kukushkin, V. M. Tkachuk, N. V. Vorobiov-Desiatovsky, *Inorg. Synth.* **1998**, *32*, 144; V. Yu. Kukushkin, Yu. A. Izotova, D. Tudela, *Inorg. Synth.* accepted for publication.

[17] V. Yu. Kukushkin, V. K. Belsky, E. A. Aleksandrova, V. E. Konovalov, G. A. Kirakosyan, *Inorg. Chem.* **1992**, *31*, 3836. V. Yu. Kukushkin, V. K. Belsky, D. Tudela, *Inorg. Chem.* **1996**, *35*, 510.

[18] G. Wagner, A. J. L. Pombeiro, V. Yu. Kukushkin, *J. Am. Chem. Soc.* **2000**, *122*, 3106; G. Wagner, M. Haukka, J. J. R. Fraústo da Silva, A. J. L. Pombeiro, V. Yu. Kukushkin, *Inorg. Chem.* **2001**, *40*, 264; C. M. P. Fereira, M. F. C. Guedes da Silva, J. J. R. Fraústo da Silva, A. J. L. Pombeiro, V. Yu. Kukushkin, R. A. Michelin, *Inorg. Chem.* **2001**, *40*, 1134; V. Yu. Kukushkin, T. B. Pakhomova, Yu. N. Kukushkin, R. Herrmann, G. Wagner, A. J. L. Pombeiro, *Inorg. Chem.* **1998**, *37*, 6511.

[19] V. Yu. Kukushkin, I. V. Ilichev, G. Wagner, J. J. R. Fraústo da

Silva, A. J. L. Pombeiro, *J. Chem. Soc., Dalton Trans.* **1999**, 3047; G. Wagner, A. J. L. Pombeiro, N. A. Bokach, V. Yu. Kukushkin, *J. Chem. Soc., Dalton Trans.* **1999**, 4083; V. Yu. Kukushkin, I. V. Ilichev, M. A. Zhdanova, G. Wagner, A. J. L. Pombeiro, *J. Chem. Soc., Dalton Trans.* **2000**, 1567; D. A. Garnovskii, V. Yu. Kukushkin, M. Haukka, G. Wagner, A. J. L. Pombeiro, *J. Chem. Soc., Dalton Trans.* **2001**, 560.

[20] M. L. Kuznetsov, N. A. Bokach, V. Yu. Kukushkin, T. Pakkanen, G. Wagner, A. J. L. Pombeiro, *J. Chem. Soc., Dalton Trans.* **2000**, 4683.

[21] K. V. Luzyanin, N. A. Bokach, V. Yu. Kukushkin, M. Haukka, A. J. L. Pombeiro, unpublished results.

[22] V. Yu. Kukushkin, I. G. Zenkevich, V. K. Belsky, V. E. Konovalov, A. I. Moiseev, E. O. Sidorov, *Inorg. Chim. Acta* **1989**, *166*, 79; V. Yu. Kukushkin, V. M. Tkachuk, *Z. Anorg. Allg. Chem.* **1992**, *613*, 123.

[23] A. L. Spek, *PLATON*, A Multipurpose Crystallographic Tool, Utrecht University, Utrecht, The Netherlands, 2000. A. L. Spek, *Acta Crystallogr., Sect. A* **1990**, *46*, C34.

[24] F. H. Allen, O. Kennard, D. G. Watson, L. Brammer, A. G. Orpen, R. Taylor, *J. Chem. Soc., Perkin Trans. 2* **1987**, S1; A. G. Orpen, L. Brammer, F. H. Allen, O. Kennard, D. G. Watson, R. Taylor, *J. Chem. Soc., Dalton Trans.* **1989**, S1.

[25] D. Tudela, *J. Chem. Educ.* **1994**, *71*, 1083.

[26] V. Yu. Kukushkin, *Zh. Neorg. Khim.* **1988**, *33*, 1905; *Russ. J. Inorg. Chem. (Engl. Transl.)* **1988**, *33*, 1085.

[27] V. K. Belsky, V. Yu. Kukushkin, V. E. Konovalov, A. I. Moiseev, V. N. Yakovlev, *Zh. Obsch. Khim.* **1990**, *60*, 2180; *J. Gen. Chem. (Engl. Transl.)*, **1990**, *60*, 1947. V. Yu. Kukushkin, V. K. Belsky, E. A. Aleksandrova, E. Yu. Pankova, V. E. Konovalov, V. N. Yakovlev, A. I. Moiseev, *Zh. Obsch. Khim.* **1991**, *61*, 318; *J. Gen. Chem. (Engl. Transl.)*, **1991**, *61*, 284.

[28] J. A. Davies, *Adv. Inorg. Chem. Radiochem.* **1981**, *24*, 115. H. B. Kagan, B. Ronan, *Rev. Heteroatom Chem.* **1992**, *7*, 92.

[29] A. Bax, S. Sabramanian, *J. Magn. Reson.* **1986**, *67*, 565.

[30] A. J. Shaka, P. B. Barker, R. Freeman, *J. Magn. Reson.* **1985**, *64*, 547.

[31] Z. Otwinowski, W. Minor, in *Methods in Enzymology*, *Volume 276*, *Macromolecular Crystallography, part A* (Eds.: C. W. Carter, Jr. and R. M. Sweet), Academic Press, **1997**, pp. 307−326.

[32] A. Altomare, M. C. Burla, M. Camalli, G. L. Cascarano, C. Giacovazzo, A. Guagliardi, A. G. G. Moliterni, G. Polidori, R. Spagna, *J. Appl. Cryst.* **1999**, *32*, 115.

[33] G. M. Sheldrick, SHELXS-97, University of Göttingen, Göttingen, Germany, **1997**.

[34] L. J. Farrugia, *J. Appl. Cryst.* **1999**, *32*, 837.

[35] G. M. Sheldrick, SHELXL-97, University of Göttingen, Göttingen, Germany, **1997**.

[36] G. M. Sheldrick, *SHELXTL* Version 5.1, Bruker Analytical X-ray Systems, Bruker AXS, Inc. Madison, Wisconsin, USA, **1998**.

Received May 14, 2001
[I01169]

Diamond-Shaped Heterometallic Complexes of Iron(II) and Copper(I) Bridged by Cyanide Groups Containing Monodentate or Bidentate Phosphanes Bound to Copper(I), Including an Alternative Structure Based on the Nature of the Bidentate Phosphane Ligand

Donald J. Darensbourg,*[a] Way-Zen Lee,[a] M. Jason Adams,[a] and Jason C. Yarbrough[a]

Keywords: Copper / Iron / P ligands / Cyanides / Bridging ligands

The diamond-shaped heterometallic cyanide-bridged complex of iron(II) and copper(I), $[CpFe(CO)(\mu\text{-}CN)_2Cu(CH_3CN)_2]_2$ (**1**), has been synthesized from the reaction of $K[CpFe(CO)(CN)_2]$ and $[Cu(CH_3CN)_4][BF_4]$ in acetonitrile. Upon the addition of 2–4 equivalents of phosphane ligands to complex **1**, the coordination geometry of the copper centers can be varied from trigonal planar as in $[CpFe(CO)(\mu\text{-}CN)_2Cu(PCy_3)]_2$ (**2**), to tetrahedral as found in $[CpFe(CO)(\mu\text{-}CN)_2Cu(PCy_3)_2]_2$ (**3**). Analogous derivatives containing other phosphane ligands, namely PMe_3, P(*p*-tolyl)$_3$, PMe_2Ph, and PPh_2Me have been synthesized as well. Prolonged exposure of complex **3** in CH_2Cl_2 to excess PCy_3 has provided the bimetallic complex $[CpFe(PCy_3)(CN)(\mu\text{-}CN)Cu(PCy_3)_2]$ (**4**), where the metal aggregate is disrupted and PCy_3 has displaced CO at the iron center. Bidentate phosphane analogs of complex **3** have been prepared by adding two equivalents of dcpe [bis(dicyclohexylphosphanyl)-ethane] or dcpp [bis(dicyclohexylphosphanyl)propane] to complex **1**. The solid-state structures of several of these diamond-shaped derivatives, in addition to complex **4**, have been determined by X-ray crystallography. The overlapping diamond-shaped $[Fe_2(CN)_4Cu_2]$ cores, which form channels within the solids, are blocked by bulky, copper-bound phosphane ligands such as PCy_3. However, in the case of the small phosphane PMe_3, or the chelating phosphanes dcpe and dcpp, these channels are not blocked by the phosphane ligands; solvent molecules occupy the channels created by the overlapping metal cores instead. Alternatively, the complex $[CpFe(CO)(CN)(\mu\text{-}CN)Cu(dcpm)]_2$ (**13**), derived from bis(dicyclohexylphosphanyl)methane(dcpm), possesses two copper(I) centers, each in a distorted trigonal coordination geometry, bridged by two dcpm ligands to form an eight-membered metallacycle with a short $Cu^I\cdots Cu^I$ separation of 2.844 Å. The third ligand completing each copper's coordination sphere is a nitrogen-bound bridging cyanide group from a $CpFe(CO)(CN)_2^-$ anion.

Introduction

The use of linkage groups for assembling multinuclear complexes has been extensively investigated. A variety of polygons of transition metal complexes has been created using different linkage groups.[1] Among these, molecular squares are the most common of the metallacyclic polygons which have been prepared and structurally characterized. Included in these are one-, two-, and three-dimensional complexes which have been synthesized employing bridging cyanide groups of $M_x(CN)_y$ building blocks.[2–25] Recently, the research groups of Rauchfuss,[26] and Long[27] have reported remarkable molecular boxes, cages, and clusters made from $M(CN)_3$ or $M_6Q_6(CN)_6$ (Q = S, Se, or Te) building blocks. Other studies ranging from the electronic communication between metal atoms, i.e. electron transfer, mixed-valence, and magnetic interactions,[28] to the understanding of cyanide's role as a respiratory inhibitor in heme-copper oxidases, involve the investigation of metal cyanide complexes.[29]

Recently, we have communicated our initial investigations of the synthesis and characterization of diamond-shaped heterometallic cyanide-bridged complexes of iron(II) and copper(I) with tricyclohexylphosphane ligands coordinated to the copper(I) centers.[30] These studies showed that the coordination geometries of the copper(I) centers in the complexes $[CpFe(CO)(\mu\text{-}CN)_2Cu(PCy_3)_n]_2$ (Cp = η^5-C_5H_5; n = 1 or 2) vary from trigonal planar (n = 1) to tetrahedral (n = 2) upon the addition of a phosphane ligand. Herein we elaborate upon these investigations employing a variety of monodentate and bidentate phosphanes. Hopefully, these results will yield the necessary knowledge to allow us to expand our studies to dimeric cyanide-bridged complexes of iron(II) and zinc(II), the latter of which may serve to mimic the double metal cyanide (DMC) catalysts employed in the homopolymerization of epoxides or the copolymerization of CO_2/epoxides.[31]

Results and Discussion

Synthesis and Infrared Spectroscopy

Upon reacting $K[CpFe(CO)(CN)_2]$ (Cp = η^5-C_5H_5) with $[Cu(CH_3CN)_4][BF_4]$ in acetonitrile at ambient temperature, a clear yellow solution of $[CpFe(CO)(\mu\text{-}CN)_2Cu(CH_3CN)_2]_2$ (**1**) and a fine pale gray solid of KBF_4 were formed immediately. Two CN and one CO absorption bands in the infrared spectrum of complex **1** were observed at higher frequencies [2125 sh, 2118**s** (ν_{CN}); 1974 vs cm^{-1}

[a] Department of Chemistry, Texas A&M University, P. O. Box 30012, College Station, Texas, 77842-3012, USA

 © WILEY-VCH Verlag GmbH, 69451 Weinheim, 2001 1434–1948/01/1111–2811 $ 17.50+.50/0

Table 1. Infrared spectroscopic data in ν_{CN} and ν_{CO} regions

Compound	Condition	ν_{CN} (cm^{-1})	ν_{CO} (cm^{-1})
$K[CpFe(CO)(CN)_2]$	CH_3CN	2094 w, 2088 w	1949 vs
	KBr	2095 w, 2085 w	1973 s, 1954 s
$[CpFe(CO)(\mu\text{-}CN)_2Cu(CH_3CN)_2]_2$ (**1**)	CH_3CN	2125 sh, 2118 s	1974 vs
	CH_2Cl_2	2137 s, 2123 s	1990 vs
	KBr	2131 sh, 2118 s	1981vs
$[CpFe(CO)(\mu\text{-}CN)_2Cu(PPh_3)_{1\ or\ 2}]_2$ (**1a**)	KBr	2118 sh, 2112 s	1964 vs
$[CpFe(CO)(\mu\text{-}CN)_2Cu(PCy_3)]_2$ (**2**)	CH_2Cl_2	2115 s	1974 vs
$[CpFe(CO)(\mu\text{-}CN)_2Cu(PCy_3)_2]_2$ (**3**)	CH_3CN	2105 s, 2095 s	1959 vs
	CH_2Cl_2	2105 s, 2093 s	1963 vs
$[CpFe(PCy_3)(CN)(\mu\text{-}CN)_2Cu(PCy_3)_2]$ (**4**)	CH_2Cl_2	2062 s, 2049 s	
$[CpFe(CO)(\mu\text{-}CN)_2Cu\{P(p\text{-tolyl})_3\}]_2$ (**5**)	CH_3CN	2120 sh, 2114 s	1970 vs
	CH_2Cl_2	2127 s, 2114 s	1983 vs
$[CpFe(CO)(\mu\text{-}CN)_2Cu\{P(p\text{-tolyl})_3\}_2]_2$ (**6**)	CH_3CN	2112 s	1964 vs
	CH_2Cl_2	2121 s, 2095 sh	1970 vs
	THF	2120 s	1968 vs
$[CpFe(CO)(\mu\text{-}CN)_2Cu(PMePh_2)]_2$ (**7**)	CH_3CN	2114 s	1970 vs
$[CpFe(CO)(\mu\text{-}CN)_2Cu(PMe_2Ph)]_2$ (**8**)	CH_3CN	2115 s	1971 vs
$[CpFe(CO)(\mu\text{-}CN)_2Cu(PMe_3)]_2$ (**9**)	CH_3CN	2115s	1971 vs
	CH_2Cl_2	2119s	1977 vs
$[CpFe(CO)(\mu\text{-}CN)_2Cu(PMePh_2)_2]_2$ (**10**)	CH_3CN	2110 m, 2095 s	1958 vs
$[CpFe(CO)(\mu\text{-}CN)_2Cu(PMe_2Ph)_2]_2$ (**11**)	CH_3CN	2110 m, 2095 s	1956 vs
$[CpFe(CO)(\mu\text{-}CN)_2Cu(PMe_3)_2]_2$ (**12**)	CH_3CN	2110 m, 2095 s	1956 vs
	CH_2Cl_2	2108 s, 2092 s	1963 vs
$[CpFe(CO)(CN)(\mu\text{-}CN)Cu(dcpm)]_2$ (**13**)	CH_2Cl_2	2101, 2092	1964
$[CpFe(CO)(\mu\text{-}CN)_2Cu(dcpe)]_2$ (**14**)	CH_2Cl_2	2121, 2111	1970
$[CpFe(CO)(\mu\text{-}CN)_2Cu(dcpp)]_2$ (**15**)	CH_2Cl_2	2111, 2093	1964
$[CpFe(CO)(\mu\text{-}CN)_2Cu(dcpb)]_{2v}$ (**16**)	CH_2Cl_2	2108, 2093	1965

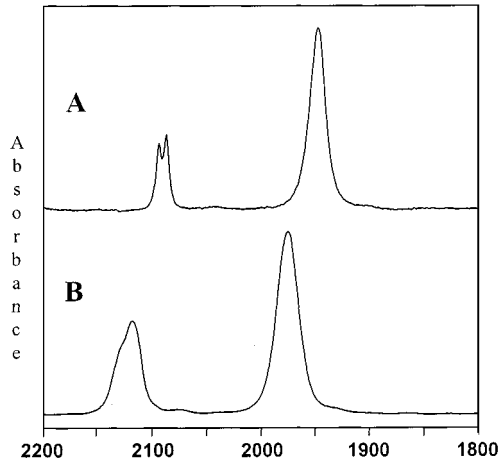

Figure 1. Infrared spectra of: **A**: [K][CpFe(CO)$(CN)_2$], and **B**: $[CpFe(CO)(\mu\text{-}CN)_2Cu(CH_3CN)_2]_2$

(ν_{CO}), Table 1] than in the parent anion $CpFe(CO)(CN)_2^-$. The absolute intensity of the ν_{CN} bands vs. that of the CO stretching vibration of **1** was increased by a factor of 2.1 times that of the corresponding bands in the parent anion (Figure 1).

The greater intensities and higher frequencies of the CN bands are evidence that the CN groups of the $CpFe(CO)(CN)_2^-$ unit are ligated to Cu^I centers in complex **1**. Two acetonitrile molecules are expected to complete each copper's coordination sphere. When the reaction was carried out in dichloromethane, free acetonitrile was observed in the infrared spectrum of the resulting solution, with the CN and CO bands being shifted to higher frequencies (Figure 2). These observations indicate that the acetonitrile molecules are dissociated from the copper(I) centers in dichloromethane solution, thereby making the metal more electron deficient. This in turn leads to a significant withdrawal of electron density from the nitrogens of the bridging cyanides to the Cu^I centers, and the frequencies of the CN and CO vibrational modes are shifted to significantly higher frequencies than those seen in complex **1**. Nevertheless, it is most likely that in this instance there are weak Cu···Cl interactions with dichloromethane. In the absence of strongly coordinating solvents, the complex was unstable under an argon atmosphere and decomposed within 3−4 h.

A turbid solution resulted immediately upon adding triphenylphosphane to an acetonitrile solution of **1**, with subsequent formation of a yellow solid after several minutes of stirring at ambient temperature. The isolated yellow solid was found to be insoluble in all common organic solvents. However, the solid-state infrared spectrum of this material (**1a**) exhibited ν_{CN} and ν_{CO} vibrational modes of lower frequencies than those observed in complex **1**, and hence indicate the binding of PPh_3 ligands at the copper(I) centers. In order to obtain an analogous complex which was soluble in organic solvent, complex **1** was reacted with tricyclohexylphosphane. In this manner, two complexes, $[CpFe(CO)(\mu\text{-}CN)_2Cu(PCy_3)]_2$ (**2**) and $[CpFe(CO)(\mu\text{-}CN)_2Cu(PCy_3)_2]_2$ (**3**), were synthesized by the reaction of **1** with two or four equivalents of PCy_3, respectively.[30] Whereas, complex **2** precipitated directly from the acetonitrile reaction solution,

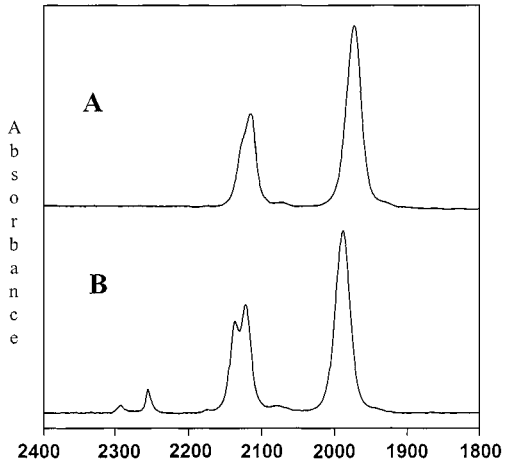

Figure 2. Infrared spectra of: **A** $[CpFe(CO)(\mu\text{-}CN)_2Cu(CH_3CN)_2]_2$, and **B**: $[CpFe(CO)(\mu\text{-}CN)_2Cu]$

complex **3** remained in solution; both derivatives were readily soluble in dichloromethane. As seen in Table 1, the ν_{CN} and ν_{CO} bands progressively shift to lower frequencies in proceeding from complex **1** to **2** and **3**, consistent with one and two equivalents of PCy_3 binding to the Cu^I centers. The subsequent addition of PCy_3 to complex **3** in dichloromethane with stirring over a period of time affords a complex devoid of any CO ligand which has been characterized as $[CpFe(PCy_3)(CN)(\mu\text{-}CN)Cu(PCy_3)_2]$ (**4**) (vide infra). Scheme 1 summarizes the sequence of reactions employed in the synthesis of **2** and **3** and other phosphane analogs, along with further reaction pathways of these derivatives.

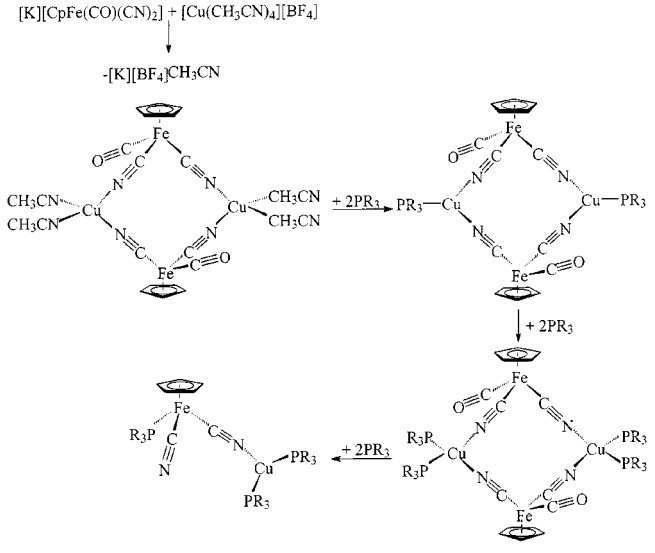

Scheme 1

In an effort to prepare soluble derivatives containing a phosphane ligand that closely mimics the electronic and steric properties of PPh_3, we synthesized the $P(p\text{-tolyl})_3$ derivatives. Upon adding two equivalents of $P(p\text{-tolyl})_3$ to complex **1** in acetonitrile, a yellow solution of $[CpFe(CO)(\mu\text{-}CN)_2Cu\{P(p\text{-tolyl})_3\}]_2$ (**5**) was obtained. Unfortunately, complex **5** was unstable in acetonitrile or dichloromethane solution, even when maintained at 10 °C. In contrast, the addition of four equivalents of $P(p\text{-tolyl})_3$ to **1** in acetonitrile resulted in the formation of a precipitate of $[CpFe(CO)(\mu\text{-}CN)_2Cu\{P(p\text{-tolyl})_3\}_2]_2$ (**6**), which was stable when redissolved in either THF or dichloromethane. The conversion of complex **6** to the bimetallic complex $[CpFe\{P(p\text{-tolyl})_3\}(CN)(\mu\text{-}CN)Cu\{P(p\text{-tolyl})_3\}]_2$, in the presence of added equivalents of $P(p\text{-tolyl})_3$ in dichloromethane (ν_{CN} = 2086 sh, 2073 s cm^{-1}) proceeded more rapidly (only four days) than the corresponding process involving **3** and PCy_3. In addition the reaction of two or four equivalents of the series of phosphanes PMe_nPh_{3-n} (n = 1, 2, or 3) with complex **1** in dichloromethane have similarly provided the mono- and bisphosphane-substituted copper(I) derivatives **7**, **9**, **11**, and **8**, **10**, **12**, respectively. As is evident from the vibrational data in Table 1, the basicity of the phosphane ligand, which varies significantly from PMe_3 to PPh_2Me, has a negligible effect on the ν_{CN} and ν_{CO} values observed. Complexes **8**, **10**, and **12** were found to react more rapidly with added equivalents of the corresponding phosphane ligand to provide the bimetallic complex than previously observed for other complexes. For example, complex **12** was quantitatively converted in the presence of PMe_3 into $[CpFe(PMe_3)(CN)(\mu\text{-}CN)Cu(PMe_3)_2]$ in two days. When eight equivalents of PMe_nPh_{3-n} (n = 1, 2, or 3) were added directly to complex **1** in dichloromethane, the infrared spectra of the products were consistent with complete disruption of the parallelogram structures with concomitant formation of the $[Cu(PMe_nPh_{3-n})_4]$-$[CpFe(CO)(CN)_2]$ salts.

In studies designed to examine the nature of the complex formed when the monodentate tricyclohexylphosphane is replaced by its bidentate analogs $Cy_2P\text{-}(CH_2)_n\text{-}PCy_2$, we synthesized the derivatives where n varies from 1 to 4 in an identical manner. Infrared spectroscopic data in the ν_{CO} and ν_{CN} regions for the derivatives of dcpm [bis(dicyclohexylphosphanyl)methane] (**13**), dcpe [1,2-bis(dicyclohexylphosphanyl)ethane] (**14**), and dcpp [bis(dicyclohexylphosphanyl)propane] (**15**) are quite similar (Table 1). Furthermore, these derivatives were shown by elemental analysis to be stoichiometrically of the same composition. The most distinguishing spectral feature noted between complex **13** and complexes **14** and **15** is the magnitude of the downfield shift of the ^{31}P NMR resonance of the bisphosphane ligand upon complexation to copper(I): whereas the ^{31}P NMR shift is significantly different from that of the free phosphane in complex **13** (by 16 ppm), in complexes **14** and **15** the chemical shift difference is only 0.9−1.2 ppm (see Table 2).

X-ray Crystal Structures

X-ray quality crystals of **2** were obtained upon the slow diffusion of acetonitrile into a dichloromethane solution of the complex over several days at 10 °C. Under similar conditions, yellow or yellow-orange crystals of complexes **3**, **6**, **12**, and **15** were obtained from THF/hexane, and orange crystals of **4**, **13**, and **14** from dichloromethane/diethyl

Table 2. ^{31}P NMR spectroscopic data

Compound[a]	δ, ppm
PCy_3	10.86
$[CpFe(CO)(\mu\text{-}CN)_2Cu(PCy_3)]_2$ (**2**)	15.16
$[CpFe(CO)(\mu\text{-}CN)_2Cu(PCy_3)_2]_2$ (**3**)	11.74
$[CpFe(PCy_3)(CN)(\mu\text{-}CN)_2Cu(PCy_3)_2]$ (**4**)	80.16, 12.00
$PMePh_2$	−26.65
$[CpFe(CO)(\mu\text{-}CN)_2Cu(PMePh_2)]_2$ (**7**)	−22.08
$[CpFe(CO)(\mu\text{-}CN)_2Cu(PMePh_2)_2]_2$ (**10**)	−20.06
PMe_2Ph	−45.01
$[CpFe(CO)(\mu\text{-}CN)_2Cu(PMe_2Ph)]_2$ (**8**)	−35.48
$[CpFe(CO)(\mu\text{-}CN)_2Cu(PMe_2Ph)_2]_2$ (**11**)	−32.95
PMe_3	−60.96
$[CpFe(CO)(\mu\text{-}CN)_2Cu(PMe_3)]_2$ (**9**)	−47.48
$[CpFe(CO)(\mu\text{-}CN)_2Cu(PMe_3)_2]_2$ (**12**)	−44.79
dcpm	−9.93
$[CpFe(CO)(CN)(\mu\text{-}CN)Cu(dcpm)]_2$ (**13**)	6.20
dcpe	2.25
$[CpFe(CO)(\mu\text{-}CN)_2Cu(dcpe)]_2$ (**14**)	3.10
dcpp	−5.55
$[CpFe(CO)(\mu\text{-}CN)_2Cu(dcpp)]_2$ (**15**)	−6.71
dcpb	−4.30
$[CpFe(CO)(\mu\text{-}CN)_2Cu(dcpb)]_2$ (**16**)	−0.82

[a] Spectra determined in dichloromethane at ambient temperature.

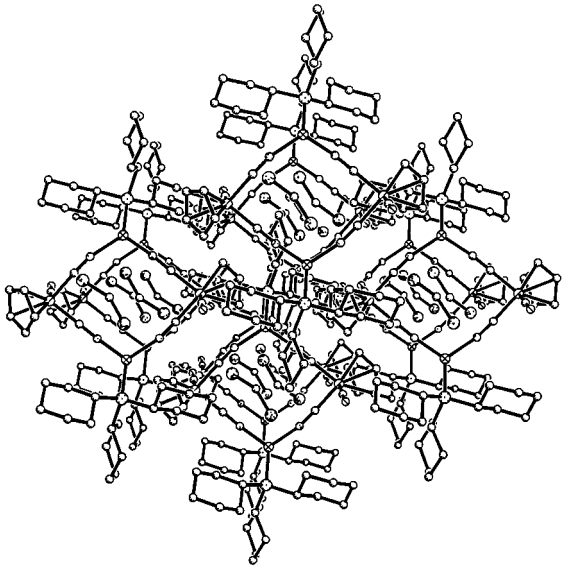

Figure 3. Crystal packing diagram of $[CpFe(CO)(\mu\text{-}CN)_2Cu(PCy_3)]_2$ (**2**)

ether. The solid-state structures of **2**, **3**, **4**, **6**, and **12**−**15** were determined by X-ray crystallographic analysis. Selected bond lengths and angles of **2**, **3**, **4**, **6**, **12**−**15** are listed in Table 3. Figure 3 presents a crystal packing diagram of complex **2**, and Figure 4 shows a thermal ellipsoid drawing of complex **3**. Complexes **2** and **3** possess a diamond-shaped motif composed of two $\eta^5\text{-}C_5H_5Fe(CO)$ fragments, two Cu^I centers, and four bridging CN groups. Due to the addition of phosphane ligands, the coordination geometry about the copper(I) centers of **2** and **3** are trigonal planar and tetrahedral, respectively. As anticipated, upon increasing the coordination number of the copper centers from three to four, i.e., proceeding from complex **2** to **3**, the average Cu−P and Cu−N bond lengths are lengthened by about 0.1 Å. As seen in Figure 4, the diamond-shaped core of complex **3** was found to be partially blocked by the cyclohexyl groups from phosphane ligands. This steric hindrance is not observed in complex **2** or in the chelated bisphosphane derivatives (vide infra). Figure 3 shows the packing diagrams for complex **2**, where solvent molecules (CH_2Cl_2) lie between the overlapping diamonds that form channels within the solids. Complex **2** is the only structurally characterized of these species that has a trigonal Cu^I center. Presumably due to the sterically encumbering PCy_3 ligand, which has a cone angle of 179°,[32] complex **2** is stabilized by filling up the coordination space of the copper centers with PCy_3. We were not able to crystallize other derivatives from solution. The insert in Figure 4 illustrates another interesting feature of the solid-state structure of **3**: the disorder of the $\eta^5\text{-}C_5H_5Fe$ fragments. This type of disorder is also found in the solid-state structure of complex **6**. This is illustrated in Figure 5, which shows that complex **6** has a structure similar to complex **3**; the ball-stick drawing of the $\eta^5\text{-}C_5H_5Fe$ disorder of complex **6** is provided as the insert of Figure 5.

Table 3. Selected bond lengths (Å) and bond angles (deg) for complexes **2**−**4**, **6** and **12**−**15**

	2	**3**	**4**	**6**	**12**	**13**	**14**	**15**
Cu−N(1)	1.957(3)	2.036(3)	1.943(9)	2.028(3)	2.032(4)	1.994(3)	1.974(5)	2.004(3)
Cu−N(2)	1.953(4)	2.020(4)	−	2.008(3)	2.010(4)		1.977(5)	1.992(3)
Cu−P(1)	2.206(2)	2.2958(10)	2.233(3)	2.2814(9)	2.2454(16)	2.2473(11)	2.2462(17)	2.2542(9)
Cu−P(2)	−	2.2622(10)	2.236(3)	2.2474(9)	2.2369(15)	2.2626(11)	2.2478(16)	2.2494(9)
Fe−C(1)	1.886(4)	1.875(5)	1.854(10)	1.923(5)	1.898(5)	1.880(4)	1.890(6)	1.898(3)
Fe−C(2)	1.897(4)	1.882(5)	1.870(13)	1.888(5)	1.901(5)	1.900(5)	1.891(6)	1.900(3)
Fe−C(3)	1.750(4)	1.737(12)	−	1.801(6)	1.731(6)	1.788(5)	1.755(6)	1.749(3)
$Fe-C_{Cp}$ (av.)	2.101	2.008	2.092	2.056	2.091	2.075	2.096	2.099
P(1)−Cu−P(2)	−	127.75(4)	139.54(11)	121.21(3)	118.71(6)	144.26(4)	92.49(6)	104.67(3)
N(1)−Cu−N(2)	109.33(13)	100.58(14)	−	106.78(11)	103.04(16)		103.93(19)	101.98(11)
Cu−N−C (av.)	160.4	166.7	166.5(9)	162.9	174.7	158.3(3)	178.9(5)	172.1(3)
Fe−C−N (av.)	175.5	178.4	172.9(10)	171.1	176.9	175.4(4)	176.9(5)	179.1(3)

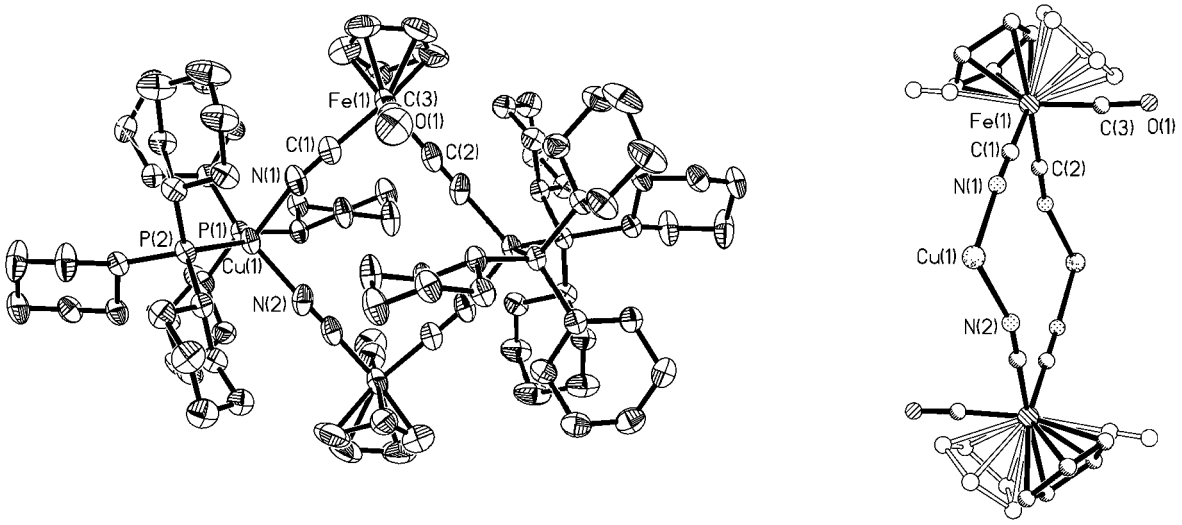

Figure 4. Thermal ellipsoid representation of $[CpFe(CO)(\mu\text{-}CN)_2Cu(PCy_3)_2]_2$ (**3**)

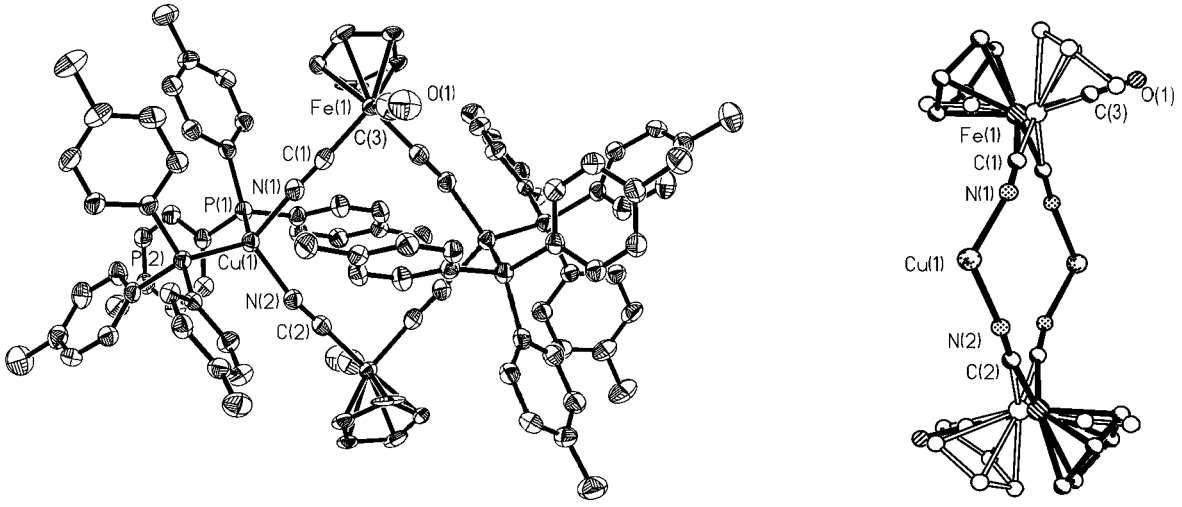

Figure 5. Thermal ellipsoid representation of $[CpFe(CO)(\mu\text{-}CN)_2Cu(P\text{-}p\text{-}totyl_3)_2]_2$ (**6**)

As previously mentioned, the prolonged exposure of complex **3** to PCy_3 in CH_2Cl_2 affords the bimetallic complex **4**, which does not contain a CO ligand bound to iron. The thermal ellipsoid representation of complex **4** is depicted in Figure 6. A tricyclohexylphosphane, a terminal CN ligand, and the bridging CN group occupy the remaining coordination sites of the CpFe moiety. The coordination geometry about the Cu^I center is trigonal, and the copper's coordination sphere is completed by the bridging CN group and two PCy_3 ligands. Apparently, complex **4** is synthesized by the substitution of CO with PCy_3 on the iron centers of **3** and the cleavage of one Cu^I-N bond on each copper center of complex **3**. The average Cu−P bond length in complex **4** (2.235 Å) is slightly shorter than those found in complex **3** (2.279 Å). Similarly, the Cu−N bond length of 1.943(9) Å is shorter than the average Cu−N bond length in **3** (2.028 Å). These bond length trends are the same as those observed in proceeding from **2** to **3**, that is, when the coordination number of copper increases from three to four. By comparing the two trigonal Cu^I centers of complexes **2** and **4**, the average Cu−P bond length in **4** (2.235 Å) is slightly longer than that in **2** [2.206(2) Å], whereas, the Cu−N bond length in **4** [1.943(9) Å] is shorter than that in **2** (1.955 Å on average). As expected, the P(I)−Cu−P(2) bond angle in complex **4** [139.54(11)°] is much larger than that found in **3** [127.75(4)°]. The bonding mode of Fe−C≡N−Cu in complex **4** is nonlinear, with Fe−C(1)−N(1) and C(1)−N(1)−Cu bond angles of 172.9(10) and 166.5(9)°, respectively.

Figure 7 shows a thermal ellipsoid drawing of $[CpFe(CO)(\mu\text{-}CN)_2Cu(PMe_3)_2]_2$ (**12**), where the basic metal cyanide core structure is similar to those seen in the other bis-bimetallic derivatives. However, in this instance the Cp and carbonyl ligands were not disordered about the $[Fe(CN)_2Cu]_2$ plane.

Furthermore, unlike the bis tricyclohexylphosphane and $P(p\text{-tolyl})_3$ analogs, the sterically less demanding PMe_3 ligands do not block the entrance to the diamond-shaped core. Instead, solvent molecules are able to occupy the channels created by the overlapping diamonds as in com-

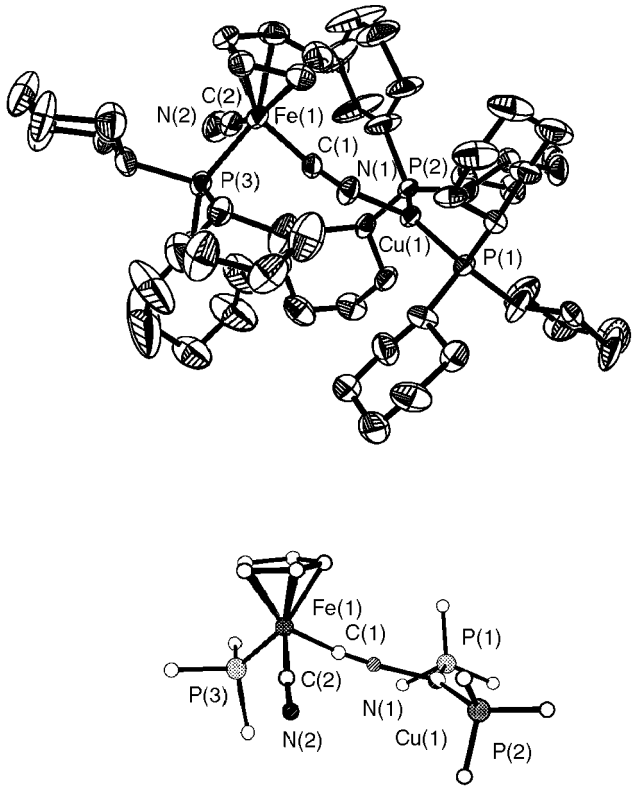

Figure 6. Thermal ellipsoid representation of $CpFe(PCy_3)(CN)(\mu\text{-}CN)Cu(PCy_3)_2$ (**4**)

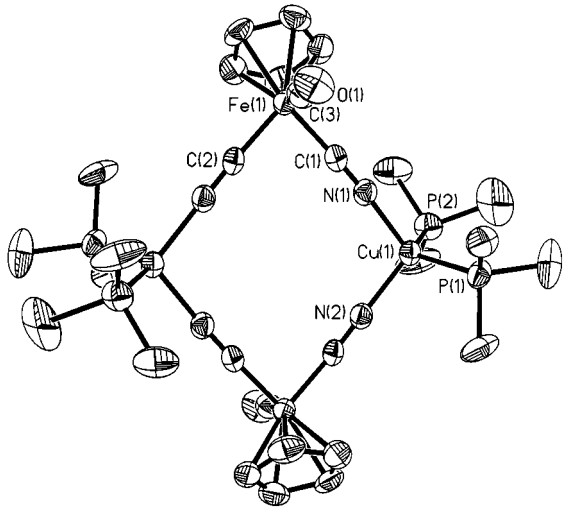

Figure 7. Thermal ellipsoid representation of $[CpFe(CO)(\mu\text{-}CN)_2Cu(PMe_3)_2]_2$ (**12**)

plex **2**. It is noteworthy that in this complex the C≡N−Cu bond angles are close to being linear, with an average bond angle of 174.7°. The corresponding average C≡N−Cu bond angles in the other crystallographically determined derivatives (complexes **2**, **3**, and **6**) cover a range of 160.4−166.7°. Although complexes **3**, **6**, and **12** have similar structures, the P−Cu−P angles and Cu−P bond lengths respond to the steric requirements of the phosphane ligands, that is, the P−Cu−P angles become more obtuse and the Cu−P bond lengths become longer with increasing phosphane cone angles (see Table 4).

A thermal ellipsoid representation of complex **13** is shown in Figure 8, and a list of selected bond lengths and angles is provided in Table 3. Unlike the bis(tricyclohexylphosphane) derivative, complex **13** consists of two Cu^I centers, each in a distorted trigonal environment, separated by 2.844 Å and bridged by the two dcpm ligands. The third ligand completing each copper center's coordination sphere is a nitrogen atom of a bridging CN group from the $CpFe(CO)(CN)_2^-$ anion. The insert in Figure 8 illustrates the distorted T-shape about the copper centers, where the P(1)−Cu(1)−P(2) angle is 144.26(4)°. Hence, like the CO ligand, one cyanide ligand of the $CpFe(CO)(CN)_2^-$ units is terminal.

As seen in Figure 8, the two $CpFe(CO)(CN)_2^-$ moieties are on opposite sides of the eight-membered metallacycle afforded by the two copper(I) atoms and the two bisphosphane ligands. The Cu−P bond lengths in complex **13** [2.2473(11) and 2.2626(11) Å] are slightly shorter than those found in the diamond-shaped bis(tricyclohexylphosphane) derivative (2.28 Å on average), where the geometry about the copper is tetrahedral with two bridging CN ligands. Similarly, the Cu−N bond length of 1.994(3) Å is shorter than the average Cu−N bond length in the bis-PCy_3 analog. These observations are to be expected in proceeding from three- to four-coordinate copper, and are also observed in the mono- and bis-tricyclohexylphosphane complexes. Interestingly, the C−N−Cu bond angle in **13** [158.3(3)°] is more acute than that found in the geometrically constrained diamond-shaped derivatives (vide infra).

Again, in an effort to conclusively define the structures of complexes **14** and **15** we have resorted to X-ray crystallography. This is of particular importance since the spectroscopic data for complexes **13**−**15** are so similar. Thermal ellipsoid drawings of complexes **14** and **15** are found in Figures 9 and 10, respectively, and lists of selected bond lengths and angles are provided in Table 3.

Table 4. Cone angles, P−Cu−P bond angles, and Cu−P bond lengths of **3**, **6**, and **12**

Compound	Cone angle (deg)	P−Cu−P (deg)	Cu−P (Å)
$[CpFe(CO)(\mu\text{-}CN)_2Cu(PCy_3)_2]_2$ (**3**)	179	127.75	2.264
$[CpFe(CO)(\mu\text{-}CN)_2Cu\{(P\text{-}p\text{-}tolyl)_3\}_2]_2$ (**6**)	145	121.21	2.279
$[CpFe(CO)(\mu\text{-}CN)_2Cu(PMe_3)_2]_2$ (**12**)	118	118.71	2.241

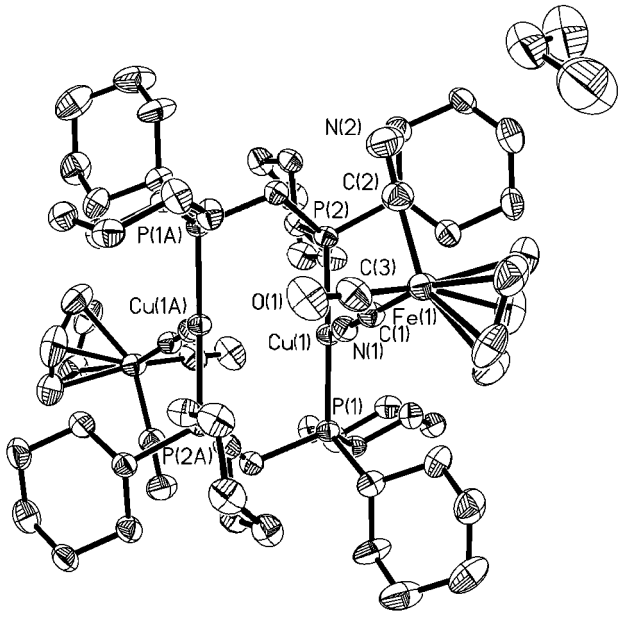

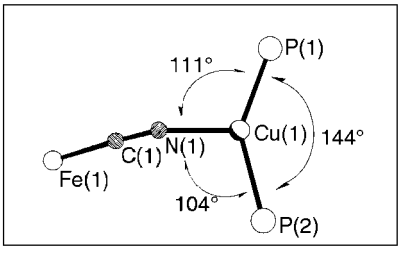

Figure 8. Thermal ellipsoid representation of complex **13**; the insert illustrates the coordination sphere about the copper(I) center

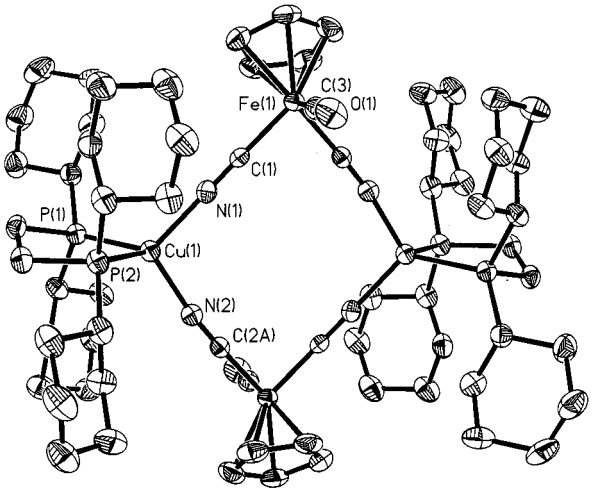

Figure 9.Thermal ellipsoid representation of complex **14**

Complex **14** crystallized with two molecules each of CH_2Cl_2 and CH_3CN, whereas complex **15** crystallized with five molecules of THF. Both derivatives possess the diamond-shaped structure previously observed in the analogous complexes containing monodentate tricyclohexylphosphane ligands. The diamond or parallelogram is formed by two iron(II) and two copper(I) atoms linked by four bridging cyanide ligands, where the carbon end of the CN group is bound to iron and the nitrogen end to copper. The coppers' coordination spheres are completed by a chelating bisphosphane ligand. Hence, upon changing the number of methylene groups between the two PCy_2 donors from one to two or three, the bisphosphanes switch from bridging to chelating with regard to their binding to the copper(I) centers. The two iron-bound terminal CO ligands lie on opposite sites of the plane defined by the four metal atoms.

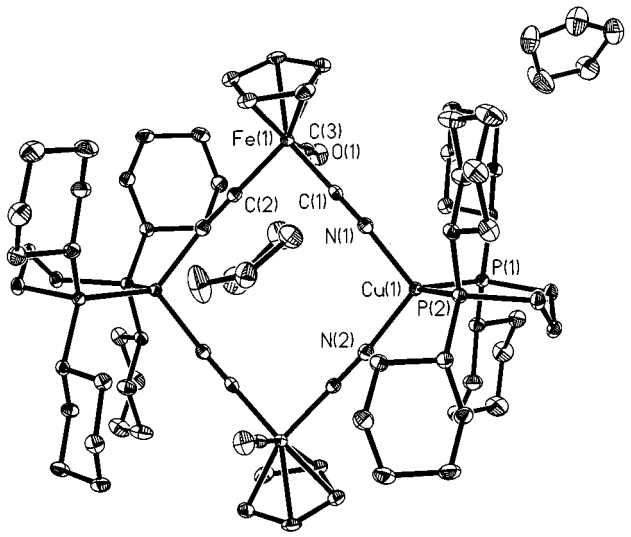

Figure 10. Thermal ellipsoid representation of complex **15**

The average Cu−N and Cu−P bond lengths were found to be 1.975(5) and 2.247(2) Å in **14**, and 1.998(3) and 2.252(1) Å in **15**, respectively. These bond parameters are quite similar to those found in complex **13**. The P−Cu−P angle in **14** at 92.49(6)° is, as expected, more acute than that seen in complex **15** [104.69(4)°] due to the change in going from a five-membered chelate ring to a six-membered chelate ring. On the other hand, the N−Cu−N angles are quite similar in the two diamond-shaped complexes at 103.93(19) and 101.93(12)°, in **14** and **15** respectively. Similarly, the C−Fe−C angles in the two parallelograms differ only slightly, 87.0(2) in **14** and 87.99(14)° in **15**. In contrast to complex **13**, where the Cu−N−C−Fe linkage is highly nonlinear, in complexes **14** and **15** which contain C−N−Cu average angles of 175.8(5) and 172.0(3)° and N−C−Fe average angles of 177.3(5) and 179.2(3)°, this unit is fairly linear.

The geometric dimensions of the Fe_2Cu_2 diamond-shaped core in complexes **14** and **15** are summarized in Figure 11. The internal area of the diamond is approximately 25 $Å^2$. As is seen in the space-filling model of **15** (Figure 12) access to the internal void space, which can accommodate a sphere with a radius up to approximately 1.04 Å, is ready available in the case of the chelated cyclohexylphosphane ligands. This is *not* the case in the analogous bis PCy_3 derivative where the cyclohexyl rings partially block the opening. Figure 13 displays a packing diagram for complex **14**, where

between the layers of overlapping diamonds, which form channels in the solids, there are solvate molecules of CH_3CN.

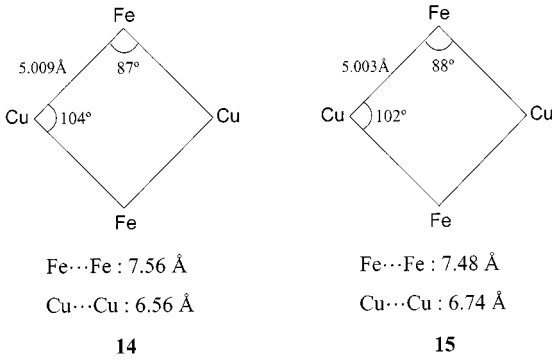

Figure 11. Metric parameters of the $Fe_2Cu_2(CN)_4$ cores of complexes **14** and **15**

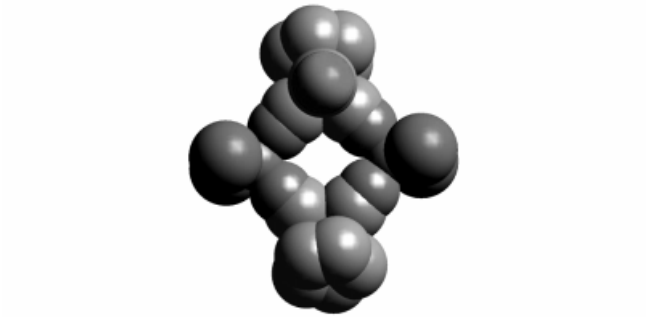

Figure 12. Space-filling model of complex **15**

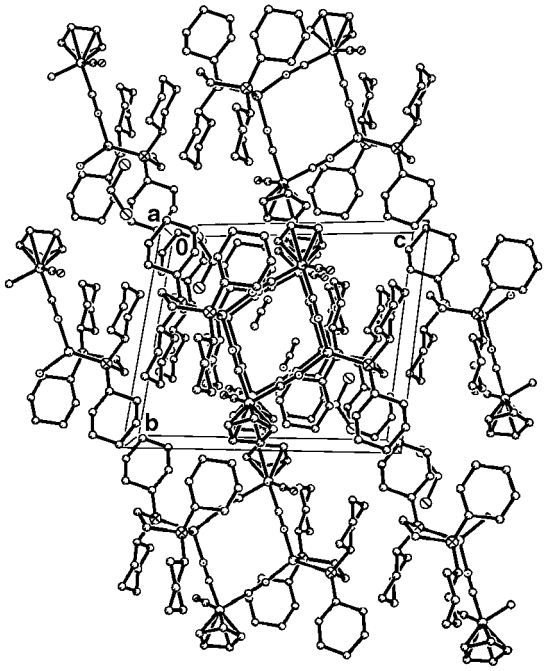

Figure 13. Packing diagram for complex **14**, indicating solvent molecules between the layers of the stacked diamond-shaped complexes

Since we have observed $[CpFe(CO)(\mu\text{-}CN)_2CuPCy_3]_2$, where the copper(I) center is trigonal, to be quite stable, it was of interest to examine the effect of extending the number of methylene units in the $Cy_2P(CH_2)_nPCy_2$ ligand to four. In this instance the bisphosphane ligand may have a greater propensity for affording linked chains of diamond-shaped moieties as opposed to chelating to a single copper(I) center. Hence, the synthesis of the derivative with $Cy_2P(CH_2)_4PCy_3$ (dcpb) (**16**) was performed in a completely analogous manner to that employed for complexes **14** and **15**. Unfortunately, we have yet to obtain X-ray quality crystals of **16**, and therefore have not been able to definitively identify its structure. However, based on the close spectral resemblance of complex **16** to complexes **14** and **15** (see Table 1), coupled with its ready solubility, we suggest it to be the seven-membered chelate bisphosphane derivative.

Solution ^{31}P NMR Spectroscopy

Table 2 lists the ^{31}P NMR spectra in CH_2Cl_2 of the heterobimetallic complexes synthesized and structurally characterized in this report. As seen in Table 2 and Figures 14A and 14B, the ^{31}P NMR resonances for complexes **2** and **3**, the mono- and bis-tricyclohexylphosphane derivatives of $[CpFe(CO)(\mu\text{-}CN)_2Cu]_2$, at ambient temperature are shifted slightly downfield from the free ligand at $\delta = 15.16$ and 11.74, respectively, and are somewhat broadened with frequency width half-height (fwhh) values of 106 and 65 Hz, respectively. This is presumably due to line broadening by

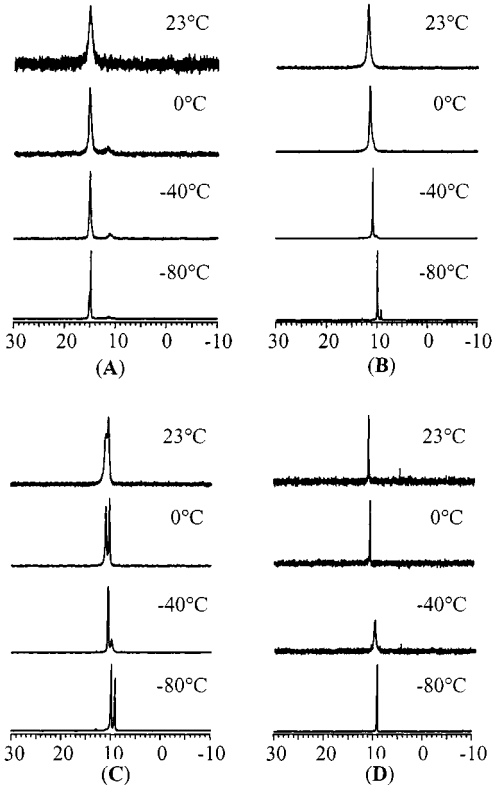

Figure 14. Variable temperature ^{31}P NMR spectra of $[CpFe(CO)(\mu\text{-}CN)_2Cu(PCy_3)]_2$ (**A**), $[CpFe(CO)(\mu\text{-}CN)_2Cu(PCy_3)_2]_2$ (**B**), $[CpFe(CO)(\mu\text{-}CN)_2Cu(PCy_3)_2]_2 + PCy_3$ (**C**), and PCy_3 (**D**)

the quadrupolar nuclei ^{63}Cu and ^{65}Cu. By way of contrast, the free PCy_3 ligand has a resonance at $\delta = 10.86$ with a fwhh of only 11 Hz at ambient temperature. Nevertheless, there is a temperature dependence of the free PCy_3 ligand with broadening being noted around −40 °C; this can be attributed to the conformation exchange of the chair and boat forms of the cyclohexyl rings (see Figure 14D).

Upon the addition of two equivalents of PCy_3 to complex **3** in dichloromethane the ^{31}P NMR spectrum exhibits resonances for both complex **3** and free PCy_3. These ^{31}P NMR signals display the same temperature behavior noted for the individually determined spectra, i.e., the sum of the spectra in Figure 14B and 14D afford that seen in Figure 14C. These ^{31}P NMR spectral results are indicative of *slow phosphane exchange* between complex **3** and PCy_3 ($<<100$ sec^{-1}). Furthermore, the infrared spectra of complexes **2** and **3** clearly indicate that there is only one principal species in pure solutions of these two derivatives, as can be seen from the overlapping spectra in the ν(CN) region in Figure 15. As previously indicated prolonged standing of the reaction solution containing complex **3** and PCy_3 affords complex **4**, where the phosphorous resonance for PCy_3 bound to iron is observed at $\delta = 80.2$.

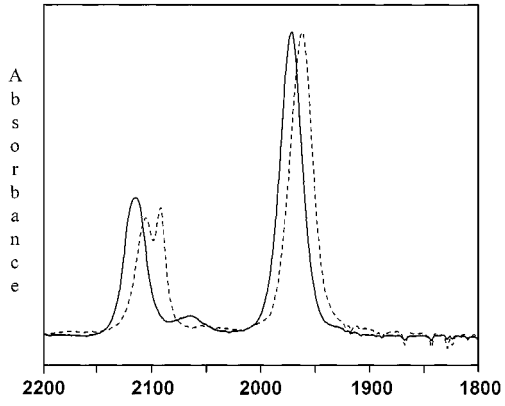

Figure 15. Superimposition of the infrared spectra of complexes **2** (——) and **3** (- - - -)

There is a trend noted in the ^{31}P NMR resonance of the methyl(phenyl)phosphane derivatives. That is, the more basic phosphane derivative shows an increased downfield shift in the complex compared to that of the free phosphane ligand (Table 2). These differences in chemical shift range from the most basic PMe_3 derivative (**9**; $\delta = 13.48$) to the least basic PPh_2Me derivative (**7**; $\delta = 4.04$). In addition, the ^{31}P NMR resonances of the derivatives containing two phosphanes per copper center all fall downfield from their one-phosphane-bound counterparts by about 2 ppm.

Concluding Remarks

Encompassed in this report are contributions to the growing body of work on the synthesis and structural characterization of metallacyclic polygons,[1] in particular those containing cyanide bridges.[2−27] Among the iron(II)/copper(I) cyanide-bridged bimetallic complexes we have synthesized, **13** is the only complex composed of an eight-membered metallacycle with a short $Cu^{I}\cdots Cu^{I}$ distance in the solid-state due to dcpm bridging the two copper(I) centers. As the number of methylene groups between the PCy_2 donors of the bisphosphane ligand is increased, the bisphosphane changes its bonding mode from bridging to chelating. Hence, the X-ray structures of complexes **14** and **15**, which contain the bisphosphane ligands dcpe and dcpp, respectively, show an Fe_2Cu_2 diamond-shaped core as seen in the monodentate phosphane derivatives **2**, **3**, **6**, and **12**, e.g., $[CpFe(CO)(\mu\text{-}CN)_2(PCy_3)_2]_2$, where the copper(I) centers are four coordinate. The diamond-shaped core can readily accommodate a sphere with a radius of up to 1.04 Å. In contrast to the bis(tricyclohexylphosphane) derivative, the cores of **12**, **14** and **15** are not blocked by cyclohexyl groups. Therefore, solvent molecules are able to occupy the channels created by the overlapping diamonds in the solids. In general the Cu−N−C−Fe linkage is nonlinear, with the Cu−N−C and Fe−C−N angles covering a range of 158.3 to 178.9° and 171.1 to 179.1°, respectively.

Experimental Section

Methods and Materials: All manipulations were performed under argon using standard Schlenk and glovebox techniques. Acetonitrile was distilled once from CaH_2 and once from P_2O_5 and then freshly distilled from CaH_2 immediately before use. Dichloromethane was dried and distilled over P_2O_5. Hexane, diethyl ether, and THF were dried in sodium benzophenone stills prior to use. The following reagents were used as received without further purification: Cyclopentadienylirondicarbonyl dimer, tetrafluoroboric acid, dimethylphenylphosphane (Aldrich); bromine (EM Science); potassium cyanide, cuprous oxide, triphenylphosphane (Fisher Scientific); tricyclohexylphosphane, trimethylphosphane, methyldiphenylphosphane, tri-*p*-tolylphosphane (Strem), bis(dicyclohexylphosphanyl)methane, dcpm (Strem), 1,2-bis(dicyclohexylphosphanyl)ethane, dcpe (Strem), 1,3-bis(dicyclohexylphosphanyl)-propane, dcpp (Aldrich), 1,4-bis(dicyclohexylphosphanyl)butane, dcpb (Aldrich). $[Cu(CH_3CN)_4][BF_4]$[33] and $K[CpFe(CO)(CN)_2]$[34] salts were prepared according to published literature procedures.

Infrared spectra were recorded on a Mattson 6021 FTIR using a 0.1 mm CaF_2-sealed cell for solutions and KBr pellets for solid samples. All ^{31}P NMR spectra were recorded on a Varian Unity Plus 300 MHz spectrometer (121.4 MHz ^{31}P) using non-deuterated dichloromethane as solvent. The magnetic field was locked with deuterium oxide, and a tube with an 85% phosphoric acid solution was used as an external reference. Variable temperature ^{31}P NMR spectra were recorded every 20 °C from +20 to −80 °C using liquid N_2 as coolant. Elemental analyses were carried out by Canadian Microanalytical Service, Ltd., Canada.

Synthesis of $[CpFe(CO)(\mu\text{-}CN)_2Cu(CH_3CN)_2]_2$ (1): Acetonitrile (10 mL) was added to a mixture of $K[CpFe(CO)(CN)_2]$ (0.2 mmol, 0.048 g) and $[Cu(CH_3CN)_4][BF_4]$ (0.2 mmol, 0.0628 g) in a 50 mL Schlenk flask. After 30 min. of stirring at ambient temperature a pale gray solid of KBF_4 precipitated from the yellow reaction mixture. The KBF_4 salt was separated from the yellow solution of **1** by filtration. The acetonitrile solution of **1** was used immediately in the following syntheses.

Synthesis of $[CpFe(CO)(\mu\text{-}CN)_2Cu(PCy_3)]_2$ (2): An acetonitrile solution of **1** prepared as described above was added to a 50 mL Schlenk flask containing 0.2 mmol of tricyclohexylphosphane (0.056 g). The crude product precipitated out as a yellow solid. Upon removal of the solvent by cannula and vacuum, the remaining solid was isolated in ca. 91% yield. X-ray quality crystals of **2** were obtained upon slow diffusion of acetonitrile into a dichloromethane solution of **2** maintained at 10 °C for several days. − $[CpFe(CO)(CN)_2Cu(PCy_3)]_2 \cdot 1.5CH_2Cl_2$: calcd. C 52.79, H 6.54, N 4.60; found C 52.90, H 7.21, N 4.36.

Synthesis of $[CpFe(CO)(\mu\text{-}CN)_2Cu(PCy_3)_2]_2$ (3). Method I: Complex **3** was synthesized as described above for complex **2** employing 0.4 mmol of PCy_3 (0.112 g). A clear yellow solution of **3** was obtained in acetonitrile. Upon removal of the solvent by vacuum, a crude product of **3** was obtained as a yellow solid (yield 92%). Yellow orange crystals of **3** were obtained by slow diffusion of hexane into a THF solution of **3**. − $[CpFe(CO)(CN)_2Cu(PCy_3)]_2 \cdot 2THF$: calcd. C 64.24, H 8.87, N 3.12; found C 63.60, H 10.13, N 2.43.

Method II: Complex **3** could also be synthesized by adding two equivalents of PCy_3 to complex **2** in dichloromethane.

Synthesis of $[CpFe(PCy_3)(CN)(\mu\text{-}CN)Cu(PCy_3)_2]$ (4): A 5 mL dichloromethane solution of PCy_3 (0.2 mmol, 0.056 g) was added to a 10 mL dichloromethane solution of complex **3** (0.1 mmol, 0.165 g). An olive solution was formed along with some gray precipitate after two weeks of stirring. The gray precipitate was separated by filtration, and complex **4** was isolated by recrystallization. X-ray quality crystals of **4** were obtained by slow diffusion of diethyl ether into a dichloromethane solution of **4**.

Synthesis of $[CpFe(CO)(\mu\text{-}CN)_2Cu(P\text{-}p\text{-}Tol_3)]_2$ (5): The synthesis of complex **5** was carried out exactly as described above for complex **2** employing tri-*p*-tolylphosphane (0.2 mmol, 0.061 g). A yellow solution of **5** resulted; unfortunately, complex **5** decomposes at ambient temperature.

Synthesis of $[CpFe(CO)(\mu\text{-}CN)_2Cu(P\text{-}p\text{-}Tol_3)_2]_2$ (6): An acetonitrile solution of **1** as described above was added to a 50 mL Schlenk flask containing 0.4 mmol of tri-*p*-tolylphosphane (0.122 g). The reaction solution was stirred for 30 min., and **6** formed as a yellow precipitate. Upon removing the solvent by cannula and vacuum, the yellow solid was isolated in 90% yield. Yellow crystals of **6** were obtained upon slow diffusion of hexane into a THF solution of **6** at 10 °C for several days. − Calcd. C 68.77, H 5.42, N 3.21; found C 68.23, H 5.50, N 3.13.

Synthesis of $[CpFe(CO)(\mu\text{-}CN)_2CuL]_2$ [L = $PMePh_2$ (7), PMe_2Ph (9), PMe_3 (11)]: A 5 mL acetonitrile solution of phosphane (0.2 mmol, 0.015 g for PMe_3, 0.028 g for PMe_2Ph, and 0.040 g for $PMePh_2$) was slowly added to a yellow acetonitrile solution of **1**. A yellow-orange solution was obtained for each phosphane derivative. Upon removing the solvent by vacuum, yellow-orange solids were isolated.

Synthesis of $[CpFe(CO)(\mu\text{-}CN)_2CuL_2]_2$ [L = $PMePh_2$ (8), PMe_2Ph (10), PMe_3 (12)]: The syntheses of complexes **8**, **10**, and **12** were carried out as described above for **7**, **9**, and **11** with 0.4 mmol of phosphane (0.030 g for PMe_3, 0.056 g for PMe_2Ph, and 0.080 g for $PMePh_2$). X-ray quality crystals were obtained by slow diffusion of hexane into a THF solution of **12**.

Synthesis of $[CpFe(CO)(CN)(\mu\text{-}CN)Cu(dcpm)]_2$ (13): A 10 mL dichloromethane solution of dcpm (0.20 mmol, 0.081 g) was added to an acetonitrile solution of **1** prepared as described above. The reaction solution was stirred for 30 min. at ambient temperature, followed by removal of the mixed solvent under vacuum to afford a yellow residue in 92% yield. Yellow-orange crystals of **13** were obtained by slow diffusion of diethyl ether into a dichloromethane solution of **13** maintained at 10 °C for several days. − $C_{66}H_{102}Cu_2Fe_2N_4O_2P_4$ (1346.24): calcd. C 58.88, H 7.64, N 4.16; found C 58.10, H 8.00, N 3.98.

Synthesis of $[CpFe(CO)(\mu\text{-}CN)_2Cu(dcpe)]_2$ (14): The synthesis of this derivative was carried out exactly as described above for complex **13** employing 0.20 mmol (0.084 g) of dcpe. The yellow-orange product was recovered upon removing the mixed solvent under vacuum. Orange crystals of **14** were obtained from CH_2Cl_2/diethyl ether maintained at 10 °C over several days. − $C_{68}H_{106}Cu_2Fe_2N_4O_2P_4 \cdot 2CH_2Cl_2$: calcd. C 54.45, H 7.18, N 3.63; found C 55.29, H 7.97, N 3.97.

Synthesis of $[CpFe(CO)(\mu\text{-}CN)_2Cu(dcpp)]_2$ (15): Alternatively, the reaction between $K[CpFe(CO)(CN)_2]$ (0.20 mmol, 0.048 g) and $[Cu(CH_3CN)_3][BF_4]$ (0.20 mmol, 0.063 g) was carried out directly in dichloromethane for 30 min. followed by filtration to remove the KBF_4 salt. Subsequently, dcpp (0.20 mmol, 0.087 g) in 10 mL of dichloromethane was added dropwise to the yellow filtrate and the solution stirred at room temperature for 30 min. to yield a yellow solution. Upon removal of the solvent under vacuum, the yellow solid was redissolved in THF for recrystallization. Yellow crystals of **15** were obtained upon slow diffusion of hexanes into a THF solution of **15** maintained at 10 °C for several days.

X-ray Crystallography: A yellow or yellow-orange crystal of **2**, **3**, or **4** was mounted on a glass fiber with epoxy cement and placed in a cold nitrogen stream at 193 K. X-ray crystallographic data of **2**, **3**, and **4** were obtained on a Siemens R3m/V single-crystal X-ray diffractometer operating at 55 kV and 30 mA, Mo-K_α (λ = 0.71073 Å) radiation equipped with a Siemens LT-2 cryostat. Diffractometer control software P3VAX 3.42 was supplied by Siemens Analytical Instruments, Inc. Crystals of **6** and **12**−**15** were coated by mineral oil and mounted on a glass fiber with apiezon grease at room temperature. The mounted crystal was then placed in a cold nitrogen stream (Oxford) maintained at 110 K on a Bruker SMART 1000 three-circle goniometer. X-ray data of **6** and **12**−**15** were obtained on a Bruker CCD diffractometer and covered more than a hemisphere of reciprocal space by a combination of three sets of exposures.

Crystal data and details of data collection for complexes **2**, **3**, **4, 6,** and **12**−**15** are provided in Table 5. The structures were solved by direct methods. Full-matrix least-squares anisotropic refinement for all non-hydrogen atoms yielded $R(F)$ and $wR(F^2)$ values as indicated in Table 5 at convergence. Hydrogen atoms were placed in idealized positions with isotropic thermal parameters fixed 1.2- or 1.5-times the value of the attached atom. Neutral atom scattering factors and anomalous scattering factors were taken from the International Tables for X-ray Crystallography Vol. C.

For complexes 2, 3, 4, 6, and 12−15, program(s) used to solve the structure: SHELXS-86 (Sheldrick[35]); program(s) used to refine the structure: SHELXL-97 (Sheldrick[36]); program(s) used for molecular graphics: SHELXTL version 5.0 (Bruker[35]); software used to prepare material for publication: SHELXTL version 5.0 (Bruker[37]).

Crystallographic data (excluding structure factors) for the structures reported in this paper have been deposited with the Cambridge Crystallographic Data Centre as supplementary publication nos. CCDC-118334 (**2**), -168366 (**3**), -168367 (**4**), -168368 (**6**),

Table 5. X-ray crystallographic data for complexes **2**−**4**, **6**, and **12**−**15**

	2	**3**	**4**	**6**	**12**	**13**	**14**	**15**
Formula	$C_{52}H_{76}Cu_2Fe_2N_4O_2P_2 \cdot 2CH_2Cl_2$	$C_{88}H_{142}Cu_2Fe_2N_4O_2P_4 \cdot 2C_4H_8O$	$C_{61}H_{104}CuFeN_2P_3 \cdot 2CH_2Cl_2$	$C_{100}H_{94}Cu_2Fe_2N_4O_2P_4 \cdot 2C_4H_8O$	$C_{28}H_{46}Cu_2Fe_2N_4O_2P_4 \cdot 2CH_2Cl_2$	$C_{33}H_{51}CuFeN_2OP_2 \cdot CH_2Cl_2$	$C_{68}H_{106}Cu_2Fe_2N_4O_2P_4 \cdot 2CH_2Cl_2 \cdot 2CH_3CN$	$C_{55}H_{55}CuFeN_2OP_2 \cdot 2.5C_4H_8O$
Formula wt. (g/mol)	1259.74	1794.92	1247.61	1890.66	1003.20	758.01	1626.19	881.40
Crystal system	Triclinic	Triclinic	Monoclinic	Triclinic	Monoclinic	Triclinic	Triclinic	Triclinic
Space group	$P\bar{1}$	$P\bar{1}$	$P2_1/c$	$P\bar{1}$	$P2_1/n$	Pi	Pi	Pi
a (Å)	9.615(8)	13.3707(9)	12.815(6)	11.6307(11)	10.799(4)	11.6437(8)	12.7117(11)	13.363(2)
b (Å)	10.700(11)	13.8757(18)	18.698(5)	13.2303(12)	11.477(4)	11.7162(8)	12.7254(11)	13.568(2)
c (Å)	14.918(11)	15.1154(16)	27.766(6)	16.3741(16)	18.081(6)	15.0748(11)	14.6351(13)	15.616(3)
α (deg)	84.06(7)°	67.049(9)	−	92.829(2)	−	104.4820(10)	89.812(2)	65.369(3)
β (deg)	82.86(6)°	69.703(7)	92.35(3)	105.674(2)	97.943(7)	107.1720(10)	69.976(2)	69.598(3)
γ (deg)	75.56(8)°	80.748(9)	−	99.244(2)	−	102.6400(10)	67.664(2)	64.211(3)
Volume (Å)^3	1471(2)	2411.2(4)	6648(4)	2383.0(4)	2219.4(13)	1804.7(2)	2035.4(3)	2268.4(7)
Z	1	1	4	1	2	2	1	2
d_{calcd} (g/cm^3)	1.422	1.236	1.247	1.317	1.501	1.395	1.327	1.290
Temperature (K)	193	193	193	110	110	110	110	110
Wavelength (Å)	0.71073	0.71073	0.71073	0.71073	0.71073	0.71073	0.71073	0.71073
Abs. coeff. mm^{-1}	1.475	0.846	0.809	0.860	1.866	1.257	1.120	0.900
Goodness of fit on F^2	1.101	0.983	0.850	1.038	0.625	1.066	0.958	0.926
R [a]	3.92	7.13	10.00	6.72	6.54	7.61	8.85	3.62
R_w [b]	5.02	15.99	19.45	8.42	10.63	21.47	22.19	8.15

[a] $R = \Sigma||F_o| - |F_c||/\Sigma F_o$. − [b] $R_w = \{[\Sigma w(F_o^2 - F_c^2)^2]/[\Sigma w(F_o^2)^2]\}^{1/2}$.

-168362 (**12**), -168363 (**13**), -168364 (**14**), -168365 (**15**). Copies of the data can be obtained free of charge on application to CCDC, 12 Union Road, Cambridge CB2 1EZ, UK [Fax: (internat.) + 44-1223/336-033; E-mail: deposit@ccdc.cam.ac.uk].

Acknowledgments

Financial support from the National Science Foundation (CHE-99−10342 and CHE 98−07975 for the purchase of X-ray equipment), the Robert A. Welch Foundation, and by the Texas Advanced Research Technology Program (Grant No. 0390−1999) is greatly appreciated.

[1] [1a] S. Leininger, B. Olenyuk, P. J. Stang, *Chem. Rev.* **2000**, *100*, 853−908. − [1b] M. Fujita, *Chem. Soc. Rev.* **1998**, *27*, 417−425. − [1c] S. Bélanger, M. H. Keefe, J. L. Welch, J. T. Hupp, *Coord. Chem. Rev.* **1999**, *190*−*192*, 29−45.

[2] S. M. Contakes, K. K. Klausmeyer, T. B. Rauchfuss, *Inorg. Chem.* **2000**, *39*, 2069−2075; S. M. Contakes, K. K. Klausmeyer, R. M. Milberg, S. R. Wilson, T. B Rauchfuss, *Organometallics* **1998**, *17*, 3633−3635.

[3] D. Williams, J. Kouvetakis, M. O'Keeffe, *Inorg. Chem.* **1998**, *37*, 4617−4620.

[4] [4a] G. N. Richardson, H. Vahrenkamp, *J. Organomet. Chem.* **2000**, *593*−*594*, 44−48. − [4b] H. Vahrenkamp, A. Geiss, G. N. Richardson, *J. Chem. Soc., Dalton Trans.* **1997**, 3643−3651.

[5] J. J. Rupp, D. F. Shriver, *Inorg. Chem.* **1967**, *6*, 755−761.

[6] J. Emri, B. Györi, A. Bakos, G. Czira, *J. Organomet. Chem.* **1976**, *112*, 325−331.

[7] C. Carini, C. Pelizzi, G. Pelizzi, G. Predieri, P. Tarasconi, F. Vitali, *J. Am. Chem. Soc. Commun.* **1990**, 613−614.

[8] J. A. Smith, J.-R. Galán-Mascarós, R. Clérac, K. R. Dunbar, *Chem. Commun.* **2000**, 1077−1078; K. R. Dunbar, R. Heitz, *Prog. Inorg. Chem.* **1997**, *93*, 283−291.

[9] W. P. Fehlhammer, M. Fritz, *Chem. Rev.* **1993**, *93*, 1243−1280.

[10] M. Adam, A. K Brimah, R. D. Fischer, L. Xing-Fu, *Inorg. Chem.* **1990**, *29*, 1597.

[11] D. J. Darensbourg, J. C. Yoder, M. W. Holtcamp, K. K. Klausmeyer, J. H. Reibenspies, *Inorg. Chem.* **1996**, *35*, 4764−4769.

[12] M. Ohba, H. Okawa, *Coord. Chem. Rev.* **2000**, *198*, 313−328.

[13] N. Mondal, M. K. Saha, B. Bag, S. Mitra, V. Gramlich, J. Ribas, M. S. E. Fallah, *J. Chem. Soc., Dalton Trans.* **2000**, 1601−1604.

[14] V. P. Fedin, A. V. Virovets, I. V. Kalinina, V. N. Ikorskii, M. R. J. Elsegood, W. Clegg, *Eur. J. Inorg. Chem.* **2000**, 2341−2343.

[15] E. Colacio, J. M. Domínguez-Vera, M. Ghazi, R. Kivekäs, J. M. Moreno, A. Pajunen, *J. Chem. Soc., Dalton Trans.* **2000**, 505−509.

[16] N. G. Connelly, O. M. Hicks, G. R. Lewis, A. G. Orpen, A. J. Wood, *J. Chem. Soc., Dalton Trans.* **2000**, 1637−1643.

[17] P. Fspinet, K. Soulantica, J. P. H. Charmant, A. G. Orpen, *Chem. Commun.* **2000**, 915−916.

[18] Y. Zhao, M. Hong, W. Su, R. Cao, Z. Zhou, A. S. C. Chan, *J. Chem. Soc., Dalton Trans.* **2000**, 1685−1686.

[19] D. G. Fu, J. Chen, X. S. Tan, L. J. Jiang, S. W. Zhang, P. J. Zheng, W. X. Tang, *Inorg. Chem.* **1997**, *36*, 220−225.

[20] M. Fritz, D. Rieger, E. Bär, G. Beck, J. Fuchs, G. Holzmann, W. P. Fehlhammer, *Inorg. Chim. Acta* **1992**, *198*−*200*, 513−526.

[21] P. Schinnerling, U. Thewalt, *J. Organomet. Chem.* **1992**, *431*, 41−45.

[22] A. Christofides, N. G. Connelly, H. J. Lawson, A. C. Loyns, A. G. Orpen, M. O. Simmonds, G. H. Worth, *J. Chem. Soc., Dalton Trans.* **1991**, 1595−1601.

[23] C. Carini, C. Pelizzi, G. Pelizzi, G. Predieri, P. Tarasconi, F. Vitali, *Chem. Commun.* **1990**, 613−614.

[24] G. Lavigne, N. Lugan, J.-J. Bonnet, *Chem. Commun.* **1987**, 957−958.

[25] H. Oshio, O. Tamada, H. Onodera, T. Ito, T. Ikoma, S. Tero-Kubota, *Inorg. Chem.* **1999**, *38*, 5686−5689.

[26] [26a] S. M. Contakes, T. B. Rauchfuss, *Angew. Chem. Int. Ed.* **2000**, *39*, 1984−1986. − [26b] K. K. Klausmeyer, S. R. Wilson, T. B. Rauchfuss, *J. Am. Chem. Soc.* **1999**, *121*, 2705−2711. − [26c] K. K. Klausmeyer, T. B. Rauchfuss, S. R. Wilson, *Angew. Chem. Int. Ed.* **1998**, *37*, 1694−1696.

[27] [27a] P. A. Berseth, J. J. Sokol, M. P. Shores, J. L. Heinrich, J. R. Long, *J. Am. Chem. Soc.* **2000**, *122*, 9655−9662. − [27b] J. L. Heinrich, P. A. Berseth, J. R. Long, *Chem. Commun.* **1998**, 1231−1232. − [27c] L. G. Beauvais, M. P. Shores, J. R. Long, *J. Am. Chem. Soc.* **2000**, *122*, 2763−2772. − [27d] M. V. Ben-

nett, M. P. Shores, L. G. Beauvais, J. R. Long, *J. Am. Chem. Soc.* **2000**, *122*, 6664−6668. − [27e] M. P. Shores, L. G. Beauvais, J. R. Long, *Inorg. Chem.* **1999**, *38*, 1648−1649.
[28] [28a] A. Geiss, H. Vahrenkamp, *Inorg. Chem.* **2000**, *39*, 4029−4036 and references therein. − [28b] C. Díaz, A. Arancibia, *Inorg. Chim. Acta* **1998**, *269*, 246−252. − [28c] J. Larionova, M. Gross, M. Pilkington, H. Andres, H. Stoeckli-Evans, H. U. Güdel, S. Decurtins, *Angew. Chem. Int. Ed.* **2000**, *39*, 1605−1609.
[29] [29a] B. S. Lim, R. H. Holm, *Inorg. Chem.* **1998**, *37*, 4898−4908. − [29b] D. M. Corsi, N. N. Murthy, V. G. Young, Jr., K. D. Karlin, *Inorg. Chem.* **1999**, *38*, 848−858.
[30] D. J. Darensbourg, W.-Z. Lee, M. J. Adams, D. L. Larkins, J. H. Reibenspies, *Inorg. Chem.* **1999**, *38*, 1378−1379.
[31] [31a] B. Le-Khac, U. S. Patent 5,482,908, **1996**. − [31b] W. J. Kruper, Jr., D. J. Swart, U. S. Patent 4,500,704, **1985**.
[32] C. A. Tolman, *Chem. Rev.* **1977**, *77*, 313−348.
[33] G. J. Kubas, in *Inorg. Synth.* (Ed.: D. F. Shriver); John Wiley and Sons: New York, 1979; Vol. 19, p. 90.
[34] [34a] C. E. Coffey, *Inorg. Nucl. Chem.* **1963**, *25*, 179. − [34b] C.-H. Lai, W.-Z. Lee, M. L. Miller, J. H. Reibenspies, D. J. Darensbourg, M. Y. Darensbourg, *J. Am. Chem. Soc.* **1998**, *120*, 10103−10114.
[35] G. Sheldrick, SHELXS-86 *Program for Crystal Structure Solution*, (1986), Institut fur Anorganische Chemie der Universitat, Tammanstraße 4, 3400 Göttingen, Germany.
[36] G. Sheldrick, SHELXL-97 *Program for Crystal Structure Refinement*, (1997), Institut fur Anorganische Chemie der Universitat, Tammanstraße 4, 3400 Göttingen, Germany.
[37] Bruker, SHELXTL version 5.0, (1999), Madison, WI, USA.

Received May 3, 2001
[I01153]

Synthesis and Crystal Structure of a Novel Binucleating Symmetrical μ-Bis(tetradentate) Schiff Base Ligand: Syntheses and Redox Properties of Dimanganese(III/III) Complexes

Uday Mukhopadhyay,[a] Larry R. Falvello,[b] and Debashis Ray*[a]

Keywords: Chelates / Redox chemistry / Manganese / Schiff bases / NMR spectroscopy / Cyclic voltammetry

A family of dinuclear manganese(III/III) complexes $[Mn_2^{III}(\mu\text{-}X)(\mu\text{-}L)(Y)_2](Z)_2$ (X = Cl, OMe, OEt; Y = H_2O; Z = Cl) (**6a**–**c**) of a new μ-bis(tetradentate) ligand, H_3L, derived from the stepwise Schiff base condensation of triethylenetetramine, acetylacetone, and salicylaldehyde has been reported for the first time. NMR spectral and single crystal X-ray structural characterizations of the ligand confirm the formation of a five-membered imidazolidine ring as a backbone to have a new type of doubly bridging binucleating ligand system. In methanol solutions both the $Mn^{III}Mn^{IV}/Mn^{III}Mn^{III}$ and $Mn^{II\text{-}I}Mn^{III}/Mn^{III}Mn^{II}$ couples are observable for the chloro-bridged complex with $E_{1/2}$ in the range of +0.49 to –0.13 V vs. saturated calomel electrode (SCE). The calculation of the comproportionation constant (K_c) from the $E_{1/2}$ values clearly point towards the role of the Mn–O(phenolate)–Mn core for thermodynamic stability of the parent dimanganese(III/III) complex.

Introduction

The field of binucleating ligands and their metal complexes has been receiving considerable attention in recent years.[1] These ligands can coordinate two of the same, or different, metal ions at a suitable predetermined distance to bind and activate a small molecule[2] between the metal centres. Such systems of transition metal complexes may be of interest in relating structures to interesting magnetic behaviours in homo- and hetero-dimetallic complexes,[3] and may mimic aspects of two-metal biosites in various proteins and enzymes.[4] Dinuclear complexes containing manganese centres in close proximity have been the subject of recent extensive investigations due to their involvement in a variety of important biochemical processes like catalytic disproportionation of H_2O_2 to H_2O and O_2 in Mn-catalase[5] and several others,[6] where the Mn_2^{III} unit is present as a redox core in the enzymatic cycle.[7] The Mn^{III}/Mn^{III} oxidation states are believed to participate in the catalytic cycle of Mn-catalase.[8] Furthermore, manganese model-compounds with Cl−Mn bonding have potential applications to the oxygen evolving complex (OEC) in Photosystem II (PSII).[9−13] Insight into the redox properties of Mn-catalase systems and the role of the Mn_2^{III} unit can be obtained from electrochemical studies of new synthetic dimanganese(III/III) complexes. Herein we describe a detailed synthetic account of the preparation of a novel binucleating ligand, its spectroscopic and X-ray structural characterisation, and synthesis of its dimanganese(III/III) complexes and their electron transfer properties.

Results and Discussion

The precursor hexadentate Schiff base ligand (**1**), formed from salicylaldehyde and triethylenetetramine, usually binds to a single metal ion in an octahedral (**2**) geometry, using two tridentate meridional (ONN) halves. However, incorporation of a seventh donor site (D) as a spacer bridging group inside this ligand framework, via an imidazolidine ring formation with a pendent salicylaldehyde group, resulted in a compartmentally fused μ-bis (tetradentate) ligand system (**3**). Here we report the synthesis and structural characterization of one such acyclic binucleating ligand and its binding property towards manganese(III) ions. This novel synthetic strategy for binucleating ligand systems is applicable to all meridionally spanning hexadentate ligands having an ethylenediamine backbone. A new symmetrical binucleating ligand, H_3L, having unsymmetrical compartments containing 1-methyl-3-oxobut-1-enyl end groups and its dimanganese(III/III) complexes are reported.

We have taken advantage of the known[14−19] imidazolidine ring formation reaction as shown in Scheme 1 to prepare the N_4O_3 Schiff base ligand. The ligand is potentially heptadentate, but has its chelating arms spread wide to allow bridging of two metal ions. Though free H_3L exits in the keto form (**4**) in the solid state, it can coordinate two metal ions in the enol form.[1a,20] The unsymmetrical "salenacac" (**5**)-winged ligand (**4**) could take up one metal ion in each wing and fold along the spacer backbone with the help of monoatomic (Cl or OR) exogenous bridging. Reaction of H_3L with $MnCl_2{\cdot}4H_2O$ in the absence or presence

[a] Department of Chemistry, Indian Institute of Technology, Kharagpur-721302, India
E-mail: dray@chem.iitkgp.ernet.in
[b] Department de Quimica Inorganica, Universidad de Zaragoza, 50009 Zaragoza, Spain
E-mail: falvello@lrf1.unizar.es
Supporting information for this article is available on the WWW under http://www.wiley-vch.de/home/eurjic or from the author.

 © WILEY-VCH Verlag GmbH, 69451 Weinheim, 2001 1434−1948/01/1111−2823 $ 17.50+.50/0

of NaOR (R = Me, Et) afforded complexes of the type $[Mn_2(\mu\text{-}L)(\mu\text{-}X)(H_2O)_2]Cl_2$ (X = Cl, OMe, OEt), where the potentially heptadentate ligand H_3L is coordinated as a μ-bis (tetradentate) N_2O_2-donor ligand with endogenous imidazolidine nitrogen and phenolic oxygen bridging.

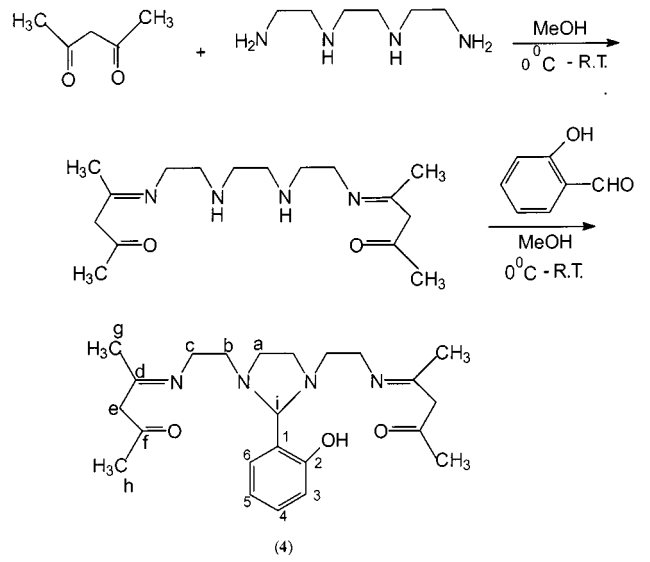

Scheme 1

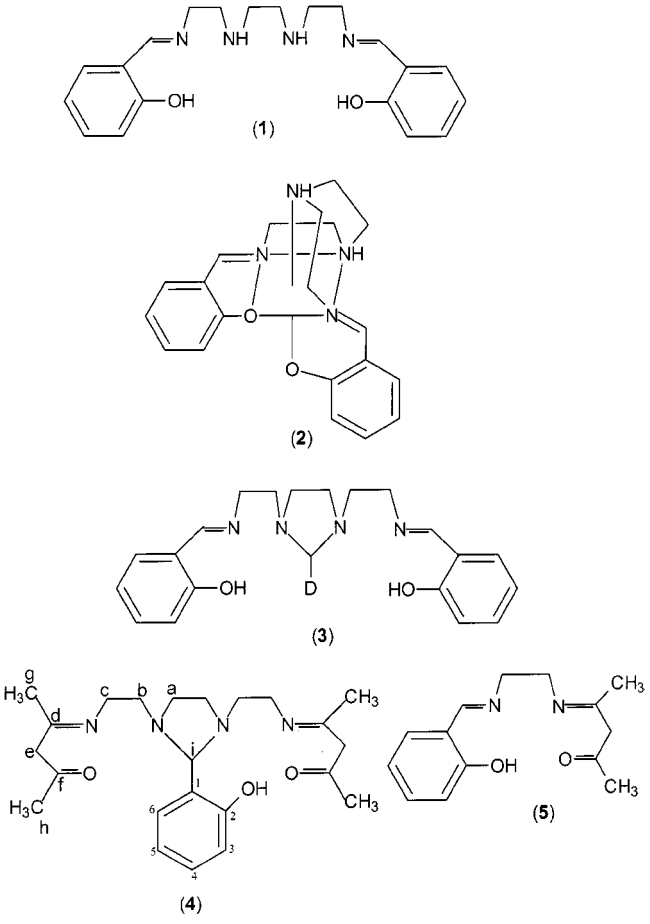

The complexation reaction in the presence of O_2 (from air) oxidizes all the Mn^{2+} centres to Mn^{3+}. During complex formation all the three protons from the phenol and enol functions are removed. The flexibility of the imidazolidine ring and the tendency of the manganese (III) centres to attain octahedral geometry appear to be the driving force for this overall non-planar arrangement of the complex. The potentially heptadentate, but functionally μ-bis (tetradentate), Schiff base ligand H_3L was prepared by a stepwise condensation reaction of trien with two equivalents of acetylacetone and salicylaldehyde in a 1:2:1 molar ratio in 78% yield (Scheme 1). The five-membered imidazolidine ring was formed at the ethylenediamine backbone with salicylaldehyde. The imidazolidine bridging-arm was therefore unique (compared to the other two ketoimine arms), as is clearly shown in the ^1H NMR spectra. ^1H and ^{13}C NMR spectral assignments for the H_3L were consistent with the proposed formulations. The infrared spectrum of the ligand showed peaks around 1605 cm^{-1}, which is characteristic of imine C=N functions. The phenolic OH resonance was observed as a broad signal at about δ = 10.7. This downfield signal can be explained by the intermolecular hydrogen bond of the phenolic OH with solvent ($CDCl_3$), water, or water of crystallization in the solid state (shown in the X-ray structure determination, vide infra). No enolic OH resonance was observed within the 20 ppm range, confirming the diketone form of H_3L in solution.

The molecular structure of H_3L was determined by X-ray crystallography. A view of the dinucleating ligand is shown in Figure 1, and selected bond lengths and angles are listed in Table 1. The ligand molecule is rendered quite rigid by the formation of a five-membered imidazolidine ring and by the presence of three very weak intermolecular hydrogen bonds with a water of crystallization [O(2)−H(2)···O(11) = 2.647 Å; O(11)−H(11A)···O(1) = 2.730 Å; O(11)−H(11B)···O(3) = 2.739 Å]. The water molecule in $H_3L{\cdot}H_2O$ sits comfortably, with the help of these hydrogen-bonding interactions, within the intermolecular hydrophilic pocket created by the keto and phenol functionalities of the ligand. Both N(1)−C(6)−C(7)−N(2) and N(3)−C(17)−C(18)−N(4) adopt gauche conformations [torsion angles: N(1)−C(6)−C(7)−N(2) = 57.5 (6) °; N(3)−C(17)−C(18)−N(4) = −55.5 (6) °]. The whole ligand structure resembles a big Y. Among the three intermolecular hydrogen bonds the bond length between phenolic hydrogen [H(2)] on one ligand molecule and oxygen [O(11)] of the water molecule is lowest 2.65 Å, and results in a highly ordered packing (Figure 2).

The molecular structure clearly shows two tetradentate non-planar compartments suitable for binding two of the same, or different, metal ions. The phenoxy hydrogen of the middle phenolate arm is not intramolecularly hydrogen bonded to one of the imidazolidine nitrogen as is the case with the H_3api ligand.[19] The observed >C=O distances of terminal acetylacetone arms are quite normal[21] for the purely keto tautomeric form in the crystalline state. The similar C−C distances within keto-imine framework also support this observation. The C=N distances also corre-

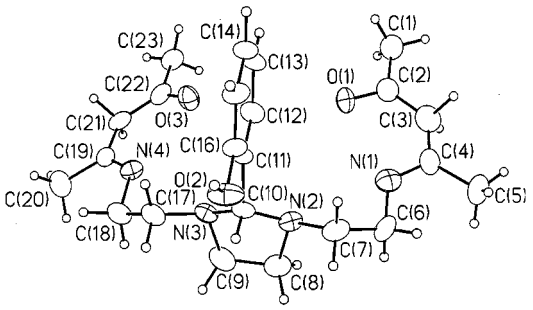

Figure 1. ORTEP plot and labelling scheme for H_3L; all atoms are shown as 50% probability ellipsoids; H atoms are omitted for clarity

Table 1. Selected bond lengths (Å) and angles (°) for $H_3L{\cdot}2H_2O$

O(1)−C(2)	1.273(6)	O(2)−C(16)	1.362(6)
O(3)−C(22)	1.256(6)	N(1)−C(4)	1.338(7)
N(1)−C(6)	1.441(7)	N(2)−C(10)	1.445(7)
N(2)−C(7)	1.453(7)	N(2)−C(8)	1.472(7)
N(3)−C(17)	1.438(6)	N(3)−C(9)	1.470(6)
N(4)−C(19)	1.483(7)	N(4)−C(18)	1.329(7)
C(1)−C(2)	1.480(7)	C(2)−C(3)	1.498(8)
C(3)−C(4)	1.382(8)	C(4)−C(5)	1.383(8)
C(6)−C(7)	1.501(8)	C(8)−C(9)	1.526(8)
C(4)−N(1)−C(6)	125.2(5)	C(10)−N(2)−C(7)	112.9(4)
C(10)−N(2)−C(8)	104.2(4)	C(7)−N(2)−C(8)	114.0(4)
C(17)−N(3)−C(9)	113.3(4)	C(10)−N(3)−C(9)	103.8(8)
C(19)−N(4)−C(18)	123.4(4)	O(1)−C(2)−C(3)	122.6(5)
O(1)−C(2)−C(1)	117.1(5)	C(3)−C(2)−C(1)	120.2(5)
C(2)−C(3)−C(4)	126.0(6)	N(1)−C(4)−C(3)	121.1(5)
N(1)−C(4)−C(5)	118.2(5)	C(3)−C(4)−C(5)	120.6(5)
N(1)−C(6)−C(7)	110.2(4)	N(2)−C(7)−C(6)	111.4(4)
N(2)−C(8)−C(9)	104.1(4)	N(3)−C(9)−C(8)	104.7(4)
N(2)−C(10)−N(3)	101.8(4)	N(2)−C(10)−C(11)	113.8(4)
N(3)−C(10)−C(11)	112.0(4)		

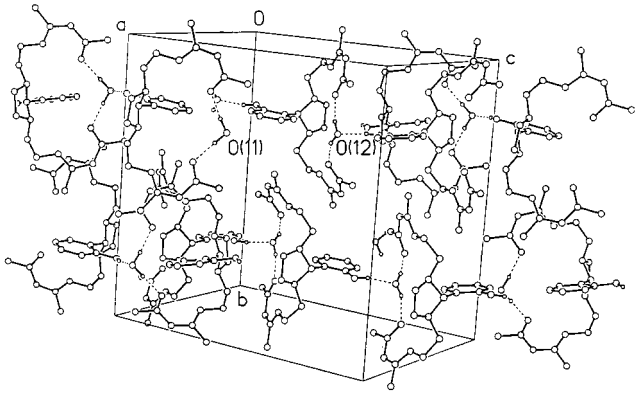

Figure 2. Packing diagram of the H_3L molecule showing hydrogen bonding with a water molecule

spond to a formal double bond.[19] The C−C and C−N distances within the imidazolidine ring are in the1.457−1.496 Å range.

Homodinuclear manganese(III) complexes with the formulation $[Mn_2^{III}(\mu\text{-}X)(\mu\text{-}L)(Y)_2](Z)_2$ (X = Cl, OMe, OEt; Y = H_2O; Z = Cl) (**6**) were prepared from reactions of Mn^{2+} with the ligand H_3L in presence and absence of bases (alkoxide), following oxidation by air. The homodinuclear complexes contain two manganese(III) ions, each coordinated by the N_2O_2 donor set of one half of the ligand. The phenolate O atom from the middle arm of the ligand acts as an endogenous bridge between the two metal centres. The exogenous alkoxide bridge and terminal Y groups complete the coordination sphere and the bi-octahedral structure. The binucleating ligand provides four donor points around each manganese(III) centre. We have so far been unable to synthesize any mononuclear complex of manganese(III) using H_3L. Those complexes could have been used as controls in comparing the change in spectral and magnetic behaviour through dinuclear complex formation. Single-crystal X-ray structure determination of a heterodinuclear assembly of copper(II)-zinc(II) inside the compartments of a similar type of ligand recently[22] established distorted square-pyramidal geometries around each metal centre. Microanalysis data for complexes **6a**−**c** (See Exp. Sect.) confirm their composition. The complexes are highly soluble in polar solvents such as methanol, dimethylformamide, and dimethyl sulfoxide, and are moderately soluble in non-polar solvents like dichloromethane and tetrahydrofuran.

The IR spectra of the complexes show strong C=N stretching frequencies of the imine functions at around 1612 cm^{-1}. The complexes have characteristic μ_2-bridging phenolic ν_{C-O} vibrations in the range 1509−1536 cm^{-1}. The terminal C−O and alkoxide bridging C−O stretching frequencies are observed at around 1295 and 1145 cm^{-1} respectively. The electronic spectra of the intimate dimanganese(III/III) complexes in methanol solutions show several intense absorptions in the near UV region (Table 2, Figure 3).

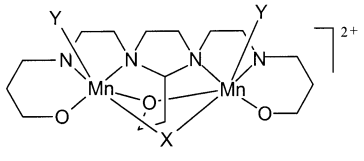

(**6**)

a : X = Cl

b : X = OMe

c : X = OEt

The moderately intense UV band near 360 nm is typical for the 2-hydroxyphenylimino chromophore.[23] The bands near 300 nm for the present complexes are due to the overlap of the azomethine transition with the charge-transfer band from bridging phenolic oxygen to the d-orbital of Mn^{III}. Absence of any inter-valence band in the 1170 nm region eliminates the possibility for a $Mn^{III}Mn^{II}$ species.[24]

In methanol solutions the complexes behave as 1:2 electrolytes (conductivity values, 180−210 $ohm^{-1}cm^2$ mol^{-1}).The complexes are paramagnetic and correspond to the trivalent states of the metals (high-spin d^4, S = 2) in these complexes. Magnetic studies of powdered samples of

Table 2. Electronic spectral and cyclic voltammetric data for $[Mn_2(\mu\text{-}L)(\mu\text{-}X)(H_2O)_2]Cl_2$

Compound	Electronic spectral data λ_{max}, nm (ε, $dm^3\ mol^{-1}\ cm^{-1}$)	Cyclic voltammetric data[a] $E_{1/2}$, V (ΔE_p, mV)
$[Mn_2(\mu\text{-}L)(\mu\text{-}Cl)(H_2O)_2](Cl)_2$	400 (2250), 340 (4500), 280 (10965), 232 (20305), 217 (20815)[b]	0.49 (90), −0.13[c]
$[Mn_2(\mu\text{-}L)(\mu\text{-}OMe)(H_2O)_2](Cl)_2$	390 (9525), 281 (18740), 235 (28580), 214 (29860)[b]	0.47 (115) [c]
$[Mn_2(\mu\text{-}L)(\mu\text{-}OEt)(H_2O)_2](Cl)_2$	383 (4555), 300 (16545), 240 (21650), 214 (26430)[c]	0.46 (100) [c]

[a] Supporting electrolyte TEAP: reference electrode SCE; $E_{1/2} = 0.5\ (E_{pa} + E_{pc})$, where E_{pa} and E_{pc} are anodic and cathodic peak potentials, respectively; $\Delta E_p = E_{pa} - E_{pc}$; scan rate 50 mV S^{-1}. – [b] In aqueous solution. – [c] In methanol solution.

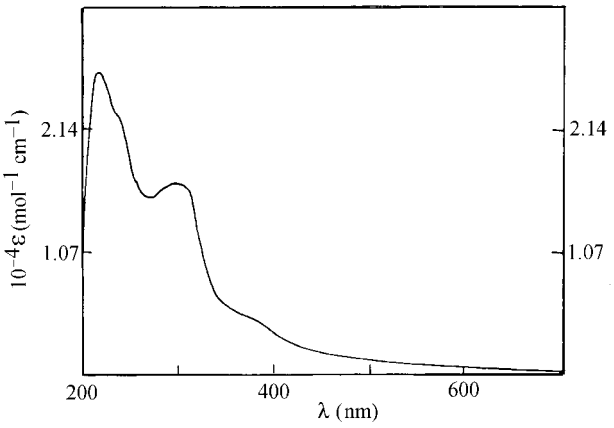

Figure 3. Electronic spectrum of $[Mn_2(\mu\text{-}L)(\mu\text{-}OEt)(H_2O)_2]Cl_2$ (**6c**) in DMF at 298 K

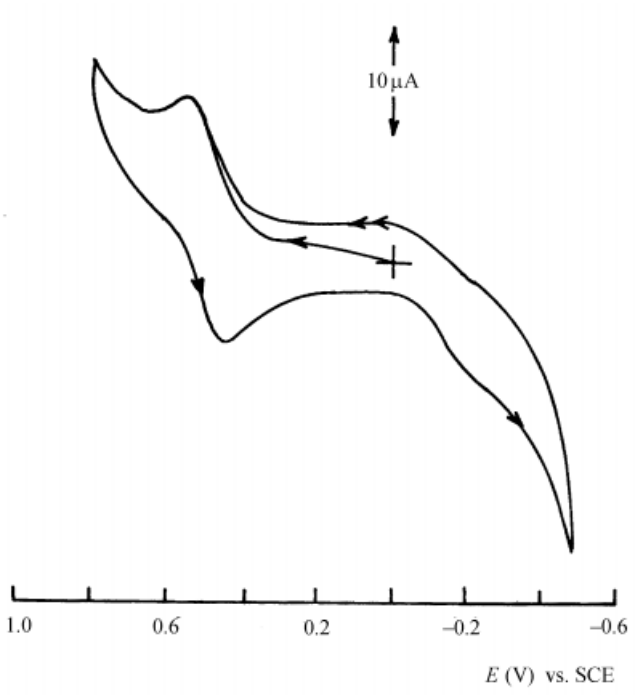

Figure 4. Cyclic voltammogram (scan rate 50 mVs^{-1}) of 10^{-3} M solutions of $[Mn_2(\mu\text{-}L)(\mu\text{-}Cl)(H_2O)_2]Cl_2$ (**6a**) in MeOH at a Pt electrode at 298 K

the complexes were carried out at room temperature using a Gouy balance. The room temperature magnetic moments (μ_{eff}) of the complexes were in the range of 4.24−4.39 μ_B per Mn at 298 K (total μ_{eff} 5.99−6.21 μ_B). The dependence of the room temperature magnetic moments on exogenous bridging is in the order Cl > OMe > OEt, clearly indicating the role of the single exogenous bridging group in varying the magnetic interactions.

The electron-transfer properties of complexes **6a**−**c** were studied in aqueous and methanol solutions by cyclic voltammetry (CV) using a platinum working-electrode. The complexes are electroactive with respect to the metal centres and exhibited two redox processes in the potential range +1.0 V *versus* a saturated calomel electrode (SCE) (tetraethylammonium perchlorate as supporting electrolyte, at 298 K). The chloro-bridged complex showed one oxidative and one reductive response on the positive and negative side of SCE, respectively (Figure 4).

The cathodic and anodic peak heights(i_{pc} and i_{pa}) are equal, and vary as the square root of the scan rate; E_{pc} and E_{pa} are virtually independent of the scan rate. The measured oxidation and reduction potentials were lower in aqueous solutions than in non-aqueous solutions. Both the processes are assumed to be metal-centred. The first quasi-reversible response on the positive side of SCE is due to the one-electron oxidation of Equation (1).

$$[Mn^{III}Mn^{IV}(\mu\text{-}L)(\mu\text{-}Cl)(H_2O)_2]^{3+} \rightleftarrows [Mn^{III}Mn^{III}(\mu\text{-}L)(\mu\text{-}Cl)(H_2O)_2]^{2+} \quad (1)$$

On further scan reversal on the negative side, the one-electron reductive couple in Equation (2) was observed.

$$[Mn^{III}Mn^{III}(\mu\text{-}L)(\mu\text{-}Cl)(H_2O)_2]^{2+} \rightleftarrows [Mn^{III}Mn^{II}(\mu\text{-}L)(\mu\text{-}Cl)(H_2O)_2]^{+} \quad (2)$$

Constant-potential coulometric- and cyclic-voltammetric current height (i_{pa}) data suggest the one-electron nature of these couples. From the separation of $E_{1/2}$ (oxidative response) and $E_{1/2}$ (reductive response) values for $[Mn_2(\mu\text{-}L)(\mu\text{-}Cl)(H_2O)_2]Cl_2$, the comproportionation constant (K_C at 298 K) of the reaction in Equation (3) was calculated to be 5.77×10^{10}, indicating that the Mn_2^{III} complex is considerably stabilized with respect to the $Mn^{III}Mn^{IV}$ and $Mn^{III}Mn^{II}$ species.

$$[Mn^{III}Mn^{IV}(\mu\text{-}L)(\mu\text{-}Cl)(H_2O)_2]^{3+} + [Mn^{III}Mn^{II}(\mu\text{-}L)(\mu\text{-}Cl)(H_2O)_2]^{+} \rightleftharpoons 2\,[Mn^{III}Mn^{III}(\mu\text{-}L)(\mu\text{-}Cl)(H_2O)_2]^{2+} \quad (3)$$

Thus, the cyclic voltammetric study gives an idea of the stability of the parent dimanganese(III/III) complexes with respect to disproportionation. A similar behaviour was reported for other binuclear manganese(III/III) complexes.[25] The reduction potential for $Mn_2^{III/IV}$ species is low compared to the other fully exogenous $(\mu\text{-O})(\mu\text{-OAc})_2$ triply bridged complexes.[26,27] The mixed-valence complexes are stable on the cyclic-voltammetric time scale. A reduction potential in acetonitrile of $E_{1/2} \approx +1.05$ V was measured for a functional model of Mn catalase possessing an alkoxo-bridged core structure.[28] The results described in this section indicate that the $Mn^{II}Mn^{III}$, Mn_2^{III} and $Mn^{III}Mn^{IV}$ oxidation states are accessible for complex **6a** in methanol.

Variation of the terminal arms of the ligand and the single exogenous bridging group to get different homo- and heterodinuclear complexes is currently under investigation. To suppress the deviation in redox potentials for successive electron transfers, charge neutralization within the complex, perhaps by proton release (from coordinated H_2O) or uptake of Cl^- (replacement of coordinated H_2O), might provide the requisite adjustment in redox potentials. Studies in that direction are also in progress.

Conclusion

It has been shown that the nitrogen-oxygen donor Schiff base ligand H_3L, with imidazolidine bridging groups, can be easily synthesized in high yields in a step-wise condensation reaction from the hexadentate precursor ligand with ethylenediamine back-bone. The ligand forms an interesting class of dimanganese complexes, and can serve as multi-electron reservoir showing stepwise electron transfer behaviour. The stability of the dimanganese(III/III) complexes of different but similar types of parent ligand such as H_3L could be compared with respect to the electrochemically generated $Mn^{III}Mn^{IV}$ and $Mn^{III}Mn^{II}$ species.

Experimental Section

Physical Measurements: Microanalyses (C, H N) were performed using a Perkin−Elmer 240 C elemental analyser. IR spectra were obtained on a Perkin−Elmer 883 spectrometer (200−4000 cm^{-1}) prepared as KBr pellets. Electronic spectra were recorded on a Shimadzu UV/Vis/NIR 3100 (190−3200 nm) (MeOH, 1 cm quartz cell) spectrometer. Magnetic susceptibilities were measured using a home built Gouy balance fitted with a polytronic DC power supply. Diamagnetic corrections for ligand susceptibilities were made using Pascal's constants. ^1H and ^{13}C NMR spectra were obtained on a Bruker AC 200 NMR spectrometer using TMS as the internal standard. Electrochemical measurements were made using a PAR model 173 potentiostat/galvanostat, 175 universal programmer, 178 electrometer, and 377-cell system. A planar Beckaman 39273 platinum-disk working-electrode, a platinum-wire auxiliary-electrode, and an aqueous saturated calomel reference electrode (SCE) were used in a three-electrode configuration. A digital series 2000 Omni Graphic recorder was used to trace the voltammograms. Electrochemical measurements were made under a dinitrogen atmosphere. All chemical data were collected at 298 K and are uncorrected for junction potentials. Solution electrical conductivity was measured using a Unitech type UI31C digital conductivity meter with a solute concentration of about 10^{-3}.

Materials: Triethylenetetramine (trien) was obtained from S.D. Fine Chem, India. Salicylaldehyde and 2,4-pentanedione were purchased from SRL, India and S.D. Fine Chem, India, respectively. All other chemicals and solvents were reagent grade materials and were used as received without further purification. Purification of methanol and preparation of tetraethylammonium perchlorate (TEAP) for electrochemical work was performed as reported in the literature.[29]

1,3-Bis[3-aza-3-(1-methyl-3-oxobut-1-enyl)-prop-3-en-1-yl]-2-(2-hydroxyphenyl)-1,3-imidazolidine (H_3L): A solution of trien (7.00 g, 47.8 mmol) in methanol (50 mL) was added to an ice-cold solution of acetylacetone (9.57 g, 95.6 mmol) in methanol (100 mL). The resulting pale-yellow solution was stirred for ca. 15 min. at 0 °C. The hexadentate precursor diketone is a yellow oily product and was not isolated for the synthesis of **4**. In the next step, a solution of salicylaldehyde (5.84 g, 47.8 mmol) in methanol (50 mL) was added to the previous solution of diketone. The yellow solution was then stirred, initially at 0 °C for 15 min., and finally at ambient temperature (30 °C) for 23 h. The solution was then evaporated to dryness to give a yellow crystalline compound. The product was isolated by filtration, washed with water and hexane, and finally dried in vacuo over fused $CaCl_2$ for a total yield of 15.46 g (78%), m.p. 85−87 °C. − $C_{23}H_{34}N_4O_3$ (414.55): calcd. C 66.64, H 8.27, N 13.52; found C 66.52, H 8.16, N 13.57. − MS (EI): *m/z* = 414 [M^+]. − IR (KBr): $\tilde{\nu}$ = 1605 cm^{-1} (vs, $\nu_{C=N}$), 1546, 1443 (s, $\nu_{C=C}$). − ^1H NMR (200 MHz, $CDCl_3$): δ = 1.76 (s, 6 H, g), 2.65 (m, 4 H, a), 2.77 (m, 8 H, b, c), 6.79 (m, 2 H, 3,5), 10.73(H, b, phenolic OH). − ^{13}C NMR (50 MHz, $CDCl_3$): δ = 18.55 (g), 28.65 (h), 42.17 (a), 50.95 (b), 52.04 (c), 89.33 (i), 95.62 (e), 116.87 (3), 118.82 (5), 120.34 (1), 130.35 (6), 130.80 (4), 158.03 (2), 162.70 (d), 194.99 (f).

Preparation of the Dimanganese(III/III) Complexes: All manipulations were carried out under aerobic conditions. Since many of the syntheses are similar, a detailed procedure is given only for a representative example.

$[Mn_2(\mu\text{-}L)(\mu\text{-}Cl)(H_2O)_2]Cl_2$: Solid $MnCl_2{\cdot}4H_2O$ (0.477 g, 2.41 mmol) was added in portions during 15 min. to a solution of H_3L (0.5 g, 1.206 mmol) in methanol (20 mL). The resulting brown solution was stirred with a magnetic stirrer in air for 1 h at ambient temperature for complete oxidation of all Mn^{2+} centres to Mn^{3+}. The solution was then evaporated to dryness to give a brown gummy mass. A solid brown powder was obtained from this mass after trituration with hexane, collection by filtration, washing thoroughly with a little cold water to remove the produced NaCl, and washing with hexane. The compound was finally dried in vacuo over P_4O_{10}. Yield 0.714 g (89%). − $C_{23}H_{35}Cl_3Mn_2N_4O_5$ (663.79): calcd. C 41.62, H 5.31, N 8.44, Mn 16.55; found C 41.55, H 5.28, N 8.50, Mn 16.59. − IR (KBr): $\tilde{\nu}$ = 3394 cm^{-1} (b), 1612 (vs), 1536 (s), 1441 (s), 1386 (s), 1298 (s).

$[Mn_2(\mu\text{-}L)(\mu\text{-}OMe)(H_2O)_2]Cl_2$: Solid $MnCl_2{\cdot}4H_2O$ (0.477 g, 2.41 mmol) was added in portions during 15 min. to a solution of H_3L (0.5 g, 1.206 mmol) and NaOMe (0.07 g, 1.30 mmol) in methanol (30 mL). The resulting brown solution was stirred with a magnetic stirrer in air for 1 h at ambient temperature. The solution was then evaporated to dryness to yield a brown gummy mass. A solid brown powder was obtained after trituration with hexane, collection by filtration and washing thoroughly with hexane. The compound was finally dried in vacuo over P_4O_{10}. Yield 0.692 g (87%). − $C_{24}H_{38}Cl_2Mn_2N_4O_6$ (659.37): calcd. C 43.72, H 5.81, N 8.49, Mn 16.66; found C 43.66, H 5.86, N 8.52, Mn 16.72. − IR (KBr): $\tilde{\nu}$ = 3400 cm^{-1} (b), 1612 (vs), 1509 (s), 1440 (s), 1385 (s), 1296 (s).

$[Mn_2(\mu\text{-}L)(\mu\text{-}OEt)(H_2O)_2]Cl_2$: This compound was prepared following the above procedure, except that ethanol was used as solvent and stirring was continued for 1 h. − $C_{25}H_{40}Cl_2Mn_2N_4O_6$ (673.39): calcd. C 44.59, H 5.99, N 8.32, Mn 16.32; found C 44.51, H 6.01, N 8.37, Mn 16.41. − IR (KBr): $\tilde{\nu}$ = 3394 cm^{-1} (b), 1610 (vs), 1510 (s), 1438 (s), 1390 (s), 1296 (s).

X-ray Crystallography: Orange prismatic crystals of ligand **1** were obtained by slow diffusion of hexane into a dichloromethane solution of H_3L. Selected crystal data and data collection parameters are given in Table 3. The unit cell parameters were determined by the usual procedure of random searching followed by indexing. The plate-like yellow crystal selected for data collection was mounted at the end of a quartz fibre and covered with a thin layer of epoxy resin. Data were collected on an Enraf−Nonius CAD-4 diffractometer with PC control,[30] using graphite-monochromated Mo-K_α radiation (λ = 0.71073 Å) by ω scans within the angular range 4.0−45.0°. The structure was solved by direct methods[31] in the monoclinic space group $P2_1/c$, which is the only space group in either the orthorhombic or monoclinic system consistent with the systematic absences found in the data. All non-hydrogen atoms were refined anisotropically. All data were used in the least-squares calculations[32] and the structure was refined to F_o^2. There was no significant residual electron density in a final difference Fourier map. The detailed experimental write-up and comments on the structure determination are given as Supplementary Material.

Table 3. Crystallographic data for $H_3L{\cdot}2H_2O$

Empirical formula	$C_{23}H_{34}N_4O_3{\cdot}H_2O$
M_r	432.56
System	Monoclinic
Space group	$P2_1/c$
a/Å	13.587(7)
b/Å	18.170(11)
c/Å	19.283(13)
β/°	90.09(8)
U/Å^3	4761(5)
Z	8
D_c/g cm^{-3}	1.207
Radiation(λ/Å)	Mo-K_α (0.71073), graphite monochromated
Crystal size/mm	0.59 × 0.34 × 0.15
T, °C	−123 ± 1
Scan method	ω-scans
θ Range for data collection/°	4.0−45.0
μ/cm^{-1}	8.3
Data, restraints, parameters	4400, 2, 582
R[a]	0.0624
R_w[b]	0.1626
Goodness of fit on F^2	1.007
Largest difference peak and trough/e Å^{-3}	0.37, −0.41
$(shift/e.s.d.)_{max}$	0.033

[a] $R = \Sigma||F_o| - |F_c||/\Sigma|F_o|$. − [b] $R_w = \Sigma w(|F_o| - |Fc|)^2/\Sigma w(F_o)^2]^{1/2}$.

Crystallographic data (excluding structure factors) for the structure reported in this paper have been deposited with the Cambridge Crystallographic Data Centre as supplementary publication no. CCDC-152200. Copies of the data can be obtained free of charge on application to CCDC, 12 Union Road, Cambridge CB2 1EZ, UK [Fax: (internat.) +44-1223/336-033; E-mail: deposit@ccdc.cam.ac.uk].

Acknowledgments

Financial assistance received from the Indian National Science Academy, New Delhi [Grant No. BS/YSP-1/3471] and the Directorate General for Higher Education, Spain [Grant No. PB95−0792], is gratefully acknowledged.

[1] [1a] P. E. Kruger, B. Moubaraki, K. S. Murray, E. R. T. Tiekink, *J. Chem. Soc., Dalton Trans.* **1994**, 2129−2134. − [1b] D. E. Fenton, H. Okawa, *J. Chem. Soc., Dalton Trans.* **1993**, 1349−1357. − [1c] A. M. Bond, M. Haga, I. S. Creece, R. Robson, J. C. Wilson, *Inorg. Chem.* **1989**, *28*, 556−559. − [1d] L. J. Farrugia, P. A. Lovatt, R. D. Peacock, *J. Chem. Soc., Dalton Trans.* **1997**, 911−912. − [1e] V. Alexander, *Chem. Rev.* **1995**, *95*, 273−342.

[2] [2a] O. Kahn, *Molecular Magnetism*, VCH, New York, Weinheim, Cambridge, **1993**, ch. 8, p. 164. − [2b] O. Kahn, *Adv. Inog. Chem.* **1995**, *43*, 179−259. − [2c] S. S. Tandon, L. K. Thompson, J. N. Brideson, *J. Chem. Soc., Chem. Commun.* **1993**, 804−806. − [2d] C. A. Reed, *Research Frontiers in Magnetochemistry* (Ed.: C. J. O'Connor), World Scientific Publishing Co., Singapore, New Jersey, London, Hong Kong, **1993**, p. 351.

[3] L. Que, Jr., A. E. True, *Prog. Inorg. Chem.* **1990**, *38*, 97−200.

[4] P. N. Howells, J. W. Kenny, J. H. Nelson, R. A. Henry, *Inorg. Chem.* **1976**, *15*, 124−129.

[5] [5a] V. L. Pecoraro, *Manganese Redox Enzymes*, VCH Publishers, New York, **1992**. − [5b] Y. Kono, I. Fridovich, *J. Biol. Chem.* **1983**, *2588*, 6015−6019. − [5c] G. S. Aldood and J. J. Perry, *J. Bacteriol.* **1986**, *168*, 563−567. − [5d] V. V. Barynin, A. I. Givebenko, *Dokl. Akad. Nauk, SSSR* **1986**, *286*, 461−464. − [5e] R. M. Fronko, J. E. Penner-Hahn, C. J. Bender, *J. Am. Chem. Soc.* **1988**, *110*, 7554−7555. − [5f] S. V. Khangulov, V. V. Barynin, S. V. Antonyk-Barynina, *Biochem. Biophys. Acta* **1990**, *1020*, 25−33. − [5g] S. V. Khangulov, V. V. Barynin, N. V. Voevodskaya, A. I. Grebenko, *Biochem. Biophys. Acta* **1990**, *1020*, 305−310. − [5h] G. S. Waldo, R. M. Franko, J. E. Penner-Hahn, *Biochemistry* **1991**, *30*, 10486−10490. − [5i] G. S. Waldo, S. Yu, J. E. Penner-Hahn, *J. Am. Chem. Soc.* **1992**, *114*, 5869−5870.

[6] [6a] M. Atta, P. Nordlund, A. Aaberg, H. Eklund, M. Fontecave, *J. Biol. Chem.* **1992**, *267*, 20682−20688. − [6b] R. Cammack, A. Chapman, W. P. Lu, A. Karagomi, D. P. Kelly, *FEBS Lett.* **1989**, *253*, 239−243.

[7] [7a] M. Delroisse, A. Rabion, F. Chardac, D. Tétard, J.-B. Verlhac, L. Fraisse, J.-L. Séris, *J. Chem. Soc., Chem. Commun.* **1995**, 949−950. − [7b] P. Mathur, M. Crowder, G. C. Dismukes, *J. Am. Chem. Soc.* **1987**, *109*, 5227−5233. − [7c] E. J. Larsen, V. L. Pecoraro, *J. Am. Chem. Soc.* **1991**, *113*, 3810−3818. − [7d] E. J. Larsen, V. L. Pecoraro, *J. Am. Chem. Soc.* **1991**, *113*, 7809−7810. − [7e] Y. Naruta, K. Maruyama, *J. Am. Chem. Soc.* **1991**, *113*, 3595−3596. − [7f] T. Nagata, Y. Ikawa, K. Maruyama, *J. Chem. Soc., Chem. Commun.* **1994**, 471−472. − [7g] Y. Nishida, M. Nasu, *Inorg. Chim. Acta* **1991**, *190*, 1−3. − [7h] U. Bossek, M. Saher, T. Weyhermueller, K. Weighardt, *J. Chem. Soc., Chem. Commun.* **1992**, 1780−1782. − [7i] H. Sakiyama, H. Okawa, R. Isobe, *J. Chem. Soc., Chem. Commun.* **1993**, 882−884. − [7j] D. R. Gamelin, M. L. Kirk, T. L. Stemmler, S.

Pal, W. H. Armstrong, J. E. Penner-Hahn, E. I. Solomon, *J. Am. Chem. Soc.* **1994**, *116*, 2392−2399. − [7k] A. Gelasco, M. L. Kirk, J. W. Kampf, V. L. Pecoraro, *Inorg. Chem.* **1997**, *36*, 1829−1837. − [7l] A. Gelasco, S. Bensiek, V. L. Pecoraro, *Inorg. Chem.* **1998**, *37*, 3301−3309. − [7m] C. Palopoli, B. Chanson, J.-P. Tuchagues, S. Signorella, *Inorg. Chem.* **2000**, *39*, 1458−1462.

[8] G. S. Waldo, J. E. Penner-Hahn, *Biochemistry* **1995**, *34*, 1507−1512.

[9] A. Boussac, A. W. Rutherford, *Biochem. Soc. Trans.* **1994**, *22*, 352−358.

[10] [10a] P. O. Sandusky, C. F. Yocum, *Biochim. Biophys. Acta* **1986**, *849*, 85−93. − [10b] C. F. Yocum, *Biochim. Biophys. Acta* **1991**, *1059*, 1−15. − [10c] K. Lindberg, L.-E. Andréasson, *Biochemistry* **1996**, *35*, 14259−14267.

[11] V. L. Pecoraro, W. M. Butler, *Acta Crystallogr., Sect. C* **1986**, *42*, 1151−1154.

[12] N. A. Law, T. E. Machonkin, J. P. McGorman, E. J. Larson, J. W. Kampf, V. L. Pecoraro, *J. Chem. Soc., Chem. Commun.* **1995**, 2015−2016.

[13] A. Rompel, J. C. Andrews, R. M. Cinco, M. W. Wemple, G. Christou, N. A. Law, V. L. Pecoraro, K. Sauer, V. K. Yachandra, M. P. Klein, *J. Am. Chem. Soc.* **1997**, *119*, 4465−4470.

[14] B. D. Sarma, J. C. Bailar Jr., *J. Am. Chem. Soc.* **1955**, *77*, 5476−5480.

[15] B. D. Sarma, K. R. Ray, R. E. Sievers, J. C. Bailar Jr., *J. Am. Chem. Soc.* **1964**, *86*, 14−16.

[16] T. Isobe, S. Kida, S. Misumi, *Bull. Chem. Soc. Jpn.* **1967**, *40*, 1862−1863.

[17] N. A. Bailey, E. D. McKenzie, J. M. Worthington, M. McPartlin, P. A. Tasker, *Inorg. Chim. Acta* **1977**, *25*, L137−L138.

[18] B. W. Tsang, C. J. Mathias, M. A. Green, *J. Nucl. Med.* **1993**, *34*, 1127−1131.

[19] L.-W. Yang, S. Liu, E. Wong, S. J. Rettig, C. Orvig, *Inorg. Chem.* **1995**, *34*, 2164−2178.

[20] P. E. Kruger, B. Moubaraki, K. S. Murray, *Polyhedron* **1997**, *16*, 2659−2665.

[21] J.-P. Costes, J.-F. Serra, F. Dahan, J.-P. Laurent, *Inorg. Chem.* **1986**, *25*, 2790−2795.

[22] U. Mukhopadhyay, L. Govindasamy, K. Ravikumar, D. Velmurugan, D. Ray, *Inorg. Chem. Commun.* **1998**, *1*, 152−154.

[23] G. Alzuet, L. Casella, M. L. Villa, O. Carugo, M. Gullotti, *J. Chem. Soc., Dalton Trans.* **1997**, 4789−4794.

[24] S.-B. Yu, C.-P. Wang, E. P. Day, R. H. Holm, *Inorg. Chem.* **1991**, *30*, 4067−4074.

[25] [25a] K. Wieghardt, V. Bossek, D. Ventur, J. Weiss, *J. Chem. Soc., Chem. Commun.* **1985**, 367−368. − [25b] J. E. Sheats, R. S. Czernuszewicz, G. C. Dismukes, A. L. Rheingold, V. Petrouleas, A. Stubbe, W. H. Armstrong, R. H. Beer, S. J. Lippard, *J. Am. Chem. Soc.* **1987**, *109*, 1435−1444.

[26] [26a] S. Mahapatra, T. K. Lal, R. Mukherjee, *Inorg. Chem.* **1994**, *33*, 1579−1580. − [26b] T. K. Lal, R. Mukherjee, *Inorg. Chem.* **1998**, *37*, 2373−2382.

[27] S. K. Mandal, W. H. Armstrong, *Inorg. Chim. Acta* **1995**, *229*, 261−270.

[28] [28a] P. J. Pessiki, S. V. Khangulov, D. M. Ho, G. C. Dismukes, *J. Am. Chem. Soc.* **1994**, *116*, 891−897. − [28b] P. J. Pessiki, G. C. Dismukes, *J. Am. Chem. Soc.* **1994**, *116*, 898−903.

[29] [29a] D. T. Sawyer, J. L. Roberts, Jr. *Experimental Electrochemistry for chemists*, Wiley, New York, **1974**, pp. 167−215. − [29b] M. Walter, L. Ramaley, *Anal. Chem.* **1973**, *45*, 165−166. − [29c] D. D. Perrin, W. L. F. Armango, D. R. Perrin, *Purification of Laboratory Chemicals*, Pergamon, Oxford, **1980**.

[30] Diffractometer control program: CAD4/PC version 2.0, **1996** Nonius bv, Delft, The Netherlands.

[31] G. M. Sheldrick, SHELXS-97: Fortran *program for crystal structure solution*, **1997**.

[32] G. M. Sheldrick, SHELXS-97: Fortran *program for crystal structure refinement*, **1997**.

Received March 19, 2001
[I01101]

Fluorine Route Synthesis of Montmorillonites Containing Mg or Zn and Characterization by XRD, Thermal Analysis, MAS NMR, and EXAFS Spectroscopy

Marc Reinholdt,*[a,b] Jocelyne Miehé-Brendlé,[a] Luc Delmotte,[a] Marie-Hélène Tuilier,[b] Ronan le Dred,[a] Robert Cortès,[c] and Anne-Marie Flank[c]

Keywords: Montmorillonite / Clays / Synthesis / Fluorine / Solid-state NMR / EXAFS spectroscopy

EXAFS spectroscopy, combined with X-ray powder diffraction, chemical and thermal analysis, scanning electronic microscopy, ^{29}Si, ^{27}Al, and ^{19}F MAS NMR spectroscopy, are used in the structural analysis of montmorillonites, synthesised in an acidic fluoride medium. Hydrothermal synthesis performed under mild conditions (493 K, autogenous pressure) enables the formation of montmorillonite clays, containing Al and Zn or Mg in the octahedral sheet. It is shown that montmorillonites can only be synthesized in a narrow range of compositions. An accurate value of the Al for Si substitution rate in the tetrahedral sheet is determined by using ^{27}Al MAS NMR spectroscopy performed under definite conditions. Some interatomic distances are determined by EXAFS spectroscopy (R_{Mg-O} = 2.11 Å, R_{Zn-O} = 2.08 Å, R_{Zn-Al} = 2.98 Å, R_{Zn-Zn} = 3.11 Å) which reveals strong local distortions in the octahedral sheet with respect to the ideal montmorillonite structure. Lengthening of the out-of-plane Zn–Si(Al) distances also shows the swelling of the whole layer in the neighbourhood of Zn. Moreover, the combination of EXAFS and ^{19}F MAS NMR spectroscopic data reveals a clustering of the divalent elements of the octahedral sheet, which is related to a possible local trioctahedral character of these materials.

Introduction

Smectites present in soils and sediments are one of the largest and most important classes of the phyllosilicate clay minerals group. Their ability to swell upon contact with water and other solvents is extensively used in two fields of application. The first one is related to the properties of adsorption (use in the selective adsorption of toxic compounds from water, detergents, organic chemistry, etc.).[1] The other one concerns pillared clays which are commonly used in the field of catalysis.[2,3] The 2:1 structure of smectites consists of two sheets of distorted SiO_4 tetrahedra connected by a sheet of $Al(M)(OH)_2O_4$ octahedra, M being a divalent element (Figure 1a). The silicon and metal atoms occupy the centre of the tetrahedra or the octahedra, with the oxygen atoms and hydroxy groups (OH) located at the corners. Smectites are divided into two groups: the dioctahedral smectites for which the octahedral sheet contains two Al(M) elements in the centre of two out of three octahedra, the third one being vacant; and the trioctahedral smectites which contain only divalent elements in the octahedral sheet without vacancies. Montmorillonite, which belongs to the former group, has been extensively studied. Among the dioctahedral smectites, the distinctive feature of montmorillonite is that transition elements are included in the octahedral sheet whereas Al can be split into the tetrahedral (Al_{IV}) and octahedral (Al_{VI}) sheets. The Al atoms are partially replaced by either Mg or Fe atoms, thereby creating a charge deficiency within the unit structure. This results in a small negative charge on the basal plane of the silica tetrahedra which is balanced by exchangeable cations present in the interlayer spacing. In natural montmorillonites these cations are usually calcium or sodium according to the weather agent associated with the formation of the mineral. The crystal structure of montmorillonite has a *C*2*mm* symmetry.

The ideal formula per half a unit cell, without tetrahedral substitution, is $R_{2x}(Al_{2(1-x)}M_{2x}\ \square)Si_4O_{10}(OH)_2$, where R represents the interlayer cations and x the layer charge ranging from 0.05 to 0.54. Natural montmorillonites usually present isomorphic substitutions in both tetrahedral and octahedral layers. Moreover, depending on the deposits, various structural compositions and particle sizes can be found. These drawbacks, combined with the presence of impurities, limit their use in some applications. One way to avoid these disadvantages is to synthesize such compounds; this enables the control of the chemical composition by fine tuning the preparative methods. Many studies have been performed in this field, as recently mentioned by Kloprogge et al., but only four papers mentioned the synthesis of pure montmorillonite.[4] The first one, by Otsubo and Kato, described Zn for Al partially substituted montmorillonite in the $ZnO-Al_2O_3-SiO_2$ system,[5] the Zn and Al atoms being located in the octahedral sheet and the Si atoms in the tetrahedral sheet. The clay has been prepared under hydrothermal conditions in an alkali medium at temperatures

[a] Laboratoire des Matériaux Minéraux, UPRES-A 7016, 3 rue A. Werner, 68093 Mulhouse Cedex, France
[b] Laboratoire de Physique et Spectroscopie Electronique, UPRES-A 7014, 4 rue des Frères Lumière, 68093 Mulhouse Cedex, France
[c] Laboratoire pour l'Utilisation du Rayonnement Electromagnétique (LURE), Bât 209D, Centre Universitaire, B. P. 34, 91898 Orsay Cedex, France

 © WILEY-VCH Verlag GmbH, 69451 Weinheim, 2001 1434–1948/01/1111–2831 $ 17.50+.50/0

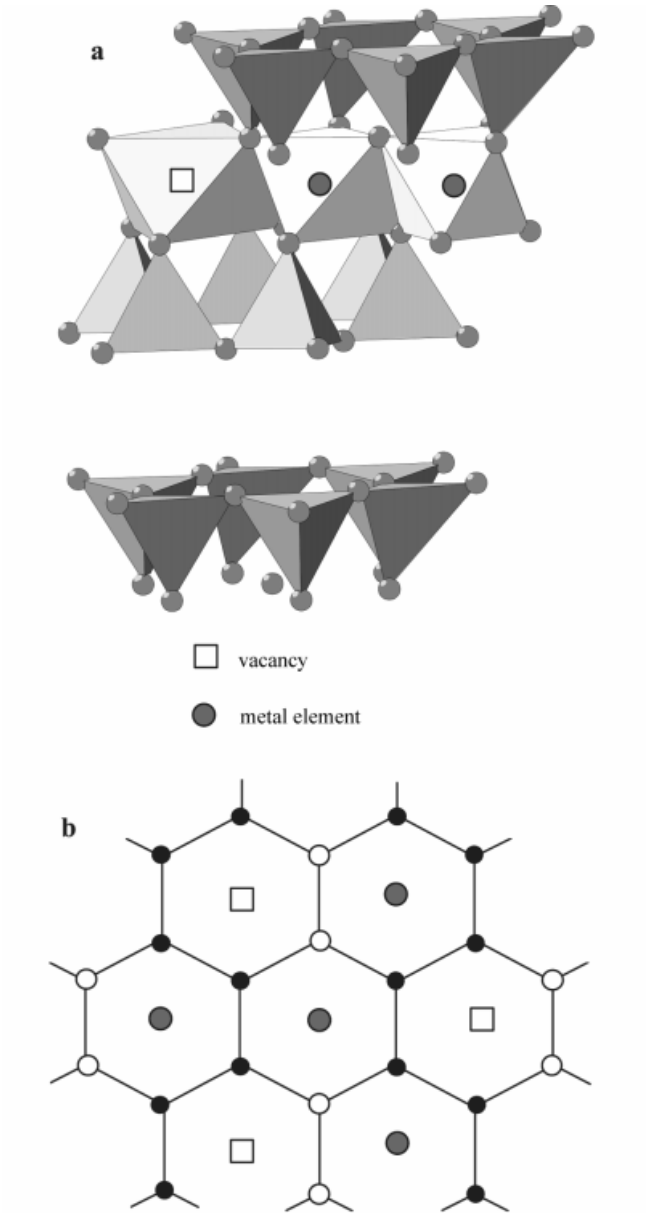

Figure 1. Layer of a 2:1 phyllosilicate (a) and hexagonal cavities (b) of the octahedral sheet of a 2:1 phyllosilicate

ranging from 423 to 573 K, over 5 to 20 h. The second synthesis, described by Harder, was carried out on the basis of the precipitation of hydroxides, in the $MgO-Al_2O_3-SiO_2$ system in an alkali to neutral medium at 276 and 293 K.[6] The same system was studied by Nakazawa et al., but syntheses were performed on magnesium aluminosilicate glass under a hydrothermal pressure of 100 Mpa.[7] A more recent work was also performed in an alkali medium, by Nagase et al., in the $MgO-Fe_2O_3-SiO_2$ system under hydrothermal conditions at 373 and 473 K for 24 h.[8] Samples were characterised by X-ray diffraction (XRD), thermal and chemical analyses, electronic microscopy, or X-ray photoelectron spectroscopy (XPS). None of these studies have brought any information about the distribution of the elements in the structure and their local environment.

The present paper deals with the synthesis of montmorillonites in the $MgO-Al_2O_3-SiO_2$ and $ZnO-Al_2O_3-SiO_2$ systems. Starting from the previously mentioned ideal formula per half a unit cell, we introduced an increasing amount of divalent element (x ranging from 0 to 1) in the hydrogel in order to establish the best conditions to obtain montmorillonite. Samples were labelled Mg($10 \times x$) or Zn($10 \times x$) (Table 1). Syntheses were performed in acidic and fluoride media. Similarly, mild conditions were previously used for the preparation of dioctahedral smectites, such as beidellite,[9,10] and trioctahedral smectites, such as stevensite.[11] In the present work, samples were characterised by XRD, thermal, and chemical analyses. Some of them were selected for further structural investigation by solid-state nuclear magnetic resonance spectroscopy (NMR) and X-ray absorption spectroscopy (XAS), in order to study the local environment of the metallic elements. An explanation of the process of formation of montmorillonite is suggested.

Table 1. Labels of the samples

Sample[a]	x	Theoretical formula[b]
M01	0.1	$Na_{0.2}(Al_{1.8}M_{0.2}\,\square)Si_4O_{10}(OH)_2$
M02	0.2	$Na_{0.4}(Al_{1.6}M_{0.4}\,\square)Si_4O_{10}(OH)_2$
M03	0.3	$Na_{0.6}(Al_{1.4}M_{0.6}\,\square)Si_4O_{10}(OH)_2$
M04	0.4	$Na_{0.8}(Al_{1.2}M_{0.8}\,\square)Si_4O_{10}(OH)_2$
M05	0.5	$Na_{1.0}(Al_{1.0}M_{1.0}\,\square)Si_4O_{10}(OH)_2$
M06	0.6	$Na_{1.2}(Al_{0.8}M_{1.2}\,\square)Si_4O_{10}(OH)_2$
M07	0.7	$Na_{1.4}(Al_{0.6}M_{1.4}\,\square)Si_4O_{10}(OH)_2$
M08	0.8	$Na_{1.6}(Al_{0.4}M_{1.6}\,\square)Si_4O_{10}(OH)_2$
M09	0.9	$Na_{1.8}(Al_{0.2}M_{1.8}\,\square)Si_4O_{10}(OH)_2$
M10	1.0	$Na_{2.0}(M_{2.0}\,\square)Si_4O_{10}(OH)_2$

[a] M represents Mg or Zn. – [b] □ Represents the vacancy.

Results

X-ray Powder Diffraction

XRD patterns of the two series of samples are characteristic of clays (Figure 2). Each diffractogram exhibits *hkl* bands at 4.45–4.48 Å (020, 110), 2.52–2.58 Å (130, 200) and 1.67–1.70 Å (210), which are typical features of smectites.[12] One or two peaks are also observed between 1.48 and 1.53 Å; they correspond to the (060) and (330) reflections. Their relative intensity is related to the dioctahedral (peak at about 1.49 Å) or trioctahedral (peak at about 1.52 Å) nature of the product, i.e. a dioctahedral compound has vacancies in the octahedral sheet and a trioctahedral one has none. The position of the (001) peak gives information about the basal spacing (d_{001}). The basal spacing is equal to the sum of the interlayer spacing and the thickness of the silicate layer, which is about 9.6 Å for a 2:1 phyllosilicate. The usual value of d_{001} is about 15 Å for natural montmorillonites under a relative humidity of $P/P_0 = 80\%$ (P represents the saturated vapour pressure over the sample at 298 K and P_0 the saturated aqueous vapour pressure at 298 K).

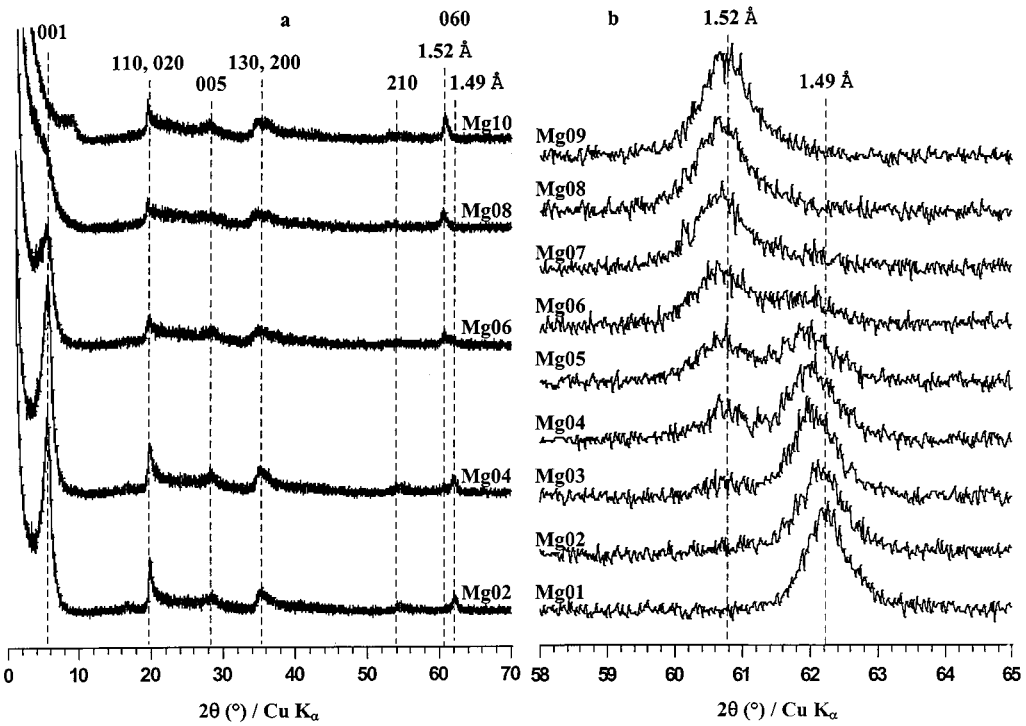

Figure 2. Comparison of the XRD patterns of synthetic clays containing various amount of Mg (P/P_0 = 80%) (a) and evolution of the position of the (060) peak with this amount (b)

A sample which has $x = 0.0$ is unambiguously identified as kaolinite (DRX and TGA-DTA). The Mg01 sample is a dioctahedral clay (d_{060} = 1.49±0.01 Å, Table 2) and the Mg02 sample could have a small trioctahedral component (see next section). Samples Mg03 to Mg06 are mixtures of di- and trioctahedral compounds. Their XRD patterns present two (060) bands, one at 1.49±0.01 Å and a second at 1.52±0.01 Å. For samples Mg07 to Mg09, d_{060} is equal to 1.52±0.01 Å. This value corresponds to trioctahedral compounds. The Mg10 sample is identified as a talc-type clay (probably stevensite) which is trioctahedral, with silicon in the tetrahedral sheet and magnesium in the octahedral sheet. The (001) peak is observed for each sample, except Mg08 and Mg09. This is characteristic of a higher disorder and a lower crystallinity of the samples. The Zn01 sample has the position of the (060) peak corresponding to a dioctahedral compound (d_{060} = 1.49±0.01 Å, Table 2). The Zn02 sample could have a little trioctahedral component (see next section). Similarly to the Mg series, the Zn03 to Zn06 samples are mixtures of di- and trioctahedral clays and the Zn07 to Zn09 samples have the structure of trioctahedral compounds (d_{060} = 1.52±0.01 Å). Each diffractogram of Zn(10 × x) samples exhibits a (001) peak, contrary to some of the Mg(10 × x) samples. The Zn10 sample is identified as a mixture of an amorphous phase and willemite (Zn_2SiO_4). The investigation of samples containing a mixture of clays was not carried out beyond this preliminary characterisation. Trioctahedral products are also dismissed because of the presence of amorphous silica, observed by NMR spectroscopy (see the paragraph about solid-state NMR spectroscopy). Consequently, only the Mg01, Mg02, Zn01, and Zn02 samples will be further characterised. Their diffractograms exhibit the characteristic *hk* bands of montmorillonite.[12] The position of the (060) peak indicates the dioctahedral nature of the sample, i.e. the presence of vacancies in the octahedral sheet, except for the Mg02 and Zn02 samples, which can have a weak trioctahedral component at 1.52 Å (Figures 2 and 3 and discussion section). As a comparison, Figure 3 (inset) shows the diffractogram of a natural clay from Camp Berteau which contains quartz. The study of the (001) peak position was performed on samples which were previously placed under a controlled humidity (P/P_0 = 80%). The d_{001} values are listed in Table 2. These values are in good agreement with those indexed in the literature for natural Na-exchanged montmorillonites (d_{001} = 15−16 Å).[13−15] The (001) peaks are more symmetrical and intense than they are for samples containing Mg.

Scanning Electronic Microscopy

The micrographs of the Mg01 sample are presented in Figure 4. The picture shows crumpled platelets that look like gypsum flower. More compact aggregates are also observed. Natural montmorillonites present this typical morphology.[16−18] The samples of Mg01, Zn01, and Zn02 have a similar morphology.

Table 2. X-ray diffraction, and thermal analysis data of samples Mg01, Mg02, Zn01, and Zn02

Sample	XRD		TGA-DTA[a]		
	d_{001} [A]	d_{060} [A]	Dehydration [K]	Dehydroxylation [K] First peak	Second peak
Mg01	16.5	1.49	350	750	930
Mg02	16.1	1.49	360	–	930
Zn01	17.4	1.49	360	750	950
Zn02	16.4	1.49	365	730	940

[a] Temperatures are taken at the inflexion point of the weight losses on the TGA curves.

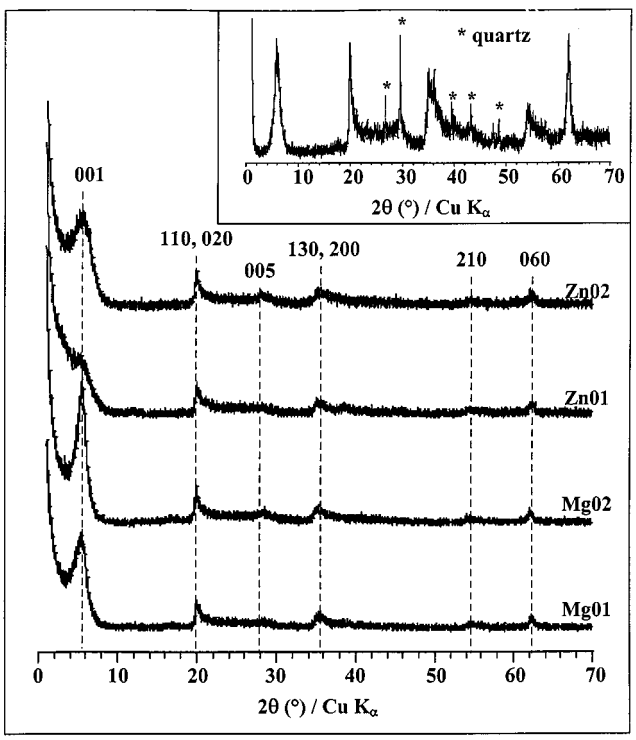

Figure 3. XRD patterns of synthetic montmorillonites containing Mg or Zn (P/P_0 = 80%); inset: diffractogram of natural montmorillonite from Camp Berteau

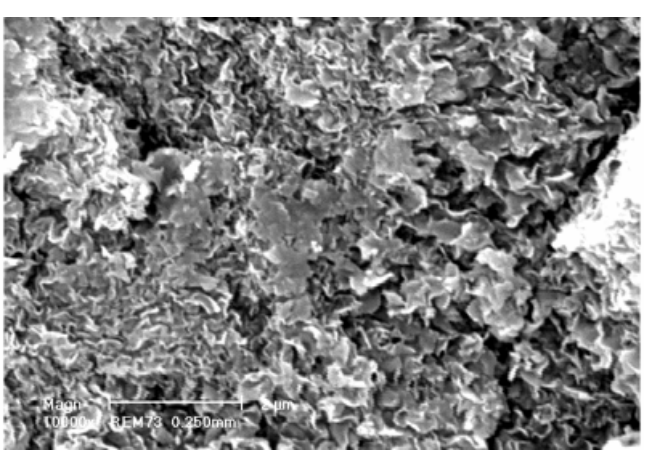

Figure 4. SEM micrograph of Zn02 sample

TGA-DTA

The curves of weight loss and heat flow versus temperature are shown in Figure 5. Each sample exhibits a main peak at 370 K corresponding to dehydration. Moreover, the Mg01, Zn01, and Zn02 samples exhibit two peaks, at about 720−760 K and 920−960 K, which are attributed to the dehydroxylation. The peaks of dehydroxylation are observed at 750 and 930 K for the Mg01 sample, 750 and 950 K for the Zn01 sample, and 730 and 930 K for the Zn02 sample (Figure 5). In the case of the Mg02 sample, only one dehydroxylation peak is observed at 930 K. The peak ranging from 920 to 960 K was already reported in the literature.[19−23] It is characteristic of natural montmorillonites. The peak ranging from 720 to 760 K was observed by Cuadros et al.[20] on DTA curves of samples coming from the deposit of "Los Trancos" in Almeria (SE Spain) and by Frost et al.[23] on ferruginous montmorillonite SWa-1 (Clay Mineral Society standard).

Chemical Analysis

The results of elemental analyses are listed in Table 3. Na and divalent element contents are higher, whereas the Al content is lower, in samples of Mg02 and Zn02 than in the Mg01 and Zn01 samples. The content of divalent element has roughly doubled in Mg02 (Zn02) with respect to Mg01 (Zn01). This is in good agreement with the theoretical compositions. It should be noted that there is a small amount of fluorine in each sample, so this element could only be considered as a local probe. The half unit cell formula was calculated for the four selected samples (last column of Table 3) on the basis of twenty two negative charges of the layer. However, chemical analysis does not enable one to determine whether Al is only in the octahedral sheet or if there is some Al in the tetrahedral sheet.

Solid-State NMR Spectroscopy

^{29}Si NMR spectroscopy, using the magic-angle spinning technique (^{29}Si MAS NMR), gives information on the Al-for-Si substitution in the tetrahedral sheet. In the case of trioctahedral products, the presence of a small quantity of amorphous silica was revealed by ^{29}Si MAS NMR spectroscopy. The ^{29}Si MAS NMR spectra of Mg01, Mg02, Zn01, and Zn02 samples (Figure 6) show signals corresponding to Si(nAl) (n ranges from 0 to 3) environments where n represents the number of tetrahedral Al atoms that are next-nearest neighbours of Si. The main peak, which appears at a chemical shift (δ) of $\delta \approx -93$ is assigned to the Si(0Al) environment, i.e. Si surrounded by three Si in the tetrahedral sheet.[24,25] The shoulder observed at $\delta \approx -90$ is attributed to the Si(1Al) environment, i.e. Si surrounded by one Al and two Si in the tetrahedral sheet. The presence of these signals indicates that Al is substituted for Si in the tetrahedral sheet, which could not be observed by chemical analysis. The shielding of the Si(0Al) site increases with the amount of Mg. The same behaviour is observed for the Zn01 and Zn02 samples but with an enhanced effect. These phenomena can be correlated to the increase of the average

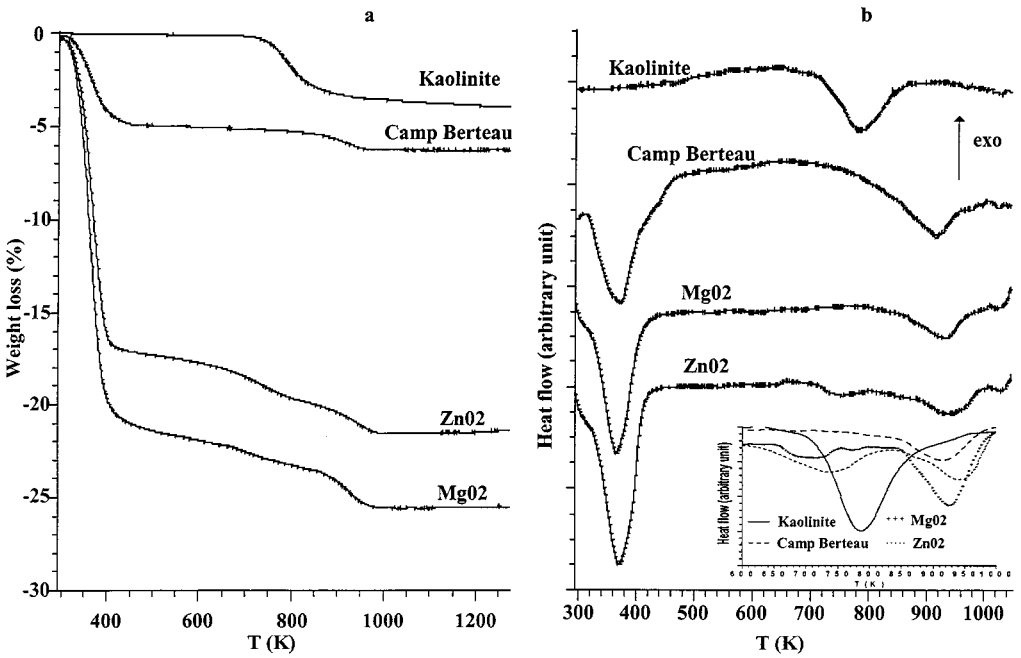

Figure 5. TG patterns of natural and synthetic clays (a) and ATD curves of the same samples (b); inset: comparison of the dehydroxylation peaks of each sample between 600 to 1000 K

Table 3. Half a unit cell formula calculated from chemical analysis for samples Mg01, Mg02, Zn01, and Zn02

Sample	Elemental analyses (mass-%)								Half a unit cell formula[a]
	Na_2O	MgO	ZnO	Al_2O_3	SiO_2	F	H_2O	sum	
Mg01	2.03	1.63	–	22.53	55.54	0.23	17.90	99.86	$Na_{0.28}[Al_{1.81}Mg_{0.18}\,\square_{1.01}]$-$[Si_{3.93}Al_{0.07}]O_{10}(OH_{1.95}F_{0.05})\cdot 3.3H_2O$
Mg02	2.34	3.40	–	19.02	55.00	0.20	19.95	99.91	$Na_{0.34}[Al_{1.64}Mg_{0.37}\,\square_{0.99}]$-$[Si_{4.00}]O_{10}(OH_{1.95}F_{0.05})\cdot 4.0H_2O$
Zn01	1.36	–	3.21	22.21	57.58	0.28	15.77	100.41	$Na_{0.17}[Al_{1.83}Zn_{0.17}\,\square_{1.00}]$-$[Si_{4.00}]O_{10}(OH_{1.94}F_{0.06})\cdot 2.8H_2O$
Zn02	1.98	–	6.90	18.30	55.70	0.20	19.25	102.33	$Na_{0.3}[Al_{1.64}Zn_{0.39}\,\square_{0.97}]$-$[Si_{4.00}]O_{10}(OH_{1.95}F_{0.05})\cdot 4.0H_2O$

[a] □ Represents the vacancy.

Si−O−Si bond angle[26] that was previously observed by Sanz and Serratosa.[24]

^{19}F MAS NMR spectroscopy confirms the substitution of fluoride ions for hydroxy groups, and reveals their environment.[11,27] Spectra (Figure 7) show several peaks with chemical shifts corresponding to various fluorine environments. In the spectrum of the Mg01 sample, two peaks are observed at δ = −133.3 and −153.0 which correspond to Al−Al−□ and Mg−Al−□ fluorine environments, respectively (□ represents a vacancy in the octahedral sheet). For the spectrum of the Mg02 sample, only the Mg−Al−□ peak is conserved at δ = −153.0 and another appears at δ = −177.0 which is characteristic of an Mg−Mg−Mg fluorine environment. The latter was previously observed for trioctahedral compounds like natural hectorite and synthetic mica-montmorillonite clay.[27] The two chemical shifts in the Zn01 and Zn02 samples are assigned to Al−Al−□ (δ = −132.8) and Zn−Al−□ (δ = −142.0 for Zn01 and δ = −142.4 for Zn02) fluorine sites, respectively.[11] The intensity of the former decreases whereas that of the latter increases as the Zn content increases. Consequently, ^{19}F MAS NMR spectroscopy shows the presence of Mg or Zn in the octahedral sheet and the presence of vacancies in the octahedral sheet.

^{27}Al MAS NMR spectroscopy indicates the localisation of Al in the structure.[24,28] The presence of Al_{VI} (δ = 2−3) and Al_{IV} (δ = 64−67) aluminium is observed in the structure (Figure 8). This is further proof for the Al-for-Si substitution in the tetrahedral sheet. The chemical shifts of Al_{VI} and Al_{IV} increase with the content of divalent element.

X-ray Absorption Spectroscopy (XAS)

The Zn *k*-edge extended X-ray absorption fine structure (EXAFS) spectra recorded from Zn01 and Zn02 montmorillonites are shown in Figure 9a, after background subtraction and conversion to *k*-space. There are no major differences between the data except for a slight enhancement of

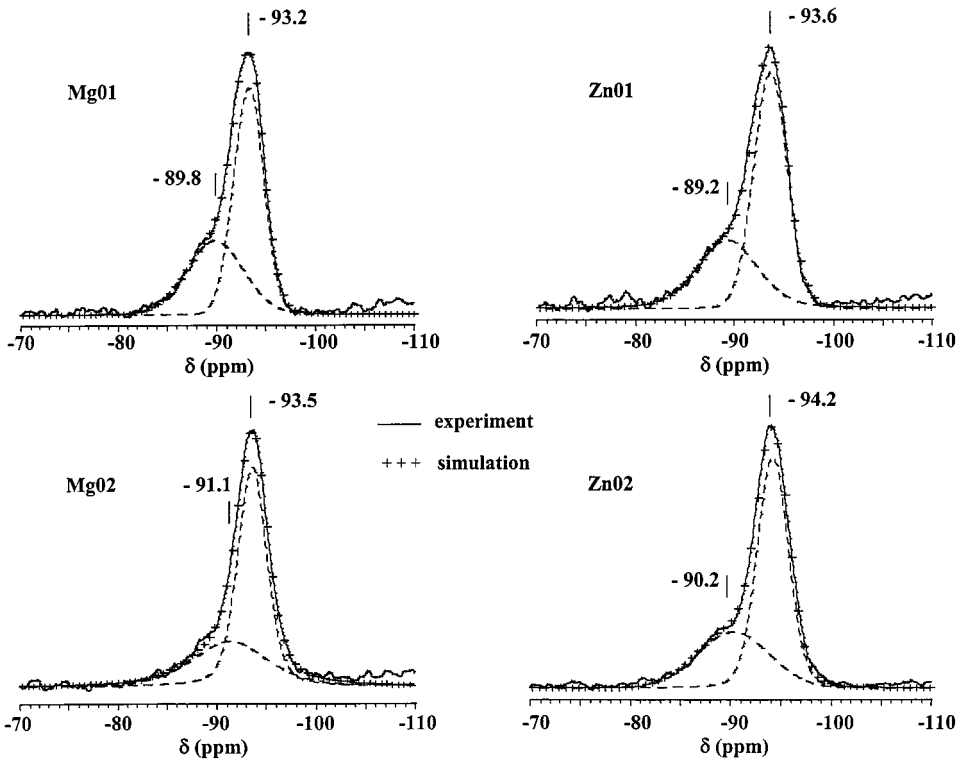

Figure 6. ^{29}Si MAS NMR spectra [standard reference $Si(CH_3)_4$] and corresponding simulations of the studied synthetic montmorillonites

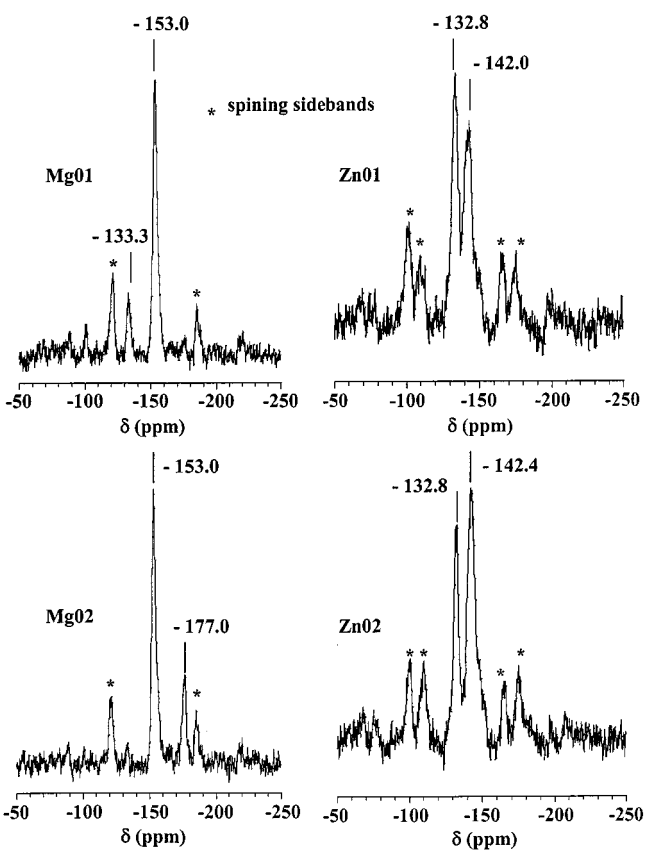

Figure 7. ^{19}F MAS NMR spectra of samples Mg01, Mg02, Zn01, and Zn02 (standard reference $CFCl_3$)

the high frequency oscillation for Zn02. The corresponding Fourier transforms (FT) between 0 and 8 Å are presented in Figure 9b. The main peak, which is assigned to the oxygen atom's nearest neighbours (NN), has the same position and amplitude for both samples. The structural parameters, derived from the simulation of the Fourier-filtered contribution of the NN peak, are reported in Table 4. Figure 10a compares the experimental and calculated curves. Zn is formed in octahedral coordination with O in agreement with the other characterisations; the average bond length is found to be 2.08 Å. The second and third peaks observed between 2 and 3.5 Å in FT (Figure 9 b) are not well separated and are related to Al and Zn next-nearest neighbours (NNN) in the octahedral sheet on one hand, and Si(Al) belonging to the tetrahedral sheets on the other hand. Some preliminary considerations have to be made before giving the results of the simulations. In the ideal montmorillonite lattice, the shortest metal−metal distance within the octahedral sheet is 2.99 Å, whereas the distance from sixfold-coordinated metal to fourfold-coordinated Si(Al) is 3.11−3.18 Å.[29] On the other hand, the average number of metallic neighbours inside the octahedral sheet is assumed to be four from the rate of vacancies (see next section), whereas the number of Si(Al) neighbours remains equal to 4 (2 per tetrahedral sheet) as in the theoretical structure. The Fourier-filtered contributions of the 2−3.5 Å region in FT are presented in Figure 10b, together with their best fits using the structural parameters of Table 4. They exhibit strong differences in the low *k*-range, which involves mainly Al and Si backscatterers. Indeed it is well known that Al's and Si's backscattering (BS) amplitudes, which are very

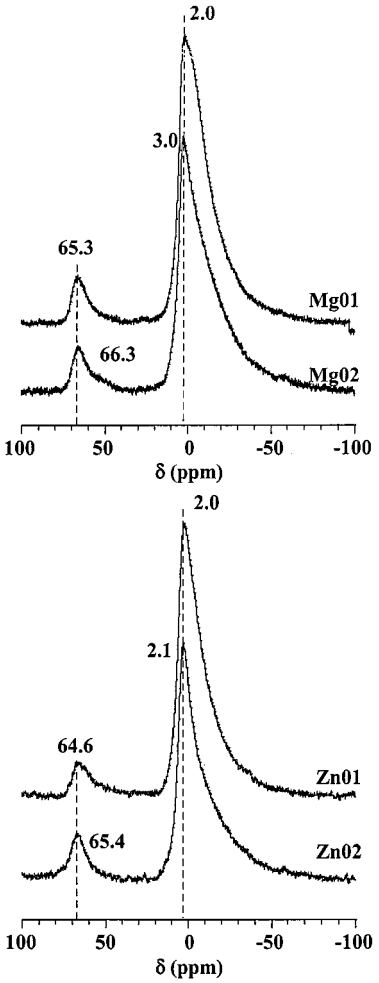

Figure 8. ^{27}Al MAS NMR spectra [standard reference $Al(H_2O)_6^{3+}$] of the studied synthetic montmorillonites

close together, present a maximum around 3−4 $Å^{-1}$ and are strongly dampened above 9−10 $Å^{-1}$ (ref.[30] and references therein). The behaviour of the Zn BS amplitude is quite different, with a minimum at low k and a maximum around 8−9 $Å^{-1}$. Therefore the high k-range of the data (Figure 10b) involves the Zn neighbours of Zn almost exclusively. The positions of the oscillations above 8 $Å^{-1}$, which are the same for Zn01 and Zn02, reveal that the metal−metal distances within the octahedral sheet do not depend on the Zn content in montmorillonite. However, the amplitude of the Zn contribution is enhanced by a factor of about one third in Zn02 with respect to Zn01. Coming back to the Si and Al contributions, the differences observed between Zn01 and Zn02, around 3−8 $Å^{-1}$, are attributed to a variation of the distance from Zn to Si(Al) belonging to the tetrahedral sheets. Following these considerations, the fits were performed by keeping the number of Si(Al) that are underneath and beyond the Zn, located in the plane of the octahedral sheet, constant and equal to four. The number of metallic neighbours inside the octahedral sheet was also kept constant and equal to four. The preferential orientation of the crystallites has not been considered in this preliminary treatment of the Zn k-edge data. An accurate determination of the absolute coordination numbers requires a careful texture analysis which has not yet been carried out.[31] Consequently, only an evaluation of the N_{Zn}/N_{Al} ratio can be deduced from the data treatment at this stage. After the interatomic distances and Debye−Waller parameters were roughly determined (with initial values of the Al and Zn coordination numbers taken to be 3 and 1, respectively) the Al/Zn ratio was varied step by step until the lowest value of the residue was obtained. In the octahedral sheet, the Zn−Al and Zn−Zn distances are found to be 2.98 and 3.11 Å for Zn01 and Zn02, respectively (Table 4). The values of 2.0 and 2.3 Zn neighbours of Zn are consistent with the amplitude of the data in the high k-range. The Zn−Si(Al) distances are found to be 3.17 and 3.25 Å in Zn01 and Zn02, respectively. The latter value is longer than the mean Al−Si distance in the ideal structure (3.15 Å). This main result clearly demonstrates that the montmorillonite lattice is submitted to more and more distortions as the Zn content is increased.

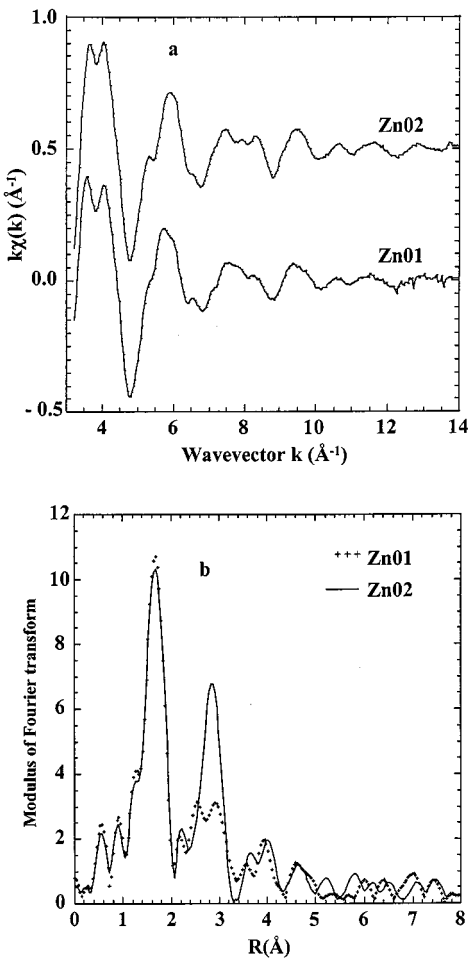

Figure 9. EXAFS data (a) and RDF (b) of synthetic montmorillonites containing Zn (samples Zn01 and Zn02)

The Mg k-edge spectra of samples Mg01 and Mg02 are presented in Figure 11a and the corresponding FT in Figure 11b. The results of the fits give a value of the Mg−O distance of 2.11 Å (Table 5) similar to the Zn−O distance.

Table 4. Structural parameters derived from Zn *K*-edge EXAFS analysis

	Sample	Shell	*N*	*R* [Å]	σ^2 [Å^2]
NN shell	Zn01	Zn−O	5.9	2.08±0.02	0.004
	Zn02	Zn−O	5.9	2.07±0.02	0.004
		Zn−Al	2.0[a]	2.98±0.04	0.007
	Zn01	Zn−Zn	2.0[a]	3.11±0.04	0.005
NNN shell		Zn−Si	4.0[b]	3.17±0.04	0.005
		Zn−Al	1.7[a]	2.97±0.04	0.006
	Zn02	Zn−Zn	2.3[a]	3.11±0.04	0.006
		Zn−Si	4.0[b]	3.25±0.04	0.005[b]

[a] The sum of N_{Zn-Al} and N_{Zn-Zn} was fixed to 4.0. − [b] Fixed parameter.

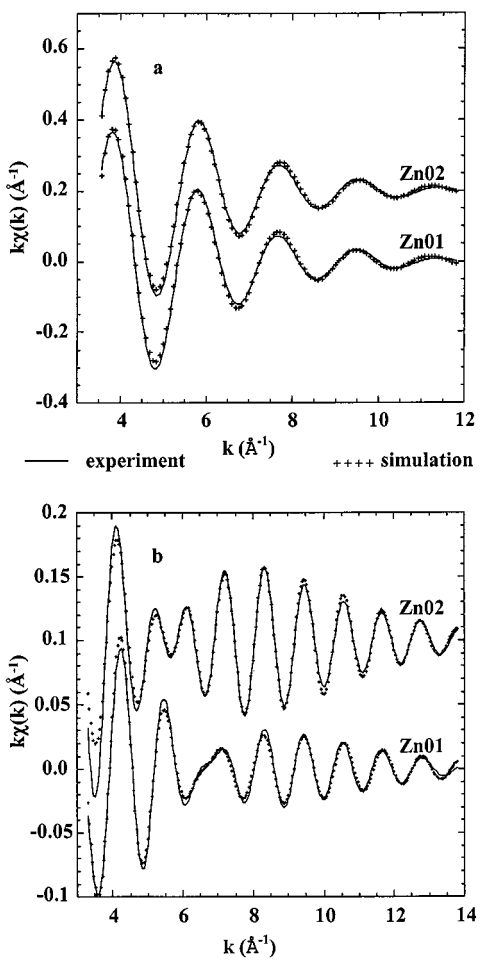

Figure 10. Best fits performed on the Fourier-filtered NN shell (a) and NNN shell (b) contributions using the parameters reported in Table 2: samples Zn01 and Zn02

Due to the short-range data (2−8 Å^{-1}) the NNN shell has not yet been investigated.

Discussion

XRD and ^{29}Si MAS NMR spectroscopic studies of the $MgO-Al_2O_3-SiO_2$ and $ZnO-Al_2O_3-SiO_2$ systems demonstrate that montmorillonite can only be synthesized in a narrow range of compositions ($x = 0.2$). The XRD patterns of Mg01, Mg02, Zn01, and Zn02 selected samples (Figure 3) are unambiguously assigned to smectites and exhibit the typical *hkl* bands of montmorillonite.[12] Moreover, the morphology of the crystal particles observed by SEM (Figure 4) are similar to those of natural montmorillonites.[16−18]

The TGA-DTA analysis (Figure 5), which gives information about the octahedral sheet, confirms this result since the dehydroxylation peak characteristic of natural montmorillonite is observed between 920 and 960 K.[19−23] The additional dehydroxylation peak, which appears in the 720−760 K range, was assigned by Cuadros et al. to the presence of kaolinite.[20] However, the characteristic exothermic contribution of kaolinite above 1173 K is not ob-

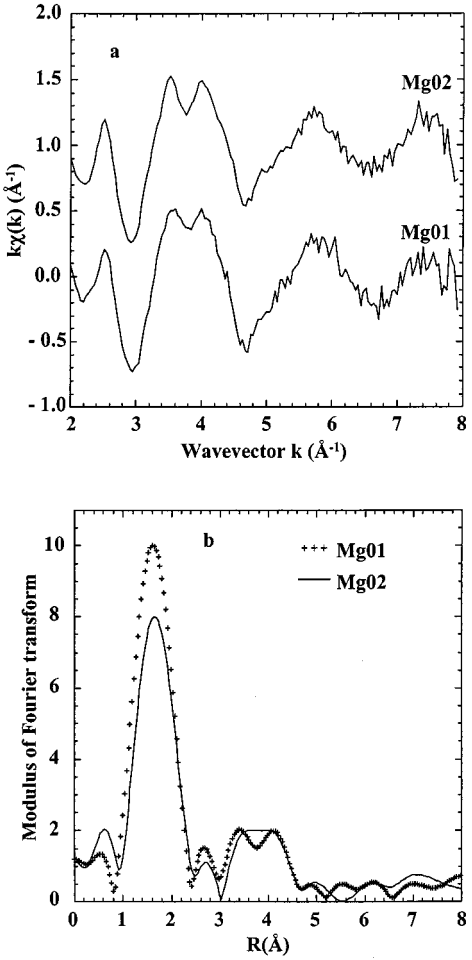

Figure 11. EXAFS data (a) and RDF (b) of synthetic montmorillonites containing Mg (samples Mg01 and Mg02)

Table 5. Structural parameters derived from Mg *K*-edge EXAFS analysis

	Sample	Shell	*N*	*R* [Å]	σ^2 [Å^2]
NN shell	Mg01	Mg−O	6	2.12±0.02	0.006
	Mg02		6	2.10±0.02	0.007

served for the four synthetic clays.[32] On the other hand, the endothermic peak observed at 720−760 K cannot be assigned to the presence of a small amount of kaolinite, because the typical endothermic contribution of kaolinite appears at higher temperatures.[20] The endothermic peak observed in our case (Figure 5) is attributed to hydroxy groups which have different octahedral metallic neighbours. In this way, Frost et al. have assigned the low-temperature dehydroxylation endotherm of a ferruginous montmorillonite to hydroxy groups associated with Fe−Fe pairs and the higher one to hydroxy neighbour Fe−Al pairs.[23] Therefore, the presence of extraneous kaolinite can be ruled out in the four analysed synthetic montmorillonites. The deviation of a random distribution of metallic atoms inside the montmorillonite lattice will be discussed below.

Both ^{29}Si and ^{27}Al MAS NMR spectroscopy gave proof that Al is partially substituted for Si in the tetrahedral sheets. Chemical analysis is not accurate enough to probe such a kind of substitution. It appears that whatever the synthetic conditions, the incorporation of small amounts of aluminium in the tetrahedral sheet (Al_{IV}) cannot be avoided. The Si/Al_{IV} ratio could not be determined by ^{29}Si MAS NMR spectroscopy because of the deviation of the statistic distribution pointed out below. Sanz and Serratosa have indeed shown that other factors exist besides the rule of Loewenstein (no Al−O−Al bond in the structure), which governs the Si and Al distribution in the tetrahedral sheet, when atoms are not randomly distributed in the layer.[24] Working on natural pyrophyllite (talc-type clay), muscovite and margarite (mica-type clays) as dioctahedral clays which have only tetrahedral substitutions, Sanz and Serratosa have reported a poor agreement between the Al_{VI}/Al_{IV} ratio determined by using ^{27}Al MAS NMR spectroscopy and those calculated from the chemical analysis and ^{29}Si MAS NMR spectroscopy.[26] Later, Goodman and Stucki noticed that ^{27}Al MAS NMR spectroscopy can be used to obtain the Al_{VI}/Al_{IV} ratio and probably, in precise experimental conditions, have accurate quantitative results in the case of natural montmorillonite.[28] The presence of paramagnetic elements in the samples of Sanz and Serratosa and the fact that the spinning rate was lower for the MAS at this time, could explain the poor agreement for ^{27}Al MAS NMR spectroscopy in their study.[24] Nowadays, the knowledge about ^{27}Al MAS NMR spectroscopic technology has improved, particularly that concerning the quantitative analysis.[33−35] The determination of the absolute Al contents in Mg01, Mg02, Zn01, and Zn02 by ^{27}Al MAS NMR spectroscopy can now be achieved. The calibration was made using well-known synthetic beidellites.[9,10] However, the determination of the Al_{VI}/Al_{IV} ratio by this technique requires complementary measurements that are currently in progress.[36]

The EXAFS study provides a determination of the NN and NNN shell distances. NN shell distances are very similar for samples Zn01 and Zn02 (2.08 Å and 2.07 Å, respectively) and for samples Mg01 and Mg02 (2.12 Å and 2.10 Å, respectively). These values have to be compared to those of an ideal montmorillonite lattice, where two types of octahedral sites exist: the first one, here called M_1, and the second one called M_2.[29] Only the M_2 octahedral site is occupied by an atom and the value of the M_2−O distance is 1.94 Å. These deviations indicate a strong distortion of the coordination polyhedron with respect to the ideal structure. In the case of the NNN shell, the values of the out-of-plane Zn−Si distance increases with the quantity of Zn contained in the octahedral sheet (3.17 Å for Zn01 and 3.25 Å for Zn02, as a comparison d_{M-Si} = 3.15 Å in the ideal lattice). The values of the Zn−Al distance deduced for samples Zn01 and Zn02 (2.98 Å and 2.97 Å, respectively) are close to those of the ideal montmorillonite lattice (2.99 Å), whereas the values deduced for the Zn−Zn distance are longer (3.11 Å for both Zn01 and Zn02). This observation confirms that the distance between two elements in the structure strongly depends on their nature.

Finally, let us consider the distribution of tri- and divalent elements within the octahedral sheet. The simulation of the backscattered contribution of the NNN of Zn reveals a surprisingly high value of the Zn/Al_{VI} ratio, which reaches 1.0/1.0 in Zn01 and 1.4/1.0 in Zn02 (Table 4). The projection of the octahedral sheet onto the (*ab*) plane has the form of a two-dimensional hexagonal network whose every third apex is vacant (Figure 1b). If we consider various arrangements of vacancies within this plane, the average coordination number of an element is four (at least 3, at most 5). Consequently, the coordination number of Zn was kept constant and equal to 4 in the simulations. The value of the octahedral substitution, which could be determined by using ^{27}Al MAS NMR spectroscopy and chemical analyses, indicates 1.8 Al for 0.2 Zn in Zn01 and 1.6 Al for 0.4 Zn in Zn02, i.e. one octahedral site out of 15 and two octahedral sites out of 15 are occupied by Zn atoms in Zn01 and Zn02, respectively. For a random distribution of the elements in the sheet, the number of Zn neighbours of Zn would be much less than one in both Zn01 and Zn02. On the other hand, the TGA-DTA study has also demonstrated a possible deviation from a random distribution of metallic atoms inside the montmorillonite lattice. The deviation from the statistical distribution and the clustering of divalent elements is also confirmed by ^{19}F MAS NMR spectroscopy that reveals unambiguously the presence of Mg−Mg−Mg arrangement around fluorine atoms in the Mg02 sample. The existence of a Mg−Mg−Mg environment and the absence of a Zn−Zn−Zn one could also be explained by a higher affinity of fluorine for Mg than Al or Zn due to the difference between the electronegativity of the elements. The clustering induces strong local distortions within the octahedral sheet that are balanced by the tetrahedral sheet substitutions. This behaviour was already observed in the octahedral sheet of a natural montmorillonite from Camp Berteau by EXAFS measurements at the Ni *k*-edge.[37]

Conclusion

Montmorillonites containing Al and exclusively Zn or Mg as divalent elements in the octahedral sheet were syn-

thesized in acidic and fluoride medium. The substitution of Al in the octahedral sheet was obtained for a narrow range of Mg or Zn contents. The elemental analysis (XRD, TGA-DTA, chemical analysis) of the synthesized materials demonstrates their major dioctahedral character. Beyond these fundamental characterisations, ^{27}Al MAS NMR spectroscopy gives an accurate value of the substitution rate of the Al for Si in the tetrahedral sheet and demonstrates that elemental analyses are not sufficient to establish the half unit cell formula. EXAFS reveals substantial increases of the bond lengths (R_{Mg-O} = 2.11 Å, R_{Zn-O} = 2.08 Å, R_{Zn-Al} = 2.98 Å, R_{Zn-Zn} = 3.11 Å) in the octahedral sheet with respect to the ideal structure. The distortions of the coordination polyhedra of divalent elements could be related to a local trioctahedral character of these materials. This interpretation can be connected with the clustering of divalent elements revealed by EXAFS and ^{19}F MAS NMR spectroscopy. It appears that the substitution and the clustering of the divalent elements induce a mismatch between the octahedral and the tetrahedral sheets, and finally a local undulation of the layer which could be compensated by Al for Si substitutions in the tetrahedral sheet. This could be the reason why montmorillonite clays without tetrahedral substitutions are seldom observed in nature. The relevant phenomena may influence the physical and the chemical properties of these clays (adsorption, catalytic efficiency, etc.).

Experimental Section

Synthesis: Two series of syntheses were performed on $MgO-Al_2O_3-SiO_2$ and $ZnO-Al_2O_3-SiO_2$ systems. The compositions of hydrogel are based on a theoretical formula of montmorillonite: $Na_{2x}[(Al_{2(1-x)}M_{2x}\ \square)Si_4O_{10}(OH,F)_2]\cdot nH_2O$. M represents the divalent element (Mg or Zn), and x ranges from 0.0 to 1.0. Samples were synthesized in an acidic fluoride medium under hydrothermal conditions using hydrogels with the following molar composition:

$$1SiO_2 : (1 - x)/4\cdot Al_2O_3 : x/2\cdot MO : x/4\cdot Na_2O : 0.05\cdot HF : 96\cdot H_2O$$

Water, hydrofluoric acid, and silicon oxide contents are the same for each synthesis. Reactants were mixed in the following order: deionized water, hydrofluoric acid (HF, 40%; BDH), sodium acetate ($NaCOOCH_3$, 99%; Fluka), zinc acetate [$Zn(COOCH_3)_2$, $2H_2O$, 98%; Prolabo] or magnesium acetate [$Mg(COOCH_3)_2\ 4H_2O$, 99%; Fluka], boehmite (Al_2O_3, 75−78%, Pural SB1; Condea), and silica (SiO_2, 99.5%, Aerosil 130; Degussa). Hydrogels were matured over 2 h at room temperature and the pH was measured (pH = 4.5−6) before hydrothermal treatment in a PTFE-lined stainless steel autoclave at 493 K for 72 h under autogeneous water pressure. After crystallisation, the autoclaves were cooled to room temperature. The pH of the supernatant was 3.5−4.5. Products were then separated by filtration, washed thoroughly with distilled water and dried at 333 K for 12 h. The samples were then ground to a fine powder form and placed under controlled humidity. This was made by keeping samples under a relative pressure P/P_0 = 80%, by using a saturated solution of NH_4Cl salt.

X-ray Powder Diffraction (XRD): The X-ray powder diffraction patterns were recorded with two diffractometers: the first one employing Cu-K_α radiation was equipped with automatic divergence slits (Philips PW1800), the second one employing either Cu-K_α or Cr-K_α radiation with fixed divergence slits (Philips PW1100). The latter enables patterns to be recorded under controlled humidity (P/P_0 = 80% RH). In both cases diffractograms were performed on powders which were only pressed on sample carriers. Information about the phase and d_{001} spacing was obtained with the APD 1700 software (Philips).

Scanning Electronic Microscopy (SEM): Starting materials were first examined by SEM with a Philips XL30 microscope in order to determine their morphology. An ethanolic suspension of the sample was left on a support covered by graphite and then evaporated. Samples were then metallized (10 or 20 nm of gold) under vacuum by sputtering.

Thermal Analysis (TGA-DTA): Measurements were carried out on samples which were previously placed under controlled humidity (P/P_0 = 80%), with a heating rate of 5 K·min^{-1} obtained by using a Setaram Labsys apparatus under a mixture of N_2 and O_2 (1 and 0.5 bars, respectively).

Chemical Analysis: A part of each sample was Na-saturated to be sure that only Na^+ cations balanced the charge. Na-saturated products were prepared as follows: 5 mL of 1 M NaCl solution was added to 0.5 g of synthetic product. The mixture was stirred at room temperature for 1 h before it was filtered. The exchange process was repeated twice. The samples were then washed with distilled water until the product was chloride-free (this was tested using $AgNO_3$ solution). The resultant product was then dried at 333 K for 12 h. Elemental analysis of Na-saturated clays was then performed by the Service Central d'Analyse of the Centre National de la Recherche Scientifique (Vernaison, France) for the following elements: Mg, Zn, Al, Si, and F.

Solid-State Nuclear Magnetic Resonance (NMR) Spectroscopy

Experiments: ^{29}Si MAS NMR spectra were obtained with a Bruker MSL-300 spectrometer at 59.63 MHz with 4 kHz spinning speed, 2 μs excitation pulses (π/2 pulse width of 4 μs) and 95 s recycle time. Chemical shifts of Si were referenced to tetramethylsilane (TMS) using a secondary standard of trimethylsilyl ester of cubic octameric silicate (Q8M8) at δ = −109.7 (the more shielded signal). ^{27}Al MAS NMR spectra were obtained with a Bruker MSL-300 spectrometer at 78.21 MHz with 10 kHz spinning speed, 0.7 μs excitation pulses (π/2 pulse width of 9 μs for an aqueous solution) and 1 s recycle time. Chemical shifts of aluminium were referenced to a 1 M $Al(NO_3)_3$ aqueous solution with a chemical shift of δ = 0. ^{19}F MAS NMR spectra were obtained with a Bruker DSX-400 spectrometer at 379.23 MHz with a Hahn echo pulse sequence (π/2 pulse − τ − π pulse − τ − acquisition),[38] 10 kHz spinning speed, π/2 pulse width of 7 μs and 20 s recycle time.

Data Analysis: After their collection, free-induction decay (FID) signals were treated following a standard procedure using the software WIN NMR (Bruker software). The FID signals were smoothed in order to reduce the background noise. Base-lines were also corrected when necessary. The ^{29}Si MAS NMR spectra were simulated with the WINFIT software.[39] The Al_{VI}/Al_{IV} ratio was calculated by determining the area of each component of the ^{27}Al MAS NMR spectra. Furthermore, the aluminium content was determined accurately by using quantitative ^{27}Al MAS NMR spectroscopic conditions.[33−36]

Extended X-ray Absorption Fine Structure (EXAFS)

Experiments: The X-ray absorption experiments were performed at the Laboratoire pour l'Utilisation du Rayonnement Electromagnétique (LURE, Orsay, France). Samples studied by EXAFS were named Mg01, Mg02, Zn01, and Zn02, see below for their selection. The Zn01 and Zn02 samples were mixed with cellulose (0.122 g of Zn01 and 0.006 g of cellulose, 0.121 g of Zn02 and 0.005 g of cellulose), and pressed (1 T and 1.5 T, respectively) in the form of pellets (less than 1 mm thickness), that were maintained between two Kapton windows. Measurements were performed on the D21 beam line of the DCI storage ring. The X-rays were monochromatized by an Si(311) two-crystal spectrometer. The X-ray absorption spectra were recorded at the Zn-*K* edge (9659 eV) from 9400 to 10900 eV (1 eV step; 1 s^{-1} per point) in transmission mode at 20 K. Measurements for the Mg (1305 eV) and Al (1559 eV) *K* edges were performed on the SA32 beam line of the Super−Aco storage ring. Powdered Mg01, Mg02, Zn01, and Zn02 samples were directly pressed on indium films deposited on a copper sheet used as a support. The X-ray absorption spectra were collected at the Mg-*K* edge between 1250 and 1560 eV (1 eV step; 4 s^{-1} per point) in fluorescence mode. X-rays were monochromatized by a spectrometer using beryl crystals. All the spectra were collected with the samples perpendicular to the beam path. Measurements were performed at room temperature in a chamber at a pressure of 10^{-9} bar.

Data Analysis: The raw data were analysed following the standard procedure by using the software designed by Michalowiz.[40] First the pre-edge and post-edge backgrounds were removed from the raw data. After conversion to *k*-space, the EXAFS spectra were k^3-weighted and Fourier-transformed using a Kaiser apodization window. The nearest neighbours (NN) and next-nearest neighbours (NNN) peaks in the Fourier transforms (FT) were assigned to the oxygen and metal backscatterers. The Fourier-filtered (FF) contribution of oxygen was simulated using a squares fit by the standard EXAFS formula in order to derive the structural parameters: the interatomic distances *R*, coordination numbers *N* and Debye−Waller (DW) parameters σ. The amplitude and phase shifts are extracted either from reference samples or theoretical calculation.[30] The Fourier-filtered contribution of the metallic NNN of Zn in the 2.0−3.3 Å range (Figure 9 b) were simulated with amplitude and phase shifts calculated by using the FEFF software.[30]

Acknowledgments

The authors are grateful to Jean-Marc Le Meins for the interesting and helpful discussions concerning crystallography and for providing Figure 1. We also thank Anne-Catherine Faust for SEM micrographs.

[1] M. Ogawa, K. Kuroda, *Chem. Rev.* **1995**, *95*, 399−438.
[2] F. Figueras, *Catal. Rev. Sci. Eng.* **1988**, *30*, 457−499.
[3] A. Clearfield, *Chem. Mater.* **1998**, *10*, 2801−2810.
[4] J. T. Kloprogge, S. Komarneni, J. E. Amonette, *Clays Clay Miner.* **1999**, *47*, 529−554,
[5] Y. Otsubo, C. Kato, *J. Chem. Soc. Jpn.* **1954**, *75*, 456−459,
[6] H. Harder, *Chem. Geol.* **1972**, *10*, 31−39,
[7] H. Nakazawa, H. Yamada, K. Yoshioka, M. Adachi, T. Fujita, *Clay Sci.* **1991**, *8*, 59−68,
[8] T. Nagase, T. Iwasaki, T. Ebina, H. Hayashi, Y. Onodera Chandra, N. Dutta, *Chem. Lett.* **1999**, *4*, 303−304,
[9] L. Huve, L. Delmotte, R. Le Dred, J. Baron, D. Saehr, *Proc. ACS Symposium on Advances in Zeolites and Pillared Clays Synthesis*, New York, **1991**.
[10] J.-F. Joly, L. Huve, R. Le Dred, D. Saehr, J. Baron, French patent no. 2673930, **1992**.
[11] F. Lhommédé, R. Le Dred, D. Saehr, J. Baron, *C. R. Acad. Sci. Paris* **1996**, *t. 322 série Iia*, 827−830.
[12] E. Maegdefrau, U. Hofmann, *Z. Kristallogr.* **1937**, *98*, 299−323.
[13] T. Watanabe, T. Sato, *Clay Sci.* **1988**, *7*, 129−138.
[14] H. Yamada, H. Nakazawa, H. Hashizume, S. Shimomura, T. Watanabe, *Clays Clay Miner.* **1994**, *42*, 77−80.
[15] E. S. Boeck, P. V. Coveney, N. T. Skipper, *J. Am. Chem. Soc.* **1995**, *117*, 12608−12617.
[16] S. P. Skaribas, P. J. Pomonis, P. Grange, B. Delmon, *Multifunctional Mesoporous Inorganic Solids* (Eds.: C. A. C. Sequeira, M. J. Hudson), Kluwer Academic Publishers, Netherlands, **1993**, p. 127−136.
[17] K. Ma, A. C. Pierre, *Colloid Surface A* **1999**, *155*, 359−372.
[18] F. Cravero, K. S. Keith, H. H. Murray, T. Toth, *Appl. Clay Sci.* **2000**, *16*, 31−43.
[19] R. Greene-Kelly, *Clay Min. Bull.* **1952**, *1*, 221−225.
[20] J. Cuadros, A. Delgado, A. Cardenete, E. Reyes, J. Linares, *Clays Clay Miner.* **1994**, *42*, 643−651.
[21] A. Garcia-Rodriguez, F. del Rey-Bueno, F. J. del Rey-Perez-Caballero, M. D. Ureña-Amate, A. Mata-Arjona, *Mater. Chem. Phys.* **1995**, *39*, 269−277.
[22] M. D. Alba, R. Alvero, A. I. Beccero, M. A. Castro, J. M. Trillo, *J. Phys. Chem. B* **1998**, *102*, 2207−2213.
[23] R. L. Frost, H. Ruan, J. T. Kloprogge, W. P. Gates, *Thermochim. Acta* **2000**, *346*, 63−72.
[24] J. Sanz, J. M. Serratosa, *J. Am. Chem. Soc.* **1984**, *106*, 4790−4793.
[25] S. R. Drachman, G. E. Roch, M. E. Smith, *Solid State Nucl. Magn.* **1997**, *9*, 257−267.
[26] G. Engelhardt, D. Michel, *High resolution solid- state NMR of silicates and zeolites*, J. Wiley & Sons, New York, **1987**, p. 129.
[27] L. Huve, L. Delmotte, P. Martin, R. Le Dred, J. Baron, D. Saehr, *Clays Clay Miner.* **1992**, *40*, 186−191.
[28] B. A. Goodman, J. W. Stucki, *Clay Miner.* **1984**, *19*, 663−667.
[29] S. I. Tsipursky, V. A. Drits, *Clay Miner.* **1984**, *19*, 177−193.
[30] J. J. Rehr, J. Mustre de Leon, S. I. Zabinsky, R. C. Albers, *J. Am. Chem. Soc.* **1991**, *113*, 5135−5145.
[31] A. Manceau, D. Chateigner, W. P. Gates, *Phys. Chem. Miner.* **1998**, *25*, 347−365.
[32] G. Suraj, C. S. P. Iyer, S. Rugmini, M. Lalithambika, *Appl. Clay Sci.* **1997**, *12*, 111−130.
[33] D. Plee, F. Borg, L. Gatineau, J. J. Fripiat, *J. Am. Chem. Soc.* **1985**, *107*, 2362−2369
[34] A. Samoson, E. Lippma, G. Engelhardt, U. Lohse, H.-G. Jerschkewitz, *Chem. Phys. Lett.* **1987**, *134*, 589−592.
[35] N. C. Nielsen, H. Bildsøe, H. J. Jakobsen, *Chem. Phys. Lett.* **1992**, *191*, 205−212.
[36] M. Reinholdt, J. Miehé-Brendlé, L. Delmotte, M.-H. Tuilier, R. Le Dred, to be published.
[37] F. Muller, G. Besson, A. Manceau, V.-A. Drits, *Phys. Chem. Miner.* **1997**, *24*, 159−166.
[38] E. L. Hahn, *Phy. Rev.* **1950**, *80*, 580−594.
[39] D. Massiot, *Winfit 990420 version*, Centre de Recherches sur les Matériaux à Haute Température, Orléans, http://crmht.cnrs-orleans.fr/Pole2/ThemeDM/default.htm
[40] A. Michalowiz, *J. Phys.* **1997**, *III − C2*, 235−237.

Received April 23, 2001
[I01143]

Structure and Magnetism of a Polycrystalline Transition Metal Soap – $Co^{II}[OOC(CH_2)_{10}COO](H_2O)_2$

Jean-Michel Rueff,[a] Norberto Masciocchi,*[b,c] Pierre Rabu,*[a] Angelo Sironi,[b] and Antoine Skoulios[a]

Keywords: Carboxylate ligands / Cobalt / Layered compounds / Magnetic properties / X-ray powder diffraction

Diaquacobalt(II) *n*-dodecane-α,ω-dioate (**2**) has been synthesized by metathesis of the corresponding potassium soap **1** and has been fully characterized by chemical and spectroscopic analysis. The crystal structure of **2** has been established by X-ray powder diffraction techniques combined with electron diffraction experiments. It crystallizes in a monoclinic cell [$P2_1/a$; a = 9.6558(8), b = 7.4793(6), c = 19.8936(2) Å, β = 95.648(9)°, V = 1429.7(3) Å^3; Z = 2] and consists of stacked layers of cobalt(II) ions connected by carboxylato bridges, thus forming chains that extend along the a axis. These layers are separated by alkyl chains arranged quasi-perpendicularly to the polar sheets. Structure analysis reveals a rare *anti-anti* conformation of the Co–OCO–Co fragments, which is thought to be responsible for the weak antiferromagnetism of the Co^{II} chains. The exchange coupling constant between the magnetic centres has been estimated as J = –2.08 K.

Introduction

Low-dimensional magnetic compounds, in which the magnetic centres are arranged in well-separated, one-dimensional rows or two-dimensional layers, for instance, may be fully understood and quantitatively analysed on theoretical grounds.[1–5] Their systematic investigation is therefore expected to provide useful information on the relationship between their properties and their chemical and crystal structures, and thus to help towards the design of novel magnetic materials, hopefully with high T_C values.

In this respect, lamellar transition metal soaps[6,7] are very appealing model compounds. As shown by systematic investigations of their X-ray powder diffraction (XRPD) fingerprints,[6,8,9] it has long been known that, like micelles[10] and liquid-crystalline phases,[11–13] these materials can adopt ordered structures, although the details of these structures have been only rarely established owing to the difficulty in growing suitable single crystals.

As established previously, grafting of dicarboxylates onto parallel metal-containing layers is expected to afford highly crystalline powders, for which a complete 3D structure may be determined,[14] and to permit control over the spin coupling if suitable magnetic metal ions are employed.[15] Accordingly, the aims of the present paper are: (i) to outline the synthesis of one long-chained cobalt(II) soap, $Co^{II}[OOC(CH_2)_{10}COO](H_2O)_2$, i.e. diaquacobalt(II) *n*-dodecane-α,ω-dioate (**2**), (ii) to describe its crystal structure in detail, as elucidated by XRPD methods combining ab initio techniques (a method recently promoted by us in the field of coordination chemistry[16]) with electron diffraction analysis, and (iii) to discuss its magnetic behaviour in terms of its chemical bonding and crystal structure.

Results and Discussion

Compound **2** was prepared as a pink powder by metathesis of the corresponding potassium soap **1** with a stoichiometric amount of cobalt(II) acetate tetrahydrate, according to the precipitation method generally used in the synthesis of heavy metal soaps.[17,18] To ensure its chemical (and magnetic) purity and the coordination state of the cobalt atoms, special care was taken in choosing the operating conditions (high purity of reactants and solvents, low concentration and temperature, strict stoichiometry). The chemical nature of the product was ascertained by a set of complementary analytical techniques and was fully confirmed by XRPD.

The room-temperature diffraction pattern of **2** contains a subset of low-angle, equidistant, sharp reflections (00*l*), indicative of a lamellar structure with a spacing of ca. 19.9 Å. This value, which is larger than that determined for *n*-dodecane (17.2 Å[19]), suggests parallel, all-*trans*-alkyl chains oriented perpendicularly to the layers. Moreover, the overall complexity of the XRPD pattern is indicative of a well-developed three-dimensional crystalline arrangement. Although too intricate to be interpreted straight away in terms of a 3D crystal lattice (using conventional cell determination procedures), the pattern was eventually indexed

[a] Institut de Physique et Chimie des Matériaux de Strasbourg, UMR 75046 CNRS-ULP-ECPM,
23 rue du Loess, 67037 Strasbourg Cedex, France
Fax: (internat.) + 33-3/88107247
E-mail: pierre.rabu@ipcms.u-strasbg.fr
[b] Dipartimento di Chimica Strutturale e Stereochimica Inorganica e Centro CNR "CSSSCMTBSO", Università di Milano,
Via Venezian 21, 20133 Milano, Italy
[c] Dipartimento di Scienze Chimiche, Fisiche e Matematiche, Università dell'Insubria,
Via Valleggio 11, 22100 Como, Italy
Fax: (internat.) + 39-02/7063-5288
E-mail: norberto.masciocchi@uninsubria.it

 © WILEY-VCH Verlag GmbH, 69451 Weinheim, 2001 1434–1948/01/1111–2843 $ 17.50+.50/0

with the aid of additional information provided by electron-diffraction experiments. Indeed, SEM observations (Figure 1) showed that **2** apparently consists of single-crystalline platelets, thus permitting electron diffraction (ED) experiments on isolated platelets oriented perpendicularly to the electron beam. A typical ED pattern contains an extended set of sharp reflections (*hk*0; all present in the XRPD trace), consistent with a rectangular two-dimensional lattice of cell parameters $a \approx 9.6$ Å and $b \approx 7.5$ Å. Using this information, along with the knowledge of the lamellar period, the XRPD pattern of **2** was indexed on the basis of a monoclinic lattice with cell parameters $a = 9.6558(8)$ Å, $b = 7.4793(6)$ Å, $c = 19.8936(2)$ Å, and $\beta = 95.648(9)°$.[20] Systematic absences pointed to $P2_1/a$ as the probable space group, which was later confirmed by a successful crystal structure determination. Interestingly, the centred rectangular sublattice ($a' = a/2 \approx 4.8$ Å, $b' = b \approx 7.5$ Å) built-up from reflections 400, 210, 020, 420, 230, 040 of the electron-diffraction patterns (Figure 2) is identical to the two-dimensional crystal lattice that describes the lateral packing of linear paraffins in the orthorhombic form,[21] and suggests a similar packing for the alkyl chains in the crystals of soap **2**. Incidentally, the intensities of these particular reflections are especially strong, as expected from the upright orientation of the alkyl chains in the platelets.

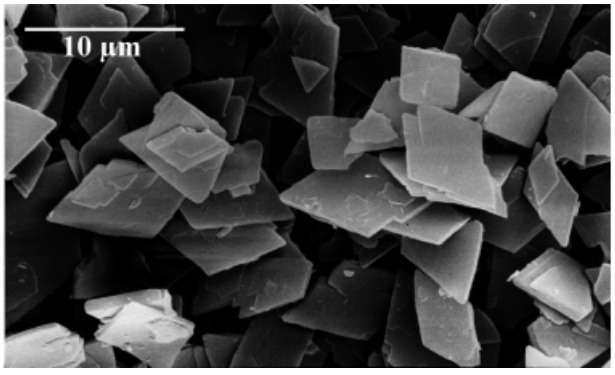

Figure 1. Morphology of powdered compound **2** as observed by scanning electron microscopy

The detailed crystal structure of **2** was established by an ab initio analysis and a Rietveld refinement of the intensity distribution in the powder X-ray diffraction patterns (see Exp. Sect.). As shown in Figure 3, the structure incorporates octahedral cobalt(II) ions *cis*-coordinated by two water molecules, as well as by one chelating [η^2-*O*,*O*] and two bridging [μ-*O*,*O*] carboxylato groups. Connected by OCO bridges in an *anti-anti* conformation (see Scheme 1), the Co atoms form $(-OCO-Co-)_n$ chains that extend in a zigzag fashion along *a*. Due to the glide symmetry operation, the chiral configuration of the Co atoms alternates along the chains. Arranged in slabs (with hydrophobic cores and polar surfaces), slightly tilted with respect to *c* and lying virtually perpendicular to the (*a*,*b*) planes, the fully extended dodecanedioato groups (bearing a chelating carboxylato

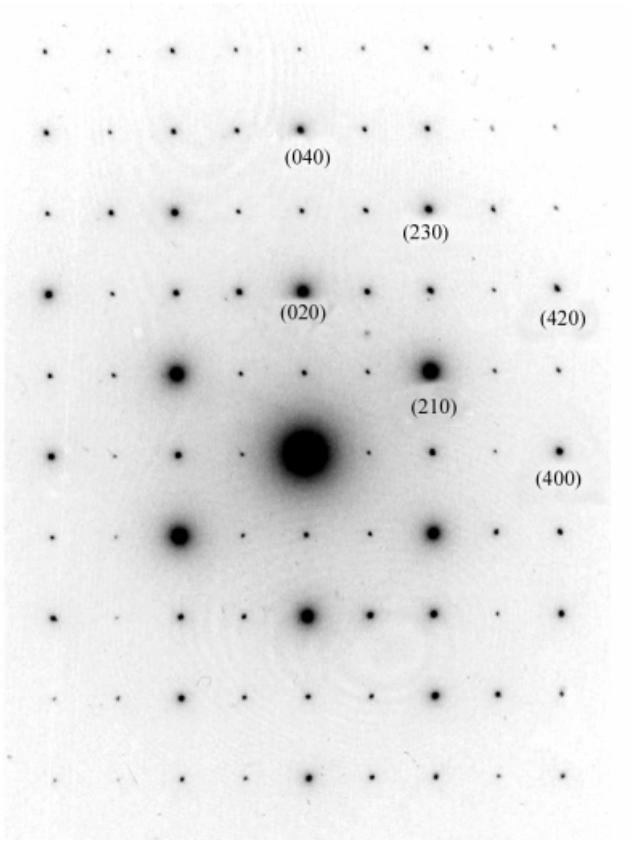

Figure 2. Electron diffraction pattern of **2** as recorded with the platelets oriented perpendicularly to the electron beam

group at one end and a bridging one at the other) connect Co atoms of opposite surfaces. These slabs are held together by hydrogen bonds between the water molecules and the carboxylic oxygen atoms, which are separated by about 2.70 Å. The separation of the Co atoms is 5.93 Å within the $(-OCO-Co-)_n$ chains, and only 5.07 Å between metal atoms of adjacent slabs (Co−O−H···O−Co).

The IR and UV data collected for **2** were readily analysed on the basis of the crystal structure. The IR spectrum features the characteristic bands of the alkyl chains in a fully stretched all-*trans* conformation. The frequency difference between the symmetric and antisymmetric carboxylate vibrations, $\Delta\nu = 128$ cm^{-1}, is smaller than that observed for the corresponding ionic potassium soap ($\Delta\nu_i \approx 150$ cm^{-1}), as befits the bidentate coordination mode of the carboxylic groups; because of the band widths, it is not possible to distinguish the chelating from the bridging mode in the structure.[22] The two broad ν(O−H) bands in the range 3200−3400 cm^{-1} can be assigned to the two hydrogen-bonded aqua ligands. The UV spectrum corroborates the quasi-regular octahedral geometry about the Co^{II} ions.[23,24] The values of Dq (950 cm^{-1}) and Racah's parameter B (846 cm^{-1}) deduced from the observed absorption bands indicate a low crystal field ($Dq/B = 1.1$), favouring the high-spin configuration observed for the metal centre (see below).

The magnetic behaviour of **2** was investigated using a SQUID magnetometer. The susceptibility χ (suitably cor-

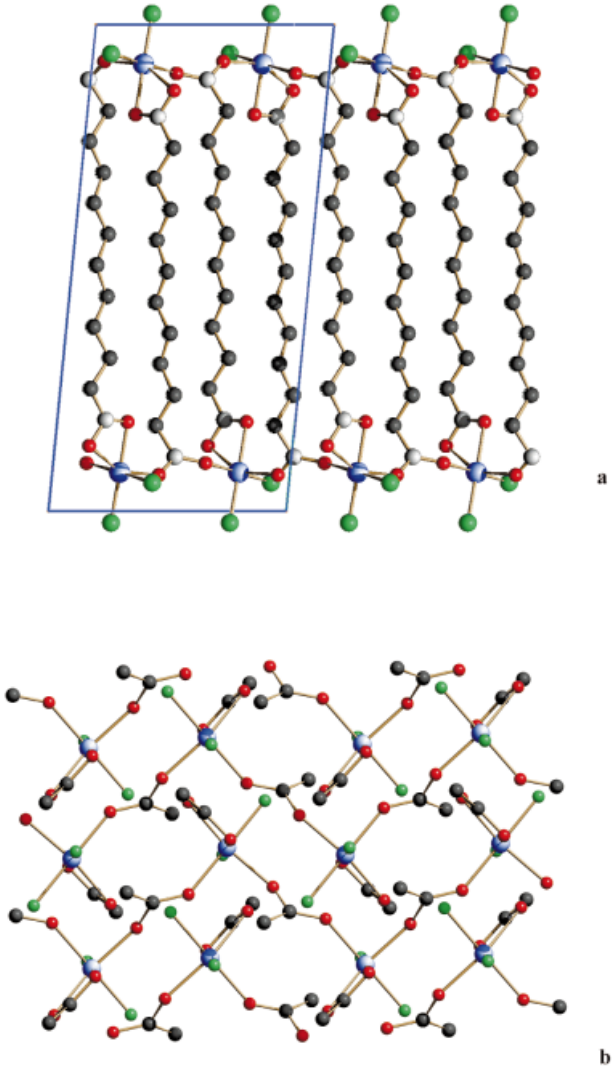

Figure 3. (a) Schematic plot (viewed down the *b* axis; horizontal axis = *a*) of the crystal structure of $Co(C_{10}H_{20}C_2O_4)(H_2O)_2$ showing the elongated organic ligands interconnecting parallel layers of octahedrally coordinated Co^{II} ions (see text); (b) a top view of the *ab* plane showing the Co^{II} chains extending along the *a* axis (horizontal) within the layers; cobalt atoms in blue; oxygen atoms of coordinated water molecules in green; for the sake of simplicity, a number of aliphatic carbon atoms have been omitted in (b)

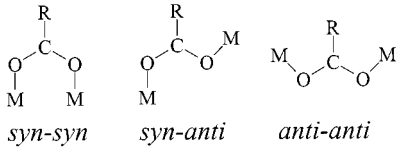

Scheme 1

rected for sample and holder diamagnetism) grows smoothly with decreasing temperature (Figure 4), according to the Curie–Weiss law $\chi = C/(T - \theta)$ at temperatures in excess of 200 K. The value of the Curie constant, $C = 3.0$ $cm^3\ K\ mol^{-1}$, is consistent with the presence of hexacoordinated high-spin Co^{II} ions ($C \approx 2.8-3.4$ $cm^3\ K\ mol^{-1}$)[25] and the negative sign of the Weiss temperature, $\theta = -19.7$ K, points, phenomenologically, to the existence of antiferromagnetic exchange interactions (also supported by the decrease of χT from 2.76 $cm^3\ K\ mol^{-1}$ at 295 K to 1.08 $cm^3\ K\ mol^{-1}$ at 2 K). The effect of spin-orbit coupling, known to be operative for Co^{II} ions,[5,25,26] most certainly also contributes to the decay of χT upon cooling; however, on no account does it explain entirely the observed decay. Firstly, the temperature dependence of the effective magnetic moment deduced from the experimental data differs from that calculated for isolated Co^{II} ions[26] (Figure 4); in particular, the χT value measured at 2 K (1.08 $cm^3\ K\ mol^{-1}$) is significantly smaller than expected (1.8 $cm^3\ K\ mol^{-1}$) for isolated Co^{II} magnetic centres. Secondly, the magnetization curve $M(H)$, saturating at $M_S = 2.2$ $\mu_B mol^{-1}$ as expected ($2-3$ $\mu_B mol^{-1}$),[5,25] is significantly lower than that predicted by Brillouin's law[25] (Figure 5).

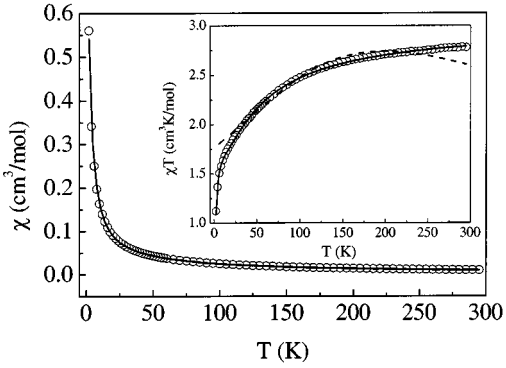

Figure 4. Temperature variation of the magnetic susceptibility of compound **2**; inset: χT vs. T variation; full lines correspond to the best fit of the experimental data with the relationship given in the text; the dashed line in the inset corresponds to the variation of $\mu_{eff}^2/8 = \chi T$ calculated from the expression given in ref.[26] for the effective moment of isolated Co^{II} ions in a weak octahedral field

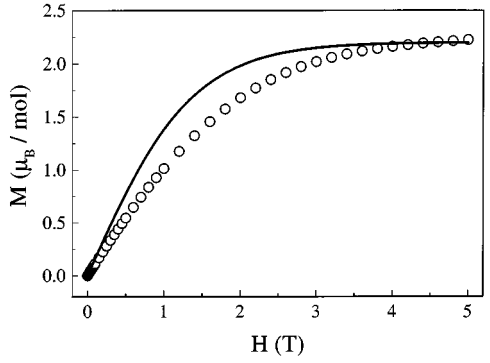

Figure 5. Magnetization vs. field curve at 2 K for compound **2**; the full line corresponds to the best fit to Brillouin's function

However weak, the antiferromagnetic coupling suggested by the experimental data most likely occurs through the carboxylato bridges along the $(-OCO-Co-)_n$ chains; although shorter, the exchange pathway through the hydrogen bonds appears to be less effective. No analytical expression is available in the literature to describe the temperature dependence of χT for chains of Co^{II} ions with spin-orbit coupling. Considering, however, that below 30 K the Co^{II}

ions generally behave as anisotropic $S = 1/2$ pseudo spins,[5,25,26] one may attempt to calculate the susceptibility by using the relationship given for Ising chains:[5,25]

$$\chi = 1/3(\chi_z + 2\chi_x)$$

with

$$\chi_z = \frac{Ng_z^2\mu_B^2}{4kT}\exp(J/2kT)$$

and

$$\chi_x = \frac{Ng_x^2\mu_B^2}{2J}\left[\tanh(J/2kT) + (J/4kT)\sec h^2(J/4kT)\right]$$

In the present case, this model turned out to be unsatisfactory as the antiferromagnetic exchange interaction is too weak to show up clearly against the spin-orbit coupling (see below) and, ultimately, because the anisotropy of the ion g tensor is too small.[5]

Nevertheless, in order to obtain an estimate of the strength of the antiferromagnetic exchange interaction, one may use the following simple phenomenological equation:[27]

$$\chi T = A\exp(-E_1/kT) + B\exp(-E_2/kT)$$

Here, $A + B$ equals the Curie constant, and E_1, E_2 represent the "activation energies" corresponding to the spin-orbit coupling and the antiferromagnetic exchange interaction. This equation adequately describes the spin-orbit coupling, which results in a splitting between discrete levels, and the exponential low-temperature divergence of the susceptibility [$\chi T \propto \exp(\alpha J/2kT)$]. Moreover, it is in excellent agreement with the experimental data obtained in the present work (Figure 4). The obtained values of $A + B = 3.0$ $cm^3\,K\,mol^{-1}$ and $E_1/k = +56.6$ K (using a least-squares fitting method) are consistent with those given in the literature for the Curie constant ($C \approx 2.8-3.4$ $cm^3\,K\,mol^{-1}$) and for the effect of spin-orbit coupling and site distortion (E_1/k of the order of $+100$ K).[25] As for the value found for the antiferromagnetic exchange interaction, it is very weak indeed ($-E_2/k = -1.03$ K), corresponding to $J = -2.06$ K according to the Ising chain approximation [see above; $\chi T \propto \exp(+J/2kT)$].

Although rare, several examples of one-dimensional systems of transition metal(II) ions have been reported in the literature,[28−32] in which the exchange effectively occurs through carboxylato bridges of various geometries (see Scheme 1). In Cu^{II} complexes, for instance, the exchange coupling is strongly antiferromagnetic with a *syn-syn* conformation,[33] very weakly so (eventually ferromagnetic[34]) with a *syn-anti* conformation,[35−37] and weak to moderately antiferromagnetic with an *anti-anti* conformation.[38] In the present work, the *anti-anti* geometry of the diaquacobalt(II) dicarboxylate appears to favour very weak antiferromagnetic interactions.

Conclusions

The cobalt compound investigated in the present work is, to the best of our knowledge, the first example of a carboxylate-bridged chain complex of Co^{II} featuring an uncommon *anti-anti* conformation to have been fully characterized both magnetically and structurally. Indeed, this *rare* coordination mode of the μ-RCOO group was only discovered thanks to XRPD, which has allowed the determination of the complete 3D structure of a transition metal soap for the first time.[39−41] The XRPD method that we used combined the power of ab initio techniques with that of selected area electron diffraction. Such coupling of complementary techniques, eventually assisted by further computational modelling,[42−44] is expected to allow the solution of more complex crystal structures in the near future, leading to the extensive use of these methods in materials science.[27,45,46] Furthermore, the magnetic properties of **2** have been analysed in detail on the basis of its crystal structure. The weak antiferromagnetism of the carboxylato-bridged Co^{II} chains (with a *cis* coordination mode of the cobalt atoms) is attributed to an *anti-anti* configuration of the bridges.

Experimental Section

General Remarks: Thermogravimetric experiments were performed using a Setaram TG92 instrument (heating rate 2 °C/min; air stream). − Mass-spectrometric measurements were performed using a Micro Mass Trio 2000 instrument (degassing of quartz crucible at 100 °C, desolvation of soap at 200 °C). − Scanning electron microscopy was performed using a JEOL JSM-840 instrument coupled with a KEVEX energy dispersion spectrometer. − Electron diffraction experiments were performed with a Philips CM12 transmission instrument equipped with a PW6594 goniometer (120 kV). − FT-IR studies were performed with an ATI Mattson Genesis computer-driven instrument (0.1 mm thick powder samples in KBr). − UV/Vis/NIR studies were performed with a Perkin−Elmer Lambda 19 instrument (spectra recorded by reflection with a resolution of 4 nm and a sampling rate of 480 nm/min). − Magnetic studies were carried out using a Quantum Design XMPMS SQUID magnetometer. Susceptibilities were measured at 0.2 T in the temperature range 1.7−295 K. The magnetization curve was determined at 2 K with an applied field ranging from 0 to 5 T. − For the powder X-ray diffraction experiments, the powder samples were cautiously deposited in the hollow of a side-loaded holder. Data were collected with a Siemens D500 diffractometer equipped with Soller slits, a primary-beam curved quartz monochromator (Co-$K_{\alpha 1}$, $\lambda = 1.78897$ Å), an Na(Tl)I scintillation detector, and a pulse height amplifier discriminator. The generator was operated at 35 kV and 30 mA. Slits used: divergence 1.0°, antiscatter 1.0°, and receiving 0.15 mm. Long overnight scans were performed in the range $2° < 2\theta < 130°$ with a $\theta/2\theta$ step-scanning mode ($\Delta 2\theta = 0.02°$ and $t = 10$ s). The indexing procedure is described in the text.

Potassium *n*-Dodecane-α,ω-dioate, $C_{12}H_{20}K_2O_4$ (1): A 0.1 N aqueous solution of KOH (5.611 g, 0.1 mol; Titrisol, Fluka) was diluted with acetone (150 mL; Carlo Erba, analytical grade) and added dropwise to a stirred solution of *n*-dodecane-α,ω-dioic acid (11.515 g, 0.05 mol; Lancaster, 99%) in acetone (500 mL) and the

mixture was refluxed for 3 h (56.5 °C). After cooling to room temperature, a white precipitate of the potassium soap had formed, which was collected by filtration, washed repeatedly with hot acetone, and dried in vacuo at room temperature for 12 h.

Diaquacobalt(II) *n*-Dodecane-α,ω-dioate, $C_{12}CoH_{24}O_6$ (2): Pure **1** (1.96 g, 6.4 mmol) was dissolved in a mixture of demineralized water (18.2 MΩcm; Millipore) and ethanol (purum; Carlo Erba) (300 mL, 1:1, v/v). The resulting solution was added dropwise to a stirred solution of $(CH_3COO)_2Co{\cdot}4H_2O$ (1.59 g, 6.4 mmol; Aldrich, 99.999%) in demineralized water (40 mL) at 20 °C. After stirring for 3 h, a pink precipitate of the diaquacobalt dicarboxylate had formed, which was collected by filtration, washed repeatedly with aqueous ethanol (1:1, v/v), and dried in vacuo at room temperature for 24 h (yield 82%). The presence of water molecules was detected by thermogravimetry (TGA) (10.8% weight loss at about 90 °C) and confirmed by mass spectrometry. The purity of the product was confirmed by elemental analysis (EA) $\{Co[OOC(CH_2)_{10}COO](H_2O)_2$: calcd. C 44.6, H 7.5; found C 44.3, H 7.5}, oxidative pyrolysis (OP) (heating in air from 20 to 700 °C at 2 °C/min, maintaining at 700 °C for 30 min to transform cobalt into Co_3O_4,[47,48] and cooling to 20 °C at 10 °C/min: calcd. Co 18.2; found 18.4), and Karl Fischer (KF) titration of water (calcd. 11.2; found 12.5) (water molecules per Co atom: 1.9 by TGA, 2.2 by KF, 1.9 by OP, and 2.1 by EA). − IR (KBr pellet): $\tilde{\nu}$ = 3401 [ν(OH−O)], 3262 [ν(OH−O)], 1670 [$\delta_b(H_2O)$], 2919 [$\nu_{as}(CH_2)$], 2850 [$\nu_s(CH_2)$], 1542 [$\nu_{as}(C{=}O)$], 1470 [$\delta_s(CH_2)$], 1414 [$\nu_s(C{-}O)$], 723 cm^{-1} [$\rho(CH_2)$]. − UV/Vis (reflectance for octahedral coordination of Co^{II}): λ = 1316 nm ($^4T_{1g} \rightarrow {}^4T_{2g}$), 714 nm ($^4T_{1g} \rightarrow {}^4A_{2g}$), 543 nm [$^4T_{1g} \rightarrow {}^4T_{1g}$(P)].

X-ray Crystallographic Study: The structure solution of **2** was initiated using EXPO,[49,50] which revealed the positions of the cobalt atom and of a few oxygen atoms bound to it. With the help of difference Fourier syntheses and geometrical modelling, approximate coordinates for *all* the remaining non-hydrogen atoms were subsequently obtained. All refinements were performed with the aid of the GSAS suite of programs,[51] by imposing steric restraints on the organic fragments, which were idealized with average literature values (C−C 1.54 Å; C−C−C 109.5°). Soft restraints were also applied to Co−O distances and C−O interactions in order to maintain plausible Co−O−C and O−C−O angles. The peak shapes were best described by the Thompson/Cox/Hastings formulation[52] of the pseudo Voigt function, with GV and LY set to zero. The experimental background was modelled by a cosine Fourier series, while systematic errors were corrected with the aid of sample-displacement angular shifts and preferred orientation corrections [with (001) pole]. Metal atoms were given a refinable isotropic displacement parameter of $U_{iso}(M)$ = 0.028(2) $Å^2$, while the *U* values of lighter atoms were arbitrarily given values of $U_{iso}(M)$ + 0.02 $Å^2$. The contribution of the hydrogen atoms to the scattered intensity was neglected. Scattering factors, corrected for real and imaginary anomalous dispersion terms, were taken from the GSAS internal library. The final Rietveld refinement plot is shown in Figure 6. Crystal Data: $C_{12}H_{24}CoO_6$, M_r = 323.25 g mol^{-1}, monoclinic, $P2_1/a$; *a* = 9.6558(8), *b* = 7.4793(6), *c* = 19.8936(2) Å, β = 95.648(9)°, *V* = 1429.7(3) $Å^3$; *Z* = 2; μ = 100.48 cm^{-1}; ρ = 1.502 g cm^{-3}. The final R_p, R_{wp}, and R_F agreement factors, for 6001 data collected in the 4−124° range (1442 reflections), were 0.125, 0.163, and 0.067, respectively. Full pattern decomposition resulted in R_p and R_{wp} values of 0.108 and 0.146, respectively. Crystallographic data (excluding structure factors) for the structure reported in this paper have been deposited with the Cambridge Crystallographic Data Centre as supplementary publication no. CCDC-156267. Copies of the data can be obtained free of charge on application to CCDC, 12 Union Road, Cambridge CB2 1EZ, U.K. [Fax: (internat.) + 44-1223/336-033; E-mail: deposit@ccdc.cam.ac.uk].

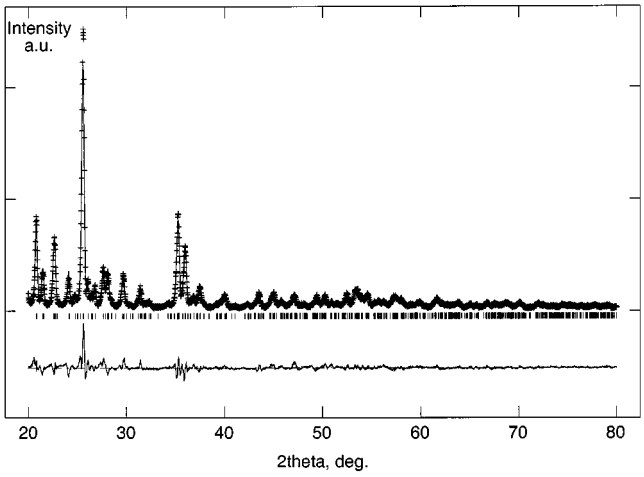

Figure 6. Rietveld refinement plot of compound **2** in the 20−80° (2θ) range, with difference plot and peak markers at the bottom; the low-angle section, dominated by the strong (001) peak, has been omitted in order to highlight the agreement at intermediate angles

Acknowledgments

This is part of the Ph.D. thesis work of one of us (J.-M. R). We thank Dr. B. Lotz of the Institut Charles Sadron, Strasbourg, France, for his contribution to the electron diffraction experiments, Prof. J. Guille of the Institut de Physique et Chimie des Matériaux de Strasbourg, Strasbourg, France, for his contribution to the scanning electron microscopy studies, and Dr. M. Drillon for helpful discussions.

[1] *Organic and Inorganic Low-Dimensional Crystalline Materials* (Eds.: P. Delhaes, M. Drillon), NATO ASI Series, B: Physics, Plenum Press, New York, **1987**.
[2] *Magnetic Properties of Layered Transition Metal Compounds* (Ed.: L. J. de Jongh), Physics and Chemistry of Materials with Low-Dimensional Structures 9A, Kluwer Academic Publishers, Dordrecht, **1990**.
[3] *Research Frontiers in Magnetochemistry* (Ed.: C. O'Connor), World Scientific Publishers, Singapure, **1993**.
[4] J. S. Miller, A. J. Epstein, W. M. Reiff, *Chem. Rev.* **1988**, *88*, 201; *Magnetic Molecular Materials* (Eds.: D. Gatteschi, O. Kahn, J. S. Miller, F. Palacio), Kluwer, Dordrecht, **1991**.
[5] O. Kahn, *Molecular Magnetism*, VCH, Weinheim, **1993**.
[6] R. D. Vold, G. S. Hattiangdi, *Ind. Eng. Chem.* **1949**, *41*, 2311 and 2320.
[7] A. Skoulios, *Ann. Phys.* **1978**, *3*, 421.
[8] T. Lomer, *Acta Crystallogr.* **1952**, *5*, 11.
[9] H. Kambe, *Bull. Chem. Soc. Jpn.* **1962**, *35*, 78.
[10] See, for example: B. K. Tyagi, R. Varma, A. Kumar, *Phys. Chem. Liq.* **1996**, *31*, 253.
[11] See, for example: H. D. Dorfler, *Mol. Cryst. Liq. Cryst. Sci. Techn. Sect A* **1995**, *258*, 73.
[12] K. Binnemans, H. Heinrich, D. Guillon, D. W. Bruce, *Liq. Cryst.* **1999**, *26*, 1717.
[13] K. Binnemans, L. Jongen, C. Görller-Walrand, W. D'Olieslager, D. Hinz, G. Meyer, *Eur. J. Inorg. Chem.* **2000**, 1429 and references therein.

[14] Z. L. Huang, M. Drillon, N. Masciocchi, A. Sironi, J. T. Zhao, P. Rabu, P. Panissod, *Chem. Mater.* **2000**, *12*, 2805.
[15] C. Hornick, P. Rabu, M. Drillon, *Polyhedron* **2000**, *19*, 259.
[16] N. Masciocchi, A. Sironi, *J. Chem. Soc., Dalton Trans.* **1997**, 4643; N. Masciocchi, A. Sironi, L. Garavaglia, G. D'Alfonso, *Angew. Chem. Int. Ed.* **2000**, *39*, 4477 and references therein.
[17] R. C. Mehrotra, R. Bohra, *Metal Carboxylates*, Academic Press, London, **1983**, p. 16.
[18] H. Kambe, *Bull. Chem. Soc. Jpn.* **1961**, *34*, 81.
[19] Orthorhombic crystal form: A. I. Kitaigorodskii, *Organic Chemical Crystallography*, Consultants Bureau, New York, **1961**.
[20] Final refined values from whole-pattern Rietveld refinement (vide infra).
[21] D. L. Dorset, *Structural Electron Crystallography*, Plenum Press, New York, **1995**.
[22] K. Nakamoto, *Infrared and Raman Spectra of Organic and Coordination Compounds*, 4th ed., Wiley Interscience, New York, **1986**, p. 231.
[23] A. B. P. Lever, *Inorganic Electronic Spectroscopy*, 2nd ed., Elsevier, Amsterdam, **1984**.
[24] L. Banci, A. Bencini, C. Benelli, D. Gatteschi, C. Zanchini, *Struct. Bonding* **1982**, *52*, 37
[25] R. L. Carlin, *Magnetochemistry*, Springer-Verlag, Berlin, Heidelberg, **1986**.
[26] F. E. Mabbs, D. J. Machin, *Magnetism and Transition Metal Complexes*, Chapman and Hall, Ltd., London, **1973**.
[27] P. Rabu, J.-M. Rueff, Z.-L. Huang, S. Angelov, J. Souletie, M. Drillon, *Polyhedron*, in press.
[28] E. Colacio, J. M. Dominguez-Vera, J. P. Costes, R. Kivekäs, J. P. Laurent, J. Ruiz, M. Sundberg, *Inorg. Chem.* **1992**, *31*, 774.
[29] D. K. Towle, S. K. Hoffmann, W. E. Hatfield, P. Singh, P. Chaudhuri, *Inorg. Chem.* **1988**, *27*, 394.
[30] J. E. Davies, B. M. Gatehouse, K. S. Murray, *J. Chem. Soc., Dalton Trans.* **1973**, 2523.
[31] K. K. Nanda, A. W. Addison, E. Sinn, L. K. Thomson, *Inorg. Chem.* **1996**, *35*, 5966.
[32] E. Colacio, J. M. Dominguez-Vera, M. Ghazi, R. Kivekäs, M. Klinga, J. M. Moreno, *Eur. J. Inorg. Chem.* **1999**, 441.
[33] B. N. Figgis, R. L. Martin, *J. Chem. Soc.* **1956**, 3837.
[34] D. K. Towle, S. K. Hoffmann, W. E. Hatfield, P. Singh, P. Chanduri, *Inorg. Chem.* **1988**, *27*, 394.
[35] R. L. Carlin, K. Kopinga, O. Kahn, M. Verdaguer, *Inorg. Chem.* **1986**, *25*, 1786.
[36] A. Fuertes, C. Miravittles, E. Escriva, E. Coronado, D. Beltran, *J. Chem. Soc., Dalton Trans.* **1986**, 1795.
[37] P. K. Coughlin, S. J. Lippard, *J. Am. Chem. Soc.* **1984**, *106*, 2328.
[38] M. Kato, Y. Muto, *Coord. Chem. Rev.* **1988**, *92*, 45.
[39] Occurring, among acyclic carboxylates, only in two polymeric derivatives: G. Liu, A. M. Arif, F. W. Bruenger, S. C. Miller, *Inorg. Chim. Acta* **1999**, *287*, 109.
[40] W. Aurangzeb, C. E. Hulme, C. A. McAuliffe, R. G. Pritchard, M. Watkinson, A. Garcia-Deibe, M. R. Bernejo, A. Sousa, *J. Chem. Soc., Chem. Commun.* **1992**, 1624.
[41] In the $[V_9O_{19}(CH_3COO)_5]^{3-}$ anion, but with much larger intermetallic distances of up to 6.86 Å: G. B. Karet, Z. Sun, W. E. Streib, J. C. Bollinger, D. N. Hendrickson, G. Christou, *Chem. Commun.* **1992**, 2249.
[42] E. Corradi, N. Masciocchi, G. Palyi, R. Ugo, A. Vizi-Orosz, C. Zucchi, A. Sironi, *J. Chem. Soc., Dalton Trans.* **1997**, 4651.
[43] N. Masciocchi, F. Ragaini, S. Cenini, A. Sironi, *Organometallics* **1998**, *17*, 1052.
[44] N. Masciocchi, A. Sironi, *Adv. X-ray Anal.* **2000**, *42*, 366.
[45] For recent examples, see ref.[10] and: M. Brinkmann, G. Gadret, M. Muccini, C. Taliani, N. Masciocchi, A. Sironi, *J. Am. Chem. Soc.* **2000**, *121*, 5147.
[46] N. Masciocchi, G. A. Ardizzoia, G. La Monica, A. Maspero, A. Sironi, *Eur. J. Inorg. Chem.* **2000**, 2507.
[47] J. Amiel, J. Besson, *Nouveau Traité de Chimie Minérale* (Ed.: P. Pascal), Masson, Paris, **1963**, p. 17.
[48] M. A. Mohamed, S. A. Halawy, M. M. Ebrahim, *J. Thermal Anal.* **1994**, *41*, 387−404.
[49] A. Altomare, M. C. Burla, G. Cascarano, G. Giacovazzo, A. Guagliardi, A. G. G. Moliterni, G. Polidori, *J. Appl. Crystallogr.* **1995**, *28*, 842.
[50] A. Altomare, M. C. Burla, M. Camalli, B. Carrozzini, G. L. Cascarano, C. Giacovazzo, A. Guagliardi, A. G. G. Moliterni, G. Polidori, R. Rizzi, *J. Appl. Crystallogr.* **1999**, *32*, 339.
[51] A. C. Larson, R. B. Von Dreele, LANSCE, MS-H805, Los Alamos National Laboratory, New Mexico, **1990**.
[52] P. Thompson, D. E. Cox, J. B. Hastings, *J. Appl. Crystallogr.* **1987**, *20*, 79.

Received April 3, 2001
[I01117]

Heptacoordinate Dimethyltin(IV)cupferronato Complexes − X-ray and Solid-State NMR Structural Analysis − Hydrogen Bond Supramolecular Self-Assembly

Andrea Deák,[a] Lajos Radics,*[a] Alajos Kálmán,*[a] László Párkányi,[a] and Ionel Haiduc*[b]

Keywords: Chelates / Hypervalent compounds / N ligands / Self assembly / Tin

Reaction of the dimeric dimethyltin(IV)cupferronato complex $[Me_2Sn(O_2N_2Ph)_2]_2$ (**1**) with 4,4′-bipyridine (bipy), pyridine (py), and 2,6-diamino-4-phenyl-1,3,5-triazine (dpt) afforded three new hepta-coordinated derivatives, [μ-(4,4′-bipy){$Me_2Sn(O_2N_2Ph)_2$}$_2$]·MeOH (**2**), $Me_2Sn(O_2N_2Ph)_2$(py) (**3**), and $[Me_2Sn(O_2N_2Ph)_2(MeOH)]$·dpt (**4**). These were characterised by X-ray structural analysis and solid-state ^{119}Sn, ^{13}C CP MAS NMR-, and multinuclear solution NMR spectroscopy. Single-crystal X-ray diffraction analysis of **2**–**4** showed that in all three compounds tin was hepta-coordinated, and the cupferronato anions were chelated to the Me_2Sn^{IV} centre in a nearly symmetrical arrangement. Compound **4** contained supramolecular self-assembled ribbons, formed by hydrogen bonds between Me_2SnO_5 moieties and pairs of dpt molecules.

Introduction

Recently, we reported the synthesis and structural characterisation of *N*-nitroso-*N*-phenylhydroxylaminato (cupferronato, $PhN_2O_2^-$, hereinafter cupf) tin(IV) complexes, such as $[Me_3Sn(cupf)]_4$ (**5**),[1] $Ph_2Sn(cupf)_2$ (**6**), $[Me_2Sn(cupf)_2]_2$ (**1**), and $Sn(cupf)_4$ (**7**).[2] We found that, depending on the number (0, 2, 3) and the nature (Me, Ph) of the substituents at the Sn^{IV} atom, the cupferronato anion displays various coordination patterns in these molecules: chelating (**6**, **1**, **7**), bridging (**5**), and bridging-chelating (**1**). As a consequence of this, the central Sn^{IV} atom assumes a penta- (**5**), hexa- (**6**), hepta- (**1**), or octacoordinate (**7**) state, respectively, and the resulting complexes display different coordination geometries at the central Sn^{IV} atom.[1,2] Bridging-chelating coordination of the cupferronato ligand to Me_2Sn^{IV} gives the dimeric species **1** (Scheme 1),[2] whereas a bridging coordination affords the tetrameric complex **5** (Scheme 2).[1]

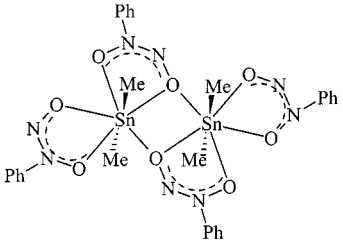

1

Scheme 1

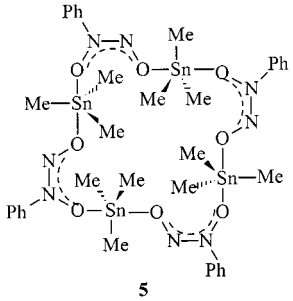

5

Scheme 2

Compound **5** seemed an attractive starting material for building supramolecular structures based upon chains of alternating trigonal planar $SnMe_3$ units with rigid linear spacers, such as 4,4′-bipyridine (4,4′-bipy). The reaction of **5** with 4,4′-bipy, however, afforded a dimethyltin derivative **2**, following tin−carbon bond redistribution (vide infra). This led us to investigate the reactions of the dimethyltin derivative **1** with 4,4′-bpy and with pyridine (py) as a model. Formation of **2** and **3** suggested that a nitrogen-donor base coordinates easily to the tin atom of a $Me_2Sn(cupf)_2$ moiety and we decided to use 2,6-diamino-4-phenyl-1,3,5-triazine (dpt) as a coordinated ligand able to participate in intermolecular hydrogen bond interactions and thus to connect the tin coordination centres into supramolecular architectures. This approach is well documented by several examples of hydrogen bond self-assembled supramolecular structures formed by interactions between amino substituents and heteroatoms.[3] From our previous experience with cobalt and nickel cupferronato adducts of dpt[4] we knew that metalcupferronates could form supramolecular structures based upon this strategy. Although only in its

[a] Institute of Chemistry, Chemical Research Center of the Hungarian Academy of Sciences,
P. O.Box 17, 1525 Budapest, Hungary
Fax: (internat.) +36−1/325−7554
E-mail: radics@nmr.chemres.hu
akalman@chemres.hu
[b] Chemistry Department Babes-Bolyai University,
3400 Cluj-Napoca, Romania
Fax: (internat.) +40−64/190−818
E-mail: ihaiduc@chem.ubbcluj.ro

 © WILEY-VCH Verlag GmbH, 69451 Weinheim, 2001 1434−1948/01/1111−2849 $ 17.50+.50/0

infancy, the combination of coordination dative and hydrogen bonds in the construction of supramolecular architectures opens a wide area of investigation, and has already provided some interesting results.[4] On the other hand, some organotin supramolecular assemblies based on hydrogen bonds are known,[6] opening a potentially broad field for novel materials of this type.

The reactions investigated in this research are illustrated in Scheme 3. The structural analyses of the products thus obtained, [μ-(4,4′-bipy){$Me_2Sn(cupf)_2$}$_2$]·MeOH (**2**), $Me_2Sn(cupf)_2(py)$ (**3**), and [$Me_2Sn(cupf)_2$(MeOH)]·dpt (**4**), are reported here. To this end, X-ray analyses of **2**−**4** were carried out and the resulting structures compared with those of **1** and **5** reported previously.[1,2]

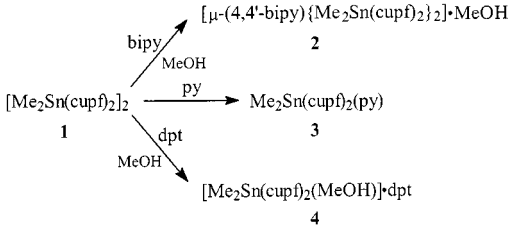

Scheme 3

Solid-state ^{119}Sn NMR spectroscopy is known to give insight into the local symmetry properties of the central tin(IV) atom, and, combined with solution ^{119}Sn NMR spectroscopic data, provides information about the structural changes occurring upon dissolution of the organotin compounds.[7] The availability of X-ray data on a set of structurally related organotin(IV) molecules (**1**−**5**) prompted us to complement the present work with the solid-state and solution NMR spectroscopic data.

Results and Discussion

Synthesis of the Complexes

The reaction of **5**, a tetrameric complex, with bipy in methanol, and the reaction of dimer **1** in *n*-heptane with bipy, followed by recrystallisation from MeOH, both yielded the solvated binuclear complex **2** (Scheme 3).

Mössbauer spectroscopic studies[8] have shown that in concentrated methanolic solution, **5** undergoes a redistribution[9] involving Sn−Me bond cleavage (Scheme 4).

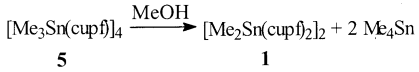

Scheme 4

Slow evaporation of a pyridine solution of **1** afforded mononuclear **3** as colourless crystals after several days. Addition of a methanolic solution of dpt to **1** in methanol readily gave **4** as a crystalline compound.

X-ray Analyses

Molecular Structures

The molecular structures of **2**−**4**, established by single-crystal X-ray diffraction, are shown in Figures 1−3, with the atom numbering schemes. The relevant geometric parameters are collected in Table 1. The data obtained for **2** reveal that the Sn^{IV} centres are heptacoordinate and located

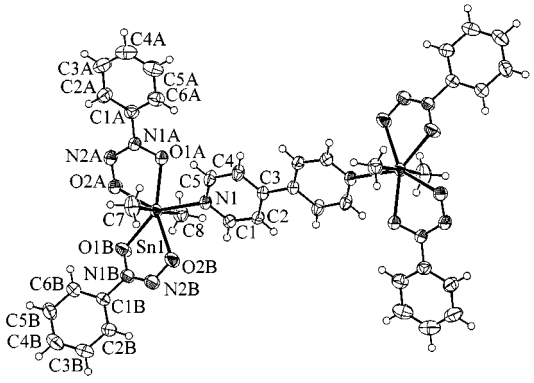

Figure 1. Molecular structure of **2**, the disordered MeOH molecules were omitted

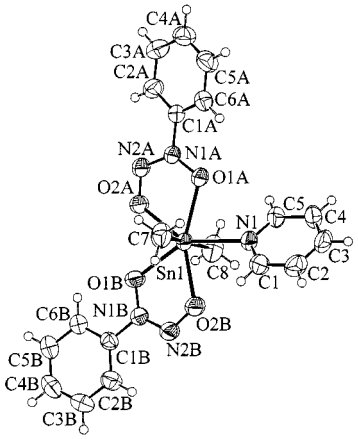

Figure 2. Molecular structure of **3**

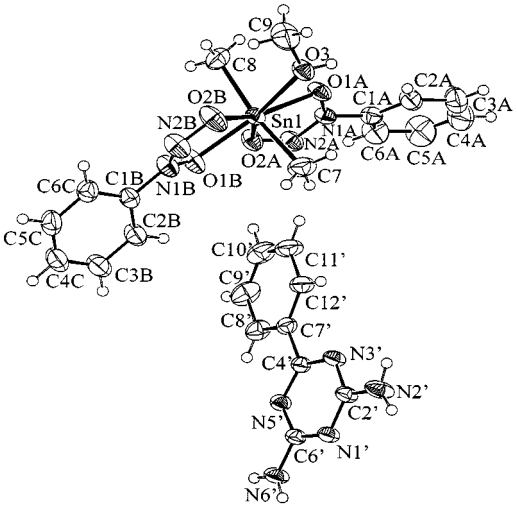

Figure 3. Molecular structure of **4**

Table 1. Selected bond lengths (Å), bond angles (°) and torsion angles (°) for **2**−**4**

	2[a]		**3**		**4**	
	L = *A*	*L* = *B*	*L* = *A*	*L* = *B*	*L* = *A*	*L* = *B*
Sn(1)−O(1*L*)	2.2831(12)	2.2769(13)	2.3104(14)	2.2306(14)	2.3435(10)	2.2012(10)
Sn(1)−O(2*L*)	2.2738(12)	2.3313(13)	2.2584(14)	2.3167(15)	2.2792(9)	2.2804(12)
Sn(1)−N(1)	2.4497(13)		2.4677(16)			
Sn(1)−O(3)					2.4119(9)	
Sn(1)−C(7)	2.123(2)			2.114(3)	2.1100(15)	
Sn(1)−C(8)	2.1124(18)			2.109(3)	2.1129(14)	
O(1*L*)−N(1*L*)	1.3134(16)	1.3132(16)	1.3168(18)	1.314(2)	1.3133(13)	1.3243(14)
O(2*L*)−N(2*L*)	1.3004(18)	1.288(2)	1.293(2)	1.287(2)	1.3025(15)	1.2948(17)
N(1*L*)−N(2*L*)	1.2852(18)	1.2896(19)	1.284(2)	1.286(2)	1.2878(14)	1.2864(16)
O(1*L*)−Sn(1)−O(2*L*)	67.51(4)	66.87(4)	67.53(5)	67.71(5)	66.12(3)	69.43(4)
C(7)−Sn(1)−C(8)		177.91(7)		174.30(9)		170.75(6)
O(1*L*)−N(1*L*)−N(2*L*)−O(2*L*)	0.4(2)	−0.4(3)	0.9(3)	0.3(3)	−0.2(2)	0.8(2)
O(1*L*)−N(1*L*)−C(1*L*)−C(6*L*)	−7.5(2)	−16.6(2)	15.7(3)	−1.8(3)	16.7(2)	−145.1(1)
N(2*L*)−N(1*L*)−C(1*L*)−C(2*L*)	−9.0(2)	−18.4(2)	18.5(3)	−1.9(3)	19.3(2)	−143.5(1)

[a] *L* = *A* and *L* = *B* represent the two different cupferronato ligands chelated to tin.

in a nearly pentagonal bipyramidal environment, with the equatorial plane defined by the O_4N donor set of the cupferronato and the bipy ligands, and the two methyl groups in the apical positions. The formation of **2** occurs through the cleavage of the dative Sn←O bonds of the dimer **1**, with the bipy ligands acting as spacers that link the two Me_2Sn^{IV} centres. One should note that the four-membered Sn_2O_2 ring, typical for all structurally characterised pentagonal bipyramidal C_2SnO_4N cores of Me_2Sn^{IV} dimers,[10] is absent in **2**. Consequently, each half of **2** contains two SnO_2N_2 units as five-membered chelate rings (*A* and *B*) with O(1*L*)−Sn(1)−O(2*L*) bite angles of 67.51(4)° (*A*) and 66.87(4)° (*B*). The lengths of the two Sn−O bond formed in ligands *A* are nearly equal (Δ = 0.009 Å), while those in ligands *B* are slightly different (Δ = 0.054 Å). It should be mentioned here that the chelating cupferronato anions in the parent **1** are isobidentate when coordinated to the dimethyltin(IV) centre (Δ = 0.076 Å), whereas the triconnective cupferronato ligands exhibit different Sn−O bond lengths (Δ = 0.148 Å). In a manner similar to the tridentate aminodicarboxylato anions in dimethyltin(IV) dimers,[10] the latter finding may be ascribed to the triconnective coordination of the cupferronato O atoms. The Sn−N bond length of 2.4450 (1) Å in **2** is slightly longer than the 2.402(2) Å observed in the polymeric $[Me_2SnCl_2(4,4'\text{-bipy})]_n$ complex.[11] There are two positionally disordered MeOH molecules in the unit cell (space group $P2_1/n$) with their O atoms in special positions (inversion centres).

Dissolution of **1** in anhydrous pyridine affords **3**, the "monomeric" form of **2**. Consequently, each tin(IV) centre retains its nearly pentagonal bipyramidal coordination. To the best of our knowledge this is the first reported case where a Me_2Sn^{IV} complex is built from C_2SnO_4N core, despite the fact that this core is known to be ubiquitous in multinuclear complexes.[7,10] The structural similarity between **3** and **2** is reflected by the practically unaltered O(1*L*)−Sn(1)−O(2*L*) bite angles [67.53(5)° for *A* and 67.71(5)° for *B*] and differential Sn−O distances (Δ = 0.052 Å for *A*, Δ = 0.086 Å for *B*). The Sn−N distance is somewhat longer than those found for dimer **2** and Me_2SnCl_2·2py (2.39 Å).[12] In a manner similar to **2**, the nitrosohydroxylaminato groups of the cupferronato anions are essentially planar in **3**, while the phenyl ring is nearly coplanar with the plane of the N(O)NO group, although the O(1*L*)−N(1*L*)−C(1*L*)−C(6*L*) and O(1*L*)−N(1*L*)−C(1*L*)−C(2*L*) torsion angles show some variation (Table 1).

The crystal lattice of **4** contains the complex $Me_2Sn(cupf)_2(MeOH)$ (**4a**) and dpt molecules. The coordination geometry of the Sn^{IV} atom in **4** was found to be closely similar to that in **2** and **3**. Coordination of the bulky dpt unit to the Me_2Sn^{IV} centre via the pyridyl nitrogen atoms is sterically hindered by the likewise bulky cupferronato ligands. Therefore, only one MeOH molecule may occupy the vacant seventh position of the coordination sphere. In this arrangement, the O atom of the MeOH molecule occupies the position of the N atom of bipy (**2**) or py (**3**). This results in a pentagonal bipyramidal C_2SnO_5 core, like the one found for the parent **1**. The latter core is known to occur both in mononuclear[13] and dinuclear[2,14] Me_2Sn^{IV} complexes, although **4** represents the first structurally characterised compound containing methanol coordinated to a dimethyltin(IV) centre.

In complex **4**, the cupferronato *A* and *B* ligands display fairly similar coordination, but remarkably different hydrogen bonding. Both *A* and *B* form five-membered inorganic SnO_2N_2 rings that assume different O(1*L*)−Sn(1)−O(2*L*) bite angles [66.12(3)° for *A* and 69.43(4)° for *B*] and unequal differential Sn−O bond lengths: Δ = 0.064 Å in ligand *A* and Δ = 0.079 Å in ligand *B*. Finally, in anion *B*, the plane of the phenyl group is markedly twisted away from the plane of the N(O)NO group with the O(1*B*)−N(1*B*)−C(1*B*)−C(6*B*) torsion angle taking a value of −145.1(1)°.

Crystal Packing and Supramolecular Organisation

The data collected in Table 2 reveal that the crystal lattices of the complexes reported in this work are supramolec-

Table 2. Selected interatomic distances (Å) and angles (°) for the hydrogen bonding and C−H···π interactions in **2**−**4**; Symmetry codes see footnotes

Compd.	D−H···A[a]	H···A (Å)	D···A (Å)	D−H···A (°)
2	C(1)−H(1)···O(2A)[b]	2.56	3.41	151
	C(2)−H(1)···O(1B)[b]	2.58	3.43	153
	C(4A)−H(4A)···π(Ph_B)[c]	2.86	3.44	121
	C(5)−H(5)···π(Ph_B)[d]	3.21	3.72	117
	C(4)−H(4)···π(Ph_B)[d]	3.24	3.72	115
	C(4A)−H(4A)···π(bipy)[e]	3.29	3.34	85
	C(1S)−H(11S)··· π(bipy)[f]	3.05	3.77	133
3	C(5)−H(5)···π(Ph_B)[g]	3.195	3.96	141
	C(7)−H(7A)···π(py)[h]	3.23	3.63	107
	C(7)−H(7B)···π(py)[h]	3.14	3.63	113
4	O(3)−H(3O)···N(3′)[i]	1.96	2.77	160
	N(2′)−H(2′A)···O(1A)[i]	2.11	2.96	171
	N(2′)−H(2′B)···O(2A)[j]	2.32	3.10	161
	N(6′)−H(6′B)···N(1′)[k]	2.18	3.02	171
	N(6′)−H(6′A)···O(2A)[l]	2.46	3.13	134
	C(4A)−H(4A)···π(Ph_{dpt})[m]	2.875	3.78	165
	C(7)−H(7B)···π(Ph_A)[n]	3.00	3.73	133
	C(9′)−H(9′)···π(Ph_B)[o]	3.09	3.78	132

[a] for intermolecular C−H···π contacts the H···ring-centroid distances must be less than 3.4 Å[15a] [b] 3/2 − *x*, 1/2 + *y*, 1/2 − *z*; [c] 1 − *x*, 1 − *y*, − *z*; [d] 1/2 + *x*, 3/2 − *y*, − 1/2 + *z*; [e] 2 − *x*, 1 − *y*, − *z*; [f] *x*, *y*, *z*; [g] 3/2 − *x*, 1/2 + *y*, 3/2 − *z*; [h] 2 − *x*, −*y*, 2 − *z*; [i] −*x* + 1, − *y* + 1, − *z*; [j] *x*, *y* − 1, *z*; [k] − *x* + 1, − *y*, − *z* + 1; [l] − *x* + 1, − *y* + 1, − *z* + 1; [m] − *x*, 1 − *y*, − *z*; [n] 1 − *x*, 1 − *y*, − *z*; [o] −1 + *x*, *y*, *z*.

ular architectures involving more than just van der Waals interactions. Thus, molecules **2** and **3** form crystal lattices stabilised by weak C−H···π intermolecular interactions. An additional interaction via weak C−H···O hydrogen bonding between individual molecules can also be observed in the crystal lattice of **2**.

Compound **4** forms an infinite supramolecular structure (Figure 4) where units of **4a** and dpt molecules are interconnected by regular N−H···O and O−H···N hydrogen bonds, mediated in part by the MeOH molecules. On the one hand, this is achieved in such a way that the MeOH molecules form short (1.96 Å) O−H···N hydrogen bonds with the neighbouring dpt units. In competition with the MeOH molecules, the dpt units, in their turn, interact with the two oxygen atoms of cupferronato anions of the **4a** complex via N−H···O hydrogen bonds (2.11 Å and 2.46 Å). The intermolecular O−H···N and N−H···O hydrogen bonds together assemble the units **4a** and dpt in infinite chains. These chains then become cross-linked to their respective symmetry-related neighbouring chains through N−H···O and N−H···N hydrogen bonds (2.32 Å and 2.18 Å, respectively) to form infinite one-dimensional double-chains (ribbons). In the supramolecular structure thus formed, the Sn···Sn separation between neighbouring **4a** units amounts to ca. 6.8 Å. It may be noted that the N−H···N hydrogen bonds between neighbouring dpt units lead to the formation of eight-membered $(N-C-N-H\cdots)_2$ rings (see Figure 4), while, using the hydrogen atoms of their NH_2 groups, the dpt units also formed N−H···O hydrogen bonds with the cupferronato O atoms of **4a** in the adjacent chain.

Alternatively, the supramolecular arrays can be described as containing pairs of hydrogen-bonded dpt molecules (via N−H···N bonds), interconnected through two separate **4a** molecules, via N−H···O bonds (to the chelate rings) and N···H−O bonds (to the coordinated methanol molecules). Therefore, the supramolecular architecture is a result of the co-operative use of hydrogen bonds and dative coordinate bonds (provided by the methanol ligand).

The neighbouring supramolecular sheets are ordered by C−H···π (Table 2) and π···π interactions. These weak C−H···π and π···π interactions influence the nature of hydrogen-bonding and vice versa.[15]

Structure Determination by NMR Spectroscopy

The structurally relevant NMR spectral parameters for **1**−**5** are collected in Table 3. (For the fully assigned, solution, ^1H, ^{13}C, and ^{119}Sn NMR parameters see the Exp. Sect. and ref.[2]).

Within a given set of related organotin complexes, the chemical shift of the ^{119}Sn nuclei has been shown to reflect the coordination number, the size of the chelate ring, and the nature of the donor atom directly bonded to the central tin(IV) atom: higher coordination numbers, larger ring sizes, and lower electronegativities of the donor atoms shift the ^{119}Sn resonance to lower frequencies.[3,16] Although an exact separation of the various contributions to the nuclear shielding is beyond current theoretical knowledge, the ^{119}Sn chemical shift values in Table 3 do, in general, follow the expected trends. The highest value of the chemical shift of tetrameric (**5**) clearly reflects its pentacoordinated geometry,[1] while the nuclear shielding found for **1**−**4** falls in the range typical of hexa- and heptacoordinated organotin complexes.[3,12] One may tentatively assume that the rela-

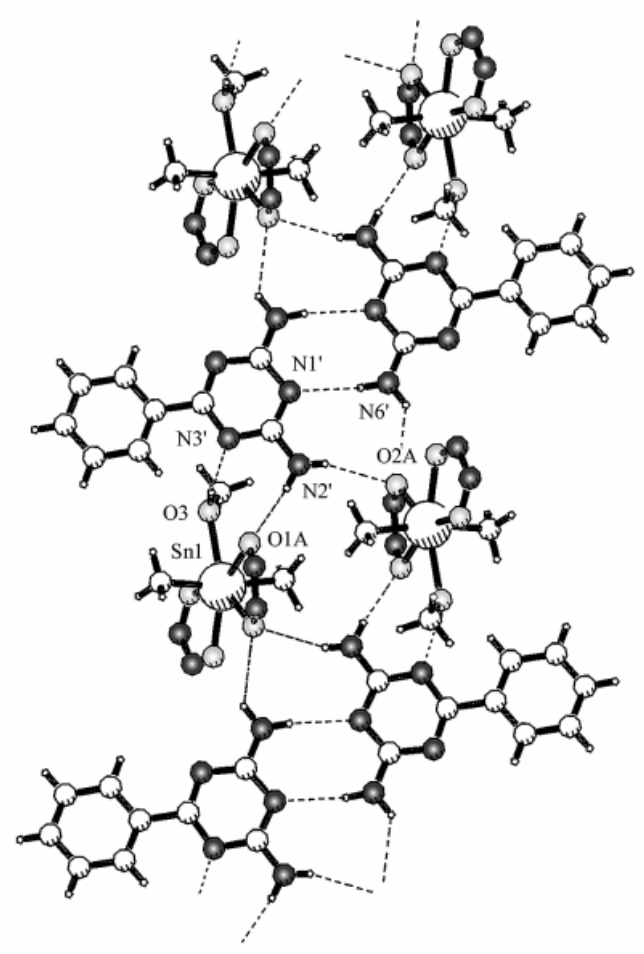

Figure 4. Section of the crystal structure of **4** showing the infinite one-dimensional double-chains (ribbons) formed through O−H···N and N−H···X (X = O, N) hydrogen bonds; the phenyl groups were omitted for clarity.

tively lower δ_i^{Sn} values observed for solid **1** and **4** are due to the higher electronegativity of the directly bonded oxygen atom as compared to the N-linkage in **2** and **3**.[16]

The chemical shift anisotropy, $\Delta\sigma$, for **1**−**4** varies in the range between +383 and +532 ppm, while it becomes negative (−262 ppm) in **5**. An analogous dissimilarity can be seen in the case of the asymmetry parameter, η: it is zero, or nearly zero, in complexes **1**−**4** while it has a substantial value (0.6) in **5**. Low values of η are known to reflect axial symmetry of the tin(IV) centre,[17] an expectation fully supported by X-ray results showing pentagonal bipyramidal coordination geometry for **1**−**4**. By contrast, the asymmetry parameter measured for **5** may be rationalised by considering the X-ray structure of this molecule.[1] It has been found that a weak, secondary, nonbonded Sn···O interaction removes the axial symmetry of the Sn^{IV} centre, which then assumes a distorted trigonal bipyramidal (TBP), pseudo hexagonal, geometry.

The magnitude of the solid state one bond tin−carbon scalar coupling, $^1J(^{119}Sn-^{13}C)$, (measured here as the frequency difference between ^{119}Sn satellite signals in the ^{13}C CP MAS spectra) can be used for estimating the Me−Sn−Me angle.[7] The coupling data obtained for **1**−**4** fall in the range ≈ 1060−1160 Hz (Table 3), and according to the Lockhart−Manders approximation,[7] give a value of 170−179°, in good overall agreement with X-ray observations. It should be noted, however, that the slight changes in the Me−Sn−Me angles show opposite trends according to whether the angles were inferred from X-ray or $^1J(^{119}Sn-^{13}C)$ coupling data (see Table 4). The value of 520 Hz measured for **5** gives 122°, in excellent agreement with the X-ray-derived average value, 120°.

Table 4. Values of Me−Sn−Me angles(°) from X-ray and from ^1J and ^2J[7a]

Compd.	Me−Sn−Me (°) X-ray	^1J(solid)[a]	^1J(solution)[a]	^2J(solution)[b]
1	173.6(1)[2]	171.6	136.3	127.3
2	177.91(7)	173	142.8	135.6
3	174.30(9)	173.8	151	145.8
4	170.75(6)	181.5	175.8	191.7
5	119.91(12)[1] [c]	121.3	110.4	109.5

[a] Me−Sn−Me (°) = ($|^1J|$ + 778)/10.7 [b] Me−Sn−Me (°) = 0.0161 ($|^2J|)^2 - 1.32(|^2J|)$ + 133.4 [c] average value

Some additional features of the ^{13}C CP MAS spectra deserve attention. Mirroring the slight changes in the steric environments of the two Sn^{IV}-bonded Me carbon atoms, the ^{13}C spectra of **1**−**4** display two methyl signals separated by 1.3−2.7 ppm (Table 3). No such effect could be resolved (at 100 MHz) in the spectrum of **5** having three, equatorially oriented, methyl groups attached to the central Sn^{IV} atom. The ^{13}C CP MAS spectrum of **4** also displays a sharp resonance at δ = 49.5 attributable to the methanol Me signal.

Table 3. Selected NMR spectral parameters of complexes **1**−**5**

Compd.	σ_i [a] Solid-state	σ_{33}	σ_{22}	σ_{11}	$\Delta\sigma$	δ_A	η	δ_i^{Sn} [b]	$^1J(^{119}Sn-^{13}C)$	$\Delta\delta^{Me}$	δ_i^{Sn}(sol.) Solution	$^1J(^{119}Sn-^{13}C)$	$^2J(^{119}Sn-^1H)$
1	184.7	464.0	47.6	−2.7	419.0	279.3	0.2	−184.7	1058±15	1.21	−185.5	680.8	77.1
2	273.2	628.1	74.5	21.2	532.4	354.9	0.2	−273.2	1073±15	2.68	−216.4	750.5	83.6
3	252.6	523.0	58.7	58.7	405.6	270.4	0.0	−252.6	1082±15	2.66	−258.5	837.6	90.5
4	246.6	502.0	70.0	70.0	383.0	255.3	0.0	−246.6	1164±15	1.36	−368.2	1103.3	113.8
5	−1.5	−173.1	81.6	136.8	−261.9	−174.6	0.6	1.5	520±10	0.0	95.9	403.8	54.9

[a] $\sigma_i = 1/3(\sigma_{33} + \sigma_{22} + \sigma_{11})$; $|\sigma_{33} - \sigma_i| > |\sigma_{11} - \sigma_i| > |\sigma_{22} - \sigma_i|$; $\Delta\sigma = \sigma_{33} - 1/2(\sigma_{11} + \sigma_{22})$; $\Delta\sigma = 3/2\delta_A$; $\delta_A = \sigma_{33} - \sigma_I$; $\eta = 3/2\ (\sigma_{22} - \sigma_{11})(\Delta\sigma)^{-1}$ [b] Chemical shifts are in ppm, coupling constants in Hz;

Dissolution of the complexes results in several changes in the spectral parameters (see Table 3) that suggest differences between the molecular conformations in the solid and solution states. The solution ^{119}Sn chemical shifts, δ^{Sn}(sol.), for **1**−**3** are fairly close to their isotropic values, δ_i^{Sn}, found in the solid state, suggesting that the coordination geometry of these complexes remains unaffected by dissolution. The marked shift to lower frequency of the ^{119}Sn resonance in **4** may be tentatively rationalised by assuming that due to the presence of DMSO in the solvent (which may replace the coordinated methanol molecule), the coordination pattern of the complex undergoes some modifications. In contrast to the near-constancy of the overall molecular geometry in the two states, as mirrored by the ^{119}Sn chemical shifts, $^1J(^{119}Sn-^{13}C)$ and in part $^2J(^{119}Sn-^1H)$, couplings suggest that the solvent-solute interactions may, in reality, give rise to some changes in the molecular geometry. As attested by the coupling data, these are highest in **1** while practically absent in **4**. For **1** we find that the Me−Sn−Me angle assumes a value of approx. 130° in solution as opposed to 170° (X-ray: 173.6°) in the solid-state (see Table 4). It seems justified to assume that so significant a decrease of the bond angles at the Sn^{IV} centre of the complex should entail further changes in the molecular conformation. However, at this stage of our work we cannot suggest a plausible correlation between the extent of solvent-induced geometrical changes and the structure of the complexes.

The δ = 1.5 measured for δ_i^{Sn} in **5** is in accordance[18] with the *trans*-TBP pentacoordinated structure of this complex (see above).[1] The ^{119}Sn resonance was shifted to higher frequency (δ = 95.9) in solution, which is best understood by assuming that the tetrameric complex dissociates into monomeric species featuring *cis*-TBP coordination geometry. This expectation seems to be supported by the reduction of the Me−Sn−Me angle from its original value of 120°, typical of planar Me_3Sn groups, to the value of 110° (see Table 4) characteristic for the pyramidal Me_3Sn arrangement as in the proposed monomer.[19]

Conclusion

Coordination of N- and O-donor molecules to the Me_2Sn^{IV} centre of dimeric **1** results in the cleavage of the stanoxanic dative Sn←O bonds, and subsequent formation of novel heptacoordinated dimethyltin(IV)cupferronato complexes (**2**−**4**). In these, the cupferronato ligands assume their typical chelating coordination pattern and are nearly symmetrically bound to the Me_2Sn^{IV} centre. An X-ray diffraction study of **4** revealed that the pentagonal bipyramidal C_2SnO_5 moiety might interact with dpt molecules through hydrogen-bonding interactions. Multinuclear solid- and solution NMR spectroscopic data of the novel complexes provide useful complementary information about structural changes accompanying the dissolution of the crystalline complexes.

Experimental Section

General Remarks: All reagents and solvents were purchased from commercial suppliers. The preparation and purification of the complexes were carried out in the open air or in a dry atmosphere, as indicated. The syntheses of **1**[2] and **5**[1] were reported previously. All other starting materials were obtained from commercial sources as pure compounds and used as received. − FT-IR spectra were recorded with a Jasco FT/IR 615 spectrometer. − NMR spectroscopy: A Varian Associates model Unity-Inova 400 NMR spectrometer was used to run the NMR spectra using TMS as the internal reference for ^{1}H, ^{13}C, and external $SnMe_4$ for ^{119}Sn spectra. Solution spectra were recorded at 30 °C using solutions of ca. 5% in $CDCl_3$. For solubility reasons, spectra for **4** were taken in a [D_6]DMSO/$CDCl_3$ (1:1) solvent mixture. Assignment of the resonances to individual sites in the molecules was inferred from ^nJ(H−H) and ^nJ(C−C) coupling patterns and, when needed, verified through standard, gradient-enhanced, homo-, and heteronuclear 2D (gDQFCOSY,[20] gHSQC[20]) experiments. − Solid-state ^{119}Sn and ^{13}C CP MAS spectra were recorded at room temperature using 7 mm rotors. Typically, two ^{119}Sn CP-MAS spectra were recorded at significantly different spinning rates, ca. 2000 and 4500 rps, respectively. The π/2 pulse width for ^{119}Sn had a value of 4.1 μs (61 kHz). A recycle delay of 20 s and a CP time of 1 ms were used, and from 30000 to 36000 transients were co-added to obtain the fits. Solid-state ^{119}Sn line-widths varied between 250 to 500 Hz. Solid-state spectral parameters (see Table 3) were inferred by iterative fitting of simulated spectra to the side band manifold of the experimental spectra. The r.m.s. errors of the fitting procedures varied between 0.12 and 0.18 suggesting a 10 to 15 ppm probable error in the values of δ_i and Δσ. However, due to limited pulse power for the uniform excitation of the wide (5000−8000 ppm) ^{119}Sn spectral range, the real errors of these parameters may be larger. ^{13}C CP MAS spectra were taken at spinning rates 3000−4000 rps using a pw90 = 4.1μs (61 KHz) carbon pulse, 5 s recycle delay, 1 ms CP time, and from 4000 to 8000 transients. In alternative runs the TOSS sequence[21] was used to remove the spinning side bands. Solids-state ^{13}C line-widths varied between 100 and 150 Hz.

(μ$_2$−4,4′-Bipyridyl)-bis[di-*N*-nitroso-*N*-phenyl-(hydroxylaminato)-dimethyltin(IV)] Methanol Solvate (2). − Method A: To a solution containing **1** (0.41 g, 0.47 mmol) in 5 mL of *n*-heptane was added a solution of bipy (0.10 g, 0.64 mmol, 35% excess) in 2 mL of *n*-heptane while stirring. Precipitation of the complex occurred immediately. After stirring for one hour at room temperature the precipitate was filtered off and washed with cold MeOH and dried in air. Yield 0.385 g, 81%. The product was recrystallized from MeOH under ambient conditions as large colourless block crystals.

Method B: To a solution containing **5** (0.3 g, 0.25 mmol) in 3 mL of MeOH was added a solution of bipy (0.156 g, 1 mmol, 300% excess) in 2 mL of MeOH while stirring. The mixture was stirred for 4 hours. After 2−3 days the compound was separated as large colourless block crystals. The crystals were filtered off, washed with cold MeOH and dried in air. Yield 0.14 g, 53%, melting point 125−126 °C. − FT-IR (KBr): $\tilde{\nu}$ = 3483 cm^{-1} (O−H) (m b), 3104−2823 (m b), 1606 (O−H) (m), 1482 (Ph) (m), 1461 (Ph) (ms), 1415(m), 1337 (N−N) (ms), 1285 (vs), 1215 (N=O) (s), 1166 (N=O) (ms), 1060 (ms), 921 (ONNO) (s), 812 (m), 761 (Ph) (s), 691 (Ph) (s), 627 (ms), 576 (SnC_2) (m), 523 (Sn−C) (m), 395 (Sn−O) (vs). − ^{1}H NMR ($CDCl_3$, 399.10 MHz, 30 °C): δ = 0.79 [m, 6 H, CH_3, $^1J(^{13}C-^1H)$ = 132.3 Hz, $^2J(^{119}Sn-^1H)$ = 83.6 Hz, $^2J(^{117}Sn-^1H)$ = 80.0 Hz, $^2J(^{115}Sn-^1H)$ = 73.6 Hz], 7.46 (m, 3 H, Ph−H3, −H4, −H5), 7.59 (m, 2 H, Py−H3, −H5), 7.96 (m, 2 H,

Table 5. Summary of X-ray diffraction data for **2**−**4**

	2	**3**	**4**
Empirical formula	$C_{38}H_{40}N_{10}O_8Sn_2\ CH_4O$	$C_{19}H_{21}N_5O_4Sn$	$C_{15}H_{20}N_4O_5Sn\ C_9H_9N_5$
Formula mass	1034.22	502.10	642.25
Crystal size [mm]	0.25 × 0.25 × 0.50	0.25 × 0.30 × 0.55	0. 35 × 0.45 × 0.60
Colour	colourless	colourless	colourless
Crystal system	monoclinic	monoclinic	triclinic
Space group	$P2_1/n$	$P2_1/n$	$P\bar{1}$
θ range for data collection (°)	2.39 ≤ θ ≤ 34.97	2.46 ≤ θ ≤ 34.96	2.36 ≤ θ ≤ 34.96
a [Å]	11.047(2)	9.746(1)	10.259(1)
b [Å]	11.395(2)	14.596(2)	11.500(1)
c [Å]	17.025(3)	14.759(2)	12.591(1)
α [°]	90	90	100.31(1)
β [°]	90.70(3)	92.51(1)	100.77(1)
γ [°]	90	90	97.33(1)
V [Å^3]	2143.0(7)	2097.5(5)	1415.7(2)
Z	2	4	2
d_{calc} [Mg/m^3]	1.603	1.590	1.507
μ [mm^{-1}]	1.230	1.253	0.953
F(000)	1040	1008	652
Index ranges (°)	−17 ≤ *h* ≤ 17	−15 ≤ *h* ≤ 15	−16 ≤ *h* ≤ 16
	0 ≤ *k* ≤ 18	0 ≤ *k* ≤ 23	−18 ≤ *k* ≤ 18
	0 ≤ *l* ≤ 27	−23 ≤ *l* ≤ 0	−20 ≤ *l* ≤ 20
No. of reflections collected	9883	9700	26352
No. of indep. reflns./R_{int}	9362/0.0067	9162/0.0092	12379/0.014
No. of obsd. reflns. $I > 2\sigma(I)$	6620	5334	10241
No. of parameters	281	264	356
GOOF	1.001	0.926	1.012
*R*1 (obsd. data)	0.0266	0.0335	0.0268
*wR*2 (all data)	0.0703	0.0786	0.0699
Largest diff. peak/ hole (e Å^{-3})	−0.392/0.670	−1.439/0.742	−0.727/1.112

Ph−H2, −H6), 8.86 (m, 2 H, Py−H2,−H6) ppm. − ^{13}C NMR ($CDCl_3$, 100.56 MHz, 30 °C): δ = 8.9 [m, CH_3, $^1J(^{119}Sn-^{13}C)$ = 750.5 Hz, $^1J(^{117}Sn-^{13}C)$ = 717.5 Hz], 119.6 (s, Ph−C2, −C6), 129.0 (s, Ph−C3, −C5), 121.5 (s, Py−C3, −C5), 140.1 (s, Ph−C1), 130.1 (s, Ph−C4), 145.7 (s, Py−C4), 150.4 (s, Py−C2, −C6). − ^{119}Sn NMR ($CDCl_3$, 149.09 MHz, 30 °C): δ = − 216.4 [br. m, Δ = 42 Hz, $^1J(^{119}Sn-^{13}C)$ = 750 Hz]. − $C_{39}H_{44}N_{10}O_9Sn_2$ (1034.26): calcd. C 45.3, H 4.3, N 13.5; found C 45.3, H 4.5, N 13.5.

Bis(*N*-nitroso-*N*-phenyl-hydroxylaminato)dimethylpyridyltin(IV) (3): Compound **1** (0.30 g. 0.347 mmol) was dissolved in 15 mL of warm pyridine and the yellow solution was stirred for several hours at room temperature. After several weeks the compound separated as large colourless block crystals. Yield 0.32 g, 91%, melting point 84−85 °C. − FT-IR (KBr): $\tilde{\nu}$ = 1487 cm^{-1} (Ph) (m), 1468 (Ph) (ms), 1342 (N−N) (ms), 1294 (vs), 1228 (N=O) (s), 1193 (N=O) (ms), 1165 (N=O) (ms), 1155 (s), 918 (ONNO) (s), 747 (Ph) (s), 700 (Ph) (s), 623 (ms), 572 (SnC_2) (m), 527 (Sn−C) (m), 395 (Sn−O). − ^{1}H NMR ($CDCl_3$, 399.10 MHz, 30 °C): δ = 0.80 [m, 6 H, CH_3, $^1J(^{13}C-^1H)$ = 132.0 Hz, $^2J(^{119}Sn-^1H)$ = 90.5 Hz, $^2J(^{117}Sn-^1H)$ = 86.5 Hz, $^2J(^{115}Sn-^1H)$ = 79.5 Hz], 7.36 (m, 2 H, Py−H3, −H5), 7.44 (m, 6 H, Ph−H3, −H5), 7.74 (m, 1 H, Py−H4), 7.98 (m, 4 H, Ph−H2, −H6), 8.81 (m, 2 H, Py−H2, −H6). − ^{13}C NMR ($CDCl_3$, 100.56 MHz, 30 °C): δ = 119.4 (s, Ph−C2,−C6), 10.0 [m, CH_3, $^1J(^{119}Sn-^{13}C)$ = 837.6 Hz, $^1J(^{117}Sn-^{13}C)$ = 802.8 Hz, $^1J(^{115}Sn-^{13}C)$ = 774.6 Hz], 123.9 (s, Py−C2, −C5), 128.9 (s, Ph−C3, −C5), 129.8 (s, Ph−C4), 136 (s, Py−C4), 140.2 (s, Ph−C1), 149.1 (s, Py−C2, −C5). − ^{119}Sn NMR ($CDCl_3$, 149.09 MHz, 30 °C): δ = − 258.5 [br. m, Δ = 75 Hz, $^1J(^{119}Sn-^{13}C)$ ≈ 835 Hz]. − $C_{19}H_{21}N_5O_4Sn$ (502.12): calcd. C 45.4, H 4.2, N 13.9; found C 45.5, H 4.4, N 13.9.

Bis(*N*-nitroso-*N*-phenyl-hydroxylaminato)methanolato-dimethyltin-(IV) 2,6-Diamino-4-phenyl-1,3,5-triazine Adduct (4): To 8 mL of methanolic solution of **1** (0.52 g, 0.60 mmol) was added dpt (0.225 g, 1.20 mmol) dissolved in 15−20 mL of warm MeOH, and the clear solution was stirred for several hours at room temperature. Precipitation of the compound occurred after 3 hours. Recrystallisation from MeOH gave the product as large colourless block crystals. Yield 0.52 g, 66.6%, m.p. 171−175 °C. − FT-IR (KBr): $\tilde{\nu}$ = 3447 cm^{-1} (O−H) (ms), 3326 (NH_2) (ms), 3224 (sh), 3154 (NH_2) (ms, br), 3062 (sh) 1661 (NH_2) (m), 1628 (O−H) (s), 1591 (ms), 1540 (C_3N_3) (vs, brd), 1524 (vs, sh), 1488 (Ph) (m), 1459 (Ph) (ms), 1436 (w), 1401 (m), 1340 (N−N) (ms), 1334 (N−N) (ms, sh), 1290 (vs), 1211 (N=O) (s), 1184 (N=O) (ms), 1166 (m), 1159 (m), 1062 (m), 1010 (m), 925 (ONNO) (s), 915(sh), 827 (m), 783(m), 755 (Ph) (s), 703 (C_3N_3), 692 (Ph) (s), 580 (SnC_2) (m), 543 (Sn−C) (b), 395 (Sn−O) (vs). − ^{1}H NMR ([D$_6$]DMSO /$CDCl_3$ (1:1), 399.10 MHz, 30 °C): δ = 0.58 [m, 6 H, CH_3, $^1J(^{13}C-^1H)$ = 132.0 Hz, $^2J(^{119}Sn-^1H)$ = 113.8 Hz, $^2J(^{117}Sn-^1H)$ = 109.2 Hz, $^2J(^{115}Sn-^1H)$ = 100.5 Hz], 6.52 (s, 4 H, dpt−NH_2), 7.41 (m, 1 H, dpt−Ph−H4), 7.45 (m, 2 H, dpt−Ph−H3, −H5), 7.48 (m, 2 H, Ph−H4), 7.53 (m, 4 H, Ph−H3, −H5), 7.96 (m, 4 H, Ph−H2, −H6), 8.29 (m, 2 H, dpt−Ph−H2, −H6). − ^{13}C NMR ([D$_6$]DMSO/$CDCl_3$ (1:1), 100.56 MHz, 30 °C): δ = 13.8 [m, CH_3, $^1J(^{119}Sn-^{13}C)$ = 1103.3 Hz, $^1J(^{117}Sn-^{13}C)$ 1055.0 Hz], 119.4 (s, Ph−C2, −C6), 127.9 (s, dpt−Ph−C2, −C6), 128.0 (s, dpt−Ph−C3, −C5), 129.3 (s, Ph−C3, −C5), 129.6 (s, Ph−C4), 131.0 (s, dpt−Ph−C4), 137.3 (s, dpt−Ph−C1), 140.7 (s, Ph−C1),

167.7 (s, dpt−C2, −C6), 170.7 (s, dpt−C4). − ^{119}Sn NMR ([D$_6$]DMSO/CDCl$_3$ (1:1), 149.09 MHz, 30 °C): δ = −368.2 [br. m, Δ = 17.5 Hz, $^1J(^{119}Sn-^{13}C)$ = 1103 Hz]. − $C_{24}H_{29}N_9O_5Sn$ (642.26): calcd. C 44.9, H 4.5, N 19.6; found C 44.8, H 4.7, N 19.6.

Solution NMR Spectroscopic Data for Tetrakis[trimethyl(*N*-nitroso-*N*-phenyl-hydroxylaminato)]tin(IV) (5): − ^{1}H NMR (CDCl$_3$, 399.10 MHz, 30 °C): δ = 0.48 [m, 9 H, CH$_3$, $^1J(^{13}C-^1H)$ = 129.6 Hz, $^2J(^{119}Sn-^1H)$ = 54.9 Hz, $^2J(^{117}Sn-^1H)$ = 52.5 Hz, $^2J(^{115}Sn-^1H)$ = 48.2 Hz], 7.46 (m, 3 H, Ph−H3, −H4, −H5), 7.93 (m, 2 H, Ph−H2, −H6). − ^{13}C NMR (CDCl$_3$, 100.56 MHz, 30 °C): δ = 129.1 (s, Ph−C3, −C5), 129.9 (s, Ph−C4), 140.3 (s, Ph−C1), 2.2 [m, CH$_3$, $^1J(^{119}Sn-^{13}C)$ = 403.8 Hz, $^1J(^{117}Sn-^{13}C)$ = 386.6 Hz], 119.1 (s, Ph−C2, −C6). − ^{119}Sn NMR (CDCl$_3$, 149.09 MHz, 30 °C): δ = 95.9 [m, Δ = 5 Hz, $^1J(^{119}Sn-^{13}C)$ = 404 Hz].

X-ray Crystallographic Study: Crystal data and refinement parameters are summarised in Table 5. Intensity data were collected on an Enraf−Nonius CAD-4 diffractometer with graphite monochromated Mo-K_α radiation (λ = 0.71073 Å) using the ω-2θ scan technique. Three standard reflections were monitored every hour; these remained constant within experimental error. The structures were solved by direct methods (SHELXS-97)[22a] and refined by full-matrix least-squares (SHELXL-97).[22b] All non-hydrogen atoms were refined anisotropically in F^2 mode. Hydrogen atomic positions were generated from assumed geometries. The riding model was applied for the hydrogen atoms. Crystallographic data (excluding structure factors) for the structures reported in this paper have been deposited with the Cambridge Crystallographic Data Center as supplementary publication nos. CCDC-162624 (**2**), CCDC-162625 (**3**) and CCDC-162626 (**4**). Copies of the data can be obtained free of charge on application to CCDC, 12 Union Road, Cambridge CB2 1EZ, UK [Fax: (internat.) +44(1223)336−033; E-mail: deposit@ccdc.cam.ac.uk].

[1] A. Deák, I. Haiduc, L. Párkányi, M. Venter, A. Kálmán, *Eur. J. Inorg. Chem.* **1999**, 1593−1596.

[2] A, Deák, M. Venter, A. Kálmán, L. Párkányi, L. Radics, I. Haiduc, *Eur. J. Inorg. Chem.* **2000**, 127−132.

[3] [3a] D. C. Sherrington, K. A. Taskinen, *Chem. Soc. Rev.* **2001**, *30*, 83−93. − [3b] A. D. Burrows, C. W. Chan, M. M. Chowdhry, J. E. McGrady, D. M. P. Mingos, *Chem. Soc. Rev.* **1995**, 329−339, and references therein.

[4] A. Deák, A. Kálmán, L. Párkányi, I. Haiduc, *Acta Crystallogr., Sect. B* **2001**, *57*, 303−310.

[5] [5a] X. Xu, S. L. James, D. M. P. Mingos, A. J. P. White, D. J. Williams, *J. Chem. Soc., Dalton Trans.* **2000**, 3783−3790. − [5b] L. Brammer, J. C. Mareque-Rivas, R. Atencio, S. Fang, F. C. Pigge, *J. Chem. Soc., Dalton Trans.* **2000**, 3855−3867. − [5c] C. B. Aakeröy, A. M. Beatty, K. R. Lorimer, *J. Chem. Soc., Dalton Trans.* **2000**, 3869−3872, and references therein.

[6] I. Haiduc, F. T. Edelmann, *Supramolecular Organometallic Chemistry*, Wiley-VCH, Weinheim, New York, **1999**, pp. 326−332.

[7] [7a] T. P. Lockhart, F. Davidson, *Organometallics* **1987**, *6*, 2471−2478. − [7b] T. P. Lockhart, W. Manders, *J. Am. Chem. Soc.* **1987**, *109*, 7015−720.

[8] Gy. Vankó, Sz. Kárpáti, A. Deák, Gy. Tarczay, A. Kálmán, I. Haiduc, A. Vértes, to be published in *Eur. J. Inorg. Chem.*

[9] [9a] M. Gielen, M. De Clerq, B. De Porter, *J. Organomet. Chem.* **1972**, *34*, 305−313. − [9b] C.-D. Hager, F. Huber, A. Silvestri, R. Barbieri, *Inorg. Chim. Acta* **1981**, *49*, 31−36.

[10] [10a] F. L. Lee, E. J. Gabe, L. E. Khoo, W. H. Leong, G. Eng, F. E. Smith, *Inorg. Chim. Acta* **1989**, *166*, 257−261. − [10b] F. Huber, H. Preut, E. Hoffmann, M. Gielen, *Acta Crystallogr., Sect. C* **1989**, *45*, 51−54. − [10c] S. Aizawa, T. Natsume, K. Hatano, S. Funahashi, *Inorg. Chim. Acta* **1996**, *248*, 215−224.

[11] S. W. Ng, *Acta Crystallogr., Sect. C* **1998**, *54*, 1393−1395.

[12] A. J. Crowe, *Drugs of the Future* **1987**, *12*, 255−275, and references therein.

[13] S. W. Ng, *Acta Crystallogr., Sect. C* **1996**, *52*, 2990−2992.

[14] A. S. Gonzalez, A. Castiñeiras, J. S. Casas, J. Sordo, U. Russo, *Inorg. Chim. Acta* **1994**, 257−260.

[15] [15a] C. Janiak, S. Deblon, H.-P. Wu, M. J. Kolm, P. Klüfers, H. Piotrowski, P. Mayer, *Eur. J. Inorg. Chem.* **1999**, 1507−1521, and references therein. − [15b] C. Janiak, *J. Chem. Soc., Dalton Trans.* **2000**, 3885−3896.

[16] [16a] J. Otera, T. Hinoishi, Y. Kawabe, R. Okawara, *Chem. Letters* **1981**, 273−274. − [16b] J. Otera, *J. Organomet. Chem.* **1981**, *221*, 57−61.

[17] B. Wrackmeyer, A. Sebald, L. H. Merwin, *Magn. Reson. Chem.* **1991**, *29*, 260−263.

[18] M. S. Rau, C. M. Kretz, G. L. Geoffroy, A. L. Rheingold, B. S. Haggerty, *Organometallics* **1994**, *13*, 1624−1634.

[19] P. G. Harrison, J. A. Richards, *J. Organomet. Chem.* **1980**, *185*, 9−51.

[20] F. J. M. van de Ven, *Multidimensional NMR in Liquids: Basic principles and experimental methods*, VCH Publishers, New York, **1995**.

[21] D. P. Raleigh, A. C. Kolbert, R. G. Griffin, *J. Magn. Reson.* **1990**, *89*, 1−12.

[22] [22a] G. M. Sheldrick, *SHELXS97-Program for Crystal Structure Determination.* − [22b] *SHELXL97-Program for the Refinement of Crystal Structures*, Universität Göttingen (Germany), **1997**.

Received May 2, 2001
[I01150]

1D Zigzag Coordination Polymers of Copper(II) and Nickel(II) with Mixed Ligands − Syntheses and Structures

Han Woong Park,[a] Soo Mi Sung,[a] Kil Sik Min,[a] Hyochoon Bang,[b] and Myunghyun Paik Suh*[a]

Keywords: Magnetic properties / N ligands / Polymers / Copper / Nickel / Self assembly

The one-dimensional coordination polymers $[Cu(NO_3)_2(2,2'\text{-bipy})(4,4'\text{-bipy})]_n{\cdot}2nCH_3OH$ (**1**) and $[Ni(tren)(4,4'\text{-bipy})]_n(ClO_4)_{2n}$ (**2**), have been synthesized by the self-assembly of a copper(II) complex of 2,2′-bipy and a nickel(II) complex of tren with 4,4′-bipy (2,2′-bipy = 2,2′-bipyridine, 4,4′-bipy = 4,4′-bipyridine, and tren = tris-(2-aminoethyl)amine). Their X-ray crystal structures show that the metal ions in **1** and **2** display a distorted octahedral coordination geometry to bind two 4,4′-bipy ligands at the *cis* positions. Each 4,4′-bipy links two $[Cu(NO_3)_2(2,2'\text{-bipy})]$ units in **1** and two $[Ni(tren)]^{2+}$ units in **2** to form 1D zigzag chains. In the structure of **1**, these chains are linked by offset π–π interactions through 2,2′-bipy ligands, giving rise to a 2D network. The pyridine rings in the 4,4′-bipy ligand are coplanar in **1** but twisted in **2**. The coordination polymer **1** shows a weak antiferromagnetic interaction between copper(II) ions with $J = -0.53$ cm^{-1} ($H = -J\sum_{i=1}^{n-1} S_{Ai}S_{A(i+1)}$).

Introduction

The construction of coordination polymers based on metal and organic building blocks is a rapidly developing area of research.[1] Coordination polymers with diverse architectures, such as linear or zigzag chains, helices, honeycombs, square grids, ladders, brick walls, and interwoven diamondoids have been extensively developed.[2] These coordination polymers attract a great deal of attention because of their interesting structural properties and potential applications to magnetism,[1f,3] electrical conductivity,[4] ion exchange,[5] separation,[1h,6] and catalysis.[7] Many important properties of coordination polymers arise from their structures and topology, and thus the rational design and construction of specific architectures are particularly important. To construct the desired framework, rigid organic building blocks are most often used.[8]

Here we report the synthesis and crystal structures of two 1D zigzag coordination polymers $[Cu(NO_3)_2(2,2'\text{-bipy})(4,4'\text{-bipy})]_n{\cdot}2nCH_3OH$ (**1**) and $[Ni(tren)(4,4'\text{-bipy})]_n(ClO_4)_{2n}$ (**2**), where the $[Cu(NO_3)_2(2,2'\text{-bipy})]$ units and $[Ni(tren)]^{2+}$ units are linked by a 4,4′-bipy ligand. The bidentate ligand 4,4′-bipy was chosen as the rigid organic building block that connects the metal ions because of its rod-like shape.[9] The coordination polymer **1** shows an antiferromagnetic interaction between the copper(II) ions.

[a] School of Chemistry and Center for Molecular Catalysis, Seoul National University,
Seoul 151-747, Republic of Korea
Fax: (internat.) +82-2/886-8516
E-mail: mpsuh@snu.ac.kr
[b] Department of Chemistry, Duksung Women's University,
Seoul 132−714, Republic of Korea

Results and Discussion

Synthesis and Properties

The 1D zigzag coordination polymer $[Cu(NO_3)_2(2,2'\text{-bipy})(4,4'\text{-bipy})]_n{\cdot}2nCH_3OH$ (**1**) was synthesized in high yield by the self-assembly of $[Cu(NO_3)_2(2,2'\text{-bipy})]$ and 4,4′-bipy in MeOH. Similarly, the 1D zigzag polymer $[Ni(tren)(4,4'\text{-bipy})]_n(ClO_4)_{2n}$ (**2**) was obtained by the self-assembly of $[Ni(CH_3CO_2)_2{\cdot}4H_2O]$, 4,4′-bipy, and tren in MeOH. Although the assemblies could have resulted in compounds with a square architecture (Schemes 1 and 2),[10] we were only able to isolate the zigzag polymers. The IR and UV/Vis spectroscopic data of **1** and **2** are summarized in Table 1.

The coordination polymer **1** is purple in the solid state, and forms a blue solution upon addition of H_2O, DMF, or DMSO as it dissociates into the building blocks. It is insoluble in most other organic solvents. The UV/Vis spectrum of **1** in the solid state shows a band at 597 nm; an aqueous solution of **1** shows λ_{max} at 678 nm ($\varepsilon = 39.9$ M^{-1}cm^{-1}), which is similar to the absorption of $[Cu(NO_3)_2(2,2'\text{-bipy})]$.[11] Compound **1** shows an OH stretching band at 3468 cm^{-1} and C=C stretching bands for the bipy rings at 1612, 1569, and 1535 cm^{-1}. By comparison with the IR spectrum of $[Cu(NO_3)_2(2,2'\text{-bipy})]$,[11] the peaks at 1612 and 1569 cm^{-1} can be assigned to those of 2,2′-bipy and the peak at 1535 cm^{-1} to that of 4,4′-bipy.

The coordination polymer **2** is pale violet in the solid state. It is soluble in H_2O, MeCN, $MeNO_2$, DMF, or DMSO, but insoluble in most other organic solvents. The diffuse reflectance spectrum of **2** shows a maximum absorption at 495 nm. When **2** is dissolved in MeCN/H_2O (1:1 v/v), however, the absorption band (λ_{max}) shifts to 552 nm ($\varepsilon = 10.6$ M^{-1}cm^{-1}), which is similar to that of $[Ni(tren)(H_2O)_2]^{2+}$ in MeCN/H_2O ($\lambda_{max} = 555$ nm, $\varepsilon = 9.3$

 © WILEY-VCH Verlag GmbH, 69451 Weinheim, 2001 1434−1948/01/1111−2857 $ 17.50+.50/0

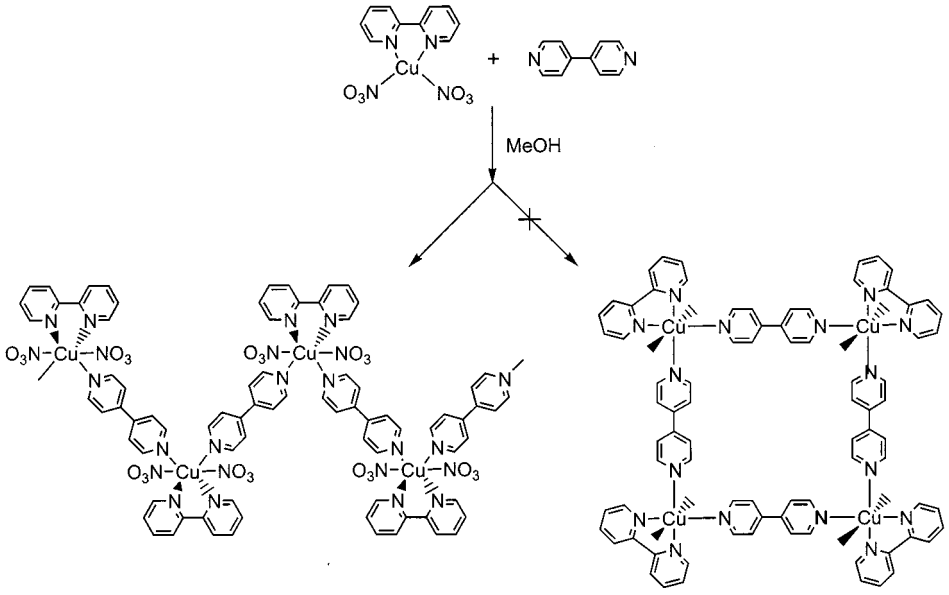

Scheme 1

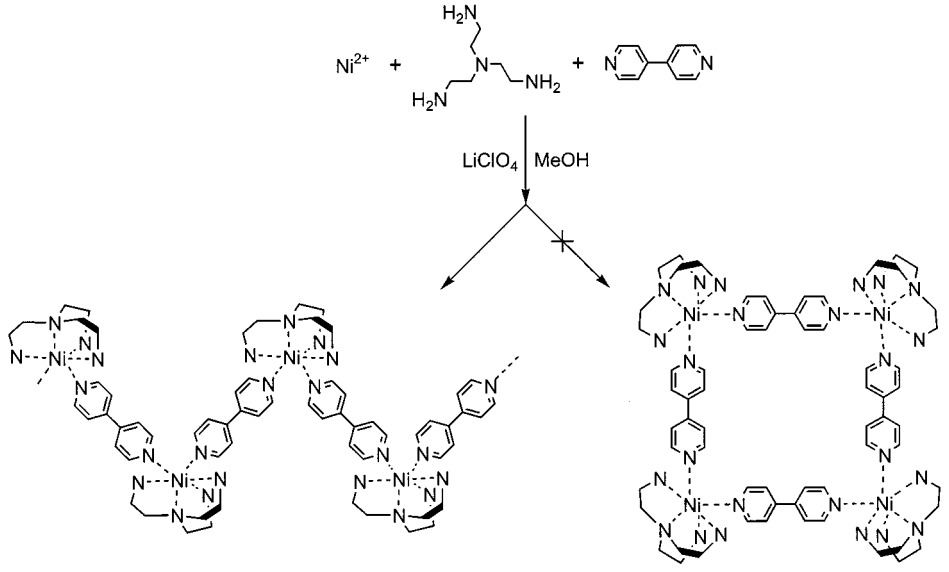

Scheme 2

Table 1. Spectral properties of the complexes

	IR [cm^{-1}][a]	UV/Vis λ_{max} [nm] (ε [M^{-1} cm^{-1}])
$[Cu(NO_3)_2(2,2'\text{-bipy})]$[b]	1610, 1570, 1490, 1275, 1035, 808	676[c]
$[Cu(NO_3)_2(2,2'\text{-bipy})(4,4'\text{-bipy})]_n \cdot 2n CH_3OH$ (**1**)	ν_{OH} 3600, 3468 ν_{py} 1612, 1569, 1535 ν_{NO_3} 1300−1400	678(39.9)[c] 597[d]
$[Ni(tren)(H_2O)_2]^{2+}$		555(9.3)[e]
$[Ni(tren)(4,4'\text{-bipy})]_n(ClO_4)_{2n}$ (**2**)	ν_{tren} 3344, 3296, 1608 ν_{py} 1535 ν_{ClO_4} 1089	495[d] 552(10.6)[f]

[a] Measured as a Nujol mull. − [b] Ref.[9] − [c] Measured in water. − [d] Diffuse reflectance spectrum. − [e] Measured with an MeCN/water solution containing 1 equiv. of $[Ni(OAc)_2 \cdot 4H_2O]$ and 1 equiv. of tren. − [f] Measured in MeCN/water.

$M^{-1}cm^{-1}$). We assume that the $[Ni(tren)]^{2+}$ moiety coordinates two water molecules in water according to the X-ray crystal structure of $[Ni(tren)(H_2O)_2]SO_4$ previously reported.[12] It is obvious that the polymeric structure decomposes into discrete units of $[Ni(tren)(H_2O)_2]^{2+}$ and 4,4′-bipy in $MeCN/H_2O$. The infrared spectrum of **2** shows strong absorption bands at 3344 cm^{-1} and 3296 cm^{-1}, which are attributed to the N−H stretching modes of the tren ligand. The NH_2 bending mode of tren appears at 1608 cm^{-1} and the C=C stretching of 4,4′-bipy at 1535 cm^{-1}.

X-ray Crystal Structure of 1

An ORTEP view of **1** is shown in Figure 1a. Table 2 shows the selected bond lengths and angles. In the structure, the copper(II) ion shows a distorted octahedral coordination geometry by binding a 2,2′-bipy and two 4,4′-bipy ligands in the equatorial positions and two nitrate anions at the axial sites. The average $Cu-N_{2,2'\text{-bipy}}$ and $Cu-N_{4,4'\text{-bipy}}$ bond lengths are 2.013(1) and 2.034(1) Å, respectively. The average Cu−O bond length involving nitrate li-

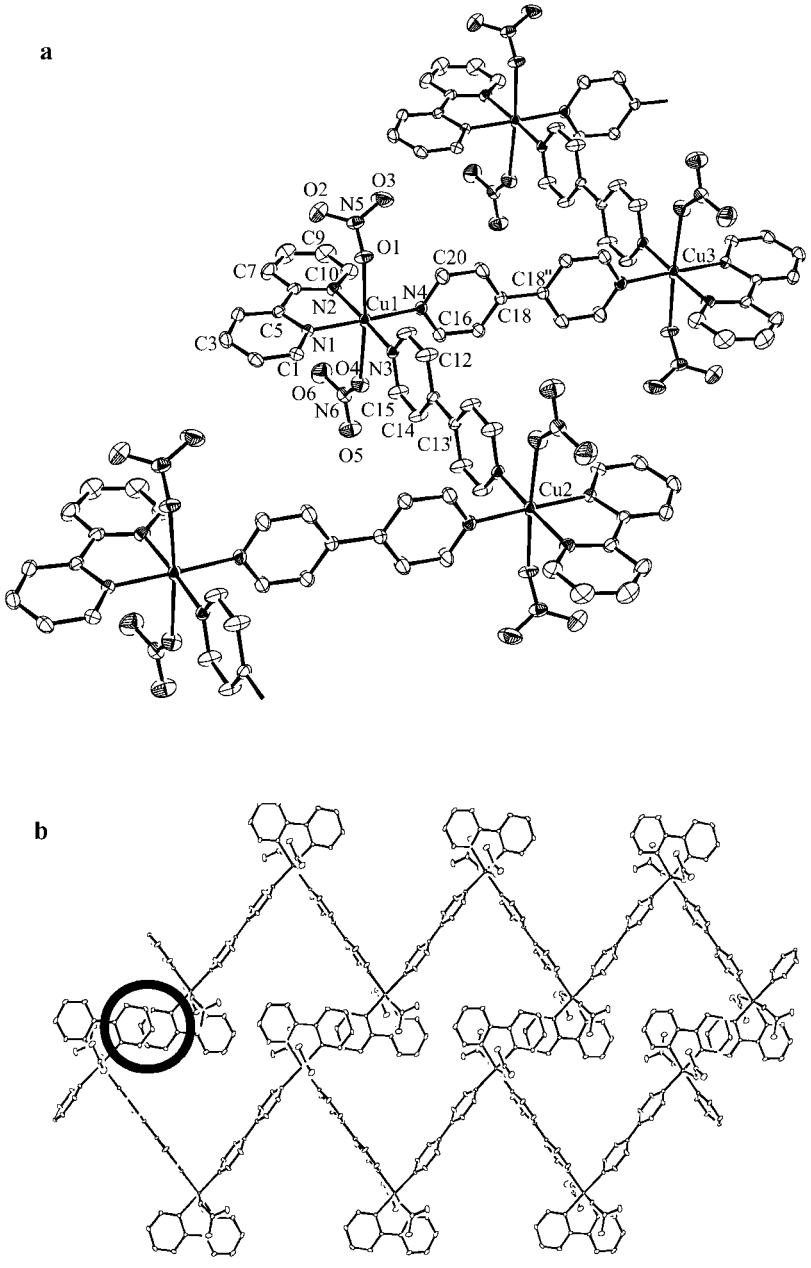

Figure 1. (a) ORTEP drawing of **1** with atomic numbering scheme (′ = 1 − *x*, −*y*, 1 − *z*; ′′ = 1 − *x*, −*y*, −*z*); thermal ellipsoids are shown at the 30% probability level; (b) extended 2D structure of **1**; the interchain offset π−π interactions are indicated by a solid circle

Table 2. Selected bond lengths [Å] and angles [°] for **1**

Cu1−N1	2.021(2)	C2−C3	1.376(5)
Cu1−N2	2.005(2)	C3−C4	1.389(5)
Cu1−N3	2.022(2)	C4−C5	1.380(4)
Cu1−N4	2.045(2)	C5−C6	1.488(4)
Cu1−O1	2.532(1)	C6−C7	1.391(5)
Cu1−O4	2.479(1)	C7−C8	1.384(6)
N1−C1	1.346(4)	C8−C9	1.359(7)
N1−C5	1.351(4)	C9−C10	1.388(6)
N2−C6	1.342(4)	C11−C12	1.381(5)
N2−C10	1.343(4)	C12−C13	1.378(4)
N3−C11	1.324(4)	C13−C13[a]	1.484(6)
N3−C15	1.341(4)	C13−C14	1.376(4)
N4−C16	1.338(4)	C14−C15	1.372(5)
N4−C20	1.330(4)	C16−C17	1.381(5)
N5−O1	1.250(3)	C17−C18	1.384(4)
N5−O2	1.246(3)	C18−C18[b]	1.489(6)
N5−O3	1.225(3)	C18−C19	1.383(5)
N6−O4	1.243(3)	C19−C20	1.386(5)
N6−O5	1.237(3)	C21−O7	1.412(5)
N6−O6	1.232(3)	C22−O8	1.263(7)
C1−C2	1.376(4)		
N1−Cu1−N2	81.20(10)	O4−N6−O5	119.2(2)
N1−Cu1−N3	94.18(10)	O4−N6−O6	120.4(2)
N1−Cu1−N4	178.35(9)	O5−N6−O6	120.3(2)
N2−Cu1−N3	174.88(10)	N1−C1−C2	122.9(3)
N2−Cu1−N4	97.23(10)	N1−C5−C4	121.4(3)
N3−Cu1−N4	87.37(10)	N1−C5−C6	114.4(3)
O1−Cu1−N1	85.64(7)	N2−C6−C5	115.3(2)
O1−Cu1−N2	89.03(8)	N2−C6−C7	121.8(3)
O1−Cu1−N3	88.42(8)	N2−C10−C9	122.0(4)
O1−Cu1−N4	93.81(8)	N3−C11−C12	123.0(3)
O4−Cu1−N1	88.13(7)	N3−C15−C14	123.2(3)
O4−Cu1−N2	93.56(8)	N4−C16−C17	122.8(3)
O4−Cu1−N3	88.46(8)	C1−C2−C3	118.7(3)
O4−Cu1−N4	92.51(8)	C2−C3−C4	119.1(3)
C1−N1−C5	118.4(3)	C3−C4−C5	119.5(3)
C1−N1−Cu1	127.3(2)	C4−C5−C6	124.1(3)
C5−N1−Cu1	114.3(2)	C5−C6−C7	122.9(3)
C6−N2−C10	118.8(3)	C6−C7−C8	118.4(4)
C6−N2−Cu1	114.7(2)	C7−C8−C9	120.0(4)
C10−N2−Cu1	126.4(2)	C8−C9−C10	119.0(4)
C11−N3−C15	116.6(3)	C11−C12−C13	120.8(3)
C11−N3−Cu1	122.6(2)	C12−C13−C14	115.8(3)
C15−N3−Cu1	120.8(2)	C12−C13−C13[a]	122.4(3)
C16−N4−Cu1	120.8(2)	C13−C14−C15	120.7(3)
C20−N4−C16	117.3(3)	C14−C13−C13[a]	121.9(3)
C20−N4−Cu1	121.6(2)	C16−C17−C18	120.5(3)
O1−N5−O2	118.7(2)	C17−C18−C18[b]	121.8(3)
O1−N5−O3	120.8(3)	C19−C18−C17	116.2(3)
O2−N5−O3	120.6(2)	C19−C18−C18[b]	122.0(3)

[a] Marked atoms are generated by the symmetry operation $1 - x$, $-y$, $1 - z$. − [b] Marked atoms are generated by the symmetry operation $1 - x$, $-y$, $-z$.

Table 3. Selected bond lengths [Å] and angles [°] for **2**

Ni1−N1	2.112(3)	N6−C16	1.332(5)
Ni1−N2	2.148(4)	C1−C2	1.503(7)
Ni1−N3	2.097(4)	C3−C4	1.479(7)
Ni1−N4	2.143(4)	C5−C6	1.519(7)
Ni1−N5	2.217(3)	C7−C8	1.362(6)
Ni1−N6	2.111(3)	C8−C9	1.387(6)
N1−C1	1.477(6)	C9−C10	1.377(6)
N1−C3	1.499(6)	C9−C12	1.473(6)
N1−C5	1.485(6)	C10−C11	1.364(6)
N2−C2	1.481(6)	C12−C13	1.367(6)
N3−C4	1.464(6)	C12−C14	1.401(6)
N4−C6	1.469(6)	C13−C16[a]	1.390(6)
N5−C7	1.353(5)	C14−C15[a]	1.378(6)
N5−C11	1.353(5)	C15−C14[b]	1.378(6)
N6−C15	1.324(5)	C16−C13[b]	1.390(6)
N1−Ni1−N2	81.33(14)	C1−N1−Ni1	105.8(3)
N1−Ni1−N3	81.58(14)	C1−N1−C3	111.3(3)
N1−Ni1−N4	82.70(14)	C1−N1−C5	113.0(4)
N1−Ni1−N5	103.53(13)	C2−N2−Ni1	110.4(3)
N1−Ni1−N6	169.10(13)	C3−N1−Ni1	110.8(3)
N2−Ni1−N3	92.99(15)	C4−N3−Ni1	109.3(3)
N2−Ni1−N4	161.45(14)	C5−N1−Ni1	105.4(3)
N2−Ni1−N5	87.68(13)	C5−N1−C3	110.3(4)
N2−Ni1−N6	98.47(13)	C6−N4−Ni1	108.8(3)
N3−Ni1−N4	93.94(16)	C7−N5−C11	115.5(3)
N3−Ni1−N5	174.88(13)	C7−N5−Ni1	129.0(3)
N3−Ni1−N6	87.55(14)	C11−N5−Ni1	115.4(3)
N4−Ni1−N5	86.95(14)	C15−N6−C16	117.6(4)
N4−Ni1−N6	98.99(14)	C15−N6−Ni1	120.9(3)
N5−Ni1−N6	87.33(13)	C16−N6−Ni1	121.4(3)
N1−C1−C2	110.8(3)	C7−C8−C9	119.6(4)
N1−C3−C4	112.4(4)	C8−C9−C10	117.2(4)
N1−C5−C6	109.8(4)	C8−C9−C12	122.3(4)
N2−C2−C1	110.8(4)	C9−C10−C11	120.3(4)
N3−C4−C3	111.5(4)	C9−C12−C13	121.7(4)
N4−C6−C5	108.8(4)	C9−C12−C14	120.7(4)
N5−C7−C8	124.0(4)	C10−C9−C12	120.5(4)
N5−C11−C10	123.4(4)	C12−C14−C15[a]	118.5(4)
N6−C15−C14[b]	123.9(4)	C12−C13−C16[a]	119.8(4)
N6−C16−C13[b]	122.5(4)	C13−C12−C14	117.6(4)

[a] Marked atoms are generated by the symmetry operation $2.5 - x$, $-0.5 + y$, $1.5 - z$. − [b] Marked atoms are generated by the symmetry operation $2.5 - x$, $0.5 + y$, $1.5 - z$.

gands is 2.505(1) Å, which is significantly longer than the equatorial Cu−N bond lengths because of a Jahn−Teller distortion. The angles N1−Cu1−N3 and N2−Cu1−N4 between 2,2′-bipy and 4,4′-bipy are greater than 90° because the chelate angle of 2,2′-bipy and the angle between two 4,4′-bipy ligands are less than 90°. The copper(II) ion lies 0.025(1) Å out of the square-coordination plane toward O4. Each 4,4′-bipy ligand links two copper(II) ions to form a zigzag chain which extends parallel to the *c* axis. The 4,4′-bipy unit is perfectly coplanar, with a dihedral angle of 0.0° between the two pyridyl ring planes. The dihedral angles between a 2,2′-bipy plane and the pyridine ring planes of 4,4′-bipy involving N3 and N4 are 87.4(1)° and 87.0(1)°, respectively. These perpendicular orientations must be attributed to the steric hindrance between the α-hydrogen atoms of the two different bipyridine ligands located at the *cis* positions. The dihedral angle between the two coordinating pyridyl ring planes involving different 4,4′-bipy ligands is 79.2(1)°. The distances Cu1···Cu2 and Cu1···Cu3 within a chain are 11.144(1) and 11.172(1) Å, respectively. The shortest interchain Cu···Cu distance is 6.980(1) Å. There are offset π−π interactions involving 2,2′-bipy groups between the zigzag chains. The centroid separation and the dihedral angle between the interacting 2,2′-bipy groups are 3.911 Å and 0.0°. The interactions propagate along the *b*−*a* direction, which leads to a 2D network structure (Figure 1b). The methanol guest molecule is involved in a hy-

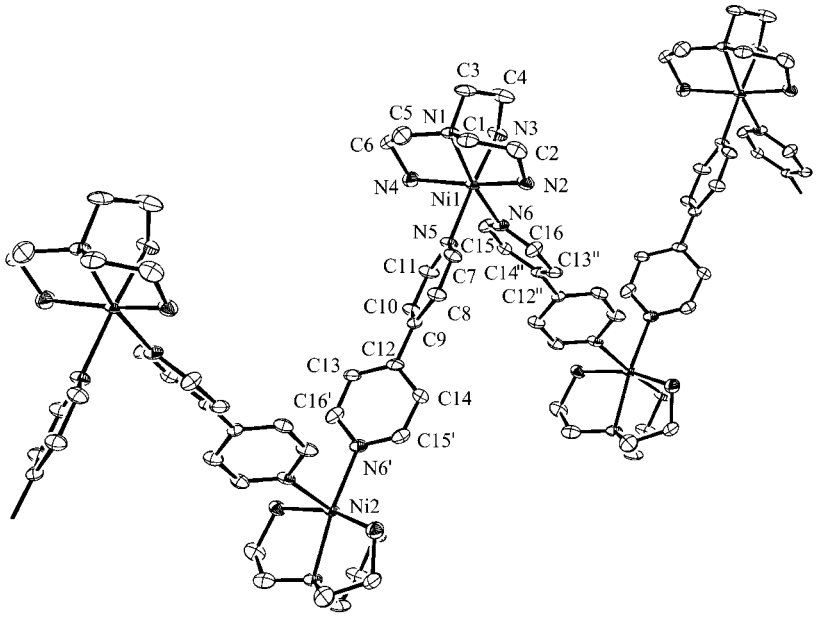

Figure 2. ORTEP drawing of **2** with atomic numbering scheme ($' = 2.5 - x, -0.5 + y, 1.5 - z$; $'' = 2.5 - x, 0.5 + y, 1.5 - z$); thermal ellipsoids are shown at the 40% probability level

drogen-bonding interaction with the oxygen atom of the coordinated nitrate anion [O5···O7($-1+x$, y, z): 2.796 Å; O5···H7A−O7: 165.5°].

X-ray Crystal Structure of 2

An ORTEP view of **2** is shown in Figure 2. Table 3 shows the selected bond lengths and angles. In the structure, the nickel(II) ion is coordinated to one tertiary and three secondary nitrogen atoms of a tren and two 4,4′-bipy ligands to form a distorted octahedral geometry. The average $Ni-N_{tren}$ and $Ni-N_{4,4'\text{-bipy}}$ bond lengths are 2.123(2) and 2.164(2) Å, respectively. The bite angles of tren are in the range 81−83°. Two 4,4′-bipy ligands coordinate a nickel(II) ion at the *cis* positions and each 4,4′-bipy ligand links adjacent $[Ni(tren)]^{2+}$ units, which gives rise to a 1D zigzag chain extending parallel to the *b* axis. In contrast to the structure of **1**, the 4,4′-bipy ligand is not planar. The dihedral angle between the two pyridyl ring planes in a 4,4′-bipy ligand is 37.9(3)°. This distortion is not unusual and has been observed with other complexes bridged by 4,4′-bipy ligands.[13] The dihedral angle between two pyridyl ring planes involving N5 and N6 is 76.8(3)°. This angle is lower than that in the structure of **1**, which must be attributed to steric hindrance with the tren ligand. The shortest Ni···Ni distance within a chain is 11.371(2) Å, and the shortest interchain Ni···Ni distance is 7.936(1) Å.

Magnetic Properties of 1

The effective magnetic moment of **1** measured at 300 K is 1.75 μ_B, in good agreement with the spin-only value of copper(II) (1.78 μ_B). The temperature dependence of the magnetic susceptibility of **1** is shown in Figure 3. The susceptibility data in the temperature range 20−300 K follow the Curie−Weiss law, where $\chi_M = C/(T - \theta)$ and $\theta = -1.8$ K. The value of $\chi_M T$ decreases as the temperature is lowered, indicating that an antiferromagnetic interaction exists between the copper(II) ions. To obtain the magnetic parameters, the magnetic susceptibility data were fitted to Equation (1), where N, β, and k are the Avogadro number, the Bohr magneton, and the Boltzmann constant, respectively.[14−15] For the simple chain made by an array of equally spaced copper(II) ions with $S = 1/2$ local spins, the spin Hamiltonian in zero-field describing the isotropic interaction between the nearest neighbor ions is expressed as Equation (2) and the magnetic susceptibility is expressed as Equation (1).[14]

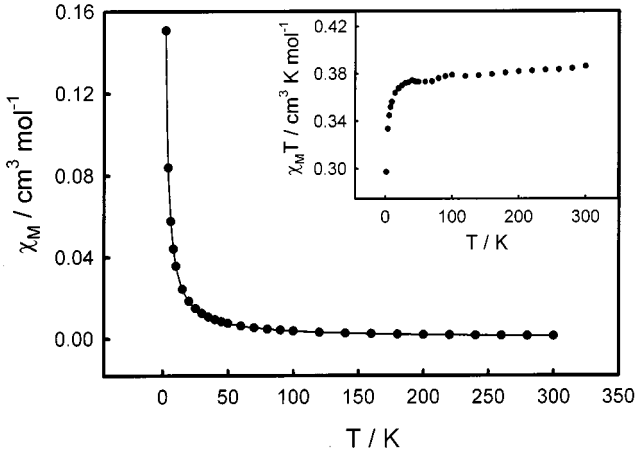

Figure 3. Plots of χ_M vs. T and $\chi_M T$ vs. T (inset) for **1**; the solid line represents the best-fit curve to Equation (1)

Table 4. Magnetic properties of various compounds bridged by 4,4′-bipy

Compounds[a]	θ [K]	J [cm^{-1}]	g	ref.
$[Cu(NO_3)_2(2,2'\text{-bipy})(4,4'\text{-bipy})]_n \cdot 2nCH_3OH$	−1.8	−0.53	2.01	This work
$[Cu_2(ClO_4)_2(dien)_2(4,4'\text{-bipy})](ClO_4)_2$	−0.4	−0.3	2.03	16
$[Cu_2(tren)_2(4,4'\text{-bipy})](BPh_4)_4$		< 1.0		17
$[Ni(Bu\text{-}dtp)_2(4,4'\text{-bipy})]_n$	−32			20

[a] Abbreviations used: dien = diethylenetriamine; Bu-dtp = dibutyldithiophosphate.

$$\chi = \frac{Ng^2\beta^2}{kT}\,\frac{0.25 + 0.074975x + 0.075235x^2}{1.0 + 0.9931x + 0.172135x^2 + 0.757825x^3}\,,\ \text{where}\ x = \frac{|J|}{kT} \quad (1)$$

$$H = -J\sum_{i=1}^{n-1} S_{Ai}S_{Ai+1} \quad (2)$$

The solid line in Figure 3 represents the best fit of the data to Equation (1), which provides $g = 2.01$ and $J = -0.53$ cm^{-1} with $R = 4.0 \times 10^{-6}$. The data are compared with those of other complexes bridged by a 4,4′-bipy ligand in Table 4. It is known that compounds bridged by 4,4′-bipy show almost no, or very weak, magnetic interactions because of the long distance of 4,4′-bipy (almost 11 Å)[16] and the weak Cu−N bond with the weak base 4,4′-bipy.[17] In addition, the C−C bond connecting two pyridine rings in 4,4′-bipy has a single bond character [the bond length of C13−C13′ is 1.484(6) Å], which breaks the conjugation of the 4,4′-bipy molecules. This also interrupts the magnetic interactions. The weak antiferromagnetic interaction in **1** must be attributed to the unfavorable π-type exchange pathway as well as the long σ-type exchange pathway for the 4,4′-bipy bridging ligand.

Experimental Section

General: All chemicals and solvents used in the syntheses were of reagent grade and were used without further purification. Infrared spectra were recorded with a Perkin−Elmer 2000 FT-IR spectrophotometer. Electronic spectra were measured with a CARY 300 Bio UV/Vis spectrophotometer. Magnetic susceptibility was measured on a Quantum Design MPMS superconducting quantum interference device (SQUID). Elemental analyses were performed by the analytical laboratory of the Seoul National University.

Safety Note: Although we have experienced no problem with the compounds reported in this work, perchlorate salts of metal complexes with organic ligands are often explosive and should be handled with great caution.

$[Cu(NO_3)_2(2,2'\text{-bipy})]$: An EtOH solution (10 mL) of $[Cu(NO_3)_2 \cdot 3H_2O]$ (4.82 g, 0.02 mol) was mixed with an EtOH solution (10 mL) of 2,2′-bipy (3.2 g, 0.02 mol). The blue precipitate formed was filtered, washed with EtOH, and dried in air. Yield: 6.19 g, 90%. − $C_{10}H_8CuN_4O_6$ (343.74): calcd. C 34.94, H 2.346, N 16.30; found C 34.78, H 2.055, N 16.35.

$[Cu(NO_3)_2(2,2'\text{-bipy})(4,4'\text{-bipy})]_n \cdot 2nCH_3OH$ (1): $[Cu(NO_3)_2(2,2'\text{-bipy})]$ (0.068 g, 0.20 mmol) was dissolved in MeOH (1 mL) in a test tube. A MeOH solution (1 mL) of 4,4′-bipy (0.031 g, 0.20 mmol) was then carefully added to the top of this blue solution, without disturbing it. A violet solid precipitated immediately at the interface of the two solutions, and violet crystals were formed over 10 days as the diffusion proceeded. These crystals were filtered, washed with MeOH, and dried in air. Yield: 0.089 g, 80%. − $C_{22}H_{24}CuN_6O_8$ (564.01): calcd. C 46.85, H 4.289, N 14.90; found C 45.28, H 3.30, N 15.93.

$[Ni(tren)(4,4'\text{-bipy})]_n(ClO_4)_{2n}$ (2): A methanol solution (10 mL) of tris-(2-aminoethyl)amine (0.63 g, 4.3 mmol) and a methanol solution (1 mL) of 4,4′-bipy (0.64 g, 4.3 mmol) were added dropwise to a methanol solution (10 mL) of $[Ni(CH_3CO_2)_2 \cdot 4H_2O]$ (1.04 g, 4.2 mmol). The solution was stirred for about 30 min. at room temperature and then a methanol solution (5 mL) of $LiClO_4$ (1.81 g, 17 mmol) was added. A pale violet precipitate formed immediately, which was filtered off, washed with methanol, and dried in vacuo. Yield: 2.07 g, 86%. The single crystals used for the X-ray diffraction study were obtained by the recrystallization of the product from a 1:1 mixture of water and MeCN. − $C_{16}H_{26}Cl_2N_6NiO_8$ (560.01): calcd. C 34.32, H 4.68, N 15.01; found C 34.34, H 4.42, N 15.36.

X-ray Diffraction Measurements: Single crystals of **1** and **2** were sealed in glass capillaries containing their mother liquor. X-ray

Table 5. Crystallographic data for **1** and **2**

	1	**2**
Formula	$C_{22}H_{24}CuN_6O_8$	$C_{16}H_{26}Cl_2N_6NiO_8$
Formula mass	564.01	560.01
Crystal system	triclinic	monoclinic
Space group	$P\bar{1}$	$P2_1/n$
a [Å]	9.3422(2)	9.449(2)
b [Å]	9.4593(2)	15.649(3)
c [Å]	14.6960(1)	15.071(3)
α [°]	80.739(1)	90
β [°]	76.790(1)	91.03(2)
γ [°]	89.212(1)	90
V [Å^3]	1247.49(4)	2228.3(7)
Z	2	4
D_{calc} [g cm^{-3}]	1.502	1.669
T [K]	293(2)	293(2)
λ [Å]	0.71073	0.71073
μ [mm^{-1}]	0.934	1.168
F(000)	582	1160
Collected	6135	3966
Unique	4182	3644
Observed	3699	2996
Parameters	316	298
GOF	1.064	0.974
R_1 (4σ data)[a]	0.0449	0.0708
wR_2 (4σ data)[b]	0.1279	0.1747

[a] $R_1 = \Sigma||F_o| - |F_c||/\Sigma|F_o|$. − [b] $wR_2 = [\Sigma w(F_o^2 - F_c^2)^2/\Sigma w(F_o^2)^2]^{1/2}$.

data were collected at room temperature using graphite monochromated Mo-K_α radiation on a Siemens CCD diffractometer for **1** and on an Enraf−Nonius CAD4 diffractometer for **2**. The orientation matrix and unit cell parameters were determined from 25 machine-centered reflections with $22.76° < 2\theta < 25.18°$. Axial photographs were used to verify the unit cell choice. Data were corrected for Lorentz and polarization effects. An absorption correction was made for **1**, but not for **2**. The crystal structures were solved by a Patterson synthesis[18] and refined by full-matrix least-squares refinement using the SHELXL-97 computer program.[19] All non-hydrogen atoms were refined anisotropically. All hydrogen atoms were positioned geometrically and refined using a riding model. The detailed crystallographic data of **1** and **2** are summarized in Table 5.

Crystallographic data (excluding structure factors) for the structures reported in this paper have been deposited with the Cambridge Crystallographic Data Centre as supplementary publication nos. CCDC-160921 (**1**) and -160922 (**2**). Copies of the data can be obtained free of charge on application to CCDC, 12 Union Road, Cambridge CB2 1EZ, UK [Fax: (internat.) +44-1223/336-033; E-mail: deposit@ccdc.cam.ac.uk).

Acknowledgments

This work was supported by the grant (1999-1-122-001-5) from the Basic Research Program of the Korea Science & Engineering Foundation and Center for Molecular Catalysis. This work was also supported in part by the Institute of Natural Science of Duksung Women's University.

[1] [1a] J.-M. Lehn, *Angew. Chem. Int. Ed. Engl.* **1990**, *29*, 1304−1319. − [1b] S. R. Batten, R. Robson, *Angew. Chem. Int. Ed.* **1998**, *37*, 1460−1494. − [1c] H. J. Choi, M. P. Suh, *J. Am. Chem. Soc.* **1998**, *120*, 10622−10628. − [1d] H. J. Choi, M. P. Suh, *Inorg. Chem.* **1999**, *38*, 6309−6312. − [1e] S. Leininger, B. Olenyuk, P. J. Stang, *Chem. Rev.* **2000**, *100*, 853−908. − [1f] K. S. Min, M. P. Suh, *J. Solid State Chem.* **2000**, *152*, 183−190. − [1g] K. S. Min, M. P. Suh, *Eur. J. Inorg. Chem.* **2001**, 449−455. − [1h] K. S. Min, M. P. Suh, *Chem. Eur. J.* **2001**, *7*, 303−313.

[2] [2a] M. Munakata, L. P. Wu, T. Kuroda-Sowa, *Adv. Inorg. Chem.* **1999**, *46*, 173−303. − [2b] A. J. Blake, N. R. Champness, P. Hubberstey, W.-S. Li, M. A. Withersby, M. Schröder, *Coord. Chem. Rev.* **1999**, *183*, 117−138. − [2c] O. M. Yaghi, H. Li, C. Davis, D. Richardson, T. L. Groy, *Acc. Chem. Res.* **1998**, *31*, 474−484. − [2d] O.-S. Jung, Y. J. Kim, Y.-A. Lee, J. K. Park, H. K. Chae, *J. Am. Chem. Soc.* **2000**, *122*, 9921−9925.

[3] H. Oshio, Y. Saito, T. Ito, *Angew. Chem. Int. Ed. Engl.* **1997**, *36*, 2673−2675.

[4] W. Kobel, M. Hanack, *Inorg. Chem.* **1986**, *25*, 103−107.

[5] [5a] O. M. Yaghi, H. Li, *J. Am. Chem. Soc.* **1996**, *118*, 295−296. − [5b] K. S. Min, M. P. Suh, *J. Am. Chem. Soc.* **2000**, *122*, 6834−6840.

[6] [6a] H. J. Choi, T. S. Lee, M. P. Suh, *Angew. Chem. Int. Ed.* **1999**, *38*, 1405−1408. − [6b] S.-I. Noro, S. Kitagawa, M. Kondo, K. Seki, *Angew. Chem. Int. Ed.* **2000**, *39*, 2082−2084.

[7] [7a] T. Sawaki, Y. Aoyama, *J. Am. Chem. Soc.* **1999**, *121*, 4793−4798. − [7b] J. S. Seo, D. Whang, H. Lee, S. I. Jun, J. Oh, Y. J. Jeon, K. Kim, *Nature* **2000**, *404*, 982−986.

[8] D. Venkataraman, S. Lee, J. Zhang, J. S. Moore, *Nature* **1994**, *371*, 591−593.

[9] [9a] S. Kitagawa, M. Kondo, *Bull. Chem. Soc. Jpn.* **1998**, *71*, 1739−1753. − [9b] P. J. Hagrman, D. Hagrman, J. Zubieta, *Angew. Chem. Int. Ed.* **1999**, *38*, 2638−2684.

[10] [10a] S. Bélanger, J. T. Hupp, C. L. Stern, R. V. Slone, D. F. Watson, T. G. Carrell, *J. Am. Chem. Soc.* **1999**, *121*, 557−563. − [10b] M. Fujita, J. Yazaki, K. Ogura, *J. Am. Chem. Soc.* **1990**, *112*, 5645−5647. − [10c] M. Fujita, F. Ibukuro, K. Yamaguchi, K. Ogura, *J. Am. Chem. Soc.* **1995**, *117*, 4175−4176. − [10d] J. Fan, J. A. Whiteford, B. Olenyuk, M. D. Levin, P. J. Stang, E. B. Fleischer, *J. Am. Chem. Soc.* **1999**, *121*, 2741−2752.

[11] I. M. Procter, B. J. Hathaway, P. G. Hodgson, *J. Inorg. Nucl. Chem.* **1972**, *34*, 3689−3697.

[12] T. Tanase, M. Doi, R. Nouchi, M. Kato, Y. Sato, K. Ishuida, K. Kobayashi, T. Sakurai, Y. Yamamoto, S. Yano, *Inorg. Chem.* **1996**, *25*, 4848−4857.

[13] [13a] L. Carlucci, G. Ciani, D. M. Proserpio, A. Sironi, *J. Chem. Soc., Chem. Commun.* **1994**, 2755−2756. − [13b] M. Kondo, T. Yoshitomi, K. Seki, H. Matsuzaka, S. Kitagawa, *Angew. Chem. Int. Ed. Engl.* **1997**, *36*, 1725−1727. − [13c] J. Lu, C. Yu, T. Niu, T. Paliwala, G. Crisci, F. Somosa, A. J. Jacobson, *Inorg. Chem.* **1998**, *37*, 4637−4640.

[14] W. E. Estes, D. P. Gavel, W. E. Hatfield, D. J. Hodgson, *Inorg. Chem.* **1978**, *17*, 1415−1421.

[15] O. Kahn, *Molecular Magnetism*, VCH Publishers, New York, **1993**.

[16] M. Julve, M. Verdaguer, J. Faus, F. Tinti, J. Mortal, A. Monge, E. Gutiérrez-Puebla, *Inorg. Chem.* **1987**, *26*, 3520−3527.

[17] M. S. Haddad, D. N. Hendrickson, J. P. Cannady, R. S. Drago, D. S. Bieksza, *J. Am. Chem. Soc.* **1979**, *101*, 898−906.

[18] G. M. Sheldrick, *Acta Crystallogr., Sect. A* **1990**, *46*, 467−473.

[19] G. M. Sheldrick, *SHELXL-97*, *Program for the Refinement of Crystal Structures*, University of Göttingen: Göttingen, Germany, **1997**.

[20] R. G. Xion, Z. Yu, J. L. Zuo, X. Z. You, *Spectrosc. Lett.* **1997**, *30*, 403−413.

Received May 23, 2001
[I01189]

Pendant Functionalised Triphosphamacrocycles

Peter G. Edwards,*[a] Florent Ingold,[a] Sudantha S. Liyanage,[a] Paul D. Newman,[a] Wai-Kwok Wong,[b] and Yang Chen[b]

Keywords: Macrocyclic ligands / Phosphanes / Molybdenum / Chromium

The selective functionalisation of a single phosphorus atom in the parent $[Mo(CO)_3(12aneP_3H_3)]$, where $12aneP_3H_3$ is 1,5,9-triphosphacyclododecane, has been achieved by deprotonation and subsequent reaction with an ether containing an alkyl halide group. Yields of the monosubstituted products are very sensitive to the reaction conditions, which must be carefully controlled in order to achieve reasonable selectivity. In addition, trisubstitution of $[M(CO)_3(12aneP_3H_3)]$ with carbon chains containing pendant donors such as ethers, thioethers, amines and phosphanes has been achieved by both deprotonation/addition ($M = Mo^0$) and hydrophosphination ($M = Cr^0$) protocols. The new compounds have been characterised by spectroscopic and analytical techniques, including X-ray crystallography, and a selection of the P_3 macrocycles released from their templates by oxidation and base digestion.

Introduction

We have previously reported the template synthesis and P-atom functionalisation of 1,5,9-triphosphacyclododecane to give a number of tritertiary derivatives ($12aneP_3R_3$), which can be liberated from their Mo^0 and Cr^0 templates by oxidation of the metal centre followed by base digestion.[1] Unlike the only other triphosphorus macrocycle known as the free ligand,[2] our synthetic procedure is stereospecific (for the *syn-syn* isomer) producing ligands with identical bridging backbone functions and hence achiral phosphorus atoms. A feature of these ligands is that they are ideally suited to coordinating a trigonal face in metal coordination polyhedra; the phosphorus atoms are clearly restricted to a mutually all *cis* arrangement which in turn locates the remaining active sites at the metal to also be mutually *cis* (at least for coordination numbers of six or less). Although a number of complexes which approximate to octahedral and tetrahedral geometries are now known for the $12aneP_3R_3$ ligand, there are others which show considerable distortions from idealised geometries as noted for the four coordinate Ni^0 [3] and five-coordinate Co^{II} systems.[4]

The enhanced stability of the metal-ligand unit formed by these macrocycles is in itself of value in the stabilisation of lower coordinate transients formed during reactions (e.g. resulting from a reductive elimination). Such reduced species might not prefer facially capping ligands and it is of interest in this context to study ligand systems that may be able to further stabilise transition states or intermediates by temporary coordination of an intrinsically labile donor, i.e. hemilabile ligands. We have previously studied acyclic phosphanes containing pendant ethers[5] and are interested to extend this approach to strongly bound ligands with a macrocyclic core, such that a section of the ligand will be bound tightly with reduced lability whilst an intrinsically labile function may provide freedom for reaction at the remaining sites and transient stabilisation. Within this theme, it is desirable to be able to selectively synthesise ligands with a chosen number of pendant functions; in this paper, we present the selective stereospecific synthesis of functionalised 1,5,9-triphosphacyclododecanes having one or three pendant ether functions, as well as related trisubstituted pendant thioether, amine or phosphane macrocycles.

Results and Discussion

Following our previous work[6] on the synthesis of tritertiary 1,5,9-triphosphacyclododecane ligands, the introduction of one ether function may be performed by the deprotonation of one secondary phosphane by a strong base (*n*BuLi), followed by the reaction of the resultant coordinated phosphide with the corresponding ether-functionalised alkyl halides (Scheme 1). The temperature at which the deprotonation is performed is critical for success in the synthesis of the mono-substituted derivative **3a**. Thus, when the reaction of the coordinated phosphide (generated in situ) with 2-bromoethyl methyl ether is performed at −78 °C the desired $[Mo(CO)_3\{12aneP_3H_2(CH_2CH_2OCH_3)\}]$ (**3a**) is formed in low yield and is difficult to isolate pure from the reaction mixture. However, when the reaction is performed at −30 °C, **3a** can be obtained in good yield (70%). Monitoring (by ^{31}P NMR spectroscopy) of the reaction mixture after addition of the alkyl halide shows resonances assignable to mono-, di- and trisubstituted macrocycles, with the undesired di- and tri- by-products being far more prevalent in the mixture at −78 °C than at −30 °C.

[a] Department of Chemistry, Cardiff University,
P.O. Box 912, Cardiff CF10 3TB, UK
Fax: (internat.) +44-29/2087-4030
E-mail: Edwardspg@cardiff.ac.uk
[b] Department of Chemistry, Hong Kong Baptist University,
Kowloon Tong, Hong Kong, China
Fax: (internat.) +8-52/2339-7348
E-mail: wkwong@hkbu.edu.hk

 © WILEY-VCH Verlag GmbH, 69451 Weinheim, 2001 1434−1948/01/1111−2865 $ 17.50+.50/0

This may reflect incomplete solubility of the lithiated complex at the lower temperature. It should be noted that these yields (70%) are only obtainable with very careful control of the stoichiometry and the reaction temperature. Indeed, reproducibility is a problem and in a series of repeat reactions, yields of less than 20% were typical. Hydrophosphination of the monoether **3a** with ethene in the presence of AIBN gave the diethyl analogue **4a**. The related reaction with tetrahydrofurfuryl chloride was less successful, and although complex **3b** could be characterised by ^{31}P NMR spectroscopy and mass spectrometry, it proved impossible to isolate the complex in a pure form — the compound was invariably contaminated with unsubstituted starting material and/or further substitution (bi- and tri-) products — and it was convenient to prepare the crude diethyl derivative (**4b**) and liberate the free macrocycle **5b**, which could then be isolated pure.

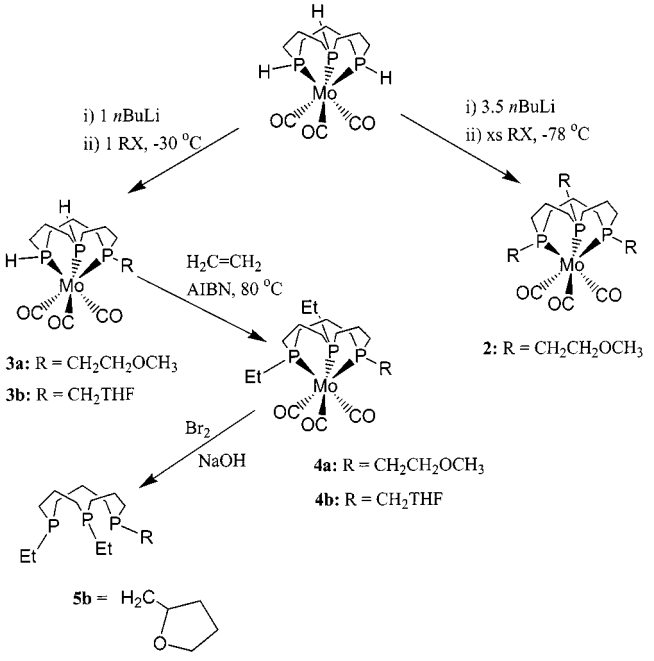

Scheme 1

The $^{31}P\{^1H\}$ NMR spectrum of **3a** appears as a first order AX_2 pattern with the two equivalent secondary phosphorus centres resonating at $\delta_P = -32$ (t, $J = 32.0$ Hz) and the unique tertiary phosphorus at $\delta_P = 3$ (d, $J = 32.0$ Hz). When the two secondary phosphanes are converted into tertiary centres on ethylation to give **4a**, the $^{31}P\{^1H\}$ NMR spectrum approximates to an AM_2 pattern with signals at $\delta_P = 5.9$ (d, $J = 31.0$ Hz, $2 \times R_2PEt$) and 4.3 (t, $J = 31.0$ Hz, $R_2PCH_2CH_2OCH_3$). A similar AM_2 pattern is observed for the tetrahydrofurfuryl macrocycle complex **4b** with $\delta_P = 5.0$ (d, $J = 30.0$ Hz, $2 \times R_2PEt$) and 4.5 (t, $J = 30.0$ Hz, R_2PCH_2THF).

In the infrared spectrum of **3a** there are two bands assignable to P−H stretches at 2355 and 2323 cm^{-1} and two bands with a shoulder for the ν(C−O) stretches reflecting the lower symmetry of **3a**.

The molecular structure of **3a** is shown in Figure 1, with significant bond lengths and angles presented in Table 1. The geometry about the Mo^0 centre is octahedral, with the major source of distortion from ideal being the disparate metal−donor bond lengths [$Mo-P_{av} = 2.491(2)$ and $Mo-C_{av} = 1.989(4)$ Å]. The average Mo−P bond length is closer to that in $[Mo(12aneP_3H_3)(CO)_3]$ [2.476(1) Å][7] than in $[Mo(12aneP_3iPr_3)(CO)_3]$ [2.527(1) Å].[8] There are no significant differences in the Mo−P bond lengths for the secondary and tertiary phosphorus donors; the $M-P_{tert}$ bond being just 0.01 Å longer than the $M-P_{sec}$ bonds. Indeed, comparison with the related C_{3v} complexes above reveals less Mo−P and Mo−C bond variation in **3a** than in these higher symmetry systems. The methoxyethyl pendant group projects over one of the carbonyl groups (C3−O3) with the result that the P1−Mo−C3 angle is expanded significantly [95.99(13)°] compared to the other *cis* angles. As is typical for $12aneP_3$ complexes of Mo^0, the P−Mo−P angles are close to, but slightly less than, 90°. This contrasts with comparable Cr^0 complexes[9] and $[CpFe(12aneP_3R_3)]^+$ [10] species, where expanded angles of greater than 90° are observed; this was anticipated as the M−P bond lengths decrease along the series $Mo^0 > Cr^0 > Fe^{II}$. As in all other structurally characterised complexes of $12aneP_3$ macrocycles, two of the chelate rings have a pseudo-chair conformation whilst the third is pseudo-boat. Other deviations from idealised geometry are small and the data are comparable to other Mo^0 complexes of this type.

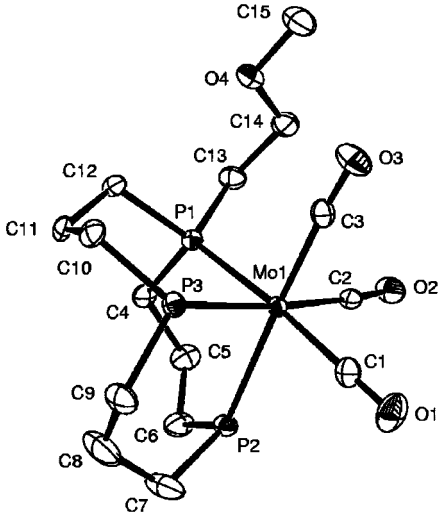

Figure 1. ORTEP representation of complex **3a**

When 3.5 mol equivalents of *n*BuLi are used followed by excess 2-bromoethyl methyl ether, the trisubstituted tertiary derivative **2** is isolated in high yield. As expected, the $^{31}P\{^1H\}$ NMR spectrum consists of a singlet at $\delta_P = 3$. The structure of the trisubstituted molybdenum complex **2** is shown in Figure 2 with selected bond lengths and angles presented in Table 2. All the bond lengths are very similar to those for complex **3a**, but, as expected for this higher symmetry complex, the angular distortions about the metal

Table 1. Selected bond lengths (Å) and angles (°) for **3a**

Mo1−C1	1.993(4)	Mo1−C2	1.993(3)	Mo1−C3	1.980(3)
Mo1−P1	2.500(3)	Mo1−P2	2.487(2)	Mo1−P3	2.4852(9)
P1−C13	1.846(4)	P1−C4	1.842(3)	P1−C12	1.839(3)
O1−C1	1.150(4)	O2−C2	1.153(3)	O3−C3	1.158(3)
O4−C15	1.428(3)	O4−C14	1.408(4)		
C2−Mo1−C1	92.34(13)	C2−Mo1−C3	89.37(12)	C1−Mo1−C3	88.9(2)
C2−Mo1−P1	87.44(10)	C1−Mo1−P1	175.12(9)	C3−Mo1−P1	95.99(13)
C2−Mo1−P2	94.37(9)	C1−Mo1−P2	85.81(13)	C3−Mo1−P2	173.63(8)
P1−Mo1−P2	89.34(10)	C2−Mo1−P3	174.65(8)	C1−Mo1−P3	92.11(9)
C3−Mo1−P3	87.75(9)	P1−Mo1−P3	88.37(5)	P2−Mo1−P3	88.91(4)

centre are generally less than those observed in **3a**. Most notably, the large *cis* angle observed in the mono-pendant derivative is not a feature in this C_3 symmetric complex. All the features are similar to those of previously reported structures of this type, including the ubiquitous chair/chair/boat conformation of the three chelate rings.

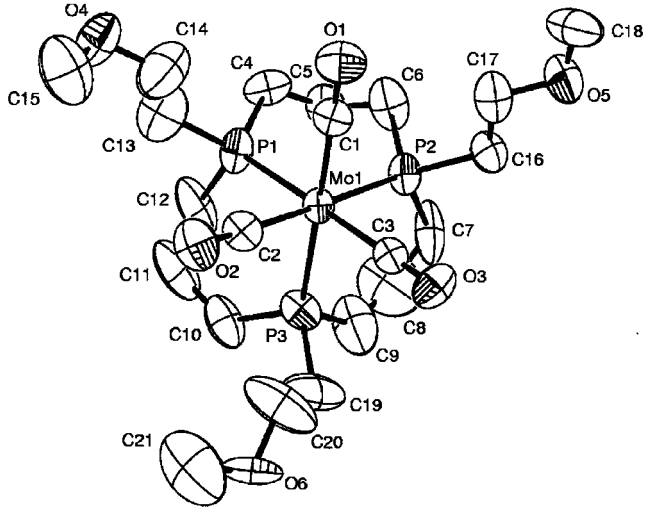

Figure 2. ORTEP representation of complex **2**

The C_3-symmetric trisubstituted macrocycles are also readily formed by radical-initiated hydrophosphinations of appropriate alkenes with $[M(CO)_3(12aneP_3H_3)]$ [M = Mo or Cr]. This method allows the direct incorporation of a range of hydrocarbyl or functionalised substituents including pendant ethers, amines, phosphanes or thioethers in high yield (Scheme 2). We have previously reported the synthesis of these pendant-donor-functionalised chromium compounds[11] although not the synthesis of the free ligands. Thus, the reaction of the coordinated secondary phosphane macrocycle with either vinyl ethyl ether or allyl methyl ether gives rise to the β- or γ-functionalised tris-ether derivatives **6a** and **6b**, respectively. These reactions may be performed readily using either $[Mo(CO)_3(12aneP_3H_3)]$ or $[Cr(CO)_3(12aneP_3H_3)]$, but are generally more efficient with the latter. The reaction of $[Cr(CO)_3(12aneP_3H_3)]$ with excess vinyl ethyl ether in toluene proceeds smoothly to the tritertiary phosphane derivative **6a**. This reaction appears to proceed by a radical-initiated mechanism as might be expected; yields are high when a radical initiator is included but are poor when performed in its absence or in the presence of a base catalyst alone. The same reaction with allyl methyl ether provides the methoxypropyl macrocycle complex, **6b**, in excellent yield.

The tris(methoxyethyl), diethyltetrahydrofurfuryl and tris(methoxypropyl) macrocycles were freed from their Mo and Cr templates by the established procedure of halogen oxidation and base digestion.[1b] As established previously, the liberation proceeds stereoselectively to give the *syn,syn* isomer exclusively; this conclusion is based on the ^{31}P NMR spectra which show singlets for both **7a** and **7b** and is confirmed by the relatively simple ^1H and ^{13}C NMR spectra. The coordination chemistry of these and the other functionalised macrocycles will be explored subsequently and will be reported at a later date. In conclusion, the versatility of the synthetic approaches described in this paper

Table 2. Selected bond lengths (Å) and angles (°) for **2**

Mo1−C2	1.959(7)	Mo1−C1	1.958(8)	Mo1−C3	1.995(7)
Mo1−P1	2.484(2)	Mo1−P2	2.489(2)	Mo1−P3	2.492(2)
P1−C13	1.801(10)	P1−C4	1.855(7)	P1−C12	1.897(9)
O1−C1	1.158(8)	O2−C2	1.148(8)	O3−C3	1.149(7)
O4−C15	1.363(9)	O4−C14	1.453(11)	O5−C17	1.410(9)
O5−C18	1.481(9)	O6−C20	1.382(14)	O6−C21	1.38(2)
C2−Mo1−C1	89.9(3)	C2−Mo1−C3	92.2(3)	C1−Mo1−C3	92.5(3)
C2−Mo1−P1	89.6(2)	C1−Mo1−P1	89.6(2)	C3−Mo1−P1	177.2(2)
C2−Mo1−P2	178.0(2)	C1−Mo1−P2	90.1(2)	C3−Mo1−P2	89.8(2)
P1−Mo1−P2	88.42(6)	C2−Mo1−P3	90.8(2)	C1−Mo1−P3	178.5(2)
C3−Mo1−P3	88.7(2)	P1−Mo1−P3	89.12(8)	P2−Mo1−P3	89.07(7)

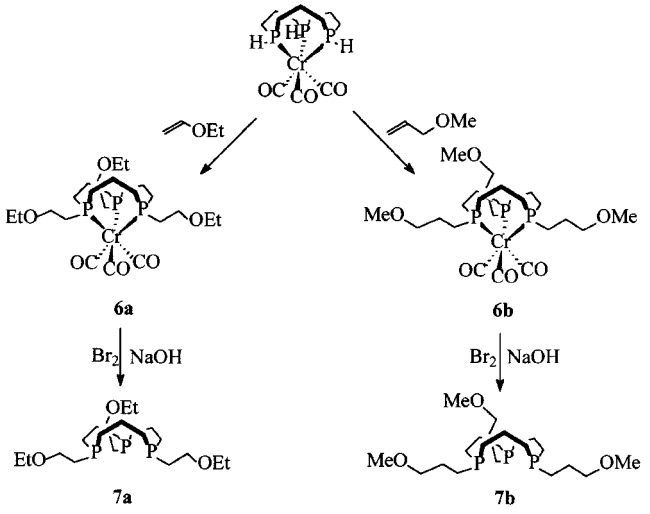

Scheme 2

enables access to a range of pendant-donor-functionalised macrocyclic triphosphanes, including selectively functionalised examples.

Experimental Section

All reactions were carried out under an atmosphere of dry nitrogen. All solvents were dried by boiling at reflux over standard drying agents. Petroleum ether had b.p. 40−60 °C. The compounds [Mo(CO)$_3$(12aneP$_3$H$_3$)] and [Cr(CO)$_3$(12aneP$_3$H$_3$)],[2] and **6a** and **6b**[11] were prepared as previously described. All other chemicals were obtained from the Aldrich Chemical Company and used without further purification, except alkyl halide reagents, which were dried over molecular sieves and deoxygenated by freeze-thaw degassing. NMR spectra were recorded on a Bruker WM400 instrument operating at 400 MHz (^{1}H), 100.6 MHz (^{13}C) or a Jeol FX-90Q instrument operating at 36.23 MHz (^{31}P). All NMR spectra were recorded in $CDCl_3$ solution unless otherwise stated, ^{1}H and ^{13}C NMR chemical shifts are quoted in ppm relative to tetramethylsilane ($\delta = 0$), ^{31}P NMR chemical shifts are quoted in ppm relative to external 85% H_3PO_4 ($\delta = 0$). All chemical shifts are positive to low field of the standards. Infrared spectra were recorded in Nujol on a Perkin−Elmer 783 infrared spectrometer. Magnetic susceptibilities were measured by the Gouy method on a Johnson−Matthey magnetic susceptibility balance, an experimental diamagnetic correction was measured for *cyclo*-(HPC$_3$H$_6$)$_3$ and applied. Mass spectra (EI) were recorded on a VG Platform II Fisons mass spectrometer. Melting points were obtained in sealed capillaries and are uncorrected.

[Mo(CO)$_3${12aneP$_3$(CH$_2$CH$_2$OCH$_3$)$_3$}] (2): *n*BuLi (3.5 equiv.) was added dropwise to a cooled (−78 °C) solution of [Mo(CO)$_3$(12aneP$_3$H$_3$)] (**1**; 2.5 g, 5.5 mmol) in THF (35 mL). The reaction mixture was allowed to warm up to −30 °C, whereupon 2-bromoethyl methyl ether (2.5 mL, 26.6 mmol) was added dropwise to the recooled (−78 °C) yellow solution and the whole allowed to warm to 20 °C. The product was purified by chromatography on silica (200 mesh) with dichloromethane as eluent. The solvent was removed to give a white solid which was crystallised from CH_2Cl_2/Et_2O. Yield: 2.63 g (83%) − ^{1}H NMR ($CDCl_3$): δ_H = 1.52 (m, 6 H, PCH$_2$C*H*$_2$CH$_2$P), 1.84 (dt, *J* = 10 and 7 Hz, 6 H, PC*H*$_2$CH$_2$OCH$_3$), 1.91 (m, 12 H, PC*H*$_2$CH$_2$C*H*$_2$P), 3.29 (s, 9 H, PCH$_2$CH$_2$OC*H*$_3$), 3.70 (dt, *J* = 13 and 7 Hz, 6 H, PCH$_2$C*H*$_2$OCH$_3$). − ^{13}C NMR ($CDCl_3$): δ_C = 20.5 (t, *J* = 7 Hz, PCH$_2$*C*H$_2$CH$_2$P), 25.6 (dd, *J* = 8 and 4 Hz, P*C*H$_2$CH$_2$*C*H$_2$P), 30.0 (m, P*C*H$_2$CH$_2$O), 58.4 (s, O*C*H$_3$), 70.2 (d, *J* = 7 Hz, *C*H$_2$O), 231.5 (m, *C*O). − ^{31}P{^{1}H} NMR ($CDCl_3$): δ_P = 3 (s). − IR (Nujol): $\tilde{\nu}$ = 1922s, 1825s cm^{-1}. − Positive-ion EI-MS: *m*/*z* = 577 [M$^+$], 549 [M − CO]$^+$. − $C_{21}H_{39}MoO_6P_3$ (576.40): calcd. C 43.75, H 6.83; found C 43.9, H 7.0.

[Mo(CO)$_3${12aneP$_3$H$_2$(CH$_2$CH$_2$OCH$_3$)}] (3a): One equivalent of *n*BuLi was added dropwise to a cooled (−78 °C) solution of [Mo(CO)$_3$(12aneP$_3$H$_3$)] (2.5 g, 5.5 mmol) in THF (35 mL). The reaction mixture was allowed to warm up to −30 °C whereupon 2-bromoethyl methyl ether was added dropwise to the yellow solution and the whole allowed to warm to room temperature (20 °C). The product was purified by chromatography on silica (200 mesh) with toluene as eluent and the resultant white solid crystallised from CH_2Cl_2/Et_2O. Yield: 0.5 g (20%). − ^{1}H NMR ($CDCl_3$): δ_H = 1.52 (m, 4 H, HPCH$_2$CH$_2$C*H*$_2$PR), 1.74 (m, 6 H, PCH$_2$C*H*$_2$CH$_2$P), 1.86 (dt, *J* = 9 and 6 Hz, 2 H, PC*H*$_2$CH$_2$OCH$_3$), 1.93 (m, 8 H, HPC*H*$_2$CH$_2$CH$_2$PR), 3.29 (s, 3 H, PCH$_2$CH$_2$OC*H*$_3$), 3.70 (dt, *J* = 13 and 7 Hz, 2 H, PCH$_2$C*H*$_2$OCH$_3$), 4.86 (d, *J* = 323 Hz, 2 H, P*H*). − ^{13}C NMR ($CDCl_3$): δ_C = 21.8 [d, *J* = 14 Hz, HPCH$_2$-*C*H$_2$CH$_2$P(CH$_2$CH$_2$OCH$_3$)], 22.1 (d, *J* = 11 Hz, HPCH$_2$*C*H$_2$-CH$_2$PH), 24.5 [dd, *J* = 40 and 9 Hz, HP*C*H$_2$CH$_2$-CH$_2$P(CH$_2$CH$_2$OCH$_3$)], 24.6 (d, *J* = 24 Hz, HPCH$_2$*C*H$_2$*C*H$_2$PH), 31.3 [d, *J* = 24 Hz, HPCH$_2$*C*H$_2$CH$_2$P(CH$_2$CH$_2$OCH$_3$)], 35.4 (d, *J* = 26 Hz, P*C*H$_2$CH$_2$OCH$_3$), 58.9 (s, PCH$_2$CH$_2$O*C*H$_3$), 69.6 (d, *J* = 9 Hz, PCH$_2$*C*H$_2$OCH$_3$). − ^{31}P{^{1}H} NMR ($CDCl_3$): δ_P = 3 (t, *J* = 32 Hz, R$_3$P), −32 (d, *J* = 32 Hz, 2 × R$_2$PH). − IR (Nujol): ν(P−H) = 2355m, 2323m; ν(C−O) = 1916s, 1831sh, 1821s cm^{-1}. − Positive-ion EI-MS: *m*/*z* = 460 [M$^+$], 432 [M − CO]$^+$. − $C_{15}H_{27}MoO_4P_3$ (460.24): calcd. C 39.14, H 5.92; found C 39.0, H 5.7.

[Mo(CO)$_3${12aneP$_3$H$_2$(CH$_2$THF)}] (3b): The complex was prepared in an analogous fashion to that for **3a** above, with tetrahydrofurfuryl chloride. The complex was not isolated pure and was used as such for the preparation of **4b**.

[Mo(CO)$_3${12aneP$_3$Et$_2$(CH$_2$CH$_2$OCH$_3$)}] (4a): A solution of **3a** (200 mg, 0.43 mmol) was placed in an autoclave with ca. 1% AIBN and the reaction mixture charged with ethene to 90 psi. After 12 h stirring at 90 °C, the autoclave was cooled to 20 °C and the excess of ethene removed. The solution was dried ($MgSO_4$) and the product purified by chromatography column on silica (200 mesh) with CH_2Cl_2 as eluent. Yield: 0.22 g (100%). − ^{1}H NMR ($CDCl_3$): δ_H = 1.08 (m, PCH$_2$*C*H$_3$), 1.7−1.2 (m, 20 H), 1.90 (q, *J* = 8 Hz, 4 H, PC*H*$_2$CH$_3$), 3.28 (s, 3 H, PCH$_2$CH$_2$OC*H*$_3$), 3.69 (dt, *J* = 11 and 7 Hz, 2 H, PCH$_2$C*H*$_2$OCH$_3$). − ^{13}C NMR ($CDCl_3$): δ_C = 8.1 (s, *C*H$_3$), 20.8 (s, PCH$_2$*C*H$_2$CH$_2$P), 23.2 (s, PCH$_2$*C*H$_2$CH$_2$P), 27.6 (dd, *J* = 13 and 9 Hz, P*C*H$_2$CH$_2$*C*H$_2$P), 29.1 (m, P*C*H$_2$CH$_2$*C*H$_2$P), 30.6 (d, *J* = 17 Hz, P*C*H$_2$CH$_3$), 34.8 (d, *J* = 20 Hz, P*C*H$_2$CH$_2$OCH$_3$), 58.3 (s, PCH$_2$CH$_2$O*C*H$_3$), 69.1 (d, *J* = 2 Hz, PCH$_2$*C*H$_2$OCH$_3$). − ^{31}P{^{1}H} NMR ($CDCl_3$): δ_P = 4.3 (t, *J* = 32 Hz, R$_2$PCH$_2$CH$_2$OCH$_3$), 5.9 (d, *J* = 32 Hz, 2 × R$_2$PEt). − IR (CH_2Cl_2): ν(C−O) = 1923s, 1825s cm^{-1}. − Positive-ion EI-MS: *m*/*z* = 516 [M$^+$], 488 [M − CO]$^+$. − $C_{19}H_{35}MoO_4P_3$ (516.35): calcd. C 44.18, H 6.84; found C 44.0, H 6.7.

[Mo(CO)$_3${12aneP$_3$Et$_2$(CH$_2$THF)}] (4b): Prepared as for **4a** using crude **3b** (≈70%). − ^{31}P{^{1}H} NMR ($CDCl_3$): δ_P = 4.5 (t, *J* = 31 Hz, R$_2$PCH$_2$CH$_2$THF), 5.0 (d, *J* = 31 Hz, 2 × R$_2$PEt). The

resultant material was used directly for the liberation and isolation of **5b**.

12aneP$_3$Et$_2$(CH$_2$THF) (5b): The ligand was released using the method defined previously.[1] It was purified by crystallisation from petroleum ether. Yield: 40%. – ^{1}H NMR ($CDCl_3$): δ_H = 2.0–0.7 (m, 34 H), 3.68 (m, $PCH_2CHCH_2CH_2CH_2O$), 3.83 (m, 2 H, PCH_2THF). – ^{13}C NMR ($CDCl_3$): δ_C = 9.9 (d, J = 12 Hz, CH_3), 19.3 (m, $PCH_2CH_2CH_2P$), 25.8 (s, CH_2-THF), 27.2 (m, $PCH2$), 29.5 (s, CH_2-THF), 33.9 (m, PCH_2CHO), 67.6 (s, $CHOCH_2$), 80.0 (d, J = 16 Hz, $CHOCH_2$). – ^{31}P{^{1}H} NMR ($CDCl_3$): δ_P = –40.4 (t, J = 16 Hz, R_2PCH_2THF), –31.9 (d, J = 16 Hz, 2 × R_2PEt).

7a: Released from the metal as previously described.[1b] Yield = 55%. – ^{1}H NMR ($CDCl_3$): δ_H = 1.10 (t, J = 7 Hz, 9 H, CH_3), 1.46 (br. m, 6 H, $PCH_2CH_2CH_2P$), 1.65 (m, 12 H, $PCH_2CH_2CH_2P$), 1.90 (br. m, 6 H, $PCH_2CH_2OCH_2CH_3$), 3.45 (q, J = 7 Hz, 6 H, $PCH_2CH_2OCH_2CH_3$), 3.72 (t, J = 7 Hz, 6 H, $PCH_2CH_2OCH_2CH_3$). – ^{13}C NMR ($CDCl_3$): δ_C = 14.0 (s, CH_3), 18.4 (m, $PCH_2CH_2CH_2P$), 27.5 (dd, J = 14 and 9 Hz, $PCH_2CH_2CH_2P$), 32.8 (m, PCH_2CH_2O), 64.1 (s, OCH_2CH_3), 65.2 (s, PCH_2CH_2O). – ^{31}P{^{1}H} NMR ($CDCl_3$): δ_P = –42.0 (s). – Positive-ion EI-MS: m/z = 438 [M^+], 365 [$M - EtOC_2H_4]^+$.

7b: Released from the metal as previously described.[1b] Yield = 68%. – ^{1}H NMR ($CDCl_3$): δ_H = 1.35 (br. m, 12 H, $PCH_2CH_2CH_2P$, $PCH_2CH_2CH_2OCH_3$), 1.58 (q, J = 8 Hz, 6 H, $PCH_2CH_2CH_2OCH_3$), 1.69 (m, 12 H, $PCH_2CH_2CH_2P$), 3.26 (s, OCH_3), 3.34 (t, J = 7 Hz, 6 H, $PCH_2CH_2CH_2OCH_3$). – ^{13}C NMR ($CDCl_3$): δ_C = 19.2 (br, $PCH_2CH_2CH_2P$), 23.2 (d, J = 7 Hz, $PCH_2CH_2CH_2O$), 27.1 (dd, J = 14 and 9 Hz, $PCH_2CH_2CH_2P$), 29.5 (d, J = 14 Hz, $PCH_2CH_2CH_2O$), 58.4 (s, OCH_3), 73.4 (d, J = 13 Hz, $PCH_2CH_2CH_2O$). – ^{31}P{^{1}H} NMR ($CDCl_3$): δ_P = –39.7 (s). – Positive-ion EI-MS: m/z = 438 [M^+], 365 [$M - EtOC_2H_4]^+$.

Crystal Data for Complex 2: $C_{21}H_{34}MoO_6P_3$, M = 571.33, T = 150(2) K, monoclinic, space group $P2_1/c$, a = 12.5069(9), b = 14.561(3), c = 15.4095(14) Å, β = 111.990(8)°, (by least-squares refinement of the setting angles for 250 reflections within θ = 1.76–24.74°), V = 2602.1(6) Å^3, Z = 4, D = 1.458 g cm^{-3}, μ(Mo-K_α) = 0.971cm^{-1}, F(000) = 1180, crystal size = 0.3 × 0.2 × 0.2 mm. All crystallographic measurements were made on an Enraf Nonius FAST area detector diffractometer. The structure was solved by direct methods[12] and refined on F_o^2 by full-matrix least-squares[13] using all unique data after correction for Lorentz and polarisation factors. All non-hydrogen atoms were refined with anisotropic thermal parameters. O6 was disordered between two half-occupied positions. Atoms C8, C13 and C14 were refined with the restraint ISOR = 0.0075. The hydrogen atoms were inserted in idealised positions with U_{iso} set at 1.5 times the U_{eq} of the parent. The weighting scheme used was $w = 1/[\sigma^2(F_o)^2 + (0.0739P)^2]$, where $P = [\mathrm{Max}(F_o)^2 + 2(F_c)^2]/3$; this gave satisfactory agreement analyses. Final R_1 (on F) and wR_2 (on F_o^2) values were 0.0789 and 0.1441 for all 3656 data and 291 parameters. The corresponding R values were 0.0543 and 0.1361 for 2467 data with $I > 2\sigma(I)$. Sources of scattering factors as given in ref.[13]

Crystallographic data (excluding structure factors) for the structure(s) included in this paper have been deposited with the Cambridge Crystallographic Data Centre as supplementary publication no. CCDC-159939. Copies of the data can be obtained free of charge on application to CCDC, 12 Union Road, Cambridge CB2 1EZ, UK [Fax: (internat.) + 44-1223/336-033; E-mail: deposit@ccdc.cam.ac.uk].

Crystal Data for Complex 3a: $C_{15}H_{27}MoO_4P_3$, M = 460.22, T = 150(2) K, monoclinic, space group $P2_1/c$, a = 10.453(19), b = 12.300(3), c = 15.777(8) Å, β = 108.41(5)°, (by least-squares refinement of the setting angles for 250 reflections within θ = 2.05–24.8°), V = 1924.7(36) Å^3, Z = 4, D = 1.588 g cm^{-3}, μ(Mo-K_α) = 0.971cm^{-1}, F(000) = 944, crystal size = 0.25 × 0.22 × 0.18 mm. All crystallographic measurements were made on an Enraf Nonius FAST area detector diffractometer. The structure was solved by direct methods[12] and refined on F_o^2 by full-matrix least-squares[13] using all unique data after correction for Lorentz and polarisation factors. All non-hydrogen atoms were anisotropic. The hydrogen atoms were inserted in idealised positions with U_{iso} set at 1.5 times the U_{eq} of the parent. The weighting scheme used was $w = 1/[\sigma^2(F_o)^2 + (0.0566P)^2]$, where $P = [\mathrm{Max}(F_o)^2 + 2(F_c)^2]/3$; this gave satisfactory agreement analyses. Final R_1 (on F) and wR_2 (on F_o^2) values were 0.0365 and 0.0834 for all 2943 data and 217 parameters. The corresponding R values were 0.0315 and 0.0790 for 2615 data with $I > 2\sigma(I)$. Sources of scattering factors as in ref.[13] Crystallographic data (excluding structure factors) for the structure(s) included in this paper have been deposited with the Cambridge Crystallographic Data Centre as supplementary publication no. CCDC-159940. Copies of the data can be obtained free of charge on application to CCDC, 12 Union Road, Cambridge CB2 1EZ, UK [Fax: (internat.) + 44-1223/336-033; E-mail: deposit@ccdc.cam.ac.uk].

Acknowledgments

We would like to thank the EPSRC (PGE and FI) and the Hong Kong Research Grants Council (WKW and CY, HKBU 874/96P) for research grants and the EPSRC crystallography service (S. J. Coles and M. B. Hursthouse) for collection of the X-ray data.

[1] [1a] S. J. Coles, P. G. Edwards, J. S. Fleming, M. B. Hursthouse, S. S. Liyanage, *Chem. Commun.* **1996**, 293–294. – [1b] S. J. Coles, P. G. Edwards, J. S. Fleming, M. B Hursthouse, S. S. Liyanage, *Inorg. Chem.* **1996**, *35*, 4563–4568.
[2] E. P. Kyba, R. E. Davis M. A. Fox, C. N. Cubb, S.-T. Lui, G. A. Reitz, V. A. Scheuler, R. P. Kashyapp, *Inorg. Chem.* **1987**, *26*, 1647–1658 and references therein.
[3] P. G. Edwards, F. Ingold, S. J. Coles, M. B. Hursthouse, *Chem. Commun.* **1998**, 545–546.
[4] P. G. Edwards, D. Jones, R. P. Tooze, unpublished results.
[5] S. J. Chadwell, S. J. Coles, P. G. Edwards, M. B. Hursthouse, *J. Chem. Soc., Dalton Trans.* **1995**, 3551–3559.
[6] S. J. Coles, P. G. Edwards, J. S. Fleming, M. B. Hursthouse, *J. Chem. Soc., Dalton Trans.* **1996**, 293–294.
[7] B. N. Diel, P. F. Brandt, R. C. Haltiwanger, M. L. J. Hackney, A. D. Norman, *Inorg. Chem.* **1989**, *28*, 2811–2816.
[8] S. J. Chadwell, P. G. Edwards, J. S. Fleming, M. B. Hursthouse, *J. Chem. Soc., Dalton Trans.* **1995**, 1139–1145.
[9] S. S. Liyanage, PhD Thesis, University of Wales, **1996**.
[10] A. J. Price, PhD Thesis, University of Wales, **2000**.
[11] P. G. Edwards, J. S. Fleming, S. S. Liyanage, *J. Chem. Soc., Dalton Trans.* **1997**, 193–197.
[12] G. M. Sheldrick, *Acta Crystallogr., Sect. A* **1990**, *46*, 467–473.
[13] G. M. Sheldrick, SHELXL-97 *Program for Crystal Structure Refinement*, University of Göttingen, Germany, **1997**.

Received March 29, 2001
[I01113]

Formation and Stereochemistry of Octahedral Cationic Hydride-Azavinylidene Osmium(IV) Complexes

Ricardo Castarlenas,[a] Miguel A. Esteruelas,*[a] Yves Jean,[b] Agustí Lledós,*[c] Enrique Oñate,[a] and Jaume Tomàs[c]

Keywords: Vinylidene ligands / Osmium / Hydrides / Density functional calculations

The complexes $[OsHCl_2(=N=CR_2)(P\textit{i}Pr_3)_2]$ [CR_2 = CMe_2 (**1**), $C^a(CH_2)_4C^bH_2(\textit{C}^a\text{-}\textit{C}^b)$ (**3**)] react with $Ag(CF_3SO_3)$ in the presence of ligands L [H_2O, $P(OMe)_3$, CO]. The reactions in the presence of water lead to $[OsHCl(=N=CR_2)(H_2O)(P\textit{i}Pr_3)_2][CF_3SO_3]$ [CR_2 = CMe_2 (**2**), $C^a(CH_2)_4C^bH_2(\textit{C}^a\text{-}\textit{C}^b)$ (**4**)], which exist as 1:1 equilibrium mixtures of the isomers **2a**/**4a** (hydride *trans* to Cl) and **2c**/**4c** (hydride *trans* to water) in the solid state and in solution. The structure of **2c** has been determined by an X-ray diffraction study. The geometry around the metal center can be described as a distorted octahedron with *trans* phosphane ligands at opposite sites of an ideal coordination plane defined by the other four ligands. The reactions in the presence of $P(OMe)_3$ afford $[OsHCl(=N=CR_2)\{P(OMe)_3\}(P\textit{i}Pr_3)_2][CF_3SO_3]$ [CR_2 = CMe_2 (**5a**), $C^a(CH_2)_4C^bH_2(\textit{C}^a\text{-}\textit{C}^b)$ (**6a**)], with the hydride and chlorine ligands *trans* disposed. Complexes **5a** and **6a** can be also obtained starting from the equilibrium mixtures of **2a** and **2c** or **4a** and **4c**, respectively, and phosphite. Compounds **5c** and **6c**, with $P(OMe)_3$ *trans* to hydride, are formed initially, and subsequently isomerize to **5a** and **6a**. Reactions under carbon monoxide give $[OsHCl(=N=CR_2)(CO)(P\textit{i}Pr_3)_2][CF_3SO_3]$ [CR_2 = CMe_2 (**7a**), $C^a(CH_2)_4C^bH_2(\textit{C}^a\text{-}\textit{C}^b)$ (**8a**)], which also contain the chlorine *trans* to the hydride ligand. A theoretical study on $[OsHCl(=N=CH_2)L(PH_3)_2]^+$ [L = H_2O, $P(OH)_3$ and CO] model complexes shows that these stereochemical preferences arise from the properties of the ligands in the plane perpendicular to the P–Os–P axis. Although the structure with the H and Cl *trans* disposed is not the most favorable when the related pentacoordinate $[OsHCl(=N=CR_2)(P\textit{i}Pr_3)_2]^+$ model complex is considered, it maximizes the interaction energy between the pentacoordinate complex and L ligand, and thus it is the most stable as a whole.

Introduction

Transition metal azavinylidene complexes have attracted a great deal of attention in recent years.[1,2] Some of them have been proposed as intermediates in the catalytic and stoichiometric reduction of nitriles[1s][1y,3] and in the ammoxidation of propylene.[1o] However, only two mononuclear hydride-azavinylidene compounds had been reported before 2000: the five-coordinate d^6 species $[MH(=N=CPh_2)(CO)(P\textit{i}Pr_3)_2]$ (M = Ru,[4] Os[5]). These hydride complexes are prepared by reaction of the corresponding chloro-hydrides $[MHCl(CO)(P\textit{i}Pr_3)_2]$ with $LiN=CPh_2$. In agreement with the strong basicity of the imido group, these compounds undergo hydrolysis in methanol or in the presence of traces of water and evolve into the orthometallated benzophenone imine derivatives $[M^aH\{NH=C(Ph)C^b_6H_4\}(CO)(P\textit{i}Pr_3)_2(\textit{M}^a\text{-}\textit{C}^b)]$ (M = Ru, Os) by a similar process to the orthopalladation.[4]

We have recently shown that the dihydride-dichloro complex $[OsH_2Cl_2(P\textit{i}Pr_3)_2]$ reacts with acetone oxime and cyclohexanone oxime to give the six-coordinate d^4 hydride-azavinylidene derivatives $[OsHCl_2(=N=CR_2)(P\textit{i}Pr_3)_2]$,[6] via the oximate intermediates $[OsH_2Cl\{\kappa\text{-}\textit{N},\kappa\text{-}\textit{O}[ON=CR_2]\}(P\textit{i}Pr_3)_2]$ [CR_2 = CMe_2, $C^a(CH_2)_4C^bH_2(\textit{C}^a\text{-}\textit{C}^b)$].[7] In contrast to $[MH(=N=CPh_2)(CO)(P\textit{i}Pr_3)_2]$, these $[OsHCl_2(=N=CR_2)(P\textit{i}Pr_3)_2]$ complexes are stable in methanol and in the presence of significant amounts of water. Despite the *cis* disposition of the hydride and azavinylidene ligands, they are also stable towards intramolecular reductive elimination to afford d^6-imine species.[6]

The N−H oxidative addition/reductive elimination equilibrium is proposed to be one of the fundamental steps in the hydroamination of olefins and alkynes catalyzed by electron-rich late transition metal centers [Equation (1)]. The $MH(NR_2)$ species are considered the key intermediates of the process.[8]

$$M + H\text{-}NR_2 \rightleftharpoons MH(NR_2) \quad (1)$$

A homogeneous catalyst must have free coordination sites that allow it to bind the substrates *cis* disposed to the reactive points of the metallic center. However, the complexes $[OsHCl_2(=N=CR_2)(P\textit{i}Pr_3)_2]$ are saturated. So, from the hydroamination point of view, the creation of a coordination vacancy stabilizing the resulting metallic fragment, without producing the intramolecular reductive elimination to Os-imine species, is by itself an objective. This fact prompted us to investigate the reactivity of $[OsHCl_2(=N=$

[a] Departamento de Química Inorgánica-Instituto de Ciencia de Materiales de Aragón, Universidad de Zaragoza-CSIC, 50009 Zaragoza, Spain
[b] Laboratoire de Chimie Physisque, Bâtiment 490, Université de Paris Sud, 91405 Orsay Cedex, France
[c] Departament de Química, Universitat Autònoma de Barcelona, 08193 Bellaterra, Barcelona, Spain

 © WILEY-VCH Verlag GmbH, 69451 Weinheim, 2001 1434−1948/01/1111−2871 $ 17.50+.50/0

$CR_2)(PiPr_3)_2]$ towards $Ag(CF_3SO_3)$ in the presence of water (a usual impurity in amines), trimethylphosphite and carbon monoxide (which are π-acceptor ligands as the olefins and alkynes) and to study the relative stability of the possible isomers resulting from the reactions.

In this paper, we report: *i*) the complexes $[OsHCl(=N=CR_2)L(PiPr_3)_2]^+$ [L = H_2O, $P(OMe)_3$, CO] and their stereochemistries, and *ii*) the factors determining the formation of these stereochemistries.

Results and Discussion

Reactions in the Presence of Water

The treatment of dichloromethane solutions of $[OsHCl_2(=N=CMe_2)(PiPr_3)_2]$ (**1**) with 1.0 equiv. of $Ag(CF_3SO_3)$ in the presence of 2.0 equiv. of water leads to blue solutions and AgCl. The solutions afford a blue solid after the solvent is removed. According to the elemental analysis and MS, the solid corresponds to the complex $[OsHCl(=N=CMe_2)(H_2O)(PiPr_3)_2][CF_3SO_3]$ (**2**). The IR, ^1H, $^{13}C\{^1H\}$, and $^{31}P\{^1H\}$ NMR spectra indicate that complex **2** exists as a 1:1 equilibrium mixture of two isomers in the solid state and in solution.

The IR spectrum in KBr shows the ν(Os−H) band of both isomers, at 2164 and 2156 cm^{-1}, along with the characteristic stretching bands of the free $CF_3SO_3^-$ anion (see Exp. Sect.),[9] in agreement with the salt character of the complex. At −90 °C in [D_2]dichloromethane, the $^{31}P\{^1H\}$ NMR spectrum contains two singlets at δ = −10.3 and −3.7, corresponding to each isomer. Raising the sample temperature leads to a slight broadening of both resonances, although they show no signs of coalescence at temperatures below 35 °C. The ^1H NMR spectrum at −90 °C agrees well with the $^{31}P\{^1H\}$ NMR spectrum. In the high-field region, it contains two hydride resonances at δ = −3.85 and 0.56, which appear as triplets with H−P coupling constants of 14.1 and 13.2 Hz, respectively. In the low-field region, the spectrum contains two singlets due to the water protons at about δ = 4.9 and four singlets corresponding to the methyl protons of the azavinylidene ligand between δ = 4.6 and 3.4, in addition to the phosphane resonances. The behavior of the resonances due to the hydride and water ligands at this temperature is the same as that of the resonances observed in the $^{31}P\{^1H\}$ NMR spectrum. However, the behavior of the resonances corresponding to the methyl groups of the azavinylidene ligand is significantly different. At −70 °C, the coalescence of two of them is observed, whereas the coalescence of the other two occurs at −30 °C.

The above-mentioned spectra indicate that both isomers have an octahedral structure, with the phosphanes occupying *trans* positions and the C=N group and the carbon atoms bonded to this group lying in a plane that is perpendicular to the P−Os−P axis. In solution, the coordination polyhedron is rigid, although the azavinylidene ligand rotates around the Os−N−C axis.

Three stereochemistries are consistent with the spectroscopic data obtained for **2** (Scheme 1): hydride *trans* to chlorine (**a**), hydride *trans* to azavinylidene (**b**), and hydride *trans* to water (**c**). In order to obtain information about the stereochemistries of the isomers of **2**, we carried out its slow crystallization in dichloromethane/diethyl ether. Unfortunately, the crystals obtained from numerous attempts were in all cases not suitable for an X-ray crystallographic study. The $CF_3SO_3^-$ counterion was therefore exchanged for BF_4^-, and in a crop we obtained a suitable crystal. The remaining crystals of the crop showed the same NMR spectra as **2**.

A view of the molecular geometry of the obtained isomer is shown in Figure 1. Selected bond lengths and angles are listed in Table 1. Although the hydride ligand could not be properly refined, the X-ray study clearly indicates that the isomer formed has the stereochemistry **c**. Thus, the coordination geometry around the osmium atom can be rationalized as being derived from a distorted octahedron, with the triisopropylphosphane ligands occupying *trans* positions [P(1)−Os−P(2) = 168.59(4)°] at opposite sites of an ideal coordination plane defined by the hydride ligand *trans* disposed to the water molecule and the chlorine *trans* disposed to the azavinylidene group [Cl−Os−N = 178.59(12)°].

The most conspicuous feature of the structure is the very short Os−N bond length of 1.829(4) Å, which is fully consistent with an Os−N double bond formulation and agrees well with the Os−N(azavinylidene) bond lengths previously reported [between 1.789(2)[6] and 1.882(6)[2d] Å]. The C−N distance [1.285(6) Å] is similar to those found in other azavinylidene transition metal complexes (about 1.30 Å)[1,2] and also agrees with the N−C bond lengths found in organic azaallenium cations (between 1.23 and 1.33 Å)[10] and in the 2-azaallenyl complexes $[Cr\{C(OEt)=N=CtBu_2\}(CO)_5]$ [1.272(5) and 1.264(5) Å],[11] $[Cr\{C(Ph)=N=CHPh\}(CO)_5]$ [1.260(4) and 1.265(4) Å],[12] and $[Ru(\eta^5\text{-}C_5H_5)\{C(CH=$

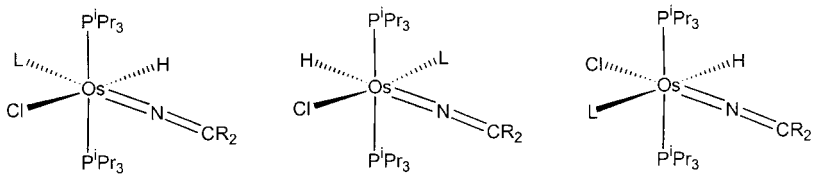

Scheme 1

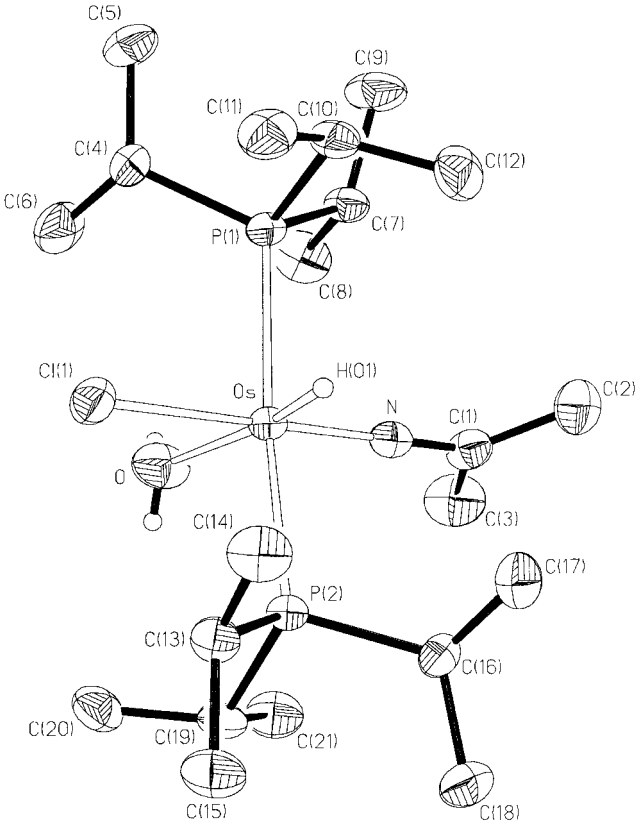

Figure 1. Molecular diagram for $[OsHCl(=N=CMe_2)(H_2O)(P\textit{i}Pr_3)_2]^+$ (**2c**); thermal ellipsoids are shown at 50% probability

Table 1. Selected bond lengths (Å) and angles (deg) for the complex $[OsHCl\{=N=C(CH_3)_2\}(H_2O)(P\textit{i}Pr_3)_2][BF_4]\cdot CH_2Cl_2$ (**2c**)

Os−Cl	2.3972(14)	Os−N	1.829(4)
Os−P(1)	2.4608(14)	N−C(1)	1.285(6)
Os−P(2)	2.4378(14)	C(1)−C(3)	1.518(8)
Os−O	2.306(4)		
Cl−Os−P(1)	88.89(4)	P(2)−Os−O	97.32(11)
Cl−Os−P(2)	90.18(4)	P(2)−Os−N	90.44(12)
Cl−Os−O	83.51(13)	O−Os−N	95.15(17)
Cl−Os−N	178.59(12)	Os−N−C(1)	176.5(4)
P(1)−Os−P(2)	168.59(4)	N−C(1)−C(2)	120.7(5)
P(1)−Os−O	93.88(11)	N−C(1)−C(3)	120.2(5)
P(1)−Os−N	90.74(12)	C(2)−C(1)−C(3)	119.0(5)

$CPh_2)=N=CPh_2\}(CO)(P\textit{i}Pr_3)]^+$ [1.283(9) and 1.252(9) Å].[13]

The Os−N−C chain is almost linear [Os−N−C(1) = 176.5(4)°] and, in agreement with the ^1H and $^{13}C\{^1H\}$ NMR spectra at low temperatures, forms a plane with C(2) and C(3) perpendicular to the best plane containing the phosphorus atoms of the phosphane ligands and the osmium atom [angle: 89.0(2)°]. A similar disposition of the azavinylidene ligand has also been found in the complex $[OsHCl_2\{=N=C^a(CH_2)_4C^bH_2)(P\textit{i}Pr_3)_2(C^a\text{-}C^b)]$ (**3**), where the azavinylidene group is also *trans* disposed to a chlorine ligand.[6]

Since experimental methods have been shown to be ineffective in solving the problem of the determination of the stereochemistry in the other isomer of **2**, we have carried out DFT geometry optimizations on the **a**, **b** and **c** isomers of the model complex $[OsHCl(=N=CH_2)(H_2O)(PH_3)_2]^+$ (**2t**). Single point CCSD(T) calculations on the B3LYP optimized geometries have also been carried out in order to refine further the obtained energetic differences between the three isomers. The results (Table 2) indicate that the stereochemistries **a** (hydride *trans* to chlorine) and **c** (hydride *trans* to water) are clearly more stable (about 20 kcal·mol^{-1}) than stereochemistry **b** (hydride *trans* to azavinylidene) and, in agreement with the spectroscopically observed 1:1 ratio between the isomers, that the difference in stability between **a** and **c** is negligible. Thus, our discussion will be focused on these two isomers. Their main geometrical parameters are listed in Table 3, and their structures are depicted in Figure 2.

Table 2. B3LYP relative energies of the **a**, **b** and **c** isomers of the $[OsHCl(=N=CH_2)L(PH_3)]^+$ (L = H_2O, $P(OH)_3$, CO) model complexes; CCSD(T)//B3LYP single point energies are given in parentheses, where available

	L = H_2O	L = $P(OH)_3$	L = CO
Isomer **a**	0.0(0.0)	0.0	0.(0.0)
Isomer **b**	19.6(21.0)	11.4	3.2(2.2)
Isomer **c**	1.1(0.4)	5.5	7.7(5.4)

A good agreement is found when the optimized structure for isomer **c** of $[OsHCl(=N=CH_2)(H_2O)(PH_3)_2]^+$ and the available X-ray structure of **2c** are compared. The coordination geometry around the Os atom is essentially well reproduced, although the Os−P distances are somewhat shorter (between 0.04 and 0.05 Å) when real phosphanes are substituted by model PH_3 phosphanes. Another minor discrepancy arises from the modeling of the azavinylidene ligand: the substitution of $N=CMe_2$ by $N=CH_2$ decreases the N−Os−O angle in complex **2t**. Our theoretical calculations do, however, allow the determination of the hydride position. The short Os−H distance, similar to that found in the pentacoordinate $[OsHCl(=N=CH_2)(PH_3)_2]^+$ complex (1.601 Å in the former vs. 1.590 Å in the latter) is noteworthy. This reflects the large *trans* influence exerted by the hydride ligand, which is also mirrored by the long Os−O distance (2.341 Å).

Structure **a** shows a distorted octahedral geometry, with almost strictly *trans* arranged phosphanes (P−Os−P = 178.1°) and the angles in the perpendicular plane ranging from 73.8° to 115.0°. The different arrangement of ligands induces some changes in the osmium−ligand distances with regard to structure **c**. Thus, with the chlorine and the strong σ-donor hydride *trans* disposed, the Os−Cl and Os−H distances are significantly longer than in isomer **c** (2.431 Å and 1.622 Å respectively). On the other hand, the Os−N and Os−O distances are shorter (1.792 Å and 2.264 Å), the former being among the smallest Os−N distances found in the literature for Os-azavinylidene complexes. The linearity

Table 3. Most relevant distances (Å) and angles (deg) for the model complexes $[OsHCl(=N=CH_2)L(PH_3)]^+$ [L = H_2O (**a**, **c**), $P(OH)_3$ (**a**), CO (**a**)]

	$[OsHCl(=N=CH_2)(H_2O)(PH_3)_2]^+$ **a**	**c**	$[OsHCl(=N=CH_2)\{P(OH)_3\}(PH_3)_2]^+$ **a**	$[OsHCl(=N=CH_2)(CO)(PH_3)_2]^+$ **a**
Os−P	2.404	2.399	2.402	2.415
Os−P	2.404	2.403	2.396	2.415
Os−N	1.792	1.809	1.839	1.846
Os−Cl	2.431	2.405	2.458	2.430
Os−L	2.264	2.341	2.396	2.009
Os−H	1.622	1.601	1.621	1.630
N−C	1.263	1.263	1.261	1.259
P−Os−P	178.08	171.46	178.86	176.07
H−Os−N	94.76	91.67	90.64	90.94
H−Os−Cl	150.28	84.53	151.51	151.84
H−Os−L	73.79	165.16	70.02	71.77
N−Os−Cl	114.95	176.12	117.85	117.22
N−Os−L	167.88	102.98	160.64	162.71
Cl−Os−L	76.61	80.79	81.49	80.07
Os−N−C	179.55	175.39	169.07	169.86

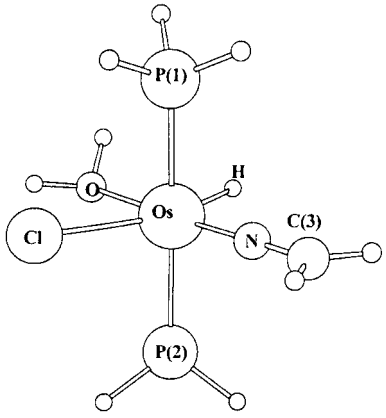

a

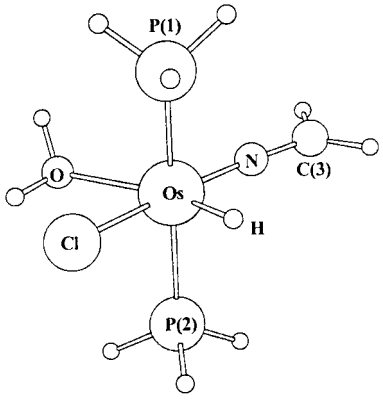

c

Figure 2. B3LYP optimized structures of the most stable isomers (**a** and **c**) of the $[OsHCl(=N=CH_2)(H_2O)(PH_3)_2]^+$ complex

of the Os-azavinylidene moiety (Os−N−C = 179.5°) should also be noted. In addition, it should be mentioned that in the calculated structures, the azavinylidene ligand is perpendicular to the P−Os−P axis, in agreement with the ^1H and $^{13}C\{^1H\}$ NMR spectra of **2** and the X-ray structure shown in Figure 1.

The spectroscopic data of **2** together with the results of the theoretical calculations strongly support that the reaction of **1** with $Ag(CF_3SO_3)$ and water leads to an equimolar mixture of the isomers shown in Equation (2). Similarly, the treatment of **3** with $Ag(CF_3SO_3)$ and water gives $[OsHCl\{=C=C^a(CH_2)_4C^bH_2\}(H_2O)(P\textit{i}Pr_3)_2(\textit{C}^a\text{-}\textit{C}^b)][CF_3SO_3]$ (**4**), which according to the IR, ^1H, $^{13}C\{^1H\}$ and $^{31}P\{^1H\}$ NMR spectra is a 1:1 mixture of the isomers **4a** and **4c**.

The IR spectrum of **4** in KBr contains two ν(Os−H) bands at 2145 and 2135 cm^{-1}. In the ^1H NMR spectrum, the hydride resonances appear at δ = −4.40 and 0.43 as triplets, with H−P coupling constants of 13.8 and 13.2 Hz, respectively. The $^{31}P\{^1H\}$ NMR spectrum shows two singlets at δ = −10.9 and 4.8.

Reactions in the Presence of Trimethylphosphite

The treatment of dichloromethane solutions of **1** at −40 °C with 1.0 equiv. of $Ag(CF_3SO_3)$ and 1.1 equiv. of trimethylphosphite leads, after 2 h at this temperature, to brown solutions and AgCl. The solutions afford a brown-orange solid after the solvent is removed. According to the elemental analysis and MS, the solid corresponds to the complex $[OsHCl(=N=CMe_2)\{P(OMe_3)\}(P\textit{i}Pr_3)_2][CF_3SO_3]$ (**5**).

In contrast to **2** and **4**, the IR spectrum of **5** in KBr shows only one ν(Os−H) band, at 2155 cm^{-1}, suggesting that in the solid state this complex exists as only one isomer. The ^1H, $^{13}C\{^1H\}$, and $^{31}P\{^1H\}$ NMR spectra in $[D_2]$dichloromethane at −40 °C also indicate that there is also only one isomer in solution. Thus, the $^{31}P\{^1H\}$ NMR spectrum contains a triplet at δ = 57.5 [$P(OMe_3)$] and a doublet at δ = 47.6 ($P\textit{i}Pr_3$). The multiplicity of the signals and the value of the P−P coupling constant (19.4 Hz) strongly support the *trans* disposition of the phosphanes, which lie *cis* to the phosphite. In the ^1H NMR spectrum the hydride ligand appears as a doublet of triplets at δ = −7.20, with

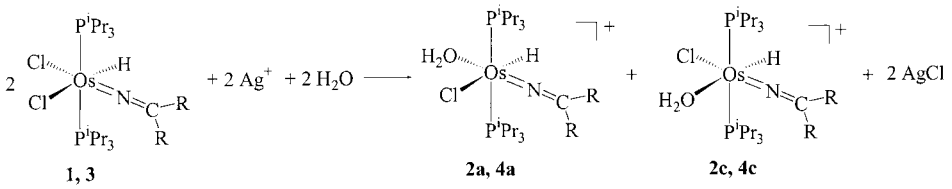

(2)

H−P coupling constants of 39.6 and 13.8 Hz, indicating that the hydride is *cis* to the phosphorus donor ligands. At temperatures higher than room temperature the decomposition of **5** to $[HP{i}Pr_3]^+$ and unidentified products is observed.

The above-mentioned spectroscopic data are consistent with the stereochemistries **a** and **b** shown in Scheme 1. In order to determine the most stable isomer of **5** DFT calculations on the model complex $[OsHCl(=N=CH_2)\{P(OH)_3\}(PH_3)_2]^+$ (**5t**) were also carried out. In this case, the results of the B3LYP calculations (Table 2) indicate that the stereochemistry **a** (hydride *trans* to chlorine) is again favored, while **b** and **c** lie higher in energy (11.4 kcal·mol^{-1} and 5.5 kcal·mol^{-1} respectively). This excludes the possibility of an equilibrium similar to that found in the previous case. So, the spectroscopic data of **5** together with the results of the theoretical calculations support that the reaction of **1** with $Ag(CF_3SO_3)$ in the presence of trimethylphosphite leads to **5a** [Equation (3)]. Similarly the treatment of **3** with $Ag(CF_3SO_3)$ and trimethylphosphite affords **6a**.

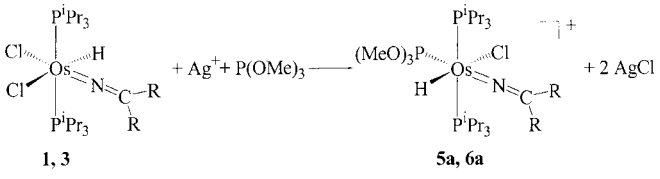

(3)

The spectroscopic data of **6a** agree well with those of **5a**. The IR spectrum in KBr shows the ν(OS−H) band at 2154 cm^{-1}. In the ^{1}H NMR spectrum in $[D_2]$dichloromethane at −40 °C, the resonance corresponding to the hydride ligand appears at δ = −7.07 as a doublet of triplets with H−P coupling constants of 40.0 and 13.2 Hz. The $^{31}P\{^1H\}$ NMR spectrum shows a triplet at δ = 59.2 and a doublet at δ = 49.1. The value of the P−P coupling constant is 12.3 Hz.

The geometrical parameters for isomer **a** of the $[OsHCl(=N=CH_2)\{P(OH)_3\}(PH_3)_2]^+$ model complex are listed in Table 3 and its structure is depicted in Figure 3. This complex can be described as a distorted octahedron with *trans* phosphanes (P−Os−P = 178.9°). In the perpendicular plane, the angles N−Os−P and Cl−Os−H are 160.6° and 151.5°, respectively. The Os−N (1.839 Å) and N−C (1.261 Å) distances and Os−C−N angle (169.7°) are consistent with the azavinylidene formulation. In agreement with the structures shown in Figure 1, the azavinylidene lies in the plane containing the osmium atom, the hydride, the chlorine and the phosphorous atom of the phosphite ligand.

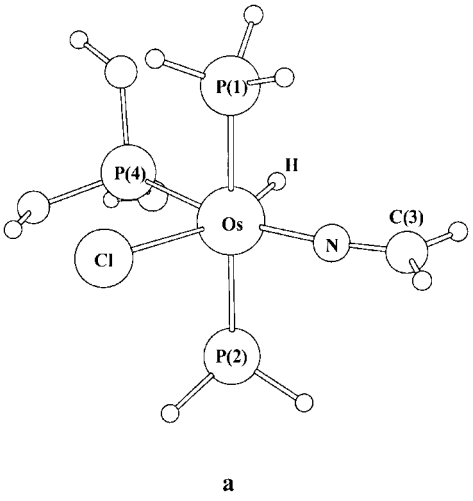

Figure 3. B3LYP optimized structure of the most stable isomer of the $[OsHCl(=N=CH_2)\{P(OH)_3\}(PH_3)_2]^+$ complex

Theoretical results also indicate that the stability of the stereochemistry of **c** (hydride *trans* to phosphite) is between those of the stereochemistries of **a** and **b**. The corresponding isomers **5c** and **6c** can be isolated from $[D_2]$dichloromethane solutions at −60 °C. Thus, the addition of 1.0 equiv. of trimethylphosphite to $[D_2]$dichloromethane solutions of the equilibrium mixtures of **2a** and **2c** or **4a** and **4c** at −60 °C gives rise to the immediate and selective formation of **5c** or **6c** [Equation (4)] (in quantitative yield, in both cases). Under these conditions the isomers **5c** and **6c** are moderately stable and slowly isomerize to **5a** or **6a**. At −20 °C, about 50% of conversion is observed after 10 min. Isomers with **b** stereochemistry are not observed during the isomerization process, in agreement with the higher energy of this stereochemistry.

The *trans* disposition of the hydride and phosphite ligands in **5c** and **6c** is strongly supported by the ^{1}H NMR

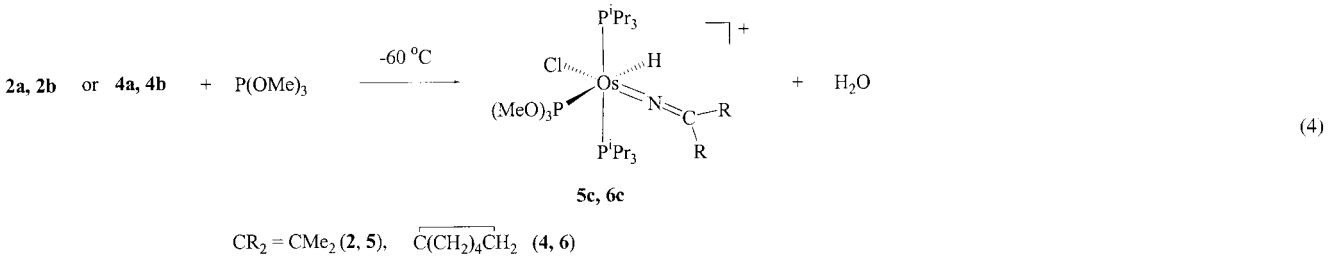

(4)

spectra of these compounds, which show a doublet of triplets at $\delta = 0.95$ (**5c**) and $\delta = 0.65$ (**6c**) with H−P coupling constants of 125.0 and 16.3 Hz (**5c**) and 122.7 and 17.7 Hz (**6c**).

Reactions Under a Carbon Monoxide Atmosphere

The reaction of **1** with $Ag(CF_3SO_3)$ under a carbon monoxide atmosphere affords only one isomer of the carbonyl derivative $[OsHCl\{=N=C(CH_3)_2\}(CO)(P\textit{i}Pr_3)_2][CF_3SO_3]$ (**7**), according to the IR, ^1H, $^{13}C\{^1H\}$, and $^{31}P\{^1H\}$ NMR spectra of the yellow solid obtained.

In the IR spectrum, the most noticeable features are the presence of a ν(Os−H) band at 1951 cm^{-1} and a ν(CO) vibration at 1981 cm^{-1}. In the high field region of the ^1H NMR spectrum, the hydride ligand appears as a triplet at $\delta = -5.74$, with an H−P coupling constant of 34.5 Hz. The $^{31}P\{^1H\}$ NMR spectrum shows a singlet at $\delta = 63.0$.

The chemical shift of the hydride ligand of **7** is similar to that of both **5a** and **6a**. At first glance, this suggests that the stereochemistry of **7** is the same as that of **5a** and **6a** (hydride *trans* to chloride), since the chemical shift of a hydride ligand is highly dependent on the *trans* effect of the ligand located *trans* to the hydride. In order to corroborate this, DFT calculations were also carried out on the model complex $[OsHCl(=N=CH_2)(CO)(PH_3)_2]^+$ (**7t**). As expected, the results of the single point CCSD(T) calculations on the B3LYP optimized geometries (Table 2) indicate that the stereochemistry **a** is the most stable. The spectroscopic data of **7** together with the results of the theoretical calculations both suggest that the reaction of **1** with $Ag(CF_3SO_3)$ under carbon monoxide atmosphere leads to **7a** [Equation (5)]. Similarly, the treatment of **3** with $Ag(CF_3SO_3)$ under a carbon monoxide atmosphere gives **8a**. These isomers are also the species formed by the reaction of **2** or **4** with carbon monoxide at −60 °C in $[D_2]$dichloromethane as solvent.

The spectroscopic data of **8a** agree well with those of **7a**. The IR spectrum of **8b** in KBr shows the ν(Os−H) band at 1940 cm^{-1} and the ν(CO) vibration at 1977 cm^{-1}. In the ^1H NMR spectrum in $[D_2]$dichloromethane, the hydride ligand appears as a triplet at $\delta = -5.56$, with an H−P coupling constant of 34.5 Hz. The $^{31}P\{^1H\}$ NMR spectrum shows a singlet at $\delta = 63.2$.

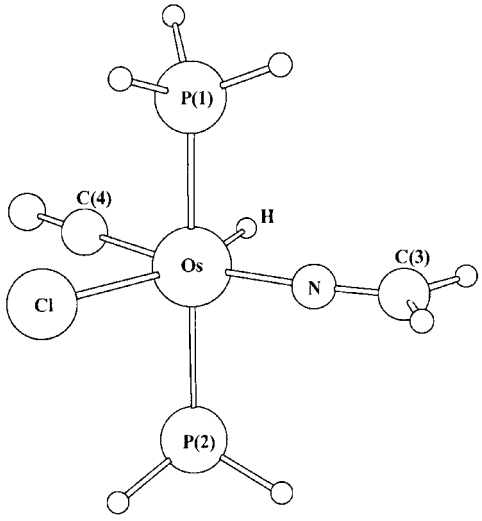

a

Figure 4. B3LYP optimized structure of the most stable isomer of the $[OsHCl(=N=CH_2)(CO)(PH_3)_2]^+$ complex

Figure 4 shows the optimized geometry at the B3LYP level for the **a** isomer of the $[OsHCl(=N=CH_2)(CO)(PH_3)_2]^+$ model complex; its main geometrical parameters are listed in Table 3. This isomer exhibits similar patterns to the $[OsHCl(=N=CH_2)(H_2O)(PH_3)_2]^+$ and

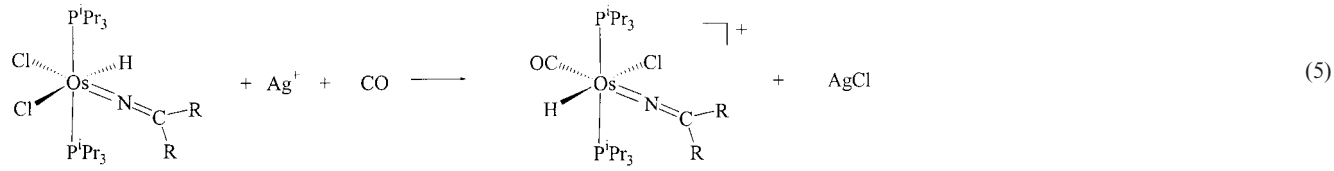

(5)

$[OsHCl(=N=CH_2)\{P(OH)_3\}(PH_3)_2]^+$ model complexes i.e. a distorted octahedral geometry where the P−Os−P angle is almost linear, although the angles between the ligands in the plane containing the H, Cl, N and C atoms clearly deviate from ideality (H−Os−Cl = 151.5°, N−Os−Cl = 162.7°). As in the $[OsHCl(=N=CH_2)\{P(OH)_3\}(PH_3)_2]^+$ complex, the Os−azavinylidene axis is slightly tilted (Os−N−C = 169.9°). The Os−N distance is the longest of our family of complexes (1.846 Å). As in the previous cases the azavinylidene ligand lies in the plane perpendicular to the P−Os−P axis.

Stereochemical Preferences of $[OsHCl(=N=CH_2)L(PH_3)_2]^+$ [L = H_2O, $P(OH)_3$ and CO] Complexes

In octahedral hexacoordinate complexes containing ligands with different electronic properties, as in $[OsHCl(=N=CH_2)L(PH_3)_2]^+$ [L = H_2O, $P(OH)_3$ and CO] model complexes, the presence of a strong σ-donor hydride will have a pronounced influence on the rest of the ligands, and the ability of a given ligand to remain *trans* to the hydride will govern the stereochemistry of the complex. To illustrate this general idea, a DFT theoretical study on $[OsHCl(=N=CH_2)(PH_3)_2]^+$ and $[OsHCl(=N=CH_2)L(PH_3)_2]^+$ [L = H_2O, $P(OH)_3$ and CO] complexes is offered in this section.

Pentacoordinate Complexes

To begin our study the parent pentacoordinate $[OsHCl(=N=CH_2)(PH_3)_2]^+$ model complex, from which the hexacoordinate $[OsHCl(=N=CH_2)L(PH_3)_2]^+$ complexes are obtained, is analyzed in some detail. The structures of the related hexacoordinate complexes (i.e. phosphanes must be equivalent by symmetry), with available NMR spectroscopic data, have been fully optimized at the DFT level of theory using the B3LYP functional. Regular square-planar pyramids and trigonal bipyramids have been taken as starting points and no symmetry constraints have been imposed in order to allow free rotation of the azavinylidene ligand. The seven initial structures that were obtained are depicted in Scheme 2.

After geometry optimization, no trigonal bipyramid is found to be stable, and they all revert to a square-planar pyramid structure. Within the square-planar pyramid's family, only two isomers are obtained (**B** and **C** according to our labelling), although **B** lies much higher in energy than **C** (by 33.8 kcal·mol^{-1}). Thus, it is obvious that despite the apparent possibility of isomerism, there is only one available structure for the pentacoordinate complex. This result agrees perfectly with the ligand site preferences in a square-planar pyramid, where the stronger σ-donor ligand tends to occupy the apical position.[14] The geometrical parameters of complex **C** are listed in Table 4, and its structure is depicted in Figure 5.

Table 4. Selected bond lengths (Å) and angles (deg) for the most stable isomer of the B3LYP optimized $[OsHCl(=N=CH_2)(PH_3)]^+$ model complex

Os−P(1)	2.411	Os−P(2)	2.411
Os−N	1.809	Os−H(1)	1.590
Os−Cl	2.328	N−C	1.263
C−H(2)	1.091	C−H(3)	1.090
H(1)−Os−P(1)	88.9	H(1)−Os−P(2)	88.9
H(1)−Os−N	94.4	H(1)−Os−Cl	109.1
P(1)−Os−P(2)	174.0	N−Os−Cl	156.5
P(1)−Os−N	92.8	N−Os−P(2)	92.8
P(2)−Os−Cl	87.8	Cl−Os−P(1)	87.8
Os−N−C	171.2	N−C−H(2)	119.8
N−C−H(3)	121.6		

Square Planar Pyramids

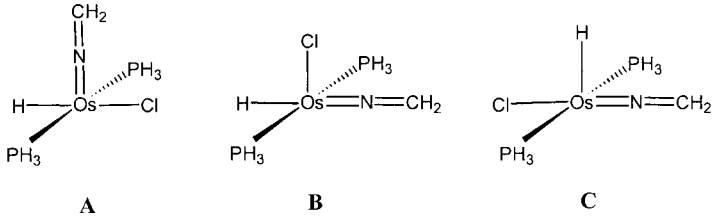

Trigonal Bipyramids

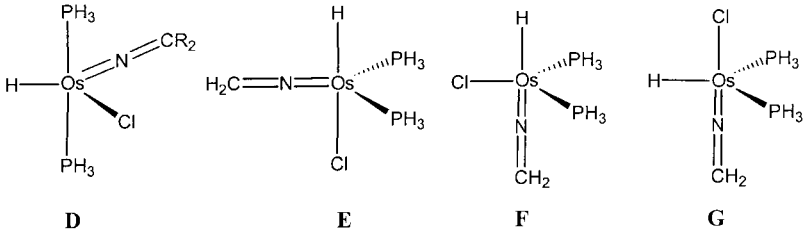

Scheme 2

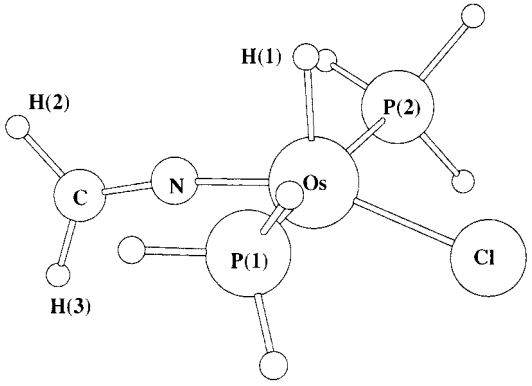

Figure 5. B3LYP optimized structure of the most stable isomer of the $[OsHCl(=N=CH_2)(PH_3)]^+$ complex

Complex **C** can be described as a slightly distorted square-planar pyramid with the strongest σ-donor hydride occupying the apical position *trans* to the vacant site. The phosphanes are located almost strictly *trans* to each other (P−Os−P = 174.0°), and the other ligands of the basal plane (azavinylidene and chloride) form an angle of 156.5°, thus making the whole structure somewhat distorted. It is noteworthy that the $Os=N=CH_2$ plane is perpendicular to the P−Os−P axis. As a matter of fact, the structure with the azavinylidene plane parallel to the P−Os−P axis, which would correspond to the transition state for the azavinylidene ligand rotation process, was found to be 9.2 kcal·mol^{-1} higher in energy than the minimum at the B3LYP// CCSD(T) level of theory.

Hexacoordinate Complexes

From the structural data and the calculated relative energies for the different isomers of $[OsHCl(=N=CH_2)L(PH_3)_2]^+$ complexes (Table 2), some initial trends may be drawn: (a) No matter what the electronic character of L (from a σ-donor H_2O ligand to a strong π-acceptor CO ligand), the structure with H *trans* to Cl turns out to be the most stable. (b) If the **b** and **c** structures are taken into account, opposite trends are found when the π-acceptor character of L is enhanced i.e. **b** is stabilized and **c** is destabilized. For the $[OsHCl(=N=CH_2)(H_2O)(PH_3)_2]^+$ complex the relative energies of **a** and **c** are similar (a difference of only 0.4 kcal·mol^{-1} is found at the CCSD(T)// B3LYP level of theory), but **c** is 5.4 kcal·mol^{-1} higher in energy than **a** in $[OsHCl(=N=CH_2)(CO)(PH_3)_2]^+$. At the same time, structure **b** is 21.0 kcal·mol^{-1} higher in energy than **a** in $[OsHCl(=N=CH_2)(H_2O)(PH_3)_2]^+$, although the difference between them is lowered to 2.2 kcal·mol^{-1} for the $[OsHCl(=N=CH_2)(CO)(PH_3)_2]^+$ complex. It should be noted at this point that even on purely thermodynamic grounds this difference might be somewhat large to allow an equilibrium between these two isomers. However, it should be possible in principle for **a** and **b** to exist simultaneously by using an even stronger π-acceptor ligand. (c) The addition of a sixth ligand to the most favorable pentacoordinate isomer (H *trans* to the empty coordination site) would lead to the **c** isomer. As a consequence, it is reasonable to suppose that this is the isomer that would be obtained under kinetic control conditions; structure **c** is indeed observed for L = $P(OMe)_3$ (**5c**, **6c**) and rapidly evolves into the isomer **a**.

To give a simple explanation of these facts, it has been assumed that, starting from the most stable pentacoordinate isomer, the corresponding hexacoordinate complexes can be obtained in two steps (of course, this has nothing to do with the actual mechanism; it is only a theoretical way of thinking). In a first step, the pentacoordinate complex is distorted towards the geometry that it would have in the hexacoordinate complex. The energy related to this distortion (ΔE_{dist}) is evaluated by simply removing the L ligand from the optimized hexacoordinate structure and calculating the B3LYP energy of the resulting fragment. In the second step, a crude interaction energy (ΔE_{int}) of the $[OsHCl(=N=CH_2)(PH_3)_2]^+$ fragment with the L ligand fragment is obtained as the difference between the sum of the energies of both fragments and the energy of the optimized hexacoordinate structure. The results of this decomposition are shown in Figures 6 and 7.

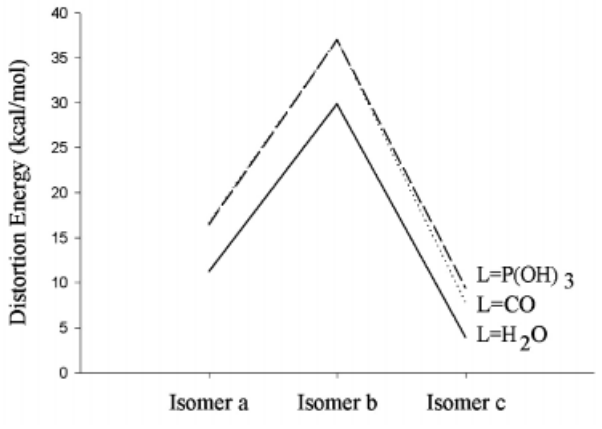

Figure 6. Distortion energies of the $[OsHCl(=N=CH_2)(PH_3)_2]^+$ fragments calculated at the B3LYP level of theory

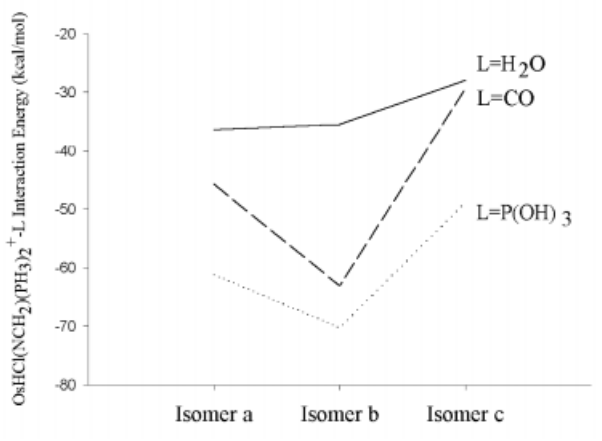

Figure 7. Interaction energies between $[OsHCl(=N=CH_2)(PH_3)_2]^+$ distorted fragments and L ligands (L = H_2O, $P(OH)_3$, CO) calculated at the B3LYP level of theory

The distortion term (Figure 6) is in fact related to the stability of the pentacoordinate fragment. This term is clearly smaller for isomer **c**, which is related to the best pentacoordinate structure previously described. The highest distortion energy arises from isomer **b**. In this fragment, the chloride ligand occupies the apical position *trans* to the vacant site, which is a very unfavorable arrangement for a square-planar pyramid. As a consequence, this would, in principle, be a factor that works against this hexacoordinate isomer. The distortion energy of isomer **a** lies in between the **b** and **c** isomers. Another interesting fact is that although the distortion energy is smaller for L = H_2O (as we shall see later, this is a consequence of the weaker interaction of water with the pentacoordinate fragment), the trends are almost identical in all cases [for L = $P(OH)_3$ and L = CO, the distortion term is not only parallel, but practically coincident]. Thus, the same consequences for the three isomers would be drawn if only this term is considered, and the energetic ordering of the hexacoordinate isomers would be **c** < **a** < **b**. It is obvious that the different behavior arises from the interaction term. Just looking at the shapes of the lines in Figure 7, it is clear that H_2O, $P(OH)_3$ and CO interact very differently with the distorted $[OsHCl(=N=CH_2)(PH_3)_2]^+$ fragment. Our theoretical results show that water interacts only weakly with the metallic fragment; the long Os−O distance in **2c** confirms this. The strongest interaction would correspond to the phosphite ligand, and carbonyl lies in between both of these. It is evident that in all cases isomer **c** is clearly disfavored, because this isomer is obtained by adding a σ-donor or a π-acceptor ligand *trans* to the strong σ-donor hydride. The strong *trans* influence exerted by this hydride would then destabilize the bond between Os and the L ligand, and this would lead to a small interaction energy. The next isomer in our ordering of interaction energies is isomer **a**. For this isomer, an equilibrium is reached between interaction and distortion, and the immediate consequence is that this is the most stable isomer as a whole. Lastly, isomer **b** exhibits a large interaction energy except for L = H_2O, but this energy is in general not enough to compensate the distortion term.

The relative interaction energies within each group (see the slope of the lines in Figure 7) follow a definite trend in enhancing the π-acceptor character of L: taking the most stable isomer **a** as the reference, the interaction energy due to isomer **b** increases, while that due to isomer **c** decreases. Again, this is a consequence of the electronic nature of the ligands, because in isomer **b** the L ligand is trans to a π-donor chloride, while in isomer **c** L is trans to a hydride. Thus, for L = H_2O, the interaction energy of isomer **c** is not very small and the distortion term can compensate nicely for the disadvantage of having an H_2O ligand *trans* to the hydride. This compensation leads to the observed equilibrium between **a** and **c**. For L = $P(OH)_3$, both hexacoordinate isomers **b** and **c** are far more unstable than isomer **a**, because in isomer **b** the interaction cannot compensate for the distortion and in isomer **c** the distortion cannot compensate for the interaction. Finally, for L = CO, the interaction term is so small for isomer **c** that the corresponding hexacoordinate structure is highly unstable, while the interaction term in **b**, although bigger than in the other cases, does not compensate for the distortion.

Concluding Remarks

Although the imido groups [$R_2C=N$] are strong bases, this study has revealed that the azavinylidene ligand of the complexes $[OsHCl_2(=N=CR_2)(P\mathit{i}Pr_3)_2]$ are stable towards hydrolysis when they are treated with $Ag(CF_3SO_3)$ in the presence of water. The reactions lead to the six-coordinate hydride-azavinylidene-osmium(IV) derivatives $[OsHCl(=N=CR_2)(H_2O)(P\mathit{i}Pr_3)_2]^+$, which are the first cationic species of this type.

Hydride-azavinylidene-osmium(IV) compounds are stable, not only towards hydrolysis of the azavinylidene, but also towards reductive elimination into imino species. It is well-known that the oxidative addition/reductive elimination equilibrium is governed by the amount of electron density at the metal. Electron-rich donor ligands favor the oxidized species, while π-acceptor ligands favor the reduced one. However, the extraction of a strong π-donor chlorine from $[OsHCl_2(=N=CR_2)(P\mathit{i}Pr_3)_2]$ and the coordination of π-acceptor ligands [i.e. CO, $P(OMe)_3$] does not induce a reductive elimination to afford the corresponding d^6-imine derivatives, but results in the formation of $[OsHCl(=N=CR_2)L(P\mathit{i}Pr_3)_2]^+$ [L = $P(OMe)_3$, CO].

Three stereochemistries are possible for complexes $[OsHCl(=N=CR_2)L(P\mathit{i}Pr_3)_2]^+$ [L = H_2O, $P(OMe)_3$, CO]: hydride *trans* to chlorine (**a**), hydride *trans* to azavinylidene (**b**) and hydride *trans* to L (**c**). Theoretical calculations indicate that structure **a** is the most favored in all cases from a thermodynamic point of view, whereas structure **c** is kinetically favored. The relative stability of structures **b** and **c** depends upon the electronic character of L. When the π-acceptor character of L increases, **b** is stabilized and **c** is destabilized; however, even with L=CO, the **b** isomer is never observed.

Experimental Section

All reactions were carried out with rigorous exclusion of air using Schlenk-tube techniques. Solvents were dried by the usual procedures and distilled under argon prior to use. The starting materials $[OsHCl_2(=N=CMe_2)(P\mathit{i}Pr_3)_2]$ (**1**) and $[OsHCl_2\{=N=C^a(CH_2)_4C^bH_2\}(P\mathit{i}Pr_3)_2(C^a\text{-}C^b)]$ (**3**) were prepared by the published method.[6] ^1H NMR spectra were recorded at 300 MHz and chemical shifts are expressed in ppm downfield from Me_4Si. $^{13}C\{^1H\}$ NMR spectra were recorded at 75.4 MHz and chemical shifts are expressed in ppm downfield from Me_4Si. $^{31}P\{^1H\}$NMR spectra were recorded at 121.4 MHz and chemical shifts are expressed in ppm downfield from 85% H_3PO_4. Coupling constants, *J* and *N*, are given in Hertz.

Preparation of $[OsHCl\{=N=C(CH_3)_2\}(H_2O)(P\mathit{i}Pr_3)_2][CF_3SO_3]$ (2a,c): A pale green solution of **1** (200 mg, 0.313 mmol) in 10 mL of acetone was treated with 81 mg (0.315 mmol) of $Ag(CF_3SO_3)$ and 12 μL (0.666 mmol) of water. The suspension was stirred for 3

hours and was filtered through Celite to remove the AgCl formed. After the solvent was removed, addition of diethyl ether yielded a blue precipitate that was washed (2 × 2 mL) with diethyl ether and dried in vacuo. The resulting blue microcrystalline solid was a mixture of two isomers with an **a**:**c** ratio of 1:1. Yield: 180 mg (74%). − $C_{22}H_{51}ClF_3NO_4OsP_2S$ (770.30): calcd. C 34.30, H 6.67, N 1.82, S 4.16; found C 34.51, H 6.52, N 1.73, S 3.99. − MS (FAB^+): *m*/*z* = 604 [$M^+ - H_2O$].

Isomer a) IR (KBr): ν(Os−H) 2164 cm^{-1} (m), ν(C=N) 1686 (m), $\nu_a(SO_3)$ 1296 (s), $\nu_s(CF_3)$ 1242 (s), $\nu_a(CF_3)$ 1174 (s), $\nu_s(SO_3)$ 1024 (s), $\delta_a(SO_3)$ 636 (s). − ^1H NMR (CD_2Cl_2, −90 °C): δ = 4.91 (br, 2 H, H_2O), 4.46 and 4.16 (both s, 6 H, $\{CH_3\}_2C=N$), 2.47 (m, 6 H, PCH), 1.30 (br. {at −40 °C dvt, J_{H-H} = 6.3, *N* = 12.6}, 36 H, PCHC*H*$_3$), −3.85 (t, J_{H-P} = 14.1, 1 H, OsH). − $^{13}C\{^1H\}$ NMR (CD_2Cl_2, −40 °C): δ = 151.0 (s, Os=N=C), 121.4 (q, J_{C-F} = 316.7, CF_3), 22.5 (vt, *N* = 24.4, PCH), 19.3 and 18.7 (both s, PCH*C*H_3), 5.1 and 2.5 (both s, $\{CH_3\}_2C=N$). − $^{31}P\{^1H\}$ NMR (CD_2Cl_2, −90 °C): δ = −10.3 (s).

Isomer c) IR (KBr): ν(Os−H) 2156 cm^{-1} (m), ν(C=N) 1671 (m), $\nu_a(SO_3)$ 1296 (s), $\nu_s(CF_3)$ 1242 (s), $\nu_a(CF_3)$ 1174 (s), $\nu_s(SO_3)$ 1024 (s), $\delta_a(SO_3)$ 636 (s). − ^1H NMR (CD_2Cl_2, −90 °C): δ = 4.85 (br, 2 H, H_2O), 3.56 and 3.45 (both s, 6 H, $\{CH_3\}_2C=N$), 2.27 (m, 6 H, PCH), 1.23 (br. {at −40 °C dvt, J_{H-H} = 6.6, *N* = 13.6}, 36 H, PCHC*H*$_3$), 0.56 (t, J_{H-P} = 13.2, 1 H, OsH). − $^{13}C\{^1H\}$ NMR (CD_2Cl_2, −40 °C): δ = 148.7 (s, Os=N=C), 121.4 (q, J_{C-F} = 316.7, CF_3), 22.7 (vt, *N* = 24.4, PCH), 18.6 and 18.3 (both s, PCH*C*H_3), −1.6 (both s, $\{CH_3\}_2C=N$). − $^{31}P\{^1H\}$ NMR (CD_2Cl_2, −90 °C): δ = −3.7 (s).

Preparation of [OsHCl{=N=C^a(CH$_2$)$_4$C^{b}H$_2$}(H$_2$O)(P*i*Pr$_3$)$_2$(*C*^{a}-*C*^{b})]-[CF$_3$SO$_3$] (4a,c): This complex was prepared as described for **2** starting from 200 mg (0.311 mmol) of **3**, 80 mg (0.311 mmol) of $Ag(CF_3SO_3)$, and 12 μL (0.666 mmol) of water. The resulting blue microcrystalline solid was a mixture of two isomers with an **a**:**c** ratio of 1:1. Yield: 180 mg (71%). − $C_{25}H_{55}ClF_3NO_4OsP_2S$ (810.37): calcd. C 37.05, H 6.84, N 1.73, S 3.96; found C 37.17, H 6.92, N 1.69, S 4.01. − MS (FAB^+): *m*/*z* = 644 [$M^+ - H_2O$].

Isomer a) IR (KBr): ν(Os−H) 2135 cm^{-1} (m), ν(C=N) 1686 (m), $\nu_a(SO_3)$ 1294 (s), $\nu_s(CF_3)$ 1247 (s), $\nu_a(CF_3)$ 1160 (s), $\nu_s(SO_3)$ 1031 (s), $\delta_a(SO_3)$ 637 (s). − ^1H NMR (CD_2Cl_2, −40 °C): δ = 4.60 (br, 2 H, H_2O), 4.13 (br, 4 H, $\{CH_2\}_2C=N$) 2.57 (m, 6 H, PCH), 2.6−2.4 (m, 6 H, Cy), 1.30 (m, 36 H, PCHC*H*$_3$), −4.40 (t, J_{H-P} = 13.8, 1 H, OsH). − $^{13}C\{^1H\}$ NMR (CD_2Cl_2, −40 °C): δ = 152.3 (s, Os=N=C), 121.4 (q, J_{C-F} = 316.7, CF_3), 28.6 and 23.6 (both s, Cy), 22.5 (vt, *N* = 24.4, PCH), 19.3 and 18.8 (both s, PCH*C*H_3), 16.2 and 13.5 (both s, $\{CH_2\}_2C=N$). − $^{31}P\{^1H\}$ NMR (CD_2Cl_2, −40 °C): δ = −10.9 (s).

Isomer c) IR (KBr): ν(Os−H) 2145 cm^{-1} (m), ν(C=N) 1671 (m), $\nu_a(SO_3)$ 1294 (s), $\nu_s(CF_3)$ 1247 (s), $\nu_a(CF_3)$ 1160 (s), $\nu_s(SO_3)$ 1031 (s), $\delta_a(SO_3)$ 637 (s). − ^1H NMR (CD_2Cl_2, −40 °C): δ = 4.48 (br, 2 H, H_2O), 3.74 (br, 4 H, $\{CH_2\}_2C=N$) 2.32 (m, 6 H, PCH), 1.23 (m, 36 H, PCHC*H*$_3$), 0.43 (t, J_{H-P} = 13.2, 1 H, OsH). − $^{13}C\{^1H\}$ NMR (CD_2Cl_2, −40 °C): δ = 149.2 (s, Os=N=C), 121.4 (q, J_{C-F} = 316.7, CF_3), 27.1 and 22.8 (both s, Cy), 22.5 (vt, *N* = 24.4, PCH), 18.9 and 18.4 (both s, PCH*C*H_3), 10.5 (br, $\{CH_2\}_2C=N$). − $^{31}P\{^1H\}$ NMR (CD_2Cl_2, −40 °C): δ = −4.8 (s).

Preparation of [OsHCl{=N=C(CH$_3$)$_2$}{P(OMe)$_3$}(P*i*Pr$_3$)$_2$]-[CF$_3$SO$_3$] (5a): A pale green solution of **1** (200 mg, 0.313 mmol), at 40 °C, in a mixture of dichloromethane (10 mL) and acetone (0.2 mL) was treated with 81 mg (0.315 mmol) of $Ag(CF_3SO_3)$ and 38 μL (0.322 mmol) of $P(OMe)_3$. The suspension was stirred for 2 h at this temperature and was then filtered through Celite to remove the AgCl formed. The resulting brown solution was evaporated to dryness at the same temperature. Addition of diethyl ether yielded a brown-orange solid that was washed (3 × 2 mL) with diethyl ether at −40 °C and dried in vacuo. Yield: 200 mg (73%). − $C_{25}H_{58}ClF_3NO_6OsP_3S$ (876.36): calcd. C 34.26, H 6.67, N 1.60, S 3.66; found C 34.05, H 6.55, N 1.70, S 3.55. − IR (KBr): ν(Os−H) 2155 cm^{-1} (m), ν(C=N) 1686 (m), $\nu_a(SO_3)$ 1276 (s), $\nu_s(CF_3)$ 1225 (s), $\nu_a(CF_3)$ 1158 (s), $\nu_s(SO_3)$ 1034 (s), $\delta_a(SO_3)$ 639 (s). − ^1H NMR (CD_2Cl_2, −40 °C): δ = 3.69 (d, J_{H-P} = 10.8, 9 H, $P\{OMe\}_3$), 2.69 (br, 6 H, $\{CH_3\}_2C=N$) 2.47 (m, 6 H, PCH), 1.32 and 1.30 (both dvt, J_{H-H} = 7.2, *N* = 15, 36 H, PCHC*H*$_3$), −7.20 (td, J_{H-P} = 39.6, J_{H-P} = 13.8, 1 H, OsH). − $^{13}C\{^1H\}$ NMR (CD_2Cl_2, −60 °C): δ = 161.5 (s, Os=N=C), 120.7 (q, J_{C-F} = 320.3, CF_3), 54.9 (d, J_{C-P} = 11.5, $P\{OMe\}_3$), 23.4 (vt, *N* = 25.3, PCH), 19.6 and 18.8 (both s, PCH*C*H_3), 17.4 (br, $\{CH_3\}_2C=N$). − $^{31}P\{^1H\}$ NMR (CD_2Cl_2, −40 °C): δ = 57.5 (t, J_{P-P} = 19.4, $P\{OMe\}_3$), 47.6 (d, J_{P-P} = 19.4, P*i*Pr$_3$). − MS (FAB^+): *m*/*z* = 728 [M^+], 604 [$M^+ - P(OMe)_3$].

Reaction of an Equilibrium Mixture of 2a and 2c with P(OMe)$_3$. Formation of 5c: A solution of an equilibrium mixture of **2a** and **2c** (30 mg, 0.040 mmol) in 0.5 mL of [D_2]dichloromethane in an NMR tube at −60 °C was treated with $P(OMe)_3$ (5 μL, 0.042 mmol). The NMR tube was sealed under argon and measurements were made immediately. − ^1H NMR (CD_2Cl_2, −60 °C): δ = 3.93 (d, J_{H-P} = 9.9, 9 H, $P\{OMe\}_3$), 3.65 (br, 6 H, $\{CH_3\}_2C=N$), 2.47 (m, 6 H, PCH), 1.28 and 1.22 (both dvt, J_{H-H} = 6.6, *N* = 13.5, 36 H, PCHC*H*$_3$), 0.95 (dt, J_{H-P} = 125.0, J_{H-P} = 16.3, 1 H, OsH). − $^{13}C\{^1H\}$ NMR (CD_2Cl_2, −60 °C): δ = 149.3 (s, Os=N=C), 120.7 (q, J_{C-F} = 320.3, CF_3), 56.5 (d, J_{C-P} = 12.0, $P\{OMe\}_3$), 23.4 (vt, *N* = 25.3, PCH), 19.4 and 18.8 (both s, PCH*C*H_3), 2.4 (br, $\{CH_3\}_2C=N$). − $^{31}P\{^1H\}$ NMR (CD_2Cl_2, −60 °C): δ = 56.2 (t, J_{P-P} = 17.8, $P\{OMe\}_3$), −8.0 (d, J_{P-P} = 17.8, P*i*Pr$_3$).

Preparation of [OsHCl{=N=C^a(CH$_2$)$_4$C^{b}H$_2$}{P(OMe)$_3$}(P*i*Pr$_3$)$_2$-(*C*^{a}-*C*^{b})][CF$_3$SO$_3$] (6a): This complex was prepared as described for **5a** starting from 200 mg (0.311 mmol) of **3**, 80 mg (0.311 mmol) of $Ag(CF_3SO_3)$, and 38 μL (0.321 mmol) of $P(OMe)_3$. Yield: 210 mg (74%). − $C_{28}H_{62}ClF_3NO_6OsP_3S$ (916.43): calcd. C 36.70, H 6.82, N 1.53, S 3.50; found C 36.55, H 6.67, N 1.65, S 3.42. − IR (KBr): ν(Os−H) 2154 cm^{-1} (m), ν(C=N) 1686 (m), $\nu_a(SO_3)$ 1276 (s), $\nu_s(CF_3)$ 1225 (s), $\nu_a(CF_3)$ 1158 (s), $\nu_s(SO_3)$ 1034 (s), $\delta_a(SO_3)$ 639 (s). − ^1H NMR (CD_2Cl_2, −40 °C): δ = 3.68 (d, J_{H-P} =10.5, 9 H, $P\{OMe\}_3$), 2.9 (br, 4 H, $\{CH_2\}_2C=N$), 2.6 (m, 6 H, PCH), 1.68 (m, 6 H, Cy), 1.4−1.2 (m, 36 H, PCHC*H*$_3$), −7.07 (td, J_{H-P} = 40.0, J_{H-P} = 13.2, 1 H, OsH). − $^{13}C\{^1H\}$ NMR (CD_2Cl_2, −60 °C): δ = 165.2 (s, Os=N=C), 120.3 (q, J_{C-F} = 320.3, CF_3), 54.9 (d, J_{C-P} = 11.5, $P\{OMe\}_3$), 28.2 and 27.0 (both s, Cy), 24.6 (m, PCH), 20.3 and 19.9 (both s, PCH*C*H_3), 17.3 (br, $\{CH_2\}_2C=N$). − $^{31}P\{^1H\}$ NMR (CD_2Cl_2, −40 °C): δ = 59.5 (t, J_{P-P} = 12.3, $P\{OMe\}_3$), 49.1 (d, J_{P-P} = 12.3, P*i*Pr$_3$). − MS (FAB^+): *m*/*z* = 768 [M^+], 644 [$M^+ - P(OMe)_3$].

Reaction of an Equilibrium Mixture of 4a and 4c with P(OMe)$_3$. Formation of 6c: This complex was prepared as described for **5c** starting from an equilibrium mixture of **4a** and **4c** (30 mg, 0.037) and $P(OMe)_3$ (5 μL, 0.042 mmol). − ^1H NMR (CD_2Cl_2, −60 °C): δ = 3.91 (d, J_{H-P} = 10.2, 9 H, $P\{OMe\}_3$), 3.87 (br, 4 H, $\{CH_2\}_2C=N$), 2.48 (m, 6 H, PCH), 1.7−1.3 (m, 6 H, CH_2 Cy), 1.29 and 1.20 (m, 36 H, PCHC*H*$_3$), 0.65 (dt, J_{H-P} = 122.7, J_{H-P} = 17.7, 1 H, OsH). − $^{13}C\{^1H\}$ NMR (CD_2Cl_2, −60 °C): δ = 149.4 (s, Os=N=C), 120.5 (q, J_{C-F} = 321.3, CF_3), 56.1 (d, J_{C-P} = 11.5, $P\{OMe\}_3$), 26.8 and 23.5 (both s, Cy), 23.0 (br, PCH), 19.5 and 18.6 (both s, PCH*C*H_3), 13.2 (br, $\{CH_2\}_2C=N$). − $^{31}P\{^1H\}$ NMR (CD_2Cl_2,

−60 °C): δ = 59.4 (t, J_{P-P} = 11.5, P{OMe}$_3$), −6.6 (d, J_{P-P} = 11.5, P*i*Pr$_3$).

Preparation of [OsHCl{=N=C(CH$_3$)$_2$}(CO)(P*i*Pr$_3$)$_2$][CF$_3$SO$_3$] (7a): A pale green solution of **1** (200 mg, 0.313 mmol) in a mixture of dichloromethane (10 mL) and acetone (0.2 mL) was treated with 81 mg (0.315 mmol) of Ag(CF$_3$SO$_3$) and was then stirred for 10 min. under a carbon monoxide atmosphere. The suspension was filtered through Celite to remove the AgCl formed and the resulting yellow solution was evaporated to dryness. Subsequent addition of diethyl ether yielded a yellow solid, which was washed with diethyl ether (3 × 2 mL) and dried in vacuo. Yield: 225 mg (86%). − $C_{23}H_{49}ClF_3NO_4OsP_2S$ (780.30): calcd. C 35.40, H 6.33, N 1.80, S 4.11; found C 35.33, H 6.12, N 1.77, S 3.80. − IR (KBr): ν(CO) 1981 cm^{-1} (s), ν(Os−H) 1950 (m), ν(C=N) 1687 (m), ν_a(SO$_3$) 1270 (s), ν_s(CF$_3$) 1236 (s), ν_a(CF$_3$) 1140 (s), ν_s(SO$_3$) 1032 (s), δ_a(SO$_3$) 637 (s). − ^{1}H NMR (CDCl$_3$, 20 °C): δ = 2.88 (m, 6 H, PCH), 2.60 (br, 6 H, {CH$_3$}$_2$C=N), 1.43 and 1.37 (both dvt, J_{H-H} = 6.9, *N* = 16.8, 36 H, PCHC*H*$_3$), −5.74 (t, J_{H-P} = 34.5, 1 H, OsH). − ^{13}C{^{1}H} NMR (CDCl$_3$, 20 °C): δ = 169.5 (t, J_{C-P} = 6.9, CO), 165.9 (t, J_{C-P} = 6.0, Os=N=C), 121.2 (q, J_{C-F} = 316.9, CF$_3$), 27.8 (vt, *N* = 29.3, PCH), 19.4 and 19.2 (both s, PCH*C*H$_3$), 18.7 (br, {*C*H$_3$}$_2$C=N). − ^{31}P{^{1}H} NMR (CDCl$_3$, 20 °C): δ = 63.0 (s, d off resonance). − MS (FAB$^+$): *m*/*z* = 632 [M$^+$].

Reaction of an Equilibrium Mixture of 2a and 2c with CO at −60 °C: CO was bubbled through a solution of an equilibrium mixture of **2a** and **2c** (30 mg, 0.040 mmol), in 0.5 mL of [D$_2$]dichloromethane in an NMR tube at −60 °C, for 5 minutes. The NMR tube was then sealed under argon and measurements were made immediately. A mixture of **2a**, **2c**, and **7a** was obtained.

Preparation of [OsHCl{=N=C^a(CH$_2$)$_4$C^{b}H$_2$}(CO)(P*i*Pr$_3$)$_2$(*C*^{a}-*C*^{b})][CF$_3$SO$_3$] (8a): This complex was prepared as described for **7a** starting from 200 mg (0.311 mmol) of **3** and 80 mg (0.311 mmol) of Ag(CF$_3$SO$_3$). Yield: 230 mg (85%). − $C_{26}H_{53}ClF_3NO_4OsP_2S$ (820.36): calcd. C 38.07, H 6.51, N 1.77, S 3.80; found C 37.75, H 6.82, N 1.51, S 3.83. − IR (KBr): ν(CO) 1977 cm^{-1} (s), ν(Os−H) 1940 (m), ν(C=N) 1687 (m), ν_a(SO$_3$) 1271 (s), ν_s(CF$_3$) 1222 (s), ν_a(CF$_3$) 1139 (s), ν_s(SO$_3$) 1031 (s), δ_a(SO$_3$) 637 (s). − ^{1}H NMR (CDCl$_3$, 20 °C): δ = 3.0−2.8 (m, 10 H, {CH$_2$}$_2$C=N and PCH), 1.9−1.7 (m, 6 H, Cy), 1.42 and 1.37 (both dvt, J_{H-H} = 7.2, *N* = 16.8, 36 H, PCHCH$_3$), −5.56 (t, J_{H-P} = 34.5, 1 H, OsH). − ^{13}C{^{1}H} NMR (CDCl$_3$, 20 °C): δ = 168.5 (t, J_{C-P} = 6.9, CO), 168.0 (t, J_{C-P} = 6.0, Os=N=C), 121.2 (q, J_{C-F} = 316.9, CF$_3$), 28.1 (br, {*C*H$_2$}$_2$C=N), 25.9 (vt, *N* = 29.5, PCH), 25.4 and 22.7 (both s, Cy), 17.2 and 17.0 (both s, PCH*C*H$_3$). − ^{31}P{^{1}H} NMR (CDCl$_3$, 20 °C): δ = 63.2 (s, d off resonance). − MS (FAB$^+$): *m*/*z* = 672 [M$^+$].

Reaction of an Equilibrium Mixture of 4a and 4c with CO at −60 °C: CO was bubbled through a solution of an equilibrium mixture of **4a** and **4c** (30 mg, 0.037 mmol) in 0.5 mL of [D$_2$]dichloromethane in an NMR tube at −60 °C for 5 minutes. Then, the NMR tube was sealed under argon and measurements were made immediately. A mixture of **4a**, **4c**, and **8a** was obtained.

X-ray Structure Analysis of Complex 2: Crystals suitable for X-ray diffraction analysis were mounted onto a glass fiber and transferred to a Bruker-Siemens P4 automatic diffractometer (173 K, Mo-K_α radiation, graphite monochromator, λ = 0.71073 Å). A summary of crystal data and refinement parameters is reported in Table 5. Accurate unit cell parameters were determined by least-squares fitting from the setting of high angle reflections. Data were collected by the ω/2θ scan method. Lorentz and polarization corrections were applied. Measuring three standards throughout the data collection monitored the decay. Corrections for decay and absorption (semiempirical psi-scan method) were applied.

Table 5. Crystal data and data collection and refinement for complex [OsHCl{=N=C(CH$_3$)$_2$}(H$_2$O)(P*i*Pr$_3$)$_2$][BF$_4$]·CH$_2$Cl$_2$ (**2c**)

	2c
Formula	$C_{21}H_{51}BClF_4NOOsP_2\cdot CH_2Cl_2$
Mol wt	792.95
Color and habit	Irregular block
Space group	Triclinic, $P\bar{1}$
a, *b*, *c* Å	9.323(4), 11.941(4), 16.249(6)
α, β, γ °	77.653(9), 82.73(1), 79.09(1)
V, Å^3	1728.2(11)
Z	2
D_{calc}, g cm^{-3}	1.524
Data Collection and Refinement	
Diffractometer	Bruker-Siemens P4
λ(Mo-K_α), Å	0.71073
Monochromator	Graphite oriented
μ, mm^{-1}	4.051
Scan type	ω/2θ
2θ range, deg	3 ≤ 2θ ≤ 50°
Temp, K	173.0(2)
No. of data collected	6385 (*h*: −10, 0; *k*: −13, 13; *l*: −19, 19)
No. of unique data	5977 (merging *R* factor 0.0526)
No. of params refined/restraints	337/2
R_1 [a] [$F^2 > 2\sigma(F^2)$]	0.0302
wR_2 [b] [all data]	0.0748
S[c] [all data]	1.052

[a] $R_1(F) = \Sigma||F_o| - |F_c||/\Sigma|F_o|$. − [b] $wR_2(F^2) = \{\Sigma[w(F_o^2 - F_c^2)^2]/\Sigma[w(F_o^2)^2]\}^{1/2}$. − [c] Goof = S = $\{\Sigma[w(F_o^2 - F_c^2)^2]/(n - p)\}^{1/2}$, where n is the number of reflections, and p is the number of refined parameters.

The structure was solved by Patterson methods and refined by full-matrix least-squares on F^2.[16] Non-hydrogen atoms were anisotropically refined and the hydrogen atoms were observed or included at idealized positions. The hydride ligand H(01) was observed in the difference Fourier maps as a peak of adequate intensity and expected geometry, but does not support an appropriate refinement, and was not included in the atom list. However, the water hydrogen atoms H(02) and H(03) were located and refined as isotropic atoms with the same distance to the O atom.

Computational Details: DFT[17] optimizations without any symmetry constraint were carried out with the Gaussian94 series of programs[18] using the B3LYP functional.[19] Furthermore, for [OsHCl(=N=CH$_2$)(PH$_3$)$_2$]$^+$, [OsHCl(=N=CH$_2$)(H$_2$O)(PH$_3$)$_2$]$^+$, [OsHCl(=N=CH$_2$){P(OH)$_3$}(PH$_3$)$_2$]$^+$ and [OsHCl(=N=CH$_2$)-(CO)(PH$_3$)$_2$]$^+$ complexes CCSD(T)[20] single-point calculations on the DFT-optimized structures were performed in order to obtain more reliable energies. A quasi-relativistic effective core potential operator was used to represent the 60 innermost electrons of the osmium atom.[21] The basis set for the osmium atom was that associated with the pseudopotential[21] with a standard valence double-ζ LANL2DZ contraction.[18] The 6-31G(d) basis set[22c] was used for all the atoms directly attached to the metal, except for the hydride atom, which was described using a 6-31G(p) basis set.[22a,22b] For the oxygen atom in the carbonyl ligand a 6-31G(d) basis was used.[22c] The rest of the atoms were described with a 6-31G basis set.[22a]

Crystallographic data (excluding structure factors) for the structure(s) reported in this paper have been deposited with the Cambridge Crystallographic Data Centre as supplementary publication no. CCDC-162318. Copies of the data can be obtained free of charge on application to CCDC, 12 Union Road, Cambridge CB2 1EZ. UK [Fax: (internat.) +44-1223/336-033; E-mail: deposit@ccdc.cam.ac.uk]

Acknowledgments

Financial support from the DGES of Spain (Projects PB98-1591 and PB98-0916-C02-01) is acknowledged. R. C. thanks the "Ministerio de Ciencia y Tecnología" for a grant.

[1] [1a] K. Farmery, M. Kilner, C. Midcalf, *J. Chem. Soc. A* **1970**, 2279−2285. − [1b] M. Kilner, C. Midcalf, *J. Chem. Soc. A* **1971**, 292−297. − [1c] J. Chatt, R. J. Dosser, F. King, G. J. Leigh, *J. Chem. Soc., Dalton Trans.* **1976**, 24352−444. − [1d] G. Erker, W. Frömberg, J. L. Atwood, W. E. Hunter, *Angew. Chem. Int. Ed. Engl.* **1984**, *23*, 68−69. − [1e] R. E. Cramer, K. Panchanatheswaran, J. W. Gilje, *J. Am. Chem. Soc.* **1984**, *106*, 1853−1854. − [1f] W. Frömberg, G. Erker, *J. Organomet. Chem.* **1985**, *280*, 343−354. − [1g] M. Green, R. J. Mercer, C. E. Morton, A. G. Orpen, *Angew. Chem. ; Int. Ed. Engl.* **1985**, *24*, 422−424. − [1h] J. E. Bercaw, D. L. Davies, P. T. Wolczanski, *Organometallics* **1986**, *5*, 443−450. − [1i] M. Bochmann, L. M. Wilson, *J. Chem. Soc., Chem. Commun.* **1986**, 1610−1611. − [1j] I. A. Latham, G. J. Leigh, G. Huttner, I. Jibril, *J. Chem. Soc., Dalton Trans.* **1986**, 377−383. − [1k] R. F. Jordan, C. S. Bajgur, W. E. Dasher, A. L. Rheingold, *Organometallics* **1987**, *6*, 1041−1051. − [1l] H. Werner, W. Knaup, M. Dziallas, *Angew. Chem. Int. Ed. Engl.* **1987**, *26*, 248−250. − [1m] A. Dormond, A. Aaliti, A. Elbouadili, C. Moise, *J. Organomet. Chem.* **1987**, *329*, 187−199. − [1n] A. R. Barron, J. E. Salt, G. Wilkinson, M. Motevalli, M. B. Hursthouse, *J. Chem. Soc., Dalton Trans.* **1987**, 2947−2954. − [1o] G. Erker, W. Frömberg, C. Krüger, E. Raabe, *J. Am. Chem. Soc.* **1988**, *110*, 2400−2405. − [1p] M. Bochmann, L. M. Wilson, M. B. Hursthouse, M. Motevalli, *Organometallics* **1988**, *7*, 1148−1154. − [1q] E. A. Maatta, Y. Du, *J. Am. Chem. Soc.* **1988**, *110*, 8249−8250. − [1r] H. M. Colquhoun, A. E. Crease, S. A. Taylor, D. J. Williams, *J. Chem. Soc, Dalton Trans.* **1988**, 2781−2786. − [1s] S. G. Feng, J. L. Templeton, *J. Am. Chem. Soc.* **1989**, *111*, 6477−6478. − [1t] H. G. Woo, T. D. Tilley, *J. Organomet. Chem.* **1990**, *393*, C6−C9. − [1u] S. L. Borkowsky, R. F. Jordan, G. D. Hinch, *Organometallics* **1991**, *10*, 1268−1274. − [1v] T. Daniel, H. Müller, H. Werner, *Inorg. Chem.* **1991**, *30*, 3118−3120. − [1x] Y. W. Alelyunas, R. F. Jordan, S. F. Echols, S. L. Borkowsky, P. K. Bradley, *Organometallics* **1991**, *10*, 1406−1416. − [1y] J. D. Debad, P. Legzdins, R. J. Batchelor, F. W. B. Einstein, *Organometallics* **1992**, *11*, 6−8. − [1z] S. G. Feng, J. L. Templeton, *Organometallics* **1992**, *11*, 1295−1303.

[2] [2a] S. G. Feng, P. S. White, J. L. Templeton, *Organometallics* **1993**, *12*, 1765−1774. − [2b] S. G. Feng, P. S. White, J. L. Templeton, *Organometallics* **1993**, *12*, 2131−2139. − [2c] H. Werner, T. Daniel, W. Knaup, O. Nürnberg, *J. Organomet. Chem.* **1993**, *462*, 309−318. − [2d] T. Daniel, W. Knaup, M. Dziallas, H. Werner, *Chem. Ber.* **1993**, *126*, 1981−1993. − [2e] S. G. Feng, P. S. White, J. L. Templeton, *J. Am. Chem. Soc.* **1994**, *116*, 8613−8620. − [2f] K. R. Powell, P. J. Pérez, L. Luan, S. G. Feng, P. S. White, M. Brookhart, J. L. Templeton, *Organometallics* **1994**, *13*, 1851−1864. − [2g] T. Daniel, H. Werner, *J. Chem. Soc., Dalton Trans.* **1994**, 221−227. − [2h] H. Werner, T. Daniel, T. Braun, O. Nürnberg, *J. Organomet. Chem.* **1994**, *480*, 145−153. − [2i] M. A. Esteruelas, F. J. Lahoz, M. Oliván, E. Oñate, L. A. Oro, *Organometallics* **1994**, *13*, 3315−3323. − [2j] S. G. Feng, P. S. White, J. L. Templeton, *Organometallics* **1995**, *14*, 5184−5192. − [2k] L. W. Francisco, P. S. White, J. L. Templeton, *Organometallics* **1996**, *15*, 5127−5136. − [2l] T. B. Gunnoe, P. S. White, J. L. Templeton, *J. Am. Chem. Soc.* **1996**, *118*, 6916−6923. [2m] H. Werner, T. Daniel, M. Müller, N. Mahr, *J. Organomet. Chem.* **1996**, *512*, 197−205. − [2n] J. A. Cabeza, I. del Rio, V. Riera, *J. Organomet. Chem.* **1997**, *548*, 255−261. − [2o] J. A. Cabeza, I. del Rio, R. J. Franco, F. Grepioni, V. Riera, *Organometallics* **1997**, *16*, 2763−2764. − [2p] J. A. Cabeza, I. del Rio, M. Moreno, V. Riera, F. Grepioni, *Organometallics* **1998**, *17*, 3027−3033. − [2q] J. A. Cabeza, I. del Rio, V. Riera, D. Ardura, *J. Organomet. Chem.* **1998**, *554*, 117−121. − [2r] C. Bois, J. A. Cabeza, R. J. Franco, V. Riera, E. Savorit, *J. Organomet. Chem.* **1998**, *564*, 201207. − [2s] P. Schollhammer, M. Pichon, K. W. Muir, F. Y. Petillon, R. Pichon, J. Talarmin, *Eur. J. Inorg. Chem.* **1999**, 221−223. − [2t] S. N. Brown, *Inorg. Chem.* **2000**, *39*, 378−381. − [2u] M. A. Jiménez-Tenorio, M. Jiménez-Tenorio, M. C. Puerta, P. Valerga, *Inorg. Chim. Acta* **2000**, *300*, 869−874. − [2v] R. Castarlenas, M. A. Esteruelas, E. Oñate, *Organometallics* **2000**, *19*, 5454−5463. − [2x] R. Castarlenas, M. A. Esteruelas, E. Gutiérrez-Puebla, E. Oñate, *Organometallics* **2001**, *20*, 1545−1554.

[3] [3a] R. C. Wade, *Catalysis of Organic Reactions* (Ed.: W. R. Moser); Marcel Dekker: New York, 1981. − [3b] L. F. Rhodes, L. M. Venanzi, *Inorg. Chem.* **1987**, *26*, 2692−2695. −

[4] C. Bohanna, M. A. Esteruelas, A. M. López, L. A. Oro, *J. Organomet. Chem.* **1996**, *526*, 73−83.

[5] T. Daniel, H. Werner, *Z. Naturforsch, B* **1992**, *47*, 1707−1710.

[6] R. Castarlenas, M. A. Esteruelas, E. Gutiérrez-Puebla, Y. Jean, A. Lledós, M. Martín, E. Oñate, J. Tomàs, *Organometallics* **2000**, *19*, 3100−3108.

[7] R. Castarlenas, M. A. Esteruelas, E. Gutiérrez-Puebla, Y. Jean, A. Lledós, M. Martín, J. Tomàs, *Organometallics* **1999**, *18*, 4296−4303.

[8] T. E. Müller, M. Beller, *Chem. Rev.* **1998**, *98*, 675−703.

[9] G. A. Lawrence, *Chem. Rev.* **1986**, *86*, 17−33.

[10] [10a] J. C. Jochims, R. Abu-El-Halawa, I. Jibril, G. Huttner, *Chem. Ber.* **1984**, *117*, 1900−1912. − [10b] M. Al-Talib, J. C. Jochims, *Chem. Ber.* **1984**, *117*, 3222−3230. − [10c] M. Al-Talib, I. Jibril, E.-U. Würthwein, J. C. Jochims, G. Huttner, *Chem. Ber.* **1984**, *117*, 3365−3373. − [10d] R. Kupfer, E.-U. Würthwein, M. Nagel, R. Allmann, *Chem. Ber.* **1985**, *118*, 643−652. − [10e] M. Al-Talib, I. Jibril, G. Huttner, J. C. Jochims, *Chem. Ber.* **1985**, *118*, 1876−1886. − [10f] M. Al-Talib, J. C. Jochims, L. Zsolnai, G. Huttner, *Chem. Ber.* **1985**, *118*, 1887−1902. − [10g] E.-U. Würthwein, R. Kupfer, R. Allmann, M. Nagel, *Chem. Ber.* **1985**, *118*, 3632−3642. − [10h] M. Krestel, R. Kupfer, R. Allmann, E.-U. Würthwein, *Chem. Ber.* **1987**, *120*, 1271−1279.

[11] F. Seitz, H. Fischer, J. Riede, *J. Organomet. Chem.* **1985**, *287*, 87−101.

[12] R. Aumann, S. Althaus, S. Krüger, P. Betz, *Chem. Ber.* **1989**, *122*, 357−364.

[13] M. A. Esteruelas, A. V. Gómez, F. J. Lahoz, A. M. López, E. Oñate, L. A. Oro, *Organometallics* **1996**, *15*, 3423−3435.

[14] A. R. Rossi, R. Hoffmann, *Inorg. Chem.* **1975**, *14*, 365−374.

[15] [15a] J. T. Poulton, M. P. Sigalas, K. Folting, W. E. Streib, O. Eisenstein, K. G. Caulton, *Inorg. Chem.* **1994**, *33*, 1476−1485. − [15b] K. G. Caulton, *New J. Chem.* **1994**, *18*, 25−41.

[16] G. M. Sheldrick, University of Göttingen, Göttingen, Germany, **1997**.

[17] R. G. Parr, W. Yang, *Density Functional Theory of Atoms and Molecules*; Oxford University Press: Oxford, U.K., **1989**.

[18] M. J. Frisch, G. W. Trucks, H. B. Schlegel, P. M. W. Gill, B. G. Johnson, M. A. Robb, J. R. Cheeseman, T. A. Keith, G. A. Petersson, J. A. Montgomery, K. Raghavachari, M. A. Al-Laham, V. G. Zakrzewski, J. V. Ortiz, J. B. Foresman, J. Cioslowski, B. B. Stefanov, A. Nanayakkara, M. Challacombe, C. Y.

Peng, P. Y. Ayala, W. Chen, M. W. Wong, J. L. Andres, E. S. Replogle, R. Gomperts, R. L. Martin, D. J. Fox, J. S. Binkley, D. J. Defrees, J. Baker, J. P. Stewart, M. Head-Gordon, C. Gonzalez, J. A. Pople, Gaussian 94; Gaussian Inc.: Pittsburgh PA, **1995**.

[19] [19a] C. Lee, W. Yang, R. G. Parr, *Phys. Rev. B* **1988**, *37*, 785−789. − [19b] A. D. Becke, *J. Chem. Phys.* **1993**, *98*, 5648−5652. − [19c] P. J. Stephens, F. J. Devlin, C. F. Chabalowski, M. J. Frisch, *J. Phys. Chem.* **1994**, *98*, 11623−11627.

[20] [20a] R. J. Bartlett, *J. Phys. Chem.* **1989**, *93*, 1697−1708. − [20b] R. J. Bartlett, J. D. Watts, S. A. Kucharski, J. Noga, *Chem. Phys. Lett.* **1990**, *165*, 513−522.

[21] P. J. Hay, W. R. Wadt, *J. Chem. Phys.* **1985**, *82*, 299−310.

[22] [22a] W. J. Hehre, R. Ditchfield, J. A. Pople, *J. Chem. Phys.* **1972**, *56*, 2257−2261. − [22b] P. C. Hariharan, J. A. Pople, *Theor. Chim. Acta* **1973**, *28*, 213−218. − [22c] M. M. Francl, W. J. Pietro, W. J. Hehre, J. S. Binkley, M. S. Gordon, D. J. DeFrees, J. A. Pople, *J. Chem. Phys.* **1982**, *77*, 3654−3665.

Received May 7, 2001
[I01162]

Bimetallic Titanocene or Zirconocene/Aluminium Complexes as Active Catalysts in Lactone Polymerization Reactions

Perdita Arndt,*[a] Anke Spannenberg,[a] Wolfgang Baumann,[a] Sigurd Becke,[b] and Uwe Rosenthal[a]

Keywords: Lactones / Sandwich complexes / Titanium / Zirconium / Aluminum / Ring-opening polymerization

The metallocene alkyne complexes [$Cp_2M(L)(\eta^2$-$Me_3SiC_2R)$] react with diisobutylaluminium hydride at room temp. by addition of $HAl(iBu)_2$ to yield the heterobimetallic complexes [{Cp_2M}(μ-η^1:η^2-$RCCSiMe_3$)(μ-H){$Al(iBu)_2$}] [{Cp_2M}: (η^5-$C_5H_5)_2Ti$, R = Ph **1**, R = $SiMe_3$ **2**; {Cp_2M}: (η^5-$C_5H_5)_2Zr$, R = $SiMe_3$ **3**; {Cp_2M}: (ebthi)Zr, R = $SiMe_3$ **4**] {ebthi: *rac*-[1,2-ethylene-1,1′-bis(η^5-tetrahydroindenyl)]}. Complexes **1**–**4** were characterized by NMR spectroscopy and **1**, **2** and **4** investigated by X-ray crystal structure analysis. Compounds **1**–**4** were tested as initiators in the ring-opening polymerization of lactones. The results are discussed in comparison to the corresponding monometallic titanocene and zirconocene alkyne complexes.

Introduction

Group 4 metallocene complexes react with organoaluminium compounds to give highly active Ziegler-type catalyst systems.[1] Nevertheless, these catalysts present some disadvantages, such as the necessity of very large amounts of MAO. An approach to overcome this problem resides in the development of new activation methods to extend these active systems to other catalytic reactions. The generation of single-component catalysts, or their direct precursors, is therefore of great current interest.[2]

The reaction of metallocene-alkyne and -alkene complexes with aluminium or boron organic compounds has been intensively investigated by Erker and Binger[3] and leads to bimetallic systems of the type [{Cp_2M^1}(μ-η^1:η^2-RCCR)(μ-X){$M^2R_2^2$}] (M^1 = Zr, Hf, X = Cl, H, M^2 = Al, Ga; M^1 = Ti, X = H, M^2 = B) containing a planar tetracoordinate carbon atom bridging between a group 4 transition metal and a main group element; [$Cp_2M(PMe_3)$(alkyne)] complexes give [{Cp_2M}(μ-η^1:η^2-RCCR)(μ-H){$Al(iBu)_2$}] with diisobutylaluminium hydride.[3f] These compounds are of current interest and have been studied extensively, although compounds with a desired activation for catalytic processes were not obtained.[4]

We report here the easy synthesis of bimetallic titanium or zirconium/aluminium compounds, starting from (η^2-alkyne) metallocene complexes (alkyne = Me_3SiC_2R, R = Ph, $SiMe_3$) and their polymerization capability in the ring-opening polymerization (ROP) of lactones in comparison to the corresponding monometallic (η^2-alkyne)compounds.[11,12]

Results and Discussion

In the reaction of [$Cp_2M(L)(\eta^2$-$RC_2SiMe_3)$] {[Cp_2M]: (η^5-$C_5H_5)_2Ti$, R = Ph, $SiMe_3$, without L; [Cp_2M]: (η^5-$C_5H_5)_2Zr$, R = $SiMe_3$, L = Py; [Cp_2M]: *rac*-(ebthi)Zr, R = $SiMe_3$, without L} with diisobutylaluminium hydride in toluene (2 h) at ambient temperature, corresponding to the investigations by Erker,[3f] the bimetallic complexes [{Cp_2M}(μ-η^1:η^2-$RCCSiMe_3$)(μ-H){$Al(iBu)_2$}] **1**–**4** are formed [Equation (1)].

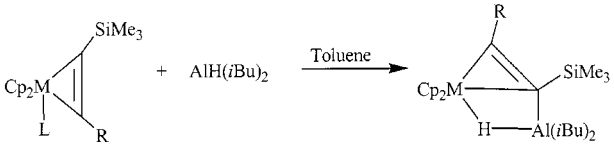

1 - 4

Cp_2M	R	L
(η5-$C_5H_5)_2Ti$	Ph	-
(η5-$C_5H_5)_2Ti$	$SiMe_3$	-
(η5-$C_5H_5)_2Zr$	$SiMe_3$	Py
rac-(ebthi)Zr	$SiMe_3$	-

Cp_2M	R	
(η5-$C_5H_5)_2Ti$	Ph	**1**
(η5-$C_5H_5)_2Ti$	$SiMe_3$	**2**
(η5-$C_5H_5)_2Zr$	$SiMe_3$	**3**
rac-(ebthi)Zr	$SiMe_3$	**4**

rac-(ebthi) = *rac*-[1,2-Ethylene-1,1'-bis(η5-tetrahydroindenyl)]

(1)

Complex **1** crystallizes from *n*-hexane as yellow prisms (m.p. 150–152 °C) and is stable in solution for some days even at higher temperatures. The corresponding bis(trimethylsilyl)-substituted compound **2** (brown-yellow crystals, m.p. 136 °C dec.) is less stable, it regenerates the starting

[a] Institut für Organische Katalyseforschung an der Universität Rostock e.V.,
Buchbinderstraße 5–6, 18055 Rostock, Germany
E-mail: perdita.arndt@ifok.uni-rostock.de
[b] Bayer AG, ZSB Zentrale Forschung, Gebäude Q 18, 51368 Leverkusen, Germany
Fax: (internat.) +49-214/302-4202
E-mail: sigurd.becke.sb@bayer-ag.de

 © WILEY-VCH Verlag GmbH, 69451 Weinheim, 2001 1434–1948/01/1111–2885 $ 17.50+.50/0

compound [$Cp_2Ti(\eta^2$-$Me_3SiC_2SiMe_3)$] in solution at higher temperatures (80 °C, 5 h). The stable analogous zirconocene complexes **3** (light yellow needles, m.p. 142 °C) and **4** (deep yellow prism, m.p. 157−158 °C) are obtained in a similar reaction. All the above complexes were characterized by NMR spectroscopy and **1**, **2** and **4** by X-ray crystal structure analysis.

Spectroscopic Data

The most characteristic proton NMR spectroscopic feature of the compounds **1**−**4** is the high-field resonances of the bridging hydrido ligands (Table 1). The resonance signals are located in the range expected for a hydrogen atom bridging the aluminium and the transition metal center[7] [broad singlets at: δ = −3.79 (**1**), δ = −4.87 (**2**), δ = −2.46 (**3**), δ = −1.27 (**4**)].

Table 1. Selected NMR spectroscopic data of complexes **1**−**4**

	1	**2**	**3**	**4**
^{1}H NMR (δ [ppm])				
Cp	5.15	5.10	5.35	
H	−3.79	−4.87	−2.46	−1.27
^{13}C NMR (δ [ppm])				
C_α, C_β (alkyne)	230.1	234.3	240.4	243.4
	105.0	123.7	138.5	149.5

The methylene groups at aluminium give broad signals in the ^{13}C NMR spectrum which become sharper upon cooling the sample, especially for complex **2**. Besides that, no changes in the NMR spectra were observed. The ^{13}C resonances of the planar-tetracoordinated carbon atom are in the expected olefinic range [δ = 105.0 (**1**), δ = 123.7(**2**), δ = 138.5 (**3**), δ = 149.5 (**4**)]. The methylene group at the aluminium is found in the ^{13}C NMR spectrum as a broad signal at room temp.

These data of complexes **1**−**4** are in good agreement with the zirconocene/aluminium complexes [{Cp_2Zr}(μ-η^1:η^2-RCCR)(μ-H){Al(*i*Bu)$_2$}] from Erker,[3a−3f,4] and the titanocene complexes [{Cp_2Ti}(μ-η^1:η^2-$RCCSiMe_3$)(μ-H)-{Al(*i*Bu)$_2$}] described by Binger[4] and show the same structural features.

X-ray Crystal Structure Analysis of Bimetallic Ti or Zr and Aluminium Compounds

It turned out that an unambiguous characterization of the compounds **1**, **2** and **4** cannot be revealed by NMR spectroscopy as the structural element of the square-planar carbon coordination geometry does not cause any remarkable features in the NMR spectra. Compounds **1**, **2** and **4** were therefore crystallized from *n*-hexane solution by cooling to −30 °C.

The X-ray crystal structures of the titanium complexes exhibit planar, bicyclic five-membered ring systems consisting of the metal atom, the hydridic hydrogen H, Al, C_β and C_α (Figure 1−3 and Table 2). The most remarkable structural element is the coordination geometry of the carbon atom C_β, which is bonded to C_α, M, Al and the Si atom of the $SiMe_3$ group, with all four bonds lying in one plane (mean deviation from the best plane through Ti, Al, Si, C_α **1**: 0.057 Å, **2**: 0 Å). The zirconium complex **4** shows a similar bicyclic ring system as the titanium complexes but in this case the planarity is distorted because of the steric hindrance of the ebthi ligand. The values found for the M−C_β bond lengths are in the expected range for such structural features.[3−5]

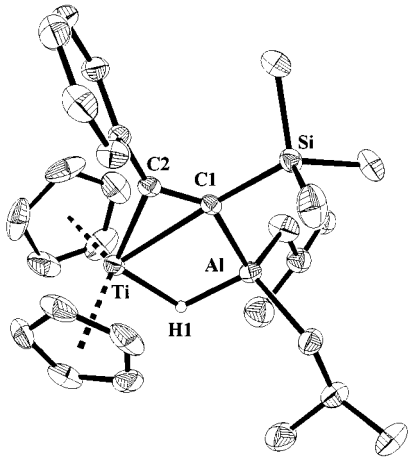

Figure 1. Molecular structure of complex **1** as an ORTEP plot at the 30% probability level; selected bond lengths (Å) and bond angles (deg):[14] Ti−Al 2.788(1), Ti−H1 1.857, Al−H1 1.628, Ti−C1 2.379(3), Ti−C2 2.111(3), C1−C2 1.315(5), Al−C1 2.098(4); Ti−H1−Al 106.1, Al−C1−Ti 76.74(11), H1−Al−C1 96.0, Ti−C1−Si 172.7(2), C1−C2−Ti 84.6(2)

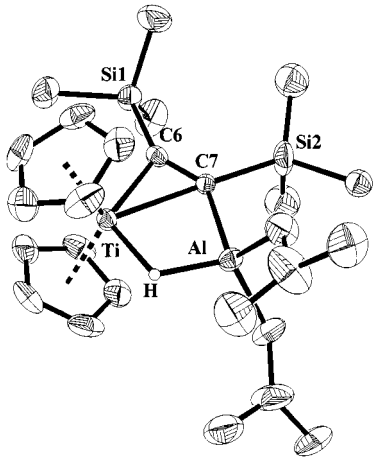

Figure 2. Molecular structure of complex **2** as an ORTEP plot at the 30% probability level; selected bond lengths (Å) and bond angles (deg):[14] Ti−Al 2.762, Ti−H 1.765, Al−H 1.624, Ti−C7 2.341(7), Ti−C6 2.127(7) C7−C6 1.311(9), Al−C7 2.145(7); Ti−H−Al 109.1, Al−C7−Ti 75.9(2), H−Al−C7 92.4, Ti−C7−Si2 177.9(4), C7−C6−Ti 82.1(5)

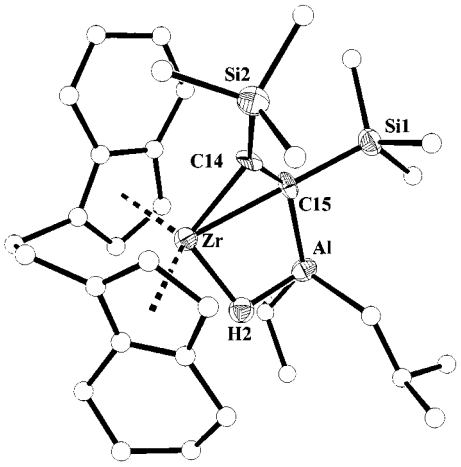

Figure 3. ORTEP view of complex **4** (for clarity only atoms regarded as significant are drawn as 30% probability ellipsoids); selected bond lengths (Å) and bond angles (deg):[14] Zr−Al 2.866(4), Zr−H2 2.048, Al−H2 1.659, Zr−C15 2.384(15), Zr−C14 2.221(13), C15−C14 1.33(2), Al−C15 2.15(2); Zr−H2−Al 100.8, Al−C15−Zr 78.3(5), H2−Al−C15 96.9, Zr−C15−Si1 174.8(9), C15−C14−Zr 80.1(9)

Table 2. Selected bond lengths [Å] and angles [°][14]

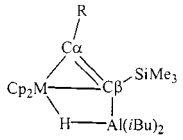	**1**	**2**	**4**
Bond lengths [Å]			
M-Al	2.788(1)	2.762	2.866(4)
M-H	1.857	1.765	2.048
Al-H	1.628	1.624	1.659
M-Cβ	2.379(3)	2.341(7)	2.384(15)
M-Cα	2.111(3)	2.127(7)	2.221(13)
Cα-Cβ	1.315(5)	1.311(9)	1.33(2)
Al-Cβ	2.098(4)	2.145(7)	2.15(2)
Bond angles [°]			
M-H-Al	106.1	109.1	100.8
Al-Cβ-M	76.74(11)	75.9(2)	78.3(5)
H-Al-Cβ	96.0	92.4	96.9
M-Cβ-Si	172.7(2)	177.9(4)	174.8(9)
Cβ-Cα-M	84.6(2)	82.1(5)	80.1(9)

Catalytic ROP of Lactones with Complexes 1−4 as Catalysts

The ROP of ε-caprolactone provides a convenient route to the synthesis of polylactones which are important for medical applications and as plastic modifiers.[6] These applications require polyesters with predictable molecular weights and low polydispersity indices, which is only possible with initiators having selectivity in terms of initiation, propagation and termination reactions.[7] For example, alkali metal alkyls or alkoxides give very fast polymerization of lactones, but inter- and intramolecular side reactions often lead to a broadening of the molecular weight distribution of the products. When aluminium alkoxides are used as initiators, the ROP has been reported to be living and generates polyesters with narrow polydispersity indices that are free of macrocycles.[8a−8c] Recently, well characterized transition metal and lanthanoid complexes containing cyclopentadienyl ligands (metallocenes) have emerged as a new class of initiators.[9] The polymerization activity (for polar monomers) was tested using mono(cyclopentadienyl)-titanium,[9] rare earth[7a] and heterobimetallic lanthanocene[7a,10a−10c] compounds. Organolanthanide complexes in general seem to be highly active and well suited as initiators for the ROP of lactones due to their Lewis acidity.[7a]

Recently, we described how (alkyne)zirconocene and titanocene complexes are capable of polymerizing ε-caprolactone with living characteristics and high yield.[11,12] (Table 3, runs 1 and 4)

The heterobimetallic complexes **1−4** are of interest in the context of the activation of catalytic systems. Polymerization reactions were carried out under the same conditions as described before;[11,12] for a high conversion it is necessary to start with a mixture of ε-caprolactone/catalyst in toluene at room temp. and add a second portion of substrate/toluene at 75 °C (Table 3, runs 2, 3 and 5). The poly-ε-caprolactone (PCL) was isolated as a colorless solid and characterized by GPC and NMR spectroscopy. The polymers formed by **1−4** are generally of high molecular weight and of moderate polydispersities ($M_w/M_n < 2.7$). The efficiency depends on the experimental conditions, with the highest value being observed for **3**.

The heterobimetallic complexes show an increase of molecular weights (runs 2 and 3, Ti) by a factor of 10 for titanium compared to their monometallic derivatives and are dependent on the metal in the metallocene unit. The lower yield of run 2 might be explained by the instability of complex **2**: as mentioned above, it forms the monometallic compound [$Cp_2Ti(\eta^2$-$Me_3SiC_2SiMe_3)$] in solution at higher temperatures (80 °C, 5 h).

The results of NMR studies of the ROP with titanocene initiators were disappointing. All subsequent steps of the catalytic cycles such as initiation, propagation and chain termination are very fast on the NMR time scale, and could not be detected. This is consistent with the results we obtained in the case of (alkyne)zirconocene catalysts (for propagation and termination)[12] and those obtained by other groups in monitoring lactone polymerization by NMR spectroscopy.[10b] Furthermore, no end-group signals were found.[12] This has been explained in other reports by the formation of a cyclic polymer as the termination step.[10a,10d] The corresponding heterobimetallic zirconocene(alkyne)/aluminium derivatives (**3**, **4**) (Table 3, runs 5, 7) show no significant changes in comparison to their monometallic example in the ROP. The NMR investigation of the ROP of ε-caprolactone with initiator **4** shows the formation of a five-membered metallacyclic spirozirconadihydrofuran complex, which was already described as the first step in the ROP of lactones by the monometallic

Table 3. Polymerization of ε-caprolactone (CL) in toluene at 75 °C by complexes **1**−**4** in comparison to the corresponding monometallic (η^2-alkyne) compounds (75 °C, toluene)

Run	Initiator	CL/initiator	Time [h]	Yield [%]	M_n(calcd.)	M_w(GPC)	M_n(GPC)	M_w/M_n	Efficiency[a]
1	$Cp_2Ti(Me_3SiC_2SiMe_3)$[11]	5 000	1	86	490 000	110 000	68 500	1.6	7.2
2	$Cp_2Ti(Me_3SiC_2SiMe_3)$-(μ-H)(Al*i*Bu)$_2$ (**2**)	10 000	1	67	764 000	942 900	390 000	2.4	1.9
3	$Cp_2Ti(Me_3SiC_2Ph)$-(μ-H)(Al*i*Bu)$_2$ (**1**)	50 000	1	97	5 535 000	1 072 000	410 000	2.6	13.5
4	$Cp_2Zr(Py)(Me_3SiC_2SiMe_3)$[11]	5 000	1	80	450 000	80 000	44 400	1.8	10.3
5	$Cp_2Zr(Me_3SiC_2SiMe_3)$-(μ-H)(Al*i*Bu)$_2$ (**3**)	5 000	1	82	460 000	67 570	48 170	1.4	9.7
6	(ebthi)$Zr(Me_3SiC_2SiMe_3)$[12]	5 100	1	34	190 000	−	−	−	−
7	(ebthi)$Zr(Me_3SiC_2SiMe_3)$-(μ-H)(Al*i*Bu)$_2$ (**4**)	5 000	1	10	57 000	52 760	39 680	1.3	1.4

[a] Efficiency is defined as the fraction of active initiators, calculated from the observed number of polymer chains relative to the theoretical ones, assuming that each metallocene initiates one polymer chain.

(zirconocene) alkyne complexes;[12] it is followed by a rapid polymerization. No influence of the HAl(*i*Bu)$_2$ was found. A control experiment with HAl(*i*Bu)$_2$ as catalyst gave no polymerization. This is in agreement with the fact that Al(*i*Bu)$_3$ has no catalytic activity for the ROP of ε-caprolactone.[13b]The catalytic activity of the titanocene heterobimetallic compounds can be explained by an interaction between the active species and the monomer by coordination of the exo- or endocyclic oxygen of ε-caprolactone to different metal units (Al, Ti). This could cause the increased rate of polymerization and high molecular weights of the resulting polylactones. Such an activation was demonstrated by Sheng[13a,13b] for rare-earth coordination initiators obtained in situ by adding trialkylaluminium to Ln compounds. Also, heterobimetallic lanthanide/lithium complexes have been found to be active in the polymerization of ε-caprolactone, as reported by Okuda.[10a] In this case, however, another activation mechanism involving an amide nitrogen atom was proposed.

Experimental Section

General: All operations were carried out under argon with standard Schlenk techniques. Solvents were freshly distilled prior to use from sodium tetraethylaluminate and stored under argon. Deuterated solvents were treated with sodium or sodium tetraethylaluminate, distilled and stored under argon. ε-Caprolactone (Aldrich) was dried over molecular sieves and degassed before use. − The following spectrometers were used: Mass spectra: AMD 402. − NMR spectra: Bruker ARX 400. Chemical shifts referenced to signals of the used solvents: [D_6]benzene (δ_H = 7.16, δ_C = 128.0). The spectra were assigned with the help of DEPT experiments. − Melting points: sealed capillaries, Büchi 535 apparatus. − Elemental analyses: Leco CHNS-932 elemental analyzer. − Gel permeation chromatographic (GPC) analyses of the polymers were performed using a Liquid Chromatograph 1090 HP [column: SDV 10^4 Å + 10^3 Å +100 Å (Polymer Standard Service), eluent: THF]. Molecular weights were corrected by universal calibration relative to polystyrene standards.

Preparation of 1: 1.2 mL (1.2 mmol) of a 1.0 M solution of AlH(*i*Bu)$_2$ in *n*-heptane was added to a solution of [$Cp_2Ti(\eta^2$-$PhC_2SiMe_3)$] (375 mg, 1.18 mmol) in 10 mL of toluene. The mixture was stirred for 2 h at room temp. and the color changed to brown. After evaporation of the solvents to dryness, the residue was washed twice with 2 mL of *n*-pentane and dissolved in *n*-hexane (60 °C). The solution was filtered, and after 12 h at room temp. yellow crystals formed. The crystals were washed with cold *n*-pentane and dried in vacuo to give 435 mg (75%) of **1**. M.p. 150 −152 °C. − ^{1}H NMR (C_6D_6, 297 K): δ = −3.79 (br., 1 H, μ-H), 0.11 (2 s, 9 H, $SiMe_3$), 0.47, 0.62 (m, 4 H, CH_2), 1.34, 1.36 (2 d, ^3J = 5.9/5.8 Hz, 12 H, CH_3), 2.35 (m, 2 H, CH), 5.13 (d, 2 H, Ph), 5.15 (s, 10 H, Cp), 6.83 (d, 2 H, Ph), 6.98 (t, 1 H, Ph). − ^{13}C{^{1}H} NMR (C_6D_6, 297 K): δ = 3.8 ($SiMe_3$), 26.8 (br., CH_2), 27.3 (CH), 28.8, 29.0 (CH_3), 104.9 (Cp), 123.8, 125.1, 128.0 (CH, Ph), 150.4 (*ipso-C*, Ph), 105.0(*C*-$SiMe_3$), 230.1 (*C*-Ph). − MS (70 eV): *m*/*z* (%) = 352 [$Cp_2Ti(\eta^2$-$PhC_2SiMe_3)]^+$, 178 [Cp_2Ti^+], 173 [$PhC_2SiMe_3]^+$, 141 [Al(*i*Bu)$_2]^+$. − $C_{29}H_{43}AlSiTi$ (494.61): calcd. C 70.42, H 8.76; found C 70.10, H 8.59.

Preparation of 2: 1.2 mL (1.2 mmol) of a 1.0 M solution of AlH(*i*Bu)$_2$ in *n*-heptane was added to a solution of [$Cp_2Ti(\eta^2$-$Me_3SiC_2SiMe_3)$] (405 mg, 1.16 mmol) in 10 mL of toluene. The mixture was stirred for 2 h at room temp. and the color changed to green-brown. After evaporation of the solvents to dryness, the oil was washed twice with 1 mL of cold *n*-pentane and dissolved in a small amount of *n*-hexane. After filtration the solvent was removed in vacuo until the first yellow-brown crystals formed. Upon cooling to −78 °C for 12 h a brown precipitate formed which was filtered off, washed with cold *n*-pentane and dried in vacuo to give 400 mg (76%) of **2**. M.p.: 136 °C (dec.). − ^{1}H NMR (C_6D_6, 297 K): δ = −4.87 (br., 1 H, μ-H), 0.29, 0.33 (2 s, 18 H, $SiMe_3$), 0.46, 0.60 (m, 4 H, CH_2), 1.30, 1.35 (2 d, ^3J = 6.5 Hz, 12 H, CH_3), 2.31 (m, 2 H, CH), 5.10 (s, 10 H, Cp). − ^{13}C{^{1}H} NMR (C_6D_6, 297 K): δ = 2.0, 3.6 ($SiMe_3$), 25.8 (br, CH_2), 25.7 (CH), 27.4, 27.5 (CH_3), 102.5 (Cp), 123.7, 234.3 (*C*-$SiMe_3$). − ^{1}H NMR ([D_8]toluene, 192 K): δ = −5.05 (br., 1 H, μ-H), 0.18, 0.18 (2 s, 18 H, $SiMe_3$), 0.43, 0.56 (br., 4 H, CH_2), 1.32, 1.40 (2 d, 12 H, CH_3), 2.30 (m, 2 H, CH), 5.10 (s, 10 H, Cp). − ^{13}C{^{1}H} NMR ([D_8]toluene, 192 K): δ = 2.0, 3.6 ($SiMe_3$), 26.5 (br., CH_2), 27.0 (CH), 28.8, 28.9 (CH_3), 103.5 (Cp), 123.7, 234.3 (*C*-$SiMe_3$). − MS (70 eV): *m*/*z* (%) =348 [$Cp_2Ti(\eta^2$-$Me_3SiC_2SiMe_3)]^+$, 178 [Cp_2Ti^+], 173 [$Me_3SiC_2SiMe_3]^+$, 141 [Al(*i*Bu)$_2]^+$. − $C_{26}H_{47}AlSi_2Ti$ (490.69): calcd. C 63.64, H 9.65; found C 63.09, H 9.23.

Preparation of 3: 1.1 mL (1.1 mmol) of a 1.0 M solution of AlH(*i*Bu)$_2$ in *n*-heptane was added to a solution of [$Cp_2Zr(Py)(\eta^2$-$Me_3SiC_2SiMe_3)$] (503 mg, 1.07 mmol) in 10 mL of toluene. The

mixture was stirred for 2 h at 40 °C and the color changed to light green. After evaporation of the solvents to dryness. the residue was solved in a small amount of *n*-hexane. Upon cooling to −78 °C for 12 h light yellow-green crystals were formed which were filtered off, washed with cold *n*-pentane and dried in vacuo to give 410 mg (71%) of **3**. M.p.: 142 °C. − ^{1}H NMR (C_6D_6, 297 K): δ = − 2.46 (br., 1 H, μ-H), 0.34, 0.35 (2 s, 18 H, $SiMe_3$), 0.39, 0.60 (m, 4 H, CH_2), 1.29, 1.34 (2 d, ^3J = 6.4 Hz, 12 H, CH_3), 2.28 (m, 2 H, CH), 5.35 (s, 10 H, Cp). − $^{13}C\{^1H\}$ NMR (C_6D_6, 297 K): δ = 3.5, 4.7 ($SiMe_3$), 26.8 (br., CH_2), 27.2 (CH), 28.6, 28.9 (CH_3), 104.6 (Cp), 138.5, 240.4 (*C*-$SiMe_3$). − MS (70 eV): *m*/*z* (%) = 534 [M^+], 220 [Cp_2Zr^+], 170 [$Me_3SiC_2SiMe_3]^+$. − $C_{26}H_{47}AlSi_2Zr$ (534.03): calcd. C 58.48, H 8.87; found C 58.23, H 8.60.

Preparation of 4: 0.7 mL (0.7 mmol) of a 1.0 M solution of $AlH(iBu)_2$ in *n*-heptane was added to a solution of [(ebthi)Zr(η^2-$Me_3SiC_2SiMe_3$)] (378 mg, 0.72 mmol) in 10 mL of toluene were added of $AlH(iBu)_2$ as a solution in *n*-heptane (1.0 M). The light yellow solution was stirred for 2 h at room temp. After evaporation to dryness. the residue was dissolved in 5 mL of *n*-hexane. After filtration and cooling to −40 °C for 12 h crystals formed, which were filtered off and dried in vacuo to give 234 mg (48%) of **4**. M.p.: 157−158 °C. − ^{1}H NMR (C_6D_6, 297 K): δ = −1.27 (br., 1 H, μ-H), 0.48, 0.50 (2 s, 18 H, $SiMe_3$), 0.63−0.72 (m, 4 H, CH_2), 1.20, 1.29, 1.38, 1.43 (4 d, ^3J = 6.4 Hz, 12 H, CH_3), 2.23 (m, 2 H, CH), 4.38, 5.51, 5.54, 6.35 (4 d, *J* = 2.5 Hz, 4 H, CH ebthi). − $^{13}C\{^1H\}$ NMR (C_6D_6, 297 K): δ = 3.5, 4.7 ($SiMe_3$), 26.8 (br., CH_2), 27.1 (CH), 28.6, 28.9 (CH_3), 99.2, 100.46, 103.0, 104.8 (CH, ebthi), 116.7, 119.2, 122.1, 124.0, 126.4, 126.2 (q-C, ebthi) 149.5, 243.4 (*C*-$SiMe_3$). − $C_{36}H_{61}AlSi_2Zr$ (668.25): calcd. C 64.71, H 9.20; found C 63.99, H 9.02.

Polymerization of ε-Caprolactone: A stirred 5 M solution of the monomer in toluene (5 mL) was heated to 75 °C and an appropriate amount of the initiator complex dissolved in toluene was added. Ten minutes later a further amount of lactone dissolved in toluene was added. After one hour the reaction mixture was worked up by dropwise addition of a tenfold volume of methanol. The poly(ε-caprolactone)s were filtered off and dried in vacuo until the weight remained constant.

PCL: ^{1}H NMR (C_6D_6, 297 K): δ = 1.5, 1.41, 1.17 (3 m, 6 H, CH_2); 2.11, 3.98 (2 t, 4 H, CH_2).

X-ray Crystallographic Study of Complexes 1, 2 and 4: Diffraction data were collected on a STOE-IPDS diffractometer using graphite-monochromated Mo-K_α radiation. Crystal data, details of the data collections and structure refinement are compiled in Table 4. The structures were solved by direct methods (SHELXS-86: G. M. Sheldrick, *Acta Crystallogr., Sect. A* **1990**, *46*, 467) and refined by full-matrix least-squares techniques against F^2 (SHELXL-93: G. M. Sheldrick, University of Göttingen, Germany, **1993**).
Crystallographic data (excluding structure factors) for the structures reported in this paper have been deposited with the Cambridge Crystallographic Data Centre as supplementary publication nos. CCDC-157428 (**1**), -157429 (**2**), -157430 (**4**). Copies of the data can be obtained free of charge on application to CCDC, 12 Union Road, Cambridge CB2 1EZ, UK [Fax (internat.): +44-1223/336-033; E-mail: deposit@ccdc.cam.ac.uk].

Table 4. Crystal data, data collection and structure refinement for compounds **1**, **2** and **4**

	1	**2**	**4**
Cryst. color	yellow	yellow	yellow
Cryst. system	orthorhombic	monoclinic	monoclinic
Space group	*Pbca*	*C*2/*m*	$P2_1$
Lattice constants			
a [Å]	9.867(2)	20.713(4)	9.448(2)
b [Å]	20.212(4)	14.630(3)	18.131(4)
c [Å]	28.261(6)	9.979(2)	11.581(2)
α [°]	90.00	90.00	90.00
β [°]	90.00	105.19(3)	108.46(3)
γ [°]	90.00	90.00	90.00
Z	8	4	2
F(000) [e]	2128	1064	716
μ [mm^{-1}]	0.392	0.416	0.401
Temp. [K]	293(2)	293(2)	293(2)
No. of rflns. (meas.)	10532	2957	5651
No. of rflns. (indep.)	2982	1562	2951
No. of rflns. (obsd.)	2290	1092	1182
No. of parameters	290	148	361
*R*1 [$I \geq 2\sigma(I)$]	0.042	0.056	0.049
w*R*2 (all data)	0.110	0.152	0.110

Acknowledgments

We thank the Deutsche Forschungsgemeinschaft (AR 321/1-1) and the Fonds der Chemischen Industrie for financial support.

[1] [1a] W. Kaminsky, K. Külper, H.-H. Brintzinger, F. R. Wild, *Angew. Chem. Int. Ed. Engl.* **1985**, *97*, 507−508; H. Sinn, W. Kaminsky, *Adv. Organomet. Chem.* **1980**, *18*, 99−150 and references therein. − [1b] M. Bochmann, *J. Chem. Soc., Dalton Trans.* **1996**, 255−270 and references therein.
[2] [2a] W. E. Piers, *Chem. Eur. J.* **1998**, *4*, 13−18. − [2b] W. E. Piers, *J. Am. Chem. Soc.* **1997**, *119*, 5132−5143. − [2c] W. E. Piers, Y. Sun, L. W. M. Lee, *Top. Catal.* **1999**, *7*, 133−143. − [2d] M. Bochmann, *Top. Catal.* **1999**, *7*, 9−22. − [2e] A. Bertuleit, M. Könemann, L. Duda, G. Erker, R. Fröhlich, *Top. Catal.* **1999**, *7*, 37−44.
[3] [3a] G. Erker, *Comments Inorg. Chem.* **1992**, *13*, 111−122. − [3b] G. Erker, R. Noe, D. Wingbergmühle, *Chem. Ber.* **1994**, *127*, 805−811. − [3c] G. Erker, M. Albrecht, K. Krüger, *Synlett* **1993**, 441−448. − [3d] G. Erker, M. Albrecht, *Organometallics* **1992**, *11*, 3517−3525. − [3e] F. Sandmeyer, Doctoral dissertation, University of Kaiserslautern, Germany, **1994**. − [3f] G. Erker, M. Albrecht, S. Werner, M. Nolte, C. Krüger, *Chem. Ber.* **1992**, *125*, 1953−1956.
[4] [4a] P. Binger, F. Sandmeyer, K. Krüger, G. Erker, *Tetrahedron* **1995**, *51*, 4277−4290. − [4b] P. Binger, F. Sandmeyer, K. Krüger, *Organometallics* **1995**, *14*, 2969- 2976.
[5] [5a] W. K. Kot, N. M. Edelstein, A. Zalkin, *Inorg. Chem.* **1987**, *26*, 1339−1942. − [5b] G. Erker, U. Hoffmann, R. Zwettler, K Krüger, *J. Organomet. Chem.* **1989**, *367*, C15−C17.
[6] [6a] H. Yasuda, E. Ihara, *Adv. Polym. Sci.* **1997**, *133*, 53−101. − [6b] G. L. Brode, J. V. Koleske, *J. Macromel. Sci., Pure Appl. Chem.* **1972**, *A6*, 1109−1115.
[7] [7a] S. Agarwal, C. Mast, K. Dehnicke, A. Greiner, *Macromol. Rapid Commun.* **2000**, *21*, 195−212. − [7b] H. Yasuda, M. Furo, H. Yamamoto, Y. Takemoto, M. Yamashita, K. Yokota, S. Miyake, A. Nakamura, *Macromolecules* **1992**, *25*, 5115−5116. − [7c] H. Yasuda, E. Ihara, *Bull. Chem. Soc. Jpn.* **1997**, *70*, 1745−1767 and references therein.
[8] [8a] T. Yasuda, T. Aida, S. Inou, *Bull. Chem. Soc. Jpn.* **1986**, *59*, 3931−3943. − [8b] J. Okuda, I. Taden, H.-C. Kang, W. Massa,

T. P. Spaniol, *Eur. J. Inorg. Chem.* **2000**, 441−445. − [8c] A. Duda, Z. Florjanczyk, A. Hofman, S. Slomkowski, S. Penczek, *Macromolecules* **1990**, *23*, 1640−1646.

[9] J. Okuda, I. L Rushkin, *Macromolecules* **1993**, *26*, 5530−5532 and references therein.

[10] [10a] K. C. Hultzsch, J. Okuda, *Macromol. Rapid Commun.* **1997**, *18*, 809−815. − [10b] K. Beckerle, K. C. Hultzsch, J. Okuda, *Macromol. Chem. Phys.* **1999**, *200*, 1702−1707. − [10c] K. C. Hultzsch, T. P. Spaniol, J. Okuda, *Organometallics* **1998**, *17*, 5836−5849. − [10d] K. C. Hultzsch, T. P. Spaniol, J. Okuda, *Angew. Chem. Int. Ed.* **1999**, *38*, 227−230.

[11] P. Arndt, D. Thomas, U. Rosenthal, *Tetrahedron Lett.* **1997**, *38*, 5467−5468.

[12] D. Thomas, P. Arndt, N. Peulecke, A. Spannenberg, R. Kempe, U. Rosenthal, *Eur. J. Inorg. Chem.* **1998**, 1351−1357.

[13] [13a] Z. Shen, X. Chen,Y. Shen, Y. Zhang, *J. Polym. Sci., Part A: Polym. Chem.* **1994**, *32*, 597- 603. − [13b] J. Zhang, Z. Gan, Z. Zhong, X. Jing, *Polym. Int.* **1998**, *45*, 60−66.

[14] Values without standard deviations were determined by the program XP (Siemens Analytical X-ray Instruments, Inc.).

Received March 2, 2001
[I01078]

On the d^6-Transition Metal Complex Formation of Electron-Rich Methylenephosphanes, a Quantum Chemical Investigation

Wolfgang W. Schoeller,*[a] Alexander B. Rozhenko,[a] and Sonja Grigoleit[a]

Keywords: Ab initio calculations / Density functional theory / Methylenephosphanes / Carbonyl complexes

d^6-Transition metal fragments $M(CO)_5$ (M = Cr, Mo, W) form mono- and binuclear complexes with methylenephosphanes. In the mononuclear complexes the metal fragment adds to the lone pair at the phosphorus atom without considerable geometrical change of the original phosphaalkene moiety. Amino substitution at the phosphorus atom yields a slightly more stable complex than amino substitution at the carbon atom. The latter substitution pattern causes an *inverse polarization* of the P–C π-bond. As a further consequence, in the corresponding transition metal complexes, the phosphorus atom is slightly pyramidalized. In the binuclear complexes the transition metal atoms tend to adopt a distorted bipyramidal arrangement at the phosphorus atom with concomitant lengthening of the P–C bond. The stretching of the P–C π-bond is required to form a second lone pair for coordination at the phosphorus atom. However, the longest P–C bonds are achieved by *C*-diamino-substituted methylenephosphanes with overall bulky alkyl groups at the phosphorus and nitrogen atoms. It has the effect of not only extending the P–C bond but also widening the angle at the phosphorus atom.

Introduction

While the earliest reports of compounds containing a P=C double bond originated from Dimroth and Hoffmann,[1] its first stable acyclic species with a localized P=C bond was described in the pioneering work of Becker and co-workers,[2] type **A**. It opened an exciting chapter in modern phosphorus chemistry and is now documented in various review articles.[3−8] It has been stated that phosphorus is related to carbon by the diagonal relationship in the periodic table of elements[8] and typical reactions of organic chemistry may well be found also in organophosphorus chemistry[9] (Scheme 1).

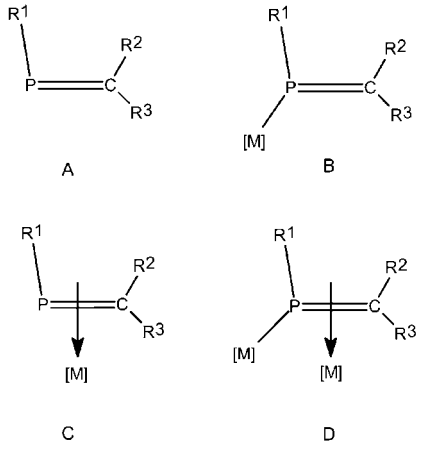

Scheme 1

An archetypal reaction of phosphaalkenes **A** is the formation of transition metal complexes,[10] as η^1-complexes, type **B** {[M] = $Cr(CO)_5$,[11] $Fe(CO)_4$,[12] $Pt(PPh_3)_2$[13]}. The X-ray crystal structure of the solid indicated that for the latter, the ligand was η^1-bonded, whereas in solution η^2-coordination, type **C**, was favoured. A rationalization for this experimental observation was not given. It was also suggested that the ligation modes are a delicate balance of various effects.[14] Other η^2-bonded complexes with Ni, Rh, and W were subsequently reported.[15] A series of η^2-ligated nickel(0) species were prepared.[16] It has been shown that for an η^2-bonded ligand, the P−C bond is longer than it is in the comparable η^1-complexes or the free ligand systems.[17,18] An η^1,η^2-complex of a phosphaalkene with two coordinated transition metal atoms {[M] = $Fe(CO)_4$}, type **D**, was first recorded by Appel et al.[19] (see also ref.[15]). Phosphaalkenes acting as an η^1-(μ_2)-four-electron donor have also been reported {[M] = $Cr(CO)_5$,[20] $CpFe(CO)_2$[21]}. In these complexes the transition metal fragments are linked to the same phosphorus atom.

It is obvious that the experimental results obtained for transition metal coordination of phosphaalkenes is very rich. Besides the η^1- and η^2-mode of coordination, bridged metal centres in an η^1-(μ_2-P) or η^2-(μ_3) manner are also known. This material has been recorded in detail in reviews.[8,15] In the present publication we analyze the principal bonding features of transition metal coordination, i.e., the η^1- and η^2-modes, for methylenephosphanes. Particular attention is given to amino-substituted methylenephosphanes, since their coordination abilities are somewhat different and they can also be considered as electron rich π-systems. We considered mono- and binuclear transition metal complex formation at the phosphorus atom. The d^6-ML_5 (L = CO; M = Cr, Mo, W) species were chosen as the transition metal fragments. Our analysis is based on the results of quantum chemical investigations at a density functional level (DFT). We note that in this instance DFT calculations are the appropriate choice for the cases studied

[a] Fakultät für Chemie der Universität Bielefeld,
Postfach 100131, 33501 Bielefeld, Germany
Fax: (internat.) + 49-(0)521/106-6467
E-mail: wolfgang.schoeller@uni-bielefeld.de

 © WILEY-VCH Verlag GmbH, 69451 Weinheim, 2001 1434−1948/01/1111−2891 $ 17.50+.50/0

at hand, due to the large size of these structures. Recent investigations on a variety of transition metal complexes with phosphorus compounds were skilfully performed by Creve et al.[22,23] These studies show that the results of density functional calculations (at the B3LYP level) are comparable to those obtained at the more elaborate CCSD(t) level. Details of the used quantum chemical methodology are given in the Theoretical Section.

Results and Discussion

a. Various Modes of Complexation

We first discuss the qualitative bonding features of the P−C π-bond. The parent methylenephosphane possesses two closely spaced frontier orbitals,[24,25] shown schematically in Scheme 2.

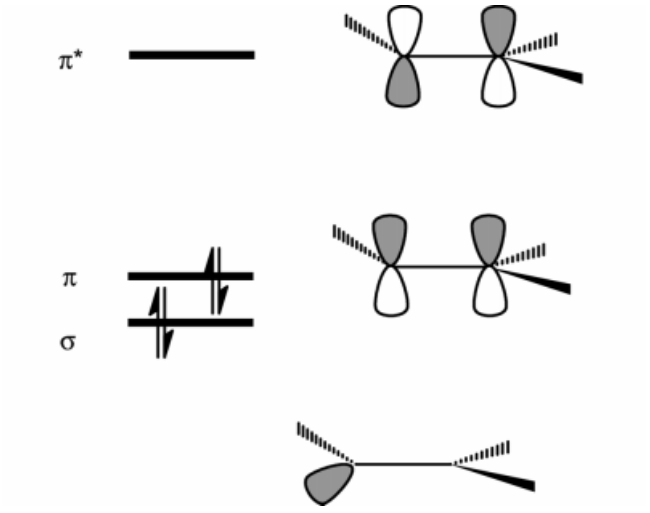

Scheme 2

In general the HOMO is the π- and the LUMO the π*-orbital. Slightly below the HOMO is the σ-orbital, constituted from the nonbonding lone pair orbital at the phosphorus atom. On the contrary in the related iminophosphanes[26,27] the HOMO is the σ- and the HOMO-1 is the π-orbital, thus the orbital sequence is reversed. This gives rise to a different chemical behaviour of methylene- vs. iminophosphanes. The latter class of compounds reveals a pseudo-carbenic behavior.[24] The levelling of frontier orbitals in the methylene- and iminophosphanes is in agreement with detailed photoelectron-spectroscopic investigations[27,28−31] and the assignment of the orbital character (σ vs. π) is performed by supplementary investigations of the UV spectra.[26,27]

The P−C π-bond (in methylenephosphane) is essentially weaker than a C−C or an N−C π-bond,[32−34] thus it can be more easily distorted by other potential π-donors, e.g., an amino group at the carbon atom. It causes a polarization of the P−C π-bond, in terms of canonical valence bond structures best described as quasi-allylic resonance, under accumulation of negative charge at the phosphorus atom.[25] Since phosphorus and carbon atoms possess comparable electronegativities,[35] the P−C π-bond is unpolarized in the parent methylenephosphane. With this we mean the coefficient at the HOMO is almost the same for both the carbon and the phosphorus atom. However, substitution by an amino group at the carbon atom causes the formation of a strong N−C π-bond, with concomitant weakening of the P−C π-bond. As a consequence negative π-charge is accumulated at the phosphorus atom by allylic resonance. In terms of frontier orbital considerations the π-bond coefficient becomes enlarged at the phosphorus atom and diminished at the carbon atom. The effect is rather strong since an N−C π-bond is stronger than a P−C π-bond. This aspect was first noted some time ago[25] and was coined as *inverse π bond polarization*, in the studies on phosphatriafulvenes.[36−38] Thus, while parent methylenephosphane possesses an unpolarized π-bond (phosphorus and carbon have similar electronegativities), in *C*-amino-substituted species the π-bond is *inversely polarized*. This concept explains the large variation in the cycloaddition behavior of the P−C double bond[39,40] and was recently summarized in a review article.[41]

What effect does it have on transition metal complex formation? This is the aim of our present study. In order to reveal the effect of π-bond polarization we included in our work the transition metal complexes of (a) the parent compound and an amino group attached (b) to the phosphorus or (c) to the carbon atom. Thus, the DFT calculations probe the various alternatives. For mononuclear transition metal complexation with a d^6-$M(CO)_5$ (M = Cr, Mo, W) fragment the bonding parameters as shown in Figure 1 were obtained.

For completeness we include the bonding parameters for the (substituted) methylenephosphanes. The transition metal fragment in our study refers to the d^6-$M(CO)_5$ fragment. In qualitative terms it possesses the frontier orbital system[42] as shown in Scheme 3.

Two doubly occupied orbitals at the transition metal centre (d_{xz}, d_{yz}) can provide electron density for the formation of a π-bond while the d_z^2-orbital can accept electrons. In more detail, on a qualitative basis this extends the common view on bonding in Fischer-type complexes[43] to the diagram in Scheme 4, with **II** referring to donation and **I** to back-donation of electron density. One expects that the amount of back-donation $\pi(ML_5)\rightarrow\pi^*(PC)$ is less compared to (phosphanyl)carbenes,[44] due to the energetically higher (antibonding) π*-orbital in methylenephosphane as compared with the corresponding empty (nonbonding) p-orbital in methylene.

The calculations indicate that the mononuclear transition metal coordination does in essence only slightly alter the geometry of the methylenephosphane. The transition metal variation insignificantly changes the bonding parameters of the (free) methylenephosphane moieties. It is in contrast to the phosphanylcarbene complexes in which complexation requires substantial changes in the geometries of the free

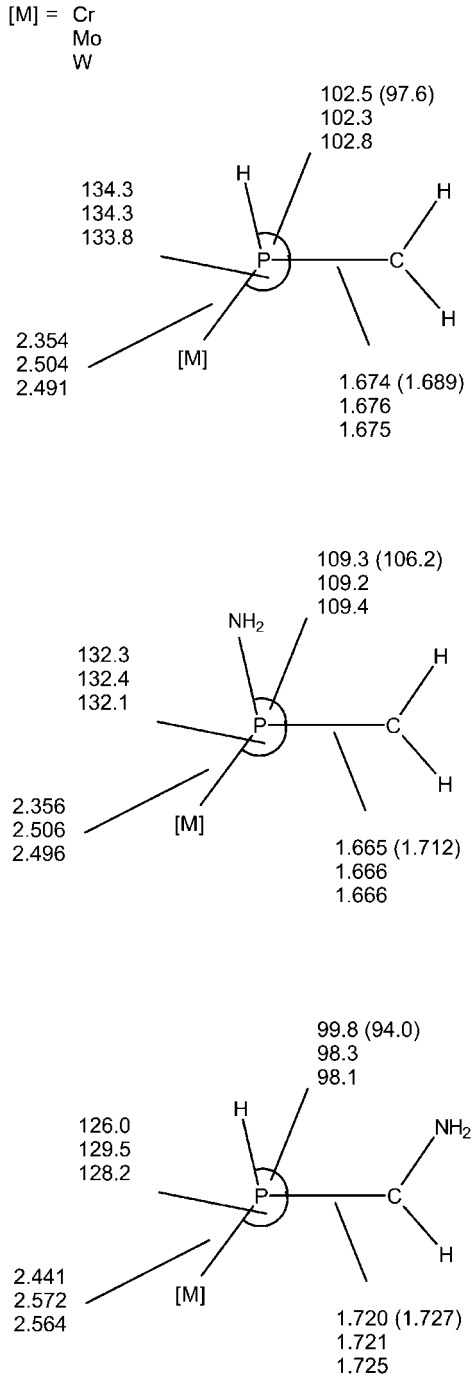

Figure 1. Relevant bonding parameters (bond lengths [Å], bond angles [°]) of η^1-transition metal complexes of methylenephosphanes

carbenes.[44] The situation for η^1-coordination is more deeply analyzed by an inspection of the energies for bonding of the transition metal fragments (Table 1). They are defined by the reactions according to Equations (1) and (2).

$$R^1P{=}CR^2R^3 \rightarrow [R^1P{=}CR^2R^3]^{\ddagger} \quad (1)$$

$$[R^1P{=}CR^2R^1]^{\ddagger} + ML_5 \rightarrow (ML_5)(R^1P{=}CR^2R^3 \quad (2)$$

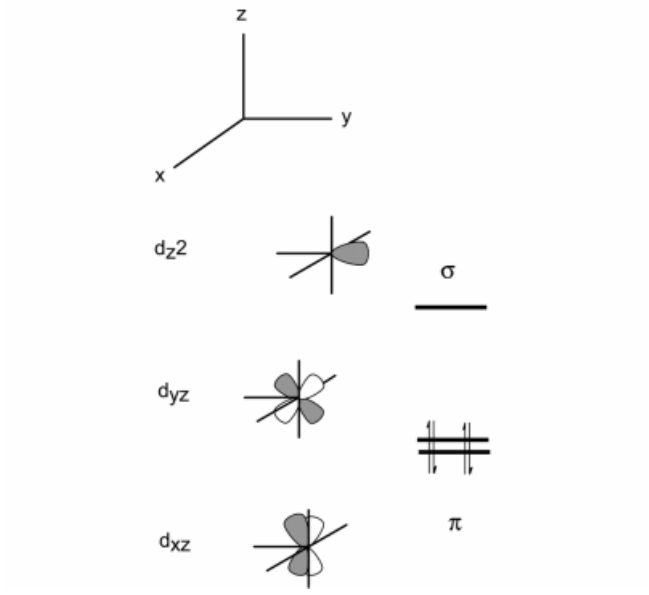

Scheme 3

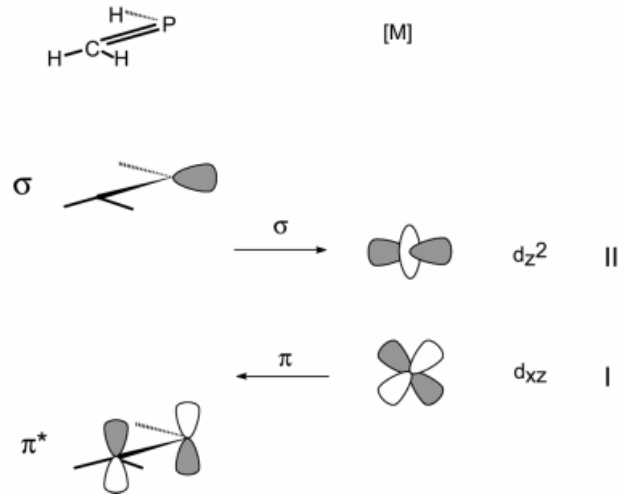

Scheme 4

The first process [Equation (1)] refers to the energy (E_{prep}) needed to bring the free ligand (methylenephosphane) towards the structure for complexation.[45] Overall the preparation energies are in the range of 1−2 kcal/mol, thus fairly small. The second process [Equation (2)] corresponds to the energy gained in the formation of the transition metal complex from its standard state. The table includes the electronic energies (ΔE, with zero-point vibrational energy correction) and the free energies (ΔG, at room temperature) for complexation. The binding energies (as given by ΔE and ΔG) are throughout exothermic and strongly superimpose the (endothermic) preparation energies. We note here that the free energies also include the entropy contributions and were determined by standard thermodynamic formulae (see Theoretical Section). The bonding situation for transition-metal complexation contrasts that of the phosphanylcarbene complexes, where both

Table 1. Energies for η^1-coordination of d^6-$M(CO)_5$ fragments

Ligand	Metal	$-\Delta E$ [kcal/mol]	$-\Delta G$ [kcal/mol]	ΔE_{prep} [kcal/mol]
$HP{=}CH_2$	Cr	26.5	16.0	1.0
	Mo	27.7	17.5	0.9
	W	31.8	21.5	1.0
$H_2N{-}P{=}CH_2$	Cr	28.2	17.2	0.7
	Mo	29.4	18.8	0.7
	W	33.5	22.9	0.7
$HP{=}CH{-}NH_2$	Cr	25.3	15.1	1.4
	Mo	27.7	18.0	1.1
	W	30.8	21.6	1.4

quantities are comparable in magnitude.[44] Overall the free energies (ΔG) are smaller in magnitude than the electronic energies (ΔE + zero-point vibrational energy corrections). There is a continuous trend in that the binding energies increase slightly from Cr to W.

The structures of the methylenephosphanes are to a degree preserved by the coordination. Amino substitution at the phosphorus atom does not essentially alter the geometry of the parent compound, the P−C bond is only slightly elongated, as compared with the parent compound. In terms of π-conjugation, the amino group at the phosphorus atom acts only as a weak π-donor toward the P−C π-bond. The case is different for amino substitution at the carbon atom. Here the P−C bond is sizeably elongated, due to effects of *inverse* π *bond polarization*. In the coordinated compounds the phosphorus atom adopts for **a** the parent methylenephosphane and **b** for its $P{-}NH_2$-substituted congener a trigonal planar arrangement. The situation is different for the $C{-}NH_2$ substitution. After coordination, the phosphorus atom becomes slightly pyramidal, in agreement with the experiments.[31,41] The sum of valence angles for *C*-amino substitution are as follows: Cr 348.9°, Mo 353.9°, W 350.9°. This matter can be touched on in the limiting structures shown in Scheme 5.

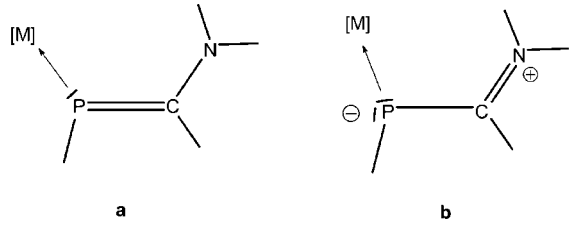

Scheme 5

In **a** the transition metal centre coordinates to the lone pair at the phosphorus atom while in **b** the transition metal fragment occupies one lone pair of the phosphorus atom which is obtained by shifting electron density from the amino group towards the P−C π-bond. In this case one lone pair is available for complexation while the other becomes stereochemically active and causes pyramidalization at the phosphorus atom.

For the *binuclear coordination*, the various modes for complexation at the phosphorus as shown in Scheme 6 are possible.

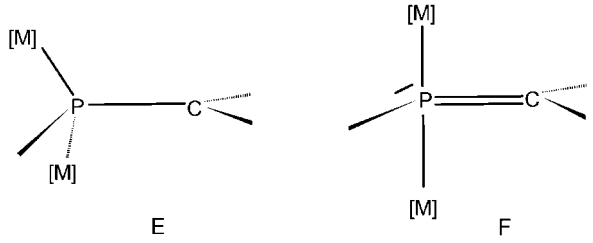

Scheme 6

In **E** the phosphorus atom adopts a tetrahedral coordination with equal bond angles [M]−P−C. In **F** the phosphorus atom adopts a trigonal bipyramid with one lone pair in an equatorial position. In principle, the stereochemical activity of the phosphorus lone pair can lead to such conformations.[46] However, the electropositive transition metal fragment would occupy the axial rather than the equatorial positions. This would be uncommon for a trigonal bipyramid. In any case, one expects for all three alternatives, **D** to **F**, a longer P−C bond than for the mononuclear cases since the phosphorus atom has now to provide a second lone pair for coordination. It becomes only available by adopting the limiting structure **b**.

A binuclear chromium complex of $F_3CP{=}C(F)NMe_2$ has been reported recently.[20] The P−[M] distances are 2.459, 2.457 Å, with Cr−P−Cr = 127.5° and Cr−P−C = 113.5, 104.6°. Thus, this structures has been addressed as a (η^1-μ_2)-4e-complex. Concomitantly the P−C bond results in a value of 1.859 Å, which is in the range of the length of a P−C single bond (exp. 1.82−1.86 Å).[47]

We have studied the binuclear case for [M] = $Cr(CO)_5$ at (*C*-amino)methylenephosphane. A Molden plot[48] of the resulting equilibrium geometry is shown in Figure 2.

Only the case where the transition metal fragment was situated *trans* to the amino group at the carbon atom was studied, in order to mimic the situation with the least steric hindrance. The P−C bond here is sizeably longer (1.784 Å) than in the parent compound or in the mononuclear congener (see Figure 1), however also essentially shorter than in the experiment.[20] Interestingly, the angles [M]−P−C are

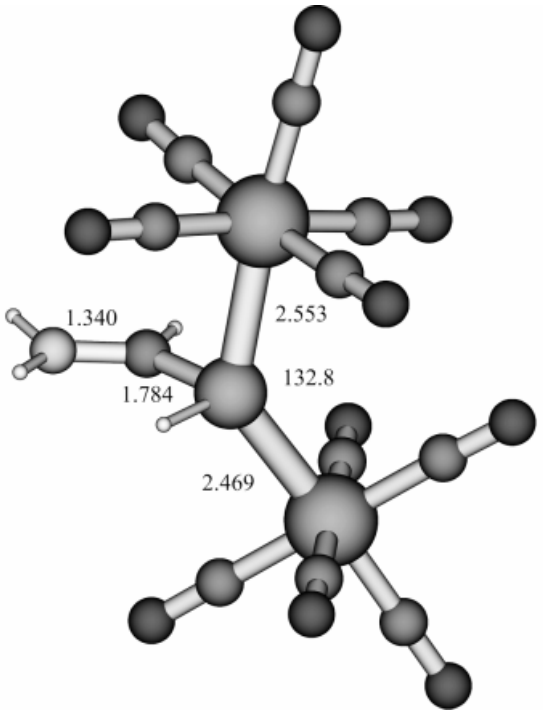

Figure 2. Molden plot of the chromium binuclear complex of *C*-aminomethylenephosphane

different (112.8, 88.2°), also the Cr−P distances are not equal (2.469, 2.553 Å) (see Figure 2). This indicates that the structure does not adopt type **D**, rather it prefers a bonding situation between **E** and **F**. In other words, the first transition metal fragment can easily coordinate to the lone pair of the phosphorus atom, however, the second transition metal fragment cannot bind strongly enough, such as to emphasise the limiting structure of **b** over **a**. It will be shown in the following section that steric effects also contribute to a further lengthening of the P−C bond in methylenephosphanes.

Accordingly, an amino group at the phosphorus atom shortens the [M]−P bond. It can be attributed to an increase of the p-character of the lone pair. On this basis the phosphorus atom changes from p^3-hybridization[32,49] (R−P−C = 90°) to sp^2-hybridization (R−P−C = 120°). This is already witnessed in the structures of the transition metal free methylenephosphanes. The amino substitution at the phosphorus atom causes an opening of the angle at P, as compared with the parent methylenephosphane. In the experimentally reported structure of the binuclear chromium complex the M−Cr distances as well as the angles of the transition metal centres with the P−C bond are almost equal. Thus, our investigations make it likely that the crucial structural effect on bicoordination is exerted by the electron-withdrawing substituent at the phosphorus atom. The energy quantities for coordination of a second $Cr(CO)_5$ fragment in addition to the η^1-complex of *C*-aminomethylenephosphane are: $\Delta E = -20.8$, $\Delta G = -8.0$, $\Delta E_{prep} = 1.4$ kcal/mol. Hence the second metal coordination is essentially less favored than the first metal coordination. The preparation energy, i.e., the energy mainly required to stretch the P−C π-bond is rather small. It is evident that the η^1/η^2- or η^1/η^1-coordination will preferentially take place for inversely polarized methylenephosphanes, since the energy contributions ΔE_{prep}, i.e., the energy to stretch the P−C π-bond can be expected to be small. Our analysis is in agreement with the wealth of experimental data available on transition metal coordination of the P−C systems.[8]

There is a further aspect that must be considered here, that is the electron distribution in the various coordination compounds. In the η^1-complexes, the $M(CO)_5$ fragments are only weakly bound to the phosphorus atom. The Wiberg bond indices yield a result for the [M]−P bond of approximately 0.5 which indicate a rather weak bond. These values are almost independent on the nature of the transition metal (Cr, Mo, W). Overall −0.4 e flow from the ligand (methylenephosphane) into the $M(CO)_5$ fragment. In other words, the latter acts only as a poor electron acceptor. Again, it is not essentially effected by the nature of the transition metal, e.g., for η^1-coordination at the *C*-aminomethylenephosphane the following Wiberg bond orders and flow of electron densities result: Wiberg bond order (Δ charge) Cr 0.411 (−0.438), Mo 0.437 (−0.374), W 0.434 (−0.376). Thus, the $Cr(CO)_5$ fragment is the slightly stronger electron acceptor, although the $W(CO)_5$ fragment binds slightly stronger to the methylenephosphanes. With respect to the electron distribution in the transition metal complexes we will now report our results on the Laplacians (Figure 3).

Figure 3 (top) views the Laplacian of the electron density of Cr bound to the phosphorus atom as well as in plane with the carbon atom. The bond-critical point is at the phosphorus atom that indicates a bond of the lone pair at P towards the transition metal centre. In comparison to the coordination of the second transition metal fragment, an essentially different electronic structure results (Figure 3, bottom). The bond-critical point is located within the triangle spanned by the atoms C, P, and Cr. It indicates that the second transition metal fragment binds simultaneously to the phosphorus and the carbon atom. Whether the second transition metal fragment coordinates according to type **E** or **F** thus depends largely on the preparation energy required to stretch the P−C π-bond.

b. Steric Effects

While it seems clear that monocoordination does not effect the P−C bond length, this, however, is the case for the addition of a second transition metal fragment, since a second lone pair at the phosphorus atom has to be provided. Alternatively in the coordination **C** to **F** the P−C π-bond is weakened. In practise the methylenephosphanes are substituted by bulky groups in order to kinetically protect the central π-bond. It is well established that the "naked" methylenephosphanes tend to undergo immediate reactions after generation.[50] To further analyze this aspect we performed quantum chemical calculations on a variety of differently substituted methylenephosphanes, at times utilizing the B3LYP/6-31g* level of approximation (see following Theoretical Section). The most important bonding para-

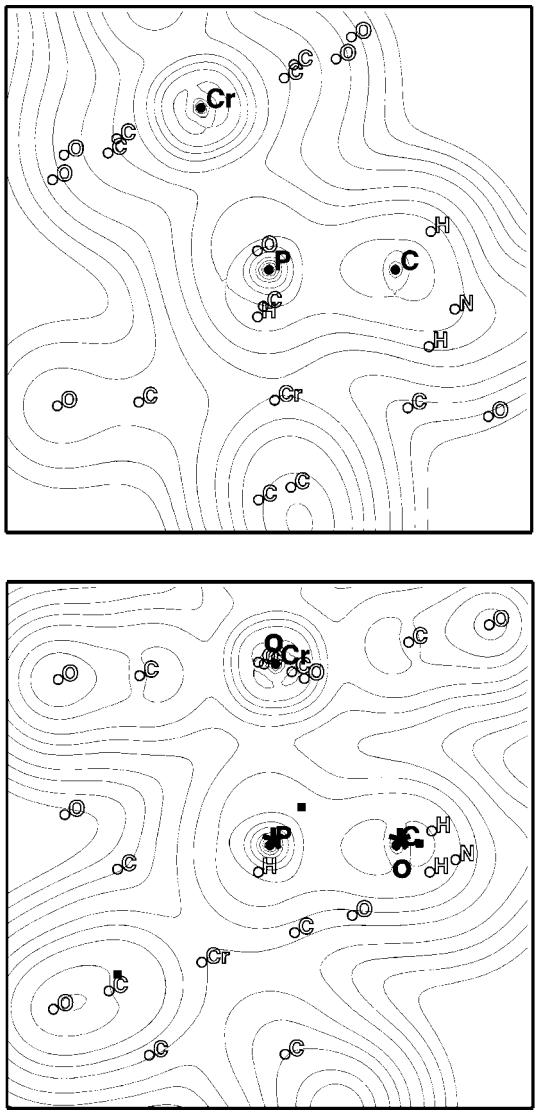

Figure 3. Laplacian of the electron density distribution for $Cr(CO)_5$ complex formation with *C*-aminomethylenephosphane; top: first transition metal fragment (with a large angle bound to the phosphorus atom); bottom: second transition metal fragment (with a small angle bound to the phosphorus atom)

meters are the P−C bond lengths and the R−P−C angles; these are collected in Table 2.

The amino groups at the carbon atom sizeably extend the P−C bond lengths. The effect is largely electronic. Two amino groups increase the P−C distance to 1.742 Å, but the further substitution by sterically demanding isopropyl groups does not essentially continue this tendency. Still the resulting equilibrium bond lengths are shorter than the largest value (1.805 Å) obtained for the binuclear metal complex.[20] According to our investigations the stretching of the P−C bond does not require much energy. Consequently the actual P−C bond lengths are determined by the bonding state in the crystal.

The alkyl substitution in the phosphaalkenes has a further effect, it induces a twisting of the π-bond. The matter is illustrated for the case R^1 = *i*Pr and $R^2 = R^3 = NiPr_2$ in a Molden plot of the computed equilibrium geometry

Table 2. Relevant bonding parameters of various alkyl-substituted phosphaalkenes (bond lengths [Å], bond angles [°]), computed at B3LYP/6-31 g(d) level

R^1(P)	R^2(C)[a]	R^3(C)[b]	P−C	R−P−C
H	H	H	1.674	97.7
H	NH_2	H	1.715	95.5
H	H	NH_2	1.721	93.8
H	NH_2	NH_2	1.742	94.5
H	NMe_2	NMe_2	1.749	96.0
Me	NMe_2	NMe_2	1.744	103.0
Me	$NiPr_2$	$NiPr_2$	1.752	103.2
*i*Pr	$NiPr_2$	$NiPr_2$	1.751	104.8
Me	H	NH_2	1.728	97.2
SiF_3	H	NH_2	1.735	94.7
CF_3	H	NH_2	1.716	97.2
F	H	NH_2	1.701	99.1

[a] *cis* to R^1(P). − [b] *trans* to R^1(P).

(Figure 4). The substituents at the phosphorus and carbon atoms exert considerable mutual steric hindrance, such as to induce rotation at the amino groups (Figure 4, top). As a further consequence, the P−C π-bond starts rotating (Figure 4, bottom).

Conclusion

The results of our investigations can be summarized as follows:

(1) For π-conjugation of an amino group with the π-bond in methylenephosphane an essential lengthening of the P−C bond is observed for the case of substitution of an amino group at the carbon atom. It is due to the stronger N−C π-bond compared with the P−C π-bond that makes the stronger N−C π-conjugation feasible. This refers to the case of *inverse polarized* PC π-bonds.

(2) The mononuclear transition metal coordination causes only slight changes in the equilibrium geometries of the free ligands, resulting in small preparation energies required for coordination. The phosphorus atom remains essentially planar. However, for the case of amino substitution at the carbon atom, the phosphorus atom accumulates negative charge. As a consequence the latter are slightly pyramidal in the coordinated compounds and [M]−P is also slightly longer compared to the other cases.

(3) For the binuclear complexes the first transition metal fragment is coordinated to the phosphorus lone pair and the second fragment to the P−C π-bond. Consequently, the second fragment is weaker bound than the first fragment. The second fragment can easily slip from η^1- to η^2-coordination.

(4) Sterically demanding alkyl groups cause a further lengthening of the P−C π-bond. Concomitantly a twisting of the P−C π-bond is induced.

Theoretical Section

All structures were fully optimized at the B3LYP[51,52] level. For the description of the metal complexes the effect-

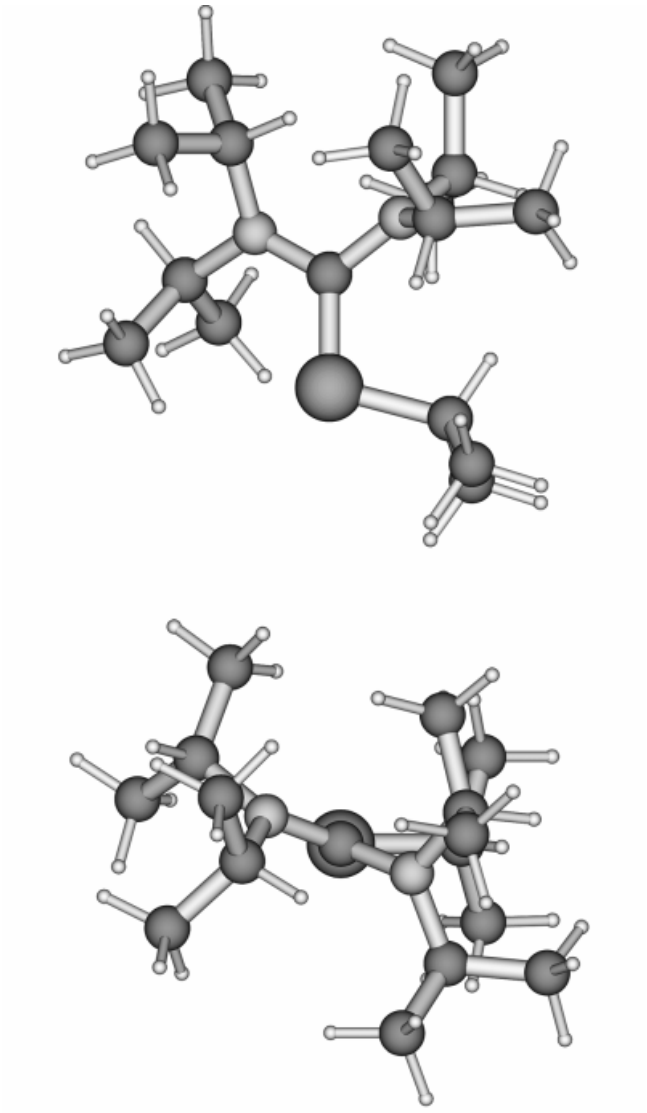

Figure 4. Molden plot of a substituted phosphaalkene (R^1 = *i*Pr; $R^2 = R^3$ = N*i*Pr$_2$)

ive core potential basis sets of Stevens, Basch, and Krauss,[53,54] were augmented by one set of polarization functions (of d-type) for the heavy (non-hydrogen) main group elements [SBK(d) basis]. The use of polarization functions is imperative to obtain a correct description of the polar [M]−P bond. All stationary points were characterized as local minima by inspection of the eigenvalues of the corresponding Hessian matrices calculated at the DFT level. The free energy contributions were evaluated using standard thermodynamic formulae and refer to contributions at 25° C (room temperature). For the cases of the uncomplexed methylenephosphanes which are substituted by bulky substituents [see Section (b)] we employed the 6-31g(d) basis set.[55] For the population analyses the NBO partitioning scheme[56] was used. Further investigations of the electron density distributions were performed with the method of "atoms in molecules".[57] All calculations were performed using the Gaussian 98 package of programs.[58]

Acknowledgments

This work has been supported by the Deutsche Forschungsgemeinschaft and the Fonds der Chemischen Industrie.

[1] K. Dimroth, P. Hoffmann, *Angew. Chem.* **1964**, *76*, 433−512; *Angew. Chem. Int. Ed. Engl.* **1964**, *3*, 384. K. Dimroth, P. Hoffmann, *Chem. Ber.* **1966**, *99*, 1325−1331.
[2] G. Becker, *Z. Anorg. Allg. Chem.* **1976**, *423*, 242−254.
[3] L. N. Markovskii, V. D. Romanenko, *Tetrahedron* **1989**, *45*, 6019−6090.
[4] R. Appel, F. Knoll, I. Ruppert, *Angew. Chem.* **1981**, *93*, 771−784; *Angew. Chem. Int. Ed. Engl.* **1981**, *20*, 731.
[5] M. Reitz, B. Weber, *Methoden Org. Chem. (Houben-Weyl)* **1982**, vol. E1, pp. 27−31.
[6] L. N. Markovskii, V. D. Romanenko, A. V. Ruban, *The Chemistry of Acyclic Twofold Coordinated Phosphorus Compounds*, Kiev, **1988** (in Russian).
[7] M. Regitz, O. J. Scherer (Eds.), *Multiple Bonds and Low Coordination in Phosphorus Chemistry*, Thieme, Stuttgart, **1990**.
[8] K. B. Dillon, F. Mathey, J. F. Nixon, *Phosphorus: The Carbon Copy*, Wiley, Chichester, **1998**.
[9] F. Mathey, *J. Organomet. Chem.* **1997**, *529*, 1; see following publications.
[10] H. Estiagh-Hosseini, H. W. Kroto, J. F. Nixon, M. J. Maah, M. J. Taylor, *J. Chem. Soc., Chem. Commun.* **1981**, 199−200.
[11] T. C. Klebach, R. Lourens, F. Bickelhaupt, C. H. Stam, A. van Herk, *J. Organomet. Chem.* **1981**, *210*, 211−221.
[12] J.-P. Majoral, R. Mathieu, A.-M. Caminade, S. Attali, M. Sanchez, *Phosphorus Sulfur* **1987**, *30*, 443.
[13] Th. A. van der Knaap, F. Bickelhaupt, H. van der Poel, G. van Koten, C. H. Stam, *J. Am. Chem. Soc.* **1982**, *105*, 1756−1757.
[14] H. W. Kroto, S. I. Klein, M. F. Meidine, J. F. Nixon, R. K. Harris, K. J. Packer, P. Reams, *J. Organomet. Chem.* **1985**, *280*, 281−287.
[15] J. F. Nixon, *Chem. Rev.* **1988**, *88*, 1327−1362.
[16] E. Niecke, H.-J. Metternich, M. Nieger, D. Gudat, P. Wenderoth, W. Malisch, C. Hahner, W. Reich, *Chem. Ber.* **1993**, *126*, 1299−1309.
[17] A. L. Spek, A. J. M. Duisenberg, *Acta Crystallogr., Sect. C* **1987**, *43*, 1216−1219.
[18] M. H. A. Benvenutti, N. Cenac, J. F. Nixon, *Chem. Commun.* **1997**, 1327.
[19] R. Appel, C. Casser, F. Knoch, *J. Organomet. Chem.* **1985**, *293*, 213−217.
[20] J. Grobe, D. Le Van, B. Krebs, R. Fröhlich, A. Schiemann, *J. Organomet. Chem.* **1990**, *389*, C29−C33.
[21] I.-P. Lorenz, W. Pohl, H. Nöth, M. Schmidt, *J. Organomet. Chem.* **1994**, *475*, 211−221.
[22] S. Creve, K. Pierloot, M. T. Nguyen, L. G. Vanquickenborne, *Eur. J. Inorg. Chem.* **1999**, 107−115.
[23] S. Creve, M. T. Nguyen, L. G. Vanquickenborne, *Eur. J. Inorg. Chem.* **1999**, 1281−1289.
[24] W. W. Schoeller, E. Niecke, *J. Chem. Soc., Chem. Commun.* **1982**, 569−570.
[25] W. W. Schoeller, *J. Chem. Soc., Chem. Commun.* **1985**, 334−335.
[26] E. Niecke, D. Gudat, W. W. Schoeller, P. Rademacher, *J. Chem. Soc., Chem. Commun.* **1985**, 1050−1051.
[27] D. Gudat, E. Niecke, W. Sachs, P. Rademacher, *Z. Anorg. Allg. Chem.* **1987**, *545*, 7−23.
[28] S. Lacombe, D. Gonbeau, J.-L. Cabioch, B. Pellerin, J.-M. Denis, G. Pfister-Guillouzo, *J. Am. Chem. Soc.* **1988**, *110*, 6964−6967.
[29] H. Bock, M. Bankmann, *Angew. Chem.* **1986**, *98*, 287−288; *Angew. Chem. Int. Ed. Engl.* **1986**, *25*, 265.
[30] G. Davis, V. von der Gönna, E. Niecke, T. Busch, W. W. Schoeller, P. Rademacher, *J. Chem. Soc., Faraday Trans.* **1984**, *90*, 2611−2618.

[31] J. Grobe, D. L. Van, U. Althoff, B. Krebs, M. Dartmann, R. Gleiter, *Heteroatom Chem.* **1991**, *2*, 385−394.
[32] W. Kutzelnigg, *Angew. Chem.* **1984**, *96*, 262−286; *Angew. Chem. Int. Ed. Engl.* **1984**, *23*, 272.
[33] M. W. Schmidt, Phi N. Truong, M. S. Gordon, *J. Am. Chem. Soc.* **1987**, *109*, 5217−5227. T. L. Windus, M. S. Gordon, *J. Am. Chem. Soc.* **1992**, *114*, 9559−9568.
[34] W. W. Schoeller, C. Begemann, U. Tubbesing, J. Strutwolf, *J. Chem. Soc., Faraday Trans.* **1997**, *93*, 2957−2962.
[35] L. Pauling, *The Nature of the Chemical Bond*, Cornell University Press, New York, **1960**.
[36] This concept (ref.[25]) has been first coined explicitely as an *inverse polarization* in the discussion on the electronic properties of phosphatriafulvenes: E. P. O. Fuchs, H. Heydt, M. Regitz, W. W. Schoeller, T. Busch, *Tetrahedron Lett.* **1989**, *30*, 5111−5114; E. Fuchs, B. Breit, H. Heydt, W. W. Schoeller, T. Busch, C. Krüger, P. Betz, M. Regitz, *Chem. Ber.* **1991**, *124*, 2843−2855.
[37] L. Weber, *Eur. J. Inorg. Chem.* **2000**, 2425−2441.
[38] L. Weber, S. Uthmann, H.-G. Stammler, B. Neumann, W. W. Schoeller, R. Boese, D. Bläser, *Eur. J. Inorg. Chem.* **1999**, 2369−2381.
[39] A. N. Chernega, A. V. Ruban, V. D. Romanenko, L. N. Markovski, A. A. Korkin, M. Yu. Antipin, Y. T. Struchkov, *Heteroatom Chem.* **1991**, *2*, 229−241.
[40] J. Grobe, D. L. Van. J. Nientedt, B. Krebs, M. Dartmann, *Chem. Ber.* **1988**, *121*, 655−664.
[41] L. Weber, *Phosphaalkenes with Inverse Electron Density*; for a full account see ref.[37].
[42] T. A. Albright, J. K. Burdett, M. H. Whangbo, *Orbital Interaction in Chemistry*, Wiley-Interscience, New York **1985**.
[43] Ch. Elschenbroich, A. Salzer, *Organometallchemie*, Teubner, Stuttgart, **1986**.
[44] W. W. Schoeller, D. Eisner, S. Grigoleit, A. B. Rozhenko, A. Alijah, *J. Am. Chem. Soc.* **2000**, *122*, 10115−10120.
[45] T. Ziegler, A. Rauk, *Theor. Chim. Acta* **1977**, *46*, 1−10. T. Ziegler, A. Rauk, *Inorg. Chem.* **1979**, *18*, 1558−1565.
[46] W. W. Schoeller, A. Sundermann, M. Reiher, *Inorg. Chem.* **1999**, *38*, 29−37, and refs. cited therein.
[47] A. F. Wells, *Structural Inorganic Chemistry*, 4th ed., Clarendon Press, Oxford, **1975**, pp. 234.
[48] G. Schaftonaar, *Molden*, www.caos.kun.nl/~schaft/molden.html.
[49] W. W. Schoeller, in: *Multiple Bonds and Low Coordination in Phosphorus Chemistry* (Eds.: M. Regitz, O. J. Scherer), Thieme Verlag, Stuttgart, **1990**.
[50] M. J. Hopkinson, H. W. Kroto, J. F. Nixon, N. P. C. Simmons, *J. Chem. Soc., Chem. Commun.* **1976**, 513−515.
[51] A. D. Becke, *J. Chem. Phys.* **1993**, *98*, 5648−5653.
[52] C. Lee, W. Yang, R. G. Parr, *Phys. Rev. B* **1988**, *37*, 785−789.
[53] W. J. Stevens, H. Basch, M. Krauss, *J. Chem. Phys.* **1984**, *81*, 6026−6033.
[54] W. J. Stevens, M. Krauss, H. Basch, P. G. Jasien, *Can. J. Chem.* **1992**, *70*, 612−630.
[55] P. C. Hariharan, J. A. Pople, *Theor. Chim. Acta* **1973**, *28*, 213−222.
[56] A. E. Reed, L. A. Curtiss, F. Weinhold, *Chem. Rev.* **1988**, *88*, 899−926.
[57] R. F. W. Bader, *Atoms in Molecules*, Clarendon Press, Oxford, **1994**.
[58] M. J. Frisch, G. W. Trucks, H. B. Schlegel, G. E. Scuseria, M. A. Robb, J. R. Cheeseman, V. G. Zakrzewski, J. A. Montgomery, R. E. Stratmann, J. C. Burant, S. Dapprich, J. M. Millam, A. D. Daniels, K. N. Kudin, M. C. Strain, O. Farkas, J. Tomasi, V. Barone, M. Cossi, R. Cammi, B. Mennucci, C. Pomelli, C. Adamo, S. Clifford, J. Ochterski, G. A. Petersson, P. Y. Ayala, Q. Cui, K. Morokuma, D. K. Malick, A. D. Rabuck, K. Raghavachari, J. B. Foresman, J. Cioslowski, J. V. Ortiz, B. B. Stefanov, G. Liu, A. Liashenko, P. Piskorz, I. Komaromi, R. Gomperts, R. L. Martin, D. J. Fox, T. Keith, M. A. Al-Laham, C. Y. Peng, A. Nanayakkara, C. Gonzalez, M. Challacombe, P. M. W. Gill, B. G. Johnson, W. Chen, M. W. Wong, J. L. Andres, M. Head-Gordon, E. S. Replogle, J. A. Pople, *Gaussian 98 (Revision A.1)*, Gaussian Inc., Pittsburgh PA, **1998**.

Received May 31, 2001
[I01221]

Reactivity of $[Ru_3(\mu_3\text{-NPh})(\mu_3\text{-CO})(CO)_9]$ towards Activated Alkynes and Diynes − Isolation of a Trinuclear Intermediate During the Formation of Bi- and Tetranuclear Products

Javier A. Cabeza,*[a] Ignacio del Río,[a] Santiago García-Granda,[b] Marta Moreno,[a] Víctor Riera,[a] María de Jesús Rosales-Hoz,[c] and Marta Suárez[a]

Keywords: Ruthenium / Imido complexes / Cluster compounds / Alkynes / Diynes

Treatment of the trinuclear imido-bridged cluster compound $[Ru_3(\mu_3\text{-NPh})(\mu_3\text{-CO})(CO)_9]$ (**1**) with activated alkynes (methyl propynoate and methyl phenylpropynoate) and diynes (diphenylbutadiyne, 2,4-hexadiyne, 1,6-diphenyloxy-2,4-hexadiyne, and 1-trimethylsilyl-1,4-pentadiyne) in hexanes at reflux temperature leads to separable mixtures of the tetranuclear and binuclear derivatives $[Ru_4(\mu_4\text{-NPh})(\mu_4,\eta^2\text{-RC}{\equiv}\text{CR}')(\mu\text{-CO})_2(CO)_9]$ and $[Ru_2\{\mu,\eta^3\text{-RC=CR}'\text{C(O)NPh}\}(CO)_6]$, respectively. While the former complexes feature a phenylimido ligand in a rather rare μ_4-coordination mode, the binuclear compounds contain acrylamido ligands that result from the coupling of a CO ligand and the original phenylimido ligand of **1** with the incoming alkyne or diyne. Surprisingly, all the products derived from diynes contain a pendant (non-coordinated) alkyne functionality. The isolation of the trinuclear derivative $[Ru_3(\mu_3\text{-NPh})(\mu_3,\eta^2\text{-PhC}{\equiv}\text{CC}{\equiv}\text{CPh})(CO)_9]$ (**9**) in the reaction of **1** with diphenylbutadiyne and the fact that its thermolysis leads to a mixture of $[Ru_4(\mu_4\text{-NPh})(\mu_4,\eta^2\text{-PhC}{\equiv}\text{CC}{\equiv}\text{CPh})(\mu\text{-CO})_2(CO)_9]$ and $[Ru_2\{\mu,\eta^3\text{-C(C}{\equiv}\text{CPh)=C(Ph)C(O)NPh}\}(CO)_6]$ support the proposal that trinuclear species containing coordinated alkyne or diyne ligands, similar to **9**, are intermediates in the synthesis of all the bi- and tetranuclear products. Only one of the two possible regioisomers of each product (that might have arisen from the asymmetry of the alkyne or diyne reagents used) is formed. The origin of this regioselectivity is also discussed.

Introduction

Carbon−nitrogen bond formation assisted by metal cluster complexes has emerged as a powerful tool for the synthesis of novel organic fragments.[1−12] The cluster precursors often contain amido (NR_2)[1,2] or imido (NR)[4−12] ligands, which constitute the nitrogen source for the synthesis of new N-containing organic fragments. In other cases, C−N bond-forming reactions have been achieved by attack of nitrogen nucleophiles (e.g. RNH_2, R_2NH) on coordinated unsaturated hydrocarbyls such as alkynyls, allenyls, etc.[3] In some cases, these assemblies have been successfully separated from the metallic core, yielding interesting heteronuclear organic molecules.[4−8]

Interesting reactions of face-capping organoimido ligands (μ_3-NR) in cluster complexes have been reported. These ligands can easily combine with a variety of other ligands such as hydrides,[13] carbenes,[5,14] acyls,[5,8] carbonyls,[7,10] methoxycarbonyls,[5] or alkynes[4,11] to give organic compounds such as imidates, amides, amines, carbamates, isocyanates, pyridinones, or ureas. In this context, Geoffroy et al. have reported on the reactivity of the trinuclear imido cluster $[Ru_3(\mu_3\text{-NPh})(\mu_3\text{-CO})(CO)_9]$ (**1**) with the internal alkynes diphenylacetylene and methylphenylacetylene.[4] These reactions afforded, among other noteworthy products, binuclear metallapyrrolidone complexes from which pyridinone or maleimide derivatives could subsequently be obtained by treating them with further alkyne or CO, respectively.[4]

Recently, our group has been paying attention to the reactivity of diynes with ruthenium carbonyl cluster complexes containing N-donor ligands.[2,15] To date, only a few reactions of ruthenium clusters with diynes have appeared in the literature,[2,15−17] though these ligands are expected to be more reactive than monoalkynes and, therefore, to offer a richer derivative chemistry.

The interesting results obtained by Geoffroy et al. in the reactions of **1** with non-activated internal alkynes[4] prompted us to study its reactivity towards activated alkynes and diynes, the aim being to prepare new derivatives made accessible by the enhanced reactivity expected for these unsaturated molecules as compared to simple non-activated monoalkynes.

We report herein the synthesis and structural characterization of a series of new bi-, tri-, and tetranuclear ruthenium cluster complexes derived from **1** and activated alkynes or diynes. The regioselectivity of the reactions, which

[a] Departamento de Química Orgánica e Inorgánica, Instituto de Química Organometálica "Enrique Moles", Universidad de Oviedo,
33071 Oviedo, Spain
Fax: (internat.) + 34-985/103446
E-mail: jac@sauron.quimica.uniovi.es
[b] Departamento de Química Física y Analítica, Universidad de Oviedo,
33071 Oviedo, Spain
[c] Departamento de Química, CINVESTAV-IPN,
Apartado Postal 14−740, 07000 México D.F., México

 © WILEY-VCH Verlag GmbH, 69451 Weinheim, 2001 1434−1948/01/1111−2899 $ 17.50+.50/0

give only one of the two possible regioisomers of each product (that might arise from the asymmetry of the alkyne or diyne reagents used) is discussed. This work also demonstrates that trinuclear alkyne or diyne complexes are intermediates in the synthesis of the final bi- and tetranuclear products.

Results and Discussion

Synthesis and Characterization of the Compounds

It has been reported that compound **1** can be prepared following different synthetic procedures, i.e. by treating $[Ru_3(CO)_{12}]$ with phenyl isocyanate,[18] nitrobenzene,[18,19] or nitrosobenzene,[20] or by treating the more reactive $[Ru_3(MeCN)(CO)_{11}]$ with nitrosobenzene.[8] However, the first three methods afford compound **1** in only moderate to low yields and it is invariably accompanied by considerable amounts of the diimido derivative $[Ru_3(\mu_3\text{-}NPh)_2(CO)_9]$. In our hands, the best yields (up to 40%) were obtained starting from $[Ru_3(MeCN)(CO)_{11}]$ and nitrosobenzene, following a modification of the published method (see Exp. Section).[8]

Treatment of a solution of **1** with an excess of methyl propynoate in refluxing hexanes afforded a mixture of compounds, from which the derivatives $[Ru_4(\mu_4\text{-}NPh)\{\mu_4,\eta^2\text{-}C(CO_2Me)\equiv CH\}(\mu\text{-}CO)_2(CO)_9]$ (**2**) and $[Ru_2\{\mu,\eta^3\text{-}C(CO_2Me)=CHC(O)NPh\}(CO)_6]$ (**3**) could be isolated by column chromatography (Scheme 1). In an analogous reaction, the compounds $[Ru_4(\mu_4\text{-}NPh)\{\mu_4,\eta^2\text{-}C(CO_2Me)\equiv CPh\}(\mu\text{-}CO)_2(CO)_9]$ (**4**) and $[Ru_2\{\mu,\eta^3\text{-}C(CO_2Me)=C(Ph)C(O)NPh\}(CO)_6]$ (**5**) were obtained by reaction of compound **1** with methyl phenylpropynoate.

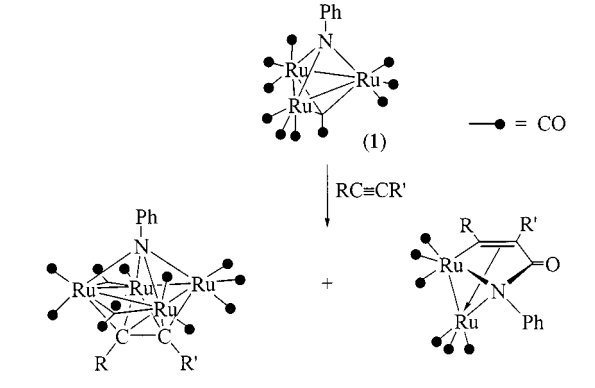

	R	R'
2	CO_2Me	H
4	CO_2Me	Ph
6	C≡CMe	Me
8	C≡CPh	Ph
11	$C{\equiv}CCH_2OPh$	CH_2OPh
12	$CH_2C{\equiv}CSiMe_3$	H

	R	R'
3	CO_2Me	H
5	CO_2Me	Ph
7	C≡CMe	Me
10	C≡CPh	Ph
13	$CH_2C{\equiv}CSiMe_3$	H

Scheme 1

The ^1H NMR spectra of the tetranuclear compounds **2** and **4** clearly indicate the absence of hydride ligands and confirm that only one molecule of alkyne is present per phenylimido ligand. Both compounds display the same pattern in the carbonyl stretching region of their IR spectra, showing the presence of terminal and bridging CO ligands. This IR pattern is analogous to that reported previously for the compounds $[Ru_4(\mu_4\text{-}NR)(\mu_4,\eta^2\text{-}PhC{\equiv}CPh)(\mu\text{-}CO)_2(CO)_9]$ (R = Ph,[21] H[22]), which were structurally characterized by X-ray diffraction methods.

As the alkyne ligands in **2** and **4** are asymmetric, an X-ray diffraction study was carried out on a single crystal of **4** in order to determine the ligand arrangement within the clusters. A molecular plot is shown in Figure 1. Selected bond lengths are listed in Table 1.

Table 1. Selected interatomic distances [Å] in compounds **4** and **8**

	4	**8**
Ru(1)−Ru(3)	2.6954(9)	2.6853(9)
Ru(1)−Ru(4)	2.6959(6)	2.684(1)
Ru(2)−Ru(3)	2.7136(6)	2.812(1)
Ru(2)−Ru(4)	2.7951(8)	2.726(1)
Ru(1)−N(3)	2.206(3)	2.201(4)
Ru(1)−C(2)	2.197(4)	2.223(5)
Ru(1)−C(1P)	2.082(4)	2.288(6)
Ru(1)−C(2P)	2.299(4)	2.076(4)
Ru(2)−N(3)	2.145(3)	2.148(4)
Ru(2)−C(1)	2.133(4)	2.114(5)
Ru(3)−N(3)	2.210(3)	2.256(4)
Ru(3)−C(1)	2.397(4)	2.407(5)
Ru(3)−C(2)	2.246(4)	2.299(5)
Ru(3)−C(2P)	1.999(4)	2.034(5)
Ru(4)−N(3)	2.255(3)	2.256(4)
Ru(4)−C(1)	2.333(4)	2.364(5)
Ru(4)−C(2)	2.270(4)	2.281(5)
Ru(4)−C(1P)	2.019(4)	2.004(5)
C(1)−C(2)	1.427(5)	1.424(7)
C(2)−C(3)	1.496(6)	1.427(4)
C(3)−C(4)	−	1.193(7)
C(3)−O(1)	1.190(5)	−
C(3)−O(2)	1.335(6)	−
C(4)−O(2)	1.444(7)	−

The four Ru atoms of **4** define a distorted square, forming a dihedral Ru(1)−Ru(3)−Ru(4)−Ru(2) angle of 19.5°. The Ru−Ru distances range from 2.695 to 2.795 Å. Two CO ligands span the Ru(1)−Ru(3) and Ru(1)−Ru(4) edges. The phenylimido ligand bridges the four metal atoms, while the alkyne ligand is positioned on the opposite face of the metal core, binding the four Ru atoms in an η^2-fashion, in such a way that it is σ-bonded to Ru(1) and Ru(2) and π-bonded to Ru(3) and Ru(4). The C(2) atom of the alkyne ligand, which bears the CO_2Me group, is attached to the three Ru atoms that bear the bridging carbonyl ligands, while the CPh fragment is bonded to Ru(2), Ru(3), and Ru(4). The cluster shell is completed by nine terminal CO ligands. The structure of **4** resembles those reported previously for the complexes $[Ru_4(\mu_4\text{-}NR)(\mu_4,\eta^2\text{-}PhC{\equiv}CPh)(\mu\text{-}CO)_2(CO)_9]$ (R = Ph,[21] H[22]), which contain a symmetrical alkyne ligand.

The μ_4-coordination mode adopted by the phenylimido ligand in **2** and **4** is rather rare. Apart from the compounds mentioned above, a series of ruthenium compounds containing μ_4-imido ligands has been prepared by Wong et al.

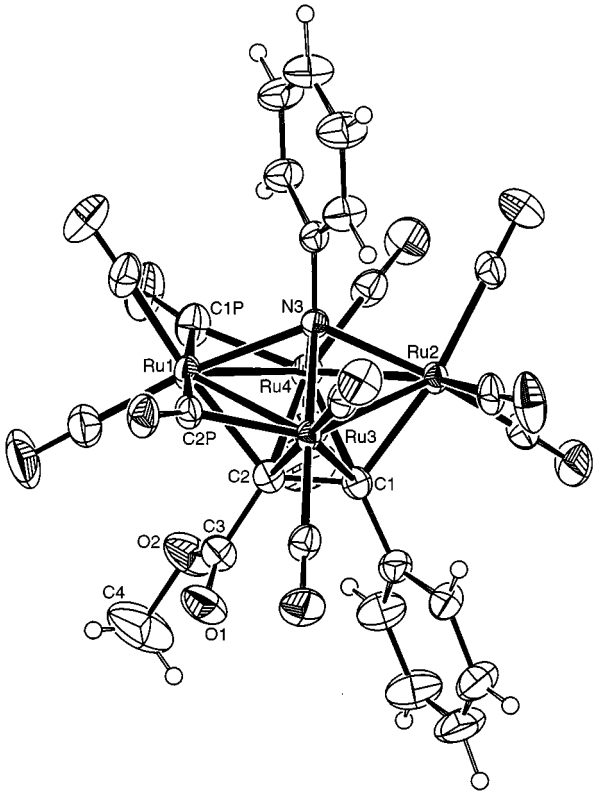

Figure 1. Molecular structure of compound **4**; ellipsoids are drawn at a 50% probability level

by deoxygenation reactions of the methoxyimido precursor $[Ru_3(\mu_3\text{-NOMe})(\mu_3\text{-CO})(CO)_9]$.[12] Further examples of μ_4-imido complexes are the heteronuclear derivative $[WO(\eta^5\text{-}C_5H_5)(\mu\text{-O})Ru_4(\mu_4\text{-NPh})(\mu_4,\eta^2\text{-CCPh})(CO)_{10}]$[23] and the iron complex $[Fe_4(\mu_4\text{-NEt})(\mu,\eta^2\text{-ONEt})(CO)_{11}]$.[24]

The other two complexes isolated from the reactions of **1** with monoalkynes are the binuclear derivatives **3** and **5**. Their elemental analyses and mass spectra clearly indicate their binuclear nature, while their ^1H NMR spectra show the incorporation of only one molecule of alkyne per phenylimido ligand. A comparison of the ^1H and ^{13}C NMR spectra of both compounds with those of other related binuclear metallapyrrolidone complexes[9,11,12a] also indicates that the CO_2Me group is attached to the C_α carbon atom. Both compounds display the same IR pattern in the carbonyl stretching region, suggesting an analogous ligand arrangement. This IR pattern is similar to that reported previously for other binuclear metallapyrrolidone ruthenium[4,11,12a] and iron[9,25] compounds. All these data are in accordance with the structures proposed for **3** and **5** in Scheme 1, and are also supported by an X-ray structural characterization of a related compound (vide infra).

Similar coupling reactions of imido ligands with CO and alkynes to give binuclear metallapyrrolidone compounds have also been reported for rhodium,[26] although in this case the coordination sphere of the metal atoms is not completed by carbonyl but by cyclopentadienyl ligands.

The reactivity of **1** towards 2,4-hexadiyne, diphenylbutadiyne, 1,6-diphenyloxy-2,4-hexadiyne, and 1-trimethylsilyl-1,4-pentadiyne was studied. To our surprise, the diyne ligands exhibited the same reactivity pattern as the monoalkynes, leading to mixtures of the tetranuclear cluster compounds $[Ru_4(\mu_4\text{-NPh})(\mu_4,\eta^2\text{-RC}\equiv\text{CR}')(\mu\text{-CO})_2(CO)_9]$ (R = C≡CMe, R′ = Me, **6**; R = C≡CPh, R′ = Ph, **8**; R = $C\equiv CCH_2OPh$, R′ = CH_2OPh, **11**; R = $CH_2C\equiv CSiMe_3$, R′ = H, **12**; Scheme 1) and the binuclear metallapyrrolidones $[Ru_2\{\mu,\eta^3\text{-RC}{=}\text{CR}'\text{C(O)NPh}\}(CO)_6]$ (R = C≡CMe, R′ = Me, **7**; R = C≡CPh, R′ = Ph, **10**; R = $CH_2C\equiv CSiMe_3$, R′ = H, **13**; Scheme 1), which could be separated by chromatographic methods. In the case of 1,6-diphenyloxy-2,4-hexadiyne, only the tetranuclear derivative **11** could be satisfactorily isolated, while the corresponding binuclear compound could not be separated from uncharacterized impurities.

Interestingly, in the reaction of **1** with diphenylbutadiyne, a novel trinuclear derivative, subsequently characterized as $[Ru_3(\mu_3\text{-NPh})(\mu_3,\eta^2\text{-PhC}\equiv\text{CC}\equiv\text{CPh})(CO)_9]$ (**9**), could be isolated in addition to the aforementioned tetranuclear and binuclear compounds **8** and **10**.

The IR spectra of the tetranuclear compounds **6**, **8**, **11**, and **12** are reminiscent of those of compounds **2** and **4**, indicating a similar ligand arrangement. This was confirmed by an X-ray diffraction study carried out on a single crystal of **8**. A molecular plot is shown in Figure 2 and selected bond lengths are listed in Table 1. For quick comparison purposes, and as far as possible, similar numbering schemes have been used for **4** and **8**. The structure of **8** is entirely analogous to that of compound **4**. Again, the car-

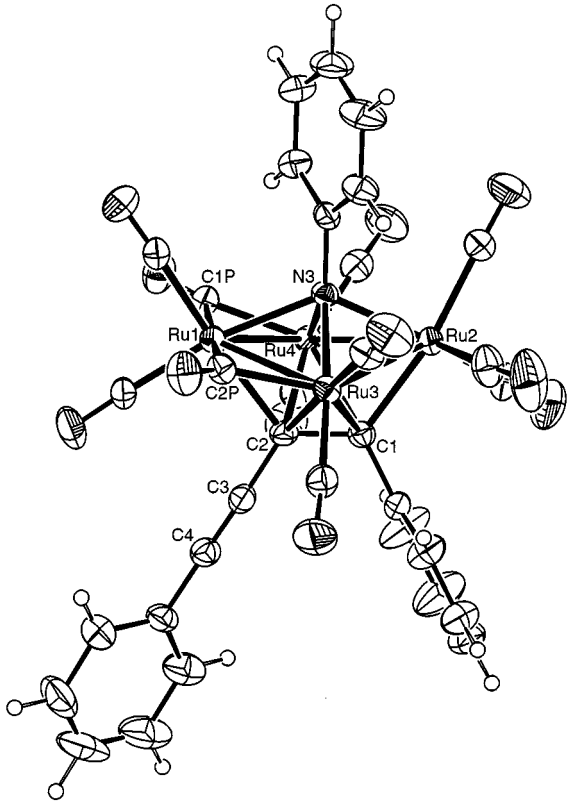

Figure 2. Molecular structure of compound **8**; ellipsoids are drawn at a 50% probability level

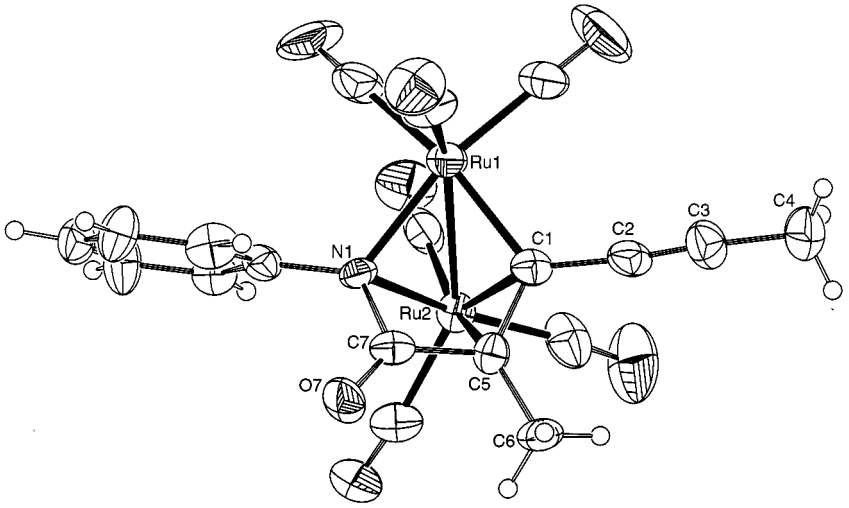

Figure 3. Molecular structure of compound **7**; ellipsoids are drawn at a 50% probability level

bon atom bearing the most electron-withdrawing substituent of the coordinated alkyne, the C≡CPh group, is bonded to the three metal atoms that bear the bridging carbonyl ligands.

The structures of the binuclear ruthenapyrrolidones **7**, **10**, and **13** are analogous to those described above for compounds **3** and **5**. The positions of the substituents attached to the C_α and C_β carbon atoms of the metallapyrrolidone fragments were unambiguously determined on the basis of their ^{13}C and ^{1}H NMR spectra (Scheme 1). These data also compare well with those reported previously for related iron[9] and ruthenium[11,12a] compounds. This structural assignment was also supported by an X-ray structure determination carried out on a single crystal of **7**.

The structure of **7** is shown in Figure 3. Selected bond lengths are listed in Table 2. The compound consists of two ruthenium atoms bridged by an acrylamido ligand, which stems from the coupling of the original imido ligand, one of the C≡C bonds of the incoming diyne, and a carbonyl ligand. The molecule can be described as a ruthenapyrrolidone fragment attached to a ruthenium atom through the Ru, N, and both C atoms of the double bond, C(1) and C(5). The carbon atom C(1), bearing the noncoordinated C≡CMe group, is also σ-bonded to Ru(1). The coordination sphere of each metal atom is completed by three terminal CO ligands. The C(1)−C(5) distance, 1.42(2) Å, is within the range typical of coordinated double bonds, while the C(1)−Ru(1) bond length, 2.05(2) Å, is shorter than that corresponding to C(1)−Ru(2), 2.26(2) Å, reflecting σ- and π-interactions, respectively. The Ru(1)−Ru(2) distance, 2.682(2) Å, is appropriate for a single metal−metal bond.

Table 2. Selected interatomic distances [Å] in compound **7**

Ru(1)−Ru(2)	2.681(2)
Ru(1)−C(1)	2.05(2)
Ru(1)−N(1)	2.12(2)
Ru(2)−C(1)	2.26(2)
Ru(2)−C(5)	2.28(2)
Ru(2)−C(7)	2.57(2)
Ru(2)−N(1)	2.16(2)
N(1)−C(7)	1.48(2)
C(1)−C(2)	1.45(3)
C(1)−C(5)	1.42(2)
C(2)−C(3)	1.15(3)
C(3)−C(4)	1.48(3)
C(5)−C(6)	1.48(3)
C(5)−C(7)	1.48(3)
C(7)−O(7)	1.20(2)

The ^{1}H and $^{13}C\{^{1}H\}$ NMR spectra of the trinuclear compound **9** show the presence of the imido ligand and indicate the incorporation of one molecule of diyne into the cluster shell. Its trinuclear nature was revealed by its elemental analysis and mass spectrum, which shows the appropriate molecular ion isotopomers. The presence of nine carbonyl ligands was also deduced from its $^{13}C\{^{1}H\}$ NMR spectrum. The 50-electron count of the cluster is consistent with the presence of only two metal−metal bonds. Unfortunately, despite many attempts, we could not obtain crystals of **9** suitable for an X-ray diffraction study and the coordination mode of the diyne could not be unambiguously determined. However, its IR spectrum compares well with that reported previously for the imido-bridged cluster $[Ru_3(\mu_3\text{-}NOPh)(\mu_3,\eta^2\text{-}PhC{\equiv}CH)(CO)_9]$,[12a] which was structurally characterized by X-ray diffraction methods and which features the same ligand arrangement as that depicted for **9** in Scheme 2.

Regioselectivity of the Products

In all the reactions reported in this article, the use of asymmetric alkynes could have led to the formation of two regioisomers for each compound. However, *only one of the two possible regioisomers is selectively formed.* Diynes can also be considered as asymmetric alkynes, since all the isolated products derived from them contain a pendant (noncoordinated) alkyne fragment.

For the metallapyrrolidone complexes, electronic rather than steric effects seem to govern the exclusive formation

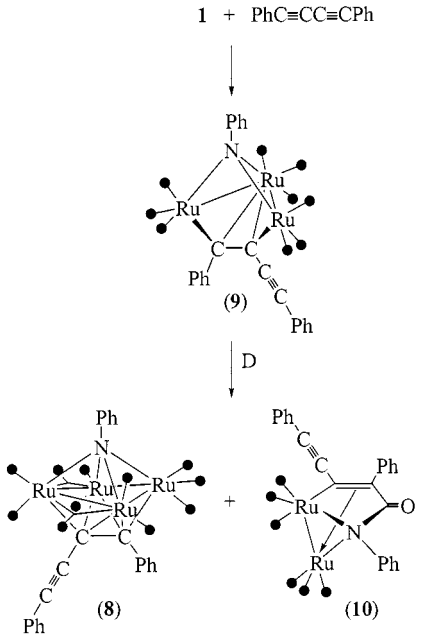

Scheme 2

of one of the two possible isomers in each case, since the group attached to the pyrrolidone C_α atom is always more electron-withdrawing than that attached to C_β, regardless of their volumes. This proposal is also in agreement with the results obtained by Geoffroy et al. for analogous derivatives, for which no explanations were given.[4]

In the case of the tetranuclear derivatives, again only one of the two possible isomers was observed in each case. In these complexes, the two alternative coordination modes of the alkynes or diynes are not expected to lead to marked differences in the spectroscopic data, and only in the compounds studied by X-ray diffraction methods could the ligand disposition be unambiguously determined. For the X-ray-characterized compounds **4** and **8**, it is found that the ruthenium atom that bears the two bridging CO ligands is attached to the carbon atom of the alkyne moiety that bears the most electron-withdrawing group, but, coincidentally, this group is also the smallest one in each case. It is also unfortunate that the two previously reported structures of related compounds are of complexes containing a symmetrical alkyne ligand, $[Ru_4(\mu_4\text{-NR})(\mu_4,\eta^2\text{-PhC}{\equiv}\text{CPh})(\mu\text{-CO})_2(CO)_9]$ (R = Ph,[21] H[22]). However, careful examination of the X-ray structures of all these tetranuclear complexes indicates that there is sufficient space at both ends of the C≡C moiety to accommodate the bulkier substituent. Therefore, electronic rather than steric effects must account for the observed regioselectivity. Accordingly, the assignment of the substituents shown in Scheme 1 for the tetranuclear derivatives is such that the most electron-withdrawing substituent of the alkyne is close to the ruthenium atom that bears the two bridging CO ligands, as found in the structurally characterized compounds **4** and **8**.

Insights into the Formation of the Bi- and Tetranuclear Compounds

The synthesis of the bi- and tetranuclear complexes appears to be initiated by coordination of the alkyne or diyne reagents to compound **1**, to generate trinuclear intermediates analogous to complex **9**. These 50-electron trimetallic intermediates seem to be highly unstable as they could only be isolated in the reaction with diphenylbutadiyne. In subsequent steps, the alkyne coordination must be followed by cluster fragmentation and C−C and C−N bond formations to afford the corresponding binuclear ruthenapyrrolidone complexes. The $Ru(CO)_x$ fragments arising from this cluster degradation would be readily trapped by the remaining trimetallic intermediates to afford the corresponding tetranuclear derivatives (Scheme 2).

This proposal is supported by the fact that compound **9** is readily converted into an approximately 1:1 mixture of compounds **8** and **10** upon heating in hexanes or after long periods in solution at room temperature. In fact, all attempts to obtain single crystals of **9** afforded compound **8** as the only crystallized species, while the IR spectrum of the remaining solution indicated the presence of the binuclear derivative **10** as the major product.

Concluding Remarks

The present work describes the synthesis of a series of bi- and tetranuclear ruthenium derivatives by treatment of a trinuclear imido-bridged compound with activated alkynes and diynes. In each case, only one of the two possible regioisomers of the product is formed. This selectivity has been rationalized on the basis of electronic effects of the groups attached to the C≡C moiety. The μ_4-coordination mode adopted by the imido ligand in the tetranuclear compounds reported herein is rather rare for ligands of this type, the number of examples hitherto reported being very limited.[12,21−24]

Surprisingly, the diynes studied in the present work invariably behaved as simple monoalkynes, leading to metal complexes containing a pendant, non-coordinated alkyne fragment. These results are to some extent at variance with those found for other triruthenium clusters in their reactions with diynes, where these ligands lead to a richer derivative chemistry than that of simple monoalkynes.[2,15−17] The isolation, characterization, and observed reactivity of the trinuclear derivative **9** has shed light on the general reaction pathway followed by trinuclear imido-bridged cluster complexes in their reactions with alkynes and diynes since compounds analogous to **9** are intermediates in the formation of the final bi- and tetranuclear products.

Experimental Section

General Remarks: Solvents were dried withn sodium diphenyl ketyl (THF, hydrocarbons) or calcium hydride (dichloromethane, acetonitrile) and were distilled under nitrogen prior to use. The reactions were carried out under nitrogen using Schlenk vacuum line techniques and were routinely monitored by solution IR spectroscopy

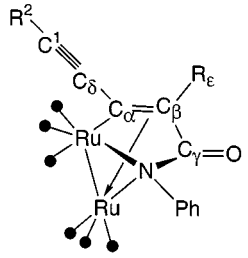

Figure 4. Carbon atom labeling scheme for the binuclear derivatives

(carbonyl stretching region) and by spot TLC (silica gel). − All reagents were purchased as analytically pure samples, except for anhydrous Me_3NO, which was obtained by azeotropic distillation of $Me_3NO{\cdot}2H_2O$ in toluene. − IR: Perkin−Elmer Paragon 1000 FT. − NMR: Bruker AC-200, AC-300, or DPX-300, room temperature, $SiMe_4$ as internal standard; carbon atom labeling scheme see Figure 4. − Microanalyses were obtained from the University of Oviedo Analytical Service. − FAB-MS were obtained from the University of Santiago de Compostela Mass Spectrometric Service; data given refer to the most abundant molecular ion isotopomer.

Synthesis of $[Ru_3(\mu_3\text{-NPh})(\mu_3\text{-CO})(CO)_9]$ (1): A solution of Me_3NO (70 mg, 0.936 mL) in dichloromethane (50 mL) was added dropwise to a solution of $[Ru_3(CO)_{12}]$ (500 mg, 0.782 mmol) in dichloromethane/acetonitrile (400 mL:15 mL) at −78 °C. An instantaneous color change from yellow to brown was observed. Once the addition was complete, the mixture was allowed to warm to room temperature and a solution of nitrosobenzene (100 mg, 0.934 mmol) in dichloromethane (10 mL) was added dropwise. After stirring for 15 min, the mixture was concentrated under reduced pressure to a volume of ca. 2 mL and the residue was transferred to a column of silica gel (10 × 2 cm). Elution with hexanes afforded first a yellow band, which contained some unchanged $[Ru_3(CO)_{12}]$, followed by a second yellow band containing 210 mg (40%) of complex **1**. − $C_{16}H_5NO_{10}Ru_3$ (674.46): calcd. C 28.50, H 0.75, N 2.08; found C 28.70, H 0.80, N 1.99. − FAB-MS: *m*/*z* = 675 [M^+]. − IR (CH_2Cl_2): ν(CO) = 2102 (d), 2070 (vs), 2029 (m), 1721 (w, br) cm^{-1}. − ^1H NMR ($CDCl_3$): δ = 7.20−7.00 (m, 5 H, Ph).

General Procedure for the Reactions of 1 with Alkynes and Diynes: In a typical reaction, a solution of **1** in hexanes (30 mL) was stirred at reflux temperature with an excess of the appropriate alkyne or diyne until complete consumption of the starting material **1** (IR monitoring). The color of the solution changed from yellow to brown. The solution was then transferred to a column of silica gel (2 × 15 cm). In each case, elution with hexanes afforded a first band that contained some unchanged starting material **1**. Subsequent elution with the appropriate eluent gave the products.

$[Ru_4(\mu_4\text{-NPh})\{\mu_4,\eta^2\text{-C(CO}_2\text{Me)}{\equiv}\text{CH}\}(\mu\text{-CO})_2(CO)_9]$ (2) and $[Ru_2\{\mu,\eta^3\text{-C(CO}_2\text{Me)}{=}\text{CHC(O)NPh}\}(CO)_6]$ (3): Reactants: **1** (52 mg, 0.077 mmol); methyl propynoate (50 μL, 0.562 mmol). Reaction time: 2 h.

Data for 2: Eluted with hexanes/diethyl ether (10:1). Second band (yellow). Yield: 7 mg (10%). − $C_{21}H_9NO_{13}Ru_4$ (887.30): calcd. C 28.42, H 1.02, N 1.58; found C 28.56, H 1.05, N 1.61. − FAB-MS: *m*/*z* = 859 [M^+ − CO]. − IR (CH_2Cl_2): ν(CO) = 2097 (m), 2061 (s), 2041 (vs), 2001 (m), 1982 (m, sh), 1907 (w), 1844 (m, br) cm^{-1}. − ^1H NMR ($CDCl_3$): δ = 6.90−6.30 (m, 5 H, Ph), 6.21 (s, 1 H, CH), 3.93 (s, 3 H, CH_3).

Data for 3: Eluted with hexanes/diethyl ether (3:1). Third band (pale green). Yield: 12 mg (27%). − $C_{17}H_9NO_9Ru_2$ (573.42): calcd. C 35.61, H 1.58, N 2.44; found C 35.98, H 1.69, N 2.35. − IR (CH_2Cl_2): ν(CO) = 2102 (m), 2076 (s), 2032 (s), 2014 (m), 1693 (m, br), 1659 (w, br) cm^{-1}. − ^1H NMR ($CDCl_3$): δ = 7.33−7.10 (m, 3 H, Ph), 6.70 (d, *J* = 7.4 Hz, 2 H, Ph), 6.12 (s, 1 H, CH), 3.78 (s, 3 H, CH_3).

$[Ru_4(\mu_4\text{-NPh})\{\mu_4,\eta^2\text{-C(CO}_2\text{Me)}{\equiv}\text{CPh}\}(\mu\text{-CO})_2(CO)_9]$ (4) and $[Ru_2\{\mu,\eta^3\text{-C(CO}_2\text{Me)}{=}\text{CPhC(O)NPh}\}(CO)_6]$ (5): Reactants: **1** (51 mg, 0.076 mmol); methyl phenylpropynoate (39 μL, 0.263 mmol). Reaction time: 2 h.

Data for 4: Eluted with hexanes/diethyl ether (10:1). Second band (yellow). Yield: 22 mg (30%). − $C_{27}H_{13}NO_{13}Ru_4$ (963.40): calcd. C 33.65, H 1.36, N 1.45; found C 33.50, H 1.29, N 1.40. − FAB-MS: *m*/*z* = 965 [M^+]. − IR (CH_2Cl_2): ν(CO) = 2095 (m), 2064 (s), 2041 (vs), 2006 (m), 1989 (m, sh), 1901 (w), 1845 (m, br) cm^{-1}. − ^1H NMR ($CDCl_3$): δ = 7.20−6.60 (m, 7 H, Ph), 6.51 (t, *J* = 7.5 Hz, 1 H, Ph), 5.42 (d, *J* = 7.5 Hz, 2 H, Ph), 3.03 (s, 3 H, CH_3).

Data for 5: Eluted with hexanes/diethyl ether (3:1). Third band (pale green). Yield: 22 mg (45%). − $C_{23}H_{13}NO_9Ru_2$ (649.52): calcd. C 42.53, H 2.02, N 2.16; found C 42.65, H 2.13, N 2.09. − FAB-MS: *m*/*z* = 651 [M^+]. − IR (CH_2Cl_2): ν(CO) = 2100 (m), 2075 (vs), 2031 (s), 2013 (m), 1712 (m, br), 1698 (m, br) cm^{-1}. − ^1H NMR ($CDCl_3$): δ = 7.38−7.08 (m, 8 H, Ph), 6.80 (d, *J* = 7.4 Hz, 2 H, Ph), 3.45 (s, 3 H, CH_3). − $^{13}C\{^1H\}$ NMR (CD_2Cl_2): δ = 194.3, 190.9, 189.2 (CO's); 173.3 (C_γ), 172.1 (C_α), 167.5 (C_δ), 146.6 (NC), 133.9 (C_ε); 130.0, 128.3, 127.6, 127.4, 126.1, 126.0 (Ph); 100.5 (C_β); 18.7 (C_1).

$[Ru_4(\mu_4\text{-NPh})(\mu_4,\eta^2\text{-MeC}{\equiv}\text{CC}{\equiv}\text{CMe})(\mu\text{-CO})_2(CO)_9]$ (6) and $[Ru_2\{\mu,\eta^3\text{-C(C}{\equiv}\text{CMe)}{=}\text{CMeC(O)NPh}\}(CO)_6]$ (7): Reactants: **1** (50 mg, 0.074 mmol); 2,4-hexadiyne (15 mg, 0.192 mmol). Reaction time: 55 min.

Data for 6: Eluted with hexanes. Second band (orange). Yield: 30 mg (46%). − $C_{23}H_{11}NO_{11}Ru_4$ (881.66): calcd. C 31.33, H 1.26, N 1.59; found C 31.29, H 1.30, N 1.48. − FAB-MS: *m*/*z* = 881 [M^+]. − IR (CH_2Cl_2): ν(CO) = 2090 (m), 2058 (s), 2034 (vs), 2001 (m), 1982 (m, sh), 1895 (w, br), 1840 (m, br) cm^{-1}. − ^1H NMR ($CDCl_3$): δ = 6.60 (t, *J* = 7.5 Hz, 2 H, Ph), 6.44 (t, *J* = 7.5 Hz, 1 H, Ph), 5.24 (d, *J* = 7.5 Hz, 2 H, Ph), 1.83 (s, 3 H, CH_3), 1.79 (s, 3 H, CH_3).

Data for 7: Eluted with hexanes/diethyl ether (10:1). Third band (pale green). Yield: 14 mg (33%). − $C_{19}H_{11}NO_7Ru_2$ (567.46): calcd. C 40.22, H 1.95, N 2.47; found C 40.01, H 1.86, N 2.39. − FAB-MS: *m*/*z* = 569 [M^+]. − IR (CH_2Cl_2): ν(CO) = 2210 (w), 2094 (m), 2067 (vs), 2022 (s), 1998 (m), 1686 (m, br) cm^{-1}. − ^1H NMR ($CDCl_3$): δ = 7.30−7.13 (m, 3 H, Ph), 6.72 (d, *J* = 7.0 Hz, 2 H, Ph), 2.36 (s, 3 H, CH_3), 2.17 (s, 3 H, CH_3). − $^{13}C\{^1H\}$ NMR (CD_2Cl_2): δ = 195.6, 191.7, 189.9 (CO's); 175.2 (C_γ), 154.4 (C_α), 147.0 (NC), 128.0, 126.2, 125.7 (Ph); 108.3 (C_δ), 98.3 (C_β), 82.2 (C_1), 16.2 (C_ε), 4.1 (C_2).

$[Ru_4(\mu_4\text{-NPh})(\mu_4,\eta^2\text{-PhC}{\equiv}\text{CC}{\equiv}\text{CPh})(\mu\text{-CO})_2(CO)_9]$ (8), $[Ru_3(\mu_3\text{-NPh})(\mu_3,\eta^2\text{-PhC}{\equiv}\text{CC}{\equiv}\text{CPh})(CO)_8]$ (9), and $[Ru_2\{\mu,\eta^3\text{-C(C}{\equiv}\text{CPh)}{=}\text{CPhC(O)NPh}\}(CO)_6]$ (10): Reactants: **1** (50 mg, 0.074 mmol); diphenylbutadiyne (25 mg, 0.124 mmol). Reaction time: 35 min.

Data for 8: Eluted with hexanes/diethyl ether (30:1). Second band (orange). Yield: 10 mg (13%). − $C_{33}H_{15}NO_{11}Ru_4$ (1005.81): calcd. C 39.41, H 1.50, N 1.39; found C 39.82, H 1.52, N 1.40. − FAB-MS: *m*/*z* = 1005 [M^+]. − IR (CH_2Cl_2): ν(CO) = 2091 (m), 2061 (s), 2036 (vs), 2006 (m), 1985 (m), 1892 (w), 1843 (m, br) cm^{-1}. −

^{1}H NMR ($CDCl_3$): δ = 7.20−6.45 (m, 13 H, Ph), 5.41 (d, *J* = 7.8 Hz, 2 H, Ph).

Data for 9: Eluted with hexanes/diethyl ether (30:1). Third band (yellow). Yield: 20 mg (32%). − $C_{31}H_{15}NO_9Ru_3$ (848.46): calcd. C 43.88, H 1.78, N 1.65; found C 44.01, H 1.90, N 1.68. − FAB-MS: *m*/*z* = 850 [M^+]. − IR (CH_2Cl_2): ν(CO) = 2095 (w), 2076 (s), 2053 (s), 2026 (s), 2006 (m), 1995 (m, sh) cm^{-1}. − ^{1}H NMR ($CDCl_3$): δ = 7.40−6.70 (m, 15 H, Ph). − $^{13}C\{^1H\}$ NMR (CD_2Cl_2): δ = 200.0 (1 CO), 199.5 (3 CO), 195.1 (2 CO), 191.3 (1 CO), 177.3 (2 CO), 161.7, 153.7, 148.4 (Ru−C), 136.0 (Ru−C), 132.2−117.9 (m, 15 CH), 111.2 (C_{ipso}), 102.3 (C_{ipso}), 97.0 (C_{ipso}).

Data for 10: Eluted with hexanes/diethyl ether (3:1). Fourth band (pale green). Yield: 14 mg (27%). − $C_{29}H_{15}NO_7Ru_2$ (691.60): calcd. C 50.36, H 2.19, N 2.03; found C 50.18, H 2.04, N 1.99. − FAB-MS: *m*/*z* = 693 [M^+]. − IR (CH_2Cl_2): ν(CO) = 2188 (w), 2094 (m), 2069 (vs), 2026 (s), 2007 (m), 1696 (m, br) cm^{-1}. − ^{1}H NMR ($CDCl_3$): δ = 7.74 (d, *J* = 7.3 Hz, 2 H, Ph), 7.49−7.16 (m, 11 H, Ph), 6.81 (d, *J* = 7.3 Hz, 2 H, Ph). − $^{13}C\{^1H\}$ NMR (CD_2Cl_2): δ = 196.1 (CO's); 175.1 (C_γ), 151.8 (C_α), 147.8 (NC), 153.4 (C_ε); 131.5, 131.4, 129.3, 129.1, 128.5, 128.3, 128.1, 127.1, 126.8, 122.8 (Ph); 110.6 (C_δ), 104.2 (C_β), 93.0 (C_1).

$[Ru_4(\mu_4\text{-NPh})(\mu_4,\eta^2\text{-PhOCH}_2C{\equiv}CC{\equiv}CCH_2OPh)(\mu\text{-CO})_2(CO)_9]$ (11): Reactants: **1** (75 mg, 0.111 mmol); 1,6-diphenyloxy-2,4-hexadiyne (58 mg, 0.222 mmol). Reaction time: 45 min. Silica gel TLC eluting with hexanes/CH_2Cl_2 (5:1), second band (orange). Yield: 14 mg (12%). − $C_{35}H_{19}NO_{13}Ru_4$ (1065.54): calcd. C 39.45, H 1.80, N 1.31; found C 39.61, H 1.88, N 1.26. − FAB-MS: *m*/*z* = 1065 [M^+]. − IR (CH_2Cl_2): ν(CO) = 2094 (m), 2062 (s), 2036 (vs), 2005 (m), 1983 (m), 1895 (w), 1846 (m, br) cm^{-1}. − ^{1}H NMR ($CDCl_3$): δ = 7.30−6.40 (m, 15 H, Ph), 4.67 (s, 2 H, CH_2), 3.38 (s, 2 H, CH_2).

$[Ru_4(\mu_4\text{-NPh})\{\mu_4,\eta^2\text{-C}(CH_2C{\equiv}CSiMe_3){\equiv}CH\}(\mu\text{-CO})_2(CO)_9]$ (12) and $[Ru_2\{\mu,\eta^3\text{-C}(CH_2C{\equiv}CSiMe_3){=}CHC(O)NPh\}(CO)_6]$ (13): Reactants: **1** (52 mg, 0.077 mmol); 1-trimethylsilyl-1,4-pentadiyne (20 μL, 0.117 mmol). Reaction time: 35 min.

Data for 12: Eluted with hexanes/diethyl ether (10:1). Second band (orange). Yield: 16 mg (22%). − $C_{25}H_{17}NO_{11}Ru_4Si$ (939.49): calcd. C 31.96, H 1.82, N 1.49; found C 32.02, H 1.88, N 1.41. − FAB-MS: *m*/*z* = 939 [M^+]. − IR (CH_2Cl_2): ν(CO) = 2091 (m), 2057 (s), 2035 (vs), 2000 (m), 1982 (m), 1897 (w), 1841 (m, br) cm^{-1}. − ^{1}H NMR ($CDCl_3$): δ = 6.61 (t, *J* = 7.5 Hz, 2 H, Ph), 6.45 (t, *J* = 7.5 Hz, 1 H, Ph), 5.27 (d, *J* = 7.5 Hz, 2 H, Ph), 4.24 (s, 1 H, CH), 2.55 (s, 2 H, CH_2), 0.21 (s, 9 H, CH_3).

Data for 13: Eluted with hexanes/diethyl ether (3:1). Third band (pale green). Yield: 12 mg (26%). − $C_{21}H_{17}NO_7Ru_2Si$ (625.24): calcd. C 40.32, H 2.74, N 2.24; found C 40.41, H 2.99, N 2.22. − IR (CH_2Cl_2): ν(CO) = 2186 (w), 2095 (m), 2069 (vs), 2022 (s), 1996 (m), 1696 (m, br) cm^{-1}. − ^{1}H NMR ($CDCl_3$): δ = 7.21−7.16 (m, 3 H, Ph), 6.78−6.71 (m, 2 H, Ph), 6.00 (s, 1 H, CH), 3.84 (d, *J* = 19.1 Hz, 1 H, CH_2), 3.68 (d, *J* = 19.1 Hz, 1 H, CH_2), 0.16 (s, 9 H, $SiMe_3$). − $^{13}C\{^1H\}$ NMR (CD_2Cl_2): δ = 192.2, 181.7 (CO's); 179.1 (C_α), 175.2 (C_γ), 156.2 (C_β), 147.7 (NC), 129.3, 127.3, 127.0 (Ph); 103.2 (C_2), 82.7 (C_1), 37.7 (C_δ), 1.2 ($SiMe_3$).

Thermolysis of 9: A solution of **9** (40 mg, 0.047 mmol) in hexanes (20 mL) was heated at reflux temperature for 3 h, whereupon the color changed from yellow to brown. It was then concentrated under reduced pressure to a volume of ca. 2 mL and applied to the top of a column of silica gel. Elution with hexanes/diethyl ether (30:1) afforded 13 mg (27%) of compound **8** as an orange solid. Subsequent elution with hexanes/diethyl ether (3:1) afforded a pale-green band, which was found to contain 10 mg (31%) of compound **10**.

Table 3. Relevant crystal and refinement data for compounds **4**, **7**, and **8**

Compound	**4**	**7**	**8**
Empirical formula	$C_{27}H_{13}NO_{13}Ru_4$	$C_{19}H_{11}NO_7Ru_2$	$C_{33}H_{15}NO_{11}Ru_4$
Molecular mass	963.66	567.43	1005.74
Crystal system	monoclinic	orthorhombic	triclinic
Space group	$P2_1/n$	*Pcab*	$P\bar{1}$
a [Å]	10.727(2)	11.403(3)	10.031(2)
b [Å]	18.576(4)	16.531(4)	13.239(3)
c [Å]	15.721(3)	22.41(2)	13.523(3)
α [°]	90	90	78.85(3)
β [°]	99.39(3)	90	79.28(3)
γ [°]	90	90	68.95(3)
V [Å^3]	3090.7(11)	4225(5)	1631.0(6)
Z	4	8	2
F(000)	1848	2208	968
$D_{calcd.}$ [g cm^{-3}]	2.071	1.784	2.048
λ(Mo-K_α) [Å]	0.71073	0.71073	0.71073
Crystal size [mm^3]	0.45 × 0.35 × 0.32	0.26 × 0.17 × 0.10	0.40 × 0.30 × 0.40
T [K]	293(2)	293(2)	293(2)
μ [mm^{-1}]	1.983	1.468	1.879
θ max [°]	24.98	25.97	24.99
Min./max. *h*, *k*, *l*	−11/12, 0/22, −18/18	−14/0, 0/20, 0/27	−11/11, −15/15, −16/0
Measured reflns.	11225	4135	5859
Unique reflns.	5431	4135	5607
Reflns. with [$I > 2\sigma(I)$]	4694	1800	4478
Parameters	406	262	439
GoF on F^2	1.076	1.086	1.109
R_1 [on *F*, $I > 2\sigma(I)$]	0.0353	0.0916	0.0306
wR_2 (on F^2, all data)	0.0869	0.3462	0.0832
Min., max Δρ, [e·Å^{-3}]	−1.385, 1.388	−1.466, 2.148	−0.657, 0.768

X-ray Crystallographic Studies: Crystal data and refinement details are summarized in Table 3. Single crystals of compounds **4**, **7**, and **8** were analyzed on a Nonius CAD4 diffractometer, equipped with a graphite crystal monochromator, using the $\omega-2\theta$ scan technique with a variable scan rate and a maximum scan time of 60 s per reflection. In all cases, Lorentz and polarization corrections were applied and data were reduced to F_o^2 values. A semiempirical absorption correction was applied based on ψ scans,[27] with correction factors in the range 0.53 to 0.40 for **4**, 0.977 to 1.011 for **7**, and 0.987 to 0.995 for **8**. The structures were solved by Patterson interpretation using the program DIRDIF-96.[28] Isotropic and full-matrix anisotropic least-squares refinements were carried out using SHELXL-97.[29] All non-H atoms were refined anisotropically. Hydrogen atom positions were geometrically calculated and refined as riding on their parent atoms. Molecular plots were generated with the EUCLID program package.[30]

Crystallographic data (excluding structure factors) for the structures reported in this paper have been deposited with the Cambridge Crystallographic Data Centre as supplementary publication nos. CCDC-164215 (**4**), CCDC-164216 (**7**), and CCDC-164217 (**8**). Copies of the data can be obtained free of charge on application to the CCDC, 12 Union Road, Cambridge CB2 1EZ, U.K. [Fax: (internat.) +44 (0)1223 336033; E-mail: deposit@ccdc.cam.ac.uk].

Acknowledgments

This work has been supported by the Spanish DGESIC (grants PB95-1042 and PB98-1555 to J.A.C., and BQU2000-0219 to S.G.-G.). M.M. thanks the Spanish Ministry of Education for a predoctoral fellowship (FPI Program).

[1] [1a] J. A. Cabeza, I. del Río, R. J. Franco, F. Grepioni, V. Riera, *Organometallics* **1997**, *16*, 2763. – [1b] J. A. Cabeza, I. del Río, M. Moreno, V. Riera, F. Grepioni, *Organometallics* **1998**, *17*, 3027.

[2] J. A. Cabeza, F. Grepioni, M. Moreno, V. Riera, *Organometallics* **2000**, *19*, 5424.

[3] See, for example: [3a]A. A. Cherkas, N. Hadj-Bagheri, A. J. Carty, E. Sappa, M. A. Pellinghelli, A. Tiripicchio, *Organometallics* **1990**, *9*, 1887. – [3b] S. M. Breckenridge, N. J. Taylor, A. J. Carty, *Organometallics* **1991**, *10*, 837.

[4] [4a] S.-H. Han, G. L. Geoffroy, A. L. Rheingold, *Organometallics* **1986**, *5*, 2561. – [4b] S.-H. Han, G. L. Geoffroy, A. L. Rheingold, *Organometallics* **1987**, *6*, 2380.

[5] G. D. Williams, R. R. Whittle, G. L. Geoffroy, A. L. Rheingold, *J. Am. Chem. Soc.* **1987**, *109*, 3936.

[6] S. Cenini, M. Pizzoti, C. Crotti, F. Porta, G. La Monica, *J. Chem. Soc., Chem. Commun.* **1984**, 1286.

[7] [7a] S. Cenini, C. Crotti, M. Pizzotti, F. Porta, *J. Org. Chem.* **1988**, *53*, 1243. – [7b] S. Bhaduri, H. Khwaja, N. Sapre, K. Sharma, A. Basu, P. G. Jones, G. Carpenter, *J. Chem. Soc., Dalton Trans.* **1990**, 1313. – [7c] D. L. Ramage, G. L. Geoffroy, A. L. Rheingold, B. S. Haggerty, *Organometallics* **1992**, *11*, 1242.

[8] S.-H. Han, J. S. Song, P. D. Mackin, S. T. Nguyen, G. L. Geoffroy, A. L. Rheingold, *Organometallics* **1989**, *8*, 2127.

[9] J.-S. Song, S.-H. Han, S. T. Nguyen, G. L. Geoffroy, A. L. Rheingold, *Organometallics* **1990**, *9*, 2386.

[10] [10a] S.-H. Han, G. L. Geoffroy, *Inorg. Chem.* **1987**, *26*, 3426. – [10b] A. Basu, S. Bhaduri, H. Khwaja, *J. Organomet. Chem.* **1987**, *319*, C28. – [10c] M. Pizzotti, F. Porta, S. Cenini, F. Demartin, *J. Organomet. Chem.* **1988**, *356*, 105.

[11] M. Pizzotti, S. Cenini, C. Crotti, F. Demartin, *J. Organomet. Chem.* **1989**, *375*, 123.

[12] [12a] E. N.-M. Ho, W.-T. Wong, *J. Chem. Soc., Dalton Trans.* **1998**, 4215 and references therein. – [12b] E. N.-M. Ho, Z. Lin, W.-T. Wong, *Chem. Eur. J.* **2001**, *7*, 258.

[13] [13a] S. Bhaduri, K. S. Gopalkrishnan, W. Clegg, P. G. James, G. M. Sheldrick, D. Stalke, *J. Chem. Soc., Dalton Trans.* **1984**, 1765. – [13b] W. Bernhardt, V. C. Schnering, H. Vahrenkamp, *Angew. Chem. Int. Ed. Engl.* **1986**, *25*, 279.

[14] G. D. Williams, G. L. Geoffroy, R. R. Whittle, A. L. Rheingold, *J. Am. Chem. Soc.* **1985**, *107*, 729.

[15] [15a] J. A. Cabeza, M. Moreno, V. Riera, M. J. Rosales-Hoz, *Inorg. Chem. Commun.* **2001**, *4*, 57. – [15b] J. A. Cabeza, I. del Río, S. García-Granda, G. Lavigne, N. Lugan, M. Moreno, P. Nombel, M. Pérez-Priede, V. Riera, A. Rodríguez, M. Suárez, J. F. van der Maelen, *Chem. Eur. J.* **2001**, *7*, 2370.

[16] See, for example: [16a] J. F. Corrigan, S. Doherty, N. J. Taylor, A. J. Carty, *Organometallics* **1992**, *11*, 3160. – [16b] J. F. Corrigan, S. Doherty, N. J. Taylor, A. J. Carty, *Organometallics* **1993**, *12*, 1365. – [16c] M. I. Bruce, P. J. Low, A. Werth, B. W. Skelton, A. H. White, *J. Chem. Soc., Dalton Trans.* **1996**, 1551. – [16d] M. I. Bruce, N. N. Zaitseva, B. W. Skelton, A. H. White, *Inorg. Chim. Acta* **1996**, *250*, 129. – [16e] M. I. Bruce, N. N. Zaitseva, B. W. Skelton, A. H. White, *J. Organomet. Chem.* **1997**, *536–537*, 93. – [16f] S. P. Tunik, E. V. Grachova, V. R. Denisov, G. L. Starova, A. B. Nikol'skii, F. M. Dolgushin, A. I. Yanovsky, Y. T. Struchkov, *J. Organomet. Chem.* **1997**, *536–537*, 339. – [16g] M. I. Bruce, B. W. Skelton, A. H. White, N. N. Zaitseva, *Russ. Chem. Bull.* **1998**, *47*, 983. – [16h] M. I. Bruce, N. N. Zaitseva, B. W. Skelton, A. H. White, *Aust. J. Chem.* **1998**, *51*, 165. – [16i] M. I. Bruce, B. W. Skelton, A. H. White, N. N. Zaitseva, *J. Organomet. Chem.* **1998**, *558*, 197. – [16j] C. J. Adams, M. I. Bruce, B. W. Skelton, A. H. White, *J. Organomet. Chem.* **1999**, *589*, 213. – [16k] C. S. W. Lau, W. T. Wong, *J. Chem. Soc., Dalton Trans.* **1999**, 2511.

[17] [17a] Unpublished results cited by: G. Lavigne, B. Bonneval, in: *Catalysis by Di- and Polynuclear Metal Cluster Complexes* (Eds.: R. D. Adams, F. A. Cotton), Wiley-VCH, New York, **1998**, p. 39. – [17b] P. Nombel, Ph.D. Thesis, Université Paul Sabatier, Toulouse, **1996**.

[18] E. Sappa, L. Milone, *J. Organomet. Chem.* **1973**, *61*, 383.

[19] S. Bhaduri, K. S. Gopalkrishnan, G. M. Sheldrick, W. Clegg, D. Stalke, *J. Chem. Soc., Dalton Trans.* **1983**, 2339.

[20] J. A. Smieja, W. L. Gladfelter, *Inorg. Chem.* **1986**, *25*, 2667.

[21] A. L. Rheingold, D. L. Staley, S.-H. Han, G. L. Geoffroy, *Acta Crystallogr., Sect. C* **1988**, *44*, 570.

[22] M. L. Blohm, W. L. Gladfelter, *Organometallics* **1986**, *5*, 1049.

[23] C.-H. Pin, Y. Chi, C. Chung, A. J. Carty, S.-M. Peng, G.-H. Lee, *Organometallics* **1998**, *17*, 4146.

[24] G. Gervasio, R. Rossetti, P. L. Stanghellini, *J. Chem. Soc., Chem. Commun.* **1977**, 387.

[25] [25a] D. Nuel, F. Dahan, R. Mathieu, *Organometallics* **1986**, *5*, 1278. – [25b] V. Crocq, J.-C. Daran, Y. Jeannin, *J. Organomet. Chem.* **1989**, *373*, 85.

[26] [26a] R. S. Dickson, R. J. Nesbit, H. Pateras, J. M. Patrick, A. H. White, *J. Organomet. Chem.* **1984**, *265*, C25. – [26b] R. S. Dickson, R. J. Nesbit, H. Pateras, W. Baimbridge, J. M. Patrick, A. H. White, *Organometallics* **1985**, *4*, 2128.

[27] A. C. T. North, D. C. Phillips, F. S. Mathews, *Acta Crystallogr., Sect. A* **1968**, *24*, 351.

[28] [28a] P. T. Beurskens, G. Beurskens, W. P. Bosman, R. de Gelder, S. García-Granda, R. O. Gould, R. Israël, J. M. M. Smits, *The DIRDIF-96 Program System*, Crystallography Laboratory, University of Nijmegen, The Netherlands, **1996**. – [28b] C. Smykalla, P. T. Beurskens, W. P. Bosman, S. García-Granda, *J. Appl. Cryst.* **1994**, *27*, 661.

[29] G. M. Sheldrick, *SHELXL97*, *version 97-2*, University of Göttingen, Germany, **1997**.

[30] A. L. Spek, *The EUCLID Package*, in: *Computational Crystallography* (Ed.: D. Sayre), Clarendon Press, Oxford, U.K., **1982**, p. 528.

Received May 25, 2001
[I01192]

A New Highly Active Diphosphane-Palladium(II) Complex as a Catalyst Precursor for the Heck Reaction

Sven Sjövall,[a] Maria H. Johansson,[a] and Carlaxel Andersson*[a]

Keywords: Palladium / Phosphanes / Catalysis / Heck reaction

The new diphosphane ligand *cis*-1,3-bis[(diphenylphosphanyl)methyl]cyclohexane (**4**) has been prepared and has allowed the synthesis of the palladium complex *cis*-[Pd(**4**)$(CO_2CF_3)_2$] (**6**). To obtain *cis* complexation of the diphosphane in **6** the cyclohexane skeleton adopts a chair conformation with a diaxial orientation of the substituents, a structure that has been verified by an X-ray structure determination. This complex efficiently catalyses the vinylation of iodo- and bromobenzenes in high yields. For the best reaction, with methyl acrylate and iodobenzene, a yield of >98% was obtained with an average turnover frequency of 11 760 h^{-1} and a turnover number of 1 176 000.

Introduction

Novel or improved homogeneous catalytic reactivities are continuously being achieved with a large variety of organometallic complexes. The main method of controlling and directing the reactivity of a metal in such a compound is by modifying the steric and/or electronic properties of the coordinated ligands.[1] The effect of using different "fine-tuned" ligands in catalysis is perhaps best illustrated by the widely studied Heck reaction,[2] the generation of sp^2-sp^2 carbon−carbon bonds by palladium-catalysed arylation of olefins with aryl halides.[3] In order to increase the catalyst efficiency in this potentially industrially important reaction a great deal of efforts have been made recently and this has led to the development of improved palladium catalysts in terms of both stability and activity.[4−10] A variety of different ligands have been investigated for these high-performing catalysts, such as sterically hindered, highly basic phosphanes,[4] carbenes,[5] cyclometallated phosphanes,[6] phosphites,[7] mono- and bis-chelating diphosphanes[8] and imines,[9] as well as more traditional Heck coupling catalysts combined with additives such as $[PPh_4]Cl$ or $PtBu_3$.[10] A key feature of several of these systems is the stabilisation of the active catalyst by either ligand chelation or steric shielding of the transition metal centre. This confers a high thermal stability on the catalyst allowing long reaction times and high reaction temperatures without noticeable catalyst deactivation. Intrigued by the delicate ligand effects in the Heck reaction we have initiated a general program aimed at the development and catalytic investigation of bidentate phosphane ligands that can potentially cyclometallate at an sp^3 carbon.

In this paper we report the synthesis of the stereospecific diphosphane *cis*-1,3-$(Ph_2PCH_2)_2C_6H_{10}$ (**4**), which is the fully aliphatic analogue to the well-known tridentate PCP ligand 1,3-$(Ph_2PCH_2)_2C_6H_4$ (**4′**).[11] Thus, by changing the ring carbons from sp^2 to sp^3, the different electronic properties of ligand **4** relative to **4′** should modify the reactivity of the resulting complex. However, when we first investigated the coordination chemistry of ligand **4** we found a totally different coordination mode, as evidenced by X-ray crystallography, from the analogous aromatic diphosphane. We also describe some preliminary results on the catalytic vinylation of aryl halides by the Pd^{II} complex synthesised herein.

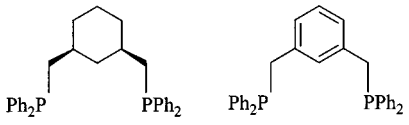

4 **4′**

Results and Discussion

Ligand Synthesis

Based on the fact that the sterically demanding substituents of *cis*-1,3-cyclohexanedicarboxylic acid (**1**) prefer an equatorial orientation,[12] we have chosen **1** as the starting material for the preparation of *cis*-1,3-bis[(diphenylphosphanyl)methyl]cyclohexane (**4**) following the procedure depicted in Scheme 1. In the initial step, **1** was reduced with an excess of BH_3 in THF yielding *cis*-1,3-bis(hydroxymethyl)cyclohexane (**2**). A good leaving group was introduced in **2** by treating it with a stoichiometric amount of trifluoromethanesulfonic anhydride in the presence of a base, giving *cis*-1,3-bis[(trifluoromethylsulfonyloxy)methyl]cyclohexane (**3**). This colourless oil undergoes decomposition within hours, even when it is stored below −18 °C, and was therefore used immediately after isolation. The reaction of **3** with 2 equiv. of $LiPPh_2$ in THF furnished phosphane **4**. An NMR spectroscopic analysis showed the phosphane to be essentially pure and, because of its high air-sensitivity, it was used without further purification. However, sulfuriz-

[a] Inorganic Chemistry, Centre for Chemistry and Chemical Engineering, Lund University,
P.O. Box 124, 221 00 Lund, Sweden

 © WILEY-VCH Verlag GmbH, 69451 Weinheim, 2001 1434−1948/01/1111−2907 $ 17.50+.50/0

ation of the phosphane, by treating it with an excess of elementary sulfur, results in the air-stable compound *cis*-1,3-bis[(diphenylphosphane sulfide)methyl]cyclohexane (**5**), which was fully characterised including elemental analysis. Clean removal of the sulfur atoms in **5** with Raney-Nickel or trichlorosilane,[13] was unsuccessful and sulfurization therefore does not provide a simple route to analytically pure **4**.

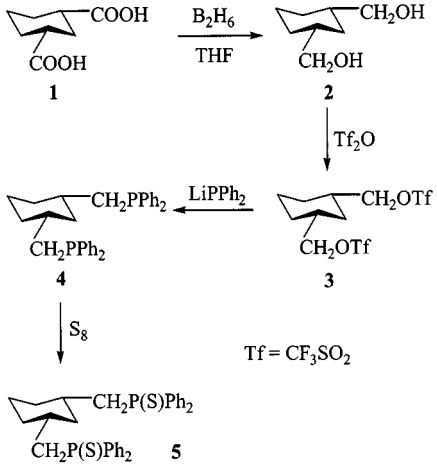

Scheme 1

The $^{13}C\{^1H\}$ NMR spectra of compounds **2**−**5** imply C_s symmetry and thus confirm the *cis* arrangement of the functional groups in the 1,3-positions of the cyclohexane ring. Hence, the respective cyclohexane skeletons give rise to four sets of signals: those of the chemically equivalent methine groups and three chemically different sets of methylene groups. Furthermore, the triflate substituents in **3** cause a significant downfield shift (to δ = 81.2) for the α-methylene group, which is in accordance with its good leaving group capacity.

Complexation

Our initial studies revealed that the choice of palladium precursor was of importance, since attempts to synthesise a monomeric palladium complex using a dihalide precursor failed. Hence, when $[PdCl_2(NCPh)_2]$ was stirred overnight with 1 equiv. of **4** in CH_2Cl_2 a yellow insoluble material was isolated in high yield. Shaw and co-workers have earlier described similar results, which they explained with the formation of a large-ring polynuclear palladium compound.[14] Instead, the preparation of a monomeric palladium complex was achieved by reacting $[Pd(CO_2CF_3)_2]$ with 1 equiv. of **4** in THF, yielding **6** as air-stable crystals in reasonable yield (Scheme 2).

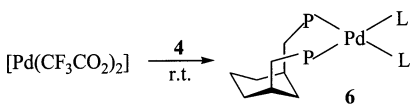

Phenyls on P omitted for clarity
L = CF_3CO_2

Scheme 2

The integral sum in the ^1H NMR spectrum of **6** suggests no displacement of hydrogen from ligand **4**. In addition, one of the protons in the cyclohexane ring is substantially shifted downfield to δ = 4.46, implying a through-space interaction with the metal centre. The $^{31}P\{^1H\}$ NMR spectrum displays a singlet, which is consistent with a mirror-plane symmetry of **6**, and the position at δ = 16.5 is in accordance with other Pd *cis*-diphosphane complexes.[15] In the $^{13}C\{^1H\}$ NMR spectrum, the C2 signal occurs as a triplet in the normal aliphatic region (δ = 28.6, $^3J_{PC}$ = 6.6 Hz). Hence, the NMR spectroscopic data is consistent with the structure shown in Scheme 2, i.e. the ligand binds to the metal centre in a *cis*-diphosphane fashion with a diaxial arrangement of the substituents on the cyclohexane ring. This energetically more demanding conformation of the cyclohexane ring, relative to the diequatorial counterpart, was not expected.[12] Moreover, the coordination mode of **4** also deviates substantially from the fully aromatic analogue 1,3-bis[(diphenylphosphanyl)methyl]benzene, which coordinates as a tridentate PCP ligand in a *trans*-configuration.[11] The reason for the reluctance of ligand **4** to activate a C−H bond, even though the spacing between its phosphorous atoms is sufficiently large for *trans*-coordination when diequatorially oriented, must be due to an improper arrangement of its C−H bonds with respect to the palladium metal centre.

An X-ray crystallographic investigation has confirmed the structure of **6**. Yellow blocks were obtained upon crystallisation by layering Et_2O onto a THF solution of **6**. A perspective view of the molecular structure is shown in Figure 1 including selected bond lengths and angles.

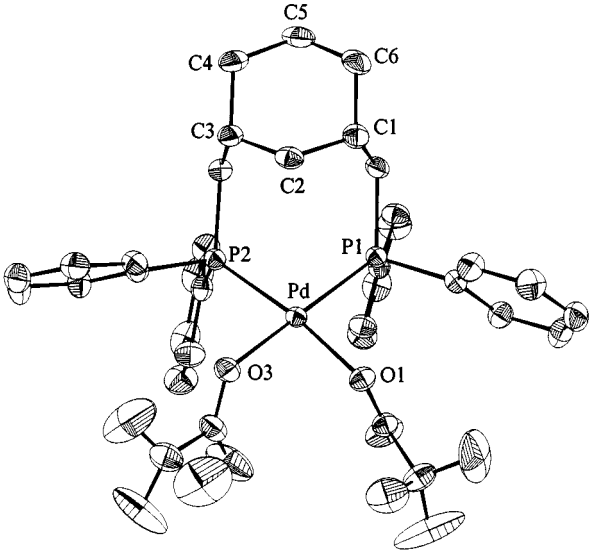

Figure 1. Perspective view (DIAMOND) of **6** (thermal ellipsoids at 30% probability); bond lengths (Å) and angles (deg) with estimated standard deviations: Pd−O1 2.086(2), Pd−O3 2.074(2), Pd−P1 2.261(1), Pd−P2 2.252(1), O1−Pd−O3 83.36(10), P1−Pd−P2 93.81(4), P1−Pd−O1 93.36(8), P1−Pd−O3 173.83(7)

Complex **6** exhibits a *cis* square-planar geometry. The congested conformation of the cyclohexane ring causes the chelate to distort the complex slightly away from an ideal geometry by widening the P1−Pd−P2 angle [93.81(4)°]. Small deviations in the bond lengths, for example for Pd−P1 [2.261(1) Å] and Pd−P2 [2.252(1) Å], illustrate the pseudo-symmetric property of **6**. The diaxial disposition of the substituents on the cyclohexane ring causes the ring to lie well above the plane of the complex (Figure 2). Note the correlation of the position of the equatorial hydrogen on C2 (Figure 2) and its downfield shift in the ^{1}H NMR spectrum of **6** (vide supra). The strained cyclohexane ring adopts the chair conformation, where the endocyclic bond angles deviate substantially from free cyclohexane (111.5°).[16]

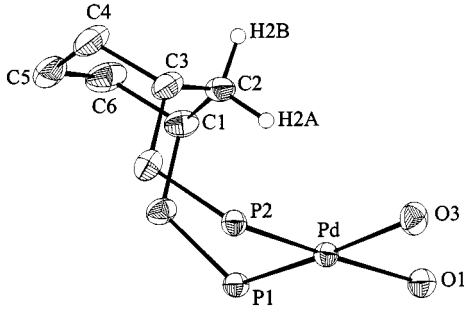

Figure 2. A plot showing the chair conformation of the cyclohexane skeleton in **6** including the hydrogens on C2; bond angles (deg) with estimated standard deviations: C1−C2−C3 115.2 (3), C2−C3−C4 109.0(3), C3−C4−C5 113.3(3), C4−C5−C6 112.2(4), C5−C6−C1 = 112.9(3), C6−C1−C2 108.8 (3)

Catalysis

As mentioned in the introduction, some chelating diphosphane-palladium(II) complexes are high-performing precatalysts for the vinylation of aryl halides (Scheme 3), as recently communicated by Shaw et al.[8a]

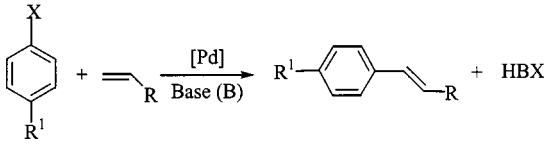

Scheme 3

Until then, the prevailing belief was that diphosphanes were unsuitable ligands in Heck catalysis.[17] Intrigued by this observation we decided to investigate complex **6** as a precatalyst for the same reaction.

As shown in Table 1, complex **6** is indeed very active in the arylation of a variety of olefins with aryl iodides and bromides. The reaction of methyl acrylate with iodobenzene is by far the most active system in the present study where a TON of 1.2×10^6 was achieved (TOF up to 1.2×10^4, Table 1, entry 2). This TON is the highest observed so far for a chelating palladium-diphosphane catalyst,[18] and also among the highest reported overall for a phosphane-containing catalyst in a high-yielding Heck reaction.[19] The screening of different bases (Na_2CO_3, NaOAc, lutidine, NBu_3 and DABCO) revealed that **6** performs best with NBu_3 as base. Of the polar solvents tested, *N*-methylpyrrolidone (NMP) was found to be superior in terms of reaction rate (entry 1), relative to *N*,*N*-dimethylformamide or *N*,*N*-dimethylacetamide, when using the same reaction conditions. The reaction can also be carried out in semi-polar and non-polar solvents, although at lower rates. However, as far as we are aware, the TONs in dioxane (333 000, entry 5) and mesitylene (320 000, entry 6) are unsurpassed.[20] The catalyst system is sensitive and to ensure high catalytic activity the efficient exclusion of air was necessary, as well as the use of pure solvents and starting materials. Complex **6** is thermally stable up to at least 140 °C, presumably due to the stabilising chelate effect, but the reactions were routinely performed at 120 °C for comparative purposes.[8a] To further verify the thermal stability of the complex we intentionally left some reactions for prolonged times: some reaction times could probably be reduced, and in no case was any noticeable formation of palladium metal observed. The catalyst remains highly active after the reaction is completed, and upon addition of more substrates the catalytic reaction resumes at essentially the same rate using the reaction conditions described (Table 1, entry 1).

As expected, both the electronic properties of the reacting olefin and steric hindrance are decisive factors for the efficiency of the catalyst: methyl acrylate gave a higher average reaction rate than styrene or *n*-butyl acrylate regardless of the aryl halide employed. However, the TONs for the arylation of *n*-butyl acrylate (495 000, entry 3) and styrene (490 000, entry 4) with iodobenzene are again among the highest reported.[6a] Complex **6** was also capable of catalysing the vinylation of relatively unreactive bromobenzenes in excellent yields (entry 7−10). Here it is also evident that an electron-withdrawing group on the aryl ring increases the reaction rate. Unfortunately, **6** is not able to convert the relatively cheaper aryl chlorides to any degree, although the effect of adding expensive promoters like [NBu_4][Br] was not tested.[21]

The trend of reactivity for iodo-, bromo- and chlorobenzenes indicates that an oxidative addition of the aryl halide to the catalyst is involved in the rate-determining step for the Heck reaction. Whether this mechanism involves a Pd^{II}/Pd^{IV} catalytic cycle, as previously suggested for other palladium-diphosphane catalysts,[8a] or not, is unclear for the moment. However, the greater efficiency of the eight-membered chelate complex **6** in catalysing the Heck reaction, compared to the previously reported four- to seven-membered ones,[8a] suggests that chelate-opening is involved in the catalytic cycle. A similar striking chelate effect on catalytic activity has been reoported by Milstein and coworkers.[4b]

In summary, ligand **4** coordinates as a normal *cis*-diphosphane, which is opposed to its fully aromatic analogue. This is made possible by the diaxial orientation of the substituents in the cyclohexane skeleton. An investigation of the catalytic activity of the resulting diphosphane-palladium

Table 1. Selected results of the Heck reaction with complex **6**; experiments conducted with 1.2 equivalents of Bu_3N in NMP except where noted

No.	Olefin (mmol)[a]	ArX (mmol)[b]	**6** (mmol) × 10^{-5}	time/temp (h)/(°C)	TON[c]	Yield (%)[d]	TOF (h^{-1})[e]
1	mac (6)	PhI (9)	6	9/120	100 000	100	11 111
2	mac (24)	PhI (36)	2	100/120	1176 000	98	11 760
3	bac (10)	PhI (15)	2	56/120	495 000	99	8 840
4	sty (10)	PhI (15)	2	54/120	490 000	98[f]	9 075
5[g]	mac (10)	PhI (15)	3	36/120	333 000	99	9 250
6[h]	mac (10)	PhI (15)	3	95/120	320 000	95	3 370
7	mac (10)	4-bba (15)	3	32/120	333 000	99	10 410
8	bac (10)	4-bba (15)	3	41/120	333 000	99	8 125
9	mac (10)	PhBr (15)	4	79/140	235 000	94	2 975
10	bac (10)	PhBr (15)	4	90/140	207 500	83	2 310

[a] mac = methyl acrylate, bac = *n*-butyl acrylate, sty = styrene. – [b] 4-bba = 4-bromobenzaldehyde. – [c] TON = Turnover number (mol product/mol catalyst). – [d] GC yield using 2-methylnaphthalene as internal standard. – [e] TOF = Turnover frequency (mol product/mol catalyst × time). – [f] *trans*-stilbene/*cis*-stilbene = 9. – [g] Dioxane as solvent. – [h] Mesitylene as solvent.

complex **6** has shown it to be by far the most active chelating diphosphane-Pd^{II} catalyst reported for the Heck reaction, and it shows an exceedingly high catalytic activity including reactions of non-activated aryl bromides. Huge TONs are also found in semi-polar or non-polar solvents, and **6** should be placed amongst the most active phosphane-containing catalysts overall for vinylation of aryl halides. We believe that the catalytic cycle is assisted by a labile chelate.

Experimental Section

All experiments with metal complexes and phosphane ligands were carried out under an atmosphere of argon or nitrogen in a Braun glovebox equipped with an inert gas purifier, or by using standard Schlenk and vacuum-line techniques. All non-deuterated solvents, reagent grade or better, were freshly distilled under a nitrogen atmosphere: Et_2O, THF, toluene, *n*-hexane, and *n*-pentane from sodium/benzophenone ketyl; CH_2Cl_2 and $CHCl_3$ from CaH_2. Deuterated solvents were used as received. Commercially available reagents was purchased from Aldrich and used without purification. The *cis*-1,3-cyclohexanedicarboxylic acid (**1**) was isolated from the commercially available *cis,trans* mixture according to a literature procedure.[22] The lithium phosphide $LiPPh_2$ was prepared by the drop-wise addition of *n*BuLi to an equimolar amount of PPh_2Cl below −60 °C, allowed to age for 2 h at room temperature, and thereafter used in situ for further reaction.

NMR spectra were recorded either on a Varian Unity 300 MHz instrument (^1H, ^{31}P, ^{19}F) or a Bruker ARX 500 MHz spectrometer (^{13}C). A ^{13}C DEPT NMR spectrum was routinely recorded for each compound. The NMR spectroscopic measurements were performed in $CDCl_3$ unless stated otherwise. ^1H and ^{13}C NMR chemical shifts are reported in ppm downfield from tetramethylsilane but were measured relative to the residual ^1H in the deuterated solvent. ^{31}P NMR chemical shifts are reported in ppm downfield from an external 85% solution of phosphoric acid. ^{19}F NMR chemical shifts are reported in ppm downfield from an external sample of $CClF_3$ in $CDCl_3$ v = virtual. NMR multiplicities are abbreviated as follows: s = singlet, d = doublet, t = triplet, q = quadruplet, m = multiplet, br = broad. Fast Atom Bombardment (FAB) mass spectroscopic data were obtained on a JEOL SX-102 spectrometer using 3-nitrobenzyl alcohol as matrix and CsI as calibrant. Gas chromatographic analyses were performed on a Varian 3300 instrument equipped with a 12-m BP-10 fused silica capillary column (0.22 ID). Elemental analyses were performed by MikroKemi AB, Uppsala, Sweden.

Except for the workup of reaction mixtures, all Heck reactions were carried out under argon. Stock solutions of catalyst were used due to low concentrations. These were freshly prepared under anaerobic conditions for each reaction and used only once. The solvents, aryl halides and bases were distilled when possible and used immediately. The olefin substrates were carefully deoxygenated by at least three freeze-pump-thaw cycles.

General Procedure for the Heck Reactions: The solvent (10 mL), aryl halide, base, olefin, 2-methylnaphthalene (internal standard) and a magnet were placed in a Schlenk tube with a screw cap. Three freeze-pump-thaw cycles were performed before the addition of an appropriate volume of the catalyst stock solution. The Schlenk tube was sealed and placed in a pre-heated, temperature-controlled oil-bath. The mixture was stirred vigorously for the desired time. Workup was achieved by pouring the cooled reaction mixture into an excess of 5% HCl (aq) and extracting with CH_2Cl_2 or Et_2O. The combined organic phases were neutralised with 10% $NaHCO_3$ (aq) and dried with $MgSO_4$. After removal of the solvent the products were analysed by ^1H NMR spectroscopy and MS; the yields were determined by GC. All of the products are known compounds.[23]

Preparation of *cis*-1,3-Bis(hydroxymethyl)cyclohexane (2): Over a period of 1.5 h, BH_3 (100 mL, 2.2 equiv. as a 1.0 M THF solution) was slowly added to an ice-cooled, stirred solution of **1** (7.75 g, 45.0 mmol) in 20 mL of THF. After the addition was completed the suspension was stirred at room temperature for an additional 2 h, and the excess hydride was thereafter carefully decomposed by the addition of 20 mL of 2 M HCl (aq). The water phase was neutralised with NaOH and about 8−10 g of K_2CO_3 was added in order to transfer the water-soluble diol to the organic phase. The organic phase was isolated and the water phase was further extracted with 2 × 10 mL of $CHCl_3$; the combined organic phases were then dried over silica. Filtration and removal of the organic solvent resulted in a highly viscous, colourless oil which solidified upon standing. Yield: 5.71 g (88%). – ^1H NMR (D_2O): δ = 0.45 (q, $^2J_{HH}$, $^3J_{HH}$ = 12.0 Hz, 1 H, CH_eH_a), 0.71 (m, 2 H, CH_2), 1.15 (m, 1 H, CH_eH_a), 1.39 (m, 2 H, CH), 1.62 (m, 4 H, CH_2), 3.41 (d, $^3J_{HH}$ = 6.3 Hz, 4 H, CH_2OH). – $^{13}C\{^1H\}$ NMR (D_2O): δ = 25.1

(s, $CH_2CH_2CH_2$), 29.3 (s, $CHCH_2CH_2$), 32.3 (s, $CHCH_2CH$), 39.4 [s, $(CH)_2CHCH_2$], 67.9 (s, CH_2OH). − MS (FAB^+): *m*/*z* = 142 [$C_8H_{14}O_2^+$]. − $C_8H_{16}O_2$ (144.21): calcd. C 66.6, H 11.2; found C 66.5, H 11.4.

Preparation of *cis*-1,3-Bis[(trifluoromethylsulfonyloxy)methyl]cyclohexane (3): A stirred suspension of **2** (1.00 g, 6.93 mmol) and pyridine (1.15 mL, 14.2 mmol) in 15 mL of CH_2Cl_2 was cooled in an ice-bath. Dropwise addition of trifluoromethanesulfonic anhydride (2.40 mL, 14.2 mmol), diluted with 10 mL of CH_2Cl_2, resulted in a yellow-tinted solution. After 30 min., the ice-bath was removed and the solution was allowed to age for an additional hour. The suspension was then filtered through a short plug of silica on a G3 glass frit and the plug was rinsed with additional CH_2Cl_2. Removal of the organic solvent on a rotary evaporator resulted in a colourless oil. The compound is too unstable for microanalysis. Yield 2.29 g (82%). − ^{1}H NMR: δ = 0.89 (q, $^2J_{HH}$, $^3J_{HH}$ = 12.0 Hz, 1 H, CH_eH_a), 1.03 (m, 2 H, CH_2), 1.37 (m, 1 H, CH_eH_a), 1.97−1.83 (m region, 6 H, CH and CH_2), 4.36 (d, $^3J_{HH}$ = 6.0 Hz, 4 H, CH_2OTf). − ^{13}C{^{1}H} NMR: δ = 24.6 (s, $CH_2CH_2CH_2$), 28.4 (s, $CHCH_2CH_2$), 31.1 (s, $CHCH_2CH$), 37.2 [s, $(CH)_2CHCH_2$], 81.2 (s, CH_2OTf), 119.0 (q, $^1J_{FC}$ = 320 Hz, CF_3). − ^{19}F NMR: δ = 51.5 (s, CF_3).

Preparation of *cis*-1,3-Bis[(diphenylphosphanyl)methyl]cyclohexane (4): A solution of **3** (2.33 g, 5.71 mmol) in 15 mL of THF was carefully added to a cooled (−60 °C) and stirred deep-red solution of $LiPPh_2$ (2.14 g, 11.4 mmol) in 15 mL of THF. The solution was allowed to reach room temperature over a period of 1 h, and stirred for an additional 18 h. The orange solution was then quenched with 5 mL of degassed water and the colourless organic phase was isolated. The water phase was further extracted with 2 × 10 mL of Et_2O and the combined organic phases were dried over silica. Filtration and removal of the solvent resulted in a viscous, almost colourless oil which partly solidified upon standing. NMR spectroscopic analysis showed the product to be essentially pure. The air-sensitivity precluded further purification and the phosphane was therefore not subjected to microanalysis. Yield: 2.52 g (92%). − ^{1}H NMR: δ = 1.41−0.84 (m region, 6 H, CH_2), 1.72 (m, 1 H, CH_2), 1.93 (m, 2 H, CH), 2.02 (d, $^3J_{HH}$ = 6.9 Hz, 4 H, CH_2P), 2.24 (m, 1 H, CH_2), 7.33 (m, 12 H, Ar), 7.43 (m, 8 H, Ar). − ^{13}C{^{1}H} NMR: δ = 26.0 (s, $CH_2CH_2CH_2$), 34.5 (d, $^3J_{PC}$ = 9.7 Hz, $CHCH_2CH_2$), 35.3 [d, $^2J_{PC}$ = 13.6 Hz, $(CH)_2CHCH_2$], 36.7 (d, $^1J_{PC}$ = 13.1 Hz, CH_2P), 43.5 (t, $^3J_{PC}$ = 9.6 Hz, $CHCH_2CH$), 128.3 (br. s, CH), 132.8 (m, CH), 133.9 (m, CH), 134.1 (m, CH), 139.4 (m, CH). − ^{31}P{^{1}H} NMR: δ = −21.3 (s).

Preparation of *cis*-1,3-Bis[(diphenylphosphane sulfide)methyl]cyclohexane (5). Sulfur (1.76 g, 6.86 mmol) was added to a solution of **4** (827 mg, 1.72 mmol) in 15 mL of toluene and the mixture was stirred for 16 h. The solution was decanted and removal of the toluene resulted in a pale yellow solid. The crude compound was loaded on a column of silica of 10 cm height. Eluting with *n*-hexane removed the remaining elementary sulfur and the white solid **5** was recovered by washing the column with CH_2Cl_2 and removing the solvent under vacuum. Yield: 759 mg (81%). − ^{1}H NMR: δ = 0.74 (m, 2 H, CH_2), 0.87 (q, $^2J_{HH}$, $^3J_{HH}$ = 11.6 Hz, 1 H, CH_eH_a), 1.12 (m, 1 H, CH_eH_a), 2.01−1.42 (m region, 6 H, CH and CH_2), 2.32 (m, 4 H, CH_2P), 7.43 (m, 12 H, Ar), 7.82 (m, 8 H, Ar). − ^{13}C{^{1}H} NMR: δ = 25.6 (s, $CH_2CH_2CH_2$), 33.0 (br. s, $CHCH_2CH_2$), 34.0 [d, $^2J_{PC}$ = 6.9 Hz, $(CH)_2CHCH_2$], 39.2 (d, $^1J_{PC}$ = 55.1 Hz, CH_2P), 43.5 (t, $^3J_{PC}$ = 10.2 Hz, $CHCH_2CH$), 128.5 (m, CH), 130.9 (m, CH), 131.3 (br. s, CH), 133.2 (d, J_{PC} = 28.2 Hz, CH), 134.2 (d, J_{PC} = 28.9 Hz, CH). − ^{31}P{^{1}H} NMR: δ = 37.1 (s). − MS (FAB^+): *m*/*z* = 544 [$C_{32}H_{34}P_2S_2^+$]. − $C_{32}H_{34}P_2S_2$ (544.69): calcd. C 70.6, H 6.3, S 11.8; found C 70.4, H 6.1, S 11.6.

Reaction of 4 with $[Pd(CO_2CF_3)_2]$. Formation of $[Pd(4)(CO_2CF_3)_2]$ (6): Phosphane **4** (25.1 mg, 52.2 μmol) and $[Pd(CO_2CF_3)_2]$ (17.4 mg, 52.2 μmol) were dissolved in 3 mL of THF. After stirring for 3 h, 12 mL of Et_2O was layered on top of the red THF solution. After 3 days yellow air-stable crystals were harvested. Yield: 20.5 mg (48%). − ^{1}H NMR (CD_2Cl_2): δ = 1.89−1.54 (m region, 7 H, CH_2), 2.25 (m, 4 H, CH_2P), 2.81 (m, 2 H, CH), 4.46 (br. d, $^2J_{HH}$ = 15.3 Hz, 1 H, CH_eH_a), 7.39 (m, 16 H, Ar), 7.82 (m, 4 H, Ar). − ^{13}C{^{1}H} NMR (CD_2Cl_2): δ = 28.3 (s, $CH_2CH_2CH_2$), 28.6 (t, $^3J_{PC}$ = 6.6 Hz, $CHCH_2CH$), 33.5−33.0 (m region, CH and CH_2), 116.4 (q, $^1J_{FC}$ = 291 Hz, CF_3), 129.0 (vt, J_{PC} = 11.1 Hz, CH), 129.7 (vt, J_{PC} = 11.1 Hz, CH), 131.9 (s, CH), 132.5 (s, CH), 132.9 (vt, J_{PC} = 10.0 Hz, CH), 133.8 (vt, J_{PC} = 11.1 Hz, CH), 160.8 (q, $^2J_{FC}$ = 36.2 Hz, C=O). − ^{31}P{^{1}H} NMR (CD_2Cl_2): δ = 16.5 (s). − ^{19}F NMR (CD_2Cl_2): δ = 52.8 (s). − MS (FAB^+): *m*/*z* = 812 [$C_{36}H_{34}F_6O_4P_2Pd^+$] (correct isotope pattern). − $C_{36}H_{34}F_6O_4P_2Pd$ (813.00): calcd. C 53.2, H 4.2; found C 53.2, H 4.2.

X-ray Crystal Structure Determination of Complex 6:[24] Crystal data and details of the data collection and refinement are given in Table 2. The intensity data were collected at 293 K with a Bruker Smart CCD system using ω scans and a rotating anode with Mo-K_α radiation (λ = 0.710 73 Å).[25] The intensities were corrected for Lorentz, polarisation and absorption effects with SADABS.[26]

Table 2. Crystallographic data

	Complex **6**
Formula	$C_{36}H_{34}F_6O_4P_2Pd$
Crystal description	Yellow prism
Crystal size (mm)	0.19 × 0.11 × 0.10
Crystal system	Triclinic
Space group	$P\bar{1}$
a (Å)	10.950(2)
b (Å)	12.174(2)
c (Å)	15.014(3)
α (°)	91.83(3)
β (°)	104.93(3)
γ (°)	114.76(3)
V (Å^3)	1733.7(6)
Z	2
D_x (Mg m^{-3})	1.557
No. of refl. used for cell parameters	7080
μ (mm^{-1})	0.698
F(000)	824
T_{min}/T_{max}	0.745/0.920
θ- range	1.4−31.7
No. of collected refl	19208
No. of unique refl.	10293
No. of observed refl., *m* [$I > 2\sigma(I)$]	7589
Parameters, *n*	442
hkl range	$-15 < h < 16$ $-17 < k < 17$ $-21 < l < 21$
R[a]	0.0486
w*R*[b]	0.1264
S[c]	1.035
(Δ/σ) max	0.002
ρ max/min (e$^-$/Å^3)	1.482/−0.958

[a] $R = \Sigma(|F_o| - |F_c|)/\Sigma|F_o|$. − [b] $wR = [\Sigma w(|F_o| - |F_c|)^2/\Sigma|F_o|^2]^{1/2}$. − [c] $S = [\Sigma w(|F_o| - |F_c|)^2/(m - n)]^{1/2}$.

The first 50 frames were collected again at the end to check for decay. No decay was observed. All reflections were merged and integrated with SAINT.[27] The structure was solved by direct methods and refined by a full-matrix least-squares calculation on F^2.[28] Non-H atoms were refined with anisotropic displacement parameters. The hydrogen atoms were constrained to their parent sites using a riding model.

Acknowledgments

We thank Mr David Dominguez-Guiteéres for helpful assistance in the laboratory. Financial support by the TFR (The Swedish Research Council for Engineering Sciences) and the NFR (The Swedish Natural Science Research Council) is gratefully acknowledged.

[1] [1a] J. P. Collman, L. S. Hegedus, J. R. Norton and R. G. Finke, *Principles and Applications of Organotransition Metal Chemistry*, University Science Book, CA, **1987**. – [1b] *Applied Homogeneous Catalysis with Organometallic Compounds* (Eds.: B. Cornils, W. A. Herrmann), VCH, Weinheim, **1996**.

[2] For excellent reviews see: [2a] I. P. Beletskaya, A. V. Cheprakov, *Chem. Rev.* **2000**, *100*, 3009−3066. – [2b] A. de Meijere, F. E. Meyer, *Angew. Chem. Int. Ed. Engl.* **1994**, *33*, 2379−2411. – [2c] V. V. Grushin, H. Alper, *Chem. Rev.* **1994**, *94*, 1047−1062.

[3] [3a] R. F. Heck, J. P. Nolley, *J. Org. Chem.* **1972**, *37*, 2320−2322. – [3b] T. Mizoroki, K. Mori, A. Ozaki, *Bull. Chem. Soc. Jpn.* **1971**, *44*, 581.

[4] [4a] M. Portnoy, Y. Ben-David, D. Milstein, *Organometallics* **1993**, *12*, 4734−4735. – [4b] Y. Ben-David, M. Portnoy, M Gozin, D. Milstein, *Organometallics* **1992**, *11*, 1995−1996.

[5] W. A. Herrmann, M. Elison, J. Fischer, C. Köcher, G. R. J. Artus, *Angew. Chem. Int. Ed. Engl.* **1995**, *34*, 2371−2374.

[6] [6a] B. L. Shaw, S. D. Perera, E. A. Staley, *Chem. Commun.* **1998**, 1361−1362. – [6b] W. A. Herrmann, C. Brossmer, T. H. Riermeier, K. Öfele, M. Beller, *Chem. Eur. J.* **1997**, *3*, 1357−1364. – [6c] W. A. Herrmann, C. Brossmer, K. Öfele, C. Reisinger, T. Priermeier, M. Beller, H. Fischer, *Angew. Chem. Int. Ed. Engl.* **1995**, *34*, 1844−1849.

[7] [7a] D. Morales-Morales, R. Redon, C. Yung, C. M. Jensen, *Chem. Commun.* **2000**, 1619−1620. – [7b] D. Morales-Morales, C. Grause, K. Kasaoka, R. Redon, R. E. Cramer, C. M. Jensen, *Inorg. Chim. Acta* **2000**, *300*, 958−963. – [7c] M. Beller, A. Zapf, *Synlett.* **1998**, 792−793. – [7d] D. A. Albisson, R. B. Bedford, P. N. Scully, *Tetrahedron Lett.* **1998**, *39*, 9793−9796.

[8] [8a] B. L. Shaw, S. D. Perera, *Chem. Commun.* **1998**, 1863−1864. – [8b] M. Ohff, A. Ohff, M. E. van der Boom, D. Milstein, *J. Am. Chem. Soc.* **1997**, *119*, 11687−11688.

[9] M. Ohff, A. Ohff, D. Milstein, *Chem. Commun.* **1999**, 357−358.

[10] [10a] A. F. Littke, G. C. Fu, *J. Org. Chem.* **1999**, *64*, 10−11. – [10b] M T. Reetz, G. Lohmer, R. Schwickardi, *Angew. Chem. Int. Ed.* **1998**, *37*, 481−483.

[11] [11a] P. R. Ashton, P. Calcagno, N. Spencer K. D. Harris, D. Philip, *Org. Lett.* **2000**, *2*, 1365−1368. – [11b] F. Gorla, L. M. Venanzi, M. Luigi, A. Albinati, *Organometallics* **1994**, *13*, 43−54. – [11c] H. Rimml, L. M. Venanzi, *J. Organomet. Chem.* **1983**, *259*, C6−C7.

[12] T. L. Westman, R. Paredes, S. B. Wallace, *J. Org. Chem.* **1963**, *28*, 3512−3518.

[13] [13a] S. R. Gilbertson, C.-W. T. Chang, *J. Org. Chem.* **1998**, *23*, 8424−8430. – [13b] M. B. Goli, S. O. Grim, *Tetrahedron Lett.* **1991**, *32*, 3631−3634.

[14] N. A. Al-Salem, W. S. McDonald, R. Markham, M. C. Norton, B. L. Shaw, *J. Chem. Soc., Dalton Trans.* **1980**, 59−63.

[15] L. E. Overman, D. J. Poon, *Angew. Chem. Int. Ed. Engl.* **1997**, *36*, 518−521.

[16] G. Mann, *Z. Chem.* **1990**, *30*, 1−9.

[17] [17a] R. F. Heck, *Vinyl Substitution with Organometallic Intermediates*, in *Comprehensive Organic Synthesis* (Eds. B. M. Trost, I. Fleming), Pergamon, Oxford, **1991**, *4*, p. 833. – [17b] W. Cabri, I. Candiani, *Acc. Chem. Res.* **1995**, *28*, 2−7.

[18] A TON of 139 000 was reported for the reaction of iodobenzene with methyl acrylate after 9 days at 95 °C with a yield of 92%. See ref.[8a]

[19] [19a] A. S. Gruber, D. Zim, G. Ebeling, A. L. Monteiro, J. Dupont, *Org. Lett.* **2000**, *2*, 1287−1290. – [19b] See ref.[9]

[20] A TON of 130 300 was reported for the reaction of iodobenzene with methyl acrylate in mesitylene after 16 h at 140 °C with a yield of 93%. See ref.[9]

[21] [21a] T Jeffery, *Tetrahedron Lett.* **1985**, *26*, 2667−2669. – [21b] T. Jeffery, *J. Chem. Soc., Chem. Commun.* **1984**, 1287−1289.

[22] A. Skita, R. Rossler, *Ber. Dtsch. Chem. Ges.* **1939**, *72B*, 265−269.

[23] T. Yoshino, Y. Nagata, E. Itoh, M. Hashimoto, T. Katoh, S. Terashima, *Tetrahedron Lett.* **1996**, *37*, 3475−3478.

[24] Crystallographic data (excluding structure factors) for the structure reported in this paper has been deposited with the Cambridge Crystallographic Data Centre as supplementary publication no. CCDC-158133. Copies of the data can be obtained free of charge on application to CCDC, 12 Union Road, Cambridge CB2 1EZ, UK [Fax: (internat.) + 44-1233/336-033; E-mail: deposit@ccdc.cam.ac.uk].

[25] BrukerAXS, *SMART*, Area Detector Control Software, Bruker Analytical X-ray System, Madison, Wisconsic, USA, **1995**.

[26] G. M. Sheldrick, *SADABS*: Program for Absorption Correction, University of Göttingen, Göttingen, Germany, **1996**.

[27] BrukerAXS, *SAINT*, Integration Software, Bruker Analytical X-ray System, Madison, Wisconsin, USA, **1995**.

[28] G. M. Sheldrick, *SHELXTL5.1*, Program for Structure Solution and Least Square Refinement, University of Göttingen, Göttingen, Germany, **1998**.

Received April 18, 2001
[I01138]

Characterization and Reactivity of Triperoxo Vanadium Complexes In Protic Solvents

Marcella Bonchio,[a] Olga Bortolini,*[b] Valeria Conte,*[c] and Stefano Moro[d]

Keywords: Mass spectrometry / Ab initio calculations / Peroxo complexes / Vanadates

ESI-MS and ^{51}V NMR techniques have been used to detect the formation of vanadium triperoxo complexes in protic solvents. RHF/6-311++G(d,p) ab initio calculations were also carried out to address the structure and the energy requirements of vanadium peroxo species formed from vanadates and hydrogen peroxide. Such studies point to a step-by-step decomposition process involving the triperoxo vanadium complex, as highlighted by ESI-MS^n experiments. The reactivity of the triperoxo compound has been examined in an alcohol/water mixture with the aim of elucidating its oxidative behavior; evidence for the formation of the HOO^- anion as an active oxidant in solution has been obtained.

Introduction

The relevance of peroxo transition metal compounds either in oxidation chemistry[1,2] or in biochemical systems[3,4] is well established. Vanadium peroxides, in particular, are effective oxidants, as demonstrated by their reactions with different inorganic and organic substrates, viz. halides, sulfur dioxide, thioethers, alkenes, alcohols and aromatic or aliphatic hydrocarbons (Scheme 1).[5,6]

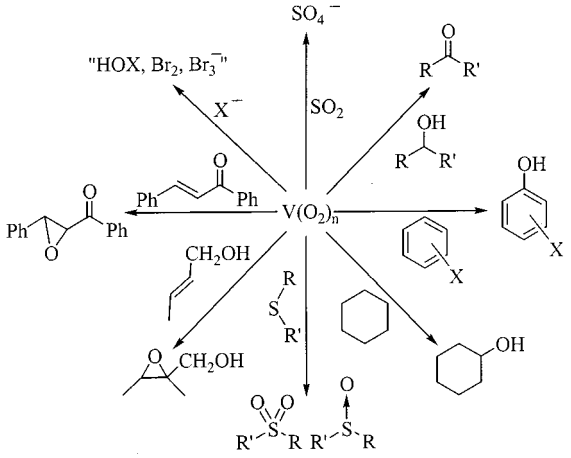

Scheme 1. Reactivity of vanadium peroxides with inorganic and organic substrates

[a] CNR C. M. R. O., Dip. Chimica Organica,
University of Padova
Via Marzolo 1, 35131 Padova, Italy,
E-mail: marcella@chor.unipd.it
[b] Dip. Chimica, University of Ferrara
Via Borsari 46 44100 Ferrara, Italy
Fax: (internat.) +39-053/240-709
E-mail: brl@unife.it
[c] I.P.P.A. Facoltà di Agraria, University of Foggia,
Via Napoli 25, 71100 Foggia, Italy
Fax: (internat.) +39-0881/740-211
E-mail: conte@chor.unipd.it
[d] Dip. Scienze Farmaceutiche, University of Padova
Via Marzolo 5, 35131 Padova, Italy
E-mail:smoro@purple.dsfarm.unipd.it

These processes, whether stoichiometric or catalytic, where the oxidant can be hydrogen peroxide or an alkyl hydroperoxide, are usually carried out under very mild conditions with good selectivities and chemical yields.

The oxidation of halides with peroxo vanadates is the rate-determining step in the peroxidative halogenation of organic substrates [Equation (1)]:[7]

$$X^- + H_2O_2 + RH + H^+ \xrightarrow{\text{V(V)-peroxides}} RX + 2H_2O \quad (1)$$

Such a process is actually a chemical model of the activity of vanadium-dependent haloperoxidases enzymes.[8,9] Recent studies have shown that in the natural haloperoxidase systems the active peroxidic intermediate for the oxidation of bromide ion is a monoperoxo vanadate stabilized by a histidine residue contained in the active site pocket.[8,9] Conversely, mimicking systems reported in the literature are usually based either on monoperoxo vanadium [10] or on divanadium triperoxo species.[11]

Monoperoxo vanadium compounds are also catalysts for the aerobic oxidation of alcohols to carbonyl compounds [Equation (2)]:

$$R_2CHOH + O_2 \xrightarrow{\text{catalyst}} R_2C{=}O + H_2O_2 \quad (2)$$

In particular, it has been observed[12] that an accumulation of hydrogen peroxide takes place during the course of the oxidation of *i*PrOH with $n Bu_4NVO_3$ in the presence of $HClO_4$ and excesses of H_2O_2 and H_2O, carried out at 40 °C under a pressure of one atmosphere of oxygen. Interestingly, the kinetic profile of this process is characterized by the presence of a periodic pattern, where the concentration of H_2O_2 oscillates as the result of a balance between subsequent production and decomposition phases. Under certain experimental conditions the efficiency of the process, defined as $([H_2O_2]t_{max} - [H_2O_2]_0)/[cat]_0$ where t_{max} is the reaction time for detection of the first maximum in the H_2O_2 concentration kinetic profile, reaches values higher than 4000.[13] Such a reaction compares well with the re-

 © WILEY-VCH Verlag GmbH, 69451 Weinheim, 2001 1434−1948/01/1111−2913 $ 17.50+.50/0

cently reported Pd^{II}-catalyzed process,[14,15] one of the most effective and environmentally friendly methods for the production of hydrogen peroxide.

It should be noted that most of the reactivity data cited above refer to mono- and diperoxo-vanadates. These species are easily formed in neutral or acid solutions upon addition of hydrogen peroxide to V^V precursors according to the equilibria in Equations (3) and (4):[16]

$$VO_2^+ + H_2O_2 \overset{K_1}{\rightleftharpoons} VO(OO)^+ + H_2O \quad (3)$$

$$VO(OO)^+ + H_2O_2 \overset{K_2}{\rightleftharpoons} VO(OO)_2 + 2\,H^+ \quad (4)$$

Nevertheless, together with mono- and diperoxo complexes, other peroxo vanadates may be formed depending upon the pH, and relative concentrations of vanadate and H_2O_2. The nature of the different complexes formed has been studied by ^{17}O and ^{51}V NMR,[17−22] Raman,[23] UV/Vis[24] spectroscopy and, more recently, by electrospray ionization mass spectrometry (ESI-MS).[25−27] The most important monomeric peroxo species are collected in Scheme 2. For the sake of simplicity throughout the paper the peroxo vanadium derivatives will be reported without the solvent molecules bound to the metal center in the first coordination sphere.

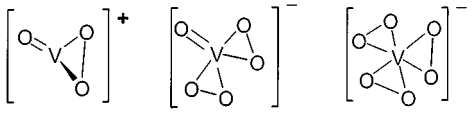

1 2 3

Scheme 2. Monomeric peroxo vanadium species with ligands or solvent molecules in the coordination sphere omitted for clarity

The spectroscopic studies cited above provided several details concerning the true structure in solution of the vanadium peroxides,[21,25] even though the actual coordination number for all of them is still uncertain. Further information on the structure of vanadium peroxo derivatives has also been obtained from theoretical calculations. As already reported, considering the coordination ability of the vanadium(V) metal center, the maximum stabilization energy for the naked monoperoxo derivative has been calculated (from both HF and DFT calculations) with three molecules of solvent (H_2O) coordinated to the metal center.[28] Moreover, particular attention has been paid to the identification of the protonation sites for complexes **1** and **2** of Scheme 2. As an example, results obtained for the diperoxo species from RHF/3-21G(*) and B3LYP/LANL2DZ DFT calculations, have indicated that between the two most favorite protonation sites, i.e. the oxo oxygen and one of the peroxidic oxygens, protonation at the latter position is by far the most favored.[29]

It should be noted that very little information, from both experimental and theoretical[30] points of view, is available on species with more than two peroxo ligands.

It has already been mentioned that mono- and diperoxo complexes are well-known as electrophilic oxygen-transfer reagents or as radical oxidants.[5,6] However, the few papers[31,32] present in the literature reporting the reactivity of triperoxo vanadates claim that these species behave as nucleophilic oxidants. In particular, the triperoxo vanadium complexes $M[V(O_2)_3]\cdot 3H_2O$ (M = Na or K) are proposed[32,33] to be efficient oxidants of α,β-unsaturated ketones to the corresponding epoxide, benzonitrile to benzamide and benzil to benzoic acid, reactions which are usually carried out with alkaline hydrogen peroxide.

In the course of our studies on the mechanism[12,13] of the aerobic vanadium-catalyzed oxidation of *i*PrOH cited above [see Equation (2)], we were faced with the possible occurrence in solution of triperoxo vanadium derivatives caused by the high concentration of hydrogen peroxide that accumulates during the reaction. Hence, we decided to analyze alcoholic solutions of vanadates in the presence of high excesses of hydrogen peroxide in more detail in order to ascertain the presence of triperoxo species, and possibly to characterize them. We have also performed reactivity studies in the same media with preformed triperoxo vanadates with the aim of elucidating their oxidative behavior. The results obtained are presented and discussed below.

Results and Discussion

Characterization

Vanadium derivatives undergo fast and favorable addition reactions with hydrogen peroxide producing peroxo complexes whose nature depends on the concentration of the reagents and on the pH. The negative-ion mode ESI mass spectra of $n Bu_4NVO_3$ (5×10^{-4} molL^{-1}) solutions in *i*PrOH containing 0.5 molL^{-1} H_2O and increasing amounts of H_2O_2 from 0.025 up to 0.35 molL^{-1}, are characterized and increasing amounts of H_2O_2 from 0.025 up to 0.35 mol·L^{-1}, are characterized by the presence of two major ions at m/z = 131 and 147. Less intense, but equally important, ionic species are found at m/z = 99, 115, 133, 149 and 165. For relatively low excesses of H_2O_2 over V^V (50−150 equivalents) the m/z = 131 ion, corresponding to the oxo diperoxo derivative,[26] is dominant, however it is progressively overtaken by the species centered at m/z = 147 as the hydrogen peroxide concentration is increased. By analogy with previous studies carried out using either ethanol or *i*PrOH as mobile phases, the system under investigation was studied in both solvents and no significant dependence on the alcohol used was observed.

The different species were identified on the basis of labeling experiments and MS^n spectra[25−27] and are summar-

ized in the inset of Figure 1. Among them, the species at m/z = 147, identified as the vanadium triperoxo derivative $[V(O_2)_3]^-$, and that at m/z = 115, assigned to the unprecedented dioxo monoperoxo compound $[O_2V(O_2)]^-$, are of particular interest. Labeling experiments were used to confirm this assignment. As expected, the replacement of water with $H_2{}^{17}O$ (ca. 50% isotope content) has no effect on the triperoxo anion, whereas formation of new peaks at m/z = 116 and 117 is observed next to the species at m/z = 115. In agreement with literature data,[5] this evidence indicates a fast exchange of the two oxo oxygens.

When the triperoxo derivative is mass selected within the ion-trap analyzer and allowed to decompose by increasingly higher tickling voltages, the CID decompositions observed are the fragmentations of one and two of the three peroxidic bridges, thus affording the oxo diperoxo derivative $[OV(O_2)_2]^-$ (m/z = 131, path **a**), and the dioxo monoperoxo

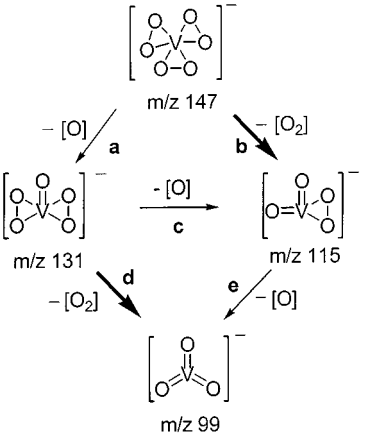

Scheme 3. Decomposition patterns of mono-, di- and triperoxo derivatives as obtained by MS^n experiments; wate-r or alcohol-containing adducts of ions at m/z = 131, 115 and 99 are not shown

derivative $[O_2V(O_2)]^-$ (m/z = 115, path **b**) of Scheme 3, including its water- and alcohol-containing homologues

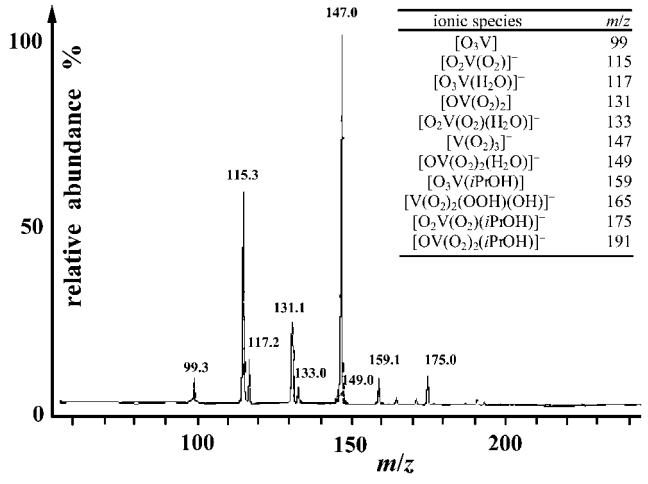

Figure 1. Negative-ion mode ESI-MS full scan spectrum of solutions of 5×10^{-4} mol·L^{-1} nBu$_4$NVO$_3$ in iPrOH-0.5 mol·L^{-1} H_2O and H_2O_2 (0.25 mol·L^{-1}); the identification of the different ions is reported in the inset

$[O_2V(O_2)(ROH)]^-$ (R=H, Et, iPr). The decomposition implicating two peroxo moieties is the most favorable pattern. This fragmentation is also the major decomposition observed with the oxo diperoxo derivative $[OV(O_2)_2]^-$, path **d** of Scheme 3.

The direct decomposition of both peroxidic bridges, formally corresponding to the expulsion of an O_2 molecule (pathways **b** and **d** of Scheme 3) probably occurs by a two-step mechanism consisting of two subsequent oxygen atom losses; this has been confirmed by experiments at increasing tickling energies.

Ab initio calculations have been carried out in order to address the structure and the energy requirements for the various intermediates detected by MS^n experiments and outlined in Scheme 3. Calculations have been carried out at the RHF/6-311++G(d,p) level of theory,[34–39] and the fully optimized species are collected in Scheme 4. The formation of all the peroxidic species results from a sequence of addition of H_2O_2, release of H_2O and proton transfer equilibria. In particular, proton-transfer processes are thermodynamically connected with the corresponding proton affinity (PA) of vanadium peroxo species, defined as the standard heat of ion dissociation to form a proton and the conjugate base in the gas phase (see Scheme 4).

The theoretical calculations showed that the addition of one molecule of hydrogen peroxide to vanadate, to form the hydroxo-monoperoxo derivative, is a favorable process with an energy balance of −76.6 kJ/mol. Similarly, the coordination of hydrogen peroxide to such a monoperoxidic adduct to produce the oxo-diperoxo species is an exothermic process by −68.5 kJ/mol. Such theoretical evidence agrees well with the experimental studies carried out on the complexation of vanadate by hydrogen peroxide, where an almost quantitative formation of mono and diperoxo vanadium complexes is observed under a range of conditions.[5]

Interestingly, the further reaction of protonated diperoxo vanadates with hydrogen peroxide yielding the triperoxo complex is clearly endothermic (see Scheme 4). In fact, the protonated triperoxo species lies 33.5 kJ/mol higher in energy than the diperoxo precursor. The capped trigonal prismatic geometry expected for the triperoxo complex[30,33] does not retain the V=O bond originally present in all mono and diperoxo vanadium complexes, and this probably destabilizes the triperoxo structure. However, the hydroperoxy-diperoxo vanadium complex can be formed in solution by protonation of the triperoxo derivative, and it could also represent one of the predominant structures of the triperoxo vanadate in alkaline solution. Moreover, the structure of this hydroperoxy-diperoxo vanadium complex may explain the peculiar oxidative behavior of vanadium species formed in highly basic solutions in the presence of large excesses of hydrogen peroxide (seebelow). The optimized structures of both protonated and unprotonated triperoxo vanadium complexes are shown in Figure 2. It should be noted that all the minimized species shown in Scheme 4 have been observed experimentally, as anions or as $[M - H]^-$ if neutrals, in the full scan ESI mass spectrum of Figure 1.

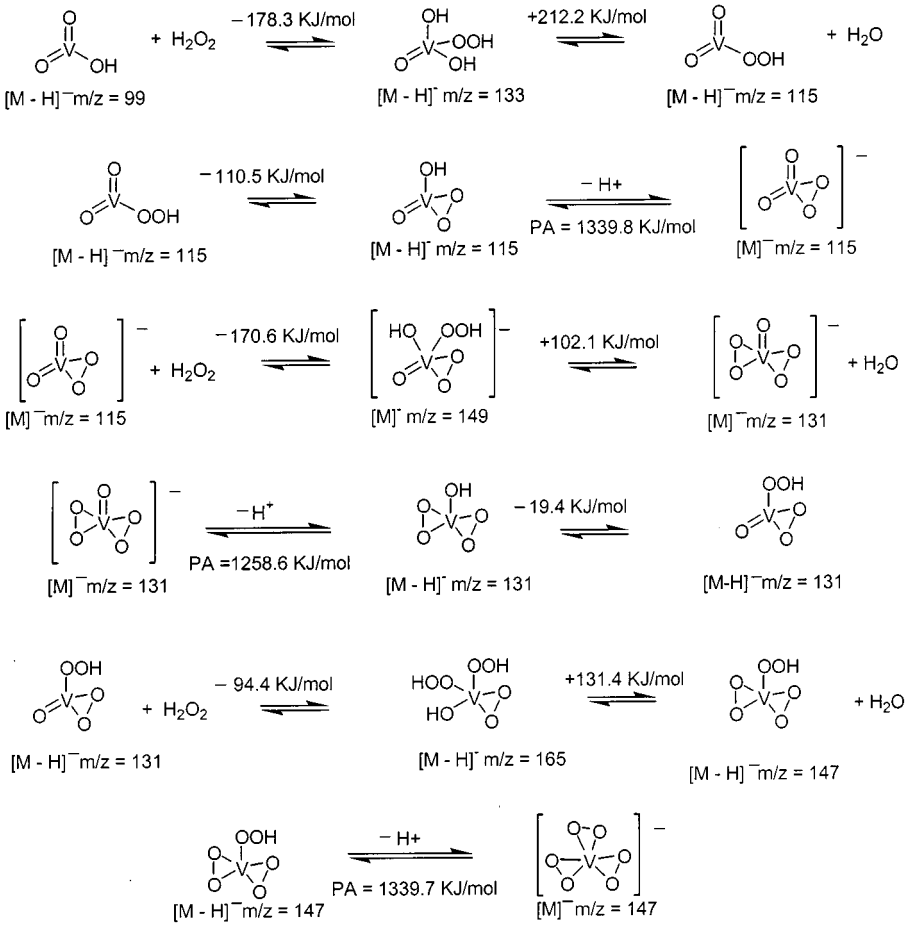

Scheme 4. Calculated relative energies (kJ/mol) for the formation of peroxo species from hydrogen peroxide and vanadate derived by RHF/6-311++G(d,p) ab initio calculations; calculated proton affinities (PA) for vanadium peroxo species, defined as the standard heat of ion dissociation to a proton and the conjugate base in the gas phase, are also included; all the species reported here have been observed experimentally, either as anions or as $[M - H]^-$ if neutrals, in the full scan ESI mass spectrum of Figure 1

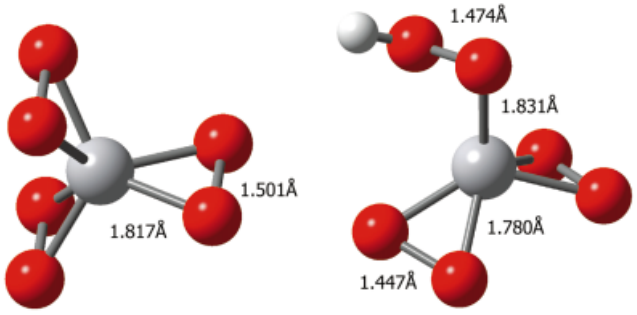

Figure 2. Structures of $[V(O_2)_3]^-$ (*left*) and of $[V(O_2)_2OOH]$ (*right*) optimized at the RHF/6-311++G(d,p) level; atomic distances are reported in Å

As pointed out in previous paragraphs, ESI-MS experiments were conducted to investigate the possible direct relationship occurring between diperoxo and triperoxo species as a function of hydrogen peroxide excess. The full-scan mass spectra of the system under investigation, recorded at different initial concentration of hydrogen peroxide, (5×10^{-4} molL^{-1} nBu$_4$NVO$_3$ in iPrOH containing 0.5 molL^{-1} H_2O, $[H_2O_2]$ from 0.025 up to 0.35 mol·L^{-1}, apparent pH ca. 7), showed that, as the concentration of H_2O_2 is increased, the vanadium diperoxo derivatives are progressively replaced by the triperoxo species. In addition, the ratio of the relative abundances of the diperoxo compounds (and related fragments) with the relative abundances of the triperoxo compounds (and related fragments) correlates linearly with the hydrogen peroxide concentration. Such a linear behavior suggests a direct equilibrium between the two peroxo species, even though a quantitative measure of the related K_{eq} is hampered by the non-equilibrium, low-pressure and solvent free conditions that pertain to ion traps.

Tracey et al.[40] have reported a thermodynamic measure of a pH dependent K_{eq} (9.4 L·mol^{-1}) in water measured in ^{51}V NMR experiments (1.0 mol·L^{-1} KCl, 2×10^{-2} mol·L^{-1} HEPES buffer, pH 6.7), referring to the equilibrium $Vl_2 + l \rightleftarrows Vl_3$ (l = peroxide). We have tried to determine the equilibrium constant for the formation of triperoxo derivatives in experimental conditions as close as possible to those employed for ESI experiments by recording ^{51}V NMR spectra in mixed solvents (alcohol/water) in the absence of buffers and without controlling the ionic strength. Under our experimental conditions, in contrast to Tracey's results, the presence of an alcohol-containing diperoxo derivative (signal at $\delta = -642$, $W_{1/2} = 240$ Hz) is

detected irrespective of the excesses of hydrogen peroxide. Furthermore, upon increasing the water content in the solvent a second signal ($\delta = -663$, $W_{1/2} = 260$ Hz) appears, probably due to a water-containing diperoxo complex. The occurrence of a slow equilibrium between these species was confirmed previously by the coalescence of these two signals at 348 K.[12] It should be noted that the high ionic strength of the solutions (buffers and/or KCl as used in Tracey's experiments) is compelling for the formation of triperoxo vanadium complexes.[41]

The observation, during ESI-MS experiments in almost neutral solutions, of the triperoxo derivative as the major ionic species in the presence of large excesses of hydrogen peroxide may be explained by the particular conditions that pertain to the electrospray ionization technique. The electrospray process of aqueous or mixed alcohol-water solutions of various analytes has been reported to produce a marked pH change in the nebulized droplets with respect to the bulk.[42,43] In particular, droplets formed under the ESI negative-ion mode may undergo a considerable pH increase, favoring the formation of the triperoxo derivative, which is stable under fairly basic conditions, as discussed below.

Reactivity

The blue-violet complex $Na[V(O_2)_3]$ has been synthesized by using a slightly modified literature procedure[31−33] (see Experimental section for details). $Na[V(O_2)_3]\cdot 3H_2O$ is not stable in aqueous solution at millimolar concentrations. Accordingly, a fast change of color from blue-violet (triperoxo vanadate) to yellow (diperoxo vanadate) is observed while preparing the solutions. The yellow solution thus obtained has a pH of about 11 due to the hydrolysis of the triperoxo derivative.[31−33] Such equilibria may be indicated schematically as in Equation (5)−(7), where the triperoxo species is reported with one end-on peroxy anion in order to unravel the hydrolysis equilibria. Indeed, the structural data available[7] indicate that such a species contains three side-on peroxo moieties. Similarly, the theoretical calculations reported above indicate that the triperoxo complex has a capped trigonal prismatic geometry with three side-on peroxo moieties.

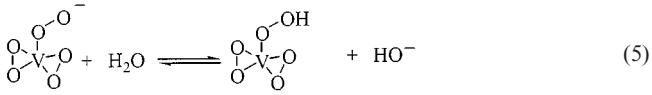

(5)

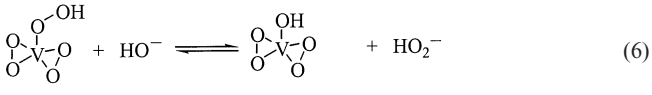

(6)

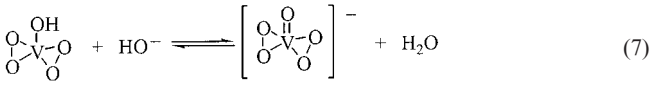

(7)

The formation of the yellow diperoxo complex from the blue triperoxo derivative has been further confirmed by ^{51}V NMR spectroscopy.[17−22] When $Na[V(O_2)_3]\cdot 3H_2O$ (1×10^{-3} mol·L^{-1}) is dissolved in aqueous solution (giving a solution of pH 11), the triperoxo complex quickly decomposes to form the diperoxo vanadium derivative identified by a signal at $\delta = -764$. On the other hand, when strongly basic water (pH 14) is used to dissolve the same amount of $Na[V(O_2)_3]\cdot 3H_2O$, the decomposition reaction described above is slowed down, although not blocked. In fact, in the ^{51}V NMR spectrum a peak is observed at $\delta = -847$ due to the triperoxo derivative together with the signal at $\delta = -764$.

The scarce data present in the literature[31,32] regarding the reactivity of triperoxo vanadium complexes indicate that they react as nucleophilic oxidants. Correspondingly, the oxidation of benzonitrile to benzamide by $Na[V(O_2)_3]\cdot 3H_2O$ and Baeyer−Villiger-type oxidations of benzil to benzoic acid, as well as the epoxidation of (*E*)-chalcone, have been reported. These authors also reported that the reduction product of the triperoxo derivative is the anionic diperoxo vanadate $[OV(O_2)_2(H_2O)]^-$.[32]

In the present work the behavior of the complex $Na[V(O_2)_3]\cdot 3H_2O$ toward cyclobutanone was studied. The triperoxo complex is almost insoluble in most organic solvents therefore its oxidative ability toward the selected substrate was examined in mixed alcohol/water solvents, even though the oxidant was still not completely dissolved at the desired concentration in this medium (see below).

When 0.45 mmol of $Na[V(O_2)_3]\cdot 3H_2O$ was allowed to react with 0.3 mmol of cyclobutanone in 2.5 mL of *i*PrOH/H_2O (2:1, heterogeneous conditions) at room temperature, complete consumption of the substrate and the formation of 4-hydroxy butyric acid as the main product were observed in about four days. It has also been confirmed that the initially formed γ-butyrolactone is not stable in the basic reaction conditions. By a careful GC check of the reaction mixture, it was observed that oxidation of *i*PrOH to acetone occurs as well as oxidation of the cyclobutanone. Thus, in order to simplify the system under analysis the solvent was changed to a mixture of CH_3OH/H_2O (1:2), where a similar oxidation of cyclobutanone to 4-hydroxy butyric acid takes place.

It is well-known that Baeyer−Villiger-type oxidations are carried out by the hydroperoxy anion.[44] It is conceivable that in the hydrolytic equilibria of Equation (5)−(7), the triperoxo vanadium species may act as a source of HOO^-. Therefore a more detailed analysis of the oxidation of cyclobutanone with $Na[V(O_2)_3]\cdot 3H_2O$ was required in order to elucidate the nature of the active nucleophilic oxidant.

Figure 3 shows the disappearance of cyclobutanone (0.12 mol·L^{-1}) as a function of time, observed under different experimental conditions. A very fast reaction (•) is observed when the substrate is reacted with basic H_2O_2 [CH_3OH/H_2O (1:2), pH 11]. On the other hand, slower processes have been observed with the triperoxo complex in CH_3OH/H_2O (1:2) (○) or in CH_3OH/H_2O (1:2; pH 11) (▲).

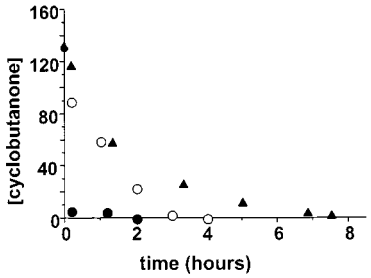

Figure 3. Behavior of cyclobutanone concentration as a function of time: (•) reaction with basic H_2O_2 in CH_3OH/H_2O (1:2), pH 11, room temp.; (○) reaction with $Na[V(O_2)_3]\cdot 3H_2O$ in CH_3OH/H_2O (1:2), room temp.; (▲) reaction with $Na[V(O_2)_3]\cdot 3H_2O$ in CH_3OH/H_2O (1:2), pH 11 (NaOH) room temp.

The behaviors detected can be explained by taking into consideration that, in all cases, the real oxidant is the hydroperoxy anion. Indeed, when the oxidant is $[V(O_2)_3]^-$, HOO^- is slowly released in solution upon hydrolysis of the vanadium triperoxide. This process [see Equation (5)−(7)] is in fact inhibited in the presence of added base. Accordingly the reaction performed at pH 11 (▲) is the slowest.

In order to verify this hypothesis further, two reactions with $Na[V(O_2)_3]\cdot 3H_2O$ in basic water (pH 14) were performed in the presence and in the absence of cyclobutanone. These processes were monitored by UV/Vis spectroscopy by measuring the decrease of the absorbance of the triperoxo vanadium complex at 561 nm. Interestingly, an identical kinetic behavior is observed both in the presence and in the absence of cyclobutanone, which is clear evidence that the substrate is not involved in the rate-determining step of the oxidation. Furthermore, taking into account that $[V(O_2)_3]^-$ decomposes to form $[OV(O_2)_2]^-$, and that the acid-base equilibria reported in Equation (5) and (7) are fast, it is likely that the ligand exchange process HO^-/HOO^- [Equation (6)], where the hydroperoxy anion is released in solution, is the rate determining step in the oxidation of cyclobutanone.

At variance with literature data,[32] our reactivity studies provide conclusive evidence that the triperoxo anion is a mere precursor of the hydroperoxy anion, which is the active species in the Baeyer−Villiger-type oxidation here examined. Furthermore, this result fits in well with the accepted knowledge that nucleophilic reactivity for d^0 metal peroxides is rarely observed.[45]

Conclusion

In summary, the association of ESI-MS spectrometry with ^{51}V NMR spectroscopy and ab initio calculations has allowed the definition of the nature and the speciation of peroxidic vanadium compounds, and in particular, of the triperoxo vanadium derivative that is formed in highly basic protic solutions in the presence of large excesses of hydrogen peroxide. Furthermore, the oxidation of cyclobutanone to 4-hydroxy butyric acid carried out with the preformed triperoxo compound in alcohol/water mixtures clearly indicates that the triperoxo complex does not itself act as a nucleophilic oxidant, but only as a source of the HOO^- anion.

Experimental Section

The synthesis of $n Bu_4NVO_3$ has been reported previously.[27,46] $Na[V(O_2)_3]$ was synthesized by using a slightly modified literature procedure:[31,33] V_2O_5 (2.6 mmol) was suspended in 1 mL of water and stirred. A large excess of hydrogen peroxide (ca. 50 equivalents, 14.8 mL of 30% v/v solution) was then added slowly and the solution stirred at 0° C until it turned dark red. Subsequently, 11 equivalents of NaOH (1.144 g) were slowly added whilst stirring at 0 °C. The reaction mixture changed color from red to yellow and, finally, to blue-violet, thus indicating the formation of the triperoxo derivative. The reaction was left at 0 °C for 30 min. and the precipitation of the complex was obtained by addition of cold ethanol (10 mL). The product was collected by filtration, washed twice with cold ethanol, dried and characterized as $Na[V(O_2)_3]\cdot 3H_2O$ (86% yield). IR (KBr): ν_{O-O} 854 cm^{-1}, ν_{V-O_2} 617 and 565 cm^{-1}. − UV/Vis: λ'_{max} = 192 nm, λ''_{max} = 560 nm (ε = 230). The active oxygen content was determined quantitatively by cerimetric titration.

The ESI-MS measurements were obtained using an LCQ instrument (Thermoquest, San Jose, CA). The peroxovanadium solutions were prepared by dissolving $n Bu_4NVO_3$ (5×10^{-4} mol·L^{-1}) in *i*PrOH (or EtOH for the experiments conducted in this solvent) in the presence of increasing amounts of H_2O_2 from 0.025 up to 0.35 mol·L^{-1}. The concentration of water was adjusted to 0.5 mol L^{-1}. The apparent pH for these solutions is about 7. For labeling experiments, $H_2{}^{17}O$ with an isotope content of ca. 50% was used ($H_2{}^{18}O$ less than 4%). Solution flow rate: 8μL min^{-1}; capillary temperature: 80 °C; spray voltage: 2.2 kV; capillary voltage: −5 to −10 V; tube lenses offset: −55 V; nebulizing gas: N_2 (40 units flow rate). The parameters related to the octapoles and detector were achieved by the automatic set-up procedure. Collision-induced decompositions of selected ions were obtained by applying a supplementary r.f. voltage (tickle voltage) to the end-cap electrodes of the ion trap (resonance activation).

All calculations were carried out with Gaussian 98,[34] running on an SGI O2 R10000 workstation. Hartree−Fock calculations were run with the 6-311++G(d,p) basis set. The latter includes the Wachters−Hay all-electron basis set for vanadium,[34,35] and the standard triply split valence basis set for H and O.[36,37] Only singlet states were considered. Harmonic vibrational frequencies were obtained from RHF/6-311++G(d,p) calculations and used to characterize local energy minima (all frequency real). Atomic charges were calculated by fitting to electrostatic potential maps (CHELPG method).[38]

Oxidation Reactions: The desired amount of cyclobutanone was dissolved in the alcoholic solvent (*i*PrOH or CH_3OH, typically 0.3 mmol in 1.5 mL *i*PrOH or CH_3OH). Subsequently, the appropriate amount of an aqueous (natural pH or basic pH obtained with NaOH) solution of $Na[V(O_2)_3]\cdot 3H_2O$ (typically 0.45−0.6 mmol) was slowly added. The reaction mixture was stirred at room temperature. The consumption of the substrate was followed by quantitative GC analysis [external standard n-C14 on a Carbowax 20M 15% on Chromosorb WAW-DMCS (1.8 m × 2 mm) column, FID detector]. Identification of the products was accomplished by ^1H NMR spectroscopy of the solid material isolated from the reaction mixtures.

Acknowledgments

We acknowledge financial support from the Italian Ministry of University and Scientific and Technological Research to the project COFIN2000: "Activation of Peroxidic Species in Innovative Selective Oxidation Processes" and from the Italian National Research Council. This work has been managed in the framework of the COST D12 project "New Catalysts for Environmentally Friendly Oxidations with H_2O_2 or O_2" D12/0027/99.

[1] H. Mimoun, *The Chemistry of Peroxides* (Ed.: S. Patai), Wiley, Chichester, U. K., **1983**; chapter 15.
[2] V. Conte, F. Di Furia, G. Modena, in *Organic Peroxides* (Ed.: W. Ando), Wiley, Chichester, U. K., **1992**; Chapter 11.2 pp.559−598
[3] N. D. Chasteen, *Vanadium in Biological Systems*; Kluwer Academic Publishers, Dordrecht, **1990**.
[4] *Metal Ions in Biological Systems. Vol.3. Vanadium and its Role in Life* (Ed.: H. Sigel), Marcel Dekker inc., New York NY, **1995**.
[5] A. Butler, M. Clague, G. E. Meister, *Chem. Rev.* **1994**, *94*, 625−638.
[6] V. Conte, F. Di Furia, G. Licini, *Appl. Catal.* **1997**, *157*, 335−361.
[7] A. Butler, J. V. Walker, *Chem. Rev.* **1993**, *93*, 1937−1944.
[8] A. Messerschmidt, R. Wever, *Proc. Natl. Acad. Sci. USA* **1996**, *93*, 392−396.
[9] A. Messerschmidt, L. Prade, R. Wever, *Biol. Chem.* **1997**, *378*, 309−315.
[10] V. Pecoraro, C. Slebodnick, B. Hamstra, *Vanadium Compounds: Chemistry, Biochemistry and Therapeutic Applications* (Eds.: D. C. Crans, A. Tracey), ACS Symposium Series 711, American Chemical Society, Washington, DC, **1998** chapter12, pp. 157−167.
[11] A. Butler, A. H. Baldwin, *Structure and Bonding − Metal sites in Proteins and Models*, Springer, Berlin, **1997**, vol.89 p.109−131.
[12] M. Bonchio, O. Bortolini, M. Carraro, V. Conte, S. Primon, *J. Inorg. Biochem.* **2000**, *80*, 191−194.
[13] M. Bonchio, O. Bortolini, V. Conte, S. Primon, *J. Chem. Soc., Perkin Trans. 2* **2001**, 763−765.
[14] R. Bortolo, D. Bianchi, R. D'Aloisio, C. Querci, M. Ricci, *J. Mol. Catal.* **2000**, *153*, 25−29.
[15] W. R. Thiel, *Angew. Chem. Int. Ed.* **1999**, *38*, 3157−3158.
[16] V. Conte, F. Di Furia, S. Moro, *J. Mol. Catal.* **1994**, *94*, 323−333 and refs. cited therein.
[17] O. W. Howarth, J. R. Hunt, *J. Chem. Soc., Dalton Trans.* **1979**, 1388−1391.
[18] O. W. Howarth, A. T. Harrison, *J. Chem. Soc., Dalton Trans.* **1985**, 1173−1177.
[19] J. S. Jaswal, A. S. Tracey, *Inorg. Chem.* **1991**, *30*, 3718−3722.
[20] V. Conte, F. Di Furia, S. Moro, *J. Mol. Catal.* **1995**, *104*, 159−169.
[21] V. Conte, F. Di Furia, S. Moro, *Inorg. Chim. Acta* **1998**, *272*, 62−67.
[22] I. Andersson, S. Angus-Dunne, O. Howarth, L. Pettersson, *J. Inorg. Biochem.* **2000**, *80*, 51−58.
[23] N. S. Campbell, A. C. Dengel, W. P. Griffith, *Polyhedron* **1989**, *8*, 1379−1386.
[24] O. Bortolini, F. Di Furia, G. Modena, P. Scrimin, *J. Mol. Catal.* **1980**, *9*, 323−334.
[25] O. Bortolini, V. Conte, F. Di Furia, S. Moro, *Eur. J. Inorg. Chem.* **1998**, 1193−1197.
[26] O. Bortolini, M. Carraro, V. Conte, S. Moro, *Eur. J. Inorg. Chem.* **1999**, 1489−1495.
[27] O. Bortolini, M. Carraro, V. Conte, S. Moro, *J. Inorg. Biochem.* **2000**, *80*, 41−49.
[28] A. Bagno, V. Conte, F. Di Furia, S. Moro, *J. Phys. Chem. A* **1997**, *101*, 4637−4640.
[29] V. Conte, F. Di Furia, S. Moro, *J. Mol. Catal.* **1997**, *120*, 93−99.
[30] T. R. Cundari, L. L. Sisterhen, C. Stylianopoulos, *Inorg. Chem.* **1997**, *36*, 4029−4034.
[31] M. N. Bhattacharjee, M. K. Chaudhuri, N. S. Islam, *Inorg. Chem.* **1989**, *28*, 2420−2423.
[32] M. Bhattacharjee, S. K. Chettri, M. K. Chaudhuri, N. S. Islam, S. R. Barman, *J. Mol. Catal.* **1993**, *78*, 143−149.
[33] M. K. Chaudhuri, S. K. Ghosh, N. S. Islam, *Inorg. Chem.* **1985**, *24*, 2706−2707.
[34] M. Frisch, G. W. Trucks, H. Schlegel, G. Scuseria, M. Robb, J. Cheeseman, V. G. Zakrzewski, J. A. Montgomery, R. E. Stratmann, J. C. Burant, S. Dapprich, J. M. Millam, A. Daniels, K. Kudin, M. Strain, O. Farkas, J. Tomasi, V. Barone, M. Cossi, R. Cammi, B. Mennucci, C. Pomelli, C. Adamo, S. Clifford, J. Ochterski, G. A. Petersson, P. Y. Ayala, Q. Cui, K. Morokuma, D. K. Malick, A. D. Rabuck, K. Raghavachari, J. B. Foresman, J. Cioslowski, J. V. Ortiz, B. B. Stefanov, G. Liu, A. Liashenko, P. Piskorz, I. Komaromi, R. Gomperts, R. L. Martin, D. J. Fox, T. Keith, M. A. Al-Laham, C. Y. Peng, A. Nanayakkara, C. Gonzalez, M. Challacombe, P. M. W. Gill, B. G. Johnson, W. Chen, M. W. Wong, J. L. Andres, M. Head-Gordon, E. S. Replogle, J. A. Pople, Gaussian 98 (revision A.6), **1998**, Gaussian, Inc, Pittsburgh, PA.
[35] A. J. H. Wachters, *J. Chem. Phys.* **1970**, *52*, 1033−1036.
[36] P. J. Hay, *J. Chem. Phys.* **1977**, *66*, 4377−4385.
[37] M. J. Frisch, J. A. Pople, J. S. Binkley, *J. Chem. Phys.* **1984**, *80*, 3265−3272.
[38] T. Clark, J. Chandrasekhar, G. W. Spitznagel, P. v. R. Schleyer, *J. Comp. Chem.* **1983**, *4*, 294−306.
[39] C. M. Breneman, K. B. Wiberg, *J. Comp. Chem.* **1990**, *11*, 361−368.
[40] A. S. Tracey, J. S. Jaswal, *Inorg. Chem.* **1993**, *32*, 4235−4243.
[41] V. Conte, D. C. Crans, unpublished.
[42] G. Wang, R. B. Cole, *Electrospray Ionization Mass Spectrometry. Fundamentals, Instrumentation and Applications* (Ed.: R. B. Cole), Wiley, New York, **1997**, chapter 4, pp. 137−174.
[43] C. L. Gatlin, F. Turecek, *Anal. Chem.* **1994**, *66*, 712−718.
[44] M. Renz, B. Meunier, *Eur. J. Org. Chem.* **1999**, 737−750.
[45] M. Bonchio, S. Calloni, F. Di Furia, G. Licini, G. Modena, S. Moro, W. A. Nugent, *J. Am. Chem. Soc.* **1997**, *119*, 6935−6936.
[46] V. W. Day, W. G. Klemperer, A. Yagasaki, *Chem. Lett.* **1990**, 1267−1270.

Received May 18, 2001
[I01180]

A Model for Trivalent Actinides in Media Containing High Carbonate Concentrations − Structural Characterization of the Lanthanide Tetracarbonate $[Co(NH_3)_6][Na(\mu\text{-}H_2O)(H_2O)_4]_2[Ho(CO_3)_4]\cdot 4H_2O$

Deborah L. Bond,[b] David L. Clark,[a] Robert J. Donohoe,[c] John C. Gordon,*[d] Pamela L. Gordon,[b] D. Webster Keogh,*[a] Brian L. Scott,[b] C. Drew Tait,[b] and John G. Watkin*[b]

Keywords: Actinides / Lanthanides / Carbonate / Coordination chemistry / Structural elucidation

The identity of the limiting Ho^{III} species in aqueous solutions with high carbonate concentrations has been determined to be $Ho(CO_3)_4^{5-}$. Single crystals of $[Co(NH_3)_6][Na(\mu\text{–}H_2O)(H_2O)_4]_2[Ho(CO_3)_4]\cdot 4H_2O$ were obtained by the addition of $[Co(NH_3)_6]^{3+}$ to an aqueous 0.04 M solution of Ho^{III} in 2.1 M Na_2CO_3. The asymmetric unit contains the anion, $[Ho(CO_3)_4]^{5-}$, a $[Co(NH_3)_6]^{3+}$ cation and two Na^+ cations, which are bound to H_2O molecules in an edge-sharing bioctahedral geometry. The $[Ho(CO_3)_4]^{5-}$ anion is eight coordinate with four bidentate carbonate ligands bound to the Ho atom. The molecule has essentially C_{2v} symmetry with two coplanar carbonates making a vane, which is perpendicular to a similar vane produced by the other two carbonate ligands. An alternative way to this view molecule is through the geometry of the C atoms, which are found in a distorted tetrahedron. The average Ho–O distance was determined to be 2.361(5) Å, while the average Ho–C distance was 2.784(6) Å. The IR and Raman spectra were determined in both the solid state and solution in order to confirm the solution speciation. The Raman data show a single CO_3^{2-} stretch for the solid at 1062 cm^{-1}. The solution data show multiple peaks with the most prominent being at 1048 cm^{-1}, which is consistent with the literature reports of an equilibrium mixture. The IR data for the solids confirm the X-ray results showing bidentate carbonate ligands by the splitting of the ν_3 band of the CO_3^{2-}. The crystal data for $[Co(NH_3)_6][Na(\mu\text{-}H_2O)(H_2O)_4]_2[Ho(CO_3)_4]\cdot 4H_2O$ are as follows: monoclinic space group $P2/n$, a = 8.7091(5) Å, b = 10.8744(6) Å, c = 15.7971(9) Å, β = 93.117(1)°, Z = 2, $R1$ = 0.0307, $wR2$ = 0.0756.

Introduction

Carbonate is commonly found in groundwater environments and has a high affinity for metal cations such as lanthanide and actinide ions; thermodynamic formation constants can often be as high as 10^{50}.[1,2] Unlike many metal ions, whose carbonate salts are relatively insoluble, carbonate complexation of the lanthanides and actinides can actually enhance solubility through the formation of highly charged anionic complexes. This enhancement of the solubility of the actinides in carbonic solutions is a serious concern for modeling the transport of these materials through the environment.[1−3] As an example, we note that there are conflicting reports on the nature of the limiting complex in trivalent lanthanide/actinide carbonate system. Recent spectroscopic studies of Cm^{III} in carbonate solution indicate that the tetra-carbonato complex $[Cm(CO_3)_4]^{5-}$ is the limiting species in the An^{III} carbonate system.[4] Other workers who have examined trivalent lanthanide systems have argued that the tris-carbonato complex $[Nd(CO_3)_3]^{3-}$ is the limiting species in the Ln^{III} carbonate system.[5] As a result, it is important to identify the structural models which could have spectroscopic tags for the environmentally relevant complexes formed in the equilibria.

Despite the reported synthesis of a number of materials, there are limited structural data for either the lanthanide or actinide metals with lower carbonate stoichiometries. The proposed lanthanide materials include: $Ln_2(CO_3)_3$, $Ln_2(CO_3)_3\cdot xH_2O$ (x = 2, 3, 8),[6−15] $M_6[Ce(CO_3)_5]\cdot xH_2O$ (M = Na, x = 12; M = $C(NH_2)_3$, x = 4),[16] $M_4[Ce(CO_3)_4]\cdot xH_2O$ (M = Na, x = 7; M = $C(NH_2)_3$, x = 6),[17] $M[Ln(CO_3)_2]$ (M = Li,[18] Na,[19,20] K,[21] Cs,[11] Tl[22]), and $M_5[Ln(CO_3)_4]$ (M = Na,[21] Tl[22]). Typically, the characterization of these materials involved X-ray powder diffraction, vibrational spectroscopy and thermogravimetric analysis. Recently, one of the first examples of a single crystal X-ray determination of a monomeric Ln^{III} tetra-carbonato complex, $[C(NH_2)_3]_5Nd(CO_3)_4(H_2O)$ was re-

[a] Los Alamos National Laboratory, Chemistry and Nuclear Materials Technology Divisions, G. T. Seaborg Institute for Transactinium Science
MS-G739, Los Alamos, NM 87545, USA
Fax: (internat.) +1-505/665-4622
E-mail: wkeogh@lanl.gov
[b] Chemistry Division, G. T. Seaborg Institute for Transactinium Science,
MS-J514, Los Alamos, NM 87545, USA
[c] Biosciences Division, G. T. Seaborg Institute for Transactinium Science,
MS-J586, Los Alamos, NM 87545, USA
[d] Nuclear Materials Technology Division, G. T. Seaborg Institute for Transactinium Science,
MS-J514, Los Alamos, NM 87545, USA

 © WILEY-VCH Verlag GmbH, 69451 Weinheim, 2001 1434−1948/01/1111−2921 $ 17.50+.50/0

ported.[23] We have also structurally characterized by single crystal X-ray techniques, $[Co(NH_3)_6][Sm(CO_3)_3(H_2O)]\cdot 4H_2O$[24] and $[Co(NH_3)_6]_6[K_2(H_2O)_{10}][Nd_2(CO_3)_8]_2\cdot 20H_2O$.[25] We sought to extend these studies by structurally characterizing additional carbonato anions, which could be found in the equilibrium systems described above. Studies were initiated with the lanthanides due to the ease of handling, the oxidation state stability and greater resistance to hydrolysis. Since the ionic radii of the lanthanides decrease across the series, we reasoned that the heavier lanthanides would be most likely to produce a mononuclear eight-coordinate tetracarbonate anion. We describe here our efforts in the synthesis and structural characterization of the limiting Ho^{III} tetracarbonate anion $[Ho(CO_3)_4]^{5-}$.

Results and Discussion

Synthesis and Electronic Spectra

The study of the holmium carbonate system is complicated by the precipitation of mineral phase carbonates of the form $Ho_2(CO_3)_3\cdot xH_2O$. The formation of this phase can be avoided by a judicious choice of metal carbonate, for example M_2CO_3 (M = Na, K, Cs, etc.), as well as controlling the total lanthanide and carbonate concentrations. The solutions were prepared by addition of $Ho(NO_3)_3\cdot xH_2O$ to 2.5 M Na_2CO_3, resulting in a yellow 0.1 M Ho^{III} solution. The Ho^{III} solution was analyzed by UV/Vis spectroscopy to identify any shift or change in intensity of the *f-f* transition compared to the Ho^{III} aquo ion. The electronic absorption spectrum was measured from 350 to 800 nm. The five most intense peaks were found at 360, 419, 450, 489, and 539 nm, with optical densities of 8.1, 2.9, 28, 1.9, and 3.5 $M^{-1}cm^{-1}$, respectively. It should be noted that the peaks at 360 and 450 nm are more intense than those of the aquo ion (ε = 1.3 and 3.1 $M^{-1}cm^{-1}$, respectively), indicating a possible lowering of the molecular symmetry.

Single Crystal X-ray Diffraction

Single crystals of $[Co(NH_3)_6][Na(\mu\text{-}H_2O)(H_2O)_4]_2[Ho(CO_3)_4]\cdot 4H_2O$ were obtained by addition of $[Co(NH_3)_6]Cl_3$ to a 0.04 M solution of Ho^{III} in 1.7 M Na_2CO_3, from which yellow orange crystals were obtained after two weeks of slow evaporation at room temperature. The data collection and crystallographic parameters are summarized in Table 1, and the selected bond lengths and angles are given in Table 2. A thermal ellipsoid drawing of $[Co(NH_3)_6][Na(\mu\text{-}H_2O)(H_2O)_4]_2[Ho(CO_3)_4]\cdot 4H_2O$ is shown in Figure 1, which also provides the atom-numbering scheme used in the tables. Figure 2 depicts the crystal matrix down the *b*-axis and shows the extensive hydrogen bonding network within the crystal.

The asymmetric unit contains the anion $[Ho(CO_3)_4]^{5-}$, a $[Co(NH_3)_6]^{3+}$ cation, two Na^+ cations, and 14 H_2O molecules, which are either bound to the Na^+ cations or found in the lattice. The metrical parameters for the $[Co(NH_3)_6]^{3+}$ ion are all within normal ranges. The $[Ho(CO_3)_4]^{5-}$ anion is eight coordinate, with four bidentate carbonate ligands bound to the Ho atom. The molecule has essentially C_{2v} symmetry with two coplanar carbonates making a vane, which is perpendicular to a similar vane produced by the other two carbonate ligands. Another view of this molecule is obtained through the geometry of the C atoms, which are found in a severely distorted tetrahedral geometry. The

Table 1. Crystal data and structure refinement for $[Ho(CO_3)_4][Co(NH_3)_6][Na(\mu\text{-}H_2O)(H_2O)_4]_2\cdot 4H_2O$

Empirical formula	$C_4H_{44}CoHoN_6Na_2O_{26}$
Molecular weight	862.29
Temperature	203(2) K
Wavelength λ (Mo-K_α)	0.71073 Å
Crystal system	monoclinic
Space group	*P*2/*n*
Unit cell dimensions	a = 8.7091(5) Å b = 10.8744(6) Å; β = 93.117(1)° c = 15.7971(9) Å
Volume	1493.87(15) $Å^3$
Z	2
Density (calculated)	1.917 Mg/m^3
Absorption coefficient	3.317 mm^{-1}
*T*min./*T*max.	0.85/0.95
F(000)	868
Crystal size	0.06 × 0.06 × 0.12 mm^3
Theta range for data collection	1.9 to 26.4°.
Index ranges	$-10 \le h \le 10$, $0 \le k \le 13$, $0 \le l \le 19$
Reflections collected	6986
Independent reflections	2945 [*R*(int) = 0.0232]
Data/restraints/parameters	2945/0/187
Goodness-of-fit on F^2	1.281
Final *R* indices [$I > 2\sigma(I)$]	*R*1 = 0.0267,[a] *wR*2 = 0.0741[b]
R indices (all data)	*R*1 = 0.0307, *wR*2 = 0.0756
Largest diff. peak and hole	0.772 and −0.504e.$Å^{-3}$

[a] $R1 = \Sigma||F_o| - |F_c||/\Sigma|F_o|$. — [b] $wR2 = \{\Sigma[w(F_o^2 - F_c^2)^2]/\Sigma[w(F_o^2)^2]\}^{1/2}$, where $w = 1/[\sigma^2(F_o^2) + (0.0397*P)^2 + 5.0273*P]$

Table 2. Selected bond lengths [Å] and angles [°] for $[Co(NH_3)_6][Na_2(H_2O)_{10}][Ho(CO_3)_4]\cdot 4H_2O$

Ho(1)−O(2)	2.386(3)	Ho(1)−C(1)	2.793(4)
Ho(1)−O(3)	2.352(3)	Ho(1)−C(2)	2.775(4)
Ho(1)−O(5)	2.357(3)	Ho(1)−O(1)	4.057(5)
Ho(1)−O(6)	2.348(3)	Ho(1)−O(2)	4.041(1)
Na(1)−O(7)	2.503(3)	Na(1)−O(10)	2.388(3)
Na(1)−O(8)	2.414(3)	Na(1)−O(11)	2.425(4)
Na(1)−O(9)	2.417(3)	Na(1)−O(9A)	2.423(3)
Na(1)−Na(1A)	3.555(3)		
O(3)−Ho(1)−O(5A)	76.99(9)	O(5)−Ho(1)−O(2)	90.86(10)
O(6)−Ho(1)−O(5)	55.73(9)	C(2A)−Ho(1)−C(2)	100.77(15)
O(6A)−Ho(1)−O(2)	169.77(9)	C(2A)−Ho(1)−C(1)	132.26(10)
O(6)−Ho(1)−O(2)	90.39(11)	C(2)−Ho(1)−C(1)	99.73(11)
O(3)−Ho(1)−O(2)	55.27(9)	C(1)−Ho(1)−C(1A)	97.42(15)
O(10)−Na(1)−O(8)	86.04(11)	O(10)−Na(1)−O(11)	176.96(14)
O(10)−Na(1)−O(9)	97.49(12)	O(8)−Na(1)−O(11)	90.95(12)
O(8)−Na(1)−O(9)	91.83(11)	O(9)−Na(1)−O(11)	83.00(13)
O(10)−Na(1)−O(9A)	93.43(12)	O(9A) −Na(1)−O(11)	89.60(12)
O(8)−Na(1)−O(9A)	177.15(13)	O(10)−Na(1)−O(7)	76.92(11)
O(9)−Na(1)−O(9A)	85.46(11)	O(8)−Na(1)−O(7)	97.06(11)
O(9)−Na(1)−O(7)	169.09(12)	O(11)−Na(1)−O(7)	103.09(13)
O(9)a−Na(1)−O(7)	85.54(11)		

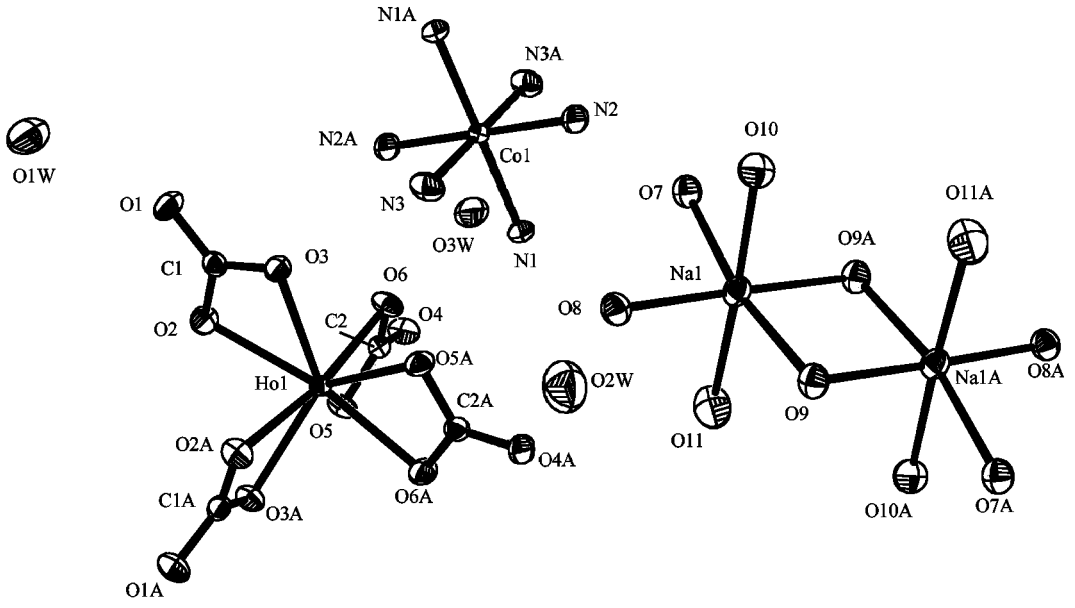

Figure 1. Thermal ellipsoid plot (50% probability) of $[Co(NH_3)_6][Na_2(H_2O)_{10}][Ho(CO_3)_4]\cdot 4H_2O$, giving the atom numbering scheme used in the tables

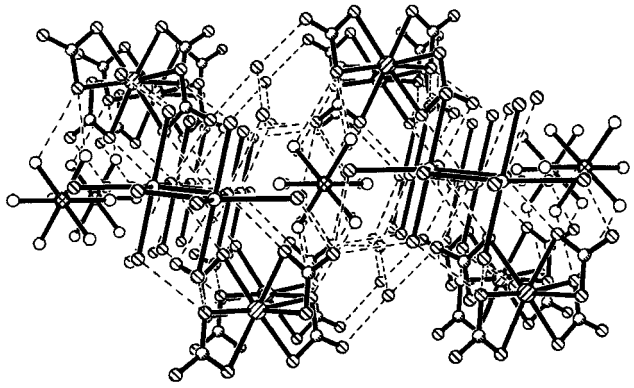

Figure 2. Ball and stick drawing depicting the crystal matrix of $[Co(NH_3)_6][Na_2(H_2O)_{10}][Ho(CO_3)_4]\cdot 4H_2O$ down the *b*-axis; the hydrogen bonding within the complex is shown by the dashed lines

average Ho−O distance was determined to be 2.361(5) Å, while the average Ho−C distance was 2.784(6) Å. As was previously stated, this is the first structural characterization of a mononuclear homoleptic carbonato complex of a trivalent lanthanide. In fact, the only structurally well characterized homoleptic lanthanide carbonate molecules are $[C(NH_2)_3]_6[Ce(CO_3)_5]\cdot 4H_2O$,[26] $La_2(CO_3)_3\cdot 8H_2O$,[27] $(La,Ce)_2(CO_3)_3\cdot 8H_2O$,[28] and $M[Ln(CO_3)_2]$ (M = K, Ln = Nd, Dy; M = Cs, Ln = Pr).[11,29,30] A comparison of the bond lengths may be made with $[Ho(oxam)_3(H_2O)_3]_4\cdot 2.75H_2O$ (**I**),[31] Ho(2,6-dihydroxybenzoato-*O*)$_2$(2,6-dihydroxybenzoato-*O*,*O*)$(H_2O)_4\cdot 2H_2O$ (**II**),[32] and $Ho(HCO_3)_3(H_2O)_4\cdot 2H_2O$ (**III**).[33] These complexes all contain terminal aquo ligands and carbonate or carboxylate groups with the Ho−O bond lengths being slightly different for Ho−$O_{(aquo)}$ and Ho−$O_{(O\text{-}R)}$. For **I** the average Ho−$O_{(aquo)}$ bond length is 2.37(1) Å, while the average for Ho−$O_{(O\text{-}R)}$ is 2.42(1) Å with values ranging from 2.362(8)−2.535(8) Å.[31] For **II** the average Ho−OH_2 distance is 2.37(1) Å, with a range for all Ho−O distances of 2.297(3)−2.486(3) Å.[32] Lastly, the average Ho−OH_2 distance in **III** is 2.36(1) Å, while the bond lengths of the bicarbonate ligands range from 2.442(9)−2.557(9) Å.[33] Clearly the bond lengths for the $Ho(CO_3)_4^{5-}$ ion are reasonable relative to other known Ho complexes. There are three main O−Ho−O angles of interest. The first type is the "bite" angle of the carbonate ligands, for example O(3)−Ho(1)−O(2), whose average is 55.5 (1)°. The other two angles are based on those between the carbonate ligands: O(3)−Ho(1)−O(5A) at 76.99(9)° and O(2)−Ho(1)−O(6A) at 169.77(9)°. An indication of the planarity between the two sets of carbonate ligands can be obtained by addition of the angles, which gives 358(1)°, quite close to the theoretical 360°. The C−Ho−C angles come in pairs and range from 132.26(11) to 97.42(15)° with the average being 107.5(2)°. The large range in the angles indicates the severe distortion from a tetrahedral geometry. The average distal C−O distance, 1.265(4) Å, is significantly shorter than the average metal-bound C−O distance, 1.301(5) Å. The O−C−O angles of the carbonate ligand deviate from the ideal value of 120°. The O−C−O angle between O atoms bound to Ho (the bite angle) averages 115.4(3)° while the remaining two O−C−O angles have opened up somewhat to 122.3(6)°. These distortions are typically found within carbonate ligands that are complexed to metal centers. The carbonate ligands are also involved with an extended hydrogen-bonding network. There are close contacts between the O atoms of the Ho carbonate ligands to the N atoms of the $[Co(NH_3)_6]^{3+}$ [average O···N is 3.09(1) Å]. The carbonate O atoms also have close contacts with the H_2O molecules in the lattice and those bound to the Na atoms [average O···O is 2.81(1) Å]. These dis-

tances are all well within the range expected for weak H-bonding interactions.[34]

Another interesting structural feature is the sodium aquo ion dimer $[Na_2(H_2O)_{10}]^{2+}$. Each of the Na atoms is six-coordinate, with four terminal and two bridging H_2O molecules; the overall geometry is best described as an edge-shared bioctahedron. The two Na atoms are separated by a reasonable 3.555(3) Å. The average Na−O distance is 2.43(1) Å with values ranging from 2.388(3) Å to 2.503(3) Å. The octahedra are distorted by an approximate 5° tilt of the axial ligands towards the center of the molecule. This distortion is further indicated by the average $O(11)-Na-O_{(cis)}$ angle of 91.7(1)°, while the average $O(10)-Na-O_{(cis)}$ angle is 88.5(1)°.

Vibrational Spectroscopy

Metal-carbonate complexation results in the splitting of the doubly degenerate e′ and e′′ modes of the free carbonate (D_{3h} symmetry). The extent of this splitting can be used to indicate whether the complexation is mono- or bidentate in nature.[35−37] This is especially true of the e′ ν_3 carbonate band composed of the asymmetric stretch of the free ligand. For bidentate complexation to a trivalent metal, the higher frequency stretch is pushed to over 1500 cm^{-1}, and the splitting between this band and the lower stretch is greater than 100 cm^{-1}. Conversely, monodentate complexation shifts the higher stretch to less than 1500 cm^{-1} and results in a splitting of less than 100 cm^{-1}. Another vibrational mode of interest, the metal−oxygen stretch, gives information on the strength of the bonding. For carbonate complexes with trivalent metals, this peak is typically in the 300−400 cm^{-1} region.[36]

Both Raman and infrared absorption (IR) measurements were performed to aid the characterization of the mode of carbonate complexation to Ho^{III}. The Raman spectrum from a single crystal of Ho^{III} carbonate is dominated by bands due to the $Co(NH_3)_6^{3+}$ moiety, with the only clear carbonate mode due to the symmetric stretch at 1062 cm^{-1}(Figure 3). The spectrum of the crystal differs from that of the parent solution, in which peaks at 1048 and 1066 cm^{-1} are observed. The latter feature is due in large part to free carbonate and obscures any measure of the tetracarbonato species, while the former demonstrates that a significant amount of the Ho in solution is a lower carbonato complex. This is consistent with earlier work that indicated an equilibrium mixture of complexes even up to 2.0 M CO_3^{2-}.[38] No Raman feature due to the Ho−O stretch could be observed, perhaps due to it being obscured by the cobalt hexaammine peak at 295 cm^{-1}, but also possibly due to the lack of covalent character of the holmium-carbonate bonding.

More carbonate bands for the $Ho(CO_3)_4^{5-}$ solid are found in the IR spectrum obtained from a ground sample prepared as a KBr pellet (Figure 4). In contrast to the Raman spectrum, the cobalt hexaammine peaks do not mask large areas of the spectral region: peaks are observed at 826, 1328 (shoulder), and 1653 cm^{-1},[36] with the latter also receiving any contribution from H_2O absorption. The remaining IR peaks are similar to those found for a holmium carbonate complex previously postulated to be the tetracarbonato species.[39] The coincidence of the IR peaks shown in the earlier work and the peaks reported here confirm that the holmium carbonato species is the same in both reports. While the nature of the species was postulated in the earlier work, water molecules directly bonded to the holmium had been postulated to sterically force the carbonates to bond in a monodentate fashion.[39] The crystal structure here shows that these water molecules are not bonded to holmium but rather to sodium, and that the carbonate bonds are indeed bidentate. The IR peaks support this bidentate bonding scheme.[35−37] Specifically, there is clearly a high frequency carbonate peak at 1519 cm^{-1}, consistent

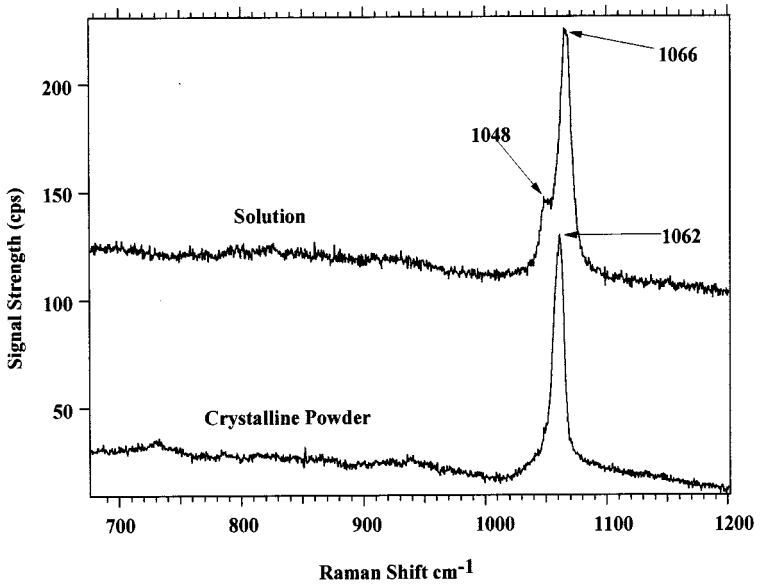

Figure 3. Raman spectra of 0.01 M Ho^{III} in 2.5 M Na_2CO_3 (upper) and solid $[Co(NH_3)_6][Na_2(H_2O)_{10}][Ho(CO_3)_4]\cdot 4H_2O$ (lower)

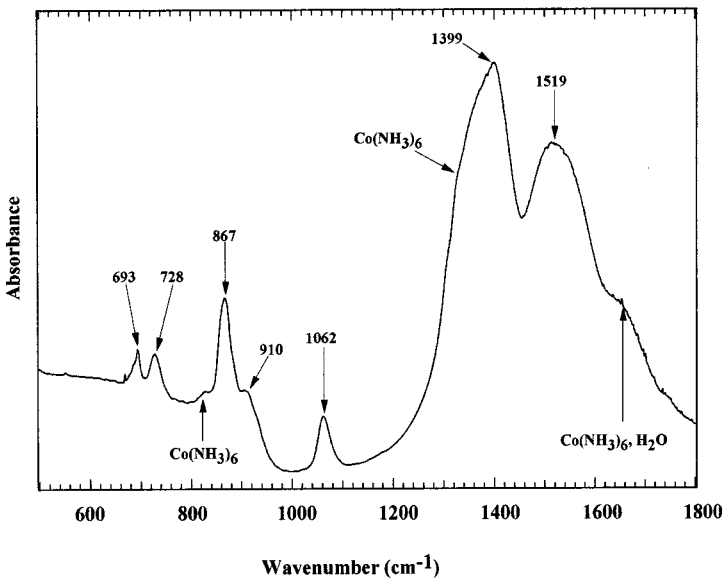

Figure 4. Infra-red spectrum of solid $[Co(NH_3)_6][Na_2(H_2O)_{10}][Ho(CO_3)_4]\cdot 4H_2O$ in a KBr matrix

with the higher asymmetric stretch from bidentate carbonate complexation. The other partner to this split e′ mode is observed at 1399 cm^{-1}, yielding a 120 cm^{-1} splitting of these peaks, consistent with bidentate complexation. To complete the vibrational description, the two peaks at 694 and 729 cm^{-1} are the result of splitting the ν_4 e′′ free carbonate bending mode upon complexation, the 867 cm^{-1} peak is the trampoline π mode, and the symmetric stretching mode can be seen at 1062 cm^{-1}, consistent with the Raman spectrum, and very close to the value observed in solution for the free carbonate ion. Therefore, the Raman and IR spectra are consistent with bidentate carbonate complexation with little covalent character.

Conclusion

The identification of the limiting complex in the Ho^{III} carbonate system under high carbonate concentration has been determined using a combination of single-crystal X-ray diffraction, electronic absorption and vibrational spectroscopy. It has been shown that the limiting complex is the mononuclear $[Ho(CO_3)_4]^{5-}$ ion. The solution from which the solid tetracarbonate was isolated was confirmed to contain an equilibrium mixture of complexes. This molecule can now be used as a structural and spectroscopic model for tetracarbonates of other Ln^{III} as well as $An^{III/IV}$ ions. However, it should be noted that this is only one structure type, and other expanded coordination environments could be observed in the larger lanthanide and actinide ions. Similar studies to determine the identity of the other species in the Ln^{III}, An^{III} and Pu^{IV} carbonate systems of importance to nuclear waste isolation and disposal programs are currently in progress.

Experimental Section

General: All operations were carried out in an open atmosphere and at room temperature. $Co(NH_3)_6Cl_3$, Na_2CO_3, and $Ho(NO_3)_3\cdot 5H_2O$ (Aldrich) were all used as received. The solution electronic absorption measurements were obtained in 1.0 cm matched quartz cells on a Perkin−Elmer Lambda 19 or Cary Model 5 spectrophotometer. Complete spectra in the range from 400 to 1000 nm as well as absorbance values at selected wavelengths were obtained. Measurements were made at 23 ± 1 °C. Raman vibrational spectra were obtained using near-infrared excitation obtained from a Ti-sapphire CW laser (752 nm, Spectra Physics Model 3900s) with detection accomplished through a CCD detector (Princeton Instruments). The Raman scattering was dispersed with a single-stage monochromator (diffraction gratings blazed at 1150 nm, 4 cm^{-1} resolution) after being prefiltered through an interference filter designed to remove Rayleigh-scattered laser light. The Raman samples were recorded in sealed 5 mm glass NMR tubes or mounted on a glass plate with silicon grease. Elemental analyses were performed with a Perkin−Elmer Series II CHNS/O Analyzer.

Preparation of Ho^{III} Carbonate Solutions: A solution of Ho^{III} (1.0 mL, 0.08 M) was prepared by dissolving $Ho(NO_3)_3\cdot 5H_2O$ (0.707 g, 1.60 mmol) in 20 mL of H_2O. The carbonate solution was then prepared by the addition of 1.0 mL of the Ho^{III} stock solution to 1.0 mL of a 4.1 M Na_2CO_3 solution. The resulting solution concentrations were 0.04 M Ho^{III} and 2.1 M Na_2CO_3.

Preparation of $[Co(NH_3)_6][Na_2(H_2O)_{10}][Ho(CO_3)_4]\cdot 4H_2O$: $Co(NH_3)_6Cl_3$ (0.4 mL, 0.2 M) was added to a solution of Ho^{III} (2.0 mL, 0.04 M) in 2.1 M Na_2CO_3. The mixture was allowed to sit open to the atmosphere for two weeks, during which time yellow-orange blocks formed. Raman: $\tilde{\nu}$ = 1064 cm^{-1}. − IR: $\tilde{\nu}$ = 694, 727, 827, 867, 907 1062, 1399 (CO_3^{2-}), 1520 (CO_3^{2-}), 1646 cm^{-1}. − $C_4H_{46}CoHoN_6Na_2O_{26}$ (864.3): calcd. C 5.56, H 5.36, N 9.12; found C 5.83, H 5.07, N 10.16.

X-ray Crystallography: A yellow-orange, irregular shaped crystal was attached to a glass fiber with a spot of silicone grease. The crystal was mounted from a matrix of mineral oil. The crystal was immediately placed on a Bruker P4/CCD/PC diffractometer, and cooled to 203 K using a Bruker LT-2 temperature device. The data were collected using a sealed, graphite monochromatized Mo-K_α X-ray source. A hemisphere of data were collected using a combination of and ω scans, with 20 second frame exposures and 0.3° frame widths. Data collection, initial indexing and cell refinement was handled using SMART[40] software. Frame integration and final cell parameter calculation were carried out using SAINT[41] software. The data were corrected for absorption using the DIFABS[42] program. Decay of reflection intensity was not observed.

The structure was solved in the space group *P*2/*n* using Direct methods and difference Fourier techniques. The initial solution revealed the holmium, cobalt, and the majority of all non-hydrogen atom positions. Several lattice water molecules were discovered during subsequent Fourier synthesis [atoms labeled O(1W) to O(3W)]. The hydrogen atoms were fixed (N−H= 0.89 Å) on the amine groups, which were allowed to rotate in order to maximize electron density at the hydrogen atom positions, and were refined with isotropic temperature factors set to 1.5 times the equivalent isotropic U of the atoms to which they are bound. The hydrogen atom positions associated with the water molecules were not considered in the structural model. The final refinement included anisotropic temperature factors on all non-hydrogen atoms, and converged to $R1 = 0.0267$ and $wR2 = 0.0741$. Structure solution, refinement, graphics, and creation of publication materials were performed using SHELXTL/NT.[43] Additional details of the data collection and structure refinement are listed in Table 1.

Further details of the crystal-structure investigation may be obtained from the Fachinformationszentrum Karlsruhe, 76344 Eggenstein-Leopoldshafen, Germany, on quoting the depository number CSD-411045.

Acknowledgments

We thank Dr. T. W. Newton and Dr. Th. Fanghänel for helpful discussions. This research was supported by the US DOE Office of Basic Energy Sciences and US DOE Office of Defense Programs, under Contract W-7405-ENG-36 with the University of California.

[1] J. Fuger, *Radiochim. Acta* **1992**, *59*, 81−91.
[2] D. L. Clark, D. E. Hobart, M. P. Neu, *Chem. Rev.* **1995**, *95*, 25−48.
[3] M. Dozol, R. Hagemann, *Pure and Appl. Chem.* **1993**, *65*, 1081−1082.
[4] T. Fanghänel, T. Konnecke, H. Weger, P. Paviet-Hartmann, V. Neck, J. I. Kim, *J. Solution Chem.* **1999**, *28*, 447−462.
[5] W. Runde, G. Meinrath, J. L. Kim, *Radiochim. Acta* **1992**, *58−59*, 93−100.
[6] S. Liu, R. Ma, R. Jiang, F. Luo, *J. Cryst. Growth* **1999**, *206*, 88−92.
[7] S. Liu, R. Ma, R. Jiang, F. Luo, *J. Cryst. Growth* **1999**, *203*, 454−457.
[8] H. Wakita, *Bull. Chem. Soc. Jpn* **1978**, *51*, 2879−2881.
[9] L. Song, M. Rongjun, *Indian J. Chem. Sect. A* **1996**, *35*, 992−994.
[10] N. Yanagihara, K. Vemulapalli, Q. Fernando, J. T. Dyke, *J. Less-Common Met.* **1991**, *167*, 223−232.
[11] A. Lossin, G. Meyer, *Z. Anorg. Allg. Chem.* **1993**, *619*, 2031−7.
[12] H. Wakita, S. Kinoshita, *Bull. Chem. Soc. Jpn.* **1979**, *52*, 428−432.
[13] R. L. N. Sastry, S. R. Yoganarasimhan, P. N. Mehrotra, C. N. R. Rao, *J. Inorg. Nucl. Chem.* **1966**, *28*, 1165−77.
[14] G. Pannetier, J. Hataf, A. Dereigne, *Bull. Chim. Soc. Fr.* **1965**, *5*, 318−321.
[15] R. G. Charles, *J. Inorg. Nucl. Chem.* **1965**, *27*, 1489−93.
[16] J. P. Jolivet, Y. Thomas, B. Taravel, V. Lorenzelli, G. Busca, *J. Mol. Struct.* **1982**, *79*, 403−8.
[17] J. P. Jolivet, Y. Thomas, B. Taravel, V. Lorenzelli, G. Busca, *J. Mol. Struct.* **1983**, *102*, 137−143.
[18] H. J. Kalz, H. Seidel, *Z. Anorg. Allg. Chem.* **1980**, *465*, 92−108.
[19] A. Mochizuki, K. Nagashima, H. Wakita, *Bull. Chem. Soc. Jpn* **1974**, *47*, 755−756.
[20] H. Schweer, H. Seidel, *Z. Anorg. Allg. Chem.* **1981**, *477*, 196−204.
[21] A. De Polignac, J. Delaunay, F. Fromage, J. Despujols, *C. R. Acad. Sci., Ser. C* **1971**, *273*, 735.
[22] H. Schweer, H. Seidel, *Z. Anorg. Allg. Chem.* **1983**, *498*, 205−217.
[23] W. Runde, M. P. Neu, C. Van Pelt, B. L. Scott, *Inorg. Chem.* **2000**, *39*, 1050−1051.
[24] D. L. Bond, D. L. Clark, R. J. Donohoe, J. C. Gordon, P. L. Gordon, D. W. Keogh, B. L. Scott, C. D. Tait, J. G. Watkin, *J. Chem. Soc., Dalton Trans.* **2000**, 1975−1980.
[25] D. L. Bond, D. L. Clark, R. J. Donohoe, J. C. Gordon, P. L. Gordon, D. W. Keogh, B. L. Scott, C. D. Tait, J. G. Watkin, *Inorg. Chem.* **2000**, *39*, 3934−3937.
[26] P. S. Voliotis, A. Rimsky, J. Faucherre, *Acta. Cryst., Sect. B* **1975**, *31*, 2607−2611.
[27] D. B. Shinn, H. A. Eick, *Inorg. Chem.* **1968**, *7*, 1340−1345.
[28] A. Dal Negro, G. Rossi, V. Tazzoli, *Am. Mineral.* **1977**, *62*, 142−146.
[29] H. J. Kalz, H. Seidel, *Z. Anorg. Allg. Chem.* **1982**, *486*, 221−228.
[30] I. Kutlu, H. J. Kalz, R. Wartchow, H. Ehrhardt, H. Seidel, G. Meyer, *Z. Anorg. Allg. Chem.* **1997**, *623*, 1753−1758.
[31] C. Papadimitriou, P. Veltsistas, J. Marek, J. D. Woollins, *Inorg. Chim. Acta* **1998**, *267*, 299−303.
[32] T. Glowiak, W. Bryska, A. Kula, A. Rzaczynska, *J. Coord. Chem.* **1999**, *48*, 477−486.
[33] W. J. Rohrbaugh, R. A. Jacobson, *Inorg. Chem.* **1974**, *13*, 2535−9.
[34] L. Pauling, *The Nature of the Chemical Bond*; 3rd ed.; Cornell University Press: Ithaca, NY, **1960**.
[35] J. P. Jolivet, T. B. Taravel, V. Lorenzelli, *J. Mol Struct.* **1980**, *60*, 93−98.
[36] K. Nakamoto *Infrared and Raman Spectra of Inorganic and Coordination Compounds*; 5th ed.; Wiley-Interscience: New York, **1997**.
[37] B. Taravel, F. Fromage, P. Delorme, V. Lorenzelli, *C. R. Acad. Sc. Paris B* **1972**, *275*, 589−592.
[38] F. Fromage, *Ann. Chim.* **1968**, *3*, 457−467.
[39] B. Taravel, F. Fromage, P. Delorme, V. Lorenzelli, *J. Mol. Struct.* **1973**, *16*, 483−498.
[40] Bruker Analytical X-ray Systems, Inc., SMART, 4.210, **1996**, Madison, Wisconsin
[41] Bruker Analytical X-ray Systems, Inc., SAINT, 4.05, **1996**, Madison Wisconsin
[42] J. Walker, J. Stuart, *J. Appl. Cryst.* **1994**.
[43] Bruker Analytical X-ray Instruments, Inc., SHELXTL/NT, 5.10, **1997**, Madison, Wisconsin.

Received November 10, 2000
[I00428]

Synthesis, Spectroscopic and Structural Studies on Six- and Eight-Coordinate Phosphane and Arsane Complexes of Titanium(IV) Halides

Richard Hart,[a] William Levason,[a] Bhavesh Patel,[a] and Gillian Reid*[a]

Keywords: Titanium / Halides / Phosphanes / Arsanes / Structure elucidation

The six-coordinate complexes [TiX_4(L-L)] [X = Cl or Br; L-L = $Ph_2PCH_2PPh_2$, $Ph_2P(CH_2)_2PPh_2$, $Ph_2P(CH_2)_3PPh_2$, *o*-$C_6H_4(PPh_2)_2$, *o*-$C_6H_4(PMe_2)_2$, $Ph_2As(CH_2)_2AsPh_2$, *o*-$C_6H_4(AsMe_2)_2$ or $MeC(CH_2AsMe_2)_3$] and the eight-coordinate complexes [TiX_4(L-L)$_2$] [L-L = *o*-$C_6H_4(PMe_2)_2$ or *o*-$C_6H_4(AsMe_2)_2$] have been prepared and characterised by solution ^1H and $^{31}P\{^1H\}$ NMR spectroscopy, IR and UV/Visible spectroscopy and microanalyses. The crystal structures of [$TiCl_4${*o*-$C_6H_4(PMe_2)_2$}], [$TiCl_4${*o*-$C_6H_4(PMe_2)_2$}$_2$], [$TiBr_4${*o*-$C_6H_4(PMe_2)_2$}$_2$], [$TiBr_4${*o*-$C_6H_4(AsMe_2)_2$}$_2$] and [$TiBr_4${$MeC(CH_2AsMe_2)_3$}] are described and permit detailed comparisons to be made between the six- and eight-coordinate species and between the phosphane and arsane species. The crystal structure of the zwitterionic [$TiCl_5(Ph_2PCH_2PHPh_2)$] is also reported.

Introduction

Recently we have been investigating the chemistry of the early transition metal ions, particularly Ti^{IV}, with thio-, seleno- and telluroether ligands. Part of the impetus for this work arises from the potential of the resultant complexes as single-source precursors for transition metal chalcogenides through CVD processes. Thus, we have reported the preparation of a wide range of six-coordinate, distorted octahedral complexes of the form [TiX_4(E-E)] (E-E = dithio- or diselenoether).[1] We have also isolated six- and seven-coordinate species involving trithio- and triselenoether ligands.[2] In the course of this work we attempted to generate eight-coordinate species of the form [TiX_4(E-E)$_2$]; however we saw no evidence at any stage for their existence either in solution or in the solid state. This prompted us to examine in some more detail the literature describing eight-coordinate Ti^{IV} complexes involving diphosphane and diarsane ligands. While a number of references to such species have been made, including, for example, [$TiCl_4${*o*-$C_6H_4(PMe_2)_2$}$_2$], [TiX_4{*o*-$C_6H_4(AsMe_2)_2$}$_2$] (X = Cl or Br) and [$TiCl_4${$Me_2P(CH_2)_2PMe_2$}$_2$],[3−8] the literature is in fact very patchy and single crystal X-ray structural data are only available for two examples: an early report by Nyholm and co-workers on [$TiCl_4${*o*-$C_6H_4(AsMe_2)_2$}$_2$],[3,4] and [$TiCl_4${$Me_2P(CH_2)_2PMe_2$}$_2$], which was reported by Cotton and co-workers in 1998.[6] The synthesis of [$TiCl_4${*o*-$C_6H_4(PMe_2)_2$}$_2$] has been reported, but structural information is limited to an X-ray powder photograph, indicating the same structure as [$TiCl_4${*o*-$C_6H_4(AsMe_2)_2$}$_2$].[5] This lack of structural data and the absence of any detailed solution studies on either the six- or eight-coordinate systems has prompted us to conduct more thorough studies on the synthesis and properties of phosphane and arsane complexes of Ti^{IV}. Our specific aims were to investigate the possibility of forming other complexes with coordination numbers greater than six and to establish the structural consequences of changing from six- to eight-coordination. In this paper we report the results of our studies, including the preparations and spectroscopic characterisation of six- or eight-coordinate Ti^{IV} halide complexes involving $Ph_2PCH_2PPh_2$, $Ph_2P(CH_2)_2PPh_2$, $Ph_2P(CH_2)_3PPh_2$, *o*-$C_6H_4(PPh_2)_2$, *o*-$C_6H_4(PMe_2)_2$, $Ph_2As(CH_2)_2AsPh_2$, *o*-$C_6H_4(AsMe_2)_2$ and $MeC(CH_2AsMe_2)_3$. The crystal structures of [$TiCl_4${*o*-$C_6H_4(PMe_2)_2$}], [$TiCl_4${*o*-$C_6H_4(PMe_2)_2$}$_2$], [$TiBr_4${*o*-$C_6H_4(PMe_2)_2$}$_2$], [$TiBr_4${*o*-$C_6H_4(AsMe_2)_2$}$_2$] and [$TiBr_4${$MeC(CH_2AsMe_2)_3$}] are also described and permit the details of the structural changes incurred upon changing the Ti^{IV} coordination to be examined. The crystal structure of the unusual zwitterionic species [$TiCl_5(PPh_2PCH_2PHPh_2)$], which was obtained as a decomposition product from a solution of [$TiCl_4(Ph_2PCH_2PPh_2)$], is also presented.

Results and Discussion

Compounds TiX_4 (X = Cl or Br) react with one molar equivalent of L-L [L-L = $Ph_2P(CH_2)_nPPh_2$ (n = 1−3), *o*-$C_6H_4(PMe_2)_2$, *o*-$C_6H_4(PPh_2)_2$, *o*-$C_6H_4(AsMe_2)_2$ or $Ph_2As(CH_2)_2AsPh_2$] in rigorously anhydrous CH_2Cl_2 solution under an N_2 atmosphere to afford the 1:1 species [TiX_4(L-L)] as orange- or red-coloured solids in good yield; the tripodal ligand $MeC(CH_2AsMe_2)_3$ gives [TiX_4{$MeC(CH_2AsMe_2)_3$}] also in high yield. The 1:2 complexes [TiX_4{*o*-$C_6H_4(PMe_2)_2$}$_2$] and [TiX_4{*o*-$C_6H_4(AsMe_2)_2$}$_2$] were obtained in good yield by similar reactions using two molar equivalents of ligand. The compounds are relatively stable as solids when stored under N_2 in a dry glove-box. However, in solution they are very susceptible to hydrolysis, rapidly decolourising. The powdered solids are also readily hydrolysed in moist air. For these

[a] Department of Chemistry, University of Southampton, Highfield, Southampton SO17 1BJ, UK
Fax: (internat.) +44-23/8059-3781
E-mail: gr@soton.ac.uk

 © WILEY-VCH Verlag GmbH, 69451 Weinheim, 2001 1434−1948/01/1111−2927 $ 17.50+.50/0

reasons all measurements were conducted using solutions freshly prepared in rigorously anhydrous solvents. IR spectra were recorded as nujol mulls and the complexes $[TiX_4(L\text{-}L)]$ show, in addition to peaks due to the coordinated phosphane or arsane ligand, up to four bands around 420−350 cm^{-1} (X = Cl) or 320−280 cm^{-1} (X = Br), consistent with the presence of the *cis*-octahedral species (theory $2a_1 + b_1 + b_2$ for C_{2v} symmetry). Similar frequencies were observed for the tetrahalo-titanium thio- and selenoether species reported earlier.[1] For the complexes $[TiX_4(L\text{-}L)_2]$ [L-L = *o*-$C_6H_4(PMe_2)_2$ or *o*-$C_6H_4(AsMe_2)_2$], IR spectroscopy shows two peaks around 315 cm^{-1} for the chloro species and ca. 290 cm^{-1} for the bromo species (theory $b_2 + e$ for D_{2d} symmetry). The frequencies for the eight-coordinate species are generally significantly lower than for their six-coordinate analogues. These data are in good agreement with the literature.[5]

Electronic spectra were recorded by diffuse reflectance owing to the highly sensitive nature of the compounds in solution. For the six-coordinate d^0 complexes $[TiCl_4(L\text{-}L)]$, two broad features are present at ca. 21,000 and ca. 28,000 cm^{-1}, which may be assigned as $\sigma(P,As) \rightarrow Ti(t_{2g})$ and $\pi(Cl) \rightarrow Ti(t_{2g})$ LMCT transitions, respectively. Although the actual symmetry at Ti is C_{2v} rather than O_h, the lifting of the degeneracy of the Ti t_{2g} orbitals does not result in resolved splittings, although it may contribute to the broadness of the bands. The spectra of the $[TiBr_4(L\text{-}L)]$ complexes are less well resolved, but features at ca. 20,000 and 23,000 cm^{-1} are assigned similarly as $\sigma(P,As) \rightarrow Ti(t_{2g})$ and $\pi(Br) \rightarrow Ti(t_{2g})$ transitions. The $\sigma(P,As) \rightarrow Ti(t_{2g})$ transition appears at slightly lower energy when X = Br than when X = Cl, an effect often observed with later transition metals.[9] The eight-coordinate $[TiX_4(L\text{-}L)_2]$ complexes have broad features at similar energies to their six-coordinate analogues, which are similarly assigned to LMCT transitions. For a D_{2d} metal centre, taking the z-axis as the principle inversion (S_4) axis, the lowest d-level is b_1 and thus the transitions are L (or X) $\rightarrow$ Ti(b_1). A careful comparison of the diffuse reflectance spectra of the corresponding $[TiCl_4(L\text{-}L)]$ and $[TiCl_4(L\text{-}L)_2]$ complexes shows two differences: (i) the bands are broader in the eight-coordinate than in the six-coordinate complexes, and (ii) the $\sigma(P,As) \rightarrow Ti$ transitions are relatively more intense than the $\pi(X) \rightarrow Ti$ transition in the former, which is reasonable since the number of P/As donors has doubled. The bands in the spectra of $[TiBr_4(L\text{-}L)_x]$ (x = 1 or 2) are very broad, but appear to show a similar trend. Whilst the six- and eight-coordinate complexes can be distinguished by their diffuse reflectance spectra when the spectra for both species are compared; the differences do not appear to be sufficiently large to assign the coordination number to a $TiX_4(L\text{-}L)_x$ complex on the basis of the spectrum of only one or the other with any confidence.

Solution NMR studies

The $^{31}P\{^1H\}$ NMR spectrum of $[TiCl_4\{o\text{-}C_6H_4(PMe_2)_2\}_2]$ in CH_2Cl_2 at room temperature is a singlet at δ = 31.5, whereas that of the poorly soluble $[TiCl_4\{o\text{-}C_6H_4(PMe_2)_2\}]$ has δ = 29.5. The corresponding ^1H NMR spectra show second order multiplets for the PMe_2 groups at δ = 1.88 ($[TiCl_4\{o\text{-}C_6H_4(PMe_2)_2\}_2]$) and 1.90 ($[TiCl_4\{o\text{-}C_6H_4(PMe_2)_2\}]$) and the spectra are essentially unchanged on cooling the solution to −90 °C. We therefore conclude that neither complex dissociates ligand under these conditions. Similar studies on $[TiBr_4\{o\text{-}C_6H_4(PMe_2)_2\}]$ reveal a single $^{31}P\{^1H\}$ NMR resonance at δ = 24.5, and addition of *o*-$C_6H_4(PMe_2)_2$ to this solution produces, in addition to a free ligand resonance at δ = −55, a new species at δ = 22.2. The $^{31}P\{^1H\}$ NMR spectrum of $[TiBr_4\{o\text{-}C_6H_4(PMe_2)_2\}_2]$ at ambient temperatures contains three resonances at δ = 24.5, 22.2 and −54, from which it is clear that $[TiBr_4\{o\text{-}C_6H_4(PMe_2)_2\}_2]$ is partially dissociated in solution into the 1:1 complex and *o*-$C_6H_4(PMe_2)_2$, and that exchange between either complex and *o*-$C_6H_4(PMe_2)_2$ is slow on the ^{31}P NMR time-scale at ambient temperatures. The ^1H NMR spectra lead to similar conclusions, although the coordinated PMe_2 resonances overlap. The $^{31}P\{^1H\}$ NMR spectrum of $[TiCl_4\{o\text{-}C_6H_4(PPh_2)_2\}]$ shows a sharp singlet at δ = 34.2, and that of $[TiCl_4\{Ph_2P(CH_2)_2PPh_2\}]$ a singlet at δ = 24.6. The spectra of the corresponding bromides and of $[TiX_4\{Ph_2P(CH_2)_3PPh_2\}]$ show only very broad resonances at lower frequency which remain broad even at −90 °C; we attribute this to reversible ligand dissociation.

For the *o*-$C_6H_4(AsMe_2)_2$ complexes only ^1H NMR spectroscopic data were available (attempts to study ligand exchange in solution by $^{13}C\{^1H\}$ NMR were unsuccessful due mainly to poor solubility). At room temperature the complex $[TiCl_4\{o\text{-}C_6H_4(AsMe_2)_2\}]$ showed a singlet $AsMe_2$ resonance at δ = 1.75, whereas $[TiCl_4\{o\text{-}C_6H_4(AsMe_2)_2\}_2]$ contained three resonances at δ = 1.8, 1.74 and 1.2. The δ = 1.2 resonance is due to free *o*-$C_6H_4(AsMe_2)_2$, and thus the spectrum shows that $[TiCl_4\{o\text{-}C_6H_4(AsMe_2)_2\}_2]$ is partially dissociated into the 1:1 complex and *o*-$C_6H_4(AsMe_2)_2$. Attempts to record spectra at −90 °C were unsuccessful due to the poor solubility of the complex at low temperatures. The spectrum obtained from $[TiBr_4\{o\text{-}C_6H_4(AsMe_2)_2\}]$ in CD_2Cl_2 at room temperature shows an $AsMe_2$ singlet at δ = 1.9 (assigned to the complex) and some free *o*-$C_6H_4(AsMe_2)_2$ at δ = 1.2. The spectrum of $[TiBr_4\{o\text{-}C_6H_4(AsMe_2)_2\}_2]$ contained broad lines at δ = 1.9 and 1.2 attributable to the 1:1 complex and free ligand; a weaker peak at δ = 1.6 is tentatively attributed to the 2:1 complex. These resonances sharpened on cooling.

Comparison of these results show that whilst the $[TiCl_4\{o\text{-}C_6H_4(PMe_2)_2\}_n]$ (n = 1 or 2) and $[TiBr_4\{o\text{-}C_6H_4(PMe_2)_2\}]$ complexes are stable in solution, the $[TiCl_4\{o\text{-}C_6H_4(AsMe_2)_2\}_2]$ and $[TiBr_4\{o\text{-}C_6H_4(PMe_2)_2\}_2]$ complexes are partially dissociated in solution into the corresponding 1:1 complex and free ligand. Greater dissociation is observed with the weaker Lewis acid $TiBr_4$: $[TiBr_4\{o\text{-}C_6H_4(AsMe_2)_2\}]$ appears to be partially dissociated into $TiBr_4$ and *o*-$C_6H_4(AsMe_2)_2$ in solution. Of the complexes of the phenyl-substituted diphosphanes, only the $[TiCl_4(L\text{-}L)]$ [L-L = $Ph_2P(CH_2)_2PPh_2$ or *o*-$C_6H_4(PPh_2)_2$] show sharp ^{31}P NMR spectra; in the corresponding brom-

ides or in $[TiCl_4\{Ph_2P(CH_2)_3PPh_2\}]$, only very broad lines, typical of rapidly exchanging systems are observed.

The $[TiX_4\{MeC(CH_2AsMe_2)_3\}]$ systems were difficult to study in solution due to their very poor solubility in chlorocarbons, and attempts to obtain $^{13}C\{^1H\}$ data were unsuccessful. However, the ^1H NMR spectroscopic data are consistent with the six-coordinate structure established crystallographically for the bromide. Both show an uncoordinated $AsMe_2$ resonance at $\delta = 0.95$, coordinated $AsMe_2$ groups (broad singlet at $\delta = 1.71$ for X = Br, and two lines of 1:1 intensity $\delta = 1.59$, 1.61 X = Cl) and corresponding CH_2 resonances near $\delta = 2.0$ (coord) and $\delta = 1.7$ (free). The spectra show that exchange between the free and coordinated arms of the tridentate arsane is slow at ambient temperatures, which contrasts with the behaviour in the trithioether analogues.[2] These conclusions are at odds with an early literature report[10] which concludes from ^1H NMR spectroscopy that $[TiCl_4\{MeC(CH_2AsMe_2)_3\}]$ is seven-coordinate with tridentate triarsane coordination. This was subsequently questioned by McAlees and co-workers[11] who reinterpreted the original NMR spectroscopic data and suggested six-coordination, with one arm of the tripod uncoordinated. Our conclusions are also supported by a single crystal X-ray structure determination (see below).

X-ray Crystallographic Studies

Crystals of $[TiCl_4\{o\text{-}C_6H_4(PMe_2)_2\}]$, $[TiCl_4\{o\text{-}C_6H_4(PMe_2)_2\}_2]$, $[TiBr_4\{o\text{-}C_6H_4(PMe_2)_2\}_2]$, $[TiBr_4\{o\text{-}C_6H_4(AsMe_2)_2\}_2]$ and $[TiBr_4\{MeC(CH_2AsMe_2)_3\}]$ were obtained from CH_2Cl_2 solution. The structure of $[TiCl_4\{o\text{-}C_6H_4(PMe_2)_2\}]$ (Figure 1) shows a discrete distorted octahedral geometry at Ti^{IV}, with the $o\text{-}C_6H_4(PMe_2)_2$ ligand chelating. The Ti−P bond lengths of 2.5733(13) and 2.5600(12) Å are in agreement with those in $[TiCl_4\{Me_2P(CH_2)_2PMe_2\}]$ [2.574(2) − 2.590(2) Å] and other six-coordinate phosphane complexes of Ti^{IV}.[12,13] The Ti−Cl distances *trans* to Cl are longer than those *trans* to P by ca. 0.2 Å, consistent with a *trans* influence on Ti^{IV} of Cl > P. A similar trend was observed for $[TiX_4(E\text{-}E)]$ (E-E = dithioether or diselenoether), where the *trans* influence was X > E, and $[TiCl_4\{Me_2P(CH_2)_2PMe_2\}]$ and $[TiCl_4\{Et_2P(CH_2)_2PEt_2\}]$.[12,13] The axial Cl(3)−Ti(1)−Cl(4) unit is tilted to lie over the $o\text{-}C_6H_4(PMe_2)_2$ ligand, with an angle of 164.25(6)°. The P−Ti−P angle in the five-membered chelate ring is constrained to be 76.05(4)°.

Crystals were also obtained for the directly comparable eight-coordinate species $[TiCl_4\{o\text{-}C_6H_4(PMe_2)_2\}_2]$, although the crystal quality was less good, resulting in higher residuals. However, the structure of this complex (Figure 2) shows crystallographic 4bar symmetry and adopts a dodecahedral stereochemistry. The Ti−Cl distance [2.503(3) Å] is 0.20−0.25 Å longer than in the six-coordinate $[TiCl_4\{o\text{-}C_6H_4(PMe_2)_2\}]$. This is substantially greater than the increase in d(Ti−P) which is ca. 0.1 Å on going from a six- to an eight-coordinate geometry. Normally one would expect an increase in coordination number to be accompanied by an increase in Ti−donor atom bond length. Indeed,

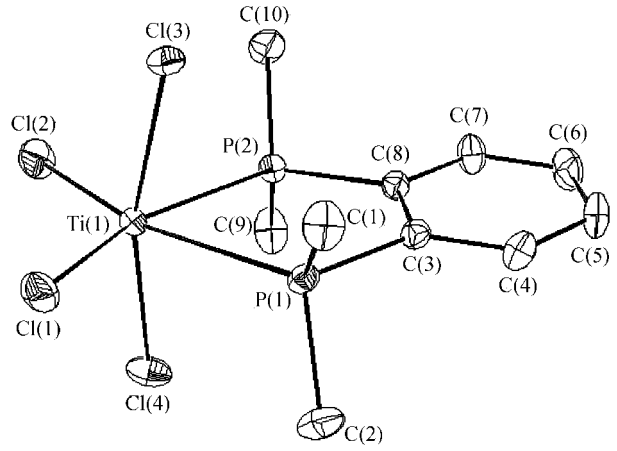

Figure 1. View of the structure of $[TiCl_4\{o\text{-}C_6H_4(PMe_2)_2\}]$ with atom numbering scheme; ellipsoids are shown at the 40% probability level; selected bond lengths (Å) and angles (°): Ti(1)−Cl(1) 2.2748(12), Ti(1)−Cl(2) 2.253(1), Ti(1)−Cl(3) 2.2975(13), Ti(1)−Cl(4) 2.2938(13); Ti(1)−P(1) 2.5733(13), Ti(1)−P(2) 2.5600(12); Cl(1)−Ti(1)−Cl(2) 114.58(5), Cl(1)−Ti(1)−Cl(3) 93.88(5), Cl(1)−Ti(1)−Cl(4) 94.23(5), Cl(1)−Ti(1)−P(1) 84.39(5), Cl(1)−Ti(1)−P(2) 160.39(5), Cl(2)−Ti(1)−Cl(3) 94.42(5), Cl(2)−Ti(1)−Cl(4) 94.44(5), Cl(2)−Ti(1)−P(1) 161.00(5), Cl(2)−Ti(1)−P(2) 84.96(5), Cl(3)−Ti(1)−Cl(4) 164.25(6), Cl(3)−Ti(1)−P(1) 82.80(4), Cl(3)−Ti(1)−P(2) 82.39(4), Cl(4)−Ti(1)−P(1) 84.59(5), Cl(4)−Ti(1)−P(2) 85.45(5), P(1)−Ti(1)−P(2) 76.05(4)

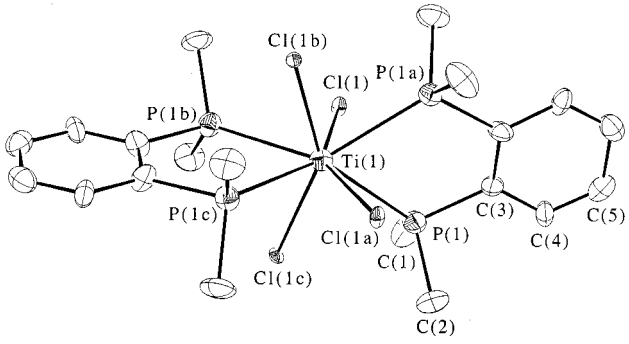

Figure 2. View of the structure of $[TiCl_4\{o\text{-}C_6H_4(PMe_2)_2\}_2]$ with atom numbering scheme; ellipsoids are shown at the 40% probability level; symmetry operators $-x, -y, z$; $1/2 - y, 1/2 + x, 1/2 - z$; $1/2 + y, 1/2 - x, 1/2 - z$; selected bond lengths (Å) and angles (°): Ti(1)−Cl(1) 2.503(3), Ti(1)−P(1) 2.654(4); Cl(1)−Ti(1)−Cl(1b) 95.23(3), Cl(1)−Ti(1)−Cl(1a) 144.85(11), Cl(1)−Ti(1)−P(1) 75.97(12), Cl(1)−Ti(1)−P(1a) 75.88(12), Cl(1)−Ti(1)−P(1b) 71.22(10), Cl(1)−Ti(1)−P(1c) 143.93(10)

this is clearly true for these systems, although the increase in bond length is different for Ti−P than for Ti−Cl. In the six-coordinate species the high *trans* influence of Cl on Ti^{IV} lengthens the Ti−P bond and indeed shortens the Ti−Cl *trans* P bond length (above). In the eight-coordinate flattened dodecahedron, however, the P−Ti−Cl angles are all less than 145°, and this will reduce the magnitude of the *trans* influence of the Cl ligands, thus accounting for some of the disparity. The P−Ti−P angle in the chelate ring is reduced to 72.7(2)° upon increasing the coordination number, a direct consequence of the longer Ti−P bond lengths.

The same geometry has been identified for $[TiCl_4\{Me_2P(CH_2)_2PMe_2\}_2]$, although in this case there is twofold crystallographic symmetry [d(Ti−P) = 2.648(1), 2.654(1) Å; d(Ti−Cl) = 2.446(1), 2.451(1) Å].[6] $[TiCl_4\{o\text{-}C_6H_4(AsMe_2)_2\}_2]$[3,4] is probably isostructural with the $[TiCl_4\{o\text{-}C_6H_4(PMe_2)_2\}_2]$ complex reported here, although few details of the crystallographic information are presented in the early reports [d(Ti−As) = 2.71(2) Å; d(Ti−Cl) = 2.46(2) Å].

The only other case where both the six- and eight-coordinate Ti^{IV} complexes of a single phosphane or arsane ligand have been structurally characterised involves $Me_2P(CH_2)_2PMe_2$. The structures of $[TiCl_4\{Me_2P(CH_2)_2PMe_2\}]$ and $[TiCl_4\{Me_2P(CH_2)PMe_2\}_2]$ were both reported by Cotton and co-workers,[6,12] although in the former the phosphane ligand is disordered, making direct comparison of the structural details more difficult.

The crystals of $[TiBr_4\{o\text{-}C_6H_4(PMe_2)_2\}_2]$ (Figure 3) and $[TiBr_4\{o\text{-}C_6H_4(AsMe_2)_2\}_2]$ (Figure 4) are isostructural with $[TiCl_4\{o\text{-}C_6H_4(PMe_2)_2\}_2]$ above, although the crystal quality was significantly better in these, leading to better structure definition and lower esd's on the geometric parameters. The Ti−Br and Ti−P distances in $[TiBr_4\{o\text{-}C_6H_4(PMe_2)_2\}_2]$ are 2.5776(9), 2.672(2) Å, respectively. The latter is in agreement with the Ti−P distance in $[TiCl_4\{o\text{-}C_6H_4(PMe_2)_2\}_2]$. The Ti−As distance in $[TiBr_4\{o\text{-}C_6H_4(AsMe_2)_2\}_2]$ is 2.7324(13) Å, similar to the value of 2.71(2) Å reported for $[TiCl_4\{o\text{-}C_6H_4(AsMe_2)_2\}_2]$.[3,4] A comparison of the Ti−P and Ti−As distances in $[TiBr_4\{o\text{-}C_6H_4(PMe_2)_2\}_2]$ and $[TiBr_4\{o\text{-}C_6H_4(AsMe_2)_2\}_2]$ shows an increase of 0.06 Å upon changing from phosphane to arsane. This is slightly less than the differences observed for some other transition metal complexes of $o\text{-}C_6H_4(PMe_2)_2$ and $o\text{-}C_6H_4(AsMe_2)_2$. For example, $[NiCl_2\{o\text{-}C_6H_4(PMe_2)_2\}_2]^+$ has a Ni−P bond length of 2.255(3) Å and $[NiCl_2\{o\text{-}C_6H_4(AsMe_2)_2\}_2]^+$ Ni−As bond lengths of 2.339(3), 2.345(3) Å,[14,15] while $[CoCl_2(o\text{-}C_6H_4(PMe_2)_2\}_2]^+$ has an average Co−P bond length of 2.261 Å and $[CoCl_2\{o\text{-}C_6H_4(AsMe_2)_2\}_2]^+$ an average Co−As bond length of 2.334 Å.[15,16]

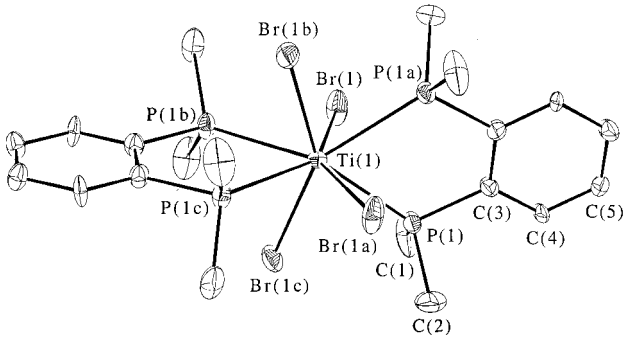

Figure 3. View of the structure of $[TiBr_4\{o\text{-}C_6H_4(PMe_2)_2\}_2]$ with atom numbering scheme; ellipsoids are shown at the 40% probability level; symmetry operators $-x, -y, z$; $y, -x, -z$; $-y, x, -z$; selected bond lengths (Å) and angles (°): Ti(1)−Br(1) 2.5776(9), Ti(1)−P(1) 2.672(2); Br(1)−Ti(1)−Br(1a) 144.70(4), Br(1)−Ti(1)−Br(1b) 95.276(13), Br(1)−Ti(1)−P(1) 75.89(7), Br(1)−Ti(1)−P(1a) 75.86(7), Br(1)−Ti(1)−P(1b) 71.22(6), Br(1)−Ti(1)−P(1c) 144.08(5)

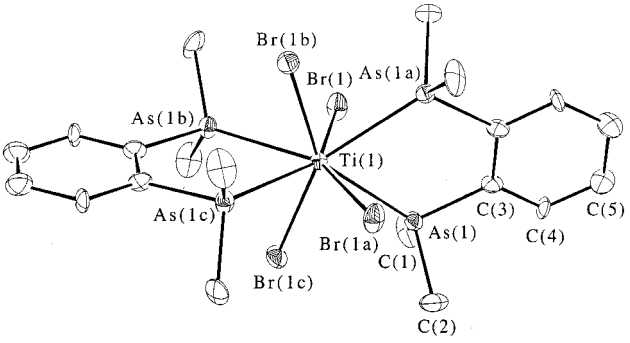

Figure 4. View of the structure of $[TiBr_4\{o\text{-}C_6H_4(AsMe_2)_2\}_2]$ with atom numbering scheme; ellipsoids are shown at the 40% probability level; symmetry operators $-x, -y, z$; $y, -x, -z$; $-y, x, -z$; selected bond lengths (Å) and angles (°): Ti(1)−Br(1) 2.5869(12), Ti(1)−As(1) 2.7324(13); Br(1)−Ti(1)−Br(1a) 144.77(6), Br(1)−Ti(1)−Br(1b) 95.26(2), Br(1)−Ti(1)−As(1) 75.98(5), Br(1)−Ti(1)−As(1a) 75.92(5), Br(1)−Ti(1)−As(1b) 70.94(4), Br(1)−Ti(1)−As(1c) 144.29(4)

The Ti^{IV} tetrahalo complexes of the tripodal $MeC(CH_2AsMe_2)_3$ were prepared in an attempt to obtain seven-coordinate species. NMR studies (above and ref.[11]) indicate that these species in fact adopt six-coordinate geometries in solution with one arm of the $MeC(CH_2AsMe_2)_3$ ligand remaining uncoordinated. A crystal structure determination was also undertaken on $[TiBr_4\{MeC(CH_2AsMe_2)_3\}]$ to establish the solid state structure. This shows that the complex adopts a distorted octahedral coordination environment at Ti^{IV}, derived from four Br ligands and two mutually *cis* As atoms from the bidentate tripodal $MeC(CH_2AsMe_2)_3$ ligand (Figure 5). The remaining As atom is uncoordinated. Hence the structures adopted in solution and in the solid state are the same. The Ti−Br distances in this species exhibit similar trends to the Ti−Cl distances in the six-coordinate $[TiCl_4\{o\text{-}C_6H_4(PMe_2)_2\}]$ complex above, with the Ti−Br(*trans*-Br) distances significantly longer than those *trans* to the *trans* As atom. Also, the Ti−Br distances in this six-coordinate species are significantly shorter than in the eight-coordinate $[TiBr_4\{o\text{-}C_6H_4(PMe_2)_2\}_2]$ complex above, while the Ti−As distances [2.680(3), 2.686(2) Å] are ca. 0.05 Å shorter than in $[TiBr_4\{o\text{-}C_6H_4(AsMe_2)_2\}_2]$. These observations parallel the differences described above for the six- and eight-coordinate $TiCl_4/o\text{-}C_6H_4(PMe_2)_2$ systems.

A small number of crystals of $[TiCl_5(Ph_2PCH_2PHPh_2)]$ were produced by partial decomposition of $[TiCl_4(Ph_2PCH_2PPh_2)]$ in CH_2Cl_2 solution, probably by hydrolysis and subsequent HCl addition. Although there was insufficient sample to permit full spectroscopic characterisation (ν_{Ti-Cl} = 360 sh, 356, 344 sh), a crystal structure was obtained. The structure shows the phosphane ligand to be coordinated to a $TiCl_5$ fragment through a single phosphorus atom (Figure 6). A proton on the other P atom (giving a phosphonium function) was located in the difference map and is also inferred to achieve charge balance. Thus this species is an unusual zwitterionic complex with a distorted octahedral Ti^{IV} coordination geometry. The Ti−P

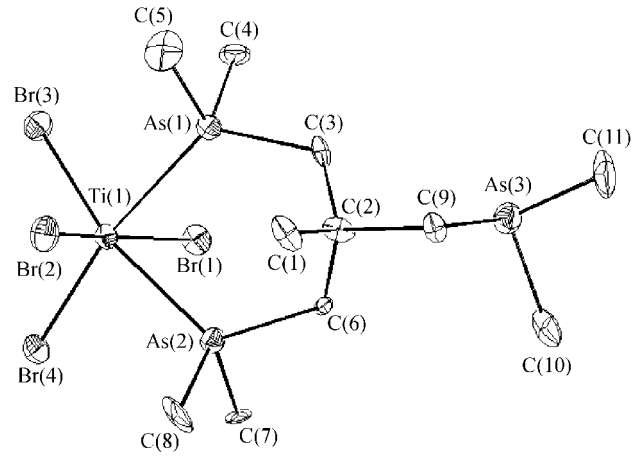

Figure 5. View of the structure of $[TiBr_4\{MeC(CH_2AsMe_2)_3\}]$ with atom numbering scheme; ellipsoids are shown at the 40% probability level; selected bond lengths (Å) and angles (°): Br(1)−Ti(1) 2.471(3), Br(2)−Ti(1) 2.445(3), Br(3)−Ti(1) 2.407(3), Br(4)−Ti(1) 2.403(3), As(1)−Ti(1) 2.680(3), As(2)−Ti(1) 2.688(3); Br(1)−Ti(1)−Br(2) 162.3(1), Br(1)−Ti(1)−Br(3) 95.93(11), Br(1)−Ti(1)−Br(4) 95.97(11), Br(1)−Ti(1)−As(1) 82.57(10), Br(1)−Ti(1)−As(2) 81.53(10), Br(2)−Ti(1)−Br(3) 94.84(12), Br(2)−Ti(1)−Br(4) 93.93(11), Br(2)−Ti(1)−As(1) 84.78(10), Br(2)−Ti(1)−As(2) 84.70(10), Br(3)−Ti(1)−Br(4) 108.29(13), Br(3)−Ti(1)−As(1) 83.36(10), Br(3)−Ti(1)−As(2) 166.30(13), Br(4)−Ti(1)−As(1) 168.4(1), Br(4)−Ti(1)−As(2) 85.39(10), As(1)−Ti(1)−As(2) 82.97(9)

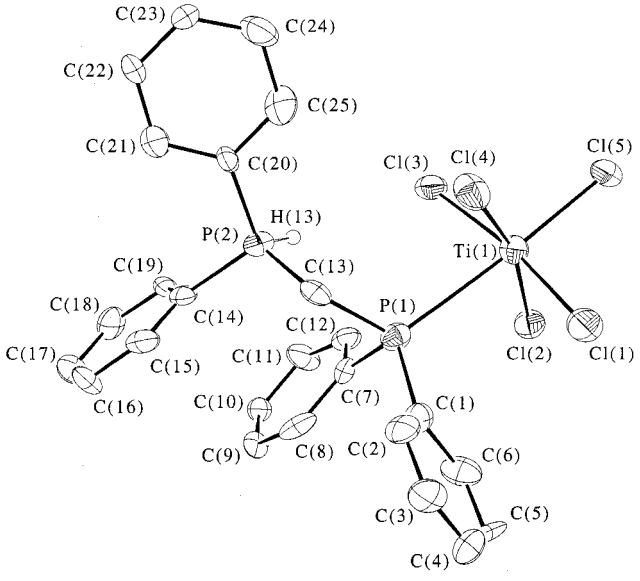

Figure 6. View of the structure of $[TiCl_5(Ph_2PCH_2PHPh_2)]$ with atom numbering scheme; ellipsoids are shown at the 40% probability level; selected bond lengths (Å) and angles (°): Ti(1)−Cl(1) 2.276(3), Ti(1)−Cl(2) 2.283(3), Ti(1)−Cl(3) 2.320(3), Ti(1)−Cl(4) 2.333(3), Ti(1)−Cl(5) 2.291(3), Ti(1)−P(1) 2.732(4); Cl(1)−Ti(1)−Cl(2) 95.67(12), Cl(1)−Ti(1)−Cl(3) 96.82(12), Cl(1)−Ti(1)−Cl(4) 93.02(13), Cl(1)−Ti(1)−Cl(5) 98.94(12), Cl(1)−Ti(1)−P(1) 176.52(13), Cl(2)−Ti(1)−Cl(3) 87.87(13), Cl(2)−Ti(1)−Cl(4) 171.2(1), Cl(2)−Ti(1)−Cl(5) 89.1(1), Cl(2)−Ti(1)−P(1) 87.62(12), Cl(3)−Ti(1)−Cl(4) 89.70(12), Cl(3)−Ti(1)−Cl(5) 164.18(13), Cl(3)−Ti(1)−P(1) 82.15(11), Cl(4)−Ti(1)−Cl(5) 90.92(12), Cl(4)−Ti(1)−P(1) 83.66(11), Cl(5)−Ti(1)−P(1) 82.20(10), P(1)−C(13)−P(2) 113.7(5)

distance in this species [2.732(4) Å] is considerably longer (by about 0.2 Å) than *d*(Ti−P) *trans* X in other six-coordinate complexes such as $[TiCl_4\{o\text{-}C_6H_4(PMe_2)_2\}]$, above, and $[TiCl_4\{Me_2P(CH_2)_2PMe_2\}]$.[12] This substantial lengthening of *d*(Ti−P) in the zwitterionic complex may arise from deactivation of the P-based lone pair on the phosphane function upon quaternization of the adjacent P centre, leading to a weaker Ti−P interaction. Notably, the Ti−Cl distance *trans* to P is not very different to the other Ti−Cl distances, unlike the examples above, $[TiCl_4\{o\text{-}C_6H_4(PMe_2)_2\}]$ and $[TiBr_4\{MeC(CH_2AsMe_2)_3\}]$, where *d*(Ti−X) *trans* P/As is significantly shorter than *d*(Ti−X) *trans* X. The angles at Ti indicate a distorted octahedral geometry, but with the Cl(1)−Ti(1)−Cl angles all greater than 90° and, correspondingly, the P(1)−Ti(1)−Cl(x) ($x = 2-5$) angles all less than 90°. The consequence of this is that the Cl atoms in the $TiCl_4$ plane are displaced towards the phosphane ligand.

Conclusions

These results show that both six- and eight-coordinate Ti^{IV} complexes of $o\text{-}C_6H_4(PMe_2)_2$ and $o\text{-}C_6H_4(AsMe_2)_2$ may be isolated. Solution NMR studies show that the six-coordinate phosphane and arsane species do not undergo fast ligand exchange. On the other hand, the eight-coordinate complexes generally dissociate a ligand and exist in solution as an equilibrium mixture of $[TiX_4(L\text{-}L)_2]$, $[TiX_4(L\text{-}L)]$, TiX_4 and L-L. Attempts to prepare seven-coordinate Ti^{IV} complexes with $MeC(CH_2AsMe_2)_3$ yielded only the six-coordinate species, with the tripodal ligand functioning as a bidentate chelate. The six- and eight-coordinate complexes $[TiCl_4\{o\text{-}C_6H_4(PMe_2)_2\}]$ and $[TiCl_4\{o\text{-}C_6H_4(PMe_2)_2\}_2]$ have been crystallographically characterised and the structural consequences of converting from six- to eight-coordinate Ti^{IV} have been established.

Experimental Section

Infrared spectra were measured as Nujol mulls between CsI plates using a Perkin−Elmer 1710 spectrometer over the range 220−4000 cm^{-1}. ^1H NMR spectra were recorded in $CDCl_3$ or CD_2Cl_2 using a Bruker AM300 or DPX400 spectrometer. $^{13}C\{^1H\}$ and $^{31}P\{^1H\}$ NMR spectra were recorded at 300 K unless otherwise stated, using a Bruker DPX400 spectrometer operating at 100.6 and 162.0 MHz, respectively, and are referenced to TMS or external 85% H_3PO_4. UV/Visible spectra were recorded by diffuse reflectance using a Perkin−Elmer Lambda19 spectrometer. Samples were diluted with $BaSO_4$. Titanium halides were obtained from Aldrich and used as received. The ligands $o\text{-}C_6H_4(PMe_2)_2$, $o\text{-}C_6H_4(PPh_2)_2$, $Ph_2As(CH_2)_2AsPh_2$, $o\text{-}C_6H_4(AsMe_2)_2$ and $MeC(CH_2AsMe_2)_3$ were prepared by literature methods,[17−20] while the other phosphane ligands were obtained from Aldrich. Dichloromethane and chloroform were dried by distillation from CaH_2 and hexane was dried by distillation from the sodium ketyl of benzophenone. Deuterated solvents were dried over molecular sieves. All preparations used rigorously anhydrous solvents and inert atmosphere techniques.

(i) [$TiCl_4(Ph_2PCH_2PPh_2)$]: $Ph_2PCH_2PPh_2$ (0.35 g, 0.91 mmol) was dissolved in dry, degassed hexane (20 cm^3) in a Schlenk flask under an atmosphere of dry N_2. $TiCl_4$ (0.1 cm^3, 0.91 mmol) was added with a syringe, resulting in immediate precipitation of a bright orange solid. The solution was stirred for ca. 30 min. and the solid filtered and dried in vacuo. Yield 0.45 g, 88%. $C_{25}H_{22}Cl_4P_2Ti$ (574.11): calcd. C 52.3, H 3.8; found C 52.0, H 3.7. − IR: ν_{Ti-Cl} = 419, 398, 385, 375 cm^{-1}. − UV/Vis ($\lambda_{max} \times 10^3$ cm^{-1}): 20.7, 28.5sh, 34.8. − ^1H NMR ($CDCl_3$, 300 K): δ = 7.0−8.0 (m, Ph), 4.0 (t, $^2J_{H-P}$ = 10 Hz, CH_2).

(ii) [$TiCl_4(Ph_2P(CH_2)_2PPh_2)$]: Method as for (i) above, orange solid, yield 0.43 g, 80%. $C_{26}H_{24}Cl_4P_2Ti$ (588.14): calcd. C 53.0, H 4.1; found C 53.7, H 4.4. − IR: ν_{Ti-Cl} = 420, 398, 385, 376 cm^{-1}. − UV/Vis ($\lambda_{max} \times 10^3$ cm^{-1}): 20.7, 26.1sh, 34.8. − ^1H NMR ($CDCl_3$, 300 K): δ = 7.1−7.9 (*m*, Ph), 3.0 (*d*, CH_2, $^2J_{H-P}$ = 13 Hz). − $^{31}P\{^1H\}$ NMR (CH_2Cl_2/CD_2Cl_2): δ = 24.6.

(iii) [$TiCl_4\{Ph_2P(CH_2)_3PPh_2\}$]: Method as for (i) above, orange solid, yield 0.49 g, 91%. $C_{27}H_{26}Cl_4P_2Ti$ (602.16): calcd. C 53.8, H 4.3; found C 53.6, H 4.4. − IR: ν_{Ti-Cl} = 417, 394, 369 cm^{-1}. − UV/Vis ($\lambda_{max} \times 10^3$ cm^{-1}): 20.7, 27.8 sh, 37.7. − ^1H NMR ($CDCl_3$, 300 K): δ = 7.2−7.8 (m, Ph), 2.7 (t, CH_2), 2.2 (q, CH_2). − $^{31}P\{^1H\}$ NMR (CH_2Cl_2): 2.3 (very broad).

(iv) [$TiCl_4\{o\text{-}C_6H_4(PPh_2)_2\}$]: Method as for (i) above, orange solid, yield 0.69 g, 81%. $C_{30}H_{24}Cl_4P_2Ti$: calcd. C 56.6, H 3.8; found C 56.3, H 3.9. − IR: ν_{Ti-Cl} = 420, 408, 386, 375 cm^{-1}. − UV/Vis ($\lambda_{max} \times 10^3$ cm^{-1}): 21.3, 26.0sh, 32.3. − ^1H NMR ($CDCl_3$, 300 K): δ = 7.0−8.2 (m, Ph). − $^{31}P\{^1H\}$ NMR ($CH_2Cl_2/CDCl_3$): δ = 34.1.

(v) [$TiCl_4\{o\text{-}C_6H_4(PMe_2)_2\}$]: Method as for (i) above, pale yellow solid, yield 0.10 g, 57%. $C_{10}H_{16}Cl_4P_2Ti$ (387.90): calcd. C 31.0, H 4.2; found C 31.2, H 4.3. − IR: ν_{Ti-Cl} = 420, 410, 382 cm^{-1}. − UV/Vis ($\lambda_{max} \times 10^3$ cm^{-1}): 22.7, 28.6, 33.0. − ^1H NMR ($CDCl_3$, 300 K): δ = 7.6 (m, *o*-C_6H_4), 1.9 (m, Me). − $^{31}P\{^1H\}$ NMR ($CH_2Cl_2/CDCl_3$): δ = 29.5.

(vi) [$TiCl_4\{Ph_2As(CH_2)_2AsPh_2\}$]: Method as for (i) above, red solid, yield 0.26 g, 86%. $C_{26}H_{24}As_2Cl_4Ti$ (676.03): calcd. C 46.2, H 3.6; found C 46.0, H 3.7. − IR: ν_{Ti-Cl} = 401, 385, 377 cm^{-1}. − UV/Vis ($\lambda_{max} \times 10^3$ cm^{-1}): 20.0, 21.7, 25.0, 32.3. − ^1H NMR ($CDCl_3$, 300 K): δ = 7.7−7.3 (m, Ph), 3.1 (s, CH_2).

(vii) [$TiCl_4\{o\text{-}C_6H_4(AsMe_2)_2\}$]: Method as for (i) above, pale orange solid, yield 0.16 g, 62%. $C_{10}H_{16}As_2Cl_4Ti$ (475.79): calcd. C 25.2, H 3.4; found C 25.4, H 3.5. − IR: ν_{Ti-Cl} = 422, 409, 384 cm^{-1}. − UV/Vis ($\lambda_{max} \times 10^3$ cm^{-1}): 21.9, 29.1, 33.0. − ^1H NMR ($CDCl_3$, 300 K): δ = 7.6 (m, *o*-C_6H_4), 1.75 (s, Me).

(viii) [$TiCl_4\{MeC(CH_2AsMe_2)_3\}$]: Method as in (i), orange solid, yield 0.22 g, 86%. $C_{11}H_{27}As_3Cl_4Ti$ (573.81): calcd. C 23.0, H 4.7; found C 23.0, H 4.9. − IR: ν_{Ti-Cl} = 400, 375, 368 cm^{-1}. − UV/Vis ($\lambda_{max} \times 10^3$ cm^{-1}): 21.1, 25.3, 27.2, 34.5. − ^1H NMR (CD_2Cl_2, 300 K): δ = 0.95 (AsMe, free), 1.23 (MeC), 1.58, 1.61 (AsMe, coordinated), 1.74 (CH_2, free), 2.15 (m, CH_2, coordinated).

(ix) [$TiCl_4\{o\text{-}C_6H_4(PMe_2)_2\}_2$]: Method as in (i), using two molar equivalents of *o*-$C_6H_4(PMe_2)_2$, golden yellow solid, yield 0.22 g, 85%. $C_{20}H_{32}Cl_4P_4Ti$ (586.08): calcd. C 41.0, H 5.5; found C 40.6, H 5.3. − IR: ν_{Ti-Cl} = 314, 302 sh cm^{-1}. − UV/Vis ($\lambda_{max} \times 10^3$ cm^{-1}): 20.8, 22.5, 24.0, 28.0. − ^1H NMR (CD_2Cl_2, 300 K): δ = 7.5−7.7 (m, *o*-C_6H_4), 1.88 (Me); (183 K): 7.7 (br, *o*-C_6H_4), 1.92 (m, Me). − $^{31}P\{^1H\}$ NMR ($CH_2Cl_2/CDCl_3$): δ = 31.5.

(x) [$TiCl_4\{o\text{-}C_6H_4(AsMe_2)_2\}_2$]: Method as in (i), using two molar equivalents of *o*-$C_6H_4(AsMe_2)_2$, bright orange solid, yield 0.30 g, 89%. $C_{20}H_{32}As_4Cl_4Ti$ (761.87): calcd. C 31.5, H 4.2; found C 31.4, H 4.0. − IR: ν_{Ti-Cl} = 323 sh, 317 cm^{-1}. − UV/Vis ($\lambda_{max} \times 10^3$ cm^{-1}): 21.6, 27.6. − ^1H NMR (CD_2Cl_2, 300 K): δ = 7.6 (m, *o*-C_6H_4), 1.8, 1.74, 1.2 (s, Me).

(xi) [$TiBr_4\{Ph_2P(CH_2)_3PPh_2\}$]: $TiBr_4$ (0.15 g, 0.41 mmol) was dissolved in refluxing, dry, degassed CH_2Cl_2 (≈30 cm^3) in a Schlenk flask under an atmosphere of N_2. After cooling to room temperature, $Ph_2P(CH_2)_3PPh_2$ (0.17 g, 0.41 mmol) in CH_2Cl_2 (5 cm^3), was added to the stirring solution with a syringe, resulting in a dark red solution. The solution was stirred for ca. 30 min., and then the solvent volume was reduced in vacuo to ca. 5 cm^3. Dry, degassed hexane (20 cm^3) was added to afford a red/orange solid. This solid was filtered, washed with hexane and dried in vacuo. Yield 0.23 g, 73%. $C_{27}H_{26}Br_4P_2Ti$ (779.97): calcd. C 41.5, H 3.3; found C 42.0, H 3.5. − IR: ν_{Ti-Br} = 313, 298, 293 cm^{-1}. − UV/Vis ($\lambda_{max} \times 10^3$ cm^{-1}): 22.5, 32.7. − ^1H NMR ($CDCl_3$, 300 K): δ = 7.2−8.3 (m, Ph), 3.0−3.6 (br, CH_2). − $^{31}P\{^1H\}$ NMR (CH_2Cl_2/CD_2Cl_2): δ = 3.5 (broad).

(xii) [$TiBr_4\{Ph_2P(CH_2)_2PPh_2\}$]: Method as for (xi) above, red solid, yield 0.26 g, 65%. − IR: ν_{Ti-Br} = 309, 299, 292 cm^{-1}. − UV/Vis ($\lambda_{max} \times 10^3$ cm^{-1}): 20.6, 25.5, 34.5. − ^1H NMR ($CDCl_3$, 300 K): δ = 6.8−7.9 (m, Ph), 4.4−4.8 (m, CH_2). − $^{31}P\{^1H\}$ NMR ($CH_2Cl_2/CDCl_3$, 300 K): δ = 13.0 (s); (200 K): δ = 15.4.

(xiii) [$TiBr_4\{o\text{-}C_6H_4(PPh_2)_2\}$]: Method as for (xi) above, red/orange solid, yield 0.26 g, 72%. $C_{30}H_{24}Br_4P_2Ti$ (813.98): calcd. C 44.2, H 2.9; found C 44.6, H 3.0. − IR: ν_{Ti-Br} = 315, 310, 304, 301 cm^{-1}. − UV/Vis ($\lambda_{max} \times 10^3$ cm^{-1}): 20.5. − ^1H NMR ($CDCl_3$, 300 K): δ = 7.0−8.3 (m, Ph, *o*-C_6H_4). − $^{31}P\{^1H\}$ NMR (CH_2Cl_2/CD_2Cl_2): δ = −10.3 (broad).

(xiv) [$TiBr_4\{o\text{-}C_6H_4(PMe_2)_2\}$]: Method as for (xi) above, orange/brown solid, yield 0.16 g, 55%. $C_{10}H_{16}Br_4P_2Ti$ (565.70): calcd. C 21.2, H 2.8; found C 21.6, H 2.9. − IR: ν_{Ti-Br} = 325 sh, 321 cm^{-1}. − UV/Vis ($\lambda_{max} \times 10^3$ cm^{-1}): 21.0, 23.3, 27.7. − ^1H NMR (CD_2Cl_2, 300 K): δ = 7.6 (m, *o*-C_6H_4), 2.03 (m, Me). − $^{31}P\{^1H\}$ NMR (CH_2Cl_2/CD_2Cl_2): δ = 24.5.

(xv) [$TiBr_4\{Ph_2As(CH_2)_2AsPh_2\}$]: Method as for (xi) above, red solid, yield 0.33 g, 78%. $C_{26}H_{24}As_2Br_4Ti$ (853.83): calcd. C 36.6, H 2.8; found C 36.3, H 3.0. − IR: ν_{Ti-Br} = 304, 295, 291, 285 cm^{-1}. − UV/Vis ($\lambda_{max} \times 10^3$ cm^{-1}): 18.9, 22.2, 28.6, 32.3. − ^1H NMR (CD_2Cl_2, 300 K): δ = 7.7−7.4 (m, Ph), 3.1 (s, CH_2).

(xvi) [$TiBr_4\{o\text{-}C_6H_4(AsMe_2)_2\}$]: Method as for (xi) above, bright red solid, yield 0.17 g, 53%. $C_{10}H_{16}As_2Br_4Ti$ (653.60): calcd. C 18.4, H 2.5; found C 18.4, H 2.5. − IR: ν_{Ti-Br} = 327, 323 cm^{-1}. − UV/Vis ($\lambda_{max} \times 10^3$ cm^{-1}): 20.0, 22.6, 27.2. − ^1H NMR (CD_2Cl_2, 300 K): δ = 7.6 (m, *o*-C_6H_4), 1.9 (s, Me), 1.2 (s, Me).

(xvii) [$TiBr_4\{MeC(CH_2AsMe_2)_3\}$]: Method as in (xi), red solid, yield 0.27 g, 72%. $C_{11}H_{27}As_3Br_4Ti$ (751.62): calcd. C 17.6, H 3.6; found C 18.1, H 3.7. − IR: ν_{Ti-Br} = 326, 313, 284 cm^{-1}. − UV/Vis ($\lambda_{max} \times 10^3$ cm^{-1}): 19.7, 21.5, 26.7, 32.3. − ^1H NMR (CD_2Cl_2, 300 K): δ = 0.96 (AsMe, free), 1.26 (MeC), 1.71 (br, AsMe, coordinated), 1.75 (CH_2, free), 2.2 (m, CH_2, coordinated).

(xviii) [$TiBr_4\{o\text{-}C_6H_4(PMe_2)_2\}_2$]: Method as in (xi), using two molar equivalents of *o*-$C_6H_4(PMe_2)_2$, bright orange solid, yield 0.16 g, 55%. $C_{20}H_{32}Br_4P_4Ti$ (763.88): calcd. C 31.4, H 4.2; found C 31.2, H 4.0. − IR: ν_{Ti-Br} = 280 br cm^{-1}. − UV/Vis ($\lambda_{max} \times 10^3$ cm^{-1}): 18.9, 21.5, 25.8, 29.0. − ^1H NMR (CD_2Cl_2, 300 K): δ = 7.6−7.8 (m, *o*-C_6H_4), 2.02 (m, Me); (−90 °C): 7.6−7.9 (m, Ph), 2.04−2.00 (m, Me), 1.32 (m, Me). − $^{31}P\{^1H\}$ NMR (CH_2Cl_2/

Table 1. Crystallographic data

Complex	$[TiCl_4\{o\text{-}C_6H_4(PMe_2)_2\}]$	$[TiCl_4\{o\text{-}C_6H_4(PMe_2)_2\}_2]$	$[TiBr_4\{o\text{-}C_6H_4(PMe_2)_2\}_2]$	$[TiBr_4\{o\text{-}C_6H_4(AsMe_2)_2\}_2]$	$[TiBr_4\{MeC(CH_2AsMe_2)_3\}]$	$[TiCl_5(Ph_2PCH_2PHPh_2)]$
Formula	$C_{10}H_{16}Cl_4P_2Ti$	$C_{20}H_{32}Cl_4P_4Ti$	$C_{20}H_{32}Br_4P_4Ti$	$C_{20}H_{32}As_4Br_4Ti$	$C_{11}H_{27}As_3Br_4Ti$	$C_{25}H_{23}Cl_5P_2Ti$
M	387.90	586.08	763.88	939.68	751.62	610.57
Crystal System	orthorhombic	tetragonal	tetragonal	tetragonal	orthorhombic	orthorhombic
Space Group	*Pbca*	$I\bar{4}$	$I\bar{4}$	$I\bar{4}$	$Pna2_1$	$P2_12_12_1$
a (Å)	13.1752(2)	9.0716(7)	9.1729(4)	9.3125(5)	23.4808(5)	10.4063(6)
b (Å)	15.3631(2)	9.0716(7)	9.1729(4)	9.3125(5)	9.4899(2)	15.3834(9)
c (Å)	16.6348(3)	16.104(1)	16.2896(8)	16.4876(9)	9.9052(2)	16.5893(11)
U (Å^3)	3367.08(8)	1325.2(2)	1370.64(9)	1429.85(12)	2207.18(7)	2655.2(2)
Z	8	2	2	2	4	4
μ(Mo-K_α) (cm^{-1})	13.10	9.75	64.02	105.08	121.05	9.59
Unique obs. reflections	3860	790	722	753	3509	5781
Obs. reflections with $[I_o > 3\sigma(I_o)]$	2461	630	586	633	1769	8136
No. of parameters	154	66	66	66	171	298
R[a]	0.037	0.083	0.044	0.048	0.047	0.060
R_w [b]	0.047	0.111	0.053	0.053	0.051	0.082

[a] $R = \Sigma(||F_{obs}|_i - |F_{calc}|_i)/\Sigma|F_{obs}|_i$. – [b] $R_w = \sqrt{[\Sigma w_i(|F_{obs}|_i - |F_{calc}|_i)^2/\Sigma w_i|F_{obs}|_i^2]}$.

$CDCl_3$): δ = 22.2 ($[TiBr_4\{o\text{-}C_6H_4(PMe_2)_2\}_2]$), 24.3 ($[TiBr_4\{o\text{-}C_6H_4(PMe_2)_2\}]$) and −55 $[o\text{-}C_6H_4(PMe_2)_2]$.

(xix) $[TiBr_4\{o\text{-}C_6H_4(AsMe_2)_2\}_2]$: Method as in (xi), using two molar equivalents of $o\text{-}C_6H_4(AsMe_2)_2$, red/purple solid, yield 0.36 g, 76%. $C_{20}H_{32}As_4Cl_4Ti$ (761.87): calcd. C 25.6, H 3.4; found C 25.2, H 3.5. – IR: ν_{Ti-Br} = 305, 301 cm^{-1}. – UV/Vis ($\lambda_{max} \times 10^3$ cm^{-1}): 18.5, 20.3, 22.7. – ^{1}H NMR (CD_2Cl_2, 300 K): see text.

X-ray Crystallography: Details of the crystallographic data collection and refinement parameters are given in Table 1. Crystals of $[TiCl_4\{o\text{-}C_6H_4(PMe_2)_2\}]$, $[TiCl_4\{o\text{-}C_6H_4(PMe_2)_2\}_2]$, $[TiBr_4\{o\text{-}C_6H_4(PMe_2)_2\}_2]$, $[TiBr_4\{o\text{-}C_6H_4(AsMe_2)_2\}_2]$ and $[TiBr_4\{MeC(CH_2AsMe_2)_3\}]$ were obtained by slow evaporation from a solution of the appropriate complex in CH_2Cl_2. The crystals of $[TiCl_5(Ph_2PCH_2PHPh_2)]$ were obtained as a hydrolysis product from $[TiCl_4(Ph_2PCH_2PPh_2)]$ in CH_2Cl_2. Data collection was performed with an Enraf–Nonius Kappa CCD diffractometer operating at 150 K, with graphite monochromated Mo-K_α radiation (λ = 0.71073 Å). Structure solution and refinement were routine.[21–24] Crystallographic data (excluding structure factors) for the structure(s) included in this paper have been deposited with the Cambridge Crystallographic Data Centre as supplementary publication no. CCDC-162704–162709. -162704: $[TiCl_4\{o\text{-}C_6H_4(PMe_2)_2\}]$, -162705: $[TiCl_4\{o\text{-}C_6H_4(PMe_2)_2\}_2]$, -162706: $[TiBr_4\{o\text{-}C_6H_4(PMe_2)_2\}_2]$, -162707: $[TiBr_4\{o\text{-}C_6H_4(AsMe_2)_2\}_2]$, -162708: $[TiBr_4\{MeC(CH_2AsMe_2)_3\}]$, -162709: $[TiCl_5(Ph_2PCH_2PHPh_2)]$. Copies of the data can be obtained free of charge on application to CCDC, 12 Union Road, Cambridge CB2 1EZ, UK [Fax: (internat.) + 44-1223/336-033; E-mail: deposit@ccdc.cam.ac.uk].

Acknowledgments

We thank the EPSRC for support and Professor M. B. Hursthouse for access to the Nonius Kappa CCD diffractometer.

[1] B. Patel, W. Levason, G. Reid, V.-A. Tolhurst and M. Webster, *J. Chem. Soc., Dalton Trans.* **2000**, 3001–3006.
[2] B. Patel, W. Levason, G. Reid, unpublished work.
[3] R. J. H. Clark, J. Lewis, R. S. Nyholm, *J. Chem. Soc.* **1962**, 2460–2465.
[4] R. J. H. Clark, J. Lewis, R. S. Nyholm, P. Pauling, G. B. Robertson, *Nature* **1961**, *192*, 222–223.
[5] R. J. H. Clark, R. H. U. Negrotti, R. S. Nyholm, *J. Chem. Soc., Chem. Commun.* **1966**, 486–487.
[6] F. A. Cotton, J. H. Matonic, C. A. Murillo, M. A. Petrukhina, *Inorg. Chim. Acta* **1998**, *267*, 173–176.
[7] D. Kepert, K. R. Trigwell, *Aust. J. Chem.* **1975**, *28*, 1245–1248.
[8] W. P. Crisp, R. L. Deutscher, D. L. Kepert, *J. Chem. Soc.* **1970**, 2199–2201.
[9] R. A. Cipriano, W. Levason, R. A. S. Mould, D. Pletcher, M. Webster, *J. Chem. Soc., Dalton Trans.* **1990**, 339–347.
[10] R. J. H. Clark, M. L. Greenfield, R. S. Nyholm, *J. Chem. Soc. A* **1966**, 1254–1259.
[11] A. J. McAlees, R. McCrindle, A. R. Woon-Fat, *Inorg. Chem.* **1976**, *15*, 1065–1074.
[12] F. A. Cotton, C. A. Murillo, M. A. Petrukhina, *J. Organomet. Chem.* **1999**, *573*, 78–86.
[13] F. A. Cotton, C. A. Murillo, M. A. Petrukhina, *J. Organomet. Chem.* **2000**, *593–594*, 1–6.
[14] C. Mahadevan, M. Seshasyee, B. L. Ramakrishna, P. T. Manoharan, *Acta Crystallogr., Sect. C* **1985**, *41*, 38–40.
[15] P. K. Bernstein, G. A. Rodley, R. Marsh, H. B. Gray, *Inorg. Chem.* **1972**, *11*, 3040–3043.
[16] L. F. Warren, M. A. Bennett, *Inorg. Chem.* **1976**, *15*, 3126–3140.
[17] A. Tzschach, W. Lange, *Chem. Ber.* **1962**, *95*, 1360–1366.
[18] R. D. Feltham, R. S. Nyholm, A. Kasenally, *J. Organomet. Chem.* **1967**, *7*, 285–288.
[19] E. P. Kyba, S.-T. Lui, R. L. Harris, *Organometallics* **1983**, *2*, 1877–1879.
[20] H. C. E. McFarlane, W. McFarlane, *Polyhedron* **1983**, *2*, 303–304.
[21] PATTY, The DIRDIF Program System, P. T. Beurskens, G. Admiraal, G. Beurskens, W. P. Bosman, S. Garcia-Granda, R. O. Gould, J. M. M. Smits, C. Smykalla. Technical Report of the Crystallography Laboratory, University of Nijmegen, The Netherlands, **1992**.
[22] teXsan: Crystal Structure Analysis Package, Molecular Structure Corporation, Texas, **1995**.
[23] H. D. Flack, *Acta Crystallogr., Sect. A* **1983**, *39*, 876–881.
[24] R. H. Blessing, *Acta Crystallogr., Sect. A* **1995**, *51*, 33–38.

Received May 17, 2001
[I01176]

Two-Step Spin Crossover in a Mononuclear Compound $[Fe(DPEA)(bim)](ClO_4)_2 \cdot 0.5\,H_2O$[DPEA = (2-Aminoethyl)-bis(2-pyridylmethyl)amine, bim = 2,2-Bisimidazole] − Crystal Structure, Magnetic Properties, Mössbauer Spectroscopy, and Photomagnetic Effects

Galina S. Matouzenko,*[a] Jean-François Létard,[b] Sylvain Lecocq,[c] Azzedine Bousseksou,[d] Laurence Capes,[b,e] Lionel Salmon,[d] Monique Perrin,[c] Olivier Kahn,[†][b] and André Collet[††][a]

Dedicated to the memory of André Collet and Olivier Kahn

Keywords: Iron / N ligands / Spin crossover / Mössbauer spectroscopy / Photomagnetism

The synthesis and characterization of the new spin crossover mononuclear complex $[Fe^{II}(DPEA)(bim)](ClO_4)_2 \cdot 0.5\,H_2O$, where DPEA = (2-aminoethyl)bis(2-pyridylmethyl)amine and bim = 2,2-bisimidazole, are reported. Variable-temperature magnetic susceptibility measurements (77–295 K) reveal the occurrence of a two-step spin transition. Two steps on the magnetic curve are separated by an inflection point at 200 K, corresponding to about 50% of the complexes that have undergone a thermal spin transition. The first step is centered at 171 K and the second one at 218 K. Mössbauer spectroscopy and X-ray analysis show that the profile of the magnetic curve is a consequence of the presence of two inequivalent iron(II) molecules in the crystal lattice. The crystal structure was resolved at 293 K (high-spin form) and at 123 K (low-spin form). Both spin-state isomers belong to the monoclinic space group $P2_1/c$ ($Z = 4$). The main differences between high-spin and low-spin isomers are found in the geometry of the $[FeN_6]$ core, the shorter Fe–N distances are seen at lower temperatures. Two inequivalent HS molecules at lattice sites **1** and **2** successively undergo a thermal spin transition. The analysis of the mean Fe–N distances for functionally different nitrogen donor atoms show that the two steps of the spin transition can be assigned to the inequivalent lattice sites. The gradual character of the spin transition at both lattice sites is accounted for in terms of intermolecular H-bonding via the perchlorate ions. At 10 K the light-induced excited spin state trapping (LIESST) effect is observed within the SQUID magnetometer cavity. Two critical temperatures T_c(LIESST) were recorded (36 K and 21 K) and are attributed to the lattice sites **1** and **2**.

Introduction

During the last few decades coordination chemistry has provided many examples of new iron(II) compounds exhibiting high-spin (HS, $^5T_2$) ↔ low-spin (LS, $^1A_1$) transitions, which have been extensively studied using various techniques.[1] The proximity of HS and LS electronic states in an isolated molecule, governed by the interplay between the electron-pairing energy and the ligand field, is a prerequisite for the occurrence of a spin transition. The change of the molecular equilibrium geometry accompanying a spin transition in the solid state occurs through intermolecular interactions, leading to more or less pronounced cooperative effects. Different intermolecular interactions such as H-bonding, π-stacking, van der Waals interactions can act as the communication link between neighboring molecules. Several theoretical models have been proposed to account for cooperativity in spin transition.[2]

The crystal structure plays an important role in the shaping of spin transition. Packing effects appear as a small perturbation on the interplay between the ligand field and the interelectronic interactions. Besides this they determine the propagation pattern of the cooperative interactions in the solid. The influence of packing effects on the spin-state of the complex is neither predictable, nor controllable and can

[†] Deceased on Dec. 7, 1999.
[††] Deceased on Oct. 26, 1999.
[a] Stéréochimie et Interactions Moléculaires (UMR CNRS and ENS-Lyon n° 5532), École Normale Supérieure de Lyon, 69364 Lyon Cedex 07, France
E-mail: Galina Matouzenko@ens-lyon.fr
[b] Laboratoire des Sciences Moléculaires, Institut de Chimie de la Matière Condensée de Bordeaux (UPR CNRS n° 9048), 33608 Pessac, France
[c] Laboratoire de Reconnaissance et Organisation Moléculaire (UMR 5078), Université Claude Bernard-Lyon 1, 69622 Villeurbanne Cedex, France
[d] Laboratoire de Chimie de Coordination (UPR CNRS n° 8241), 31077 Toulouse Cedex, France
[e] Motorola centre de recherche, Espace technologique Saint Aubin, 91193 Gif, France

 © WILEY-VCH Verlag GmbH, 69451 Weinheim, 2001 1434−1948/01/1111−2935 $ 17.50+.50/0

lead to different situations. One such situation involves the existence of several polymorphic modifications with differing magnetic behavior for a single compound.[3,4] Recently, we have isolated, under the same experimental conditions, three polymorphic modifications of the [Fe(DPPA)$(NCS)_2$] complex, where DPPA = (3-aminopropyl)bis(2-pyridylmethyl)amine.[4] A detailed study has revealed that one polymorph undergoes a gradual spin transition, the second remains high-spin at temperatures down to 4.5 K and the third exhibits a spin transition with hysteresis. Another situation arises when several crystallographically independent iron(II) sites co-exist in the same unit cell. The structural distinctions among iron(II) complexes can result in their different magnetic behavior. In the iron(II) complex $[Fe(mtz)_6](BF_4)_2$ (mtz = 1-methyl-1*H*-tetrazole), one site remains in the HS form until 4.2 K and the second undergoes a thermal spin transition.[5] Two lattice sites can be selectively converted into their spin isomers at low temperature by irradiating light at different frequencies. A similar feature was observed for $[Fe(etz)_6](BF_4)_2$ (etz = 1-ethyl-1*H*-tetrazole).[6] In the crystal of the iron(II) complex of C_3-cyclotriveratrylene ligand,[7] one site is occupied by LS species, whereas the other shows a temperature-independent mixture of HS and LS states. In the spin-equilibrium complex $[Fe(tren)](ClO_4)_2 \cdot {}^2/_3H_20$ [tren = tetrakis(2-pyridylmethyl)ethylendiamine)], one of two cation sites has a greater HS content, and both sites act quasi independently in the HS $\leftrightarrow$ LS conversion.[8] In the recently reported compound $[Fe(btr)_3](ClO_4)_2$ (btr = 4,4′-bis-1,2,4-triazole), the presence of two slightly different Fe^{II} sites generates the two-step spin transition with a plateau.[9] Another case of the two-step transition is represented by [Fe(5-NO_2-sal-N(1,4,7,10)] (the ligand results from the Schiff base condensation of 5-nitrosalicylaldehyde with tetraazadecane), in which two inequivalent lattice sites appear as a result of the structural phase transition on cooling.[10]

Here we report on the detailed characterization of a new spin transition complex $[Fe(DPEA)(bim)](ClO_4)_2 \cdot 0.5\ H_2O$, with DPEA = (2-aminoethyl)bis(2-pyridylmethyl)amine and bim = 2,2-bisimidazole (Scheme 1). The single-crystal X-ray structure at 293 K (HS form) and 123 K (LS form), magnetic susceptibility, Mössbauer spectra and photomagnetism of this complex are investigated. The presence of two inequivalent molecules in the crystal lattice both undergoing thermal spin conversion results in a two-step magnetic behavior. The LIESST (light-induced excited spin state trapping)[11] experiments reveal a partial conversion of the LS state into the HS state for both sites.

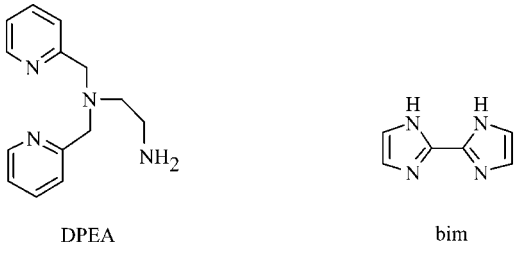

DPEA bim

Scheme 1. Representation of the DPEA and bim ligands

Results

Description of the Structure

The crystal structures of $[Fe(DPEA)(bim)](ClO_4)_2 \cdot 0.5\ H_2O$ in both HS and LS states were resolved by X-ray crystallography at 293 K and 123 K, respectively. The X-ray analysis did not reveal a change in the space group over the temperature range 123−293 K, and both spin-state forms belong to the monoclinic space group $P2_1/c$ (Z = 4). The unit cell contains two crystallographically independent iron(II) sites **1** and **2** (Figure 1), occurring in equal amounts in general positions. Selected bond lengths and angles are given in Table 1 and Table 2, respectively. The $[FeN_6]$ core is formed by two imino nitrogen atoms of 2,2-bisimidazole and by four nitrogen atoms of the tetradentate DPEA ligand. The latter is coordinated to the iron(II) atom via two pyridine nitrogen atoms in apical positions and by two aliphatic amino groups in adjacent positions. Thus, due to the meridionally arranged DPEA pyridine rings, both inequivalent iron(II) complexes represent the achiral *mer* isomer, as was also observed for $[Fe(DPEA)(NCS)_2]$.[12] Despite some

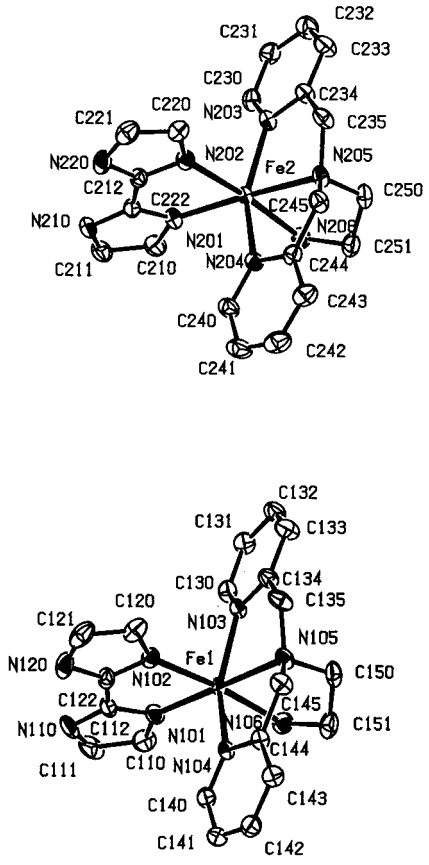

Figure 1. ORTEP view of the two inequivalent $[Fe(DPEA)(bim)](ClO_4)_2 \cdot 0.5\ H_2O$ molecules of the unit cell at 293 K (ellipsoids enclose 20% probability)

Table 1. Selected bond lengths [Å] for [Fe(DPEA)(bim)]-$(ClO_4)_2$·0.5 H_2O

	T = 293 K	T = 123 K
Fe(1)−N(101)	2.130(4)[a]	1.996(2)[a]
Fe(1)−N(102)	2.233(4)	2.040(3)
Fe(1)−N(103)	2.181(3)	1.979(2)
Fe(1)−N(104)	2.208(3)	1.989(3)
Fe(1)−N(105)	2.209(3)	1.991(2)
Fe(1)−N(106)	2.173(4)	2.012(3)
Fe(2)−N(201)	2.134(4)	1.993(2)
Fe(2)−N(202)	2.253(4)	2.060(3)
Fe(2)−N(203)	2.143(4)	1.964(2)
Fe(2)−N(204)	2.177(3)	1.977(2)
Fe(2)−N(205)	2.211(3)	1.994(2)
Fe(2)−N(206)	2.194(4)	2.021(3)

[a] Estimated standard deviations in the least significant digits are given in parentheses.

Table 2. Selected angles [deg] for [Fe(DPEA)(bim)]$(ClO_4)_2$·0.5 H_2O

	T = 293 K	T = 123 K
N(101)−Fe(1)−N(102)	77.5(2)[a]	80.7(1)[a]
N(101)−Fe(1)−N(103)	105.2(2)	98.1(1)
N(101)−Fe(1)−N(104)	101.7(2)	96.9(1)
N(101)−Fe(1)−N(105)	178.5(2)	179.6(1)
N(101)−Fe(1)−N(106)	99.2(2)	94.1(1)
N(102)−Fe(1)−N(103)	93.6(2)	92.9(1)
N(102)−Fe(1)−N(104)	87.6(2)	89.0(1)
N(102)−Fe(1)−N(105)	101.2(2)	99.3(1)
N(102)−Fe(1)−N(106)	174.0(2)	174.0(1)
N(103)−Fe(1)−N(104)	152.7(2)	165.0(1)
N(103)−Fe(1)−N(105)	75.6(2)	81.5(1)
N(103)−Fe(1)−N(106)	92.1(2)	90.8(1)
N(104)−Fe(1)−N(105)	77.4(2)	83.6(1)
N(104)−Fe(1)−N(106)	88.3(2)	88.7(1)
N(105)−Fe(1)−N(106)	82.1(2)	86.0(1)
N(201)−Fe(2)−N(202)	77.0(2)	80.5(1)
N(201)−Fe(2)−N(203)	107.9(2)	98.8(1)
N(201)−Fe(2)−N(204)	98.9(2)	95.6(1)
N(201)−Fe(2)−N(205)	176.1(2)	179.3(1)
N(201)−Fe(2)−N(206)	99.2(2)	93.8(1)
N(202)−Fe(2)−N(203)	92.6(2)	91.9(1)
N(202)−Fe(2)−N(204)	89.0(2)	90.2(1)
N(202)−Fe(2)−N(205)	101.8(2)	99.5(1)
N(202)−Fe(2)−N(206)	174.7(2)	174.0(1)
N(203)−Fe(2)−N(204)	152.8(2)	165.6(1)
N(203)−Fe(2)−N(205)	75.9(2)	81.9(1)
N(203)−Fe(2)−N(206)	92.1(2)	90.9(1)
N(204)−Fe(2)−N(205)	77.3(2)	83.7(1)
N(204)−Fe(2)−N(206)	88.0(2)	88.5(1)
N(205)−Fe(2)−N(206)	81.8(2)	86.2(1)

[a] Estimated standard deviations in the least significant digits are given in parentheses.

differences in the corresponding bond lengths and angles of the two inequivalent $[FeN_6]$ octahedrons, their configurations are the same at both temperatures.

(a) High-Spin Complex Structure (T = 293 K)

The similar $[FeN_6]$ octahedrons in the two inequivalent molecules are strongly distorted. The two Fe−N distances involving the 2,2-bisimidazole ligand are rather different [site **1**: Fe1−N101 = 2.130(4) Å, Fe1−N102 = 2.233(4) Å; site **2**: Fe2−N201 = 2.134(4) Å, Fe2−N202 = 2.253(4) Å]. The Fe−N(DPEA) bond lengths also differ considerably for the aromatic and aliphatic nitrogen donor atoms within each site and between both sites (see Table 1). The corresponding N−Fe−N angles at both lattice sites are rather similar (Table 2). They fall within 75.6(2)−107.9(2)° for adjacent nitrogen atoms and 152.8(2)−178.5(2)° for opposite nitrogen atoms, instead of 90 and 180° that would be observed in an ideal octahedron. The largest deviations from 90° are observed in the five-membered chelate rings (see Table 2). Evidently, this severe distortion of the $[FeN_6]$ core from O_h symmetry is due to the steric constraints caused by the coordination of the tetradentate and bidentate ligands.

The large values of the equivalent isotropic displacement parameter at room temperature reflect a disorder of the perchlorate anions and the solvent water molecules in the crystal. The disordered character of the packing of the ClO_4 groups is also displayed in the variation of the distances and angles. The Cl−O bond lengths in four ClO_4 groups arising from two sites are in the range 1.277(6)−1.420(5) Å. The angles Cl−O−Cl fall within the range 98.4(5)−120.6(6)°, instead of 109° for an ideal tetrahedron. It has not been possible to split the atom positions into several different orientations.

The crystal packing of [Fe(DPEA)(bim)]$(ClO_4)_2$·0.5 H_2O consists of alternate layers originating from the Fe1 and Fe2 molecule sets parallel to the *bc* plane. Figure 2 shows a projection of the structure along the *b* axis. Each layer can be considered as being formed by the columns of complex cations along the *b* direction. The columns of the complex cations at lattice sites **1** and **2** result from the symmetry operations ($-x$, $-{}^1/_2 + y$, ${}^1/_2 - z$) and ($1 - x$, $-{}^1/_2 + y$, ${}^1/_2 - z$), respectively. The nearest complexes in the columns are linked by π-stacking interactions resulting from a par-

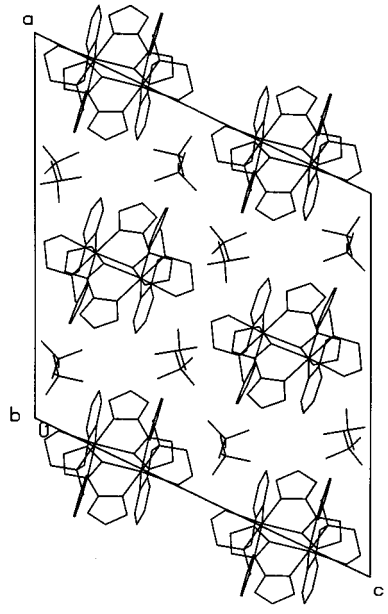

Figure 2. Projection of the molecular structure along the *b* axis at 293 K

Table 3. Intermolecular C···C contacts [Å] shorter than van der Waals distances (3.6 Å) and selected Fe−Fe distances for $[Fe(DPEA)(bim)](ClO_4)_2 \cdot 0.5\ H_2O$

	293 K	123 K
C(130)···C(143)[1] [a]	3.549(8)[b]	3.410(5)[b]
C(130)···C(144)[1]	3.597(8)	3.490(5)
C(131)···C(140)[1]	3.497(8)	3.563(5)
C(131)···C(141)[1]	3.544(9)	3.598(5)
C(132)···C(141)[1]	3.597(9)	3.461(5)
C(230)···C(243)[2]		3.471(5)
C(230)···C(244)[2]		3.519(5)
C(231)···C(240)[2]	3.417(8)	3.387(5)
C(231)···C(241)[2]	3.444(9)	3.455(5)
C(232)···C(241)[2]		3.447(5)
Fe(1)−Fe(1)[1]	7.455(1)	7.413(1)
Fe(1)−Fe(1)[3]	10.349(2)	10.232(2)
Fe(1)−Fe(1)[4]	11.258(2)	11.501(2)
Fe(1)[1]−Fe(1)[3]	14.093(3)	13.676(3)
Fe(2)−Fe(2)[5]	7.417(1)	7.394(1)
Fe(2)−Fe(2)[6]	10.208(2)	10.027(2)
Fe(2)−Fe(2)[7]	9.764(2)	9.460(2)
Fe(2)[5]−Fe(2)[6]	14.936(3)	14.863(3)

[a] Key: ([1]) $-x, -1/2 + y, 1/2 - z$; ([2]) $1 - x, -1/2 + y, 1/2 - z$; ([3]) $x, 3/2 - y, 1/2 + z$; ([4]) $-x, 1 - y, 1 - z$; ([5]) $1 - x, 1/2 + y, 1/2 - z$; ([6]) $x, 1/2 - y, 1/2 + z$; ([7]) $1 - x, 1 - y, 1 - z$. [b] Estimated standard deviations in the least significant digits are given in parentheses.

tial overlap of the pyridine rings of the DPEA ligand, which can be illustrated by the corresponding C···C intermolecular contacts (see Table 3). The dihedral angles between the stacked pyridine planes of the adjacent molecules are 9.6(4) and 20.2(4)° at lattice sites **1** and **2**, respectively. Each column is surrounded by perchlorate anions, yielding the electrically neutral layers of molecules. The solvent water molecules are inserted between the layers. The cohesion within a layer, as well as between neighboring layers is achieved by numerous H-bonds involving the oxygen atoms of the perchlorate ions. Moreover, these indirect H-bonds are realized either by means of the same oxygen atom of the perchlorate ion, or by the different ones. Detailed information on the hydrogen-bonding interactions is listed in Table 4.

(b) Low-Spin Complex Structure (T = 123 K)

The comparison of the HS and LS complex structures shows that the molecular configuration of the two forms essentially remains unchanged. The main difference between them involves the variation of the octahedral geometry of the $[FeN_6]$ core. The HS → LS transition is accompanied by the shortening of the Fe−N bond lengths, the degree of which is dependent on the chemical nature of the nitrogen atoms. In the LS complex two Fe−N(bim) distances are shorter by 0.134 Å (Fe1−N101) and 0.193 Å (Fe1−N102) at lattice site **1**, relative to 0.141 Å (Fe2−N201) and 0.193 Å (Fe2−N202) at lattice site **2**. The reduction of the Fe−N(DPEA) mean distances to the aromatic and aliphatic nitrogen atoms at both lattice sites are 0.211 Å (Fe1−N_{arom}) and 0.190 Å (Fe1−N_{aliph}), and 0.190 Å (Fe2−N_{arom}) and 0.195 Å (Fe2−N_{aliph}). The N−Fe−N angles, which are significantly distorted in the HS complex, are closer to 90° and 180° in the LS complex. The range of the N−Fe−N angles for both lattice sites in the LS $[FeN_6]$ core is 80.5(1)−99.5(1)° and 165.0(1)−179.6(1)°. Clearly, the HS → LS transition is followed by the rearrangement of the $[FeN_6]$ octahedron into a more regular geometry.

The perchlorate anion positions, which are disordered at high temperatures, are far less perturbed at low temperature. The Cl−O distances are in the range 1.372(4)−1.445(3) Å. The Cl−O−Cl angles range from 104.9(2) to 113.4(4)°, and approach the regular tetrahedron value. The disordered nature of the solvent water molecules, which is noted at room temperature, is also reduced at low temperatures.

The crystal packing in the LS complexes is similar to that in the HS state, but more compact. This is consistent with the decrease in the volume of the unit cell by 5.66% and the increase in the density from 1.600 to 1.696 g/cm^3 on lowering the temperature to 123 K. In the columns of the

Table 4. Interatomic distances [Å] and angles [deg] for the hydrogen-bonding interactions for $[Fe(DPEA)(bim)](ClO_4)_2 \cdot 0.5\ H_2O$

D−H···A[a]	D−H	H···A[b]	D···A[b]	D−H···A[b]
293 K				
N(106)−H(10A)···O(42)[1]	0.900	2.546(14)	3.277(13)	138.7(3)
N(106)−H(10B)···O(23)[2]	0.900	2.424(8)	3.197(8)	144.1(2)
N(110)−H(110)···O(13)[2]	0.860	2.512(10)	3.135(9)	130.0(2)
N(120)−H(120)···O(20)[3]	0.860	2.449(9)	3.044(8)	126.9(2)
N(120)−H(120)···O(22)[3]	0.860	2.401(11)	3.151(9)	144.8(3)
N(206)−H(20A)···O(33)[4]	0.900	2.360(10)	3.144(9)	145.6(3)
N(206)−H(20B)···O(10)[2]	0.900	2.288(10)	3.104(10)	150.6(5)
N(210)−H(210)···O(13)[5]	0.860	2.246(9)	3.056(9)	157.1(2)
N(220)−H(220)···O(13)[5]	0.860	2.289(9)	3.086(9)	154.3(2)
C(111)−H(111)···O(30)[6]	0.930	2.563(11)	3.430(11)	155.2(3)
C(150)−H(15B)···O(23)[1]	0.970	2.594(8)	3.426(8)	143.9(2)
C(211)−H(211)···O(40)[7]	0.930	2.565(12)	3.337(11)	140.7(3)
C(233)−H(233)···O(42)[8]	0.930	2.548(16)	3.465(16)	168.7(3)
C(245)−H(24A)···O(12)[4]	0.970	2.412(11)	3.348(10)	162.1(3)
C(250)−H(25B)···O(12)[4]	0.970	2.549(11)	3.474(10)	159.3(3)
O(600)−H(600)···O(43)[7]	1.081	2.36(4)	3.15(2)	129(4)
123 K				
N(106)−H(10A)···O(41)[1]	0.900	2.549(6)	3.375(7)	159.5(1)
N(106)−H(10B)···O(23)[2]	0.900	2.280(5)	3.094(5)	150.3(1)
N(110)−H(110)···O(13)[2]	0.860	2.599(6)	3.229(6)	131.1(1)
N(120)−H(120)···O(20)[3]	0.860	2.222(5)	2.877(5)	132.8(2)
N(120)−H(120)···O(22)[3]	0.860	2.502(6)	3.219(6)	141.4(1)
N(206)−H(20A)···O(33)[4]	0.900	2.441(4)	3.197(6)	141.8(1)
N(206)−H(20B)···O(10)[2]	0.900	2.262(4)	3.126(4)	160.7(1)
N(210)−H(210)···O(13)[5]	0.860	2.158(5)	2.950(5)	152.9(1)
N(220)−H(220)···O(10)[5]	0.860	2.558(5)	3.316(5)	148.5(1)
N(220)−H(220)···O(13)[5]	0.860	2.308(5)	3.075(5)	147.6(1)
C(111)−H(111)···O(30)[6]	0.930	2.508(5)	3.355(5)	151.5(2)
C(210)−H(21A)···O(31)[7]	0.930	2.523(5)	3.426(5)	163.6(1)
C(221)−H(221)···O(31)[9]	0.930	2.547(5)	3.278(5)	135.8(1)
C(232)−H(232)···O(21)[8]	0.930	2.547(5)	3.317(5)	140.5(1)
C(233)−H(233)···O(42)[8]	0.930	2.386(6)	3.262(6)	156.9(1)
C(245)−H(24A)···O(12)[4]	0.970	2.401(5)	3.299(5)	153.8(1)
C(250)−H(25B)···O(12)[4]	0.970	2.514(5)	3.413(5)	154.2(1)
O(600)−H(601)···O(43)[7]	1.080	2.50(2)	3.30(1)	130(2)

[a] Symmetry operations: ([1]) $x, 1.5 - y, 0.5 + z$; ([2]) $-x, 0.5 + y, 0.5 - z$; ([3]) $-x, 1 - y, -z$; ([4]) $1 - x, 1 - y, 1 - z$; ([5]) $x, 0.5 - y, -0.5 + z$; ([6]) $-x, -0.5 + y, 0.5 - z$; ([7]) $x, -1 + y, z$; ([8]) $1 - x, -0.5 + y, 0.5 - z$; ([9]) $x, 1.5 - y, -0.5 + z$. [b] Estimated standard deviations in the least significant digits are given in parentheses.

cation complexes, the interplanar distances between the overlapping pyridine rings of the DPEA ligand are slightly reduced relative to the HS structure, as can be seen from the C···C intermolecular distances (Table 3). The dihedral angles between the adjacent stacked pyridine rings in the LS structure are reduced to 5.7(4) and 15.3(4)° at lattice sites **1** and **2**, respectively. It appears that in the LS structure the overlap between pyridine rings is more effective. As in the case of the HS form, no direct intermolecular interactions between the complexes from the different columns have been detected. The cohesion between the columns of complexes within a layer, as well as between the columns from neighboring layers, is maintained by numerous H-bonds. Data on the hydrogen-bonding interactions are listed in Table 4.

Magnetic Susceptibility Data

Variable-temperature magnetic susceptibility data were collected in both cooling and warming modes in the temperature range 290−77 K and are presented as $\chi_M T$ versus T plots in Figure 3. This magnetic behavior indicates a gradual spin transition between high-spin ($S = 2$) and low-spin ($S = 0$) electronic states. At 290 K, the magnitude of $\chi_M T$ is 3.13 $cm^3 \cdot mol^{-1} \cdot K$ ($\mu_{eff} = 5.01\ \mu_B$) which corresponds to a quintet spin-state. This value continuously decreases on cooling to 77 K, to reach a value of 0.02 $cm^3 \cdot mol^{-1} \cdot K$ ($\mu_{eff} = 0.40\ \mu_B$), which is close to the expected temperature-independent paramagnetism value for singlet spin state iron(II) complexes. Furthermore, the absence of residual paramagnetism at low temperatures, as confirmed by Mössbauer spectroscopy (vide infra), suggests that the spin transition is practically complete. Examination of the shape of the magnetic curve reveals that the spin transition takes place in two steps, separated by an inflection point at about 200 K. Approximately 50% of the complexes undergo a thermal spin transition at this temperature. The high-temperature and low-temperature steps are centered at about 218 and 171 K, respectively.

Mössbauer Spectroscopy

The temperature-dependent ^{57}Fe Mössbauer spectra of [Fe(DPEA)(bim)]$(ClO_4)_2 \cdot 0.5\ H_2O$ were recorded between 80 and 295 K. Figure 4 shows six relevant spectra obtained in the cooling mode. Fitting parameters for all spectra are given in Table 5. The low- and high-temperature spectra are characteristic for the LS and HS states of iron(II). According to the X-ray study (vide supra), the crystal lattice of [Fe(DPEA)(bim)]$(ClO_4)_2 \cdot 0.5\ H_2O$ incorporates two inequivalent iron(II) molecules with slightly different $[FeN_6]$ core geometries. The Mössbauer spectra also clearly agree with the presence of two spin crossover sites in the system.

The thermal variations of the quadrupole splitting and the isomer shift of the HS and LS doublets are shown in Figure 5. The thermal variation of the isomer shift of the LS and HS1 doublets is linear and follows the classical 2nd order Doppler shift law. The isomer shift of the HS2 doublet remains approximately constant between 80 and 295 K. The range of values (2.00−1.81 $mm \cdot s^{-1}$ for the first site and 2.4−2.0 $mm \cdot s^{-1}$ for the second site) of the quadrupole splitting ΔE_Q(HS) between 170 and 295 K is indicative of a strong distortion from cubic symmetry. This is also seen from the X-ray data, and suggests that the orbital levels are not degenerate. The orbital energy splittings can be obtained through the analysis of the thermal variation of the quadrupole splitting.[13] The ratio of the average energy splittings between the fundamental and first excited orbital states for the two sites ($\Delta E1$ and $\Delta E2$) gives a rough estimate of the relative degree of their distortion and can be evaluated from both the Ingalls's model[13] and ref.[10] and ref.[14] The ratio $\Delta E2/\Delta E1 = 0.74$ is obtained {$\Delta E = 570$ and 420 cm^{-1} and $\Delta E_Q(0\ K) = 2.06$ and 2.59 mm/s for sites **1** and **2**, respectively} when the thermal variation of the quadrupole splitting is fitted to the Ingalls's model[13] {$\Delta E_Q(T) = \Delta E_Q(0\ K) \times \tanh[\Delta E/2K_BT]$}. The same value for the ratio $\Delta E2/\Delta E1 = p_1/p_2 = 0.7$ was obtained from the slopes ($p_1 = 2 \cdot 10^{-3}$ $mm \cdot s^{-1} \cdot K^{-1}$ and $p_2 = 1.36 \cdot 10^{-3}$ $mm \cdot s^{-1} \cdot K^{-1}$) of the thermal variation of ΔE_Q(HS).[10,14] In systems with two non-equivalent Fe^{II} sites, the Mössbauer spectra would be expected to reveal two clearly separated quadrupole doublets. However, because of the temperature variation of the quadrupole splitting[10,14] and the similar

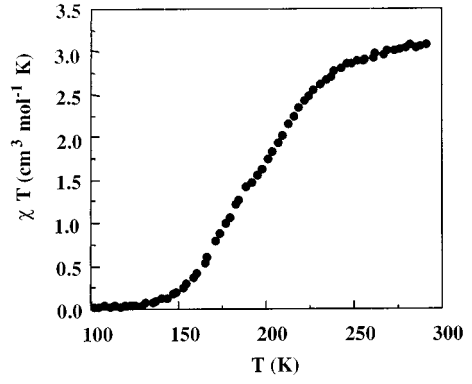

Figure 3. Thermal variation of $\chi_M T$ for [Fe(DPEA)(bim)]$(ClO_4)_2 \cdot 0.5\ H_2O$

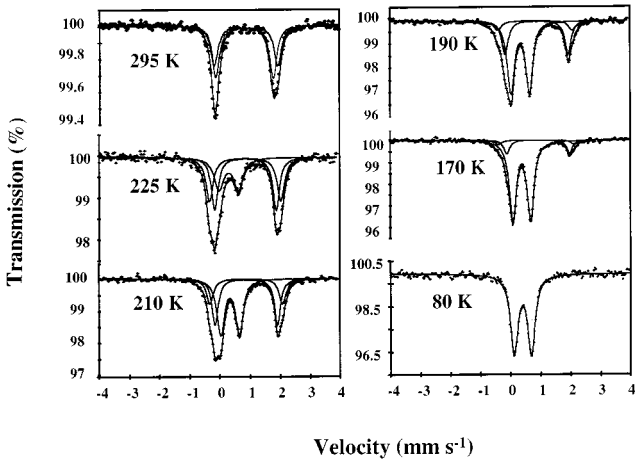

Figure 4. Selected Mössbauer spectra of [Fe(DPEA)(bim)]$(ClO_4)_2 \cdot 0.5\ H_2O$ recorded in the cooling mode. The solid lines represent fitted curves

Table 5. Least-squares-fitted Mössbauer data for $[Fe(DPEA)(bim)](ClO_4)_2 \cdot 0.5\ H_2O$

T	LS[a][b]			HS(1)			HS(2)			A_{HS1}/A_{tot}	A_{HS2}/A_{tot}	A_{LS}/A_{tot}
	δ	ΔE_Q^{LS}	$\Gamma/2$	δ	ΔE_Q^{HS}	$\Gamma/2$	δ	ΔE_Q^{HS}	$\Gamma/2$			
[K]	[mm·s^{-1}]	[mm·s^{-1}]	[mm·s^{-1}]	[mm·s^{-1}]	[mm·s^{-1}]	[mm·s^{-1}]	[mm·s^{-1}]	[mm·s^{-1}]	[mm·s^{-1}]	(%)	(%)	(%)
295	–	–	–	0.90(4)	1.81(8)	0.24(4)	0.96(4)	2.0(1)	0.28(4)	55(7)	45(7)	0
225	0.45(4)	0.61(4)	0.36(4)	0.99(1)	1.96(8)	0.24(4)	0.98(1)	2.2(1)	0.30(4)	41(7)	29(7)	30(1)
210	0.47(1)	0.60(1)	0.28(1)	1.00(1)	2.00(4)	0.24(2)	1.00(1)	2.3(1)	0.26(4)	33(3)	21(3)	46(1)
190	0.485(4)	0.59(3)	0.26(1)	1.01(1)	2.03(4)	0.25(2)	0.97(4)	2.4(2)	0.30(8)	28(2)	10(2)	62(1)
170	0.493(4)	0.57(1)	0.262(4)	1.02(3)	2.00(4)	0.22(4)	0.97(8)	2.4(2)	0.3(1)	12(2)	5(2)	83(1)
80	0.520(8)	0.55(1)	0.286(8)	–	–	–	–	–	–	0	0	100

[a] δ, isomer shift; ΔE_Q, quadrupole splitting; Γ half-height width of line; A/A_{tot}, area ratio. – [b] Error bars are given in parentheses; isomer shift values refer to metallic iron at 300 K.

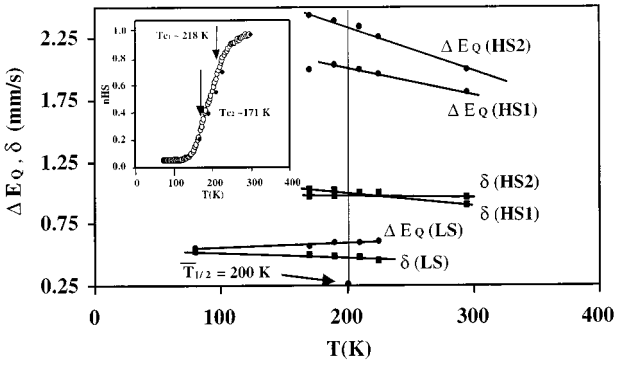

Figure 5. Thermal variation of the quadrupole splitting and the isomer shift of the HS and LS doublets obtained from the Mössbauer measurements of $[Fe(DPEA)(bim)](ClO_4)_2 \cdot 0.5\ H_2O$. In the inset: the thermal variation of the HS fraction (n_{HS}) obtained from magnetic susceptibility measurements (○) and the relative area of the HS component in the Mössbauer spectra (•)

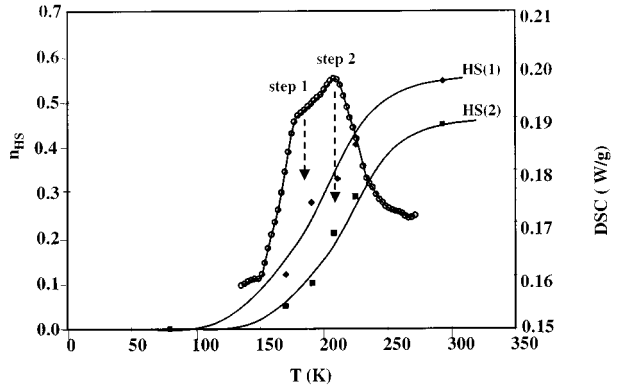

Figure 6. Thermal variation of the HS fractions for both lattice sites (◆ and ■) obtained by Mössbauer spectroscopy and the DSC curve (○) for $[Fe(DPEA)(bim)](ClO_4)_2 \cdot 0.5\ H_2O$

symmetries of the sites **1** and **2**, the two complexes cannot be easily separated. At high temperatures, the quadrupole splittings for the two sites with similar geometry almost merge, resulting in essentially one doublet.

On cooling, the $[Fe(DPEA)(bim)](ClO_4)_2 \cdot 0.5\ H_2O$ complex undergoes the HS → LS transition. On spin conversion the spectra show the co-existence of the HS and LS isomers, with strongly temperature-dependent relative intensities. At 80 K, the spectrum consists of one quadrupole doublet with typical parameters for the iron(II) LS state (Table 5), and the HS → LS transition at both **1** and **2** sites is complete, as seen by the absence of a residual HS fraction. The temperature at which 50% of the complexes undergo thermal spin transition is found to be close to 200 K. Curves showing the thermal variation of the total high-spin fraction n_{HS}, as determined from Mössbauer measurements and independently from magnetic susceptibility data, are in reasonable agreement as shown in the inset of Figure 5. In order to confirm the two-step character of the spin crossover, DSC measurements were carried out (Figure 6). Two peaks around 170 and 220 K are observed, which corresponds to the transition temperatures found from the thermal variation of the high-spin fraction for the two sites of the system obtained by Mössbauer spectroscopy (Figure 6). This confirms the two-step character of the spin transition in the present complex.

Photomagnetic Properties

The LIESST experiments were performed at 10 K on a very thin layer of powder sample. The weight was estimated by comparing the thermal spin crossover curve with the curve recorded with a heavier and accurately weighed sample. The sample was irradiated using different wavelengths accessible with the Laser-Diode (830±15 nm) and with the Kr^+ Laser; i.e. single-line 530.9 nm, multi-lines 647.1−676.4 nm and 752.3−799.3 nm.

At 10 K, the magnetic response of the sample without irradiation was diamagnetic (LS state). Irradiation with the wavelengths accessible with the Kr^+ Laser or the Laser-Diode resulted in a rapid increase of the magnetic response (Figure 7). This peculiar behavior may be assigned to a conversion into the HS state, according to the well-known LIESST effect.[11] It is worth noting that independent of the wavelengths used, the power applied and the irradiation time, the highest LS → HS conversion reached was about 40%. The optimal conversion was obtained with the multilines 647.1−676.4 nm at a power of 20 mW/cm^2 and after 2 hours of irradiation. In contrast, the irradiation of the compound at 830 nm induced only 5% of HS state, whereas tetrazole iron(II) derivatives exhibited a reverse-LIESST ef-

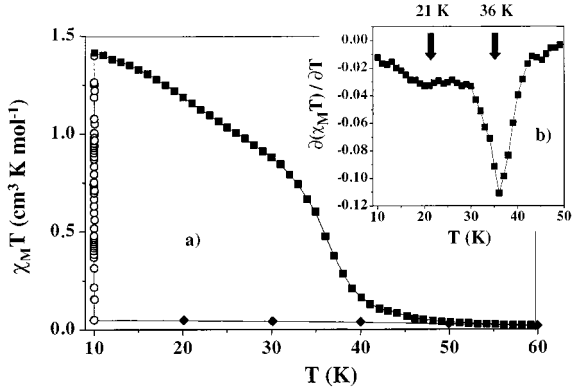

Figure 7. a) Temperature-dependence of $\chi_M T$ for [Fe(DPEA)(bim)]$(ClO_4)_2$·0.5 H_2O: (◆) data recorded in the cooling mode without irradiation; (○) data recorded with irradiation for 2 h at 10 K; (■) data recorded in the warming mode (0.3 K min^{-1}) after light irradiation was applied for two hours, then turned off. b) Derivative $\partial(\chi_M T)/\partial T$

fect instead.[15][11b] The most straightforward explanation for this difference is that the weak $^5T_2 \rightarrow {}^5E$ absorption band is totally overlapped by the intense ^{1}MLCT band involving the aromatic rings of the organic ligand.

We have recently proposed that the capacity of a compound to retain the light-induced HS information may be estimated through the determination of the T_c(LIESST) value.[16] By using the same procedure, we recorded the photomagnetic properties of [Fe(DPEA)(bim)]$(ClO_4)_2$·0.5 H_2O. After 2 hours of irradiation at 10 K, a photostationary limit was reached. The light was turned off and the temperature was slowly increased (0.3 K·min^{-1}). Figure 7 shows the temperature dependence of $\chi_M T$, which gradually decreases until 30 K and then rapidly drops to a value close to zero around 50 K. The $\partial(\chi_M T)/\partial T$ versus T plot reveals a clear minimum at a temperature of 36 K and also a second minimum is present around 21 K. This suggests that for both sites **1** and **2** the LS → HS conversion occurs under light-irradiation. The shape of the $\partial(\chi_M T)/\partial T$ vs. T plot nevertheless indicates a more effective LS → HS conversion for the site with the T_c(LIESST) at 36 K than for the site at 21 K.

Figure 8 shows the HS → LS relaxation curve recorded at 10 K. These data reveal a strong deviation from the single exponential law. The time-dependence of the high-spin fraction γ_{HS} is fast at first and then slows down. This behavior has been previously reported[17] and attributed to the local non-homogeneities of the iron(II) environment in the [FeN_6] core. Hauser et al.[17a] have proposed an analysis of the $\gamma_{HS}(t)$ curves based upon a distribution of relaxation rates $k_{HL}(T)$ and a corresponding repartition of the activation energy. In the [Fe(DPEA)(bim)]$(ClO_4)_2$·0.5 H_2O case, the situation is more complicated due to the population of sites **1** and **2**; i.e. each site may possess an exponential decay and hence the HS → LS relaxation curves may follow the bi-exponential law [Equation (1)].

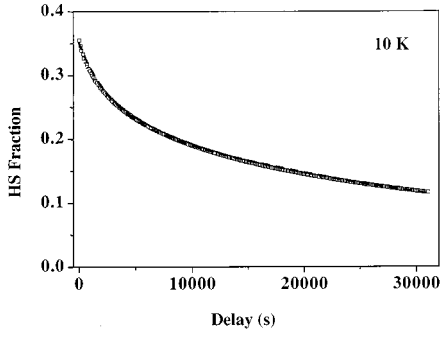

Figure 8. The HS → LS relaxation curve recorded at 10 K. The dashed line represents the fitted curve

$$\gamma_{HS} = A_1 \exp(-k_{HL}^1 t) + A_2 \exp(-k_{HL}^2 t) \quad (1)$$

The solid line shown in Figure 8 results from the least-squares fit of the relaxation data to Equation (1). It can be seen that a good fit of the data has been found with the biexponential law. The numerical fit results in values of $2.3 \cdot 10^{-5}$ s^{-1} and $3.4 \cdot 10^{-4}$ s^{-1} for k_{HL}, and of 0.24 and 0.11 for pre-exponential factors. Note that this relaxation curve can also be fitted by using a Gaussian distribution of activation energy centered at 50 cm^{-1} with a standard deviation of 12 cm^{-1} and a pre-exponential factor of $6.5 \cdot 10^{-2}$ s^{-1}. This gives a k_{HL} value of $5 \cdot 10^{-5}$ s^{-1}. However, the large standard deviation that arises in the latter case suggests that the bi-exponential analysis related to the two independent lattice sites is the more likely scenario.

Discussion

Relation Between the Structure and Spin Transition Properties

The synthesis and investigation of the title complex were undertaken with the aim of modifying the spin transition properties of the complex *mer*-[Fe(DPEA)$(NCS)_2$].[12] The latter manifests a sharp spin conversion close to the first-order transition. We expected that the replacement of two NCS groups by a bidentate ligand more predisposed to the intermolecular H-bonding, might enhance the cooperativity and eventually lead to a spin transition with hysteresis. The 2,2-bisimidazole molecule, containing two NH groups, was selected for this purpose. To the best of our knowledge, there are no data regarding iron(II) spin transition complexes with 2,2-bisimidazole in the literature. Contrary to expectation, the [Fe(DPEA)(bim)]$(ClO_4)_2$·0.5 H_2O complex exhibits a very gradual two-step spin transition which was revealed by the magnetic measurements, Mössbauer spectroscopy and differential scanning calorimetry. To date, there have been three reports in the literature describing the two-step behavior in spin crossover systems. The first one arises from the static density waves of HS complexes in the crystal lattice with a unique crystallographic Fe^{II} site.[18] The second one relates to binuclear complexes.[19] It is known that 2,2-bisimidazole can act not only as a bidentate chelating ligand but also as a bridging tetradentate one.[20] The third reason for the two-step behavior may be due to the presence of two inequivalent sites in the crystal lattice.

The X-ray analysis of [Fe(DPEA)(bim)]$(ClO_4)_2$·0.5 H_2O shows that the unit cell contains two inequivalent molecules with analogous configurations. The average Fe−N distances at both lattice sites **1** and **2** are almost identical and equal to 2.189 and 2.185 Å at 293 K, and 2.001 and 2.002 Å at 123 K, respectively. The closeness of the mean Fe−N distances in both inequivalent HS molecules does not allow the two steps of the spin transition, which arise on cooling, to be attributed to lattice sites **1** and **2**. In order to address this question we must analyze separately the bond lengths for three pairs of functionally distinct nitrogen atoms, which form the first coordination sphere of iron(II), namely, imidazolic imine, pyridinic imine and aliphatic amine types. In the HS state, the mean Fe−N(imidazole), Fe−N(pyridine), and Fe−N(amine) distances are 2.182, 2.195, and 2.191 Å, respectively at lattice site **1**, compared with 2.194, 2.160, and 2.203 Å, respectively at lattice site **2**. In other words, the mean Fe−N(pyridine) distance is shorter by 0.035 Å at site **2**, whereas the mean Fe−N(imidazole) and Fe−N(amine) distances at this same site are both longer by 0.012 Å. The occurrence of the spin transition depends on the magnitude of the ligand field strength, and the ligand field strength depends on the metal−ligand distance (as $\approx 1/r^5$) and on the nature of the donor atoms. Three functionally distinct types of nitrogen donor atoms contribute, in differing degrees, to the overall magnitude of the ligand field.[1d] The main contribution arises from the aromatic pyridine ligands, participating in both σ- and π-bonding interactions and favoring the LS state in iron(II) complexes. The contribution of the imine nitrogen atoms of 2,2-bisimidazole is much weaker due to the lack of aromaticity. Indeed, the $[Fe(bim)_3]SO_4$ complex is paramagnetic.[21] The ligand field produced by the aliphatic amine nitrogen atoms is still weaker and is entirely determined by σ interactions. It is clear that the spin transition sequence at lattice sites **1** and **2** is dependent on the difference in the Fe−N(pyridine) distances. The shorter mean Fe−N(pyridine) distance at lattice site **2** (by 0.035 Å) ensures a stronger overall ligand field and can be regarded as favoring the higher temperature spin conversion. However, it is unlikely that the inflection point near 200 K separates two successive and independent spin transitions. As it follows from the Mössbauer data, it results from the overlap of two gradual spin processes with close transition temperatures. Under such conditions the X-ray study near the inflection point, which proved to be useful in the case of the two sharp steps separated by a plateau,[9,10] cannot distinguish spin states at two lattice sites.

It could be noted that the order-disorder transition of both the solvent molecules and the perchlorate anions on cooling might also be a reason for the different change in spin state for the two sites. However, the intrinsic structural distinction of the two Fe^{II} sites found from the X-ray data, and resulting in the difference in the overall ligand field (also displayed by the two values of the crystal field distortion parameter) seems to be a more likely explanation for the two-step transition behavior.

The X-ray analysis confirms that our goal of generating a branched network of intermolecular links in the crystal lattice has been attained (Table 3 and Table 4). Nevertheless, the spin transition is rather gradual. Let us consider the structural features responsible for cooperative interactions in [Fe(DPEA)(bim)]$(ClO_4)_2$·0.5 H_2O. The layers of Fe1 and Fe2 molecules alternate parallel to the *bc* plane, forming two similar interpenetrating sublattices (Figure 2). The cooperativity within a sublattice is assured by two different types of intermolecular interactions. The pyridine rings of the DPEA ligand of neighboring complexes partially overlap resulting in the columns of π-stacked molecules extended along the *b* direction. The Fe−Fe distances in columns for two HS sublattices, 7.455(1) and 7.417(1) Å, are rather short in comparison with the values for several other spin-crossover systems.[22] At 123 K, the C···C intermolecular contacts become shorter and some new contacts appear (Table 3), probably due to a more parallel arrangement of the pyridine rings. The second type of intermolecular interactions is represented by hydrogen-bonds (Table 4), forming a branched network. The H-bonds propagate preferentially in the *a* and *c* directions where they link the complexes of neighboring columns from the same or from different sublattices. The H-bonds between the molecules within the columns are less numerous. All hydrogen-bonds between the complexes are indirect and pass through the oxygen atoms of the perchlorate anions. As a result, the corresponding Fe−Fe distances are rather long and vary in the range 9.764(2)−14.936(3) Å within the HS sublattices and 9.466(2)−20.234(5) Å between them. The majority of the H-bonds involve the atoms belonging to the second coordination sphere of the Fe^{II} ion. Only four of the sixteen hydrogen-bonds include the nitrogen atoms directly linked to Fe^{II} and can be represented schematically as N−H···O(ClO_4) or N−H···O(ClO_4)···H−C. At 123 K, several new H-bonds appear but the overall network essentially does not change relative to the HS state. The indirect character of the hydrogen-bonds and the non-branched one-dimensional system of the intermolecular π-stacking do not provide a good basis for a strong cooperativity resulting in a gradual spin transition in [Fe(DPEA)(bim)]$(ClO_4)_2$·0.5 H_2O. It can reasonably be concluded that the various ways referred to above of propagating intermolecular interactions are responsible for the anisotropy in the unit cell contraction (2.15, 0.03, and 1.94% for the *a*, *b*, and *c* axes, respectively) on cooling.

Two distinct iron(II) lattice sites are also manifested in the LIESST process. The HS conversion after light irradiation at 10 K results in the two minima in the $\partial(\chi_M T)/\partial T$ versus T plot (Figure 7). The corresponding T_c(LIESST) values are 21 K and 36 K, with a less pronounced minimum for the first temperature. This shows that the relaxation at one of the two lattice sites is faster than at the other. The lifetime of the HS species at 10 K was recorded over a 10-hour period. As has already been reported for other spin crossover compounds exhibiting a LIESST effect, the HS → LS relaxation curves deviate markedly from single exponential behavior. The numerical data can be fitted both by

using a Gaussian distribution of activation energy and with a biexponential decay that considers two independent lattice sites. In this latter case, the numerical analysis shows that one of the two lifetimes is very short. This may explain why the HS conversion does not exceed 40%. In fact, the photostationary point reached after irradiation is due to a critical balance between light population and HS → LS relaxation.

According to the theory of nonadiabatic multiphonon relaxation,[23] the characteristic features of the relaxation rate constant are a temperature-independent tunneling rate at low temperatures and a thermally activated process at elevated temperatures. At low temperatures, the lifetimes of the HS species depend on both the Huang−Rhys factor, S, which is a measure of the horizontal displacement of the potential wells of the HS and LS states, and the energy gap $\Delta E°_{HL}$ HL between the lowest vibronic levels of the HS and LS states. Hauser et al.[24] proposed that S does not vary to a large extent within the series of $[FeN_6]$ compounds, whereas the energy difference and thus the reduced energy gap $p = \Delta E°_{HL}/h\omega$ varies from $p < 1$ for samples with $T_{1/2}$ below 100 K to $p > 10$ for LS compounds. The thermal spin transitions in $[Fe(DPEA)(bim)](ClO_4)_2 \cdot 0.5\ H_2O$ located at 171 K for lattice site **1** and at 218 K for site **2** correspond to a higher $\Delta E°_{HL}$ HL (and thus p) value for site **2**. Note that the Δr_{HL} values recorded by X-ray diffraction are similar for the two lattice sites (0.188 and 0.183 Å), and hence S can be assumed to be quasi constant. According to the inverse energy-gap law reported for $[FeN_6]$ core compounds, the increase in the p factor between the two lattice sites enables the faster relaxation to be attributed to lattice site **2**. Consequently, T_c(LIESST) around 21 K corresponds to the relaxation of site **2**, and that at 36 K to site **1**. The relaxation rates estimated at 10 K with both the biexponential fit and the Gaussian distribution are in the range $10^{-4}-10^{-5}\ s^{-1}$. These values, as well as those observed recently for other $[FeN_6]$ compounds[17b] exceed the values predicted by the inverse energy-gap law[24] with $S \approx 50$. Generally, this discrepancy can be accounted for by large changes in the Fe−N bond lengths, which do not agree with the theoretical approximations. The Δr_{HL} change (≈ 0.19 Å) for $[Fe(DPEA)(bim)](ClO_4)_2 \cdot 0.5\ H_2O$ is in the same range as for other $[FeN_6]$ core compounds (0.16−0.21 Å). It is clear that the LIESST effect is controlled by many parameters, which are not all identified yet. More extensive studies should be carried out.

Experimental Section

Materials: All reagents and solvents used in this study are commercially available and were used without further purification. All syntheses involving Fe^{II} species were carried out in deoxygenated solvents under an inert atmosphere of N_2 using glovebox techniques. (2-Aminoethyl)bis(2-pyridylmethyl)amine (DPEA) was obtained according to the procedure we have recently reported.[12] 2,2-Bisimidazole (bim) was prepared as described previously.[25] ^1H NMR spectra were recorded in $CDCl_3$ on a Bruker AC200 spectrometer operating at 200 MHz. Elemental analyses (C, H N, Cl, and Fe determination) were performed at the Service Central de Microanalyse du CNRS in Vernaison.

Caution: The perchlorate salts of metal complexes with organic ligands are potentially explosive. Only small quantities of the compound should be prepared and handled with much care!

Synthesis of the Iron(II) Complex: $Fe(ClO_4)_2 \cdot 6\ H_2O$ (72.6 mg, 0.2 mmol) was dissolved in 8 mL of ethanol/methanol (5:1 mixture) and 2,2-bisimidazole (26.8 mg, 0.2 mmol) was added to it. A yellow solution was formed. After the addition of (2-aminoethyl)bis(2-pyridylmethyl)amine (48.4 mg, 0.2 mmol) in 2 mL of the same mixture of alcohols, the solution turned red-brown. The solution was filtered and allowed to stand overnight at room temperature, affording yellow-brown crystals of $[Fe(DPEA)(bim)](ClO_4)_2 \cdot 0.5\ H_2O$ which were collected by filtration, washed with ethanol, and dried in vacuum. The crystal used in the X-ray structure determination was selected from this sample. Yield: 56%. − $C_{20}H_{25}Cl_2FeN_8O_{8.5}$ (640.2): calcd. C 37.52, H 3.94, N 17.50, Cl 11.08, Fe 8.72; found C 37.68, H 3.98, N 17.74, Cl 11.22, Fe 8.77.

Magnetic Properties: Magnetic susceptibility measurements were carried out using two instruments: (i) A Manics DSM-8 fully automated Faraday-type magnetometer equipped with an DN-170 Oxford Instruments continuous-flow cryostat and a BE 15f Bruker electromagnet operating at ca. 0.8 Tesla and in the 80−300 K temperature range; (ii) a MPMS-55 QuantumDesign SQUID magnetometer operating at ca. 2 Tesla in the 2−300 K temperature range. Data were corrected for the magnetization of the sample holder and for diamagnetic contributions.

LIESST experiments were realized using a Spectra-Physics series 2025 Ker^+ laser system coupled through an optical fiber to the cavity of a MPMS-55 Quantum Design SQUID magnetometer. The wavelengths at 830±15 nm were generated using a Laser Diode SDS-2360-L2. The measurements were performed on a very thin layer of powder sample. The weight was estimated by comparing the thermal spin crossover curve with that for a heavier and accurately weighed sample.

Mössbauer Spectra: The variable-temperature Mössbauer measurements were obtained on a constant-acceleration spectrometer with a 50 mCi source of ^{57}Co (Rh matrix). The isomer shift values (δ) are given with respect to metallic iron at room temperature. The absorber was a sample of microcrystalline powder enclosed in a 2 cm diameter cylindrical plastic sample holder, the size of which had been determined to optimize the absorption. The variable-temperature spectra were obtained in the range 80−305 K, using a MD306 Oxford cryostat, the thermal scanning was monitored by an Oxford ITC4 servocontrol device (±0.1 K). Fitting parameters for all spectra (Table 5) were obtained by using a least-squares computer program.[26] The standard deviations of statistical origin are given in parentheses. As a Mössbauer fitting criteria, in order to get correct parameters of the Mössbauer spectra components for the present compound, it was important to find a good starting point for the fitting procedure. The spectrum at 210 K was selected for this goal, since it is the only case where two components of the HS state can be separated, even visually. Once this spectrum fits well, the starting points of the fitting procedure for other spectra were obtained smoothly and continuously varying the Mössbauer parameters.

Differential Scanning Calorimetry (DSC): Calorimetric measurements were obtained with a NETZSCH DSC-204 differential scanning calorimeter. The instrument was calibrated at solid cyclohexane transition and melting temperatures, and at the mercury melt-

ing temperature. 27 mg of the sample was used in an aluminium sample-holder. An identical aluminium holder was used as a reference. The scan rate of the measurements in the cooling and heating modes was 10 K·min^{-1}. The temperature values are measured with a ±0.4 K accuracy and the uncertainty on the enthalpy values is ±2%. All results were analyzed with an integrated PROTEUS Analysis computational program.

Solution and Refinement of the X-ray Structure: A Nonius Kappa CCD diffractometer was used for data collection. The selected crystal was mounted on a thin glass fiber. Two collections were made: one at the room temperature and the second at 123 K after a very slow decrease of the temperature with a cold nitrogen gas flow at a rate of 0.3 K·min^{-1}. From 10 frames with 1° steps, the initial set of cell parameters was obtained for each measurement. A total of 42881 reflections were collected at room temperature, of which 12124 unique reflections were used for the structure determination. The second collection at 123 K involved 45394 measured reflections of which 11793 unique reflections were used for the hypothesis and refinement. The structures were solved by direct method using the SHELXS-97 program.[27] The structures were then refined by the least-squares method using the SHELXL-97[28] with anisotropic temperature factors for all non-H atoms. The hydrogen atoms were introduced at calculated positions and refined riding on their carrier atoms. The final R factor [with $I > 2\sigma(I)$] has a value of 0.077 and 0.056 for both structures. Crystal data and refinement results are summarized in Table 6. The perspective view of the asymmetric unit containing two complex cations (Figure 1) has been calculated with PLATON.[29]

Crystallographic data for the structures reported in this paper have been deposited with the Cambridge Crystallographic Data Centre as supplementary publication no. CCDC- 162786 for structure at 293 K and CCDC-162787 for structure at 123 K. Copies of the data can be obtained free of charge on application to CCDC, 12 Union Road, Cambridge CB2 1EZ, UK [Fax: (internat.) + 44−1223/336-033; E-mail:deposit@ccdc.cam.ac.uk].

Acknowledgments

We deeply thank Professor J. J. McGarvey for his helpful suggestions to the present work. We are grateful for financial support from the European Commission for granting the TMR-Network "Thermal and Optical Switching of Spin States (TOSS)", Contract No. ERB-FMRX-CT98−0199. We thank J.-F. Meunier for technical assistance in the Mössbauer spectroscopy, magnetic and DSC measurements.

Table 6. Crystallographic Data for [Fe(DPEA)(bim)]-$(ClO_4)_2$·0.5 H_2O

	T = 293 K	T = 123 K
chem formula	$C_{40}H_{50}N_{16}Cl_4O_{17}Fe_2$	
fw	1280.46	
a, Å	21.146(4)	20.692(4)
b, Å	13.692(3)	13.688(3)
c, Å	20.398(4)	20.003(4)
β, deg	115.82(3)	117.72(3)
V, Å^3	5316(2)	5015(2)
Z	4	4
space group	$P2_1/c$	$P2_1/c$
λ, Å	0.71073	0.71073
ρ_{calc}, g·cm^{-3}	1.600	1.696
μ, cm^{-1}	8.31	8.81
R[a] $[I > 2\sigma(I)]$	0.077	0.056
wR_2[b] $[I > 2\sigma(I)]$	0.211	0.136

[a] $R = \Sigma(|F_o| - |F_c|)/\Sigma|F_o|$. − $wR = \{\Sigma[w(F_o^2 - F_c^2)^2]/\Sigma[w(F_o)^2]\}^{1/2}$.

[1] [1a] H. A. Goodwin, *Coord. Chem. Rev.* **1976**, *18*, 293−325. − [1b] P. Gütlich, *Struct. Bonding* **1981**, *44*, 83−164. − [1c] E. König, G. Ritter, S. K. Kulshreshtha, *Chem. Rev.* **1985**, *85*, 219−234. − [1d] H. Toftlund, *Coord. Chem. Rev.* **1989**, *94*, 67−108. − [1e] P. Gütlich, A. Hauser, *Coord. Chem. Rev.* **1990**, *97*, 1−22. − [1f] J. Zarembowitch, O. Kahn, *New J. Chem.* **1991**, *15*, 181−190. − [1g] E. König, *Struct. Bonding.* **1991**, *76*, 51−152. − [1h] P. Gütlich, A. Hauser, H. Spiering, *Angew. Chem. Ed. Engl.* **1994**, *33*, 2024−2053. − [1i]O. Kahn, *Molecular Magnetism*; VCH: New York **1993**. − [1j]O. Kahn, E. Codjovi, *Phil. Trans. R. Soc. Lond. A* **1996**, *354*, 359−379.

[2] [2a] C. P. Slichter, H. G. Drikamer, *J. Chem. Phys.* **1972**, *56*, 2142−2160. − [2b] R. Zimmermann, E. König, *J. Phys. Chem. Solids* **1977**, *38*, 779−788. − [2c] P. S. Rao, P. Ganguli, B. R. McGarvey, *Inorg. Chem.* **1981**, *20*, 3682−3688. − [2d] N. Sasaki, T. Kambara, *J. Chem. Phys.* **1981**, *74*, 3472−3481. − [2e] S. Ohnishi, S. Sugano, *J. Phys. C* **1981**, *14*, 39−47. − [2f] H. Spiering, E. Meissner, C. P. Köhler, E. F. Müller, P. Gutlich, *Chem. Phys.* **1982**, *68*, 65−71. − [2g] H. Spiering, N. Willenbacher, *J. Phys. Condens. Matter* **1989**, 10089−10105.

[3] [3a] E. König, K. Madeja, *Inorg. Chem.* **1967**, *6*, 48−55. − [3b] E. König, K. Madeja, K. J. Watson, *J. Am. Chem. Soc.* **1968**, *90*, 1146−1153. − [3c] A. Ozarowski, B. R. McGarvey, A. B. Sarkar, E. Drake, *Inorg. Chem.* **1988**, *27*, 627−635.

[4] G. S. Matouzenko, A. Bousseksou, S. Lecocq, P. J. van. Koningsbruggen, M. Perrin, O. Kahn, A. Collet, *Inorg. Chem.* **1997**, *36*, 5869−5879.

[5] [5a]P. Poganiuch, S. Decurtins, P. Gütlich, *J. Am. Chem. Soc.* **1990**, *112*, 3270−3278. − [5b] L. Wiehl, *Acta Crystallogr., Sect. B* **1993**, *49*, 289−303.

[6] R. Hinek, H. Spiering, D. Schollmeyer, P. Gûtlich, A. Hauser, *Chem. Eur. J.* **1996**, *2*, 1427−1434.

[7] G. Matouzenko, G. Vériot, J. P. Dutasta, A. Collet, J. Jordanov, F. Varret, M. Perrin, S. Lecocq, *New J. Chem.* **1995**, *19*, 881−885.

[8] H. R. Chang, J. K. McCusker, H. Toftlund, S. R. Wilson, A. X. Trautwein, H. Winkler, D. N. Hendrickson, *J. Am. Chem. Soc.* **1990**, *112*, 6814−6827.

[9] Y. Garcia, O. Kahn, L. Rabardel, B. Chansou, L. Salmon, J. P. Tuchagues, *Inorg. Chem.* **1999**, *38*, 4663−4670.

[10] D. Boinnard, A. Bousseksou, A. Dworkin, J. M. Savariault, F. Varret, J. P. Tuchagues, *Inorg. Chem.* **1994**, *33*, 271−281.

[11] [11a] S. Decurtins, P. Gütlich, C. P. Köhler, H. Spiering, A. Hauser, *Chem. Phys. Lett.* **1984**, *105*, 1−4. − [11b] S. Decurtins, P. Gütlich, K. M. Hasselbach, H. Spiering, A. Hauser, *Inorg. Chem.* **1985**, *24*, 2174−2178.

[12] G. S. Matouzenko, A. Bousseksou, S. Lecocq, P. J. van Koningsbruggen, M. Perrin, O. Kahn, A. Collet, *Inorg. Chem.* **1997**, *36*, 2975−2981.

[13] R. Ingalls, *Phys. Rev.* **1964**, *133A*, 787−795.

[14] A. Ducouret-Cérèse, F. Varret, *J. Phys. (Paris)* **1988**, *49*, 661−666.

[15] A. Hauser, *Chem. Phys. Lett.* **1986**, *124*, 543−548.

[16] J.-F. Létard, L. Capes, G. Chastanet, N. Moliner, S. Létard, J.-A. Real, O. Kahn, *Chem. Phys. Lett.* **1999**, *313*, 115−120.

[17] [17a] A. Hauser, J. Adler, P. Gütlich, *Chem. Phys. Lett.* **1988**, *152*, 468−472. − [17b] T. Buchen, P. Gütlich, *Chem. Phys. Lett.* **1994**, *220*, 262−266. − [17c] In LB film: J.-F. Létard, O. Nguyen, H. Soyer, C. Mingotaud, P. Delhaès, O. Kahn, *Inorg. Chem.* **1999**, *38*, 3020−3021. − [17d] A. Roubeau, J. G. Haasnoot, J. Linares, F. Varret, *Mol. Cryst. and Liq. Cryst.* **1999**, *335*, 541−550.

[18] [18a] H. Köppen, E. W. Müller, C. P. Köhler, H. Spiering, E. Meissner, P. Gütlich, *Chem. Phys. Lett.* **1982**, *91*, 348−352. − [18b] A. M. Greenaway, C. J. O'Connor, A. Schrock, E. Sinn,

Inorg. Chem. **1979**, *18*, 2692−2695. − [18c] M. Mikami, M. Konno, Y. Saito, *Chem. Phys. Lett.* **1979**, *63*, 566−569. − [18d] K. Kaji, M. Sorai, *Thermochim. Acta* **1985**, *88*, 185−190. − [18e] R. Jakobi, H. Spiering, P. Gütlich, *J. Phys. Chem. Solids* **1992**, *53*, 267−275. − [18f] C. P. Köhler, R. Jakobi, E. Meissner, L. Wiehl, H. Spiering, P. Gütlich, *J. Phys. Chem. Solids* **1990**, *51*, 239−247. − [18g] H. Spiering, T. Kohlhaas, H. Romstedt, A. Hauser, C. Bruns-Yilmaz, J. Kusz, P. Gütlich, *Coord. Chem. Rev.* **1999**, *190−192*, 629−647.

[19] [19a] J. A. Real, H. Bolvin, A. Bousseksou, A. Dworkin, O. Kahn, F. Varret, J. Zarembowitch, *J. Am. Chem. Soc.* **1992**, *114*, 4650−4658. − [19b] J. A. Real, I. Castro, A. Bousseksou, M. Verdaguer, R. Burriel, M. Castro, J. Linares, F. Varret, *Inorg. Chem.* **1997**, *36*, 455−464.

[20] [20a] S. W. Kaiser, R. B. Saillant, P. G. Rasmussen, *J. Am. Chem. Soc.* **1975**, *97*, 425−426. − [20b] S. W. Kaiser, R. B. Saillant, W. M. Butler, P. G Rasmussen, *Inorg. Chem.* **1976**, *15*, 2681−2694. − [20c] M. S. Haddad, D. H. Hendrickson, *Inorg. Chem.* **1978**, *17*, 2622−2625. − [20d] P. G. Rasmussen, O. H. Bailey, J. C. Bayon, *Inorg. Chem.* **1984**, *23*, 338−344.

[21] F. Holmes, K. M. Jones, E. G. Torrible, *J. Chem. Soc.* **1961**, 4790−4793.

[22] [22a] B. Gallois, J. A. Real, C. Hauw, J. Zarembowitch, *Inorg. Chem.* **1990**, *29*, 1152−1158. − [22b] J.-F. Létard, P. Guionneau, L. Rabardel, J. A. K. Howard, A. E. Goeta, D. Chasseau, O. Kahn, *Inorg. Chem.* **1998**, *37*, 4432−4441. − [22c] P. Guionneau, J.-F. Létard, D. S. Yufit, D. Chasseau, G. Bravic, A. E. Goeta, J. A. K. Howard, O. Kahn, *J. Mater. Chem.* **1999**, *9*, 985−994.

[23] E. Buhks, G. Navon, M. Bixon, J. Jortner, *J. Am. Chem. Soc.* **1980**, *102*, 2918−2923.

[24] [24a] A. Hauser, A. Vef, P. J. Adler, *Chem. Phys.* **1991**, *95*, 8710−8717. − [24b] A. Hauser, *Comment. Inorg. Chem.* **1995**, *17*, 17−39.

[25] H. Debus, *Annalen.* **1859**, *107*, 199−208.

[26] F. Varret, *Proceedings of the International Conference on Mössbauer Effect Applications.* Jaipar, India, **1981**; Indian National Science Academy: New Delhi, **1982**.

[27] G. M. Sheldrick, *SHELXS-97*, *Program for Crystal Structure Determination*; University of Göttingen: Germany, **1997**.

[28] G. M. Sheldrick, *SHELXL-97*, *Program for Crystal Structure Refinement*; University of Göttingen: Germany, **1997.**

[29] A. L. Spek, *PLATON, A Multipurpose Crystallographic Tool*; Utrecht University: Utrecht, The Netherlands, **1999**.

Received May 17, 2001
[I01178]

Silylimido Complexes of Niobium and Tantalum at the Limit of π-Bond Saturation

Andrea Schorm[a] and Jörg Sundermeyer*[a]

Dedicated to Professor Ernst-G. Jäger on the occasion of his 65th birthday

Keywords: Niobium / Tantalum / N ligands / Cyclopentadienyl ligands / Rearrangements

Convenient strategies towards the synthesis of silylimido niobium and -tantalum complexes of the metallocene and half-sandwich type are reported. Bent metallocenes [(η^5-C_5H_5)$_2$M(NSiMe$_3$)Cl] (M = Nb: **1a**; Ta: **1b**) and [(η^5-C_5H_5)$_2$M(NSiMe$_3$)(η^1-C_5H_5)] (M = Nb: **2a**; Ta: **2b**) are synthesized by reaction of [M(NSiMe$_3$)Cl$_3$(py)$_2$] with 2 or 3 equiv. NaCp, respectively. Half-sandwich type silylimido complexes [(η^5-C_5Me_5)M(NSiMe$_3$)Cl$_2$] (M = Nb: **3a**; Ta: **3b**) cannot selectively be obtained from the (pyridine)(silylimido) precursor complexes. However, their synthesis is accomplished by reaction of [(η^5-C_5Me_5)MCl$_4$] with LiN(SiMe$_3$)$_2$. On the other hand pyridine silylimido complexes are perfect starting materials for the synthesis of the related hydridotris(pyrazolyl)borato complexes [Tp*M(NSiMe$_3$)Cl$_2$] [M = Nb: **4a**; Ta: **4b**; Tp* = κ^3-HB(3,5-Me$_2$pz)$_3$]. A comparative study of the σ,π-donor capability of isoelectronically related *tert*-butyl- and trimethylsilylimido ligands in complexes [(η^5-C_5H_5)$_2$Ta(NR)(η^1-C_5H_5)] (R = SiMe$_3$: **2b**; *t*Bu: **2c**) is presented. With respect to solid-state structural investigations and solution variable-temperature NMR-spectroscopic studies on the dynamic exchange process of η^5- and η^1-bonded cyclopentadienyl rings in **2b**,**c**, *tert*-butlyimido ligands are better donors than silylimido ligands, and both are better donors towards a d^0 metal center than an η^5-C_5H_5 ligand.

Introduction

The last two decades have witnessed an increasing interest in the organometallic chemistry of transition metal complexes containing imido ligands [NR]$^{2-}$.[1] Half-sandwich imido complexes of group-5 metals containing the fragment [(η^5-$C_5R'_5$)M(NR)] have been investigated in their relationship with bent metallocenes of group-4 metals.[2] The concept of the cyclopentadienyl imido ligand analogy[3] was introduced to explain the surprising similarities in structural features and reactivity of both complex classes and led to new catalytic systems.[4] Variation of the ancillary substituent R at the imido function [NR]$^{2-}$ offers a tool for the fine tuning of the steric demand and electronic properties of these ligands. In previous studies we and others have established the chemistry of organoimido complexes (R = alkyl, aryl) of type [(η^5-$C_5R'_5$)M(NR)X$_2$],[2,5] [(η^5-$C_5R'_5$)$_2$M(NR)X][5a,5k,6] and [Tp*M(NR)Cl$_2$][7,22] (M = Nb, Ta, X = anionic ligand). Less reports are available, by far, for corresponding silylimido complexes of niobium and tantalum:[8] the key compounds are [M(NSiMe$_3$)Cl$_3$(py)$_2$] reported by Doherty et al.[9], [Nb{(η^5-C_5H_4)CMe$_2$(η^5-C_5H_4)}(NSiMe$_3$)Cl], a representative of a silylimido *ansa*-metallocene complex reported by Green and co-workers[10] and [Cp*Ta(NSi*t*Bu$_3$)Cl$_2$], which was synthesized and tested by Stryker et al.[4b] as an interesting catalyst for olefin polymerization reactions. Our interest in developing silylimido compounds stems from their potential to act as precursors for heterobimetallic complexes containing bridging nitrido ligands.[11] We believe that electronic saturation of all empty d orbitals of a d^0-metal center by interaction with a set of strong σ- and, especially, π-donor ligands might be a good strategy in order to direct the attack of a nucleophile, for example fluoride or chloride, towards the silicon atom of the silylimido ligand instead of the d^0-metal center. We anticipate that π-bond saturation of a Lewis-acidic metal center might increase the selectivity in condensation reactions with other reactive metal compounds. Therefore we set out to systematically synthesize a series of new silylimido complexes of half-sandwich, bent metallocene and tris(pyrazolyl)borate types. Furthermore we intended to receive experimental data from crystal structure analyses and variable-temperature NMR-spectroscopic studies in order to compare the donor capability of *tert*-butyl- and silylimido ligands in isoelectronically related compounds.

Results and Discussion

Preparative Studies

The starting compounds [M(NSiMe$_3$)Cl$_3$(py)$_2$] (M = Nb, Ta) are readily prepared from the metal pentachlorides and (Me$_3$Si)$_2$NH.[9] All our attempts to synthesize half-sandwich complexes by treatment of these pyridine complex precursors with an equimolar amount of NaCp or LiCp* in THF or toluene failed. This is in contrast to the results of Otero et al. who recently described that [(η^5-C_5H_5)Nb(N*t*Bu)Cl$_2$] can be obtained in 80% yield by reaction of [Nb(N*t*Bu)Cl$_3$(py)$_2$] with NaCp in THF[12]. In agree-

[a] Fachbereich Chemie der Universität Marburg,
Hans-Meerwein-Straße, 35032 Marburg, Germany
E-mail: jsu@chemie.uni-marburg.de

 © WILEY-VCH Verlag GmbH, 69451 Weinheim, 2001 1434−1948/01/1111−2947 $ 17.50+.50/0

ment with our report on this class of cyclopentadienyl imido complexes[5a] the selectivity of the reaction is increased, when 2 equiv. of NaCp are treated with the pyridine silylimido precursors. We were able to synthesize the corresponding bent metallocenes $[(\eta^5\text{-}C_5H_5)_2M(NSiMe_3)Cl]$ (M = Nb: **1a**; Ta: **1b**), which were isolated as yellow powders in good yields (Scheme 1). The cyclopentadienyl protons in silylimido complex **1a** (δ = 6.14) are less shielded compared to the corresponding (*tert*-butylimido)niobium complex (δ = 5.74)[5a]. A similar trend is found for the silylimido tantalum complex **1b** and its *tert*-butylimido derivative. This is the first experimental evidence, that the donor strength of $NCMe_3$ is superior to that of $NSiMe_3$.

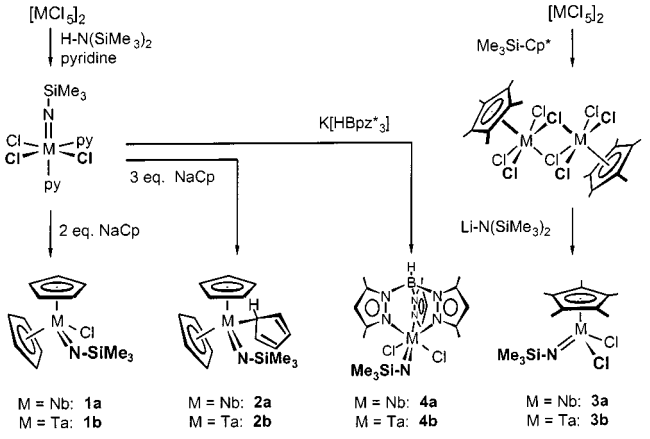

Scheme 1

In previous work Green and co-workers examined the reaction of $[(\eta^5\text{-}C_5H_5)Nb(N\textit{t}Bu)Cl_2]$ with NaCp in THF at room temperature leading to the blue d^0-metal compound $[(\eta^5\text{-}C_5H_5)_2Nb(N\textit{t}Bu)(\eta^1\text{-}C_5H_5)]$. The latter was structurally characterized and the dynamic exchange between σ- and π-bonded cyclopentadienyl rings was examined.[13] We prepared the corresponding silylimido niobium and -tantalum complexes $[(\eta^5\text{-}C_5H_5)_2M(NSiMe_3)(\eta^1\text{-}C_5H_5)]$ (M = Nb: **2a**; Ta: **2b**) by reaction of $[M(NSiMe_3)Cl_3(py)_2]$ (M = Nb, Ta) with 10 equiv. of NaCp. The large excess is needed for complete conversion to the highly π-bond-saturated products. Their variable-temperature NMR-spectroscopic study is described below.

In order to have two isoelectronically and structurally related complexes for a comparative study of the σ,π-donor capability of $NCMe_3$ vs. $NSiMe_3$ ligands, the alkylimido complex $[(\eta^5\text{-}C_5H_5)_2Ta(N\textit{t}Bu)(\eta^1\text{-}C_5H_5)]$ (**2c**) was synthesized by reaction of $[(\eta^5\text{-}C_5H_5)_2Ta(N\textit{t}Bu)Cl]$[5a] with 1 equiv. of NaCp or by reaction of $[Ta(N\textit{t}Bu)Cl_3(py)_2]$ with 3 equiv. of NaCp in THF.

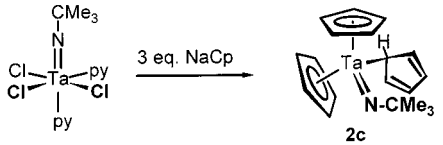

Finally we intended to obtain hitherto unknown silylimido complexes of the half-sandwich type $[(\eta^5\text{-}C_5Me_5)M(NSiMe_3)Cl_2]$ (M = Nb: **3a**; Ta: **3b**) as well as their related tris(pyrazolyl)borato derivatives $[Tp^*M(NSiMe_3)Cl_2]$ [M = Nb: **4a**; Ta: **4b**; Tp* = κ^3-HB(3,5-Me_2pz)$_3$]. It was found that a silylimido ligand may be introduced to preformed half-sandwich complexes $[(\eta^5\text{-}C_5Me_5)MCl_4]$[14] (M = Nb, Ta). By applying ultrasound the reaction of $[(\eta^5\text{-}C_5H_5)MCl_4]$ (M = Nb, Ta) with $LiN(SiMe_3)_2$ in toluene (40 °C) leads to the pale yellow condensation products **3a** and **3b**. Bis(trimethylsilyl)amido complex intermediates[15] were not observed spectroscopically under these conditions.

EHMO calculations support the statement that the monoanionic 6-electron donor ligands Tp and Tp* [Tp = κ^3-HBpz$_3$; Tp* = κ^3-HB(3,5-Me_2pz)$_3$] possess similar σ,2π-bonding interactions with metal d orbitals as an η^5-cyclopentadienyl group.[16] Therefore these ligands can be envisaged as cyclopentadienyl ligand equivalents with a very high steric demand.[17] According to our procedure developed for the synthesis of $[Tp^*M(N\textit{t}Bu)Cl_2]$ (M = Nb, Ta)[7] we treated $[M(NSiMe_3)Cl_3(py)_2]$ (M = Nb, Ta)[9] with 1 equiv. of KTp* in THF and isolated $[Tp^*M(NSiMe_3)Cl_2]$ (M = Nb: **4a**, Ta: **4b**) in good yields. The 2:1 ratio of chemically equivalent ^{1}H and ^{13}C nuclei of the Tp* ligand reflects the C_s symmetry of complexes **4a** and **4b**. Because of the quadrupole moment of the ^{93}Nb nucleus (I = 9/2, 100%) ^{29}Si NMR signals of all niobium complexes described in this paper are too broad to be detected under standard conditions. The corresponding silylimido tantalum complexes reveal ^{29}Si NMR signals in the range of δ_{Si} = −4.9 (**2b**), −2.4 (**3b**), −2.3 (**1b**) and −1.5 (**4b**). As expected, by increasing the strength and number of σ,π-donor ligands the ^{29}Si nucleus becomes more shielded. In oscillators with a linear M=N−Si backbone the ν(M=N) and ν(N−Si) vibrational modes are probably coupled.[18] Therefore in most literature reports, assignments of the stretching modes ν(M=N−Si) of imido niobium or -tantalum complexes are not reported. By synthesis of the analogous *tert*-butyl- and silylimido complexes and by comparing their IR absorptions in the region 900−1300 cm^{-1} we were able to assign the stretching frequencies ν_{sym}(M=N−E) (E = C, Si). Vibrational absorptions are shifted towards lower wavenumbers due to the higher atomic mass of silicon versus carbon. Because of the coupling of vibrational modes IR data seems to be too insignificant to compare the donor strength via bond orders of the silyl- and *tert*-butylimido ligands.

Molecular Structures

In order to evaluate the σ,π-donor strength of the two imido ligands, $NCMe_3$ and $NSiMe_3$, single crystals of two isoelectronically related complexes $[(\eta^5\text{-}C_5H_5)_2Ta(NEMe_3)(\eta^1\text{-}C_5H_5)]$ (E = Si **2b**; C **2c**) were grown. Yellow needles of **2b** crystallized from a saturated hexane solution at −30 °C whereas cubic crystals of **2c** were obtained from acetonitrile. The results of the X-ray analyses are shown in Figure 1 and Figure 2.

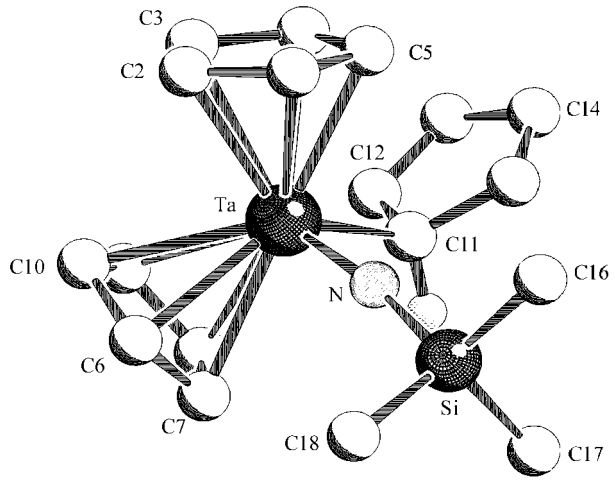

Figure 1. Molecular structure of **2b**; selected bond lengths [Å] and angles [°]: Ta−N(1) 1.796(7), Ta−C(11) 2.291(8), N(1)−Si 1.701(8), Ta−X(1) 2.168, Ta−X(2) 2.185, Ta−C(1) 2.449(9), Ta−C(2) 2.461(10), Ta−C(3) 2.523(9), Ta−C(4) 2.500(9), Ta−C(5) 2.438(9), Ta−C(6) 2.410(9), Ta−C(7) 2.457(9), Ta−C(8) 2.530(9), Ta−C(9) 2.547(10), Ta−C(10) 2.485(10), Ta−C(11) 229.1(8); Ta−N(1)−Si 171.9(5), X(1)−Ta−X(2) 125.9, X(1)−Ta−N(1) 111.7, X(1)−Ta−C(11) 117.0, X(2)−Ta−N(1) 111.3, X(2)−Ta−C(11) 102.8; X(1) is the centroid of the ring C(1)−C(5); X(2) is the centroid of the ring C(6)−C(10)

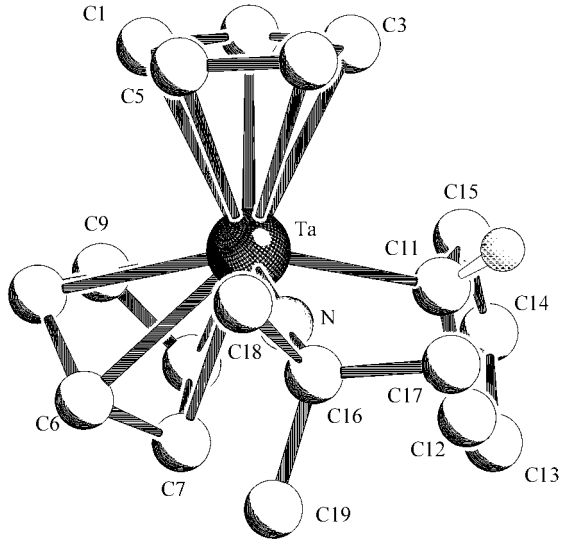

Figure 2. Molecular structure of **2c**; selected bond lengths [Å] and angles [°]: Ta−N(1) 1.761(5), Ta−C(11) 2.308(6), N(1)−C(16) 1.450(9), Ta−X(1) 2.199, Ta−X(2) 2.192, Ta−C(1) 2.510(7), Ta−C(2) 2.573(7), Ta−C(3) 2.525(6), Ta−C(4) 2.474(8), Ta−C(5) 2.417(8), Ta−C(6) 2.444(6), Ta−C(7) 2.447(7), Ta−C(8) 2.518(7), Ta−C(9) 2.570(7), Ta−C(10) 2.483(7), Ta−C(11) 2.308(6), Ta−N(1)−C(16) 175.2(5), X(1)−Ta−X(2) 124.2, X(1)−Ta−N(1) 113.1, X(1)−Ta−C(11) 102.3, X(2)−Ta−N(1) 112.3, X(2)−Ta−C(11) 107.2; X(1) is the centroid of the ring C(1)−C(5); X(2) is the centroid of the ring C(6)−C(10)

Both complexes **2b** and **2c** reveal a pseudotetrahedral coordination sphere at the tantalum atom defined by the centroids of two η^5-bonded cyclopentadienyl ligands X(1) and X(2), C(11) of the η^1-bonded cyclopentadienyl ring and the nitrogen atom N(1) of the imido ligand. They crystallize in different conformers with respect to the rotation about the Ta−C(11) bond. It is evident that the silylimido ligand, being less basic and also sterically less demanding than its carbon counterpart, forms a longer bond to the metal center: Ta−N(1)$SiMe_3$ 179.6(7) pm versus Ta−N(1)*t*Bu 176.1(5) pm. This is in agreement with the view that the dianion $[NSiMe_3]^{2-}$ is a weaker donor than $[NCMe_3]^{2-}$. The shorter Ta−N(1) bond of *tert*-butylimido complex **2c** corresponds with a longer distance Ta−C(11) 230.8(6) pm and longer distances of the tantalum atom to the centroids Ta−X(1) 219.9 and Ta−X(2) 219.2 pm of both η^5-C_5H_5 rings, whereas a longer Ta−N(2) bond of the silylimido complex **2b** corresponds with shorter distances Ta−C(11) 229.1(8), Ta−X(1) 216.8 and Ta−X(2) 218.5 pm. Steric ligand repulsion, but also the stronger σ,π-donor capability of the more π-basic alkylimido ligand, seem to be responsible for this trend. Due to the strong *trans* influence of the imido ligands Ta−C, the distances of the η^5-C_5H_5 ligands are not equivalent, the ones *trans* to Ta−N are longer. This is a typical structural feature of the imido half-sandwich complexes.[19] The angle between the ring centroids X(1)−Ta−X(2) of **2c** (124.2°) and **2b** (125.9°) are significantly smaller than in other bent tantalocenes.[6] This is probably due to steric repulsion. In both compounds **2b** and **2c** four ligands, with a potential for one σ- and two π-bonds and a maximum electron count of 6, are competing for π-interactions with a limited set of empty metal s, p and d orbitals. Orbital-symmetry restrictions are limiting the number of π-type interactions in a tetrahedral transition metal complex to five: two strong π-bonds are generated by the *e* set and three weaker π-bonds by the t_2 set of metal orbitals.[20] Four σ- and five π-bonding electron pairs would also be in agreement with the 18 valence electrons rule. If in a π-bond-saturated pseudo-tetrahedral molecule more than five orbitals of π-symmetry (p orbitals at N atoms or e_1-group orbitals of η^5-C_5H_5 rings) are available at the 4 ligands, electron density essentially remains in nonbonding orbitals (lone pairs) centered at the ligands, and only the strongest π-interactions dominate the π-bond regime.[21] Our structural data indicates that both dianionic $[NR]^{2-}$ ligands (R = $SiMe_3$, CMe_3) possess a stronger π-donor capability towards the relatively hard d^0-metal center than the more polarizable, softer and sterically more demanding ligand $[C_5H_5]^-$ that is released into a σ-bonding mode.

In π-bond-saturated complexes **2b**,**c** the Ta−N bond order, based on its length, is about 2. With respect to orbital symmetry and electron count considerations a higher Ta−N bond order is expected for the octahedral complex **4b**. In order to check this proposal, colorless cubic crystals of **4b** were grown from acetonitrile and submitted for an X-ray structural analysis. The molecular structure of **4b** is presented in Figure 3.

The tantalum center is octahedrally coordinated by three *fac*-binding nitrogen atoms of the Tp* ligand, by two chlorine atoms and one nitrogen atom of the silylimido ligand. The tantalum−imido bond Ta−N(1) 176.7(6) pm in **4b** is short compared with Ta−N(1) 179.6(7) pm in **2b**. This is in agreement with the assumption, that the silylimido ligand

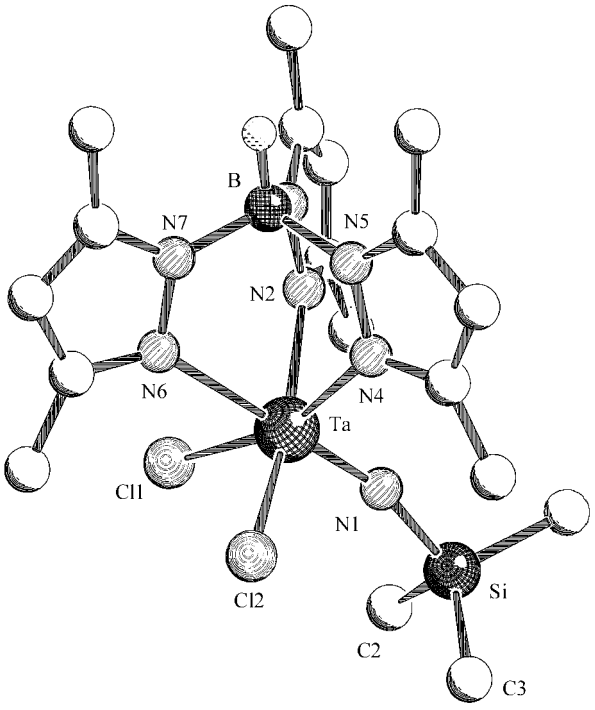

Figure 3. Molecular structure of **3b**; selected bond lengths [Å] and angles [°]: Ta−N(1) 1.767(6), Ta−N(2) 2.176(6), Ta−N(4) 2.201(6), Ta−N(6) 2.387(6), Ta−Cl(1) 2.373(2), Ta−Cl(2) 2.367(2), Si−N(1) 1.742(6), B−N(3) 1.550(11), B−N(5) 1.527(11), B−N(7) 1.515(12); Ta−N(1)−Si 164.8(4), N(1)−Ta−N(2) 97.9(3), N(1)−Ta−N(4) 97.8(3), N(1)−Ta−N(6) 179.5(3), N(1)−Ta−Cl(1) 96.8(2), N(1)−Ta−Cl(2) 96.29(19)

of [Tp*Ta(NSiMe$_3$)Cl$_2$] is more involved in π-bonding to the metal center than **2b**. The higher Ta−N bond order is a consequence of the lower π-bond saturation due to a weaker set of donor ligands in **4b**. It is worth noting that a shorter Ta−N bond corresponds with a longer N−Si bond: N(1)−Si 174.2(6) pm in **4b** vs. N(1)−Si 170.1(8) pm in **2b**. This is a result of an unequal competition of the electrophilic centers, the d^0-metal atom and the SiMe$_3$ substituent, for the electron density at the nitrogen atom of the nitrido bridge. The Ta−N−Si axis 164.8(4)° of **4b** deviates considerably from linearity, presumably a result of the steric requirement imposed by the bulky trimethylsilyl group and the Tp* ligand. Deviations from M−N−C linearity in the range 160−180° are not specific for the evaluation of bond orders.[21] There is no correlation of bond order and angle; e.g. the more π-saturated **2b** has a lower Ta−N bond order but a higher angle Ta−N(1)−Si(1) 171.9(5)°. The strong *trans* influence of the imido ligand is evident in the longer tantalum−pyrazol distance Ta−N(6) 238.7(6) pm *trans* to the imido ligand when compared with the *cis*-bonded pyrazol groups Ta−N(2) 217.6(6) pm and Ta−N(4) 220.1(6) pm. This is in agreement with other structurally characterized tris(pyrazolyl)borato complexes [Tp*Ta(NDip)Cl$_2$][22] and [Tp*Mo(N*t*Bu)$_2$Cl].[7]

Variable-Temperature NMR-Spectroscopic Studies

In solutions of π-bond-saturated complexes with σ- and π-bonded enyl ligands of the same type, ligand fluxionality is expected. The potential of the electronically flexible imido ligand to act as either a 4- or 6-electron donor [NR]$^{2-}$ should support the fluxional rearrangement of the σ- and π-bonded cyclopentadienyl ligands by lowering the energy barriers between the η^1-, η^3- and η^5-coordination modes. In agreement with the experiments of Green et al. on the related complex [(η^5-C$_5$H$_5$)$_2$Nb(NCMe$_3$)(η^1-C$_5$H$_5$)][13] variable-temperature ^{1}H-NMR spectroscopic studies, which are shown in Figure 4 and Figure 5, reveal the dynamic behavior of the cyclopentadienyl ligands in complexes **2b** and **2c**.

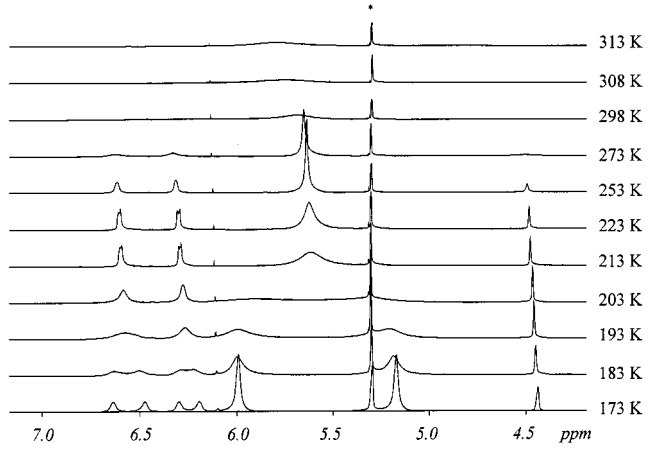

Figure 4. Variable-temperature ^{1}H NMR spectra of [(η^5-C$_5$H$_5$)$_2$Ta(NSiMe$_3$)(η^1-C$_5$H$_5$)] (**2b**) (400 MHz, CD$_2$Cl$_2$), showing the dynamic behavior of the C$_5$H$_5$ ligand; the asterisk denotes the solvent resonance

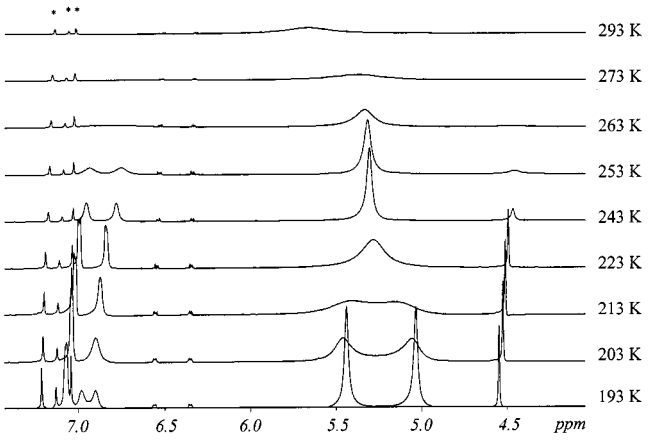

Figure 5. Variable-temperature ^{1}H NMR spectra of [(η^5-C$_5$H$_5$)$_2$Ta(N*t*Bu)(η^1-C$_5$H$_5$)] (**2c**) (400 MHz, [D$_8$]toluene), showing the dynamic behavior of the C$_5$H$_5$ ligand; the asterisks denote the solvent resonances

Three fluxional processes shown in Scheme 2 and Scheme 3 are observed for **2b** and **2c**: The rotation of the σ-C$_5$H$_5$ ligand about the Ta−C$_{ipso}$ bond, the metallotropic migration of the tantalum center between the σ-C$_5$H$_5$ ring

carbon atoms, and the σ,π-exchange of the cyclopentadienyl ligands.

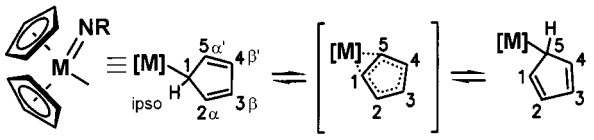

Scheme 2. 1,2-Metallotropic rearrangement by 1,5-sigmatropic shift of [M] (M = Nb, Ta)

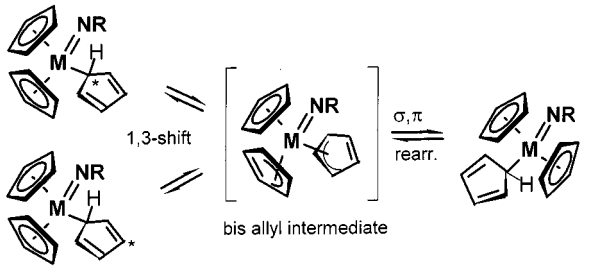

Scheme 3. 1,3-Shift of [M] and σ,π-rearrangement via the allyl intermediate (M = Nb, Ta)

In the slow-exchange-limiting ^{1}H NMR spectrum of **2b** at 173 K two resonances of the η^5-C_5H_5 ligands at δ = 6.02 and 5.20 and five resonances of the σ-C_5H_5 ligand at δ = 6.66, 6.50, 6.32, 6.22, 4.46 are separated. This is consistent with a hindered rotation about the Ta−C_{ipso} bond on the NMR time scale. The same separation is observed for *tert*-butylimido complex **2c** but at a higher coalescence temperature. Upon raising the temperature a pairwise coalescence of the signals of both η^5-C_5H_5 ligands and of the σ-C_5H_5 olefinic protons H_α, $H_{\alpha'}$, H_β, $H_{\beta'}$ is observed, while H_{ipso} remains unchanged, as expected for a system with free rotation about the Ta−C_{ipso} bond. Experimental data of dynamic exchange processes and their coalescence temperatures for complexes **2b** and **2c** are listed in Table 1. The assignment of H_α and $H_{\alpha'}$ is based on the assumption that due to their closer position to the tantalum center, their chemical shift difference will be larger than between H_β and $H_{\beta'}$.

There is a trend in that the three exchange processes originating from a hindered rotation about the Ta−C_{ipso} bond, have higher coalescence temperatures for *tert*-butylimido complex **2c** than for the silylimido complex **2b**. This is probably due to the higher degree of RN→M π-donation and to the greater steric demand of the *tert*-butylimido versus silylimido ligand. The free activation enthalpy of rotation about the Ta−C_{ipso} bond reveals $\Delta G^{\neq}(T_C)$ values in the range 37.5−40.6 kJmol^{-1} (**2b**) and 40.7−41.9 kJmol^{-1} (**2c**) depending on the type of exchanging nuclei chosen for this estimation (Table 1). These barriers are slightly lower than 43.4 kJ mol^{-1} reported by Green for the sterically slightly more hindered complex $[(\eta^5\text{-}C_5H_5)_2Nb(NCMe_3)(\eta^1\text{-}C_5H_5)]$.[13] It is evident that in the sterically less hindered silylimido complex **2b**, rotation is less hindered. On the other hand, the lower coalescence temperatures for the σ,π-exchange of silylimido complex **2b** suggests that the stronger donor $[NCMe_3]^{2-}$ promotes the ring slippage into an η^3- and finally the η^1-cyclopentadienyl bonding mode more readily than the weaker donor $[NSiMe_3]^{2-}$. In our complexes the migration of the tantalum atom between the carbon atoms of σ-C_5H_5 could occur by either a metallotropic 1,3-shift via such η^3-allyl intermediates or by a concerted 1,2-shift, a process that could also be envisaged as a symmetry-allowed 1,5-sigmatropic rearrangement. According to Cotton et al. a 1,2-shift mechanism will lead to a faster initial broadening of the resonances assigned to the H_α and $H_{\alpha'}$ resonances relative to the *ipso* hydrogen atom, while initial broadening of the resonances assigned to H_β and $H_{\beta'}$ would be indicative of a 1,3-shift mechanism. In agreement with our variable-temperature NMR spectra we favor the 1,2-shift mechanism. We are facing the same problem discussed for $[(\eta^5\text{-}C_5H_5)_2Nb(NCMe_3)(\eta^1\text{-}C_5H_5)]$[13] since we are not able to fully resolve the coupled fluxional processes associated with the Ta−C_{ipso} rotation on our NMR time scale in order to obtain quantitative results of the rate constants of the metallotropic migration.

Conclusion

A series of new silylimido niobium and -tantalum complexes of half-sandwich and metallocene type has been synthesized. To the best of our knowledge the donor strength of isoelectronically related trimethylsilyl- and *tert*-butylimido complexes has not been evaluated by experimental methods before. M−N bond lengths and, in a less pronounced manner, dynamic exchange of η^1- and η^5-coordinated cyclopentadienyl ligands in isoelectronic compounds of the formula $[(\eta^5\text{-}C_5H_5)_2M(NEMe_3)(\eta^1\text{-}C_5H_5)]$ (M = Nb, Ta; E = C, Si) indicate that *tert*-butylimido ligands are stronger donors than their silylimido counterparts. This might have been expected from the standpoint of N-basicity or proton affinity of the corresponding amines that is, to a certain extent, reflecting the donor strength of the ligand.

Table 1. Coalescence temperatures T_c, rate constants k and free activation enthalpies $\Delta G^0(T_C)$ for the Ta−C_{ipso} bond rotation process in **2b** and **2c**

Exchanging nuclei	$[(\eta^5\text{-}C_5H_5)_2Ta(NSiMe_3)(\eta^1\text{-}C_5H_5)]$ **2b**				$[(\eta^5\text{-}C_5H_5)_2Ta(N\textit{t}Bu)(\eta^1\text{-}C_5H_5)]$ **2c**			
	Δν [Hz]	T_c [K]	k [s^{-1}]	ΔG [kJmol^{-1}]	Δν [Hz]	T_c [K]	k [s^{-1}]	ΔG [kJmol^{-1}]
H_β, $H_{\beta'}$	40.0	193	177.7	38.3	32.0	203	142.2	40.7
H_α, $H_{\alpha'}$	64.0	193	284.3	37.5	64.0	213	284.3	41.6
η^5,η^5-C_5H_5	328.1	223	1457.7	40.6	164.1	223	729.1	41.9
η^5,η^1-C_5H_5	−	293±5	−	−		273±5	−	−

By this study we extend the series of isolobal, highly π-bond-saturated organometallic complexes of group-4 −7 metals with a set of competing cyclopentadienyl and imido ligands. The isolobal relationship among the complexes shown in Scheme 4 is based on the cyclopentadienyl imido ligand analogy.[3]

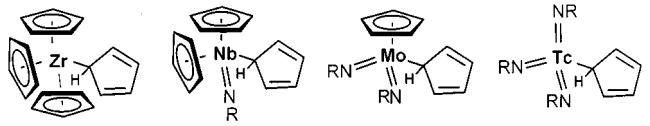

Atwood | Green (Nb) this study (Ta) | Sundermeyer (Mo, W) | Burrell

Scheme 4. Isolobally related π-bond-saturated molecules based on the cyclopentadienyl-imido ligand analogy; references: Atwood,[23] Green,[13] Sundermeyer,[24] Burrell[25]

Experimental Section

Materials and Methods: All manipulations were performed under dry argon 4.8. Solvents were rigorously dried, distilled and stored over 3 Å and 4 Å molecular sieves before use. All air-sensitive compounds were stored in glove boxes MB 150B-G-II and Lab Master 130 (MBraun) under nitrogen. − Melting points (uncorrected) were determined with a melting point apparatus Büchi-SMP 20. − The ^{1}H, ^{13}C and ^{29}Si NMR spectra were recorded with a Bruker ARX200, a Bruker AMX300 and a Bruker DRX400 at 25 °C if not indicated otherwise. All ^{13}C NMR spectra are proton-decoupled. The signals of solvents were used as internal standards for the ^{1}H and ^{13}C NMR spectra: CD_2Cl_2 (δ = 5.32; 54.2), $CDCl_3$ (δ = 7.24; 77.0), C_6D_6 (δ = 7.15; 128.0) and C_7D_8 (δ = 2.03; 20.4). Tetramethylsilane served as an external standard for the ^{29}Si NMR spectra. − The IR spectra were recorded with a Nicolet 510 M FT spectrometer. All solids were recorded as Nujol mulls between KBr plates. − Elemental analyses were performed in the microanalytical laboratories of the Chemistry Department at Marburg University. − EI mass spectra were recorded with a Varian MAT CH7 (70 eV) and APCI mass spectra were recorded with a Hewlett Packard HP 5989 B spectrometer. − The X-ray structure analyses were performed with an Enraf Nonius CAD4 diffractometer. Crystallographic data (excluding structure factors) for the structures reported in this paper have been deposited with the Cambridge Crystallographic Data Centre as supplementary publication no. CCDC-132475 (**2b**), -132476 (**2c**), and -132477 (**4b**). Copies of the data can be obtained free of charge on application to CCDC, 12 Union Road, Cambridge, CB2 1EZ, UK [Fax: (internat.) + 44-1223/336-033; E-mail: deposit@ccdc.cam.ac.uk]. Starting materials: Niobium and tantalum pentachloride were products of H. C. Starck GmbH & Co. KG. The following compounds were prepared as described in the literature: $Na(C_5H_5)$,[26] $Li(C_5Me_5)$,[27] $Me_3Si(C_5Me_5)$,[28] $LiN(SiMe_3)_2$,[29] KTp*,[30] $[(\eta^5\text{-}C_5Me_5)MCl_4]$,[14] $[M(NSiMe_3)Cl_3(py)_2]$ (M = Nb, Ta)[9].

$[(\eta^5\text{-}C_5H_5)_2Nb(NSiMe_3)Cl]$ (1a): A mixture of $[Nb(NSiMe_3)Cl_3(py)_2]$ (250 mg, 0.56 mmol) and NaC_5H_5 (104 mg, 1.18 mmol) was dissolved in 20 mL of THF at −78 °C. After 1 h, the temperature was allowed to reach 25 °C and the color of the mixture turned from yellow to brown. After 2 h of stirring, the volatiles were removed in vacuo. The brown residue was extracted into 25 mL of toluene and the solution was filtered. Part of the solvent of the filtrate was evaporated to leave 10 mL, which was layered with 7 mL of hexane and stored at −30 °C to afford **1a** as a yellow powder. Yield: 65 mg (0.19 mmol, 30%); m.p. 156 °C. − ^{1}H NMR (300 MHz, C_6D_6): δ = 0.02 [s, 9 H, $Si(CH_3)_3$], 5.81 (s, 10 H, C_5H_5). − ^{1}H NMR (200 MHz, $CDCl_3$): δ = − 0.03 [s, 9 H, $Si(CH_3)_3$], 6.14 (s, 10 H, C_5H_5). − ^{13}C NMR (75 MHz, C_6D_6): δ = 0.5 [s, $Si(CH_3)_3$], 112.5 (s, C_5H_5). − IR (Nujol): $\tilde{\nu}$ = 3086 vw, 1634 vw ν(C=C), 1377 s, 1262 m, 1246 s, 1078 vs ν(Nb=N−Si), 1067 vs, 951 w, 835 vs, 812 vs, 793 vs, 748 m, 687 w, 633 w cm^{-1}. − $C_{13}H_{19}ClNNbSi$ (345.75): calcd. C 45.16, H 5.54, N 4.05; found C 44.36, H 5.60, N 3.74. − EI-MS (70 eV, EI): *m/z* (%) = 346 (74) [M^+], 311 (12) [M^+ − Cl]. − APCI-MS (CH_3CN): *m/z* (%) = 346 (100) [M^+].

$[(\eta^5\text{-}C_5H_5)_2Ta(NSiMe_3)Cl]$ (1b): A mixture of $[Ta(NSiMe_3)Cl_3(py)_2]$ (250 mg, 0.47 mmol) and NaC_5H_5 (87 mg, 0.99 mmol) was dissolved in 25 mL of THF at −78 °C. After 2 h, the temperature was allowed to reach 25 °C and the color of the mixture turned brown. After 2 h of stirring, the volatiles were removed in vacuo. The brown residue was extracted into 30 mL of *n*-hexane, the solution was filtered and reduced in volume. **1b** was obtained at −30 °C as a yellow powder. Yield: 100 mg (0.23 mmol, 45%); m.p. 145 °C. − ^{1}H NMR (200 MHz, C_6D_6): δ = − 0.09 [s, 9 H, $Si(CH_3)_3$], 5.78 (s, 10 H, C_5H_5). − ^{1}H NMR (300 MHz, $CDCl_3$): δ = − 0.06 [s, 9 H, $Si(CH_3)_3$], 6.13 (s, 10 H, C_5H_5). − ^{13}C NMR (75 MHz, $CDCl_3$): δ = 1.5 [s, $Si(CH_3)_3$], 111.4 (s, C_5H_5). − ^{29}Si NMR (78 MHz, C_6D_6): δ = −2.3 [s, $Si(CH_3)_3$]. − IR (Nujol): $\tilde{\nu}$ = 3137 vw, 3122 w, 3082 w, 1638 vw, 1611 m ν(C=C), 1528 m, 1456 vs, 1435 vs, 1395 w, 1377 s, 1368 s, 1261 s, 1244 s, 1113 vs ν(Ta=N−Si), 1080 vs, 1026 vs, 920 m, 855 br, 801 br, 745 vs, 706 vs, 631 vs, 606 m cm^{-1}. − $C_{13}H_{19}ClNSiTa$ (433.79): calcd. C 35.99, H 4.41, N 3.23; found C 35.99, H 4.98, N 3.01. − EI-MS (70 eV): *m/z* (%) = 433 (55) [M^+], 418 (100) [M^+ − CH_3].

$[(\eta^5\text{-}C_5H_5)_2Nb(NSiMe_3)(\sigma\text{-}C_5H_5)]$ (2a): A mixture of $[Nb(NSiMe_3)Cl_3(py)_2]$ (300 mg, 0.68 mmol) and an excess of NaC_5H_5 (595 mg, 6.75 mmol) was dissolved in 25 mL of THF at −78 °C. After 2 h, the temperature was allowed to reach 25 °C. After 2 h of stirring at 25 °C, the volatiles of the light-brown reaction mixture were removed completely and the residue was extracted into 30 mL of *n*-hexane. The solution was filtered and reduced in volume to 7 mL and stored for 1 week at −30 °C to give **2a** as a yellow, microcrystalline solid. Yield: 100 mg (0.27 mmol, 30%); m.p. 132 °C. − ^{1}H NMR (400 MHz, CD_2Cl_2, 298 K): δ = 0.01 [s, 9 H, $NSi(CH_3)_3$], 5.64 (br. s, 10 H, $\eta^5\text{-}C_5H_5$), 6.27 (br. s, 5 H, $\eta^1\text{-}C_5H_5$). − ^{1}H NMR (400 MHz, CD_2Cl_2, 173 K): δ = −0.11 [s, 9 H, $NSi(CH_3)_3$], 5.09 (br. s, 5 H, $\eta^5\text{-}C_5H_5$), 5.14 (br. s, 1 H, C-H_{ipso}), 5.99 (br. s, 5 H, $\eta^5\text{-}C_5H_5$), 6.26 (m, br, 2 H, C-$H_{\beta,\beta'}$), 6.49 and 6.61 (m, 2 H, C-$H_{\alpha,\alpha'}$). − ^{13}C NMR (75 MHz, CD_2Cl_2, 298 K): δ = 1.5 [s, $NSi(CH_3)_3$], 111.0 (s, $\eta^5\text{-}C_5H_5$), 132.9 (br. s, $C_{\beta,\beta'}$), 133.9 (br. s, $C_{\alpha,\alpha'}$), C_{ipso} is not observed. − ^{13}C NMR (100 MHz, CD_2Cl_2, 173 K): δ = 0.3 [s, $NSi(CH_3)_3$], 55.5 (s, C_{ipso}), 109.0 and 110.7 (br. s, $\eta^5\text{-}C_5H_5$), 121.15 and 119.4 (br. s, $C_{\beta,\beta'}$), 136.3 and 141.0 (br. s, $C_{\alpha,\alpha'}$). − IR (Nujol): $\tilde{\nu}$ = 3102 m, 3079 m, 3065 w, 1624 vw, 1607 m ν(C=C), 1383 s, 1366 m, 1300 w, 1262 vs, 1244 vs, 1128 vw, 1080 vs ν(Nb=N−Si), 1030 vs, 972 m, 909 vw, 883 s, 835 vs, 801 vs, 752 s, 737 vs, 714 s, 693 w, 685 w, 633 m, 625 m, 611 vw cm^{-1}. − $C_{18}H_{24}NNbSi$ (375.39): calcd. C 57.59, H 6.44, N 3.73; found C 57.22, H 6.23, N 3.44. − EI-MS (70 eV): *m/z* (%) = 375 (26) [M^+], 310 (37) [M^+ − C_5H_5].

$[(\eta^5\text{-}C_5H_5)_2Ta(NSiMe_3)(\sigma\text{-}C_5H_5)]$ (2b): **2b** was prepared analogously to **2a** by treating $[Ta(NSiMe_3)Cl_3(py)_2]$ (300 mg, 0.56 mmol) with NaC_5H_5 (496 mg, 5.63 mmol). The reaction time was 20 h at 25 °C. Yellow needles of **2b** were obtained from *n*-hexane at −30 °C. Yield: 100 mg (0.216 mmol, 38%); m.p. 135 °C. − ^{1}H NMR (400 MHz, CD_2Cl_2, 298 K): δ = −0.01 [s, 9 H, $NSi(CH_3)_3$], 5.71

(br. s, 10 H, η^5-C_5H_5), 5.91 (br. s, 5 H, η^1-C_5H_5). − ^{1}H NMR (400 MHz, CD_2Cl_2, 173 K): δ = −0.13 [s, 9 H, NSi(CH_3)$_3$], 4.46 (br. s, 1 H, C-H_{ipso}), 5.20 (br. s, 5 H, η^5-C_5H_5), 6.02 (br. s, 5 H, η^5-C_5H_5), 6.22 and 6.32 (m, br, 2 H, C-$H_{\beta,\beta'}$), 6.50 and 6.66 (m, 2 H, C-$H_{\alpha,\alpha'}$). − ^{13}C NMR (100 MHz, CD_2Cl_2, 233 K): δ = 1.3 [s, NSi(CH_3)$_3$], 57.2 (s, C_{ipso}), 108.8 (s, η^5-C_5H_5), 122.4 (br. s, $C_{\beta,\beta'}$), 141.4 (br. s, $C_{\alpha,\alpha'}$). − ^{13}C NMR (100 MHz, CD_2Cl_2, 173 K): δ = 0.7 [s, NSi(CH_3)$_3$], 56.3 (s, C_{ipso}), 106.6 and 107.7 (br. s, η^5-C_5H_5), 120.8 and 122.5 (br. s, $C_{\beta,\beta'}$), 138.1 and 143.5 (br. s, $C_{\alpha,\alpha'}$) − ^{29}Si NMR (78 MHz, C_6D_6): δ = −4.9 [s, Si(CH_3)$_3$]. − IR (Nujol): $\tilde{\nu}$ = 3103 vw, 3080 w, 3064 vw, 1634 w ν(C=C), 1441 vw, 1398 m, 1261 s, 1244 vs, 1117 vs ν(Ta=N−Si), 1086 s, 1023 vs, 969 m, 910 m, 818 vs, br, 742 vs, 714 m, 630 m cm^{-1} − $C_{18}H_{24}ClNSiTa$ (463.43): calcd. C 46.65, H 5.22, N 3.02; found C 46.18, H 5.72, N 3.01 − EI-MS (70 eV): *m*/*z* (%) = 463 (78) [M^+], 398 (60) [M^+ − C_5H_5], 383 (100) [M^+ − C_5H_5−CH_3].

X-ray Structure Analysis of 2b:[31] $C_{18}H_{24}NSiTa$, M_r = 463.43, tetragonal, space group $P4_2/n$ (no. 105), $a = b$ = 19.978(1), c = 8.868(1) Å, V = 3539.7(4) Å^3, Z = 8, $\rho_{calcd.}$ = 1.739 g cm^{-3}, λ(Mo-K_α) = 0.71073 Å, μ = 6.272 mm^{-1}, T = 203(2) K. A pale yellow crystal 0.60 × 0.20 × 0.20 mm was used to record 2791 intensities to θ = 24.96°, of which 2637 ($R_{int.}$ = 0.0788) were unique and 2229 were observed [$I > 2\sigma(I)$]. An empirical absorption correction was applied on the basis of ψ-scans, with the transmission minimum at 36.7%. The structure was solved by direct methods (SHELXS-97) and subjected to full-matrix least-squares refinement on F^2 (SHELXL-97). All non-hydrogen atoms were refined anisotropically; H atoms were geometrically positioned (riding model) with a 1.5-fold isotropic U value of the equivalent U value of the corresponding C atom. Refinement proceeded with 198 parameters to R = 0.0509; wR_2 = 0.1485 for all data, GooF = 1.045; w^{-1} = [$\sigma^2(F_o^2)$ + (0.1114P)^2 + 8.3375P] where P = [F_o^2 + 2F_c^2]/3; maximum/minimum residual electron densities 2.356/−1.213 e/Å^3.

[(η^5-C_5H_5)$_2$Ta(N*t*Bu)(σ-C_5H_5)] (2c): [Ta(N*t*Bu)Cl$_3$(py)$_2$] (300 mg, 0.58 mmol) and 3.5 equiv. of NaC_5H_5 (181 mg, 2.03 mmol) were dissolved in 30 mL of THF at −78 °C. The stirred mixture was allowed to reach 25 °C within 2 h and stirred for another 20 h at this temperature. Volatiles were removed in vacuo, the product extracted into 30 mL of *n*-hexane and insoluble material was removed by decanting the solution after centrifugation. After reducing the volume of the solvent, cubic crystals of **2c** crystallized at −30 °C. Yield: 180 mg, (0.40 mmol, 70%); m.p. 125 °C. − ^{1}H NMR (400 MHz, C_7D_8, 263 K): δ = 0.97 [s, 9 H, NC(CH_3)$_3$], 4.38 (br. s, 1 H, C-H_{ipso}), 5.24 (s, 10 H, η^5-C_5H_5), 6.65 (br. s, 4 H, C-$H_{\alpha,\alpha',\beta,\beta'}$). − ^{1}H NMR (400 MHz, C_7D_8, 193 K): δ = 1.00 [s, 9 H, NC(CH_3)$_3$], 4.45 (br. s, 1 H, C-H_{ipso}), 4.93 (br. s, 5 H, η^5-C_5H_5), 5.34 (br. s, 5 H, η^5-C_5H_5), 6.80 and 6.88 (s, 2 H, C-$H_{\beta,\beta'}$), 6.94 and 7.10 (s, 2 H, C-$H_{\alpha,\alpha'}$). − ^{13}C NMR (75 MHz, C_6D_6, 298 K): δ = 32.3 [s, NC(CH_3)$_3$], 66.1 [s, NC(CH_3)$_3$], 107.0−117.6 (br. s, η^5-C_5H_5 and η^1-C_5H_5). − IR (Nujol): $\tilde{\nu}$ = 3104 vw, 3082 w, 3069 vw, 1630 vw, 1611 m, ν(C=C), 1541 vw, 1524 vw, 1449 vs, 1439 vs, 1385 s, 1366 m, 1352 vs, 1262 vs, br, 1211 vs ν(Ta=N−C), 1086 vs, br, 1025 vs, br, 970 vs, 899 vs, 792 vs, br, 739 vs, 714 s, 631 s, 544 m, 527 vs cm^{-1} − $C_{19}H_{24}NTa$ (447.36): calcd. C 51.01, H 5.41, N 3.13; found C 50.94, H 5.39, N 3.12 − EI-MS (70 eV): *m*/*z* (%) = 447.0 (17) [M^+], 382 (5) [M^+ − C_5H_5], 367 (60) [M^+ − C_5H_5−CH_3].

X-ray Structure Analysis of 2c:[31] $C_{19}H_{24}NTa$, M_r = 447.36, tetragonal, space group $I4_1/amd$ (no. 141), $a = b$ = 19.7571(8), c = 8.6796(8) Å, V = 3388.0(4) Å^3, Z = 8, $\rho_{calcd.}$ = 1.754 g cm^{-3}, λ(Mo-K_α) = 0.71073 Å, μ = 6.482 mm^{-1}, T = 197(2) K. A yellow cubic crystal 0.30 × 0.20 × 0.20 mm was used to record 3627 intensities to θ = 26.26°, of which 3426 ($R_{int.}$ = 0.0432) were unique and 2903 were observed [$I > 2\sigma(I)$]. An empirical absorption correction was applied on the basis of ψ-scans, with the transmission minimum at 24.7%. The structure was solved by direct methods (SHELXS-97) and subjected to full-matrix least-squares refinement on F^2 (SHELXL-97). All non-hydrogen atoms were refined anisotropically; H atoms were geometrically positioned (riding model) with a 1.5-fold isotropic U value of the equivalent U value of the corresponding C atom. Refinement proceeded with 183 parameters to R = 0.0464; wR_2 = 0.1236 for all data, GooF = 1.098; w^{-1} = [$\sigma^2(F_o^2)$ + (0.1776P)^2 + 64.5121P] where P = [F_o^2 + 2F_c^2]/3; maximum/minimum residual electron densities 1.055/−3.939e/Å^3.

[(η^5-C_5Me_5)Nb(NSiMe$_3$)Cl$_2$] (3a): [(η^5-C_5Me_5)NbCl$_4$] (250 mg, 0.68 mmol) and LiN(SiMe$_3$)$_2$ (124 mg, 0.74 mmol) were suspended in 30 mL of toluene at room temperature. The color immediately changed from yellow to green. The suspension was treated with ultrasound (40 h/40 °C water bath). LiCl and other insoluble material were removed by centrifugation. The solvent was completely removed in vacuo and the yellow residue dissolved in 10 mL of *n*-hexane. At −30 °C the crystalline product **3a** precipitated. Yield: 85 mg (0.22 mmol, 30%); m.p. 165 °C. − ^{1}H NMR (300 MHz, C_6D_6): δ = 0.18 [s, 9 H, NSi(CH_3)$_3$], 1.93 [s, 15 H, C_5(CH_3)$_5$]. − ^{13}C NMR (75 MHz, C_6D_6): δ = 1.9 [s, Si(CH_3)$_3$], 12.7 [s, C_5(CH_3)$_5$], 120.6 [s, C_5(CH_3)$_5$]. − IR (Nujol): $\tilde{\nu}$ = 3148 m, br, 1618 w ν(C=C), 1306 w, 1262 vs, 1093 vs, br ν(Nb=N−Si), 1020 vs, 974 w, 918 w, 876 w, 845 m, 801 s, 723 m, 588 w cm^{-1} − $C_{13}H_{24}Cl_2NNbSi$ (386.24): calcd. C 40.42, H 6.26, N 3.63; found C 40.97, H 5.47, N 4.41 − EI-MS (70 eV): *m*/*z* (%) = 355 (2) [M^+ − 2CH_3] − APCI-MS (CH_3CN): *m*/*z* (%) = 387 (8) [M^+], 315 (100) [M^+ − 2Cl].

[(η^5-C_5Me_5)Ta(NSiMe$_3$)Cl$_2$] (3b): 3b was synthesized analogously to **3a** from [(η^5-C_5Me_5)$TaCl_4$] (250 mg, 0.55 mmol) and LiN(SiMe$_3$)$_2$ (101 mg, 0.60 mmol). Yellow microcrystalline **3b** precipitated from *n*-hexane at −30 °C. Yield: 100 mg (40 mg, 0.08 mmol) of **3b**; m.p. 202 °C. − ^{1}H NMR (300 MHz, C_6D_6): δ = 0.18 [s, 9 H, NSi(CH_3)$_3$], 1.93 [s, 15 H, C_5(CH_3)$_5$]. − ^{13}C NMR (75 MHz, C_6D_6): δ = 2.4 [s, NSi(CH_3)$_3$], 11.7 [s, C_5(CH_3)$_5$], 121.9 [s, C_5(CH_3)$_5$] − ^{29}Si NMR (78 MHz, C_6D_6): δ = −2.4 [s, NSi(CH_3)$_3$]. − IR (Nujol): $\tilde{\nu}$ = 3110 m, br, 3050 m, br, 1617 w ν(C=C), 1262 vs, 1080 vs, br ν(Ta=N−Si), 1022 vs, br, 862 s, 799 vs, br, 702 s, 687 s, 662 s, 631 m, 588 w cm^{-1} − $C_{13}H_{24}Cl_2NSiTa$ (474.28): calcd. C 32.92, H 5.10, N 2.95; found C 34.93, H 5.58, N 2.94 − EI-MS (70 eV): *m*/*z* (%) = 439 (2) [M^+ − Cl], 330 (100) [M^+ − Cl−Me_3SiCl].

[Tp*Nb(NSiMe$_3$)Cl$_2$] (4a): To 300 mg (0.68 mmol) of [Nb(NSiMe$_3$)Cl$_3$(py)$_2$] and 231 mg (0.69 mmol) of KTp* was added 30 mL of THF at −78 °C. After warming up (1 h) the solution, it was stirred for 1 d at 25 °C and the solvent completely removed in vacuo. The residue was extracted into 30 mL of toluene, and KCl and other insoluble side products were separated by filtration. Toluene was removed in vacuo and the residue crystallized from MeCN at −30 °C to give yellow cubic crystals of **4a**. Yield: 315 mg (0.58 mmol, 85%); m.p. 296 °C. − ^{1}H NMR (300 MHz, C_6D_6): δ = 0.40 [s, 9 H, NSi(CH_3)$_3$], 1.87 [s, 6 H, pz_A-C(5)−CH_3], 2.09 [s, 3 H, pz_B-C(5)−CH_3], 2.64 [s, 6 H, pz_A-C(3)−CH_3], 2.87 [s, 3 H, pz_B-C(3)−CH_3], 5.31 [s, 2H pz_A, C(4)-H], 5.54 [s, 1 H, pz_B-C(4)-H]. − ^{13}C NMR (75 MHz, C_6D_6): δ = 1.4 [s, NSi(CH_3)$_3$], 12.2 [s, pz_B-C(5)-CH_3], 12.5 [s, pz_A-C(5)-CH_3], 15.0 [s, pz_B-C(3)-CH_3], 16.6 [s, pz_B-C(3)-CH_3], 107.1 [s, pz_A, C(4)], 107.6 [s, pz_B, C(4)], 142.9 [s, pz_A, C(3)], 145.8 [s, pz_B, C(3)], 152.7 [s, pz_A, C(5)], 153.8 [s, pz_B, C(5)]. − IR (Nujol): $\tilde{\nu}$ = 3339 m ν(C−H_{pz}), 3288 m, br, 3130 m, 2733 w, 2542 vs ν(B−H), 2362 w, 2212 w, 1572 s, 1541 vs ν(C−N_{pz}), 1524 m, 1381 vs, 1366 vs, 1252 vs, 1202 vs, 1090 vs, br ν(Nb=

N−Si), 1043 vs, 982 s, 941 s, 841 vs,br, 799 vs, br, 777 s, 694 s, 662 s, 596 vw, 522 m, 478 s cm^{-1} − $C_{18}H_{31}BCl_2NNbSi$ (548.21): calcd. C 39.44, H 5.70, N 17.89; found C 39.27, H 5.80, N 17.47 − EI-MS (70 eV): *m*/*z* (%) = 547 (19) [M^+], 532 (13) [$M^+ - CH_3$], 511 (100) [$M^+ - Cl$].

[Tp*Ta(NSiMe$_3$)Cl$_2$] (4b): 4b was synthesized analogously to **4a** from [Ta(NSiMe$_3$)Cl$_3$(py)$_2$] (300 mg, 0.56 mmol) and KTp* (193 mg, 0.57 mmol). Colorless cubic crystals were obtained at −30 °C from MeCN. Yield: 250 mg (0.39 mmol, 70%); m.p. 310 °C. − ^{1}H NMR (300 MHz, C_6D_6): δ = 0.44 [s, 9 H, NSi(CH_3)$_3$], 1.83 [s, 6 H, pz$_A$-C(5)−CH_3], 2.05 [s, 3 H, pz$_B$-C(5)−CH_3], 2.70 [s, 6 H, pz$_A$-C(3)−CH_3], 2.86 [s, 3 H, pz$_B$-C(3)−CH_3], 5.29 [s, 2H pz$_A$, C(4)-*H*], 5.65 [s, 1 H, pz$_B$-C(4)-*H*]. − ^{13}C NMR (75 MHz, C_6D_6): δ = 1.5 [s, NSi(*C*H$_3$)$_3$], 12.2 [s, pz$_B$-C(5)-*C*H$_3$], 12.4 [s, pz$_A$-C(5)-*C*H$_3$], 15.3 [s, pz$_B$-C(3)-*C*H$_3$], 17.0 [s, pz$_B$-C(3)-*C*H$_3$], 107.6 [s, pz$_A$, *C*(4)], 108.0 [s, pz$_B$, *C*(4)], 143.7 [s, pz$_B$, *C*(3)], 146.0 [s, pz$_A$, *C*(3)], 153.9 [s, pz$_A$, *C*(5)], 154.4 [s, pz$_B$, *C*(5)] − ^{29}Si NMR (78 MHz, C_6D_6): δ = −1.5 [s, N*Si*(CH$_3$)$_3$]. − IR (Nujol): $\tilde{\nu}$ = 3288 m ν(C−H$_{pz}$), 3130 m, br, 2544 vs ν(B−H), 2362 vw, 2226 w, 1574 m, 1545 vs ν(C−N$_{pz}$), 1451 vs, 1414 vs, 1383 vs, 1366 vs, 1250 vs, 1215 m, 1202 vs, 1123 vs, br, 1074 vs ν(Ta=N−Si), 1044 vs, 982 m, 941 s, 847 vs, br, 801 vs, br, 694 m, 662 m cm^{-1} − $C_{18}H_{31}BCl_2NSiTa$ (636.25): C 33.98, H 4.91, N 15.41; found C 33.75, H 5.02, N 15.33 − EI-MS (70 eV): *m*/*z* (%) = 635 (61) [M^+], 620 (100) [$M^+ - CH_3$].

X-ray Structure Analysis of 4b:[31] $C_{22}H_{31}BCl_2N_9SiTa$, M_r = 447.36, triclinic, space group $P\bar{1}$ (no. 2), a = 10.075(2), b = 10.256(2), c = 15.635(4) Å, α = 79.29(2), β = 80.17(2), γ = 82.30(2)°, V = 1555.5(4) Å^3, Z = 2, $\rho_{calcd.}$ = 1.521 g cm^{-3}, λ(Mo-K_α) = 0.71073 Å, μ = 3.771 mm^{-1}, T = 193(2) K. A yellow cubic crystal 0.40 × 0.20 × 0.10 mm was used to record 6115 intensities to θ = 24.97°, of which 5449 ($R_{int.}$ = 0.0595) were unique and 2229 were observed [$I > 2\sigma(I)$]. An empirical absorption correction was applied on the basis of ψ-scans, with the transmission minimum at 70.4%. Structure solution and refinement: The structure was solved by direct methods (SHELXS-97) and subjected to full-matrix least-squares refinement on F^2 (SHELXL-97). All non-hydrogen atoms were refined anisotropically; H atoms were geometrically positioned (riding model) with a 1.5-fold isotropic U value of the equivalent U value of the corresponding C atom. Refinement proceeded with 198 parameters to R = 0.0493; wR_2 = 0.1043 for all data, GooF = 1.002, $w^{-1} = [\sigma^2(F_o^2) + (0.0522P)^2]$ where $P = [F_o^2 + 2F_c^2]/3$; maximum/minimum residual electron densities 1.075/−1.530 e/Å^3.

Acknowledgments

We gratefully acknowledge support of this work by the Deutsche Forschungsgemeinschaft, Schwerpunktprogramm "Nitridobrücken", Grant Su 127/6−3 and by the Fonds der Chemischen Industrie. We also thank H. C. Starck GmbH & Co. KG for a donation of $NbCl_5$ and $TaCl_5$.

[1] [1a] W. A. Nugent, J. M. Mayer, *Metal-Ligand Multiple Bonds*, Wiley, New York, **1988**. − [1b] D. E. Wigley, *Progr. Inorg. Chem.*, Vol. 42, (Ed.: K. D. Karlin), Wiley, New York, **1994**, pp 239−482.

[2] [2a] D. N. Williams, J. P. Mitchell, A. D. Poole, U. Siemeling, W. Clegg, D. C. R. Hockless, P. A. O'Neil, V. C. Gibson, *J. Chem. Soc. Dalton Trans.* **1992**, 739−751. − [2b] A. D. Poole, V. C. Gibson, W. Clegg, *J. Chem. Soc., Chem. Commun.* **1992**, 237−239. − [2c] U. Siemeling, V. C. Gibson, *J. Organomet. Chem.* **1992**, *426*, C25−C27. − [2d] J. K. Cockcroft, V. C. Gibson, J. A. K. Howard, A. D. Poole, U. Siemeling, C. Wilson, *J. Chem. Soc. Chem. Commun.* **1992**, 1668−1669.

[3] Selected references for cyclopentadienyl imido complex analogy: [3a] D. S. Williams, M. H. Schofield, J. T. Anhaus, R. R. Schrock, *J. Am. Chem. Soc.* **1990**, *112*, 6728−6729. − [3b] D. S. Williams, M. H. Schofield, R. R. Schrock, *Organometallics* **1993**, *12*, 4560−4571. − [3c] V. C. Gibson, *J. Chem. Soc., Dalton Trans.* **1994**, 1607−1618. − [3d] J. Sundermeyer, D. Runge, *Angew. Chem.* **1994**, *106*, 1328−1331; *Angew. Chem. Int. Ed. Engl.* **1994**, *33*, 1255−1257. − [3e] D. S. Glueck, J. C. Green, R. I. Michelman, I. N. Wright, *Organometallics* **1992**, *11*, 4221−4225.

[4] [4a] M. P. Coles, C. I. Dalby, V. C. Gibson, I. R. Little, E. L. Marshall, M. H. Ribeiro da Costa, S. Mastroianni, *J. Organomet. Chem.* **1999**, *591*, 78−87. − [4b] D. M. Antonelli, A. Leins, J. M. Stryker, *Organometallics* **1997**, *16*, 2500−2502. − [4c] S. Scheuer, J. Fischer, J. Kress, *Organometallics* **1995**, *14*, 2627−2629. − [4d] M. P. Coles, C. I. Dalby, V. C. Gibson, W. Clegg, M. R. J. Elsegood, *J. Chem. Soc., Chem. Commun.* **1995**, 1709−1711. − [4e] D. S. La, J. B. Alexander, D. R. Cefalo, D. D. Graf, A. H. Hoveyda, R. R. Schrock, *J. Am. Chem. Soc.* **1998**, *120*, 9720−9721. − [4f] R. R. Schrock, *Acc. Chem. Res.* **1990**, *23*, 158−165. − [4g] E. A. Kretzschmar, J. Kipke, J. Sundermeyer, *Chem. Commun.* **1999**, 2381−2382.

[5] [5a] S. Schmidt, J. Sundermeyer, *J. Organomet. Chem.* **1994**, *472*, 127−138. − [5b] V. C. Gibson, D. N. Williams, W. Clegg, D. C. R. Hockless, *Polyhedron* **1989**, *8*, 1819−1820. − [5c] M. Jolly, J. P. Mitchell, V. C. Gibson, *J. Chem. Soc., Dalton Trans.* **1992**, 1331−1332. − [5d] D. M. Antonelli, M. L. H. Green, P. Mountford, *J. Organomet. Chem.* **1992**, *438*, C4−C8. − [5e] A. D. Poole, D. N. Williams, A. M. Kenwright, V. C. Gibson, W. Clegg, D. C. R. Hockless, P. A. O'Neil, *Organometallics* **1993**, *12*, 2549−2555. − [5f] C. D. Wood, S. J. McLain, R. R. Schrock, *J. Am. Chem. Soc.* **1979**, *101*, 3210−3222. − [5g] M. R. Churchill, H. J. Wasserman, P. A. Belmonte, R. R. Schrock, *Organometallics* **1982**, *1*, 559−561. − [5h] J. M. Mayer, C. J. Curtis, J. E. Bercaw, *J. Am. Chem. Soc.* **1983**, *105*, 2651−2660. − [5i] M. P. Coles, C. I. Dalby, V. C. Gibson, I. R. Little, E. L. Marshall, M. H. Ribeiro da Costa, S. Mastroianni, *J. Organomet. Chem.* **1999**, *591*, 78−87. − [5j] M. I. Alcalde, M. P. Gomez-Sal, P. Royo, *Organometallics* **1999**, *18*, 546−554. − [5k] L. Djakovitch, W. A. Herrmann, *J. Organomet. Chem.* **1998**, *562*, 71−78. − [5l] W. A. Herrmann, W. Baratta, E. Herdtweck, *Angew. Chem.* **1996**, *108*, 2098−2100; *Angew. Chem. Int. Ed. Engl.* **1996**, *35*, 1951−1953.

[6] [6a] D. M. Antonelli, W. P. Schaefer, G. Parkin, J. E. Bercaw, *J. Organomet. Chem.* **1993**, *462*, 213−220. − [6b] A. Antinolo, S. Garcia-Lledo, J. Martinez de Ilarduya, A. Otero, *J. Organomet. Chem.* **1987**, *335*, 85−90. − [6c] R. E. Blake, Jr., D. M. Antonelli, L. M. Henling, W. P. Schaefer, K. I. Hardcastle, J. E. Bercaw, *Organometallics* **1998**, *17*, 718−725. − [6d] A. Antinolo, P. Espinosa, M. Fajardo, P. Gómez-Sal, C. López-Mardomingo, A. Martin-Alonso, A. Otero, *J. Chem. Soc., Dalton Trans.* **1995**, 1007−1013. − [6e] A. Antinolo, F. Carillo-Hermosilla, A. Otero, M. Fajardo, A. Garcés, P. Gómez-Sal, C. López-Mardomingo, A. Martin, C. Miranda, *J. Chem. Soc., Dalton Trans.* **1998**, 59−65.

[7] [7a] J. Sundermeyer, J. Putterlik, M. Foth, J. S. Field, N. Ramesar, *Chem. Ber.* **1994**, *127*, 1201−1212. − [7b] A. Antinolo, F. Caprillo-Hermosilla, J. Fernández-Baeza, M. Lanfranchi, A. Lara-Sánchez, A. Otero, E. Palomares, M. A. Pellinghelli, A. M. Rodriguez, *Organometallics* **1998**, *17*, 3015−3019.

[8] [8a] D. C. Bradley, M. B. Hursthouse, K. M. A. Malik, A. J. Nielson, G. B. Chota Vuru, *J. Chem. Soc., Dalton Trans.* **1984**, 1069−1072. − [8b] A. Antinolo, A. Otero, F. Urbanos, S. Garcia-Blanco, S. Martinez-Carrera, J. Sanz-Aparicio, *J. Organomet. Chem.* **1988**, *350*, 25−34. − [8c] H. C. L. Abbenhuis, N. Feiken, D. M. Grove, J. T. B. H. Jastrzebski, J. Kooijman, P. van der Sluis, W. J. J. Smeets, A. L. Spek, G. van Koten, *J. Am. Chem. Soc.* **1992**, *114*, 9773−9781.

[9] C. M. Jones, M. E. Lerchen, C. J. Church, B. M. Schomber, N. M. Doherty, *Inorg. Chem.* **1990**, *29*, 1679−1682.
[10] N. J. Bailey, J. A. Cooper, H. Gailus, M. L. H. Green, J. T. James, M. A. Leech, *J. Chem. Soc., Dalton Trans.* **1997**, 3579−3584.
[11] [11a] N. M. Doherty, S. C. Critchlow, *J. Am. Chem. Soc.* **1987**, *109*, 7906−7908. − [11b] S. C. Critchlow, M. E. Lerchen, R. C. Smith, N. M. Doherty, *J. Am. Chem. Soc.* **1988**, *110*, 8071−8075. − [11c] S. C. Critchlow, R. C. Smith, N. M. Doherty, in *Atomic and Molecular Processing of Electronic and Ceramic Materials: Preparation, Characterization, and Properties*; (Eds.: I. A. Aksay, G. L. McVay, T. G. Stoebe, J. F. Wager), Material Research Society: Pittsburgh, PA, **1988**, 153−158. − [11d] C. E. Pohl-Ferry, J. W. Ziller, N. M. Doherty, *J. Chem. Soc. Chem. Commun.* **1999**, 1815−1816.
[12] A. Antinolo, M. Fajardo, C. Huertas, A. Otero, S. Prashar, A. M. Rodriguez, *J. Organomet. Chem.* **1999**, *585*, 154−161.
[13] M. L. H. Green, D. M. Michaelidou, P. Mountford, A. G. Suarez, L.-L. Wong, *J. Chem. Soc., Dalton Trans.* **1993**, 1593−1597.
[14] [14a] T. Okamoto, H. Yasuda, A. Nakamura, *Organometallics* **1988**, *7*, 2266−2273. − [14b] J. de la Mata, R. Fandos, M. Gomez, P. Gomez-Sal, S. Martinez-Carrera, P. Royo, *Organometallics* **1990**, *9*, 2846−2850. − [14c] W. A. Herrmann, W. Kalcher, H. Biersack, I. Bernal, M. Creswick, *Chem. Ber.* **1981**, *114*, 3558−3571.
[15] [15a] D. H. Harris, M. F. Lappert, in *Organometallic Chemistry Reviews: Organosilicon Reviews*, (Eds.: D. Seyferth, A. G. Davies, E. O. Fischer, J. F. Normant, O. A. Reutov), Elsevier, Amsterdam, **1976**, 13−102. − [15b] M. F. Lappert, P. P. Power, A. R. Sanger, R. C. Srivastava, *Metal and Metalloid Amides*, Ellis Horwood, Chichester, U. K., **1980**, Chapter 8.
[16] M. D. Curtis, K.-B. Shiu, W. M. Butler, J. C. Huffman, *J. Am. Chem. Soc.* **1986**, *108*, 3335−3343.
[17] Reviews on Tp(*) complexes: [17a] S. Trofimenko, *Progr. Inorg. Chem.*, Vol. 34, (Ed.: S. J. Lippard), Wiley, New York, **1986**, *34*, S. 115−210; [17b] S. Trofimenko, *Chem. Rev.* **1993**, *93*, 943−980. − [17c] S. Trofimenko, *The Coordination Chemistry of Polypyrazolylborate Ligands*, Imperial College Press, London, **1999**.
[18] K. S. Heinselman, V. M. Miskowski, S. J. Geib, L. C. Wang, M. D. Hopkins, *Inorg. Chem.* **1997**, *36*, 5530−5538.
[19] See e. g.: [19a] J. Sundermeyer, U. Radius, Ch. Burschka, *Chem. Ber.* **1992**, *125*, 2379−2384. − [19b] S. Schmidt, J. Sundermeyer, F. Möller, *J. Organomet. Chem.* **1994**, *475*, 157−166.
[20] The relative effectiveness of π-bonding due to three t_2 and two *e* orbital interactions is 3 x 1/3 (t_2) and 2 x 1 (*e*): K. F. Miller, R. A. D. Wentworth, *Inorg. Chem.* **1979**, *18*, 984−988.
[21] [21a] G. Parkin, A. van Asselt, D. J. Leahy, L. Whinnery, N. G. Hua, R. W. Quan, L. M. Henling, W. P. Schaefer, B. D. Santarsiero, J. E. Bercaw, *Inorg. Chem.* **1992**, *31*, 82−85. − [21b] K. A. Jørgensen, *Inorg. Chem.* **1993**, *32*, 1521−1522.
[22] J. M. Boncella, M. L. Cajigal, A. S. Gamble, K. A. Abboud, *Polyhedron* **1996**, *15*, 2071−2078.
[23] R. D. Rogers, R. Vann Bynum, J. L. Atwood, *J. Am. Chem. Soc.* **1978**, *100*, 5238−5239.
[24] U. Radius, J. Sundermeyer, K. Peters, H.-G. v. Schnering, *Eur. J. Inorg. Chem.* **2001**, 1617−1623.
[25] A. K. Burrell, *Organometallics* **1992**, *11*, 3501−3503.
[26] R. L. Pruett, *Preparative Inorganic Reactions*, Vol. 2, (Ed.: W. L. Jolly), Interscience Publishers, Wiley, New York, **1965**, 198.
[27] F. X. Kohl, P. Jutzi, *Organomet. Synth.*, Vol. 3, (Eds. R. B. King, J. J. Eisch), Elsevier, Oxford, **1986**, 489−491. The lithiated Cp* is obtained by deprotonation of Cp*H with *n*-BuLi in *n*-hexane.
[28] H. Yamamoto, H. Yasuda, K. Tatsumi, K. Lee, A. Nakamura, J. Chen, Y. Kai, N. Kasai, *Organometallics* **1989**, *8*, 105−119.
[29] The lithiated amine $LiN(SiMe_3)_2$ is obtained by deprotonation with *n*-BuLi in hexane.
[30] S. Trofimenko, *J. Am. Chem. Soc.* **1967**, *89*, 6288−6294.
[31] The following programs were used: [31a] G. M. Sheldrick, SHELXS-97, *Program for Determination of Crystal Structures*, University of Goettingen, **1997**. − [31b] G. M. Sheldrick, SHELXL-97, *Program for Refinement of Crystal Structures*, University of Goettingen, **1997**. − [31c] A. Spek, PLATON, *Program Package for Calculations of Crystal Structure Data*, University of Utrecht, **1997**. − [31d] E. Keller, SCHAKAL-97, *A Program for Graphic Representation of Crystal Structures*, University of Freiburg, **1997**.

Received January 10, 2001
[I01011]

Synthesis and Host−Guest Properties of Multi-Crown Dendrimers towards Sodium Pertechnetate and Mercury(II) Chloride

Holger Stephan,*[a] Hartmut Spies,[a] Bernd Johannsen,[a] Karsten Gloe,*[b] Marius Gorka,[c] and Fritz Vögtle*[c]

Dedicated to Prof. Peter Mühl (Dresden) on the occasion of his 70th birthday

Keywords: Dendrimers / Crown compounds / Pertechnetate / Mercury / Solvent extraction

Multi-crown dendrimers of four different generations have been synthesized by grafting 4, 8, 16, and 32 benzo[15]-crown-5 units at the periphery of POPAM dendrimers. The binding of sodium pertechnetate and mercury(II) chloride by the multi-crown dendrimers has been studied by liquid-liquid extraction using the radioactive probes $^{22}Na^+$, $^{99}TcO_4^-$, and $^{203}Hg^{2+}$. The third- and fourth-generation dendrimers **3** and **4**, in particular, are capable of extracting mercury(II) with high efficiency (ca. 12 Hg^{II} ions per dendrimer molecule, even at low generation). It has been shown that the guest molecules investigated are preferentially encapsulated inside the dendrimers.

Introduction

Due to their unique topology, dendrimers show unusual guest-binding behaviour,[1] and there are almost unlimited possibilities for the structural modification of dendritic hosts. In principle, dendrimers can accommodate different kinds of guests, such as anionic species,[2] metal ions,[3] and neutral substrates,[4] either within the porous interior or at the exterior of the multifunctional periphery. Furthermore, there is an almost infinite variability regarding the solubility behaviour. Thus, water-soluble unimolecular micelles have been developed, having a hydrophobic interior and hydrophilic shells, which are capable of encapsulating hydrophobic guests.[5] Recently, oligoethyleneoxy-modified polypropyleneamine dendrimers (POPAM dendrimers) possessing hydrophilic interiors and exteriors were shown to function as water-soluble hosts for hydrophilic xanthene dyes.[6] On the other hand, hydrophilic guests can be transported from water into an organic phase or liquid carbon dioxide by the use of inverted unimolecular micelles based on a POPAM skeleton with grafted aliphatic and fluorinated chains.[7] Such hydrophobic dendrimers have been discussed as a new generation of extractants.[8] This stems mainly from the unique ability of dendrimers to encapsulate a multitude of guests. In this context, dendritic hosts have been propagated as nanoscopic reactors for environmental remediation.[9] Additionally, dendrimers are gaining in importance in the development of novel diagnostic and therapeutic agents with high specific activities.[10] For both applications, dendrimers based on multiple 1,4,7-triazacyclononane derivatives seem to be very promising.[11] These molecules coordinate multiple Cu^{2+} and Ni^{2+} ions, whereby each triazacyclononane unit can be loaded with the metal ions under investigation. Likewise, cascade molecules having up to 21 diaza[18]crown-6 moieties have been reported.[12] These dendrimers were shown to extract alkali metal ions in a generation-independent manner. The experimental results indicated only 1:1 complexes of the crown subunits with Cs^+, without any sandwich species.

Herein, we present the synthesis of multi-crown dendrimers having a different structure. Specifically, benzo[15]-crown-5 units have been grafted onto the periphery of four generations of POPAM dendrimers (Scheme 1). The combination of protonated amine nitrogen atoms in the dendrimer core, which can bind anions, together with cation-active crown ether moieties, represents an approach for the simultaneous binding of cations and anions. The host−guest properties of these dendrimers **1**−**4** have been investigated by liquid-liquid extraction. Sodium pertechnetate, as a typical contaminant of nuclear waste,[13] and mercury(II) chloride, as a pollutant of chloride-containing effluents of incineration processes,[14] were selected as guests for our studies.

Results and Discussion

The new dendritic family consists of four different generations of benzo-crown-modified polypropyleneamine

[a] Institut für Bioanorganische und Radiopharmazeutische Chemie, Forschungszentrum Rossendorf,
Postfach 510119, 01314 Dresden, Germany
Fax: (internat.) + 49-(0)351/260-3232
E-mail: h.stephan@fz-rossendorf.de
[b] Institut für Anorganische Chemie der Technischen Universität Dresden,
Mommsenstraße 13, 01062 Dresden, Germany
Fax: (internat.) + 49-(0)351/463-7287
E-mail: Karsten.Gloe@chemie.tu-dresden.de
[c] Kekulé-Institut für Organische Chemie und Biochemie der Universität Bonn,
Gerhard-Domagk-Straße 1, 53121 Bonn, Germany
Fax: (internat.) + 49-(0)228/73-3495
E-mail: voegtle@uni-bonn.de
Supporting information for this article is available on the WWW under http://www.wiley-vch.de/home/eurjic or from the author.

 © WILEY-VCH Verlag GmbH, 69451 Weinheim, 2001 1434−1948/01/1111−2957 $ 17.50+.50/0

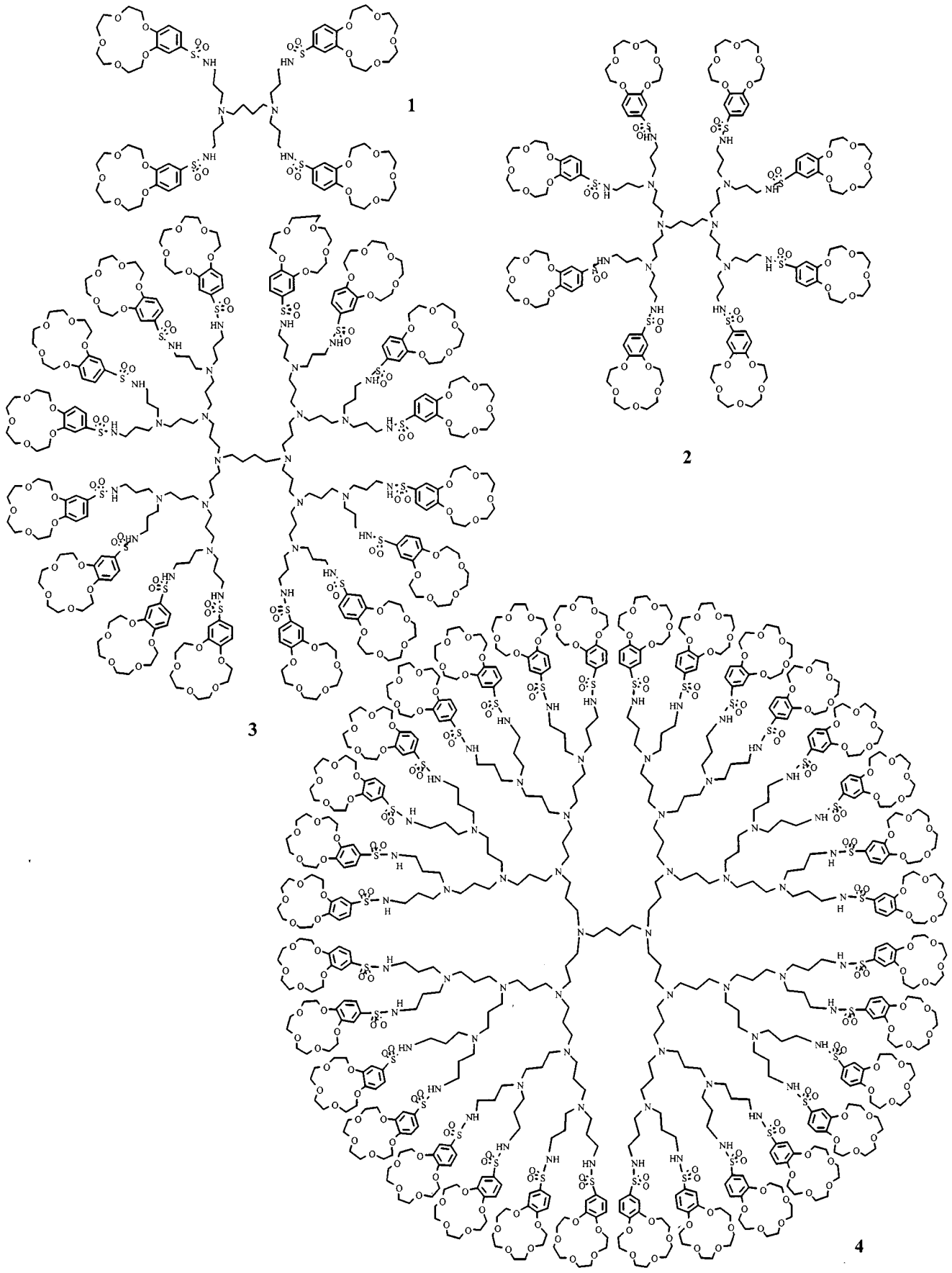

Scheme 1. Constitutions of the investigated multi-crown dendrimers

(POPAM, PPI) dendrimers. They were synthesized by treating amine-functionalized POPAM dendrimers with 1 equiv. (with respect to the primary amino groups of the dendrimer) of benzo[15]crown-5-4′-sulfonyl chloride in the presence of triethylamine (Scheme 2). The monofunctionalized multi-crown dendrimers **1**−**4** were characterized by ^1H and ^{13}C NMR spectroscopy as well as by MALDI-TOF mass spectrometry.[15] Dendrimers **1**−**4** were found to be soluble in common organic solvents but not in water. The melting points of the products ranged from 74 °C (**1**) to 85 °C (**4**).

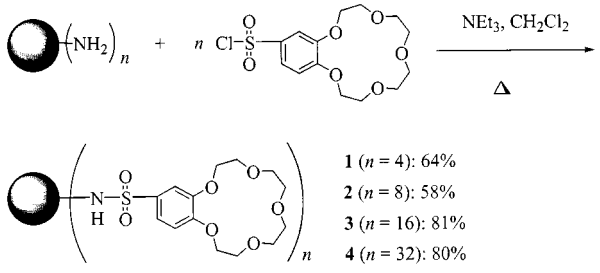

Scheme 2. Preparation of multi-crown dendrimers

The synthesized multi-crown dendrimers were found to exhibit good solubility in solvents of low polarity, such as dichloromethane and chloroform, making them attractive as extractant and carrier molecules for separation processes. Solvent extraction was thus chosen to characterize the host−guest properties. In all cases, the experimental parameter of interest was the distribution ratio *D*, defined as the quotient of the relative amounts of the species present in the organic and aqueous phases. Aqueous solutions of sodium pertechnetate and mercury(II) chloride were extracted with solutions of the multi-crown dendrimers in chloroform. Excellent coalescence behaviour and the rapid attainment of extraction equilibria (within a few minutes) was observed.

The extraction of pertechnetate by the multi-crown dendrimers was investigated as a function of dendrimer concentration at pH = 7.5 (see Figure 1). As expected, the extraction efficiency increases with increasing dendrimer generation.[16] This finding is consistent with the results of pertechnetate extraction studies using urea- and methyl-orange-functionalized dendrimers,[10c,10d] confirming that the anion is bound by protonated tertiary amine groups in the interior of the dendrimer. Analysis of the organic phase revealed that no sodium ions were co-extracted, indicating that the crown ether moieties at the periphery of the dendrimer were not involved under the experimental conditions used.[17] Further insight into the extraction mechanism was gained by studying the effect of pH on the distribution ratio D_{TcO_4}.

Figure 2 summarizes the extraction of pertechnetate by the third-generation crown-ether dendrimer **3** as a function of pH and dendrimer concentration. The highest efficacy was obtained at pH = 5.4,[18] at which most of the tertiary amine groups should be protonated.[19] Increasing the pH led to a decrease in the efficiency of the pertechnetate extraction, in agreement with the decreasing degree of protonation of the dendrimer. It is worth mentioning that the buffer composition plays only a minor role. Likewise, the presence of a competing anion such as chloride[20] has only a small influence on the extraction of pertechnetate. At pH < 11, sodium ions were not extracted into the organic phase. Thus, we conclude that in this pH range the binding of pertechnetate occurs mainly by electrostatic attraction of the protonated amine groups. The peripheral groups play only a minor role. This was corroborated by the results of control experiments using dendrimers bearing 3,4-dimethoxybenzenesulfonamide peripheral groups.[21] Only at pH > 12 was the co-extraction of sodium ions observed. We found that the extraction efficacy of sodium pertechnetate from sodium hydroxide solution using dendrimer **3** was rather poor (Figure 2). However, it is known that benzo[15]-crown-5 shows only a weak affinity in the binding and extraction of sodium ions.[22] Despite this, the multi-benzo[15]crown-5 dendrimers investigated show considerable sodium uptake when the dendrimer concentration is increased and the hydrophobic picrate counterion is used (see Figure 3). As expected, the sodium uptake increases with increasing dendrimer generation. The introduction of more suitable crown ether units such as cyclohexano[18]-

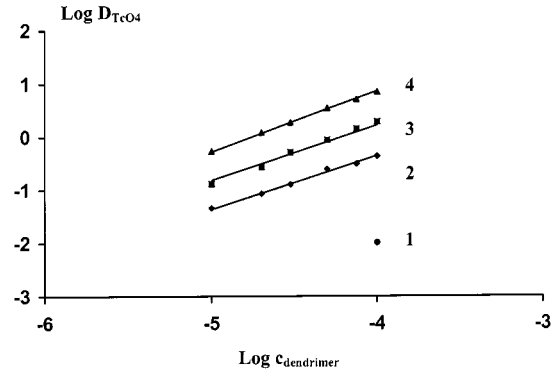

Figure 1. Variation of log D_{TcO_4} with dendrimer concentration for the extraction of pertechnetate with dendrimers **1**−**4**; c_{NaTcO_4} = 1×10^{-5} M, pH = 7.5 (TRIS/HCl buffer), $c_{dendrimer} = 1 \times 10^{-5}$ to 1×10^{-4} M in $CHCl_3$

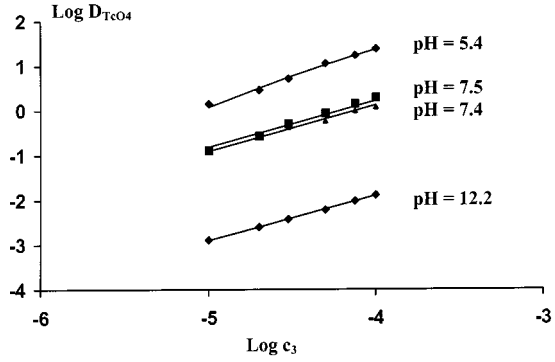

Figure 2. Variation of log D_{TcO_4} with pH for the extraction of pertechnetate with **3**; $c_{NaTcO_4} = 1 \times 10^{-5}$ M, pH = 5.4 (MES/NaOH), 7.4 (HEPES/NaOH), 7.5 (TRIS/HCl), 12.2 (1.5×10^{-2} M NaOH), $c_3 = 1 \times 10^{-5}$ to 1×10^{-4} M in $CHCl_3$

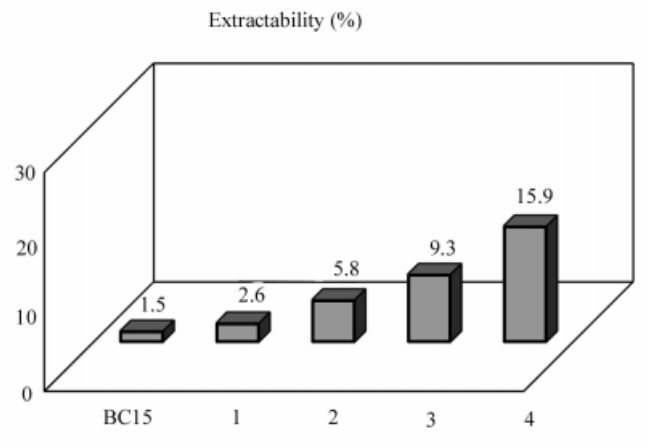

Figure 3. Extractability of sodium ions by benzo-15-crown-5 (BC15) and dendrimers **1**−**4**; $c_{NaOH} = 1.5 \times 10^{-2}$ M, $c_{HPic} = 1.5 \times 10^{-2}$ M, $c_{ligand} = 1 \times 10^{-3}$ M in $CHCl_3$

crown-6[23] at the periphery of the dendrimers can be expected to lead to higher sodium ion extraction efficiency.

Interestingly, in all cases, the slopes of the lines in the log D_{TcO_4}/log $c_{dendrimer}$ plots (Figures 1 and 2) were unity, indicating a clean 1:1 composition (pertechnetate:dendrimer) of the extracted complexes.[24] This finding is mainly attributable to the experimental conditions used. The concentration of the dendrimer was equimolar or in excess with respect to the pertechnetate concentration, which is a prerequisite for obtaining reliable information about the stoichiometries of the extracted complexes.[25] On the other hand, an excess of the dendrimer with respect to the pertechnetate concentration favours the formation of some partially loaded host−guest species. This is clearly evident from Figure 4.

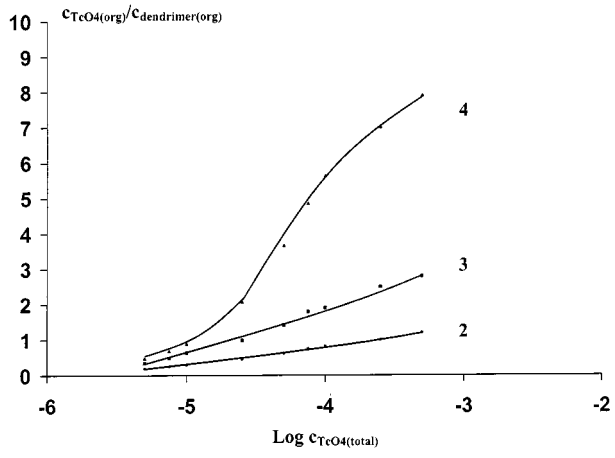

Figure 4. Variation of ratio $c_{TcO_4(org)}/c_{dendrimer(org)}$ with log $c_{TcO_4(total)}$ for the extraction of pertechnetate with dendrimers **2**−**4**; $c_{TcO_4} = 5 \times 10^{-6}$ to 5×10^{-4} M, pH = 5.4 (MES/NaOH), $c_{dendrimer} = 1 \times 10^{-5}$ in $CHCl_3$

Thus, at low pertechnetate concentration, the ratio $c_{TcO_4(org)}/c_{dendrimer(org)}$ is ≤ 1. The higher the generation of the dendrimer and the concentration of pertechnetate, the higher the loading capacity of the dendrimer with pertechnetate. At a total pertechnetate concentration of 5×10^{-4} M, approximately eight pertechnetate anions are extracted into the organic phase per fourth-generation dendrimer **4**.

Multi-crown dendrimers are also capable of extracting mercury(II) ions from chloride-containing solutions. The same trends were observed as in the case of pertechnetate extraction. As shown in Figure 5, the extraction efficiency of mercury(II) ions increases with increasing dendrimer generation. Benzo[15]crown-5 shows only a poor ability to transfer mercury(II) ions into an organic phase.

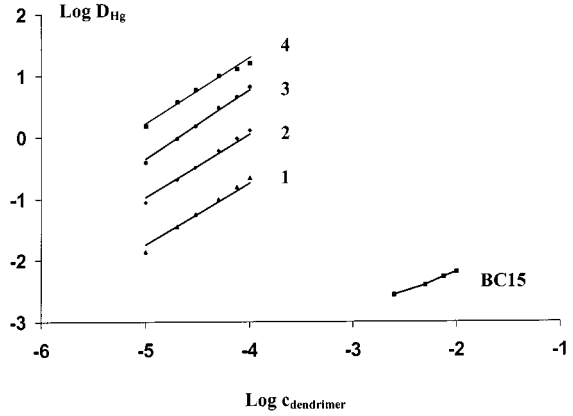

Figure 5. Variation of log D_{Hg}^{II} with dendrimer concentration for the extraction of mercury(II) with dendrimers **1**−**4** and benzo-15-crown-5 (BC15); $c_{HgCl_2} = 1 \times 10^{-5}$ M, pH = 7.5 (TRIS/HCl buffer), $c_{dendrimer} = 1 \times 10^{-5}$ to 1×10^{-4} M in $CHCl_3$, c_{BC15} 1×10^{-3} to 1×10^{-2} M in $CHCl_3$

The different extraction behaviour of multi-crown dendrimers as compared to benzo[15]crown-5 is not caused by a dendritic effect. Apparently, it is determined by the binding mode. Benzo[15]crown-5 is known as a weak extraction agent for $HgCl_2$.[22b] In general, mercury(II) prefers nitrogen and sulfur as donor atoms.[26] Hence, POPAM dendrimers are ideally suited to the binding and extraction of mercury(II) in the presence of chloride. Both neutral undissociated $HgCl_2$ as well as anionic $HgCl_3^-$ and $HgCl_4^{2-}$ may be bound by unprotonated and protonated tertiary amine groups, respectively.[27] The third- and fourth-generation dendrimers **3** and **4** in particular were found to be capable of extracting mercury(II) ions with high efficiency. Furthermore, these dendrimers can be loaded with a multitude of mercury(II) species. Thus, we found that the third-generation dendrimer **3** could accommodate approximately 12 Hg^{II} guests per molecule when mercury(II) was extracted from an aqueous solution ($c_{HgCl_2} = 5 \times 10^{-2}$ M; pH = 7.5; TRIS/HCl buffer) using only a low dendrimer concentration ($c_{\mathbf{3}} = 5 \times 10^{-5}$ M in $CHCl_3$).

Conclusion

It has been demonstrated that novel multi-crown dendrimers are easily accessible by grafting benzo[15]crown-5 units at the periphery of POPAM dendrimers. These multi-

crown dendrimers of four different generations, having 4, 8, 16, and 32 crown moieties at the exterior, are most soluble in organic solvents of low polarity and may serve as a new kind of carrier molecules for transport processes. Extraction studies performed with sodium pertechnetate and mercury(II) chloride have shown that the guest molecules are mainly bound in the interior of the polyamine skeleton. The crown ether units are rather inferior in terms of their complexation behaviour. Replacing the benzo[15]crown-5 units by more suitable [18]crown-6 moieties would seem to be an interesting line of future research, not only with regard to binding metal salts, but also for the complexation of biologically relevant substrates such as amino acids in their zwitterionic forms.

Experimental Section

General Remarks: All synthetic experiments were routinely carried out under dry nitrogen. Starting materials (POPAM dendrimers, generations 1 to 4) were purchased from Aldrich. Benzo[15]crown-5-4′-sulfonyl chloride was prepared according to a published procedure.[28] − NMR-spectroscopic data were obtained at 400 MHz with a Bruker AM 400 spectrometer (for ^{1}H and ^{13}C NMR spectra, the $CDCl_3$ signals were used as an internal reference; shifts are quoted with respect to TMS). − MALDI-TOF mass spectra were obtained with a TofSpec E & SE instrument from Micromass, Manchester.

General Synthetic Procedure for the Multi-Crown Dendrimers 1−4: 1/*n* equiv. of the starting polypropyleneamine dendrimer-$(NH_2)_n$ and 1.1·*n* equiv. of triethylamine were dissolved in dry dichloromethane (150 mL) (where *n* is the number of primary amino groups on the dendrimer). The mixture was heated to reflux, whereupon a solution of *n* equiv. of benzo[15]crown-5-4′-sulfonyl chloride in dichloromethane (50 mL) was added dropwise. The reaction mixture was stirred for 3−5 d under reflux under argon. The solvent was then removed in vacuo, the residue was taken up in dichloromethane, and the resulting solution was thoroughly washed with water, aq. sodium hydrogen carbonate solution, and again water (three times). After drying the organic phase with sodium sulfate and evaporation of the solvent, the multi-crown dendrimers were obtained as bright-yellow solids.

4-Cascade:1,4-diaminobutane[4-*N*,*N*,*N*′,*N*′]:(1-azabutylidene)^1: benzo[15]crown-5-4′-sulfonamide (1): Reaction procedure as described above. Amounts of reagents used to obtain the 4-cascade: 1,4-diaminobutane[4-*N*,*N*,*N*′,*N*′]:(1-azabutylidene)^1:aminopropane (0.20 g, 0.63 mmol), triethylamine (0.28 g, 2.77 mmol), benzo[15]crown-5-4′-sulfonyl chloride (0.93 g, 2.53 mmol). We obtained 0.66 g (0.40 mmol, 64%) of a bright-yellow solid; m.p. 74−76 °C. − ^{1}H NMR (400 MHz, $CDCl_3$, 25 °C): δ = 1.39−1.65 (br, 12 H, CH_2), 2.25−2.43 (br, 12 H, CH_2N), 2.79−2.92 (br, 8 H, CH_2NHSO_2), 3.61−3.75 (m, 32 H, OCH_2), 3.76−3.91 (m, 16 H, OCH_2), 4.01−4.21 (m, 16 H, OCH_2), 6.82−6.92 (d, 4 H, CH_{ar}), 7.25−7.32 (s, 4 H, CH_{ar}), 7.35−7.45 (d, 4 H, CH_{ar}). − ^{13}C NMR (62.9 MHz, $CDCl_3$, 25 °C): δ = 25.1 ($CH_2CH_2NHSO_2$), 25.6 (CH_2CH_2N), 42.9 (CH_2NHSO_2), 53.1, 53.5 (CH_2N), 68.9, 69.0, 69.2, 70.2, 70.3, 71.2, 71.2 (OCH_2), 111.1, 111.9, 121.9, 135.9, 149.1, 154.9 (CH_{ar}). − MALDI-TOF MS (matrix: 2,5-DHB; $CHCl_3$/EtOH, 3:1): *m*/*z* (%) = 1659.2 (100) $[M + Na]^+$, 1636.1 (60) $[M]^+$, 1306.6 (8) [M − crown]$^+$, 846.1 (37) $[M/2 + 2CH_2]^+$. − $C_{72}H_{112}N_6O_{28}S_4$: 1638.0.

8-Cascade:1,4-Diaminobutane[4-*N*,*N*,*N*′,*N*′]:(1-azabutylidene)^2: benzo[15]crown-5-4′-sulfonamide (2): Reaction procedure as described above. Amounts of reagents used to obtain the 8-cascade: 1,4-diaminobutane[4-*N*,*N*,*N*′,*N*′]:(1-azabutylidene)^2:aminopropane (0.23 g, 0.30 mmol), triethylamine (0.26 g, 2.64 mmol), benzo[15]-crown-5-4′-sulfonyl chloride (0.88 g, 2.40 mmol). We obtained 0.58 g (0.17 mmol, 58%) of a bright-yellow solid; m.p. 79−80 °C. − ^{1}H NMR (400 MHz, $CDCl_3$, 25 °C): δ = 1.32−1.61 (br, 28 H, CH_2), 2.21−2.41 (br, 36 H, CH_2N), 2.75−2.92 (br, 18 H, CH_2NHSO_2), 3.55−3.75 (br, 64 H, OCH_2), 3.80−3.92 (br, 32 H, OCH_2), 4.00−4.20 (m, 32 H, OCH_2), 6.82−6.93 (d, 8 H, CH_{ar}), 7.25−7.32 (s, 8 H, CH_{ar}), 7.35−7.43 (d, 8 H, CH_{ar}). − ^{13}C NMR (62.9 MHz, $CDCl_3$, 25 °C): δ = 24.0 ($CH_2CH_2NHSO_2$), 25.9 (CH_2CH_2N), 42.6 (CH_2NHSO_2), 51.7, 51.9, 52.6 (CH_2N), 68.9, 69.0, 69.19, 70.2, 70.3, 71.16, 71.19 (OCH_2), 111.05, 111.86, 121.91, 135.89, 149.12, 154.89 (CH_{ar}). − MALDI-TOF MS (matrix: 2,5-DHB; $CHCl_3$/EtOH, 3:1): *m*/*z* (%) = 3434.3 (100) $[M + Na]^+$, 3411.7 (47) $[M + H]^+$, 3082.2 (9) [M − crown]$^+$, 1734.7 (32) $[M/2 + 2\ CH_2]^+$. − $C_{152}H_{240}N_{14}O_{56}S_8$: 3413.4.

16-Cascade:1,4-Diaminobutane[4-*N*,*N*,*N*′,*N*′]:(1-azabutylidene)^3: benzo[15]crown-5-4′-sulfonamide (3): Reaction procedure as described above. Amounts of reagents used to obtain the 16-cascade: 1,4-diaminobutane[4-*N*,*N*,*N*′,*N*′]:(1-azabutylidene)^3:aminopropane (0.23 g, 0.14 mmol), triethylamine (0.25 g, 2.46 mmol), benzo[15]-crown-5-4′-sulfonyl chloride (0.82 g, 2.24 mmol). We obtained 0.77 g (0.11 mmol, 81%) of a bright-yellow solid; m.p. 80−82 °C. − ^{1}H NMR (400 MHz, $CDCl_3$, 25 °C): δ = 1.45−1.65 (br, 60 H, CH_2), 2.21−2.58 (br, 84 H, CH_2N), 2.78−2.95 (br, 32 H, CH_2NHSO_2), 3.65−3.81 (br, 128 H, OCH_2), 3.82−3.97 (br, 64 H, OCH_2), 4.03−4.21 (br, 64 H, OCH_2), 6.82−6.92 (d, 16 H, CH_{ar}), 7.25−7.32 (s, 16 H, CH_{ar}), 7.35−7.45 (d, 16 H, CH_{ar}). − ^{13}C NMR (62.9 MHz, $CDCl_3$, 25 °C): δ = 24.3 ($CH_2CH_2NHSO_2$), 26.1 (CH_2CH_2N), 42.6 (CH_2NHSO_2), 51.8−52.5 (CH_2N), 68.9, 69.0, 69.2, 70.2, 70.3, 71.2, 71.2 (OCH_2), 111.1, 111.9, 121.9, 135.9, 149.1, 154.9 (CH_{ar}). − MALDI-TOF MS (matrix: THAP; $CHCl_3$/EtOH, 3:1): *m*/*z* (%) = 6969.9 (87) $[M]^+$, 6992.6 (69) $[M + Na]^+$, 3512.1 (40) $[M/2 + CH_2]^+$. − $C_{312}H_{496}N_{30}O_{112}S_{16}$: 6973.0.

32-Cascade:1,4-diaminobutane[4-*N*,*N*,*N*′,*N*′]:(1-azabutylidene)^4: benzo[15]crown-5-4′-sulfonamide (4): Reaction procedure as described above. Amounts of reagents used to obtain the 32-cascade: 1,4-diaminobutane[4-*N*,*N*,*N*′,*N*′]:(1-azabutylidene)^4:aminopropane (0.24 g, 0.07 mmol), triethylamine (0.25 g, 2.46 mmol), benzo[15]-crown-5-4′-sulfonyl chloride (0.82 g, 2.24 mmol). We obtained 0.77 g (0.06 mmol, 80%) of a bright-yellow solid; m.p. 84−85 °C. − ^{1}H NMR (400 MHz, $CDCl_3$, 25 °C): δ = 1.41−1.72 (br, 124 H, CH_2), 2.19−2.67 (br, 180 H, CH_2N), 2.79−2.92 (br, 64 H, CH_2NHSO_2), 3.49−3.75 (br, 256 H, OCH_2), 3.76−3.91 (m, 128 H, OCH_2), 4.01−4.21 (br, 128 H, OCH_2), 6.72−6.92 (br, 32 H, CH_{ar}), 7.23−7.32 (br, 32 H, CH_{ar}), 7.35−7.45 (br, 32 H, CH_{ar}). − ^{13}C NMR (62.9 MHz, $CDCl_3$, 25 °C): δ = 26.0 ($CH_2CH_2NHSO_2$), 26.0 (CH_2CH_2N), 42.4 (CH_2NHSO_2), 51.7−52.8 (CH_2N), 68.9, 69.0, 69.2, 70.2, 70.3, 71.2, 71.2 (OCH_2), 111.1, 111.9, 121.9, 135.9, 149.1, 154.9 (CH_{ar}). − $C_{632}H_{1008}N_{62}O_{224}S_{32}$: 14085.

Liquid-Liquid Extraction Procedure: Extraction studies were performed at 25 ± 1 °C in 2-mL microcentrifuge tubes by mechanical shaking.[29] The phase ratio $V_{(org)}/V_{(w)}$ was 1:1 (0.5 mL each); the shaking period was 30 min. The extraction equilibrium was attained within this period. All samples were centrifuged after extraction. The pertechnetate and metal concentrations in both phases

were determined radiometrically using β-emission ($^{99}TcO_4^-$; Beckman LS 6000 LL liquid scintillation counter) and γ-radiation [^{22}Na, ^{203}Hg; Cobra II/Canberra Packard NaI(Tl) scintillation counter]. The pH of the aqueous solution was adjusted using 0.05 M 2-(*N*-morpholino)ethanesulfonic acid (MES)/NaOH (pH = 5.4), *N*-(2-hydroxyethyl)piperazine-*N*′-(2-ethanesulfonic acid) (HEPES)/NaOH (pH = 7.4), and tris(hydroxymethyl)aminomethane (TRIS)/HCl buffer (pH = 7.5).

Acknowledgments

We thank the Sächsisches Ministerium für Wissenschaft und Kunst (project no. 7533-844-98/4) and the BMBF ("Funktionelle supramolekulare Systeme für diagnostische Anwendungen") for support of this work, and Roche Diagnostics GmbH, Penzberg (Dr. H.-P. Josel, Dr. J. Herrmann) for co-operation.

[1] [1a] D. A. Tomalia, A. M. Naylor, W. A. Goddard III, *Angew. Chem.* **1990**, *102*, 119−157; *Angew. Chem. Int. Ed. Engl.* **1990**, *29*, 138−176. − [1b] G. R. Newkome, C. N. Moorefield, F. Vögtle, *Dendritic Molecules: Concepts, Syntheses, Perspectives*, VCH, New York, **1996**. − [1c] O. A. Matthews, A. N. Shipway, J. F. Stoddart, *Prog. Polym. Sci.* **1998**, *23*, 1−56. − [1d] Y. Kim, S. C. Zimmerman, *Curr. Opin. Chem. Biol.* **1998**, *2*, 733−742. − [1e] M. Fischer, F. Vögtle, *Angew. Chem.* **1999**, *111*, 934−995; *Angew. Chem. Int. Ed.* **1999**, *38*, 884−905. − [1f] A. W. Bosman, H. M. Jannsen, E. W. Meijer, *Chem. Rev.* **1999**, *99*, 1665−1688. − [1g] K. Inoue, *Prog. Polym. Sci.* **2000**, *25*, 453−571. − [1h] F. Vögtle, S. Gestermann, R. Hesse, H. Schwierz, B. Windisch, *Prog. Polym. Sci.* **2000**, *25*, 987−1041. − [1i] D. Smith, F. Diederich, *Top. Curr. Chem.* **2000**, *210*, 184−227. − [1j] S. Hecht, J. M. J. Fréchet, *Angew. Chem.* **2001**, *113*, 76−94; *Angew. Chem. Int. Ed.* **2001**, *40*, 74−91. − [1k] R. Haag, *Chem. Eur. J.* **2001**, *7*, 327−335.

[2] [2a] A. M. Naylor, W. A. Goddard III, G. E. Kiefer, D. A. Tomalia, *J. Am. Chem. Soc.* **1989**, *111*, 2339−2341. − [2b] J. F. G. A. Jansen, E. W. Meijer, *J. Am. Chem. Soc.* **1995**, *117*, 4417−4418. − [2c] A. Archut, G. C. Azzellini, V. Balzani, L. De Cola, F. Vögtle, *J. Am. Chem. Soc.* **1998**, *120*, 187−191. − [2d] C. Valerio, E. Alonso, J. Ruiz, J. C. Blais, D. Astruc, *Angew. Chem.* **1999**, *111*, 1855−1859; *Angew. Chem. Int. Ed.* **1999**, *38*, 1747−1751. − [2e] A. W. Kleij, R. van de Coevering, R. J. M. Klein Gebbink, A.-M. Noordman, A. L. Spek, G. van Koten, *Chem. Eur. J.* **2001**, *7*, 181−192.

[3] [3a] M. Zhao, R. M. Crooks, *J. Am. Chem. Soc.* **1998**, *120*, 4877−4878. − [3b] L. Balogh, D. A. Tomalia, *J. Am. Chem. Soc.* **1998**, *120*, 7355−7356. − [3c] R. J. M. Klein Gebbink, A. W. Bosman, M. C. Feiters, E. W. Meijer, R. J. M. Nolte, *Chem. Eur. J.* **1999**, *5*, 65−69. − [3d] B. Jendrusch-Borkowski, J. Awad, F. Wasgestian, *J. Inclusion Phenom.* **1999**, *35*, 355−359. − [3e] F. Vögtle, S. Gestermann, C. Kauffmann, P. Ceroni, V. Vicinelli, V. Balzani, *J. Am. Chem. Soc.* **2000**, *122*, 10398−10404. − [3f] V. Balzani, P. Ceroni, S. Gestermann, M. Gorka, C. Kauffmann, M. Maestri, F. Vögtle, *Chem. Phys. Chem.* **2000**, *4*, 224−227. − [3g] C. Larré, B. Donnadien, A.-M. Caminade, J.-P. Majoral, *Chem. Eur. J.* **1998**, *4*, 2031−2036. − [3h] S. M. Cohen, S. Petoud, K. N. Raymond, *Chem. Eur. J.* **2001**, *7*, 272−279.

[4] [4a] S. Mattei, P. Seiter, F. Diederich, V. Gramlich, *Helv. Chim. Acta* **1995**, *78*, 1904−1912. − [4b] P. Wallimann, P. Seiler, F. Diederich, *Helv. Chim. Acta* **1996**, *79*, 779−788. − [4c] S. Mattei, P. Wallimann, B. Kenda, W. Amrein, F. Diederich, *Helv. Chim. Acta* **1997**, *80*, 2391−2417. − [4d] G. R. Newkome, B. D. Woosley, E. He, C. N. Moorefield, R. Güther, G. R. Baker, G. H. Escamilla, J. Merrill, H. Luftmann, *Chem. Commun.* **1996**, 2337−2338. − [4e] G. Pistolis, A. Mallearis, D. Tsiourvas, C. M. Paleos, *Chem. Eur. J.* **1999**, *5*, 1440−1444.

[5] [5a] G. R. Newkome, C. N. Moorefield, G. R. Baker, M. J. Saunders, S. H. Grossman, *Angew. Chem.* **1991**, *103*, 1207−1209; *Angew. Chem. Int. Ed. Engl.* **1991**, *30*, 1178−1181. − [5b] C. J. Hawker, K. L. Wooley, J. M. J. Fréchet, *J. Chem. Soc., Perkin Trans. 1* **1993**, 1287−1297.

[6] M. W. P. L. Baars, R. Kleppinger, M. H. J. Koch, S.-L. Yeu, E. W. Meijer, *Angew. Chem.* **2000**, *112*, 1341−1344; *Angew. Chem. Int. Ed.* **2000**, *39*, 1285−1288.

[7] [7a] S. Stevelmans, J. C. M. van Hest, J. F. G. A. Jansen, A. A. F. J. van Boxtel, E. M. M. de Brabander-van den Berg, E. W. Meijer, *J. Am. Chem. Soc.* **1996**, *118*, 7398−7399. − [7b] A. I. Cooper, J. D. Londono, G. Wignall, J. B. McClain, E. T. Samulski, J. S. Lin, A. Dobrynin, M. Rubinstein, A. L. C. Burke, J. M. J. Fréchet, *Nature* **1997**, *389*, 368−371. − [7c] M. W. P. L. Baars, P. E. Froehling, E. W. Meijer, *Chem. Commun.* **1997**, 1959−1960.

[8] B. A. Moyer, in *Comprehensive Supramolecular Chemistry* (Eds.: J. L. Atwood, J. E. D. Davies, D. D. MacNicol, J.-M. Lehn, G. W. Gokel), Pergamon, Oxford, UK, **1996**, vol. 1, p. 377−416.

[9] L. Balogh, D. R. Swanson, D. A. Tomalia, M. S. Diallo, W. A. Goddard III, *219th ACS National Meeting, San Francisco*, March 26−30, **2000**, Abstract 291.

[10] [10a] C. Bieniarz, in *Encyclopedia of Pharmaceutical Technology*, Marcel Dekker, New York, **1998**, vol. 18, p. 55−89. − [10b] C. Wu, M. W. Brechbiel, R. W. Kozak, O. A. Gansow, *Bioorg. Med. Chem. Lett.* **1994**, *4*, 449−454. − [10c] H. Stephan, H. Spies, B. Johannsen, L. Klein, F. Vögtle, *Chem. Commun.* **1999**, 1875−1876. − [10d] H. Stephan, H. Spies, B. Johannsen, C. Kauffmann, F. Vögtle, *Org. Lett.* **2000**, *2*, 2343−2346.

[11] P. D. Beer, D. Gao, *Chem. Commun.* **2000**, 443−444.

[12] T. Nagasaki, O. Kimura, M. Ukon, S. Arimori, I. Hamachi, S. Shinkai, *J. Chem. Soc., Perkin Trans. 1* **1994**, 75−81.

[13] K. L. Nash, R. E. Barrans, R. Chiarizia, M. L. Dietz, M. P. Jensen, P. G. Rickert, B. A. Moyer, P. V. Bonnesen, J. C. Bryan, R. A. Sachleben, *Solv. Extr. Ion Exch.* **2000**, *18*, 605−631.

[14] K. Gloe, H. Stephan, O. Heitzsch, H. Braun, T. Kind, in *Hydrometallurgy − Fundamentals, Technology and Innovations* (Eds.: J. B. Hiskey, G. W. Warren), Soc. Min. Metall. Expl., Littletown, Colorado, **1993**, p. 845−859.

[15] MALDI-TOF spectra of multi-crown dendrimers **1**−**3** are available as Supporting Information; see footnote on the first page of this article.

[16] The extractability of pertechnetate using benzo[15]crown-5 ($c = 1 \times 10^{-2}$ M in $CHCl_3$) was lower than 1% under the experimental conditions used.

[17] Co-operative pertechnetate anion−sodium cation binding has been described for a tripodal tris(amidobenzo[15]crown-5) ligand; see: P. D. Beer, P. K. Hopkins, J. D. McKinney, *Chem. Commun.* **1999**, 1253−1254.

[18] At pH < 5, the solubility of lipophilic POPAM dendrimers in the aqueous phase is noticeably increased. This is obviously due to the higher hydrophilicity of the higher protonation state. Thus, dendrimers incorporating amino groups are rather unsuitable as extractants in more acidic media.

[19] For the protonation mechanism of POPAM dendrimers, see: [19a] G. J. M. Koper, M. H. P. van Genderen, C. Elissen-Roman, M. W. P. L. Baars, E. W. Meijer, M. Borkovec, *J. Am. Chem. Soc.* **1997**, *119*, 6512−6521. − [19b] R. C. van Duijvenbode, M. Borkovec, G. J. M. Koper, *Polymer* **1998**, *39*, 2657−2664.

[20] In the case of TRIS/HCl buffer (pH = 7.5), the chloride concentration is 4.2×10^{-2} M, which represents a huge excess over the pertechnetate concentration (ratio Cl^-/TcO_4^- = 4200:1).

[21] Dendrimers bearing 3,4-dimethoxybenzene peripheral groups extract pertechnetate with comparable efficiency as multi-crown dendrimers. Thus, at pH = 7.4, the third-generation 3,4-dimethoxybenzene-functionalized dendrimer ($c_{dendrimer} = 1 \times 10^{-4}$ M) extracts 42.1% of the pertechnetate into the or-

ganic phase. The analogous multi-crown dendrimer **3** extracts 54.1% of the pertechnetate under the same experimental conditions.

[22] [22a] R. M. Izatt, K. Pawlak, J. S. Bradshaw, R. L. Bruening, *Chem. Rev.* **1995**, *95*, 2529−2586. − [22b] K. Gloe, P. Mühl, A. I. Kholkin, M. Meerbote, J. Beger, *Isotopenpraxis* **1981**, *18*, 170−175.

[23] [23a] P. V. Bonnesen, B. A. Moyer, D. J. Presley, V. S. Armstrong, T. J. Haverlock, R. M. Counce, R. A. Sachleben, *Oak Ridge National Laboratory (ORNL) Report TM 13241*, **1996**. − [23b] R. A. Leonard, C. Conner, M. W. Liberatore, P. V. Bonnesen, D. J. Presley, B. A. Moyer, G. J. Lumetta, *Sep. Sci. Technol.* **1999**, *34*, 1043−1068.

[24] Points in Figures 1, 2, and 4 represent the experimental data; lines were calculated for 1:1 complex formation using a nonlinear regression program. For this program, see: M. Petrich, L. Beyer, K. Gloe, P. Mühl, *Anal. Chim. Acta* **1990**, *228*, 229−234.

[25] K. Gloe, P. Mühl, *Isotopenpraxis* **1979**, *15*, 236−239.

[26] K. Gloe, H. Stephan, R. Jacobi, J. Beger, *Solv. Extr. Res. Dev. (Jpn.)* **1995**, *2*, 18−25.

[27] For the experimental conditions used ($c_{\text{chloride}} = 4.2 \times 10^{-2}$ M; $c_{HgCl_2} = 1 \times 10^{-5}$ M), the following distribution of mercury(II) species was calculated: $HgCl_2$ (71%), $HgCl_3^-$ (17%), $HgCl_4^{2-}$ (12%). For stability constants of chloromercury(II) complexes, see: N. M. Rice, M. R. Smith, *J. Appl. Chem. Biotechnol.* **1975**, *25*, 379−402.

[28] L. N. Markovskii, D. M. Rudkevich, I. V. Kal'chenko, *J. Org. Chem. USSR (Engl. Transl.)* **1989**, *25*, 1803−1807.

[29] K. Gloe, P. Mühl, *Isotopenpraxis* **1983**, *19*, 257−260.

Received February 26, 2001
[I01071]

Platinum(II) Complexes of 2-(Dimethylamino)ethylselenolate − Donor−Acceptor Inter-Ligand Interactions as Evident from Experimental and TD-DFT Computational Analysis

Sandip Dey,[a] Vimal K. Jain,*[a] Axel Knoedler,[b] Wolfgang Kaim,[b] and Stanislav Zalis[c]

Keywords: Platinum / Selenium / NMR spectroscopy / Density functional calculations

Several platinum(II) complexes of 2-(dimethylamino)ethaneselenolate with the formulae, $[PtCl(SeCH_2CH_2NMe_2)(PR_3)]$ (**1**), $[PtPh(SeCH_2CH_2NMe_2)(PnBu_3)]$ (**2**), $[Pt_2Ph_2(Cl)(SeCH_2CH_2NMe_2)(PnBu_3)_2]$ (**3**), $[Pt_2Cl_3(SeCH_2CH_2NMe_2)(PR_3)_2]$ (**4**), $[Pt(SeCH_2CH_2NMe_2)_2(P–P)]$ (**5**), $[Pt_2(SeCH_2CH_2NMe_2)_2(P–P)_2]^{++}$ (**6**), and $[Pt(SeCH_2CH_2NMe_2)(PPh_3)]_n[PF_6]_n$ (**7**) have been synthesized and characterized by elemental analysis, UV/Vis and NMR (^1H, ^{31}P, ^{77}Se, ^{195}Pt) spectroscopy. The stereochemistry of these complexes (**1**–**7**) has been deduced from NMR spectroscopic data. A weak absorption in the UV/Vis spectrum of **1** has been assigned to a ligand (Se)-to-ligand (PR_3) charge transfer (LLCT), supported by TD-DFT calculations. The structures of $[PtCl(SeCH_2CH_2NMe_2)(PPh_3)]$ and $[Pt_2Ph_2(Cl)(SeCH_2CH_2NMe_2)(PnBu_3)_2]$ have been established by single crystal X-ray diffraction analysis. Each platinum atom in the latter is coordinated to four different ligands and $Me_2NCH_2CH_2Se$ behaves as μ_2-bridging and is also simultaneously chelated to one of the platinum atoms.

Introduction

Platinum group metal chalcogenolates have attracted considerable attention during the last 15 years or so due to their wide structural diversity[1] and relevance in catalysis,[2−5] and as a result of being precursors for the synthesis of metal chalcogenides[6−8] for electronic devices.[9] The area of metal chalcogenolates has been dominated by molecules containing the M−SR linkage.[1] In most cases these molecules have been isolated as non-volatile, insoluble (or sparingly soluble) polymers, thus making them inconvenient as precursors for the synthesis of metal chalcogenides. Although several strategies have been adopted to suppress polymerisation, the use of hybrid ligands containing both soft chalcogen and hard N donor atoms has been quite successful, such as pyridine-2-thiolate[10] or aliphatic mercapto amines.[11−14] The continued current interest in selenium containing inorganic materials[15] and in pursuance of our program on the design and development of molecular precursors, we explored some chemistry of internally functionalized selenolates, viz. pySe[16] and $Me_2NCH_2CH_2Se^-$.[8] Herein we now report the synthesis, spectroscopy, electrochemistry, structures, and DT-DFT calculations of platinum complexes derived from the latter ligand.

[a] Novel Materials & Structural Chemistry Division, Bhabha Atomic Research Center (B.A.R.C.), Mumbai-400085, India
[b] Institut für Anorganische Chemie, Universität Stuttgart, Pfaffenwaldring 55, 70569 Stuttgart, Germany
[c] J. Heyrovsky Institute of Physical Chemistry, Academy of Sciences of the Czech Republic, Dolejskova 3, 18223 Prague, Czech Republic

Results and Discussion

Synthesis and Spectroscopy

Treatment of $[Pt_2Cl_2(\mu\text{-}Cl)_2(PR_3)_2]$ with two equivalents of $NaSeCH_2CH_2NMe_2$, prepared by the reductive cleavage of the Se−Se bond in $(Me_2NCH_2CH_2Se)_2$ with sodium borohydride, afforded dimethylaminoethylselenolate complexes of the type $[PtCl(\eta^2\text{-}SeCH_2CH_2NMe_2)(PR_3)]$ (**1**) [PR_3 = PEt_3 (**1a**), $PnPr_3$ (**1b**), $PnBu_3$ (**1c**), PMe_2Ph (**1d**), or $PMePh_2$ (**1e**)] (Scheme 1). The analogous triphenylphosphane complex, $[PtCl(SeCH_2CH_2NMe_2)(PPh_3)]$ (**1f**) can be readily prepared by the reaction of $PtCl_2(PPh_3)_2$ with one equivalent of $NaSeCH_2CH_2NMe_2$.

The ^1H NMR spectra of **1** showed the expected integration and peak multiplicities. The selenolate proton resonances, i.e., $SeCH_2$, NMe_2, NCH_2 were flanked with platinum satellites with ^3J(Pt-H) being 24−27, 14−18, and 36−42 Hz, respectively. The observed magnitudes of ^3J(Pt-H) can be compared with platinum complexes containing neutral $RSeCH_2CH_2NMe_2$ ligands.[17,18] The ^{31}P NMR spectra of **1** exhibited single resonances flanked with ^{195}Pt satellites. The magnitude of ^1J(Pt-P), (3434−3662 Hz) indicates that the phosphane ligand is *trans* to the nitrogen atom of the chelated $[SeCH_2CH_2NMe_2]^-$ group.[16,19,20] The $^{195}Pt\{^1H\}$ NMR spectra of these complexes displayed a doublet due to coupling with a single ^{31}P nucleus. The doublet appeared in a narrow range of δ = −4266 to −4308. As is evident from Table 1, there is shielding of the ^{195}Pt resonances as the phosphane ligand is changed from PMe_2Ph to $PMePh_2$ through PPh_3. A similar trend is evident for ^{77}Se and ^{31}P chemical shifts which, however, showed deshielding. The ^{77}Se NMR resonances for **1** appeared as a triplet owing to the coupling with the ^{195}Pt nucleus. The resonance for **1f**, however, appeared as a broad signal and

 © WILEY-VCH Verlag GmbH, 69451 Weinheim, 2001 1434−1948/01/1111−2965 $ 17.50+.50/0

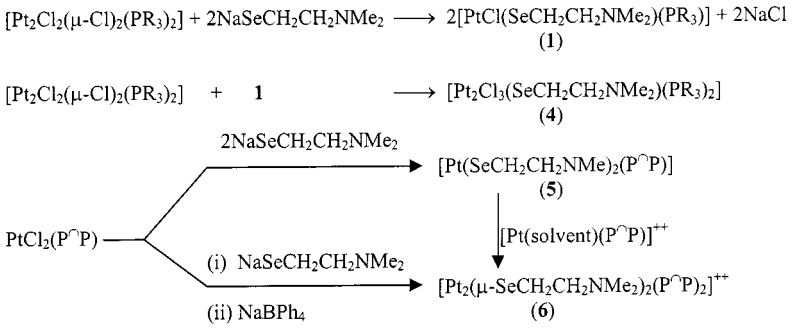

Scheme 1

Table 1. $^{31}P\{^1H\}$, $^{77}Se\{^1H\}$ and $^{195}Pt\{^1H\}$ NMR spectroscopic data (δ in ppm, *J* in Hz) for dimethylaminoethaneselenolate complexes of platinum(II)

Complex	$^{195}Pt\{^1H\}$ δ	$^1J(^{195}Pt\text{-}^{31}P)$	$^{77}Se\{^1H\}$ δ	$^1J(^{195}Pt\text{-}^{77}Se)$	$^{31}P\{^1H\}$	$^1J(^{195}Pt\text{-}^{31}P)$
[PtCl(SeCH$_2$CH$_2$NMe$_2$)(PEt$_3$)] (**1a**)	−4308(d)	3407	140.1	147	4.5	3434
[PtCl(SeCH$_2$CH$_2$NMe$_2$)(P*n*Pr$_3$)] (**1b**)	−4283(d)	3400	138.5	129	−4.7	3415
[PtCl(SeCH$_2$CH$_2$NMe$_2$)(P*n*Bu$_3$)] (**1c**)	−4284(d)	3394	137.8	138	−4.0	3416
[PtCl(SeCH$_2$CH$_2$NMe$_2$)(PMe$_2$Ph)] (**1d**)	−4266	3439	164(d)	123	−21.8	3454
				^2J(Se-P) = 24		
[PtCl(SeCH$_2$CH$_2$NMe$_2$)(PMePh$_2$)] (**1e**)	−4293(d)	3555	190.6(d)	104	−6.8	3571
				^2J(Se-P) = 30		
[PtCl(SeCH$_2$CH$_2$NMe$_2$)(PPh$_3$)] (**1f**)	−4305	3658	218.6(br)	−	7.4	3662
[Pt(Ph)(SeCH$_2$CH$_2$NMe$_2$)(P*n*Bu$_3$)] (**2**)	−4245	3845	−	−	−3.1	3834
[Pt$_2$(Ph)$_2$Cl(SeCH$_2$CH$_2$NMe$_2$)(P*n*Bu$_3$)$_2$] (**3**)	−4295	3776	−	−	−1.0	3783
	−4073	3761	−	−	−4.2	3829
[Pt$_2$Cl$_3$(SeCH$_2$CH$_2$NMe$_2$)(PEt$_3$)$_2$] (**4a**)	−	−	−	−	5.1	3203
					3.5	3355
[Pt$_2$Cl$_3$(SeCH$_2$CH$_2$NMe$_2$)(PMe$_2$Ph)$_2$] (**4b**)	−	−	−	−	−21.0	3581
					−22.4	3359
[Pt(SeCH$_2$CH$_2$NMe$_2$)$_2$(dppm)] (**5a**)	−4251(t)	2429	78.0	294	−52.9	2412
[Pt(SeCH$_2$CH$_2$NMe$_2$)$_2$(dppe)] (**5b**)	−4958(t)	2884	29.3	264	46.7	2859
				J(Se-P) = 11		
[Pt(SeCH$_2$CH$_2$NMe$_2$)$_2$(dppp)] (**5c**)	−4913(t)	2783	53.5	279	−1.8	2849
[Pt$_2$(SeCH$_2$CH$_2$NMe$_2$)$_2$(dppm)$_2$][BPh$_4$]$_2$ (**6a**)	−4065(d,d)	2738	255.0	472	−39.3(d)	2286
						J(P-P) = 65
					−44.8(d)	2745
						J(P-P) = 65
[Pt$_2$(SeCH$_2$CH$_2$NMe$_2$)$_2$(dppe)$_2$][BPh$_4$]$_2$ (**6b**)	−4680(d,d)	2852	276.6	385	47.3	2822
					36.9	3158
[Pt$_2$(SeCH$_2$CH$_2$NMe$_2$)$_2$(dppp)$_2$][BPh$_4$]$_2$ (**6c**)	−4534(d,d)	2706	309.8	316	−1.8(d)	2676
						J(P-P) = 31
					−13.7(d)	3048
						J(P-P) = 31
[Pt(SeCH$_2$CH$_2$NMe$_2$)(PPh$_3$)]$_n$[PF$_6$]$_n$ (**7**)	−4071(d) (major)	3323	49.8	−	5.3 (major)	3330
	−3854 (minor)	3337	17.9	−	3.1 (minor)	3353

hence platinum coupling could not be resolved. The magnitude of $^1J(^{195}Pt\text{-}^{77}Se)$ is comparable to that of the values reported for mononuclear platinum selenolates.[16,21,22] The appearance of a single resonance in ^{77}Se NMR spectra suggests that the phosphane is *cis* to the selenium atom as the $^2J(^{77}Se\text{-}^{31}P)_{cis}$ couplings are usually small (> 10 Hz).[22,23] However, such couplings are slightly larger for **1d** and **1e** (24 and 30 Hz, respectively) and could thus be resolved in the ^{77}Se NMR spectra.

Reaction of [Pt$_2$Ph$_2$(μ-Cl)$_2$(P*n*Bu$_3$)$_2$] with two equivalents of NaSeCH$_2$CH$_2$NMe$_2$, affords a mixture of products, [PtPh(SeCH$_2$CH$_2$NMe$_2$)(P*n*Bu$_3$)] (**2**) and [Pt$_2$Ph$_2$(Cl)-(SeCH$_2$CH$_2$NMe$_2$)(P*n*Bu$_3$)$_2$] (**3**). Compound **3** appears to be an intermediate product in the reaction, which on further reaction with NaSeCH$_2$CH$_2$NMe$_2$ yields **2**. The calculated values of C, H, and N for the two are not significantly different, hampering an unambiguous identification of **2** and **3**. The two can, however, be separated by repeated

recrystallization. The NMR spectroscopic data for **2** can be compared with **1** as described above. Although the magnitude of ^1J(Pt-P) is greater (418 Hz) than that of **1c**, it is in compliance with $ArPt^{II}$ complexes in which the phosphane is *trans* to nitrogen, e.g. $[Pt_2R_2(\mu\text{-}N{-}N)_2(PR_3)_2]$ (R = Me or aryl, N−N = pyrazole).[24] The ^{31}P and ^{195}Pt NMR spectra of **3** exhibited two separate resonances attributable to "$PtPhCl(PnBu_3)$" and "$PtPh(Se{-}N)(PnBu_3)$" fragments. The magnitude of ^1J(Pt-P) suggests that the phosphane ligand is *trans* to Cl in the former and *trans* to N in the latter fragment.[25] This stereochemistry is unambiguously established by X-ray structural analysis (see later).

The chloro analogue of **3**, $[Pt_2Cl_3(SeCH_2CH_2NMe_2)(PR_3)_2]$ (**4**) [PR_3 = PEt_3 (**4a**), PMe_2Ph (**4b**)] can be obtained readily by treatment of $[Pt_2Cl_2(\mu\text{-}Cl)_2(PR_3)_2]$ with **1** in 1:2 molar ratio. The ^{31}P NMR spectra of a freshly prepared solution exhibited two singlets each flanked with platinum satellites. The signal of lower frequency may be attributed to the phosphane attached to the metal atom containing the chelating Se−N ligand. The magnitude of ^1J(Pt-P) coupling associated with this signal is reduced (≈ 90 Hz) relative to that of the corresponding mononuclear complex. The second resonance at higher frequency may be assigned to the phosphane coordinated to the metal atom containing two chlorines and the selenium atom. Similar NMR spectroscopic data have been reported for $[Pt_2Cl_3(\mu\text{-}Sepy)(PR_3)_2]$.[16] Although the spectra of **4b** did not change with time, **4a** slowly isomerised in solution to establish an equilibrium with another species **4a′**. Thus, a $CDCl_3$ solution of **4a**, after 2 h, displayed four resonances (δ = 5.1, 3.4, 3.1, 2.4), each showing platinum satellites, the intensity of which changed with time until an equilibrium is reached after two days. No change occurs after a week. It is likely that the "$PtCl_2(PR_3)$" fragment of **4a** isomerises from *cis*-"$PtCl_2$" to the *trans*-"$PtCl_2$" configuration, a structure observed for palladium complex, $[Pd_2Cl_3(Sepy)(PR_3)_2]$.[16] Thus, the second set of resonances (δ = 3.1, ^1J(Pt-P) = 3504 Hz; δ = 2.4, ^1J(Pt-P) 3218 Hz) may be attributed to **4a′** in which "$PtCl_2$" has a *trans* configuration.

Reaction of $PtCl_2(P{-}P)$ with two equivalents of $NaSeCH_2CH_2NMe_2$ yields, mononuclear $[Pt(SeCH_2CH_2NMe_2)_2(P{-}P)]$ (**5**) [P−P = dppm (**5a**), dppe (**5b**), dppp (**5c**)] as yellow crystalline solids. The NMR spectra (^{31}P, ^{77}Se, ^{195}Pt) (Table 1) are similar to several organochalcogenolates $[Pt(ER)_2(P{-}P)]$ reported by us.[16,21,23,26] These complexes have been assigned a *cis* configuration. Unlike **1**, the $Me_2NCH_2CH_2Se$ in **5** acts in monodentate fashion i.e., binding through selenium only. This mode of binding can readily be identified from ^1H NMR spectra. The NMe_2 protons in **5** appear at δ ≈ 2.0 with the absence of ^{195}Pt couplings whereas in **1** they appear at δ ≈ 2.7 with ^{195}Pt couplings. When the reaction is carried out in 1:1 stoichiometry in the presence of $NaBPh_4$ (Scheme 1), a new series of binuclear complexes, $[Pt_2(SeCH_2CH_2NMe_2)_2(P{-}P)_2][BPh_4]_2$ (**6**) [P−P = dppm (**6a**), dppe (**6b**), dppp (**6c**)] could be isolated. Complex **6** can also be prepared, as pale yellow fibrous crystals, by the reaction of **5** with $[Pt(solvent)_2(P{-}P)][BPh_4]_2$. The ^{77}Se NMR spectra exhibited single resonances suggesting that two bridging selenolate ligands are equivalent. The signals are deshielded with increased ^1J(Pt-Se) in comparison to the corresponding resonance for **5**. However the $^{31}P\{^1H\}$ (Figure 1) and $^{195}Pt\{^1H\}$ (Figure 2) spectra showed two sets of resonances, and doublet of doublets, respectively; a pattern indicative of non-equivalence of phosphorus nuclei of the P−P ligand. The spectra of **6a** and **6c** further showed phosphorus coupling, thus each signal appeared as a doublet (Figure 1). The X-ray structures of several mononuclear compounds $[M(ER)_2(P{-}P)]$ (E = S or Se, M = Pd or Pt) have been reported.[13,23] The structures reveal that in thiolates the two M−S distances are nearly identical,[13,23] but for selenolates the two M−Se distances differ markedly[21,23,26] (e.g. $Pt(Sepy)_2(dppe)$ Pt−Se = 2.498, 2.433 Å).[26] Similar differences in Pt−E distances in binuclear complexes $[Pt_2X_2(\mu\text{-}ER)_2(PR_3)_2]$ (ER = SeEt, $SeCH_2Ph$)[19,27] are reported. The selenolato ligands form an asymmetric Pt_2Se_2 ring[19,27] whereas the thiolates give a symmetrical Pt_2S_2 fragment.[28] On chelation of $M(ER)_2(P{-}P)$ with another metal centre, binuclear complexes such as $[M_2(ER)_2(P{-}P)_2]^{++}$ [11,13] (M = Pd or Pt) are formed when E = S a symmetrical M_2E_2 bridge forms as shown by the X-ray structure of $[M_2(\mu\text{-}SC_5H_9NMe)_2(dppe)_2][BPh_4]_2$[13] where M−S distances are nearly equivalent. Accordingly all phosphorus nuclei become chemically equivalent and display only one ^{31}P NMR resonance.[11,13,21,23] In case of binuclear cationic selenolate complexes, as observed for $[Pt_2Cl_2(\mu\text{-}SeR)_2(PR_3)_2]$,[19,27] the M−Se bridge may be asymmetric (**I**) due to different M−Se distances consequently making the

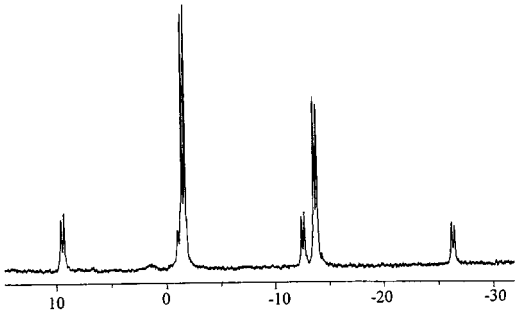

Figure 1. $^{31}P\{^1H\}$ NMR spectrum of $[Pt_2(SeCH_2CH_2NMe_2)_2(dppp)_2][BPh_4]_2$ (**6c**) in $CDCl_3$

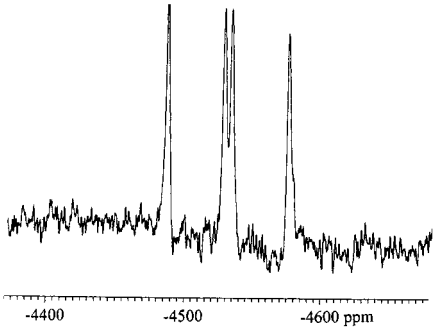

Figure 2. $^{195}Pt\{^1H\}$ NMR spectrum of $[Pt_2(SeCH_2CH_2NMe_2)_2(dppp)_2][BPh_4]_2$ (**6c**) in $CDCl_3$

phosphorus nuclei magnetically different. The two inequivalent phosphorus nuclei are coupled together to give doublets in the ^{31}P NMR spectra of **6a** and **6c**. The magnitude of ^{2}J(P-P) couplings are in accordance with the literature values.[29] The absence of ^{2}J(P-P) in **6b** might be due to different signs of ^{3}J(P-P), ^{2}J(P-P) coupling operating through P−C−C−P and P−Pt−P routes, respectively.[30] The intensity of two resonances (Figure 1) is significantly different. This can be attributed to the difference in the magnitude of T_1 of two sites, as reported earlier.[30]

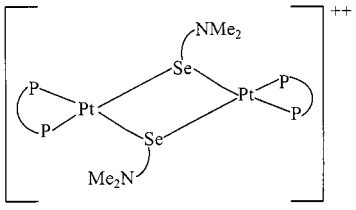

I

Treatment of **1f** with $AgPF_6$ affords $[Pt(SeCH_2CH_2NMe_2)(PPh_3)]_n[PF_6]_n$ (**7**). The ^{31}P, ^{77}Se, and ^{195}Pt spectra exhibited two separate resonances in approximately a 2:1 ratio. The ^{1}J(Pt-P) in ^{31}P and ^{195}Pt NMR spectra are comparable, indicating that both the species have similar configuration. Recently we have reported the structure of $[\{Pd(SeCH_2CH_2NMe_2)Cl\}_n]$ which is a trimer ($n = 3$) in which the chelated Se−N ligand bridges another palladium atom through Se.[8] The observed two signals may be interpreted for dimeric (**II**) and trimeric (**III**) forms in which each platinum is bonded to two Se atoms, one N and one PPh_3 in nearly similar environments.

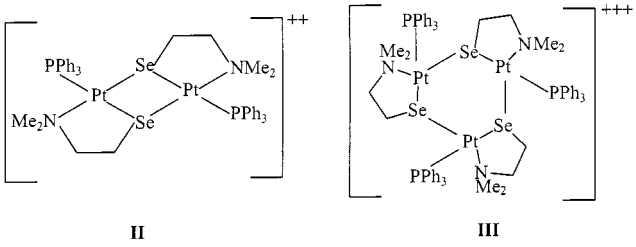

II **III**

Absorption Spectra and Electrochemistry

The absorption spectra of the complexes $[PtCl(SeCH_2CH_2NMe_2)(PR_3)]$ in CH_2Cl_2 solution are characterised by a very weak band at 400−430 nm (Figure 3, Table 2). The band is hypsochromically shifted on replacing the phenyl substituents on the PR_3 group by donating alkyl groups. As will be confirmed by TD-DFT calculations (see below) this absorption is due to a ligand (Se)-to-ligand (PR_3) charge transfer (LLCT) transition. The geometry obviously allows only rather poor orbital overlap, resulting in very weak yet well discernible bands (Figure 3). A similar band with $\varepsilon = 80\ mol^{-1}\cdot dm^3\cdot cm^{-1}$ at 514 nm has been reported for the palladium analogue $[PdCl(SeCH_2CH_2NMe_2)(PPh_3)]$.[8] Allowed transitions occur only at higher energies with $\lambda_{max} < 300$ nm, in agreement with theory. The dinuclear species $[Pt_2Ph_2(Cl)(SeCH_2CH_2NMe_2)(PnBu_3)_2]$ does not allow a detectable Se-to-P*n*Bu$_3$ transition in the visible or near UV region(Table 2).

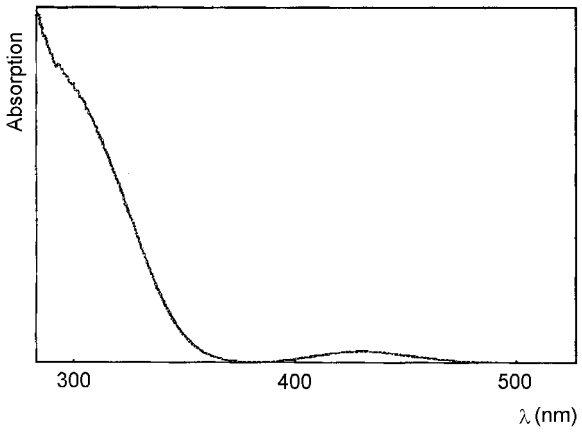

Figure 3. UV/Vis spectrum of $[PtCl(SeCH_2CH_2NMe_2)(PPh_3)]$ (**1f**) in CH_2Cl_2

Table 2. UV/Vis absorption data of some platinum complexes recorded in CH_2Cl_2

Complex	λ_{max} (nm)
$[PtCl(SeCH_2CH_2NMe_2)(PEt_3)]$ (**1a**)	284, 405
$[PtCl(SeCH_2CH_2NMe_2)(PMe_2Ph)]$ (**1d**)	283, 405
$[PtCl(SeCH_2CH_2NMe_2)(PMePh_2)]$ (**1e**)	266 sh, 273 sh, 293 sh, 418
$[PtCl(SeCH_2CH_2NMe_2)(PPh_3)]$ (**1f**)	268 sh, 275 sh, 300 sh, 430

According to cyclic voltammetry in CH_2Cl_2/0.1 $mol\cdot dm^{-3}$ Bu_4NPF_6 the Pt^{II} complexes **1** and **3** are oxidised irreversibly. The peak potentials for **1** show little variation (0.83−0.89 V vs. ferrocene/ferrocenium), confirming that it is primarily the selenolate part (HOMO) which loses an electron and not the PR_3^- ligating platinum centre. The bridging selenolate in compound **3** is hard to oxidise as illustrated by the anodic peak potential of 1.13 V for irreversible oxidation.

Electronic Structure Calculations on 1f

The ADF/BP calculated one-electron scheme of the $[PtCl(SeCH_2CH_2NMe_2)(PPh_3)]$ complex is schematically given in Figure 4. The composition of important molecular

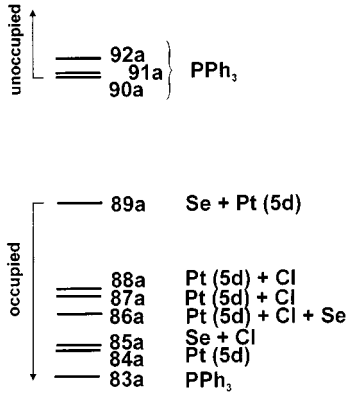

Figure 4. ADF/BP calculated qualitative MO scheme of **1f**

Table 3. ADF/BP calculated one-electron energies and percentage composition of selected highest occupied and lowest unoccupied molecular orbitals of [PtCl($SeCH_2CH_2NMe_2$)(PPh_3)] (**1f**) expressed in terms of composing fragments

MO	*E* [eV]	Prevailing Character	Pt	PPh_3	Se	Cl	N
Unoccupied							
92a	−1.87	PPh_3	3 (d)	90	2	2	
91a	−2.06	PPh_3	2 (d)	94			
90a	−2.11	d_{Pt} + PPh_3 + Se	13 (d)	63	9	3	3
Occupied							
89a	−4.05	Se + d_{Pt}	29 (d)	−	58	10	−
88a	−5.37	d_{Pt}	11 (s); 57(d)	1	7	23	−
87a	−5.45	d_{Pt} + Cl	5 (s); 42(d)	3		43	
86a	−5.70	Cl + Se + d_{Pt}	1(p); 19 (d)		25	50	
85a	−6.16	Cl + Se	3(p); 4 (d)	4	46	34	
84a	−6.25	d_{Pt}	78 (d)	10	3	2	
83a	−6.60	PPh_3	6 (d)	72	10	3	2

orbitals is summarised in Table 3. The highest molecular orbital 89a is formed mainly from a Se *p* orbital with some additional metal contribution. Pt 5*d* and Cl 3*p* orbitals contribute significantly to the next lower lying occupied MOs. The set of the lowest lying unoccupied molecular orbitals, 90a, 91a, and 92a, is to a large extent located on the PPh_3 fragment. The composition of the occupied MOs of the [PtCl($SeCH_2CH_2NMe_2$)(PH_3)] model (Table 4) corresponds to those of the PPh_3 complex. The lowest lying molecular orbital is delocalised; PH_3 localised unoccupied MOs lie at a rather high energy. The excitation energies listed in Table 5 were calculated for the [PtCl($SeCH_2CH_2NMe_2$)(PH_3)] model with different DFT program configurations. In agreement with the experiments, there is one very weak transition (HOMO→LUMO, oscillator strength $< 10^{-3}$) at low energy, set apart by more than 1 eV from the following singlet transitions (Table 5). The calculated excitation energies of about 2.4 eV (corresponding to ca. 500 nm) are in broad agreement with the 400−430 nm observed for various substituted derivatives (Table 2). This conspicuous absorption must be formulated mainly as ligand (Se)-to-ligand (PR_3) charge transfer, as has been proposed previously for palladium analogues.[8]

Table 4. ADF/BP calculated one-electron energies and percentage composition of selected highest occupied and lowest unoccupied molecular orbitals of model complex [PtCl($SeCH_2CH_2NMe_2$)(PH_3)] expressed in terms of composing fragments

MO	*E* [eV]	Prevailing Character	Pt	PH_3	Cl	Se
Unoccupied						
49a	−0.77	PH_3	17(d)	68		10
48a	−0.83	PH_3	7(d)	47		30
47a LUMO	−2.23	delocalized	28 (d)	20	11	28
Occupied						
47a HOMO	−4.30	Se + d_{Pt}	28 (d)	2	9	62
46a	−5.58	d_{Pt}	18 (s); 71(d)	−	4	7
45a	−5.71	d_{Pt} + Cl	2 (s); 27(d)	−	61	5
44a	−5.85	Cl + Se + d_{Pt}	1(p); 16 (d)	−	57	24
43a	−6.10	Se + Cl	7 (d)	1	36	52
42a	−6.40	d_{Pt}	85 (d)	11	−	−

Crystal Structures of 1f and 3

An ORTEP plot of **1f** with the crystallographic numbering scheme is shown in Figure 5, and Table 6 summarises essential data. The geometry around the platinum atom is essentially square planar with the atoms P, Cl, Se, and N defining the coordination sphere. The phosphane ligand is *trans* to the nitrogen atom of the chelating selenolate group as inferred from the NMR spectroscopic data. The five-membered chelate ring (Pt−Se−C−C−N) exists in a puckered conformation with the carbon atoms C(19) and C(20) lying on opposite sides of the mean plane. The structure of **1f** is isomorphous to its palladium analogue, [PdCl($SeCH_2CH_2NMe_2$)(PPh_3)][8] and various bond lengths and angles in the two structures are comparable.

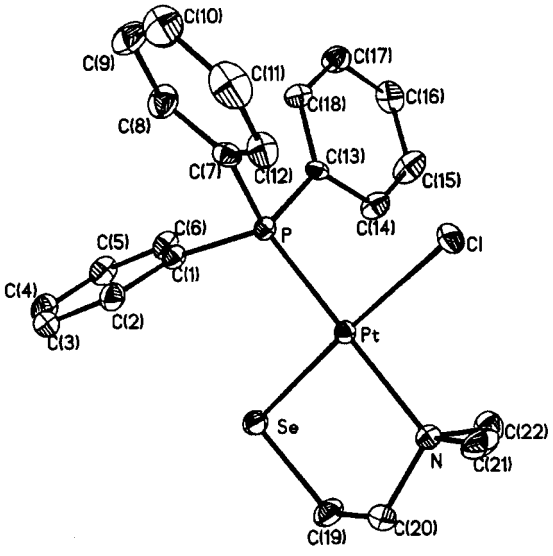

Figure 5. Molecular structure of [PtCl($SeCH_2CH_2NMe_2$)(PPh_3)] (**1f**) with crystallographic numbering scheme

Table 5. Selected calculated lowest TD DFT singlet excitation energies (eV) for [PtCl($SeCH_2CH_2NMe_2$)(PH_3)]

State	Main character	ADF/BP		G98/B3LYP	
		Transition energy [eV]	Oscillator strength	Transition energy [eV]	Oscillator strength
$^1A_1$	HOMO → LUMO	2.24	0.0004	2.53	0.0006
$^1A_1$	HOMO → LUMO +1	3.55	0.001	3.71	0.002
$^1A_1$	HOMO − 1 → LUMO	3.58	0.002	3.95	0.005
$^1A_1$	HOMO → LUMO + 2	3.67	0.010	4.08	0.012
$^1A_1$	HOMO −4 → LUMO	4.71	0.082	5.09	0.190

Table 6. Selected bond lengths [Å] and bond angles [°] with esd's for [PtCl(SeCH$_2$CH$_2$NMe$_2$)(PPh$_3$)] (**1f**)

Pt−N	2.161 (5)	N−C(20)	1.501 (8)
Pt−P	2.2292 (15)	N−C(21)	1.485 (8)
Pt−Se	2.3773(7)	N−C(22)	1.486 (8)
Pt−Cl	2.3788 (15)	C(19)−C(20)	1.502 (9)
Se−C(19)	1.953 (6)	P−C (av)	1.830
N−Pt−P	174.57 (14)	C(20)−N−C(21)	107.1 (5)
N−Pt−Se	87.02 (14)	C(20)−N−C(22)	109.5 (5)
P−Pt−Se	91.07 (4)	C(21)−N−C(22)	106.6 (5)
N−Pt−Cl	90.61 (15)	Pt−N−C(21)	114.9 (4)
P−Pt−Cl	90.89 (6)	Pt−N−C(22)	107.2 (4)
Se−Pt−Cl	174.92 (4)	Pt−N−C(20)	111.3 (4)
Pd−Se−C(19)	95.9 (2)	N−C(20)−C(19)	112.2 (5)
		Se−C(19)−C(20)	108.9 (4)

The molecular structure of [Pt$_2$Ph$_2$(Cl)(SeCH$_2$CH$_2$NMe$_2$)(P*n*Bu$_3$)$_2$] (**3**), established by the X-ray diffraction method, is illustrated in Figure 6. Selected bond lengths and bond angles are given in Table 7. The structure consists of two distorted square planar platinum atoms which are held together by a bridging selenolate centre. The two square planes of the platinum atoms are inclined to each other through a Pt(1)−Se−Pt(2) angle of 111.69 (5)°. Each platinum atom is coordinated to four different ligand atoms. The Pt(1) centre is coordinated to Ph, Cl, PBu$_3$, and the selenium atom, the latter being mutually *trans*. The Pt(2) atom is bound to the chelating Me$_2$NCH$_2$CH$_2$Se ligand and to the other PBu$_3$ and Ph groups. The phosphane is *trans* to the nitrogen atom whereas Se is *trans* to Ph. The Pt−Se distances in **1f** [2.3788(15) Å] and **3** [2.4793(14) and 2.4562(12) Å] are significantly different, although these distances are in agreement with the standard values. The longer Pt−Se distances in **3** compared with that of **1f** reflect greater *trans* influence of Ph and PBu$_3$ than the chloride.

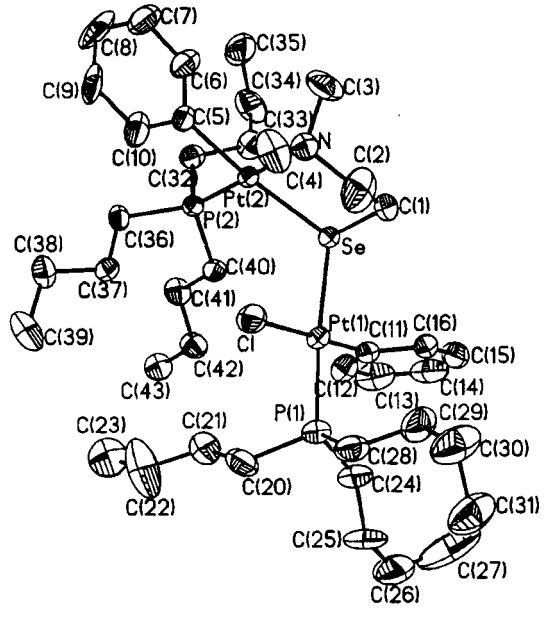

Figure 6. ORTEP plot of [Pt$_2$Ph$_2$Cl(SeCH$_2$CH$_2$NMe$_2$)(P*n*Bu$_3$)$_2$] (**3**) with crystallographic numbering scheme

Table 7. Selected bond lengths [Å] and bond angles [°] with esd's for [Pt$_2$Ph$_2$(Cl)(SeCH$_2$CH$_2$NMe$_2$)(P*n*Bu$_3$)] (**3**)

Pt(1)−Se	2.4793(14)	Pt(2)−Se	2.4562(12)
Pt(1)−P(1)	2.235(3)	Pt(2)−P(2)	2.227(2)
Pt(1)−Cl	2.432(3)	Pt(2)−N	2.177(9)
Pt(1)−C(11)	2.010(10)	Pt(2)−C(5)	2.039(10)
Se−C(1)	1.931(12)	N−C(2)	1.542(18)
C(11)−Pt(1)−P(1)	92.1(3)	C(5)−Pt(2)−N	90.7(3)
C(11)−Pt(1)−Cl	178.4(3)	C(5)−Pt(2)−P(2)	88.5(3)
P(1)−Pt(1)−Cl	88.20(11)	P(2)−Pt(2)−N	178.9(2)
C(11)−Pt(1)−Se	85.1(3)	C(5)−Pt(2)−Se	174.0(3)
P(1)−Pt(1)−Se	175.23(8)	N−Pt(2)−Se	87.2(2)
Cl−P(1)−Se	94.69(8)	P(2)−Pt(2)−Se	93.64(7)
Pt(1)−Se−Pt(2)	111.69(8)	Pt(2)−N−C(2)	109.2(7)
Pt(1)−Se−C(1)	101.7(4)	Se−C(1)−C(2)	110.7(9)
		Pt(2)−Se−C(1)	95.3(4)

The comparable *trans* influence of PBu$_3$ and Ph groups is evident from the ^1J(Pt-P) values from NMR spectra. Other distances, Pt−P, Pt−Cl, Pt−N, and Pt−C are well in agreement with those reported in the literature.[16,21,23,26]

Experimental Section

All the reactions were carried out under a nitrogen atmosphere in dry, distilled analytical grade solvents to prevent oxidation of the oxygen sensitive selenolate ions. The complexes K$_2$[PtCl$_4$], *cis*-[PtCl$_2$(PPh$_3$)$_2$], *cis*-[PtCl$_2$(P−P)], *trans*-[Pt$_2$Cl$_2$(μ-Cl)$_2$(PR$_3$)$_2$], and the mixture of *cis*- and *trans*-[Pt$_2$Ph$_2$(μ-Cl)$_2$(P*n*Bu$_3$)$_2$] (P−P = dppm, dppe, dppp; PR$_3$ = PEt$_3$, P*n*Pr$_3$, P*n*Bu$_3$, PMe$_2$Ph, PMePh$_2$) were prepared by the literature methods.[31,32,33] Melting points were determined in capillary tubes and are uncorrected. Microanalyses were performed by the Analytical Chemistry Division of B.A.R.C. ^{1}H, ^{31}P{^{1}H}, ^{77}Se{^{1}H}, and ^{195}Pt{^{1}H} NMR spectra were recorded on a Bruker DPX-300 NMR spectrometer operating at 300, 121.49, 57.31, 64.52 MHz, respectively. Chemical shifts are relative to internal chloroform peak (δ = 7.26) for ^{1}H, external 85% H$_3$PO$_4$ for ^{31}P, Me$_2$Se for ^{77}Se, and Na$_2$PtCl$_6$ for ^{195}Pt. UV/Vis absorption spectra were recorded on a Bruins Instruments Omega 10 spectrophotometer. Cyclic voltammetry was carried out at 100 mV/s scan rate in dichloromethane/0.1 M Bu$_4$NPF$_6$ using a three electrode configuration (glassy carbon working electrode, Pt counter electrode, Ag/AgCl reference) and a PAR 273 potentiostat and function generator. The ferrocene/ferrocenium couple served as internal reference.

Ground state electronic structure calculations on [PtCl(SeCH$_2$CH$_2$NMe$_2$)(PPh$_3$)] have been done by density-functional theory (DFT) methods using the ADF2000.01[34,35] and Gaussian 98[36] program packages. The lowest excited states were calculated by the time dependent DFT (TD-DFT) method (both ADF and G98 programs) for the model system [PtCl(SeCH$_2$CH$_2$NMe$_2$)(PH$_3$)]. Within the ADF program, Slater type orbital (STO) basis sets of double-ζ quality with polarisation functions within the phenyl rings and triple-ζ for the rest of the system were employed. The inner shells were represented by the frozen core approximation (1s for C, N 2p for Cl, 3p for Se, and 1s−4d for Pt were kept frozen). The following density functionals were used within ADF: The local density approximation (LDA) with VWN parameterisation of electron gas data or the functional including Becke's gradient correction[37] to the local exchange expression in conjunction

with Perdew's gradient correction[38] to the LDA expression (ADF/BP). The scalar relativistic (SR) zero order regular approximation (ZORA) was used within the study. Within Gaussian-98 Dunning's polarized valence double-ζ basis sets[39] were used for C, N, Cl, and H atoms; quasirelativistic effective core pseudopotentials and a corresponding optimized set of basis functions was employed for Pt[40] and Se.[41] Becke's three parameter hybrid functional with the Lee, Yang, and Parr correction functional (B3LYP)[42] was used in Gaussian 98 calculations (G98/B3LYP). The calculation on the model system $[PtCl(SeCH_2CH_2NMe_2)(PH_3)]$ was done with the experimental geometry of the PPh_3 complex with an optimized structure of the PH_3 ligand.

1. Preparation of $[PtCl(SeCH_2CH_2NMe_2)(PEt_3)]$ (1a): To a freshly prepared methanolic solution (5 cm^3) of $NaSeCH_2CH_2NMe_2$ [prepared from $(Me_2NCH_2CH_2Se)_2$ (99.7 mg, 0.32 mmol) and $NaBH_4$ (25.4 mg, 0.67 mmol)] was added a dichloromethane solution (20 cm^3) of $[Pt_2Cl_2(\mu\text{-}Cl)_2(PEt_3)_2]$ (247.7 mg, 0.32 mmol). The reaction mixture was stirred at room temperature for 4 h. The solvents were evaporated under reduced pressure and the residue was extracted with dichloromethane (3×7 cm^3), the solution was passed through a Florisil column and the solvent removed in vacuo. The residue was recrystallised from hexane (yield 210 mg, 65%). All other mononuclear complexes $[PtCl(SeCH_2CH_2NMe_2)(PR_3)]$ (PR_3 = P*n*Pr$_3$, P*n*Bu$_3$, PMe_2Ph, $PMePh_2$) were prepared in a similar manner. Pertinent data are summarized in Table 8.

2. Preparation of $[PtCl(SeCH_2CH_2NMe_2)(PPh_3)]$ (1f): Prepared analogously as described in method **5** by using $[PtCl_2(PPh_3)_2]$ (268.8 mg, 0.34 mmol) $NaSeCH_2CH_2NMe_2$ [prepared from $(Me_2NCH_2CH_2Se)_2$ (54.4 mg, 0.18 mmol) and $NaBH_4$ (14.0 mg, 0.37 mmol)]. The residue was washed thoroughly with diethyl ether to remove liberated triphenylphosphane and then recrystallised from CH_2Cl_2/acetone mixture as yellow-orange crystals (yield 158 mg, 72%).

3. Preparation of $[PtPh(SeCH_2CH_2NMe_2)(PnBu_3)]$ (2) and $[Pt_2Ph_2Cl(SeCH_2CH_2NMe_2)(PnBu_3)_2]$ (3): Prepared analogously

Table 8. Physical, analytical and ^1H NMR spectroscopic data for dimethylaminoethaneselenolate complexes of platinum(II)

Complex	Recrystallisation solvent (% yield)	M.p. (^0C)	Analysis:Found (calcd) (%) C	H	N	^1H NMR spectroscopic data δ
$[PtCl(SeCH_2CH_2NMe_2)(PEt_3)]$ (**1a**)	hexane (65)	63	23.6 (24.0)	5.3 (5.0)	2.6 (2.8)	1.40 [d,t, 7.6 Hz (t), 17 Hz (d) PCH_2Me]; 1.86 [d,q, 7.6 Hz (q), 17 Hz (d) PCH_2-]; 2.33 [t, 6.1 Hz, ^3J(Pt-H) = 27 Hz, $SeCH_2$]; 2.75 [d, ^4J(P-H) = 2.6 Hz, ^3J(Pt-H) = 17 Hz, NMe_2]; 2.86 [d, t, 1.7 Hz (d) ^4J(P-H), J(H-H) = 7 Hz; ^3J(Pt-H) = 36 Hz, NCH_2]
$[PtCl(SeCH_2CH_2NMe_2)(PnPr_3)]$ (**1b**)	hexane (72)	87	28.3 (28.8)	6.0 (5.8)	2.8 (2.6)	1.04 (t, 7.2 Hz, PCH_2CH_2Me); 1.52−1.67 (m, PCH_2CH_2-); 1.75−1.87 (m, PCH_2-); 2.33 [t, 6.2 Hz, ^3J(Pt-H) = 27 Hz, $SeCH_2$]; 2.74 [d, ^4J(P-H) = 2.5 Hz, ^3J(Pt-H) = 15 Hz, NMe_2]; 2.85 [t, d, ^4J(P-H) = 1.5, 6 Hz (d), ^3J(Pt-H) = 37 Hz, NCH_2-]
$[PtCl(SeCH_2CH_2NMe_2)(PnBu_3)]$ (**1c**)	hexane (80)	46	32.2 (32.9)	6.3 (6.4)	2.1 (2.4)	0.85 (t, 7.1 Hz, P $CH_2CH_2CH_2Me$); 1.30−1.50 (m, $PCH_2CH_2CH_2$-); 1.72−1.80 (m, PCH_2-); 2.24 [t, 6.2 Hz, ^3J(Pt-H) = 27 Hz, $SeCH_2$]; 2.67 [d, ^4J(P-H) = 2.6 Hz, ^3J(Pt-H) = 14 Hz, NMe_2]; 2.78 [d, t, ^4J(P-H) = 1.5, 5 Hz (t), ^3J(Pt-H) = 36 Hz, NCH_2-]
$[PtCl(SeCH_2CH_2NMe_2)(PMe_2Ph)]$ (**1d**)	CH_2Cl_2/hexane (69)	156	27.3 (27.7)	3.9 (4.1)	2.5 (2.7)	1.80, 1.81 [each d, ^2J(P-H) = 11.2 Hz, ^3J(Pt-H) = 40 Hz, PMe_2]; 2.23 (br, $SeCH_2$); 2.70 [d, ^3J(P-H) = 2.2 Hz, NMe_2]; 2.85 [br, ^3J(Pt-H) = 38 Hz, NCH_2]; 7.34 (br), 7.67 (br) (Ph)
$[PtCl(SeCH_2CH_2NMe_2)(PMePh_2)]$ (**1e**)	CH_2Cl_2/hexane (45)	199(d)	34.5 (35.1)	3.7 (4.0)	2.2 (2.4)	2.23 [d, J(P-H) = 11.2, ^3J(Pt-H) = 32 Hz, PMe]; 2.21 ($SeCH_2$, merged with PMe resonance) 2.83 [d, ^4J(P-H) = 2.8 Hz, ^3J(Pt-H) = 18 Hz, NMe_2]; 2.99 [d, t, 1.6 Hz (d) ^4J(P-H), J(H-H) = 6.1 Hz; ^3J(Pt-H) = 38 Hz, NCH_2]; 7.38−7.43 (m) (Ph)
$[PtCl(SeCH_2CH_2NMe_2)(PPh_3)]$ (**1f**)	CH_2Cl_2/acetone (72)	235(d)	40.4 (41.0)	3.5 (3.9)	2.1 (2.2)	2.21 [t, 6.2 Hz ^3J(Pt-H) = 24 Hz, $SeCH_2$]; 2.88 [d, ^4J(P-H) = 2.8 Hz, ^3J(Pt-H) = 17 Hz, NMe_2]; 3.08 [d, t, (d) ^4J(P-H) = 1.5 Hz, J(H-H) = 6.2 Hz; ^3J(Pt-H) = 42 Hz, NCH_2]; 7.33−7.49 (m) 7.68−7.49 (m) (Ph)
$[PtPh(SeCH_2CH_2NMe_2)(PnBu_3)]$ (**2**)	hexane (40)	147	41.6 (42.2)	6.7 (6.8)	1.1 (2.2)	0.89 (t, 7.2 Hz, $PCH_2CH_2CH_2Me$); 1.34 (m, $PCH_2CH_2CH_2$-); 1.50 (m, PCH_2CH_2-); 2.33 [d, ^4J(P-H) = 1.9 Hz, ^3J(Pt-H) = 27 Hz, NMe_2]; 2.45 (t, 6 Hz, $SeCH_2$); 2.99 [t, d, ^4J(P-H) = 2.2 Hz; J(H-H) = 5.5 Hz, ^3J(Pt-H) = 38 Hz, NCH_2-], 6.89−7.00 (m), 7.45−7.48 (m) (Ph)
$[Pt_2Ph_2(Cl)(SeCH_2CH_2NMe_2)(PnBu_3)_2]$ (**3**)		153	41.6 (42.3)	6.8 (6.6)	1.0 (1.2)	0.90 (m, $PCH_2CH_2CH_2Me$); 1.26−1.88 (m, $PCH_2CH_2CH_2$-); 2.01 (s, NMe_2); 2.20 (br, $SeCH_2$), 2.43 (br, NCH_2), 7.38−7.57 (m, Ph)
$[Pt_2Cl_3(SeCH_2CH_2NMe_2)(PEt_3)_2]$ (**4a**)	hexane (80)	187	21.1 (21.7)	4.2 (4.6)	1.7 (1.6)	1.16 (m, PCH_2Me); 1.82−2.16 (m; PCH_2-); 2.63 (br, $SeCH_2$); 2.79 (br, NMe_2) 3.02 (br, NCH_2).
$[Pt_2Cl_3(SeCH_2CH_2NMe_2)(PMe_2Ph)_2]$ (**4b**)	hexane (87)	102	25.7 (26.0)	3.5 (3.5)	1.3 (1.5)	1.64, 1.83, 1.88, 2.04 (each d, 11.5 Hz PMe_2), 2.55 [d, ^4J(P-H) = 2.3 Hz], 3.00 [d, ^4J(P-H) = 2.8 Hz, NMe_2 1:1], 3.58 (br., NCH_2), 2.64 (br, $SeCH_2$), 7.32−7.54(m), 7.76−7.83 (m) (Ph)
$[Pt(SeCH_2CH_2NMe_2)_2(dppm)]$ (**5a**)	acetone/hexane (62)	154	44.2 (44.9)	4.8 (4.8)	3.0 (3.2)	1.96 (s, NMe_2); 2.42 (br, $SeCH_2$); 2.59 (br, NCH_2); 4.35 [t, ^2J(P-H) = 10.4 Hz; ^3J(Pt-H) = 44 Hz, PCH_2-]; 7.39−7.47 (m), 7.82−7.89 (m) (Ph)
$[Pt(SeCH_2CH_2NMe_2)_2(dppe)]$ (**5b**)	acetone/hexane (60)	184	44.8 (45.6)	4.9 (4.9)	3.0 (3.1)	2.03 (s, NMe_2); 2.15−2.56 (m, NCH_2, $SeCH_2$, PCH_2); 7.51 (br), 7.88−7.96 (m) (Ph)
$[Pt(SeCH_2CH_2NMe_2)_2(dppp)]$ (**5c**)	acetone/hexane (75)	162	44.7 (46.2)	4.8 (5.1)	2.0 (3.1)	1.88 (s, NMe_2); 1.94−2.96 (overlapping resonance due to NCH_2, $SeCH_2$, PCH_2) 7.29−7.82 (m, Ph)
$[Pt_2(SeCH_2CH_2NMe_2)_2(dppm)_2][BPh_4]_2$ (**6a**)	CH_2Cl_2/hexane (65)	84	60.6 (60.6)	5.0 (5.0)	1.1 (1.3)	2.47 (br, NMe_2); 2.74 (br, $SeCH_2$); 2.82 (br, NCH_2); 4.04 [t, ^2J(P-H) = 11 Hz PCH_2-]; 6.75−6.93 (m), 7.23−7.62 (m) (Ph)
$[Pt_2(SeCH_2CH_2NMe_2)_2(dppe)_2][BPh_4]_2$ (**6b**)	acetone/hexane (72)	126	60.3 (61.0)	5.2 (5.1)	1.4 (1.3)	1.80−1.95 (br, PCH_2); 2.34 (s, J(Pt-H) = 16 Hz NMe_2); 2.61 (br, $SeCH_2$); 3.05 [br, ^3J(Pt-H) = 45 Hz NCH_2]; 6.77−6.91 (m), 7.18−7.31 (m), 7.37−7.69 (m) (Ph)
$[Pt_2(SeCH_2CH_2NMe_2)_2(dppp)_2][BPh_4]_2$ (**6c**)	acetonehexane (60)	195	60.5 (61.3)	5.1 (5.2)	1.1 (1.3)	1.68 (br, PCH_2); 2.17 (s, NMe_2); 2.25 (br, CH_2-CH_2P), 2.49 (br, $SeCH_2$); 3.07 [br, J(Pt-H) = 46 Hz, NCH_2]; 6.87−7.06 (m); 7.42−7.64 (m) (Ph)
$[Pt(SeCH_2CH_2NMe_2)(PPh_3)]_n[PF_6]_n$ (**7**)						2.79 (s, NMe_2 + NCH_2 base of the peak broadened); 2.30 (br, $SeCH_2$); 7.34−7.70 (m) Ph.

as described in method **1** from $[Pt_2Ph_2(\mu\text{-}Cl)_2(PnBu_3)_2]$ (99.5 mg, 0.10 mmol) and $NaSeCH_2CH_2NMe_2$ [prepared from $(Me_2NCH_2CH_2Se)_2$ (32 mg, 0.11 mmol) and $NaBH_4$ (8.9 mg, 0.23 mmol)]. The ^{31}P and ^{195}Pt NMR spectra of this product exhibited three resonances. The product on recrystallization from hexane gave colourless crystals of $[PtPh(SeCH_2CH_2NMe_2)(PnBu_3)]$ (yield 29 mg, 24%). The supernatant solution on repeated recrystallization from hexane containing ≈ 5% benzene afforded $[Pt_2Ph_2(Cl)(SeCH_2CH_2NMe_2)(PnBu_3)_2]$ (54 mg, 48%).

4. Preparation of $[Pt_2Cl_3(SeCH_2CH_2NMe_2)(PEt_3)_2]$ (4a): Solid $[PtCl(SeCH_2CH_2NMe_2)(PEt_3)]$ (17.7 mg, 0.04 mmol) was mixed with $[Pt_2Cl_2(\mu\text{-}Cl)_2(PEt_3)_2]$ (13.5 mg, 0.02 mmol) in $CDCl_3$ (0.5 cm^3) in an NMR tube. After a few days the solution was dried in vacuo, the pale yellow product was washed with hexane and dried in vacuo (yield 25.0 mg, 80%).

5. Preparation of $[Pt(SeCH_2CH_2NMe_2)_2(dppe)]$ (5b): To a stirred methanolic solution (5 cm^3) of $NaSeCH_2CH_2NMe_2$ [prepared from $(Me_2NCH_2CH_2Se)_2$ (92.8 mg, 0.31 mmol) and $NaBH_4$ (23.8 mg, 0.63 mmol)] solid $[PtCl_2(dppe)]$ (201.5 mg, 0.30 mmol) was added. To this mixture dry acetone (20 cm^3) was added whereupon a yellow solution formed which was stirred for 3 h at room temperature. The solvents were stripped off under vacuum and the residue was extracted with acetone (3×7 cm^3) and filtered. The filtrate was reduced to a minimum volume (5 cm^3), a few drops of hexane were added to yield yellow crystals of the title complex (yield 163 mg, 60%).

The complexes $[Pt(SeCH_2CH_2NMe_2)_2(P-P)]$ (P−P = dppm, dppe) were prepared in an analogous manner.

6. Preparation of $[Pt_2(SeCH_2CH_2NMe_2)_2(dppm)_2][BPh_4]_2$ (6a): a) A dichloromethane suspension of (20 cm^3) of $[PtCl_2(dppm)]$ (248.9 mg, 0.38 mmol) was added to a stirred methanolic solution (5 cm^3) of $NaSeCH_2CH_2NMe_2$ [prepared from $(Me_2NCH_2CH_2Se)_2$ (59.2 mg, 0.20 mmol) and $NaBH_4$ (15.5 mg, 0.41 mmol)]. After 1 h of stirring a methanolic solution of $NaBPh_4$ (133.5 mg, 0.39 mmol) was added and the whole mixture was stirred for 3 h. Solvents were evaporated in vacuo and the residue was extracted with dichloromethane and passed through a Florisil column. The solvent was evaporated in vacuo, the residue was washed with hexane and recrystallised from a CH_2Cl_2/hexane mixture (yield 261 mg, 65%). Other cationic complexes $[Pt_2(SeCH_2CH_2NMe_2)_2(P-P)_2][BPh_4]_2$ (P−P = dppe, dppp) were prepared in a similar way.

b) To a methanolic suspension (8 cm^3) of $[PtCl_2(dppm)]$ (215.7 mg, 0.33 mmol) a methanolic solution (3 cm^3) of $NaBPh_4$ (114.2 mg, 0.33 mmol) was added and stirred for 1 h whereupon a pale yellow solution formed. To this a freshly prepared methanolic solution of $NaSeCH_2CH_2NMe_2$ [prepared from $(Me_2NCH_2CH_2Se)_2$ (51.4 mg, 0.17 mmol), $NaBH_4$ (13.2 mg, 0.35 mmol)] and 20 cm^3 of dichloromethane was added and stirred. After 3 h the solvents were stripped off under vacuum. The residue was extracted with dichloromethane (3×7 cm^3) and passed through a Florisil column. The volume of the solution was reduced to 5 cm^3. Recrystallisation from CH_2Cl_2/hexane mixture gave yellow solid (yield 216 mg, 62%).

7. Preparation of $[Pt(SeCH_2CH_2NMe_2)(PPh_3)]_n[PF_6]_n$ (7): An acetone solution (15 cm^3) of $AgPF_6$ (51 mg, 0.21 mmol) was added to solid $[PtCl(SeCH_2CH_2NMe_2)(PPh_3)]$ (116 mg, 0.20 mmol) with stirring. Silver chloride immediately precipitated with concomitant colour change from orange to pale yellow. The reactants were stirred at room temperature for 4 h. Precipitated AgCl was filtered through celite and the solvent was evaporated in vacuo. The yellow residue was examined by NMR spectroscopy.

Crystallography: X-ray data of an orange crystal of $[PtCl(SeCH_2CH_2NMe_2)(PPh_3)]$ (**1f**) (0.2×0.2×0.2 mm) and a colourless crystal of $[Pt_2Ph_2Cl(SeCH_2CH_2NMe_2)(PnBu_3)_2]$ (**3**) (0.3×0.3×0.3 mm) were collected at 173(2) K on a Siemens P3 diffractometer using graphite monochromated Mo-K_α radiation (λ = 0.71073 Å), employing the ω-2θ scan technique. The unit cell parameters (Table 9) were determined from 25 reflections each, measured by random search routine. The intensity data were

Table 9. Crystal data and structure refinement for $[PtCl(SeCH_2CH_2NMe_2)(PPh_3)]$ (**1f**) and $[Pt_2Ph_2Cl(SeCH_2CH_2NMe_2)(PnBu_3)_2]$ (**3**)

	1f	**3**
Empirical formula	$C_{22}H_{25}ClNPSePt$	$C_{43}H_{68}ClNP_2SePt_2$
Molecular mass	643.90	1165.55
Crystal system,	Monoclinic,	Triclinic,
Space group	$P2_1/n$	$P\bar{1}$
Unit cell dimensions:		
a [Å]	9.4299(19)	9.3083(19)
b [Å]	19.972(4)	15.859(3)
c [Å]	11.704(2)	16.587(3)
α [°]		108.96(3)
β [°]	95.19(3)	97.55(3)
γ [°]		93.32(3)
V [Å^3]	2175.6(8)	2282.5(8)
Z	4	4
D_c [Mg·m^{-3}]	1.966	1.924
Absorption coefficient μ [mm^{-1}]	8.326	7.938
F(000)	1232	1300
Range for data collection [°]	2.03 to 30.00	1.55 to 30.00
Refinement method	Full-matrix least-squares on $F^2>0$	Full-matrix least-squares on $F^2>0$
Reflections collected/unique	7797/6351	14091/13328
Data/restraints/parameters	6351/0/244	13328/0/419
Goodness of fit on F^2	0.937	1.092
Final R indices	$R1$ = 0.0444, $wR2$ = 0.1151	$R1$ = 0.0357, $wR2$ = 0.0838
R indices (all data)	$R1$ = 0.0574, $wR2$ = 0.1263	$R1$ = 0.0996, $wR2$ = 0.1798
Largest diff. peak and hole [e·Å^{-3}]	2.000 and −5.602	2.340 and −2.075

corrected for Lorentz polarisation and absorption effects. The structures were solved using direct methods, the mononuclear complex proved to be isostructural with the previously reported palladium analogue.[8] The non-hydrogen atoms were refined anisotropically except for the methyl carbon atoms C(23) and C(43). These two atoms were treated within a disorder model [0.62 and 0.38 for C(23) and C(23A), 0.93 and 0.07 for C(43) and C(43A)]; each of the adjacent methylene carbon atoms C(22) and C(42) was refined using two different sets of hydrogen atoms. Three of the n-butyl groups and the phenyl ligands exhibit high standard deviations, presumably due to thermal motion.

Acknowledgments

We thank Dr. J. P. Mittal and Dr. P. Raj for encouragement of this work. We are also grateful to Dr. P. K. Mathur, Head, Analytical Chemistry Division, BARC for providing the microanalysis of the compounds. Support for this work from BMBF (Project IND 99/060), the DFG, FCI (Frankfurt am Main), the Ministry of Education of the Czech Republic, and the DLR (Bonn) for KONTAKT Project CZE 00/013 is gratefully acknowledged.

[1] [1a] I. G. Dance, *Polyhedron* **1986**, *5*, 1037−1104. − [1b] P. J. Blower, J. R. Dilworth, *Coord. Chem. Rev.* **1987**, *76*, 121−185.
[2] K. Osakada, Y. Ozawa, K. Yamamoto, *J. Chem. Soc., Dalton Trans.* **1991**, 759−764.
[3] W. D. Jones, M. R. Chim, *J. Am. Chem. Soc.* **1994**, *116*, 198−203.
[4] J. R. Dilworth, N. Wheatley, *Coord Chem. Rev.* **2000**, *199*, 89−158.
[5] J. Real, M. Pages, A. Polo, J. F. Pinella, A. Alvarez-Larena, *Chem. Commun.* **1999**, 277−278.
[6] S. Narayan, V. K. Jain, K. Panneerselvam, T. H. Lu, S. F. Tung, *Polyhedron* **1999**, *18*, 1253−1258.
[7] A. Singhal, V. K. Jain, R. Misra, B. Varghese, *J. Mat. Chem.* **2000**, 1121−1124.
[8] S. Dey, V. K. Jain, S. Chaudhury, A. Knoedler, F. Lissner, W. Kaim, *J. Chem. Soc., Dalton Trans.* **2001**, 723−728.
[9] [9a] Y. Tonomura, J. Handa, Mitsubishi Paper Mills Ltd., *Jpn. Pat.* **1991**, 03126035, *Chem. Abstr.* **1991**, *115*, 218921. − [9b] T. Oota, K. Yoshioka, T. Akyama, S. Mori, *Jpn. Pat.* **1995**, 7205548, *Chem. Abstr.* **1995**, *123*, 325855j.
[10] [10a] E. S. Raper, *Coord. Chem. Rev.* **1996**, *153*, 199−255. − [10b] E. S. Raper, *Coord. Chem. Rev.* **1997**, *165*, 475−567.
[11] M. Capdevila, P. Gonzalez-Duarte, C. Foces-Foces, F. H. Cano, M. Martinez- Ripoll, *J. Chem. Soc., Dalton Trans.* **1990**, 143−149.
[12] M. Capdevila, W. Clagg, P. Gonzalez-Duarte, I. Mira, *J. Chem. Soc., Dalton Trans.* **1992**, 173−181.
[13] M. Capdevila, W. Clegg, P. Gonzalez-Duarte, B. Harris, I. Mira, J. Sola, I. C. Taylor, *J. Chem. Soc., Dalton Trans.* **1992**, 2817−2826.
[14] S. Marchal, V. Moreno, G. Aullon, S. Alvarez, M. Quiros, M. Font. Bardia, X. Solans, *Polyhedron* **1999**, *18*, 3675−3682.
[15] [15a] M. A. Malik, P. O' Brien, D. J. Otway, *Phosphorus, Sulfur, Silicon* **1998**, *136−138*, 431−446. − [15b] M. Bochmann, *Chem. Vap. Deposition* **1996**, *2*, 85−96.
[16] S. Narayan, V. K. Jain, B. Varghese, *J. Chem. Soc., Dalton Trans.* **1998**, 2359−2366.
[17] V. K. Jain, S. Chaudhury, R. Bohra, *Polyhedron* **1993**, *12*, 2377−2385.
[18] S. Chaudhury, V. K. Jain, R. P. Patel, *J. Chem. Res. (S)* **1996**, 486−487.
[19] V. K. Jain, S. Kannan, R. J. Butcher, J. P. Jasinski, *Polyhedron* **1995**, *14*, 3641−3647.
[20] A. Singhal, V. K. Jain, *Polyhedron* **1995**, *14*, 285−291.
[21] V. K. Jain, S. Kannan, R. J. Butcher, J. P. Jasinski, *J. Chem. Soc., Dalton Trans.* **1993**, 1509−1513.
[22] V. K. Jain, S. Kannan, E. R. T. Tiekink, *J. Chem. Res. (S)* **1994**, 85.
[23] A. Singhal, V. K. Jain, B. Varghese, E. R. T. Tiekink, *Inorg. Chim. Acta.* **1999**, *285*, 190−196.
[24] A. Singhal, V. K. Jain, S. Kannan, *J. Organomet. Chem.* **1993**, *447*, 317−322.
[25] A. Singhal, PhD Thesis, Mumbai University **1996**.
[26] N. K. Lokanath, D. Gowda, S. J. Prasad, S. M. Anandalwar, S. Narayan, V. K. Jain, *Analytical Science* **2000**, *17*, 565−566.
[27] S. Dey, V. K. Jain, B. Varghese, *J. Organomet. Chem.* **2001**, *623*, 48−55.
[28] V. K. Jain, S. Kannan, R. J. Butcher, J. P. Jasinski, *J. Organomet. Chem.* **1994**, *468*, 285−290.
[29] H. C. Clark, A. B. Goel, V. K. Jain, K. G. Tyers, C. S. Wong, *J. Organomet. Chem.* **1987**, *321*, 123−134.
[30] P. S. Pregosin, R. W. Kunz, *^{31}P and ^{13}C NMR of Transition Metal Phosphane complexes*, Springer Verlag, New York **1979**.
[31] F. R. Hartley, *The Chemistry of Platinum and Palladium*, Wiley, New York **1973**.
[32] J. Chatt, R. G. Willkins, *J. Chem. Soc.* **1951**, 2532−2533.
[33] A. C. Smithies, M. Rycheck, M. Orchin, *J. Organomet. Chem.* **1968**, *12*, 199−202.
[34] C. F. Guerra, J. C. Snijders, G. Te Velde, E. J. Baerends, *Theor. Chim. Acta.* **1998**, *99*, 391−403.
[35] S. J. A. van Gisbergen, J. G. Snijders, E. J. Baerends, *Comput. Phys. Commun.* **1999**, 118−122.
[36] M. J. Frisch, G. W. Trucks, H. B. Schlegel, G. E. Scuseria, M. A. Robb, J. R. Cheeseman, V. G. Zakrzewski, J. A. Montgomery, R. E. Startmenn, J. C. Burant, S. Dapprich, J. M. Millan, A. D. Daniels, K. N. Kudin, M. C. Strain, O. Farkas, J. Tomasi, V. Barone, M. Cossi, R. Cammi, B. Mennucci, C. Pomelli, C. Adamo, S. Clifford, J. Ochterski, G. A. Petersson, P. Y. Ayala, Q. Cui, K. Morokuma, D. K. Malick, A. D. Rabuck, K. Raghavachari, J. B. Foresman, J. Ciolowski, J. V. Ortiz, B. B. Stefanov, G. Liu, A. Liashenko, P. Piskorz, I. Komaromi, R. Gomperts, R. L. Martin, D. J. Fox, T. Keith, M. A. Al-Laham, C. Y. Peng, A. Narayakkara, C. Gonzalez, M. Challacombe, P. M. W. Gill, B. G. Johnson, W. Chen, M. W. Wong, J. L. Andres, M. Head-Gordon, E-S Replogle, J. A. Pople, *Gaussian 98*, *Revision A 7*; Gaussian Inc. Pittsburgh, PA **1998**.
[37] A. D. Becke, *Phys. Rev.* **1998**, *A, 38*, 3098−3105.
[38] J. P. Perdew, *Phys. Rev.* **1986**, *A33*, 8822−8829.
[39] D. E. Woon, T. H. J. Dunning, *J. Chem. Phys.* **1993**, *98*, 1358−1371.
[40] D. Andrae, U. Haeussermann, M. Dolg, H. Stoll, H. Preuss, *Theor. Chim. Acta* **1990**, *77*, 123−141.
[41] A. Bergner, M. Dolg, W. Kuechle, H. Stoll, H. Preuss, *Mol. Phys.* **1993**, *80*, 1431−1441.
[42] P. J. Stephens, F. J. Devlin, C. F. Cabalowski, M. J. Frisch, *J. Phys. Chem.* **1994**, *98*, 11623−11627.

Received April 2, 2001
[I01118]

Medium and Temperature Effects on the Redox Chemistry of Cytochrome *c*

Gianantonio Battistuzzi,[a] Marco Borsari,[a] and Marco Sola*[a]

Keywords: Cytochrome *c* / Electrochemistry / Thermodynamics / Ionic strength

Cytochromes *c* (cytc) are ubiquitous heme-containing metalloproteins that shuttle electrons in a variety of electron-transport chains, most often central to the production of the chemical energy necessary for cell life. The reduction potential ($E^{\circ\prime}$) of the $Fe^{3+/2+}$ couple is central to the physiological role of these species in that it influences the thermodynamic and kinetic features of electron-exchange reactions with redox partners. In the last two decades, voltammetric techniques exploiting the heterogeneous electron exchange between cytc and solid electrodes have proved to be particularly valuable for the determination of $E^{\circ\prime}$ values for these species and for characterizing the mechanistic and kinetic aspects of the redox process for the various cytc conformers under a variety of solution conditions. The understanding of how, and to what extent, different molecular factors control the $E^{\circ\prime}$ value in these species has been the subject of much debate. First coordination sphere effects on the heme iron and the interactions of the heme group with the surrounding polypeptide chain and the solvent are the main factors affecting $E^{\circ\prime}$ in cytc. These interactions are sensitive to medium effects such as the pH and the nature and ionic composition of the solvent. $E^{\circ\prime}$ is also strongly affected by the temperature. This article summarizes the authors' work on the effects on the selective stabilization of the two redox states of class I cytochromes *c* exerted by acid-base equilibria, general ionic strength effects, specific anion binding, the presence of non-aqueous solvents, and the temperature. The temperature dependence of $E^{\circ\prime}$ allows the determination of the enthalpy and entropy changes that accompany protein reduction. These parameters have proved to be informative with regard to the interplay between first coordination sphere effects and electrostatics at the heme–protein interface, including solvent dipoles, which mainly affect the reduction enthalpy, and solvent reorganization effects and differences in protein dynamics between the two oxidation states, which control the reduction entropy instead.

Introduction

Biological electron-transport (ET) chains in photosynthetic and aerobic and anaerobic respiratory processes are the main source of chemical energy in living systems.[1,2] Electron flow occurs among membrane-bound multi-com-

[a] Department of Chemistry, University of Modena and Reggio Emilia,
Via Campi 183, 41100 Modena, Italy
Fax: (internat.) + 39-059/373-543
E-mail: sola@unimo.it
URL: http://www.chimica.unimo.it/websola/bioichemgroup.html

Gianantonio Battistuzzi obtained his Ph.D. in Chemistry from the University of Modena (Italy) in 1996, under the supervision of Prof. M. Sola, working on the purification and the characterization of the solution behavior of electron-transfer metalloproteins. After a period in the laboratories of Professors H. Witzel and B. Krebs at the University of Münster, he held a postdoctoral position at the University of Modena, where he was appointed Assistant Professor of Inorganic Chemistry in 1999. His main research interest lies in the understanding of the molecular and solution factors influencing the thermodynamics of the reduction of electron-transfer metalloproteins, in particular cytochromes c and blue copper proteins, through a combination of electrochemical and spectroscopic techniques.

Marco Borsari obtained his Ph.D. in Chemistry from the University of Modena (Italy) in 1992, working with Prof. G. Gavioli on the characterization of the electrochemical behavior of sulfur-containing organic molecules and the determination of the nature and stability of metal complexes in solution through voltammetric and polarographic techniques. In 1992, he was appointed Assistant Professor of Physical Chemistry at the University of Modena and Reggio Emilia (Italy) and started working on the electrochemistry of metalloproteins with Marco Sola. He also established collaborations with the groups of I. Bertini and H. B. Gray. His main research activity has been directed towards the study of the redox properties of electron-transport proteins and redox enzymes, with a particular focus on the thermodynamics of the electron-transfer processes in cytochromes, blue copper, and iron–sulfur proteins.

Marco Sola obtained his Ph.D. in Chemistry from the University of Parma (Italy) in 1987. Between 1985 and 1991 he was a member of the group of I. Bertini and C. Luchinat in Florence working on NMR of paramagnetic metalloproteins. He spent 1988 as a research associate at the California Institute of Technology, Pasadena, CA, with H. B. Gray, working on iron–sulfur proteins involved in biological electron transport. From 1992, he independently pursued the characterization of the redox properties of electron-transport proteins, and with M. Borsari initiated the bio-electrochemistry group at the University of Modena. In 1992, he was also appointed Associate Professor of Chemistry at the University of Basilicata, Potenza, Italy. He then moved to the University of Bologna (1994–1997) and afterwards returned to the University of Modena, where he became Full Professor of General and Inorganic Chemistry in 2000. His main research interests have focused on structure–function relationships in redox metalloproteins and, more recently, on the issue of how the protein matrix and medium effects control the reduction potentials of cytochromes, blue copper, and iron–sulfur proteins.

MICROREVIEWS: This feature introduces the readers to the authors' research through a concise overview of the selected topic. Reference to important work from others in the field is included.

 © WILEY-VCH Verlag GmbH, 69451 Weinheim, 2001 1434–1948/01/1212–2989 $ 17.50+.50/0

ponent protein complexes that feature a variety of mono- or polynuclear metal centers (heme, type I and type II copper, and Fe-S) capable of switching between two stable oxidation states. Electrons are shuttled between these complexes by mobile carriers, which may be either organic molecules (e.g. the ubiquinone/ubihydroquinone system) or small metalloproteins such as cytochromes *c*, blue copper proteins, and iron-sulfur proteins.[1,2]

Cytochromes *c* (cytc) are ubiquitous species: their remarkable stability in vitro and ease of purification[2−5] made them the system of choice for an impressive amount of biophysical research on biological ET.[4,5] In their native form, these monomeric proteins contain one or more heme groups covalently bound to the polypeptide chain through two thioether bonds involving two cysteines; in addition, two residues (either His,Met or His,His) serve as axial ligands to the heme iron. The latter thus resides in a six-coordinate (distorted octahedral) geometry and has a typical low-spin state. Cytochromes *c* can be classified into four subclasses on the basis of their structural properties.[4] The most widely studied species belong to class I, found in both eukaryotes and prokaryotes, which are small positively charged globular proteins (M_r = 10−15 kDa) possessing a His,Met pair of axial heme iron ligands and are characterized by a largely preserved polypeptide folding. These species constitute the main focus of this article. The mitochondrial species shuttle electrons between the last two membrane-bound components of the electron-transfer chain of oxidative phosphorylation, namely ubiquinol-cytochrome *c* reductase and cytochrome *c* oxidase, whereas the species from photosynthetic bacteria, generally denoted as cytochromes c_2, act as electron donors to the photooxidized photosynthetic reaction center.[2−5]

Class III cytochromes *c* are multiheme proteins of bacterial origin featuring bis(histidine) coordination.[4−6] Classes II and IV include cytochromes *c*′, in which the heme iron is high-spin pentacoordinate with an axial histidine ligand, and bacterial tetraheme proteins containing either bis(His) or His,Met-coordinated heme.[4,5]

As for any other redox protein, the reduction potential ($E^{\circ\prime}$) is a key property of cytc. On the one hand, it regulates the biological function influencing both the thermodynamic and kinetic aspects of electron-exchange reactions with redox partners, as a result of which extensive work has been devoted to unravelling the complex interplay of molecular factors and medium effects that modulate it. On the other hand, $E^{\circ\prime}$ can be profitably exploited as a tool for the investigation of several aspects of the solution chemistry of cytc. In fact, the reduction potential of cytc is remarkably sensitive to any changes in the properties of the heme and the protein matrix, and can nowadays be measured with relative ease thanks to the development of direct electrochemical (voltammetric) techniques for redox proteins.

This article summarizes the authors' work on both the above aspects, which are closely related, focusing mainly on how the $E^{\circ\prime}$ of cytc is influenced by the ionic composition and pH of the aqueous medium, by the presence of organic solvents, and on temperature effects. The temperature dependence of $E^{\circ\prime}$ allows the determination of the enthalpy and entropy changes that accompany reduction of oxidized cytc: these parameters have proved to be informative with regard to understanding the molecular factors that control the reduction potential in these species. This aspect will also be covered in detail. No details are given here of the theoretical and experimental aspects of the voltammetric techniques or of the operational conditions that allow the attainment of fast heterogeneous electron transfer between the freely diffusing protein in solution and the solid electrode, for which the reader is referred to the original literature.[7−11] It is worth mentioning, however, that under the conditions of variable pH, temperature, and solvent composition employed in these studies, the electrochemical processes involving cytc at surface-modified gold electrodes were invariably found to be one-electron, electrochemically reversible or quasi-reversible, and diffusion-controlled (as an example, a typical cyclic voltammogram of freely diffusing native cytochrome *c* obtained on a 4-mercaptopyridine surface modified gold electrode at pH = 7 is shown in Figure 1, a). These conditions warrant that the electron transfer between the protein and the electrode is fast and that no protein adsorption and denaturation occurs at the electrode surface. Therefore, the half-wave potentials obtained from the voltammograms can be confidently assumed to represent the thermodynamic $E^{\circ\prime}$ values.

I. The Reduction Potential of the Native Form of Class I Cytochromes *c*

The native His,Met-ligated form (state III) of class I cytochromes *c* from mitochondrial and bacterial sources has reduction potentials in the range of +0.2 to +0.38 V (vs. SHE) (all the potential values reported herein are referred to the standard hydrogen electrode, SHE).[4,12] Two main factors have been recognized as contributing to these remarkably positive $E^{\circ\prime}$ values. One is the π-electron accepting character of the thioether sulfur atom of the methionine axially bound to the iron, which stabilizes the reduced (Fe^{2+}) state.[12−14] The other is the poor accessibility of the solvent to the heme and its burial within a hydrophobic pocket, which induce a further significant enthalpic stabilization of the ferrous over the ferric state.[12] Against this background, electrostatic interactions of the charge at the redox center with net charges and polar groups on the protein and solvent dipoles are responsible for the fine-tuning of $E^{\circ\prime}$.[4,5,15−18] Theoretical and experimental approaches have been directed towards an understanding of how and to what extent these interactions modulate $E^{\circ\prime}$ in cytochromes *c*.[4,5] Models for the calculation of the electrostatic interaction energies of the heme with polar and charged residues and solvent dipoles were able to reproduce the differences in $E^{\circ\prime}$ among cytc from different sources.[18−20] Evidence has been obtained from experiments involving chemical modification, site-directed mutagenesis, and specific anion binding[4,21−25] that modification of internal net charges, such as those of the heme propionates, induces variations in $E^{\circ\prime}$ (50−65 mV per charge) that

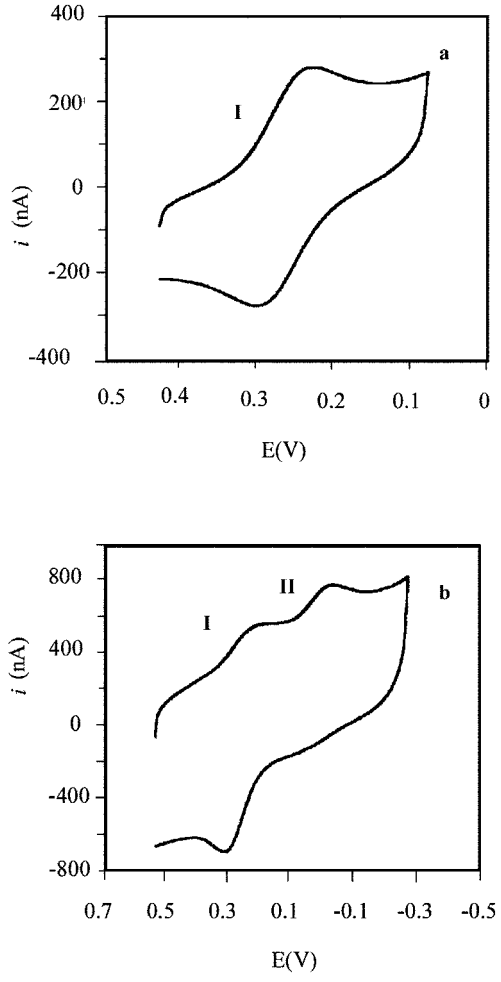

Figure 1. Cyclic voltammograms of beef heart cytochrome *c* at a 4-mercaptopyridine surface modified gold disc electrode: (a) pH = 7, $T = 293$ K, sweep rate 50 mV s^{-1}, protein concentration 0.17 mM; (b) pH = 9.13, $T = 293$ K, sweep rate 50 mV s^{-1}, protein concentration 0.25 mM; I and II refer to the waves of the native and alkaline conformers, respectively; supporting electrolyte 0.1 M sodium acetate (reproduced by permission from G. Battistuzzi et al., *Biochemistry* **1999**, *38*, 7900−7907; copyright American Chemical Society, 1999)

are more pronounced than those due to surface charges (10−30 mV per charge). The overall effect depends on several factors, such as the heme−charge distance and the dielectric properties of the intervening medium, which can be described by an "effective dielectric constant"; the latter is different for each particular interaction and involves contributions from both the solvent and the protein.[4,16,21−23,25]

Our recent work on the thermodynamics of cytc reduction, carried out by means of variable-temperature $E^{\circ\prime}$ measurements (see Section II), has elucidated the role of entropic effects in determining the reduction potential. Reduction entropy is likely to be largely controlled by differences in dynamic and solvation properties between the two redox states, although no detailed understanding of the factors involved at a molecular level has yet been achieved. However, it is clear that this thermodynamic contribution strongly affects $E^{\circ\prime}$[12] and may contribute to the differences in $E^{\circ\prime}$ between cytc from different sources, as found for other classes of electron-transport metalloproteins.[26,27]

A wealth of data is now available on the way in which the pH, temperature, ionic composition, and dielectric constant of the solvent influence the electrostatic interactions at the heme−protein/solvent interface, axial coordination to the heme iron, and the dynamic and solvation properties of both redox forms, and hence how they ultimately affect $E^{\circ\prime}$. These effects, which constitute the focus of this review, indicate that the properties of the medium exert a critical influence on the redox behavior of cytochrome *c* in vitro and, in principle, may also affect its function in vivo.

II. Temperature Dependence of $E^{\circ\prime}$: Reduction Thermodynamics

The redox behavior of class I cytochromes *c* is temperature-sensitive. The reduction potential of the conformers for which the voltammetric signal due to the Fe^{3+}/Fe^{2+} couple falls in the potential range accessible in diffusion-controlled direct electrochemistry experiments at surface-modified gold or graphite electrodes (from +1.3 to −0.60 V), namely the native His,Met-ligated form (state III) and the alkaline His,Lys-ligated form (state IV), invariably decreases with increasing temperature between 5 and 65 °C. However, the $E^{\circ\prime}/T$ profiles are pH-dependent and differ slightly for species from different sources.[12,28−37] In particular, the $E^{\circ\prime}$ of the native form of cytc from mammalian mitochondria shows a monotonic linear decrease with increasing temperature at slightly acidic and neutral pH values (Figure 2, a), whereas at higher pH values the $E^{\circ\prime}$ vs. T plot clearly becomes biphasic with a transition point at approximately 50 °C (Figure 2, b). This behavior has been ascribed to a reversible conformational transition between two states of the oxidized native form involving fractional proton loss on going from the low-T to the high-T conformer,[33] which is indeed consistent with the decrease in the transition point temperature observed with increasing pH.[12] Spectroscopic studies indicate that the low-T and high-T native conformers are not significantly different in the surroundings of the heme.[12] An additional effect of increasing temperature is a depression of the pK_a for the alkaline transition (see Section III.2).

The $E^{\circ\prime}/T$ profiles for the native form of class I cytc from plant mitochondria and photosynthetic bacteria are similar to those outlined above, but show some interesting differences (Figure 3).[12,28] In particular: (i) the transition between the low-T and high-T native forms occurs at lower pH values and lower temperatures (35−40 °C), (ii) the temperature of the transition point decreases with increasing pH, (iii) the T-induced decrease in the pK_a for the alkaline transition is more marked as compared to that of their mammalian analogues (for these species, formation of the alkaline form can be observed at pH values as low as 7−7.5 at temperatures of approximately 35−40 °C).[12,28]

The temperature dependence of $E^{\circ\prime}$ can be profitably exploited to measure the thermodynamic parameters of cytc

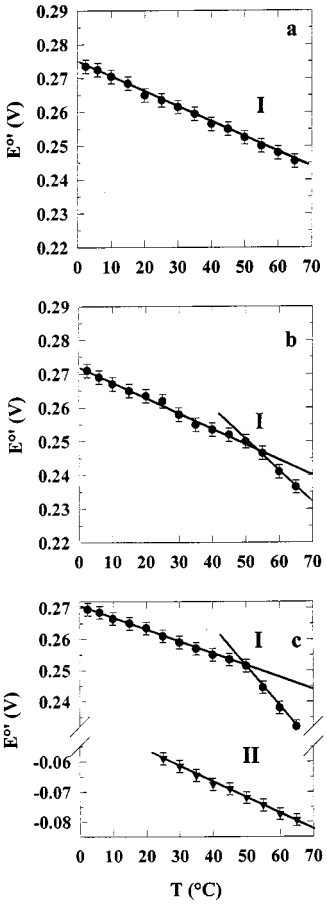

Figure 2. Temperature dependence of the reduction potential of beef heart cytochrome *c* at pH = 6.9 (a), 7.5 (b), and 8.3 (c); supporting electrolyte 0.1 M sodium chloride; solid lines are least-squares fits to the data points; I and II refer to the waves of the native and alkaline conformers, respectively (reproduced by permission from G. Battistuzzi et al., *Biochemistry* **1997**, *36*, 16247−16258; copyright American Chemical Society, 1997)

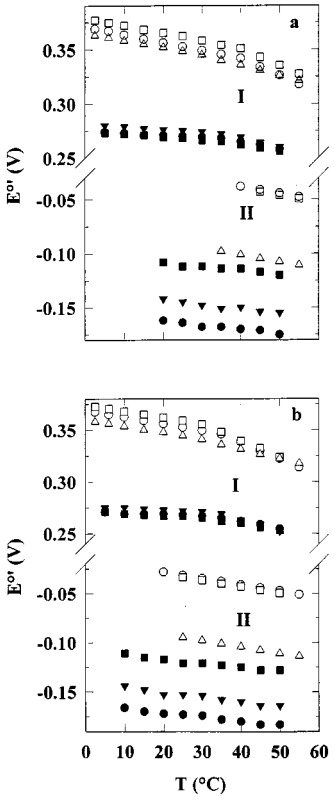

Figure 3. Temperature dependence of the reduction potentials of bacterial and plant cytochromes *c*: (a) pH = 7.5 (plant), 7 (bacterial); (b) pH = 8.5;[12,28] plant cytochromes *c*: spinach (■), cucumber (●), sweet potato (▲); bacterial cytochromes c_2: *Rps. palustris* (□), *Rb. sphaeroides* (○), *Rb. capsulatus* (Δ); supporting electrolyte 0.1 M NaCl in 10 mM phosphate buffer; least-squares fits to the data points are omitted for clarity; I and II refer to the reduction potentials of wave I (native cytc) and wave II (alkaline cytc), respectively

reduction. In particular, the use of a so-called "non-isothermal" electrochemical cell, in which the reference electrode (SCE) is kept at constant temperature while the half-cell containing the working electrode and the junction to the reference electrode is under thermostatic control,[38] allows determination of the standard entropy ($\Delta S^{\circ\prime}_{rc}$) and enthalpy ($\Delta H^{\circ\prime}_{rc}$) changes associated with reduction of the oxidized protein.[12,28,30−37] In particular, with this experimental configuration, the reaction entropy for reduction of the oxidized form is given by the following Equation.[34,38−40]

$$\Delta S^{\circ\prime}_{rc} = S^{\circ\prime}_{red} - S^{\circ\prime}_{ox} = nF\,(dE^{\circ\prime}/dT)$$

Thus, $\Delta S^{\circ\prime}_{rc}$ can be determined from the slope of the plot of $E^{\circ\prime}$ versus temperature, which turns out to be linear under the hypothesis that $\Delta S^{\circ\prime}_{rc}$ is constant over the limited temperature range investigated. With the same assumption, the enthalpy change ($\Delta H^{\circ\prime}_{rc}$) can be obtained from the Gibbs−Helmholtz equation, namely from the slope of the $E^{\circ\prime}/T$ versus $1/T$ plot.

Analysis of the thermodynamic parameters of protein reduction for several mitochondrial and bacterial class I cytochromes *c* (Table 1) allowed further insight to be gained into the interplay between the enthalpic and entropic contributions to the reduction potential (see ref.[12] for an overview on the available thermodynamic data for cytc reduction determined by several authors using a variety of techniques under different solution conditions). It can clearly be seen that the high reduction potentials of these species are largely enthalpic in origin, arising from the remarkably negative $\Delta H^{\circ\prime}_{rc}$ values, which can confidently be ascribed to the stabilization of the ferroheme by ligand binding interactions and the hydrophobicity of the heme environment.[12,28−30] Conversely, the entropic term invariably disfavors protein reduction ($\Delta S^{\circ\prime}_{rc} < 0$),[12,32] yielding a negative contribution to the $E^{\circ\prime}$ values. The entropic term is generally smaller than the enthalpic term, but it nevertheless plays an important role in the modulation of the reduction potential in these species.[12,28−30] Solvent reorganization effects and changes in protein flexibility, the latter expressed as the sum of the conformational (vibrational, torsional) degrees of freedom, associated with reduction of

cytc play a major role in determining the $\Delta S^{\circ\prime}_{rc}$ values.[3,12,28–31] In particular, the entropy loss upon reduction is consistent with the decreased flexibility of the reduced state as compared to the ferri form determined by NMR in solution.[41–45] However, it is still the case that the contribution of the reduction-induced changes in the H-bonding network within the hydration sphere of the molecule remains largely uncharacterized.

Table 1. Reduction potentials for the native and alkaline forms of class I cytochromes *c*, and $\Delta H^{\circ\prime}_{rc}$ [kJ·mol^{-1}] and $\Delta S^{\circ\prime}_{rc}$ [J·mol^{-1}·K^{-1}] values determined from the temperature dependence of the reduction potential (from refs.[12,28])

cyt *c*	pH	$E^{\circ\prime}_{N}$[a]	$E^{\circ\prime}_{A}$[a]	$\Delta S^{\circ\prime}_{rc}$[b] native	$\Delta S^{\circ\prime}_{rc}$[b] alkaline	$\Delta H^{\circ\prime}_{rc}$[b] native	$\Delta H^{\circ\prime}_{rc}$[b] alkaline
beef heart	6.9	+0.263		−44		−38	
	7.5	+0.262		−43		−38	
				−96		−55	
	8.3	+0.261	−0.075[c]	−37	−50	−36	−9
				−125		−65	
spinach	7.0	+0.268		−29		−35	
				−58		−43	
	7.5	+0.268	−0.112	−27	−33	−34	+1
				−58		−43	
	8.4	+0.267	−0.121	−20	−40	−32	0
				−58		−43	
cucumber	7.0	+0.271		−23		−33	
				−58		−44	
	7.5	+0.270	−0.164	−19	−38	−32	+4
				−64		−46	
	8.5	+0.268	−0.173	−13	−41	−30	+4
				−64		−46	
sweet potato	7.0	+0.274		−31		−36	
				−77		−50	
	7.6	+0.274	−0.145	−24	−41	−34	+2
				−79		−51	
	8.4	+0.272	−0.153	−17	−47	−31	+1
				−106		−59	
cyt c_2							
Rps. palustris	7	+0.362		−67	−62	−55	−14
				−151		−81	
	8.5	+0.359	−0.056	−60	−62	−52	−13
				−152		−80	
Rb. sphaeroides	7	+0.354		−69	−63	−55	−13
				−152		−81	
	9	+0.353	−0.054	−63	−61	−53	−13
				−154		−82	
Rb. capsulatus	7	+0.347		−66	−60	−52	−9
				−94		−61	
	9	+0.345	−0.095	−58	−61	−50	−9
				−89		−60	

[a] Subscripts N and A denote native and alkaline forms, respectively. – [b] At 25 °C. Measurements were performed in 10 mM phosphate buffer, 0.1 M NaCl. Values in the upper and lower rows for the native species refer to the low-T (N_1) and high-T (N_2) conformers, respectively. Average errors in the $\Delta H^{\circ\prime}_{rc}$ and $\Delta S^{\circ\prime}_{rc}$ values are ±2 kJ·mol^{-1} and ±6 J·mol^{-1}·K^{-1}, respectively. – [c] $E_{1/2}$ value at 55 °C for an electrochemically quasi-reversible wave (ΔE_p = 0.07 V).

A similar balance between the enthalpic and entropic contributions to the $E^{\circ\prime}$ value of cytc has been observed for all the other classes of high-potential electron-transport metalloproteins, namely blue copper proteins and high-potential iron–sulfur proteins (HiPIPs).[26,27,46,47] Therefore, it is apparent that Nature uses the same strategy to control the reduction potential of these species; the reasons for this are still unclear and define a fascinating field for future investigations.

The alkaline conformer(s) of cytc are characterized by lower (negative) $E^{\circ\prime}$ values as compared to the native conformers (Table 1). This decrease in $E^{\circ\prime}$ is almost entirely enthalpic in origin, since the $\Delta S^{\circ\prime}_{rc}$ values for this form are found to be comparable to those for the native form, whereas the $\Delta H^{\circ\prime}_{rc}$ values are much less negative (Table 1) (see Section III.2.a for details).[12,48]

III. Acid-Base Equilibria

Acid-base equilibria involving ionizable groups such as axial ligands, heme propionates, and distal residues influence the electronic properties of the heme, axial heme ligation, and polypeptide folding. Therefore, the reduction potential of class I cytc is remarkably pH-dependent.[4,5,28,49,50]

III.1. Equilibria Occurring Between Acidic and Neutral pH Values

The native His,Met-ligated form (state III) transforms into a low-pH conformer (state II) with an apparent pK_a of 2.5. In this conformer, the axial ligands are protonated and are detached from the iron (which indeed becomes high-spin): the free coordination positions are most likely occupied by water molecules.[4,5] The $E^{\circ\prime}$ of this form cannot be determined owing to the worsening of the electrochemical response at low pH caused by protonation of the promoter adsorbed onto the electrode surface and the probable disruption of the adsorbed layer.[49]

At intermediate pH values (approximately from pH = 5 to 8), the pH dependence of the reduction potential of native cytc is species-dependent. In particular, no acid/base equilibria affect the redox properties of mitochondrial (mammalian and plant) cytc in this pH range. In fact, His26 (present in all eukaryotic cytc) and the heme propionate-7 are characterized by low pK_a values. In particular, the former residue, which controls the accessibility of the solvent to the hydrophobic core of cytc influencing the global protein stability and that of the ligating Met80,[51] has a pK_a value lower than 3.6 in horse heart cytc, probably due to its non-polar environment,[4,51,52] which is maintained also in the plant proteins.[53] The pK_a of the heme propionate-7 in oxidized mammalian cytochromes *c* is lower than 4.5.[4,50] In contrast, the $E^{\circ\prime}$ values of some bacterial cytochromes c_2 have been found to be sensitive to the pro-

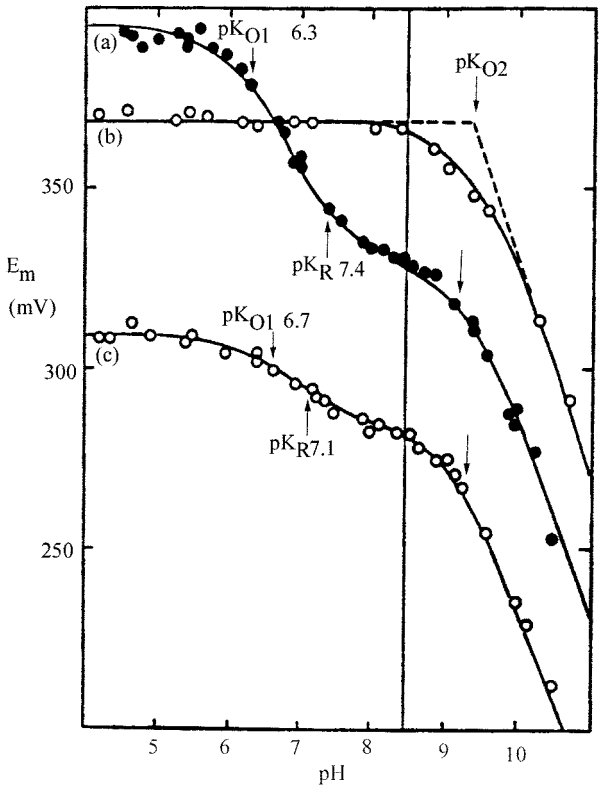

Figure 4. pH dependence of the reduction potentials of cytochromes c_2 from: (a) *Rm. vannielii*, (b) *Rps. viridis*, (c) *Rb. capsulatus* (reproduced by permission from G. R. Moore, G. W. Pettigrew *Cytochromes c: Evolutionary, Structural and Physicochemical aspects*, Springer-Verlag, Berlin, **1990**)

tonation state of a non-ligated histidine residue[4,16,22,50,54] or heme propionate, the pK_a of which falls in the range 6−8 (Figure 4).[4,50] The deprotonation of an ionizable residue induces the typical sigmoidal decrease in $E°'$ because of the electrostatic stabilization of the oxidized form due to the decrease of the overall positive charge of the protein: the extent of the change in $E°'$ depends on the solvation properties of the residue, the distance from the heme, and the properties of the intervening medium.

III.2. The Alkaline Transition

The moderate affinity of the axial methionine sulfur for the ferric ion in the native form of cytochrome *c* renders this residue susceptible to substitution by endogenous ligand(s) at high pH, leading to the "alkaline" isomer(s) (state IV), in which the iron retains the low-spin ferric state.[4,5,12,28−30,48,49,55−60] The spectroscopic and redox changes induced by this equilibrium have been exploited to determine the thermodynamics and kinetics of the isomerization, to identify the nature of the substituting ligands, and to determine the role of the residues neighboring the heme in the relative stabilization of the two conformers. The overall reaction turns out to be a two-step process, in which a fast residue deprotonation triggers a slow and thermodynamically favored conformational change leading to the replacement of the methionine by a surface lysine in axial heme ligation, with an apparent pK_a in the range 8.5−9.5 depending on the species.[4,5] The ionizable residue has not yet been unambiguously identified, and no information is available on the structural features of the alkaline conformers. The existence of two alkaline isomers in a pH-dependent ratio suggests that at least two Lys residues can replace the methionine at high pH.[28,30,48,56−59]

The alkaline conformers of cytc give rise to a single voltammetric wave (wave II) (Figure 1, b), which is diffusion-controlled and chemically irreversible at the potential sweep rates employed for detection of the voltammetric wave for native cytc (wave I) (20−200 mVs^{-1}). The reduction potentials of the alkaline isomers of various cytc's are lower than those of the native forms by 0.3−0.5 V (falling in the range −0.05 to −0.18 V) (Figure 2, c, and Figure 3).[12,28,29,48,49,55] It has been found that this remarkable decrease in the reduction potential is mainly due to the different coordination properties of methionine and lysine: the latter is a stronger donor ligand that selectively stabilizes the ferric form.[12] The chemical irreversibility of wave II is due to the fact that the reduced alkaline conformer is unstable and tends to transform rapidly into the reduced native form through the uptake of a proton. With increasing sweep rate, the reduced alkaline isomer has no time to transform prior to re-oxidation, and indeed the intensity of the anodic counterpart of wave II becomes comparable to that of the cathodic peak using scan rates higher than 0.6 V s^{-1} (for beef heart cytc).[12]

Upon increasing the pH in the range 7.5−10.5, the cathodic peak current of wave II increases to the detriment of that of native cytc, while the sum of the two currents remains constant. Moreover, at each pH value, the cathodic peak currents of both waves (as well as their $E°'$ values) are independent of the potential sweep rate in the range 0.02−1 Vs^{-1}.[48] Individual peak intensities simply depend on the root square of the scan rate, as expected for diffusion-controlled processes.[48] Thus, waves I and II turn out not to be "kinetic waves" (in the range of potential sweep rates used) and, at each pH value, their currents are those determined by the chemical equilibrium between the native and alkaline forms.[48,61] Therefore, the measured currents can be used to determine the apparent equilibrium constants. The current intensity (*i*) of the cathodic peak of wave I was measured as a function of pH at different temperatures from 5 to 65 °C.[48] The fit of the sigmoidal decrease of *i* with increasing pH to a one-proton equilibrium equation yields the apparent pK value (pK_{app}) for the alkaline transition at a given temperature (Figure 5). This value was found to decrease from 9.8 to 8.6 on increasing the temperature from 5 to 65 °C at 0.1 M ionic strength (acetate).[48] The latter effect is a direct consequence of the endothermicity of the overall process of the alkaline isomerization (see Section III.2.a).

It is worthy of note that the alkaline transition is also greatly influenced by the properties of the medium. The pK_{app} decreases with decreasing dielectric constant of the medium, as noted in mixed water/dimethyl sulfoxide solutions (see Section V).[29] This effect is of potential relevance

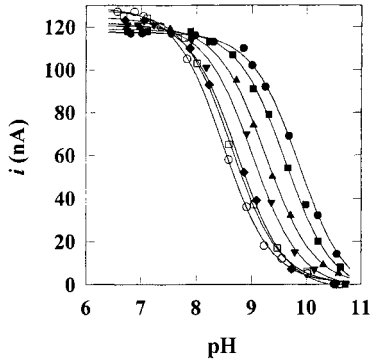

Figure 5. pH dependence of the current intensity of the cathodic peak (*i*) of wave I for beef heart cytochrome *c* at different temperatures in sodium acetate at I = 0.1 M; T [°C] = 5 (●), 10 (■), 20 (▲), 30 (▼), 40 (◆), 50 (□), and 60 (○); the pH values were corrected for temperature; solid lines are fits to a conventional one-proton equilibrium equation (reproduced by permission from G. Battistuzzi et al., *Biochemistry* **1999**, *38*, 7900−7907; copyright American Chemical Society, 1999).

from a physiological point of view since it has been reported that there is a decrease in the dielectric constant near the surface of phospholipid membranes and that the alkaline form of cytochrome *c* is involved in the interaction with synthetic anion phospholipid vesicles.[62,63] Interestingly, monoclonal antibody binding studies indicate that only the native form is present in live cells, where cytochrome *c* acts as an electron shuttle near the inner mitochondrial membrane, whereas the presence of the alkaline isomers has been detected in apoptotic and necrotic cells.[64] The alkaline isomers are formed in the early stages of apoptosis and necrosis, possibly as a result of the translocation of cytochrome *c* through the mitochondrial membrane (or of its association with membranes altered during the process of death). It is therefore possible that the phospholipid-induced conformational changes associated with the formation of the alkaline isomers are connected with the signaling role of cytochrome *c* during apoptosis, although experimental evidence seems to indicate that these isomers are not involved in the interaction with Apaf-1 to form apoptosomes.[63,64]

The pK_{app} for the alkaline transition also increases with increasing ionic strength (see Section III.2.a).[48] This is likely to be one of the factors that hampers separation of the alkaline form in the crystal state from the usually high ionic strength solutions (ammonium sulfate) used in the crystallization procedure.

Upon increasing the pH beyond 10, another state (state V) becomes accessible, in which a hydroxide ion is probably axially bound to the heme iron.[56] The remarkably low reduction potential of this species is outside the potential window accessible with the present techniques.

III.2.a The Thermodynamics of the Alkaline Transition

The thermodynamic parameters of the alkaline transition have been investigated in some detail.[48,65−67] We have measured the apparent equilibrium constant (K_{app}) of the alkaline transition (AT) of beef heart cytochrome *c* by means of pH titrations of the current intensities in cyclic voltammetry experiments. These were carried out at different temperatures (from 5 to 65 °C) and at different ionic strengths (I = 0.01−0.2 M).[48] The ionic strength of the solution was varied using acetate, which has been found not to bind specifically to beef (and horse) heart cytc, but rather to simply exert an ionic atmosphere effect (see Section IV).[23]

The temperature profile of the pK_{app} values was found to be biphasic (Figure 6). Two distinct sets of $\Delta H^{\circ\prime}_{AT}$ and $\Delta S^{\circ\prime}_{AT}$ values were obtained below and above approximately 40 °C (Table 2). In the low-temperature range, the process is endothermic and is accompanied by a small positive entropy change, whereas at higher temperatures it becomes less endothermic and involves a moderate entropy loss. Ligand substitution should not be responsible for the endothermicity of the process, given the higher affinity of the lysine nitrogen atom for the ferric ion as compared to the methionine sulfur atom. Therefore, other factors, such as transition-induced changes in the hydrogen-bond network (also including ordered water molecules on the protein surface) and in the electrostatic interactions between the metal site and the protein environment and the solvent must be responsible for the positive $\Delta H^{\circ\prime}_{AT}$ values. The slightly positive or negative $\Delta S^{\circ\prime}_{AT}$ values cannot be easily rationalized. In fact, this isomerization has been proposed to involve a number of processes, which would increase the number of degrees of freedom of the molecule, such as the net release of a proton, the formation of multiple conformers,[56−59] the opening of the heme crevice through the disruption of two key stabilizing interactions on the protein surface,[67] and the probable disruption of a hydrogen-bond network involving the internal water molecule and protein residues due to the detachment of Met80.[68] Therefore, other opposing (structure-making) processes must be operative, which most probably involve a rearrangement of the solvation sphere of the protein (in a way

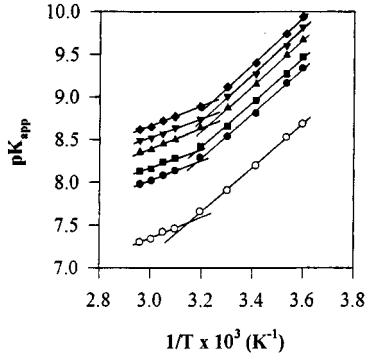

Figure 6. Apparent pK values for the alkaline transition of beef heart cytochrome *c* as a function of 1/T at various ionic strengths (sodium acetate); I = 0.01 M (●), 0.02 M (■), 0.05 M (▲), 0.1 M (▼), and 0.2 M (◆); the pK values extrapolated to I = 0 (○) are true thermodynamic equilibrium constants; solid lines are least-squares fits to the data points (reproduced by permission from G. Battistuzzi et al., *Biochemistry* **1999**, *38*, 7900−7907; copyright American Chemical Society, 1999)

Table 2. Thermodynamic parameters for the alkaline transition (AT) of beef heart ferricytochrome *c* at various ionic strengths obtained from the pK_{app} vs. $1/T$ plots of Figure 6 (from ref.[48])

I [M][a]	$f(I)$	$\Delta H^{\circ\prime}_{AT}$ [kJ·mol^{-1}][b] low-T[c]	high-T	$\Delta S^{\circ\prime}_{AT}$ [J·mol^{-1}·K^{-1}][b] low-T	high-T
0[d]	0	+49	+23	+12	−70
0.01	0.063	+52	+23	+8	−86
0.02	0.076	+52	+22	+5	−90
0.05	0.096	+52	+24	+1	−88
0.1	0.109	+52	+21	−1	−100
0.2	0.12	+53	+22	0	−98

[a] Sodium acetate. − [b] Average errors in the $\Delta H^{\circ\prime}_{AT}$ and $\Delta S^{\circ\prime}_{AT}$ values are ±2 kJ·mol^{-1} and ±6 J·mol^{-1}·K^{-1}, respectively. − [c] Enthalpy and entropy values in the low-T and high-T ranges refer to the N_1 and N_2 conformers, respectively (see text). − [d] Data obtained from the pK_a values extrapolated at $f(I) = 0$ at various temperatures (see Figure 6). These values are true standard thermodynamic parameters.

which is presently unknown, but that might involve formation of internally hydrogen-bonded ordered molecular arrays within the hydrophobic heme crevice or a net release of water molecules from the hydration sphere of the protein to the bulk solvent) and/or a suppression of vibrational, rotational, and torsional motions in the A form as compared to the N form. However, no clear definition of the molecular details of the processes underlying the entropy change is yet available.

The change in transition thermodynamics observed above approximately 40 °C is most likely the result of the thermal transition of native ferricytochrome *c* from a low-T to a high-T conformer, which occurs at alkaline pH values at a comparable temperature (see Section II). Thus, it is apparent that the transitions of the two native conformers to the corresponding alkaline forms are thermodynamically distinct processes. It is suggested that this difference either arises from peculiar transition-induced changes in the hydration sphere of the protein or is due to the preferential binding of different lysines to the heme iron in the two temperature ranges. Extrapolation of the K_{app} values at zero ionic strength allowed determination of the thermodynamic equilibrium constants (K_a) at each temperature, and hence of the "true" standard thermodynamic parameters of the transition. The pK_a value at 25 °C was found to be 8.0. A pK_{app} value of 14.4 was calculated for the alkaline transition of ferrocytochrome *c* at 25 °C and I = 0.1 M. The much greater relative stabilization of the native state in the reduced as compared to the oxidized form turns out to be almost entirely enthalpic in origin, and is most likely due to the greater affinity of the methionine sulfur for the Fe^{II} ion.[48]

The pK_{app} values for the alkaline transition of cytc are influenced by the ionic strength in a fashion that can be explained, at least qualitatively, by the finite-ion version of the Debye−Hückel theory,[48] analogously to the ionic strength dependence of the reduction potential (see Section IV). In particular, the pK_{app} values measured at different ionic strengths were found to conform to Equation (1).

$$pK_{app} = pK_a + 0.5(z^2_{cytH} - z^2_{cyt^-}) \cdot \frac{\sqrt{I}}{1+6\sqrt{I}} = pK_a + 0.5(z^2_{cytH} - z^2_{cyt^-}) \cdot f(I) \quad (1)$$

Here, z_{cytH} and z_{cyt^-} are the net charges of the neutral and alkaline forms, respectively (Figure 7).[4,69] The slope of the plots (approximately +10) is almost twice that expected from the net charges of the native and alkaline forms, namely $0.5\cdot(6^2 - 5^2) = +5.5$. This difference is most likely due to the intrinsic limits of the Debye−Hückel theory as applied to a complex electrolyte such as a protein (see below), although it might also be due to the specific binding of one acetate ion to a surface site of the alkaline form. In fact, although the acetate ion was shown not to interact specifically with neutral cytc, nothing is known about its interaction with the alkaline conformer.

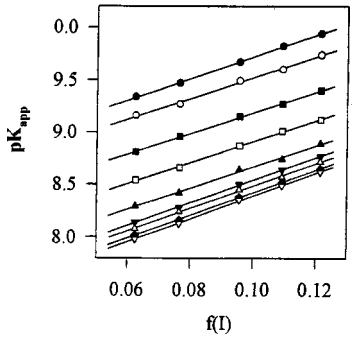

Figure 7. Apparent pK values for the alkaline transition of beef heart cytochrome *c* as a function of $f(I) = \sqrt{I}/(1 + 6\sqrt{I})$ at various temperatures; T [°C] = 5 (●), 10 (○), 20 (■), 30 (□), 40 (▲), 50 (▼), 55 (Δ), 60 (◆), 65 (▽); solid lines are least-squares fits to the data points (reproduced by permission from G. Battistuzzi et al., *Biochemistry* **1999**, *38*, 7900−7907; copyright American Chemical Society, 1999)

Comparison of the $\Delta H^{\circ\prime}_{AT}$ and $\Delta S^{\circ\prime}_{AT}$ values at different ionic strengths (Table 2) indicates that the increase in the pK_{app} values with increasing ionic strength is almost entirely entropic in origin. Thus, the expected selective stabilization of the native conformer (which has one more positive charge than the alkaline form) by the negative ionic atmosphere that surrounds the protein has little or no effect. This result cannot be readily rationalized at present owing to the uncertainty regarding the factors responsible for the transition entropy.

IV. The Effects of the Ionic Composition of the (Aqueous) Medium on $E^{\circ\prime}$

The ionic composition of the medium is known to affect the interaction of cytc with redox partners[70] and phospholipid membranes.[71] Salt-induced effects on the reduction potential of cytc are of two types: (i) changes in the activity coefficients of both redox states, known as "general" ionic strength effects; (ii) specific protein−anion interactions at surface sites (cytc is positively charged at neutral pH). The former effect is related to the shielding of the protein charge

by the surrounding "ionic atmosphere", which is greater for the oxidized state since it bears the greater positive charge. As a consequence, the oxidized state will be selectively stabilized with respect to the reduced state, leading to a decrease in the reduction potential with increasing ionic strength (see Section IV.2). A combination of the Nernst and extended Debye−Hückel equations, using a model in which the protein behaves as a low dielectric cavity bearing a net charge uniformly distributed on the surface, with no specific ion−protein interactions, yields Equation (2) for the changes in $E^{\circ\prime}$ of cytc induced by the ionic atmosphere.[4,72,73]

$$E^0 = E^0_{I=0} + 2.303 \cdot \frac{RT}{nF} \cdot \left[z^2_{red} - z^2_{ox}\right] \cdot \frac{0.5 \cdot \sqrt{I}}{1 + 0.33 \cdot a \cdot \sqrt{I}} \quad (2)$$

Here, I is the ionic strength, $E^\circ_{I=0}$ is the reduction potential extrapolated to zero ionic strength, z_{red} and z_{ox} are the charges of the reduced and oxidized protein, and a is the "ion-size parameter", defined as the mean distance of closest approach between the protein and an ion of opposite charge belonging to the ionic atmosphere. The value of a lies between the sum of the crystallographic radii and the sum of the solvated radii. An a value of 18 Å has been used for bovine ferricytochrome *c*. By defining Equation (3), Equation (2) becomes Equation (4) which predicts a linear decrease in E° with increasing $f(I)$, with a slope given by $0.059 \cdot (z^2_{red} - z^2_{ox})$.

$$f(I) = (0.5\sqrt{I})/(1 + 0.33a\sqrt{I}) \quad (3)$$

$$E^\circ = E^\circ_{I=0} + 0.059(z^2_{red} - z^2_{ox})f(I) \quad (4)$$

Despite the roughness of the model, especially regarding the dielectric properties of the polypeptide matrix, this approach proved to be surprisingly effective in describing the ionic strength dependence of $E^{\circ\prime}$ for native and chemically modified class I cytochromes *c*.[21−23,69,72−74] This might be ascribed, at least in part, to the facts that these species are roughly spherical, that there are only subtle oxidation state induced structural changes[42,46,75] (which fits with an implicit assumption of the model), and that the metal center is almost totally embedded in the protein matrix. Indeed, we found that the Debye−Hückel theory works less well for the cucumber basic protein (which possesses a type I copper center), in which the metal site is more exposed to the solvent (hence the dielectric constant of the metal environment can no longer be regarded as low and homogeneous) and which shows more pronounced oxidation state induced changes in solvation properties and a stronger asymmetry in charge distribution as compared to cytochrome *c*.[76,77]

Specific binding of anions to surface sites of cytc (intended as more or less localized surface regions of positively charged potential),[78] occurring either on one or both redox states, would result in a decrease in the net positive protein charge, related to the charge of the anion and the number of protein-bound anions. This would alter the slope of the $E^{\circ\prime}/f(I)$ profile as compared to the free protein. Therefore, the above equations were exploited to detect specific anion−cytc interactions and to determine the stoichiometry of binding for a wide variety of anions either occurring in biological systems in vivo (such as Cl^-, HPO_4^{2-}, HCO_3^-), or used as components of buffer systems in vitro (NO_3^-, SO_4^{2-}, citrate^{3-}, oxalate^{2-}).[21−23] Several anions were found to possess peculiar binding properties,[78,79] often including sequential binding due to the presence of multiple protein binding sites with different affinities for the anion.[21−23] In parallel, these studies allowed evaluation of the electrostatic effect on $E^{\circ\prime}$ resulting from anion-induced neutralization of net positive protein surface charge(s). In the following we will briefly illustrate some details of the binding properties of biologically important anions and the relationships between surface charges and $E^{\circ\prime}$ which were obtained with this approach.

IV.1. Specific Anion Binding Effects

IV.1.a. Anion−Protein Binding Stoichiometries

Some examples of the $E^{\circ\prime}$ vs. $f(I)$ plots obtained for bovine and horse heart cytochromes *c* interacting with different anions are shown in Figure 8. Linear plots are invariably obtained, according to Equation (4), showing either a constant slope or biphasic behavior. The latter plots, which yield two sets of protein charges at low and high anion concentrations, are interpreted as being indicative of sequential anion binding. The protein charges obtained from the slopes of the plots allowed an estimate to be made of the number of anions bound to the two redox states of bovine and horse heart cytc, which are listed in Table 3[23] [it is worth noting that evaluation of *two* unknowns, z_{red} and z_{ox}, from only *one* experimental parameter ($z^2_{red} - z^2_{ox}$) can only be achieved by introducing a number of constraints on the charge values, for which the reader is referred to the original literature].[21−23] The main results can be summarized as follows: (i) all anions other than acetate interact specifically with both proteins, (ii) in many cases, the number of anions bound per protein molecule increases with increasing anion concentration, indicating sequential anion binding due to the presence of low and high affinity sites, (iii) chloride and phosphate bind to both species to a greater extent as compared to the other anions and show different binding stoichiometries toward the two closely sequence-related proteins (97% identity). In particular, one less chloride ion binds to the bovine protein as compared to the equine species: it is tempting to attribute this effect to the presence of one less lysine residue in the bovine species as compared to the horse species (a Gly residue in the former replaces Lys60 in the latter). However, since Lys60 is proposed as not being directly involved in the anion binding sites,[69,80] the observed effect is likely to be due to a decrease in the overall positive charge of bovine cytc and to a change in the distribution of the surface electrostatic potential.

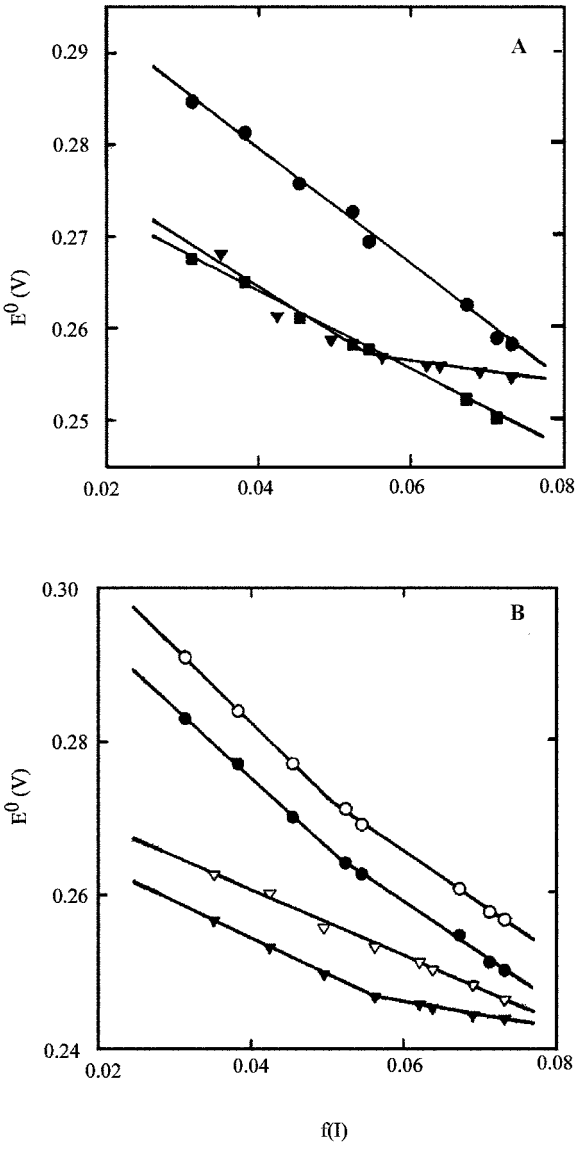

Figure 8. Selected $E^{\circ\prime}$ vs. $f(I)$ plots for horse and bovine heart cytochromes *c* in the presence of various anions: (A) bovine protein with acetate (●), sulfate (▼), bicarbonate (■); (B) bovine protein with chloride (●) and oxalate (▼); horse protein with chloride (○) and oxalate (▽); solid straight lines are fits to Equation (4) (reproduced by permission from G. Battistuzzi et al., *Eur. J. Biochem.* **1996**, *241*, 208−214; copyright Blackwell Science Ltd., 1996)

The presence of two phosphate binding sites on the horse protein at low anion/protein molar ratios was also indicated by different approaches, some of which involved chemical modification of surface lysines.[69,79,81−85] With increasing anion concentration, the electrochemical data indicate the binding of a third phosphate anion (except to the reduced horse protein). As also indicated by ion chromatography data,[69] phosphate displays a distinct binding preference toward the oxidized forms of both proteins as compared to the reduced forms. This is in contrast to chloride, which shows the opposite behavior. This indicates that for both proteins the lysine-based binding sites for the two anions are different and are subject to different reduction-induced changes that affect anion affinity. In addition, phosphate, unlike chloride, binds to a greater extent to the bovine cytochrome, in spite of the smaller positive charge as compared to the horse species. No obvious explanation for this effect can be offered at present. As noted elsewhere,[69] these facts demonstrate that even a few amino acid substitutions perturb the positive surface potential field of the protein in such a way as to significantly alter the number, magnitude, and/or location of the potential energy minima for anion interaction.

Only one bicarbonate ion binds to both of these proteins, in agreement with studies of chemical modification of surface lysines, from which it was proposed that lysines 72 and/or 73 and 86 and/or 87 are involved in anion binding.[79] It is possible that one of the nitrate binding sites corresponds to the bicarbonate site, in view of the structural similarity of the two anions.

Sulfate and citrate show the same binding properties. For both proteins and redox states, the number of anions bound per protein molecule increases from one to two with increasing anion concentration. This suggests the presence of two protein sites with different affinities for the two anions in both of the cytochromes, possibly corresponding to those for phosphate, given the close similarity of sulfate and phosphate in terms of geometry, dimensions, and charge. Consistently, citrate has previously been shown to have at least one binding site in common with phosphate.[67,79,86]

Given that a number of anions show different binding stoichiometries toward horse and bovine cytc, which are highly sequence-related, the anion binding data for a bacterial cytochrome c_2 from *Rps. palustris* (which shows only about 38% sequence identity with the mitochondrial species) were expected to be quite distinctive. However, it has been found that, although some anions such as chloride, phosphate (at concentrations below 0.06−0.08 M), acetate, and oxalate do indeed show peculiar binding properties toward different species (e.g. chloride does not bind to the bacterial species), many others, including perchlorate, bicarbonate, nitrate, phosphate (at concentrations above 0.06−0.08 M), sulfate, and citrate exhibit the same binding stoichiometries (Table 3).[21−23] These two groups of anions do not differ in their structural and charge characteristics, or in their ability to form hydrogen bonds, hence intrinsic anion properties are not responsible for this distinct behavior. Therefore, the invariance of the binding data for the latter group of anions is most probably a consequence of the fact that the binding sites are maintained in the different species: this would suggest the existence of (a) more or less extended region(s) of relatively conserved electrostatic potential in the three cytochromes. It is known that the distribution of lysines around the perimeter of the heme crevice at the "front" of the molecule is largely retained in eukaryotic cytochromes *c* and bacterial cytochromes c_2, which also share the main features of the overall polypeptide folding.[87−91] This also appears to be the case for *Rps. palustris* cytochrome c_2.[21] No other regions show analogous similarities in the location of lysine residues. As a consequence, the "frontside" region of these cytochromes,

Table 3. Number *n* of specifically bound anions for horse and bovine heart cytochromes *c* and *Rps. palustris* cyt c_2, determined from the ionic strength dependence of the redox potential in the presence of various anions, according to Equation (2); $T = 25$ °C; measurements for chloride, perchlorate, nitrate, and sulfate were carried out at pH = 7; for the basic anions the pH varied from 8 to 9.3 depending on anion concentration; in the case of sequential anion binding, values in the upper and lower rows refer to low and high anion concentrations, respectively (from refs.[21−23])

Anion	Bovine cyt *c*			Horse cyt *c*			*Rps. palustris* cyt c_2		
	c [M]	n_{ox}	n_{red}	*c* [M]	n_{ox}	n_{red}	*c* [M]	n_{ox}	n_{red}
Cl^-		1	2		2	3		0	0
	> 0.04	2	3	> 0.04	3	4			
ClO_4^-		1	1		1	0		1	1
				> 0.02	1	1			
HCO_3^-		1	1		1	0		1	1
				> 0.02	1	1			
CH_3COO^-		0	0		0	0		1	1
NO_3^-		1	2		1	2		1	2
HPO_4^{2-}		3	2		2	2		1	1
	> 0.08	3	3	> 0.06	3	2	> 0.06	3	3
SO_4^{2-}		1	1		1	1		1	1
	> 0.08	2	2	> 0.08	2	2	> 0.1	2	1 (2)
$C_2O_4^{2-}$		1	1		1	1		2	1 (2)
	> 0.06	2	2				> 0.08	3	3
$citrate^{3-}$		1	1		1	1		1	1
	> 0.1	2	2	> 0.1	2	2	> 0.08	2	2

which has been proposed to correspond to the likely site of interaction with physiological oxidoreductases,[91−94] should also serve as a site of interaction with a number of anions. Accordingly, the proposed binding site for the bicarbonate ion to the horse protein[79] as well as the common binding site for phosphate and citrate (''Phosphate Site I'' formed by Lys86, Lys87, and Lys88)[79,81,82] fall in this region. As a consequence, the sites for chloride and acetate, as well as the additional low-affinity site(s) for phosphate, are probably located elsewhere.

IV.1.b. Relationships between Surface Charges and $E^{\circ\prime}$

The role of net surface charges in determining the reduction potential in redox metalloproteins has been the subject of much debate.[16,18,95−98] In the various protein families, net charges contribute to the $E^{\circ\prime}$ value only by approximately 10−30 mV per charge, depending on their location with respect to the metal center. These data were obtained through mutation or chemical modification of surface residues and pH titration studies. This moderate effect can mainly be attributed to the screening of the coulombic interaction by the dielectric effect of water. However, recent work from this laboratory[99] has shown that enthalpy-entropy compensation phenomena also contribute in minimizing the resulting $E^{\circ\prime}$ change.

Anion binding to specific surface sites of cytochrome *c* may be exploited as an additional tool to monitor the effect of changes in charge on the $E^{\circ\prime}$ value.[21−23] In fact, since NMR and X-ray data indicate that increasing anion concentrations induce only minor structural modifications, which leave the overall protein folding and conformational flexibility of the molecule largely unaffected,[44,100] it is reasonable to assume that the $E^{\circ\prime}$ change caused by specific anion binding is mainly electrostatic in origin, due to the partial neutralization of positive surface charges. The relationships between $E^{\circ\prime}$ and charge were obtained as follows.[21−23] When only one anion is bound per protein molecule, in both redox states, extrapolation of the linear $E^{\circ\prime}$ vs. $f(I)$ plot to $f(I) = 0$ allows determination of the $E^{\circ\prime}$ value at zero ionic strength ($E^{\circ\prime}_{I=0}$) for the protein, the surface charge of which is decreased by that of the bound anion. The value $E^{\circ\prime}_{I=0}$ for the ion-free protein is taken as that extrapolated in the plot for the non-binding anion (acetate and chloride for the mitochondrial and bacterial species, respectively). The difference between $E^{\circ\prime}_{I=0}$ for the ion-free and the electrostatically perturbed protein ($\Delta E^{\circ\prime}_{I=0}$) yields an estimate of the fall in reduction potential due to the neutralization of *n* positive surface charges (at zero ionic strength). The $\Delta E^{\circ\prime}_{I=0}$ and $dE^{\circ\prime}/dq \cdot (dE^{\circ\prime}/dq$ = change in $E^{\circ\prime}$ per unit charge) values obtained for the three cytochromes studied are listed in Table 4. A number of observations can be made. First, the $dE^{\circ\prime}/dq$ values for the multiply charged anions, such as sulfate, oxalate, and citrate, interacting with the mitochondrial species range from 14.6 to 16.5 mV. They are intermediate between the theoretical value of 12 mV predicted by the smeared charge model for a sphere of radius 1.5 nm in water[4] and 23 mV determined from a comparison of the reduction potentials of a series of proteins bearing different charges.[101] They compare very well with the $dE^{\circ\prime}/dq$ value at zero ionic strength of 11−14 mV determined from mutation of surface lysines,[102] while they appear to be somewhat higher than the 5−10 mV estimated from chemical modification and pH titration studies.[4] Second, the $dE^{\circ\prime}/dq$ values for the two monovalent anions, perchlorate and bicarbonate, are somewhat greater, especially those for the latter ion (24 and 25 mV for beef and horse heart cytc, respectively). This may be due to a closer approach of these anions to the heme, consistent with the existence of a specific ''bicarbonate site''.[79]

Table 4. $\Delta E^{\circ\prime}_{I=0}$ and $dE^{\circ\prime}/dq$ values (see text) for beef and horse heart cytochromes *c* and *Rps. palustris* cytochrome c_2 determined upon anion binding to one site in both redox states of the proteins (from refs.[21−23])

Anion	$\Delta E^{\circ\prime}_{I=0}$ [mV]			$dE^{\circ\prime}/dq$		
	horse	bovine	*Rps. palustris* cyt c_2	horse	bovine	*Rps. palustris* cyt c_2
ClO_4^-	21	20	23	21	20	23
HCO_3^-	25	24	33	25	24	33
SO_4^{2-}	31	31	31	15.5	15.5	15.5
$C_2O_4^{2-}$	33	33	–	16.5	16.5	–
$citrate^{3-}$	44	45	41	14.6	15	14
CH_3COO^-	–	–	28	–	–	28
HPO_4^{2-}	–	–	32	–	–	16

Overall, the $dE^{\circ\prime}/dq$ values determined using the present approach are in line with those previously estimated for mutated or chemically modified species. The picture that emerges is that the effect of alteration of one net surface charge of the protein on the reduction potential of the heme, although being small, as discussed above, is measurable and is also significant at physiological ionic strengths. Thus, besides the general ionic strength effects related to the charge shielding of the protein as a whole due to the surrounding ionic atmosphere, the ionic composition of the medium may also induce protein charge neutralization at specific site(s), which determines an additional alteration (decrease) in the reduction potential. Hence, the salt effects on the rate of electron transfer between cytochrome *c* and redox partners may not only be due to changes in orientation and/or distance of the redox centers in the complex, but a contribution may also arise from changes in the driving force.

IV.1.c. Effects on the Alkaline Transition

Recently, the thermodynamic parameters of the alkaline transition of beef heart ferricytochrome *c* have been measured using the procedure illustrated in Section II.2.a in the presence of various sulfate concentrations.[103] Sulfate is known to bind specifically to cytochrome *c* in a sequential manner at two surface sites.[23] It has been found that the effects of such a specific binding reflect the thermodynamics of the transition and can be satisfactorily interpreted within the frame of the Debye−Hückel theory with simple electrostatic considerations. In particular, the increase in the thermodynamic pK_a values (extrapolated to $I = 0$) upon sequential sulfate binding turns out to be a fully enthalpic effect, which can be accounted for, at least qualitatively, simply by considering the coulombic effects of charge modification due to the formation of ionic couple(s) on the protein surface. In particular, according to Equation (1), the pK_{app} values increase linearly with increasing $f(I)$ (Figure 9). It is worthy of note that: (i) the discontinuity in the pK_{app} vs. $f(I)$ plot corresponds to the sulfate concentration (0.08 M) above which the number of sulfate anions specifically bound to the protein is known to increase from one to two;[23] (ii) the measured slopes are in close agreement with those expected from the decrease in protein charge upon binding of one and two binegative anions to both the alkaline and neutral isomers. These two observations, taken together, clearly indicate that the biphasic profile of the pK_a values as a function of sulfate concentration is the result of the electrostatic effect of sequential anion binding to protein surface sites.

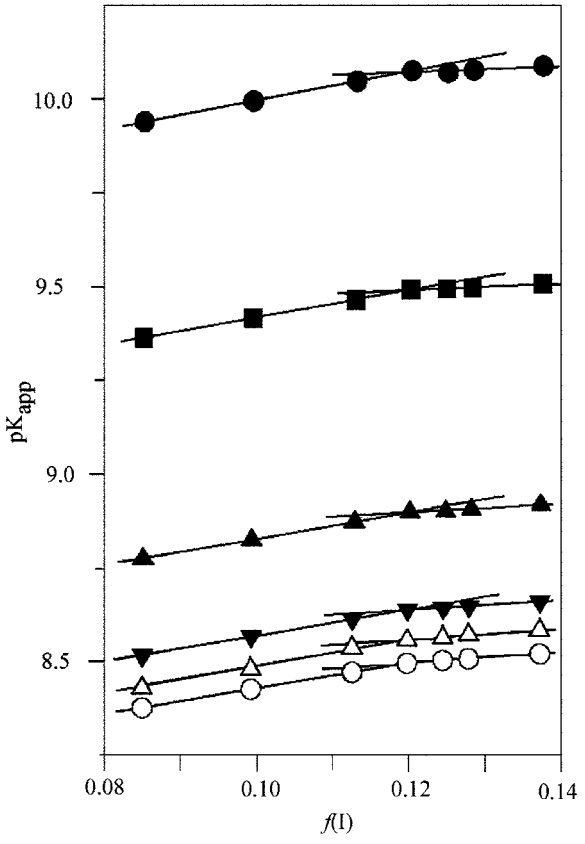

Figure 9. Apparent p*K* values for the alkaline transition of beef heart cytochrome *c* as a function of $f(I) = \sqrt{I}/(1 + 6\sqrt{I})$ (sodium sulfate) at various temperatures; *T* [°C] = 5 (●), 20 (■), 40 (▲), 50 (▼), 55 (Δ), 60 (○); solid lines are least-squares fits to the data points (reproduced by permission from G. Battistuzzi et al., *Arch. Biochem. Biophys.* **2001**, *386*, 177−122; copyright Academic Press, 2001)

IV.2. General Ionic Strength ("Ionic Atmosphere") Effects

The reduction potential of native beef heart cytochrome *c* has been measured as a function of the temperature in the presence of increasing concentrations of the non-binding

anion acetate, in order to quantify the influence of the general ionic strength effect, namely of non-specific electrostatic interactions due to the ionic atmosphere that surrounds the protein, on the thermodynamics of protein reduction.[30] Most of the previous investigations on salt-induced effects on the physicochemical properties of cytochromes *c* were carried out using either phosphate or chloride to adjust the ionic strength of the solution, which, as seen above, do in fact bind specifically to both redox states of cytochrome *c*.[21−23,69,79] The $E^{\circ\prime}/T$ profiles at different ionic strengths and the $E^{\circ\prime}/f(I)$ plots at different temperatures measured at three pH values (7, 8, and 9) are shown in Figure 10 and Figure 11, respectively. At pH = 7 and 8, the reduction enthalpy and entropy become less negative with decreasing ionic strength. The reduction entropy extrapolated to zero ionic strength is approximately zero, indicating that in the absence of the screening effects of the salt ions on the network of the electrostatic interactions at the protein−solvent interface, the solvation properties and the conformational flexibilities of the two redox states are comparable. At the same pH values, the reduction potential of cytc slightly decreases with increasing ionic strength at constant temperature (Figure 11). For example, $\Delta E^{\circ\prime}{}_{IS} = (E^{\circ\prime})_{I=0.1\,M} - (E^{\circ\prime})_{I=0\,M} = -0.035$ V at 25 °C, which corresponds to a $\Delta\Delta G^{\circ\prime}{}_{IS}$ value of +3.3 kJ·mol^{-1}.[30] Since X-ray and NMR studies have shown that salt effects do not alter the overall protein folding and the conformational flexibility of cytc,[100,104−106] the positive $\Delta\Delta G^{\circ\prime}{}_{IS}$ value can mainly be attributed to the selective stabilization of the ferri form by the exclusively electrostatic effects of the salt ions. Such a free energy change turns out to be composed of a $\Delta\Delta H^{\circ\prime}{}_{IS}$ [$= (\Delta H^{\circ\prime})_{I=0.1\,M} - (\Delta H^{\circ\prime})_{I=0\,M}$] term of −8.5 kJ·mol^{-1} and a $T\Delta\Delta S^{\circ\prime}{}_{IS}$ term of −11.8 kJ·mol^{-1} (analogous quantitative relationships between the enthalpic and entropic terms hold at the other pH values and temperatures).[30] Enthalpy-entropy compensation phenomena in the hydration of biopolymers[107−111] must be taken into account to identify the molecular effect responsible for the positive value of $\Delta\Delta G^{\circ\prime}{}_{IS}$. In particular, since the salt-induced changes in the hydration sphere of the two redox states of cytc are likely to be responsible for the negative $T\Delta\Delta S^{\circ\prime}{}_{IS}$ term, a compensating enthalpic effect of the same sign and magnitude should contribute to the measured $\Delta\Delta H^{\circ\prime}{}_{IS}$. Thus, once the compensating enthalpic and entropic effects of the change in solvation properties are factorized out, the measured $\Delta\Delta G^{\circ\prime}{}_{IS}$ value of +3.3 kJ·mol^{-1} turns out to be entirely due to a $\Delta\Delta H^{\circ\prime}$ term attributable to the electrostatic effect of the negatively charged ionic atmosphere that surrounds cytc, which should indeed stabilize the ferri form (which bears a greater positive charge than the reduced state). This would nicely explain why at pH = 7 the $E^{\circ\prime}$ vs. $f(I)$ plot follows the simple electrostatic model of the extended Debye−Hückel equation [Equation (4)], yielding a negative slope that at most temperatures is that expected for the unperturbed protein ($z_{red} = 5+$ and $z_{ox} = 6+$). Notably, at pH = 8, the gradient of such a slope decreases, and at pH = 9 it becomes positive (Figure 11, b, c).[30] We attribute this effect to the specific binding of the hydroxide ion to surface sites of the protein, which results in a decrease in the positive charge of both redox states. The positive slope at pH = 9 would indicate that such a binding occurs preferentially to the oxidized form, as observed elsewhere for a number of anions.[21−23,69]

V. The Effects of Non-Aqueous Solvents

Solvent−solute interactions play a significant role in determining the reduction potentials of redox metalloproteins, affecting both the enthalpic and entropic contributions to the free energy change of the reduction process.[26,27,29] Some theoretical models reproduce the experimental $E^{\circ\prime}$ values of families of homologous ET proteins reasonably well, treating the solvent as a dielectric continuum.[95,112−115]

It has been proposed that there is a decrease in the dielectric constant near the surface of the cell membrane, which induces conformational transitions in some proteins that are central to their physiological role.[116−118] The behavior of cytochrome *c* has been investigated in mixed water/alcohol solutions of low average dielectric constant and at low pH, conditions that, in principle, simulate those in the proximity of the inner mitochondrial membrane.[116,119,120] Two alcohol-induced conformational transitions have been detected at intermediate and high alcohol concentrations. The former leads to a compact species which retains most of the secondary structure of the native state but lacks most features of the tertiary structure (molten globular state), whereas the latter is a more helical state that differs from the extensively unfolded state obtained at high concentrations of strong denaturants such as guanidine hydrochloride or urea.[116] Much less is known about the effects of other organic solvents, or about the redox properties of cytochrome *c* in not purely aqueous media in general. We have investigated the redox behavior of bovine heart cytc in mixed water/dimethyl sulfoxide (DMSO) solutions containing up to 40% (v/v) DMSO. We used cyclic voltammetry, under varying conditions of temperature and pH, and we also monitored the effects on protein conformation by means of ^{1}H NMR and circular dichroism.[29] The main observations can be summarized as follows. The redox behavior of cytc in solutions containing less than 10% DMSO is very similar to that in water. An increase in the proportion of DMSO induces a number of effects, which are different for the native and alkaline forms. Regarding the native form, at constant temperature, its $E^{\circ\prime}$ decreases to a similar extent as that determined in aqueous solution following an increase in temperature reproducing the same dielectric constant as that of the mixed solvent. This indicates that the effect of DMSO on $E^{\circ\prime}$ is mainly determined by the decrease in the average dielectric constant of the solvent. It would appear that DMSO does not significantly alter the protein conformation, as indicated by the absence of appreciable DMSO-induced changes in the hyperfine-shifted ^{1}H NMR resonances and CD spectra of native cytc. Regarding

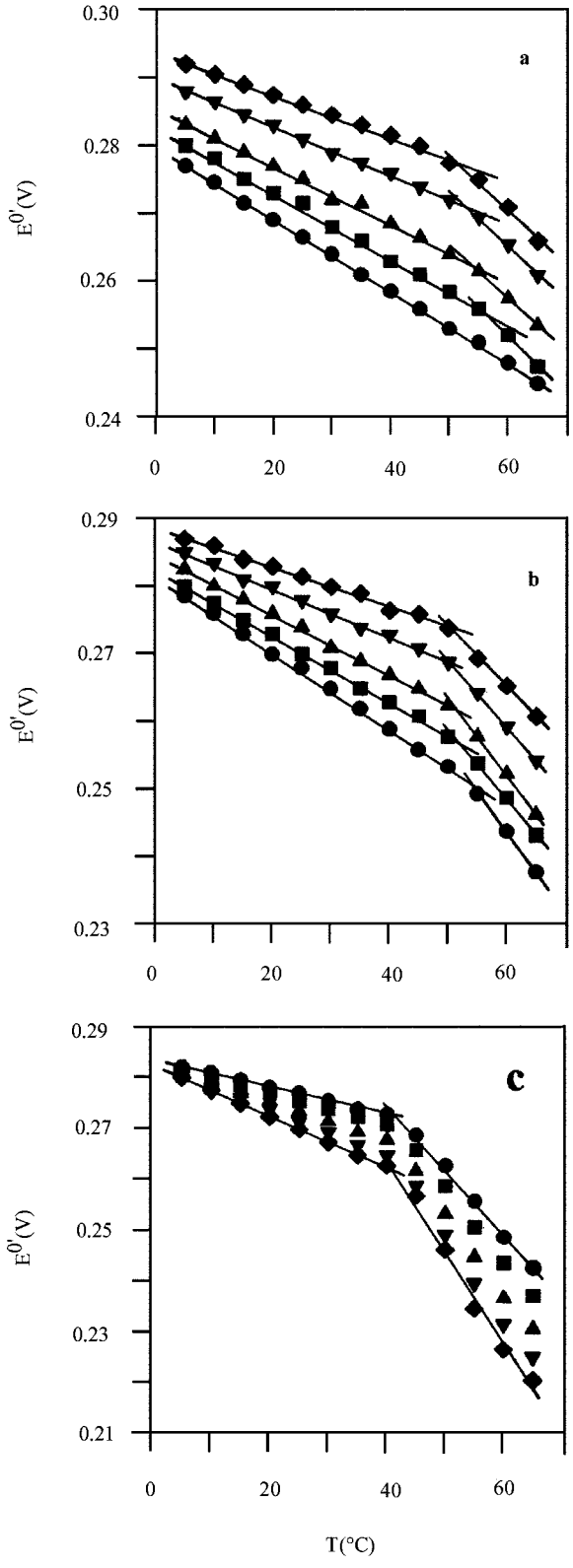

Figure 10. Temperature dependence of the reduction potential of beef heart cytochrome *c* at various ionic strengths (sodium acetate); I = 0.01 M (◆), 0.02 M (▼), 0.05 M (▲), 0.1 M (■), and 0.2 M (●); (a) pH = 7, (b) pH = 8, (c) pH = 9; solid lines are least-squares fits to the data points [those for intermediate ionic strength in (c) are omitted for clarity] (reproduced by permission from G. Battistuzzi et al., *J. Biol. Inorg. Chem.* **1999**, *4*, 601−607; copyright Springer, 1999)

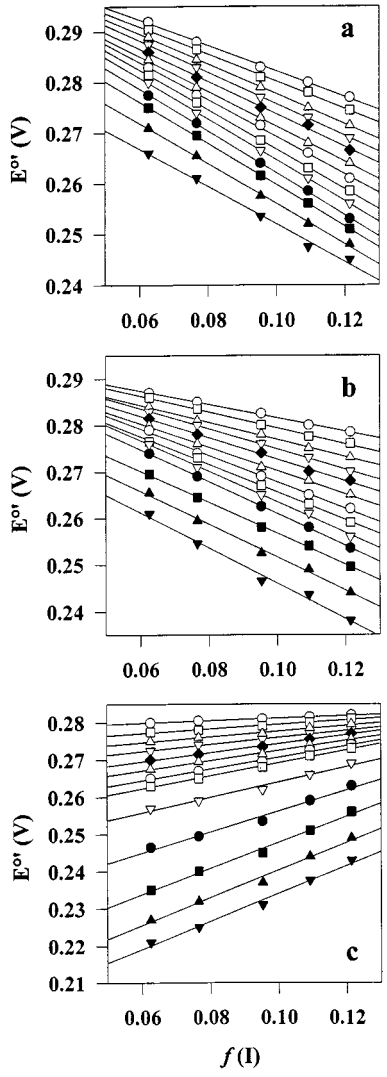

Figure 11. Reduction potential of beef heart cytochrome *c* as a function of $f(I) = \sqrt{I}/(1 + 6\sqrt{I})$ at various temperatures; T [°C] = 5 (○), 10 (□), 15 (Δ), 20 (▽), 25 (◆), 30 (Δ), 35 (○), 40 (□), 45 (▽), 50 (●), 55 (■), 60 (▲), 65 (▼); (a) pH = 7, (b) pH = 8, (c) pH = 9; solid lines are least-squares fits to the data points (reproduced by permission from G. Battistuzzi et al., *J. Biol. Inorg. Chem.* **1999**, *4*, 601−607; copyright Springer, 1999)

the alkaline form(s), at constant pH, the electrochemical wave corresponding to the alkaline conformer(s) of cytc (wave II) increases in intensity to the detriment of wave I (Figure 12). This is paralleled by a decrease in the apparent pK_a value for the transition of native cytc to the alkaline form, estimated from the pH dependence of the peak currents (not shown). Moreover, the electrochemical reversibility of wave II increases (Figure 12) and detectable changes are observed in the ^{1}H NMR and CD spectra of the alkaline form. These data indicate that, in contrast to the native form, DMSO affects to some extent the conformation of alkaline cytc and stabilizes both redox states of this form to the detriment of the native form. The latter effect is not unexpected since the alkaline species is less positively charged and therefore should be preferentially stabilized over the neutral species by a decrease in solvent polarity.

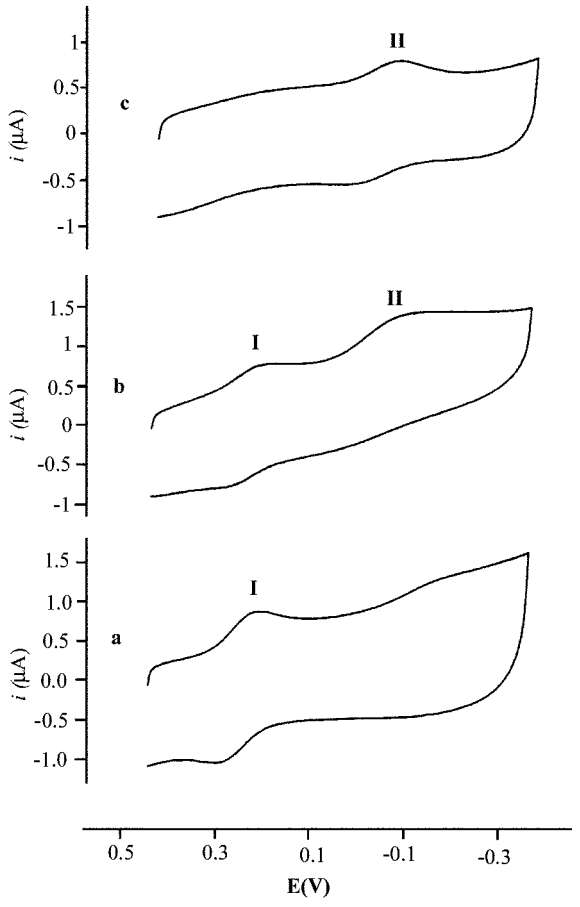

Figure 12. Cyclic voltammograms for bovine heart cytc at a 4-mercaptopyridine surface-modified gold electrode in (a) water, pH = 6.7; (b) 30% DMSO, pH* = 6.1; (c) 40% DMSO, pH* = 6.3; scan rate 50 mVs^{-1}; waves I and II are due to native and alkaline cytc, respectively; protein concentration 0.2 mM; T = 55 °C (this fairly high temperature allows the effects of DMSO on the current and reversibility of wave II to be better visualized) (reproduced by permission from G. Battistuzzi et al., *Inorg. Chim. Acta* **1998**, *272*, 168−175; copyright Elsevier Science S.A., 1998)

The highly homologous horse heart cytc was previously found to behave in a similar manner in water/methanol mixtures at pH = 6.[121]

[1] J. A. Cowan, *Inorganic Biochemistry: An Introduction*, Wiley-VCH, New York, **1996**.
[2] H. B. Gray, W. R. Ellis, in *Bioinorganic Chemistry* (Eds.: I. Bertini, H. B. Gray, S. J. Lippard, J. S. Valentine), University Science Books, Mill Valley, CA, **1994**, chapter 6, p. 315−363.
[3] L. Banci, I. Bertini, A. Rosato, G. Varani, *J. Biol. Inorg. Chem.* **1999**, *4*, 824−837.
[4] G. R. Moore, G. W. Pettigrew, *Cytochromes c: Evolutionary, Structural and Physicochemical aspects*, Springer-Verlag, Berlin, **1990**.
[5] R. Scott, A. G. Mauk, *Cytochrome c: A Multidisciplinary Approach*, University Science Books, Sausalito, CA, **1996.**
[6] G. W. Pettigrew, G. R. Moore, *Cytochromes c: Biological Aspects*, Springer-Verlag, Berlin, **1987**.
[7] F. A. Armstrong, *Struct. Bonding* **1990**, *72*, 137−222.
[8] F. M. Hawkridge, I. Taniguchi, *Comments Inorg. Chem.* **1995**, *17*, 163−187.
[9] M. J. Eddowes, H. A. O. Hill, *J. Am. Chem. Soc.* **1979**, *101*, 4461−4464.
[10] H. A. O. Hill, N. I. Hunt, *Methods Enzymol.* **1993**, *227*, 501−522.
[11] A. M. Bond, *Inorg. Chim. Acta* **1994**, *226*, 293−340.
[12] G. Battistuzzi, M. Borsari, M. Sola, F. Francia, *Biochemistry* **1997**, *36*, 16247−16258.
[13] J. C. Marchon, T. Mashiko, C. A. Reed, in *Electron Transport and Oxygen Utilization* (Ed.: H. Chien), Elsevier, Amsterdam, **1982**, p. 67−72.
[14] F. A. Tezcan, J. R. Winkler, H. B. Gray, *J. Am. Chem. Soc.* **1998**, *120*, 13383−13388.
[15] M. R. Gunner, E. Alexov, E. Torres, S. Lipovaca, *J. Biol. Inorg. Chem.* **1997**, *2*, 126−134.
[16] A. G. Mauk, G. R. Moore, *J. Biol. Inorg. Chem.* **1997**, *2*, 119−125.
[17] P. J. Stephens, D. R. Jollie, A. Warshel, *Chem. Rev.* **1996**, *96*, 2491−2513.
[18] A. Warshel, A. Papazyan, I. Muegge, *J. Biol. Inorg. Chem.* **1997**, *2*, 143−152.
[19] A. K. Churg, A. Warshel, *Biochemistry* **1986**, *25*, 1675−1681.
[20] N. K. Rogers, *Prog. Biophys. Mol. Biol.* **1986**, *48*, 37−66.
[21] G. Battistuzzi, M. Borsari, M. Sola, *Arch. Biochem. Biophys.* **1997**, *339*, 283−290.
[22] G. Battistuzzi, M. Borsari, D. Dallari, S. Ferretti, M. Sola, *Eur. J. Biochem.* **1995**, *233*, 335−339.
[23] G. Battistuzzi, M. Borsari, D. Dallari, I. Lancellotti, M. Sola, *Eur. J. Biochem.* **1996**, *241*, 208−214.
[24] R. L. Cutler, A. M. Davies, S. Creighton, A. Warshel, G. R. Moore, M. Smith, A. G. Mauk, *Biochemistry* **1989**, *28*, 3188−3197.
[25] S. P. Rafferty, L. L. Pearce, P. D. Barker, J. G. Guillemette, C. M. Kay, M. Smith, A. G. Mauk, *Biochemistry* **1990**, *29*, 9365−9369.
[26] G. Battistuzzi, M. Borsari, L. Loschi, F. Righi, M. Sola, *J. Am. Chem. Soc.* **1999**, *121*, 501−506.
[27] G. Battistuzzi, M. Borsari, A. L. Macedo, J. J. G. Moura, P. Rodrigues, M. Sola, *J. Biol. Inorg. Chem.* **2000**, *5*, 748−760.
[28] G. Battistuzzi, M. Borsari, J. A. Cowan, C. Eicken, L. Loschi, M. Sola, *Biochemistry* **1999**, *38*, 5553−5562.
[29] G. Battistuzzi, M. Borsari, G. Rossi, M. Sola, *Inorg. Chim. Acta* **1998**, *272*, 168−175.
[30] G. Battistuzzi, M. Borsari, L. Loschi, M. Sola, *J. Biol. Inorg. Chem.* **1999**, *4*, 601−607.
[31] S. Benini, M. Borsari, S. Ciurli, A. Dikiy, M. Lamborghini, *J. Biol. Inorg. Chem.* **1998**, *3*, 371−382.
[32] P. Bertrand, O. Mbarki, M. Asso, L. Blanchard, F. Guerlesquin, M. Tegoni, *Biochemistry* **1995**, *34*, 11071−11079.
[33] T. Ikeshoji, I. Taniguchi, F. M. Hawkridge, *J. Electroanal. Chem.* **1989**, *270*, 297−308.
[34] K. B. Koller, F. M. Hawkridge, *J. Am. Chem. Soc.* **1985**, *107*, 7412−7417.
[35] K. B. Koller, F. M. Hawkridge, *J. Electroanal. Chem.* **1988**, *239*, 291−306.
[36] I. Taniguchi, T. Funatsu, M. Iseki, H. Yamaguchi, K. Yasukouchi, *J. Electroanal. Chem.* **1985**, *193*, 295−302.
[37] I. Taniguchi, M. Iseki, T. Eto, K. Toyosawa, H. Yamaguchi, K. Yasukouchi, *Bioelectrochem. Bioenerg.* **1984**, *13*, 373−383.
[38] E. L. Yee, R. J. Cave, K. L. Guyer, P. D. Tyma, M. J. Weaver, *J. Am. Chem. Soc.* **1979**, *101*, 1131−1137.
[39] E. L. Yee, M. J. Weaver, *Inorg. Chem.* **1980**, *19*, 1077−1079.
[40] V. T. Taniguchi, N. Sailasuta-Scott, F. C. Anson, H. B. Gray, *Pure Appl. Chem.* **1980**, *52*, 2275−2281.
[41] P. Baistrocchi, L. Banci, I. Bertini, P. Turano, K. L. Bren, H. B. Gray, *Biochemistry* **1996**, *35*, 13788−13796.
[42] L. Banci, I. Bertini, H. B. Gray, C. Luchinat, T. Redding, A. Rosato, P. Turano, *Biochemistry* **1997**, *36*, 9867−9877.
[43] L. Banci, I. Bertini, J. G. Huber, G. A. Spyroulias, P. Turano, *J. Biol. Inorg. Chem.* **1999**, *4*, 21−31.

[44] L. Banci, I. Bertini, T. Redding, P. Turano, *Eur. J. Biochem.* **1997**, *256*, 271−278.
[45] L. Banci, G. Gori-Savellini, P. Turano, *Eur. J. Biochem.* **1997**, *249*, 716−723.
[46] A. Soriano, D. Li, S. Bian, A. Agarwal, J. A. Cowan, *Biochemistry* **1996**, *35*, 12479−12486.
[47] H. A. Heering, Y. B. M. Bulsink, W. R. Hagen, T. E. Meyer, *Biochemistry* **1995**, *34*, 14675−14686.
[48] G. Battistuzzi, M. Borsari, L. Loschi, M. Martinelli, M. Sola, *Biochemistry* **1999**, *38*, 7900−7907.
[49] G. Battistuzzi, M. Borsari, S. Ferretti, M. Sola, E. Soliani, *Eur. J. Biochem.* **1995**, *232*, 206−213.
[50] G. R. Moore, D. E. Harris, F. A. Leitch, G. W. Pettigrew, *Biochim. Biophys. Acta* **1984**, *764*, 331−342.
[51] W. Qin, R. Sanishvili, B. Plotkin, A. Schejter, E. Margoliash, *Biochim. Biophys. Acta* **1995**, *1252*, 87−94.
[52] J. S. Cohen, W. R. Fischer, A. N. Schechter, *J. Biol. Chem.* **1974**, *249*, 1113−1118.
[53] H. Ochi, Y. Hata, N. Tanaka, M. Kakudo, T. Sakurai, S. Aihara, Y. Morita, *J. Mol. Biol.* **1983**, *166*, 407−418.
[54] G. W. Pettigrew, R. G. Bartsch, T. E. Meyer, M. D. Kamen, *Biochim. Biophys. Acta* **1978**, *503*, 509−523.
[55] P. D. Barker, A. G. Mauk, *J. Am. Chem. Soc.* **1992**, *114*, 3619−3624.
[56] S. Döpner, P. Hildebrandt, F. I. Rosell, A. G. Mauk, *J. Am. Chem. Soc.* **1998**, *120*, 11246−11255.
[57] J. C. Ferrer, J. G. Guillemette, R. Bogumil, S. C. Inglis, M. Smith, A. G. Mauk, *J. Am. Chem. Soc.* **1993**, *115*, 7507−7508.
[58] X. Hong, D. W. Dixon, *FEBS Lett.* **1989**, *246*, 105−108.
[59] F. I. Rosell, J. C. Ferrer, A. G. Mauk, *J. Am. Chem. Soc.* **1998**, *120*, 11234−11245.
[60] G. Taler, A. Schejter, G. Navon, I. Vig, E. Margoliash, *Biochemistry* **1995**, *34*, 14209−14212.
[61] K. S. Nicholson, I. Shain, *Anal. Chem.* **1964**, *36*, 706−723.
[62] P. J. Spooner, A. Watts, *Biochemistry* **1991**, *30*, 3871−3879.
[63] P. J. Spooner, A. Watts, *Biochemistry* **1992**, *31*, 10129−10138.
[64] R. Jemmerson, J. Liu, D. Hansauer, K.-P. Lam, A. Mondino, R. D. Nelson, *Biochemistry* **1999**, *38*, 3599−3609.
[65] M. T. Wilson, C. Greenwood, *Eur. J. Biochem.* **1971**, *22*, 11−18.
[66] A. Schejter, P. George, *Biochemistry* **1965**, *3*, 1045−1049.
[67] N. Osheroff, D. Borden, W. H. Koppenol, E. Margoliash, *J. Biol. Chem.* **1980**, *255*, 1689−1697.
[68] A. Schejter, T. L. Luntz, T. I. Koshy, E. Margoliash, *Biochemistry* **1992**, *31*, 8336−8343.
[69] D. Gopal, G. S. Wilson, R. A. Earl, M. A. Cusanovich, *J. Biol. Chem.* **1988**, *263*, 11652−11656.
[70] F. Millett, M. A. Miller, L. Green, B. Durham, *J. Bioenerg. Biomembr.* **1995**, *27*, 341−351.
[71] T. Heimburg, D. Marsh, *Biophys. J.* **1995**, *68*, 536−546.
[72] T. Goldkorn, A. Schejter, *Arch. Biochem. Biophys.* **1976**, *177*, 39−45.
[73] R. Margalit, A. Schejter, *Eur. J. Biochem.* **1973**, *32*, 492−499.
[74] I. Aviram, Y. P. Myer, A. Schejter, *J. Biol. Chem.* **1981**, *256*, 5540−5544.
[75] L. Banci, I. Bertini, K. L. Bren, H. B. Gray, P. Sompornpisut, P. Turano, *Biochemistry* **1997**, *36*, 8992−9001.
[76] G. Battistuzzi, M. Borsari, L. Loschi, M. Sola, *J. Biol. Inorg. Chem.* **1997**, *2*, 350−359.
[77] J. M. Guss, E. A. Merritt, R. P. Phizackerley, H. C. Freeman, *J. Mol. Biol.* **1996**, *262*, 686−705.
[78] C. O. Arean, G. R. Moore, G. Williams, R. J. P. Williams, *Eur. J. Biochem.* **1988**, *173*, 607−615.
[79] N. Osheroff, D. L. Brautigan, E. Margoliash, *Proc. Natl. Acad. Sci. USA* **1980**, *77*, 4439−4443.
[80] G. R. Moore, G. C. S. Eley, G. Williams, in *Advances in Inorganic and Bioinorganic Mechanisms* (Ed.: A. G. Sykes), Academic Press, New York, **1984**, chapter 1, p. 1.
[81] D. L. Brautigan, S. Ferguson-Miller, E. Margoliash, *J. Biol. Chem.* **1978**, *253*, 130−139.
[82] D. L. Brautigan, S. Ferguson-Miller, G. E. Tarr, E. Margoliash, *J. Biol. Chem.* **1978**, *253*, 140−148.
[83] S. Ferguson-Miller, D. L. Brautigan, E. Margoliash, *J. Biol. Chem.* **1978**, *253*, 149−159.
[84] E. Stellwagen, R. G. Shulman, *J. Mol. Biol.* **1973**, *75*, 683−695.
[85] J. K. Dethmers, S. Ferguson-Miller, E. Margoliash, *J. Biol. Chem.* **1979**, *254*, 11973−11981.
[86] G. H. Barlow, E. Margoliash, *J. Biol. Chem.* **1966**, *241*, 1473−1477.
[87] S. Sogabe, T. Ezoe, N. Kasai, M. Saeda, A. Uno, M. Miki, K. Miki, *FEBS Lett.* **1994**, *345*, 5−8.
[88] M. M. Benning, G. Wesemberg, M. S. Caffrey, R. G. Bartsch, T. E. Meyer, M. A. Cusanovich, I. Rayment, H. M. Holden, *J. Mol. Biol.* **1991**, *220*, 673−685.
[89] F. R. Salemme, S. T. Freer, Ng. H. Xuong, R. A. Alden, J. Kraut, *J. Biol. Chem.* **1973**, *248*, 3910−3921.
[90] M. M. Benning, T. E. Meyer, H. M. Holden, *Arch. Biochem. Biophys.* **1994**, *310*, 460−466.
[91] F. R. Salemme, J. Kraut, M. D. Kamen, *J. Biol. Chem.* **1973**, *248*, 7701−7716.
[92] J. Hall, X. Zha, B. Durham, P. O'Brien, B. Vieira, D. Davis, M. Y. Okamura, F. Millet, *Biochemistry* **1987**, *26*, 4494−4500.
[93] J. E. Long, B. Durham, M. Y. Okamura, F. Millet, *Biochemistry* **1989**, *28*, 6970−6974.
[94] C. Weber, B. Michel, H. R. Bosshard, *Proc. Natl. Acad. Sci. USA* **1987**, *84*, 6687−6691.
[95] H.-X. Zhou, *J. Biol. Inorg. Chem.* **1997**, *2*, 109−113.
[96] I. Bertini, G. Gori-Savellini, C. Luchinat, *J. Biol. Inorg. Chem.* **1997**, *2*, 114−118.
[97] Q. Zeng, E. T. Smith, D. M. Kurtz, R. A. Scott, *Inorg. Chim. Acta* **1996**, *242*, 245−251.
[98] F. A. Armstrong, *J. Biol. Inorg. Chem.* **1997**, *2*, 139−142.
[99] M. Sola, unpublished results.
[100] R. Sanishvili, K. W. Volz, E. M. Westbrook, E. Margoliash, *Structure* **1995**, *3*, 707−716.
[101] D. C. Rees, *Proc. Natl. Acad. Sci. USA* **1985**, *82*, 3082−3085.
[102] M. S. Caffrey, M. A. Cusanovich, *Arch. Biochem. Biophys.* **1991**, *285*, 227−230.
[103] G. Battistuzzi, M. Borsari, A. Ranieri, M. Sola, *Arch. Biochem. Biophys.* **2001**, *386*, 117−122.
[104] Y. Feng, S. W. Englander, *Biochemistry* **1990**, *29*, 3505−3509.
[105] L. Banci, I. Bertini, T. Reddig, P. Turano, *Eur. J. Biochem.* **1998**, *256*, 271−278.
[106] G. Liu, C. A. Grygon, T. E. Spiro, *Biochemistry* **1989**, *28*, 5046−5050.
[107] W. Blokzijl, J. B. N. F. Engberts, *Angew. Chem. Int. Ed. Engl.* **1993**, *32*, 1545−1579.
[108] E. Grunwald, *J. Am. Chem. Soc.* **1986**, *108*, 5726−5731.
[109] R. Lumry, S. Rajender, *Biopolymers* **1970**, *9*, 1125−1227.
[110] N. Matubayasi, L. H. Reed, R. M. Levy, *J. Phys. Chem.* **1994**, *98*, 10640−10649.
[111] B. Lee, G. Graziano, *J. Am. Chem. Soc.* **1996**, *118*, 5163−5168.
[112] P. J. Stephens, D. R. Jollie, A. Warshel, *Chem. Rev.* **1996**, *96*, 2491−2513.
[113] A. K. Churg, A. Warshel, *Biochemistry* **1986**, *25*, 1675−1681.
[114] R. Langen, G. M. Jensen, U. Jacob, P. J. Stephens, A. Warshel, *J. Biol. Chem.* **1992**, *267*, 25625−25627.
[115] H.-X. Zhou, *J. Am. Chem. Soc.* **1994**, *116*, 10362−10375.
[116] V. E. Bychkova, A. F. Dujsekina, S. I. Klenin, E. I. Tiktopulo, V. N. Uversky, O. B. Ptitsyn, *Biochemistry* **1996**, *35*, 6058−6063.
[117] F. G. Van der Goot, J. M. Gonzales-Mañas, J. H. Lakey, F. Pattus, *Nature* **1991**, *354*, 408−410.
[118] O. B. Ptitsyn, *Adv. Protein Chem.* **1995**, *47*, 83−229.
[119] P. Fan, C. Bracken, J. Baum, *Biochemistry* **1993**, *32*, 463−479.
[120] K. Shiraki, K. Nishikawa, Y. Goto, *J. Mol. Biol.* **1995**, *245*, 180−192.
[121] H. R. Drew, R. E. Dickerson, *J. Biol. Chem.* **1978**, *253*, 8420−8427.

Received March 14, 2001
[I01098]

Rhodium-Catalysed Carbonylation of Methanol Using a New Multifunctional Ligand − Isolation and Structural Characterisation of the Macrocycle $[Rh_2I_6(CO)_2(C_6H_4N_3CH_2CO_2C_4H_2SCO_2CH_2C_6H_4N_3)]_2$

Christophe M. Thomas,[a] Antonia Neels,[a] Helen Stœckli-Evans,[a] and Georg Süss-Fink*[a]

Dedicated in profound gratitude to Professor Max Herberhold on the occasion of his 65th birthday

Keywords: Rhodium / Nitrogen ligands / Macrocycles / Carbonylation

The new multifunctional ligand thiophene-2,5-bis(carboxylatomethylenebenzotriazole) (**1**) reacts with $[RhCl(CO)_2]_2$ to give the rhodium complex $[RhCl(CO)(\mathbf{1})]_2$ (**2**), which was found to catalyse efficiently the iodide-mediated carbonylation of methanol. The macrocyclic carbonyliodorhodium complex $[Rh_2I_6(CO)_2(\mathbf{1})]_2$ (**3**) was isolated from the catalytic mixture and structurally characterised.

The carbonylation of methanol to give acetic acid is one of the most important homogeneously catalysed industrial processes.[1] The catalytic reaction requires the use of iodide promoters which convert methanol, prior to carbonylation, into the actual substrate methyl iodide.[2] The classical Monsanto process is based on soluble rhodium catalysts.[3] It is well established that the anion $[RhI_2(CO)_2]^-$ is the active species in the catalytic process, the rate-determining step of which is the oxidative addition of CH_3I to give $[RhI_3(CH_3)(CO)_2]^-$.[4] There have been many attempts to modify the complex $[RhI_2(CO)_2]^-$ with suitable ligands which can increase the susceptibility of the Rh^I centre towards oxidative addition of methyl iodide.[5] Our approach consisted in developing multifunctional ligands based on benzotriazole and thiophene units in order to improve the catalytic activity of the rhodium catalyst.

The multifunctional ligand thiophene-2,5-bis(carboxylatomethylenebenzotriazole) (**1**) is easily accessible by classical condensation methods[6] from hydroxymethylbenzotriazole and 2,5-thiophene dicarboxylic acid (Scheme 1). It can be isolated in 62% yield as a white microcrystalline powder.

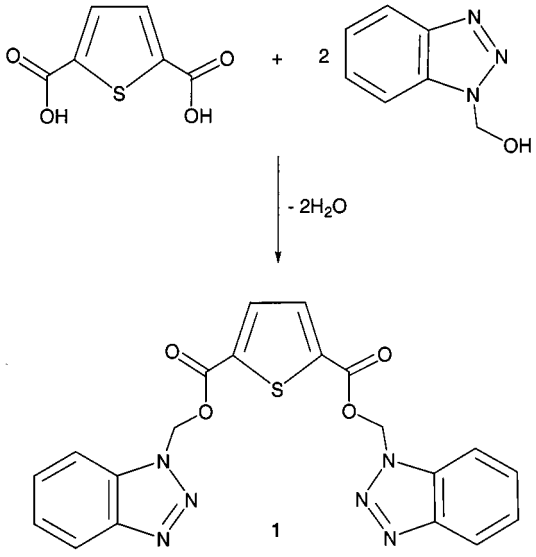

Scheme 1

Compound **1** was found to coordinate easily to rhodium through the 3-N atom of the triazole unit. The reaction of **1** with $[RhCl(CO)_2]_2$ in toluene at room temperature gives the rhodium(I) complex $[RhCl(CO)(\mathbf{1})]_2$ (**2**) quantitatively as an air-stable yellow solid (Scheme 2). This compound is moderately soluble in acetone and toluene, but only sparingly soluble in alcohols and insoluble in alkanes. Microanalytical and NMR spectroscopic data are consistent with the composition proposed, the dimeric nature of the molecule clearly follows from the ESI mass spectrum which shows the molecular peak at $m/z = 1220$. Complex **2** exhibits two

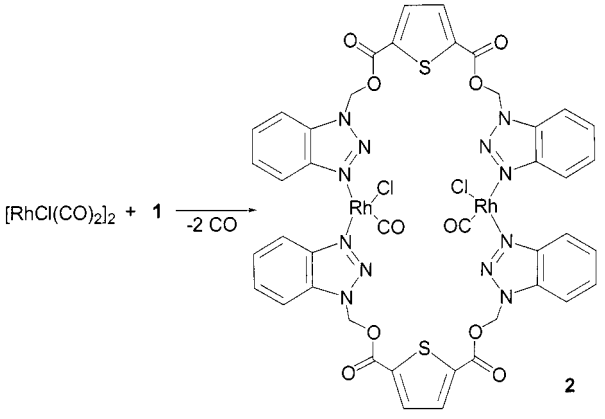

Scheme 2

[a] Institut de Chimie, Université de Neuchâtel,
Case postale 2, 2007 Neuchâtel, Switzerland
Fax: (internat.) +41-32/718-2511
E-mail: georg.suess-fink@unine.ch

 © WILEY-VCH Verlag GmbH, 69451 Weinheim, 2001 1434−1948/01/1212−3005 $ 17.50+.50/0

strong ν(CO) absorptions in the IR spectrum, as expected for a *cisoid* arrangement of the two terminal carbonyl ligands.[7] The yellow colour is indicative of square-planar, noninteracting rhodium centres.[8] Macrocycles of similar types, for example $[Rh_2Cl_2(CO)_2\{\mu\text{-}(Ph_2P)_2py\}_2]$[9] and $[Rh_2(CO)_2Cl_2\{Ph_2P(CH_2)P(S)Ph_2\}_2]$,[7] have been reported previously for rhodium but never used as catalysts.

Complex **2** catalyses the iodide-promoted carbonylation of methanol to give acetic acid and methyl acetate with much higher catalytic activities than that of the classical $[RhCl(CO)_2]_2$ catalyst. The catalytic reaction is performed with a methanol/methyl iodide/water (58%, 26%, 16%) mixture at 170 °C under a CO pressure of 25 bar, the catalyst/substrate ratio being 1:2000. After 20 min., the catalytic turnover number (mol CH_3COOH plus mol CH_3COOCH_3 per mol **2**) is found to be 700 (catalytic turnover frequency 35 min^{-1}). $[RhCl(CO)_2]_2$ gives a catalytic turnover number of 400 (catalytic turnover frequency 20 min^{-1}) under the same conditions. A similar increase of the catalytic activity with respect to that of $[RhCl(CO)_2]_2$ has been observed for the triethylphosphane complex $[RhCl(CO)(PEt_3)_2]$.[5f]

From the reaction mixture of the catalytic reaction we isolated the red-brown complex **3** by crystallisation of the organometallic residue from acetone. Compound **3** is directly accessible in high yield from the reaction of **2** with methyl iodide and carbon monoxide (1 bar) in acetone solution. It contains iodo ligands and a *transoid* dicarbonyl arrangement, giving rise to a single ν(CO) absorption in the infrared spectrum. It was suggested for complexes containing phosphane ligands that the dissociation of the phosphane may occurred during the catalytic process. In our case there is clearly a Rh−N bond cleavage. The facile conversion of **2** into **3** under ambient conditions demonstrates that fragmentation, ligand dissociation and rearrangement occur easily.

In the single-crystal X-ray structure analysis[10] **3** turns out to be a macrocycle containing two dinuclear iodo-bridged Rh^{III} units (Scheme 3). The four rhodium atoms have a distorted octahedral coordination geometry: they are coordinated to the 3-N atoms of the benzotriazole units of

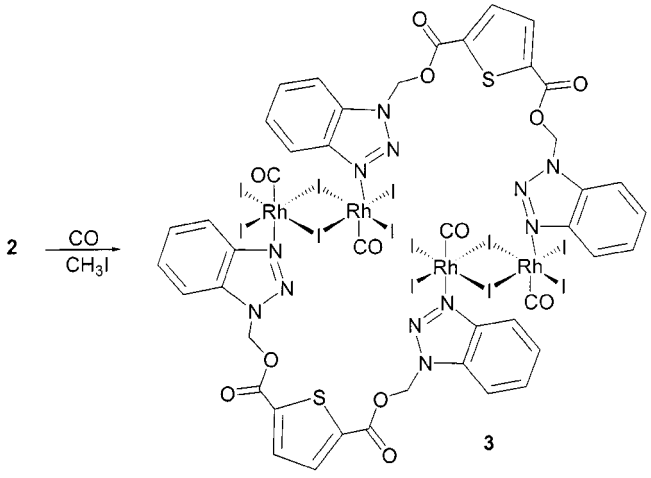

Scheme 3

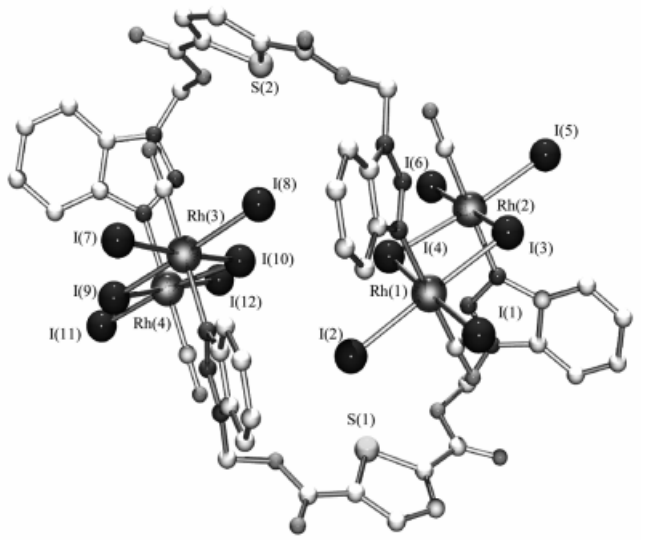

Figure 1. Molecular structure of complex **3** (hydrogen atoms and solvent molecules omitted for clarity); selected bond lengths [Å]: Rh(1)−N(12) 2.128(11), Rh(2)−N(1) 2.139(10), Rh(3)−N(6) 2.091(11), Rh(4)−N(7) 2.102(11), Rh(1)-(C1) 1.864(16), Rh(2)−C(2) 1.851(14), Rh(3)−C(3) 1.867(16), Rh(4)−C(4) 1.840(12), Rh(3)−I(8) 2.6056(14), Rh(3)−I(10) 2.6922(13), Rh(1)−Rh(2) 3.8854, Rh(3)−Rh(4) 3.9098

1 (Figure 1). The four rhodium−nitrogen bonds are almost equal in length. The two planar $Rh_2(\mu_2\text{-}I)_2$ rings are arranged perpendicular with respect to the cycle formed by the four rhodium atoms and the two ligands, Rh(1)−**1**−Rh(2)−Rh(3)−**1**−Rh(4). The bond lengths and angles for each Rh_2I_6 unit are similar to those reported by Forster[11] for $[Rh_2I_6(MeCO)_2(CO)_2]^{2-}$ and by Dilworth[12] for $[Rh_2I_6(Ph_2PC_6H_4SMe)_2]$.

In contrast to the rhodium(I) macrocycle **2**, the rhodium(III) macrocycle **3** does not catalyse the carbonylation of methanol: the low catalytic activity observed (TON 100 after 20 min., TOF 5 min^{-1}) when **3** is used as the catalyst precursor is due to a partial decomposition of **3** to give $[RhI_2(CO)_2]^-$. This is in line with what has been observed for other iodo-bridged dirhodium(III) complexes.[13]

To the best of our knowledge, **2** is the first macrocyclic dirhodium complex involved in the carbonylation of methanol. It is possible that the better catalytic performance of **2** with respect to that of the classical species $[RhI_2(CO)_2]^-$ is due to its macrocyclic nature.

Experimental Section

General: Solvents were dried and distilled under nitrogen prior to use. All reactions were carried out under nitrogen, using standard Schlenk techniques. All other reagents were purchased (Fluka) and used as received. Nuclear magnetic resonance spectra were recorded using a Varian Gemini 200 BB instrument or a Bruker AMX 400 spectrometer and referenced to the signals of the residual protons in the deuterated solvents. ^1H NMR: internal standard solvent, external standard TMS; ^{13}C NMR: internal standard solvent, external standard TMS. Infrared spectra were recorded with a Perkin−Elmer 1720X FT-IR spectrometer as KBr pellets. Micro-

analyses were carried out by the Laboratory of Pharmaceutical Chemistry, University of Geneva, Switzerland.

1: A solution of 2,5-thiophenedicarboxylic acid (1.72 g, 10 mmol), *N*,*N*-dicyclohexylcarbodiimide (2.3 g, 11 mmol), 4-(dimethylamino)pyridine (122 mg, 1 mmol), 4-pyrrolidinopyridine (148 mg, 1 mmol) and hydroxymethylbenzotriazole (3.3 g, 22 mmol) in CH_2Cl_2 (40 mL) was allowed to stand at room temperature under nitrogen, until the esterification was complete. The resulting solution was filtered to remove *N*,*N*-dicyclohexyl urea and the filtrate was concentrated under reduced pressure. The residue was chromatographed on silica gel (80 g), eluting with hexane/ether (1:1) to afford 2.7 g (62%) of **1** as a white solid. $C_{20}H_{14}N_6O_4S$ (434.4): calcd. C 55.29, H 3.25, N 19.35; found C 55.25, H 3.27, N 19.31. − FT-IR (4000−400 cm^{-1}): $\tilde{\nu}$ = 3029vw, 2979w, 1749s, 1709vs, 1532m, 1452m, 1280s, 1240s, 1159m, 1069s, 989m, 743s, 543m, 493m cm^{-1}. − FAB-MS (positive ion): *m*/*z* = 435 [M^+]. − ^{1}H NMR ([D$_6$]acetone): δ = 8.07 (m, 4 H), δ = 7.87 (s, 2 H), δ = 7.68 (t, 2 H), δ = 7.37 (t, 2 H), δ = 6.99 (s, 4 H). − ^{13}C NMR ([D$_6$]acetone): δ = 160.46, 146.31, 138.28, 134.73, 132.95, 128.94, 124.97, 120.44, 110.17, 68.82.

2: A solution of $[RhCl(CO)_2]_2$ (100 mg, 0.26 mmol) and **1** (248 mg, 0.57 mmol) in toluene (20 mL) was stirred at room temperature for 2 h. The solution was filtered then evaporated to dryness. The resulting yellow solid was washed with ether (10 mL) and dried under vacuum (240 mg, 77%). $C_{42}H_{28}Cl_2N_{12}O_{10}Rh_2S_2$ (1201.6): calcd. C 41.98, H 2.35, N 13.99; found C 42.25, H 2.27, N 13.81. − FT-IR (4000−400 cm^{-1}): $\tilde{\nu}$ = 3035vw, 2975w, 2086s, 2013vs, 1727vs, 1529m, 1455m, 1237s, 1159m, 1070s, 984m, 746s, 493m cm^{-1}. − ESI-MS: *m*/*z* = 1220 [M + H_2O]. − ^{1}H NMR ([D$_6$]acetone): δ = 8.35 (d, 4 H), δ = 8.20 (d, 4 H), δ = 7.91 (s, 4 H), δ = 7.80 (m, 4 H), δ = 7.67 (m, 4 H), δ = 7.09 (s, 8 H). − ^{13}C NMR ([D$_6$]acetone): δ = 183.52, 160.35, 145.89, 138.18, 135.74, 133.42, 129.58, 125.98, 120.09, 111.66, 70.16.

3: Complex **2** (100 mg, 0.08 mmol), ethanoic acid (1 mL) and iodomethane (1 mL) were dissolved in acetone (20 mL) under an atmosphere of carbon monoxide. After heating at reflux for 1 h, the resulting brownish solution was filtered and then the solvent was evaporated to dryness. The remaining red-brown solid was washed with ether and dried in vacuo (388 mg, 59%). Crystals suitable for X-ray diffraction analysis were grown by slow evaporation of an acetone solution. FT-IR (4000−400 cm^{-1}): $\tilde{\nu}$ = 3035vw, 2975w, 2059s, 1729vs, 1524m, 1455m, 1246s, 1076s, 746s, 519m cm^{-1}. − ^{1}H NMR ([D$_6$]DMSO): δ = 8.65 (d, 4 H), δ = 8.53 (d, 4 H), δ = 8.01−7.88 (m, 12 H), δ = 7.15 (s, 8 H). − ^{13}C NMR ([D$_6$]DMSO): δ = 192.53, 160.26, 147.04, 138.56, 134.93, 133.40, 129.21, 125.50, 120.11, 111.66, 70.28.

Catalytic Runs: In a typical experiment, $[RhCl(CO)_2]_2$ (24 mg, 0.06 mmol) and **1** (53 mg, 0.12 mmol) were dissolved in methanol (4.46 mL). Iodomethane (11 mmol) and water (200 mmol) were added to this solution, and the mixture was placed in a 100 mL stainless steel autoclave. After purging three times with CO, the autoclave was pressurised with carbon monoxide (25 bar) and heated to 170 °C with vigorous stirring of the reaction mixture (900 rpm). After 20 min., the autoclave was cooled to room temperature, and the pressure was released. The solution was filtered and analysed by GC.

Crystal Structure Determination of 3:[10] A black crystal of compound **1** was mounted on a Stoe Imaging Plate Diffractometer System (Stoe & Cie, 1995) equipped with a one-circle goniometer and a graphite-monochromator. Data collection was performed at −120 °C using Mo-K_α radiation (λ = 0.71073 Å). 190 exposures (3 min. per exposure) were obtained at an image plate distance of 70 mm with $0 < \theta < 190°$ and with the crystal oscillating through 1° in θ. The resolution was D_{min} − D_{max} 12.45−0.81 Å. Crystallographic data are reported in Table 1. The structure was solved by direct methods using the program SHELXS-97[14] and refined by full-matrix least-squares on F^2 with SHELXL-97.[15] The hydrogen atoms were included in calculated positions and treated as riding atoms using the SHELXL-97 default parameters. The compound crystallises with 7.5 molecules of acetone per asymmetric unit. The solvent molecule with an occupancy of 0.5 is strongly disordered and therefore all atom positions have been refined isotropically. An absorption correction using DIFABS in PLATON99[16] was applied (T_{min} = 0.185, T_{max} = 0.656). The figures were drawn with ORTEP-32.[17]

Table 1. Crystallographic data for **3**

Empirical formula	$C_{66.5}H_{73}I_{12}N_{12}O_{19.5}Rh_4S_2$
Molecular mass	3350.93
Temperature [K]	153(2)
Crystal system	triclinic
Space group	$P\bar{1}$
a [Å]	27.693(2)
b [Å]	14.3087(13)
c [Å]	13.6096(11)
α [°]	103.300(10)
β [°]	80.091(10)
γ [°]	79.420(10)
Volume [Å^3]	5027.9(7)
Z	2
D_c [g cm^{-3}]	2.213
Wavelength [Å]	0.71073(Mo-K_α)
μ [min^{-1}]	4.434
F (000)	3120
θ range [°]	1.84−25.83
Unique refl. with $I > 2\sigma(I)$	11752
Final *R*1, *wR*2 (observed data)[a]	0.0578, 0.1600
No. of variables	740
GOF	1.009
Residual density (max/min) [eÅ^{-3}]	2.941/-2.508

[a] $R1 = [\Sigma(||F_o| - |F_c||)/\Sigma|F_o|]$; $wR^2 = \{[\Sigma(w(F_o^2 - F_c^2)^2]/\Sigma(wF_o^4)]^{1/2}\}$

[1] K. Weissermel, H.-J. Arpe, *Industrial Organic Chemistry*, 3rd Edition, VCH, Weinheim, **1997**.

[2] G. W. Parshall, S. D. Ittel, *Homogeneous Catalysis*, 2nd Edition, Wiley-Interscience, New York, **1992**, p. 96.

[3] [3a] M. Gauss, A. Seidel, P. Torrence and P. Heymans, in *Applied Homogeneous Catalysis with Organometallic Compounds* (Eds.: B. Cornils and W. A. Herrmann), VCH, Weinheim Basel, **1996**, p. 104. − [3b] M. J. Howard, M. D. Jones, M. S. Roberts, S. A. Taylor, *Catal. Today* **1993**, *18*, 325−354. − [3c] F. E. Paulik, J. F. Roth, *Chem. Commun.* **1968**, 1578. − [3d] J. F. Roth, J. H. Craddock, A. Hershman, F. E. Paulik, *Chem. Technol.* **1971**, 600−605. − [3e] K. K. Robinson, A. Hershman, J. H. Craddock, J. F. Roth, *J. Catal.* **1972**, *27*, 389−396. − [3f] F. E. Paulik, A. Hershman, W. R. Knox, J. F. Roth, Monsanto Company, *US Pat.* **1973**, 3769329.

[4] [4a] T. W. Dekleva, D. Forster, *Adv. Catal.* **1986**, *34*, 81−130. − [4b] P. M. Maitlis, A. Haynes, G. J. Sunley, M. J. Howard, *J. Chem. Soc., Dalton Trans.* **1996**, 2187−2196.

[5] [5a] R. W. Wegman, A. G. Abatjoglou, A. M. Harrison, *J. Chem. Soc., Chem. Commun.* **1987**, 1891−1892. − [5b] A. Bader, E. Lindner, *Coord. Chem. Rev.* **1991**, *108*, 27−110. −

[5c] M. S. Balakrishna, R. Klein, S. Uhlenbrock, A. A. Pinkerton, R. G. Cavell, *Inorg. Chem.* **1993**, *32*, 5676−5681. − [5d] M. J. Baker, M. G. Giles, A. G. Orpen, J. Taylor, R. J. Watt, *J. Chem. Soc., Chem. Commun.* **1995**, 197−198. − [5e] J. R. Dilworth, J. R. Miller, N. Wheatley, M. J. Baker, G. Sunley, *J. Chem. Soc., Chem. Commun.* **1995**, 1579−1581. − [5f] J. Rankin, A. D. Poole, A. C. Benyei, D. J. Cole-Hamilton, *Chem. Commun.* **1997**, 1835−1836. − [5g] C.-A. Carraz, E. J. Ditzel, A. G. Orpen, D. D. Ellis, P. G. Pringle, G. J. Sunley, *Chem. Commun.* **2000**, 1277−1278.

[6] [6a] A. Hassner, L. Krepski, V. Alexanian, *Tetrahedron* **1978**, *34*, 2069−2076. − [6b] A. Hassner, V. Alexanian, *Tetrahedron Lett.* **1978**, *46*, 4475−4478. − [6c] E. F. V. Scriven, *Chem. Soc. Rev.* **1983**, *12*, 129−161.

[7] T. C. Blagborough, R. Davis, P. Ivison, *J. Organomet. Chem.* **1994**, *467*, 85−94.

[8] A. L. Balch, B. Tulyathan, *Inorg. Chem.* **1977**, *16*, 2840−2845.

[9] A. L. Balch, H. Hope, F. E. Wood, *J. Am. Chem. Soc.* **1985**, *107*, 6936−6941.

[10] Crystallographic data (excluding structure factors) for the structure reported in this paper have been deposited with the Cambridge Crystallographic Data Centre as supplementary publication no. CCDC-160381 (**3**). Copies of the data can be obtained free of charge on application to CCDC, 12 Union Road, Cambridge CB2 1EZ, UK [Fax: (internat.) +44-1223/336-033; E-mail: deposit@ccdc.cam.ac.uk].

[11] G. W. Adamson, J. J. Daly, D. Forster, *J. Organomet. Chem.* **1974**, *71*, C17−C19.

[12] J. R. Dilworth, D. Morales, Y. Zheng, *J. Chem. Soc., Dalton. Trans.* **2000**, 3007−3015.

[13] H. Adams, N. A. Bailey, B. E. Mann, C. P. Manuel, C. M. Spencer, A. G. Kent, *J. Chem. Soc., Dalton. Trans.* **1988**, 489−496.

[14] G. M. Sheldrick, *Acta Crystallogr., Sect. A* **1990**, *46*, 467−473.

[15] G. M. Sheldrick, (1997). *SHELXL-97*, *Program for crystal structure refinement*, University of Göttingen, Germany.

[16] A. L. Spek, *Acta Crystallogr., Sect. A* **1990**, *46*, C34−C36.

[17] L. J. Farrugia, *J. Appl. Cryst.* **1997**, *30*, 565.

Received June 22, 2001
[I01224]

New Pyridine−Imidazoline Ligands for Palladium-Catalyzed Copolymerization of Carbon Monoxide and Styrene

Amaia Bastero,[a] Aurora Ruiz,[a] Carmen Claver,*[a] and Sergio Castillón[b]

Keywords: N ligands / Palladium / Copolymerization / Stereochemistry / Nitrogen heterocycles

C_1-symmetrical pyridine–imidazoline ligands have been synthesised and used in the preparation of Pd^{II} complexes of general formula [PdMe(NCMe)(N-N′)][BAr′$_4$] [Ar′ = 3,5-$(CF_3)_2C_6H_3$]. The introduction of electronically different substituents in the imidazoline moiety determines the coordination position of the methyl group in the cationic complexes, which are catalyst precursors for the copolymerization of carbon monoxide and 4-*tert*-butylstyrene (TBS). Interestingly, the use of a precatalyst with a different stereochemistry provides copolymers with a different stereoregularity.

Introduction

Chelating nitrogen ligands have been reported to be the most efficient for the Pd-catalyzed alternating copolymerization of carbon monoxide and styrene.[1−6] Catalysts containing planar, achiral ligands give syndiotactic copolymers with high stereocontrol.[3,7,8] This stereoregularity has been attributed to a chain-end control due to the interaction of the growing chain with the incoming styrene unit, which inserts exclusively in a 2,1-fashion.[3] Enantiomerically pure C_2-symmetrical N-N ligands yield highly isotactic copolymers due to the strict enantiomorphic site control provided by the chiral ligand.[9−11]

To the best of our knowledge there is only one example of a C_1-symmetrical bisnitrogen ligand. Surprisingly, the use of (*S*,*S*)-4,5-dihydro-4-methoxymethyl-3-phenyl-2-(2-pyridyl)oxazole provides a syndiotactic copolymer. It has been proposed that, due to a pronounced site-selective coordination of the olefin, the influence of the chirality of the growing chain is more efficient than the enantiosite control.[9,12,13] The related C_1-symmetrical phosphane−oxazoline ligands provide isotactic poly(styrene-*alt*-CO). It seems that with these ligands the enantioface discrimination is determined by the site-selective coordination of the olefin (*trans* to the P atom) and a secondary insertion of the incoming styrene units.[12]

Recently it has been reported that electronic effects in palladium catalysts modified with chiral ferrocenyldiphosphanes may increase the differentiation of the two coordinating P atoms and change the catalytic activity in the enantioselective copolymerization of carbon monoxide and propene dramatically.[14]

[a] Departament de Química Física i Inorgànica, Universitat Rovira i Virgili,
Pl. Imperial Tàrraco 1, 43005 Tarragona, Spain
Fax: (internat.) +34-977/559-563
E-mail: claver@quimica.urv.es
[b] Departament de Química Analítica i Química Orgànica, Universitat Rovira i Virgili,
Pl. Imperial Tàrraco 1, 43005 Tarragona, Spain

In this paper we show that the stereochemistry of the [PdMe(NCMe)(N-N′)][BAr′$_4$] complexes can be modified by changing the electronic properties of the C_1-symmetrical pyridine−imidazoline ligands. This fact influences the stereoregularity of the CO/TBS copolymers.

Results and Discussion

The pyridine−imidazoline ligand **1a** was prepared similarly to the oxazolines by reaction of 2-cyanopyridine with *meso*-1,2-diphenylethylenediamine but using $YbOTf_3$ as catalyst.[15,16] Further reaction of **1a** with BnBr, TsCl or Tf_2O, provided the 1-substituted-4,5-dihydro-4,5-diphenyl-2-(2-pyridyl)-imidazoles **1b**−**d**, respectively, in a racemic manner (Figure 1).[16] The neutral [PdClMe(N-N′)] complexes **2a**−**d** were isolated from the stoichiometric reaction of [PdClMe(cod)] (cod = 1,5-cyclooctadiene) and the ligands **1a**−**d** in anhydrous toluene.[17,18] The cationic palladium complexes [PdMe(NCMe)(N-N′)][BAr$_4$′] (**3a**−**d**) were prepared following reported procedures.[19]

The stereochemistry of the neutral complexes **2a**−**d** was assigned by means of NOE experiments at room temperature, showing that all the complexes have the methyl group coordinated *trans* to the pyridine ring. This is also confirmed by the downfield shift in the ^{1}H NMR spectra of the proton H_6, next to the N-pyridine atom, which is indicative of the presence of the chloride ligand in a *cis* position.[17] However, the cationic compounds [Pd(Me)(NCMe)(N-N′)][BAr′$_4$] (**3a**−**d**) show a different stereochemistry depending on the ligand. The ^{1}H NMR spectra of **3c**−**d** at

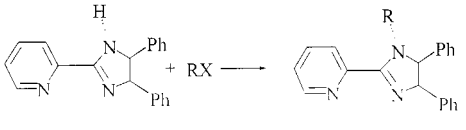

1a **1b** R = Bn
c R = Ts
d R = Tf

Figure 1. Synthesis of the pyridine-imidazoline ligands

 © WILEY-VCH Verlag GmbH, 69451 Weinheim, 2001 1434−1948/01/1212−3009 $ 17.50+.50/0

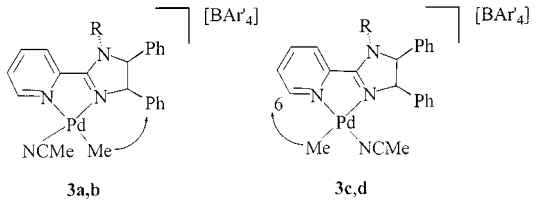

Figure 2. NOE difference experiments show the stereochemistry of the complexes

room temperature show a downfield shift of the Pd−Me signal to around δ = 1.[19] NOE difference experiments at room temperature allowed the determination of the stereochemistry of these complexes and showed that in the complexes **3a**−**b** the methyl group is *trans* to the pyridine moiety whereas it is *cis* in the complexes **3c**−**d** (Figure 2). Therefore the use of different substituents (R) with electron-donor or electron-withdrawing character results in an effective electronic determination in the methyl coordination. The methyl group is always coordinated *trans* to the less basic nitrogen of the ligand.

Under copolymerization conditions the coordination of carbon monoxide and the migratory insertion of the methyl group take place to form an acyl species; the styrene coordinates in the vacant position. The electronic effects of these ligands could therefore affect the steroregularity of the copolymer obtained with the catalytic precursors. The new Pd^{II} complexes with imidazoline-containing ligands were tested as catalysts for the alternating CO/TBS copolymerization. In a typical experiment **3a**−**d** were placed in chlorobenzene under 1 bar CO and TBS was added (Table 1).

Table 1. Alternating CO/TBS copolymerization catalysed by [PdMe(NCMe)(N-N′)][BAr′$_4$][a]

Entry	Precursor	Productivity[b] [g(gPd × h)$^{-1}$]	Stereoregularity (*l* diads) [%]	M_N (M_W/M_N)
1	**3a**	2	65	42200 (1.1)
2	**3b**	8.9	52	49750 (1.5)
3	**3c**	7	15	59250 (1.2)
4	**3d**	12.8	18	39700 (1.5)

[a] Reaction conditions: 0.0125 mmol catalyst, [TBS]/[cat] = 620, 5 mL chlorobenzene, p(CO) = 1 bar, 24 h at room temperature. [b] Productivity calculated from the isolated copolymer.

As Table 1 shows, introducing electron-withdrawing groups (entries 3 and 4) leads to a greater proportion of *u* diads giving highly syndiotactic copolymers. With the substituents H and Bn (entries 1 and 2 respectively) such a clear effect is not observed, probably due to the smaller electronic differentiation of the two rings (pyridine and imidazoline), although there is a bigger proportion of *l* diads. The degree of stereoregularity was evaluated from the ^{13}C NMR spectrum of the copolymers by integrating the signals in the region of the methylene carbon atom using the epimerized copolymer as reference (Figure 3). The molecular weights were high and similar in all the cases. In general, we did not find any relation between the nature of the R substituent and the activity of the catalytic systems.

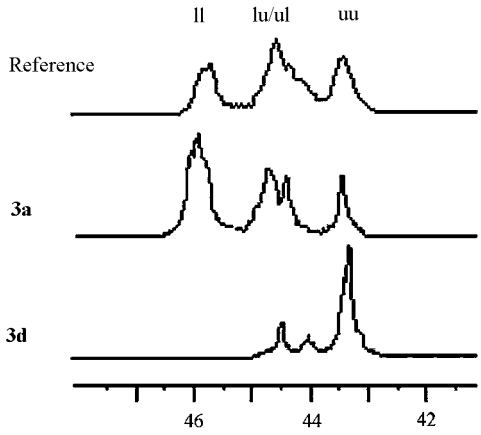

Figure 3. Comparative ^{13}C NMR spectrum of the copolymers in the region of the methylene carbon atom using the epimerized copolymer as reference

In conclusion, we have prepared pyridine−imidazoline ligands with several substituents in the imidazoline moiety and their related [Pd(Me)(NCMe)(N-N′)][BAr$_4$′] complexes. Interestingly, the nature of the substituents determines the stereochemistry of the complexes. The Pd^{II} complexes are active as catalysts in the CO/TBS copolymerization reaction and show that the electronic properties of the ligands strongly influence the stereoregularity of the copolymers. We are currently studying how this electronic discrimination affects the different steps of the catalytic reaction.

Acknowledgments

We thank the Spanish Ministerio de Educación y Cultura for the financial support (DGES PB-97-0407-C05-01, DGES PB-98-0315 and 2FD97-1565) and the Ministerio de Ciencia y Tecnología for awarding a research grant (to A. B.).

[1] P. Corradini, C. De Rosa, A. Panunzi, G. Petrucci, P. Pino, *Chimia* **1990**, *44*, 52−54.
[2] M. Barsacchi, G. Consiglio, L. Medici, G. Petrucci, U. W. Suter, *Angew. Chem. Int. Ed. Engl.* **1991**, *30*, 989−991.
[3] M. Brookhart, F. C. Rix, J. M. DeSimone, J. C. Barborak, *J. Am. Chem. Soc.* **1992**, *114*, 5894−5895.
[4] E. Drent, P. H. M. Budzelaar, *Chem. Rev.* **1996**, *96*, 663−681.
[5] K. Nozaki, T. Hiyama, *J. Organomet. Chem.* **1999**, *576*, 248−253.
[6] B. Milani, G. Mestroni, *Comments Inorg. Chem.* **1999**, *20*, 301−326.
[7] A. Bastero, A. Ruiz, J. A. Reina, C. Claver, A. M. Guerrero, F. A. Jalón, B. R. Manzano, *J. Organomet. Chem.* **2001**, *619*, 287−292.
[8] C. Carfagna, G. Gatti, D. Martini, C. Pettinari, *Organometallics* **2001**, *20*, 2175−2182.
[9] M. Brookhart, M. I. Wagner, G. G. A. Balavoine, H. A. Haddou, *J. Am. Chem. Soc.* **1994**, *116*, 3641−3642.
[10] S. Bartolini, C. Carfagna, A. Musco, *Macromol. Rapid. Commun.* **1995**, *16*, 9−14.
[11] M. T. Reetz, G. Haderlein, K. Angermund, *J. Am. Chem. Soc.* **2000**, *122*, 996−997.

[12] A. Aeby, G. Consiglio, *Inorg. Chim. Acta* **1999**, *296*, 45−51.

[13] A. Aeby, A. Gsponer, M. Sperrle, G. Consiglio, *J. Organomet. Chem.* **2000**, *603*, 122−127.

[14] C. Gambs, S. Chaloupka, G. Consiglio and A. Togni, *Angew. Chem. Int. Ed.* **2000**, *39*, 2486−2488.

[15] J. V. Allen, S. J. Coote, G. J. Dawson, C. G. Frost, C. J. Martin, J. M. J. Williams, *J. Chem. Soc., Perkin Trans.* **1994**, *1*, 2065−2072.

[16] 2-Cyanopyridine and *meso*-1,2-diphenylethylenediamine were refluxed in chlorobenzene during 72 h using $YbOTf_3$ as catalyst. ^{1}H NMR (400 MHz, $CDCl_3$, room temp.): δ = 8.63 (ddd, ^3J = 5.0, ^4J = 1.8, ^5J = 1.1 Hz, 1 H, H_6), 8.36 (dt, ^3J = 7.7, ^4J = 1.1, ^5J = 1.1 Hz, 1 H, H_3), 7.81 (td, ^3J = 7.7, ^4J = 1.8 Hz, 1 H, H_4), 7.40 (ddd, ^3J = 7.7, ^3J = 5.0, ^4J = 1.1 Hz, 1 H, H_5), 7.02−6.94 (m, 10 H, $H_{arom.}$), 5.51 (s, 2 H, CHN); $C_{20}H_{17}N_3$ (299.37): calcd. C 80.2, H 5.4, N 14; found C 79.3, H 5.0, N 13.8.

[17] Selected data for **1d** as an example: ^{1}H NMR (300 MHz, $CDCl_3$, room temp.): δ = 8.78 (ddd, ^3J = 4.8, ^4J = 1.8, ^5J = 1.0 Hz, 1 H, H_6), 7.96 (dt, ^3J = 7.7, ^4J = 1.0, ^5J = 1.0 Hz, 1 H, H_3), 7.87 (td, ^3J = 7.7, ^4J = 1.8 Hz, 1 H, H_4), 7.49 (ddd, ^3J = 7.7, ^3J = 4.8, ^4J = 1.0 Hz, 1 H, H_5), 7.11−6.99 (m, 10 H, $H_{arom.}$), 5.98 (d, ^3J = 8.7 Hz, 1 H, CHN), 5.92 (d, ^3J = 8.7 Hz, 1 H, CHN); $C_{21}H_{16}F_3N_3O_2S$ (431.43): calcd. C 58.46, H 3.74, N 9.74, S 7.43; found C 58.85, H 3.82, N 9.42, S 7.28.

[18] R. E Rülke, J. M Ernsting, A. L Spek, C. J. Elsevier, P. W. N. M. van Leeuwen, K. Vrieze, *Inorg. Chem.* **1993**, *32*, 5769−5778.

[19] Selected data for **2d** as an example: ^{1}H NMR (400 MHz, $CDCl_3$, room temp.): δ = 9.27 (ddd, ^3J = 5.1, ^4J = 1.7, ^5J = 0.8 Hz, 1 H, H_6), 8.32 (ddd, ^3J = 7.9, ^4J = 1.2, ^5J = 0.8 Hz, 1 H, H_3), 8.15 (td, ^3J = 7.9, ^4J = 1.7 Hz, 1 H, H_4), 7.83 (ddd, ^3J = 7.9, ^3J = 5.1, ^4J = 1.2 Hz, 1 H, H_5), 7.24−6.69 (m, 10 H, H_{arom}), 6.11 (s, 2 H, CHN), 0.45 (s, 3 H, Pd−CH_3); $C_{22}H_{19}ClF_3N_3O_2PdS$ (588.32): calcd. C 45.0, H 3.3, N 7.1; found C 45.4, H 3.8, N 6.5.

[20] The standard synthesis is described in ref. 7. As representative examples **3b** and **3d** are chosen. Selected data for **3b**: ^{1}H NMR (300 MHz, $CDCl_3$, room temp.): δ = 8.44 (dd, ^3J = 5.2, ^4J = 1.8 Hz, 1 H, H_6), 7.98 (dd, ^3J = 8.1, ^4J = 1.0 Hz, 1 H, H_3), 7.86 (td, ^3J = 8.1, ^4J = 1.8 Hz, 1 H, H_4), 7.72 (s, 8 H, H_{arom}), 7.53 (s, 4 H, H_{arom}), 7.43 (ddd, ^3J = 8.1, ^4J = 5.2, ^5J = 1.0 Hz, 1 H, H_5), 7.36−6.77 (m, 15 H, H_{arom}), 5.54 (d, ^3J = 11.7 Hz, 1 H, CHN), 5.43 (d, ^3J = 11.7 Hz, 1 H, CHN), 5.11 (d, ^2J = 17.6 Hz, 1 H, CH_2), 4.45 (d, ^2J = 17.6 Hz, 1 H, CH_2), 2.27 (s, 3 H, CH_3CN), 0.56 (s, 3 H, Pd−CH_3); $C_{62}H_{41}BF_{24}N_4Pd$ (1415.2): calcd. C 52.6, H 2.9, N 3.9; found C 50.8, H 2.9, N 3.4. Selected data for **3d**: ^{1}H NMR (400 MHz, $CDCl_3$, room temp.): δ = 8.51 (dt, ^3J = 5.6, ^4J = 0.8 Hz, 1 H, H_6), 8.41 (ddd, ^3J = 7.8, ^4J = 1.4, ^5J = 0.8 Hz, 1 H, H_3), 8.24 (td, ^3J = 7.8, ^4J = 1.5 Hz, 1 H, H_4), 7.76 (ddd, ^3J = 7.8, ^3J = 5.6, ^4J = 1.4 Hz, 1 H, H_5), 7.72 (s, 8 H, H_{arom}), 7.53 (s, 4 H, H_{arom}), 7.2-6.64 (m, 10 H, H_{arom}), 6.09 (d, ^3J = 8.0 Hz, 1 H, CHN), 6.01 (d, ^3J = 8.0 Hz, 1 H, CHN), 1.5 (s, 3 H, CH_3CN), 1.06 (s, 3 H, Pd−CH_3); $C_{56}H_{34}BF_{27}N_4O_2PdS$: calcd. C 46.2, H 2.4, N 3.8, S 2.2; found C 48.3, H 2.4, N 3.7, S 2.3.

Received August 7, 2001
[I01300]

Bent Metallocenes of Germanium, Tin, and Lead with Aminoboratabenzene Ligands − Crystal Structures of E[3,5-$Me_2C_5H_3BN(SiMe_3)_2$]$_2$ (E = Ge, Sn, and Pb)[‡]

Xiaolai Zheng[a] and Gerhard E. Herberich*[a]

Keywords: Boron / Metallocenes / Sandwich compounds / Germanium / Tin / Lead

The reaction of GeI_2, $SnCl_2$, or $PbCl_2$ with two equivalents of lithium aminoboratabenzenes in diethyl ether affords the new sandwich compounds Pb(3,5-$Me_2C_5H_3BNMe_2$)$_2$ (**4**) and E[3,5-$Me_2C_5H_3BN(SiMe_3)_2$]$_2$ (**5:** E = Ge, **6:** E = Sn, **7:** E = Pb). While compound **4** undergoes a redox ligand coupling reaction at ambient temperature to give lead black and ligand dimers, the bis(trimethylsilyl)amino compounds **5**–**7** are thermally stable, and coupling products are only detected under the conditions of mass spectrometry. This difference in stability can be attributed to the different perturbation effects which the *B*-amino groups exert on the electronic properties of the boratabenzene rings. Crystal structure determinations reveal that the compounds **5**–**7** possess a monomeric bent-sandwich geometry in the solid state with facially bonded boratabenzenes. The E–C distances span rather large ranges [**5:** 2.320–2.939(4) Å; **6:** 2.519–3.033(9) Å; **7:** 2.632–3.054(7) Å]; the central element E is always particularly close to one of the two α-C atoms and displays intermediate E–B distances.

Introduction

Compared to sandwich complexes of the transition metals, group 14 metallocenes exhibit a more ionic bonding character of the metal−ligand interactions and minimal involvement of the metal d orbitals. These features give rise to loose electronic demands and flexible bonding situations, which have well been documented in recent years with the observation of great structural diversity in this family of compounds.[1−3]

In the solid state, group 14 metallocenes can essentially be classified into three types (Figure 1). Bridging μ-η^5:η^5 cyclopentadienyl ligands (type **A**) exist in all three polymorphic modifications of the parent plumbocene, Pb(C_5H_5)$_2$, with the structural motifs of a zigzag chain,[4] of a toluene/solvated sinusoidal chain,[5] and of a hexameric aggregate.[5] Utilization of lighter homologues[6,7] and/or of sterically demanding cyclopentadienyl ligands[8−10] affords the most frequently encountered bent sandwich structures (type **B**);[1] in some cases, extra short intermolecular interactions are present among neighboring molecules in the lattice.[11] Finally, high steric congestion may cause a parallel alignment of the two cyclopentadienyl rings, resulting in a linear sandwich geometry (type **C**).[12−15] The first group 14 metallocene with parallel ring ligands to be discovered was decaphenylstannocene Sn(C_5Ph_5)$_2$,[12] and the first linear germanocene and plumbocene were E[(C_5Me_4)($SiMe_2tBu$)]$_2$ (E = Ge, Pb).[13] Interestingly, in the case of decamethylsilicocene Si(C_5Me_5)$_2$ two independent isomers are observed in the crystal structure, one with parallel pentamethylcyclopentadienyl ligands and the other one with a bent geometry.[16]

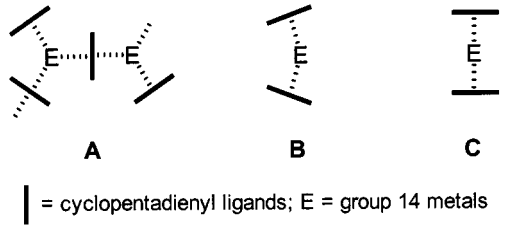

Figure 1. Three structural types of group 14 metallocenes

As aromatic anionic ligands with some similarity to cyclopentadienides, boratabenzenes have drawn substantial research interest recently.[17,18] However, boratabenzene compounds of p-block elements are still quite rare.[19−22] In previous work, we have synthesized the bis(1-methylboratabenzene) compounds E(C_5H_5BMe)$_2$ (**1**: E = Ge; **2**: E = Sn; **3**: E = Pb).[19] X-ray diffraction studies showed that the lead compound **3** possesses a bent geometry locally and forms a tetrameric packing aggregate with short intermolecular contacts which indicate a specific interaction between the lead atoms and the most negatively charged α-carbons of the boratabenzenes of neighboring molecules. In this paper, we describe the synthesis and characterization of the bis(aminoboratabenzene) compounds **4**−**7** using 1-(dimethylamino)-3,5-dimethylboratabenzene and 1-[bis(trimethylsilyl)amino]-3,5-dimethylboratabenzene as ligands. A comparison of their spectroscopic and structural data with those of the known 1-methylboratabenzene analogues provides insight into the electronic and steric effects of the *B*-bonded substituents on group 14 metal−boratabenzene complexes.

[‡] Borabenzene Derivatives, 36. − Part 35: X. Zheng, G. E. Herberich, *Organometallics* **2001**, *20*, 3097−3100.

[a] Institut für Anorganische Chemie, Technische Hochschule Aachen
52056 Aachen, Germany
Fax: (internat.) + 49-241/8092288
E-mail: gerhard.herberich@ac.rwth-aachen.de

 © WILEY-VCH Verlag GmbH, 69451 Weinheim, 2001 1434−1948/01/1212−3013 $ 17.50+.50/0

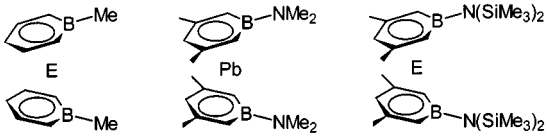

1: E = Ge
2: E = Sn
3: E = Pb

4

5: E = Ge
6: E = Sn
7: E = Pb

Results and Discussion

Syntheses

Salt-metathetical reactions were used in the present work to synthesize the bis(aminoboratabenzene) compounds of the group 14 elements. We had previously reported the synthesis of $Pb(C_5H_5BMe)_2$ (**3**) from lithium 1-methylboratabenzene and $PbCl_2$ in a 2:1 molar ratio.[19] The analogous reaction of lithium 1-(dimethylamino)-3,5-dimethylboratabenzene with $PbCl_2$ at −30 °C produced $Pb(3,5\text{-}Me_2C_5H_3BNMe_2)_2$ (**4**) as a red oil. The formation of the targeted compound was verified by ^1H, ^{11}B, and ^{13}C NMR spectroscopy. Unfortunately, **4** is thermally unstable at ambient temperature and decomposes completely within hours to give lead black as well as an oily mixture of ligand coupling products. To avoid thermal decomposition, all manipulations must be performed at temperatures lower than −20 °C. A similar oxidative coupling reaction had previously been observed when a pinene-fused aminoboratabenzene ion was treated with CuI.[23]

The different stabilities of **3** and **4** seem to arise from the different electronic perturbations of the *B*-amino substituents on the boratabenzene ligands.[24−27] In general, considerable π-interactions exist between the nitrogen and the boron for 1-(dialkylamino)boratabenzenes.[24] This B−N π-interaction is antibonding with respect to the intra-ring B−C π-conjugation, which consequently makes aminoboratabenzenes somewhat similar to the open pentadienyl ligand.[25] Using cyclopentadienide ions as reference, Ashe et al.[26] evaluated the pK_a values of several boracyclohexadienes (or dihydroborinines), the conjugate acids of the corresponding boratabenzene ions, in DMSO by means of NMR spectroscopic methods. The pK_a of 1-methylboracyclohexa-2,5-diene is lower than 12.5 whereas that of 1-(diisopropylamino)boracyclohexa-2,5-diene reaches 17.8 (cf. pK_a = 18.0 for CpH[28]). In other words, 1-(dimethylamino)-boratabenzene is considerably more basic than 1-methylboratabenzene, and hence should be more prone to oxidation and oxidative ligand coupling.

We then chose 1-[bis(trimethylsilyl)amino]-3,5-dimethylboratabenzene as the ligand. From the viewpoint of electronic effects, the polarizing positive Si centers stabilize the nitrogen lone-pair and weaken the B−N π-conjugation; as a consequence, this ligand is expected to be less basic and less nucleophilic than the *B*-(dimethyamino) analogue. The reduced π-conjugation is evidenced by the B−N bond length in the crystal structure of $ScCl[3,5\text{-}Me_2C_5H_3BN(SiMe_3)_2]_2$ [1.471(3) Å] which is considerably longer than that of the η^6-bonded 1-(dialkylamino) ligand in $[ScCl(3,5\text{-}Me_2C_5H_3BNMe_2)]_2$ [1.417(3) Å].[29] Further support comes from the ^{11}B NMR spectroscopic data of the relevant compounds as will be discussed in some detail below. From the viewpoint of steric effects, the bulky *B*-bis(trimethylsilyl)amino substituent of the ligand is expected to enhance the kinetic stability of its complexes.

The bis[1-bis(trimethylsilyl)amino-3,5-dimethylboratabenzene] compounds **5**−**7** can be obtained in good yields (63−85%) from a suitable dihalide (GeI_2, $SnCl_2$, or $PbCl_2$) and 2 equivalents of $Li[3,5\text{-}Me_2C_5H_3BN(SiMe_3)_2]$ using diethyl ether as the solvent. All three compounds can be crystallized from pentane at −30 °C as large prisms. Since the previously known 1-methyl compounds **1** and **2** are liquids, the new compounds **5** and **6** of germanium and tin are the first crystalline bis(boratabenzene) derivatives of these elements. While **5** and **6** are pale yellow, the lead compound **7** is orange red; they are thermally stable at room temperature but quite sensitive to moisture and oxygen.

Spectroscopic Data

The new compounds were characterized by multinuclear NMR spectroscopy and electron-impact mass spectrometry (EIMS). The ^{11}B NMR chemical shifts for **1**−**7** are collected in Table 1, together with data for the related lithium boratabenzenes. On going from germanium to lead, the chemical shifts $\delta(^{11}B)$ move to high field and are, for the lead−boratabenzene compounds, very close to the chemical shifts of the corresponding lithium boratabenzenes.[29,30] This increase (**5** < **6** < **7**) indicates an increasing electrostatic contribution to the metal−ligand interactions for the heavier homologues, which reduces the transfer of electron density from the ligand to the cationic center. Moreover, a survey of the ^{11}B NMR spectroscopic data also provides an insight into the influence of the *B*-bonded substituents on the electronic properties of the ligands. In the case of 1-[bis(trimethylsilyl)amino]-3,5-dimethylboratabenzene, the polarizing influence of the positive silicon centers, as well as the steric demand of the *B*-substituent, diminishes the π-interaction in the B−N bond.[29] Therefore, the ^{11}B chemical shifts of its compounds are located between those of

Table 1. ^{11}B NMR chemical shift data for **1**−**7**[a]

Compound	$\delta(^{11}B)$	ref.
$Ge(C_5H_5BMe)_2$ (**1**)	41	[19]
$Sn(C_5H_5BMe)_2$ (**2**)	38	[19]
$Pb(C_5H_5BMe)_2$ (**3**)	36.1	[19]
$Li(C_5H_5BMe)_2$	36	[30]
$Ge[Me_2C_5H_3BN(SiMe_3)_2]_2$ (**5**)	37.8	this work
$Sn[Me_2C_5H_3BN(SiMe_3)_2]_2$ (**6**)	36.3	this work
$Pb[Me_2C_5H_3BN(SiMe_3)_2]_2$ (**7**)	35.2	this work
$Li[Me_2C_5H_3BN(SiMe_3)_2]$	34.5	[29]
$Pb(Me_2C_5H_3BNMe_2)_2$ (**4**)	32	this work
$Li(Me_2C_5H_3BNMe_2)$	31.6	[29]

[a] Chemical shifts were measured in CD_2Cl_2 for group 14 metal compounds and in $[D_8]$THF for lithium boratabenzenes.

the 1-methylboratabenzene and those of the 1-(dimethylamino)-3,5-dimethylboratabenzene compounds.

The ^{119}Sn and ^{207}Pb NMR chemical shifts for the relevant compounds are listed in Table 2. $\delta(^{119}Sn)$ for **6** is located at $\delta = -1592$ and the $\delta(^{207}Pb)$ for **7** at $\delta = -2890$. Both values are slightly more negative than those of the 1-methylboratabenzene analogues [**2**: $\delta(^{119}Sn) = -1535$, **3**: $\delta(^{207}Pb) = -2579$],[19] and far less negative than those of the cyclopentadienyl analogues [e.g., $Sn(C_5H_5)_2$:[31] $\delta(^{119}Sn) = -2199$, $Pb(C_5H_5)_2$:[32] $\delta(^{207}Pb) = -5030$].[34] As discussed in our earlier paper, these dramatic differences can qualitatively be related to the different donor properties of the ligand anions (mainly influencing σ_{dia}) and to the different HOMO/LUMO gaps (influencing σ_{para}).[19]

The EIMS data for **5**−**7** are summarized in Table 3. All three compounds exhibit very weak parent peaks {$[EL_2 - 1]^+$, $I_{rel} < 1\%$; E = Ge, Sn, Pb; L = 3,5-$Me_2C_5H_3BN(SiMe_3)_2$} and feature two sequential losses of the boratabenzene ligands. The most abundant peaks belong to the cations EL^+ or L^+. It is interesting to note that the fragments L_2^+ and $[L_2 - Me]^+$ are also present in the mass spectra. This observation indicates that oxidative ligand coupling reactions are taking place under the conditions of mass spectrometry.

Table 2. ^{119}Sn and ^{207}Pb NMR chemical shift data

Compound	$\delta(^{119}Sn)$	$\delta(^{207}Pb)$
$E(C_5H_5BMe)_2$ (**2** and **3**)	−1535[19]	−2584[19]
$E[Me_2C_5H_3BN(SiMe_3)_2]_2$ (**6** and **7**)	−1592	−2890
$E(C_5H_5)_2$	−2199[31]	−5030[32]
$E(C_5Me_5)_2$	−2121[33]	−4390[32]
$E[(C_5Me_4(SiMe_2Bu^t)]_2$	−2204[13c]	−4595[13c]
$E(C_5Ph_5)_2$ [a]	−2215[32]	−6150[32]

[a] Chemical shifts were measured in the solid state.

Table 3. Mass spectroscopic data for **5**−**7**[a]

Fragment	*m/z* (I_{rel} [%]) **5** (E = Ge)	**6** (E = Sn)	**7** (E = Pb)
$[EL_{2-}1]^+$	602 (< 1)	647 (< 1)	735 (< 1)
L_2^+	528 (1)	528 (2)	528 (20)
$[L_2 - Me]^+$	513 (1)	513 (13)	513 (80)
EL^+	338 (100)	384 (100)	472 (30)
L^+	264 (30)	264 (48)	264 (100)
E^+	74 (3)	120 (4)	208 (1)

[a] E = Ge, Sn, Pb; L = [3,5-$Me_2C_5H_3BN(SiMe_3)_2$].

Crystal Structures of E[3,5-$Me_2C_5H_3BN(SiMe_3)_2]_2$ (E = Ge, Sn, Pb)

The crystal structures of the compounds **5**−**7** were determined by X-ray diffraction methods (Table 4 and 5). The germanium compound **5** (Figure 2) crystallizes in the monoclinic space group $P2_1/c$ ($Z = 4$) whereas the tin compound **6** and the lead compound **7** (both with an overall structure very similar to that of **5** and therefore not shown) adopt the triclinic space group $P\bar{1}$ ($Z = 4$) with two independent, but quite similar molecules per asymmetric unit. The latter two compounds are isomorphous in the solid state.

All three structures are of a bent-sandwich type, and no specific intermolecular interactions between neighboring molecules are observed. The two boratabenzene ligands are orientated in such a way that the two voluminous bis(trimethylsilyl)amino groups are related to each other with rotational angles of 147−162° so as to minimize repulsive interactions. The B−N bond lengths [1.46−1.49(1) Å] are comparatively long, and the interplanar angles between the best boratabenzene C_5B plane and the amino NSi_2 plane are quite large. Both observations indicate rather weak π-interactions between the boron and the nitrogen.

The central elements display a rather asymmetric bonding to the boratabenzene rings. This is evidenced by the fact that the metal-to-carbon/boron distances span a very large range, especially in the case of the germanium compound [**5**: 2.320−2.939(4) Å; **6**: 2.519−3.033(9) Å, **7**: 2.632−3.054(7) Å]. Note that the E−B distances are even slightly shorter than some of the E−C distances despite the larger covalent radius of the boron atom. In such a situation, a statement about ligand hapticity would seem quite arbitrary, but we may safely state that the ligand is facially coordinated to the central element.

Table 4. Selected bond lengths (Å) for **5**−**7**

	5		**6**			**7**			
Ge−C12	2.321(4)	Sn1−C12	2.540(9)	Sn2−C32	2.534(8)	Pb1−C12	2.644(6)	Pb2−C32	2.632(6)
Ge−C13	2.467(4)	Sn1−C13	2.616(10)	Sn2−C33	2.634(9)	Pb1−C13	2.706(7)	Pb2−C33	2.702(7)
Ge−C14	2.637(4)	Sn1−C14	2.783(9)	Sn2−C34	2.784(10)	Pb1−C14	2.853(7)	Pb2−C34	2.862(6)
Ge−C15	2.913(4)	Sn1−C15	3.024(8)	Sn2−C35	3.027(9)	Pb1−C15	3.034(6)	Pb2−C35	3.043(6)
Ge−C16	2.939(4)	Sn1−C16	3.017(8)	Sn2−C36	3.030(9)	Pb1−C16	3.049(6)	Pb2−C36	3.046(7)
Ge−B1	2.739(5)	Sn1−B1	2.898(9)	Sn2−B3	2.914(9)	Pb1−B1	2.973(7)	Pb2−B3	2.953(7)
Ge−C22	2.320(4)	Sn1−C22	2.530(8)	Sn2−C42	2.519(9)	Pb1−C22	2.642(6)	Pb2−C42	2.634(6)
Ge−C23	2.454(4)	Sn1−C23	2.620(9)	Sn2−C43	2.624(10)	Pb1−C23	2.704(7)	Pb2−C43	2.714(7)
Ge−C24	2.612(4)	Sn1−C24	2.787(9)	Sn2−C44	2.787(10)	Pb1−C24	2.851(7)	Pb2−C44	2.840(6)
Ge−C25	2.874(4)	Sn1−C25	3.008(9)	Sn2−C45	3.029(9)	Pb1−C25	3.047(6)	Pb2−C45	3.040(7)
Ge−C26	2.908(4)	Sn1−C26	3.033(8)	Sn2−C46	3.013(9)	Pb1−C26	3.049(6)	Pb2−C46	3.054(7)
Ge−B2	2.736(5)	Sn1−B2	2.907(9)	Sn2−B4	2.907(9)	Pb1−B2	2.968(7)	Pb2−B4	2.948(7)
N1−B1	1.486(6)	N1−B1	1.464(12)	N3−B3	1.476(12)	N1−B1	1.480(9)	N3−B3	1.481(8)
N2−B2	1.474(6)	N2−B2	1.458(12)	N4−B4	1.494(11)	N2−B2	1.466(9)	N4−B4	1.486(8)

Table 5. Structural data related to the best least-squares planes for **5**−**7**[a]

Compound	**5**	**6**	**7**
Max. deviation from C_5B planes [Å]	0.072 (C*n*2)	0.055 (C*n*2)	0.047 (C*n*2)
Tilt angle of the sandwich unit [°]	43	51	51
Metal distance to best C_5B plane [Å]	2.179	2.375	2.456
Rotational angle between ligands[b] [°]	162	148	147
Slip distortion[c] [Å]	0.56	0.51	0.43

[a] The data are averaged where applicable. − [b] The rotational angle of the two boratabenzene ligands A and B is defined as the angle between the projections of the two exocyclic B−N bond vectors onto the C_5B plane of the ligand A. − [c] The slip distortion is defined as the distance between the projection of the central metal onto the C_5B plane and the geometric center of the C_5B ring.

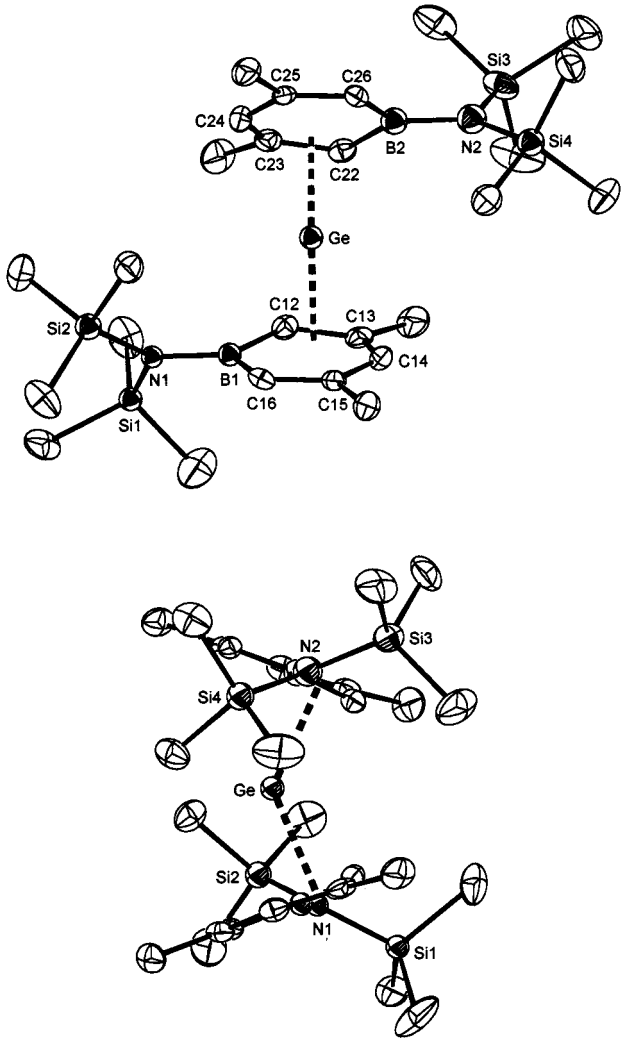

Figure 2. Front and side views (Platon plots[35] at the 30% probability level) of the molecular structure of **5**

The slip distortions, defined as the distances between the projections of the central metals onto the ligand C_5B planes and the geometric centers of the C_5B rings, are 0.56 Å for **5**, 0.51 Å for **6**, and 0.43 Å for **7** on average. These slip distortions are essentially directed toward one of the two ortho-carbon atoms (C*n*2), as can readily be seen from the extremely short E−C*n*2 and at the same time rather long E−C*n*6 distances. The rings also display substantial deviations from planarity. In all cases, the C*n*2 atoms show the largest vertical displacements [0.043−0.056 Å] from the best C_5B planes and toward the central elements.

The π-electron distribution of the boratabenzene ring and the intra-ring B−C bond polarization concentrate negative charge onto the α-carbons.[19−21,25] A symmetric slip toward the boron atom would indicate a largely ionic interaction as in the case of $Mg(C_5H_5BMe)_2$.[25] On the other hand, the combination of an asymmetric slip toward one of the two α-carbon atoms with a partial localization of the ring π-electron system would be expected in cases with significant covalent orbital interactions, as for instance for 2-$(Me_3Sn)C_5H_5BMe$.[20] The Ge compound **5** displays the most asymmetric coordination of the central atom, and the intra-ring bond lengths [cf. B1−C12 1.515(7), C12−C13 1.428(6), C13−C14 1.388(6), C14−C15 1.411(6), C15−C16 1.374(6), B1−C16 1.523(6) Å] show some localization of the π-electron system. The situation is still far from a fully localized diene system, but we may safely conclude that covalent orbital interactions contribute significantly to the bonding in this case. On the other hand, the Pb compound **7** shows a less asymmetric slip, and the intra-ring distances [cf. B1−C12 1.532(10), C12−C13 1.403(9), C13−C14 1.396(10), C14−C15 1.400(10), C15−C16 1.385(9), B1−C16 1.514(10) Å] show barely significant differences which exclude any pronounced localization of the π-electron system. Hence electrostatic interactions are more important in this case.

The tilt angles of the sandwich units are remarkably large in all three structures. For instance, an averaged interplanar angle of 51° is found for the lead compound **7**. In comparison, the sterically less demanding compound bis(1-methylboratabenzene)lead (**3**) possesses a smaller tilt angle of 44° despite the marked short intermolecular interactions in the structure.[19] Although it is generally accepted that steric congestion may cause a decrease of the bending angle of the group 14 sandwich compounds, a rationalization of the molecular geometries based solely on this line seems insufficient. Recent ab initio calculations on the parent stannocene and plumbocene predict very small energy gaps between the bent and linear forms.[36] In addition, accumulating experimental evidence tends to support the notion that the molecular shapes of this family of compounds are strongly affected by lattice forces, as one would expect for soft structural parameters. A pertinent example is the fact

that decaisopropylplumbocene $Pb(C_5Pri_5)_2$ [10a] is bent, whereas the less highly substituted hexaisopropyl analogue $Pb(C_5H_2Pri_3)_2$ [15] is linear.

Concluding Remarks

This paper presents work on bis(aminoboratabenzene) compounds of divalent group 14 elements. We found that the thermal stability of the plumbocene analogues decreases in the order **3** > **7** > **4**. This sequence parallels the basicity of the corresponding boratabenzene ligands and suggests that the stability is tunable by varying the *B*-bonded groups.

Crystal structure analyses reveal a monomeric bent-sandwich structure for the compounds **5**−**7**. The molecules possess rather large tilt angles, implying that the bulky substituents of the ligands do not necessarily result in less bent molecular geometries for group 14 metallocenes. In all three structures, the metal−ligand bonding is surprisingly asymmetric with large slip distortions. This observation, together with the synopsis of the ^{11}B NMR spectroscopic data, suggests that the metal−ligand interactions comprise large electrostatic contributions for this family of compounds which increase on going from Ge to Pb.

Experimental Section

General: All manipulations were carried out under an inert atmosphere of nitrogen by means of standard Schlenk techniques. Pentane was distilled from Na/K alloy, toluene from sodium, and Et_2O from sodium benzophenone ketyl solution. Anhydrous GeI_2, $SnCl_2$, and PbI_2 were used as received from commercial sources. The lithium salts $Li(3,5\text{-}Me_2C_5H_3BNMe_2)$[29,37] and $Li[3,5\text{-}Me_2C_5H_3BN(SiMe_3)_2]$[29] were prepared according to established procedures. Electron-impact mass spectra were recorded on a Finnigan MAT-95 at a nominal electron energy of 70 eV. Elemental analyses were performed at the Analytische Laboratorien, 51779 Lindlar, Germany.

NMR spectra were recorded on a Varian Unity 500 (^1H: 500 MHz; ^{13}C: 125.7 MHz; ^{11}B: 160.4 MHz; ^{119}Sn: 186.5 MHz; ^{207}Pb: 104.6 MHz), a Varian Mercury 200 (^1H: 200 MHz; ^{13}C: 50.3 MHz), or a PMR Firenze spectrometer (^{11}B: 27.9 MHz). Chemical shifts are given in ppm and are referenced to TMS for ^1H and ^{13}C, to $BF_3{\cdot}OEt_2$ for ^{11}B, to $SnMe_4$ for ^{119}Sn, and to $PbMe_4$ for ^{207}Pb. In the case of ^{207}Pb, a solution of $PbEt_4$ (17%, δ = 74.8)[38] in CD_2Cl_2 was used as external standard.

Synthesis of Bis(1-dimethylamino-3,5-dimethylboratabenzene)lead (4): $Li(3,5\text{-}Me_2C_5H_3BNMe_2)$ (0.53 g, 3.42 mmol) in ether (10 mL) was added to a suspension of $PbCl_2$ (0.48 g, 1.71 mmol) in ether (10 mL) at −30 °C. The reaction mixture was stirred at this temperature for 24 h to give a red solution. After removal of the solvent under high vacuum at −30 °C, cold pentane (15 mL, −78 °C) was injected to the residue and a precipitate of LiCl was filtered off quickly. All the solvent was pumped off from the filtrate to give **4** (ca. 0.6 g, 70%) as a red oil that can be stored at −78 °C for weeks. Upon standing at room temperature, compound **4** decomposes to give lead black and a pale yellow oil; this oil contains the ligand-coupling products and consists mainly (ca. 80%) of the 4,4′-isomer.

Data for 4: ^1H NMR (200 MHz, $CDCl_3$, −20 °C): δ = 2.10 (s, 2 × 3-/5-Me), 2.90 (s, 2 × NMe_2), 4.97 (s, 2 × 2-/6-H), 6.10 (s, 2 × 4-H). − $^{13}C\{^1H\}$ NMR (50 MHz, $CDCl_3$, −20 °C): δ = 24.3 (3-/5-Me), 39.0 (NMe_2), 109.3 (C-4), 114.1 (br, C-2,6), 148.5 (C-3,5). − ^{11}B NMR (28 MHz, $CDCl_3$, external $BF_3{\cdot}OEt_2$, −20 °C): δ = 32.

Data for the 4,4′-Isomeric Ligand-coupling Product: ^1H NMR (200 MHz, $CDCl_3$, 20 °C): δ = 1.91 (s, 3-/3′-/5-/5′-Me), 2.83 (s, 2 × NMe_2), 3.23 (s, 4-/4′-H), 5.96 (s, 2-/2′-/6-/6′-H). − $^{13}C\{^1H\}$ NMR (50 MHz, $CDCl_3$, 20 °C): δ = 26.6 (3-/5-Me), 39.1 (NMe_2), 52.5 (C-4,4′), 127.0 (br, C-2,2′,6,6′), 159.2 (C-3,3′,5,5′).

Synthesis of Bis[1-bis(trimethylsilyl)amino-3,5-dimethylboratabenzene]germanium (5): $Li[3,5\text{-}Me_2C_5H_3BN(NSiMe_3)_2]$ (0.64 g, 2.36 mmol) in ether (10 mL) was added dropwise to GeI_2 (0.39 g, 1.18 mmol) in ether (10 mL) at 0 °C. The system was allowed to warm to ambient temperature and stirring was continued for 6 h to give a yellow slurry. After the solvent had been completely removed under vacuum, pentane (30 mL) was added to the residue. A white precipitate of LiCl was removed by filtration and washed with pentane (2 × 5 mL). The combined filtrate was concentrated and cooled to −30 °C for 3 days to give **5** (0.52 g, 73%) as pale yellow crystals. The compound is extremely sensitive to moisture and air.

Data for 5: ^1H NMR (500 MHz, CD_2Cl_2, 20 °C): δ = 0.20 (s, 4 $SiMe_3$), 2.06 (s, 2 × 3-/5-Me), 5.32 (t, *J* = 1.5 Hz, 2 H, 4-H), 5.44 (d, *J* = 1.5 Hz, 2 × 2-/6-H). − $^{13}C\{^1H\}$ NMR (126 MHz, CD_2Cl_2, 20 °C): δ = 4.7 ($SiMe_3$), 25.1 (3-/5-Me), 117.9 (C-4), 122.0 (br, C-2,6), 147.8 (C-3,5). − ^{11}B NMR (160 MHz, CD_2Cl_2, external $BF_3{\cdot}OEt_2$, 20 °C): δ = 37.8. − $C_{26}H_{54}B_2GeN_2Si_4$ (601.3): calcd. C 51.94, H 9.05, N 4.66; found C 51.69, H 9.23, N 4.55.

Synthesis of Bis[1-bis(trimethylsilyl)amino-3,5-dimethylboratabenzene]tin (6): $Li[3,5\text{-}Me_2C_5H_3BN(NSiMe_3)_2]$ (231 mg, 0.85 mmol) in ether (10 mL) was added dropwise to $SnCl_2$ (80 mg, 0.42 mmol) in ether (5 mL) at 0 °C. The system was allowed to warm to ambient temperature and stirring was continued for 6 h to give a yellow slurry. After the solvent had been completely removed under vacuum, pentane (20 mL) was added to the residue. A white precipitate of LiCl was removed by filtration and washed with pentane (5 mL). The combined filtrate was concentrated and cooled to −30 °C overnight to give **6** (0.17 g, 63%) as pale yellow crystals. The compound is sensitive to moisture and air.

Data for 6: ^1H NMR (500 MHz, CD_2Cl_2, 20 °C): δ = 0.21 (s, 4 × $SiMe_3$), 2.10 (s, 2 × 3-/5-Me), 5.32 (t, *J* = 1.2 Hz, 2 × 4-H), 5.51 (d, *J* = 1.2 Hz, 2 × 2-/6-H). − $^{13}C\{^1H\}$ NMR (126 MHz, CD_2Cl_2, 20 °C): δ = 4.9 ($SiMe_3$), 24.9 (3-/5-Me), 113.7 (C-4), 123.8 (br, C-2,6), 148.1 (C-3,5). − ^{11}B NMR (160 MHz, CD_2Cl_2, external $BF_3{\cdot}OEt_2$, 20 °C): δ = 36.3. − ^{119}Sn NMR (186 MHz, CD_2Cl_2, external $SnMe_4$, 20 °C): δ = −1592. − $C_{26}H_{54}B_2N_2Si_4Sn$ (647.4): calcd. C 48.24, H 8.41, N 4.33; found C 48.14, H 8.40, N 4.17.

Synthesis of Bis[1-bis(trimethylsilyl)amino-3,5-dimethylboratabenzene]lead (7): $Li[3,5\text{-}Me_2C_5H_3BN(NSiMe_3)_2]$ (0.56 g, 2.06 mmol) in ether (20 mL) was added dropwise to a suspension of $PbCl_2$ (0.28 g, 1.02 mmol) in ether (10 mL) at −78 °C. The system was allowed to warm to ambient temperature and stirring was continued for 6 h to give an orange slurry. After the solvent had been completely removed under vacuum, pentane (30 mL) was added to the residue. A white precipitate of LiCl was removed by filtration and washed with pentane (2 × 5 mL). The combined filtrate was concentrated to ca. 5 mL and cooled to −30 °C to afford **7** (0.64 g, 85%) as large orange-red crystalline blocks which are sensitive to moisture and air.

Table 6. Crystal data, data collection parameters, and convergence results for **5**−**7**

	5	**6**	**7**
Empirical formula	$C_{26}H_{54}B_2GeN_2Si_4$	$C_{26}H_{54}B_2N_2Si_4Sn$	$C_{26}H_{54}B_2N_2PbSi_4$
Molecular weight	601.28	647.39	735.89
Crystal system	monoclinic	triclinic	triclinic
Space group	$P2_1/c$ (No. 14)	$P\bar{1}$ (No. 2)	$P\bar{1}$ (No. 2)
a [Å]	10.877(2)	14.806(5)	14.913(4)
b [Å]	27.330(8)	15.345(4)	15.394(3)
c [Å]	12.178(4)	16.060(3)	16.036(3)
α [deg]		89.54(3)	89.57(2)
β [deg]	96.13(2)	103.49(3)	103.45(2)
γ [deg]		90.41(2)	90.36(2)
V [Å^3]	3599(2)	3548(2)	3580(1)
Z	4	4	4
$d_{calcd.}$ [g/cm^3]	1.11	1.21	1.37
F(000)	1288	1360	1488
μ [cm^{-1}]	9.86	8.71	48.94
Absorption correction	empirical	none	empirical
Max./min. transmission	0.998/0.943		1.000/0.417
θ range [deg]	3.0−26.0	3.0−25.0	3.0−26.0
Temperature [K]	223	213	233
Crystal size [mm]	0.60 × 0.50 × 0.45	0.30 × 0.30 × 0.25	0.40 × 0.34 × 0.18
Reflections collected	10206	16361	15020
Reflections unique	7021 (R_{int} = 0.079)	12415 (R_{int} = 0.068)	13984(R_{int} = 0.030)
Reflections observed	3994	5956	8016
Criterion for observation	$I > 2\,\sigma(I)$	$I > 2\,\sigma(I)$	$I > 2\,\sigma(I)$
Variables	332	663	663
R_1,[a] observed (all data)	0.058 (0.131)	0.070 (0.164)	0.040 (0.089)
wR_2,[b] observed (all data)	0.111 (0.128)	0.137 (0.161)	0.085 (0.093)
GOF[c]	0.923	0.898	0.923
Max. resd. density [e/Å^3]	0.53	1.12 (close to Sn)	2.03 (close to Pb)

[a] $R_1 = \|\|F_o\| - |F_c\|\|/|F_o|$. − [b] $wR_2 = [w(F_o^2 - F_c^2)^2/w(F_o^2)^2]^{1/2}$, where $w = 1/[\sigma^2(F_o^2) + (aP)^2]$ and $P = [\max(F_o^2,0) + 2F_c^2]/3$. − [c] GOF = $[w(F_o^2 - F_c^2)^2/(n - p)]^{1/2}$.

Data for 7: ^{1}H NMR (500 MHz, CD_2Cl_2, 20 °C): δ = 0.20 (s, 4 $SiMe_3$), 2.19 (s, 2 × 3-/5-Me), 5.32 (t, J = 1.8 Hz, 2 × 4-H), 5.41 (d, J = 1.8 Hz, 2 × 2-/6-H). − $^{13}C\{^1H\}$ NMR (126 MHz, CD_2Cl_2, 20 °C): δ = 5.0 ($SiMe_3$), 24.6 (3-/5-Me), 113.5 (C-4), 125.0 (br, C-2,6), 148.5 (C-3,5). − ^{11}B NMR (160 MHz, CD_2Cl_2, external $BF_3{\cdot}OEt_2$, 20 °C): δ = 35.2. − ^{207}Pb NMR (105 MHz, CD_2Cl_2, external $PbEt_4$, relative to $PbMe_4$, 20 °C): δ = −2890. − $C_{26}H_{54}B_2N_2PbSi_4$ (735.9): calcd. C 42.44, H 7.40, N 3.81; found C 41.27, H 7.51, N 3.72.

X-ray Crystal Structure Determinations of 5−7: Data collection was performed on an ENRAF-Nonius CAD4 diffractometer with Mo-K_α radiation (graphite monochromator, λ = 0.71073 Å) using the ω-2θ scan mode. Crystal data, data collection parameters, and convergence results are listed in Table 6. Empirical absorption corrections on the basis of azimuthal scans[39] were applied to the data sets of **5** and **7** before merging symmetry-related reflections. The structure of **5** was solved by direct methods whereas the solutions for compounds **6** and **7** were obtained by conventional heavy atom methods.[40] All three structures were refined on reflection intensities (F^2) with the SHELXL-97 program.[41] In the final structural models, non-hydrogen atoms were refined with the anisotropic displacement parameters while hydrogen atoms were included as riding with fixed displacement parameters [C−H = 0.98 Å, U_{iso}(H) = 1.3 U_{eq}(C)].[42]

Acknowledgments

We thank Dr. U. Englert for helpful advice with the X-ray structure determinations. This work was generously supported by the Deutsche Forschungsgemeinschaft and the Fonds der Chemischen Industrie.

[1] [1a] P. Jutzi, N. Burford, *Chem. Rev.* **1999**, *99*, 969−990. − [1b] P. Jutzi, N. Burford, in *Metallocenes*, vol. 1 (Eds.: A. Togni, R. L. Halterman), Wiley-VCH, Weinheim, Germany, **1998**, p. 3−54. − [1c] P. Jutzi, *J. Organomet. Chem.* **1990**, *400*, 1−17. − [1d] P. Jutzi, *Adv. Organomet. Chem.* **1986**, *26*, 217−295.

[2] [2a] M. A. Beswick, J. S. Palmer, D. S. Wright, *Chem. Soc. Rev.* **1998**, *27*, 225−232. − [2b] M. A. Beswick, H. Gornitzka, J. Kärcher, M. E. G. Mosquera, J. S. Palmer, P. R. Raithby, C. A. Russel, D. Stalke, A. Steiner, D. S. Wright, *Organometallics* **1999**, *18*, 1148−1153. − [2c] D. R. Armstrong, M. J. Duer, M. G. Davidson, D. Moncrieff, C. A. Russell, C. Stourton, A. Steiner, D. Stalke, D. S. Wright, *Organometallics* **1997**, *16*, 3340−3351. − [2d] M. A. Beswick, N. L. Cromhout, C. N. Harmer, P. R. Raithby, C. A. Russel, J. S. B. Smith, A. Steiner, D. S. Wright, *Chem. Commun.* **1996**, 1977−1978.

[3] [3a] J. Satgé, P. Rivière, M. Rivière-Baudet, in *Comprehensive Organometallic Chemistry II* (Eds.: E. W. Abel, F. G. A. Stone, G. Wilkinson), vol. 2 (volume Ed.: A. G. Davies), Pergamon Press, Oxford, U. K., **1995**, p. 137−216. − [3b] A. G. Davies, in *Comprehensive Organometallic Chemistry II* (Eds.: E. W. Abel,

F. G. A. Stone, G. Wilkinson), vol. 2 (volume Ed.: A. G. Davies), Pergamon Press, Oxford, U. K., **1995**, p. 217−303. − [3c] P. G. Harrison, in *Comprehensive Organometallic Chemistry II* (Eds.: E. W. Abel, F. G. A. Stone, G. Wilkinson), vol. 2 (volume Ed.: A. G. Davies), Pergamon Press, Oxford, U. K., **1995**, p. 305−319.

[4] [4a] J. S. Overby, T. P. Hanusa, V. G. Young, Jr., *Inorg. Chem.* **1998**, *37*, 163−165. − [4b] C. Panattoni, G. Bombieri, U. Croatto, *Acta Crystallogr.* **1966**, *21*, 823−826.

[5] M. A. Beswick, C. Lopez-Casideo, M. A. Paver, P. R. Raithby, C. A. Russell, A. Steiner, D. S. Wright, *Chem. Commun.* **1997**, 109−110.

[6] [6a] J. V. Scibelli, M. D. Curtis, *J. Am. Chem. Soc.* **1973**, *95*, 924−925. − [6b] M. Grenz, E. Hahn, W.-W. du Mont, J. Pickardt, *Angew. Chem.* **1984**, *96*, 69−70; *Angew. Chem. Int. Ed. Engl.* **1984**, *23*, 61.

[7] [7a] E. O. Fischer, H. Grubert, *Z. Naturforsch., Teil B* **1956**, *11*, 423−424. − [7b] J. L. Atwood, W. E. Hunter, A. H. Cowley, R. A. Jones, C. A. Stewart, *J. Chem. Soc., Chem. Commun.* **1981**, 925−927.

[8] [8a] A. H. Cowley, P. Jutzi, F. X. Kohl, J. G. Lasch, N. C. Norman, E. Schlüter, *Angew. Chem.* **1984**, *96*, 603−604; *Angew. Chem. Int. Ed. Engl.* **1984**, *23*, 616. − [8b] P. Jutzi, B. Hielscher, *Organometallics* **1986**, *5*, 1201−1204. − [8c] P. Jutzi, E. Schlüter, M. B. Hursthouse, A. M. Arif, R. L. Short, *J. Organomet. Chem.* **1986**, *299*, 285−295.

[9] [9a] H. Schumann, C. Janiak, E. Hahn, J. Loebel, J. J. Zuckerman, *Angew. Chem.* **1985**, *97*, 765; *Angew. Chem. Int. Ed. Engl.* **1985**, *24*, 773. − [9b] H. Schumann, C. Janiak, E. Hahn, C. Kolax, J. Loebel, M. D. Rausch, J. J. Zuckerman, M. J. Heeg, *Chem. Ber.* **1986**, *119*, 2656−2667.

[10] [10a] H. Sitzmann, *Z. Anorg. Allg. Chem.* **1995**, *621*, 553−556. − [10b] D. J. Burkey, T. P. Hanusa, *Organometallics* **1995**, *14*, 11−13. − [10c] W. W. Schoeller, O. Friedrich, A. Sundermann, A. Rozhenko, *Organometallics* **1999**, *18*, 2099−2106.

[11] W. J. Evans, R. D. Clark, K. J. Forrestal, J. W. Ziller, *Organometallics* **1999**, *18*, 2401−2402.

[12] M. J. Heeg, C. Janiak, J. J. Zuckerman, *J. Am. Chem. Soc.* **1984**, *106*, 4259−4261.

[13] [13a] S. P. Constantine, P. B. Hitchcock, G. A. Lawless, G. M. de Lima, *Chem. Commun.* **1996**, 1101−1102. − [13b] S. P. Constantine, P. B. Hitchcock, G. A. Lawless, *Organometallics* **1996**, *15*, 3905−3906. − [13c] S. P. Constantine, H. Cox, P. B. Hitchcock, G. A. Lawless, *Organometallics* **2000**, *19*, 317−326.

[14] H. Sitzmann, R. Boese, P. Stellberg, *Z. Anorg. Allg. Chem.* **1996**, *622*, 751−755.

[15] D. J. Burkey, T. P. Hanusa, J. C. Huffman, *Inorg. Chem.* **2000**, *39*, 153−155.

[16] T. J. Lee, J. E. Rice, *J. Am. Chem. Soc.* **1989**, *111*, 2011−2017.

[17] For reviews on borabenzene chemistry, see: [17a] G. E. Herberich, in *Advances in Boron Chemistry* (Ed.: W. Siebert), The Royal Society of Chemistry, Cambridge, U. K., **1997**, Special Publication No. 201, p. 211−223. − [17b] G. E. Herberich, H. Ohst, *Adv. Organomet. Chem.* **1986**, *25*, 199−236. − [17c] A. J. Ashe III, S. Al-Ahmad, X. Fang, *J. Organomet. Chem.* **1999**, *581*, 92−97.

[18] For further leading references on borabenzene chemistry, see: [18a] A. J. Ashe III, S. Al-Ahmad, X. Fang, J. W. Kampf, *Organometallics* **2001**, *20*, 468−473. − [18b] D. H. Woodmansee, X. Bu, G. Bazan, *Chem. Commun.* **2001**, 619−620. − [18c] X. Zheng, G. E. Herberich, *Organometallics* **2000**, *19*, 3751−3753.

[19] G. E. Herberich, X. Zheng, J. Rosenplänter, U. Englert, *Organometallics* **1999**, *18*, 4747−4752.

[20] G. E. Herberich, J. Rosenplänter, B. Schmidt, U. Englert, *Organometallics* **1997**, *16*, 926−931.

[21] U. Englert, G. E. Herberich, J. Rosenplänter, *Z. Anorg. Allg. Chem.* **1997**, *623*, 1098−1102.

[22] G. E. Herberich, H. J. Becker, C. Engelke, *J. Organomet. Chem.* **1978**, *153*, 265−270.

[23] G. E. Herberich, U. Englert, B. Ganter, M. Pons, R. Wang, *Organometallics* **1999**, *18*, 3406−3413.

[24] G. E. Herberich, B. Schmidt, U. Englert, T. Wagner, *Organometallics* **1993**, *12*, 2891−2893.

[25] X. Zheng, U. Englert, G. E. Herberich, J. Rosenplänter, *Inorg. Chem.* **2000**, *39*, 5579−5585.

[26] A. J. Ashe III, J. W. Kampf, C. Müller, M. Schneider, *Organometallics* **1996**, *15*, 387−393.

[27] G. C. Bazan, W. D. Cotter, Z. J. A. Komon, R. A. Lee, R. J. Lachicotte, *J. Am. Chem. Soc.* **2000**, *122*, 1371−1380.

[28] F. G. Bordwell, *Acc. Chem. Res.* **1988**, *21*, 456−463.

[29] G. E. Herberich, U. Englert, A. Fischer, J. Ni, A. Schmitz, *Organometallics* **1999**, *18*, 5496−5501.

[30] G. E. Herberich, B. Schmidt, U. Englert, *Organometallics* **1995**, *14*, 471−480.

[31] R. K. Harris, J. D. Kennedy, W. McFarlane, in *NMR and the Periodic Table* (Eds.: R. K. Harris, B. E. Mann), Academic Press, London, U. K., **1978**, p. 351.

[32] C. Janiak, H. Schumann, C. Stader, B. Wrackmeyer, J. J. Zuckerman, *Chem. Ber.* **1988**, *121*, 1745−1751.

[33] P. Jutzi, B. Hielscher, *J. Organomet. Chem.* **1985**, *291*, C25−C27.

[34] [34a] B. Wrackmeyer, *Annu. Rep. NMR Spectrosc.* **1985**, *16*, 73−186. − [34b] B. Wrackmeyer, K. Horchler, *Annu. Rep. NMR Spectrosc.* **1990**, *22*, 249−306. − [34c] B. Wrackmeyer, A. Sebald, L. H. Merwin, *Magn. Reson. Chem.* **1991**, *29*, 260−263.

[35] A. L. Spek, *Acta Crystallogr., Sect. A* **1990**, *46*, C34.

[36] D. R. Armstrong, M. A. Beswick, N. L. Cromhout, C. N. Harmer, D. Moncrieff, C. A. Russell, P. R. Raithby, A. Steiner, A. E. H. Wheatley, D. S. Wright, *Organometallics* **1998**, *17*, 3176−3181.

[37] G. E. Herberich, U. Englert, M. U. Schmidt, R. Standt, *Organometallics* **1996**, *15*, 2707−2712.

[38] J. D. Kennnedy, W. McFarlane, G. S. Pyne, *J. Chem. Soc., Dalton Trans.* **1977**, 2332−2339.

[39] A. C. T. North, D. C. Phillips, F. S. Mathews, *Acta Crystallogr., Sect. A* **1968**, *24*, 351−359.

[40] G. M. Sheldrick, *SHELXS-97*, *Program for Structure Solution*, University of Göttingen, Göttingen, Germany, **1997**.

[41] G. M. Sheldrick, *SHELXL-97*, *Program for Structure Refinement*, University of Göttingen, Göttingen, Germany, **1997**.

[42] Crystallographic data (excluding structure factors) for the structures reported in this paper have been deposited with the Cambridge Crystallographic Data Centre as supplementary publications nos. CCDC-164368 (**5**), CCDC-164369 (**6**), and CCDC-164370 (**7**). Copies of the data can be obtained free of charge on application to the CCDC, 12 Union Road, Cambridge CB2 1EZ, U. K. [Fax: (internat.) +44-1223/336-033; E-mail: deposit@ccdc.cam.ac.uk].

Received June 1, 2001
[I01201]

Reactivity of Coordinated Nitriles − Formation of the Acetamidine Complex *cis*-[$(PMe_3)_2Pt\{1\text{-}MeTy(-H)\}\{CH_3C(NH)NH_2\}]^+$ from the 1-Methylthyminate Compound *cis*-[$(PMe_3)_2Pt\{1\text{-}MeTy(-H)\}(CH_3CN)]^+$ − Synthesis, Characterisation, and X-ray Structures

Bruno Longato,*[a,b] Giuliano Bandoli,[c] Adele Mucci,[d] and Luisa Schenetti[d]

Keywords: Platinum / Nucleobases / Phosphanes / N ligands

1-Methylthymine (1-MeTy) reacts reversibly with the hydroxo complexes *cis*-$[(PMe_3)_2Pt(\mu\text{-}OH)]_2X_2$ ($X^- = NO_3$; ClO_4) in various solvents (S = CH_3CN, H_2O, DMSO) to give the thyminate derivatives *cis*-$[(PMe_3)_2Pt\{1\text{-}MeTy(-H)\}(S)]X$ that have been isolated as pure compounds when S is CH_3CN. The single-crystal X-ray structure of *cis*-$[(PMe_3)_2Pt\{1\text{-}MeTy(-H)\}(CH_3CN)]ClO_4$ shows that the N(3)-platinated nucleobase acts as a monodentate ligand and a molecule of CH_3CN completes the coordination sphere of the metal. Crystals of the acetamidine derivative *cis*-$[(PMe_3)_2Pt\{1\text{-}MeTy(-H)\}\{CH_3C(NH)NH_2\}]X$ were isolated from an acetonitrile solution of this complex, in the presence of small amounts of water, after several months at room temperature, separated in 5–10% yield. The X-ray analysis of the perchlorate salt shows a configuration of the amidine ligand consistent with a formal *trans* addition of NH_3 to the CN triple bond of the coordinated nitrile. The acetamidine complex was formed in high yield (70%), in a few weeks, when aqueous solution of NH_3 was added to *cis*-$[(PMe_3)_2Pt\{1\text{-}MeTy(-H)\}(CH_3CN)]^+$ dissolved in CH_3CN. Side products of this reaction are the ammonia complex *cis*-$[(PMe_3)_2Pt\{1\text{-}MeTy(-H)\}(NH_3)]^+$, which was also obtained as pure compound, acetamide, and other platinum containing species. All the isolated complexes were characterised by elemental analysis, IR, and multinuclear NMR spectroscopy.

Introduction

The coordination of nitriles to electron-withdrawing transition metals results in an enhanced electrophilicity of the nitrile carbon, making it susceptible to nucleophilic attack. Reactions of nitriles with protic nucleophiles such as water, alcohols, and ammonia (or amines) generate the corresponding amides, $H_2N-C(O)R$, imino esters (or imino ethers), $HN=C(OR')R$, and amidines, $HN=C(R)NH_2$, respectively.[1,2]

The products of the reactions of Pt^{II}-coordinated nitriles with water and alcohols have been investigated in details, whereas only a few reports deal with the characterization of amidine complexes.[3−5] The first example of structurally authenticated acetamidine [$HN=C(CH_3)NH_2$] complex of platinum was the dication *trans*-$[Pt(NH_3)_2\{CH_3C(NH)NH_2\}_2]^{2+}$, initially formulated as the octahedral species *trans*-$[Pt(NH_3)_4(CH_3CN)_2]^{2+}$.[6] Very recently, Bertani and co-workers have reported the characterisation of the bis-amidine *trans*-$[PtCl_2\{CH_3C(NH)NHMe\}_2]$, obtained by reacting the acetonitrile complex *trans*-$[PtCl_2(CH_3CN)_2]$ with the primary amine $MeNH_2$, under very mild conditions.[7]

Following our interest in the study of model nucleobases with phosphane analogues of *cis-platin*,[8−14] we came across the nitrile complex *cis*-$[(PMe_3)_2Pt\{1\text{-}MeTy(-H)\}(CH_3CN)]^+$, **1**, containing the N(3)-deprotonated 1-methylthymine ligand [1-MeTy(−H)]. Complex **1** is formed by condensation of the dinuclear hydroxo compound *cis*-$[(PMe_3)_2Pt(\mu\text{-}OH)]_2^{2+}$ with N(1)-substituted methylthymine (1-MeTy), in acetonitrile. We found that when this cationic acetonitrile complex was left in the reaction mixture for several months at room temperature, the acetamidine derivative *cis*-$[(PMe_3)_2Pt\{1\text{-}MeTy(-H)\}\{CH_3C(NH)NH_2\}]^+$, **2**, separated as pure colourless crystalline solid, whereas the solution became yellow. Such a transformation, which implies the formal addition of NH_3 to the coordinated acetonitrile, occurred in low yield (5−10%) and was accompanied by the formation, in addition to free acetamide, of the ammonia complex *cis*-$[(PMe_3)_2Pt\{1\text{-}MeTy(-H)\}(NH_3)]^+$, **3**, and other platinum-containing products.

In this paper we report on the synthesis and the characterisation of these new thyminate complexes showing that the acetamidine derivative **2** can be conveniently prepared by addition of aqueous NH_3 to the acetonitrile complex **1**.

[a] Dipartimento di Chimica Inorganica, Metallorganica ed Analitica, Universitá di Padova,
Via Marzolo 1, 35131 Padova, Italy
Fax: (internat.) + 39-049/8275161
E-mail: longato@chim02.chin.unipd.it
[b] Centro di Studio sulla Stabilitá e Reattivitá dei Composti di Coordinazione, CNR, c/o Dipartimento di Chimica Inorganica, Metallorganica ed Analitica, Universitá di Padova,
Via Marzolo 1, 35131 Padova, Italy
[c] Dipartimento di Scienze Farmaceutiche, Universitá di Padova,
Via Marzolo 5, 35131 Padova, Italy
[d] Dipartimento di Chimica, Universita' di Modena e Reggio Emilia,
Via Campi 183, 41110 Modena, Italy

 © WILEY-VCH Verlag GmbH, 69451 Weinheim, 2001 1434−1948/01/1212−3021 $ 17.50+.50/0

Along with a detailed multinuclear NMR analysis of the isolated compounds, the X-ray structures of *cis*-$[(PMe_3)_2Pt\{1\text{-}MeTy(-H)\}(CH_3CN)]ClO_4$ and *cis*-$[(PMe_3)_2Pt\{1\text{-}MeTy(-H)\}\{CH_3C(NH)NH_2\}]ClO_4$ were obtained, defining the stereochemistry of the amidine ligand in solution as well as in the solid state.

Results and Discussion

Synthesis and Characterisation of the Thyminate Complexes *cis*-$[(PMe_3)_2Pt\{1\text{-}MeTy(-H)\}(CH_3CN)]X$ ($X^- = ClO_4$, **1a**; NO_3, **1b**)

The dinuclear hydroxo complex *cis*-$[(PMe_3)_2Pt(\mu\text{-}OH)]_2^{2+}$ reacted with a stoichiometric amount of 1-MeTy in H_2O, DMSO, or CH_3CN, to give the mononuclear species *cis*-$[(PMe_3)_2Pt\{1\text{-}MeTy(-H)\}(S)]^+$ (S = solvent molecule), resulting from the deprotonation of the nucleobase, according to the following reaction [Equation (1)]:

$$^1/_2\ cis\text{-}[(PMe_3)_2Pt(\mu\text{-}OH)]_2^{2+} + 1\text{-}MeTy + S \rightleftarrows cis\text{-}[(PMe_3)_2Pt\{1\text{-}MeTy(-H)\}(S)]^+ + H_2O \quad (1)$$

The reaction occurred at room temperature in a few hours and was essentially quantitative when anhydrous acetonitrile was used as the solvent, whereas it was incomplete in dimethylsulfoxide or water. The position of the equilibrium could be easily deduced from the ^{31}P NMR spectrum of the reaction mixture since the reagent is characterized by a sharp singlet at δ ca. −25, flanked by the ^{195}Pt satellites, which was substituted by an AB multiplet when the product was formed. The chemical shifts and the coupling constants are dependent on the solvent, as shown in Table 1.

Table 1. ^{31}P NMR spectroscopic data of *cis*-$[(PMe_3)_2Pt\{1\text{-}MeTy(-H)\}(S)]^+$ (S = solvent molecule)

Solvent S	δ_P; $^1J_{PPt}$ (Hz)	δ_P; $^1J_{PPt}$ (Hz)	$^2J_{PP}$ (Hz)
CD_3CN	−31.10 (2944)	−29.59 (3809)	27.5
$[D_6]$DMSO	−23.16 (3169)	−29.12 (3892)	25.6
D_2O	−26.05 (3171)	−30.11 (3885)	26.4

Thus, the ^{31}P NMR spectrum of a $5\cdot10^{-2}$ M solution of the perchlorate salt *cis*-$[(PMe_3)_2Pt(\mu\text{-}OH)]_2(ClO_4)_2$ in CD_3CN containing the nucleobase in 1:2 molar ratio, after equilibration (a few hours at ambient conditions), showed the complete disappearance of the resonance at δ = −25.6, which was replaced by a sharp AB multiplet at δ = −29.6 ($^1J_{PPt}$ = 3810 Hz) and −31.1 ($^1J_{PPt}$ = 2944 Hz) with $^2J_{PP}$ 27.5 Hz, attributable to the thyminato complex *cis*-$[(PMe_3)_2Pt\{1\text{-}MeTy(-H)\}(CH_3CN)]ClO_4$, **1a**.

When the reaction was carried out in $[D_6]$DMSO, at the equilibrium ca. 10% of the starting hydroxo complex remained unchanged, suggesting a relatively lower stability of the thyminate complex in this solvent. In line with the presence of different types of donor atoms *trans* to the PMe_3 ligands, the ^{31}P NMR spectrum of the product shows well separated doublets ($^2J_{PP}$ = 25.6 Hz), at δ = −23.1 ($^1J_{PPt}$ = 3169 Hz) and −29.1 ($^1J_{PPt}$ = 3892 Hz). The deprotonation of the nucleobase is evidenced in the proton spectrum by the disappearance of the N(3)H resonance at δ = 11.2 and the concomitant shift to higher field of the H(6) resonance, which is observed as a 1:3:3:1 quadruplet ($^4J_{HH} \approx 1$ Hz) at δ = 7.40, slightly shielded with respect to the free base (δ = 7.49).[9]

Although to a minor extent, the deprotonation of the thymine occurs also in aqueous solution. In this solvent, the perchlorate is insoluble and therefore the corresponding nitrato salt was used. The stoichiometric amount of 1-MeTy added to a $4.1\cdot10^{-2}$ M solution of *cis*-$[(PMe_3)_2Pt(\mu\text{-}OH)]_2(NO_3)_2$ in D_2O dissolved in 2.5 h at ambient temperature. The ^{31}P NMR spectrum of the resulting colourless solution exhibits an intense AB pattern (Table 1), tentatively attributed to the aqua complex *cis*-$[(PMe_3)_2Pt\{1\text{-}MeTy(-H)\}(H_2O)]^+$, and the singlet of the unchanged hydroxo complex having an intensity of about 18% of the total resonances. In addition, at the equilibrium, very weak resonances in the range δ = −25 to −32 are detectable. Since the thyminate ion can also act as a bidentate ligand,[15] these signals could be due to the presence of small concentrations of polynuclear complexes of the type *cis*-$[(PMe_3)_2Pt\{1\text{-}MeTy(-H)\}]_n^{n+}$ or, alternatively, to other species related to the acidic character of the water molecule coordinated to the metal centre. It is worth noting that addition of a small amount of CH_3CN (1−2%) to the D_2O solution resulted in the immediate appearance of the multiplet due to the complex *cis*-$[(PMe_3)_2Pt\{1\text{-}MeTy(-H)\}(CH_3CN)]^+$ as the only detectable species.

As anticipated, in anhydrous CH_3CN the reaction 1 was essentially complete and the solvent complex *cis*-$[(PMe_3)_2Pt\{1\text{-}MeTy(-H)\}(CH_3CN)]^+$ could be isolated by addition of diethyl ether. The IR spectrum of the perchlorate salt, **1a**, shows the weak absorptions at 2332 and 2371 cm^{-1}, typical values for the η^1-coordinated CH_3CN in platinum(II) complexes, and the carbonyl bands of the thyminate ligand at 1653 and 1591 cm^{-1}. The $\{^1H\}$-^{31}PNMR spectrum (at 161 MHz) in CD_3CN shows an AB system at δ = −29.6 and −31.1 (Table 1), flanked by the ^{195}Pt satellites, due to the chemical non-equivalence of the phosphane ligands. In the corresponding ^1H NMR spectrum the PMe_3 resonances are observed as two doublets at δ = 1.78 ($^2J_{HP}$ = 11.3 Hz; $^3J_{HPt}$ = 30 Hz) and δ = 1.63 ($^2J_{HP}$ = 11.8 Hz; $^3J_{HPt}$ = 42 Hz). The first resonance is attributable to the methyl groups of the phosphane resonating at higher field, as deduced from inverse detection experiments. However, attempts to discriminate between the two PMe_3 ligands with respect to the nucleobase, through NOE experiments, were unsuccessful. The nitrile methyl resonance (δ = 2.03) does not differ significantly from the value of the free ligand indicating that replacement of the CH_3CN molecule by the solvent upon dissolution of compound had occurred. The lability of the acetonitrile ligand was confirmed by dissolving the complex in $[D_6]$DMSO. In this solvent the ^{31}P NMR spectrum of **1a** displays a main set of resonances due to the species *cis*-$[(PMe_3)_2Pt\{1\text{-}MeTy(-H)\}(DMSO)]^+$ (Table 1) and a weak AB multiplet ($^2J_{PP}$ = 25.9 Hz) at δ = −29.4 ($^1J_{PPt}$ = 3960 Hz) and −30.9

($^1J_{PPt}$ = 2985 Hz), which accounts for ca. 5% of the mixture, attributable to the incomplete replacement of the nitrile molecule on the coordination sphere of the metal. Moreover, as a consequence of the reversibility of reaction (1), **1a** decomposes immediately in water with precipitation of *cis*-$[(PMe_3)_2Pt(\mu\text{-}OH)]_2(ClO_4)_2$ that is, unlike the nitrate salt, insoluble in water.

The dissolution of the acetonitrile complexes **1a** and **1b** in [D_6]DMSO or D_2O (for **1b**) caused a remarkable shift to lower field of one of the two PMe_3 resonances in the ^{31}P NMR spectra, while the second one changed only slightly (Table 1). Whereas these changes are in agreement with the replacement of the labile CH_3CN ligand by the solvent, the attribution of the resonances is not obvious. It is generally assumed that in square-planar Pt^{II} complexes the phosphane *trans* to a labile ligand experiences the highest value of the one-bond $^{31}P-^{195}Pt$ coupling. For the complexes *cis*-$[(PMe_3)_2Pt\{1\text{-}MeTy(-H)\}(S)]^+$ (Table 1) we found that the larger value of $^1J_{PPt}$ was associated with the less shielded phosphane in the case of CD_3CN (δ = 29.6, $^1J_{PPt}$ = 3809 Hz) but in [D_6]DMSO and D_2O the opposite was observed.

Characterisation of the Acetamidine Complexes *cis*-$[(PMe_3)_2Pt\{1\text{-}MeTy(-H)\}\{CH_3C(NH)NH_2\}]X$ (X = ClO_4, 2a; NO_3, 2b)

When the reaction mixture of *cis*-$[(PMe_3)_2Pt(\mu\text{-}OH)]_2(ClO_4)_2$ (ca. 0.1 M) and 1-MeTy in CH_3CN [Equation (1)] was left at room temperature for several weeks, the colourless solution, became yellow, and colourless crystals started to precipitate. In some months (4−7) small amounts (5−10%) of the new complex *cis*-$[(PMe_3)_2Pt\{1\text{-}MeTy(-H)\}\{CH_3C(NH)NH_2\}]ClO_4$, **2a**, were formed as a crystalline solid that was characterised by elemental analysis, multinuclear NMR spectroscopy, and single-crystal X-ray diffraction methods. The compound was insoluble in acetonitrile and in chlorinated solvents, whereas it dissolved in DMSO and water. The proton spectrum (400 MHz) in [D_6]DMSO exhibits the resonances of the phosphane methyl groups as doublets (δ = 1.58 and 1.48, $^2J_{HP}$ = 11 Hz) with unresolved Pt-satellites and a single set of resonances for the thymine and the amidine ligands. The acetamidine resonances are observed as broad singlets at δ = 7.37 for the imino proton, at δ = 7.24 and 6.95 for the amino protons, and as a sharp singlet at δ = 1.93 for the CH_3 group. The assignments of the NH resonances were obtained through inverse detected $^1H,^{15}N$ heteronuclear multiple quantum coherence experiments (HMQC).[16]

As shown in Figure 1, a, the two NH resonances at higher field correlate with the same ^{15}N resonance at δ = −274 ($^1J_{NH}$ = 90 Hz), whereas that at δ = 7.37, partially overlapping with the thymine H(6) multiplet, correlates with a second ^{15}N resonance at δ = −241 ($^1J_{NH}$ = 80 Hz). This latter ^{15}N resonance displays (Figure 1, b) an additional splitting (ca. 60 Hz) due to the coupling with the ^{31}P nucleus in *trans* position. Moreover, the imino proton displays an H,H coupling (3 Hz) with the NH_2 proton at δ = 7.24, as confirmed through a COSY experiment. This finding suggests a *trans* relationship between the NH_2 group and the imino proton and, in particular, a zigzag arrangement between the imino proton and the NH_2 proton at δ = 7.24.

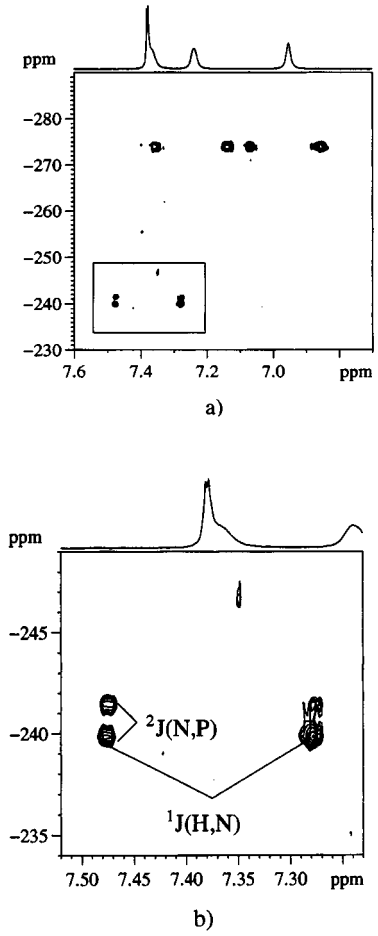

Figure 1. Inverse-detected $^1H,^{15}N$ shift-correlated spectrum of **2a** in [D_6]DMSO obtained with a HMQC experiment without decoupling during the acquisition: a) complete spectrum of the NH region; b) expanded region corresponding to the imino proton

In the inverse detected $^1H,^{195}Pt$ heteronuclear multiple bond correlation experiment (HMBC),[17] the imino proton at δ = 7.37 shows a correlation with the ^{195}Pt signal at δ = −4633 (Figure 2, a), confirming the involvement of the imino group in the coordination to the metal centre.

Figure 2, b, displays that the same ^{195}Pt resonance is also detected through the phosphane proton resonances, demonstrating that the imino nitrogen and the phosphane ligands are bonded to the same metal centre. The left trace in Figure 2 represents the $\{^1H\}$-^{195}Pt spectrum obtained by direct acquisition and, due to the low resolution used in the experimental conditions, the resonance appears as a triplet, whereas the $\{^1H\}$-^{31}P spectrum allowed us to detect two different $^1J_{PPt}$ coupling constants. The phosphane resonances exhibit, in fact, very similar chemical shifts and coupling constants (δ = −28.80 and −29.25; $^1J_{PPt}$ = 3088 and 3125 Hz, respectively) in agreement with the presence of similarly hybridized nitrogen atoms in a *trans* position. As shown in Figure 3, the ^{195}Pt satellites, in spite of the rela-

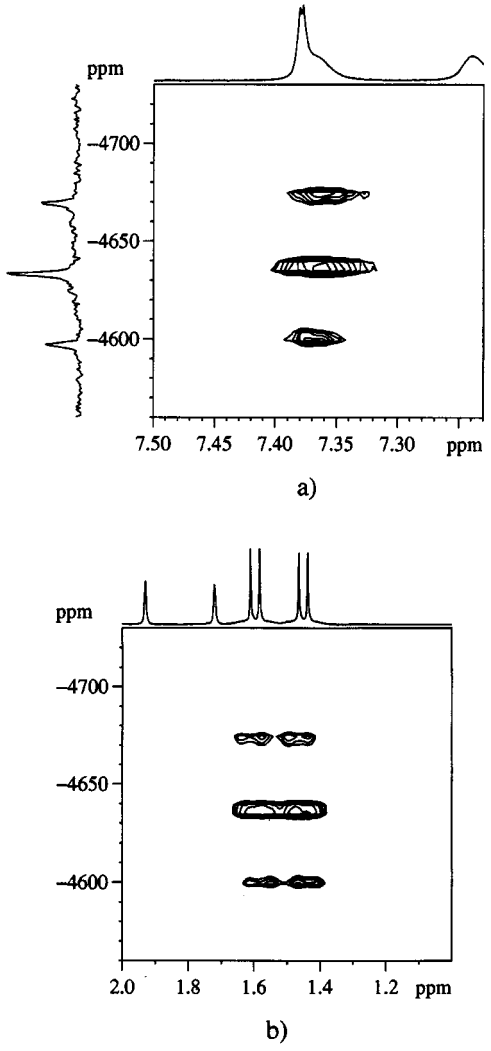

Figure 2. Inverse-detected ^{1}H,^{195}Pt shift-correlated spectrum of **2a** in [D_6]DMSO obtained through a HMBC experiment without decoupling during the acquisition: a) imino proton region and b) phosphane methyl region. The upper trace corresponds to the proton spectrum and the left trace corresponds to the ^{195}Pt spectrum

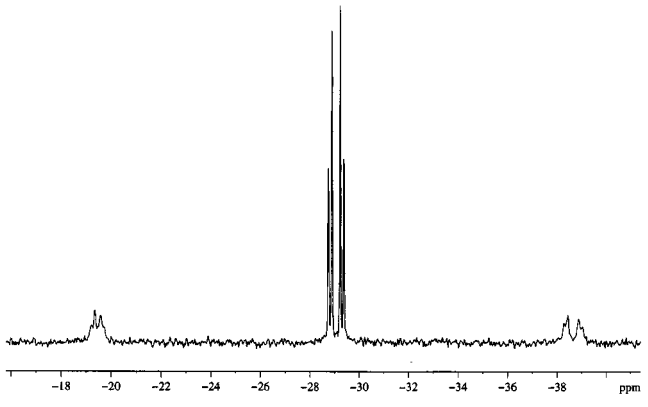

Figure 3. $\{^{1}H\}$-^{31}P NMR at 162 MHz of *cis*-[$(PMe_3)_2$Pt{1-MeTy(−H)}{$CH_3C(NH)NH_2$}]ClO_4 (**2a**) in [D_6]DMSO

tively high field used (162 MHz), were particularly well resolved.

X-ray Structure Analyses of *cis*-[$(PMe_3)_2$Pt-{1-MeTy(−H)}(CH_3CN)]ClO_4, 1a, and *cis*-[$(PMe_3)_2$Pt-{1-MeTy(−H)}{$CH_3C(NH)NH_2$}]ClO_4, 2a

The identification of the atoms and the molecular structures of **1a** and **2a** are depicted in Figure 4 and Figure 5,

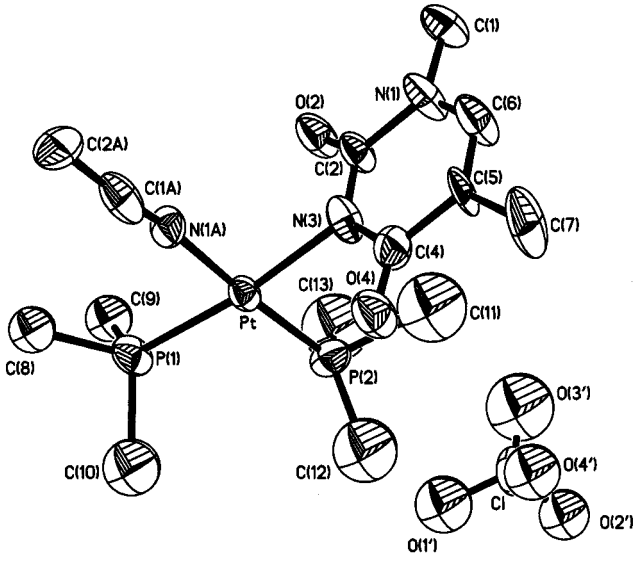

Figure 4. ORTEP drawing of the molecular structure of *cis*-[$(PMe_3)_2$Pt{1-MeTy(−H)}(CH_3CN)]ClO_4, **1a**, along with atomic numbering system. Non-hydrogen atoms are presented as thermal ellipsoids at 35% probability levels

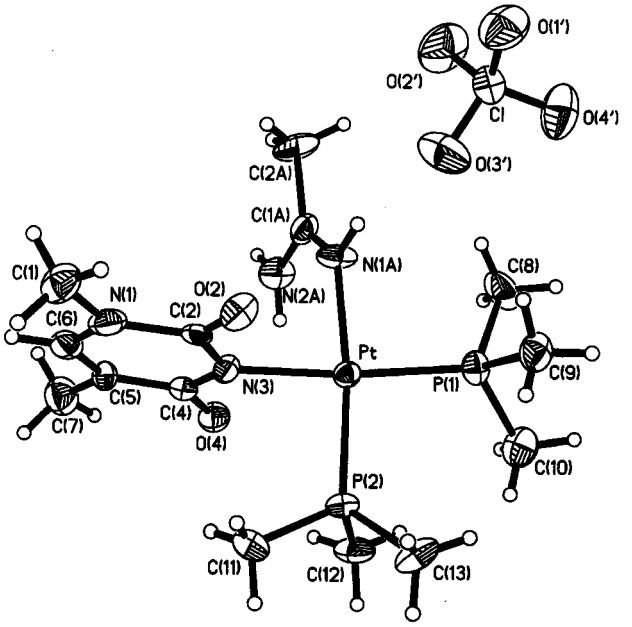

Figure 5. ORTEP drawing of the molecular structure of *cis*-[$(PMe_3)_2$Pt{1-MeTy(−H)}{$CH_3C(NH)NH_2$}]ClO_4 **2a**, along with atomic numbering system. Non-hydrogen atoms are presented as thermal ellipsoids at 35% probability levels, whereas hydrogen atoms are drawn as spheres of arbitrary size

Table 2. Selected bond lengths [Å], intramolecular separations [Å] and angles [°] in *cis*-[$(PMe_3)_2$Pt{1-MeTy(−H)}(CH_3CN)]ClO_4, **1a**, and *cis*-[$(PMe_3)_2$Pt{1-MeTy(−H)}{$CH_3C(NH)NH_2$}]ClO_4 **2a**. Standard deviations are given in parentheses

Compound	**1a**	**2a**
Pt−P(1)	2.268(5)	2.263(3)
Pt−P(2)	2.232(5)	2.259(3)
Pt−N(3)	2.12(1)	2.097(9)
Pt−N(1A)	2.05(1)	2.09(1)
P(1) ··· P(2)	3.347	3.361
P(2) ··· N(3)	3.04	3.07
N(3) ··· N(1A)	2.86	2.81
P(1)−Pt−P(2)	96.1(2)	95.2 (3)
P(1)−Pt−N(3)	173.2(5)	172.0(7)
P(1)−Pt−N(1A)	89.1(4)	90.5(3)
P(2)−Pt−N(3)	88.5(4)	92.6(7)
P(2)−Pt−N(1A)	174.3(4)	173.2(3)
N(3)−Pt−N(1A)	86.5(5)	84.1(5)

respectively, and the main bond lengths and angles are summarised in Table 2.

In both complexes the platinum exhibits a distorted square-planar coordination in which the bond angles around the metal range from 86.5(5) to 96.1(2)° in **1a** and from 84.1(5) to 95.2(3)° in **2a**, their sum being 360.2° and 362.4°, respectively. The common portion of the two structures are roughly superimposable, with an r.m.s. deviation (derived from the BMFIT program)[18] of 0.13 Å when the fitting is performed without the methyl groups. The thymine ring forms a dihedral angle of 89.3(4)° in **1a** and 103.0(3)° in **2a** with the coordination plane, and the acetamidine group in **2a** lies nearly orthogonal to the mean square plane [dihedral angle 111.2(3)°]. In both compounds no effective hydrogen bonds occur and the complexes are built up by the juxtaposition at van der Waals distances of well separated Pt^{II} monocations and perchlorate counter anions. This

Table 3. Geometry of the possible weak hydrogen bonds in **2a**

D−H···A	H···D [Å]	H···A [Å]	D−H···A[°]
N(2A)−H(1AA) ···- O(4)	2.20	2.93	141.3
N(2A)−H(1AB) ···- O(2A)[a]	2.10	2.85	146.1
N(1A)−H(1AC) ···- O(3′)	2.30	3.14	165.5

[a] Refers to the atom in the position x, $y-1$, z.

is despite the fact that the shortest intramolecular (2.93 Å) and intermolecular (2.85 Å) separations in **2a** (Table 3 and Figure 6) seem to be of some significance.

The Pt−P distances are comparable to the mean value of 2.27(4) Å derived from 65 Pt−PMe_3 data retrieved from Cambridge Crystallographic Data Base,[19] while the Pt−N(3) distances [2.12(1) and 2.10(1) Å in **1a** and **2a**, respectively] are greater than the value of 2.03 Å found for Pt−N (thyminate or uracilate) distances in four mononuclear, but uncharged, Pt^{II} complexes.[20−23] Similarly, in **1a** the Pt−N(acetonitrile) distance [2.05(1) Å] is remarkably longer than the mean value [1.97(3) Å] derived from 12 X-ray determinations.[19] The Pt−N(acetamidine) distance of **2a** [2.09(1) Å] is also longer than the value of 1.96 Å found in the diamminebis(acetamidine)platinum(II) dichloride.[6]

Reactivity of the Coordinated Nitrile in the Cationic Complex *cis*-[$(PMe_3)_2$Pt{1-MeTy(−H)}(CH_3CN)]$^+$

Amidine complexes are formally derived by nucleophilic attack of amines on metal-coordinated nitriles. It has recently been reported that the neutral acetonitrile complex *trans*-$PtCl_2(CH_3CN)_2$ reacts with $MeNH_2$, under very mild conditions, to give the bis-amidine product *trans*-$PtCl_2${(*Z*)-N(H)=C(NHMe)CH_3}$_2$.[7] The X-ray structure shows that the organic ligands assume the (*Z*) configuration corresponding to the *trans*-addition of the amine fragments to the CN triple bond (Scheme 1).

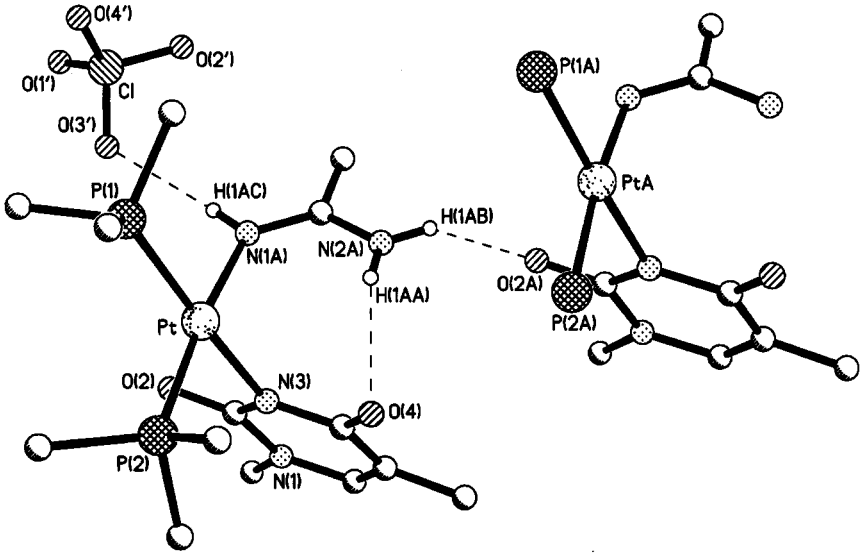

Figure 6. The interactions involving the acetamidine group in **2a**

Scheme 1

The same stereochemistry of the acetamidine groups was early established for the cationic amino complex *trans*-$[Pt(NH_3)_2\{CH_3C(NH)NH_2\}_2]^{2+}$ [6] and is now confirmed for complex **2a** in the solid state as well as in solution.

The separation of the acetamidine compound **2a** as crystalline colourless solid from the reaction mixture of 1-MeTy and *cis*-$[(PMe_3)_2Pt(\mu\text{-}OH)]_2^{2+}$ in CH_3CN requires several months at ambient conditions, and the yield is poor. The NMR analysis of the solution, after separation of the solid, removal of the volatiles and dissolution of the yellow residue in $[D_6]$DMSO, indicates the formation of a very complex mixture of products among which acetamide is one of the main components.

Under the experimental conditions in which we observe the conversion of **1** into **2**, the formation of acetamide is easily predictable since the initial solution contains the nitrile molecule, activated through the coordination to the metal centre, and a stoichiometric amount of water resulting from the condensation reaction (1). The hydrolysis of the nitrile to acetamide, therefore, was expected to be the first step of the transformation of the CH_3CN complex into the amidine derivative. The resulting acetamide is likely the source of the ammonia required for the formation of the amidine ligand.

Comparative experiments in which variable amounts of water were added to solutions of **1a** in CH_3CN indicate an increased concentration of acetamide in the reaction mixture after a few weeks, whereas the conversion of complex **1** into **2** had occurred to a small extent (ca. 1−2%). This result is in line with expectations, if we consider the catalytic properties of platinum complexes on the hydrolysis of nitriles to amides.

Amides, in turn, can undergo hydrolysis with formation of free NH_3, or its conjugate acid, depending on the pH. Moreover, the coordination of acetamide to a metal centre, either in the neutral[24] or deprotonated form, is well documented, in particular in the case of platinum.[25] Preliminary experiments indicate that the hydroxo complex *cis*-$[(PMe_3)_2Pt(\mu\text{-}OH)]_2(NO_3)_2$ does react with $CH_3C(O)NH_2$, leading to the deprotonation of the amide and the coordination of the resulting anion.[26]

Complex **2** can be obtained in relatively good yield by addition of aqueous NH_3 to the acetonitrile complex **1** in CH_3CN. Within a few weeks at room temperature, crystals of the pure **2a** (yield 44%) separated from a solution of *cis*-$[(PMe_3)_2Pt\{1\text{-}MeTy(-H)\}(CH_3CN)]ClO_4$ containing an excess of NH_3. The NMR analysis of the colourless solution, after removal of the solid **2a**, indicated the complete conversion of **1a** into the amidine derivative **2a** (ca. 70% of the mixture of products, on the basis of the ^{31}P spectrum) together with the ammonia complex *cis*-$[(PMe_3)_2Pt\{1\text{-}MeTy(-H)\}(NH_3)]^+$ (ca. 16%) and another species (ca. 14%) that has not yet been fully characterised.

This ammonia complex was isolated as a pure compound with the composition *cis*-$[(PMe_3)_2Pt\{1\text{-}MeTy(-H)\}(NH_3)]NO_3\cdot H_2O$, **3**, and characterised by multinuclear NMR spectroscopy. It was isolated from a solution of **1b** after addition of excess aqueous NH_3. In the proton spectrum, in $[D_6]$DMSO, the NH_3 resonance is seen as a broad singlet at $\delta = 4.0$, with unresolved platinum satellites. The presence of ammonia in the coordination sphere of the metal was confirmed by means of $^1H,^{15}N$ HMQC experiments in which the ^{15}N signal at $\delta = -381.6$, attributable to the NH_3 ligand, correlates with the proton signal at $\delta = 4.0$, and shows couplings with protons ($^1J_{HN} = 70$ Hz) and ^{31}P nuclei ($^2J_{NP} \approx 50$ Hz; $^3J_{HP} = 5$ Hz). Moreover, in the $^1H,^{195}Pt$ HMBC spectrum the NH_3 and PMe_3 protons correlate with the ^{195}Pt resonance at $\delta = -4653$. The chemical non-equivalence of the phosphanes (in *trans* position to the nucleobase and to the NH_3 ligands, respectively) is proved by the presence of two distinct resonances in the proton spectrum (at $\delta = 1.48$ and 1.66), flanked by well-resolved (90 MHz) ^{195}Pt satellites ($^2J_{HP} = 11.2$; $^3J_{HPt} = 33$ Hz), and by the presence of an AB multiplet [at $\delta = -29.0$ ($^1J_{PPt} = 3237$ Hz) and −32.0 ($^1J_{PPt} = 3084$ Hz) with $^2J_{PP} = 25.6$ Hz] in the ^{31}P spectrum.

Conclusion

In this paper we have reported a further example of reactivity of a dinuclear hydroxo complex of platinum(II) stabilized by phosphanes towards model nucleobases. As previously shown for *N*(1)-methylcytosine,[8,12] *N*(9)-substituted adenine,[11] and guanine,[13] the dimeric species *cis*-$[(PMe_3)_2Pt(\mu\text{-}OH)]_2^{2+}$ deprotonates the *N*(1)-substituted thymine, leading to the platination of the nucleobase at the N(3) position. In the isolated complex **1a** the thyminate moiety acts as monodentate ligand leaving the fourth position around the metal centre available for the coordination of a solvent molecule. A similar binding mode of the thymine was early shown in the interaction with the hydroxo complex *cis*-$[(dppf)Pt(\mu\text{-}OH)]_2^{2+}$ [dppf = 1,1′-bis(diphenylphosphanyl)ferrocene].[9]

Fortuitous circumstances of leaving the nitrile complex *cis*-$[(PMe_3)_2Pt\{1\text{-}MeTy(-H)\}(CH_3CN)]ClO_4$ in the presence of small amounts of water for a long period of time, allowed the separation of X-ray quality crystals of the amidine derivative *cis*-$[(PMe_3)_2Pt\{1\text{-}MeTy(-H)\}\{CH_3C(NH)NH_2\}]ClO_4$. This reaction represents the first example of a direct (i.e. in absence of metal-coordinated[6] or added ammonia) conversion of a nitrile group into an amidine. Such a transformation occurred in low yield with the concomitant formation of a yellow solution containing several not fully characterised products. The ^{31}P NMR spectrum

exhibits a plethora of PMe_3 resonances among which only those of the amidine and ammonia complexes, **2** and **3**, have so far been attributed.

Both **2** and **3** were isolated as pure compounds by simple addition of aqueous NH_3 to acetonitrile solution of *cis*-$[(PMe_3)_2Pt\{1\text{-}MeTy(-H)\}(CH_3CN)]^+$. The replacement of the acetonitrile ligand by NH_3 in **1** is immediate, and the formation of **3** appears to be quantitative (by ^{31}P NMR). In contrast, the formation of the amidine complex **2** from **1**, in the presence of added ammonia, is a slow process. At room temperature, in fact, the separation of crystals of *cis*-$[(PMe_3)_2Pt\{1\text{-}MeTy(-H)\}\{CH_3C(NH)NH_2\}]ClO_4$ requires several weeks (4−6). This is likely due to the high stability of the ammonia complex *cis*-$[(PMe_3)_2Pt\{1\text{-}MeTy(-H)\}(NH_3)]^+$. We observed that CD_3CN solutions of the isolated compound **3**, warmed at 50 °C for one week, appeared unchanged. Whether this complex is an intermediate in the transformation of the nitrile complex **1** into the acetamidine derivative **2** is, at the moment, an open question.

Experimental Section

Reagents and Chemicals: Reagent grade chemicals were used as received unless otherwise stated. The complex *cis*-$[(PMe_3)_2Pt(\mu\text{-}OH)]_2(NO_3)_2$ was synthesized as previously reported.[8] 1-MeTy was purchased from Sigma Chemical Company.

Instrumentation: ^1H, ^{31}P, ^{13}C, ^{195}Pt, and ^{15}N NMR spectra were obtained with a Bruker AMX 400-WB spectrometer operating at 400.13, 161.98, 100.61, 85.88, and 40.56 MHz, respectively, and/or on a JEOL 90Q spectrometer. The external references are H_3PO_4 (85% w/w in H_2O) for ^{31}P, Na_2PtCl_4 in D_2O (adjusted to δ = −1628 from Na_2PtCl_6) for ^{195}Pt, CH_3NO_2 in $CDCl_3$ (50% v/v) for ^{15}N. Proton and carbon resonances are referred to internal TMS. The parameters used for HMQC and HMBC experiments are similar to those previously reported.[14] IR spectra in the range 4000−400 cm^{-1} were recorded as KBr pellets with a Perkin−Elmer 283 spectrophotometer.

Syntheses of the Complexes

Preparation of *cis*-$[(PMe_3)_2Pt(\mu\text{-}OH)]_2(ClO_4)_2$: Addition of $NaClO_4{\cdot}H_2O$ (0.20 g, 0.48 mmol) to a solution of *cis*-$[(PMe_3)_2Pt(\mu\text{-}OH)]_2(NO_3)_2$ (0.410 g, 0.48 mmol) caused the immediate precipitation of a white solid, which was collected by filtration, washed with H_2O, and dried under vacuum. The yield of *cis*-$[(PMe_3)_2Pt(\mu\text{-}OH)]_2(ClO_4)_2$ was 438 mg (98%). − $C_6H_{19}ClO_5P_2Pt$ (463.7): calcd. C 15.54, H 4.13; found C 15.6, H 4.15. The complex, insoluble in water, dissolved in DMSO and CH_3CN; it was slightly soluble in CH_2Cl_2 and $CHCl_3$. ^1H NMR in $[D_6]$DMSO: δ = 3.46 (s, 1 H, OH), 1.52 (d, $^2J_{HP}$ 11.7 Hz, $^3J_{HPt}$ 36 Hz, 18 H, PMe_3). − $\{^1H\}^{31}P$ NMR in $[D_6]$DMSO: δ = −24.4 (s, $^1J_{PPt}$ 3358 Hz); in CD_3CN −25.5 ($^1J_{PPt}$ 3416 Hz).

Caution: The perchlorate is a potential explosive!

***cis*-$[(PMe_3)_2Pt\{1\text{-}MeTy(-H)\}(CH_3CN)]ClO_4$ (1a):** A mixture of *cis*-$[(PMe_3)_2Pt(\mu\text{-}OH)]_2(ClO_4)_2$ (263 mg, 0.283 mmol) and 1-MeTy (79.4 mg, 0.567 mmol) was dissolved in CH_3CN (12 mL) at room temperature and stirred for 24 h. The resulting solution was filtered to eliminate a trace amount of a black powder, and concentrated to a final volume of 2 mL. Addition of Et_2O afforded a white precipitate, which was recovered by filtration, and recrystallised from CH_3CN/Et_2O. The yield of the pure **1a** was 261 mg (74%). − $C_{14}H_{28}ClN_3O_6P_2Pt$ (626.9): calcd. C 26.82, H 4.47, N 6.70; found C 26.83, H 4.43, N 6.49. − ^1H NMR at 90 MHz in CD_3CN δ = [1-MeTy(−H) resonances] 7.15 [quadruplet, J_{HH} ca 1 Hz, 1 H, H(6)], 3.26 (singlet, 3 H, NCH_3), 1.72 (doublet, J_{HH} ca 1 Hz, 3 H, CH_3); 1.93 (s, 3 H, CH_3CN); 1.59 (d, $^2J_{HP}$ 11.7 Hz, $^3J_{HPt}$ 36 Hz, 9 H, PMe_3); 1.49 (d, $^2J_{HP}$ 11.7 Hz, $^3J_{HPt}$ 36 Hz, 9 H, PMe_3). − $\{^1H\}^{31}P$ NMR at 36.23 Mz in CD_3CN: δ = −29.7 ($^1J_{PPt}$ 3809 Hz) and −31.1 ($^1J_{PPt}$ 2944 Hz) with $^2J_{PP}$ 27 Hz. − ^1H NMR in $[D_6]$DMSO: [1-MeTy(−H) resonances] 7.40, [d $^4J_{HH}$ 1.2 Hz, H(6); 3.20, (s, NCH_3), 1.83 (d, $^4J_{HH}$ 1.2 Hz, $CH_3(5)$] 2.03 (s, 3 H, CH_3CN); 1.59 (d, $^2J_{HP}$ 11.7 Hz, 9 H, PMe_3); 1.53 (d, $^2J_{HP}$ 12 Hz, 9 H, PMe_3). $\{^1H\}^{31}P$ NMR at 36.23 Mz in $[D_6]$DMSO: δ = −23.1 ($^1J_{PPt}$ 3169 Hz) and −29.1 ($^1J_{PPt}$ 3892 Hz) with $^2J_{PP}$ 25.6 Hz. $\{^1H\}^{195}Pt$ in $[D_6]$DMSO: δ = −4695, dd.

***cis*-$[(PMe_3)_2Pt\{1\text{-}MeTy(-H)\}(CH_3CN)]NO_3$ (1b):** With the procedure described for **1a**, the nitrate derivative **1b** was prepared from *cis*-$[(PMe_3)_2Pt(\mu\text{-}OH)]_2(NO_3)_2$ (350 mg, 0.41 mmol) and 1-MeTy (115 mg, 0.82 mmol). The yield of the recrystallised product was 338 mg (70%). − $C_{14}H_{28}N_4O_5P_2Pt$ (589.4): calcd. C 28.53, H 4.79, N 9.50, found C 28.17, H 4.78, N 9.31. The spectroscopic data (^1H and ^{31}P NMR) are the same as those of **1a**. The elemental analysis and the ^{31}P NMR spectrum of the isolated solid indicate the presence of small amounts (ca. 3%) of unchanged *cis*-$[(PMe_3)_2Pt(\mu\text{-}OH)]_2(NO_3)_2$.

***cis*-$[(PMe_3)_2Pt\{1\text{-}MeTy(-H)\}\{CH_3C(NH)NH_2\}]ClO_4$ (2a). − a):** A suspension of *cis*-$[(PMe_3)_2Pt(\mu\text{-}OH)]_2(ClO_4)_2$ (212 mg, 0.23 mmol) and 1-MeTy (64 mg, 0.45 mmol) in CH_3CN (10 mL) was stirred at room temperature for 12 h. The resulting colourless solution was left at room temperature in the dark for 6 months during which time a colourless solid was formed while the solution became yellow. The crystalline product, separated by filtration, washed with CH_3CN, and dried under vacuum, was 26 mg (yield 8.8%). − $C_{14}H_{31}ClN_4O_6P_2Pt$ (643.9): calcd. C 26.11, H 4.85, N 8.70; found C 26.02, H 4.68, N 8.73. − ^1H NMR (400 MHz) in $[D_6]$DMSO δ = [1-MeTy(−H) resonances] 7.38 [q, J_{HH} 1 Hz, 1 H, H(6)], 3.19 (s, 3 H, NCH_3), 1.72 (d, J_{HH} 1 Hz, 3 H, CH_3); [$CH_3C(NH)NH_2$ resonances] 7.37 (broad singlet, 1 H, NH), 7.24, (br. s, 1 H, NH_2), 6.95 (br. s, 1 H, NH_2), 1.93 (s, 3 H, CH_3); 1.58 (d, $^2J_{HP}$ 11 Hz, 9 H, PMe_3) and 1.48 (d, J_{HP} 11 Hz, 9 H, PMe_3). − $\{^1H\}^{31}P$ NMR at 162 MHz in $[D_6]$DMSO: δ = −28.82 ($^1J_{PPt}$ 3100 Hz) and −29.27 ($^1J_{PPt}$ 3119 Hz) with $^2J_{PP}$ 23 Hz. − $^{13}C\{^1H\}$ at 100.6 MHz, in $[D_6]$DMSO δ = [1-MeTy(−H) resonances] 171.0 C(4)O, 154.0 C(2)O, 140.0 C(6), 106.0 C(5); 35.9 NCH_3, 12.5 $CH_3(5)$; PMe_3 14.0 (d, J_{CP} ca 40 Hz); $CH_3C(NH)NH_2$ resonances: 167.0 and 20.8. $\{^1H\}^{195}Pt$: δ = −4633, apparent triplet.

b): A suspension of *cis*-$[(PMe_3)_2Pt(\mu\text{-}OH)]_2(ClO_4)_2$ (228 mg, 0.245 mmol) and 1-MeTy (68.5 mg, 0.49 mmol) in CH_3CN (8 mL) was stirred at room temperature for a few hours. The resulting solution was then divided in 3 portions (labelled A, B, and C) the first of which was left as a reference. To the fraction B (1 mL) 25.2 mg of H_2O [molar ratio $(H_2O)/(Pt)$ = 20] was added. To the fraction C (2.0 mL) 62.7 mg of an aqueous solution of NH_3 {25% w/w; [molar ratio $(NH_3)/(Pt)$ = 7.5]} was added. After 6 weeks at ca. 20 °C samples A and B appeared as colourless solutions whereas fraction C contained well shaped prismatic crystals of pure **2a** that were separated, washed with CH_3CN and dried under vacuum (35 mg, yield 44%). The mother liquor was evaporated under vacuum, the residue dissolved in $[D_6]$DMSO and analysed by NMR. The ^{31}P spectrum of this residue showed major components to be

the species **2a** (ca. 60%), **3** (14%), and a third species characterised by a broad singlet (line width 8 Hz) at δ = −30.05, flanked by ^{195}Pt satellites ($^1J_{PPt}$ = 2963 Hz), whose relative intensity was 18% of the total resonances. Moreover, a number of very weak resonances in the range δ = −28 to −31 were also detectable. From the corresponding ^{1}H NMR spectrum, the presence of small amounts of free nucleobase and acetamide were also detected.

c): A solution of **1a**, obtained reacting *cis*-$[(PMe_3)_2Pt(\mu\text{-}OH)]_2(ClO_4)_2$ (137 mg; 0.147 mmol) and 1-MeTy (41 mg, 0.29 mmol) in CH_3CN (5 mL), was divided in 3 portions. One of them was left as reference sample (A), to the second (B) was added water (molar ratio H_2O/Pt = 34) and to the third sample (C) was added aqueous NH_3 (molar ratio: H_2O/Pt = 70; NH_3/Pt = 9.2). After 4 weeks at ca. 30 °C the resulting colourless solutions were evaporated under vacuum and the residues dissolved in [D$_6$]DMSO. The ^{31}P NMR analysis of the reference solution A indicated only a minor conversion of the initial species **1a** into **2a** (1−2%) and the presence of small amounts (a few %) of other platinum containing species. Trace amounts of acetamide were identified in the corresponding ^{1}H spectrum. In the sample B, free acetamide was the major component of the mixture whereas the molar ratio of the complexes **1a** and **2a** was approximately 1.3. Sample C contained the acetamidine complex **2a** as the dominant component (ca. 80%) of the mixture of products, whereas complex **1** appeared to have completely reacted.

***cis*-[(PMe$_3$)$_2$Pt{1-MeTy(−H)}(NH$_3$)]NO$_3$ (3):** A mixture of *cis*-$[(PMe_3)_2Pt(\mu\text{-}OH)]_2(NO_3)_2$ (161 mg, 0.19 mmol) and 1-MeTy (55 mg, 0.39 mmol) in DMSO (3.5 mL) was stirred at room temperature for 12 h, and the resulting colourless solution, containing trace amounts a black solid, was filtered. Addition of aqueous NH_3 (25% w/w, 50 μL, 0.67 mmol) gave **3** in quantitative yield (by ^{31}P NMR). The compound was isolated by addition of CH_3CN (6 mL) and precipitated with Et_2O (30 mL). The white solid recovered by filtration and dried under vacuum was purified by dissolution in the minimum volume of hot CH_3CN, filtered and left to crystallise at room temperature. The yield of colourless crystals, having the composition $[(PMe_3)_2Pt\{1\text{-}MeTy(-H)\}(NH_3)]NO_3\cdot H_2O$, was 175 mg, 79%. − $C_{12}H_{30}N_4O_6P_2Pt$ (583.4): calcd. C 24.70, H 5.18, N 9.60; found C 24.71, H 5.08, N 9.46. − ^{1}H NMR (90 MHz) in CD_3CN δ = [1-MeTy(−H)] 7.10 [q, $^4J_{HH}$ 1.4 Hz, 1 H, H(6)], 3.20 (s, 3 H, NCH_3), 1.74 (s, 3 H, CH_3); 3.7 (very broad singlet, 3 H, NH_3); 2.20 (s, 2 H, H_2O); 1.69 (d, $^2J_{PH}$ 11 Hz, $^3J_{HPt}$ 34 Hz, 9 H, PMe_3) and 1.23 (d, J_{PH} 11 Hz, $^3J_{HPt}$ 34.7 Hz, 9 H, PMe_3). − ^{1}H NMR at 400 MHz in in [D$_6$]DMSO: [1-MeTy(−H)] 7.35 [s, H(6)], 3.17 (s, NCH_3), 1.72 (s, CH_3); 4.03 (broad singlet, 3 H, NH_3); 3.31 (s, H_2O); 1.65 (d, $^2J_{PH}$ 11 Hz, 9 H, PMe_3) and 1.48 (d, J_{PH} 11 Hz, 9 H, PMe_3). − $\{^1H\}^{31}$P NMR at 162 MHz in [D$_6$]DMSO: AB multiplet at δ = −29.5 ($^1J_{PPt}$ 3342 Hz) and −32.5 ($^1J_{PPt}$ 3076 Hz) with $^2J_{PP}$ 26 Hz. $\{^1H\}^{195}$Pt NMR in [D$_6$]DMSO: δ = −4653.

X-ray Data Collection, Structure Solution, and Refinement of 1a and 2a:[27] The experimental X-ray data are summarized in Table 4 and some metrical parameters for both structures are reported in Table 2. Further details are provided in Supporting Information. The crystals [milk-white, opaque, wedged-shaped **1a**, and colourless, transparent cuboids **2a**] proved of sufficient size to collect data on a Nicolet R3m/V four-circle diffractometer, using the ω − 2θ technique. Unfortunately, the crystal quality of **1a** was poor and significant crystal decomposition was observed during the course of data collection (up to 20% in intensity). The structures were solved by Patterson methods using the SHELXTL/PC[28] and refined using the SHELXL-93 package.[29] Refinement of the crystal structure of **1a** was not satisfactory and it was hampered by some disorder of the ClO_4^- ions. No disorder model was found to be adequate and consequently some high residual electron density peaks (up to 1.2 e·Å^{-3}) lie in the vicinity of the Cl atom, as evidenced by the final Fourier map. In addition, the phosphane methyl

Table 4. Crystal data and structure refinement for *cis*-$[(PMe_3)_2Pt\{1\text{-}MeTy(-H)\}(CH_3CN)]ClO_4$, **1a**, and *cis*-$[(PMe_3)_2Pt\{1\text{-}MeTy(-H)\}]\{CH_3C(NH)NH_2\}]ClO_4$, **2a**

Compound	**1a**	**2a**
Empirical formula	$C_{14}H_{28}ClN_3O_6P_2Pt$	$C_{14}H_{31}ClN_4O_6P_2Pt$
Molecular mass	626.87	643.91
Temperature [K]	293(2)	293(2)
Wavelength [Å]	0.71073	0.71073
Crystal system	Monoclinic	Orthorhombic
Space group	$P\,2_1/c$ (no. 14)	$Pna2_1$ (no. 33)
Unit cell dimensions		
a [Å]	11.184(4)	28.091(6)
b [Å]	16.610(5)	6.731(1)
c [Å]	12.990(4)	12.568(3)
β [°]	106.45(3)	90
V [Å^3]	2314(1)	2376(1)
$D_{calcd.}$ [Mg m^{-3}]; Z	1.799; 4	1.800; 4
Absorption coefficient [mm^{-1}]	6.35	6.19
θ Range for data collection [°]	2.2−24.0	2.2−28.0
Independent reflections	3403	2993
Observed reflections	2293	2034
Refinement method	Full-matrix least-squares on F^2	Full-matrix least-squares on F^2
Data/ parameters	3403/195	2420/133
Goodness-of-fit on F^2	0.965	0.981
Final R indices [$I > 2\sigma(I)$]	$R1$[a]= 0.066	$R1$[a] = 0.032
	$WR2$[b] = −0.163	$WR2$[b] = 0.072
Largest difference peak and hole [eÅ^{-3}]	1.91, − 3.07	1.08, − 1.07

[a] $R1 = \Sigma||F_o| - |F_c||/\Sigma|F_o|$. − [b] $wR2 = [\Sigma[w(|F_o|^2 - |F_c|^2)^2]/\Sigma[w(|F_o|^2)]]^{1/2}$.

groups carbons of **1a** suffer from high temperature factors (up to 21.7 Å^2) and the P−C distances (comprised in the large range 1.79−1.91 Å) of high e.s.d.'s. Due to the fact that the refinement was not satisfactory, with relatively high values for the *R* indices, only the bond lengths and angles in the coordination sphere around Pt are discussed for the complex **1a**.

Acknowledgments

This work was financially supported by the Ministero dell'Universita′ e della Ricerca Scientifica e Tecnologica (MURST; Progetto Finalizzato).

[1] B. N. Storhoff, H. C. Lewis, *Coord. Chem. Rev.* **1977**, *23*, 1−29.
[2] R. A. Michelin, M. Mozzon, R. Bertani, *Coord. Chem. Rev.* **1996**, *147*, 299−338.
[3] R. Ros, J. Renaud, R. Roulet, *J. Organomet. Chem.* **1976**, *104*, 393−400.
[4] L. Calligaro, R. A. Michelin, P. Uguagliati, *Inorg. Chim. Acta* **1983**, *76*, L83−L87.
[5] C. A. Amodio, K. B. Nolan, *Inorg. Chim. Acta* **1986**, *113*, 27−30.
[6] N. C. Stephenson, *J. Inorg. Nucl. Chem.* **1962**, *24*, 801−808.
[7] R. Bertani, D. Catanese, R. A. Michelin. M. Mozzon, G. Bandoli, A. Dolmella, *Inorg. Chem. Commun.* **2000**, *3*, 16−18.
[8] G. Trovo′, G. Bandoli, U. Casellato, B. Corain, M. Nicolini, B. Longato, *Inorg. Chem.* **1990**, *29*, 4616−4621.
[9] G. Bandoli, G. Trovo′, A. Dolmella, B. Longato, *Inorg. Chem.* **1992**, *31*, 45−51.
[10] G. Trovo′, G. Valle, B. Longato, *J. Chem. Soc., Dalton Trans.* **1993**, 669−673.
[11] G. Trovo′, G. Bandoli, M. Nicolini, B. Longato, *Inorg. Chim. Acta* **1993**, *211*, 95−99.
[12] L. Schenetti, G. Bandoli, A. Dolmella, G. Trovo′, B. Longato, *Inorg. Chem.* **1994**, *33*, 3169−3176.
[13] B. Longato, G. Bandoli, G. Trovo′, E. Marasciulo, G. Valle, *Inorg. Chem.* **1995**, *34*, 1745−1750.
[14] L. Schenetti, A. Mucci, B. Longato, *J. Chem. Soc., Dalton Trans.* **1996**, 299−303.
[15] B. Lippert, *Progr. Inorg. Chem.* **1989**, *37*, 1−97.
[16] A. Bax, R. H. Griffey, B. L. Hawkins, *J. Magn. Reson.* **1983**, *55*, 301−315.
[17] A. Bax, M. F. Summers, *J. Am. Chem. Soc.* **1986**, *108*, 2093−2094.
[18] S. C. Nyburg, *Acta Crystallogr.* **1974**, *B30*, 251−253.
[19] F. N. Allen, J. E. Davies, J. J. Galloy, O. Johnson, O. Kennard, C. F. Macrae, E. M. Mitchell, G. F. Mitchell J. M. Smith, D. G. Watson, *J. Chem. Inf. Comput. Sci.* **1991**, *31*, 187−204; CCDC Version 5.18, October **1999**.
[20] D. Neugebauer, B. Lippert, *J. Am. Chem. Soc.* **1982**, *104*, 6596−6601.
[21] H. Schöllhorn, U. Thewalt, B. Lippert, *Inorg. Chim. Acta* **1985**, *106*, 177−180.
[22] O. Renn, B. Lippert, H. Schöllhorn, U. Thewalt, *Inorg. Chim. Acta* **1990**, *167*, 123−130.
[23] H. Rauter, E. C. Hillgeris, A. Erxleben, B. Lippert, *J. Am. Chem. Soc.* **1994**, *116*, 616−624.
[24] R. Cini, F. P. Intini, L. Maresca, C. Pacifico, G. Natile, *Eur. J. Inorg. Chem.* **1998**, 1305−1312.
[25] A. Erxleben, I. Mutikainen, B. Lippert, *J. Chem. Soc., Dalton Trans.* **1994**, 3667−3675.
[26] B. Longato, unpublished results.
[27] Crystallographic data (excluding structure factors) for the structures reported in this paper have been deposited with the Cambridge Crystallographic Data Centre as supplementary publication no. CCDC-162408 and 162409. Copies of the data may be obtained free of charge on application to CCDC, 12 Union Road, Cambridge CB2 1EZ, UK [fax: (internat.) + 44(0)1223/336033; E-mail: deposit@ccdc.cam.ac.uk].
[28] G. M. Sheldrick, *SHELXTL/PC Version 5.03*, Siemens Analytical X-ray Instruments Inc., Madison, WI, **1994**.
[29] G. M. Sheldrick, *SHELXL-93*, Program for the Refinement of Crystal Structures, University of Göttingen, Germany, **1993**.

Received June 7, 2001
[I01207]

The $[M_2(CO)_8]$ Complexes of the Cobalt Group

Gabriel Aullón*[a] and Santiago Alvarez[a]

Keywords: Carbonyl complexes / Cobalt / Rhodium / Iridium / DFT calculations / Metal-metal interactions

A theoretical study of the carbonyl complexes $[M_2(CO)_8]$ of the group 9 metals (M = Co, Rh, Ir) is presented. Three isomers were found for each metal, with the relative stabilities and energies differing from one metal to another, and two transition states corresponding to their interconversion processes were identified. The minima in the potential energy surface have been fully characterized through a vibrational analysis and the Raman-active metal–metal stretching frequencies, as well as infrared-active carbonyl stretching frequencies. The combination of theoretical, structural, and vibrational data is expected to be useful for the correct characterization of the Rh and Ir complexes for which no experimental structural data have been reported so far.

Introduction

Transition-metal carbonyl complexes constitute a reference set of compounds that have played a crucial role in the development and understanding of modern transition metal chemistry.[1] Dinuclear carbonyls, for instance, are paradigmatic examples used to illustrate the predictive power of the electron counting rules in regard with the existence of metal−metal bonds. Those complexes also constitute the simplest possible realization of a metal cluster and have allowed us to theoretically analyze the effect of the ligands' orientation on metal−metal bonding and their influence in stability.[2,3]

In the particular case of the dicobalt complex $[Co_2(CO)_8]$, a structure with two bridging and six terminal carbonyl groups has been found in the solid state (**1a**).[4,5] The geometry around the metal may be described as square pyramidal with the basal plane comprising two bridging and two terminal carbonyls. With this arrangement, the metal atom obeys the 18-electron rule, completing a pseudo-octahedral coordination sphere with a so-called *bent* metal−metal bond,[5,6] consistent with its diamagnetic behavior.

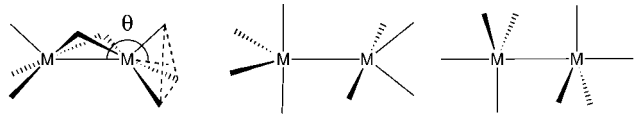

C_{2v} D_{2d} D_{3d}

1a **1b** **1c**

Evidence for the existence of other structures for $[Co_2(CO)_8]$ was early reported by Bor and Noack, based on the study of the carbonyl region of its infrared spectrum, from which they proposed the presence of at least two isomeric forms.[7−9] The first form was associated with the same structure found in the solid state, namely a bridged form with idealized C_{2v} symmetry (**1a**). A second unbridged form with D_{3d} symmetry was proposed, analogous to that found for the isoelectronic $[Fe_2(CO)_8]^{2-}$ anion in the solid state. Later, the existence of a third isomer with eight terminal ligands was detected by infrared spectroscopy.[10−12] Raman spectroscopy also shows the presence of three forms in solution.[13] In summary, it is currently accepted that the vibrational spectra of $[Co_2(CO)_8]$ is consistent with the existence of three isomers: C_{2v} (**1a**), D_{2d} (**1b**), and D_{3d} (**1c**).

No crystal structure has been reported so far for the analogous compounds with other group 9 metals, although some interesting data have been reported in the literature. A bridged form **1a** was proposed for $[Rh_2(CO)_8]$ from its infrared[14−16] and electronic[17] spectra, which are consistent with the existence of two bridging carbonyls. In contrast, no bridging carbonyl groups appear in the infrared spectrum of $[Ir_2(CO)_8]$, for which the unbridged form has been proposed.[18] In both cases, the isomers seem to be unstable toward the formation of tetranuclear species.[19]

Substitution of carbonyls by ER_3 ligands [e.g., PR_3, $P(OR)_3$, or AsR_3] may provide some hints about the structures of the parent compounds. Hence, the $[Co_2(CO)_6(ER_3)_2]$ complexes appear in the D_{3d} structure (**1c**) in the solid state,[20−28] and their conversion in solution into the C_{2v} form has been observed by infrared spectroscopy.[29−31] A similar interconversion has been reported for $[Co_2(CO)_7(ER_3)]$ complexes.[29,32] Rhodium[15,33−35] and iridium[36] complexes of type $[M_2(CO)_{8-n}(ER_3)_n]$ also present an equilibrium between bridged and unbridged forms.

In this paper we present a systematic density functional (DFT) study[37,38] of the $[M_2(CO)_8]$ complexes (M = Co, Rh, or Ir) in an attempt to contribute to a better interpretation of the experimental data available for these complexes. We will focus not only on the calculation of molecular geometries, but also on the relative energies of the three isomers, and on the barriers for their interconversion. We also

[a] Departament de Química Inorgànica and Centre de Recerca en Química Teòrica, Universitat de Barcelona,
Diagonal 647, 08028 Barcelona, Spain
E-mail: gabriel.aullon@qi.ub.es
santiago.alvarez@qi.ub.es

Supporting information for this article is available on the WWW under http://www. eurjic.com or from the author.

 © WILEY-VCH Verlag GmbH, 69451 Weinheim, 2001 1434−1948/01/1212−3031 $ 17.50+.50/0

intend to provide some hints for the characterization of the different tautomers from the vibrational spectra, mostly in the carbonyl stretching and metal-metal stretching regions.

Results

Molecular Structure

Density functional calculations were performed on complexes with the formula $[M_2(CO)_8]$ (M = Co, Rh, or Ir), considering in each case the three possible isomers corresponding to idealized symmetries C_{2v}, D_{2d}, and D_{3d} (**1**). The main structural parameters for the optimized structures are presented in Table 1.

Table 1. Calculated structural parameters for the three optimized isomers of $[M_2(CO)_8]$ complexes with M = Co, Rh, and Ir. All distances in Å, angles in degrees, mean experimental values (refs. [4,5]) in parentheses

Isomer	Parameter[a]	Co	Rh	Ir
C_{2v} (**1a**)	M−M	2.545 (2.538)	2.830	2.827
	$M-C_{eq}$	1.821 (1.837)	1.985	1.962
	$M-C_{ax}$	1.816 (1.821)	1.997	1.940
	$M-C_{bg}$	1.960 (1.946)	2.106	2.127
	$M-M-C_{eq}$	110.3 (112.7)	112.8	109.9
	$M-M-C_{ax}$	126.5 (123.8)	123.0	126.7
	$C_{eq}-M-C_{ax}$	105.7 (105.0)	105.5	105.8
	$C_{eq}-M-C_{eq}$	93.2 (93.3)	92.7	93.5
	$C_{bg}-M-C_{ax}$	95.5 (95.1)	94.8	94.8
	$C_{bg}-M-C_{bg}$	84.1 (86.0)	82.5	79.2
	$M-C_{bg}-M$	81.0 (81.4)	84.4	83.3
	θ	196.5 (193.1)	192.9	197.6
D_{2d} (**1b**)	M−M	2.619	2.882	2.921
	$M-C_{eq}$	1.812	1.973	1.936
	$M-C_{ax}$	1.795	1.941	1.936
	$M-M-C_{eq}$	124.0	120.5	118.1
	$M-M-C_{ax}$	77.1	78.4	79.7
	$C_{eq}-M-C_{ax}$	97.1	95.9	94.8
D_{3d} (**1c**)	M−M	2.671	2.851	2.901
	$M-C_{eq}$	1.814	1.975	1.946
	$M-C_{ax}$	1.789	1.934	1.926
	$M-M-C_{eq}$	85.3	85.1	84.8
	$C_{eq}-M-C_{eq}$	119.3	119.3	119.2

[a] Notation: eq = equatorial (D_{2d} and D_{3d}) or basal (C_{2v}); ax = axial (D_{2d} and D_{3d}) or apical (C_{2v}); bg = bridge (C_{2v}).

The optimized geometry of the bridged form of $[Co_2(CO)_8]$ (**1a**) is in good agreement with the experimental data, such as the Co−Co distance (2.545 Å calculated, 2.536 and 2.539 Å experimental) and the pyramidality angle for the apical ligand (100.6° calcd., 100.1° exp.). These data are consistent with a description of the coordination sphere of the metal atom as a square pyramid. The structural parameters calculated here are very similar to those previously reported by Ziegler,[39] only a shorter Co−Co distance was found by us, in better agreement with the experimental value. The orientation of the terminal carbonyl triads (defined by an angle θ of 196.5°, **1a**) is slightly different from the experimental values (193.1±0.5°), but well within the range of experimental values found for the analogous $[Co_2(\mu\text{-}CO)_2(CO)_{6-n}L_n]$ complexes (188° < θ < 212°, Table 2). As predicted for the isoelectronic iron carbonylate,[3] the experimental data for the homoleptic complexes $[Co_2(\mu\text{-}CO)_2(CO)_6]$ and $[Co_2(\mu\text{-}CNR)_2(CNR)_6]$ present a linear correlation between the orientation angle θ and the Co−Co bond length (Figure 1, black circles), corresponding to Equation (1) (regression coefficient $r = 0.958$).

$$Co-Co = 4.187 - 0.00857\cdot\theta \quad (1)$$

It thus seems obvious that substitution of the carbonyls by the bulkier isocyanide ligands should favor a larger outward bending of the terminal ligands and shorten the Co−Co distance (which in turn would affect the Co−Co stretching vibration, see below). A similar behavior was found for the isoelectronic mixed ligand complexes $[Co_2(\mu\text{-}CO)_2(CO)_{6-n}L_n]$ (Figure 1, white circles), although some dispersion appears probably due to the bidentate nature of the non-carbonyl ligands. Although the available data is scarcer for Rh and Ir, their complexes follow a similar trend [Figure 1, squares, regression coefficient $r = 0.976$, Equation (2)].

$$M-M = 4.092 - 0.00697\cdot\theta \quad (2)$$

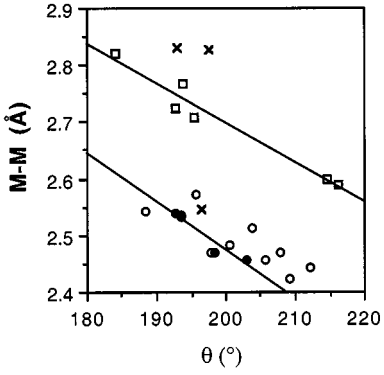

Figure 1. Scatterplot of the experimental values of the orientation angle of the terminal carbonyl groups (θ, see **1**) and the Co−Co distance for the family of $[Co_2(\mu\text{-}CO)_2(CO)_{6-n}L_n]$ complexes; the black circles and the solid line correspond to homoleptic complexes $[Co_2(\mu\text{-}CO)_2(CO)_6]$ and $[Co_2(\mu\text{-}CNR)_2(CNR)_6]$, white circles to the rest of Co complexes in Table 2, squares to Rh and Ir compounds, and crosses to calculated data (Table 1)

Two unbridged forms of symmetries D_{2d} and D_{3d} were also found to be minima in the potential energy surface. The Co−Co bond length in these two isomers is significantly longer than in the bridged one. In the D_{2d} isomer (**1b**), the axial ligands form angles of less than 90° with the equatorial plane, indicating the presence of a weak semibridging interaction (Co···C = 2.83 Å and $Co-Co-C_{ax}$ = 77.1°), similar to that observed in the optimized isoelectronic anion $[Fe_2(CO)_8]^{2-}$ (2.87 Å and 76° for the same parameters),[3] and in $[Mn_2(CO)_8]$ (2.74 Å and 82°).[58]

We have found no D_{2d} structures for carbonyl complexes in the chemical literature, but D_{2d} structures have been proposed for the isoelectronic compounds $[M_2(PF_3)_8]$ (M =

Table 2. Structural data for $[M_2(\mu\text{-}CO)_2L_6]$ complexes of zero-valent metals of the cobalt group with the C_{2v} (**1a**) structure

Compound[a]	M−M [Å]	θ [°]	refcode	ref.
$[Co_2(\mu\text{-}CO)_2(CO)_6]$	2.536	193.6	FOHDEL04	[4,5]
$[Co_2(\mu\text{-}CO)_2(CO)_6]$	2.539	192.6		
$[Co_2(\mu\text{-}CNXyl)_2(CNXyl)_6]$	2.469	198.5	LIDVOJ	[40]
$[Co_2(\mu\text{-}CN\textit{t}Bu)_2(CN\textit{t}Bu)_6]$	2.457	203.1	TBICCO10	[41]
$[Co_2(\mu\text{-}CO)_2(CO)_4(\mu\text{-}dppa)]$	2.457	205.6	PPACCP	[42]
$[Co_2(\mu\text{-}CO)_2(CO)_4(\mu\text{-}dmstb)]$	2.471	207.8	PAYKUV	[43]
$[Co_2(\mu\text{-}CO)_2(CO)_4(\mu\text{-}dmars)]$	2.482	200.5	FARSCO10	[44]
$[Co_2(\mu\text{-}CO)_2(CO)_4(dppe)]$	2.541	188.4	BUVSIU	[45]
$[Co_2(\mu\text{-}CO)_2(CO)_4(\mu\text{-}dppbf)]$	2.573	195.8	ROBKIC	[46]
$[Co_2(\mu\text{-}CO)_2(CO)_2(\mu\text{-}dppa)_2]$	2.424	209.1	YEZMOF	[47]
$[Co_2(\mu\text{-}CO)_2(CO)_2(\mu\text{-}dppm)_2]$	2.443	212.2	HANSUK	[48]
$[Co_2(\mu\text{-}CO)_2(CO)_2(\mu\text{-}deppm)]$	2.513	203.7	VAKCEP	[49]
$[Co_2(\mu\text{-}CO)_2(CO)_4(dppp)]$	2.532	193.6	YAWMIS	[50]
$[Co_2(\mu\text{-}CO)_2(CO)_2(dmpv)_2]$	2.471	197.9	YIGXUH	[51]
$[Rh_2(\mu\text{-}CO)_2(CO)_3(PPh_3)_3]$	2.769	193.9	BOPLAT10	[52,53]
$[Rh_2(\mu\text{-}CO)_2(CO)_2(dppp)_2]$	2.709	195.5	CEBBOA	[54]
$[Rh_2(\mu\text{-}CO)_2(CO)_2(dppp)_2]$	2.725	192.7		
$[Rh_2(\mu\text{-}CO)_2(triphos)_2]$	2.822	184.1	FOHMOE	[55]
$[Ir_2(\mu\text{-}CNXyl)_2(CNXyl)_2(\mu\text{-}dmpm)_2$	2.600	214.6	GEFNAG10	[56,57]
$[Ir_2(\mu\text{-}CNXyl\{BH_3\})_2(CNXyl)_2(\mu\text{-}dmpm)_2]$	2.589	216.2	KAXNIG	[57]

[a] Abbreviations: deppm = bis(2-(diethylphosphanyl)ethylphenylphosphanyl)methane; dmars = 1,2-bis(dimethylarsanyl)tetrafluorocyclobutene; dmpv = dimethylphosphanylbenzenevanadium; dmstb = bis(dimethylstibino)methane; dppa = bis(diphenylphosphanyl)amine; dppbf = 4,6-bis(diphenylphosphanyl)dibenzofuran; dppe = 1,2-bis(diphenylphosphanyl)ethane; dppm = bis(diphenylphosphanyl)methane; dppp = 1,3-bis(diphenylphosphanyl)propane; triphos = 1,1,1-tris(diphenylphosphanylmethyl)ethane.

Rh, Ir) based on their ^{19}F- and ^{31}P NMR spectra. Also, an approximate Rh−Rh distance of ≈ 2.88 Å has been estimated from X-ray diffraction of a poor crystal,[59] in agreement with the calculated value of 2.882 Å for the corresponding carbonyl complex. In contrast, ^1H and ^{31}P NMR spectra of complexes with bulkier ligands, $[M_2\{P(OR)_3\}_8]$ (M = Co, Rh), suggest a D_{3d} symmetry.[60−62]

A third isomer of $[M_2(CO)_8]$ (D_{3d} symmetry, **1c**) with trigonal bipyramidal coordination around the metal atoms was also found to be a minimum in the potential energy surface. Such a structure is found in isoelectronic compounds of the type $[M_2(CO)_6(ER_3)_2]$ (M = Co,[20−28] Rh,[63] and Ir[64]), and the most relevant structural parameters are shown in Table 3. The metal−metal distances in the optimized structures agree well with the experimental data for Co (calcd.: 2.671, exp.: 2.639−2.671 Å) and Rh (calcd.: 2.851, exp.: 2.817−2.827 Å). The equatorial carbonyls are bent towards the second metal atom (i.e., $M-M-C_{eq}$ angles of less than 90°) for the three metals, and the calculated values are also in good agreement with the experimental ones. The present results for Co agree, within chemical accuracy, with those reported by Ziegler,[39] both in the Co−Co distance (2.634 Å) and the pyramidality angle (85.1°).

Energy Minima and Transition States

The relative energies of the minima and transition states of each metal are presented in Table 4. The three isomers shown in **1** correspond to minima in the potential energy surfaces of the three metals, according to the analysis of calculated vibrational frequencies (see below). As summarized in the introductory section, there is spectroscopic evidence for the coexistence, in solution, of different isomers of the compounds under study, in agreement with the similar energies found in our calculations. However, for such intramolecular reactions to occur thermally, a low activation-

Table 3. Structural data for compounds with the D_{3d} structure and the general formula $[M_2(CO)_6(L)_2]$, where L is a ligand *trans* to the metal−metal bond

Compound	M−M [Å]	$M-M-C_{eq}$ [°]	refcode	ref.
$[Co_2(CO)_6(AsPh_3)_2]$	2.639	86.2	GOGJAN01	[20,21]
$[Co_2(CO)_6(P\{C_6H_4SO_3\}_3)_2]^{6-}$	2.645	85.8	PIGBUC	[22]
$[Co_2(CO)_6(P\{O\textit{i}Pr\}_3)_2]$	2.654	86.5	ZENCUQ	[23]
$[Co_2(CO)_6(PPh_2\{C_4F_4AsMe_2\})_2]$	2.663	85.9	ACBPCO	[24]
$[Co_2(CO)_6(PBu_3)_2]$	2.665	87.7	CBUPCO01	[25,26]
$[Co_2(CO)_6(PPh_2\{CH_2COPh\})_2]$	2.666	85.0	WELMOP	[27]
$[Co_2(CO)_6(PMe_3)_2]$	2.671	86.6	DIVZOX	[28]
$[Rh_2(CO)_6(P\textit{i}Pr_3)_2]$	2.817	83.4	FOFREX	[63]
$[Rh_2(CO)_6(P\{C_5H_9\}_3)_2]$	2.827	84.6	FOFRAT	[63]

Table 4. Calculated energies of the stationary points in the potential energy surfaces of $[M_2(CO)_8]$ (M = Co, Rh, Ir). All data are in kcal·mol^{-1}

Compound	Co	Rh	Ir
Minima			
C_{2v} (**1a**)	1.48	0.00	5.97
D_{2d} (**1b**)	0.00	2.78	0.00
D_{3d} (**1c**)	5.81	8.17	3.53
Transition states			
$C_{2v} \rightleftarrows D_{2d}$ (**2a**)	2.96	4.69	7.91
$D_{2d} \rightleftarrows D_{3d}$ (**2b**)	8.41	10.92	7.43

energy is needed. We have located only two transition states connecting the three minima, indicating two isomerization pathways: **1a** → **1b** and **1b** → **1c** (for schematic energy diagrams see Figure 2). No transition state could be located between C_{2v} and D_{3d} isomers (**1a** → **1c**), indicating that their interconversion must proceed through a D_{2d} intermediate **1b**.

The results of our calculations indicate that the unbridged D_{2d} (**1b**) structure is the most stable one for Co and Ir, but for Rh it is the C_{2v} isomer (**1a**), with **1b** ≈ 2.8 kcal·mol^{-1} above the minimum. Nevertheless, the energy differences between the three isomers are relatively small in most cases, as previously found for the isoelectronic $[Fe_2(CO)_8]^{2-}$ anion.[3] Noack studied the interconversion of bridged to unbridged forms of the cobalt complex in paraffin/alkane solutions between 69 and 295 K,[9] and estimated a reaction enthalpy of about −1.3±0.1 kcal·mol^{-1}, compared with a calculated value of −1.5 kcal·mol^{-1}. The isomerization was monitored through the infrared intensities of the 2044 (or 1857) and 2025 cm^{-1} absorption bands of the bridged and unbridged forms, respectively. A second isomerization ($D_{2d} \rightarrow D_{3d}$) process can be expected according to our results, with a reaction enthalpy of +5.8 kcal·mol^{-1} and low energy barriers (Table 4).

The ligand rearrangement that takes place along the $C_{2v} \rightleftarrows D_{2d}$ path is schematically illustrated in **2a**. Through such a pathway, the bridging and basal CO ligands of the C_{2v} structure (labeled 2, 3, and 4 in **2a**) occupy axial and equatorial positions of the trigonal bipyramid coordination spheres of the D_{2d} isomer. Since the apical ligand (labeled 1 in **2a**) of the C_{2v} isomer also occupies an equatorial position of the D_{2d} trigonal bipyramid, successive rearrangement steps result in exchange of the three types of CO ligands of the C_{2v} structure. Therefore, the $C_{2v} \rightleftarrows D_{2d}$ interconversion is consistent with the observation of a single NMR signal for the carbonyl ligands. This process has a tiny calculated energy barrier of 3.0 kcal·mol^{-1} for $[Co_2(CO)_8]$, lower than the upper limit measured by infrared spectroscopy in hexane matrices at 84 K where interactions with matrix molecules exist ($\Delta G^{\ddagger} \approx 6.4 \pm 0.4$ kcal·mol^{-1}).[12] The complex $[Co_2(CO)_8]$ has been observed to be fluxional at room temperature, even in the solid state, as seen by the equivalence of all carbonyl ligands in the ^{13}C NMR spectrum.[65] An activation energy for the exchange of bridging and terminal carbonyls has been estimated at 11.7±0.6 kcal·mol^{-1}. The $D_{2d} \rightleftarrows D_{3d}$ conversion (**2b**) for $[Co_2(CO)_8]$ has an energy barrier

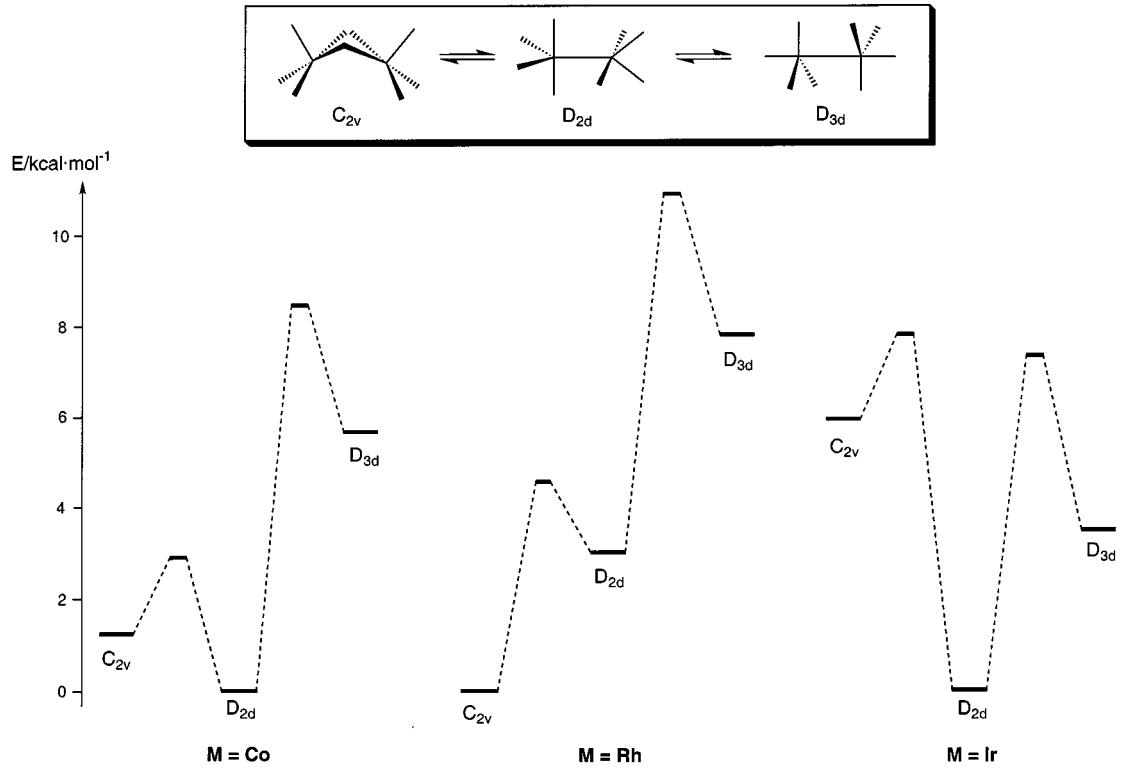

Figure 2. Diagram of the relative energies [in kcal·mol^{-1}] for the differents isomers of the $[M_2(CO)_8]$ complexes (M = Co, Rh, Ir)

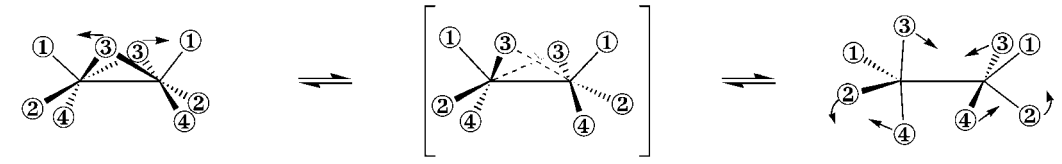

2a

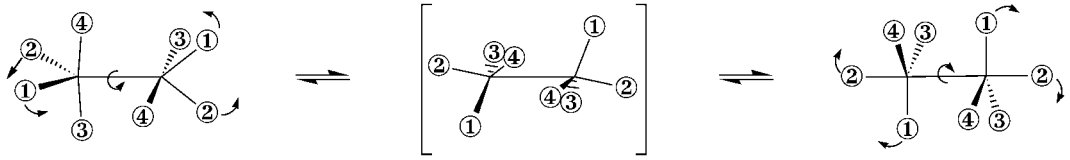

2b

of 8.4 kcal·mol^{-1}, and the reverse process has an energy barrier of 2.6 kcal·mol^{-1}. The experimental observation is that this transformation is extremely facile in hexane at 84 K.[12]

For $[Rh_2(CO)_8]$, the most stable structure is that with the bridged C_{2v} symmetry, as previously suggested from infrared and UV/Visible spectroscopic data. In contrast, our calculations for the Ir complex clearly predict the unbridged D_{2d} structure to be the most stable one, in agreement with the absence of absorption bands in the bridging CO region of the infrared spectrum. According to our calculations, the Rh complex presents a low barrier for the $C_{2v} \rightarrow D_{2d}$ transformation (4.7 kcal·mol^{-1}), although this isomerization cannot be experimentally observed due the formation of larger clusters.[15,16,19] The $D_{2d} \rightarrow D_{3d}$ transformation presents a barrier of about 8.1 kcal·mol^{-1}. For the Ir complex, the larger stability of the intermediate D_{2d} structure and the calculated energy barriers of about 7−8 kcal·mol^{-1} allow us to predict that a fluxional process should be observable.

Vibrational Analysis

Metal−Metal Stretching Vibrations

We have studied the vibrational frequencies for the three isomers (**1**): C_{2v}, D_{2d}, and D_{3d}. In all cases they have no imaginary frequencies, and all three structures are minima in the potential energy surface, as found previously in studies on the isoelectronic dianion $[Fe_2(CO)_8]^{2-}$.[3] The calculated metal−metal stretching frequencies of the three isomers are shown in the Table 5. An interesting finding is the existence of a linear correlation between the optimized M−M distance and the corresponding stretching frequency for the three isomers in the case of the Co and Ir complexes [regression coefficients $r = 0.990$ and 0.992, Equation (3) and Equation (4), respectively]. The same trend is found for Rh but the correlation is poorer.

Table 5. Theoretical M−M stretching frequencies, ν_{MM} [cm^{-1}] for the three isomers of $[M_2(CO)_8]$, and experimental Raman values for M = Co (refs. [13,66])

Structure	$[Co_2(CO)_8]$ calcd.	$[Co_2(CO)_8]$ exp.	$[Rh_2(CO)_8]$ calcd.	$[Ir_2(CO)_8]$ calcd.
C_{2v}	221	235−239[a] 229−231[b]	183	163
D_{2d}	179	185−186[a]	150	128
D_{3d}	162	157−159[a]	148	131

[a] Solution. − [b] Solid state.

$$\tilde{\nu}_{CoCo} = 1392 - 450 \cdot d_{Co-Co} \quad (3)$$

$$\tilde{\nu}_{Ir-Ir} = 1261 - 389 \cdot d_{Ir-Ir} \quad (4)$$

For $[Co_2(CO)_8]$, the $\tilde{\nu}_{Co-Co}$ band in the solid state[13] appears at 229 cm^{-1}, a value that is consistent with a metal−metal bond supported by two carbonyl bridging ligands,[1] although it appears shifted to 235−239 cm^{-1} in solution. This band can be unequivocally assigned to the C_{2v} isomer, structurally characterized in the solid state, according to our calculated value (221 cm^{-1}), since the corresponding vibration for the two other isomers is expected at significantly lower wavenumbers. Two additional bands appear in solution,[13] at 185 and 158 cm^{-1}. The most intense peak, at 185 cm^{-1}, corresponds to the predominant species in solution, which can be assigned to a D_{2d} structure according to the present computational results (calculated value 179 cm^{-1}) and in excellent agreement with this being the most stable isomer in our calculations. The intensity of the band observed in solution at 158 cm^{-1} increases upon warming[13] and can be assigned to the D_{3d} structure according to the present results (calculated value 162 cm^{-1}). No Raman data have been reported for the analogous Rh and Ir compounds. The calculated frequencies in these cases allow for a clear-cut assignment of the Raman stretching bands that appear at different temperatures to the three isomers: C_{2v}, D_{2d}, and D_{3d} (see Table 5). The successive appearance of the C_{2v}, D_{2d}, and D_{3d} isomers upon warming is consistent with the theoretical finding that the two transition states located allow no direct conversion of the C_{2v} and D_{3d} isomers, but requires going through the D_{2d} intermediate.

Table 6. Calculated and experimental infrared stretching frequencies in the carbonyl region for $[M_2(CO)_8]$ complexes. Relative intensities given in parenthesis (maximum = 100; for some experimental data: *vs* = very strong; *s* = strong, *m* = medium; *w* = weak; *sh* = shoulder)

C_{2v}	B_2	A_1	B_1	B_2	A_1	B_1	A_1	Notes[a]
Co	1823 (46)	1838 (18)	1993 (0)	2002 (82)	2001 (100)	2022 (100)	2067 (1)	calcd.
	1868 (46)	1878 (18)	2013 (1)	2020 (84)	2021 (100)	2048 (90)	2086 (1)	calcd. (f)
	1857 (42)	1868 (27)	–	2048 (78)	2050 (19)	2076 (100)	2117 (1)	(a)
	1857 (s)	1866 (sh)	–	2042 (vs)	2044 (vs)	2071 (vs)	2112 (w)	(b, c)
	1831 (s)	1844 (s)	–	2025 (s)	2025 (s)	2070 (sh)	2111 (w)	(d)
	1828 (w)	1848 (w)	–	2017 (s)	2031 (s)	2065 (sh)	2107 (m)	(e)
Rh	1816 (51)	1829 (17)	1985 (4)	1991 (86)	1992 (100)	2016 (93)	2051 (3)	calcd.
	1830 (m)	1852 (w)	–	2038 (s)	2043 (s)	2060 (s)	–	(g)
	1845 (s)	1860 (m)	–	–	2061 (s)	2086 (s)	–	(h, i)
Ir	1786 (43)	1800 (23)	1986 (2)	1992 (86)	1997 (100)	2022 (91)	2059 (2)	calcd.
D_{2d}	E	A_1	E	B_2	B_2	A_1		
Co	1957 (21)	1979 (–)	1994 (92)	1971 (3)	2010 (100)	2067 (–)		calcd.
	–	–	2028 (83)[b]	2051 (26)	2073 (59)	–		(a)
	–	–	2023 (vs)	2031 (m)	2069 (vs)	2107		(b, c)
Rh	1953 (10)	1968 (–)	1981 (100)	1976 (18)	1998 (69)	2053 (–)		calcd.
Ir	1958 (0)	1972 (–)	1982 (36)	1982 (100)	2011 (36)	2069 (–)		calcd.
	–	–	2040	2052	2065	–		(g)
D_{3d}	E_g	A_{2u}	E_u	A_{1g}	A_{2u}	A_{1g}		
Co	1962 (–)	1966 (1)	1980 (89)	1998 (–)	2017 (100)	2065 (–)		calcd.
	1992 (–)	1996 (12)	2009 (100)	2016 (–)	2050 (82)	2090 (–)		calcd. (f)
	1999 (24)[b]	2043 (26)	2033 (85)[b]	–	2059 (74)	–		(a)
	1991	–	–	–	2059	–		(b)
Rh	1962 (–)	1959 (5)	1970 (100)	1987 (–)	2024 (79)	2051 (–)		calcd.
Ir	1958 (–)	1963 (12)	1972 (100)	1991 (–)	2035 (67)	2062 (–)		calcd.

[a] (a) Argon matrix at 8 K (solid sample);[12] (b) Hexane solution at 77 K;[12] (c) Paraffin hydrocarbon solvents at variable temperature;[7,8] (d) KBr disk;[67] (e) Spinning-cell FT-Raman (solid state);[66] (f) Calculated with ADF package and BP functional;[58] (g) Co-condensation reaction with CO at 10–15 K (solid sample) for rhodium[16] and iridium;[18] (h) Liquid paraffin-heptane at high pressure of CO (430–490 atm, 243–293 K);[14,15] (i) Adamantane solution at 77 K.[68] – [b] The band appears as a doublet.

Vibrational Spectra in the Carbonyl Region

The second part of our vibrational analysis focused on the carbonyl stretching frequencies (Table 6) since this region of the infrared spectrum is used as a diagnostic tool for carbonyl complexes. The main characteristic of this spectral zone is the number of infrared-active $\tilde{\nu}_{CO}$ modes, although group-theoretical predictions may be not fulfilled because of the existence of allowed bands with low-intensity. The presence of CO bands below 1850 cm^{-1} can be considered as a fingerprint of the presence of bridging carbonyl groups. This feature is clearly present in the calculated spectra for the three metals, as well as in the experimental data of the Co and Rh complexes. In the terminal carbonyl stretching region, two of the three intense bands expected for the C_{2v} isomer are practically coincident and only two peaks should be observed, whereas three bands seem to appear in the D_{2d} form, probably due to intensity stealing between the two B_2 modes. In summary, the three isomers can in principle be identified from the pattern of the CO stretching bands for any of the three metals. These patterns are as follows: (a) the C_{2v} isomer must present two bridging frequencies below 1850 cm^{-1} and three intense bands around 2000–2030 cm^{-1}; (b) the D_{2d} isomer does not present bands below 1900 cm^{-1} but three bands around 2000 cm^{-1} spanning a range of at most 29 cm^{-1}; (c) the D_{3d} isomer does not present bands below 1900 cm^{-1} but has two bands around 2000 cm^{-1}, separated by 37 (for Co) to 63 cm^{-1} (for Ir).

The infrared spectra reported for $[Co_2(CO)_8]$ and $[Rh_2(CO)_8]$ are assigned to the C_{2v} structure, because of the presence of two bridging carbonyl stretching bands between 1820 and 1870 cm^{-1}, together with a set of three strong bands in solid state between 2010 and 2090 cm^{-1}. A similar pattern is found in solution, except that only two terminal carbonyl bands are observed in the case of Rh. The spectra of $[Co_2(CO)_8]$ in an argon matrix at 8 K and in a hexane solution at 77 K, however, are consistent with the pattern expected for the D_{2d} isomer. The spectrum reported in the literature for $[Ir_2(CO)_8]$ can probably be assigned to the D_{2d} isomer, given the absence of bridging carbonyls and the relatively small splitting of the terminal CO bands (25 cm^{-1}, compared to a calculated range of 29 cm^{-1}). With the proposed assignments, deviations of the calculated frequencies relative to the experimental ones of less than 3% result. Interestingly, the isomers that best account for the experimental spectra of the Rh and Ir complexes, and for the Co complex at low temperatures, are those found in our calculations to be the most stable ones.

Conclusions

In the present theoretical work we have analyzed three structures of the dinuclear carbonyl complexes $[M_2(CO)_8]$ (M = Co, Rh, and Ir). The three isomers are stationary points in the corresponding energy surfaces, with the D_{2d} structure being the most stable one for Co and Ir, and C_{2v} the most stable for Rh. However, the other isomers are not very different in energy and are separated by relatively small energy barriers. The calculated structural parameters of the optimized structures are in good agreement with the available experimental data.

Two transition states are found for fluxional process and our calculations show a sequence of transformations $C_{2v} \rightarrow D_{2d} \rightarrow D_{3d}$ without direct pathway connecting the C_{2v} and D_{3d} structures. The conversion between the C_{2v} and D_{2d} isomers has smaller energy barriers for Co and Rh. For the Ir complex, slower processes are to be expected, given the higher calculated energy barriers.

The analysis of the M−M stretching region of the vibrational spectra for the three isomers shows a linear correlation between the M−M wavenumber and the distance for M = Co and Ir. For each of the three metals the M−M stretching of the C_{2v} isomer appears at higher frequencies than the D_{2d} and D_{3d} ones. The calculated peaks show an excellent agreement with the experimental Raman spectrum for Co. In the carbonyl stretching region, two bands are expected at low frequencies for the C_{2v} bridged isomer (1780−1840 cm^{-1}, characteristic of bridging carbonyls), together with three bands between 1995 and 2025 cm^{-1}. For the unbridged D_{2d} and D_{3d} isomers, very similar infrared spectra are expected between 1950 and 2100 cm^{-1}. In all cases, the calculated frequencies differ from the experimental ones by less than 3%.

Experimental Section

Computational Details: Density functional calculations were carried out using the GAUSSIAN94 package.[69] The hybrid B3LYP-DFT method was applied, in which the Becke three parameters exchange functional[70] and the Lee−Yang−Parr correlation functional[71] were used. The double-ζ basis set for the valence and outermost core orbitals combined with pseudo-potentials known as LANL2DZ were used for all the atoms.[72][73] The geometries were fully optimized using gradient techniques. The calculated frequencies shown in this paper are not corrected with any factor to reproduce experimental ones. The zero-point energies of minima and transition states were also calculated, but the relative energies change by less than 10%.

Structural Analysis: Structural data was searched through the Cambridge Structural Database (Version 5.19, February 2000).[74] Our search included compounds with several cores having metal atoms of group 9.

Supporting Information: Tables containing atomic coordinates of structures $[M_2(CO)_8]$ (M = Co, Rh, and Ir) for the three energy minima (**1a**, **1b**, and **1c**) and for the transition states (**2a**, **2b**). This material is available free of charge via the Internet, see also footnote on the first page of this article.

Acknowledgments

Financial support to this work was provided by the Dirección General de Enseñanza Superior (DGES) through grant PB98-1166-C02-01 and by Comissionat per a Universitats i Recerca (Generalitat de Catalunya) through grant SGR99-0046. The computing resources at the Centre de Supercomputació de Catalunya (CESCA) were made available in part through a grant of Fundació Catalana per a la Recerca (FCR) and Universitat de Barcelona. The authors are indebted to A. Solé for discussions.

[1] C. E. Housecroft, *Metal−Metal Bonded Carbonyl Dimers and Clusters*, Oxford University Press, Oxford, **1996**.
[2] S. Alvarez, G. Aullón, in: *Metal Clusters in Chemistry, Vol. 1* (Eds.: P. Braunstein, L. A. Oro, P. R. Raithby), Wiley-VCH, Weinhein, **1999**, p. 308 (Chapter 17).
[3] G. Aullón, S. Alvarez, *Organometallics* **2001**, *20*, 818.
[4] G. G. Sumner, H. P. Klug, L. E. Alexander, *Acta Crystallogr.* **1964**, *17*, 732.
[5] P. Leung, P. Coppens, *Acta Crystallogr., Sect. B* **1983**, *39*, 535.
[6] A. A. Low, K. L. Kunze, P. J. MacDougall, M. B. Hall, *Inorg. Chem.* **1991**, *30*, 1079.
[7] K. Noack, *Spectrochim. Acta* **1963**, *19*, 1925.
[8] G. Bor, *Spectrochim. Acta* **1963**, *19*, 2065.
[9] K. Noack, *Helv. Chim. Acta* **1964**, *47*, 1064.
[10] G. Bor, K. Noack, *J. Organomet. Chem.* **1974**, *64*, 367.
[11] G. Bor, U. K. Dietler, K. Noack, *J. Chem. Soc., Chem. Commun.* **1976**, 914.
[12] R. L. Sweany, T. L. Brown, *Inorg. Chem.* **1977**, *16*, 415.
[13] S. Onaka, D. F. Shriver, *Inorg. Chem.* **1976**, *15*, 915.
[14] R. Whyman, *Chem. Commun.* **1970**, 1194.
[15] R. Whyman, *J. Chem. Soc., Dalton Trans.* **1972**, 1375.
[16] A. J. L. Hanlan, G. A. Ozin, *J. Am. Chem. Soc.* **1974**, *96*, 6324.
[17] A. J. L. Hanlan, G. A. Ozin, H. B. Gray, *Inorg. Chem.* **1979**, *18*, 1790.
[18] A. J. L. Hanlan, G. A. Ozin, *J. Organomet. Chem.* **1979**, *179*, 57.
[19] F. Oldani, G. Bor, *J. Organomet. Chem.* **1983**, *246*, 309.
[20] P. Macchi, L. Garlaschelli, S. Martinengo, A. Sironi, *Inorg. Chem.* **1998**, *37*, 6263.
[21] P. Macchi, D. M. Proserpio, A. Sironi, *J. Am. Chem. Soc.* **1998**, *120*, 13429.
[22] T. Bartik, B. Bartik, B. E. Hanson, K. H. Whitmire, I. Guo, *Inorg. Chem.* **1993**, *32*, 5833.
[23] D. H. Farrar, A. J. Lough, A. J. Poe, T. A. Stromnova, *Acta Crystallogr., Sect. C* **1995**, *51*, 2008.
[24] F. W. B. Einstein, R. Kirkland, *Acta Crystallogr., Sect. B* **1978**, *34*, 1690.
[25] R. F. Bryan, A. R. Manning, *Chem. Commun.* **1968**, 1316.
[26] J. A. Ibers, *J. Organomet. Chem.* **1968**, *14*, 423.
[27] P. Braunstein, D. G. Kelly, Y. Dusausoy, D. Bayeul, M. Lanfranchi, A. Tiripicchio, *Inorg. Chem.* **1994**, *33*, 233.
[28] R. A. Jones, M. H. Seeberger, A. L. Stuart, B. R. Whittlesey, T. C. Wright, *Acta Crystallogr., Sect. C* **1986**, *42*, 399.
[29] G. Capron-Cotigny, R. Poilblanc, *Bull. Soc. Chem. Fr.* **1967**, 1440.
[30] A. R. Manning, *J. Chem. Soc., A* **1968**, 1135.
[31] A. R. Manning, *J. Chem. Soc., A* **1968**, 1665.
[32] P. Szabó, L. Fekete, G. Bor, Z. Nagy-Magos, L. Markó, *J. Organomet. Chem.* **1968**, *12*, 245.
[33] R. Whyman, *Chem. Commun.* **1970**, 230.
[34] C. O′Connor, G. Yagupsky, D. Evans, G. Wilkinson, *Chem. Commun.* **1968**, 420.
[35] D. Evans, G. Yagupsky, G. Wilkinson, *J. Chem. Soc., A* **1968**, 2660.
[36] R. Whyman, *J. Organomet. Chem.* **1970**, *24*, C35.
[37] R. G. Parr, W. Yang, *Density-functional Theory of Atoms and Molecules*, Oxford University Press, NewYork, **1989**.
[38] T. Ziegler, *Chem. Rev.* **1991**, *91*, 651.
[39] E. Folga, T. Ziegler, *J. Am. Chem. Soc.* **1993**, *113*, 5169.

[40] P. A. Leach, S. J. Geib, J. A. Corella II, G. F. Warnock, N. J. Cooper, *J. Am. Chem. Soc.* **1994**, *116*, 8566.
[41] W. E. Carroll, M. Green, A. M. R. Galas, M. Murray, T. W. Turney, A. J. Welch, P. Wodward, *J. Chem. Soc., Dalton Trans.* **1980**, 80.
[42] J. Ellermann, N. Geheeb, G. Zoubek, G. Thiele, *Z. Naturforsch., Teil B* **1977**, *32*, 1271.
[43] A. M. Hill, W. Levason, M. Webster, I. Albers, *Organometallics* **1997**, *16*, 5641.
[44] W. Harrison, J. Trotter, *J. Chem. Soc. A* **1971**, 1607.
[45] P. Braunstein, I. Pruskil, G. Predieri, A. Tiripicchio, *J. Organomet. Chem.* **1983**, *247*, 227.
[46] E. M. Vogl, J. Bruckmann, C. Krüger, M. W. Haenel, *J. Organomet. Chem.* **1996**, *520*, 249.
[47] D. Pohl, J. Ellermann, F. A. Knoch, M. Moll, W. Bauer, *J. Organomet. Chem.* **1994**, *481*, 259.
[48] D. J. Elliot, D. G. Holah, A. N. Hughes, V. R. Magnuson, I. M. Moser, R. J. Puddephatt, *Bull. Soc. Chim. Fr.* **1992**, *129*, 676.
[49] S. A. Laneman, F. R. Fronczek, G. G. Stanley, *Inorg. Chem.* **1989**, *28*, 1206.
[50] S.-J. Lu, F. Yang, H.-Y. Fu, *Jiegou Huaxue (J. Struct. Chem.)* **1993**, *12*, 405.
[51] C. Elschenbroich, B. Metz, B. Neumüller, E. Reijerse, *Organometallics* **1994**, *13*, 5072.
[52] H.-S. Shieh, A. S. C. Chan, *Am. Cryst. Assoc., Ser. 2* **1983**, *11*, 32.
[53] A. S. C. Chan, H.-S. Shieh, J. R. Hill, *J. Chem. Soc., Chem. Commun.* **1983**, 688.
[54] B. R. James, D. Mahajan, S. J. Rettig, G. M. Williams, *Organometallics* **1983**, *2*, 1452.
[55] C. Allevi, M. Golding, B. T. Heaton, C. A. Ghilardi, S. Midollini, A. Orlandini, *J. Organomet. Chem.* **1987**, *326*, C19.
[56] J. Wu, P. E. Fanwick, C. P. Kubiak, *J. Am. Chem. Soc.* **1988**, *110*, 1319.
[57] J. Wu, P. E. Fanwick, C. P. Kubiak, *J. Am. Chem. Soc.* **1989**, *111*, 7812.
[58] T. A. Barckholtz, B. E. Bursten, *J. Am. Chem. Soc.* **1998**, *120*, 1926.
[59] M. A. Bennett, R. N. Johnson, T. W. Turney, *Inorg. Chem.* **1976**, *15*, 2938.
[60] E. L. Muetterties, F. J. Hirsekorn, *J. Am. Chem. Soc.* **1973**, *95*, 5419.
[61] E. L. Muetterties, F. J. Hirsekorn, *J. Am. Chem. Soc.* **1974**, *96*, 7920.
[62] R. Mathieu, J. F. Nixon, *J. Chem. Soc., Chem. Commun.* **1974**, 147.
[63] Y. Tomotake, T. Matsuzaki, K. Murayama, E. Watanabe, K. Wada, T. Onoda, *J. Organomet. Chem.* **1987**, *320*, 239.
[64] T. Takano, T. Deguchi, M. Ishino, S. Nakamura, *J. Organomet. Chem.* **1986**, *309*, 209.
[65] B. E. Hanson, M. J. Sullivan, R. J. Davis, *J. Am. Chem. Soc.* **1984**, *106*, 251.
[66] S. H. R. Brienne, R. D. Markwell, S. M. Barnett, I. S. Butler, J. A. Finch, *Appl. Spectrosc.* **1993**, *47*, 1131.
[67] M. Ishii, H. Ashbahs, E. Hellner, G. Schmidt, *Ber. Bunsenges. Phys. Chem.* **1979**, *83*, 1026.
[68] J. H. B. Chenier, M. Histed, J. A. Howard, H. A. Joly, H. Morris, B. Mile, *Inorg. Chem.* **1989**, *28*, 4114.
[69] *Gaussian 94 (Revision E.1)*, M. J. Frisch, G. W. Trucks, H. B. Schlegel, P. M. W. Gill, B. G. Johnson, M. A. Robb, J. R. Cheeseman, T. A. Keith, G. A. Petersson, J. A. Montgomery, K. Raghavachari, M. A. Al-Laham, V. G. Zakrzewski, J. V. Ortiz, J. B. Foresman, J. Cioslowski, B. B. Stefanov, A. Nanayakkara, M. Challacombe, C. Y. Peng, P. Y. Ayala, W. Chen, M. W. Wong, J. L. Andrés, E. S. Replogle, R. Gomperts, R. L. Martin, D. J. Fox, J. S. Binkley, D. J. Defrees, J. P. Baker, J. P. Stewart, M. Head-Gordon, C. Gonzalez, J. A. Pople, Gaussian Inc., Pittsburgh, PA, **1995**.
[70] A. D. Becke, *J. Chem. Phys.* **1993**, *98*, 5648.
[71] C. Lee, W. Yang, R. G. Parr, *Phys. Rev. B* **1988**, *37*, 785.
[72] T. H. Dunning Jr., P. J. Hay, *Modern Theoretical Chemistry*, Plenum, New York, **1976**.
[73] P. J. Hay, W. R. Wadt, *J. Chem. Phys.* **1985**, *82*, 299.
[74] F. H. Allen, O. Kennard, *Chem. Des. Autom. News* **1993**, *8*, 31.

Received March 23, 2001
[I01107]

Magnesium Versus Zinc Coordination to Multidentate Schiff Base Ligands

Andrea Erxleben*[a] and Dinah Schumacher[a]

Keywords: Magnesium / Zinc / Schiff bases / N,O ligands

The reactions of two mononuclear zinc complexes, $[Zn(HL^1)(H_2O)_2]$, **1**, and $[ZnL^4(H_2O)]$, **7**, (H_3L^1 = Schiff base derived from 3-formylsalicylic acid and glycine, H_2L^4 = Schiff base derived from 2,6-diformyl-4-methylphenol and 1,2-diaminoethane), with Mg^{2+} has been studied. These complexes contain binucleating Schiff base ligands and have vacant coordination sites. For both compounds, substitution of zinc by magnesium has been observed in DMSO. Likewise, the Zn complex of H_2L^2 (Schiff base derived from salicylaldehyde and glycine) can be converted into the corresponding Mg compound. The following complexes were characterized by single-crystal X-ray analysis: $[MgL^3(H_2O)_3]$, **4**, $[MgL^2(H_2O)_2]_n$, **5**, $[Mg(sal)_2(H_2O)_2]$, **6**, and $[MgL^4(H_2O)(CH_3OH)]$, **8** (H_2L^3 = Schiff base derived from 5-bromosalicylaldehyde and glycine, Hsal = salicylaldehyde). The tri- and tetradentate *N,O* ligands H_2L^3 and H_2L^4 form discrete complex molecules in the solid state, while a carboxylate-bridged polymeric structure is formed by H_2L^2. In **4** and **8** the aqua ligands hydrogen bond with the deprotonated phenolate and carboxylate oxygen atoms, resulting in the formation of dimers. In **6** two aqua ligands, two phenolate oxygens and two aldehyde oxygens give rise to an O_6 coordination sphere.

Introduction

Magnesium and zinc are indispensable elements in biology. They are involved in several biochemical processes and are essential cofactors required for the activation of a variety of enzymes. To date, a large number of coordination compounds of Zn have been prepared, many of which represent low-molecular-weight model compounds for Zn enzymes.[1−11] By contrast, Mg complexes have received much less attention.[12−19] Relative to other biologically relevant cations, Mg is unique in that it possesses the smallest ionic radius and the highest charge density. Furthermore, Mg^{2+} shows a strong tendency to bind six water molecules in the inner coordination sphere as manifested by the wide range of crystal structures containing the octahedral $[Mg(H_2O)_6]^{2+}$ dication.[12] Consequently, the presence of hexahydrated Mg^{2+} as the counterion in the crystal structure of $[Mg(H_2O)_6][\{Zn_2L(CH_3CO_2)\}_2(\mu_3\text{-}OH)_2]\cdot 6H_2O$ (H_3L = Schiff base derived from 2,6-diformyl-4-methylphenol and glycine) previously reported by us was not unusual.[20] However, in nonaqueous solution (DMSO) substitution of zinc by magnesium was observed and the heteronuclear complex $[MgZnL]^+$ was identified in solution.

As part of our ongoing study on dinucleating Schiff base ligands[21] we have now investigated Zn and Mg coordination to H_3L^1, as well as to the salen derivative H_2L^4. The ability of the deprotonated phenolic oxygen atoms of *N,N*-ethylenebis(salicylideneimine), H_2salen, to bridge two metal ions has been known for a long time. Several examples of neutral salen complexes acting as bidentate oxygen-donor ligands, and forming adducts of the type $[(ML)M']^{n+}$ or $[(ML)_2M']^{n+}$ (M = transition metal ion, M′ = transition metal, alkali or alkaline earth metal ion) are documented in the literature.[22] Fukuhara et al. and Carbonaro et al. showed that Mg reacted with Cu(salpd), Ni(salpd)[23] and Ni(salen)[24] to give di- and trinuclear complexes [H_2salpd = *N,N*-propylenebis(salicylideneimine)]. Besides the formation of heteronuclear compounds, metal substitution has been observed for transition metal complexes of salen and related ligands: Co was replaced by Cu in [Co(salen)],[25] while Ni substituted Cu in [Cu(amben)] [H_2amben = *N,N′*-ethylenebis(2-aminobenzaldimine)].[26]

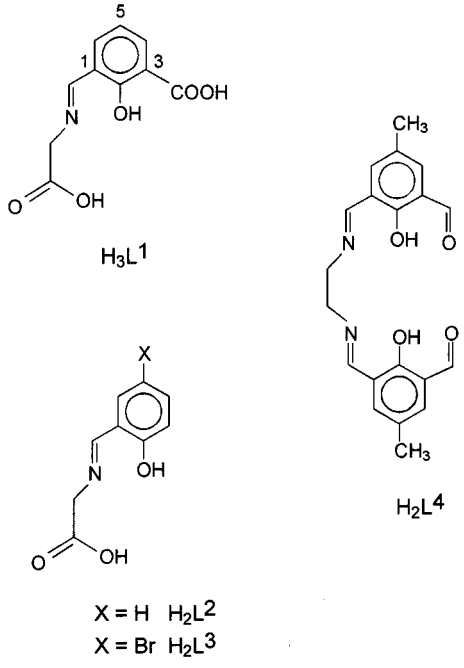

Here we report on the reaction of $[Zn(HL^1)(H_2O)_2]$, $[ZnL^2(H_2O)]$ and $[ZnL^4(H_2O)]$ with Mg^{2+}, leading to the conversion of the Zn complexes into the corresponding Mg compounds. The crystal structures of $[MgL^3(H_2O)_3]$,

[a] Fachbereich Chemie der Universität Dortmund,
Otto-Hahn-Straße 6, 44221 Dortmund, Germany
Fax: (internat.) + 49-(0)231/755−3797
E-mail: aerx@platon.chemie.uni-dortmund.de

 © WILEY-VCH Verlag GmbH, 69451 Weinheim, 2001 1434−1948/01/1212−3039 $ 17.50+.50/0

$[MgL^2(H_2O)_2]_n$, $[Mg(sal)_2(H_2O)_2]$ (Hsal = salicylaldehyde) and $[MgL^4(H_2O)(CH_3OH)]$ are presented.

Results and Discussion

Reaction of $[Zn(HL^1)(H_2O)_2]$ and $[ZnL^2(H_2O)]$ with Mg^{2+}

Metal complexes of Schiff bases are generally easily accessible in high yields in a one-step synthesis, by condensation of an aldehyde with an amine in the presence of the metal ion. Despite the well-known susceptibility of imine bonds to hydrolysis, metal complexes of Schiff bases are usually resistant towards hydrolytic cleavage, and as a result the syntheses can be carried out in aqueous solutions.[27] Reaction of 3-formylsalicylic acid with glycine and $Zn(CH_3CO_2)_2$ in ethanol/water gave a pale yellow precipitate of $[Zn(HL^1)(H_2O)_2]$ (**1**). Formation of the Schiff base complex is seen by the ^1H NMR spectrum displaying a singlet for the azomethine proton at $\delta = 8.49$. In the infrared spectrum characteristic bands at 1653 and 1617 cm^{-1} which are assigned to CO and C=N vibrations are observed. In analogy to compound **4** (see below), the polydentate ligand is assumed to coordinate to Zn via the deprotonated phenolic oxygen, the imine nitrogen and the aliphatic carboxylate group. The aromatic carboxyl group is protonated and not coordinated, as deduced from the ^1H NMR spectrum featuring a sharp resonance at $\delta = 16.11$. The assignment of the aromatic carboxyl proton was confirmed by an HMBC experiment that indicated coupling between the proton and the ring carbon C2 at $\delta = 170.0$. Since **1** is only sparingly soluble in most common solvents, attempts to crystallize this compound were unsuccessful.

Complex **1** is potentially suitable to bind a second metal ion through the aromatic carboxyl group and the (bridging) phenolate oxygen. It was reacted with $MgCl_2 \cdot 6H_2O$ in DMSO and the reaction was monitored by ^1H NMR spectroscopy (Figure 1). On addition of increasing amounts of $MgCl_2$ new singlets appear at $\delta = 16.97$ and $\delta = 8.25$. By comparison with a genuine sample prepared by the reaction of 3-formylsalicylic acid with glycine and $Mg(CH_3CO_2)_2$, the new resonances can be assigned to the azomethine and carboxyl protons of the mononuclear magnesium complex of H_3L^1 (**2**).[28] Conversion of **1** into **2** is complete after addition of two equivalents Mg^{2+}. As in the case of **1**, crystallization of **2** is hampered by its low solubility, however, coordination through the chelating ligand side-arm and protonation of the aromatic carboxyl group is consistent with the NMR spectroscopic data and the X-ray structures of the related Mg compounds **4** and **5** (see below).

Metal ion exchange is also observed for the Zn complex of H_2L^2, **3**. Addition of one equivalent Mg^{2+} leads to ca. 30% conversion of **3** into the corresponding Mg compound.

The reaction of **1** and **3** with $MgCl_2 \cdot 6H_2O$ deserves some further comments. Obviously, in DMSO Mg^{2+} competes efficiently with Zn^{2+} for the binding sites of the chelate ligand. Mg coordination is probably supported by the use of a nonaqueous reaction medium. The dielectric properties of the solvent are known to have a crucial influence on the coordination behavior of metal ions. Recently, the dependence of water-(monodentate)ligand exchange reactions of Mg complexes on the dielectric constant has been studied theoretically by Lim and co-workers.[29] They demonstrated that water-carboxylate exchange can take place in media with a low ε, while it is thermodynamically unfavorable in aqueous solutions. In general, the basicity of negatively charged oxygen donors increases significantly with decreasing solvent polarity.[30] Consequently, M^{2+}/O^- binding is stabilized in a medium with a low dielectric constant. Unfortunately, the low solubilities of **1** and **3** prevent studies in other solvents (for the effect of small amounts of water added to the DMSO solution, see below).

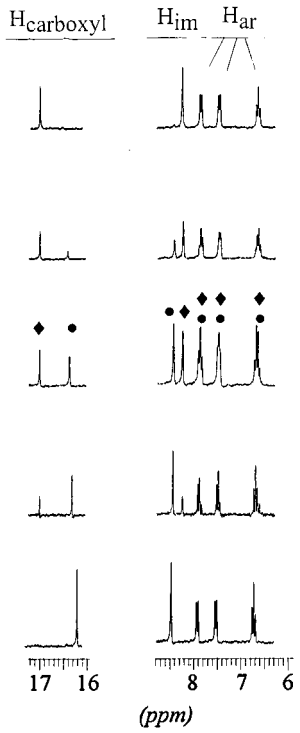

Figure 1. Reaction of **1** with Mg^{2+} in [D$_6$]DMSO. Proton NMR spectra ($\delta = 6-9$ and $\delta = 16-17$) of **1** (bottom) and after addition of 0.7, 1.0, 1.3 and 2.0 equiv. of $MgCl_2$ (top). **1** (•), **2** (◆).

Solid-State Structures of $[MgL^3(H_2O)_3]$, $[MgL^2(H_2O)_2]_n$ and $[Mg(sal)_2(H_2O)_2]$

Tridentate coordination of the Schiff base ligand via the deprotonated phenolic oxygen, the aliphatic carboxylate group and the imine nitrogen has been verified by X-ray crystallography for the magnesium complexes $[MgL^3(H_2O)_3]$ (**4**) and $[MgL^2(H_2O)_2]_n$ (**5**). A perspective view of the complex molecule of **4** is displayed in Figure 2, selected bond lengths and angles are listed in Table 1. Due to the narrow bite of the chelating Schiff base ligand, Mg assumes a distorted octahedral coordination geometry with the angles around Mg ranging from 76.7 to 98.9°. The bond lengths are normal, Mg−O(water) distances compare well with those found in other Mg aqua complexes. The ligand deviates significantly from the planar conformation that might be expected, the aromatic ring is inclined at 20.61(5)°

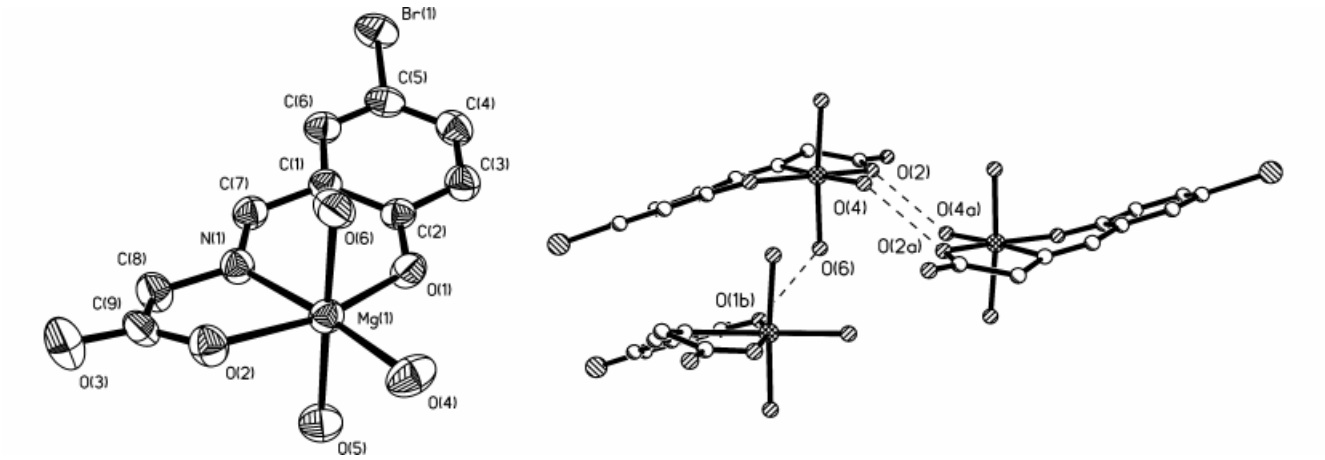

Figure 2. Molecular structure of **4** and details of intermolecular H-bonding interactions. Hydrogen atoms are omitted for clarity.

Table 1. Bond lengths [Å], angles [°] and hydrogen-bonding interactions [Å] in **4**

Mg(1)−N(1)	2.127(2)	Mg(1)−O(1)	2.018(2)
Mg(1)−O(2)	2.103(2)	Mg(1)−O(4)	2.032(2)
Mg(1)−O(5)	2.108(2)	Mg(1)−O(6)	2.080(2)
N(1)−Mg(1)−O(1)	86.79(9)	N(1)−Mg(1)−O(2)	76.71(8)
O(1)−Mg(1)−O(2)	163.22(9)	O(1)−Mg(1)−O(4)	98.92(9)
O(1)−Mg(1)−O(5)	93.43(9)	O(2)−Mg(1)−O(4)	97.64(9)
O(2)−Mg(1)−O(6)	87.83(8)	O(5)−Mg(1)−O(6)	174.87(9)
O(1)···O(5)[a]	2.937(3)	O(1)···O(6)[b]	2.721(3)
O(2)···O(4)[c]	2.777(3)	O(3)···O(4)[d]	2.971(3)
O(3)···O(5)[e]	2.954(3)	O(3)···O(6)[f]	2.786(3)

[a] $x, -y + 1/2, z + 1/2$. − [b] $x, -y + 1/2, z - 1/2$. − [c] $-x - 1, -y + 1, -z$. − [d] $-x - 1, y + 1/2, -z - 1/2$. − [e] $x, -y + 1/2 + 1, z + 1/2$. − [f] $x, -y + 1/2 + 1, z - 1/2$.

to the plane defined by the three donor atoms. In the crystal lattice two molecules dimerize via two hydrogen bonds involving the coordinating carboxylate oxygens O(2) and the aqua ligands O(4).

Adjacent dimers form stacks along the crystallographic z-axis that are stabilized by hydrogen-bonding interactions between the phenolate oxygen and the aqua ligands O(5) and O(6). The metal ions are indirectly bridged through the phenolate oxygen as H-bonding takes place between O(1) and the Mg-bound water molecules. Further H bonding occurs between the carboxylate oxygen O(3) and the water ligands O(4), (O5) and O(6).

In contrast to **4**, the Mg complex derived from the related ligand H_2L^2 is polymeric in the solid state. Figure 3 gives a view of the X-ray structure of $[MgL^2(H_2O)_2]_n$ (**5**), selected bond lengths, angles and hydrogen-bonding interactions are summarized in Table 2. The asymmetric unit comprises the Schiff base ligand that is bonded to Mg via the three donor sites and the two aqua ligands. Adjacent $MgL^2(H_2O)_2$ entities are linked through carboxylate bridges in a *syn-anti* fashion forming infinite chains extending in the z-direction. The C(9)−O(2) [1.264(3) Å] and C(9)−O(3) [1.256(3) Å] distances indicate full delocalization of the carboxylate negative charge. The Mg(1)−O(2) and Mg(1)−O(3) bond lengths differ only slightly [2.120(2) and 2.085(2) Å]. Again, the phenolic oxygen is involved in hydrogen-bonding interactions. Neighboring chains are connected through hydrogen bonds involving the aqua ligand O(5) and the phenolate oxygen O(1), as well as the carboxylate oxygens O(2) and O(3).

The X-ray structure of the bis(salicylaldehydato) complex $[Mg(sal)_2(H_2O)_2]$, **6**, is depicted in Figure 4. This complex was obtained as a by-product during the synthesis of **5**. As pointed out above, Schiff base formation is generally quantitative and the coordination of metal ions renders imine bonds resistant towards hydrolytic cleavage. Thus, in the case of the Zn complexes dissociation to the aldehyde and amine due to the presence of water was not observed. However, as for Mg, slow decomposition of the complex during crystallization results in hydrolysis of the ligand and the formation of the aldehyde complex. In the centrosymmetric molecule of **6**, the deprotonated salicylaldehydes act as chelating, bidentate ligands, and two water molecules complete the octahedral coordination sphere around the Mg atom. Salicylaldehyde and the metal ion are located on a mirror plane and the Mg−O(water) bond coincides with a crystallographic twofold axis of symmetry. Thus, except for O(1)−Mg(1)−O(2) and O(1)−Mg(1)−O(2a), ideal 90° values are observed for the valence angles around Mg. Due to the chelating coordination mode of the ligand, the O(1)−C(7)−C(1) bond angle involving the aldehyde carbon increases to 128.1(7)°. In the crystal lattice the neutral complex molecules form layers parallel to the crystallographic ac plane. Adjacent layers are linked through hydrogen bonds involving the water ligands, as well as the carbonyl and phenolate oxygens (Table 3). Thus, again the deprotonated phenolic oxygen acts as an H bond acceptor. The structure of **6** is in contrast with that of $[Mg(salicylate)_2(H_2O)_4]$ and [Mg(*p*-aminosalicylate)$(H_2O)_4$] reported in the literature.[18,19] In the latter complexes the salicylate ligands act as monodentate O-donors and bind to the Mg atom through one carboxylate oxygen, while the phenolic groups are protonated and do not take part in the coordination.

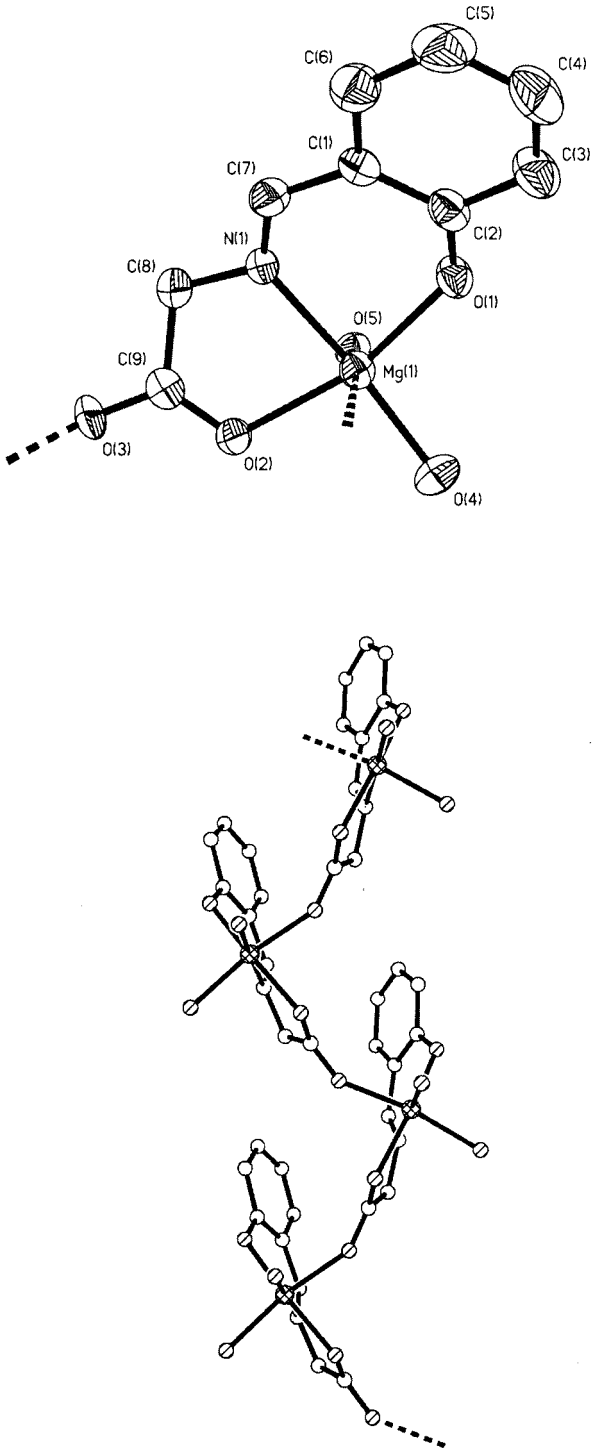

Figure 3. Asymmetric unit of the crystal structure of **5** with the atom numbering scheme and a section of the polymer. Hydrogen atoms are omitted for clarity.

Table 2. Bond lengths [Å], angles [°] and hydrogen-bonding interactions [Å] in **5**

Mg(1)−N(1)	2.105(2)	Mg(1)−O(1)	2.017(2)
Mg(1)−O(2)	2.120(2)	Mg(1)−O(4)	2.024(2)
Mg(1)−O(5)	2.159(2)	Mg(1)−O(3) [a]	2.085(2)
N(1)−Mg(1)−O(1)	86.18(8)	N(1)−Mg(1)−O(2)	77.30(8)
O(1)−Mg(1)−O(2)	162.84(8)	O(1)−Mg(1)−O(4)	98.85(8)
O(1)−Mg(1)−O(5)	100.23(8)	O(2)−Mg(1)−O(4)	97.69(8)
O(2)−Mg(1)−O(3)[a]	83.60(7)	O(3)−Mg(1)−O(5)[a]	166.40(8)
O(1)···O(5)[b]	2.716(2)	O(2)···O(4)[c]	3.089(3)
O(2)···O(5)[d]	2.789(3)	O(3)···O(4)[d]	2.798(3)
O(3)···O(4)[e]	2.846(3)	O(4)···O(5)[c]	2.815(3)

[a] $x, -y - 1/2, z - 1/2$. − [b] $x, -y + 1/2, z - 1/2$. − [c] $-x, y - 1/2, -z + 1/2$. − [d] $-x, -y, -z + 1$. − [e] $x, -y - 1/2, z + 1/2$.

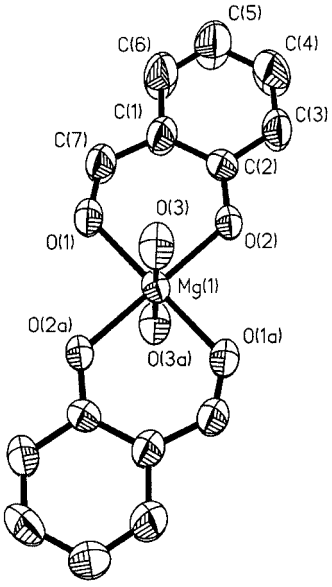

Figure 4. Molecular structure of **6**. Hydrogen atoms are omitted for clarity.

Table 3. Bond lengths [Å], angles [°] and hydrogen-bonding interactions [Å] in **6**

Mg(1)−O(1)	2.044(5)	Mg(1)−O(2)	2.049(4)
Mg(1)−O(3)	2.056(5)		
O(1)−Mg(1)−O(2)	89.0(2)	O(1)−Mg(1)−O(2)[a]	91.0(2)
O(1)···O(3)[a]	2.899(5)	O(2)···O(3)[a]	2.903(4)
O(2)···O(3)[b]	2.830(4)		

[a] $-x - 1, -y, -z$. − [b] $-x - 1/2 - 1, -y + 1/2, -z$.

Substitution of Zn^{2+} by Mg^{2+} in a Salen-Type Complex

As outlined in the introduction, metal ion exchange and the formation of adducts are observed when first row transition metal complexes of salen are treated with hetero metals. The Zn[31] and Mg[32] complexes of salen have been known for a long time, however, no studies on the formation of adducts, or metal ion substitution have been carried out. We have used the mononuclear Zn complex of the salen derivative H_2L^4, $[ZnL^4(H_2O)]$,[33] **7**, and investigated its reaction with Mg^{2+}. In principle, **7** provides an O_4 coordination site to bind Mg to form a heteronuclear complex. As evident from the solid-state structure of **6**, chelation through the phenolate and aldehyde oxygens is a possible binding mode. However, in the ^1H NMR spectrum (Fig-

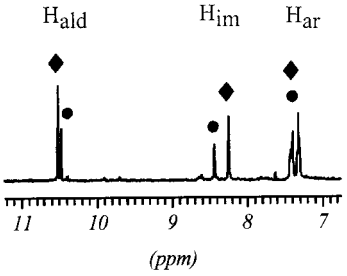

Figure 5. ^{1}H NMR spectrum (δ = 7−11) of **7** in [D_6]DMSO after addition of 2 equiv. of $MgCl_2$. **7** (•), **8** (◆). Peaks of very low intensity at δ = 10.39, 9.90, 9.70, 8.61 and δ = 7.63 result from hydrolysis of the imine ligand due to traces of water.

ure 5), the new set of signals that emerges after the addition of $MgCl_2 \cdot 6H_2O$ to a solution of **7** in DMSO is unambiguously assigned to the Mg complex [MgL^4] (**8**), resulting from metal ion exchange as found for complexes **1** and **3**. Complex **8** was identified by preparation of a genuine sample from H_2L^4 and $MgCl_2$. When two equivalents of $MgCl_2$ are added, approximately 62% of **7** is converted into **8**. Small amounts of water shift the equilibrium between **7** and **8** towards the formation of the Zn complex: on addition of 2.5% D_2O to the DMSO solution, the percentage of **8** is halved. The conversion of **8** back into **7** in the presence of water reflects the high affinity of Mg for aqua ligands.

It might be speculated that the substitution reaction proceeds via the heteronuclear Zn,Mg complex as an intermediate, although no evidence for its existence (or lack thereof) is seen from the NMR spectra. It is worth noting that **7** and **8** are nonlabile on the NMR time-scale, since mixtures of the respective complex and the "free" ligand give two distinct sets of resonances. Dissociation to the ligand and solvated metal ions was not observed in the spectra of pure **7** or **8** in DMSO.

The structure of **8** has been determined by single-crystal X-ray analysis. In the solid state the molecules of [$MgL^4(H_2O)(CH_3OH)$] form centrosymmetric dimers via hydrogen-bonding between the water ligand and the phenolic oxygen (Figure 6).

The hydrogen bonds are reinforced by stacking interactions of the aromatic rings (stacking distance ≈ 3.5 Å). As expected, the Schiff base ligand assumes an essentially planar configuration. The dihedral angles between the phenolic rings and the four donor atoms are 8.5(1) and 12.0(1) °. The rigid nature of the chelating ligand causes a significant distortion of the octahedral coordination geometry (range of valence angles around Mg: 78.5−107.9 °). Coordination of Mg^{2+} causes a shift of the $\tilde{\nu}$(C=O) and $\tilde{\nu}$(C=N) IR bands from 1688 and 1645 cm^{-1} [34] to 1655 and 1609 cm^{-1}, respectively.

Conclusions

In conclusion we have demonstrated that in complexes with *N,O* ligands, Zn is susceptible to substitution by Mg^{2+} when DMSO is used as the nonaqueous solvent. The presence of small amounts of water decreases the yield of the Mg complex significantly due to the high affinity of Mg for aqua ligands. The quantity of the Mg complex formed in DMSO is comparable for all ligand systems described here (ca. 30% Mg complex formed on addition of equimolar amounts of $MgCl_2$ to the respective Zn Schiff base complex).

Furthermore we have isolated and structurally characterized three Mg Schiff base complexes, namely [$MgL^4(H_2O)(CH_3OH)$], [$MgL^3(H_2O)_3$], and polymeric [$MgL^2(H_2O)_2]_n$. Schiff bases have been extensively used in transition metal chemistry, while main-group imine complexes are considerably less abundant. The coordination chemistry of alkaline earth metals has generally received far less attention than the coordination chemistry of transition metals. Thus, it is

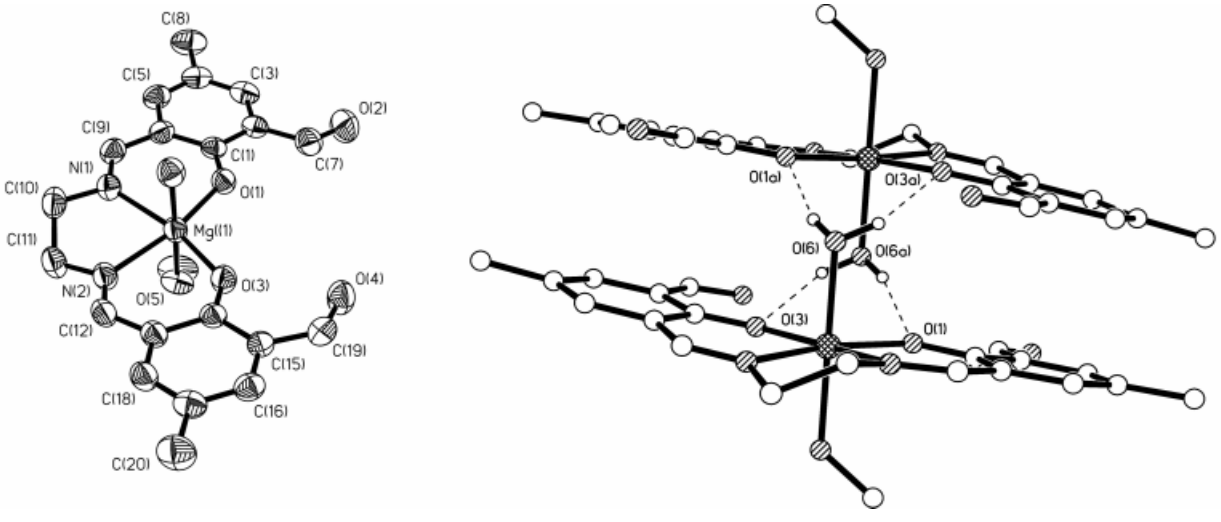

Figure 6. Molecular structure of **8** and arrangement of two molecules with H-bonding interactions indicated. Hydrogen atoms were located in the Fourier-difference map, but for clarity only the hydrogen atoms involved in H-bonding are shown.

our aim to further increase the number of Mg compounds by varying the versatile Schiff base ligands.

Experimental Section

Materials and Methods: 3-Formylsalicylic acid[35] and 2,6-diformyl-4-methylphenol[36] were prepared according to the literature procedures. H_2L^4 was prepared by reaction of 2,6-diformyl-4-methylphenol and 1,2-diaminoethane in $CHCl_3$ and subsequent evaporation of the solvent according to a slightly modified literature procedure.[34] All chemicals and solvents were of reagent grade and used without further purification. – ^{1}H NMR spectra were recorded on a Varian Mercury spectrometer at 200.13 MHz., the HMBC experiment on a Bruker DRX 400 spectrometer. – Infrared spectra of KBr pellets were measured on a Bruker IFS 28 FT-spectrometer.

Complex 1: 3-Formylsalicylic acid (84 mg, 0.51 mmol), glycine (34 mg, 0.45 mmol) and $Zn(CH_3CO_2)_2{\cdot}2H_2O$ (151 mg, 0.69 mmol) were stirred in ethanol/water (1:1, 30 mL) for 3 h. The resulting precipitate was filtered off, washed with ethanol and dried at 40 °C overnight to give $[Zn(HL^1)(H_2O)_2]$, **1** as a yellow powder (98 mg, 0.30 mmol, 68%). – IR (KBr): $\tilde{\nu}$ = 3071, 2925, 1653 (CO), 1617 (C=N), 1566, 1519, 1471, 1399, 1296, 1243, 1097, 1076, 1005, 959 cm^{-1}. – ^{1}H NMR [$(CD_3)_2SO$]: δ = 3.96 (s, 2 H, CH_2), 6.73 (t, J = 7.6 Hz, 1 H, CH_{arom}), 7.54 (d, J = 7.8 Hz, 1 H, CH_{arom}), 7.93 (d, J = 7.8 Hz, 1 H, CH_{arom}), 8.49 (s, 1 H, HC=N), 16.11 (s, 1 H, COOH). – ^{13}C NMR [$(CD_3)_2SO$]: δ = 59.5 (CH_2), 117.6 (C_{arom}), 121.6 (C_{arom}), 132.4 (C_{arom}), 147.3 (C_{arom}), 155.0 (C_{arom}), 167.7 (C=N), 170.0 (C_{arom}), 173.6 (COOH), 177.0 (Ar-COOH). – $C_{10}H_{11}NO_7Zn$ (322.56): calcd. C 37.2, H 3.4, N 4.3; found C 36.8, H 3.5, N 4.3.

Table 4. Bond lengths [Å], angles [°] and hydrogen-bonding interactions [Å] in **8**

Mg(1)–N(1)	2.140(2)	Mg(1)–N(2)	2.137(2)
Mg(1)–O(1)	1.979(1)	Mg(1)–O(3)	1.985(1)
Mg(1)–O(5)	2.147(2)	Mg(1)–O(6)	2.141(2)
N(1)–Mg(1)–O(1)	87.35(6)	N(1)–Mg(1)–N(2)	78.50(6)
O(1)–Mg(1)–O(3)	107.89(5)	O(1)–Mg(1)–N(2)	165.22(6)
O(1)–Mg(1)–O(5)	89.90(6)	O(3)–Mg(1)–O(5)	91.94(6)
O(3)–Mg(1)–O(6)	89.06(6)	O(5)–Mg(1)–O(6)	178.47(6)
O(1)···O(6)[a]	2.788(2)	O(3)···O(6)[a]	3.057(2)
O(4)···O(5)[b]	2.721(2)	O(4)···O(6)[a]	2.939(2)

[a] $-x, -y + 1, -z$. – [b] $x, -y + 1/2 + 1, z - 1/2$.

Complex 2: 3-Formylsalicylic acid (83 mg, 0.50 mmol), glycine (38 mg, 0.51 mmol), $Mg(CH_3CO_2)_2{\cdot}4H_2O$ (107 mg, 0.50 mmol) and KOH (56 mg, 1.00 mmol) were reacted in ethanol/water (5:1, 30 mL). After 3 days a yellow precipitate of $[Mg(HL^1)(H_2O)_2]$, **2**, was filtered off, washed with ethanol and dried at 40 °C overnight (65 mg, 0.23 mmol, 46%). – IR (KBr): $\tilde{\nu}$ = 3395, 1659 (CO), 1613 (C=N), 1546, 1495, 1464, 1436, 1401, 1314, 1220, 1154 cm^{-1}. – $C_{10}H_{11}NO_7Mg$ (281.47): calcd. C 42.7, H 3.9, N 5.0; found C 42.3, H 3.8, N 4.9.

Complex 3: Salicylaldehyde (117 mg, 0.96 mmol), sodium glycinate hydrate (111 mg, 0.97 mmol) and $Zn(NO_3)_2{\cdot}6H_2O$ (900 mg, 3.03 mmol) were reacted in methanol (20 mL) for 6 h at room temperature and afforded a pale yellow precipitate of composition $ZnL^2{\cdot}1.5H_2O$, **3** (116 mg, 0.43 mmol, 45%). – IR (KBr): $\tilde{\nu}$ = 3277, 3064, 2909, 1654 (CO), 1611 (C=N), 1581, 1476, 1405, 1282, 1197, 1158, 1076, 1040, 796, 767 cm^{-1}. – ^{1}H NMR [$(CD_3)_2SO$]: δ = 3.88 (s, 2 H, CH_2), 6.41 (t, J = 7.2 Hz, 1 H, CH_{arom}), 6.59 (d, J = 8.5 Hz, 1 H, CH_{arom}), 7.12 (t, J = 7.2 Hz, 2 H, CH_{arom}), 8.34 (s, 1 H, HC=N). – $C_9H_{10}NO_{4.5}Zn$ (269.57): calcd. C 40.1, H 3.7, N 5.2; found C 40.0, H 3.5, N 5.1.

Complex 4: 5-Bromosalicylaldehyde (201 mg, 1.00 mmol), sodium glycinate hydrate (115 mg, 1.00 mmol) and $Mg(NO_3)_2{\cdot}6H_2O$ (769 mg, 3.00 mmol) were stirred in methanol (20 mL) for 3 h. Addition of water (10 mL) yielded a yellow precipitate that was filtered off and washed with Et_2O. Recrystallization from methanol/water (4:1, 50 mL) gave pale yellow needles of $[MgL^3(H_2O)_3]$, **4** (140 mg, 0.42 mmol, 42%). – IR (KBr): $\tilde{\nu}$ = 3410, 2911, 1657 (CO), 1607 (C=N), 1532, 1469, 1395, 1381, 1285, 1174 cm^{-1}. – ^{1}H NMR [$(CD_3)_2SO$]: δ = 3.79 (s, 2 H, CH_2), 6.34 (d, J = 8.9 Hz, 1 H, CH_{arom}), 7.05 (d, J = 8.9 Hz, 1 H, CH_{arom}), 7.17 (s, 1 H, CH_{arom}), 8.01 (s, 1 H, HC=N). – $C_9H_{12}BrMgNO_6$ (334.41): calcd. C 32.3, H 3.6, N 4.2; found C 32.3, H 3.7, N 4.1.

Table 5. Crystallographic data for **4**, **5**, **6** and **8**

	4	**5**	**6**	**8**
Empirical formula	$C_9H_{12}BrMgNO_6$	$C_9H_{11}MgNO_5$	$C_{14}H_{14}MgO_6$	$C_{21}H_{24}MgN_2O_6$
Molecular mass	334.42	237.50	302.56	424.73
Crystal system	monoclinic	monoclinic	monoclinic	monoclinic
Space group	$P2_1/c$	$P2_1/c$	$C2/m$	$P2_1/c$
a [Å]	16.755(1)	15.465(1)	7.379(1)	12.905(3)
b [Å]	9.844(1)	7.543(1)	7.400(1)	13.574(3)
c [Å]	7.681(1)	9.148(1)	13.017(1)	12.880(3)
β [°]	97.43(1)	106.24(1)	90.95(1)	112.95(3)
V [Å^3]	1256.2(2)	1024.6(2)	710.7(2)	2077.6(8)
Z	4	4	2	4
$\rho_{calcd.}$ [g cm^{-3}]	1.768	1.540	1.414	1.358
Measured reflections	5289	1858	1042	5367
Independent reflections	3070	1858	636	5367
Observed reflections [$I > 2\sigma(I)$]	2020	948	464	2621
R_1 [$I > 2\sigma(I)$][a]	0.038	0.039	0.082	0.043
wR_2 [$I > 2\sigma(I)$][b]	0.108	0.071	0.227	0.089

[a] $R_1 = \Sigma||F_o| - |F_c||/\Sigma|F_o|$. – [b] $wR_2 = [\Sigma w(F_o^2 - F_c^2)^2/\Sigma w(F_o^2)^2]^{1/2}$; $w^{-1} = \sigma^2(F_o^2) + (aP)^2$; $P = (F_o^2 + 2F_c^2)/3$ with a = 0.0783 for **4**, 0.0393 for **5**, 0.1297 for **6** and 0.0522 for **8**.

Complex 5: 5 was prepared in an analogous manner to **4** from salicylaldehyde (117 mg, 0.96 mmol), sodium glycinate hydrate (111 mg, 0.97 mmol) and $Mg(NO_3)_2 \cdot 6H_2O$ (735 mg, 2.87 mmol). yield: 53%. X-ray suitable crystals of $[MgL^2(H_2O)_2]_n$ (**5**) were obtained by recrystallization from methanol. − IR (KBr): $\tilde{\nu}$ = 3383, 1658 (CO), 1574, 1539, 1471, 1452, 1406, 1334, 1298, 1193 cm^{-1}. − ^1H NMR [$(CD_3)_2SO$]: δ = 3.84 (s, 2 H, CH_2), 6.28 (t, J = 7.2 Hz, 1 H, CH_{arom}), 6.46 (d, J = 8.5 Hz, 1 H, CH_{arom}), 7.04 (t, J = 7.1 Hz, 2 H, CH_{arom}), 8.08 (s, 1 H, HC=N). − $C_9H_{11}MgNO_5$ (237.50): calcd. C 45.5, H 4.7, N 5.9; found C 45.8, H 4.7, N 5.9.

Complex 6: Salicylaldehyde (351 mg, 2.88 mmol), sodium glycinate hydrate (333 mg, 2.89 mmol) and $Mg(NO_3)_2 \cdot 6H_2O$ (2.20 g, 8.58 mmol) were stirred in methanol (36 mL) overnight. The solution was evaporated to dryness and complex **5** was extracted with water. The residue was dissolved in methanol. After a few days microcrystals of $[Mg(sal)_2(H_2O)_2] \cdot 0.5H_2O$, **6**·$0.5H_2O$ formed (82 mg, 0.26 mmol, 18%). − IR (KBr): $\tilde{\nu}$ = 3455, 2887, 2795, 1661 (CO), 1606 (ring), 1531, 1449, 1333, 1201, 1179, 1152, 1124 cm^{-1}. − ^1H NMR [$(CD_3)_2SO$]: δ = 6.34 (t, br, 1 H, CH_{arom}), 7.26 (t, br, 2 H, CH_{arom}), 7.45 (d, J = 8.5 Hz, 1 H, CH_{arom}), 9.19 (s, 1 H, HC=O). − $C_{14}H_{15}MgO_{6.5}$ (311.58): calcd. C 53.9, H 4.9; found C 53.7, H 4.7.

Recrystallization from methanol yielded pale yellow needles of $[Mg(sal)_2(H_2O)_2]$, **6** suitable for X-ray analysis.

Complex 7:[33] H_2L^4 (215 mg, 0.61 mmol), $NaOCH_3$ (66 mg, 1.22 mmol) and $ZnCl_2$ (83 mg, 0.61 mmol) were stirred in methanol (20 mL) at room temperature. After 10 min unchanged H_2L^4 was filtered off. Addition of water resulted in the precipitation of $[ZnL^4(H_2O)]$, **7** (110 mg, 0.25 mmol, 41%). − IR (KBr): $\tilde{\nu}$ = 3262, 2921, 1664 (CO), 1609 (C=N), 1532, 1449, 1389, 1231, 1029 cm^{-1}. − ^1H NMR [$(CD_3)_2SO$]: δ = 2.22 (s, 6 H, CH_3), 3.81 (s, 4 H, CH_2), 7.39 (s, 2 H, CH_{arom}), 7.48 (s, 2 H, CH_{arom}), 8.53 (s, 2 H, HC=N), 10.55 (s, 2 H, HC=O). − $C_{20}H_{20}N_2O_5Zn$ (433.78): calcd. C 55.4, H 4.7, N 6.5; found C 55.0, H 4.7, N 6.5.

Complex 8: 8 was prepared in an analogous manner to **7** from H_2L^4 (554 mg, 1.55 mmol), $NaOCH_3$ (168 mg, 3.11 mmol) and $MgCl_2 \cdot 6H_2O$ (315 mg, 1.55 mmol) in a 69% yield. Recrystallization from methanol afforded orange-yellow cubes of $[MgL^4(H_2O)(CH_3OH)]$ suitable for X-ray analysis. − IR (KBr): $\tilde{\nu}$ = 3438, 2900, 1655 (CO), 1609 (C=N), 1539, 1522, 1463, 1386, 1231, 1032 cm^{-1}. − ^1H NMR [$(CD_3)_2SO$]: δ = 2.19 (s, 6 H, CH_3), 3.70 (s, 4 H, CH_2), 7.32 (s, 2 H, CH_{arom}), 7.41 (s, 2 H, CH_{arom}), 8.26 (s, 2 H, HC=N), 10.53 (s, 2 H, HC=O). − $C_{21}H_{24}MgN_2O_6$ (424.74): C 59.3, H 5.7, N 6.6; found C 58.9, H 5.8, N 6.5.

Metal Ion Substitution: Solutions of **7** (10 mM), **1** and **3** (2 mM due to lower solubility) in $(CD_3)_2SO$ were treated with aliquots of a solution of $MgCl_2 \cdot 6H_2O$. NMR spectra were run 10 to 30 minutes after addition of $MgCl_2$. For a representative sample no change of the spectrum was observed over 24 h.

X-ray Crystallography: Crystal data for compounds **4, 5, 6** and **8** were collected at room temperature on an Enraf−Nonius-KappaCCD diffractometer[37] using graphite-monochromated Mo-K_α radiation (λ = 0.71069 Å). For data reduction and cell refinement the programs DENZO and SCALEPACK were used.[38] The structures were solved by conventional Patterson (**4**) or direct (**5**, **6** and **8**) methods and subsequent Fourier syntheses, and refined by full-matrix least-squares on F^2 using the SHELXTL PLUS and SHELXL-93 programs.[39] All non-hydrogen atoms were refined anisotropically. Hydrogen atoms of **4**, **5**, and **8** were located in the final Fourier-difference maps (except for those of the aqua ligands in **4**) and refined isotropically. For **6** carbon-bound hydrogen atoms were placed at calculated positions and given fixed isotropic temperature factors. Crystallographic data (excluding structure factors) for the structures reported in this paper have been deposited with the Cambridge Crystallographic Data Centre as supplementary publication no. CCDC-161094 (**4**), -161095 (**5**), -161096 (**6**) and 161097 (**8**). Copies of the data can be obtained free of charge on application to CCDC, 12 Union Road, Cambridge CB2 1EZ, UK [Fax: (internat.) +44−1223/336−033; E-mail: deposit@ccdc.cam.ac.uk].

Acknowledgments

This work was supported by the Ministerium für Schule, Wissenschaft und Forschung, NRW (Lise-Meitner-Habilitationsstipendium to A. E.) and the Fonds der Chemischen Industrie (FCI). We thank Professor Bernhard Lippert for his support.

[1] R. H. Prince, in Comprehensive Coordination Chemistry; (Ed.: G. Wilkinson), Pergamon Press: Oxford, **1987**; Vol. 5, pp 925−1045 and references therein.
[2] A. Looney, G. Parkin, R. Alsfasser, M. Ruf, H. Vahrenkamp, *Angew. Chem. Int. Ed. Engl.* **1992**, *31*, 92−93.
[3] P. Chaudhuri, C. Stockheim, K. Wieghardt, W. Deck, R. Gregorzik, H. Vahrenkamp, B. Nuber, J. Weiss, *Inorg. Chem.* **1992**, *31*, 1451−1457 and references therein.
[4] S. Uhlenbrock, B. Krebs, *Angew. Chem. Int. Ed. Engl.* **1992**, *31*, 1647−1648.
[5] H. Adams, N. A. Bailey, D. E. Fenton, Q.-Y. He, *J. Chem. Soc., Dalton Trans.* **1996**, 2857−2865.
[6] E. Kimura, Y. Kodama, T. Koike, M. Shiro, *J. Am. Chem. Soc.* **1995**, *117*, 8304−8311.
[7] X.-M. Chen, Y.-X. Tong, T. C. W. Mak, *Inorg. Chem.* **1994**, *33*, 4586−4588.
[8] C. Bazzicalupi, A. Bencini, A. Bianchi, V. Fusi, L. Mazzanti, P. Paoletti, B. Valtancoli, *Inorg. Chem.* **1995**, *34*, 3003−3010.
[9] J. W. Yun, T. Tanase, S. J. Lippard, *Inorg. Chem.* **1996**, *35*, 7590−7600.
[10] M. Yamami, M. Tanaka, H. Sakiyama, T. Koga, K. Kobayashi, H. Miyasaka, M. Ohba, H. Okawa, *J. Chem. Soc., Dalton Trans.* **1997**, 4595−4601.
[11] F. Meyer, P. Rutsch, *Chem. Commun.* **1998**, 1037−38.
[12] D. E. Fenton, in Comprehensive Coordination Chemistry; (Ed.: G. Wilkinson); Pergamon Press: Oxford, **1987**; Vol. 3, pp 1−80 and references therein.
[13] J. W. Yun, T. Tomoaki, L. E. Pence, S. J. Lippard, *J. Am. Chem. Soc.* **1995**, *117*, 4407−4408.
[14] H. Schmidbaur, I. Bach, D. L. Wilkinson, G. Müller, *Chem. Ber.* **1989**, *122*, 1433−1438.
[15] P. Ghosh, G. Parkin, *Inorg. Chem.* **1996**, *35*, 1429−1430.
[16] B.-H. Ye, T. Mak, I. D. Williams, X.-Y. Li, *J. Chem. Soc., Dalton Trans.* **1998**, 1935−1936.
[17] J. Huskens, A. D. Sherry, *Inorg. Chem.* **1996**, *35*, 5137−5143.
[18] L. B. Cole, E. M. Holt, *Inorg. Chim. Acta* **1989**, *160*, 195−203.
[19] S. R. Drake, K. D. Sanderson, M. B. Hursthouse, K. M. A. Malik, *Inorg. Chem.* **1993**, *32*, 1041−1044.
[20] J. Hermann, A. Erxleben, *Inorg. Chim. Acta* **2000**, *304*, 125−129.
[21] [21a] A. Erxleben, J. Hermann, *J. Chem. Soc., Dalton Trans.* **2000**, 569−575. − [21b] A. Erxleben, *Inorg. Chem.* **2001**, *40*, 208−213. − [21c] A. Erxleben, *Inorg. Chem.* **2001**, *40*, 412−414.
[22] L. Sacconi, F. Mani, A. Bencini, in Comprehensive Coordination Chemistry; (Ed.: G. Wilkinson); Pergamon Press: Oxford, **1987**; Vol. 5, Chapter 50, p 197 and references therein.
[23] C. Fukuhara, K. Tsuneyoshi, N. Matsumoto, S. Kida, M. Mikuriya, M. Mori, *J. Chem. Soc., Dalton Trans.* **1990**, 3473−3479.

[24] L. Carbonaro, M. Isola, P. La Pegna, L. Senatore, *Inorg. Chem.* **1999**, *38*, 5519−5525.
[25] D. J. Kitko, K. E. Wiegers, S. G. Smith, R. S. Drago, *J. Am. Chem. Soc.* **1977**, *99*, 1410−1416.
[26] S. Busse, H. Elias, J. Fischer, M. Poggemann, K. J. Wannowius, R. Boca, *Inorg. Chem.* **1998**, *37*, 3999−4005.
[27] D. L. Leussing, in Metal Ions in Biological Systems; H. Sigel, (Ed.: Marcel Dekker), New York, **1976**; Vol. 5, pp 2−77.
[28] Although replacement of water ligands by solvent molecules is to be considered in DMSO, for simplicity the same notation is used for the solution-state and solid-state structures of the complexes throughout the manuscript.
[29] T. Dudev, J. A. Cowan, C. Lim, *J. Am. Chem. Soc.* **1999**, *121*, 7665−7673.
[30] H. Sigel, D. B. McCormick, *Acc. Chem. Res.* **1970**, *3*, 201−208.
[31] D. Hall, F. H. Moore, *J. Chem. Soc. A* **1966**, 1822−1824.
[32] P. Pfeiffer, E. Breith, E. Lübbe, T. Tsumaki, *Justus Liebigs Ann. Chem.* **1933**, *503*, 84−130.
[33] K. Manseki, H. Imadzu, T. Kobayashi, H. Sakiyama, M. Sakamoto, Y. Nishida, A. Matsumoto, Y. Sadaoka, H. Okawa, *Kidorui* **1998**, *32*, 282−283.
[34] H. Okawa, S. Kida, *Bull. Chem. Soc. Jpn.* **1972**, *45*, 1759−1764.
[35] J. C. Duff, E. J. Bills, *J. Chem. Soc.* **1932**, 1987.
[36] R. R. Gagné, C. L. Spiro, T. J. Smith, C. A. Hamann, W. R. Thies, A. K. Shiemke, *J. Am. Chem. Soc.* **1981**, *103*, 4073−4081.
[37] KappaCCD package, Nonius, Delft, The Netherlands, **1997**.
[38] Z. Otwinowsky, W. Minor, DENZO and SCALEPACK, *Methods Enzymol.* **1997**, *276*, 307−326.
[39] G. M. Sheldrick, SHELXTL-PLUS (VMS), Siemens Analytical X-ray Instruments, Inc., Madison, WI, **1990**; SHELXL-93, *Program for crystal structure refinement*, University of Göttingen, Germany, **1993**.

Received April 5, 2001
[I01122]

Gas-Phase Structures and Acidities of the Sulfur Oxoacids $H_2S_nO_6$ (n = 2−4) and $H_2S_2O_7$[‡]

André H. Otto[a] and Ralf Steudel*[a]

Keywords: Sulfur oxoacids / Acidity / Superacidic systems / ab initio calculations / Thermodynamics

The gas-phase geometries, dipole moments, enthalpies, and Gibbs free energies of dithionic acid $H_2S_2O_6$, trithionic acid $H_2S_3O_6$, tetrathionic acid $H_2S_4O_6$, and disulfuric acid $H_2S_2O_7$ have been determined by ab initio MO calculations at various levels of theory. The most stable conformations of $H_2S_2O_6$ and $H_2S_2O_7$ are of C_2 symmetry, the other two acids are of C_1 symmetry. The gas-phase acidities defined as $\Delta G°_{298}$ of the deprotonation reaction obtained at the {MP2/6-311++ G(3df, 3pd)//MP2/6-31+ G(d) + ZPVE[HF/6-31+ G(d)]} level are as follows [kJ·mol^{-1}]: $H_2S_2O_6$ 1180, $H_2S_3O_6$ 1162, $H_2S_4O_6$ 1156, $H_2S_2O_7$ 1171. All four acids are much stronger than fluorosulfuric acid and chlorosulfuric acid in the gas phase. The decomposition of $H_2S_2O_7$ into SO_3 and H_2SO_4 is slightly endothermic and the same holds for the decomposition of $H_2S_3O_6$ into SO_3 and $H_2S_2O_3$, but the reaction of $H_2S_2O_6$ to SO_2 and H_2SO_4 is strongly exothermic. The structures of the monoanions $HS_2O_6^-$, $HS_3O_6^-$, $HS_4O_6^-$, and $HS_2O_7^-$ are characterized by intramolecular hydrogen bonds.

Introduction

Sulfur forms numerous ternary oxoacids $H_2S_mO_n$ where the oxidation numbers of the sulfur atom(s) are between −1 and +6.[1] Most of these compounds are unstable at ambient temperatures and have been detected only in aqueous solution (as anions) or in the vapour phase by mass spectrometry. Consequently, the structures and physical properties of almost all sulfur oxoacids have remained unknown for a long time.[2] More recently high-level ab initio MO calculations of a number of these compounds provided, for the first time, the gas-phase structures and, in some cases, the gas-phase acidities of H_2SO,[3] H_2SO_2,[3] H_2SO_3,[3] H_2SO_4,[3,4] H_2SO_5,[5] H_2S_2O,[6] $H_2S_2O_2$,[7] $H_2S_2O_3$,[5] $H_2S_2O_4$,[8] and H_2S_3O.[9] In this work we report on the gas-phase structures and acidities of three disulfonic acids $H_2S_nO_6$ (n = 2−4) and of disulfuric acid $H_2S_2O_7$.

Disulfuric acid is an industrial chemical prepared in huge amounts as an intermediate in the production of sulfuric acid from SO_3 and water. The sulfur trioxide from the contact process is absorbed into concentrated sulfuric acid with the formation of polysulfuric acids that are subsequently hydrolysed to give H_2SO_4:[10]

$$x\,SO_3 + H_2SO_4 \rightarrow H_2S_{x+1}O_{3x+4} \quad (1)$$

$$H_2S_{x+1}O_{3x+4} + x\,H_2O \rightarrow (x+1)\,H_2SO_4 \quad (2)$$

If x = 1, disulfuric acid is formed. Its structure is unknown but its gas-phase acidity has recently been determined by density functional calculations, at the B3LYP/6-311+ G(d, p) level of theory[11], as $\Delta G°_{298}$ = 1147 kJ·mol^{-1}. This enthalpy applies to the deprotonation reaction resulting in the gaseous monoanion $HS_2O_7^-$. The structure of this anion is known from X-ray crystallography of a number of salts, e.g. $[NO_2][HS_2O_7]$[12] and $[Se_4][HS_2O_7]_2$.[13] The connectivity of the anion is $HO-SO_2-O-SO_2^-$ but the structures of the two salts are characterized by strong intermolecular O−H···O hydrogen bonds.

The disulfonic acids $H_2S_nO_6$ with n = 2, 3, 4, ... occur in various natural habitats[14] as well as in industrial processes.[15] Consequently, they play a role in the global sulfur cycle. However, neither their structures nor their gas-phase acidities are known. The acidity of aqueous dithionic acid $H_2S_2O_6$ has recently been determined as pK_a = 1.9,[16] but no data for the other acids are available. The structures of the monoanions $HS_nO_6^-$ are also unknown since no corresponding salts have ever been isolated. However, a number of salts containing the dianions $S_nO_6^{2-}$ have been analyzed by X-ray crystallography.[17] From these studies it follows that the acids should have the connectivities $HO-SO_2-S_{n-2}-SO_2-OH$ (n = 2−4). In other words, all these molecules contain at least one sulfur−sulfur bond.

Calculations

Ab initio molecular orbital calculations were performed with CBS-Q,[18] G2(MP2),[19] and an MP2 treatment[20] elaborated in our group. The G2(MP2) method is a modified version of G2[21] and is almost as accurate as the G2 method, but at a substantially reduced computational expense.

The Complete Basis Set (CBS) model CBS-Q utilizes the "dagger" 6-31G† basis set[22] trying to overcome some deficiencies in the standard 6-31G(d) basis set. CBS-Q consists

[‡] Sulfur Compounds, 220. − Part 219: K. Hassenberg, J. Pickardt, R. Steudel, *Eur. J. Org. Chem.* **2001**, 2815−2817.

[a] Institut für Chemie, Technische Universität Berlin, Sekr. C2, 10623 Berlin, Germany
Fax (internat.) +49−(0)30/3142 6519
E-mail: steudel@schwefel.chem.tu-berlin.de

Supporting information for this article is available on the WWW under http://www.eurjic.com or from the author.

 © WILEY-VCH Verlag GmbH, 69451 Weinheim, 2001 1434−1948/01/1212−3047 $ 17.50+.50/0

of the following steps: Geometry optimization at the HF/6-31G† level, thermal corrections using wavenumbers obtained at the same level and scaled by a factor of 0.918, reoptimization at the MP2/6-31G† level followed by energy calculations using a large basis set in combination with HF and MP2. The next steps are MP4(sdq) and QCISD(T) calculations applying medium size basis sets. Then the CBS extrapolation is made and empirical corrections are added to obtain the final thermodynamic data.

The excellent performance of both CBS-Q and G2(MP2) in predicting gas-phase acidities of small molecules is well established.[23]

For an effective estimation of Brønsted acidities, a special MP2 treatment is elaborated. This approach consists of MP2/6-31+ G(d) geometry optimizations followed by MP2/6-311++ G(3df, 3pd) energy calculations while the thermal corrections were obtained from HF/6-31+ G(d) wavenumbers scaled by 0.9.

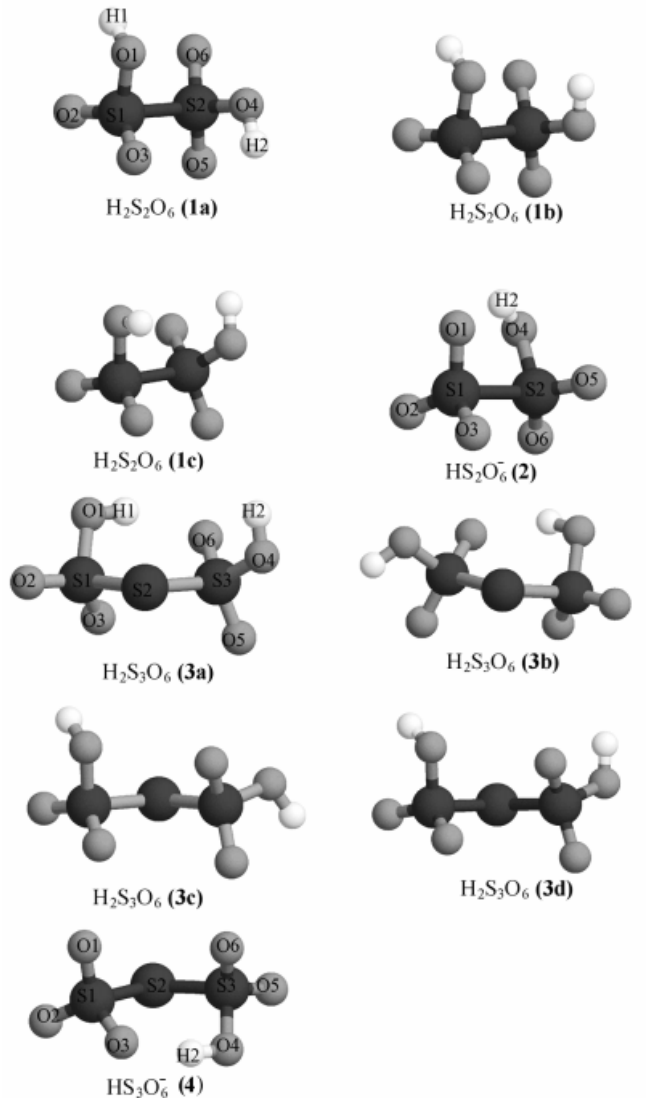

Figure 1. Conformations of the sulfur oxoacids $H_2S_nO_6$ (n = 2, 3) and of their anions as well as numbering of atoms in the most stable conformers

For details of the quantum chemical methods see ref.[24] To allow for the thermal corrections to the Gibbs free energy of the proton a value of −0.010654 hartree (−28 kJ·mol^{-1}) was used.

All calculations were carried out on a Cray J90 or on a Linux workstation using the GAUSSIAN program system.[25]

Results and Discussion

Molecular Structures

Dithionic Acid $H_2S_2O_6$

Three conformations of $H_2S_2O_6$ (**1a**−**1c**) were found to be minima on the potential energy surface (PES) of $(SO_3H)_2$. These structures are shown in Figure 1. Basically, they are rotational isomers which differ mainly by the signs and values of the torsion angles at the three axes H−O−S−S, (H)O−S−S−O(H), and S−S−O−H. The signs of these torsion angles, if one goes from one hydrogen atom to the other, are termed *motifs* which are used in the following tables to identify the different rotamers. In all three $H_2S_2O_6$ molecules the trigonal-pyramidal SO_3 groups are staggered. The conformers **1a** and **1b** are of C_2 symmetry while **1c** is of C_1 symmetry.

The geometrical parameters of the most stable isomer **1a** are listed in Table 1. The enthalpy and Gibbs energy differ-

Table 1. Geometrical parameters of $H_2S_2O_6$ (**1a**, C_2, motif + + +) and $HS_2O_6^-$ (**2**, C_1) calculated at the MP2/6-31+ G(d) level (internuclear distances in pm, bond angles and torsion angles in °). For numbering of atoms see Figure 1

Parameter	**1a** HO−SO_2−SO_2−OH	**2** HO−SO_2−SO_2−O^-
H1−O1	98.5	−
S1−O1	162.3	149.2
S1−O2	145.6	147.5
S1−O3	145.3	147.4
S1−S2	219.2	226.6
S2−O4	162.3	166.5
H2−O4	98.5	98.9
S2−O5	145.6	147.3
S2−O6	145.3	146.9
O1−H2	296.1	209.6
H1−O1−S1	109.4	−
O1−S1−O2	109.9	115.6
O1−S1−O3	106.1	116.4
O2−S1−O3	125.0	117.3
O1−S1−S2	99.2	96.0
O2−S1−S2	106.9	103.2
O3−S1−S2	106.7	103.9
S1−S2−O4	99.2	96.2
S1−S2−O5	106.9	109.2
S1−S2−O6	106.7	116.0
O4−S2−O5	109.9	108.1
O4−S2−O6	106.1	104.6
O5−S2−O6	125.0	119.7
S2−O4−H2	109.4	104.7
H1−O1−S1−S2	80.8	−
O1−S1−S2−O4	61.7	−40.8
S1−S2−O4−H2	80.8	37.1

Table 2. Relative enthalpies and Gibbs free energies [kJ·mol^{-1}] of the isomers of dithionic acid $H_2S_2O_6$ (**1**)

Species	Motif	Symmetry	MP2/6-31+ G(d)[a]		MP2/6-311++ G(3df, 3pd)[b]		CBS-Q		G2(MP2)	
			$\Delta H°_{298}$	$\Delta G°_{298}$	$\Delta H°_{298}$	$\Delta G°_{298}$	$\Delta H°_{298}$	$\Delta G°_{298}$	$\Delta H°_{298}$	$\Delta G°_{298}$
1a	+++	C_2	0.0	0.0	0.0	0.0	0.0	0.0	0.0	0.0
1b	−++	C_1	3.5	1.4	6.1	4.1	7.2	5.1	6.4	4.4
1c	−+−	C_2	10.2	9.4	13.2	12.4	14.0	14.0	14.3	13.6

[a] MP2/6-31+ G(d) +ZPVE[HF/6-31+ G(d)]. − [b] MP2/6-311++ G(3df, 3pd)//MP2/6-31+ G(d) +ZPVE[HF/6-31+ G(d)].

ences between the three conformers calculated at various levels of theory are shown in Table 2.

At the highest level, conformer **1b** is 4 kJ·mol^{-1} less stable than **1a**, and **1c** is 13 kJ·mol^{-1} less stable. None of these molecules seem to contain intramolecular hydrogen bonds, since the shortest O···H contacts are 256 pm in **1a**, 252 pm in **1b**, and 246 pm in **1c**. These distances are roughly equivalent to the van der Waals distance between oxygen and hydrogen atoms. For comparison, the length of the weak hydrogen bond in the gaseous water dimer $(H_2O)_2$ is 200 pm.[1a] The calculated bond lengths O−H and S−O as well as the bond angles show the expected values. Interestingly, the S−S bond (219.2 pm) is considerably longer than the single bond length of 205 pm observed in H_2S_2 and in S_8. This fact is in line with the evidence that S−S distances depend on the coordination numbers (CNs) of the two atoms and increase with higher CNs. An even longer S−S bond of 226.6 pm is calculated for the monoanion $HS_2O_6^-$ (**2**) the structural parameters of which are also listed in Table 1. This anion is of C_1 symmetry and, in contrast to **1a**−**1c**, contains an O···H hydrogen bond of length 209.6 pm (O1···H2). For the anion of potassium dithionate ($K_2S_2O_6$) the S−S bond length has been determined by X-ray crystallography as 214 pm (S−O 145 pm, S−S−O 105°, O−S−O 114°).[17]

Trithionic Acid $H_2S_3O_6$

Trithionic acid is also termed as sulfane disulfonic acid since it is formally a derivative of sulfane H_2S as the following formula shows: $S(SO_3H)_2$. Four conformational isomers (rotamers) were located as minima on the PES. The structures of these isomers (**3a**−**3d**) are shown in Figure 1; they are all of symmetry C_1 and differ mainly by the values and signs of the four torsion angles H1−O−S−S, (H1)O−S−S−S, S−S−S−O(H2), and S−S−O−H2. The signs of these angles (*motifs*) are given in Table 3. The most stable species **3a** is characterized by a weak intramolecular hydrogen bond between O6 and H1 (length 201.0 pm). Isomer **3b** is 5 kJ·mol^{-1} less stable than **3a** and also contains a hydrogen bond (O3···H2) with a length of 200.6 pm. In contrast, the shortest intramolecular O···H contacts in **3c** and **3d** are 243 and 248 pm, respectively. These rotamers are 19 and 20 kJ·mol^{-1}, respectively, less stable than **3a** (Gibbs energies; see Table 3).

The geometrical parameters of the stable isomer **3a**, together with those of the monoanion $HS_3O_6^-$ (**4**), are given in Table 4.

While the O−H and S−O bond lengths as well as the bond angles show the normal values, the two S−S bonds of **3a** (212.2 and 214.4 pm) are not equivalent, probably as a result of the hydrogen bond which makes the two SO_3H groups inequivalent. An even larger difference between the two S−S bonds is calculated for the anion **4** (208.3 and 226.3 pm) which is characterized by a strong hydrogen bond that is 172.8 pm (O3···H2; see Figure 1) in length; this is about the same length as observed for the hydrogen bonds in ice I (176 pm).[1a] For the anion of potassium trithionate ($K_2S_3O_6$) the two S−S distances have been determined by X-ray crystallography as 215 pm.[17]

Attempts to optimize the geometry of the zwitterion $HO_3S-S^+(H)-SO_3^-$ at the MP2/6-31+G(d) level of theory led to the dissociation of this tautomer of trithionic acid into thiosulfuric acid, $H_2S_2O_3$, and sulfur trioxide.

Tetrathionic Acid $H_2S_4O_6$

Ten rotational isomers were located as minima on the PES of $H_2S_4O_6$. Seven of these species are of C_1 symmetry and three are of C_2 symmetry; their structures are shown in Figure 2. To characterize these rotamers we once again use the motif which in this case represents the signs of the five torsional angles H1−O−S−S, (H1)O−S−S−S, S−S−S−S, S−S−S−O(H2), and S−S−O−H2. The structures **5a**−**5d** as well as **5f** contain one intramolecular hydrogen bond each which are of the lengths 190.5 pm (**5a**), 187.8

Table 3. Relative enthalpies and Gibbs free energies [kJ·mol^{-1}] of the isomers of trithionic acid $H_2S_3O_6$ (**3**)

Species	Motif	Symmetry	MP2/6-31+ G(d)[a]		MP2/6-311++ G(3df, 3pd)[b]	
			$\Delta H°_{298}$	$\Delta G°_{298}$	$\Delta H°_{298}$	$\Delta G°_{298}$
3a	− + − +	C_1	0.0	0.0	0.0	0.0
3b	− + − −	C_1	1.5	5.2	1.7	5.4
3c	− − + +	C_1	20.2	20.4	19.0	19.2
3d	+ − + +	C_1	20.6	21.1	19.2	19.8

[a] MP2/6-31+ G(d) +ZPVE[HF/6-31+ G(d)]. − [b] MP2/6-311++ G(3df, 3pd)//MP2/6-31+ G(d) +ZPVE[HF/6-31+ G(d)].

Table 4. Geometrical parameters of $H_2S_3O_6$ (**3a**, C_1, motif $-+-+$) and $HS_3O_6^-$ (**4**, C_1) calculated at the MP2/6-31+ G(d) level (internuclear distances in pm, bond angles and torsion angles in °). For numbering of atoms see Figure 1

Parameter	**3a** HO−SO_2−S− SO_2−OH	**4** HO−SO_2−S− SO_2−O^-
H1−O1	99.1	−
S1−O1	161.2	147.0
S1−O2	144.8	147.4
S1−O3	145.4	149.6
S1−S2	214.4	226.3
S2−S3	212.2	208.3
S3−O4	162.4	162.0
H2−O4	98.4	100.6
S3−O5	144.5	146.3
S3−O6	146.9	146.3
O6···H1	201.0	
O3···H2		172.8
H1−O1−S1	108.0	−
O1−S1−O2	106.0	117.2
O1−S1−O3	109.1	114.8
O2−S1−O3	125.0	114.9
O1−S1−S2	103.0	106.1
O2−S1−S2	103.9	98.7
O3−S1−S2	107.6	101.9
S1−S2−S3	96.9	100.5
S2−S3−O4	98.1	103.2
S2−S3−O5	111.6	107.2
S2−S3−O6	107.4	110.5
O4−S3−O5	105.9	105.3
O4−S3−O6	107.9	108.5
O5−S3−O6	123.0	120.6
S3−O4−H2	109.4	106.3
H1−O1−S1−S2	−72.0	−
O1−S1−S2−S3	69.1	−81.8
S1−S2−S3−O4	−153.1	−59.5
S2−S3−O4−H2	83.2	53.2

pm (**5b**), 188.6 pm (**5c**), 201.2 pm (**5d**), and 191.5 pm (**5f**). For the other five species the shortest O···H contacts were calculated as 241 pm or longer.

At the highest level of theory employed, the three species **5a**−**5c** practically have identical Gibbs energies (see Table 5) while the other molecules are 8−22 kJ·mol^{-1} less stable.

The geometrical parameters of the most stable species **5a** are given in Table 6. The most interesting data are those of the S−S bonds. As expected, the central S−S bond (202.7 pm) is considerably shorter than the other two (212.9 and 216.5 pm) as a result of the higher CNs within the sulfonic groups. The S−S−S−S torsion angle of 80.9° is quite normal for sulfur chains.[26]

For the monoanion $HS_4O_6^-$, three rotational isomers of C_1 symmetry (**6a**−**6c**) were found as local minima on the PES. Their structures are shown in Figure 3 and their relative enthalpies are given in Table 7.

The more stable structures **6a** and **6b** contain hydrogen bonds of length 162.0 and 159.8 pm, respectively, while no such bond is present in isomer **6c**. The geometrical parameters of **6a** are given in Table 6. The lengths of the S−S bonds show an interesting pattern: while the central bond (203.6 pm) has changed little compared to the free acid **5a**

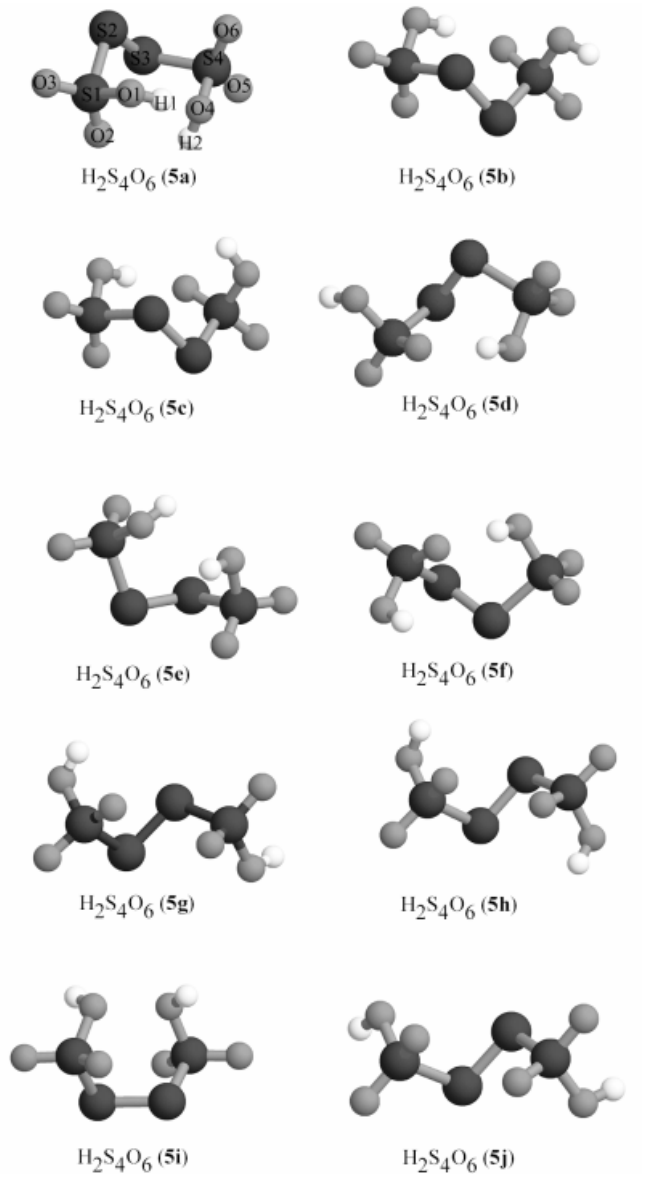

Figure 2. Conformations of the sulfur oxoacid $H_2S_4O_6$ as well as numbering of atoms in the most stable conformers

(202.7 pm), the bond in the S−SO_3H group (213.8 pm) has shortened by 2.7 pm and the bond S−SO_3^- (220.8 pm) has increased in length by 8 pm on deprotonation. For the anion of potassium tetrathionate the S−S bond lengths have been determined by X-ray crystallography as 202 pm (central bond) and 212 pm (terminal bonds); the S−S−S bond angles were found as 102° and 104°.[17]

Disulfuric Acid $H_2S_2O_7$

The structure of the disulfuric acid molecule **7** is of C_2 symmetry as shown in Figure 3. Only one minimum was located on the PES. This structure is stabilized by two hydrogen bonds of length 204.3 pm. The geometrical parameters of $H_2S_2O_7$ **7** as well as of its monoanion **8** are given in Table 8. The anion is characterized by a strong but asymmetric hydrogen bond of length 178.6 pm (symmetry C_1;

Table 5. Relative enthalpies and Gibbs free energies [kJ·mol^{-1}] of the isomers of tetrathionic acid $H_2S_4O_6$ (**5**)

Species	Motif	Symmetry	MP2/6-31+ G(d)[a]		MP2/6-311++ G(3df, 3pd)[b]	
			$\Delta H°_{298}$	$\Delta G°_{298}$	$\Delta H°_{298}$	$\Delta G°_{298}$
5a	− + − + +	C_1	0	0	5	0
5b	+ − + + +	C_1	5	10	0	1
5c	− + + − +	C_1	5	11	1	2
5d	− − + + +	C_1	15	17	11	8
5e	+ − + − +	C_2	17	15	16	9
5f	+ − − + +	C_1	12	20	8	11
5g	− + + + +	C_1	28	22	24	13
5h	− + + + −	C_2	28	22	24	13
5i	+ + − + +	C_2	19	19	18	14
5j	+ + + + +	C_1	30	31	26	22

[a] MP2/6-31+ G(d) +ZPVE[HF/6-31+ G(d)]. − [b] MP2/6-311++ G(3df, 3pd)//MP2/6-31+ G(d) +ZPVE[HF/6-31+ G(d)].

Table 6. Geometrical parameters of the $H_2S_4O_6$ (**5a**, C_1, motif − + − + +) and $HS_4O_6^-$ (**6a**, C_1, motif − + − +) calculated at the MP2/6-31+G(d) level (internuclear distances in pm, bond angles and torsion angles in °). For numbering of atoms see Figure 2

Parameter	**5a** HO−SO_2−S−S−SO_2−OH	**6a** HO−SO_2−S−S−SO_2−O^-
H1−O1	99.2	102.3
S1−O1	161.4	160.0
S1−O2	146.2	146.4
S1−O3	145.0	146.2
S1−S2	216.5	213.8
S2−S3	202.7	203.6
S3−S4	212.9	220.8
S4−O4	166.0	150.4
H2−O4	98.7	−
S4−O5	145.6	147.5
S4−O6	145.0	147.4
O4···H1	190.5	162.0
H1−O1−S1	108.0	109.7
O1−S1−O2	108.9	105.8
O1−S1−O3	105.7	109.9
O2−S1−O3	124.3	121.5
O1−S1−S2	101.4	103.4
O2−S1−S2	108.3	104.9
O3−S1−S2	105.9	109.8
S1−S2−S3	102.4	103.9
S2−S3−S4	101.6	101.8
S3−S4−O4	100.6	102.3
S3−S4−O5	104.7	100.2
S3−S4−O6	112.1	106.2
O4−S4−O5	108.5	114.0
O4−S4−O6	102.8	113.6
O5−S4−O6	125.4	117.9
S4−O4−H2	109.4	−
H1−O1−S1−S2	−69.5	−56.6
O1−S1−S2−S3	101.7	83.3
S1−S2−S3−S4	−80.9	−80.6
S2−S3−S4−O4	64.8	66.4
S3−S4−O4−H2	66.0	−

Figure 3). The calculated anion structure is in reasonable agreement with the X-ray structure of $[Se_4][HS_2O_7]_2$ if one takes into account the fact that there are interanionic hydrogen bonds in the solid-state structure which are absent in the free ion. The S−O−S bridge is asymmetric with

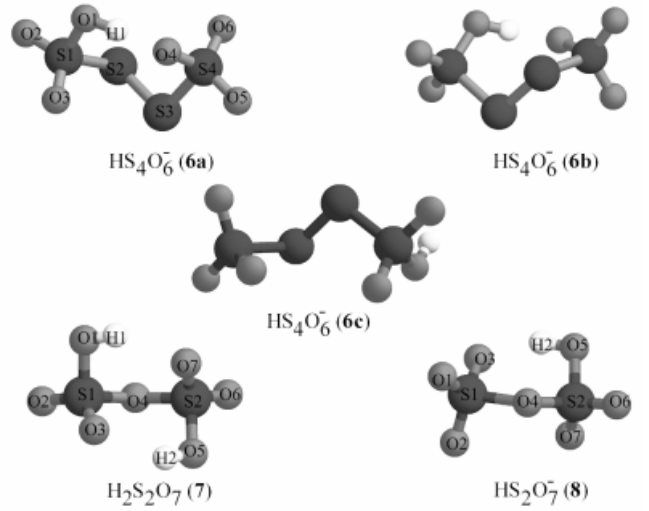

Figure 3. Conformations of the anion $HS_4O_6^-$, the acid $H_2S_2O_7$ and its anion $HS_2O_7^-$, as well as numbering of atoms in the most stable conformers

bond lengths of 160.2 pm and 184.1 pm and a bond angle of 120.5°; the experimental values are: 160(2) pm, 167(2) pm, 123(1)°.[13]

Acidities

The gas-phase acidities of the four acids investigated in this work are listed in Table 9. Only the most stable conformers were used. The acidities are defined as the enthalpies or Gibbs energies of the deprotonation reaction at 298 K. As a reference the acidity of gaseous sulfuric acid is used which has been calculated at the G2 level of theory[3] as $\Delta H°_{298} = 1305$ and $\Delta G°_{298} = 1268$ kJ·mol^{-1} in excellent agreement with experimental studies. Acids that have a higher acidity than sulfuric acid are termed superacids. The results in Table 9 demonstrate that both disulfuric acid and all the polythionic acids, including dithionic acid, are superacids that are stronger proton donors than HSO_3F, HSO_3Cl and $HClO_4$. They are surpassed only by a few extremely superacidic molecules like $HSO_3F{\cdot}SO_3$, $H_2S_3O_{10}$, and $HSO_3F{\cdot}SbF_5$.[11] Figure 4 shows a comparison of the acidities of sulfur-containing superacids.

Table 7. Relative enthalpies and Gibbs free energies [kJ·mol^{-1}] of the isomers of the anions $HS_4O_6^-$ (**6**)

Species	Motif	Symmetry	MP2/6-31+ G(d)[a]		MP2/6-311++ G(3df, 3pd)[b]	
			$\Delta H°_{298}$	$\Delta G°_{298}$	$\Delta H°_{298}$	$\Delta G°_{298}$
6a	− + − +	C_1	0.0	0.0	0.0	0.0
6b	+ + − +	C_1	10.5	10.6	8.4	8.4
6c	+ + + +	C_1	71.7	63.5	74.4	66.3

[a] MP2/6-31+ G(d) +ZPVE[HF/6-31+ G(d)]. − [b] MP2/6-311++ G(3df, 3pd)//MP2/6-31+ G(d) +ZPVE[HF/6-31+ G(d)].

Table 8. Geometrical parameters of $H_2S_2O_7$ (**7**, C_2) and $HS_2O_7^-$ (**8**, C_1) calculated at the MP2/6-31+ G(d) level (internuclear distances in pm, bond angles and torsion angles in °). For numbering of atoms see Figure 3

Parameter	**7** HO−SO_2−O−SO_2−OH	**8** HO−SO_2−O−SO_2−O^-
H1−O1	99.2	−
S1−O1	159.7	146.5
S1−O2	143.7	146.4
S1−O3	146.1	149.0
S1−O4	168.5	184.1
S2−O4	168.5	160.2
S2−O5	159.7	162.4
H2−O5	99.2	100.0
S2−O6	143.7	145.6
S2−O7	146.1	146.0
O3···H2	204.3	178.6
H1−O1−S1	108.4	−
O1−S1−O2	107.6	117.9
O1−S1−O3	110.1	115.9
O2−S1−O3	124.1	115.8
O1−S1−O4	101.5	98.1
O2−S1−O4	105.5	103.8
O3−S1−O4	105.6	100.6
S1−O4−S2	117.0	120.5
O4−S2−O5	101.5	102.0
S2−O5−H2	108.4	105.0
O4−S2−O6	105.5	107.3
O4−S2−O7	105.6	110.7
H1−O1−S1−O4	−63.1	−
O1−S1−O4−S2	73.7	−155.5
S1−O4−S2−O5	73.7	63.8
O4−S2−O5−H2	−63.1	−49.4

It is obvious from this data that the acidity increases with increasing anion size. This may be rationalized by the better stabilization of the excess negative charge and this stabilization should be easier the larger the anion becomes with regard to the total number of electrons.[27] Similar observations have been made before with peroxosulfuric acid and chlorosulfuric acid.[5]

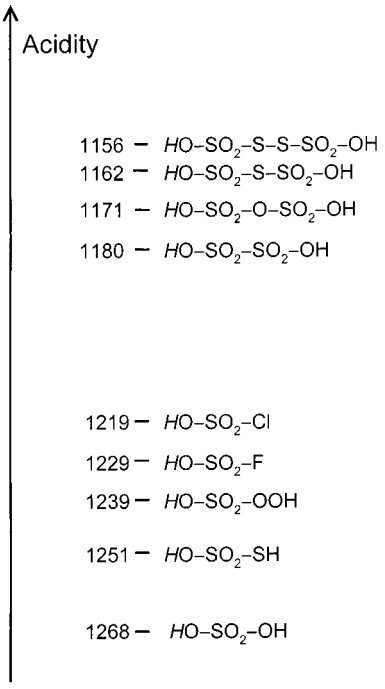

Figure 4. Gas phase acidities of the sulfur oxoacids $H_2S_nO_6$ (n = 2, 3, 4) and $H_2S_2O_7$ compared to the acidities of other superacidic proton donors. The values of $\Delta G°_{298}$ [kJ·mol^{-1}] for the deprotonation reaction are given

According to our previous experience[5] the acidities calculated at the CBS-Q level agree with those from the G2(MP2) level within 10 kJ·mol^{-1}. Therefore, we consider our acidity of disulfuric acid of 1169 kJ·mol^{-1} ($\Delta G°_{298}$) as

Table 9. Gas phase acidities [kJ·mol^{-1}] and dipole moments [Debye] of the polythionic acids HO−SO_2−S_n−SO_2−OH (n = 0, 1, 2) (**1**, **3**, **5**) and disulfuric acid HO−SO_2−O−SO_2−OH (**7**)

Species	MP2		CBS-Q		G2(MP2)		MP2[a]
	$\Delta H°_{298}$	$\Delta G°_{298}$	$\Delta H°_{298}$	$\Delta G°_{298}$	$\Delta H°_{298}$	$\Delta G°_{298}$	μ
HO−SO_2−SO_2−OH (**1a**)	1214	1180	1204	1171	1215	1182	2.66
HO−SO_2−S−SO_2−OH (**3a**)	1188	1162					5.04
HO−SO_2−S−S−SO_2−OH (**5a**)	1182	1156					1.48
HO−SO_2−O−SO_2−OH (**7**)	1205	1171	1203	1169			2.28

[a] MP2/6-311++ G(3df, 3pd)//MP2/6-31+ G(d).

more reliable than the literature value[11] of 1147 kJ·mol^{-1} obtained by B3LYP calculations. It has been shown[28] that B3LYP provides accurate Brønsted acidities only in combination with large basis sets.

Stabilities

Since heating can easily decompose all the acids investigated in this work, we have calculated the Gibbs energies ($\Delta G°_{298}$) of some typical dissociation reactions. The data in Table 10 show that the decomposition of dithionic acid to sulfuric acid and sulfur dioxide is exothermic. This reaction has in fact been observed in aqueous solution.[29] The decomposition of trithionic acid into sulfur trioxide and thiosulfuric acid is slightly endothermic. This also holds for the decomposition of disulfuric acid into sulfuric acid and SO_3. However, in the case of $H_2S_3O_6$ other redox reactions are also possible.

Table 10. Stabilities ($\Delta G°_{298}$) of the polythionic acids HO−SO_2−S_n−SO_2−OH (n = 0, 1) (**1**, **3**) and disulfuric acid (**7**) HO−SO_2−O−SO_2−OH with respect to the decomposition into lower acids and SO_2 or SO_3

Decomposition	MP2[a]	CBS-Q	G2(MP2)
$H_2S_2O_6$ (**1a**) → H_2SO_4 + SO_2	−121	−116	−122
$H_2S_3O_6$ (**3a**) → $H_2S_2O_3$ + SO_3	21		
$H_2S_2O_7$ (**7**) → H_2SO_4 + SO_3	15	32	

[a] MP2/6-311++ G(3df, 3pd)//MP2/6-31+ G(d) + ZPVE[HF/6-31+ G(d)].

The calculated enthalpies $H°$ and Gibbs energies $G°$ of the 24 conformers corresponding to the four sulfur oxoacids and their anions are given in Table 11S while Table 12S contains the data from which the stabilities have been determined. These Tables are available as Supplementary Information (see also first page of this article).

Conclusions

The four sulfur oxo acids HO−SO_2−SO_2−OH (**1**), HO−SO_2−S−SO_2−OH (**3**), HO−SO_2−S−S−SO_2−OH (**5**), and HO−SO_2−O−SO_2−OH (**7**), as well as their monoanions, were investigated by ab initio MO calculations at various levels to obtain their structures as well as their enthalpies and Gibbs energies from which the thermodynamics of the deprotonation reactions, at 298 K, were calculated. In most cases several different conformations were located as minima on the PES. The monoanions and some of the acid molecules are stabilized by intramolecular hydrogen bonds. The sulfonic acid groups are always staggered to each other. The S−S bonds are scattered over the range 202.7−226.6 pm with long distances occurring between sulfur atoms of CN = 4 and short distances with sulfur of CN = 2. All other structural parameters show normal values. Unexpectedly, the gas-phase acidities of these acids are much higher than that of sulfuric acid. Therefore, these species may be termed as superacids. The decomposition of dithionic acid **1** to sulfur dioxide and sulfuric acid is strongly exothermic. Tetrathionic acid is even stronger than disulfuric acid.

Acknowledgments

This work was supported by the Deutsche Forschungsgemeinschaft, the Verband der Chemischen Industrie, and the Konrad-Zuse-Zentrum für Informationstechnologie Berlin.

[1] [1a] R. Steudel, *Chemie der Nichtmetalle*, 2nd ed., de Gruyter, Berlin, **1998**, p. 298−307. − [1b] N. N. Greenwood, A. Earnshaw, *Chemistry of the Elements*, 2nd ed., Butterworth, Oxford, **1997**, p. 706−721.
[2] Experimental structure determinations are available only for H_2SO_4 and H_2SO_5.
[3] A. H. Otto, R. Steudel, *Eur. J. Inorg. Chem.* **2000**, 617−624.
[4] J. R. Rustad, D. A. Dixon, J. D. Kubicki, A. R. Felmy, *J. Phys. Chem. A* **2000**, *104*, 4051−4057.
[5] R. Steudel, A. H. Otto, *Eur. J. Inorg. Chem.* **2000**, 2379−2386.
[6] [6a] R. Steudel, Y. Drozdova, R. H. Hertwig, W. Koch, *J. Phys. Chem.* **1995**, *99*, 5319−5324. − [6b] A. Königshofen, M. Behnke, M. Hoverath, J. Hahn, *Z. Anorg. Allg. Chem.* **2000**, *625*, 1779−1786.
[7] K. Miaskiewicz, R. Steudel, *J. Chem. Soc., Dalton Trans.* **1991**, 2395−2399.
[8] Y. Drozdova, R. Steudel, R. H. Hertwig, W. Koch, T. Steiger, *J. Phys. Chem. A* **1998**, *102*, 990−996.
[9] Y. Drozdova, R. Steudel, *Chem. Eur. J.* **1995**, *1*, 193−198.
[10] H. Müller, U. Sander, U. Rothe, R. Kola, *Ullmanns Encycl. Ind. Chem.* **1994**, *25*, 635.
[11] I. A. Koppel, P. Burk, I. Koppel, I. Leito, T. Sonoda, M. Mishima, *J. Am. Chem. Soc.* **2000**, *122*, 5114−5124.
[12] J. W. M. Steeman, C. H. MacGillavry, *Acta Crystallogr.* **1954**, *7*, 402−404.
[13] I. D. Brown, D. B. Crump, R. J. Gillespie, *Inorg. Chem.* **1971**, *10*, 2319−2323.
[14] *Autotrophic Bacteria* (Eds.: H. G. Schlegel, B. Bowien), Science Tech Publ., Madison, and Springer, Berlin, **1989.**
[15] *Environmental Technologies to Treat Sulfur Pollution* (Eds.: P. N. L. Lens, L. Hulshoff Pol), IWA Publ., London, **2000**.
[16] T. Meissner, F. Eisenbeiss, B. Jastorff, *J. Chromatogr. A* **1999**, *838*, 81−88.
[17] A. F. Wells, *Structural Inorganic Chemistry*, 5th ed., Clarendon, Oxford, **1984**, pp. 725, 733.
[18] J. W. Ochterski, G. A. Petersson, J. A. Montgomery, Jr., *J. Chem. Phys.* **1996**, *104*, 2598−2519.
[19] L. A. Curtiss, K. Raghavachari, J. A. Pople, *J. Chem. Phys.* **1993**, *98*, 1293−1298.
[20] A manuscript dealing with a comprehensive test of this method is in preparation.
[21] L. A. Curtiss, K. Raghavachari, G. W. Trucks, J. A. Pople, *J. Chem. Phys.* **1991**, *94*, 7221−7230.
[22] [22a] G. A. Petersson, A. Bennett, T. G. Tensfeldt, M. A. Al-Laham, W. A. Shirley, J. Mantzaris, *J. Chem. Phys.* **1988**, *89*, 2193−2218. − [22b] G. A. Petersson, M. A. Al-Laham, *J. Chem. Phys.* **1991**, *94*, 6081−6090
[23] J. W. Ochterski, G. A. Petersson, K. B. Wiberg, *J. Am. Chem. Soc.* **1995**, *117*, 11299−11308.
[24] J. B. Foresman, A. E. Frisch, *Exploring Chemistry with Electronic Structure Methods*, 2nd ed., Gaussian, Inc., Pittsburgh, PA, **1996**.
[25] M. J. Frisch, G. W. Trucks, H. B. Schlegel, P. M. W. Gill, B. G. Johnson, M. A. Robb, J. R. Cheeseman, T. A. Keith, G. A.

Petersson, J. A. Montgomery, K. Raghavachari, M. A. Al-Laham, V. G. Zakrzewski, J. V. Ortiz, J. B. Foresman, J. Cioslowski, B. B. Stefanov, A. Nanayakkara, M. Challacombe, C. Y. Peng, P. Y. Ayala, W. Chen, M. W. Wong, J. L. Andres, E. S. Replogle, R. Gomperts, R. L. Martin, D. J. Fox, J. S. Binkley, D. J. Defrees, J. Baker, J. P. Stewart, M. Head-Gordon, C. Gonzalez, J. A. Pople, *GAUSSIAN 94 Revisions D.2* (Cray) and *E.1* (workstation), Gaussian, Inc., Pittsburgh, PA, **1995**.

[26] R. Steudel, *Angew. Chem.* **1975**, *87*, 683−692; *Angew. Chem. Int. Ed. Engl.* **1975**, *14*, 655−664.
[27] C. A. Reed, *Acc. Chem. Res.* **1998**, *31*, 133−139.
[28] P. Burk, I. A. Koppel, I. Koppel, I. Leito, O. Travnikova, *Chem. Phys. Lett.* **2000**, *323*, 482−489.
[29] J. Meyer, *Z. Anorg. Allg. Chem.* **1935**, *222*, 337−344.

Received May 22, 2001
[I01185]

$[(C_9H_7)YbI(DME)_2]$, the First Indenyl Half-Sandwich Complex of Divalent Ytterbium

Alexander A. Trifonov,*[a] Eugenii N. Kirillov,[a] Sebastian Dechert,[b] Herbert Schumann,*[b] and Mikhail N. Bochkarev[a]

Keywords: Indenyl complexes / Structure determination / Ytterbium / Sandwich complexes

The reaction of the naphthalene ytterbium(II) complex $(\mu\text{-}C_{10}H_8)[YbI(DME)_2]_2$ (**1**) with indene proved to be a convenient synthetic route to the novel indenyl half-sandwich ytterbium(II) complex $[(C_9H_7)YbI(DME)_2]$ (**2**), which is a monomer in the solid state and stable in DME solution, although it rearranges in THF to give the symmetric derivatives $[(C_9H_7)_2Yb(THF)_2]$ and $[YbI_2(THF)_2]$. The reaction of **2** with equimolar amounts of C_5H_5Na in DME yields $[(C_5H_5)_2Yb(DME)]$ and $[(C_9H_7)_2Yb(DME)]$.

Introduction

Although the first tris(indenyl)lanthanide complexes were synthesized more than 30 years ago,[1] the interest in indenyllanthanide compounds, especially concerning the nature of the metal-ligand bond and the characteristics of their molecular structures, still continued in the following decades. In the last years, a new wave of interest in this class of compounds was caused by the numerous reports on the high catalytic activity of analogous complexes of the early d-transition metals in α-olefin polymerization.[2,3]

Despite the attention which Ln^{II} complexes with η^5-bonded aromatic carbocyclic ligands attracted as prospective catalysts for the polymerization of both non-polar and polar monomers,[4−7] the number of indenyllanthanide(II) complexes is still very limited and their catalytic potential only scarcely investigated.

Although the synthesis of the first indenyl complex of divalent ytterbium, $[(C_9H_7)_2Yb(THF)_2]$, obtained by ligand exchange between $(C_6F_5)_2Yb$ and indene was described in 1985,[8] the structure of this complex was not determined until 1993.[9] The corresponding DME-coordinated complex $[(C_9H_7)_2Yb(DME)]$ was isolated as an unexpected product in 98% yield from the reaction of $[(CH_3)_2C(1\text{-}C_9H_6)_2]Na_2$ with $YbCl_3$, although the authors were actually intending to synthesize the $(CH_3)_2C$-bridged *ansa*-bis(indenyl) complex $[(CH_3)_2C(1\text{-}C_9H_6)_2YbCl]$.[10] The ethylene-bridged *ansa*-bis(indenyl) complexes *rac*-$[(CH_2)_2(1\text{-}C_9H_6)_2Yb(THF)_2]$ and *rac*-$[(CH_2)_2\{1\text{-}(4,7\text{-}(CH_3)_2C_9H_4\}_2\text{-}Yb(THF)_2]$ have been isolated in poor yields starting from $YbCl_3$ and $[(CH_2)_2(1\text{-Ind})_2]Li_2$ [Ind = C_9H_6, 4,7-$(CH_3)_2C_9H_4$], and subsequent reduction of the product by sodium metal.[10] The ytterbocenes $[\{1\text{-}(HSiR_2)\text{-}2\text{-}R'\text{-}C_9H_5\}_2Yb(L)_2]$ (R = Me, Ph; R′ = H, Me; L = donor ligand), obtained by a silylamine elimination reaction from $HSiR_2$-substituted indenes and $Yb[N(SiMe_3)_2]_2(THF)_2$ as well as their fluxional behaviour in solution have also been described.[11] A structurally characterized bisindenyl complex of divalent samarium, $[(C_9H_7)_2Sm(THF)]$, was prepared in high yields by metathesis of $SmI_2(THF)_2$ and C_9H_7K.[12] The Yb^{II} and Sm^{II} derivatives, $(Me_2NCH_2CH_2C_9H_6)_2Ln$ (Ln = Sm, Yb) containing the donor-functionalized 2-dimethylaminoethylindenyl ligands were synthesized by Qian et al.[13]

Halogen-functionalized half-sandwich complexes of Yb^{II} are of essential practical interest since they might serve as suitable precursors for the synthesis of mixed-ligand derivatives. Up to now, only very few compounds of this type such as $[Cp^*YbI(THF)_2]$[14] and $[(1,2\text{-}Me_2NCH_2CH_2)_2\text{-}C_5H_3]YbI(THF)_2$ [15] are known, probably due to the pronounced tendency of heteroleptic Ln^{II} compounds to equilibrate in solution to the corresponding symmetric derivatives.[16] Since half-sandwich indenyllanthanide(II) halide complexes are still unknown, we tried to synthesize the mixed indenyl iodide complex of divalent ytterbium.

Results and Discussion

Naphthalene complexes of ytterbium[17,18] proved to be suitable precursors for the preparation of various Yb^{II} and Yb^{III} derivatives. In particular, these complexes readily react with CH and EH acidic compounds affording the corresponding derivatives of divalent ytterbium in good yields.[17] Thus, the reaction of $(\mu\text{-}C_{10}H_8)[YbI(DME)_2]_2$ (**1**) with indene was proposed as a convenient method for the preparation of indenylytterbium(II) iodide. In contrast to a metathetical pathway, the formation of an alkali halide, which very often hampers the synthesis of organolanthanide complexes, is avoided.

[a] G. A. Razuvaev Institute of Organometallic Chemistry of Russian Academy of Sciences, Tropinina 49, 603950 Nizhny Novgorod GSP-445, Russia
Fax: (internat.) +7-8312/661-497
E-mail: trif@imoc.sinn.ru
[b] Institut für Chemie der Technischen Universität, Straße des 17. Juni 135, 10623 Berlin, Germany
Fax: (internat.) +49-(0)30/3142-2168
E-mail: schumann@chem.tu-berlin.de

 © WILEY-VCH Verlag GmbH, 69451 Weinheim, 2001 1434−1948/01/1212−3055 $ 17.50+.50/0

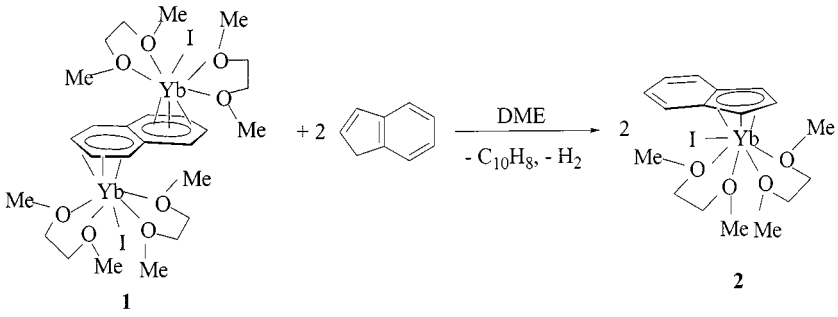

Scheme 1

The reaction of (μ-$C_{10}H_8$)[YbI(DME)$_2$]$_2$ (**1**) with indene in DME occurs at room temperature with progressive dissolution of **1**, evolution of hydrogen and formation of free naphthalene, and is complete within ca. 4 hours. Ruby-red diamagnetic crystals of [C_9H_7YbI(DME)$_2$] (**2**) separate at 0 °C from the filtered and concentrated reddish-brown DME solution with yields of 76% (Scheme 1).

Complex **2** has been characterized by elemental analysis, IR spectroscopy, magnetic measurements and by single crystal X-ray diffraction. It dissolves in DME, THF and pyridine, but is stable only in DME solution. A ligand rearrangement occurs in THF or pyridine yielding equimolar amounts of the symmetric compounds [(C_9H_7)$_2$Yb(THF)$_2$] and YbI$_2$(THF)$_4$ [Equation (1)].

$$2\,(C_9H_7)YbI(DME)_2\,(\mathbf{2}) \rightarrow (C_9H_7)_2Yb(THF)_2 + YbI_2(THF)_2 \qquad (1)$$

Complex **2** is diamagnetic corresponding to the Yb^{2+} oxidation state.[19] The ^{1}H and ^{13}C NMR spectra recorded in [D_8]THF or [D_5]pyridine show a complex pattern of signals due to simultaneous or exclusive presence of the ligand exchange products.

The single crystal X-ray diffraction study of complex **2** − the crystal and structure refinement data are listed in Table 1 − shows monomeric molecules (Figure 1) with the ytterbium atom coordinated in a distorted octahedral fashion to one iodine atom, the five-membered ring part of the indenyl ligand, and the four oxygen atoms of the two DME molecules. The fact that the distances of the ytterbium atom to three of the carbon atoms [C(1), C(2), and C(3)] forming the coordinating cyclopentadienyl part of the indenyl ligand are shorter than the remaining two Yb−C(4) and Yb−C(9) distances, indicate a certain transition from an η^5- to an η^3-bonding mode. This is also consistent with a ring slippage of 0.27 Å. In contrast to **2**, the bis(indenyl) complexes [(C_9H_7)$_2$Yb(DME)][9] and [(C_9H_7)$_2$Yb(THF)$_2$][10] show a distorted tetrahedral ligand arrangement with slightly shorter Yb−ring centroid and Yb−O distances (Yb−C_g: 2.43/2.45 Å; Yb−O: 2.41/2.38 Å).

To examine the utility of complex **2** for the synthesis of mixed ligand complexes of divalent ytterbium, we reacted **2** in DME with equimolar amounts of sodium cyclopentadienide, which did not result in the formation of the expected [(C_5H_5)Yb(C_9H_7)], but instead gave a mixture of the two ligand-exchanged products [(C_5H_5)$_2$Yb(DME)] and [(C_9H_7)$_2$Yb(DME)]. This result corresponds to that reported by Roesky et al.,[21] who isolated [Li(THF)$_3${μ^2−η^8−C_8H_8)}Sm(C_8H_8)] after the reaction of [(C_8H_8)SmI(THF)$_2$] with (1,4-$R_2C_8H_6$)Li$_2$ [R = 2-(dimethylsilyl)-*N*,*N*-dimethylaniline], formed by ligand rearrangement, instead of a heteroleptic complex. Both examples demonstrate a facile transfer of multi-η-bonded anionic carbocyclic ligands from one lanthanide centre to another, a chemical behaviour which already has been observed with cyclopentadienyl complexes of the lanthanides [Equation (2)].[22−24]

$$2\,(C_9H_7)YbI(DME)_2\,(\mathbf{2}) + 2\,C_5H_5Na \rightarrow (C_9H_7)_2Yb(DME) + (C_5H_5)_2Yb(DME) + 2\,NaI \qquad (2)$$

Table 1. Crystal data and structure refinement for **2**

Empirical formula	$C_{17}H_{27}IO_4Yb$
M_r [g mol^{-1}]	595.33
Crystal system	orthorhombic
Space group	*Pca*2$_1$ (No. 29)
Unit cell dimensions	
a [Å]	14.1633(3)
b [Å]	10.0847(3)
c [Å]	14.1803(3)
α = β = γ [°]	90
V [Å^3]	2025.41(9)
Z	4
$\rho_{calcd.}$ [g/cm^3]	1.952
μ (Mo-K_α) [mm^{-1}]	6.156
F(000)	1136
Crystal dimensions [mm^3]	0.38 × 0.30 × 0.24
Data collection θ range [°]	2.02−27.50
h	−17/18
k	−13/8
l	−18/18
Collected/unique reflections	14717/4573
R_{int}	0.0637
Reflections with $I > 2\sigma(I)$	3772
Max./min. transmission	0.3631/0.1218
Goodness-of-fit on F^2	1.023
Final *R* indices [$I > 2\sigma(I)$]	R_1 = 0.0363, wR_2 = 0.0645
R indices (all data)	R_1 = 0.0531, wR_2 = 0.0695
Absolute structure parameter	0.017(11)
Larg. Diff. peak and hole [e/Å^3]	1.040/−1.443

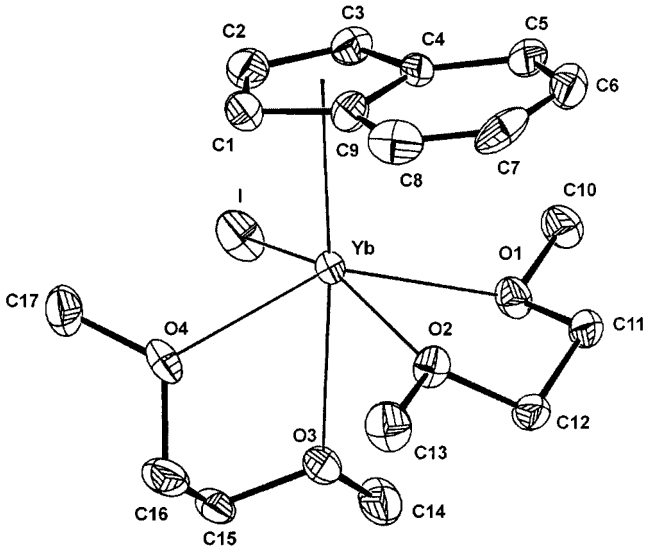

Figure 1. ORTEP drawing[20] and numbering scheme of the molecular structure of **2** (50% probability thermal ellipsoids); all hydrogen atoms have been omitted for clarity; selected bond lengths (Å) and angles (°) [Cg is defined by the ring atoms C(1), C(2), C(3), C(4), C(9)]: Yb(1)−Cg 2.533(3), Yb−C(1) 2.789(8), Yb−C(2) 2.689(8), Yb−C(3) 2.734(7), Yb−C(4) 2.889(7), Yb−C(9) 2.914(8), Yb−I 3.1423(7), Yb−O(1) 2.431(5), Yb−O(2) 2.437(5), Yb−O(3) 2.573(5), Yb−O(4) 2.472(4); Cg−Yb−I 105.37(9), Cg−Yb−O(1) 107.15(16), Cg−Yb−O(2) 100.66(14), Cg−Yb−O(3) 172.29(16), Cg−Yb−O(4) 105.7(2), O(1)−Yb−O(2) 66.92(17), O(1)−Yb−O(3) 78.48(17), O(1)−Yb−O(4) 143.4(2), O(2)−Yb−O(3) 76.48(17), O(2)−Yb−O(4) 91.54(17), O(3)−Yb−O(4) 67.5(2), O(1)−Yb−I 96.38(14), O(2)−Yb−I 152.41(11), O(3)−Yb−I 78.76(13), O(4)−Yb−I 90.08(12); ring slippage (Å): Cg 0.274

Experimental Section

All experiments were performed in evacuated tubes using standard Schlenk techniques, thus excluding traces of air and water. THF, DME, and toluene were purified by distillation from sodium/benzophenone ketyl. [D_5]pyridine was dried with CaH_2 and condensed in vacuum prior to use. Commercially available indene (Dalhim Ltd.) was used after drying with CaH_2 and subsequent distillation. Compound **1** was prepared from $YbI_2(THF)_2$, $C_{10}H_8$ and Li according to literature methods.[18] IR spectra were recorded as Nujol mulls on a Specord M80 spectrophotometer. NMR spectra were recorded in [D_8]THF or [D_5]pyridine at 298 K using a Bruker DPX 200 spectrometer. Chemical shifts for ^1H and ^{13}C spectra were referenced internally using the residual solvent resonances and reported relative to tetramethylsilane.

[(C9H7)YbI(DME)2] (2): A solution of indene (1.91 g, 16.44 mmol) in DME (10 mL) was slowly added to a suspension of **1** (8.92 g, 8.19 mmol) in DME (50 mL) at room temperature with vigorous stirring. The suspended **1** disappeared within 4 h. The resulting solution was filtered and slowly concentrated in vacuum at room temperature until crystallization started. The concentrate was then cooled to 0 °C and left overnight. The mother liquor was decanted from ruby-red crystals of **2**, which were washed with cold DME and dried in vacuum. Yield: 3.70 g (76%). − IR (Nujol): $\tilde{\nu}$ = 3060 (w), 1340 (s), 1320 (m), 1250 (m), 1200 (m), 1125 (s), 980 (m), 870 (s), 750 (s), 720 (s), 700 cm^{-1} (s). − $C_{17}H_{27}IO_4Yb$ (595.34): calcd. C 34.30, H 4.57, I 21.33, Yb 29.07; found C 33.84, H 4.11, I 20.95, Yb 29.50.

Ligand Exchange of 2 in THF: Compound **2** (0.78 g, 1.31 mmol) was dissolved in THF (15 mL) at room temperature. Within 1 h a pale yellow precipitate formed. The precipitate was separated by filtration, washed with cold THF and dried in vacuo yielding $YbI_2(THF)_2$ (0.33 g, 88%). Hexane (5 mL) was then slowly added to the mother liquor, and the resulting solution was cooled to 0 °C and left overnight. Ruby-red crystals of [$(C_9H_7)_2Yb(THF)_2$] (0.30 g, 83%) were isolated after filtration. − ^1H NMR (200 MHz, [D_8]THF): δ = 5.74 [d, ^3J(H,H) = 3.2 Hz, 2 H, aryl-H^1,H^3], 6.20 [t, ^3J(H,H) = 3.2 Hz, 1 H, aryl-H^2], 6.62−6.67 (m, 2 H, aryl-H^5, H^6), 7.29−7.34 (m, 2 H, aryl-H^7, H^8). − ^{13}C NMR (50.3 MHz, [D_8]THF) δ = 94.0 (aryl-C^1, C^3), 116.6 (aryl-C^2 and aryl-C^5,C^6), 120.4 (aryl-C^4,C^7), 127.1 (aryl-C^8,C^9).

Reaction of 2 with NaCp: A solution of NaC_5H_5 (0.33 g, 3.75 mmol) in DME (15 mL) was slowly added to a solution of **2** (2.26 g, 3.79 mmol) in DME (30 mL) precooled to 0 °C with vigorous stirring. The reaction mixture was allowed to warm up to room temperature, was then stirred for 12 h and filtered. The resulting brown solution was concentrated in vacuum until the growth of green crystals started and was then cooled to 0 °C. 0.4 g (54%) of [$(C_5H_5)_2Yb(DME)$] was isolated. The IR and ^1H NMR spectra as well as the microanalytical data were in agreement with those given previously.[25] Long term cooling or condensation of hexane into the solution decanted from the precipitated [$(C_5H_5)_2Yb(DME)$] resulted in the simultaneous growth of both green and ruby-red crystals. Parts of the red crystals were separated manually and found to be [$(C_9H_7)_2Yb(DME)$]. − ^1H NMR (200 MHz, [D_8]THF): δ = 3.26 (s, 6 H, OCH_3, DME), 3.49 (s, 4 H, CH_2O, DME), 5.73 [d, ^3J(H,H) = 3.3 Hz, 2 H, aryl-H^1,H^3], 6.19 [t, ^3J(H,H) = 3.2 Hz, 1 H, aryl-H^2], 6.62−6.68 (m, 2 H, aryl-H^5,H^6), 7.30−7.35 (m, 2 H, aryl-H^4,H^7). − ^{13}C NMR (50.3 MHz, [D_8]THF): δ = 59.3 (OCH_3, DME), 72.8 (CH_2O, DME), 94.0 (aryl-C^1, C^3), 116.6 (aryl-C^2 and aryl-C^5,C^6), 120.4 (aryl-C^4,C^7), 127.1 (aryl-C^8,C^9).

Crystal Structure Determination: Data were collected on a Siemens SMART CCD diffractometer (graphite monochromated Mo-K_α radiation, λ = 0.71073 Å) with area-detector by use of ω scans at 173 K. The structure was solved by direct methods using SHELXS-97[26] and refined on F^2, using all reflections, with SHELXL-97.[27] All non-hydrogen atoms were refined anisotropically. The hydrogen atoms were placed in calculated positions and assigned to an isotropic displacement parameter of 0.08 $Å^2$. The idealized methyl groups were allowed to rotate about their X−C bond. The absolute structure parameter was determined according to Flack[28] with SHELX-97. SADABS[29] was used to perform area-detector scaling and absorption corrections. The maximum and minimum transmission factors are summarized in Table 1. The PLATON program[30] was used for the geometric analysis of the structure.

Crystallographic Data (excluding structure factors) for the structure reported in this paper have been deposited with the Cambridge Crystallographic Data Centre as supplementary publication no CCDC-164375 (**2**). Copies of the data can be obtained free of charge on application to CCDC, 12 Union Road, Cambridge CB2 1EZ, UK [Fax: (internat.) +44-1223/336-033; E-mail: deposit@ccdc.cam.ac.uk].

Acknowledgments

This work was supported by the Russian Foundation of Basic Research (RFBR Grant No. 99-03-32905), as well as the Deutsche Forschungsgemeinschaft and the Fonds der Chemischen Industrie.

[1] M. Tsutsui, H. J. Guisling, *J. Am. Chem. Soc.* **1969**, *91*, 3175−3178.
[2] M. Bochmann, *J. Chem. Soc., Dalton Trans.* **1996**, 255−270.
[3] H. G. Alt, A. Köppl, *Chem. Rev.* **2000**, *100*, 1205−1221.
[4] H. Yasuda, H. Tamai, *Prog. Polym. Sci.* **1993**, *18*, 1097−1139.
[5] W. J. Evans, I. Bloom, W. E. Hunter, J. L. Atwood, *J. Am. Chem. Soc.* **1981**, *103*, 6507−6508.
[6] E. Ihara, M. Nodono, K. Katsura, Y. Adachi, H. Yasuda, M. Yamagashira, H. Hashimoto, N. Kanehisa, Y. Kai, *Organometallics* **1998**, *17*, 3945−3956.
[7] A. V. Khvostov, A. I. Sizov, B. M. Bulychev, S. Ya. Knyajanski, V. K. Belsky, *J. Organomet. Chem.* **1998**, *559*, 97−105.
[8] G. B. Deacon, R. H. Newham, *Aust. J. Chem.* **1985**, *38*, 1757−1765.
[9] J. Z. Jin, Z. S. Jin, W. Q. Chen, Y. Zhang, *Chinese J. Struct. Chem. (Jiegou Huaxue)* **1993**, *12*, 241−245.
[10] A. V. Khvostov, B. M. Bulychev, V. K. Belsky, A. I. Sizov, *J. Organomet. Chem.* **1999**, *584*, 164−170.
[11] M. G. Klimpel, W. A. Herrmann, R. Anwander, *Organometallics* **2000**, *19*, 4666−4668.
[12] W. J. Evans, T. S. Gummersheimer, T. J. Boyle, J. W. Ziller, *Organometallics* **1994**, *13*, 1281−1284.
[13] C. Qian, H. Li, J. Sun, W. Nie, *J. Organomet. Chem.* **1999**, *585*, 59−62.
[14] S. P. Constantine, G. M. De Lima, P. B. Hitchcock, J. M. Keates, G. A. Lawless, *Chem. Commun.* **1996**, 2421−2422.
[15] I. L. Fedushkin, S. Dechert, H. Schumann, *Organometallics* **2000**, *19*, 4066−4076.
[16] G. Heckmann, M. Niemeyer, *J. Am. Chem. Soc.* **2000**, *122*, 4227−4228.
[17] M. N. Bochkarev, A. A. Trifonov, E. A. Fedorova, N. S. Emelyanova, T. A. Basalgina, N. S. Emelyanova, G. S. Kalinina, G. A. Razuvaev, *J. Organomet. Chem.* **1989**, *372*, 217−224.
[18] M. N. Bochkarev, I. L. Fedushkin, R. B. Larichev, *Russ. Chem. Bull.* **1996**, *45*, 2443−2445.
[19] W. J. Evans, M. A. Hozbor, *J. Organomet. Chem.* **1987**, *326*, 299−306.
[20] L. Zolnai, H. Pritzkow, *ZORTEP ORTEP Program for PC*, Universität Heidelberg, **1994**.
[21] T. G. Wetzel, S. Dehnen, P. W. Roesky, *Organometallics* **1999**, *18*, 3835−3842.
[22] T. Akhnoukh, J. Müller, K. Qiao, X.-F. Li, R. D. Fischer, *J. Organomet. Chem.* **1991**, *408*, 47−58.
[23] D. Stern, M. Sabat, T. J. Marks, *J. Am. Chem. Soc.* **1990**, *112*, 9558−9575.
[24] G. Desurmont, Y. Li, H. Yasuda, *Organometallics* **2000**, *19*, 1811−1813.
[25] F. Calderazzo, R. Pappalardo, S. Losi, *J. Inorg. Nuclear Chem.* **1966**, *28*, 987−991.
[26] G. M. Sheldrick, *SHELXS-97 Program for the Solution of Crystal Structures*; Universität Göttingen, **1990**.
[27] G. M. Sheldrick, *SHELXL-97 Program for the Refinement of Crystal Structures*; Universität Göttingen, **1997**.
[28] H. D. Flack, *Acta Crystallogr., Sect. A* **1983**, *39*, 876−881.
[29] G. M. Sheldrick, *SADABS Program for Empirical Absorption Correction of Area Detector Data*; Universität Göttingen, **1996**.
[30] A. L. Spek, *PLATON A Multipurpose Crystallographic Tool*; Utrecht University, **2000**.

Received June 6, 2001
[I01206]

New Carbaalanes − $(AlMe)_8(CCH_2Me)_5(C{\equiv}C{-}Me)$ and the THF Adduct $(AlMe)_8(CCH_2Me)_5H{\cdot}2THF$

Werner Uhl,*[a] Frank Breher,[a] Alphonse Mbonimana,[a] Jürgen Gauss,[b] Detlev Haase,[c] Arne Lützen,[c] and Wolfgang Saak[c]

Keywords: Aluminium / Carbaalanes / Clusters / Quantum-chemical calculations / NMR spectroscopy

The hydroalumination of $Me_2Al{-}C{\equiv}C{-}Me$ with a large excess of Me_2AlH afforded the *arachno*-carbaalane $(AlMe)_8(CCH_2Me)_5H$ (**4**) by the release of $AlMe_3$. **4** is almost insoluble in noncoordinating solvents and could not be purified by recrystallization. On an attempt to recrystallize **4** from a THF solution, the adduct $(AlMe)_8(CCH_2Me)_5H{\cdot}2THF$ (**5**) was isolated as the first stable ether adduct of a carbaalane. Crystal structure determination revealed a cube of eight aluminium atoms, five faces of which are bridged by $C{-}CH_2Me$ groups. The sixth face is μ_2-bridged by a hydrogen atom, and two opposite aluminium atoms of this face are coordinated by one THF ligand each. When the excess of dimethylaluminium hydride was reduced and the starting compounds were employed in a 1:2.1 molar ratio, an incomplete hydroalumination reaction led to the formation of the carbaalane $(AlMe)_8(CCH_2Me)_5(\mu\text{-}C{\equiv}C{-}Me)$ (**6**), in which the bridging hydrogen atom of **4** is replaced by an alkynido group. ^{27}Al NMR spectroscopic data of all the characterized carbaalanes are reported and supplemented by ^{27}Al NMR chemical shift calculations.

Introduction

Carbaalanes[1] constitute a new class of compounds containing clusters of aluminium and carbon atoms. They are easily obtained by hydroalumination of dialkylaluminium alkynides using an excess of the corresponding dialkylaluminium hydride.[2−4] Two completely different structure types have so far been observed. One may be described by a cube of eight aluminium atoms (**1**, Scheme 1), the six faces of which are occupied by five $C{-}CH_2{-}R$ groups and one hydrido or alkynido ligand. Compound **2** (Scheme 1) may be derived from this cubic arrangement, but it has a unique structure with one vertex unoccupied and possesses only seven aluminium atoms. The three remaining Al_4 faces are still occupied by $C{-}CH_2{-}R$ groups, while the open site of the cluster is coordinated by one hydrogen atom and two alkenido ligands containing C=C double bonds. This structure results from an incomplete hydroalumination reaction, and the formal addition of one equivalent of ethylaluminium dihydride to complete the Al_8 cube is missing. The second principal type of carbaalane has a *closo*-configuration on the basis of its structure and electron count (**3**; Scheme 1) and is a remarkable analogue of the *closo*-borate anion $[B_{11}H_{11}]^{2-}$.[5] The bonding situation in the carbaalanes has been studied by quantum-chemical calculations.[4] They revealed a delocalized multi-centre bonding with only weak direct Al−Al interactions. We report herein on the synthesis and structure of further carbaalane derivatives and their characterization by ^{27}Al NMR spectroscopy.

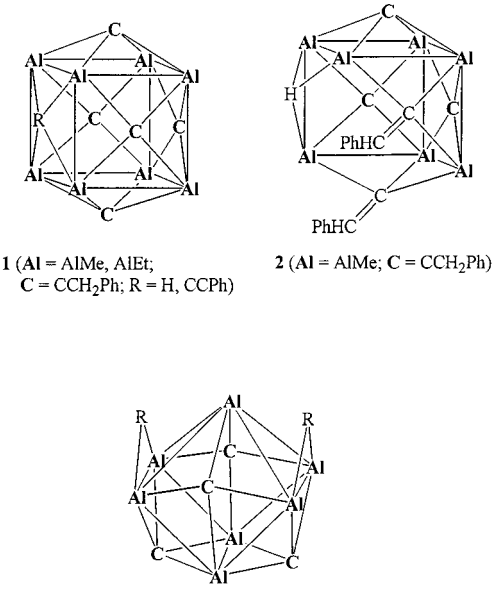

Scheme 1

Results and Discussion

Synthesis of $(AlMe)_8(CCH_2Me)_5H$ (4) and its THF Adduct (5)

The reaction of dimethyl(propynyl)aluminium with a large excess of dimethylaluminium hydride has been re-

[a] Fachbereich Chemie der Philipps Universität, Hans-Meerwein-Straße, 35032 Marburg, Germany
Fax: (internat.) + 49-(0)6421/2825653
[b] Institut für Physikalische Chemie, Universität Mainz, 55099 Mainz, Germany
[c] Fachbereich Chemie der Carl von Ossietzky Universität, Postfach 2503, 26111 Oldenburg, Germany

 © WILEY-VCH Verlag GmbH, 69451 Weinheim, 2001 1434−1948/01/1212−3059 $ 17.50+.50/0

ported by our group only recently.[4] As a main product, we isolated the heptaaluminium carbaalane $(AlMe)_7(CCH_2Me)_4H_2$ in 63% yield, which possesses the *closo*-structure **3** shown in Scheme 1. In all of these reactions, we observed the formation of a hitherto uncharacterized by-product [**4**; Equation (1)], which is almost insoluble in nonpolar solvents such as pentane or toluene and could not be purified by recrystallization. It was isolated as an amorphous and highly pyrophoric powder in about 30% yield. Owing to its insolubility and unknown purity, **4** was characterized only by its ^1H NMR spectrum, which was recorded from a very dilute solution in $[D_6]$benzene. The data obtained were clearly indicative of an *arachno*-type structure similar to compound **1** in Scheme 1. Two resonances of equal intensity were observed for the methyl groups attached to aluminium in a quite normal range ($\delta = -0.20$ and -0.15). The signal of the hydrogen atom bridging an Al_4 face of the cluster is shifted downfield ($\delta = 5.68$) compared to that in dialkylaluminium hydrides containing μ_2-bridging hydrogen atoms in four- or six-membered heterocycles.[6] A similar shift has been observed in all carbaalanes isolated to date. Two triplets ($\delta = 1.04$ and 1.33) and two quadruplets ($\delta = 1.93$ and 2.33), each pair with an intensity ratio of 4:1, were observed for the ethyl substituents of the cluster carbon atoms. These observations are in accordance with the proposed *arachno* structure, in which four of these substituents are adjacent to the hydrogen-bonded face, while one is opposite to this face.

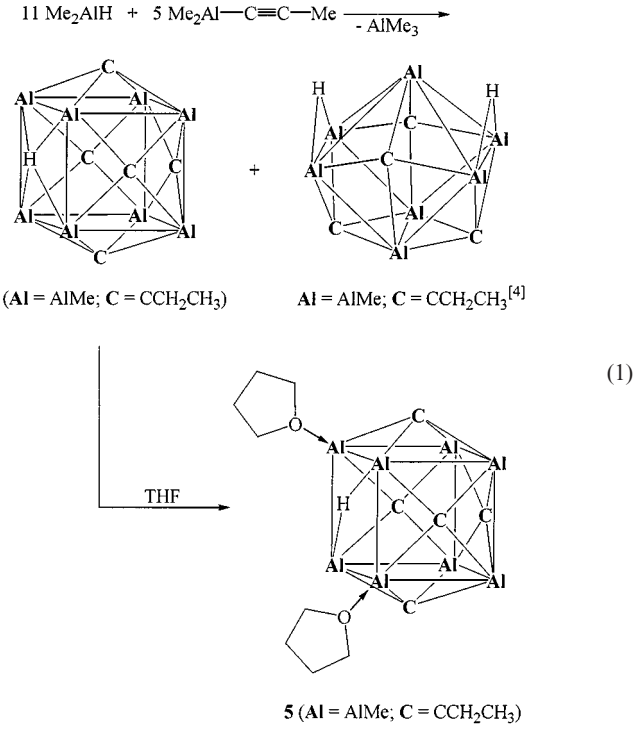

(1)

All attempts to recrystallize **4** from dilute solutions in noncoordinating solvents failed. In some cases, we were able to successfully recrystallize carbaalanes from THF, in which they are usually quite soluble and they do not form any kind of stable THF adduct. Clearly, the aluminium atoms of the carbaalanes are such weak Lewis acids that the coordination of THF molecules even at the open faces of these clusters has never previously been observed. Upon treatment of **4** with THF and slow evaporation of the solvent at room temperature, we obtained colourless crystals. However, an X-ray structure determination (see below) showed that a THF adduct of compound **4** had been formed in which two opposite aluminium atoms of the hydrogen-bonded face of the cluster were each coordinated by one THF molecule [**5**; Equation (1)]. The ether molecules are tightly bound to the aluminium atoms, and no dissociation was observed upon storing of the crystals in vacuo at 10^{-3} Torr and 50 °C. Compound **5** is thermally very stable and does not decompose at temperatures below 260 °C. The NMR spectroscopic characterization in $[D_8]$THF at room temperature showed two quite narrow singlets due to the methyl groups attached to aluminium, two triplets and two quadruplets (each pair with an intensity ratio of 4:1) due to the ethyl substituents bound to the cluster carbon atoms, and one singlet due to the bridging hydrogen atom. The chemical shift of the latter ($\delta = 4.19$) shows the most significant deviation from the resonances of the starting compound **4** and is closer to the shifts normally observed for alkylaluminium hydrides. The cluster carbon atoms exhibit chemical shifts of $\delta = 20.5$ and 21.5, which are strongly downfield shifted compared to the resonances normally observed with coordinatively saturated aluminium atoms ($\delta = -8.8$ and -9.4 for the terminal methyl groups) and may be caused by the particular delocalized bonding situation in these clusters. Two resonances were observed in the ^{27}Al NMR spectrum ($\delta = 155$ and 56), which are discussed in more detail below. Two THF molecules were detected for each formula unit of **5**, in accordance with the result of the crystal structure determination. More complicated NMR spectra were expected in view of the molecular symmetry detected in the solid state, indicating a fast exchange process in THF solution at room temperature. This process is frozen only at very low temperatures, and at -110 °C a splitting of both methyl resonances was observed [$\delta = -0.41$ and -0.56 (coalescence at about 225 K) and $\delta = -0.49$ and -0.51 (coalescence at about 202 K)]. The activation barrier was estimated[7] from these data to be about 45 kJ mol^{-1}.

A crystal structure determination of **5** revealed a structure similar to that of **1**[2,4] (Figure 1) with a cube of eight aluminium atoms. However, two opposite aluminium atoms of the hydrogen-bonded face are coordinated by a THF molecule. The Al−C distances to the terminal methyl groups (average 196.8 pm) do not depend on the coordination sphere of the aluminium atoms and are shorter than those within the cluster (203.8 to 213.3 pm). The Al−Al separations are 293.4 pm at the hydrogen-bonded face and 258.3 pm for the remaining eight edges of the Al_8 cube. The latter are similar to those observed for 3c−2e Al−X−Al interactions (X = H, CH_3)[8] and are shorter than those of Al−Al single bonds in tetraalkyldialuminium(4) derivatives $R_2Al-AlR_2$.[9] All these parameters were similarly determined in carbaalanes of type **1**.[2,4] The most notable devi-

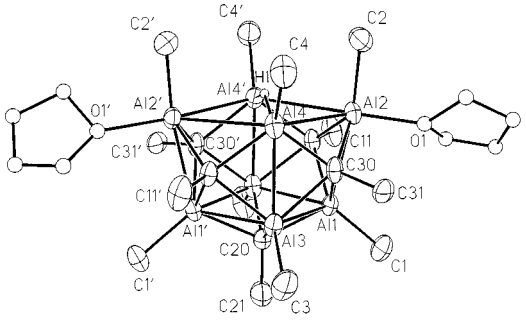

Figure 1. Molecular structure and numbering scheme for compound **5**; thermal ellipsoids are drawn at a 40% probability level; methyl groups have been omitted for clarity; hydrogen atoms are drawn with arbitrary radii; selected bond lengths (pm): Al-1−C-1 196.8(3), Al-2−C-2 197.5(4), Al-3−C-3 196.4(3), Al-4−C-4 196.3(3), Al-1−C-10 210.7(3), Al-1−C-20 205.7(2), Al-1−C-30 209.4(3), Al-2−O-1 197.9(2), Al-2−C-10 204.4(3), Al-2−C-30 205.5(3), Al-3−C-20 203.8(2), Al-3−C-30 211.5(3), Al-3−C-10′ 213.3(3), Al-4−C-30 204.8(3), Al-4−C-10′ 205.7(3), Al-4−H-1 173(1), Al-1−Al-2 259.3(1), Al-1−Al-3 258.4(1), Al-1−Al-3′ 258.4(1), Al-2−Al-4 293.0(1), Al-2−Al-4′ 293.7(1), Al-3−Al-4 257.1(1); C-10′ and Al-3′ were generated by $-x + 3/2$, y, $-z + 1/2$

ation from these recently published structures is a greater distortion of the hydrogen-bonded face with strongly differing transannular Al−Al distances of 483.2 pm (Al2−Al2′, unsupported) and 331.8 pm (Al4−Al4′, hydrogen bonded). The latter distance resembles that in the trimeric compound $[(Me_3C)_2AlH]_3$ containing a six-membered Al_3H_3 heterocycle with three μ_2-bridging hydrogen atoms.[10] The THF molecules are bound to the aluminium atoms Al2 and Al2′ with relatively long Al−O "dative" distances of 197.9 pm.[11] The oxygen atoms of the ether molecules lie slightly below the plane spanned by the four aluminium atoms of the hydrogen-bonded face of the cluster (37.6 pm; angle Al2′···Al2−O1 9.6°). Owing to this lateral coordination of THF, the Al(2)−C bonds are almost perpendicular to this plane (angle Al2′···Al2−C2 94.5°; for comparison Al4′···Al4−C4 54.4°).

Synthesis of $(AlMe)_8(CCH_2Me)_5(\mu\text{-}C{\equiv}C{-}Me)$ (6)

In a further reaction, we reduced the excess of dimethylaluminium hydride from about 6:1 required for the synthesis of **4** and **5** according to Equation (1) to a molar ratio of only 2.1:1. Once again, a strongly exothermic reaction was observed on stirring a mixture of the hydride and the alkynide at room temperature without a solvent and a bright-yellow solid precipitated. After 1 h at room temperature, all volatile components ($AlMe_3$) were distilled off in vacuo and the yellow residue was recrystallized from warm toluene. Bright-yellow crystals of compound **6** were isolated in 39% yield after cooling to −30 °C [Equation (2)]. According to the NMR spectra, the mother liquors still contained considerable quantities of **6**, but in all cases we were unable to isolate a second pure fraction. Compound **6** was identified as the carbaalane $(AlMe)_8(CCH_2Me)_5(\mu\text{-}C{\equiv}C\text{-}Me)$, which is similar to compound **4** but has a bridging propynido group instead of the bridging hydrogen atom. The formation of **6** according to Equation (2) requires a stoichiometric ratio of the starting compounds of 1 (alkynide) to 1.7 (hydride). Thus, we still employed a slight excess of the hydride, but further reduction of the hydride concentration did not result in an improved yield of **6**.

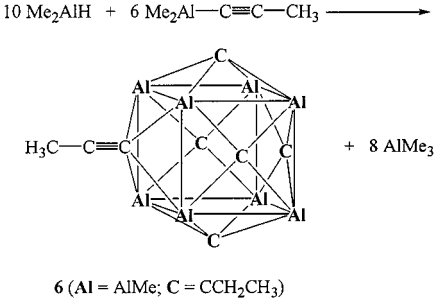

(2)

An absorption at 2019 cm^{-1} was detected in the IR spectrum due to the stretching vibration of the C≡C triple bond. Compared to the corresponding vibration of the starting compound $Me_2Al{-}C{\equiv}C{-}Me$ (2109 cm^{-1}),[4] a shift of about 90 cm^{-1} to lower wavenumbers was observed. An even lower value (1957 cm^{-1}) was found for a similar compound with benzyl instead of ethyl groups bound to the cluster carbon atoms.[4] In this case, the weakening of the C≡C triple bond, which may be caused by the particular μ_4-bridging arrangement in the cluster, was also verified by an increased C−C bond length and by quantum chemical calculations.[4] NMR spectroscopic characterization proved quite difficult owing to the very low solubility of **6** in organic solvents. In contrast to compound **4**, small quantities of **6** could be dissolved and handled in THF at room temperature without the formation of a stable ether adduct; thus, all spectra were recorded in dilute $[D_8]$THF solutions. The terminal methyl groups attached to aluminium exhibit two equivalent resonances in the expected ranges of the ^1H and ^{13}C NMR spectra ($\delta = -0.36$, -0.44 and $\delta = -7.7$, -8.9, respectively). The cluster carbon atoms resonate at $\delta = 21.5$ and 17.5, which, as discussed above, is further downfield than expected, and a shift of $\delta = 88.2$ was observed for the bridging carbon atom of the propynido ligand ($\delta = 117.0$ in the benzyl compound cited above).[4] Only one resonance was observed in the ^{27}Al NMR spectrum ($\delta = 153$); a shoulder may be present at $\delta \approx 130$ owing to a marked asymmetry of this signal (see below). A crystal structure determination of **6** revealed a strong disorder of the propyne group, which partially occupies all faces of the Al_8 cube (not shown). As a result of this disorder, an almost undistorted cube of eight aluminium atoms is obtained, with an average Al−Al distance of 265.8 pm; this represents a reasonable mean value between the three different distances expected for a regular structure, as discussed previously for compound **5** and the corresponding benzyl derivative.[4]

In contrast to the dimethylaluminium starting compounds, the sterically slightly more shielded ethyl derivatives diethylaluminium hydride and diethylaluminium propynide do not react exothermically at room temperature. The mixture was heated to 50 °C without a solvent for 18 h

to complete the reaction. As expected, triethylaluminium was formed, which was distilled off in vacuo. An orange residue remained, which, according to its ^{1}H NMR spectrum, contained a carbaalane cluster accompanied by a considerable amount of impurities. However, we did not succeed in isolating a pure component by recrystallization or sublimation. Moreover, the sterically more shielded diisopropyl derivatives did not react exothermically at room temperature and had to be stirred at 50 °C for 18 h to complete the reaction. Owing to the low volatility of triisobutylaluminium, the mixture was subsequently heated in vacuum to 80 °C for 2 h to completely remove this by-product. The oily, light-yellow residue was redissolved in diisopropyl ether. After several weeks at −70 °C, only trace amounts of a colourless solid (**7**) were isolated. On the basis of the results of the NMR spectroscopic characterization (see Exp. Sect.), we suppose that **7** has a *closo*-type structure (Scheme 2) with two opposite Al−Al edges bridged by hydrogen atoms. As required by such a structure, we observed three clearly resolved ^{27}Al NMR resonances (see below). Single crystals suitable for a crystal structure determination were not obtained. A concentrated solution of bis(*tert*-butyl)aluminium hydride and the corresponding propynylaluminium compound in toluene was heated for 20 h at 50 °C. NMR spectroscopic monitoring of the reaction showed the complete consumption of the starting compounds, but no evidence was found for the formation of a carbaalane cluster. Despite many attempts to recrystallize the crude product from various solvents, we did not succeed in isolating any pure component of the mixture.

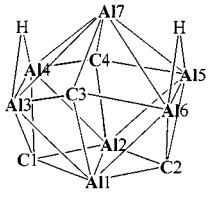

7 (**Al** = Al*i*Pr; **C** = CCH_2CH_3)

Scheme 2

^{27}Al NMR Spectra of Carbaalanes

For the first time, we have investigated the ^{27}Al NMR spectra of carbaalanes in a systematic manner. ^{27}Al NMR shifts are known to be very sensitive to the coordination sphere at the central aluminium atoms, and coordination numbers of three, four, five, or six give characteristic shifts of $\delta \approx 270$, 170, 120, and 0, respectively.[12] Furthermore, ^{27}Al NMR chemical shifts, in combination with quantum chemical NMR shift calculations, have previously been shown to be useful for the identification and characterization of aluminium cluster compounds.[13−15] However, the unequivocal interpretation of ^{27}Al NMR spectra is difficult owing to the quadrupole moment of aluminium and the usually broad line width of the resonances. The overlap of signals often prevents a clear assignment, especially in those cases in which chemically different aluminium atoms are present, as in the carbaalanes.

To facilitate the interpretation of the experimental spectra, we performed quantum chemical ^{27}Al NMR shift calculations for most of the carbaalanes under consideration and in this way investigated the usefulness of ^{27}Al NMR spectroscopy for the identification and characterization of carbaalanes. The results of the experimental and the computational investigations are summarized in Table 1. Experimentally, only one broad resonance is observed for most carbaalanes; this is in line with the calculations, which yield values within the rather narrow range of $\delta = 150$ to 210 for the ^{27}Al chemical shifts of all the considered carbaalanes. In some cases, shoulders could be identified, but it seems that in most cases these result from strong anisotropies of the main resonances.

As expected, the *arachno*-type compounds exhibit two Al NMR signals, which are found experimentally at around $\delta = 80$ and 140, while the calculations predict values around $\delta = 160$ and 180 to $\delta = 210$. According to the calculations, the ^{27}Al signal at lower field corresponds to the aluminium atoms close to either the bridging hydrogen atom or the bridging CCR group. The signal shows a slight, though not very pronounced, dependence on the bridging group. The resonances at higher field on the other side are due to the remaining aluminium cluster atoms. They appear to be rather insensitive to the nature of the bridging group and the substituents at the carbon atoms in the cluster.

In principle, the more open alkenido derivatives have five distinct aluminium atoms. The calculations predict ^{27}Al NMR signals for these in the range $\delta = 155$ to 172. Only for the F-containing derivative are higher values of $\delta = 184$ and 200 found for the aluminium atoms close to the bridging fluorine atom. Experimentally, very broad resonances with one (R = H) or two maxima (R = F) are observed. One of the resonances of the fluorine derivative has quite an unusual chemical shift of $\delta = -28$.

For the *closo* form, the calculations again predict values in the range of $\delta = 150$ to 170. The experimental value of $\delta = 157$ for one of the carbaalanes seems to be in satisfactory agreement with the theoretical predictions. However, three clearly resolved resonances ($\delta = 145$, 79, and −38) are observed for **7**.

Overall, it appears that the ^{27}Al NMR spectra of carbaalanes typically consist of one broad resonance, for which a clear assignment, even with the aid of quantum chemical shift calculations, is rather difficult. Our experimental and computational results also suggest that the sensitivity of the ^{27}Al NMR shifts to structural features of the carbaalanes is not very pronounced and that ^{27}Al NMR spectroscopy is not a particularly promising tool for future investigations of such compounds.

Experimental Section

General: All procedures were carried out under purified argon in dried solvents (toluene and THF over Na/benzophenone; *n*-pent-

Table 1. Experimental and computed ^{27}Al NMR spectroscopic data of carbaalanes (104.3 MHz, δ in ppm relative to $[Al(H_2O)_6]^{3+}$ as an external standard, $W_{1/2}$ in Hz, shoulders with uncertain chemical shifts in italics; the asterisk* denotes uncertain values as a consequence of impurities)

	Al	C	R	δ ($W_{1/2}$)	$\delta_{computed}$	Solvent	Ref.
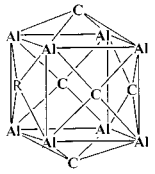	AlMe	CCH_2Ph	H	142 (10200); *100*	159-164 (4x), 176-180 (2x), 209-215 (2x)	C_6D_6	[2]
	AlEt	CCH_2Ph	H	130; 85 (10900)	–	C_6D_6	[4]
	AlMe	CCH_2Ph	C≡CPh	*130*; 80 (6300)	162-166 (4x), 173-175 (2x), 206-209 (2x)	C_6D_6	[4]
	AlMe	CCH_2CH_3	C≡CCH_3 (**6**)	153 (3100); *130*	163-166 (4x), 187-191 (4x)	OC_4D_8	–
	AlMe	CCH_2Ph	F	62 (6500); -20 (13000)*	–	C_6D_6	[16]
	AlMe	CCH_2CH_3	H/THF (**5**)	155 (3700); 56 (6800)	160-163 (4x), 195-203 (4x)	OC_4D_8	–
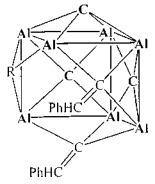	AlEt	CCH_2Ph	H	*170*; 149 (8800); *100*	159-172	C_6D_6	[3]
	AlEt	CCH_2Ph	F	*110*; 74 (12000); *20*, -28 (10000)	152, 160, 168, 184, 200	C_7D_8	[16]
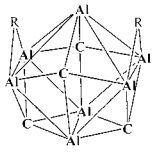	AlEt	CCH_2Ph	C≡CPh, H	*110*; 66 (4500)	156-171	C_6D_6	[3]
	AlMe	CCH_2CH_3	H	157 (4200); very broad base (up to ~ 60 ppm)	155, 164-170 (6x)	C_6D_6	[4]
	Al*i*Pr	CCH_2CH_3	H (**7**)	145 (6900); 79 (5600); -38 (> 10000)	–	C_6D_6	–

ane and *n*-hexane over $LiAlH_4$). The compounds $Me_2Al-C\equiv C-CH_3$,[4] Me_2Al-H,[17] Et_2Al-H,[17] iPr_2Al-H,[17] tBu_2Al-H,[10] Et_2Al-Cl,[17] iPr_2Al-Br,[17] and tBu_2Al-Cl[18] were synthesized according to literature procedures. – ^1H and ^{13}C NMR shifts were assigned on the basis of ^1H, ^{13}C, HH-COSY, HMQC, and HMBC spectra. Shifts are reported on the δ scale in ppm relative to residual nondeuterated solvent signals (^1H) or the signals of the deuterated solvent (^{13}C) as internal standards, or relative to $[Al(H_2O)_6]^{3+}$ (^{27}Al) as an external standard.

Synthesis of $(AlMe)_8(CCH_2Me)_5H$ (4): Dimethylpropynylaluminium (0.604 g, 6.29 mmol) was dissolved in excess dimethylaluminium hydride (2.301 g, 39.6 mmol) and the solution was stirred at room temperature. A strongly exothermic reaction occurred after some minutes and a colourless solid precipitated. After stirring for 2 h, all volatile components were distilled off in vacuo. The vessel containing the residue was thoroughly evacuated to 10^{-3} Torr and then the dried product was redissolved in toluene (40 mL). After filtration and cooling to −30 °C, an amorphous, extremely pyrophoric precipitate of the product **4** was deposited. The mother liquor contained a *closo*-carbaalane derivative similar to **3**, the isolation and characterization of which has been reported previously. Owing to its low solubility, **4** could not be purified by recrystallization from noncoordinating solvents. Yield of the crude product: 0.201 g (29% based on propynylaluminium). – ^1H NMR (very dilute solution in C_6D_6, 200 MHz, 298 K): δ = −0.20 and −0.15 (2 s, 12 H each, AlMe), 1.04 (t, 12 H, $^3J_{HH}$ = 7.3 Hz, CH_3 of ethyl), 1.33 (t, 3 H, $^3J_{HH}$ = 7.5 Hz, CH_3 of ethyl opposite to bridging H), 1.93 (q, 8 H, $^3J_{HH}$ = 7.3 Hz, CH_2 of ethyl), 2.33 (q, 2 H, $^3J_{HH}$ = 7.5 Hz, CH_2 of ethyl opposite to bridging H), 5.68 (s, 1 H, AlH).

Synthesis of $(AlMe)_8(CCH_2Me)_5H{\cdot}2THF$ (5): Compound **4** was dissolved in THF. The solution was slowly concentrated under slightly reduced pressure at room temperature over several weeks to yield single crystals of the THF adduct **5**. M.p. (argon, sealed capillary): 260 °C (dec.). – ^1H NMR ([D$_8$]THF, 500 MHz, 300 K): δ = −0.44 (s, 12 H, methyl at Al-1, Al-3), −0.43 (s, 12 H, methyl at A-l2, Al-4 of the hydrogen-bonded face), 1.04 (t, 12 H, $^3J_{HH}$ = 7.3 Hz, CH_3 of ethyl), 1.05 (t, 3 H, $^3J_{HH}$ = 7.3 Hz, CH_3 of ethyl opposite to the bridging hydrogen atom), 1.99 (q, 8 H, $^3J_{HH}$ = 7.3 Hz, CH_2 of ethyl), 2.05 (q, 2 H, $^3J_{HH}$ = 7.3 Hz, CH_2 of ethyl opposite to the bridging hydrogen atom), 4.19 (s, 1 H, AlH); coordinated THF: δ = 1.77 and 3.62 (each m), part of the THF was replaced by [D$_8$]THF and was detected as free THF in solution. – ^1H NMR ([D$_8$]THF, 400 MHz, 165 K): δ = −0.49 and −0.51 (2 s, 6 H each, methyl of Al-1, Al-3), −0.41 and −0.56 (2 s, 6 H each, methyl of Al-2, Al-4), 3.98 (s, 1 H, AlH), broad resonances of the ethyl groups at δ = 1.0 and 1.9. – ^{13}C NMR ([D$_8$]THF, 125.8 MHz, 300 K): δ = −9.4 and −8.8 (AlMe); 20.5 (cluster carbon atom C-20, see Figure 1), 21.5 (cluster carbon atoms C-10 and C-30), 23.1 (CH_3 of ethyl, C-12 and C-32), 24.35 (CH_2 of ethyl, C-11 and C-31), 24.40 (CH_3 of ethyl, C-22), 24.5 (CH_2 of ethyl, C-21), 68.2 (CO of coordinated THF), 26.4 (C_β of THF). – ^{13}C NMR ([D$_8$]THF, 100.6 MHz, 202 K): δ = −10.6, −10.3, −8.5, and −7.8 (AlMe). – ^{27}Al NMR: See Table 1. – IR (CsBr, paraffin): $\tilde{\nu}$ = 1616 m (νAlH), 1458 vs, 1376 vs paraffin; 1314 s, 1269 m (δCH_3), 1196 m, 1176 s, 1078 m, 1066 m, 1025 s, 1004 s, 920 m, 874 s, 801 s (νCC, νCO, δCH_3) 721 vs, 679 vs [br. νAlC(Me)] 465 m, 426 m, 388 m, 344 m, 301 m, 275 m (νAlC, δCC). – $C_{31}H_{66}Al_8O_2$ (686.7): calcd. Al 31.4; found Al 31.2.

Synthesis of $(AlMe)_8(CCH_2Me)_5(\mu\text{-}C\equiv C-Me)$ (6): Dimethylpropynylaluminium (1.665 g, 17.3 mmol) was treated with dimethylaluminium hydride (2.102 g, 36.2 mmol, 2.1 equiv.) without a solvent at room temperature. After about 1 min, a strongly exothermic reaction occurred and a bright-yellow solid precipitated. The mixture was stirred for 1 h and then all volatile components were re-

moved in vacuo. The yellow residue was redissolved in warm toluene (50 mL). The yellow, air-sensitive product was isolated after cooling the solution to −30 °C. Yield: 0.654 g (39%), m.p. (argon, sealed capillary): 240 °C (dec.). − ^{1}H NMR ([D$_8$]THF, 500 MHz, 300 K): δ = −0.44 (s, 12 H, methyl groups of the aluminium atoms at the bottom of the cluster), −0.36 (s, 12 H, methyl groups of the aluminium atoms of the propynido-bridged face), 1.03 (t, 12 H, $^3J_{HH}$ = 7.3 Hz, CH$_3$ of ethyl), 1.08 (t, 3 H, $^3J_{HH}$ = 7.3 Hz, CH$_3$ of the ethyl group opposite to the bridging propynido group), 1.99 (q, 8 H, $^3J_{HH}$ = 7.3 Hz, CH$_2$ of ethyl), 2.07 (q, 2 H, $^3J_{HH}$ = 7.3 Hz, CH$_2$ of the ethyl group opposite to the bridging propynido group), 2.41 (s, 3 H, CH$_3$ of the propynido ligand). − ^{13}C NMR ([D$_8$]THF, 125.8 MHz, 300 K): δ = −8.9 and −7.7 (AlMe), 8.8 (CH$_3$ of the propynido ligand), 17.5 (cluster carbon atom opposite to the bridging propynido ligand), 21.5 (remaining cluster carbon atoms), 23.5 (CH$_3$ of ethyl), 24.1 (CH$_2$ of ethyl opposite to the propynido bridge), 24.3 (CH$_3$ of the ethyl group opposite to the propynido bridge), 25.0 (CH$_2$ of ethyl)*, 88.2 (bridging C of the C≡C triple bond), 162.3 (β-C of C≡C triple bond); *obscured by solvent signal. − ^{27}Al NMR: See Table 1. − IR (CsBr, paraffin): ṽ = 2019 m, 2010 m (νC≡C, splitting possibly caused by Fermi resonance) 1460 vs, 1377 vs (paraffin) 1322 s, 1186 vs, 1082 m, 1067 m, 1031 vs, 879 vs, 788 m (νCC, δCH$_3$), 663 vs [br. νAlC(Me)] 437 m, 402 w, 344 w (νAlC). − $C_{26}H_{54}Al_8$ (582.6): calcd. Al 37.1; found Al 37.2.

Synthesis of Et$_2$Al−C≡C−Me:[19] A mixture of *n*-butyllithium (15.0 mL, 1.6 M solution in *n*-hexane, 24.0 mmol) and *n*-pentane (20 mL) was cooled to −70 °C. Dried (P_4O_{10}) gaseous propyne was then passed over the solution for half an hour. A colourless solid precipitated. The resulting suspension was allowed to warm to room temperature and stirred until the gas evolution had ceased. A solution of diethylaluminium chloride (2.601 g, 21.6 mmol, 0.9 equiv.) in *n*-pentane (20 mL) was then added dropwise at room temperature. The mixture was stirred for 1 h and filtered. The solvent was removed in vacuo and the oily residue was employed directly for further reactions without purification. Yield: 1.955 g (73% based on Et$_2$AlCl). − ^{1}H NMR (C_6D_6, 300 MHz, 300 K): δ = 0.43 (q, 4 H, $^3J_{HH}$ = 8.1 Hz, CH$_2$), 1.25 (s, 3 H, C≡C−CH$_3$), 1.39 (t, 6 H, $^3J_{HH}$ = 8.1 Hz, CH$_3$ of ethyl). − ^{13}C NMR (C_6D_6, 75.5 MHz, 300 K): δ = 2.4 [AlC(Et)], 5.3 (CH$_3$ of propyne), 9.6 (CH$_3$ of ethyl), 86.3 and 134.5 (C≡C). − ^{27}Al NMR (C_6D_6, 104.3 MHz, 300 K): δ = 146 ($W_{1/2}$ = 4000 Hz). − IR (CsBr, paraffin): ṽ = 2149 s, 2101 vs (νC≡C), 1463 vs (paraffin), 1407 s, 1393 s (δCH$_3$), 1375 s (paraffin) 1303 vw, 1227 w, 1194 w, 1167 w, 1101 w, 1056 s, 988 vs, 974 sh, s, 951 s, 919 m, 899 s, 868 m, 808 m, (br. νCC, δCH$_3$) 656 vs (br. νAlC), 541 s, 469 sh, s, 406 s, br., 346 s, 312 m (νAlC, δCC).

Synthesis of *i*Pr$_2$Al−C≡C−Me: A solution of *n*-butyllithium (15.6 mL, 1.6 M in *n*-hexane, 25.0 mmol) and *n*-hexane (20 mL) was cooled to −70 °C. Dried (P_4O_{10}) gaseous propyne was passed over the solution for half an hour. A colourless solid precipitated. The mixture was then allowed to warm to room temperature and stirred until the gas evolution (butane, excess propyne) had ceased. A solution of diisopropylaluminium bromide (4.568 g, 23.7 mmol, 0.95 equiv.) was then added dropwise at room temperature. The resulting suspension was stirred for 3 h, then filtered, and all volatile components were removed from the filtrate in vacuo. The waxy residue was employed without further purification. Yield: 2.179 g (61% based on *i*Pr$_2$AlBr). − ^{1}H NMR (C_6D_6, 200 MHz, 300 K): δ = 0.76 (septet, 2 H, $^3J_{HH}$ = 7.5 Hz, AlCH), 1.32 (s, 3 H, C≡C−CH$_3$), 1.41 (d, 12 H, $^3J_{HH}$ = 7.5 Hz, CH$_3$ of isopropyl). − ^{13}C NMR (C_6D_6, 50.3 MHz, 300 K): δ = 5.9 (CH$_3$ of propyne), 12.1 [br., AlC(*i*Pr)], 21.1 (CH$_3$ of isopropyl), 136.8 (C≡C); only one resonance of the C≡C triple bond was detected. − ^{27}Al NMR (C_6D_6, 104.3 MHz, 300 K): δ = 138 ($W_{1/2}$ = 5000 Hz). − IR (CsBr, paraffin): ṽ = 2149 w, 2098 vs (νC≡C), 1461 vs, 1377 vs (paraffin), 1305 w, 1261 m, 1206 w, 1169 sh, w, 1120 m, 1055 s, 1028 sh, m, 972 s, 957 s, 910 w, 873 s, 835 w, 801 m, (br. νCC, δCH$_3$), 723 m,

Table 2. Crystal data, data collection parameters, and structure refinement of compounds **5** and **6**[a]

	5	**6**
Formula	$C_{31}H_{66}Al_8O_2$	$C_{26}H_{56}Al_8$
Crystal system	monoclinic	tetragonal
Space group	*P*2/*n*; No. 13 [20]	*I*4/*m*; No. 87 [20]
Z	2	2
Temperature [K]	193(2)	193(2)
$d_{calcd.}$ [g/cm^3]	1.175	1.172
a [pm]	1059.7(1)	1061.62(5)
b [pm]	1093.6(1)	1061.62(5)
c [pm]	1689.7(3)	1464.21(9)
β [°]	97.63(2)	90
V [10^{-30} m^3]	1940.8(5)	1650.2(2)
μ [mm^{-1}]	0.236	0.262
Crystal size [mm]	0.40 × 0.34 × 0.31	0.36 × 0.36 × 0.34
Diffractometer	STOE IPDS	
Radiation	Mo-K_α radiation; graphite monochromator	
Range [°]	2.15 to 25.93	3.84 to 25.84
Index ranges	$-12 \le h \le 12$	$-12 \le h \le 12$
	$-13 \le k \le 13$	$-13 \le k \le 12$
	$-20 \le l \le 20$	$-17 \le l \le 17$
Independent reflections	3758 [*R*(int) = 0.0406]	828 [*R*(int) = 0.0414]
Reflections $F > 4\sigma(F)$	2987	685
Parameters	257	55
$R = \Sigma\|\|F_o\| - \|F_c\|\|/\Sigma\|F_o\|$ $[F > 4\sigma(F)]$	0.0511	0.0553
$wR^2 = [\Sigma w(F_o^2 - F_c^2)^2/\Sigma w(F_o^2)^2]^{1/2}$ (all data)	0.1539	0.1831
Max./min. residual [10^{30} e/m^3]	0.896/−0.567	0.318/−0.648

[a] Programs: SHELXTL-Plus, SHELXL-97;[21] solutions by direct methods; full-matrix refinement with all independent structure factors.

699 w, 622 vs (br. νAlC), 563 sh, m, 532 s, 457 s, 402 m, 350 m (νAlC, δCC).

Reaction of *i*Pr$_2$Al−H with *i*Pr$_2$Al−C≡C−Me: Diisopropylpropynylaluminium (1.090 g, 7.17 mmol) was treated with diisopropylaluminium hydride (3.466 g, 30.4 mmol) and the resulting mixture was heated to 50 °C for 18 h. In order to distil off triisopropylaluminium, the mixture was heated in vacuo to 80 °C for 2 h. The oily, light-yellow residue was treated with diisopropyl ether. After filtration, the solution was cooled to −70 °C to furnish a small quantity of a colourless solid (**7**) after several weeks. Yield: <1%. − ^{1}H NMR (C_6D_6, 500 MHz, 300 K, the numbering scheme is given in Scheme 2): ethyl groups at C-1 and C-2: δ = 1.19 (t, 6 H, $^3J_{HH}$ = 7.4 Hz, CH_3)*, 2.18 (q, 4 H, $^3J_{HH}$ = 7.4 Hz, CH_2); ethyl groups at C-3 and C-4: δ = 1.19 (t, 6 H, $^3J_{HH}$ = 7.4 Hz, CH_3)*, 2.18 (q, 4 H, $^3J_{HH}$ = 7.4 Hz, CH_2); isopropyl groups at Al-1 and Al-2: δ = 0.90 (m, 2 H, $^3J_{HH}$ = 7.7 Hz, AlCH), 1.46 (d, 12 H, $^3J_{HH}$ = 7.7 Hz, CH_3); isopropyl groups at Al-3, Al-4, Al-5, and Al-6: δ = 0.85 and 0.95 (2 m, each 2 H, $^3J_{HH}$ = 7.7 Hz, AlCH), 1.37 and 1.38 (2 d, each 12 H, $^3J_{HH}$ = 7.7 Hz, CH_3); isopropyl group at Al-7: δ = 0.46 (septet, 1 H, $^3J_{HH}$ = 7.7 Hz, AlCH), 1.41 (d, 6 H, $^3J_{HH}$ = 7.7 Hz, CH_3); 4.53 (s, 2 H, AlH) (*assignments may be interchanged). − ^{13}C NMR (C_6D_6, 125.8 MHz, 300 K): ethyl groups at C-1, C-2, C-3, and C-4: δ = 21.2 and 23.1 (CH_2), 23.9 and 25.3 (CH_3); cluster carbon atoms C-1 to C-4: δ = 18.0 and 27.0; isopropyl groups at Al-1 and Al-2: δ = 13.0 or 13.3 (AlC, uncertain), 21.0 (CH_3); isopropyl groups at Al-3, Al-4, Al-5, Al-6: δ = 6.2 and 10.3 (AlC), 21.6 and 21.8 (CH_3); isopropyl group at Al-7: δ = 9.8 (AlC), 21.7 (CH_3). − ^{27}Al NMR: See Table 1.

Synthesis of (Me$_3$C)$_2$Al−C≡C−Me: Li−C≡C−Me was synthesized as described above (5.3 mL of a 1.6 M solution of *n*-butyllithium in *n*-hexane, 8.48 mmol). A solution of bis(*tert*-butyl)aluminium chloride (1.490 g, 8.44 mmol) in *n*-hexane (20 mL) was added and the mixture was stirred at room temperature for 3 h. After filtration and concentration, a colourless solid was obtained upon cooling the solution to −30 °C. The product was further purified by recrystallization from *n*-hexane. Yield: 1.172 g (77%, based on *t*Bu$_2$AlCl); m.p. (argon, sealed capillary): 96 °C (dec.). − ^{1}H NMR (C_6D_6, 200 MHz, 300 K): δ = 1.31 (s, 18 H, CMe_3), 1.49 (s, 3 H, C≡C−CH_3). − ^{13}C NMR (C_6D_6, 100.6 MHz, 300 K): δ = 5.6 (CH_3 of propyne), 18.4 [br., AlC(*t*Bu)], 31.8 (CH_3 of *tert*-butyl), 135.6 (C≡C); only one resonance of the C≡C triple bond was detected. − ^{27}Al NMR (C_6D_6, 104.3 MHz, 300 K): δ = 130 ($W_{1/2}$ = 5000 Hz). − IR (CsBr, paraffin): $\tilde{\nu}$ = 2092 vs, 2058 w, 2047 w (νC≡C), 1464 vs, 1378 vs (paraffin), 1308 m, 1262 m, 1178 m, 1127 w, 1043 m, 1002 s, 966 s, 939 s, 891 w, 846 w, 812 vs (νCC, δCH$_3$), 722 s, 663 vw, 631 w, 587 vs (νAlC), 541 s, 442 vs, 418 vs, 356 vs (νAlC, δCC).

Crystal Structure Determinations: Single crystals of compounds **5** and **6** were obtained by very slow concentration of solutions in THF at room temperature over several weeks. Crystal data and structure refinement parameters are given in Table 2.[22] The carbon atoms of the THF molecules and one ethyl group (C-31, C-32) of compound **5** showed a disorder; these atoms were refined in split positions. Compound **6** is severely disordered and the propynido group is distributed over all six faces of the cluster.

Quantum Chemical Calculations: The structures of the carbaalanes **1** (with Al = AlMe and R = CCPh as well as H, respectively), **2**, **3** (with Al = AlMe and AlEt, respectively), **4**, and **6** were optimized at the density-functional theory (DFT) level[23] employing the Becke−Perdew (BP86) functional[24] together with an auxiliary basis set approximation for the Coulomb energy (RI-DFT).[25] A polarized split-valence basis SV(P)[26] was used in all calculations, with the parentheses indicating that polarization functions have been considered only for non-hydrogen atoms as well as the hydrogen bonds.

^{27}Al NMR chemical shifts were computed employing the gauge-including atomic orbital (GIAO) Hartree−Fock self-consistent-field (HF-SCF) method[27] using a polarized double-zeta (dzp) basis[28] for Al, C, and F and a DZ basis for all nonbridging hydrogen atoms. Relative shifts were obtained with $[AlH_4]^-$ as an internal reference and a δ(^{27}Al) value for $[AlH_4]^-$ of δ = 101 [28] (the absolute shielding computed for $[AlH_4]^-$ at the GIAO-HF-SCF/dzp level is 517.1 ppm). For the parent system of **5** (all ethyl and methyl groups replaced by hydrogens), the accuracy of the calculated shifts was checked in GIAO-HF-SCF calculations using a larger polarized triple-zeta (TZP) basis,[26] as well as in electron-correlated calculations using second-order Møller−Plesset perturbation theory, i.e. GIAO-MP2.[29] According to these calculations, the accuracy of the computed shift can be estimated to be in agreement with previous ^{27}Al NMR chemical shift calculations on aluminium cluster compounds within δ = 20−30.[13,14] All calculations were carried out with the TURBOMOLE program package.[30]

Acknowledgments

We are grateful to the Deutsche Forschungsgemeinschaft and the Fonds der Chemischen Industrie for generous financial support.

[1] W. Uhl, F. Breher, *Eur. J. Inorg. Chem.* **2000**, 1.
[2] W. Uhl, F. Breher, *Angew. Chem.* **1999**, *111*, 1578; *Angew. Chem. Int. Ed.* **1999**, *38*, 1477.
[3] W. Uhl, F. Breher, A. Lützen, W. Saak, *Angew. Chem.* **2000**, *112*, 414; *Angew. Chem. Int. Ed.* **2000**, *39*, 406.
[4] W. Uhl, F. Breher, J. Grunenberg, A. Lützen, W. Saak, *Organometallics* **2000**, *19*, 4536.
[5] O. Volkov, W. Dirk, U. Englert, P. Paetzold, *Z. Anorg. Allg. Chem.* **1999**, *625*, 1193; E. H. Wong, L. Prasad, E. J. Gabe, M. G. Gatter, *Inorg. Chem.* **1983**, *22*, 1143.
[6] $(Me_2AlH)_3$: δ = 2.92; $(Et_2AlH)_3$: δ = 2.75; $(iPr_2AlH)_3$: δ = 2.71. O. T. Beachley, Jr., L. Victoriano, *Organometallics* **1988**, *7*, 63.
[7] H. Günther, *NMR-Spektroskopie*, Georg Thieme Verlag, Stuttgart, **1983**, p. 229.
[8] R. G. Vranka, E. L. Amma, *J. Am. Chem. Soc.* **1967**, *89*, 3121; J. C. Huffman, W. E. Streib, *J. Chem. Soc., Chem. Commun.* **1971**, 911; A. Almenningen, G. A. Anderson, F. R. Forgaard, A. Haaland, *Acta Chem. Scand.* **1972**, *26*, 2315.
[9] W. Uhl, *Z. Naturforsch. B., Chem. Sci.* **1988**, *43*, 1113; R. J. Wehmschulte, K. Ruhlandt-Senge, M. M. Olmstead, H. Hope, B. E. Sturgeon, P. P. Power, *Inorg. Chem.* **1993**, *32*, 2983; N. Wiberg, K. Amelunxen, T. Blank, H. Nöth, J. Knizek, *Organometallics* **1998**, *17*, 5431.
[10] W. Uhl, *Z. Anorg. Allg. Chem.* **1989**, *570*, 37.
[11] A. Haaland, in *Coordination Chemistry of Aluminum* (Ed.: G. H. Robinson), VCH, New York, **1993**; W. Uhl, M. Koch, S. Pohl, W. Saak, W. Hiller, M. Heckel, *Z. Naturforsch., Teil B* **1995**, *50*, 635.
[12] R. Benn, A. Rufińska, H. Lehmkuhl, E. Janssen, C. Krüger, *Angew. Chem.* **1983**, *95*, 808; *Angew. Chem. Int. Ed. Engl.* **1983**, *22*, 779; R. Benn, A. Rufińska, *Angew. Chem.* **1986**, *98*, 851; *Angew. Chem. Int. Ed. Engl.* **1986**, *25*, 861; J. F. Hinton, R. W. Briggs in *NMR and the Periodic Table* (Eds.: R. K. Harris, B. E. Mann), Academic Press, London, **1978**.
[13] J. Gauss, U. Schneider, R. Ahlrichs, C. Dohmeier, H. Schnöckel, *J. Am. Chem. Soc.* **1993**, *115*, 2402.
[14] C. Klemp, M. Bruns, J. Gauss, U. Häussermann, G. Stösser, L. Van Wüllen, M. Jansen, H. Schnöckel, *J. Am. Chem. Soc.* in press.

[15] C. Dohmeier, H. Schnöckel, C. Robl, U. Schneider, R. Ahlrichs, *Angew. Chem.* **1993**, *105*, 1714; *Angew. Chem. Int. Ed. Engl.* **1993**, *32*, 1655.
[16] W. Uhl, F. Breher, B. Neumüller, J. Grunenberg, A. Lützen, W. Saak, *Organometallics*, in press.
[17] H. Lehmkuhl, K. Ziegler, in *Methods of Organic Chemistry (Houben-Weyl)*, 4th ed., Thieme-Verlag, Stuttgart, **1970**; vol. XIII/4, pp. 58−59.
[18] W. Uhl, J. Wagner, D. Fenske, G. Baum, *Z. Anorg. Allg. Chem.* **1992**, *612*, 25.
[19] The synthesis of $Et_2Al-C\equiv C-Me$ by a very complicated route has been reported previously; its characterization was incomplete: H. Demarne, P. Cadiot, *Bull. Soc. Chim. Fr.* **1968**, 205; A. Almenningen, L. Fernholt, A. Haaland, *J. Organomet. Chem.* **1978**, *155*, 245; see ref.[14].
[20] *International Tables for Crystallography, Space Group Symmetry* (Ed.: T. Hahn), Kluwer Academic Publishers, Dordrecht, Boston, London, **1989**, vol. A.
[21] *SHELXTL-Plus, Release 4.2* for Siemens R3 Crystallographic Research Systems, Siemens Analytical X-ray Instruments Inc., Madison, USA, **1990**; G. M. Sheldrick, *SHELXL-97*, *Program for the Refinement of Crystal Structures*, Universität Göttingen, **1997**.
[22] The crystallographic data for **5** and **6** (excluding structure factors) have been deposited with the Cambridge Crystallographic Data Centre as supplementary publication nos. CCDC-160388 (**5**) and -160389 (**6**). Copies of the data can be obtained free of charge on application to The Director, CCDC, 12 Union Road, Cambridge CB2 1EZ, U.K. [Fax: (internat.) +44 (0)1223 336033; E-mail: deposit@chemcrys.cam.ac.uk].
[23] See, for example: R. G. Parr, W. Yang, *Density-Functional Theory of Atoms and Molecules*, Clarendon Press, New York, **1989**, and references therein.
[24] A. D. Becke, *Phys. Rev.* **1998**, *A38*, 3098; J. P. Perdew, *Phys. Rev.* **1996**, *B33*, 8822.
[25] K. Eichkorn, O. Treutler, H. Öhm, M. Häser, R. Ahlrichs, *Chem. Phys. Lett.* **1995**, *240*, 283.
[26] A. Schäfer, H. Horn, R. Ahlrichs, *J. Chem. Phys.* **1992**, *97*, 2571.
[27] R. Ditchfield, *Mol. Phys.* **1974**, *27*, 789; K. Wolinski, J. F. Hinton, P. Pulay, *J. Am. Chem. Soc.* **1990**, *112*, 8251; M. Häser, R. Ahlrichs, H. P. Baron, P. Weis, H. Horn, *Theoret. Chim. Acta* **1992**, *83*, 455.
[28] H. Nöth, *Z. Naturforsch., Teil B* **1980**, *35*, 119.
[29] J. Gauss, *Chem. Phys. Lett.* **1992**, *191*, 614; M. Kollwitz, J. Gauss, *Chem. Phys. Lett.* **1996**, *260*, 639.
[30] R. Ahlrichs, M. Bär, M. Häser, H. Horn, C. Kölmel, *Chem. Phys. Lett.* **1989**, *162*, 165.

Received June 8, 2001
[I01209]

Structural Investigations of Sulfite-Bridged Binuclear Complexes of Platinum(II) and Palladium(II)

Roland Krieglstein,[a] Dietrich K. Breitinger,*[a] and Günther Liehr[a]

Keywords: Palladium / Platinum / O,S ligands / Structure elucidation / Vibrational spectroscopy

Although analogous platinum(II) and palladium(II) compounds usually show similar chemical behaviour, different reaction products have been obtained on reaction of ethane-1,2-diamine bissulfitometallates(II) with the diaqua ethane-1,2-diamine metal(II) complexes of Pt and Pd. – The crystal structures of bis(μ-sulfito-1κS:2κO)bis[(ethane-1,2-diamine)-platinum(II)] trihydrate $[(en)Pt(SO_2O)_2Pt(en)]\cdot 3\,H_2O$ (**1**) with parallel μ-(S:O) sulfite bridges, and of bis[(ethane-1,2-diamine)-μ-(S:O)-sulfitopalladium(II)] trihydrate $[(en)Pd(SO_2O)(OO_2S)Pd(en)]\cdot 3\,H_2O$ (**2**) with antiparallel bridges, have been determined by single-crystal X-ray structure analyses. In both compounds the complex units are held together mainly by a complicated network of hydrogen bonds including the hydrate water molecules. – In contrast to the complex molecules in **1** with parallel bridges, the complex units of **2** possess an inversion centre. As a result the mutual exclusion rule reduces the number of bands in each of the vibrational spectra of **2** to half that in the spectra of **1**. This effect is most clearly seen in the number of the valence vibrations $\nu(MN_2)$; the Raman spectrum of **1** displays four relatively strong bands, whereas the Raman spectrum of **2** shows only two, as expected. Further, features of the vibrational spectra are in agreement with the findings of the crystal and molecular structures. Thus, the *trans*-influence exerted by the *S*-coordinated sulfites onto the M–N bonds in the *trans*-position induces a significant lengthening and weakening of these bonds relative to the M–N bonds *trans* to oxygen. In the Raman spectrum of **1** the valence vibrations of the PtN_2 group *trans* to sulfur are clearly lowered in frequency.

Introduction

Our group has been involved with the syntheses, crystal structures, and vibrational spectra of the sulfito complexes of the platinum-group metals for some time. In these studies particular attention has been paid towards the effects of the *trans*-influence of the sulfite ligands.

It has been shown by X-ray structure analysis and vibrational spectroscopy that the anions in the compounds $K_2[M^*(SO_3)_2]$ (M* = Pd and Pt) are coordination polymers in which the metal atoms are connected by pairs of sulfite groups forming parallel μ-(S:O) bridges.[1,2]

After the preparation of a non-polymeric trinuclear cobalt complex with triple parallel μ-(S:O) bridges,[3] it seemed feasible to form related dinuclear sulfite-bridged complexes of the platinum-group metals involving the isolated repeat units in the above mentioned coordination polymers. A possible synthetic pathway would be the condensation of the cation *cis*-$[L_2M^*(OH_2)_2]^{2+}$ and the anion *cis*-$[L_2M^*(SO_3)_2]^{2-}$ to yield the neutral complex $[L_2M^*(SO_2O)_2M^*L_2]$. It was not possible to use a complex with $L = NH_3$ as a terminating ligand for this purpose (as in the case of the above cobalt complex), since it was previously found that the anion *cis*-$[Pd(SO_3)_2(NH_3)_2]^{2-}$ undergoes *cis*-*trans*-isomerisation in aqueous solution.[1a] Hence, the chelating ligand ethane-1,2-diamine (en), which prevents this rearrangement, was chosen as terminating ligand. The preparation of the complexes $[(en)M^*(OH_2)_2]^{2+}$ and $[(en)M^*(SO_3)_2]^{2-}$ are well-documented (see ref.[4]).

Based on limited IR[5] and Raman spectra,[6] the existence of a palladium complex with antiparallel double sulfite bridges has already been suggested.

Although analogous platinum and palladium compounds usually show similar chemical behaviour in their reactions of the aqua complexes $[(en)M^*(OH_2)_2]^{2+}$ with the disulfitometallates $[(en)M^*(SO_3)_2]^{2-}$, different final reaction products are obtained. For M* = Pt, the complex bis(μ-sulfito-1κS:2κO)bis[(ethane-1,2-diamine)platinum(II)] trihydrate $[(en)Pt(SO_2O)_2Pt(en)]\cdot 3\,H_2O$ (**1**) with parallel bridges is formed, and for M* = Pd, the species bis[(ethane-1,2-diamine)-μ-(S:O)-sulfitopalladium(II)] trihydrate $[(en)Pd(SO_2O)(OO_2S)Pd(en)]\cdot 3\,H_2O$ (**2**) with antiparallel bridges is formed (see Scheme 1).

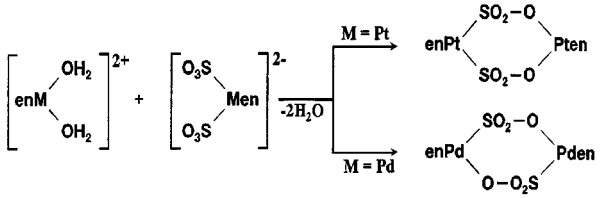

Scheme 1

Results and Discussion

Crystal Structure Analyses

Both complexes **1** and **2** could be obtained as single crystals by recrystallisation from aqueous media, under care-

[a] Institute of Inorganic Chemistry,
University of Erlangen-Nürnberg,
Egerlandstraße 1, 91058 Erlangen, Germany
Fax: (internat.) + 49-9131/85 27387
E-mail: Breitinger@chemie.uni-erlangen.de

 © WILEY-VCH Verlag GmbH, 69451 Weinheim, 2001 1434–1948/01/1212–3067 $ 17.50+.50/0

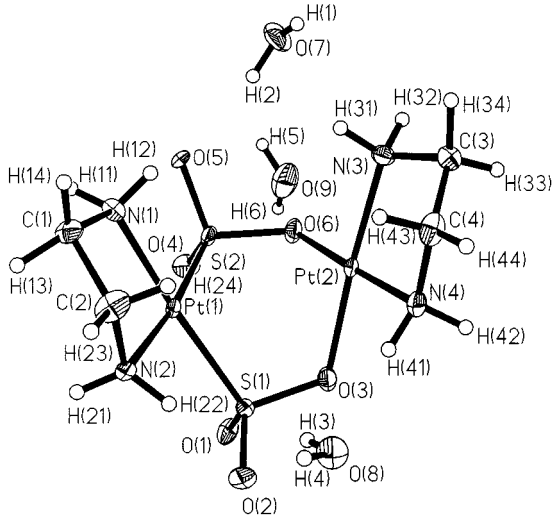

Figure 1. ORTEP plot of the dinuclear complex unit of **1**

fully controlled conditions (see Exp. Sect.). Table 4 lists the relevant crystallographic data.

Figure 1 shows the molecular structure of the dinuclear complex unit of **1**, including one set of the three independent water molecules.

Bond lengths and angles for both compounds are presented in Table 1 and Table 2.

All bond lengths and angles in the complex unit $[(en)Pt(SO_3)_2Pt(en)]$ of **1** (with no crystallographically imposed symmetry) are as expected. Thus, the chemically equivalent Pt−N bonds in each of the two different chelate rings, as well as the chemically equivalent Pt−S and Pt−O bonds are the same within their e.s.d's. However, the averaged Pt(1)−N bonds [$\bar{r}$ = 2.09(1) Å] are significantly longer than the Pt(2)−N bonds [$\bar{r}$ = 2.02(1) Å], clearly showing the differences in the *trans*-influence of sulfite when coordinated through sulfur and oxygen. Further, the angles N−Pt(1)−N [81.9(4)°] and N−Pt(2)−N [84.2(5)°] deviate substantially from 90°. This is also suggested by the sequences $\nu_s > \nu_{as}$ of the valence frequencies of the two PtN_2 entities in the Raman spectrum of **1**.[7]

The S(1)−O(3) and S(2)−O(6) bonds, which form part of the sulfite bridges in **1**, are clearly longer [$\bar{r}$ = 1.533(8) Å] relative to the four terminal S−O bonds [$\bar{r}$ = 1.468(9) Å], which do not deviate significantly from each other. This is similar to the findings in the structure of $K_2[Pd(SO_3)_2]\cdot H_2O$.[1b] The bonding data of these μ-(S:O) bridging sulfite ligands are similar to those in the less precisely determined structure of a dinuclear organometallic complex $[Pt_2(\mu\text{-}SO_3)(\mu\text{-}SO_2)(COD)_2]$ (COD = cycloocta-1,5-diene).[8]

Both μ-(S:O)-bridged platinum atoms display an approximately square-planar environment comprising pairs of nitrogen atoms *cis* to one another, and pairs of sulfur and oxygen atoms at Pt(1) and Pt(2), respectively. The five atoms in each of these groups deviate from the respective least-squares plane by a maximum of 0.099 Å for the $Pt(1)N_2S_2$ group, and by a maximum of 0.025 Å for the $Pt(2)N_2O_2$ group (see Table 3).

The central ring $Pt(1)(S-O)_2Pt(2)$ in **1** adopts a boat conformation in contrast to the chair conformation in **2**.

In **1** two molecules are arranged around an inversion centre such that their Pt(2) atoms are 3.0441(9) Å apart (Figure 2). This is a remarkably short distance. The conformations of the two en ligands within one molecule are different. However, due to the inversion centre between the two molecules, their symmetry-related en-rings adopt δ- and λ-conformations, respectively.

Table 1. Bond lengths and angles of **1**; e.s.d.'s are given in parentheses

Bond lengths [Å]		N(2)−Pt(1)−S(2)	172.8(3)
Pt(1)−N(1)	2.08(1)	N(3)−Pt(2)−N(4)	84.2(5)
Pt(1)−N(2)	2.10(1)	O(3)−Pt(2)−O(6)	88.9(4)
Pt(2)−N(3)	2.02(1)	N(3)−Pt(2)−O(3)	176.0(4)
Pt(2)−N(4)	2.01(1)	N(3)−Pt(2)−O(6)	94.3(4)
Pt(1)−S(1)	2.244(3)	N(4)−Pt(2)−O(3)	92.6(4)
Pt(1)−S(2)	2.243(3)	N(4)−Pt(2)−O(6)	178.1(4)
Pt(2)−O(3)	2.044(9)	Pt(1)−S(1)−O(1)	116.3(4)
Pt(2)−O(6)	2.070(9)	Pt(1)−S(1)−O(2)	110.9(4)
S(1)−O(1)	1.475(9)	Pt(1)−S(1)−O(3)	105.1(4)
S(1)−O(2)	1.471(9)	O(1)−S(1)−O(2)	109.9(6)
S(1)−O(3)	1.528(8)	O(1)−S(1)−O(3)	108.3(5)
S(2)−O(4)	1.461(9)	O(2)−S(1)−O(3)	105.6(5)
S(2)−O(5)	1.463(9)	Pt(1)−S(2)−O(4)	114.7(4)
S(2)−O(6)	1.537(8)	Pt(1)−S(2)−O(5)	108.0(4)
N(1)−C(1)	1.50(2)	Pt(1)−S(2)−O(6)	108.6(4)
N(2)−C(2)	1.49(2)	O(4)−S(2)−O(5)	111.3(6)
N(3)−C(3)	1.48(2)	O(4)−S(2)−O(6)	106.9(5)
N(4)−C(4)	1.48(2)	O(5)−S(2)−O(6)	107.2(5)
C(1)−C(2)	1.49(2)	S(1)−O(3)−Pt(2)	119.1(5)
C(3)−C(4)	1.48(2)	S(2)−O(6)−Pt(2)	113.8(5)
Pt(2)−Pt(2)[a]	3.0441(9)	Pt(1)−N(1)−C(1)	110.9(8)
Pt(1)−Pt(2)	3.1263(7)	C(2)−N(2)−Pt(1)	106.8(8)
Bond angles [°]		Pt(2)−N(3)−C(3)	108.7(8)
N(1)−Pt(1)−N(2)	81.9(4)	C(4)−N(4)−Pt(2)	108.3(8)
S(1)−Pt(1)−S(2)	92.8(1)	N(1)−C(1)−C(2)	111(1)
N(1)−Pt(1)−S(1)	171.7(3)	C(1)−C(2)−N(2)	108(1)
N(1)−Pt(1)−S(2)	91.1(3)	N(3)−C(3)−C(4)	108(1)
N(2)−Pt(1)−S(1)	94.4(3)	C(3)−C(4)−N(4)	108(1)

[a] $1-x, 2-y, 1-z$.

Table 2. Bond lengths and angles of **2**; e.s.d.'s are given in parentheses

Bond lengths [Å]		O(3)−Pd−N(2)	172.3(2)
Pd−N(1)	2.079(4)	O(3)−Pd−N(1)	90.6(1)
Pd−N(2)	2.019(4)	S−Pd−O(3)	93.5(1)
Pd−S	2.229(1)	Pd−S−O(1)	111.6(1)
Pd−O(3)	2.043(3)	Pd−S−O(2)	109.2(1)
S−O(1)	1.466(3)	Pd−S−O(3)[a]	110.1(1)
S−O(2)	1.479(3)	O(1)−S−O(2)	111.2(2)
S−O(3)[a]	1.501(3)	O(1)−S−O(3)[a]	105.5(2)
N(1)−C(1)	1.484(6)	O(2)−S−O(3)[a]	109.1(2)
N(2)−C(2)	1.492(6)	Pd−O(3)−S[2]	128.0(2)
C(1)−C(2)	1.493(7)	Pd−N(1)−C(1)	109.4(3)
Bond angles [°]		Pd−N(2)−C(2)	108.9(3)
N(2)−Pd−N(1)	82.8(2)	N(1)−C(1)−C(2)	106.9(4)
S−Pd−N(1)	175.8(1)	N(2)−C(2)−C(1)	108.3(4)
S−Pd−N(2)	93.1(1)		

[a] $1-x, 1-y, 1-z$.

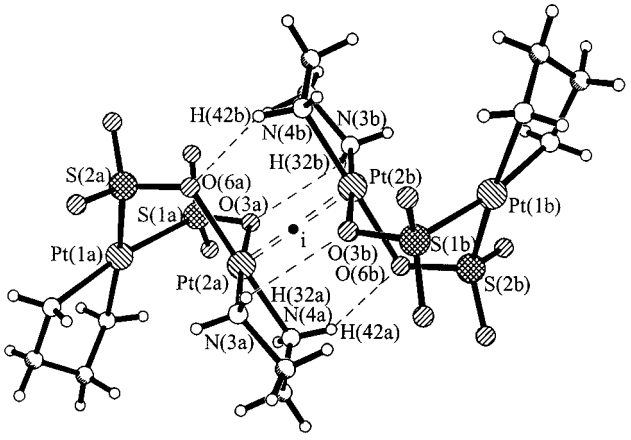

Figure 2. Arrangement of the complex units of **1** into dimers

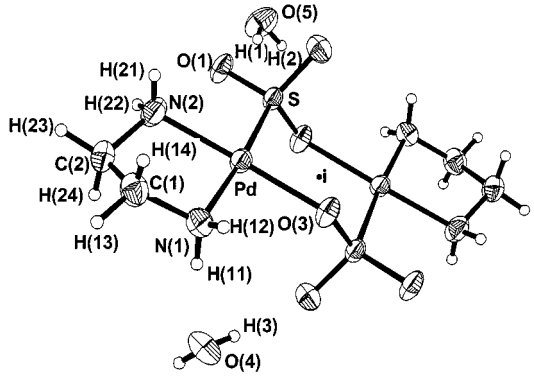

Figure 3. ORTEP plot of the dinuclear complex unit of **2**

Table 3. Deviation from the least-square planes through the metal atoms and their environments in **1** and **2**

$Pt(1)N_2S_2$ plane of **1**		$Pt(2)N_2O_2$ plane of **1**		PdN_2SO plane of **2**	
Pt(1)	−0.049(3)	Pt(2)	−0.025(4)	Pd	0.021(1)
N(1)	0.099(4)	N(3)	0.016(5)	N(1)	0.045(2)
N(2)	−0.072(4)	N(4)	−0.004(5)	N(2)	−0.053(2)
S(1)	0.083(4)	O(3)	0.016(5)	S	0.037(1)
S(2)	−0.061(4)	O(6)	−0.003(5)	O(3)	−0.050(2)

The above-mentioned short intermolecular Pt···Pt distance may suggest that metal-to-metal interactions could contribute to the cohesion of the molecules in the lattice. Square-planar complexes of d^8-metals that are stacked in columns or chains, with overlapping d_{z^2} orbitals, are well-known. Thus, chain-structured Krogmann salts (obtained by partial oxidation of $K_2[Pt(CN)_4]$) show Pt−Pt distances between 2.87 and 2.96 Å, in comparison with the distance of 2.78 Å in platinum metal.[9] In the structure of **1** there are no such chain-like arrangements, but only isolated pairs of close Pt atoms in antiparallel (inversion correlated) N_2PtO_2 groups. A situation similar to that in **1** is found in $[(NH_3)_2Pt(OH)_2Pt(NH_3)_2]CO_3{\cdot}2\,H_2O$, where an intermolecular metal-to-metal distance of 3.167(1) Å is found.[10] In this case, the authors precluded attractive interactions between the platinum atoms, since they deviate from the least-squares planes, containing the atoms coordinated to the Pt atoms, such that the Pt···Pt distance increases. Consequently, the cohesion within a pair of complex units is attributed to four hydrogen bonds N−H···O.

Similarly, in **1** the platinum atom Pt(2) is shifted from the least-squares plane through the ligand atoms N(3), N(4), O(3) and O(6) by 0.031(5) Å, such that the Pt···Pt distance increases again. Once more, four hydrogen−bonds, N−H···O, apparently hold the two molecules together. Although these individual hydrogen−bonds, with O···N distances of 2.98(1) and 2.99(1) Å, and unfavourable bond angles are considered to be weak, their cooperation effects the cohesion in these pairs of molecules.

Thus, a complex network of these hydrogen bonds, and of further hydrogen bonds involving the water molecules, hold the constituents of this crystal structure together.

The remarkably poor stability of the crystals in air under ambient conditions can be attributed to the fewer appropriate partners available for hydrogen bonding with the lattice water molecule $H_2O(9)$. Further, one of the two hydrogen bonds [N(4)···O(9)] with a distance of 2.96(1) Å is weak. These facts are in accordance with the findings of the TGA/DTA analysis of the substance. They show that the loss of just one water molecule per formula unit occurs at a temperature as low as 30 °C; the further loss of two lattice water molecules occurs by about 140 °C.

The molecular structure of **2** is shown in Figure 3. The respective bond lengths and angles are presented in Table 2.

The two palladium centres in **2** are μ-(S:O) bridged by two sulfite groups in an antiparallel arrangement. The coordination around these equivalent Pd atoms is square-planar, with two non-equivalent nitrogen atoms *cis* to one another, one oxygen atom and one sulfur atom. The five atoms deviate from the ideal plane by a maximum of 0.05 Å (see Table 3). The $(Pd-S-O)_2$ ring adopts a chair conformation, in contrast to the central ring in the platinum compound **1** (see above). Since the molecules in **2** are centrosymmetric, their equivalent Pd(en) rings adopt opposite δ- and λ-conformations, respectively. While the oxygen atom O(4) of one lattice water molecule is located on a C_2-axis (Wyckoff 4e), the second water molecule and all the other atoms are distributed on general sites (Wyckoff 8f).

The Pd−N(2) bond [2.019(4) Å] is significantly shorter than Pd−N(1) bond [2.079(4) Å]. It is also shorter than the analogous Pd−N bonds in $Na_2[Pd(SO_3)_2en]\cdot 4\,H_2O$ [2.084(2) Å].[11] Both these examples serve to emphasise the effect of the *trans*-influence of the sulfite ligands, albeit to a different extent (dependent on the total charge and coordination mode). As discussed for **1**, this is as a result of the lower *trans*-influence of the bridging oxygen atom, as compared with sulfur, on the Pd−N(2) bond in the position *trans* to it.

The influence of the ligand in the *trans*-position also affects the Pd−O bond. Here, this bond, with the less efficient nitrogen atom *trans* to it, is significantly shorter [2.043(3)

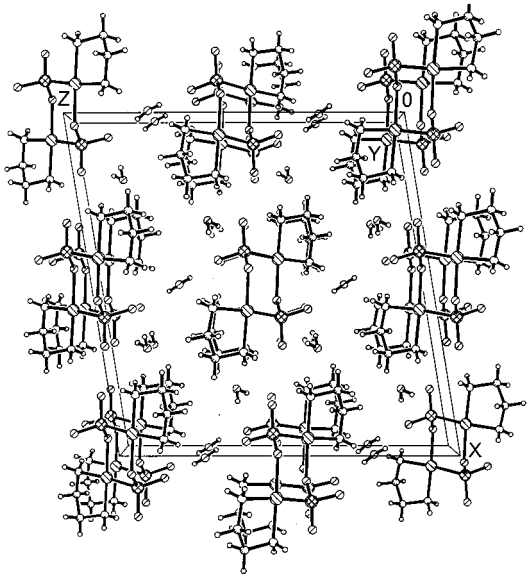

Figure 4. Molecular packing in the crystal structure of **2**

Å] than that in $K_2[Pd(SO_3)_2]\cdot H_2O$ where a sulfur atom is in the *trans*-position [2.121(3) Å].[1b]

As expected, the Pd−S bond in **2** is clearly shorter [2.229(1) Å] than that in the complex $Na_2[Pd(SO_3)_2(en)]\cdot 4\,H_2O$ [2.269(1) Å],[11] involving monodentate *S*-coordinated sulfite ligands in an anionic complex species. After the bond-valence approach,[12] weakening of one bond causes an increase of the bond orders and hence the decrease of the bond lengths in adjacent bonds. Thus, lowering of the bond order on going from almost S−O double bonds in $Na_2[Pd(SO_3)_2(en)]\cdot 4\,H_2O$ to S−O single bonds in the sulfite bridges of **2**, leads to the shortening of the Pd−S bonds. In $K_2[Pd(SO_3)_2]\cdot H_2O$, with bidentate bridging sulfite ligands, the Pd−S bonds are similarly short [2.241(1) Å].[1b]

The overall arrangement of the chair-shaped molecules in the crystal lattice of **2** is such that the hydrophilic regions of the complexes (NH_2 and SO_2 groups) approach each other. Thus, a complicated network of hydrogen bonds between these hydrophilic segments of the dinuclear complex units, and between the complexes and water molecules can be formed. Also, the intermolecular distances between the hydrophobic parts of the complexes (CH_2 groups) are short (see Figure 4).

Spectrometry

UV/Vis Spectra: The reaction between $[Pd(en)(OH_2)_2]^{2+}$ and $[Pd(SO_3)_2(en)]^{2-}$ was followed by UV/Vis spectrometry (see Figure 5). However, from the spectra it is not certain whether the dinuclear complex $[(en)Pd(SO_2O)_2Pd(en)]$ is formed first, followed by the isomerisation to $[(en)Pd(SO_2O)(OO_2S)Pd(en)]$, or whether the mononuclear complex $[(en)Pd(SO_3)(H_2O)]$ is formed (generated by the partial dissociation of the anion and recoordination of the released sulfite to the cation), which condenses prior to the crystallisation of **2**.

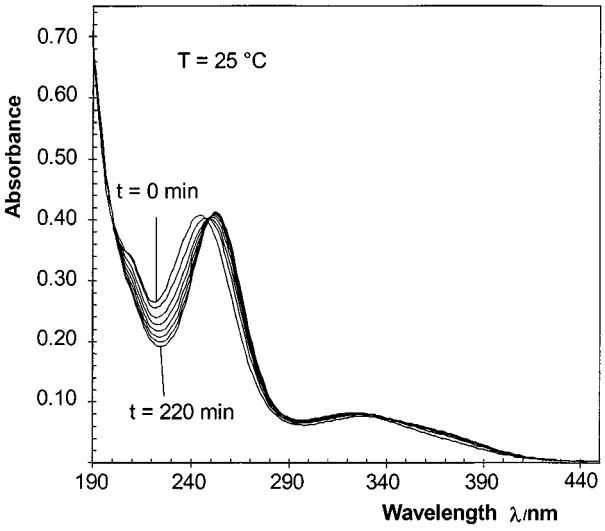

Figure 5. Time-dependent UV spectra of the reaction mixture yielding **2**

IR and Raman Spectra: The molecule of **2** (crystallographic symmetry $\bar{1}$ − C_i) has an inversion centre, in contrast to the complex unit in **1** on a general position. As a result, the mutual exclusion rule reduces the number of bands in each of the vibrational spectra of **2** to one half of that in **1**, i.e. both IR and Raman spectra of **2** are simpler. This fact is most clearly seen in the region of the valence vibrations $\nu(MN_2)$. Thus, the Raman spectrum of **1** displays four rather strong bands [two interpenetrating $\nu_s(MN_2)$/$\nu_{as}(MN_2)$ doublets] around 500 cm^{-1}, whereas the spectrum of **2** shows only two bands (see Figure 6). With respect to the differences in the Pt−N bond lengths at Pt(1) and Pt(2) (*trans*-influence), the higher doublet (574/490 cm^{-1}) is assigned to the valence vibrations of the $Pt(2)N_2$ group *trans* to oxygen and the lower one (517/442 cm^{-1}) to the $Pt(1)N_2$ fragment *trans* to sulfur. Since the angles in both PtN_2 groups are substantially smaller than 90° [81.9 and 84.2° at Pt(1) and Pt(2), respectively], the frequency sequence of their valence vibrations is always $\nu_s(PtN_2) > \nu_{as}(PtN_2)$ (cf. the reasoning in ref.[7]).

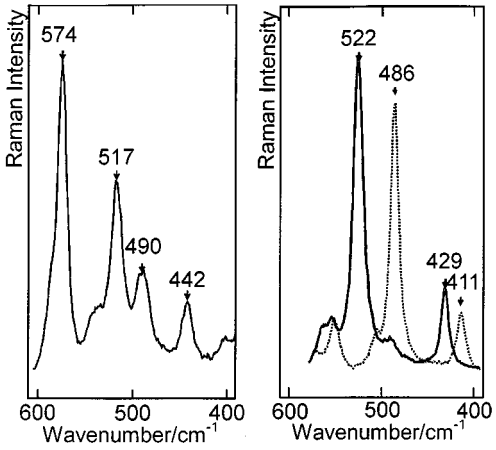

Figure 6. Raman spectra of the $\nu(MN_2)$ ranges of **1** (left), and of **2** (right) and its N-deuterated isotopomer (dotted)

In the IR spectra the result of these structural features are by far less obvious since the valence vibrations $\nu(MN_2)$ are weak. Further, these vibrations are obscured by the complex system of intense bands originating from the splitting of the deformation vibrations $\delta_{as}(SO_3)$ by the present bonding mode, with concomitant symmetry lowering, and by correlation coupling. In addition, librational modes of the three different water molecules contribute to the complexity of this spectral region. The special bonding mode also leads to three regions of valence vibrations $\nu(SO_3)$; $\nu_{as}(SO_2)$ (coarsely around 1150 cm^{-1}), $\nu_s(SO_2)$ (1050 cm^{-1}) and ν(SO) (ca. 900 cm^{-1}); for details see ref.[7] The latter vibrations are very strong in both the IR and Raman spectra of **1** and **2.** However, the bands of the SO_2 fragments are strong and broad in the IR spectra, but are of different intensity in the Raman spectra. It should be mentioned that the valence vibrations ν(CC) and ν(CN), as well as the wagging modes $\omega(NH_2)$ and $\omega(CH_2)$ of the chelate rings are expected to be in the same spectral region. Hence, a definite assignment of all the bands is difficult.

Due to the low solubilities of **1** and **2** in H_2O under ambient conditions, and its almost insoluble nature in common organic solvents, it was not possible to obtain Raman and NMR spectra of solutions.

Conclusion

On reaction of the cations $[(en)M^*(OH_2)_2]^{2+}$ and anions $[(en)M^*(SO_3)_2]^{2-}$, the expected dinuclear complex $[(en)M^*(SO_2O)_2M^*(en)]$ (in **1**) with two parallel μ-(S:O) sulfite bridges really forms in the case of M* = Pt. Thus, the repeat unit $M^*(SO_2O)_2M^*$, previously found in polymeric complexes of the type $K_2[M^*(SO_3)_2]$, is now available in an isolated stabilised form. In the case of M* = Pd, the kinetically labile starting materials probably symmetrise in two steps to form $[(en)Pd(SO_3)(OH_2)]$, prior to the condensation to the dinuclear unit $[(en)Pd(SO_2O)(OO_2S)Pd(en)]$ (in **2**) with antiparallel μ-(S:O) sulfite bridges. Seemingly, the latter is the thermodynamically controlled product, whereas in the reaction of the inert platinum(II) complexes the kinetically controlled product is formed.

These findings also raise the question of the existence of coordination polymers $^1_\infty[M^*(SO_2O)(OO_2S)]^{2-}$, with these antiparallel bridged repeat units, and also of polymers with counter-current bridges of each type, for instance $^1_\infty[M^*(SO_2O)_2M^*(OO_2S)_2]^{4-}$.

The molecular structures clearly reveal the differences of the *trans*-influence of S- and O-coordinated sulfite ligands in the same complex species. These differences and the different symmetries (non-centrosymmetric **1** vs. centrosymmetric **2**) also imprint the vibrational spectra.

Experimental Section

General Remarks: Elemental analyses for C, H, N, and S were performed using the analyser Carlo Erba Model 1108. Platinum and palladium were determined as residues after simultaneous TGA/DTA runs using the thermal analyser TA Instruments Model SDT 2960 (reference Al_2O_3).

Time-dependent UV/Vis spectra were scanned using the spectrometer HP 8452 A.

IR spectra on KBr pellets were taken with the FTIR spectrometer ATI Mattson Infinity controlled by the soft-ware package WinFirst 3.0.

Raman spectra of the pure substances in capillaries, excited with a Spectra Physics Stabilite 2014 Ar^+ laser (514.5 nm, 100 to 150 mW), were recorded using the spectrometer DILOR XY (multichannel detection) controlled by the software system XY 2.0.

X-ray structure determinations were performed with data sets collected on a four-circle diffractometer Enraf−Nonius CAD4 Mach 3, after the determination of the space groups on the basis of Weissenberg photographs. Details of the data collections for the compounds **1** and **2** are compiled in Table 4. The structures were solved with Patterson techniques and refined on F^2 using the program SHELX97.[13] In the last step of the structure refinement of **1**, the H atoms were considered with restraints for the bond lengths r(O−H), r(N−H), and r(C−H) (0.85, 0.90, and 0.96 Å, respectively), and for the bond angles in H_2O and in the H_2N groups (107 and 109°, respectively). The isotropic displacement factors of the H atoms were taken as the 1.2-fold of the equivalent U_{eq} values of the respective neighbouring atoms O, N, and C. In the case of **2** the H atoms were included in the refinement without restraints and with individual isotropic displacement factors, with the exception of the H_2O molecules (restraints 0.85 Å and 107°). − Due to the instability and the strong absorption of **1**, its structure is less accurate than that of **2**.

Crystallographic data (excluding structure factors) for the structures reported in this paper have been deposited with the Cambridge Crystallographic Data Centre as supplementary publication no. CCDC-148274 and CCDC-148275. Copies of the data can be obtained free of charge on application to CCDC, 12 Union Road, Cambridge CB2 1EZ, UK [Fax: (internat.) + 44−1223/336-033; E-mail: deposit@ccdc.cam.ac.uk].

$[(en)Pt(SO_2O)_2Pt(en)]\cdot 3\,H_2O$ (1): $[PtCl_2(en)]$ (0.326 g, 1.00 mmol) was dissolved in 10 mL of H_2O whilst heating. After cooling to about 30 °C, $AgNO_3$ (19.9 mL of a 0.1 M solution, 1.99 mmol) was added. The mixture was stirred at room temperature in the dark for at least 8 h in order for the reaction to reach completion. The precipitated AgCl was then filtered off and washed twice with 10 mL of H_2O. The combined filtrates must be completely clear and colourless. The resulting solution of $[Pt(en)(OH_2)_2]^{2+}$ was combined with a solution of $K_2[Pt(SO_3)_2(en)]\cdot 2\,H_2O$[4] (0.519 g, 0.980 mmol) in 10 mL of H_2O and kept in a refrigerator for 3 h. The reaction product deposited as a lemon-yellow, microcrystalline precipitate. To complete precipitation, 200 mL of acetone was added; the product was filtered off, washed with 20 mL of acetone, dried in an air flow, and recrystallised from 15 mL of boiling water. Yield: 0.415 g (0.587 mmol), 60.0% of the dihydrate. − $C_4H_{20}N_4O_8S_2Pt_2$: calcd. C 6.80, H 2.85, N 7.93, S 9.08, Pt 55.22; found C 7.03, H 2.77, N 7.75, S 8.82, Pt 56.4.

In order to grow single crystals, about 200 mg of the compound was dissolved in 8 to 10 mL of hot H_2O. This solution was placed in an appropriate vial and put into a well-isolated Dewar flask, so that slow cooling could take place over several days; after about a week lemon-yellow crystal platelets of the trihydrate **1**, with edge lengths of 0.2 to 1.0 mm had grown. − $C_4H_{22}N_4O_9S_2Pt_2$: calcd. C 6.63, H 3.06, N 7.73, S 8.85, Pt 53.76; found C 6.72, H 2.87, N 7.70, S 8.64, Pt 55.2.

$[(en)Pd(SO_2O)(OO_2S)Pd(en)]\cdot 3\,H_2O$ (2): $[PdCl_2(en)]$ (0.2373 g, 1.000 mmol) was dissolved in 10 mL of boiling H_2O; after cooling

Table 4. Data for crystal structure determinations of **1** and **2**; e.s.d.'s are given in parentheses

	1	**2**
Empirical formula	$C_4H_{22}N_4Pt_2O_9S_2$	$C_4H_{22}N_4Pd_2O_9S_2$
Formula mass	724.6	547.2
Crystal system	Monoclinic	Monoclinic
Space group	$P\,2_1/n$	$C\,2/c$
a [Å]	10.064(1)	17.4340(2)
b [Å]	12.486(2)	5.3276(9)
c [Å]	13.099(3)	17.016(2)
β [°]	109.52(1)	99.386(9)
Z	4	4
D_c [g·cm^{-3}]	3.102	2.330
F_{000}	1336	1080
V [Å^3]	1551.4(5)	1559.8(4)
Colour	Yellow	Yellow
Diffractometer	Enraf−Nonius CAD 4 − Mach 3 four circle	Enraf−Nonius CAD 4 − Mach 3 four circle
X-Radiation, λ [Å]	Mo-K_α, graphite monochromatic, 0.71073	Mo-K_α, graphite monochromatic, 0.71073
Crystal size [mm]	0.3×0.2×0.05	0.20×0.06×0.05
Data collect. temp. [K]	173	Ambient
Data collecting mode	ω −2θ scan	ω −2θ scan
2θ -range	5.0° ≤ 2θ ≤ 48°	5.7° ≤ 2θ ≤ 50°
$h\ k\ l$ range	−11/11, 0/14, −14/14	−20/20, 0/6, −20/20
Reflections measured	5104	3069
unique	2426	1375
observed	2130 ($I \geq 4\sigma\ (I)$]	1134 ($I \geq 4\sigma\ (I)$]
μ (Mo-K_α) [cm^{-1}]	183.3	26.2
Absorption correction	ψ -scans	ψ -scans
$T_{max}/T_{min}/T_{mean}$	99.7%/23.46%/66.67%	99.78%/73.76%/87.15%
GooF	1.050	1.051
$R(F)$ (all reflections)	0.049	0.036
$R(F)$ (observed reflections only)	0.042	0.024
$R_w(F^2)$ (all reflections)	$R_w(F^2) = 0.122$ $w = 1/[\sigma^2(F) + (A\cdot P)^2 + B\cdot P]$ $P = [\mathrm{Max}(F_0^2, 0) + 2\cdot F_c^2]/3$ $A = 0.0871$, $B = 2.52$	$R_w(F^2) = 0.057$ $w = 1/[\sigma^2(F) + (A\cdot P)^2 + B\cdot P]$ $P = [\mathrm{Max}(F_0^2, 0) + 2\cdot F_c^2]/3$ $A = 0.0241$, $B = 0.00$

to about 30 °C, $AgClO_4$ (0.413 g, 1.99 mmol) in 20 mL of H_2O was added. After stirring at room temperature in the dark for 4 h, AgCl that had precipitated was filtered off and washed twice with 10 mL of H_2O. The clear and colourless solution of $[Pd(en)(OH_2)_2](ClO_4)_2$ was cooled with ice and mixed with $K_2[Pd(SO_3)_2(en)]\cdot 2\,H_2O$[4] (0.432 g, 0.980 mmol) in 10 mL of H_2O (0 °C); the reaction mixture turned lemon-yellow within a few seconds. After stirring for 10 s, the precipitated $KClO_4$ was filtered off and washed twice with 5 mL of cold H_2O. The combined yellow filtrate was poured into 200 mL of cooled acetone, the formed yellow precipitate was filtered off, washed with a few mL of cold acetone, dried for a short time in air, and finally over P_4O_{10} in a desiccator under ambient pressure. This procedure yielded 0.346 g (0.654 mmol), 65.4% of a dihydrate. − $C_4H_{20}N_4O_8S_2Pd_2$: calcd. C 9.08, H 3.81, N 10.59, S 12.12, Pd 40.22; found C 9.16, H 3.87, N 10.5, S 12.2, Pd 41.9.

On diffusion of acetone vapour into a solution of 0.100 g of the dihydrate in 5 mL of H_2O, at ambient temperature in the dark, yellow prismatic crystals of the trihydrate **2** grew on the glass walls within some days. − $C_4H_{22}N_4O_9S_2Pd_2$: calcd. C 8.78, H 4.05, N 10.24, S 11.72, Pd 38.90; found C 8.91, H 3.90, N 10.0, S 11.3, Pd 37.6.

Acknowledgments

The authors thank the Verband der Chemischen Industrie − Fonds der Chemischen Industrie, Frankfurt/Main, and the Universitätsbund Erlangen-Nürnberg for financial support, and DEGUSSA, Hanau, for gifts of the platinum-group metals.

[1] [1a] W. Haegler, Thesis, University of Erlangen-Nürnberg, **1979**. − [1b] D. Messer, D. K. Breitinger, W. Haegler, *Acta Crystallogr., Sect. B* **1979**, *35*, 815.
[2] G. Bauer, Thesis, University of Erlangen-Nürnberg, **1979**.
[3] B. Ballet, A. Bino, S. Cohen, H. Rubin, T. Zor, *Inorg. Chim. Acta* **1991**, *188*, 91.
[4] R. Krieglstein, Thesis, University of Erlangen-Nürnberg, **1997**.
[5] R. Eskenazi, J. Raskovan, R. Levitus, *J. Inorg. Nucl. Chem.* **1965**, *27*, 371.
[6] M. Raidel, Thesis, University of Erlangen-Nürnberg, **1985**.
[7] R. Krieglstein, D. K. Breitinger, *J. Mol. Struct.* **1997**, *408/409*, 379.
[8] D. H. Farrar, R. R. Gukathasan, *J. Chem. Soc., Dalton Trans.* **1989**, 557.
[9] F. A. Cotton, G. Wilkinson, *Advanced Inorganic Chemistry*, 5th Ed., John Wiley & Sons, New York − Chichester − Brisbane − Toronto − Singapore, **1988**, p. 1094.
[10] B. Lippert, C. J. L. Lock, B. Rosenberg, M. Zvagulis, *Inorg. Chem.* **1978**, *17*, 2971.
[11] D. K. Breitinger, G. Schottner, M. Raidel, H. P. Beck, *Z. Anorg. Allg. Chem.* **1986**, *539*, 18.
[12] I. D. Brown, D. Altermatt, *Acta Crystallogr., Sect. B* **1985**, *41*, 244.
[13] G. S. Sheldrick, *SHELX97*, *Program for Crystal Structure Refinement*, University of Göttingen, Germany, **1997**.

Received December 14, 2000
[O00473]

The Hydrothermal Synthesis, Crystal Structures and Thermal Stability of the Novel One- and Two-Dimensional Thioantimonate(III) Compounds $[Co(tren)]Sb_2S_4$ and $[Ni(tren)]Sb_2S_4$

Ralph Stähler[a] and Wolfgang Bensch*[a]

Keywords: Sulfur / Antimony / Solvothermal synthesis / Crystal structure / Thermoanalytical measurements

Two novel thioantimonate(III) compounds $[Co(C_6H_{18}N_4)]Sb_2S_4$ (**1**) and $[Ni(C_6H_{18}N_4)]Sb_2S_4$ (**2**) were synthesised under solvothermal conditions by reacting the transition metal, Sb and S in a 50% solution of tris(2-aminoethyl)amine (tren). The use of a tetradentate amine yields incompletely shielded transition metal cations which in turn are able to form bonds to the sulfur atoms of thioantimonate(III) anions. Compound **1** crystallises in the orthorhombic space group *Pbca*, a = 13.886(3) Å, b = 11.452(2) Å, c = 20.549(4) Å, V = 3268(1) Å^3, Z = 8 and compound **2** crystallises in the monoclinic space group $P2_1/n$, a = 6.906(1) Å, b = 22.822(5) Å, c = 10.347(2) Å, β = 103.17(3)°, V = 1587.9(6) Å^3, Z = 4. The $^2_\infty[Sb_2S_4^{2-}]$ anion in compound **1** is formed by an SbS_3 and an SbS_4 unit sharing a common corner. Two SbS_4 units have a common edge to form an Sb_2S_2 heterocycle. Four such Sb_2S_2 rings are at the corners of a two-dimensional square-like net. Interconnection of the rings by SbS_3 pyramids yields $Sb_{10}S_{10}$ rings with pores measuring 10·8.4 Å in diameter. The pores are filled by the $[Co(tren)]^{2+}$ cations. The $[Co]^{2+}$ cation is in a trigonal bipyramidal environment of four N atoms of the tren ligand and one S atom of the SbS_3 pyramid. The one-dimensional $^1_\infty[Sb_2S_4^{2-}]$ chain anion in **2** is built by two corner-sharing SbS_3 units. The $[Ni]^{2+}$ cation is in an octahedral environment consisting of four N atoms of the tren ligand and two S atoms of the anion. An $NiSb_2S_3$ heteroring in a twist conformation is formed with an unusually large Ni–S(1)–Sb(1) angle of 121.73(3)°. For the $[Co]^{2+}$ (d^7) cation no significant energy differences can be expected for the trigonal bipyramidal and octahedral coordination, and due to the geometrical requirements of the tetradentate ligand the former environment is preferred. In contrast, for $[Ni]^{2+}$ (d^8) an octahedral environment is energetically favoured over the trigonal bipyramidal arrangement. Both compounds start to decompose under an Ar atmosphere at about 250 °C. For **1** two not well resolved steps are observed, whereas **2** decomposes in one step. In the X-ray powder patterns of the grey products Sb_2S_3, Co/NiSbS and Co/NiS could be identified.

Introduction

Compared to the large number of thioantimonate(III) compounds with A^+ (A = alkali metal), EA^{2+} (EA = earth alkali metal) or organic ammonium cations as charge balancing ions only a few compounds are known in which a transition metal is integrated within the anionic framework of the main group thiometallates. In $[M(NH_3)_6]Cu_8Sb_3S_{13}$ the Cu_8S_{13} cores are linked by Sb atoms resulting in the formation of channels that are occupied by transition metal hexamine complexes.[1] Adamantane-like $[Ge_4S_{10}]^{4-}$ units have been linked by tetrahedral Mn^{II},[2] copper[3] or dimers like $[Ag_2]^+$ and $[Cu_2]^+$.[4] Other examples are copper antimony sulfides prepared at elevated temperatures such as $Cu_{12}Sb_4S_{13}$,[5] Cu_3SbS_4,[6] Cu_3SbS_3,[7–9] $CuSbS_2$,[10] and $[Cu_2SbS_3]\cdot(en)_{0.5}$ synthesised by the solvothermal route.[11] Applying solvothermal conditions it was also possible to incorporate a complex cation $[Co(en)_3]^{2+}$ into a thioantimonate(III) framework.[12] During the last few years we have synthesised and characterised layered thioantimonates(III) with general formula $Mn_2Sb_2S_5\cdot L$ (L = methylamine, ethylamine, 1,3-diaminopropane, *N*-methyl-1,3-diaminopropane and diethylenetriamine) with Mn^{II} being part of the Sb_2S_5 network.[13–15]

For syntheses using elements as starting materials very basic solutions are needed to dissolve and mobilise the elements. Organic amines are useful solvents with high pH values. However, the amines usually coordinate to the transition metal cations (TM^{n+}) preventing their incorporation into the thioantimonate(III) network. A way of enhancing the probability that the TM^{n+} ions are integrated into the thiometallate network is the use of multidentate amines which coordinate the TM^{n+} ion but leave one or two coordination sites free for bonds to the S atoms of the M_xS_y moieties (M = main group element). According to this idea the tetradentate amine tris(2-aminoethyl)amine (tren) seems to be a good candidate: transition metal cations that prefer an octahedral environment are coordinated by the four N atoms of the tren ligand leaving two coordination sites to form bonds to the S atoms of the thiometallate framework. Such ligated $[TM(tren)]^{n+}$ complexes may be described as geometrically constrained structure-directing agents.

Based on these considerations we synthesised and characterised two novel thioantimonate(III) compounds, two-dimensional $[Co(tren)]Sb_2S_4$ and one-dimensional $[Ni(tren)]Sb_2S_4$, both exhibiting new and exciting thioantimonate(III) networks.

[a] Institut für Anorganische Chemie, Universität Kiel
Olshausenstraße 40, 24098 Kiel, Germany
Fax: (internat.) + 49-(0)431/880-1520
E-Mail: wbensch@ac.uni-kiel.de

 © WILEY-VCH Verlag GmbH, 69451 Weinheim, 2001 1434–1948/01/1212–3073 $ 17.50+.50/0

Results and Discussion

In the new compound $[Co(tren)]Sb_2S_4$ (**1**) the $[Co]^{2+}$ ion is coordinated by four N atoms of the tren ligand, with Co−N distances ranging from 2.077(2) to 2.263(2) Å (see Table 1) and by one S atom of the $^2_\infty[Sb_2S_4^{2-}]$ anion yielding a trigonal bipyramidal environment (Figure 1). As expected the longer Co−N(1) bond is *trans* to the Co−S(1) bond [distance: 2.3539(7) Å].[14] The $^2_\infty[Sb_2S_4^{2-}]$ anion is built up from the Sb(1) and Sb(2) atoms, each being in a different geometrical environment of S atoms. The Sb(1) atom has bonds to three S atoms [S(1) to S(3)] forming the typical SbS_3 trigonal pyramid. The Sb(1)−S bond lengths are between 2.3899(7) and 2.4655(6) Å, indicating single bonds. The S(1) atom of the $Sb(1)S_3$ pyramid has a bond to the $[Co]^{2+}$ ion and the two other S atoms are bound to the Sb(2) atom. The Sb(2) atom has a shorter bond to S(3) [2.4577(7) Å] and a longer bond of 2.8784(8) Å to S(2a). The environment of Sb(2) is completed by S(4) at a distance of 2.3991(8) Å and the symmetry related S(4b) atom at 2.7084(7) Å yielding an $Sb(2)S_4$ unit. The two long Sb(2)−S distances are longer than expected for single bonds, which usually lie between about 2.4 and 2.6 Å, but they are significantly shorter than the typical so-called secondary bonds with Sb−S distances above about 2.9 Å. The two long Sb(2)−S bonds are in *trans* position to each other [angle: S(2a)−Sb(2)−S(4b): 174.95(2)°]. Taking into account the Sb^{III} $6s^2$ lone pair the environment may be described as distorted trigonal bipyramidal. We note that SbS_4 units are not uncommon and Sb−S distances between 2.4 and 2.85 Å were reported, for example, for $Cs_2Sb_8S_{13}$,[17] $(CH_3NH_3)_2Sb_8S_{13}$,[18] $Cs_5Sb_8S_{18}(HCO_3)$,[19] and $[Fe(C_4H_{13}N_3)_2]Sb_6S_{10}\cdot 0.5H_2O$.[20]

Two $Sb(2)S_4$ units share a common edge to form an Sb_2S_2 heteroring. Four such Sb_2S_2 heterorings are at the corners of a square-like net and are each joined by four $Sb(1)S_3$ pyramids yielding a two-dimensional thioantimonate(III) layer within the *ab* plane (Figure 2). The interconnection of the Sb_2S_2 rings and the pyramids yields large $Sb_{10}S_{10}$ rings with pores having a diameter of 10.19 × 8.388 Å (shaded area in Figure 2) measured between symmetry related Sb(1) atoms. The cavities of the rings are filled by the $[Co(tren)]^{2+}$ cations.

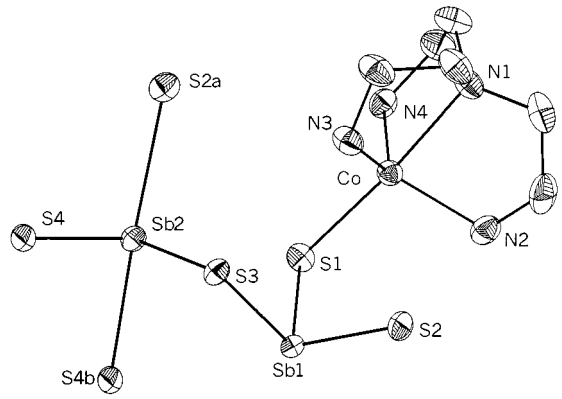

Figure 1. View of the $[Co(tren)]Sb_2S_4$ unit with labelling and displacement ellipsoids drawn at the 50% probability level; the symmetry codes are given in Table 1; hydrogen atoms are omitted for clarity

Table 1. Selected distances [Å] and angles [°] for $[Co(tren)]Sb_2S_4$

Sb(1)−S(1)	2.4165(7)	Sb(1)−S(2)	2.3899(7)
Sb(1)−S(3)	2.4655(6)	Sb(2)−S(2)[a]	2.8784(8)
Sb(2)−S(3)	2.4577(7)	Sb(2)−S(4)	2.3991(8)
Sb(2)−S(4)[b]	2.7084(7)	Co−S(1)	2.3539(7)
Co−N(1)	2.263(2)	Co−N(2)	2.077(2)
Co−N(3)	2.082(2)	Co−N(4)	2.092(2)
S(1)−Sb(1)−S(2)	103.05(2)	S(1)−Sb(1)−S(3)	96.53(2)
S(2)−Sb(1)−S(3)	95.71(3)	S(2)[a]−Sb(2)−S(3)	88.31(2)
S(2)[a]−Sb(2)−S(4)	93.39(2)	S(2)[a]−Sb(2)−S(4)[b]	174.95(2)
S(3)−Sb(2)−S(4)	99.15(2)	S(3)−Sb(2)−S(4)[b]	93.38(3)
S(4)−Sb(2)−S(4)[b]	91.04(2)	Co−S(1)−Sb(1)	106.95(3)
N(1)−Co−S(1)	175.32(6)	N(2)−Co−S(1)	105.35(7)
N(3)−Co−S(1)	98.38(6)	N(4)−Co−S(1)	98.70(6)
N(1)−Co−N(2)	79.30(9)	N(1)−Co−N(3)	79.37(8)
N(1)−Co−N(4)	79.11(8)	N(2)−Co−N(3)	120.85(9)
N(2)−Co−N(4)	108.54(8)	N(3)−Co−N(4)	120.36(9)
long Sb−S bonds [Å]			
Sb(1)−S(4)[b]	3.6103(8)	Sb(2)−S1	3.4765(9)

[a] Symmetry code: $0.5 - x$, $0.5 + y$, z. − [b] $-x$, $1 - y$, $-z$.

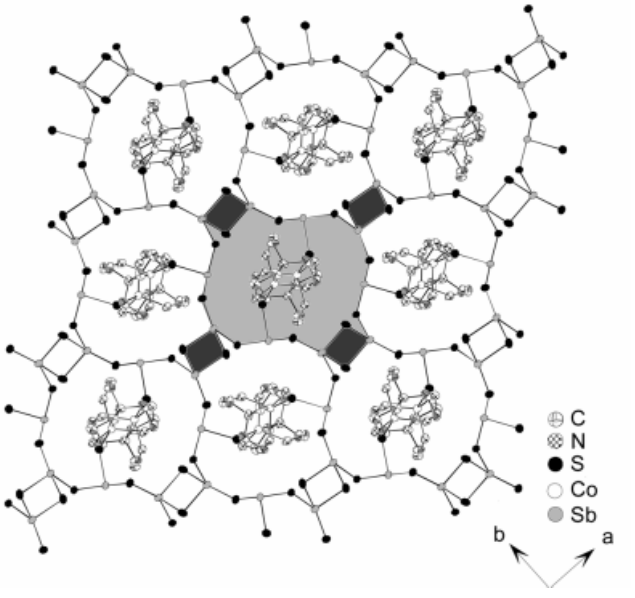

Figure 2. The crystal structure of $[Co(tren)]Sb_2S_4$ viewed along [001]; the Sb_2S_2 and the $Sb_{10}S_{10}$ heterorings are highlighted by shaded areas; the probability ellipsoids are drawn at the 50% level; hydrogen atoms are omitted for clarity

The layers are stacked parallel to the *c* axis to form channels containing the cations, with H···S contacts between 2.566 and 2.723 Å and angles N−H···S ranging from 150.24 to 164.63° indicating weak hydrogen bonding (Table 2).

Table 2. Selected H···S distances [Å] and angles [°]

$[Co(tren)]Sb_2S_4$				$[Ni(tren)]Sb_2S_4$			
N2−H1N2	2.566	154.30	S1[a]	N1−H2N1	2.594	146.62	S1[b]
N3−H2N3	2.723	164.63	S2[c]	N4−H1N4	2.834	161.26	S1[b]
N4−H1N4	2.626	150.24	S3[c]	N1−H1N1	2.615	166.86	S4[d]

[a] Symmetry code: $-x+1, -y+1, -z$. − [b] $-x+1, -y, -z+1$. − [c] $-x+1/2, y+1/2, z$. − [d] $x+1, y, z$.

The Sb atoms complete their coordination spheres by so-called secondary bonds to S atoms: one contact is observed for Sb(1) [3.6103(8) Å to S(4b)] and one for Sb(2) [3.4765(9) Å to S(1)] (Figure 3: A and B; Table 1). Taking these contacts into account the environment of Sb(1) may be viewed as a ψ-trigonal bipyramid (Figure 3, A) and that of Sb(2) as a distorted ψ-octahedron (Figure 3, B).

In $[Ni(tren)]Sb_2S_4$ the $[Ni]^{2+}$ ion is coordinated by four N atoms of the tren ligand with Ni−N distances ranging between 2.085(2) and 2.115(2) Å (see Table 3) and by two S atoms of the $^1_\infty[Sb_2S_4^{2-}]$ anion, yielding an octahedral coordination (Figure 4). The Ni−N bond lengths lie within the range reported in the literature.[21−23] The Ni−S bond lengths are 2.4306(8) Å for Ni−S(1) and 2.642(1) Å for Ni−S(4). An analysis of the geometry about the cation reveals why the Ni−S(4) distance is elongated: the S(1) and S(4) atoms have neighbouring N atoms at a distance of about 3.2−3.5 Å. A shortening of the Ni−S(4) bond to about 2.4 Å would bring the S(4) atom in closer contact to the N atoms leading to strong repulsive interactions. To avoid these repulsive forces the geometry at the $[Ni]^{2+}$ centre, as well as that of the anion, must be distorted, which is energetically unfavourable.

The thioantimonate(III) anion acts as a bidentate ligand to form an $NiSb_2S_3$ heteroring exhibiting the twist conformation (Figure 4). An interesting feature within the ring is the relatively large Ni−S(1)−Sb(1) angle of 121.73(3)°. In the overwhelming number of cases the angles around the

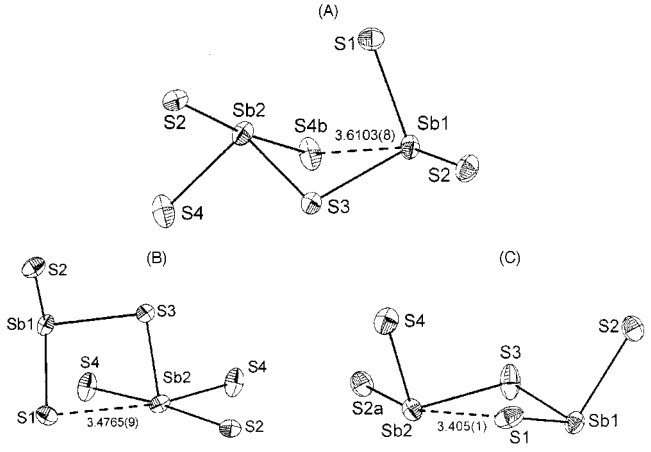

Figure 3. The environments of the Sb atoms with their long secondary bonds (dotted lines); (A and B) $[Co(tren)]Sb_2S_4$; (C) $[Ni(tren)]Sb_2S_4$; the numbers are the interatomic distances in Å

Table 3. Selected distances [Å] and angles [°] for $[Ni(tren)]Sb_2S_4$

Sb(1)−S(1)	2.3676(9)	Sb(1)−S(2)	2.4652(8)
Sb(1)−S(3)	2.4456(9)	Sb(2)−S(2)[a]	2.486(1)
Sb(2)−S(3)	2.4599(9)	Sb(2)−S(4)	2.3549(8)
Ni−S(1)	2.4306(8)	Ni−S(4)	2.642(1)
Ni−N(1)	2.097(2)	Ni−N(2)	2.115(2)
Ni−N(3)	2.085(2)	Ni−N(4)	2.105(2)
S(1)−Sb(1)−S(2)	103.03(3)	S(1)−Sb(1)−S(3)	100.19(4)
S(2)−Sb(1)−S(3)	93.16(3)	S(2)[a]−Sb(2)−S(3)	89.89(3)
S(2)[a]−Sb(2)−S(4)	97.02(3)	S(3)−Sb(2)−S(4)	102.03(3)
Ni−S(1)−Sb(1)	121.73(3)	Sb(1)−S(2)−Sb(2)[b]	96.27 (3)
Sb(1)−S(3)−Sb(2)	98.34(3)	Sb(2)−S(4)−Ni	102.64(3)
N(1)−Ni−N(2)	82.03(9)	N(1)−Ni−N(3)	94.1(1)
N(1)−Ni−N(4)	92.3(1)	N(2)−Ni−N(3)	83.6(1)
N(2)−Ni−N(4)	82.5(1)	N(3)−Ni−N(4)	163.8(1)
N(1)−Ni−S(1)	90.39(7)	N(2)−Ni−S(1)	169.95(7)
N(3)−Ni−S(1)	103.62(7)	N(4)−Ni−S(1)	91.22(8)
N(1)−Ni−S(4)	173.81(7)	N(2)−Ni−S(4)	91.79(7)
N(3)−Ni−S(4)	84.74(8)	N(4)−Ni−S(4)	87.23(8)
S(1)−Ni−S(4)	95.79(3)		
long Sb−S bonds [Å]			
Sb(2)−S(1)	3.405(1)		

[a] Symmetry code: $-1+x, y, z$. − [b] $1+x, y, z$.

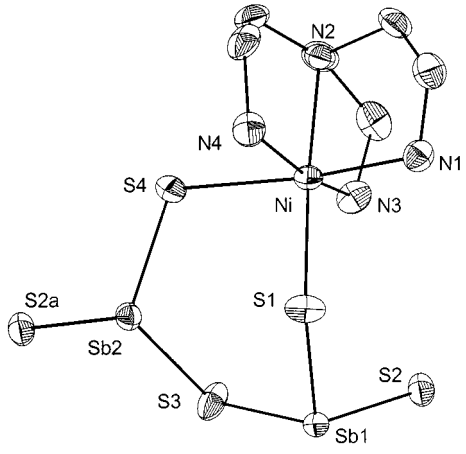

Figure 4. $[Ni(tren)]Sb_2S_4$ with the $NiSb_2S_3$ heteroring, labelling and displacement ellipsoids drawn at the 50% level; the hydrogen atoms are omitted for clarity

S atoms are between about 90 and 110°. For silicates, strong deviations of the Si−O−Si angles from the strain-free angle of about 140° are accompanied by an enhanced isotropic (U_{eq}) and/or anisotropic displacement parameter.[24] For S(1) the U_{eq} is comparable with those of the other atoms, but the U_{11} parameter is more than twice the U_{22} and U_{33} components. However, it should be noted that the U_{22} of S(3) is also large despite a relatively "normal" Sb(1)−S(3)−Sb(2) angle of 98.34(3)°, hence a straightforward relationship as for silicates is not obvious, and a rigorous analysis of many such thioantimonates(III) is required to establish such a relationship.

The anionic part of the structure, $^1_\infty[Sb_2S_4^{2-}]$, is composed of two corner-sharing SbS_3 pyramids formally yielding an Sb_2S_5 unit. The Sb−S distances are between

2.3549(8) and 2.486(1) Å, typical for single bonds. The Sb_2S_5 unit is interconnected via the S(2) atom into one-dimensional chains running parallel to the *a* axis (see Figure 5). These chains are arranged in a simple hexagonal rod packing. The coordination sphere of Sb(2) is completed by a secondary bond to S(1) of 3.405(1) Å forming a distorted ψ-trigonal bipyramid (Figure 3, C; Table 3). For the Sb(1) atom no S atoms are found at distances less than 4 Å. Three short intermolecular H···S distances (Table 2) with distances ranging from 2.594 to 2.834 Å and N−H···S angles between 146.62° and 166.86° are observed, which may indicate weak hydrogen bonding.

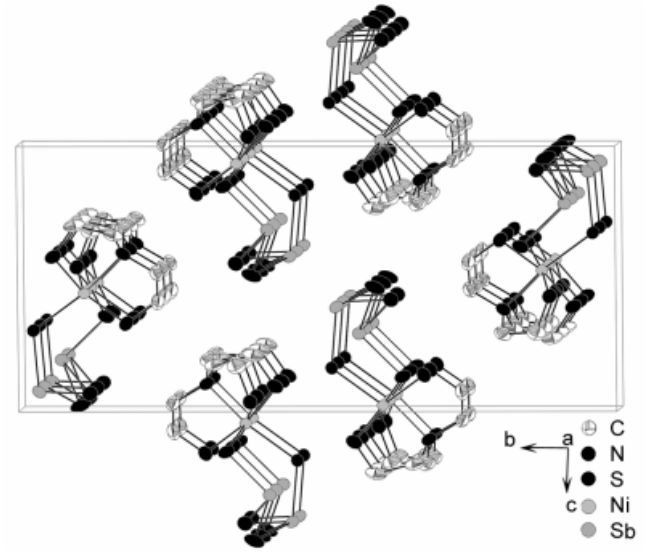

Figure 5. Crystal structure of [Ni(tren)]Sb_2S_4 viewed along [100]; the probability ellipsoids are drawn at the 50% level; hydrogen atoms are omitted for clarity

The $[Co]^{2+}$ cation has a d^7 electronic configuration. Simple considerations suggest that the energy differences between the trigonal bipyramidal and octahedral coordination should be negligible. Therefore, it can be assumed that the geometrical requirements of the tetradentate ligand force the formation of the trigonal bipyramidal environment. For $[Ni]^{2+}$, with a d^8 electronic configuration, the octahedral environment is energetically favoured over the trigonal bipyramidal arrangement.

Thermal Investigations

[Co(tren)]Sb_2S_4: The DTA-TG curve is shown in Figure 6. Decomposition starts at T_{onset} = 262 °C. A weight loss occurs in two steps on heating. These steps are accompanied by two strong endothermic signals in the DTA curve with peak temperatures T_p = 270 °C and T_p = 295 °C. The total loss of weight amounts to $-\Delta m_{1+2}$ = 23.8% ($-\Delta m_1$ = 15.8%, $-\Delta m_2$ = 8%). If the tren ligand is extruded during thermal decomposition a value of $-\Delta m_{theo(tren)}$ = 25.3% is expected. C, H and N were all found in the grey residue (C: 0.4%; H: 0.5%; N: 0.2%; CHN_{sum} = 1.1%) suggesting that the decomposition reaction is more complex. In the decomposition product Sb_2S_3, CoS and CoSbS was identified by X-ray powder diffraction (XRD).

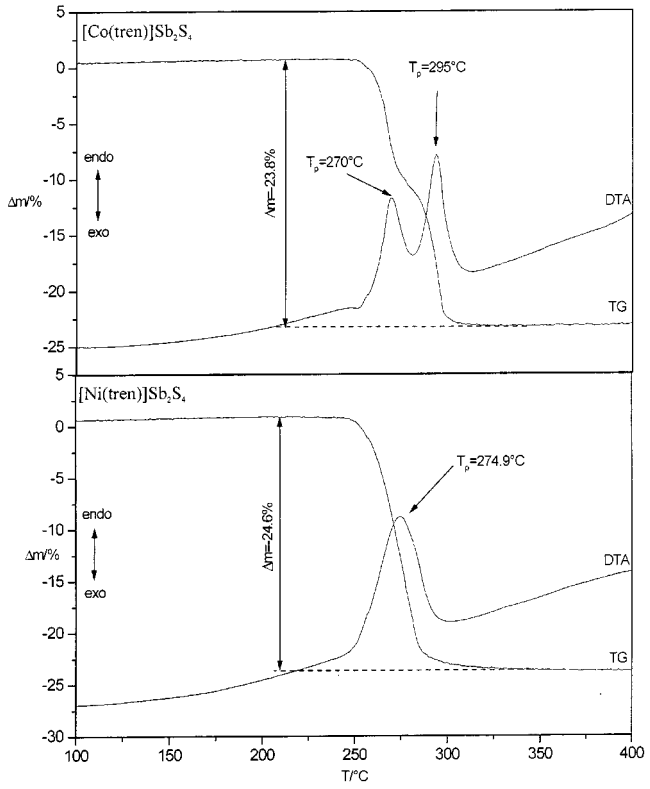

Figure 6. DTA and TG curves of [Co(tren)]Sb_2S_4 (atmosphere: argon; weight: 75.10 mg powdered crystals; heating rate: 3 °C/min) and [Ni(tren)]Sb_2S_4 (atmosphere: argon; weight: 68.50 mg; heating rate: 3 °C/min; T_p = peak temperature)

In a further experiment the decomposition was stopped at 270 °C. In the X-ray powder pattern Sb_2S_3, CoS, CoSbS and a small amount of a fourth phase were identified. The weight loss between T_p = 270 °C and T_p = 295 °C may be attributed to the decomposition of the unknown phase accompanied by the emission of C, H and N as well as S (C: 5.061%; H: 0.876%; N: 3.242%; CHN_{sum} = 9.179%). In the IR spectrum of the residue no C−H, C−N, C−C or N−H vibrations could be detected.

[Ni(tren)]Sb_2S_4: A significantly different behaviour is observed for the Ni compound. As can be seen in Figure 6 the sample decomposes in one step with an endothermic signal in the DTA curve at T_p = 274.9 °C (T_{onset} = 254 °C). The loss of weight is $-\Delta m$ = 24.6% which is similar to the value calculated for the emission of the tren ligand ($-\Delta m_{theo(tren)}$ = 25.4%). In the black residue small amounts of C, H and N could be found (C: 0.3%; H: 0.3%; N: 0.2%; CHN_{sum} = 0.8%). No C−H, C−N, C−C or N−H vibrations could be detected in the IR spectrum. NiS, Sb_2S_3 and NiSbS could be identified by X-ray powder diffraction.

Raman Spectroscopy

The changes of the bonding properties of a lone pair atom are best detected from changes in the bond angles, as interatomic bond lengths are only affected slightly.[25,26]

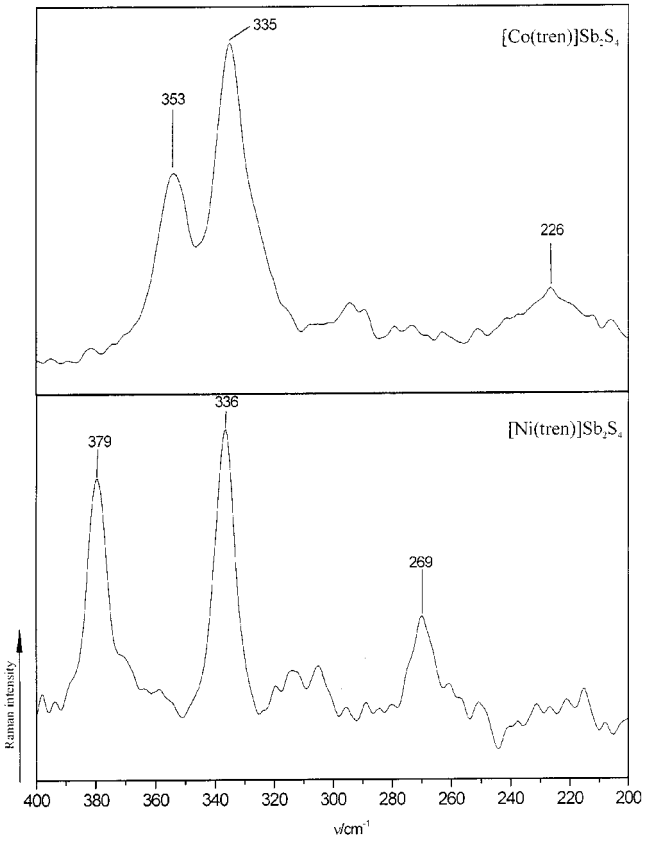

Figure 7. Raman spectra of $[Co(tren)]Sb_2S_4$ and $[Ni(tren)]Sb_2S_4$

This means that the local environment of the Sb^{III} ions does not lead to significant alterations of the Sb−S distances. In the Raman spectra, however, the different bonding properties of the two title compounds become apparent (Figure 7). For $[Co(tren)]Sb_2S_4$ two intense bands located at 353 and 335 cm^{-1} are observed, in accordance with the observation that all Sb^{III} ions have a $(3 + n)$ coordination [$n = 1$ for Sb(1) and $n = 2$ for Sb(2)]. For the Ni compound one Raman band is located at 379 cm^{-1} which can be assigned to $Sb(1)S_3$; a band at lower frequency of 336 cm^{-1} is due to the $Sb(2)S_4$ unit. The lower Raman frequencies obtained for the Co compound reflect the decreased bonding interactions within the $[SbS_3^{3-}]$ units. The Raman bands at 226 cm^{-1} (Co compound) and 269 cm^{-1} (Ni compound) are assigned to Co−S/Ni−S vibrations. The assignment of the Sb−S modes is in accordance with the results reported by Pfitzner for Cu_3SbS_3 and $(CuI)_2Cu_3SbS_3$.[27] In the former compound two maxima were observed at 321 and 290 cm^{-1} reflecting the weaker bonding interaction due to the (3 + 5) environment. In the latter compound the $[SbS_3^{3-}]$ anion has no next-nearest S atoms, yielding Raman bands at 362 and 339 cm^{-1}. For $Mn_2Sb_2S_4$ with one Sb^{III} atom in a sixfold and the other Sb^{III} atom in a sevenfold environment of S atoms the Raman bands occur at even lower frequencies and are located between about 280 and 310 cm^{-1}.[28]

Experimental Section

Synthesis: $[Ni(tren)]Sb_2S_4$ was first prepared by reacting elemental Ni, Sb and S in an aqueous solution of tren under solvothermal conditions in a Teflon-lined steel autoclave (inner volume: 30 mL). In a typical synthesis 1 mmol of Ni (0.0586 g), 1 mmol of Sb (0.1217 g) and 3 mmol of S (0.0962 g) were added to 10 mL of a 50% aqueous tren solution. The mixture was heated at 140 °C for 8 days then cooled to room temperature within 3 h. The reaction mixture was filtered, washed with water and acetone and cleaned in an ultrasonic bath. The product consists of green square-like crystals of the title compound as the major phase and a grey microcrystalline powder as the minor phase which is amorphous to X-rays. In the by-product the elements Ni, S, and Sb were identified by an EDAX analysis. Stirring the reaction mixture during the synthesis gave a phase-pure product using the same ratio of starting materials as under static conditions. C, H N analysis: calcd. C 12.49, H 3.15, N 9.72; found C 12.24, H 3.05, N 9.60.

$[Co(tren)]Sb_2S_4$: Dark black squares of $[Co(tren)]Sb_2S_4$ were prepared by reacting a mixture of elemental Co (0.059 g, 1 mmol), Sb (0.121 g, 1 mmol) and S (0.096 g, 3 mmol) in an aqueous solution of 50% tren (10 mL) (Merck Chemical). The synthesis was performed in a Teflon-lined steel autoclave, which was heated to 140 °C, held at this temperature for 7 days and then cooled to room temperature within 3 h. The products were filtered off, washed with water and dried under vacuum. The yield was 70% based on Co. Stirring the solution during the synthesis gave nearly 100% yield based on Co (Co/Sb/S = 1:1:3) in an aqueous solution of 10 mL tren (50%) at 140 °C. Calcd. C 12.49, H 3.14, N 9.71; found C 12.14, H 3.14, N 9.17. NB The differences between the applied starting material ratio and the 1:2:4 ratio in the solid products is due to unknown antimony sulfide species dissolved in the solution.

Structure Determination: Intensities were collected on a STOE Imaging Plate Diffraction System (IPDS) and a STOE AED-II four-circle diffractometer using monochromated Mo-K_α radiation (λ = 0.71073 Å). The intensities were corrected for Lorentz, polarisation and absorption effects. Structure solution was performed using SHELXS-97.[29] Refinement was done against F^2 using SHELXL-97.[30] All heavy atoms were refined anisotropically. The hydrogen atoms were positioned with idealised geometry and refined with fixed isotropic displacement parameters using a riding model. Technical details of data acquisition and refinement results are summarised in Table 4.

Thermoanalytical Measurements: Thermoanalytical measurements were performed using a DTA-TG device STA 429 from Netzsch. All measurements were performed under an argon atmosphere (flow rate 50 mL min^{-1}) with Al_2O_3 crucibles and heating rates of 3 K min^{-1}.

Raman Spectroscopy: Raman spectra were measured in the region from 100 to 3500 cm^{-1} with a Bruker IFS 66 Fourier transform Raman spectrometer (wavelength: 514.5 nm, 20 K).

X-ray Powder Diffractometry: The X-ray powder patterns were recorded on a STOE Stadi-P diffractometer (Co-$K_{\alpha 1}$, Cu-$K_{\alpha 1}$ radiation, λ = 1.788965 and 1.540598 Å, respectively) in transmission geometry.

Crystallographic data (excluding structure factors) for the structures reported in this paper have been deposited with the Cambridge Crystallographic Data Centre as supplementary publication nos. CCDC-162040 for $[Ni(tren)]Sb_2S_4$ and CCDC-162041 for $[Co(tren)]Sb_2S_4$. Copies of the data can be obtained free of charge on application to CCDC, 12 Union Road, Cambridge

Table 4. Technical details of data acquisition and selected refinement results for $[Co(tren)]Sb_2S_4$ and $[Ni(tren)]Sb_2S_4$

Empirical formula	$[Co(C_6H_{18}N_4)]Sb_2S_4$	$[Ni(C_6H_{18}N_4)]Sb_2S_4$
Colour, habit	black squares	dark green squares
Crystal size	0.3 × 0.1 × 0.1 mm	0.3 × 0.02 × 0.1 mm
Molecular weight	576.91 g/mol	576.69 g/mol
Crystal system	orthorhombic	monoclinic
Space group	*Pbca*	$P2_1/n$
Calculated density	2.345 g/cm^3	2.412 g/cm^3
a	13.886(3) Å	6.906(1) Å
b	11.452(2) Å	22.822(5) Å
c	20.549(4) Å	10.347(2) Å
β	90.00 °	103.17(3) °
V	3267.9(11) A^3	1587.9(6) A^3
Z	8	4
Temperature	293 *K*	293 *K*
Scan range	$5° \leq 2\theta \leq 56°$	$5.4° \leq 2\theta \leq 56°$
	$-17 \leq h \leq 18$	$0 \leq h \leq 9$
	$-15 \leq k \leq 15$	$0 \leq k \leq 30$
	$-24 \leq l \leq 25$	$-13 \leq l \leq 13$
Measured reflections	31348	4246
Independent reflections	3766	3827
Reflections with $F_o > 4\sigma(F_o)$	3345	3251
μ	4.78 mm^{-1}	5.06 mm^{-1}
$R_{int.}$	0.030	0.016
Absorption correction	face-indexed	face-indexed
Min./max. trans.	0.3609/0.5848	0.3693/0.6770
Extinction coefficient[a]	none	$x = 0.00050(10)$
Weight[b]	$y = 0.0242$, $z = 2.1033$	$y = 0.0205$, $z = 0.7594$
*R*1 $[F_o > 4\sigma(F_o)]$	0.0197	0.0187
*R*1 (all reflections)	0.0249	0.0306
*wR*2 $[F_o > 4\sigma(F_o)]$	0.0437	0.0449
*wR*2 (all reflections)	0.0456	0.0468
Δρ	−0.67/0.66 e/Å^3	−0.41/0.71 e/Å^3
Goodness of fit	1.072	1.038

[a] $F^* = F_c(k[1 + 0.001 \cdot x \cdot F_c^2 \cdot \lambda^3/\sin(2\theta)]^{-0.25})$. − [b] $w = 1/[\sigma^2(F_o^2) + (yP)^2 + zP]$; $P = (\max(F_o^2,0) + 2F_c^2)/3$.

CB2 1EZ, UK [Fax: (internat.) +44-1223/336-033; E-mail: deposit@ccdc.cam.ac.uk].

Acknowledgments

This work has been supported by the State of Schleswig-Holstein and the Fonds der Chemischen Industrie.

[1] G. L. Schimek, J. W. Kolis, G. J. Long, *Chem. Mater.* **1997**, *9*, 2776−2785.
[2] C. L. Cahill, J. B. Parise, *Chem. Mater.* **1997**, *9*, 807−811.
[3] K. Tan, A. Darovsky, J. B. Parise, *J. Am. Chem. Soc.* **1995**, *117*, 7039−7040.
[4] C. L. Bowes, W. U. Huynh, S. J. Kirkby, A. Malek, G. A. Ozin, S. Petrov, M. Twardowski, D. Young, R. L. Bedard, T. Broach, *Chem. Mater.* **1996**, *8*, 2147−2152.
[5] A. Pfitzner, M. Evain, V. Petricek, *Acta Crystallogr., Sect. B* **1997**, *53*, 337−345.
[6] J. Garin, E. Parthe, H. R. Oswald, *Acta Crystallogr., Sect. B* **1972**, *28*, 3672−3674.
[7] A. Pfitzner, *Z. Anorg. Allg. Chem.* **1994**, *620*, 1992−1997.
[8] S. Karup-Møller, E. Makovicky, *Am. Mineral.* **1974**, *59*, 889−895.
[9] E. Makovicky, T. Balic-Zunic, *Can. Mineral.* **1995**, *33*, 655−663.
[10] M. F. Razmara, C. M. B. Henderson, R. A. D. Pattrick, *Mineral. Mag.* **1997**, *61*, 79−88.
[11] A. V. Powell, S. Boissiere, A. M. Chippindale, *J. Chem. Soc., Dalton Trans.* **2000**, *22*, 4192−4195.
[12] H.-O. Stephan, M. G. Kanatzidis, *J. Am. Chem. Soc.* **1996**, *118*, 12226−12227.
[13] W. Bensch, M. Schur, *Eur. J. Solid State Inorg. Chem.* **1996**, *33*, 1149−1160.
[14] M. Schur, C. Näther, W. Bensch, *Z. Naturforsch.* **2001**, *56b*, 79−84.
[15] L. Engelke, R. Stähler, M. Schur, C. Näther, W. Bensch, *Z. Anorg. Allg. Chem.* **2001**, in preparation.
[16] R. Demuth, F. Kober, Grundlagen der Komplexchemie, Frankfurt am Main, **1992**, *2*, 145−150.
[17] K. Volk, H. Schäfer, *Z. Naturforsch.* **1979**, *34b*, 1637−1640.
[18] X. Wang, F. Liebau, *J. Solid State Chem.* **1994**, *111*, 385−389.
[19] G. L. Schimek, J. W. Kolis, *Inorg. Chem.* **1997**, *36*, 1689−1693.
[20] R. Stähler, C. Näther, W. Bensch, *Eur. J. Inorg. Chem.* **2001**, *7*, 1835−1840.
[21] W. Bensch, C. Näther, R. Stähler, *Chem. Commun.* **2001**, *5*, 477−478.
[22] J. Ellermeier, W. Bensch, *Monatsh. Chem.* **2001**, *132*, 565−573.
[23] R. Stähler, C. Näther, W. Bensch, *Acta Crystallogr., Sect. C* **2001**, *57*, 26−27.
[24] F. Liebau, Structural Chemistry of Silicates, Springer Verlag, Germany, **1985**, p. 24 ff.
[25] X. Wang, F. Liebau, *Acta Crystallogr., Sect. B* **1996**, *52*, 7−15.
[26] X. Wang, F. Liebau, *Z. Kristallogr.* **1996**, *211*, 437−439.
[27] A. Pfitzner, *Chem. Eur. J.* **1997**, *3*, 2032−2038.
[28] A. Pfitzner, D. Kurowski, *Z. Kristallogr.* **2000**, *215*, 373−376.
[29] G. M. Sheldrick, *SHELXS-97*, Universität Göttingen, **1997**.
[30] G. M. Sheldrick, *SHELXL-97*, Universität Göttingen, **1997**.

Received April 25, 20001
[I01145]

Speciation of Al^{III} in Blood Serum − The Al^{III}−Citrate−Phosphate Ternary System

Andrea Lakatos,[a] Ferenc Evanics,[b] György Dombi,[b] Roberta Bertani,[c] and Tamás Kiss*[d]

Keywords: Aluminium / Citric acid / Inorganic phosphate / Speciation of blood serum / NMR spectroscopy / Bioinorganic chemistry

Time-dependent speciation studies have been carried out on the ternary Al^{III}–citrate (A)–phosphate (B) system in order to clarify the solution state of Al^{III} in blood serum. The potentiometric results indicate that ternary complexes predominate both in freshly prepared mixtures and at equilibrium. The ternary species AlAB and $AlABH_{-1}$ and the binary species $AlAH_{-1}$ and $AlBH_{-1}$ are present at physiological pH. As the solution ages the amount of the trinuclear species $[Al_3(AH_{-1})_3(OH)]^{4-}$ increases at the expense of the mononuclear binary and ternary complexes. ^{31}P NMR spectra measured at neutral pH provide corroborating evidence of the formation of the ternary complexes AlAB and $AlABH_{-1}$ and binary species $AlBH_{-1}$ and Al_2BH_{-3} found potentiometrically. Time-dependent ^1H NMR measurements show that monodentate phosphate can slowly displace citrate from the otherwise very stable structure of the trinuclear species $[Al_3(AH_{-1})_3(OH)]^{4-}$. At blood serum concentrations [$c(Al^{III})$ = 3 μM], Al^{III} is mostly bound to citrate either in binary species or in the ternary species formed with phosphate. However, with increasing Al^{III} concentrations binding to phosphate becomes more important.

Introduction

The toxicity of aluminium is recognized as the cause of various neurological disorders, including dialysis dementia and other skeletal and haematological disorders.[1,2] Its involvement in Alzheimer's disease (AD) is rather controversial, although it is largely accepted that Al^{III} is not a causative agent but may serve as a risk factor by inducing conformational changes in neuropeptides, leading to the enhanced formation of plaques and tangles, the common markers of AD.[3,4] To understand the toxic effects of Al^{III}, it is important to know the chemical forms in which Al^{III} can enter the organism or in which it is present in natural waters, soil waters, biological fluids, and tissues. The absorption, excretion, tissue retention, and deposition of Al^{III} depend on the properties of the Al^{III} complexes formed with exogenous and endogenous biological ligands. After absorption in the body, Al^{III} is transported via the blood stream to the target organs. The main carrier of Al^{III} in blood serum is transferrin;[3−5] albumin, the other high molecular mass (h.m.m.) protein, is not an efficient aluminium binder.[6] Transferrin binds about 80% of the total Al^{III}; the remaining 20% is complexed by the low molecular mass (l.m.m.) bioligands present in blood serum.[7] As regards the most important l.m.m. Al^{III} binders, the picture is rather controversial. Dayde et al.,[8] Jackson,[9] and Harris[7] propose inorganic phosphate, while Clevette and Orvig,[10] Duffield et al.,[11] and Öhman and Martin[12,13] suggest that citrate is the main Al^{III} binder. The main reasons for the divergent results are the kinetically rather sluggish equilibration of the Al^{III}−citrate system and the very slow ligand-exchange processes of the citrate complexes of Al^{III}.[14−16] In freshly prepared solutions of Al^{III} and citrate, 1:1 mononuclear species are present; these polymerize to the trinuclear complex $[Al_3(AH_{-1})_3OH]^{4-}$ in rather slow processes. In the presence of a large excess of the ligand, 1:2 complexes predominate and the trinuclear species is of less importance. At pH 7.4 and a metal ion-to-ligand ratio of 1:1, besides the aforementioned trinuclear complex, the mononuclear species $[Al(AH_{-1})]^-$ and $[Al(AH_{-1})OH]^{2-}$ are present in solution; at higher ligand excesses, the bis complexes $[Al(AH_{-1})(A)]^{4-}$ and $[Al(AH_{-1})_2]^{5-}$ are formed.[14−17]

The Al^{III}−phosphate system can only be studied directly in a fairly acidic pH range, because at pH > 4 $AlPO_4$, or, more precisely, a mixed hydroxo-phosphato complex precipitates. To estimate the binding constants of Al^{III}−phosphate species at physiological pH, linear free-energy relationships (LFER) have been used. Harris[7] and Atkari et al.[18] concluded that the predominant species at pH

[a] Biocoordination Chemistry Research Group of the Hungarian Academy of Sciences, University of Szeged,
P. O. Box 440, 6701 Szeged, Hungary
[b] Department of Pharmaceutical Analytical Chemistry, University of Szeged,
P. O. Box 35, Szeged, Hungary
[c] Centro di Studio sulla Chimica e Tecnologia dei Composti Metallorganici degli Elementi di Transizione, CNR,
Via Marzolo 9, 35131 Padova, Italy
[d] Department of Inorganic and Analytical Chemistry, University of Szeged,
P. O. Box 440, 6701 Szeged, Hungary
E-mail: tkiss@chem.u-szeged.hu

 © WILEY-VCH Verlag GmbH, 69451 Weinheim, 2001 1434−1948/01/1212−3079 $ 17.50+.50/0

7.4 is the mixed hydroxo complex $Al(PO_4)(OH)^-$, but they obtained values differing by approximately an order of magnitude for the binding constant of this species.

All the models proposed for the biological speciation of Al^{III} only take into account binary species of Al^{III} with l.m.m. bioligands. However, biological systems invariably contain many potential binder ligands and hence the formation of ternary complexes may also be very important. Since the main potential l.m.m. Al^{III} binders in blood serum are citrate and phosphate, the formation of their ternary species would seem to be a very logical assumption. For this reason, we have studied the Al^{III}−citrate (A)−phosphate (B) ternary system. As a consequence of the slow oligomerization processes, time-dependent speciation measurements could be carried out. The time-dependent species distribution can give a more accurate description of the Al^{III} speciation in blood serum as Al^{III} does not generally attain thermodynamic equilibrium in biological fluids because of its very sluggish ligand-exchange reactions.

Results and Discussion

Time-Dependent Potentiometric Study

Potentiometric titrations were carried out in order to determine the protonation constants of the two ligands and the concentrations of their solutions. The proton complex formation constants obtained in this way are reported in Table 1.

For the Al^{III}-containing samples, as for the binary Al^{III}−citrate system,[16] very sluggish electrode responses were observed in the slightly acidic and neutral pH ranges. Thus, instead of carrying out normal titrations, the Al^{III}-containing samples were analysed using the batch method described in the Exp. Sect.. The time course of the pH changes proved to be dependent on the starting pH of the samples: starting at pH < 5.6, the hydrogen ion concentration increases with time, while above this pH it decreases. Similar behaviour was observed for the binary Al^{III}−citrate system[16] and was explained in terms of the slow oligomerization of the mononuclear complexes with formation of the trinuclear species $[Al_3(AH_{-1})_3OH]^{4-}$. While the oligomerization of the semi-protonated mononuclear complexes is accompanied by the release of protons in the acidic pH range, at basic pH the mixed hydroxo species oligomerize with the liberation of hydroxide ions.[16] This explanation seems to be applicable to the ternary system as well (vide supra). For each sample, the zero-time data (the pH values corresponding to the time of mixing of the components) were extrapolated from the first three minutes of the pH changes.

Through a combination with the potentiometric data obtained at the same time, a series of titration curves was created. Some selected curves obtained at an Al^{III}−citrate−phosphate ratio of 1:1:1 are depicted in Figure 1. The main differences between the titration curves relating to different times are seen in the pH range 3−5.6, the range of formation of the trinuclear citrato complex. At higher pH, in contrast to the results obtained for the Al^{III}−citrate system, no measurable time dependence was observed. The titration curve obtained after 30 h represents the equilibrium state. At an Al^{III}−citrate−phosphate ratio of 1:1:4, the time-induced changes are not so spectacular, due to the large excess of phosphate, which may partly suppress the oligomerization processes and also buffer the pH effect of the oligomerization.

In the evaluation of the titration curves corresponding to the equilibrium state, the stability constants of the binary complexes in the Al^{III}−citrate system were regarded as known values; we used the results obtained earlier in a time-dependent speciation study of the binary Al^{III}−citrate system.[16] For the binary Al^{III}−phosphate species, our basis was the speciation model proposed by Atkari.[19] For this system, pH equilibrium could be attained in less than 5 min for each point and thus normal titrations were carried out for speciation description. The applied model, however, gives practically no information on the species formed at pH > 4, since the formation of a precipitate of alumi-

Table 1. Stability constants of proton and Al^{III} binary complexes of citrate (A) and phosphate (B) and ternary complexes of citrate and phosphate at 25 °C and I = 0.2 M (KCl)

log K[a]/log β Al^{III}−citrate[16]		Al^{III}−phosphate[19]		Al^{III}−citrate−phosphate	
$K([HA]^{2-})$	5.57(2)	$K([HB]^{2-})$	11.52(1)		
$K([H_2A]^-)$	4.27(2)	$K([H_2B]^-)$	6.63(1)		
$K([H_3A])$	2.87(3)	$K([H_3B])$	1.86(1)		
$[AlAH]^+$	10.18	$[AlBH_2]^{2+}$	19.65	$[AlABH_2]^-$	28.46(4)
[AlA]	7.85	$[AlBH]^+$	17.60	$[AlABH]^{2-}$	25.02(7)
$[AlAH_{-1}]^-$	4.27	[AlB]	13.50	$[AlAB]^{3-}$	19.68(6)
$[AlAH_{-2}]^{2-}$	−1.77	$[AlBH_{-1}]^-$	8.37	$[AlABH_{-1}]^{4-}$	12.03(7)
$[AlA_2]^{3-}$	12.73	$[Al_2B]^{3+}$	17.42		
$[AlA_2H_{-1}]^{4-}$	7.81	$[Al_2BH_{-2}]^+$	11.05	fitting (Δ cm^3)[b]	0.0083
$[AlA_2H_{-2}]^{5-}$	0.4	$[Al_2BH_{-3}]$	6.9		
$[Al_3A_3H_{-4}]^{4-}$	16.34				

[a] log K values are the logarithms of the stepwise protonation constants, which are numerically the same as the negative logarithms of the acidity constants pK_a of the corresponding species; ±3 S.D. values are given in parentheses. − [b] Average difference between the experimental and calculated titration curves, expressed in cm^3 of titrant.

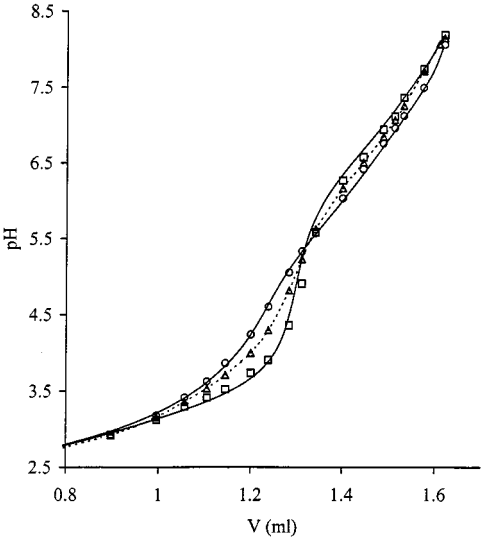

Figure 1. Titration curves (plotted as mL titrant KOH versus pH) of the Al^{III}−citrate−phosphate system at a ratio of 1:1:1, c_{Al} = 0.004 M and at different times after mixing of the reactants: (O) immediately after mixing (zero time), (Δ) 40 min after mixing, (□) at equilibrium (after 30 h); the solid curve was calculated using the stability constants reported in Table 1; the intermediate dashed curve serves only to join the titration points and does not represent any theoretical model

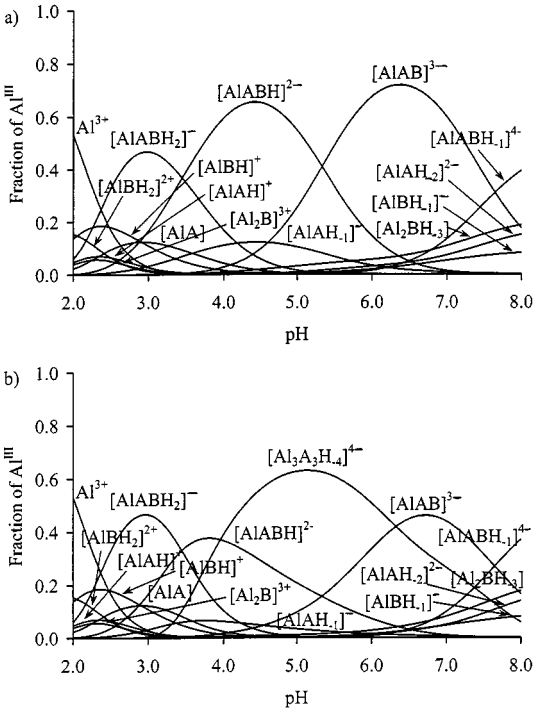

Figure 2. Species distribution curves as a function of pH for the Al^{III}−citrate−phosphate system at a 1:1:4 ratio, c_{Al} = 0.004 M and at different times after sample preparation: (a) immediately after mixing, (b) at equilibrium (after 30 h)

nium(III) phosphate does not allow potentiometric studies above this pH. For data evaluation in the neutral and slightly basic pH ranges, the stability constants of the Al^{III}−phosphate complexes [AlB] (log β = 13.50) and $[AlBH_{-1}]^-$ (log β = 7.20) estimated by LFER calculations[18] were used. In addition to the binary citrato and phosphato complexes, the formation of ternary Al^{III}−citrate−phosphate species was assumed in the speciation calculations. The species distribution calculated using the stability constants obtained for the ternary system at equilibrium showed that the amount of the Al^{III}−phosphate complex $[AlBH_{-1}]^-$ was negligible. In contrast, NMR spectroscopy indicated the presence of a considerable amount of this binary Al^{III}−phosphate complex at neutral pH (see later). This led to the conclusion that the stability constant of the complex $[AlBH_{-1}]^-$ (log β = 7.2) obtained by means of LFER calculations[18] may be underestimated. It should be noted here that Harris[7] suggested a stability constant one order of magnitude higher (log β = 8.37) for this species. When this value was used in the model calculations, the fitting of the experimental titration data were slightly improved. The speciation model obtained and the stability constants of the complexes are listed in Table 1. The titration curves corresponding to the zero-time data were fitted well if the sole formation of mononuclear complexes was assumed and the trinuclear complex $[Al_3(AH_{-1})_3OH]^{4-}$ was excluded from the speciation model. Speciation curves of the complexes formed on mixing of the components and in the equilibrium state are depicted in Figure 2.

Both immediately after mixing and at equilibrium, the ternary complexes $[AlABH_2]^-$, $[AlABH]^{2-}$, $[AlAB]^{3-}$, and $[AlABH_{-1}]^{4-}$ predominate in the system over the entire pH range. In addition to these complexes, as Figure 2 indicates, the concentration of the trinuclear species $[Al_3(AH_{-1})_3OH]^{4-}$ increases with time at the expense of the initially formed mononuclear binary and ternary complexes. In fresh solutions, the trinuclear species is hardly formed, while at equilibrium it is the predominant complex over a wide pH range. It can also be seen that at physiological pH (7−7.4) most of the Al^{III} is bound in the ternary complexes $[AlAB]^{3-}$ and $[AlABH_{-1}]^{4-}$, but that significant amounts of the binary phosphato complexes $[Al_2BH_{-3}]$ and $[AlBH_{-1}]^-$ are also present. Because of the excess of phosphate, the mononuclear and trinuclear binary citrato complexes are somewhat less important at an Al^{III}−citrate−phosphate ratio of 1:1:4. In the absence of citrate, Al^{III}−phosphate precipitates under neutral to alkaline conditions as a solid of variable composition, $Al(PO_4)_f(OH)_{3(1-f)}$, where the value of f varies from 1 to 0 as a function of the pH and concentration of the solution.[13] Detailed solubility measurements led Martin and Öhman[13] to conclude that $f = 0.75$ at pH 7.4; thus, the precipitate may be described as $Al(PO_4)_{0.75}(OH)_{0.75}$ and characterized by $\log K_{SO} = [Al^{3+}][PO_4^{3-}]^{0.75}/[H]^{0.75} = -11.1$. In the presence of citrate (at Al^{III}−citrate ratios of at least 1:1 and up to a maximum tenfold phosphate excess), the solutions are clear even at higher concentrations (0.04 and 0.1 M).[13] However, besides the proposed soluble Al^{III}−phosphate complexes $[Al_2BH_{-3}]$ and $[AlBH_{-1}]^-$, this Al^{III}−hydroxide−phosphate precipitate dissolves to form not only ternary Al^{III}−citrato−phosphato−hydroxo complexes, but probably also outer-sphere complexes with the

binary Al^{III}−citrate species through electrostatic and/or hydrogen-bonding interactions. This interpretation may explain our observation that potentiometry indicates the formation of a greater amount of ternary complexes than is suggested by NMR spectroscopy (vide infra).

As regards the ternary complexes, the complexation starts with the formation of $[AlABH_2]^-$ in acidic solution. In this complex, both ligands are coordinated to Al^{III}, probably each in a monoprotonated form. Thus, the complex should be written as $[AlCitH(HPO_4)]^-$. Here, the citrate binds to Al^{III} as a tridentate ligand through one terminal and the central carboxylate group and also the protonated hydroxy group (as in the binary species $[AlAH]^+$ [16]) and the hydrogen phosphate coordinates to Al^{III} as a monodentate ligand. The other terminal carboxylic group of the citrate ion is protonated and unbound. Further deprotonations occur on the coordinated hydroxy group and the unbound terminal carboxylate group with formation of the complexes $[Al(Cit)(HPO_4)]^{2-}$ and $[Al(CitH_{-1})(HPO_4)]^{3-}$. The ternary species $[AlABH_{-1}]^{4-}$ eventually formed can exist in two microforms: $[Al(CitH_{-1})(PO_4)]^{4-}$, with the phosphate coordinated to Al^{III} as a trivalent ligand with all hydroxy groups in deprotonated form, and $[Al(CitH_{-1})(HPO_4)(OH)]^{4-}$, which is a mixed hydroxo species.

NMR Spectroscopic Measurements

The formation of ternary Al^{III}−citrate−phosphate species was also unambiguously demonstrated by NMR spectroscopy. For correct NMR signal assignment, we first studied the Al^{III}−phosphate system. Figure 3, a, shows the ^{31}P NMR spectrum recorded at pH ≈ 2.2 and an Al^{III}−phosphate ratio of 1:2. The intense sharp signal at δ = 1.03 is due to free phosphate, while the other resonances can be attributed to the complexed ligand. Although a number of authors have investigated the Al^{III}−phosphate system, the assignment of the ^{31}P NMR signals remains uncertain. Akitt et al.[20,21] attributed these signals to differently protonated mononuclear 1:1 and 1:2 species and a polynuclear complex. Feng and Waki[22] assumed the presence of coordination isomers. The authors generally agree that, in the presence of excess ligand, the signal at δ = −6.37, which is the closest to the signal of the free ligand, is due to a bis-Al^{III}−phosphate complex. Our results for an Al^{III}−phosphate solution at a metal ion-to-ligand ratio of 1:4 and pH ≈ 2.2 support this assumption, since the intensity of the signal in question is increased compared to that in the spectrum recorded at a metal ion-to-ligand ratio of 1:2 and also relative to the other signals in the spectrum (not shown). For the ternary Al^{III}−citrate−phosphate system, the formation of binary Al^{III}−citrate species results in a higher phosphate excess than in the citrate-free solution under the same conditions, which favours formation of the bis-Al^{III}−phosphate complex. This is reflected in an increased intensity of the resonance at δ = −6.37 (Figure 3, b). Akitt et al.[21] also detected this signal at more acidic pH, and assigned it to a highly protonated 1:2 complex, AlB_2H_6. However, the formation of this species with the phosphate in fully protonated form is highly questionable, especially at pH ≈ 2. No similar bis complex has been found at acidic pH in any potentiometric study. As regards the other signals in the spectrum (see Figure 3, a), by analogy with the Al^{III}−phosphinate system, Feng and Waki[22] established that the coordination mode of the ligand (proceeding from the signal of the free ligand to higher fields) varies in the following order: monodentate, bidentate, and bridged coordination. To summarize the literature results and those from our own experiments, and additionally taking into account our potentiometric findings, the signals in the spectrum depicted in Figure 3, a, could be assigned as follows: free phosphate: δ = 1.03; highly protonated bis complex with monodentate phosphate coordination: δ = −6.37; monodentate phosphate-coordinated species $[AlBH_2]^{2+}$ and $[AlBH]^+$: δ = −6.91; the complex $[AlBH]^+$ with the ligand coordinated in a bidentate fashion and the binuclear phosphate and/or hydroxide-bridged complex $[Al_2B]^{3+}$: δ = −11.42 (the shape of the resonance suggests the presence of two overlapping signals belonging to two different species). The signal at δ = −16.42 was assigned by Akitt et al.[21] to another polynuclear (most probably trinuclear) complex. Feng and Waki[22] could not detect this latter species in less concentrated solution (0.025 M). At the millimolar concentrations employed in our potentiometric study, the formation of this polynuclear complex is probably negligible.

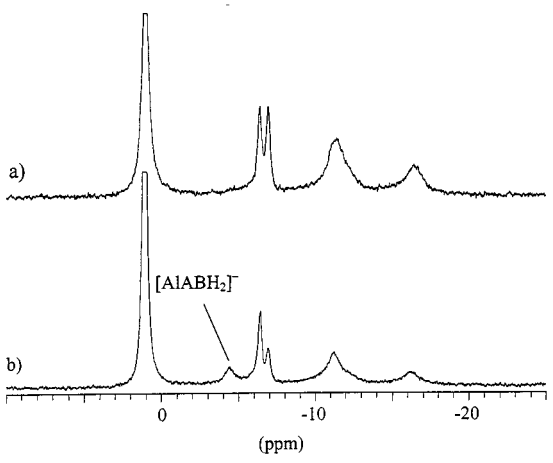

Figure 3. ^{31}P NMR spectra measured at pH ≈ 2.2 in a solution of (a) Al^{III}−phosphate at a 1:2 ratio and (b) Al^{III}−citrate−phosphate at a 1:1:2 ratio; c_{Al} = 0.04 M

Besides the aforementioned signals, in the spectrum of the citrate-containing solution at pH ≈ 2.2 a new ^{31}P resonance is seen at δ = −4.41; this could clearly be assigned to the ternary complex $[AlABH_2]^-$. On the basis of the chemical shift of this signal in the complex $[AlABH_2]^-$, the phosphate group must be coordinated in a monodentate fashion. On increasing the pH of the samples, the resonance of the ternary complexes is shifted downfield, which indicates that there is a rapid proton-exchange between the differently protonated ternary species. At pH ≈ 3, the resonances corresponding to the ternary complexes $[AlABH_2]^-$ and $[AlABH]^{2-}$ (δ = −4.2) and the monodentate phosphate-

coordinated binary complex $[AlBH]^+$ ($\delta = -5.64$) can be assigned unambiguously, but a small amount of the complex $[Al_2B]^{3+}$ is also present, giving a broad signal centred at around $\delta = -11$. At higher pH, due to the poor resolution of the spectra (the signals are broad and merged) the signals are extremely difficult to assign. This is well-illustrated by the spectrum recorded at pH ≈ 7.4 (Figure 4), where the very broad signals at $\delta = -3.7$, -9.3, and -13.9 were attributed to the ternary complexes $[AlAB]^{3-}$ and $[AlABH_{-1}]^{4-}$, the mononuclear 1:1 complex $[AlBH_{-1}]^-$, and the dinuclear complex $[Al_2BH_{-3}]$, respectively. Since no spectra of the binary Al^{III}−phosphate system could be recorded because of precipitation at this pH, signals were assigned on the basis of their relative intensities, taking into account the potentiometric speciation results and the spectra measured in the acidic pH range. The pattern of the signals, however, may suggest the presence of coordination isomers, possibly including the bidentate phosphate-coordinated isomer of the ternary complex and the proposed outer-sphere complexes of the Al^{III}−hydroxide−phosphate precipitate formed with the binary Al^{III}−citrate species (vide supra).

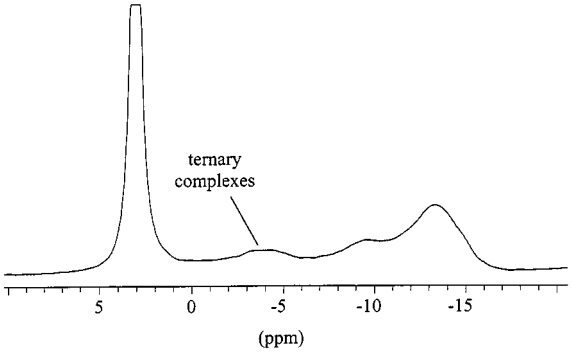

Figure 4. ^{31}P NMR spectrum recorded for the Al^{III}−citrate−phosphate system at a metal ion-to-ligand ratio of 1:1:2 and pH ≈ 7.4; $c_{Al} = 0.04$ M

In the ^1H NMR spectra of the same solutions, only the AB quadruplet of free citrate can be unambiguously assigned. The resonances of the other complexes present are merged into one very broad signal in the chemical shift range $\delta = 3.0-2.4$, probably as a consequence of the quadrupole effect of ^{27}Al nuclei and the relatively fast exchange reactions between these complexes. The resolution of the spectra was not improved even at low temperatures (5−10 °C). In the pH range of formation of the trinuclear complex $[Al_3(AH_{-1})_3OH]^{4-}$, its signals are well-separated and easily discerned as a result of its rigid structure and slow proton- and ligand-exchange reactions.[23] Figure 5 shows the ^1H NMR spectrum obtained at pH ≈ 7.4, which clearly indicates the slow formation of the trinuclear complex.

Since the primary aim of this work was to characterize the behaviour of the Al^{III}−citrate−phosphate system under physiological conditions, we attempted to obtain quantitative information from ^1H and ^{31}P NMR measurements. For a quantitative evaluation of the spectrum, a known amount of dioxane was added to a solution of the

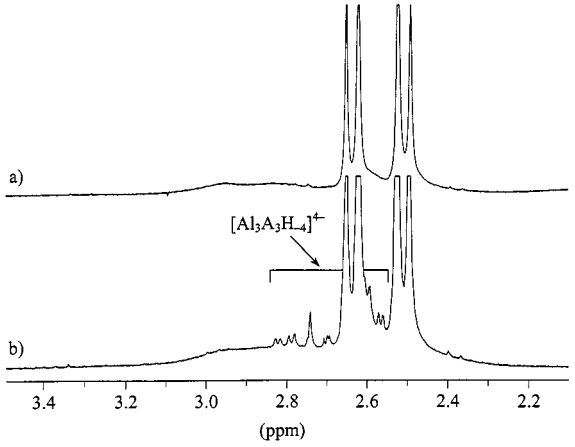

Figure 5. ^1H NMR spectra of the Al^{III}−citrate−phosphate system at a metal ion-to-ligand ratio of 1:1:2 and pH ≈ 7.4: (a) in freshly prepared solution, (b) at equilibrium; $c_{Al} = 0.04$ M

Al^{III}−citrate−phosphate 1:1:2 system under thermodynamic equilibrium at pH ≈ 7.4 and the amount of free citrate was calculated from the ^1H NMR spectrum using the deconvolution method. About 43% of the citrate was found to be free, while 57% was complexed in binary and ternary species. Since the ratio of Al^{III}−citrate in these solutions was 1:1, and since potentiometry indicates that only 1:1 Al^{III}−citrato species exist in the system, an amount of Al^{III} equivalent to the free citrate (43%) should be complexed in the binary Al^{III}−phosphato species. We should mention here that the ^{27}Al NMR spectrum of this solution featured one very broad resonance centred at $\delta \approx 3$, suggesting the formation of complexes containing Al^{III} in an octahedral environment, and gave no indication of the presence of free $[Al(OH)_4]^-$ (no signal at $\delta = -80$), i.e. no uncomplexed Al^{III} in the sample. Integration of the signals due to the free and the complexed phosphate in the ^{31}P NMR spectrum of the same solution revealed that ca. 65% of the phosphate was free and ca. 35% was in complexed form. This means that about 70% of the Al^{III} was bound in phosphate-containing complexes (including the ternary species), as the ratio of Al^{III}−phosphate in the sample was 1:2. The ^1H and ^{31}P NMR spectra revealed that ca. 43% of the total Al^{III} was bound in binary Al^{III}−phosphato species, ca. 30% in binary Al^{III}−citrato complexes, and ca. 27% in ternary complexes. In contrast, the speciation calculations indicate 58% in ternary complexes. This difference in the results of NMR and potentiometry may be explained partly by the relatively high degree of error in the percentage values calculated from the NMR measurements due to the rather poor quality of the spectra, and partly by the assumption of the formation of outer-sphere complexes (vide supra), which cannot be clearly observed by NMR spectroscopy.

These results indicate that (although a full quantitative speciation description of the Al^{III}−citrate−phosphate system could not be given) under the conditions (concentrations and metal ion-to-ligand ratios) of our NMR measurements, the binding abilities of the ligands citrate and phos-

phate to complexed Al^{III} are practically the same at physiological pH.

Reaction of the Trinuclear Species in the Presence of Inorganic Phosphate

The most characteristic species of the Al^{III}–citrate speciation is the trinuclear complex $[Al_3(AH_{-1})_3OH]^{4-}$. This is the predominant complex in equimolar Al^{III}–citrate solution between pH 4 and 9, i.e. in the range including physiological pH. The solid-state structure of the complex has been determined by X-ray crystallography[24] and the same rather asymmetric binding mode was confirmed by solution ^1H and ^{13}C NMR studies.[23] This raises the question as to what happens to this very stable and kinetically rather inert species in the presence of phosphate. Is phosphate able to decompose the trinuclear species? To answer this question, a twofold excess of phosphate (pH 7.4) was added to a 0.1 M solution of the trinuclear complex adjusted to pH 7.4. A slight increase ($\approx$ 0.2 pH unit) in the pH of the solution was observed and the spectral changes over time were monitored by ^1H, ^{31}P, and ^{13}C NMR. The ^1H NMR spectrum shows that the very characteristic proton spectrum (Figure 6, a) of the trinuclear complex collapses in the presence of phosphate (Figure 6, b), and that citrate is slowly partially displaced by phosphate as the AB quadruplet of free citrate clearly appears in the spectrum recorded after five days (Figure 6, c).

In the ^{31}P NMR spectrum of the same sample, a sharp signal initially appeared at $\delta = -1.8$, besides the resonance of the free phosphate. The intensity of this signal slowly decreased and it disappeared completely at equilibrium.

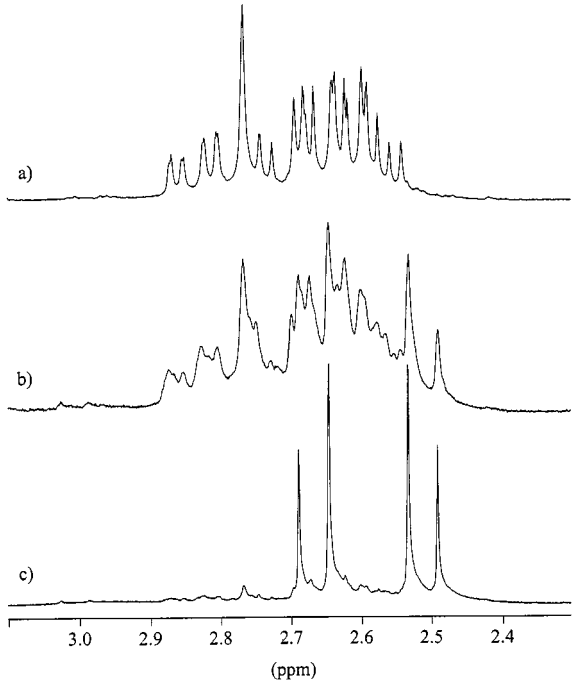

Figure 6. Decomposition of the trinuclear Al^{III}–citrate complex in the presence of a twofold excess of phosphate as monitored by ^1H NMR spectroscopy: (a) spectrum of the trinuclear species, (b) 10 h and (c) 5 days after the addition of phosphate; $c_{complex}$ = 0.1 M

The pattern of the equilibrium spectrum was the same as that obtained when Al^{III} was added to a solution of a mixture of citrate and phosphate (see Figure 4). The signal at $\delta = -1.8$ may presumably be assigned to a mixed-ligand complex formed as an intermediate species during decomposition of the trinuclear complex. The signals of this intermediate complex can easily be recognized in the ^{13}C NMR spectrum of the above solution. Besides the signals of the trinuclear complex (δ = 41.80, 42.90, 43.67, 44.98, 45.95, 46.24, 73.37, 75.51, 75.68, 177.18, 177.64, 177.89, 177.92, 178.19, 178.45, 180.78, 182.75, and 182.89),[16] 14 new resonances appear at δ = 41.83, 43.77, 45.51, 46.10, 46.46, 73.10, 75.25, 177.43, 177.73, 177.91, 178.88, 179.44, 180.85, and 183.29, which suggests that the intermediate species is most probably an oligonuclear mixed-ligand complex with a relatively asymmetric structure. During the formation of this complex, phosphate may be incorporated into the structure of the trinuclear complex $[Al_3(AH_{-1})_3OH]^{4-}$, replacing one or more of the coordinated donor groups of one of the citrate molecules. The ligand exchange between the trinuclear complex $[Al_3(AH_{-1})_3OH]^{4-}$ and the intermediate species is slow on the NMR time scale.

Modelling of Blood Serum

As one of the aims of the work was to determine whether citrate or phosphate is the primary l.m.m. Al^{III} binder in blood serum, we constructed the species distribution at plasma concentrations by using the speciation model and the stability constants obtained from the potentiometric measurements (Figure 7). For the calculations, the serum model suggested by Harris[7] was used: c(phosphate) = 1.1 mM, c(citrate) = 99 μM; the other l.m.m. constituents of blood serum, such as lactate, oxalate, amino acids, etc.,[7] have significantly lower affinities for Al^{III} and their participation in Al^{III} binding can therefore be neglected. This was assumed in all previous modelling calculations.[8–13] The total Al^{III} concentration was taken as 3 μM, which is in the range of serum concentrations observed for patients on haemodialysis.[7] In the calculations, we also took into account the fact that only ca. 20% of the total Al^{III} in the serum is bound to l.m.m. biomolecules while ca. 80% is bound to the h.m.m. components, mostly to transferrin[7] (vide supra). Figure 7 shows that at biologically relevant Al^{III} concentrations ($c_{Al}^{III} \approx$ 3 μM, of which only 0.6 μM is bound to l.m.m. components) the mononuclear complexes predominate and ternary species are formed in significant amounts. The oligomerization processes are strongly suppressed. At physiological pH, 51% of the Al^{III} is bound to citrate in the complex $[AlAH_{-2}]^{2-}$, ca. 28% is bound in the ternary species $[AlAB]^{3-}$ and $[AlABH_{-1}]^{4-}$, and ca. 21% is bound in the binary species with phosphate, $[AlBH_{-1}]^{-}$. If, however, we envisage an Al overload case, when the serum Al^{III} level can increase up to 100 μM, assuming a complete saturation of transferrin the distribution of Al^{III} between the h.m.m. and l.m.m. fractions of serum is 26:74%. The distribution of Al^{III} between citrate, phosphate binary, and citrate–phosphate ternary complexes becomes ca. 32%, 51%, and 17%, respectively. Interestingly, at increasing Al^{III}

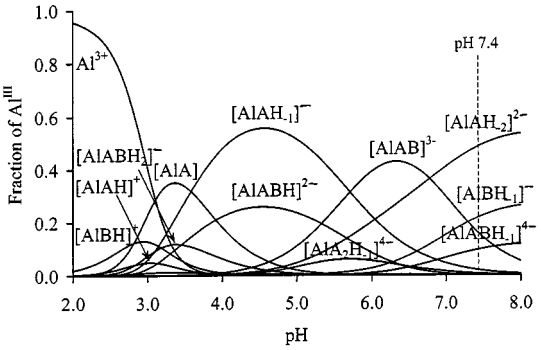

Figure 7. Species distribution curves for complexes formed in the Al^{III}−citrate−phosphate system at serum concentrations ($c_{Al} = 6 \times 10^{-7}$ M, $c_{citrate} = 99 \times 10^{-6}$ M, $c_{phosphate} = 1.1 \times 10^{-3}$ M, see text)

concentrations, phosphate becomes the more important binder.

Citrate-bound Al^{III} (either in binary or in ternary species) has been observed directly in blood plasma by Sadler et al. by means of ^1H NMR spectroscopy.[25] In a more recent study, Bantan et al.[26] investigated the speciation of l.m.m. Al^{III} complexes in human serum taken from eight healthy volunteers by means of fast liquid chromatography and electrospray techniques. In agreement with our results, they found that the main l.m.m. Al^{III} species present in the serum were binary Al^{III}−citrate and Al^{III}−phosphate and ternary Al^{III}−citrate−phosphate complexes. The distribution of these complexes varied from individual to individual.

Conclusions

This work has clearly demonstrated that the assumption of ternary complex formation may be of great importance in the modelling of biological systems. In the ternary Al^{III}−citrate−phosphate system under model conditions, the ternary species dominate, especially in freshly prepared solutions. Gradual increases in the concentrations of the trinuclear species over time are observed. This has been confirmed by time-dependent NMR spectral measurements. At physiological pH and millimolar concentrations, most of the Al^{III} is bound in the ternary complexes $[AlAB]^{3-}$ and $[AlABH_{-1}]^{4-}$, but some Al^{III} is also bound in the binary species involving citrate or phosphate. The trinuclear species $[Al_3(AH_{-1})_3OH]^{4-}$ slowly decomposes in the presence of excess phosphate, indicating that monodentate phosphate is not a negligible Al^{III} binder and that the trinuclear citrato species is not completely stable under these conditions. The latter is nevertheless relatively inert as the partial citrate replacement by excess phosphate reaches equilibrium only after several days.

At normal blood serum concentrations and physiological pH, Al^{III} is bound partly in mononuclear ternary complexes but mostly in the mixed Al^{III}−citrate−hydroxo complex $[AlAH_{-2}]^{2-}$.

Experimental Section

Reagents: Citric acid of the highest available purity was purchased from Sigma; the phosphate used was the highest quality monopotassium salt from Fluka. The ligands were used without further purification. Their purities were checked and the precise concentrations of their solutions were determined by the Gran method.[27] An Al^{III} stock solution was prepared from recrystallized $AlCl_3 \cdot 6H_2O$; its metal concentration was determined gravimetrically following conversion into the oxinate. The stock solution contained 0.1 M HCl to prevent hydrolysis of the aluminium.

Potentiometric Measurements: The stability constants of the proton complexes of the ligands were determined by pH-potentiometric titrations of 10.0 cm^3 samples. The ligand concentration was 0.004 M. The titrations were performed using 0.2 M carbonate-free KOH solution of known concentration under a purified argon atmosphere. The ionic strength of all solutions for potentiometric measurements was adjusted to 0.2 M with KCl and the samples were thermostatted at 25.0 ± 0.1 °C.

In this work, only the Al^{III}−citrate−phosphate ternary system was analysed; stability constants for the binary systems were taken from our previous studies.[16,18,19] The time-dependent speciation measurements were performed using the batch technique, in a similar manner as described for the Al^{III}−citrate binary system.[16] After appropriate amounts of stock solutions of the ligand and base had been mixed with the Al^{III} solution, the pH of the resulting mixture was recorded at given times until thermodynamic equilibrium of the system had been obtained (ca. 30 h). The procedure was repeated for different starting pH values, whereby titration curves relating to different times were obtained. The measurements were carried out at Al^{III}−citrate−phosphate ratios of 1:1:1 and 1:1:4 in 10.0 cm^3 solutions with intense stirring under argon atmosphere. The pH range studied was 2−8. For each ratio, the time-dependent changes were monitored for 20 different samples. However, in order to increase the reliability of the speciation description of the system at thermodynamic equilibrium and to reduce the uncertainties in the calculated stability constants, twice as many samples were prepared, but every second one was only analysed 30 h after mixing, when pH equilibrium had been attained. The stability constants listed in Table 1 were calculated from the total number of batch points (40 points for each metal ion ligand composition). In the case of the Al^{III}−phosphate binary system,[18,19] pH equilibrium could be attained within 5 min for each point and the normal titration procedure was used to obtain the stability constants for the complexes formed. The pH was measured with an Orion 710A precision digital pH-meter with a Metrohm combined glass electrode, which was calibrated for hydrogen ion concentration according to Irving et al.[28]

The concentration stability constants $\beta_{pqrs} = [M_pA_qB_rH_s]/[M]^p[A]^q[B]^r[H]^s$ were calculated with the aid of the computer program PSEQUAD.[29] The stability constants used for the hydroxo species of Al^{III} were taken from ref.[30] and corrected to $I = 0.2$ M using the Davies equation: −5.49 for $[AlH_{-1}]^{2+}$, −13.54 for $[Al_3H_{-4}]^{5-}$, −97.2 for $[Al_{13}H_{-32}]^{7-}$, and −23.40 for $[AlH_{-4}]^{-}$.

NMR Spectroscopy: ^1H, ^{31}P, and ^{13}C NMR spectra were recorded at 25 °C on Bruker AM360 and DMX500 spectrometers. For the ^1H and ^{13}C NMR spectra, chemical shifts were referenced to the signal of TMS as an external standard, while for the ^{31}P NMR spectra 85% orthophosphoric acid was used as an external standard. The samples were prepared in D_2O and the pH was adjusted with concentrated NaOD and DCl, using the relationship pH =

pD + 0.4. The concentrations of the solutions were 0.04−0.1 M in Al^{III}; samples with Al^{III}−phosphate ratios of 1:1, 1:2, and 1:4 and Al^{III}−citrate−phosphate ratios of 1:1:1, 1:1:2, and 1:1:4 were investigated. Unless otherwise stated, all NMR measurements were made on thermodynamically equilibrated samples. − ^{27}Al NMR spectra were measured on a Bruker AM200 instrument at 25 °C. Chemical shifts were recorded with respect to $Al(H_2O)_6^{3+}$. Solutions containing 0.1 M Al^{III} and having a metal ion-to-ligand ratio of 1:1:2 were prepared in water, to which 10% D_2O was added to provide a lock signal.

Acknowledgments

This work was carried out within the framework of the COST D8 collaboration and was supported by the Hungarian Research Fund (OTKA 23776/97) and the Hungarian Ministry of Education (FKFP 0013/97).

[1] M. Nicolini, P. F. Zatta, B. Corain (Eds.), *Aluminum in Chemistry, Biology and Medicine*, Harwood Academic Publishers, Switzerland, **1994**, vol. 2.
[2] R. A. Yokel, M. S. Golub (Eds.), Research Issues in Aluminum Toxicity, *J. Toxicol. Environm. Health* **1996**, *48*, 527−683.
[3] R. B. Martin, J. Savory, S. Brown, R. L. Bertholf, M. R. Wills, *Clin. Chem.* **1987**, *33*, 405−407.
[4] W. R. Harris, J. Sheldon, *Inorg. Chem.* **1990**, *29*, 119−124.
[5] G. de Jong, C. C. A. Ammerloan, W. L. van Mort, H. G. van Eijh, G. L. van Landeghem, P. C. D'Haese, M. E. de Broe, *Biometals* **1995**, *8*, 352−356.
[6] S. J. A. Fatemi, D. J. Williamson, G. R. Moore, *J. Inorg. Biochem.* **1992**, *46*, 35−40.
[7] W. R. Harris, *Clin. Chem.* **1992**, *38*, 1809−1818.
[8] S. Dayde, M. Filella, G. Berthon, *J. Inorg. Biochem.* **1990**, *38*, 241−259.
[9] G. E. Jackson, *Polyhedron* **1990**, *9*, 163−170.
[10] D. J. Clevette, C. Orvig, *Polyhedron* **1990**, *9*, 151−161.
[11] J. R. Duffield, K. Edwards, D. A. Evans, D. M. Morrish, R. A. Vole, D. R. Williams, *J. Coord. Chem.* **1991**, *23*, 277−290.
[12] R. B. Martin, *Acc. Chem. Res.* **1994**, *27*, 204−210.
[13] L. O. Öhman, R. B. Martin, *Clin. Chem.* **1994**, *40*, 598−601.
[14] L. O. Öhman, S. Sjöberg, *J. Chem. Soc., Dalton Trans.* **1983**, 2513−2517.
[15] L. O. Öhman, *Inorg. Chem.* **1988**, *27*, 2565−2570.
[16] A. Lakatos, I. Bányai, P. Decock, T. Kiss, *Eur. J. Inorg. Chem.* **2001**, 461−469.
[17] J. E. Gregor, H. K. J. Powell, *Aust. J. Chem.* **1986**, *39*, 1851−1864.
[18] K. Atkári, T. Kiss, R. Bertani, R. B. Martin, *Inorg. Chem.* **1996**, *35*, 7089−7094.
[19] K. Atkári, Diploma Work, Debrecen, **1994**.
[20] J. W. Akitt, N. N. Greenwood, G. D. Lester, *J. Chem. Soc. (A)* **1971**, 2450−2457.
[21] M. A. Wilson, P. J. Collin, J. W. Akitt, *Anal. Chem.* **1989**, *61*, 1253−1259.
[22] Q. Feng, H. Waki, *Polyhedron* **1991**, *10*, 659−665.
[23] A. Bodor, I. Bányai, I. Tóth, *Coord. Chem. Rev.*, submitted.
[24] T. L. Feng, P. L. Gurian, M. D. Healy, A. R. Barron, *Inorg. Chem.* **1990**, *29*, 408−411.
[25] J. D. Bell, G. Kubal, S. Radulovic, P. J. Sadler, A. Tucker, *Analyst* **1993**, *118*, 241−244.
[26] T. Bantan, R. Milacic, B. Mitrovic, B. Pihlar, *J. Anal. At. Spectrom.* **1999**, *14*, 1743−1748.
[27] G. Gran, *Acta Chem. Scand.* **1950**, *4*, 559−575.
[28] H. M. Irving, M. G. Miles, L. D. Pettit, *Anal. Chim. Acta* **1967**, *38*, 475−481.
[29] L. Zékány, I. Nagypál, G. Peintler, PSEQUAD for Chemical Equilibria, Technical Software Distribution, Baltimore, **1991**.
[30] L. O. Öhman, S. Sjöberg, *Acta Chem. Scand., Ser. A* **1982**, *36*, 47−53.

Received May 7, 2001
[I01160]

Thermodynamics of Complexation of Cadmium(II) by Open-Chain N-Donor Ligands in Dimethyl Sulfoxide Solution

Clara Comuzzi,[a] Michela Grespan,[a] Andrea Melchior,[a] Roberto Portanova,[a] and Marilena Tolazzi*[a]

Keywords: Cadmium / Ammine complexes / Solvent effects / Calorimetry / Thermodynamics

Thermodynamic parameters for the complexation of Cd^{II} by the amines *n*-butylamine (*n*-but), ethylenediamine (en), *N*,*N*′-dimethylethylenediamine (dmen), *N*,*N*,*N*′-trimethylethylenediamine (trmen), *N*,*N*,*N*′,*N*′-tetramethylethylenediamine (tmen), diethylenetriamine (dien), *N*,*N*′′-dimethyldiethylenetriamine (dmdien), and *N*,*N*,*N*′,*N*′′,*N*′′-pentamethyldiethylenetriamine (pmdien) have been determined in dimethyl sulfoxide (DMSO) solution by potentiometric and calorimetric techniques at 298 K and 0.1 mol dm^{-3} ionic strength (NEt_4ClO_4). Only mononuclear complexes are formed, in which the polyamines act predominantly as chelating agents. All the complexes are enthalpy-stabilized, whereas the entropy changes counteract the complexation. The steric requirements of the donors have a strong influence on the stoichiometry and nature of the Cd^{II} complexes formed. Comparisons are made with data reported for some of these systems in water and with available data on silver(I) complexation by the same amines in DMSO, the latter showing that the selectivity of the ligands towards metal ions is also influenced by *N*-alkylation.

Introduction

In the last few years, many papers have been published concerning the complexation of transition and f-block metal ions by a number of multidentate polyamines.[1−9] The aim of this work has been to improve knowledge on the coordination chemistry of hard and soft metal ions with N-donor ligands in aprotic solvents of varying donating ability, as well as to investigate the strong influence of the basicities and steric properties of the ligands on the thermodynamic stability and nature of the complexes formed. These studies have also attracted renewed interest as the coordination properties of open-chain polyamines towards different cations have been used as models allowing direct comparison with the corresponding macrocyclic systems.[10]

In particular, the papers published by our group concerning complexation of the transition metal ions silver(I) and cobalt(II)[3a−3f] have shown that the coordination properties of polyamines towards these ions may be modulated through adjustment of the alkyl chain length between the donor atoms or through nitrogen functionalization. Methylation of nitrogens leads to a decrease in the thermodynamic stability of the corresponding metal complexes due to the decreased σ-donor ability of *N*-methylated groups. Nitrogen functionalization may also lead to molecular crowding and to an increase in the radii of the complexes; such steric effects may strongly affect the selectivity pattern in metal coordination. As far as cobalt(II) complexes are concerned, different *N*-alkylation of polyamines has important effects on the dioxygen affinity of these complexes.[3f,10]

[a] Dipartimento di Scienze e Tecnologie Chimiche, Università di Udine,
Via Cotonificio 108, 33100 Udine, Italy
Fax: (internat.) +39−0432−558803
E-mail: tolazzi@dstc.uniud.it

In this context, and as an extension of previous work, we have now undertaken an investigation on the complexation of Group 12 dications by a series of open-chain and cyclic polyamines in aprotic solvents. Especially interesting comparisons should be possible between the monovalent d^{10} acceptor silver(I), with very soft character, and the divalent very soft Hg^{2+} or moderately soft Cd^{2+}. Moreover, despite the fact that complexation of Group 12 dications has been extensively studied in the past[11−14] and in more recent years,[15] scant thermodynamic data are available concerning their coordination by simple, open-chain N-donor ligands.[13h,14]

In this paper, we report the first results concerning the complexation of Cd^{II} by the differently *N*-methylated mono- and polyamines *n*-butylamine (*n*-but), ethylenediamine (en), *N*,*N*′-dimethylethylenediamine (dmen), *N*,*N*,*N*′-trimethylethylenediamine (trmen), *N*,*N*,*N*′,*N*′-tetramethylethylenediamine (tmen), diethylenetriamine (dien), *N*,*N*"-dimethyldiethylene triamine (dmdien), and *N*,*N*,*N*′,*N*′′,*N*′′-pentamethyldiethylenetriamine (pmdien) in the aprotic solvent dimethyl sulfoxide (DMSO).

In order to investigate both the influence of the solvent on Cd^{II} complexation as well as the selectivity of these ligands toward metal ions, comparisons are made with available data for the same systems in water[14] and with previously obtained data concerning Ag^{I} complexation by some of these polyamines.[3a−3e]

Potentiometric and calorimetric measurements have been used to obtain the free energies and enthalpies of the reactions, respectively. All measurements were performed at 298 K in an ionic medium adjusted to 0.1 mol dm^{-3} with NEt_4ClO_4 as the neutral salt. FT-IR spectroscopy has been used to provide insight into the coordination modes of the ligands.

 © WILEY-VCH Verlag GmbH, 69451 Weinheim, 2001 1434−1948/01/1212−3087 $ 17.50+.50/0

Table 1. Overall stability constants and thermodynamic functions for the reaction $Cd^{2+} + jL \rightleftarrows CdL_j^{2+}$ in DMSO at 298 K and $I = 0.1$ mol dm^{-3}, and for that in water;[14] the errors quoted correspond to three standard deviations

Ligand	Complex	$\log\beta_j$	$-\Delta G°_{\beta j}$/kJmol^{-1}	$-\Delta H°_{\beta j}$/kJmol^{-1}	$-T\Delta S°_{\beta j}$/kJmol^{-1}
n-but 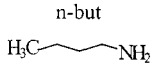	CdL	2.6(0.2)	14.8(1.2)	24.1(0.9)	9.3
	CdL_2	4.2(0.2)	24.0(1.1)	58(3)	34
	CdL_3	6.0(0.3)	34.2(1.7)	71(3)	36.8
en 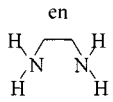	CdL	5.88(0.01)	33.62(0.02)	52.2(0.5)	19
	CdL_2	11.40(0.02)	65.1(0.1)	96.9(0.4)	31.8
	CdL_3	15.81(0.02)	90.2(0.1)	147.1(0.1)	56.9
dmen 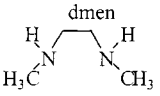	CdL	5.22(0.02)	29.8(0.1)	43.8(0.5)	14
	CdL_2	9.61(0.01)	55.0(0.1)	90.0(0.5)	35
	CdL_3	11.09(0.04)	63.3(0.2)	143.1(1.4)	79.8
trmen 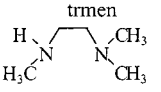	CdL	4.13(0.02)	23.6(0.1)	39.0(0.4)	15.4
	CdL_2	6.39(0.02)	36.5(0.1)	78.6(0.3)	42.1
tmen 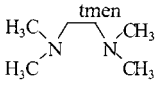	CdL	3.1(0.03)	17.7(0.2)	35.7(0.9)	18
dien 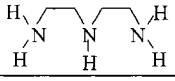	CdL	8.46(0.05)	48.3(0.3)	65.3(0.9)	17
	CdL_2	17.18(0.08)	98.2(0.3)	137.2(0.8)	39
dmdien 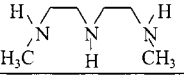	CdL	7.51(0.08)	42.8(0.5)	60.2(0.9)	17.4
	CdL_2	13.42(0.09)	76.6(0.5)	109.7(0.9)	33.1
pmdien 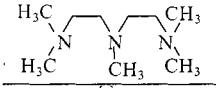	CdL	3.80(0.03)	21.7(0.2)	43.5(1.2)	21.8
en[a] water 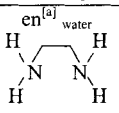	CdL	5.4	30.79	25	–5.79
	CdL_2	9.87	56.28	55.6	–0.68
	CdL_3	12.2	69.56	82.4	12.84
dmen[b] water 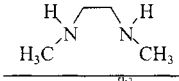	CdL	5.28			
	CdL_2	8.90			
	CdL_3	10.8			
trmen[b] water 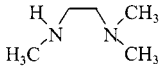	CdL	4.56			
	CdL_2	6.73			
	CdL_3	7.7			
tmen[b] water 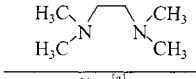	CdL	3.97			
	CdL_2	5.37			
dien[a] water 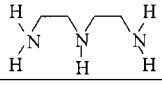	CdL	8.3	47.33	41	-6.33
	CdL_2	13.7	78.12		

[a] $\mu = 0.1$, $T = 298$ K; [b] $\mu = 1.0$, $T = 298$ K.

Results

Computer treatment of the potentiometric experimental data shows that for all the systems the best fit is obtained when the formation of successive mononuclear complexes is taken into account. The overall stability constants obtained from the potentiometric data minimization procedures, with the corresponding error limits, are listed in Table 1 for the reactions $Cd^{2+} + jL \rightleftarrows CdL_j^{2+}$ ($j = 1-3$ for L = *n*-but, en, dmen; $j = 1,2$ for L = trmen, dien, dmdien; $j = 1$ for L = tmen and pmdien).

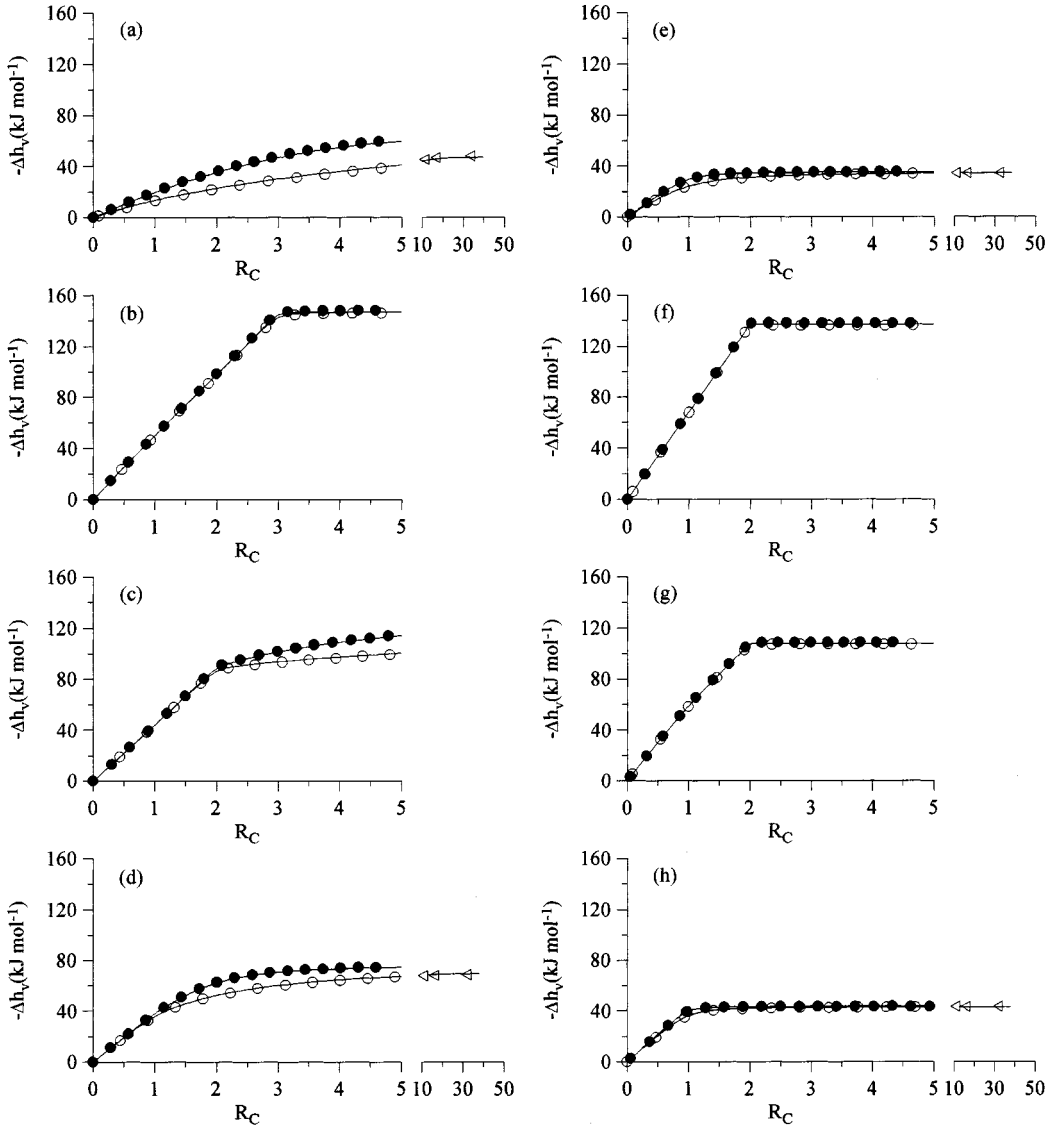

Figure 1. The total molar enthalpy changes, Δh_v, as a function of $R_c = C_L/C_M$ for Cd^{II}- polyamine systems in DMSO: (a) *n*-but (○) 5.05, (•) 19.90 mmol dm^{-3} in Cd^{2+}; (b) en, (○) 5.05, (•) 19.90 mmol dm^{-3} in Cd^{2+}; (c) dmen, (○) 5.10, (•) 19.98 mmol dm^{-3} in Cd^{2+}; (d) trmen, (○) 5.10, (•) 19.98 mmol dm^{-3} in Cd^{2+}; (e) tmen, (○) 5.05, (•) 19.90 mmol dm^{-3} in Cd^{2+}; (f) dien, (○) 5.05, (•) 19.98 mmol dm^{-3} in Cd^{2+}; (g) dmdien, (○) 5.10, (•) 20.05 mmol dm^{-3} in Cd^{2+}; (h) pmdien, (○) 5.05, (•) 20.05 mmol dm^{-3} in Cd^{2+}; the open triangles represent part of the "reverse" titrations; only some of the experimental points, chosen at random, have been plotted; the solid lines have been calculated from the values of β_j and $\Delta H^\circ_{\beta j}$ in Table 1

From an examination of the shape of the curves reproduced in Figure 1, some conclusions can be drawn about the coordinated species formed, which are fully consistent with the information obtained from analysis of the potentiometric data.

For the diamine en, the shape of the thermogram is consistent with the formation of three successive complexes of high stability. For the dmen system, the calorimetric curves indicate the formation of a third complex of lower stability in addition to two highly stable mononuclear species. The overlapping of the complexation curves up to $R_c = 2$ for the triamines dien and dmdien is indicative of the formation of two successive complexes of high stabilities and the lack of heat evolution at $R_c > 2$ clearly indicates that no more complexes are formed beyond the second one. The fit between the experimental and calculated curves is quite good.

Figure 2 depicts the FT-IR spectra of a series of solutions containing the same concentration (about 50 mmol dm^{-3}) of Cd^{2+} and different ligand-to-metal ratios R_c for the Cd^{II}-dmen system, chosen as a representative example.

Figure 3 shows log β_{jCd} plotted as a function of log β_{jAg} to allow better visualization of the comparison between the behaviour of the two ions.

Discussion

All the complexation reactions are strongly exothermic whereas the entropy terms oppose the reactions (Table 1).

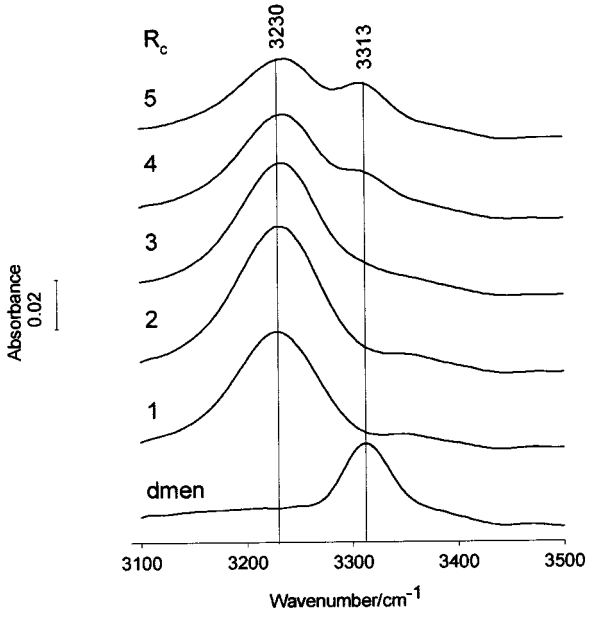

Figure 2. FT-IR spectra of solutions containing 50 mmol dm^{-3} cadmium(II) and different dmen/metal ratios, R_c

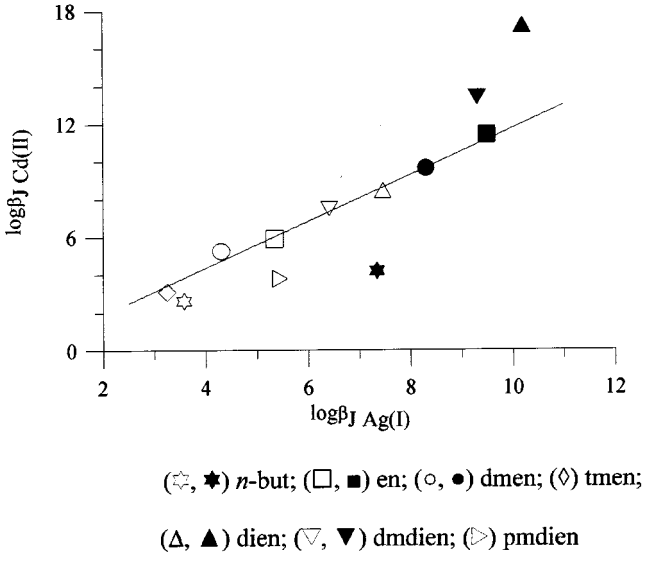

Figure 3. The log β_j relationship of the complexation of cadmium(II)- and silver(I)-amines; open symbols refer to ML, filled symbols to ML_2 species

The negative enthalpy values are typical of reactions involving the complexation of metal ions by neutral ligands in aprotic solvents.[3,5] The negative entropy values are in line with the fact that the release of solvent molecules from the coordination sphere of the metal ions does not compensate the decrease in internal entropy of the ligand and the negative entropy change due to the loss of translational entropy of the reagents upon complexation.[16] Data are available for a few of these species in aqueous solution.[14] Cd^{2+} is hexasolvated in both DMSO and water with the solvent molecules in a regular octahedral arrangement.[16]

The complexes are characterized by lower stabilities in water than in DMSO when primary and secondary amines are involved. Moreover, the complexes are always more enthalpy-stabilized in DMSO than in water, while in the latter solvent the entropy terms are favourable or, when negative, much less unfavourable. This trend is at variance with what might be expected on the basis of the thermodynamic parameters for the transfer of Cd^{2+} from water to DMSO ($\Delta G^{\circ}_{\text{transfer water}\rightarrow\text{ DMSO}} = -60.4$ kJ mol^{-1} [17]) and may be attributed to a greater solvation, through hydrogen bonding, of amines in water than in DMSO.[16] For the complexes with the tertiary amines trmen and tmen the opposite is observed as they are more stable in water than in DMSO; hydrogen bonds are only formed to a limited extent (for trmen) or not at all (for tmen) and therefore the greater solvation of the metal ion in DMSO prevails in governing the trend in the stabilities.

Cd^{II}-*n*-but System: The upper limit of Cd^{II} complexation is the fourth complex in both water and aprotic solvents when charged halides and thiocyanate ligands are involved.[15c,16] With these ligands, the behaviour of which has been extensively studied, a switch from an octahedral to a tetrahedral configuration has been shown to take place in DMSO as well as in water, which occurs at the second or third step of complexation, respectively.[16] The only data available in the literature for Cd^{II} monoamine systems in water relate to methylamine[14] and show that four successive mononuclear complexes are also formed in this case. In DMSO, only three successive mononuclear complexes are detected for the Cd^{II}-*n*-but system, despite the fact that the mildly soft character of Cd^{II} becomes hard in DMSO[16] and its affinity towards the hard N-atom is enhanced accordingly. Evidently, the steric requirements of this bulky ligand prevent the monodentate *n*-but from forming higher Cd^{II} complexes.

The only available data concerning Cd^{II} complexation by uncharged amines in DMSO do not allow suitable comparisons as they refer to the very bulky tri-*N*-butylamine,[13f] which is only able to form one mononuclear complex, whereas data relating to secondary monoamines show that they are able to form three successive complexes with the Group 12 dication Hg^{II} in DMSO.[13i] Interesting features emerge on analyzing the values of the thermodynamic functions. The more exothermic stepwise enthalpy value of the second complexation step, $\Delta H\,(K_2)$, as compared with $\Delta H\,(K_1)$, is probably due to the occurrence of particularly extensive desolvation in the first step of complexation: the enthalpy needed for desolvation causes $\Delta H\,(K_1)$ to be less exothermic than $\Delta H\,(K_2)$ in spite of the greater exothermicity associated with Cd^{II}-amine bond formation in the first step.

A switch in the coordination seems to take place at the third complexation step; indeed, the rupture of the solvate shell generally results in the liberation of more solvent molecules than would occur in the case of a simple substitution. Consequently, this step will be characterized by an abnormally large entropy gain while, on the other hand, the

extensive desolvation will absorb extra energy thereby resulting in an abnormally unfavourable enthalpy change.[16]

The low enthalpy gain and the slight counteracting effect of the entropy term associated with the third complexation step are consistent with this hypothesis.

Cd^{II}-diamine Systems: The $[CdL]^{2+}$ complexes of the various primary, secondary, and tertiary diamines are all more stable than the corresponding *n*-but complex. Furthermore, their enthalpies and entropies of formation are more exothermic and more negative, respectively, than the corresponding ΔH°_1 and ΔS°_1 values with the unidentate amine. This indicates the formation of chelate complexes with all the investigated diamines.

It can be seen in Table 1 that the $\log \beta_1$ values decrease smoothly as the number of methyl groups is increased on going from primary to secondary diamines (and triamines; see below), while the decrease in both stability and exothermicity is much more evident when tertiary groups are present. Evidently, for primary and secondary diamines, the decrease in stability is primarily due to the different basicities of the N-atoms, which decrease in the order $NH_2 > -NHR > -NR_2$.[18] The huge decrease in the thermodynamic stability and exothermicity shown by Cd^{II}-trmen and, in particular, -tmen systems can readily be explained in terms of the greater steric crowding resulting from complete *N*-methylation leading to decreased strength and marked elongation of the M−N bonds.[19] The steric requirements of the ligands evidently play an important role in determining the nature and stoichiometry of the complexes formed; this is even more clearly evidenced by the absence of higher complexes beyond the first one using the bulky tmen (or pmdien when triamines are considered).

The stability constants available in the literature relating to Cd^{II} complexation by dmen, trmen, and tmen in water at $\mu = 1.0$[14] are listed in Table 1. It should be noted that steric requirements also strongly influence the stoichiometry of the species formed in water as dmen and trmen form three successive mononuclear complexes while only two species are formed by the bulkier tmen.

The high values of the stability constants relating to the formation of the second complex and the high exothermicities of the reactions $ML + L \rightleftarrows ML_2$ suggest that both ligands are bidentate in these complexes. A reasonable question about this assumption may be raised in view of the high K_1/K_2 value associated with the Cd^{II}-trmen system. The highly exothermic value of the stepwise $\Delta H\,(K_2)$ favours chelation; in fact, if rough values of $-22\ kJ\ mol^{-1}$ and $-18\ kJ\ mol^{-1}$, respectively, are calculated for the formation of one $Cd^{II}-NHR$ and one $Cd^{II}-NR_2$ bond of a diamine chelate (on the basis of the mean enthalpy values relating to Cd^{II}-dmen and Cd^{II}-tmen complex formation), then the stepwise value of $\Delta H\,(K_2) = -39.6\ kJ\ mol^{-1}$ found for the Cd^{II}-trmen system [calculated: $-22 + (-18) = -40\ kJ\ mol^{-1}$] is wholly consistent with the hypothesis that both the $-NR_2$ and $-NHR$ groups coordinate to the metal ion in the formation of the $[Cd(trmen)_2]^{2+}$ complex.

Chelation is certainly also achieved when the $[Cd(en)_3]^{2+}$ complex is formed. For the $[Cd(dmen)_3]^{2+}$ system, the abrupt decrease in K_3 might be viewed as an indication of a possible rearrangement of the ligands in this third complexation step. In reality, this is an example illustrating the fact that a determination of the complete thermodynamics of complexation is necessary in order to ensure a reliable interpretation of the reactions involved; the values of the enthalpy and entropy terms are, in fact, in line with a bidentate behaviour of dmen in the $[Cd(dmen)_3]^{2+}$ complex.

Independent FT-IR spectroscopic measurements were carried out in order to corroborate the conclusions drawn from thermodynamic data. The interactions of the amino groups with the metal ions were studied by observing the bathochromic shift of the NH stretching modes of primary (at 3360 and 3300 cm^{-1}) and secondary (at 3313 cm^{-1}) groups in DMSO when Cd^{II} ions were added to amine solutions.[3g] Figure 2 shows the spectra of a series of solutions containing Cd^{II} and different dmen-to-metal ratios, R_c. It can be seen that up to $R_c = 3$ only the band due to the bonded amine (at 3230 cm^{-1}) is present, while the band due to the free amino group is present only when $R_c > 3.0$, clearly indicating that all the $-NH$ groups are coordinated to the Cd^{II} ion in each of the complexation steps. Similar measurements were also carried out for the other diamine (and triamine, see below) systems and confirmed the hypotheses suggested on the basis of the thermodynamic data.

Cd^{II}-triamine Systems: The higher values of the stability constants and the higher exothermicities associated with the formation of the $[CdL]^{2+}$ complexes of the triamines dien and dmdien, compared with those of the corresponding diamines, indicate that these ligands are tridentate, forming two fused five-membered chelate rings. The same arguments discussed in detail for the Cd^{II}-diamine systems can also be applied to the Cd^{II}-triamine systems to account for the decrease in stability and exothermicity observed on going from primary to tertiary triamines. In particular, it should be stressed that in this case as well, and to an even greater extent, the values of the stability constants and enthalpy gains for Cd^{II}-pmdien differ greatly from the values found for the secondary dmdien, further supporting the statement that, in addition to the decreased basicity of the amino groups, steric crowding plays a very important role in determining the coordinating abilities of the amines. The thermodynamic parameters for the Cd^{II}-pmdien system show better agreement with a bidentate coordination for this ligand; no additional information could be obtained by independent spectroscopic measurements.

The Cd^{II} ion is certainly hexacoordinated ion in the ML_2 complexes with the other triamines. This is unequivocally indicated by the thermodynamic parameters and was confirmed by independent FT-IR measurements run on the Cd^{II}-dien and -dmdien systems, which did not show the presence of uncoordinated amino groups up to $R_c > 2$ (see above for details). Evidently, a certain "preorganization" of the diamines and triamines is responsible for their ability to saturate the coordination sphere of the Cd^{II} ion, which is not achieved using monoamines.

It should be noted that $[Cd(dien)_2]^{2+}$ is formed alongside $[Cd(dien)]^{2+}$ as a result of the higher stability constant relating to the second complexation step ($\log K_2 = 8.74$), which is not seen in water. This result may be explained by considering that in Cd^{II} complexation by dien the desolvation of the species involved occurs mainly in the first step of complexation; this is confirmed by the lower enthalpy gain and the unfavourable entropy term associated with the formation of the ML complex as compared to the stepwise terms relating to the formation of the ML_2 species [$\Delta H(K_2) = -72$, $T\Delta S(K_2) = -22.3$ kJ mol^{-1}].

Cd^{II}- vs. Ag^{I}-amines Complexation: In Figure 3, the stabilities of the 1:1 and 1:2 Cd^{II}-amine complexes are plotted against the corresponding stabilities of the $[AgL]^+$ and $[AgL_2]^+$ species[3a−3e] in DMSO. The positive slope (1.2) of the line, calculated by taking into account the $\log \beta_1$ values for all the amines except *n*-but and pmdien (for the reasons discussed below), indicates that the stabilities of the 1:1 Cd^{II}-amine complexes are invariably greater than those of the corresponding Ag^{I} complexes (although almost of the same order of magnitude in the case of tmen); this probably reflects the higher affinity of the N atom for the soft-hard borderline divalent acceptor Cd^{II} than for the very soft univalent Ag^{I} ion. The linearity evident in Figure 3 seems to indicate that the different coordination structures of the two metal ions in DMSO, octahedral for Cd^{II} and tetrahedral for Ag^{I},[16] does not play a significant role in the ML complexation by the polyamines en, dmen, tmen, dien, and dmdien.

In the case of the bulkier *n*-but and pmdien, however, the selectivity of the ligands changes and Ag^{I} complexation becomes more favourable than Cd^{II} complexation. The steric hindrance of the ligands, together with the different structures of the metal ion solvates, is likely to be responsible for this behaviour. In fact, the environment of a tetrahedrally coordinated metal ion is less crowded compared with an octahedral structure[15c] and may allow enough space for the steric bulk of the *n*-but or pmdien molecules to no longer be significant.

In line with this hypothesis is the fact that pmdien is able to act as a terdentate ligand in the $[AgL]^+$ complex,[3e] while bidentate ligation is more reasonable in the $[CdL]^{2+}$ species (see the above discussion).

Furthermore, the $\log \beta_2$ values for the dmen and en systems fall on the line shown in Figure 3, indicating that the same arguments invoked to explain the trends observed for their ML (M = Cd, Ag) species can also be applied in rationalizing the behaviour of their ML_2 complexes.

Considering the dien and dmdien ML_2 compounds, the huge increase in stability of the Cd^{II} complexes with respect to their Ag^{I} counterparts certainly stems from the fact that terdentation is also achieved in the second complexation step using Cd^{II}. This is not possible in the case of $[AgL_2]^+$ as the maximum coordination number of silver(I) in solution is usually four.[20]

Conclusions

Cd^{II} complexes with open-chain N-donors in DMSO have been shown to be stable. Hexacoordination of the metal ion is achieved with primary and secondary polyamines. Complexation by primary and secondary amines is favoured in DMSO compared to that in water due to the less extensive hydrogen bonding of the amines in the aprotic solvent. The greater solvation of the metal ion in DMSO prevails in governing the stability trend in the case of the Cd^{II}-trmen and -tmen systems, the complexes being more stable in water than in DMSO.

The *N*-functionalization of the ligands has a strong influence not only on the stoichiometry and the nature of the Cd^{II} complexes formed but, very interestingly, on the selectivity of the ligands towards metal ions as well, as shown by a comparison with the available data on silver(I) complexation by the same amines.

Experimental Section

Warning! Although metal perchlorates solvated by DMSO are generally explosive under certain conditions,[11,21] no problems were encountered when handling $Cd(ClO_4)_2 \cdot 6DMSO$. Nevertheless, as a precaution, the salt should only be prepared in small quantities. Great caution has been exercised when handling DMSO solutions of poisonous cadmium salts, since they are easily carried through the skin by DMSO, which penetrates lipid tissues at an astonishing rate. Moreover, DMSO dissolves many natural and synthetic polymers.[11,21] These solvent properties were, of course, taken into account when designing the apparatus (e.g. the ion-selective cadmium electrode was externally covered by Teflon), particularly so as to ensure good personal and environmental protection.

General Remarks: $Cd(ClO_4)_2 \cdot 6DMSO$ was prepared by precipitation from an almost saturated solution of the hydrated salt (Aldrich; 98%) in dimethyl sulfoxide by the addition of diethyl ether. It was collected by filtration and dried in vacuo for several days at 50 °C. The compound was characterized as $Cd(ClO_4)_2 \cdot 6DMSO$ by elemental analysis and by titration of Cd^{II} with EDTA[22] using Eriochrome Black T as indicator. The molar conductivity of a 1.00 mmol dm^{-3} solution of $Cd(ClO_4)_2$ in DMSO (about 75 Ω^{-1} M^{-1} cm^2) was measured with a Metrohm 712 conductometer and was found to be in good agreement with the accepted value for 1:2 elecrolytes in DMSO.[23] Dimethyl sulfoxide (Fluka, > 99%) was purified by distillation according to the described procedure[3a] and stored over 4 Å molecular sieves. The ligands *n*-but, en, dmen, trmen, tmen, dien, and pmdien (Aldrich, >97%) were purified by fractional distillation.[24] The ligand dmdien was synthesized and purified as described previously.[25,26] Its purity (> 99%) was checked by GC mass spectrometry and ^{1}H NMR measurements. Cd^{II} perchlorate stock solutions were prepared by dissolving weighed amounts of the adducts in anhydrous DMSO and their concentrations were checked by titration with EDTA.[22] The supporting salt NEt_4ClO_4 was recrystallized twice from methanol and dried at 110 °C. The solutions of the ligands were prepared by dissolving weighed amounts in DMSO and were standardized by thermometric titration with standard $HClO_4$ solutions. All standard solutions were prepared and stored in an MB Braun 150 glove box under a controlled atmosphere containing less than 1 ppm of

water. The water content in the solutions, typically 10−20 ppm, was determined using a Metrohm 684 KF coulometer.

Potentiometric Measurements: All measurements were carried out in the aforementioned MB Braun 150 glove box in a thermostatted cell maintained at 298.0 ± 0.1 K. The experimental data required for the determination of the stability constants of the Cd^{II}-polyamine complexes were the equilibrium concentrations of the cadmium ion, which were obtained from the e.m.f. data of a galvanic cell. For this purpose, a Weiss WCDIOOI Cd ion selective electrode with a Teflon body was used as the working electrode and a Metrohm 6.0718.000 silver electrode was used as the reference. To Cd^{II} solutions in the concentration range $2.00 < c^0_{Cd} < 20.00$ mmol dm^{-3}, ligand solutions of known concentration were added and the free cadmium(II) concentration was measured after each addition of titrant. Some titrations were carried out in duplicate to verify the reproducibility of the systems. Equilibrium was typically reached in 2−5 minutes. The Nernstian response of the Cd electrode was checked in the range $10^{-2} < [Cd^{II}] < 10^{-6}$ mmol dm^{-3}. The computer program Hyperquad[27] was used to calculate the stability constants.

Calorimetric Measurements: A Tronac model 87−558 precision calorimeter was employed to measure the heats of reaction. The calorimeter was calibrated by titrating tris(hydroxymethyl)aminomethane (tham) with a standard solution of HCl in water. The experimental value of the heat of neutralization of tham was found to be $\Delta H° = -47.59$ kJ mol^{-1}, in good agreement with the accepted value of -47.53 ± 0.13 kJ mol^{-1}.[14]

The calorimetric titrations were performed at 298.00 ± 0.02 K by adding known volumes of ligand solutions ($50 < c^0_L < 200$ mmol dm^{-3}) to 20 mL of cadmium(II) solution ($2.00 < c^0_{Cd} < 20.0$ mmol dm^{-3}). In order to reach higher ligand-to-metal ratios so as to confirm that no higher complexes beyond the reported ones were formed by *n*-but, trmen, tmen, and pmdien, "reverse" calorimetric titrations were carried out for the relevant systems. In these titrations, Cd^{II} ion solutions (100 mmol dm^{-3}) were added to solutions of ligand (≈ 30 mmol dm^{-3}).

For each titration run, *n* experimental values of the total heat produced in the reaction vessel ($Q_{ex,j}$ $j = 1$ to n) were calculated as a function of the amount of titrant added. These values were only corrected for the heat of dilution of the titrant ($Q_{dil,j}$), which was determined separately. The heat of dilution of the titrate was found to be negligible in the metal ion concentration range used. The net heat of reaction at the *j*th point ($Q_{r,j}$) was obtained from the difference $Q_{r,j} = Q_{ex,j} - Q_{dil,j}$.

The quantity Δh_v, the total heat per mol of metal ion, was defined and calculated by dividing the net heat of reaction by the number of mol of metal ion in the calorimetric vessel. The enthalpy and entropy changes of the identified complexes were calculated using a Fortran program, MQ90,[28] with $q_{r,j}$ ($= Q_{r,j} - Q_{r,j-1}$) or Δh_v as the error-carrying variables.

FT-IR Measurements: The FT-IR measurements were made using a Bio-Rad FTS40 spectrometer (maximum resolution 4 cm^{-1}; 16 scans). A cell with barium fluoride windows (thickness of 32 μm) was used. The cell was filled and sealed in a glove box and then transferred to the spectrometer.

Acknowledgments

This work has been supported by the Ministero dell'Università e della Ricerca Scientifica e Tecnologica (MURST, Rome) within the program COFIN 2000. We thank Mr. Pierluigi Polese for technical assistance.

[1] B. G. Cox., J. Garcia-Rosas, H. Schneider, *J. Am. Chem. Soc.* **1981**, *103*, 1384.
[2] H. K. Chantooni, I. M. Kolthoff, *J. Solut. Chem.* **1985**, *14*, 1.
[3] [3a] A. Cassol, P. Di Bernardo, P. L. Zanonato, R. Portanova, M. Tolazzi, *J. Chem. Soc., Dalton Trans.* **1987**, 657. – [3b] A. Cassol, P. Di Bernardo, P. L. Zanonato, R. Portanova, M. Tolazzi, G. Tomat, *J. Chem. Soc., Dalton Trans.* **1988**, 1781. – [3c] A. Cassol, P. Di Bernardo, P. L. Zanonato, R. Portanova, M. Tolazzi, G. Tomat, V. Cucinotta, D. Sciotto, *J. Chem. Soc., Faraday Trans. I* **1989**, *85*(*8*), 2445. – [3d] A. Cassol, P. Di Bernardo, P. L. Zanonato, R. Portanova, M. Tolazzi, G. Tomat, *J. Chem. Soc., Faraday Trans.* **1990**, *86*(*16*), 2841. – [3e] C. Comuzzi, V. Novelli, R. Portanova, M. Tolazzi, *Supramol. Chem.* **2001**, *13*(*3*), 455. – [3f] C. Comuzzi, M. Grespan, P. Polese, R. Portanova, M. Tolazzi, *Inorg. Chim. Acta*, submitted. – [3g] A. Cassol, P. Di Bernardo, R. Portanova, M. Tolazzi, G. Tomat, P. L. Zanonato, *J. Chem. Soc., Dalton Trans.* **1992**, 469. – [3h] Z. Wang, G. R. Choppin, P. Di Bernardo, P. L. Zanonato, R. Portanova, M. Tolazzi, *J. Chem. Soc., Dalton Trans.* **1993**, 2791. – [3i] A. Cassol, G. R. Choppin, P. Di Bernardo, R. Portanova, M. Tolazzi, G. Tomat, P. L. Zanonato, *J. Chem. Soc., Dalton Trans.* **1993**, 1695. – [3j] P. Di Bernardo, G. R. Choppin, R. Portanova, P. L. Zanonato, *Inorg. Chim. Acta* **1993**, *207*, 85. – [3k] A. Cassol, P. Di Bernardo, R. Portanova, M. Tolazzi, P. L. Zanonato, *Inorg. Chim. Acta* **1997**, *262*, 1997.
[4] A. F. De Namor, *J. Chem. Soc., Faraday Trans. 1* **1988**, *84*(*7*), 2441.
[5] F. Arnaud-Neu, *Chem. Soc. Rev.* **1994**, 235.
[6] A. Lewandowski, A. Szukalska, M. Galinski, *J. Chem. Soc., Faraday Trans.* **1995**, *91*(*7*), 1097 and refs. therein.
[7] S.-I. Ishiguro, K. Kato, R. Takahashi, S. Nakasone, *Rare Earths* **1995**, *27*, 61.
[8] N. Heidari, A. Thaler, H. Schneider, B. G. Cox, *Inorg. Chim. Acta* **1998**, *279*, 186.
[9] A. Thaler, N. Heidari, B. G. Cox, H. Schneider, *Inorg. Chim. Acta* **1999**, *286*, 160.
[10] I. Bertini, L. Messori, G. Galub, H. Cohen, D. Meyerstein, *Inorg. Chim. Acta* **1995**, *235*, 5.
[11] S. Ahrland, I. Persson, *Acta Chem. Scand., Ser. A* **1980**, *34*, 645.
[12] S.-I. Ishiguro, K. Ozutsumi, *Inorg. Chem.* **1990**, *29*, 1117.
[13] [13a] S. Ahrland, N.-O. Bjork, *Acta Chem. Scand., Ser. A* **1974**, *28*, 823. – [13b] S. Ahrland, N.-O. Bjork, *Acta Chem. Scand., Ser. A* **1976**, *30*, 265. – [13c] M. Sandstrom, I. Persson, S. Ahrland, *Acta. Chem. Scand., Ser. A* **1978**, *32*, 607. – [13d] S. Ahrland, T. Berg, P. Blaunstein, *Acta Chem. Scand., Ser. A* **1978**, *32*, 933. – [13e] M. Kodama, E. Kimura, *J. Chem. Soc., Dalton Trans.* **1978**, 1081. – [13f] S. Ahrland, E. Avsar, T. Berg, *J. Organomet. Chem.* **1979**, *181*, 17. – [13g] S. Ahrland, S.-I. Ishiguro, A. Marton, I. Persson, *Acta Chem. Scand., Ser. A* **1985**, *39*, 227. – [13h] S.-I. Ishiguro, K. Ozutsumi, H. Ohtaki, *Bull. Chem. Soc. Jpn.* **1987**, *60*, 531. – [13i] I. Persson, B. Schneider, *Inorg. Chim. Acta* **1989**, *158*, 245. – [13j] R. Bhula, P. Osvath, D. C. Weatherburn, *Coord. Chem. Rev.* **1988**, *91*, 89.
[14] A. E. Martell, R. M. Smith, R. J. Motekaitis, "*Critically Selected Stability Constants of Metal Complexes Database*", version 5.0, **1998**.
[15] [15a] H. Suzuki, S.-I. Ishiguro, H. Ohtaki, *J. Chem. Soc., Faraday Trans.* **1990**, *86*(*12*), 2179. – [15b] A. Bencini, A. Bianchi, P. Paoletti, P. Paoli, *Coord. Chem. Rev.* **1992**, *120*, 29. – [15c] M. Koide, H. Suzuki, S.-I. Ishiguro, *J. Chem. Soc., Faraday Trans.* **1995**, *91*(*21*), 3851. – [15d] H. Adams, R. Bastida, D. E. Fenton, A. Macias, S. E. Spey, L. Valencia, *J. Chem. Soc., Dalton Trans.* **1999**, 4131. – [15e] P. Arrauz-Mascaros, R. Lopez-Garzou, M. D. Gutierrez-Valero, M. L. Godino-Salido, J. M. Moreno, *Inorg. Chim. Acta* **2000**, *304*, 137. – [15f] D. J. R.

Brook, S. Fornell, J. E. Stevens, B. Noll, T. H. Koch, W. Eisfeld, *Inorg. Chem.* **2000**, *34*, 562. – [15g] G. J. Grant, M. W. Jones, K. D. Loveday, D. G. Van Derveer, W. T. Pennington, C. T. Eagle, L. F. Mehne, *Inorg. Chim. Acta* **2000**, *300–302*, 250. – [15h] C. Bazzicalupi, A. Bencini, A. Bianchi, V. Fedi, C. Giorgi, P. Paoletti, L. Tei, B. Valtancoli, *Inorg. Chim. Acta* **2000**, *300–302*, 653. – [15i] M. Di Vaira, F. Mani, P. Stoppiani, *Inorg. Chim. Acta* **2000**, *303*, 61. – [15j] M. B. Inoue, I. C. Muñoz, M. Inoue, Q. Fernando, *Inorg. Chim. Acta* **2000**, *300–302*, 206. – [15k] G. Park, N. Ye, R. D. Rogers, M. W. Brechbiel, R. P. Planalp, *Polyhedron* **2000**, *19*,1155.

[16] S. Ahrland, in *The Chemistry of Non-Aqueous Solvents* (Ed.: J. J. Lagowsky), Academic Press, New York, **1978**, *vol. 5a.*

[17] C. Kalidas, G. Hefter, Y. Marcus, *Chem. Rev.* **2000**, *100*(*3*), 819.

[18] [18a] A. Mucci, R. Domain, R. L. Benoit, *Can. J. Chem.* **1980**, *58*, 953. – [18b] R. L. Benoit, M. J. Mackinnon, L. Bergeron, *Can. J. Chem.* **1981**, *59*, 1501.

[19] D. Mayerstein, *Coord. Chem. Rev.* **1999**, *185–186*, 141 and refs. therein.

[20] N. R. Thomson, in *Comprehensive Inorganic Chemistry*, Vol. 3 (Eds.: J. C. Bailar, Jr., A. F. Trotman-Dickenson), Pergamon, Oxford, **1973**, p. 111.

[21] D. Martin, H. G. Hauthal, "*Dimethyl Sulfoxide*", Van Nostrand Reinhold, Wokingham, Berkshire, **1975**, pp. 448–449.

[22] A. I. Vogel, in *Textbook of Quantitative Chemical Analysis*, 5th edn., Longman Group UK, **1989**.

[23] W. J. Geary, *Coord. Chem. Rev.* **1971**, *7*, 81

[24] D. D. Perrin, W. L. F. Amarego, D. R. Perrin, in *Purification of Laboratory Chemicals*, 2nd edn., Pergamon, Oxford, **1980**.

[25] R. M. Clay, S. Corr, M. Micheloni, P. Paoletti, *Inorg. Chem.* **1985**, *24*, 3330.

[26] D. W. White, B. A. Karcher, R. A. Jacobson, J. K. Verkade, *J. Am. Chem. Soc.* **1979**, 4921.

[27] P. Gans, A. Sabatini, A. Vacca, *Talanta* **1996**, *43*, 1739.

[28] The program MQ90 was made available to R. P. by the courtesy of Prof. S.-I. Ishiguro.

Received May 7, 2001
[I01161]

Nucleophilic Attack of Carbanions on Cationic Platinum(II) Nitrile Complexes Affording Stable η^1-Imine Enol and η^1-Enamine Coordinated Fragments

Maria E. Cucciolito,*[a] Vincenzo De Felice,[b] Federico Giordano,[a] Ida Orabona,*[a] and Francesco Ruffo[a]

Keywords: Platinum / Carbanions / Nucleophilic addition / Nitrile complexes / Enaminodiones

Cationic nitrile platinum(II) complexes of formula [PtMe(RCN)(bipy)]$^+$ undergo nucleophilic addition of carbanions $^-$CH(COX)(COY) (X, Y= Me, OMe), $^-$CH(CO_2Me)CN and $^-$CH$(CN)_2$ to afford neutral products. According to the nature of the nucleophile, the organic ligand fragment displays either an imino enol or an enamine isomeric structure. The Pt–N bond can be cleaved upon reaction with acids with formation of the corresponding β-enaminodione.

Introduction

Nucleophilic attack on coordinated nitriles is an agile way for the formation of several organic functions.[1,2] For example, the addition of water,[1] alcohols,[1] amines,[1] nitrones[3] and oximes[4] to metal-bonded nitriles gives rise to the corresponding amidato, imidoester, amidine, oxadiazoline and iminoacylated oxime groups. With several metals (e.g. W, Co, Ir, Rh, Ru, Pt) stable complexes can be isolated.[1]

Within this field of research, d^8 ions exhibit a very rich chemistry. For example, Michelin[1,5] and Natile[6] have carried out extensive studies on the attack of amines and alcohols to Pd^{II} and Pt^{II} nitrile complexes, with important implications for asymmetric synthesis[7] and medicine.[8]

On the other hand, a correspondingly thorough investigation of the species involved in the addition of carbanions to d^8 metal-bound nitriles has not been developed, although this is a convenient catalytic route to β-enaminodiones.[1,2] As far as we know, only one group has investigated the attack of carbanions, for example $^-$CH$(COMe)_2$, on platinum(II) nitrile complexes.[9] The reaction was generally accompanied by acyl migration and the formation of neutral products containing a bidentate *N,O*-chelated moiety, such as [Pt{N(COMe)C(Ph)CHC(Me)O^a}(*Pt*−*O*^{a})]. The acyl migration could be prevented with retention of the chelated fragment [Pt{NHC(Ph)C(COMe)C(Me)O^a}(*Pt*−*O*^{a})]. Similar Pd^{II} and Ni^{II} complexes were also prepared[10] by an alternative method, the addition of β-enaminodiones, for example $H_2NC(Et)=C(COMe)_2$, to suitable metal precursors.

Aiming to extend the knowledge within this field, we investigated the reaction of carbanions with complexes of formula [PtMe(RCN)(bipy)]$^+$. As described below, in all cases the nucleophile easily attacks the coordinated nitrile, and different structural types are obtained according to the nature of the carbanions.

The solid-state characterisation of a representative product, as well as reactions involving the functionalised coordinated fragment, have also been carried out.

Results and Discussion

Addition of Carbanions to [PtMe(RCN)(bipy)]BF_4 Complexes. Characterisation of the Products

Five carbanions of general formula $^-$CH(COX)(COY) were used, $^-$CH$(COMe)_2$ (**a**), $^-$CH(COMe)(CO_2Me) (**b**), $^-$CH$(CO_2Me)_2$ (**c**), $^-$CH(CO_2Me)(CN) (**d**) and $^-$CH$(CN)_2$ (**e**). In most cases the cationic platinum(II) precursor was [PtMe(MeCN)(bipy)]BF_4 (**1,** bipy = 2,2′-bipyridine), although in some experiments the related complexes [PtMe(PhCN)(bipy)]BF_4 (**2**), [PtMe(MeCN)(phen)]BF_4 (**3**, phen = 1,10-phenanthroline) and [PtMe(MeCN)(dmphen)]BF_4 (**4**, dmphen = 2,9-dimethyl-1,10-phenanthroline) were used. The latter was chosen in order to see the effect of the steric hindrance of the chelating ligand.

When an acetonitrile suspension of the Pt^{II} complexes was allowed to react with an excess of the appropriate nucleophile, the colour of the reaction mixture turned from yellow to orange-red within a few minutes. The metal products could be isolated in good yields as microcrystalline powders according to standard procedures. Only when the chelate was the hindered dmphen was the yield low, possibly due to the pronounced crowding in the square-planar coordination plane.

The new complexes are soluble in chlorinated solvents, although very poorly in the case of the cyano derivatives derived from **d** and **e**. Characterisation was carried out by IR and NMR spectroscopy, elemental analysis and, in one representative case, by X-ray diffractometry.

In principle, nucleophiles can react with cationic nitrile-containing platinum(II) complexes either by substitution or

[a] Dipartimento di Chimica, Università di Napoli "Federico II", Complesso Universitario di Monte S. Angelo, Via Cintia, 80126, Napoli, Italy
E-mail: cucciolito@chemistry.unina.it
orabona@chemistry.unina.it
[b] Facoltà di Scienze MM.FF.NN., Università del Molise, Via Mazzini 8, 86170, Isernia, Italy

 © WILEY-VCH Verlag GmbH, 69451 Weinheim, 2001 1434−1948/01/1212−3095 $ 17.50+.50/0

by attacking the ligand, with formation of a corresponding metal-bonded organic fragment. The following NMR spectroscopic features allow us to confirm that all the reactions involved the attack of the anion on the nitrile with formation of a square-panar product:

i) the presence of a peak for the σ-bonded Pt−Me group with ^{195}Pt satellites of the appropriate intensities ($^{2}J_{Pt-H}$ = 80−85 Hz).[11]

ii) a singlet weakly coupled to ^{195}Pt around δ = 2.3 attributable to the methyl group of a Me−C−N−Pt fragment ($^{4}J_{Pt-H}$ = 8 Hz) in the case of the acetonitrile precursor. When benzonitrile was used, the aromatic region contained the expected Ph pattern.

iii) the presence of other singlets attributable to CO_2Me and COMe groups, when present in the reacting nucleophile. In the case of symmetric carbanions, i.e. X = Y, these groups are equivalent even at 213 K.

iv) the non-equivalence of the two halves of the chelating ligand, according to the absence of a mirror plane orthogonal to the square-planar coordination plane. The $^{3}J_{Pt-H}$ coupling constants of the protons H6 (12−16 Hz) and H6′ (45−50 Hz) of bipy are significantly different. On the grounds of the higher trans influence of Me groups with respect to N atoms, these values are compatible with the presence of a Me and an N atom trans to N1 and N1′ respectively. Analogously, the H2 and H9 protons of phen split to a different extent, and the smaller coupling is attributable to the hydrogen trans to Me.

When the nucleophile contains at least one carbonyl function (**a**−**d**), the product resulting from the addition can exist in an equilibrium between the following isomers:[12] keto enamine (**I**), enamine with N−H···O hydrogen bonds (**II**) and imino enol (with either O−H···N, **III**, or O−H···O hydrogen bonds, **III′**), as depicted in Scheme 1.

Structures such as **I** seem to contribute little to our products since the ^{1}H NMR spectra lack a signal attributable to the CH proton that was originally present in the nucleophiles. Instead, a broad singlet is present at very low field (δ = 9.5−12), which disappears in a couple of hours when a few drops of CD_3OD are added to a $CDCl_3$ solution of the complexes. The position of this peak is typical of a proton involved in a hydrogen bond,[13] as is found in isomers of types **II**, **III** and **III′**.

Further structural information was obtained from the IR spectra of the complexes in chloroform solution. More precisely, in the products derived from acetylacetone (X= Y= Me, **1a** and **2a**), the COMe signals were found below 1570 cm^{-1}. A similarly significant lowering of the carbonyl frequencies suggests that an imino enol (isomer **III′**) is present, which forms an O−H···O chelating moiety. An IR band at 2500 cm^{-1} is in agreement with this linkage. The electronic delocalisation within the dicarbonyl moiety would account for the equivalence of the carbonyl functions in the NMR spectra (see point iii, above).

Analogously, the COMe stretching in **1b** (X= Me, Y= OMe) is found at 1568 cm^{-1}, while the CO_2Me signal lies at 1670 cm^{-1}. This suggests that an imino enol isomer is favoured here as well, even though a distinction between **III** and **III′** appears to be quite difficult. In fact, the lowering of the CO_2Me stretching mode at 1670 cm^{-1} can also be ascribed to the conjugation in the organic fragment, rather than to the possible formation of a hydrogen bond.[10]

It should be noted that the organic moiety present in complexes **1a, 1b** and **2a** is strongly related to the above-

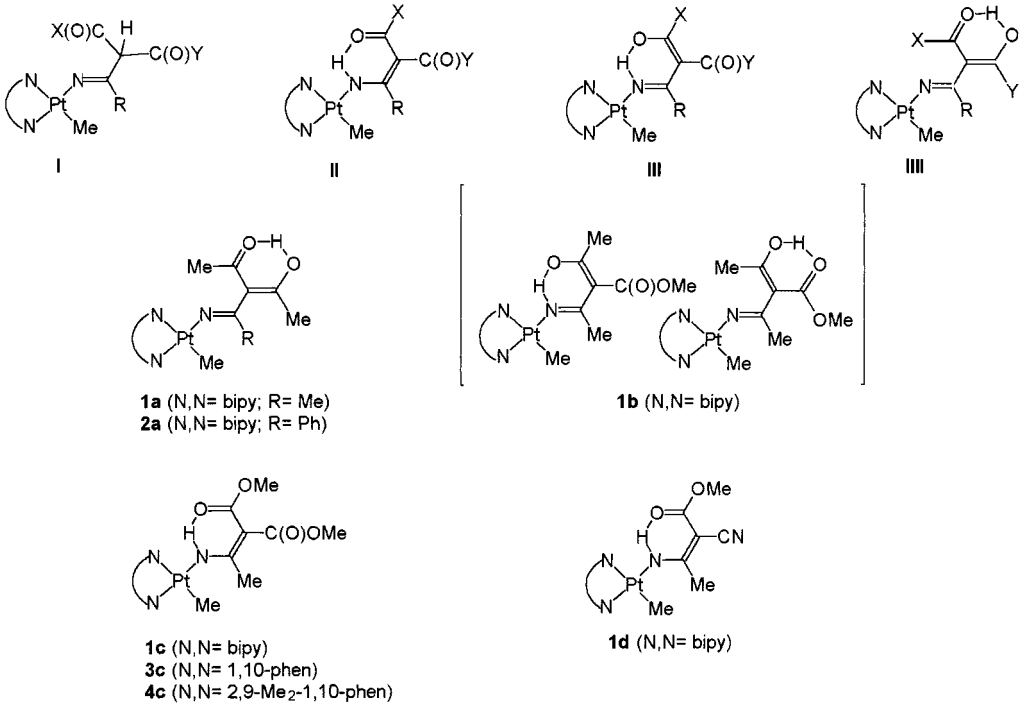

Scheme 1

mentioned chelated fragments [M{NHC(R)C(COMe)-C(Me)O[a]}(*M-O[a]*)].[1,2,9,10] In the latter cases, the ligand binds the metal by forming a six-membered ring. In **1a, 1b** and **2a** the lack of an easily accessible coordination site prevents chelation through the oxygen atom, which therefore binds the mobile proton. As far as we know, these are the first examples of β-imino enols bonded to a d^8 ion in an η^1 fashion.

When the carbonyl group does not belong to a ketonic function (**c**,**d**), an enolic form of the product is no longer possible,[13] and hence the isomeric forms **III** and **III′** can be ruled out. In keeping with this hypothesis, the IR spectra of **1c**, **1d 3c**, and **4c** (Scheme 1) show N−H bands in the range 3230−3320 cm^{-1}. This band disappears upon addition of deuterium oxide to a chloroform solution of the complexes. The two carbonyl stretchings in **1c** appear at 1670 and 1610 cm^{-1}. The difference of ca. 60 cm^{-1} can be attributed to the fact that only one of them is involved in a hydrogen bond N−H···O[13] according to a type **II** structure (Scheme 1). The carbonyl groups are equivalent on the NMR time scale, as expected by site exchange through conformational rearrangements.

Analogous considerations hold true for **3c** and **4c**, which contain phen and dmphen as chelating ligands, respectively.

For complex **1d**, derived from the attack of $^{-}CH(CO_2Me)CN$, an enamine type **II** isomer seems favoured in chloroform solution. In addition to the above-mentioned N−H band (3250 cm^{-1}) and to a sharp signal at 2180 cm^{-1} (CN), the IR spectrum also displays the carbonyl stretching shifted to 1640 cm^{-1}. This frequency is in agreement with the involvement of this moiety in a N−H···O hydrogen bond.

Finally, when the nucleophile does not contain a carbonyl group, i.e. $^{-}CH(CN)_2$ (**e**), the formation of a hydrogen bond in the product **1e** (Scheme 2) is obviously not possible. In this case the absence of a methinic -$CH(CN)_2$ signal in the ^1H NMR spectrum rules out a keto enamine form (**I** in Scheme 2). The presence of a broad signal at δ = 6.5, which slowly disappears upon addition of CD_3OD, suggests the presence of an N−H bond,[5] which is confirmed by the corresponding IR stretching at 3316 cm^{-1}. Furthermore, the two non-equivalent nitriles give rise to two strong signals at 2195 and 2167 cm^{-1}, respectively. Thus, in this case the most stable structure is the enamine (type **II** in Scheme 2).

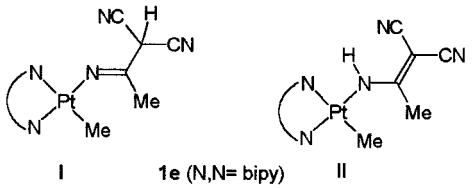

I 1e (N,N= bipy) II

Scheme 2

Solid-State Structure of 1a

The molecular structure of **1a** is shown in Figure 1, and bond parameters of interest are listed in Table 1.

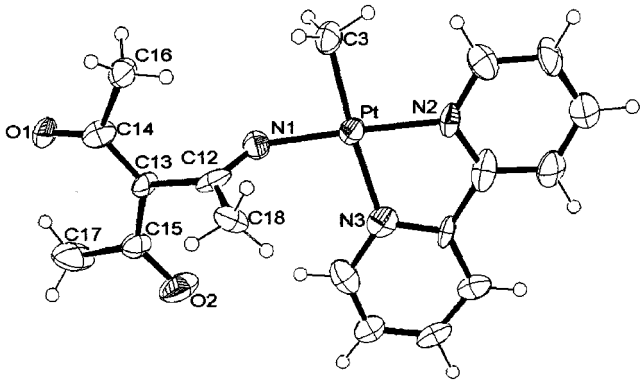

Figure 1. The molecular structure of **1a**

Table 1. Selected distances (Å) and angles(°) with their standard deviations in parentheses

Pt−N(1)	2.01(2)	C(12)−C(13)	1.53(3)
Pt−N(2)	2.01(2)	C(12)−C(18)	1.48(3)
Pt−N(3)	2.06(2)	C(13)−C(14)	1.39(3)
Pt−C(3)	2.00(2)	C(13)−C(15)	1.44(3)
O(1)−C(14)	1.24(3)	C(14)−C(16)	1.54(3)
O(2)−C(15)	1.25(3)	C(15)−C(17)	1.53(4)
N(1)−C(12)	1.29(2)		
N(1)−Pt−N(2)	173.9(6)	C(12)−C(13)−C(14)	122(2)
N(1)−Pt−N(3)	96.8(7)	C(12)−C(13)−C(15)	111(2)
N(1)−Pt−C(3)	86.6(8)	C(14)−C(13)−C(15)	127(2)
N(2)−Pt−N(3)	78.4(6)	O(1)−C(14)−C(13)	127(2)
N(2)−Pt−C(3)	98.1(8)	O(1)−C(14)−C(16)	117(2)
N(3)−Pt−C(3)	175.8(6)	C(13)−C(14)−C(16)	116(2)
Pt−N(1)−C(12)	129(2)	O(2)−C(15)−C(13)	121(2)
N(1)−C(12)−C(13)	118(2)	O(2)−C(15)−C(17)	120(2)
N(1)−C(12)−C(18)	123(2)	C(13)−C(15)−C(17)	119(2)
C(13)−C(12)−C(18)	119(1)		

The metal complex displays a square-planar geometry with the platinum lying out of the plane defined by the coordinated atoms by 0.05 Å.

The distances Pt−N(2) [2.01(2) Å] and Pt−N(3) [2.08(3) Å] are different and reflect the higher *trans* influence of Me with respect to the nitrogen function.

The most relevant feature of the structure is the electronic distribution within the ligand fragment resulting from the addition. It should be noted that: (i) atoms C(12), C(13), C(14) and C(15) are hybridised sp^2; (ii) N(1)−C(12) [1.29(3) Å] is a double bond, while C(12)−C(13) [1.53(4) Å] is a single bond; (iii) the atoms C(12), C(13), C(14), C(15), C(16), C(17), O(1) and O(2) lie in the same plane within 0.02 Å. This plane forms an angle of 76.3(5)° with the plane Pt−N(1)−C(12)−C(13)−C(18); (iv) C(13)−C(14) and C(13)−C(15) are intermediate between a single and a double bond; (v) the C(14)−O(1) and C(15)−O(2) bond lengths are characteristic of the carboxyl group.

These features, which indicate π-electron delocalisation within the planar dicarbonyl moiety, allow us to state that an imino enol isomer is also present in the solid state, al-

though not of type **III**, which implies the complete planarisation of the whole fragment including N(1) and C(18). This conformation seems in any case to be ruled out by the presence of a short methyl−methyl contact. The crystal structure shows a *transoid* conformation of the oxygen atoms, which makes it different also from the *cisoid* form **III′** found in solution, where an intramolecular hydrogen bond is present. In the solid state, the enolic H is statistically shared by O(1) and O(2). One of these positions is stabilised by the formation of the H bond O(2)−H···Cl [O(2)−Cl 2.86 Å] with a Cl atom of the solvent molecule CH_2Cl_2 in one of the two alternative sites of occupancy (see Exp. Sect.). On the other hand, when the hydrogen is linked to O(1), an intermolecular hydrogen bond is established with N(1) [O(1)−H···N(1), O(1)−N(1) 2.91 Å], and in this case the solvent lies far from the complex in order to minimise the steric contacts.

In conclusion, crystal forces stabilise a molecular structure in the solid state which is different from that found in solution, even though the main bonding properties are retained.

Reactions of 1c

The reaction of **1c** with protic acids were examined. Reaction with $HBF_4{\cdot}Et_2O$, which contains a non-coordinating anion, was very fast. The spectroscopic features of the product are similar to those displayed by the parent complex, except for a new signal at δ = 4.89 integrating for one proton. This evidence can be interpreted as the protonation of **1c**, with formation of a cationic product. Actually, in a type **II** structure (Scheme 3) the nitrogen atom has a lone pair, which can be protonated to form **1c′**. The large difference in chemical shift (5 ppm) between the hydrogen atoms bound to N can be ascribed to the fact that only one is involved in a hydrogen bond. It should be noted that **1c′** can be obtained independently by reacting $H_2NC(Me)=C(CO_2Me)_2$ with [PtClMe(bipy)] in the presence of one equivalent of $AgBF_4$.

The β-enaminodione can be liberated by reacting **1c** with HCl, which contains a coordinating anion. In this case, the formation of an intermediate product was followed by cleavage of the organic molecule and coordination of the chloride anion affording the stable complex [PtCl(Me)(bipy)] (Scheme 3).

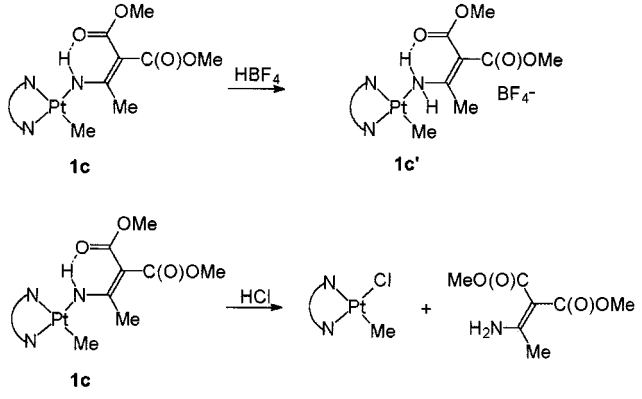

Scheme 3

Conclusion

In this study we have demonstrated that nitriles (RCN) coordinated to square-planar cationic Pt^{II} complexes easily undergo nucleophilic attack by carbanions. The structure of the resulting organic ligand moiety can be controlled by varying the nature of the nucleophile. When it contains a ketonic function, imino enoles coordinated in an η^1 fashion are attained. In the other cases, an enamine structure is favoured.

It should also be noted that the same nucleophiles react with five-coordinated olefin complexes of formula $[PtMe(RCN)(N,N\text{-chelate})(olefin)]^+$ by simply substituting the axial nitrile.[14] This finding confirms once again the great influence of the coordination environment on the stability and reactivity of Pt^{II} complexes.

The reaction of a protic acid HX affords the corresponding β-enaminodione, which is either still coordinated to the metal centre or is obtained free, according to the coordinating ability of the X^- anion.

Experimental Section

All experiments were carried out under a nitrogen atmosphere using standard Schlenk techniques. Solvents and reagents were of AnalaR grade and were used without further purification, unless otherwise stated. THF was dried and distilled from Na/benzophenone. The carbanions,[15] [PtClMe(*N*,*N*-chelate)][16,17] and $[PtMe(MeCN)(N,N\text{-chelate})]BF_4$ [18] were prepared according to literature procedures.

^{1}H NMR spectra were recorded on a Varian XL-200 spectrometer. $CDCl_3$, CD_3NO_2 and $C_2D_2Cl_4$ were used as solvents and $CHCl_3$ (δ = 7.26), CD_2HNO_2 (δ = 4.33) and C_2DHCl_4 (δ = 5.98) as internal standard. ^{13}C NMR spectra were recorded on a Varian XL-200 (^{13}C: 50.3 MHz). $^{13}CDCl_3$ (δ = 77) and $^{13}CD_3NO_2$ (δ = 62.8) were used as internal standard. The following abbreviations are used for describing NMR multiplicities: s, singlet; d, doublet; dd, doublet of doublets; t, triplet; m, multiplet; br, broad signal. Infrared spectra were recorded on a JASCO FT/IR 430 spectrometer.

[PtMe(PhCN)(bipy)]BF_4 (2): $AgBF_4$ (0.107 g, 0.550 mmol) and benzonitrile (0.100 mL, 1.00 mmol) were added to a cooled dichloromethane solution (10 mL) of [PtClMe(bipy)] (0.201 g, 0.500 mmol). After 1 h of stirring AgCl was removed by filtration and the solvent was evaporated under vacuum. The residue was washed with diethyl ether (2 × 5 mL) and dried. The yield was almost quantitative (0.270 g, 97.1%). − $C_{18}H_{16}BF_4N_3Pt$ (556.24): calcd. C 38.87, H 2.90, N 7.55; found C 39.03, H 2.95, N 7.52. − ^{1}H NMR (200 MHz, CD_3NO_2): δ = 1.11 (s, $^2J_{Pt-H}$ = 75 Hz, 3 H, Pt-Me), 7.73 (m, 3 H, PhCN), 7.90 (m, 2 H, PhCN), 8.07 (dd, 2 H, H5 and H5′-bipy), 8.40 (m, 4 H, H3,H3′,H4 and H4′-bipy), 8.98 (d, $^3J_{Pt-H}$ = 16 Hz, 1 H, H6-bipy), 8.98 (d, $^3J_{Pt-H}$ = 60 Hz, 1 H, H6′-bipy). − ^{13}C NMR (CD_3NO_2): δ = −13.1 ($^1J_{Pt-C}$ = 678 Hz, Pt-Me), 110.9 (C1-PhCN), 120.7 (C≡N), 124.8 (C3-bipy), 125.4 ($^3J_{Pt-C}$ = 33 Hz, C3′-bipy), 129.0 ($^3J_{Pt-C}$ = 55 Hz, C5′-

bipy), 130.0 (C5-bipy), 131.1 (C3 and C5-PhCN), 135.0 (C2 and C6-PhCN), 136.8 (C4-PhCN), 141.9 and 142.4 (C4 and C4′-bipy), 149.4 ($^2J_{Pt-C}$ = 25 Hz, C6-bipy), 150.8 ($^2J_{Pt-C}$ = 51 Hz, C6′-bipy), 154.8 and 159.9 (C2 and C2′-bipy).

Complexes 1a−e, 3c, 4c. − General Procedure: A THF suspension (6 mL) of the appropriate carbanion (2.0 mmol) was added to an acetonitrile solution (2 mL) of [PtMe(MeCN)(*N*,*N*-chelate)]BF_4 (0.200 mmol). The mixture was stirred for 30 min. The solvent was then removed under vacuum and the residue extracted with dichloromethane (4 × 5 mL). The extracts were filtered through Celite, then concentrated to 1−2 mL. An orange-red crystalline product was obtained by adding diethyl ether (yield: 80−90%).

1a: $C_{18}H_{21}N_3O_2Pt$ (506.38): calcd. C 42.69, H 4.18, N 8.30; found C 42.44, H 4.26, N 8.18. Yield: 0.091 g, 90%. − ^{1}H NMR ($CDCl_3$): δ = 0.86 (s, $^2J_{Pt-H}$ = 84 Hz, 3 H, Pt-Me), 2.28 (s, $^4J_{Pt-H}$ = 8 Hz, 3 H, MeCN), 2.34 (s, 6 H, MeCO), 7.50 (m, 2 H, H5 and H5′-bipy), 8.15 (m, 4 H, H3,H3′,H4 and H4′-bipy), 8.62 (d, $^3J_{Pt-H}$ = 12 Hz, 1 H, H6-bipy), 8.97 (d, $^3J_{Pt-H}$ = 44 Hz, 1 H, H6′-bipy), 12.05 (br, 1 H, OH). − ^{13}C NMR ($CDCl_3$): δ = −15.1 ($^1J_{Pt-C}$ = 780 Hz, Pt-Me), 28.5 ($^3J_{Pt-C}$ = 81 Hz, *Me*CN), 31.5 (*Me*CO), 115.9 [*C*($COMe)_2$], 122.6 and 123.5 (C3 and C3′-bipy), 127.0 and 127.6 (C5 and C5′-bipy), 138.1 (C4 and C4′-bipy), 147.8 and 148.6 (C6 and C6′-bipy), 154.1 and 157.9 (C2 and C2′-bipy), 174.4 (Me*C*N), 196.5 (Me*C*O) − IR($CHCl_3$): ν̃= 2476 (O−H···O), 1557 (COMe) cm^{-1}.

1b: $C_{18}H_{21}N_3O_3Pt$ (522.38): calcd. C 41.39, H 4.05, N 8.04; found C 41.19, H 4.15, N 8.23. Yield: 0.090 g, 86%. − ^{1}H NMR ($CDCl_3$): δ = 0.84 (s, $^2J_{Pt-H}$ = 80 Hz, 3 H, Pt-Me), 2.32 (s, $^4J_{Pt-H}$ = 8 Hz, 3 H, MeCN), 2.34 (s, 3 H, MeCO), 3.72 (s, 3 H, MeOCO), 7.50 (m, 2 H, H5 and H5′-bipy), 8.15 (m, 4 H, H3,H3′,H4 and H4′-bipy), 8.58 (d, $^3J_{Pt-H}$ = 16 Hz, 1 H, H6-bipy), 8.96 (d, $^3J_{Pt-H}$ = 44 Hz, 1 H, H6′-bipy), 12.1 (br, 1 H, OH). − ^{13}C NMR ($CDCl_3$): δ = −15.1 ($^1J_{Pt-C}$ = 769 Hz, Pt-Me), 28.5 ($^3J_{Pt-C}$ = 80 Hz, *Me*CN), 29.7 (*Me*CO), 50.3 (*Me*OCO), 102.4 [*C*(COMe)(CO_2Me)], 122.8 and 123.7 (C3 and C3′-bipy), 126.9 and 127.4 (C5 and C5′-bipy), 138.1 (C4 and C4′-bipy), 147.4 and 148.5 (C6 and C6′-bipy), 154.2 and 157.9 (C2 and C2′-bipy), 172.6 (MeO*C*O), 174.5 (Me*C*N), 191.9 (Me*C*O) − IR ($CHCl_3$): ν̃= 2471 (O−H···O), 1670 (CO_2Me), 1568 (COMe) cm^{-1}.

1c: $C_{18}H_{21}N_3O_4Pt$ (538.38): calcd. C 40.16, H 3.93, N 7.80; found C 40.30, H 4.04, N 7.69. Yield: 0.090 g, 84%. − ^{1}H NMR ($CDCl_3$): δ = 0.93 (s, $^2J_{Pt-H}$ = 82 Hz, 3 H, Pt-Me), 2.37 (s, $^4J_{Pt-H}$ = 8 Hz, 3 H, MeCN), 3.73 (s, 6 H, MeOCO), 7.50 (m, 2 H, H5 and H5′-bipy), 8.10 (m, 4 H, H3,H3′,H4 and H4′-bipy), 8.71 (d, $^3J_{Pt-H}$ = 16 Hz, 1 H, H6-bipy), 9.06 (d, $^3J_{Pt-H}$ = 46 Hz, 1 H, H6′-bipy), 10.1 (br, 1 H, NH). − ^{13}C NMR ($CDCl_3$): δ = −15.1 ($^1J_{Pt-C}$ = 776 Hz, Pt-Me), 28.2 ($^3J_{Pt-C}$ = 77 Hz, *Me*CN), 50.3 (*Me*OCO), 87.5 [*C*(CO_2Me)$_2$], 122.5 and 123.3 (C3 and C3′-bipy), 127.0 and 127.5 (C5 and C5′-bipy), 137.9 and 138.0 (C4 and C4′-bipy), 147.7 and 148.9 (C6 and C6′-bipy), 154.2 and 158.1 (C2 and C2′-bipy), 171.1 (MeO*C*O), 173.8 (Me*C*N) − IR ($CHCl_3$): ν̃= 3227 (N−H···O), 1670 (CO_2Me), 1610 (CO_2Me) cm^{-1}.

1d: $C_{17}H_{18}N_4O_2Pt$ (505.35): calcd. C 40.40, H 3.59, N 11.09; found C 40.26, H 3.67, N 11.29. Yield: 0.081 g, 80%. − ^{1}H NMR ($C_2D_2Cl_4$): δ = 0.94 (s, $^2J_{Pt-H}$ = 80 Hz, 3 H, Pt-Me), 2.33 (s, 3 H, MeCN), 3.73 (s, 3 H, MeOCO), 7.53 (t, 1 H, H5-bipy), 7.62 (t, 1 H, H5′-bipy), 8.08 (m, 4 H, H3,H3′,H4 and H4′-bipy), 8.62 (d, $^3J_{Pt-H}$ = 16 Hz, 1 H, H6-bipy), 9.06 (d, $^3J_{Pt-H}$ = 44 Hz, 1 H, H6′-bipy), 9.65 (br, 1 H, NH) − IR ($CHCl_3$): ν̃ = 3250 (N−H···O), 2180 (CN), 1640 (CO_2Me) cm^{-1}.

1e: $C_{16}H_{15}N_5Pt$ (472.33): calcd. C 40.69, H 3.20, N 14.82; found C 40.93, H 3.09, N 14.62. Yield: 0.076 g, 80%. − ^{1}H NMR ($CDCl_3$): δ = 0.98 (s, 3 H, $^2J_{Pt-H}$ = 80 Hz, Pt-Me), 2.28 (s, $^4J_{Pt-H}$ = 8 Hz, 3 H, MeCN), 6.55 (br, 1 H, NH), 7.56 (t, 1 H, H5-bipy), 7.72 (t, 1 H, H5′-bipy), 8.15 (m, 4 H, H3,H3′,H4 and H4′-bipy), 8.68 (d, $^3J_{Pt-H}$ = 12 Hz, 1 H, H6-bipy), 9.13 (d, $^3J_{Pt-H}$ = 52 Hz, 1 H, H6′-bipy) − IR ($CHCl_3$): ν̃ = 3316 (N−H), 2195 (CN), 2167 (CN) cm^{-1}.

3c: $C_{20}H_{21}N_3O_4Pt$ (562.40): calcd. C 42.71, H 3.76, N 7.47; found C 42.88, H 3.61, N 7.53. Yield: 0.094 g, 84%. − ^{1}H NMR ($CDCl_3$): δ = 1.09 (s, $^2J_{Pt-H}$ = 82 Hz, 3 H, Pt-Me), 2.41 (s, 3 H, MeCN), 3.76 (s, 6 H, MeOCO), 7.80 (dd, 1 H, H3-phen), 7.85(dd, 1 H, H8-phen), 7.99 (s, 2 H, H5 and H6-phen), 8.58 (d, 1 H, H4-phen), 8.67 (d, 1 H, H7-phen), 8.98 (d, 1 H, H2-phen), 9.31 (d, $^3J_{Pt-H}$ = 44 Hz, 1 H, H9-phen), 10.2 (br, 1 H, NH). − ^{13}C NMR ($CDCl_3$): δ = −16.1 ($^1J_{Pt-C}$ = 780 Hz, Pt-Me), 28.3 ($^3J_{Pt-C}$ = 73 Hz, *Me*CN), 50.4 (*Me*OCO), 87.5 [*C*(CO_2Me)$_2$], 125.5 and 126.0 (C3 and C8-phen), 127.5 and 127.4 (C5 and C6-phen), 130.1 and 130.9 (C10 and C12-phen), 136.8 and 137.2 (C4 and C7-phen), 148.0 and 148.7 (C2 and C9-phen), 171.2 (MeO*C*O), 174.0 (Me*C*N) − IR ($CHCl_3$): ν̃= 3229 (N−H···O), 1669 (CO_2Me), 1609 (CO_2Me) cm^{-1}.

4c: $C_{22}H_{25}N_3O_4Pt$ (590.46): calcd. C 44.75, H 4.27, N 7.12; found C 44.92, H 4.16, N 7.25. Yield: 0.103 g, 87.0%. − ^{1}H NMR ($CDCl_3$): δ = 1.12 (s, $^2J_{Pt-H}$ = 84 Hz, 3 H, Pt-Me), 2.40 (s, $^4J_{Pt-H}$ = 8 Hz, 3 H, MeCN), 2.74 (s, 3 H, Me-dmphen), 2.97 (s, $^4J_{Pt-H}$ = 4 Hz, 3 H, Me-dmphen), 3.69 (s, 6 H, MeOCO), 7.57 (d, 2 H, H3 and H8-dmphen), 7.78 (s, 2 H, H5 and H6-dmphen), 8.33 (d, 2 H, H4 and H7-dmphen), 10.1 (br, 1 H, NH). − ^{13}C NMR ($CDCl_3$): δ = −19.3 ($^1J_{Pt-C}$ = 755 Hz, Pt-Me), 25.8 and 27.8 (Me-dmphen), 28.5 ($^3J_{Pt-C}$ = 75 Hz, *Me*CN), 50.3 (*Me*OCO), 87.5 [*C*(CO_2Me)$_2$], 125.6 and 126.2 (C3 and C8-dmphen), 126.4 and 127.1 (C5 and C6-dmphen), 136.3 (C4 and C7-dmphen), 161.9 and 164.2 (C2 and C9-dmphen), 171.1 (MeO*C*O), 173.5 (Me*C*N) − IR ($CHCl_3$): ν̃= 3228 (N−H···O), 1668 (CO_2Me), 1609 (CO_2Me) cm^{-1}.

Complex 2a: This complex was prepared as above, but with THF as solvent. Yield: 0.091 g, 80%. − $C_{23}H_{23}N_3O_2Pt$ (568.45): calcd. C 48.60, H 4.08, N 7.39; found C 48.49, H 4.15, N 7.52. − ^{1}H NMR ($CDCl_3$): δ = 0.76 (s, $^2J_{Pt-H}$ = 81 Hz, 3 H, Pt-Me), 2.00 (s, 6 H, MeCO), 7.10 (m, 3 H, PhCN), 7.40 (m, 2 H, H5 and H5′-bipy), 7.62 (m, 2 H, PhCN), 8.10 (m, 4 H, H3,H3′,H4 and H4′-bipy), 8.43 (d, $^3J_{Pt-H}$ = 12 Hz, 1 H, H6-bipy), 8.86 (d, $^3J_{Pt-H}$ = 43 Hz, 1 H, H6′-bipy), 11.9 (br, 1 H, OH). − ^{13}C NMR ($CDCl_3$): δ = −14.4 (Pt-Me), 31.4 (*Me*CO), 116.3 [*C*($COMe)_2$], 122.6 and 123.6 (C3 and C3′-bipy), 126.9 and 127.3 (C5 and C5′-bipy), 128.3 and 128.7 (C2, C3, C5 and C6-PhCN), 137.6 (C4 and C4′-bipy), 142.0 (C4-PhCN), 147.6 and 148.7 (C6 and C6′-bipy), 153.6 and 157.6 (C2 and C2′-bipy), 176.3 (Ph*C*=C), 197.3 (Me*C*O) − IR ($CHCl_3$): ν̃= 2475 (O−H···O), 1542 (COMe) cm^{-1}.

Complex 1c′: (a) HBF_4·Et_2O (0.016 g, 0.10 mmol) was added to a chloroform solution (5 mL) of **1c** (0.054 g, 0.10 mmol). The colour of the solution turned from orange to yellow, and the solvent was removed under vacuum affording the product **A** in quantitative yield (0.062 g).

(b) A deuteronitromethane solution (1 mL) of $AgBF_4$ (0.010 g, 0.050 mmol) and $NH_2C(Me)=C(COMe)_2$ (0.010 g, 0.059 mmol) was added to solid [PtClMe(bipy)] (0.020 g, 0.050 mmol). After one hour of stirring AgCl was removed by filtration through a short column of Celite, and the filtrate transferred into an NMR tube. The spectrum was identical to that of the product **1c′** obtained as in (a) above. ^{1}H NMR (CD_3NO_2): δ = 0.82 (s, 3 H, $^2J_{Pt-H}$ =

80 Hz, Pt-Me), 2.57 (s, $^4J_{Pt-H}$ = 12 Hz, 3 H, MeCN), 3.92 (s, 6 H, MeOCO), 4.89 (s, 1 H, NH), 7.8 (m, 2 H, H5 and H5′-bipy), 8.4 (m, 4 H, H3,H3′,H4 and H4′-bipy), 8.59 (d, 1 H, H6-bipy,), 9.01 (d, $^3J_{Pt-H}$ = 52 Hz, 1 H, H6′-bipy), 11.1 (br, 1 H, NH).

X-ray Crystallographic Determination of 1a: Details of the structure analysis are listed in Table2. The compound was recrystallised from dichloromethane/toluene. X-ray data were collected at room temperature on an Enraf−Nonius CAD4-F automatic diffractometer using Mo-K_α graphite-monochromated radiation and operating in the ω/θ scan mode. The unit cell parameters were obtained by a least-squares fitting of the setting values of 25 reflections in the θ range 12°≤ θ ≤14°. Three monitoring reflections, measured every 500 reflections, showed an intensity decay of about 12% for which a linear correction was applied. In addition to the corrections for Lorentz and polarisation factors, a semiempirical correction for absorption was applied[19] (max and min. values of the transmission factor were 1.3 and 1.0). The structure was solved by routine application of the Patterson and Fourier techniques and refined by a full-matrix least-squares procedure minimising the quantity $\Sigma w(|F_o| - |F_c|)^2$ with $w^{-1} = [\sigma^2(F_0)+(0.02F_0)^2+4]$, where σ is derived from counting statistics. A molecule of CH_2Cl_2 per molecule of complex allowed the calculated density to fit the measured value (by flotation). However, scrutiny of the Fourier difference map showed the solvent molecule to be distributed over two different sites and only the position of the four Cl atoms could be located and refined with isotropic thermal parameters. All non-hydrogen atoms were refined anisotropically. The H atoms were placed in calculated positions and included, but not refined, in the last refinement cycles with isotropic thermal parameters equal to those of the carrier atoms. The final Fourier difference map showed no peaks greater than 1.5 e·Å^{-3}. All calculations were performed with the Enraf−Nonius SDP set of programs.[20]

Table 2. Crystal and data collection details for **1a**

Crystal size	0.05 × 0.20 × 0.30 mm
Formula	$PtO_2N_3C_{18}H_{21}\cdot CH_2Cl_2$
Molecular weight	591.41
System	triclinic
Space group	$P\bar{1}$
a	8.187(2) Å
b	12.561(3) Å
c	12.743(3) Å
α	61.34(2)°
β	74.56(2)°
γ	82.26(2)°
V	1108(3) Å^3
Z	2
D_{calc}	1.77 g/cm^3
D_{obs}	1.78 g/cm^3
Radiation	Mo-K_α (0.71073 Å)
μ	66.5 cm^{-1}
Temperature	23 ±1°
Corrections	Lorentz-polarization linear decay (from 1.000 to 1.064 on *I*) reflection averaging (agreement on *I* = 4.0%) empirical absorption (from 1.000 to 1.315 on *I*)
θ_{max}	27°
Parameters refined	233
No independent reflections	4966
No reflections above 3σ	1705
Unweighted agreement factor	0.049
Weighted agreement factor	0.063
Esd of obs. of unit weight	1.06

Crystallographic data (excluding structure factors) for the structure reported in this paper have been deposited with the Cambridge Crystallographic Data Centre as supplementary publication no. CCDC-167118. Copies of the data can be obtained free of charge on application to CCDC, 12 Union Road, Cambridge CB2 1EZ, UK [Fax: (internat.) +44-1223/336-033; E-mail: deposit@ccdc.cam.ac.uk].

Acknowledgments

The authors thank the Consiglio Nazionale delle Ricerche, the MURST (Programmi di Ricerca Scientifica di Rilevante Interesse Nazionale, Cofinanziamento 2000−2001), and the Centro Interdipartimentale di Metodologie Chimico-Fisiche, Università di Napoli "Federico II" for NMR and X-ray facilities.

[1] R. A. Michelin, M. Mozzon, R. Bertani, *Coord. Chem. Rev.* **1996**, *147*, 299−338.
[2] B. Corain, M. Basato, A. C. Veronese, *J. Mol. Catal.* **1993**, *81*, 133−155.
[3] J. Wagner, M. Haukka, J. J. R. Fraùsto da Silva, A. J. L. Pombeiro, V. Y. Kukushkin, *Inorg. Chem.* **2001**, *40*, 264−271.
[4] V. Y. Kukushkin, T. B. Pakhomova, Y. N. Kukushkin, R. Herrmann, G. Wagner, A. J. L. Pombeiro, *Inorg. Chem.* **1998**, *37*, 6511−6517.
[5] R. Bertani, D. Catanese, R. A. Michelin, M. Mozzon, G. Bandoli, A. Dolmella, *Inorg. Chem. Commun.* **2000**, *3*, 16−18 and references therein.
[6] R. Cini, P. A. Caputo, F. P. Intini, G. Natile, *Inorg. Chem.* **1995**, *34*, 1130−1137 and references therein.
[7] U. Belluco, R. Bertani, F. Meneghetti, R. A. Michelin, M. Mozzon, G. Bandoli, A. Dolmella, *Inorg. Chim. Acta* **2000**, *300−302*, 912−921.
[8] M. Coluccia, A. Nassi, F. Roseto, A. Boccarelli, M. A. Mariggiò, D. Giordano, F. P. Intini, P. Caputo, G. Natile, *J. Med. Chem.* **1993**, *36*, 510−512.
[9] T. Uchiyama, K. Takagi, K. Matsumoto, S. Ooi, Y. Nakamura, S. Kawaguchi, *Bull. Chem. Soc. Jpn.* **1981**, *54*, 1077−1084.
[10] M. Basato, U. Vettori, A. C. Veronese, A. Grassi, G. Valle, *Inorg. Chem.* **1998**, *37*, 6737−6745.
[11] V. G. Albano, D. Braga, V. De Felice, A. Panunzi, A. Vitagliano, *Organometallics* **1987**, *5*, 517−525.
[12] M. Calligaris, L. Randaccio, in *Comprehensive Coordination Chemistry* (Eds.: G. Wilkinson, R. D. Gillard, J. A. McCleverty), Pergamon Press: Oxford, England, **1987**, vol. 2.
[13] B. Couchoron, J. Le Saint, P. Courtot, *Bull. Soc. Chim. Fr.* **1983**, *II*, 66−72.
[14] V. De Felice, M. L. Ferrara, I. Orabona, F. Ruffo, *J. Organomet. Chem.* **1996**, *519*, 75−82.
[15] P. Ham, A. J. Pearson, T. R. Perrior, C. W. Ong, D. C. Rees, *J. Chem. Soc., Perkin Trans. 1* **1982**, 1527−1534.
[16] H. C. Clark, L. E. Manzer, *J. Organomet. Chem.* **1973**, *59*, 411−428.
[17] M. E. Cucciolito, V. De Felice, A. Panunzi, A. Vitagliano, *Organometallics* **1989**, *8*, 1180−1187.
[18] A. Sanchez, C. Castellari, A. Panunzi, A. Vitagliano, V. De Felice, *J. Organomet. Chem.* **1990**, *388*, 243−252.
[19] A. C. T. North, D. C. Phillips, F. S. Mathews, *Acta Crystallogr., Sect. A* **1968**, *24*, 351−359.
[20] B. Frenz, Crystallographic Computing 5, Oxford University Press, **1991**, *11*, 126−135.

Received May 21, 2001
[I01181]

Relaxivity Studies on a Gadolinium(III) Complex of a Macrocyclic DTPA Derivative

Emrin Zitha-Bovens,[a] Luce Vander Elst,[b] Robert N. Muller,[b] Herman van Bekkum,[a] and Joop A. Peters*[a]

Keywords: Chelates / Contrast agents / Gadolinium / Macrocyclic ligands / NMR spectroscopy

The dinuclear Gd^{3+} complex of the 30-membered cyclic DTPA derivative, cy(DTPA-en-DTPA-en), was studied by various NMR spectroscopic techniques in order to evaluate the parameters governing its relaxivity. The values obtained were compared with those for Gd(DTPA-BMA), which is an acyclic mononuclear analogue. Because of the increase in molecular weight the relaxivity r_1 =5.25 $s^{-1}mM^{-1}$ (20 MHz, 37 °C) is higher than that of the monomeric analogue (4.2 $s^{-1}mM^{-1}$). The rotational correlation time at 298 K, τ_R^{298} was determined to be 175–188 ps, which is significantly higher than that expected, based on the increase in the molecular volume of the acyclic compared to the cyclic compound. Possibly, the cyclic nature of the ligand induces steric constraints in Gd[cy(DTPA-en-DTPA-en)], which reduce the local mobility. The water exchange rate for this complex (k_{ex}^{298} = 2.9×10^5 s^{-1}) is somewhat smaller than that of Gd(DTPA-BMA) (k_{ex}^{298} = 4.5×10^5 s^{-1}), which suggests that the water exchange rates are different in the various isomers of acyclic Gd-DTPA-bisamides.

Introduction

Chelates of Gd^{3+} have found widespread application as contrast agents for MRI (Magnetic Resonance Imaging).[1−3] The paramagnetic Gd^{3+} ion in these compounds has an enhancing effect on the relaxation rate of the water protons in its proximity, which may lead to an increase in the quality of the images and a decrease of the recording time. The encapsulation of Gd^{3+} into a strongly chelating ligand is necessary, since the Gd^{3+} aquo ion is highly toxic, whereas the chelates are not. The currently commercially available MRI contrast agents are derivatives of either the acyclic DTPA (DTPA = diethylenetriamine-*N*,*N*,*N*′,*N*′′,*N*′′-pentaacetate) or the macrocyclic ligand DOTA (DOTA = 1,4,7,10-tetraazacyclododecane-1,4,7,10-tetraacetate). Both types of Gd^{3+} complexes have been shown to be very suitable for this application, because of their high in vivo thermodynamic and kinetic stabilities. It is important that the chelating ligand leaves enough space on the Gd^{3+} ion for the coordination of a water molecule, which exchanges with the bulk to provide an overall reduction of the water proton relaxation rate.

The overwhelming success of the MRI contrast agents and the rapid development of the MRI technique have given rise to a continuing demand for new generations of contrast agents that are more effective and selective. Extensive studies in this field have shown that higher relaxivities, r_1 (enhancement of the water proton relaxation rate, expressed in $s^{-1}mM^{-1}$ Gd^{3+}), may be achieved, for example, by: (i) the design of the environment of the water coordination site, so that the water exchange rate will not limit the overall relaxivity ($\tau_m < T_{1m}$, with τ_m being the residence time of a water molecule in the first coordination sphere, and T_{1m} its proton longitudinal relaxation time), or (ii) an increase of the molecular weight of the compounds, in order to increase τ_R and thus the relaxivity, or (iii) by attaching substituents onto the ligand so that a higher tissue specificity is obtained.

Here, we report on a comprehensive study of the parameters that govern the relaxivity of the dinuclear Gd^{3+} complex of the 30-membered macrocycle cy(DTPA-en-DTPA-en),[4,5] also referred to as L (see Figure 1), using variable temperature ^{17}O and ^2H NMR spectroscopic measurements, and ^1H NMR longitudinal relaxation rate measurements at variable magnetic fields (NMRD profiles).

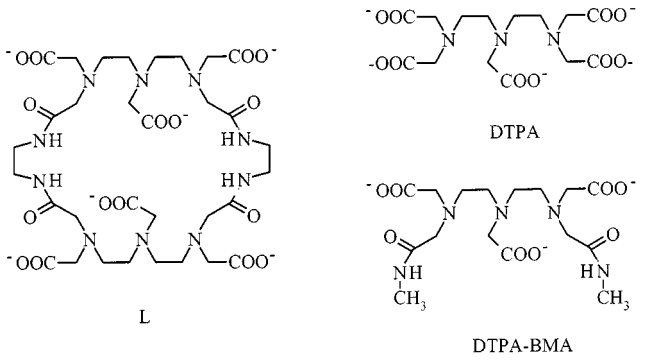

Figure 1. Chemical structure of the cy(DTPA-en-DTPA-en) ligand (L), DTPA and DTPA-BMA

[a] Laboratory of Applied Organic Chemistry and Catalysis, Delft University of Technology
Julianalaan 136, 2628 BL Delft, Netherlands
Fax: (internat.) + 31-15/2784289
E-mail: J.A.Peters@tnw.tudelft.nl
[b] NMR Laboratory, Department of Organic Chemistry, University of Mons-Hainaut
7000 Mons, Belgium
Fax: (internat.) + 32-65/373520
E-mail: robert.muller@umh.ac.be

 © WILEY-VCH Verlag GmbH, 69451 Weinheim, 2001 1434−1948/01/1212−3101 $ 17.50+.50/0

Ligand L can be considered as a cyclic dimer of DTPA-bis(methylamide) (DTPA-BMA) and features several interesting aspects which may be of relevance to its relaxivity: (i) the distance between the two Gd^{3+} ions in the dinuclear complex is relatively small (7.1 Å),[6] which might result in magnetic coupling and a concomitant effect on the electronic relaxation, (ii) Gd_2L has a higher molecular weight than Gd(DTPA-BMA), which may result in a smaller tumbling rate and (iii) intramolecular fluctuations are reduced due to the cyclic nature of the ligand. Furthermore, the number of diastereomeric pairs is reduced from 4 to 2 upon the 'cyclization' of DTPA-BMA[5] and, therefore, this compound may afford information on possible differences in water exchange rates between the various diastereomers of Gd^{3+} complexes of DTPA derivatives. Recently, it has been shown that subtle differences in the coordination geometry of the lanthanide ion in chelates, with macrocyclic derivatives of cyclen, has a profound effect on the rate of exchange between the bound water and the bulk.[7–12]

Results and Discussion

NMRD Measurements

The complex Gd_2L was investigated by water ^1H longitudinal relaxation time measurements at several temperatures (5, 15, 25, 37, and 45 °C) and magnetic field strengths varying between 2.5×10^{-4} T and 1.2 T (NMRD) in order to assess the relaxation processes in this system (see Figure 2). The profiles were fitted using the Solomon–Bloembergen–Morgan equations, to obtain the inner-sphere relaxation, along with the Freed equations for the outer-sphere contribution. Using these well-established procedures[13] may afford the values of the parameters that determine the overall relaxivity of Gd_2L. Since the NMRD curves are rather featureless and the number of parameters is large, first τ_m and τ_R were determined independently using other techniques. Previous studies have shown that variable temperature ^{17}O NMR spectroscopy is a very suitable technique for evaluating accurate values for water exchange rates.[13] Discrepancies often exist between τ_R values obtained from ^{17}O NMR spectroscopy and those obtained from NMRD. Therefore, these values were determined independently with the use of ^2H longitudinal relaxation rates. The advantage of ^2H relaxation for the determination of τ_R is that it is fully controlled by quadrupolar interactions (see below), while for the ^{17}O longitudinal relaxation, a dipole-dipole contribution also has to be taken into account.[14]

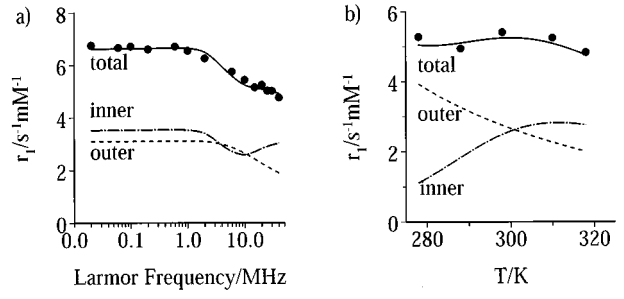

Figure 2. (a) NMRD profile of Gd_2L at 310 K. The lines are calculated using the values for the parameters as mentioned in Table 1. (b) Temperature dependence of the relaxivity of Gd_2L at 20 MHz

Variable Temperature ^2H NMR Spectroscopy

The cyclic ligand L deuterated at the methylene moieties of the acetate groups was synthesized in a similar manner to the unlabeled compound[4] which is by condensation of the bisamide of DTPA and ethylenediamine with DTPA-bisanhydride. However, deuterated DTPA was now used as the starting compound. The latter was obtained by refluxing a solution of DTPA in D_2O at pD 10.6 for 24 hours.[15] Subjecting the cyclic ligand L to similar reaction conditions leads to the hydrolysis of the amide bonds.[16]

The ^2H longitudinal relaxation time T_1 of La_2L, the diamagnetic analogue of the Gd^{3+} complex under study, was measured at different temperatures (see Figure 3). The rotational correlation time (τ_R) was calculated from the data using Equation (1), where χ is the quadrupolar coupling constant ($\chi = 1.06\times10^6$ rad s^{-1}) and η is an asymmetry factor which is negligible for the C-^2H bond. From the temperature dependence of the rotational correlation times, the values of $\tau_R^{298} = 175$ ps and an activation energy $E_R = 22.1$ kJ mol^{-1} were calculated using Equation (2).

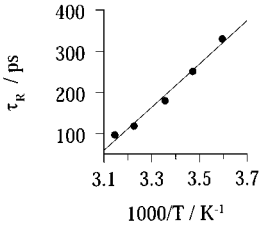

Figure 3. Temperature dependence of τ_R of La_2L, as determined from ^2H longitudinal relaxation rates as calculated from the experimental T_1 values using Equation (1)

$$\frac{1}{T_1}\left(^2H\right) = \frac{3\pi^2}{10}\frac{2I+3}{I^2(2I-1)}\chi^2\left(1+\eta^2/3\right)\tau_R \quad (1)$$

$$\tau_R = \tau_R^{298}\exp\left(\frac{E_R}{R}\left(\frac{1}{T}-\frac{1}{298.15}\right)\right) \quad (2)$$

Variable Temperature ^{17}O NMR Spectroscopy

The water exchange rate ($k_{ex} = \tau_m^{-1}$) of Gd_2L was determined from a variable temperature ^{17}O NMR spectroscopic study (chemical shifts and longitudinal and transversal relaxation rates). The total set of data (see Figure 4) enables the determination of a number of parameters including the rotational correlation time (τ_R), the hyperfine coupling constant ($A/\hbar$), and parameters concerning the electronic relaxation, τ_V (the correlation time for the zero-field splitting),

E_V (the activation energy for the latter process) and Δ^2 (the trace of the square of the zero-field splitting tensor).

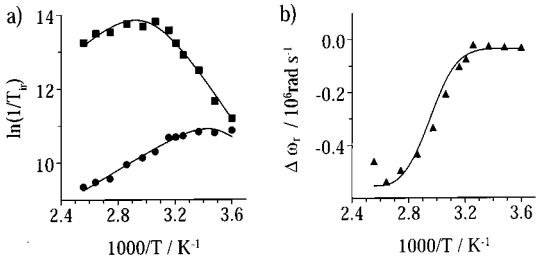

Figure 4. Temperature dependence of the reduced ^{17}O (a) transverse (filled squares) and longitudinal (filled circles) relaxation rates, expressed as $\ln(1/T_{ir})$, and (b) chemical shifts (filled triangles), $\Delta\omega_r$.

Simultaneous Fitting of NMRD and ^{17}O NMR Spectroscopic Data

The NMRD data of Gd_2L (Figure 2) together with the ^{17}O NMR spectroscopic data (Figure 4) was submitted for a least-squares fitting procedure. The advantage of a simultaneous fitting is that it puts constraints on the common parameters. Additional constraints were introduced by fixing the water hydration number (q) of each Gd^{3+} at 1, the quadrupolar coupling constant $[\chi(1 + \eta^{2/3})^{1/2}]$ at 7.58 MHz, the distance of closest approach of a water proton to a Gd^{3+} center (a_{GdH}) at 3.5 Å, and the inner sphere Gd−H distance (r_{GdH}) at 3.1 Å. In Table 1, the parameters as determined from the multiparameter fit are compared with those of the acyclic complexes $Gd(DTPA)^{2-}$ and Gd(DTPA-BMA).[17] Three parameters for the cyclic dinuclear complex Gd_2L differ significantly from those of its acyclic mononuclear counterparts, namely, $A/\hbar$, τ_R, and k_{ex}^{298}.

The relatively low value found for the scalar coupling constant ($A/\hbar = -3.2\times10^6$ rad s^{-1}, see Table 1) may indicate that there is effectively less water bound to the paramagnetic center. The hydration number, q, is an average taken over the different isomers, which are characterized by their respective lifetime in aqueous solution. Because of the crowding in the cyclic ligand, it is very well possible that the averaged value of q is smaller than one. Overestimation of the (fixed) hydration number in the fitting procedure can result in a lower value for $A/\hbar$. Assuming that $A/\hbar = -3.9\times10^6$ rad s^{-1} for a Gd^{3+}-bound ^{17}O nucleus,[13,15] the data would indicate that $q = 0.8$, which is in good agreement with previous results based on Dy^{3+} induced water ^{17}O shifts.[5]

Table 1. Comparison of parameters obtained from simultaneous fitting of ^{17}O NMR spectroscopic and NMRD data with some literature data

	DTPA[17]	DTPA-BMA[17]	L
k_{ex}^{298} (10^6 s^{-1})	3.3 ± 0.2	0.45 ± 0.01	0.29 ± 0.02
$\Delta H^{\neq}$ (kJ mol^{-1})	51.6 ± 1.4	47.6 ± 1.1	44.8 ± 2.2
τ_R (ps)	58 ± 11	66 ± 11	188 ± 9
E_R (kJ mol^{-1})	17.3 ± 0.8	21.9 ± 0.5	19.0 ± 1.3
τ_v (ps)	25 ± 1	25 ± 1	21 ± 2
E_v (kJ mol^{-1})	1.6 ± 1.8	3.9 ± 1.4	1[a]
$A/\hbar$ (10^6 rad s^{-1})	−3.8 ± 0.2	−3.8 ± 0.2	−3.2 ± 0.5
C_{os}	0.18 ± 0.04	0.11 ± 0.04	0.05 ± 0.08
Δ^2 (10^{20} s^{-2})	0.46 ± 0.02	0.41 ± 0.02	0.51 ± 0.07
δg_L^2 (10^{-2})[b]	1.2 ± 0.3	0.8 ± 0.2	2.0 ± 0.9
D_{GdH}^{298} (10^{-10} m^{2}s^{-1})	20 ± 3	23 ± 2	23 ± 1
$E_{D\ GdH}$ (kJ mol^{-1})	19.4 ± 1.8	12.9 ± 2.1	20.4 ± 1.0
r_{GdO} (Å)	2.20 ± 0.09	2.12 ± 0.04	2.09 ± 0.02
$\chi(1+\eta^2/3)^{1/2}$ (MHz)	7.58	7.58	7.58[a]

[a] Parameter fixed in fitting procedure. – [b] Parameter that determines the spin rotation contribution of the longitudinal electronic relaxation.[13]

The value of the rotational correlation time (τ_R^{298}) follows the general trend of the relative molecular masses of the complexes. The value found from the simultaneous fitting was in good agreement with the value determined by ^2H NMR spectroscopy (see above). It should be noted that the ^1H water relaxation rate of Gd_2L solutions at 200 MHz was linearly dependent on the concentration of the paramagnetic compound in solution. Over the concentration range in which the ^{17}O and ^2H NMR spectroscopic measurements and the NMRD profiles were recorded (200, 50 and 1 mM of Gd^{3+}, respectively), a correlation coefficient of 0.99 was calculated for T_1 as a function of the concentration. This justifies the use of the data that were obtained via the different techniques in a simultaneous fitting procedure.

It is surprising that the increase of τ_R^{298} upon going from Gd(DTPA-BMA) to GdL_2 is not linearly proportional with the increase in molecular weight. The molecular mass of the dimeric compound is two times higher than that of the DTPA-BMA complex, and the molar volume, as estimated from molecular mechanics using the HyperChem program on the Gd_2L complex (1857 Å^3) is 1.7 times higher than that of Gd(DTPA-BMA) (1084 Å^3). Based on these data, and the Debye−Stokes−Einstein relationship, a value for τ_R^{298}, of about 112 ps would be expected for Gd_2L. The value of 175 ps for τ_R^{298} as found by ^2H NMR spectroscopy that is in agreement with the results of the fitting of the ^{17}O NMR spectroscopic data, is significantly higher. Therefore, features other than the molar volume must be involved in the rotational correlation time of these complexes. Possibly, the τ_R^{298} value of Gd(DTPA-BMA) is not only determined by the global rotation, but has an additional contribution of relatively fast local motions. It may be expected that the mobility decreases upon going from the acyclic Gd(DTPA-BMA) to its macrocyclic dimer Gd_2L, which may explain the unexpectedly high τ_R^{298} value for the latter compound. This is in line with the ratio of the τ_R values for $Gd(DOTA)^-$ and $Gd(DTPA)^{2-}$, which is 1.3, whereas the molecular volumes of these complexes are about equal (982 Å^3 and 937 Å^3, respectively).

The water exchange rate k_{ex}^{298} for the dimeric Gd_2L ligand is somewhat smaller than for DTPA-BMA. The cyclic nature of the ligand limits the number of isomers that are existing in solution.[5] Recently, it was shown that for Ln^{3+} complexes of cyclen derivatives the water exchange rate can vary significantly for the different isomers of a complex in solution.[7−11] So, the reduction of the number of isomers

in the present case may explain a different overall water exchange rate than was observed for the acyclic monomeric counterpart.

The relatively low exchange rate of the inner sphere water molecules in Gd_2L limits the transfer of inner sphere relaxation towards the bulk solution. This effect is manifested clearly in Figure 2, b, which displays the relaxivity at 20 MHz as a function of the temperature. The inner and outer sphere contributions to the relaxivity have an opposite temperature dependence; the outer sphere term increases with a decrease in the temperature. Upon decreasing the temperature below 30 °C the relaxivity levels off, because the effect of the increase in τ_R is quenched by slow water exchange. The water exchange is slowed down (and the inner sphere relaxivity decreases) to the extent where the outer sphere relaxivity, which increases on lowering the temperature, becomes predominant.

Finally, the NMRD profile recorded from an aqueous solution of the Gd_2L compound containing 4% Human Serum Albumin (HSA), at 37 °C, was identical to the curve obtained in the absence of HSA, indicating that there is no interaction with albumin.

Conclusion

The 'cyclo-dimerisation' of Gd(DTPA-BMA) towards Gd_2L has some particular effects on the relaxivity properties. First, the increase in molar volume (with a factor of 1.7) resulted in a much higher increase in the rotational correlation time (factor of 2.7), suggesting a reduction in the local mobility of the complex as induced by the cyclic nature of the ligand. Moreover, the water exchange rate, k_{ex}^{298} is somewhat smaller for Gd_2L than for Gd(DTPA-BMA), which may be due to a difference in the isomer distribution in aqueous solution. The exchange rate of the inner sphere water molecule with the bulk, limits the relaxivity to such an extent that, at low temperature (5 °C), the outer sphere term becomes predominant. The electronic relaxation does not seem to be influenced by the cyclo-dimerization. Apparently, the interaction between the neighboring Gd^{3+} ions is negligible. Finally, it can be stated that the design of rigid cyclic ligands can lead to an increase in τ_R, which is favorable for higher relaxivity values. A drawback is that the water exchange can become so slow, that the effect of τ_R is counteracted. The challenge is to find an optimum for both parameters.

Experimental Section

General Remarks: All chemicals were purchased from ACROS Chimica, except the lanthanide chlorides that were purchased from Aldrich Chemical Co. All compounds were used without further purification.

NMR Spectroscopy: The ^1H and ^{13}C NMR spectra were recorded on a Varian INOVA-300 or a Varian VXR-400 spectrometer. *Tert*-butyl alcohol was used as an internal standard (methyl signal at $\delta = 1.2$ (^1H NMR) and $\delta = 31.2$ (^{13}C NMR). The variable temperature ^{17}O NMR spectroscopic measurements were performed with H_2O solutions at a magnetic field of 7.05 T on a Varian INOVA 300 spectrometer. The samples were enclosed in a sealed NMR tube under argon atmosphere. The ^1H signal of *tert*-butyl alcohol was used as an internal reference, to correct the ^{17}O NMR chemical shift for the Bulk Magnetic Susceptibility (BMS) shift contribution. The BMS shift had to be taken into account since the measurements were performed in an unlocked configuration.

Longitudinal relaxation rates, $1/T_1$, were measured using the inversion-recovery method, and transversal relaxation rates, $1/T_2$, were obtained via the Carr−Purcell−Meiboom−Gill spin-echo technique. At each temperature, the spectral parameters were measured for both a sample with 0.1 M dinuclear Gd^{3+} complex and a sample of acidified water (pH 5.2) under exactly the same conditions.

^2H longitudinal relaxation rates were measured at 4.7 T on a Bruker MSL-200−15 spectrometer using a broadband probe. The solvent (water) was deuterium depleted. The 90° and 180° pulse lengths were 9 and 18 μs, respectively.

The exact Gd^{3+} contents of the NMR samples were determined by ICP. The pH values of the NMR samples were measured at room temperature with a calibrated micro-combination probe (Aldrich Chemical Co.) and a Corning 125 pH meter. No corrections were made for deuterium isotope effects.

Relaxivity Measurements: The $1/T_1$ NMRD (Nuclear Magnetic Relaxation Dispersion) profiles were recorded at different temperatures on a FCS Research Relaxometer using the field cycling method, covering a continuum of magnetic fields from 2.5×10^{-4} to 1.2 T (corresponding to a proton Larmor Frequency range of 0.01−50 MHz). The absolute uncertainty in the $1/T_1$ values for the NMRD measurements was about 2%. The spin-lattice relaxation rates at 20 MHz were also measured on a Minispec Bruker PC-20 spin analyzer.

Computer Calculations: Experimental variable-temperature ^{17}O NMR spectroscopic and NMRD data were fitted with a computer program written by Dr. É. Tóth and Dr. L. Helm (University of Lausanne, Switzerland) using the Micromath Scientist program version 2.0 (Salt Lake City, UT, USA). Molecular volumes were calculated with the use of the HyperChem program (version 6.0, HyperCube Inc., Gainsville FL, USA).

Synthesis of the Ligands: The ligand L was synthesized following Carvalho et al.[4] Purification was done via ion exchange chromatography (DOWEX 1×8−200, OAc^- form, elution with a gradient of HOAc).[5] Ligand L with deuterated methylene groups in the acetate functions was synthesized in an analogous way starting from DTPA, deuterated at the corresponding positions. The latter was obtained using the procedure of Wheeler and Legg.[15] H_5DTPA (0.42 g) was dissolved in 15 mL D_2O, and the pD was adjusted to 10.6 by addition of solid K_2CO_3. The solution was refluxed for 24 h. After cooling, the reaction mixture was acidified to pD 2 using concentrated HCl. The solution obtained was concentrated under reduced pressure, and the solid KCl was filtered off. Upon addition of 2-propanol to the filtrate, the deuterated compound precipitated, and was filtered off. The yield of $[D_{10}]H_5DTPA$ was 0.27 g (67%). The degree of acetate methylene deuteration (>99%) was determined from the integrals in the ^1H NMR spectrum. The compound was converted into the bis-anhydride compound by reflux in an acetic anhydride/pyridine mixture.

Preparation of the Dinuclear Gd_2L Complex: The gadolinium complex of the macrocyclic ligand L was prepared by adding an aque-

ous solution of $GdCl_3 \cdot 6H_2O$ dropwise to a solution of the ligand in water (molar ratio $GdCl_3$:L = 2:1) while keeping the pH at about 6. Salts were removed by ultrafiltration over a UTC-60 membrane (Toray Industries, Tokyo, Japan) under a pressure of 20 bar N_2. Finally, the aqueous solution was freeze dried. The complex was tested for the absence of free lanthanides using an arsenazo III indicator.

Acknowledgments

This work was performed in the framework of the EU COST actions D8 and D18 and was financially supported by the EU BIOMED program (MACE network). We are grateful to Dr. É. Tóth (University of Lausanne, Switzerland) for providing the Scientist files.

[1] A. E. Merbach, É. Tóth (Eds.), *The Chemistry of Contrast Agents in Medical Magnetic Resonance Imaging*, John Wiley & Sons, Chichester, **2001**.
[2] P. Caravan, J. J. Ellison, T. J. McMurry, R. B. Lauffer, *Chem. Rev.* **1999**, *99*, 2293−2352.
[3] J. A. Peters, J. Huskens, D. J. Raber, *Progr. Nucl. Magn. Reson. Spectrosc.* **1996**, *28*, 283−350.
[4] J. F. Carvalho, S.-H. Kim, C. A. Chang, *Inorg. Chem.* **1992**, *31*, 4065−4068.
[5] E. Bovens, M. A. Hoefnagel, E. Boers, H. Lammers, H. van Bekkum, J. A. Peters, *Inorg. Chem.* **1996**, *35*, 7679−7683.
[6] S. T. Frey, C. A. Chang, J. F. Carvalho, A. Varadarajan, L. M. Schulze, K. L. Pounds, W. DeW. Horrocks, Jr., *Inorg. Chem.* **1994**, *33*, 2882- 2889.
[7] S. Aime, A. Barge, M. Botta, A. S. De Sousa, D. Parker, *Angew. Chem. Int. Ed.* **1998**, *37*, 2673−2674.
[8] F. A. Dunand, S. Aime, A. E. Merbach, *J. Am. Chem. Soc.* **2000**, *122*, 1506−1512.
[9] S. Aime, A. Barge, J. L. Bruce, M. Botta, J. A. K. Howard, J. M. Moloney, D. Parker, A. S. de Sousa, M. Woods, *J. Am. Chem. Soc.* **1999**, *121*, 5762−5771.
[10] M. Woods, S. Aime, M. Botta, J. A. K. Howard, J. M. Moloney, M. Navet, D. Parker, M. Port, O. Rousseaux, *J. Am. Chem. Soc.* **2000**, *122*, 9781−9762.
[11] S. Zhang, Z. Kovacs, S. Burgess, S. Aime, E. Terreno, A. D. Sherry, *Chem. Eur. J.* **2001**, *7*, 288−296.
[12] D. M. Corsi, L. Vander Elst, R. N. Muller, H. van Bekkum, J. A. Peters, *Chem. Eur. J.* **2001**, *7*, 1383−1389.
[13] É. Tóth, L. Helm, A. E. Merbach in *The Chemistry of Contrast Agents in Medical Magnetic Resonance Imaging* (Eds.: É. Tóth, A. E. Merbach), John Wiley & Sons, Chichester, **2001**, Ch. 2.
[14] L. Vander Elst, F. Maton, S. Laurent, F. Seghi, F. Chapelle, R. N. Muller, *Magn. Reson. Med.* **1997**, *38*, 604−614.
[15] W. D. Wheeler, J. I. Legg, *Inorg. Chem.* **1985**, *24*, 1292−1297.
[16] H. Lammers, F. Maton, D. Pubanz, M. W. van Laren, H. van Bekkum, A. E. Merbach, R. N. Muller, J. A. Peters, *Inorg. Chem.* **1997**, *36*, 2527−2538.
[17] D. H. Powell, O. M. Ni Dhubhghaill, D. Pubanz, L. Helm, Y. S. Lebedev, W. Schlaepfer, A. E. Merbach, *J. Am. Chem. Soc.* **1996**, *118*, 9333−9346.
[18] J. A. Peters, E. Zitha-Bovens, D. M. Corsi, C. F. G. C. Geraldes in *The Chemistry of Contrast Agents in Medical Magnetic Resonance Imaging* (Eds.: É. Tóth, A. E. Merbach), John Wiley & Sons, Chichester, **2001**, Ch. 8.

Received May 25, 2001
[I01191]

3,7,10-Trichalcogenaoctasila[3.3.3]propellanes

U. Herzog*[a] and G. Rheinwald[b]

Keywords: Silanes / Sulfur / Selenium / Tellurium / Polycycles

The reaction of hexakis(trimethylsilyl)disilane with acetyl chloride and aluminum chloride yields hexakis(chlorodimethylsilyl)disilane (**5a**) under carefully controlled reaction conditions. Treatment of **5a** with either H_2S/NEt_3 or Li_2E (E = Se, Te) gives the dodecamethyl-3,7,10-trichalcogenaoctasila-[3.3.3]propellanes $Si_2(SiMe_2)_6E_3$ (**6a** E = S, **6b** E = Se, **6c** E = Te). The products have been characterized by multinuclear NMR spectroscopy (^1H, ^{13}C, ^{29}Si, ^{77}Se, ^{125}Te). The central silicon atoms are very deshielded in comparison with other compounds containing an $Si(Si)_4$ unit due to their incorporation into three five-membered rings. The molecular structures of **5a** and **6a** are reported revealing an elongated central Si–Si bond in **5a** of 2.3865(11) Å and three different spatial orientations of the $SiMe_2Cl$ groups in each $Si(SiMe_2Cl)_3$ unit. In **6a** all three five-membered rings Si_4S adopt *envelope* conformations with the four silicon atoms in one plane. A view of the Si_8S_3 skeleton along the central silicon–silicon bond of **6a** resembles a three-blade propeller.

Introduction

In previous investigations we have shown that the reaction of 1,1,2,2-tetrakis(chlorodimethylsilyl)dimethyldisilane (**1**) with either H_2S/NEt_3 or Li_2E (E = Se, Te) yields exclusively the 3,7-dichalcogenahexasilabicyclo[3.3.0]octanes [**2a**–**c**; Equation (1)].[1]

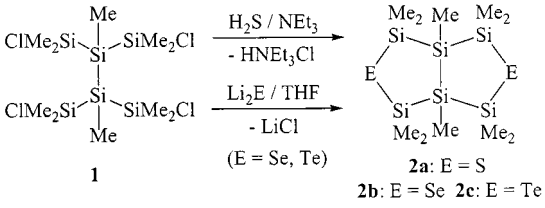

(1)

The formation of these compounds underlines the general observation that the formation of five-membered heterocycles is preferred in the systems silicon-sulfur, -selenium and -tellurium.[2,3] The facile formation of the bicyclic systems tempted us to apply these reactions to the synthesis of the corresponding tricyclic ring systems, which can be described as [3.3.3]propellanes (**3a**, Scheme 1).

It should be mentioned that carbon-based [3.3.3]propellanes have been known for some time[4,5] and even a naturally occurring sesquiterpene, modhephene (**3b**),[6,7] containing this tricyclic skeleton has been described. Molecular structures have been reported for modhephenediol (**3c**, 2,3-dihydroxy-2,4,4,8-tetramethyl[3.3.3]propellane,[6]) and [3.3.3]-propellane-2,8,9-trione (**3d**).[8]

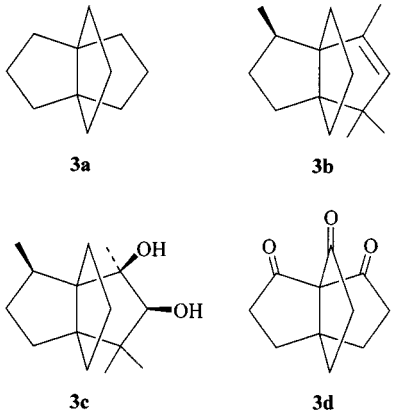

Scheme 1

Results and Discussion

Formation and Structure of Hexakis(chlorodimethylsilyl)disilane (5a)

The formation of 3,7,10-trichalcogenaoctasila[3.3.3]propellanes requires an octasilane skeleton with six chlorodimethylsilyl units connected to a central disilane. This compound, hexakis(chlorodimethylsilyl)disilane (**5a**), can be prepared in three steps starting from tetrakis(trimethylsilyl)-silane by the formation of hypersilylpotassium developed by Marschner[9] [Equation (2)] and a subsequent oxidative dimerization of the hypersilanyl anion [Equation (3)].

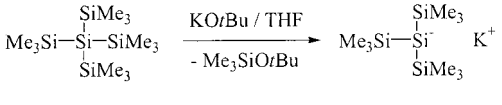

(2)

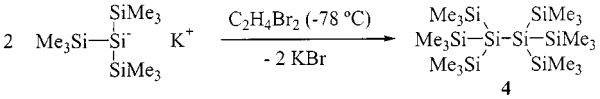

(3)

[a] Institut für Anorganische Chemie der TU Bergakademie Freiberg,
Leipziger Str. 29, 09596 Freiberg, Germany
[b] Institut für Chemie, Lehrstuhl Anorganische Chemie,
TU Chemnitz,
Straße der Nationen 62, 09111 Chemnitz, Germany

 © WILEY-VCH Verlag GmbH, 69451 Weinheim, 2001 1434–1948/01/1212–3107 $ 17.50+.50/0

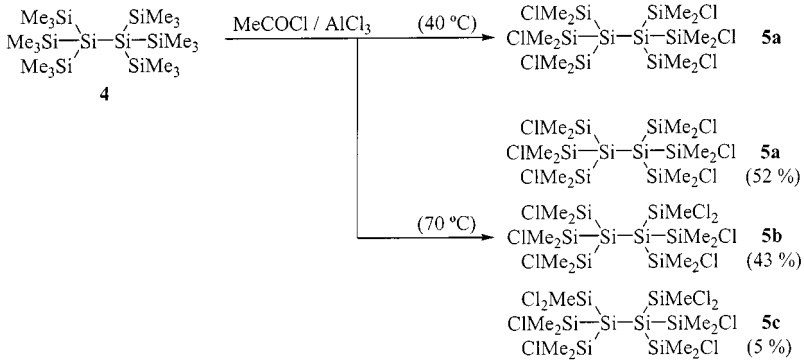

(4)

The molecular structure of the formed hexakis(trimethylsilyl)disilane (**4**) has been reported previously[10,11] revealing an elongated central Si−Si bond of 2.40 Å.

The treatment of **4** with acetyl chloride and aluminum chloride in hexane yields the desired hexachlorinated octasilane **5a** under optimized reaction conditions. Slightly higher reaction temperatures also led to the formation of the higher chlorinated octasilanes **5b** and **5c** [Equation (4)].

The molecular structure of **5a** is shown in Figure 1 and 2 and selected bond lengths and angles are summarized in Table 1. The structure of **5a** is a rare example of a successful crystal structure determination of a methylchlorooligosilane because most compounds of this class are liquids or low melting solids which are highly soluble in all organic solvents. The central silicon−silicon bond of **5a** (Si1−Si5) is, at 2.3865(11) Å, longer than the other Si−Si bonds but slightly shorter than that in **4**. In both $Si(SiMe_2Cl)_3$ units one chlorine substituent occupies a more axial position with respect to the central Si−Si bond (Cl3, Cl4) while the other two are equatorial. This reduces the steric overcrowding resulting in a slightly shorter central Si−Si bond than in **4**. A closer look reveals that in each $Si(SiMe_2Cl)_3$ unit there are three different $SiMe_2Cl$ groups which can be distinguished by their different dihedral angles Cl−Si−Si−Si (see Table 1). A comparison of the two $Si(SiMe_2Cl)_3$ units shows that the silyl units containing Si(2) and Si(8) have a similar orientation, as is the case for Si(3) and Si(7) and Si(4) and Si(6). A look at the Si−Si−Si angles shows that all the Si−Si(1)−Si(5) ands Si(1)−Si(5)−Si angles are larger than the tetrahedral angle of 109.5°, while all the Si−Si−Si angles within each $Si(SiMe_2Cl)_3$ unit are smaller. This is a result of the mutual repulsion of the two $Si(SiMe_2Cl)_3$ units connected by the central Si−Si bond. By comparing the angles C−Si−C (107.93−112.18°, average 109.68°) and C−Si−Si (112.18−117.41°, average 114.30°) with the angles C−Si−Cl (104.94−107.03°, average 106.00°) and Cl−Si−Si (102.97−109.18°, average 105.68°) it can be clearly seen that a methyl group occupies more space than a chlorine substituent.

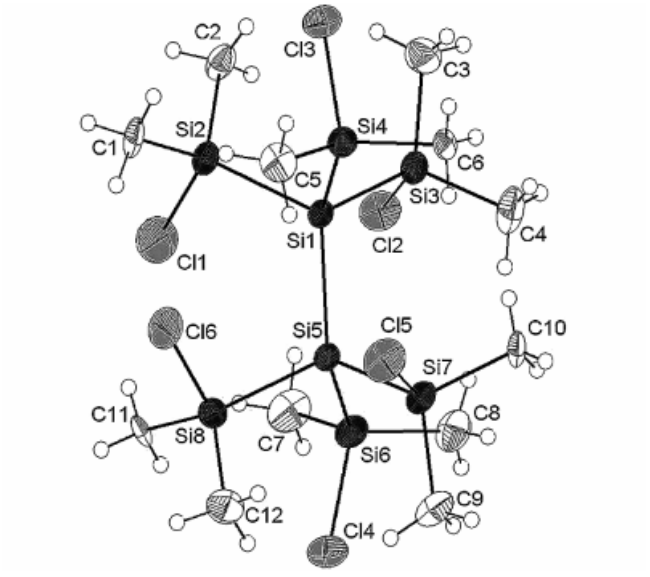

Figure 1. Molecular structure of **5a**

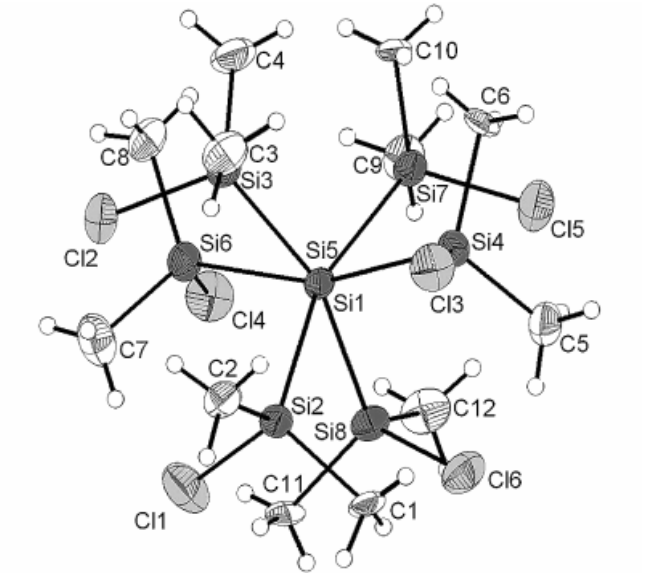

Figure 2. Molecular structure of **5a** viewed along the Si1−Si5 bond

Table 1. Selected bond lengths (Å) and angles (°) of **5a**

Atoms	Distances	Atoms	Angles
Si(1)−Si(2)	2.3754(11)	Si(2)−Si(1)−Si(3)	104.64(4)
Si(1)−Si(3)	2.3597(12)	Si(2)−Si(1)−Si(4)	104.27(4)
Si(1)−Si(4)	2.3597(10)	Si(3)−Si(1)−Si(4)	105.31(4)
Si(1)−Si(5)	2.3865(11)	Si(2)−Si(1)−Si(5)	117.20(4)
Si(5)−Si(6)	2.3658(10)	Si(3)−Si(1)−Si(5)	110.48(4)
Si(5)−Si(7)	2.3676(11)	Si(4)−Si(1)−Si(5)	113.88(4)
Si(5)−Si(8)	2.3617(12)	Si(6)−Si(5)−Si(1)	116.16(4)
Si(2)−Cl(1)	2.0621(12)	Si(7)−Si(5)−Si(1)	112.14(4)
Si(3)−Cl(2)	2.0911(11)	Si(8)−Si(5)−Si(1)	112.50(4)
Si(4)−Cl(3)	2.0865(11)	Si(6)−Si(5)−Si(7)	105.57(4)
Si(6)−Cl(4)	2.1002(12)	Si(6)−Si(5)−Si(8)	104.09(4)
Si(7)−Cl(5)	2.0778(11)	Si(7)−Si(5)−Si(8)	105.45(4)
Si(8)−Cl(6)	2.0764(12)	Si(1)−Si(2)−Cl(1)	109.18(5)
Si(2)−C(1)	1.883(3)	Si(1)−Si(3)−Cl(2)	104.78(5)
Si(2)−C(2)	1.879(3)	Si(1)−Si(4)−Cl(3)	103.21(4)
Si(3)−C(3)	1.857(4)	Si(5)−Si(6)−Cl(4)	102.97(5)
Si(3)−C(4)	1.854(4)	Si(5)−Si(7)−Cl(5)	106.98(5)
Si(4)−C(5)	1.849(4)	Si(5)−Si(8)−Cl(6)	106.97(5)
Si(4)−C(6)	1.885(3)	Si(4)−Si(1)−Si(5)−Si(6)	−157.81(5)
Si(6)−C(7)	1.849(4)	Si(3)−Si(1)−Si(5)−Si(7)	81.97(5)
Si(6)−C(8)	1.867(4)	Si(2)−Si(1)−Si(5)−Si(8)	−39.67(5)
Si(7)−C(9)	1.856(4)	Si(5)−Si(1)−Si(2)−Cl(1)	−31.78(6)
Si(7)−C(10)	1.882(3)	Si(5)−Si(1)−Si(3)−Cl(2)	68.92(5)
Si(8)−C(11)	1.870(3)	Si(5)−Si(1)−Si(4)−Cl(3)	−174.49(5)
Si(8)−C(12)	1.861(3)	Si(1)−Si(5)−Si(8)−Cl(6)	−33.29(6)
		Si(1)−Si(5)−Si(7)−Cl(5)	68.48(6)
		Si(1)−Si(5)−Si(6)−Cl(4)	−167.52(5)

Table 2. ^{29}Si, ^{77}Se, ^{125}Te, ^{13}C and ^{1}H NMR spectroscopic data (ppm, Hz) of the [3.3.3]propellanes $Si_2(SiMe_2)_6E_3$ (E = S, Se, Te)

	compound	δ_{Si}	δ_E	δ_C	δ_H
6a	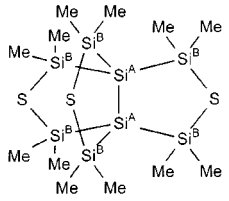	A: −84.52 B: 19.78 $^1J_{SiSi}$: 54.2	–	6.11 $^1J_{SiC}$: 47.5	0.61
6b	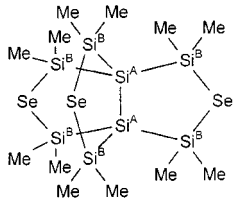	A: −73.22 B: 14.96 $^1J_{SiSi}$: 48.6	Se: −189 $^1J_{SiSe}$: 110.8 $^2J_{SiSe}$: 24.8 $^3J_{SiSe}$: 13.6	5.89	0.72
6c	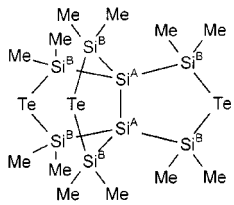	A:−52.36 B: −5.26 $^1J_{SiSi}$: 45.3	Te: −622 $^1J_{SiTe}$: 284.3	5.64	0.99

3,7,10-Trichalcogenaoctasila[3.3.3]propellanes

The reaction of **5a** with either H_2S/NEt_3 in hexane or Li_2E (E = Se, Te) prepared in situ from the chalcogens and $LiBEt_3H$ in THF yielded the expected dodecamethyl-3,7,10-trichalcogenaoctasila[3.3.3]propellanes **6a−c** [Equation (5) and (6)]:

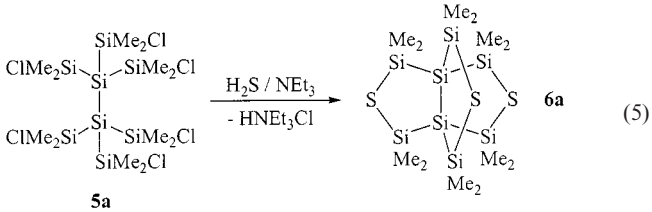

(5)

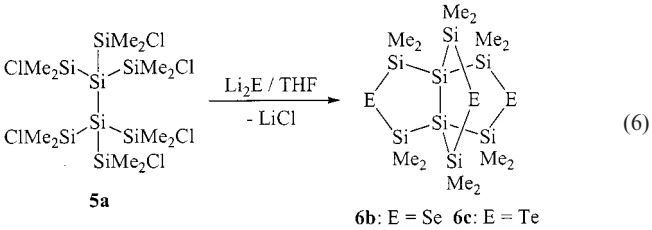

(6)

The NMR spectroscopic data of the propellanes **6a−c** are given in Table 2. While the δ_{Si} values of the $SiMe_2$ units are similar to those in the corresponding monocyclic five-membered rings $(SiMe_2)_4E$[12] and the bicyclo[3.3.0]octanes **2a−c**, the NMR chemical shifts of the central Si atoms are remarkable. Compared with other compounds containing $Si(Si)_4$ units like $Si(SiMe_3)_4$ (δ_{Si} = −135.5[13]), $Si_2(SiMe_3)_6$ (**4**, δ_{Si} = −129.5[9]) or even chloro-substituted derivatives like $Si(SiMe_2Cl)_4$ (δ_{Si} = −113.9[14]) and $Si_2(SiMe_2Cl)_6$ (**5a**, δ_{Si} = −111.62) the chemical shifts found in the propellanes **6a−c** are shifted significantly to lower field, especially in the cases of the heavier chalcogens (Se, Te; see Figure 3).

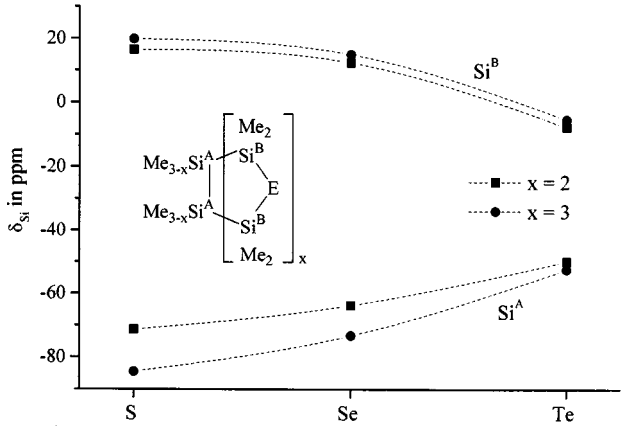

Figure 3. ^{29}Si NMR chemical shifts in bicyclo[3.3.0]octanes (**2a−c**) [1] and [3.3.3]propellanes (**6a−c**) for E = S, Se, Te

It has been observed before that the formation of five-membered rings in the silicon chalcogen systems is always accompanied by a strong low-field shift of the ^{29}Si NMR signals, which increases from sulfur to tellurium in the case of oligosilanyl units.[3] In the cases of the central silicon atoms in the propellanes **6a−c** these atoms are incorporated into three five-membered rings causing these unusual low-

field shifts. Furthermore, compared to the bicyclo[3.3.0]octanes **2b**−**c**[1] the ^{77}Se and the ^{125}Te NMR signals of the propellanes **6b**−**c** are shifted to lower field by 89 ppm (Se) and 114 ppm (Te), despite the same first and second coordination sphere around the chalcogen atoms.

Compound **6a** was characterized by its mass spectrum and also by an X-ray structure analysis. Figure 4 shows the molecular structure of **6**, and some bond lengths and angles are given in Table 3.

In contrast to **5a** all the Si−Si bond lengths are in the usual range. All three five-membered rings adopt almost ideal envelope conformations with dihedral angles Si−Si(1)−Si(5)−Si of −4.8 to −5.2° and envelope angles of 44.57(6)° [Si_4S ring including S(1)], 46.52(6)° [Si_4S ring including S(2)] and 45.28(8)° [Si_4S ring including S(3)]. This is slightly more than in the organic [3.3.3]propellane modhephenediol (**3c**) with envelope angles of 37−42°[6] and close to the envelope angles in the bicyclo[3.3.0]octane derivative **2a** [42.34(4)° and 44.35(3)° [1]]. In contrast to the structure of **2a**, however, all three five-membered rings in **6a** are folded in the same rotatory sense resembling an almost ideal three-blade propeller (Figure 5). The angles at the sulfur atoms in **6a** are, at 101.5−102.4°, close to the values in **2a**. The same holds for the Si−Si and the Si−S bond lengths. Due to the formation of the five-membered rings all Si−Si−Si angles including the Si(1)−Si(5) bond are smaller than the tetrahedral angle (101.5−102.6°) resulting in Si−Si−Si angles of more than 109.5° within the $Si_3Si(1)$ and $Si_3Si(5)$ units (in the range of 115.1−116.4°).

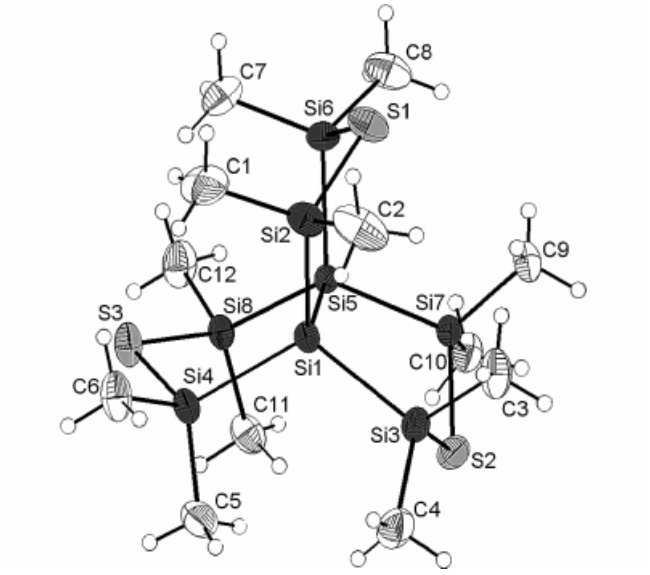

Figure 4. Molecular structure of **6a**

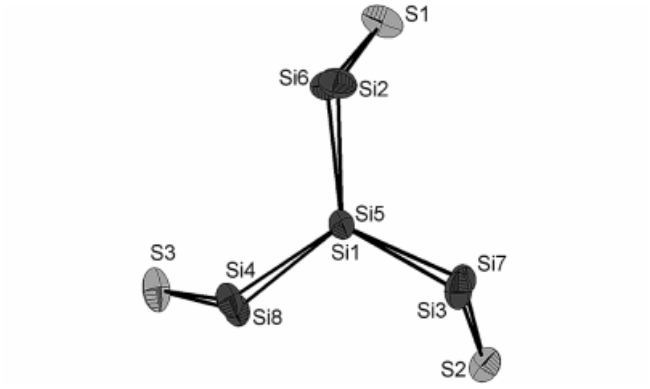

Figure 5. The silicon and sulfur skeleton of **6a** viewed along the central Si−Si bond

Table 3. Selected bond and distances (Å) and angles (°) of **6a**

Atoms	Distances	Atoms	Angles
Si(1)−Si(2)	2.3564(17)	Si(2)−S(1)−Si(6)	102.40(7)
Si(1)−Si(3)	2.3543(15)	Si(3)−S(2)−Si(7)	101.53(6)
Si(1)−Si(4)	2.3621(17)	Si(4)−S(3)−Si(8)	101.65(7)
Si(1)−Si(5)	2.3487(16)	Si(2)−Si(1)−Si(3)	115.41(7)
Si(5)−Si(6)	2.3416(15)	Si(2)−Si(1)−Si(4)	116.39(7)
Si(5)−Si(7)	2.3416(16)	Si(3)−Si(1)−Si(4)	115.24(6)
Si(5)−Si(8)	2.3395(17)	Si(2)−Si(1)−Si(5)	101.89(6)
Si(2)−S(1)	2.1501(18)	Si(3)−Si(1)−Si(5)	102.60(6)
Si(3)−S(2)	2.1541(18)	Si(4)−Si(1)−Si(5)	102.02(6)
Si(4)−S(3)	2.1492(16)	Si(6)−Si(5)−Si(1)	102.58(6)
Si(6)−S(1)	2.1479(18)	Si(7)−Si(5)−Si(1)	101.55(6)
Si(7)−S(2)	2.1543(15)	Si(8)−Si(5)−Si(1)	101.80(6)
Si(8)−S(3)	2.1401(18)	Si(6)−Si(5)−Si(7)	115.15(6)
Si(2)−C(1)	1.871(5)	Si(6)−Si(5)−Si(8)	116.37(6)
Si(2)−C(2)	1.854(5)	Si(7)−Si(5)−Si(8)	115.91(6)
Si(3)−C(3)	1.856(5)	Si(1)−Si(2)−S(1)	106.34(7)
Si(3)−C(4)	1.868(4)	Si(1)−Si(3)−S(2)	105.49(6)
Si(4)−C(5)	1.864(4)	Si(1)−Si(4)−S(3)	106.15(7)
Si(4)−C(6)	1.861(5)	Si(5)−Si(6)−S(1)	104.89(6)
Si(6)−C(7)	1.855(4)	Si(5)−Si(7)−S(2)	104.80(6)
Si(6)−C(8)	1.868(5)	Si(5)−Si(8)−Cl(6)	105.50(7)
Si(7)−C(9)	1.860(4)	Si(4)−Si(1)−Si(5)−Si(8)	−4.95(7)
Si(7)−C(10)	1.865(4)	Si(3)−Si(1)−Si(5)−Si(7)	−5.21(8)
Si(8)−C(11)	1.867(4)	Si(2)−Si(1)−Si(5)−Si(8)	−4.79(7)
Si(8)−C(12)	1.868(4)		

Experimental Section

General: All NMR spectra were recorded on a Bruker DPX 400 in $CDCl_3$ solution and TMS as internal standard for ^{1}H, ^{13}C and ^{29}Si. External Ph_2Se_2 (δ_{Se} = 460) and Ph_2Te_2 (δ_{Te} = 422) in $CDCl_3$ were used as standards for ^{77}Se and ^{125}Te. In order to obtain a sufficient signal-to-noise ratio of ^{29}Si NMR spectra for obtaining $^1J_{SiC}$, $^1J_{SiSi}$, $^{1,2,3}J_{SiSe}$ or $^1J_{SiTe}$ satellites ^{29}Si INEPT spectra were also recorded. ^{77}Se and ^{125}Te spectra were determined using an IGATED pulse program.

Mass spectra were measured on a Hewlett Packard 5971 (ionization energy: 70 eV, column: 30 m × 0.25 mm × 0.25 μm, phenylmethylpolysiloxane, column temperature: 80 °C (3 min)/20 K/min, flow: He 0.5 mL/min).

Starting Materials: H_2S (N25, Air Liquide), Se, Te, triethylamine, 1 M $LiBEt_3H$ in THF (Super Hydride), were commercially available. $Si(SiMe_3)_4$ was prepared as described in ref.[21] THF was distilled from sodium/potassium alloy prior to use. The other solvents were dried over KOH or sodium wire. All reactions were carried out under argon using standard Schlenk techniques.

Crystal Structure Analysis: X-ray structure analysis measurements were performed on a Bruker SMART CCD. Crystal data of **5a** and

Table 4. Crystal data of **5a** and **6a** as well as data collection and refinement details

	5a	**6a**
Chemical formula	$C_{12}H_{36}Cl_6Si_8$	$C_{12}H_{36}S_3Si_8$
Molecular weight	617.83	501.31
Crystal system	monoclinic	monoclinic
Space group	$P2_1/n$	$C2/c$
Unit cell dimensions, Å, °	a = 10.9820(6)	a = 14.6972(19)
	b = 17.0125(10)	b = 12.0174(14)
	c = 17.2780(11)	c = 31.930(4)
	β = 100.401(2)	β = 100.812(2)
Volume in Å^3; Z	3175.0(3); 4	5539.4(12); 8
Density (calcd.) in g/cm^3	1.292	1.202
Linear absorption coeff., mm^{-1}	0.845	0.612
Radiation used	Mo-K_α	Mo-K_α
Temperature	173(2) K	173(2) K
Scan method	ω scans	ω scans
Absorption correction	empirical	empirical
Max./min. transmission	0.9202/0.6773	0.9138/0.8144
Measured reflections	14079	12037
Independent reflections	6291	6510
Observed reflections	4435	3151
Index range	$-13 \le h \le 12$	$-19 \le h \le 19$
	$-23 \le k \le 4$	$-16 \le k \le 8$
	$-22 \le l \le 22$	$-15 \le l \le 42$
R(int)	0.0341	0.0713
θ range for collection, °	1.69−29.36	1.30−29.47
Completeness to θ_{max} %	72.1	84.6
Refinement method	full-matrix least-squares on F^2	full-matrix least-squares on F^2
Final R_1/wR^2 [$I > 2\,\sigma(I)$][a]	0.0368/0.0900	0.0532/0.1030
R_1/wR^2 (all data) [a]	0.0643/0.1008	0.1493/0.1279
No. of reflections/parameters used	6291/379	6510/220
H-locating and refining	difmap/refall	geom./constr.
Goodness-of-fit (S)[b] on F^2	1.000	0.904
Max./min. e-density in e/Å^3	0.472/-0.410	0.545/-0.421

[a] $R_1 = \Sigma(||F_o| - |F_c||)/\Sigma|F_o|$, $wR^2 = [\Sigma[w(F_o^2 - F_c^2)^2]/\Sigma(wF_o^4)]^{1/2}$, $w = 1/[\sigma^2(F_o^2) + (aP)^2 + bP]$ where $P = (F_o^2 + 2F_c^2)/3$, a = 0.0530, b = 0.5866 (**5a**), a = 0.053, b = 0 (**6a**). − [b] $S = [\Sigma w(F_o^2 - F_c^2)^2]/(n - p)^{1/2}$, n = number of reflections, p = parameters used.

6a as well as data collection and refinement details are given in Table 4. The unit cell dimensions were determined with the program SMART.[15] The program SAINT[15] was used for data integration and refinement of the unit cell parameters. The space group was determined with the aid of the programs ABSEN[16] (**5a**) and XPREP[15] (**6a**). All data were corrected for absorption using SADABS.[17] The structures were solved using direct methods [SIR97[18] (**5a**), SHELX97[19] (**6a**)], refined using least-squares methods (SHELX-97) and drawn using Diamond.[20] The ellipsoids of the non-hydrogen atoms are at the 50% probability level. The hydrogen atoms on the methyl groups in **6a** were refined as constrained groups, whereas all hydrogen atoms in **5a** could be located from the difference map and fully refined.

Crystallographic data (excluding structure factors) for the structures in this paper have been deposited with the Cambridge Crystallographic Data Centre as supplementary publication nos. CCDC-164379 (**5a**) and -164380 (**6a**). Copies of the data can be obtained, free of charge, on application to CCDC, 12 Union Road, Cambridge CB2 1EZ, UK [Fax: (internat.) +44-1223/336-033, E-mail: deposit@ccdc.cam.ac.uk].

Hexakis(trimethylsilyl)disilane, $Si_2(SiMe_3)_6$ (4): $Si(SiMe_3)_4$ was reacted in THF with KO*t*Bu and the resulting $KSi(Me_3Si)_3$ solution was treated with $C_2H_4Br_2$ as described in ref.[9] After removal of the solvent the product was a mixture of **4** and approximately 25% $Si(SiMe_3)_4$. The two compounds were separated by sublimation in vacuo at 130 °C for 6 h. The residue of the sublimation was almost pure **4** in 72% yield, which could be used without further purification. ^{1}H NMR: δ = 0.274; ^{13}C NMR: δ = 4.38 ($^1J_{SiC}$ = 42.3 Hz); ^{29}Si NMR: δ = −9.55 ($SiMe_3$, $^1J_{SiSi}$ = 53.0 Hz), −130.13 ($SiSi_4$). − GC/MS: *m*/*z* (%) = 494 (4) [M$^+$], 479 (4) [M − Me], 421 (3) [$Me_{15}Si_7$], 406 (5) [$Me_{14}Si_7$], 305 (2) [$Me_{11}Si_5$], 273 (11) [Me_7Si_6], 247 (22) [Me_9Si_4], 232 (100) [Me_8Si_4], 199 (15), 173 (12) [$Me_5Si_3CH_2$], 131 (13) [Me_5Si_2], 73 (62) [Me_3Si].

Hexakis(chlorodimethylsilyl)disilane, $Si_2(SiMe_2Cl)_6$ (5a): Compound **4** (1.36 g, 2.75 mmol) was dissolved in 20 mL hexane and anhydrous aluminum chloride (3.00 g, 22.5 mmol) was added. Acetyl chloride (1.6 g, 20 mmol) was slowly added to this stirred mixture. After stirring overnight the reaction mixture was heated to 40 °C for one hour and the hexane phase was separated. Removal of the solvent in vacuo yielded 0.70 g (1.13 mmol, 41%) of pure crystalline **5a**, m.p.: 257 °C; ^{1}H NMR: δ = 0.845; ^{13}C NMR: δ = 8.05 ($^1J_{SiC}$ = 48.7 Hz); ^{29}Si NMR: δ = 29.06 ($SiMe_2Cl$, $^1J_{SiSi}$ = 56.9 Hz), −111.62 ($SiSi_4$). − GC/MS: *m*/*z* (%) = 601 (2) [M − Me], 581 (1) [M − Cl], 523 (44) [$Me_{10}Cl_5Si_7$], 488 (21) [$Me_{10}Cl_4Si_7$], 395 (9) [$Me_8Cl_3Si_6$], 380 (15) [$Me_7Cl_3Si_6$], 309 (13) [$Me_6Cl_3Si_4$], 272 (42) [$Me_6Cl_2Si_4$], 209 (18) [Me_6ClSi_3], 174 (13) [Me_6Si_3], 131 (26) [Me_5Si_2], 93 (37) [Me_2ClSi], 73 (100) [Me_3Si].

If the reaction mixture was heated to 70 °C, a mixture of **5a** (52%), $(ClMe_2Si)_3Si-Si(SiClMe_2)_2(SiCl_2Me)$ (**5b**; 43%) and

$(Cl_2MeSi^C)(ClMe_2Si^B)_2Si^A-Si^A(Si^BClMe_2)_2(Si^CCl_2Me)$ (**5c**; 5%) was obtained after removal of the solvent hexane.

$(ClMe_2Si^C)_3Si^A-Si^B(Si^DClMe_2)_2(Si^ECl_2Me)$ (5b): ^{13}C NMR: δ = 8.03 (Si^CMe_2), 7.69 (Si^DMe_2), 13.02 (Si^EMe); ^{29}Si NMR: δ = −111.23 (Si^A), −104.08 (Si^B), 28.88 (Si^C), 27.85 (Si^D), 36.98 (Si^E). − GC/MS: *m*/*z* (%) = 623 (2) [M − Me], 543 (27) [$Me_9Cl_6Si_7$], 508 (28) [$Me_9Cl_5Si_7$], 415 (10) [$Me_7Cl_4Si_6$], 400 (24) [$Me_6Cl_4Si_6$], 309 (31) [$Me_6Cl_3Si_4$], 272 (13) [$Me_6Cl_2Si_4$], 209 (19) [Me_6ClSi_3], 159 (22) [Me_5Si_3], 131 (29) [Me_5Si_2], 93 (61) [Me_2ClSi], 73 (100) [Me_3Si].

$(Cl_2MeSi^C)(ClMe_2Si^B)_2Si^A-Si^A(Si^BClMe_2)_2(Si^CCl_2Me)$ (5c): ^{29}Si NMR: δ = −111.23 (Si^A), 27.75 (Si^B), 36.21 (Si^C).

Dodecamethyl-3,7,10-trithiaoctasila[3.3.3]propellane, $Si_2(SiMe_2)_6S_3$ (6a): Compound **5a** (0.23 g, 0.37 mmol) was dissolved in 30 mL hexane and NEt_3 (0.35 mL, 2.5 mmol) was added while a stream of dried H_2S was bubbled through the stirred solution. After stirring overnight the reaction mixture was filtered. Removal of the solvent from the filtrate yielded 0.14 g (0.28 mmol, 76%) of pure **6a** as a colorless crystalline residue. Single crystals of **6a** were grown from a solution in hexane, m.p.: 225 °C (decomp.).

6a: GC/MS: *m*/*z* (%) = 500 (25) [M^+], 485 (6) [M − Me], 441 (8) [$Me_9Si_7S_3CH_2$], 427 (29) [$Me_9Si_7S_3$], 395 (3) [$Me_9Si_7S_2$], 351 (6) [$Me_7Si_6S_2CH_2$], 337 (7) [$Me_7Si_6S_2$], 293 (6) [$Me_5Si_5S_2CH_2$], 277 (10) [Me_7Si_5S], 262 (8) [Me_6Si_5S], 247 (15) [Me_5Si_5S], 233 (11) [$Me_5Si_4SCH_2$], 189 (11) [Me_7Si_3], 131 (13) [Me_5Si_2], 73 (100) [Me_3Si].

Dodecamethyl-3,7,10-triselenaoctasila[3.3.3]propellane, $Si_2(SiMe_2)_6Se_3$ (6b) and Dodecamethyl-3,7,10-tritelluraoctasila[3.3.3]propellane, $Si_2(SiMe_2)_6Te_3$ (6c): A solution of **5a** (0.31 g, 0.50 mmol) in 1 mL THF was slowly added to a suspension of Li_2E (E = Se, Te) prepared from 1.5 mmol elemental E and 3 mL of a 1 M solution of $Li[BEt_3H]$ in THF. In the case of the tellurium compound the reaction was carried out at −30 °C to prevent Si−Si bond cleavage reactions. After stirring for 30 min the solvent was removed in vacuo and replaced by 10 mL hexane. Filtration from precipitated lithium salts and removal of the solvents yielded the propellanes **6b** and **6c** as colorless crystalline residues in 62 and 25% yield, respectively.

Acknowledgments

The authors thank the Deutsche Forschungsgemeinschaft for financial support. Special thanks are given to Prof. H. Lang, Chair of Inorganic Chemistry, TU Chemnitz for the access to the X-ray facility used to determine the single crystal structures.

[1] U. Herzog, U. Böhme, E. Brendler, G. Rheinwald, *J. Organomet. Chem.* **2001**, *630*, 139−148.
[2] U. Herzog, U. Böhme, G. Roewer, G. Rheinwald, H. Lang, *J. Organomet. Chem.* **2000**, *602*, 193−207.
[3] U. Herzog, G. Rheinwald, *J. Organomet. Chem.* **2001**, *627*, 23−36.
[4] L. Fitjer, A. Kanschik, M. Majewski, *Tetrahedron Lett.* **1985**, *26*, 5277−5280.
[5] L. Fitjer, A. Kanschik, M. Majewski, *Tetrahedron* **1994**, *50*, 10867−10878.
[6] L. H. Zalkow, R. N. Harris III, D. van Derveer, *J. Chem. Soc., Chem. Commun.* **1978**, 420−421.
[7] L. Fitjer, A. Kanschik, M. Majewski, *Tetrahedron Lett.* **1988**, *29*, 5525−5528.
[8] T. Prange, *J. Chem. Soc., Chem. Commun.* **1977**, 430−431.
[9] C. Marschner, *Eur. J. Inorg. Chem.* **1998**, 221−226.
[10] H. Bock, J. Meuret, K. Ruppert, *Angew. Chem.* **1993**, *105*, 413−415; *Angew. Chem. Int. Ed. Engl.* **1993**, *32*, 414−416.
[11] F. R. Fronczek, P. D. Lickiss, *Acta Crystallogr., Sect. C* **1993**, *49*, 331−333.
[12] H. Stüger, M. Eibl, *Phosphorus, Sulfur, and Silicon* **1992**, *65*, 29−32.
[13] M. Ishikawa, J. Iyoda, H. Ikeda, K. Kotake, T. Hashimoto, *J. Am. Chem. Soc.* **1981**, *103*, 4845−4850.
[14] K. Trommer, U. Herzog, G. Roewer, *J. Prakt. Chem.* **1997**, *339*, 637−641.
[15] *Bruker AXS Inc.*, Madison, WI, USA, **1998**.
[16] P. McArdle, *J. Appl. Cryst.* **1996**, *29*, 306.
[17] G. M. Sheldrick, *SADABS V2.01, Program for Empirical Absorption Correction of Area Detector Data*, University of Göttingen, Germany, **2000**.
[18] A. Altomare, M. C. Burla, M. Camalli, G. L. Cascarano, C. Giacovazzo, A. Guagliardi, A. G. G. Moliterni, G. Polidori, R. Spagna, *J. Appl. Cryst.* **1999**, *32*, 115−119.
[19] G. M. Sheldrick, *SHELX97, Programs for Crystal Structure Analysis (Release 97−2)*, University of Göttingen, Germany **1997**.
[20] *Diamond 2.1:* K. Brandenburg, Crystal Impact GbR, Bonn, Germany, **1999**.
[21] H. Gilman, C. L. Smith, *J. Am. Chem. Soc.* **1964**, *86*, 1454.

Received May 31, 2001
[I01199]

Photoinduced C−H Activation and Catalytic Carbonylation of Benzene − New Features of a Tris(pyrazolyl)methanesulfonato (Tpms) Rhodium(I) Complex

Wolfgang Kläui,*[a] Daniel Schramm,[a] and Wilfried Peters[a]

Keywords: Rhodium / Tripodal ligands / N ligands / C−H activation / Carbonylation / Homogeneous catalysis / Aldehydes

Irradiation of [(Tpms)Rh(CO)(PMe_3)] (**1**) in benzene or [D_6]benzene affords the rhodium(III) compounds [(Tpms)Rh(H)(C_6H_5)(PMe_3)] (**2**) and [(Tpms)Rh(D)(C_6D_5)(PMe_3)] (**2-d_6**) respectively. The k_H/k_D ratio for the formation of **2** and **2-d_6** was found to be 1.1. The complexes **2** and **2-d_6** are stable in protic solvents. When a solution of **1** in benzene is irradiated under carbon monoxide pressure, benzaldehyde is formed catalytically with turnover numbers of up to 20. The formation of **2** and [(Tpms)Rh(H)(COC_6H_5)(PMe_3)] (**4**) under catalytic conditions allows the proposal of a catalytic cycle.

Introduction

Since the first reports on C−H bond activation in 1965,[1] the transition-metal-catalysed activation of alkanes and arenes has become one of the most challenging fields of organometallic chemistry.[2] Bergman was the first to observe the oxidative addition of cyclohexane to the Cp*Rh(PMe_3) fragment in 1982,[3] which led to the development of similar complexes with ligands such as tris(pyrazolyl)borates (Tp, Tp*).[4,5] So far none of the above-mentioned complexes has been reported to catalytically functionalize hydrocarbons or arenes by C−H activation. Until now carbonylation reactions based on tripodal rhodium(I) systems like [Tp*Rh(CO)(C_2H_4)] only produced stoichiometric amounts of insertion products.[5b] The catalytic carbonylation of arenes and alkanes is, however, known with Vaska-type catalysts like [RhCl(CO)(PPh_3)$_2$][6] and analogous compounds.[7,8]

We have recently reported[9] the synthesis of the novel tris(pyrazolyl)methanesulfonate ligand (Tpms), a monoanionic tripodal nitrogen ligand. TpmsRh^I compounds show a coordination chemistry which resembles that of analogous tris(pyrazolyl)borato compounds. Moreover, they are hydrolytically stable and soluble in polar protic solvents.[10]

We describe here the C−H activation of benzene and [D_6]benzene with [(Tpms)Rh(CO)(PMe_3)] leading to the rhodium(III) complexes [(Tpms)Rh(R)(C_6R_5)(PMe_3)] (R = H, D) that catalyse the formation of benzaldehyde from benzene and carbon monoxide.

Results and Discussion

Photoactivation of [(TpmsRh(CO)(PMe_3)] (1)

The photolysis of the bright yellow [(TpmsRh(CO)(PMe_3)] (**1**) offers a convenient method for the generation of a coordinatively unsaturated intermediate which can then undergo the oxidative addition of C−H bonds. Although **1** is only moderately soluble in benzene, irradiation leads to a quantitative conversion into the C−H activation product [(TpmsRh(H)(C_6H_5)(PMe_3)] (**2**). However, due to its low solubility in less polar solvents we have not yet found the correct reaction conditions for the C−H activation of saturated hydrocarbons.

Preparation of [(TpmsRh(H)(C_6H_5)(PMe_3)] (2) and [(TpmsRh(D)(C_6D_5)(PMe_3)] (2-d_6)

The UV/Vis spectrum of [(TpmsRh(CO)(PMe_3)] (**1**) shows a band at 232 nm (ε = 17000 L·mol^{-1}·cm^{-1}), which is typical for the Tpms ligand, and a charge transfer band at 355 nm (ε = 2000 L·mol^{-1}·cm^{-1}). In order to prevent possible photochemical reactions of the pyrazoles, **1** is irradiated in Pyrex vessels ($\lambda > 290$ nm) which serve as a cut-off filter. The yellow suspension of **1** in benzene gradually clears as the reaction proceeds leading to the whitish hydrido compound [(TpmsRh(H)(C_6H_5)(PMe_3)] (**2**) (Figure 1). The reaction is complete within one hour. When the reaction is performed in a 1:1 mixture of benzene/[D_6]benzene, **2** and [(TpmsRh(D)(C_6D_5)(PMe_3)] (**2-d_6**) are formed in a ratio of 1:0.9 (i.e. k_H/k_D = 1.1). This indicates that there is only a very small kinetic isotope effect.[11]

Both **2** and **2-d_6** are soluble in benzene, toluene, and in polar organic solvents like THF and acetone. In wet solvents like acetone no decomposition is observed within hours at ambient temperatures. However, the hydrido compound **2** reacts with a stoichiometric amount of CCl_4 to

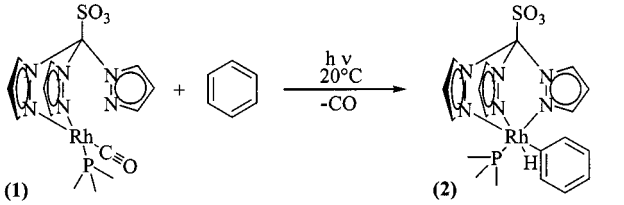

Figure 1. C−H activation of benzene with [(TpmsRh(CO)(PMe_3)] (**1**)

[a] Institut für Anorganische Chemie und Strukturchemie der Universität Düsseldorf,
Universitätsstraße 1, 40225 Düsseldorf, Germany
E-mail: klaeui@uni-duesseldorf.de

 © WILEY-VCH Verlag GmbH, 69451 Weinheim, 2001 1434−1948/01/1212−3113 $ 17.50+.50/0

give the corresponding chloro compound [(TpmsRh(Cl)(C_6H_5)(PMe_3)] (**3**) and chloroform within a few hours.

The ^{1}H NMR spectrum of the benzene activation product **2** shows a signal pattern consistent with a compound of C_1 symmetry. The most prominent signal is a doublet of doublets found at $\delta = -16.30$ for the hydride bound to the rhodium atom. The coupling constants to rhodium ($^1J_{RhH} = 26.0$ Hz) and phosphorous ($^2J_{PH} = 32.3$ Hz) are within the range found for similar Cp*[12] and Tp*[13] compounds. All the pyrazole protons (see Figure 2 for numbering scheme) show coupling to the hydride and the phosphorous. Due to limitations of the spectral resolution ($\approx$ 0.2 Hz) only the *trans* couplings are observable. This allows a complete assignment of all protons by selective decoupling, COSY and NOESY-experiments (see Exp. Sect.).

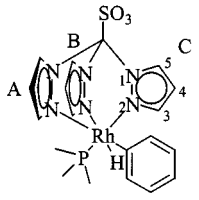

Figure 2. Schematic structure of the C_1 symmetrical complex [(TpmsRh(H)(C_6H_5)(PMe_3)] (**2**)

The deuteride bound to the rhodium in the [D_6]benzene activation product **2-*d*$_6$** can be found as a doublet of doublets in the ^{2}H NMR spectrum at $\delta = -16.1$. Due to the differences in the magnetogyric ratio, the coupling constants are smaller by a factor of 6.5 ($^1J_{RhD} = 4$ Hz, $^2J_{PD} = 5$ Hz). Therefore no H−D coupling can be resolved in the ^{1}H NMR spectrum.

In the IR spectra of **2** and **2-*d*$_6$** the characteristic $\nu_{(Rh-H)}$ band is found at $\tilde{\nu} = 2085$ cm^{-1}, whereas the $\nu_{(Rh-D)}$ band can be observed at $\tilde{\nu} = 1500$ cm^{-1}. The frequency ratio caused by the different masses of H and D is close to the theoretical value of $\approx$1.41.

The mass spectra show peaks at $[M - 1]^+$ for **2** and $[M - 2]^+$ for **2-*d*$_6$**. This indicates that the hydrido and deuterido ligands are lost under FAB conditions.

Catalytic Carbonylation of Benzene

A suspension of [(TpmsRh(CO)(PMe_3)] (**1**) in benzene was irradiated with a 125 W medium pressure mercury arc. The reaction was conducted in a Pyrex ($\lambda > 290$ nm) vessel equipped with Teflon seals and valves allowing us to maintain a carbon monoxide pressure of three to four atmospheres. The carbonylation proceeds without a significant induction period (Figure 3). This indicates that the primary photoprocess is fast under catalytic conditions. In the beginning the turnover frequency (TOF) is about 3 h^{-1}, which is in the same range as found for the Vaska-type compound [RhCl(CO)(PMe_3)$_2$] under similar conditions.[7a] The analogous complex [Tp*Rh(CO)(PMe_3)][14] produces only sub-

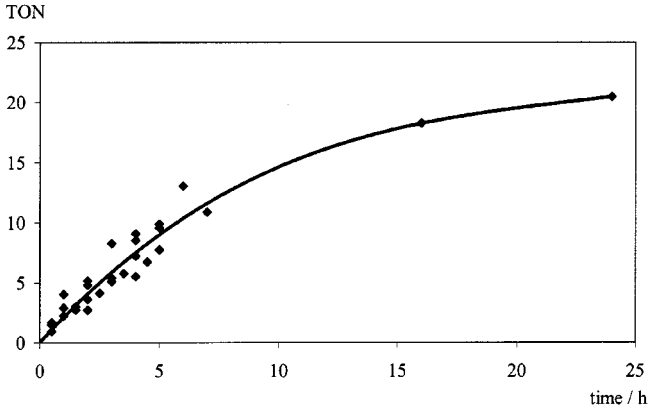

Figure 3. Time-dependence of the catalytic carbonylation of benzene

stoichiometric amounts of benzaldehyde within 5 hours under similar conditions.

The maximum turnover of 20 is reached after about 24 h. At that point only small amounts of the catalytically active hydride species can still be found in the reaction mixture. In addition secondary photoreactions of the benzaldehyde take place. This was also observed in the analogous reaction with [RhCl(CO)(PMe_3)$_2$] as catalyst.[8]

Intermediates and Mechanism

After a short time the benzene activation product **2** and the carbon monoxide insertion product [(TpmsRh(H)(COC_6H_5)(PMe_3)] (**4**) can be identified by NMR spectroscopy. The most characteristic signal of **4** is a doublet of doublets for the hydrido ligand found at $\delta = -14.88$. The coupling constants as well as the spectral appearance are almost identical to those found for **2** indicating the structural relationship between **2** and **4**. This allows us to propose a catalytic cycle for the carbonylation of benzene with [(TpmsRh(CO)(PMe_3)] (**1**) as precursor (Figure 4).

The irradiation of the carbonyl compound **1** probably results in the formation of an unsaturated 14-electron complex, which reacts with benzene to give the hydridophenyl compound **2**. We exclude an associative mechanism as we could show that **1** does not undergo oxidative addition without irradiation. For the Vaska-type compound [RhCl(CO)(PMe_3)$_2$] an associative mechanism was proposed to be more likely than a dissociative one.[7d]

The next step, leading to the CO insertion product **4**, again does not happen without irradiation. When complex **2** is stirred under carbon monoxide pressure without irradiation, the rhodium(I) compound **1** is recovered and no traces of **4** or benzaldehyde are observed. The reason for this is that **2** is a coordinatively saturated complex where one of the ligands has to be abstracted in order to add and insert CO. This is most likely to occur by a change of the tripod's denticity, as Tpms is known to act as a bi- or tridentate ligand in rhodium chemistry.[10]

^{1}H and ^{31}P NMR studies of the reaction mixture show that **2** and **4** exist in a ratio of 3:1 throughout the catalysis,

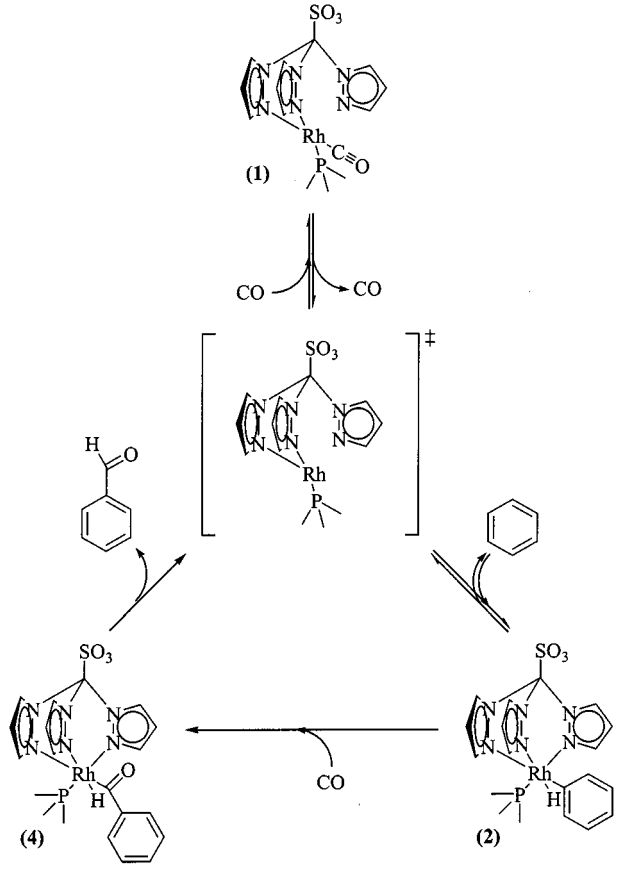

Figure 4. Proposed catalytic cycle for the photoinduced carbonylation of benzene

while only traces of **1** are found. This indicates that the Tpms ligand stabilises the catalytic intermediates **2** and **4** in a steady state at ambient temperatures. This is in clear contrast to the $[RhCl(CO)(PMe_3)_2]$ catalyst where the intermediates of the catalytic cycle revert thermally to the starting material.[15]

Conclusions

The compound $[(TpmsRh(CO)(PMe_3)]$ (**1**) readily activates benzene under irradiation to give $[(TpmsRh(H)(C_6H_5)(PMe_3)]$ (**2**), which is the first example of a $TpmsRh^{III}$ complex. The analogous reaction with $[D_6]$benzene affords $[(TpmsRh(D)(C_6D_5)(PMe_3)]$ **(2-*d*$_6$)**. Both compounds are stable in protic solvents. The kinetic isotope effect (k_H/k_D = 1.1) is similar to that found for the [Cp*Rh(PMe_3)] fragment.[11a]

To the best of our knowledge, $[(TpmsRh(CO)(PMe_3)]$ (**1**) is the only known catalyst with a tripodal ligand which is active in the catalytic carbonylation of benzene. The low steric bulk of the tripod and the phosphane help to keep the metal centre accessible while inhibiting intramolecular C−H activation. Therefore **1** produces efficiencies which are similar to those observed for the Vaska-type catalyst $[RhCl(CO)(PMe_3)_2]$.

Compound **1** provides a push-pull system of a highly basic phosphane and the weakly donating Tpms, which can act as a bi- or tridentate ligand. This unique blend allows the stabilisation of both planar Rh^I and octahedral Rh^{III} complexes. This is the main reason why the hydridophenyl complex **2** and the hydridobenzoyl compound $[(TpmsRh(H)(COC_6H_5)(PMe_3)]$ (**4**) are stable enough to be identified from the catalytically active reaction mixture.

Experimental Section

General Remarks: The compound $[(TpmsRh(CO)(PMe_3)]$ (**1**), was synthesised as previously reported.[10] All other reagents were commercial samples and were used as received. All reactions were carried out under nitrogen using standard Schlenk techniques unless stated otherwise. All solvents were purified and degassed by standard procedures. Filtration was done with 1 μm membrane filters (regenerated cellulose, Schleicher & Schuell). Reactions under 3−4 atm. pressure were performed in glass tubes equipped with Teflon seals and valves. All operations in glass vessels at elevated pressures should be done using effective body and face protection! Irradiation was done with a medium pressure mercury arc Philips HPK 125 (125 W, $\lambda > 230$ nm). Turnover numbers (TON) and turnover frequencies (TOF) are based on the molar ratio of benzaldehyde/catalyst. One dimensional ^1H, ^{31}P, and ^{13}C NMR spectra were recorded with Bruker DRX 200 (at 296 K) or Bruker DRX 500 (at 300 K) spectrometers. Two dimensional NOESY and COSY as well as one dimensional ^2H, ^1H $\{^1H\}$and ^1H $\{^{31}P\}$ NMR spectra were recorded with a Bruker DRX 500 spectrometer. The chemical shifts (δ) are given in ppm referenced to the solvent $[D_6]$benzene at δ = 7.16.[16] Infrared spectra were recorded using a Bruker IFS 66 FT spectrometer. FAB mass spectra were recorded on a Finnigan MAT 8200 using a NBA matrix with addition of NaI. Elemental analyses were performed using a Perkin−Elmer CHN-2400/II elemental analyser. GC analysis was done with a HP-5890 series II chromatograph with a FID-detector and a MSD 5970 integrator. All concentrations were determined by comparison to calibration curves obtained with actual samples of benzaldehyde in benzene.

Hydridophenyltrimethylphosphane[tris(pyrazol-1-yl)methanesulfonato]rhodium(III), $[(TpmsRh(H)(C_6H_5)(PMe_3)]$ (2): A suspension of **1** (10 mg, 0.020 mmol) in 10 mL of benzene was stirred in a Pyrex vessel in a water bath at room temperature. The mixture was irradiated for one hour. Addition of pentane precipitated 12 mg of a light grey solid. − ^1H NMR (500 MHz, C_6D_6): δ = −16.30 (dd, $^1J_{RhH}$ = 26.0 Hz, $^2J_{PH}$ = 32.3 Hz, 1 H, hydrido-*H*), 0.65 [dd, $^2J_{PH}$ = 10.1 Hz, $^3J_{RhH}$ = 1.2 Hz, 9 H, $P(CH_3)_3$], 5.31 (ddd, $^3J_{HH}$ = 3.0 Hz, $^3J_{HH}$ = 2.0 Hz, $^4J_{PH}$ = 1.1 Hz, 1 H, C-pyrazolyl C^4H), 5.56 (dd, $^3J_{HH}$ = 3.0 Hz, $^3J_{HH}$ = 2.0 Hz, 1 H, A-pyrazolyl C^4H), 5.69 (ddd, $^3J_{HH}$ = 3.0 Hz, $^3J_{HH}$ = 2.0 Hz, $^4J_{HH}$ = 0.4 Hz, 1 H, B-pyrazolyl C^4H), 6.85 (db, $^3J_{HH}$ = 2.0 Hz, 1 H, A-pyrazolyl C^3 *H*), 6.96 (db, $^3J_{HH}$ = 2.0 Hz, 1 H, C-pyrazolyl C^3H), 7.05 (m, 5 H, C_6H_5), 7.10 (db, $^3J_{HH}$ = 2.0 Hz, 1 H, B-pyrazolyl C^3H), 9.36 (ddd, $^3J_{HH}$ = 3.0 Hz, $^4J_{RhH}$ = 0.7 Hz, $^5J_{PH}$ = 1.5 Hz, 1 H, C-pyrazolyl C^5H), 9.52 (dd, $^3J_{HH}$ = 3.0 Hz, $^4J_{RhH}$ = 0.7 Hz, 1 H, A-pyrazolyl C^5H), 9.64 (ddd, $^3J_{HH}$ = 3.0 Hz, $^4J_{RhH}$ = 0.6 Hz, $^5J_{HH}$ = 0.6 Hz, 1 H, B-pyrazolyl C^5H). − ^{13}C $\{^1H\}$ NMR (500 MHz, C_6D_6): δ = 15.8 [d, $^1J_{PC}$ = 35 Hz, $P(CH_3)_3$], 90.3 (s, *C*-SO_3), 104.7 (s, A-pyrazolyl C^4), 104.8 (s, C-pyrazolyl C^4), 105.0 (s, B-pyrazolyl C^4), 121.5, 126.0, 126.1 (s, phenyl *C*), 126.2 (d, J_{RhC} = 2 Hz, phenyl *C*), 135.0 (s, C-pyrazolyl C^5), 135.3 (s, A-pyrazolyl C^5), 135.5 (s, B-pyrazolyl C^5), 141.2 (s, B-pyrazolyl C^3), 143.0 (s,

A-pyrazolyl C^3), 143.4 (s, C-pyrazolyl C^3). − ^{31}P {^{1}H} NMR (200 MHz, C_6D_6): δ = 10.3 (d, $^1J_{RhP}$ = 145 Hz). − IR (KBr): $\tilde{\nu}$ = 3176 cm^{-1} (m, pyrazolyl C−H), 3052 (w, phenyl C−H), 2963, 2909 [w, P(CH)$_3$ C−H], 2085 (m, Rh−H), 1569 (m, phenyl), 1521 (s, C=C), 1420 (s, P−C), 1081, 1058, 1038 (s, S=O). − MS (FAB$^+$): *m*/*z* (%) = 549 (4.3) [M − H]$^+$.

Deuteropentadeuteriophenyltrimethylphosphane[tris(pyrazol-1-yl)-methanesulfonato]rhodium(III), [(TpmsRh(D)(C_6D_5)(PMe_3)] (2-*d*$_6$): **2-*d*$_6$** was prepared in the same way as **2**, using [D$_6$]benzene as a solvent and irradiating for 100 minutes. Addition of pentane precipitated 12 mg of a light grey solid. − ^{1}H NMR (200 MHz, C_6D_6): δ = 0.64 [dd, $^2J_{PH}$ = 10.0 Hz, $^3J_{RhH}$ = 1.0 Hz, 9 H, P(C*H*$_3$)$_3$], 5.30 (ddd, $^3J_{HH}$ = 3.0 Hz, $^3J_{HH}$ = 2.0 Hz, $^4J_{PH}$ = 1.1 Hz, 1 H, C-pyrazolyl C^4*H*), 5.55 (dd, $^3J_{HH}$ = 3.0 Hz, $^3J_{HH}$ = 2.0 Hz, 1 H, A-pyrazolyl C^4*H*), 5.68 (dd, $^3J_{HH}$ = 3.0 Hz, $^3J_{HH}$ = 2.0 Hz, 1 H, B-pyrazolyl C^4*H*), 6.83 (db, $^3J_{HH}$ = 2.0 Hz, 1 H, A-pyrazolyl C^3*H*), 6.95 (db, $^3J_{HH}$ = 2.0 Hz, 1 H, C-pyrazolyl C^3*H*), 7.10 (dd, $^3J_{HH}$ = 2.0 Hz, $^3J_{RhH}$ = 0.5 Hz,1 H, B-pyrazolyl C^3*H*), 9.37 (ddd, $^3J_{HH}$ = 3.0 Hz, $^4J_{RhH}$ = 0.7 Hz, $^5J_{PH}$ = 1.5 Hz, 1 H, C-pyrazolyl C^5*H*), 9.53 (dd, $^3J_{HH}$ = 3.0 Hz, $^4J_{RhH}$ = 0.5 Hz, 1 H, A-pyrazolyl C^5*H*), 9.65 (dd, $^3J_{HH}$ = 3.0 Hz, $^4J_{RhH}$ = 0.5 Hz, 1 H, B-pyrazolyl C^5*H*). − ^{2}H NMR (500 MHz, C_6H_6): δ = −16.1 (dd, $^1J_{RhD}$ = 4 Hz, $^2J_{PD}$ = 5 Hz, 1 D, deuterido-*D*), 7.1 (br. s, 5 D, C_6D_5). − ^{31}P {^{1}H} NMR (200 MHz, C_6D_6): δ = 10 (dt, $^1J_{RhP}$ = 144 Hz, $^2J_{PD}$ = 4 Hz). − IR (KBr): $\tilde{\nu}$ = 3176 cm^{-1} (m, pyrazolyl C−H), 2963, 2909 [w, P(CH)$_3$ C−H], 2264 (w, phenyl C−D), 1533 (m, phenyl), 1521 (s, C=C), 1500 (m, Rh−D), 1420 (s, P−C), 1081, 1058, 1038 (s, S=O). − MS (FAB$^+$): *m*/*z* (%) = 554 (4.8) [M − D]$^+$.

Determination of the k_H/k_D Ratio: A suspension of **1** (20 mg, 0.040 mmol) in a mixture of benzene (10 mL) and [D$_6$]benzene (10 mL) was stirred in a Pyrex vessel in a water bath at room temperature. The mixture was irradiated for 100 minutes. After the solution was evaporated, the residue was dissolved in [D$_6$]benzene and analysed by ^{1}H NMR spectroscopy. The integration ratios of the hydrido signal of **2** at δ = −16.30 (1.0 H) and the signals of the protons bound to the pyrazoles of the ligand allows the calculation of the ratio k_H/k_D to be 1.1. The ratio did not change within 12 hours, which rules out a thermal equilibration of **2** with [D$_6$]benzene.

Chlorophenyltrimethylphosphane[tris(pyrazol-1-yl)methanesulfonato]rhodium(III), [(TpmsRh(Cl)(C_6H_5)(PMe_3)] (3): Tetrachloromethane (1 mL) was added to a solution of **2** (22 mg, 0.040 mmol) in 15 mL of benzene. The reaction mixture was stirred overnight and the solvents evaporated to dryness to yield **3** as a light grey solid (23 mg). − ^{1}H NMR (200 MHz, C_6D_6): δ = 0.62 [dd, $^2J_{PH}$ = 10.8 Hz, $^3J_{RhH}$ = 0.8 Hz, 9 H, P(C*H*$_3$)$_3$], 5.31 (ddd, $^3J_{HH}$ = 3.0 Hz, $^3J_{HH}$ = 2.3 Hz, $^4J_{PH}$ = 1.8 Hz, 1 H, pyrazolyl C^4*H*), 5.50 (dd, $^3J_{HH}$ = 3.0 Hz, $^3J_{HH}$ = 2.5 Hz, 1 H, pyrazolyl C^4*H*), 5.63 (dd, $^3J_{HH}$ = 3.0 Hz, $^3J_{HH}$ = 2.2 Hz, 1 H, pyrazolyl C^4*H*), 6.60 (db, $^3J_{HH}$ = 2.5 Hz, 1 H, pyrazolyl C^3*H*), 7.04 (m, 5 H, C_6H_5), 7.21 (m,1 H, pyrazolyl C^3*H*), 7.44 (dd, $^3J_{HH}$ = 2.2 Hz, $^3J_{RhH}$ = 0.7 Hz, 1 H, pyrazolyl C^3*H*), 9.24 (ddd, $^3J_{HH}$ = 3.0 Hz, $^4J_{RhH}$ = 0.8 Hz, $^5J_{PH}$ = 1.8 Hz, 1 H, pyrazolyl C^5*H*), 9.44 (dd, $^3J_{HH}$ = 3.0 Hz, $^4J_{RhH}$ = 0.8 Hz, 1 H, pyrazolyl C^5*H*), 9.58 (dd, $^3J_{HH}$ = 3.0 Hz, $^4J_{RhH}$ = 0.8 Hz, 1 H, pyrazolyl C^5*H*). − ^{13}C {^{1}H} (500 MHz, C_6D_6): δ = 12.8 [d, $^1J_{PC}$ = 35 Hz, P(*C*H$_3$)$_3$], 90.0 (s, *C*-SO$_3$), 105.5 (s, pyrazolyl *C*^{4}), 105.6 (s, pyrazolyl *C*^{4}), 105.7 (s, pyrazolyl *C*^{4}), 122.6, 124.2, 125.8 (s, phenyl *C*), 126.1 (db, J_{RhC} = 3 Hz, phenyl *C*), 135.0 (s, pyrazolyl *C*^{5}), 135.4 (s, pyrazolyl *C*^{5}), 135.5 (s, pyrazolyl *C*^{5}), 142.3 (s, pyrazolyl *C*^{3}), 143.4 (s, pyrazolyl *C*^{3}), 143.6 (s, pyrazolyl *C*^{3}). − ^{31}P {^{1}H} NMR (200 MHz, C_6D_6): δ = 7.6 (d, $^1J_{RhP}$ = 127 Hz). − IR (KBr): $\tilde{\nu}$ = 3171 cm^{-1} (m, pyrazolyl C−H), 3059 (w, phenyl C−H), 2962, 2910 [w, P(CH)$_3$ C−H], 1569 (m, phenyl), 1522 (s, C=C), 1422 (s, P−C), 1099, 1070, 1054, 1021 (s, S=O). − MS (FAB$^+$): *m*/*z* (%) = 607 (7.1) [M + Na]$^+$, 549 (1.3) [M − Cl]$^+$. − $C_{19}H_{23}ClN_6O_3PRhS$ (584.8): calcd. C 39.02, H 3.96, N 14.37; found C 39.28, H 3.74, N 14.09.

Catalysis and Preparation of Benzoylhydridotrimethylphosphane-[tris(pyrazol-1-yl)methanesulfonato]rhodium(III), [(TpmsRh(H)-(COC_6H_5)(PMe_3)] (4): A suspension of **1** (10 mg, 0.020 mmol) in 20 mL benzene was stirred in a Pyrex vessel equipped with Teflon seals and valves and pressurised with 3−4 atm. of carbon monoxide. The reaction mixture was irradiated for 0.5 to 24 hours in a water bath at room temperature. At regular intervals, samples for gas chromatographic analysis were taken. The solvent was finally removed under reduced pressure yielding a red brown solid, from which **4** could not be isolated as a pure compound. The crude product contains **2**, **4**, traces of **1** and traces of Rh^0 carbonyl compounds. − ^{1}H NMR (200 MHz, C_6D_6): δ = −14.88 (dd, $^1J_{RhH}$ = 24.2 Hz, $^2J_{PH}$ = 35.6 Hz, 1 H, hydrido-*H*), 0.74 [dd, $^2J_{PH}$ = 10.6 Hz, $^3J_{RhH}$ = 1.2 Hz, 9 H, P(C*H*$_3$)$_3$], 5.6−5.9 (m, 3 H, pyrazolyl C^4*H*), 7.1 (m, 5 H, C_6H_5), 8.1−8.4 (m, 3 H, pyrazolyl C^3*H*), 9.30 (ddd, $^3J_{HH}$ = 3.1 Hz, $^4J_{RhH}$ = 0.8 Hz, $^5J_{PH}$ = 1.6 Hz, 1 H, pyrazolyl C^5*H*), 9.52 (dd, $^3J_{HH}$ = 3.1 Hz, $^4J_{RhH}$ = 0.7 Hz, 1 H, pyrazolyl C^5*H*), 9.60 (db, $^3J_{HH}$ = 3.1 Hz, 1 H, pyrazolyl C^5*H*). − ^{31}P {^{1}H} NMR (200 MHz, C_6D_6): δ = 9.3 (d, $^1J_{RhP}$ = 146 Hz).). − MS (FAB$^+$): *m*/*z* (%) = 577 (9.1) [M − H]$^+$, 549 (9.5) [M − CO − H]$^+$.

Acknowledgments

This work was supported by the Fonds der Chemischen Industrie. W. K. thanks Degussa AG, Hanau, for a loan of rhodium chloride.

[1] J. Chatt, J. M. Davidson, *J. Chem. Soc.* **1965**, 843−855.
[2] [2a] C. L. Hill, *Activation and Functionalization of Alkanes*, Wiley, New York, **1989**. − [2b] J. A. Davies, P. L. Watson, A. Greenberg, J. F. Liebman, *Selective Hydrocarbon Activation*, VCH Publishers, New York, **1990**. − [2c] J. B. Asbury, K. Hang, J. S. Yeston, J. G. Cordaro, R. G. Bergman, T. Lian, *J. Am. Chem. Soc.* **2000**, *122*, 12870−12871 and references cited therein.
[3] A. H. Janowicz; R. G. Bergman, *J. Am. Chem. Soc.* **1982**, *104*, 352−354.
[4] [4a] J. K. Hoyano, W. A. G. Graham, *J. Am. Chem. Soc.* **1982**, *104*, 3723−3725. − [4b] W. D. Jones, F. J. Feher, *J. Am. Chem. Soc.* **1984**, *106*, 1650−1663. − [4c] W. D. Jones, F. J. Feher, *Acc. Chem. Res.* **1989**, *22*, 91−100. − [4d] N. Dunwoody, S.-S. Sun, A. J. Lees, *Inorg. Chem.* **2000**, *39*, 4442−4451.
[5] [5a] C. K. Ghosh, W. A. G. Graham, *J. Am. Chem. Soc.* **1987**, *109*, 4726−4727. − [5b] C. K. Ghosh, W. A. G. Graham, *J. Am. Chem. Soc.* **1989**, *111*, 375−376. − [5c] P. E. Bloyce, J. Mascetti, A. J. Rest, *J. Organomet. Chem.* **1993**, *444*, 223−233. − [5d] J. S. Yeston, B. K. McNamara, R. G. Bergman, C. B. Moore, *Organometallics* **2000**, *19*, 3442−3446. − [5e] C. Slugovc, I. Padilla-Martínez, S. Sirol, E. Carmona, *Coord. Chem. Rev.* **2001**, *213*, 129−157.
[6] [6a] A. J. Kunin, R. Eisenberg, *J. Am. Chem. Soc.* **1986**, *108*, 535−536. − [6b] A. J. Kunin, R. Eisenberg, *Organometallics* **1988**, *7*, 2124−2129.
[7] [7a] T. Sakakura, M. Tanaka, *Chem. Lett.* **1987**, 249−252. − [7b] T. Sakakura, M. Tanaka, *Chem. Lett.* **1987**, 1113−1116. − [7c] H. Moriyama, T. Sakakura, A. Yabe, M. Tanaka, *J. Mol. Cat.* **1990**, *60*, L9−L12. − [7d] G. P. Rosini, W. T. Boese, A. S. Goldman, *J. Am. Chem. Soc.* **1994**, *116*, 9498−9505. − [7e] G. P. Rosini, K. Zhu, A. S. Goldman, *J. Organomet. Chem.* **1995**, *504*, 115−121.

[8] T. Sakakura, T. Sodeyama, K. Sasaki, K. Wada, M. Tanaka, *J. Am. Chem. Soc.* **1990**, *112*, 7221−7229.
[9] W. Kläui, M. Berghahn, G. Rheinwald, H. Lang, *Angew. Chem.* **2000**, *112*, 2590−2592; *Angew. Chem. Int. Ed.* **2000**, *39*, 2464−2466.
[10] W. Kläui, D. Schramm, W. Peters, G. Rheinwald, H. Lang, *Eur. J. Inorg. Chem.* **2001**, 1415−1424.
[11] [11a] W. D. Jones, F. J. Feher, *J. Am. Chem. Soc.* **1986**, *108*, 4814−4819. − [11b] D. D. Wick, K. A. Reynolds, W. D. Jones, *J. Am. Chem. Soc.* **1999**, *121*, 3974−3983.
[12] W. D. Jones, V. L. Kuykendall, *Inorg. Chem.* **1991**, *30*, 2615−2622.
[13] [13a] W. D. Jones, E. T. Hessell, *J. Am. Chem. Soc.* **1992**, *114*, 6087−6095. − [13b] M. Paneque, P. J. Pérez, A. Pizzano, M. L. Poveda, S. Taboada, M. Trujillo, E. Carmona, *Organometallics* **1999**, *18*, 4304−4310.
[14] V. Chauby, C. Serra Le Berre, P. Kalck, J.-C. Daran, G. Commenges, *Inorg. Chem.* **1996**, *35*, 6354−6355.
[15] S. E. Boyd, L. D. Field, M. G. Partridge, *J. Am. Chem. Soc.* **1994**, *116*, 9492−9497.
[16] H. Günther, *NMR Spectroscopy − Second Edition*, Wiley, New York **1994**

Received June 11, 2001
[I01211]

Synthesis, Structure and Physical Properties of Tetrabutylammonium Salts of Nickel Complexes with the New Ligand dcbdt = 4,5-dicyanobenzene-1,2-dithiolate, $[Ni(dcbdt)_2]^{z-}$ (z = 0.4, 1, 2)

Dulce Simão,[a] Helena Alves,[b] Dulce Belo,[b] Sandra Rabaça,[b] Elsa Branco Lopes,[b] Isabel Cordeiro Santos,[b] Vasco Gama,[b] Maria Teresa Duarte,[a] Rui Teives Henriques,[a,b] Horácio Novais,[a] and Manuel Almeida*[b]

Keywords: S ligands / Charge transfer / Nickel / Cyclic voltammetry / Magnetic properties

The synthesis and characterization of the new aromatic *ortho*-dithiol, 4,5-dicyanobenzene-1,2-dithiol (**3**) is reported. This compound was used to prepare tetrabutylammonium salts of novel nickel complexes; the nickel(II) salt $(n\mathrm{Bu_4N})_2[Ni(dcbdt)_2]$ (**4**), the nickel(III) salt $(n\mathrm{Bu_4N})_2[Ni(dcbdt)_2]_2$ (**5**), and the partially oxidized $Ni^{III/IV}$ salt $(n\mathrm{Bu_4N})_2[Ni(dcbdt)_2]_5$ (**6**). (dcbdt = 4,5-dicyanobenzene-1,2-dithiolate). The Ni^{II} complex presents a square-planar coordination geometry and is diamagnetic, while in the paramagnetic Ni^{III} complex the $Ni(dcbdt)_2$ units are strongly dimerized with the metal atom in a square-pyramidal coordination geometry and its magnetic susceptibility follows a singlet-triplet model with an antiferromagnetic coupling J = 897 K. The partially oxidized $Ni^{III/IV}$ complex **6** presents a weakly temperature-dependent paramagnetism of $5–6\cdot10^{-4}$ emu/mol and a room-temperature electrical conductivity of 0.15 S/cm following a semiconducting regime.

Introduction

Bis(dithiolene) transition metal complexes, showing a variety of coordination geometries and oxidation states, have been extensively studied since the 1960s,[1] and they have been widely used as building blocks for molecular compounds with conducting and or magnetic properties.[2] Among the simple examples of such complexes are the $M(mnt)_2$ complexes based on the ligand mnt = 1,2-dicyanoethene-1,2-dithiolate, also known as maleonitriledithiolate (Scheme 1), first prepared in 1955 by Bähr and Schleitzer.[3] These simple $M(mnt)_2$ complexes have provided the basis of compounds with very interesting properties such as metallic conductivity,[4] magnetic chains in compounds also having conducting chains based on other donor species,[5] and even ferroelectric behaviour.[6] However, it is believed that more extended and delocalized π-ligands of this type would make the different oxidation states more accessible, favouring electron transport in the solid, and offering a richer variety of structures. Indeed, other bis(dithiolene) complexes with delocalized sulfur-rich ligands have provided the bases for many other metallic and even superconducting systems.[2]

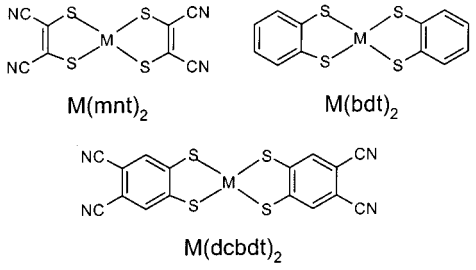

Scheme 1

In order to explore chemical modifications on electron charge-transfer solids containing the $M(mnt)_2$ complexes, we decided to prepare analogous dicyanodithio complexes with the more extended and aromatic ligand 4,5-dicyanobenzene-1,2-dithiol (**3**), (H_2dcbdt), whose preparation was not previously described. Preliminary data on a gold complex with this ligand, $(n\mathrm{Bu_4N})_2[Au(dcbdt)_2]_5$, was recently reported by us.[7] In this paper we report the synthesis of the ligand and the preparation and characterization of the tetrabutylammonium salts of three different nickel complexes, $[Ni(dcbdt)_2]^{z-}$ (z = 0.4, 1, 2).

Results and Discussion

The key compound for the synthesis of the ligand is 4,5-dichloro-1,2-dicyanobenzene (**1**) that can be obtained from 4,5-dichlorophthalic anhydride,[8] and is actually commercially available. The followed synthetic procedure involved the preparation of the aromatic dibenzyl sulfide,[9] 1,2-bis(*S*-benzylthio)-4,5-dicyanobenzene (**2**), in 71% yield (m.p. 189–190 °C), followed by a mild cleavage with the assistance of anhydrous aluminium chloride[10] (Scheme 2) to obtain **3** in 53% yield [m.p. 100 °C (dec.)].

[a] Departamento de Engenharia Química,
Instituto Superior Técnico
Av. Rovisco Pais, 1049-001 Lisboa, Portugal
Fax: (internat.) + 351-218490844
E-mail: dulce@alfa.ist.utl.pt
[b] Departamento de Química, Instituto Tecnológico Nuclear
Estrada Nacional no. 10, 2685-953 Sacavém, Portugal
Fax: (internat.) + 351-219941455
E-mail: malmeida@itn.pt

 © WILEY-VCH Verlag GmbH, 69451 Weinheim, 2001 1434–1948/01/1212–3119 $ 17.50+.50/0

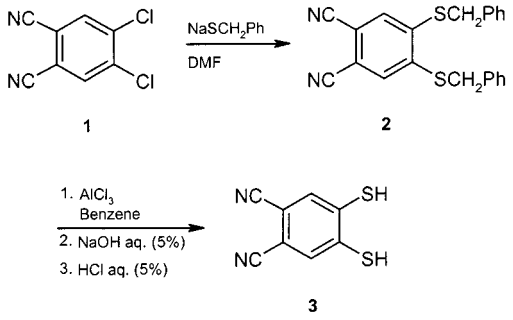

Scheme 2

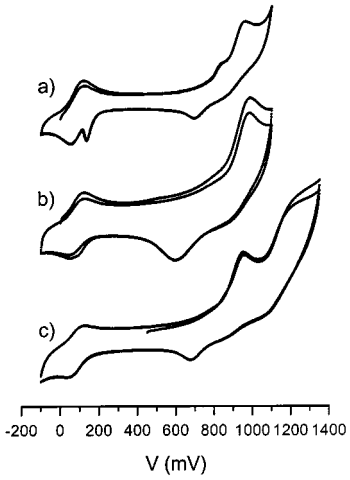

Figure 1. Cyclic voltammograms of $(n\mathrm{Bu_4N})_2[\mathrm{Ni(dcbdt)_2}]_2$ (**5**) in acetonitrile solution (ref. $Ag/AgNO_3$) at different scan rates: a) 50 mV/s; b) 500 mV/s; c) 100 mV/s

The nickel(II) complex of the ligand 4,5-dicyanobenzene-1,2-dithiol was obtained by the reaction of the dithiolate with nickel chloride, in an aqueous/alcoholic solvent mixture, and precipitated in the form of the tetrabutylammonium salt $(n\mathrm{Bu_4N})_2[\mathrm{Ni(dcbdt)_2}]$ (**4**) (Scheme 3), following the usual procedure for other bis(dithiolene) complexes.[11] This complex could be oxidized to Ni^{III}, $(n\mathrm{Bu_4N})_2[\mathrm{Ni(dcbdt)_2}]_2$ (**5**), with iodine in acetone solutions (yield 44%, m.p. 244−245 °C). Further electrochemical oxidation of **5** led to a mixed Ni^{III}/Ni^{IV} compound $(n\mathrm{Bu_4N})_2[\mathrm{Ni(dcbdt)_2}]_5$ (**6**).

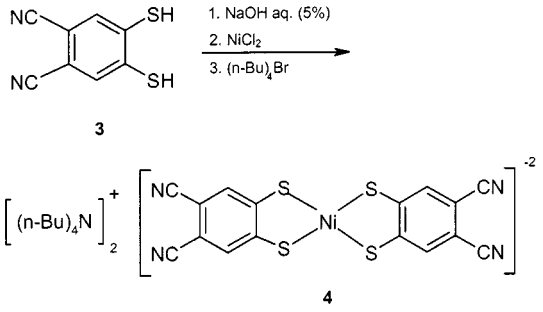

Scheme 3

The cyclic voltammetry of $(n\mathrm{Bu_4N})_2[\mathrm{Ni(dcbdt)_2}]_2$ (**5**) in acetonitrile showed different redox processes (Figure 1). One pair of reversible waves at 0.08 V vs. $Ag/AgNO_3$ was always present, as in $(n\mathrm{Bu_4N})_2[\mathrm{Ni(dcbdt)_2}]$ (**4**), and it was ascribed to the couple Ni^{II}/Ni^{III}. This value should be compared with the corresponding one for the compound with the unsubstituted benzodithiolate ligand (bdt), $Ni(bdt)_2$ (−1.05 V),[12] showing that the two cyano groups stabilize the dianionic state. In fact, while the $Ni(bdt)_2^-$ complex was obtained by oxidation of the dianion in air, obtaining $Ni(dcbdt)_2^-$ from the dianion required iodine as the oxidizing agent.

At more positive potentials a series of irreversible waves were observed with oxidation peaks at 0.83, 0.94, and 1.2 V, and reductions at 1.08, 0.89, and 0.68 V. The first oxidation wave became less prominent at higher scan rates (above 100 mV/s), while the corresponding reduction wave changed position from 0.70 to 0.50 V as the rate increased from 50 to 3000 mV/s. For slow scanning rates (50−100 mV/s) with amplitudes above 0.9 and below 1.2 V, there was an additional reduction peak at 0.120 V, typical of the formation upon oxidation of adsorbed species on the electrode (Figure 1, a). This peak was no longer observed at a scan rate of 500 mV/s and above (Figure 1, b) or for sweeps of 1.2 V or above (Figure 1, c).

This suggests that the process at 0.94/0.89 V led to the formation of insoluble $[\mathrm{Ni(dcbdt)_2}]_5^{2-}$ at the electrode. In fact from dichloromethane solutions of the monoanionic complex $(n\mathrm{Bu_4N})_2[\mathrm{Ni(dcbdt)_2}]_2$ (**5**), crystals of $(n\mathrm{Bu_4N})_2[\mathrm{Ni(dcbdt)_2}]_5$ (**6**) were obtained by electrocrystallization, using similar conditions to those previously described to obtain the gold analogue.[7] The higher potential process is probably the full oxidation to Ni^{IV}, while the waves at 0.83/0.68 with a very rate-sensitive reduction peak were associated with the process $[\mathrm{Ni(dcbdt)_2}]_2^{-2}/[\mathrm{Ni(dcbdt)_2}]_2^-$, coupled to some other reaction.

The direct comparison of this with cyclic voltammetry data obtained with $(n\mathrm{Bu_4N})_2[\mathrm{Ni(dcbdt)_2}]$ (**4**) was not possible due to the much lower solubility of compound **4**. The results for compound **4** present the same pair of reversible waves at 0.086 V, and the two similar pairs of waves at higher oxidation potentials. However, the waves at 0.83/ca. 0.68 V and the reduction wave ascribed to electrode deposition were not observed. This may be due only the lower solubility of **4**.

Compound **5** probably exists in solution as the dimer $[\mathrm{Ni(dcbdt)_2}]_2^{2-}$ as suggested by the solid-state X-ray structure with quite short dimerization bonds (see below). This

proposal is also supported by the comparison of the conductivity of **4** and **5** in acetonitrile solutions. If compound **5** were fully dissociated, the conductivity of an equimolar solution of **4** should have been twice that of **5**, but we found values of 57.5 and 22.7 μS/cm, respectively, for 0.2 mM solutions at 18 °C, giving a higher ratio and denoting the presence of the less mobile dimer.

The crystals obtained for compounds **4** and **5** enabled the crystal-structure determination by X-ray diffraction, but those of **6** were of insufficient quality for diffraction work. An ORTEP view of the complex anions in **4** and **5** is depicted in Figure 2, showing the atomic labelling scheme. Selected bond lengths for these compounds are presented in Table 1.

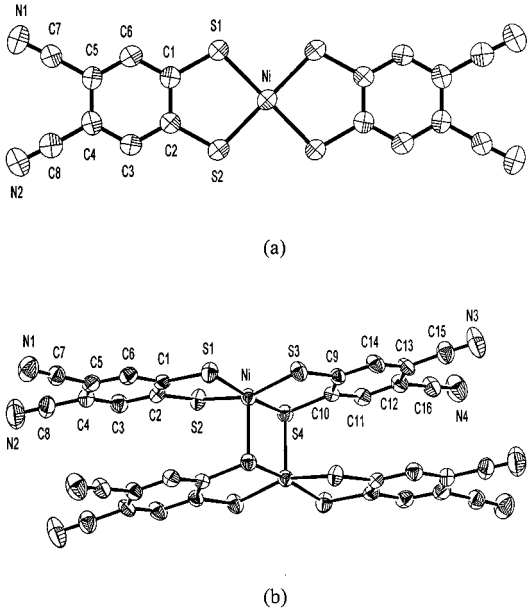

Figure 2. ORTEP diagrams and atomic numbering scheme of the complexes; a) $[Ni(dcbdt)_2]^{2-}$ in **4** and b) $[Ni(dcbdt)_2]^{-}$ in **5**, with thermal ellipsoids at 40% probability level

In complex **4** the Ni atom is located at an inversion centre, and the dianion $[Ni(dcbdt)_2]^{2-}$ presents a perfectly planar geometry, since all atoms lie in a mirror plane. The Ni−S bond lengths, Ni−S(2) 2.1736(15) Å and Ni−S(1) 2.1658(16) Å, are in the typical range, 2.16−2.18 Å, of other bis(dithio)Ni^{II} complexes,[13−16] namely for $Ni(bdt)_2$ where the distances are 2.166−2.172 Å.[16] The crystal structure of **4** shows $[Ni(dcbdt)_2]^{2-}$ layers with the complex in mirror planes at $y = 0$ and $y = 1/2$, which are separated by cation layers (Figure 3) preventing any short anion−anion interactions.

In **5** the Ni^{III} complex presents a strong dimerization of the $[Ni(dcbdt)_2]^{-}$ units that are related by an inversion centre (Figure 2) between the two nickel atoms. In the $[Ni(dcbdt)_2]_2^{2-}$ units, besides the equatorial Ni−S bonds at distances Ni−S(1) 2.2050(17) Å, Ni−S(2) 2.2023(16) Å, Ni−S(3) 2.1993(16) Å, Ni−S(4) 2.1792(16) Å, there are two Ni−S(4)* bonds at 2.3965(16) Å.

As shown by the side view of the dimer $[Ni(dcbdt)_2]_2^{2-}$ in Figure 4, the ligand where one sulfur atom is coordinating two metal atoms is almost planar [the largest deviations being the S(3) 0.072 Å and S(4) 0.083 Å] and the Ni atom lies only 0.08 Å from its average plane. In contrast, the other ligand presents a more considerable distortion with the coordinating sulfur atoms S1 and S2 deviated in opposite directions (0.063 and −0.127, respectively) and the Ni atom −0.39 Å from its average plane. Thus the four coordinating sulfur atoms are not coplanar and present a significant tetrahedral distortion with deviations of ±0.137 Å from their average plane, while the Ni atom deviates 0.286 Å from the average plane of the four sulfur atoms. The average plane of the two ligands makes a dihedral angle of 9.39(17)°.

Table 1. Selected bond lengths [Å] for $[Ni(dcbdt)_2]$ complexes

	$[Ni(dcbdt)_2]^{2-}$	$[Ni(dcbdt)_2]_2^{2-}$
Ni−S(1)	2.1658(16)	2.2050(17)
Ni−S(2)	2.1736(15)	2.2023(16)
Ni−S(3)		2.1993(16)
Ni−S(4)		2.1792(16)
Ni−S(4)[a]		2.3965(16)
S(1)−C(1)	1.729(6)	1.738(5)
S(2)−C(2)	1.725(6)	1.732(5)
S(3)−C(9)		1.734(5)
S(4)−C(10)		1.752(5)
C(1)−C(6)	1.384(7)	1.409(7)
C(1)−C(2)	1.424(8)	1.414(7)
C(2)−C(3)	1.394(7)	1.398(7)
C(6)−C(5)	1.388(7)	1.380(7)
C(3)−C(4)	1.389(7)	1.377(7)
C(5)−C(4)	1.403(8)	1.401(7)
C(5)−C(7)	1.436(8)	1.450(7)
C(4)−C(8)	1.441(8)	1.448(8)
C(7)−N(1)	1.144(7)	1.134(7)
C(8)−N(2)	1.135(6)	1.130(7)
C(9)−C(14)		1.394(7)
C(9)−C(10)		1.406(7)
C(10)−C(11)		1.376(6)
C(14)−C(13)		1.385(7)
C(11)−C(12)		1.374(7)
C(13)−C(12)		1.411(7)
C(13)−C(15)		1.447(8)
C(12)−C(16)		1.444(7)
C(15)−N(3)		1.125(7)
C(16)−N(4)		1.131(7)

[a] $-x,-y,-z+1$.

The dimerization of bis(dithiolene)metal(III) complexes, with the metal atom presenting a square-pyramidal coordination geometry, is frequent in similar complexes of other metals such as Fe and Co.[1,17,18] For bis(dichalcogenato)-nickel complexes such a clear dimeric structure was only found in a few bis(diselenolato)Ni complexes, as the neutral $Ni^{IV}(ddds)_2$ complex (ddds = 5,6-dihydro-1,4-dithiin-2,3-diselenolate),[19] the partially oxidised $Me_4N[Ni(dsise)_2]_2^{+}$ (dsise = 1,3-dithio-2-selenenido-4,5-diselenolate),[20] and the Ni^{III} complex $nBu_4N[Ni(dsit)_2]$ (dsit = 1,3-dithiole-2-thione-4,5-diselenolate).[21] With complex $Ni(mnt)_2^{-}$ a much weaker tendency towards a metal-over-sulfur packing has been reported in the compounds $(pet)_3[Ni(mnt)_2]_2$,[22] $(PPh_3Me)[Ni(mnt)_2]$,[23] and $NEt_4[Ni(mnt)_2]$,[24] where the

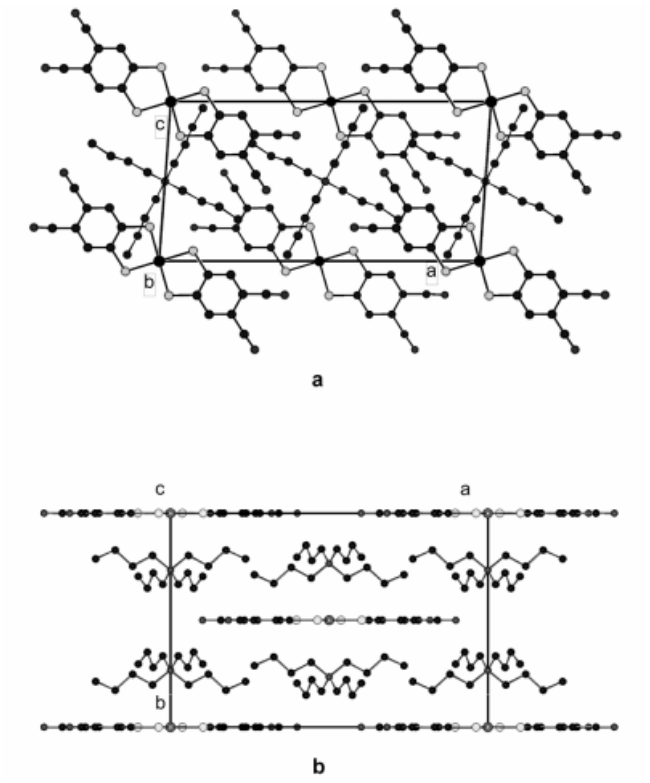

Figure 3. Crystal structure of $(n\mathrm{Bu_4N})_2\mathrm{Ni(dcbdt)_2}$ (**4**): (a) viewed along the *b* axis, and (b) viewed along the *c* axis

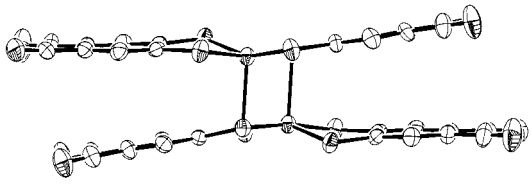

Figure 4. Side view of the dimer $[\mathrm{Ni(dcbdt)_2}^-]_2$ in **5**

apical Ni−S distances are much larger, 3.85, 3.59, and 3.69 Å, respectively, and the $\mathrm{Ni(mnt)_2}$ units remain almost planar. To the best of our knowledge, this is the first time that a clearly dimerized structure was found in a bis(dithio)$\mathrm{Ni^{III}}$ complex. Furthermore, it should be noticed that in this case, when compared with other dimerized bis(dichalcogenide) complexes, the apical bond is quite short and almost comparable to the equatorial ones.

The crystal structure of **5** is shown in Figure 5. Along the axes *c* and *b* the dimerized anions and the cations are alternating. However, along *a* the $[\mathrm{Ni(dcbdt)_2}]_2^{2-}$ dimers are arranged in chains, due to several weak interactions, connecting two $[\mathrm{Ni(dcbdt)_2}]^-$ units of adjacent dimers side by side, namely the hydrogen bonds N(3)···H(3*) and N(3*)···H(3) at 2.612 Å and 156.6°, and S(1)···H(11) at 3.188 Å and 149.9°, and a short contact S(3)···S(3*) at 3.784 Å, (see Figure 6).

While the dianionic complex **4** is diamagnetic, the monoanionic complex **5**, with $\mathrm{Ni^{III}}$, is expected to be paramagnetic with $S = {}^1/_2$. However, the strong dimerization

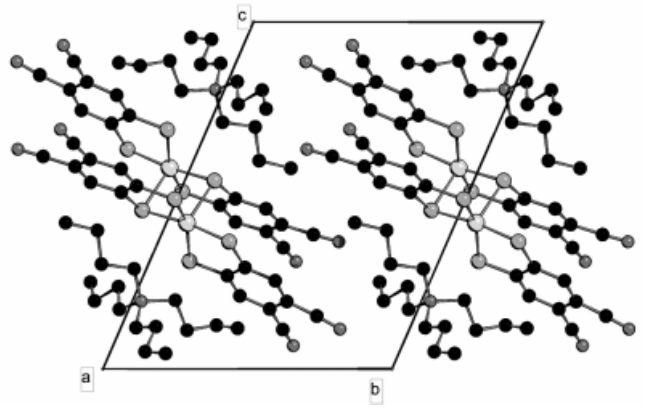

Figure 5. Crystal structure of $(n\mathrm{Bu_4N})_2[\mathrm{Ni(dcbdt)_2}]_2$ (**5**) viewed along the *a* axis

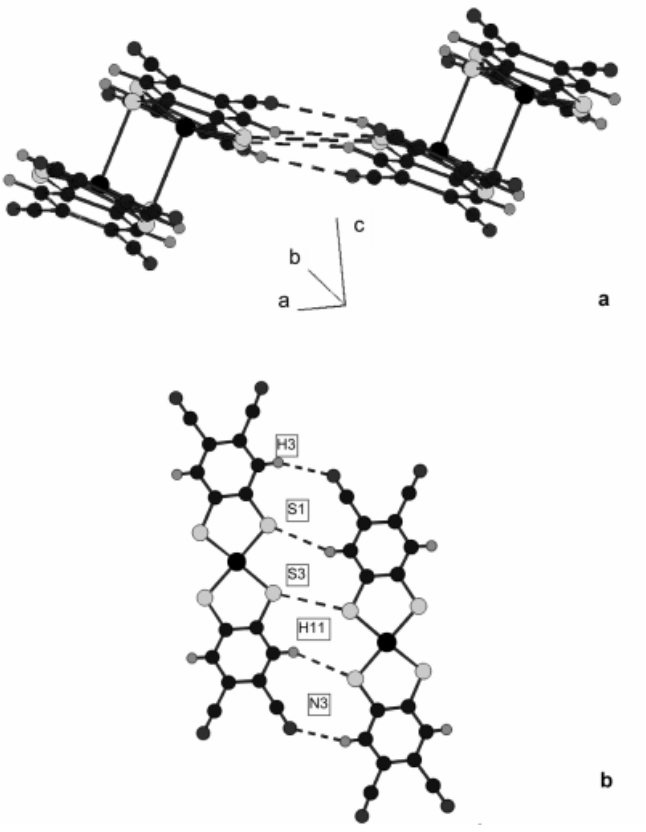

Figure 6. Chain of $[\mathrm{Ni(dcbdt)_2}^-]_2$ dimers in **5** connected along *a* by S···S contacts and N···H and S···H hydrogen bonds: a) side view; b) detail of two $[\mathrm{Ni(dcbdt)_2}]^-$ units of adjacent dimers viewed perpendicularly to their average plane with indication of the short contacts connecting them

of the $[\mathrm{Ni(dcbdt)_2}]^-$ units, as frequently observed in other dimerized Fe complexes, can lead to a strong antiferromagnetic coupling of the $S = {}^1/_2$ states expected for a isolated square planar coordination.[17,22,25]

The EPR spectra of **5**, both as a powder or as a frozen solution, show rhombic symmetry, with *g* values of 2.210, 2.0421, and 2.0064, for acetone solution at 110 K.

$(n\mathrm{Bu_4N})_2[\mathrm{Ni(dcbdt)_2}]_5^{-2}$ also shows an EPR signal, as expected for a partially oxidized $Ni^{III/IV}$ compound, but this signal is visible only at low temperature, as an almost isotropic broad signal, 300G wide and centred at $g = 2.025$ at 8 K.

The paramagnetic susceptibility of $(n\mathrm{Bu_4N})_2[\mathrm{Ni(dcbdt)_2}]_2$, obtained from raw data after a correction for diamagnetism estimated from tabulated Pascal constants as $4.2\cdot10^{-4}$ emu/mol, was ca. $5\cdot10^{-4}$ emu/mol at room temperature and showed a strong decrease upon cooling, reaching a minimum around 100 K (Figure 7). At lower temperatures the magnetic susceptibility became dominated by a Curie tail of impurities and increased again. The paramagnetic susceptibility data could be accurately fitted by a model, considering in addition to the Curie tail and a temperature-independent term a contribution due to the dimers of $S = {}^1/_2$ spins, following a singlet-triplet law as given by the Bleaney−Jones equation.[26]

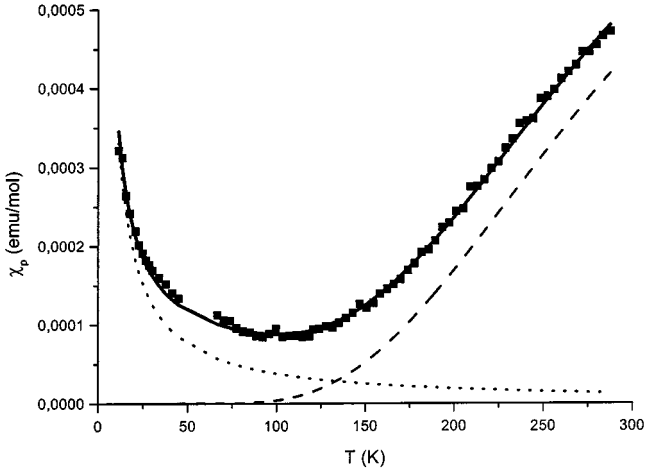

Figure 7. Paramagnetic susceptibility χ_p of $(n\mathrm{Bu_4N})_2[\mathrm{Ni(dcbdt)_2}]_2$ (**5**) as a function of the temperature T: the continuos line is a fit by Equation (1), the dotted line being the Curie tail contribution, corresponding to ca. 0.9% of $S = {}^1/_2$ spins and the dashed line the singlet-triplet contribution of the dimers (see text)

$$\chi_P = A + C/T + (Ng^2\mu_B^2/k_BT)[\exp(-2J/k_BT) + 3]^{-1} \quad (1)$$

with $A = 50(2)\cdot10^{-6}$ emu/mol, $J = 447(4)$ K, $g = 2.79(4)$, and $C = 0.00339(5)$ emu/mol·K corresponding to approximately 0.90% of $S = {}^1/_2$ spins (see Figure 7).

As it can be seen in Figure 7, the fit to our data is very good, but it is worth noting that the g value obtained is too high compared with known isolated Ni^{III} complex, and is above the EPR value obtained for this compound. However, the EPR signal that was visible only at low temperature, where the contribution was negligible, was due to the isolated Ni^{III} species associated with the Curie tail, rather than with the triplet state for which there are no EPR data in dimers of Ni^{III} species.

The J value obtained is quite large and can be compared to those reported for other $Ni(mnt)_2^-$ compounds such as $Cs[Ni(mnt)_2]\cdot H_2O$,[4c] $(pet)_3[Ni(mnt)_2]_2$,[22] $(PPh_3Me)[Ni(mnt)_2]$,[27] and $NEt_4[Ni(mnt)_2]$,[27] where the susceptibility data were also fitted to a similar singlet-triplet model with J values of 197, 226, 352, and 446 K, respectively. It is worth noting that the g values obtained by the fit in the last three compounds are also significantly larger than typical ones for similar isolated Ni^{III} complexes.

The paramagnetic susceptibility of **6**, obtained after a correction for diamagnetism, estimated from tabulated Pascal constants as $6.8\cdot10^{-4}$ emu/mol, is ca. $7\cdot10^{-4}$ emu/mol at room temperature and shows an almost temperature-independent behaviour down to ca. 70 K (Figure 8). Below this temperature there is an increase of susceptibility upon cooling that is ascribed to a Curie tail of impurities (or most likely defects). As shown in Figure 8, this Curie tail is relatively large and corresponds to ca. 5.6% $S = {}^1/_2$ spins. Subtracting this Curie tail from our experimental data an intrinsic susceptibility contribution was obtained that remained almost constant at least above 20 K with values in the range $5-7\times10^{-4}$ emu/mol. This behaviour is comparable to that previously found also in the partially oxidised gold analogue $(n\mathrm{Bu_4N})_2[\mathrm{Au(dcbdt)_2}]_5$ where the susceptibility was smaller (ca. $3-4\times10^{-4}$ emu/mol) as well as the Curie tail (ca. 0.7% of $S = {}^1/_2$ spins).

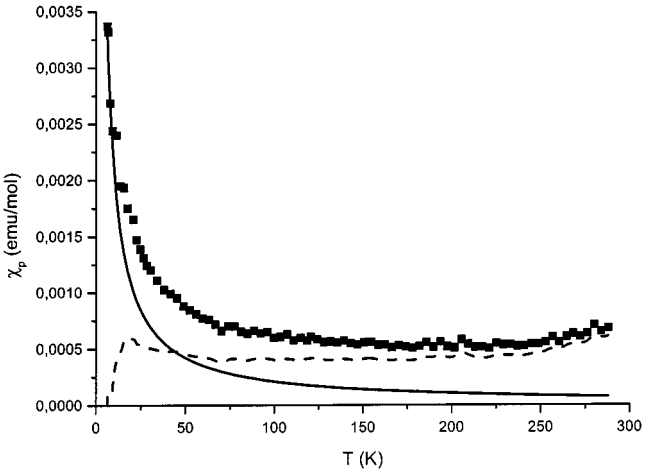

Figure 8. Paramagnetic susceptibility χ_p of $(n\mathrm{Bu_4N})_2[\mathrm{Ni(dcbdt)_2}]_5$ (**6**) as a function of the temperature T: the lines are a decomposition in a Curie tail, corresponding to ca. 5.6% of $S = {}^1/_2$ spins (full line) and the intrinsic susceptibility (− − −)

Although this behaviour of the paramagnetic susceptibility is reminiscent of a Pauli contribution, such a possibility is ruled out by the relatively low electrical resistivity as discussed below, and instead it should be seen as the result of complex antiferromagnetic interactions between the Ni^{III} states. The electrical conductivity, σ, of $(n\mathrm{Bu_4N})_2[\mathrm{Ni(dcbdt)_2}]_5$ (**6**), measured in single crystals is $\sigma_{rt} \approx 0.15$ S/cm at room temperature, following a thermally activated

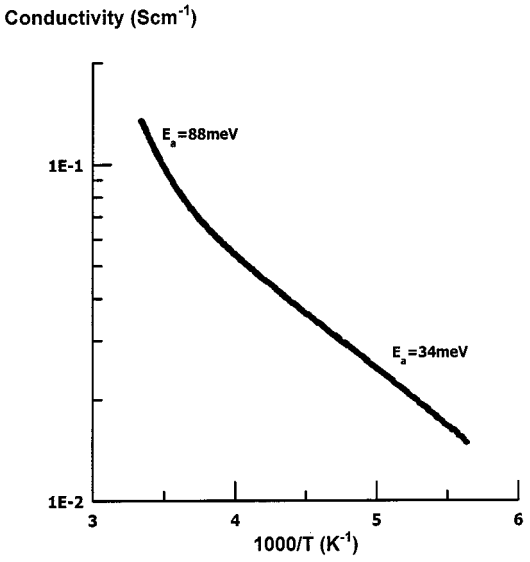

Figure 9. Electrical conductivity of $(n\mathrm{Bu_4N})_2[\mathrm{Ni(dcbdt)_2}]_5$ (**6**) single crystals as a function of the inverse temperature

semiconducting behaviour (Figure 9). The plot of logσ versus $1/T$ shows an activation energy of 88 meV at higher temperatures that decreases upon cooling, and was reduced to 34 meV below 250 K. This variation could be attributed to a change from an intrinsic to an extrinsic semiconducting regime upon cooling. The electrical conductivity of this compound was not as large as that of the gold analogue $(n\mathrm{Bu_4N})_2[\mathrm{Au(dcbdt)_2}]_5$, where the room-temperature value was $\sigma_{rt} \approx 11$ S/cm, with a smaller activation energy of 13.5 meV.[7] The thermoelectric power measurements in crystals of $(n\mathrm{Bu_4N})_2[\mathrm{Ni(dcbdt)_2}]_5$ indicated a value of $S_{rt} = -170$ μV/K at room temperature, also following a semiconducting behaviour with more negative values upon cooling in contrast to the gold analogue where the room-temperature thermopower value was rather small, $S_{rt} = -6$ μV/K, and slowly increased upon cooling, reaching a maximum of 20 μV/K at 120 K.[7] It was not possible to solve the crystal structure of $(n\mathrm{Bu_4N})_2[\mathrm{Ni(dcbdt)_2}]_5$ due to the poor diffracting quality of the crystals, and in the absence of the structure it was only possible to speculate about the reason for this difference in the electrical properties of the Ni and Au compounds. However, besides a possible stacking of the $\mathrm{Ni(dcbdt)_2}$ units in a more irregular way than in the Au analogue, but in a similar structure, the smaller conductivity and the larger activation energy observed in the Ni compound most probably reflects the different band filling.

Conclusion

In summary, we synthesized a new aromatic *ortho*-arenedithiol, which allowed the preparation of a new bis(dithiolate)nickel complex, that could exist in a broad range of oxidation states, dianionic, monoanionic, or mixed between monoanionic and neutral. The monoanionic complex presents a dimerisation of the $\mathrm{Ni(dcbdt)_2}$ units, the strongest found so far in an $\mathrm{Ni^{III}}$ complex. The partially oxidised compound $(n\mathrm{Bu_4N})_2[\mathrm{Ni(dcbdt)_2}]_5$ behaves as a semiconductor. This new dcbdt ligand opens the way for the preparation of a new family of transition metal complexes with other metallic elements such as Au, Pt, Pd, Cu, Co, and Fe. The use of the nickel complex as an electron acceptor in the preparation of different new charge-transfer salts is presently under way.

Experimental Section

General: Elemental analyses were performed by the analytical services of IST and ITN. − ^{1}H and ^{13}C NMR: Varian (300 MHz), [D$_6$]DMSO as solvent, TMS as internal standard. − IR: Perkin-Elmer 1330. − UV/Vis/NIR: Cary 5G Varian spectrophotometer. − MS: Fourier Transform Ion Cyclotron Resonance apparatus (EXTREL FTMS 2001) operated with a YAG laser source. − 4,5-Dichloro-1,2-dicyanobenzene was synthesized by literature methods.[8] DMF, acetonitrile, and dichloromethane were distilled from phosphorus pentoxide, while benzene was distilled from sodium. All other reagents were used without purification.

Synthesis of 1,2-Bis(*S*-benzylthio)-4,5-dicyanobenzene (2): To a suspension of sodium hydride (1.2 g, 51 mmol) in dry DMF (80 mL), phenylmethanethiol (6 ml, 51 mmol) was added under argon while keeping the temperature between 10 and 15 °C. At room temperature, **1** (5 g, 25 mmol) (Aldrich, TCI) was then added in small portions. The reaction mixture was left overnight under argon with stirring. The product was collected by filtration and recrystallized from $CHCl_3$/MeOH to give **2** as pale yellow needles. Yield 71%, m.p. 189−190 °C. − $C_{22}H_{16}N_2S_2$ (372.50): calcd. C 70.94, H 4.34, N 7.52, S 17.21; found C 70.28, H 4.44, N 7.42, S 16.91. − IR (KBr): $\tilde{\nu}$ = 3080 cm^{-1}, 2220, 1560, 1490, 1455, 1340, 1235, 1110. − ^{1}H NMR (CD_2Cl_2): δ = 7.47 (s, 2 H), 7.34 (m, 10 H), 4.24 (s, 4 H). − ^{13}C NMR (CD_2Cl_2): δ = 144.2, 135.0, 130.4, 129.3, 128.4, 115.8, 112.2, 37.9. − MS (EI, 70 eV): *m*/*z* (%) = 372 (13) [M$^+$], 281 (15), 203 (25), 91 (100), 83 (58).

Synthesis of 4,5-Dicyanobenzene-1,2-dithiol (3): A solution of **2** (3.0 g, 8.05 mmol) in dry benzene (100 mL) was added dropwise to a suspension of finely powdered anhydrous $AlCl_3$ (4.3 g, 32.2 mmol) in dry benzene (50 mL) and the mixture was stirred under argon at room temperature for 96 h. Ice/water was added (120 mL) and the organic layer was separated and washed successively with water and 5% aq. NaOH (3 × 80 mL). Upon acidification with 5% aq. HCl a yellowish solid precipitated that was filtered to give **3**. Yield 53%, m.p. 100 °C (dec.). − $C_8H_4N_2S_2$ (192.25): calcd. C 49.97, H 2.10, N 14.57, S 33.36; found C 50.78, H 2.02, N 13.93, S 32.76. − IR (KBr): $\tilde{\nu}$ = 3080 cm^{-1}, 2540, 2230, 1570, 1460, 1340, 1220. − ^{1}H NMR ([D$_6$]acetone): δ = 8.05 (s, 2 H), 3.84 (s, 2 H). − ^{13}C NMR ([D$_6$]acetone): δ = 141.0, 134.0, 116.1, 112.3.

Synthesis of $(n\mathrm{Bu_4N})_2[\mathrm{Ni(dcbdt)_2}]$ (4): Compound **3** (0.2 g, 1.04 mmol) was dissolved in 5 mL of NaOH aq. (5%). A solution of $n\mathrm{Bu_4NBr}$ (0.34 g, 1.05 mmol) in EtOH/H_2O (1:1) (5 mL) was added, followed by a solution of $NiCl_2{\cdot}6H_2O$ (0.12 g, 0.5 mmol) in the same solvent. The mixture was cooled and filtered, and the precipitate was washed with EtOH. The crude material was recrystallized from EtOH to give **4** as red needles. Yield 17%, m.p. 261−262 °C. − $C_{48}H_{76}N_6NiS_4$ (924.11): calcd. C 62.37, H 8.30, N 9.09, S 13.88; found C 62.38, H 8.28, N 8.92, S 13.62. − UV/Vis (CH_2Cl_2): λ (ε [Mcm^{-1}]) = 251.9 (31800), 281.6 (50700), 319.8 (52200), 406.0 (28700). − IR (KBr): $\tilde{\nu}$ = 3060 cm^{-1}, 2960−2860,

2220, 1530, 350. − ^{1}H NMR ([D$_6$]DMSO): δ = 7.24 (s, 4 H), 3.19 (t, 16 H, *J* = 8.5, *J* = 8.5), 1.57 (m, 16 H), 1.31 (m, 16 H), 0.93 (t, 24H *J* = 7.2, *J* = 7.2). − ^{13}C NMR ([D$_6$]DMSO): δ = 128.7, 120.8, 118.0, 101.6, 57.5, 23.0, 19.1, 13.4.

Synthesis of (*n*Bu$_4$N)$_2$[Ni(dcbdt)$_2$]$_2$ (5): To a solution of **4** (0.17 g, 0.18 mmol) in acetone (100 mL) was added a solution of I_2 (70.1 mg, 0.28 mmol) in 5 ml of the same solvent. EtOH was added and the solution was slowly concentrated to give **5** as dark green needles. Yield 44%, m.p. 244−245 °C. − $C_{64}H_{80}N_{10}Ni_2S_8$ (1363.28): calcd. C 56.35, H 5.93, N 10.28, S 18.83; found C 55.85, H 6.03, N 10.13, S 18.39. − UV/Vis (CH_2Cl_2): λ (ε [mcm]) = 274.5 (7400), 319.8 (6000), 352.3 (4900), 854.3 (1400). − IR (KBr): $\tilde{\nu}$ = 3070 cm^{-1}, 2970, 2220, 1530, 420. − ^{1}H NMR ([D$_6$]acetone): δ = 7.98 (s, 4 H), 3.44 (t, 8 H, *J* = 7.8, *J* = 7.8), 1.85 (m, 8 H), 1.46 (m, 8 H), 0.99 (t, 12 H, *J* = 7.1, *J* = 7.1). − ^{13}C NMR ([D$_6$]acetone): δ = 135.5, 128.4, 123.9, 102.8, 47.1, 24.5, 20.5, 13.9. − MS: *m*/*z* (%) = 437.86 (100), 438.89 (14.9), 439.87 (48.83), 440.89 (9.49) 441.88 (10.63) 442.90 (1.82), 443.91 (2.02) [Ni(dcbdt)$_2^-$], 685.88 (4.33) 687.89(5.31) 689.89 (2.80) [Ni$_2$(dcbdt)$_3$]$^-$.

Synthesis of (*n*Bu$_4$N)$_2$[Ni(dcbdt)$_2$]$_5$ (6): A solution of **5** (19.4 mg, 28.4 μmol) in dichloromethane (20 mL) was placed in a two-compartment electrocrystallisation cell, separated by a glass frit, with platinum electrodes. Employing galvanostatic conditions (ca. 1.5 μA/cm^2) for 5 d, dark brown thin needle-shaped crystals, with typical dimensions up to 2 × 0.1 × 0.05 mm, grew on the anode surface. The product was collected and washed with dichloromethane. M.p. > 240 °C. − $C_{112}H_{92}N_{22}Ni_5S_{20}$ (2680.81): calcd. C 50.18, H 3.46, N 11.49, S 23.92; found C 50.31, H 3.38, N 11.47, S 23.52.

Electrochemical Measurements: Cyclic voltammetry data were obtained using an EG&G Princeton Applied Research Electrochemical workstation. The measurements were performed at 20 °C in acetonitrile containing 0.1 M tetra-*n*-butylammonium perchlorate as supporting electrolyte with platinum working and counter-electrode and either a 0.1 M Ag/AgNO$_3$ or a calomel reference electrode and scan rates in the range 50−3000 mV s^{-1}.

X-ray Crystallographic Study: Data collection for both crystals of **4** and **5** was performed with an Enraf Nonius CAD4 diffractometer with graphite-monochromated Mo-K_α radiation (λ = 0.71069) at room temperature. Intensities were collected by the ω-2θ scan technique. The structures were solved by directed methods using SHELXS86[28] and refined with SHELXL97.[29] All non-hydrogen atoms were anisotropically refined by a full-matrix least-squares method. The hydrogen atoms were placed at calculated positions riding on the parent carbon atoms. Details of data collection and refinement are presented in Table 2. Molecular and crystal graphics were prepared with ORTEPIII[30] and SCHAKAL-97.[31] Crystallographic data (excluding structure factors) for the structures reported in this manuscript have been deposited with the Cambridge Crystallographic Data Centre. The deposition numbers are CCDC-154018 and -154019 for (*n*Bu$_4$N)$_2$[Ni(dcbdt)$_2$] and (*n*Bu$_4$N)[Ni(dcbdt)$_2$], respectively. Copies of the data can be obtained free of charge on application to CCDC, 12 Union Road, Cambridge CB2 1EZ, UK [Fax: (internat.) + 44-1223/336-033; E-mail: deposit@ccdc.cam.ac.uk].

EPR Measurements: EPR spectra in the range 4−300 K were obtained with an X-Band Bruker ESP 300E spectrometer equipped with a microwave bridge ER041XK, a rectangular cavity operating in T102 mode, a Bruker variable-temperature unit, an Oxford ESR-900 cryostat, and a field controller ER 032M system. The modulation amplitude was kept well below the line-width and the microwave power well below saturation.

Magnetic Susceptibility Measurements: Magnetic susceptibility measurements in the range 4−300 K were performed using a longitudinal Faraday system (Oxford Instruments) with a 7 T superconducting magnet under a magnetic field of 5 T and forward and reverse field gradients of 1 T/m. Polycrystalline samples (8−12 mg) were placed inside a previously calibrated thin-wall Teflon bucket. The force was measured with a microbalance (Sartorius S3D-V). Under these conditions the magnetisation was found to be proportional to the applied magnetic field.

Electrical Transport Measurements: Electrical conductivity and thermoelectric power measurements of selected single crystals were performed in the range 120−320 K, using a measurement cell attached to the cold stage of a closed-cycle helium refrigerator. In a first step, thermopower was measured using a slow AC (ca. 10^{-2} Hz) technique,[32] by attaching to the extremities of an elongated sample, with platinum paint (Demetron 308A), two 60 μm diameter 99.99% pure Au wires (Goodfellow Metals) thermally anchored to two quartz reservoirs, in a previously described apparatus,[33] operated by computer control.[34] In a second step, electrical resistivity measurements of the same sample were performed using a four-probe technique. Two extra Au wires were placed on the sample, in order to achieve a four-in-line contact configuration. Measurements were done imposing through the sample a current of 1 μA at low frequency (77 Hz) and measuring the voltage drop with a lock-in amplifier.

Acknowledgments

This work was partially supported by Fundação para a Ciência e Tecnologia (Portugal) under contracts PRAXIS XXI 2/2.1/QUI/203/94 and POCTI/1999/Qui/35452. H. A., D. B. and S. R. thank PRAXIS for their PhD grants. This work also benefited from COST action D14/0003/99.

[1] [1a] H. B. Gray, *Transition Met. Chem.* **1965**, *1*, 239−287. − [1b] G. N. Schrauzer, *Transition Met. Chem.* **1968**, *4*, 299−335. − [1c] J. A. McCleverty, *Prog. Inorg. Chem.* **1968**, *10*, 49. − [1d] D. Coucuvanis, *Prog. Inorg. Chem.* **1970**, *11*, 233. − [1e] R. Eisenberg, *Prog. Inorg. Chem.* **1970**, *12*, 295−369. − [1f] S. Alvarez, V. Ramon, R. Hoffman, *J. Am. Chem. Soc.* **1985**, *107*, 6253. − [1g] R. P. Burns, C. A. McAuliffe, *Adv. Inorg. Chem. Radiochem.* **1986**, *22*, 303−348.

[2] [2a] L. Alcácer, H. Novais, in *Extended Linear Chain Compounds*, vol. 3 (Ed.: J. S. Miller), Plenum Press, New York, **1983**, chapter 6, p. 319−351. − [2b] P. Cassoux, L. Valade, H. Kobayashi, A. Kobayashi, R. A. Clark, A. E. Underhill, *Coord. Chem. Rev.* **1991**, *110*, 115−160.

[3] G. Bähr, H. Schleitzer, *Chem. Ber.* **1955**, *88*, 1771.

[4] [4a] A. E. Hunderhill, M. M Ahmad, *J. Chem. Soc., Chem. Commun.* **1981**, 67−68. − [4b] A. Braude, K. Carneiro, C. S. Jacobsen, K. Mortensen, D. J. Turner, A. E. Underhill, *Phys. Rev. B.* **1987**, *35*, 7835. − [4c] A. E. Underhill, P. I. Clemenson, M. B. Hursthouse, R. L. Short, G. J. Ashwell, I. M. Sandy, K. Carneiro, *Synth. Met.* **1987**, *19*, 953−958.

[5] [5a] M. Almeida, R. T. Henriques, in *Handbook of Organic Conductive Molecules and Polymers* (Ed.: H. S. Nalwa), John Wiley and Sons, Chichester **1997**, vol. 1, chapter 2, p. 7. − [5b] V. Gama, R. T. Henriques, G. Bonfait, M. Almeida, S. Ravy, J. P. Pouget, L. Alcácer, *Mol. Cryst Liquid Cryst.* **1993**, *234*, 171−178.

[6] A. T. Coomber, D. Beljonne, R. H. Friend, J. L. Bredas, A. Charlton, N. Robertson, A. E. Underhill, M. Kurmoo, P. Day, *Nature* **1996**, *380*, 144.

[7] H. Alves, D. Simão, E. B. Lopes, D. Belo, V. Gama, M. T. Duarte, H. Novais, R. T. Henriques, M. Almeida, *Synth. Met.*, in press.

Table 2. Crystallographic data for $[Ni(dcbdt)_2]$ complexes

	$(nBu_4N)_2[Ni(dcbdt)_2]$	$(nBu_4N)_2[Ni(dcbdt)_2]_2$
Empirical formula	$C_{48}H_{76}N_6S_4Ni$	$C_{64}H_{80}N_{10}S_8Ni_2$
Crystal colour, habit	red, needle	green, needle
Molecular mass	924.1	681.64
Crystal system	monoclinic	triclinic
Space group	*C*2/*m*	$P\bar{1}$
Lattice constants [Å, °]	*a* =19.665(2)	*a* = 9.5061(10)
	b = 13.398(1)	*b* = 13.127(3)
	c = 9.758(1)	*c* = 16.045(3)
		α = 66.213(10)
	β = 94.16(1)	β = 85.715(10)
		γ = 70.363(10)
V [Å^3]	2564.2(4)	1721.2(5)
Z	2	1
ρ(calcd.) [Mg/m^3]	1.197	1.315
μ [mm^{-1}]	0.578	0.835
F(000)	996	718
θ range [°]	1.84−26.99.	1.78−26.97
Index ranges (*h*, *k*, *l*)	−25/25, −1/17, 12/1	−12/12, −16/15, −20/0
Reflections collected	3675	7712
Independent reflections	2881 [*R*int = 0.0439]	7441 [*R*int = 0.0547]
Data/parameters	2881/154	7441/398
Goodness-of-fit on F^2	0.965	1.054
Final *R* indices [$I > 2\sigma(I)$]	*R* = 0.0687	*R* = 0.0781
	*wR*2 = 0.0957	*wR*2 = 0.1088
Δρ: max./min. [e·Å^{-3}]	0.272/−0.297	0.248/−0.288

[8] D. Wöhrle, M. Eskes, K. Shigehara, A. Yamada, *Synthesis* **1993**, *32*, 3705.

[9] A. M. Richter, V. Engels, N. Beye, *Z. Chem.* **1989**, *29*, 444.

[10] D. E. L. Carrington, K. Clark, R. M. Scrowston, *J. Chem. Soc. C* **1971**, 3262.

[11] R. Williams, E. Billig, J. H. Waters, H. B. Gray, *J. Am. Chem. Soc.* **1966**, *88*, 43

[12] M. J. Baker-Hawkes, E. Billig, H. B. Gray, *J. Am. Chem. Soc.* **1966**, *88*, 4870−4875.

[13] N. C. Shiødt, P. Sommer Larsen, T. Bjørnholm, M. Folmer Nielsen, J. Larsen, K. Bechgaard, *Inorg. Chem.* **1995**, *34*, 3688−94.

[14] C. Mahadevan, M. Seshasayer, A. Radha, P. T. Manoharan, *Acta Crystallogr., Sect. C* **1984**, *40*, 2032.T. Yamamura, H. Arai, H. Kurihara, R. Kuroda, *Chem. Lett.* **1990**, 1975.

[15] E. Ribera, C. Rovira, J. Veciana, J. Tarrés, E. Canadell, R. Rousseau, E. Molins, M. Mas, J-P. Schoeffel, J.-P. Pouget, J. Morgado, R. T. Henriques, M. Almeida, *Chem. Eur. J.* **1999**, *5*, 2025.

[16] D. Sellmann, S. Funfgelder, F. Knoch, M. Moll, *Z. Naturforsch., Teil B* **1991**, *46*, 1601.

[17] J. V. Rodrigues, I. C. Santos, V. Gama, R. T. Henriques, J. C. Waerenborgh, M. T. Duarte, M. Almeida, *J. Chem. Soc., Dalton Trans.* **1994**, 2655−2660.

[18] [18a] W. C. Hamilton. I. Bernal, *Inorg. Chem.* **1967**, *6*, 2003. − [18b] A. L. Balch. I. G. Dance, R. H. Holm, *J. Am. Chem. Soc.* **1968**, *90*, 1139.

[19] H. Fujiwara, E. Ojima, H. Kobayashi, T. Courcet, I. Malfant, P. Cassoux, *Eur. J. Inorg. Chem.* **1998**, *11*, 1631−39.

[20] R.-M. Olk, R. Kirmse, E. Hoyer, C. Faulmann, P. Cassoux, *Z. Anorg. Alllg. Chem.* **1994**, *620*, 90.

[21] J. P. Cornelissen, J. G. Haasnoot, J. Reedijk, C. Faulmann, J.-P. Legros, P. Cassoux, P. J. Nigrey, *Inorg. Chim. Acta* **1992**, *202*, 131−139.

[22] J. Morgado, I. C. Santos, L. F. Veiros, R. T. Henriques, M. T. Duarte, M. Almeida, L. Alcácer, *J. Mat. Chem.* **1997**, *7*, 2387−2392.

[23] C. J. Firch Jr., *Acta Crystallogr.* **1966**, *20*, 107.

[24] A. Kobayashi, Y. Sasaki, *Bull. Chem. Soc. Jpn.* **1977**, *50*, 2650.

[25] V. Gama, I. C. Santos, G. Bonfait, R. T. Henriques, M. T. Duarte, J. C. Waerenborgh, L. Pereira, J. M. P. Cabral, M. Almeida, *Inorg. Chem.* **1992**, *31*, 2598−2604.

[26] R. L. Carlin, *Magnetochemistry*, Springer-Verlag, Berlin, **1986**.

[27] J. F. Veiher, L. R. Melby, R. E. Benson, *J. Am. Chem. Soc.* **1964**, *86*, 4329.

[28] *SHELXS86*: G. M. Sheldrick, *Acta Crystallogr., Sect. A* **1990**, *46*, 467−473.

[29] G. M. Sheldrick, *SHELXL97*, *A Program for Crystal structure refinement*, University of Göttingen, Germany, **1997**.

[30] M. N. Burnett, C. K. Johnson, *ORTEPIII*, Report ORNL-6895, Oak Ridge National Laboratory, Tennessee, USA, **1996**.

[31] E. Keller, *SCHAKAL-97*, *A Computer Program for the Representation of Molecular and Crystallographic Models*, Kristallographisches Institut der Universität Freiburg i. Br., Germany, **1997**.

[32] P. M. Chaikin, J. F. Kwak, *Rev. Sci. Instrum.* **1975**, *46*, 218.

[33] M. Almeida, S. Oostra, L. Alcácer, *Phys. Rev. B* **1984**, *30*, 2839−2845.

[34] E. B. Lopes, *INETI-Sacavém*, internal report, **1991**.

Received January 22, 2001
[I01029]

Nickel Complexes Based on Thiophenedithiolate Ligands − Magnetic Properties of Metallocenium Salts

Dulce Belo,[a] Helena Alves,[a] Sandra Rabaça,[a] Laura Cristina Pereira,[a] Maria Teresa Duarte,[b] Vasco Gama,[a] Rui Teives Henriques,[a] Manuel Almeida,*[a] Elisabet Ribera,[c] Concepció Rovira,[c] and Jaume Veciana[c]

Keywords: S ligands / Coordination chemistry / Magnetic properties / Nickel

The nickel complex nBu$_4$N[Ni(α-tpdt)$_2$] (**2**) (α-tpdt = 2,3-thiophenedithiolate) has been prepared and characterized. A salt of this monoanionic paramagnetic complex, [Fe(Cp*)$_2$][Ni(α-tpdt)$_2$] (**3**), was obtained with decamethylferrocene, crystallizing in the monoclinic space group $P2_1/a$ with a = 15.443(3), b = 10.237(1), c = 20.360(2) Å, β = 107.54(1)°, V = 3069.1(7) Å^3, Z = 4. Its structure consists of alternating cationic and anionic layers, with short interlayer contacts defining alternating cation–anion chains. Magnetic characterization of **3** at low applied magnetic fields revealed an antiferromagnetic transition at T_N = 2.56 K. Below T_N, **3** displays a metamagnetic behaviour with a critical field of 0.07 T at 1.6 K. The magnetic properties of this compound are compared with those of the analogous salts with diamagnetic gold dithiolate [Fe(Cp*)$_2$][Au(α-tpdt)$_2$] (**4**), and diamagnetic decamethylcobaltocenium, [Co(Cp*)$_2$][Ni(α-tpdt)$_2$] (**5**), which are also reported. This comparison shows that the ferromagnetic interactions observed in **3** are due to cation–anion intrachain interactions.

Introduction

Square-planar bis(dithiolene) transition metal complexes have attracted considerable interest, essentially in their use as building blocks for constructing molecular materials. They are versatile units that can have a wide range of oxidation states, coordination geometries, and magnetic moments.[1] To date they have been used to generate several interesting and unusual properties, such as metallic behaviour[2] or even superconductivity,[3,4] third-order nonlinear optical properties, and cooperative magnetic properties such as ferromagnetism[5] or metamagnetism.[6]

In a recent paper, we reported the preparation of gold complexes based on three different thiophenedithiolate ligands.[7] They were viewed as the first members of a new larger family of complexes with different transition metals. These complexes have a high potential for use as building blocks in the preparation of novel molecular materials with interesting conducting or magnetic properties.

In this paper, we report the synthesis and characterization of the first nickel complex belonging to this series in the form of a tetrabutylammonium salt, nBu$_4$N[Ni(α-tpdt)$_2$], where α-tpdt = 2,3-thiophenedithiolate (Scheme 1). The synthesis, crystal structure, and magnetic properties of the decamethylferrocenium charge-transfer (CT) salt are also reported and are compared with those of the analogous salts with the diamagnetic acceptor (A) [Fe(Cp*)$_2$][Au(α-tpdt)$_2$] and the diamagnetic donor (D) [Co(Cp*)$_2$][Ni(α-tpdt)$_2$].

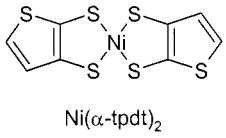

Ni(α-tpdt)$_2$

Scheme 1

Results and Discussion

The synthesis of nBu$_4$N[Ni(α-tpdt)$_2$] was carried out following a procedure (Scheme 2) similar to that described previously for the gold analogue.[7] The thiophenedithiolate ligands were obtained from 5,6-thieno[2,3-*d*]-1,3-dithiol-2-one (**1**) in methanol solution by cleavage with potassium methoxide. The ligand solution thus obtained, without isolation of the intermediate, was immediately added to a solution of nickel dichloride in methanol to give the nickel species, which precipitated as the green tetrabutylammonium salt nBu$_4$N[Ni(α-tpdt)$_2$] (**2**) upon treatment with nBu$_4$NI followed by stirring in air at ice-bath temperature. The precipitate was washed with methanol and purified by recrystallization from acetone/2-propanol to give air-stable crystals. The final yield was 89%. Elemental analysis results

[a] Instituto Tecnológico e Nuclear,
Estrada nacional no. 10, 2686−953 Sacavém, Portugal
Fax: (internat.) + 351-21/994-1455
E-mail: malmeida@itn1.itn.pt
[b] Instituto Superior Técnico,
Av. Rovisco Pais, 1049−001 Lisboa, Portugal
Fax: (internat.) + 351-21/841-7862
E-mail: teresa.duarte@ist.utl.pt
[c] Institut de Ciència de Materials de Barcelona (CSIC), Campus Universitari de Bellaterra,
08193 Cerdanyola, Spain
Fax: (internat.) + 34-93/5805729
E-mail: cun@icmab.es

 © WILEY-VCH Verlag GmbH, 69451 Weinheim, 2001 1434−1948/01/1212−3127 $ 17.50+.50/0

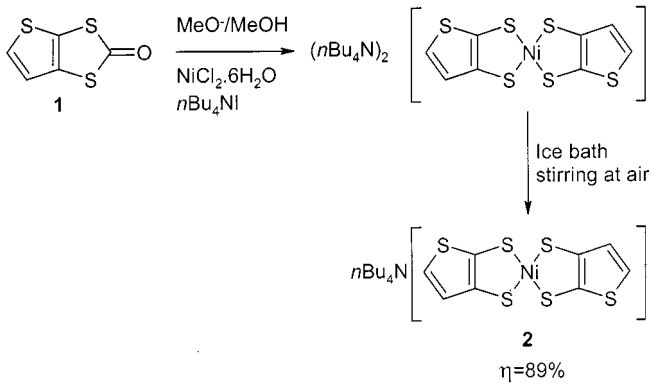

Scheme 2

correspond to a 1:1 stoichiometry for the nBu$_4$N salts of the nickel complex, thus indicating that Ni^{II} is oxidized during the synthesis.

Cyclic voltammetry of **2** in acetonitrile shows a pair of symmetric reversible redox waves at $E_{1/2} = -0.562$ V vs. Ag/AgCl, corresponding to the couple [Ni(α-tpdt)$_2$]$^{2-}$/[Ni(α-tpdt)$_2$]$^-$. At higher potentials, a pair of reversible waves is seen at $E_{1/2} = 0.253$ V, corresponding to the couple [Ni(α-tpdt)$_2$]$^-$/[Ni(α-tpdt)$_2$]. Similar voltammograms and almost identical potentials are observed in dichloromethane solution.

Oxidation potentials indicate that it is easier to obtain the neutral species in the case of the nickel complex than for the gold analogue, for which the couples Au^{II}/Au^{III} and Au^{III}/Au^{IV} were found under the same conditions at −1.62 V and 0.456 V, respectively.[7] In fact, solutions of compound **2** are rather unstable in air and decompose to give a fine precipitate, faster than in the case of the Au analogue.

In spite of the fact that well-formed single crystals are easily obtained, the crystal structure of **2**, with cell parameters $a = 9.4801(19)$, $b = 18.7867(24)$, $c = 9.6185(20)$ Å, $\beta = 119.336(23)°$, $V = 1493(1)$ Å^3, could not be solved due to severe twinning problems.

Ni^{III}, having a d^7-electronic configuration, in the square-planar coordination anticipated for [Ni(α-tpdt)$_2$]$^-$, is expected to be paramagnetic with $S = {}^1/_2$. This was confirmed by EPR and magnetization measurements.

The powder EPR spectrum of salt **2** at 7.5 K is shown in Figure 1, a. The spectrum observed in frozen acetone solutions, as shown in Figure 1, b, gives similar g values, with a structure corresponding to a rhombic anisotropy with

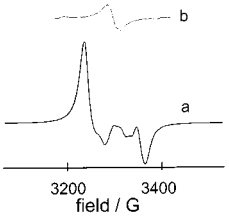

Figure 1. EPR spectra of compound **2**: (a) powder at 7.5 K, (b) acetone solution at 60 K

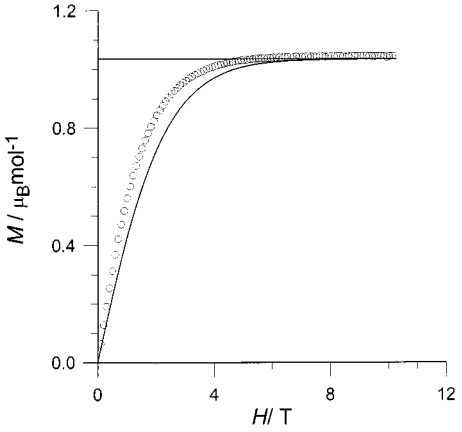

Figure 2. Magnetization of compound **2** as a function of the field at 1.6 K

values of $g_1 = 2.11492$, $g_2 = 2.04992$, $g_3 = 1.99611$. Single-crystal data show a single line of width 20 G at 8 K.

The static paramagnetic susceptibility of compound **2** follows the Curie−Weiss law with $\theta = 2.1$ K and indicates an effective magnetic moment, μ_{eff}, of 1.76 μ_B. The presence of slight ferromagnetic interactions in this compound, as denoted by the small positive θ value, is confirmed by the magnetization field dependence at 1.6 K (Figure 2), which shows a saturation magnetization of 1.04 $N\mu_B$. This is approached more rapidly than predicted by the Brillouin function for an $S = {}^1/_2$ spin system with an average $<g> = 2.06$ (thin solid curve). In most cases, the salts of metal-bis(dichalcogenide) monoanionic complexes with diamagnetic cations exhibit antiferromagnetic interactions, while in the case of compound **2** the coupling between the complexes is ferromagnetic. However, the absence of a crystal structure precludes a discussion of the contacts that give rise to the ferromagnetic interactions. In view of this, efforts towards the determination of the structure of compound **2** will be made.

The CT salt **3** and the corresponding analogues with decamethylcobaltocenium, [Co(Cp*)$_2$][Ni(α-tpdt)$_2$] (**4**), and gold-bis(thiophenedithiolate), [Fe(Cp*)$_2$][Au(α-tpdt)$_2$] (**5**), were obtained as small crystals by addition of equimolar solutions of a decamethylmetallocene salt and nBu$_4$N-[M′(α-tpdt)$_2$], respectively, under anaerobic conditions. Single crystals suitable for structural and physical studies were obtained by slow evaporation of the solvent from saturated acetonitrile solutions.

The crystal structure of compound **3** was solved. It crystallizes in the monoclinic space group $P2_1/a$ with $Z = 4$. Crystal and experimental data are summarized in Table 2. The systematic absences confirm the space group as $P2_1/a$. In the asymmetric unit, we found two half-[Fe(Cp*)$_2$]$^+$ fragments, the Fe atoms lying in special positions (centres of symmetry), and one acceptor molecule, [Ni(α-tpdt)$_2$], the Ni atom residing far from any special position. A significant disorder was observed in the methyl groups of the Cp* fragments; several disorder models were tried but none seemed to bring any improvement in the structure refine-

ment, not by lowering the e.s.d. in the bond lengths and angles nor by lowering the *R* values. Thus, the Me groups were allowed to refine anisotropically with an ISOR restraint of 0.02.

The Cp rings of the donor adopt a staggered conformation, as is commonly found. The $[Ni(\alpha\text{-tpdt})_2]^-$ anion adopts only a *trans* (*E*) configuration in the crystal, in analogy with the salt of a gold complex with the similar non-aromatic ligand dtpdt, $n Bu_4N[Au(dtpdt)_2]$.[7] The Ni−S bond lengths observed in the Ni complex, with average values of 2.156 Å (see Table 1), are in a good agreement with the values reported for other Ni^{III} dithiolates.[8−10] The $[Ni(\alpha\text{-tpdt})_2]^-$ anion is almost planar with a small chair-type distortion (Figure 3).

The crystal structure of **3** consists of alternating layers of donors, $[Fe(Cp^*)_2]^+$, and acceptors, $[Ni(\alpha\text{-tpdt})_2]^-$, extending parallel to the *a*,*b* plane. This is illustrated in Figure 4, which shows a projection of the crystal structure along the *a* axis. Unlike the donor layers, in which the cations are quite isolated from each other, in the acceptor layers relatively short interionic AA distances are found involving S atoms of the central NiS_4 fragment and a C atom of the thiophenic fragment of the ligand, as shown in Figure 5. The S···C separations are 3.723 and 3.751 Å, exceeding the sum of the van der Waals radii (3.450 Å) by 8 and 9%, respectively. Short interlayer interionic DA distances are also seen, involving C atoms of the Cp rings and the S atom of the thiophenic fragment from the acceptors, as shown in Figure 4 (dashed lines). These S···C distances are 3.530 and 3.610 Å, exceeding the sum of the van der Waals radii by 2 and 5%, respectively. These contacts form another set of layers composed of parallel alternating DA chains, as shown in Figure 6, and the chains in adjacent layers are almost perpendicular to each other, extending along directions alternating from $2\boldsymbol{b} + \boldsymbol{c}$ to $2\boldsymbol{b} - \boldsymbol{c}$ (Figure 7).

Table 1. Selected bond lengths and angles for $[Fe(Cp^*)_2][Ni(\alpha\text{-tpdt})_2]$ (**3**)

	d (Å)
Ni−S(1)	2.154(3)
Ni−S(2)	2.162(4)
Ni−S(3)	2.150(3)
Ni−S(4)	2.160(4)
S(1)−C(1)	1.703(13)
S(2)−C(2)	1.745(11)
S(3)−C(3)	1.736(12)
S(4)−C(4)	1.716(12)
S(5)−C(6)	1.703(14)
S(5)−C(1)	1.725(11)
S(6)−C(8)	1.732(16)
S(6)−C(3)	1.719(12)
C(1)−C(2)	1.387(14)
C(2)−C(5)	1.455(14)
C(3)−C(4)	1.346(15)
C(4)−C(7)	1.492(15)
C(5)−C(6)	1.361(15)
C(7)−C(8)	1.341(18)

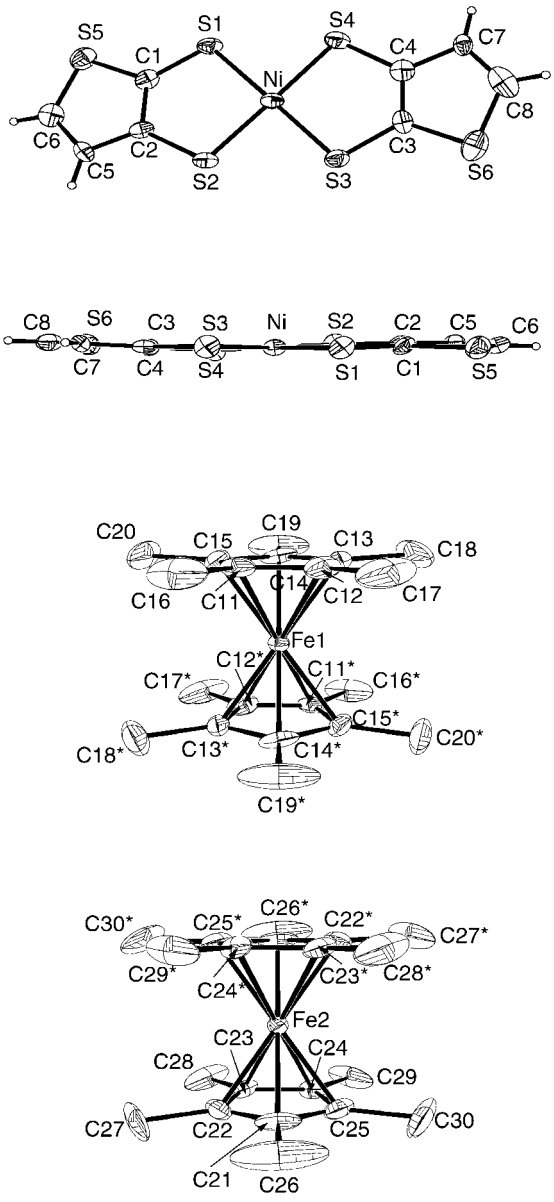

Figure 3. ORTEP diagram and atomic numbering scheme of compound **3** with thermal ellipsoids drawn at a 20% probability level; the high thermal vibration of the methyl groups is due to the disorder referred to in the text

The linear chain-based layers, extending parallel to the *b*,*c* plane (*bc* layers) are connected by the acceptor−acceptor interactions shown in Figure 5 forming a 3D network. Two chains from adjacent layers are shown in Figure 7 along with one anionic *ac* layer. The S···C contacts are slightly shorter in the *b*,*c* layers than in the *a*,*b* layers. However, in this case it is not possible to predict which ones dominate the magnetic interactions, as this also depends on the spin densities of the atoms involved in the contacts.

In view of this crystal structure, if the *ab* intralayer (AA) and *bc* intralayer (DA) contacts are different in nature, a complex magnetic behaviour can be expected for compound **3**, where both the donor and acceptor units are paramag-

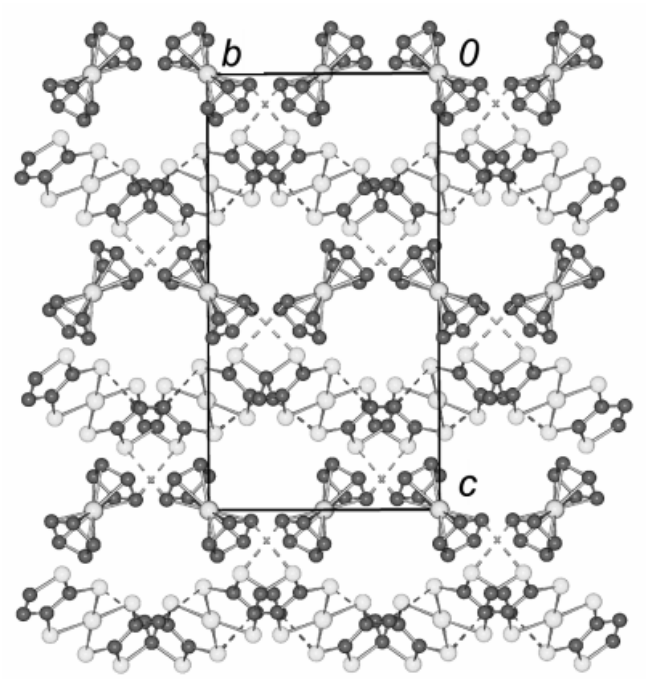

Figure 4. Crystal structure of **3** viewed along the *a* axis showing alternating layers of donors, $[Fe(Cp^*)_2]^+$, and acceptors, $[Ni(\alpha\text{-tpdt})_2]^-$, extending parallel to the *a*,*b* plane

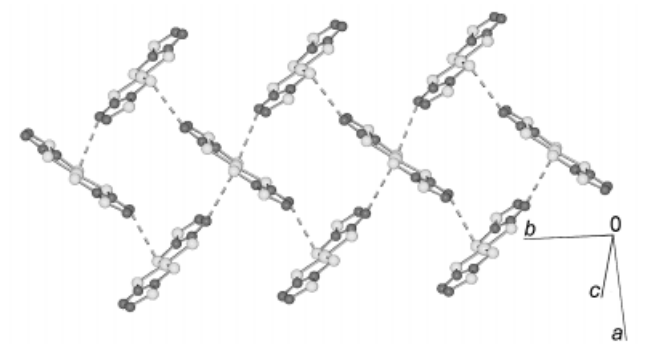

Figure 5. Layers of $[Ni(\alpha\text{-tpdt})_2]^-$ in **3** showing the closest S···C contacts

netic species with localized $S = {}^1/_2$ spins. The nature of these interactions can be better understood through studying the magnetic properties of the two other analogous CT salts **4** and **5**, in which one of the species, either the donor, as $[Co(Cp^*)_2]^+$, or the acceptor, as $[Au(\alpha\text{-tpdt})_2]^-$, is diamagnetic.

For compound **4**, the crystal structure could not be refined due to lower quality of the crystals, but the X-ray diffraction data reveal a monoclinic unit cell with parameters of $a = 15.370(3)$, $b = 10.233(2)$, $c = 20.450(3)$ Å, $\beta = 108.41(3)°$, indicating that it is isostructural with **3**. In the case of **5**, it was not possible to determine the unit cell parameters.

The temperature dependence of the product of the static paramagnetic susceptibility χ_P and the absolute temperature T, $\chi_P T$, for compounds **3**, **4**, and **5** is shown in Figure 8. In the latter two cases, $\chi_P T$ decreases upon cooling

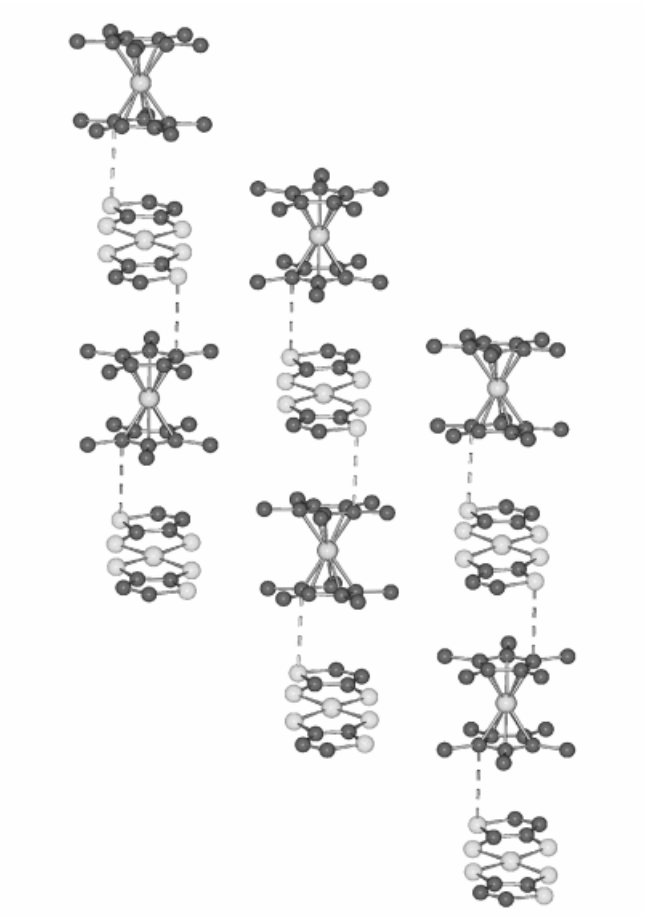

Figure 6. Partial view of the crystal structure of **3** showing the parallel alternating DA chains

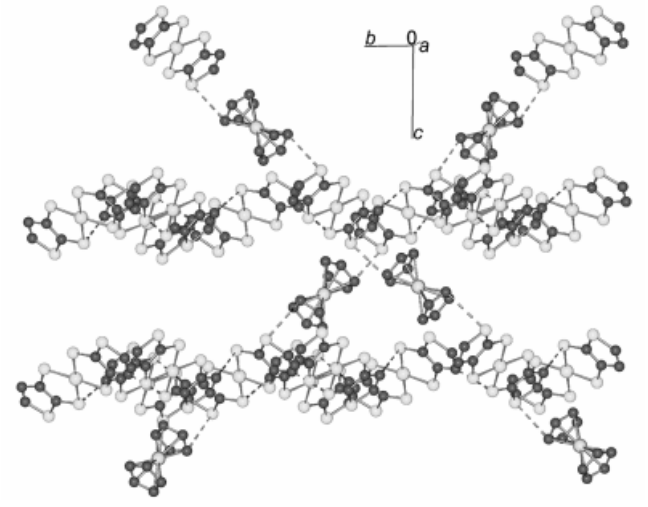

Figure 7. Partial view of the crystal structure of **3** illustrating the orthogonal DA chain directions

indicating that for the CT salt **4** the AA interactions are antiferromagnetic and that for compound **5** the DD interactions are antiferromagnetic. In the case of **3**, a broad minimum was observed at 130 K, and at lower temperatures a faster increase upon cooling was detected, indicating that

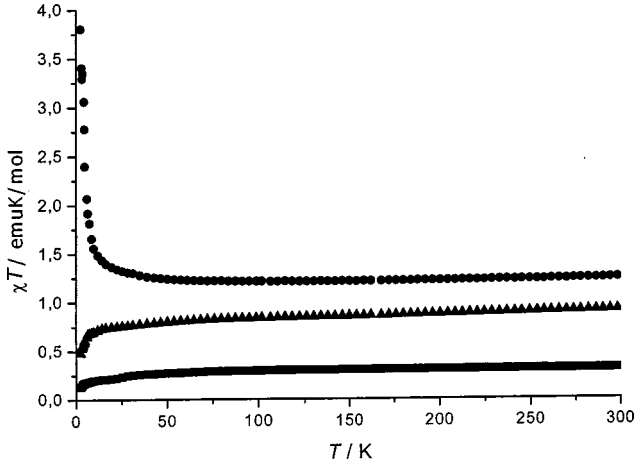

Figure 8. Temperature dependence of the product of the absolute temperature, T, with the static paramagnetic susceptibility, χ_P, for salts **3** (circles), **4** (triangles), and **5** (squares)

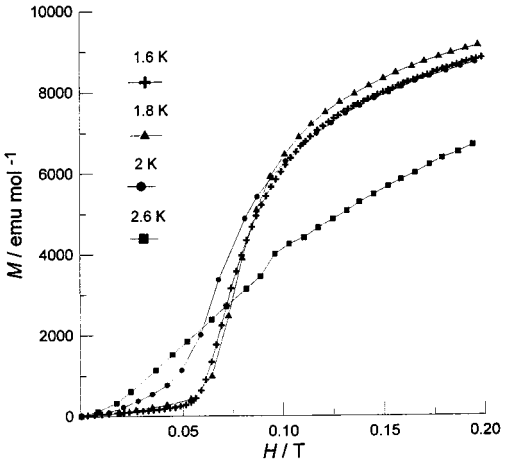

Figure 10. Magnetisation field dependence of compound **3**, at different temperatures indicated

under these conditions the dominant interactions are ferromagnetic.

At low temperatures, a field-dependent behaviour was observed in the magnetization temperature dependence of compound **3**, as shown in Figure 9. At low fields, e.g. at 15 mT, a maximum in the magnetization was observed at 2.5 K, indicating the existence of an antiferromagnetic transition. On increasing the applied magnetic field, the maximum shifts towards lower temperatures and at 30 mT it occurs at 2.35 K. At fields of greater than 70 mT the maximum is suppressed, suggesting a metamagnetic behaviour. The Neél temperature of the antiferromagnetic transition in this compound was determined by low-field (1 Oe) AC magnetic susceptibility measurements through the observation of a sharp maximum at $T_N = 2.56$ K (inset in Figure 9). Below 2.6 K, the isothermal magnetization (Figure 10) shows a sigmoidal field dependence, confirming the existence of a metamagnetic transition. At 1.6 K, the critical field H_C, defined as the maximum of dM/dH, is 70 mT. Above 7 T, the magnetization becomes almost saturated, attaining a value of 2.45 μ_B/mol at 12 T. This value is close to the predicted value of 2.44 $N\mu_B$, with $g_{Ni} = 2.07$[1a] and $g_{Fe} = 2.81$.[11] The different measurements of DC magnetization as a function of temperature at several magnetic field strengths and of AC susceptibility as a function of field and temperature led to the tentative phase diagram shown in Figure 11.

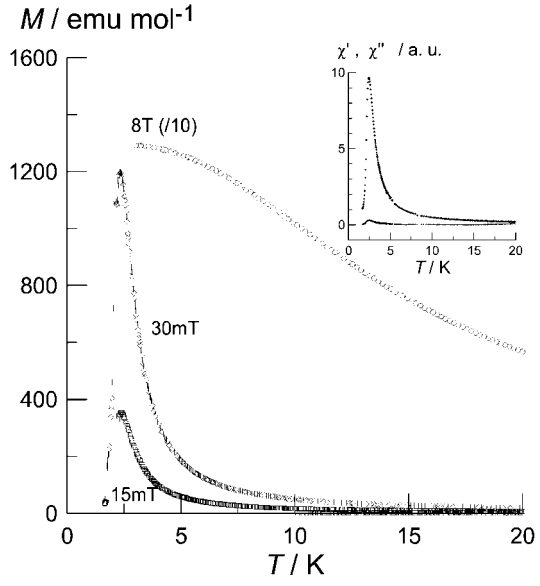

Figure 9. Magnetization temperature dependence of compound **3** under different applied magnetic fields as indicated; the inset shows the AC susceptibility, χ_{AC}, vs. T

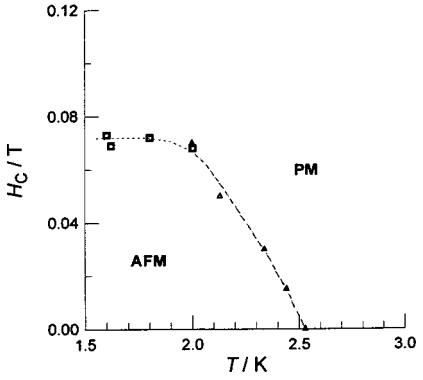

Figure 11. Critical field temperature dependence for compound **3**

Metamagnetism results from the existence of magnetic anisotropy. For compound **3**, this anisotropy can only be assigned to a different magnetic nature of the S···C contacts in the *b*,*c* layers, corresponding to DA contacts from the alternating 1D DA chains, and in the *a*,*b* layers, corresponding to the AA contacts in the acceptor layers. The negative θ value obtained for the isostructural CT salt **4** suggests that in the *a*,*b* layers the AA interactions are antiferromagnetic, which would imply that the DA interactions from the *b*,*c* layers are ferromagnetic. It is envisaged that this could be confirmed by single-crystal experiments, since if the linear chains in the *b*,*c* plane show a ferromagnetic coupling, then an antiferromagnetic behaviour should be observed along a perpendicular direction. Unfortunately,

however, it has not yet been possible to grow crystals large enough to perform such experiments.

In order to achieve a better understanding of the magnetic behaviour of the CT salt **3**, efforts will be made to obtain large single crystals. This should also allow a more detailed study of the phase diagram, which we hope to report in a subsequent publication along with the analogous salts with the donors $[Mn(Cp^*)_2]^+$ ($S = 1$) and $[Cr(Cp^*)_2]^+$ ($S = {}^3/_2$).

Conclusion

In conclusion, we have prepared and characterized a new nickel complex $[Ni(\alpha\text{-tpdt})_2]^-$, based on a thiophenedithiolate ligand that was previously described as coordinating a gold atom. The nBu$_4$N$^+$ salt of this complex shows ferromagnetic interactions, a full understanding of which will require a crystal structure determination. From this complex, decamethylmetallocenium-based CT salts have been obtained. $[Fe(Cp^*)_2][Ni(\alpha\text{-tpdt})_2]$ displays a metamagnetic behaviour with $T_N = 2.56$ K and a critical field of 70 mT at 1.6 K. Comparison of the magnetic properties of this compound with those of analogous salts with the diamagnetic acceptor $[Au(\alpha\text{-tpdt})_2]^-$ and the diamagnetic donor $[Co(Cp^*)_2]^+$ indicates that the metamagnetism is associated with the existence of ferromagnetically coupled alternating DA chains, forming layers in the *b*,*c* plane, together with antiferromagnetically acceptor-coupled layers in the perpendicular *a*,*b* plane.

The possibility of combining this complex with suitable donors to prepare conducting materials with paramagnetic anions as well as new magnetic materials is currently being explored and will be reported in due course.

Experimental Section

General Remarks: All manipulations were carried out with the exclusion of air under nitrogen or argon (CV), unless stated otherwise. The starting ketone, 5,6-thieno[2,3-*d*]-1,3-dithiol-2-one, and the tetrabutylammonium salt of gold(III) bis(2,3-thiophenedithiolate), nBu$_4$N[Au(α-tpdt)$_2$], were prepared following the method used in ref.[7] All solvents were purified following standard procedures. Other chemicals were obtained commercially and were used without further purification. − Column chromatography was carried out on silica gel S (0.063−0.2 mm). − UV/vis spectra were recorded on a Cary 5G spectrophotometer (Varian). − IR spectra were recorded on a Perkin−Elmer 577 spectrophotometer. − ^{1}H NMR: Bruker Aspect 3000 (300 MHz for ^{1}H), CD_2Cl_2 as solvent, TMS as internal reference. − MALDI mass spectra were obtained in time-of-flight linear mode on a Kratos Kompact MALDI 2 K probe apparatus (Kratos Analytical) operated through pulsed extraction of the ions. − Cyclic voltammetry data were obtained using an EG&G PAR 263A potentiostat galvanostat on a cell equipped with a double KCl (3 M) bridge. Measurements were made at room temperature in dichloromethane and acetonitrile solutions containing nBu$_4$NPF$_6$ as the supporting electrolyte at a scan rate of 100 mV/s, using platinum wire working and counterelectrodes and an Ag/AgCl reference electrode.

Tetrabutylammonium Salt of Nickel(III) Bis(2,3-thiophenedithiolate), nBu$_4$N[Ni(α-tpdt)$_2$] (2): To a stirred solution of potassium methoxide in methanol (10 mL, 2 M) was added 5,6-thieno[2,3-*d*]-1,3-dithiol-2-one (**1**) (100 mg, 0.57 mmol). The resulting yellow solution was filtered and the filtrate was added to a solution of nickel dichloride (107.7 mg, 0.29 mmol) in methanol (2 mL) yielding a red mixture. The inorganic precipitate was removed and the supernatant was added to a solution of tetrabutylammonium iodide (207.4 mg, 0.58 mmol) in methanol (1 mL). No visible change occurred while the solution was kept under an inert atmosphere. When it was stirred open to the air in an ice bath, the colour changed to green and a dark-green crystalline precipitate appeared. This solid was collected by filtration and recrystallized from acetone/2-propanol to afford dark-green, plate-like crystals. Stirring was maintained in all steps until no further modification was observed. Yield 151 mg (89%). − $C_{24}H_{40}NNiS_6$ (593.7): calcd. C 48.56, H 6.79, N 2.36, S 32.40; found C 49.01, H 6.51, N 2.38, S 32.93. − UV/vis (CH_3CN): $\lambda_{max.}$ = 672, 989 nm. − M.p. 130 °C (dec.). − IR (KBr): $\tilde{\nu}$ = 380, 390 (m, Ni−S), 500 (m), 700 (m), 780 (m), 875 (m), 1140 (s), 1345 (s), 1460 (m), 3035−3085 (m, C−H arom.). − MS: *m*/*z* (%) = 243 [M$^+$], 350 [M$^-$].

Decamethylferrocinium Salt of Nickel(III) 2,3-Thiophenedithiolate, [Fe(Cp*)$_2$][Ni(α-tpdt)$_2$] (3): Saturated solutions of nBu$_4$N[Ni(α-tpdt)$_2$] (30.8 mg, 52 μmol) and $[Fe(Cp^*)_2]BF_4$ (58.1 mg, 0.14 mmol) in acetonitrile were mixed under an inert atmosphere with stirring. Almost immediately, a dark-green crystalline precipitate appeared. This microcrystalline powder was then recrystallized from acetonitrile to afford dark-green plates. Crystals suitable for X-ray measurements were obtained by slow evaporation of the solvent from acetonitrile solutions. Yield 24 mg (69%). − $C_{28}H_{34}FeNiS_6$ (677.5): calcd. C 49.64, H 5.06, S 28.39; found C 49.71, H 6.00, S 28.16.

Decamethylferrocinium Salt of Gold(III) 2,3-Thiophenedithiolate, [Fe(Cp*)$_2$][Au(α-tpdt)$_2$] (4): This compound was obtained according to the same method as used to prepare **3**, using nBu$_4$N[Au(α-tpdt)$_2$] instead of nBu$_4$N[Ni(α-tpdt)$_2$]. Yellow-gold needle-shaped crystals were obtained in 76% yield. − $C_{28}H_{34}AuFeS_6$ (815.8): calcd. C 41.23, H 4.20, S 23.58; found C 40.72, H 4.28, S 23.51.

Decamethylcobaltocinium Salt of Nickel(III) 2,3-Thiophenedithiolate, [Co(Cp*)$_2$][Ni(α-tpdt)$_2$] (5): This compound was obtained according to the same method as used to prepare **3**, using $[Co(Cp^*)_2]PF_6$ instead of $Fe(Cp^*)_2BF_4$. Dark-green, plate-like crystals were obtained in 34% yield. − $C_{28}H_{34}CoNiS_6$ (680.6): calcd. C 49.42, H 5.04, S 28.26; found C 49.03, H 5.13, S 27.91.

EPR Spectroscopy: EPR spectra in the range 4−300 K were obtained with an X-band Bruker ESP 300E spectrometer equipped with an ER041XK microwave bridge, a rectangular cavity operating in T102 mode, a Bruker variable-temperature unit, an Oxford Instruments ESR-900 cryostat, and an ER 032M field controller system. The modulation amplitude was kept well below the line width and the microwave power well below saturation.

Magnetic Susceptibility: Magnetic measurements were performed using either a longitudinal Faraday system (Oxford Instruments) with a 7 T superconducting magnet for static susceptibility measurements in the range 2−300 K, or a Maglab 2000 system (Oxford Instruments) for DC magnetization and AC susceptibility at fields of up to 12 T at temperatures down to 1.5 K. The Faraday system was used with a magnetic field of 2 T and forward and reverse field gradients of 5 T/m. A polycrystalline sample (10−15 mg) was placed inside a previously calibrated thin-walled Teflon® bucket. The force was measured with a microbalance (Sartorius S3D-V). The Maglab 2000 system was used for magnetization measurements

of similar polycrystalline samples at different magnetic fields using an extraction technique, and for AC susceptibility measurements using an AC field of 1 Oersted.

X-ray Crystallographic Study: The crystal structure was solved by direct methods.[12] Non-hydrogen atoms were refined anisotropically. Hydrogen atoms were placed in calculated positions and refined as riding on their parent carbon atoms. Further details of the crystal structure determination are given in Table 2. Graphical representations were generated using ORTEP III[13] (Figure 4) and SCHAKAL-97[14] (Figure 5−Figure 7). Experimental details such as atomic coordinates, bond lengths, and angles are available as Supporting Information. Crystallographic data (excluding structure factors) for the structure of $Fe(Cp^*)_2[Ni(\alpha\text{-tpdt})_2]$ reported in this paper have been deposited with the Cambridge Crystallographic Data Centre under the depository number CCDC-152949. Copies of the data can be obtained free of charge upon application to CCDC, 12 Union Road, Cambridge CB2 1EZ, U.K. [Fax: (internat.) + 44-(0)1223/336033; E-mail: deposit@ccdc.cam.ac.uk].

Table 2. Crystallographic data for $[Fe(Cp^*)_2][Ni(\alpha\text{-tpdt})_2]$ (**3**)

Cmpd.	$Fe(Cp^*)_2[Ni(\alpha\text{-tpdt})_2]$
Crystal system	Monoclinic
Crystal colour/Shape	Dark-green plates
Space group	$P2_1/a$
Lattice constants [Å, °]	a = 15.443(3)
	b = 10.237(1)
	c = 20.360(2)
	β = 107.54(1)
Volume [Å^3]	3069.1(7)
Z	4
Empirical formula	$C_{28}H_{34}FeNiS_6$
Molecular mass	677.47
Density (calcd.) [Mg/m^3]	1.466
Absorption coefficient [mm^{-1}]	1.511
F(000)	1408
Diffractometer	Enraf−Nonius CAD4
Wavelength	Mo-K_α (0.71069 Å)
T [K]	293(2)
θ range[°]	2.10 to 27.04
Index range (h,k,l)	−19/1, −1/13, −25/26
Scan type	ω−2θ
Program for data collection	CAD4 software
Data reduction	Process-MOLEN
No. of collected reflns.	8208
No. of independent reflns.	6640
Max. and min. transmission	0.9996/0.9172
Structure solution	Direct methods
Structure refinement	Full-matrix least-squares
Programs used	SHELXS-86
	SHELXL-97
Goodness-of-fit on F^2	1.026
No of refined parameters	328
R [$I > 2\sigma(I)$]	0.0976
wR_2 [$I > 2\sigma(I)$]	0.1215

Acknowledgments

This work was partially supported by the Fundação para a Ciência e Tecnologia (Portugal) under contracts PRAXIS XXI 2/2.1/QUI/203/94 and POCTI/1999/QUI/35452 and by the Comisión Interministerial de Ciencia y Tecnología (MAT2000-1388-C03-01) and the Generalitat de Catalunya (2000SGR-00114) (Spain). The collaboration between the team members of Sacavém and Barcelona was supported under the CSIC-ICCTI bilateral agreement and by COST action D14.

[1] [1a] J. A. McCleverty, *Prog. Inorg. Chem.* **1968**, *10*, 29. − [1b] D. Coucouvanis, *Prog. Inorg. Chem.* **1970**, *11*, 233. − [1c] R. Eisenberg, *Prog. Inorg. Chem.* **1970**, *12*, 295. − [1d] L. Alcácer, H. Novais, in: *Extended Linear Chain Compounds*, Vol. 3 (Ed.: J. S. Miller), Plenum Press, New York, **1983**, chapter 6, p. 319. − [1e] S. Alvarez, R. Vicente, R. Hoffman, *J. Am. Chem. Soc.* **1985**, *107*, 6253−6277.

[2] [2a] A. E. Underhill, M. Ahamadà, *J. Chem. Soc., Chem. Commun.* **1981**, 67−68. − [2b] M. M. Ahamad, D. J. Turner, A. E. Underhill, C. S. Jacobsen, K. Mortensen, K. Carneiro, *Phys. Rev. B* **1984**, *29*, 4796.

[3] P. Cassoux, L. Valade, in: *Inorganic Materials*, 2nd edn. (Eds.: D. W. Bruce, D. O'Hare), John Wiley and Sons, Chichester, **1996**, p. 1−64.

[4] P. Cassoux, J. S. Miller, in: *Chemistry of Advanced Materials* (Eds.: L. V. Interrante, M. J. Hampden-Smith) Wiley-VCH, New York, **1998**, p. 19−72.

[5] I. D. Parker, R. H. Friend, P. I. Clemenson, A. E. Underhill, *Nature (London)* **1986**, *324*, 547−548.

[6] [6a] V. Gama, D. Belo, S. Rabaça, I. C. Santos, H. Alves, M. T. Duarte, J. C. Warenborg, R. T. Henriques, *Eur. J. Inorg. Chem.* **2000**, *9*, 2101−2110; W. E. Broderick, J. A. Thompson, B. M. Hoffman, *Inorg. Chem.* **1991**, *30*, 2958−2960. − [6b] V. Gama, S. Rabaça, C. Ramos, D. Belo, I. C. Santos, M. T. Duarte, *Mol. Cryst. Liq. Cryst.* **1999**, *335*, 81−90.

[7] D. Belo, H. Alves, E. B. Lopes, M. T. Duarte, V. Gama, R. T. Henriques, M. Almeida, A. Pérez-Benítez, C. Rovira, J. Veciana, *Chem. Eur. J.* **2001**, *7*, 511−519.

[8] W. E. Broderick, J. A. Thompson, M. R. Godfrey, M. Sabat, B. M. Hoffman, *J. Am. Chem. Soc.* **1989**, *111*, 7656−7659.

[9] C. Mahadevan, M. Seshasayer, P. Kuppusamy, P. T. Manoharan, *J. Cryst. Spectrosc. Res.* **1985**, *15*, 305−316.

[10] E. Ribera, C. Rovira, J. Veciana, J. Tarrés, E. Canadell, R. Rousseau, E. Molins, M. Mas, J.-P. Schoeffel, J.-P. Pouget, J. Morgado, R. T. Henriques, M. Almeida, *Chem. Eur. J.* **1999**, *5*, 2025−2039.

[11] J. S. Miller, J. C. Calabrese, H. Rommelmann, S. R. Chittipeddi, J. H. Zhang, W. M. Reiff, A. J. Epstein, *J. Am. Chem. Soc.* **1987**, *109*, 769−781.

[12] [12a] G. M. Sheldrick, *Acta Crystallogr., Sect. A* **1990**, *46*, 467. − [12b] G. M. Sheldrick, *SHELXL-93 − Program for the Refinement of the Crystal Structures*, University of Göttingen, Germany, **1993**. − [12c] G. M. Sheldrick, *SHELXL-97 − Program for the Refinement of the Crystal Structures*, University of Göttingen, Germany, **1997**, release 97−2.

[13] P. McArdle, *J. Appl. Cryst.* **1995**, *28*, 65.

[14] E. Keller, *SCHAKAL-97 − A Computer Program for the Graphical Representation of Molecular and Crystallographic Models*, Krystallographisches Institut der Universität Freiburg, Hebelstrasse 25, D-79104 Freiburg, Germany.

Received July 5, 2001
[I01251]

A New Trinuclear Oxovanadium(V) Complex with DMPP Ligands – Synthesis and Structural Characterization in the Solid State and in Aqueous Solution

Fernando Avecilla,*[a] Carlos F. G. C. Geraldes,[b,c] and M. Margarida C. A. Castro*[b,c]

Keywords: Oxo ligands / Vanadium / N ligands / NMR Spectroscopy / Cluster compounds

A new trinuclear oxovanadium(V) complex with the anionic dmpp ligand (Hdmpp = 3-hydroxy-1,2-dimethyl-4-pyridinone), $[V_3O_6(dmpp)_3(H_2O)](H_2O)_2$, was isolated from the reaction of Hdmpp, KOH and sodium metavanadate at pH 4.5. The solid state structure of the $[V_3O_6(H_2O)(dmpp)_3](H_2O)_2$ complex, investigated by X-ray diffraction methods, was found to contain a cyclic trinuclear metal cluster. This complex crystallises in the monoclinic system: $P2_1/n$, a = 9.5324(7) Å, b = 16.4107(11) Å and c = 18.0638(12) Å, β = 91.1010(10)°, V = 2825.3(3) Å^3, Z = 4 and $R_1(wR_2)$ = 0.0704 (0.2025). Two of the vanadium atoms (V1 and V3) are six-coordinated, with distorted octahedral geometries, and the other one (V2) is five-coordinated with a distorted square pyramidal geometry. The cyclic V_3O_4 framework has one oxygen atom bridging two vanadium atoms in two V–O–V groups, V1–O4–V2 and V2–O5–V3, and two oxygens bridging the V1–V3 atoms, V1–O6–V3 and V1–O12–V3. IR data confirm the crystallographic results, showing the characteristic V=O band in the 973–935 cm^{-1} frequency range. This compound has three bands corresponding to V=O stretching, indicative of different chemical environments around the vanadium atoms in the solid state. The ES mass spectrum in aqueous solution displays an intense peak corresponding to the $[V_3O_6(dmpp)_3(H_2O)+2H^+]^{2+}$ fragment. ^{51}V and ^1H NMR spectroscopy were used to study this complex in aqueous solution. The dissolution of the crystalline $[V_3O_6(dmpp)_3(H_2O)](H_2O)_2$ compound in water, under aerobic conditions at pH 4.2, gave one intense broad signal at δ = –490 in the ^{51}V NMR spectrum, which is attributed to a major species present in solution. The observation of only one ^{51}V NMR signal, instead of the three expected from the different chemical environments of each vanadium atom present in the solid, is consistent with a fast (in the NMR timescale) dynamic equilibrium equalising their environments. This involves a fast exchange between O8, O10 and O12 as mono- or bifunctional oxygen atoms, as well as the H_2O molecule, which acts in another fast equilibrium coordinating the vanadium atom that has a dmpp ligand with one bifunctional oxygen atom. The trinuclear oxovanadium(V) complex is relatively stable in water in the pH range 2.5–5.0. However, dissociation of the complex occurs at higher pH, leading to various hydrolysis products, which include mononuclear complex species with 1:1 and 1:2 metal-to-ligand stoichiometries, and monomeric and oligomeric species of free vanadium(V).

Introduction

Vanadium inorganic salts like sodium metavanadate and vanadyl sulfate have demonstrated insulino-mimetic effects in a variety of tissues.[1] However, due to their poor absorption, high doses of these salts are required and toxicity occurs. For this reason, they are not used in the treatment of diabetes, although some recent clinical studies were carried out with oral administration of these compounds in very low concentrations.[2–4] The insulino-mimetic properties exhibited by vanadium (V^{IV} and V^V) have led to an intensive search for a vanadium complex to be used as an effective oral substitute of insulin. The complex bis-maltolato-oxovanadium ^{IV} (BMOV)[5,6] seems to be, at present, one of the most promising compounds in this field. The ligand 3-hydroxy-1,2-dimethyl-4-pyridinone (Hdmpp) (see chemical structure in Scheme 1), currently used in the treatment of iron-overload under the name deferiprone,[7] forms a V^{IV} complex which, although not as soluble as BMOV, allows the optimization of the lipophylic-hydrophylic balance by changing the substituent group at the N atom, thus controlling its absorption into the cells.[8,9]

Oxovanadium complexes are attracting interest due to their biological relevance[10,11] as insulino-mimetics, as models of the vanadium coordination modes in biological systems (haloperoxidases, amavadine, tunichrome),[12] due

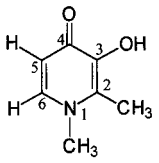

Scheme 1

[a] Departamento de Química Fundamental, Universidade da Coruña,
Campus de A Zapateira s/n 15071, A Coruña, Spain
[b] Departamento de Bioquímica, Faculdade de Ciências e Tecnologia, Universidade de Coimbra,
Apartado 3126, 3000 Coimbra, Portugal
[c] Centro de Neurociências, Universidade de Coimbra,
3000 Coimbra, Portugal

Supporting information for this article is available on the WWW under http://www. eurjic.com or from the author.

 © WILEY-VCH Verlag GmbH, 69451 Weinheim, 2001 1434–1948/01/1212–3135 $ 17.50+.50/0

to their effects on the activity of several enzymes,[13,14] and also due to their application as catalysts.[15]

Vanadium(IV) and vanadium(V) coordinate polydentate ligands, with N and O donor atoms in most cases, resulting in complexes of different stoichiometries and structures depending on ligand design, pH, metal-to-ligand ratio and total vanadium concentration.[16–18] The vanadium(V) species present in solution have been largely identified by potentiometric[19,20] and combined potentiometric/^{51}V NMR spectroscopic[21] studies, and vanadium(IV) species have been studied by EPR spectroscopy as well.[22] The solid state structures of vanadium complexes have been determined by using X-ray crystallography[23] and EXAFS.[8] Vanadium(V), in particular, has stereochemically flexible coordination geometries ranging from tetrahedral and octahedral to trigonal pyramidal and pentagonal bipyramidal, which are thermodynamically plausible.[24] It can also form mono- and polynuclear[25] oxovanadium complexes.

The biological properties of vanadium complexes are strongly dependent on their solution structures. The examination of the structural and chemical selectivity of complexes with di- or polyfunctional ligands[26–34] is an important contribution to understanding the modes of action of vanadium in biological systems.[35,36] Thus, the study of their behaviour in an aqueous medium at different pH values is necessary to obtain the structures of the different species, as well as their thermodynamic and kinetic stabilities.[37] In this work, we report the synthesis and structural characterisation, both in the solid state and in aqueous solution, of a new oxovanadium(V) complex containing three anionic dmpp ligands and a cyclic trinuclear cluster.

Results and Discussion

Synthesis of the Complex $[V_3O_6(dmpp)_3(H_2O)](H_2O)_2$

3-Hydroxy-1,2-dimethyl-4-pyridinone (0.174 g, 1.25 mmol) in 5 mL of water was added to KOH (0.07 g, 1.25 mmol) in 5 mL of water and sodium metavanadate (0.169 g, 1.25 mmol)in 5 mL of water. The pH was raised to 4.5 with a solution 2 M HCl. The black crystals, which came out of solution, were isolated by filtration and dried under *vacuum*. The yield was 0.160 g (48% based on V). Anal. Calcd. (found) for $C_{21}H_{30}O_{15}N_3V_3$: calcd. C 35.2 (34.9), H 4.2 (4.1), N 5.9 (5.8). ES mass spectrum, $[V_3O_6(C_7H_9O_2N)_3(H_2O) + 2\,H^+]^{2+}$: $m/z = 342$.

IR Spectroscopic Data

The IR spectrum of the complex $[V_3O_6(dmpp)_3(H_2O)](H_2O)_2$ obtained in KBr pellets showed the characteristic V=O band in the frequency range 973–935 cm^{-1}. This compound exhibits three bands corresponding to V=O stretching, indicative of a different chemical environment around the vanadium atoms in the solid state. In addition, the V–O–V stretching modes were observed at about 640–510 cm^{-1}, in agreement with those reported in the literature.[38] The spectrum exhibits a set of four bands in the 1625–1450 cm^{-1} range, characteristic of pyridinones.[39]

IR spectroscopy provides information on the ligands chelated to the vanadium atoms but is less informative about the nuclearity of the complex.

Crystallographic Results

The X-ray crystal structure with an atomic numbering scheme for the crystalline $[V_3O_6(dmpp)_3(H_2O)](H_2O)_2$ complex is shown in Figure 1 and the bond lengths and angles are in Table 2. It contains a cyclic trinuclear oxovanadium(V) complex, $[V_3O_6(dmpp)_3(H_2O)]$, with three anionic dmpp ligands, three oxo groups, three oxygen atom bridges and one H_2O molecule. The other two H_2O molecules are included in the asymmetric unit. Oxygen atom bridges link the three vanadium atoms and each one is coordinated to one oxo group. Two vanadium atoms (V1 and V3) are six-coordinated, exhibiting a distorted octahedral geometry and one (V2) is five-coordinated with a distorted square pyramidal geometry, with the vanadium atom (V2) 0.4197 Å from the basal plane defined by O4, O5, O9 and O10 (Figure 2). In addition to the oxo group, V1 is chelated by three dmpp oxygen atoms (O7, O8 and O12, this one acting as a bridging atom between V3 and V1), V2 and V3 are chelated by two dmpp oxygen atoms (V2 by O9 and O10, V3 by O11 and O12). The V3 atom is also coordinated to one H_2O molecule.

All the vanadium atoms have a strong V=O bond, and the values for the V1–O1, V2–O2 and V3–O3 distances are compatible with those found in other similar structures.[23] This complex has a dmpp oxygen atom (O12 in V3) that is *trans* and five dmpp oxygen atoms (O7 and O8 in V1, O9 and O10 in V2, and O11 in V3) that are *cis* relative to the strong V=O bond in each vanadium atom.[25,40–42] The dmpp oxygen atoms belonging to the enolic groups are deprotonated (O7, O9 and O11). The V3–O12 bond is longer than the V–O bonds to the other

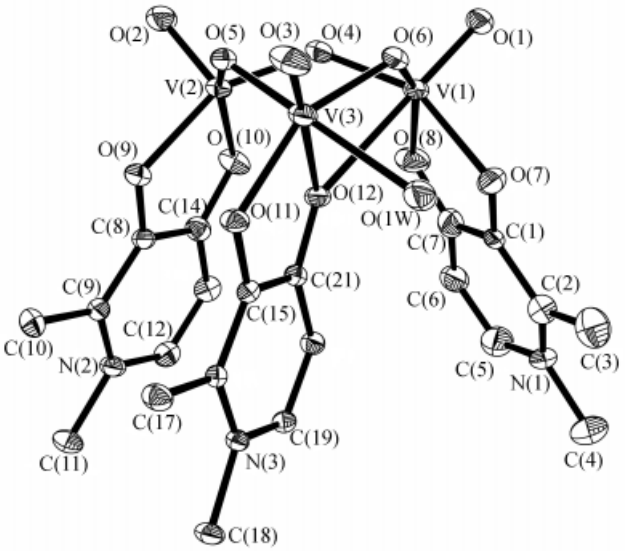

Figure 1. X-ray crystal structure of the complex $[V_3O_6(dmpp)_3(H_2O)]$ showing the atomic numbering scheme. Hydrogen atoms have been omitted for simplicity. The ORTEP plot is at the 30% probability level.

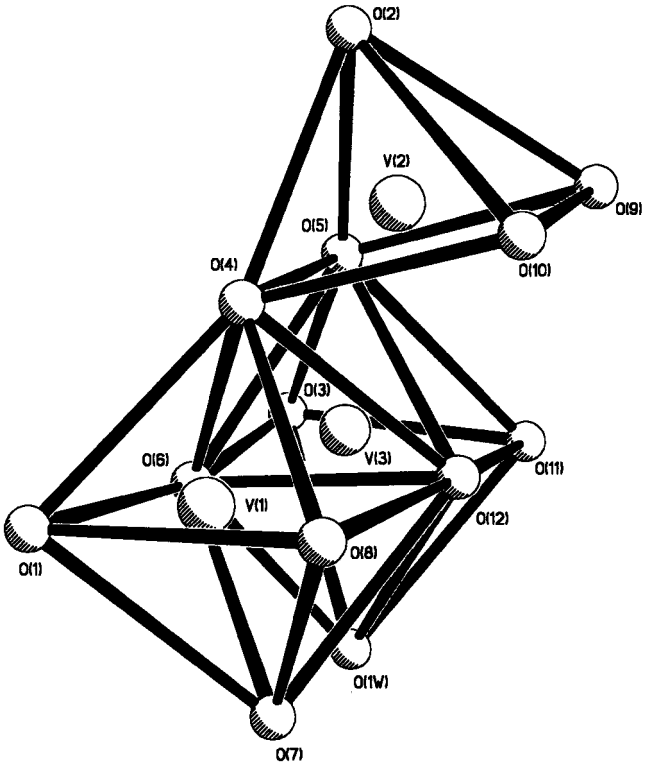

Figure 2. Coordination polyhedron in the crystal structure of the vanadium cluster in trimeric species $[V_3O_6(dmpp)_3(H_2O)]$.

ketonic groups, V1−O8 and V2−O10, (V1−O8 [2.008(4) Å], V2−O10 [2.004(4) Å] and V3−O12 [2.204(4) Å]. In addition, all these V−O bond lengths are longer than those to the enolate groups (V1−O7 [1.980(4) Å], V2−O9 [1.962(3) Å] and V3−O11 [1.909(3) Å].[43] These bond length values are all in the range of the bond lengths reported in the literature for other known polynuclear vanadium(V) complexes.[25,40−43]

The trinuclear complex contains the cyclic V_3O_4 framework.[23] This framework exhibits only one oxygen bridging two vanadium atoms in two V−O−V groups, V1−O4−V2 and V2−O5−V3, and two oxygens bridging the V1−V3 atoms, the oxo bridge V1−O6−V3 and the formal ketonic oxygen atom O12 of one dmpp. From the X-ray results one could not unambiguously distinguish between a keto-O12 and an enolate-O12 structure for this bifunctional binding group, as the C−O bond lengths to the formal keto and enolate oxygens in each C−O−V−O−C cycle are almost the same (eg. C21−O12 [1.309(5) Å], C15−O11 [1.336(5) Å], for the V3 cycle). It is possible that the π electronic cloud is delocalized among all the atoms that form each C−O−V−O−C cycle, giving an intermediate character to all the formal ketonic and enolic oxygen atoms of each dmpp. As expected, the doubly bridging dmpp oxygen atom (O12) gives V−O bond lengths [2.204(3), 2.450(3) Å] longer than the V−O distance for the bridging oxygen atoms (O6) [1.794(3), 1.857(3) Å]. The average value of the V−O−V bond lengths (V1−O4−V2, V2−O5−V3 and V3−O6−V1) is 1.82(3) Å, which is similar to that obtained for other polynuclear vanadium compounds.[44−46]

The three V−O−V bond angles, in the cyclic V_3O_4 framework, involving single bridging oxygen atoms are very similar (V1−O4−V2 = 125.61(18)°, V2−O5−V3 = 120.39(17)° and V1−O6−V3 = 119.22(17)°]. The V−O−V bond angle in the V1−O12−V3 fragment [84.98(10)°] is quite different.

Figure 3 shows an upper view of the complex along an axis perpendicular to the pseudo-plane defined by the three vanadium atoms, illustrating how the complex has lost C_{3v} symmetry. The anionic dmpp ligand bound to V3 has rotated relative to the equivalent positions of the other two ligands in the cluster, becoming almost parallel to the dmpp ligand at V2 and perpendicular to the one at V1. Its O12 oxygen binds to V1, and V3 binds a water molecule in a *cis* position relative to V3=O3, pointing outwards. V2 keeps the five coordination, as an extra water molecule *trans* to V2=O2 would be sterically hindered by the opposing dmpp ring. The methyl group at V3 points outwards, and those at V1 and V2 point t*rans* to one another.

Solution Studies

The behaviour of the crystalline compound $[V_3O_6(dmpp)_3(H_2O)](H_2O)_2$ in aqueous solution and in the presence of oxygen was investigated using ^{51}V and ^{1}H NMR and EPR spectroscopy. A freshly prepared 2 mM aqueous solution of the crystalline complex, with pH = 4.2, was grey in colour. Immediately after its preparation, this solution gave no EPR signal (data not shown), showing that all three the vanadium atoms present in the crystalline structure were in the +5 oxidation state. The ^{51}V NMR spectrum of this solution (Figure 4b) shows one single

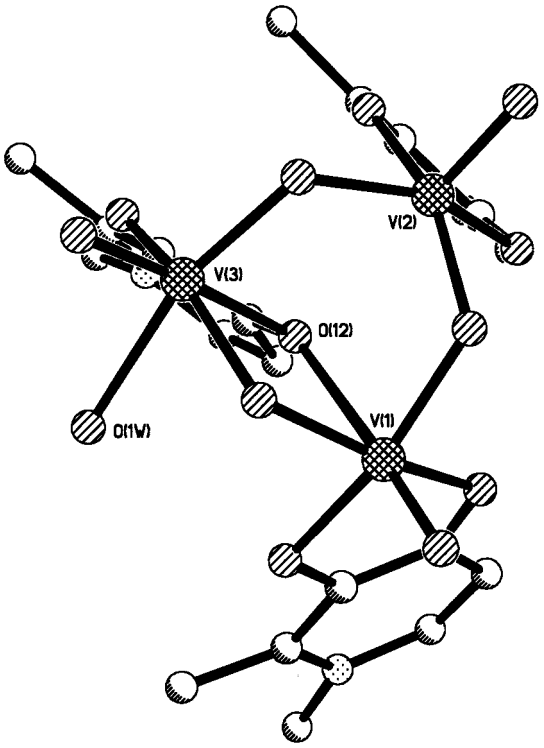

Figure 3. Upper view of the complex $[V_3O_6(dmpp)_3(H_2O)]$.

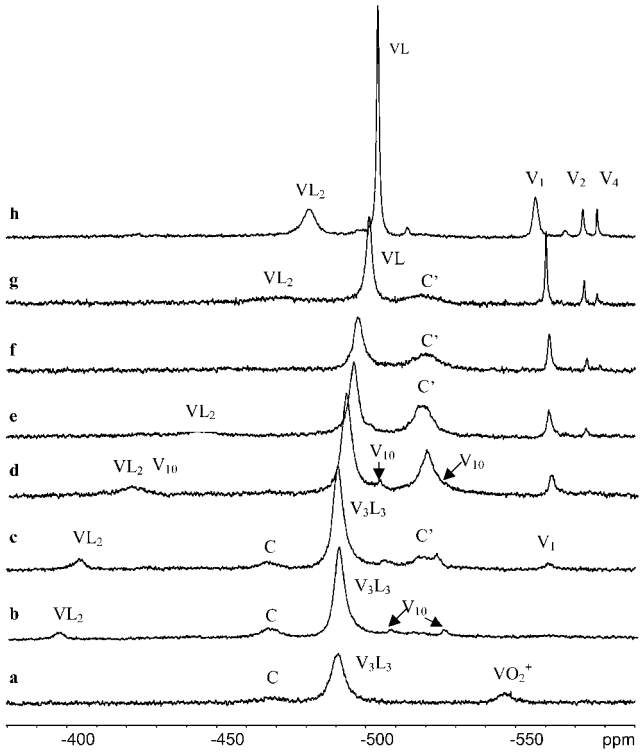

Figure 4. ^{51}V NMR spectra, at 22.0 ± 0.5 °C, of a freshly prepared 2 mM aqueous solution of the crystalline complex $[V_3O_6(dmpp)_3(H_2O)](H_2O)_2$ under aerobic conditions at a) pH = 2.8; b) pH = 4.2; c) pH = 4.7; d) pH = 5.6; e) pH = 6.1; f) pH = 6.4; g) pH = 6.9; h) pH = 7.8.

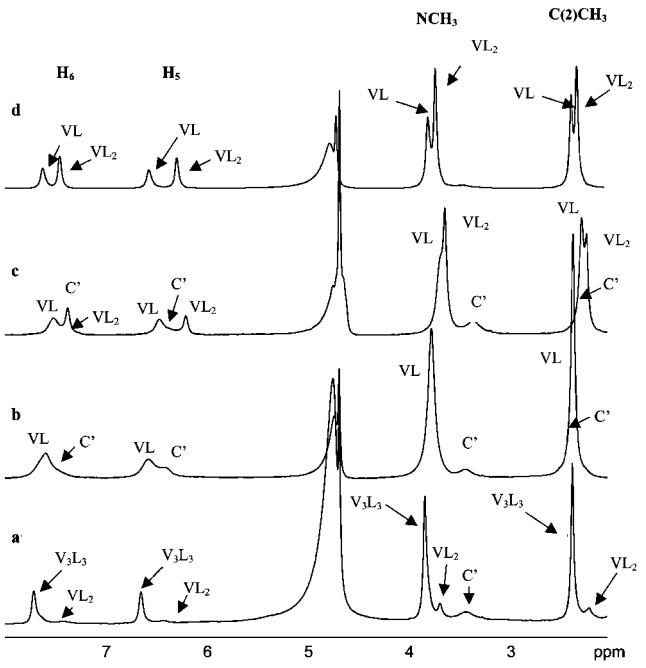

Figure 5. ^{1}H NMR spectra, at 22.0 ± 0.5 °C, of a freshly prepared 2 mM D_2O solution of the crystalline complex $[V_3O_6(dmpp)_3(H_2O)](H_2O)_2$ under aerobic conditions at a) pH = 3.6; b) pH = 5.3; c) pH = 6.8; d) pH = 8.4.

broad signal at δ = −490 (line width of 525 Hz), assigned to the cyclic trimer $[V_3O_6(dmpp)_3(H_2O)]$ (V_3L_3) as the major species present in solution. The observation of only one ^{51}V NMR signal, instead of the three expected from the different chemical environments of each V-dmpp unit present in the crystal structure, reflects the increased effective symmetry acquired by the cyclic trimer species in solution. The equivalence of its three monomer units should result from the presence of a dynamic equilibrium in solution in fast exchange conditions (in the NMR timescale). In this equilibrium, the dmpp ligand oxygen atoms bridging between two vanadium atoms of the cluster (O12 bridge between V1 and V3, O8 between V1 and V2 and O10 between V2 and V3) change their coordination between mono- and bifunctional when the compound is dissolved in water. On the other hand, the H_2O molecule acts in another fast equilibrium, coordinating the vanadium atom that has a dmpp ligand with one bifunctional oxygen atom. Thus, the presence of the polydentate oxygen donor anionic ligand (dmpp) allows the oxygen atoms to act as monofunctional or bifunctional donors.[23] The ES spectrum of the trimer in aqueous solution at pH = 4.3 exhibits an intense peak *m*/*z* = 342, corresponding to the cationic complex $[V_3O_6(dmpp)_3(H_2O)+2H^+]^{2+}$.

Additional studies of the trinuclear oxovanadium(V) complex in solution were carried out in order to investigate its stability as a function of pH, using ^{51}V (Figure 4) and ^{1}H (Figure 5) NMR spectroscopy. These spectra were compared with ^{51}V and ^{1}H NMR spectra of aqueous solutions of vanadate and dmpp at different pH and metal-to-ligand ratios (see illustrative examples at Figure 6). Figure 4 shows ^{51}V NMR spectra of a 2 mM aqueous solution of the crystalline complex at different pH values. These spectra were assigned by comparison with the ^{51}V NMR spectra of the vanadate/ dmpp aqueous solutions at the same pH values, as well as on the basis of literature data.[9,21c,27] The spectral features indicate that in the pH range 2.8−5.3 the major species present in solution is the trimer $[V_3O_6(dmpp)_3(H_2O)]$, corresponding to the dominant ^{51}V NMR peak, with very small shift changes with pH, from δ = −488 (pH 2.8−3.6) to δ = −490 (pH 3.9−5.3). Some low intensity signals are also present in the ^{51}V NMR spectra in this pH range (see Figure 4a−c), which correspond to very minor species in solution. Some of these are free vanadium(V) species: dioxovanadium(V) cation (VO_2^+), δ = −543 [21c] at pH 2.8, the monovanadate (V_1), δ = −560[21c] at pH 4.7, and two of the three decavanadate (V_{10}) signals, δ = −506 and δ = −523 [27] at pH 4.2 and 4.7. At pH < 3.9, the cyclic trimer is practically the only complex present in solution (besides the species C). However, above this pH value, a small signal of the mononuclear 1:2 complex (VL_2) is also seen at high frequency (δ = −396 and δ = −405 at pH 4.2 and 4.7, respectively). According to previous studies, this complex occurs at this pH range predominantly in its monoprotonated form $[VO_2H(dmpp)_2]$.[9] At these pH values a small resonance (VL) of the mononuclear 1:1 $[VO_2(dmpp)(H_2O)_2]$ complex, if present, is hidden by the signal of the trinuclear cationic complex.[9] Its ^{51}V shift at pH 2.8−4.7 is δ = −491, and at pH 5.3 is δ = −494 (see Figure 6a). A broad signal at δ = −468 is also

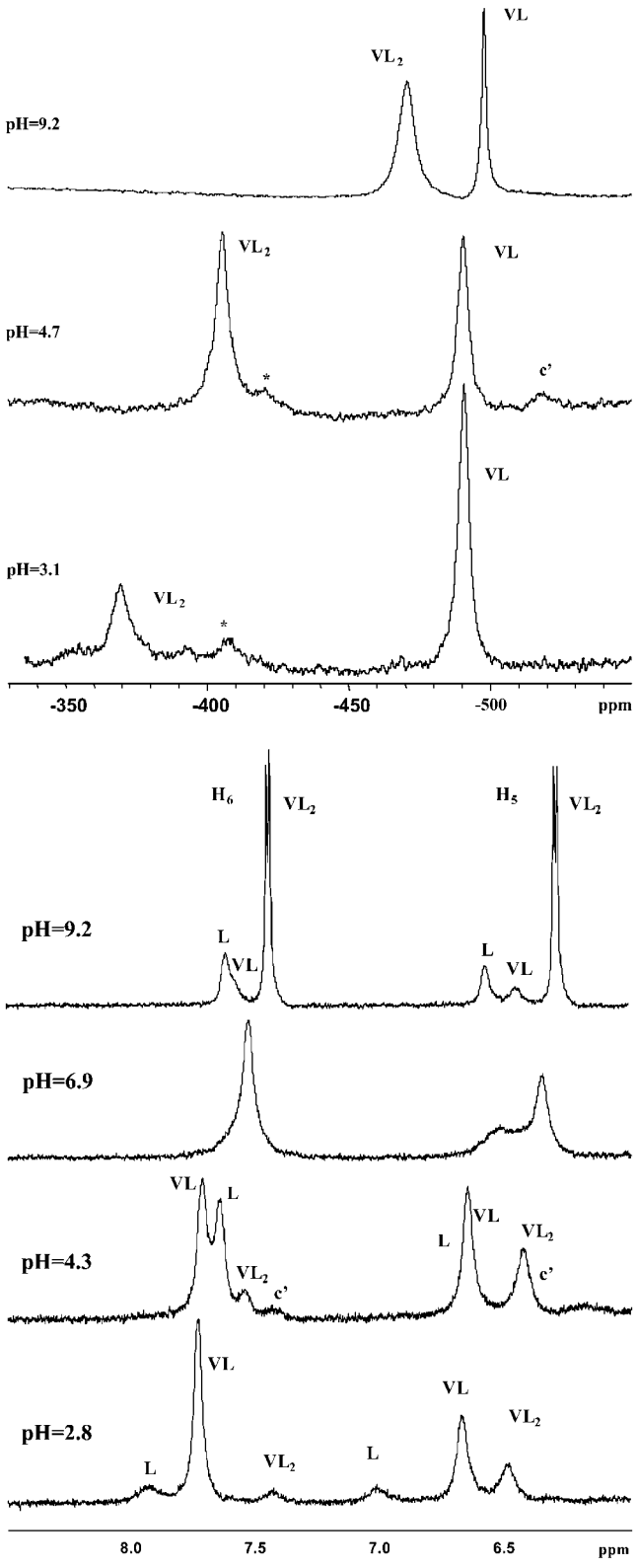

Figure 6. ^{51}V (top) and ^{1}H (bottom) NMR spectra, at 22.0 ± 0.5 °C, of a 3 mM: 6 mM vanadate-dmpp solution at different pH values.

seen between pH 2.8 and 5.3, corresponding to another complex labelled as C, and a new signal at δ = −519 appears at pH > 3.9, corresponding to another complex, labelled as C′. Both complexes C and C′ were not characterised.

Above pH 5.3 (Figure 4d−h), decomposition of the trinuclear oxovanadium(V) complex takes place, which is replaced by the two mononuclear complexes VL and VL_2, whose ^{51}V NMR resonances are shifted to lower frequency when the pH increases, as they become deprotonated.[9] From pH 5.6 to 7.8, the ^{51}V shifts of VL and VL_2 change from δ = −493 and δ = −424 to δ = −504 and δ = −480, respectively. The signal of complex C disappears at pH 5.6 and the signal at δ = −519, corresponding to complex C′, reaches a maximum intensity at pH ≈ 6 and disappears at pH 7.8. The signals of decavanadate stay very small (Figure 4d,e) and new resonances corresponding to other free vanadium(V) oligomeric species also appear: the divanadate V_2 (δ = −572) and tetravanadate V_4 (δ = −578) (Figure 4f−h). Above pH 7 the colour of the solution changes to yellow and at pH 7.8 only the signals corresponding to the mono- (δ = −556), di- (δ = −572) and tetravanadate (δ = −577) species, and those assigned to the two mononuclear complexes VL (δ = −504) and VL_2 (δ = −480) are observed. According to previous studies, these complexes occur at this pH in their deprotonated forms $[VO_2(dmpp)(H_2O)(OH)]^-$ and $[VO_2(dmpp)_2]^-$, respectively.[9]

^{51}V NMR spectra of aqueous solutions of vanadate and dmpp were obtained as a function of pH in the 2.3 to 9.2 range, at 3 mM vanadate concentrations and at 1:1, 1:2 and 1:5 metal-to-ligand ratios. Figure 6 (top) shows a few illustrative examples at the 1:2 ratio. VL and VL_2 predominate over the entire pH and metal-to-ligand ranges studied, and their shifts change with pH in accordance with what was found in the trimer solution. In the pH range 2.3−6.9, their intensities are much higher in the spectra of the vanadate-dmpp mixtures than in those of the trimer. Complex C′ (at δ = −519) is also present between pH 4.0 and 6.4, but complex C (at δ = −468) is not, as it is only present in vanadate/dmpp mixtures with excess vanadate (data not shown). Although this observation points to the possibility that C may be a dimeric complex, the characterisation of complexes C and C′, as well as of the signals at δ = −420 to −405 and at δ = −350, observed at acid pH [see Figure 6 (top)], and the detailed interpretation of the pH dependence of the ^{51}V shifts of the VL and VL_2 complexes in terms of the species previously observed by potentiometry[9] will be the subject of a future publication.

^{1}H NMR spectra were also obtained from a 2 mM D_2O solution of the crystalline complex at different pH values (Figure 5). These spectra were assigned by comparison with those of solutions of vanadate and dmpp, at 3 mM vanadate concentrations and at 1:1 and 1:2 metal-to-ligand ratios, obtained as a function of pH [see Figure 6 (bottom), for some representative spectra] and by comparison of the intensities of the ^{51}V and ^{1}H signals of the different complexes. The spectrum at pH 3.6 (Figure 5a) shows four intense signals (H_6 at δ = 7.72, H_5 at δ = 6.66, N−CH_3 at δ = 3.86 and C(2)−CH_3 at δ = 2.40, data not shown) from the trinuclear complex V_3L_3, the major species in solution. The symmetry

of the spectrum again reflects the equivalence of the three monomer units in solution. These signals are in slow exchange on the NMR timescale with the very weak signals from the complexes VL_2 and C. The signals of the V_3L_3 complex are shifted to higher frequencies relative to the respective signals of the free Hdmpp ligand at pH 7 (H_6 at $\delta = 7.53$, H_5 at $\delta = 6.41$, $N-CH_3$ at $\delta = 3.68$ and $C(2)-CH_3$ at $\delta = 2.30$, data not shown), due to complexation. However, the trimer has very similar shifts to the 1:1 monomer VL [see Figure 6 (bottom)], possibly because the coordination of the V^V ion is similar in both compounds and the relative orientations of the pyridinone rings in the trimer, near the edge of their respective dipolar shift cones, lead to negligible intramolecular ring current effects. At pH 5.3, the signals broaden and the spectrum (Figure 5b) is quite similar to that of a 1:1 vanadate/ dmpp solution, except for the relative intensities of the complexes present, in agreement with dissociation of the complex and the presence of the mononuclear complexes resulting from its hydrolysis, with relative intensities $VL > C' >> VL_2$. At pH 6.8 (Figure 5c) the signals of the complexes present, $VL > VL_2 >> C'$, start to sharpen and at pH 8.4 (Figure 5d) only the VL and VL_2 complexes are present. The protons of the VL_2 complex are shifted to lower frequency relative to those of the VL complex, due to the mutual effect of the pyridinone ring currents in an octahedral complex. Comparison with the ^1H NMR spectra of free Hdmpp solutions at the same pH values showed that no free ligand could be detected at any pH studied. The results from ^1H NMR spectroscopy are, therefore, in good agreement with those obtained by ^{51}V NMR spectroscopy.

Figure 6 (bottom) shows the aromatic region of the ^1H NMR spectra of a 3 mM:6 mM vanadate-dmpp solution at some of the pH values between 2.8 and 9.2. At this metal-to-ligand ratio of 1:2, it was found that, while at pH 2 to 2.8 the relative concentrations of the species are $VL >> VL_2 \approx L$, at pH 4 to 5 VL decreases and L increases, so that $VL \approx L > VL_2 >> C'$. Above pH 5, L and VL decrease and VL_2 becomes the dominant species. The complex C′ is only present in the range of pH 4.0 to 5.6, and complex C is not detected at low pH. For a 1:1 metal-to-ligand ratio (3 mM: 3 mM vanadate-dmpp, data not shown), VL is the dominant species at pH 2 (92%), with $VL >> VL_2$, and VL slowly decreases its percentage up to pH 5 (80% VL), with $VL >> VL_2 > C'$. Above pH 5, VL continues to decrease, VL_2 increases more sharply and C′ disappears. The detailed interpretation of the pH dependence of the distribution of the VL and VL_2 species by NMR spectroscopy and potentiometry[9] will be presented in a future publication.

Thus, the differences observed in the ^{51}V and ^1H NMR spectra of a V_3L_3 solution and a vanadate-dmpp 1:1 solution in the pH range of 2.5−5.0, where the trimer is stable in solution, can be summarised as follows: slightly different ^{51}V shifts of V_3L_3 and VL, sharper proton resonances of VL at the same pH values, smaller relative intensity of VL_2 and larger relative intensity of C′ in the trimer solution, and presence of species C at low pH in the trimer solution, which is not present in the vanadate-dmpp 1:1 solution.

The stability of the solution structure of the trinuclear complex at pH 4.2 with time was also studied by ^{51}V NMR spectroscopy. The spectra obtained (see Supporting Information, Figure 1S) show that there are no changes in the signal corresponding to the $[V_3O_6(dmpp)_3(H_2O)]$ complex (see Figure 4b), even 5 days after the dissolution of the crystalline compound in water and in the presence of oxygen, which indicates that the structure of the trinuclear oxovanadium(V) complex is stable in solution at this pH. The low intensity signals also present decrease their intensity somewhat.

Thus, we can conclude that the major species resulting from the dissolution of the crystalline compound in water, under aerobic conditions and at pH 2.5−5.0, is a trinuclear oxovanadium(V) cationic complex, which is relatively stable in this pH range. However, when the pH increases above 5.0, dissociation of the complex takes place with the appearance in solution of various hydrolysis products, including free V^V oligomeric species and the mononuclear V^V species with metal to ligand ratios of 1:1 and 1:2.

Experimental Section

Reagents: Sodium metavanadate, $NaVO_3$, and the ligand 3-hydroxy-1,2-dimethyl-4-pyridinone (Hdmpp) were purchased from Sigma and ACROS Organics, respectively, and used without further purification. D_2O (99.9 atom% D), DCl and NaOD were obtained from Cambridge Isotope Laboratories. All the experiments were carried out in aqueous solution and under aerobic conditions.

Methods: IR Spectroscopy: Vibrational spectra were obtained in potassium bromide pellets on a Bruker Vector 22 MIR spectrometer. − Elemental Analysis: Analyses for C, H and N were performed using a Carlo Erba EA 1108 elemental analyser. − Mass Spectrometry: A mass spectrum was obtained in aqueous solution on a LC/NS Mass Spectrometer Finnigan Navigator with ES(+) ion mode and direct injection. − NMR Spectroscopy: ^{51}V and ^1H NMR spectra were recorded on a Varian Unity-500 Spectrometer operating at 131.404 MHz and 499.824 MHz, respectively, using a 5 mm broad band probe, at 22.0±0.5 °C. The pH of the D_2O solutions was adjusted with DCl and CO_2-free NaOD using a Crison MicropH 2002 pH-meter with an Ingold 405-M5 combined electrode. ^{51}V NMR chemical shifts were externally referenced to a $VOCl_3$ solution at $\delta = 0$. The ^{51}V NMR acquisition parameters were: 33 KHz spectral width, 25 μs pulse width, 0.5 s acquisition time and 10 Hz line broadening. A pre-saturation pulse sequence was used for ^1H NMR spectra to eliminate the residual water signal. − EPR Spectroscopy: The EPR spectrum of the freshly prepared aqueous solution of the crystalline compound $[V_3O_6(dmpp)_3(H_2O)](H_2O)_2$ was obtained at room temperature on a Bruker ESP300E spectrometer, operating at 9.77 GHz. The frequency was calibrated with diphenylpycryl-hydrazyl (dpph) and the magnetic field using Mn^{2+} in MgO.

X-ray Crystallography: Selected crystallographic data are shown in Table 1. Three dimensional X-ray data were collected at low temperature (173 K) in the range $1.68 < 2\theta < 28.32°$ on a Siemens SMART 1000 CCD diffractometer by the Ω-scan method. Complex scattering factors were taken from the program package

Table 1. Crystallographic data for the complex $[V_3O_6(Hdmpp)_3(H_2O)](H_2O)_2$

Empirical formula	$C_{21}H_{30}N_3O_{15}V_3$
Formula mass	717.30
Crystal system	monoclinic
Space group	$P2_1/n$
a (Å)	9.5324(7)
b (Å)	16.4107(11)
c (Å)	18.0638(12)
α (deg)	90
β (deg)	91.1010(10)
γ (deg)	90
V (Å^3)	2825.3(3)
Z	4
T (K)	193
λ (Å)	0.71073
$D_{calcd.}$ (gcm^{-3})	1.686
$F(000)$	1464
No. of reflns collected	19434
No. of indep reflns.	6989
R_1 [a]	0.0704
wR_2(all data)	0.2025
Largest diff peak and hole (e·Å^{-3})	2.04, −0.887

[a] $R_1 = \Sigma||F_0| - |F_c||/\Sigma[|F_0|$, $wR_2 = \{\Sigma[w(||F_0|^2 - |F_c|^2|)^2]/\Sigma[w(F_0^4)]\}^{1/2}$.

SHELXTL.[48] The structure was solved by direct methods and refined by using full-matrix least-squares methods on F^2. The data were processed and corrected for Lorentz and polarisation effects and for absorption (semi-empirical method). The non-hydrogen atoms were refined with anisotropic thermal parameters in all cases. The hydrogen atoms of the H_2O molecules were refined with isotropic thermal parameters. The other hydrogen atoms were refined to carbon, which were placed in idealised positions and refined by using a riding mode. A final difference Fourier map showed no residual density outside −0.887 to +2.041; the highest peaks in this case suggested the presence of a residual density in the middle of one pyridinone group but its assignment was not possible. Selected bond lengths and bond angles appear in Table 2.

Crystallographic data (excluding structure factors) for the structure reported in this paper have been deposited with the Cambridge Crystallographic Data Centre as supplementary publication no. CCDC-160778. Copies of the data can be obtained free of charge on application to CCDC, 12 Union Road, Cambridge CB2 1EZ, UK [Fax: (internat.) +44−1223/336−033; E-mail: deposit@ccdc.cam.ac.uk].

Supporting Information: ^{51}V NMR spectra (131.404 MHz, 22.0 ± 0.5 °C) of $[V_3O_6(dmpp)_3(H_2O)](H_2O)_2$ in aqueous solution (2 mM, pH = 4.2) in the presence of oxygen, as a function of time (10 minutes to 5 days) (Figure 1S).

Acknowledgments

We thank Fundação para a Ciência e Tecnologia, Portugal (Project SAPIENS QUI/35368/99) for financial support. Servicios Generales de Apoyo a la Investigación (SXAIN) de la Universidad de A Coruña are also thanked for carrying out the elemental analysis, IR spectra and X-ray crystallographic data and Xunta de Galicia and University of A Coruña for two grants to F.A. to visit the University of Coimbra. This work was carried out within the Working Group "Vanadium Compounds as Insulin-Mimetic Agents" of the COST D8 Action of the E. U.

Table 2. Selected bond lengths (Å) and angles (deg) in $[V_3O_6(Hdmpp)_3(H_2O)](H_2O)_2$ with estimated standard deviation in parentheses

Bond lengths			
V(1)−O(1)	1.599(3)	V(3)−O(3)	1.609(4)
V(1)−O(6)	1.794(3)	V(3)−O(5)	1.813(3)
V(1)−O(4)	1.817(3)	V(3)−O(6)	1.857(3)
V(1)−O(7)	1.980(4)	V(3)−O(11)	1.909(3)
V(1)−O(8)	2.008(4)	V(3)−O(12)	2.204(3)
V(1)−O(12)	2.450(3)	V(3)−O(1 W)	2.180(4)
V(2)−O(2)	1.613(4)	O(7)−C(1)	1.433(7)
V(2)−O(4)	1.795(3)	O(8)−C(7)	1.259(7)
V(2)−O(5)	1.824(4)	O(9)−C(8)	1.325(5)
V(2)−O(9)	1.962(3)	O(10)−C(14)	1.310(6)
V(2)−O(10)	2.004(4)	O(11)−C(15)	1.336(5)
		O(12)−C(21)	1.309(5)
Bond angles			
O(1)−V(1)−O(6)	103.03(17)	O(4)−V(2)−O(9)	153.53(15)
O(1)−V(1)−O(4)	103.18(17)	O(5)−V(2)−O(9)	88.57(14)
O(6)−V(1)−O(4)	93.88(15)	O(2)−V(2)−O(10)	102.7(2)
O(1)−V(1)−O(7)	102.01(17)	O(4)−V(2)−O(10)	86.67(15)
O(6)−V(1)−O(7)	90.56(17)	O(5)−V(2)−O(10)	152.79(15)
O(4)−V(1)−O(7)	152.69(16)	O(9)−V(2)−O(10)	79.36(14)
O(1)−V(1)−O(8)	100.36(18)	O(3)−V(3)−O(5)	102.16(19)
O(6)−V(1)−O(8)	156.20(15)	O(3)−V(3)−O(6)	105.34(17)
O(4)−V(1)−O(8)	84.93(17)	O(5)−V(3)−O(6)	92.03(14)
O(7)−V(1)−O(8)	80.33(19)	O(3)−V(3)−O(11)	95.80(16)
O(1)−V(1)−O(12)	1767.19(17)	O(5)−V(3)−O(11)	100.14(14)
O(6)−V(1)−O(12)	74.47(12)	O(6)−V(3)−O(11)	152.82(14)
O(4)−V(1)−O(12)	78.40(12)	O(3)−V(3)−O(12)	172.09(16)
O(7)−V(1)−O(12)	76.89(13)	O(5)−V(3)−O(12)	83.65(14)
O(8)−V(1)−O(12)	82.04(13)	O(6)−V(3)−O(12)	79.86(13)
O(2)−V(2)−O(4)	103.26(18)	O(11)−V(3)−O(12)	77.54(12)
O(2)−V(2)−O(5)	103.6(2)	V(2)−O(4)−V(1)	125.61(18)
O(4)−V(2)−O(5)	94.01(15)	V(3)−O(5)−V(2)	120.39(17)
O(2)−V(2)−O(9)	101.69(17)	V(1)−O(6)−V(3)	119.22(17)
		V(3)−O(12)−V(1)	84.98(10)

[1] Y. Shechter, *Diabetes* **1990**, *39*, 1.
[2] A. B. Goldfine, F. Folli, P. E. Patti, D. C. Simonson, C. R. Kahn, *Can. J. Physiol. Pharmacol.* **1994**, *72*, (Suppl. 3), 11.
[3] N. Cohen, M. Halberstam, P. Shlimovich, C. J. Chang, H. Shamoon, L. Rossetti, *J. Clin. Invest.* **1995**, *95*, 2501.
[4] S. M. Brichard, J. Henquin, *TiPs* **1995**, *16*, 265.
[5] J. H. McNeil, V. G. Yuen, H. R. Hoveyda, C. Orvig, *J. Med. Chem.* **1992**, *35*, 1489.
[6] [6a] P. Caravan, L. Gelmini, N. Glover, F. G. Herrinh, H. Li, J. H. McNeill, S. J. Rettig, I. A. Setyawati, E. Shuter, Y. Sun, A. S. Tracey, V. G. Yuen and C. Orvig, *J. Am. Chem. Soc.* **1995**, 117, 12759. − [6b] G. R. Hanson, Y. Sun, C. Orvig, *Inorg. Chem.* **1996**, *35*, 6507.
[7] V. Berdoukas, P. Bentley, H. Frost, H. P. Schnebli, *Lancet* **1993**, *341*, 1088.
[8] J. Burgess, B. Castro, C. Oliveira, M. Rangel, W. Schlindwein, *Polyhedron* **1997**, *16*, 789.
[9] M. M. C. A. Castro, C. F. G. C. Geraldes, P. Gameiro, E. Pereira, B. Castro, M. Rangel, *J. Inorg. Biochem.* **2000**, *80*, 177.
[10] K. H. Thompson, J. H. McNeill, C. Orvig, in *Topics in Biological Inorganic Chemistry* (Eds.: M. J. Clarke, P. J. Sadler), Springer−Verlag, Heidelberg, **1999**, Vol. 2, p.139.
[11] H. Sigel, A. Sigel, *Metal Ions in Biological Systems* Marcel Dekker, New York, **1995**, Vol. 31.
[12] D. Rehder, *Angew. Chem. Int. Ed. Engl.* **1991**, 30, 148.
[13] N. D. Chasteen, *Struct. Bonding (Berlin)* **1983**, *53*, 105.
[14] T. Ramasarma, F. L. Crane, *Curr. Top. Cell. Regul.* **1981**, *20*, 247.
[15] Q. Chen, J. Zubieta, *Coord. Chem. Rev.* **1992**, 114, 107.

[16] G. Asgedom, A. Sreedhara, J. Kivikoski, J. Valkonen, E. Kolehmainen, C. P. Rao, *Inorg. Chem.* **1996**, *35*, 5674.
[17] D. C. Crans, R. W. Marshman, M. S. Gottelieb, O. P. Anderson, M. M. Miller, *Inorg. Chem.* **1992**, *31*, 4939.
[18] [18a] D. Rehder, W. Priebsch, M. von Oeynhausen, *Angew. Chem. Int. Ed. Engl.* **1989**, *28*, 1221. – [18b] M. Bashirpoor, H. Schmidt, C. Schulzke, D. Rehder, *Chem. Ber./Recueil* **1997**, *130*, 651.
[19] K. H. Tytko, J. Mehmke, *Z. Anorg. Allg. Chem.* **1983**, *503*, 67.
[20] A. A. Ivakin, L. D. Kurbatova, M. V. Kruchinina, N. I. Medvedeva, *Z. Neorg. Khim.* **1986**, *31*, 388.
[21] [21a] L. Pettersson, B. Hedman, I. Andersson, N. Ingri, *Chem. Scr.* **1983**, *22*, 254. – [21b] L. Pettersson, I. Andersson, B. Hedman, *Chem. Scr.* **1985**, *25*, 309. – [21c] L. Pettersson, B. Hedman, A.-M. Nenner, I. Andersson, *Acta Chem. Scand., Ser. A* **1985**, *39*, 499.
[22] D. C. Crans, F. Jiang, O. P. Anderson, S. M. Miller, *Inorg. Chem.* **1998**, *37*, 6645.
[23] F. Jiang, P. A. Oren, S. M. Miller, J. Chen, M. Mahroof-Tahir, D. C. Crans, *Inorg. Chem.* **1998**, *37*, 5439.
[24] K. H. Thompson, J. H. McNeill, C. Orvig, *Chem. Rev.* **1999**, *99*, 2561.
[25] Y. Sun, M. Melchior, D. A. Summers, R. C. Thompson, S. J. Rettig, C. Orvig, *Inorg. Chem.* **1998**, *37*, 3119.
[26] Y. Chang, Q. Chen, M. I. Khan, J. Salta, J. Zubieta, *J. Chem. Soc., Chem. Commun.* **1993**, 1872.
[27] O. W. Howarth, M. J. Jarrold, *Chem. Soc., Dalton Trans.* **1978**, 503.
[28] R. Codd, T. W. Hambley, P. A. Lay, *Inorg. Chem.* **1995**, 34, 877.
[29] M. I. Khan, Q. Chen, H. Höpe, S. Parkin, C. J. O′Connor, J. Zubieta, *Inorg. Chem.* **1993**, *32*, 2929.
[30] M. I. Khan, Q. Chen, D. P. Goshorn, J. Zubieta, *Inorg. Chem.* **1993**, *32*, 672.
[31] M. I. Khan, Q. Chen, D. P. Goshorn, H. Höpe, S. Parkin, J. Zubieta, *J. Am. Chem. Soc.* **1992**, *114*, 3341.
[32] Q. Chen, J. Zubieta, *Inorg. Chim. Acta* **1992**, 198.
[33] Q. Chen, J. Zubieta, *Inorg. Chim. Acta* **1992**, 95.
[34] D. C. Crans, F. Jiang, Q. Chen, O. P. Anderson, M. M. Miller, *Inorg. Chem.* **1997**, *36*, 1038.
[35] W. J. Ray Jr., D. C. Crans, J. Zheng, J. W. Burgner II, H. Deng, M. Mahroof-Tahir, *J. Am. Chem. Soc.* **1995**, 117, 6015.
[36] M. Melchior, K. H. Thompson, J. M. Jong, S. J. Rettig, E. Shuter, V. G. Yuen, Y. Zhou, J. H. McNeil, C. Orvig, *Inorg. Chem.* **1999**, *38*, 2288.
[37] Y. Sun, B. R. James, S. J. Rettig, C. Orvig, *Inorg. Chem.* **1996**, *35*, 1667.
[38] D. Schulz, T. Weyhermüller, K. Wieghardt, B. Nuber, *Inorg. Chim. Acta* **1995**, *240*, 217.
[39] [39a] A. R. Katritzky, R. A. Jones, *J. Chem. Soc.* **1960**, 2947. – [39b] A. R. Katritzky, R. A. Jones, *Spectrochim, Acta* **1961**, *17*, 64. – [39c] B. D. Batts, E. Spinner, *Aust. J. Chem.* **1976**, *22*, 2581. – [39d] M. M. Finnegan, T. G. Lutz, W. O. Nelson, A. Smith, C. Orvig, *Inorg. Chem.* **1987**, *26*, 2171.
[40] K. Isobe, S. I. Ooi, Y. Nakamura, S. Kawaguchi, H. Kuroya, *Chem. Lett.* **1975**, 35.
[41] C. R. Cornman, J. Kampf, M. S. Lah, V. L. Pecoraro, *Inorg. Chem.* **1992**, *31*, 2035.
[42] X. Li, M. S. Lah, V. L. Pecoraro, *Inorg. Chem.* **1988**, *27*, 4657.
[43] M. R. Caira, J. M. Haigh, L. R. Nassimbeni, *J. Inorg. Nucl. Chem.* **1972**, *24*, 3171.
[44] I. Cavaco, J. Costa-Pessoa, M. T. Duarte, P. M. Matias, R. T. Henriques, *Polyhedron* **1993**, *12*, 1231.
[45] W. Priebsch, D. Rehder, M. von Oeynhausen, *Chem. Ber.* **1991**, *124*, 761.
[46] H. Rieskamp, P. Gietz, R. Mattes, *Chem. Ber.* **1976**, *109*, 2090.
[47] E. Heath, O. W. Howarth, *J. Chem. Soc., Dalton Trans.* **1981**, 1105.
[48] G. M. Sheldrick, *SHELXTL* Bruker Analytical X-ray System, Madison, WI **1997**, Ver. 5.01.

Received July 20, 2001
[I01277]

The Role of the Apical Donor in the Decomposition of Copper(II) Benzoate under DOW-Phenol Conditions

Wim Buijs,[a] Peter Comba,*[b] Danny Corneli,[b] Ynze Mengerink,[a] Hans Pritzkow,[b] and Martina Schickedanz[c]

Keywords: DOW-phenol process / Methylated pyridines / Halogenated pyridines / Pyrolysis / Paddle-wheel / Aniline

The synthesis and characterization of copper(II) benzoates with the apical donors pyridine, 2-CH_3-pyridine, 2,4-$(CH_3)_2$-pyridine, 2,6-$(CH_3)_2$-pyridine, 2-fluoropyridine, 2-chloropyridine, 2-bromopyridine, 3-bromopyridine, 2,5-dibromopyridine, 3,5-dibromopyridine, and aniline, starting from copper(II) benzoate, is reported. Single-crystal X-ray structures of the products with four apical ligands show the usual paddle-wheel structure of copper(II) carboxylates; in the case of aniline no paddle-wheel dicopper(II) benzoate could be isolated. The products of thermal decomposition of the pure copper(II) compounds were analyzed by HPLC, LC-MS, and GCFID, and the expected DOW-phenol products were found in all cases other than that of aniline. This supports the assumption that a paddle-wheel dicopper(II) benzoate is required for the DOW-phenol reaction. Generally, high *ortho*-selectivities (to phenyl benzoate and phenol; the selectivity increases with increasing basicity) are obtained, in good agreement with earlier findings on the role of the base. Small but significant steric effects are observed in the series of methylated pyridine donors and the monohalogenated pyridine donors used as apical ligands; with the two dibromopyridine donors there are large steric effects and the DOW-phenol reaction is partially suppressed. With halogenated pyridine donors as apical ligands, a $Cu^{[I]}$-catalyzed process occurs, leading to dehalogenation.

Introduction

The selective oxidation of hydrocarbons in the liquid phase is a major challenge in fundamental and applied research.[1−3] Generally, free-radical chain mechanisms dominate, and only in a few cases (xylene and toluene derivatives) is a high selectivity towards the corresponding acids obtained. Various approaches have been proposed to overcome these problems but, so far, these have led to only limited success. We have tried to avoid unselective free-radical chain oxidation reactions by adopting an approach that utilizes oligonuclear metal complexes in the oxygenation of hydrocarbons. The starting point for our studies was the DOW-phenol process. This converts benzoic acid into phenol under copper(II) catalysis and this reaction may be considered as a regioselective hydroxylation.[4] In the DOW-phenol process (Scheme 1), benzoic acid is oxidized at $T >$ 180 °C with moist air and copper(II) to give phenyl benzoate and CO_2; the reduced copper(I) is reoxidized by dioxygen; hydrolysis of the phenyl benzoate then yields the desired phenol and benzoic acid [Equations (1)−(5)].[4]

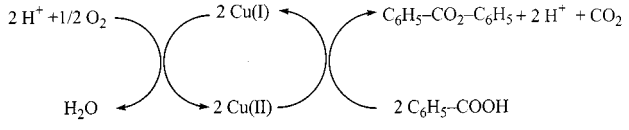

Scheme 1

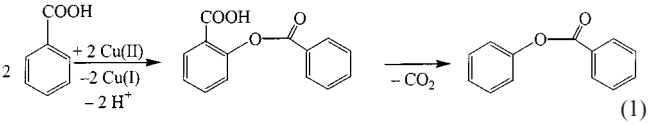

(1)

$$2\,Cu^{II} + 2\,ArCOOH \rightarrow ArCO_2Ar + 2\,H^+ + CO_2 + 2\,Cu^{I} \quad (2)$$

$$2\,Cu^{I} + 1/2\,O_2 + 2\,H^+ \rightarrow 2\,Cu^{II} + H_2O \quad (3)$$

$$ArCO_2Ar + H_2O \rightarrow ArOH + ArCOOH \quad (4)$$

Overall:

$$ArCOOH + 1/2\,O_2 \rightarrow ArOH + CO_2 \quad (5)$$

The main reaction in the catalytic process (Scheme 1) is the thermal decomposition of copper(II) benzoate to *o*-benzoyloxybenzoic acid. Rapid decarboxylation leads to phenyl benzoate [Equation (1)]. The amount of CO_2 produced is directly proportional to the amount of copper(II) involved in the stoichiometric decomposition and its quantification can be used to study the kinetics of the process. Phenyl benzoate is hydrolyzed with steam to yield phenol [Equation (4)]. The overall reaction is sensitive to solvents. In anhydrous benzoic acid solutions, the *ortho*-selectivity of the benzoyloxybenzoic acid formation is only about 50% (45% *meta*-benzoyloxybenzoic acid, 5% *para*-benzoyloxybenzoic acid).[5]

[a] DSM Research,
P. O. Box 18, 6160 MD Geleen, The Netherlands
[b] Anorganisch-Chemisches Institut der Universität Heidelberg,
Im Neuenheimer Feld 270, 69120 Heidelberg, Germany
Fax: (internat.) + 49-(0)6221/546617
E-mail: comba@akcomba.oci.uni-heidelberg.de
[c] Organisch-Chemisches Institut der Universität Heidelberg,
Im Neuenheimer Feld 270, 69120 Heidelberg, Germany

 © WILEY-VCH Verlag GmbH, 69451 Weinheim, 2001 1434−1948/01/1212−3143 $ 17.50+.50/0

Table 1. Overview of the results of the thermal decomposition of copper(II) benzoates with substituted pyridines and aniline at 230 °C with various apical ligands

Apical donor	Conversion[a] (%)	DOW Phenol product (%)[b] *ortho*	*meta*	*para*	Reduced (%)[b]	Benzene (%)[c]
pyridine	40.9	99.9	0.1	–	–	–
2-CH_3-pyridine	12.4	98.5	1.3	0.2	–	–
2,4-$(CH_3)_2$-pyridine	6.6	97.8	1.8	0.4	–	–
2,6-$(CH_3)_2$-pyridine	3.8	95.7	3.5	0.8	–	1.3
aniline	0.7[d]	93.9	5.2	0.9	–	4.0
2-F-pyridine[e]	17.7	89.2	5.6	5.2	–	8.8
2-Cl-pyridine	31.4	94.8	2.7	2.5	4.5	–
2-Br-pyridine	21.5	95.1	2.5	2.4	1.4	–
3-Br-pyridine	59.3	98.1	1.3	0.6	14.3	–
2,5-Br_2-pyridine	4.1	66.7	31.0	2.3	3.3[f]	–
3,5-Br_2-pyridine	11.6	99.2	0.8	–	12.0[g]	–

[a] With respect to copper benzoate. – [b] Reduced products in mol % copper benzoate (dimer). – [c] mol % relative to the total benzoic acid in the starting material. – [d] Most likely due to the salicylic acid reaction; aniline was completely converted to *N*-phenyl benzamide (HPLC and LC-MS). – [e] Results obtained at 250 °C; no reaction occurred at 230 °C. – [f] Products: 2-benzoyloxypyridine, 2-hydroxypyridine (approx. 1:1). – [g] Products: pyridine, 3-benzoyloxypyridine, 3-hydroxypyridine (approx. 2:2:1.5).

Results and Discussion

Thermal Decomposition of Copper(II) Benzoate with Substituted Pyridine Donors or Aniline at the Apical Sites of the Paddle-Wheel Dicopper(II) Compounds

The influence of substituted pyridine donors bearing electron-withdrawing or electron-donating groups was studied to investigate the role of the donors at the apical sites of the paddle-wheel dicopper(II) complexes in the DOW-phenol process (see Scheme 2). Copper(II) benzoate with various pyridine donors (different substitution patterns) and with aniline was pyrolyzed in a sealed silica tube (stoichiometric reaction; see Exp. Sect.). Table 1 summarizes the identified DOW-phenol products recovered following the pyrolyses of the copper(II) compounds.

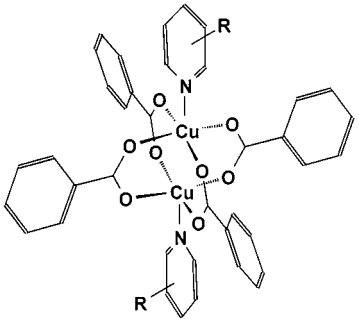

Scheme 2

An important observation is that all the apical donors studied show high *ortho*-selectivities, except for 2,5-dibromopyridine. This is in line with earlier observations on the effect of base in the DOW-phenol reaction.[5] In the series pyridine, 2-methylpyridine, 2,4-dimethylpyridine, and 2,6-dimethylpyridine, both the conversion and the *ortho*-selectivity decrease, from 40.9% to 3.8% and from 99.9% to 95.7%, respectively. Since the basicity in this series of pyridines follows the order pyridine < 2-methylpyridine < 2,4-dimethylpyridine ≈ 2,6-dimethylpyridine, both the conversion and the *ortho*-selectivity might have been expected to increase, as was observed with Mg^{II} benzoate.[5] However, the pyridine donors coordinate to Cu^{II} whereas Mg^{II} benzoate merely acts as a simple base. The electronic effect of the pyridine donors influences the thermal stability and hence the reactivity: the more electron-donating the pyridine donor is, the less effectively Cu^{II} will be able to abstract electrons from benzoate. If, however, the electrophile resulting from a benzoate is formed, the steric effect of the methylated pyridine donors may slightly decrease the probability of an *ortho*-attack at the corresponding pyridinium benzoate.

The halogenated pyridine donors constitute another interesting series. Unfortunately, their conversion cannot be compared directly with that of the methylated pyridine donors because they are also subject to reduction, which produces additional Cu^{II}.[6] This reaction seems to be comparable to the reduction of halogenated hydrocarbons.[7] The scope and limitations of the catalytic reduction are reported separately.[6]

The use of 2-fluoropyridine did not lead to any reaction at 230 °C. However, at 250 °C a fast substitution reaction of benzoate on the fluoride was observed prior to the DOW-phenol reaction. The resulting *ortho*-selectivity of approximately 89% cannot be assigned to 2-fluoropyridine, but mainly to 2-benzoyloxypyridine and HF instead.[6]

The other halogenated pyridine donors show *ortho*-selectivities of 66.7% (2,5-dibromopyridine), 94.8% (2-chloropyridine), 95.1% (2-bromopyridine), 98.1% (3-bromopyridine), and 99.2% (3,5-dibromopyridine). We believe that in these cases, both electronic and steric effects play a similar role to that observed with the methylated pyridine donors, albeit to a less pronounced extent. Despite the increasing size of the substituents, a chloro or a bromo substituent in the 2-position of the pyridine has a similar effect on the *ortho*-selectivity as two methyl groups in the 2,6-positions. This

might be due to the fact that only one side of the benzoate in a pyridinium benzoate is accessible for the coupling reaction. Moreover, a bromo substituent in the 3-position of pyridine has a similar effect as a methyl group in the 2-position. Comparing the pyridine donors with two bromo substituents in the 2,5- and 3,5-positions, a large steric effect on the *ortho*-selectivity due to the second bromine in the 2-position is evident.

For the series of monohalogenated pyridine donors, the relative amount of reduced material (given as mol % of additional copper benzoate; see Table 1) is comparatively small with respect to the observed conversion, but it is high for the dibromopyridine donors. For the latter, this correlates with the observed conversion ratios. The total conversion may therefore be interpreted as follows. The steric demand of dibromo-substituted pyridine donors in the apical positions leads to a slow DOW-phenol reaction; the resulting $Cu^{[I]}$ leads to a comparably high reduction and substitution rate to yield reduced and substituted pyridine donors and Cu^{II}; the DOW-phenol reaction then also proceeds with pyridine and benzoate-substituted pyridines. The observed selectivities for the two dibromopyridine ligands support this. With 3,5-dibromopyridine, a comparatively large amount of pyridine is formed and the observed *ortho*-selectivity is 99.2%, similar to that seen with pyridine itself. With 2,5-dibromopyridine, the major product is a pyridine substituted at the 2-position and reduced at the 5-position. This secondary ligand still leads to substantial steric hindrance, and the resulting *ortho*-selectivity of 66.7% is close to that observed for Cu^{II} benzoate in the absence of base and water.[5]

The apical donor aniline blocks the DOW-phenol reaction completely. Phenyl benzoate was not detected. Instead, the quantitative formation of *N*-phenyl benzamide was observed. Since this co-elutes with phenyl benzoate in the HPLC procedure used, LC-MS, including a peak purity check, was applied to enable a quantitative determination. On adding pyridine donors to a Cu^{II} benzoate solution in acetone, the paddle-wheel structure remained intact, whereas with aniline a distinct color change was observed and no paddle-wheel dicopper(II) compound could be isolated. The failure to observe DOW-phenol chemistry with aniline supports the interpretation that paddle-wheel structures of copper(II) benzoate are a requirement for the DOW-phenol reaction.[5]

With three donors, namely 2,6-dimethylpyridine, aniline, and 2-fluoropyridine, benzene was detected as an additional product of the stoichiometric DOW-phenol reactions. Benzene is a common by-product in the DOW-phenol process, but its formation is generally attributed to $Cu^{[I]}$, reaction at the reactor wall, and high temperatures ($\geq$ 250 °C). However, in the three cases where benzene was found (Table 1), $[Cu^{[I]}]$ is low and no metal reactor wall was present. With 2,6-dimethylpyridine and aniline, the reaction temperature was as low as 230 °C. Therefore, apart from in the case of 2-fluoropyridine, our interpretation of the benzene production is that a relatively strong base must be present.[8] In the case of 2-fluoropyridine, the elevated temperature might be the most important factor.

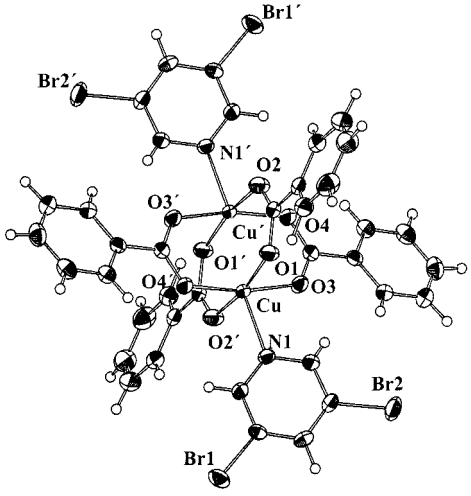

Figure 1. ORTEP[12] plot of $[Cu_2(\mu\text{-}O_2C{-}C_6H_5)_4(3,5\text{-}Br{-}C_5H_3N)_2]$ (compound **1**)

Molecular Structures of Copper(II) Benzoates with Apical Donors

For all the apical donors studied, except for aniline, dicopper(II) species with stoichiometries in agreement with the expected paddle-wheel structures were isolated. The X-ray crystal structures of the four structurally characterized dicopper(II) benzoates (see Figure 1, Table 2) are essentially identical and, as expected for copper(II), do indeed represent paddle-wheel compounds. They consist of centrosymmetric dicopper(II) units, in which each copper(II) ion is coordinated by four oxygen atoms of the four bridging carboxylate groups (see Figure 1, Scheme 2, and Table 2). The copper−copper distances range from 2.626 Å to 2.678 Å. The angle between the two planes through the two copper(II) centers and two benzoates ranges from 88.92° to 89.80°. The two pyridine rings are parallel, except in compound **2**, where their ring planes intersect at an angle of 79.23°. No paddle-wheel-type copper(II) benzoate could be isolated with aniline. Aniline seems to destroy the copper(II) benzoate fragment and this leads to the formation of unidentified mononuclear copper(II) species.

CO_2 Measurements

The pyrolyses of copper(II) benzoate in sealed silica tubes in the absence of oxygen, with all the pyridine derivatives used in this study, produce CO_2. The cumulative formation of CO_2 as a function of time with copper(II) benzoate alone reaches a constant value of approximately 66% with respect to the stoichiometrically expected amount (Figure 2; approximately 50% *o*-selectivity in the formation of the benzoyloxybenzoic acid, see above[5]). With the methylated and halogenated pyridine donors, the production of CO_2 increases significantly [see Figure 2; with pyridine 109% and with 3-bromopyridine 108% was obtained; 100% CO_2

Table 2. Selected distances [Å] and angles [deg.] for tetrakis(benzoato-μ-*O*,*O*′)bis(3,5-dibromopyridine)dicopper(II) (compound **1**), tetrakis(benzoato-μ-*O*,*O*′)bis(3-bromopyridine)dicopper(II) (compound **2**), tetrakis(benzoato-μ-*O*,*O*′)bis(2,5-dibromopyridine)dicopper(II) (compound **3**), and tetrakis(benzoato-μ-*O*,*O*′)bis(2-chloropyridine)dicopper(II) (compound **4**)

Selected bond lengths [Å]	Compound **1**	Compound **2**	Compound **3**	Compound **4**
Cu...Cu′	2.6264(6)	2.6775(6)	2.6585(8)	2.6475(6)
Cu-N1	2.206(2)	2.176(3)	2.262(3)	2.235(9)
Cu′-N1′	2.206(2)	2.159(3)	1.966(2)	2.214(10)
Cu-O1	1.9615(19)	1.947(3)	1.958(2)	1.960(2)
Cu-O2′	1.9748(19)	1.952(2)	1.976(2)	1.970(2)
Cu-O3	1.9624(19)	1.979(2)	1.960(2)	1.961(2)
Cu-O4′	1.9633(19)	2.034(2)	1.951(2)	1.963(2)
Cu′-O1′	1.9615(19)	2.018(2)	1.958(2)	1.960(2)
Cu′-O2	1.9748(19)	1.965(2)	1.976(2)	1.970(2)
Cu′-O3′	1.9624(19)	1.945(2)	1.960(2)	1.961(2)
Cu′-O4	1.9633(19)	1.952(3)	1.951(2)	1.963(2)
Selected valence angles [deg]				
O1-Cu-O4′	89.15(8)	90.20(11)	89.70(11)	89.92(10)
O4′-Cu-O2′	88.83(8)	90.16(11)	87.86(11)	89.80(12)
O2′-Cu-O3	90.82(9)	87.48(11)	89.22(11)	88.49(11)
O3-Cu-O1		89.99(11)	90.51(11)	89.28(9)
O1′-Cu′-O4		88.39(11)		
O4-Cu′-O2		90.40(11)		
O2-Cu′-O3′		89.47(11)		
O3′-Cu′-O1′		89.94(11)		
O1-Cu-N1	100.77(8)	93.83(12)	104.57(10)	97.7(4)
O4′-Cu-N1	94.75(8)	86.14(11)	101.07(10)	87.8(3)
O2′-Cu-N1	90.41(8)	92.48(11)	88.17(10)	97.0(4)
O3-Cu-N1	96.66(8)	114.20(12)	90.82(10)	104.2(3)
O1′-Cu′-N1′		88.03(10)		95.1(4)
O4-Cu′-N1′		93.43(11)		95.3(4)
O2-Cu′-N1′		111.53(11)		94.3(4)
O3′-Cu′-N1′		91.62(11)		96.7(4)
O1-Cu-Cu′	89.14(6)	84.56(8)	87.79(7)	83.69(6)
Ó4-Cu-Cu′	83.86(6)	86.05(8)		
O2′-Cu-Cu′	79.66(6)	89.34(7)	79.66(8)	84.28(7)
O3-Cu-Cu′	84.85(6)	81.17(8)		85.52(6)
O1′-Cu′-Cu		77.80(7)		
Ó4′-Cu-Cu′		78.54(7)	88.88(7)	82.53(7)
O2-Cu′-Cu		82.63(7)		
O3′-Cu′-Cu		88.60(7)	78.80(7)	
N1-Cu-Cu′		164.58(9)	164.02(8)	177.4(4)
N1′-Cu′-Cu		165.83(8)		170.2(3)

corresponds to the stoichiometric amount of copper(I) generated in one reduction cycle (see Scheme 1)].

There are various explanations for this behavior. An important observation is that after the pyrolysis with pyridine, elemental copper is found in the reaction vessel. This indicates that copper(I), formed during the reduction of the halogenated pyridines and the ensuing DOW-phenol process, undergoes disproportionation to copper(0) and copper(II) [Equation (6)]. The resulting copper(II) leads to additional CO_2 production [Equation (1) and Scheme 1].

$$2\,Cu^{I} \rightarrow Cu^{0} + Cu^{II} \qquad (6)$$

Moreover, pyridine catalyzes the decarboxylation of aromatic acids.[8] The copper(II) compound with 3-bromopyridine leads to an even larger excess of CO_2, although no elemental copper could be found after the reaction. This may be related to the detection of reduced pyridines by HPLC. After the usual decomposition of copper(II) benzoate, copper(I) is re-oxidized to copper(II) by the halopyridines [Equation (7)]. The complete reduction of halogenated pyridine derivatives in a catalytic reaction is prohibited by the precipitation of copper(I) halides.[7] These processes are described in detail in a separate publication.[6]

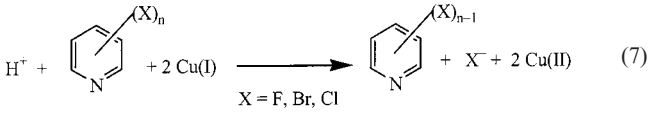

(7)

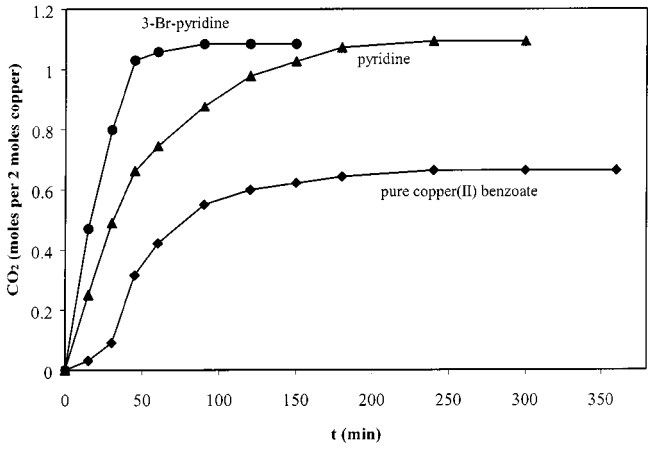

Figure 2. Cumulative CO_2 formation during the pyrolysis of various copper(II) benzoates with apical donors (stoichiometric reaction under argon; for conditions, see Exp. Sect.)

Experimental Section

Materials: Copper(II) benzoate was obtained from DSM and was used without purification. All other compounds were purchased from Sigma or Aldrich and were used without further purification. The purity ranges were 97−99%.

Syntheses of the Copper(II) Compounds

$[Cu_2(\mu_2\text{-}O_2C-C_6H_5)_4(3,5\text{-}Br-C_5H_3N)_2]$ (1): 3,5-Dibromopyridine (1.00 g, 4.22 mmol) was added to a solution of copper(II) benzoate (1.37 g, 2.12 mmol) in dry acetone (50 mL). After 24 h, the turquoise-green precipitate was collected by filtration, washed with Et_2O, and dried in vacuo. Yield: 1.55 g (67.4%). − IR (KBr): $\tilde{\nu}$ = 3060 [ν(C−H)], 1626 [ν(C=N)], 1600 [ν(C=C)], 1574 [$\nu_{asym.}$ (C=O, COO^-)], 1406 [$\nu_{sym.}$ (C=O, COO^-)], 1022 [ν(aryl-Br)] cm^{-1}. − $C_{38}H_{26}Br_4Cu_2N_2O_8$ (1085.34): calcd. C 42.03, H 2.41, N 2.58; found C 42.09, H 2.61, N 2.51.

$[Cu_2(\mu_2\text{-}O_2C-C_6H_5)_4(3\text{-}Br-C_5H_4N)_2]$ (2): 3-Bromopyridine (1.50 g, 9.81 mmol) was added to a solution of copper(II) benzoate (2.05 g, 3.17 mmol) in dry acetone (50 mL). The reaction mixture was heated at 60 °C for 24 h. The turquoise-green precipitate was then collected by filtration, washed with Et_2O, and dried in vacuo. Yield: 2.13 g (72.4%). − IR (KBr): $\tilde{\nu}$ = 3066 [ν(C−H)], 1628 [ν(C=N)], 1616 [ν(C=C)], 1572 [$\nu_{asym.}$ (C=O, COO^-)], 1402 [$\nu_{sym.}$ (C=O, COO^-)], 1028 [ν(aryl-F)] cm^{-1}. − $C_{38}H_{28}Cu_2Br_2N_2O_8$ (927.54): calcd. C 49.21, H 3.04, N 3.02, Br 17.23; found C 49.19, H 3.37, N 2.87, Br 16.47.

$[Cu_2(\mu_2\text{-}O_2C-C_6H_5)_4(2,5\text{-}Br-C_5H_3N)_2]$ (3): 2,5-Dibromopyridine (2.00 g, 8.44 mmol) was added to a solution of copper(II) benzoate (2.74 g, 4.43 mmol) in dry acetone (50 mL). The reaction mixture was heated at 60 °C for 24 h. The solvent was then removed under reduced pressure, and the residue was washed with petroleum ether (30 mL) and dried in vacuo. Yield: 2.59 g (56.3%). − IR (KBr): $\tilde{\nu}$ = 3063 [ν(C−H)], 1625 [ν(C=N)], 1600 [ν(C=C)], 1570 [$\nu_{asym.}$ (C=O, COO^-)], 1410 [$\nu_{sym.}$ (C=O, COO^-)], 1070 [ν(aryl-Br)] cm^{-1}. − $C_{38}H_{26}Br_4Cu_2N_2O_8$ (1085.34): calcd. C 42.03, H 2.41, N 2.58, Br 29.45; found C 42.48, H 2.72, N 2.57, Br 28.50.

$[Cu_2(\mu_2\text{-}O_2C-C_6H_5)_4(2\text{-}Cl-C_5H_4N)_2]$ (4): 2-Chloropyridine (2.00 g, 17.61 mmol) was added to a solution of copper(II) benzoate (3.71 g, 5.72 mmol) in dry acetone (100 mL). The reaction mixture was heated at 60 °C for 24 h. The solvent was then removed under reduced pressure, and the residue was washed with petroleum ether (30 mL) and dried in vacuo. Yield: 2.46 g (51.25%). − IR (KBr): $\tilde{\nu}$ = 3062 [ν(C−H)], 1626 [ν(C=N)], 1616 [ν(C=C)], 1572 [$\nu_{asym.}$ (C=O, COO^-)], 1406 [$\nu_{sym.}$ (C=O, COO^-)], 1270 [ν(aryl-Cl)] cm^{-1}. − $C_{38}H_{28}Cu_2Cl_2N_2O_8$ (838.65): calcd. C 54.42, H 3.37, N 3.34; found C 54.48, H 3.50, N 3.13.

$[Cu_2(\mu_2\text{-}O_2C-C_6H_5)_4(2\text{-}Br-C_5H_4N)_2]$: 2-Bromopyridine (2.70 g, 17.09 mmol) was added to a solution of copper(II) benzoate (5.00 g, 7.72 mmol) in dry acetone (100 mL). The reaction mixture was heated to 60 °C for 24 h. The solvent was then removed under reduced pressure, and the residue was washed with petroleum ether (30 mL) and dried in vacuo. Yield: 4.7 g (65.64%). − IR (KBr): $\tilde{\nu}$ = 3063 [ν(C−H)], 1625 [ν(C=N)], 1600 [ν(C=C) =], 1570 [$\nu_{asym.}$ (C=O, COO^-)], 1410 [$\nu_{sym.}$ (C=O, COO^-)], 1070 [ν(aryl-Br)] = cm^{-1}. − $C_{33}H_{24}BrCu_2NO_8$ (769.55): calcd. C 51.50, H 3.14, N 1.82, Br 10.38; found C 51.52, H 3.46, N 1.84, Br 10.11.

$[Cu_2(\mu_2\text{-}O_2C-C_6H_5)_4(2\text{-}F-C_5H_4N)_2]$: 2-Fluoropyridine (1.00 g, 10.30 mmol) was added to a solution of copper(II) benzoate (2.34 g, 5.16 mmol) in dry acetone (50 mL). The reaction mixture was heated at 60 °C for 24 h. The solvent was then removed under reduced pressure, and the residue was washed with petroleum ether (30 mL) and dried in vacuo. Yield: 2.53 g (53.73%). − IR (KBr): $\tilde{\nu}$ = 3070 [ν(C−H)], 1628 [ν(C=N)], 1610 [ν(C=C)], 1574 [$\nu_{asym.}$ (C=O, COO^-)], 1404 [$\nu_{sym.}$ (C=O, COO^-)], 1270 [ν(aryl-F)] cm^{-1}. − $C_{38}H_{28}Cu_2F_2N_2O_8$ (805.74): calcd. C 56.64, H 3.50, N 3.48; found C 56.58, H 3.87, N 3.10.

$[Cu(\mu_2\text{-}O_2C-C_6H_5)_2(H_2N-C_6H_5)]_n$: To a suspension of copper(II) benzoate (1.00 g, 1.54 mmol) in petroleum ether (30 mL) was added aniline (0.29 g, 3.11 mmol). After 24 h, the green precipitate was collected by filtration, washed with Et_2O, and dried in vacuo. Yield: 1.10 g (80.65%). − IR (KBr): $\tilde{\nu}$ = 3312 [ν(N−H)], 3066 [ν(C−H)], 1596 [ν(C=C)], 1548 [$\nu_{asym.}$ (C=O, COO^-)], 1490 [$\nu_{sym.}$ (C=O, COO^-)] cm^{-1}. − $C_{40}H_{34}Cu_2N_2O_8$ (797.81): calcd. C 60.22, H 4.30, N 3.51; found C 59.16, H 4.59, N 3.72.

$[Cu_2(\mu_2\text{-}O_2C-C_6H_5)_4(C_5H_5N)_2]$: Pyridine (1.22 g, 15.42 mmol) was added to a solution of copper(II) benzoate (5.00 g, 7.72 mmol) in dry acetone (100 mL). The reaction mixture was heated at 60 °C for 24 h. The green precipitate was then collected by filtration, washed with EtOH, and dried in vacuo. Yield: 3.6 g (60.60%). − IR (KBr): $\tilde{\nu}$ = 3063 [ν(C−H)], 1628 [ν(C=N)], 1600 [ν(C=C)], 1572 [$\nu_{asym.}$ (C=O, COO^-)], 1405 [$\nu_{sym.}$ (C=O, COO^-)] cm^{-1}. − $C_{38}H_{30}Cu_2N_2O_8$ (769.76): calcd. C 59.29, H 3.93, N 3.64; found C 59.05, H 4.01, N 3.43.

$[Cu_2(\mu_2\text{-}O_2C-C_6H_5)_4(2\text{-}CH_3-C_5H_4N)_2]$: 2-Methylpyridine (1.44 g, 15.44 mmol) was added to a solution of copper(II) benzoate (5.00 g, 7.72 mmol) in dry acetone (100 mL). The reaction mixture was heated at 60 °C for 24 h. The green precipitate was then collected by filtration, washed with Et_2O, and dried in vacuo. Yield: 3.55 g (57.63%). − IR (KBr): $\tilde{\nu}$ = 3066 [ν(C−H)], 2932 [ν(C−H, CH_3)], 1630 [ν(C=N)], 1600 [ν(C=C)], 1574 [$\nu_{asym.}$ (C=O, COO^-)], 1404 [$\nu_{sym.}$ (C=O, COO^-)] cm^{-1}. − $C_{40}H_{34}Cu_2N_2O_8$ (797.81): calcd. C 60.22, H 4.30, N 3.51; found C 60.27, H 4.38, N 3.46.

$[Cu_2(\mu_2\text{-}O_2C-C_6H_5)_4\{2,4\text{-}(CH_3)_2-C_5H_3N\}_2]$: 2,4-Dimethylpyridine (1.65 g, 15.44 mmol) was added to a solution of copper(II) benzoate (5.00 g, 7.72 mmol) in dry acetone (100 mL). The reaction mixture was heated at 60 °C for 24 h. The green precipitate was then collected by filtration, washed with Et_2O, and dried in vacuo.

Table 3. Crystallographic data for tetrakis(benzoato-μ-*O*,*O*′)bis(3,5-dibromopyridine)dicopper(II) (compound **1**), tetrakis(benzoato-μ-*O*,*O*′)bis(3-bromopyridine)dicopper(II) (compound **2**), tetrakis(benzoato-μ-*O*,*O*′)bis(2,5-dibromopyridine)dicopper(II) (compound **3**), and tetrakis(benzoato-μ-*O*,*O*′)bis(2-chloropyridine)dicopper(II) (compound **4**)

Compound	**1**	**2**	**3**	**4**
Empirical formula	$C_{38}H_{26}Br_4Cu_2N_2O_8$	$C_{38}H_{28}Br_2Cu_2N_2O_8$	$C_{38}H_{26}Br_4Cu_2N_2O_8$	$C_{38}H_{28}Cl_2Cu_2N_2O_8$
Molecular mass	1085.33	927.52	1085.33	838.60
Crystal size [mm^3]	0.48 x 0.40 x 0.20	0.27 x 0.23 x 0.22	0.28 x 0.24 x 0.09	0.48 x 0.34 x 0.16
Crystal system	Triclinic	Monoclinic	Triclinic	Monoclinic
spacc group	*P*-1	$P2_1/c$	*P*-1	$P2_1/n$
a (Å)	10.1935(2)	17.5158(2)	10.0911(1)	10.3650(2)
b (Å)	10.6326(1)	10.5161(1)	10.2947(1)	10.3761(1)
c (Å)	10.6556(2)	19.9834(2)	19.2761(3)	17.1173(2)
α (deg)	64.091(1)	90	97.216(1)	90
β (deg)	81.185(1)	97.423(1)	92.919(1)	100.073(1)
γ (deg)	68.511(1)	90	106.133(1)	90
V ($Å^3$)	966.57(3)	3650.05(7)	1900.64(4)	1812.56(4)
Z	1	4	2	2
Reflections collected / unique (*R*int)	11640 / 4639 (0.027)	49013 / 8983 (0.049)	23541 / 8991 (0.039)	18358 / 4413 (0.046)
$Density_{calcd.}$ [g cm^{-3}]	1.865	1.688	1.896	1.537
Absorption coefficient [mm^{-1}]	5.288	3.410	5.378	1.376
F(000)	530	1848	1060	852
Goodness-of-fit on *R*1 [$I>2\sigma(I)$]	0.987	1.047	0.977	1.062
*wR*2 (all data)	0.0332	0.0458	0.0342	0.0472
Largest diff. peak and hole [e /$Å^{-3}$]	0.0886	0.1361	0.0901	0.1484
	0.797 / -0.671	1.919 / -2.402	0.899 / -1.199	0.630 / -0.646

Yield: 2.60 g (40.76%). − IR (KBr): $\tilde{\nu}$ = 3062 [ν(C−H)], 2928 [ν(C−H, CH_3)], 1632 [ν(C=N)], 1598 [ν(C=C)], 1574 [$\nu_{asym.}$ (C=O, COO^-)], 1402 [$\nu_{sym.}$ (C=O, COO^-)] cm^{-1}. − $C_{42}H_{38}Cu_2N_2O_8$ (825.86): calcd. C 61.08, H 4.64, N 3.39; found C 60.97, H 4.62, N 3.24.

$[Cu_2(\mu_2\text{-}O_2C{-}C_6H_5)_4\{2,6\text{-}(CH_3)_2{-}C_5H_3N\}_2]$: 2,6-Dimethylpyridine (1.65 g, 15.44 mmol) was added to a solution of copper(II) benzoate (5.00 g, 7.72 mmol) in dry acetone (100 mL). The reaction mixture was heated at 60 °C for 24 h. The solvent was then removed under reduced pressure, and the residue was washed with petroleum ether (30 mL) and dried in vacuo. Yield: 3.24 g (58.38%). − IR (KBr): $\tilde{\nu}$ = 3062 [ν(C−H)], 2928 [ν(C−H, CH_3)], 1632 [ν(C=N)], 1598 [ν(C=C)], 1574 [$\nu_{asym.}$ (C=O, COO^-)], 1402 [$\nu_{sym.}$ (C=O, COO^-)] cm^{-1}. − $C_{35}H_{29}Cu_2NO_8$ (718.52): calcd. C 58.50, H 4.68, N 1.95; found C 58.69, H 4.63, N 1.98.

Pyrolyses: The pure copper(II) benzoate salts with the apical donors (150 mg in each case) were heated for 7 h at 230 °C in sealed silica tubes. The tubes were filled under argon. Since in the case of copper(II) benzoate with 2-fluoropyridine no reaction occurred at 230 °C, this experiment was repeated at 250 °C. After cooling to ambient temperature, the tubes were opened and the products were analyzed by HPLC. In the case of the halogenated pyridines, the products were also analysed by LC-MS.

Positive-ion ESI-MS data were obtained on an HP1100 quadrupole LC-MS system (Agilent Technologies, Waldbronn, Germany). Mass spectra were obtained in full scan mode from m/z = 50−1000 amu at a fragmentor voltage of 70 V and a capillary voltage of 3000 V. The drying gas flow was 10 L/min and the drying gas temperature was 350 °C.

For reversed-phase HPLC, the black solids produced were dissolved in acetonitrile (2 mL) and then injected into an HP 1090 chromatograph with a Nucleosil 120−5 C18 column (500 × 4 mm) at 50 °C. The products were eluted with a gradient made up of different mixtures of eluents A and B [eluent A: 1 M H_3PO_4 (45 mL), conc. acetic acid (2 mL), and 1 M NaOH (35 mL) were added to water (1500 mL) and the pH of the solution was adjusted to 3.2 with 1 M NaOH; after the addition of acetonitrile (200 mL), the mixture was made up with water to give 2000 mL of eluent A; eluent B: 1 M H_3PO_4 (20 mL), conc. acetic acid (2 mL), and 1 M NaOH (60 mL) were added to water (60 mL) and the pH of the solution was adjusted to 6.6 with 1 M NaOH; after the addition of acetonitrile (1200 mL), the mixture was made up with water to give 2000 mL of eluent B]. A DAD (L-3000 Hitachi) was used for detection at 254 nm.

GC analyses were performed using a Hewlett−Packard series 5890 gas chromatograph, equipped with a 30 m fused silica Megabore column (G. & W. Scientific) with a 5 μm DBI stationary phase. The products were identified with an FID detector; nitrogen was used as the carrier gas. − Elemental analyses were obtained from the microanalytical laboratory of the chemical institutes of the University of Heidelberg. Infrared spectra (KBr pellets) were measured with a Perkin−Elmer 16PC FT-IR instrument.

X-ray Crystallography: Crystallographic data are presented in Table 3; all structural data have been deposited with the Cambridge Crystallographic Data Centre (CCDC) as supplementary publication nos. CCDC-152937−152940. Copies of the data can be obtained free of charge on application to The Director, CCDC, 12 Union Road, Cambridge CB2 1EZ, U.K. [Fax: (internat.) +44 (1223) 336-033; E-mail: deposit@ccdc.cam.ac.uk]. Crystal data

were collected on a Bruker AXS SMART 1000 diffractometer with a CCD area detector (Mo-K_α radiation, graphite monochromator, $\lambda = 0.71073$ Å) at −100 °C, using the SMART suite of programs.[7] The reflection intensities were integrated using SAINT and corrected for absorption using SADABS.[9,10] The structures were solved by direct methods and refined by full-matrix least-squares methods based on F^2 with all reflections, using the SHELXTL programs.[11]

Acknowledgments

Financial support by DSM Research, Geleen, The Netherlands is gratefully acknowledged.

[1] R. A. Sheldon, J. K. Kochi, *Metal-Catalyzed Oxidations of Organic Compounds*, Academic Press, New York, **1981**.
[2] B. Cornils, W. A. Hermann, *Applied Homogeneous Catalysis with Organometallic Compounds*, Wiley-VCH, Weinheim, New York, **2000**.
[3] B. Meunier (Ed.), *Metal-Oxo and Metal-Peroxo Species in Catalytic Oxidations, Structure and Bonding*, Vol. 97, Springer-Verlag, Berlin/Heidelberg, **1999**.
[4] W.W. Kaeding, A. T. Shulgin, *J. Org. Chem.* **1962**, *27*, 3551.
[5] W. Buijs, *J. Mol. Cat. A: Chem.* **1999**, *146*, 237.
[6] W. Buijs, P. Comba, D. Corneli, Y. Mengerink, R. Peters, *Eur. J. Inorg. Chem.* **2001**, 3151−3154, see following article in this issue.
[7] W. Buijs, *Cat. Today* **1996**, *27*, 159.
[8] L. Artok, H. H. Schobert, *J. Anal. Appl. Pyr.* **2000**, *54*, 215.
[9] SMART and SAINT NT V5.0, *Area control and integration software*, Bruker AXS, Madison, Wisconsin, **1999**.
[10] G. M. Sheldrick, SADABS, *Program for scaling and correcting of area detector data*, University of Köln, **1998**.
[11] G. M. Sheldrick, SHELXTL V5.1, Bruker AXS, Madison, USA, **1998**.
[12] C. K. Johnson, ORTEP: *A Thermal Ellipsoid Plotting Program*, Oak Ridge National Laboratory, **1965**.

Received August 1, 2001
[I01296]

Catalytic Dehalogenation of Halogenated Pyridine Donors under DOW-Phenol Conditions

Wim Buijs,[a] Peter Comba,*[b] Danny Corneli,[b] Ynze Mengerink,[a] and Ron Peters[a]

Keywords: DOW-phenol process / Halogenated pyridines / Reductions / Nucleophilic substitutions

Various halogenated pyridines (2-fluoropyridine, 2-chloropyridine, 2-bromopyridine, 3-bromopyridine, 2,5-dibromopyridine, and 3,5-dibromopyridine) are subject to catalytic reduction and substitution under DOW-phenol conditions; copper(I) benzoate is shown to play a key role in these processes. In the absence of copper(I), the halogenated pyridines do not react with benzoic acid, while after precipitation of copper(I) halide the dehalogenation process stops. Marked differences are observed between the copper(I)-catalyzed dehalogenation of the halopyridines and the previously reported dehalogenation of halogenated aromatics. While the copper(I)-catalyzed substitution of haloaryl compounds by benzoate makes only a minor contribution to the overall dehalogenation process, substitution of halopyridine compounds is at least as important as the reduction reaction. Furthermore, the reaction with halopyridine compounds is regioselective, in contrast to that with halogenated aryl compounds.

Introduction

Many halogenated hydrocarbons are hazardous due to their tendency to accumulate in the body and the resultant damage of nerves and hepar.[1] Halogenated hydrocarbons are widely used as solvents and monomers for polymer production. Furthermore, halogenated compounds are produced in various combustion processes, including (natural) wood burning and the combustion of waste. TCDD, 2,3,7,8-tetrachlorodibenzo[1,4]dioxin, known as the "Seveso dioxin", is a well-known representative of the latter group.[1] Halogenated compounds have also played a role in parasite control (DDT).[2] The transformation of halogenated hydrocarbons into less harmful compounds is still a challenge in chemistry. Among the methods currently used industrially, electrochemical dehalogenation and decomposition by iron catalysts are well-known processes.[3,4] A recent discovery was that chlorinated and brominated hydrocarbons can be catalytically reduced under DOW-phenol conditions,[5] and this was confirmed in our investigation of the role of different apical donors on the DOW-phenol process.[6] We have investigated this process in some detail and report here the scope of this novel catalytic reaction.

Results

The catalytic reduction of halogenated hydrocarbons under DOW-phenol conditions consists of two steps:

(i) Copper(I) is oxidized by the halogenated pyridines to copper(II) [Equation (1)].

(ii) Copper(II) is reduced to copper(I) during the thermal decomposition of copper(II) benzoate (DOW-phenol reaction) [Equation (2)].

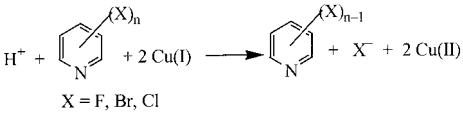

(1)

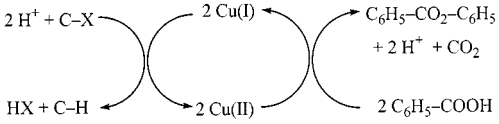

(2)

Another possible route for the dehalogenation of the halogenated pyridines is the nucleophilic substitution of a halogen atom by a benzoate [Equation (3)].

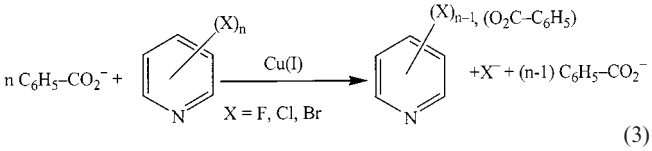

(3)

During a catalytic cycle, a halogen in a carbon−halogen bond is substituted by a benzoate and, in acidic solution, one molecule of HX is produced. The reaction stops when all halogenated substrates are reduced or substituted, or when the copper catalyst has completely precipitated as the $Cu^{[I]}$ halide.

Table 1 gives an overview of the results obtained in the thermal decomposition of the copper(II) benzoates with apical donors. Apart from the expected DOW-phenol product, i.e. phenyl benzoate, pyridine, *ipso*-benzoate substituted

[a] DSM Research,
P. O. Box 18, 6160 MD Geleen, Netherlands
[b] Anorganisch-Chemisches Institut der Universität Heidelberg,
Im Neuenheimer Feld 270, 69120 Heidelberg, Germany
Fax: (internat.) + 49-(0)6221/546617
E-mail: comba@akcomba.oci.uni-heidelberg.de

 © WILEY-VCH Verlag GmbH, 69451 Weinheim, 2001 1434−1948/01/1212−3151 $ 17.50+.50/0

Table 1. Overview of the results for the thermal decomposition of the pure complexes [Cu_2(benzoate)$_4$(*n*-X-pyridine)$_2$] at 230 °C (HPLC and LC-MS)

Apical donor	DOW Phenol phenyl benzoate	Cu^I products pyridine	*n*-$ArCO_2$-pyridine	*n*-HO-pyridine	Benzoic acid
2-F-pyridine[a]	3.6	0.3	42.1	3.9	25.9
2-Cl-pyridine	7.0	1.0	36.5	3.1	25.8
2-Br-pyridine	4.4	2.2	32.1	2.9	23.8
3-Br-pyridine	12.2	9.3	13.9	3.2	10.2
2,5-Br_2-pyridine	0.5[b]	0.5	28.6	3.3	20.8
3,5-Br_2-pyridine	1.9	1.4	25.2	3.2	9.8

[a] 250 °C (no reaction occurred at 230 °C); 3.4% of benzene was also produced. – [b] No phenyl benzoate was observed, but a mixture of the precursor *o*-, *p*-, and *m*-benzoyloxybenzoic acids; *ortho*-selectivity: 66.7%.

pyridines, and hydroxypyridine are obtained. Dehalogenation appears to be essentially complete in these experiments. The results demonstrate the scope of the reaction: F-, Cl-, and Br-substituted pyridine ligands undergo reduction and substitution by benzoate under DOW-phenol conditions. Substitution follows the order F > Cl > Br in the series of 2-halopyridine ligands, with relative molar amounts of the substituted products amounting to 99%, 94%, and 87%, respectively. The reduction shows an opposite trend, with relative amounts of pyridine of 1%, 6%, and 13%, respectively. In the case of 3-bromopyridine, the reduction and substitution processes both account for approximately 50% of the overall reaction. Similar behavior is observed for the dibromopyridine donors: the observed monobenzoyloxypyridine compounds are the result of a reduction and substitution cycle. A double reduction process yields pyridine, while a double substitution yields dibenzoyloxypyridine. Both are observed by LC-MS, albeit at very low levels. Hydroxypyridine products, resulting from hydrolysis, are also detected. Phenol, i.e. the hydrolysis product of phenyl benzoate, is not observed. In the case of 2-fluoropyridine, a significant amount of benzene is also obtained, which is probably formed as a decomposition product due to the relatively high temperature (250 °C).

Discussion

Comparing the different pyridine substrates, three issues need clarification: 1) the order of the halogens in both substitution and reduction, 2) the order of reactivity in the series of brominated pyridines with respect to their regiochemistry, and 3) the observation that phenol, the hydrolysis product of phenyl benzoate, is not present in the reaction mixtures, while the hydroxypyridines are present in all the mixtures.

A possible explanation for these issues emerges from the proposed mechanism.[5] One electron is donated by Cu^I to the carbon–halogen bond, possibly involving the temporary formation of a cuprate. A second Cu^I donates an electron to the carbon, leading formally to a carbanion stabilized by two Cu^{II} centers. The resulting halide might form a Cu^{II}·X·Cu^{II} bridge. The Cu^{II}-stabilized carbanion is then protonated by benzoic acid and eliminated from the Cu^{II} coordination sphere. Alternatively, a benzoate might act as a nucleophile after the donation of the first electron to the carbon–halogen bond, leading to net overall nucleophilic substitution of the original halogen by a benzoate. In this case, the role of Cu^I is to improve the leaving group ability of the halogen. The tentative mechanism is shown in Figure 1.

Important features are the properties of the reactive intermediates and transition states, i.e. the radicals and carbanions derived from the substrates. Quantum mechanical calculations are a useful tool for the investigation of the properties of such species. Semi-empirical calculations (PM3) were used for an efficient comparison of the entire series. DFT calculations (BP level) on the series of monohalogenated pyridines gave essentially the same results. Computational details are given in the Exp. Sect.. Table 2 lists the computed electrostatic charges on the corresponding C-atoms of the 2- and 3-halogenated pyridines.

2-Fluoropyridine has by far the highest positive charge, +0.858, on the C2 atom, followed by 2-chloro- and 2-bromopyridine, with charges of +0.504 and +0.305. 3-Bromopyridine, on the other hand, has a negative charge on the C3 atom (−0.634). If the nucleophilic substitution can be correlated with the positive charge on the relevant carbon atoms, the proposed order by PM3 would be: 2-fluoropyridine > 2-chloropyridine > 2,5-dibromopyridine (2) > 2-bromopyridine > 3-bromopyridine > 2,5-dibromopyridine (5) > 3,5-dibromopyridine. This order is indeed observed for the series of 2-halopyridines. 2,5-Dibromopyridine is a special case with its two different carbon–bromine bonds. The C2 atom is positively charged, this charge being roughly equal to that on the C2 atom of 2-bromopyridine, while its C5 atom is even more negatively charged than the C3 atom of 3-bromopyridine. Therefore, 2,5-dibromo- and 3,5-dibromopyridine fit well in this sequence, being intermediate between the 2-bromo- and 3-bromopyridines.

If the reduction can be correlated with the negative charge on the corresponding pyridine anion, then the order predicted by PM3 calculations would be: 3-pyridine anion (−1.489) ≈ 5-bromo-3-pyridine anion (−1.467) ≈ 2-bromo-5-pyridine anion (−1.464) > 2-pyridine anion (−0.893) ≈ 5-bromo-2-pyridine anion (−0.840). This order

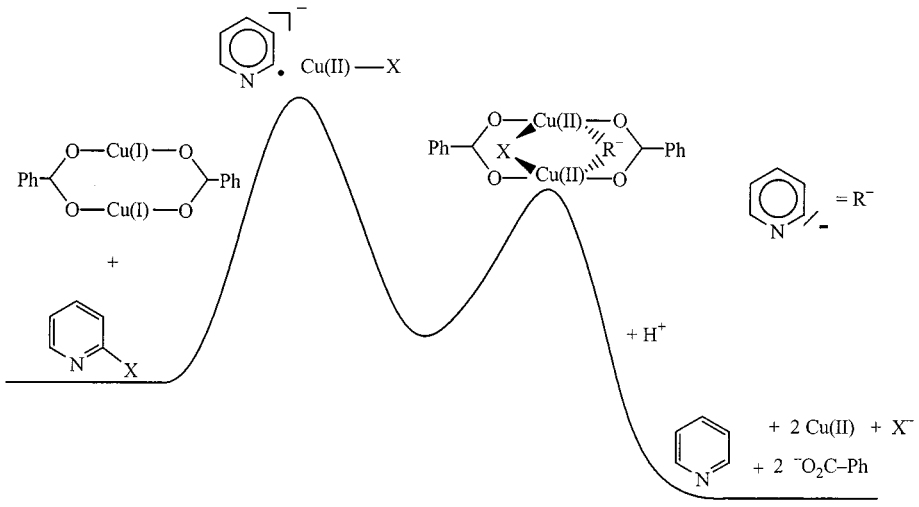

Figure 1. Proposed mechanism for the reduction of halogenated pyridines under DOW-phenol conditions

Table 2. Electrostatic charges of the halogenated pyridines, pyridyl radicals, and pyridine anions; computations were carried out at the PM3 and BP levels

pyridine substrate	PM3 electrostatic charge	BP electrostatic charge
2-fluoropyridine	+0.858	+0.718
2-chloropyridine	+0.504	+0.437
2-bromopyridine	+0.305	+0.413
3-bromopyridine	−0.634	−0.299
2,5-dibromopyridine 2-position 2,5-dibromopyridine 5-position	+0.338	
−0.651		
3,5-dibromopyridine	−0.747	
2-pyridyl radical	−0.089	+0.038
3-pyridyl radical	−0.439	−0.299
2-bromo-5-pyridyl radical	−0.428	
5-bromo-2-pyridyl radical	+0.084	
5-bromo-3-pyridyl radical	−0.497	
2-pyridine anion	−0.893	−0.793
3-pyridine anion	−1.489	−1.188
2-bromo-5-pyridine anion	−1.464	
5-bromo-2-pyridine anion	−0.840	
5-bromo-3-pyridine anion	−1.467	

indeed explains the different reduction yields, i.e. of 9.3% for 3-bromopyridine and of 2.2% for 2-bromopyridine. A similar pattern is observed for 2,5-dibromopyridine (0.5%) and 3,5-dibromopyridine (1.4%), although the double reduction yields are rather low. This also leads to speculation concerning the major product derived from the two dibromopyridines; that arising from 2,5-dibromopyridine should be 2-benzoyloxypyridine (28.6%), whereas the corresponding product from 3,5-dibromopyridine should be 3-benzoyloxypyridine (25.2%).

Conclusion

(i) Semi-empirical quantum chemical calculations are an excellent tool for interpreting the observed order of the halogens in the substitution reaction of 2-halopyridines; the opposite order for the reduction might be a simple consequence of the preference for substitution, while the next steps (pyridyl radical, pyridine anion) become increasingly independent of the leaving group in the proposed mechanism.

(ii) The difference between the regioisomers 2-bromo- and 3-bromopyridine can be adequately explained, both in terms of substitution and reduction.

(iii) At first sight, it might seem surprising that the hydrolysis products hydroxypyridines are observed, while phenol is not. However, with the benzoyloxypyridines intramolecular base hydrolysis is possible, whereas with phenyl benzoate it is not.

Finally, we would like to comment on the behavior of the halopyridines as compared with that of the haloaromatics. With the latter, no indication was found for a major contribution of the nucleophilic substitution reaction and no regioselectivity was observed.[5] An appealing explanation is that the benzene ring is an electron-rich aromatic system in comparison with the pyridine ring. Therefore, nucleophilic

substitution is more likely to occur on the electron-poor pyridine system than on benzene. Moreover, the reaction mixtures composed of benzoic acid, Cu^{I} benzoate, and a haloaryl compound are rather acidic, whereas the mixtures composed of benzoic acid, Cu^{I} benzoate, and a halopyridine are basic, at least locally. The final step in the reduction requires a proton. Therefore, the reduction should be easier in the more acidic environment. Fortunately, halogenated pyridines are not produced in very large quantities because the observed regioselectivity has to be considered as a disadvantage for an environmental technology.

Experimental Section

Materials and Analytical Procedures: Copper(II) benzoate was prepared from copper(II) sulfate and sodium benzoate. All other compounds were purchased from Sigma or Aldrich and were used without further purification. − **Pyrolyses:** The pure copper(II) benzoate salts with the apical donors (150 mg in each case) were heated for 7 h at 230 °C in sealed silica tubes. The tubes were filled under argon. Since in the case of copper(II) benzoate with 2-fluoropyridine no reaction occurred at 230 °C, this experiment was repeated at 250 °C. After cooling to ambient temperature, the tubes were opened and the products were analyzed by HPLC. In the case of the halogenated pyridines, the products were also analyzed by LC-MS. − **Electrospray MS:** Positive-ion ESI-MS data were obtained on an HP1100 quadrupole LC-MS system (Agilent Technologies, Waldbronn, Germany). Mass spectra were obtained in full scan mode from m/z = 50−1000 amu at a fragmentor voltage of 70 V and a capillary voltage of 3000 V. The drying gas flow was 10 L/min and the drying gas temperature was 350 °C. − **Reversed-Phase HPLC:** For reversed-phase HPLC, the black solids produced were dissolved in acetonitrile (2 mL) and then injected into an HP 1090 chromatograph with a Nucleosil 120−5 C18 column (500 × 4 mm) at 50 °C. The products were eluted with a gradient made up of different mixtures of eluents A and B [eluent A: 1 M H_3PO_4 (45 mL), conc. acetic acid (2 mL) and 1 M NaOH (35 mL) were added to water (1500 mL) and the pH of the solution was adjusted to 3.2 with 1 M NaOH; after the addition of acetonitrile (200 mL) the mixture was made up with water to give 2000 mL of eluent A; eluent B: 1 M H_3PO_4 (20 mL), conc. acetic acid (2 mL), and 1 M NaOH (60 mL) were added to water (60 mL) and the pH of the solution was adjusted to 6.6 with 1 M NaOH; after the addition of acetonitrile (1200 mL) the mixture was made up with water to give 2000 mL of eluent B]. A DAD (L-3000 Hitachi) was used for detection at 254 nm.

Computational Details

All calculations were carried out using the Titan molecular modeling suite of programs.[8] All molecules and fragments were geometry-optimized using the semi-empirical PM3 method. These structures were used as input data for a geometry optimization at the BP level (DFT), using the LACVP* basis set for Br and 6−31 G* for all other elements. DFT calculations were carried out only for the monohalogenated pyridines. The DFT results were in full accord with the PM3 results.

Acknowledgments

Financial Support by DSM Research, Geleen, The Netherlands, is gratefully acknowledged.

[1] C. Bliefert, *Polychlorierte Dibenzodioxine, Dibenzofurane und Biphenyle*, VCH, Weinheim, **1994**, p. 276.
[2] C. Bliefert, *Pestizide*, VCH, Weinheim, **1994**, p. 332.
[3] D. Schmal, P. J. Van Duin, A. De Jong, *Elektrochem. Energ. Umwelttech.* **1991**, *124*, 241.
[4] S. V. Ho, D. E. McKenzie, R. G. Orth, *Patent WO 9704868*, **1997**.
[5] W. Buijs, *Cat. Today* **1996**, *27*, 159.
[6] W. Buijs, P. Comba, D. Corneli, Y. Mengerink, H. Pritzkow, M. Schickedanz, *Eur. J. Inorg. Chem.* **2001**, 3143−3149, preceding article in this issue.
[7] W. Buijs, *J. Molec. Cat. A: Chemical* **1999**, *146*, 237.
[8] Wavefunction, Inc., 18401 Von Karman Avenue Suite 370, Irvine, CA 92612, USA; Schrödinger, Inc., 1500 SW First Avenue, Suite 1180, Portland, OR 97201, USA.

Received August 1, 2001
[I01297]

A Tripodal Triaminostannate as a Metal Nucleophile: Synthesis of Transition Metal−Tin Heterodimetallic Complexes

Matthias Lutz,[a,b] Bernd Findeis,[a] Matti Haukka,[b] Tapani A. Pakkanen,*[b] and Lutz H. Gade*[a]

In memoriam Sallaraisa Pulkkinen

Keywords: Tin / Metal−metal interactions / N ligands / Transition metals

The coordination capability of the previously reported triamidostannate [MeSi{$SiMe_2N(4\text{-}CH_3C_6H_4)$}$_3$SnLi($OEt_2$)] (**1**) as a precursor for transition metal–tin heterodimetallic complexes is presented. Whereas reaction with CH_3I, Me_3SiCl, or Me_3SnCl yielded the derivatives [MeSi{$SiMe_2N(4\text{-}CH_3C_6H_4)$}$_3$Sn–R] (R = Me, **2**; Me_3Si, **3**; Me_3Sn, **4**), demonstrating the nucleophilic properties of the stannate(II), its complexation to transition metal centres was achieved by halide substitution with [$CuCl(PPh_3)]_4$, [$CpM(CO)_2X$] (M = Fe, X = Cl; M = Ru, X = Br), [$CpM(CO)_3Cl$] (M = Mo, W) and *trans*(Cl)-[$RuCl_2(bpy)(CO)_2$] to give [MeSi{$SiMe_2N(4\text{-}CH_3C_6H_4)$}$_3$-Sn–$Cu(PPh_3)$] (**5**), [MeSi{$SiMe_2N(4\text{-}CH_3C_6H_4)$}$_3$Sn–$M(CO)_2Cp$ (M = Fe: **6**; Ru: **7**)], [MeSi{$SiMe_2N(4\text{-}CH_3C_6H_4)$}$_3$Sn–$M(CO)_2Cp$] (M = Mo: **8**; W: **9**) and [(MeSi{$SiMe_2N(4\text{-}CH_3C_6H_4)$}$_3$Sn)$_2$Ru(bpy)$(CO)_2$] (**10**), of which **6**, **9** and **10** were characterized by X-ray diffraction.

Introduction

Transition metal−tin heterodimetallic complexes were among the first metal−metal bonded compounds to be studied in detail,[1] and since the pioneering work of the 1960's a great number of such complexes have been synthesized and characterized.[2] Apart from the fundamental aspect of bonding between transition metals and main group metals, the fact that the formation and transformation of transition metal−main group metal bonds are crucial steps in a variety of catalytic processes as well as semiconductor growth has created a great deal of interest.[4,5] In spite of the multitude of known transition metal−tin compounds, some transition metal complex fragments, notably the more highly oxidizing species, do not form stable dimetallic complexes with tin fragments. In order to suppress degenerative intramolecular redox reactions, an appropriate ligand shell for the group 14 element has to be chosen.

The tripodal amido ligands developed by us[6] were found to be ideally suited for the synthesis of group 14 triamidometallates, in particular triamidostannates.[7−9] These triamidostannates were found to bind to potentially highly oxidizing metal centres such as the tetravalent group 4 metals[10] as well as Ag^{I}, Au^{II} and Au^{III} to give thermally stable heterometallic compounds.[11−13] The electronegative nitrogen substituents at divalent group 14 metal centres thus appear to stabilize the metals with respect to oxidation by a heterometal centre to which they are bonded.

In view of the relative chemical inertness to oxidation by transition metals of the triamidostannates and the facile variability of their peripheral tripodal amido unit, we have recently begun to explore their properties as monoanionic "ligands" in transition metal chemistry, along with their isoelectronic neutral group 15 analogues.[14] In this work we present a detailed study of the coordination capability of the previously reported triamidostannate [MeSi{$SiMe_2N(4\text{-}CH_3C_6H_4)$}$_3$SnLi($OEt_2$)] (**1**).[11]

Results and Discussion

The properties of the amidostannate complex [MeSi{$SiMe_2N(4\text{-}CH_3C_6H_4)$}$_3$SnLi($OEt_2$)] (**1**)[11] as a metal nucleophile were initially tested by reaction with CH_3I, Me_3SiCl, and Me_3SnCl. Stirring the reagents in toluene whilst warming the reaction mixture from −20 °C to ambient temperature gave the corresponding coupling products as thermally stable solids in moderate to high yields (Scheme 1).

Elemental analyses and the ^1H, ^{13}C and ^{29}Si NMR spectroscopic data are in agreement with their formulation as [MeSi{$SiMe_2N(4\text{-}CH_3C_6H_4)$}$_3$Sn−R] (R = Me, **2**; Me_3Si, **3**; Me_3Sn, **4**); the molecular structures are depicted in Scheme 1. All three compounds display the expected threefold symmetry in solution as indicated by the signal patterns in the NMR spectra.

Reaction of **1** with 0.25 molar equivalents of [$CuCl(PPh_3)]_4$ in toluene at room temperature immediately gave the Sn−Cu complex [MeSi{$SiMe_2N(4\text{-}CH_3C_6H_4)$}$_3$Sn−

[a] Laboratoire de Chimie Organométallique et de Catalyse (UMR 7513), Institut Le Bel, Université Louis Pasteur, 4, rue Blaise Pascal, 67070 Strasbourg, France
Fax: (internat.) +33-390/241-531
E-mail: gade@chimie.u-strasbg.fr
[b] Department of Chemistry, University of Joensuu, 80101 Joensuu, Finland
Fax: (internat.) +358-13/251-3344
E-mail: Tapani.Pakkanen@joensuu.fi

 © WILEY-VCH Verlag GmbH, 69451 Weinheim, 2001 1434−1948/01/1212−3155 $ 17.50+.50/0

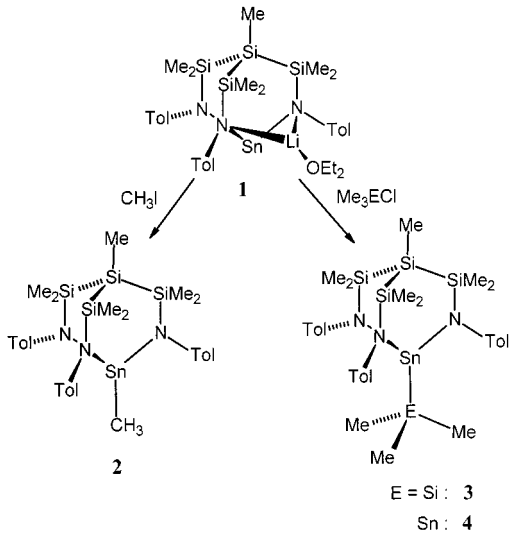

Scheme 1. Reaction of the triaminostannate with metal and non-metal electrophiles to give Sn−element bonds

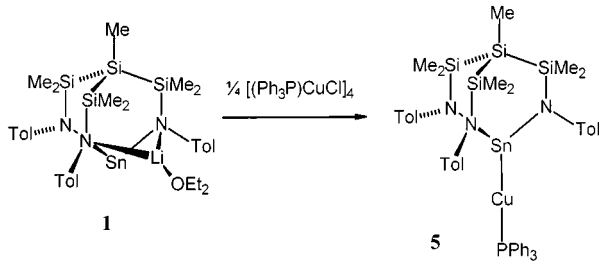

Scheme 2. Synthesis of the Cu−Sn compound **5**

Cu(PPh$_3$)] (**5**) (Scheme 2).[15] The formation of a Sn−Cu bond in this complex is supported by the observation of $^{117/119}$Sn satellites in the ^{31}P NMR spectra, which appear at room temperature as an averaged $^2J(^{117/119}\text{Sn-}^{31}\text{P})$ coupling satellite pattern associated with the ^{31}P NMR resonance at $\delta = 0.7$. The characteristic $^{117/119}$Sn-^{31}P splitting pattern [$^2J(^{117/119}\text{Sn-}^{31}\text{P})$ = 634.2 Hz/662.8 Hz] could be observed upon lowering the temperature to 205 K. The Cu−Sn compound apparently does not undergo detectable redistribution reactions in solution and thus resembles more closely the previously characterized analogous Au−Sn complex[12] than the Ag−Sn compound bearing the same triamidostannate unit.[11]

As we have previously performed studies of group 4/8 heterodimetallic complexes[16] in which the early transition metal is coordinated by the amido tripod employed in the synthesis of **1**, it was of interest to find out whether the corresponding group 14 derivatives are accessible and how their structures and properties are related to the early transition metal derivatives. [MeSi{SiMe$_2$N(4-CH$_3$C$_6$H$_4$)}$_3$SnLi(OEt$_2$)] (**1**) reacts with [CpM(CO)$_2$X] (M = Fe, X = Cl; M = Ru, X = Br) to afford the corresponding heterodimetallic complexes [MeSi{SiMe$_2$N(4-CH$_3$C$_6$H$_4$)}$_3$Sn−

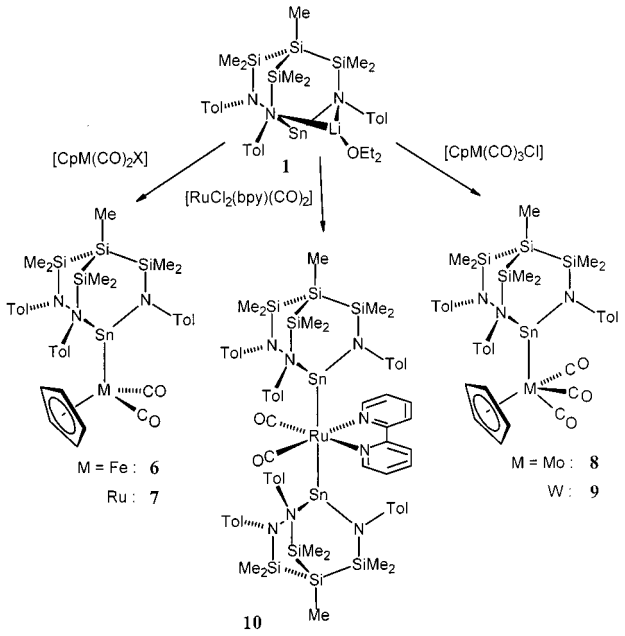

Scheme 3. Synthesis of transition metal−tin heterodimetallic complexes **6**−**10**

M(CO)$_2$Cp] (M = Fe: **6**; Ru: **7**; Scheme 3). They were characterized by ^{1}H, ^{13}C, and ^{29}Si NMR spectroscopy, infrared spectroscopy, and elemental analysis. The NMR spectra recorded at 295 K established the effective threefold symmetry of the heterodinuclear complexes in solution and thus indicated a rapid internal rotation of the molecules around the metal−metal axis. Cooling of these solutions led to the broadening of the resonances at 200 K but it was not possible to reach the low temperature limit corresponding to a frozen internal rotation on the NMR time scale. In the CO stretching region of the IR spectrum, [MeSi{SiMe$_2$N(4-CH$_3$C$_6$H$_4$)}$_3$Sn−M(CO)$_2$Cp] exhibits two bands of approximately equal intensity (**6**: 2016 and 1971 cm^{-1}; **7**: 2031 and 1981 cm^{-1}). These values are lower than those of CpM(CO)$_2$X (M = Fe, X = Cl: 2050, 2004 cm^{-1} in toluene; M = Ru, X = Br: 2049, 1999 cm^{-1} in toluene) (see Table 1), due to coordination of the two strongly σ-donating and weakly π-accepting amidostannyl ligands causing an increased π back-donation to the CO ligands.

In order to establish the details of the molecular structure of the type of group 8-tin complex discussed above, a single crystal X-ray structure analysis of compound **6** was carried out. The molecular structure of **6** is shown in Figure 1, along with the principal bond lengths and angles. The tripod amide-tin unit is characterized by its rigid cage structure as found in related tin complexes previously characterized by us. The peripheral tolyl groups adopt a "lampshade" arrangement to make space for the CpFe(CO)$_2$ fragment bonded through a metal−metal bond. The Sn−Fe bond length found in **6** [2.5146(3) Å] is similar to those found in structurally related Fe−Sn heterodimetallics, such as [Cp(CO)$_2$Fe−SnPh$_3$] (2.533 Å),[17] [Cp(CO)$_2$Fe−SnCl$_3$] [2.467(1) Å],[18] [Cp(CO)$_2$Fe−SnBr$_3$] [2.462(2) Å],[19]

Table 1. Comparison of CO stretching frequencies

Compound	ν_{CO} [cm^{-1}]	Compound	ν_{CO} [cm^{-1}]
[(η^5-C_5H_5)Fe(CO)$_2$Cl]	2050, 2004[a]	(**6**)	2016, 1971[a]
[(η^5-C_5H_5)Ru(CO)$_2$Br]	2049, 1999[a]	(**7**)	2030, 1981[a]
[(η^5-C_5H_5)Mo(CO)$_3$Cl]	2054, 1977, 1959[a]	(**8**)	2021, 1954, 1937[a]
[(η^5-C_5H_5)W(CO)$_3$Cl]	2046, 1960, 1943[a]	(**9**)	2018, 1944, 1930[a]
trans-[Cl$_2$Ru(CO)$_2$(bpy)]	2065, 2004[b]	(**10**)	2039, 1990[a]

[a] Measured in toluene. − [b] Measured in CH_2Cl_2.

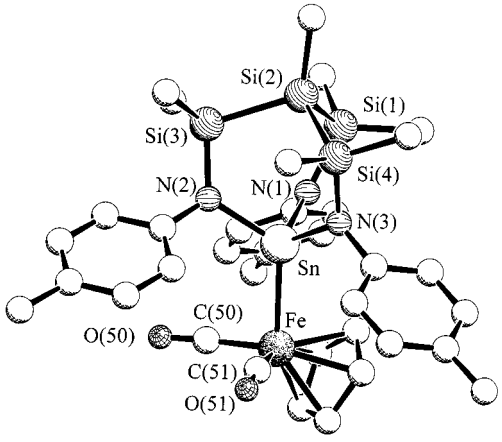

Figure 1. View of the molecular structure of **6**; principal bond lengths (Å) and angles (°): N(1)−Sn(1) 2.0652(17), N(2)−Sn(1) 2.0885(17), N(3)−Sn(1) 2.0785(18), Fe(1)−C(28) 2.099(2), Fe(1)−C(29) 2.101(2), Fe(1)−C(30) 2.088(2), Fe(1)−C(31) 2.098(2), Fe(1)−C(32) 2.102(2), Fe(1)−Sn(1) 2.5146(3), Fe(1)−C(50) 1.763(3), Fe(1)−C(51) 1.760(2) C(50)−O(50) 1.148(3), C(51)−O(51) 1.151(3); N(1)−Sn(1)−N(2) 100.81(7), N(1)−Sn(1)−N(3) 103.73(7), N(2)−Sn(1)−N(3) 99.41(7), N(1)−Sn(1)−Fe(1) 114.18(5), N(2)−Sn(1)−Fe(1) 113.13(5), N(3)−Sn(1)−Fe(1) 122.54(5), C(50)−Fe(1)−Sn(1) 89.46(8), C(51)−Fe(1)−Sn(1) 94.37(7), O(50)−C(50)−Fe(1) 177.6(2), O(51)−C(51)−Fe(1) 173.3(2)

[$Cp(CO)_2Fe]_2SnCl_2$ [2.492(8) Å],[20] [$Cp(CO)_2Fe$−Sn{N*t*Bu)$_2$SiMe}$_2$Me] [2.532(2) Å],[21] [$Cp(CO)_2$Fe{Sn(N*t*Bu)$_2$SiMe}$_2$] [2.605(2) Å],[21] [$Cp(CO)_2Fe]_2Sn(N_3)_2$ [2.504(1) Å][22] and [$Cp(CO)_2Fe$−Sn($SiMe_3NCH_2)_3CCH_3$] [2.539(1) Å].[24] The Sn−Fe−C(carbonyl) bond angles are nearly perpendicular [89.46(8)° and 94.37(7)°] and resemble those in [$Cp(CO)_2Fe$−Sn($SiMe_3NCH_2)_3CCH_3$].[24]

In analogy to the formation of the Fe−Sn and Ru−Sn complexes, compound **1** reacts with the group 6 metal complexes [CpM(CO)$_3$Cl] (M = Mo, W) to afford the corresponding heterodimetallic complexes [MeSi{$SiMe_2$N(4-$CH_3C_6H_4$)}$_3$Sn−M(CO)$_2$Cp] (M = Mo: **8**; W: **9**) (Scheme 3). However, their NMR spectral patterns recorded at room temperature differ considerably from those found for the Fe and Ru analogues. The ^{1}H NMR spectrum exhibits two singlets for the $SiMe_2$ groups (**8**: δ = 0.58, 0.62; **9**: δ = 0.54, 0.62), two singlets for the $CH_3(C_6H_4)$ groups (**8**: δ = 2.17, 2.19; **9**: δ = 2.12, 2.15), and four doublets for the aromatic protons (**8**: δ = 6.94, 7.05, 7.18, 7.21; **9**: δ = 6.88, 7.03, 7.14, 7.20). In addition, two ^{13}C NMR carbonyl resonances (**8**: δ = 224.7, 230.0; **9**: δ = 213.5, 217.4) and three ^{29}Si NMR signals [**8**: δ = −89.0 (SiMe), 1.9, 2.4 ($SiMe_2$); **9**: δ = −89.1 (SiMe), 1.7, 2.2 ($SiMe_2$)] have been detected at room temperature. It is thus clear that the internal rotation around the metal−metal bond axis is frozen out on the NMR time scale at 295 K. This is a consequence of the sterically more encumbered coordination sphere around the group 6 metal bearing an additional carbonyl ligand with respect to **6** and **7**.

In a series of high temperature ^{1}H NMR spectra of **8** and **9** coalescence of the proton resonances was observed and the high temperature limit attained at 340 K for **8** and at 350 K for **9**. At these temperatures the ^{1}H NMR spectra of both compounds show one singlet for the $SiMe_2$ groups (**8**: δ = 0.52; **9**: δ = 0.51), one singlet for the $CH_3(C_6H_4)$ groups (**8**: δ = 2.16; **9**: δ = 2.17), and two doublets for the aromatic protons (**8**: δ = 6.94, 7.13; **9**: δ = 6.94, 7.14), whereas only one ^{13}C NMR carbonyl resonance (**8**: δ = 224.9; **9**: δ = 213.7) has been observed. Coalescence of the $SiMe_2$ and $CH_3(C_6H_4)$ resonances is observed at T_c = 313 K (**8**), and T_c = 316 K (**9**), and an activation enthalpy for the rotation around the Sn−M bond of $\Delta G^{\neq}$ = 67.8 ± 1.0 kJ·mol^{-1} (**8**) and 68.3 ± 1.0 kJ·mol^{-1} (**9**) may be estimated based on these data.

The different dynamic behaviour in solution of the group 6 tricarbonyl derivatives in comparison with the group 8 dicarbonyl complexes made a detailed structural characterization desirable. To this end a single crystal X-ray diffraction study of compound **9** was carried out. The molecular structure of **9** is depicted in Figure 2 along with the principal bond lengths and interbond angles.

The overall molecular structure resembles that of **6**, the triamidotin unit being structurally very similar. The Sn−W bond length in **9** [2.7826(2) Å] is comparable to those found in structurally related W−Sn heterodimetallics, such as [$Cp(CO)_3W-SnCl_2$(*t*Bu)] (2.752 Å),[25] [(Ph_2Si−O−$SiPh_2$)O_2Sn(*t*Bu)−W(CO)$_3$Cp] (2.779 Å and 2.761 Å),[26] [$Cp(CO)_3W-SnCl_2-${Os(CO)$_4$}$_2$Os(CO)$_4$Cl] (2.756 Å),[27] [$Ph_3Sn-W(Cp)_2-SnCl$(*t*Bu)$_2$] (2.811 Å and 2.794 Å)[28] and [IHg−W(Cp)$_2$−SnPh$_3$] (2.768 Å).[17] The Sn−W−C(carbonyl) bond angles are 75.79(9)°, 74.83(9)°, and 126.44(10)° and reflect the steric hindrance around the W centre. The W−C distances of the two carbonyl ligands pointing towards the tin fragment are virtually identical [C(50)−W(1): 1.996(4) Å; C(51)−W(1): 1.987(3) Å] to that of the carbonyl pointing away from the W−Sn bond [C(52)−W(1): 2.002(3) Å].

In the synthesis of complexes **6**−**9** the triamidostannate was reacted with transition metal monohalide complexes to

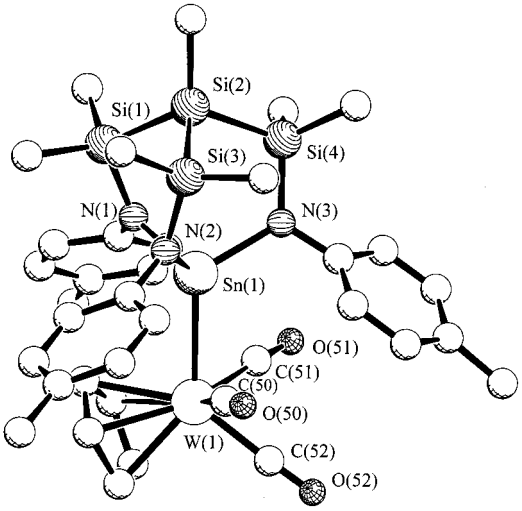

Figure 2. View of the molecular structure of **9**; principal bond lengths (Å) and angles (°): N(1)−Sn(1) 2.084(2), N(2)−Sn(1) 2.068(3), N(3)−Sn(1) 2.078(3), W(1)−C(28) 2.316(3), W(1)−C(29) 2.345(3),W(1)−C(30) 2.355(3), W(1)−C(31) 2.340(3), W(1)−C(32) 2.319(3), W(1)−Sn(1) 2.7826(2), W(1)−C(50) 1.996(4), W(1)−C(51) 1.987(3), W(1)−C(52) 2.002(3), C(50)−O(50) 1.140(4), C(51)−O(51) 1.146(4), C(52)−O(52) 1.135(4); N(1)−Sn(1)−N(2) 100.30(10), N(1)−Sn(1)−N(3) 101.64(10), N(2)−Sn(1)−N(3) 102.51(10), N(1)−Sn(1)−W(1) 114.47(7), N(2)−Sn(1)−W(1) 116.95(7), N(3)−Sn(1)−W(1) 118.30(7), C(50)−W(1)−Sn(1) 75.79(9), C(51)−W(1)−Sn(1) 74.83(9), C(52)−W(1)−Sn(1) 126.44(10), O(50)−C(50)−W(1) 174.8(3), O(51)−C(51)−W(1) 174.2(3), O(52)−C(52)−W(1) 177.4(3)

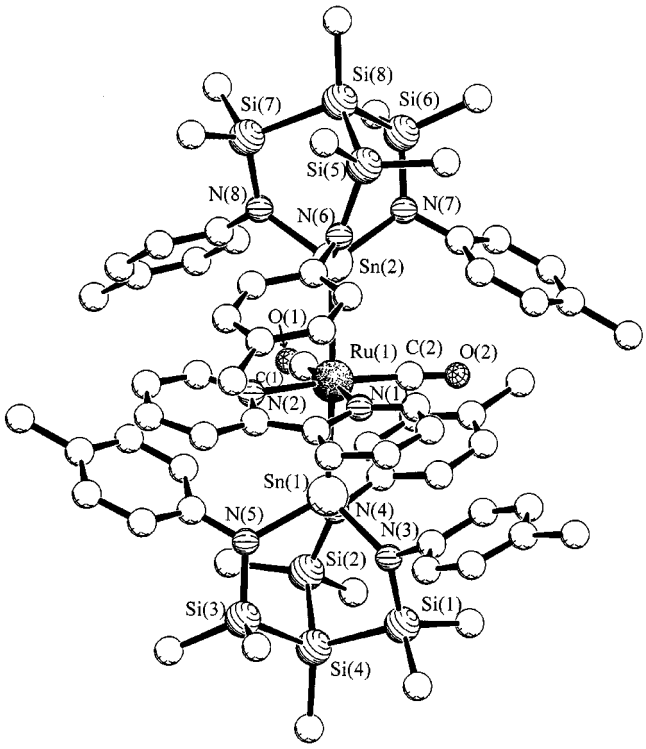

Figure 3. View of the molecular structure of **10**; principal bond lengths (Å) and angles (°): N(3)−Sn(1) 2.098(4), N(4)−Sn(1) 2.107(4), N(5)−Sn(1) 2.113(3), N(6)−Sn(2) 2.098(4), N(7)−Sn(2) 2.109(3), N(8)−Sn(2) 2.113(4), Ru(1)−N(1) 2.117(4), Ru(1)−N(2) 2.113(3), Ru(1)−Sn(1) 2.7085(5), Ru(1)−Sn(2) 2.7324(5), Ru(1)−C(1) 1.863(5), Ru(1)−C(2) 1.877(5), C(1)−O(1) 1.148(6), C(2)−O(2) 1.148(5); N(3)−Sn(1)−N(4), N(3)−Sn(1)−N(5) 101.61(14), N(4)−Sn(1)−N(5) 97.10(14), N(6)−Sn(2)−N(7) 96.40(14), N(6)−Sn(2)−N(8) 99.45(14), N(7)−Sn(2)−N(8) 100.26(14), Sn(1)−Ru(1)−Sn(2) 174.26(2), N(1)−Ru(1)−Sn(1) 91.67(10), N(2)−Ru(1)−Sn(1) 90.25(10), N(1)−Ru(1)−Sn(2) 93.98(10), N(2)−Ru(1)−Sn(2) 90.12(10), N(1)−Ru(1)−N(2) 76.15(15), C(1)−Ru(1)−C(2) 87.6(2), C(1)−Ru(1)−N(1) 173.35(18), C(2)−Ru(1)−N(2) 171.80(19), O(1)−C(1)−Ru(1) 174.3(4), O(2)−C(2)−Ru(1) 176.9(5)

form a single metal−metal bond. To extend this synthetic approach, a coupling with a "difunctional" transition metal complex (bearing two displaceable halide ligands) was attempted. Reaction of *trans*(Cl)-[$RuCl_2(bpy)(CO)_2$][30] with two molar equivalents of **1** in THF afforded the trinuclear complex **10** in moderate yield (Scheme 3). Its NMR spectroscopic data (^1H, ^{13}C, ^{29}Si) indicate a local threefold symmetry of the stannate fragment in solution. The IR spectrum of **10** shows two equally intense bands in the CO stretching region at 2039 and 1990 cm^{-1}, which can be assigned to $\nu_s(CO)$ and $\nu_{as}(CO)$, respectively. The strongly σ-donating and weakly π-accepting amidostannyl ligands shift the wavenumbers to smaller values than those of *trans*(Cl)-[$RuCl_2(bpy)(CO)_2$] (2065, 2004 cm^{-1} in CH_2Cl_2) (see Table 1). It is noteworthy that the reaction of *trans*(Cl)-[$RuCl_2(bpy)(CO)_2$] with one molar equivalent of **1** instantaneously yields **10** and 0.5 molar equivalent of unchanged *trans*(Cl)-[$RuCl_2(bpy)(CO)_2$]. The substitution of the second chloro ligand therefore appears to be accelerated by the strong trans effect of the triamidostannate bonded to the ruthenium centre upon the first substitution step. This trinuclear complex is the first of its type using the triamidostannate cages and was therefore structurally characterized by X-ray diffraction.

The molecular structure of **10** is depicted in Figure 3, along with the principal bond lengths and angles. The two $[MeSi\{SiMe_2N(4\text{-}CH_3C_6H_4)\}_3Sn]^-$ ligands are bonded to the Ru centre in a nearly linear fashion [Sn(1)−Ru−Sn(2): 174.26(2) °] and are staggered with respect to their tolyl groups. The Ru−Sn bond lengths of 2.7085(5) and 2.7324(5) Å are slightly longer than the typical values for Ru−Sn bonds (2.55−2.69 Å).[31] Similar structural parameters have been recently described in the closely related compound $[Ru(SnPh_3)_2(CO)_2(i\text{Pr-DAB})]$ (*i*Pr-DAB = *N*,*N*′-diisopropyl-1,4-diaza-1,3-butadiene),[32] where Ru−Sn bond lengths of 2.686(2) and 2.691(2) Å, and an Sn−Ru−Sn bond angle of 173.45(7)° were found. The shorter carbonyl C−O bond lengths [1.133(22) and 1.123(20) Å] in the precursor complex *trans*(Cl)-[$RuCl_2(bpy)(CO)_2$][30] compared to those of **10** [1.148(6) and 1.148(5) Å] may be due to the strong σ-donation of the stannyl ligands in the latter and confirm the results obtained by IR spectroscopy. The pyridine rings in the bpy subunit are slightly twisted with respect to each other, probably due to the steric demand of the tolyl groups [torsional angles: N(1)−C(14)−C(15)−N(2): 1.1(6)° and C(13)−C(14)−C(15)−C(16): 2.8(8)°].

Conclusion

This study has not only established new types of transition metal−tin complexes but introduced the monoanionic triamidostannate $[MeSi\{SiMe_2N(4\text{-}CH_3C_6H_4)\}_3Sn]^-$ as a "ligand" in transition metal chemistry. This system is isoelectronic to the neutral group 15 analogues but, due to its charge, gives access to structures which are complementary to those of phosphane, arsane or stibane complexes. A particularly interesting aspect of its chemistry is the *trans* effect of the stannate established for the substitution of the two *trans* disposed chloro ligands in the synthesis of **10**. Along with further aspects of the structural chemistry it is this point which we are currently studying in the context of the potential of the stannates in homogeneous catalysis.

Experimental Section

General: All manipulations were performed under argon (desiccant P_4O_{10}, Granusic®, J.T. Baker) on a high vacuum line using standard Schlenk techniques, or in a glovebox. All reaction flasks were heated prior to use using three evacuation-refill cycles. Solvents and solutions were transferred by needle-septa techniques. Solvents were dried according to standard methods and saturated with argon. The deuterated solvents used for the NMR spectroscopic measurements were degassed by three successive "freeze−pump−thaw" cycles and stored over 4 Å molecular sieves. Solids were separated from suspensions by filtration through dried Celite. The ^1H, ^{13}C, ^{29}Si and ^{31}P NMR spectra were recorded on a Bruker AC 200, a Bruker Avance 250 and a Bruker AMX 400 FT NMR spectrometer, respectively. ^1H and ^{13}C data are listed in parts per million [ppm] relative to tetramethylsilane and were referenced using the residual protonated solvent peak (^1H) or the carbon resonance (^{13}C). ^{29}Si data are listed in ppm relative to tetramethylsilane as an external standard. ^{31}P data are listed in ppm relative to 85% H_3PO_4 as an external standard. Infrared spectra were recorded on a Nicolet Magna IRTM 750 spectrometer. Elemental analyses were carried out with a Leco CHNS-932 microanalyzer and a CE-instruments EA 1110 CHNS-O microanalyzer, respectively. The compounds $[CpFe(CO)_2Cl]$,[33] $[CpRu(CO)_2Br]$,[34] *trans*-$[RuCl_2(bpy)(CO)_2]$,[35] $[CpMo(CO)_3Cl]$,[36] $[CpW(CO)_3Cl]$,[36] $[CuCl(PPh_3)]_4$ [37] and $[MeSi\{SiMe_2N(4\text{-}CH_3C_6H_4)\}_3SnLi(OEt_2)]$[11] were prepared according to published procedures. All other chemicals used as starting materials were obtained commercially and used without further purification.

Preparation of $[MeSi\{SiMe_2N(p\text{-Tol})\}_3SnCH_3]$ (2): Methyl iodide (30 μL, 67.4 mg, 0.475 mmol) was added to a solution of $[MeSi\{SiMe_2N(p\text{-Tol})\}_3SnLi(OEt_2)]$ (**1**) (348 mg, 0.474 mmol) in 15 mL of toluene at −20 °C. The reaction mixture was subsequently warmed to ambient temperature, centrifuged, and the filtrate evaporated to dryness. The colourless, microcrystalline residue was washed twice with cold pentane and then dried in vacuo. Yield: 307 mg (97%). − ^1H NMR (200.13 MHz, C_6D_6, 295 K): δ = 0.03 (s, 3 H, $SnCH_3$), 0.20 (s, 3 H, $SiCH_3$), 0.57 [s, 18 H, $Si(CH_3)_2$], 2.10 (s, 9 H, $CH_3C_6H_4$), 6.88 (d, $^3J_{H,H}$ = 8.1 Hz, 6 H, Tol-$H^{2,6}$), 6.98 (d, 6 H, Tol-$H^{3,5}$). − $^{13}C\{^1H\}$ NMR (50.32 MHz, C_6D_6, 295 K): δ = −15.0 ($SiCH_3$), −9.3 ($SnCH_3$), 3.4 [$Si(CH_3)_2$], 20.7 ($CH_3C_6H_4$), 125.9 (Tol-$C^{2,6}$), 130.1 (Tol-$C^{3,5}$), 130.9 (Tol-C^4), 147.6 (Tol-C^1). − $^{29}Si\{^1H\}$ NMR (39.76 MHz, C_6D_6, 295 K): δ = −91.3 ($SiCH_3$), 4.3 [$Si(CH_3)_2$]. − $C_{29}H_{45}N_3Si_4Sn$ (666.73): calcd. C 52.24, H 6.80, N 6.30; found C 52.57, H 6.97, N 6.41.

Preparation of $[MeSi\{SiMe_2N(p\text{-Tol})\}_3Sn-SiMe_3]$ (3) and $[MeSi\{SiMe_2N(p\text{-Tol})\}_3Sn-SnMe_3]$ (4): Me_3SiCl or Me_3SnCl (0.475 mmol) was added to a solution of $[MeSi\{SiMe_2N(p\text{-Tol})\}_3SnLi(OEt_2)]$ (**1**) (365 mg, 0.490 mmol) in 15 mL of toluene at −20 °C. The reaction mixture was subsequently warmed to ambient temperature, centrifuged, and the filtrate evaporated to dryness. The colourless, microcrystalline residue was washed twice with cold pentane and then dried in vacuo. Yields: **3**: 341 mg, 96%; **4**: 388 mg, 97%.

3: ^1H NMR (200.13 MHz, C_6D_6, 295 K): δ = −0.34 [s, 9 H, $SnSi(CH_3)_3$], 0.21 (s, 3 H, $SiCH_3$), 0.59 [s, 18 H, $Si(CH_3)_2$], 2.10 (s, 9 H, $CH_3C_6H_4$), 6.91 (d, $^3J_{H,H}$ = 8.1 Hz, 6 H, Tol-$H^{2,6}$), 7.05 (d, 6 H, Tol-$H^{3,5}$). − $^{13}C\{^1H\}$ NMR (50.32 MHz, C_6D_6, 295 K): δ = −14.4 ($SiCH_3$), 0.3 [$Si(CH_3)_3$], 3.4 [$Si(CH_3)_2$], 20.7 ($CH_3C_6H_4$), 125.2 (Tol-$C^{2,6}$), 130.0 (Tol-$C^{3,5}$), 130.2 (Tol-C^4), 150.3 (Tol-C^1). − $^{29}Si\{^1H\}$ NMR (39.76 MHz, C_6D_6, 295 K): δ = −87.0 ($SiCH_3$), 2.1 [$Si(CH_3)_2$], 9.6 [$Si(CH_3)_3$]. − $C_{31}H_{51}N_3Si_5Sn$ (724.88): calcd. C 51.37, H 7.09, N 5.80; found C 51.86, H 7.24, N 5.91.

4: ^1H NMR (200.13 MHz, C_6D_6, 295 K): δ = −0.26 [s, 9 H, $SnSn(CH_3)_3$], 0.22 (s, 3 H, $SiCH_3$), 0.60 [s, 18H, $Si(CH_3)_2$], 2.10 (s, 9 H, $CH_3C_6H_4$), 6.91 (d, $^3J_{H,H}$ = 8.4 Hz, 6 H, Tol-$H^{2,6}$), 6.98 (d, $^3J_{H,H}$ = 8.4 Hz, 6 H, Tol-$H^{3,5}$). − $^{13}C\{^1H\}$ NMR (50.32 MHz, C_6D_6, 295 K): δ = −8.4 ($SiCH_3$), 3.5 [$Si(CH_3)_2$], 15.6 [$Sn(CH_3)_3$], 20.7 ($CH_3C_6H_4$), 124.9 (Tol-$C^{2,6}$), 130.1 (Tol-$C^{3,5}$), 130.2 (Tol-C^4), 150.0 (Tol-C^1). − $^{29}Si\{^1H\}$ NMR (39.76 MHz, C_6D_6, 295 K): δ = −87.3 ($SiCH_3$), 2.0 [$Si(CH_3)_2$]. − $C_{31}H_{51}N_3Si_4Sn_2$ (815.49): calcd. C 45.66, H 6.30, N 5.15; found C 45.80, H 6.54, N 5.33.

$[MeSi\{SiMe_2N(4\text{-}CH_3C_6H_4)\}_3Sn-Cu(PPh_3)]$ (5): Precooled (−40 °C) toluene (10 mL) was added to a mixture of solid $[MeSi\{SiMe_2N(p\text{-Tol})\}_3SnLi(OEt_2)]$ (**1**) (376 mg, 0.51 mmol) and solid $[CuCl(PPh_3)]$ (186 mg, 0.51 mmol). The stirred solution was subsequently warmed to ambient temperature, the LiCl which precipitated removed by filtration and the concentrated filtrate (1 mL) stored for several days at −30 °C. The colourless crystals of compound **5** were collected after decanting of the mother liquor and dried in vacuo. Yield: 349 mg (43%). − ^1H NMR (250.13 MHz, C_6D_6, 295 K): δ = 0.38 (s, 3 H, $SiCH_3$), 0.73 [s, 18 H, $Si(CH_3)_2$], 2.05 (s, 9 H, $CH_3C_6H_4$), 6.52 (d, $^3J_{H,H}$ = 8.3 Hz, 6 H, $H^{2,6}$ of $CH_3C_6H_4$), 6.85−6.96 (m, 15 H, PPh_3), 7.02 (d, $^3J_{H,H}$ = 8.3 Hz, 6 H, $H^{3,5}$ of $CH_3C_6H_4$). − $^{13}C\{^1H\}$ NMR (62.89 MHz, C_6D_6, 295 K): δ = −13.9 ($SiCH_3$), 4.2 [$Si(CH_3)_2$], 20.9 ($CH_3C_6H_4$), 125.7, 126.7, 128.6, 129.3, 129.8, 132.9, 134.0, 152.6 (all tol and PPh_3). − $^{29}Si\{^1H\}$ NMR (49.69 MHz, C_6D_6, 295 K): δ = −88.7 ($SiCH_3$), −3.4 [$Si(CH_3)_2$]. − $^{31}P\{^1H\}$ NMR (81.03 MHz, C_6D_6, 295 K): δ = 0.70 (br, PPh_3). − $^{31}P\{^1H\}$ NMR (81.03 MHz, [D_8]toluene, 205 K): δ = 6.6 [$^2J(^{117/119}Sn-^{31}P)$ = 634.2/662.8 Hz, PPh_3]. $C_{46}H_{57}CuN_3PSi_4Sn$ (984.68): calcd. C 56.52, H 5.88, N 4.30; found C 56.19, H 5.73, N 4.29.

$[MeSi\{SiMe_2N(4\text{-}CH_3C_6H_4)\}_3Sn-Fe(\eta^5\text{-}C_5H_5)(CO)_2]$ (6): A mixture of solid $[(\eta^5\text{-}C_5H_5)Fe(CO)_2Cl]$ (116 mg, 0.55 mmol) and $[MeSi\{SiMe_2N(4\text{-}CH_3C_6H_4)\}_3SnLi(OEt_2)]$ (**1**) (400 mg, 0.55 mmol) was dissolved at room temperature in toluene (15 mL) and stirred for 3 h. The solution was filtered through Celite and the residue was extracted with toluene (10 mL). After complete removal of the solvent, a bright yellow, crystalline solid was obtained, which was subsequently washed with pentane (10 mL) and dried in vacuum (yield: 308 mg, 68%). Suitable crystals for the structure determination could be obtained from a saturated solution of **6** (100 mg) in benzene (0.5 mL) at room temperature. − ^1H NMR (200.13 MHz, C_6D_6, 295 K): δ = 0.28 (s, 3 H, $SiCH_3$), 0.62 [s, 18 H, $Si(CH_3)_2$], 2.16 (s, 9 H, $CH_3C_6H_4$), 3.43 (s, 5 H, C_5H_5), 7.01 (d, $^3J_{H,H}$ = 8.0 Hz, 6 H, $H^{2,6}$ of $CH_3C_6H_4$), 7.19 (d, $^3J_{H,H}$ = 8.0 Hz, 6 H, $H^{3,5}$

of $CH_3C_6H_4$). – $^{13}C\{^1H\}$ NMR (50.32 MHz, C_6D_6, 295 K): δ = −14.6 (Si*C*H$_3$), 3.8 [Si(*C*H$_3$)$_2$], 20.8 (*C*H$_3$C$_6$H$_4$), 81.8 (*C*$_5$H$_5$), 128.9 (C^{2,6}), 129.7 (C^{3,5}), 131.4 (C^4), 149.7 (C^1), 212.8 (CO). – $^{29}Si\{^1H\}$ NMR (39.76 MHz, C_6D_6, 295 K): δ = −90.0 (*Si*CH$_3$), 0.8 [*Si*(CH$_3$)$_2$]. – IR (toluene): ν(CO) = 2016, 1971 cm^{-1}. – $C_{35}H_{47}FeN_3O_2Si_4Sn$ (828.65): calcd. C 50.73, H 5.72, N 5.07; found C 50.83, H 5.91, N 5.23.

[MeSi{SiMe$_2$N(4-CH$_3$C$_6$H$_4$)}$_3$Sn−Ru(η^5-C$_5$H$_5$)(CO)$_2$] (7): An analogous procedure described to prepare **6**, with 61.8 mg (0.21 mmol) of [(η^5-C$_5$H$_5$)Ru(CO)$_2$Br] and 150 mg (0.21 mmol) of [MeSi{SiMe$_2$N(4-CH$_3$C$_6$H$_4$)}$_3$SnLi(OEt$_2$)] (**1**) dissolved in 10 mL of toluene, afforded compound **7** (100 mg, 56%) as a yellow, crystalline solid. – ^{1}H NMR (250.13 MHz, C_6D_6, 295 K): δ = 0.29 (s, 3 H, SiC*H*$_3$), 0.63 [s, 18 H, Si(C*H*$_3$)$_2$], 2.16 (s, 9 H, C*H*$_3$C$_6$H$_4$), 3.88 (s, 5 H, C$_5$*H*$_5$), 7.01 (d, $^3J_{H,H}$ = 7.8 Hz, 6 H, H^{2,6} of CH$_3$C$_6$H$_4$), 7.16 (d, $J_{H,H}$ = 7.8 Hz, 6 H, H^{3,5} of CH$_3$C$_6$H$_4$). – $^{13}C\{^1H\}$ NMR (62.89 MHz, C_6D_6, 295 K): δ = −14.6 (Si*C*H$_3$), 3.8 [Si(*C*H$_3$)$_2$], 20.8 (*C*H$_3$C$_6$H$_4$), 84.6 (*C*$_5$H$_5$), 128.8 (C^{2,6}), 129.7 (C^{3,5}), 130.5 (C^4), 149.9 (C^1), 199.4 (CO). – $^{29}Si\{^1H\}$ NMR (49.69 MHz, C_6D_6, 295 K): δ = −89.7 (*Si*CH$_3$), 0.7 [*Si*(CH$_3$)$_2$]. – IR (toluene): ν(CO) = 2030, 1981 cm^{-1}. – $C_{35}H_{47}N_3O_2RuSi_4Sn$ (873.88): calcd. C 48.11, H 5.42, N 4.81; found C 48.39, H 5.80, N 4.46.

[MeSi{SiMe$_2$N(4-CH$_3$C$_6$H$_4$)}$_3$Sn−Mo(η^5-C$_5$H$_5$)(CO)$_3$] (8): A solution of [(η^5-C$_5$H$_5$)Mo(CO)$_3$Cl] (38.3 mg, 0.14 mmol) in toluene (2 mL) was added at −78 °C to a vigorously stirred solution of [MeSi{SiMe$_2$N(4-CH$_3$C$_6$H$_4$)}$_3$SnLi(OEt$_2$)] (**1**) (100 mg, 0.14 mmol) in toluene (2 mL). The solution was slowly warmed up to room temperature over a period of 12 h and subsequently filtered through Celite. The solvent was removed under reduced pressure and the resulting residue was washed with pentane (1 mL). Compound **8** (74.6 mg, 61%) was obtained as a pale orange, microcrystalline solid. – ^{1}H NMR (400.13 MHz, [D$_8$]toluene, 290 K): δ = 0.26 (s, 3 H, SiC*H*$_3$), 0.58 [s, 12 H, Si(C*H*$_3$)$_2$], 0.62 [s, 6 H, Si(C*H*$_3$)$_2$], 2.17 (s, 6 H, C*H*$_3$C$_6$H$_4$), 2.19 (s, 3 H, C*H*$_3$C$_6$H$_4$), 4.07 (s, 5 H, C$_5$*H*$_5$), 6.94 (d, $^3J_{H,H}$ = 7.8 Hz, 4 H, H^{2,6} of CH$_3$C$_6$H$_4$), 7.05 (d, $^3J_{H,H}$ = 7.8 Hz, 2 H, H^{2,6} of CH$_3$C$_6$H$_4$), 7.18 (d, $^3J_{H,H}$ = 7.8 Hz, 4 H, H^{3,5} of CH$_3$C$_6$H$_4$), 7.21 (d, $^3J_{H,H}$ = 7.8 Hz, 2 H, H^{3,5} of CH$_3$C$_6$H$_4$). – ^{1}H NMR (400.13 MHz, [D$_8$]toluene, 340 K): δ = 0.24 (s, 3 H, SiC*H*$_3$), 0.52 [s, 18 H, Si(C*H*$_3$)$_2$], 2.16 (s, 9 H, C*H*$_3$C$_6$H$_4$), 4.19 (s, 5 H, C$_5$*H*$_5$), 6.94 (d, $^3J_{H,H}$ = 7.8 Hz, 6 H, H^{2,6} of CH$_3$C$_6$H$_4$), 7.13 (d, $^3J_{H,H}$ = 7.8 Hz, 6 H, H^{3,5} of CH$_3$C$_6$H$_4$). – $^{13}C\{^1H\}$ NMR (100.63 MHz, [D$_8$]toluene, 290 K): δ = −14.2 (Si*C*H$_3$), 4.1, 4.2 [Si(*C*H$_3$)$_2$], 20.9 (*C*H$_3$C$_6$H$_4$), 89.7 (*C*$_5$H$_5$), 117.1, 117.2 (C^4), 129.0, 129.1 (C^{2,6}), 130.8, 131.0(C^{3,5}), 148.3, 149.8 (C^1), 224.7, 230.0 (CO). – $^{13}C\{^1H\}$ NMR (100.63 MHz, [D$_8$]toluene, 340 K): δ = −14.6 (Si*C*H$_3$), 4.1 [Si(*C*H$_3$)$_2$], 20.6 (*C*H$_3$C$_6$H$_4$), 89.6 (*C*$_5$H$_5$), 117.8 (C^4), 129.8 (C^{2,6}), 131.4(C^{3,5}),149.8 (C^1), 224.9 (CO). – $^{29}Si\{^1H\}$ NMR (49.69 MHz, [D$_8$]toluene, 295 K): δ = −89.1 (*Si*CH$_3$), 1.9, 2.4 [*Si*(CH$_3$)$_2$]. – IR (toluene): ν(CO) = 2021 (s), 1954 (m), 1937 (s) cm^{-1}. – $C_{36}H_{47}MoN_3O_3Si_4Sn$ (896.76): calcd. C 48.22, H 5.28, N 4.69; found C 48.60, H 5.42, N 4.87.

[MeSi{SiMe$_2$N(4-CH$_3$C$_6$H$_4$)}$_3$Sn−W(η^5-C$_5$H$_5$)(CO)$_3$] (9): An analogous procedure described to prepare **8**, with 251 mg (0.68 mmol) of [(η^5-C$_5$H$_5$)W(CO)$_3$Cl] and 500 mg (0.68 mmol) of [MeSi{SiMe$_2$N(4-CH$_3$C$_6$H$_4$)}$_3$SnLi(OEt$_2$)] (**1**) dissolved in 20 mL of toluene, afforded compound **9** (504 mg, 75%) as a yellow, crystalline solid. Suitable crystals for the structure determination could be obtained from a saturated solution of **9** (100 mg) in benzene (0.5 mL) at room temperature. – ^{1}H NMR (400.13 MHz, [D$_8$]toluene, 290 K): δ = 0.21 (s, 3 H, SiC*H*$_3$), 0.54 [s, 12 H, Si(C*H*$_3$)$_2$], 0.58 [s, 6 H, Si(C*H*$_3$)$_2$], 2.12 (s, 6 H, C*H*$_3$C$_6$H$_4$), 2.15 (s, 3 H, C*H*$_3$C$_6$H$_4$), 4.02 (s, 5 H, C$_5$*H*$_5$), 6.88 (d, $^3J_{H,H}$ = 7.8 Hz, 4 H, H^{2,6} of CH$_3$C$_6$H$_4$), 7.03 (d, $^3J_{H,H}$ = 8.1 Hz, 2 H, H^{2,6} of CH$_3$C$_6$H$_4$), 7.14 (d, $^3J_{H,H}$ = 7.8 Hz, 4 H, H^{3,5} of CH$_3$C$_6$H$_4$), 7.20 (d, $^3J_{H,H}$ = 8.1 Hz, 2 H, H^{3,5} of CH$_3$C$_6$H$_4$). – ^{1}H NMR (400.13 MHz, [D$_8$]toluene, 350 K): δ = 0.24 (s, 3 H, SiC*H*$_3$), 0.51 [s, 18 H, Si(C*H*$_3$)$_2$], 2.17 (s, 9 H, C*H*$_3$C$_6$H$_4$), 4.22 (s, 5 H, C$_5$*H*$_5$), 6.94 (d, $^3J_{H,H}$ = 7.8 Hz, 6 H, H^{2,6} of CH$_3$C$_6$H$_4$), 7.14 (d, $^3J_{H,H}$ = 7.8 Hz, 6 H, H^{3,5} of CH$_3$C$_6$H$_4$). – $^{13}C\{^1H\}$ NMR (100.63 MHz, [D$_8$]toluene, 295 K): δ = −14.4 (Si*C*H$_3$), 4.0, 4.1 [Si(*C*H$_3$)$_2$], 20.8 (*C*H$_3$C$_6$H$_4$), 88.2 (*C*$_5$H$_5$), 128.6, 128.8 (C^{2,6}), 129.0, 130.1 (C^{3,5}), 130.5, 130.9 (C^4), 148.4, 149.9 (C^1), 213.5, 217.4 (CO). – $^{13}C\{^1H\}$ NMR (100.63 MHz, [D$_8$]toluene, 350 K): δ = −14.6 (Si*C*H$_3$), 4.1 [Si(*C*H$_3$)$_2$], 20.8 (*C*H$_3$C$_6$H$_4$), 88.2 (*C*$_5$H$_5$), 126.3 (C^{2,6}), 129.6 (C^{3,5}), 129.9 (C^4), 131.4 (C^1), 213.7 (CO). – $^{29}Si\{^1H\}$ NMR (49.69 MHz, [D$_8$]toluene, 295 K): δ = −89.1 (*Si*CH$_3$), 1.7, 2.2 [*Si*(CH$_3$)$_2$]. – IR (toluene): ν(CO) = 2018 (s), 1944 (m), 1930 (s) cm^{-1}. – $C_{36}H_{47}N_3O_3Si_4SnW$ (984.67): calcd. C 43.91, H 4.81, N 4.27; found C 43.98, H 4.83, N 4.21.

[(MeSi{SiMe$_2$N(4-CH$_3$C$_6$H$_4$)}$_3$Sn)$_2$−Ru(bpy)(CO)$_2$] (10): A solution of [MeSi{SiMe$_2$N(4-CH$_3$C$_6$H$_4$)}$_3$SnLi(OEt$_2$)] (200 mg, 0.27 mmol) in THF (30 mL) was added at −40 °C to solid [*trans*-RuCl$_2$(bpy)(CO)$_2$] (52.4 mg, 0.14 mmol), resulting in an immediate change of colour from pale yellow to deep orange. The reaction mixture was warmed up to ambient temperature over a period of 4 h and subsequently filtered through Celite. Removal of the solvent in vacuum, extraction of the residue with toluene (30 mL), and concentration of the solution to about 3 mL yielded a microcrystalline powder after storage at −50 °C. The supernatant solution was removed by decantation and the solid was washed with pentane (5 mL) and dried in vacuum to yield **10** (147 mg, 66%) as a deep orange solid. Suitable crystals for the structure determination could be obtained from a saturated solution of **10** (80 mg) in benzene (0.5 mL) at room temperature. – ^{1}H NMR (250.13 MHz, [D$_8$]THF, 295 K): δ = −0.08 (s, 6 H, SiC*H*$_3$), −0.04 [s, 36 H, Si(C*H*$_3$)$_2$], 2.39 (s, 18 H, C*H*$_3$C$_6$H$_4$), 6.29 (dt, $^3J_{H,H}$ = 5.7, $^4J_{H,H}$ = 1.1 Hz, 2 H, H$^{5,5'}$ of bipy), 6.47 (d, $^3J_{H,H}$ = 8.2 Hz, 12 H, H^{2,6} of CH$_3$C$_6$H$_4$), 6.71 (d, $^3J_{H,H}$ = 8.2 Hz, 12 H, H^{3,5} of CH$_3$C$_6$H$_4$), 7.04 (dd, $^3J_{H,H}$ = 5.7, $^4J_{H,H}$ = 1.1 Hz, 2 H, H$^{6,6'}$ of bipy), 7.32 (d, $^3J_{H,H}$ = 7.8 Hz, 2 H, H$^{3,3'}$ of bipy), 7.45 (dt, $^3J_{H,H}$ = 7.8, $^4J_{H,H}$ = 1.6 Hz, 2 H, H$^{4,4'}$ of bipy). – $^{13}C\{^1H\}$ NMR (62.89 MHz, [D$_8$]THF, 295 K): δ = −13.7 (Si*C*H$_3$), 4.2 [Si(*C*H$_3$)$_2$], 21.3 (*C*H$_3$C$_6$H$_4$), 117.5 (bipy), 123.0 (bipy), 124.6 (bipy), 128.2 (tol), 130.1 (tol), 137.7 (bipy), 151.1 (tol), 153.8 (tol), 154.4 (bipy), 199.1 (CO). – $^{29}Si\{^1H\}$ NMR (49.69 MHz, [D$_8$]THF, 295 K): δ = −81.4 (*Si*CH$_3$), 3.0 [*Si*(CH$_3$)$_2$]. – $^{119}Sn\{^1H\}$ NMR (149.21 MHz, [D$_8$]THF, 295 K): δ = −123.9 (N$_3$*Sn*Ru). – IR (toluene): ν(CO) = 2039, 1990 cm^{-1}. – $C_{68}H_{92}N_8O_2RuSi_8Sn_2$ (1616.66): calcd. C 50.52, H 5.74, N 6.93; found C 50.15, H 5.64, N 6.49.

X-ray Crystallographic Study of 6, 9 and 10: The X-ray diffraction data were collected with a Nonius KappaCCD diffractometer using Mo-K_α radiation (λ = 0.71073 Å) and the Collect[38] data collection program. The Denzo and Scalepack[39] programs were used for cell refinements and data reduction. The structures were solved by Patterson methods using the DIRDIF-99[40] and the WinGX graphical user interface.[41] A multi-scan absorption correction based on equivalent reflections (XPREP in SHELXTL v. 5.1)[42] was applied to **6** and **9** (T_{max}/T_{min} were 0.2529/0.2166 and 0.2766/0.2206, respectively). Structural refinements were carried out with the SHELXL-97 program.[40] All hydrogens were placed in an idealised position and constrained to ride on their parent atom. The crystallographic data are summarised in Table 2. The molecular structures of the complexes along with principal bond lengths and angles are presented in Figure 1−3.

Table 2. Crystal data and structure refinement for **6**, **9** and **10**

	6	**9**	**10**
Molecular formula	$C_{35}H_{47}FeN_3O_2Si_4Sn\cdot 1/2C_6D_6$	$C_{36}H_{47}N_3O_3Si_4SnW$	$C_{68}H_{12}N_8O_2RuSi_8Sn_2\cdot 2C_6D_6$
M_r	870.73	984.67	1784.95
Temperature	120(2) K	120(2) K	150(2) K
Wavelength	0.71073 Å	0.71073 Å	0.71073 Å
Crystal system	Triclinic	Monoclinic	Triclinic
Space group	$P\bar{1}$	$P2_1/n$	$P\bar{1}$
Z	2	4	2
Unit cell dimensions	a = 10.97620(10) Å	a = 11.33020(10) Å	a = 14.2978(2) Å
	b = 11.36830(10) Å	b = 21.5079(2) Å	b = 15.4300(2) Å
	c = 17.6453(3) Å	c = 16.5450(2) Å	c = 20.9716(3) Å
	α = 88.1369(6)°	α = 90°	α = 89.9010(7)°
	β = 79.2840(6)°	β = 92.6662(4)°	β = 83.4869(7)°
	γ = 72.5050(7)°	γ = 90°	γ = 69.0371(8)°
Volume	2062.68(4) Å^3	4027.47(7) Å^3	4288.77(10) Å^3
$D_{calcd.}$	1.402 g cm^{-1}	1.624 g cm^{-1}	1.382 g cm^{-1}
Absorption coefficient	1.108 mm^{-1}	3.630 mm^{-1}	0.912 mm^{-1}
F(000)	894	1952	1824
Crytal size	0.30 × 0.20 × 0.20 mm	0.30 × 0.20 × 0.20 mm	0.20 × 0.10 × 0.10 mm
θ range for data collection	2.11 to 27.53°	2.03 to 27.49°	2.69 to 25.32°
Limiting indices	$-14 \le h \le 14$	$-14 \le h \le 13$	$-17 \le h \le 17$
	$-14 \le k \le 14$	$-27 \le k \le 27$	$-18 \le k \le 18$
	$-22 \le l \le 22$	$-21 \le l \le 21$	$-25 \le l \le 25$
Reflections collected	31634	49083	30106
Independent reflections ($R_{int.}$)	9382 (0.0360)	9238 (0.0528)	15558 (0.0466)
Refinement method	Full-matrix least-squares on F^2	Full-matrix least-squares on F^2	Full-matrix least-squares on F^2
Data/restraints/parameters	9382/0/452	9238/0/443	15558/0/930
$T_{min/max}$	0.8087/0.7321	0.27659/0.22064	0.9144/0.8387
Goodness-of-fit on F^2	1.062	1.063	1.056
Final R indices	R_1 = 0.0299	R_1 = 0.0288	R_1 = 0.0436
[$I > 2\sigma(I)$]	wR_2 = 0.0649	wR_2 = 0.0661	wR_2 = 0.0810
R indices (all data)	R_1 = 0.0398	R_1 = 0.0377	R_1 = 0.0820
	wR_2 = 0.0688	wR_2 = 0.0703	wR_2 = 0.0932
Largest diff. Peak and hole	0.554 and −0.622 e·Å^{-3}	1.195 and −2.031 e·Å^{-3}	0.682 and −0.612 e Å^{-3}

Crystallographic data (excluding structure factors) for the structures reported in this paper have been deposited with the Cambridge Crystallographic Data Centre as supplementary publication nos. CCDC-165210 (**6**), -165211 (**9**) and -165212 (**10**). Copies of the data can be obtained free of charge on application to CCDC, 12 Union Road, Cambridge CB2 1EZ, UK [Fax: (internat.) +44-1223/336-033; E-mail: deposit@ccdc.cam.ac.uk].

Acknowledgments

We thank the European Union (TMR program, network MECATSYN), the Deutsche Forschungsgemeinschaft (SFB 347), the CNRS (France) and the Fonds der Chemischen Industrie for financial support.

[1] [1a] N. S. Vyazankin, G. A. Rauvaev, O. A. Kruglaya, G. S. Semchikova, *J. Organomet. Chem.* **1966**, *6*, 474. – [1b] J. P. Collman, F. D. Vastine, W. R. Roper, *J. Am. Chem. Soc.* **1966**, *88*, 5035. – [1c] J. Lewis, A. R. Manning, J. R. Miller, J. M. Wilson, *J. Chem. Soc. A* **1966**, *12*, 1663. – [1d] R. M. Sweet, C. J. Fritchie, R. A. Schunn, *Inorg. Chem.* **1967**, *6*, 749. – [1e] J. V. Kingston, J. W. S. Jamieson, G. Wilkinson, *J. Inorg. Nucl. Chem.* **1967**, *29*, 133. – [1f] R. F. Bryan, *J. Chem. Soc. A* **1967**, *1*, 192. – [1g] F. J. A. Des Tombe, G. J. M. Van der Kerk, H. M. J. C. Creemers, M. J. C. Henricus, J. G. Noltes, *Chem. Commun.* **1966**, *24*, 914. – [1h] J. V. Kingston, *Inorg. Nucl. Chem. Lett.* **1968**, *4*, 65. – [1i] A. R. Manning, *J. Chem. Soc. A* **1968**, *3*, 651.

[2] M. S. Holt, W. L. Wilson, J. H. Nelson, *Chem. Rev.* **1989**, *89*, 11.

[3] K. M. Mackay, B. K. Nicholson, in *Comprehensive Organometallic Chemistry* (Eds.: G. Wilkinson, F. G. A. Stone, E. W. Abel), Pergamon Press: New York, **1982**; Vol 6, p. 1043.

[4] *Applied Homogeneous Catalysis with Organometallic Compounds* (Eds.: B. Cornils, W. A. Herrmann), VCH, Weinheim, **1996**.

[5] G. B. Stringfellow, N. I. Buchan, C. A. Larsen, in *Materials Research Society Symposia Proceedings* (Eds.: R. Hull, J. M. Gibson, D. A. Smith), Materials Research Society: Pittsburgh, PA, **1987**; Vol. 94, p. 245.

[6] [6a] L. H. Gade, N. Mahr, *J. Chem. Soc., Dalton Trans.* **1993**, 489. – [6b] L. H. Gade, C. Becker, J. W. Lauher, *Inorg. Chem.* **1993**, *32*, 2308. – [6c] H. Memmler, L. H. Gade, J. W. Lauher, *Inorg. Chem.* **1994**, *33*, 3064. – [6d] M. Schubart, B. Findeis, L. H. Gade, W.-S. Li, M. McPartlin, *Chem. Ber.* **1995**, *128*, 329.

[7] K. W. Hellmann, P. Steinert, L. H. Gade, *Inorg. Chem.* **1994**, *33*, 3859.

[8] K. W. Hellmann, L. H. Gade, O. Gevert, P. Steinert, J. W. Lauher, *Inorg. Chem.* **1995**, *34*, 4069.

[9] H. Memmler, U. Kauper, L. H. Gade, D. Stalke, J. W. Lauher, *Organometallics* **1996**, *15*, 3637.

[10] M. Lutz, B. Findeis, M. Haukka, T. A. Pakkanen, L. H. Gade, *Organometallics* **2001**, *20*, 2505.

[11] M. Contel, K. W. Hellmann, L. H. Gade, I. Scowen, M. McPartlin, M. Laguna, *Inorg. Chem.* **1996**, *35*, 3713.

[12] B. Findeis, M. Contel, L. H. Gade, M. Laguna, M. C. Gimeno, I. J. Scowen, M. McPartlin, *Inorg. Chem.* **1997**, *36*, 2386.

[13] B. Findeis, L. H. Gade, I. J. Scowen, M. McPartlin, *Inorg. Chem.* **1997**, *36*, 960.
[14] L. H. Gade, B. Findeis, O. Gevert, H. Werner, *Z. Anorg. Allg. Chem.* **2000**, *626*, 1030.
[15] Examples of structurally characterized Sn−Cu complexes: [15a] M. A. Beswick, C. J. Belle, M. K. Davies, M. A. Halcrow, P. R. Raithby, A. Steiner, D. S. Wright, *Chem. Commun.* **1996**, 2619. − [15b] R. E. Allan, A. Bashall, J. S. Palmer, M. McPartlin, M. E. G. Mosquera, J. M. Rawson, A. E. H. Wheatley, D. S. Wright, *Chem. Commun.* **1997**, 1975. − [15c] J. Klett, K. W. Klinkhammer, M. Niemeyer, *Chem. Eur. J.* **1999**, *5*, 2531.
[16] [16a] S. Friedrich, H. Memmler, L. H. Gade, W.-S. Li, M. McPartlin, *Angew. Chem.* **1994**, *106*, 705; *Angew. Chem. Int. Ed. Engl.* **1994**, *33*, 676. − [16b] B. Findeis, M. Schubart, C. Platzek, L. H. Gade, I. J. Scowen, M. McPartlin, *Chem. Commun.* **1996**, 219. − [16c] G. Jansen, M. Schubart, B. Findeis, L. H. Gade, I. J. Scowen, M. McPartlin, *J. Am. Chem. Soc.* **1998**, *120*, 7239. For a review see: [16d] L. H. Gade, *Angew. Chem.* **2000**, *112*, 2768; *Angew. Chem. Int. Ed.* **2000**, *37*, 2658.
[17] R. F. Bryan, *J. Chem. Soc. A* **1967**, 192.
[18] P. T. Greene, R. F. Bryan, *J. Chem. Soc. A* **1970**, 1696.
[19] G. A. Melson, P. F. Stokely, R. F. Bryan, *J. Chem. Soc. A* **1970**, 2247.
[20] J. E. O'Connor, E. R. Corey, *Inorg. Chem.* **1967**, *5*, 968.
[21] M. Veith, L. Stahl, V. Huch, *Organometallics* **1993**, *12*, 1914.
[22] M. J. Hampden-Smith, D. Lei, E. N. Duesler, *J. Chem. Soc., Dalton Trans.* **1990**, 2953.
[23] M. K. Cooper, P. J. Guerney, M. McPartlin, *J. Chem. Soc., Dalton Trans.* **1982**, 757.
[24] K. W. Hellmann, S. Friedrich, L. H. Gade, W.-S. Li, M. McPartlin, *Chem. Ber.* **1995**, *128*, 29.
[25] K. Jurkschat, U. Kaltenbrunner, M. Schurmann, *Z. Kristallogr.* **1999**, *214*, 473.
[26] J. Beckmann, K. Jurkschat, U. Kaltenbrunner, N. Pieper, M. Schurmann, *Organometallics* **1999**, *18*, 1586.
[27] D. B. Firfiray, A. Irving, J. R. Moss, *Chem. Commun.* **1990**, 377.
[28] S. Seebald, G. Kickelbick, F. Möller, U. Schubert, *Chem. Ber.* **1996**, *129*, 1131.
[29] S. Seebald, B. Mayer, U. Schubert, *Inorg. Chem.* **1995**, *34*, 5285.
[30] M. Haukka, J. Kiviaho, M. Ahlgrén, T. A. Pakkanen, *Organometallics* **1995**, *14*, 825.
[31] Cambridge Structural Data Base, University of Cambridge, 2001.
[32] M. P. Aarnts, M. P. Wilms, K. Peelen, J. Fraanje, K. Goubitz, F. Hartl, D. J. Stufkens, E. J. Baerends, A. Vlcek, Jr., *Inorg. Chem.* **1996**, *35*, 5468.
[33] P. M. Treichel, J. P. Stenson, *Inorg. Synth.* **1970**, *12*, 36.
[34] R. J. Haines, A. L. Preez, *J. Chem. Soc., Dalton Trans.* **1972**, 944.
[35] J. M. Kelly, C. M. O'Connell, J. G. Vos, *Inorg. Chim. Acta* **1982**, *64*, L75.
[36] M. S. Wrighton, D. S. Ginley, *J. Am. Chem. Soc.* **1975**, *97*, 4246.
[37] F. Cariati, L. Naldini, *Gazz. Chim. Ital.* **1965**, *95*, 3.
[38] Collect: Data Collection Software, Enraf − Nonius, Delft, The Netherlands, **1999**.
[39] Z. Otwinowski, W. Minor, *Processing of X-ray Diffraction Data Collected in Oscillation Mode, Methods in Enzymology, Volume 276*, *Macromolecular Crystallography, Part A*, (Eds.: C. W. Carter, Jr. and R. M. Sweet), Academic Press, **1997**, p. 307−326.
[40] G. M. Sheldrick, SHELXS97, Program for Crystal Structure Determination, University of Göttingen, Germany, **1997**.
[41] L. J. Farrugia, WinGX v1.61 − A Windows Program for Crystal Structure Analysis, University of Glasgow, Glasgow, **1998**.
[42] G. M. Sheldrick, SHELXTL Version 5.1, Bruker Analytical X-ray Systems, Bruker AXS, Inc. Madison, Wisconsin, USA, **1998**.

Received June 18, 2001
[I01218]

Synthesis, Structural Characterization, Solvatochromism, and Electrochemistry of Tetra-Osmium Carbonyl Clusters Containing Azo-Ligands

Yat Li,[a] Zhen-Yang Lin,[b] and Wing-Tak Wong*[a]

Keywords: Electrochemistry / Solvatochromism / Azo-compounds / Osmium / Cluster compounds

The reaction of $[Os_4(\mu\text{-}H)_4(CO)_{12}]$ with 4-(2-pyridylazo)-*N*,*N*-dimethylaniline (PNNDA) in dichloromethane afforded the new clusters $[Os_4(\mu\text{-}H)_4(CO)_{11}\{NC_5H_4(N{=}N)C_6H_4NMe_2\}]$ (**1**) and $[Os_4(\mu\text{-}H)_4(CO)_{10}\{\eta^2\text{-}NC_5H_4(N{=}N)C_6H_4NMe_2\}]$ (**2**) in 34% and 15% yields, respectively. Upon heating in toluene under reflux, compound **1** converted into **2** in 80% yield. The MLCT transition of compound **2** shows strong solvent dependency, displaying unusually large positive solvatochromism in different organic solvents. Treatment of $[Os_4(\mu\text{-}H)_4(CO)_{12}]$ with 2-(5-bromo-2-pyridylazo)-5-(diethylamino)-phenol (Br-PADAP) in dichloromethane gives $[Os_4(\mu\text{-}H)_3(CO)_{10}\{\mu\text{-}\eta^3\text{-}Et_2NC_6H_3(O)(N{=}N)C_5NH_3Br\}]$ (**3**). The O–H bond activation is observed and the azo-ligand behaves as a five-electron donor. The clusters $[Os_4(\mu\text{-}H)_2(CO)_{10}\{\mu\text{-}\eta^3\text{-}NC_5H_4(N{=}N)C_5H_4N\}]$ (**4**) and $[Os_4(\mu\text{-}H)_4(CO)_{10}\{\mu\text{-}\eta^2\text{-}NC_5H_4(N{=}N)C_5H_4N\}]_2$ (**5**) were isolated from the reaction of $[Os_4(\mu\text{-}H)_4(CO)_{10}(NCMe)_2]$ with 2,2′-azopyridine and 3,3′-azopyridine, respectively. In compound **4**, both pyridine and azo nitrogen atoms were found to coordinate to the cluster core. Dehydrogenation was also observed in this compound. For compound **5**, two tetra-osmium metal cores were connected by two azo ligands through their pyridyl nitrogen atoms to form a novel cyclic structure. The redox properties of the compounds described herein were investigated by means of cyclic voltammetry and controlled potential coulometry. Both compound **2** and **5** exhibit a reversible cathodic wave, which indicates that they undergo addition of one electron without significant structural changes. Furthermore, compound **5** displays an electronic interaction between two redox centers, the extra electrons are believed to delocalize throughout the cyclic structure.

Introduction

The activation of strong multiple-bonded organic substrates using polynuclear metal complexes is an interesting facet of cluster reactivity. The cleavage of N=N bond in organic diazenes to give metal imido (nitrene) complexes is an important chemical transformation.[1−5] Metal imido complexes have been shown to be potential intermediates for metal-prompted organic transformations involving the formation of nitrogen-carbon bonds. As a result, the chemistry of carbonyl clusters containing azo ligands has been extensively studied in recent years.[6−18] Previously, we reported that $[Os_3(CO)_{10}(NCMe)_2]$ reacts with 2-(5-bromo-2-pyridylazo)-5-(diethylamino)phenol at room temperature to give $[Os_3(CO)_{10}\{\mu\text{-}N(H)(C_5H_3NBr)\}\{\mu\text{-}N(C_{10}H_{13}NO)\}]$,[19] containing two types of amido moieties, in which N=N cleavage of the azo ligand was observed. In an attempt to synthesize tetra-osmium imido complexes by the N=N cleavage of azo ligands, we were able to prepare some new tetra-osmium carbonyl clusters containing azo ligands. However, no cleavage of the N=N bond of these compounds by thermal or photochemical methods was observed. These compounds exhibit interesting solvatochromism and electrochemistry. The redox behavior of the clusters $M_3(CO)_{12}$ (M = Fe, Ru, Os) has been extensively studied.[20−23] To the best of our knowledge, the electrochemical behavior of tetra-osmium carbonyl clusters is rarely reported. The correlation between the structure and the redox properties of these compounds was also described.

[a] Department of Chemistry, The University of Hong Kong, Pokfulam Road, Hong Kong, P. R. China
Fax: (internat.) + 852-2547/2933 or + 852-2857/1586
E-mail: wtwong@hkucc.hku.hk
[b] Department of Chemistry, The University of Science and Technology, Clear Water Bay, Hong Kong, P. R. China

Results and Discussion

The preparation of compounds **1**−**5** is summarized in Scheme 1 and Scheme 2. These compounds have been fully characterized by elemental analyses, infrared, ^{1}H NMR, and mass spectroscopic methods. The infrared spectra of compounds **1**−**5** revealed that only terminal carbonyl ligands were present, and the mass spectra exhibit molecular ion envelopes that agree with the formulae of the compounds, with stepwise loss of terminal carbonyl ligands. Their molecular structures were established by single crystal X-ray diffraction analyses.

The molecular ion peak was not observed in the mass spectrum of **1** due to fragmentation during the ionization process. However, it exhibits an intense daughter peak at m/z = 1073 attributed to $[M^+ - PNNDA]$, and is followed by peaks corresponding to the successive loss of carbonyl groups. The chelation of the azo ligand is supported by the ^{1}H NMR spectroscopic data. The ^{1}H NMR spectrum of **1** shows two sets of multiplets for the aromatic protons at δ = 6.84−8.01. Two sets of singlets at δ = 2.04 and 1.67 correspond to the methylene protons of the azo-ligand. The

 © WILEY-VCH Verlag GmbH, 69451 Weinheim, 2001 1434−1948/01/1212−3163 $ 17.50+.50/0

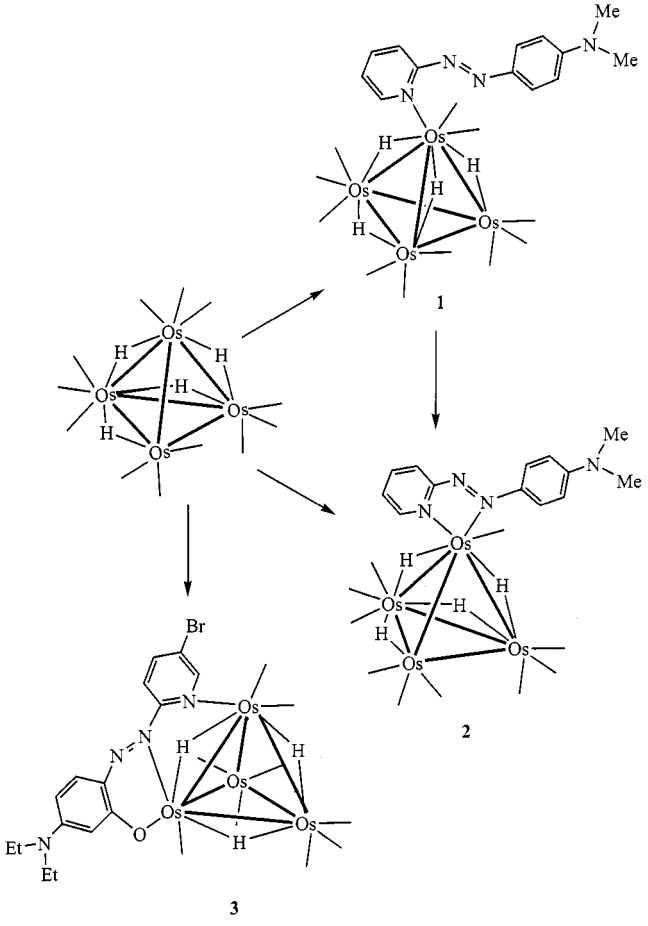

Scheme 1

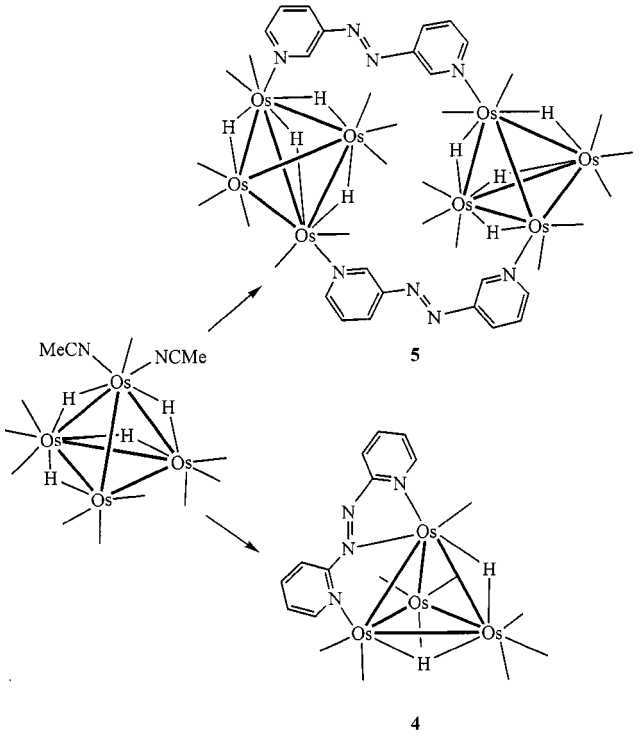

Scheme 2

^{1}H NMR cannot give a clear assignment of four hydrides in the tetra-osmium core due to the fluxional behavior of hydrides at room temperature, which is common in tetra-osmium systems.[24−25] Therefore, a variable-temperature ^{1}H NMR study from 233 to 298 K was conducted for **1**. At 233 K, the broad hydride peaks resolved into two sets of sharp singlet peaks at $\delta = -18.10, -18.63, -24.01$ and at $\delta = -16.93, -17.95, -18.86, -25.53$, with an integral ratio of 2:1:1 and 1:1:1:1, respectively. This indicates the presence of two possible isomers in solution, namely **1a** and **1b**, due to a different bridging hydride disposition. As the temperature is raised to 253 K, the ratio of **1b** to **1a** gradually increases from 0.4 to 0.5. This suggests that isomer **1a** is more favored in solution at a higher temperature.

The molecular structure of **1** is depicted in Figure 1 and selected bond lengths, and angles are summarized in Table 1. Four osmium atoms define a distorted tetrahedron with eleven carbonyl ligands terminally bonded to the metal centers. The Os(2)−Os(3) and Os(2)−Os(4) [2.819(1) and 2.809(1) Å] lengths of compound **1** are comparable to the corresponding values observed in the parent cluster $[Os_4(\mu\text{-}H)_4(CO)_{10}(NCMe)_2]$.[26] The hydride bridged Os−Os bonds are significantly elongated,[27] within the range [2.928(1)-3.022(1) Å]. The hydrides bridging the Os(1)−Os(3) and Os(1)−Os(4) are chemically equivalent, which give a sharp singlet with double integral value in low temperature ^{1}H NMR spectra. Hence, it is believed that the solid-state structure of **1** obtained by X-ray crystallography is the structure of isomer **1a**. The azo-ligand terminally coordinated to Os(1) through the pyridyl nitrogen N(1) with a mirror plane bisects along the azo ligand and Os(1) atom. The Os(1)−N(1) bond length [2.17(2) Å] is not significantly different from the equivalent Os−N distance found in other osmium-pyridine containing complexes.[28] The N(2)−N(3) bond [1.26(2) Å] is slightly lengthened compared to other azo ligands in the tri-osmium system[29] due to the electron donating aniline group, consistent with its assignment as a N−N double bond. The torsion angle defined by C(16)−N(2)−N(3)−C(17) is 178(2)°, indicating that the *trans* configuration of the ligand remains almost intact upon coordinating to the cluster framework. The dihedral angle between the pyridyl and phenyl rings is 8.08°.

Upon heating under reflux in toluene, compound **1** converted into **2** in 80% yield. Substitution of a carbonyl ligand on Os(1) by azo nitrogen was observed. The ^{1}H NMR of **2** is similar to **1**, with three broad peaks in hydride region. A variable-temperature ^{1}H NMR study was conducted for **2** from 223 to 298 K. At 223 K, the broad peaks resolved into four sets of sharp hydride signals, each with the relative intensity 1:1:1:1, indicating the presence of four isomers (namely **2a**, **2b**, **2c**, and **2d**) in solution, see Figure 2. The ratio of **2a/2b/2c/2d** is 1:2:5:8. The molecular structure of compound **2** is illustrated in Figure 3 and the relevant bond parameters are listed in Table 1. A chloroform molecule, as a solvent of crystallization, is present in the crystal lattice. The basic metal architecture of **1** is retained in compound **2**. The azo ligand coordinated to Os(1) through the pyridyl nitrogen N(1) and the azo nitrogen N(3) atom.

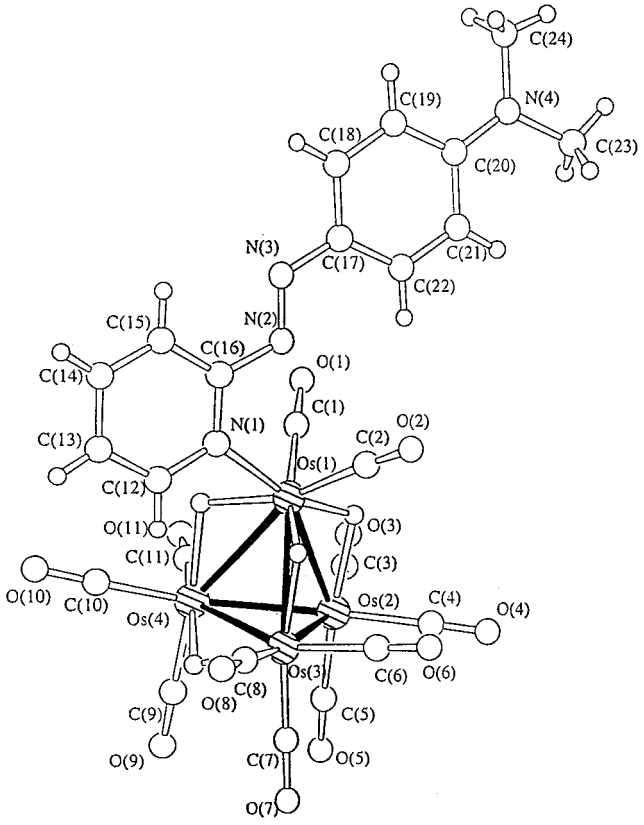

Figure 1. The molecular structure of clusters $[Os_4(\mu\text{-}H)_4(CO)_{11}\{NC_5H_4(N{=}N)C_6H_4NMe_2\}]$ (**1**) showing the atom numbering scheme

Os(1)−N(1)−C(15)−N(2)−N(3) form a metallacyclic five-membered ring with a mean deviation of 0.022Å from the least-square plane. The N(1)−Os(1)−N(3) coordination is asymmetric, with Os(1)−N(1) and Os(1)−N(3) bond lengths of 2.078(6) Å and 2.111(7), respectively, and a N(1)−Os(1)−N(3) angle of 75.0(3)°. The N(2)−N(3) length [1.290(9) Å] is almost identical to **1**, indicating a retained double bond character. Upon coordination of azo nitrogen, the pyridyl and phenyl rings are twisted with respect to each other to a greater extent, with a dihedral angle of 11.8°.

The molecular structure of **3** is shown in Figure 4 and some important bond lengths and angles are listed in Table 1. The azo-ligand was found to bridge the edge Os(1)−Os(2) of the Os_4 distorted tetrahedron, affording a five-membered ring containing Os(1), Os(2), N(2), C(15), and N(1) and a six-membered ring containing Os(2), O(11), C(21), C(16), N(3), and N(2), respectively. These rings had a maximum deviation of 0.205 Å and 0.192 Å from the least-square planes, respectively. The dihedral angle between two metallacyclic rings is 25.5°. The Os(1)−Os(2) bond [2.7816(6) Å] is slightly shorter than the hydride bridged Os−Os bonds. The O−H bond cleavage is observed in **3**. This bonding mode of the azo ligand is very similar to that found in the tri-osmium cluster $[(\mu\text{-}H)Os_3(CO)_9\{\mu\text{-}\eta^3\text{-}Et_2NC_6H_3(O)(N{=}N)C_5NH_3Br\}]$.[29] The N(2)−N(3) bond length [1.32(1) Å] is comparable to the N=N bonds in **1** and **2**, indicating no involvement of the π-electrons of the N=N bond. The pyridyl and phenyl rings are highly twisted with respect to each other, with a dihedral angle of 60.3° due to the bond strain. The characteristic 60 cluster-valence electron count was observed with the azo-ligand acting as a five-electron donor. Only three bridging hydrides were found in the metal core, confirmed by ^{1}H NMR spectroscopy, with three sharp peaks of equal intensity observed in the hydride region.

The molecular structure of **4** is depicted in Figure 5 and the relevant bond lengths and angles are listed in Table 1. It has a structure similar to compound **2** in terms of ligand coordination, however, the involvement of the other pyridyl ring was observed. The coordination of the azo-ligand, acting as a six-electron donor, resulted in a pair of hydrides being eliminated rather than a carbonyl ligand being substituted. Such elimination is not commonly observed in osmium chemistry. The presence of only two hydrides on the metal core is supported by ^{1}H NMR spectroscopic data, with two sharp singlets of equal intensity observed in hydride region. The ligand bridged Os(1)−Os(3) bond length [2.8145(8) Å] is slightly shorter than the hydride bridged Os−Os bonds. Os(1)−Os(3)−N(4)−C(16)−N(3) and Os(1)−N(1)−C(15)−N(2)−N(3) form two metallacyclic five-membered rings, with a mean deviation of 0.034Å and 0.159Å, respectively, from the least square planes. The Os(3)−N(4) bond [2.18(1) Å] is significantly lengthened compared to Os(1)−N(1) bond [2.06(1) Å] and Os(1)−N(3) bond [2.05(1) Å], owing to the bond strain. The two pyridyl rings are not coplanar, with a dihedral angle upon coordination to the metal framework of 16.2° between them. The bite angle N(1)−Os(1)−N(3) of chelating azo-ligand is 75.3(5)°, which is comparable to **2** [N(1)−Os(1)−N(3) 75.0(3)°] and $[Os_3(CO)_{10}(bipy)]$ [N−Os−N 75.6(9)°].[30]

Although the ligand system of **5** is very similar to **4**, they have totally different reaction pathways towards the tetra-osmium cluster. The molecular structure of **5** is illustrated in Figure 6 and the relevant parameters are listed in Table 1. Four tetrahydrofuran molecules, as a solvent of crystallization, were found in the crystal lattice. Two tetra-osmium metal cores are connected by two azo-ligands through their pyridyl nitrogen atoms N(1) and N(4) to form a novel cyclic structure. A similar cyclic structure was observed in the tri-osmium cluster system.[31] Cluster **5** possesses a C_i symmetry, with the center of inversion at the central point of the square involving Os(3), Os(4), Os(3)*, and Os(4)*. The Os(1)−N(1) [2.18(2) Å] and Os(2)−N(4)* [2.13(2) Å] bond lengths are lengthened relative to other Os−N dative bonds because of the large steric hindrance in the cyclic structure. The two pyridyl rings are twisted with a dihedral angle of 24.5°. The two tetra-osmium sets of atoms with their associated carbonyl ligands do not approach each other very closely; the nearest contact is O(3)···O(3)* [5.48(3) Å] and the shortest Os···Os distance between clusters is Os(2)···Os(2)* [7.940(2) Å]. This novel cyclic structure opens the possibility of encapsulating some alkali or oxophilic metal ions. The supramolecular system so formed will be useful for the studies of redox active host towards metal ion sensing applications. The steric effect may be the main

Table 1. Selected bond lengths [Å] and angles [°] for compounds **1**−**5**

	1	**2**	**3**	**4**	**5**
Os(1)−Os(2)	2.928(1)	3.0080(4)	2.7816(6)	2.8718(8)	2.977(2)
Os(1)−Os(3)	2.985(1)	2.9781(4)	3.0117(6)	2.8145(8)	2.993(2)
Os(1)−Os(4)	3.022(1)	2.9753(4)	2.7903(6)	2.8742(8)	2.747(2)
Os(2)−Os(3)	2.819(1)	2.8202(4)	2.9896(6)	2.9089(8)	3.005(1)
Os(2)−Os(4)	2.809(1)	2.9425(5)	2.9224(7)	2.7494(8)	3.013(1)
Os(3)−Os(4)	2.954(1)	2.7857(4)	2.7655(6)	2.8477(8)	2.832(1)
Os(1)−N(1)	2.17(2)	2.078(6)	2.143(9)	2.06(1)	2.18(2)
Os(1)−N(2)	–	–	2.132(1)	–	–
Os(1)−N(3)	4.45	2.111(7)	–	2.05(1)	–
Os(2)−N(4)	–	–	–	–	2.13(2)
Os(3)−N(4)	–	–	–	2.18(1)	–
Os(2)−O(11)	–	–	2.138(7)	–	–
N(2)−N(3)	1.26(2)	1.290(9)	1.32(1)	1.34(2)	1.28(3)
C(12)−Br(1)	–	–	1.89(1)	–	–
Os(2)−Os(1)−Os(3)	56.95(3)	56.212(9)	61.99(1)	61.53(2)	60.44(4)
Os(2)−Os(1)−Os(4)	56.32(3)	58.91(1)	63.27(2)	57.17(2)	63.38(4)
Os(3)−Os(1)−Os(4)	58.92(3)	55.80(1)	56.78(2)	60.07(2)	58.94(4)
Os(1)−Os(2)−Os(3)	62.56(3)	61.36(1)	62.79(1)	58.27(2)	60.05(3)
Os(1)−Os(2)−Os(4)	63.54(3)	59.99(1)	58.51(1)	61.46(2)	54.59(4)
Os(3)−Os(2)−Os(4)	63.33(3)	57.77(1)	55.77(1)	60.35(2)	56.15(3)
Os(1)−Os(3)−Os(2)	60.49(3)	62.43(1)	55.22(1)	60.21(2)	59.51(4)
Os(1)−Os(3)−Os(4)	61.16(3)	62.05(1)	57.57(1)	61.01(2)	56.19(4)
Os(2)−Os(3)−Os(4)	58.16(3)	63.32(1)	60.89(2)	57.05(2)	62.07(4)
Os(1)−Os(4)−Os(2)	60.15(3)	61.10(1)	58.22(2)	61.37(2)	62.03(4)
Os(1)−Os(4)−Os(3)	59.93(3)	62.15(1)	65.65(2)	58.93(2)	64.87(4)
Os(2)−Os(4)−Os(3)	58.51(3)	58.91(1)	63.35(2)	62.60(2)	61.78(4)
Os(2)−Os(1)−N(1)	–	–	84.3(3)	–	98.8(6)
Os(1)−Os(2)−N(4)	–	–	–	–	147.7(6)
Os(4)−Os(1)−N(1)	99.7(5)	–	–	–	–
N(1)−Os(1)−N(3)	–	75.0(3)	–	75.3(5)	–
N(2)−Os(2)−O(11)	–	–	82.1(3)	–	–

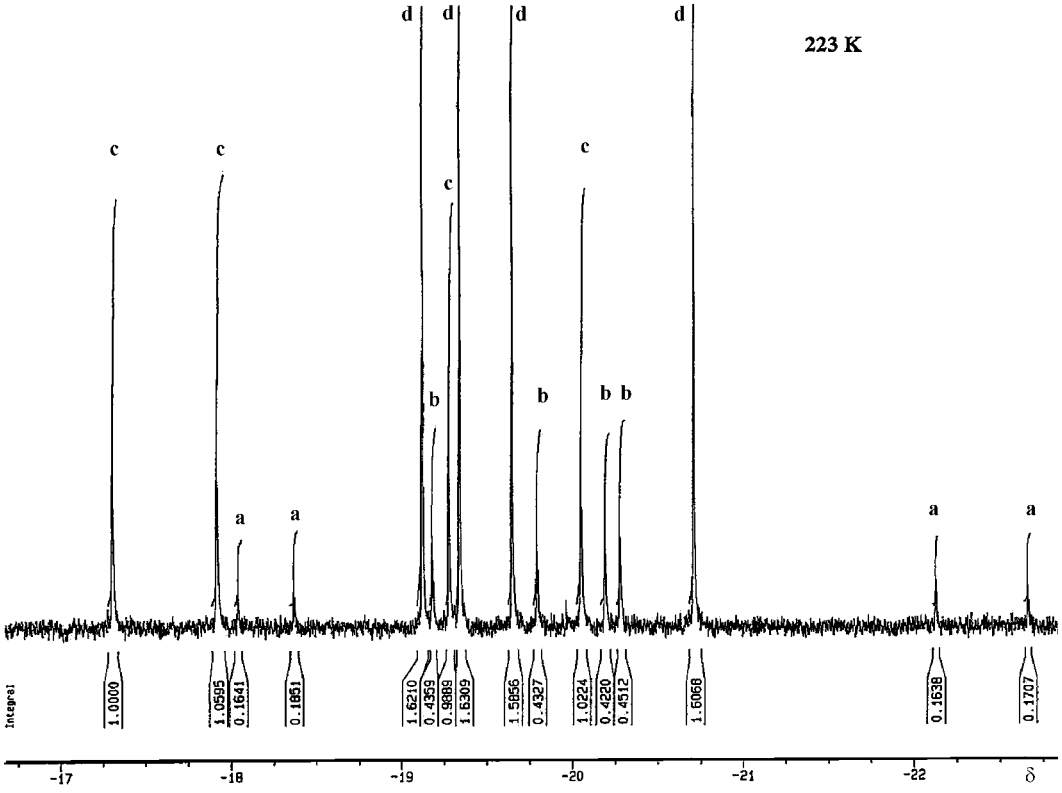

Figure 2. The low temperature (223 K) ^{1}NMR spectra of $[Os_4(\mu\text{-}H)_4(CO)_{10}\{\eta^2\text{-}NC_5H_4(N{=}N)C_6H_4NMe_2\}]$ (**2**) in the hydride region

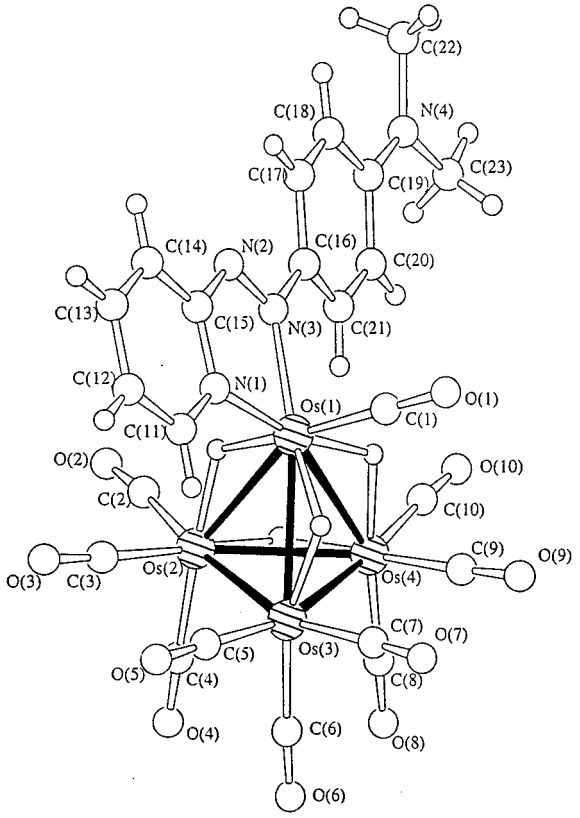

Figure 3. The molecular structure of clusters $[Os_4(\mu\text{-}H)_4(CO)_{10}\{\eta^2\text{-}NC_5H_4(N{=}N)C_6H_4NMe_2\}]$ (**2**) showing the atom numbering scheme

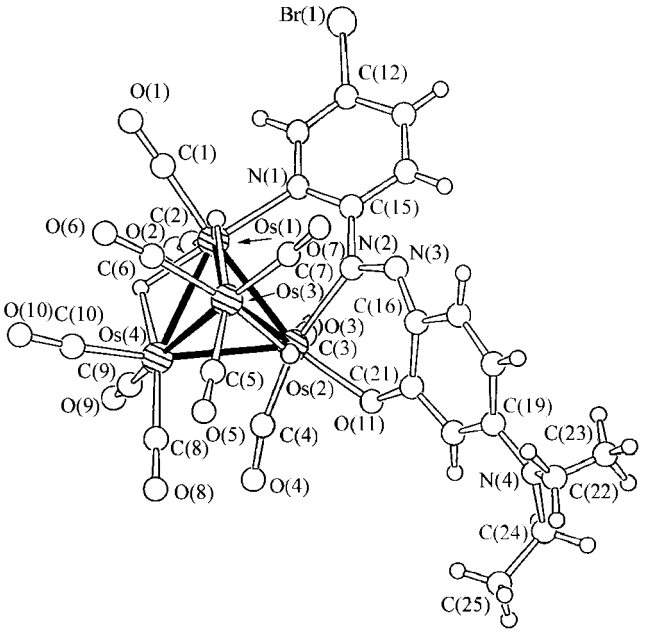

Figure 4. The molecular structure of clusters $[Os_4(\mu\text{-}H)_3(CO)_{10}\{\mu\text{-}\eta^3\text{-}Et_2NC_6H_3(O)(N{=}N)C_5NH_3Br\}]$ (**3**) showing the atom numbering scheme

reason for the cyclic structure not being observed in the reaction of 2,2′-azopyridine. 3,3′-Azopyridine provides a much larger separation between the two metal cores due to the direction of pyridine nitrogen lone pair electrons.

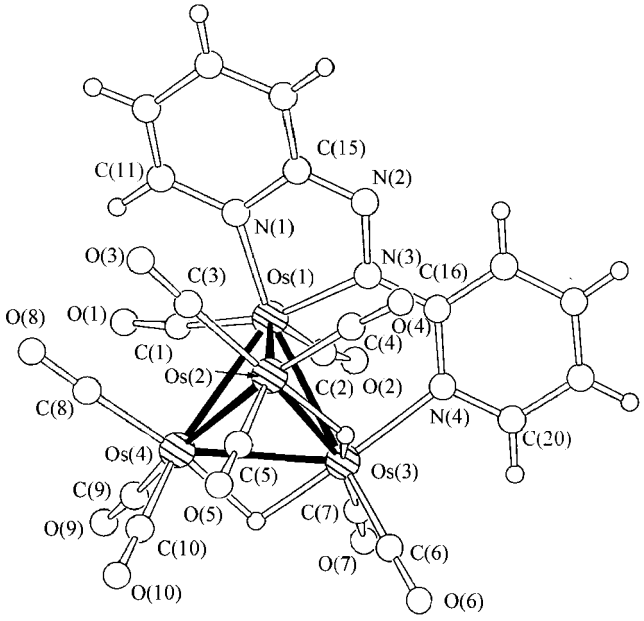

Figure 5. The molecular structure of clusters $[Os_4(\mu\text{-}H)_2(CO)_{10}\{\mu\text{-}\eta^3\text{-}NC_5H_4(N{=}N)C_5H_4N\}]$ (**4**) showing the atom numbering scheme

Solvatochromism

Compounds **1**−**5** show a variety of intense colors in the solid state, which prompted us to examine them by optical spectroscopy. Based on the experimental geometry, molecular orbital calculations at the B3LYP level of density functional theory were carried out for these compounds to examine the characteristics of the molecular orbitals in the frontier region. Similar to trinuclear osmium clusters,[32−33] the highest occupied molecular orbital (HOMO) of these compounds is mainly metal based, and the lowest unoccupied molecular orbital (LUMO) mostly based on the organic moiety.[34] The intense color of these compounds undoubtedly arises from a strong absorption due to metal-to-ligand charge transfer (M.L.C.T.) transitions.[32,34] These compounds exhibit solvatochromic absorptions in the visible region, contributed by changes in the metal-ligand bond polarity between the ground and excited states and specific solvent-solute and induced dipolar interaction.[35−40] The optical spectral parameters for a range of solvents are summarized in Table 2.

Compounds **1**−**3**, demonstrated a positive solvatochromism,[41−42] where the dipole moment of ground state (μ_g) is smaller than the excited state (μ_e). On MLCT transition, polar solvents were found to be better at stabilizing the excited state of the molecule. The red shift in absorption energies from *n*-hexane to dichloromethane was due to the increasing polarity of the organic solvents. The exceptionally large solvatochromism was observed in compound **2** (Figure 7), due to the smaller energy gap of HOMO−LUMO electronic transition. The contour plots of the lowest unoccupied (LUMO) and the highest occupied (HOMO) molecular orbitals of **2** are illustrated in Figure 8. The molecular orbital calculations showed that N(2) has a

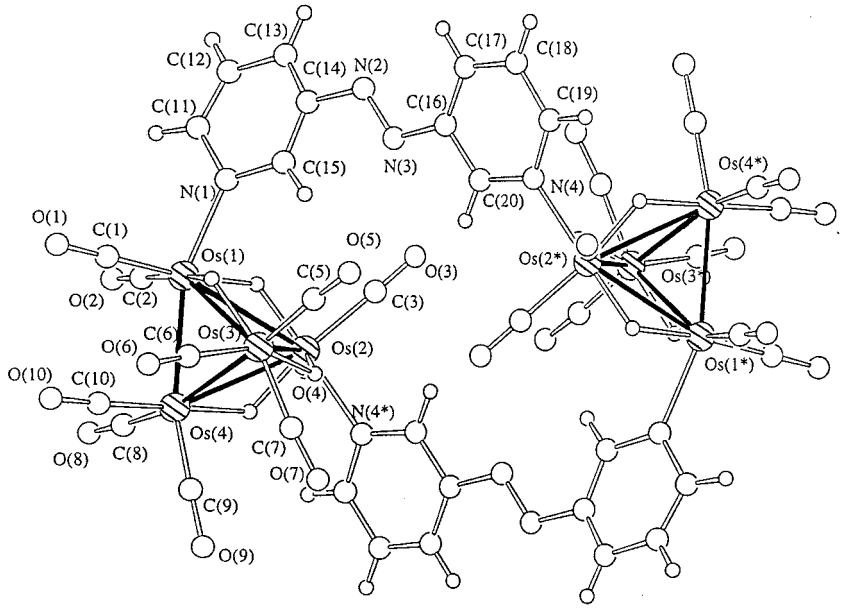

Figure 6. The molecular structure of clusters $[Os_4(\mu\text{-}H)_4(CO)_{10}\{\mu\text{-}\eta^2\text{-}NC_5H_4(N{=}N)C_5H_4N\}]_2$ (**5**) showing the atom numbering scheme

Table 2. Electronic absorption spectroscopic data for compounds **1**–**5**

Compounds	λ_{max} (nm) ε ($dm^3 \cdot mol^{-1} \cdot cm^{-1}$) *n*-hexane	acetone	dichloromethane
1	480[a]	497 (16000)	497 (18000)
2	504 (11000)	572 (15000)	577 (13000)
3	482 (5000)	522 (4000)	524 (4000)
4	613 (3000)	600 (2000)	607 (2000)
5	–	330 (34000)	306 (57000)

[a] Limited solubility for accurate determination of ε value.

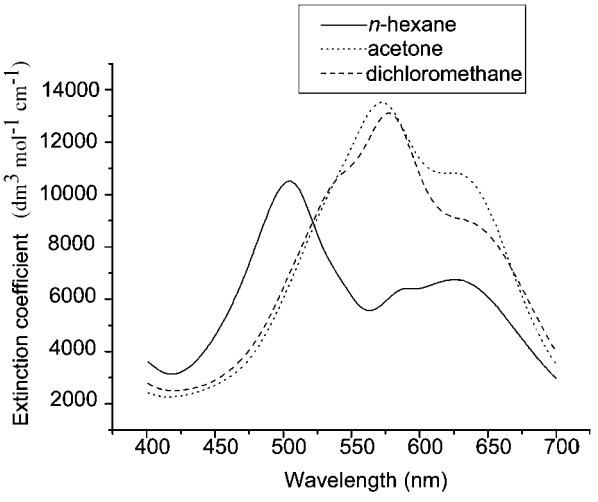

Figure 7. The electronic absorption spectrum of $[Os_4(\mu\text{-}H)_4(CO)_{10}\{\eta^2\text{-}NC_5H_4(N{=}N)C_6H_4NMe_2\}]$ (**2**) in a range of organic solvents

lone pair of electrons whose maximum electron density points away from the central cluster unit. This lone pair is greatly affected by the solvent environment. The interac-

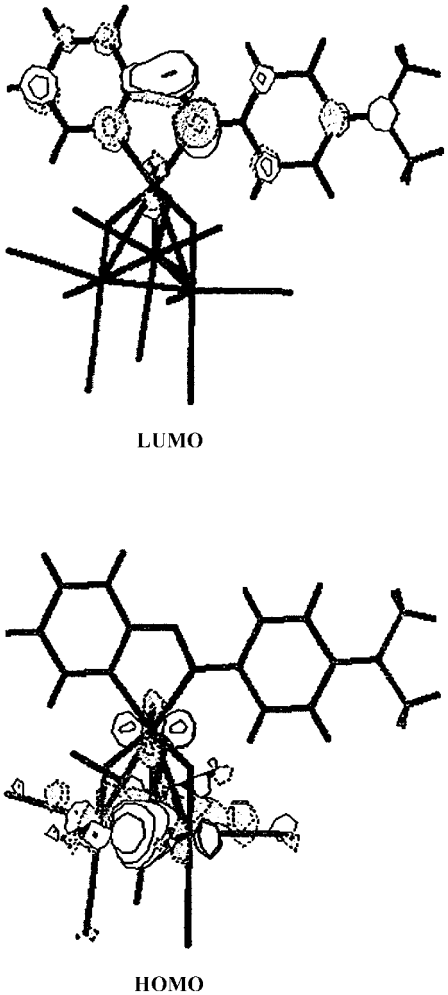

Figure 8. The contour plots of the lowest unoccupied- (LUMO) and the highest occupied (HOMO) molecular orbitals calculated for $[Os_4(\mu\text{-}H)_4(CO)_{10}\{\eta^2\text{-}NC_5H_4(N{=}N)C_6H_4NMe_2\}]$ (**2**)

tions with the polar solvents pull the electron density away from the N(2) center, lowering the orbital energy of the LUMO, which contains significant N(2)−N(3) π* character. As a result, the MLCT transition will shift to a lower energy (red shift) in polar solvents. Compound **2** has a much lower energy MLCT absorption than compound **1**. It is believed that more extensive ligand coordination to the cluster core leads to a smaller HOMO−LUMO energy gap.

Compound **4** showed some degree of solvent dependence; however, it was random with respect to the solvent polarity. Compound **4** had a low energy absorption band at around 600 nm due to the extensive coordination of ligand. Compound **5** exhibited a strong featureless intraligand π→π* absorption band at around 300 nm, along with an analogous band observed in the absorption spectrum of free ligand 3,3′-azopyridine under the same conditions. As shown in Table 1, some degree of negative solvatochromism shift was detected for **5**. Apart from π→π* transition, no indication of a low-energy band was attributed to an MLCT transition.

Electrochemistry

In order to investigate the redox properties of these new azo-ligands containing tetra-osmium compounds, the electrochemistry of compounds **1−5** was examined. Cyclic voltammetry and controlled potential coulometry were carried out at 298 K in a standard three-electrode system (glassy carbon/carbon cloth working electrode, platinum auxiliary electrode, and $Ag/AgNO_3$ reference electrode)[43] using a 0.1 M tetrabutylammonium hexafluorophosphate/dichloromethane solution as supporting electrolyte. The results of voltammetric experiments are summarized in Table 3.

Table 3. Electrochemical data for compounds **1−5**

Compounds[a]	Oxidation E_{pa2} [V][b]	E_{pa1} [V][b]	Reduction E_{pc1} [V][b]	E_{pc2} [V][b]
1	−	0.64	−1.25	−
2	0.93	0.49	(−0.94)[c]	−1.27
3	−	0.72	−1.17	−
4	−	0.52	−	−
5	−	0.55	(−1.06)[c]	−1.68

[a] ca. 10^{-3} M cluster in 0.1 M TBAHFP in dichloromethane at 298 K, the working electrode was a glassy carbon electrode, the auxiliary electrode and the reference electrode were a platinum wire and $Ag/AgNO_3$ (0V) under the same conditions, calibrated with ferrocene. Scan rate was 100 mVs^{-1}. − [b] E_{pa} and E_{pc} are the anodic and cathodic potentials, respectively. − [c] Values in parentheses are $E_{1/2}$, half-wave potential values.

Compound **1** exhibits an irreversible cathodic wave (E_{pc}) and anodic wave (E_{pa}) at −1.25 and 0.64 V vs. $Ag/AgNO_3$ in dichloromethane, respectively. Applying a working potential (E_w) at −1.4 V, controlled potential coulometry showed that two faraday/mole of **1** was involved in this reduction step. On the basis of the relative peak currents of the cathodic and anodic waves, the oxidation process is assigned as a one-electron step. Two-electron addition to compound **1** is believed to afford a 62e compound, which would be unstable, with consequent metal−metal bond cleavage, leading to metal carbonyl fragments of lower nuclearity. It conforms to a ECEC or EEC mechanism.[44]

Compounds **1** and **2** have the same ligand system, their cyclic voltammograms were expected to be similar. Interestingly, the incorporation of the azo group in the cluster framework led to great changes in the electrochemical behavior of **2**. The cyclic voltammograms of **2** consist of a reversible and an irreversible cathodic wave at −0.94 and −1.27 V, respectively. Controlled potential coulometry at the first reduction step (E_w = −1.09 V) indicates that this cathodic process consumes 1 faraday/mole of **2**. Analysis of the cyclic voltammetric responses relating to the cathodic peak of **2**, with scan rate varying from 50 to 500 mVs^{-1}, indicates that the peak current ratio i_{pa}/i_{pc} remains close to unity. The current function (proportional to $i_{pc}/v^{1/2}$) is essentially constant and the peak-to-peak separation lies between 80−100 mV. This trend is parallel with the ferrocene under the same experimental conditions. Thus, we assume that the first reduction step proceeds by an essentially reversible electron transfer process. This implies that any structural change of **2** accompanying the single-electron transfer is chemically reversible and rapid with respect to the time scale of the electrochemical experiment. The irreversible nature of the second cathodic wave showed that the reduction of compound **2** followed an EEC mechanism. In addition, two anodic waves at 0.49 and 0.93 V were found. The similarity of the relative peak heights for the waves within a given voltammogram points to the same number of electrons being involved in the oxidation and reduction of **2**. Two irreversible one-electron oxidations in **2** were assigned to follow the ECEC process. There is a 310 mV positive and 150 mV negative shift upon coordination of azo group in cathodic and anodic wave values, respectively. It shows that both reduction and oxidation processes are more likely to occur. It is believed that the extensive ligand coordination lowers the HOMO−LUMO energy gap and hence gives a lower redox potential for compound **2**. This is consistent with the UV/Vis spectroscopic data. Furthermore, it is reasonable to suggest that the reversible step of **2** is due to the presence of a metallacyclic five-membered ring unit.

The cyclic voltammograms of **3** contained an irreversible cathodic wave at E_{pc} = −1.17 V vs. $Ag/AgNO_3$, along with a small return oxidation at −0.56 V. The region where the weak oxidation wave appears was initially empty, with the wave appearing after the cathodic wave was traversed. The ΔE_p values remained virtually unchanged on varying the scan rates from 50 to 1000 $mV \cdot s^{-1}$. An irreversible anodic wave is also located at E_{pa} = 0.72 V. The irreversible nature of both oxidation and reduction presumably derives from an irreversible chemical reaction that follows the redox reaction (EC process). Controlled potential coulometry was run at 0.87 V for **3**, showing that one electron is removed for each molecule. Based on the relative peak heights, the cathodic wave is tentatively assigned to have consumed two electrons. For compound **4**, only one irreversible anodic wave was located at E_{pa} = 0.54 V vs. $Ag/AgNO_3$ within the

solvent limit. Controlled potential coulometry at the oxidation step (E_w = 0.67 V) shows that the anodic process consumes one electron per molecule. Compounds **3** and **4** have a similar ligand disposition, however, the former is much harder to oxidize than the latter due to the presence of a strong electron-withdrawing bromine ligand. Moreover, although compound **4** is extensively coordinated by the azo-ligand, the oxidation potential is comparable to **2**. This suggested that the aniline is an effective electron-donating ligand that makes oxidation easier.

Compound **5** is a cyclic structure consisting of two tetra-osmium metal cores connected by two azo-ligands. Although compounds **1** and **5** have a similar ligand system, they show different redox behavior. It is believed that there is an electronic interaction between two redox centers. The cyclic voltammogram of **5** is shown in Figure 9. A quasi-reversible and an irreversible cathodic wave were observed at E_{pc} = −1.06 and −1.68 V vs. $Ag/AgNO_3$. In addition, an irreversible anodic wave occurred at E_{pa} = 0.55 V. Applying a working potential at 0.8 V, controlled potential coulometry indicates that two faraday/mole of **5** is involved in the oxidation step. The other redox waves were assumed to involve one electron per molecule according to the relative peak heights in the voltammogram. The large potential difference between the first and second reduction peaks (over 600 mV) implies that there is good electronic interaction between the two tetra-osmium metal cores, through the azo-ligand in this novel cyclic structure. This kind of electronic interaction also appears in some organometallic dimers.[45−50]

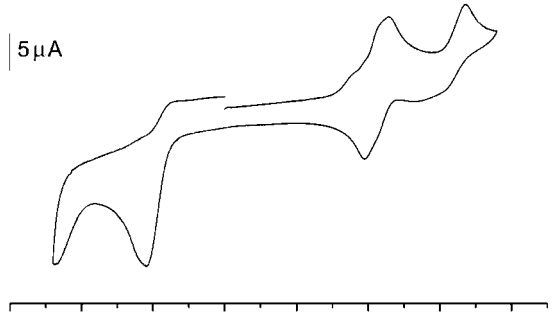

Figure 9. Cyclic voltammogram of $[Os_4(\mu\text{-}H)_4(CO)_{10}\{\mu\text{-}\eta^2\text{-}NC_5H_4(N{=}N)C_5H_4N\}]_2$ (**5**) in CH_2Cl_2 containing 0.1 mol·dm^{-3} Bu_4NPF_6; glassy carbon working electrode, platinum auxiliary electrode and $Ag/AgNO_3$ reference electrode (Ag^+ 0.1 mol·dm^{-3}; scan rate, 100 mV·s^{-1})

There is a completely charged delocalization over two redox centers, while the azo-ligand acts as a conductor. As one metal core receives one electron, the cyclic structure become more electron rich, making the second reduction of another metal core more difficult. The cyclic structure exhibits remarkably flexible redox behavior comparable to **2**, able to accommodate the addition of one electron without gross structural changes. Furthermore, it shows that both reduction and oxidation are more likely to occur in compound **5** than in compound **1**, as the extra charge is shared by two metal cores through the bridging azo-ligands. This is consistent with the 190 mV positive and 90 mV negative shift in cathodic and anodic wave values in comparison to the corresponding value observed in **1**.

Experimental Section

General: All reactions and manipulations were carried out under argon using standard Schlenk techniques, except for the chromatographic separations. Solvents were purified by standard procedures and distilled prior to use.[51] Reactions were monitored by both IR spectroscopy and analytical thin-layer chromatography (Merck Kieselgel 60 F_{254}) and the products were separated by thin-layer chromatography on plates coated with silica (Merck Kieselgel 60 F_{254}).

Materials: All chemicals, unless otherwise stated, were purchased commercially and used as received. $[Os_4(\mu\text{-}H)_4(CO)_{12}]$,[52−54] $[Os_4(\mu\text{-}H)_4(CO)_{10}(NCMe)_2]$,[26] ligand 2,2′-azopyridine,[55] and 3,3′-azopyridine[55] were prepared by literature methods.

Instrumentation: Infrared spectra were recorded on a Bio-Rad FTS-135 IR spectrometer, using 0.5 mm calcium fluoride solution cells. − ^{1}H NMR and ^{1}H-^{1}H COSY spectra were obtained on a Bruker DPX300 spectrometer using CD_2Cl_2 and referenced to $SiMe_4$ (δ = 0), variable-temperature ^{1}H NMR spectra on a Bruker DPX500 spectrometer. − Positive ionization fast atom bombardment (FAB) mass spectra were recorded on a Finnigan MAT 95 mass spectrometer, using *m*-nitrobenzyl alcohol as matrix solvent. − Electronic absorption spectra were obtained with a Hewlett−Packard 8453 diode array UV/Vis spectrophotometer, using quartz cells, with 1 cm path length at room temperature. − Microanalyses were performed by Butterworth Laboratories, UK.

Reaction of $[Os_4(\mu\text{-}H)_4(CO)_{12}]$ with 4-(2-Pyridylazo)-*N*,*N*-dimethylaniline: The complex $[Os_4(\mu\text{-}H)_4(CO)_{12}]$ (110 mg, 0.1 mmol) was dissolved in dichloromethane (50 cm^3) and stirred with one equivalent of 4-(2-pyridylazo)-*N*,*N*-dimethylaniline (22.6 mg, 0.1 mmol) at 0 °C. Two equivalent of trimethylamine *N*-oxide (Me_3NO) were added dropwise over 20 min. After the reaction had proceeded at ambient temperature for 18 h, the initial yellow solution changed to dark brown. The solvent was removed under reduced pressure and the residue subjected to TLC with *n*-hexane/dichloromethane (1:1, v/v) as eluent. Two new products were isolated, in the following order of elution: dark red $[Os_4(\mu\text{-}H)_4(CO)_{11}\{NC_5H_4(N{=}N)C_6H_4NMe_2\}]$ (**1**, R_f = 0.85, 44 mg, 0.034 mmol, 34%). IR [ν(CO)/cm^{-1}, *n*-hexane]: $\tilde{\nu}$ = 2091 w, 2060 s, 2051 m, 2032 m, 2005 m, 1985 m. − ^{1}H NMR (CD_2Cl_2): at 298 K δ = −24.06 (s, 1 H, Os−H), −18.65 (s, 1 H, Os−H), −18.06 (s, 2 H, Os−H), 1.67 (s, 3 H, methyl), 2.04 (s, 3 H, methyl), 6.84 (m, 4 H, pyridyl), 8.01 (m, 4 H, phenyl); at 233 K, **1a:** δ = −24.01 (s, 1 H, Os−H), −18.63 (s, 1 H, Os−H), −18.10 (s, 2 H, Os−H); **1b:** δ = −25.53 (s, 1 H, Os−H), −18.86 (s, 1 H, Os−H), −17.95 (s, 1 H, Os−H), −16.93 (s, 1 H, Os−H). − MS (positive FAB): *m*/*z* (%) = 1073 [M$^+$ − PNNDA]. − $C_{24}H_{18}N_4O_{11}Os_4$ (1299.3): calcd. C 22.20, H 1.39, N 4.31; found C 22.3, H 1.5, N 4.2; and dark blue (**2**, R_f = 0.7, 19 mg, 0.015 mmol, 15%). − IR [ν(CO)/cm^{-1}, *n*-hexane]: $\tilde{\nu}$ = 2087 w, 2077 m, 2050 vs, 2019 s, 2000 s, 1983 m. − ^{1}H NMR (CD_2Cl_2): at 298 K δ = −19.64 (br. s, Os−H), −19.28 (br. s, Os−H), −18.71 (br. s, Os−H), 2.82[s, 6 H, methyl], 6.95 (d, J_{HH} = 9.4 Hz, 2 H, phenyl], 7.60 (d, J_{HH} = 6.4 Hz, 1 H, pyridyl], 8.28 (m, 3 H, pyridyl and phenyl), 8.52 (d, J_{HH} = 8.1 Hz, 1 H, pyridyl], 9.36 (d, J_{HH} = 5.4 Hz, 1 H, pyridyl]; at 223 K, **2a:** δ = −20.06 (s, 1 H, Os−H),

−19.28 (s, 1 H, Os−H), −17.92 (s, 1 H, Os−H), −17.31 (s, 1 H, Os−H); **2b:** δ = −20.71 (s, 1 H, Os−H), −19.65 (s, 1 H, Os−H), −19.34 (s, 1 H, Os−H), −19.13 (s, 1 H, Os−H); **2c:** δ = −20.28 (s, 1 H, Os−H), −20.19 (s, 1 H, Os−H), −19.79 (s, 1 H, Os−H), −19.18(s, 1 H, Os−H); **2d:** δ = −22.66 (s, 1 H, Os−H), −22.13 (s, 1 H, Os−H), −18.37 (s, 1 H, Os−H), −18.04 (s, 1 H, Os−H). − MS (positive FAB): *m*/*z* (%) = 1271 $[M]^+$. − $C_{23}H_{18}N_4O_{10}Os_4$ (1271.3): calcd. C 21.73, H 1.43, N 4.41; found C 21.6, H 1.3, N 4.4.

$[Os_4(\mu\text{-}H)_3(CO)_{10}\{\mu\text{-}\eta^3\text{-}Et_2NC_6H_3(O)(N{=}N)C_5NH_3Br\}]$ (3): The complex $[Os_4(\mu\text{-}H)_4(CO)_{12}]$ (110 mg, 0.1 mmol) was dissolved in dichloromethane (50 cm^3) and mixed with one equivalent of 2-(5-bromo-2-pyridylazo)-5-(diethylamino)phenol (34.9 mg, 0.1 mmol) at 0 °C. Two equivalent of trimethylamine *N*-oxide were added dropwise. The yellow mixture was stirred for 12 h, which resulted in the formation of a deep purple solution. The solvent was pumped off and the residue purified by chromatography on TLC plates with *n*-hexane/diethyl ether (3:2, v/v) as eluent. Recrystallization from dichloromethane/*n*-hexane afforded purplish-red crystals. (R_f = 0.4, 11 mg, 0.008 mmol, 8%). − IR [ν(CO)/cm^{-1}, *n*-hexane]: $\tilde{\nu}$ = 2087 w, 2055 s, 2026 s, 2010 s. − ^{1}H NMR (CD_2Cl_2): δ = −20.58 (s, 1 H, Os−H), −16.43 (s, 1 H, Os−H), −13.17 (s, 1 H, Os−H), 1.32 (m, 6 H, CH_3), 3.50 (m, 4 H, CH_2), 5.99 (d, J_{HH} = 2.5 Hz, 1 H, phenyl), 6.47 (dd, J_{HH} = 9.8 Hz, 1 H, phenyl), 7.04 (d, J_{HH} = 9.4 Hz, 1 H, phenyl), 7.09 (d, J_{HH} = 9.2 Hz, 1 H, pyridyl), 7.80 (dd, J_{HH} = 9.0 Hz, 1 H, pyridyl), 9.05 (d, J_{HH} = 8.2 Hz, 1 H, pyridyl). − MS (positive FAB): *m*/*z* (%) = 1392 $[M]^+$. − $C_{25}H_{19}BrN_4O_{11}Os_4$ (1392.2): calcd. C 21.57, H 1.38, N 4.02; found C 21.7, H 1.5, N 3.9.

$[Os_4(\mu\text{-}H)_2(CO)_{10}\{\mu\text{-}\eta^3\text{-}NC_5H_4(N{=}N)C_5H_4N\}]$ (4): The complex $[Os_4(\mu\text{-}H)_4(CO)_{10}(NCMe)_2]$ (110 mg, 0.1 mmol) was dissolved in dichloromethane (50 cm^3) and stirred with one equivalent of 2,2′-azopyridine (18.4 mg, 0.1 mmol) at ambient temperature. After 5 h, the solvent was removed under reduce pressure. The residue was purified by chromatography on TLC plates with *n*-hexane/dichloromethane (1:1, v/v) as eluent. Recrystallization from chloroform/*n*-hexane afforded blue crystals. (R_f = 0.3, 15 mg, 0.012 mmol, 12%). − IR [ν(CO)/cm^{-1}, *n*-hexane]: $\tilde{\nu}$ = 2083 m, 2068 w, 2047 s, 2035 s, 2021 w, 2001 vs, 1977 w. − ^{1}H NMR (CD_2Cl_2): δ = −21.02 (s, 1 H, Os−H), −13.02 (s, 1 H, Os−H), 6.49 (td, J_{HH} = 6.6 Hz, 1 H, pyridyl), 7.25 (td, J_{HH} = 6.8 Hz, 2 H, pyridyl), 7.97 (m, 2 H, pyridyl), 8.17 (d, J_{HH} = 8.3 Hz, 1 H, pyridyl), 8.76 (d, J_{HH} = 5.7 Hz, 1 H, pyridyl), 8.83 (d, J_{HH} = 6.8 Hz, 1 H, pyridyl). − MS (positive FAB): *m*/*z* (%) = 1227 $[M]^+$. − $C_{20}H_{10}N_4O_{10}Os_4$ (1227.2): calcd. C 19.57, H 0.82, N 4.57; found C 19.7, H 0.9, N 4.5.

$[Os_4(\mu\text{-}H)_4(CO)_{10}\{\mu\text{-}\eta^2\text{-}NC_5H_4(N{=}N)C_5H_4N\}]_2$ (5): The complex $[Os_4(\mu\text{-}H)_4(CO)_{10}(NCMe)_2]$ (110 mg, 0.1 mmol) was dissolved in dichloromethane (50 cm^3) and stirred with one equivalent of 3,3′-azopyridine (18.4 mg, 0.1 mmol) at ambient temperature. After 24 h, the initial yellow solution changed to dark brown. The solvent was then remove in vacuo and the residue was purified by chromatography on TLC plates with *n*-hexane/dichloromethane (1:1, v/v) as eluent. Recrystallization from tetrahydrofuran/*n*-hexane afforded brown crystals. (R_f = 0.45, 29.5 mg, 0.012 mmol, 12%). − IR [ν(CO)/cm^{-1}, dichloromethane]: $\tilde{\nu}$ = 2074m, 2047s, 2028vs, 2001s, 1976w. − ^{1}H NMR (CD_2Cl_2): δ = −20.09 (s, 2 H, Os−H), −17.05 (s, 2 H, Os−H), −16.46 (s, 2 H, Os−H), −15.53 (s, 2 H, Os−H), 7.50 (dd, J_{HH} = 8.2 Hz, 2 H, pyridyl), 7.71 (dd, J_{HH} = 8.0 Hz, 2 H, pyridyl), 8.34 (dt, J_{HH} = 6.9 Hz, 2 H, pyridyl), 8.62 (dt, J_{HH} = 8.6 Hz, 2 H, pyridyl), 9.10 (d, J_{HH} = 2.1 Hz, 2 H, pyridyl), 9.24 (td, J_{HH} = 5.2 Hz, 4 H, pyridyl), 9.52 (d, J_{HH} = 1.9 Hz, 2 H, pyridyl). − MS (positive FAB): *m*/*z* (%) = 2458 $[M]^+$. − $C_{40}H_{24}N_8O_{20}Os_8$ (2458.3): calcd. C 19.54, H 0.98, N 4.56; found C 19.4, H 1.0, N 4.6.

Electrochemical Studies: Electrochemical measurements were performed with EG&G Princeton Applied Research (PAR) Model 273A potentiostat, connected to an interfaced computer employing PAR 270 electrochemical software. Cyclic voltammograms were obtained using a gas (argon) sealed two-compartment cell equipped

Table 4. Crystal data and data collection parameters for compounds **1**−**5**

	1	**2**	**3**	**4**	**5**
Empirical formula	$C_{24}H_{18}N_4O_{11}Os_4$	$[C_{23}H_{18}N_4O_{10}Os_4]\cdot 1CHCl_3$	$[C_{25}H_{19}N_4O_{11}Br_1Os_4]\cdot 1CH_2Cl_2$	$C_{20}H_{10}N_4O_{10}Os_4$	$[C_{40}H_{24}N_8O_{20}Os_8]\cdot 4C_4H_8O$
Molecular mass	1299.23	1390.59	1477.08	1227.12	2746.70
Crystal color, habit	red, block	blue, block	purple, block	blue, block	brown, block
Crystal dimensions [mm]	0.22 × 0.22 × 0.10	0.22 × 0.17 × 0.14	0.22 × 0.19 × 0.12	0.23 × 0.12 × 0.22	0.23 × 0.22 × 0.25
Crystal system	monoclinic	triclinic	triclinic	monoclinic	monoclinic
Space group	$P2_1/n$ (no. 14)	$P\bar{1}$ (no. 2)	$P\bar{1}$ (no. 2)	$P2_1/n$ (no. 14)	$P2_1/n$ (no. 14)
a [Å]	8.2310(8)	9.8510(9)	9.792(1)	12.243(1)	13.104(1)
b [Å]	27.885(1)	12.644(1)	11.709(1)	12.472(1)	16.423(1)
c [Å]	13.8710(8)	15.557(1)	17.632(1)	16.621(1)	17.853(1)
α [Å]		67.020(5)	77.40(1)		
β [Å]	105.710(5)	81.690(5)	77.02(1)	93.40(1)	107.40(2)
γ [Å]		69.110(5)	68.33(1)		
U [$Å^3$]	3064.8(3)	1666.6(3)	1810.2(3)	2533.5(3)	3666.3(6)
Z	4	2	2	4	2
D_c [g cm^{-3}]	2.816	2.771	2.710	3.217	2.488
μ(Mo-K_α) [cm^{-1}]	165.82	154.86	152.97	200.46	138.70
Reflections collected	19241	19107	11225	15648	22910
Unique reflections	7074	7480	7789	5956	8538
Observed reflections [I>1.5σ(I)]	4098	6262	5890	4783	3713
R	0.053	0.034	0.039	0.055	0.066
R_w	0.061	0.043	0.041	0.065	0.054
Goodness of fit, *S*	1.09	1.33	1.13	1.82	1.09

with a glassy carbon working electrode (Bioanalytical), a platinum wire auxiliary electrode (Aldrich), and an $Ag/AgNO_3$ reference electrode (Bioanalytical) at room temperature; 0.1 mol·dm^{-3} *n*-tetrabutylammonium hexafluorophosphate (TBAHFP) in anhydrous deoxygenated CH_2Cl_2 was used as a supporting electrolyte. Ferrocene was added at the end of each experiment as an internal standard. Potential data (vs. $Ag/AgNO_3$) were checked against the ferrocene (0/+1) couple; under the actual experimental conditions the ferrocene/ferrocenium couple is located at +0.13 V. Bulk electrolyses were carried out in a gas-tight cell consisting of three chambers separated at the bottom by fine frits, with a carbon cloth (80 mm^2) working electrode in the middle, and $Ag/AgNO_3$ reference and Pt gauze auxiliary electrodes in the lateral chambers. The working potentials (E_w) for reduction and oxidation processes were ca. 0.15 V more negative and more positive than the corresponding electrode potential (E_p), respectively; all coulometric experiments were performed in duplicate.

Crystallography: Crystals suitable for X-ray analyses were glued on glass fibers with epoxy resin or sealed in a 0.3 mm glass capillary. Intensity data were collected at ambient temperature using a Bruker SMART CCD 1000 diffractometer with graphite monochromated Mo-K_α radiation using ω scan type. Details of the intensity data collection and crystal data are given in Table 4. The data were corrected for Lorentz and polarization effects. The structure were solved by direct methods[56] and expanded using Fourier techniques.[57] Some non-hydrogen atoms were refined anisotropically, while the rest were refined isotropically. Hydrogen atoms were included but not refined. All calculations were performed by using the teXsan[58] crystallographic software package of Molecular Structure Corporation.

Crystallographic data (excluding structure factors) for the structures reported in this paper have been deposited with the Cambridge Crystallographic Data Centre as supplementary publication nos. CCDC-163743 to CCDC-163747. Copies of the data can be obtained free of charge on application to CCDC, 12 Union Road, Cambridge CB2 1EZ, UK. [Fax: (internat.) +44 (0)1223/336033; E-mail: deposit@ccdc.cam.ac.uk].

Acknowledgments

We gratefully acknowledge financial support from the Hong Kong Research Grants Council and the University of Hong Kong. Y. Li acknowledges the receipt of a postgraduate studentship, administered by the University of Hong Kong.

[1] A. K. Ghosh, P. Majumdar, L. R. Falvello, G. Mostafa, S. Goswani, *Organometallics* **1999**, *18*, 5086−5090.
[2] M. A. Aubart, R. G. Bergman, *Organometallics* **1999**, *18*, 811−813.
[3] S. D. Gray, J. L. Thorman, V. A. Adamian, K. M. Kadish, L. K. Woo, *Inorg. Chem.* **1998**, *37*, 1−4.
[4] F. Y. Petillon, P. Scholhammer, J. Talarmin, *Inorg. Chem.* **1999**, *38*, 1954−1955.
[5] M. A. Lockwood, P. E. Fanwick, O. Eisenstein, I. P. Rothwell, *J. Am. Chem. Soc.* **1996**, *118*, 2762−2763.
[6] B. Hansert, M. Tasi, A. Tiripicchio, M. T. Camellini, H. Vahrenkamp, *Organometallics* **1991**, *10*, 4070−4073.
[7] M. Tasi, A. K. Powell, H. Vahrenkamp, *Chem. Ber.* **1991**, *124*, 1549−1557.
[8] H. Bantel, B. Hansert, A. K. Powell, M. Tasi, H. Vahrenkamp, *Angew. Chem. Int. Ed. Eng.* **1989**, *28*, 1059−1060.
[9] J. A. Smieja, J. E. Gozum, W. L. Gladfelter, *Organometallics* **1987**, *6*, 1311−1317.
[10] B. Hansert, H. Vahrenkamp, *Chem. Ber.* **1993**, *126*, 2017−2022.
[11] B. Hansert, H. Vahrenkamp, *Chem. Ber.* **1993**, *126*, 2023−2026.
[12] B. Hansert, A. K. Powell, H. Vahrenkamp, *Chem. Ber.* **1991**, *124*, 2697−2704.
[13] E. J. Wucherer, M. Tasi, B. Hansert, A. K. Powell, M. T. Garland, J. F. Halet, J. Y. Saillard, H. Vahrenkamp, *Inorg. Chem.* **1989**, *28*, 3564−3572.
[14] Y. K. Au, K. K. Cheung, W. T. Wong, *Inorg. Chim. Acta* **1995**, *238*, 193−195.
[15] F. S. Kong, W. T. Wong, *J. Organomet. Chem.* **1999**, *589*, 180−190.
[16] J. A. Smieja, J. E. Gozum, W. L. Gladfelter, *Organometallics* **1986**, *5*, 2154−2155.
[17] B. Hansert, H. Vahrenkamp, *Chem. Ber.* **1993**, *126*, 2011−2016.
[18] K. Majumder, S. M. Peng, Samaresh Bhattacharya, *J. Chem. Soc., Dalton Trans.* 2001, 284−288.
[19] W. T. Wong, T. S. Wong, *J. Organomet. Chem.* **1997**, *542*, 29−33.
[20] J. C. Cyr, J. A. DeGray, D. K. Gosser, E. S. Lee, P. H. Rieger, *Organometallics* **1985**, *4*, 950−951.
[21] J. E. Cyr, P. H. Rieger, *Organometallics* **1991**, *10*, 2153−2159.
[22] T. M. Bockman, J. K. Kochi, *J. Am. Chem. Soc.* **1987**, *109*, 7725−7735.
[23] D. Osella, L. Pospisil, J. Fiedler, *Organometallics* **1993**, *12*, 3140−3144.
[24] Y. Y. Choi, W. T. Wong, *J. Organomet. Chem.* **1999**, *573*, 189−201.
[25] K. S. Y. Leung, Y. Li, *Inorg. Chem. Commun.* **1999**, *2*, 599−603.
[26] Y. Y. Choi, PhD Thesis, The University of Hong Kong, **1998**.
[27] M. R. Churchill, R. A. Lashewycz, *Inorg. Chem.* **1979**, *18*, 1926−1930.
[28] B. F. G. Johnson, J. Lewis, W. J. H. Nelson, M. A. Pearsall, P. R. Raithby, M. J. Rosales, *J. Chem. Soc., Dalton Trans.* **1987**, 327−333.
[29] T. S. Wong, unpublished results.
[30] N. E. Leadbeater, J. Lewis, P. R. Raithby, G. N. Ward, *J. Chem. Soc., Dalton Trans.* **1997**, 2511−2516.
[31] A. J. Deeming, C. Whittaker, A. J. Arce, Y. D. Sanctis, *J. Organomet. Chem.* **1997**, *540*, 67−76.
[32] W. Y. Wong, S. Chan, W. T. Wong, *J. Organomet. Chem.* **1995**, *493*, 229−237.
[33] W. Y. Wong, W. T. Wong, *J. Chem. Soc., Dalton Trans.* **1996**, 1853−1856.
[34] C. E. Housecroft, personal communication.
[35] B. F. G. Johnson, F. J. Lahoz, J. Lewis, N. D. Prior, P. R. Raithby, W. T. Wong, *J. Chem. Soc., Dalton Trans.* **1992**, 1701−1708.
[36] M. M. Zulu, A. J. Lees, *Inorg. Chem.* **1988**, *27*, 3325−3331.
[37] J. Granifo, M. E. Vargas, E. S. Dodsworth, D. H. Farrar, S. S. Fielder, A. B. P. Lever, *J. Chem. Soc., Dalton Trans.* **1996**, 4369−4378.
[38] E. S. Dodsworth, A. B. P. Lever, *Inorg. Chem.* **1990**, *29*, 499−503.
[39] P. Suppan, N. Ghoneim (Eds.), *Solvatochromism*, The Royal Society of Chemistry, (London) **1997**.
[40] C. Reichardt, *Chem. Rev.* **1994**, *94*, 2319−2358.
[41] F. Effenberger, F. Wurthner, *Angew. Chem. Int. Ed. Engl.* **1993**, *32*, 719−721.
[42] E. Buncel, S. Rajagopal, *Acc. Chem. Res.* **1990**, *23*, 226−231.
[43] J. Heinze, *Angew. Chem. Int. Ed. Eng.* **1984**, *11*, 831−847.
[44] S. R. Drake, *Polyhedron* **1990**, *9*, 455−474.
[45] D. Osella, L. Milone, C. Nervi, M. Ravera, *J. Organomet. Chem.* **1995**, *488*, 1−7.
[46] D. Osella, O. Gambino, C. Nevi, M. Ravera, D. Bertolino, *Inorg. Chim. Acta* **1993**, *206*, 155−161.
[47] D. Osella, J. Hanzlik, *Inorg. Chim. Acta.* **1993**, *213*, 311−317.

[48] J. Hock, A. M. W. C. Thompson, J. A. McCleverty, M. D. Ward, *J. Chem. Soc., Dalton Trans.* **1996**, 4257−4263.
[49] R. D. Adams, B. Qu, *J. Organomet. Chem.* **2001**, *620*, 303−307.
[50] R. D. Adams, B. Qu, *J. Organomet. Chem.* **2001**, *619*, 271−274.
[51] D. D. Perrin, W. L. F. Armarego, Purification of Laboratory Chemicals, 3rd ed., Pergamon, Oxford, **1988**.
[52] H. D. Kaesz, S. A. R. Knox, J. W. Koepke, R. B. Saillant, *J. Chem. Soc., Chem. Commun.* **1971**, 477.
[53] B. F. G. Johnson, J. Lewis, P. R. Raithby, G. M. Scheldrick, K. Wong, *J. Chem. Soc., Dalton Trans.* **1978**, 673−676.
[54] C. Zuccaro, G. Pampaloni, F. Calderazzo, *Inorg. Synth.* **1989**, *26*, 293−295.
[55] E. V. Brown, G. R. Granneman, *J. Am. Chem. Soc.* **1975**, *97*, 621−627.
[56] *SHELXS86*: G. M. Sheldrick, in: *Crystallographic Computing 3* (Eds. G. M. Sheldrick, C. Kruger, R. Goddard), Oxford University Press, **1985**, pp. 175−189.
[57] *DIRDIF94*: P. T. Beurskens, G. Admiraal, G. Beurskens, W. P. Bosman, R. de Gelder, R. Israel, J. M. M. Smits, **1994**; *The DIRDIF-94 program system*, Technical Report of the Crystallography Laboratory, University of Nijmegen, The Netherlands.
[58] *TeXsan*: Crystal Structure Analysis Package, Molecular Structure Corporation (**1985** and **1992**).

Received May 21, 2001
[I01184]

Reactivity of Sterically Unencumbered Transient Nitrilium Phosphanylide Complexes Towards 1-Piperidinocarbonitrile: A Case Study[‡]

Rainer Streubel,*[a] Udo Schiemann,[a] Ngoc Hoa Tran Huy,[b] and François Mathey*[b]

Dedicated to Professor Hans-Georg Schnöckel on the occasion of his 60th birthday

Keywords: Nitrogen heterocycles / NMR spectroscopy / Phosphorus heterocycles / P ligands / Tungsten

The thermal decomposition of the 7-phosphanorbornadiene complexes **6a**,**b** in xylene at 120 °C in the presence of two equivalents of 1-piperidinocarbonitrile yielded the 2*H*-1,3,2-azaphosphole complexes **11a**,**b** and the 2*H*-1,4,2-azaphosphole complexes **12a**–**c** in ratios of 7:4 (**11a**:**12a**) and 1:5 (**11b**:**12b**). Remarkably, the two atropisomers **12b** and **12c** were obtained (ratio: 5:1) in the case of the *P*-phenyl-substituted 2*H*-1,4,2-azaphosphole complex. Interestingly, the product ratios of both reactions were approximately the same if neat 1-piperidinocarbonitrile was used as the solvent. The reaction of complexes **6a,b** with $Cu^{I}Cl$ and 1-piperidinocarbonitrile, with exclusion of light, also furnished the 2*H*-1,3,2-azaphosphole complexes **11a,b** as the main products. In the case of complex **6a**, a by-product was detected by ^{31}P NMR spectroscopy but could not be isolated. Complexes **11a,b**, **12a** and **13** were purified by column chromatography at low temperature and characterized by NMR and MS spectroscopic means and elemental analysis, whereas only a 1:1 mixture of **12b** and **12c** could be characterized.

Introduction

Nitrilium phosphanylide complexes with bulky substituents at the phosphorus have recently become established as new building blocks in N,P-heterophosphole synthesis and their reactivity towards different trapping reagents such as alkynes,[2] nitriles[3] or phosphaalkynes[4] has been explored. So far, their generation has relied on the use of the 2*H*-azaphosphirene complexes **1a,b** and can be achieved either thermally or photochemically;[5] the mild reaction conditions of the latter being synthetically very useful. The majority of these three-component reactions profit from transylidation reactions yielding the *P*-bis(trimethylsilyl)methyl- and *P*-pentamethylcyclopentadienyl-substituted nitrilium phosphanylide tungsten complexes **2a**,**b** as transient species.[3] Of special interest are those cases where dialkylamino-substituted nitriles such as 1-piperidinocarbonitrile were used as trapping reagent and solvent (**i**; Scheme 1), thus affording selectively the 2*H*-1,3,2-diazaphosphole complexes **3a**[3b] and **3b**;[3c] if toluene solutions were used (**ii** and **iii**; Scheme 1) then intramolecular reactions also took place. Depending on the substituent at the phosphorus center two different by-products were thus formed: the 2*H*-azaphosphirene complex **4**[3b] in the case of **2a** (route **ii**) or the C,N,P-cage compound **5**[3c] in the case of **2b** (route **iii**). So far, no dimerization of complexes **2a**,**b** has been observed in solution, although we obtained a dimer by melting the 2*H*-azaphosphirene complex **1a**.[6]

Very recently we demonstrated that transient nitrilium phosphanylide complexes with less bulky substituents at the phosphorus, such as **9a**,**b**, are accessible by thermal decomposition of the 7-phosphanorbornadiene complexes **6a**,**b** in the presence of 1-piperidinocarbonitrile; the reactive intermediates **9a**,**b** were trapped with dimethylacetylene dicarboxylate, thus yielding the 2*H*-1,2-azaphosphole complexes **10a**,**b** as the main products (Scheme 2).[1] Remarkably, in these reactions no Δ^3-oxazaphospholene complexes were formed from the [3+2] cycloaddition of **9a**,**b** with the C−O π-system of DMAD, as observed earlier for **2a**,**b**.[7,8] This finding provided the first evidence for the different reactivities of sterically unencumbered and encumbered nitrilium phosphanylide complexes.

Because of our interest in exploiting the chemistry of nitrilium phosphanylide complexes using this new and easy access, we decided to study the reactions of the 7-methyl- and 7-phenyl-phosphanorbornadiene complexes **6a**,**b** with 1-piperidinocarbonitrile, which should be a good model system. The quest for the generation of transient 2*H*-azaphosphirene complexes will also be discussed.

Results and Discussion

The thermal decomposition of the 7-phosphanorbornadiene complexes **6a**,**b**[9] in xylene in the presence of two

[‡] Chemistry of Nitrilium Phosphanylide Complexes, 15. − Part 14: Ref.[1]

[a] Institut für Anorganische und Analytische Chemie der Technischen Universität Braunschweig,
Postfach 3329, 38023 Braunschweig, Germany
Fax: (internat.) + 49-531/391-5387
E-mail: r.streubel@tu-bs.de
[b] Laboratoire Hétéroéléments et Coordination, UMR 7653 CNRS, DCPH, Ecole Polytechnique,
91128 Palaiseau Cedex, France
Fax: (internat.) + 33-169/333990

 © WILEY-VCH Verlag GmbH, 69451 Weinheim, 2001 1434−1948/01/1212−3175 $ 17.50+.50/0

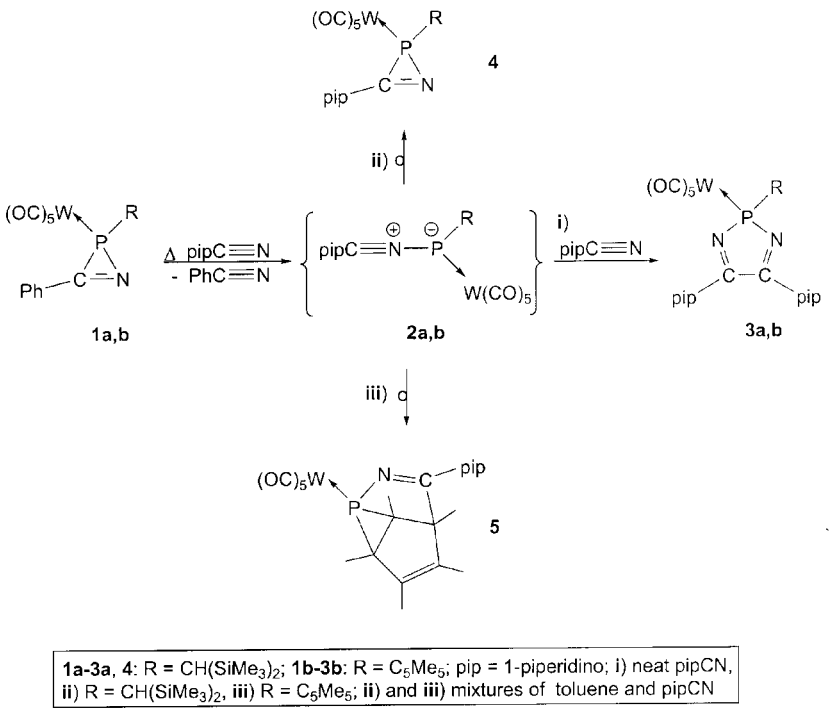

Scheme 1. Generation and reactions of bulky substituted nitrilium phosphanylide complexes

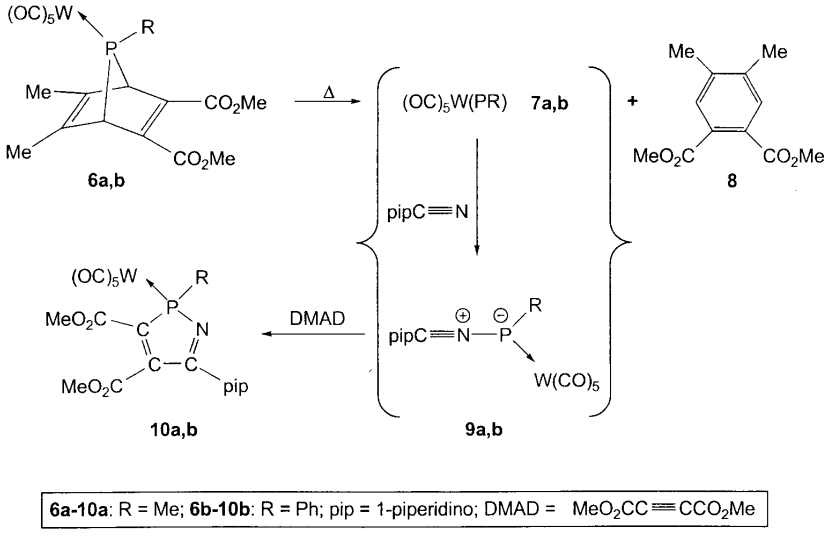

Scheme 2. Trapping reaction of nitrilium phosphanylide complexes **9a**,**b** with DMAD

equivalents of 1-piperidinocarbonitrile at 120 °C yielded the 2*H*-1,3,2-azaphosphole complexes **11a**,**b** and, surprisingly, the 2*H*-1,4,2-azaphosphole complexes **12a**,**b** *and* **12c** (Scheme 3). The ratios of the two regioisomers **11** and **12** were 7:4 (**11a**:**12a**) and 1:5 (**11b**:**12b**), as determined by ^{31}P NMR spectroscopy. Remarkably, the *P*-phenyl-substituted 2*H*-1,4,2-azaphosphole complex was obtained as a mixture of two atropisomers **12b**,**c** (5:1 ratio), in contrast to the methyl derivative **12a**. The complexes **11a,b** and **12a** were separated by double low-temperature column chromatography, whereas only a 1:1 mixture of **12b**,**c** could be isolated. According to the spectroscopic data of complexes **12b**,**c** we propose that the atropisomerism originates from differently orientated C(2)-bonded pyramidal piperidino nitrogen centers, which can be *cisoid* or *transoid* with respect to the pentacarbonyltungsten group and which have a hindered rotation around the C(2)−N bond (Figure 1). According to monitoring of the reaction by ^{31}P NMR spectroscopy, 2*H*-azaphosphirene complexes were not formed under these conditions.

Astonishingly, the deviation from the formerly observed product ratios was less than 5% if neat 1-piperidinocarbonitrile was used as solvent. The appropriate *P*-phenyl-substituted 2*H*-azaphosphirene complex was eventually de-

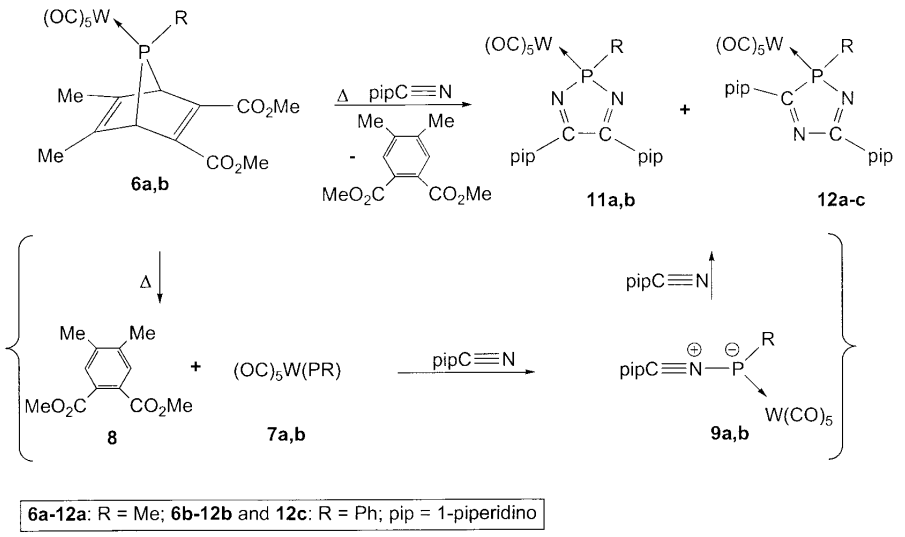

Scheme 3. Thermal decomposition of 7-phosphanorbornadiene complexes **6a**,**b** in neat 1-piperidinocarbonitrile or 1-piperidinocarbonitrile toluene solutions

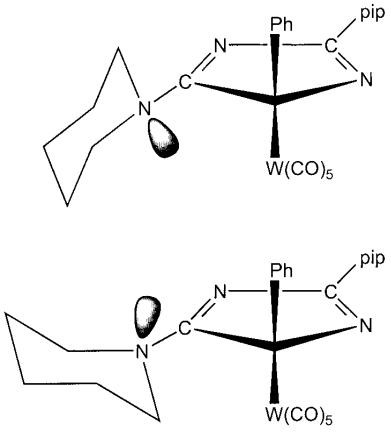

Figure 1. Proposed structures for the atropisomeric 2*H*-1,2,4-diazaphosphole complexes **12b**,**c**

tected in very small amounts (< 3% according to the ^{31}P NMR spectrum; δ = −47.9) only in the case of complex **1b**; the related *P*-bis(trimethylsilyl)methyl-substituted 2*H*-azaphosphirene complex was observed at δ = −70.3.[3b]

Because of the known thermal instability of 2*H*-azaphosphirene complexes, we decided to carry out a preliminary study on the use of Cu^{I}Cl as catalyst for the decomposition,[10] and were thus able to lower the temperature substantially to 65−70 °C. Although we performed the reaction of the complexes **6a**,**b** with 1-piperidinocarbonitrile — with and without exclusion of light[11] — the ^{31}P NMR spectra showed no further evidence for 2*H*-azaphosphirene complexes. Remarkably, the reaction of complex **6b** with 1-piperidinocarbonitrile and catalytic amounts of Cu^{I}Cl in toluene at 70 °C and with exclusion of light furnished the 2*H*-1,3,2-azaphosphole complex **11b** selectively. In the case of complex **6a** the 2*H*-1,3,2-azaphosphole complex **11a** and a complex **13** were formed in a 6:4 ratio (Scheme 4). Unfortunately, the latter complex could not be isolated by column chromatography due to decomposition. Nevertheless, a comparison of the ^{31}P NMR spectroscopic data of complex **13** [δ = 73.2, $J(^{31}P,^{31}P)$ = 25.6, $^{1}J(^{183}W,^{31}P)$ = 217.9 Hz; δ = 68.7, $J(^{31}P,^{31}P)$ = 25.6, $^{1}J(^{183}W,^{31}P)$ = 259.7 Hz] with {2,5-bis[bis(trimethylsilyl)methyl]-4,6-diphenyl-2,5-dihydro-1,3-diaza-2,5-diphosphinine-κP^2]}pentacarbonyltungsten(0)[6] [δ = 79.9, $J(^{31}P,^{31}P)$ = 15.3, $^{1}J(^{183}W,^{31}P)$ = 266.1 Hz; δ = −0.6, $J(^{31}P,^{31}P)$ = 15.3 Hz] provides some evidence for the constitution of complex **13** as the head-to-tail dimer of complex **9a**.

As expected, the ^{13}C NMR spectra of the 2*H*-1,3,2-azaphosphole complexes **11a,b** showed one resonance for the PN*C* imino carbon atoms of the ring between δ = 160.7 and 161.6 with coupling constant magnitudes $|J(^{31}P,^{13}C)|$ of ca. 2.5−6.4 Hz; the data of the complexes **14a**[3b] and **14b**[3c] are also listed in Table 1 for comparison. Three resonances were observed for the methylene carbon atoms of the 1-piperidino substituent, as expected for such 2*H*-1,3,2-azaphosphole complexes.[3b,3c] More surprising were the ^{13}C NMR spectra of the 2*H*-1,4,2-azaphosphole complexes **12a**−**c** (Table 2). Here the resonances for both types of imino carbon atoms were observed in a comparably narrow range between δ = 160 and 185 and the coupling constant magnitudes $|J(^{31}P,^{13}C)|$ were also considerably smaller (ca. 2−15 Hz) than those observed for the derivatives **15a**,[3b] **15b**[5] and **15c**[12] [values between δ = 195 and 200 (P*C*N) and δ = 163 and 170 (PN*C*); $|J(^{31}P,^{13}C)|$ ca. 1−30 Hz]. Therefore, we could only make tentative assignments in the present study. As expected, each 1-piperidino substituent of **12a**−**c** shows more than three resonances for the methylene carbon atoms, although in some cases only collapsed signals were observed.

Within each class of compounds the bulky substituted derivatives **14** and **15** tend to have ^{31}P resonances at significantly lower field; for example, the resonances of **15a**,[3b] and **15b**[5] are observed in the range δ = 110−123 with characteristic coupling constants $|J(^{183}W,^{31}P)|$ of 228−234 Hz, whereas **12a**−**c** were observed in the range δ = 70−80 with

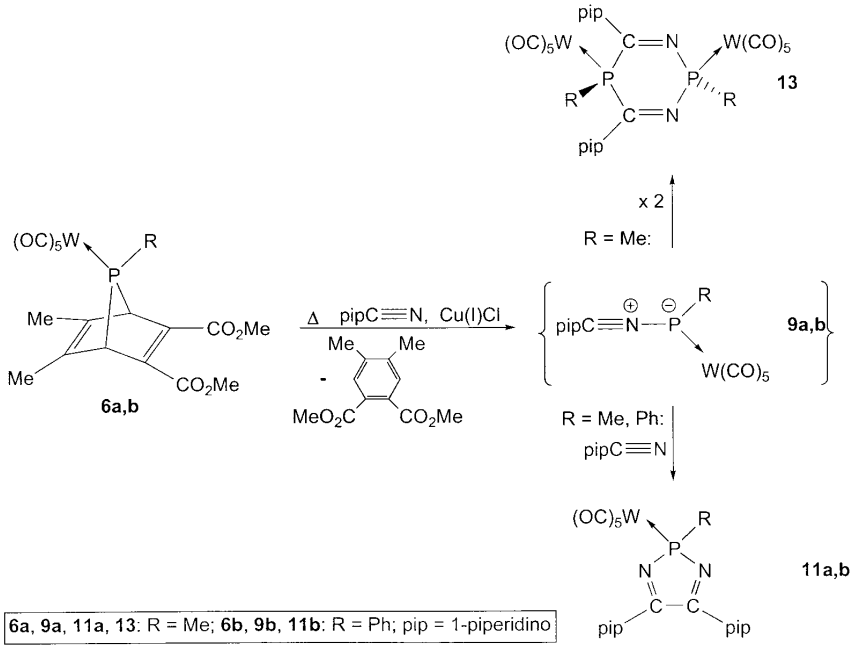

Scheme 4

Table 1. Selected ^{31}P and ^{13}C NMR spectroscopic data of the 2*H*-1,3,2-diazaphosphole tungsten complexes **11a**,**b** and **14a**[3b] and **14b**[3c] ($CDCl_3$, δ in [ppm]; *J* in [Hz]; pip = 1-piperidino)

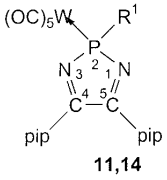

11,14

Comp.	R^1	δ ^{31}P	^1J(W,P)	δ $^{13}C^{4/5}$	$^{(2+3)}J$(P,C)
11a	Me	125.2	262.4	161.3	5.9
11b	Ph	125.6	270.1	160.7	5.8
14a	$CH(SiMe_3)_2$	133.2	264.3	160.7	6.4
14b	C_5Me_5	137.7	278.1	161.6	2.5

Table 2. Selected ^{31}P and ^{13}C NMR spectroscopic data of the 2*H*-1,4,2-diazaphosphole tungsten complexes **12a**−**c** and **15a**,[3b] **15b**[5] and **15c**[12] ($CDCl_3$, δ in [ppm]; *J* in [Hz], #: not resolved, bis = $CH(SiMe_3)_2$, *Z* = CO_2Et, pip = 1-piperidino)

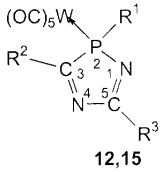

12,15

Comp.	R^1	R^2	R^3	δ ^{31}P	^1J(W,P)	δ $^{13}C^3$	*J*(P,C)	δ $^{13}C^5$	*J*(P,C)
12a	Me	pip	pip	70.6	248.5	185.6	2.6	167.3	3.9
12b	Ph	pip	pip	80.3	257.2	160.4	11.0	159.9	5.2
12c	Ph	pip	pip	78.8	254.0	165.6	15.2	169.2	4.2
15a	bis	Ph	Ph	110.6	227.9	198.5	22.3	169.5	5.1
15b	bis	Z	Ph	122.4	233.6	195.6	29.8	167.2	7.0
15c	bis	Ph	pip	110.6	227.9	199.9	22.1	163.4	#

coupling constants $|J(^{183}W,^{31}P)|$ of 248−258 Hz. These differences in the chemical shifts and the tungsten-phosphorus couplings seem to be mainly caused by different steric interactions of the organic substituents at the phosphorus center and the pentacarbonyltungsten group.

EI mass spectrometric experiments revealed that these 2*H*-1,3,2-azaphosphole and 2*H*-1,4,2-diazaphosphole complexes preferentially lose carbon monoxide and show cleavage of the C−N bonds between the different heterocyclic ring systems subsequent to the ionisation process; this behavior has also been observed for the bulky substituted derivatives **14**[3b,3c] and **15**.[3,5,12]

In conclusion, we have shown that the chemistry of nitrilium phosphanylide complexes can be further exploited using 7-methyl- and 7-phenyl-phosphanorbornadiene complexes and 1-piperidinocarbonitrile, thus providing a new access to 2*H*-1,3,2-azaphosphole and 2*H*-1,4,2-diazaphosphole complexes. Furthermore, we obtained new insights into the reactivity of nitrilium phosphanylide complexes that are sterically unencumbered at phosphorus, and we provide first evidence for the transient formation of a *P*-phenyl-substituted 2*H*-azaphosphirene complex.

Experimental Section

General Procedures: All reactions and manipulations were carried out under an atmosphere of deoxygenated dry nitrogen, using standard Schlenk techniques with conventional glassware, and solvents were dried according to standard procedures. NMR spectra were recorded on a Bruker AC-200 spectrometer (200 MHz for ^1H; 50.3 MHz for ^{13}C; 81.0 MHz for ^{31}P) with [D]chloroform and

[D_6]benzene as both solvent and internal standard; shifts are given relative to external tetramethylsilane (^{1}H, ^{13}C) or 85% H_3PO_4 (^{31}P). Mass spectra were recorded on a Finnigan Mat 8430 (70 eV); apart from the *m*/*z* values of the molecule ions, only *m*/*z* values with intensities of more than 20% are given. Infrared spectra were recorded on a Biorad FT-IR 165 (selected data given). Melting points were obtained on a Büchi 535 capillary apparatus. Elemental analyses were performed by using a Carlo Erba analytical gas chromatograph. The κ*P* notation differentiates between *P*- and *N*-coordination of the appropriate heterocycle to the metal.

Procedure for the Synthesis of the Diazaphosphole Complexes 11a,b and 12a−c: Compound **1a** (0.45 g, 0.85 mmol) or **1b** (0.56 g, 0.85 mmol) and 1-piperidinocarbonitrile (0.2 mL, 1.7 mmol), dissolved in 5 mL of xylene, were heated for 3.5−4 h at 120 °C with slow stirring. When the reaction was complete (as monitored by ^{31}P NMR spectroscopy), the solution was evaporated to dryness in vacuo (ca. 0.01 mbar), and the residue subjected to low-temperature column chromatography on silica (−32 °C, *n*-hexane/diethyl ether, 10:1). The eluates were evaporated to dryness in vacuo (ca. 0.01 mbar), and the residues recrystallised from *n*-pentane at −20 °C.

Pentacarbonyl[2-methyl-2*H*-1,3,2-diazaphosphole-4,5-di(1-piperidino)-κ*P*]tungsten(0) (11a): Yield: 210 mg (42%), m.p. 108 °C. (decomp.); ^{13}C{^{1}H} NMR ($CDCl_3$): δ = 22,8 (s, $NCH_2CH_2\mathit{C}H_2$), 24.4 (s, $NCH_2\mathit{C}H_2CH_2$), 25.5 [d, ^1J(P,C) = 27.5 Hz, PCH_3), 50.0 (s, $N\mathit{C}H_2CH_2CH_2$), 161.3 [d, $^{(2+3)}J$(P,C) = 5.9 Hz, PN=*C*], 196.3 [d, ^2J(P,C) = 8.0, ^1J(W,C) = 125.6 Hz, *cis*-CO], 200.4 [d, ^2J(P,C) = 22.9 Hz, *trans*-CO]; ^{31}P{^{1}H} NMR ($CDCl_3$): δ = 125.2 [s, ^1J(W,P) = 264.4 Hz); ^{31}P NMR ($CDCl_3$): δ = 125.2 [q, ^2J(P,H) = 6.8, ^1J(W,P) = 264.4 Hz]; MS (EI, ^{184}W): *m*/*z* (%) = 590 (51) [M^+], 562 (19) [$(M - CO)^+$], 534 (46) [$(M - 2CO)^+$], 506 (62) [$(M - 3CO)^+$], 478 (66) [$(M - 4CO)^+$], 450 (100) [$(M - 5CO)^+$], 84 (30) [$C_5H_{10}N^+$]; $C_{18}H_{23}N_4O_5PW$ (590.2): calcd. C 36.63, H 3.93, N 9.49; found C 36.42, H 3.78, N 9.39.

Pentacarbonyl[2-methyl-2*H*-1,4,2-diazaphosphole-3,5-di(1-piperidino)-κ*P*]tungsten(0) (12a): Yield: 130 mg (26%), m.p. 94 °C. (decomp.); ^{13}C{^{1}H} NMR ($CDCl_3$): δ = 21.8 [d, ^1J(P,C) = 20.3 Hz, PCH_3], 22.8 (br. s, $NCH_2CH_2\mathit{C}H_2$), 24.1 (s, $NCH_2\mathit{C}H_2\mathit{C}H_2$), 24.4 (s, $NCH_2\mathit{C}H_2CH_2$), 25.0 (s, $NCH_2CH_2\mathit{C}H_2$), 25.8 (s, $NCH_2\mathit{C}H_2CH_2$), 43.8 (s, $N\mathit{C}H_2CH_2CH_2$), 47.6 (s, $N\mathit{C}H_2CH_2CH_2$), 49.8 (s, $N\mathit{C}H_2CH_2CH_2$), 50.6 [d, ^3J(P,C) = 5.5 Hz, $N\mathit{C}H_2CH_2CH_2$], 167.3 [d, $^{(2+3)}J$(P,C) = 3.9 Hz, PN=*C*], 185.6 [d, $^{(1+4)}J$(P,C) = 2.6 Hz, P=*C*N], 196.5 [d, ^2J(P,C) = 7.1 Hz, *cis*-CO], 200.0 [d, ^2J(P,C) = 22.1 Hz, *trans*-CO]; ^{31}P{^{1}H} NMR ($CDCl_3$): δ = 70.6 [s, ^1J(W,P) = 248.5 Hz]; ^{31}P NMR ($CDCl_3$): δ = 70.6 [q, ^2J(P,H) = 6.3, ^1J(W,P) = 248.5 Hz]; MS (*neg.*-CI, NH_3, ^{184}W): *m*/*z* (%) = 589 (100) [$(M - H)^-$], 324 (42) [$W(CO)_5$]; (*pos.*-CI, NH_3, ^{184}W): *m*/*z* (%) = 591 (85) [$(M + H)^+$]; $C_{18}H_{23}N_4O_5PW$ (590.2): calcd. C 36.63, H 3.93, N 9.49; found C 36.48, H 3.81, N 9.43.

{Pentacarbonyl[2-phenyl-2*H*-1,3,2-diazaphosphole-4,5-di(1-piperidino)-κ*P*]tungsten(0)} (11b): Yield: 338 mg (61%), m.p. 127 °C. (decomp.); ^{13}C{^{1}H} NMR ($CDCl_3$): δ = 23.2 (s, $NCH_2CH_2\mathit{C}H_2$), 24.2 (s, $NCH_2\mathit{C}H_2CH_2$), 48.8 (s, $N\mathit{C}H_2CH_2CH_2$), 127.3 [d, ^2J(P,C) = 9.7 Hz, *o*-Ph], 128.6 [d, ^3J(P,C) = 12.4 Hz, *m*-Ph], 129.4 [d, ^4J(P,C) = 1.9 Hz, *p*-Ph], 136.9 [d, ^1J(P,C) = 43.5 Hz, *i*-Ph], 160.7 [d, ($^{(2+3)}J$(P,C) = 5.8 Hz, PN=*C*], 195.5 [d, ^2J(P,C) = 8.1 Hz, *cis*-CO], 199.6 [d, ^2J(P,C) = 23.7 Hz, *trans*-CO]; ^{31}P{^{1}H} NMR ($CDCl_3$): δ = 126.3 [s, ^1J(W,P) = 272.0 Hz]; ^{31}P NMR ($CDCl_3$): δ = 126.3 [t, ^3J(P,H) = 9.6, ^1J(W,P) = 272.0 Hz]; MS (EI, ^{184}W): *m*/*z* (%) = 652 (42) [M^+], 624 (6) [$(M - CO)^+$], 596 (4) [$(M - 2CO)^+$], 568 (33) [$(M - 3CO)^+$], 540 (35) [$(M - 4CO)^+$], 512 (100) [$(M - 5CO)^+$], 84 (25) [$C_5H_{10}N^+$]; $C_{23}H_{25}N_4O_5PW$ (652.3): calcd. C 42.35, H 3.86, N 8.59, found C 41.85, H 3.82, N 8.49.

A 1:1 mixture of complexes **12b**,**c** was obtained, which was slightly contaminated with **12a** (ca. 10%); the mixture was analyzed by spectroscopic means and elemental analysis.

{Pentacarbonyl[2-phenyl-2*H*-1,4,2-diazaphosphole-3,5-bis(1-piperidino)-κ*P*]tungsten(0)} (12b,c): ^{13}C{^{1}H} NMR ($CDCl_3$): δ = 23.7 (br. s, $NCH_2CH_2\mathit{C}H_2$), 24.0 (br. s, $NCH_2CH_2\mathit{C}H_2$), 24.4 (br. s, $NCH_2\mathit{C}H_2CH_2$), 24.6 (br. s, $NCH_2\mathit{C}H_2CH_2$), 25.2 (br. s, $NCH_2\mathit{C}H_2CH_2$), 25.8 (br. s, $NCH_2\mathit{C}H_2CH_2$), 46.9 (s, $N\mathit{C}H_2CH_2CH_2$), 47.8 (br. s, $N\mathit{C}H_2CH_2CH_2$), 48.8 (br. s, $N\mathit{C}H_2CH_2CH_2$), 49.7 (s, $N\mathit{C}H_2CH_2CH_2$), 49.9 (s, $N\mathit{C}H_2CH_2CH_2$), 50.9 [d, ^3J(P,C) = 5.7 Hz, $N\mathit{C}H_2CH_2CH_2$], 127.7 [d, ^2J(P,C) = 10.6 Hz, *o*-Ph], 128.9 [d, ^2J(P,C) = 9.9 Hz, *o*-Ph], 131.2 [d, ^4J(P,C) = 2.1 Hz, *p*-Ph], 129.9 [d, ^3J(P,C) = 13.5 Hz, Ph], 130.2 (s, *p*-Ph), 131.2 [d, ^1J(P,C) = 41.5 Hz, *i*-Ph], 131.5 [d, ^3J(P,C) = 8.8 Hz, *m*-Ph], 133.3 [d, ^1J(P,C) = 31.6 Hz, *i*-Ph], 159.9 [d, *J*(P,C) = 5.1 Hz, N=*C*], 160.4 [d, *J*(P,C) = 11.0 Hz, N=*C*], 165.6 [d, *J*(P,C) = 15.1 Hz, N=*C*], 169.2 [d, *J*(P,C) = 4.0 Hz, N=*C*], 195.5 [d, ^2J(P,C) = 7.3 Hz, *cis*-CO], 196.4 [d, ^2J(P,C) = 7.4 Hz, *cis*-CO], 198.5 [d, ^2J(P,C) = 25.9 Hz, *trans*-CO], 200.0 [d, ^2J(P,C) = 23.4 Hz, *trans*-CO]; ^{31}P{^{1}H} NMR ($CDCl_3$): δ = 80.3 [s, ^1J(W,P) = 257.2 Hz]; ^{31}P{^{1}H} NMR ($CDCl_3$): δ = 78.8 [s, ^1J(W,P) = 254.0 Hz]; $C_{23}H_{25}N_4O_5PW$ (652.3): calcd. C 42.35, H 3.86, N 8.59, found C 42.05, H 3.83, N 8.51.

Acknowledgments

We are grateful to H.-M. Schiebel (TU Braunschweig) for mass spectrometric experiments and the Deutsche Forschungsgemeinschaft and the Fonds der Chemischen Industrie for financial support.

[1] R. Streubel, U. Schiemann, P. G. Jones, N. H. Tran Huy, F. Mathey, *Angew. Chem.* **2000**, *112*, 3845−3847; *Angew. Chem. Int. Ed.* **2000**, *39*, 3686−3688.
[2] [2a] R. Streubel, H. Wilkens, A. Ostrowski, C. Neumann, F. Ruthe, P. G. Jones, *Angew. Chem.* **1997**, *109*, 1549−1550; *Angew. Chem. Int. Ed. Engl.* **1997**, *36*, 1492−1493; [2b] U. Rohde, F. Ruthe, P. G. Jones, R. Streubel, *Angew. Chem.* **1999**, *111*, 158−160; *Angew. Chem. Int. Ed.* **1999**, *38*, 215−217; [2c] H. Wilkens, A. Ostrowski, J. Jeske, F. Ruthe, P. G. Jones, R. Streubel, *Organometallics* **1999**, *18*, 5627−5642.
[3] [3a] H. Wilkens, J. Jeske, P. G. Jones, R. Streubel, *Chem. Commun.* **1997**, 2317−2318; [3b] H. Wilkens, F. Ruthe, P. G. Jones, R. Streubel, *Chem. Eur. J.* **1998**, *4*, 1542−1553; [3c] R. Streubel, U. Schiemann, N. Hoffmann, Y. Schiemann, P. G. Jones, D. Gudat, *Organometallics* **2000**, *19*, 475−481.
[4] F. G. N. Cloke, P. B. Hitchcock, U. Schiemann, R. Streubel, J. F. Nixon, D. J. Wilson, *Chem. Commun.* **2000**, 1659−1660.
[5] R. Streubel, H. Wilkens, F. Ruthe, P. G. Jones, *Chem. Commun.* **1999**, 2127−2128.
[6] R. Streubel, H. Wilkens, F. Ruthe, P. G. Jones, *Chem. Commun.* **2000**, 2453−2454.
[7] H. Wilkens, F. Ruthe, P. G. Jones, R. Streubel, *Chem. Commun.* **1998**, 1529−1530.
[8] U. Schiemann, PhD Thesis, Technische Universität Braunschweig, Braunschweig 2001.
[9] A. Marinetti, F. Mathey, J. Fischer, A. Mitschler, *J. Chem. Soc., Chem. Commun.* **1982**, 667−668.
[10] A. Marinetti, F. Mathey, *Organometallics* **1984**, *3*, 456−461.
[11] A. Marinetti, F. Mathey, J. Fischer, A. Mitschler, *Nouv. J. Chim.* **1984**, *8*, 453−457.
[12] R. Streubel, H. Wilkens, P. G. Jones, *Chem. Eur. J.* **2000**, *7*, 3997−4000.

Received August 31, 2001
[I01336]

Cationic Five-Coordinate Bis(butadiene)iridium(I) Complexes from the Highly Labile *cis*-$[Ir(\eta^2\text{-}C_8H_{14})_2(acetone)_2]^+$ Cation as the Precursor

Marco Bosch,[a] Kerstin Ilg,[a] and Helmut Werner*[a]

Dedicated to Professor Rudolf Taube on the occasion of his 70th birthday

Keywords: Acetone complexes / Alkene ligands / Iridium / P ligands / Arsenic / Antimony

The cation *cis*-$[Ir(\eta^2\text{-}C_8H_{14})_2(acetone)_2]^+$, which is generated in situ from $[Ir(\mu\text{-}Cl)(\eta^2\text{-}C_8H_{14})_2]_2$ (**1**) and $AgPF_6$ in acetone, reacts with butadiene at room temperature to give the five-coordinate complex $[Ir(s\text{-}cis\text{-}\eta^4\text{-}C_4H_6)_2(\eta^2\text{-}C_8H_{14})]PF_6$ (**3**). The cyclooctene ligand of **3** is only weakly coordinated and easily displaced by P*i*Pr$_3$, As*i*Pr$_3$ and Sb*i*Pr$_3$ to afford the compounds $[Ir(s\text{-}cis\text{-}\eta^4\text{-}C_4H_6)_2(E\textit{i}Pr_3)]PF_6$ (**5**–**7**) in excellent yields. Alternatively, **5**–**7** can be prepared from $[IrCl(s\text{-}cis\text{-}\eta^4\text{-}C_4H_6)_2]$ (**4**) by stepwise treatment with $AgPF_6$ and E*i*Pr$_3$ (E = P, As, Sb). The X-ray crystal structure analysis of **5** revealed a square-pyramidal geometry of the cation with the phosphane ligand in the apical position.

Introduction

In the course of our investigations on the ability of sulfonatorhodium(I) compounds to catalyze C−C coupling reactions of olefins and other unsaturated substrates,[1] we recently found that the monomeric triflatorhodium(I) complex $[Rh\{\eta^2\text{-}O_2S(O)CF_3\}(P\textit{i}Pr_3)_2]$ is an active catalyst for the polymerization of butadiene.[2] Moreover, we observed that if instead of the bis(phosphane) compound the dimeric bis(cyclooctene) derivative $[Rh\{\mu\text{-}O_2S(O)CF_3\}(\eta^2\text{-}C_8H_{14})_2]_2$ is treated with C_4H_6, the five-coordinate bis(butadiene) complex $[Rh\{\eta^1\text{-}OS(O)_2CF_3\}(\eta^4\text{-}C_4H_6)_2]$ is formed, and this complex reacts with bulky phosphanes to give the corresponding cations $[Rh(\eta^4\text{-}C_4H_6)_2(PR_3)]^+$ in excellent yields by ligand displacement.[3] Since these cations readily undergo intramolecular C−C coupling reactions and are intermediates in the formation of the unusual cyclotetramer *cis*,*cis*,*trans*,*trans*-1,5,9,13-$C_{16}H_{24}$,[4] we became interested to find out whether analogous bis(butadiene)iridium(I) compounds would be accessible and what their reactivity compared to the rhodium counterparts is. In this paper we report the generation of the highly reactive bis(cyclooctene)iridium(I) cation *cis*-$[Ir(\eta^2\text{-}C_8H_{14})_2(acetone)_2]^+$ and its smooth conversion into cationic five-coordinate bis(butadiene) derivatives.

Results and Discussion

Our attempts to start the stepwise synthesis of the target compounds $[Ir(\eta^4\text{-}C_4H_6)_2(PR_3)]^+$ from the preparation of $[Ir\{\mu\text{-}O_2S(O)CF_3\}(\eta^2\text{-}C_8H_{14})_2]_2$, the analogue of the above-mentioned rhodium complex $[Rh\{\mu\text{-}O_2S(O)CF_3\}(\eta^2\text{-}C_8H_{14})_2]_2$, failed. Treatment of a suspension of $[Ir(\mu\text{-}Cl)(\eta^2\text{-}C_8H_{14})_2]_2$ (**1**) in acetone with two equivalents of AgO_3SCF_3 afforded a mixture of products which could not be separated either by fractional crystallization or chromatographic techniques.

Following earlier work by Schrock[5] and Muetterties,[6] we therefore used the dimeric chloro derivative **1** as the starting material. This compound reacts with $AgPF_6$ (molar ratio 1:2) in acetone to give an orange solution from which, even by evaporation of the solvent under very mild conditions, no analytically pure compound could be isolated. If, however, [D$_6$]acetone was used as the solvent, both the ^{1}H and the ^{13}C NMR spectra of the solution indicated that a bis(cyclooctene)iridium(I) cation had been generated. Although the NMR spectroscopic data did not allow us to determine the number of [D$_6$]acetone molecules coordinated to the metal center, we assume, in analogy to the more stable, isolated complex *cis*-$[Rh(\eta^2\text{-}C_8H_{14})_2(acetone)_2]PF_6$,[7] that the coordination geometry corresponds to a square plane with the cyclooctene and the [D$_6$]acetone ligands in *cis* positions (see Scheme 1). We note that in the ^{13}C NMR spectrum of **2** there is only one signal for the C=O moiety and one signal for the CH_3 carbon indicating that, at room temperature, a fast exchange between free and coordinated [D$_6$]acetone takes place.

Passing a slow stream of butadiene through a solution containing the in situ generated cation **2** for ten seconds, in the presence of excess cyclooctene, led to a quick change of color from orange to pale-yellow. After addition of pentane, a white, moderately air-sensitive solid precipitated which analyzed as $[Ir(s\text{-}cis\text{-}\eta^4\text{-}C_4H_6)_2(\eta^2\text{-}C_8H_{14})]PF_6$ (**3**). The ^{1}H NMR spectrum of **3** displays three well-separated resonances for the butadiene protons at δ = 6.10, 3.50 and 1.48 of which those for the *exo* and *endo* protons of the terminal CH_2 groups are split into doublets of doublets. The signal for the olefinic protons of the coordinated cyclooctene appears at δ = 5.66 and is thus shifted about 2.2 ppm down-

[a] Institut für Anorganische Chemie der Universität Würzburg
Am Hubland, 97074 Würzburg, Germany
Fax: (internat.) + 49-931/888-4623
E-mail: helmut.werner@mail.uni-wuerzburg.de

 © WILEY-VCH Verlag GmbH, 69451 Weinheim, 2001 1434−1948/01/1212−3181 $ 17.50+.50/0

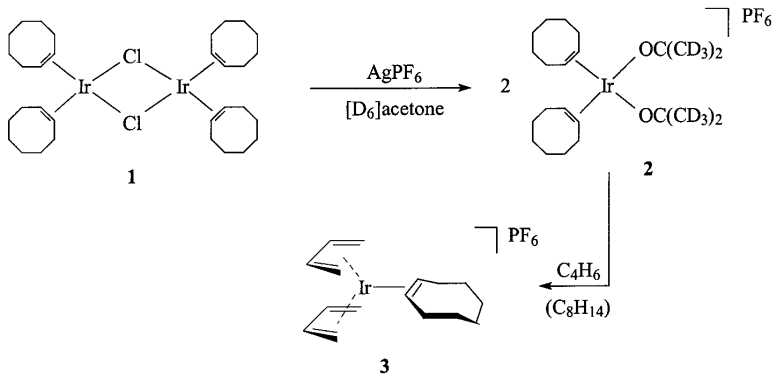

Scheme 1

field relative to **2**. A similar downfield shift is also observed in the ^{13}C NMR spectrum for the signal of the CH=CH carbon atoms of C_8H_{14}, which appears at $\delta = 81.9$ for **3** but at $\delta = 62.7$ for **2**. The increased electron density at the five-coordinate iridium(I) center of **3** could explain these observations.

The cyclooctene ligand of **3** is not strongly coordinated and can therefore be displaced by a better donor such as P*i*Pr$_3$ (Scheme 2). However, treatment of a solution of **3** in dichloromethane with *one* equivalent of the phosphane did not lead to a complete conversion and, after removal of the solvent, afforded a 1:1 mixture of **3** and **5**. An almost quantitative yield of the substitution product **5** could be achieved upon the addition of a second equivalent of P*i*Pr$_3$ to the 1:1 mixture of **3** and **5**. An alternative procedure to prepare **5** consists of the stepwise reaction of the mononuclear precursor **4**[8] with $AgPF_6$ and an equimolar amount of P*i*Pr$_3$. The yield here is also excellent. Compound **5** is a white solid that can be handled in air for a short period of time and can be stored under argon for weeks without decomposition. Similarly to **3**, the ^1H NMR spectrum of **5** displays three signals of equal intensity for the C_4H_6 protons and the ^{13}C NMR spectrum shows two resonances for the butadiene carbon atoms, one of which is split into a doublet due to ^{13}C-^{31}P coupling.

The molecular structure of the triisopropylphosphane complex **5** was determined by X-ray crystallography. There are two independent molecules, **5a** and **5b**, in the unit cell, of which **5a** is shown in Figure 1. The coordination geometry around the iridium center is square-pyramidal with the CH_2 groups of the butadiene ligands at the base of the pyramid. The apical position of the cationic species is occupied by the phosphorus atom of the P*i*Pr$_3$ ligand. The C−C bond lengths of the C_4H_6 moieties together with the bond angles C(1)−C(2)−C(3), C(4)−C(3)−C(2), C(5)−C(6)−C(7) and C(8)−C(7)−C(6) (all ≈120°) clearly indicate an η^4-coordination mode for the diene molecules. The distances between the metal and the CH and CH_2 units lie in the ranges 2.215(11)−2.205(11) and 2.184(11)−2.167(12) Å, respectively, and are quite similar to those found in other

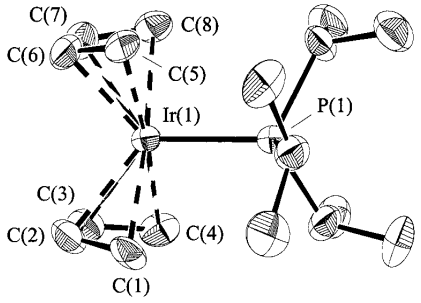

Figure 1. Molecular structure of **5a** (hydrogen atoms and anionic ligand omitted for clarity; there are two independent molecules **5a** and **5b** in the unit cell, the data for **5b** are given after the diagonal lines); principle bond lengths [Å] and angles [°] with estimated standard deviations in parentheses: Ir(1)−C(1) 2.206(11)/2.224(13), Ir(1)−C(2) 2.167(12)/2.166(12), Ir(1)−C(3) 2.184(11)/2.179(12), Ir(1)−C(4) 2.215(11)/2.216(11), Ir(1)−C(5) 2.205(11)/2.219(12), Ir(1)−C(6) 2.161(12)/2.187(13), Ir(1)−C(7) 2.178(13)/2.178(13), Ir(1)−C(8) 2.209(12)/2.212(12), C(1)−C(2) 1.424(18)/1.419(19), C(2)−C(3) 1.448(19)/1.436(19), C(3)−C(4) 1.414(18)/1.384(19), C(5)−C(6) 1.381(18)/1.418(19), C(6)−C(7) 1.430(19)/1.435(19), C(7)−C(8) 1.389(19)/1.388(18), Ir(1)−P(1) 2.394(3)/2.389(3); C(1)−Ir(1)−P(1) 90.4(3)/90.5(4), C(4)−Ir(1)−P(1) 94.4(4)/94.9(4), C(5)−Ir(1)−P(1) 91.1(3)/90.3(3), C(8)−Ir(1)−P(1) 95.1(4)/95.3(4), C(1)−C(2)−C(3) 116.8(12)/119.2(12), C(2)−C(3)−C(4) 117.5(12)/118.4(12), C(5)−C(6)−C(7) 118.4(12)/119.2(12), C(6)−C(7)−C(8) 118.5(12)/117.3(12)

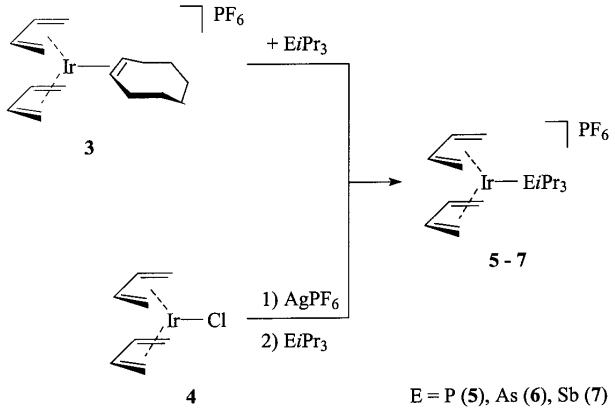

Scheme 2

bis(diene)iridium(I) compounds.[9] Both butadiene ligands are nearly planar, as indicated by the torsional angles of −1.7(17)° for the plane [C(1)−C(2)−C(3)−C(4)] and 1.9(18)° for [C(6)−C(7)−C(8)−C(9)]. However, the two planes of the butadienes are not parallel to each other but tilted by 14.6(3)° which could be due to steric repulsion between the bulky phosphane and the diene systems. The Ir−P distance of 2.394(3) Å in **5a** is relatively long compared with the distances of [IrH(s-cis-η⁴-C_4H_6)(PiPr$_3$)$_2$] (2.30−2.32 Å)[10] and several square-planar iridium(I) compounds containing $trans$-[Ir(PiPr$_3$)$_2$] (average Ir−P distance 2.34 Å) as a molecular building block.[11]

The cycloocteneiridium(I) complex **3** also reacts with two equiv. of AsiPr$_3$ or SbiPr$_3$ in dichloromethane at room temperature. The substitution products **6** and **7** (see Scheme 2) can also be formed from **4**, $AgPF_6$ and triisopropylarsane or -stibane in the molar ratio of 1:1:1. Compounds **6** and **7** are white solids, with properties that are quite similar to those of the triisopropylphosphane analogue **5**. With regard to the ^{1}H NMR spectroscopic data of **6** and **7**, we note that the signal of the *endo* protons H_a (for assignment see Figure 2) appears at lower field than that of **5** while the resonances for the protons H_b and H_c are observed slightly upfield compared with the triisopropylphosphane counterpart.

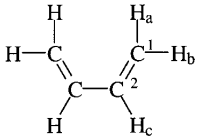

Figure 2. Assignment of the diene protons and carbon atoms in compounds **3**, **5**−**7**

The cations [Ir(s-cis-η⁴-C_4H_6)$_2$(EiPr$_3$)]$^+$ (E = P, As, Sb) are not only thermally quite stable (the PF_6^- salts decompose at about 150 °C) but, in contrast to the rhodium analogue [Rh(s-cis-η⁴-C_4H_6)$_2$(PiPr$_3$)]$^+$, they do not react upon heating by coupling of the two diene units to give an isomeric octadienediyliridium(III) derivative. We have already mentioned that the cationic bis(butadiene)rhodium(I) complex readily undergoes an intramolecular C−C coupling process in refluxing dichloromethane leading to [Rh(η³:η³-C_8H_{12})(PiPr$_3$)]$^+$, which is an intermediate in the rhodium-catalyzed cyclotetramerization of butadiene.[4] However, under the same conditions the iridium cations are completely inert and, even after stirring solutions of **5**, **6** or **7** in refluxing CH_2Cl_2 or CH_3NO_2 for 10−12 h, the starting materials could be quantitatively re-isolated. This inert behavior of the five-coordinate iridium(I) species is not only different to that of [Rh(s-cis-η⁴-C_4H_6)$_2$(PiPr$_3$)]$^+$ but also in contrast to the reactivity of some bis(butadiene)molybdenum and -ruthenium compounds which, in the presence of a Lewis base, undergo an intramolecular C−C coupling reaction.[12] Finally, we note that unlike [Rh(s-cis-η⁴-C_4H_6)$_2$(PiPr$_3$)]$^+$ the iridium counterpart does not react with excess PiPr$_3$ by either displacement of one of the diene ligands or attack of the phosphane at the coordinated butadiene to give a phosphoniumbutenylmetal cation.[3] The chemistry of diolefinrhodium(I) and diolefiniridium(I) compounds really is, as shown by several other examples,[13] not the same at all.

Experimental Section

All experiments were carried out under an atmosphere of argon by Schlenk techniques. The commercially available starting materials AgO_3SCF_3, $AgPF_6$ and butadiene were used without further purification. PiPr$_3$ was purchased from Strem Chemicals. The complexes [Ir(μ-Cl)(η²-C_8H_{14})$_2$]$_2$ (**1**)[14] and [IrCl(s-cis-η⁴-C_4H_6)$_2$] (**4**)[8] were prepared as described in the literature. The preparation of AsiPr$_3$ and SbiPr$_3$ was carried out as described for the n-propyl analogues.[15] NMR spectra were recorded at room temperature on Bruker AC 200 and Bruker AMX 400 instruments, unless otherwise stated. Abbreviations used: s, singlet; d, doublet; t, triplet; quin, quintet; sept, septet; m, multiplet; br, broadened signal. Melting and decomposition points were measured by differential thermal analysis (DTA).

Generation of cis-[Ir(η²-C_8H_{14})$_2$([D$_6$]acetone)$_2$]PF$_6$ (2): A suspension of **1** (60 mg, 0.07 mmol) in [D$_6$]acetone (1 mL) was treated with $AgPF_6$ (34 mg, 0.13 mmol) and stirred for 1 h at room temperature. A white solid precipitated, which was removed by filtration, and the clear orange solution was investigated by NMR spectroscopy. ^{1}H NMR (400 MHz, [D$_6$]acetone): δ = 2.57 (br. s, 4 H, CH of C_8H_{14}), 2.06 (br. s, 4 H, =CHCH_2 of C_8H_{14}), 1.61 (m, 4 H, CH_2 of C_8H_{14}), 1.42 (m, 12 H, CH_2 of C_8H_{14}), 1.24 (m, 4 H, CH_2 of C_8H_{14}); ^{13}C NMR (100.6 MHz, [D$_6$]acetone): δ = 206.6 (s, C=O of [D$_6$]acetone), 62.7 (s, CH of C_8H_{14}), 29.8 [sept, ^1J(D,C) = 19.3 Hz; CD_3 of [D$_6$]acetone], 29.6, 28.3, 26.7 (all s, CH_2 of C_8H_{14}); ^{19}F NMR (376.4 MHz, [D$_6$]acetone): δ = −72.3 [d, ^1J(P,F) = 709.4 Hz]; ^{31}P NMR (162.0 MHz, [D$_6$]acetone): δ = −144.1 [sept, ^1J(F,P) = 709.4 Hz].

Preparation of [Ir(s-cis-η⁴-C_4H_6)$_2$(η²-C_8H_{14})]PF$_6$ (3): A suspension of **1** (207 mg, 0.23 mmol) in acetone (10 mL) was treated with $AgPF_6$ (117 mg, 0.46 mmol) and stirred for 1 h at room temperature. The solution was filtered, and cyclooctene (100 μL, 0.77 mmol) was added to the filtrate. After stirring for 2 min, a slow stream of butadiene was passed through the solution for 10 s. The gaseous diene was replaced by argon, the pale-yellow solution was stirred for 30 min at room temperature and then concentrated to ca. 2 mL in vacuo. Addition of pentane (20 mL) resulted in the precipitation of a white solid, which was separated from the mother liquor, washed with pentane (3 × 5 mL) and dried in vacuo; yield 114 mg (89%); m.p. 103 °C (decomp); ^{1}H NMR (200 MHz, [D$_6$]-acetone): δ = 6.10 (m, 4 H, H_c), 5.66 (m, 2 H, CH of C_8H_{14}), 3.50 [dd, ^3J(H,H) = 8.0, ^2J(H,H) = 1.8 Hz, 4 H, H_b], 2.50 (m, 2 H, CHCH_2 of C_8H_{14}), 2.17, 1.97, 1.87, 1.78, 1.57 (all m, 10 H, CH_2 of C_8H_{14}), 1.48 [dd, ^3J(H,H) = 9.0, ^2J(H,H) = 1.8 Hz, 4 H, H_a]; for the assignment of the butadiene protons and carbon atoms see Figure 2; ^{13}C NMR (100.6 MHz, [D$_6$]acetone, 308 K): δ = 87.9 (s, C^2), 81.9 (s, CH of C_8H_{14}), 49.8 (s, C^1), 32.6, 29.6, 26.8 (all s, CH_2 of C_8H_{14}); ^{19}F NMR (376.4 MHz, [D$_6$]acetone, 308 K): δ = −72.2 [d, ^1J(P,F) = 705.5 Hz]; ^{31}P NMR (162.0 MHz, [D$_6$]acetone, 308 K): δ = −144.1 [sept, ^1J(F,P) = 705.5 Hz]; $C_{16}H_{26}F_6IrP$ (555.6): calcd. C 34.59, H 4.72; found C 34.34, H 4.56.

Preparation of [Ir(s-cis-η⁴-C_4H_6)$_2$(PiPr$_3$)]PF$_6$ (5): a) A solution of **3** (87 mg, 0.16 mmol) in CH_2Cl_2 (10 mL) was treated with PiPr$_3$ (30 μL, 0.16 mmol) and stirred for 1 h at room temperature. After removal of the solvent in vacuo, the colorless solid residue was

washed with pentane (5 mL) and dried in vacuo. Since the ^1H and ^{13}C NMR spectroscopic data showed that the product is a 1:1 mixture of **3** and **5**, the residue was dissolved in CH_2Cl_2 (10 mL) and treated again with P*i*Pr$_3$ (30 μL, 0.16 mmol). After stirring for 30 min, pentane (20 mL) was added to afford a colorless suspension. The solvent was decanted, the residue was washed with pentane (3 × 5 mL) and dried in vacuo. White solid; yield 88 mg (91%).

b) A suspension of **4** (125 mg, 0.37 mmol) in acetone (15 mL) was treated with $AgPF_6$ (94 mg, 0.37 mmol) and the mixture stirred for 1 h at room temperature. After removal of the solvent in vacuo, the residue was suspended in CH_2Cl_2 (10 mL). The resulting suspension was treated with P*i*Pr$_3$ (72 μL, 0.37 mmol) and stirred for 1 h at room temperature. Filtration of the mixture afforded a clear orange-yellow solution which was concentrated to ca. 2 mL in vacuo. Addition of pentane (10 mL) led to the precipitation of a white solid, which was separated from the mother liquor, washed with pentane (3 × 5 mL) and dried in vacuo. Yield 206 mg (92%); m.p. 152 °C (decomp); ^1H NMR (400 MHz, [D$_3$]nitromethane): δ = 5.64 (m, 4 H, H$_c$), 3.25 [dd, ^3J(H,H) = 7.8, ^2J(H,H) = 2.3 Hz, 4 H, H$_b$], 2.78 (m, 3 H, PC*H*CH$_3$), 1.43 [dd, ^3J(P,H) = 14.1, ^3J(H,H) = 7.4 Hz, 18 H, PCHC*H*$_3$], 1.09 [ddd, ^3J(H,H) = ^3J(P,H) = 8.9, ^2J(H,H) = 2.3 Hz, 4 H, H$_a$]; for the assignment of the butadiene protons and carbon atoms see Figure 2; ^{13}C NMR (100.6 MHz, [D$_3$]nitromethane): δ = 82.2 (s, C^2), 39.8 [d, ^2J(P,C) = 4.1 Hz, C^1], 29.1 [d, ^1J(P,C) = 27.5 Hz, P*C*HCH$_3$], 20.7 [d, ^2J(P,C) = 2.0 Hz, PCH*C*H$_3$]; ^{19}F NMR (376.4 MHz, [D$_3$]nitromethane): δ = −72.6 [d, ^1J(P,F) = 706.9 Hz]; ^{31}P NMR (162.0 MHz, [D$_3$]nitromethane): δ = 11.2 (s, P*i*Pr$_3$), −144.6 [sept, ^1J(F,P) = 706.9 Hz, PF_6^-]; $C_{17}H_{33}F_6IrP_2$ (605.6): calcd. C 33.72, H 5.49; found C 33.56, H 5.21.

Preparation of [Ir(*s-cis*-η^4-C$_4$H$_6$)$_2$(As*i*Pr$_3$)]PF$_6$ (6): This was prepared as described for **5** (method a), from **3** (93 mg, 0.17 mmol) and two portions of As*i*Pr$_3$ (33 μL, 0.17 mmol). White solid; yield 98 mg (90%). Alternatively, **6** could also be prepared as described for **5** (method b), from **4** (125 mg, 0.37 mmol), $AgPF_6$ (94 mg, 0.37 mmol) and As*i*Pr$_3$ (73 μL, 0.37 mmol) as starting materials. White solid; yield 229 mg (95%); m.p. 156 °C (decomp); ^1H NMR (400 MHz, [D$_3$]nitromethane): δ = 5.58 (m, 4 H, H$_c$), 3.21 [dd, ^3J(H,H) = 7.8, ^2J(H,H) = 2.3 Hz, 4 H, H$_b$], 2.90 [sept, ^3J(H,H) = 7.1 Hz, 3 H, AsC*H*CH$_3$], 1.47 [d, ^3J(H,H) = 7.1 Hz, 18 H, AsCHC*H*$_3$], 1.22 [dd, ^3J(H,H) = 7.9, ^2J(H,H) = 2.3 Hz, 4 H, H$_a$]; for the assignment of the butadiene protons and carbon atoms see Figure 2; ^{13}C NMR (100.6 MHz, [D$_3$]nitromethane): δ = 81.0 (s, C^2), 37.0 (s, C^1), 29.6 (s, As*C*HCH$_3$), 21.0 (s, AsCH*C*H$_3$); ^{19}F NMR (376.4 MHz, [D$_3$]nitromethane): δ = −73.3 [d, ^1J(P,F) = 706.4 Hz]; ^{31}P NMR (162.0 MHz, [D$_3$]nitromethane): δ = −144.6 [sept, ^1J(F,P) = 706.4 Hz]; $C_{17}H_{33}AsF_6IrP$ (649.6): calcd. C 31.43, H 5.12; found C 31.19, H 5.45.

Preparation of [Ir(*s-cis*-η^4-C$_4$H$_6$)$_2$(Sb*i*Pr$_3$)]PF$_6$ (7): This was prepared as described for **5** (method a), from **3** (76 mg, 0.14 mmol) and two portions of Sb*i*Pr$_3$ (27 μL, 0.14 mmol). White solid; yield 85 mg (89%). Alternatively, **7** could also be prepared as described for **5** (method b), from **4** (203 mg, 0.60 mmol), $AgPF_6$ (153 mg, 0.60 mmol) and Sb*i*Pr$_3$ (120 μL, 0.60 mmol) as starting materials. White solid; yield 388 mg (93%); m.p. 150 °C (decomp); ^1H NMR (400 MHz, [D$_3$]nitromethane): δ = 5.54 (m, 4 H H$_c$), 3.07 [dd, ^3J(H,H) = 7.6, ^2J(H,H) = 2.2 Hz, 4 H, H$_b$], 2.92 [sept, ^3J(H,H) = 7.4 Hz, 3 H, SbC*H*CH$_3$], 1.55 [d, ^3J(H,H) = 7.4 Hz, 18 H, SbCHC*H*$_3$], 1.29 [dd, ^3J(H,H) = 7.6, ^2J(H,H) = 2.2 Hz, 4 H, H$_a$]; for the assignment of the butadiene protons and carbon atoms see Figure 2; ^{13}C NMR (100.6 MHz, [D$_3$]nitromethane): δ = 79.0 (s, C^2), 32.4 (s, C^1), 22.0 (s, SbCH*C*H$_3$), 21.6 (s, Sb*C*HCH$_3$); ^{19}F NMR (376.4 MHz, [D$_3$]nitromethane): δ = −73.3 [d, ^1J(P,F) = 706.4 Hz]; ^{31}P NMR (162.0 MHz, [D$_3$]nitromethane): δ = −144.6 [sept, ^1J(F,P) = 706.4 Hz]; $C_{17}H_{33}F_6IrPSb$ (696.4): calcd. C 29.32, H 4.78; found C 29.14, H 5.17.

Thermolysis Experiments: Solutions of **5** (45 mg, 0.07 mmol), **6** (50 mg, 0.08 mmol) and **7** (63 mg, 0.09 mmol) in [D$_3$]nitromethane (0.5 mL) were stirred for 6 h at 60 °C. During this time no change of color of the solutions could be observed. The ^1H and ^{31}P NMR spectra revealed that in all cases no reaction had taken place.

Determination of the X-ray Crystal Structure of 5: Single crystals were grown by slow diffusion of pentane (10 mL) into a saturated solution of **5** in acetone (2 mL) at room temperature. The white crystalline product was washed with pentane (2 × 2 mL) and dried under a stream of argon. Crystal data (from 23 reflections, 10.00° < Θ < 15.00°): triclinic; space group $P\bar{1}$ (No. 2); a = 9.929(2), b = 12.295(3), c = 17.370(4) Å, α = 89.91(3)°, β = 89.92(3)°, γ = 89.92(3)°; V = 2120.7(7) Å^3, Z = 4; $d_{calcd.}$ = 1.897 g cm^{-3}; μ(Mo-K_α) = 6.497 mm^{-1}; crystal size 0.19 × 0.16 × 0.15 mm; Enraf−Nonius CAD4, Mo-K_α radiation (0.71073 Å), graphite monochromator; T = 193(2) K; ω/Θ-scan, max. 2Θ = 44.92°; 5964 reflections measured, 5508 independent ($R_{int.}$ = 0.0435), 4470 with $I > 2\sigma(I)$. Intensity data were corrected for Lorentz and polarization effects and an empirical absorption correction was applied. The structure was solved by direct methods (SHELX-97).[16] Atomic coordinates and anisotropic thermal parameters of the non-hydrogen atoms were refined by full-matrix least-squares method on F^2 (program package SDP (Enraf−Nonius) and SHELXL-97).[17] The asymmetric unit of **5** contains two formula units, each consisting of two moieties: a cationic iridium complex and a PF_6^- counterion. Both the PF_6^- ions are disordered occupying in both cases two geometrically independent positions. The site occupancy factors were refined with restrains on U_{ij} to values of 0.49:0.51 and 0.48:0.52, respectively. The positions of all hydrogen atoms were calculated according to ideal geometry and refined by using the riding method. Conventional R = 0.0461 [for 4470 reflections with $I > 2\sigma(I)$], and weighted wR_2 = 0.1342 for all 5964 located reflections; reflection/parameter ratio 10.0; residual electron density +1.997/−2.739 eÅ^{-3}.

Crystallographic data (excluding structure factors) for **5** have been deposited with the Cambridge Crystallographic Data Centre as supplementary publication no. CCDC-169995. Copies of the data can be obtained free of charge on application to CCDC, 12 Union Road, Cambridge CB2 1EZ, UK [Fax: (internat.) +44-1223/336-033; E-mail: deposit@ccdc.cam.ac.uk].

Acknowledgments

This work was supported by the Deutsche Forschungsgemeinschaft (SFB 347), BASF AG, and the Fonds der Chemischen Industrie. We are also grateful to the latter in particular for a PhD grant (to K. I.). Moreover, we thank Mrs. R. Schedl and Mr. C. P. Kneis (DTA and elemental analysis), Mrs. M.-L Schäfer and Dr. W. Buchner (NMR spectra), and Dr. J. Wolf for helpful advice.

[1] H. Werner, M. Bosch, C. Hahn, F. Kukla, M. Laubender, M. Manger, M. E. Schneider, B. Weberndörfer, B. Windmüller, *J. Chem. Soc., Dalton Trans.* **1998**, 3549−3558.
[2] [2a] M. E. Schneider, H. Werner, 10th International Symposium on Homogeneous Catalysis, Princeton, **1996**; [2b] M. E. Schneider, Dissertation, Universität Würzburg, **1996**.
[3] M. Bosch, M. Laubender, B. Weberndörfer, H. Werner, *Chem. Eur. J.* **1999**, *5*, 2203−2211.

[4] M. Bosch, M. Brookhart, K. Ilg, H. Werner, *Angew. Chem.* **2000**, *112*, 2388−2391; *Angew. Chem. Int. Ed.* **2000**, *39*, 2304−2307.
[5] R. R. Schrock, J. A. Osborn, *J. Am. Chem. Soc.* **1971**, *93*, 3089−3090.
[6] A. C. Sievert, E. L. Muetterties, *Inorg. Chem.* **1981**, *20*, 489−501.
[7] B. Windmüller, J. Wolf, H. Werner, *J. Organomet. Chem.* **1995**, *502*, 147−161.
[8] A. L. Onderdelinden, A. van der Ent, *Inorg. Chim. Acta* **1972**, *6*, 420−426.
[9] [9a] T. C. van Soest, A. van der Ent, E. C. Royers, *Cryst. Struct. Commun.* **1973**, *3*, 527−529; [9b] J. Müller, B. Passon, *Z. Naturforsch., Teil B* **1982**, *37*, 1358−1359; [9c] J. Müller, W. Hähnlein, B. Passon, *Z. Naturforsch., Teil B* **1982**, *37*, 1573−1579; [9d] J. Müller, C. Friedrich, T. Akhnoukh, K. Qiao, *J. Organomet. Chem.* **1994**, *476*, 93−99.
[10] G. del Piero, G. Perego, M. Cesari, *Gazz. Chim. Ital.* **1975**, *105*, 520−537.
[11] [11a] R. W. Lass, P. Steinert, J. Wolf, H. Werner, *Chem. Eur. J.* **1996**, *2*, 19−23; [11b] H. Werner, R. W. Lass, O. Gevert, J. Wolf, *Organometallics* **1997**, *16*, 4077−4088; [11c] K. Ilg, H. Werner, *Organometallics* **1999**, *18*, 5426−5428; [11d] K. Ilg, H. Werner, *Angew. Chem.* **2000**, *112*, 1691−1694; *Angew. Chem. Int. Ed.* **2000**, *39*, 1632−1634; [11e] H. Werner, K. Ilg, B. Weberndörfer, *Organometallics* **2000**, *19*, 3145−3153.
[12] [12a] D. N. Cox, R. Roulet, *J. Organomet. Chem.* **1988**, *342*, 87−95; [12b] D. N. Cox, R. Roulet, *Organometallics* **1985**, *4*, 2001−2005; [12c] R. Poli, L.-S. Wang, *J. Am. Chem. Soc.* **1998**, *120*, 2831−2842.
[13] R. S. Dickson, *Organometallic Chemistry of Rhodium and Iridium*, Academic Press, London, **1983**.
[14] A. L. Onderdelinden, A. van der Ent, *Inorg. Synth.* **1973**, *14*, 92−95.
[15] S. Samaan, in *Methoden der Organischen Chemie (Houben-Weyl)* (Ed.: E. Müller), 4th Ed., Thieme, Stuttgart, **1978**, Vol. XIII/8, p. 45 and 445.
[16] G. M. Sheldrick, *Acta Crystallogr., Sect. A* **1990**, *46*, 467−473.
[17] G. M. Sheldrick, *A Program for Crystal Structure Refinement*, University of Göttingen, **1993**.

Received July 20, 2001
[I01274]

Seven-Coordinate d^0 and d^{10} Ions − Computational and Experimental Studies on Tris(tropolonato)metal(III)−TOPO Adducts

Jerzy Narbutt,*[a] Marian Czerwiński,[b] and Jadwiga Krejzler[a]

Keywords: Chelates / Thallium / Yttrium / Coordination chemistry / Density-functional calculations / Hypervalent compounds

The stabilities of molecular adducts between tris(tropolonato)metal(III) chelates of some tripositive ions of Groups 3 and 13 and trioctylphosphane oxide (TOPO) were studied using both theoretical and experimental methods. Density-functional calculations were used to optimise the structure and characterise tris(tropolonates) of scandium and yttrium, a series of model chelates of gallium, indium, thallium, scandium, and yttrium, as well as the 1:1 adducts of these chelates with trimethylphosphane oxide. The calculated energy of adduct formation decreased in the order: Y > Sc > Tl > In. Stability constants of the 1:1 (and some 1:2) TOPO adducts in solution, determined by synergistic solvent extraction of metal tropolonates, decreased in the same order. Both methods show that gallium does not increase its coordination number (CN) above six. The chelates of d^{10} ions (CN 6) and their adducts (CN 7) are less stable than the corresponding d^0 species, because the former are hypervalent compounds with no higher-lying metal *n*d orbitals participating in bonding, while the latter have easily accessible vacant $(n-1)$d orbitals. A significant distortion of the chelate structure makes the adducts of smaller ions less stable. Examination of bonding molecular orbitals in the adducts shows an unusual origin of the metal–TOPO bond, which may be due to a contribution from π-bonding. Differences in some characteristics of indium and thallium compounds can be explained by relativistic properties of thallium.

Introduction

Metal ions with high coordination numbers (CN) continue to attract interest,[1,2] and the reason is not purely academic. The ability of a metal ion in a complex to increase its CN makes it possible to form inner-sphere adducts, to exchange ligands by an associative mechanism, to affect catalytic properties of the compound, etc. Inner-sphere solvation of metal complexes influences their behaviour in solution, which is of importance in different fields such as e.g. metal ion controlled biological processes and processes of separation of metal ions.

The coordination stereochemistry of metal complexes depends on the relations between geometrical and electrostatic factors on one side, and the electronic configuration of the metal ions on the other.[3] Geometrical models consider not only the size of the metal ion and ligand atoms, but also the ligand structure.[3,4] For example, the bite in rigid bidentate ligands and the intraligand strain affect the coordination environment of the ion.[3,5,6] Electrostatic metal−ligand attraction and ligand−ligand repulsion in the coordination polyhedron, which depend on the charges on the ion and on the ligand atoms, also affect the geometry of the complex and the strength of metal−ligand bonds. Generally, the weaker and longer the bonds, i.e. the easier the deformation of the coordination polyhedron, the greater the tendency to increase the CN by coordination of (an) additional ligand(s).[7] For less stable metal chelates, the role of ligand structure, in particular of bite size, is less pronounced.[6] The electronic configuration of the metal ion is also important in this connection. The effect of d-orbital population in transition metal ions on their CN was recently discussed in terms of the angular overlap model.[2]

The major objective of this work was to explain how the tendency to increase CN of a central metal ion in neutral chelates with bidentate ligands is influenced by properties of the ion, in particular its radius and electron configuration. Particularly interesting in this respect was the comparison of d^{10} and d^0 ions whose $(n-1)$d orbitals were either completely filled or vacant. We expected that d^0 ions with $(n-1)$d orbitals easily accessible for hybridisation would attain CN = 7 more readily than d^{10} ions with distant vacant *n*d orbitals.[8]

The metal ions selected were trivalent gallium, indium, and thallium from Group 13, as well as scandium and yttrium from Group 3. The tropolonate anion, $C_7H_5O_2^-$ − a short-bite bidentate ligand − made it possible for the ions to reach CN > 6.[6] Trioctylphosphane oxide (TOPO) − a very strong electron donor − was an auxiliary neutral monodentate ligand. Practical interest in studying such systems stemmed from the application of indium tropolonates and other α-diketonates for labelling blood cells with radioindium to be used in nuclear medicine,[9] while gallium tro-

[a] Department of Radiochemistry, Institute of Nuclear Chemistry and Technology,
Dorodna 16, 03195 Warsaw, Poland
Fax: (internat.) + 48-22/8111-532
E-mail: jnarbut@orange.ichtj.waw.pl
[b] Chemistry Institute, Pedagogical University,
Al. Armii Krajowej 13/15, 42201 Czestochowa, Poland
E-mail: czerwinski@ichn.ch.pwr.wroc.pl
Supporting Information for this article is available on the WWW under http://www.eurjic.com or from the author.

 © WILEY-VCH Verlag GmbH, 69451 Weinheim, 2001 1434−1948/01/1212−3187 $ 17.50+.50/0

polonate was not effective in this respect.[10] Other reasons for our interest were relativistic properties of thallium and scarcity of data on its mixed-ligand complexes.[1,11,12]

Both quantum chemistry calculations and an experimental technique were used in our studies. Theoretical calculations based on Density-Functional Theory (DFT), particularly suitable for studying metal complexes,[13] were carried out for the chelates and adducts. We obtained information on their structure, energy and charge distribution, and verified our hypothesis on the role of electronic configuration of the ion. The calculated (DFT) energies of adduct formation correlate well with the experimental stability constants of the metal tropolonate − TOPO adducts in solution, determined by solvent extraction, and considered as a measure of the tendency of a metal ion to increase its CN over six.

Computational Details

Density-functional calculations were carried out both on the metal(III) tris(chelates) (CN = 6) and on their 1:1 adducts (CN = 7). To save computer resources, only two tris(-tropolonato)metal(III) structures were optimised, and then the whole system was modelled. In order to reproduce symmetry of chelate rings in tris(chelato)metal(III) complexes, as well as their quasi-aromatic character (in the original complex they are coupled with the seven-membered ring of tropolone) the simple bidentate anionic ligand O−CH=CH−O$^-$ (denoted as αdik)[14] was selected as a model for tropolonate, while trimethylphosphane oxide (denoted as TMPO or B) replaced TOPO. Additionally, to check the reliability of the model with the radical anionic ligand another system was studied consisting of Sc and Y chelates (and their TMPO adducts) with a molecular ligand, O=CH−CH$_2$−O$^-$. All the calculations were based on the DFT method as implemented in the GAUSSIAN-94 program.[15] The Lanl2dz double-ζ basis set,[16] Becke three-parameter functional (B3LYP),[17] and Berny geometry-optimisation algorithm[18] were used. The charge density was obtained from Mulliken overlap and bonding population analysis.[19] The calculations were performed by using relativistic effective core potential, which retained the outer shells (e.g. $5d^{10}6s^26p^1$ shells of the Tl atom) in the valence space, replacing the rest of electrons by relativistic effective potentials. The basis sets for the metals were supplemented with polarisation functions taken from Andzelm et al.[20]

CAS SCF Calculations

In order to evaluate the tendency of the d^0 and d^{10} ions to reach a valence state corresponding to CN = 7, we carried out multi-configurational self-consistent-field calculations with the complete active space self-consistent-field (CAS SCF)[21] approach. Promotion energies, defined as differences between the calculated energies of the ground and excited states, were calculated for single isolated atoms. The active space with seven electrons distributed over eight orbitals was taken for the CAS SCF calculations; this led to 2352 configuration states. The calculations were carried out for the ground state and the two lowest excited states of the atoms, of total multiplicity two. All the numerical calculations were carried out using supercomputers: Cray T3E, Cray J90, and Cray Y-MP.

Results

Geometry Optimisation and Charge Distribution

Firstly the optimisations of geometry of the chelates [ML$_3$] (where L = trop or αdik; Table 1), of a free TMPO molecule, and of their adducts [ML$_3$·TMPO] (Table 2) were performed. The coordination polyhedra of the chelates were D_3-twisted trigonal antiprisms (Figure 1a).

Optimisation of systems consisting of [ML$_3$] and TMPO, starting with the previously optimised structures, resulted in stable [ML$_3$·TMPO] adducts with CN = 7, of significantly distorted structures for Sc, Y, In, and Tl^{III} ions (Figure 1b). The smallest Ga^{III} ion preserved a CN = 6 in the adduct by breaking one of the six Ga−O^L bonds (Table 2).

Formation of the M−O^B bond was accompanied by a charge (electron density) transfer from TMPO to [ML$_3$]. Its magnitude is given by the Δq value (Table 2), which is equal to the total charge on each of the two components in the

Table 1. Optimised geometry of the chelates [M(trop)$_3$] and [M(αdik)$_3$], charge distribution on their atoms and Mulliken bond population (GAUSSIAN 94 with potential B3LYP in the basis Lanl2dz)

	Calculated geometry[a] and charge distribution						Literature data[b]			
	M−O	O−O$_{bite}$	OMO	q_M	q_{OL}	q_{M-OL}	M−O	O−O$_{bite}$	OMO	r_i [c]
Sc(trop)$_3$	210.9	251.5	73.2	1.227	−0.490	0.156	210	252	74	74.5
Sc(αdik)$_3$	213.3	258.9	74.8	1.270	−0.422	0.155				
Y(trop)$_3$	228.1	255.2	68.0	1.347	−0.501	0.147	−	−	−	90
Y(αdik)$_3$	230.9	264.3	69.8	1.404	−0.430	0.160				
Ga(αdik)$_3$	198.9	260.5	81.8	1.205	−0.410	−	196.7	255.8	81.1	62.0
In(αdik)$_3$	213.4	266.4	77.2	1.448	−0.446	0.177	213.4	260.7	75.3	80.0
Tl(αdik)$_3$	231.7	277.9	73.7	1.353	−0.407	0.134	−	−	−	88.5

[a] Distances in pm; the C−O and C−C distances in each [M(trop)$_3$] and [M(αdik)$_3$] are equal to 131.8(1) and 149.1(2), and to 131.7(1) and 142.9(1) pm, respectively; the bite angle, OMO, in deg. [b] Distances [pm] and bite angles [deg] for crystalline tropolonates; ref.[22] [c] Shannon ionic radii for six coordination [pm]; ref.[23]

Table 2. Optimised geometry of the [ML_3·TMPO] adducts, charge distribution on their atoms and Mulliken bond population (GAUSSIAN 94 with potential B3LYP in the basis Lanl2dz)

	Calculated geometry and charge distribution in the adducts[a]									
	Range M−O^L	M−O^B	MOP	q_M	q_{O^L}[b]	q_{O^B}	Δq[c]	q_{M-O^L}[b]	q_{M-O^B}	$q_{P=O}$[d]
Sc(trop)$_3$·B	211.8−227.8	208.0	136.7	1.209	−0.466	−0.795	0.203	−	−	−
Sc(αdik)$_3$·B	213.7−231.5	206.7	138.7	1.245	−0.401	−0.803	0.220	0.159	0.136	0.291
Y(trop)$_3$·B	230.5−241.5	225.4	136.3	1.340	−0.484	−0.795	0.195	−	−	−
Y(αdik)$_3$·B	232.2−244.8	222.7	139.9	1.342	−0.414	−0.802	0.210	0.154	0.140	0.298
Ga(αdik)$_3$·B	190.3−302.3[e]	189.7	−	−	−	−	−	−	−	−
In(αdik)$_3$·B	214.0−241.8	204.6	137.4	1.484	−0.428	−0.855	0.185	0.150	0.160	0.276
Tl(αdik)$_3$·B	234.6−244.3	226.1	132.5	1.383	−0.403	−0.808	0.184	0.119	0.117	0.306

[a] Distances, angles and charges as in Table 1. [b] The average values for six O^L atoms and/or six M−O^L bonds; for the actual values see Supporting Information; [c] The total charge-transfer from TMPO to chelate. [d] $q_{P=O}$ = 0.494 in free TMPO molecule. [e]] Broken Ga−O bond; open chelate ring.

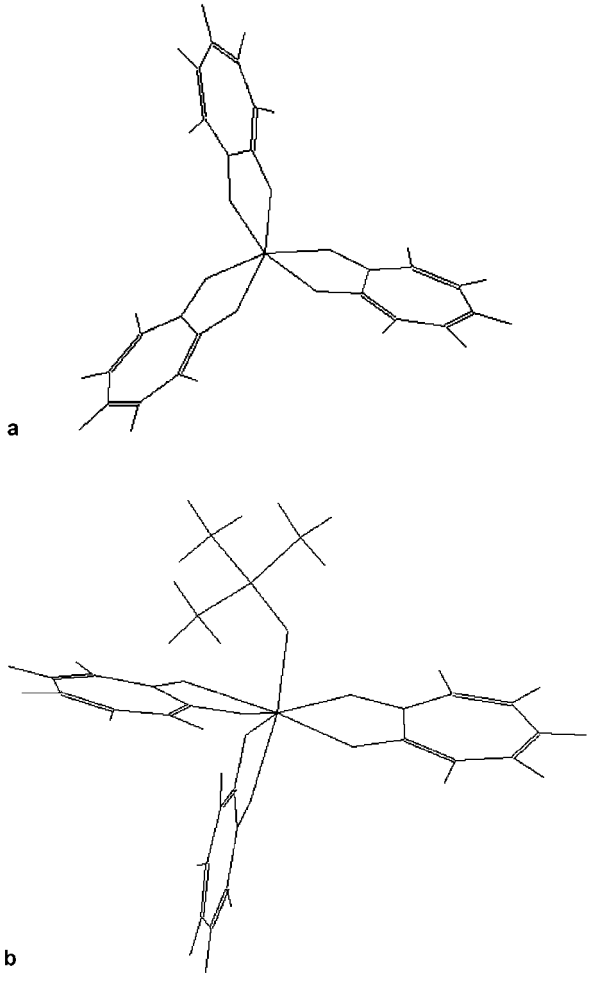

Figure 1. Stick models of the optimised structures: (a) [Sc(trop)$_3$] chelate; (b) [Sc(trop)$_3$·TMPO] adduct

adduct. The dipole moments of the adducts were much greater than that of TMPO alone, and the TMPO molecule in the adduct was strongly polarised. In the Supporting Information the computed coordinates and total charges of all atoms in the Sc, Y, (Ga), In, and Tl^{III} chelates and adducts studied, the dipole moments, and other data are reported.

Energy Calculations

Energies of Chelate Formation and Adduct Formation and Their Components

The respective ΔE_{ch} and ΔE_{ad} values were calculated after full optimisation of all the components, and computing their total energies with the same Lanl2dz basis set. The use of polarisation functions had little effect on the results of the calculations (Table 3, footnote c).

The bond analysis developed by Ziegler and Rauk[24] made possible an insight into the character of metal−ligand interactions in the complexes studied. The energy of adduct formation could be separated into contributions related to the energy of structure distortion, ΔE_d, for both components of the adduct, and the energy of interaction, ΔE_{int}, between the distorted components. In our system, $\Delta E_{d,ch}$ reflects significant changes in the chelate structure upon adduct formation, involving rearrangement of the first coordination sphere of the metal ion, and $\Delta E_{d,B}$ − a slight deformation of the TMPO structure when in the adduct. Further separation of the ΔE_{int} term is also possible into orbital interaction energies (charge transfer) and steric interactions (Pauli repulsion and Coulomb electrostatic terms), the former being the main stabilising factor in some adducts [Equation (1)].[25]

$$\Delta E_{ad} = \Delta E_{d,ch} + \Delta E_{d,B} + \Delta E_{int} \quad (1)$$

The values $\Delta E_{d,ch}$ and $\Delta E_{d,B}$ were calculated (Table 3) as the differences between the total bond energies of the [M(αdik)$_3$] (and TMPO) molecules in their distorted and optimised structures.[26] The ΔE_{int} values were obtained with the use of Equation (1). However, because these values might be in error due to calculating their components with the use of different basis sets, we independently calculated another set of $\Delta E_{int}'$ values, equal to the differences between the total energies of the adduct and of its subunits −

Table 3. Calculated (GAUSSIAN 94 with potential B3LYP in the basis Lanl2dz) formation energies of chelates and adducts [M(αdik)$_3$·TMPO], distortion energies of the chelates and TMPO, and the energy of interaction between the components of the adducts

Chelate	ΔE_{ch}	ΔE_{ad} [a]	$\Delta E_{d,ch}$	$\Delta E_{d,B}$	ΔE_{int}	$\Delta E_{int}'$	E^{σ} [b]	E^{π} [c]
	Formation energies and their components [kJ mol^{-1}]						Orbital energies [a.u.][d]	
Sc(trop)$_3$		−87.5						
Sc(αdik)$_3$	−2328	−95.5	81.0	7.0	−183	−188	−0.4099	−0.2936
Y(trop)$_3$		−93.0						
Y(αdik)$_3$	−1077	−120	59.0	7.0	−186	−183	−0.4135	−0.2943
Ga(αdik)$_3$	−657	[−42][e]	–	–	–	–	–	–
In(αdik)$_3$	−639	−74.2	114	7.7	−196	−196	−0.4132	−0.2904
Tl(αdik)$_3$	−353	−82.6	54.5	7.0	−144	–	−0.4129	−0.2897

[a] The respective ΔE_{ad} values calculated using one (and two) polarisation function(s) are equal to: −70 kJ mol^{-1} for In; −80 kJ mol^{-1} for Tl; −98 (−99) kJ mol^{-1} for Sc; and −123 (−122) kJ mol^{-1} for Y. [b] Energies of bonding molecular orbitals in the adducts; σ-type bonds; the average energies for α and β spins. [c] π-type bonds; the average energies for α and β spins and for five different MOs, including the indium adduct. [d] 1 a.u. = 2262 kJ mol^{-1}. [e] Broken Ga−O bond; open chelate ring.

chelate and TMPO − all in the same structure, optimised for the adduct.[27] The results, except for thallium where the procedure was not convergent, are presented in Table 3. The reasonable agreement between both sets of data makes the ΔE_{int} values convincing.

Promotion Energies

Data were calculated for the metal atoms by using the CAS SCF method. The ground and excited states of each atom are well represented by single determinants (the coefficients of the SCF configurations being greater than 0.8). The ground state was characterised by the $s^2p^3d^2$ configuration, the excited states by $s^2p^2d^3$. High values of ca 330 kJ mol^{-1}, corresponding to the transfer of one electron from the ground-state p orbital to the lowest excited-state d orbital, were obtained for isolated atoms of In and Tl. In contrast, the respective values for the Group 3 atoms were either much lower (ca 100 kJ mol^{-1} for Sc), or even negative (−5 kJ mol^{-1} for Y). In our opinion, the difference between the above data obtained for the d- and p-block metal atoms well characterises the change CN = 6 → CN = 7, which relates to the formation of the 1:1 TOPO adducts by the respective chelates.

Molecular Orbitals

In order to characterise the [ML$_3$]−TMPO bonds by the electron density localised in the bond region, i.e. between the O^B and M atoms (q_{M-O^B} Table 2), the population and the energy of all occupied molecular orbitals (MO) in the adducts were calculated after full optimisation of the structures. To find the original MOs of [M(αdik)$_3$] and TMPO, which contribute to formation of the adduct bond, the respective data including some vacant MOs were also calculated for TMPO and the chelates. All the calculated MOs of the chelates and TMPO (Supporting Information), and of the adducts (Figure 2) were examined with the use of MOLDEN,[28] a program for visualisation. Tables 1 and 2 show M−O bond populations in the chelates and adducts, respectively, and Table 3 shows the average energies of bonding MOs (σ and π) in the adducts.

Solvent Extraction Studies

Solvent extraction is a technique particularly useful for characterising molecular adducts formed in solution by amphiphilic neutral metal chelates and neutral hydrophobic ligands, e.g. TOPO.[6] If a metal ion, M^{m+}, and a bidentate organic ligand in the anionic form, L^-, in aqueous solution combine, the neutral chelate formed, ML_m, may then be transferred to an immiscible organic phase on bringing the solutions into contact. The equilibrium can be described by an extraction constant, where square brackets denote the molar concentrations[29] of the given species, and subscripts "org" and "aq" refer to the organic and aqueous phase, respectively [Equation (2)].

$$K_{ex} = \frac{[ML_m]_{org}[H^+]^m_{aq}}{[M^{m+}]_{aq}[HL]^m_{org}} \quad (2)$$

The transfer can be enhanced by formation (in the organic phase; the subscripts omitted) of molecular adducts [ML_m·iB] where B denotes an auxiliary neutral hydrophobic ligand, e.g. TOPO [Equation (3)].

$$ML_m + iB \rightleftarrows ML_m \cdot iB \quad (3)$$

The stability constants, $\beta_{m,i}$, of the adducts, equal to the equilibrium constants of reactions (3), are expressed in terms of molar concentrations, assuming the solution to be ideal associated. This assumption is reasonable in view of trace concentration of the chelate. The distribution ratio of the metal is given by Equation (4).

$$D = \frac{[ML_m]_{org} + \sum_i [ML_m \cdot iB]_{org}}{[M^{m+}]_{aq} + \sum_j [ML_j^{m-j}]_{aq}} \quad (4)$$

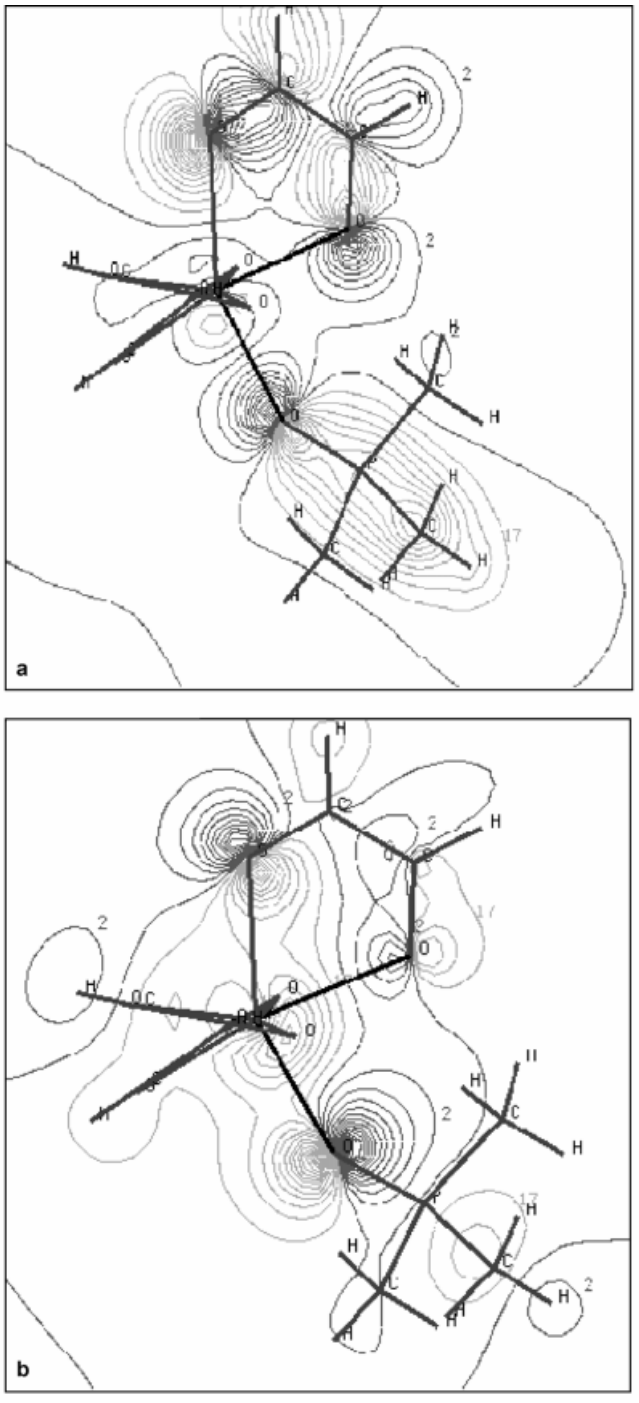

Figure 2. 3D contours of selected bonding molecular orbitals in the [Y(αdik)$_3$·TMPO] adduct: (a) σ symmetry, $E = -0.4006$ a.u.; (b) π symmetry, $E = -0.2874$ a.u.

In the case of two adducts ML_m·B and ML_m·2B predominating in the organic phase Equation (4) can be rearranged to Equation (5), where D_0 denotes the distribution ratio in the absence of TOPO in the system, and [B] − the molar concentration of free TOPO in the organic phase at equilibrium.

Only in the case of gallium, which is extracted from HCl solutions as solvates, $Ga(TOPO)_nCl_3$, D_0 denotes the distribution ratio at the same TOPO concentration, but in the absence of tropolone in the system. In the cases when D was independent of pH and of the concentration of HL (plateau region, when the only form of the metal in the aqueous phase was the uncharged chelate, ML_m), D_0 was equal to partition constant, P, defined as the ratio of molar concentrations of ML_m in both phases. The chelate partition constants were determined directly for Sc and Y, and indirectly for Tl as specified below. The distribution ratio D of thallium(III) has been found to decrease with time. After a fast decrease during the first few minutes, reflecting the transfer of Tl(trop)$_3$ from the organic to the aqueous phase, a further continuous, but rather slow drop in D was observed, with the rate practically constant (the half-time being 13−16 min) in the pH range studied (2.0−4.6). This slow decrease was presumably due to the hydration of the uncharged chelate molecule in the aqueous phase, followed by fast hydrolysis of the hydrated thallium(III) species. The hydration is a first-order reaction, followed by further fast transfer of Tl(trop)$_3$ from the organic to the aqueous phase to sustain the transient equilibrium described with the equilibrium constant $P = [Tl(trop)_3]_{org}\,[Tl(trop)_3]_{aq}^{-1}$. The transfer is thus a first-order reaction as well, and the organic phase concentration of the chelate is (in the interval of the continuous slow drop in D) a function of time (t): $[Tl(trop)_3]_{org} = C^0 \cdot e^{-\lambda t}$, where C^0 is an extrapolated value equal to a hypothetical concentration of the chelate in the organic phase at time zero, assuming the hydration had not started, but the transfer equilibrium had already been established. Provided that the volumes of the organic and aqueous phases are equal to each other, $P = C^0(C_{tot} - C^0)^{-1}$, where C_{tot} denotes the real initial concentration of the chelate in the organic phase. Extrapolation of the experimental $\log[Tl(trop)_3]_{org}$ values to $t = 0$ from the time interval where the dependence was found linear, made it possible for us to evaluate the partition constant for [Tl(trop)$_3$], and the "true" distribution constants when TOPO was present in the system.

$$\frac{D}{D_0} = 1 + \beta_{m,1}[B] + \beta_{m,2}[B]^2 \quad (5)$$

Figure 3 shows the logarithms of the relative distribution ratios, $\log(D/D_0)$ or $\log(D/P)$, of metal tropolonates studied, plotted against the total TOPO concentration (C_B). The solid curves are the best-fit functions (weighted least squares), except for the highest C_B values for Tl and Y. The observed increase in D with increasing TOPO concentration means that the chelates, except for [Ga(trop)$_3$],[30] formed adducts with TOPO. However, because of significant tropolone−TOPO association in the organic phase:

$$HL + B \xrightarrow{K_{as}} HL \cdot B \quad (6)$$

where K_{as} denotes the association constant, $[B] < C_B$ and therefore, to calculate adduct stability constants, we must

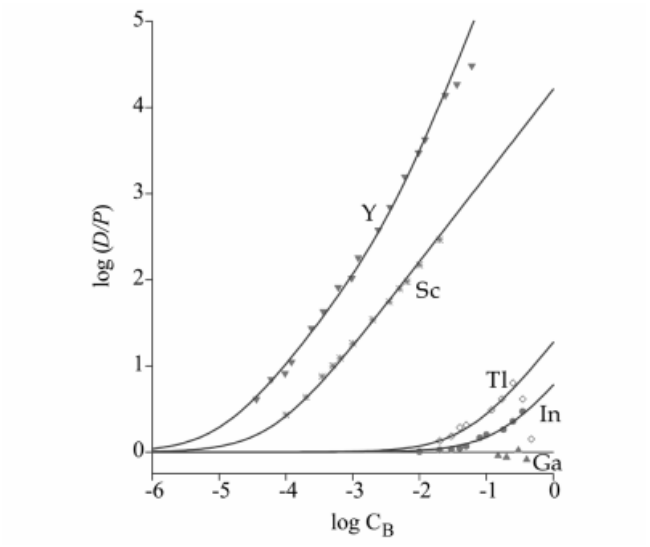

Figure 3. Effect of total molar concentration of TOPO, C_B, on the distribution of tropolonates of gallium, indium, and thallium(III) between carbon tetrachloride and various aqueous phases, and tropolonates of scandium and yttrium between toluene and water at 298.2 K (see Exp. Sect.); in the case of In and Ga, P denotes the distribution ratio, D_0, determined in the absence of either TOPO or tropolone, respectively; the solid lines are the best-fit curves

account for this effect. In contrast, we may neglect a decrease in TOPO concentration due to adduct formation, because of the large excess of TOPO with respect to the metal ions. Thus, the actual [B] values can be calculated[31] as a function of C_{HL}, C_B, K_{as}, and P_{HL}, where C_{HL} denotes the total concentration of tropolone, and P_{HL} – its partition constant (at low experimental pH the dissociation of tropolone in the aqueous phase is negligible). The P_{HL} values were either determined spectrophotometrically (3.9 for the CCl_4/water system), or evaluated (10 for toluene/water). The association constants of the tropolone–TOPO adduct were either determined from the distribution data[32] of tropolone in the solvent–TOPO/water system at pH = 2 (K_{as} = 2.7 ± 0.3 mol^{-1} dm^3 in CCl_4), or estimated based on the former value and on the data of ref.[32] (K_{as} = 5 mol^{-1} dm^3 in toluene).

Equation (5) correctly describes the system when the changes in the concentration of B do not affect the $M^{n+} \rightleftarrows ML_n$ equilibrium, i.e. where $D_0 = P$, which is the case for Sc, Y, and Tl. The decrease in the concentration of free tropolone, [HL], in the experiments with In(trop)$_3$ results (at low pH) in some dissociation of the chelate, accompanied by a decrease in the D values. That is because at sufficiently low pH, when the concentration of any charged chelate, $[ML_j]^{m-j}$, in the aqueous phase is negligible in relation to M^{m+}, the extraction equilibrium can be described with the Equation (7) obtained by the transformation of Equation (2).

$$D = K_{ex}[HL]_{org}^{m}[H^+]_{aq}^{-m} \quad (7)$$

The TOPO–tropolone association decreases the original $[HL]_{org,0}$ value to $[HL]_{org}$, therefore the values $D[HL]_{org}^{-m}[H^+]_{aq}^{m}$ and $D_0[HL]_{org,0}^{-m}[H^+]_{aq,0}^{m}$, are to be substituted for D and D_0, respectively, in Equation (5).[31] With this substitution, and assuming that (1) D and D_0 were measured at the same pH, (2) only one TOPO–tropolone associate (1:1) was formed in the organic phase, and (3) a large excess of HL existed with respect to M^{m+}; we could rearrange Equation (5) to Equation (8).

$$\frac{D}{D_0}\left(\frac{C_{HL}}{C_{HL} - C_B + [B]}\right)^m = 1 + \beta_{m,1}[B] + \beta_{m,2}[B]^2 \quad (8)$$

The stability constants (Table 4) were calculated in this way by putting free TOPO concentrations for [B], and by weighted least-squares fitting, Equation (5) for Sc^{3+}, Y^{3+}, and Tl^{3+} ions; and Equation (8) for In^{3+}.

Discussion

Reliability of the Model

The αdik ligand has 23 valence electrons, but their number on the four atoms (O and C) in the 5-membered chelate ring, 21, is the same as that in the tropolonate ligand which has the even number of all valence electrons. The αdik ligand has a high symmetry in the optimised chelate structure, the same as the tropolonate ligand. Although the optimised structures of [M(αdik)$_3$] and [M(trop)$_3$] chelates (M = Sc, Y) and the charge distribution on their atoms had appeared similar (Table 1), a question arose, as to whether the αdik ligand, a radical, was a reliable model for tropolonate. Additional calculations were thus carried out for scandium and yttrium chelates with another similar ligand, O=CH–CH$_2$–O$^-$ (L′), which has an even number of electrons. However, the optimised 5-membered chelate rings formed by L′ appeared asymmetric, with the M–O$^{L'}$ distances differing by ca. 20% from each other, and also with two different C–O distances. Two hydrogen atoms at one of the carbon atoms were located out-of-plane of the ligand rings. Also some other differences between [ML′$_3$] and [M(trop)$_3$], greater than those between [M(αdik)$_3$] and [M(trop)$_3$], allowed us to conclude that the αdik ligand, although a radical, is a good model for tropolonate, and is better than L′.

Another question concerns the possible inadequacy of the computation method used for thallium, the heavy relativistic metal. In fact, the DFT calculations with the use of pseudo-relativistic potentials can hardly be considered as fully relativistic, and their use for heavy metal compounds may result in, e.g. overestimated metal–ligand distances.[33] At the moment, the quality of the computation method used can be verified indirectly (see below). As long as fully relativistic calculations in such extensive systems are extremely troublesome and time consuming, we have to accept the results obtained.

Table 4. Experimental values of partition constants of metal tropolonates, stability constants of their adducts with TOPO, and Gibbs free energies of the 1:1 adducts formation (25 °C, molar concentration scale; energies in kJ mol^{-1}; the uncertainties are equal to two standard deviations)

Chelate	Solvent	P	log $\beta_{3,1}$ [a]	log $\beta_{3,2}$ [a]	ΔG_{ad} (1:1)
$Sc(trop)_3$ [b]	toluene	0.381 ± 0.007	4.27 ± 0.03	− [c]	−24.4 ± 0.2
$Y(trop)_3$	toluene	0.0020 ± 0.0003	4.99 ± 0.05	7.39 ± 0.08	−28.5 ± 0.3
$Ga(trop)_3$	CCl_4	38 ± 3	no adduct	−	−
$In(trop)_3$	CCl_4	39 ± 3	0.97 ± 0.10	1.86 ± 0.10	−5.5 ± 0.6
$Tl(trop)_3$	CCl_4	6.8 ± 0.7	1.35 ± 0.08	(0.3 ± 5.9)[c]	−7.7 ± 0.4

[a] Calculated using Equation (5) for Sc, Y, and Tl, and Equation (8) for In. [b] The data from ref.[6], corrected for TOPO−tropolone association. [c] The $\beta_{3,2}$ value could not be determined because of either insufficient TOPO concentration in the experiment (Sc) or the antagonistic effect in solvent extraction at higher TOPO concentrations (Tl).

Structures

The optimised distances and angles in $[Sc(trop)_3]$ correspond very well with the experimental data for the crystalline complex (Table 1). A good agreement was also found between the parameters calculated for $[M(\alpha dik)_3]$ chelates (M = Sc, Ga, In) and the experimental data for crystalline tropolonates[22] and other α-diketonates.[34] Because of no experimental data are available for α-diketonates of thallium(III) (and Y), their aqua complexes can be used for comparison. The $Tl^{III}-O$ distance calculated for $[Tl(\alpha dik)_3]$ is greater (by 4%) than the experimental values in octahedral hexahydrates, both in solution and in the solid (221 to 225.5 pm[35]), while the corresponding differences for Sc,[36] Ga, and In[37] (Y forms octahydrates) are smaller, below 2%.

The analysis of the optimised coordination polyhedra in the adducts (CN = 7)[5] shows that TMPO attacks the chelate molecule (CN = 6; D_3) from the side of its open trigonal face. The coordination of the seventh ligand is accompanied by significant rearrangements in the chelate structure (Table 2). To make room for this ligand, the three αdik ligands have to be contracted, turned, and spread apart (Figure 1b), followed by a decrease in their bite angles and an elongation of the $M-O^L$ bonds. The chelate rings are nonsymmetrically deformed, the three $M-O^L$ bonds adjacent to the $M-O^B$ bond being elongated much more than those opposite the bond were. The extent of distortion of chelate molecules depends on the metal ion radius. The smallest distortion has been found for chelates of large Tl^{3+} and Y^{3+}; the angle between two αdik ligands (medians) adjacent to the $M-O^B$ bond increased by ca 15% in relation to the original one (120°) in the chelates. There are three short (290−320 pm) O^B-O^L distances, one intermediate (330−336 pm), and two long (390−450 pm) in the distorted structures (intermediate between C_{3v} and C_{2v}). For the intermediate-size In^{3+} and Sc^{3+}, the angle between the two αdik ligands increased by ca 22%. There are three or four short (280−310 pm) O^B-O^L distances, one or two intermediate (340−365 pm), and one long (ca 415 pm) in the distorted structures (intermediate between C_{2v} and D_{5h}).

According to the calculations, binding of TMPO by the smallest Ga^{3+} ion in $[Ga(\alpha dik)_3]$ is accompanied by breaking one $Ga-O^L$ bond and opening the chelate ring. Such a picture has not been experimentally confirmed for $[Ga(trop)_3]$, but has been confirmed for another, less stable chelate $[Ga(tta)_3]$ (Htta = 2-thenoyltrifluoroacetone), which forms a TOPO adduct.[31] In no case Ga^{3+} increases its CN to seven. The nonexistence of $[Ga(trop)_3]$−TOPO adducts may explain the difference in the ability of tris(tropolonates) of gallium and indium to label blood cells[9,10] by an associative reaction within the cell.

Energies

We expected the energy of $[ML_3]$ formation to be affected by two factors: (1) the charge-to-radius ratio of the metal ion, and (2) the availability of vacant d orbitals of the metal ion for hybridisation to a valence state corresponding to CN = 6. The order of decreasing ΔE_{ch} values calculated for the $[M(\alpha dik)_3]$ chelates, Sc > Y > Ga > In > Tl (Table 3), shows that the d^0 ions form much more stable chelates than d^{10} ions, while the expected decrease in chelate stability with increasing ionic radius can be observed only within each group. Thus, the effect of electron configuration prevails over that of radius.

The calculated ΔE_{ad} values give the following order of adduct stability in the gas phase: In < Tl < Sc < Y. This sequence reproduces the experimental order of Gibbs free energies of adduct formation in solution,[38] $\Delta G_{ad} = -RT \ln \beta_{3,1}$. The differences between the ΔE_{ad} and ΔG_{ad} values result from the differences in the reaction media, temperature (0 and 273.2 K), and above all from the entropy term that contributes to ΔG_{ad} only, and can be large.[39] With all these differences, the correlation between ΔE_{ad} for $[M(\alpha dik)_3]$ and ΔG_{ad} for $[M(trop)_3]$ (Tables 3 and 4) is quite reasonable. Moreover, the differences between the values for the two tropolonates (of yttrium and scandium), $\Delta(\Delta E_{ad}) = -5.5$ kJ mol^{-1} and $\Delta(\Delta G_{ad}) = -4.2$ kJ mol^{-1}, are fairly similar.

The experimental data on the 1:1 and 1:2 TOPO adducts of metal tropolonates (CN = 7 and 8) correspond well with the data on anionic $[M(trop)_4]^-$ complexes;[6,40] more stable for Y and Sc, and less stable for In.[40] Much greater stability of the adducts of the d-block than p-block metal ions betokens the primary importance of electron config-

uration of the metal center. Only further, in each group, is the adduct stability differentiated according to the radii of metal ions. Moreover, the sequences of ΔE_{ad} values are reversed when compared with those of ΔE_{ch}, i.e. the effect of ionic radius on the stability of the adducts (CN = 7) is opposite to that observed for the chelates (CN = 6).[41] This can be explained in terms of differences in distortion energies of the chelates formed by small and large ions of the same charges upon coordination of the seventh ligand. These differences are due to stronger $M-O^L$ bonds and the lesser flexibility of ligands in the chelates of small ions.[6] Greater distortion energies observed for the chelates of small ions (Sc, In) compared to those of large ions (Y, Tl) (Table 3) overcompensate the stronger attraction of the ligand by the small cations.

Character of the M−O Bonds; Hypervalence

Less stable $[ML_3]$ chelates and $[ML_3{\cdot}TMPO]$ adducts of the d^{10} ions do not necessarily imply that the high-lying (cf. the calculated promotion energies) virtual *n*d orbitals of the $(n-1)d^{10}$ ions participate in bonding. General considerations suggest that the use of these distant *n*d orbitals in bonding is unlikely.[42] Molecular orbitals of such a complex with e.g. six ligands can be formed using only four orbitals of the central ion (s and p) and six ligand orbitals. Thus, four bonding and four antibonding MOs are formed, and the two ligand orbitals remain nonbonding. This results in a lowering of the average bond order and a decrease in the electron population in the $M-O^L$ bond region, therefore in less stable hypervalent (or hypercoordinate) complexes.[42] The binding of the seventh ligand to the hypervalent chelate should additionally decrease the electron population of the $M-O^L$ bonds in the adduct by $^1/_7$. This has been observed for In and Tl, where the $M-O^L$ populations in the TMPO adducts are about 14% less than those in the corresponding chelates (Tables 1 and 2), in contrast to the Sc and Y adducts, where the $M-O^L$ populations remain practically the same as those in the chelates. Therefore, we suppose that the adducts formed by In and Tl chelates are also hypercoordinate, with their bonding MOs formed only from the *n*s and *n*p orbitals of the d^{10} ions, with no participation of either filled $(n-1)$d or virtual *n*d orbitals. In contrast, Sc and Y chelates form stronger "normal" adducts with seven bonding MOs in which the vacant $(n-1)$d orbitals of the metal do participate. Indeed, the analysis of charge distribution on the metal ions (q_M in Tables 1 and 2) shows that the d-block ions accept some electron density from TMPO in the adducts, in contrast to the p-block metals that increase their positive charge in the adducts. Also, the analysis of the electron population of basis metal AOs contributing to bonding ($M-O^L$) MOs in the chelates betokens a contribution from the d orbitals of scandium and yttrium, but none from those of indium and thallium. The same has been observed in the case of the adducts ($M-O^B$ bonding). The expansion coefficients of the bonding MOs show that the d orbitals of Sc and Y in the adducts accept practically the whole charge equal to the difference (ca. 0.03 a.u.) between the Δq values calculated for the adducts of d-block and p-block metals (Table 2).

Rather high electron population in the $In-O^L$ bonds (the population on the $Tl-O^L$ bonds is low, as expected) can be explained in terms of incomplete screening from nuclear charge by the filled d^{10} shell, which increases the effective charge on the p-block ion, and also the population of the bonds. This is in line with the high negative $\Delta E_{d,ch}$ and ΔE_{int} values for In (Table 3). The lack of unoccupied $(n-1)$d indium orbitals able to accept the electron density makes the $M-O^L$ charge separation in $[In(\alpha dik)_3]$ the highest (Table 1), i.e. the smallest shift of electron density from the ligands to the metal ion. On the other hand, particularly strong stabilisation of thallium 6s and $6p_{1/2}$ orbitals, due to the presence of filled 4f shell and relativistic effects,[43] should result in a greater shift of electron density from the ligands to these orbitals, which is the reason for the low positive charge on the Tl^{III} ion in the chelate, and for the small electron population of the $Tl-O^L$ bonds.

In all the adducts, the $M-O^B$ bond is significantly shorter than the $M-O^L$ bonds, though this is not reflected in the bond populations (Table 2). A possible reason for shortening the $M-O^B$ bond is its partially π-bond character, as discussed below. Its lower electron population can be due in turn to the lack of charge on the TMPO ligand, whereas the αdik ligands are negatively charged. In any case, the In and Tl adducts studied give us an interesting case of hypervalent bonding strengthened by π-bonding.

Molecular Orbitals

The examination of the system, by means of MOLDEN, shows that there exist sets of lower lying multi-centred bonding MOs of σ symmetry, responsible for the formation of TMPO adducts of yttrium and scandium chelates. In the yttrium adduct, these strongly bonding MOs (ca. −1.0 a.u.) are formed from the MOs of the chelate (−0.957 a.u.) and TMPO (−0.923 a.u.), with the contribution from AOs of the metal (s and p, ca. 25%) and oxygen atoms only. In the scandium adduct, these MOs (ca. −1.3 a.u.) are weakly bonding because they are formed almost entirely from the metal orbitals. The indium and thallium adducts have no bonding MOs in the region of lower energies. The only orbitals in the latter (ca. −0.75 a.u.) are practically pure, occupied AOs (d) of thallium, while there is no contribution from indium AOs in the former.

In all the adducts there are higher lying (ca. −0.41 a.u.) bonding MOs of σ symmetry (Figure 2a). They are more strongly delocalised (apart from mainly the O atoms, they also extend to the C atoms), and are formed with the participation of occupied orbitals of σ symmetry, the HOMO (ca. −0.22 a.u.) of the chelates and the HOMO−2 (−0.3317 a.u.) of TMPO. Unexpectedly, the latter does not describe a lone electron pair on the O^B atom, but the σ-electron pair of the O=P bond. The energy gain is due to redistribution of the electron densities of both MOs over the delocalised orbitals. This rather unusual picture can be explained assuming that (1) the lone electron pairs on the O^B atom participate in another bonding, and (2) the O^B

atom changes its valence state and hybridisation from sp^2 in the free TMPO molecule to sp^3 or rather sp^m in the adduct (*m* is a fractional value smaller than 3). The former assumption is in line with the short O^B-O^L distances. The latter explains why the shift of electron density from the P=O to the $M-O^B$ bond region is large (Table 2). The most important, however, is the observation that the contribution from the metal AOs to these multi-centred bonding MOs in the adducts is quite different for the d- and p-block metals. This contribution is equal to about 7% from the d orbitals of Sc and Y, but none from those of In and Tl, in line with the hypothesis of hypervalent character of their adducts.

The expected additional bonding between TMPO and the chelates has been exemplified by another set of bonding MOs found in each adduct, higher lying (ca. −0.29 a.u.), of symmetry typical for π-type interactions (Figure 2b). These MOs are greatly delocalised; their electron density extends over the whole adduct molecule, in particular the O^B and O^L atoms. These MOs are formed from orbitals of the same symmetry, presumably with the chelate LUMO localised mainly on the O^L atoms (ca. −0.13 a.u.), and the TMPO doubly degenerate HOMO (−0.2336 a.u.) that accommodates two lone electron pairs localised on the TMPO oxygen atom. This π-type interaction between the two lone electron pairs and the αdik ligands enhances the deformation of the adduct molecule and increases the MOP angle to 130−140°, as calculated.

The energies of both σ- and π-type bonding MOs in the adducts (Table 3) are closer to the energies of the original MOs in TMPO, not in the chelates. This is in line with the earlier conclusion (based on Δq values) that the TMPO electrons are mainly responsible for the TMPO − chelate bonding. The moderate asymmetry of this bond together with the results of bond population analysis (Table 2) shows that both the extent of covalence and of the ionic character determine the bond character.

Conclusions

Both density-functional calculations and experimental data show that the coordination number of the central metal ion in the studied neutral chelates with bidentate ligands increases from six to seven (or even eight) upon formation of inner-sphere molecular adducts with a monodentate strong electron-donor ligand. Noteworthy is a good correspondence between the computational and experimental data both in structural parameters of the chelates and in the energies of adduct formation. The method used permits not only the calculation of reasonable values of the energies, but also their separation into contributions related to mutual interactions of electron clouds of both components, and to the structural distortion of the components that accompany adduct formation.

The tendency to increase the CN from 6 to 7 depends strongly on the metal ion, in particular on its radius and electron configuration − the larger the radius, i.e. the larger the space accessible to the seventh donor atom, the smaller the energy required for distortion of the chelate structure, and in consequence the greater the tendency to form adducts. The energy of chelate distortion strongly differentiates the metal ions with respect to adduct stability. If the ion is too small, the chelate does not form adducts at all, as exemplified by gallium tropolonate.

On the other hand, much greater tendency to increase the CN by metal ions of d-block than those of p-block points out the problem of high energy gaps between the *n*s, *n*p, and *n*d orbitals, which is not the case with empty $(n-1)$d orbitals in the d^0 ions. High promotion energy makes it rather unlikely that the distant virtual *n*d orbitals could be used for hybridisation, corresponding to CN = 5 and more. Instead, the assumption on the formation by p-block metal ions of hypervalent compounds, with no participation in bonding of metal d orbitals, satisfactorily explains why the chelates (CN = 6) of d^{10} metal ions and their TOPO adducts (CN = 7 or 8) are less stable than the related compounds of d^0 ions.

The analysis of the molecular orbitals calculated for the adducts and for their components allows the identification of the orbitals contributing to adduct formation, and the description of the bond between the components as having both σ- and π-type character. The σ-type bond is formed with no participation of the lone electron pair on the donor oxygen atom in the TOPO molecule but of another pair already engaged in double bonding, therefore, in order to form the bond, the oxygen atom must change its original hybridisation. The π-type bonds are formed by transferring electron density from the lone electron pairs of the TOPO oxygen atom to the vacant orbitals on the donor oxygen atoms of the bidentate ligands. This additional π-bonding strengthens the bond and stabilises the adduct.

Some unexpected characteristics calculated for the compounds of d^{10} ions, especially of indium, are probably due to the occupancy of the metal $(n-1)$d orbitals, which hinder the transfer of electron density to the metal ions, in contrast to the compounds of d^0 ions. Quite effective transfer of electron density to the thallium(III) ion can be explained in terms of the relativistic properties of this heavy metal.

Experimental Section

General Remarks: Distribution ratios were calculated from direct measurements of specific radioactivity of both phases using an NaI(Tl) well-type detector (^{72}Ga and ^{114m}In), and a Geiger−Müller counter (^{90}Y, ^{204}Tl). The radiotracers were supplied by the Centre for Isotope Production at Swierk, Poland. Tropolone, 1-hydroxycyclohepta-3,5,7-trien-2-one, Htrop (98%, Aldrich), was used as received. TOPO (p.a., Merck) was purified[6] by repeated (up to six times) washing its concentrated stock solutions in heptane or toluene with 5% aqueous sodium carbonate solution and water. Carbon tetrachloride (p.a., POCh Gliwice) was washed and distilled. Toluene (p.a., POCh Gliwice) was used as received. Doubly distilled water was used throughout. Distribution of tropolone between water (pH = 2) and carbon tetrachloride (+ TOPO) was studied by shaking the solutions followed by absorbance measurements of

dilute aqueous solutions of tropolone (original and at equilibrium) in quartz cells at 345 nm at pH = 1. − pH: Orion 720A with a glass-calomel combination electrode calibrated against standard reference buffers. UV/Vis: Beckman DU-68.

Solvent Extraction Procedure: The organic phase was prepared immediately before extraction. After the radiotracer was added to the equilibrated aqueous phase, the pH was adjusted with either H_2SO_4 (Tl: pH = 2.6) or HCl (Ga: 2 mol dm^{-3}; In: pH = 1.5; Y: pH = 4.5) and the system was re-equilibrated. Thallium(I) was previously oxidised in 2 mol dm^{-3} H_2SO_4 with $Na_2S_2O_8$ (10^{-3} mol dm^{-3} Ag^+).[44] The concentration of indium and thallium carriers was kept in the range 10^{-5}−10^{-4} mol dm^{-3}, that of scandium and gallium in the range 10^{-6}−10^{-5} mol dm^{-3}, and ^{90}Y was carrier-free. The initial concentration of tropolone in carbon tetrachloride was either 0.1 mol dm^{-3} (Tl) or 0.01 mol dm^{-3} (Ga and In), and in toluene either 0.01 mol dm^{-3} (Y) or 0.02 mol dm^{-3} (Sc). The phases were shaken for 30 min until the distribution equilibrium was attained, separated, and then the specific activities of aliquots were measured. The loaded (Sc, In) organic phase was contacted again with a freshly pre-equilibrated aqueous phase containing no metal and the procedure was repeated. The *D* values (see Supporting Information) determined in both extraction and back-extraction steps differed from each other by less than 5%.

The partition constant and "true" distribution ratios for Tl(trop)$_3$ were determined in back-extraction experiments with the thallium-loaded organic phase and fresh, no thallium-containing, aqueous phase of pH ≈ 2.6. The phases were continually shaken and the aliquot samples were collected at ca. 5−10 min intervals in the range from 10 to 45 min (see Supporting Information). Partition constants of the other tropolonates have been determined independently in the plateau regions,[6] i.e. $4 < pH < 6$. The data for scandium are taken from our recent paper.[6] The extraction experiments were carried out at 298.2 ± 0.2 K.

Acknowledgments

We thank Professor J. Konarski (Poznan) and Dr. J. Burgess (Leicester) for their critical reading of the manuscript and for valuable comments. The research was supported in part originally by the Polish Committee for Scientific Research (KBN) under grant nr. 3 T09A 016 09 and then by the Institute of Nuclear Chemistry and Technology. The numerical calculations were carried out at the Interdisciplinary Centre for Mathematical and Computational Modelling, Warsaw, and the Poznan Supercomputing & Networking Centre. We acknowledge obtaining access to the computer resources and the kind cooperation of the staff.

[1] S. Musso, G. Anderegg, H. Rüegger, C. W. Schläpfer, V. Gramlich, *Inorg. Chem.* **1995**, *34*, 3329−3338.
[2] [2a] W. O. Koch, J. T. Kaiser, H-J. Krüger, *Chem. Commun.* **1997**, 2237−2238. [2b] R. Meier, M. Boddin, S. Mitzenheim, V. Schmid, T. Schönherr, *J. Inorg. Biochem.* **1998**, *69*, 249−252.
[3] P. Comba, *Coord. Chem. Rev.* **1993**, *123*, 1−48.
[4] R. D. Hancock, A. E. Martell, *Chem. Rev.* **1989**, *89*, 1875−1941.
[5] D. L. Kepert, *Inorganic Stereochemistry*, Springer Verlag, Berlin, **1982**, chapters 1 and 8, pp. 1−6 and 92−111.
[6] J. Narbutt, J. Krejzler, *Inorg. Chim. Acta* **1999**, *286*, 175−180.
[7] T. V. Healy, in *Solvent Extraction Research* (Eds.: A. S. Kertes, Y. Marcus), Wiley-Interscience, **1969**, p. 257−279.
[8] R. J. H. Clark, D. L. Kepert, R. S. Nyholm, J. Lewis, *Nature* **1963**, *199*, 559−562.
[9] R. D. Abeysinghe, B. L. Ellis, R. C. Hider, J. B. Porter, *Eur. J. Nucl. Med.* **1994**, *21*, 1141−1147.
[10] G. Karanikas, M. Rodriguez, S. Granegger, H. Sinzinger, *Appl. Radiat. Isot.* **1999**, *50*, 505−511.
[11] D. G. Tuck, in *Chemistry of Aluminium, Gallium, Indium and Thallium* (Ed.: A. J. Downs), Blackie Academic & Professional, London, **1993**, chapter 8, p. 430−473.
[12] J. Glaser, *Adv. Inorg. Chem.* **1995**, *43*, 1−78.
[13] [13a] R. J. Deeth, *Struct. Bond.* **1995**, *82*, 1−42. [13b] M. Czerwinski, *Int. J. Quantum Chem.* **1999**, *72*, 39−51.
[14] Neither the double bond nor the negative charge was fixed on the ligand; the electron density was distributed on the atoms of the chelate in the course of the optimisation procedure.
[15] M. J. Frisch, G. W. Trucks, H. B. Schlegel, P. M. W. Gill, B. G. Johnson, M. A. Robb, J. R. Cheeseman, T. Keith, G. A. Petersson, J. A. Montgomery, K. Raghavachari, M. A. Al-Laham, V. G. Zakrzewski, J. V. Ortiz, J. B. Foresman, J. Cioslowski, B. B. Stefanov, A. Nanayakkara, M. Challacombe, C. Y. Peng, P. Y. Ayala, W. Chen, M. W. Wong, J. L. Andres, E. S. Replogle, R. Gomperts, R. L. Martin, D. J. Fox, J. S. Binkley, D. J. Defrees, J. Baker, J. P. Stewart, M. Head-Gordon, C. Gonzalez, J. A. Pople, *GAUSSIAN 94*, *Revision D.3*, Gaussian, Inc., Pittsburgh PA, **1995**.
[16] [16a] P. J. Hay, W. R. Wadt, *J. Chem. Phys.* **1985**, *82*, 270, 299. [16b] W. R. Wadt, P. J. Hay, *J. Chem. Phys.* **1985**, *82*, 284.
[17] [17a] A. D. Becke, *J. Chem. Phys.* **1988**, *88*, 52. [17b] C. Lee, W. Yang, R. G. Parr, *Phys. Rev. B* **1988**, *37*, 786. [17c] A. D. Becke, *J. Chem. Phys.* **1993**, *98*, 5648.
[18] H. B. Schlegel, *J. Comp. Chem.* **1982**, *3*, 214.
[19] R. S. Mulliken, *J. Chem. Phys.* **1955**, *23*, 1833, 1841, 2388, 2343.
[20] J. Andzelm, M. Klobukowski, E. Radzio-Andzelm, Y. Saki, H. Tatewaki, in *Gaussian Basis Sets for Molecular Calculations* (Ed.: S. Huzinaga), Elsevier, New York, **1984**, chapter 1.
[21] B. O. Roos, in *Methods of Computational Molecular Physics* (Eds.: G. H. F Dierksen, S. Wilson), Reidel, Dordrecht, The Netherlands, **1979**.
[22] [22a] T. J. Anderson, M. A. Neuman, G. A. Melson, *Inorg. Chem.* **1974**, *13*, 158−163; [22b] F. Nepveu, F. Jasanada, L. Walz, *Inorg. Chim. Acta* **1993**, *211*, 141−147.
[23] R. D. Shannon, *Acta Crystallogr., Sect. A* **1976**, *32*, 751−767.
[24] T. Ziegler, A. Rauk, *Inorg. Chem.* **1979**, *18*, 1558, 1755.
[25] A. Bérces, *Chem. Eur. J.* **1998**, *4*, 1297−1304.
[26] The total energies of the distorted structures were calculated for both components of the same geometry as they had in the adduct with the optimised structure. This means that all the atoms belonging to one of the adduct components were removed, preserving the interatomic distances and angles in the other, and then the energy was calculated for the remaining system of total charge equal to zero. Then the same procedure was repeated for the other component.
[27] The total energies of the adduct components (subunits − chelate and TMPO) were calculated after moving away the subunits (the distance of 600 pm was thought sufficient to neglect the effects of all interactions between the two components − electrostatic, charge transfer etc.) In this new system the M−O^B bond was broken, but the geometry of the subunits was maintained the same as that in the adduct. The total charges (Δq) on all the atoms of the separated subunits were equal to zero, contrary to the case when in the adduct.
[28] G. Shaftenaar, *Molden*, CAOS/CAMM Center Nijmegen, The Netherlands, **1991**.
[29] This concentration extraction constant correctly describes the system, provided the concentrations are low enough and the activity coefficients are close to one.
[30] Under the conditions of the experiment with gallium (2 mol dm^{-3} HCl as the aqueous phase) not only [Ga(trop)$_3$], but also solvated chloride, [$GaCl_3$·3TOPO], was extracted into the organic phase at higher TOPO concentrations. After deducting the contribution from the latter from the *D* values, we obtained

a set of corrected D values for gallium, each very close to D_0 (equal to 0.905) over the whole range of TOPO concentrations studied (Figure 2). This shows that [Ga(trop)$_3$] formed no TOPO adducts.

[31] M. Yamada, S. Suganuma, I. Tanaka, T. Sekine, *Bull. Chem. Soc. Jpn.* **1999**, *72*, 2703−2711.

[32] T. Sekine, T. Saitou, H. Iga, *Bull. Chem. Soc. Jpn.* **1983**, *56*, 700−704.

[33] [33a] P. Schwerdtfeger, G. A. Heath, M. Dolg, M. A. Bennett, *J. Am. Chem. Soc.* **1992**, *114*, 7518; [33b] T. Nakajima, T. Suzumura, K. Hirao, *Chem. Phys. Lett.* **1999**, *304*, 271.

[34] [34a] C. A. Matsuba, W. O. Nelson, S. J. Rettig, C. Orvig, *Inorg. Chem.* **1988**, *27*, 3935 −3939; [34b] W. O. Nelson, S. J. Rettig, C. Orvig, *Inorg. Chem.* **1989**, *28*, 3153−3157.

[35] [35a] J. Glaser, G. Johansson, *Acta Chem. Scand., Ser. A* **1981**, *35*, 639−644; [35b] J. Blixt, J. Glaser, J. Mink, I. Persson, P. Persson, M. Sandström, *J. Am. Chem. Soc.* **1995**, *117*, 5089−5104.

[36] P. Lindqvist-Reis, L. Eriksson, I. Persson, M. Sandström, unpublished data.

[37] P. Lindqvist-Reis, A. Munoz-Páez, S. Díaz-Moreno, S. Pattanaik, I. Persson, M. Sandström, *Inorg. Chem.* **1998**, *37*, 6675−6683.

[38] The differences in log$\beta_{3,1}$ caused by the use of either toluene (when studying Sc and Y chelates) or CCl_4 (In and Tl chelates) may be neglected because the expected corrections are probably less than 0.2 unit (see ref.[32]).

[39] Y. Takazawa, H. Itabashi, H. Kawamoto, *Anal. Sci.* **1999**, *15*, 83−86.

[40] E. L. Muetterties, C. M. Wright, *J. Am. Chem. Soc.* **1965**, *87*, 4706−4717.

[41] This inverse relationship between the stability of the chelates (CN = 6) and of their adducts (CN = 7) is in line with the general empirical rule "the stronger chelate the weaker its adduct", well known in solvent extraction (ref.[7]).

[42] [42a] A. E. Reed, P. v. R. Schleyer, *J. Am. Chem. Soc.* **1990**, *112*, 1434; [42b] Kin-ya Akiba, in *Chemistry of Hypervalent Compounds* (Ed.: Kin-ya Akiba), Wiley-VCH, New York, **1999**, chapters 1 and 2, p. 1−47.

[43] P. Pyykkö, *Chem. Rev.* **1988**, *88*, 563−594.

[44] A. I. Busev, V. G. Tipcova, *Zh. Anal. Khim.* **1958**, *13*, 180−185.

Received November 21, 2000
[I00441]